Available online at www.sciencedirect.com
SCIENCE DIRECT®
Polyhedron 23 (2004) 1–4
POLYHEDRON
www.elsevier.com/locate/poly

X-ray structure and ^{77}Se, ^{31}P and ^{13}C MAS NMR of the dinuclear complex 1,2-*bis*(selenourea)-1\κSe, 2\κSe-1,2-*bis*(trimethylphosphine)digold(I) chloride

Mohammed. Fettouhi *, Mohamed I. M. Wazeer *, Saeed Ahmad, Anvarhusein A. Isab *

Department of Chemistry, King Fahd University of Petroleum and Minerals, P.O. Box 1703, Dhahran 31261, Saudi Arabia

Received 20 May 2003; accepted 14 July 2003

Abstract

The single crystal X-ray structure of the compound $[(Me_3P\text{-}Au\text{-}Selenourea)_2^{2+}\ 2Cl^-]$ has been determined. The $[Me_3P\text{-}Au\text{-}(selenourea)]$ units are dimerized and adopt a binuclear structure characterized by a metal–metal interaction (Au–Au:3.0386(5) Å) and a torsion angle of 69.71(2)°. Hydrogen bonding takes place between the selenourea ligands and the chloride ions. The principal components of the ^{77}Se, ^{31}P and ^{13}C shielding tensors were determined from solid-state NMR data.
© 2003 Elsevier Ltd. All rights reserved.

Keywords: Crystal structure; Gold complex; Selenourea; MAS NMR

1. Introduction

There has been a considerable recent interest in the study of gold(I) phosphine complexes of the type R_3PAuL, because of the successful use of auranofin for the treatment of rheumatoid arthritis [1,2]. In addition, auranofin and a number of gold(I) complexes of Ph_3P have been reported to have anticancer activity [3,4]. We have been investigating the coordination chemistry of >C=S and >C=Se ligands with d^{10} metal ions in an attempt to examine their mode of binding and to study their physical properties. In this regard, we have recently reported the characterization of several R_3PAuTu complexes (Tu, thiourea) [5]. Numerous studies have shown, that heavy metal toxicity is lower in the case of selenium based gold drugs and understanding the structure of such complexes will help in the characterization of their biochemical mechanism [6]. In this context and since the crystallographic data related to Au–selenourea complexes are relatively scarce [7], we have undertaken the X-ray structure determination, as well as the solid state NMR characterization of the title compound $[(Me_3P\text{-}Au\text{-}SeU)_2^{2+}\ 2Cl^-]$ (where SeU = selenourea). We report herein its X-ray crystal structure and the results of the ^{77}Se, ^{31}P and ^{13}C solid state NMR investigations.

2. Experimental

Selenourea (Seu) MeOD, Me_2S and all solvents were obtained from Fluka-Aldrich Chemical Co., Germany. $HAuCl_4 \cdot 3H_2O$ and trimethylphosphine were obtained from Strem Chemical Co., USA.

2.1. Synthesis of the complex

The title compound was prepared as reported earlier [8]. Single crystals suitable for X-ray diffraction analysis were grown from an acetonitrile solution.

2.2. X-ray data collection and structure determination

A colorless octahedral crystal of the complex $[(Me_3P\text{-}Au\text{-}SeU)_2^{2+}\ 2Cl^-]$ was mounted on a glass fiber.

* Corresponding authors. Tel.: +966-3-860-2941; fax: +966-3-860-4277.
E-mail addresses: fettouhi@kfupm.edu.sa (M. Fettouhi), miwazeer@kfupm.edu.sa (M.I.M. Wazeer), aisab@kfupm.edu.sa (A.A. Isab).

0277-5387/$ - see front matter © 2003 Elsevier Ltd. All rights reserved.
doi:10.1016/j.poly.2003.07.014

Diffraction data were recorded at 24 °C, on a Bruker-Axs Smart Apex system equipped with graphite monochromatized Mo Kα radiation ($\lambda = 0.71073$ Å). The data were collected using SMART [9]. The data integration was performed using SAINT [10]. An empirical absorption correction was carried out using SADABS [11]. The structure was solved with direct methods and refined by full matrix least square methods based on F^2, using the structure determination and graphics package SHELXTL [12], based on SHELX 97 [13]. Hydrogen atoms were included at calculated positions using a riding model. For the NH_2 groups, sp^2 hybridization was assumed for the nitrogen atoms. Crystallographic data are given in Table 1. Selected bond lengths and angles are given in Table 2. The ORTEP atomic labelling scheme is given in Fig. 1.

2.3. Solid state NMR

Natural abundance ^{13}C solid state NMR spectra were obtained on a JEOL LAMBDA 500 spectrometer operating at 125.65 MHz (11.74 T), at an ambient temperature of 25 °C. Samples were packed into 6 mm zirconium oxide rotors. Cross polarization and high power decoupling were employed. A pulse delay of 7.0 s and a contact time of 5.0 ms were used in the CPMAS experiments. The magic angle spinning rates were from 2000 to 5000 Hz. Carbon chemical shifts were referenced to TMS by setting the high frequency isotropic peak of solid adamantane to 38.56 ppm. Solid state cross-polarization magic-angle spinning (CP/MAS) $^{31}P\{^1H\}$ NMR spectra were obtained at ambient temperature on the same spectrometer, operating at a frequency of 202.35 MHz. A contact time of 3 ms was used with a proton pulse width of 6 μs, with a recycle delay of 10 s. Approximately 500 FID's were collected and transformed with a line broadening of 50 Hz. Chemical shifts were referenced using an external sample of solid PPh_3

Table 1
Crystallographic data for $[(Me_3P\text{-}Au\text{-}SeU)_2^{2+}\ 2Cl^-]$

Formula	$(C_8H_{26}Au_2N_4P_2Se_2)^{2+}\ 2Cl^-$
Formula weight	863.02
Crystal system	tetragonal
Space group	$P\bar{4}2_1c$
Temperature (K)	297
λ (Å)	0.71073
ρ_{calc} (g cm^{-3})	2.650
μ (mm^{-1})	17.308
$F(000)$	1568
a (Å)	10.7588(6)
c (Å)	18.6845(14)
V (Å^3)	2162.8(2)
Z	4
θ Range (°)	2.18–28.29
Index ranges	$-11 \leqslant h \leqslant 13,\ -14 \leqslant k \leqslant 11,$ $-24 \leqslant l \leqslant 23$
$N_{collect}$	13268
N_{indep}	2648
N_{obs}	2403 ($I_{obs} > 2\sigma(I)$)
$R(I_{obs} > 2\sigma(I))$	0.0235
wR_2	0.0495
S	1.003
$(\Delta/\sigma)_{max}$	0.001
ρ_{max} (e Å^{-3})	0.853
ρ_{min} (e Å^{-3})	−1.014

Table 2
Selected bond lengths (Å) and bond angles (°) for $[(Me_3P\text{-}Au\text{-}SeU)_2^{2+}\ 2Cl^-]$

Bond distances	
Au1–P1	2.2648(16)
Au1–Se1	2.4360(6)
Au1–Au1[a]	3.0386(5)
Se1–C1	1.881(6)
P1–C4	1.795(6)
P1–C2	1.799(7)
P1–C3	1.807(6)
C1–N2	1.314(7)
C1–N1	1.319(7)
Bond angles	
P1–Au1–Se1	175.06(4)
P1–Au1–Au1[a]	97.49(4)
Se1–Au1–Au1[a]	86.622(17)
C1–Se1–Au1	100.34(17)
C4–P1–C2	102.9(4)
C4–P1–C3	106.2(4)
C2–P1–C3	105.5(3)
C4–P1–Au1	113.9(2)
C2–P1–Au1	112.8(3)
C3–P1–Au1	114.6(3)
N2–C1–N1	118.7(5)
N2–C1–Se1	123.4(4)
N1–C1–Se1	117.9(4)

[a] Symmetry operation $(-x+2, -y+2, z)$.

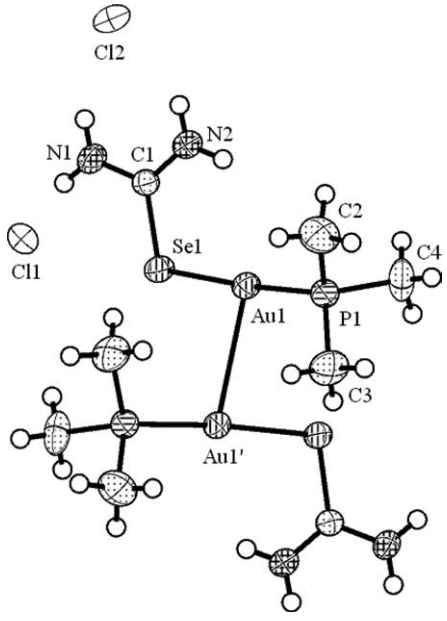

Fig. 1. Structure of $[(Me_3P\text{-}Au\text{-}SeU)_2^{2+}\ 2Cl^-]$, showing the numbering scheme. Displacement ellipsoids are drawn at the 50% probability level. Atoms of the second half have the symmetry $(-x+2, -y+2, z)$.

($\delta = -8.40$ ppm from 85% H_3PO_4). The CPMAS ^{77}Se spectrum of [$(Me_3P\text{-}Au\text{-}SeU)_2^{2+}$ $2Cl^-$] was obtained on the same instrument operating at a frequency of 95.35 MHz. A contact time of 5 ms with proton pulse width of 6.0 μs and a recycle delay of 12 s were used. The sample was spun at 3 and 5 kHz at the magic angle, to determine the isotropic peak. Approximately 5000 scans were employed. ^{77}Se chemical shifts are referenced using an external ammonium selenate sample by setting its isotropic peak to 1040.2 ppm [14], relative to liquid Me_2Se at 23 °C. The CPMAS spectra (selenone carbons, ^{31}P and ^{77}Se) containing spinning side-band manifolds were analyzed using a program based on Maricq and Waugh [15] and developed by Durham University, U K using an iterative method.

3. Results and discussion

3.1. X-ray structure of [$(Me_3P\text{-}Au\text{-}SeU)_2^{2+}$ $2Cl^-$]

The crystal structure of the compound is depicted in Fig. 1. Selected bond distances and bond angles are given in Table 2. The compound crystallizes in a tetragonal unit cell and a non-centrosymmetric space group $P\bar{4}2_1c$. The asymmetric unit contains one [Me_3P-Au-SeU] moiety that dimerizes and adopts a binuclear structure characterized by a metal–metal interaction (Au–Au:3.0386(5) Å). The metal–metal weak bond distance is within the range found in other binuclear species [16–19]. The dimer is located on a twofold axis, hence generating symmetrical [Me_3P-Au-SeU] units with a torsion angle of 69.71(2)°, calculated as the dihedral angle between the (Au1′, Au1, P1, Se1) and (Au1, Au1′, P1′, Se1′) least square mean planes. The coordination at the gold atom deviates from the perfect linearity (P1–Au1–Se1:175.06(4)°) and the Au–P bond distance (2.2648(16) Å) is within the range found in related compounds [7] while the Au1–Se1 bond length (2.4360(6) Å) is significantly longer than the one observed in the mononuclear triphenylphosphine complex (2.412(2) Å) [7]. The Au–P–C and the C–P–C bond angles range from 112.8(3)° to 114.6(3)° and 102.9(4)° to 106.2(4)°, respectively. The absence of a bridging ligand imposing such a metal–metal interaction [7,20], the bending of the P–Au–Se unit and the lengthening of the Au–Se bond suggest the occurrence of a significant dimerization through a metal–metal interaction as found in other complexes [17]. In this case, the dimerization is not hindered by the steric effect of the ligand. However, such a steric hindrance takes place significantly in the monomeric triphenyl phosphine gold complex [7], preventing the gold atoms from coming into bonding range in the absence of a bridging ligand. The two Cl^- ions of the asymmetric unit, lying on two C2 axes, respectively, have nonbonding contacts with the two nitrogen atoms of the selenourea ligands. The N Cl^- distances are in the range of 3.306–3.333 Å, suggesting hydrogen bonding.

3.2. MAS NMR studies

The room temperature ^{77}Se CPMAS spectrum of the complex is shown in Fig. 2. The spectrum shows a set of spinning side-bands arising from the large shielding anisotropy. The selenium is considered as an isolated nucleus, the interaction with ^{13}C at natural abundance is below the detection limit. With a line broadening of 50 Hz, we were unable to resolve the two bond P–Se coupling ($^2J_{P\text{–}Se}$). Hence we could not perform spinning side-band analysis to obtain tensor parameters corresponding to the two spin states of phosphorus, which would yield the sum and difference of the shielding tensor and dipolar tensor. We assume that ^{77}Se chemical shift anisotropy is substantially greater, than the dipolar coupling constant over the P–Se distance of 4.7 Å. Moreover at the rotor speed of 4.5 kHz, we were, most probably, spinning out the dipolar coupling. The fact that we were able to get a good fit for the ^{77}Se spinning side-band manifold intensities with the calculated intensities justifies the above assumption.

The principal components of the ^{77}Se, ^{31}P and ^{13}C (selenone carbon) chemical shift tensors σ_{ii} were calculated from spinning side-band intensities employing an iterative computer program. Nuclear magnetic shielding tensors of selenourea and the complex [$(Me_3P\text{-}Au\text{-}SeU)_2^{2+}$ $2Cl^-$] are shown in Table 3, along with the span, which is the breadth of the chemical shift tensor and the skew, which describes the shape of the powder pattern [21]. The ^{13}C and ^{31}P chemical shift tensors are believed to have an error of ± 1 ppm and that of ^{77}Se is ± 4 ppm. It is known [22], that span reflects the distortion of molecular structure from ideal tetrahedral, while the skew parameter reflects the asymmetry of the electron density distribution about the atom.

It is seen that the ^{77}Se isotropic shift moves 25 ppm downfield whereas ^{13}C isotropic shift moves 4.4 ppm upfield upon complexation. However, when tensor components are considered, a large downfield shift of 98 ppm

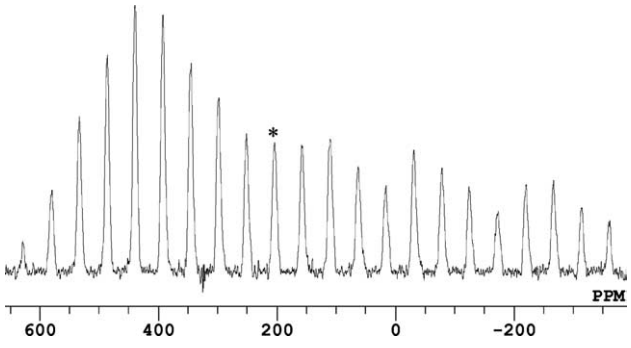

Fig. 2. Room temperature ^{77}Se CPMAS spectrum of [$(Me_3P\text{-}Au\text{-}SeU)_2^{2+}$ $2Cl^-$]. * Denotes the isotropic peak.

Table 3
Nuclear Magnetic Shielding tensors[a] of selenourea and $[(Me_3P\text{-}Au\text{-}SeU)_2^{2+}\ 2Cl^-]$

Compound	Nucleus	δ_{iso}[b]	σ_{11}	σ_{22}	σ_{33}	Ω[c]	κ[d]
SeU	^{13}C	175.1	−255	−203	−67	188	0.45
SeU[e]	^{77}Se	180.4	−300	−230	+529	829	0.83
Complex	^{13}C	170.7	−256	−196	−59	197	0.39
Complex	^{77}Se	205.2	−578	−394	+361	939	0.60
Complex	^{31}P	+7.3	−17.6	−13.8	+9.5	27.1	0.72

[a] Given in ppm, except for κ, which is dimensionless.
[b] δ_{iso} is obtained from the isotropic peak of an MAS sample.
[c] Span $\Omega = \sigma_{33} - \sigma_{11}$.
[d] Skew $\kappa = 3(\sigma_i - \sigma_{22})/\Omega$.
[e] From [1], δ_{iso} is the weighted average position of the 5 different crystallographic sites.

is observed for the ^{77}Se shielding tensor σ_{11}, while 16 ppm upfield shift and 12 ppm downfield shift were observed for the shielding tensors σ_{22} and σ_{33}, respectively on complexation of selenourea. The greater paramagnetic contribution, due to possible π bonding between Se and Au, is leading to lesser shielding along the Se–Au axis. Hence the molecular axis containing the Au–Se bond can be associated with the principal value of σ_{11} of the ^{77}Se chemical shift tensor. The symmetry around Se in the SeU ligand decreases upon complexation and this is borne out by the decrease in the skew parameter.

Studies on the chemical shift tensors of carbonyl carbons have shown [23], that the principal axes of the tensor σ_{33} is perpendicular to the carbonyl sp^2 plane and the principal axes associated with σ_{22} and σ_{11} components are ca. 10° and 80° off the C═O bond, respectively. For the selenone carbon, we observe a very small change in the σ_{11} component, whereas both σ_{22} and σ_{33} components are deshielded by ca. 7 ppm upon complexation. So it is plausible, that there exists a parallel between chemical shift tensor directions and molecular geometry in selenone compounds and the carbonyl system. The ^{31}P shielding tensor span, Ω, is rather small in comparison to that in four coordinate systems [24]. The skew value of 0.72 shows the ^{31}P chemical shift tensor has a near tetrahedral shape.

4. Supplementary material

Crystallographic data, tables of atomic coordinates, thermal parameters, bond lengths and bond angles have been deposited with the Cambridge Crystallographic Data Centre, CCDC, with the deposition No. 205930. Copies of this information may be obtained free of charge from the Director, CCDC, 12 Union Road, Cambridge CB2 1EZ, UK (fax: +44 1223 336 033; email: deposit@ccdc.cam.ac.uk or http://www.ccdc.cam.ac.uk).

Acknowledgements

We gratefully acknowledge King Fahd University of Petroleum and Minerals, Dhahran, Saudi Arabia for the financial support to acquire our new Buker-axs Smart Apex X-ray diffraction system and also to the Research Committee for providing funds under the project No. CY/NMRSTUDIES/214.

References

[1] C.F. Shaw III, Chem. Rev. 99 (1999) 2589.
[2] S.L. Best, P.J. Sadler, Gold Bull. 29 (1996) 2987.
[3] C.K. Mirabelli, R.K. Johnson, C.M. Sung, L. Faucette, K. Muirhead, S.T. Crooke, Cancer Res. 45 (1985) 32.
[4] P.J. Sadler, M. Nasr, V.L. Narayanan, in: M.P. Hacker, E.B. Douple, I.H. Kirakhoff (Eds.), Platinum Coordination Complexes in Cancer Chemotherapy, Martinus Nijhoff, Boston, MA, 1984, p. 290.
[5] A.A. Isab, M.B. Fettouhi, Saeed Ahmad, L. Ouahab, Polyhedron 22 (2003) 1349.
[6] R.F. Stockel, E. Dumas, Gold Bull. 21 (1988) 1.
[7] P.G. Jones, C. Thone, Chem. Ber 124 (1991) 2725.
[8] S. Ahmad, A.A. Isab, Transition Met. Chem. 28 (2003) 540.
[9] SMART APEX software (5.05) for SMART APEX detector, Bruker Axs Inc. Madison. WI.
[10] SAINT software (5.0) for SMART APEX detector, Bruker Axs Inc. Madison. WI.
[11] SADABS program for absorption correction for SMART APEX detector, Bruker Axs Inc. Madison. WI, based on R. Blessing, Acta. Cryst. A, 51 (1995) 33.
[12] SHELXTL NT (5.10) structure determination and molecular graphics package, Bruker Axs Inc. Madison. WI.
[13] G.M. Sheldrick, (1997) University of Gottingen, Germany.
[14] M.J. Collins, C.I. Ratcliffe, J.A. Ripmeester, J. Magn. Reson 68 (1986) 172.
[15] M. Maricq, J. Waugh, J. Chem. Soc. 70 (1979) 3300.
[16] F.B. Stocker, D. Britton, Acta. Cryst. C 56 (2000) 798.
[17] S. Ahrland, K. Dreisch, B. Noren, A. Oskarsson, Acta. Chem. Scan. A 41 (1987) 173.
[18] S. Friedrichs, P.G. Jones, Acta. Cryst. C 55 (1999) 1625.
[19] M.S. Hussain, A.R. Al-Arfaj, M.N. Akhtar, A.A. Isab, Polyhedron 15 (1996) 2781.
[20] A.A. Mohamed, J.A. Krause Bauer, A.E. Bruce, M.R.M. Bruce, Acta. Cryst. C 59 (2003) m84.
[21] J. Mason, Solid State Nucl. Magn. Reson. 2 (1993) 285.
[22] M.J. Potrzebowski, J. Blaszcyk, M.W. Wieczrek, J. Klinowski, J. Phys. Chem. A 101 (1997) 8077.
[23] T.G. Oas, C.J. Hartzell, T.J. McMahon, G.P. Drobny, F.W. Dahlquist, J. Am. Chem. Soc. 109 (1987) 5956.
[24] R.K. Harris, I.J. McNaught, P. Reams, K.J. Packer, Magn. Reson. Chem. 29 (1991) S60.

Available online at www.sciencedirect.com
SCIENCE DIRECT®
Polyhedron 23 (2004) 5–14
POLYHEDRON
www.elsevier.com/locate/poly

Synthesis and spectroscopic characterization of new cobalt(III) complexes with 5-methyl-3-formyl pyrazole 3-hexamethyleneiminyl thiosemicarbazone (HMPz3Hex): X-ray crystallographic identification of HMPz3Hex and $[Co(MPz3Hex)_2]Br \cdot H_2O$ with evidence for unusual rotation about the azomethine double bond of the ligand on complexation with cobalt(III)

Dhiman Kumar Sau [a], Ray J. Butcher [b], Siddhartha Chaudhuri [c], Nityananda Saha [a,*]

[a] *Department of Chemistry, University of Calcutta, 92 A.P.C. Road, Kolkata 700009, India*
[b] *Department of Chemistry, Howard University, 2400 Sixth Street N.W, Washington, DC 20059, USA*
[c] *RSIC, Bose Institute, Kolkata 700009, India*

Received 22 May 2003; accepted 14 August 2003

Abstract

The coordinating properties of the title ligand, 5-methyl-3-formyl pyrazole 3-hexamethyleneiminyl thiosemicarbazone (HMPz3Hex), synthesized and characterized (elemental analysis, MS, IR, ^1H and ^{13}C NMR and X-ray crystallography) for the first time, are reported by solid-state isolation of cobalt(III) complexes, $[Co(MPz3Hex)_2]X \cdot nH_2O$ ($X = Cl$, Br, NO_3, ClO_4 or BF_4; $n = 1$ to 2). The reported complex species have been spectroscopically characterized with X-ray structural identification of $[Co(MPz3Hex)_2]Br \cdot H_2O$. IR and NMR data ($^1H$ and ^{13}C) for the free ligand and its Co^{III} complexes confirm that the ligand, HMPz3Hex, behaves as a uninegative anion with NNS tridentate function via the pyrazolyl *tert*-nitrogen, azomethine nitrogen and thiol sulfur. Electronic spectral data recommend a distorted octahedral environment for the six-coordinate Co^{III} species. X-ray crystallography of $[Co(MPz3Hex)_2]Br \cdot H_2O$ ($C2/c$, monoclinic), has shown unambiguously that the crystallographic asymmetric unit consists of a $[Co(MPz3Hex)_2]^+$ cation and one Br^- anion with one H_2O molecule as solvent of crystallization. The two NNS ligands coordinate orthogonally to the central Co^{III} ion with *mer*-configuration. A critical scrutiny of the X-ray data of free HMPz3Hex ($Pna2_1$, orthorhombic) and $[Co(MPz3Hex)_2]Br \cdot H_2O$ indicates that an unusual rotation about the azomethine (C=N) double bond occurs during complexation with Co^{III}. A plausible reaction mechanism for the same has been proposed. Sulfur is involved in a C(7)–H(7)···S(1) intramolecular contact restricting the conformation of the ligand both in free and its complexed form.
© 2003 Elsevier Ltd. All rights reserved.

Keywords: Synthesis; Spectroscopy; Pyrazolyl thiosemicarbazone; Cobalt(III) complexes; X-ray crystallography

1. Introduction

The well-documented biological activities of heterocyclic N(4)-substituted thiosemicarbazones have prompted further investigation on the coordination chemistry of such ligands during the past several years [1–3], with the recommendation that structural variation of the N(4)-substituent on the thiosemicarbazone (tsc)

* Corresponding author. Present address: University of Kalyani, Kalyani 741235, WB, India. Tel.: +91-033-2350-8386; fax: +91-033-2582-8282.
E-mail addresses: nsaha2@yahoo.com, n.saha@cucc.ernet.in (N. Saha).

0277-5387/$ - see front matter © 2003 Elsevier Ltd. All rights reserved.
doi:10.1016/j.poly.2003.09.007

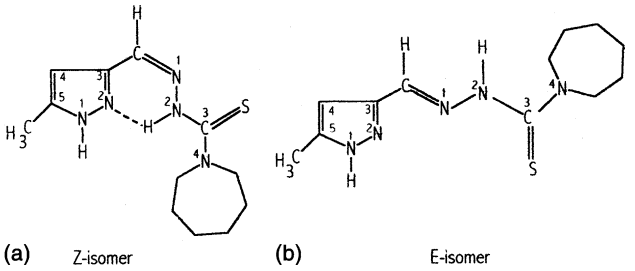

Fig. 1. Methyl-3-formyl pyrazole 3-hexamethyleneiminyl thiosemicarbazone (HMPz3Hex).

moiety as well as modification of the heterocyclic ring might bring out significant enhancement of the biological properties of such new metal ion complexes, often with novel structural information. As a part of our comprehensive efforts [4–12] towards synthesis and structural characterization of new materials containing bio-relevant pyrazolyl thiosemicarbazones, the present paper reports the synthesis, spectroscopic and structural properties of new cobalt(III) complexes with 5-methyl-3-formyl pyrazole 3-hexamethyleneiminyl thiosemicarbazone (HMPz3Hex) (Fig. 1) with X-ray crystallographic identification of the free ligand, HMPz3Hex, and a representative Co(III) species $[Co(MPz3Hex)_2]Br \cdot H_2O$.

2. Experimental

2.1. Preparation of 5-methyl-3-formyl pyrazole 3-hexamethyleneiminyl thiosemicarbazone

All chemicals of AR grade were used without further purification. The title ligand, HMPz3Hex, was synthesized for the first time in our laboratory by a similar, but appropriately modified method [4], followed by final *trans*amination [15,16] of *S*-methyl dithiocarbazate of 5-methyl-3-formyl pyrazole (HMPzSMe) (2.14 g, 10 mmol) with hexamethyleneimine (Fluka) (0.99 g, 10 mmol) in EtOH (30 cm^3) at water bath temperature. The white crystalline product was filtered off and dried over fused $CaCl_2$. The compound (Yield: 2.0 g, 75%) melts at 204 °C (from EtOH) (Found: C, 54.4; H, 7.2; N, 26.3%. Calc. for $C_{12}H_{19}N_5S$: C, 54.3; H, 7.2; N, 26.4%). EIMS: m/z 265 (M^+, 65%).

2.2. Preparation of cobalt(III) complexes: $[Co(MPz3Hex)_2]X \cdot nH_2O$ ($X = Cl$, Br, NO_3, ClO_4 or BF_4; $n = 1$ to 2)

To the title ligand (0.530 g; 2 mmol) dissolved in 1:1 EtOH–MeOH (40 cm^3), an EtOH (20 cm^3) solution of the corresponding hydrated cobalt(II) salt (1 mmol) was added dropwise under hot condition (ca. 40–50 °C). The resulting wine red mixture (pH ≅ 4.0) was boiled under reflux over a water bath for 1.5 h. The coloured solution, upon slow evaporation at RT (~30 °C), yielded a nearly brown crystalline cobalt(III) complex in each case. The complex was filtered off, washed with 1:1 MeOH–EtOH and dried over fused $CaCl_2$ at room temperature. Yield: 60–70%.

2.2.1. Preparation of $[Co(MPz3Hex)_2]Br \cdot H_2O$

The same procedure, as outlined above, was adopted for the preparation and isolation of reddish brown crystals of the desired the cobalt(III) complex (yield: 0.48 g, 70%) using the $CoBr_2 \cdot 6H_2O$ (0.327 g, 1 mmol); X-ray quality crystals of this complex were successfully grown from EtOH–MeOH mixture (1:1) on slow evaporation at room temperature (~303 K).

2.3. Physical measurements

Elemental analyses (C, H and N) using a Perkin–Elmer CHNS/O analyzer 2400 and magnetic measurements in the polycrystalline state in a PAR 155 sample vibrating magnetometer were carried out at the Indian Association for the Cultivation of Science (IACS), Kolkata. The cobalt contents of the complexes were determined gravimetrically as anhydrous $CoSO_4$, except for the perchlorate complex, where the metal was determined as $CoHg(SCN)_4$ after decomposing the complex with a conc. HNO_3–H_2SO_4 mixture. Molar conductances of complexes were measured in methanol with a Systronic Model 304 digital conductivity meter. IR spectra (4000–200 cm^{-1}) were recorded in a JASCO FT-IR model 420 with KBr pellets at the University of Burdwan, Burdwan. The electronic spectra in methanol (ca. 298 K) and the diffuse reflectance spectra were recorded in a Hitachi U-3501 spectrophotometer. ^1H and ^{13}C NMR spectra were recorded in d^6-DMSO with a Bruker AM 300L (300 MH_z) superconducting FT-NMR. The mass spectrum (EIMS) of the ligand was recorded with a Jeol JMS-D 300 spectrometer at the Indian Institute of Chemical Biology (IICB), Kolkata.

2.4. Structure determination

The crystal data, X-ray diffraction data collection and refinement information, for the free ligand, HMPz3Hex, and its cobalt(III) complex, $[Co(MPz3Hex)_2]Br \cdot H_2O$, are summarized in Table 1. Both the structures were solved using the program SHELXS [17]. All non-hydrogen atoms were refined anisotropically. The hydrogen atoms, either located from difference electron density maps or fixed geometrically, were included in the structure factor calculations. Full-matrix least-squares refinement of the structures were carried out using the program SHELXL [18–20].

Table 1
Crystal data for HMPz3Hex (**I**) and $[Co(MPz3Hex)_2]Br \cdot H_2O$ (**II**)

Compound	Ligand **I**	Complex **II**
Crystal data		
Empirical formula	$C_{12}H_{19}N_5S$	$C_{24}H_{38}N_{10}S_2OCoBr$
Formula weight	265.38	685.60
T (K)	296(2)	293(2)
Crystal system	orthorhombic	monoclinic
Space group	$Pna2_1$	$C2/c$
a (Å)	13.217(1)	22.615(2)
b (Å)	9.274(1)	16.628(2)
c (Å)	11.373(2)	16.623(2)
α (°)	90	90
β (°)	90	90.671(8)
γ (°)	90	90
Unit cell volume (Å^3)	1394.1(3)	6250.5(10)
Z	4	8
Data collection		
Diffractometer	Bruker P4	Bruker P4
λ (Mo Kα) (Å)	0.71073	0.71073
d_{calcd} (g cm^{-3})	1.264	1.457
μ (mm^{-1})	0.224	1.997
Reflections collected	1642	7236
Independent reflections	1642 ($R_{int} = 0.000$)	7065 ($R_{int} = 0.019$)
Absorption correction	none	SHELXS
Maximum and minimum transmission		0.8163 and 0.4440
Structure refinement		
Refinement method	full-matrix least-squares on F^2	full-matrix least-squares on F^2
Observed reflections [$I > 2\sigma(I)$]	1642	7065
Number of parameters	183	405
Number of restraints	1	3
Goodness-of-fit on F^2	1.008	1.013
$R[I > 2\sigma(I)]$	0.0419	0.0584
wR2	0.0970	0.1213

3. Results and discussion

3.1. Characterization of 5-methyl-3-formyl pyrazole 3-hexamethyleneiminyl thiosemicarbazone

The title ligand, HMPz3Hex, has been characterized by elemental analyses (C, H and N), NMR (^{1}H and ^{13}C – discussed along with those of the Co(III) complexes) and mass spectrum. The mass fragmentation data (M^+; $m/z = 265$) are compatible with the proposed molecular formula, $C_{12}H_{19}N_5S$. The proposed structure of the ligand has also been authenticated by X-ray crystallography (discussed later).

3.2. Characterization of the cobalt(III) complexes

All the cobalt(III) complexes gave satisfactory C, H, N and Co analyses (Table 2) conforming to the general composition, $[Co(MPz3Hex)_2]X \cdot nH_2O$ (X = Cl, Br, NO_3, ClO_4 or BF_4); the complexes are all diamagnetic as expected. The molar conductance values ($\Lambda_M = 80.3$ to 85.1 $\Omega^{-1}\,cm^2\,mol^{-1}$) in MeOH (303 K) identify the species as 1:1 electrolytes.

Table 2
Colours, conductivity and analytical data for cobalt(III) complexes

Compound	Colour	Analytical data (%)				Λ_M[a]
		C Found (calc.)	H Found (calc.)	N Found (calc.)	Co Found (calc.)	
$[Co(MPz3Hex)_2]Cl \cdot H_2O$	brown	45.0(44.9)	5.9(5.9)	21.6(21.8)	9.1(9.2)	85.1
$[Co(MPz3Hex)_2]Br \cdot H_2O$	reddish brown	42.1(42.0)	5.4(5.5)	20.2(20.4)	8.5(8.6)	80.3
$[Co(MPz3Hex)_2]NO_3 \cdot 2H_2O$	deep brown	42.1(42.0)	5.7(5.8)	22.3(22.5)	8.5(8.6)	83.4
$[Co(MPz3Hex)_2]ClO_4 \cdot 2H_2O$	reddish brown	39.8(39.8)	5.4(5.5)	19.3(19.4)	8.2(8.2)	82.1
$[Co(MPz3Hex)_2]BF_4 \cdot 2H_2O$	reddish brown	40.5(40.6)	5.6 (5.5)	19.5(19.7)	8.4 (8.3)	83.3

[a] Molar conductivity ($\Omega^{-1}cm^2mol^{-1}$) of ca. 10^{-3} M solution in MeOH at 30 °C.

3.3. Spectroscopy

Assignments of selected characteristic IR bands (4000–200 cm^{-1}) for the free ligand (HMPz3Hex) and its cobalt(III) complexes, compiled in Table 3, indicate the bonding sites of the primary ligand molecule when complexed with the cobalt(III) ion. A negative shift of the band assigned to ν(CH=N) of the free ligand (1563 cm^{-1}) to a lower value (1500–1508 cm^{-1}) in its complexes, is consistent with coordination of the azomethine nitrogen to the central cobalt(III) ion; the bands at 445–473 cm^{-1} in the complexes are then assignable to ν(Co–N) [4,8,13,14,21]. A second band at 1480 cm^{-1} assignable to ν(C=N) of the pyrazole ring is shifted positively with a split band (1550–1574 cm^{-1}) in each of the complexes; this is because while coordinating to the cobalt(III) ion, the ligand molecule undergoes deprotonation, generating a double bond between N(2) and C(3) of its tsc moiety (Fig. 1). Moreover, the bands at 1003 and 634 cm^{-1} for ν(N–N) and in-plane deformation, respectively, of the pyrazole ring, are shifted to higher wave numbers on complexation; the positive shifts indicate the participation of the pyrazolyl ring nitrogen (tertiary) in complexation [4,8,13,14,21]. An intense band at 869 cm^{-1} assigned to ν(C=S) of the free ligand is found to have been shifted to a lower frequency region by ca. $\Delta\nu > 69$ cm^{-1} indicating that thiol sulfur participates as a coordinating site [4,8,13,14,21]. Moreover, the appearance of new bands at the 342–352 and 273–288 cm^{-1} regions in the spectra of the complexes substantiates the proposed bonding sites of the thiol sulfur and pyrazolyl ring nitrogen (tertiary), respectively.

The diffuse reflectance spectra of all the reported cobalt(III) complexes are very similar, exhibiting four bands in the 11 710–11 876, 14 881–15 773, 20 408–21 322 and 23 753–24 272 cm^{-1} regions which may be assigned as $^1A_{1g} \rightarrow {}^3T_{1g}$, $^1A_{1g} \rightarrow {}^3T_{2g}$, $^1A_{1g} \rightarrow {}^1T_{1g}$ and $^1A_{1g} \rightarrow {}^1T_{2g}$ transitions, respectively, in an octahedral symmetry [8], although CT bands in the 19 800–24 500 cm^{-1} range seem to have been mixed with the d–d transition bands; the observed lower energy bands are not split to a large extent. The electronic spectra of the MeOH solutions of the complexes exhibit two intense-bands in the region 37 104–41 154 cm^{-1} ($\log\varepsilon = 4.18-4.47$) and 30 796–30 818 cm^{-1} ($\log\varepsilon = 4.46 - 4.49$) attributable to intraligand CT bands ($\pi \rightarrow \pi^*$ and $n \rightarrow \pi^*$, respectively). The spectra also exhibit a shoulder at 25 000–25 978 cm^{-1} ($\log\varepsilon = 3.56 - 4.07$) which may be due to $S \rightarrow Co^{III}$ charge transfer (LMCT) bands. The absence of bands corresponding to $d \rightarrow d$ transitions may be due to the masking of $d \rightarrow d$ bands by strong CT bands [4,5].

The ^{1}H NMR (in d^6-DMSO) spectral data (Table 4) reveal that the free ligand molecule in solution exists in isomeric forms [1,22–27], i.e., *Z*- and *E*-forms (Fig. 1). The *Z*:*E* ratio in DMSO is ca. 2:1; whereas, in the solid state the molecule exists only in the *Z*-form, being stabilized with intramolecular hydrogen bonding (Fig. 1(a)). In solution the higher value of the ^{1}H chemical shift (δ_H 10.67) corresponding to the iminyl hydrogen (^{2}NH) indicates the presence of an intramolecular hydrogen bond stabilizing the *Z*-form. The predominance of the *Z*-isomer is possibly due to the bulky group on the N(4)-position of the substituted tsc moiety. A slightly higher value of the ^{13}C chemical shift corresponding to one of the two neighbouring carbons of nitrogen in the hexamethyleneiminyl moiety can be thought to be due to intramolecular C–H···S contacts [^{13}C NMR: C7, δ 52.6; C12, δ 51.4]. In solution the transformation from *Z*- to *E*-form is believed to occur via the reaction mechanism (Fig. 3) proposed showing the rotation about the azomethine double bond owing to its fluxional nature which is, perhaps, due to the electron withdrawing nature of the azomethine carbon (sp^2-hybridised and directly attached to the aromatic pyrazole ring, as well as the azomethine double bond being in conjugation with the aromatic double bond). The higher value of the ^{13}C chemical shift (Table 4) assigned to the azomethine carbon (δ_c 146.4) indicates its electron deficient nature which favours the reaction mechanism from step I to II (Fig. 3) involving the loss of the azomethine double bond character momentarily and then rotation about the C–^{1}N bond takes place followed by proton transfer from azomethine carbon to imine nitrogen (^{2}N) giving rise to the *trans*-isomer (*E*-form) in solution. An earlier communication from this laboratory [11] reported an unusual finding that the azomethine hydrogen of a similar type of ligand had been replaced by an ethoxy group while complexed with

Table 3
Selected IR bands (cm^{-1}) of the ligand and its cobalt(III) complexes

Compound[a]	ν(CH=N)(azom)	ν(C=N)(Pz)	ν(N–N)(Pz)	ν(C=S)	ν(ipdef.)(Pz)	ν(Co–N)(azom)	ν(Co–N)(Pz)	ν(Co–S)
HMPz3Hex	1563	1480	1003	869	634			
$[Co(MPz3Hex)_2]Cl$	1500	1560	1040	800	650	445	288	352
$[Co(MPz3Hex)_2]Br$	1508	1550	1040	750	680	461	278	350
$[Co(MPz3Hex)_2]NO_3$	1508	1569	1051	755	688	462	273	346
$[Co(MPz3Hex)_2]ClO_4$	1508	1574	[b]	800	690	471	274	342
$[Co(MPz3Hex)_2]BF_4$	1500	1570	[b]	750	680	473	276	343

[a] Water molecule(s) of crystallization have been omitted from this and the subsequent table.
[b] Not well defined as masked by $\nu(ClO_4)$ and $\nu(BF_4)$.

Table 4
Selected ^{1}H and ^{13}C NMR data of the ligand and its cobalt(III) complexes in d^6-DMSO; values given in δ (ppm) relative to TMS

Compound	^{1}H assignments					^{13}C assignments					
	Imino proton	Position of pyrazole ring protons			Methine proton	Thioamide carbon	Pyrazole carbon				Azomethine carbon
		^{1}N–H	^{4}C–H	$5CH_3$			^{3}C	^{4}C	^{5}C	$5CH_3$	
HMPz3Hex	10.67	12.84	6.32	2.25	8.10	177.8	132.2	105.8	140.0	10.2	146.4
	7.34	12.55	6.22	2.18	7.99						
$[Co(MPz3Hex)_2]Cl$		13.61	6.43	2.27	8.38						
$[Co(MPz3Hex)_2]Br$		13.67	6.47	2.27	8.38	178.6	142.3	105.9	145.5	11.0	151.3
$[Co(MPz3Hex)_2]NO_3$		13.61	6.44	2.26	8.28	178.7	142.3	105.9	145.6	11.1	151.4
$[Co(MPz3Hex)_2]ClO_4$		13.61	6.43	2.26	8.29						
$[Co(MPz3Hex)_2]BF_4$		13.60	6.43	2.26	8.29						

copper(II). This fact provides a good support for the electron attracting nature of the azomethine carbon. The ^{1}H NMR data of the complexes, when compared with those of the free ligand, point to the following: (i) the ^{1}H shift corresponding to the imine ^{2}NH of the moiety tsc at δ 10.67 (7.34) disappears after complexation, indicating that the ligand molecule undergoes deprotonation followed by coordination to the metal ion through the thiolato sulfur atom; (ii) maximum downfield shift occurs with the methine proton (azomethine C*H*) appearing at δ 8.28–8.38 in the complexes, corresponding to δ 7.99 (8.10) in the free ligand, as expected due to coordination of the azomethine nitrogen to the central cobalt(III) ion; and (iii) the shifting of the ^{4}CH (the pyrazole ring) from δ 6.32 (6.22) (free ligand) to δ 6.39–6.47 in the case of the complexes indicating the coordination site of the pyrazolyl nitrogen (tertiary, ^{2}N). Comparison of the ^{13}C NMR spectra of the uncomplexed ligand with those of its cobalt(III) complexes reveals that the thioamide carbon [^{3}C(S)] shifts slightly downfield from δ_c 177.8 (free ligand) to ca. δ_c 178.6 (in the complexes) showing a coordination through the thiolato sulfur. The significant downfield shift occurs with the azomethine carbon appearing at ca. δ_c 151.3 in the complexes corresponding to δ_c 146.4 in the free ligand as expected due to coordination of the azomethine nitrogen to the metal ion and also the maximum downfield shifting of the ^{3}C ring (pyrazole) carbon from δ_c 132.2 (free ligand) to ca. δ_c 142.3 in the complexes is quite reasonable with the proposition that the neighbouring ^{2}N (pyrazole) coordinates strongly with the central atom; moreover, downfield shifts of the ^{5}C ring carbon and its methyl carbon (pyrazole) support the proposed pyrazolyl *tert*-nitrogen (^{2}N) as a coordination site.

Both the ^{1}H and ^{13}C NMR spectra thus provide excellent support for the bonding characteristics of the primary ligand (HMPz3Hex) in forming complexes with the cobalt(III) ion through the pyrazolyl ring nitrogen (tertiary), azomethine nitrogen and the thiolato sulfur atom [4,5,8,13,14,22–27].

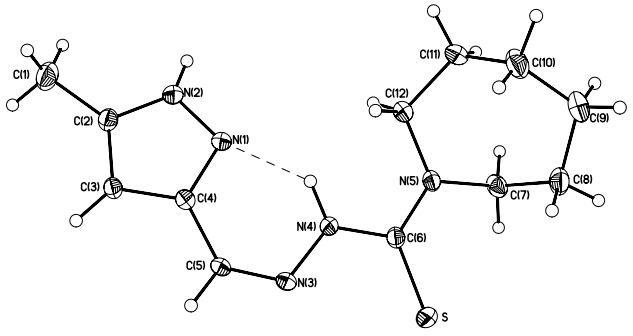

Fig. 2. ORTEP-3 diagram of HMPz3Hex with 50% thermal ellipsoids.

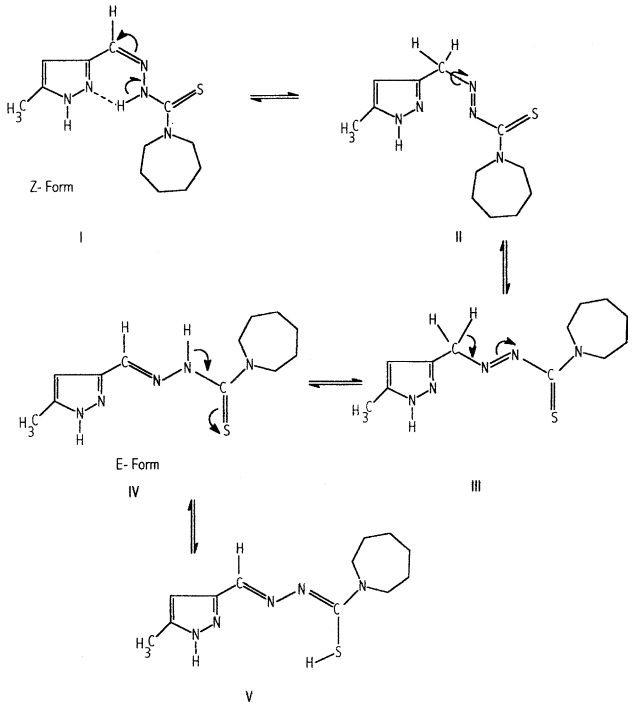

Fig. 3. Reaction mechanism showing the rotation about the azomethine double bond owing to the fluxional nature of the bond.

3.4. Structural determinations of HMPz3Hex and $[Co(MPz3Hex)_2]Br \cdot H_2O$

Figs. 2 and 4 are ORTEP [28] diagrams of the free ligand and the complex $[Co(MPz3Hex)_2]Br \cdot H_2O$, respectively, together with the atom numbering schemes. The crystallographic asymmetric unit in the complex comprises of a $[Co(MPz3Hex)_2]^+$ cation, a Br^- anion and a molecule of water of crystallization. Some selected bond distances, nonbonded contacts, bond angles and torsion angles in the two examined structures are compiled in Table 5.

Two molecules (A and B) of the tridentate ligand [5-methyl-3-formyl pyrazole 3-hexamethyleneiminyl thiosemicarbazone] coordinate to the Co(III) ion to form four five-membered chelate rings [Co–N(1A)–C(4A)–C(5A)–N(3A), Co–N(1B)–C(4B)–C(5B)–N(3B), Co–N(3A)–N(4A)–C(6A)–S(1A) and Co–N(3B)–N(4B)–C(6B)–S(1B)]. The two azomethine nitrogen atoms [N(3A) and N(3B)] are *trans* to each other while the pyrazolyl ring nitrogen atoms [N(1A) and N(1B)] and the thiolato sulfurs [S(1A) and S(1B)] are in the *cis* positions.

The C(6)–S(1) double bond distance of 1.681(3) Å in the free ligand is comparable to those found in other similar heterocyclic N(4)-substituted thiosemicarbazones [29,30]. This bond lengthens to 1.741(5) and 1.746(5) Å in ligands A and B, respectively, in the complex, indicating a conversion to single bonds; this has been observed for other Co(III) complexes with similar thiosemicarbazone ligands with NNS donor sites [8,31]. A concurrent shortening of the N(4)–C(6) bonds, from 1.363(4)Å in the free ligand to 1.324(6) Å [ligand A] and 1.319(6) Å [ligand B] in the complex, shows that deprotonation of the imine nitrogen [N(4)] results in a conversion from thione to thiol sulfur. Deprotonation of the imine nitrogen is further corroborated by the closing of the N(3)–N(4)–C(6) angle by about 9° in the complex. Whereas, in nickel(II) and copper(II) complexes of similar ligands, where the imine nitrogen is not deprot-

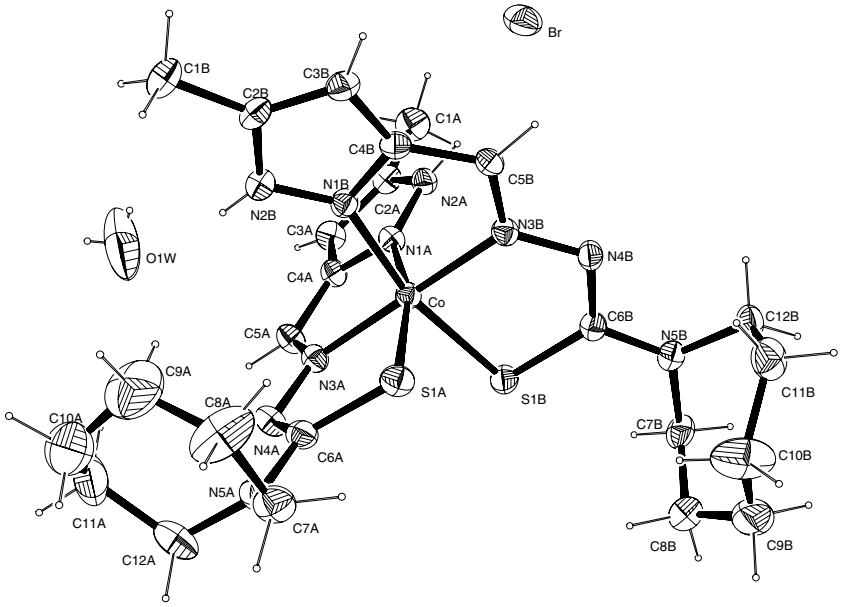

Fig. 4. ORTEP-3 diagram of $[Co(MPz3Hex)_2]Br \cdot H_2O$ with 50% thermal ellipsoids.

Table 5
Characteristic bond lengths (Å), bond angles (°) and torsion angles(°) of HMPz3Hex (**I**) and $[Co(MPz3Hex)_2]Br.H_2O$ (**II**)

	Free ligand (**I**)	Complex (**II**)	
		Ligand A	Ligand B
Bond distances			
Co–S(1)		2.215(1)	2.217(1)
Co–N(1)		1.969(4)	1.953(3)
Co–N(3)		1.898(3)	1.905(3)
N(1)–N(2)	1.341(4)	1.347(5)	1.342(6)
C(4)–C(5)	1.455(4)	1.437(7)	1.449(7)
C(5)–N(3)	1.278(4)	1.278(6)	1.281(6)
N(3)–N(4)	1.372(3)	1.374(5)	1.382(5)
N(4)–C(6)	1.363(4)	1.324(6)	1.319(6)
C(6)–S(1)	1.681(3)	1.741(5)	1.746(5)
C(6)–N(5)	1.342(4)	1.349(6)	1.357(6)
Selected nonbonded contacts			
S(1)–N(1)	5.278(3)	4.153(4)	4.142(4)
S(1)–N(3)	2.742(3)	2.793(4)	2.804(4)
N(1)–N(3)	2.965(4)	2.509(5)	2.508(5)
N(1)–N(4)	2.639(4)	3.877(5)	3.885(5)
Bond angles			
N(1)–C(4)–C(5)	121.4(3)	113.0(4)	110.3(4)
C(4)–C(5)–N(3)	129.2(3)	115.5(4)	114.2(4)
C(5)–N(3)–N(4)	116.4(3)	118.8(4)	119.0(4)
N(3)–N(4)–C(6)	120.5(3)	111.5(3)	111.6(3)
N(4)–C(6)–S	121.1(2)	123.4(4)	123.8(4)
N(4)–C(6)–N(5)	114.6(2)	117.6(4)	117.2(4)
S–C(6)–N(5)	124.3(2)	119.0(4)	119.0(4)
Torsion angles			
N(3)–N(4)–C(6)–S(1)	5.8(4)	−4.8(5)	2.1(5)
N(3)–N(4)–C(6)–N(5)	−175.1(3)	175.8(4)	−179.1(3)
S(1)–C(6)–N(5)–C(7)	7.7(7)	14.4(7)	−3.8(5)
C(5)–N(3)–N(4)–C(6)	−174.6(3)	−177.2(4)	178.0(4)
C(4)–C(5)–N(3)–N(4)*	3.3(5)	175.5(4)	−177.1(4)
N(1)–C(4)–C(5)–N(3)	−7.0(5)	−1.6(6)	−4.2(6)
Bond angles around the Co(III) ion			
S(1A)–Co–N(1A)	165.90(11)	S(1B)–Co–N(1B)	166.43(11)
S(1A)–Co–N(3A)	85.18(12)	S(1B)–Co–N(3B)	85.36(11)
N(1A)–Co–N(3A)	80.89(15)	N(1B)–Co–N(3B)	81.07(14)
S(1A)–Co–N(1B)	89.02(11)	S(1B)–Co–N(1A)	91.38(11)
S(1A)–Co–N(3B)	93.12(11)	S(1B)–Co–N(3A)	94.91(11)
N(1A)–Co–N(3B)	100.79(14)	N(1B)–Co–N(3A)	98.66(14)
S(1A)–Co–S(1B)	92.02(6)	N(1A)–Co–N(1B)	90.88(15)
N(3A)–Co–N(3B)	178.29(15)		

onated, the corresponding endocyclic bond angles are wider: 119.0(3)° in octahedral $[Ni(HMPzNBu_2)_2](ClO_4)_2$ [7], and 117.2(2)° in square pyramidal $[Cu(HMPz4BM)(NO_3)_2]$ [10]. The relevant C–S bond distances is 1.699(4) Å, with the N–C bond distance being 1.355(5) Å in the nickel(II) complex [7]. The corresponding distances in the copper(II) complex are 1.724(3) and 1.354(3) Å [10]. In the present complex, the release of the iminyl hydrogen in the ligand during complexation is, perhaps, facilitated by the harder acid character of the cobalt(III) ion compared to the nickel (II) and the copper(II) ions.

In the complex, the cobalt(III) ion has a distorted octahedral coordination with each of the two tridentate ligands, A and B, coordinating to the metal ion through the pyrazolyl nitrogen, N(1), the azomethine nitrogen, N(3), and the thiol sulfur, S(1). The geometrical requirements of coordination result in a significant closing of the C(4)–C(5)–N(3) and N(1)–C(4)–C(5) angles by about 15° and 10°, respectively, as indicated in Table 5. The tridentate ring systems [Co–S(1)–C(6)–N(4)–N(3)–C(5)–C(4)–C(3)–C(2)–N(2)–N(1)] of the chromophores in the complex are practically planar; the maximum deviation from planarity is +0.110(5) Å for C(6A) in ligand A and −0.212(4) Å for C(2B) in ligand B. The coordinating ligands A and B are nearly orthogonal to each other while bonding to Co(III) resulting in a meridonial structure with a dihedral angle of 86.78(5)°

between them. The three individual rings, in both the ligands, namely, the pyrazole and the two five-membered chelate rings, are individually almost planar with small dihedral angles between them; the maximum dihedral angle is observed between the chelate ring Co–S(1)–C(6)–N(4)–N(3) and the pyrazole ring N(1)–C(4)–C(3)–C(2)–N(2) in both the ligands, being 3.77(12)° in ligand A and 9.53(14)° in ligand B.

The most interesting feature of the complex formation is an unusual rotation about the azomethine C=N double bond to form the Co–N(1)–C(4)–C(5)–N(3) chelate ring This is indicated by the torsion angles C(4)–C(5)–N(3)–N(4), which are 3.3(5)° in the free ligand, and 175.5(4)° (ligand A) and −177.1(4)° (ligand B) in the complex (identified by an asterisk in Table 5). The expected rotation about either the N(3)–N(4) bond or the N(4)–N(6) bond does not take place during complexation as indicated by the torsional angles C(5)–N(3)–N(4)–C(6) and N(3)–N(4)–C(6)–N(5), respectively, which remain practically the same in the ligand, both in its free and complexed forms (Table 5). The unexpected rotation about the azomethine double bond, C(5)–N(3), during complexation can be explained by the reaction mechanism proposed in Fig. 3. The feasibility of this mechanism is due to the electron attracting character of the azomethine carbon, C(6). The electron attracting nature of this carbon atom has already been documented in a complex of a similar ligand with a copper(II) ion [11].

The transient conversion of the C=N double bond to a single bond allows the rotation of the thiosemicarbazone moiety about this bond so that the sulfur atom, S, is in a *cis* position with respect to the pyrazolyl nitrogen (tertiary), N(1), in order to cater to the requirement of complexation. The C(5)–N(3) bond distance, which is 1.278(4) Å in the free ligand, resumes its double bond character in the complex with bond distances of 1.278(6) Å in ligand A and 1.281(6) Å in ligand B.

Figs. 5 and 6 show the hydrogen bonds and C–H···X contacts in the free ligand and its Co(III) complex; the geometrical details are listed in Table 6. As has been observed in other similar structures [7,10], S(1) is involved in a C(7)–H(7)···S(1) intramolecular contact which practically restricts the conformation of the ligand about the C(6)–N(5) bond, both in its free and complexed forms. The torsion angle about the C(6)–N(5) bonds varies between −3.8(5)° and 14.4(7)° (Table 5). The *Z*-isomeric conformation of the free ligand is stabilised by an intramolecular N(4)–H(4)···N(1) hydrogen bond. This finding is exactly in agreement with the cases of similar thiosemicarbazone type ligands, with one exception, namely, 2-acetylpyridine 3-hexamethyleneiminyl thiosemicarbazone which is crystallographically different and has been reported earlier [29,30]. The crystal structure of the free ligand is further stabilised by the formation of a pair of bifurcated hydrogen bonds; the pyrazolyl secondary nitrogen, N(2), contributes a hydrogen atom which is shared by the azomethine nitrogen, N(3), and the thione sulfur, S(1), of a glide related moiety. In the complex, the pyrazolyl secondary nitrogen, N(2A), of one of the ligands forms a N(2A)–H(2A)···Br hydrogen bond with a bromine ion. The corresponding nitrogen from the other ligand forms a N(2B)–H(2B)···O(1W) hydrogen bond with the water

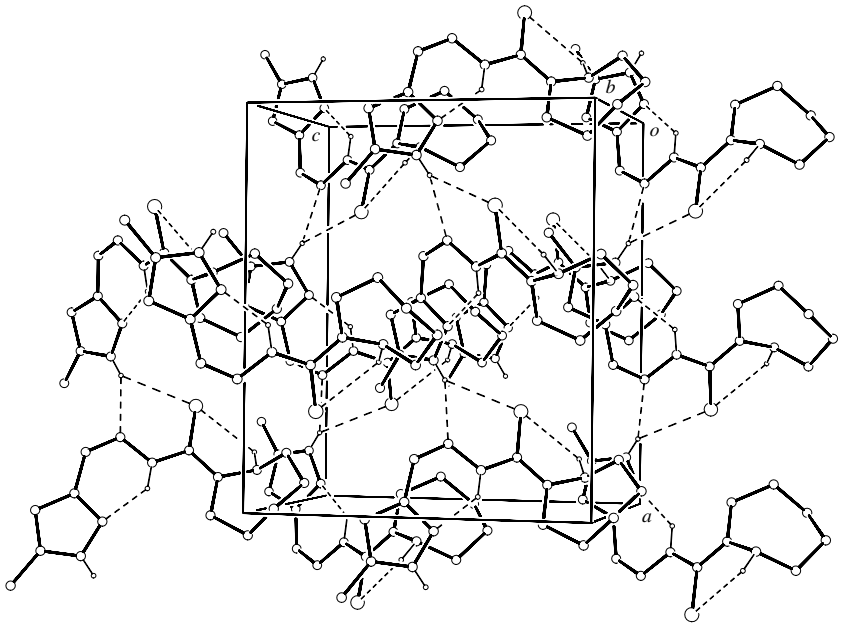

Fig. 5. Crystal structure of HMPz3Hex showing the unit cell contents. The dashed lines show the hydrogen bonds (five dashes) and C–H···X contacts (seven dashes).

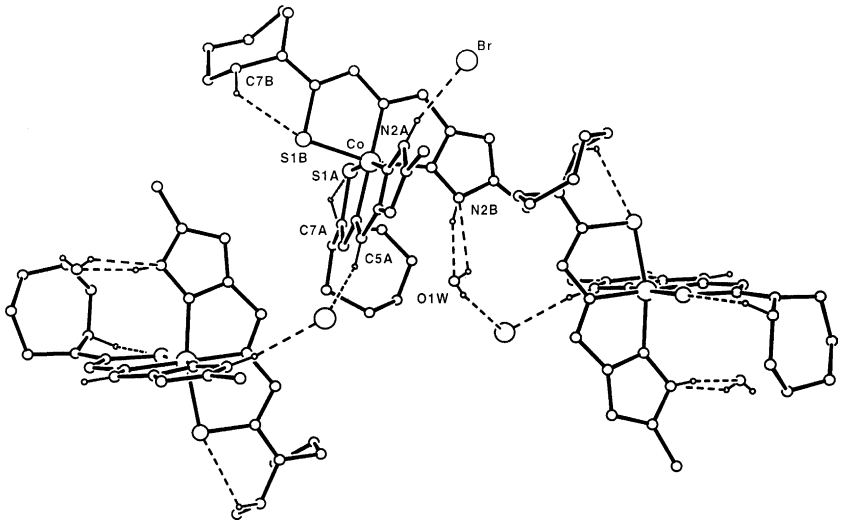

Fig. 6. Schematic diagram showing the hydrogen bonds (five dashes) and C–H···X contacts (seven dashes) in the crystal structure of $[Co(MPz3Hex)_2]Br \cdot H_2O$.

Table 6
Hydrogen bonds and C–H···X contacts

D–H···A	D–H (Å)	D···A (Å)	H···A (Å)	∠D–H···A (°)
Free ligand				
N(2)–H(2)···S(1)[(i)]	0.78(4)	3.358(3)	2.75(4)	137(4)
N(2)–H(2)···N(3)[(i)]	0.78(4)	3.003(4)	2.29(4)	152(4)
N(4)–H(4)···N(1)	0.94(4)	2.639(4)	1.87(4)	137(3)
C(7)–H(7B)···S(1)	0.97	2.593	3.036(4)	108
Complex				
N(2A)–H(2A)···Br	0.88(5)	3.173(5)	2.32(5)	165(3)
N(2B)–H(2B)···O(1W)	0.80(5)	2.780(11)	2.01(5)	162(5)
O(1W)–H(1W1)···N(2B)	0.54(6)	2.780(11)	2.55(5)	109(7)
O(1W)–H(1W2)···Br[(ii)]	0.54(5)	3.257(10)	2.81(5)	142(6)
C(5A)–H(5AA)···Br[(iii)]	0.93	3.619(5)	2.90	135
C(7A)–H(7AA)···S(1A)	0.97	2.993(6)	2.56	107
C(7B)–H(7BB)···S(1B)	0.97	2.990(5)	2.56	107

Symmetry equivalents: (i) $-1/2+x$, $1/2-y$, z; (ii) $1/2-x$, $-1/2+y$, $1+1/2-z$ and (iii) x, $-y$, $1/2+z$.

of crystallization; the water molecule, in its turn, is the donor in an O(1W)–H(11W)···N(2B) hydrogen bond with the same nitrogen. This leads to a situation where a pair of atoms, N(2B) and O(1W), are doubly hydrogen bonded to each other with both atoms playing the roles of donor as well as acceptor. The second hydrogen atom, H(12W), from the water molecule participates in an O(1W)–H(12W)···Br hydrogen bond. In addition, the bromide ion is the acceptor in a C(5A)–H(5AA)···Br contact with an azomethine carbon atom, C(5A).

4. Conclusion

The present study shows that the bio-relevant pyrazolyl thiosemicarbazone, NNS tridentate ligand, HMPz3Hex (Fig. 1), undergoes deprotonation during complexation with cobalt(III) and forms a *bis*-ligated complex, with the two ligands coordinating with the central metal ion orthogonally in the distorted octahedral environment, while azomethine nitrogens are in *trans* and sulfur atoms are in *cis*-positions (*mer*-configuration). Comparison of the X-ray crystallographic data of both the free ligand and its cobalt(III) complex brings out an interesting feature of the complex formation that the thiosemicarbazone moiety (tsc) of the ligand undergoes unexpected rotation about the azomethine double bond joining tsc and pyrazole moieties together, by the driving force for complexation with cobalt(III).

5. Supplementary material

Crystallographic data for the structures reported here have been deposited with the Cambridge

Crystallographic Data Centre, CCDC numbered 201868 and 201869. Copies of these information may be obtained free of charge from The Director, CCDC Data Centre, 12 Union Road, Cambridge, CB2 1EZ, UK (fax: +44-1223-336033; E-mail: deposit@ccdc.cam.ac.uk or www:http://www.ccdc.cam.ac.uk).

Acknowledgements

Financial support from UGC (India) to one of the authors (D.K.S.), in the form of a Teacher Fellowship, is gratefully acknowledged. The authors thank Prof. (Mrs.) A. Chatterjee of the Department of Chemistry, University of Calcutta, for providing NMR spectral data.

References

[1] D.X. West, S.B. Padhye, P.B. Sonawane, Struct. Bond. 76 (1991) 1.
[2] A.E. Liberta, D.X. West, Biometals 5 (1992) 121.
[3] D.X. West, A.E. Liberta, S.B. Padhye, R.C. Chikate, P.B. Sonawane, A.S. Kumbhar, R.G. Yerande, Coord. Chem. Rev. 123 (1993) 49.
[4] N.C. Saha, A. Seal, R.J. Butcher, N. Saha, J. Indian Chem. Soc. 78 (2001) 601.
[5] N.C. Saha, R.J. Butcher, S. Chaudhuri, N. Saha, Polyhedron 21 (2002) 779.
[6] N.C. Saha, A. Saha, R.J. Butcher, S. Chaudhuri, N. Saha, Inorg. Chim. Acta 339C (2002) 348.
[7] N.C. Saha, R.J. Butcher, S. Chaudhuri, N. Saha, Polyhedron 22 (2003) 383.
[8] D.K. Sau, N. Saha, R.J. Butcher, S. Chaudhuri, Trans. Met. Chem. 28 (2003) 229.
[9] N. Saha, N. Mukherjee, Polyhedron 3 (1984) 1135.
[10] D.K. Sau, R.J. Butcher, S. Chaudhuri, N. Saha, Mol. Cell. Biochem. (2003), in press.
[11] P. Bera, R.J. Butcher, N. Saha, Chem. Lett. (1998) 559.
[12] P. Bera, N. Saha, S. Kumar, D. Banerjee, R. Bhattacharya, Trans. Met. Chem. 24 (1999) 425.
[13] P. Bera, R.J. Butcher, S. Chaudhuri, N. Saha, Polyhedron 21 (2002) 1.
[14] A. Mitra, T. Banerjee, P. Raychowdhury, S. Chaudhuri, P. Bera, N. Saha, Polyhedron 16 (1997) 3735.
[15] J.P. Scovill, Phosphorus Sulfur and Silicon 60 (1991) 15.
[16] Klayman, J.P. Scovill, J.F. Bartosevich, C.J. Mason, J. Med. Chem. 22 (1979) 1367.
[17] G.M. Sheldrick, SHELXS 97, Program for the Automatic Solution of Crystal Structures, Universität Göttingen, Göttingen, Germany, 1997.
[18] G.M. Sheldrick, SHELXL 97, Program for the Refinement of Crystal Structure, Universität Göttingen, Göttingen, Germany, 1997.
[19] D.T. Cromer, J.T. Weber, in: International Tables for X-ray Crystallography, vol. 4, Kynoch Press, Birmingham, England, 1994 (Table 2.2A).
[20] J.A. Ibers, W.C. Hamilton, Acta. Crystallogr. 17 (1964) 781.
[21] N. Saha, N. Mukherjee, Synth. React. Inorg. Met.-Org. Chem. 14 (1984) 1151.
[22] G.F. de Sousa, D.X. West, C.A. Brown, J.K. Swearingen, J. Valdés-Martínez, R.A. Toscano, S. Herñandez-Ortega, M. Hörner, A.J. Bortoluzzi, Polyhedron 19 (2000) 841.
[23] E. Bermejo, Carballo, A. Castiñeiras, R.R. Domínguez, C. Maichle- Mössmer, J. Strähle, D.X. West, Polyhedron 18 (1999) 3695.
[24] D.X. West, M.A. Lockwood, A.E. Liberta, X. Chen, R.D. Willett, Trans. Met. Chem. 18 (1993) 221.
[25] D.X. West, C.S. Carlson, C.P. Galloway, A.E. Liberta, C.R. Daniel, Trans. Met. Chem. 15 (1990) 91.
[26] D.X. West, B.L. Mokijewski, H. Gebremedhin, T.J. Romack, Trans. Met. Chem. 17 (1992) 384.
[27] P.S. Kalsi, Spectroscopy of Organic Compounds, 3rd ed., New Age International Publishers, New Delhi, 1998, p. 318.
[28] L.J. Farrugia, J. Appl. Crystallgr. 30 (1997) 565, ORTEP-3.
[29] D.X. West, G.A. Bain, R.J. Butcher, J.P. Jasinski, Y. Li, R.Y. Pozdniakiv, J. Valdés-Martínez, R.A. Toscano, S. Hersimnandez-Ortega, Polyhedron 15 (1996) 665.
[30] J. Vald/'es-Mart/'inez, S. Herñandez-Ortega, D.X. West, J.S. Ives, G.A. Bain, Z. Kristallogr. 213 (1998) 246.
[31] D.X. West, M.A. Lockwood, A. Castineiras, Trans. Met. Chem. 22 (1997) 447.

Available online at www.sciencedirect.com
SCIENCE DIRECT®
Polyhedron 23 (2004) 15–21
POLYHEDRON
www.elsevier.com/locate/poly

Syntheses and crystal structures of ferrocene-containing enaminones and their copper complexes

Yao-Cheng Shi [a,*], Hua-Mei Yang [a], Wen-Bin Shen [b], Chao-Guo Yan [a], Xiao-Ya Hu [a]

[a] School of Chemistry, Yangzhou University, Yangzhou 225002, PR China
[b] Analytical Center, China Pharmaceutical University, Nanjin 210009, PR China

Received 2 July 2003; accepted 29 August 2003

Abstract

Six ferrocene-containing enaminones $[C_5H_5FeC_5H_4C(O)CH=C–(NHAr)R]$ (**HL^1**, $R=CH_3$, $Ar=C_6H_5$; **HL^2**, $R=CH_3$, $Ar=2\text{-}CH_3C_6H_4$; **HL^3**, $R=CH_3$, $Ar=2,6\text{-}(CH_3)_2C_6H_3$; **HL^4**, $R=C_6H_5$, $Ar=C_6H_5$; **HL^5**, $R=C_6H_5$, $Ar=2\text{-}CH_3C_6H_4$; **HL^6**, $R=C_6H_5$, $Ar=2,6\text{-}(CH_3)_2C_6H_3$) and their copper(II) complexes (**I**, $L_2^1Cu{\cdot}2H_2O$; **II**, L_2^2Cu; **III**, L_2^3Cu; **IV**, $L_2^4Cu{\cdot}2H_2O$; **V**, $L_2^5Cu{\cdot}2H_2O$) have been synthesized and characterized by elemental analyses, ^{1}HNMR, IR and UV spectroscopies. Their structures have been determined by the X-ray crystallography of enaminone **HL^6** and complex **I**.
© 2003 Elsevier Ltd. All rights reserved.

Keywords: Ferrocene; Enaminone; Ligand; Copper; Complex; X-ray crystallography

1. Introduction

In the last few decades enaminones and enaminecarbaldehydes have been widely investigated because of their applications in the synthesis of heterocyclic compounds [1] and plentiful reaction chemistry [2] and coordination chemistry [3]. Therefore, enaminones of the type $[R'C(O)CHC(NHAr)R]$ constitute an important class. Recently non-metallocene complexes of Group IV metals have attracted much interest as possible alternatives for olefin polymerization catalysts using N_4-macrocycles, porphrins, tripodal amides, mixed cyclopentadienyl-amides and Schiff bases as spectator ligands [5–7]. Because the anions $[R'C(O)CHC(NAr)R]^-$ generated from the above enaminones offer potential isoelectronic alternatives to the cyclopentadienyl-based anion and can be used as good chelating ligands for copper complexes that exhibit catalytic activity [3,8], organometallic enaminones of the new type $[C_5H_5FeC_5H_4C(O)CH=C(NHAr)R]$ have been studied. To our knowledge, so far no article on organometallic enaminones has appeared, and herein we report the syntheses and structures of the ferrocenyl enaminones and their copper complexes.

2. Experimental

2.1. Reagents and general procedures

All chemicals used were of reagent grade. Toluene and THF were distilled from Na/benzophenone under dinitrogen atmosphere. Absolute ethanol for sodium ethoxide was distilled from Na/diethyl phthalate. DMF, ethyl acetate and ethyl benzoate were redistilled before use. Other commerial chemicals were used without further purification. Acetylferrocene was synthesized from ferrocene according to the literature method [9]. Progress of the reactions was monitored by TLC. ^{1}H NMR spectra were determined with a Bruker Avance 500 spectrometer using TMS as external standard in $CDCl_3$. IR spectra were recorded on a Perkin–Elmer 402 as KBr disks in the range of 400–4000 cm^{-1}. UV spectra were measured with a Shimadzu UV-240 spectrometer using a solution in DMF. Analyses for C, H and N were performed on an Elementa Vario EL III instrument.

* Corresponding author. Tel.: +86-514-7857939; fax: +86-514-7857939.
E-mail address: yzssyc@yzcn.net (Y.-C. Shi).

0277-5387/$ - see front matter © 2003 Elsevier Ltd. All rights reserved.
doi:10.1016/j.poly.2003.08.017

Melting points were measured on a Yanagimoto apparatus and were uncorrected.

2.2. Syntheses of enaminones

2.2.1. Syntheses of β-diketones *1* and *2*

Modified literature syntheses were used [10,11]. A solution of sodium ethoxide (8.85 g, 130 mmol), acetylferrocene (16.42 g, 72 mmol) and ethyl acetate (11.45 g, 130 mmol) in 60 ml of THF was refluxed under nitrogen for 2 h. The yellow solid was filtered, washed with THF and acidified with aqueous acetic acid to give the β-diketone **1** (16.14 g, 83%) as a red solid. M.p. 97 °C (lit: 97–97.5 °C) [10]. UV (nm, in DMF): $\lambda_{max}(\varepsilon \times 10^4)$ 261 (1.02), 308 (1.12).

The similar reaction of sodium ethoxide (4.08 g, 60 mmol), acetylferrocene (7.98 g, 35 mmol) and ethyl benzoate (5.56 g, 37 mmol) in 60 ml of THF for 2 h after the above-mentioned workup and extraction with CH_2Cl_2 (three times, each 20 ml) gave the combined organic layer. The mixture was dried with anhydrous $CaCl_2$ and then the solvent of the filtrate was removed to give a purple–red oil, which was separated with the eluant (CH_2Cl_2: petroleum ether, 2:1) by vacuum liquid chromatography (VLC). A main band was collected to afford the β-diketone **2** (5.81 g, 50%) as a purple–red solid. M.p. 106 °C (lit: 106–107 °C) [11]. UV (nm, in DMF): $\lambda_{max}(\varepsilon \times 10^4)$ 268 (0.85), 332 (0.64), 360 (0.65).

2.2.2. Syntheses of enaminones

$[C_5H_5FeC_5H_4C(O)CH=C(NHAr)CH_3]$ (Ar = C_6H_5, **HL[1]**). Aniline (1.86 g, 20 mmol) was added to a solution of β-diketone **1** $[C_5H_5FeC_5H_4C(O)CH_2C(O)\ CH_3]$ (2.7 g, 10 mmol) and a catalytic trace amount of p-TsOH (≈10 mg) in 20 ml of toluene, and then the mixture was refluxed with a Dean-Stark apparatus to remove water for 2 h. The solvent was evaporated under vacuum, and the residue was recrystallized from petroleum ether (60–90 °C) to afford 2.76 g (80%) of **HL[1]** as a red crystalline solid. M.p. 120–121 °C. *Anal.* Found: C, 69.60; H, 5.52; N, 3.72. Calc. for $C_{20}H_{19}NFeO$: C, 69.58; H, 5.55; N, 4.06%. IR (KBr disk): ν(NH) 3084 (s), ν(C=O) and ν(C=C) 1582 (vs, br) cm^{-1}. UV (nm, in DMF): $\lambda_{max}(\varepsilon \times 10^4)$ 259 (8.7), 275 (1.5) (B-band); 328 (1.9) (K-band). ^1H NMR ($CDCl_3$): δ 2.15 (s, 3H, CH_3), 4.24 (s, 5H, C_5H_5), 4.58 (s, 2H, 2 (H^3, H^4) of C_5H_4 ring), 4.83 (s, 2H, 2 (H^2, H^5) of C_5H_4 ring), 5.54 (s, 1H, CH), 7.10–7.37 (m, 5H, C_6H_5), 12.64 (s, 1H, NH).

$[C_5H_5FeC_5H_4C(O)CH=C(NHAr)CH_3]$ (Ar = 2-$CH_3C_6H_4$, **HL[2]**). The similar reaction of 2-methylaniline (2.14 g, 20 mmol) and β-diketone **1** (10 mmol) afforded 2.83 g (80%) of **HL[2]** as a red crystalline solid. M.p. 96–97 °C. *Anal.* Found: C, 70.24; H, 5.70; N, 3.85. Calc. for $C_{21}H_{21}FeNO$: C, 70.21; H, 5.89; N, 3.90%. IR (KBr disk): ν(NH) 3080 (s), ν(C=O) 1601 (vs), ν(C=C) 1554 (vs) cm^{-1}. UV (nm, in DMF): $\lambda_{max}(\varepsilon \times 10^4)$ 274 (0.9) (B-band), 333 (1.2) (K-band). ^1H NMR ($CDCl_3$): δ 1.99 (s, 3H, CH_3), 2.33 (s, 3H, CH_3), 4.21 (s, 5H, C_5H_5), 4.41 (s, 2H, 2 (H^3, H^4) of C_5H_4 ring), 4.79 (s, 2H, 2 (H^2, H^5) of C_5H_4 ring), 5.54 (s, 1H, CH), 7.12–7.27 (m, 4H, C_6H_4), 12.44 (s, 1H, NH).

$[C_5H_5FeC_5H_4C(O)CH=C(NHAr)CH_3]$ (Ar = 2,6-$(CH_3)_2C_6H_3$, **HL[3]**). The similar reaction of 2,6-dimethylaniline (2.42 g, 20 mmol) and β-diketone **1** (10 mmol) afforded 2.99 g (80%) of **HL[3]** as a red crystalline solid. M.p. 114–116 °C. *Anal.* Found: C, 70.81; H, 6.04; N, 3.27. Calc. for $C_{22}H_{23}FeNO$: C, 70.79; H, 6.21; N, 3.75%. IR (KBr disk): ν(NH) 3079 (w), ν(C=O) 1603 (vs), ν(C=C) 1553 (vs) cm^{-1}. UV (nm, in DMF): $\lambda_{max}(\varepsilon \times 10^4)$ 265 (1.51) (B-band), 330 (1.36) (K-band). ^1H NMR ($CDCl_3$): δ 1.73 (s, 3H, CH_3), 2.26 (s, 6H, $2CH_3$ of benzene ring), 4.21 (s, 5H, C_5H_5), 4.41 (s, 2H, 2 (H^3, H^4) of C_5H_4 ring), 4.82 (s, 2H, 2 (H^2, H^5) of C_5H_4 ring), 5.57 (s, 1H, CH), 7.10–7.15 (m, 3H, C_6H_3), 12.03 (s, 1H, NH).

$[C_5H_5FeC_5H_4C(O)CH=C(NHAr)C_6H_5]$ (Ar = C_6H_5, **HL[4]**). The similar reaction of aniline (0.93g, 10 mmol) and β-diketone **2** $[C_5H_5FeC_5H_4C(O)CH_2C(O)\ C_6H_5]$ (1.66 g, 5 mmol) afforded 1.71 g (84%) of **HL[4]** as a deep red crystalline solid. M.p. 118–120 °C. *Anal.* Found: C, 73.29; H, 5.00; N, 3.02. Calc. for $C_{25}H_{21}$ FeNO: C, 73.72; H, 5.20; N, 3.44%. IR (KBr disk): ν(NH) 3087 (s), ν(C=O) 1589 (vs), ν(C=C) 1567 (vs) cm^{-1}. UV (nm, in DMF): $\lambda_{max}(\varepsilon \times 10^4)$ 369 (1.06) (K-band). ^1H NMR ($CDCl_3$): δ 4.25 (s, 5H, C_5H_5), 4.57 (s, 2H, 2 (H^3, H^4) of C_5H_4 ring), 4.87 (s, 2H, 2 (H^2, H^5) of C_5H_4 ring), 5.77 (s, 1H, CH), 6.75–7.13 (3m, 5H, NC_6H_5), 7.27–7.44 (m, 5H, C_6H_5), 12.43 (s, 1H, NH).

$[C_5H_5FeC_5H_4C(O)CH=C(NHAr)C_6H_5]$ (Ar = 2-$CH_3C_6H_4$, **HL[5]**). The similar reaction of 2-methylaniline (1.07 g, 10 mmol) and β-diketone **2** (5 mmol) afforded 1.71 g (81%) of **HL[5]** as a light red crystalline solid. M.p. 138–140 °C. *Anal.* Found: C, 73.98; H, 5.22; N, 2.88. Calc. for $C_{26}H_{23}FeNO$: C, 74.12; H, 5.50; N, 3.32%. IR (KBr disk): ν(NH) 3082 (s), ν(C=O) 1591 (vs), ν(C=C) 1567 (vs) cm^{-1}. UV (nm, in DMF): $\lambda_{max}(\varepsilon \times 10^4)$ 274 (1.32) (B-band), 369 (1.03) (K-band). ^1H NMR ($CDCl_3$): δ 2.48 (s, 3H, CH_3), 4.27 (s, 5H, C_5H_5), 4.50 (s, 2H, 2 (H^3, H^4) of C_5H_4 ring), 4.90 (s, 2H, 2 (H^2, H^5) of C_5H_4 ring), 5.70 (s, 1H, CH), 6.40–7.50 (4m, 9H, (C_6H_4, C_6H_5)), 12.26 (s, 1H, NH).

$[C_5H_5FeC_5H_4C(O)CH=C(NHAr)C_6H_5]$ (Ar = 2,6-$(CH_3)_2C_6H_3$, **HL[6]**). The similar reaction of 2,6-dimethylaniline (1.21 g, 10 mmol) and β-diketone **2** (5 mmol) was refluxed for four days. After removal of the solvent, the deep-red oil obtained was chromatographed on a silica gel column with $CH_2Cl_2$and petroleum ether (3:1). The second band was collected and further recrystallized from petroleum ether (60–90 °C) afforded 1.31 g (46%) of **HL[6]** as a deep red crystalline solid. M.p. 153–154 °C. *Anal.* Found: C, 74.89; H, 5.67; N, 2.79. Calc. for $C_{27}H_{25}FeNO$: C, 74.49; H, 5.79; N, 3.22%. IR (KBr

disk): ν(NH) 3080 (w), ν(C = O) 1586 (vs), ν(C = C) 1567 (vs) cm^{-1}. UV (nm, in DMF): $\lambda_{max}(\varepsilon \times 10^4)$ 365 (1.45) (K-band). ^1H NMR ($CDCl_3$): δ 2.21 (s, 6H, $2CH_3$), 4.24 (s, 5H, C_5H_5), 4.46 (s, 2H, 2 (H^3, H^4) of C_5H_4 ring), 4.87 (s, 2H, 2 (H^2, H^5) of C_5H_4 ring), 5.70 (s, 1H, CH), 6.93–7.33 (2m, 8H, (C_6H_3, C_6H_5)), 12.22 (s, 1H, NH).

2.3. Syntheses of copper complexes

A solution of 1 mmol of the appropriate ligand (except enaminone **HL^6**) in absolute ethanol (10 ml) was added dropwise to a stirred solution of 0.5 mmol of hydrated copper acetate in the same solvent (10 ml). The mixture was stirred for 24 h at room temperature and then filtered to afford the crude product. The resulting solid was recrystallized from CH_2Cl_2 and petroleum ether to give the corresponding complex.

Complex **I** as a black solid, yield: 0.335 g (85%). M.p. 201–202 °C (dry sample). *Anal.* Found: C, 60.82; H, 4.71; N, 3.14. Calc. for $C_{40}H_{40}N_2O_4Fe_2Cu$: C, 60.97; H, 5.12; N, 3.55%. IR (KBr disk): ν(OH) 3436 (m, br), ν(C = O) 1562 (s), ν(C = C) 1513 (vs) cm^{-1}. UV (nm, in DMF): $\lambda_{max}(\varepsilon \times 10^4)$ 275 (2.5), 358 (3.4) (K-band), 450 (0.49) (CT-band).

Complex **II** as a black red solid, yield: 0.312 g (80%). M.p. 209.5–210.5 °C. *Anal.* Found: C, 64.75; H, 5.21; N, 3.33. Calc. for $C_{42}H_{40}N_2O_2Fe_2Cu$: C, 64.67; H, 5.17; N, 3.59%. IR (KBr disk): ν(C = O) 1561 (s), ν(C = C) 1512 (vs) cm^{-1}. UV (nm, in DMF): $\lambda_{max}(\varepsilon \times 10^4)$ 275 (2.9), 355 (4.3) (K-band), 447 (0.50) (CT-band).

Complex **III** as a purple red solid, yield: 0.331 g (82%). M.p. 213–214.5 °C. *Anal.* Found: C, 65.30; H, 5.16; N, 3.04. Calc. for $C_{44}H_{44}N_2O_2Fe_2Cu$: C, 65.40; H, 5.49; N, 3.47%. IR (KBr disk): ν(C = O) 1557 (s), ν(C = C) 1513 (vs) cm^{-1}. UV (nm, in DMF): $\lambda_{max}(\varepsilon \times 10^4)$ 278 (2.4), 351 (3.2) (K-band), 447 (0.37) (CT-band).

Complex **IV** as a black solid, yield: 0.379 g (83%). M.p. 203.5–205 °C (dry sample). *Anal.* Found: C, 65.51; H, 4.47; N, 3.14. Calc. for $C_{50}H_{44}N_2O_4Fe_2Cu$: C, 65.84; H, 4.86; N, 3.07%. IR (KBr disk): ν(OH) 3439 (w, br), ν(C = O) 1550 (m), ν(C = C) 1509 (vs) cm^{-1}. UV (nm, in DMF): $\lambda_{max}(\varepsilon \times 10^4)$ 379 (3.5) (K-band).

Complex **V** as a black red solid, yield: 0.376 g (80%). M.p. 222.5–223.5 °C (dry sample). *Anal.* Found: C, 66.85; H, 5.06; N, 3.18. Calc. for $C_{52}H_{48}N_2O_4Fe_2Cu$: C, 66.43; H, 5.15; N, 2.98%. IR (KBr disk): ν(OH) 3430 (w, br), ν(C = O) 1580 (m), ν(C = C) 1513 (vs) cm^{-1}. UV (nm, in DMF): $\lambda_{max}(\varepsilon \times 10^4)$ 378 (2.67) (K-band).

2.4. Crystal structure determinations

Single crystals of enaminone **HL^6** for X-ray analysis were obtained by slow evaporation of its solution in CH_2Cl_2 and petroleum ether at room temperature. Single crystals of complex **I** for structure determination were obtained by further recrystallization from CH_2Cl_2 and ethanol. X-ray data of both compounds were measured on an Enraf–Nonius CAD4 diffractometer using graphite-monochromated Mo K_α radiation ($\lambda = 0.71073$ Å) at 293 K. The structures were solved by direct methods and refined by full-matrix least-squares methods based on F^2 with anisotropic thermal parameters for all non-hydrogen atoms [12]. A summary of the data collection and structure refinement parameters is given in Table 1. Selected bond distances (Å) and angles (°) are listed in Tables 2 (enaminone **HL^6**) and 3 (complex **I**).

3. Results and discussion

3.1. Syntheses of enaminones and their complexes

Syntheses of enaminones and their complexes are represented in Schemes 1 and 2. Reaction of the β-diketone **1** or **2** [$C_5H_5FeC_5H_4C(O)CH_2C(O)R$] (R = CH_3, C_6H_5) and an excess of an appropriate aniline [H_2NAr] (Ar = Ph, 2-$CH_3C_6H_4$, 2,6-$(CH_3)_2C_6H_3$) in the presence of a catalytic trace amount of *p*-toluenesulfonic acid in refluxing toluene via removal of water using a Dean–Stark apparatus affords the corresponding enaminones in satisfactory yields. For enaminones **HL^4**, **HL^5** and **HL^6**, in view of the electronic and steric effects of the phenyl and ferrocenyl groups, it may be expected that the anilines attack the carbonyl with the Ph substituent. This conclusion is further supported by X-ray diffraction analysis on the enaminone **HL^6** (see below). Also because of steric hindrance from the N-phenyl and C-phenyl groups, reaction of the β-diketone **2** with 2,6-dimethylaniline is incomplete and accordingly enaminone **HL^6** is obtained only in moderate yield. Except **HL^6**, each enaminone can react with the copper(II) ion forming the corresponding neutral complex with the release of HOAc. TLC analyses of all the complexes show that each exists as a single isomer. However, because of the steric hindrance of **HL^6**, all attempts to synthesize the corresponding complex $\mathbf{L^6_2}Cu{\cdot}xH_2O$ were unsuccessful and the starting materials were recovered.

Analytical data of all the new complexes listed in Section 2 suggest that they may be formulated as $\mathbf{L^1_2}Cu{\cdot}2H_2O$, $\mathbf{L^2_2}Cu$, $\mathbf{L^3_2}Cu$, $\mathbf{L^4_2}Cu{\cdot}2H_2O$ and $\mathbf{L^5_2}Cu{\cdot}2H_2O$, respectively.

3.2. ^1H NMR spectra of enaminones

The ^1H NMR spectral data of the enaminones are presented in Section 2. The spectra of the free ligands display two singlets at δ 4.41–4.58 and 4.79–4.90 ppm, with the integration corresponding to 2H attributed to the H^3/H^4 and H^2/H^5 protons of the substituted cyclopentadienyl ring. Another singlet signal with the integration corresponding to 5H at δ 4.21–4.27 ppm is due

Table 1
Crystallographic data for **HL⁶** and **I**

	HL⁶	**I**
Formula	$C_{27}H_{25}FeNO$	$C_{40}H_{40}Fe_2N_2O_4Cu$
Formula weight	435.33	787.98
Crystal size (mm)	$0.30 \times 0.30 \times 0.20$	$0.3 \times 0.3 \times 0.2$
Crystal system	monoclinic	orthorhombic
Space group	$P2_1/c$	$Pbcn$
Unit cell dimensions		
a(Å)	8.3000(17)	12.910(3)
b(Å)	13.320(3)	19.280(4)
c(Å)	20.410(4)	27.620(6)
α(°)	90.00	90.00
β(°)	101.66(3)	90.00
γ(°)	90.00	90.00
V (Å^3)	2209.9(8)	6875(2)
Z	4	8
D_c(g cm^{-1})	1.308	1.521
F(0 0 0)	912	3176
T (K)	293(2)	293(2)
μ(Mo K$_\alpha$) (mm^{-1})	0.700	1.487
Scan mode	$\omega - 2\theta$	$\omega - 2\theta$
θ Range (°)	1.84; 24.97	2.16; 24.96
Limiting indices	$0 \leqslant h \leqslant 9$, $0 \leqslant k \leqslant 15$, $-24 \leqslant l \leqslant 23$	$0 \leqslant h \leqslant 15$, $0 \leqslant k \leqslant 22$, $0 \leqslant l \leqslant 32$
Absorption correction	PSI-scan	PSI-scan
Reflections collected	4158	5996
Independent reflections [$I > 2.0\sigma$ (I)]	3872	5996
Refinement method	full-matrix least-squares on F^2	full-matrix least-squares on F^2
Number of parameters refined	271	436
Final R indices [$I > 2.0\sigma$ (I)]	R_1, 0.0485; wR_2, 0.1427	R_1, 0.0944; wR_2, 0.1910
R indices (all data)	R_1, 0.1059; wR_2, 0.1690	R_1, 0.3446; wR_2, 0.3014
Goodness-of-fit	1.016	0.931
Largest difference peak and hole (e Å^{-3})	0.228 and −0.221	0.546 and −0.552

Table 2
Selected bond distances (Å) and angles (°) for **HL⁶**

Bond distances			
H–N	0.85(0)	C(1)–C(15)	1.516(7)
N–C(3)	1.349(5)	C(2)–C(13)	1.473(8)
C(3)–C(4)	1.367(5)	C(3)–C(45)	1.493(5)
C(4)–C(5)	1.408(5)	C(5)–C(34)	1.482(5)
O–C(5)	1.250(4)	C(14)–N	1.443(8)
Bond angles			
N–C(3)–C(4)	121.2(3)	N–C(3)–C(45)	118.4(3)
C(3)–C(4)–H	117.9(3)	O–C(5)–C(4)	123.0(3)
C(3)–C(4)–C(5)	124.2(3)	O–C(5)–C(34)	119.0(3)
C(5)–C(4)–H	117.9(3)	C(4)–C(5)–C(34)	117.9(3)
C(3)–N–C(14)	127.3(3)	N–H···O	135
C(3)–N–H	116.3(3)		

Table 3
Selected bond distances (Å) and angles (°) for **I**

Bond distances			
Cu–O(1)	1.92(1)	Cu–O(2)	1.89(1)
Cu–N(1)	1.95(1)	Cu–N(2)	1.99(1)
N(1)–C(2)	1.28(2)	N(2)–C(6)	1.31(2)
O(1)–C(4)	1.31(1)	O(2)–C(8)	1.31(2)
N(1)–C(14)	1.45(2)	N(2)–C(26)	1.42(2)
Bond angles			
O(1)–Cu–O(2)	154.1(5)	C(2)–N(1)–Cu	124.9(1)
O(1)–Cu–N(1)	92.1(5)	C(2)–N(1)–C(14)	117.4(1)
O(1)–Cu–N(2)	93.1(5)	C(14)–N(1)–Cu	117.5(1)
O(2)–Cu–N(1)	91.6(5)	C(6)–N(2)–Cu	123.1(1)
O(2)–Cu–N(2)	94.1(5)	C(6)–N(2)–C(26)	118.4(1)
N(1)–Cu–N(2)	155.5(5)	C(26)–N(2)–Cu	118.4(1)

to the unsubstituted cyclopentadienyl ring protons. For enaminones **HL¹**, **HL²** and **HL³**, the methyl protons of the C(O)CHC(NHAr)CH_3 moiety show a singlet corresponding to 3H at δ 1.73–2.15 ppm. The methyl protons of the NHAr moiety also show a singlet corresponding to 3H and 6H for **HL²** and **HL⁵** and for **HL³** and **HL⁶** at δ 2.21–2.48 ppm, respectively. For each ligand, the vinylic proton as a singlet appears at δ 5.54–5.70 ppm, and the relative integrated intensity ratio of this peak to other peaks shows that there is only one H atom bonded to the α-C atom in the C(O)C$_\alpha$HC(NHAr)R moiety. The aromatic protons of the ligands exhibit multiplets corresponding to 5H, 4H and 3H for **HL¹**, **HL²** and **HL³** and 10H, 9H and 8H for **HL⁴**, **HL⁵** and **HL⁶** at δ 6.40–7.44 ppm, respectively. The spectra of all ligands display a singlet signal at δ 12.03–12.64 ppm, which is assigned to the enamino NH and disappears in the presence of D_2O. The downfield position of this signal may mainly arise from the intramolecular hydrogen bonding as shown in Scheme 1. Obviously, the above evidence is in agreement with the proposed structure of the ligands and also supported by the crystal structure of enaminone **HL⁶** [2a,3c].

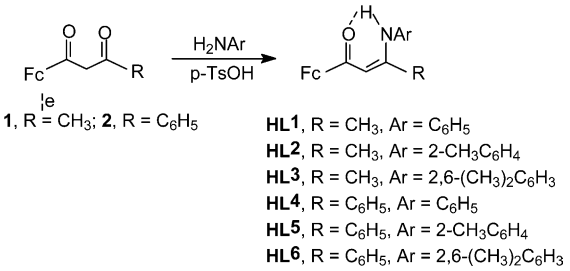

Scheme 1. Syntheses of enaminones.

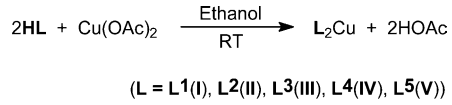

Scheme 2. Syntheses of complexes.

3.3. Crystal structure

3.3.1. Crystal structure of HL⁶

As mentioned above, enaminones with the general formula [R′C(O)CHC(NHAr)R] may have the following four isomers: *cis*-s-*cis*, *cis*-s-*trans*, *trans*-s-*cis* and *trans*-s-*trans* in which *cis* and *trans* refer to two possible geometric arrangements for the carbon–carbon double bond and s-*cis* and s-*trans* to both isomerisms about the carbon–carbon single bond between the carbon–carbon and carbon–oxygen double bonds [2a]. Owing to very few X-ray diffraction studies, so far the structure of enaminones [R′C(O)CHC(NHAr)R] has resulted in inconsistencies and remains uncertain [2b,4]. Therefore, a single crystal X-ray analysis on **HL⁶** was carried out to determine the structure of the new enaminones. The molecular structure of **HL⁶** together with the atomic numbering is shown in Fig. 1. As seen from Fig. 1, **HL⁶** in the solid state belongs to the *cis*-s-*cis* isomer. All atoms in the skeleton O=C–C=C–N can be regarded as sp^2 hybridized. As shown by the comparison of the C=O, C–C, C=C and C–N distances (Table 2) with the corresponding pure double or single bond distances C(sp^2)=O ≈1.20, C(sp^2)–C(sp^2) ≈ 1.48, C(sp^2)=C(sp^2) ≈ 1.33 and C(sp^2)–N (sp^2) ≈ 1.44 Å, **HL⁶** exhibits partial delocalization of the O=C–C=C–N system. That the H···O distance of 1.971 Å is significantly shorter than the sum of the van der walls radii (2.60 Å) indicates the existence of intramolecular hydrogen bonding; this is also in accordance with spectroscopic data. The plane of the skeleton and the plane of the substituted cyclopentadienyl ring only form a dihedral angle of 13.6°, whereas the skeleton with the N-benzene ring and C-benzene ring makes two angles of 74.4 and 116.9° to avoid the steric repulsions. Therefore, in the solid state, neither the N-benzene ring nor the C-benzene ring is involved in the conjugation of the skeleton, whereas the substituted cyclopentadienyl ring may in part conjugate with the enaminonic system [3c,4a].

3.3.2. Crystal structure of complex *I*

In view of *cis* or *trans* isomerism of donor atoms and planar or tetrahedral coordination geometry of the central metal ion, as well as anti or syn arrangement of the ferrocenyl groups with respect to the plane with the central metal ion and donor atoms, four-coordinate copper(II) complexes may possess eight stereoisomers: planar-*cis*-anti, planar-*cis*-syn, planar-*trans*-anti, planar-*trans*-syn, tetrahedral-*cis*-anti, tetrahedral-*cis*-syn, tetrahedral-*trans*-anti and tetrahedral-*trans*-syn [13,14]. Therefore, to further establish their structures and to provide more structural evidence for the new complexes, the crystal structure of complex **I** was determined. The molecular structure of the new copper complex **I** together with the atomic numbering is shown in Fig. 2. The metal atom displays a tetrahedral coordination geometry surrounded by two nitrogen atoms and two oxygen atoms of two deprotonated ligands (L^-), so complex **I** exists only in the tetrahedral-*trans*-syn form, which is further supported by the above-described TLC. More interestingly, against usual expectation, both

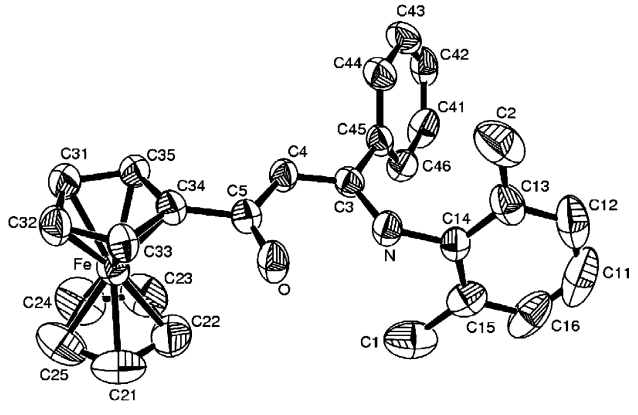

Fig. 1. Molecular structure of enaminone **HL⁶** together with the atomic numbering. Hydrogen atoms are omitted for clarity.

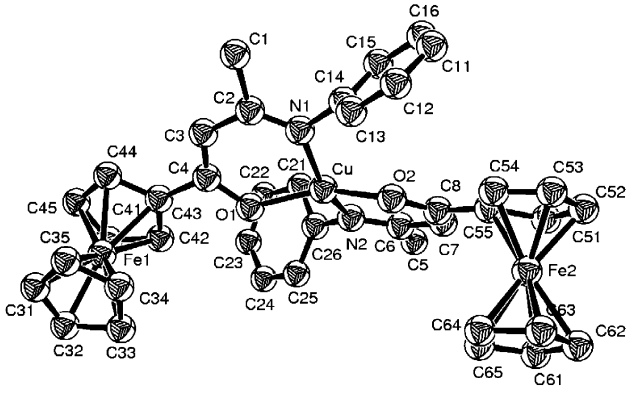

Fig. 2. Molecular structure of complex **I** together with the atomic numbering. Hydrogen atoms and water molecules are omitted for clarity.

ferrocenyl groups in complex **I** are syn to each other. In view of the Fe···Fe distance of 10.502 Å, it may be concluded that one ferrocenyl group in complex **I** does not interact sterically with the other and therefore the syn isomer can be isolated, whereas the corresponding anti-isomer cannot be found. As expected, both six-membered chelate rings are planar. Angles O(1)–Cu–N(1) and O(2)–Cu–N(2), which are 92.1(5) and 94.1(5)°, are slightly larger than the corresponding values observed in related structures [15,16]. Values of angles O(1)–Cu–O(2) and N(1)–Cu–N(2) are 154.1(5) and 155.5(5)°, therefore indicating that the coordination geometry about the copper ion is tetrahedral as mentioned above. The bonds between the copper atom and the donor sites of the deprotonated ligand are within the range of values normally found for these bonds [15,16]. Interestingly, the Cu–O distances (Cu–O(1) = 1.92(1); Cu–O(2) = 1.89(1) Å) are significantly different from each other whereas the Cu–N distances (Cu–N(1) = 1.95(1); Cu–N(2) = 1.99(1) Å) are similar. The structural features of two $\mathbf{L}^-$ ions (Table 3) are as follows. One exhibits N(1)–C(2), C(2)–C(3), C(3)–C(4) and O(1)–C(4) bond distances of 1.28(2), 1.42(2), 1.35(2) and 1.31(2) Å, and the other shows N(2)–C(6), C(6)–C(7), C(7)–C(8) and O(2)–C(8) bond distances of 1.31(2), 1.42(2), 1.36(2) and 1.31(2) Å whereas the corresponding bond distances of **HL⁶** are 1.349(5), 1.367(5), 1.408(5) and 1.250(4) Å. These suggest that the O=C–C=C–N system of the complex has more delocalization than that of the corresponding ligand [16]. It should be pointed out that the water molecules in complex **I** are non-coordinate and disordered.

3.4. IR spectra

The important IR data of the enaminones and the complexes are given in Section 2. The band at ≈3080 cm^{-1} in the spectrum of each ligand is due to *v*(NH) and does not occur in that of the corresponding complex. This suggests that the enaminones are bonded to copper ions in the monoanionic form. Moreover, the strong bands assignable to stretching vibrations of the skeleton C=O and C=C groups, which are observed at 1585–1603 and 1552–1567 cm^{-1} in the ligands, are all red-shifted to the region 1550–1580 and 1510–1513 cm^{-1} in the complexes [3c,7a]. This is because the complexes possess resonance forms as shown in Fig. 3, which lead to a decrease in double bond character of the C=O and C=C groups [17]. As expected, the spectra of complexes **I**, **IV** and **V** display a broad and weak band at ≈3430 cm^{-1} due to the presence of *v*(OH) of lattice water molecules. Further, this has been confirmed by another band appearing at about 600 cm^{-1} [18,19]. Also this is consistent with the above-described X-ray crystal structure determination and elemental analyses data.

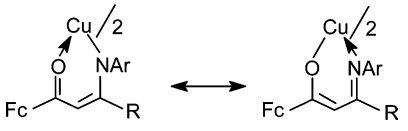

Fig. 3. Resonance forms of copper complexes.

3.5. UV spectra

The UV spectral data of the enaminones and the complexes are listed in Section 2. In the UV spectra, complexes **I**, **II** and **III** show three maxima at ≈275, 350 and 450 nm while for complexes **IV** and **V** each exhibits one maxima at ≈378 nm. The shortest wavelength absorption which is due to the B-band of cyclopentadienyl or benzene rings, displays a red shift compared with the corresponding ligand [20]. Unlike other ligands, only **HL¹** exhibits the respective B-band for the cyclopentadienyl ring and benzene ring. On the other hand, the longer wavelength band in the region 350–379 nm may be attributed to the $(\pi \rightarrow \pi^*)$ transition (viz. K-band) while the corresponding absorption in each ligand is observed in the region 328–369 nm. Therefore, compared with those absorptions of the corresponding ligands, the K-bands of all the complexes also show red shifts. Because deprotonated ligands bonded to the central metal ions strengthen the conjugative effect of the skeleton as shown in Fig. 3, red shifts of K-bands in the complexes are observed, whereas slightly decreased bonding of the cyclopentadienyl groups of the complexes results in a bathochromic shift of the B-band of the cyclopentadienyl group, which is also supported by the X-ray crystallography of enaminone **HL⁶** and complex **I** [20,21]. Furthermore, unlike the corresponding ligands, complexes **I**, **II** and **III** exhibit an intense absorption band in the region 450–447 nm which may be assignable to a ligand-to-metal charge transfer transition [22]. However for complexes **IV** and **V** no charge transfer transitions are observed. Finally, because weak d–d transtions in ferrocene-containing complexes are obscured by much more intense UV transitions from a different nature, the ligand field absorptions in these complexes cannot be resolved.

4. Conclusion

Reaction of the ferrocene-containing β-diketone $[C_5H_5FeC_5H_4C(O)CH_2C(O)R]$ (**1**, R = CH_3; **2**, R = C_6H_5) and the corresponding aniline $[H_2NAr]$ (Ar = Ph, 2-$CH_3C_6H_4$, 2,6-$(CH_3)_2C_6H_3$) in the presence of a catalytic amount of *p*-toluenesulfonic acid yields a series of *cis*-s-*cis* enaminones $[C_5H_5FeC_5H_4C(O)CH=C(NH Ar)R]$ (**HL¹**–**HL⁶**). Reaction of enaminones **HL¹**–**HL⁵** and copper acetate affords tetrahedral-*trans*-syn complexes **I**–**V** in which each of the enaminones coordinates to the copper ion as a monoanionic bidentate ligand via

carbonyl oxygen and enamine nitrogen atoms after deprotonation.

5. Supplementary material

Full crystallographic data (CCDC No. 200938 for enaminone **HL**[6] and CCDC No. 207417 for complex **I**) have been deposited at the Cambridge Crystallographic Database Centre and are available on request from the Director, CCDC, 12 Union Road, Cambridge, CB2 1EZ, UK (Fax: +44-1223-336-033; Email:deposit@ccdc.cam.ac.uk or http://www.ccdc.cam.ac.uk).

Acknowledgements

We thank the National Nature Science Foundation of China (No. 20175023) and Yangzhou University (No. D0009107) for financial support of this work.

References

[1] (a) L.F. Tietze, A. Bergmann, G. Brill, K. Brüggemann, U. Hartfiel, E. Voβ, Chem. Ber. 122 (1989) 83;
(b) H. Iida, Y. Yuasa, C. Kibayashi, J. Chem. Soc., Chem. Comm. (1981) 114.
[2] (a) J.V. Greenhill, Chem. Soc. Rev. 6 (1977) 277;
(b) L. Kozerski, Tetrahedron 32 (1976) 1299.
[3] (a) J. Mrosset, C. Floriani, M. Mazzanti, A.C. Villa, C. Guastini, Inorg. Chem. 29 (1990) 3991;
(b) M. Kwiatkowski, A. Olechnowicz, J. Mrozinski, D.M. Ho, E. Deutsch, Inorg. Chim. Acta 158 (1989) 37;
(c) H. Iida, Y. Yuasa, C. Kibayashi, Y. Iitaka, J. Chem. Soc., Dalton Trans. (1981) 2212.
[4] (a) P. Gilli, V. Bertolasi, V. Ferretti, G. Gilli, J. Am. Chem. Soc. 122 (2000) 10405;
(b) G.O. Dudek, G.P. Volpp, J. Am. Chem. Soc. 85 (1963) 2697.
[5] G.J.P. Britovsek, Angew. Chem., Int. Ed. Engl. 38 (1999) 428.
[6] M.J. Bochmann, J. Chem. Soc., Dalton Trans. (1996) 255.
[7] (a) A.A. Osowole, J.A.O. Woods, O.A. Odunola, Synth. React. Inorg. Met. Org. Chem. 32 (2002) 783;
(b) J. Kim, J.W. Hwang, Y. Kim, M.H. Lee, Y. Han, Y. Do, J. Organomet. Chem. 620 (2001) 1;
(c) S. Doherty, R.J. Errington, N. Housley, J. Ridland, W. Clegg, M.R.J. Elsegood, Organometallics 18 (1999) 1018.
[8] C.W. Ho, W.C. Cheng, M.C. Cheng, S.M. Peng, K.F. Cheng, C.M. Che, J. Chem. Soc., Dalton Trans. (1996) 405.
[9] P.J. Graham, G.W. Parshall, M.L. Peterson, G.M. Whitman, J. Am. Chem. Soc. 79 (1957) 3416.
[10] V. Weinmayr, Naturwiss 45 (1958) 311.
[11] (a) C.E. Cain, T.A. Mashburn Jr., C.R. Hauser, J. Org. Chem. 26 (1960) 1030;
(b) C.R. Hauser, J.K. Lindsay, J. Org. Chem. 22 (1957) 482.
[12] G.M. Sheldrick, SHLXTL, Software Reference Manual, Bruker Analytical X-ray Systems, Madison, WI, USA, 1996.
[13] G.E. Gurr, Inorg. Chem. 3 (1964) 614.
[14] R.D. Archer, Inorg. Chem. 2 (1963) 292.
[15] J.P. Costes, J.F. Serra, F. Dahan, J.P. Laurent, Inorg. Chem. 25 (1986) 2790.
[16] M.B. Cingi, A.C. Villa, A.G. Manfredotti, C. Guastini, M. Nardelli, Acta Crystallogr. Sect. B 28 (1972) 1075.
[17] Y.C. Shi, W.B. Shen, H.M. Yang, H.B. Song, X.Y. Hu, Polyhedron 22 (2003), in press.
[18] M.A. El-Gahami, Synth. React. Inorg. Met.-Org. Chem. 32 (2002) 1143.
[19] K. Nakamoto, Infrared and Raman Spectra of Inorganic and Coordination Compounds, third ed., John Wiley, New York, 1978.
[20] Y.C. Shi, Q.B. Song, X.L. Wu, Y.X. Ma, Polyhedron 13 (1994) 2101.
[21] Y.C. Shi, Y.M. Liang, X.L. Wu, Q.B. Song, G.S. Huang, Y.X. Ma, J. Coord. Chem. 33 (1994) 295.
[22] B.N. Figgis, Introduction to Ligand Fields, John Wiley, New York, 1976.

Available online at www.sciencedirect.com
SCIENCE DIRECT®
Polyhedron 23 (2004) 23–31
POLYHEDRON
www.elsevier.com/locate/poly

Synthesis, characterization and magnetochemical studies of some copper(II) complexes derived from *n*-salicylidene-*n*-alkanoylhydrazins: X-ray crystal and molecular structure of bis [monochloro-(μ-*n*-salicylidenemyristoylhydrazine)ono (−1)] dicopper(II)

Magdi F. Iskander [a,*], Laila El-Sayed [a], Nahed M.H. Salem [a], Wolfgang Haase [b], Hans Jorg Linder [c], Sabine Foro [c]

[a] *Chemistry Department, Faculty of Science, Alexandria University, P.O. Box 426, Ibrahimia, Alexandria 21321, Egypt*
[b] *Institut fur Physikalische Chemie, AG Kondensierte Materie, Fachbereich Chemie, Technische Universitat Darmstadt, Petersenstrasse 20, D-64287 Darmstadt, Germany*
[c] *Institute fur Organische Chemie, TU - Darmstadts Petersenster 22, Darmstadt, Germany*

Received 19 June 2003; accepted 1 September 2003

Abstract

Three types of copper(II) complexes, $[Cu(HL)Cl \cdot H_2O] \cdot xH_2O$, $[\{Cu(HL)Cl\}_2]$ and $[\{Cu(L)\}_2]$, derived from *N*-Salicylidene-*n*-alkanoylhydrazines (H_2L) have been synthesized and characterized by elemental analyses, infrared spectra and field desorption mass spectra as well as variable temperature magnetic susceptibility measurements. The X-ray molecular structure of bis[monochloro(μ-*N*-salicylidene myristoylhydrazine)ONO′(−1)]dicopper(II) showed that this complex is a centrosymmetric dimer in which each copper(II) is in a distorted square pyramidal environment and coordinated in the equatorial plane to the ONO mononegative tridentate acylhydrazone ligand. The fourth coordination site is occupied by the symmetry related phenoxy oxygen of the other monomeric unit. The chloride ion occupies the fifth axial coordination site. Magnetic susceptibility measurements at different temperatures (5–298 K) showed that the hydrated chloro complexes $[Cu(HL)Cl \cdot H_2O] \cdot xH_2O$ are monomeric and no spin–spin interaction was detected, while the anhydrous chloro complexes $[\{Cu(HL)Cl\}_2]$ are dimeric and exhibit strong antiferromagnetic coupling with $-2J$ values the range 466–477 cm^{-1}. The neutral complexes $[\{Cu(L)\}_2]$ also show antiferromagetic behaviour with $-2J$ varying from 170 to 243 cm^{-1}.
© 2003 Elsevier Ltd. All rights reserved.

Keywords: *N*-salicylidene-*n*-alkanoylhydrazines; Copper(II) complexes; Magnetochemical studies; Bis[monochloro(μ-*N*-salicylidenemyristoylhydrazine) ONO′(−1)]dicopper(II); X-ray crystal and molecular structure

1. Introduction

N-salicylideneacylhydrazines show a wide spectrum of biological activities [1–6]. The cytotoxicity of these acylhydrazones and their transition metal(II) complexes against T-cell leukaemia and human colon adenocarcinoma cell lines were recently evaluated [5,6]. As *N*-salicylideneacylhydrazines can act towards transition and non-transition metal ions either as neutral, mono- or dinegative ONO tridentate ligands [5,7–12], their biological activities appear to be associated with their ability to bind essential metal ions in vivo [1–6]. QSAR analysis revealed that the cytotoxicity of *n*-alkanoylhydrazones and their copper(II) complexes are dominated by the transport factor as measured by log the octanol/water partition coefficient (*P*) [5], while for the aroylhydrazone series, both electronic factors, as measured by the Hammett sigma parameter (σ), and transport factors (log *P*) play a key role in the observed cytotoxicity [6].

* Corresponding author. Tel.: +20-3-3911794; fax: +20-3-4911794.
E-mail address: m.iskander@link.net (M.F. Iskander).

0277-5387/$ - see front matter © 2003 Elsevier Ltd. All rights reserved.
doi:10.1016/j.poly.2003.09.022

Moreover, the biological activities of metal(II), especially copper(II), complexes were found more significantly active than the metal free ligands [1–6].

In this paper, we report the synthesis and characterization of some novel lipophilic copper(II) complexes derived from *N*-salicylidene-*n*-alkanoylhydrazines. The X-ray crystal and molecular structure of bis [monochloro-(*N*-salicylidenemyristoyl-hydrazine)ONO(−1)] dicopper(II) has been determined and the magnetic properties of the different types of the prepared copper(II) complexes will be discussed.

2. Results and discussion

2.1. Synthesis

Condensation of *n*-alkanoylhydrazines with salicylaldehyde in methanol afforded the corresponding *N*-salicylidene-*n*-alkanoylhydrazines, (H_2L), (**1**, $n = 0$, 4, 5, 6, 12 and 16). The reaction of **1a**–**1d** (Scheme 1) with copper(II) chloride gave the green monomeric chloro complexes $[Cu(HL)Cl \cdot H_2O] \cdot xH_2O$ (**2a**–**2d**) (Scheme 2), while with **1e**−**1f** the anhydrous brown dimeric chloro complexes (**3e**–**3f**) (Scheme 3) were isolated. Similar to other ONO tridentate *N*-salicylideneacylhydrazines, the reaction of **1a**–**1f** with copper(II) acetate in methanol, using a 1:1 molar ratio, gave the neutral dimeric copper(II) complexes $[\{Cu(L)\}_2]$, where L refers to the hydrazone dianion [2,5–7,13]. The elemental analyses of the prepared copper(II) complexes are listed in Table 1.

2.2. Mass spectra

The electron impact (EI) mass spectra of **1a**–**1f** display the corresponding molecular ion peak together with other fragments originated from both *N*-salicylidene and *n*-alkanoylhydrazine residues. The field desorption (FD) mass spectra of both hydrated and anhydrous chloro complexes, Table 2, show peaks corresponding to $[L]^+$, $[\{Cu(L)\}]^+$, $[\{Cu(L)Cl\}_2 - Cl]^+$ and $[\{Cu(L)\}_2]^+$. The relative abundances of these ions, Table 2, suggest the higher stability of the dimeric species $[\{Cu(L)\}_2]^+$ relative to the corresponding monomeric species $[\{Cu(L)\}^+]$ in the gas phase. On the other hand, the field desorption

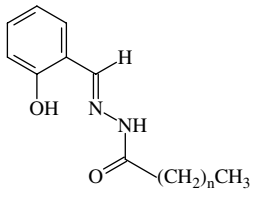

	n
1a	0
1b	4
1c	5
1d	6
1e	12
1f	16

(1)

Scheme 1.

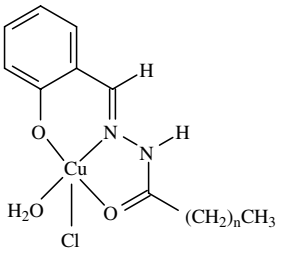

	n
2a	0
2b	4
2c	5
2d	6

(2)

Scheme 2.

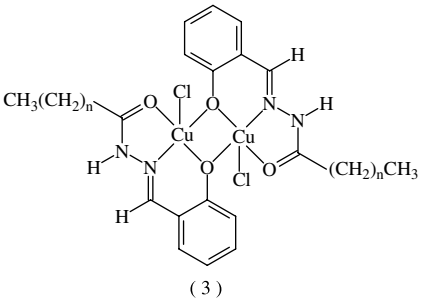

	n
3a	12
3b	16

(3)

Scheme 3.

(FD) mass spectra of neutral complexes $[\{Cu(L)\}_2]$ ($n = 4$, 5, 6, 12 and 16), Table 2, show only the molecular ion peak at $m/z = 590$, 618, 646, 815 and 927 corresponding to the dimeric species $[\{Cu(L)\}_2]^+$.

2.3. Infrared spectra

The infrared spectra of the metal free ligands (**1a**–**1f**), are more or less similar and show a series of bands at ca. 3200, 1670, 1620, 1540 and 1280 cm^{-1} due to ν(N–H), amide I [ν(C=O)], ν(C=N), amide II [δ(NH)] and amide III [ν(C–N)] bands, respectively [14]. The recorded spectra reveal the predominance of the ketoamide tautomer in the solid state. The infrared spectra of both hydrated monomeric (**2a**–**2d**) and anhydrous dimeric chloro complexes (**3a** and **3b**) show bands at ca. 3220, 1625, 1600, 1550 and 1330 cm^{-1} due to ν(N–H), amide I [ν(C=O)], ν(C=N), amide II (δ(N–H) and amide III [ν(C–N)] bands, respectively. Both amide I [ν(C=O)] and ν(C=N) are shifted to lower frequencies, while the amide III band appears at higher frequencies relative to those of the corresponding metal free ligands. The recorded spectra indicate that the *n*-alkanoylhydrazone in these complexes behaves as a mononegative ONO tridentate ligand. The spectra of the neutral dimeric complexes $[\{Cu(L)\}_2]$, on the other hand, lack absorptions due to ν(N–H), amide I [ν(C=O)] and amide II [δ(N–H)] bands, but show intense bands at ca. 1615 cm^{-1} due to an asymmetric vibration of the conjugated C=N–N=C residue [5,7,15]. The recorded spectra suggest the deprotonation of both phenolic and enolimide

Table 1
Elemental analyses of copper(II) complexes derived from *N*-salicylidene-*n*-alkanoylhydrazines

Complex number	R	Found (calculated) (%)		
		C	H	N
(i) $[Cu(HL)Cl \cdot H_2O] \cdot xH_2O$ (**2**)				
2a	CH_3	36.54 (36.74)	3.78 (3.77)	9.46 (9.52)
2b	$(CH_2)_4CH_3$ ($x = 1$)	42.83 (42.39)	5.04 (5.75)	8.02 (7.61)
2c	$(CH_2)_5CH_3$ ($x = 0.5$)	44.80 (45.04)	5.44 (5.94)	7.72 (7.50)
2d	$(CH_2)_6CH_3$ ($x = 1$)	45.83 (45.45)	5.79 (6.36)	7.51 (7.07)
(ii) $[\{Cu(HL)Cl\}_2]$(**3**)				
3a	$(CH_2)_{12}CH_3$	56.65 (56.74)	7.32 (7.48)	6.05(6.30)
3b	$(CH_2)_{16}CH_3$	59.83 (59.98)	8.37 (8.25)	5.47 (5.59)
(iii) $[\{Cu(L)\}_2]$(**4**)				
4a	CH_3	54.20 (54.09)	3.24 (3.36)	11.57 (11.69)
4b	$(CH_2)_4CH_3$	52.87 (52.78)	5.45 (5.45)	9.40 (9.47)
4c	$(CH_2)_5CH_3$	54.06 (54.27)	5.80 (5.86)	9.11 (9.04)
4d	$(CH_2)_6CH_3$	55.76 (55.63)	6.28 (6.22)	8.51 (8.65)
4e	$(CH_2)_{12}CH_3$	61.62 (61.81)	7.96 (7.90)	6.80 (6.87)
4f	$(CH_2)_{16}CH_3$	64.34 (64.69)	8.85 (8.69)	5.92 (6.04)

groups, and the *n*-alkanoylhydrazone in this type of complex acts as an ONO tridentate dianion.

2.4. X-ray structure of bis[monochloro(N-salicylidenatomyristoylhydrazine)ONO(−1)] dicopper(II)

The crystal data and structure refinement parameters are given in Table 3. The structure of **3a** together with

Table 2
Field desorption (FD) mass spectra of $[\{Cu(L)\}_2]$, $[Cu(L)Cl \cdot H_2O] \cdot xH_2O$ and $[\{Cu(L)Cl\}_2]$ complexes

Complex	*m/z* (R.A)	Assignments
(i) $[Cu(HL)Cl \cdot H_2O] \cdot xH_2O$ (**2**)		
2b $CH_{24}CH_3$	234 (100)	$[H_2L + H]^+$
	333 (3)	$[Cu(HL)Cl]^+$
	589 (10)	$[\{Cu(L)\}_2]^+$
	630 (10)	$[\{Cu(HL)Cl\}_2 - Cl]^+$
	664 (5)	
2c $CH_{25}CH_3$	249 (22)	$[H_2L + H]^+$
	310(15)	$[Cu(HL)]^+$
	618 (100)	$[\{Cu(HL)Cl\}_2 - 2Cl]^+$
	900 (32)	$[\{Cu(L)\}_3]^+$
2d $CH_{26}CH_3$	263 (18)	$[H_2L + H]^+$
	324(18)	$[Cu(HL)]^+$
	720	$[\{Cu(L)Cl\}_2 - 2Cl]^+$
(ii) $[\{Cu(HL)Cl\}_2]$ (**3**)		
3a $CH_{212}CH_3$	346 (2)	$[H_2L + H]^+$
	407 (4)	$[Cu(HL)]^+$
	814(100)	$[\{Cu(HL)Cl\}_2 - 2Cl]^+$
3b $CH_{216}CH_3$	403 (5)	$[H_2L + H]^+$
	464(15)	$[Cu(HL)]^+$
	928 (100)	$[\{Cu(HL)Cl\}_2 - 2Cl]^+$
(iii) $[\{Cu(L)\}_2]$ (**4**)		
4b $CH_{24}CH_3$	590 (100)	$[\{Cu(L)\}_2]^+$
4c $CH_{25}CH_3$	618 (100)	$[\{Cu(L)\}_2]^+$
4d $CH_{26}CH_3$	646 (100)	$[\{Cu(L)\}_2]^+$
4e $CH_{212}CH_3$	815 (100)	$[\{Cu(L)\}_2]^+$
4f $CH_{216}CH_3$	927 (100)	$[\{Cu(L)\}_2]^+$

Table 3
Crystallographic data and structure refinement parameters for **3a**

Empirical formula	$C_{21}H_{33}ClCuN_2O_2$
Formula weight	444.48
Temperature (K)	299(2)
Wavelength (Å)	0.71093
Crystal system	triclinic
Space group	$P\bar{1}$
Unit cell dimensions	
a (Å)	6.488(2)
b (Å)	8.602(1)
c (Å)	20.605(3)
α (°)	93.03(1)
β (°)	96.13(2)
γ (°)	101.20(2)
Volume (Å^3)	1118.4(4)
Z, Calculated density (Mg/m^3)	2, 1.320
Absorption coefficient (mm^{-1})	1.113
F(000)	470
Crystal size (mm)	0.8 × 0.1 × 0.09
θ range for data collection (°)	1.99–25.97
Limiting indices	$-7 \leqslant h \leqslant 1$, $-10 \leqslant k \leqslant 10$, $-25 \leqslant l \leqslant 25$
Reflections collected/unique	4777/4362 [$R_{int} = 0.0168$]
Completeness to $\theta = 25.97$ (%)	100.0
Absorption correction	empirical from Psi-scan
Maximum and minimum transmission	0.9221 and 0.6584
Refinement method	full-matrix least-squares on F^2
Data/restraints/parameters	4362/0/343
Goodness-of-fit on F^2	1.038
Final *R* indices [$I > 2\sigma(I)$]	$R_1 = 0.0397$, $wR_2 = 0.1025$
R indices (all data)	$R_1 = 0.0610$, $wR_2 = 0.1120$
Largest differential peak and hole (e Å^{-3})	0.625 and −0.654

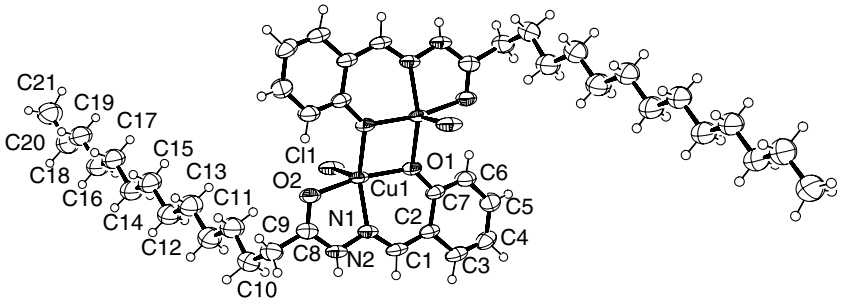

Fig. 1. X-ray molecular structure of **3a** (**3**, $n = 12$).

Table 4
Selected bond lengths (Å) and angles (°) for **3a**

Bond lengths (Å)		Bond angles (°)	
Copper(II) polyhedron			
Cu1–O1	1.9558(18)	O1–Cu–O1#	79.16(8)
Cu1–O2	2.0045(19)	O1–Cu–N1	90.20(8)
Cu1–N1	1.950(2)	O2–Cu–N1	80.61(8)
Cu1–O1#	1.9881(17)	O2–Cu–O1#	104.39(8)
Cu1–Cl1	2.4516(8)	O1–Cu–O2	164.50(8)
Cu1–Cu1#	3.0498(8)	N1–Cu–O1#	155.81(8)
		Cl1–Cu–O1	100.57(6)
		Cl1–Cu–O1#	103.20(6)
		Cl1–Cu–O2	93.35(6)
		Cl1–Cu–N1	100.07(6)
Monoanionic hydrazone ligand			
O1–C7	1.348(3)	O1–C7–C2	121.6(2)
C7–C2	1.424(3)	C7–C2–C1	124.6(2)
C2–C1	1.429(4)	C2–C1–N1	123.4(2)
C1–N1	1.285(3)	C1–N1–N2	119.4(2)
N1–N2	1.376(3)	N1–N2–C8	116.1(2)
N2–C8	1.331(4)	N2–C8–O2	119.6(2)
C8–O2	1.249(3)	N2–C8–C9	117.0(2)
C8–C9	1.484(4)	C9–C8–O2	123.4(3)
Hydrogen bonds			
Cl1···HN2	2.3118 (0.0352)	Cl1···H–N2	172.56 (3.28)

Symmetry transformation used to generate equivalent atoms: # $(-x, -y, -z+1)$.

the atom numbering scheme are shown in Fig. 1, and some selected bond distances and angles are listed in Table 4. This complex is a centrosymmetric dimer in which each copper(II) is coordinated in the equatorial plane to the *N*-salicylidene *n*-alkanoylhydrazine through the deprotonated phenolic oxygen (O1), imine nitrogen (N1) and ketoamide oxygen (O2). The fourth coordination site is occupied by the symmetry related phenoxy oxygen of the other monomeric unit, while the chloride ion is in the axial coordination site. The coordination polyhedron around each copper(II) is best described as (4 + 1) distorted square pyramidal. This is in agreement with the value of the tetragonality parameter $\tau = [(\beta - \alpha)/60] = 0.14$ where α and β are N1–Cu–O1# (155.81°) and O1–Cu–O2 (164.50°) angles, respectively [16,17]. In this dimer, the two chloride ions are in *trans* positions with respect to each other and are perpendicular to the Cu_2O_2 plane with angles O1–Cu–Cl and O2–Cu–Cl of 100.57° and 93.35°, respectively. The Cu· · · ·Cu separation (3.0398 (8) Å) in the Cu_2O_2 moiety is similar to other related dimeric copper(II) complexes with mononegative ONO tridentate acylhydrazones [5,9,10,18]. The Cu1–O1–Cu1# bridging angle (100.84°) compares favourably with that reported for [{Cu(HStbu)Cl}$_2$] (100.9°) (HStbu refers to the *N*-salicylidene-*t*-butanoylhydrazine mononegative anion) [5], but higher than that of [{Cu(HSbzh)Cl}$_2$] (99.1°) (HSbzh) refers to the *N*-salicylidenebenzoylhydrazine mononegative anion) [18]. The two chloride ions in each dimer form short contacts with two other symmetrically related dimers. Thus the dimeric units are linked together via two N2H···Cl1 hydrogen bonds forming a supramolecular structure which consist of a chain of double chains of hydrogen bonds as shown in Fig. 2.

2.5. Magnetic studies

The room temperature magnetic moments of the hydrated chloro copper(II) complexes (**2a**–**2d**) (1.85–1.92 μ_B), Table 5, are within the range expected for magnetically diluted mononuclear copper(II) complexes [19]. The variation of χ_M over the temperature range [5–298 K] reveals no substantial deviation from Curie–Weiss behaviour. The θ values recorded for these complexes, Table 5, are within the range (−2.8 to −4.0 K), indicating very weak antiferromagnetic magnetic intermolecular interaction. The magnetic data, Table 5, suggest that these hydrated chloro complexes exist, in solid state, as discrete monomers, in agreement with the previously reported X-ray molecular structure of **2a** (**2**, $n = 0$) [10]. In this complex, the central copper(II) is in a distorted square pyramidal environment. The monoanionic tridentate hydrazone ligand is coordinated to the Cu(II) in the equatorial plane while the fourth coordination site is occupied by a water molecule. The fifth axial coordination site is occupied by the chloride ion [10]. A similar structure

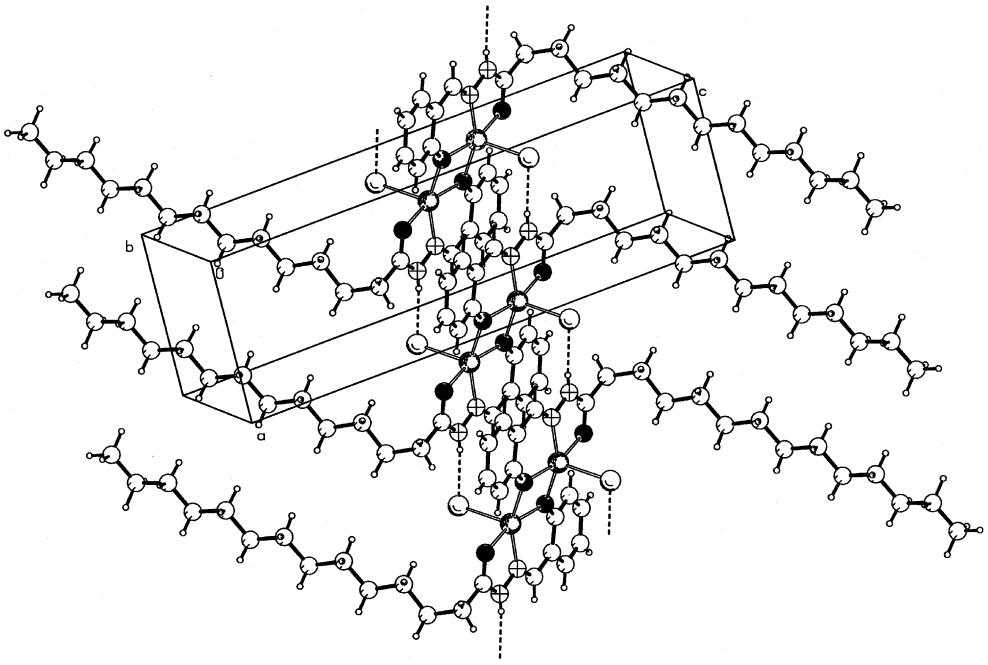

Fig. 2. Hydrogen bonds in **3a** (**3**, $n = 12$).

Table 5
The best fit magnetic parameters for copper(II) complexes derived from *N*-salicylidene-*n*-alkanoylhydrazines

Complex	μ_{eff}/Cu (298 K) (μ_B)	$-2J$ (cm^{-1})	g	θ (K)	ρ (%)
(i) $[Cu(HL)Cl \cdot H_2O] \cdot xH_2O$ (**2**)					
2a	1.85		2.10	−7.5	
2b	1.92		2.10	−5.7	
2c	1.85		2.12	−4.8	
2d	1.91		2.10	−5.4	
(ii) $[\{Cu(HL)Cl\}_2]$ (**3**)					
3a	1.20	477	2.31		1.90
3b	1.22	466	2.25		1.96
(iii) $[\{Cu(L)\}_2]$ (**4**)					
4a	1.58	170	2.04		1.90
4b	1.57	235	2.09	−18.5	3.40
4c	1.60	217	2.09	−20.0	3.50
4d	1.60	194	2.05	−20.0	1.90
4e	1.56	243	2.05	−10.0	2.80
4f	1.53	181	2.06	−19.6	1.71

can be adopted for the other hydrated chloro complexes.

The anhydrous chloro complexes **3a** and **3b** (**3**, $n = 12$ and 16) show room temperature magnetic moments (1.20 and 1.22 μ_B) much lower than expected for spin only values [19]. The variation of χ_M and μ_{eff} recorded for **3a** (**3**, $n = 16$) with temperature, Fig. 3, suggest strong antiferromagnetic interaction between the copper(II) centers in the dimeric structure shown in Fig. 1. Similar behaviour was also observed for **3b** (**3**, $n = 12$). The recorded variable temperature magnetic susceptibility data were fitted to the modified Bleaney–Bowers equation [20]:

$$\chi_M = (1-\rho)\frac{2N_L\mu_B^2 g^2 \exp(2J/kT)}{k(T-\theta)(1+3\exp(2J/kT))} + \rho\frac{2N_L\mu_B^2 g^2}{4kT} + 2N_\alpha, \quad (1)$$

where N_α is the temperatue independent paramagnetism (60×10^{-6} cm^3 mol^{-1} per Cu(II)), ρ is the mole fraction of monomeric impurity and θ is a correction term for interdimer interaction [21,22]. Other terms have their usual meaning. The best fit values of $2J$, g, ρ and are listed in Table 5.

The $-2J$ values measured for **3a** (477 cm^{-1}) and **3b** (466 cm^{-1}) are more or less similar, implying similar

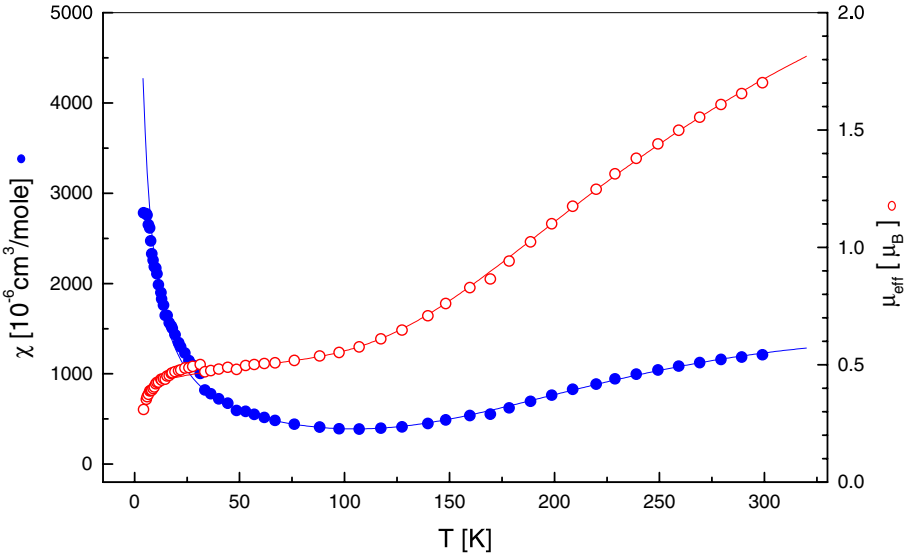

Fig. 3. Magnetic susceptibilities χ_M (•) and magnetic moments (○) vs. temperature for **3a** (**3**, $n = 12$). Solid lines represent the best least square fit to Eq. (1) with $2J = -477$, $g = 2.31$ and $\rho = 1.90\%$.

structures. However, these $-2J$ values, Table 5, are higher than that reported for other similar dichloro dicopper(II) complexes with *N*-salicylidenearoylhydrazines (406–452 cm^{-1}) [13,18].

The X-ray structures of **3a** (Fig. 1), [{Cu(HSbh)Cl}$_2$] [18] and [{Cu(HStbu)Cl}$_2$] [5] revealed that these five coordinate dichloro dicopper(II) complexes belong to a coplanar (distorted square pyramidal) rather than parallel planar (distorted trigonal bipyramidal) type [23]. In this type the extent of antiferromagnetic interaction, as measured by singlet–triplet separation ($-2J$), increases on increasing either Cu–O–Cu bridge angles or Cu···Cu separation, but shows a pronounced decrease as the dihedral angle between the Cu_2O_2 plane and that of the remaining ligand increases [24]. In both **3a** and [{Cu(HSbh)Cl}$_2$], this dihedral angle is more or less similar with an average value of 25.8°. Accordingly the higher $-2J$ value recorded for **3a** (477 cm^{-1}) relative to that of [{Cu(HSbh)Cl}$_2$] (452 cm^{-1}) [13,18] can be related to the increase in both Cu–O–Cu angle (100.84°) and Cu···Cu separation (3.0398 Å) of **3a** as compared with the Cu–O–Cu angle (99.10) and Cu···Cu separation (3.0290 Å) of [{Cu(HSbh)Cl}$_2$].

At room temperature (298 K), the neutral copper(II) complexes [{Cu(L)}$_2$] show low lying magnetic moments (1.53–1.60 μ_B), and the magnetic susceptibility measurements within the temperature range 4.2–298 K recorded for these neutral complexes indicate antiferromagnetic exchange coupling between two copper(II) centers. The variation of χ_M and μ_{eff} as a function of T recorded for the neutral copper(II) complex derived from *N*-salicylidenestearoylhydrazine is shown in Fig. 4. The magnetic susceptibility curve shows a broad maximum around 120 K then rapidly decreases to a minimum at 50 K as the temperature is lowered. This type of temperature dependence is expected for antiferromagnetic coupled copper(II) binuclear complexes. The further increase in χ_M as the temperature is lowered is due to the presence of paramagnetic mononuclear impurity.

The variable temperature magnetic susceptibility data collected for neutral copper(II) complexes [{Cu(L)}$_2$] were fitted in the Bleaney–Bowers equation (Eq. (1)) and the best fit magnetic parameters (g, $2J$, θ and ρ) are included in Table 5. Similar to other copper(II) complexes with dinegative *N*-salicylideneacylhydrazines [13,25] and other dinegative ONO tridentate Schiff bases [24], the antiferromagnetic behaviour of these copper(II) complexes confirm their dimeric nature. Dimerization of copper(II) complexes with dinegative tridentate *N*-salicylideneacylhydrazones usually occurs via the phenoxy oxygen as shown in structure **4** (Scheme 4) [13,25]. However, Leukov et al. [26,27] showed that dimerization may also occur via oxazine oxygens (Scheme 5) (**5**). The calculated exchange parameter ($-2J$) of the phenoxy bridged isomer lies in the range $230 < -2J < 520$ cm^{-1} while $25 < -2J < 125$ cm^{-1} was reported for an oxazine oxygen bridged isomer [27]. The $-2J$ values recorded in the present work for [{Cu(L)}$_2$] complexes, Table 5, varies from 170 to 243 cm^{-1}. This range is lower than that expected for other neutral dicopper(II) complexes with dinegative ONO tridentate ligands where dimerization occurs via phenoxy oxygens [13,24,25] but is still higher than the range proposed by Leukov et al. for oxazine bridged isomers. Thus, the results of the present magnetic measurements cannot provide non-equivocal evidence for the structure of these neutral copper(II)

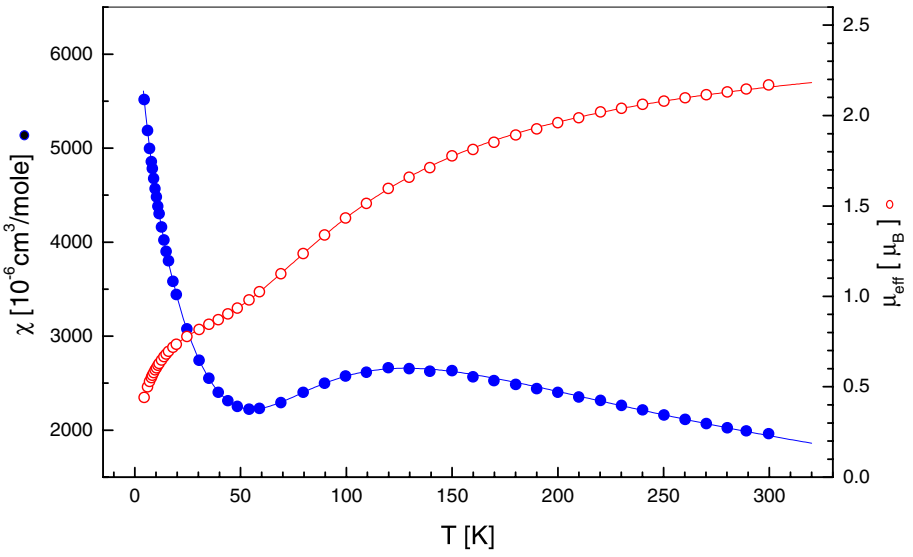

Fig. 4. Magnetic susceptibilities χ_M (•) and magnetic moments (○) vs. temperature for **4f** (**4**, $n = 16$). Solid lines represent the best least square fit to Eq. (1) with $2J = -181$, $g = 2.06$, $\theta = -19.6$ and $\rho = 1.71\%$.

complexes. Meanwhile, the X-ray molecular structures reported for all dimeric copper(II) complexes with *N*-salicylideneacylhydrazines with different degrees of deprotonation indicate dimerization through the phenoxy oxygen [5,9–12,18]. To the best of our knowledge there is no X-ray structure reported for an oxazine oxygen bridged complex. This may favour structure (**4**) for the dimeric neutral copper(II) [{Cu(L)}$_2$] complexes where dimerization occurs via phenoxy oxygens (**4**) rather than oxazine oxygens (**5**). The lower $-2J$ values recorded for **4a**–**4f**, Table 5, relative to the dicopper(II) complexes derived from other *N*-salicylideneacylhydrazines [13,18,25] may be related to an increase in the dihedral angle between the Cu_2O_2 plane and that of the remaining ligand resulted, most probably, from the hydrophobic interactions between the *n*-alkyl chains within the crystal lattice. The actual structure of this type of dicopper(II) complex, however, must remain in doubt until a complete X-ray molecular structure is available.

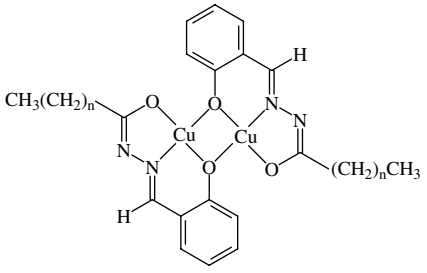

	n
4a	0
4b	4
4c	5
4d	6
4e	12
4f	16

(4)

Scheme 4.

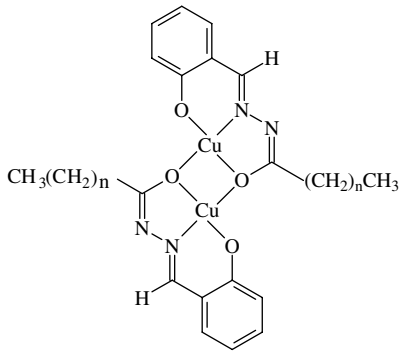

(5)

Scheme 5.

3. Experimental

3.1. Preparation of n-alkanoylhydrazines and N-salicylidene-n-alkanoylhydrazines (*1a*–*1f*)

N-alkanoylhydrazines were prepared, as previously described [5,28], by the hydrazinolysis of fatty acid methyl esters in methanol. The corresponding *N*-salicylidene-*n*-alkanoylhydrazines (**1a**–**1f**) were prepared by the condensation of salicylaldehyde with *n*-alkanoylhydrazine in methanol [5,28], (**1a**, m.p. = 200–202 °C; **1b**, m.p. = 123–124 °C; **1c**, m.p. = 110°C; **1d**, m.p. = 103–104 °C; **1e**, m.p. = 106–108 °C; **1f**, m.p. = 114 °C).

3.2. Preparation of dimeric neutral copper(II) complexes [{Cu(L)}$_2$] (*2b*–*2f*)

A solution of *N*-salicylidene-*n*-alkanoylhydrazine (**1b**–**1f**) (5.0 mmol) in dry methanol (40 cm^3) was added

to a solution of copper(II) acetate monohydrate (5.1 mmol) in dry methanol. The reaction mixture was heated under reflux with constant stirring for ca. 15 min. On cooling the formed green complex was filtered, washed with hot methanol and then dried in vacuo.

3.3. Preparation of monomeric hydrated monochloro copper(II) complexes $[Cu(HL)Cl \cdot H_2O] \cdot xH_2O$ (**3b**–**3d**)

To a solution of $CuCl_2 \cdot 2H_2O$ (5.0 mmol) in dry methanol (20 cm^3), a solution of *N*-salicylidene-*n*-alkanoylhydrazine (5.0 mmol) in dry methanol (30 cm^3) was added dropwise with constant stirring. The reaction mixture was stirred at room temperature for 1 h and the formed complex was filtered, washed successively with dry methanol and ether then dried in air.

3.4. Preparation of anhydrous dimeric monochloro copper(II) complexes $[\{Cu(HL)Cl\}_2]$ (**3a** and **3b**)

A solution of *N*-salicylidene-*n*-alkanoylhydrazine (**1e** or **1f**) (5.0 mmol) in absolute ethanol (50 cm^3) was added dropwise to a solution of $CuCl_2 \cdot 2H_2O$ (5.0 mmol) in absolute ethanol (20 cm^3). The reaction mixture was then heated under reflux for 10 min. On cooling, the crystalline anhydrous chloro copper(II) complex (**3a** or **3b**) which separated out was filtered, washed with dry diethylether then dried in vacuum.

3.5. Physical measurements

Infrared spectra were recorded on a Perkin–Elmer 1430 Data system and/or a Perkin–Elmer (FT-IR spectrophotometer) PARAGON 1000 PC infrared spectrophotometer. Calibration of frequency reading was made with polystyrene film. Solid samples were examined as KBr discs. Electron impact and field desorption mass spectra on Finnigan Mat 212 (70 eV) instrument. Magnetic susceptibilities of powdered dried samples were recorded on a Faraday-type magnetometer using a sensitive computer controlled D-200 Cahn RG microbalance in the temperature range 4.2–298 K. The magnetic field applied was ~1.5 T. Details of the apparatus have been described elsewhere [29]. Experimental susceptibility data were corrected for the underlying diamagnetism using Pascal's constants [20].

3.6. X-ray crystal and molecular structure

X-ray diffraction measurements were carried out on an Oxford diffraction Xcalibur (TM) single crystal X-ray diffractometer with a Sapphire CCD detector. The structure of **3a** was solved by a direct method using SHELXS 97 [30] and refined by a full-matrix least squares method on all F^2 data using SHELXL 97 [31] programs.

4. Supplementary material

Atomic coordinates, equivalent isotropic displacement parameters, hydrogen coordinates, isotropic displacement parameters, anisotropic displacement parameters and a complete list of bond distances and bond angles of **3a** have been deposited with the Cambridge Crystallographic Data Center as supplementary publication no. CCDC 211370. Copies of this information may be obtained free of charge from the Director, CCDC, 12 Union Road, Cambridge, CB2 IEZ, UK (fax: +44-1223-336033; e-mail: deposit@ccdc.cam.ac.uk or http://www.ccdc.cam.ac.uk).

Acknowledgements

Thanks are due to BMBF/Forschungszentrm, Jülich, ÖA-IB/Wo WTZ for supporting this bilateral project.

References

[1] A.A. Aruffo, T.B. Murphy, D.K. Johnson, N.J. Rose, V. Schomaker, Inorg. Chim. Acta 67 (1982) L25.
[2] D.K. Johnson, T.B. Murphy, N.J. Rose, W.H. Goodwin, L. Pickart, Inorg. Chim. Acta 67 (1982) 159.
[3] L. Pickart, W.H. Goodwin, W. Burgua, T.B. Murphy, D.K. Johnson, Biochem. Pharmacol. 32 (1983) 3868.
[4] M. Mohan, A. Kumar, M. Kumar, N.K. Jha, Inorg. Chim. Acta 136 (1987) 65.
[5] L.L. Koh, O.L. Kon, K.W. Loh, Y.C. Long, J.D. Ranford, A.L.C. Tan, Y.Y. Tjan, J. Inorg. Biochem. 72 (1998) 155.
[6] E.W. Ainscough, A.M. Brodie, W.A. Denny, G.J. Finlay, S.A. Gothe, J.D. Ranford, J. Inorg. Biochem. 77 (1999) 125.
[7] M.F. Iskander, A.M. El-Aggan, L.S. Refaat, L. El-Sayed, Inorg. Chim. Acta 14 (1975).
[8] A.A. Aruffo, T.B. Murphy, D.K. Johnson, N.J. Rose, Schomaker, Acta Crystallogr. C 40 (1984) 1164.
[9] S.C. Chan, L.L. Koh, P.-K. Leung, J.D. Ranford, K.Y. Sim, Inorg. Chim. Acta 236 (1995) 101.
[10] E.W. Ainscough, A.M. Brodie, A.J. Dobbs, J.D. Ranford, J.M. Waters, Inorg. Chim. Acta 267 (1998) 27.
[11] N.R. Sangeetha, K. Baradi, R. Gupta, C.K. Pal, V. Manivannan, S. Pal, Polyhedron 18 (1999) 1425.
[12] N.R. Sangetha, S. Pal, J. Chem. Crystallogr. 29 (1999) 278.
[13] M.F. Iskander, T.E. Khalil, R. Werner, W. Haase, I. Svoboda, H. Fuess, Polyhedron 19 (2000) 949.
[14] C. Colonna, J.-P. Doucet, A. Cosse-barbi, Trans. Met. Chem. 20 (1995) 338.
[15] L. El-Sayed, M.F. Iskander, J. Inorg. Nucl. Chem. 33 (1971) 435.
[16] A.W. Addison, T.N. Rao, J. Reedijk, J. Van Rijn, G.C. Verschoor, J. Chem. Soc., Dalton Trans. (1984) 1349.
[17] M. Zoeteman, E. Bouwman, R.A.G. de Graaff, W.L. Driessen, J. Reedijk, P. Zanello, Inorg. Chem. 29 (1990) 3487.
[18] W. Haase, K. Griesar, M.F. Iskander, Y. Galyametdinov, Mol. Mater. 3 (1993) 115.
[19] B.J. Hathaway, in: G. Wilkinson, R.D. Gillard, J.A. McCleverty (Eds.), Copper in Comprehensive Coordination Chemistry, vol. 5, Pergamon, Oxford, 1987.
[20] O. Kahn, Molecular Magnetism, VCH, New York, 1993.

[21] K.T. McGregor, J.A. Barnes, W.E. Hatfield, J. Am. Chem. Soc. 95 (1973) 7993.
[22] S. Sikraw, I. Brouche-Waksman, O. Kahn, Inorg. Chem. 23 (1984) 490.
[23] T.C. Higgns, M. Helliwell, E.J.L. McInnes, F.E. Mabbs, C.J. Harding, C.D. Garner, J. Chem. Soc., Dalton Trans. (1997) 927.
[24] M. Melnik, Coord. Chem. Rev. 42 (1982) 259.
[25] J.M. Dance, M.T. Do, P. Gambardella, R.H. De, A. Santos, E. Medina, F.G. Manrique, M.S. Palacios, Inorg. Chim. Acta 162 (1989) 239.
[26] S.I. Levchenkov, I.N. Shcherbakov, V.V. Lukov, J.A. Kogan, Russ. J. Coord. Chem. 23 (4) (1997) 293.
[27] V.V. Lukov, S.I. Levchenkov, V.A. Kogan, Russ. J. Coord. Chem. 24 (12) (1998) 887.
[28] H. Ohta, Bull. Chem. Soc. Jpn. 33 (2) (1960) 202.
[29] S. Gerhring, P. Fleichhauer, H. Paulus, W. Haase, Inorg. Chem. 23 (1993) 54.
[30] G.M. Sheldrick, Acta Crystallogr. A 46 (1990) 467.
[31] G.M. Sheldrick, SHELXL 97, Program for Crystal Structure Refinement, University of Göttingen, Göttingen, Germany, 1997.

Available online at www.sciencedirect.com
SCIENCE DIRECT®
Polyhedron 23 (2004) 33–39
POLYHEDRON
www.elsevier.com/locate/poly

Mono- and dizinc complexes of diporphyrins with flexible spacers of variable length

Joanna Borowiec, Irena Trojnar, Stanisław Wołowiec *

Faculty of Chemistry, Rzeszów University of Technology, 6 Powstańców Warszawy Ave., Rzeszów 35-959, Poland

Received 3 July 2003; accepted 1 September 2003

Abstract

The di- and mono-zinc(II) complexes of diporphyrins (D) were synthesized, in which two porphyrin halves were covalently linked through a variable length hydrocarbon spacer ($-CH_2)_n-$, where $n = 2$–4, D2–D4, respectively) attached via the *ortho* oxygen atom of the *meso*-phenyl ring. Three *p*-tolyl substituents were attached to other *meso* positions of both porphyrins. The zinc(II) complexes were studied by 1-D and 2-D COSY and NOESY ^{1}H NMR spectroscopy. The stability constants of dizincdiporphyrins with azaaromatic ligands: pyridine (py), pyrazine (pyr), and 4,4′-bipyridyl (bipy) were determined by spectrophotometric titration. The discriminating factor for stability of dinuclear complexes with diazaaromatic ligands was the length of the diporphyrin spacer. The formation constant for ZnTTP with pyr and bipy were very close to that for py, whereas they were about 1.3 orders of magnitude larger for **D2Zn$_2$**-pyr, **D3Zn$_2$**-bipy, and **D4Zn$_2$**-bipy complexes which was attributed to the formation of nitrogen base bridged species. The monozincdiporphyrin complexes were demonstrated to be a convenient starting material for synthesis of heterodimetallodiporphyrins. The Zn(II)/Cu(II)diporphyrin complex was synthesized and characterized by EPR spectroscopy.
© 2003 Elsevier Ltd. All rights reserved.

Keywords: Diporphyrins; Zinc(II) complexes; Nitrogen base ligation; Stability constants

1. Introduction

Diporphyrins are suitable ligands that are able to coordinate two metal ions. This feature renders them good candidates for synthesis of dinuclear complexes, which can be applied as bifunctional catalysts, especially in the case when two different catalytic metal ions are incorporated. The diporphyrins linked with rigid spacers attached to *meso* positions were studied in detail [1–7]. The most explored were those with *ortho*-, *meta*- or *para*-phenylene [1,2] and pillard diporphyrins, in which biphenylene, anthracene, xanthene and 1,10-phenanthroline were attached to *meso* positions of the porphyrin subunits [3–7]. Some heterodimetallodiporphyrins containing for example Mn(III)/Cu(II) and Al(III)/Co(II) metal ion pairs were characterized structurally [3,7]. Synthesis of heterodimetallodiporphyrins requires the insertion of the metal ion under stoichiometric control. In this paper, we have described the synthetic route for obtaining the di- and monozinc complexes of the diporphyrins with flexible spacers. Two porphyrin halves are linked via *meso* positions at which phenyl substituents are connected by variable length hydrocarbons attached to the *ortho* oxygen. The monozincdiporphyrins are useful starting materials for synthesis of heterodimetallodiporphyrins, which was exemplified by the mixed-metal Zn(II)/Cu(II)diporphyrin complex, characterized by EPR spectroscopy.

2. Experimental

2.1. Syntheses

2.1.1. General syntheses

The 5-(*ortho*-hydroxyphenyl)-10,15,20-tris(*p*-tolyl)-porphyrin (**H$_2$TTP-*o*-OH**) and diporphyrins with variable-length hydrocarbon spacers **S** attached to the peripheral oxygen of two porphyrin macrocycles:

* Corresponding author. Tel.: +17-865-1657; fax: +17-854-3655.
E-mail address: sw@prz.rzeszow.pl (S. Wołowiec).

0277-5387/$ - see front matter © 2003 Elsevier Ltd. All rights reserved.
doi:10.1016/j.poly.2003.09.021

(H_2TTP-*o*-OCH_2)$_2$(CH_2)$_n$: **D2H$_4$** ($n = 0$, **S** = 2), **D3H$_4$** ($n = 1$, **S** = 3) and **D4H$_4$** ($n = 2$, **S** = 4) were synthesized as described previously [8–12]. The 5,10,15,20-tetra(*p*-tolyl)porphyrin (**TTPH$_2$**) was obtained as a side-product and its zinc(II) complex (**TTPZn**) was used for comparative purposes.

*2.1.2. Mono- and bis-zinc(II)diporphyrin complexes (DSH$_2$Zn, DSZn$_2$, **S** = 2, 3 and 4)*

The insertion of the zinc(II) ion into diporhyrins **DSH$_4$** was performed on the 30–75 μmol scale (50–100 mg of diporphyrins were used) by stepwise addition of ca. 0.1 M zinc(II) chloride in methanol into a refluxing solution of **DSH$_4$** in chloroform containing potassium carbonate (about 1 g). The progress of reaction was monitored by TLC on silicagel using 65/35 v/v% dichloromethane/hexane eluent The chromatographic mobility decreased in order: **DSH$_4$** > **DSZnH$_2$** > **DSZn$_2$** in every case. The insertion procedure was continued until the near disappearance of starting **DSH$_4$** was noticed. Separation of **DSZnH$_2$** and **DSZn$_2$** was achieved by column chromatography on silicagel using dichloromethane/hexane eluent; traces of **DSH$_4$** were eluted with 30% CH_2Cl_2, while fractions eluted with 35% and 45% CH_2Cl_2 contained almost pure of **DSZnH$_2$** and **DSZn$_2$**, respectively. The second fractions were re-chromatographed using the same conditions in order to obtain high-purity **DSZnH$_2$**. Total yields of the products of insertion were close to 100% (45% and 50% for **DSZnH$_2$** and **DSZn$_2$**, respectively). The free ligands **DSH$_4$** were recoverable by the demetallation procedure based on the extraction of a chloroform solution of **DSZnH$_2$** and/or **DSZn$_2$** with 2 M HCl 1:1 H_2O: CH_3OH within 1 h with about 20% loss of diporhyrin, which in those conditions gave starting ***o*-HOTTPH$_2$** and other products, which were easy to separate from **DSH$_4$** due to their chromatographic immobility under standard conditions. The complexes have been identified on the basis of their ^{1}H NMR spectra. Resonances were assigned using standard ^{1}H COSY and NOSEY experiments. The numbering scheme of the ligands is presented in Fig. 1.

2.1.3. Synthesis of D2ZnCu

To the solution of **D2ZnH$_2$** (35 mg, 2.4×10^{-2} mmol) in chloroform (50 cm^3) containing 1 g K_2CO_3 under reflux, 1.8-fold molar excess of $CuCl_2$ was added dropwise as a 0.058 M methanolic solution. The color of the mixture changed from pink-purple to orange-red. The products of reaction were separated chromatographically on silicagel. The first compound eluted with 35% CH_2Cl_2/hexane (v/v) was $D2Cu_2$ (15 mg, 1.0×10^{-2} mmol, 42%), identified by comparison with an authentic sample of the complex obtained in a separate synthesis, while **D2ZnCu** was eluted with CH_2Cl_2 (yield 18 mg, 1.2×10^{-2} mmol, 50%).

D2ZnCu was demetallated by stirring of a chloroform solution (20 cm^3) of the complex with 2 M HCl H_2O/CH_3OH (20 cm^3) for 2 h, followed by chromatographic separation of **D2H$_4$**, which was identified easily by its ^{1}H NMR spectrum.

2.2. Analytical data

2.2.1. D4H$_4$

^{1}H NMR ($CDCl_3$, 298 K); chemical shift (ppm) (intensity, multiplicity, assignment, coupling constant): −2.85 (4H, s, NH), −0.23 (4H, t, CH_2(2)), 2.56 (4H, t, CH_2(1)), 2.65 (12H, s, 2x(*p*-CH_3(1))), 2.68 (6H, s, CH_3 (*p*-CH_3(2))), 6.02 (2H, d, m_6-H, $J(m_6\text{-}p) = 7.4$ Hz), 6.84 (2H, ddd, *p*-H, $J(p\text{-}m_5) = 8.0$ Hz, $J(p\text{-}o_5) = 1.9$ Hz), 6.97 (2H, dd, m_5-H, $J(m_5\text{-}o_5) = 7.5$ Hz), 7.40–7.56 (12H, m, m_1-m_4-H), 7.73 (2H, dd, o_5-H), 7.92–8.11 (12H, m, o_1-o_4-H), 8.40 and 8.65 (4H and 4H, d and d, 2(8)-H, 3(7)-H, $J(2,3) = 4.7$ Hz), 8.82 (8H, s, 12,13,17,18-H).

RF = 0.60.

2.2.2. D4Zn$_2$

^{1}H NMR ($CDCl_3$, 298 K); chemical shift (ppm) (intensity, multiplicity, assignment, coupling constant):

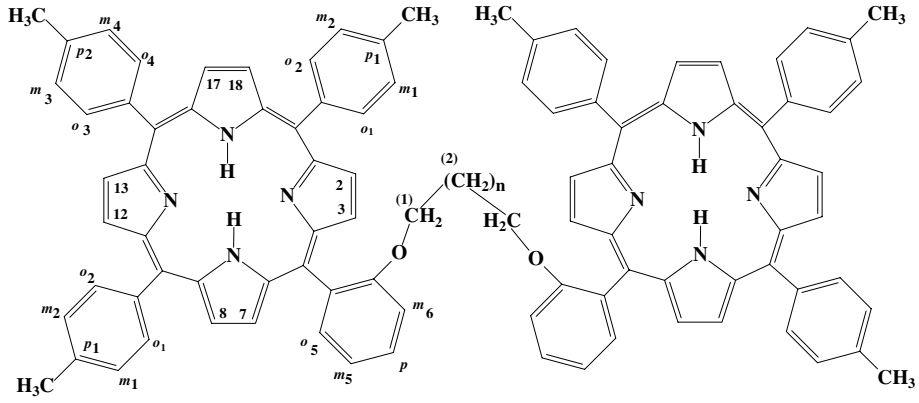

Fig. 1. The numbering scheme in diporphyrin. The variable length spacers **S** = 2 ($n = 0$), **S** = 3 ($n = 1$) and **S** = 4 ($n = 2$).

−0.29 (4H, t, CH_2(2)), 2.59 (4H, t, CH_2(1)), 2.65 (12H, s, 2x(*p*-CH_3(1))), 2.69 (6H, s, *p*-CH_3(2)), 6.00 (2H, d, m_6-H, $J(m_6\text{-}p) = 7.5$ Hz), 6.66 (2H, ddd, *p*-H, $J(p\text{-}m_5) = 8.1$ Hz, $J(p\text{-}o_5) = 1.9$ Hz), 6.77 (2H, dd, m_5-H, $J(m_5\text{-}o_5) = 7.1$ Hz), 7.37–7.57 (12H, m, m_1-m_4-H), 7.63 (2H, dd, o_5-H), 7.88–8.12 (12H, m, o_1-o_4-H), 8.38 and 8.75 (4H and 4H, d + d, 2(8)-H, 3(7)-H, $J(2,3) = 4.7$ Hz), 8.91 (8H, AB spectrum, $\delta_A = 8.89$, $\delta_B = 8.91$, 12(18)-H, 3(17)-H, $J(12,13) = 4.7$ Hz).

RF = 0.44.

UV–Vis: 422 (4.6×10^5, Soret band), 510 (5.2×10^3), 550 (2.7×10^4), 592 (4.9×10^3).

2.2.3. $D4ZnH_2$

^{1}H NMR ($CDCl_3$, 298 K); chemical shift (ppm) (intensity, multiplicity, assignment, coupling constant): −2.88 (2H, s, NH), −0.24 (4H, m, CH_2(2,2′)), 2.48 (4H, m, CH_2(1,1′)), 2.65 (12H, s, 2x(*p*-CH_3(1,1′))), 2.68 and 2.69 (3H and 3H, s and s, *p*-CH_3(2) and *p*-CH_3(2′)), 5.79 (2H, d, m_6-H, $J(m_6\text{-}p) = 8.1$ Hz), 6.18 (2H, d, $m_{6'}$-H, $J(m_{6'}\text{-}p') = 8.1$ Hz), 6.44 (2H, ddd, *p*-H, $J(p\text{-}m_5) = 8.1$ Hz, $J(p\text{-}o_5) = 1.9$ Hz), 6.64 (2H, dd, m_5-H, $J(m_5\text{-}o_5) = 7.5$ Hz), 6.96 (2H, ddd, *p*′-H, $J(p\text{-}m_5) = 8.1$ Hz, $J(p'\text{-}o_{5'}) = 1.9$ Hz), 7.02 (2H, dd, $m_{5'}$-H, $J(m_{5'}\text{-}o_{5'}) = 7.1$ Hz), 7.48–7.57 (12H, m, m_1-m_4-H + $m_{1'}$-$m_{4'}$-H), 7.68 (2H, dd, o_5-H), 7.78 (2H, dd, $o_{5'}$-H), 7.88.- 8.12 (12H, m, o_1-o_4-H + $o_{1'}$-$o_{4'}$-H), 8.17, 8.61 (2H + 2H, d + d, 2(8)-H, 3(7)-H, $J(2,3) = 4.7$ Hz), 8.55, 8.77 (2H + 2H, d + d, 2′(8′)-H, 3′(7′)-H, $J(2',3') = 4.7$ Hz), 8.79 (4H, AB spectrum, $\delta_A = 8.78$, $\delta_B = 8.80$, 12(18)-H, 3(17)-H, $J(12,13) = 4.7$ Hz), 8.91 (4H, AB spectrum, $\delta_A = 8.89$, $\delta_B = 8.93$, 12′(18′)-H, 3′(17′)-H, $J(12',13') = 4.7$ Hz).

RF = 0.56.

UV–Vis: 421 (4.3×10^5, Soret band), 510 (4.3×10^3), 550 (2.5×10^4), 592 (4.3×10^3).

2.2.4. $D3H_4$

^{1}H NMR ($CDCl_3$, 298 K); chemical shift (ppm) (intensity, multiplicity, assignment, coupling constant): −2.76 (4H, s, NH), 0.60 (2H, q, CH_2(2)), 2.71 (12H, s, 2x(*p*-CH_3(1))), 2.72 (6H, s, CH_3 (*p*-CH_3(2))), 2.77 (4H, t, 2xCH_2(1)), 5.82 (2H, d, m_6-H, $J(m_6\text{-}p) = 8.0$ Hz), 6.58 (2H, ddd, *p*-H, $J(p\text{-}m_5) = 8.0$ Hz, $J(p\text{-}o_5) = 1.5$ Hz), 6.96 (2H, dd, m_5-H, $J(m_5\text{-}o_5) = 8.4$ Hz), 7.51–7.57 (12H, m, m_1-m_4-H), 7.77 (2H, dd, o_5-H), 8.03–8.14 (12H, m, o_1-do_4-H), 8.56 and 8.73 (4H + 4H, d and d, 2(8)-H, 3(7)-H, $J(2,3) = 4.8$ Hz), 8.86 (8H, s, 12,13,17,18-H).

RF = 0.73.

2.2.5. $D3Zn_2$

^{1}H NMR ($CDCl_3$, 298 K); chemical shift (ppm) (intensity, multiplicity, assignment, coupling constant): 0.61 (2H, q, CH_2(2)), 2.71 (18H, s, 2x(*p*-CH_3(1) + *p*-CH_3(2))), 2.76 (4H, t, 2xCH_2(1)), 5.76 (2H, d, m_6-H, $J(m_6\text{-}p) = 8.1$ Hz), 6.41 (2H, dd, *p*-H, $J(p\text{-}m_5) = 8.1$ Hz), 6.82 (2H, dd, m_5-H, $J(m_5\text{-}o_5) = 8.0$ Hz), 7.50–7.58 (12H, m, m_1-m_4-H), 7.73 (2H, d, o_5-H), 8.03–8.16 (12H, m, o_1-o_4-H), 8.53 and 8.82 (4H + 4H, d and d, 2(8)-H, 3(7)-H, $J(2,3) = 4.4$ Hz), 8.96 (8H, s, 12,13,17,18-H).

RF = 0.63.

UV–Vis: 420 (4.2×10^5, Soret band), 520 (4.0×10^3), 561(2.3×10^4), 601(3.9×10^3).

2.2.6. $D3ZnH_2$

^{1}H NMR ($CDCl_3$, 298 K); chemical shift (ppm) (intensity, multiplicity, assignment, coupling constant): −2.79 (2H, s, NH), 0.59 (2H, m, CH_2(2)), 2.69 (2H, m, CH_2(1)), 2.71 (18H, s, 2x(*p*-CH_3(1) + *p*-CH_3(2))), 2.83 (2H, t, CH_2(1′)), 5.59 + 5.95 (1H + 1H, d + d, m_6-H + $m_{6'}$-H, $J(m_6\text{-}p) = 8.0$ Hz, $J(m_{6'}\text{-}p') = 8.0$ Hz), 6.30 + 6.65 (1H + 1H, dd + dd, *p*-H + *p*′-H, $J(p\text{-}m_5) = 8.0$ Hz, $J(p'\text{-}m_{5'}) = 8.1$ Hz), 6.75 + 6.98 (1H + 1H, dd + dd, m_5-H + $m_{5'}$-H, $J(m_5\text{-}o_5) = 8.0$ Hz, $J(m_{5'}\text{-}o_{5'}) = 8.0$ Hz), 7.49-7.59 (12H, m, m_1-m_4-H + $m_{1'}$-$m_{4'}$-H), 7.65 + 7.86 (1H + 1H, d + d, o_5-H + $o_{5'}$-H), 8.02–8.16 (12H, m, o_1-o_4-H + $o_{1'}$-$o_{4'}$-H), 8.39, 8.71 (4H, d + d, AB spectrum, 2(8)-H, 3(7)-H), 8.69, 8.86 (4H, d + d, AB spectrum, 2′(8′)-H, 3′(7′)-H), 8.85 and 8.98 (4H and 4H, s and s, 12,13,17,18-H and 12′,13′,17′,18′-H).

RF = 0.68.

UV–Vis: 421 (4.0×10^5, Soret band), 519 (4.0×10^3), 561 (2.0×10^4), 595 (3.7×10^3).

2.2.7. $D2H_4$

^{1}H NMR ($CDCl_3$, 298 K); chemical shift (ppm) (intensity, multiplicity, assignment, coupling constant): −2.73 (4H, s, NH), 2.68 (12H, s, 2x(*p*-CH_3(1))), 2.71 (6H, s, CH_3 (*p*-CH_3(2))), 3.34 (4H, s, 2xCH_2), 5.82 (2H, dd, *p*-H, $J(p\text{-}m_5) = 8.1$ Hz, $J(p\text{-}m_6) = 8.1$ Hz), 5.88 (2H, d, m_6-H), 6.43 (2H, dd, m_5-H, $J(m_5\text{-}o_5) = 8.0$ Hz), 7.46–7.59 (12H, m, m_1-m_4-H), 7.61 (2H, d, o_5-H), 8.00–8.15 (12H, m, o_1-o_4-H), 8.50 and 8.73 (4H and 4H, d and d, AB spectrum, 2(8)-H, 3(7)-H, $J(2,3) = 4.7$ Hz), 8.86 (8H, s, 12,13,17,18-H).

RF = 0.63.

2.2.8. $D2Zn_2$

^{1}H NMR ($CDCl_3$, 298 K); chemical shift (ppm) (intensity, multiplicity, assignment, coupling constant): 2.66 (6H, s, CH_3 (*p*-CH_3(2))), 3.34 (4H, s, 2xCH_2), 2.69 (12H, s, 2x(*p*-CH_3(1))), 5.91 (2H, dd, *p*-H, $J(p\text{-}m_5) = 8.0$ Hz, $J(p\text{-}m_6) = 8.0$ Hz), 5.93 (2H, d, m_6-H), 6.43 (2H, dd, m_5-H, $J(m_5\text{-}o_5) = 8.0$ Hz), 7.45 (2H, d, o_5-H), 7.46-7.59 (12H, m, m_1-m_4-H), 7.98–8.14 (12H, m, o_1-o_4-H), 8.50 and 8.81 (4H and 4H, d and d, AB spectrum, 2(8)-H, 3(7)-H, $J(2,3) = 4.7$ Hz), 8.93 (8H, AB spectrum, $\delta_A = 8.92$, $\delta_B = 8.94$, 12(18), 13(17) – H, $J(12,13) = 4.7$ Hz).

RF = 0.45.

UV–Vis: 420 (4.3×10^5, Soret band), 510 (3.6×10^3), 548 (2.5×10^4), 586 (6.3×10^3).

2.2.9. D2ZnH$_2$

^{1}H NMR ($CDCl_3$, 298 K); chemical shift (ppm) (intensity, multiplicity, assignment, coupling constant): −2.76 (2H, s, NH), 2.66 (12H, s, 2x(p-CH_3(1)) + 2x(p-CH_3(1′))), 2.69 (6H, s, CH_3 (p-CH_3(2)) + CH_3(p-CH_3(2′))), 3.29 and 3.31 (2H and 2H,s and s, CH_2(1) + CH_2(1′)), 5.86–6.06 (4H, m, p-H + m_6-H + p'-H + $m_{6'}$-H, $J(p\text{-}m_5) = 8.0$ Hz, $J(p\text{-}m_6) = 8.0$ Hz, $J(p'\text{-}m_5) = 8.0$ Hz, $J(p'\text{-}m_{6'}) = 8.0$ Hz), 6.26–6.51 (4H, m, m_5-H + $m_{5'}$-H), 7.40–7.60 (12H, m, m_1-m_4-H, o_5-H, and $o_{5'}$-H), 7.98–8.13 (12H, m, o_1- o_4-H), 8.37 and 8.69 (2H and 2H, d and d, AB spectrum, 2(8)-H, 3(7)-H, $J(2,3) =$ 4.7 Hz), 8.59 and 8.82 (2H and 2H, d and d, AB spectrum, 2′(8′)-H, 3′(7′)-H, $J(2',3') = 4.7$ Hz), 8.83 (4H, s, 12,13,17,18-H), 8.92 (4H, s, 12′,13′,17′,18′-H).

RF = 0.50.

UV–Vis: 420 (3.6×10^5, Soret band), 516 (7.5×10^3), 549 (1.5×10^4), 589 (4.0×10^3), 646 (1.4×10^3).

2.2.10. D2ZnCu

MS (ESI): m/e: (**1**$^+$) 1496 (40%); (**1**-Zn + 3H) 1434 (100%).

2.3. Spectrophotometric titration of $DSZn_2$ with nitrogen bases

Formation constants of PZnL (where P is the porphyrin subunit in **DSZn$_2$** or TTP, and L = pyridine (py), pyrazine (pyr) or 4,4′-bipyridyl (bipy)) have been obtained by spectrophotometric titration of **DSZn$_2$** (concentration 3.00×10^{-5} mol/dm^3) with L (concentration varied in the 3.00×10^{-5}–0.1 mol/dm^3 range) with the assumption that no other species are present in the equilibrium except those defined by reaction scheme

$$\mathrm{PZn} + \mathrm{L} \Longleftrightarrow \mathrm{PZnL}$$

Stability constants were calculated from the general formula

$$K = \frac{(\varepsilon_1 C_{\mathrm{Zn}} - A)(\varepsilon_1 - \varepsilon_2)}{(A - \varepsilon_2 C_{\mathrm{Zn}})[C_{\mathrm{L}}^0(\varepsilon_1 - \varepsilon_2) - \varepsilon_1 C_{\mathrm{Zn}} - A]},$$

derived from initial equations:

$$C_1 + C_2 = C_{\mathrm{Zn}},$$

$$C_{\mathrm{L}}^0 = C_{\mathrm{L}} + C_2,$$

$$K = \frac{C_2}{C_1 C_{\mathrm{L}}},$$

$$A = \varepsilon_1 C_1 + \varepsilon_1 C_2,$$

where C_1 and C_2 are concentrations of PZn starting complex and PZnL adduct, respectively, C_{L}^0 is total concentration of L, C_{L} is concentration of free L, ε_1 and ε_1 are extinction coefficients of PZn and PZnL, respectively, A is the value of absorbance at the monitoring wavelength, and K is the formation constant. The monitoring wavelength corresponding to Q-bands was chosen for every case.

2.4. Methods and instruments

^{1}H NMR spectra were obtained with a Bruker AMX300 spectrometer operating in the quadrature mode at 300 MHz. The residual peaks of deuterated solvents were used as internal standards. ^{1}H COSY and NOESY spectra were obtained using standard pulse sequences as described before [10]. UV–Vis spectra were recorded on Beckman DU 640 instrument. EPR spectra were obtained with a Bruker ESP300E at X band for frozen solutions (77 K) in CH_2Cl_2/toluene 1/3 v/v. The mass spectrum was obtained on a Finnigan MAT TSQ 700 spectrometer by the ESI method at 4.5 kV ionization potential and 250 °C capillary temperature in chloroform.

3. Results and discussion

3.1. ^{1}H NMR studies of DSH_4, $DSZn_2$ and $DSZnH_2$

It has been demonstrated previously that the ring current effect imposed by a porphyrin macrocycle caused an upfield shift of the adjacent second porphyrin in diporhyrins [10,12]. It is especially pronounced in the case of a peripheral *meso*-phenyl substituent to which the spacer is attached (Table 1). A simple comparison of the chemical shifts of m_6-H, p-H, m_5-H and o_5-H in the diporphyrins studied here with those for the mono-porphyrin reference compound (Table 1) shows that: (i) the upfield shift decreases in order $m_6 > p > m_5 > o_5$ for **S** = 3 and 4, and $p > m_6 > m_5 > o_5$ for **S** = 2, (ii) the upfield shift of m_6-H decreases with increasing spacer length, i.e., in order of **S**; $2 \cong 3 > 4$, (iii) the same relationship holds for **DSZn$_2$** complexes as well as for **DSZnH$_2$** and (iv) introducing one zinc(II) ion into the porphyrin subunit induces considerable differentiation of the chemical shifts of the two porphyrin subunits, which can be exemplified by Δ (where Δ is the chemical shift difference between the corresponding resonances of linking 5-phenyl and pyrrole β-H protons in PH_2 and PZn porphyrin halves (see Fig. 2)). In the case of **D3ZnH$_2$** and **D4ZnH$_2$** Δ decreases in the order:

D3ZnH$_2$: $m_6(0.36) > p(0.35) > m_5 = \beta_{2,3}$ $(0.23) > o_5(0.21) > \beta_{12,13}(0.18)$.

D4ZnH$_2$: $p(0.52) > m_6(0.39) > m_5(0.28) > \beta_{2,3}(0.13) o_5$ $(0.10) > \beta_{12,13}(0.09)$.

The largest values of Δ for **D4ZnH$_2$** indicate that the ring current effect is most pronounced in this case. On the other hand the Δ values for **D2ZnH$_2$** are very small

Table 1
Relevant ^{1}H NMR data of **DSH$_4$**, **DSZnH$_2$** and **DSZn$_2$**

Entry	Compound	Chemical shift (ppm) (chemical shift difference related to reference[a])			
		m_6	p	m_5	o_5
1	**TTP-*o*-PrBr**[a]	7.32	7.76	7.37	8.04
2	**D2H$_4$**	5.88 (−1.44)	5.82 (−1.84)	6.43 (−0.94)	7.61 (−0.43)
3	**D2Zn$_2$**	5.93 (−1.39)	5.91 (−1.85)	6.43 (−0.94)	7.45 (−0.59)
4	**D3H$_4$**	5.82 (−1.50)	6.58 (−1.18)	6.96 (−0.41)	7.77 (−0.27)
5	**D3Zn$_2$**	5.76 (−1.56)	6.41 (−1.35)	6.82 (−0.55)	7.73 (−0.31)
6	**D3ZnH$_2$**	5.95 (−1.37)	6.65 (−1.11)	6.98 (−0.39)	7.86 (−0.18)
		5.59 (−1.73)	6.30 (−1.46)	6.75 (−0.62)	7.65 (−0.39)
7	**D4H$_4$**	6.02 (−1.30)	6.84 (−0.92)	6.97 (−0.40)	7.73 (−0.31)
8	**D4Zn$_2$**	6.00 (−1.32)	6.66 (−1.10)	6.77 (−0.60)	7.63 (−0.41)
9	**D4ZnH$_2$**	5.79 (−1.53)	6.44 (−1.32)	6.64 (−0.73)	7.68 (−0.36)
		6.18 (−1.14)	6.96 (−0.80)	7.02 (−0.35)	7.78 (−0.26)

[a] The chemical shifts were related to reference compound of C_{2v} effective symmetry; 5-(*ortho*-(3-bromopropoxy)phenyl)-10,15,20-tris(*para*-methylphenyl)porphyrin (entry 1, **TTP-*o*-PrBr**).

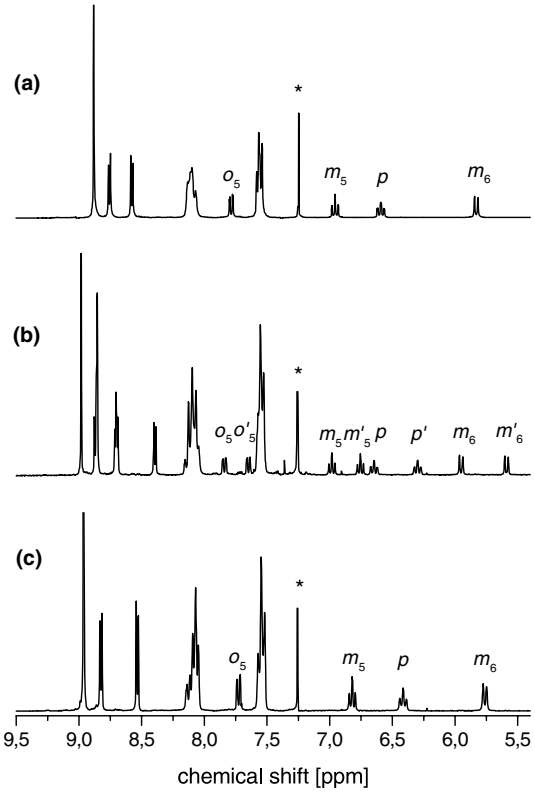

Fig. 2. Relevant fragments of the ^{1}H NMR spectra of **D3H$_4$** (a); **D3ZnH$_2$** (b) and **D3Zn$_2$** (c). The residual $CHCl_3$ resonance is labelled with an asterisk. The resonances labelled with $\prime$ at trace B were tentatively attributed to the PZn part of **D3ZnH$_2$**.

and the corresponding resonances of 5-*meso*-phenyl substituents almost overlap. These features suggest that in all **DSZnH$_2$** the two porphyrin subunits are in face-to-face conformation, however, in the case of $\mathbf{S} = 2$ the average conformation is slightly different from those for $\mathbf{S} = 3$ and 4.

3.2. Coordination of nitrogen aromatic ligands into dizincdiporphyrins

Coordination of pyridine-type bases into PZn causes red shift of the Soret band and a 14 nm red shift of the Q-band centered at about 550–560 nm. The titration of PZn indicated well-resolved isosbestic points for all studied systems at the concentration of L up to 10^{-2} M (Fig. 3). Above that concentration of L a further red shift (1–2 nm) of the Q-band could be detected, typical for formation of PML_2 (P – porphyrin or phthalocyanine) [13] with a very small change of extinction at the analytical wavelength. In order to avoid overlapping equilibrium related to the formation of bis-ligand $PZnL_2$ complexes only the points for base concentration below 10^{-3} M were used for the calculation of formation constants. The values of ε_1 and ε_2 were taken from

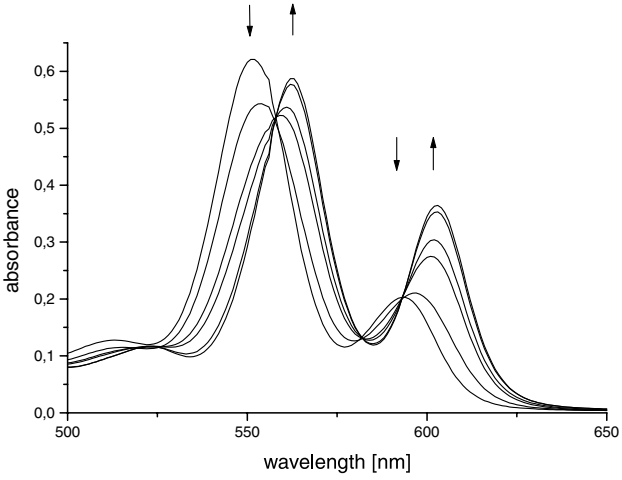

Fig. 3. The Q-band regions of UV–Vis spectra of the solutions containing **D4Zn$_2$** ($c = 2.2 \times 10^{-5}$ mol dm^{-3}) and pyr in CH_2Cl_2. Vertical arrows indicate absorbance changes upon addition of pyr, whose concentrations are (from top to bottom at 550 nm): 0; 3.0×10^{-5}; 6.0×10^{-5}; 2.5×10^{-4}; 5.0×10^{-3} and 0.10 mol $\times$ dm^{-3}.

Table 2
Formation constants of PZnL complexes (where L = py, pyr and bipy) determined by spectrophotometric titration of PZn in methylene dichloride at 298 K

Entry	Starting complex	log K (K – formation constant in mol/dm^3) (EM (mol dm^{-3}))		
		py	pyr	bipy
1	**TTPZn**	3.61 (3.68)[a]	3.90	3.20
2	**D2Zn$_2$**	3.35	4.61 (0.00065)	3.22
3	**D3Zn$_2$**	3.63	4.90 (0.0012)	4.63 (0.017)
4	**D4Zn$_2$**	3.65	3.83	5.19 (0.062)
5	**D4ZnH$_2$**	3.03	3.10	3.12

[a] Determined in benzene solution [14].

experimental data at an analytical wavelength chosen at the maximum of two Q-bands of PZnL. The calculated data on K are collected in Table 2. The formation constants of PZnL, where L = py are in every case close to that of TTPZnL. Pyrazine and bipyridyl form in some cases considerably stronger complexes, which was attributed to an entropic factor due to the bridging mode of coordination of the ligands. Thus, the best fit between size of heteroaromatic base and length of spacer was obtained for bipy and **D4Zn$_2$**, while for pyr the best fit was in the case of **D3Zn$_2$** and **D2Zn$_2$**. The complementarity between host (dizincdiporphyrin) and bidentate ligand (here pyr or bipy) can be rationalized using the concept of effective molarity [15] expressed as

$$\mathrm{EM} = K/K_i^2,$$

where K_i is the microscopic equilibrium constant for binding of monodentate ligand into metal ion.

This approach was successfully applied for quantification of oligopyridyl ligands to butadiyne-linked porphyrin dimers, trimers and tetramers [16]. The best host–guest complementarity was found in the case of a relatively rigid cyclic diporphyrin with bipy, resulting in EM as large as 76 mol dm^{-3}, while in the case of the corresponding linear diporphyrin the EM was merely 0.5 mol dm^{-3}.

Here the EMs were calculated using experimental K_i obtained as the formation constant for binding bidentate ligand into TTPZn (entry 1 in Table 2). The values of EM are listed in Table 2. Obtained EM are much lower in comparison with those found for well-fitted host–guest pairs based on rigid cyclic oligoporphyrins [16], which seems reasonable considering the flexibility of the diporhyrins studied here. Nevertheless, the best complementarity within the **D4Zn$_2$**/bipy and **D3Zn$_2$**/pyr pairs is clearly seen.

3.3. Synthetic route to heterodimetallodiporphyrin D2ZnCu

The insertion of Cu(II) ion into **D2ZnH$_2$** was accompanied by partial replacement of Zn(II) with Cu(II) resulting in the formation of two species: **D2ZnCu** and **D2Cu$_2$**. The complexes were identified by their EPR spectra (Fig. 4). The **D2Cu$_2$** complex was obtained in an independent synthesis by insertion of Cu(II) into **D2H$_4$**. The mixed-metal **D2ZnCu** was identified by MS measurement. Moreover, the complexes were demetallated and the identity of **D2H$_4$** was verified by its ^{1}H NMR spectrum. The EPR spectrum of **D2Cu$_2$** is composed of broad lines, probably due to weak interaction between the two copper(II) centers and does not show superhyperfine coupling with nitrogen donors [17]. The characteristic feature of **D2ZnCu** is the presence of 18 lines of superhyperfine structure related to two distinct $g_\perp$, typical for monomeric copperporphyrins [17].

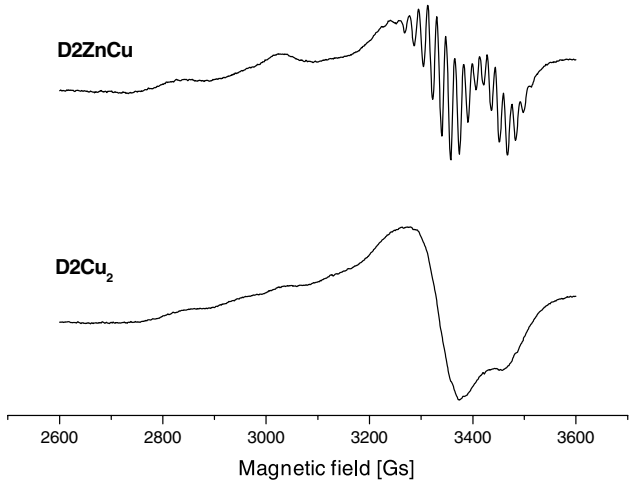

Fig. 4. EPR spectra of **D2ZnCu** and **D2Cu$_2$** in CH_2Cl_2/toluene glass in 77 K.

4. Conclusion

We have presented the successful method of synthesis and separation of mono-zinc diporphyrin complexes, which are useful starting materials for the synthesis of heterodimetallodiporphyrins. Heterometallodiporphyrins with flexible spacers of tunable length and geometry may be used as catalysts in many reactions, depending on the metal ions incorporated. The most promising is the application of diiron(II)diporphyrins in activation of dioxygen and oxygen atom

transfer from diferryldiporphyrins into dienes. Especially interesting seems to study the influence of different metal ions in Fe(II)/M(II)diporphyrin complexes on the chemoselectivity of such catalytic reaction.

References

[1] A. Osuka, S. Nakajima, T. Nagata, K. Maruyama, K. Toriumi, Angew. Chem., Int. Ed. Engl. 30 (1991) 582.
[2] R. Paolesse, R.K. Pandey, T.P. Forsyth, L. Jaquinod, K.R. Gerzevske, D.J. Nurco, M.O. Senge, S. Licoccia, T. Boschi, K.M. Smith, J. Am. Chem. Soc. 118 (1996) 3869.
[3] R. Guilard, S. Brandes, A. Tabard, N. Bouhmaida, C. Lecomte, P. Richard, J.M. Latour, J. Am. Chem. Soc. 116 (1994) 10202.
[4] J.P. Fillers, K.C. Ravichandran, I. Abdalmuhdi, A. Tulinsky, C.K. Chang, J. Am. Chem. Soc. 108 (1986) 417.
[5] C.J. Chang, Y. Deng, A.F. Heyduk, C.K. Chang, D.G. Nocera, Inorg. Chem. 39 (2000) 959.
[6] C. Pascard, J. Guilhem, S. Chardon- Noblat, J.P. Sauvage, New J. Chem. 17 (1993) 331.
[7] R. Guillard, M.A. Lopez, A. Tabard, P. Richard, C. Lecomte, S. Brandes, J.E. Hutchison, J.P. Collman, J. Am. Chem. Soc. 114 (1992) 9869.
[8] R.G. Little, J.A. Anton, P.A. Loach, J.A. Ibers, J. Heterocycl. Chem. 12 (1975) 343.
[9] R.G. Little, J. Heterocycl. Chem. 15 (1978) 203.
[10] S. Wołowiec, L. Latos-Grażyński, Inorg. Chem. 33 (1994) 3576.
[11] S. Wołowiec, Polyhedron 16 (1997) 3779.
[12] S. Wołowiec, Polyhedron 17 (1998) 1295.
[13] T. Baldacchini, F. Monacelli, Inorg. Chim. Acta 295 (1999) 200.
[14] C.J. Miller, P. Hambright, Inorg. Chem. 9 (1976) 958.
[15] A.J. Kirby, Adv. Phys. Org. Chem. 17 (1980) 183.
[16] H.L. Anderson, S. Anderson, J.K.M. Sanders, J. Chem. Soc., Perkin Trans. I (1995) 2231.
[17] M. Chikira, H. Kon, R.A. Hawley, K.M. Smith, J. Chem. Soc., Dalton Trans. (1979) 245.

Available online at www.sciencedirect.com
SCIENCE DIRECT®
Polyhedron 23 (2004) 41–47
POLYHEDRON
www.elsevier.com/locate/poly

Cobalt(III) complexes of 2-hydroxyacetophenone N(4)-phenyl semicarbazone containing heterocyclic coligands: syntheses, structure and spectral studies

A. Sreekanth, U.L. Kala, Chandini R. Nayar, M.R. Prathapachandra Kurup *

Department of Applied Chemistry, Cochin University of Science and Technology, Kochi 682 022, Kerala, India

Received 6 May 2003; accepted 3 September 2003

Abstract

An interesting series of four novel mixed ligand Co(III) complexes of 2-hydroxyacetophenone 4-phenyl semicarbazone (H_2L), heterocyclic base, B [1,10-phenanthroline (phen), piperidine (pip) and pyrrolidine (pyrr)] and azide/thiocyanate (X) with a general formula [$CoLB_xX$] (where $x = 1$ for phen and 2 for pip and pyrr) were prepared. They were characterized by a variety of physicochemical techniques. All the four complexes are diamagnetic indicating that the cobalt is in a d^6 strong field. The tridentate character of the semicarbazone in all cases is inferred from IR spectra. The structure of the compound $CoLphenN_3$ is solved by single crystal X-ray diffraction. It shows that the compound crystallizes in the orthorhombic system, [space group is *P 21 21 21*, $a = 10.6590(8)$ Å, $b = 11.9150(16)$ Å, $c = 19.1650(4)$ Å, $Z = 4$]. The coordination geometry around the cobalt is distorted octahedral with tridentate L^{2-}, bidentate phenanthroline and unidentate azido anion. The azido nitrogens and phenanthroline hydrogens form intermolecular hydrogen bonds to give a sandwich type of packing to the molecule.
© 2003 Elsevier Ltd. All rights reserved.

Keywords: Cobalt(III); Semicarbazone; 2-Hydroxyacetophenone; NMR spectra; IR spectra; Electronic spectra; X- ray crystal structure

1. Introduction

In the quest of exploring the chelating behavior of some ONS and NNS donor thiosemicarbazones in several metal complexes, we could acquire more information about their nature of coordination and related structural, spectral and biological properties [1–5]. Recently, we have reported the spectral and structural studies of Co(III) complexes containing N(4)-substituted thiosemicarbazones [6]. Thiosemicarbazones and their metal complexes have been the subject of extensive investigations because of their potential pharmacological properties and a wide variation in their modes of bonding and stereochemistry whereas their semicarbazone analogs received much less attention. However, semicarbazones are reported to possess versatile structural features [7] and very good antifungal and antibacterial properties [8,9]. Spectral studies of some complexes of furfuraldehyde semicarbazone were recently reported [10]. So we considered it worthwhile to extend our studies to semicarbazones, which are structurally similar to thiosemicarbazones, except that they have an oxygen atom in place of sulfur. Herein we report the synthesis and spectral studies of a new ligand 2-hydroxyacetophenone N(4)-phenyl semicarbazone (Scheme 1) and its four Co(III) complexes containing heterocyclic bases, 1,10-phenanthroline, piperidine and pyrrolidine. The crystal structure of the compound $CoLphenN_3$ (**1**) is also reported.

2. Experimental

2.1. Materials

1,10-Phenanthroline, pyrrolidine and piperidine were purchased from Merck and used as received. 4-Phenyl semicarbazide (Fluka), 2-hydroxyacetophenone (CDH)

* Corresponding author. Tel.: +91-484-575804; fax: +91-484-577595.
E-mail addresses: sreekanth@cusat.ac.in (A. Sreekanth), mrp@cusat.ac.in (M.R. Prathapachandra Kurup).

0277-5387/$ - see front matter © 2003 Elsevier Ltd. All rights reserved.
doi:10.1016/j.poly.2003.09.029

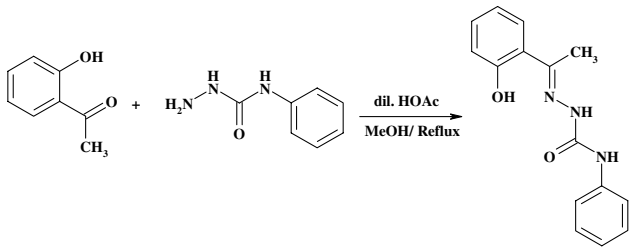

Scheme 1.

and cobalt acetate (BDH) were used without further purification. All solvents obtained commercially were distilled before use.

2.2. Syntheses of compounds

2.2.1. Synthesis of ligand H_2L

The ligand was prepared from a methanolic solution of 4-phenyl semicarbazide and 2-hydroxyacetophenone in acidic medium. 4-Phenyl semicarbazide (0.151 g; 1 mmol) dissolved in hot methanol (50 ml) was added to a solution of 2-hydroxyacetophenone (0.136 g, 1 mmol) in the same solvent. Two drops of concentrated acetic acid was added to the reaction mixture to change the pH. Then the reaction mixture was refluxed for 3 h on a water bath and cooled to room temperature. The product formed was filtered off and washed with methanol to obtain an off-white crystalline compound. M.p. 188–189 °C. Yield 70%. *Anal.* Calc. for $C_{15}H_{15}N_3O_2$: C, 66.90; H, 5.61; N 15.60. Found: C, 66.70; H, 5.57; N, 15.6%. ^{1}H NMR, DMSO-d_6, 500 Hz: $\delta = 12.79$ (s, br, 1H, OH); $\delta = 7.52$ (d, $J = 8$ Hz, 1H, H-3); $\delta = 6.89$ (d, $J = 7.9$ Hz, 1H, H-4); $\delta = 7.25$ (t, $J = 7.3$ Hz, 1H, H-5); $\delta = 6.87$ (d, $J = 7.6$ Hz, 1H, H-6); $\delta = 2.23$ (s, 3H, methyl); $\delta = 9.87$ (s, 1H, N(3)H); $\delta = 8.89$ (s, 1H, N(4)H); $\delta = 7.57$ (d, $J = 7.3$ Hz, 2H, H-11 and H15); $\delta = 7.32$ (t, $J = 7.7$ Hz, 2H, H12 and H14); $\delta = 7.01$ (t, $J = 7.3$ Hz, 1H, H13). ^{13}C NMR, DMSO-d_6, 125 Hz: $\delta = 152.79$ C9; 151.20 C7; 13.90 C8; 158.80 C1; 121.09 C2; 128.70 C3; 119.37 C4; 131.12 C5; 117.86 C6; 140.05 C10; 110.37 C11 and C15; 129.73 C12 and C14; 123.12 C13.

2.2.2. Syntheses of complexes

The complexes $[CoLB_xX]$ were prepared by the following general method. A hot methanolic solution (30 ml) of $Co(CH_3COO)_2 \cdot 5H_2O$ (0.458 g, 2 mmol) was added to a mixture of H_2L (0.598 g, 2 mmol) and appropriate heterocyclic base (2 mmol phen and 4 mmol pip and pyrr) in the same solvent. The resulting green solution was stirred for 10 min. To this 2 mmol NaN_3/KCNS was added and refluxed for 20 min. Then microcrystalline powders of the complexes were separated out which were filtered and washed with methanol, water and diethyl ether. They were then dried over P_4O_{10} in vacuo. *Anal.* Calc. for $[CoLphenN_3]$: C, 58.59; H, 4.58; N, 18.85; Co, 9.91. Found: C, 58.11; H, 4.04; N 19.02; Co, 9.63%. *Anal.* Calc. for [CoLphenNCS]: C, 59.57; H, 3.75; N, 14.89; Co, 10.44. Found: C, 59.27; H, 4.24; N 14.79; Co, 10.36%. *Anal.* Calc. for $[CoLpip_2N_3]$: C, 55.76; H, 6.55; N 20.81; Co, 10.94. Found: C, 55.92; H, 6.62; N, 20.21; Co, 11.16%. *Anal.* Calc. for $[CoLpyrr_2N_3]$: C, 54.12; H, 6.12; N, 21.95; Co, 11.54. Found: C, 54.89; H, 6.02; N 21.83; Co, 11.8%.

2.3. Physical methods

Molar conductance measurements of the complexes were carried out in DMF solvent at 28 ± 2 °C on a Centuary CC-601 digital conductivity meter with a dip type cell and platinum electrode. Approximately 10^{-3} M solutions were used. The magnetic susceptibility measurements were made using a simple Gouy balance at room temperature using mercury tetrathiocyanatocobaltate(II), $Hg[Co(NCS)_4]$ as calibrant. Microanalysis of carbon, hydrogen and nitrogen content of the ligand and the metal complexes was carried out using a Heraeus Elemental Analyzer at CDRI, Lucknow, India. Electronic spectra were recorded on a Shimadzu UV-160A spectrophotometer. IR spectra were recorded as KBr pellets on a Perkin–Elmer model 1620 FT IR spectrophotometer. Metal estimation was done by the AAS method on a Varian spectrometer AA-10/20. NMR spectra were obtained in a Bruker DRX 500 instrument

Table 1
Crystal data and structure refinement for compound **1**

Empirical formula	$C_{27}H_{21}CoN_8O_2$
Formula weight, M	548.45
Temperature, T (K)	293(2)
Wavelength, Mo Kα (Å)	0.70930
Crystal system	orthorhombic
Space group	*P 21 21 21*
Unit cell dimensions	
A (Å) and α (°)	10.6590(8) and 90
B (Å) and β (°)	11.9150(16) and 90
C (Å) and γ (°)	19.1650(4) and 90
Volume, V (Å^3)	2430.0(4)
Z and calculated density, ρ(mg/m^3)	4 and 1.497
Absorption coefficient, μ (mm^{-1})	0.749
$F(000)$	1128
Crystal size (mm)	$0.35 \times 0.30 \times 0.05$
θ Range for data collection (°)	2.01–24.93
Limiting indices	$0 \leqslant h \leqslant 12, 0 \leqslant k \leqslant 14, 0 \leqslant l \leqslant 22$
Reflections collected/unique	2281/2281 [$R_{int} = 0.000$]
Completeness to 2θ	24.93 (93.8%)
Maximum and minimum transmission	1.000 and 0.935
Goodness-of-fit on F^2	1.124
Final R indices [$I > 2\sigma(I)$]	$R_1 = 0.0376$, $wR_2 = 0.0779$
R Indices (all data)	$R_1 = 0.0508$, $wR_2 = 0.0886$
Largest difference peak and hole (e Å^{-3})	0.335 and −0.401

using DMSO-d_6 as solvent at the Sophisticated Instruments Facility, IISc, Bangalore, India.

2.4. X-ray crystallography

A dark brown orthorhombic crystal of $CoLphenN_3$ (**1**) having approximate dimensions $0.35 \times 0.3 \times 0.05$ mm was sealed in a glass capillary, and intensity data were measured at room temperature (293 K) on a Nonius MACH3 diffractometer equipped with graphite-monochromated Mo Kα ($\lambda = 0.7093$ Å) radiation. The crystallographic data along with details of structure solution refinements are given in Table 1. The intensity data were collected by the ω-scan mode within $2.01° < \theta < 24.93°$ for *hkl* ($0 \leqslant h \leqslant 12$, $0 \leqslant k \leqslant 14$, $0 \leqslant l \leqslant 22$) in the monoclinic system. The trial structure was obtained by direct methods using SHELXS 97 [11] and refined by full-matrix least-squares on F^2 (SHELXL 97) [12]. The non-hydrogen atoms were refined with anisotropic thermal parameters. All the hydrogen atoms were geometrically fixed and allowed to refine using a riding model.

3. Results and discussions

The principal ligand H_2L was synthesized by the direct condensation of 2-hydroxyacetophenone with 4-phenyl semicarbazide. The elemental analysis is in good accordance with the proposed structure. 2-Hydroxyacetophenone N(4)-phenyl semicarbazone can exist either as the keto or enol form or an equilibrium mixture of the two since it has an amide –NH–C(=O) function. However, the IR and NMR spectra of H_2L indicate that in solid state it remains in the keto form. The IR spectra of complexes, however, does not show any intense absorption band at 1696 cm^{-1} due to the carbonyl stretching of the semicarbazone moiety. This shows that in solution, it converts to the enol form and coordinates to the metal in the enolate form.

Four new complexes are readily formed by the reaction of the ligand and heterocyclic base with cobaltous acetate followed by a metathetical displacement of the acetate anion by azide or thiocyanate anions. It is found that cobalt(II) is getting oxidized to cobalt(III) in all the complexes.

The elemental analysis corresponds to a general formula $[CoLB_xX]$ for all complexes. The principal ligand H_2L undergoes double deprotonation to form L^{2-} and acts as a tridentate ligand thus occupying three positions of an octahedral geometry. In the case of [CoLphenX], phenanthroline acts as a bidentate ligand and occupies the fourth and fifth positions. The azido or thiocyanato group occupies the sixth position. In the case of the complexes with piperidine and pyrrolidine, two molecules of heterocyclic base complete the fifth and sixth position of the six coordinate geometry. Room temperature magnetic susceptibility measurements of the complexes reveal that all compounds are diamagnetic indicating the oxidation of cobalt(II) to cobalt(III). All complexes are found to be non-conducting in DMF solution.

3.1. NMR spectrum of H_2L

The ^1H and ^{13}C NMR spectra of H_2L were recorded in DMSO-d_6 as solvent. The tentative structure of the compound H_2L and the ^1H NMR spectral assignments are given in Fig. 1. In the ^1H NMR spectrum, the signal for N(2)H is observed at $\delta = 9.87$ which is consistent with hydrogen bonding to the oxygen of DMSO-d_6 [13,14]. The N(4)H is observed as a singlet at $\delta = 8.89$. The OH proton is observed at $\delta = 12.79$. These values are in agreement with salicylaldehyde and 2-hydroxyacetophenone thiosemicarbazones [2,6]. Upon addition of D_2O the intensities of these signals significantly decrease, confirming the assignments. A singlet at $\delta = 2.23$ is attributed to the methyl protons which are chemically and magnetically equivalent. Aromatic protons of both rings appear within the range 6–8 ppm with coupling constants around 7 Hz.

The assignments made from ^{13}C NMR spectrum of the ligand are shown in Fig. 2.

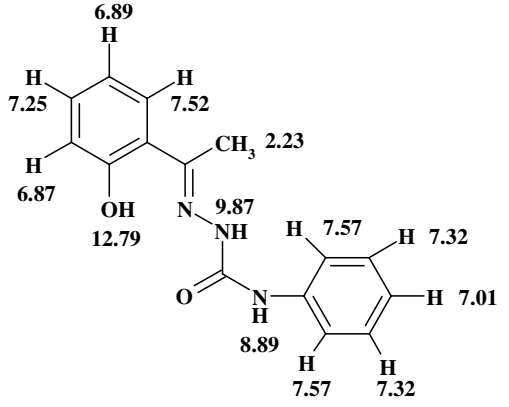

Fig. 1. ^1H NMR spectral assignments of the compound H_2L.

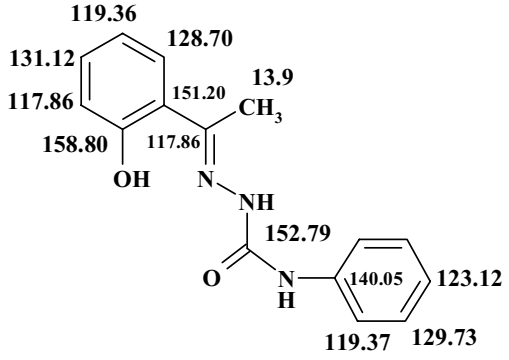

Fig. 2. ^{13}C NMR spectral assignment of the compound H_2L.

3.2. X-ray diffraction studies

Dark brown X-ray quality single crystals of compound **1** $CoLphenN_3$ were grown by slow evaporation of the compound from DMF solution. The molecular structure of compound **1** along with atomic labelling is given in Fig. 3, and selected bond lengths and bond angles are summarized in Table 2. The cobalt atom is six coordinate and has a distorted octahedral geometry. The three donor atoms of the semicarbazone, *viz* phenolato oxygen, azomethine nitrogen, enolate oxygen, constitute a meridional arrangement around the cobalt atom, along with the phenanthroline nitrogens and terminal azido group. The Co–O(1) and Co–O(2) bond lengths are 1.866(4) and 1.914(3) Å and the Co–N bond lengths are 1.856(4) Å (azomethine) and 1.961(4) Å (phen). The fifth and sixth positions of the distorted octahedral geometry are occupied by the second nitrogen of 1,10-phenanthroline, N(4) and the unidentate azide ion N(1). The bond length Co–N(4) is found to be 1.968(5) Å (slightly larger value) and Co–N(1) is 1.926(4) Å. These bond length values agree with that of a bipyridyl analog of a cobalt complex of a thiosemicarbazone compound reported elsewhere [6]. The shorter $Co–N_{azomethine}$ bond length indicates that the azomethine nitrogen coordinates more strongly than the phenanthroline nitrogen. The difference in bond lengths can be attributed to the difference in the extent of π-back bonding between the phenanthroline and semicarbazone moiety. However the comparatively larger bond distance of Co–N(5) supports the lack of significant out-of-plane π-bonding. The azido group has practically a linear configuration with a N(1)–N(2)–N(3) bond angle of 174.7(6)° and bond length N(1)–N(2) 1.214(6) Å slightly longer than N(2)–N(3) 1.147(7) Å.

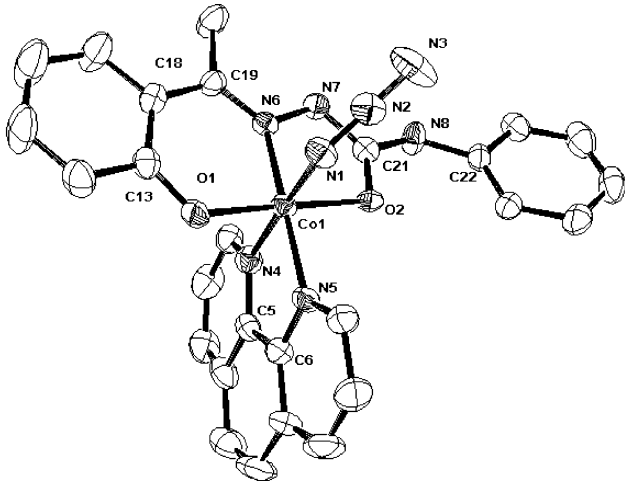

Fig. 3. ORTEP diagram for compound **1**, displacement ellipsoids are drawn at the 54% probability level and hydrogen atoms are removed for clarity.

Table 2
Bond lengths and angles of compound **1**

Bond lengths	
Co(1)–N(6)	1.856(4)
Co(1)–O(1)	1.866(4)
Co(1)–O(2)	1.914(3)
Co(1)–N(1)	1.926(4)
Co(1)–N(5)	1.961(4)
Co(1)–N(4)	1.968(5)
O(1)–C(13)	1.316(6)
O(2)–C(21)	1.290(7)
N(1)–N(2)	1.214(6)
N(2)–N(3)	1.147(7)
Bond angles	
N(6)–Co(1)–O(1)	95.97(17)
N(6)–Co(1)–O(2)	84.82(16)
O(1)–Co(1)–O(2)	177.82(17)
N(6)–Co(1)–N(1)	89.9(2)
O(1)–Co(1)–N(1)	89.90(19)
O(2)–Co(1)–N(1)	92.14(18)
N(6)–Co(1)–N(5)	175.37(19)
O(1)–Co(1)–N(5)	86.50(16)
O(2)–Co(1)–N(5)	92.57(16)
N(1)–Co(1)–N(5)	94.0(2)
N(6)–Co(1)–N(4)	93.04(19)
O(1)–Co(1)–N(4)	89.10(18)
O(2)–Co(1)–N(4)	88.83(17)
N(1)–Co(1)–N(4)	177.0(2)
N(5)–Co(1)–N(4)	83.08(19)
C(13)–O(1)–Co(1)	124.1(3)
C(21)–O(2)–Co(1)	107.5(3)
N(2)–N(1)–Co(1)	118.2(4)
N(3)–N(2)–N(1)	174.7(6)
C(1)–N(4)–Co(1)	129.0(4)
C(5)–N(4)–Co(1)	112.1(4)
C(10)–N(5)–C(6)	118.0(5)
C(10)–N(5)–Co(1)	129.4(4)
C(6)–N(5)–Co(1)	112.5(4)
C(19)–N(6)–N(7)	117.9(4)
C(19)–N(6)–Co(1)	129.1(4)
N(7)–N(6)–Co(1)	112.9(3)

But the Co–N(1)–N(2) bond angle is 118.2(4)° showing bent coordination and the Co–N(1) bond length is 1.926(4) Å. The bond angles N(1)–Co–N(4) 177.0(2)° and N(5)–Co–N(4) 83.08(19)° indicate distortion from octahedral geometry.

It is found that hydrogen bonding, π–π stacking and C–H–π interactions affect the molecular packing [16–18] (Table 3). The phenanthroline proton H(1) forms an intramolecular hydrogen bond with N(6) of the same molecule, [C(1)H···N(6) 2.48 Å], while H(10) forms an intermolecular hydrogen bond with the N(7) nitrogen of the neighboring molecular unit [C(10)H··· N(7) 2.50 Å]. A hydrogen bond from H(9) links one molecule to the azido nitrogen N(3) of the neighboring molecule [C(9)H···N(3) 2.50 Å]. The intramolecular hydrogen bond influences the geometry of the molecule. However, the two intermolecular hydrogen bonds lead to a "sandwich" type of packing, resulting in centrosymmetric architecture (Fig. 4). This arrangement gives a

Table 3
H-bonding, CH–π and π–π interaction parameters of compound **1**

D–H–A	D–H (Å1)	H–A (Å)	D–A (Å)	∠D–H–A (°)
N(8)–H(8)···N(1)[a]	0.81	2.14	2.92	165
N(8) – H(8)···N(2)[a]	0.81	2.58	3.30	150
Intra C(1)–H(1)···N(6)	0.99	2.48	3.01	114
C(9)–H(9)···N(3)	0.99	2.50	3.08	157
Intra C(10)–H(10)···N(7)	0.99	2.50	3.08	118
C(10)–H(10)···N(7)[b]	0.99	2.47	3.42	162
Intra C(27)–H(27)···O(2)	0.86	2.39	2.94	123
X–H(I)–Cg(J)	H–Cg (Å)	X–Cg (Å)	∠X–H–Cg (°)	
C(8)–H(8)–Cg(4)[c]	3.1269	3.9480	157.21	
C(12)–H(12)–Cg(5)[e]	2.4889	3.5302	169.23	
C(24)–H(24)–Cg(2)[d]	3.1792	3.4850	100.17	
C(26)–H(26)–Cg(1)[d]	3.1518	3.8242	123.43	
Centroids	Cg···Cg distance (Å)	Equivalent position codes		
Cg(1)–Cg(2)[f]	3.8583	f: $1-X$, $-1/2+Y$, $1/2-Z$		
Cg(3)–Cg(5)[g]	3.7875	g: $1/2+X$, $1/2-Y$, $-Z$		

Equivalent position codes a: $-x$, $1/2+y$, $1/2-z$; b: $-x$, $-1/2+y$, $1/2-z$; c: $1-x$, $1/2+y$, $1/2-z$; d: $-1/2+x$, $1/2-y$, $-z$; e: $1+x$, y, z. D, donor; A, acceptor and Cg, Centroid.

Cg(1) = N(4), C(1), C(2), C(3), C(4), C(5); Cg(2) = N(5), C(6), C(7), C(8), C(9), C(10); Cg(3) = C(4), C(5), C(6), C(7), C(11), C(12); Cg(4) = C(13), C(14), C(15), C(16), C(17), C(18); Cg(5) = C(22), C(23), C(24), C(25), C(26), C(27).

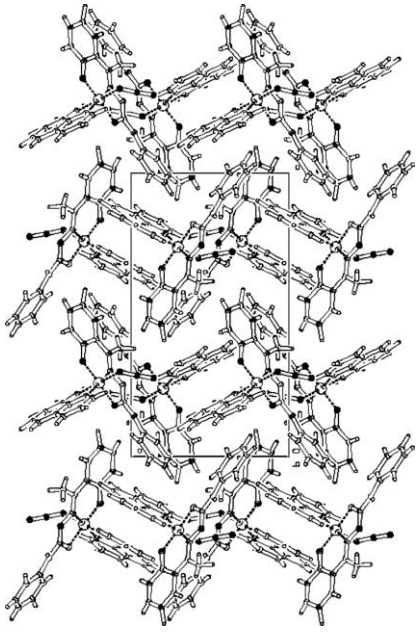

Fig. 4. Packing diagram for compound **1** viewed along a axis.

polar nature to the region between the semicarbazone planes. The non-polar phenanthroline groups of two neighboring sandwich units assemble via a π–π stacking interaction. The aromatic rings of two neighboring sandwich units are arranged in an off-set fashion in which the Cg(1) ring interacts with the Cg(2) ring of the neighboring unit and is separated by an average face-to-face distance of 3.8583 Å. The packing is further assisted by the π–π interactions between the Cg(3) ring of phen and the Cg(5) ring of the semicarbazone of the neighboring group at a Cg–Cg distance of 3.7875 Å. The network of hydrogen bonds and π–π stacking interactions leads to a two-dimensional arrangement of molecular units in a periodic fashion in the unit cell lattice. The 2-D chains are assembled into a 3-D network *via* CH–π interactions.

3.3. Electronic and IR spectra

Electronic spectral data of the ligand and its complexes are presented in Table 4. The semicarbazone and its complexes show bands in the range 46 300–30 000 cm^{-1} due to $\pi \rightarrow \pi^*$ and $n \rightarrow \pi^*$ transitions. Charge transfer bands were observed in the range 32 000–23 000 cm^{-1} which is rather too broad and is explained as the combination of $O \rightarrow Co$, and $N \rightarrow Co$ LMCT transitions. For low spin Co(III) complexes, there are two spin allowed transitions at relatively low energy, $^1A_{1g} \rightarrow {}^1T_{1g}$, $^1A_{1g} \rightarrow {}^1T_{2g}$. We have assigned them to be the bands at ~20 370 [$^1A_{1g} \rightarrow {}^1T_{1g}$] and 25 900 cm^{-1} [$^1A_{1g} \rightarrow {}^1T_{2g}$]. There are additional spin-forbidden transitions $^1A_{1g} \rightarrow {}^3T_{1g}$ and $^1A_{1g} \rightarrow {}^3T_{2g}$ at higher energies and these are usually complicated by overlap of interligand and charge transfer transitions. $^1A_{1g} \rightarrow {}^3T_{2g}$ is the most difficult to assign because this weak spin-forbidden band is always at the onset of other high-energy intense bands [19,20].

The observed spectra fitted to the corresponding Tanabe–Sugano diagram enabled us to obtain D_q values for the complexes. In addition we have evaluated the electronic repulsion parameter B. The value of B is found to be less than that of free ion B' (1100 cm^{-1}). This is attributed to the nephalauxetic effect. The ne-

Table 4
Electronic spectral assignments, λ (cm^{-1}) for H_2L and its cobalt(III) complexes

Compound	d–d	LMCT	$n \rightarrow \pi^*$	$\pi \rightarrow \pi^*$	B	β	D_q (cm^{-1})
H_2L			30 120, 34 260, 374 530	43 103, 46 296			
$CoLphenN_3$ (**1**)	17 241, 20 725, 25 806	29 411, 31 695	31 250, 33 557	40 000, 45 662	497.0	0.45	2239.20
CoLphenNCS (**2**)	17 035, 20 408, 26 041	24 783, 31 887	33 333, 33 788	48 309	520.7	0.47	2056.37
$CoLpip_2N_3$ (**3**)	17 285, 20 345, 26 109	23 364, 24 630	30 864, 34 364	44 240	549.7	0.49	2089.43
$CoLpyrr_2N_3$ (**4**)	20 004, 25 940	28 011	34 364	41 153	552.2	0.52	2016.97

Table 5
IR spectral assignment for compounds **1**–**4**

Compound	ν(C=N)	$\nu(N_3)$/NCS	$\nu(Co–N)_{azomethine}$	ν(NH)	ν(Co–O)	Bands due to heterocyclic bases
H_2L	1621 s			3327 b, 1030 m		
$CoLphenN_3$ (**1**)	1593 s	2020 s	529 m	3249 b, 1104 m	720 w	1497 s, 1433 s,f 1360 m, 842 m
CoLphenNCS (**2**)	1594 s	2105 s, 696 m	534 m	3250 b, 1149 m	751 w	1498 s, 1431 s, 1332, 844 m
$CoLpip_2N_3$ (**3**)	1598 s	2017 s	542 m	3280 b, 1029 m	746 w	1109 m, 619 m
$CoLpyrr_2N_3$ (**4**)	1592 s	2096 s, 2029 s	525 m	3300 b, 1157 m	752 w	1057 w, 893 w

phalauxetic ratio β is also calculated and is found to be less than unity. D_q values are in good agreement with low spin Co(III) complexes.

The significant bands observed in the IR spectra of H_2L and its complexes are presented in Table 5. The IR spectra of the complexes do not exhibit a broad absorption band at 3420 cm^{-1}, which is due to the O–H stretching modes of phenolic oxygen, indicating deprotonation during coordination. Weak bands in the region 720–755 cm^{-1} indicate the presence of a Co–O bond, resulting from coordination of the phenolic oxygen [9,15]. Besides, the shifting of the band due to the Ar–O group to lower frequencies indicates the weakening of the Ar–O bond due to coordination. A band around 1696 cm^{-1} attributable to the ν(C=O) stretching in the ligand spectrum is absent in the spectra of all complexes which indicates the coordination in the enolate form. A sharp band at 1621 cm^{-1} in the spectrum of H_2L is shifted to lower frequencies by 30–40 cm^{-1} in the spectra of the complexes which indicates coordination via the azomethine nitrogen. This band is broad and intense compared to that of the ligand and can be attributed to overlapping of the bands of the newly formed N=C bond stretching. The spectra of the complexes exhibit a systematic shift in the position of bands in the region 1600–1350 cm^{-1} due to ν(C=C) and ν(C=N) vibrational modes and their mixing patterns are different from those present in the ligand spectrum. Coordination of the bases is indicated by the presence of weak bands in the 410–485 cm^{-1} region. The presence of the terminal azido group in the coordination sphere is evident from a strong and sharp absorption peak at ~2050 cm^{-1}. The slight lowering in values is assumed to be the result of its coordination with Co(III) [21,22]. There are bands at 2105 and 696 cm^{-1} in the spectra of compound **2** due to the N-coordinated thiocyanato group.

4. Supplementary data

Crystallographic data for the structural analysis has been deposited with the Cambridge Crystallographic Data center, CCDC 204600 for compound $CoLphenN_3$. Copies of this information may be obtained free of charge from The Director, CCDC, 12 Union Road, Cambridge, CB2, IEZ, UK (fax: +44-1223-336-033; e-mail: deposit@ccdc.cam.ac.uk or http://www.ccdc.cam.ac.uk).

Acknowledgements

U.L.K. thanks the University Grants Commission, Bangalore, India, for financial assistance in the form of a Teacher Fellowship. C.R.N. thanks the Cochin University of Science and Technology for the award of Junior Research Fellowship. The authors are also thankful to the National Single Crystal X-ray Diffraction Facility, IIT, Bombay, India for single crystal X-ray crystallographic data and Sophisticated Instruments Facility, IISc, Bangalore for NMR data.

References

[1] A. Sreekanth, S. Sivakumar, M.R.P. Kurup, J. Mol. Struct. 655 (2003) 47.
[2] P. Bindu, M.R.P. Kurup, T.R. Satyakeerthy, Polyhedron 18 (1999) 321.
[3] R.P. John, A. Sreekanth, M.R.P. Kurup, A. Usman, I.A. Razak, H.K. Fun, Spectrochim. Acta 59A (2003) 1349.
[4] A. Sreekanth, R.P. John, M.R.P. Kurup, in: XXXVth International Conference on Coordination Chemistry (ICCC35), P4.005, Heidelberg, Germany, July 21–26, 2002, p. 543.
[5] C.K. Alphonsa, M.R.P. Kurup, Synth. React. Inorg. Met. Org. Chem. 29 (1999) 805.

[6] R.P. John, A. Sreekanth, M.R.P. Kurup, S.M. Mobin, Polyhedron 21 (2002) 2515.
[7] M. Akkurt, S. Ozfuric, S. Ide, Anal. Sci. 16 (2000) 667.
[8] J.R. Dimmock, R.N. Puthucode, J.M. Smith, M. Hetherington, J.W. Quail, U. Pugazhenthi, J. Med. Chem. 39 (1996) 3984.
[9] J.R Dimmock, K.K. Sidhu, S.D. Tumber, S.K. Basran, M. Chen, J.W. Quail, Eur. J. Med. Chem. 30 (1995) 287.
[10] G. Ibrahim, M.A. Khan, G.M. Bouet, Transit. Met. Chem. 27 (2002) 34.
[11] G.M. Sheldrick, SHELXS 97, Program for the Solution of Crystal Structures, University of Göttingen, Göttingen, Germany, 1997.
[12] G.M. Sheldrick, SHELXL 97, Program for the Solution of Crystal Structures, University of Göttingen, Göttingen, Germany, 1997.
[13] I.C. Mendes, L.R. Teixeira, R. Lima, T.G. Carneiro, H. Beraldo, Transit. Met. Chem. 24 (1999) 655.
[14] H. Beraldo, W.F. Nacif, D.X. West, Spectrochim. Acta 57A (2001) 1847.
[15] R.P. John, Ph.D. Thesis, Cochin University of Science and Technology, Kochi, India.
[16] A. Castiñeiras, A.G.S. Zafra, M. Gonzalez-Perez, D.C. Lazarte, J.N. Gutierrez, Inorg. Chem. 41 (2002) 6956.
[17] B.H. Ye, X.M. Chen, G.Q. Xue, L.N. Ji, J. Chem. Soc., Dalton Trans. (1998) 2827.
[18] C. Janiak, J. Chem. Soc., Dalton Trans. (2000) 3885.
[19] M.B. Ferrari, G.G. Fava, C. Pelizzi, P. Tarasconi, J. Chem. Soc., Dalton Trans. (1992) 2153.
[20] M.B. Ferrari, G.G. Fava, C. Pelosi, M.C. Rodriguez-Argüelles, P. Tarasconi, J. Chem. Soc., Dalton Trans. (1995) 3035.
[21] D.X. West, J.K. Swearingen, J. Vadés-Martínez, S. Hernández-Ortega, A.K. El-Sawaf, F. van Meurs, A. Castiñeiras, I. Garcia, E. Bermejo, Polyhedron 18 (1999) 2919.
[22] A.L. Balch, L.A. Fosset, R.R. Guimerans, M.M. Olmstead, P.E. Reed, F.E. Wood, Inorg. Chem. 25 (1986) 1248.

Available online at www.sciencedirect.com
SCIENCE DIRECT®
Polyhedron 23 (2004) 49–53
POLYHEDRON
www.elsevier.com/locate/poly

Characterization and crystal structure of lanthanide cryptates of a ligand derived from 2,6-diformyl-pyridine

Xue-Lei Hu, Yi-Zhi Li, Qin-Hui Luo *

State Key Laboratory of Coordination Chemistry, Coordination Chemistry Institute, Nanjing University, 22 Hankou Rd., 210093, PR China

Received 19 June 2003; accepted 3 September 2003

Abstract

Seven lathanide cryptates $[LnL](NO)_3 \cdot nH_2O$ ($n = 1$–3; Ln = La, Ce, Pr, Sm, Eu, Gd, Tb) were synthesized by the reactions of lanthanide nitrates with free ligand L (L was derived from the (2 + 3) condensation of 2,6-diformyl-pyridine (*dfp*) with tris-(2-aminoethyl) amine (*tren*)) and characterized by physical methods. ES-MS spectra show that except for La(III) cryptate, the other six are all stable in solution. The crystal structure of the Eu(III) cryptate showed a tricapped prismatic coordination geometry.
© 2003 Elsevier Ltd. All rights reserved.

Keywords: Lanthanide; Cryptate; Crystal structure; ES-MS

1. Introduction

There has been a great deal of interest in design and synthesis of lanthanide complexes [1–5] due to their unique properties and many valuable applications [6], such as fluorescent probes in biological systems [7], magnetic resonance imaging and as contrast agents in clinical NMR images [8] as well as chemical logics in molecular information processing [9]. Cryptand ligands containing appropriate binding sites of suitable size and shape have been designed to form lanthanide cryptates [10,11]. The europium(III) cryptates are of particular interest in view of their novel photophysical properties [12], and several reports on their syntheses and properties have appeared [13,14]; for example, the luminescence properties of solutions of Eu(III) cryptates with 2,2-bipyridine and pyridine N-oxide units have been studied in detail [15–18]. A cryptand L synthesized by condensation of 2,6-diformyl-pyridine (*dfp*) with tris-(2-aminoethyl) amine (*tren*) has been reported [19], but its lanthanide cryptates and their crystal structure reported to date are few. Generally, the lanthanide cryptates are obtained by template synthesis involving alkali, alkali-earth [20] or lanthanide ions [21] as templating agents. We failed to obtain the lanthanide cryptates of ligand L by the template method. On the other hand, we obtained seven lanthanide cryptates $[LnL](NO)_3 \cdot nH_2O$ (Ln = La, Ce, Pr, Sm, Eu, Gd, Tb) (Scheme 1) by directly reacting the free ligand L with the corresponding lanthanide nitrates. The crystal structure of the Eu(III) cryptate displays a tricapped prismatic coordination geometry which is different from the structure of the sodium cryptate with the same ligand [22] and those of other lanthanide cryptates [20]. The ES-MS spectra of the seven cryptates show that, except for La (III) cryptate, all complex cations are stable in the solution.

2. Experimental

2.1. Materials

All starting chemicals were of reagent grade. Hydrated lanthanide nitrate was prepared by dissolving Ln_2O_3 (99.99%) in an excess amount of nitric acid. Tris(2-aminoethyl)amine [23] and 2,6-diformyl-pyridine [24] were prepared by literature methods. Cryptand L was prepared by the condensation of *dfp* with *tren* as described in the literature [19]. Their physical constants and spectroscopic data are in agreement with previously reported values.

* Corresponding author. Tel.: +86253594030; fax: +86253317761.
E-mail address: qhluo@jlonline.com (Q.-H. Luo).

0277-5387/$ - see front matter © 2003 Elsevier Ltd. All rights reserved.
doi:10.1016/j.poly.2003.09.024

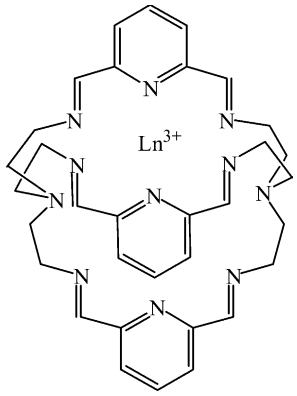

Scheme 1. The chemical formulas of the complex cations, Ln = Eu (III), La (III), Ce (III), Pr (III), Sm (III), Gd (III), Tb(III).

2.2. Preparation of the compounds

[EuL](NO₃)₃·H₂O (1): $Eu(NO_3)_3 \cdot 6H_2O$ (0.054 g, 0.12 mmol) in 20 ml MeCN was added to a boiling solution of L (0.059 g 0.1 mmol) in 150 ml MeCN. After refluxing for 12 h, the orange product was filtered out and washed with MeCN and Et_2O, and then dried. Red solid 0.078 g were obtained. Yield: 82%. (*Anal.* Calc. for $C_{33}H_{41}N_{14}O_{10}Eu$ (M_w 945.74): C, 41.91; H, 4.37; N, 20.73. Found: C, 41.63; H, 4.75; N, 21.11%.) IR (cm^{-1}): 1641 (s, ν(C=N)); 1383 (s, $\nu(NO_3^-)$), UV–Vis (λ_{max}/nm (ε/dm^3 mol^{-1} cm^{-1}), H_2O): 215 (1 00 200), 246 (40 800), 317 (20 700), 330 (17 000). Λ_M(H_2O, 293 K): 412 S cm^2 mol^{-1}. Red block-like crystals suitable for X-ray diffraction were obtained by diffusion of Et_2O into MeOH/DMF solution over 1 week.

The cryptates $[LaL](NO_3)_3 \cdot 2H_2O$ (**2**), $[CeL](NO_3)_3 \cdot 2H_2O$ (**3**), $[PrL](NO_3)_3 \cdot 3H_2O$ (**4**), $[SmL](NO_3)_3 \cdot 2H_2O$ (**5**), $[GdL](NO_3)_3 \cdot 2H_2O$ (**6**), $[TbL](NO_3)_3 \cdot 2H_2O$ (**7**) were prepared by a similar procedure as for **1**, except that the corresponding lanthanide(III) nitrates were used instead of $Eu(NO)_3 \cdot 6H_2O$.

[LaL](NO₃)₃·2H₂O (2): Yellow tiny crystals. Yield: 75%. (*Anal.* Calc. for $C_{33}H_{43}N_{14}O_{11}La$ (M_w 951.91): C, 41.69; H, 4.56; N, 20.63. Found: C, 41.25; H, 4.18; N, 20.66%.), IR (cm^{-1}): 1641 (s, ν(C=N)); 1384 (s, $\nu(NO_3^-)$), UV–Vis (λ_{max}/nm (ε/dm^3 mol^{-1} cm^{-1}), H_2O): 208 (68 700), 246 (20 430), 316 (10 200), 330 (8300). Λ_M(H_2O, 293 K): 409 S cm^2 mol^{-1}.

[CeL](NO₃)₃·2H₂O (3): Orange solid. Yield: 75%. (*Anal.* Calc. for $C_{33}H_{43}N_{14}O_{11}Ce$ (M_w 970.71) C, 41.64; H, 4.55; N, 20.60. Found: C, 41.85; H, 4.89; N, 20.35%.), IR (cm^{-1}): 1640 (s, ν(C=N)); 1383 (s, $\nu(NO_3^-)$), UV–Vis (λ_{max}/nm (ε/dm^3 mol^{-1} cm^{-1}), H_2O): 207 (97 600), 249 (25 400), 316 (12 200), 329 (9700). Λ_M(H_2O, 293 K): 425 S cm^2 mol^{-1}.

[PrL](NO₃)₃·3H₂O (4): Yellow solid. Yield: 80%. (*Anal.* Calc. for $C_{33}H_{45}N_{14}O_{12}Pr$ (M_w 970.71) C, 40.83; H, 4.67; N, 20.20. Found: C, 41.15; H, 4.25; N, 20.68%.) IR (cm^{-1}): 1642 (s, ν(C=N)); 1384 (s, $\nu(NO_3^-)$), UV–Vis (λ_{max}/nm (ε/dm^3 mol^{-1} cm^{-1}), H_2O): 207 (120 000), 245 (30 600), 316 (14 200), 329 (10 400). Λ_M(H_2O, 293 K): 406 S cm^2 mol^{-1}.

[SmL](NO₃)₃·2H₂O (5): Orange solid. Yield: 83%. (*Anal.* Calc. for $C_{33}H_{43}N_{14}O_{11}Sm$ (M_w 962.15) C, 41.20; H, 4.50; N, 20.38. Found: C, 41.35; H, 4.55; N, 20.55%.) IR (cm^{-1}): 1641 (s, ν(C=N)); 1383 (s, $\nu(NO_3^-)$), UV–Vis (λ_{max}/nm (ε/dm^3 mol^{-1} cm^{-1}), H_2O): 209 (92 000), 247 (24 700), 316 (11 500), 328 (9800). Λ_M(H_2O, 293 K): 399 S cm^2 mol^{-1}.

[GdL](NO₃)₃·2H₂O (6): Yellow solid. Yield: 75%. (*Anal.* Calc. for $C_{33}H_{43}N_{14}O_{11}Sm$ (M_w 969.04) C, 40.90; H, 4.47; N, 20.24. Found: C, 40.58; H, 4.56; N, 20.70%.) IR (cm^{-1}): 1634 (s, ν(C=N)); 1383 (s, $\nu(NO_3^-)$), UV–Vis (λ_{max}/nm (ε/dm^3 mol^{-1} cm^{-1}), H_2O): 211 (97 300), 249 (21 500), 318 (11 600), 329 (10 200). Λ_M(H_2O, 293 K): 405 S cm^2 mol^{-1}.

[TbL](NO₃)₃·2H₂O (7): Orange solid. Yield: 74%. (*Anal.* Calc. for $C_{33}H_{43}N_{14}O_{11}Tb$ (M_w 970.72) C, 40.84; H, 4.46; N, 20.20. Found: C, 41.40; H, 4.43; N, 20.67%.) IR (cm^{-1}): 1638 (s, ν(C=N)); 1384 (s, $\nu(NO_3^-)$), UV–Vis (λ_{max}/nm (ε/dm^3 mol^{-1} cm^{-1}), H_2O): 205 (94 500), 246 (22 500), 317 (15 600), 330 (9500). Λ_M(H_2O, 293 K): 441 S cm^2 mol^{-1}.

2.3. Physical measurements

Elemental analysis of C, H, N were performed on a Perkin–Elmer 240c analytical instrument. The molar electrical conductivities in aqueous solution containing 10^{-4} mol l^{-1} complexes were measured at 25 ± 0.1 °C using a BSD-A conductometer (Jangsu, China). Electronic spectra were recorded on a UV-3100 spectrophotometer. IR spectra were measured using KBr discs with a vector 22 FI-IR spectrophotometer. Electrospray mass spectrum (ES-MS) was determined on a Finnigan LCQ ES-MS mass spectrograph using methanol as the mobile phrase with a sample concentration of about 1.0 mmol dm^{-3}. The diluted solution was electrosprayed at a flow rate of 5×10^{-6} dm^3 min^{-1} with a needle voltage of +4.5 kV. The temperature of the heated capillary in the interface was 200 °C and a fuse silica sprayer was used.

2.4. Crystal structure determination

Diffraction intensity data were collected on a SMART-CCD area-detector diffractometer at 293 K using graphite monochromatic Mo Kα radiation ($\lambda = 0.71073$ Å). Data reduction and cell refinement were performed by SMART and SAINT programs [25]. The structure was solved by direct methods (Bruker SHELXTL) and refined on F^2 by full-matrix least-squares (Bruker SHELXTL) using all unique data [26]. The non-H atoms in the structure were treated as anisotropic. Hydrogen atoms were located geometrically and refined in the riding mode.

3. Results and discussion

3.1. Synthesis and characterization

We have tried to synthesize lanthanide cryptates by the condensation of *dfp* with *tren* in the presence of Ln^{3+} or alkali-earth metal ions as templates by previous methods, but pure products could not be obtained. An effective method has been developed by reacting free ligand with the lanthanide nitrate. However, by the same procedure, we could not get pure products of the cryptates of the heavier lanthanides, which may be due to mismatch of their ionic size with the cavity of the ligand.

The conductivities of all the seven lanthanide cryptates are in the range of 399–412 S cm^2 mol^{-1}, typical for a 1:3 electrolyte [27] and consistent with the chemical formulas from elemental analysis. The IR spectra of all cryptates show the characteristic vibrations of the C=N bond (1634–1642 cm^{-1}) and nitrate ions (~1384 cm^{-1}). The vibration frequency of the observed C=N bond shifts to longer wavelength by 5–13 cm^{-1}in contrast to that of the free ligand (1647 cm^{-1}) [19]. The intense absorptions in the electronic spectra of the cryptates at 200–240 and 310–330 nm are designated to the π–π^* transitions of the pyridyls and C=N groups, respectively.

3.2. Electrospray mass spectra

ES-MS data are listed in Table 1. There, except for **2**, the ES-MS spectra of all cryptates show common features, and the spectra are composed of two to three simple peaks. The dominant peaks are assigned to the formation of $[ML]^{3+}$ (M = Eu, Ce, Pr, Sm, Gd, Tb) and the other peak clusters are due to $[ML]^{3+}$ that captures one to two nitrate anions forming $[ML(NO_3)]^{2+}$ or $[ML(NO_3)_2]^{+}$. The simplicity of the spectra can be attributed to the thermodynamic and kinetic stability of the cryptates. For example, Fig. 1(a) shows the positive-ion ES mass spectrum of **1** $[EuL](NO_3)_3 \cdot H_2O$. The base peak at $m/z = 247.5$ corresponds to $[EuL]^{3+}$. The peaks at $m/z = 402.1$ can be assigned to the species $[EuL(NO_3)]^{2+}$. The isotopic distribution of the peak at $m/z = 247.5$ is shown in Fig. 1(a). From the numbers

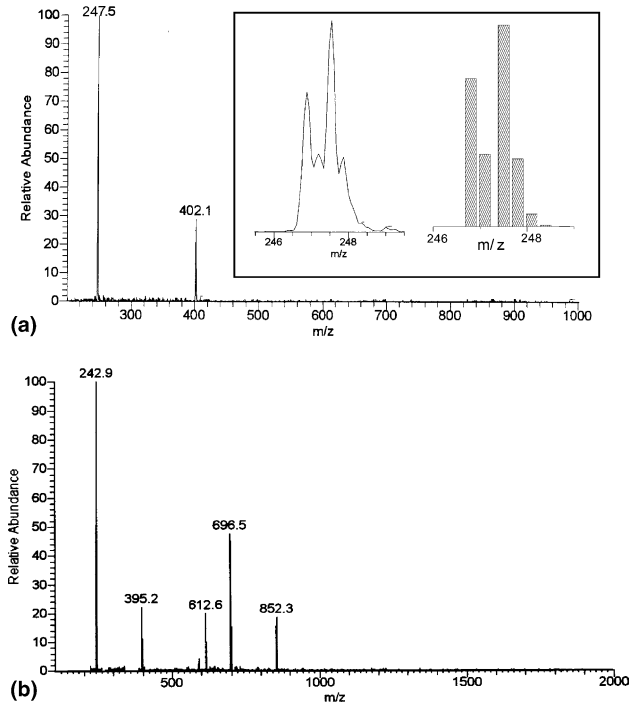

Fig. 1. The ES-MS spectra of cryptates **1** and **2** in MeOH solution: (a) cryptate **1** (inset: the isotopic distribution of the peak at $m/z = 247.5$; left: experimental pattern; right: calculated pattern); (b) cryptate **2**.

Table 1
ES-MS spectroscopic data for the cryptates **1**–**7**

No.	Cryptate	Peak (m/z)	Relative abundance (%)	Assignment
1	$[EuL](NO_3)_3 \cdot H_2O$	247.5	100	$[EuL]^{3+}$
		402.1	29	$[EuL(NO_3)]^{2+}$
2	$[LaL](NO_3)_3 \cdot 2H_2O$	242.9	100	$[LaL]^{3+}$
		395.2	23	$[LaL(NO_3)]^{2+}$
		612.6	20	$[NaL]^{+}$
		696.5	47	$[Na_2L(NO_3)]^{+}$
		852.3	19	$[LaL(NO_3)_2]^{+}$
3	$[CeL](NO_3)_3 \cdot 2H_2O$	243.2	100	$[CeL]^{3+}$
		395.7	11	$[CeL(NO_3)]^{2+}$
4	$[PrL](NO_3)_3 \cdot 3H_2O$	243.7	100	$[PrL]^{3+}$
		396.3	18	$[PrL(NO_3)]^{2+}$
		854.3	10	$[PrL(NO_3)_2]^{+}$
5	$[SmL](NO_3)_3 \cdot 2H_2O$	247.3	100	$[SmL]^{3+}$
		402.7	22	$[SmL(NO_3)]^{2+}$
6	$[GdL](NO_3)_3 \cdot 2H_2O$	249.1	100	$[GdL]^{3+}$
		403.8	19	$[GdL(NO_3)]^{2+}$
7	$[TbL](NO_3)_3 \cdot 2H_2O$	249.5	100	$[TbL]^{3+}$
		405.7	29	$[TbL(NO_3)]^{2+}$

and isotopic abundances of the atoms in $[EuL]^{3+}$, a revised program is used to calculated the pattern which is in good agreement with the experimental one (Fig. 1(a) inset). For the six cryptates, no peak of free ligand or ligand fragments is observed, showing that the cryptates and the ligand are rather stable in solution. For **2**, the ES-MS spectra (Fig. 1(b)) are more complicated. Besides the species of $[LaL]^{3+}$ and $[LaL(NO_3)]^{2+}$, two peaks at $m/z = 612.5$ and at $m/z = 696.5$ are designed to $[NaL]^{+}$ and $[Na_2L(NO_3)]^{+}$, respectively, implying that the cryptand can bind the Na^{+} ion to form an inclusion complex. The Na^{+} is present in a trace amount. The dissociation of the La^{+} ion implies that the cryptate is less stable than the other six. Because of its larger radius, La^{3+} in the ligand cage is not so stable as Eu^{3+} so that the binding of the ligand to La^{3+} is weaker than those of other lanthanide ions.

Table 2
Crystal data of the complex $[EuL]NO_3 \cdot 0.5H_2O$

Empirical formula	$C_{33}H_{40}N_{14}O_{9.5}Eu$
Crystal system	trigonal
Space group	*R*-3*c*
a, *b*, *c* (Å)	14.709(1), 14.709(1), 32.167(3)
α, β, γ (°)	90, 90, 120
V (Å^3)	6027.1(8)
$D_{calcd.}$ (g/cm^3)	1.548
F(000)	2850
Crystal size (mm)	$0.20 \times 0.20 \times 0.30$
Temperature (K)	293
μ(Mo Kα) (mm^{-1})	1.631
2θ range (°)	2–25
Reflections collected	9636
Independent reflections	1189
Observed reflections	757
Index ranges	$-17 \leqslant h \leqslant 17k$; $-17 \leqslant k \leqslant 9$; $-38 \leqslant l \leqslant 37$
w^{-1}	$1/[\sigma^2(F_o^2) + (0.0240P)^2 + 1.880P]$; $P = (F_o^2 + 2F_c^2)/3$
Goodness-of-fit on F^2	1.02
Final R_1, wR_2 $[I > 2\sigma]$	0.0419, 0.0919

Table 3
Selected bond distances (Å) and angles (°) of $[EuL](NO_3)_3 \cdot 0.5H_2O$[a]

Bond distances			
Eu1–N1	2.597(3)	Eu1–N2	2.559(5)
Eu1–N1A	2.597(3)	Eu1–N2A	2.559(5)
Eu1–N1B	2.597(3)	Eu1–N2B	2.559(5)
Eu1–N1C	2.597(3)	Eu1···N3	3.768(5)
Eu1–N1D	2.597(3)	Eu1···N3A	3.768(5)
Eu1–N1E	2.597(3)		
Bond angles			
N1–Eu1–N2	63.28(8)	N1C–Eu1–N2B	63.28(8)
N1–Eu1–N1A	80.78(12)	N1E–Eu1–N2B	72.95(7)
N1–Eu1–N2A	72.96(7)	N1D–Eu1–N2B	137.96(7)
N1–Eu1–N1B	80.78(12)	N1C–Eu1–N1E	80.78(12)
N1–Eu1–N2B	137.97(7)	N1C–Eu1–N1D	80.78(12)
N1–Eu1–N1C	145.91(13)	N1E–Eu1–N1D	80.78(12)
N1–Eu1–N1E	126.56(15)	N1A–Eu1–N2	137.97(7)
N1–Eu1–N1D	84.07(15)	N2–Eu1–N2A	120.00(1)
N1B–Eu1–N1E	84.07(15)	N1B–Eu1–N2	72.96(7)
N1A–Eu1–N2A	63.28(8)	N2–Eu1–N2B	120.00(1)
N1A–Eu1–N1B	80.78(12)	N1C–Eu1–N2	137.97(7)
N1A–Eu1–N1C	84.07(15)	N1E–Eu1–N2	63.28(8)
N1A–Eu1–N1E	145.91(13)	N1D–Eu1–N2	72.96(7)
N1B–Eu1–N1D	145.91(13)	N1A–Eu1–N2B	72.96(7)

[a] Symmetry transformation used to generate equivalent atoms: (i) $1-y, 1+x-y, z$ (N1A, N2A); (ii) $-x+y, 1-x, z$ (N1B, N2B); (iii) $-1/3+y, 1/3+x, 5/6-z$ (N1C, N3A); (iv) $2/3+x-y, 4/3-y, 5/6-z$ (N1D); (v) $2/3-x, 1/3-x+y, 5/6-z$ (N1E).

3.3. Crystal structure of the cryptate

The crystal data of **1** are listed in Table 2. Selected bond distances and bond angles are listed in Table 3. In the complex **1** (Fig. 2(a)), the central cation Eu1 is lo-

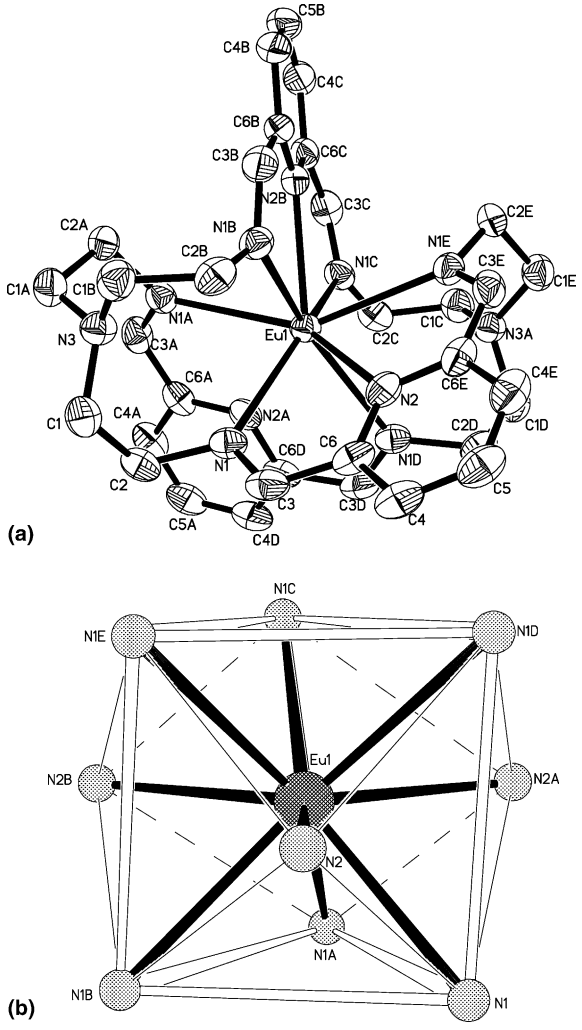

Fig. 2. (a) A perspective view of the $[EuL]^{3+}$cation; (b) the structure of the coordination polyhedron. Symmetry transformation used to generate equivalent atoms: (i) $1-y, 1+x-y, z$ (N1A, N2A); (ii) $-x+y, 1-x, z$ (N1B, N2B); (iii) $-1/3+y, 1/3+x, 5/6-z$ (N1C, N3A); (iv) $2/3+x-y, 4/3-y, 5/6-z$ (N1D); (v) $2/3-x, 1/3-x+y, 5/6-z$ (N1E).

cated in the center of the macrocycle and coordinated by three pyridyl nitrogen atoms (N2, N2A and N2B) and six imino nitrogens (N1, N1A, N1B, N1C, N1D, N1E) to form a tricapped prism (Fig. 2(b)). The complex cation has a threefold axis through Eu1 and the two bridgehead nitrogen atoms (N3, N3A). The average bond length between Eu1 and nitrogen atoms of the pyridine groups is 2.559 Å, being slightly shorter than those for the imino groups (2.598 Å). The average length of Eu1–N (bridgehead) is 3.768 Å. No interaction between Eu1 and N(bridgehead) is observed. The coordination polyhedron of **1** can be described approximately as a tricapped prism. The upper and basal planes of the prism, which are approximately parallel, are composed of the imino nitrogen atoms (N1, N1A, N1B and N1C, N1D, N1E, respectively). The distance between the two planes is 3.446 Å. The distance between Eu1 and the upper plane is 1.723 Å. The three pyridyl nitrogen atoms are located at the capping positions. Eu1 is located in the symmetrical center of the prism. The distances of Eu1 to each least squares prism plane is approximately 0.964 Å. The tricapped prism structure is different from the unsymmetrical structure of sodium cryptate with the same ligand [22] and those of phenol-based lanthanide cryptates [13,20,21], in which the central ions are located at one side of the macrocycles. The present Eu(III) cryptate is located at the inversion center of the cavity of the macrocycle in order to satisfy the requirement of a higher coordination number of the lanthanide ion. To our knowledge, this is the first crystal structure of a lanthanide cryptate derived from 2,6-pyridyl-dicarboxaldehyde.

4. Supplementary data

Supplementary data are available from The Director, CCDC, 12 Union Road, Cambridge CB2 1EZ, UK (fax: +44-1223-336033; E-mail: deposit@ccdc.cam.ac.uk or www: http://www.ccdc.cam.ac.uk) on request, quoting the deposition number CCDC-208092.

Acknowledgements

This work was supported by the National Natural Science Foundation of China.

References

[1] V. Alexander, Chem. Rev. (1995) 273.
[2] C. Piguet, J.-C.G. Bünzli, Chem. Soc. Res. 18 (1999) 347.
[3] Q.-Y. Chen, Q.-H. Luo, X.-L. Hu, M.-C. Shen, J.-T. Chen, Chem. Eur. J. 8 (2002) 3984.
[4] G.F. de Sá, O.L. Malta, C. de Mello Donegá, A.M. Simas, R.L. Longo, P.A. Santa-Cruz, E.F. da Silva Jr., Coord. Chem. Rev. 196 (2000) 165.
[5] B.H. Bakker, M. Goes, N. Hoebe, H.J. Van Ramesdonk, J.W. Verhoeven, M.H.V. Werts, J.W. Hofstraat, Coord. Chem. Res. 208 (2000) 3.
[6] S. Aime, M. Botta, M. Fasano, E. Terreno, Chem. Soc. Rev. 27 (1998) 19.
[7] J.-M. Lehn, D.D. Macnicol, J.L. Atwood, J.E. Davies, D.N. Reinhoudt, F. Vogtl (Eds.), Comprehensive Supramolecular Chemistry, vol. 10, Pergamon, Oxford, 1996 (Ch. 17).
[8] A. Beeby, S.W. Botchway, I.M. Clarkson, S. Faulkner, A.W. Parker, D. Parker, J.A. Gareth Williams, J. Photochem. Photobiol. B 57 (2000) 83.
[9] T. Gunnlaugsson, D.A. MacDonail, D. Parker, Chem. Commun. (2000) 93.
[10] Q.-Y. Chen, Q.-H. Luo, Z.-L. Wang, J.-T. Chen, Chem. Commun. (2000) 1033.
[11] Q.-Y. Chen, Q.-H. Luo, L.-M. Zheng, Z.-L. Wang, J.-T. Chen, Inorg. Chem. 41 (2002) 605.
[12] G. Vicentini, L.B. Zinner, J. Zukerman-Schpector, K. Zinner, Coord. Chem. Rev. 196 (2000) 353.
[13] Q.-Y. Chen, C.-J. Feng, Q.-H. Luo, C.-Y. Duan, X.-S. Yu, Y.-J. Liu, Eur. J. Inorg. Chem. (2001) 1067.
[14] C. Bazzicalupi, A. Bencini, E. Berni, A. Bianchi, C. Giorgi, V. Fusi, B. Valtancoli, C. Lodeiro, A. Roque, F. Pina, Inorg. Chem. 40 (2001) 6172.
[15] B. Alpha, J.-M. Lehn, G. Mathis, Angew. Chem., Int. Ed. Engl. 26 (1987) 266.
[16] C.O. Paul-Roth, J.-M. Lehn, J. Guilhem, C. Pascard, Helv. Chim. Acta 78 (1995) 1895, and references therein.
[17] J.-M. Lehn, J.-B.R. de Vains, Helv. Chim. Acta 75 (1992) 1221.
[18] C. Galaup, C. Picard, H. Autiero, D. Aspe, Helv. Chim. Acta 82 (1999) 544.
[19] D.J. Marrs, V. Mckee, J. Nelson, Q. Lu, C.J. Harding, Inorg. Chim. Acta 211 (1993) 195.
[20] M.G. Drew, O.W. Howarth, C.J. Harding, N. Martin, J. Nelson, J. Chem. Soc., Chem. Commun. (1995) 903.
[21] C.-J. Feng, Q.H. Luo, C.-Y. Duan, M.-C. Shen, Y.-J. Liu, J. Chem. Soc., Dalton Trans. (1998) 1377.
[22] V. Mckee, M.R.J. Dorrity, J.F. Malone, D. Marrs, J. Nelson, J. Chem. Soc., Chem. Commun. (1992) 383.
[23] E. Kimura, S. Young, J.P. Collman, Inorg. Chem. 9 (1970) 1187.
[24] C.J. Gray, F.A. Hart, J. Chem. Soc., Dalton Trans. (1987) 2289.
[25] SMART and SAINT, Area Detector Control and Integration Software. Siemens Analytical X-Ray Systems, Inc., Madison, WI, USA, 1996.
[26] G.M. Sheldrick, SHELXTL V5.1 Software Reference Manual, Bruker AXS, Madison, WI, USA, 1997.
[27] W.J. Geary, Coord. Chem. Rev. 7 (1971) 81.

Available online at www.sciencedirect.com
SCIENCE DIRECT®
Polyhedron 23 (2004) 55–58
POLYHEDRON
www.elsevier.com/locate/poly

Neutral coordination frameworks with host–guest properties constructed by dicopper(II) units and 4,7-phenanthroline

Hui Huang, Shu-Yan Yu *, Hong-Bo Liu, Mei Shi

State Key Laboratory of Polymer Physics and Chemistry, and Joint Laboratory Polymer Science and Materials, Center for Molecular Science, Institute of Chemistry, Chinese Academy of Sciences, Beijing 100080, PR China

Received 22 April 2003; accepted 5 September 2003

Abstract

Reaction of $[Cu_2(O_2CR)_4]$ [R = Me(**1**), Ph(**2**)] with 4,7-phenanthroline produced neutral coordination frameworks $\{[Cu_2(O_2CR)_4](C_{12}N_2H_8)\}_n$ showing inclusion behavior toward solvent molecules; through variation of the equatorial ligands of the dimetal units, the channels size and host–guest properties of the coordination polymers can be controlled.
© 2003 Elsevier Ltd. All rights reserved.

Keywords: Copper; 4,7-Phenanthroline; Coordination framework; Host–guest properties; Polymers; Extended structures

1. Introduction

Crystal engineering of coordination polymers is of considerable interest in the area of materials chemistry [1]. The coordination-driven assembly of these polymers has shown high promise in various potential applications, such as molecular recognition, catalysis, gas storage and molecular magnetization [2,3]. However, most of the assembled structures are complicated and restricted by the choice of counter cations or anions, which can occupy part of the space within the framework [4]. To avoid such drawback, attention has been paid to construct neutral coordination frameworks with dimetal units [5]. Notably, constructing channels with various size and shapes in this type of polymers can be finely tuned by a suitable choice of both equatorial and axial ligands on the dimetal units. While much study is focused on changing the axial ligands, such as 4,4-bipyridine [3d], less attention has been paid to altering the equatorial ligands. The latter approach has many advantages: (1) as the equatorial ligands can be selective in the synthesis of dimetal units, it is very easy to design the size and the shapes of the channels; (2) it is a very efficient way to extend the size of the channels because the distance between adjacent layers can be increased by using lucky equatorial ligands. Herein, we report the preparation, crystal structures and properties of a novel coordination framework constructed with the neutral dimetal units $[Cu_2(O_2CR)_4]$ (R = Me, Ph) and the rigid aromatic ligand 4,7-phenanthroline (L) [6]. Furthermore, this ligand has been successfully employed in self-assembly of molecular crowns in our laboratory [7].

2. Experimental

4,7-Phenanthroline and $Cu(CH_3COO)_2$ were obtained commercially. $Cu(C_6H_5COO)_2$ was prepared according to a published method [8]. Other materials were of the highest available purity and used without further treatment.

2.1. Synthesis

2.1.1. $\{[Cu_2(O_2CCH_3)_4](C_{12}N_2H_8)\}_n$ (**1**)

A buffer layer of *p*-xylene (5 ml) was carefully layered over a solution of 4,7-phenanthroline (14.4 mg, 0.080

* Corresponding author. Fax: +86-10-6255-9373.
E-mail address: syu@iccas.ac.cn (S.-Y. Yu).

0277-5387/$ - see front matter © 2003 Elsevier Ltd. All rights reserved.
doi:10.1016/j.poly.2003.09.014

mmol) in *p*-xylene (10 ml), and a layer of $Cu(O_2CCH_3)_2 \cdot H_2O$ (16.0 mg, 0.08 mmol) in methanol (10 ml) was carefully placed on top of the buffer layer. Green, cube-like crystals were harvested after several days in ca. 60% yield based on $Cu(O_2CCH_3)_2 \cdot H_2O$. *Anal.* Calc. for $C_{20}H_{20}Cu_2N_2O_8$: C, 44.20, H, 3.71, N, 5.14. Found: C, 44.11, H, 3.62, N, 5.17%.

2.1.2. $\{[Cu_2(O_2CC_6H_5)_4](C_{12}N_2H_8)(C_8H_{10})\}_n$ (2)

As above, a buffer of *p*-xylene (5 ml) was carefully layered over a solution of 4,7-phenanthroline (14.4 mg, 0.080 mmol) in *p*-xylene (10 ml), and a layer of $Cu(O_2CC_6H_5)_2$ (36.9 mg, 0.080 mmol) in methanol (10 ml) was carefully placed on top of the buffer layer. Green, cube-like crystals were harvested after several days in ca. 65% yield based on $Cu(O_2CC_6H_5)_2$. *Anal.* Calc. for $C_{24}H_{19}CuNO_4$: C, 59.92, H, 4.78, N, 3.49. Found: C, 59.88, H, 4.71, N, 3.52%.

2.2. X-ray single-crystal analysis

Intensity data were collected on a Rigaku R-AXIS RAPID IP area detector diffractometer with graphite monochromated Mo Kα radiation (50 kV, 300 mA). Crystal parameters and refinement results for both compounds are summarized in Table 1. Empirical absorption corrections were employed. The structure was solved by SHELXTL [9]. The final refinement was done by full-matrix least squares based on F^2 with anisotropic thermal parameters for all non-hydrogen atoms, and the hydrogen atoms were generated geometrically.

Table 1
Crystallographic data for compounds **1** and **2**

	1	**2**
Empirical formula	$C_{20}H_{20}Cu_2N_2O_8$	$C_{48}H_{38}Cu_2N_2O_8$
M_r	543.46	897.93
Crystal system	triclinic	monoclinic
Space group	$P\bar{1}$	*C2/c*
Crystal color, habit	green, block	green, block
Crystal dimensions (mm)	$0.32 \times 0.20 \times 0.16$	$0.32 \times 0.20 \times 0.15$
Unit cell dimensions		
a (Å)	8.0084(7)	28.451(4)
b (Å)	11.5685(10)	9.4789(10)
c (Å)	13.1368(10)	20.536(3)
α (°)	86.515(5)	90
β (°)	77.686(10)	129.380
γ (°)	89.912(9)	90
U (Å^3)	1186.78(17)	4280.9(9)
Z	2	4
D_{calc} (Mg m^{-3})	1.521	1.393
F (000)	552	1848
Radiation	Mo Kα	Mo Kα
λ (Å)	0.71073	0.71073
μ (mm^{-1})	1.837	1.050
θ (max)	27.41	27.42
Number of data collected	5696	8412
Number of unique data	4331	4761
R_{int}	0.0413	0.0498
Number of observed data ($I \geqslant \sigma(I)$)	2736	2387
Number of variables	289	271
S (all data)	1.035	0.819
R ($I \geqslant \sigma(I)$)	0.0612	0.0481
R_w (all data)	0.0961	0.1031

3. Results and discussion

Fig. 1(a) shows the structural unit of **1.** In the centrosymmetric dicopper units, each Cu (II) ion has four oxygens of different carboxylate groups in the equatorial positions, and an infinite chain along the [−1, 1, −1] axis is formed by linking consecutive dimetal units with bridging 4,7-phenanthroline ligands. Fig. 2(a) shows that along the chain each $Cu_2(OOCCH_3)_4$ paddle wheel is rotated by ca. 45° with respect to its nearest neighbor.

The molecular packing of complex **1** is shown in Fig. 3(a). Normally, the arrangement of paddle wheels belonging to neighboring layers give rise to a channel system, and the size of the void is $\approx 8.0(5) \times 5.57(6)$ Å, which can accommodate some solvent molecules as guests [10]. However, the channels in the framework of **1** are void. Owing to the alternate rotation of the paddle wheels, the actual size of the channel is even smaller. Thus, the size of the channel is not large enough to accommodate solvent molecules as guests.

For controlling the actual size of the channel in the framework to absorb some guests, we substituted R = Me with R = Ph in order to enlarge the distance between two adjacent layers. The X-ray structure of **2** (Fig. 1(b)) shows that this structure also contains centrosymmetric dinuclear Cu units with the paddle-wheel cage unit. The bridging 4,7-phenanthroline ligand coordinates two neighbor dimetal units to form an extended structure along the *c*-axis. Along the chain, the conformations of successive $[Cu_2(O_2CPh)_4]$ units are alike, as distinct from the conformation of the chain in **1**.

Fig. 3(b) shows the molecular packing of **2**. The *p*-xylene molecules are trapped in the channels formed by the paddle wheels between adjacent layers. The size of the void is $\approx 14.22(6) \times 5.57(5)$ Å, which is sufficiently large to include the solvent molecules as guests.

However, not only *p*-xylene molecules but also methanol molecules exist in the mixture during preparation. It is very notable that the neutral coordination framework of **2** can selectively absorb *p*-xylene molecules as guests, which may involve favorable edge to face C–H interactions. The distance between the center of the *p*-xylene molecule and the center of the just adjacent

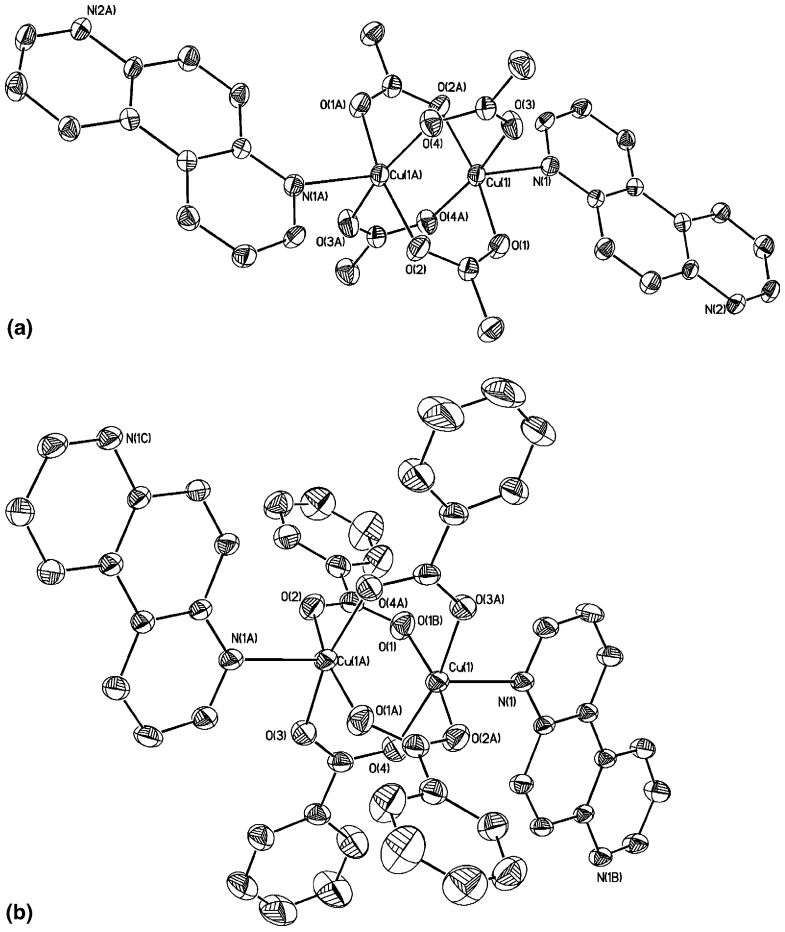

Fig. 1. (a) The structural unit of **1**. (b) The structural unit of **2**.

phenylene ring to which the *p*-xylene molecule is about perpendicular is 5.026 Å. It suggests a strong edge-to-face interaction (the standard distance of T-shaped orientation is 4.99 Å and the energy of that that interaction is −2.3 kcal mol^{-1}) [11].

In conclusion, we have succeeded in controlling the size of the pore and the host–guest properties in a neutral coordination framework by changing the substituents in a $[Cu_2(O_2CR)_4]$ unit. Further investigation will be extended to other multiple-bonded dimetal units [6] (e.g. Mo_2^{4+}, Rh_2^{4+}, Ru_2^{4+}, etc.) with larger substituted aromatic R groups so as to constitute larger channels for the accommodation of various organic guests.

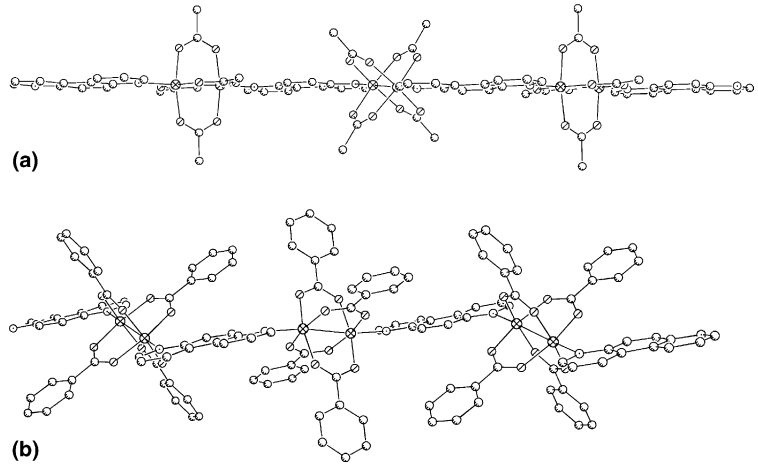

Fig. 2. (a) An infinite chain along the [−1, 1, −1] axis of **1**. (b) An infinite chain along the *c*-axis of **2**.

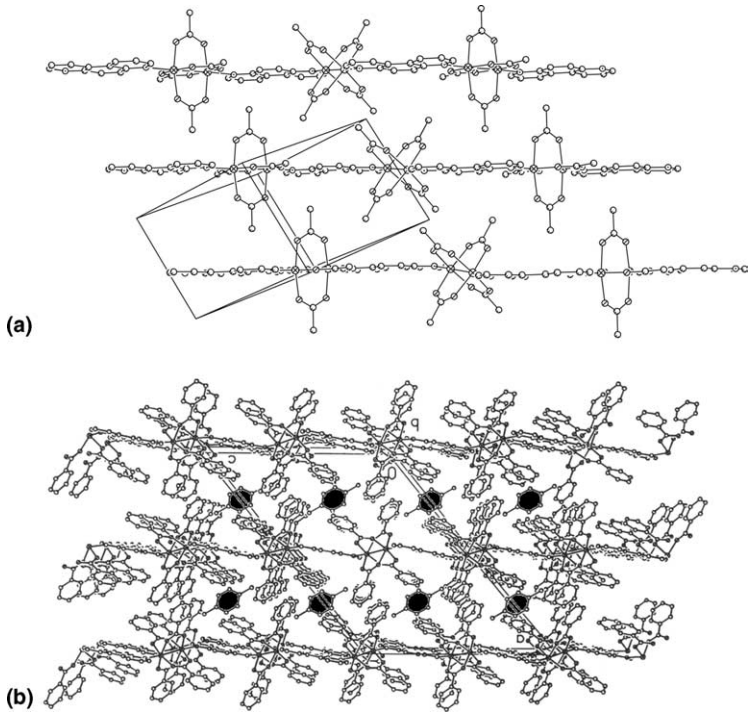

Fig. 3. (a) Molecular packing structure along the [−1, 1, −1] axis of **1**. (b) Molecular packing structure along the *c*-axis of **2** showing channels occupied by *p*-xylene molecules (the dark labelling).

4. Supplementary material

Supplementary data are available from The Director, CCDC, 12 Union Road, Cambridge CB2 1EZ, UK (fax: +44-1223-336033; E-mail: deposit@ccdc.cam.ac.uk or www:http://www.ccdc.cam.ac.uk) on request, quoting the deposition numbers 192173 and 192174.

Acknowledgements

This work is supported by grants of the National Nature Science Foundation of China No. 90206013.

References

[1] (a) B. Moulton, M.J. Zaworotko, Chem. Rev. 101 (2001) 1629;
(b) M.E. Davis, Nature 417 (2002) 813.
[2] (a) Y.-Q. Tian, C.-X. Cai, Y. Ji, X.-Z. You, S.-M. Peng, G.-H. Lee, Angew. Chem. Int. Ed. 41 (2002) 1384;
(b) R.-G. Xiong, X.-Z. You, B.F. Abrahams, E.-L. Xue, C.-M. Chen, Angew. Chem. Int. Ed. 40 (2001) 4422.
[3] (a) M. Fujita, Y.J. Kwon, S. Washizu, K. Ogura, J. Am. Chem. Soc. 116 (1994) 1151;
(b) S.-Y. Yu, M. Fujita, K. Yamaguchi, J. Chem. Soc., Dalton Trans. (2001) 3415;
(c) K. Biradha, C. Seward, M.J. Zaworotko, Angew. Chem. Int. Ed. 38 (1999) 492;
(d) H. Gudbjartson, K. Biradha, K.M. Poirier, M.J. Zaworotko, J. Am. Chem. Soc. 121 (1999) 2599;
(e) M. Eddaoudi, J. Kim, N. Rosi, D. Vodak, J. Wachter, M. O'Keeffe, O.M. Yaghi, Science 295 (2002) 469.
[4] H. Li, M. Eddaoudi, M. O'Keeffe, O.M. Yaghi, Nature 402 (1999) 276.
[5] (a) F.A. Cotton, R.A. Walton, Multiple Bonds Between Metal Atoms, Oxford University Press, Oxford, 1993;
(b) S.A. Bourne, J.-J. Lu, A. Mondal, B. Moulton, M.J. Zaworotko, Angew. Chem. Int. Ed. 40 (2001) 2111;
(c) S.M.-F. Lo, S.S.-Y. Chui, L.-Y. Shek, Z.-Y. Lin, X.X. Zhang, G.-H. Wen, I.D. Willianms, J. Am. Chem. Soc. 122 (2000) 6293;
(d) S.R. Batten, B.F. Hoskins, B. Moubaraki, K.S. Murray, R. Robson, Chem. Commun. (2000) 1095.
[6] (a) C.V.K. Sharma, A. Clearfield, J. Am. Chem. Soc. 122 (2000) 4395;
(b) S. Lopez, S.W. Keller, Inorg. Chem. 38 (1999) 1883;
(c) D. Hagrman, P.J. Zapf, J. Zubieta, Chem. Commun. (1998) 1283.
[7] S.-Y. Yu, H. Huang, H.-B. Liu, Z.-N. Chen, R. Zhang, M. Fujita, Angew. Chem. Int. Ed. 42 (2003) 686.
[8] J. Lewis, Y.C. Lin, L.K. Royston, R.C. Thompson, J. Chem. Soc., Dalton Trans. (1965) 6464.
[9] SHELXTL, Version 5.1, Bruker AXS Inc., Madison, WI, USA, 1999.
[10] O. Kristiansson, L.-E. Tergenius, J. Chem. Soc., Dalton Trans. (2001) 1415.
[11] (a) B.J. MeNelis, L.C. Nathan, C.J. Clark, J. Chem. Soc., Dalton Trans. (1999) 1831;
(b) C. Janiak, J. Chem. Soc., Dalton Trans. (2000) 3885.

Available online at www.sciencedirect.com
SCIENCE DIRECT®
Polyhedron 23 (2004) 59–62
POLYHEDRON
www.elsevier.com/locate/poly

A silica immobilized cobalt complex: absorption of dioxygen and the redox ability in aqueous solution

Jian Gao, Ralph A. Zingaro *, Ming Z. Gao

Department of Chemistry, Texas A&M University, College Station, TX 77842-3012, USA

Received 3 March 2003; accepted 8 September 2003

Abstract

A new dioxygen carrier supported on a solid matrix has been synthesized through the tethering of a dinuclear chelating ligand to the surface of mesoporous silica. The material thus prepared is extremely efficient for the selective absorption of dioxygen from gaseous mixtures. In aqueous solution, this material displays good catalytic ability for the disproportionation of H_2O_2.
© 2003 Elsevier Ltd. All rights reserved.

Keywords: Immobilization; Silica support; Cobalt(II) complexes; H_2O_2

1. Introduction

During the past two decades, a number of dinuclear metal complexes have been reported to serve as dioxygen carriers for the chemical separation of dioxygen from other gases [1]. A dicobalt complex having polyamine moieties has been found to rank among the best of the chemical dioxygen carriers [2]. However, in aqueous solution, all dioxygen–dicobalt(II) complexes undergo degradation to form inert Co_2(III) complexes [3]. This observation has been attributed to the formation of H_2O_2 with concurrent reduction of dissolved oxygen during the redox processes. On the other hand, solid oxygen selective absorbents play a very important role in gas separation [4], gas sensor [5] and as reactants towards O_2-contaminated reducing gases in a catalytic reactor [6]. Furthermore, recyclable dinuclear complexes are of use in the industrial disposal of H_2O_2 [7]. Therefore, the design and synthesis of supported inorganic–organic materials [8–10] are applicable in this area. This is attributed to the active Si–OH sites on silica surface, which can covalently bind to organic functional groups. In this report, a generic approach to the design and synthesis of heterogenized dicobalt–hexacyclen complexes is described. The O_2 absorption ability and catalytic properties of the material are also described.

2. Experimental

2.1. Material and equipment

Mesoporous silica was synthesized according to methods described in the literature [11]. Prior to the binding procedure, it was washed with 1 N HNO_3, and thoroughly rinsed with water and then dried at 473 K in vacuo (24 h). Other materials were purchased from the Aldrich Chemical Company and were of analytical grade.

Metal analyses were performed using EDTA titration: Co(II) ions on the solid support were separated by adding $HClO_4$ (0.1 M aqueous solution). After removing the solid from the system, the resulting solution and washings were neutralized by adding NaOH (0.1 M aqueous solution) and the metal ion concentration was determined by titration. The electronic spectrum of the hexacyclen dicobalt(II) complex (in methanol) was measured using a Shimadzu UV-365 spectrophotometer. The diffusion reflection spectrum (DRS) of the solid catalyst was measured with SiO_2 serving as a reference. The temperature programmed desorption (TPD) product were detected with a quadrupole mass spectrometer, model LZL-203.

* Corresponding author. Tel.: +1-4098452731; fax: +1-4098454719.
E-mail address: zingaro@mail.chem.tamu.edu (R.A. Zingaro).

0277-5387/$ - see front matter © 2003 Elsevier Ltd. All rights reserved.
doi:10.1016/j.poly.2003.09.016

2.2. Preparation of bromopropyl-trimethoxysilane (BPTS) modified silica support

2.0 g of silica was treated with 2.0 mmol of BPTS in 10 ml of dry MeCN in the presence of 0.5 ml Et_3N. After the reaction had proceeded for a period of 2 h, the solid material was removed by filtration and washed with 30 ml of MeCN (10 ml × 3). This material was extracted with MeCN using a Soxhlet apparatus to remove unreacted species and was then dried in vacuo for 1 h. *Anal*. Calc. for 1 mmol (BPTS)/g SiO_2: C, 3.13; Br, 6.95. Found: C, 1.51; H, 1.06; N,<0.5; Br, 3.35%.

2.3. Preparation of hexacyclen functionalized silica

The solid material obtained in the above step was suspended in 10 ml of MeCN, and to this 2.0 mmol of *N*-bisdien in 10 ml MeCN was added dropwise in the presence of 2.5 mmol Et_3N. The mixture was allowed to react for 8 h at 60 °C and then the solid was filtered off, washed three times with MeCN and dried in vacuo at 60 °C for 2 h. *Anal.* Calc. for 1 mmol (hexacyclen)/g SiO_2: C, 13.57; N, 6.33. Found: C, 7.62; H, 2.13; N, 3.17%; Br, <0.1%.

2.4. Preparation of immobilized dicobalt(II) complexes

To the hexacyclen functionalized material in 10 ml of MeCN, 2.0 mmol of hexacyclen in 10 ml of MeCN was added dropwise in the presence of 2.5 mmol Et_3N. The mixture was allowed to react for 8 h at 60 °C and then 4.0 mmol of $Co(II)(ClO_4)_2$ in 5 ml of MeOH was added. After the reaction had proceeded for 0.5 h, the color of the solid material changed to deep purple, indicating that Co(II) was immobilized on the surface. *Anal*. Calc. for 1 mmol hexacyclen–Co(II) complex/g SiO_2: Co, 6.39. Found: Co, 2.30%.

2.5. Measurement of the O_2 volume in absorption

The O_2 absorption by the solid material in dry and aqueous solution was measured by determining the volume of gaseous dioxygen absorbed from a mixture of N_2 and O_2 (50%). To a 50 ml three-neck flask was added 200 mg of the solid. A modified procedure and apparatus, which were described previously [12], was employed.

2.6. TPD-MS (mass spectral) experiments

In the TPD-MS experiments, 850 mg of solid material were loaded on a quartz micro-reactor and the two sides were packed with asbestos fiber. Before the adsorption of O_2, the solid sample was treated by heating to 373 K under vacuum (1.0×10^{-4} Pa) for 2 h. The absorption was measured at 298 K by the injection of a gaseous mixture of O_2, N_2 and CO_2 (0.5 mmol, respectively). Following a 2 h period of absorption, the excess of O_2 was removed by evacuation to 1.0×10^{-4} Pa. The catalyst was ramped at a linear heating rate of 8 K/min. The desorbed gases were analyzed using a quadrupole mass spectrometer at $m/e = 32$ (for O_2), 28 (N_2) and 44 (CO_2), respectively.

2.7. Study of catalase-like activity

The disproportionation reaction was carried out in air at 20 °C in a 50 ml reactor containing a stirring bar. To 14.85 ml H_2O was added a sample of the supported complex (0.005 mmol, 25.0 mg solid sample) and the flask was sealed with a rubber septum. Hydrogen peroxide (1.33 mmol, 0.150 ml) was injected through the septum with a syringe. The reactor was connected to a graduated gas burette filled with water and dioxygen evolution was measured at 1 min time intervals by volumometry. The initial rates observed were expressed as mol Ms^{-1} by taking the volume of the solution (15 ml) into account and were calculated from the maximum slope of curve describing evolution of O_2 versus time.

3. Results and discussion

3.1. Synthesis of the immobilized solid material

The surface reaction is described in Scheme 1. The degree of loading of grafted macrocycles was calculated from elemental analyses. The amount of support was chosen so as to give a theoretical loading of 1.0 mmol hexacyclen/g. However, the true loading was about 24.6% (mmol/gSiO_2). The graft of Co(II) ions onto the surface was conducted by simply charging the modified silica with a stoichiometric amount of $Co(II)(ClO_4)_2 \cdot 6H_2O$ in MeCN under argon. After refluxing for 6 h, the solid acquired a purple color (**3**). The Co(II) content in the final material was determined by titration, and the formation of the supported dinuclear complexes was clearly indicated. The comparison of the DRS of the supported complex **4** with that of the corresponding untethered dicobalt–hexacyclen–O_2 adducts [13] revealed a similar absorption maximum at 380 nm (Fig. 1), further indicating that the supported dicobalt complex material had been formed.

3.2. Selective absorption of O_2 on the dry solid and from aqueous solution

In the initial experiment, the solid supported dicobalt complex was studied as an oxygen carrier. The absorption of O_2 was determined by the method described in Section 2. As shown in Fig. 2, after the absorption and evacuation procedures were repeated more than ten

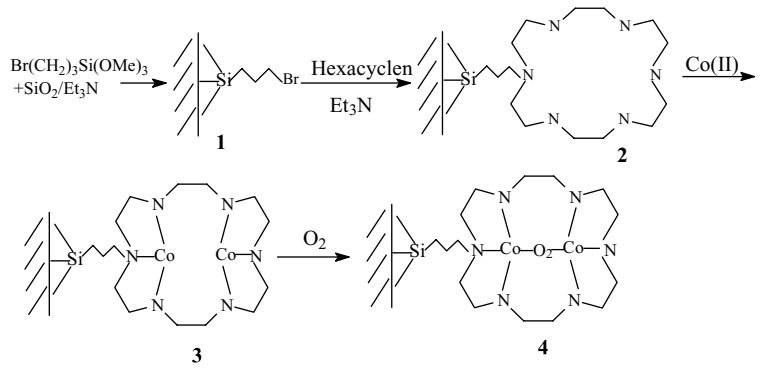

Scheme 1.

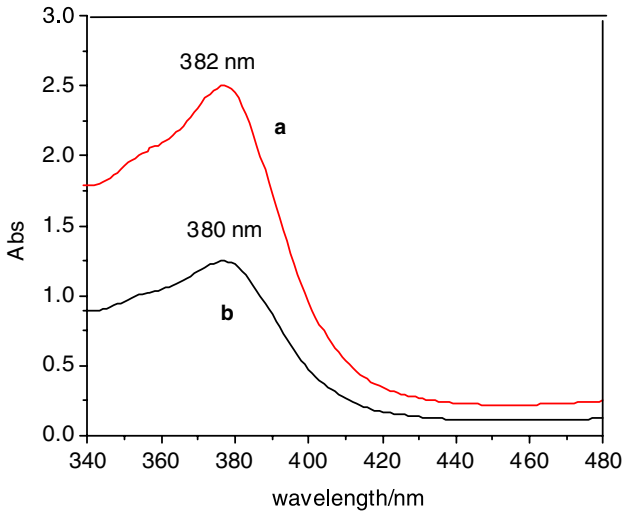

Fig. 1. DRS spectra (a) of the solid sample and the solution absorption spectra (b) of the complex precursor.

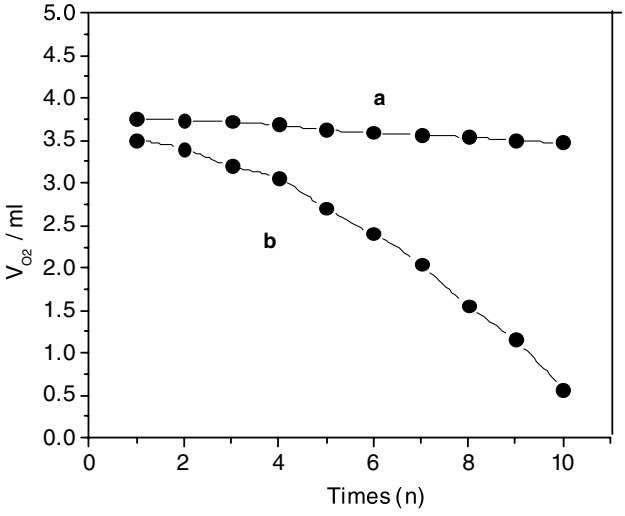

Fig. 2. Variation of the absorption ability (ml of O_2 at 25 °C) of the solid sample in dry (a) and aqueous (b) conditions with the recycling times.

times, no obvious loss of absorption volume, V_{O2}, was noted. This observation suggests the occurrence of a reversible oxygenation process. The reversibility results from variation in the pressure of O_2 and the temperature of the system during evacuation. However, when this experiment was conducted in the presence of H_2O (by introducing 5 ml H_2O to the above system), at pH 8.0, the color of the sample changed from the initial purple Co(II) color to a brownish-red indicating the formation of Co(III). The brownish-red colored species results from the formation of cobalt–polyamine–dioxygen complex [3,13]. After several repetitions, the solid material becomes inert towards the absorption and release of O_2.

3.3. Selective absorption of O_2 from a gaseous mixture

A temperature programmed desorption mass spectrum was employed to observe the selective absorption of O_2 from a gaseous mixture by the solid material. As is shown in Fig. 3, with an increase in temperature, one peak at ca. 368 K was observed for $m/e = 32$. The result

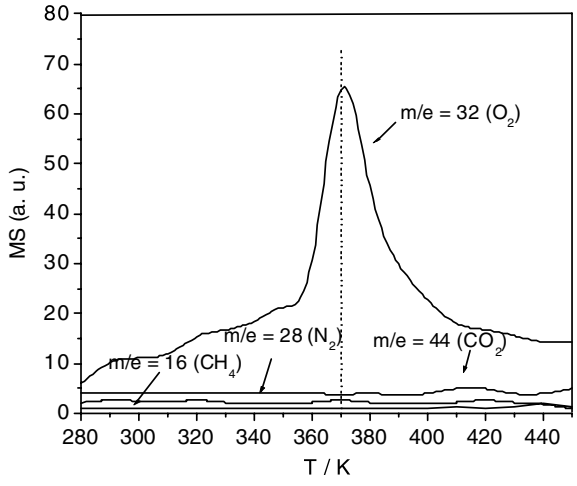

Fig. 3. TPD-MS profiles of the solid sample monitored at $m/e = 32$, 28 and 44, respectively.

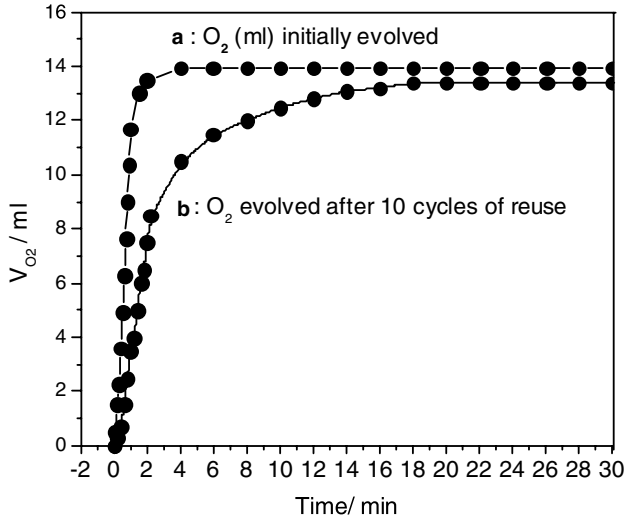

Fig. 4. The H_2O_2 dismutation curve of the immobilized dicobalt(II) complex in aqueous solution.

indicated that O_2 molecules are physico-chemically absorbed on the silica surface by binding to the coordination unsaturated Co(II) ions. Mass profiles monitored at 16, 28 and 44 reveal that this material does not absorb CH_4, N_2 or CO_2.

3.4. Catalytic activity in disproportionation of H_2O_2

The catalytic activity of this material was tested by measuring the dioxygen evolution with a Co(II) complex (supported):H_2O_2 ratio of 1:500. This condition was found to be optimal in a controlled reaction process. The amount of residual hydrogen peroxide (measured by iodometric titration) was compared with the amounts of dioxygen formed (as calculated from volumometry) and was found to satisfy the stoichiometry implied by equation: $2H_2O_2 \rightarrow 2H_2O + O_2$. The time course of oxygen evolution for the catalysis is shown in Fig. 4. The evolution profile suggests the involvement of a quick catalytic process occurring at the initial stage followed by a very short term of a slow catalytic process. The fast catalytic rate calculated graphically was 0.132 $M(O_2)$/min. The dioxygen evolution ceased after 10 min. At this stage the evolved dioxygen correspond to 100% decomposition of hydrogen peroxide. When more H_2O_2 was added, the disproportionation reaction rate resumed, indicating the supported dicobalt complex still functioned as an active catalyst.

4. Concluding remarks

A new dicobalt complex bound to a solid silica matrix functions as an effective and selective oxygen absorbent and is capable of recycling O_2 more than 10 times without loss of activity. This type of immobilization provides the possibility for the prevention of degradation of the active centers. This is an intrinsic problem encountered by oxygen carriers in water solution. This result indicates that this material can be of practical value in the separation of O_2 from gaseous mixtures. In water solution, this material displays effective catalytic activity towards the disproportionation of H_2O_2. This effectiveness is due to the redox reaction from Co(II) to Co(III) which occurs in aqueous solution. It was proposed that any residual hydrogen peroxide formed during industrial processes can be decomposed prior to disposal through the application of immobilized transtion metal complexes.

Acknowledgements

Thanks are due to the Robert A. Welch Foundation of Houston, Texas for financial support.

References

[1] J.M. Lehn, S.H. Pine, E. Watanabe, A.K. Willard, J. Am. Chem. Soc. 99 (1977) 6766.
[2] J.M. Lehn, Pure Appl. Chem. 52 (1980) 2441.
[3] S. Fallab, P.R. Mitchell, in: Advances in Inorganic and Bioinorganic Mechanisms, vol. 3, Academic Press, New York, 1984, p. 311.
[4] D.R. Corbin, PCT Int. Appl. (2002) 16.
[5] F. Gora, S. Malkmus, C. Modes, A. Kipka, PCT Int. Appl. (2002) 3.
[6] M. Schwartz, J.H. White, A.F. Sammells, PCT Int. Appl. (1997) 86.
[7] P. Dhaese, Chem. Today (1996) 19.
[8] B.R. Bodagard, J.N. Burstyn, Chem. Commun. (2001) 647.
[9] R.J. Clarke, I.J. Shannon, Chem. Commun. (2001) 1936.
[10] S. Abramson, M. Lasperas, A. Galarneau, D. Desplantier-Giscard, D. Brunel, Chem. Commun. (2000) 1773.
[11] C.T. Kresge, M.E. Loenowicz, W.J. Roth, J.C. Vartuli, J.S. Beck, Nature 359 (1992) 710.
[12] F. Calderazzo, F.A. Cotton, Inorg. Chem. 1 (1962) 30.
[13] R.J. Motekaitis, A.E. Martell, J. Am. Chem. Soc. 110 (1988) 7715.

Available online at www.sciencedirect.com
SCIENCE DIRECT®
Polyhedron 23 (2004) 63–69
POLYHEDRON
www.elsevier.com/locate/poly

Synthesis, structural characterisation and thermal decomposition of [{Pt(dppf)(2-SPy)}{BF_4}](dppf = 1,1′-bisdiphenylphosfinoferrocene and 2-SPy = 2-mercaptopyridine) – a source for a Fe–Pt containing alloy

V.D. de Castro [a], Geraldo M. de Lima [a,*], Arilza O. Porto [a,*], Helmuth G.L. Siebald [a], José D. de Souza Filho [a], J.D. Ardisson [b], José D. Ayala [a], Gabriella Bombieri [c]

[a] *Departamento de Química, Universidade Federal de Minas Gerais – UFMG, Avenida Antonio Carlos 6627, Belo Horizonte MG 31270-901, Brazil*
[b] *CDTN, Belo Horizonte MG 31270-901, Brazil*
[c] *Istituto di Chimica Farmaceutica della Università di Milano, Milano, Italy*

Received 28 May 2003; accepted 8 September 2003

Abstract

The reaction of 2-PySK with [Pt(dppf)Cl_2] [dppf = 1,1′-bis(diphenylphosfinoferrocene and 2-PyS = 2-mercaptopyridine] produced Pt(dppf)(2-SPy)$_2$ (**1**) and its subsequent reaction with $SnBu_2(BF_4)_2$ or $SnBu_3(BF_4)$ yielded [{Pt(dppf)(2-SPy)}{BF_4}] (**2**). Compounds **1** and **2** were fully characterised by multinuclear NMR [^{1}H, ^{13}C{^{1}H}, ^{31}P{^{1}H} and ^{195}Pt{^{1}H}] and ^{57}Fe Mössbauer spectroscopies. In addition the structure of **2** was determined by X-ray crystallographic studies, which can be summarised as follows: monoclinic $P2_1/c$, $a = 9.9291(9)$ Å, $b = 22.270(4)$ Å, $c = 16.919(2)$ Å, $\gamma = 103.6(9)°$, $V = 3636.2(8)$ Å^3 and $Z = 4$. Finally, a thermal decomposition study was carried out with **2** in three different atmosphere: oxygen, nitrogen or hydrogen. The residues were characterised by X-ray powder diffraction (XRD), X-ray electron probe microanalysis (EPMA), scanning electron microscopy (SEM) and ^{57}Fe Mössbauer spectroscopy. The results have shown the formation of a disordered $Pt_{1-x}Fe_x$ based alloy when the pyrolysis process was performed in H_2, simultaneously with small amount of Fe(II) and Fe(III) phosphides. Furthermore, in oxygen and nitrogen the thermal decomposition of **2** produced metallic agglomerates of Pt dispersed in a combination of Fe(II) and Fe(III) phosphates in O_2, and an intricate mixture of sulphides and phosphides in N_2.
© 2003 Elsevier Ltd. All rights reserved.

Keywords: Pyrolysis; Organometallic compounds; Iron–platinum compounds

1. Introduction

The compound [Fe(η^5-$C_5H_4PPh_2$)$_2$], dppf, still plays an important role in organometallic chemistry [1]. The coordination versatility of this metalloligand is highly remarkable. Actually, the various coordinating modes of dppf just reflect its ability to change conformation in order to match the steric demands of the surrounding molecular environment. However, in most examples it is η^2 bonded to metal centres. So far more than 250 structures determined by X-ray crystallography, containing the dppf fragment, have been deposited at CCDC (version 5.24 of April 2003).

The considerable research attention granted to dppf relates to: (i) the various coordination modes towards metallic anions [2], (ii) the catalytic activity of the complexes [3] and (iii) the chemotherapeutic potential for cancer treatment of some derivatives [4].

Our research interest towards dppf concerns the preparation of well characterised Pt(II) [5], Ru(II), and its Sn(II)-containing heterometallic derivatives in order to obtain oxides and Fe/Pt/Sn or Fe/Ru/Sn containing alloys. For that, thermal decomposition of single source organometallic precursors has received special attention from us in the last two years [6]. Heterometallic

* Corresponding authors. Tel.: +553134995744; fax: +553134995720.
E-mail address: gmlima@dedalus.lcc.ufmg.br (G.M. de Lima).

0277-5387/$ - see front matter © 2003 Elsevier Ltd. All rights reserved.
doi:10.1016/j.poly.2003.09.017

derivatives of dppf seems to be attractive since it possesses different metallic species close enough to interact and produce synergetic effects which can result in interesting properties. Therefore, this work reports the thermal decomposition of [{Pt(dppf)(SPy)}{BF_4}] (**2**) carried out in oxygen, nitrogen and hydrogen. The residues were studied by X-ray powder diffraction (XRD), scanning electron microscopy (SEM), X-ray electron probe microanalysis (EPMA) and ^{57}Fe Mössbauer spectroscopy.

2. Experimental

2.1. Synthesis and characterisation of metal complexes

The synthetic work was conducted in an atmosphere of dry N_2. All solvents were treated by the appropriate method in order to remove moisture and oxygen, prior to use. All chemicals unless stated were obtained from Aldrich or Strem Co. NMR spectra were recorded in $CDCl_3$, at 400 MHz, ^{1}H, 100.62 MHz; ^{13}C{^{1}H}, 50.29 MHz; ^{31}P{^{1}H}, 161.92 MHz; ^{195}Pt{^{1}H}, 86.00 MHz using a Bruker DPX-400 spectrometer equipped with an 89 mm wide-bore magnet. ^{13}C and ^{1}H shifts are reported relative to $SiMe_4$, ^{31}P to H_3PO_4 and ^{195}Pt to K_2PtCl_4. Carbon and hydrogen elemental analyses were performed on a Perkin–Elmer PE-2400 CHN-analyses using tin sample-tubes. The X-ray diffraction data were collected using a Enraf Nonius FR590 with SMART CCD area detector and graphite–graphite-monochromated Mo Kα.

2.2. Synthesis of Pt(dppf)(2-SPy)$_2$ (1)

To a Schlenk-flask containing a suspension of 0.88 g (5.90 mmol) of 2-PySK and 20 ml of thf, was slowly added a thf solution of [Pt(dppf)Cl_2], 2.42 g (2.95 mmol in 15 ml). Within 4 h of stirring the thf was removed in vacuum and CH_2Cl_2 (30 ml) was added in order to extract the product, originating an orange solution and KCl which was separated by filtration. A yellow solid was obtained after removing the solvent and re-crystallisation in CH_2Cl_2/toluene (1:1, 30 ml). Yield based in [Pt(dppf)Cl_2]: 70% (2.00 g, 2.07 mmol). Mp 180(d) °C. ^{1}H NMR δ 6.2–7.5(m) (Py and Ph), 4.4(s) and 4.2(s) (Cp); ^{13}C{^{1}H} NMR δ 168, 147, 137, 125, 115 (Py), δ 134–127 (Ph and Cp); ^{31}P{^{1}H} δ 16.87 ^1J(^{31}P–^{195}Pt) = 3139 Hz; ^{195}Pt{^{1}H} δ −4684 ^1J(^{31}P–^{195}Pt) = 3195 Hz. Elemental analysis for $C_{44}H_{38}FeP_2PtN_2S_2$, found (calc): C, 57.41(58.35); H, 3.99(4.01); N, 2.99(3.09)%.

2.3. Synthesis of [{Fe(η^5-$C_5H_4PPh_2$)$_2$Pt(SPy)}{BF_4}] (2)

To a solution of $AgBF_4$, 42 mg (0.22 mmol) in thf (20 ml), was added 70 mg (0.22 mmol) of $SnBu_3Cl$ in thf. The clear solution remained stirring for 30 mim in dark. The AgCl formed was filtered off by cannula and the solution transferred to another Schlenk-flask containing 210 mg (0.22 mmol) of Pt(dppf)(2-SPy)$_2$ in thf (20 ml). After 15 h of stirring the solvent was removed and the residue was washed with *n*-hexane, extracting $SnBu_3$-SPy. The resultant golden-yellow solid was re-crystallised in toluene (30 ml) affording X-ray quality crystals. Yield 69% (144 mg, 0.150 mmol). Mp 215(d) °C. ^{1}H NMR δ 7.9–6.6 (m) (Py and Ph), 4.9(s) and 4.4(s) (Cp); ^{13}C{^{1}H} NMR δ 166, 145, 136, 125, 119 (Py), δ 134–128 (Ph and Cp); ^{31}P{^{1}H} δ 17.27 ^1J(^{31}P–^{195}Pt) = 3162 Hz and δ 11.56 ^1J(^{31}P–^{195}Pt) = 3609 Hz; ^{195}Pt{^{1}H} δ −3500. Elemental analysis for $C_{39}H_{32}BF_4FeP_2PtS$, found(calc): C, 49.78(49.49); H, 2.81(2.78); N, 1.39(1.38)%. The same product was obtained using $SnBu_2Cl_2$ (50 mg, 0.16 mmol).

2.4. X-ray structure determination of 2

The structure was solved by direct methods with SIR-92 [7] and the refinements were carried out using SHELXL 97 [8], minimising on the weighted *R* factor *wR*2. Further details are given in Table 1. All non-H atoms are anisotropic. The ORTEP drawing shows the non-H atoms as 50% thermal vibration ellipsoids. The crystals were obtained by slow evaporation of a toluene solution of **2**. The BF_4^- group showed to be very disordered.

Table 1
Crystal data and structure refinement for **2**

	2
Empirical formula	$C_{39}H_{32}BF_4FeP_2PtS$
Formula weight	946.41
Temperature (K)	263(2)
Wavelength	0.71073
Crystal system	monoclinic
Space group	$P2_1/c$
Unit cell dimensions	
a (Å)	9.9291(9)
b (Å)	22.270(4)
γ (°)	103.605(9)
c (Å)	16.919(2)
Volume (Å^3)	3636.2(8)
Calculated density (g cm^{-3})	2.298
Z	4
Absorption coefficient	4.438
$F(000)$	1856
Crystal size (mm)	$0.45 \times 0.25 \times 0.08$
Theta range for data collection	2.48–28.54
Limiting indices	$h = 0$–13; $k = -29$–0; $l = -22$–22
Reflections collected/unique	9260/6317
Refinement method	Full-matrix least-squares on F^2
Final R indices [$I > 2\sigma(I)$]	$R_1 = 0.032$, $wR_2 = 0.066$
R indices (all data)	$R_{1=0.078}$, $wR_2 = 0.076$
CCDC reference	192715

2.5. Thermal analysis of **2**

In order to determine the range of temperature of degradation of **2**, thermogravimetric analysis (TG) with simultaneous differential thermal analysis (DTA) experiments were performed in a TA Instruments SDT 2960 with a heating rate of 5 °C/min until 900 °C in oxygen.

2.6. Pyrolysis of **2**, chemical, structural and morphological characterisation of the residue

Thermal decomposition of **2** was carried out in a tube furnace in N_2, O_2 and H_2, using a heating rate of 5 °C/min until a final temperature of 900 °C employing a gas flux of 100 ml/min. The decomposed products were characterised by XRD, SEM, ^{57}Fe Mössbauer spectroscopy and EPMA.

X-ray powder diffraction was executed in a Rigaku Geigerflex using a Cu Kα radiation ($\lambda = 1.54178$ Å). A scan rate of 4°/min in the 2θ range from 4° to 100° was used. In those samples containing platinum its main diffraction line at 39.76° (1 1 1) was used as internal standard for angle calibration.

The scanning electron micrographs was recorded in a JEOL JSM-840A equipment and the electron probe X-ray microanalysis were carried out in a JXA 89000 RL wavelength dispersive/energy dispersive combined microanalyser. For the SEM images and X-ray microanalysis the samples were recovered with a thin film of gold and carbon, respectively, deposited by sputtering.

^{57}Fe Mössbauer measurements were obtained in order to identify the Fe oxidation states and number of different sites in the decomposed materials by using a conventional apparatus with ^{57}Co as source of γ-radiation, kept at room temperature.

3. Results and discussion

Organometallic compounds are good candidates for single source precursors for thermal decomposition because they decompose at low temperature, producing metallic oxides, metallic particles or inorganic salts. Following our interest in this research area, we have attempted to prepare a Pt/Fe/Sn derivative, as described in Scheme 1, to be employed as an source for the trimetallic containing materials. Firstly, the reaction of [Pt(dppf)Cl_2] with 2-PySK produced the bimetallic derivative [Pt(dppf)$(SPy)_2$] (**1**) (see Scheme 1) that was used as a S and N electron donor ligand towards another metal centre. Organotin(IV) Lewis acid were chosen due to the great Sn–N affinity observed in other complexes [9]. However, instead of a simple coordination reaction, it was observed an exchange of 2-PyS$^-$ ligand between Pt(II) and Sn(IV) atoms.

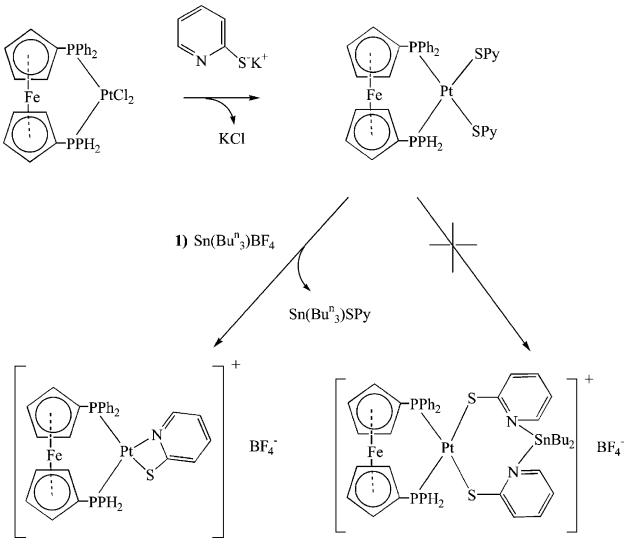

Scheme 1. Pathway of the preparation of compound **1**.

Similar interchange was also detected when the reaction of [$SnPh_3SPy$] with [Pt$(PPh_3)_2Cl_2$] was performed in order to obtain a bimetallic complex where Pt(II) was coordinated through the S donor centre. However, two separated compounds $SnPh_3Cl$ and [Pt$(PPh_3)_2(SPy)_2$] [10] were isolated and identified.

Compounds **1** and **2** are air and moisture stable golden-yellow products, readily soluble in CH_2Cl_2 and toluene, and they showed satisfactory results of elemental analysis. NMR spectroscopic measurements were carried out using a $CHCl_3/CDCl_3$ solutions. For both compounds the ^{13}C and ^{1}H NMR spectra exhibited the expected resonances for Cp, Ph and Py groups. Compound **1** displayed a single signal at δ 16.9 [$^1J(^{31}P–^{195}Pt) = 3139$ Hz] in the ^{31}P NMR spectrum, and a peak at δ −4684 [$^1J(^{31}P–^{195}Pt) = 3195$ Hz] in the ^{195}Pt NMR spectrum. It possesses a smaller $^{31}P–^{195}Pt$ coupling constant, 3195Hz compared to the starting material [Pt(dppf)Cl_2], 3768 Hz. The latter is a consequence of the better π-acceptor character of S compared to Cl which causes a decrease in the Pt–P bond strength.

The ^{31}P NMR spectrum of **2** revealed two signals at δ 17.3 [$^1J(^{31}P–^{195}Pt) = 3162$ Hz] and 11.6 [$^1J(^{31}P–^{195}Pt) = 3609$ Hz]. Moreover, it was detected a coupling constant between the two non-equivalent phosphorus at 17 Hz. The first set of chemical shifts and coupling constants are similar to the signals displayed by **1**. Therefore, it might be assigned to the P atom *trans* to S of the –SPy moiety and the remaining signal can be attributed the other P atom *trans* to N. A broad resonance centred at δ −3500 was detected in the ^{195}Pt NMR spectrum, resulting from a complicated coupling pattern of ^{195}Pt with the non-equivalent ^{31}P nuclei.

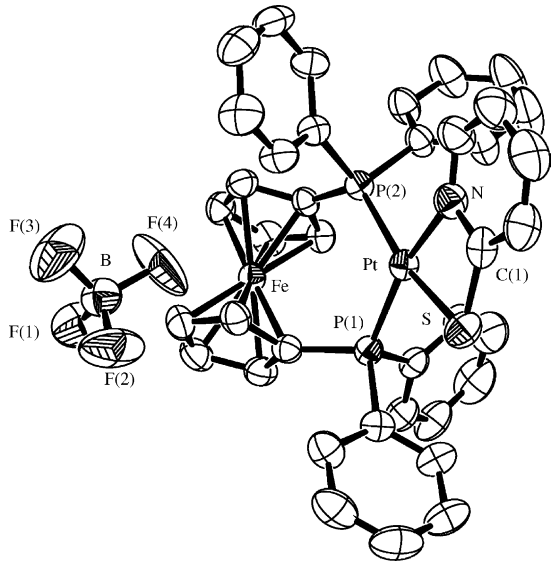

Fig. 1. Molecular structure of **2** determined by X-ray crystallography.

Table 2
Selected bond lengths (Å) and angles (°) for **2**

Bond lengths	
Pt–N	2.1160(4)
Pt–P(1)	2.2521(11)
Pt–P(2)	2.2910(11)
S–C(1)	1.7470(5)
Pt–S	2.3635(12)
Bond angles	
N–Pt–P(1)	164.07(14)
P(1)–Pt–P(2)	99.09(5)
P(1)–Pt–S	95.09(6)
S–C(1)–N	110.00(3)
N–Pt–P(2)	96.82(14)
N–Pt–S	69.00(14)
P(2)–Pt–S	165.81(6)

A single-crystal X-ray experiment confirmed the structure of **2** to be composed of $Pt(dppf)(SPy)^+$ cations and BF_4^- anions, with no direct contact between the two fragments, Fig. 1. The Pt(II) atom lies in the centre of a distorted square where it is bonded to both S {Pt–S, 2.3641(15) Å} and N {Pt– N, 2.113(5) Å} of the pyridyl group. These bond length and angles {N– Pt–S 69.00(14)°, P(1)–Pt–P(2) 99.09(5)°, S–C(1)–N 110.00(3)°} are very close to the ones observed for $[\{Pt(PPh_3)_2(SPy)\}\{PF_6\}]$ [11] (Table 2).

The coordination position of the fluorine atoms in the BF_4^- group was very disordered, similarly to other reported results [11].

3.1. Thermal analysis

Compound **2** displayed a highly exothermic decomposition process in a pseudo single step, which started at 300 °C and finished at 800 °C. The initial loss of weight at 60 °C was subtracted from the curve in order to disregard the loss of solvent. In this step the complex loses 54.2% of the weight. After 400 °C, the material continues to decompose losing at the end, 800 °C, 47% of mass, leaving a final residue containing 7.2% of the initial amount, which suggests that an appreciable amount of material was lost to the gas phase.

3.2. X-ray electron probe microanalysis

The chemical composition of the residues was determined by EPMA in different regions of the samples in order to evaluate their level of homogeneity. The presence of carbon peaks in all residues is a consequence of the deposit of graphite at the sample's surface.

Two different regions were identified in the residues obtained in oxygen: a bright one, formed by agglomerates of metallic platinum (approximately 10 μm in size) dispersed in an amorphous media, dark region, constituted basically of P, Fe and O, Fig. 2. No sulphur was identified in this sample. A similar situation was revealed for the residue obtained in N_2, Fig. 3(b), however, the particles of platinum are much smaller than the previous one. Moreover, in this case it was noticed only a trace of oxygen, and the major components were Fe, P and S. The residue from decomposition of **2** in H_2 has not shown oxygen or sulphur, but only Pt, P and Fe, Fig. 3(c). The nature of the species formed could only be tentatively identified with the support of XRD and ^{57}Fe Mössbauer spectroscopies.

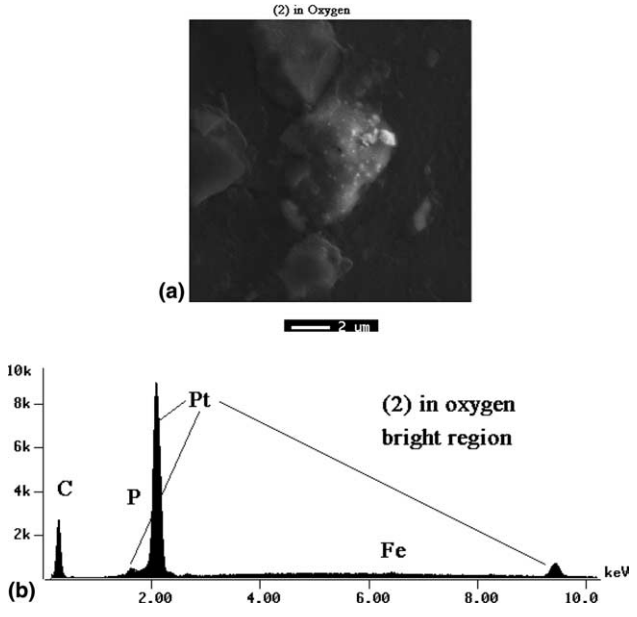

Fig. 2. The image and the dispersive energy X-ray microanalysis (EPMA) of **2** decomposed in O_2.

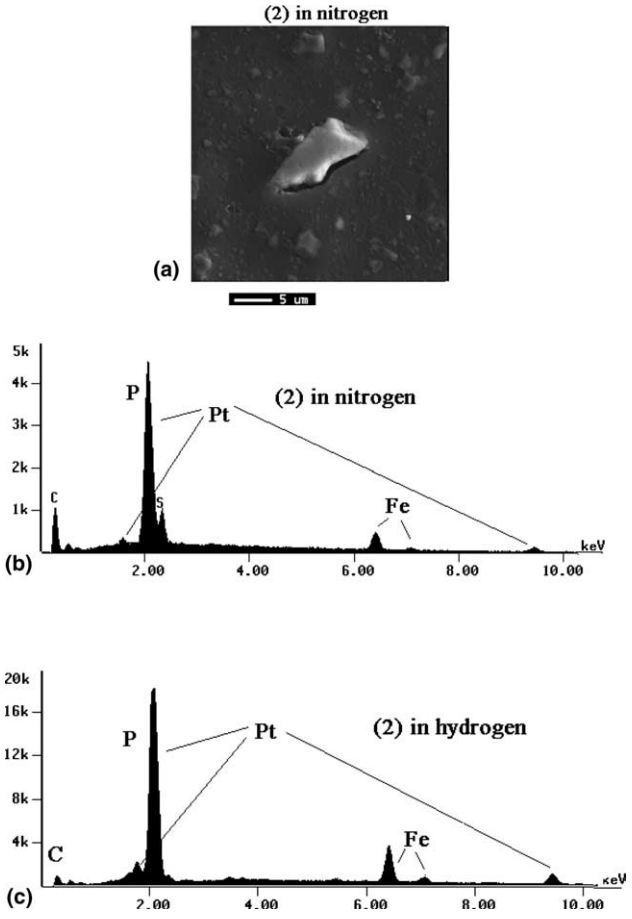

Fig. 3. (a) The image and the EPMA of **2** decomposed in N_2 (b) and H_2 (c).

3.3. X-ray powder diffraction

X-ray diffraction measurements were executed in order to identify the pyrolysis residues of **2**, Fig. 4. The diffractogram of the decomposed material in oxygen, Fig. 4(a) revealed lines at $2\theta = 39°$, 46°, 67° and 81°; corresponding, as indicated by the Miller index to the diffraction planes (1 1 1), (2 0 0), (2 2 0) and (3 1 1) to metallic platinum (Cubic, $Fm3m$, $a = 3.923$ Å) {04-0802} [12]. The high intensity of the Pt diffraction lines suggests the production of large and well formed particles of platinum as observed in the electron backscaterred image. The other diffraction lines can be clearly attributed to the formation of $FePO_4$ and $Fe_3(PO_4)_2$ [13] and it is in accordance to the EPMA and ^{57}Fe Mössbauer spectroscopic results.

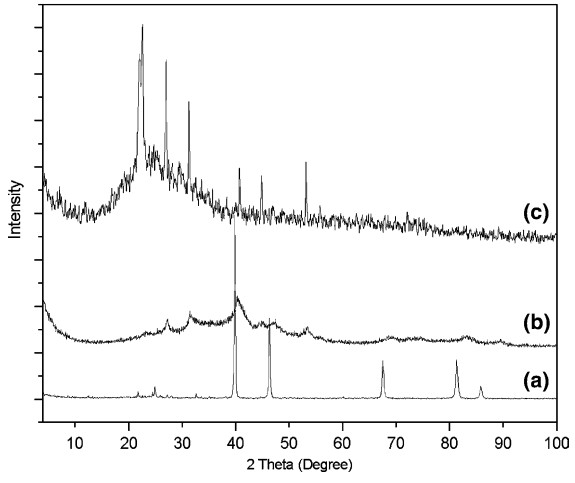

Fig. 4. XRD pattern of **2** decomposed in O_2 (a), N_2 (b) and H_2 (c).

Much more broader Pt diffraction lines (1 1 1), (2 0 0), (2 2 0) and (3 1 1) were revealed for the residue prepared in N_2, in consequence of the lower crystallinity of the decomposed material. The much less intense lines at approximately $2\theta = 28°$, 47° and 56° might be attributed to the cubic FeS [14a] {pyrite form – 06-0710} and those at $2\theta = 32°$ and 53° which are also observed in the diffractogram of the sample decomposed in H_2, can be associated to the orthorhombic FeP_4 [14b] {34-0996i}, Fig. 4(b). On the basis of the EPMA analysis there is no oxygen in the sample which frustrate the presence of phosphate anions. Therefore, it is reasonable to assume that Fe(II) and Fe(III) are in the form of sulphide and phosphide. The diffraction pattern of the product obtained in H_2 has shown lines, at $2\theta = 25°$, 31°, 32° and 53°, corresponding to orthorhombic FeP_4, as before, and the diffractions at $2\theta = 41°$ and 46°, may be associated to the planes (1 0 0) and (2 0 0) of the Pt–Fe alloy (cubic – 29-0718). The intense line at $2\theta = 24°$ is probably related to the alloy as well since other similar materials with different stoichiometry present diffraction lines at angles smaller than 30° [12].

3.4. ^{57}Fe Mössbauer experiments

The room temperature ^{57}Fe Mössbauer spectroscopy experiments supported the identification of iron compounds and its oxidation state, Fig. 5 and Table 3.

For the starting material, **2**, it was observed the presence of Fe(II) to which the parameters $\delta = 0.40(2)$ mm s^{-1} and $\Delta = 2.25(3)$ mm s^{-1} relates very well with the classical values reported for ferrocene, [$FeCp_2$], $\delta = 0.44(2)$ mm s^{-1} and $\Delta = 2.38(3)$ mm s^{-1} and the dppf $\delta = 0.42(2)$ mm s^{-1} and $\Delta = 2.30(3)$ mm s^{-1} [15], Fig. 5(a). The ^{57}Fe Mössbauer spectrum of the residue prepared in O_2, Fig. 5(b) displayed two signals with the corresponding parameters, $\delta = 0.30(2)$ mm s^{-1}, $\Delta = 0.44(3)$ mm s^{-1} and $\delta = 0.37(2)$ mm s^{-1}, $\Delta = 0.98(3)$ mm s^{-1} assigned to the presence of Fe(III), 63%, and Fe(II), 37%, respectively, that are in the form of phosphates [13]. Two sites of Fe(II), $\delta = 0.25(2)$ mm s^{-1}, $\Delta = 1.49(3)$ mm s^{-1} (14%) and $\delta = 0.37(2)$ mm s^{-1}, $\Delta = 0.80(3)$ mm s^{-1} (43%) and one site of Fe(III) $\delta = 0.29(2)$ mm s^{-1}, $\Delta = 0.23(3)$ mm s^{-1} (43%) were

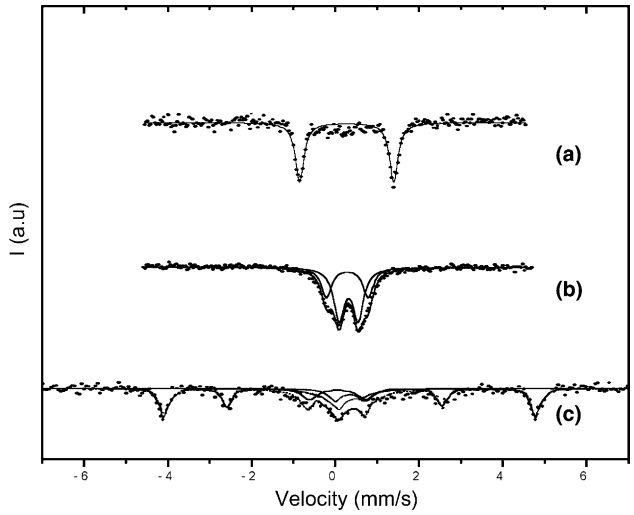

Fig. 5. ^{57}Fe Mössbauer spectra of **2** and the corresponding residues obtained in O_2 (a), N_2 (b), and H_2(c).

found in the material obtained in N_2, Fig. 5(c). The iron species are associated to the sulphide and phosphide, as attested by the other results. Finally, the sample obtained in H_2 presents signals related to Fe(II), $\delta = 0.36(2)$ mm s^{-1}, $\Delta = 0.83(3)$ mm s^{-1} (12%), and Fe(III) with $\delta = 0.26(2)$ mm s^{-1}, $\Delta = 0.12(3)$ mm s^{-1} (11%). These cations are in the form of orthorhombic phosphide FeP_4 as the XRD pointed out. The more remarkable is the sextet with $\delta = 0.26(2)$ mm s^{-1}, $\Delta = 0.19(3)$ mm s^{-1} and a hyperfine field (B_{hf}) = 27 T (77%), which indicates some form of metallic iron, Fig. 5(e). It was attributed to a disordered $Pt_{1-x}Fe_x$ phase on the basis of the ^{57}Fe Mössbauer parameters of

Table 3
^{57}Fe Mössbauer parameters for the complex **2** and the residue of decomposition of **2** under O_2 (a), N_2 (b) and H_2 (d)

Sample	Fe oxidation state	IS (mm s^{-1})	QS (mm s^{-1})	Area (%)
2	Fe(II)	0.40	2.25	100
O_2	Fe(III)	0.30	0.44	63
	Fe(II)	0.37	0.98	37
N_2	Fe(III)	0.30	0.44	43
	Fe(II)	0.25	1.49	14
	Fe(II)	0.37	0.80	43
H_2	Fe	0.26	0.19	77
	Fe(III)	0.26	0.12	11
	Fe(II)	0.36	0.83	12

The experimental errors associated to IS and QS are 0.02, 0.03, respectively.

other Fe/Pt alloys [16] and the data of metallic iron $\delta = 0.29(2)$ mm s^{-1}, $\Delta = 0.14(3)$ mm s^{-1} and $B_{hf} = 28$ T. The experiments of ^{57}Fe Mössbauer have shown the formation of different sites of iron which can not be directly attributed to any particular compound without the help of other techniques. However, it is clear that a very different iron phase is formed in the sample decomposed in H_2, that is very similar to the pattern exhibited for iron containing alloys. No further evidence was found for the formation of iron carbides, carbonates or oxides, at least as major products.

3.5. Scanning electron microscopy

The SEM images, Fig. 6, were obtained for each residue in order to investigate the level of homogeneity

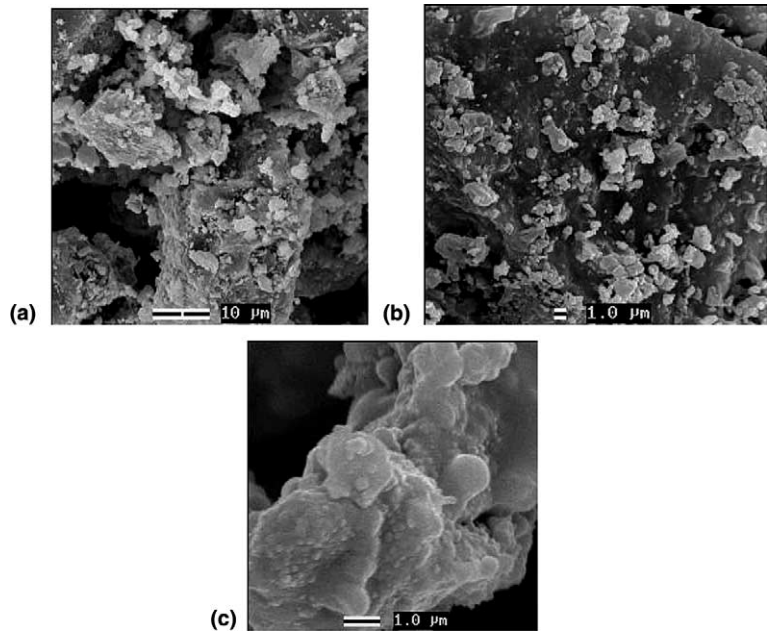

Fig. 6. Electron scanning micrographs of **2** decomposed in O_2 (a), N_2 (b) and H_2 (c).

and the presence of metallic agglomerates. No considerable difference is observed for the decomposed material in O_2, Fig. 6(a), or N_2, Fig. 6(b). It is obvious since the grains correspond to the presence of metallic platinum. The major difference consists in the nature of the dark and amorphous material that in the first case consists of a mixture of Fe(II) and Fe(III) phosphates and in the second product it is associated to a complex combination of Fe(II) and Fe(III) phosphides or sulphides. Also, the size of the particles obtained in oxygen vary from 40 to 70 μm whist in nitrogen it is much smaller. In the case of **2** decomposed in H_2 a more compact and homogenous material was obtained and seems to be formed by very big grains (100–200 μm).

4. Conclusions

In this work the synthesis and structural characterisation of [{Pt(dppf)(SPy)}{BF_4}] (**2**) was described. The thermal behaviour of **2** was studied by simultaneous TG/DTA measurements. The preparation of products of decomposition of **2** in O_2, N_2 and H_2 was investigated and the obtained residue was fully characterised by XRD, SEM, EPMA and ^{57}Fe Mössbauer spectroscopy. The results have attested the formation of a disordered $Pt_{1-x}Fe_x$ alloy when the pyrolysis process was performed in H_2. However, the procedure also produced Fe(II) and Fe(III) containing materials, as contaminants. The degradation product of **2** in O_2 and N_2 consisted of metallic platinum and again Fe(II) and Fe(III) species.

5. Supplementary data

Crystallographic data for the structural analysis of compound **1** have been deposited at the Cambridge Crystallographic Data Centre, 12 Union Road, Cambridge, CB2 1 EZ, UK, and are available free of charge from the Director on request quoting the deposition number CCDC 192715 (fax: 44-1223-336033; e-mail: deposit@ccdc.cam.ac.uk or www: http://www.ccdc.cam.ac.uk).

Acknowledgements

We thank TWAS – Third World Academy of Science (Research Grant Agreement 00-229 RG/CHE/LA) and CNPq-Brazil for the financial support. The present work was partially developed at the Laboratório de Microscopia Eletrônica e Microanálise (LMA) – Física, Química, Geologia-UFMG and CDTN-CNEN financed by FAPEMIG (Project CEX 1074/95).

References

[1] G. Bandoli, A. Dolmella, Coord. Chem. Rev. 209 (2000) 161.
[2] W.-Y Yeh, Y.J. Cheng, M.Y. Chiang, Organometallics 16 (1997) 918.
[3] K.S. Chan, T.S.A. Hor, in: A. Togni, T. Hayashi (Eds.), Ferrocenes – Homogenous Catalysis, Organic Synthesis and Material Science, VHC, Weinheim, 1995, p. 3.
[4] M. Viotte, B. Gautheron, I. Nifantév, L.G. Kuz'mina, Inorg. Chim. Acta 253 (1996) 71.
[5] G.M. de Lima, C.A.L. Filgueiras, M.T.S. Giotto, Y.P. Mascarenhas, Transition Met. Chem. 26 (1995) 380.
[6] (a) A.G. Pereira, A.O. Porto, G.M. de Lima, G.G. Silva, H.G.L. Siebald, J.L. Neto, Phys. Chem. Chem. Phys. 4 (2002) 4528;
(b) G.A.A. Costa, M.C. Silva, A.C.B. Silva, G.M. de Lima, R.M. Lago, M.T.C. Sansiviero, Phys. Chem. Chem. Phys. 2 (2000) 5708.
[7] (a) G.M. Sheldrick, SHELXL 5.0, Siemens Analytical Instruments, Madison, WI, 1994;
(b) A. Altomare, G. Cascarano, C. Giacovazzo, A. Guagliardi, J. Appl. Cryst. 26 (1993) 343.
[8] (a) G.M. Sheldrick, SHELXL 96, University of Göttingen, Germany, 1996;
(b) G.M. Sheldrick, SHELXL 97. Program for Refinement of Crystal Structures, University of Göttingen, Germany, 1997.
[9] (a) I. Omae, Organotin Chemistry, Elsevier, Amsterdan, 1989;
(b) G. Wilkinson, F.G.A. Stone, E.W. Abel (Eds.), Comprehensive Organometallic Chemistry, vol. 3, Pergamon Press, Oxford, 1982, p. 1043.
[10] V.D. de Castro, G.M. de Lima, C.A.L. Filgueiras, M.T.P. Gambardella, N.L. Speziali, Main Group Met. Chem. 24 (2001) 761.
[11] S. Wang, R.J. Staples, J.P. Fackler Jr., Acta Crystallogr., Sect. C 50 (1994) 889.
[12] All the XRD data are related to JCPDS – ICDD – 1997.
[13] (a) R. Jones, P.F. Kelley, C.P. Warrens, D.J. Willians, J.D. Wollins, J. Chem. Soc., Chem. Commun. (1986) 711, J. Chem. Soc., Chem. Commun. (1988) 1569;
(b) O.L. Casagrande Jr., A.E. Gerbase, F.C. Stedile, F.O.V. da Cunha, L. Amaral, I.J.R. Baumvol, Polyhedron 16 (1997) 171.
[14] (a) T. Douglas, D.P.E. Dickson, S. Betteridge, J. Charnock, E.D. Garner, S. Mann, Science 269 (1995) 54;
(b) M. Sugitani, N. Kinomura, M. Koizumi, S. Kume, J. Solid State Chem. 26 (1978) 195.
[15] (a) I.R. Butler, W.R. Cullen, J. Trotter, Organometallics 4 (1985) 972;
(b) G.M. de Lima, C.A.L. Filgueiras, A. Abras, Hyperfine Interactions 83 (1994) 183.
[16] (a) T. Goto, H. Utzugi, A. Kashiwakura, J. Magn. Magn. Mat. 104–107 (1992) 2051;
(b) U. Gonser, S. Nasu, W. Kappes, J. Magn. Magn. Mat. 10 (1979) 244;
(c) J.G. Na, J. Mat. Sci. Lett. 19 (2000) 1171.

Available online at www.sciencedirect.com
SCIENCE DIRECT®
Polyhedron 23 (2004) 71–75
POLYHEDRON
www.elsevier.com/locate/poly

Reactivity behavior of (hydroxy)diorganotin(IV)methanesulfonates with ionic nucleophiles – synthesis and structural characterization of novel diorganostannate salts, $[R_2Sn(\mu\text{-}OH)(OSO_2Me)(ONO_2)]_2 2Bu_4N$

Ravi Shankar [a,*], Mukesh Kumar [a], Raj K. Chadha [b], Suraj P. Narula [c]

[a] Department of Chemistry, Indian Institute of Technology, Hauz Khas, New Delhi 110016, India
[b] The Scripps Research Institute, BCC-159, 10555N Torrey Pines Road, La Jolla, CA 92037, USA
[c] Department of Chemistry, Punjab University, Chandigarh 160014, India

Received 3 June 2003; accepted 8 September 2003

Abstract

The reaction of $R_2Sn(OH)OSO_2Me$ [R = *n*-Pr (**1a**), or *n*-Bu (**1b**)] with one equivalent of Bu_4NNO_3 in CH_2Cl_2 proceeds via nucleophilic addition of NO_3^- ion to the Lewis acidic tin center and results in the formation of novel diorganostannates, $[R_2Sn(\mu\text{-}OH)(OSO_2Me)(ONO_2)]_2 2Bu_4N$ [R = *n*-Pr (**2a**), *n*-Bu(**2b**)]. The molecular structure of **2b** comprises of hydroxy-bridged dimer with monodentate methanesulfonate and nitrate groups bonded to each tin atom. Analogous reactions of the tin precursor, **1b** with strong nucleophiles such as Bu_4NX ($X = F^-$, OAc^-) and RLi (R = *n*-Bu, Me) favor ionic metathesis pathway involving $Sn–OSO_2Me$ bond cleavage. This approach provides a simple and facile synthetic route for triorganotin oxides, $(R_2R'Sn)_2O$ ($R = R' = n$-Bu, $R = n$-Bu, $R' =$ Me).
© 2003 Published by Elsevier Ltd.

Keywords: Diorganostannate; Methanesulfonate; Ionic metathesis; Organotin oxide

1. Introduction

The property of diorganotin (IV) compounds, R_2SnX_2 (X = halogen) to act as Lewis acids has been frequently utilized to synthesize a large number of trihalodiorganostannates, $[R_2SnX_3]^-$ [1] as well as tetrahalodiorganostannates, $[R_2SnX_4]^{2-}$ [2]. Recently, Tudela et al. [3] have reported solvent dependence on the formation of these class of compounds. It has been shown that the reaction of Me_2SnBr_2 with Et_4NBr in $CHCl_3$/hexane mixture yields $[Me_2SnBr_4](Et_4N)_2$ while $[Me_2SnBr_3](Et_4N)$ is exclusively formed in water. Extensive studies have been reported on selective anion binding capability of "tailormade" organotin hosts with high nuclearity tin centers as Lewis acids [4]. This has led to the isolation of wide structural diversity of diorganostannate derivatives. In contrast, anionic tin derivatives bearing functional ligands other than halogen on the tin atom are much less known. The identity of 'ate' complexes, $[Bu_2SnI_2H]Li$ and $[Bu_2SnIHBr]MgBr$ generated in situ has been gleaned by ^{119}Sn NMR spectroscopy and their utility in regio/stereoselective reduction of various enals and aliphatic alkynes has been reported [5]. The diorganostannates bearing carboxylate ligands such as, $[R_2Sn(O_2C)_2C_5H_3N{\cdot}X]Et_4N$ ($X = Cl^-$, F^-) [6] and $[Me_2Sn(OAc)_3]Me_4N$ [7] have also been structurally characterized and examined for their antitumor activity.

In recent years, we have been interested in the development of new synthetic strategies for functional organotin derivatives and reported on the preparation

* Corresponding author. Tel.: +91-11-26596421/26591513; fax: +91-11-26862620/26581102.
E-mail addresses: shankar@netearth.iitd.ac.in, ravi1@dms.iitd.ernet.in (R. Shankar).

0277-5387/$ - see front matter © 2003 Published by Elsevier Ltd.
doi:10.1016/j.poly.2003.09.010

and structural characterization of (hydroxy)diorganotin (IV)methanesulfonates, $R_2Sn(OH)OSO_2Me$ (R = *n*-Pr, *n*-Bu, etc.) [8]. The reaction chemistry of these bifunctional tin compounds has attracted our attention. It has been demonstrated that the selective dehydration reaction involving Sn–OH group with carboxylic acids results in the isolation of diorganotin carboxylates [9], which are not accessible by classical route. Another interesting aspect concerns the reactivity of these tin precursors towards the ionic nucleophiles. In the present work, preliminary investigations on this aspect have been undertaken. While the reaction of **1a** or **1b** with Bu_4NNO_3 results in the isolation of novel diorganostannate derivatives, **2a** or **2b**, the use of strong nucleophiles such as Bu_4NX ($X = F^-$, OAc^-) and RLi (R = *n*-Bu, Me) favor ionic metathesis reaction involving $Sn–OSO_2Me$ bond cleavage. The results obtained from these studies are reported herein.

2. Results and discussion

The synthesis of $[R_2Sn(\mu\text{-}OH)(OSO_2Me)(ONO_2)]_2\,2Bu_4N$ [R = *n*-Pr (**2a**), *n*-Bu (**2b**)] is accessible from the reaction of (hydroxy)diorganotin methanesulfonates (**1a** or **1b**) with one equivalent of tetra-*n*-butylammonium nitrate (Eq. (1)). These compounds are moderately sensitive to moisture and are soluble in common organic solvents such as chloroform, dichloromethane, methanol, acetonitrile, etc.

$$2R_2Sn(OH)OSO_2Me + 2Bu_4NNO_3 \xrightarrow{RT/8\text{–}10\ h} [R_2Sn(\mu\text{-}OH)(OSO_2Me)(ONO_2)]_2 2Bu_4N$$
$$R = n\text{-Pr}\ (\mathbf{2a}),\ n\text{-Bu}\ (\mathbf{2b}) \qquad (1)$$

The single crystals of **2b** suitable for X-ray structure were obtained upon cooling solution of the compound in dichloromethane at 4 °C for several days. The compound crystallizes with two independent molecules in the unit cell of which only one is shown in Fig. 1. The relevant crystal data are given in Table 1, while selected bond distances and angles are given in Table 2. The anion in each molecule adopts a centrosymmetric hydroxy-bridged dimeric structure with highly distorted octahedral geometry around each tin atom. The SnO_4 coordination sphere formed by two bridging OH, a monodentate methanesulfonate and a nitrate group is planer (360° ± 1). Principle differences between the two molecules in the unit cell appear in the Sn–O (methanesulfonate and nitrate) bond distances and O–Sn–O/C–Sn–C angles. A comparison of these metrical parameters with those of the precursor [Sn–O (methanesulfonate) = 2.410(4) Å] [8] reveals significant elongation of Sn–O (methanesulfonate) bond distance in the stannate [Sn(1A)–O(2A) = 2.451(6)/Sn(1B)–O(2B) = 2.552(7) Å] and suggests appreciable ionic character. The angle C(5A)–Sn(1A)–C(1A) = 159.6(3)°/C(5B)–Sn(1B)–C(1B) = 153.3(4)° is much larger than observed in the tin precursor **1b** [C–Sn–C = 151.4(3)°]. Secondary interactions such as intramolecular hydrogen bonding [O(3A)···H–O(1A) = 2.694 Å, O(3B)···H–O(1B) = 2.780 Å] as well as intermolecular C–H···O

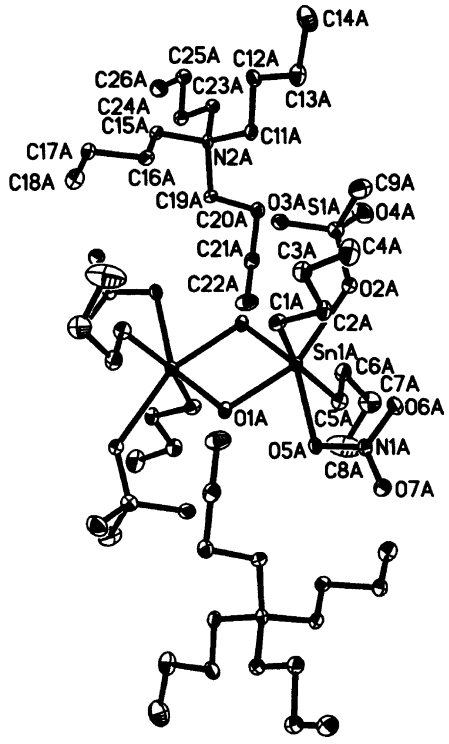

Fig. 1. ORTEP view of one independent molecule of **2b**, showing 30% probability ellipsoids. Hydrogen atoms have been omitted for clarity.

Table 1
Summary for crystallographic data for **2b**[a]

Empirical formula	$C_{25}H_{58}N_2O_7SSn$
Formula weight	648.48
T (°C)	173(2) K
λ (Å)	0.71073
Crystal system	triclinic
Space group	$P\bar{1}$ (no. 2, Ci^1)
a (Å)	11.9775(18)
b (Å)	13.610(2)
c (Å)	22.857(3)
α (°)	81.360(2)
β (°)	75.527(3)
γ (°)	67.153(2)
V (Å^3)	3318.8(9)
Z	4
ρ_{calcd} (Mg m^{-3})	1.298
μ (mm^{-1})	0.872
Final R indices	$R_1 = 0.0735$
$[I > 2\sigma(I)]$	$wR_2 = 0.1938$
R indices (all data)	$R_1 = 0.1250$, $wR_2 = 0.2241$

[a] $R_1 = (\sum |\|F_o\| - \|F_c\|| / \sum \|F_o\|)$, $wR_2 = [\sum w(F_o^2 - F_c^2)^2 / \sum [w(F_o^2)^2]]^{1/2}$, $s = [\sum w(F_o^2 - F_c^2)^2 / n - p]^{1/2}$.

Table 2
Selected bond lengths (Å) and angles (°) for the two independent molecules of **2b**[a]

Bond lengths			
Sn(1A)–C(1A)	2.139(8)	Sn(1B)–C(1B)	2.150(9)
Sn(1A)–O(1A)	2.130(5)	Sn(1B)–O(1B)	2.136(5)
Sn(1A)–C(5A)	2.117(8)	Sn(1B)–C(5B)	2.105(9)
Sn(1A)–O(5A)	2.418(5)	Sn(1B)–O(5B)	2.383(6)
Sn(1A)–O(2A)	2.451(6)	Sn(1B)–O(2B)	2.552(7)
Sn(1A)–O(1A)#1	2.118(5)	Sn(1B)–(1B)#2	2.104(6)
Bond angles			
C(5A)–Sn(1A)–C(1A)	159.6(3)	C(5B)–Sn(1B)–C(1B)	153.3(4)
O(1A)#1–Sn(1A)–O(1A)	71.8(2)	O(1B)#2–Sn(1B)–O(1B)	71.8(3)
O(1A)–Sn(1A)–O(5A)	74.95(18)	O(1B)#2–Sn(1B)–O(5B)	74.2(2)
O(5A)–Sn(1A)–O(2A)	130.95(18)	O(5B)–Sn(1B)–O(2B)	136.6(2)
O(1A)#1–Sn(1A)–O(2A)	82.4(2)	O(1B)–Sn(1B)–O(2B)	77.5(2)

[a] #1 $-x+2, -y+1, -z$, #2 $-x, -y+2, -z+1$.

interaction [C(11B)–H(11D)···O(7A) = 2.506 Å, C(15A)–H(15B)···O(7B) = 2.458 Å] have also been observed. Similar interactions have been previously reported in organotin carboxylates derived from ferrocenyl carboxylic acid [10].

The IR spectra (KBr) of **2a** and **2b** reveal two bands at 1485–1490 and 1384–1388 cm^{-1} due to $\nu_a NO_2$ and $\nu_s NO_2$, respectively, and suggest unidentate coordination mode of the nitrate group [11]. The strong absorptions due to νSO_3 mode appear at 1205–1210 and 1050–1060 cm^{-1}. The absence of additional splitting of these bands may be attributed to the monodentate character of methanesulfonate group [12]. ^1H NMR spectrum of each compound identifies Pr_2Sn/Bu_2Sn, Bu_4N and SMe groups in 1:1:1 integrated ratio and conforms to the structural composition. ^{119}Sn NMR spectra in $CDCl_3$ show four distinct signals spanning a broad chemical shift range and appear at δ −155, −159, −191, −234 (for **2a**) and −157, −159, −194, −234 (for **2b**). The ^{119}Sn NMR chemical shift values and spectral intensity of the signals between δ −155 and −195 show a close resemblance to those of parent tin precursors, **1a** and **1b**, while the appearance of a new upfield signal at δ −234 may be ascribed to the stannates (**2a** and **2b**). These results coupled with the lack of $^2J(^{119}Sn–O–^{117}Sn)$ coupling may suggest a fast equilibrium in solution between the precursor tin compound and the product. Such phenomena have been reported in a few studies related to the formation of stannate derivatives [13]. No change in the δ ^{119}Sn NMR values was observed upon addition of another equivalent amount of Bu_4NNO_3 to **1a** or **1b** suggesting that the tin precursor binds only one NO_3^- ion.

Nucleophilicity of the anionic reagents has been found to substantially alter the reaction chemistry of the tin precursors. This is evident by studying the reactions of **1b** with Bu_4NX (F, OAc) or RLi (*n*-Bu, Me). These reactions invariably proceed via an ionic metatheses pathway involving the cleavage of Sn–OSO_2Me bond. The products obtained in these reactions are shown as:

$$2Bu_2Sn(OH)OSO_2Me + 2Bu_4NX \rightarrow [Bu_2Sn(X)]_2O + 2Bu_4NOSO_2Me + H_2O \quad (X = F, OAc) \quad (2)$$

$$2Bu_2Sn(OH)OSO_2Me + 2RLi \rightarrow (Bu_2RSn)_2O + 2LiOSO_2Me + H_2O \quad (R = n\text{-}Bu, Me) \quad (3)$$

The identity of these products has been confirmed by comparison of IR, ^1H, and ^{119}Sn NMR spectral data with those of the known compounds previously reported in literature [14].

A final comment concerns the formation of the stannates, **2a** and **2b.** Complexation of the NO_3^- ion to the tin center of **1a** or **1b** can be rationalized by considering coordinative dissociation of bridging bidentate methanesulfonate in the tin precursors [8]. It appears that the nucleophilicity of NO_3^- and $MeSO_3^-$ ions being comparable [15] inhibits the ionic metathesis pathway. Nevertheless, the use of organometallic reagents such as RLi may also be of significant synthetic utility in the formation of mixed triorganotin oxides. This aspect is presently being investigated in our laboratory.

3. Experimental

All reactions were conducted in an inert atmosphere of nitrogen. Solvents were dried using standard techniques (dichloromethane and *n*-hexane over P_2O_5, diethyl ether over sodium benzophenone). Glassware was dried in an oven at 110–120 °C and further flame dried under vacuum prior to use. The precursors, (hydroxy)di-*n*-propyl/di-*n*-butyltin(IV)methanesulfonates [8] and di-*n*-propyltin oxide [16] were prepared using literature methods, while the reagents such as Bu_4NX (X = NO_3, F, OAc) and RLi (R = Bu, Me) were obtained commercially (Aldrich). ^1H, ^{13}C and ^{119}Sn NMR spectra

were recorded on Bruker DPX-300 at 300, 75.46 and 111.88 MHz, respectively. ^{1}H and ^{13}C chemical shifts are quoted with respect to the residual protons of the solvent, while ^{119}Sn NMR data are given using tetramethyltin as internal standard. The IR spectra were recorded on Nicolet protégé 460 E.S.P. spectrophotometer using KBr optics. Elemental analysis (C, H and N) was performed on a Perkin–Elmer model 2400CHN elemental analyzer. Tin was estimated gravimetrically [17].

3.1. Reactions of (hydroxy)diorganotin methanesulfonate with tetrabutylammonium nitrate

To a stirred suspension of (hydroxy)di-*n*-propyltin(IV)methanesulfonate (0.69 g, 2.16 mmol) or (hydroxy)di-*n*-butyltin(IV)methanesulfonate (0.75 g, 2.16 mmol) in dichloromethane (~50 ml) was added a solution of Bu_4NNO_3 (0.65 g, 2.16 mmol) in the same solvent. The clear reaction mixture was stirred for 12–15 h. at room temperature. The resulting solution was concentrated under vacuum and *n*-hexane was added. A white solid, thus obtained in each case was filtered and dried in vacuum.

3.1.1. [n-Pr$_2$Sn(μ-OH)(OSO$_2$Me)(ONO$_2$)]$_2$2Bu$_4$N (**2a**)

Yield: (85%), m.p. 80–83 °C. ^{1}H NMR ($CDCl_3$): δ 3.33 (t, 8H, NCH_2), 2.77 (s, 3H, SMe), 1.78 (m, 16H, $Sn(CH_2)_2 + NCH_2CH_2$), 1.50 (m, 8H, $N(CH_2)_2CH_2$), 1.01 (t, 18H, $Sn(CH_2)_2CH_3 + N(CH_2)_3CH_3$). $^{13}C\{^{1}H\}$ NMR ($CDCl_3$): 58.3 (NCH_2), 39.2 (SMe), 29.2 ($SnCH_2$), 18.1 ($SnCH_2CH_2$), 12.2 ($Sn(CH_2)_2CH_3 + N(CH_2)_3CH_3$), 23.5 ($NCH_2CH_2$), 19.3 $N(CH_2)_2CH_2$. ^{119}Sn NMR ($CDCl_3$): δ −155, −159, −191, −234. IR (KBr, cm^{-1}): 3420 (νOH), 1487, 1386 (νNO_2), 1209, 1054 (νSO_3), 784 (SME). *Anal.* Calc. for $C_{23}H_{54}N_2O_7SSn$: C, 44.37; H, 8.68; N, 4.50; Sn, 19.29. Found: C, 44.10; H, 8.75; N, 4.61; Sn, 19.91%.

3.1.2. [n-Bu$_2$Sn(μ-OH)(OSO$_2$Me)(ONO$_2$)]$_2$2Bu$_4$N (**2b**)

Yield: (90%), m.p. 72–75 °C. ^{1}H NMR ($CDCl_3$): δ 3.33 (t, 8H, NCH_2), 2.77 (s, 3H, SMe), 1.65 (m, 16H, $Sn(CH_2)_2 + NCH_2CH_2$), 1.45 (m, 12H, $N(CH_2)_2CH_2 + Sn(CH_2)_2CH_2$), 1.03 (t, 12H, $N(CH_2)_3CH_3$), 0.93 (t, 6H, $Sn(CH_2)_3CH_3$). $^{13}C\{^{1}H\}$ NMR ($CDCl_3$): δ 58.3 (NCH_2), 39.2 (SMe), 26.5 ($SnCH_2$), 23.5 ($SnCH_2CH_2 + NCH_2CH_2$), 18.1 ($Sn(CH_2)_2CH_2$), 12.2 ($Sn(CH_2)_2CH_3 + N(CH_2)_3CH_3$, 23.5 ($NCH_2CH_2$), 19.3 ($Sn(CH_2)_2CH_2 + N(CH_2)_2CH_2$), 13.2 ($Sn(CH_2)_3CH_3 + N(CH_2)_3CH_3$). ^{119}Sn NMR ($CDCl_3$): δ −157, −159, −194, −234. IR (KBr, cm^{-1}): 3400 (νOH), 1487, 1384 (νNO_2), 1210, 1058 (νSO_3), 784 (SME). *Anal.* Calc. for $C_{25}H_{58}N_2O_7SSn$: C, 46.15; H, 8.92; N, 4.30; Sn, 18.46. Found: C, 46.91; H, 8.33; N, 4.21; Sn, 18.01%.

3.2. Reactions of (hydroxy)di-n-butyltin methanesulfonate with Bu$_4$NX (X = F$^-$, OAc$^-$)

To a stirred suspension of (hydroxy)di-*n*-butyltin methanesulfonate, **1b** (0.62 g, 1.79 mmol) in dichloromethane was added Bu_4NF (1.79 ml (1.0 M/THF), 1.79 mmol). The resulting clear solution was stirred for 8–10 h at room temperature. Thereafter the reaction mixture was concentrated under vacuum and diethyl ether was added to precipitate a white solid identified as tetra-*n*-butyl ammonium methanesulfonate, Bu_4NOSO_2Me. Solvent was evaporated from the ether solution to afford $[Bu_2Sn(F)]_2O$ as a white solid. The reaction of **1b** (0.62 g, 1.79 mmol) with Bu_4NOAc (0.53 g, 1.79 mmol) was performed by following a similar procedure as above. *n*-Hexane was added to precipitate the salt Bu_4NOSO_2Me which was filtered and dried under vacuum. The compound $[Bu_2Sn(OAc)]_2O$ was isolated from the concentrated hexane solution as a white solid.

3.2.1. Bu$_4$NOSO$_2$Me

Yield: (45%), ^{1}H NMR ($CDCl_3$): δ 3.31 (t, 8H, NCH_2), 2.75 (s, 3H, SMe), 1.66 (m, 8H, NCH_2CH_2), 1.44 (m, 8H, $N(CH_2)_2CH_2$) 1.01 (t, 12H, CH_3). IR (KBr, cm^{-1}): 2960, 2932 (νCH), 1240, 1193, 1058 (νSO_3), 784 (SME). *Anal.* Calc. for $C_{17}H_{39}NO_3S$: C, 60.53; H, 11.57; N, 4.15; Found: C, 61.01; H, 11.43; N, 4.21%.

3.2.2. [Bu$_2$Sn(F)]$_2$O

Yield: (41%), m.p. 137–140 °C (Lit. 140 °C). ^{1}H NMR ($CDCl_3$): δ 0.92 (t, 6H, CH_3), 1.20 (m, 8H, $(CH_2)_2CH_3$), 1.54 (m, 4H, $SnCH_2$). ^{119}Sn NMR ($CDCl_3$): δ −160. IR (KBr, cm^{-1}): 2959, 2928, 2857 (νCH), 660 (νSn–O–Sn). *Anal.* Calc. for $C_{16}H_{36}OF_2Sn_2$: C, 36.78; H, 6.89. Found: C, 36.60; H, 6.75%.

3.2.3. [Bu$_2$Sn(OAc)]$_2$O

Yield: (51%), m.p. 52–53 °C (Lit. 54 °C). ^{1}H NMR ($CDCl_3$): δ 1.89 (s, 3H, OAc), 0.86 (t, 6H, CH_3), 1.30 (m, 8H, $(CH_2)_2CH_3$), 1.57 (m, 4H, $SnCH_2$). ^{119}Sn NMR ($CDCl_3$): δ −215, −226. IR (KBr, cm^{-1}): 2961, 2926, 2870 (νCH), 1636, 1559 ($\nu_a CO_2$), 1372 ($\nu_s CO_2$), 639 (νSn–O–Sn). *Anal.* Calc. for $C_{20}H_{42}O_5Sn_2$: C, 39.86; H, 6.97. Found: C, 39.60; H, 6.74%.

3.3. Reactions of (hydroxy)di-n-butyltin methanesulfonate (**1b**) with RLi (R = n-Bu, Ph)

To a stirred solution of **1b** (0.75 g, 2.16 mmol) in diethyl ether (~75 ml) was added *n*-BuLi (3.45 ml, 1.6 M/hexane, 2.16 mmol) or MeLi (2.16 ml, 1.0 M/THF, 2.16 mmol) at 25 °C. The reaction mixture was stirred for 12 h and subsequently hydrolyzed by 25 ml of water. The organic layer was extracted in each case and kept on anhydrous sodium sulfate. Evaporation of solvent ether

gave $(Bu_3Sn)_2O$ or $(Bu_2Me)_2SnO$ as colorless viscous liquids.

3.3.1. $(Bu_3Sn)_2O$

Yield: (55%): b.p. 205–210 °C/10 mm (Lit. 210–214 °C/10 mm). ^{1}H NMR ($CDCl_3$): δ 0.90 (t, 6H, CH_3), 1.37 (m, 8H, $(CH_2)_2CH_3$), 1.65 (m, 4H, $SnCH_2$). ^{119}Sn NMR ($CDCl_3$): δ 85.6. IR (KBr, cm^{-1}): 2961, 2926, 2870 (νCH), 689 (νSn–O–Sn). *Anal.* Calc. for $C_{24}H_{54}OSn_2$: C, 48.16; H, 9.03. Found: C, 47.95; H, 9.21%.

3.3.2. $(Bu_2MeSn)_2O$

Yield: (50%): b.p. 180–185 °C/10 mm. ^{1}H NMR ($CDCl_3$): δ 0.91 (t, 6H, CH_3), 1.40 (m, 8H, $(CH_2)_2CH_3$), 1.71 (m, 4H, $SnCH_2$), 1.85 (s, 3H, $SnCH_3$). ^{119}Sn NMR ($CDCl_3$): δ 95.0. IR (KBr, cm^{-1}): 2963, 2927, 289 (CH), 680 (νSn–O–Sn). *Anal.* Calc. for $C_{18}H_{42}OSn_2$: C, 42.02; H, 8.17. Found: C, 42.11; H, 8.10%.

3.4. X-ray crystallography

A colorless, block shaped crystal was mounted along with the largest dimension and data were collected on a Bruker SMART APEX diffractometer equipped with a molybdenum sealed tube and a highly oriented graphite monochromator. There were no systematic absences in the data, therefore space group $P\bar{1}$ was assumed and later confirmed by successful refinement of the structure. The structure was solved by direct methods using SHELXTL-PC [18,19]. All non-hydrogen atoms were refined anisotropically by the full matrix least-square method. The function was minimized to $\sum w(\|F_o\| - \|F_c\|)^2$. Hydrogen atoms were included in the ideal position with fixed isotropic U values equal to 1.2 times that of the atom they are attached to. A weighting scheme of the form $w = 1/[\sigma^2(F_o^2) + (aP)^2 + bP]$ with $a = 0.1185$ and $b = 0.00$ was used. (P is defined as $\max(F_o^2, 0) + 2F_c^2/3$.) An extinction correction was also applied. The refinement converged to the R indices given in Table 1. All calculations were done on an IBM compatible PC using Windows-NT operating system.

4. Supplementary data

Crystallographic data for the structural analysis have been deposited with the Cambridge Crystallographic Data Center, CCDC No. 204117 for compound **2b**. Copies of this information may be obtained free of charge from The Director, CCDC, 12 Union Road, Cambridge CB2 1EC, UK (Fax: +44-1223-336033; E-mail: deposit@ccdc.cam.ac.uk or www: http://www.ccdc.cam.ac.uk).

Acknowledgements

M.K. is grateful to CSIR New Delhi for senior research fellowship.

References

[1] E.M. Garcia, A.G. Sanchez, A. Castineiras, J.S. Casas, J. Sordo, J. Organomet. Chem. 469 (1994) 41.
[2] J. Ouyang, Y. Zu, L.E. Khoo, J. Organomet. Chem. 561 (1998) 143.
[3] D. Tudela, M. Diaz, D.A. Alvaro, J. Ignacic, L. Seijo, V.K. Belsky, Organometallics 20 (2001) 654 (and references cited therein).
[4] (a) P.D. Beer, P.A. Gale, Angew. Chem. Int. Ed. 40 (2001) 486; (b) M. Shulte, M. Schurmann, K. Jurkschat, Chem. Eur. J. 7 (2001) 347; (c) R. Altmann, O. Gausset, D. Horn, K. Jurkschat, M. Schurmann, M. Fontani, P. Zanello, Organometallics 19 (2000) 430; (d) F.P. Schmidtchen, M. Berger, Chem. Rev. 97 (1997) 1609.
[5] (a) T. Suwa, I. Shibata, A. Baba, Organometallics 18 (1999) 3965; (b) I. Shibata, T. Suwa, A. Baba, J. Am. Chem. Soc. 123 (2001) 4101.
[6] (a) R. Willem, M. Biesemans, M. Boualam, A. Delmotte, A. EI Khloufi, M. Gielen, Appl. Organomet. Chem. 7 (1993) 311; (b) S.W. Ng, V.G. Kumar Das, J. Holecek, A. Lycka, M. Gielen, M.G.B. Drew, Appl. Organomet. Chem. (1997) 1139.
[7] T.P. Lockhart, J.C. Calabrese, F. Davidson, Organometallics 6 (1987) 2479.
[8] S.P. Narula, S. Kaur, R. Shankar, S. Verma, P. Venugopalan, S.K. Sharma, R.K. Chadha, Inorg. Chem. 38 (1999) 4777.
[9] R. Shankar, M. Kumar, S.P. Narula, R.K. Chadha, J. Organomet. Chem. 671 (2003) 35.
[10] V. Chandrasekhar, S. Nagendran, S. Bansal, A.W. Cordes, A. Vij, Organometallics 21 (2002) 3297.
[11] K. Nakamoto, Infrared and Raman Spectra of Inorganic and Coordination Compounds, 5th ed., Wiley, New York, 1997, p. 87.
[12] (a) P.A. Yeats, J.R. Sams, F. Aubke, Inorg. Chem. 11 (1972) 2634; (b) E. Hochberg, E.H. Abott, Inorg. Chem. 117 (1978) 506.
[13] D. Dakternieks, H. Zhu, Organometallics 11 (1992) 3820.
[14] (a) A.G. Davies, L. Smith, P.J. Smith, W. Mc Farlane, J. Organomet. Chem. 29 (1971) 245; (b) Y. Maeda, R. Okawara, J. Organomet. Chem. 10 (1967) 247; (c) D.C. Gross, Inorg. Chem. 28 (1989) 2355; (d) S.J. Blunden, R. Hill, J. Organomet. Chem. 333 (1987) 317; (e) Wm.J. Considine, J.J. Ventura, B.G. Kushlefsky, A. Ross, J. Organomet. Chem.1 (1964) 299.
[15] F.A. Carey, R.J. Sundberg, Advanced Organic Chemistry (Part A), 4th ed., Kluwer Academic/Plenum, New York, 2000, p. 291.
[16] R.K. Ingham, S.D. Rosenberg, H. Gilman, Chem. Rev. 60 (1960) 459.
[17] A.I. Vogel, Textbook of Quantitative Chemical Analysis, 5th ed., Longman, London, 1989, p. 474.
[18] SMART (Ver 5.6). Software for data collection on CCD Detector System. Bruker X-ray Analytical Instruments, Madison, WI, 1995.
[19] SHELXTL-PC. (Ver 5.1) G.M. Sheldrick, Bruker X-ray Analytical Instruments, Inc. Madison, WI, 1990.

Available online at www.sciencedirect.com
SCIENCE DIRECT®
Polyhedron 23 (2004) 77–82
POLYHEDRON
www.elsevier.com/locate/poly

Effect of free and chelating phosphine coordination environments on the NiS_2P_2 chromophore: synthesis, NMR and other spectral studies. Crystal and molecular structures of (*N*,*N*-dipropyldithiocarbamato)di(triphenylphosphine)nickel(II) perchlorate and (*N*,*N*-dipropyldithiocarbamato)1,2-bis((diphenylphosphino)ethane)nickel(II) tetraphenylborate

B. Arul Prakasam [a], Kuppukkannu Ramalingam [a,*], M. Saravanan [a], Gabriele Bocelli [b], Andrea Cantoni [b]

[a] *Department of Chemistry, Annamalai University, Annamalainagar 608 002, India*
[b] *IMEM, CNR, Parma, Italy*

Received 26 July 2003; accepted 9 September 2003

Abstract

Planar $[Ni(dnpdtc)(PPh_3)_2]$ $ClO_4 \cdot PPh_3$ (**1**) and $[Ni(dnpdtc)(dppe)]BPh_4 \cdot H_2O$ (**2**) (dnpdtc = *N*,*N*-dipropyldithiocarbamate, dppe = 1,2-bis(diphenylphosphino)ethane) complexes were prepared and characterized by elemental analysis, electronic, IR and NMR spectra and their structures were determined by single crystal X-ray crystallography. Both the complexes were diamagnetic. IR spectra of the two compounds show isobidentate coordination of the dithiocarbamate moiety. The important stretching mode characteristic of the thioureide bond occurs at 1536 and 1526 cm^{-1} for **1** and **2**, respectively. The BVS data support the highly covalent nature of the Ni–S interaction. NMR spectra of the complexes show very large (~20 ppm) ^{31}P chemical shifts in both compounds. The most important $N^{13}CS_2$ chemical shifts appear at 199.17 and 201.88 ppm for **1** and **2**, respectively. Structural implications are very large for **2** compared to **1** when free phosphines are replaced by chelating dppe with the P–Ni–P angle shrinking to approximately 12°.
© 2003 Elsevier Ltd. All rights reserved.

Keywords: Nickel; Dithiocarbamate; PPh_3; Dppe; X-ray crystal structure; NMR

1. Introduction

Divalent nickel complexes of dithiocarbamates with different substituents contain planar diamagnetic MS_4 chromophores. Ni(II)dithiocarbamates are borderline acceptors and they prefer to react with soft Lewis bases such as phosphines and hard bases such as nitrogenous ligands [1,2]. The symbiotically induced softness and the electronic effects of the substitutents on the dithiocarbamate ligands were found to be important in deciding the reactivity [3,4]. On reaction with phosphines, they form complexes with a NiS_2P_2 chromophore which are again planar and diamagnetic in nature [5–7]. Synthetic and structural studies on $[Ni(dtc)Cl(PPh_3)]$ and $[Ni(dtc)(PPh_3)_2]ClO_4$ complexes, where dtc = $S_2CN(C_2H_5)_2$, $S_2CNH(C_2H_4OH)$, $S_2CN(C_2H_4OH)_2$, $S_2CN(C_4H_8O)$, $S_2CN(C_5H_{10})$ have been reported from our laboratory [8]. The effect of alkyl substitutents in the metal dithiocarbamates have been investigated earlier [9]. In order to understand the influence of free and chelating phosphines on the NiS_2P_2 chromophore and on the thioureide C–N bond, in this paper, we report the synthesis, spectral and structural characterization of two new complexes, $[Ni(dnpdtc)(PPh_3)_2]ClO_4 \cdot PPh_3$ (**1**), and $[Ni(dnpdtc)(dppe)]BPh_4$ (**2**) where, dnpdtc = *N*,*N*-dipropyldithiocarbamate.

* Corresponding author. Tel.: +91-413-2202-834; fax: +91-414-422-265.
E-mail addresses: krauchem@yahoo.com, krchem@rediffmail.com (K. Ramalingam).

0277-5387/$ - see front matter © 2003 Elsevier Ltd. All rights reserved.
doi:10.1016/j.poly.2003.09.013

2. Experimental

All the reagents and solvents employed were commercially available analytical grade materials and were used as supplied, without further purification. IR spectra were recorded on an ABB Bomem MB 104 spectrophotometer (range 4000–400 cm^{-1}) as KBr pellets. The UV–vis spectra were recorded in CH_2Cl_2 on a U-2001 spectrophotometer. NMR spectra were recorded on a Bruker AMX 400 spectrometer at room temperature, using $CDCl_3$ as solvent.

2.1. Preparation of complexes

2.1.1. Bis(triphenylphosphine)(N,N-dipropyldithiocarbamato)nickel(II) perchlorate

*2.1.1.1. [Ni(dnpdtc)(PPh$_3$)$_2$]ClO$_4$ (**1**).* A mixture of $Ni(dnpdtc)_2$ (210 mg, 0.5 mmo1), PPh_3(520 mg, 2 mmol), $NiCl_2 \cdot 6H_2O$ (120 mg, 0.5 mmol) and NH_4ClO_4 (115 mg, 1 mmol) was refluxed for about 2 h in methanol–dichloromethane solvent mixture (50:50, 50 cm^3), and was then concentrated to ca. 25 cm^3. The purple-red solution obtained was filtered and was left for evaporation. The fine single crystals suitable for X-ray structural analysis were obtained by repeated recrystallization from the same solvent mixture (yield 60%, 520 mg, dec. 178 °C). *Anal.* Calc. for $C_{61}H_{59}ClNNiO_4P_3S_2$: C, 65.34; H, 5.30; N, 1.25. Found: C, 65.12; H, 5.14; N, 1.17%.

2.1.2. 1,2-Bis((diphenylphosphino)ethane)(N,N-dipropyldithiocarbamato)nickel(II) tetraphenylborate

*2.1.2.1. [Ni(dnpdtc)(dppe)]BPh$_4$ · H$_2$O (**2**).* A mixture of $Ni(dnpdtc)_2$ (420 mg, 1 mmol), dppe (790 mg, 2 mmol), $NiCl_2 \cdot 6H_2O$ (240 mg, 1 mmol) and $NaBPh_4$ (680 mg, 2 mmol) was refluxed for about 3 h in methanol–dichloromethane solvent mixture (50:50, 50 cm^3). The solution was then concentrated to ca. 25 cm^3. The purple-red solution obtained was filtered and was kept for evaporation. After 2 days a purple-red coloured solid separated out and was recrystallized from methanol–dichloromethane mixture. Single crystals suitable for X-ray structural analysis were obtained by repeated recrystallization from the same solvent mixture (yield 65%, 1.2 g, dec. 182 °C). *Anal.* Calc. for $C_{57}H_{58}BNNiOP_2S_2$: C, 70.67; H, 6.03; N, 1.44. Found: C, 70.12; H, 5.97; N, 1.32%.

2.2. X-ray crystallography

Details of the crystal data, data collection and refinement parameters for **1** and **2** are summarized in Table 1. Intensity data were collected at ambient temperature (295 K) on Philips PW 100 (for **1**) and SMART

Table 1
Crystal data, data collection and refinement parameters for [Ni(dnpdtc)(PPh$_3$)$_2$]ClO$_4$ and [Ni(dnpdtc)(dppe)]BPh$_4$

Compound	[Ni(dnpdtc)(PPh$_3$)$_2$]ClO$_4$ · PPh$_3$ (**1**)	[Ni(dnpdtc)(dppe)]BPh$_4$ · H$_2$O (**2**)
Empirical formula	$C_{61}H_{59}ClNNi_{O4}P_3S_2$	$C_{57}H_{58}BNNiOP_2S_2$
Formula weight	1121.3	968.6
Colour	purple-red	purple-red
Habit	needle	column, irregular
Crystal dimensions (mm)	$0.20 \times 0.29 \times 0.36$	$0.17 \times 0.24 \times 0.29$
Crystal system	triclinic	triclinic
Space group	$P\bar{1}$	$P\bar{1}$
a (Å)	13.787 (2)	9.460 (2)
b (Å)	17.625 (2)	14.526 (2)
c (Å)	12.350 (3)	21.083 (2)
α (°)	99.88 (3)	108.360 (2)
β (°)	99.09 (3)	101.370 (3)
γ (°)	74.57 (2)	90.400 (3)
U (Å^3)	2829.9 (9)	2688.3 (7)
Z	2	2
D_c (g cm^{-3})	1.316	1.197
μ cm^{-1} (L)	5.96	5.36
$F(000)$	1172	1020
λ (Å)	Mo Kα (0.71069)	Mo Kα (0.71069)
θ range (°)	3.03–30.02	1.04–30.47
Scan type	ω-2θ	ω-2θ
Index ranges	$-19 \leqslant h \leqslant 19$, $-24 \leqslant k \leqslant 24$, $0 \leqslant l \leqslant 15$	$-12 \leqslant h \leqslant 13$, $-20 \leqslant k \leqslant 14$, $-29 \leqslant l \leqslant 28$
Reflections collected	16 150	12 357
Observed reflections $F_o > 4\sigma(F_o)$	6791	7900
Weighting scheme	$W = 1/[\sigma^2(F_o^2) + (0.0447P)^2 + 0.00P]$, where $P = (F_o^2 + 2F_c^2)/3$	$W = 1/[\sigma^2/(F_o^2) + (0.0968P)^2 + 0.00P]$, where $P = (F_o^2 + 2F_c^2)/3$
Number of parameters refined	894	836
Final R, R_w (observed, data)	0.0414, 0.0890	0.0510, 0.1409
GOOF	0.816	0.904

Table 2
Bond distances (Å) and angles (°) for $[Ni(dnpdtc)(PPh_3)_2]ClO_4$ and $[Ni(dnpdtc)(dppe)]BPh_4$

$[Ni(dnpdtc)(PPh_3)_2]ClO_4$ **(1)**		$[Ni(dnpdtc)(dppe)]BPh_4 \cdot H_2O$ **(2)**	
Bond distances			
Ni(1)–P(31)	2.1919(10)	Ni(1)–P(12)	2.1607(9)
Ni(1)–S(3)	2.2094(9)	Ni(1)–P(15)	2.1715(7)
Ni(1)–S(2)	2.2120(10)	Ni(1)–S(2)	2.1931(8)
Ni(1)–P(12)	2.2253(10)	Ni(1)–S(3)	2.2108(9)
S(2)–C(4)	1.722(3)	S(2)–C(4)	1.718(3)
S(3)–C(4)	1.727(3)	S(3)–C(4)	1.715(3)
C(4)–N(5)	1.304(3)	C(4)–N(5)	1.314(4)
N(5)–C(9)	1.464(4)	N(5)–C(6)	1.477(4)
N(5)–C(6)	1.478(3)	N(5)–C(9)	1.492(5)
Bond angles			
P(31)–Ni(1)–S(3)	93.56(4)	P(12)–Ni(1)–P(15)	86.50(3)
P(31)–Ni(1)–S(2)	171.99(3)	P(12)–Ni(1)–S(2)	94.72(3)
S(3)–Ni(1)–S(2)	78.61(4)	P(15)–Ni(1)–S(2)	167.70(4)
P(31)–Ni(1)–P(12)	98.41(4)	P(12)–Ni(1)–S(3)	172.06(3)
S(3)–Ni(1)–P(12)	167.99(3)	P(15)–Ni(1)–S(3)	100.32(3)
S(2)–Ni(1)–P(12)	89.45(4)	S(2)–Ni(1)–S(3)	79.49(3)
C(4)–S(2)–Ni(1)	85.65(9)	C(4)–S(2)–Ni(1)	85.25(10)
C(4)–S(3)–Ni(1)	85.60(9)	C(4)–S(3)–Ni(1)	84.74(10)
N(5)–C(4)–S(2)	124.8(2)	N(5)–C(4)–S(3)	125.3(2)
N(5)–C(4)–S(3)	126.6(2)	N(5)–C(4)–S(2)	124.4(2)
S(2)–C(4)–S(3)	108.60(14)	S(3)–C(4)–S(2)	110.21(16)
C(4)–N(5)–C(9)	120.7(2)	C(4)–N(5)–C(6)	122.7(3)
C(4)–N(5)–C(6)	121.9(3)	C(4)–N(5)–C(9)	120.9(3)
C(9)–N(5)–C(6)	117.3(2)	C(6)–N(5)–C(9)	116.1(3)
N(5)–C(6)–C(7)	111.7(3)	N(5)–C(6)–C(7)	111.8(3)

AXS (for **2**) diffractometers using graphite monochromated Mo Kα radiation ($\lambda = 0.71069$ Å). Lorentz and polarization corrections were applied. The structures were solved by direct methods using SHELXS-97 [10] and were refined by SHELXL-97 [11]. All the non-hydrogen atoms were refined anisotropically and all the hydrogen atoms were refined isotropically. Selected bond lengths and bond angles are given in Table 2.

3. Results and discussion

3.1. IR spectral studies

The IR spectrum of **1** shows the thioureide ν_{C-N} band at 1536 cm^{-1} and that of compound **2** at 1526 cm^{-1}. The mesomeric shift of electrons from the dithiocarbamate moiety towards the metal centre increases the contribution of the polar thioureide form in both the cases. This is reflected in the shift in ν_{C-N} values to higher wave numbers compared with that observed in the parent complex at 1508 cm^{-1}. The ν_{C-S} band appears at 1091 cm^{-1} for **1** and 999 cm^{-1} for **2** without any splitting, supporting the bidentate coordination of the dithiocarbamate moiety [12].

3.2. NMR spectral studies

NMR spectra were recorded at room temperature using TMS as an internal reference. For all the compounds $CDCl_3$ was used as solvent. The ^{13}C NMR spectra were recorded in the proton decoupled mode. The ^{1}H, ^{13}C and ^{31}P NMR chemical shift values are given in Table 3 with splitting patterns.

Table 3
NMR spectral data (chemical shift values in ppm)

Compound	NMR	PPh_x	BPh_4	CH_3	β-CH_2	α-CH_2	–PCH_2CH_2P–	$S_2^{13}CN$
1	^{1}H	7.20–7.60(m)		0.81(t)	1.61(m)	3.50(t)		
	^{13}C	128–137		11.06	20.70	51.13		199.17
	^{31}P	31.0						
2	^{1}H	7.10–7.60(m)	6.7–6.9	0.88(t)	1.62(m)	3.49(t)	1.91(t)	
	^{13}C	121–136	163–165	11.12	20.71	51.27	25.80	201.88
	^{31}P						60.80	

Where $x = 3$ for compound **1** and 2 for compound **2**.

3.2.1. ^{1}H NMR

For compound **1**, the methyl group protons resonate at 0.81 ppm as a triplet. The methylene protons were observed at 1.61 and 3.50 ppm. Of these two signals, the triplet at 3.50 ppm was assigned to α-CH_2 protons and the multiplet at 1.61 ppm was assigned to β-CH_2 protons. A multiplet in the region of 7.20–7.60 ppm was due to aromatic protons. For compound **2**, apart from the propyl group signals (the splitting pattern was the same as observed for compound **1**), a triplet in the upfield region of 1.91 ppm was assigned to methylene protons present in the chelating phosphine. In the downfield region, two sets of signals were obtained for aromatic protons of PPh_3 and BPh_4.

3.2.2. ^{13}C NMR

The chemical shifts of thioureide carbon (N–$^{13}CS_2$) were observed at 199.17 and 201.88 ppm for complexes **1** and **2**, respectively. The slight upfield shift from the normal chemical shift values of $Ni(dtc)_2$ complexes (206–210 ppm) [13] is supported by the higher ν_{C-N} values observed for complexes **1** and **2** in the present study. This was due to the mesomeric shift of electron density from the dithiocarbamate moiety towards the metal centre. This supports the bidentate coordination of the dithiocarbamate and the strong back bonding in both the compounds. For compound **2**, the low intensity signals in the region of 163–165 ppm were due to BPh_4 aromatic carbons.

3.2.3. ^{31}P NMR

^{31}P NMR for compound **1** shows a signal at 31 ppm and is assigned to coordinated phosphorus. The free PPh_3 phosphorus resonates at the more upfield region of −5.8 ppm. For compound **2**, the signal at 60.8 ppm is assigned to the phosphorus of the chelating phosphine [14]. The very high deshielding for the coordinated phosphorus in both the cases compared with the free phosphines indicates the drift of electron density from the phosphorus towards the metal centre. The shift is phenomenal with the free dppe chemical shift being observed at 40 ppm [15].

3.3. BVS calculations

For the two complexes, BVS values were calculated by two procedures [16,17]. The values are 3.0646 (B/OK), 2.9338 (OK/B); 3.2629 (B/OK), 3.1602 (OK/B) for the two complexes **1** and **2**, respectively. In both the complexes, the values are higher than the expected formal oxidation state of +2. The higher value observed in the present set of compounds supports the fact that the Ni–S, Ni–P bonds are more covalent and the back bonding effects are very highly pronounced [18].

3.4. Structural analysis

The ORTEP diagram of **1** is shown in Fig. 1. Two units of $[Ni(dnpdtc)(PPh_3)_2]ClO_4 \cdot PPh_3$ are present in the unit cell. It is interesting to note that a free triphenylphosphine molecule is also present along with the complex in the unit cell. The NiS_2P_2 chromophore is not of perfect square planar geometry because of the small bite angle associated with the dithiocarbamate moiety [78.61(4)°]. The Ni–P distances [2.1919(10) and 2.2253(10) Å] show asymmetry, as reported earlier for similar compounds [8]. The planarity of the molecule is in keeping with the observed diamagnetism of the complex. The asymmetry in the Ni–P distances and the observed large P–Ni–P bond angle is due to the bulkiness of the PPh_3 group. The C–S bond lengths are 1.722(3) and 1.727(4) Å, which are shorter than the single bond length of 1.81 Å and higher than the C=S distance of 1.69 Å. The observed intermediate value between the single and double bond distances indicates a partial double bond character. The short thioureide C–N distance, 1.304(3) Å, indicates that the π electron density is delocalized over the S_2CN moiety and that this bond has a strong double bond character. This is also confirmed by the fact that the two S–C–N angles are much greater than that of the S–C–S (108.60(14)°) angle.

There is a shortening of the Ni–P distances for the *N*,*N*-dipropyl analogue [2.1919(10) and 2.2253(10) Å] compared to its *N*,*N*-diisopropyl analogue [2.215(2) and 2.224(3) Å] [19]. Also, the S–Ni–S angle decreases in the *N*,*N*-diisopropyl compound [77.7(1) Å] compared to that in the *N*,*N*-dipropyldithiocarbamate analogue [78.61(4) Å] indicating a reduced steric requirement of the isopropyl compound. In $[Ni(dnpdtc)(PPh_3)_2]ClO_4$

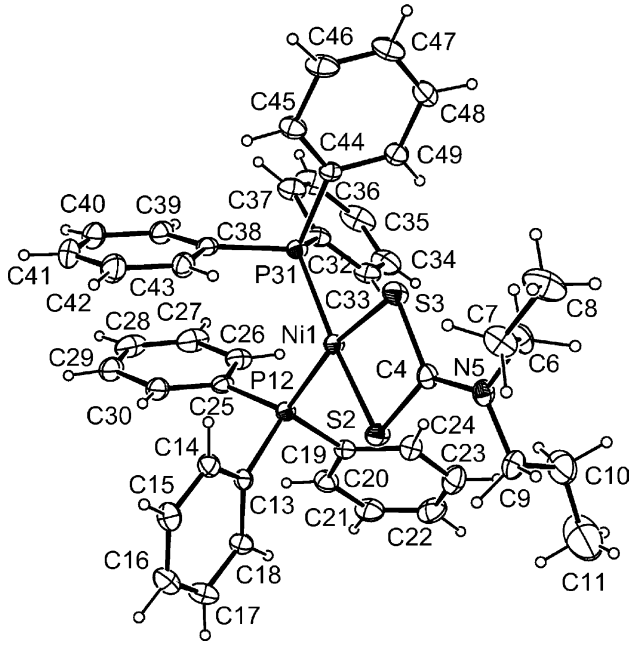

Fig. 1. ORTEP diagram for compound **1** (PPh_3 is omitted for clarity).

(**1**) the thioureide C–N distance is 1.304(3) Å and in $[Ni(dipdtc)(PPh_3)_2]ClO_4$ it is 1.321(11) Å, the observed reduction of the thioureide distance in **1** shows the effective π back bonding of the phosphines in **1**. The Cl–O distances vary from 1.340 to 1.421 Å and the O–Cl–O angles vary from 107.8° to 112.5° in **1** indicating the distortion from tetrahedral geometry. The phenyl rings show normal bond parameters. The P–C bond distances are also normal with an average value of 1.8286 Å. The C–P–C angles deviate appreciably from the ideal tetrahedral angle of 109.5° and the resultant crowding of the phenyl rings causes the P–C–C angles to be asymmetric.

$[Ni(dnpdtc)(dppe)]BPh_4$ (**2**) is monomeric with two molecules per unit cell. The ORTEP diagram of the molecule is shown in Fig. 2. The molecule is approximately planar, in keeping with the observed diamagnetism. The Ni–S [2.1931(8) and 2.2108(9) Å] and C–S [1.718(3) and 1.715(3) Å] bonds are symmetric, showing that the negative charge on the dithiocarbamate ligand is equally distributed all over the two donor atoms as found in **1**. One molecule of water is found in the unit cell. The short thioureide C–N distance of 1.314(4) Å indicates that the electron density is delocalized over the S_2CN moiety and this bond has partial double bond character. The bond lengths and bond angles of $[Ni(dipdtc)(dppe)]^+$ reported from our laboratory [19] show a similarity in thioureide C–N distance [(1.314(4) Å] in **2**, and 1.316(8) Å in $[Ni(dipdtc)(dppe)]^+$). The *N*,*N*-dipropyl complexes (**1**) and (**2**) exhibit a relatively larger steric influence compared to the diisopropyl analogue. In **2**, the P–Ni–P angle is 86.50(3)° which is smaller than that in the diisopropyl analogue: 87.3(1)°.

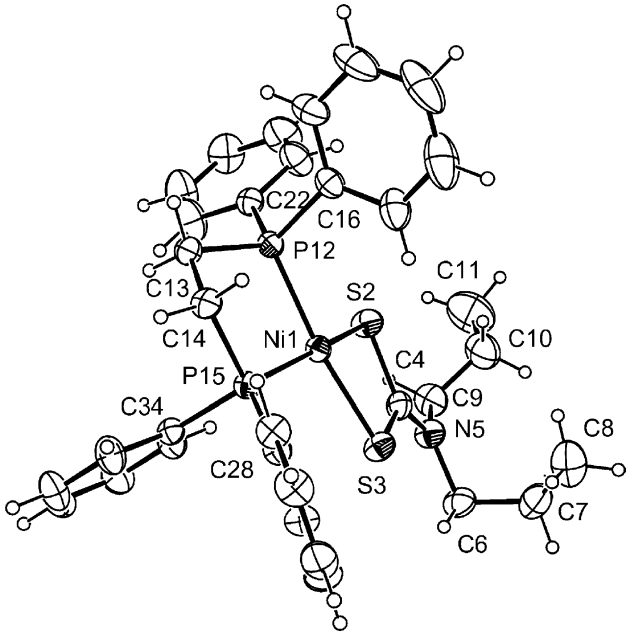

Fig. 2. ORTEP diagram for compound **2** (BPh_4 and H_2O are omitted for clarity).

Comparison of **1** and **2** shows that S–Ni–S bite angles [78.61(4)° versus 79.49(3)°] and the Ni–S–C angles [85.625° versus 84.995°] are very similar. On the other hand, a significant difference is observed in the P–Ni–P angles that are subtended by dppe, a bidentate ligand, being about 12° smaller than that found in **1**, where the PPh_3 groups exert higher steric hindrance. Thus, the P–Ni–P angles show a large change and are influenced by the bulkiness of the nature of the phosphines. The thioureide C–N bond is **1** is shorter than the bond in **2**. The significant shortening is a clear manifestation of mesomeric shift of electron density towards nickel through the thioureide C–N bond in **1** compared to **2**. Though the Ni–P bonds in **2** are relatively shorter than those in **1**, the back bonding effects are felt more pronounced in **1** and hence the corresponding thioureide bond shows a shortening of its length. As a result of the reduced P–Ni–P chelated angle in **2**, the S–Ni–S angle increases by 0.49° compared to **1**. Hence, both electronic and steric influences of dppe over PPh_3 are exemplified by compound **2** with respect to the compound **1**.

4. Supplementary data

Supplementary data are available from The Director, CCDC, 12 Union Road, Cambridge CB2 1EZ, UK (fax: +44-1223-336033; E-mail: deposit@ccdc.cam.ac.uk or www:http://www.ccdc.cam.ac.uk) on request, quoting the deposition number(s) CCDC 211258 and CCDC 211259.

References

[1] A. Chakravorty, Prog. Inorg. Chem. 7 (1966) 83.
[2] J.P. Fackler Jr., W.C. Seidel, Inorg. Chem. 8 (1969) 1631.
[3] C.K. Jorgensen, Inorg. Chem. 3 (1964) 1201.
[4] K. Ramalingam, G. Aravamudan, V. Venkatachalam, Bull. Chem. Soc. Japan. 66 (1993) 1554.
[5] J.A. McCleverty, N.J. Morrison, J. Chem. Soc., Dalton Trans. (1976) 541.
[6] D. Lachenal, Inorg. Nucl. Chem. Lett. 11 (1975) 101.
[7] R.P. Burns, F.P. McCullough, C.A. McAuliffe, Adv. Inorg. Chem. Radiochem. 23 (1980) 211.
[8] K. Ramalingam, G. Aravamudan, M. Seshasayee, Inorg. Chim Acta 128 (1987) 231.
[9] G. Polzonetti, C. Preti, G. Tosi, Polyhedron 5 (1986) 1969.
[10] G.M. Sheldrick, Acta Crystallogr. A 46 (1990) 467.
[11] G.M. Sheldrick, SHELX-97 Programs for Crystal Structure Analysis (Release 97-2), University of Göttingen, Germany.
[12] F. Bonati, R. Ugo, J. Organomet. Chem. 110 (1967) 257.
[13] H.L.M. Van Gaal, J.W. Diesveld, F.W. Pijpers, Van der Linden, Inorg. Chem. 18 (1979) 11,3251.
[14] Robert M. Silverstein, Francis X. Webster, Spectrometric Identification of Organic Compounds, 6th ed., p. 294.

[15] Philip E. Garrou, Chem. Rev. 229 (1981) 81.
[16] N.E. Brese, M.O'. Keeffe, Acta Crystallogr. B 47 (1991) 192.
[17] M.O'. Keeffe, N.E. Brese, J. Am. Chem. Soc. 113 (1991) 3226.
[18] S.P. Summers, K.A. Abboud, S.R. Farrah, G.J. Palenik, Inorg. Chem. 33 (1994) 88.
[19] V. Venkatachalam, K. Ramalingam, T.C.W. Mak, L.B. Sheng, Polyhedron 15 (8) (1996) 1295.

Available online at www.sciencedirect.com
SCIENCE DIRECT®
Polyhedron 23 (2004) 83–95
POLYHEDRON
www.elsevier.com/locate/poly

2-Pyridinealdoxime [(py)CHNOH] in manganese(II) carboxylate chemistry: mononuclear, dinuclear, tetranuclear and polymeric complexes, and partial transformation of (py)CHNOH to picolinate(−1) ☆

Constantinos J. Milios [a], Elena Kefalloniti [a], Catherine P. Raptopoulou [b], Aris Terzis [b], Albert Escuer [c], Ramon Vicente [c,*], Spyros P. Perlepes [a,*]

[a] *Department of Chemistry, University of Patras, GR 26504 Patras, Greece*
[b] *Institute of Materials Science, NCSR "Demokritos", GR 15310 Aghia Paraskevi Attikis, Greece*
[c] *Departament de Quimica Inorganica, Universitat de Barcelona, Diagonal 647, E-08028 Barcelona, Spain*

Received 16 July 2003; accepted 10 September 2003

Abstract

The preparation and crystal structures of four Mn^{II} carboxylate complexes containing 2-pyridinealdoxime, (py)CHNOH, are reported. The 1:1 reaction between $Mn(O_2CPh)_2 \cdot 2H_2O$ and (py)CHNOH in MeCN, followed by evaporation of the resulting solution, redissolution of the residue in $CHCl_3$ and precipitation with Et_2O leads to isolation of $[Mn_4(O_2CPh)_6\{(py)CO_2\}_2\{(py)CHNOH\}_2] \cdot 0.6CHCl_3$ (**1** · 0.6$CHCl_3$). The most interesting synthetic feature is the in situ formation of the picolinate(−1) ligand, $(py)CO_2^-$. The centrosymmetric tetranuclear cluster consists of an exactly planar zig-zag array of Mn^{II} ions and is held together by four *syn*, *syn* $\eta^1{:}\eta^2{:}\mu_2$ and two $\eta^1{:}\eta^2{:}\mu_3$ $PhCO_2^-$ groups, two $\eta^1{:}\eta^2{:}\mu_2$ $(py)CO_2^-$ ligands and two *N*,*N*′-bidentate chelating (py)CHNOH molecules. The 1:4:7 $[Mn_3^{II,III,III}O(O_2CPh)_6(pyr)_2(H_2O)]$/$Me_3SiCl$/(py)CHNOH reaction mixture in MeCN (pyr = pyridine) yields the 1D coordination polymer $[Mn(O_2CPh)\{(py)CO_2\}\{(py)CHNOH\}]_n$ (**2**), in which the partial (py)CHNOH → $(py)CO_2^-$ transformation has again occurred. In each chain the Mn^{II} ions are bridged by *syn*, *anti* carboxylate groups of the $\eta^1{:}\eta^1{:}\eta^1{:}\mu_2$ $(py)CO_2^-$ ligands, while the monodentate $PhCO_2^-$ group and the *N*,*N*′-bidentate chelating (py)CHNOH molecule complete the octahedral coordination at each metal ion. The 1:3 reaction between $Mn(O_2CMe)_2 \cdot 4H_2O$ and (py)CHNOH in EtOH leads to the isolation of the dinuclear complex $[Mn_2(O_2CMe)_2\{(py)CO_2\}_2\{(py)CHNOH\}_2]$ (**3**); crystallography reveals again the partial (py)CHNOH → $(py)CO_2^-$ transformation. The dinuclear molecule is located at a centre of symmetry; the Mn^{II} ions are bridged by two oxygen atoms from the two symmetry-related $\eta^1{:}\eta^1{:}\mu_2$ $(py)CO_2^-$ ligands, whose nitrogen atoms are ligated to different metal ions. Each Mn^{II} ion is further coordinated by a monodentate $MeCO_2^-$ group and a *N*,*N*′-bidentate chelating (py)CHNOH molecule. Reaction of $Mn(hfac)_2 \cdot 3H_2O$ (hfacH = hexafluoroacetylacetone) with 1 equivalent of (py)CHNOH in CH_2Cl_2 yields complex $[Mn(O_2CCF_3)_2\{(py)CHNOH\}_2]$ (**4**); the $CF_3CO_2^-$ ligand is one of the decomposition products of the $hfac^-$ ligand. The Mn^{II} ion in **4** is coordinated by two monodentate $CF_3CO_2^-$ groups and two *N*,*N*′-bidentate chelating (py)CHNOH ligands in a *cis–cis–trans* fashion. The four complexes have been characterised by IR spectroscopy; characteristic bands are discussed in terms of the known structures and the coordination modes of the ligands. Variable-temperature magnetic susceptibility and EPR studies indicate weak antiferromagnetic exchange interactions in **1**.
© 2003 Published by Elsevier Ltd.

Keywords: Crystal structures; Manganese(II) carboxylate chemistry; Magnetochemistry; Metal-assisted reactions; 2-Pyridinealdoxime complexes

1. Introduction

Manganese carboxylate chemistry is of great current interest from several viewpoints, including bioinorganic chemistry and molecular magnetism. In the former area,

☆ This work is dedicated to the memory of our young inorganic chemistry colleague Spyridoula Kasselouri.

* Corresponding authors. Tel.: +34-3-402-1264; fax: +34-3-490-7725 (R. Vicente), Tel.: +30-2610-997146; fax: +30-2610-997118 (S.P. Perlepes).

E-mail addresses: rvicente@kripto.qui.ub.es, ramon.vicente@qi.ub.es (R. Vicente), perlepes@patreas.upatras.gr (S.P. Perlepes).

0277-5387/$ - see front matter © 2003 Published by Elsevier Ltd.
doi:10.1016/j.poly.2003.09.009

small Mn carboxylate clusters are found at the active sites of a variety of metallobiomolecules [1]; for example, the water oxidising complex (WOC) of photosystem II contains a tetranuclear Mn carboxylate cluster whose structure and mechanism of function have not yet been fully elucidated [2]. Thus, synthetic Mn_4 molecular clusters have been sought as models of the WOC [3–5]. Most of these have many structural/physical/spectroscopic properties similar to those of the WOC, but no synthetic species currently seems to reproduce the properties (especially the functional ones) of the catalytic active site in all ways. In the molecular magnetism arena, it has been discovered that some Mn carboxylates clusters can function as single-domain nanomagnets at very low temperatures [6–9]. These complexes have been called single-molecule magnets (SMMs) to reflect the fact that their magnetic properties are due to a combination of two intramolecular properties (and not to intermolecular exchange interactions and long-range ordering), namely a high-spin ground state and a large magnetoanisotropy, the latter reflected in a large and negative value of the zero-field splitting parameter, D [6,7]. Several groups, including our group [10–12], are actively developing methods to high-nuclearity, high-spin Mn molecular species that might be new SMMs.

There is currently a renewed interest in the coordination chemistry of oximes [13,14]. These efforts are driven by a number of considerations, including the solution of pure chemical problems [15–19], the desire to provide useful bioinorganic models (oximes may be considered to be reasonable models for the biologically important imidazole donor group of the amino acid histidine) [20], the development of new oxygen activation catalysts [21], the application of metal/oxime systems as simple and efficient catalysts for the hydrolysis of organonitriles [22], the mechanistic study of corrosion inhibition by Acorga P5000 (a modern corrosion inhibitor) on iron surfaces [23] and the employment of oximate ligands in the synthesis of homometallic [10–12,24] and heterometallic [25] clusters with interesting magnetic properties. For example, the pure chemical interest in the coordination chemistry of oximes arises from the ability of the oximate(−1) group (–C=N–O$^-$) to stabilise higher oxidation states of metals, e.g. Ni^{III} or Ni^{IV} [26,27], and the fact that the activation of oximes by transition metal centres towards further reactions seems to be an emergent area of modern synthetic chemistry [13,14]. In contrast to the great number of studies concerning metal complexes of simple oximes and salicylaldoxime [12,15–19,23–25], very little is known about complexes of pyridyloximes [28], although this class of compounds could offer unique features in terms of structural and physical properties.

We have recently embarked on a programme aiming at the amalgamation of the above two areas, namely the use of pyridyloxime ligands in manganese carboxylate cluster chemistry, in order to explore the influence of the ligands on the cluster identity; the main objectives are the access to new structural types of clusters with interesting magnetic properties and the study of Mn-mediated reactions of the oxime group. Reaction schemes involving di-2-pyridyl ketone oxime, $(py)_2CNOH$ (Fig. 1), and various Mn carboxylate sources in the presence of X^- led [11] to the new family of valence-trapped, mixed-valent complexes $[Mn_2^{II}Mn_2^{III}(O_2CR)_2X_2\{(py)_2CNO\}_2\{(py)_2CO_2\}_2]$(X = Cl,Br;$(py)_2CO_2^{2-}$ = the *gem*-diolate(−2) form of di-2-pyridyl ketone); it has been of great interest that an appreciable quantity of the oxime ligand undergoes transformation to yield the coordinated dianion of the *gem*-diol form of di-2-pyridyl ketone. The mechanism of this transformation probably involves reaction(s) of the electrophilically activated coordinated oxime group [11]. The use of phenyl 2-pyridyl ketone oxime, (ph)(py)CNOH (Fig. 1), in Mn carboxylate chemistry has yielded [10] the novel clusters $[Mn_4^{II}Mn_4^{III}O_2(OH)_2(O_2CR)_{10}\{(ph)(py)CNO\}_4]$; the core of these complexes has a unique topology consisting of two linked $\{Mn_2^{II}Mn_2^{III}(\mu_3\text{-}O)(\mu_3\text{-}OH)\}^{7+}$ units. The above prior results with 2-pyridyloximes encouraged us to proceed to the use of 2-pyridinealdoxime ((py)CHNOH, Fig. 1) to Mn carboxylate chemistry, and we have thus been exploring the reactions of (py)CHNOH with suitable Mn starting materials. The results of this investigation are reported here. It is worth mentioning that (py)CHNOH has been used only sparingly in Mn chemistry to date. The only known compounds comprise two heterometallic complexes and one homometallic coordination polymer. The chain $[Mn_2^{III}(saltmen)_2Ni\{(py)CHNO\}_2(pyr)_2]_n(ClO_4)_{2n}$ (saltmen^{2-} = *N*,*N*′-(1,1,2,2-tetramethylethylene) bis(salicylideneiminate)) shows evidence for single-chain magnet behaviour; the 2-pyridinealdoximate(−1) ligand in this 1D complex bridges two adjacent Mn^{III} and Ni^{II} ions [29]. The dinuclear complex $[LCr^{III}\{(py)CHNO\}_3Mn^{II}](ClO_4)_2$, where L is 1,4,7-trimethyl-1,4,7-triazacyclononane, is composed of two pseudooctahedral

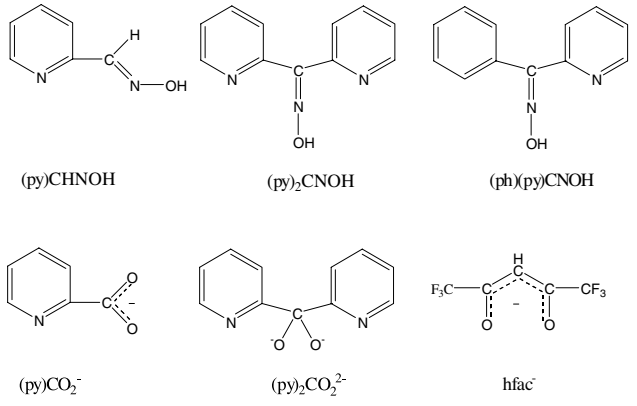

Fig. 1. Some of the ligands discussed in the text; note that (py) $_2CO_2^{2-}$ does not exist as a free species but exists only in its metal complexes.

polyhedra which are joined by three oximato (=N–O$^-$) groups [30]. Complex $[Mn(SO_4)\{(py)CHN\,OH\}(H_2O)]_n$ is a double-chain polymer in which the Mn^{II} ions are bridged by μ_3-SO_4^{2-} ligands [31].

2. Experimental

2.1. General and physical measurements

All manipulations were performed under aerobic conditions using materials (reagent grade) and solvents as received. $Mn(O_2CPh)_2 \cdot 2H_2O$ [32] and $[Mn_3O(O_2CPh)_6(pyr)_2(H_2O)]$ [33] were prepared as described elsewhere.

Microanalyses (C, H, N) were performed by the University of Ioannina (Greece) Microanalytical Laboratory using an EA 1108 Carlo Erba analyser. IR spectra (4000–450 cm^{-1}) were recorded on a Perkin–Elmer 16 PC FT spectrometer with samples prepared as KBr pellets. Magnetic susceptibility measurements were carried out for a polycrystalline sample of complex **1** (vide infra) in the range 2–300 K using a SQUID susceptometer; the applied magnetic field was 0.1 T. Diamagnetic corrections were applied to the observed paramagnetic susceptibilities using Pascal's constants. Solid-state EPR spectra in the 77–300 K temperature range were recorded on a Bruker ES200 spectrometer at X-band frequency.

2.2. Compound preparation

2.2.1. $[Mn_4(O_2CPh)_6\{(py)CO_2\}_2\{(py)CHNOH\}_2] \cdot 0.6CHCl_3$ (**1** $\cdot$ 0.6$CHCl_3$)

A colourless solution of $Mn(O_2CPh)_2 \cdot 2H_2O$ (0.33 g, 1.0 mmol) in MeCN (20 ml) was treated with solid (py)CHNOH (0.12 g, 1.0 mmol). The solid soon dissolved. The resulting yellow solution was evaporated under reduced pressure, and the residue redissolved in $CHCl_3$ (20 ml) to give an orange solution. This was layered with Et_2O (40 ml). After several days, large yellow prisms were formed; they were collected by filtration, washed with Et_2O and dried in air. Yield: 72% (based on total Mn). The dried sample analysed as solvent-free. *Anal*. Calc. for $C_{66}H_{50}N_6O_{18}Mn_4$: C, 55.2; H, 3.5; N, 5.9. Found: C, 55.4; H, 3.4; N, 6.0%. Selected IR data (KBr pellet, cm^{-1}): 3446mb, 3020w, 2926w, 1602s, 1555sh, 1544s, 1476w, 1404s, 1068w, 1024m, 776w, 720s, 674m.

2.2.2. $[Mn(O_2CPh)\{(py)CO_2\}\{(py)CHNOH\}]_n$ (**2**)

To a stirred deep brown solution of $[Mn_3O(O_2CPh)_6(pyr)_2(H_2O)]$ (0.34 g, 0.3 mmol) in MeCN (30 ml) was added Me_3SiCl (0.16 ml, 1.2 mmol) dropwise to give a solution of essentially the same colour. No immediate precipitate was observed, but slow formation of a dark brown solid began soon after. When precipitation was judged complete (2–3 h), the powder was removed by filtration. The filtrate was treated with (py)CHNOH (0.24 g, 2.0 mmol) under reflux. The dark brown–green solution slowly faded to orange over the course of 1 h. The homogeneous orange solution was layered with Et_2O (60 ml). Slow mixing yielded orange crystals of X-ray quality, which were collected by filtration, washed with Et_2O and dried in air. Yield: 43% (based on total Mn). *Anal.* Calc. for $C_{19}H_{15}N_3O_5Mn$: C, 54.3; H, 3.6; N, 10.0. Found: C, 54,1; H, 3.7; N, 10.2%. Selected IR data (KBr pellet, cm^{-1}): 3442mb, 3064w, 1610m, 1588s, 1564m, 1474w, 1394s, 1332w, 1148w, 1092w, 1054m, 1012w, 918m, 892w, 830w, 782w, 766m, 714m, 674m, 490m.

2.2.3. $[Mn_2(O_2CMe)_2\{(py)CO_2\}_2\{(py)CHNOH\}_2]$ (**3**)

Solid (py)CHNOH (0.09 g, 0.7 mmol) was added to a stirred, colourless solution of $Mn(O_2CMe)_2 \cdot 4H_2O$ (0.06 g, 0.25 mmol) in EtOH (20 ml). The resulting yellow solution was allowed to stand undisturbed at 5 °C for several days. Well-formed, X-ray quality yellow crystals appeared, which were collected by filtration, washed with Et_2O and dried in vacuo over silica gel. Yields as high as 75% were obtained. *Anal.* Calc. for $C_{28}H_{26}N_6O_{10}Mn_2$: C, 46.9; H, 3.7; N, 11.7%. Found: C, 46.5; H 3.7; N, 11.5%. Selected IR data (KBr pellet, cm^{-1}): 3442mb, 1602m, 1548sb, 1478m, 1416s, 1330m, 1308w, 1258w, 1048s, 1010w, 924w, 888w, 782m, 678sh, 668m, 656s, 638w, 618w, 522w, 488w.

2.2.4. $[Mn(O_2CCF_3)_2\{(py)CHNOH\}_2]$ (**4**)

To a pale yellow slurry of $Mn(hfac)_2 \cdot 3H_2O$ (0.47 g, 1.0 mmol) in CH_2Cl_2 (20 ml) was added dropwise a colourless solution of (py)CHNOH (0.12 g, 1.0 mmol) in the same solvent (10 ml). The reaction mixture colour changed slightly from pale yellow to darker yellow. This was stirred for about 10 min, a small quantity of undissolved material removed by filtration and the filtrate layered with *n*-hexane (60 ml). Slow mixing yielded yellow crystals (some of them were of X-ray quality), which were collected by filtration, washed with Et_2O and dried in air. The yield was typically 40%. *Anal.* Calc. for $C_{16}H_{12}N_4O_6F_6Mn$: C, 36.6; H, 2.3; N, 10.7. Found: C, 36.9; H, 2.4; N, 10.5%. Selected IR data (KBr pellet, cm^{-1}): 3428mb, 1668s, 1602m, 1508m, 1448m, 1328m, 1310m, 1206s, 1144s, 1038s, 890m, 840m, 780m, 678w, 640w.

2.3. X-ray crystallographic studies

Crystals of complexes **2**, **3** and **4** were mounted in air, while a crystal of complex **1** $\cdot$ 0.6$CHCl_3$ was mounted in a capillary filled with drops of mother liquid. Diffraction measurements for **1** $\cdot$ 0.6$CHCl_3$, **3** and **4** were made on a Crystal Logic Dual goniometer diffractometer using graphite-monochromated Mo radiation. Data for

complex **2** were collected on a $P2_1$ Nicolet diffractometer upgraded by Crystal Logic using Ni-filtered Cu radiation. Complete crystal data and parameters for data collection and processing are reported in Table 1. Unit cell dimensions were determined and refined by using the angular settings of 25 automatically centred reflections in the ranges $11° < 2\theta < 23°$ (**1** · 0.6$CHCl_3$, **3** and **4**) and $22° < 2\theta < 54°$ (**2**). In all cases, three standard reflections, monitored every 97 reflections, showed less than 3% fluctuation and no decay. Lorentz, polarisation and Ψ-scan absorption (except for **3**) corrections were applied using CRYSTAL LOGIC software.

The structures were solved by direct methods using SHELXS-86 [34] and refined by full-matrix least squares techniques on F^2 with SHELXL-93 [35]. For **2**, **3** and **4**, all hydrogen atoms – except those on the methyl carbon (C(14)) in **3** which were introduced at calculated positions as riding on their bonded atom – were clearly visible in subsequent Fourier maps and refined isotropically. For **1** · 0.6$CHCl_3$, all hydrogen atoms – except HO(11) which was located by difference maps and refined isotropically – were placed in ideal, calculated positions riding on their respective carbon atoms. All non-hydrogen atoms were refined using anisotropic thermal parameters, except those of the solvate $CHCl_3$ molecule in **1** · 0.6$CHCl_3$ which were refined isotropically with occupation factors fixed at 10.3; the fluorine atoms of the $–CF_3$ groups in **4** were found disordered and refined anisotropically over two positions with occupation factors summing one.

3. Results and discussion

3.1. Syntheses

The reaction that we initially investigated was that between $Mn(O_2CPh)_2 \cdot 2H_2O$ and (py)CHNOH. Treatment of a solution of $Mn(O_2CPh)_2 \cdot 2H_2O$ with one equivalent of (py)CHNOH in MeCN, followed by evaporation of the resulting solution, redissolution of the residue in $CHCl_3$ and layering the solution with Et_2O allowed yellow crystals of the product to be obtained in a form suitable for crystallography. The product was identified as the interesting new tetranuclear cluster $[Mn_4(O_2CPh)_6\{(py)CO_2\}_2\{(py)CHNOH\}_2] \cdot 0.6CHCl_3$

Table 1
Crystallographic data for complexes **1** · 0.6$CHCl_3$, **2**, **3** and **4**

	1 · 0.6$CHCl_3$	**2**	**3**	**4**
Formula	$C_{66.6}H_{50.6}N_6O_{18}Cl_{1.8}Mn_4$	$C_{19}H_{15}N_3O_5Mn$	$C_{28}H_{26}N_6O_{10}Mn_2$	$C_{16}H_{12}N_4O_6F_6Mn$
Formula weight	1506.53	420.28	716.42	525.24
Crystal colour, habit	yellow, prism	yellow, prism	orange, prism	yellow, prism
Crystal dimensions (mm)	0.16 × 0.20 × 0.50	0.10 × 0.10 × 0.30	0.15 × 0.28 × 0.50	0.10 × 0.30 × 0.50
Crystal system	monoclinic	orthorhombic	monoclinic	triclinic
Space group	$P2_1/n$	$Pcab$	$P2_1/n$	$P\bar{1}$
a (Å)	18.825(7)	17.720(6)	9.526(5)	9.439(7)
b (Å)	17.012(7)	21.869(7)	8.761(4)	14.15(1)
c (Å)	11.045(4)	9.612(3)	18.701(9)	9.291(8)
α (°)				93.90(3)
β (°)	90.23(1)		99.61(2)	118.82(3)
γ (°)				97.27(2)
V (Å^3)	3537(2)	3725(2)	1539(1)	1067(1)
Z	2	8	2	2
D_{calc} (g cm^{-3})	1.415	1.499	1.546	1.635
μ (mm^{-1})	0.837	6.090	0.886	0.711
Radiation (λ, Å)	Mo Kα (0.71073)	Cu Kα (1.54180)	Mo Kα (0.71073)	Mo Kα (0.71073)
Temperature (K)	298	298	298	298
Scan mode/speed (°min^{-1})	$\theta - 2\theta/3.0$	$\theta - 2\theta/1.5$	$\theta - 2\theta/3.5$	$\theta - 2\theta/3.6$
$2\theta_{max}$ (°)	48.5	124.8	50.0	50.0
Reflections collected	6020	2820	5222	3996
Unique reflections (R_{int})	5698 (0.0131)	2818 (0.0351)	2663 (0.0361)	3745 (0.0107)
Data with $I > 2\sigma(I)$	3865	2273	2062	3201
Parameters refined	450	313	250	398
$[\Delta/\sigma]_{max}$	0.003	0.002	0.011	0.016
$(\Delta\rho)_{max}, (\Delta\rho)_{min}$ (e Å^{-3})	0.647, −0.290	0.256, −0.529	0.810, −0.386	0.272, −0.259
Goodness-of-fit (on F^2)	1.019	1.111	1.145	0.796
R_1[a]	0.0521	0.0415	0.0639	0.0322
wR_2[b]	0.1376	0.1034	0.1578	0.0934

[a] $R_1 = \sum(|F_o| - |F_c|)/\sum|F_o|$.
[b] $wR_2 = \{\sum[w(F_o^2 - F_c^2)^2]/\sum[w(F_o^2)^2]\}^{1/2}$, $w = 1/[\sigma^2(F_o^2) + (aP)^2 + bP]$, where $P = [\max(F_o^2, 0) + 2F_c^2]/3$.

($\mathbf{1}\cdot 0.6CHCl_3$). The most remarkable feature of this reaction is the in situ formation of the picolinate(−1) ligand, $(py)CO_2^-$ (Fig. 2). The following experimental points should be mentioned at this point: (a) the 1:1 reaction between $Mn(O_2CPh)_2\cdot 2H_2O$ and (py)CHNOH in MeOH under strictly anaerobic conditions affords a solid, whose analytical data correspond to the formula $Mn(O_2CPh)_2\{(py)CHNOH\}_2$ and IR spectrum confirms the absence of $(py)CO_2^-$. (b) No colour change, indicative of oxidation of Mn^{II} to Mn^{III}, was observed during the preparation/crystallisation of **1**. (c) The partial $(py)CHNOH \rightarrow (py)CO_2^-$ transformation noticed in **1** was also observed in the reactions of other Mn carboxylate sources with (py)CHNOH (vide infra), and (d) analogous reactions of Co^{II} or Ni^{II} carboxylates and the oxime did not give any evidence [36] for the formation of picolinate(−1). The above experimental facts do not provide us with a clear mechanistic view. Without any mechanistic implication, we suggest that the formation of **1** is triggered by hydrolysis of an amount of (py)CHNOH to the corresponding aldehyde, 2-pyridinealdehyde ((py)CHO), followed by oxidation of the latter to picolinic acid, (py)COOH, which is deprotonated by the excess of $PhCO_2^-$s present in the reaction mixture. This simplified transformation scheme is shown in Fig. 2. The difference between regular and metal-mediated conditions lead us to the belief that the transformation is Mn^{II}-assisted and probably involves the reaction of electrophilically activated coordinated oxime group [14,37].

It has been demonstrated that direct hydrolysis of oximes to carbonyl compounds proceeds slowly in low yields and is subject to side reactions [13,14]. Attanasi et al. [37] have proposed a facile method for this conversion based on copper(II)-assisted hydrolysis, which is not reductive or oxidative in nature but involves the reaction of the electrophilically activated, coordinated oxime group with water. In general, the conversion of oximes into the parent carbonyl compounds requires reductive or oxidative cleavages, strongly basic or acidic media [13,14]. Oximes can be converted to the corresponding aldehydes or ketones by treatment with, among other reagents, microwave irradiation on clay (Clayan), on wet sodium periodate impregnated silica gel or in the presence of $BiCl_3$, $CuCl_2$ in MeCN, aqueous $NaHSO_3$, $KMnO_4$-aqueous MeCN, Amberlyst 15 and acetone, alkaline H_2O_2 and with $Me_3NH^+CrO_3Cl^-$ [38].

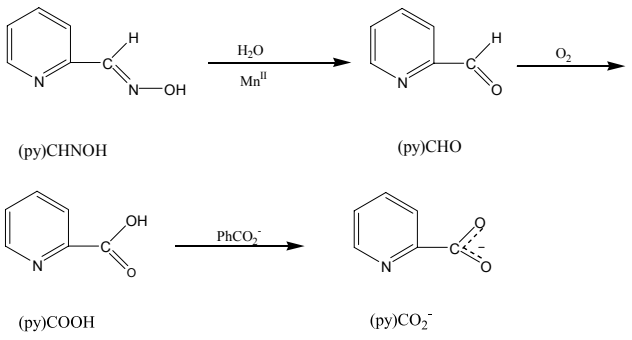

Fig. 2. A simplified view for the partial transformation of 2-pyridinealdoxime to picolinate(−1) during the preparation of complexes **1**–**3**.

Oxidation of aldehydes to carboxylic acids is one of the most common oxidation reactions in organic chemistry [38] and has been carried out with many oxidising agents, the most popular of which is MnO_4^- in acidic, basic or neutral solution. Aldehydes are also oxidised to carboxylic acids by atmospheric oxygen, but the actual direct oxidation product is the peroxy acid RCO_3H ($(py)CO_3H$ in our case), which with another molecule of aldehyde disproportionates to give two molecules of acid ((py)COOH in our case).

Since single-crystal X-ray crystallography (vide infra) revealed the existence of the interesting tetranuclear cluster **1** and the $(py)CHNOH \rightarrow (py)CO_2^-$ transformation, we sought to prepare the acetate analogue of **1**. Our main goals were to determine whether this would be isostructural with the benzoate species and (if they are isostructural) to access any influence of the alkyl vs. aryl difference on magnetochemical properties. A completely analogous reaction scheme with that used for **1** was initially employed, i.e., the 1:1 $Mn(O_2CMe)_2\cdot 4H_2O$/(py)CHNOH mixture in MeCN. This yielded a solid with poor crystallinity. 1:1 reactions of (py)CHNOH with $Mn(O_2CMe)_2\cdot 4H_2O$ in other solvents, including alcohols, have also been carried out, but attempts to crystallographically characterise the products have all been unsuccessful to date. The isolation of the dinuclear product $[Mn_2(O_2CMe)_2\{(py)CO_2\}_2\{(py)CHNOH\}_2]$ (**3**) came about from the employment of excess of (py)CHNOH, i.e., Mn^{II}: (py)CHNOH = 1:2.5–3.0, in EtOH. X-ray crystallography revealed again the partial $(py)CHNOH \rightarrow (py)CO_2^-$ transformation! Since the two systems that lead to **1** and **3** are clearly not analogous, the difference in stoichiometry is not surprising; the $(py)CHNOH + (py)CO_2^-$:Mn^{II} ratio in the formula of **3** is 2:1 (whereas it is 1:1 in **1**), and we attribute this to the excess of (py)CHNOH used in the synthesis of the acetate complex.

With the identity of **3** established, its benzoate version was sought. Note that since only a dinuclear species was being sought, excess of oxime was added. Several 1:2 and 1:3 $Mn(O_2CPh)_2\cdot 2H_2O$/(py)CHNOH reaction mixtures were studied using various conditions, but almost all led to a mixture of **1** and a yet unidentified product. Since the RCO_2^-:Mn^{II} ratio in **1** is higher than that in **3** (1.5:1 vs. 1:1), methods to reduce the benzoate concentration were examined. Use of $MnCl_2\cdot 4H_2O$, $Mn(NO_3)_2\cdot 6H_2O$ or $Mn(ClO_4)_2\cdot 6H_2O$ as starting materials, followed by addition of one equivalent of NaO_2CPh, complicated the reaction mixtures. The carboxylate-abstraction reagent Me_3SiCl [39,40] was our

next choice; this reagent forms the silyl ester as shown in Eq. (1). Treatment of $Mn(O_2CPh)_2 \cdot 2H_2O$ with 2–3 equivalents of

$$Me_3SiCl + RCO_2^- \rightarrow RCO_2SiMe_3 + Cl^- \quad (1)$$

Me_3SiCl and 2–2.5 equivalents of (py)CHNOH in alcohols or MeCN gave orange powders whose analytical data were consistent with the formulation $Mn(O_2CPh)\{(py)CO_2\}\{(py)CHNOH\}$. The rather low solubility and platelike crystallinity of the material precluded a crystallographic investigation. Somewhat to our surprise, the preparation and crystallisation of this orange compound were achieved by the reaction of the mixed-valence compound $[Mn_3^{II,III,III}O(O_2CPh)_6\ (pyr)_2(H_2O)]$ [33] with 4 equivalents of Me_3SiCl and ~7 equivalents of (py)CHNOH (Mn:oxime ≈1:2, in fact the actual Mn:oxime ratio is lower, e.g. 1:3, because a small quantity of a dark brown, Mn-containing solid was removed prior to the addition of the oxime) in MeCN. The advantage of the present procedure is its slow crystallisation of product upon layering with Et_2O and the well-formed nature of the resulting crystals that have proven excellent diffractors of X-rays. The product was crystallographically identified as the coordination polymer $[Mn(O_2CPh)\{(py)CO_2\}\{(py)CHNOH\}]_n$ (**2**) rather than the expected dinuclear species $[Mn_2(O_2CPh)_2\ \{(py)CO_2\}_2\{(py)CHNOH\}_2]$; note that the partial (py) CH NOH → $(py)CO_2^-$ transformation again occurred. The fading of the reaction solution after the addition of the oxime and the Mn^{II} nature of **2** both require reduction of Mn^{III} to have occurred; the source of the reducing equivalent is probably solvent, solvent impurities or excess ligand, facilitated by the strongly oxidising nature of Mn^{III} [32].

Complex $[Mn(O_2CCF_3)_2\{(py)CHNOH\}_2]$ (**4**) was not prepared from the reaction of a trifluoroacetate-based Mn starting material and (py)CHNOH. However, we have incorporated this compound in the present work because it does contain a carboxylate ligand! Treatment of $Mn(hfac)_2 \cdot 3H_2O$ (hfac = hexafluoroacetylacetonate) with one equivalent of (py)CHNOH in CH_2Cl_2, followed by stirring of the slurry, leads to a yellow solution that can be layered with *n*-hexane to give **4** in 40% yield. Single-crystal X-ray diffraction unambiguously established that this complex contains monodentate $CF_3CO_2^-$ ligands. The origin of the trifluoroacetate ligands is intriguing, and the $hfac^- \rightarrow CF_3CO_2^-$ transformation has been confirmed in at least two cases [41,42]. The $CF_3CO_2^-$ ligand should be one of the decomposition products of the $hfac^-$ ligand (Eq. (2)). β-Diketones have been known to undergo the retro-Claisen condensation reaction to produce a ketone and a carboxylate when strong bases are present. The (py)CHNOH ligand could function as the base to promote the decomposition of the hfacH molecule [41].

$$CF_3COCH_2COCH_3 \xrightarrow{H_2O/base} CF_3CO_2^- + CH_3COCF_3 \quad (2)$$

It has been previously suggested that hfacH reacts with H_2O to form initially a "dihydrate", i.e. $hfacH \cdot 2H_2O$ [43]; however, later rigorous studies by Christou's group demonstrated [44,45] that this reaction is far from simple. These latter researchers have demonstrated that hfacH reacts with H_2O to yield the tetraol $F_3CC(OH)_2CH_2C(OH)_2CF_3$, which can act as ligand in transition metal chemistry at various degrees of deprotonation. Ultimately, the pH of the reaction solution seems to have a profound effect on the nature of the product and how the $hfac^-$ ligand is cleaved [42].

3.2. Description of structures

Selected interatomic distances and angles for complexes **1** · 0.6$CHCl_3$, **2**, **3** and **4** are listed in Tables 2–5, respectively.

Complex **1** · 0.6$CHCl_3$ crystallises in monoclinic space group $P2_1/n$. Its structure consists of the tetranuclear $[Mn_4(O_2CPh)_6\{(py)CO_2\}_2\{(py)CHNOH\}_2]$ species (Fig. 3) and lattice $CHCl_3$ molecules; the latter will not be further discussed. The tetranuclear molecule lies on a crystallographic inversion centre, resulting in an exactly planar zig-zag array of Mn^{II} atoms. The bridging system comprises four *syn*,*syn* $\eta^1:\eta^1:\mu_2$ $PhCO_2^-$ groups, two $\eta^1:\eta^2:\mu_3$ $PhCO_2^-$ groups (those containing atoms O(41), O(42) and O(41′), O(42′)) and two $\eta^1:\eta^1:\mu_2$ picolinate(−1) ligands. Each outer metal ion (Mn(1), Mn(1′)) is chelated by a single (py)CHNOH molecule bound in a *N*,*N*′-bidentate fashion and forming a five-membered ring. Atoms Mn(1) and Mn(2) are bridged by one $\eta^1:\eta^1:\mu_2$ $PhCO_2^-$ group, the "triatomic" part of one $\eta^1:\eta^2:\mu_3$ $PhCO_2^-$ group and one $\eta^1:\eta^2:\mu_2$ $(py)CO_2^-$ ligand, while two oxygen atoms (O(42), O(42′)) from the $\eta^1:\eta^2:\mu_3$ $PhCO_2^-$ ligand and its symmetry partner doubly bridge atoms Mn(2) and Mn(2′). The Mn(1)···Mn(2′) pair is bridged by one $\eta^1:\eta^1:\mu_2$ $PhCO_2^-$ group and the "triatomic" part of the same μ_3 benzoate that bridges Mn(1) and Mn(2). The central Mn(2)O(42)Mn(2′)O(42′) core is strictly planar due to the presence of the inversion centre in the middle of the core, with an Mn(2)–O(42)–Mn(2′) angle of 103.1(1)° and a Mn(2)···Mn(2′) separation of 3.460(2) Å. This separation is shorter than the Mn(1)···Mn(2) (3.557(2) Å) and Mn(1)···Mn(2′) (4.522(2) Å) separations presumably due to the greater number (two) of monoatomic bridges.

The Mn^{II} atoms are octahedrally coordinated, their chromophores being *cis*-$Mn(1)N_2O_4$ and $Mn(2)NO_5$. Both polyhedra are distorted; the main distortions arise from the chelating rings with the narrow N(11)–Mn(1)–N(12) (69.8(2)°) and O(1)–Mn(2)–N(1) (74.1(1)°) bond

Table 2
Selected interatomic distances (Å) and angles (°) for $[Mn_4(O_2CPh)_6\{(py)CO_2\}_2\{(py)CHNOH\}_2]\cdot 0.6CHCl_3$ (**1**$\cdot 0.6CHCl_3$)[a]

Interatomic distances			
Mn(1)···Mn(2)	3.557(2)	Mn(1)–N(11)	2.302(5)
Mn(1)···Mn(2′)	4.522(2)	Mn(1)–N(12)	2.383(6)
Mn(1)···Mn(1′)	7.364(3)	Mn(2)–O(1)	2.233(3)
Mn(2)···Mn(2′)	3.460(2)	Mn(2)–O(22)	2.102(3)
Mn(1)–O(1)	2.224(3)	Mn(2)–O(32)	2.050(3)
Mn(1)–O(21)	2.147(3)	Mn(2)–O(42)	2.140(3)
Mn(1)–O(31)	2.129(3)	Mn(2)–O(42′)	2.278(3)
Mn(1)–O(41)	2.202(4)	Mn(2)–N(1)	2.235(4)
Interatomic angles			
Mn(1)–O(1)–Mn(2)	105.9(1)	N(11)–Mn(1)–N(12)	69.8(2)
Mn(2)–O(42)–Mn(2′)	103.1(1)	O(1)–Mn(2)–O(22)	89.0(1)
O(1)–Mn(1)–O(21)	83.3(1)	O(1)–Mn(2)–O(32)	163.5(1)
O(1)–Mn(1)–O(31)	94.3(1)	O(1)–Mn(2)–O(42)	96.4(1)
O(1)–Mn(1)–O(41)	111.6(1)	O(1)–Mn(2)–O(42′)	88.1(1)
O(1)–Mn(1)–N(11)	159.1(2)	O(1)–Mn(2)–N(1)	74.1(1)
O(1)–Mn(1)–N(12)	95.3(2)	O(22)–Mn(2)–O(32)	98.2(1)
O(21)–Mn(1)–O(31)	175.4(1)	O(22)–Mn(2)–O(42)	92.1(1)
O(21)–Mn(1)–O(41)	83.1(1)	O(22)–Mn(2)–O(42′)	168.3(1)
O(21)–Mn(1)–N(11)	86.3(2)	O(22)–Mn(2)–N(1)	100.1(1)
O(21)–Mn(1)–N(12)	104.1(2)	O(32)–Mn(2)–O(42)	98.1(2)
O(31)–Mn(1)–O(41)	94.2(1)	O(32)–Mn(2)–O(42′)	87.6(1)
O(31)–Mn(1)–N(11)	97.2(2)	O(32)–Mn(2)–N(1)	89.9(2)
O(31)–Mn(1)–N(12)	80.1(2)	O(42)–Mn(2)–O(42′)	77.0(1)
O(41)–Mn(1)–N(11)	84.9(2)	O(42)–Mn(2)–N(1)	164.3(1)
O(41)–Mn(1)–N(12)	152.9(2)	O(42′)–Mn(2)–N(1)	90.0(1)

[a] Symmetry transformations used to generate equivalent atoms: (′) $-x+1,-y,-z$.

Table 3
Selected interatomic distances (Å) and angles (°) for $[Mn(O_2CPh)\{(py)CO_2\}\{(py)CHNOH\}]_n$ (**2**)[a]

Interatomic distances			
Mn···Mn#1	5.855(2)	Mn–N(1)	2.301(3)
Mn–O(1)	2.168(2)	Mn–N(2)	2.324(3)
Mn–O(2)	2.092(3)	Mn–N(3)	2.317(3)
Mn–O(4)	2.106(3)		
Interatomic angles			
O(1)–Mn–O(2)	88.3(1)	O(2)–Mn–N(3)	104.8(1)
O(1)–Mn–O(4)	97.3(1)	O(4)–Mn–N(1)	90.9(1)
O(1)–Mn–N(1)	72.8(1)	O(4)–Mn–N(2)	166.7(1)
O(1)–Mn–N(2)	94.1(1)	O(4)–Mn–N(3)	97.1(1)
O(1)–Mn–N(3)	159.0(1)	N(1)–Mn–N(2)	85.9(1)
O(2)–Mn–O(4)	97.8(1)	N(1)–Mn–N(3)	91.8(1)
O(2)–Mn–N(1)	160.1(1)	N(2)–Mn–N(3)	70.1(1)
O(2)–Mn–N(2)	89.4(1)		

[a] Symmetry transformations used to generate equivalent atoms: #1 $-x,-y+1/2,z+1/2$.

angles. The Mn–N and Mn–O bond lengths agree well with values expected for high-spin Mn^{II} [30,31,46–50]. The bridging Mn–$O_{picolinate}$ distances are symmetric (2.224(3), 2.233(3) Å), whereas the analogous Mn–$O_{benzoate}$ distances are asymmetric (2.140(3), 2.278(3) Å). The two bridging oxygens are essentially planar ($\Sigma^{o}O(1)=357.5°$, $\Sigma^{o}O(42)=355.7°$). An intramolecular hydrogen bond is present in **1**$\cdot 0.6CHCl_3$ with the oxime oxygen, O(11), as donor and the uncoordinated picolinate oxygen, O(2), as acceptor; its dimensions are O(11)···O(2) 2.564 Å, HO(11)···O(2) 1.382 Å and O(11)–HO(11)···O(2) 162.9°.

There is a rather small family of tetranuclear manganese(II) clusters [51–62], which mainly adopt the cubane, planar rhomboidal, zig-zag, adamantane-like and pair-of-dimer topologies. Complex **1** joins a small family of manganese(II) picolinate complexes [47–50] and it is only the second such complex comprising the $(py)CO_2^-$ ligand in the rare $\eta^1{:}\eta^2{:}\mu_2$ coordination mode, the first example being the 2D coordination polymer $[Mn(N_3)\{(py)CO_2\}(H_2O)]_n$ [47].

Views of the structure of complex **2** are shown in Figs. 4 and 5. The compound contains zig-zag chains of repeating $[Mn(O_2CPh)\{(py)CO_2\}\{(py)CHNOH\}]$ units.

Table 4
Selected interatomic distances (Å) and angles (°) for $[Mn_2(O_2CMe)_2\{(py)CO_2\}_2\{(py)CHNOH\}_2]$ (**3**)[a]

Interatomic distances			
Mn ⋯ Mn′	3.633(2)	Mn–N(1)	2.307(5)
Mn–O(2)	2.204(4)	Mn–N(2)	2.298(5)
Mn–O(2′)	2.210(4)	Mn–N(3′)	2.265(5)
Mn–O(4)	2.107(4)		
Interatomic angles			
Mn–O(2)–Mn′	110.8(2)	O(2′)–Mn–N(2)	158.0(2)
O(2)–Mn–O(2′)	69.2(2)	O(2′)–Mn–N(3′)	73.1(2)
O(2)–Mn–O(4)	95.0(2)	O(4)–Mn–N(1)	166.0(2)
O(2)–Mn–N(1)	90.4(2)	O(4)–Mn–N(2)	95.7(2)
O(2)–Mn–N(2)	123.2(2)	O(4)–Mn–N(3′)	91.8(2)
O(2)–Mn–N(3′)	142.3(2)	N(1)–Mn–N(2)	70.6(2)
O(2′)–Mn–O(4)	101.5(2)	N(1)–Mn–N(3′)	91.9(2)
O(2′)–Mn–N(1)	92.5(2)	N(2)–Mn–N(3′)	92.8(2)

[a] Symmetry transformations used to generate equivalent atoms: (′) $-x+1, -y, -z$.

Table 5
Selected bond distances (Å) and angles (°) for $[Mn(O_2CCF_3)_2\{(py)CHNOH\}_2]$ (**4**)

Bond distances			
Mn–O(3)	2.147(2)	C(13)–O(3)	1.232(3)
Mn–O(5)	2.101(2)	C(13)–O(4)	1.229(3)
Mn–N(1)	2.287(2)	C(15)–O(5)	1.225(3)
Mn–N(2)	2.287(3)	C(15)–O(6)	1.212(4)
Mn–N(3)	2.289(2)	N(2)–O(1)	1.380(2)
Mn–N(4)	2.286(3)	N(4)–O(2)	1.388(3)
Bond angles			
O(3)–Mn–O(5)	90.6(1)	O(5)–Mn–N(4)	96.5(1)
O(3)–Mn–N(1)	88.0(1)	N(1)–Mn–N(2)	71.4(1)
O(3)–Mn–N(2)	96.9(1)	N(1)–Mn–N(3)	90.5(1)
O(3)–Mn–N(3)	171.4(1)	N(1)–Mn–N(4)	91.5(1)
O(3)–Mn–N(4)	100.2(1)	N(2)–Mn–N(3)	90.6(1)
O(5)–Mn–N(1)	172.0(1)	N(2)–Mn–N(4)	155.3(1)
O(5)–Mn–N(2)	101.0(1)	N(3)–Mn–N(4)	71.4(1)
O(5)–Mn–N(3)	92.1(1)		

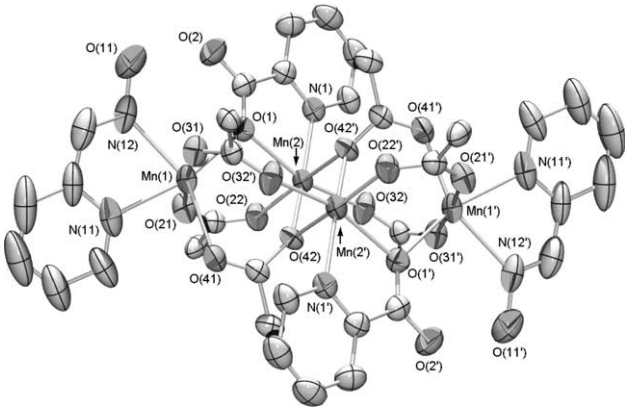

Fig. 3. An ORTEP plot at the 30% probability level of complex $\mathbf{1}\cdot 0.6CHCl_3$. Primed and unprimed atoms are related by the crystallographic inversion centre. Only the *ipso* carbon atoms of the phenyl groups of the benzoate ligands are shown.

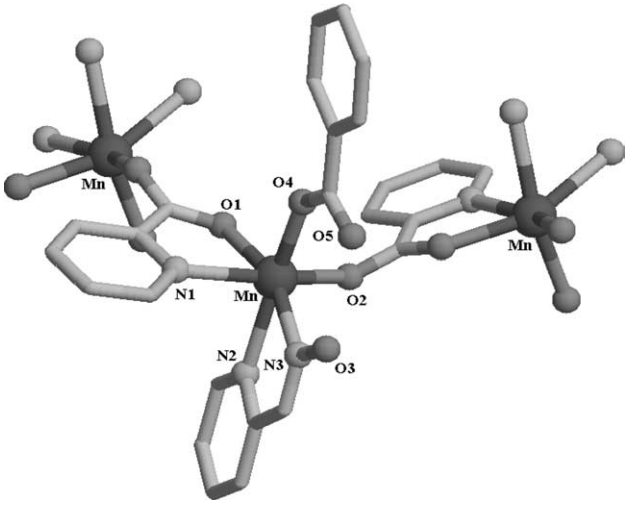

Fig. 4. A very small section of the polymeric chain of complex **2** emphasising the coordination sphere of the Mn^{II} atom.

The polymeric chain extends along the *c* axis of the *Pcab* space group. In each chain the Mn^{II} atoms are bridged by *syn*, *anti* carboxylato groups of the $\eta^1{:}\eta^1{:}\eta^1{:}\mu_2$ picolinate(−1) ligands. The Mn^{II} atom is octahedrally coordinated to one oxygen atom (O(4)) from the monodentate $PhCO_2^-$ group, two nitrogen atoms (N(2),

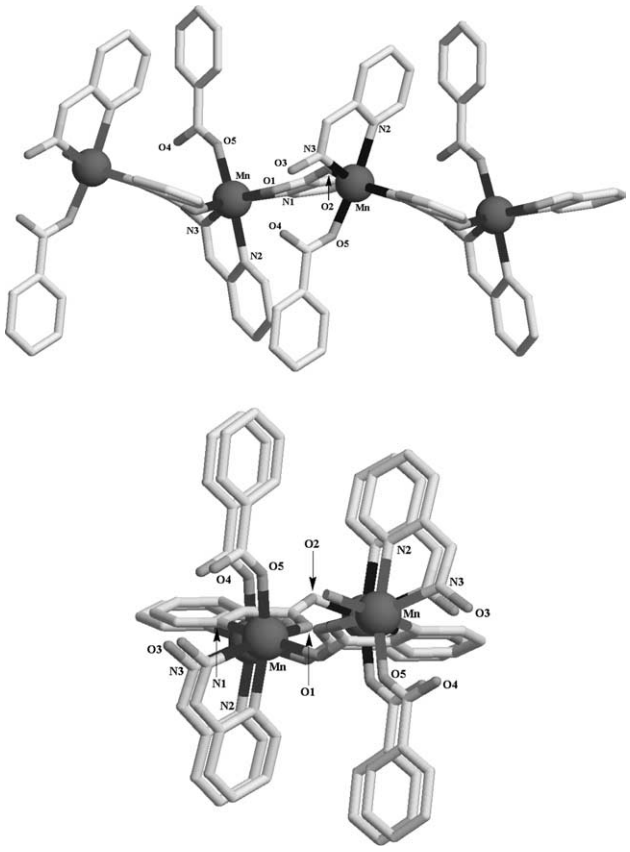

Fig. 5. Views of complex **2** along *b* axis (up) and *c* axis (down).

N(3)) from the chelating neutral 2-pyridinealdoxime molecule, one nitrogen and one oxygen (N(1), O(1)) from a picolinate(−1) ligand and to one oxygen atom (O(2)) from a neighbouring picolinate(−1) ligand; thus, the chromophore is *fac*-MnN_3O_3. The Mn–O and Mn–N bond lengths are in the narrow 2.092(3)–2.168(2) and 2.301(3)–2.324(3) Å ranges, respectively. Inspection of the bond angles listed in Table 3 shows that the octahedral coordination sphere of Mn is distorted. The intrachain Mn···Mn distance is 5.855(1) Å, slightly outside the typical range (5.2–5.8 Å) reported for singly *syn*, *anti* carboxylate-bridged Mn^{II} atoms [63]. A strong intrachain hydrogen bond is present in **2** with the oxime oxygen, O(3), as donor and the uncoordinated benzoate oxygen, O(5), as acceptor; its dimensions are O(3)···O(5) 2.489 Å, HO(3)···O(5) 1.440 Å, O(3)–HO(3)···O(5) 175.9°.

Complex **2** joins a small family of structurally characterised, neutral, 1D coordination polymers containing six-coordinate Mn^{II} sites; representative examples are described in [64–68]. It is also the first example in manganese(II) picolinate chemistry in which the $(py)CO_2^-$ ion adopts the $\eta^1{:}\eta^1{:}\eta^1{:}\mu_2$ coordination mode, i.e., chelating one Mn^{II} atom through its nitrogen and one carboxylate oxygen, and bridging an adjacent Mn^{II} atom through its second carboxylate oxygen.

An ORTEP plot of complex **3** is shown in Fig. 6. Its structure consists of a dinuclear $[Mn_2(O_2CMe)_2\{(py)CO_2\}_2\{(py)CHNOH\}_2]$ molecule located at a centre of symmetry. The two Mn^{II} atoms are bridged by two oxygen atoms (O(2), O(2′)) from the two symmetry-related $\eta^1{:}\eta^2{:}\mu_2$ $(py)CO_2^-$ ligands, the nitrogen atoms of which are ligated to Mn and Mn′. Each Mn^{II} atom is further coordinated by a monodentate acetate ion and a *N*,*N*′-chelating (py)CHNOH ligand, completing a distorted octahedral coordination at each metal. The central MnO(2)Mn′O(2′) core is strictly planar due to the presence of the inversion centre in the middle of the core. As for $\mathbf{1}\cdot 0.6CHCl_3$, the bridging $Mn–O_{picolinate}$ distances are symmetric (2.204(4), 2.210(4) Å). The Mn···Mn′ distance of 3.633(2) Å is somewhat longer than the analogous Mn(2)···Mn(2′) distance in $\mathbf{1}\cdot 0.6CHCl_3$ (Fig. 3) reflecting the different nature of the monoatomic bridge (picolinate versus benzoate); in accord with this the corresponding Mn–O–Mn angle in **3** (110.8(2)°) is larger than that in $\mathbf{1}\cdot 0.6CHCl_3$ (103.1(1)°). The Mn–N and Mn–O bond lengths are normal [30,31,46–50]. The bridging oxygen is perfectly planar ($\Sigma^{o}O(2) = 360°$).

An intramolecular hydrogen bond is present in **3** with the oxime oxygen, O(1), as donor and the "free", i.e., uncoordinated, acetate oxygen, O(5), as acceptor; its dimensions are O(1)···O(5) 2.479 Å, HO(1)···O(5) 1.602 Å and O(1)–HO(1)···O(5) 153.3°.

The structure of complex **4** consists of well-separated $[Mn(O_2CCF_3)_2\{(py)CHNOH\}_2]$ molecules (Fig. 7). The Mn^{II} atom is coordinated by two monodentate trifluoroacetates and two *N*,*N*′-bidentate chelating (py)CHNOH molecules. The six-coordinate molecule is the

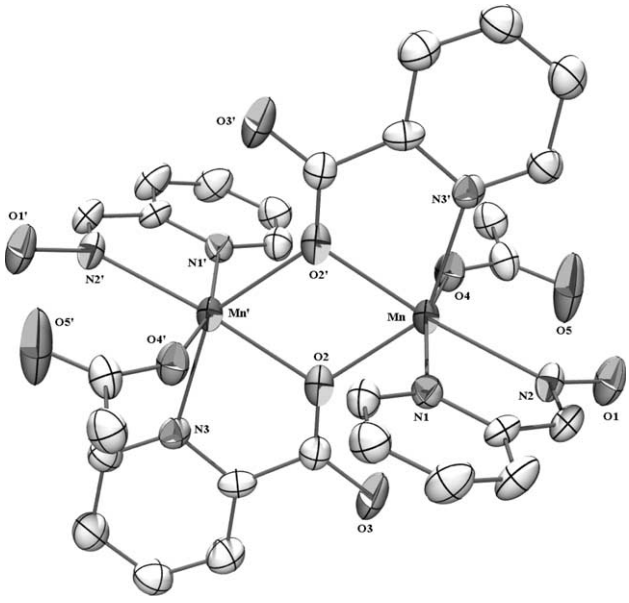

Fig. 6. An ORTEP plot at the 30% probability level of complex **3**. Primed and unprimed atoms are related by the crystallographic inversion centre. The carbon atoms are not labelled for clarity.

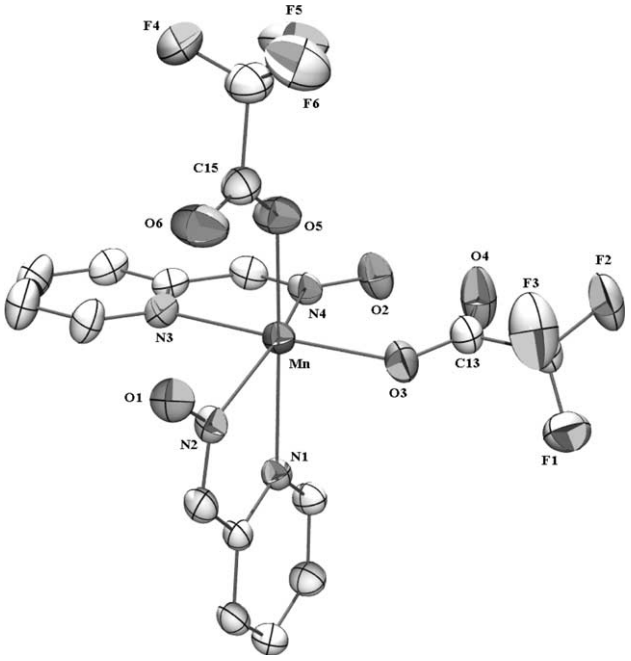

Fig. 7. ORTEP representation of the molecule of complex **4** at the 30% probability level. The plot has derived considering the positions of the F atoms with the larger occupation, i.e., 70% for F(1), F(2), F(3) and 60% for F(4), F(5), F(6).

cis–cis–trans isomer considering the positions of the oxygen, pyridyl nitrogen and oxime nitrogen atoms, respectively. The molecule has no imposed symmetry, although it approximates closely to C_2 symmetry, the C_2 axis bisecting the O(3)–Mn–O(5) angle. The four Mn–N bond lengths are almost identical (2.286(3)–2.289(2) Å). Angular distortions from octahedral geometry are primarily a consequence of the chelating oxime ligands and their restricted bite angles. There are two intramolecular hydrogen bonds with the uncoordinated oxime oxygens as donors and the "free" carboxylate oxygens as acceptors. Their dimensions are: O(1)···O(6) 2.582 Å, HO(1)···O(6) 1.612 Å, O(1)–OH(1)···O(6) 145.7° and O(2)···O(4) 2.571 Å, HO(2)···O(4) 1.697 Å, O(2)–HO(2)···O(4) 177.3°.

Complex **4** represents a new addition to the very small family of Mn^{II} complexes possessing monodentate $CF_3CO_2^-$ ligands [69,70]. Complex $[Mn(O_2CCF_3)_2(bpy)_2]$ [70] comes closest to reproduce the structural features of **4**; it has chelating 2,2′-bipyridine molecules instead of (py)CHNOH molecules.

3.3. Characteristic IR bands

A common, characteristic feature in the IR spectra of **1**–**4** is the appearance of a medium broad band at 3446–3428 cm^{-1} assignable [71] to ν(OH) of the (py)CHNOH ligand. The broadness and relatively low frequency of this band are both indicative of hydrogen bonding. Several bands appear in the 1670–1350 cm^{-1} range. Contributions from RCO_2^- (R = Me, Ph, CF_3) and/or picolinate $\nu_{as}(CO_2)$ and $\nu_s(CO_2)$ would be expected in this region, but overlap with the stretching vibrations of the aromatic rings renders assignments difficult. It seems that the frequencies of the $\nu_s(CO_2)$ bands of $PhCO_2^-/MeCO_2^-$ and $(py)CO_2^-$ coincide in the spectra of **1** (1404 cm^{-1}), **2** (1394 cm^{-1}) and **3** (1416 cm^{-1}). The bands at 1544, 1564 and 1548 cm^{-1} in **1**, **2** and **3**, respectively, are assigned to the $\nu_{as}(CO_2)_{PhCO_2^-/MeCO_2^-}$ vibration [72,73]. The difference Δ ($\Delta = \nu_{as}(CO_2) - \nu_s(CO_2)$) for **1** is 140 cm^{-1}, less than that for NaO_2CPh (184 cm^{-1}), as expected for the bridging modes of benzoate ligation [72]. The value of this parameter is 170 cm^{-1} for **2** and 132 cm^{-1} for **3**, less than the corresponding value for NaO_2CPh (184 cm^{-1}) and NaO_2CMe (164 cm^{-1}), respectively. These low Δ values might be interpreted as indicating bidentate (bridging or chelating) benzoate/acetate groups [72]; however, the crystal structures of both complexes reveal the presence of monodentate carboxylate groups. This disagreement with the spectroscopic criterion of Deacon and Phillips [72] is presumably due to the uncoordinated carboxylate oxygen's involvement (O(5) in Figs. 4 and 6) in hydrogen-bonding linkages [72,74] with the oxime group.

In the IR spectrum of NaO_2CF_3, the $\nu_{as}(CO_2)$ and $\nu_s(CO_2)$ bands appear at 1680 and 1457 cm^{-1}, respectively, i.e., $\Delta = 223$ cm^{-1} [72], while the corresponding bands for KO_2CCF_3 are at 1678 and 1437 cm^{-1} ($\Delta = 241$ cm^{-1}) [72]. In the spectrum of **4**, the bands at 1668 and 1448 cm^{-1} are assigned to $\nu_{as}(CO_2)$ and $\nu_s(CO_2)$; the Δ value (220 cm^{-1}) is not as large as expected ($\Delta > 260$ cm^{-1}) for monodentate trifluoroacetate ligands [72]. This is again due to the fact that the carboxylate oxygens (O(4), O(6) in Fig. 7) not coordinated to Mn^{II} are hydrogen bonded to the oxime groups, giving what can be regarded as a "pseudo-bridging" arrangement [72]. In addition, the $\nu_{as}(CO_2)$ and $\nu_s(CO_2)$ frequencies of **4** are sufficiently close to those of the alkali metal trifluoroacetates to raise the possibility of anion ($CF_3CO_2^-/Br^-$) exchange [72].

3.4. Magnetic properties and EPR spectra of *1*

Solid state variable-temperature (2–300 K) magnetic susceptibility (χ_M) studies were performed on a polycrystalline sample of compound **1** in a 0.1 T field. The data are plotted as $\chi_M T$ and χ_M versus T in Fig. 8. The χ_M versus T curve shows a maximum at approximately 5 K, indicative of weak antiferromagnetic coupling [60]. The room-temperature $\chi_M T$ value is 16.1 cm^3 mol^{-1} K, somewhat lower than the expected value of $\chi_M T = 17.5$ cm^3 mol^{-1} K for four $S = 5/2$ uncoupled spins with $g = 2$. The $\chi_M T$ product decreases steadily with decreasing temperature and tends to zero at very low

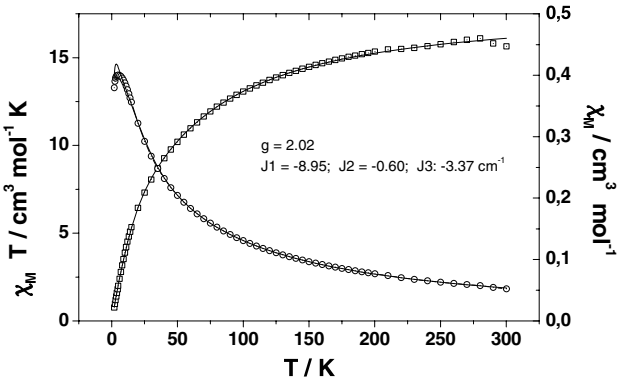

Fig. 8. Plots of $\chi_M T$ and χ_M vs. T for the tetranuclear complex **1**.

temperatures, indicating an overall antiferromagnetic behaviour. Since the spins carriers are all d^5 Mn^{II} ions, and therefore orbital singlet (S) ions, only the isotropic part of the exchange interaction was considered and the contribution of the zero-field splitting was neglected [60].

For a molecule such as **1** a total of five exchange parameters J_{ij} are required to cover each possible pairwise exchange interaction between Mn^{II} ions i and j; a sixth parameter $J_{11'}$ (the numbering scheme is the same as that shown in Fig. 3) is assumed to be zero, given the large distance and superexchange pathway involved ($Mn(1)\cdots Mn(1') = 7.364(3)$ Å). However, due to symmetry, a total of three exchange parameters are enough to cover each possible pairwise interaction. The magnetic model that was used is shown graphically in Fig. 9. Inspection of the molecular structure of **1** reveals that the three exchange pathways can be described as follows: The first one, J_1, refers to the interaction between Mn(1) and Mn(2) (and their symmetry equivalents) mediated by one monoatomic picolinate O-bridge, one *syn*, *syn* bidentate bridging $PhCO_2^-$ group and the "triatomic" part of one $\eta^1{:}\eta^2{:}\mu_3$ $PhCO_2^-$ group. The second one, J_2, refers to the interaction between Mn(1) and Mn(2′) (and their symmetry equivalents) mediated by one *syn, syn* bidentate bridging $PhCO_2^-$ group and the "triatomic" part of the same μ_3 $PhCO_2^-$ that bridges Mn(1) and Mn(2). The third exchange pathway, represented by J_3, refers to the $Mn(2)\cdots Mn(2')$ interaction mediated by two monoatomic benzoate O-bridges. Best-fit parameters, obtained by means of the full-matrix diagonalisation program CLUMAG [75] and applying the Hamiltonian given in Eq. (3) (where S_1, S_2, S_3 and S_4 correspond to Mn(1), Mn(2), Mn(2′) and Mn(1′), respectively),

$$H = -J_1(S_1S_2 + S_3S_4) - J_2(S_1S_3 + S_2S_4) - J_3(S_2S_3) \quad (3)$$

are $J_1 = -8.95$ cm^{-1}, $J_2 = -0.60$ cm^{-1}, $J_3 = -3.37$ cm^{-1} and $g = 2.02$ ($R = 5.1 \times 10^{-5}$).

The g parameter presents a value very close to 2.0, in accord with the presence of Mn^{II} ions which do not exhibit spin-orbit coupling [67]. The obtained J values are in agreement with qualitative magnetostructural correlations found in Mn^{II} complexes. J values reported in the literature with *only* carboxylate groups as bridging ligands are always small and negative, between approximately −0.2 and −5 cm^{-1} [67,76,77], indicating weak antiferromagnetic coupling. The J_2 value is well within the reported range. The carboxylate group involving O(41) and O(42) can be considered as poorly efficient to transmit the superexchange interaction between Mn(1) and Mn(2′) due to the quasi orthogonal arrangement, evidenced by the Mn(1)–O(41)–O(42)–Mn(2′) dihedral angle of 88.0°; this may explain the very low J_2 value, since only one *syn*, *syn* carboxylate bridge is operative (the group involving O(31) and O(32′)). DFT calculations on Mn–$(OR)_2$–Mn systems indicate a strong dependence of the antiferromagnetic coupling as function of the Mn–O–Mn bond angle below 98° and weak, but increasing, antiferromagnetic response for Mn–O–Mn bond angles in the 98°–110° range [78]. Thus, on the basis of the Mn(2)–O(42)–Mn(2′) angle of 103.1(1)°, the weak antiferromagnetic coupling J_3 (−3.37 cm^{-1}) is understandable. The fact that the J_1 value is outside the reported range (−0.2 to −5 cm^{-1}) may be due to the different carboxylate bridges involved (picolinate and benzoate).

The X-band EPR spectrum of a polycrystalline sample of **1** (Fig. 10) consists of an isotropic featureless signal centred at $g = 2$ (linewidth 390 G), and one weak half-field signal centred at $g = \sim 4$. The spectrum remains unchanged in the 77–300 K range. Such a spectrum is typical for magnetically interacting Mn^{II} ions in the solid state [61].

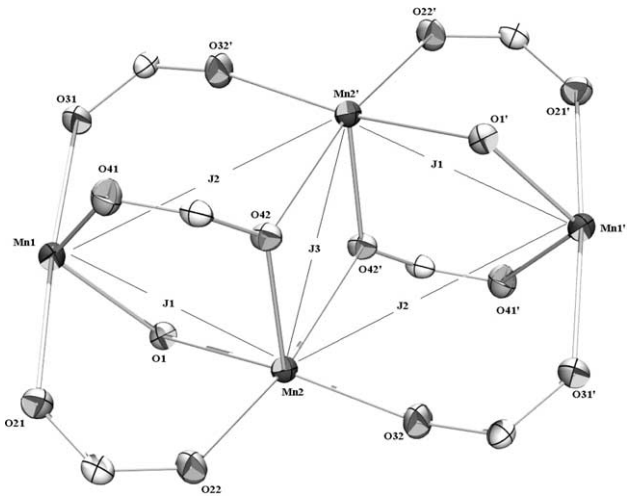

Fig. 9. Assignment of J values to $Mn\cdots Mn$ interactions for the magnetic model used for **1**. The numbering scheme used for the Mn^{II} ions is the same with that used in Fig. 3. Atoms O(1) and O(1′) are the μ_2 picolinate(−1) oxygens, while all the rest oxygen atoms belong to benzoate ligands.

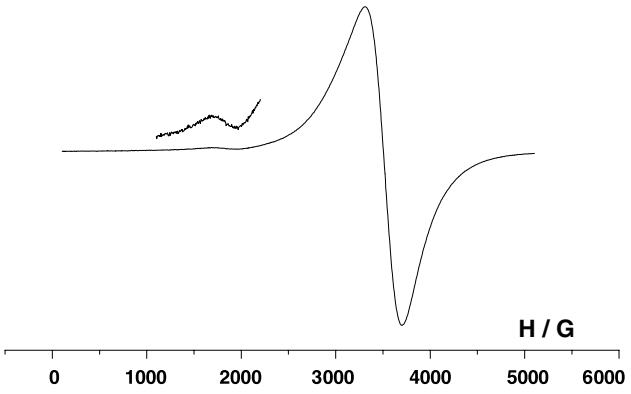

Fig. 10. Room temperature X-band EPR spectrum of a powdered sample of complex **1**.

4. Conclusions

The initial use of the pyridylaldoxime ligand (py)CHNOH in Mn^{II} carboxylate chemistry has provided accessto three new Mn^{II} complexes with interesting structures and properties: one dinuclear (**3**), one tetranuclear (**1**) and one polymeric (**2**). In all three cases, a Mn^{II}-assisted partial (py)CHNOH $\rightarrow$ (py)CO_2^- transformation has been observed. In view of this transformation, we strongly believe that the activation of 2-pyridyloximes by 3d-metals centres towards further reactions will become a fruitful area of research. The formation of the trifluoroacetate ligands and their incorporation in complex **4** are also interesting and warrant further study and expansion to other 3d-metals and β-diketonates. Since (py)CHNOH has been previously shown by others to be capable of acting as a anionic, i.e. (py)$CHNO^-$, bridging ligand, our current activity is directed towards the isolation of Mn (at various oxidation levels) carboxylate clusters containing (py)$CHNO^-$; parallel studies with Fe^{III}, Co^{II}, Ni^{II} and Cu^{II} carboxylates are also in progress. Results at the time of writing reveal that the nature of (py)$CHNO^-$ makes it a versatile ligand for a variety of objectives/advantages, including μ_2 and μ_3 behaviour, high-nuclearity cluster formation, linking of clusters into polymeric arrays, 3d–4f mixed-metal chemistry and ferromagnetic exchange interactions.

5. Supplementary material

Crystallographic data in CIF format have been deposited at the Cambridge Crystallographic Data Centre with CCDC Nos. 214660 (**1** · 0.6$CHCl_3$), 214661 (**2**), 214662 (**3**) and 214663 (**4**). Copies of this information may be obtained free of charge from The Director, CCDC, 12 Union Road, Cambridge, CB2 1EZ, UK (fax: +44-1223-336033; e-mail: deposit@ccdc.cam.ac.uk or http://www.ccdc.cam.ac.uk).

Acknowledgements

This research was supported by the Research Committee of the University of Patras (K. CARATHEODORY Program No. 1941 to S.P.P.) and by the Spanish Ministerio de Ciencia y Tecnología, BQU2000/0791 project.

References

[1] V.L. Pecoraro (Ed.), Manganese Redox Enzymes, VCH, New York, 1992.
[2] P. Jordan, P. Fromme, H.T. Witt, O. Klukas, W. Saenger, N. Krauss, Nature 411 (2001) 909.
[3] S. Wang, M.S. Wemple, J. Yoo, K. Folting, J.C. Huffman, K.S. Hagen, D.N. Hendrickson, G. Christou, Inorg. Chem. 39 (2000) 1501 (and references therein).
[4] C.E. Dube, D.W. Wright, S. Pal, P.J. Bonitatebus, W.H. Armstrong, J. Am. Chem. Soc. 120 (1998) 3704.
[5] R.M. Cinco, A. Rompel, H. Visser, G. Aromi, G. Christou, K. Sauer, M.P. Klein, V.K. Yachandra, Inorg. Chem. 38 (1999) 5988.
[6] G. Christou, D. Gatteschi, D.N. Hendrickson, R. Sessoli, MRS Bull. 25 (2000) 66.
[7] D. Gatteschi, R. Sessoli, Angew. Chem., Int. Ed. 42 (2003) 268.
[8] J. Yoo, E.K. Brechin, A. Yamaguchi, M. Nakano, J.C. Huffman, A.L. Maniero, L.-C. Brunel, K. Awaga, H. Ishimoto, G. Christou, D.N. Hendrickson, Inorg. Chem. 39 (2000) 3615.
[9] E.K. Brechin, C. Boskovic, W. Wernsdorfer, J. Yoo, A. Yamaguchi, E.C. Sañudo, T.R. Concolino, A.L. Rheingold, H. Ishimoto, D.N. Hendrickson, G. Christou, J. Am. Chem. Soc. 24 (2002) 9710.
[10] C.J. Milios, E. Kefalloniti, C.P. Raptopoulou, A. Terzis, R. Vicente, N. Lalioti, A. Escuer, S.P. Perlepes, Chem. Commun. (2003) 819.
[11] C.J. Milios, C.P. Raptopoulou, A. Terzis, R. Vicente, A. Escuer, S.P. Perlepes, Inorg. Chem. Commun. 6 (2003) 1056.
[12] C.J. Milios, C.P. Raptopoulou, A. Terzis, F. Lloret, R. Vicente, S.P. Perlepes, A. Escuer, Angew. Chem., Int. Ed., in press.
[13] V.Yu. Kukushkin, D. Tudela, A.J.L. Pombeiro, Coord. Chem. Rev. 156 (1996) 333.
[14] V.Yu. Kukushkin, A.J.L. Pombeiro, Coord. Chem. Rev. 181 (1999) 147.
[15] P. Chaudhuri, M. Hess, T. Weyhermüller, E. Bill, H.-J. Haupt, U. Flörke, Inorg. Chem. Commun. 1 (1998) 39.
[16] Y.N. Kukushkin, V.K. Krylov, S.F. Kaplan, M. Calligaris, E. Zangrando, A.J.L. Pombeiro, V.Yu. Kukushkin, Inorg. Chim. Acta 285 (1999) 116.
[17] N.A. Bokach, M. Haukka, A.J.L. Pombeiro, S.N. Morozkina, V.Yu. Kukushkin, Inorg. Chim. Acta 336 (2002) 95.
[18] E. Bill, C. Krebs, M. Winter, M. Gerdan, A.X. Trautwein, U. Flörke, H.-J. Haupt, P. Chaudhuri, Chem. Eur. J. 3 (1997) 193.
[19] V. Zerbib, F. Robert, P. Gouzerh, J. Chem. Soc., Chem. Commun. (1994) 2179.
[20] D.T. Rosa, J.A. Krause Bauer, M.J. Baldwin, Inorg. Chem. 40 (2001) 1606.
[21] M.J. Goldcamp, S.E. Robinson, J.A. Krause Bauer, M.J. Baldwin, Inorg. Chem. 41 (2002) 2307.
[22] M.N. Kopylovich, V.Yu. Kukushkin, M. Haukka, J.J.R. Frausto da Silva, A.J.L. Pombeiro, Inorg. Chem. 41 (2002) 4798.
[23] J.M. Thorpe, R.L. Beddoes, D. Collison, C.D. Garner, M. Helliwell, J.M. Holmes, P.A. Tasker, Angew. Chem., Int. Ed. 38 (1999) 119.
[24] P. Chaudhuri, M. Hess, E. Rentschler, T. Weyhermüller, U. Flörke, New J. Chem. (1998) 553.

[25] P. Chaudhuri, F. Birkelbach, M. Winter, V.V. Staemmler, P. Fleischhauer, W. Haase, U. Flörke, H.-J. Haupt, J. Chem. Soc., Dalton Trans (1994) 2313.
[26] H.-J. Krüger, G. Peng, R.H. Holm, Inorg. Chem. 30 (1991) 734.
[27] A.N. Singh, A. Chakravorty, Inorg. Chem. 19 (1980) 969.
[28] H. Saarinen, M. Orama, Acta Chem. Scand. 52 (1998) 1209.
[29] R. Clérac, H. Miyasaka, M. Yamashita, C. Coulon, J. Am. Chem. Soc. 124 (2002) 12837.
[30] S. Ross, T. Weyhermüller, E. Bill, K. Wieghardt, P. Chaudhuri, Inorg. Chem. 40 (2001) 6656.
[31] J.-L. Song, J.-G. Mao, H.-Y. Zeng, R.K. Kremer, Z.-C. Dong, Inorg. Chem. Commun. 6 (2003) 891.
[32] M.W. Wemple, H.-L. Tsai, S. Wang, J.P. Claude, W.E. Streib, J.C. Huffman, D.N. Hendrickson, G. Christou, Inorg. Chem. 35 (1996) 6437.
[33] J.B. Vincent, H.-R. Chang, K. Folting, J.C. Huffman, G. Christou, D.N. Hendrickson, J. Am. Chem. Soc 109 (1987) 5703.
[34] G.M. Sheldrick, SHELXS-86, Structure Solving Program, University of Göttingen, Göttingen, Germany, 1986.
[35] G.M. Sheldrick, SHELXL-93, Crystal Structure Refinement, University of Göttingen, Göttingen, Germany, 1993.
[36] C.J. Milios, Th. Stamatatos, A. Terzis, S.P. Perlepes, unpublished results.
[37] O. Attanasi, S. Garperoni, C. Carletti, J. Prakt. Chem. 322 (1980) 1063.
[38] M.B. Smith, J. March, Advanced Organic Chemistry, 5th ed., Wiley, New York, 2001, pp. 812, 813, 917, 1177.
[39] S.P. Perlepes, A.G. Blackman, J.C. Huffman, G. Christou, Inorg. Chem. 30 (1991) 1665.
[40] E. Libby, K. Folting, C.J. Huffman, J.C. Huffman, G. Christou, Inorg. Chem. 32 (1993) 2549.
[41] S. Wang, Z. Pang, K.D.L. Smith, Y.-S. Hua, C. Deslippe, M.J. Wagner, Inorg. Chem. 34 (1995) 908.
[42] S.R. Drake, A. Lyons, D.J. Otway, D.J. Williams, Inorg. Chem. 33 (1994) 1230.
[43] M.F. Richardson, W.F. Wagner, D.E. Sands, J. Inorg. Nucl. Chem. 30 (1968) 1275.
[44] E. Bouwman, J.C. Huffman, E.B. Lobkovsky, G. Christou, Inorg. Chem. 31 (1992) 4436.
[45] E. Bouwman, K. Caulton, G. Christou, K. Folting, C. Gasser, D.N. Hendrickson, J.C. Huffman, E.B. Lobkovski, J.D. Martin, P. Michel, H.-L. Tsai, Z. Xue, Inorg. Chem. 32 (1993) 3463.
[46] A.J. Tasiopoulos, N.C. Harden, K.A. Abboud, G. Christou, Polyhedron 22 (2003) 133.
[47] M.A.S. Goher, M.A.M. Abu-Youssef, F.A. Mautner, A. Popitsch, Polyhedron 11 (1992) 2137.
[48] M.A.S. Goher, M.A.M. Abu-Youssef, F.A. Mautner, A. Popitsch, Polyhedron 12 (1993) 1751.
[49] N. Okabe, M. Koizumi, Acta Crystallogr., Sect. C 54 (1998) 288.
[50] M.G. Barandika, Z.E. Serna, M.K. Urtiaga, J.I.R. De Larramendi, M.I. Arriortua, R. Cortes, Polyhedron 18 (1999) 1311.
[51] K.S. Murray, Adv. Inorg. Chem. 43 (1995) 261.
[52] S. Brooker, V. McKee, J. Chem. Soc., Chem. Commun. (1989) 619.
[53] S.C. Shoner, P.P. Power, Inorg. Chem. 31 (1992) 1001.
[54] H. Sakiyama, K. Tokuyama, Y. Matsumura, H. Okawa, J. Chem. Soc., Dalton Trans. (1993) 2329.
[55] D.A. Bardwell, J.C. Jeffery, M.D. Ward, J. Chem. Soc., Dalton Trans. (1995) 3071.
[56] S. Brooker, V. McKee, T. Metcalfe, Inorg. Chim. Acta 246 (1996) 171.
[57] P. Sobota, J. Utko, S. Szafert, Z. Janas, T. Glowiak, J. Chem. Soc., Dalton Trans. (1996) 3469.
[58] M.-X. Li, G.-Y. Xie, S.-L. Jin, Y.-D. Gu, M.-Q. Chen, J. Liu, Z. Xu, X.-Z. You, Polyhedron 15 (1996) 535.
[59] A. Gelasco, A. Askenas, V.L. Pecoraro, Inorg. Chem. 35 (1996) 1419.
[60] L.E. Pence, A. Caneschi, S.J. Lippard, Inorg. Chem. 35 (1996) 3069.
[61] S. Theil, R. Yerande, R. Chikate, F. Dahan, A. Bousseksou, S. Padhye, J.-P. Tuchagues, Inorg. Chem. 36 (1997) 6279.
[62] R.A.III Reynolds, D. Coucouvanis, Inorg. Chem. 37 (1998) 171.
[63] C. Policar, F. Lambert, M. Cesario, I. Morgenstern-Badarau, Eur. J. Inorg. Chem. (1999) 2201 (and references therein).
[64] G.S. Papaefstathiou, R. Vicente, C.P. Raptopoulou, A. Terzis, A. Escuer, S.P. Perlepes, Eur. J. Inorg. Chem. (2002) 2488.
[65] H.-Y. Shen, D.-Z. Liao, Z.-H. Jiang, S.P. Yan, B.-W. Sun, G.-L. Wang, X.-K. Yao, H.-G. Wang, Polyhedron 17 (1998) 1953.
[66] R. Cortes, M. Drillon, X. Solans, L. Lezama, T. Rojo, Inorg. Chem. 36 (1997) 677.
[67] B. Albela, M. Corbella, J. Ribas, I. Castro, J. Sletten, H. Stoeckli-Evans, Inorg. Chem. 37 (1998) 788 (and references therein).
[68] M. Lubben, A. Meetsma, B.L. Feringa, Inorg. Chim. Acta 230 (1995) 169.
[69] K. Hubner, H.W. Roesky, M. Noltemeyer, R. Bohra, Chem. Ber. 124 (1991) 515.
[70] M. Andruh, K. Hubner, M. Noltemeyer, H.W. Roesky, Z. Naturforsch., Teil B 48 (1993) 591.
[71] K.W. Nordquest, D.W. Phelps, W.F. Little, D.J. Hodgson, J. Am. Chem. Soc. 98 (1976) 1104.
[72] G.B. Deacon, R.J. Phillips, Coord. Chem. Rev. 33 (1980) 227.
[73] G.S. Papaefstathiou, A. Escuer, M. Font-Bardia, S.P. Perlepes, X. Solans, R. Vicente, Polyhedron (2002) 2027.
[74] S.P. Perlepes, E. Libby, W.E. Streib, K. Folting, G. Christou, Polyhedron 11 (1992) 923.
[75] D. Gatteschi, L. Pardi, Gazz. Chim. Ital. 123 (1993) 231.
[76] V. Tangoulis, G. Psomas, C. Dendrinou-Samara, C.P. Raptopoulou, A. Terzis, D. Kessissoglou, Inorg. Chem. 35 (1996) 7655.
[77] H. Iikura, T. Nagata, Inorg. Chem. 37 (1998) 4702 (and references therein).
[78] E. Ruiz, S. Alvarez, P. Alemany, Chem. Commun. (1998) 2767.

Available online at www.sciencedirect.com
SCIENCE DIRECT®
Polyhedron 23 (2004) 97–102
POLYHEDRON
www.elsevier.com/locate/poly

Synthesis and hypodentate Cu(II) complexes of new tripodal tetraamine ligands incorporating a long pendant arm

Natasha J. Lundin, Ian G. Hamilton, Allan G. Blackman *

Department of Chemistry, University of Otago, P.O. Box 56, Dunedin, New Zealand

Received 16 July 2003; accepted 13 September 2003

This paper is dedicated to Professor George Christou on the happy occasion of his 50th birthday

Abstract

The synthesis and characterisation of the new aliphatic tripodal amine ligands apba (*N*-(5-aminopentyl)-*N,N*-bis(2-aminoethyl)amine) and ahba (*N*-(6-aminohexyl)-*N,N*-bis(2-aminoethyl)amine) are reported. The tetrahydrochloride salts of these ligands, as well as that of the previously reported ligand abba (*N*-(4-aminobutyl)-*N,N*-bis(2-aminoethyl)amine), react with $CuCO_3 \cdot Cu(OH)_2$ to give complexes in which the tripodal ligand coordinates to the Cu(II) ion in a hypodentate fashion, with the longest arm of the tripodal ligand remaining protonated and unbound in all cases. The crystal structure of $[Cu(abbaH)Cl_2]Cl \cdot 2H_2O \cdot CH_3OH$ reveals a five-coordinate Cu(II) ion in a slightly distorted square pyramidal geometry.
© 2003 Elsevier Ltd. All rights reserved.

Keywords: Hypodentate; Tripodal amine ligand; Cu(II) complexes; Crystal structure; Five-coordinate

1. Introduction

The stereochemical features peculiar to tripodal tetradentate amine ligands have led to their use in a wide variety of inorganic systems. Six-coordinate octahedral complexes containing such ligands invariably display *cis* geometries, and the inequivalence of the remaining two coordination sites in such complexes has been utilised in numerous studies aimed at monitoring the stereochemical outcome of ligand substitution reactions in Co(III) complexes containing these ligands [1–4]. The steric constraints imposed by such ligands often result in trigonal bipyramidal geometries for five-coordinate systems [5–7], while the rare examples of four-coordinate complexes containing tripodal ligands display distorted tetrahedral geometries [8,9], owing to the inability of these ligands to accommodate a square planar geometry. Of the fully aliphatic tripodal tetradentate amine ligands, the C_{3v} symmetric ligands tren (tris(2-aminoethyl)amine) and trpn (tris(3-aminopropyl)amine), in which all three arms are the same length, have been known for many years [10,11], and it is only in relatively recent times that ligands of lower symmetry have been prepared and their complexes studied (Fig. 1). These ligands generally bind to a single transition metal ion using all four nitrogen donor atoms, although examples of hypodentate coordination [12], in which the ligand binds using less than its full complement of donor atoms, have been reported [13–18]. A number of the ligands outlined in Fig. 1 contain 4-aminobutyl or 5-aminopentyl arms [19–22] and can potentially form seven- or eight-membered chelate rings on binding to a metal ion, but their coordination chemistry has not been investigated to date. In this paper we report the synthesis of the new tripodal ligands apba (*N*-(5-aminopentyl)-*N,N*-bis(2-aminoethyl)amine) and ahba (*N*-(6-aminohexyl)-*N,N*-bis(2-aminoethyl)amine), as well as an alternative synthesis of abba (*N*-(4-aminobutyl)-*N,N*-bis(2-aminoethyl)amine). Although capable of forming complexes containing large chelate rings, these ligands display hypodentate coordination in Cu(II) complexes, with the longest arm remaining protonated and unbound in all cases. These findings are confirmed by a

* Corresponding author. Tel.: +64-3-479-7931; fax: +64-3-479-7906.
E-mail address: blackman@alkali.otago.ac.nz (A.G. Blackman).

0277-5387/$ - see front matter © 2003 Elsevier Ltd. All rights reserved.
doi:10.1016/j.poly.2003.09.030

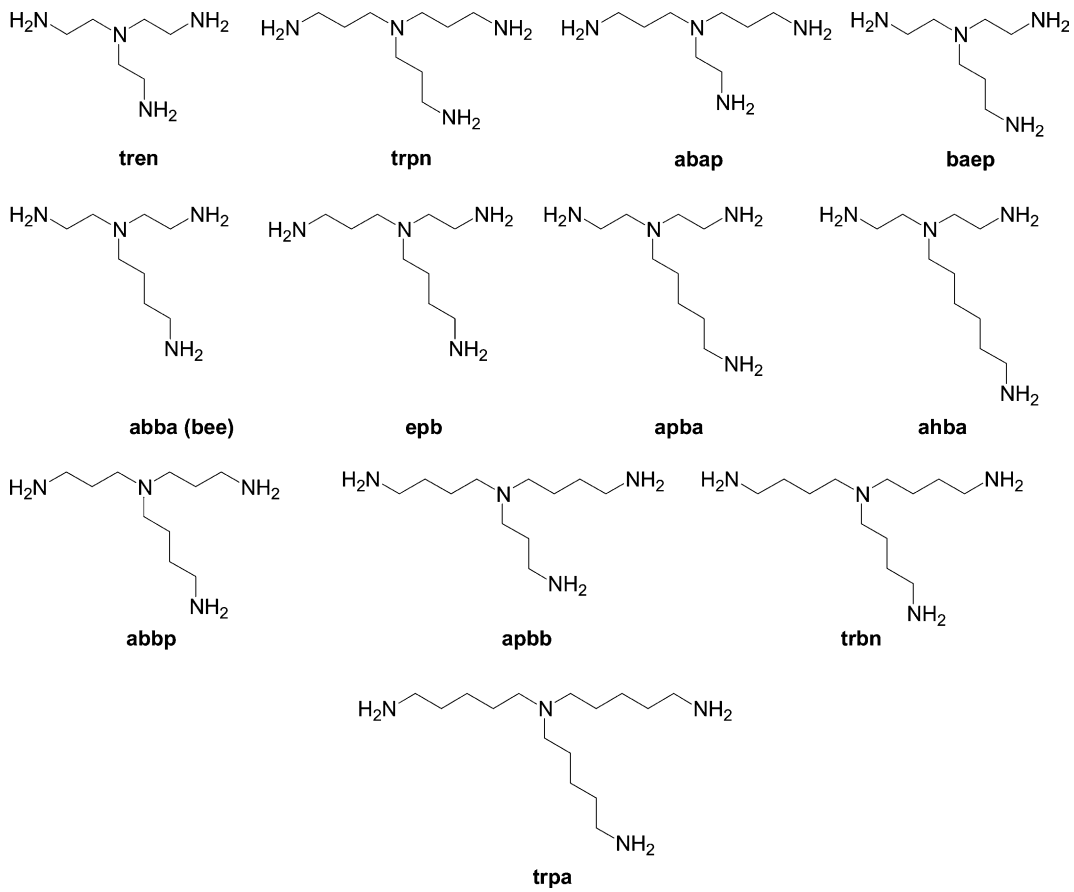

Fig. 1. Structures of the known aliphatic tripodal tetraamine ligands. References to their synthesis are as follows: abap [29], baep [31], abba [19], epb [20], apba, this work, ahba, this work, abbp [21], apbb [21], trbn [21], trpa [22].

crystal structure of the complex $[Cu(abbaH)Cl_2]Cl \cdot CH_3OH \cdot 2H_2O$.

2. Experimental

2.1. General

All chemicals used were LR grade or better. ^{13}C and ^{1}H NMR spectra were obtained in D_2O solution on a Varian Inova 300 MHz spectrometer at 25 °C. Chemical shifts are reported relative to NaTSP (^{1}H, 0.00 ppm) or dioxane (^{13}C, 67.8 ppm) as internal references. Elemental analyses were performed by the Campbell Microanalytical Laboratory, University of Otago. Electrospray mass spectra were recorded on a Shimadzu LCMS-QP800α spectrometer.

Diphthaloyldiethylenetriamine was prepared as described [19]. *N*-(4-bromobutyl)phthalimide and *N*-(6-bromohexyl)phthalimide were prepared by adaptation of the method used for the synthesis of *N*-(2-bromoethyl)phthalimide [23] (recrystallisation from cyclohexane and ethanol, respectively), while *N*-(5-bromopentyl) phthalimide was prepared according to a literature method [24].

2.2. Ligand syntheses: general procedure

An equimolar mixture of diphthaloyldiethylenetriamine and the appropriate bromoalkylphthalimide was heated at ~190 °C for 30 min with constant stirring. Following cooling, the glassy brown solid was ground to a powder and heated under reflux in 8 M HCl overnight. The solution was cooled and the precipitated phthalic acid removed by filtration. The filtrate was reduced to a yellow oil (rotary evaporator), which was diluted to 1 L with water and loaded onto a Dowex 50W-X2 (H^+ form) column. This was washed with 1 M HCl and the product was removed on elution with 3 M HCl. Removal of the solvent (rotary evaporator) gave the crude product which was recrystallised from hot ethanol (a small amount of ether was added to the cooled solution to induce crystallisation if necessary) to give the pure ligand tetrahydrochloride as a white powder.

2.2.1. *N-(4-aminobutyl)-N,N-bis(2-aminoethyl)amine tetrahydrochloride (abba·4HCl)*

Diphthaloyldiethylenetriamine (31.0 g, 85.3 mmol), *N*-(4-bromobutyl)phthalimide (24.6 g, 87.2 mmol), 8 M HCl (600 mL). Yield: 11.0 g (40.3%). Found: C, 29.6; H, 8.3; N, 16.9; Cl, 43.9. Calc. for $C_8H_{26}N_4Cl_4$: C, 30.0; H,

8.2; N, 17.5; Cl, 44.3%. ^{1}H NMR (D_2O), δ_H: 1.8 (m, 4H), 3.08 (t, $J = 6$ Hz, 2H), 3.36 (t, $J = 6$ Hz, 2H), 3.56 (m, 8H) ppm. ^{13}C NMR (D_2O), δ_C: 21.8, 25.0, 35.1, 40.1, 50.9, 54.5 ppm. MS (ESI): m/z 175 (MH^+).

2.2.2. *N-(5-aminopentyl)-N,N-bis(2-aminoethyl)amine tetrahydrochloride (apba · 4HCl)*

Diphthaloyldiethylenetriamine (23.1 g, 63.6 mmol), *N*-(5-bromopentyl)phthalimide (19.2 g, 64.8 mmol), 8 M HCl (190 mL). Yield: 8.02 g (37.7%). Found: C, 32.2; H, 8.4; N, 16.4; Cl, 42.0. Calc. for $C_9H_{28}N_4Cl_4$: C, 32.3; H, 8.4; N, 16.8; Cl, 42.4%. ^{1}H NMR(D_2O), δ_H: 1.51 (m, 2H), 1.78 (m, 2H), 1.87 (m, 2H), 3.06 (t, $J = 7.5$ Hz, 2H), 3.39 (t, $J = 8.7$ Hz, 2H), 3.56 (m, 4H), 3.66 (m, 4H) ppm. ^{13}C NMR (D_2O), δ_C: 23.3, 23.4, 26.9, 34.3, 39.8, 50.2, 54.4 ppm. MS (ESI): m/z 189 (MH^+).

2.2.3. *N-(6-aminohexyl)-N,N-bis(2-aminoethyl)amine tetrahydrochloride (ahba · 4HCl)*

Diphthaloyldiethylenetriamine (4.57 g, 12.6 mmol), *N*-(6-bromohexyl)phthalimide (3.99 g, 12.9 mmol) 8 M HCl (100 mL). Yield: 1.14 g (26.0%). Found: C, 34.7; H, 9.1; N, 15.9; Cl, 40.7. Calc. for $C_{10}H_{30}N_4Cl_4$: C, 34.5; H, 8.7; N, 16.1; Cl, 40.7%. ^{1}H NMR (D_2O), δ_H: 1.47 (m, 4H), 1.72 (m, 2H), 1.83 (m, 2H), 3.03 (t, $J = 7.8$ Hz, 2H), 3.35 (t, $J = 8.4$ Hz, 2H), 3.57 (m, 4H), 3.64 (m, 4H) ppm. ^{13}C NMR (D_2O), δ_C: 23.5, 25.78, 25.81, 27.1, 34.3, 39.9, 50.1, 54.6 ppm. MS (ESI): m/z 203 (MH^+).

2.3. Complex syntheses

Caution! Although we have experienced no difficulties with the perchlorate complexes described below, the usual care afforded all perchlorate species should be taken in their preparation and handling.

2.3.1. *[Cu(abbaH)Cl$_2$]Cl · 2H$_2$O · CH$_3$OH*

A suspension of abba · 4HCl (0.50 g, 1.6 mmol) and $CuCO_3 \cdot Cu(OH)_2$ (0.17 g, 0.77 mmol) in acetonitrile (50 mL) was heated under reflux for 2 h. The solution was allowed to cool, and the resulting green powder was removed by filtration. The powder was dissolved in the minimum volume of methanol and slow diethyl ether diffusion over three days gave bright blue needles suitable for X-ray diffraction. These crystals lose solvent readily and the analytical data thus refer to the desolvated material $[Cu(abbaH)Cl_2]Cl \cdot 2H_2O$ (0.21 g, 36%). Found: C, 24.7; H, 7.0; N, 14.2; Cl, 28.2. Calc. for $C_8H_{27}N_4Cl_3CuO_2$: C, 25.2; H, 7.1; N, 14.7; Cl, 27.9%.

2.3.2. *[Cu(apbaH)Cl(ClO$_4$)]ClO$_4$*

A suspension of apba · 4HCl (0.50 g, 1.5 mmol) and $CuCO_3 \cdot Cu(OH)_2$ (0.17 g, 0.77 mmol) in MeOH (20 mL) was heated under reflux for 2 h to give a deep green solution which was then hot filtered. Addition of $LiClO_4$ to the filtrate gave rapid formation of blue microcrystals. Following cooling in the freezer, the product was filtered off, washed with diethyl ether and dried in a vacuum desiccator. (0.29 g, 40%). Found: C, 22.2; H, 5.3; N, 11.2; Cl, 22.3. Calc. for $C_9H_{25}N_4Cl_3CuO_8$: C, 22.2; H, 5.2; N, 11.5; Cl, 21.8%.

2.3.3. *[Cu(ahbaH)Cl(ClO$_4$)]ClO$_4$*

A suspension of ahba · 4HCl (0.50 g, 1.4 mmol) and $CuCO_3 \cdot Cu(OH)_2$ (0.15 g, 0.68 mmol) in MeOH (20 mL) was heated under reflux for 2 h to give a deep green solution which was then hot filtered. Addition of $LiClO_4$ to the filtrate and storage in the freezer gave the product as blue microcrystals, which were then washed with diethyl ether and dried in a vacuum desiccator (0.27 g, 40%). Found: C, 24.1; H, 5.7; N, 11.0; Cl, 21.7. Calc. for $C_{10}H_{27}N_4Cl_3CuO_8$: C, 24.0; H, 5.4; N, 11.2; Cl, 21.2%.

2.4. X-ray crystallography

Data for $[Cu(abbaH)Cl_2]Cl \cdot 2H_2O \cdot CH_3OH$ were collected at −115 °C on a Siemens SMART system using graphite monochromated Mo Kα radiation with exposures over 0.3°. Data were corrected for Lorentz and polarisation effects using SAINT [25]. The structure was solved by direct methods using SIR-97 [26] running within the WinGX package [27], with the resulting Fourier map revealing the location of all non-hydrogen atoms. Weighted full matrix refinement on F^2 was carried out using SHELXL-97 [28] with all non-hydrogen atoms being refined anisotropically. Hydrogen atoms were included in calculated positions and were refined as riding atoms with individual (or group, if appropriate) isotropic displacement parameters. O3 was found to be disordered over two sites, with approximately 60:40 occupancy. Disorder of O2 was also evidenced by large thermal parameters, but this was not investigated further. Details of the crystal, data collection and structure refinement are given in Table 1.

3. Results and discussion

3.1. Synthesis of the tripodal ligands

The tetrahydrochloride salts of the ligands abba, apba and ahba were prepared in moderate yields in an analogous fashion to similar tripodal tetraamine ligands, by the solventless reaction of a melt of the appropriate bromoalkylphthalimide with diphthaloyldiethylenetriamine, followed by deprotection in refluxing HCl (Scheme 1) [19,20,29–31]. In our hands, this appears to be an easier method of preparing tripodal ligands than the alternative procedure involving synthesis of the appropriate trinitrile and subsequent reduction with $LiAlH_4$/H_2SO_4 [32,33]. Purification of the crude ligands was

Table 1
Crystal data and structure refinement for $[Cu(abbaH)Cl_2]Cl \cdot CH_3OH \cdot 2H_2O$

Empirical formula	$C_9H_{27}C_{l3}CuN_4O_3$
Formula weight	409.24
Temperature (K)	158(2)
Wavelength (Å)	0.71069
Crystal system	monoclinic
Space group	*P*2(1)/*n*
Unit cell dimensions	
a (Å)	6.247(5)
b (Å)	20.122(5)
c (Å)	15.729(5)
β (°)	92.734(5)
Volume (Å^3)	1974.9(18)
Z	4
Density (calculated) (Mg/m^3)	1.376
Absorption coefficient (mm^{-1})	1.521
F(0 0 0)	852
Crystal size (mm)	$0.44 \times 0.38 \times 0.28$
Theta range for data collection (°)	2.40–26.42
Index ranges	$-7 \leqslant h \leqslant 4$, $-24 \leqslant k \leqslant 25$, $-19 \leqslant l \leqslant 19$
Reflections collected	24 811
Independent reflections	3999 [$R_{int} = 0.0216$]
Completeness to theta = 26.42° (%)	98.7
Absorption correction	semi-empirical from equivalents
Maximum and minimum transmission	1.000 and 0.911
Refinement method	full-matrix least-squares on F^2
Data/restraints/parameters	3999/0/184
Goodness-of-fit on F^2	1.150
Final *R* indices [$I > 2\sigma(I)$]	$R_1 = 0.0566$, $wR_2 = 0.1671$
R indices (all data)	$R_1 = 0.0636$, $wR_2 = 0.1704$
Largest differential peak and hole (e Å^{-3})	1.196 and −0.685

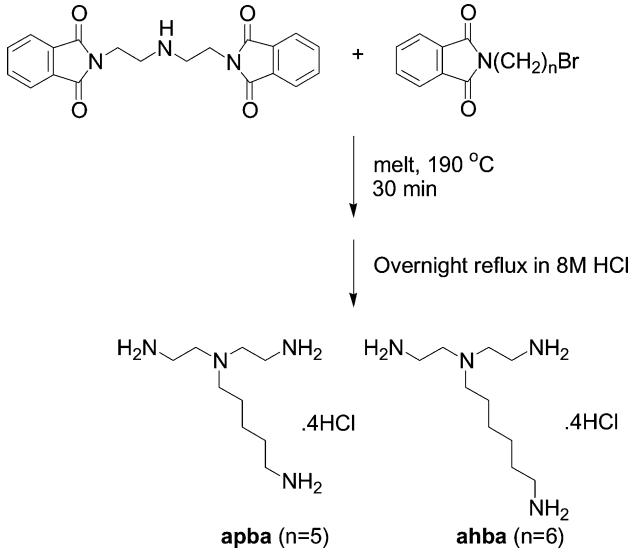

Scheme 1. The synthetic method used to prepare apba · 4HCl and ahba · 4HCl.

achieved by chromatography on Dowex 50W-X2 cation exchange resin (elution with 3M HCl) and the tetrahydrochloride salts of the pure ligands were obtained as white powders on recrystallisation from ethanol. Elemental analysis, mass spectral and ^1H and ^{13}C NMR data were consistent with the structures given in Fig. 1.

3.2. Synthesis of metal complexes

The tetrahydrochloride salts of abba, apba and ahba react with half a mole equivalent of $CuCO_3 \cdot Cu(OH)_2$ in either acetonitrile (abba) or methanol (apba, ahba), to give dissolution of the metal salts and production of bright green solutions. A green abba complex precipitated from the acetonitrile solution on cooling and the blue complex $[Cu(abbaH)Cl_2]Cl \cdot 2H_2O \cdot CH_3OH$ was isolated following recrystallisation from methanol. The green solutions obtained from the reaction of both apba and ahba in methanol slowly turned blue on cooling, and addition of $LiClO_4$ to these solutions gave the complexes $[Cu(apbaH)Cl(ClO_4)]ClO_4$ and $[Cu(ahbaH)Cl(ClO_4)]ClO_4$, respectively. Microanalytical data for all complexes were consistent with the presence of three counterions (Cl^- or ClO_4^-), strongly suggesting that the tripodal ligands were coordinating in a hypodentate fashion with a protonated pendant arm remaining uncoordinated to the metal ion. This was confirmed by the X-ray structure of $[Cu(abbaH)Cl_2]Cl \cdot CH_3OH \cdot 2H_2O$.

3.3. Crystal structure of $[Cu(abbaH)Cl_2]Cl \cdot CH_3OH \cdot 2H_2O$

Crystallographic data for $[Cu(abbaH)Cl_2]Cl \cdot CH_3OH \cdot 2H_2O$ are given in Table 1, bond lengths and

Table 2
Bond lengths (Å) and angles (°) for $[Cu(abbaH)Cl_2]Cl \cdot 2H_2O \cdot CH_3OH$

Bond lengths			
Cu(1)–N(1)	1.997(5)	Cu(1)–N(2)	2.015(4)
Cu(1)–N(3)	2.095(4)	Cu(1)–Cl(2)	2.3221(14)
Cu(1)–Cl(3)	2.541(2)	N(2)–C(4)	1.482(6)
N(3)–C(1)	1.477(7)	N(3)–C(3)	1.487(7)
N(3)–C(5)	1.491(6)	O(1)–C(9)	1.414(8)
N(4)–C(8)	1.491(7)	C(4)–C(3)	1.509(7)
C(7)–C(8)	1.521(7)	C(7)–C(6)	1.515(7)
N(1)–C(2)	1.475(8)	C(2)–C(1)	1.517(9)
C(5)–C(6)	1.522(7)		
Bond angles			
N(1)–Cu(1)–N(2)	160.20(18)	N(1)–Cu(1)–N(3)	85.05(19)
N(2)–Cu(1)–N(3)	83.81(17)	N(1)–Cu(1)–Cl(2)	93.19(14)
N(2)–Cu(1)–Cl(2)	92.40(13)	N(3)–Cu(1)–Cl(2)	162.05(11)
N(1)–Cu(1)–Cl(3)	95.86(13)	N(2)–Cu(1)–Cl(3)	102.31(13)
N(3)–Cu(1)–Cl(3)	101.10(11)	Cl(2)–Cu(1)–Cl(3)	96.85(5)
C(4)–N(2)–Cu(1)	111.6(3)	C(1)–N(3)–C(3)	113.8(4)
C(1)–N(3)–C(5)	111.2(4)	C(3)–N(3)–C(5)	112.7(4)
C(1)–N(3)–Cu(1)	105.2(3)	C(3)–N(3)–Cu(1)	101.4(3)
C(5)–N(3)–Cu(1)	111.8(3)	N(2)–C(4)–C(3)	108.5(4)
C(8)–C(7)–C(6)	111.8(4)	C(2)–N(1)–Cu(1)	109.2(4)
N(4)–C(8)–C(7)	110.5(4)	N(1)–C(2)–C(1)	107.2(4)
N(3)–C(1)–C(2)	109.8(4)	N(3)–C(5)–C(6)	115.8(4)
N(3)–C(3)–C(4)	109.4(4)	C(7)–C(6)–C(5)	111.2(4)

angles are given in Table 2, and Fig. 2 shows an ORTEP [34] diagram of the $[Cu(abbaH)Cl_2]^+$ cation. The structure consists of a five-coordinate Cu(II) ion coordinated to two chloride ligands and three nitrogen atoms of the abba ligand in a slightly distorted square pyramidal geometry ($\tau = 0.03$) [35], with the three nitrogen atoms and one chloride ion occupying the basal plane. The remaining *N* atom of the abba ligand is protonated, as evidenced by the presence of three chloride ions in the structure, and remains uncoordinated to the metal ion. The copper ion lies approximately 0.32 Å above the basal plane defined by the atoms N1, Cl2, N2 and N3. The axial Cu1–Cl3 bond (2.541(2) Å) is significantly longer than the Cu1–Cl2 bond (2.3221(14) Å), as has been found in a number of other five-coordinate Cu(II) complexes [36]. The Cu1–N1–C2–C1–N3 chelate ring adopts a symmetric skew λ conformation while the Cu1–N3–C3–C4–N2 chelate ring exists in an asymmetric envelope δ conformation [37]. The dangling aminobutyl chain displays an *anti* conformation about all C–C and C–N bonds, and the protonated terminal nitrogen atom is involved in hydrogen-bonding to both Cl3 and Cl4 of a neighbouring molecule (N4···Cl3 = 3.209(5) Å, N4···Cl4 = 3.106(6) Å) and the oxygen atom of the methanol of crystallisation (N4···O1 = 2.827(7) Å). N1 and N2 also participate in hydrogen-bonding interactions with chloride counterions.

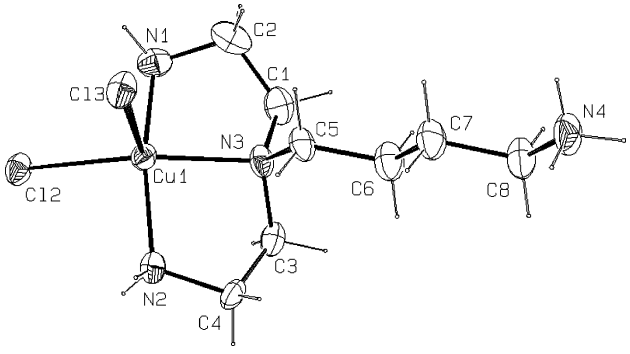

Fig. 2. ORTEP diagram of the $[Cu(abbaH)Cl_2]^+$ cation. Ellipsoids are drawn at the 50% probability level.

3.4. Discussion

The stability of five- and six-membered chelate rings in coordination complexes is usually explained in terms of the chelate effect, in which a positive entropy term renders chelation thermodynamically favourable [38]. However, the process of chelation becomes less entropically favourable for systems in which chelate rings containing more than six atoms can be formed, and such rings are also inherently strained. In agreement with this, a search of the Cambridge Structural Database [39] revealed 9891 metal complexes containing the chelated $-N(CH_2)_2N-$ fragment and 2762 containing the chelated $-N(CH_2)_3N-$ fragment, but only 140, 59 and 6 containing the chelated $-N(CH_2)_4N-$, $-N(CH_2)_5N-$ and $-N(CH_2)_6N-$ fragments, respectively. In the majority of these latter complexes, the large chelate rings are incorporated in macrocyclic or cryptand ligands, and this preorganisation undoubtedly aids chelation. The moderate steric constraints afforded by the tripodal ligands abba, apba and ahba are apparently not sufficient to

enforce chelation of the longest pendant arm of these ligands, and they thus coordinate to Cu(II) in a hypodentate fashion. However, it is interesting to note in this respect that when abba is incorporated into a Schiff-base macrocycle, all four N atoms coordinate to Cu(II) in the resulting complex [20].

X-ray quality crystals of $[Cu(apbaH)Cl(ClO_4)]ClO_4$ and $[Cu(ahbaH)Cl(ClO_4)]ClO_4$ could not be obtained and thus the exact geometries of these complexes remain uncertain. However, the presence of three counterions, as shown by elemental analysis, strongly suggests both complexes to be hypodentate, with either a five-coordinate (coordinated chloride and perchlorate) or four-coordinate (coordinated chloride) Cu(II) ion and a non-coordinated protonated aminoalkyl arm.

The presence of non-coordinated nitrogen atoms in the hypodentate complexes described herein affords several synthetic opportunities, as these complexes can potentially be used as building blocks for the synthesis of polymetallic species. The non-coordinated nitrogen atom can bind to another metal ion following deprotonation, or it can be used to prepare novel Schiff-base ligands through condensation with an appropriate carbonyl functionality. We are currently investigating these possibilities.

4. Supplementary material

Crystallographic data for $[Cu(abbaH)Cl_2]Cl \cdot CH_3OH \cdot 2H_2O$ (CCDC 214721) have been deposited with the Cambridge Crystallographic Data Centre. A copy of this information may be obtained free of charge from The Director, CCDC, 12 Union Road, Cambridge, CB2 1EZ, UK (fax: +44-1223-3360333; e-mail: deposit@ccdc.cam.ac.uk; www: http://www.ccdc.cam.ac.uk).

Acknowledgements

We thank Professor Ward Robinson and Dr. Jan Wikaira (University of Canterbury) for X-ray data collection.

References

[1] N.E. Brasch, D.A. Buckingham, C.R. Clark, A.J. Rogers, Inorg. Chem. 37 (1998) 4865.
[2] N.E Brasch, D.A. Buckingham, C.R. Clark, J. Simpson, Inorg. Chem. 35 (1996) 7728.
[3] D.A. Buckingham, C.R. Clark, W.S. Webley, Inorg. Chem. 30 (1991) 466.
[4] D.A. Buckingham, C.R. Clark, M.J. Gaudin, Inorg. Chem. 27 (1988) 293.
[5] D.B. Leznoff, B.-Y. Xue, R.J. Batchelor, F.W.B. Einstein, B.O. Patrick, Inorg. Chem. 40 (2001) 6026.
[6] R.T. Stibrany, J.A. Potenza, H.J. Schugar, Acta Cryst. C 49 (1993) 1561.
[7] M.J. Scott, S.C. Lee, R.H. Holm, Inorg. Chem. 33 (1994) 4651.
[8] E.V. Rybak-Akimova, A.Y. Nazarenko, S.S. Silchenko, Inorg. Chem. 38 (1999) 2974.
[9] X. Xu, C.S. Allen, C.-L. Chuang, J.W. Canary, Acta Cryst. C 54 (1998) 600.
[10] E. Ristenpart, Ber. 20 (1896) 2526.
[11] F.G. Mann, W.J. Pope, J. Chem. Soc. (1926) 489.
[12] E.C. Constable, in: K.D. Karlin (Ed.), Progress in Inorganic Chemistry, vol. 42, Wiley, New York, 1994, pp. 95–100.
[13] The cation of the complex $[Co(tren)_2][Co(CO)_4]_2$ contains two hydodentate tren ligands, but the pendant arms are not protonated J.C. Mareque Rivas, L. Brammer, Acta Cryst. C 54 (1998) 757.
[14] K. Sakai, Y. Yamada, T. Tsubomura, Inorg. Chem. 35 (1996) 3163.
[15] M.S. Davies, R.R. Fenton, F. Huq, E.C.H. Ling, T.W. Hambley, Aust. J. Chem. 53 (2000) 451.
[16] C.-H. Chen, J. Cai, X.-M. Chen, Acta Cryst. C 58 (2002) m59.
[17] R.L. Fanshawe, A. Mobinikhaledi, C.R. Clark, A.G. Blackman, Inorg. Chim. Acta, 307 (2000) 26.
[18] I.P.Y. Shek, T.-C. Lau, W.-T. Wong, J.-L. Zuoc, New J. Chem. 23 (1999) 1049.
[19] H. Keypour, S. Salehzadeh, Trans. Met. Chem. 25 (2000) 205.
[20] H. Keypour, S. Salehzadeh, R.G. Pritchard, R.V. Parish, Inorg. Chem. 39 (2000) 5787.
[21] M. Niitsu, H. Sano, K. Samejima, Chem. Pharm. Bull. 40 (1992) 2958.
[22] F.J. Weigert, J. Org. Chem. 43 (1978) 622.
[23] G.G. Wubbels, A.M. Halverson, J.D. Oxman, V.H. De Bruyn, J. Org. Chem. 50 (1985) 4499.
[24] J.F. Constant, B.M. Carden, J. Lhomme, J. Heterocyclic Chem. 22 (1985) 1035.
[25] SAINT, Version 4, Siemens Analytical X-ray Systems, Inc., Madison, WI, 1996.
[26] A. Altomare, M.C. Burla, M. Camalli, G.L. Cascarano, C. Giacovazzo, A. Guagliardi, A.G.G. Moliterni, G. Polidori, R. Spagna, J. Appl. Cryst. 32 (1999) 115.
[27] L.J. Farrugia, J. Appl. Cryst. 32 (1999) 837.
[28] G.M. Sheldrick, SHELXL-97, Program for the Refinement of Crystal Structures, University of Göttingen, 1997.
[29] R.L. Fanshawe, A.G. Blackman, Inorg. Chem. 34 (1995) 421.
[30] M. Streater, P.D. Taylor, R.C. Hider, J. Porter, J. Med. Chem. 33 (1990) 1749.
[31] R.J. Geue, A.M. Sargeson, R. Wijesekera, Aust. J. Chem. 46 (1993) 1021.
[32] A.M. Dittler-Klingemann, F.E. Hahn, Inorg. Chem. 35 (1996) 1996.
[33] C. Ochs, F.E. Hahn, T. Lügger, Eur. J. Inorg. Chem. (2001) 1279.
[34] ORTEP3 for Windows L.J. Farrugia, J. Appl. Crystallogr. 30 (1997) 565.
[35] A. Addison, T. Rao, J. Reedijk, J. van Rijn, G. Verschoor, J. Chem. Soc., Dalton Trans. (1984) 1349.
[36] B.J. Hathaway, in: G. Wilkinson, R.D. Gillard, J.A. McCleverty (Eds.), Comprehensive Coordination Chemistry, vol. 5, Pergamon, Oxford, 1987, p. 606, Ch. 53.
[37] C.J. Hawkins, Absolute Configurations of Metal Complexes, Wiley, New York, 1971.
[38] A.E. Martell, R.D. Hancock, R.J. Motekaitis, Coord. Chem. Rev. 133 (1994) 39.
[39] Cambridge Structural Database, Version 5.24, November 2002.

Available online at www.sciencedirect.com
SCIENCE DIRECT®
Polyhedron 23 (2004) 103–108
POLYHEDRON
www.elsevier.com/locate/poly

New one- and two-dimensional rhodium–tin polynuclear complexes, synthesis, properties and structural characterization

Florian P. Pruchnik [a,*], Zbigniew Ciunik [a], Mirosław Pruchnik [b]

[a] *Faculty of Chemistry, University of Wrocław, Joliot-Curie 14, PL-50-383 Wrocław, Poland*
[b] *Institute of Theoretical Physics, University of Wrocław, pl. M. Borna 9, 50-204 Wrocław, Poland*

Received 26 June 2003; accepted 16 September 2003

Abstract

Reactions of $[Sn(CH_2CH_2CN)_4]$ and $[Sn_2(CH_2CH_2CN)_6]$ with $[Rh_2Cl_2(CO)_4]$ give pentanuclear complex $[Sn\{CH_2CH_2CNRhCl(CO)_2\}_4]\cdot CH_2Cl_2$ (**1**) and hexanuclear compound $[Sn_2\{CH_2CH_2CNRhCl(CO)_2\}_4(CH_2CH_2CN)_2]\cdot CHCl_3$ (**2**). In acetone solution complex **2** slowly decomposes giving $[Rh_6(CO)_{16}]$ (**3**). X-ray structures of the compounds have been determined. In complexes **1** and **2** in the solid state square planar entities $[NRhCl(CO)_2]$ relatively strongly interact giving one-dimensional and two-dimensional compounds. In complex **2** the ditin moiety possesses an unexpected eclipsed conformation.
© 2003 Elsevier Ltd. All rights reserved.

Keywords: Organotin complexes; Organorhodium complexes; Organorhodiumtin complexes; One-dimensional compounds; Two-dimensional compounds; Rhodium carbonyl complexes

1. Introduction

Metal complexes containing bridging ligands often form polynuclear one- and two-dimensional polymeric compounds. They have recently been intensely investigated because of their interesting structure and physicochemical properties [1–4]. Investigation of organotin(IV) compounds in turn results from application of $[SnR_nX_{4-n}]$ in organic syntheses, for preparation of SnO_2 films and coatings on glass, in catalysis [5–7], as biocidal [5,6] and antitumor agents [8–12], etc. Functionalized alkyl and aryl complexes of tin(IV) have been much less investigated than the unsubstituted organometallic tin compounds. Organotin compounds containing 2-cyanoethyl ligands are interesting because they can be easily prepared electrochemically from a tin cathode and acrylonitrile [11,13,14] and may be used for preparation of amino, amido and carboxylic derivatives. The mononuclear compound $[Sn(CH_2CH_2CN)_4]$ is potentially a tetradentate lignd and the binuclear compound of tin(III), $[Sn_2(CH_2CH_2CN)_6]$, a hexadentate ligand coordinating via CN groups. In this paper, we describe the syntheses, structures and properties of pentanuclear one-dimensional complex $[Sn\{CH_2CH_2CNRhCl(CO)_2\}_4]\cdot CH_2Cl_2$ (**1**) and hexanuclear $[Sn_2\{CH_2CH_2CNRhCl(CO)_2\}_4(CH_2CH_2CN)_2]\cdot CHCl_3$ (**2**), a two-dimensional rhodium–tin compound which in solutions slowly decomposes giving $[Rh_6(CO)_{16}]$ (**3**).

2. Results and discussion

Reaction of $[Sn(CH_2CH_2CN)_4]$ and $[Sn_2(CH_2CH_2CN)_6]$ with $[Rh_2Cl_2(CO)_4]$ in carbon monoxide atmosphere in polar solvents give compounds with $[RhCl(CO)_2]$ moieties coordinated with the N atoms of the tin compounds. The complexes $[Sn\{CH_2CH_2CNRhCl(CO)_2\}_4]\cdot CH_2Cl_2$ (**1**) and $[Sn_2\{CH_2CH_2CNRhCl(CO)_2\}_4(CH_2CH_2CN)_2]\cdot CHCl_3$ (**2**), were obtained in dichloromethane and chloroform, respectively. It was not possible to obtain complexes containing a lower or higher number of rhodium entities. In reactions at molar ratios of tin(IV) or ditin(III) complex to dirhodium(I) compound in the range 1:1–1:3, always complexes **1** and

* Corresponding author. Tel./fax: +48-71-204-232.
E-mail address: pruchnik@wchuwr.chem.uni.wroc.pl (F.P. Pruchnik).

0277-5387/$ - see front matter © 2003 Elsevier Ltd. All rights reserved.
doi:10.1016/j.poly.2003.09.033

2 are formed. They are stable in the solid state under CO atmosphere at room temperature, however, in air **1** decomposes over several days and **2** in one day. They are soluble in organic polar solvents, e.g., dichloromethane, chloroform, acetone, acetonitrile. The solutions in carbon monoxide atmosphere are stable for several days. However, in solutions under inert atmosphere or in air compound **2** decomposes with deposition of dark brown compounds. Decomposition of compound **1** is slower. Complex **2** in acetone solution after several days at room temperature is reduced giving black crystals as the main product and an unidentified brown compound. The black compound was identified as the known hexanuclear cluster $[Rh_6(CO)_{16}]$ (**3**) [15,16]. The molecular structures of complexes **1**, **2** and **3** are shown in Figs. 1–3 and details of X-ray data collected are summarized in Table 1. Tables 2–4 contain selected bond lengths and angles for compounds **1**–**3** and in Table 5 hydrogen bonds parameters for complex **2** are given.

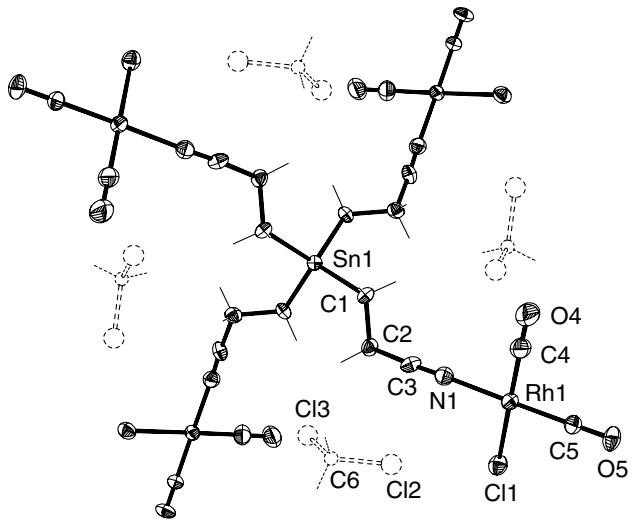

Fig. 1. ORTEP representation of **1** showing solvate molecules.

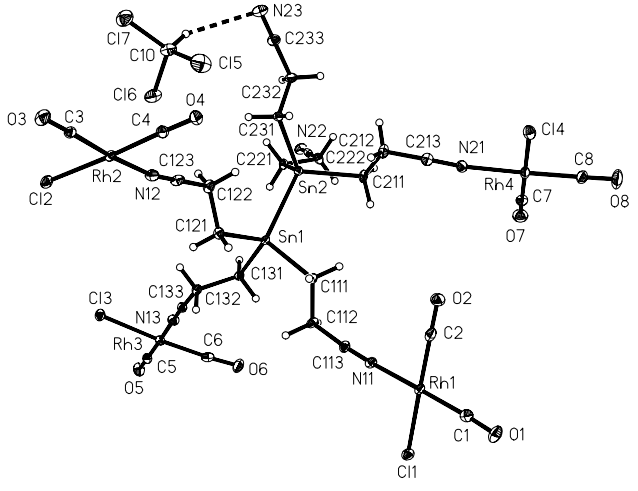

Fig. 2. ORTEP representation of complex **2**.

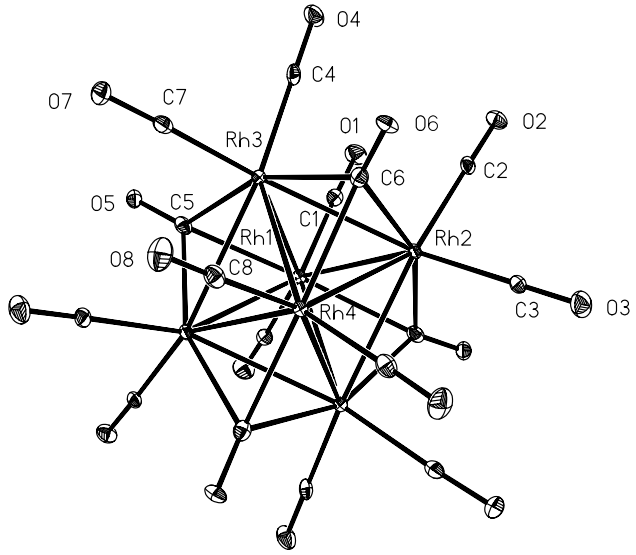

Fig. 3. ORTEP diagram showing the atom labelling scheme for the complex $[Rh_6(CO)_{16}]$ (**3**).

Compound **1** consists of discrete units $[Sn\{C_2H_4CNRhCl(CO)_2\}_4]$ of $\bar{4}$ tetrahedral symmetry with $RhCl(CO)_2$ entities coordinated through N atoms of the bridging 2-cyanoethyl ligands (Fig. 1). The Rh atoms have square-planar coordination. Compound **1** is a one-dimensional polymer linked along the [0 0 1] direction via Rh–Rh bonds (Fig. 4). The Rh–Rh distances are equal 3.134(2) Å. They are considerably shorter than those in $[Rh_2Cl_2(CO)_4]$ (3.31 Å) [7]. The neighboring square-planar $NRhCl(CO)_2$ entities are parallel with a staggered conformation. The N–Rh–Rh–N torsion angle is equal to 68.4(6)°. The disordered CH_2Cl_2 molecules (the respective occupancy parameter is equal to 0.25) occupy channels between linear chain polymers along the fourfold axes (Figs. 4 and 5). Complex **1** can also crystallize from other solvents giving analogous compounds with solvent molecules of crystallization in the channels.

The structure of **2** consists of a binuclear tin(III) unit with both tin(III) central atoms residing in a distorted tetrahedral coordination (Fig. 2). Three rhodium(I) atoms are coordinated with three 2-cyanoethyl ligands connected with the Sn(1) atom and one rhodium atom with the CH_2CH_2CN ligand bound with Sn(2). The Sn(1)–Sn(2) distance (2.7500(6) Å) is slightly shorter than that in $[Sn_2(CH_2CH_2CN)_6]$ [11]. The C–Sn and C–N distances as well as C–Sn–C and C–Sn–Sn angles are almost the same for complex **2** and for $[Sn_2(CH_2CH_2CN)_6]$. The following average distances were determined: Sn–C 2.176(7) Å, CH_2–CH_2 1.528(9) Å, CH_2–CN 1.464(9) Å, C–N 1.142(8) Å, Rh–N 2.063(5) Å, Rh–Cl 2.3423(17) Å and Rh–C 1.852(8) Å. It is interesting that the conformation of the tin moieties is

Table 1
Crystal data and structure refinement for complexes $[Sn\{CH_2CH_2CNRhCl(CO)_2\}_4]CH_2Cl_2$ (**1**), $[Sn_2(CH_2CH_2CN)_6\{RhCl(CO)_2\}_4]$ $CHCl_3$ (**2**) and $[Rh_6(CO)_{16}]$ (**3**)

Emperical formula	$C_{20}H_{16}N_4O_8Cl_4Rh_4SnCH_2Cl_2$	$C_{26}H_{24}N_6O_8Cl_4Rh_4Sn_2CHCl_3$	$C_{16}O_{16}Rh_6$
Formula weight	1197.44	1458.74	1065.62
T (K)	100(2)	100(2)	100(2)
λ (Å)	0.71073	0.71073	0.71073
Crystal system	tetragonal	triclinic	monoclinic
Space group	$P4/ncc$	$P\bar{1}$	$C2/c$
a (Å)	15.1445(10)	9.2146(9)	16.523(2)
b (Å)	15.1445(10)	12.9421(10)	9.6650(9)
c (Å)	18.380(3)	19.7750(16)	16.7419(16)
α (°)	90	102.920(7)	
β (°)	90	92.385(7)	117.889(17)
γ (°)	90	94.828(7)	
V (Å^3)	4215.6(7)	2286.0(3)	2363.1(4)
Z	4	2	4
D_{calc} (Mg m^{-3})	1.887	2.119	2.995
μ (mm^{-1})	2.536	2.942	4.172
$F(000)$	2272	1384	1976
Crystal size (mm)	$0.18 \times 0.15 \times 0.13$	$0.13 \times 0.10 \times 0.07$	$0.16 \times 0.10 \times 0.10$
θ range (°)	3.49–25.99	3.73–28.40	4.19–28.39
Ranges of h, k, l	−18 to 18, −18 to 18, −14 to 22	−8 to 12, −16 to 17, −26 to 26	−21 to 19, −12 to 12, −21 to 21
Reflections collected	23865	15837	7851
Individual reflections (R_{int})	2080 (0.0875)	10060 (0.0374)	2758 (0.0449)
Data/parameters	2080/105	10060/487	2758/174
Goodness-of-fit (F^2)	1.383	1.047	1.097
Final R_1/wR_2 indices($I > 2\sigma_I$)	0.0979/0.2070	0.0410/0.0927	0.0316/0.0826
Largest diffraction peak/hole (e Å^{-3})	2.166/−0.991	3.104/−1.306	2.228/−1.255

Table 2
Selected bond lengths (Å) and angles (°) for complex **1**

Rh(1)–C(4)	1.857(14)	C(1)–C(2)	1.520(15)
Rh(1)–C(5)	1.864(13)	C(2)–C(3)	1.488(16)
Rh(1)–N(1)	2.059(10)	C(4)–Rh(1)–C(5)	89.0(5)
Rh(1)–Cl(1)	2.352(3)	C(4)–Rh(1)–N(1)	92.8(5)
Rh(1)–Rh(1i)	3.1335(19)	C(5)–Rh(1)–N(1)	175.8(5)
Sn(1)–C(1ii)	2.167(11)	C(4)–Rh(1)–Cl(1)	178.9(5)
Sn(1)–C(1)	2.167(11)	C(5)–Rh(1)–Cl(1)	90.9(4)
Sn(1)–C(1iii)	2.167(11)	N(1)–Rh(1)–Cl(1)	87.2(3)
Sn(1)–C(1iv)	2.167(11)	C(4)–Rh(1)–Rh(1i)	92.9(5)
O(4)–C(4)	1.133(16)	C(5)–Rh(1)–Rh(1i)	91.6(4)
O(5)–C(5)	1.117(14)	N(1)–Rh(1)–Rh(1i)	92.1(3)
N(1)–C(3)	1.116(15)	Cl(1)–Rh(1)–Rh(1i)	88.20(8)

Symmetry transformations used to generate equivalent atoms; i: $y+1/2, x-1/2, -z+1/2$; ii: $-y, x-1/2, -z$; iii: $-x+1/2, -y-1/2, z$; iv: $y+1/2, -x, -z$; v: $-y+1/2, x-1, z$; vi: $y+1, -x+1/2, z$.

eclipsed. The C–Sn–Sn–C torsion angles are very small: C(121)–Sn(1)–Sn(2)–C(231) 4.8(2)°, C(111)–Sn(1)–Sn(2)–C(211) 7.5(2)° and C(131)–Sn(1)–Sn(2)–C(221) 8.6(2)°. The eclipsed conformation was also found for $[Sn_2(CH_2CH_2CN)_6]$. However, all known alkyl ditin(III) $[Sn_2R_6]$ compounds have staggered conformation [5,6,17]. The calculation of the structure of $[Sn_2(CH_2CH_2CN)_6]$ using PM3, MP2 and DFT B3LYP methods indicated that the eclipsed conformation is more stable in comparison with the staggered one [11]. Thus the stabilization of the eclipsed conformation of this complex results from electronic reasons and steric effects do not play a decisive role. Compound **2** is a

Table 3
Selected bond lengths (Å) and angles (°) for complex **2**

Sn(1)–C(121)	2.166(6)	Rh(3)–C(5)	1.858(7)
Sn(1)–C(111)	2.177(6)	Rh(3)–N(13)	2.052(5)
Sn(1)–C(131)	2.178(6)	Rh(3)–Cl(3)	2.3308(16)
Sn(1)–Sn(2)	2.7500(6)	Rh(4)–C(7)	1.850(8)
Sn(2)–C(231)	2.170(6)	Rh(4)–N(21)	2.062(5)
Sn(2)–C(211)	2.179(6)	Rh(4)–Cl(4)	2.3423(17)
Sn(2)–C(221)	2.185(5)	C(121)–Sn(1)–C(111)	102.9(2)
Rh(1)–C(1)	1.854(7)	C(121)–Sn(1)–C(131)	108.1(2)
Rh(1)–C(2)	1.863(7)	C(111)–Sn(1)–C(131)	106.7(2)
Rh(1)–N(11)	2.062(5)	C(121)–Sn(1)–Sn(2)	116.74(16)
Rh(1)–Cl(1)	2.3402(16)	C(111)–Sn(1)–Sn(2)	110.54(16)
Rh(2)–C(3)	1.853(6)	C(131)–Sn(1)–Sn(2)	111.22(16)
Rh(2)–C(4)	1.860(7)	C(231)–Sn(2)–C(211)	109.4(2)
Rh(2)–N(12)	2.074(5)	C(231)–Sn(2)–C(221)	107.6(2)
Rh(2)–Cl(2)	2.3558(16)	C(211)–Sn(2)–C(221)	108.5(2)

Table 4
Selected bond lengths (Å) for complex **3**

Rh(1)–C(1i)	1.913(5)	Rh(2)–C(2)	1.918(5)
Rh(1)–C(1)	1.913(5)	Rh(2)–C(6)	2.214(5)
Rh(1)–C(5i)	2.198(5)	Rh(2)–Rh(4)	2.7581(6)
Rh(1)–C(5)	2.198(5)	Rh(2)–Rh(3)	2.7593(7)
Rh(1)–Rh(3i)	2.7610(5)	Rh(2)–Rh(3i)	2.7607(5)
Rh(1)–Rh(3)	2.7610(5)	Rh(3)–Rh(2i)	2.7607(5)
Rh(1)–Rh(2)	2.7632(6)	Rh(3)–Rh(4)	2.7668(5)
Rh(1)–Rh(2i)	2.7632(6)	Rh(4)–Rh(2i)	2.7581(6)
Rh(2)–C(3)	1.918(5)	Rh(4)–Rh(3i)	2.7668(5)

Table 5
Lengths (Å) and angles (°) of the hydrogen bonds for complex **2**

D–H···A	D···A	H···A	D–H···A
C(10)–H(10)···N(23)	3.381(10)	2.55	142
C(111)–H(11B)···N(22i)	3.220(8)	2.84	104
C(122)–H(12C)···N(22i)	3.380(9)	2.59	139
C(212)–H(21D)···N(22i)	3.486(9)	2.58	155

Symmetry transformations used to generate equivalent atoms; (none): x, y, z; (i): $1 + x, y, z$.

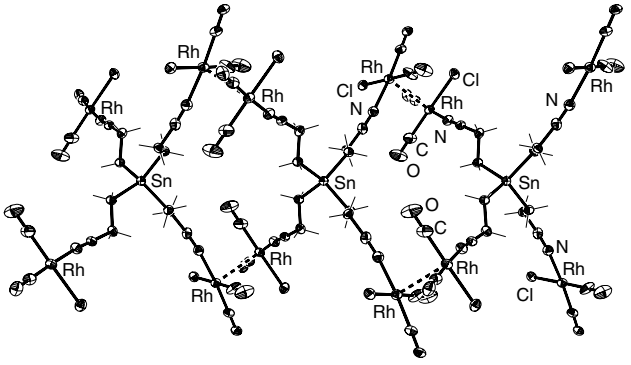

Fig. 4. ORTEP diagram showing the one-dimensional structure of **1**.

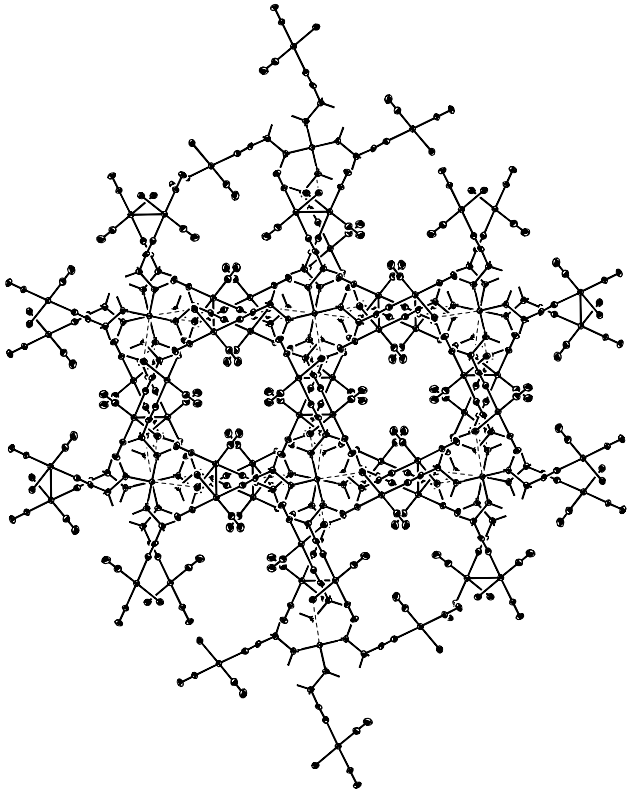

Fig. 5. View of **1** along the *c*-axis.

two-dimensional polymer containing $[Sn_2\{CH_2CH_2CNRhCl(CO)_2\}_4(CH_2CH_2CN)_2]$ units linked via three Rh–Rh bonds with three other monomers (Fig. 6). They

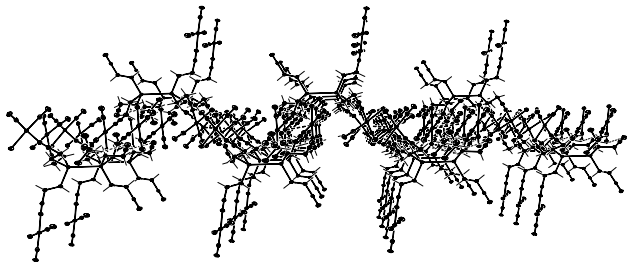

Fig. 6. View of a polymeric layer of **2** along the [0 0 1] direction.

form a puckered polymeric layer perpendicular to the [110] direction. All Rh–Rh junctions are centrosymmetric. It results in parallel and eclipsed orientations of the Rh square coordination entities. The Rh–Rh distances are different: Rh1–Rh1$(3 - x, 1 - y, 2 - z)$ 3.277(1) Å, Rh2–Rh2$(3 - x, 1 - y, 1 - z)$ 3.203(1) Å and Rh4–Rh4 $(2 - x, -y, 2 - z)$ 3.679(1) Å. The crystal structure of compound **2** is also stabilized by hydrogen bonds formed between the CH group of chloroform and the N(23) atom of a 2-cyanoethyl ligand (3.381(10) Å) and between α-CH_2 groups and the N(22i) atom (3.220(8) Å). The interaction between metal atoms of square planar complexes is characteristic for coordination compounds with d^8 electronic configuration [7]. This type of interaction can lead to the formation of column-like conductors and semiconductors. In the case of complexes **1** and **2** owing to this interaction one-dimensional and two dimensional compounds are formed. Formation of one-dimensional carbonyl rhodium(I) compounds containing Rh–Rh infinite bonds was found in complexes $[RhX(CO)_2(NCR)]$ [18], $[RhX(CO)_2(H_2NR)]$ [19] and $[Rh(CO)_2(N–N)][RhX_2(CO)_2]$ (N–N = 2,2′-bipyridine and 1,10-phenanthroline and their derivatives) [20].

The structure of complex **3** has been determined by Corey et al. [15] and recently by Farrah et al. [16]. The structure of **3** consists of discrete hexanuclear octahedral clusters (Fig. 3, Table 4). The average Rh–Rh distances and C–O bonds for terminal carbonyl ligands are slightly shorter and Rh–C bonds slightly longer than those reported by Corey et al. [15]. The following average distances were found: Rh–Rh = 2.7618(7) Å, for the terminally bonded carbonyls, Rh–C = 1.916(6) Å, C–O = 1.130(6) Å, and for bridging μ_3-CO ligands, Rh–C = 2.194(5) Å, C–O = 1.154(6) Å. The compound prepared by Farrah et al. [16] crystallized in the $P2_1/c$ space group and Rh–Rh average bond length in this crystal is slightly shorter (2.75(1) Å). Preparation of complexes of hexakis(2-cyanoethyl)ditin containing hexanuclear clusters coordinated with C–N groups was unsuccessful. Decomposition of complex **2** always leads to the cluster **3**. Reactions of the tin complex $[Sn_2(CH_2CH_2CN)_6]$ with compound **3** in acetone and acetonitrile were also unsuccessful. This most likely results from the relatively strong Rh–CO bond and less stable Rh–NC bond.

In solutions the Rh–Rh interactions are split and complexes **1** and **2** in solutions dissociate to the pentanuclear and hexanuclear compounds: [Sn{CH_2CH_2CN $RhCl(CO)_2$}$_4$] and [Sn_2\{$CH_2CH_2CNRhCl(CO)_2$\}$_4$(CH_2 CH_2CN)$_2$]. Triplets of Sn*CH*$_2$ and *CH*$_2$CN methylene protons with resolved $^{119/117}$Sn satellites for complex **1** are observed at 1.53 ppm ($^3J(^1H–^1H) = 8.2$ Hz, $^2J(^{119/117}Sn–^1H) = 52.0$ Hz) and 2.99 ppm ($^3J(^{119/117}Sn–^1H) = 49.6$ Hz) and for complex **2** at 1.68 ppm ($^3J(^1H–^1H) = 8.2$ Hz, $^2J(^1H–^{119/117}Sn) = 43.0$ Hz) and 2.97 ppm ($^3J(^1H–^{119/117}Sn) = 50.0$ Hz). The chemical shifts of α- and β-methylene groups for complexes **1** and **2** are ca. 0.06 and 0.13 ppm larger than for [Sn(CH_2CH_2CN)$_4$] and [Sn_2(CH_2CH_2CN)$_6$] [11]. The $^2J(^{119}Sn–^1H)$ coupling constants in tin(IV), SnR_2X_2 and SnR_3X, compounds depend on C–Sn–C angles [21–23]. The low values of $^2J(^{119/117}Sn–^1H)$ indicate that in polar solvents in compounds **1** and **2** tin atoms have tetrahedral coordination. Coordination of four rhodium(I) moieties with NC groups changes the dynamic properties of the 2-cyanoethyl ligands in complex **2**, as evidenced by ^{1}H NMR spectra in $(CD_3)_2CO$ and CD_2Cl_2 at lower temperatures. In deuterated acetone at room temperature both Sn*CH*$_2$ and *CH*$_2$CN signals are resolved, but at 273 K the *CH*$_2$CN signal becomes broader, at 253 K it loses resolution and at 233 K both signals are not resolved. The spectrum of [Sn_2(CH_2CH_2CN)$_6$] in $(CD_3)_2CO$ is resolved in this range of temperatures [11]. Very similar changes in the spectra were found in solution of complex **2** in CD_2Cl_2 in the same range of temperatures.

3. Experimental

3.1. Physical measurements and materials

Infrared spectra (KBr pellets) were recorded on a Bruker IFS 113v, ^{1}H NMR spectra were taken on a Bruker AMX 300. The amounts of tin and rhodium were determined using ICP-AES method on a ARL 3410.

The reagents, acrylonitrile (Aldrich), tin (POCH, Poland) and sodium hydroxide (POCH) were used as received. Complexes [Sn(CH_2CH_2CN)$_4$] [13,14] and [Sn_2(CH_2CH_2CN)$_6$] [11] were prepared according to the literature procedures from a sacrificial tin cathode in inert atmosphere and [$Rh_2Cl_2(CO)_4$] [24] in carbon monoxide atmosphere.

3.2. Preparation of [Sn{$CH_2CH_2CNRhCl(CO)_2$}$_4$]·CH_2Cl_2 (1)

A mixture of [Sn(CH_2CH_2CN)$_4$] (0.0336 g, 0.1 mmol) and [$Rh_2Cl_2(CO)_4$] (0.0778 g, 0.2 mmol) was dissolved in dichloromethane (5 cm^3) under CO atmosphere at room temperature and left for two days. The orange crystalline product [Sn{$CH_2CH_2CNRhCl(CO)_2$}$_4$]·CH_2Cl_2 (**1**) was filtered off and washed with cold dichloromethane and dried in vacuo. Yield: 0.066 g, 55%. *Anal.* Calcd. for: $C_{21}H_{18}Cl_6N_4O_8Rh_4Sn$: C, 21.06; H, 1.52; N, 4.68; Cl, 17.76. Found: C, 20.87; H, 1.44; N, 4.52; Cl, 17.58%. IR (KBr, cm^{-1}): 3005 wm, 2940 m, 2922 m, 2288 s (ν_{CN}), 2116 s (ν_{CO}), 2096 vs (ν_{CO}), 2040 vs (ν_{CO}), 2024 vs (ν_{CO}), 200sh s (ν_{CO}), 1988 s (ν_{CO}), 1420 ms, 1408 ms, 1318 s, 1260 mw, 1152 m, 1112 m, 998 m, 924 mw, 888 w, 868 w, 802 mw, 690 s, 680 ms, 664 s, 632 s, 612 s, 496 s, 464 s, 444 ms. ^{1}H NMR: ($(CD_3)_2CO$, 293 K): δ 1.53 ppm (t, *CH*$_2$Sn, $^3J(^1H–^1H) = 8.2$ Hz, $^2J(^{119/117}Sn–^1H) = 52.0$ Hz), 2.99 ppm (t, *CH*$_2$CN, $^3J(^{119/117}Sn–^1H) = 49.6$ Hz).

3.3. Preparation of [Sn_2(CH_2CH_2CN)$_6${$RhCl(CO)_2$}$_4$]·$CHCl_3$ (2)

A mixture of [Sn_2(CH_2CH_2CN)$_6$] (0.0562 g, 0.1 mmol) and [$Rh_2Cl_2(CO)_4$] (0.0778 g, 0.2 mmol) was dissolved in chloroform (5 cm^3) under CO atmosphere at room temperature and left for one day. The yellow crystalline product [Sn_2(CH_2CH_2CN)$_6${$RhCl(CO)_2$}$_4$]·$CHCl_3$, (**2**). was filtered off and washed with cold dichloromethane and dried in vacuo. Yield: 0.069 g, 47%. *Anal.* Calcd. for: $C_{27}H_{25}Cl_7N_6O_8Rh_4Sn_2$: C, 22.23; H, 1.73; N, 5.76; Cl, 17.02; Rh, 28.22; Sn, 16.28. Found: C, 22.07, H, 1.53; N, 5.52; Cl, 16.83; Rh, 27.95; Sn, 16.46%. IR (KBr, cm^{-1}): 3007 wm, 2944 m, 2925 m, 2289 s (ν_{CN}), 2241 m (ν_{CN}), 2090 vs (ν_{CO}), 2023 vs (ν_{CO}), 2005sh s (ν_{CO}), 1422 ms, 1415 sh ms, 1296 w, 1262 vw, 1237 w, 1156 w, 1144 w, 1103 vw, 996mw, 885 wm, 868 mm, 805 vw, 762 s, 749 s, 702 vw, 678 s, 658 m, 612 s, 582 vw (ν_{SnC}), 501 s, 451 s. ^{1}H NMR: ($CDCl_3$, 293 K): δ 1.63 (t, *CH*$_2$Sn, $^3J(^1H–^1H) = 7.1$ Hz, $^2J(^1H–^{119/117}Sn) = 41.2$ Hz), 2.84 (t, *CH*$_2$CN, $^3J(^1H–^{119/117}Sn) = 62.5$ Hz); (CD_2Cl_2, 293 K): δ 1.57 (t, *CH*$_2$Sn, $^3J(^1H–^1H) = 7.5$ Hz, $^2J(^1H–^{119/117}Sn) = 41.3$ Hz), 2.81 (t, *CH*$_2$CN, $^3J(^1H–^{119/117}Sn) = 65.0$ Hz); ($(CD_3)_2CO$, 293 K): δ 1.68 (t, *CH*$_2$Sn, $^3J(^1H–^1H) = 8.2$ Hz, $^2J(^1H–^{119/117}Sn) = 43.0$ Hz), 2.97 (t, *CH*$_2$CN, $^3J(^1H–^{119/117}Sn) = 50.0$ Hz); (CD_3CN, 293 K): δ 1.46 (t, *CH*$_2$*Sn*, $^3J(^1H–^1H) = 8.1$ Hz, $^2J(^1H–^{119}Sn) = 43.9$ Hz, $^2J(^1H–^{117}Sn) = 42.1$ Hz), 2.65 (t, *CH*$_2$CN, $^3J(^1H–^{119}Sn) = 53.0$ Hz, $^3J(^1H–^{117}Sn) = 51.0$ Hz).

3.4. X-ray crystallographic measurements

Crystals of **1** and **2** used for X-ray structure determination were obtained in reactions of [Sn(CH_2CH_2 CN)$_4$] and [Sn_2(CH_2CH_2CN)$_6$] with [$Rh_2Cl_2(CO)_4$] at room temperature in dichloromethane and chloroform, respectively. All measurements were performed at low temperature using an Oxford Cryosystem device on a Kuma KM4CCD κ-axis diffractometer with graphite-monochromated Mo Kα radiation. The crystal was positioned at 65 mm from the CCD camera. 612 frames

were measured at 0.75° intervals with a counting time of 12 s. Accurate cell parameters were determined and refined by a least-squares fit of the 3300 strongest reflections. The data were corrected for Lorentz and polarization effects. No absorption correction was applied. Data reduction and analysis were carried out with the Oxford Diffraction (Poland) Sp. zoo (formerly Kuma Diffraction Wrocław, Poland) programs. The structure was solved by direct methods (program SHELXS-97 [25]) and refined by the full-matrix least-squares method on all F^2 data using the SHELXL-97 [26] programs. Non-hydrogen atoms were refined with anisotropic thermal parameters; hydrogen atoms were included from the geometry of molecules and were fixed.

4. Supplementary data

Crystallographic data for the structures reported in this paper (excluding structure factors) have been deposited at the Cambridge Crystallographic Data Centre and allocated the deposition Nos. 192924 (**1**), 192923 (**2**) and 192922 (**3**). Copies of this information may be obtained free of charge from The Director, CCDC, 12 Union Road, Cambridge CB2 1EZ, UK (fax: +44-1223-336033; e-mail: deposit@ccdc.cam.ac.uk or http://www.ccdc.cam.ac.uk).

References

[1] M. Fischer, F. Vögtle, Angew. Chem., Int. Ed. Engl. 38 (1999) 885.
[2] P. Nguyen, P. Gomez-Elipe, I. Manners, Chem. Rev. 99 (1999) 1515.
[3] V. Balzani, A. Juris, M. Venturi, S. Campagna, S. Serroni, Chem. Rev. 96 (1996) 759.
[4] N. Armaroli, Chem. Soc. Rev. 30 (2001) 113.
[5] A.G. Davies, in: G. Wilkinson, F.G.A. Stone, E.W. Abel (Eds.), Comprehensive Organometallic Chemistry, Pergamon Press, Oxford, 1995 (Ch. 6).
[6] P.J. Smith, Chemistry of Tin, Blackie Academic & Profesional, London, 1998.
[7] F.P. Pruchnik, Organometallic Chemistry of the Transition Elements, Plenumn Press, New York, 1990.
[8] A.J. Crowe, in: B. Keppler (Ed.), Metal Complexes in Cancer Chemotherapy, VCH, Weinheim, New York, 1993, p. 369.
[9] M. Gielen, M. Biesemans, D. de Vos, R. Willem, J. Inorg. Biochem. 79 (2000) 139.
[10] M. Gielen, Appl. Organometal. Chem. 16 (2002) 481, and references therein.
[11] F.P. Pruchnik, M. Bańbuła, Z. Ciunik, H. Chojnacki, B. Skop, M. Latocha, T. Wilczok, J. Inorg. Biochem. 90 (2002) 149.
[12] F.P. Pruchnik, M. Bańbuła, Z. Ciunik, H. Chojnacki, M. Latocha, B. Skop, T. Wilczok, Appl. Organometal. Chem. 16 (2002) 587.
[13] A.P. Tomilov, L.V. Kaabak, Zh. Prikl. Khim. 32 (1959) 2600.
[14] O.R. Brown, E.R. Gonzalez, A.R. Wright, Electrochim. Acta 18 (1973) 555.
[15] E.R. Corey, L.F. Dahl, W. Beck, J. Am. Chem. Soc. 85 (1963) 1202.
[16] D.H. Farrah, E.V. Grachova, A. Lough, C. Patirana, A.J. Poë, S.P. Tunik, J. Chem. Soc., Dalton (2001) 2015.
[17] H. Puff, B. Breuer, G. Gehrke-Brinkmann, P. Kind, H. Reuter, W. Schuh, W. Wald, G. Weidenbrück, J. Organometal. Chem. 363 (1989) 265.
[18] R. Ugo, M. Fiore, Inorg. Chim. Acta 2 (1969) 463.
[19] L.M. Vallarino, S.W. Sheargold, Inorg. Chim. Acta 36 (1979) 243.
[20] F.P. Pruchnik, K. Wajda, J. Organometal. Chem. 164 (1979) 71.
[21] T.P. Lockhart, W.F. Manders, Inorg. Chem. 25 (1986) 892.
[22] B. Wrackmeyer, Annu. Rep. NMR Spectrosc. 38 (1999) 203.
[23] M. Nath, S. Pokharia, R. Yadav, Coord. Chem. Rev. 215 (2001) 99.
[24] F.P. Pruchnik et al., Syntheses of Organometallic Compounds. Transition Metals, PWN, Warsaw, 1993.
[25] G.M. Sheldrick, SHELXS-97: Program for Solution of Crystal Structures, University of Göttingen, Göttingen, 1997.
[26] G.M. Sheldrick, SHELXL-97: Program for Crystal Structure Refinement, University of Göttingen, Göttingen, 1997.

Available online at www.sciencedirect.com
SCIENCE DIRECT®
Polyhedron 23 (2004) 109–114
POLYHEDRON
www.elsevier.com/locate/poly

New polynuclear aluminium oxoalkoxides: molecular structures of $Al_{11}(\mu_4\text{-}O)_2(\mu_3\text{-}O)_2(\mu\text{-}O)_2(\mu\text{-}OPr^n)_{10}(\mu\text{-}OPr^i)_2(\mu\text{-}ROH)_2(OPr^i)_8(OR)$, $R = Pr^{n,i}$ and $Al_5Mg_4(\mu_4\text{-}O)_2(\mu_3\text{-}O)(\mu\text{-}OH)_3(\mu\text{-}OPr^i)_8(\mu,\eta^2\text{-}acac)_4(\eta^2\text{-}acac)_2$

Zoya A. Starikova [a], Vadim G. Kessler [b,*], Nataliya Ya. Turova [c], Dmitriy E. Tcheboukov [c], Evgeniya V. Suslova [c], Gulaim A. Seisenbaeva [b], Alexandr I. Yanovsky [a]

[a] A.N. Nesmeyanov Institute of Organoelement Compounds, Russian Academy of Sciences, 117813 Moscow, Russia
[b] Department of Chemistry, SLU, Box 7015, S-75007 Uppsala, Sweden
[c] Department of Chemistry, M.V.Lomonosov Moscow State University, 119899 Moscow, Russia

Received 26 June 2003; accepted 18 September 2003

Abstract

Prolonged storage of solutions in the $Al(OPr^i)_3$–$Ta(OPr^i)_5$–^{i}PrOH system containing additional ^{n}PrOH leads to crystallization with minor yields of a new aluminium oxopropoxide, $Al_{11}O_6(OPr^n)_{10}(OPr^i)_{10}(OR)(ROH)_2$ ($R = Pr^i$, Pr^n) (**1**). Interaction of $Al(OPr^i)_3$ with $Mg(acac)_2$ (in a 1:1 ratio) in toluene on refluxing leads to formation of $Al_5Mg_4O_3(OH)_3(OPr^i)_8(acac)_6 \cdot 0.5PhMe$ (**2**) in minor yields. Both molecules contain two pentanuclear cores $[M_5(\mu_4\text{-}O)(\mu_3\text{-}O)(\mu\text{-}OX)_6(Y)_4]$ ($X = H$, Pr^n, $Y = OPr^i$, acac/2) and differ only in the manner in which they are attached to each other, i.e. via the central $[Al(\mu_3\text{-}O)_2(\mu\text{-}O)_2(OR)]$ unit in **1**, and via a common [Al–(μ_3-O)] edge and an additional (μ-OH)-group in **2**. The core structures in the molecules of aluminium and iron oxoalkoxides are discussed.
© 2003 Elsevier Ltd. All rights reserved.

Keywords: Oxoalkoxides; Aluminium; Precursor hydrolysis; X-ray; Structure studies

1. Introduction

The interest revealed recently to the homo- and heterometallic oxoalkoxides is due to their specific role as direct precursors of oxide materials in Sol–Gel Technology and also to the fundamental interest to new possible types of oligomeric "cluster" aggregates [1].

Aluminum isopropoxide belongs to the best studied and most commonly applied derivatives of this metal. The data on its oxoderivatives has been, however, quite limited. There have only been reports on the crystalline oxoalkoxochloride, $Al_4(\mu_4\text{-}O)(OPr^i)_5[H(OPr^i)_2]Cl_4$, (earlier described as "$AlCl(OPr^i)_2$" [2]), and a complex of aluminum oxoisopropoxide with ammonia, $[Al_{10}(\mu_4\text{-}O)_2(\mu_3\text{-}O)_4(\mu\text{-}OPr^i)_6(OPr^i)_{12}(NH_3)_8]$ [3]. At the same time, at present a considerable number of oxoalkoxide derivatives of other alcohols have been reported including, for example, decameric oxoethoxide, $[Al_{10}(\mu_4\text{-}O)_2(\mu_3\text{-}O)_2(\mu\text{-}OEt)_{14}(OEt)_8]$, formed on decomposition of the polymeric $Al(OEt)_3$ ("crystalline aluminium ethoxide") [4] and also a series of oxo-isobutoxides and trifluoroethoxides such as $[Al_4(\mu_4\text{-}O)(\mu\text{-}OR)_5(OR)_5(ROH)]$ ($R = Bu^i$ [5,6], CH_2CF_3 [6,7]), $[Al_5(\mu_5\text{-}O)(\mu\text{-}OBu^i)_8(OBu^i)_5]$, $[Al_8(\mu_4\text{-}O)_2(\mu\text{-}OH)_2(\mu\text{-}OBu^i)_{10}(OBu^i)_8]$, reported recently by Bradley and co-workers [6] as the products of controlled partial hydrolysis or thermolysis. A number of other tetra- and pentanuclear complexes, where a part of the alkoxide ligands has been replaced by different OR-groups, have also been reported. Among the heteroleptic

* Corresponding author. Tel.: +46-18-671541; fax: +46-18-673476.
E-mail address: vadim.kessler@kemi.slu.se (V.G. Kessler).

0277-5387/$ - see front matter © 2003 Elsevier Ltd. All rights reserved.
doi:10.1016/j.poly.2003.09.031

oxoalkoxides it is important to mention also the recently reported pentanuclear alkoxide hydride $[H_5Al_5(\mu_5\text{-}O)(\mu\text{-}OBu^i)_8]$ [8].

2. Experimental

All the operations were carried out in dry argon or nitrogen atmosphere using a vacuum line or a glove box. The alcohols were dried by distillation over the corresponding aluminium alkoxides and the hydrocarbons by distillation over metallic sodium or $LiAlH_4$. Crystalline samples of $Al(OPr^i)_3$ were obtained by the action of alcohol on liquid freshly distilled isopropoxide. Its m.p. was 140 °C [9]. $Mg(acac)_2$ was obtained by the action of Mg metal on excess of acetylacetone and purified by recrystallization from toluene. IR spectra of nujol mulls were registered with a Perkin–Elmer FT-IR spectrometer 1720 X. ^1H NMR spectra were recorded for the $CDCl_3$ solutions on a Bruker 400 MHz spectrometer at 30 °C. Mass-spectra were recorded using a JEOL JMS-SX/SX-102A mass-spectrometer applying electron beam ionization ($U = 70$ eV) with direct probe introduction.

2.1. Synthesis and isolation of *1* and *2*

A crop of single crystals of $Al_{11}O_6(OPr^n)_{10}(OPr^i)_{10}(OR)(ROH)_2$ ($R = Pr^i$, Pr^n) (**1**) was formed after prolonged storage of a solution containing 0.75 g (3.65 mmol) $Al(OPr^i)_3$ and 2.6 g (5.5 mmol) $Ta(OPr^i)_5$ in 15 ml ^{i}PrOH after addition of 8 ml ^{n}PrOH and subsequent storage at ~0 °C. The low yield of this product precluded its further characterization. Elemental analysis for **1**: found: C, 45.9; H 9.1; Al, 17.2. Calc. for $C_{69}H_{163}Al_{11}O_{29}$: C, 47.2; H, 9.3; Al, 16.9%.

A crop of single crystals of $Al_5Mg_4(\mu_4\text{-}O)_2(\mu_3\text{-}O)(\mu\text{-}OH)_3(\mu\text{-}OPr^i)_8(\mu,\eta^2\text{-acac})_4(\eta^2\text{-acac})_2 \cdot 0.5PhMe$ (**2**) was obtained in the following experiment: $Al(OPr^i)_3$ (0.24 g, 1.2 mmol) and $Mg(acac)_2$ (0.26 g, 1.2 mmol) were dissolved in 3 ml of toluene and subjected to reflux for about 1 h. The solution was diluted with an additional 1.5 ml toluene and left for crystallization at −30 °C overnight. The needle-shaped crystals formed (about 0.1 g) were shown to be the initial $Mg(acac)_2$. They were separated by decantation and the mother liquor was concentrated to about one fourth of the initial volume and left at room temperature for one month. A number of large (up to 1.5 mm) rod-shaped single crystals of **2** were formed and isolated by removal of solvent by syringe and dried in vacuo. Found: C, 46.1; H, 7.0%. Calculated for $Al_5Mg_4O_3(OH)_3(OC_3H_7)_8(O_2C_5H_7)_6(C_7H_8)_{0.5}$: C, 47.2; H, 7.2. IR, cm^{-1}: 3523 m, 1611 s, 1412 w, 1373 s, 1284 w sharp, 1268 m sharp, 1159 s, 1081 w, 1019 s, 1003 sh, 929 s, 844 sh, 824 m, 754 s, 731 w, 665 m, 637 m, 618 m, 595 w, 567 m, 544 m, 505 m, 490 sh, 447 w, 419 m. MS, *m/z* (I), interpretation: 567(0.3), $Mg_3(acac)_5^+$, 509(0.4), $Mg_3(acac)_4(OC_3H_6)^+$, 444(0.5), $Mg_2(acac)_4^+$, 345(2.8), $Mg_2(acac)_3^+$, 324(2.1), $Al(acac)_3^+$, 299(2.2), $Al_2(acac)_2(OH)(OCH_2)^+$, 279(24.8), $MgAl(acac)_2(OCH_2)^+$, 245(21.3), $[Mg_2(acac)_2\text{–}H]^+$, 225(97.1) $Al(acac)_2^+$, 222(100), $Mg(acac)_2^+$, 207(100), $[Mg(acac)_2\text{–}CH_3]^+$, 187(100), $MgAl(OH)_2(O^iPr)(CH_3CO)^+$, 157 (100), $MgAl(OH)(O^iPr)(OCH_2)^+$, 125(31.1), $[Al(acac)\text{–}H]^+$, 123(100), $Mg(acac)^+$. NMR ^1H, ppm: 7.22 (doublet, C*H*, toluene), 7.16(doublet, C*H*, toluene), 5.36 (singlet, C*H*, acac), 5.33(singlet, C*H*, acac), 5.26(singlet, C*H*, acac), 4.24(septet, C*H*, O^{i}Pr), 4.08(septet, C*H*, O^{i}Pr), 3.88(septet, C*H*, O^{i}Pr), 3.59(septet, C*H*, O^{i}Pr), 1.98(singlet, CH_3, toluene), 1.82(singlet, CH_3, acac), 1.75(singlet, CH_3, acac), 1.70(singlet, CH_3, acac), 1.29(doublet, CH_3, O^{i}Pr), 1.22(doublet, CH_3, O^{i}Pr), 1.18(doublet, CH_3, O^{i}Pr), 1.09(doublet, CH_3, O^{i}Pr), 1.06(doublet, CH_3, O^{i}Pr), 0.95(doublet, CH_3, O^{i}Pr), 0.86(doublet, CH_3, O^{i}Pr), 0.64(doublet, CH_3, O^{i}Pr).

Table 1
Comparison of Al–O bond lengths in aluminium oxoalkoxides

Compound	Al–OR in [AlO_4]	Al–OR in [AlO_5]	Al–OR in [AlO_6]	Al–(μ-O)	Al–(μ_3-O)	Al–(μ_4-O)
1	*t* 1.748(13) μ 1.79–1.81	*t* 1.75(2)–1.79(2) μ 1.81–1.89	*t* 1.62(3) μ 1.92–2.07	1.82–1.92	1.73–1.84	1.83–1.96
$Al_{10}O_4(OEt)_{22}$ [4]	*t* 1.71 μ 1.75–1.78	*t* 1.73 μ 1.81–1.88	*t* 1.76 μ 1.92–2.00		1.75–1.83	1.83–1.91
2		μ 1.81–1.86	μ 1.85–1.87	Al–(μ-OH) 1.81–1.91	1.78–1.81	1.81–1.82 (Al) 1.97–1.98 (Mg)
$Al_8O_2(OH)_2(O^iBu)_{18}$ [6]		*t* 1.69–1.77 μ 1.77–1.91		1.81–1.79		1.82–1.91
$Al_4O(OCH_2CF_3)_{10}(CF_3CH_2OH)$ [6,7]		*t* 1.69–1.72 μ 1.82–1.89				1.87–1.90
$Al_4O(OBu^i)_{10}(Bu^iOH)$ [5,6]		*t* 1.71–1.82 μ 1.83–1.87				1.88

2.2. Crystallography

For the details of the data collection and treatment see Table 2. The structures were solved by standard direct methods. The majority of the non-hydrogen atoms were located directly from the initial solutions and completed using difference Fourier syntheses. All non-hydrogen atoms (except for the propoxide groups based on C(4), C(5), C(9) and C(10) in **1**, which were subjected to rotational disorder that could not be successfully resolved, and the highly disordered toluene molecule in **2**, where only isotropic refinement was possible) were refined first in isotropic and then in anisotropic approximation. The positions of the hydrogen atoms connected to the carbon atoms were calculated geometrically and included into the final cycles of refinement in riding isotropic approximation with the temperature factors $U = 1.2$ Uiso of the corresponding C atom for the CH and $U = 1.5$ Uiso for the CH_3 groups. The hydrogen atom of the solvating alcohol molecule could not be located in a reliable way in the difference Fourier syntheses and was supposed to be attached to the oxygen atom O(10), demonstrating relatively longer distances to the corresponding Al atoms. The hydrogen atoms of the hydroxide groups in **2** were located in difference Fourier syntheses and included into the final solution in isotropic approximation. In the determination of the structure of **2** the automatic solution contained only one type of metal atom, but systematically longer metal–oxygen distances for four of them permitted to suppose that magnesium atoms occupied these positions. The introducing of Mg into them resulted in a very strong decrease in *R*-factors, supporting the chosen model. An additional confirmation for this choice is provided by the sum of the formal charges in the structure, corresponding to the presence of five trivalent and four divalent metal atoms and by the evidently analogous placement of the four Mg atoms in the molecule (symmetric in observation, while not supported by the formal crystallographic symmetry elements). All calculations were performed on a personal computer using the SHELXTL-NT program package [10].

Table 2
Crystal data and the diffraction experiment details for compounds **1** and **2**

	1	**2**
Formula weight	1753.77	1461.42
Crystal system	monoclinic	tetragonal
Space group	*I*2/*a*	*I*4(1)/*a*
μ (mm^{-1})	0.168	0.177
R_1	0.0669	0.0676
wR_2	0.1783	0.1881
a (Å)	26.597(5)	37.329(6)
b (Å)	12.431(3)	37.329(6)
c (Å)	31.639(6)	22.775(5)
α (°)	90	90
β (°)	98.57(3)	90
γ (°)	90	90
V ($Å^3$)	10344(4)	31736(10)
T (K)	293(2)	295(2)
Z	4	16
Number of independent reflections (R_{int})	1440 (0.0284)	5444 (0.0558)
Number of observed reflections ($I > 2\sigma(I)$)	1102	3539

3. Results and discussion

Formation of oxogroups in the structures of compounds **1** and **2** occurs apparently via decomposition of the bimetallic complexes – isopropoxides of aluminium and tantalum in the first case and alkoxoacetylacetonates of aluminium and magnesium in the second. It is well known that the bimetallic alkoxides are much easier decomposable via, for example, ether elimination, than the homometallic derivatives [1]. In the $Al(OPr^i)_3$–$Ta(OPr^i)_5$–^{i}PrOH system a drastic increase in solubility of the components has been observed in the composition range from 1:1 to 1:2. The individuality of the liquid heterometallic complexes of these compositions has been confirmed by the mass-spectrometric studies [11]. Crystallization of **1** occurred only on addition to the solution the alcohol with normal chain structure – ^{n}PrOH. The duration of this process permits to suppose that uncontrolled hydrolysis might be involved in this case, the oxoalkoxide **1** being the least soluble compound in this multi-component system.

It has earlier been found out that the interaction of $Al(OPr^i)_3$ with $Mg(acac)_2$ in 2:1 ratio in toluene in the presence of 2 additional equivalents of Hacac leads to almost quantitative formation of $Mg(\mu\text{-}OPr^i)_4[Al(acac)_2]_2$ [12]. In the present work, the same reaction was carried out in 1:1 ratio in the absence of additional acetylacetone. Cooling down of the solution initially subjected to reflux led to crystallization of approximately half of the initial $Mg(acac)_2$, and changed the ratio of the components to 1:2. Long-term storage of the mother liquor led to formation of a small crop of single crystals of $Al_5Mg_4O_3(OH)_3(OPr^i)_8(acac)_6 \cdot 0.5PhMe$ (**2**). It can be supposed that the formation of **2** (according to its stoichiometry) might be due to decomposition of bimetallic alkoxo-acetylacetonate complexes formed in solution. The presence of hydroxide groups in its molecule cannot be taken as an ultimate proof of involvement of uncontrolled hydrolysis in this case, as, for example, a hydroxide complex $Al_8O_2(OH)_2(OBu^i)_{18}$ has been obtained by Abrachams et al. [6] under anhydrous conditions on distillation of an aseotrop of toluene and alcohol from $Al_4O(OBu^i)_{10}$(^{i}BuOH). The positive effect of bases on such decomposition processes as, for example, ether elimination is well known resulting in often

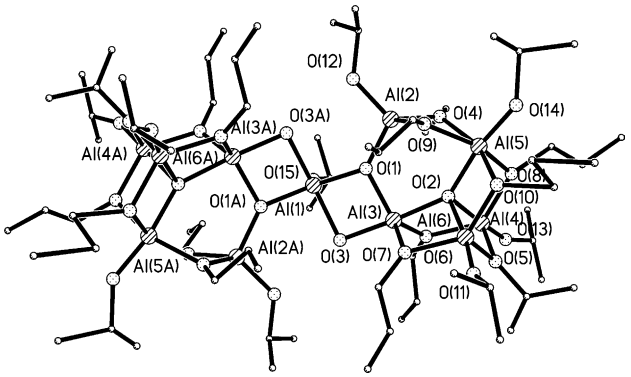

Fig. 1. Molecular structure of $Al_{11}(\mu_4\text{-}O)_2(\mu_3\text{-}O)_2(\mu\text{-}O)_2(\mu\text{-}OPr^n)_{10}(\mu\text{-}OPr^i)_2(\mu\text{-}ROH)_2(OPr^i)_8(OR)$ (**1**).

rather deep transformation of the bimetallic species formed [13].

The molecule of $Al_{11}(\mu_4\text{-}O)_2(\mu_3\text{-}O)_2(\mu\text{-}O)_2(\mu\text{-}OPr^n)_{10}(\mu\text{-}OPr^i)_2(\mu\text{-}ROH)_2(OPr^i)_8(OR)$, R = Pr^i, Pr^n (**1**) (Fig. 1, Table 3) contains two pentanuclear cores $[Al_5(\mu_4\text{-}O)(\mu_3\text{-}O)(\mu\text{-}O)(\mu\text{-}OR)_6(OR)_4]$, connected to each other via a central $[Al(\mu_3\text{-}O)_2(\mu\text{-}O)_2(OR)]$ group. In the latter the Al(1) atom has trigonal bipyramidal coordination, where the μ–O(3) and μ–O(3A) atoms occupy the axial positions. The bonds around the μ_3-O(1) oxogroups are arranged in one plane (the sum of bond angles being 359.7). The aluminium atoms in the pentanuclear cores display tetrahedral, Al(2), trigonal bipyramidal, Al(3, 4, 6), and octahedral, Al(5), coordination. Four metal atoms – all except Al(3), connected to the central group via two oxo-bridges, – each bear one terminal OR-group. Metal atoms in the core are coordinating one μ_4-O(2), six μ-OR-groups and one bridging alcohol molecule –O(10). It is very important to note that 10 of the 12 bridging OR-groups have normal structure hydrocarbon groups. This fact explains supposedly the absence of information in the literature on aluminium oxoalkoxides containing only OPr^i-groups. [1] The alcohol molecule RO(10)H could be identified by comparably longer Al–O distances (see Table 3).

The same kind of pentanuclear cores have been observed earlier in the structure of the decanuclear oxoethoxide, $[Al_{10}(\mu_4\text{-}O)_2(\mu_3\text{-}O)_2(\mu\text{-}OEt)_{14}(OEt)_8]$ [4]. The difference between the structures of 10- and 11-nuclear complexes consists only in that in the first one the cores are connected via two μ_3-O-groups (forming a four-member ring $[Al_2O_2]$), and in the second – via an additional fragment containing one more (the 11th) aluminium atom (in the central $[Al(\mu_3\text{-}O)_2(\mu\text{-}O)_2(OR)]$ group).

The molecule of $Al_5Mg_4(\mu_4\text{-}O)_2(\mu_3\text{-}O)(\mu\text{-}OH)_3(\mu\text{-}OPr^i)_8(\mu, \eta^2\text{-acac})_4(\eta^2\text{-acac})_2 \cdot 0.5PhMe$ (**2**) (Fig. 2,

[1] Partial substitution for *n*-chain structure alkoxide groups has been reported earlier to permit isolation of such crystalline derivatives as $Ti_3O(OPr^i)_9(OMe)$ [14] and $Ti_{11}O_{13}(OPr^i)_{13}(OEt)_5$ [15].

Table 3
Selected bond lengths and angles in the structure of **1**

Bond lengths			
Al(1)–O(1)	1.839(13)	Al(3)–O(2)	1.848(16)
Al(1)–O(3)	1.919(10)	Al(3)–O(3)	1.821(14)
Al(1)–O(15)	1.78(3)	Al(3)–O(6)	1.810(13)
Al(2)–O(1)	1.733(11)	Al(3)–O(7)	1.858(14)
Al(2)–O(4)	1.793(14)	Al(4)–O(2)	1.931(15)
Al(2)–O(9)	1.807(14)	Al(5)–O(2)	1.829(1)
Al(2)–O(12)	1.748(13)	Al(6)–O(2)	1.961(15)
Al(3)–O(1)	1.835(11)	Al(5) O(10)	1.920(14)
Al(3) O(7)	1.804(16)	Al(6) O(10)	1.853(13)
Bond angles			
O(1)–Al(1)–O(3)	79.4(5)	O(2)–Al(3)–O(3)	176.1(6)
O(1)–Al(2)–O(4)	109.4(6)	O(2)–Al(3)–O(7)	81.4(7)
O(1)–Al(2)–O(12)	109.6(7)	O(10)–Al(6)–O(11)	103.6(6)
O(4)–Al(2)–O(9)	86.8(8)	Al(1)–O(1)–Al(3)	100.1(7)
O(9)–Al(2)–O(12)	119.7(6)	Al(3)–O(2)–Al(5)	147.8(7)
O(1)–Al(3)–O(2)	94.0(7)	Al(3)–O(2)–Al(4)	99.7(8)
O(1)–Al(3)–O(3)	82.1(6)	Al(4)–O(2)–Al(5)	102.9(7)

Table 4) also contains five-nuclear cores, in which two aluminium atoms, connected to the μ_4-O, are replaced by Mg ones. It is to be noted that one of them – Mg (7) or Mg (8) conserves the trigonal bipyramidal coordination of the corresponding Al atoms, while the second one turns out to be octahedrally coordinated [Mg (6) or Mg(9)]. Both Mg atoms and one Al atom [(4) or Al(5)] coordinate one acac-group each. One of the latter contains only monodentate oxygen atoms [η^2-coordinated to Mg(6) or Mg(9)], while the two other contain one μ_2-O atom each. In addition, one of the μ-OR groups in the core is replaced by a μ-O group [O(7) or (12)s]. The major structural difference of **2** in comparison with the above mentioned aluminium alkoxides lies in the fact that the two cores in it are connected via a common edge Al(3)-[μ_3-O(8)] (containing the Al atom not connected to μ_4-O) and an additional μ-OH bridge. The sum of bonding angles at O(8) is 360°. The metal–oxygen

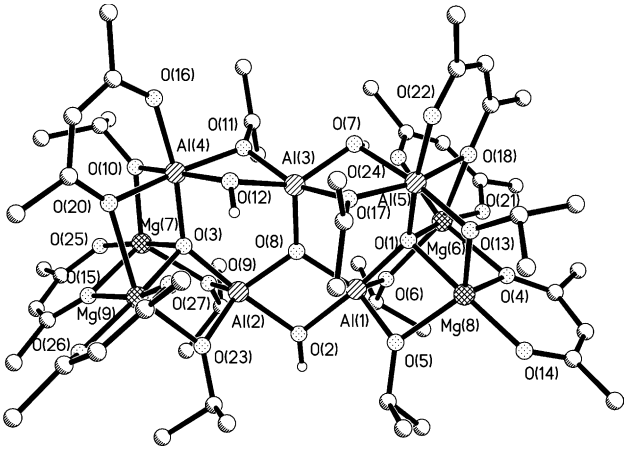

Fig. 2. Molecular structure of $Al_5Mg_4(\mu_4\text{-}O)_2(\mu_3\text{-}O)(\mu\text{-}OH)_3(\mu\text{-}OPr^i)_8(\mu, \eta^2\text{-acac})_4(\eta^2\text{-acac})_2 \cdot 0.5PhMe$ (**2**).

Table 4
Selected bond lengths and angles in the structure of **2**

Bond lengths			
Al(1)–O(8)	1.810(6)	Mg(6)–O(1)	1.977(7)
Al(1)–O(1)	1.817(6)	Mg(6)–O(21)	1.987(10)
Al(1)–O(5)	1.819(7)	Mg(6)–O(24)	2.067(9)
Al(1)–O(6)	1.827(7)	Mg(6)–O(6)	2.079(7)
Al(1)–O(2)	1.883(6)	Mg(6)–O(4)	2.216(8)
Al(2)–O(23)	1.804(7)	Mg(6)–O(18)	2.345(9)
Al(2)–O(8)	1.808(6)	Mg(7)–O(3)	1.977(6)
Al(2)–O(3)	1.812(6)	Mg(7)–O(10)	1.978(7)
Al(2)–O(9)	1.815(7)	Mg(7)–O(25)	1.985(10)
Al(2)–O(2)	1.908(6)	Mg(7)–O(15)	2.021(9)
Al(3)–O(8)	1.783(6)	Mg(7)–O(9)	2.025(7)
Al(3)–O(12)	1.814(8)	Al(1)–Al(2)	2.879(4)
Al(3)–O(7)	1.811(8)	Al(1)–Mg(6)	2.948(4)
Al(3)–O(17)	1.843(8)	Al(2)–Mg(7)	2.894(4)
Al(3)–O(11)	1.845(7)	Mg(6)–Mg(8)	3.086(5)
Bond angles			
O(8)–Al(1)–O(1)	96.3(3)	O(1)–Mg(6)–O(21)	170.6(4)
O(8)–Al(1)–O(5)	125.6(3)	O(1)–Mg(6)–O(24)	103.4(3)
O(1)–Al(1)–O(5)	86.1(3)	O(21)–Mg(6)–O(24)	85.8(4)
O(8)–Al(1)–O(6)	124.3(3)	O(1)–Mg(6)–O(6)	74.9(2)
O(1)–Al(1)–O(6)	85.2(3)	O(21)–Mg(6)–O(6)	106.4(4)
O(5)–Al(1)–O(6)	110.1(3)	O(24)–Mg(6)–O(6)	97.3(3)
O(8)–Al(1)–O(2)	78.1(3)	O(1)–Mg(6)–O(4)	80.4(3)
O(1)–Al(1)–O(2)	174.4(3)	O(21)–Mg(6)–O(4)	90.2(4)
O(5)–Al(1)–O(2)	97.5(3)	O(24)–Mg(6)–O(4)	164.7(3)
O(6)–Al(1)–O(2)	97.3(3)	O(6)–Mg(6)–O(4)	97.9(3)
O(23)–Al(2)–O(8)	124.9(3)	O(24)–Mg(6)–O(18)	79.3(3)
O(23)–Al(2)–O(3)	85.0(3)	O(6)–Mg(6)–O(18)	143.3(3)
O(8)–Al(2)–O(3)	97.1(3)	O(4)–Mg(6)–O(18)	88.3(3)
O(23)–Al(2)–O(9)	111.0(3)	O(1)–Mg(6)–O(18)	70.6(3)
O(8)–Al(2)–O(9)	124.1(3)	O(21)–Mg(6)–O(18)	109.7(4)
O(23)–Al(2)–O(2)	98.1(3)	O(3)–Mg(7)–O(25)	175.5(4)
O(8)–Al(2)–O(2)	77.6(3)	O(10)–Mg(7)–O(25)	104.8(4)
O(3)–Al(2)–O(2)	174.7(3)	O(3)–Mg(7)–O(15)	85.7(4)
O(9)–Al(2)–O(2)	97.2(3)	O(10)–Mg(7)–O(15)	114.0(3)
O(23)–Al(2)–Al(1)	118.1(3)	O(25)–Mg(7)–O(15)	90.1(4)
O(8)–Al(3)–O(12)	109.1(3)	O(3)–Mg(7)–O(9)	76.0(3)
O(8)–Al(3)–O(7)	109.1(3)	O(10)–Mg(7)–O(9)	127.7(3)
O(12)–Al(3)–O(7)	141.8(3)	O(25)–Mg(7)–O(9)	103.9(3)
O(8)–Al(3)–O(17)	99.4(3)	O(15)–Mg(7)–O(9)	108.7(3)
O(12)–Al(3)–O(17)	97.4(4)	Al(2)–Al(1)–Mg(8)	149.20(14)
O(7)–Al(3)–O(17)	77.4(4)	Mg(8)–Al(1)–Mg(6)	63.88(11)
O(8)–Al(3)–O(11)	101.4(3)	Mg(7)–Al(2)–Mg(9)	64.08(12)
O(12)–Al(3)–O(11)	76.0(3)	Al(1)–Al(2)–Mg(7)	146.85(14)
O(7)–Al(3)–O(11)	95.4(3)	Al(5)–Al(3)–Al(4)	172.33(14)
O(17)–Al(3)–O(11)	159.2(3)	Mg(7)–Al(4)–Mg(9)	61.85(13)

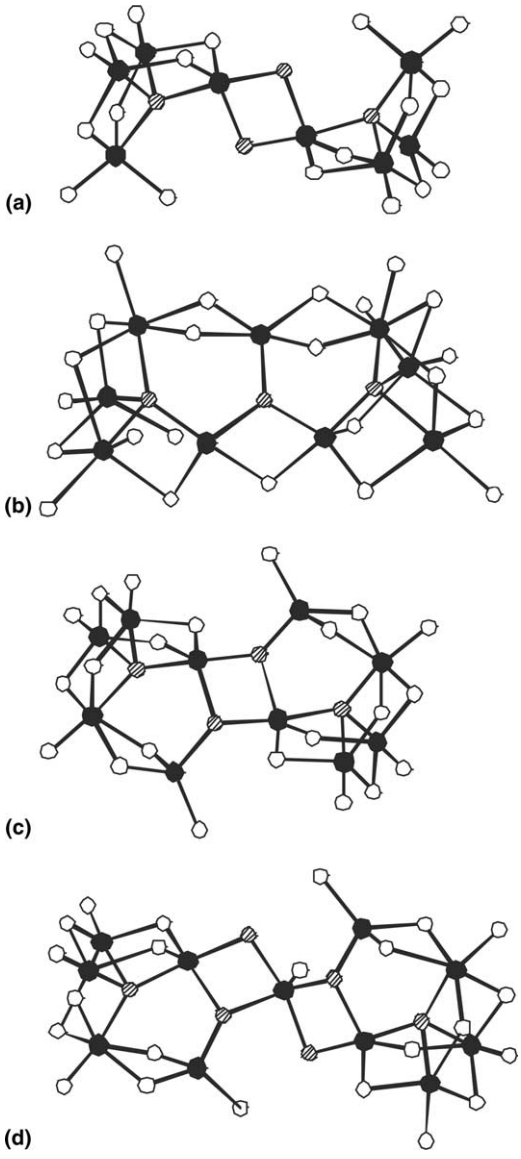

Fig. 3. Comparison of the metal–oxygen cores in the molecules of eight- (a), nine- (b), 10- (c) and 11-nuclear (d) oxoalkoxides – $[Al_4(\mu_4\text{-}O)(\mu\text{-}OH)(\mu\text{-}OBu^i)_5(OBu^i)_4]_2$ [6] $Al_5Mg_4O_3(OH)_3(OPr^i)_8(acac)_6 \cdot 0.5PhMe$, $[Al_{10}(\mu_4\text{-}O)_2(\mu_3\text{-}O)_2(\mu\text{-}OEt)_{14}(OEt)_8]$ [4], $Al_{11}O_6(OPr^n)_{10}(OPr^i)_{10}(OR)(ROH)_2$ ($R = Pr^i$, Pr^n).

skeleton of the pentanuclear cores in **2** does not differ from those in the 10- and 11-nuclear complexes and the structure as a whole turns out to be analogous to that of the recently reported nine-nuclear iron oxoethoxide $Fe_9(\mu_4\text{-}O)_2(\mu_3\text{-}O)(\mu\text{-}OEt)_{15}(OEt)_6 \cdot EtOH$ [16].

The Al–OR bond lengths in the molecule of **1** increase regularly with the increase in the coordination number of the metal atom (Table 1) and differ only negligibly from those found in the molecules of decaaluminium oxoethoxide or tetranuclear $Al_4(\mu_4\text{-}O)(OR)_{10}$ (R), $R = Bu^i$, CF_3CH_2 [5,6]. At the same time in the molecule of **2** (and its structural analog $Fe_9O_3(OEt)_{21} \cdot EtOH$ [16]) one can hardly find the same kind of correlation due, supposedly to considerable steric tension in this highly condensed structure.

Combinations of two structural fragments close to the described pentanuclear cores is observed also in other molecules. Thus, for example, the structure of $[Al_8(\mu_4\text{-}O)_2(\mu\text{-}OH)_2(\mu\text{-}OBu^i)_{10}(OBu^i)_8]$ [6] can be considered as a derivatization of the decanuclear analog of the oxoethoxide, where the fifth aluminium atom, not connected to μ_4-O, is missing (Fig. 3(a)). The two molecular structures described in this work permit the completion of the structural series of aluminium oxoalkoxides – from octamer to undecamer (Fig. 3).

4. Supplementary material

Supplementary data are available from the CCDC, 12 Union Road, Cambridge, CB2 1EZ, UK (fax: +44-1223-336033; e-mail: deposit@ccdc.cam.ac.uk or www: http://www.ccdc.cam.ac.uk) on request, quoting the deposition numbers 205865 and 205866 for compounds **1** and **2**, respectively.

Acknowledgements

The authors express their gratitude to Suresh Gohil for the assistance with the mass-spectrometric and Rolf Andersson with NMR experiments. Financial support of the Swedish Scientific Research Council and Royal Swedish Academy of Sciences is gratefully acknowledged.

References

[1] N.Ya. Turova, E.P. Turevskaya, V.G. Kessler, M.I. Yanovskaya, The Chemistry of Metal Alkoxides, Kluwer Academic Publishers, Boston/Dordrecht/London, 2002.
[2] N. Ya. Turova, A.I. Yanovsky, V.G. Kessler, N.I. Kozlova, Yu.T. Struchkov, Russ. J. Inorg. Chem. 36 (1991) 1404.
[3] U.M. Tripathi, A. Schier, H. Schmidbaur, Z. Naturforsch. B 53 (1998) 434.
[4] A.I. Yanovsky, N.Ya. Turova, N.I. Kozlova, Yu.T. Struchkov, Koord. Khim. 13 (1987) 149 (in Russian).
[5] R.A. Sinclair, W.B. Gleason, R.A. Newmark, J.R. Hill, S. Hunt, P. Lyon, J. Stevens, in: Ll. Hench, J.K. West (Eds.), Chem. Proc. Adv. Mater., Wiley, New york, 1992, p. 207.
[6] I. Abrahams, D.C. Bradley, H. Chudzynska, M. Motevalli, R.A. Sinclair, J. Chem. Soc., Dalton Trans. (2002) 259.
[7] S.A. Sangokoya, W.T. Rennigton, J. Byers-Hill, G.H. Robinson, R.D. Rogers, Organometallics 12 (1993) 2429.
[8] M. Cesari, Gazz. Chim. Ital. 110 (1980) 365.
[9] N.Ya. Turova, V.A. Kozunov, A.I. Yanovsky, N.G. Bokii, Yu.T. Struchkov, J. Inorg. Nucl. Chem. 41 (1979) 5.
[10] SHELXTL-NT Reference Manual, Bruker AXS, 1998.
[11] D.E. Chebukov, N.Ya. Turova, A.I. Belokon', Russ. J. Inorg. Chem. 44 (1990) 807.
[12] V.G. Kessler, S. Gohil, S. Parola, J. Chem. Soc. (2002) 544.
[13] N.Ya. Turova, V.G. Kessler, S.I. Kucheiko, Polyhedron 10 (1991) 2617.
[14] V.W. Day, T.A. Eberspacher, Y. Chen, J. Hao, W.G. Klemperer, Inorg. Chim. Acta 229 (1995) 391.
[15] V.W. Day, T.A. Eberspacher, W.G. Klemperer, C.W. Park, J. Am. Chem. Soc. 115 (1993) 8469.
[16] M. Veith, F. Grätz, V. Huch, Eur. J. Inorg. Chem. (2001) 367.

Available online at www.sciencedirect.com
SCIENCE DIRECT®
Polyhedron 23 (2004) 115–123
POLYHEDRON
www.elsevier.com/locate/poly

Novel mercury(II) complexes of 1,3-dithiole-2-thiones containing the 2-pyridyl moiety: syntheses, X-ray crystal structures and solution behavior

Hye Jin Nam, Ha-Jin Lee, Dong-Youn Noh *

Department of Chemistry, Seoul Women's University, Seoul 139-774, Republic of Korea

Received 7 July 2003; accepted 19 September 2003

Abstract

The mercury(II) complexes of 5-pyridin-2-yl-5,6-dihydro-[1,3]dithiolo[4,5-*b*][1,4]dithiin-2-thione (2PyEDT-DTT: **1**), [Hg(2PyEDT-DTT)X_2] (X = Cl (**2a**), Br (**2b**) and I (**2c**)) were obtained from the reaction of HgX_2 and 2PyEDT-DTT. These complexes adopt a dimeric arrangement of [Hg(2PyEDT-DTT)X_2]$_2$ through intermolecular Hg···N and Hg···S interactions. According to the FT-IR/UV–Vis/NMR spectroscopy data, these intermolecular interactions are cleaved in media containing trace H_2O. [Hg(2PyDT-DTT)$_2$] (**3**; 2PyDT-DTT: 5-(1-pyridin-2-yl-vinylsulfanyl)-2-thioxo-[1,3]dithiole-4-thiolate) was isolated from the filtrate of **2**. The Hg(II) ion is located in a center of symmetry and adopts a distorted octahedral geometry with four sulfur atoms (two from the thiolate groups and two from the sulfide groups) and two nitrogen atoms from the pyridyl group. The time-dependent solution UV–Vis and ^{1}H NMR measurements showed the transformation of 2PyDT-DTT to 2PyEDT-DTT caused by trace H_2O in organic solvents.
© 2003 Elsevier Ltd. All rights reserved.

Keywords: Mercury(II); 1,3-Dithiol-2-thione; Pyridyl; ^{1}H NMR; Solid UV

1. Introduction

The coordination chemistry of mercury(II) with N-, O- and S-donors has been extensively studied so far as its versatile coordination modes [1] and biological applications [2] are concerned. The mercury(II) ion has a large polarizability and, therefore, shows a specific affinity to S-donor ligands such as dithiocarbamate [2g], alkylthiolate [3], thione [4] and thioether [5]. Moreover, mixed N-/S-donor systems such as heterocyclic thiones [6] exhibit various coordination modes to the mercury(II) ion. Given their capacity to act as an S-donor, 1,3-dithiol-2-thione derivatives have been used to make complexes of Hg(II), Ag(I) and Cu(I) ions [7]. In these complexes, the sulfur atoms in the sulfide and thione moieties participate as S-donors. Mercury(II) compounds, such as mercury acetate, have also been routinely used in the modification of the thione moiety in 1,3-dithiol-2-thiones to create the corresponding thioketone, which is frequently used in the phosphite-based coupling reaction for tetrathiafulvalene (TTF) derivatives [8].

In our previous papers, we reported on the various coordination modes of the mercury(II) ion with S-donors: i.e. the bi-mercury complex of three- and four-coordination with 1,2-dithiolate ligand [9a], an unusual three-coordinated mercury(II)–thiolate complex [9b] and a dimeric [Hg(μ-Cl)Cl(dPhEDT-DTT)]$_2$ (dPhEDT-DTT: 2,3-dihydro-2,3-diphenyl-1,3-dithiolo[4,5-e][1,4] dithiin-6-thione) complex with a tetrahedral (μ-Cl)$_2$ $HgClS_{thione}$ core [9c]. Here, we report on the synthetic and structural investigation of mercury(II) complexes with the mixed N-/S-donor ligands, 2PyEDT-DTT (5-pyridin-2-yl-5,6-dihydro-[1,3]dithiolo[4,5-*b*][1,4] dithiine-2-thione) and 2PyDT-DTT (5-(1-pyridin-2-yl-vinylsulfanyl)-2-thioxo-[1,3]dithiole-4-thiolate) performed by X-ray crystal structure analysis and FT-IR spectroscopy. The transformation of 2PyDT-DTT from/to 2PyEDT-DTT in a solution state was investigated by means of time-dependent UV/Vis and ^{1}H NMR spectroscopies.

* Corresponding author. Tel.: +82-2-970-5656; fax: +82-2-970-5972.
E-mail address: dynoh@swu.ac.kr (D.-Y. Noh).

0277-5387/$ - see front matter © 2003 Elsevier Ltd. All rights reserved.
doi:10.1016/j.poly.2003.09.028

2. Experimental

2.1. Materials

All chemicals and solvents used in the syntheses were of reagent grade and used without further purification. The solvents used for the spectroscopic measurements were purified according to the literature method [10].

2.2. Measurements

The melting point was measured using an LA9100 electrothermal digital melting point apparatus. Elemental analyses were performed at the Korea Basic Science Institute (KBSI), Seoul. Infrared spectra were recorded on a MIDAC Prospect FT-IR spectrophotometer using the KBr pellet and/or Nujol mull methods. Electronic spectra were obtained on an HP 8452 diode array spectrophotometer and a Shimadzu Double-Beam UV-2100 spectrophotometer for the liquid and solid-state measurements, respectively. ^{1}H NMR spectra were recorded on a 300 MHz Bruker AC-250 spectrometer in $CDCl_3$ and DMSO-d_6.

2.3. Syntheses

2.3.1. 2PyEDT-DTT (**1**)

To a suspension of oligo(1,3-dithiole-2,4,5-trithione) (0.59 g, 3.0 mmol) [11,12] in benzene (50 ml) was added 2-vinylpyridine (0.32 ml, 3.0 mmol). After refluxing for 1 h at 80 °C, the hot solution was filtered and decolorized with activated charcoal (3.0 g). The brown solution was purified by column chromatography on silica gel with chloroform as the eluent. The yellow product was washed with EtOH and dried in a high vacuum. Yield 48%; mp 109–110 °C (decomp); FABMS (*m*/*z*) 302 ($M^+ + 1$); ^{1}H NMR ($CDCl_3$, ppm) δ 3.60(1H, dd), 3.85(1H, dd), 4.86(1H, dd), 7.30(1H, m), 7.45(1H, d), 7.76(1H, dt), 8.62(1H, d); ^{13}C NMR ($CDCl_3$, ppm) δ 34.763, 49.139, 122.738, 123.340, 123.512, 123.958, 137.268, 150.032, 156.532, 208.159; IR (KBr, cm^{-1}) 1581m, 1566m (py C=N), 1485m, 1467ms, 1430m (py C=C), 1055vs (C=S), 786m, 751ms, 608m (py C–H); λ_{max}(CH_3CN, nm): 214(st), 268(m), 406(m).

2.3.2. Hg(2PyEDT-DTT)X_2 (**2**)

To a 20 ml CH_2Cl_2 solution of **1** (0.15 g, 0.50 mmol) was added HgX_2 (0.50 mmol, 0.14 g for X = Cl; 0.18 g for X = Br; 0.23 g for X = I) dissolved in CH_3CN with stirring at room temperature. The red crystals formed from the mixture after standing for two days were filtered and washed with MeOH, and then dried *in vacuo*.

*Hg(2PyEDT-DTT)Cl_2 (**2a**)*. Yield 69%; mp 140–141 °C (decomp); *Anal*. Calc. for $C_{10}H_7NS_5Cl_2Hg$: C 20.95, H 1.23, N 2.44, S 27.91; Found: C 20.82, H 1.34, N 2.21, S 27.39%; IR (Nujol, cm^{-1}) 1583m, 1568m (py C=N), 1463s, 1455s, 1432m (py C=C), 1027s (C=S), 784m, 745ms, 610w (py C–H).

*Hg(2PyEDT-DTT)Br_2 (**2b**)*. Yield 70%; mp 125–126 °C (decomp); *Anal*. Calc. for $C_{10}H_7NS_5Br_2Hg$: C 18.16, H 1.07, N 2.12, S 24.19; Found: C 18.76, H 1.30, N 2.28, S 23.87%; IR (Nujol, cm^{-1}) 1583m, 1568m (py C=N), 1465s, 1453s, 1433m (py C=C), 1024s (C=S), 783m, 744ms, 611m (py C–H).

*Hg(2PyEDT-DTT)I_2 (**2c**)*. Yield 74%; mp 125–126 °C (decomp); *Anal*. Calc. for $C_{10}H_7NS_5I_2Hg$: C 15.86, H 0.93, N 1.85, S 21.13; Found: C 15.84, H 0.93, N 1.74, S 21.03%; IR (Nujol, cm^{-1}) 1590mw, 1568mw (py C=N), 1476s, 1467s, 1432m (py C=C), 1023s (C=S), 780m, 753ms, 615m (py C–H).

Table 1
Crystal data and structure refinement parameters

	2PyEDT-DTT	Hg(2PyEDT-DTT)Br_2	Hg(2PyEDT-DTT)I_2	Hg(2PyDT-TT)$_2$
Empirical formula	$C_{10}H_7NS_5$	$C_{10}H_7Br_2HgNS_5$	$C_{10}H_7I_2HgNS_5$	$C_{10}H_6Hg_{0.5}NS_5$
Formula weight	301.47	661.88	755.86	400.75
Crystal system	monoclinic	triclinic	triclinic	triclinic
Space group	$P2_1/n$ (No. 14)	$P\bar{1}$ (No. 2)	$P\bar{1}$ (No. 2)	$P\bar{1}$ (No. 2)
a (Å)	11.6753(19)	7.854(2)	8.219(2)	8.179(2)
b (Å	6.0102(18)	8.734(2)	8.785(3)	9.1270(10)
c (Å)	18.132(3)	13.594(5)	13.826(3)	9.2650(10)
α (°)	90.0	90.03(3)	79.16(3)	96.860(10)
β (°)	108.540(14)	102.12(2)	77.66(3)	109.970(10)
γ (°)	90.0	116.61(2)	62.61(3)	90.370(10)
V (Å^3)	1206.3(5)	810.4(4)	861.3(4)	644.56(19)
Z	4	2	2	2
ρ_{calcd} (Mg m^{-3})	1.660	2.713	2.915	2.065
μ (mm^{-1})	0.928	15.055	13.111	6.795
F(000)	616	608	680	386
Crystal size (mm)	0.10 × 0.15 × 0.50	0.20 × 0.23 × 0.38	0.30 × 0.30 × 0.50	0.15 × 0.15 × 0.20
$R_1(wR_2)$ [$I > 2\sigma(I)$]	0.0752 (0.1963)	0.0382 (0.0985)	0.0583 (0.1607)	0.0326 (0.0947)
$R_1(wR_2)$ (all data)	0.0762 (0.1980)	0.0389 (0.0990)	0.0589 (0.1614)	0.0328 (0.0950)

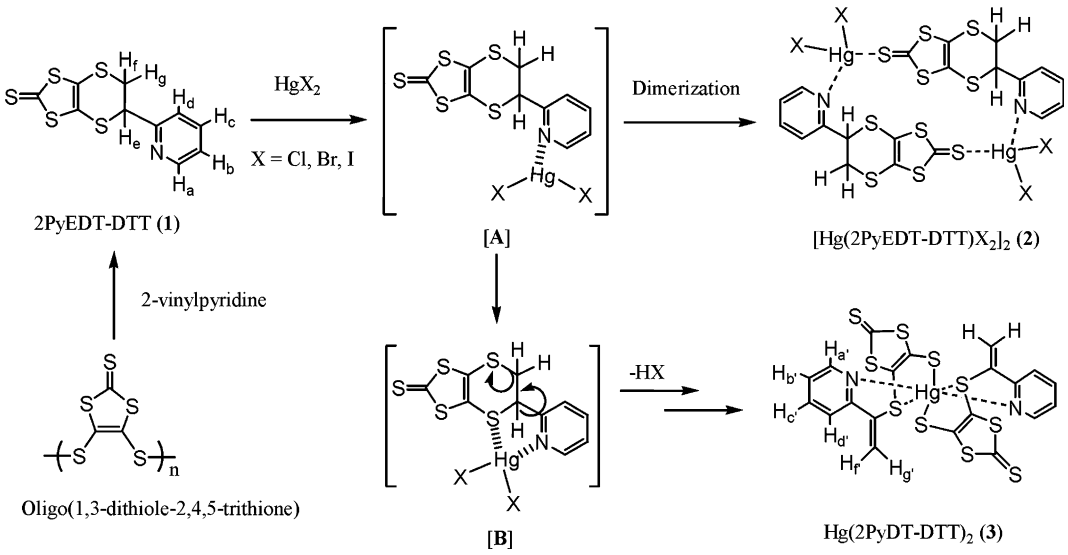

Scheme 1. Proposed routes to the products (**2**) and (**3**).

2.3.3. Hg(2PyDT-DTT)$_2$ (3)

After filtration of **2**, the filtrate was concentrated slowly in air. The yellow crystals collected from the filtrate were washed with MeOH and dried *in vacuo*. The chemical composition of the complexes obtained from the filtrates of **2** was identical regardless of which halide ion was used. Yield 6% (X = Cl), 5% (X = Br) and 3% (X = I); mp 162–163 °C (decomp); *Anal.* Calc. for $C_{20}H_{12}N_2S_{10}Hg$: C 29.93, H 1.51, N 3.49, S 39.88; Found: C 29.85, H 1.56, N 3.41, S 39.24%; IR (Nujol, cm^{-1}) 1583m, 1563m (py C=N), 1462ms, 1443m, 1429m (py C=C), 1058vs (C=S), 917ms (=CH_2), 788m, 748m, 623mw (py C–H).

2.4. X-ray crystal structure determinations

The X-ray crystal data were collected on an Enraf–Nonius CAD-4 diffractometer with graphite-monochromated Mo Kα radiation ($\lambda = 0.71073$ Å) at 293(2) K. The structures were solved by the direct method (compound **1**) or the heavy-atom method (compounds **2** and **3**) with SHELXS 86 [13] and refined by full-matrix least-squares analysis on F^2 with SHELXS-93 [14]. Atomic scattering factors for all non-hydrogen atoms were supplied by the SHELXS-86 system [13]. The crystallographic data collection and refinement details are summarized in Table 1.

3. Results and discussion

3.1. Synthesis

2PyEDT-DTT (**1**) was synthesized by employing the [2 + 4] cycloaddition reaction of oligomeric 1,3-dithiole-2,4,5-trithione and 2-vinylpyridine under the modified reaction condition (Scheme 1), and obtained in a higher yield (48%) than the reported one (20%) [15]. The 2-pyridyl compound thus prepared was fully characterized by spectroscopic methods and X-ray crystal structure analysis (Fig. 1). The preparation of its Hg(II) complexes **2** was achieved at room temperature (RT) with a 1:1 molar ratio of HgX_2 (X = Cl, Br and I) and **1** in a mixed solvent of acetonitrile and methylene chloride. After the filtrates of **2** were left to stand for an extended period of time, **3** was unexpectedly obtained, regardless of the halide ion being used (Scheme 1). This was confirmed by elemental analysis and X-ray structure analysis as will be discussed below. The total yield of **3** was about 3–6%, while that of **2** was 69–74% at RT, irrespective of the amount of HgX_2 used. However, the yields of **2** and **3** were strongly dependent upon the reaction temperature: When the reaction was performed at 60 °C, the yield of **3** (synthesized from $HgCl_2$) increased to 21%, while that of **2a** went down to 5%, indicating that **2a** is a major product at RT, but a minor product at 60 °C. On the other hand, the yields of **3** (synthesized from $HgBr_2$ and HgI_2) were almost unchanged (5%) even at 60 °C, with those of **2b** and **2c** being 3% and 32%, respectively. This indicates that **2c** is a major

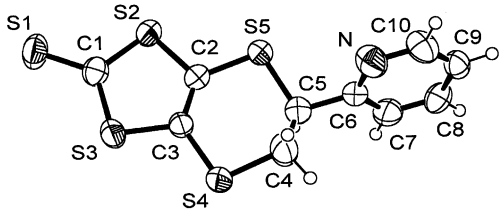

Fig. 1. Molecular structure of 2PyEDT-DTT (**1**) with the atomic numbering scheme.

product both at RT and at 60 °C. This observation can be understood based on the principle of *hard and soft acid and base* [16]: Hg(II) and the chloride ion are the most unfavorable couple among the three halide complexes, so that the elimination of HCl would be expected to be the most favorable process and would therefore give **3** as a major product at 60 °C instead of **2a**. However, in the case of HgI_2, the I_2HgSN core in **2c** is the most favorable soft acid–soft base combination, so that **2c** is still the major product even at the more elevated reaction temperature. It is noticeable, however, that the total recovery of **2** and **3** was decreased at 60 °C. The same trend was found when a mixed solvent consisting of methanol and acetone was used both at RT and at 60 °C.

Based on these observations, it can be conjectured that the formation of complexes **2** and **3** occurs via two intermediate states, [**A**] and [**B**], as shown in Scheme 1. The involvement of intermediate [**A**] can be proposed based on the assumption that the pyridyl group is a stronger Lewis base than the sulfur atoms in the thione and sulfide moieties. When the intermediate [**A**] is dimerized by adopting a sulfur atom in a thione moiety as the fourth coordination of the mercury(II) ion, it forms the dimeric complex **2**. On the other hand, when the fourth coordination of the mercury(II) ion is found in a sulfide moiety of the same molecule, it proceeds to another transition state [**B**]. In this state, the hydrogen atom in between the coordinating sulfur and nitrogen atoms becomes more acidic due to the electron donation of $S \rightarrow Hg(II)$ and $N \rightarrow Hg(II)$. Consequently, the cleavage of the C–S bond induced by the deprotonation of the acidic proton results in the ring-opening of the 1,3-dithiin moiety, which is accompanied by the formation of a C=C bond.

3.2. X-ray structure analysis of *2b* and *2c*

The crystal data and structure refinement parameters of **2b** and **2c** are shown in Table 1 and the selected bond lengths and angles are listed in Table 2. The X-ray crystal structures obtained from the diamond-shaped

Table 2
Selected bond lengths (Å) and angles (°) for 2PyEDT-DTT and Hg(2PyEDT-DTT)X_2 (X = Br and I)

	2PyEDT-DTT	Hg(2PyEDT-DTT)Br_2	Hg(2PyEDT-DTT)I_2
Bond lengths			
Hg–X(1)		2.4974(13)	2.6524(13)
Hg–X(2)		2.4451(15)	2.6179(14)
Hg–S(1)		2.670(3)	2.711(4)
Hg–N#		2.510(7)	2.590(12)
S(1)–C(1)	1.633(6)	1.680(8)	1.672(12)
S(2)–C(1)	1.718(6)	1.689(8)	1.700(12)
S(2)–C(2)	1.735(6)	1.741(8)	1.721(13)
S(3)–C(1)	1.722(6)	1.698(8)	1.692(12)
S(3)–C(3)	1.741(5)	1.747(8)	1.744(12)
S(4)–C(3)	1.740(6)	1.745(8)	1.736(13)
S(4)–C(4)	1.803(7)	1.797(9)	1.795(14)
S(5)–C(2)	1.743(6)	1.732(9)	1.739(12)
S(5)–C(5)	1.774(7)	1.809(10)	1.795(15)
N–C(6)	1.331(9)	1.336(12)	1.320(17)
N–C(10)	1.329(9)	1.324(12)	1.362(17)
C(2)–C(3)	1.337(8)	1.327(12)	1.354(17)
C(4)–C(5)	1.412(11)	1.498(13)	1.50(2)
C(5)–C(6)	1.514(9)	1.524(12)	1.510(17)
C(6)–C(7)	1.361(9)	1.378(13)	1.38(2)
C(7)–C(8)	1.356(9)	1.385(14)	1.40(2)
C(8)–C(9)	1.351(9)	1.353(16)	1.34(2)
C(9)–C(10)	1.375(9)	1.371(15)	1.34(2)
Bond angles			
N#–Hg–X(2)		98.15(18)	96.1(3)
N#–Hg–X(1)		93.64(17)	93.1(3)
X(1)–Hg–X(2)		147.50(5)	149.53(5)
N#–Hg–S(1)		110.62(18)	109.7(3)
X(2)–Hg–S(1)		113.72(7)	112.60(9)
X(1)–Hg–S(1)		89.80(7)	91.20(8)
C(1)–S(1)–Hg		116.8(3)	118.3(4)
S(1)–C(1)–S(2)	123.7(4)	119.0(5)	118.0(7)
S(1)–C(1)–S(3)	124.0(4)	126.1(5)	127.3(7)
S(2)–C(1)–S(3)	112.3(3)	114.9(5)	114.6(7)

Symmetry transformations used to generate equivalent atoms: # $-x+2, -y, -z$ (X = I) and $-x+1, -y+1, -z$ (X = Br).

single crystals are demonstrated in Figs. 2 and 3. From the structural analysis results, it was revealed that **2b** is isostructural with **2c** and that they form a head-to-tail type dimeric arrangement with the general formula $[Hg(\mathbf{1})X_2]_2$ (X = Br, I). The mercury(II) ions in these complexes are tetrahedrally coordinated by two bromides (or iodides), one sulfur atom from a thione moiety and one nitrogen atom from the neighboring pyridyl group. Such a coordination mode results in a structural deformation of the coordinated **1**. That is, the C(1)═S(1) bond length (1.680(8) Å for **2b** and 1.672(12) Å for **2c**) is longer than that of the free ligand (**1**) (1.633(6) Å). Furthermore, the difference between the two angles around the C(1) atom (S(1)–C(1)–S(2) and S(1)–C(1)–S(3)) of 7.1° (**2b**) and 9.3° (**2c**) is comparable to the situation of the corresponding angles of free ligand (**1**) which are almost identical (123.7(4)° and 124.0(4)°). This is due to the coordination of S(1) to Hg(II). The Hg···S(1) bond lengths of **2b** (2.670(3) Å) and **2c** (2.711(4) Å) are somewhat longer than the sum of the covalent radii of S and Hg (2.50 Å), but shorter than the sum of the van der Waals radii (3.53 Å) [1b]. The Hg···N# bond lengths of **2b** (2.510(7) Å) and **2c** (2.590(12) Å) are in between the sum of the covalent radii (2.23 Å) and the van der Waals radii (3.28 Å) [1b] of N and Hg. These facts indicate that the intermolecular Hg···S(1) and Hg···N# interactions are relatively significant. In terms of the coordination mode, however, it is worthwhile to consider that $[Hg_2(EDT\text{-}DTT)_2Cl_4]_n$ (EDT-DTT: 4,5-ethylenedithio-1,3-dithiole-2-thione: $C_5H_4S_5$) possesses a one-dimensional polymeric structure with a penta-coordinated Hg(II) ion [7b]. The sulfur atom in the 1,4-dithiin ring of the EDT-DTT ligand coordinates to Hg(II), and this kind of coordination mode is also observed in the corresponding Ag(I) and Cu(I) complexes [7]. However, this coordination mode is not observed in the case of **2b** and **2c**. Instead, a N atom in a pyridine moiety coordinates to Hg(II). The sulfur atom from a thione moiety coordinates to Hg(II) and the Hg···S distance in both **2b** and **2c** is much longer than that in $[Hg_2(EDT\text{-}DTT)_2Cl_4]_n$ (2.454(2) Å). These observations strongly suggest that the intermolecular Hg···S(1) and Hg···N# interactions in **2b** and **2c** could be cleaved in the solution state as will be discussed below.

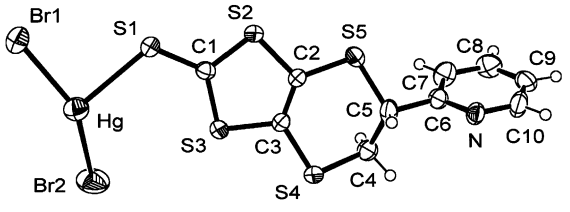

Fig. 2. Molecular structure of Hg(2PyEDT-DTT)Br_2 (**2b**) with the atomic numbering scheme. Complex **2c** is isostructural with **2b**.

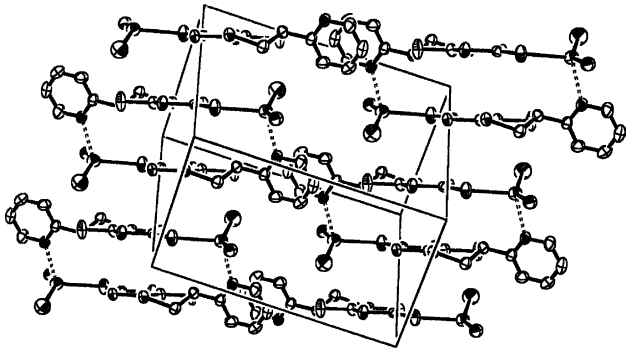

Fig. 3. Crystal structure of Hg(2PyEDT-DTT)Br_2 (**2b**) showing the dimeric arrangement with intermolecular Hg···N interaction (dashed lines). Hydrogen atoms are omitted for clarity.

3.3. X-ray structure analysis of 3

The crystal data and structural refinements for **3** are given in Table 1 and the selected bond lengths and angles are listed in Table 3. As shown in the ORTEP drawing (Fig. 4), the Hg(II) ion is situated in the inversion center with a distorted octahedral geometry, directly linked to two thiolates, two sulfides and two nitrogen atoms from the pyridyl moiety. This complex has a short Hg–S(4) bond of 2.3743(17) Å, whose distance is in between those of the three-coordinated Hg(II)–thiolate complexes such as mononuclear $Hg(SC_6H_5)_3$ (2.448(3) Å) [17] and $[Hg(S\text{-}2,4,6\text{-}Pr^i_3C_6H_2)_3]^{1-}$ (2.442(4) Å) [2e], and those of the two-coordinated ones such as $[Hg(S\text{-}2,4,6\text{-}Pr^i_3C_6H_2)_2]$ (2.322(6) Å) [2e]. Moreover, the Hg···S(5) distance (3.0195(17) Å) is apparently shorter than the Hg···S(sulfide) distance (3.271(2) Å) of $[Hg_2(EDT\text{-}DTT)_2Cl_4]_n$ [7b] and the van der Waals distance (3.53 Å) [1b]. The intramolecular Hg···N distance (2.794 Å) of **3**, however, is much longer than the reported Hg···$N_{pyridyl}$ distances (2.560(3)–2.595(4) Å) [18] and the covalent distance (2.23 Å) [1b]. Moreover, the S(5)–Hg–N angle (64.53(5)°) deviates significantly from 90°, whereas the S(4)–Hg–N angle (88.46(5)°) is quite close to 90°. Based on these findings, it can be supposed that this structure would not be stable in the solution state, even though it exhibits a stable molecular structure in the solid state.

3.4. Infrared spectroscopy

The influence of H_2O on **2** was investigated by FT-IR, and the FT-IR spectra of **2a** in different matrices and with different H_2O contents are demonstrated in Fig. 5. The FT-IR spectrum of **2a** measured in Nujol (Fig. 5(a)) is different from that of the free ligand **1** (Fig. 5(L)) in two main regions: the C═S absorption band of the free ligand **1** (1055 cm^{-1}) shifted to 1023–1027 cm^{-1} (**2**), and the change in the ring stretching vibrations of the pyridyl

Table 3
Selected bond lengths (Å) and angles (°) for $Hg(2PyDT\text{-}DTT)_2$ (**3**)

Bond lengths			
Hg–S(4)	2.3743(17)	Hg–S(5)	3.0195(17)
S(1)–C(1)	1.644(6)	S(2)–C(1)	1.726(7)
S(2)–C(3)	1.757(6)	S(3)–C(1)	1.719(7)
S(3)–C(2)	1.741(6)	S(4)–C(2)	1.727(6)
S(5)–C(3)	1.748(6)	S(5)–C(4)	1.779(6)
C(2)–C(3)	1.357(9)	C(4)–C(5)	1.325(9)
Bond angles			
S(4)#–Hg–S(5)	98.97(5)	S(4)–Hg–S(5)	81.03(5)
C(3)–S(5)–C(4)	102.3(3)	S(1)–C(1)–S(3)	122.7(4)
S(1)–C(1)–S(2)	124.8(4)	S(3)–C(1)–S(2)	112.5(3)

Symmetry transformation used to generate equivalent atoms: # $-x+1, -y+1, -z+1$.

group (1400–1600 cm^{-1}). These are surely due to changes in the intermolecular Hg···S and Hg···N interactions, as confirmed in the X-ray structure analysis. The H_2O content in the KBr pellet of **2a** was controlled semi-quantitatively and identified in its FT-IR spectra by the intensity change of the scissoring mode of H_2O observed at around 1620 cm^{-1} (denoted by # in Fig. 5). As the H_2O content increases from (b) to (d) in Fig. 5, the intensity of the free C=S vibration peak at 1055 cm^{-1} (denoted by $*$ in Fig. 5) also increases, whereas that of the coordinated C=S vibration peak at 1027 cm^{-1} (denoted by + in Fig. 5) decreases. Finally, in the spectrum of (d), the peaks are identical to that of ligand (L) except for the broad H_2O peak. The same trend is observed in the ring stretching vibrations of the pyridyl group in the 1400–1600 cm^{-1} range: the ring stretching peaks of the pyridyl group at 1584, 1568, 1468, 1452, 1433 cm^{-1} (Fig. 5(b)) are changed to those of the free ligand at 1583, 1566, 1486, 1469, 1431 cm^{-1} (Fig. 5(d)). From these observations, it can be surmised that due to the trace amount of H_2O in the KBr pellet, the intermolecular Hg···S and Hg···N interactions in **2** are cleaved and that **2** is possibly decomposed into its components, HgX_2 and **1**. These intermolecular interactions, however, have been revealed to be unaffected by increasing temperature up to 50 °C. In the case of complex **3**, the strong peak at 1058

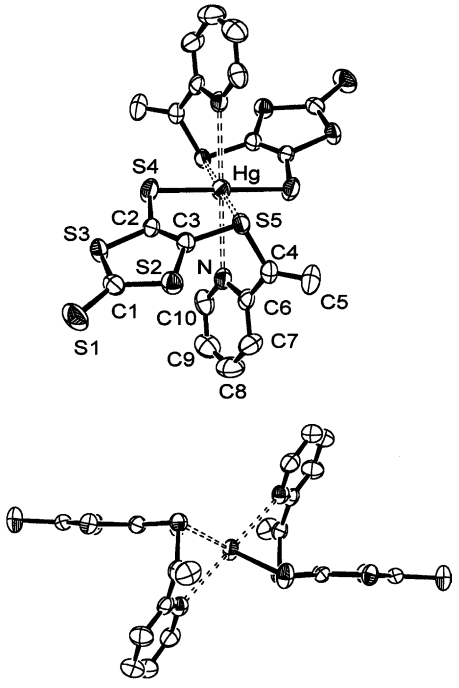

Fig. 4. Molecular structure of $Hg(2PyDT\text{-}DTT)_2$ (**3**) with the atomic numbering scheme (top) and its side view (bottom). Hydrogen atoms are omitted for clarity.

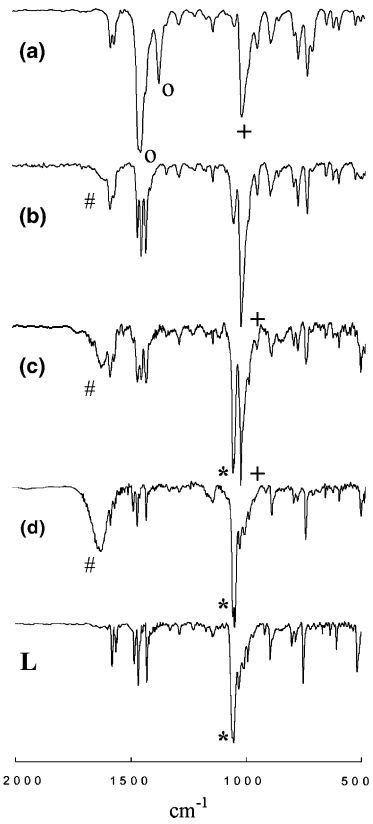

Fig. 5. Influence of H_2O on the intermolecular Hg···S bond in complex **2a**: the spectra in Nujol mull (a) and KBr pellet ((b), (c) and (d)) with different H_2O contents. The complexes **2b** and **2c** revealed the same results as that of **2a** in the FT-IR spectral studies. ($*$: H_2O; ○: Nujol; #: free C=S stretching; +: C=S stretching coordinated to Hg).

Table 4
Electronic spectral data for $n \rightarrow \pi^*$ (C=S) transition in various media[a]

Compound	λ_{max} (nm)						Time (day)
	$BaSO_4$	MeOH	MeCN	THF	DMSO	$CDCl_3$	
2PyEDT-DTT **(1)**	430	406	406	408	412	406	0
Hg(2PyEDT-DTT)Cl_2 **(2a)**[b]	453	406	406	408	412	406	0
Hg(2PyDT-DTT)$_2$ **(3)**	397	398	400	394	396	394	0
		402	402	398	400	400	1
		406	406	408	412	406	4

[a] Measured at room temperature.
[b] Complexes **2b** and **2c** give the same results as those of **2a**.

cm^{-1} was identified as a C=S vibrational peak of the 2PyDT-DTT ligand, which is free from intermolecular interaction with Hg(II). Additionally, a newly formed vinylidene peak was observed at 917 cm^{-1}.

3.5. Electronic absorption spectroscopy

The electronic transition spectra of **2** and **3** were measured in several liquid and solid media, in which the characteristic $n \rightarrow \pi^*$ transitions of the C=S moiety in **2a** and **3** are listed and compared with those of **1** in Table 4. The $n \rightarrow \pi^*$ transition of **2a** was observed at 406 nm in acetonitrile, which is surprisingly identical with that of the free ligand (**1**). On the other hand, the corresponding transition for solid **2a** (453 nm) measured in a $BaSO_4$ matrix was observed at a higher wavelength than that of solid **1** (430 nm). This blue-shift surely indicates the coordination of the sulfur atom in the C=S moiety to the Hg(II) ion in the solid state. In the solution state, however, the intermolecular Hg···S and Hg···N interactions would be cleaved as soon as the complex is dissolved in the organic solvent. Considering these observations in the light of the IR results, the trace amount of water in the solvents might play an important role in the cleavage of the intermolecular interactions. More interesting results were found for **3**. The $n \rightarrow \pi^*$ transitions were observed near 397 nm for both the solid and liquid forms of **3**, possibly because there were no intramolecular interactions in the C=S moiety. Within four days in a solution state, however, the original $n \rightarrow \pi^*$ transition of **3** exhibited a blue-shift, which resulted in their final values being the same as those of **1**. It is suggested that the 2PyDT-DTT ligand in **3**, formed by deprotonation as proposed in Scheme 1, gradually returned to its original form **1** in the solution state. This transformation can be regarded as being promoted by trace water present in the solvent. More systematic evidence of this transformation was obtained in the time-dependent ^1H NMR study.

3.6. ^1H NMR spectroscopy

The ^1H NMR spectrum of **1** exhibits a total of seven peaks, four of which can be attributed to the protons in the 2-pyridyl group (Fig. 6(e)) and three to those in the ethylene group. As expected from the electronic spectroscopy, the ^1H NMR spectra of **2** measured in $CDCl_3$ and DMSO-d_6 were completely identical to those of the free ligand (**1**), indicating the rapid cleavage of the intermolecular Hg···S and Hg···N interactions in the solvents (see Table 5). Complex **3** showed two sets of ^1H NMR peaks; one set from the free ligand (**1**) and the other from **3**. With the possibility that **3** may contain

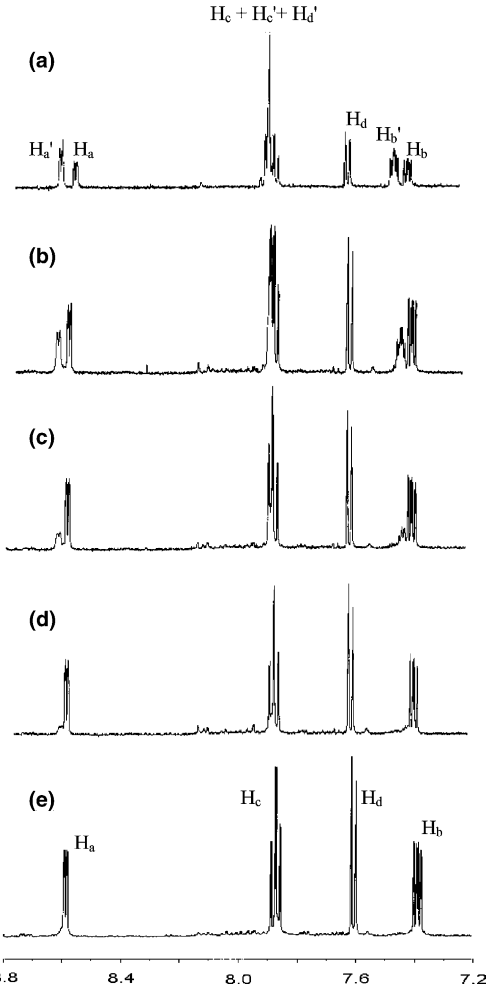

Fig. 6. Time-dependent ^1H NMR spectra of (**3**) in DMSO-d_6 measured after (a) 0 days, (b) 1 day, (c) 4 days and (d) 14 days, compared with (**1**) (e) (see Scheme 1 for the assignments of the different protons).

Table 5
^{1}H NMR spectral data of the complexes measured in DMSO-d_6 (in ppm)[a]

Complex	H_a	H_b	H_c	H_d	H_e	H_f	H_g	$H_{a'}$	$H_{b'}$	$H_{c'}$	$H_{d'}$	$H_{f'}$	$H_{g'}$
PyEDT-DTT (**1**)	8.58	7.38	7.86	7.59	5.13	3.88	3.80						
Hg(2PyEDT-DTT)X_2 (**2**)	8.58	7.39	7.87	7.60	5.13	3.88	3.80						
Hg(2PyDT-DTT)$_2$ (**3**)[b]	8.58	7.39	7.87	7.61	5.14	3.87	3.81	8.62	7.46	7.92	7.87	6.31	5.66

[a] Measured at 303 K. See Scheme 1 for the hydrogen labelling.
[b] Measured just after the sample was dissolved in DMSO-d_6.

some proportion of **1** having already been excluded by the FT-IR, UV–Vis and X-ray structure analyses, as well as by the elemental analysis, it is likely that complex **3** reaches the equilibrium state (Eq. (1)) rapidly after it is dissolved in NMR solvents. Therefore, between 7.2 and 8.8 ppm where the pyridyl protons are observed, two sets of NMR peaks corresponding to the free ligand and **3** were observed, as shown in Fig. 6(a). The initial molar ratio of **1** to **3** is calculated as being 0.7, based upon the intensity ratio of H_a/H'_a and H_b/H'_b.

$$\mathrm{Hg(II)} + 2\mathbf{1} \Longleftrightarrow \mathbf{3} + 2\mathrm{H}^+ \quad (1)$$

This equilibrium slowly moved backward and, finally, the peaks of **3** ($H_{a'}$–$H_{d'}$ in Fig. 6) completely shifted to those of **1** (H_a–H_d in Fig. 6) after 14 days. The two peaks corresponding to $=CH_2$ in the vinylidene group of **3** ($\delta = 6.31$ and 5.66 ppm) also gradually diminished, while those corresponding to $–CH_2–$ and –CH– in the ethylene group ($\delta = 3.87$, 3.81 and 5.14 ppm) intensified.

4. Conclusion

We synthesized the dimeric mercury(II) complexes ([Hg(2PyEDT-DTT)X_2]$_2$ where X = Cl, Br and I) through the reaction of mercury halides and pyridine-containing 1,3-dithiol-2-thione (2PyEDT-DTT). In these complexes, the tetrahedrally-coordinated mercury(II) ion forms intermolecular Hg···S and Hg···N interactions with S- and N-donors. It was revealed by FT-IR investigation that these interactions are easily destroyed by trace H_2O resulting in the Hg(II) ion and the free ligand (2PyEDT-DTT). As a product of the mercuration of 2PyEDT-DTT, the Hg(2PyDT-DTT)$_2$ complex was isolated, wherein the mercury(II) ion is octahedrally coordinated to form the N_2HgS_4 core. This complex is reversibly transformed to 2PyEDT-DTT and Hg(II) in solvents as evidenced by the time-dependent UV–Vis and ^{1}H NMR measurements.

5. Supplementary data

Supplementary data for the structural analyses are available from The Director, CCDC, 12 Union Road, Cambridge, CB2 1EZ, UK (fax: +44-1223-336033; E-mail: deposit@ccdc.cam.ac.uk or www:http://www.ccdc.cam.ac.uk) on request, quoting the deposition numbers 212796–212799 for the complexes **1**, **2b**, **2c** and **3**, respectively.

Acknowledgements

We gratefully acknowledge the financial support provided by the Ministry of Science and Technology (MOST) through the Women's University Research Fund (98-N6-03-01-A-08).

References

[1] (a) G.J. Grant, Mercury: Inorganic & Coordination Chemistry, in: R.B. King (Ed.), Encyclopedia of Inorganic Chemistry, vol. 4, Wiley, Chichester, 1994, p. 2136;
(b) J.G. Wright, M.J. Natan, F.M. McDonnell, D.M. Ralston, T.V. O'Halloran, Prog. Inorg. Chem 38 (1990) 323.
[2] (a) G. Fleissner, P.M. Kozlowski, M. Vargek, J.W. Bryson, T.V. O'Halloran, T.G. Spiro, Inorg. Chem. 38 (1999) 3523;
(b) G. Fleissner, M.D. Reigle, T.V. O'Halloran, T.G. Spiro, J. Am. Chem. Soc. 120 (1998) 12690;
(c) L.M. Utschig, J.W. Bryson, T.V. O'Halloran, Science 268 (1995) 380;
(d) J.G. Wright, H.T. Tsang, J.E. Penner-Hahn, T.V. O'Halloran, J. Am. Chem. Soc. 112 (1990) 2434;
(e) E.S. Gruff, S.A. Koch, J. Am. Chem. Soc. 112 (1990) 1245;
(f) S.P. Watton, J.G. Wright, F.M. MacDonnell, J.W. Bryson, M. Sabat, T.V. O'Halloran, J. Am. Chem. Soc. 112 (1990) 2824;
(g) A.M. Bond, R. Colton, A.F. Hollenkamp, B.F. Hoskins, K. McGregor, J. Am. Chem. Soc. 109 (1987) 1969.
[3] (a) G.A. Bowmaker, I.G. Dance, B.C. Dobson, D.A. Rogers, Inorg. Chem. 20 (1981) 1487;
(b) J.P. Fackler Jr., D. Coucouvanis, J. Am. Chem. Soc. 88 (1966) 3913.
[4] (a) Z. Popovic, Z. Soldin, D. Matkovic-Calogovic, G. Pavlovic, M. Rajic, G. Giester, Eur. J. Inorg. Chem. (2002) 171;
(b) N.A. Bell, T.N. Branston, W. Clegg, L. Parker, E.S. Raper, C. Sammon, C.P. Constable, Inorg. Chim. Acta 319 (2001) 130;
(c) Z. Popovic, D. Matkovic-Calogovic, J. Hasic, D. Vikic-Topic, Inorg. Chim. Acta 285 (1999) 208;
(d) E.S. Raper, J.R. Creighton, N.A. Bell, W. Clegg, L. Cucurull-Sanchez, Inorg. Chim. Acta 277 (1998) 14.
[5] F. Cecconi, C.A. Ghilardi, S. Midollini, A. Orlandini, Inorg. Chim. Acta 269 (1998) 274.
[6] (a) E.S. Raper, Coord. Chem. Rev. 165 (1997) 475;
(b) E.S. Raper, Coord. Chem. Rev. 153 (1996) 199;
(c) Z. Popovic, D. Matkovic-Calogovic, Z. Soldin, G. Pavlovic, N. Davidovic, D. Vikic-Topic, Inorg. Chim. Acta. 294 (1999) 35;

(d) M. Hong, W. Su, R. Cao, W. Zhang, J. Lu, Inorg. Chem. 38 (1999) 600.
[7] (a) J.L. Zuo, J.F. Bai, Z. Shen, X.Z. You, H.K. Fun, K. Chinnakali, C.M. Che, Inorg. Chim. Acta 292 (1999) 117;
(b) Q.H. Wang, D.L. Long, J.S. Huang, Polyhedron 17 (1998) 3665;
(c) J. Dai, M. Munakata, L.P. Wu, T. Kuroda-Sowa, Y. Suenaga, Inorg. Chim. Acta 258 (1997) 65;
(d) J. Dai, M. Munakata, T. Kuroda-Sowa, Y. Suenaga, L.P. Wu, M. Yamamoto, Inorg. Chim. Acta 255 (1997) 163.
[8] (a) D.Y. Noh, H.J. Lee, J. Hong, A.E. Underhill, Tetrahedron Lett. 37 (1996) 7603;
(b) H.J. Lee, D.Y. Noh, Bull. Korean Chem. Soc. 19 (1998) 340.
[9] (a) D.Y. Noh, A.E. Underhill, M.B. Hursthouse, Chem. Commun. (1997) 2211;
(b) Y.Y. Kim, H.J. Lee, H.J. Nam, D.Y. Noh, Bull. Korean Chem. Soc. 22 (2001) 17;
(c) H.J. Lee, H.J. Nam, D.Y. Noh, Bull. Korean Chem. Soc. 20 (1999) 1368.
[10] D.D. Perrin, W.L.F. Armarego, Purification of Laboratory Chemicals, third ed., Pergamon Press, Oxford, UK, 1988.
[11] (a) O.Ya. Neilands, Ya.Ya. Katsens, Ya.N. Kreitsberga, Zh. Org. Khim. 25 (1989) 658;
(b) O.Ya. Neilands, Ya.Ya. Katsens, Ya.N. Kreitsberga, Russian Patent # SU1428753, 1988.
[12] O.Ya. Neilands, Ya.Ya. Katsens, Ya.N. Kreitsberga, Chem. Abstr. 110 (1989) 95252.
[13] G.M. Sheldrick, SHELXS-86, A Program for Structure Determination, University of Gottingen, Germany, 1986.
[14] G.M. Sheldrick, SHELXS-93, A Program for Structure Refinement, University of Gottingen, Germany, 1993.
[15] W. Xu, D. Zhang, H. Li, D. Zhu, J. Mater. Chem. 9 (1999) 1245.
[16] C.E. Housecroft, A.G. Sharpe, Inorganic Chemistry, Prentice-Hall, Englewood Cliffs, NJ, 2001, p. 166.
[17] G. Christou, K. Folting, J.C. Huffman, Polyhedron 3 (1984) 1247.
[18] D.C. Bebout, D.E. Ehmann, J.C. Trinidad, K.K. Crahan, M.E. Kastner, D.A. Parrish, Inorg. Chem. 36 (1997) 4257.

Available online at www.sciencedirect.com
SCIENCE DIRECT®
Polyhedron 23 (2004) 125–133
POLYHEDRON
www.elsevier.com/locate/poly

Rotational barriers in dialkylaminochlorophosphines: methyl-substituted piperidinochlorophenylphosphines

Jason Anagnostis, Mark M. Turnbull *

Carlson School of Chemistry and Biochemistry, Clark University, 950 Main St., Worcester, MA 01610, USA

Received 19 July 2003; accepted 22 September 2003

Abstract

Barriers to rotation about the P–N bond in a series of substituted piperidinochlorophenylphosphines were measured. The barriers for piperidine, 2-methylpiperidine and *cis*-2,6-dimethylpiperidine are the same within experimental error. The thermal condensation of the corresponding bis(piperidino)phosphine oxides with $Mo(CO)_6$ show that only the *cis*-2,6-dimethyl compound produces significant quantities of the $[R_2NPO]_4[Mo(CO)_4]_2$ complex. These observations are explained in terms of the steric requirements of the various amines and aminophosphines via cone angle measurements. Condensation of the mixed phosphine oxide, $(^iPr_2N)(Et_2N)PHO$, with $Mo(CO)_6$ produces $[Et_2NPO]_4[Mo(CO)_4]_2$.
© 2003 Elsevier Ltd. All rights reserved.

Keywords: Rotational barriers; Polyphosphoxane; Cage complexes; Cone angles

1. Introduction

Since the initial discovery by Wong et al. [1] of the condensation reaction between bis(di-isopropylamino)phosphine oxide and molybdenum hexacarbonyl to produce the polycyclic Cage complex $(CO)_4Mo[^iPr_2NPO]_4Mo(CO)_4$ (**1**) (Fig. 1, $R = {}^iPr$), a number of related complexes of the general formula $L_aM[R_2NPO]_nM'L'_b$ have been prepared (M, M′ = Cr, Mo, W, Fe, Ni, Pd, Pt, Cu, Ag, none; L′ = CO, Cl, Br, I; R_2N = various secondary amino groups; $n = 3$–6) [2–6]. The complexes can be prepared by four pathways: direct synthesis by reaction of two diphosphine-substituted metal complexes [2], substitution of one metal for another in a Cage [4], reaction of a metal complex with a cyclotriphosphoxane [3,5], and direct thermal condensation of a bis(dialkylamino)phosphine oxide with $M(CO)_6$ (M = Cr, Mo, W) [2,3,5].

The latter route to these Cage complexes exhibited an apparent steric dependence as the reaction was successful only when large secondary amino groups, such as diisopropyl and dicyclohexyl, were employed. With less hindered amino substituents such as dimethyl-, diethyl-, and dibenzylamino, no Cage complexes could be isolated and only traces were observed spectroscopically [2]. The proposed mechanism for the thermal condensation involves initial coordination to the metal center by the diaminophosphine oxide (in its phosphinous acid tautomeric form, $\mathbf{I_1}$) followed by elimination of one molecule of dialkylamine to generate the coordinated phosphinidene oxide ($\mathbf{I_2}$). Condensation of the P=O functions and addition of a second metal atom leads to the observed products [2] (see Scheme 1).

The key step appears to be the elimination of the dialkylamine to produce the coordinated phosphinidene oxide ($\mathbf{I_2}$) and the observed requirement for bulky amines suggests that the step is driven by the relief of steric strain in intermediate $\mathbf{I_1}$.

We previously examined the steric requirements of the various alkyl substituents by variable temperature NMR experiments to determine the barrier to rotation about the P–N bond on the related dialkylaminochlorophenylphosphines [7]. We had reasoned that, within a homologous family of compounds, the electronic contributions to the barrier would remain constant and any differences observed would result from the steric bulk of

* Corresponding author. Tel.: +1-508-793-7116/7167; fax: +1-508-793-8861.
E-mail address: mturnbull@clarku.edu (M.M. Turnbull).

0277-5387/$ - see front matter © 2003 Elsevier Ltd. All rights reserved.
doi:10.1016/j.poly.2003.09.027

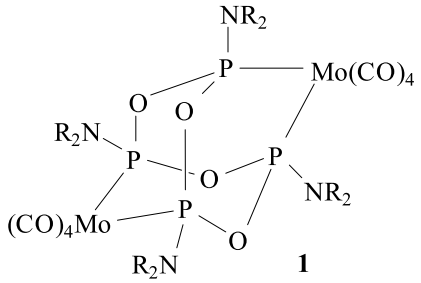

Fig. 1. The structure of the Cage complexes **1**.

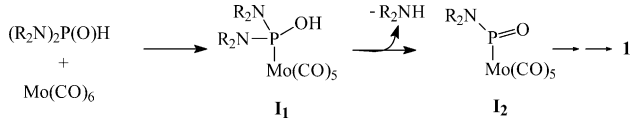

Scheme 1. Proposed mechanism for the synthesis of **1**.

the alkyl substituents. The barriers for the dialkylamino groups studied, Me_2N–, Et_2N–, Bz_2N–, $^iPr_2N$– and C-hex_2N–, fell into two distinct classes. Those with primary alkyl groups had rotational barriers of 11.6 ± 0.1 kcal/mol, while those with secondary alkyl groups had barriers of 13.4 ± 0.2 kcal/mol. Only those amino groups exhibiting the higher barrier were observed to produce Cage complexes by thermal condensation, suggesting that the steric bulk requirement in the diaminophosphine oxides for the formation of **1** was correct. However, we wished to test whether this correlation of barrier to P–N bond rotation in the dialkylaminochlorophenylphosphines would have predictive value for the success of the Cage-forming thermal condensations. Thus, we undertook the present study where we determined the barrier to rotation about the P–N bond in the series $(R_2N)PhPCl$ [R_2N = piperidine (pip), (±)-2-methylpiperidine (Mepip), *cis*-2,6-dimethylpiperidine (Me_2pip), 2,2,6,6-tetramethylpiperidine (Me_4pip)] and examined the reaction of the corresponding phosphine oxides, $(R_2N)_2P(O)H$, with $Mo(CO)_6$.

2. Experimental

All reactions were carried out under argon using Schlenk technique. CH_2Cl_2 was distilled from CaH_2, toluene from Na metal, and Et_2O and THF from Na/benzophenone ketyl. Amines were distilled just prior to use from KOH. PCl_3 and $PhPCl_2$ were purchased from Aldrich and used as received. IR spectra were recorded on a PE-1600 or PE Paragon 500 spectrophotometer. NMR spectra are reported at r.t. (unless otherwise noted) and were recorded on a Bruker AC-200 spectrometer. ^1H and ^{13}C NMR spectra were referenced to the solvent while ^{31}P NMR spectra were referenced to external Ph_3P (broadband proton decoupled unless otherwise noted). All values are given in ppm [s, singlet; d, doublet; t, triplet and br, broad]. Diisopropylaminophenylchlorophosphine (**2e**) was prepared as previously described [7]. Elemental analyses were performed at the Instrumentation Center, University of New Hampshire. Computer simulations of NMR spectra were performed on a VAX system using the KUBO program [8].

2.1. Cone angle measurements

Cone angle measurements on phosphines were carried out using CPK models according to the procedure of Tolman [9], and measurements on amines were carried out according to the procedure of Seligson and Trogler [10]. In both cases, the individual half-angles were measured and the value of the cone angle calculated as

$$\Theta = 2/3 \sum_i \theta_i. \quad (1)$$

Measurements on trigonal amines are reported as fan angles [11]. In these cases, only two measurements θ_i were possible since there were only two substituents on the N-atom in addition to the metal. Θ was calculated in the same fashion. In all cases, the sleekest conformation (that conformation resulting in the smallest value of Θ) was used.

2.2. Chlorophenylpiperidinophosphine (*2a*)

Dichlorophenylphosphine (0.905 g, 5 mmol) was dissolved in 20 ml of CH_2Cl_2 and cooled to −78 °C. Piperidine (0.861 g, 10 mmol) was added dropwise with stirring. The reaction mixture was allowed to warm to r.t. and stirred for an additional 3 h. The resulting white suspension was diluted with Et_2O (6 ml) and filtered. The filtrate was evaporated to dryness under reduced pressure to give a pale yellow oil, 1.07 g (93%). *Anal.* Calc. for $C_{11}H_{15}NPCl$: C, 58.03; H, 6.64; N, 6.15. Found: C, 57.18; H, 6.02; N, 5.85%. *Note*. Repeated attempts failed to give better results, presumably due to the ease of hydrolysis of the compound. ^{31}P NMR (d_6-acetone): δ 140.1 (s). ^{13}C NMR (d_6-acetone): δ 140.1 (d, $J = 28$ Hz), 131.2 (d, $J = 16$ Hz), 130.6 (s), 129.4 (s), 50.4 (br s), 27.2 (s), 24.5 (s). ^1H NMR ($CDCl_3$): δ 7.7 (m, 2H, *o*-Ph) 7.4 (m, 3H, *m-p*-Ph) 3.0 (br, 4H, NCH_2) 1.5 (br s, 6H, $NCH_2CH_2CH_2$). IR(neat): 3040w, 2900s br, 1040s, 745s, 690s cm^{-1}. *Note*. IR spectra for the chlorophenylpiperidinophosphines are all quite similar with minor changes in the alkyl CH stretching region and the appearance of a band at 1375 cm^{-1} for the methyl-substituted compounds.

The remaining dialkylaminophenylchlorophosphines were prepared in similar fashion on scales of 5–11 mmol. Yield and NMR data are reported below.

*2.2.1. Chloro(2-methylpiperidino)phenylphosphine (**2b**) mixed diastereomers*

Yield: 1.1 g (70%). *Anal.* Calc. for $C_{12}H_{17}NPCl$: C, 59.63; H, 7.09; N, 5.79. Found: C, 59.93; H, 7.20; N, 5.54%. ^{31}P NMR (d_6-acetone): δ 136.9 (s, major), 136.3 (s, minor). ^{13}C NMR (d_6-acetone): δ 140.2 (d, $J = 29$ Hz, major), 140.1 (d, $J = 26$ Hz, minor), 131.9 (br s, minor), 129.5 (br s, major), 129.1 (s), 127.9 (s); Major diasteromer: 55.2 (d, $J = 12.3$ Hz), 46.5 (s), 33.6 (s), 27.0 (d, $J = 4.0$ Hz), 21.4 (s), 19.3 (d, $J = 4.2$ Hz); minor diastereomer: 54.7 (d, $J = 7.1$ Hz), 44.4 (s), 32.5 (d, $J = 9.0$ Hz), 26.8 (s), 19.8 (s), 17.7 (d, $J = 7.0$ Hz). ^1H NMR (d_6-acetone): δ 7.7 (m, 2H, *o*-Ph) 7.4 (m, 3H, *m-p*-Ph) 3.7/3.4 (br, 1H, NCH) 3.1/2.9 (br, 2H, NCH_2) 1.9–1.2 (br m, 9H).

*2.2.2. Chloro(cis-2,6-dimethylpiperidino)phenylphosphine (**2c**)*

Yield: 1.9 g (83%). *Anal.* Calc. for $C_{13}H_{19}NPCl$: C, 61.06; H, 7.49; N, 5.47. Found: C, 60.78; H, 7.41; N, 5.72%. ^{31}P NMR (d_6-acetone): δ 141.4 (s). ^{13}C NMR (d_6-acetone): δ 140.0 (d, $J = 27$ Hz), 130.5 (d, $J = 20$ Hz), 129.3 (s), 128.1 (s) 53.4 (br s), 52.8 (d, $J = 18$ Hz), 31.1 (d, $J = 8.1$ Hz), 30.8 (s), 22.6 (d, $J = 8.6$ Hz), 18.1 (s), 13.2 (s). ^1H NMR ($CDCl_3$): δ 7.75 (m, 2H, *o*-Ph) 7.4 (m, 3H, *m-p*-Ph) 3.7 (br, 2H, NC*H*) 1.8–1.2 (br m, 6H, $NCH_2CH_2CH_2$) 1.3 (d, $J = 9.0$ Hz, 3H, CH_3) 1.1 (d, $J = 7.1$ Hz, 3H, CH_3).

*2.2.3. Chloro(2,2,6,6-tetramethylpiperidino)phenylphosphine (**2d**)*

Yield: 1.01 g (64%). *Anal.* Calc. for $C_{51}H_{23}NPCl$: C, 63.49; H, 8.17; N, 4.93. Found: C, 63.40; H, 8.26; N, 4.78%. ^{31}P NMR (d_6-acetone): δ 126.8 (s). ^{13}C NMR (d_6-acetone): δ 139.9 (d, $J = 29$ Hz), 130.1 (d, $J = 23$ Hz) 129.2 (s) 129.0 (s) 62.8 (d, $J = 10.6$ Hz), 59.6 (d, $J = 30$ Hz), 42.2 (s), 40.3 (s), 37.3 (d, $J = 33$ Hz), 33.8 (s), 31.1 (s), 30.9 (s), 17.3 (s). ^1H NMR ($CDCl_3$): δ 7.6 (m, 2H, *o*-Ph) 7.2 (m, 3H, *m-p*-Ph) 1.6, 1.45, 1.3, 0.9 (br singlets, 18H, piperidine protons).

*2.3. Bis(piperidino)phosphine oxide (**3a**)*

PCl_3 (1.80 g, 13 mmol) was dissolved in 30 ml of CH_2Cl_2 and cooled to −78 °C. With stirring, piperidine (6.69 g, 78 mmol) was added dropwise. The reaction mixture was then allowed to warm to r.t. and stirred an additional 5 h. Et_2O (40 ml) was added and the resulting slurry was filtered. The filtrate was evaporated to dryness under reduced pressure and the resulting gum was redissolved in 50 ml of CH_2Cl_2. With stirring, 15 ml of 5% aqueous $NaHCO_3$ was added slowly, followed by an additional 50 ml of H_2O. The layers were separated and the organic layer dried over anhydrous $MgSO_4$. The mixture was filtered and the solvent removed from the filtrate under reduced pressure to give an off-white waxy solid, 1.06 g (37%). *Anal.* Calc. for $C_{10}H_{21}N_2OP$: C, 55.54; H, 9.79; N, 12.95. Found: C, 55.91; H, 9.61; N, 12.68%. IR(neat): 2950–2850s, 2340m, 1230s cm^{-1}. ^{31}P NMR ($CDCl_3$): δ 18.0 (s). ^{13}C NMR ($CDCl_3$): δ 46.0 (d, $J = 16$ Hz), 25.5 (d, 5.5 Hz), 24.1 (s). ^1H NMR ($CDCl_3$): δ 6.6 (d, $J = 573$ Hz, 1H, PH), 3.05 (br, 4H, NCH_2), 1.4 (br, 6H, $NCH_2CH_2CH_2$).

*2.4. Bis(2-methylpiperidino)phosphine oxide (**3b**) (mixed diastereomers)*

The diastereomeric mixture **3b** was prepared in a manner analogous to **3a** on a 22-mmol scale. Yield: 3.35 g (59%). *Anal.* Calc. for $C_{12}H_{25}N_2OP$: C, 58.99; H, 10.31; N, 11.47. Found: C, 55.91; H, 9.61; N, 12.68%. IR(neat): 2950–2850s, 2335m, 1235s cm^{-1}. ^{31}P NMR (d_6-acetone): δ 16.2 (s), 15.5 (s), 14.7 (s). ^1H NMR ($CDCl_3$): 6.7 (d, 3 peaks, $J = 570$ Hz, PH), 4.0–2.6 (br, m) 1.8–1.1 (br, m) 1.2 (d, $J = 6.9$ Hz, CH_3).

*2.5. Bis(2,6-dimethylpiperidino)phosphine oxide (**3c**)*

Compound **3c** was prepared in a manner analogous to **3a** on a 34-mmol scale, except that a solution of 2,6-dimethylpiperidine (40 ml, 30% by volume) in H_2O was used in the hydrolysis step in place of aqueous $NaHCO_3$. Yield: 3.63 g (40%). IR(neat): 2950–2850s, 2345m, 1240s cm^{-1}. ^{31}P NMR (d_6-acetone): δ 20.2 (s). ^{13}C NMR ($CDCl_3$): δ 44.7 (d, $J = 14$ Hz), 44.3 (d, $J = 5.1$ Hz), 30.5 (s), 22.6 (s), 14.1 (s). ^1H NMR ($CDCl_3$): δ 6.6 (d, $J = 656$ Hz, PH), 3.7 (m, NCH_2) 1.6 (m, $NCH_2CH_2CH_2$), 1.30 (d, $J = 7$ Hz, CH_3), 1.29 (d, $J = 7$ Hz, CH_3). *Note*. This compound has been reported previously [5], but spectroscopic data were not given.

*2.6. Diethylaminodiisopropylaminophosphine oxide (**3f**)*

PCl_3 (7.34 g, 53 mmol) was dissolved in 150 ml of CH_2Cl_2 and cooled to −78 °C. Diisopropyl amine (10.83 g, 107 mmol) was added dropwise with stirring. The reaction mixture was allowed to warm to r.t. and stirred an additional 3 h. The resulting white slurry was filtered and the filtrate evaporated to dryness under reduced pressure. The residue was redissolved in 100 ml of CH_2Cl_2, cooled to −78 °C and diethylamine (4.52 g, 60 mmol) was added dropwise. The solution was again allowed to warm to r.t., stirred an additional 3 h and the resulting suspension filtered. The filtrate was evaporated to dryness under reduced pressure and the residue dissolved in 50 ml of THF. With stirring, H_2O (0.29 g, 16 mmol) was added along with solid $NaHCO_3$ (1.43 g, 16 mmol). After stirring for 2 h, the resulting suspension was filtered and dried over $MgSO_4$. The mixture was filtered and the solvent removed from the filtrate under reduced pressure to give a clear, viscous oil, 1.38 g

(11.2%). *Anal.* Calc. for $C_{10}H_{25}N_2OP$: C, 54.52; H, 11.43; N, 12.71. Found: C, 54.32; H, 11.21; N, 12.46%. IR(neat): 2980–2830s, 2330m, 1235s cm^{-1}. ^{31}P NMR ($CDCl_3$): δ 12.3. ^{13}C NMR ($CDCl_3$): δ 44.1 (d, $J = 3.9$ Hz), 37.3 (d, $J = 5.7$ Hz), 23.2 (s), 22.7 (s), 13.7 (s). ^1H NMR ($CDCl_3$): δ 6.9 (d, $J = 561$ Hz), 3.4 (observed d of quin, $J_d = 14$ Hz, $J_{quin} = 6.4$ Hz), 3.0 (observed hex, $J = 6.5$ Hz), 1.2 (d, $J = 6.0$ Hz), 1.15 (d, $J = 6.5$ Hz), 1.1 (t, $J = 7.0$ Hz).

2.7. Reaction of phosphine oxides with $Mo(CO)_6$

The various phosphine oxides (**3a**–**c**,**f**, 5–6 mmol scale) were combined with $Mo(CO)_6$ (0.5 equivalents) in toluene (20 ml) and heated to reflux. Heating was continued for up to 48 h, or until no sign of starting material remained, and aliquots were removed every 4–8 h to monitor the reaction progress by ^{31}P NMR and IR. Reaction with **3a** did not show any signs of Cage formation. Reaction with **3b** showed traces of the desired Cage complex **3b** [^{31}P NMR (toluene/d_6-acetone): δ 151.2(s)] among a complex pattern of signals, but attempts to isolate the material from the reaction mixture were unsuccessful. Products were purified by chromatography on silica gel followed by recrystallization from acetone as described previously [2].

2.7.1. $(CO)_4Mo[(2,6\text{-dimethylpiperidino})PO]_4Mo(CO)_4$ (**1c**)

Yield: 0.49 g (35%). ^{31}P NMR (d_6-acetone): δ 150.4. NMR data agree with those reported previously [5].

2.7.2. $(CO)_4Mo[(diethylamino)PO]_4Mo(CO)_4$ (**1f**)

Yield: 0.46 g (36%). *Anal.* Calc. for $C_{24}H_{40}N_4O_{12}P_4Mo_2$: C, 32.30; H, 4.52; N, 6.28. Found: C, 32.61; H, 4.68; N, 6.12%. IR(KBr): 2970–2880m, 2025s, 1930vs br cm^{-1}. ^{31}P NMR (d_6-acetone): δ 150.6. ^{13}C NMR (d_6-acetone): δ 40.0(s), 15.4 (s). ^1H NMR (d_6-acetone): δ 3.4 (quar, $J = 6.8$ Hz), 1.1 (t, $J = 6.8$ Hz).

3. Results

3.1. Dialkylaminochlorophenylphosphines

3.1.1. Synthesis and characterization

The compounds (R_2N)PhPCl **2a**–**e** were prepared by reaction of $PhPCl_2$ with two equivalents of the appropriate amine in 60–90% yield (Scheme 2).

$$PhPCl_2 + 2\ R_2NH \longrightarrow \underset{\mathbf{2}}{(R_2N)PhPCl}$$

(R_2N = **a**, pip; **b**, 2-Mepip; **c**, 2,6-Me_2pip; **d**, 2,2,6,6-Me_4pip; **e**, $^iPr_2N$)

Scheme 2. Synthesis of the aminochlorophenylphosphines.

The compounds were characterized by IR, NMR and combustion analysis. The $^{31}P\{^1H\}$ NMR spectra showed the expected singlets in the 125–140 ppm range except for **2b** where two singlets were observed (4.5:1 ratio) for the two diastereomers resulting from the chiral centers at P and the tertiary carbon. The ^1H NMR spectra for all compounds were complex as a result of a combination of restricted rotation about the P–N bond and the similar values of coupling constants for $^3J_{H-H}$ and $^3J_{P-H}$. The observed spectra were in agreement with the proposed structures, but complete correlation and assignment was not attempted since the ^{13}C NMR spectra were to be used for determination of the P–N rotational barrier.

The ^{13}C NMR spectrum of **2a** showed the expected resonances for the phenyl substituent with the ipso and ortho carbons appearing as doublets due to coupling to the phosphorus atom. The chemical shifts and coupling constants of the phenyl carbons did not change significantly in the series **2a**–**e**. Three signals were seen for the piperidine ring and assigned as the 2(6)-, 3(5)- and 4-carbons in accordance with the method of Eliel [12] (see Fig. 2(a) for numbering scheme). The chemical shifts of these carbons were then used along with Eliel's parameters for axial and equatorial methyl substituents on piperidine rings to assist in assigning the spectra of the remaining aminochlorophenylphosphines.

Assignment of the room temperature spectrum of **2d** was made based on calculated values using Eliel's parameters [12] and the observed chemical shifts from **2a**, Fraser and Grindley's [13] study of *N*-nitroso methylpiperidines and the use of the INEPT pulse sequence for distinguishing methyl and methine carbons from methylene carbons. Fraser and Grindley observed that carbons *syn* to an exocyclic substituent on the piperidine nitrogen were shifted upfield relative to their *anti* counterparts. Aminophosphines have been previously shown, by both experimental observation and molecular modeling studies, to have planar nitrogen atoms and to exist predominantly in conformations where the lone pair on the phosphorus is orthogonal to the nitrogen lone pair [14] (see Fig. 2(b)). The presence of the two geminal pairs of methyl substituents facilitated the assignment by ensuring that there was one each axial and equatorial methyl group on C2 and C6. Thus, the doublets at 62.8 and 59.6 ppm were assigned as C6 (*anti*) and C2 (*syn*), respectively, in agreement with both their

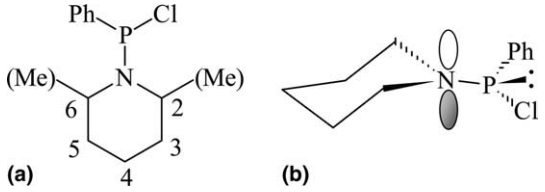

Fig. 2. Structure and geometry of the piperidinochlorophenylphosphine.

predicted chemical shifts and the magnitudes of their $^2J_{PNC}$ coupling constants (see Variable Temperature NMR Studies, below). The signals at 37.3 and 30.9 ppm were similarly assigned to C3 and C5, respectively, and that at 17.3 to C4 as a result of the strong shielding by the two γ-axial methyl substituents. The methyl groups were observed at 42.3 and 40.3 (equatorial) and 33.8 and 31.1 (axial) ppm.

Subsequent assignment of the room temperature ^{13}C NMR spectrum of **2c** was straightforward. Unlike **2d**, where the room temperature spectrum represented the low-temperature limit, in **2c** the room temperature spectrum was nearer to the high temperature limit (although with some unresolved P–N–C coupling). The *cis*-dimethyl substituents were assumed to be in the axial position based upon Fraser and Grindley's [13] observations in the nitrosopiperidine compounds, the work of Tavares and co-workers [14a] on piperidine amides, and the observed conformation of the 2,6-Me_2pip rings in the crystal structures of the chromium and molybdenum complexes of Wong and co-workers [5]. In addition, the chemical shifts were calculated for both the diaxial and diequatorial conformations, and the predicted values for the diaxial conformation agreed much better with the observed values. The diastereotopic methine carbons were assigned to a broad signal at 53.4 and a broad doublet at 52.8 ppm ($J = 18$ Hz). The C-3 and C-5 carbons were observed at 31.1 and 30.0 ppm and C-4 was shifted strongly upfield to 13 ppm by the two axial methyl groups (22.6 and 22.1 ppm).

The ^{13}C NMR spectrum of **2b**, the 2-Mepip compound, was more complicated due to the presence of two diastereomers, each of which has two distinct conformations with the phosphorus and nitrogen lone pairs orthogonal (see Fig. 3). In addition, the different rotomers were anticipated to have unequal populations. Structures **2b**-1 and **2b**-2 represent the two rotomers of one diastereomer while **2b**-3 and **2b**-4 represent the rotomers of the second diastereomer. We presumed that rotomers **2b**-1 and **2b**-3 would be the higher population forms for their respective diastereomers due to the reduced steric interactions between the methyl substituents and the phenyl and chloro groups on the phosphorus.

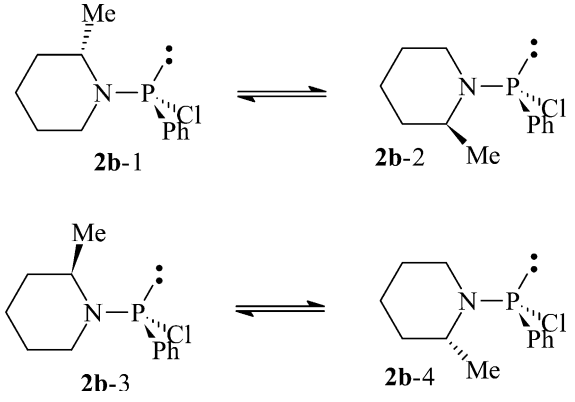

Fig. 3. Rotomers and diastereomers of **2b**.

Signals for all six carbons in each diastereomer were observed at room temperature with sufficiently different intensities to assign them to major and minor products (relative intensities ranging from 4:1 to 5:1). The resonances for the major isomer were assigned as: 54.7 (C-2) 46.5 (C-6) 33.6 (C-3) 27.0 (C-5) 21.4 (C-4) and 19.3 (Me) (coupling constants and resonances for the minor isomer are given in the experimental). Assignments for the major and minor isomers agreed well with the nitroso compound of Fraser and Gridley [13] and calculated values [12].

3.2. Variable temperature ^{13}C NMR and P–N rotational barriers

^{13}C NMR spectra were obtained for **2a**–**e** from 326 to 190 K or until the spectrum ceased to change (for **2d** and **2e**) in 5–12 °C intervals (smaller near the coalescence temperature). The carbon atoms α to the piperidine nitrogen were chosen for simulation based upon previous work demonstrating the correlation between conformation about the P–N bond and the $^2J_{PNC}$ coupling constant [15]. At the low temperature limit, aminophosphines adopt a conformation where the phosphorus and nitrogen lone pairs are orthogonal, resulting in a structure where one α-C is *syn*-periplanar to the phosphorus lone pair and one α-C is *anti*-periplaner to it. The *syn*-C exhibits a $^2J_{PNC}$ of +23 to 45 Hz while the *anti*-C exhibits a $^2J_{PNC}$ of −5 to −15 Hz. The opposite signs of the coupling constants are clearly demonstrated by the average coupling constants in the high temperature spectra which typically fall in the 10–20 Hz range. Poor solubility for **2c** at low temperature in d_6-acetone prevented obtaining the low temperature limiting spectrum, however, the full range of spectra were obtained in $CDCl_3$. Data were collected on **2e** in both d_6-acetone and $CDCl_3$ to determine the effect of the solvent on the observed barrier to rotation about the P–N bond. High temperature limiting spectra for **2d** and **2e** were not obtained below the boiling point of the solvent. Individual spectra were analyzed and exchange pairs for simulation were assigned as previously described in accordance with the known difference in sign and magnitude of the $^2J_{PNC}$ coupling constants [7,14]. The chemical shifts and coupling constants for the low- and high-temperature limiting spectra of the α-carbons used in the simulations are given in Table 1.

Spectra were simulated using the KUBO program of Saunders [8] and agreement between simulated and experimental spectra was determined by eye. At very low (<30 Hz) and very high (>20 000 Hz) frequencies, changes of up to 20% in the rotational frequency produced negligible change in the simulated spectra and

Table 1
Low- and high-temperature limiting ^{13}C NMR data for **2a**,**c**,**d**,**e**[a] Chemical shifts (ppm) and ($^2J_{PNC}$ coupling constants) [Hz]

Compound	Solvent	Low temperature	High temperature
2a	d_6-acetone	52.5 (32), 47.5 (−10.0)	50.5 (11.5)
2c	$CDCl_3$	55.1 (+43.9), 49.2 (−12.2)	53.4 (16.1)
		54.6 (+44.0), 48.7 (−14.0)	52.8 (15.3)
2d	d_6-acetone	62.8 (−10.6), 59.6 (+30.0)	[b]
2e	$CDCl_3$	52.0 (−12.0), 45.1 (+22.8)	[b]

[a] Simulations of spectra for **2b** were not carried out. See text below.
[b] Not observed below the boiling point of the solvent.

data outside that range was not used in determining the rotational barriers. In addition, nonlinearity was observed at very low and high rotational rates, but this leads to compensating errors in $\Delta H^{\ddagger}$ and $\Delta S^{\ddagger}$ so that the values of $\Delta G^{\ddagger}$ obtained are still reliable [16]. We estimate the error in the rotational rate of individual spectra to be within 5%. Standard Eyring plots of $1/T$ versus $\ln k/T$ for each series of spectra gave $\Delta H^{\ddagger}$ and $\Delta S^{\ddagger}$ from which $\Delta G^{\ddagger}$ (298 K) was calculated. The activation barriers were also calculated based on the coalescence temperatures and low temperature limiting frequency separation of the exchanging resonances [17]. All data are given in Table 2.

The values for the P–N rotational barrier derived from the coalescence temperature are in agreement with those derived from the Eyring plots when the difference in temperature is taken into account. Attempts to simulate the variable temperature spectra of **2b** were unsuccessful due to the low percentage of the minor conformers (**2b**-2 and **2b**-4) and overlap of the signals from the two diastereomers, especially as those signals broadened at temperatures above the low temperature limit. Large changes in rotational rate throughout the temperature range made minimal changes in the simulated spectrum leading to unacceptably high error. The reported coalescence temperature is that of maximum width for the overlapped signals for both the primary α-carbon and the secondary α-carbon. Comparison of the values for the rotational barrier of the diisopropylamino compound, **2e**, in acetone and $CDCl_3$ showed no difference within experimental error and the data collected in $CDCl_3$ agree with the report of Burdon et al. [18], therefore allowing us to compare the barrier for **2c** (measured in $CDCl_3$) with the other Me_n piperidine compounds.

3.3. Reaction of bis(dialkylamino)phosphine oxides with $Mo(CO)_6$

The phosphine oxides **3a**–**c**,**f** were prepared by standard techniques. Attempts to prepare **3d** (using Me_4pipH) were unsuccessful. We were unable to produce the needed bis(Me_4pip)$_2$PCl precursor; only (Me_4pip)PCl_2 was isolated even using a 10-fold excess of Me_4pipH and prolonged reaction times, presumably due to steric congestion. The phosphine oxides were then combined with $Mo(CO)_6$ in refluxing toluene (see Scheme 3) and the reactions monitored for the formation of the corresponding Cage complexes via their characteristic ^{31}P NMR (∼150 ppm) and IR (2010-2020 cm^{-1}) signatures.

No trace of **1a** was detected in the reaction of **3a** even after 48 h. Reaction of **3b** produced traces of a com-

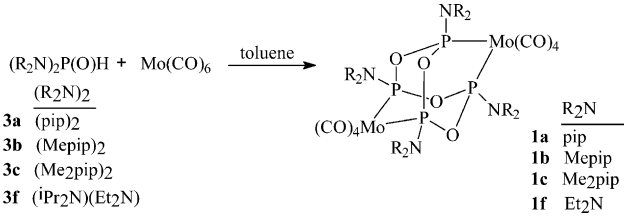

Scheme 3. Synthesis of the Cage complexes **1**.

Table 2
Activation parameters and P–N rotational barrier estimates for **2a**–**e**

Compound (solvent)	Coalescence temperature (K)	$\Delta G_c^{\ddagger}$ (kcal/mol)	$\Delta H^{\ddagger}$ (kcal/mol)	$\Delta S^{\ddagger}$ (cal/mol K)	$\Delta G^{\ddagger}$ (298 K) (kcal/mol)	r^2
2a (acetone)	255	11.6	8.19	−12.9	12.03	0.9986
2b (acetone)	261	11.7			[a]	
2c ($CDCl_3$)	249	11.3	8.91	−10.2	11.95	0.9931
2d (acetone)	>325	>15.6	12.38	−12.1	15.95	0.9912
2e (acetone)					13.3[b]	
2e ($CDCl_3$)	290	13.1	12.16	− 3.51	13.21	0.9864

[a] $\Delta G^{\ddagger}$ could not be obtained reliably. See text below.
[b] Value taken from [7].

pound presumed to be **1b** as part of a complex mixture (based on the ^{31}P NMR spectrum of the reaction mixture which showed a resonance at δ 151.2 ppm), although we were unsuccessful in isolating the material. However, reaction of **3c** yielded the corresponding Cage **1c** in fair yield after purification. Reaction of the mixed compound **3f**, containing one diisopropylamino and one diethylamino substituent, gave uniformly the diethylamino-substituted compound **1f**, also in fair yield. No sign of the diisopropyl group was observed in either the ^{1}H or ^{13}C NMR spectra after purification and only one singlet was observed in the ^{31}P NMR in the 150 ppm region ($\delta = 150.6$ ppm).

3.4. Cone angle measurements

The cone angles [9] of the various amines and bis(dialkylamino)phosphines (see Table 3) were measured according to the method of Seligson and Trogler [10] who first applied the technique to amines. An M–N bond length of 2.2 Å and an M–P bond length of 2.28 Å were used in the measurements for consistency with published data. There is some disagreement over the appropriate technique for measuring cone angles in relation to the appropriate conformation for the molecule. The predominant method involves placing the molecule in its sleekest conformation [9] and this model has been used, although there is frequently evidence to indicate that the molecules do not typically occur in those conformations, such as the known gearing of the isopropyl groups in some diisopropyl-aminophosphines [18]. Measurements of PH_3, PMe_3, NH_3 and NMe_3 were used to calibrate the models and agreed with published data [9,10] within ±3°. Fan angles [11] were also measured for the amines where the H-atom has been removed and the N-atom was in a trigonal planar geometry (R_2N–M). Measurements were reproducible within ±3° and averages are reported.

Table 3
Cone and fan angles for amines and bis(dialkylamino)phosphinous acids (°)

Compound	Tet-amine[a]	Trig-amine[b]	Phosphine[a]
Piperidine	119	93	124
2-Methylpiperidine (eq)	129	107	
2-Methylpiperidine (ax)	130	93	127, 137, 141[c]
2,6-Dimethylpiperidine (eq)	139	120	
2,6-Dimethylpiperidine (ax)	142	93	145
Diisopropylamine	140	99	151

[a] Cone angle for the phosphine or the tetrahedral neutral amine (R_2NH) with the metal coordinated in the equatorial position for piperidine and substituted piperidines.
[b] Fan angle for the trigonal amine (R_2N).
[c] Values for three different diastereomers.

4. Discussion

Hindered rotation about the P–N bond in a variety of aminophosphines and aminophosphine oxides has been observed by NMR techniques for more than three decades [19]. More recently, the use of a wide variety of alkyl and aryl substituents on the nitrogen atom has confirmed the principle that within a particular class of phosphorus compounds, the barrier is principally dependent upon the steric congestion around the P-atom [20]. Based on our previous results [7], we were surprised to find that the P–N rotational barriers in compounds **2a**–**c** are the same (within experimental error). The unsubstituted-, monomethyl- and dimethylpiperidine compounds **2a**–**c** all have a barrier to P–N rotation that is in agreement with the values previously observed for $Ph(R_2N)PCl$ compounds [7] where R was a primary alkyl substituent [$\Delta G^{\ddagger}$ (298 K) = 11.6 ± 0.1 kcal/mol] in spite of the fact that **2b** has one secondary alkyl substituent and **2c** has two secondary alkyl substituents. Compound **2d** has two tertiary alkyl substituents and, as expected, exhibits a barrier significantly higher than previously observed for compounds with two secondary substituents [$\Delta G^{\ddagger}$ (298 K) = 13.4 ± 0.2 kcal/mol] [7]. Due to the lack of high temperature data, we suggest that the value of $\Delta G^{\ddagger}$ given in Table 2 for **2d** represents a lower limit.

Cone angle measurements (Table 3) indicated that the various amines should have significantly different steric requirements, and therefore, we would expect different rotational barriers for the corresponding aminochlorophenylphosphines. However, the variability of cone angle in a variety of ligands, as observed in crystal structures, has been demonstrated clearly by Müller and Mingos [21] in their work on determining cone angles based on the crystallographic data. In their measurements of cone angles via geometric calculation, they found that although the mean values agreed with those determined by Tolman's method [9], there was great variability from one structure to the next as a result of the actual ligand conformation in the molecule and the standard deviations of the average values were significant (typically 5°). For example, they found that the average observed cone angle for PEt_3 was 137.3(5.0)° compared to the Tolman cone angle of 132° ± 2°, but the range of observed angles was 126.6°–159.4°. Most interesting was Müller and Mingos' observation that the cone angles observed in X-ray structures for the "very bulky" P(c-Hex)$_3$ ligand [ave = 160.1(5.1)°; range = 146.2°–171.7°] were actually significantly less than that proposed by Tolman [9]. Similar observations have been made by Smith and Coville [22] for phosphite ligands.

Examination of the crystal structures of **1** (R_2N = *cis*-2,6-dimethylpiperidine) and its related metal complexes all show the methyl substituents to be in the *cis*-diaxial conformation. Although surprising at first, this is in

agreement with the assignments of the ^{13}C NMR chemical shifts for the piperidine ring carbons for both the 2-methyl- and 2,6-dimethylpiperidine compounds, suggesting that it is the axial conformation that predominates in solution as well. In addition, it is observed that the nitrogen atoms are generally planar, or nearly so, in crystal structures of aminophosphines [23] unless restricted by incorporation of the nitrogen atom into a ring, or by interactions with neighboring groups. We remeasured the steric volume for the various amines replacing the tetrahedral nitrogen atoms with trigonal nitrogen atoms. These measurements are based on the fan angle measurements of Bagnall and Li [11] who determined steric requirements for a variety of ligands, not just those with pseudo-tetrahedral geometry. With the piperidine nitrogen in a trigonal hybridization, methyl substituents in the axial position on the α-carbons *do not occupy any additional volume relative to the cone swept out by rotation about the N–M bond!* The same is not true for substituents in the equatorial position. With this realization, it is clear that the rotational barrier study is in agreement with the steric requirements of the sp^2 hybridized nitrogen in the piperidinophosphines.

Cone angle measurements were also made on the phosphinous acids with the various amine substituents. In all cases, trigonal nitrogen atoms were used and, in the case of substituted piperidines, the methyl groups were placed in the axial position. In these molecules, there is an increase in cone angle with increasing substitution on the piperidine ring due to interactions between the substituents, even with axial substituents. There are three possible diastereomers of the bis(2-methylpiperidino) compound, **3b**, and all three were observed by ^{31}P NMR. The cone angles for the three diastereomers are quite different, with the chiral isomer showing the largest value.

Based solely on the results of the rotational barrier study, we did not expect any of the phosphine oxides **3a**–**c** to produce measurable quantities of the associated Cage complexes, **1**, upon reaction with $Mo(CO)_6$. However, previous experiments had also suggested that the presence of secondary alkyl substituents on the amine nitrogen was sufficient for the success of the thermal condensation and, in fact, traces of product from the reaction with $(Et_2N)_2P(O)H$ had been observed via ^{31}P NMR [2,5]. In addition, the cone angle measurements on the phosphinous acids indicated that the P–N rotational barriers, as determined in the aminochlorophenylphosphines, were not a good measure of the steric requirements of the phosphinous acids.

Reaction with **3c** does produce Cage **1c** in fair yield, but the yield is lower than observed with either $(^{i}Pr_2N)_2P(O)H$ or $(c\text{-}Hex_2N)_2P(O)H$ [2]. This suggests that while secondary alkyl substituents on the nitrogen may be sufficient to promote the condensation, the yield is still dependent on the relief of steric strain in some intermediate (presumably $\mathbf{I_1}$, Scheme 1). The reduced steric congestion in the Me_2pip compound, **3c**, compared to the other secondary amines, raises the activation barrier to the formation of the coordinated phosphinidene oxide ($\mathbf{I_2}$) and hence reduces the yield. This difference is, perhaps, not surprising in light of the known difference in steric requirements of piperidine itself relative to open chain analogues as has been observed by ^1H NMR shifts in cobaloxime complexes [24]. The observation of traces of the Mepip complex **1b** in the ^{31}P NMR of the reaction mixture with **3b**, but no Cage product in the reaction of the pip compound **3a**, also supports this hypothesis. It is possible that only the most sterically crowded diastereomer of **3b** produces Cage under these reaction conditions.

Finally, the success of the reaction with **3c** in spite of its low rotational barrier prompted our attempt to prepare the diethylamino-substituted Cage complex **1f** using the mixed aminophosphine oxide, **3f**. We believed that the diisopropyl amino substituent would provide sufficient crowding to promote the conversion of $\mathbf{I_1}$ to $\mathbf{I_2}$, the step in the mechanism which we have proposed to be rate limiting [2,5]. Moreover, we reasoned that if the reaction was indeed driven by the relief of steric strain, loss of the diisopropylamino group should be greatly preferred over loss of the diethylamino group. The isolation of **1f** in yields comparable to those observed in the synthesis of **1c** justified these predictions.

5. Conclusions

It is clear that the barrier to rotation about the P–N bond in dialkylaminochlorophenylphosphines is not a useful predictor of the results of the thermal condensation of bis(dialkylamino)phosphine oxides with $Mo(CO)_6$. Cone angle measurements show that the steric bulk of the amine is strongly dependent upon the geometry at the nitrogen atom. The interaction between the two amino substituents in the bis(dialkylamino)phosphine oxides is significant and therefore comparison to monoamino complexes is not reliable. However, the successful synthesis of the diethylamino-substituted Cage compound **1f** from the mixed bis(dialkylamino)phosphine oxide provides a new route to the synthesis of Cage complexes with less bulky substituents. Previous work on these Cage complexes has shown that they have highly selective and unique reactivity with oxidizing agents [25]. The structure and stability of the products of these reactions appeared to be strongly dependent on the steric environment around the metal centers. Thus, the ability to synthesize Cage complexes with smaller dialkylamino substituents will provide a means to further study the mechanism of these reactions and to probe the use of the complexes as templates for organic synthesis. In addition, work on the preparation of Cage complexes with smaller amino

substituents via the use of Me_4pip in mixed phosphine oxides similar to **3f** is in progress.

Acknowledgements

We are grateful to Prof. Edward Wong for helpful discussions and Mr. Joel Norton for assistance with construction of the cone angle device. Financial support for J.A. was received from the US Department of Education through a GAANN fellowship.

References

[1] E.H. Wong, M.M. Turnbull, E.J. Gabe, F.L. Lee, Y. Le Page, J. Chem. Soc., Chem. Commun. (1983) 776.
[2] E.H. Wong, M.M. Turnbull, K.D. Hutchinson, C. Valdez, E.J. Gabe, F.L. Lee, Y. Le Page, J. Am. Chem. Soc. 110 (1988) 8422.
[3] E.H. Wong, X. Sun, E.J. Gabe, F.L. Lee, J.-P. Charland, Organometallics 10 (1991) 3010.
[4] H. Yang, E.H. Wong, A.L. Rheingold, B.E. Owens-Watermire, B.S. Haggerty, Organometallics 13 (1994) 4825.
[5] X. Sun, E.H. Wong, M.M. Turnbull, A.L. Rheingold, B.E. Waltermire, R.L. Ostrander, Organometallics 14 (1995) 83.
[6] H. Yang, G.P.A. Yap, A.L. Rheingold, E.H. Wong, Inorg. Chim. Acta 287 (1999) 223.
[7] D.S. Bader, M.M. Turnbull, Polyhedron 9 (1990) 2619.
[8] M. Saunders, Tetrahedron Lett. (1963) 1699.
[9] C.A. Tolman, Chem. Rev. 77 (1977) 313.
[10] A.L. Seligson, W.C. Trogler, J. Am. Chem. Soc. 113 (1991) 2520.
[11] K.W. Bagnall, X.-f. Li, J. Chem. Soc., Dalton Trans. (1982) 1365.
[12] E.J. Eliel, in: G.C. Levy (Ed.), Topics in Carbon-13 NMR Spectroscopy, Wiley, New York, 1979.
[13] R.R. Fraser, T.B. Grindley, Can. J. Chem. 53 (1975) 2465.
[14] (a) A. Rauk, D.F. Taveres, M.A. Khan, A.J. Borkent, J.F. Olson, Can. J. Chem. 61 (1983) 2572;
(b) V. Marathias, M.M. Turnbull, R.L. Abdon II, B.P. Coppola, Polyhedron 11 (1992) 2759.
[15] (a) M.-P. Simmonnin, R.-M. Lequan, F.W. Wehrli, J. Chem. Soc., Chem. Commun. (1972) 1204;
(b) J.H. Hargis, W.B. Jernnings, S.D. Worley, M.S. Tolley, J. Am. Chem. Soc. 102 (1980) 13;
(c) W.B. Jennings, D. Rangall, S.D. Worley, J.H. Hargis, J. Chem. Soc., Perkin Trans. II (1981) 1411.
[16] (a) W.E. Stewart, T.H. Siddall, Chem. Rev. 70 (1970) 517;
(b) M.B. Robin, F.A. Bovey, H. Basch, in: J. Zabicky (Ed.), The Chemistry of Amides, John Wiley, London, 1970.
[17] H.S. Gutkowsky, C.H. Holm, J. Chem. Phys. 25 (1956) 1228.
[18] J. Burdon, J.C. Hotchkiss, W.B. Jennings, Tetrahedron Lett. 49 (1973) 4919.
[19] (a) D. Imbery, H. Friebolin, Z. Natursforsch., Teil B 23 (1968) 759;
(b) A.H. Cowley, M.J.S. Dewar, W.R. Jackson Jr., W.B. Jennings, J. Am. Chem. Soc. 92 (1870) 5206;
(c) D. Daternieks, R. Di Giacomo, Phos. Sul. Rel. Elem. 24 (1985) 217.
[20] (a) X. Ma, J. Zhang, Phos. Sul. Sil. Rel Elem. 53 (1990) 233;
(b) M. Weissenbacher, T. Sturm, H. Kalchhauser, K. Kratky, W. Weissensteiner, Monat. fur Chem. 133 (2002) 991;
(c) B. Wrackmeyer, C. Kohler, W. Milius, J.M. Grevy, Z. Garcia-Hernandez, R. Contreras, Heteroatom Chem. 13 (2002) 667.
[21] T.E. Müller, D.M. Mingos, Trans. Met. Chem. 20 (1995) 533.
[22] J.M. Smith, N.J. Coville, Organometallics 20 (2001) 1210.
[23] (a) In addition to the structures reported in Refs. [1–6], see for example: A. Bayer, U. Thewalt, B. Rieger, Eur. J. Inorg. Chem. (2002) 199;
(b) J. Borm, G. Huttner, O. Orama, J. Organomet. Chem. 306 (1986) 29;
(c) J. Borm, G. Huttner, L. Zsolnai, K. Evertz, H. Berke, J. Organomet. Chem. 327 (1987) 223;
(d) A.M. Arif, A.H. Cowley, N.C. Norman, A.G. Orpen, M. Pakulski, Organometallics 7 (1988) 309;
(e) A.H. Cowley, D.M. Giolando, C.M. Nunn, M. Pakulski, D. Westmoreland, N.C. Norman, J. Chem. Soc., Dalton Trans. (1988) 2127;
(f) P. Le Floch, L. Ricard, F. Mathey, Bull. Soc. Chim. Fr. 131 (1994) 330;
(g) H.R.G. bender, E. Niecke, M. Nieger, H. Westermann, Z. Anorg. Allg. Chem. 620 (1994) 1194.
[24] N. Bresciani-Pahor, M. Forcolin, L.G. Marzilli, L. Randaccio, M.F. Summers, P.J. Toscano, Coord. Chem. Rev. 63 (1985) 1.
[25] M.M. Turnbull, C. Valdez, E.H. Wong, E.J. Gabe, F.L. Lee, Inorg. Chem. 31 (1992) 208.

Available online at www.sciencedirect.com
SCIENCE DIRECT®
Polyhedron 23 (2004) 135–143
POLYHEDRON
www.elsevier.com/locate/poly

Efficient syntheses of 4′-(2-thienyl)- and 4′-(3-thienyl)-2,2′:6′,2″-terpyridine: preparation and characterization of Fe(II), Ru(II), Os(II) and Co(II) complexes

Edwin C. Constable *, Robyn Handel, Catherine E. Housecroft *, Markus Neuburger, Emma R. Schofield, Margareta Zehnder

Department of Chemistry, Institut fuer Anorganische Chemie, University of Basel, Spitalstrasse 51, CH-4056 Basel, Switzerland

Received 24 July 2003; accepted 22 September 2003

Abstract

Efficient and convenient methods for the preparation of thienyl-substituted 2,2′:6′,2″-terpyridines are reported. The formation and characterization of Fe(II), Ru(II), Os(II) and Co(II) complexes containing the isomeric ligands 4′-(2-thienyl)-2,2′:6′,2″-terpyridine (**1**) and 4′-(3-thienyl)-2,2′:6′,2″-terpyridine (**3**) are described. The crystal structure of **3** is reported. During studies of possible routes to ligands **1** and **3**, the reactions of thiophene-2-carbaldehyde or thiophene-3-carbaldehyde with 2-acetylpyridine under basic conditions led to 3-(2-thienyl)-1,5-bis(2-pyridyl)-2-(2-pyridylcarbonyl)cyclohexane-1,5-diol or 3-(3-thienyl)-1,5-bis(2-pyridyl)-2-(2-pyridylcarbonyl)cyclohexane-1,5-diol, respectively. These compounds have been fully characterized and their crystal structures have been determined.
© 2003 Elsevier Ltd. All rights reserved.

1. Introduction

2,2′:6′,2″-Terpyridines (tpy = 2,2′:6′,2″-terpyridine) are versatile building blocks in metallosupramolecular chemistry. A wide range of functional groups can be introduced as substituents and used to control self-assembly processes and/or the properties of the complexes which result upon coordination to metal centres [1–5]. We have shown that ruthenium(II) complexes containing 4′-(2-thienyl)-2,2′:6′,2″-terpyridine (**1**) or 2,5-bis(2,2′:6′,2″-terpyridin-4′-yl)thiophene (**2**) possess unusually long-lived ^{3}MLCT states which facilitate efficient energy transfer between metal centres [6,7]. In other studies, we have utilized complexes of **1** in studies of ligand exchange processes leading to the establishment of dynamic combinatorial libraries [8]. In this paper, we report efficient and convenient methods for the preparation of thienyl-substituted 2,2′:6′,2″-terpyridines using a one-pot method. We also report new aspects of the coordination chemistry of ligand **1** and its positional isomer 4′-(3-thienyl)-2,2′:6′,2″-terpyridine (**3**). This ligand is of interest in having a pendant sulfur-containing substituent which can be used to attach complexes to gold surfaces, and may be used as an assembly motif for the construction of a variety of novel architectures [9–11].

2. Experimental

2.1. General

Infrared spectra were recorded on Mattson Genesis or Shimadzu FTIR 8300 Fourier-transform spectrophotometers with samples in compressed KBr discs or as solids using a Golden Gate ATR. ^{1}H and ^{13}C NMR spectra were recorded on Bruker AM 250, AC 300, AV 300, AM 400, DRX 500 or AV 600 spectrometers; the proton numbering for the ligands is shown in the structure diagrams.

* Corresponding authors. Tel.: +41-61-267-1001; fax: +41-61-267-1015 (E.C. Constable), Tel.: +41-61-267-1008; fax: +41-61-267-1018 (C.E. Housecroft).

E-mail addresses: constable@ubaclu.unibas.ch (E.C. Constable), catherine.housecroft@unibas.ch (C.E. Housecroft).

0277-5387/$ - see front matter © 2003 Elsevier Ltd. All rights reserved.
doi:10.1016/j.poly.2003.09.019

UV/VIS measurements were recorded using Perkin–Elmer Lambda 19 or Shimadzu UV 3101PC spectrophotometers in acetonitrile at a concentration of $\sim 10^{-4}$ mol dm^{-3}. Luminescence spectra were recorded on Shimadzu RF 5301PC or Perkin–Elmer LS50B spectrofluorophotometers. FAB and EI mass spectra were recorded on Kratos MS 50, 890, 902, Profile or VG 70-250 or Prospec instruments. Time-of-flight (MALDI) spectra were recorded using a PerSeptive Biosystems Voyager-RP Biospectrometry Workstation using dihydroxybenzoic acid as matrix with C_{60} as the internal reference. Electrospray mass spectra (ES MS) were recorded using a Finnigan Mat LCT or LCQ mass spectrometer. Electrochemical measurements were performed with Autolab PGSTAT 20 or 30 systems using platinum or glassy-carbon working and auxiliary electrodes with an Ag/AgCl electrode as reference or a silver wire as pseudo-reference using purified acetonitrile as solvent and 0.1 M [^{n}Bu$_4$N][BF$_4$] as supporting electrolyte. Potentials are quoted versus the ferrocene/ferrocenium couple (Fc/Fc$^+$ = 0.0 V), and all potentials were referenced to internal ferrocene added at the end of each experiment.

2.2. Preparation of 4′-(2-thienyl)-2,2′:6′,2″-terpyridine (1)

2-Acetylpyridine (0.271 ml, 6.3 mmol) was added dropwise to a solution of KO^{t}Bu (1.06 g, 9.5 mmol) in dry THF (40 ml) and the mixture stirred at room temperature for 30 min to give a creamy yellow suspension, after which thiophene-2-carbaldehyde (0.277 ml, 3.1 mmol) in dry THF was added. The solution turned red and was stirred for 20 h at room temperature, after which time a solution of NH_4OAc (5.0 g) in 2:1 EtOH/AcOH (60 ml) was added and the reaction mixture heated to reflux for 5 h. The reaction mixture was then cooled to room temperature, poured onto ice (50 g) and treated with water (100 ml) to give a pale yellow precipitate that was collected by filtration and dried to give **1**. The filtrate was extracted with $CHCl_3$; removal of the organic solvent gave a brown oil that was purified by column chromatography (4% Et_2NH, toluene, Al_2O_3) to give a small additional amount of **1** (total yield 0.612 g, 62%), m.p. 185 °C; ^{1}H NMR ($CDCl_3$) δ 8.73 (dd, $J = 2.0$, 4.9 Hz, 2H, H^6), 8.70 (s, 2H, H$^{3'}$), 8.64 (d, $J = 7.8$ Hz, 2H, H^3), 7.87 (dd, $J = 7.8$, 8.0 Hz, 2H, H^4), 7.78 (dd, $J = 1.2$, 3.6 Hz, 1H, H^{3S}), 7.44 (dd, $J = 1.2$, 5.1 Hz, 1H, H^{5S}), 7.35 (ddd, $J = 1.0$, 2.0, 7.8 Hz, 2H, H^5), 7.16 (dd, $J = 3.6$, 5.1 Hz, 1H, H^{4S}); ^{13}C NMR ($CDCl_3$) δ 156.1, 156.0, 149.1, 143.4, 141.9, 136.8, 128.2, 127.1, 125.8, 123.9, 121.3, 117.1; *m/z* 315 (M), 38 (M + Na) (MALDI-TOF), 315.0829 calc. for $C_{19}H_{13}N_3S$, 315.0830 (HRMS-EI); $\bar{\nu}_{max}$/cm^{-1} 1600 s, 1572 s, 1565 s, 1549 s, 1520 m, 1466 s, 1445 m, 1413 s, 1358 m, 1269 m, 1071 w, 1039 m, 990 w, 893 w, 879 w, 834 w, 782 s, 742 m, 732 m, 671 m, 658 w, 623 m, 568 m; λ_{max}/nm ($CHCl_3$) 231 (ε/M^{-1} cm^{-1} 19.1×10^3), 253 (22.4×10^3), 284 (34.9×10^3).

2.3. Preparation of 4′-(3-thienyl)-2,2′:6′,2″-terpyridine (3)

2.3.1. Method 1

A solution of 2-acetylpyridine (2.00 ml, 0.018 mol), 3-thiophenecarbaldehyde (1.00 g, 0.009 mol) and NaOH (3.00 g, 0.051 mol) in H_2O (50 ml) and EtOH (350 ml) was stirred for 24 h after which the solvent was removed in vacuo, and the residue dissolved in CH_2Cl_2 (300 ml). The CH_2Cl_2 solution was washed with water (3×250 ml), dried ($MgSO_4$) and the solvent removed to give an orange oil which was used in the cyclization step without further purification.

This oil was dissolved in a solution of NH_4OAc (7.00 g, 0.091 mol) in EtOH (150 ml) and the mixture heated to reflux for 12 h, after which the solvent was removed in vacuo, and the residue purified by column chromatography (4% Et_2NH, toluene, Al_2O_3). The first yellow fraction was collected and recrystallized from toluene to give cubic yellow crystals of **3** (yield 0.25 g, 10 %), m.p. 233–233.5 °C.

2.3.2. Method 2

The method was as for compound **1** but using thiophene-3-carbaldehyde (0.277 ml, 3.1 mmol) and omitting the final extraction of the filtrate (yield 522 mg, 52%). (Found: C, 72.13; H, 4.33; N, 13.15. $C_{19}H_{13}N_3S$ requires C, 72.36; H, 4.15; N, 13.32%); ^{1}H NMR ($CDCl_3$) δ 8.73 (dd, 2H, $J = 4.9$, 2.0 Hz, H^6), 8.70 (s, 2H, H$^{3'}$), 8.66 (dd, 2H, $J = 8.0$, 1.0 Hz, H^3), 7.94 (dd, 1H, $J = 2.9$, 1.5 Hz, H^{2S}) 7.88 (dt, 2H, $J = 8.0$, 7.8, 2.0 Hz, H^4), 7.71 (dd, 1H, $J = 4.9$, 1.5 Hz, H^{4S}), 7.46 (dd, 1H, $J = 4.9$, 2.9 Hz, H^{5S}), 7.35 (ddd, 2H, $J = 7.8$, 4.9, 1.0 Hz, H^5); ^{13}C NMR ($CDCl_3$) δ 156.1, 155.9, 148.9, 144.7, 138.9, 137.0, 126.6, 126.3, 123.9, 123.7, 121.4, 118.2; *m/z* 315 (M) (MALDI-TOF);. $\bar{\nu}_{max}$/cm^{-1} 1600 s, 1572 s, 1565 s, 1549 s, 1520 m, 1466 s, 1445 m, 1413 s, 1358 m, 1269 m, 1071 w, 1039 m, 990 w, 893 w, 879 w, 834 w, 782 s, 742 m, 732 m, 671 m, 658 w, 623 m, 568 m; λ_{max}/nm ($CHCl_3$) 227 (ε/M^{-1} cm^{-1} 50.7×10^3), 253 (66.6×10^3), 278 (81.8×10^3).

2.4. Preparation of 1,5-bis(2-pyridyl)-3-(2-thienyl)penta-1,5-dione (4) and 3-(2-thienyl)-1,5-bis(2-pyridyl)-2-(2-pyridylcarbonyl)cyclohexane-1,5-diol (5)

A solution of 2-acetylpyridine (3.8 ml, 34 mmol) in EtOH (150 ml) was stirred with thiophene-2-carbaldehyde (0.8 ml, 8.56 mmol) and aqueous NaOH (25 ml, 2 M) for 24 h. The solvent was then reduced to half its original volume and equal volume of water was added, precipitating an orange gum and a white solid. The solid

was separated by filtration and the gum was redissolved in CH_3OH and more water added. This was continued until all of the gum had solidified. The solid consisted of two compounds which were separated by chromatography (15% Et_2NH, hexanes, silica gel) and identified as the dione **4** (0.71 g, 25%) and the condensation product **5** (1.17 g, 30%).

Compound **4**: m.p. > 215 °C (dec.); ^{1}H NMR ($CDCl_3$) δ 8.60 (dm, 2H, H^{6py}), 7.93 (dm, 2H, H^{3py}), 7.72 (ddd, 2H, H^{4py}), 7.38 (ddd, 2H, ddd, H^{5py}), 7.03 (d, H, $H^{5thienyl}$), 6.94 (d, H, $H^{3thienyl}$), 6.82 (dd, H, dd, $H^{4thienyl}$), 4.51 (quin, H, $J = 7.2$, H^{CH}), 3.7 (m, 4H, H^{CH2}); *m/z* 336 (M) (EIMS); $\bar{\nu}_{max}/cm^{-1}$ 3098 m, 3067 w, 3011 w, 2952 w, 2879 m, 1692 s, 1582 m, 1566 m, 1467 w, 1434 m, 1409 m, 1353 s, 1280 s, 1246 s, 1208 m, 1145 m, 1129 w, 1092 w, 1058 w, 1042 m, 995 s, 969 m, 853 m, 781 s, 743 m, 723 s, 701 m, 610 m, 597 m, 533 m.

Compound **5**: m.p. 183–184 °C; ^{1}H NMR ($CDCl_3$, see text for comments on assignments of aromatic protons) δ 8.53 (dm, 1H, H^6), 8.45 (dm, 1H, $H^{6'}$), 8.27 (dm, 1H, $H^{6''}$), 7.77 (d, 1H, H^3), 7.69 (ddd, 1H, H^4), 7.57 (d, 1H, $H^{3''}$), 7.51–7.49 (m, 2H, $H^{3',4'}$), 7.41 (ddd, 1H, $H^{4''}$), 7.20 (m, 1H, $H^{5'}$), 7.15 (ddd, 1H, H^5), 6.89–6.83 (m, 3H, $H^{5'', 5S, 3S}$), 6.61 (dd, 2H, $H^{4S,OH}$), 6.24 (s, 1H, H^{OH}), 5.38 (d, 1H, H^a), 4.44 (ddd, 1H, H^b), 3.10 (d, 1H, H^e), 2.73 (dd, 1H, H^d), 2.26 (dt, 1H, H^c), 2.01 (dm, 1H, H^f); *m/z* 459 (M) (MALDI-TOF); $\bar{\nu}_{max}/cm^{-1}$ 3052 w, 2915 w, 1687 s, 1588 s, 1570 m, 1469 m, 1434 s, 1414 m, 1397 m, 1378 m, 1349 m, 1320 m, 1302 m, 1272 m, 1243 w, 1216 m, 1136 m, 1085 m, 1045 w, 993 m, 967 w, 880 w, 850 w, 774 s, 745 m, 689 s, 618 w, 545 w, 521 w.

3-(3-Thienyl)-1,5-bis(2-pyridyl)-2-(2-pyridylcarbonyl) cyclohexane-1,5-diol (**7**). The method of preparation was as above using thiophene-3-carbaldehyde (0.8 ml, 8.56 mmol) to give **7** (1.17 g, 30%) m.p. 214–215 °C; ^{1}H NMR ($CDCl_3$, see text for comments on assignments of aromatic protons) δ 8.53 (d, 1H, H^6), 8.49 (d, 1H, $H^{6'}$), 8.26 (d, 1H, $H^{6''}$), 7.70 (d, 1H, H^3), 7.68 (ddd, 1H, H^4), 7.58 (d, 1H, $H^{3''}$), 7.50 (ddd, 1H, $H^{4'}$), 7.47 (d, 1H, $H^{3'}$), 7.41 (ddd, 1H, $H^{4''}$), 7.20 (m, 1H, $H^{5'}$), 7.13 (m, 1H, H^5), 7.03 (overlapping dd, 2H, $H^{2S,4S}$), 6.93 (dd, $J = 4.9$, 2.9 Hz, 1H, H^{5S}), 6.87 (m, 1H, $H^{5''}$), 6.53 (br s, H, H^{OH}), 6.23 (s, H, H^{OH}), 5.42 (d, 1H, H^a), 4.24 (ddd, 1H, H^b), 3.06 (d, 1H, H^e), 2.67 (dd, 1H, H^d), 2.14 (dt, 1H, H^c), 2.01 (dm, 1H, H^f); *m/z* 459 (M) (MALDI-TOF); $\bar{\nu}/cm^{-1}$ 3385 w, 3094 w, 3052 w, 2913 w, 1689 s, 1588 s, 1570 m, 1469 m, 1434 s, 1415 m, 1396 m, 1355 m, 1322 m, 1302 m, 1273 m, 1243 w, 1216 m, 1141 w, 1122 m, 1084 m, 1050 w, 993 m, 673 w, 774 s, 746 m, 656 m, 618 w, 540 w.

2.5. Preparation of $[Co(\mathbf{3})_2][PF_6]_2$

A solution of **3** (31.2 mg, 0.099 mmol) and $[Co(H_2O)_6][BF_4]_2$ (15 mg, 0.048 mmol) in CH_3CN/CH_3OH (1:1, 50 ml) was stirred for 10 min. at room temperature to give a pink-red solution. Aqueous NH_4PF_6 was added to precipitate **2** as a brown solid (47 mg, 100%). *m/z* (ESMS) 344 $\{M - 2PF_6\}^{2+}$; $\bar{\nu}_{max}/cm^{-1}$ 1616 m, 1554 w, 1527 w, 1469 w, 1434 m, 1346 m, 1259 w, 1218 w, 1161 w, 1049 w, 1045 w, 821 s [PF_6], 783 s, 744 m, 729 m, 682 m, 655 m, 617 m, 551 s; λ_{max}/nm (MeCN): 285 (ε/M^{-1} cm^{-1} 52 000), 314 (38 000), 364sh (7320), 516 (2150); ^{1}H NMR (CD_3CN) δ 93.5 (4H, tpy), 55.3 (4H, tpy), 44.4 (4H, tpy), 32.6 (4H, tpy), 14.7 (2H, thienyl), 13.1 (2H, thienyl), 9.47 (2H, thienyl), 9.22 (4H, tpy) (see text for assignments).

2.6. Preparation of $[Fe(\mathbf{1})_2][PF_6]_2$

A solution of ligand **1** (15.0 mg, 0.048 mmol) and $[Fe(H_2O)_6][BF_4]_2$ (8.0 mg, 0.023 mmol) in CH_3CN/CH_3OH (1:1, 20 ml) was stirred for 10 min at room temperature to give a purple solution. Aqueous NH_4PF_6 was added to precipitate $[Fe(\mathbf{1})_2][PF_6]_2$ as a purple solid (yield 22.5 mg, 100%). *m/z* (MALDI-TOF MS) 687 $\{M - 2PF_6\}^+$; *m/z* (MALDI-TOF MS) (calc.) 686 (687, $[M - 2PF_6]^+$); $\bar{\nu}_{max}$ (neat solid, cm^{-1}) 1613 m, 1468 w, 1432 m, 1400 w, 1245 w, 841 s, 788 m, 753 w, 723 w, 557 m; λ_{max}/nm (MeCN): 283 (ε/M^{-1} cm^{-1} 43 300), 327 (49 300), 456 (23 000); δ_H (CD_3CN) 9.10 (s, 4H, $H^{3'}$), 8.62 (d, 4H, H^3), 8.30 (dd, 2H, H^{3S}), 7.90 (overlapping ddd, 4H, H^4; dd, 2H, H^{5S}), 7.47 (dd, 2H, H^{4S}), 7.21 (d, 4H, H^6) 7.08 (dd, 4H, H^5).

2.7. Preparation of $[Fe(\mathbf{3})_2][PF_6]_2$

$(NH_4)_2Fe(SO_4)_2$ (13.5 mg, 0.034 mmol) was added to a solution of ligand **3** (30.8 mg, 0.097 mmol) in MeCN/MeOH (1:1; 20 ml). The solution was stirred at room temperature for 10 min, and the product was precipitated as a dark purple solid by adding aqueous NH_4PF_6. Yield (33 mg, 99 %). *m/z* (FAB MS) 831 $\{M - PF_6\}^+$, 343 $\{M - 2PF_6\}^{2+}$; $\bar{\nu}_{max}$ (neat solid, cm^{-1}) 1616 m, 1542 w, 1527 w, 1469 w, 1434 m, 1396 w, 1373 w, 1245 w, 1211 w, 825 s (PF_6), 783 s, 756 m, 729 m, 655 m, 617 m, 555 s (PF_6); λ_{max}/nm (MeCN): 569 (ε/M^{-1} cm^{-1} 26 000), 368sh (8400), 322 (57 800), 286 (71 400); ^{1}H NMR (CD_3CN) δ 9.20 (s, 4H, $H^{3'}$), 8.64 (d, $J = 8.03$ Hz, 4H, H^3), 8.60 (dd, $J = 3.01$, 1.33 Hz, 2H, H^{2S}), 8.16 (dd, $J = 5.01$, 1.33 Hz, 2H, H^{4S}), 7.94 (dt, $J = 1.33$, 7.36 Hz, 4H, H^4), 7.89 (d, $J = 3.01$, 2H, H^{5S}), 7.22 (d, $J = 5.68$ Hz, 4H, H^6), 7.10 (dt, $J = 1.33$, 5.68 Hz, 4H, H^5).

2.8. Preparation of $[Ru(\mathbf{3})_2][PF_6]_2$

Ligand **3** (308.5 mg, 0.979 mmol) and $RuCl_3.3H_2O$ (128.3 mg, 0.489 mmol) were suspended in ethane-1, 2-diol (10 ml). After adding four drops of *N*-ethylmorpholine, the reaction mixture was heated in a microwave oven (600 W) for 4 min. A red solution

resulted. The product was precipitated by addition of aqueous NH_4PF_6, collected on Celite and removed by dissolution in MeCN. The solvent was removed in vacuo and the product purified by column chromatography (SiO_2 eluting with MeCN/saturated aqueous KNO_3/H_2O, 20:1:3). The red solid product was isolated in 35% (176.5 mg) yield. *m/z* (MALDI-TOF MS) 1044 $\{M + Na\}^+$, 732 $\{M - 2PF_6\}^+$; $\bar{\nu}_{max}$ (neat solid, cm^{-1}) 1612 w, 1542 w, 1523 w, 1465 w, 1434 m, 1391 m, 1326 m, 1242 w, 1211 w, 1029 w, 879 m, 829 s (PF_6), 779 s, 752 m, 729 m, 651 m, 621 m, 555 m (PF_6), 516s; λ_{max}/nm (MeCN): 493 sh, 310, 285; emission (MeCN, 298 K, nm) $\lambda_{490} = 675$, 700; ^{1}H NMR (CD_3CN) δ 9.03 (s, 4H, $H^{3'}$), 8.67 (d, 4H, H^3), 8.48 (dd, 2H, H^{2S}), 8.08 (dd, 2H, H^{4S}), 7.97 (dt, 4H, H^4), 7.85 (d, 2H, H^{5S}), 7.45 (d, 4H, H^6), 7.20 (dt, 4H, H^5).

2.9. Preparation of [Os(3)$_2$][PF$_6$]$_2$

Ligand **3** (30.0 mg, 0.095 mmol) and K_2OsCl_6 (14.1 mg, 0.045 mmol) were suspended in ethane-1,2-diol (10 ml). After adding eight drops of *N*-ethylmorpholine, the reaction mixture was heated in a microwave oven (600 W) for 4 min, giving a dark brown solution. The product was precipitated by adding aqueous NH_4PF_6, collected on Celite and removed by dissolution in MeCN. The solvent was removed in vacuo and the product purified by column chromatography (SiO_2 eluting with MeCN/saturated aqueous KNO_3/H_2O, 14:2:1). The brown solid product was isolated in 43% (21.3 mg) yield. *m/z* (MALDI-TOF MS) 820 $\{M - 2PF_6\}^+$; $\bar{\nu}_{max}$ (neat solid, cm^{-1}) 1616 w, 1477 w, 1434 m, 1367 s, 1338 s, 1161 w, 1095 w, 1029 w, 918 w, 883 w, 825 s (PF_6), 786 m, 756 m, 725 w, 651 w, 621 w, 559 m (PF_6); λ_{max}/nm (MeCN): 671, 493, 315, 286; emission (MeCN, 298 K, nm) $\lambda_{490} = 742$; ^{1}H NMR (CD_3CN) δ 9.06 (s, 4H, $H^{3'}$), 8.66 (d, 4H, H^3), 8.40 (dd, 2H, H^{2S}), 8.05 (dd, 2H, H^{4S}), 7.83 (dt, 4H, H^4), 7.80 (d, 2H, H^{5S}), 7.32 (d, 4H, H^6), 7.12 (dt, 4H, H^5).

2.10. Preparation of [Ru(tpy)(3)][PF$_6$]$_2$

[Ru(tpy)Cl_3] (24 mg, 0.054 mmol) and ligand **3** (15 mg, 0.048 mmol) were added to ethane-1,2-diol (25 ml). After adding four drops of *N*-ethylmorpholine, the reaction mixture was heated in a microwave oven (600 W) for 4 min after which time, the mixture was cooled. The product was precipitated by adding aqueous NH_4PF_6, and purified by column chromatography (SiO_2 eluting with MeCN/saturated aqueous KNO_3/H_2O, 14:2:1). The one major fraction was collected and the volume of the solution was reduced to about half in vacuo, and aqueous NH_4PF_6 was added to precipitate the product which was filtered and collected on Celite. The residue was dissolved in MeCN; distilled H_2O was added carefully until a precipitate was obtained. This precipitate was again filtered and collected on Celite and was dried overnight under high vacuum. The product was isolated as an orange-red solid (40 mg, 89%). *m/z* (MALDI-TOF MS) 650 $\{M - 2PF_6\}^+$, 417 $\{M - tpy - 2PF_6\}^+$; $\bar{\nu}_{max}$ (KBr, cm^{-1}) 1614 m, 1466 w, 1449 m, 1435 m, 1388 m, 1368 w, 1287 w, 1244 w, 1031 w, 840 s (PF_6), 784 m, 767 m, 558 m (PF_6); λ_{max}/nm (MeCN): 484 (ε/M^{-1} cm^{-1} 44 900), 308 (67 600), 284 (44 900); ^{1}H NMR (CD_3CN) δ 9.00 (s, 2H, $H^{3'}$(**6**)), 8.74 (s, 2H, $H^{3'}$(tpy)), 8.64 (d, 2H, H^3(**6**)), 8.49 (d, 2H, H^3(tpy)), 8.45 (dd, 1H, H^{2S}), 8.41 (dd, 1H, $H^{4'}$(tpy)), 8.04 (dd, 1H, H^{4S}), 7.93 (ddd, 4H, H^4(**6** + tpy)), 7.82 (dd, 1H, H^{5S}), 7.43 (d, 2H, H^6(**6**)), 7.33 (d, 2H, H^6(tpy)), 7.16 (dd, 4H, H^5(**6** + tpy)). Electrochemical data: see text.

2.11. Preparation of [Os(tpy)(3)][PF$_6$]$_2$

[Os(tpy)Cl_3] (20 mg, 0.022 mmol) and ligand **3** (6 mg, 0.019 mmol) were added to ethane-1,2-diol (25 ml). Four drops of *N*-ethylmorpholine were added, the reaction mixture was heated in a microwave oven (600 W, 4 min), and then cooled. The product was precipitated with aqueous NH_4PF_6, and purified by column chromatography (SiO_2, MeCN/saturated aqueous KNO_3/H_2O, 14:2:1). The one major fraction was collected, and the solution was reduced in volume. The product was precipitated with aqueous NH_4PF_6, filtered and collected on Celite. The residue was dissolved in MeCN and distilled H_2O was added to produce a precipitate which was filtered, collected on Celite and dried overnight under high vacuum. The product was isolated as a brown solid (17 mg, 87%). *m/z* (MALDI-TOF MS) 739 $\{M - 2PF_6\}^+$; λ_{max}/nm (MeCN): 661 (ε/M^{-1} cm^{-1} 1400), 484 (5600), 312 (20 100), 274 (12 400); ^{1}H NMR (CD_3CN) δ 9.02 (s, 2H, $H^{3'}$(**6**)), 8.75 (d, 2H, H^3(tpy)), 8.64 (d, 2H, H^3(**6**)), 8.47 (s, 2H, $H^{3'}$(tpy)), 8.36 (dd, 1H, H^{2S}), 7.92 (dd, 1H, $H^{4'}$(tpy)), 8.01 (dd, 1H, H^{4S}), 7.83 (dd, 1H, H^{5S}), 7.78 (ddd, 4H, H^4(**6** + tpy)), 7.29 (d, 2H, H^6(**6**)), 7.21 (d, 2H, H^6(tpy)), 7.09 (dd, 4H, H^5(**6** + tpy)). Electrochemical data: see text.

2.12. Crystal structure determinations

Data were collected on a CAD4 diffractometer. The structures were solved and refined by direct methods using standard techniques as indicated in Table 1 using the programmes SIR 92 [12] and CRYSTALS [13]; a Chebychev polynomial weighting scheme was used [14]. Diagrams and supplementary material were prepared using the above programmes together with ORTEP-3 for Windows [15] and PLATON [16,17]. In **5**, the pyridyl rings exhibited a rotational disorder that was modelled by partial occupancies (0.72:0.28 and 0.53:0.47) of N and C atoms about the interannular bond. In the case of **7**, the thienyl ring was disordered, with two rotamers differing in the orientation being present; this disorder

Table 1
Crystallographic data for **5**, **7**, and **3**

	5	**7**	**3**
Molecular formula	$C_{29}H_{26}N_3O_3S$	$C_{29}H_{26}N_3O_3S$	$C_{19}H_{13}N_3S$
Formula weight	454.58	454.58	315.398
Crystal system	triclinic	triclinic	orthorhombic
Space group	$P\bar{1}$	$P\bar{1}$	*Pnab*
a (Å)	6.0679(6)	6.0675(4)	10.854(2)
b (Å)	10.201(1)	10.1245(6)	11.625(2)
c (Å)	19.155(5)	19.276(2)	12.173(2)
α (°)	97.145(15)	97.931(7)	90
β (°)	95.554(14)	95.966(7)	90
γ (°)	105.058(9)	104.831(5)	90
V (Å^3)	1125.7(3)	1121.7(2)	1535.8(4)
Z	2	2	4
T (K)	293	293	293
Number of reflections	4007	4463	2015
Number of independent reflections	3889	4329	1891
Number of observed reflections	3117	3929	1351
	$I > 3\sigma(I)$	$I > 3\sigma(I)$	$I > 3\sigma(I)$
μ (mm^{-1})	0.17	0.15	0. 20
Final *R* (observed)	0.0642	0.0615	0.0419
Final R_w (observed)	0.0790	0.0591	0.0466

was modelled with partial occupancies of 1:1 for all ring atoms.

3. Results and discussion

3.1. Ligand synthesis

We have previously described the synthesis of the 2-thienyl-functionalized ligand **1**, which was obtained in 40% yield from a one-pot reaction of 2-acetylpyridine and thiophene-2-carbaldehyde in the presence of ammonium acetate [7]. Although the yield in this reaction was low, in our hands attempts to prepare **1** by Kröhnke [18] methodology using the enone 1-(2-pyridyl)-1-oxoprop-2-enylthiophene (readily prepared in good yield from 2-acetylpyridine and thiophene-2-carbaldehyde) were unsuccessful or very low-yielding although an unspecified ''modified'' Kröhnke approach has been reported [19]. In the course of attempts to optimize the yield of **1** and to develop general methods for other 4′-aryl-2,2′:6′,2″-terpyridines, we have investigated a number of other approaches.

3.2. The 1,5-dicarbonyl route and the solid-state structures of 5 and 7

One of the approaches that we have shown to be successful for the synthesis of 4′-phenyl-2,2′:6′,2′-terpyridine is the preparation of 4-phenyl-1,5-di(2-pyridyl)pentane-1,5-dione from the reaction of benzaldehyde with an excess of 2-acetylpyridine followed by oxidative cyclization with ammonium acetate under aerobic conditions [20]. We have, however, shown that in the case of other aromatic aldehydes, the 1,5-dicarbonyl compound is the minor product compared to other cyclic condensation products.

The reaction of thiophene-2-carbaldehyde with an excess of 2-acetylpyridine in basic (aqueous ethanolic NaOH) conditions resulted in the formation of a mixture of two compounds, identified as the desired 1,5-dicarbonyl 1,5-bis(2-pyridyl)-3-(2-thienyl)penta-1,5-dione (**4**) and the 3:1 cyclic condensation product 3-(2-thienyl)-1,5-bis(2-pyridyl)-2-(2-pyridylcarbonyl)cyclohexane-1,5-diol (**5**) (Scheme 1). The isolated yield of **4** was only 25% and the reaction sequence offered no advantage in terms of yield or convenience over the previously described one-pot method. A similar reaction with thiophene-3-carbaldehyde gave small amounts of the 1,5-dicarbonyl compound **6** and the 3:1 cyclohexane derivative 3-(3-thienyl)-1,5-bis(2-pyridyl)-2-(2-pyridylcarbonyl)cyclohexane-1,5-diol (**7**) as the major product (Scheme 1). All of these compounds were fully characterized by spectroscopic and mass spectrometric methods (see Section 2).

The new compounds **5** and **7** are worthy of some additional discussion and both have been further characterized by crystal structure determinations. We have previously published details of the assignment of the ^{1}H NMR spectrum of a derivative related to **5** and **7**, but with the thienyl substituent replaced by a 4-^{t}BuC$_6$H$_4$ group [21]. The ^{1}H NMR spectra of ligands **5** and **7** exhibit resonances assigned to the two sets of geminal protons H$^{c/d}$ and H$^{e/f}$ (see Scheme 1) with a characteristic coupling constant ($^2J = 14$–15 Hz). In addition, two hydroxy resonances are observed for **7**, one broadened through exchange with the solvent, and the other sharp as a result of hydrogen-bonding with the

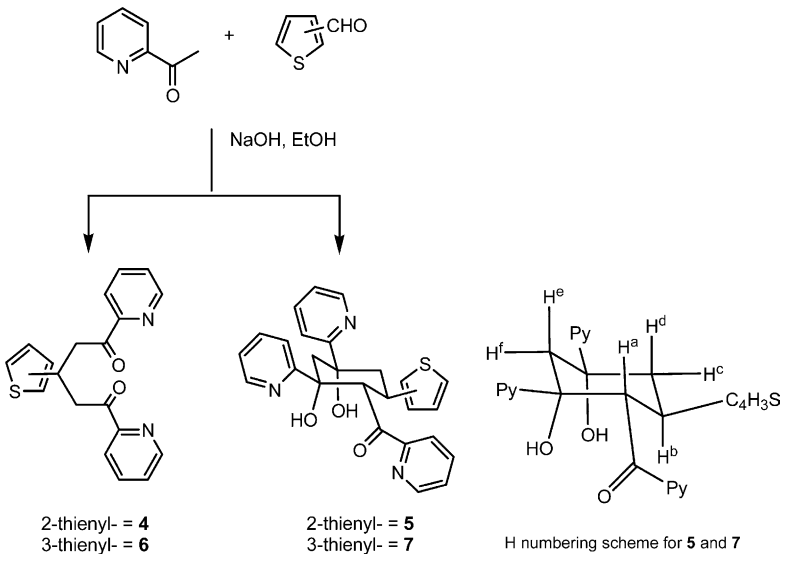

Scheme 1.

adjacent carbonyl group. In the case of **5**, integration shows that the more broadened OH signal lies under the thienyl H^4 peak. The aromatic signals were assigned by COSY NMR spectroscopy which allowed differentiation between the signals belonging to different pyridine rings (distinguished in the experimental section by use of prime marks), but did not permit their absolute assignment.

Slow evaporation of methanolic solutions of **5** and **7** afforded colourless, cubic crystals of X-ray quality. The solid-state X-ray determinations of the two compounds were very similar and confirmed the structures. The structure of compound **5** is shown in Fig. 1. The only constitutional difference between **5** and **7** lies in the position of substitution of the thienyl ring. In both compounds all of the aromatic substituents are in the favoured equatorial positions, resulting in a (1*RS*, 2*SR*, 2*RS*, 5*RS*) configuration. All bond lengths and angles lie in the normal ranges. The O···O and OH···O distances between the two hydroxy-groups are 2.732(3) and 1.87(3) Å for **5**, and 2.729(3) and 1.89(2) Å for **7**, respectively, which support the ^{1}H NMR spectroscopic data in suggesting that these groups are hydrogen-bonded. Both enantiomers of the chiral compounds **5** and **7** are present in the unit cell. Rotational disorder of the thienyl ring of **7** leads to 53% and 47% occupancy of two rotamers, distinguished by the location of the sulfur atom with respect to adjacent substituents, although compound **5** shows no such disorder.

Attempts to prepare **1** or **3** from **5** or **7**, respectively, by reaction with ammonium acetate were unsuccessful.

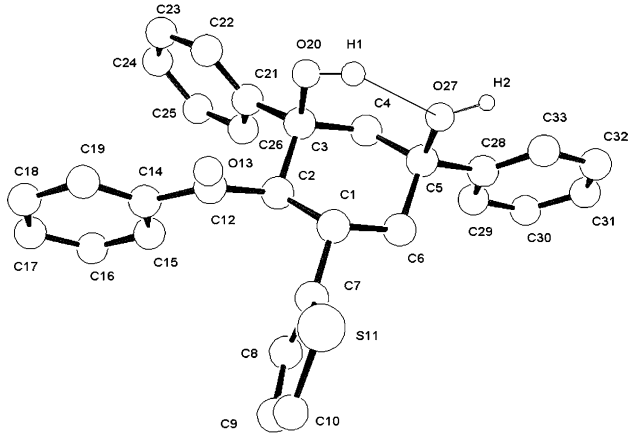

Fig. 1. Solid-state structure of **5** showing the numbering scheme adopted. Hydrogen atoms involved in hydrogen bonding are included in the diagram; all other H atoms are omitted for clarity. Selected bond distances: S(11)–C(7) = 1.696(2), S(11)–C(10) = 1.679(3), O(13)–C(12) = 1.209(3), O(20)–C(3) = 1.429(3), O(27)–C(5) = 1.434(4), O(20)–H(1) = 0.95(3), O(27)–H(2) = 0.96(3) Å.

3.3. Modified one-pot synthesis of *1* and *3* and the solid-state structure of *3*

We finally adopted a modification of the one-pot synthetic method originally described by Calzaferri [22] in which 2-acetylpyridine is converted to the enolate by reaction with potassium tert-butoxide, followed by reaction with half an equivalent of the aromatic aldehyde. Subsequently, the reaction mixture is treated with ammonium acetate in ethanolic acetic acid. Using this method, compounds **1** and **3** were obtained in 62% and 52% yield from thiophene-2-carbaldehyde and thiophene-3-carbaldehyde, respectively. Extraction and column chromatographic purification gave the desired ligands analytically pure.

Compound **3** shows a parent ion in its mass spectrum and the ^{1}H NMR spectrum is fully in accord with the

structure proposed. The solid state structure of **3** is presented in Fig. 2. The thiophene rings exhibited a rotational disorder and only one rotamer is shown in the Figure. The tpy-domain adopts the expected transoid conformation of the pyridine rings. In the solid state, the pyridine rings are almost coplanar, with a torsion angle of only 4.5° between the terminal and central rings. The average deviation of the disordered thienyl ring from the plane of the central group is only 6.0°. The C–C and C–N bond lengths in the pyridine rings lie within expected ranges as do the average C–C and C–S distances within the disordered thienyl ring. In the lattice, the molecules form a herring-bone pattern with classical π-stacking interactions between terminal pyridine rings of adjacent ligands.

3.4. Complexes of 1 and 3 with Co(II), Fe(II), Ru(II) and Os(II)

We have previously published details of the complexes $[Co(\mathbf{1})_2][PF_6]_2$ [8], $[Ru(\mathbf{1})_2][PF_6]_2$, $[Os(\mathbf{1})_2][PF_6]_2$, $[Ru(tpy)(\mathbf{1})][PF_6]_2$ and $[Os(tpy)(\mathbf{1})][PF_6]_2$ [7]. Here, we add to this series by reporting the preparation and characterization of $[Fe(\mathbf{1})_2][PF_6]_2$, and of the 4′-(3-thienyl)-2,2′:6′,2′-terpyridine-containing complexes $[Co(\mathbf{3})_2][PF_6]_2$, $[Fe(\mathbf{3})_2][PF_6]_2$, $[Ru(\mathbf{3})_2][PF_6]_2$, $[Os(\mathbf{3})_2][PF_6]_2$, $[Ru(tpy)(\mathbf{3})][PF_6]_2$ and $[Os(tpy)(\mathbf{3})][PF_6]_2$. Each complex containing ligand **3** is an isomer of the corresponding complex containing ligand **1**, differing only in the position of the sulfur atom in the thienyl ring. One of our interests in thienyl-derivatized bis(tpy) metal complexes is their adsorption properties on surfaces. With the sulfur donor in the 3- rather than 2-position, the complex is better suited sterically for interaction through S-donation to the surface.

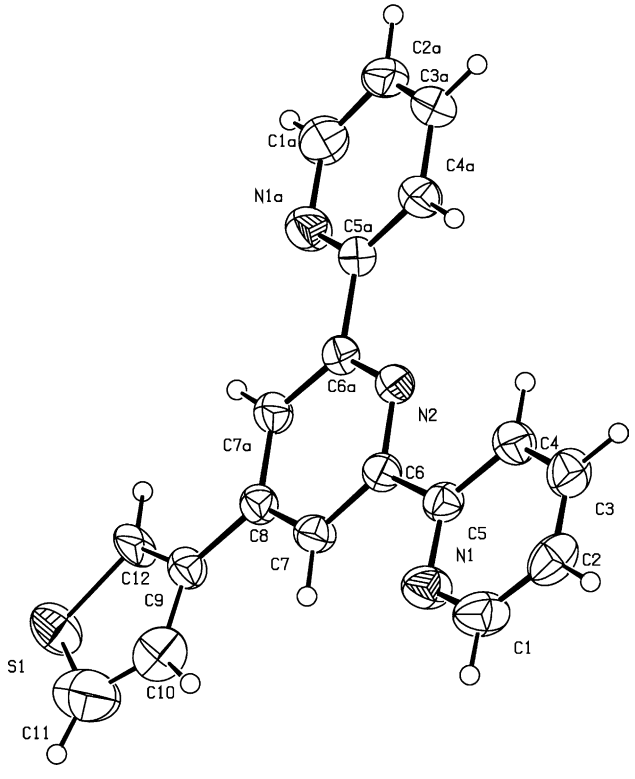

Fig. 2. Solid state structure of **3** showing the atom numbering scheme adopted. Only one conformation of the disordered thiophene ring is shown. Selected bond distances: S(1)–C(11) = 1.686(11), S(1)–C(12) = 1.664(4), N(1)–C(1) = 1.338(3), N(1)–C(5) = 1.335(2), N(2)–C(6) = 1.338(1) Å.

The diamagnetic complex $[Fe(\mathbf{1})_2]^{2+}$ was prepared in quantitative yield as the $[PF_6]^-$ salt from iron(II) tetrafluoroborate and ligand **1**, followed by precipitation with $[NH_4][PF_6]$. The highest mass peak in the MALDI-TOF mass spectrum was at *m/z* 687 corresponding to the $[M - 2PF_6]^+$; the isotopic pattern of the envelope matched that calculated. The ^1H NMR spectrum of $[Fe(\mathbf{1})_2]^{2+}$ is consistent with a symmetrical complex. On going from $[Fe(\mathbf{1})_2]^{2+}$ to $[Fe(\mathbf{3})_2]^{2+}$, there are negligible changes in the ^1H NMR spectrum for signals assigned to the tpy protons. The thiophene region in the ^1H NMR spectrum of $[Fe(\mathbf{1})_2]^{2+}$ is characterized by signals at δ 8.30, 7.90 and 7.47 assigned on the basis of the coupling constants and chemical shifts to H^{3S}, H^{5S} and H^{4S}, respectively. The signal for H^{5S} is unaffected on going from $[Fe(\mathbf{1})_2]^{2+}$ to $[Fe(\mathbf{3})_2]^{2+}$, but the signal for H^{4S} shifts from δ 7.47 to 8.16 in response to the change in position of the ring S atom. The doublet of doublets at δ 8.30 assigned to H^{3S} in $[Fe(\mathbf{1})_2]^{2+}$ is replaced by a doublet of doublets at δ 8.60 assigned to H^{2S} in $[Fe(\mathbf{3})_2]^{2+}$. The highest mass peak at *m/z* 831 in the FAB mass spectrum of $[Fe(\mathbf{3})_2][PF_6]_2$ is consistent with $[M - PF_6]^+$.

The homoleptic complexes $[Ru(\mathbf{3})_2]^{2+}$ and $[Os(\mathbf{3})_2]^{2+}$ were prepared by the reaction of $RuCl_3 \cdot 3H_2O$ or $K_2[OsCl_6]$ with **3** in ethane-1,2-diol under microwave conditions in the presence of *N*-ethylmorpholine as reducing agent. These strategies are similar to those previously reported for the syntheses of $[Ru(\mathbf{1})_2]^{2+}$ and $[Os(\mathbf{1})_2]^{2+}$ [7]. Both complexes were isolated as the $[PF_6]^-$ salts. As for the Fe(II) complex, the ^1H NMR spectra of $[Ru(\mathbf{3})_2]^{2+}$ and $[Os(\mathbf{3})_2]^{2+}$ are consistent with symmetrical species. Fig. 3 illustrates the effect that coordination of ligand **3** to each group 8 metal(II) centre has on the chemical shifts of the protons in the tpy part of the ligand; values of $(\delta_{free\ ligand} - \delta_{complex})$ are plotted for each proton. Proton H^6 is affected the most and shifts to significantly lower frequency as ligand **3** forms $[M(\mathbf{3})_2]^{2+}$, the magnitude of the change following the sequence Fe > Os > Ru. These shift correlations are a good qualitative measure of the change in coordination environment of the ligand upon coordination to the metal ion. The upfield shift of H^6 is due to the proton lying above the shielding region of a pyridine ring of the other tpy ligand. Fig. 3 shows that the δ value of tpy protons H^3 and H^4 are scarcely influenced by coordination. The signal assigned to H^5 shifts slightly to lower

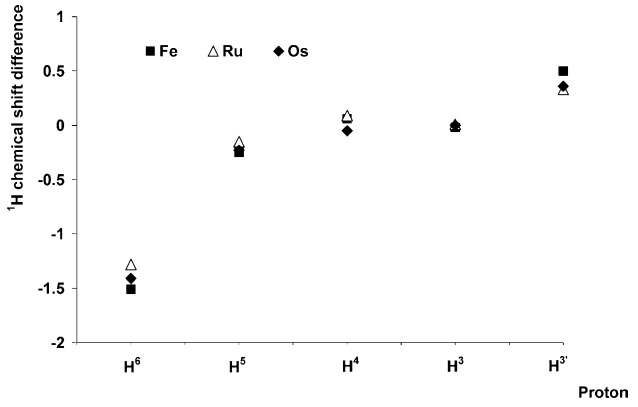

Fig. 3. Changes in the ^{1}H NMR chemical shifts ($\delta_{\text{free ligand}(CDCl_3)} - \delta_{\text{complex}(CD_3CN)}$) for the tpy proton signals on going from free ligand **3** to $[Fe(\mathbf{3})_2]^{2+}$, $[Ru(\mathbf{3})_2]^{2+}$ and $[Os(\mathbf{3})_2]^{2+}$.

frequency, while that for H$^{3'}$ (the only proton in the central ring of the tpy part of the ligand) shifts to higher frequency with the magnitude of the change following the order Fe > Os > Ru.

The paramagnetic complex $[Co(\mathbf{3})_2]^{2+}$ was prepared in quantitative yield by the reaction of $[Co(H_2O)_6][BF_4]_2$ with ligand **3** followed by anion exchange to yield $[Co(\mathbf{3})_2][PF_6]_2$. The highest mass peak in the electrospray mass spectrum came at $m/z = 344$ and the isotope pattern was consistent with the formulation $[M - 2PF_6]^{2+}$. In the ^{1}H NMR spectrum (Fig. 4), all signals were paramagnetically shifted and, although broadened, were well-resolved with the exception of the lowest frequency signal at δ 93.5. The Co(II) ion (d^7) may be high or low-spin, and in complexes derived from $[Co(tpy)_2]^{2+}$, the proton chemical shift range for the tpy protons is characteristic of the spin state [8,23]. In $[Co(\mathbf{3})_2]^{2+}$, the ^{1}H NMR spectrum showed signals over the range δ 9.22–93.5, indicative of low-spin Co(II). The signals at δ 93.5, 55.3, 44.4 and 32.6 in the ^{1}H NMR spectrum of $[Co(\mathbf{3})_2]^{2+}$ are at similar shifts to those assigned by COSY [24] to protons H^6, H^3, H$^{3'}$ and H^5 in $[Co(tpy)_2]^{2+}$ (δ 99.8, 57.2, 48.2, 34.5 for the $[PF_6]^-$ salt in CD_3CN), and we therefore assign these signals to the corresponding protons in $[Co(\mathbf{3})_2]^{2+}$. In $[Co(tpy)_2]^{2+}$, a signal at δ 8.91 has been assigned by COSY [24] to proton H^4. In the spectrum of $[Co(\mathbf{3})_2]^{2+}$, two broadened peaks appear at δ 9.47 and 9.22 with relative integrals 1:2. The signal at δ 9.22 is assigned to tpy H^4. The signals in the spectrum at δ 14.7, 13.1 and 9.4 with relative integrals 1:1:1 are assigned to the three thienyl protons but it has not been possible to unambiguously assign the peaks to individual protons. The presence of the paramagnetic Co(II) centre causes significant shifting of the signals for all protons in coordinated ligand **3** compared to their shifts in the diamagnetic Fe(II), Ru(II) and Os(II) analogues.

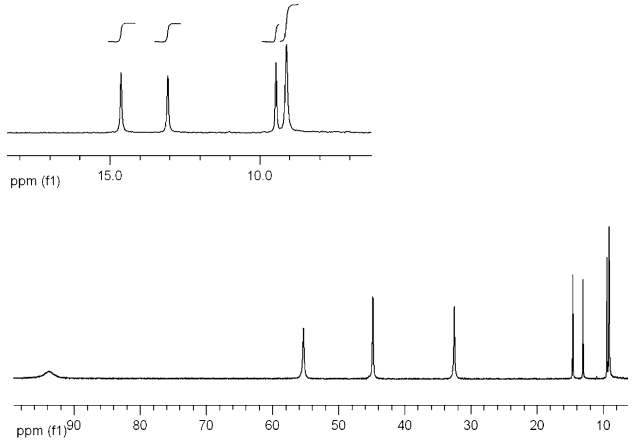

Fig. 4. The 250 MHz ^{1}H NMR spectrum of $[Co(\mathbf{3})_2][PF_6]_2$ (CD_3CN, room temperature). The expansion shows the region of the thienyl protons and the tpy H^4 proton.

The mixed-ligand complexes $[Ru(tpy)(\mathbf{3})]^{2+}$ and $[Os(tpy)(\mathbf{3})]^{2+}$ were prepared by reactions of $[M(tpy)Cl_3]^{3+}$ (M = Ru or Os) with ligand **3** under reducing conditions (*N*-ethylmorpholine). The complexes were isolated in good yields as the hexafluorophosphate salts. In the MALDI-TOF mass spectra of $[Ru(tpy)(\mathbf{3})][PF_6]_2$ and $[Os(tpy)(\mathbf{3})][PF_6]_2$, the highest mass peaks at $m/z = 650$ and 739, respectively, corresponded to $\{M - 2PF_6\}^+$ and showed the correct isotopic distribution for this formulation. The ^{1}H NMR spectrum of $[Ru(tpy)(\mathbf{3})]^{2+}$ is a superimposition of the corresponding spectra for $[Ru(tpy)_2]^{2+}$ and $[Ru(\mathbf{3})_2]^{2+}$ and the spectrum could be assigned accordingly. Similarly, the signals in the ^{1}H NMR spectrum of $[Os(tpy)(\mathbf{3})]^{2+}$ could be assigned by comparison with the spectra for $[Os(tpy)_2]^{2+}$ and $[Os(\mathbf{3})_2]^{2+}$. In both heteroleptic complexes, therefore, the ligands have little or no influence on one another.

Electrochemical data for CH_3CN solutions of $[Ru(tpy)(\mathbf{3})][PF_6]_2$ and $[Os(tpy)(\mathbf{3})][PF_6]_2$ were recorded (versus Fc/Fc^+). For each of the ruthenium and osmium complexes, a fully reversible metal-centred redox wave occurs at +0.88 and +0.52 V, respectively, and is assigned to the M^{3+}/M^{2+} process. The ease of oxidation is therefore, as expected, Os(II) > Ru(II). The metal redox processes are shifted to less positive potentials compared to the corresponding $[M(tpy)_2]^{2+}$ complexes [25,26], indicating that the thienyl group is electron-donating. Quasi-reversible ligand-based electrochemical processes are observed for $[Ru(tpy)(\mathbf{3})]^{2+}$ at −1.52 and −1.82 V, and for $[Os(tpy)(\mathbf{3})]^{2+}$ at −1.65, −1.87 and −2.25 V.

4. Conclusion

We have developed an efficient method for the preparation of 4′-(2-thienyl)-2,2′:6′,2″-terpyridine and 4′-(3-thienyl)-2,2′:6′,2″-terpyridine; the latter was structurally characterized. During the synthesis development, the cyclic condensation products 3-(2-thienyl)-1,5-bis

(2-pyridyl)-2-(2-pyridylcarbonyl)cyclohexane-1,5-diol (**5**) and 3-(3-thienyl)-1,5-bis(2-pyridyl)-2-(2-pyridylcarbonyl)cyclohexane-1,5-diol (**7**) were isolated and structurally characterized. The formation and characterization of paramagnetic Co(II) and diamagnetic Fe(II), Ru(II) and Os(II) complexes containing 4′-(2-thienyl)- and 4′-(3-thienyl)-2,2′:6′,2′-terpyridine ligands have been described.

5. Supplementary material

Full crystallographic details have been deposited in CIF format with the Cambridge Crystallographic Data Centre. Copies of the data can be obtained free of charge on request from the CCDC, 12 Union Road, Cambridge CB2 1EZ, UK (fax: +44-1223-336408, email: deposit@ccdc.cam.ac.uk or www at http://www.ccdc.cam.ac.uk.) quoting the deposition numbers CCDC 210433 (**3**), 210434 (**5**) and 210435 (**7**).

Acknowledgements

We thank the University of Basel and Schweizerischer Nationalfonds zur Förderung der wissenschaftlichen Forschung for financial support of this work.

References

[1] M. Heller, U.S. Schubert, Eur. J. Org. Chem. (2003) 947.
[2] R.A. Fallahpour, Synthesis (2003) 155.
[3] U.S. Schubert, C. Eschbaumer, Angew. Chem. Int. Ed. 41 (2002) 2893.
[4] G.F. Swiegers, T.J. Malefetse, Chem. Rev. 100 (2000) 3483.
[5] E.C. Constable, Adv. Inorg. Chem. Radiochem. 30 (1987) 69.
[6] E.C. Constable, C.E. Housecroft, E.R. Schofield, S. Encinas, N. Armaroli, F. Barigelletti, F. Flamigni, E. Figgemeier, J.G. Vos, Chem. Commun. (1999) 869.
[7] S. Encinas, L. Flamigni, F. Barigelletti, E.C. Constable, C.E. Housecroft, E. Schofield, E. Figgemeier, D. Fenske, M. Neuburger, J.G. Vos, M. Zehnder, Chem. Eur. J. 8 (2002) 137.
[8] E.C. Constable, C.E. Housecroft, T. Kulke, C. Lazzarini, E. Schofield, Y. Zimmermann, J. Chem. Soc., Dalton Trans. (2001) 2864.
[9] T. Matsuura, H. Sakaguchi, Y. Shimoyama, J. Mater. Sci. 14 (2003) 353.
[10] J. Noh, E. Ito, T. Araki, M. Hara, Surf. Sci. 532 (2003) 1116.
[11] G.J. Su, H.M. Zhang, L.J. Wan, C.L. Bai, Surf. Sci. 531 (2003) L363.
[12] SIR 92: A. Altomare, G. Cascarano, G. Giacovazzo, A. Guagliardi, M.C. Burla, G. Polidori, M. Camalli, J. Appl. Cryst. 27 (1994) 435.
[13] CRYSTALS Issue 11: D.J. Watkin, C.K. Prout, J.R. Carruthers, P.W. Betteridge, R.I. Cooper, Chemical Crystallography Laboratory, University of Oxford, Oxford, UK, 1999.
[14] J.R. Carruthers, D.J. Watkin, Acta Crystallogr., Sect. A 35 (1979) 698.
[15] ORTEP-3 for Windows: L.J. Farrugia, J. Appl. Cryst. 30 (1997) 565.
[16] A.L. Spek, Acta Crystallogr., Sect. A 46 (1990) C34.
[17] L.J. Farrugia, PLATON for Windows, University of Glasgow, 2003.
[18] F. Kröhnke, Synthesis (1976) 1.
[19] L-X. Zhao, T-S. Kim, S-H. Ahn, T-H. Kim, E. Kim, W-J. Cho, H. Choi, C-S. Lee, J-A. Kim, T.C. Jeong, C. Chang, E-S. Lee, Bioorg. Med. Chem. Lett. 11 (2001) 2659.
[20] E.C. Constable, J. Lewis, M.C. Liptrot, P.R. Raithby, Inorg. Chim. Acta 178 (1990) 47.
[21] E.C. Constable, P. Harverson, D.R. Smith, L. Whall, Polyhedron 16 (1997) 3615.
[22] W. Spahni, G. Calzaferri, Helv. Chim. Acta 67 (1984) 450.
[23] E.C. Constable, C.P. Hart, C.E. Housecroft, Appl. Organomet. Chem. 17 (2003) 383.
[24] E.C. Constable, C.E. Housecroft, K.J. Kulicke, Y. Tao, in preparation.
[25] M. Maestri, N. Armaroli, V. Balzani, E.C. Constable, A.M.W. Cargill Thompson, Inorg. Chem. 34 (1995) 2759.
[26] E.C. Constable, A.M.W. Cargill Thompson, J. Chem. Soc., Dalton Trans. (1994) 1409.

Available online at www.sciencedirect.com
SCIENCE DIRECT®
Polyhedron 23 (2004) 145–154
POLYHEDRON
www.elsevier.com/locate/poly

Eight-coordinate stereochemistries of U(IV) catecholate and aquo complexes ☆

Benjamin P. Hay *, Jamal Uddin, Timothy K. Firman

Chemical Sciences Division, Pacific Northwest National Laboratory, MS: K1-83, P.O. Box 999, Richland, WA 99352, USA

Received 28 July 2003; accepted 22 September 2003

Abstract

An extended MM3 model has been used to identify all low energy configurations for U(IV) complexes with catecholate and aquo ligands. Both stochastic and systematic conformational analyses of $[U(cat)_n(OH_2)_{8-2n}]^{4-2n}$ complexes, $n = 1$–4, establish that 20 of the 67 possible stereochemistries are minima on the MM3 potential surface. The stable stereochemistries are reported for each stoichiometry and, where possible, the results are compared with experimental data and with the predictions from prior repulsion energy calculations.
© 2003 Published by Elsevier Ltd.

Keywords: Eight-coordinate; Stereochemistry; Dodecahedron; Square antiprism; Bicapped trigonal prism; Molecular mechanics

1. Introduction

Research on computer-aided molecular design has led to the development of HostDesigner, the first computer software specifically created for the discovery of host molecules for metal ions [1]. The use of this software requires the definition of geometries that represent optimal arrangements of one or more binding sites about the metal ion of interest. One design strategy consists of placing two or more bidentate ligands on the metal and then using the software to identify molecular fragments that are suitable for bridging between the bidentate components. In this case the geometry of the initial metal complex must be defined. It is desirable to use all low energy configurations of the metal complex as input geometries to ensure that potentially viable architectures are not overlooked in the building process. Identification of these configurations can be problematic.

Consider the case where the coordination sphere will be filled with some combination of bidentate ligands and water. If the bidentate ligands are identical and symmetric (in other words, the two binding sites are equivalent) then there are only a limited number of possible configurations at low coordination numbers. For example, in an octahedral system with a coordination number of six there are two ways to place two bidentate ligands and only one way to place three bidentate ligands [2]. The situation becomes much more complex at higher coordination numbers where there may be several polyhedra and each polyhedron may exhibit multiple stereoisomers, and nonequivalent coordination sites.

This issue was brought to our attention when we considered the strategy of designing ligands for 8-coordinate U(IV) by connecting two or more catecholate groups that had been pre-positioned on the metal ion. Prior studies suggest that there are three polyhedra that should be considered for eight-coordinate U(IV) complexes: the square antiprism (SAP), the dodecahedron (DOD), and the bicapped trigonal prism (BTP) [3–9]. An enumeration of all possible ways to place one to four symmetrical bidentate ligands onto these three polyhedra, assuming vacant vertices are occupied by an identical type of unidentate ligand and excluding the optical

☆ Supplementary data associated with this article can be found, in the online version, at doi:10.1016/j.poly.2003.09.026.

* Corresponding author. Tel.: +1-509-372-6239; fax: +1-509-375-6631.
E-mail address: ben.hay@pnl.gov (B.P. Hay).

0277-5387/$ - see front matter © 2003 Published by Elsevier Ltd.
doi:10.1016/j.poly.2003.09.026

isomers, reveals that there are 130 distinct stereoisomers [11]! Which of these many possibilities actually represent stable configurations for U(IV) catecholate and aquo complexes?

This question may be addressed with force field calculations. Early analyses of eight-coordinate stereochemistries for [M(unidentate)$_8$] complexes were performed with a simple model in which the total repulsion energy in the inner coordination sphere was computed by applying $1/r^n$ potential functions between all pairs of points on the surface of a sphere [3,4a]. Such calculations have been extended to complexes containing bidentate ligands by keeping the distance between the pairs of atoms in the same chelate ring constant and used to analyze the stereochemistries of [M(bidentate)$_2$(unidentate)$_4$] and [M(bidentate)$_4$] complexes; providing one basis for the assignment of likely stereoisomers for these stoichiometries [4b–4e].

Molecular mechanics models, which mimic some of the features of the repulsion energy models, also can be used to evaluate the structures of high-coordinate metal complexes and to identify their stable stereochemistries [12]. Herein, we report the use of an extended MM3 model to perform conformational analyses of all stoichiometries for 8-coordinate U(IV) complexes with aquo and catecholate ligands. All stable stereochemistries are reported for each stoichiometry and, where possible, the results are compared with experimental data and with the predictions from prior repulsion energy calculations.

2. Methods

Molecular mechanics calculations were carried out using the MM3 program, [1] which has been modified to support "points-on-a-sphere" metal atom types [13]. The default parameter set was modified to allow treatment of the U(IV)-catecholate interactions and U(IV)-aquo interactions. With one exception, the U–O$_{cat}$ bond stretch, the parameters used for the U(IV)-catecholate interactions were taken directly from a prior study of Fe(III)-catecholate complexes [14]. The aquo ligand, which was modeled as a neutrally charged oxygen atom, also required the assignment of only U–O$_{aquo}$ bond stretch parameters. Extrapolating from Badger's rules [15], we estimate that U–O stretching force constants, k_r, should fall in the range of 1.0–1.5 mdyn/Å^2 over the range of 2.25–2.35 Å. After assigning the U–O$_{cat}$ interaction the upper limit of $k_r = 1.5$ mdyn/Å^2, an ideal length, $r_0 = 2.29$ Å, was assigned by adjusting r_0 to obtain the best fit to the U–O distances in the [U(cat)$_4$]$^{4-}$ crystal structure [16]. After assigning the U–O$_{aquo}$ interaction the lower limit of $k_r = 1.0$ mdyn/Å^2, an ideal length, $r_0 = 2.33$ Å, was assigned by interpolating a probable U–O distance from known [Ln(OH$_2$)$_8$]$^{3+}$ structures (see Section 3.2), and then adjusting r_0 to yield this U–O distance in a calculated square antiprism [U(OH$_2$)$_8$]$^{4+}$ model complex.

Extensive conformational searches on [U(OH$_2$)$_8$]$^{4+}$, [U(cat)(OH$_2$)$_6$]$^{2+}$, [U(cat)$_2$(OH$_2$)$_4$], [U(cat)$_3$(OH$_2$)$_2$]$^{2-}$, and [U(cat)$_4$]$^{4-}$ were carried out using Saunders' stochastic search algorithm as implemented in MM3 [17]. In each cycle of this algorithm, each atom is randomly displaced by up to a maximum distance of 2.0 Å, the resulting structure is energy minimized, and, if the optimized structure is unique, it is stored. Each conformer search was stopped after 10,000 cycles, after which no new conformers were being generated. Energy minimizations were done with the block diagonal Newton–Raphson method followed by the full-matrix Newton–Raphson method using a convergence criterion of RMS force of 0.0001 kcal mol^{-1} Å^{-1}. The absence of negative eigenvalues in the Hessian matrix was used to confirm that the calculated geometries were minima on the MM3 potential surface.

Given the random nature of the conformational analyses, it is possible that some minima might be overlooked. To exclude this possibility, we systematically built all possible SAP and DOD stereoisomers using the graphical user interface, Molden [18], and performed MM3 optimizations from these starting coordinates. During the building process, catecholate ligands were placed onto the edges of SAP and DOD polyhedra obtained from [U(OH$_2$)$_8$]$^{4+}$ calculations such that the U–O–C–C dihedral angles were either 0 or 180°.

An extended MM3 parameter file and Cartesian coordinates for the optimized structures are available as supplemental data.

3. Results and discussion

3.1. Idealized polyhedra

Three ideal polyhedra for 8-coordinate complexes – SAP, DOD, and BTP – are illustrated in Fig. 1. The SAP structure has D_{4d} symmetry. All eight vertices are identical. The 16 edges divide equally between two types, *s* along the square faces and *l* along the lateral edges [3]. The DOD structure has D_{2d} symmetry. It is composed of a pair of interpenetrating tetrahedra, one elongated tetrahedron giving rise to four *A* vertices and one flattened tetrahedron giving rise to four *B* vertices. The 18 edges are distributed among four classes: *a* (2 edges), *b* (4 edges), *m* (4 edges) and *g* (8 edges) [3]. The BTP has

[1] MM3 (96). The program may be obtained from Tripos Associates, 1699 S. Hanley Road, St. Louis, MO 63144 for commercial users, and it may be obtained from the Quantum Chemistry Program Exchange, Mr. Richard Counts, QCPE, Indiana University, Bloomington, IN 47405, for noncommercial users.

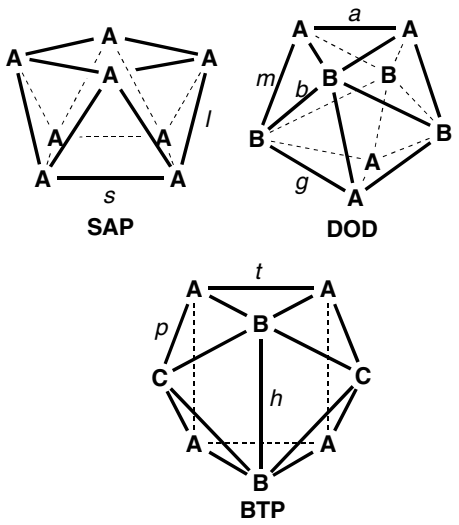

Fig. 1. Ideal polyhedra for coordination number eight. The square antiprism (SAP) and dodecahedron (DOD) are given with edge and vertex notations following the Hoard and Silverton convention [3]. The bicapped trigonal prism (BTP) is given with edge notation following the Porai-Koshits and Aslanov convention [7].

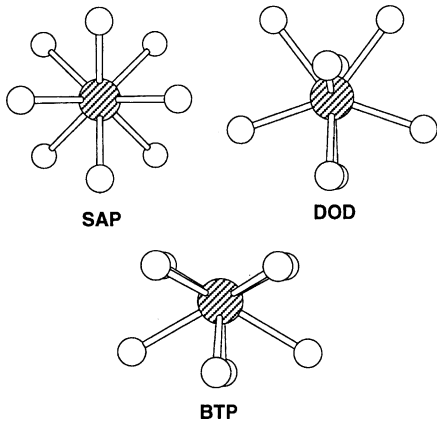

Fig. 2. Geometries for $[U(OH_2)_8]^{4+}$ obtained with the MM3 model. U–O distances, the edge lengths, and the angles formed between the U–O vectors and a symmetry axis: SAP form, U–O_A = 2.36 Å, s = 2.82 Å, l = 2.95 Å, θ = 57.7° (S_8 axis); DOD form, U–O_A = 2.37 Å, U–O_B = 2.36 Å, m = 2.77, g = 2.88 Å, a = 2.85 Å, b = 3.50 Å, Å, θ_A = 37.0°, θ_B = 71.5° (S_4 axis); BTP form, U–O_A = U–O_B = 2.36 Å, U–O_C = 2.39 Å, t = 2.87 Å, p = 2.71 Å, h = 3.37, θ_A = 69.4°, θ_B = 45.5°, θ_C = 60.0° (C_2 axis).

C_{2v} symmetry. It is composed of a trigonal prism that is capped on two of the rectangular faces giving rise to four A vertices, two B vertices and two C vertices. The 17 edges are distributed among three classes: t (6 edges), p (8 edges), and h (3 edges) [7,8].

3.2. Octaaquo complex – $[U(OH_2)_8]^{4+}$

Oxygen atoms were used to represent the aquo ligands in the U(IV) complexes. This approach, which has been used successfully in prior studies [13a,19], maintains the inner coordination sphere, but eliminates the potential for multiple minima associated with different hydrogen atom orientations. The van der Waals interactions between these charge–neutral oxygen atoms, which are equivalent to those used in the MM3 force field to model alcohol and ether oxygen atoms in organic compounds, provides a reasonable approximation of the forces present within the inner coordination sphere.

The random conformational search of the $[U(OH_2)_8]^{4+}$ complex yields a single minimum energy structure. Of the three ideal polyhedra shown in Fig. 1, only the SAP form is stable. The DOD form is located as a transition state when the initial coordinates are given in strict D_{2d} symmetry. The BTP structure is not a stationary point on the MM3 potential surface, but can be obtained by imposing D_{3h} symmetry on the trigonal prism portion of the structure during optimization. On removal of the symmetry constraints, the BTP structure optimizes to the SAP form. The relative energies for these three structures, shown in Fig. 2, are 0 kcal/mol (SAP), 0.30 kcal/mol (DOD), and 2.83 kcal/mol (BTP).

The MM3 results are consistent with those obtained from prior repulsion energy calculations for eight points on a sphere. In the earliest calculations, which focused on the SAP and DOD polyhedra, the geometries were optimized within the limitations of symmetry constraints [3,4a]. Although absolute energy differences were not reported, these calculations suggested that the SAP and DOD forms were very close in energy. Subsequently, repulsion energy calculations were used to generate a potential surface revealing that the DOD form is actually a transition state between two possible SAP forms [4e]. The BTP form has not been discussed in the repulsion energy calculation studies. It has been noted, however, that the BTP form is unlikely to represent a sterically stable polyhedron and that it should distort toward the SAP geometry if symmetry restrictions are removed [9].

No structures have been reported that contain an octaaquo U(IV) complex. However, there are 10 crystal structures that contain octaaquo ions for the smaller lanthanide metal ions, from Gd(III) to Lu(III) [20–28]. The Shannon ionic radii (CN = 8) for these metal ions range from 1.05 to 0.98 Å, bracketing the corresponding value of 1.00 Å for U(IV) [29]. A plot of the average M–O distance versus Shannon ionic radius (CN = 8) was linear (M–O distance = 1.463 + 0.897 × ionic radius, r = 0.979). Interpolation gives the U(IV)–O_{aquo} distance of 2.36 Å that served as a basis for assigning the MM3 stretching parameters.

Half of the lanthanide complexes exhibit the SAP geometry and the other half exhibit the DOD geometry. The higher energy BTP geometry is not observed. Comparison of the geometric parameters calculated for U(IV) with those observed in the lanthanide complexes,

Table 1
Comparison of calculated $[U(OH_2)_8]^{4+}$ geometries with those observed in octaaquo lanthanide complexes[a]

Metal	Type	SIR	$M–O_A$	$M–O_B$	θ_A	θ_B
Tb(III) [20]	SAP	1.040	2.39 ± 0.03		57 ± 3	
Dy(III) [21]	SAP	1.027	2.39 ± 0.02		57 ± 4	
Yb(III) [22]	SAP	0.985	2.32 ± 0.04		58 ± 8	
Lu(III) [23]	SAP	0.977	2.34 ± 0.03		57 ± 3	
Lu(III) [24]	SAP	0.977	2.33 ± 0.03		57 ± 7	
U(IV) this work	SAP	1.000	2.36		57.7	
Gd(III) [25]	DOD	1.053	2.45 ± 0.01	2.35 ± 0.01	34 ± 1	76 ± 1
Gd(III) [26]	DOD	1.053	2.43 ± 0.03	2.39 ± 0.03	37 ± 5	72 ± 4
Er(III) [27]	DOD	1.004	2.39 ± 0.04	2.34 ± 0.03	37 ± 4	72 ± 4
Yb(III) [28]	DOD	0.985	2.37 ± 0.04	2.32 ± 0.02	37 ± 5	72 ± 4
Lu(III) [26]	DOD	0.977	2.38 ± 0.04	2.32 ± 0.02	36 ± 5	72 ± 4
U(IV) this work	DOD	1.000	2.37	2.36	37.0	71.5

Table 1, establishes that the simple model used here well reproduces the shapes of these polyhedra. Although the model used in this study, as well as repulsion energy models [4e], do not predict that the DOD polyhedron to be a local minimum, they do predict a small difference in energy between the SAP and DOD forms. This small energy difference could allow other factors such as intra- and inter-molecular hydrogen bonding to stabilize the DOD form in the crystal lattice. In addition, although the lanthanide-aquo ligand interaction is more ionic than covalent in character, directional bonding at the metal center, not included in the MM3 model, could also play a role in stabilizing the DOD stereochemistry [10].

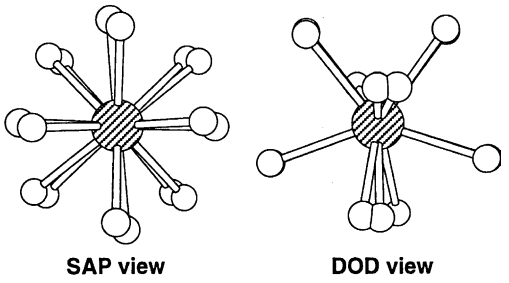

Fig. 3. Superposition of the SAP and DOD stereochemistries from Fig. 2 illustrates the similarity in these two geometries. In the SAP view, the SAP structure is oriented with the square planes parallel to the plane of the page. In the DOD view, the DOD structure is oriented with four oxygen atoms in the plane of the page and four oxygen atoms in the vertical plane perpendicular to the page.

3.3. General comments on catecholate complexes

Examination of the Cambridge Structural Database [30] reveals that catecholate ligand exhibits an average bite of 2.61 ± 0.06 Å when coordinated to a metal ion in tris- and tetrakis–catecholate complexes. Comparison of this value with the edge lengths calculated for the three $[U(OH_2)_8]^{4+}$ polyhedra (with U–O distances ranging from 2.36 to 2.39 Å) shows that the catecholate bite is too small to span even the shortest edges in these polyhedra, which are 2.82 Å in the SAP, 2.77 Å in the DOD, and 2.71 Å in the BTP. It follows that the structures calculated for catecholate complexes will contain polyhedra that are distorted, to some extent, from the polyhedra shown in Fig. 2.

This raises the problem of how to identify which stereochemistry is present. The three $[U(OH_2)_8]^{4+}$ polyhedra shown in Fig. 2 are actually not that different in shape. For example, when the idealized SAP and DOD forms are superimposed in Fig. 3, it is clear that even a perfect SAP geometry can appear to be a distorted DOD from a certain perspective, and vice versa. Even worse, if a molecule has an inner sphere geometry intermediate between these two forms, it is exceedingly difficult, to classify the polyhedron accurately by visual inspection alone. In the superposition shown in Fig. 3, the average distance between corresponding pairs of oxygen atoms is 0.38 Å and the movement required to convert the SAP to the DOD form is $\leqslant 10°$ for any U–O vector. Superposition of the SAP and BTP forms or DOD and BTP forms yield similar results.

One approach for distinguishing between the SAP, BTP, and DOD forms involves calculating the dihedral angles between the normal vectors of selected adjacent triangular faces [7,8,31]. Application of this method is not straightforward. One must correctly identify all edges in the polyhedron. As noted above, the three polyhedra in question actually have different numbers of edges and which pairs of ligands constitute an edge must be determined. In addition, before the assignment can be made, it is necessary to correctly select which edges are shape-determining for the structure. There may be more than one way to choose them, resulting in the possibility of ambiguous assignments [9].

An alternate approach involves attempting to superimpose the inner sphere atoms of an observed polyhedron onto to those of an ideal polyhedron [32]. Once the optimal superposition has been achieved by least squares fitting, the deviation, taken as the root-mean-squared distance (rmsd) between corresponding atom pairs, provides a single criterion that measures how well the observed polyhedron conforms to the ideal polyhedron.

During this process, all possible pairings of atoms from the two sets are considered and the best superposition is retained. When there are several possible ideal polyhedra, the one that yields the best superposition with the observed structure is the polyhedron that most closely resembles the observed structure.

The superposition method was used to assign the polyhedra of the calculated catecholate complexes by comparing their inner sphere geometry to the ideal polyhedra calculated for $[U(OH_2)_8]^{4+}$ (Fig. 2). Prior to performing these superpositions, all U–O distances were normalized to 1.0 Å [9]. Thus, this method of determining similarity to an ideal polyhedron is based on the degree of correspondence between the U–O vectors in the distorted polyhedron and those in the ideal polyhedron. This is equivalent to analyzing only the O–U–O angles while excluding variation in U–O distances.

Conformational analyses of $[U(cat)(OH_2)_6]^{2+}$, $[U(cat)_2(OH_2)_4]$, $[U(cat)_3(OH_2)_2]^{2-}$, and $[U(cat)_4]^{4-}$ identified 20 stable structures. The stereochemistries of these structures were assigned by first identifying which ideal polyhedron gave the best fit to the inner sphere and then noting which edges were spanned by the catecholate ligands. The inner sphere geometry in the majority of these structures most closely resembles the SAP polyhedron. The DOD polyhedron gave the best fit in

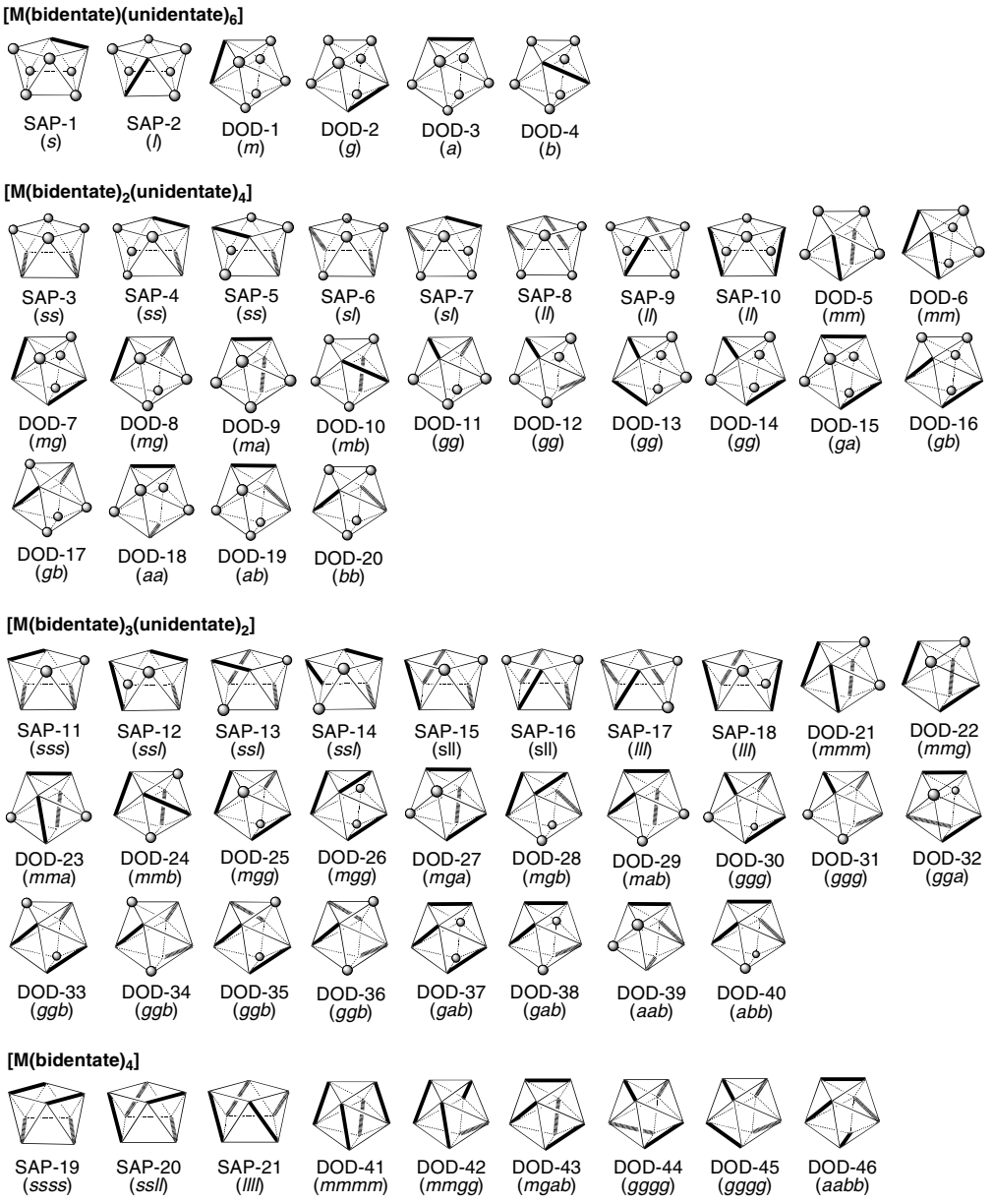

Fig. 4. Views of the 67 distinct stereochemistries, excluding optical isomers, that can be formed by placing identical unidentate ligands and identical symmetric bidentate ligands onto SAP and DOD polyhedra. The edges spanned by the bidentate ligands, given beneath each ID, are indicated by bold lines. The central M is omitted for clarity.

only a couple of instances, while the BTP polyhedron never gave the best fit. This result confirms that the BTP does not represent a sterically favorable arrangement of ligands about the metal ion.

Excluding optical isomers, there are 67 possible stereochemistries for SAP and DOD polyhedra [11]. These are illustrated in Fig. 4. Only 20 of these stereochemistries were located by the conformational analyses. To exclude the possibility that some stereochemistries might have been missed, we systematically constructed all possible SAP and DOD stereoisomers on a graphical user interface and used these structures as starting points for MM3 optimizations. This systematic analysis gave identical results to those obtained from the random conformational searches. No additional structures were obtained for any stoichiometry. In all cases, the alternative starting configurations either collapsed to those already located in the random searches or yielded structures that were transition states.

The results of the stereochemical analyses of the catecholate complexes are summarized in Table 2. Three-dimensional views of each structure are presented in Figs. 5–8. Further details for each stoichiometry are provided below.

3.4. The mono catecholate stoichiometry, $[U(cat)(OH_2)_6]^{2+}$

This stoichiometry has two possible SAP forms and four possible DOD forms (Fig. 4). The MM3 analysis yields only the two SAP stereochemistries shown in Fig. 5. The SAP-1 stereochemistry, in which the catecholate ligand spans the shorter *s* edge of a square face, is 0.52 kcal/mol more stable than the SAP-2 stereochemistry, in which the catecholate ligand spans the longer *l* edge of a triangular face. This result is consistent with the concept that a more stable complex is obtained when the bite of a bidentate ligand most closely matches the edge length of the polyhedron. None of the DOD forms are minima on the MM3 potential surface. However, the analysis of the $[U(OH_2)_8]^{4+}$ case suggests that distortion to DOD forms could be accomplished without substantial energetic penalty.

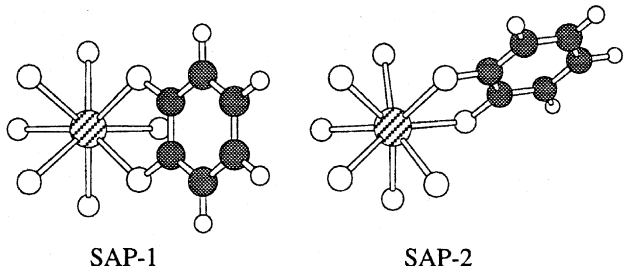

Fig. 5. MM3 geometries for the two stable stereochemistries of $[U(cat)(OH_2)_6]^{2+}$.

No crystal structures have been reported [30] for any complex with the stoichiometry $[M(cat)(OH_2)_6]$. In addition, prior stereochemical analyses for any [M(bidentate)(unidentate)$_6$] complex have not been reported.

Table 2
Stable stereochemistries for $[U(cat)_n(OH_2)_{8-2n}]^{4-2n}$ complexes, $n = 1$–4

Complex	ID[a]	Edges	Sym	Rel. E[b]	Δ(SAP)[c]	Δ(DOD)[c]	Δ(BTP)[c]
$[U(cat)(OH_2)_6]^{2+}$	SAP-1	*s*	C_s	0.00	0.045	0.128	0.112
	SAP-2	*l*	C_2	0.52	0.047	0.139	0.136
$[U(cat)_2(OH_2)_4]$	SAP-3	*ss*	C_{2v}	0.00	0.069	0.117	0.092
	SAP-4	*ss*	C_2	0.03	0.063	0.108	0.131
	SAP-5	*ss*	C_2	0.18	0.051	0.112	0.128
	SAP-6	*sl*	C_1	0.68	0.063	0.107	0.117
	SAP-7	*sl*	C_1	0.76	0.075	0.101	0.111
	SAP-8	*ll*	C_2	1.15	0.082	0.113	0.139
	SAP-9	*ll*	D_2	1.19	0.067	0.131	0.141
	SAP-10	*ll*	C_s	1.50	0.053	0.135	0.117
$[U(cat)_3(OH_2)_2]^{2-}$	SAP-11	*sss*	C_1	0.00	0.073	0.095	0.109
	SAP-12	*ssl*	C_2	0.67	0.058	0.139	0.135
	DOD-22	*mmg*	C_1	0.68	0.094	0.074	0.127
	SAP-13	*ssl*	C_2	1.16	0.058	0.136	0.138
	SAP-15	*sll*	C_1	1.43	0.083	0.111	0.124
	SAP-17	*lll*	C_1	1.79	0.096	0.114	0.145
	SAP-16	*sll*	C_s	1.98	0.065	0.126	0.097
	SAP-18	*lll*	C_2	2.34	0.066	0.107	0.123
$[U(cat)_4]^{4-}$	DOD-41	*mmmm*	D_2	0.00	0.089	0.069	0.122
	SAP-21	*llll*	D_4	2.70	0.101	0.125	0.158

[a] Labels correspond to the stereochemistries depicted in Fig. 4.
[b] Relative energy in kcal/mol.
[c] Δ = rmsd, in Å, for the superposition of the inner sphere structure onto the inner sphere structures of the SAP, DOD, and BTP forms of $[U(OH_2)_8]^{4+}$ shown in Fig. 2. Prior to performing the superpositions, all U–O distances are first normalized to 1.0 Å.

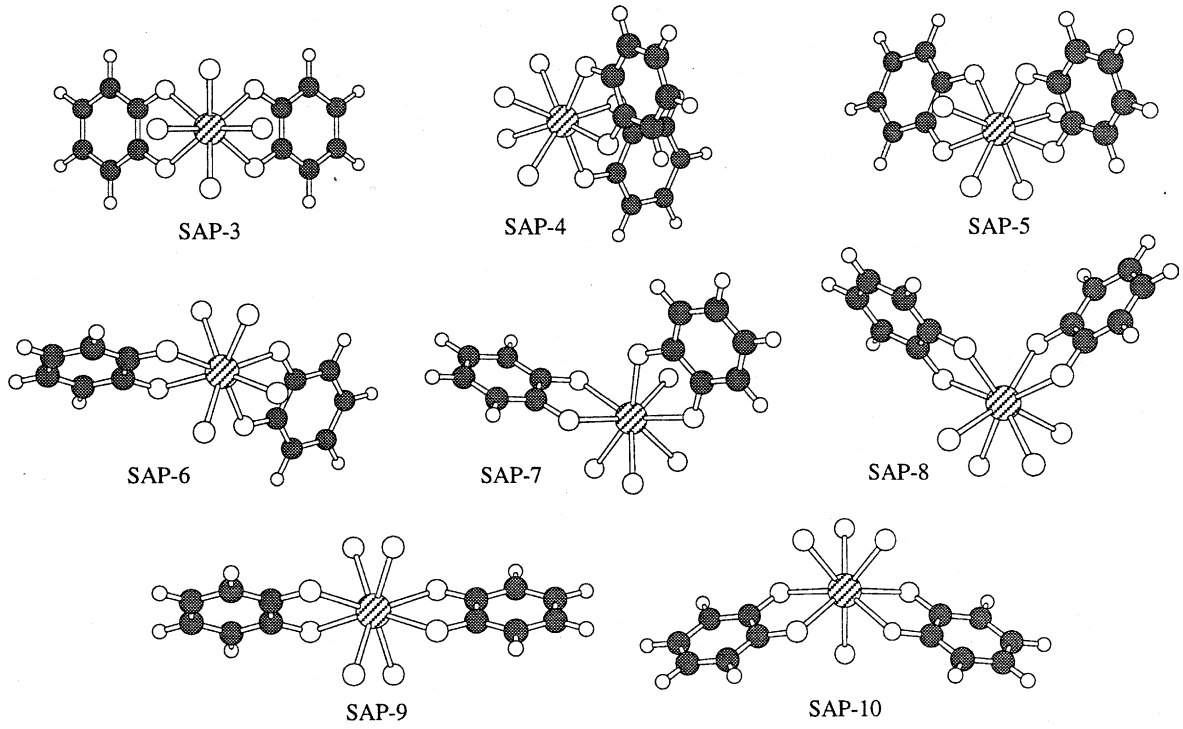

Fig. 6. MM3 geometries for the eight stable stereochemistries of $[U(cat)_2(OH_2)_4]$.

3.5. The bis catecholate stoichiometry, $[U(cat)_2(OH_2)_4]$

This stoichiometry has eight possible SAP forms and 16 possible DOD forms (Fig. 4). As with the $[U(OH_2)_8]^{4+}$ and $[U(cat)(OH_2)_6]^{2+}$ complexes, the MM3 analysis yields local minima that have polyhedra that are most similar to the SAP form. All eight possible SAP stereochemistries, shown in Fig. 6, are obtained. The relative energies span a range of 1.5 kcal/mol. The relative stabilities, which follow the order *ss* < *sl* < *ll*, again confirm the energetic preference for the catecholate ligand to occupy the shorter *s* edges of the SAP polyhedron.

No crystal structures have been reported [30] for any complex with the stoichiometry $[M(cat)_2(OH_2)_4]$. However, the results can be compared with prior stereochemical analyses of the $[M(bidentate)_2(unidentate)_4]$ stoichiometry [4b,4e]. Repulsion energy calculations were used to examine seven possible stereoisomers corresponding to SAP-3, SAP-4, SAP-5, SAP-8, SAP-9, SAP-10, and DOD-9. Plots of the repulsion energy for these forms as a function of the bite/M–L distance shows that at a value of 1.12, corresponding to the U(IV)-catecholate complexes, the stability of these forms is SAP-3 ~ SAP-4 < SAP-5 < DOD-9 ~ SAP-9 < SAP-10 < SAP-8, very similar to the ordering obtained here (see Table 2). Both models predict the forms with three *ss* edges are lower in energy than the forms with three *ll* edges. The DOD-9 form is a transition state on MM3 potential surface. When the geometry optimization is started from the DOD-9 stereochemistry, an SAP-7 form is obtained. The DOD-9 transition state is 0.52 kcal/mol higher in energy than the SAP-7 form.

3.6. The tris catecholate stoichiometry, $[U(cat)_3(OH_2)_2]^{2-}$

This stoichiometry has eight possible SAP forms and 20 possible DOD forms (Fig. 4). MM3 analysis yields a total of eight local minima (7 SAP and 1 DOD), shown in Fig. 7. Although these tris-catecholate structures are on average showing higher degrees of distortion from the ideal polyhedra than the structures presented above, the superposition method identifies seven of the structures to be closer to the SAP form and one of the structures to be closer to the DOD form. This is the first case where the inner sphere geometry, which in this case can be viewed as either a distorted DOD-22 or a distorted SAP-14, more closely resembles the DOD form (see Δ values in Table 2). The relative energies span a range of 2.34 kcal/mol. The relative stability order with respect to chelated edge lengths is *sss* < *ssl* ~ *mmg* (*ssl*) < *ssl* < *sll* < *lll* < *sll* < *lll*, again showing a clear preference for the chelate rings to span the shorter edge lengths.

No structures have been reported [30] for any complex with the stoichiometry $[M(cat)_3(OH_2)_2]$. In addition, prior stereochemical analyses of any $[M(bidentate)_3(unidentate)_2]$ complex have not been reported.

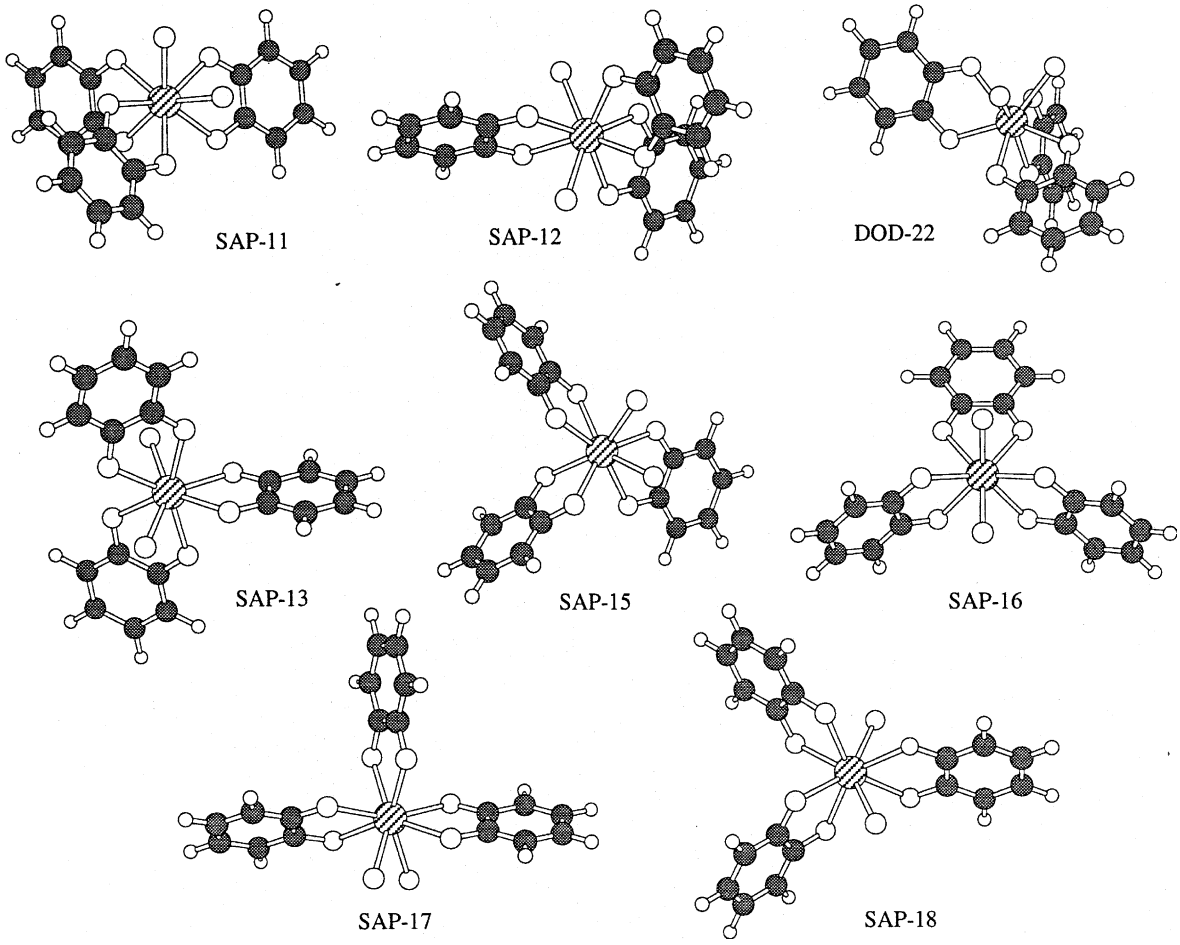

Fig. 7. MM3 geometries for the eight stable stereochemistries of $[U(cat)_3(OH_2)_2]^{2-}$.

3.7. The tetrakis catecholate stoichiometry, $[U(cat)_4]^{4-}$

This stoichiometry has three possible SAP forms and six possible DOD forms (Fig. 4). MM3 analysis yields only two local minima, shown in Fig. 8. The most stable form is a distorted DOD with D_2 symmetry in which the ligands span *m* edges. The nature of the distortion is illustrated in Fig. 9. Each of the catecholates is slightly twisted around an axis passing through the center of the catecholate ligand and the metal ion. This distortion is quantified by the dihedral angle, Φ, defined by the $m-a-m$ edges (see Fig. 1). An ideal D_{2d} DOD would have a value of $\Phi = 0°$. The calculated D_2 form has $\Phi = 18.7°$. As shown in Fig. 9, the ideal D_{2d} form is a transition state on the MM3 potential surface lying between two D_2 enantiomers. The potential surface is very flat in this region, the D_{2d} form is only 0.03 kcal/mol above the two D_2 minima.

The other stable structure is 2.69 kcal/mol higher in energy than the D_2 DOD form. It is a distorted SAP geometry with D_4 symmetry in which the ligands span *l* edges. This form can be viewed as a four-bladed propeller analogous to the three-bladed propeller that occurs in [M(bidentate)$_3$] complexes [4e].

The MM3 analysis predicts that DOD-41 should be the predominant stereochemistry for the $[U(cat)_4]^{4-}$ complex. This prediction is confirmed by crystal structures for a series of tetrakis catecholate complexes with Hf(IV), Ce(IV), Gd(III), U(IV), and Th(IV), all of which exhibit the DOD-41 form [16,33]. The chelate bite to M–O bond length ratio is similar in these structures, ranging from 1.10 to 1.17, with a value of 1.12 for U(IV). The experimental U–O_A and U–O_B distances are 2.39 and 2.36 Å. For comparison, the MM3 model yields values of 2.38 and 2.37 Å, respectively, qualitatively reproducing the elongation of the U–O_A distances. The experimental bite, 2.65 Å, is well reproduced by the model, 2.66 Å. The X-ray structure also exhibits the twist distortion predicted by the model. However, with a value of $\Phi = 5.5°$, it lies closer to the ideal D_{2d} polyhedron than to the calculated D_2 structure. In this case, there are four $[Na(OH_2)_4]^+$ counter-cations about each $[U(cat)_4]^{4-}$ complex. Each sodium ion sits above a *g* edge and is coordinated to an oxygen atom from each of

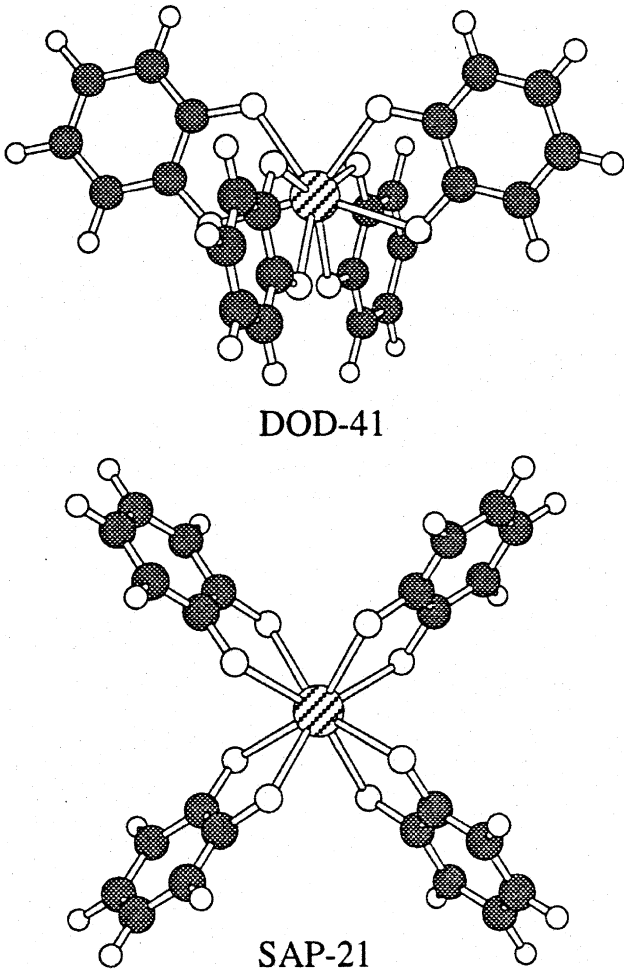

Fig. 8. MM3 geometries for the two stable stereochemistries of $[U(cat)_4]^{4-}$.

the two catecholates sharing that edge (see Fig. 10). Given the flat nature of the potential surface, the variation in Φ could easily result from these environmental effects.

The results reported here are also completely consistent with prior analyses of the stereochemistry for [M(bidentate)$_4$] complexes. Repulsion energy calculations have been used to generate potential surfaces for the [M(bidentate)$_4$] complex at different bite/M–L ratios

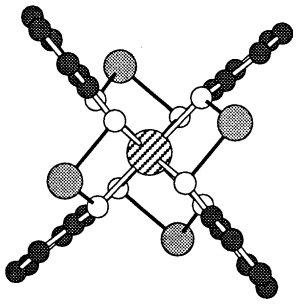

Fig. 10. A view of the $[U(cat)_4]^{4-}$ complex in the crystal structure [16] showing the location of the four sodium cations.

[4c,4d,4e]. When the ratio is 1.0, the D_{2d} DOD (DOD-41, *mmmm*) is the only stable form. As the ratio increases to 1.1, two D_2 DOD minima appear on either side of a D_{2d} DOD saddle point (see Fig. 9). On further increase of the ratio to 1.2, the D_2 DOD forms have become distorted D_2 SAP forms (SAP-19, *ssss*) and additional minima, corresponding to the optical isomers of D_4 SAP (SAP-21, *llll*), have appeared. Our analysis of the $[U(cat)_4]^{4-}$ complex, with a bite/M–L ratio of 1.12, yields results that are intermediate between the reported results for ratios of 1.1 and 1.2.

4. Summary and conclusions

An extended MM3 model was used to identify all low energy configurations for U(IV) complexes with catecholate and aquo ligands. Both stochastic and systematic conformational analyses of $[U(cat)_n(OH_2)_{8-2n}]^{4-2n}$ complexes, $n = 1$–4, establish that 20 of the 67 possible stereochemistries are minima on the MM3 potential surface. In the majority of these structures, the inner coordination sphere most resembles an SAP polyhedron. With one to three catecholates, the most stable structures are those in which the catecholates span the shorter *s* edge of the square face. With four catecholates, the most stable structure is a DOD form in which the catecholates span the *m* edges. Where comparisons are possible, we have shown that the extended MM3 model gives structures and relative energies that are consistent with available

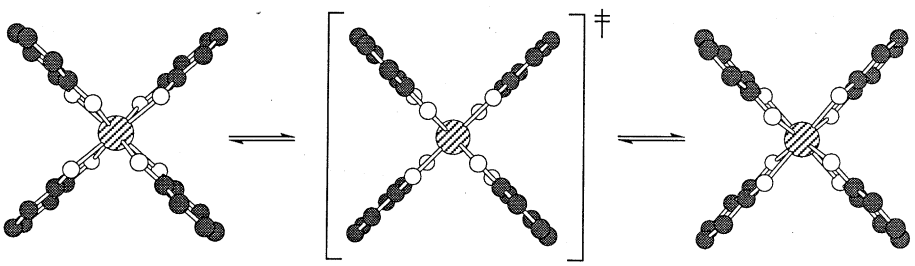

Fig. 9. Two D_2 DOD structures, the lowest energy forms for $[U(cat)_4]^{4-}$, interconvert via a D_{2d} transition state that is only 0.03 kcal/mol higher in energy.

experimental data. In addition, the MM3 model yields results that are consistent with prior repulsion energy calculations. This study has shown that conformational analysis with a simple force field model is an efficient way to identify the optimal arrangements for a set of ligands about a metal ion, thereby providing a basis for rational design of effective host structures. Work is now in progress to use the results from this study as a design basis for U(IV) hosts composed of catecholate binding sites.

5. Supplementary data

Cartesian coordinates for each structure and the MM3 parameter files are available.

Acknowledgements

This research was supported by Grants No. 73759 and 82773 of the Environmental Management Science Program of the Office of Science, US Department of Energy (DOE). The research was performed at the Pacific Northwest National Laboratory (PNNL), operated by Battelle for the DOE under contract DE-AC06-76RLO 1830.

References

[1] (a) B.P. Hay, T.K. Firman, Inorg. Chem. 41 (2002) 5502;
(b) HostDesigner is available at no cost from the website http://hostdesigner.emsl.pnl.gov.
[2] D.L. Kepert, Prog. Inorg. Chem. 23 (1977) 1.
[3] J.L. Hoard, J.V. Silverton, Inorg. Chem. 2 (1963) 235.
[4] (a) D.L. Kepert, J. Chem. Soc. (1965) 4737;
(b) D.G. Blight, D.L. Kepert, Theor. Chim. Acta 11 (1968) 51;
(c) D.G. Blight, D.L. Kepert, Inorg. Chem. 11 (1972) 1556;
(d) D.L. Kepert, Prog. Inorg. Chem. 24 (1978) 179;
(e) D.L. Kepert, in: G. Wilkinson, R.D. Gillard, J.A. McCleverty (Eds.), Comprehensive Coordination Chemistry, vol. 1, Pergamon, Oxford, 1987, pp. 83–95.
[5] S.J. Lippard, Prog. Inorg. Chem. 8 (1967) 109.
[6] E.L. Muetterties, C.M. Wright, Q. Rev. Chem. Soc. 21 (1967) 109.
[7] M.A. Porai-Koshits, L.A. Aslanov, Zh. Strukt. Khim. 13 (1972) 266.
[8] M.A. Porai-Koshits, L.A. Aslanov, J. Struct. Chem. (Engl Transl.) 13 (1972) 244.
[9] M.G.B. Drew, Coord. Chem. Rev. 24 (1977) 179.
[10] J.K. Burdett, R. Hoffman, R.C. Fay, Inorg. Chem. 17 (1978) 2553.
[11] C.W. Haigh, Polyhedron 15 (1996) 605.
[12] (a) B.P. Hay, Inorg. Chem. 30 (1991) 2876;
(b) B.P. Hay, Coord. Chem. Rev. 126 (1993) 177.
[13] (a) B.P. Hay, L. Yang, N.L. Allinger, J.-H. Lii, J. Mol. Struct. (THEOCHEM) 428 (1998) 203;
(b) B.P. Hay, O. Clement, G. Sandrone, D.A. Dixon, Inorg. Chem. 37 (1998) 5887.
[14] (a) B.P. Hay, D.A. Dixon, R. Vargas, J. Garza, K.N. Raymond, Inorg. Chem. 40 (2001) 3922;
(b) M.B. Bluhm, B.P. Hay, S.K. Sanggoo, E.A. Dertz, K.N. Raymond, Inorg. Chem. 41 (2002) 5475.
[15] R.M. Badger, J. Chem. Phys. 3 (1935) 710.
[16] S.R. Sofen, K. Abu-Dari, D.P. Freyberg, K.N. Raymond, J. Am. Chem. Soc. 100 (1978) 7882.
[17] M. Saunders, J. Am. Chem. Soc. 109 (1987) 3150.
[18] G. Schaftenaar, J.H. Noordik, J. Comput.-Aided Mol. Des. 14 (2000) 123.
[19] B.P. Hay, J.R. Rustad, J. Am. Chem. Soc. 116 (1994) 6316.
[20] C.J. Kepert, B.W. Skelton, A.H. White, Aust. J. Chem. 47 (1994) 391.
[21] R.D. Rogers, Inorg. Chim. Acta 133 (1987) 347.
[22] F.J. Waller, A.G.M. Barrett, D.C. Braddock, D. Ramprasad, R.M. McKinnell, A.J.P. White, D.J. Williams, R. Ducray, J. Org. Chem. 64 (1999) 2910.
[23] R.D. Rogers, E.J. Voss, Inorg. Chim. Acta 133 (1987) 181.
[24] R.D. Rogers, J. Coord. Chem. 16 (1988) 415.
[25] M. Bukowska-Strzyzewska, A. Tosik, Acta Cryst. B 38 (1982) 265.
[26] R.D. Rogers, L.K. Kurihara, Inorg. Chim. Acta 130 (1987) 131.
[27] R.D. Rogers, A.N. Rollins, J. Chem. Cryst. 24 (1994) 531.
[28] H. Hassaballa, J.W. Steed, P.C. Junk, M.R.J. Elsegood, Inorg.Chem. 37 (1998) 4666.
[29] R.D. Shannon, Acta Cryst. A 32 (1979) 751.
[30] Cambridge Structural Database System: F.H. Allen, S.A. Bellard, B.A. Brice, A. Cartwright, A. Doubleday, H. Higgs, T. Hummelink, B.G. Hummelink-Peters, O. Kennard, W.D.S. Motherwell, J.R. Rodgers, D.G. Watson, Acta Cryst. B 35 (1979) 2331.
[31] E.L. Mutterties, L.J. Guggenberger, J. Am. Chem. Soc. 96 (1974) 1748.
[32] W.A. Dollase, Acta Cryst. A 30 (1974) 513.
[33] (a) S.R. Sofen, S.R. Cooper, K.N. Raymond, Inorg. Chem. 18 (1979) 1611;
(b) G.E. Freeman, K.N. Raymond, Inorg. Chem. 24 (1985) 1410.

Available online at www.sciencedirect.com
SCIENCE DIRECT®
Polyhedron 23 (2004) 155–160
POLYHEDRON
www.elsevier.com/locate/poly

Pyridyl benzimidazole, benzoxazole, and benzothiazole platinum complexes

Xiao-Feng He [a], Christopher M. Vogels [a], Andreas Decken [b], Stephen A. Westcott [a,*]

[a] Department of Chemistry, Mount Allison University, Sackville, Canada NB E4L 1G8
[b] Department of Chemistry, University of New Brunswick, Fredericton, Canada NB E3B 5A3

Received 29 June 2003; accepted 24 September 2003

Abstract

Oxidative cyclization of 1,2-phenylenediamine, 2-aminophenol, and 2-aminothiophenol with pyridine carboxaldehydes affords the corresponding benzimidazole, benzoxazole, and benzothiazole pyridyl ligands. Addition of these compounds (L_P) to $[PtCl_2(coe)]_2$ (coe = *cis*-cyclooctene) or K_2PtCl_4 gives didentate *cis*-$PtCl_2(L_P)$ or monodentate *cis*-$PtCl_2(L_P)_2$ in moderate to high yields. Crystals of *cis*-dichloro(2-pyrid-2-ylbenzothiazole)platinum(II) (**1c**) as the CH_2Cl_2 solvate were triclinic, space group $P\bar{1}$, $a = 7.8715(6)$ Å, $b = 9.9873(7)$ Å, $c = 10.5883(8)$ Å, $\alpha = 104.149(1)°$, $\beta = 103.754(1)°$, $\gamma = 96.864(1)°$, $Z = 2$. *cis*-dichlorodi(2-pyrid-3-ylbenzoxazole)platinum(II) (**2b**) crystallized with a molecule of THF and H_2O and were monoclinic, space group $C2/c$, $a = 18.698(10)$ Å, $b = 16.325(10)$ Å, $c = 8.853(6)$ Å, $\beta = 90.149(17)°$, $Z = 4$.
© 2003 Elsevier Ltd. All rights reserved.

Keywords: Platinum; Imine; Benzimidazole; Benzoxazole; Benzothiazole; Pyridine

1. Introduction

Cisplatin, *cis*-$[PtCl_2(NH_3)_2]$, is one of the most effective chemotherapeutic agents currently used for the treatment of ovarian, bladder, and testicular cancer [1–3]. The drug has to be administered intravenously, however, and has dose-limiting side effects such as severe renal toxicity, neurotoxicity, and emesis, arising, in part, from the low solubility of cisplatin in water. These problems, along with the observation that cancer cells treated with cisplatin acquire resistance to the drug, have provided an impetus for research focused on the development of a more effective platinum drug that can be administered orally and with reduced side effects. Cisplatin acts by making intra- and interstrand cross-links with DNA, resulting in a halt of replication and leading to programmed cell death. Structural analogues of cisplatin, however, react with DNA the same way as the parent drug and therefore cause similar biological effects [1]. Indeed, to be considered for clinical evaluation, a new platinum drug should have activity different from that of cisplatin and eliminate multi-factorial drug resistance. Therefore, it is unlikely that future platinum drug candidates will adhere to the classical structure-activity relationships for cisplatin analogues. Toward this objective, we have begun to prepare platinum complexes containing biologically active carrier groups [4,5]. In this study we report the synthesis and characterization of platinum complexes containing pyridyl benzimidazole derivatives.

2. Experimental

2.1. General

Reagents and solvents were purchased from Aldrich Chemicals and used as received. Platinum salts were obtained from Precious Metals Online Ltd. The melting points were determined using a Mel-Temp apparatus and they are uncorrected. The infrared spectra were obtained using a Mattson Genesis FT-IR spectrometer in nujol and are reported in cm^{-1}. NMR spectra were

* Corresponding author. Tel.: +506-364-2372; fax: +506-364-2313.
E-mail address: swestcott@mta.ca (S.A. Westcott).

0277-5387/$ - see front matter © 2003 Elsevier Ltd. All rights reserved.
doi:10.1016/j.poly.2003.09.020

recorded with a Jeol JNM-GSX270 FT NMR (^{1}H 270 MHz) spectrometer. Chemical shifts (δ) are reported in ppm relative to internal TMS and coupling constants (J) in Hz. Multiplicities are reported as singlet (s), doublet (d), triplet (t), multiplet (m), broad (br), and overlapping (ov). Elemental analyses were performed by Chemisar Laboratories Inc. (Guelph, ON) and Desert Analytics (Tucson, AZ). $[PtCl_2(coe)]_2$ was prepared by an established method [6,7].

2.2. Syntheses

2.2.1. Preparation of cis-dichloro(2-pyrid-2-ylbenzimidazole)platinum(II) (**1a**)

2-Pyrid-2-ylbenzimidazole (55 mg, 0.28 mmol) in 10 ml of CH_2Cl_2 was added dropwise to a stirred solution of $[PtCl_2(coe)]_2$ (105 mg, 0.14 mmol) in 10 ml of CH_2Cl_2. The reaction was allowed to proceed for 3 h, at which point a yellow precipitate formed and was collected by suction filtration. Yield: 59 mg, 46%. Mp 238 °C (decomposition). *Anal.* Calc. for $C_{12}H_9N_3Cl_2Pt$: C, 31.24; H, 1.97; N, 9.11. Found: C, 31.57; H, 1.82; N, 8.98%. ^{1}H NMR (dmso-d_6): δ 9.47 (d, $J = 5$ Hz, 1H), 8.78 (d, $J = 8$ Hz, 1H), 8.44 (m, 1H), 8.33 (m, 1H), 7.79 (d, $J = 8$ Hz, 2H), 7.52–7.40 (ov m, 2H). IR (nujol): 3165, 3110, 2922, 2856, 1614, 1462, 1377, 1308, 1265, 1236, 1151, 1063, 823, 750, 739, 654.

2.2.2. Preparation of cis-dichloro(2-pyrid-2-ylbenzoxazole)platinum(II) (**1b**)

2-Pyrid-2-ylbenzoxazole (55 mg, 0.28 mmol) in 10 ml of CH_2Cl_2 was added dropwise to a stirred solution of $[PtCl_2(coe)]_2$ (105 mg, 0.14 mmol) in 10 ml of CH_2Cl_2. Within 1 h a red precipitate had formed that was collected by suction filtration. Yield: 101 mg, 78%. Mp 210 °C (decomposition). *Anal.* Calc. for $C_{12}H_8N_2Cl_2OPt \cdot 0.5CH_2Cl_2$: C, 29.74; H, 1.80; N, 5.55. Found: C, 29.67; H, 1.80; N, 6.26%. ^{1}H NMR (dmso-d_6): δ 9.46 (d, $J = 5$ Hz, 1H), 8.69 (d, $J = 8$ Hz, 1H), 8.48 (t, $J = 8$ Hz, 1H), 8.36 (d, $J = 8$ Hz, 1H), 8.10 (d, $J = 8$ Hz, 1H), 7.97 (t, $J = 5$ Hz, 1H), 7.72–7.64 (ov m, 2H). IR (nujol): 2914, 2858, 1549, 1462, 1377, 1306, 1273, 1147, 972, 897, 816, 781, 746, 681, 609.

2.2.3. Preparation of cis-dichloro(2-pyrid-2-ylbenzothiazole)platinum(II) (**1c**)

2-Pyrid-2-ylbenzothiazole (30 mg, 0.14 mmol) in 10 ml of CH_2Cl_2 was added dropwise to a stirred solution of $[PtCl_2(coe)]_2$ (50 mg, 0.07 mmol) in 10 ml of CH_2Cl_2. After 1 h, the mixture was stored at 5 °C overnight and the resultant orange precipitate was collected by suction filtration and dried under vacuum. Yield: 49 mg, 73%. Mp 244 °C (decomposition). *Anal.* Calc. for $C_{12}H_8N_2Cl_2PtS \cdot CH_2Cl_2$: C, 27.72; H, 1.79; N, 4.97. Found: C, 28.08; H, 1.48; N, 5.14%. ^{1}H NMR (dmso-d_6): δ 9.68 (d, $J = 8$ Hz, 1H), 9.52 (d, $J = 5$ Hz, 1H), 8.55 (d, $J = 8$ Hz, 1H), 8.45–8.41 (ov m, 2H), 7.89 (t, $J = 8$ Hz, 1H), 7.77–7.68 (ov m, 2H). IR (nujol): 2922, 2868, 1714, 1606, 1462, 1377, 1309, 1261, 1157, 1076, 970, 760, 723.

2.2.4. Preparation of cis-dichlorodi(2-pyrid-3-ylbenzimidazole)platinum(II) (**2a**)

2-Pyrid-3-ylbenzimidazole (102 mg, 0.52 mmol) in 10 ml of ethanol was added dropwise to a stirred solution of potassium tetrachloroplatinate (II) (109 mg, 0.26 mmol) in 10 ml of water. The mixture was heated gently at 40 °C for 1 h. The yellow precipitate was collected and washed with wet ethanol (2×3 ml). Yield: 122 mg, 71%. Mp 240 °C (decomposition). *Anal.* Calc. for $C_{24}H_{18}N_6Cl_2Pt \cdot 2H_2O$: C, 41.62; H, 3.20; N, 12.13. Found: C, 41.77; H, 2.61; N, 11.84%. ^{1}H NMR (dmso-d_6): δ 9.68 (s, 2H), 8.90 (m, 2H), 8.68 (m, 2H), 7.68 (m, 6H), 7.29 (m, 4H). IR (nujol): 3150, 2916, 2858, 2725, 2671, 1712, 1608, 1462, 1377, 1315, 1281, 1228, 1153, 1072, 970, 820, 739, 723, 692.

2.2.5. Preparation of cis-dichlorodi(2-pyrid-3-ylbenzoxazole)platinum(II) (**2b**)

2-Pyrid-3-ylbenzoxazole (102 mg, 0.52 mmol) in 10 ml of ethanol was added dropwise to a stirred 10 ml water solution of potassium tetrachloroplatinate (II) (109 mg, 0.26 mmol). After 1 h of heating gently at 40 °C, a beige precipitate was collected by suction filtration and washed with wet ethanol (2×3 ml). Yield: 124 mg, 72%. Mp 170 °C (decomposition). *Anal.* Calc. for $C_{24}H_{16}N_4Cl_2O_2Pt$: C, 43.78; H, 2.45; N, 8.51. Found: C, 43.67; H, 2.26; N, 8.32%. ^{1}H NMR (dmso-d_6): δ 9.70 (s, 2H), 9.02 (d, $J = 5$ Hz, 2H), 8.72 (d, $J = 8$ Hz, 2H), 7.89 (t, $J = 8$ Hz, 4H), 7.69 (t, $J = 8$ Hz, 2H), 7.55–7.45 (ov m, 4H). IR (nujol): 2926, 2856, 1713, 1608, 1541, 1462, 1377, 1304, 1242, 1115, 1063, 972, 934, 891, 754, 723, 687, 623.

2.2.6. Preparation of cis-dichlorodi(2-pyrid-3-ylbenzothiazole)platinum(II) (**2c**)

Potassium tetrachloroplatinate (II) (55 mg, 0.13 mmol) was dissolved in 10 ml of water and a 10 ml ethanol solution of 2-pyrid-3-ylbenzothiazole (59 mg, 0.28 mmol) was added dropwise. The reaction was stirred and heated gently at 40 °C for 1 h. The precipitate was collected by suction filtration and washed with wet ethanol (2×3 ml) to afford a yellow solid. Yield: 83 mg, 91%. Mp 290 °C (decomposition). *Anal.* Calc. for $C_{24}H_{16}N_4Cl_2PtS_2$: C, 41.74; H, 2.34; N, 8.11. Found: C, 41.68; H, 2.24; N, 7.75%. ^{1}H NMR (dmso-d_6): δ 9.66 (s, 2H), 8.98 (m, 2H), 8.66 (m, 2H), 8.27–8.19 (ov m, 4H), 7.67–7.45 (ov m, 6H). IR (nujol): 2920, 2856, 1504, 1462, 1377, 1315, 1248, 1196, 1074, 1032, 984, 895, 812, 762, 729, 687.

*2.2.7. Preparation of cis-dichlorodi(2-pyrid-4-ylbenzimidazole)platinum(II) (**3a**)*

2-Pyrid-4-ylbenzimidazole (50 mg, 0.26 mmol) in 10 ml of ethanol was added dropwise to a stirred solution of potassium tetrachloroplatinate (II) (54 mg, 0.13 mmol) in 10 ml of water. The mixture was heated gently at 40 °C for 1 h. The brown precipitate was collected and washed with wet ethanol (2 × 3 ml). Yield: 56 mg, 66%. Mp 220 °C (decomposition). *Anal.* Calc. for $C_{24}H_{18}N_6Cl_2Pt \cdot 1.5H_2O$: C, 42.17; H, 3.10; N, 12.30. Found: C, 42.15; H, 2.77; N, 11.86%. ^{1}H NMR (dmso-d_6): δ 8.95 (d, $J = 5$ Hz, 4H), 8.15 (d, $J = 5$ Hz, 4H), 7.67 (m, 4H), 7.31–7.28 (ov m, 4H). IR (nujol): 3150, 2908, 2858, 2725, 1712, 1618, 1462, 1377, 1317, 1147, 1063, 966, 843, 744, 723, 609.

*2.2.8. Preparation of cis-dichlorodi(2-pyrid-4-ylbenzoxazole)platinum(II) (**3b**)*

2-Pyrid-4-ylbenzoxazole (24 mg, 0.12 mmol) in 10 ml of ethanol was added dropwise to a stirred solution of potassium tetrachloroplatinate (II) (26 mg, 0.06 mmol) in 10 ml of water. After 1 h of heating gently at 40 °C, a brown precipitate was collected by filtration and washed with wet ethanol (2 × 3 ml). Yield: 27 mg, 69%. Mp 310 °C (decomposition). *Anal.* Calc. for $C_{24}H_{16}N_4Cl_2O_2Pt \cdot 1.5H_2O$: C, 42.06; H, 2.79; N, 8.17. Found: C, 41.83; H, 2.30; N 8.01%. ^{1}H NMR (dmso-d_6): δ 9.05 (d, $J = 8$ Hz, 4H), 8.17 (d, $J = 8$ Hz, 4H), 7.94–7.86 (ov m, 4H), 7.56–7.49 (ov m, 4H). IR (nujol): 2939, 2910, 2860, 2725, 1714, 1622, 1603, 1541, 1462, 1377, 1302, 1234, 1078, 1051, 931, 891, 839, 814, 764, 752, 723, 694, 621.

*2.2.9. Preparation of cis-dichlorodi(2-pyrid-4-ylbenzothiazole)platinum(II) (**3c**)*

Potassium tetrachloroplatinate (II) (100 mg, 0.24 mmol) was dissolved in 10 ml of water and 2-pyrid-4-ylbenzothiazole (102 mg, 0.48 mmol) in 10 ml of ethanol was added dropwise. The reaction was stirred and heated gently at 40 °C for 1 h. The precipitate was collected by suction filtration and washed with wet ethanol (2 × 3 ml) to afford a yellow solid. Yield: 141 mg, 85%. Mp 244 °C (decomposition). *Anal.* Calc. for $C_{24}H_{16}N_4Cl_2PtS_2 \cdot 1.5H_2O$: C, 40.16; H, 2.67; N, 7.81. Found: C, 39.96; H, 2.22; N, 7.46%. ^{1}H NMR ($CDCl_3$): δ 9.06 (d, $J = 8$ Hz, 2H), 8.90 (d, $J = 5$ Hz, 2H), 8.13 (t, $J = 8$ Hz, 2H), 7.99–7.93 (ov m, 6H), 7.58–7.47 (ov m, 4H). IR (nujol): 2918, 2856, 1714, 1614, 1462, 1377, 1311, 1167, 976, 835, 764, 723, 557.

2.3. X-ray data

Crystals of **1c** and **2b** were grown from saturated CH_2Cl_2 and wet THF solutions, respectively, at 5 °C. Single crystals were coated with Paratone-N oil, mounted using a glass fibre and frozen in the cold stream of the goniometer. A hemisphere of data were collected on a Bruker AXS P4/SMART 1000 diffractometer using ω and ϕ scans with a scan width of 0.3° and 30 s (**1c**) and 40 s (**2b**) exposure times. The detector distance was 6 cm. The data were reduced [8] and corrected for absorption [9]. The structure was solved by direct methods and refined by full-matrix least squares on F^2 [10]. All non-hydrogen atoms were refined anisotropically. Hydrogen atoms were located in Fourier difference maps and refined isotropically.

3. Results and discussion

3.1. Ligands

2-Arylbenzimidazoles, -oxazoles, and -thiazoles are a remarkably important class of biologically active compounds [11–16]. For instance, a recent study has shown that 2-(4-aminophenyl)-benzothiazole displays unusual anticancer activity originally discovered in a regimen designed for screening tyrosine kinase inhibitors [11]. More potent analogues have since been prepared and their biological profiles are unlike that of any known anticancer agent [12]. Analysis of the structure activity relationships identified the benzothiazole unit as being essential for potent activity. Likewise, potent fungicides derived from benzimidazole have recently been reported [13].

Our interest in generating platinum complexes with biologically active carrier ligands therefore prompted us to make complexes containing arylbenzimidazole, and related benzoxazole and benzothiazole groups. In this study we have focused on making monodentate and bidentate pyridine derivatives which are readily prepared by the oxidative cyclization of the appropriate Schiff bases [17–19].

3.2. Platinum complexes

Addition of 2-thiophen-2-ylbenzimidazole derivatives (L_T) to organic soluble $[PtCl_2(coe)]_2$ (coe = *cis*-cyclooctene, [6,7]) resulted in complexes of the type *trans*-$PtCl_2(coe)L_T$, where the benzimidazole ligand coordinates to the metal in an η^1-fashion *via* the imine moiety. No interaction of the thiophene unit with the metal centre was observed in these cases [20]. However, addition of analogous 2-pyridin-2-ylbenzimidazole derivatives (L_P) to $[PtCl_2(coe)]_2$ gave didentate complexes of the type *cis*-$PtCl_2(L_P)$ (**1a–c**) in moderate yields (46–78%), where coordination occurs, as expected, through the pyridine and imine nitrogens (Scheme 1) [19].

Complexes **1a–c** have been characterized using a number of physical methods, including ^{1}H NMR spectroscopy. A significant downfield shift is observed for the sp^2 hydrogen alpha to the nitrogen of the pyridine ring, upon coordination of the ligand to the metal. For

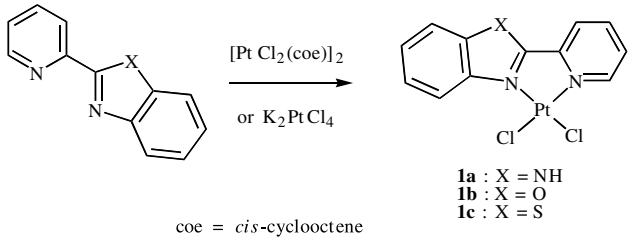

Scheme 1.

instance, the doublet at δ 8.73 ppm for the 2-pyrid-2-ylbenzimidazole ligand in dmso-d_6 shifts to 9.47 ppm in complex **1a**. Similar trends are also observed in **1b** and **1c**. The low solubility of these complexes in common organic solvents precluded the acquisition of ^{13}C NMR data.

Binding of benzimidazole derivatives to a number of other metals has been reported previously [19,21–25], where coordination of the ligand occurs predominantly through the imine nitrogen. For complex **1a** the FT-IR spectrum shows a distinct N–H stretch at 3165 cm^{-1} compared to that for the free ligand, which appears as a broad band at 3056 cm^{-1}. The low frequency and broadness of the absorption band for the free ligand has been attributed to a considerable amount of hydrogen bonding between the NH group and the pyridine nitrogen of a neighbouring molecule in the solid state [21]. Related palladium complexes containing pyridine imidazolines [26] have been used as catalysts in the copolymerization of CO/4-*tert*-butylstyrene and lanthanide complexes with substituted bis(benzimidazolyl)pyridines have been investigated for their luminescent properties [27].

Although we were unable to obtain single crystals of **1a**, we have characterized complex **1c** by an X-ray diffraction study to confirm the N,N-chelation mode (Fig. 1). Crystallographic data are given in Table 1 and

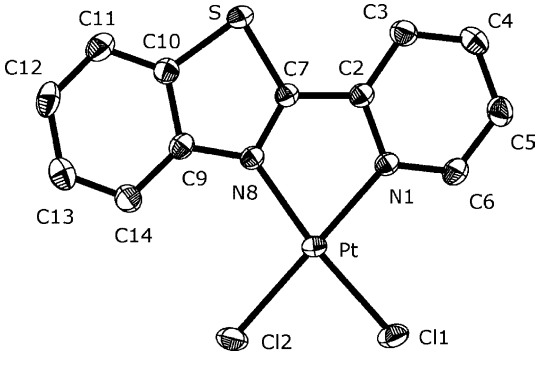

Fig. 1. The structure of **1c** showing the atomic labeling scheme and 30% probability displacement ellipsoids with hydrogen atoms omitted for clarity.

Table 1
Crystallographic data collection parameters for **1c** and **2b**

Complex	**1c** · CH_2Cl_2	**2b** · THF · H_2O
Formula	$C_{13}H_{10}Cl_4N_2PtS$	$C_{28}H_{26}Cl_2N_4O_4Pt$
fw	563.18	748.52
Crystal system	triclinic	monoclinic
Space group	$P\bar{1}$	$C2/c$
a (Å)	7.8715(6)	18.698(10)
b (Å)	9.9873(7)	16.325(10)
c (Å)	10.5883(8)	8.853(6)
α (°)	104.149(1)	
β (°)	103.754(1)	90.149(17)
γ (°)	96.864(1)	
V (Å^3)	769.9(1)	2702(3)
Z	2	4
ρ_{calcd} (Mg m^{-3})	2.429	1.840
Crystal size (mm)	$0.075 \times 0.10 \times 0.45$	$0.1 \times 0.15 \times 0.6$
Temperature (K)	173(1)	198(1)
Radiation	Mo-Kα ($\lambda = 0.71073$)	Mo-Kα ($\lambda = 0.71073$)
μ (mm^{-1})	9.933	5.433
Total reflections	5538	5897
Total unique relections	3425	2230
Number of variables	230	187
R_{int}	0.0153	0.0665
θ range (°)	2.06–27.49	1.66–24.99
Largest difference peak/hole (e Å^{-3})	1.313/−1.613	2.966/−1.785
GoF on F^2	1.110	1.117
R_1[a] ($I > 2\sigma(I)$)	0.0166	0.0402
wR_2[b] (all data)	0.0435	0.1080

[a] $R_1 = \sum||F_o| - |F_c||/\sum|F_o|$.
[b] $wR_2 = \left(\sum[w(F_o^2 - F_c^2)^2]/\sum[wF_o^4]\right)^{1/2}$, where $w = 1/[\sigma^2(F_o^2) + (0.0219 * P)^2 + (0.4739 * P)]$ (**1c**) and $w = 1/[\sigma^2(F_o^2) + (0.0746 * P)^2]$ (**2b**), where $P = (\max(F_o^2, 0) + 2 * F_c^2)/3$.

selected bond distances and angles shown in Table 2. As expected, coordination of the ligand occurs through the two nitrogen atoms. The platinum pyridyl benzothiazole fragment is planar with the nitrogen–platinum bonds of 2.019(2) (pyridine) and 2.041(2) (imine) being similar to those reported in other iminopyridine platinum systems [28,29]. Slightly longer Pt–N bond distances are observed in related five coordinate Pt(II) [30,31] and Pt(IV) complexes [32]. The C(7)–N(8) distance is 1.309(4) and in the range of accepted carbon–nitrogen double bonds found in benzothiazoles [19,33,34].

We also decided to prepare complexes of the type *cis*-$PtCl_2(L_P)_2$ with 2-pyridin-3-yl- and 2-pyridin-4-ylbenzimidazole derivatives (Scheme 2). Reactions were carried out with K_2PtCl_4 to ensure stereospecific formation of the *cis* isomer [35]. Once again, a downfield shift is observed in the ^1H NMR spectra for the sp^2 hydrogens alpha to the nitrogen of the pyridine ring upon coordination of the pyridine to the metal. For example, a singlet is observed at δ 9.68 ppm for complex **2a** compared to that of free 2-pyrid-3-ylbenzimidazole (9.34

Table 2
Selected bond lengths (Å) and angles (°) for **1c** and **2b**

1c		**2b**	
Bond lengths			
Pt–N(1)	2.019(2)	Pt–N(1)	2.033(5)
Pt–N(8)	2.041(2)	Pt–Cl	2.2943(17)
Pt–Cl(1)	2.2774(7)	N(1)–C(2)	1.321(7)
Pt–Cl(2)	2.2871(7)	N(1)–C(6)	1.341(7)
N(1)–C(6)	1.331(4)	C(7)–N(8)	1.286(8)
N(1)–C(2)	1.352(3)	C(7)–O	1.361(7)
C(7)–N(8)	1.309(4)	N(8)–C(9)	1.384(7)
C(7)–S	1.698(3)	C(10)–O	1.379(8)
N(8)–C(9)	1.393(3)	C(9)–C(10)	1.394(9)
C(10)–S	1.722(3)		
Bond angles			
		N(1)#1–Pt–N(1)	89.1(3)
N(1)–Pt–N(8)	80.33(9)	N(1)#1–Pt–Cl	176.68(12)
N(1)–Pt–Cl(1)	93.12(7)	N(1)–Pt–Cl	89.54(17)
N(8)–Pt–Cl(1)	173.33(7)	Cl–Pt–Cl#1	92.01(9)
N(1)–Pt–Cl(2)	178.95(6)	C(2)–N(1)–C(6)	119.5(5)
N(8)–Pt–Cl(2)	99.06(7)	C(2)–N(1)–Pt	118.9(4)
Cl(1)–Pt–Cl(2)	87.52(3)	C(6)–N(1)–Pt	121.6(4)
N(1)–C(2)–C(3)	122.6(3)	N(1)–C(2)–C(3)	122.2(5)
N(8)–C(7)–C(2)	119.7(2)	N(1)–C(6)–C(5)	121.0(5)
N(8)–C(7)–S	116.5(2)	N(8)–C(7)–O	115.2(5)
C(2)–C(7)–S	123.8(2)	N(8)–C(7)–C(3)	126.9(6)
C(7)–N(8)–C(9)	111.1(2)	C(7)–N(8)–C(9)	105.7(5)
C(7)–S–C(10)	89.25(13)	O–C(10)–C(14)	129.4(6)
		O–C(10)–C(9)	107.8(5)
		C(7)–O–C(10)	103.7(5)

ppm). Similar trends were observed for the other compounds (**2b,c** and **3a–c**). The N–H stretch was observed in the FT-IR spectrum at 3150 cm^{-1} for both complexes **2a** and **3a**.

An X-ray diffraction study on **2b** was carried out to confirm the formation of a *cis* geometry. The molecular structure is shown in Fig. 2, where the ligands are bound to the metal via the pyridine nitrogen with a typical distance of 2.033(5). Bond distances and angles within the benzoxazole ring are consistent with those reported previously [36,37]. The two planar benzoxazole groups are 77.3° to one another, presumably to relieve steric crowding within these bulky molecules.

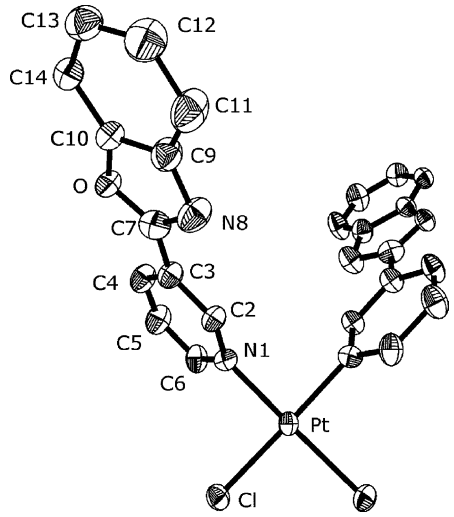

Fig. 2. The structure of **2b** showing the atomic labeling scheme and 30% probability displacement ellipsoids with hydrogen atoms omitted for clarity.

4. Conclusions

We have prepared and characterized *cis* dichloroplatinum complexes containing biologically relevant 2-pyridylbenzimidazole, oxazole, and thiazole derivatives. Chelating didentate complexes are formed with 2-pyrid-2-ylbenzimidazole compounds where coordination to the metal occurs via the pyridine and ring imine nitrogens. Future work in this area will investigate the cytotoxicities of these complexes against cisplatin-sensitive and cisplatin-resistant cells, the results of which will be published in due course.

Acknowledgements

Thanks are extended to the Research Corporation (Cottrell College Science Award), the Canada Research Chairs program/Canadian Foundation Innovation/Atlantic Innovation Fund, and Mount Allison University for financial support. We also thank Dan Durant and Roger Smith for expert technical assistance and anonymous reviewers for helpful comments.

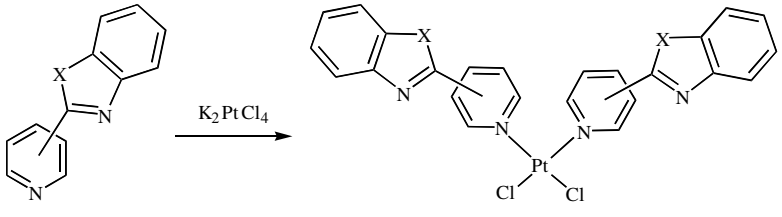

2, 3a : X = NH
2, 3b : X = O
2, 3c : X = S

Scheme 2.

References

[1] E.R. Jamieson, S.J. Lippard, Chem. Rev. 99 (1999) 2467.
[2] J. Reedijk, Chem. Rev. 99 (1999) 2499.
[3] E. Wong, C.M. Giandomenico, Chem. Rev. 99 (1999) 2451.
[4] L.G. Nikolcheva, C.M. Vogels, R.A. Stefan, H.A. Darwish, S.J. Duffy, R.J. Ireland, A. Decken, R.H.E. Hudson, S.A. Westcott, Can. J. Chem. 81 (2003) 269.
[5] A.S. King, L.G. Nikolcheva, C.R. Graves, A. Kaminski, C.M. Vogels, R.H.E. Hudson, R.J. Ireland, S.J. Duffy, S.A. Westcott, Can. J. Chem. 80 (2002) 1217.
[6] C.M. Vogels, H.L. Wellwood, T.L. Hennigar, K. Biradha, M.J. Zaworotko, S.A. Westcott, Can. J. Chem. 77 (1999) 1196.
[7] S. Otto, A. Andreas, L.I. Elding, Dalton Trans. (2003) 2519.
[8] SAINT 6.02, Bruker AXS, Inc., Madison, WI, USA (1997–1999).
[9] G.M. Sheldrick, SADABS, Bruker AXS, Inc., Madison, WI, USA, 1999.
[10] G.M. Sheldrick, SHELXTL 5.1, Bruker AXS, Inc., Madison, WI, USA, 1997.
[11] D.-F. Shi, T.D. Bradshaw, S. Wrigley, C.J. McCall, P. Lelieveld, I. Fichtner, M.F.G. Stevens, J. Med. Chem. 39 (1996) 3375.
[12] T.D. Bradshaw, S. Wrigley, D.-F. Shi, R.J. Schultz, K.D. Paull, M.F.G. Stevens, Br. J. Cancer 77 (1998) 745.
[13] M. Lezcano, W. Al-Soufi, M. Novo, E. Rodríguez-Nüñez, J.V. Tato, J. Agric. Food Chem. 50 (2002) 108.
[14] Z.-P. Zhuang, M.-P. Kung, A. Wilson, C.-W. Lee, K. Plössl, C. Hou, D.M. Holtzman, H.F. Kung, J. Med. Chem. 46 (2003) 237.
[15] G. Wells, J.M. Berry, T.D. Bradshaw, A.M. Burger, A. Seaton, B. Wang, A.D. Westwell, M.F.G. Stevens, J. Med. Chem. 46 (2003) 532.
[16] D.J. Skalitzky, J.T. Marakovits, K.A. Maegley, A. Ekker, X.-H. Yu, Z. Hostomsky, S.E. Webber, B.W. Eastman, R. Almassy, J. Li, N.J. Curtin, D.R. Newell, A.H. Calvert, R.J. Griffin, B.T. Golding, J. Med. Chem. 46 (2003) 210.
[17] J. Chang, K. Zhaob, S. Pana, Tetrahedron Lett. 43 (2002) 951.
[18] K.J. Duffy, A.T. Price, E. Delorme, S.B. Dillon, C. Duquenne, C. Erickson-Miller, L. Giampa, Y. Huang, R.M. Keenan, P. Lamb, N. Liu, S.G. Miller, J. Rosen, A.N. Shaw, H. Smith, K.J. Wiggall, L. Zhang, J.I. Luengo, J. Med. Chem. 45 (2002) 3576.
[19] J. Gangopadhyay, S. Sengupta, S. Bhattacharyya, I. Chakraborty, A. Chakravorty, Inorg. Chem. 41 (2002) 2616.
[20] X.-F. He, C.M. Vogels, A. Decken, S.A. Westcott, Can. J. Chem. 81 (2003) 861.
[21] T.R. Harkins, J.L. Walter, O.E. Harris, H. Freiser, J. Am. Chem. Soc. 78 (1956) 260.
[22] K. Müller-Buschbaum, C.C. Quitmann, Inorg. Chem. 42 (2003) 2742.
[23] M. Hossain, S.K. Chattopadhyay, S. Ghosh, Polyhedron 16 (1997) 143.
[24] M. Maji, P. Sengupta, S.K. Chattopadhyay, G. Mostafa, C.H. Schwalbe, S. Ghosh, J. Coord. Chem. 54 (2001) 13.
[25] K.W. Nordquest, D.W. Phelps, W.F. Little, D.J. Hodgson, J. Am. Chem. Soc. 98 (1976) 1104.
[26] A. Bastero, A. Ruiz, C. Claver, B. Milani, E. Zangrando, Organometallics 21 (2002) 5820.
[27] S. Petoud, J.-C.G. Bünzli, K.J. Schenk, C. Piguet, Inorg. Chem. 36 (1997) 1345.
[28] J.G. Hinman, C.R. Baar, M.C. Jennings, R.J. Puddephatt, Organometallics 19 (2000) 536.
[29] C.R. Baar, H.A. Jenkins, M.C. Jennings, G.P.A. Yap, R.J. Puddephatt, Organometallics 19 (2000) 4870.
[30] C.R. Baar, M.C. Jennings, J.J. Vittal, R.J. Puddephatt, Organometallics 19 (2000) 4150.
[31] F. Di Bianca, G. Bandoli, A. Dolmella, S. Antonaroli, B. Crociani, J. Chem. Soc., Dalton Trans. (2002) 212.
[32] C.R. Baar, L.P. Carbray, M.C. Jennings, R.J. Puddephatt, J.J. Vittal, Organometallics 20 (2001) 408.
[33] G.R. Julius, S. Cronje, A. Neveling, C. Esterhuysen, H.G. Raubenheimer, Helv. Chim. Acta 85 (2002) 3737.
[34] H.G. Raubenheimer, E.K. Marais, S. Cronje, C. Esterhuysen, G.J. Kruger, J. Chem. Soc., Dalton Trans. (2000) 3016.
[35] F.R. Hartley, The Chemistry of Platinum and Palladium, Wiley, New York, 1973.
[36] C. Lambert, I. Lopez-Solera, P.R. Raithby, Organometallics 15 (1996) 452.
[37] I. Claustro, G. Abate, E. Sanchez, J.H. Acquaye, Inorg. Chim. Acta 342 (2003) 29.

Available online at www.sciencedirect.com
SCIENCE DIRECT®
Polyhedron 23 (2004) 161–168
POLYHEDRON
www.elsevier.com/locate/poly

Synthesis, characterization and bio-activity of *S*-2-picolyldithiocarbazate (S2PDTC), some of its Schiff bases and their Ni(II) complexes and X-ray structure of *S*-2-picolyl-β-*N*-(2-acetylpyrrole)dithiocarbazate

Karen A. Crouse [a,*], Kar-Beng Chew [a], M.T.H. Tarafder [a,1], A. Kasbollah [a,2], A.M. Ali [b], B.M. Yamin [c], H.-K. Fun [d]

[a] *Department of Chemistry, University Putra Malaysia, 43400 Serdang, Selangor, Malaysia*
[b] *Laboratory of Molecular and Cell Biology, Institute of Biosciences, University Putra Malaysia, 43400 Serdang, Selangor, Malaysia*
[c] *School of Chemical Sciences and Food Technology, University Kebangsaan Malaysia, 43600 Bangi, Selangor, Malaysia*
[d] *X-ray Crystallography Unit, School of Physics, University Sains Malaysia, 11800 Minden, Penang, Malaysia*

Received 3 June 2003; accepted 29 September 2003

Abstract

A new dithiocarbazate ligand, *S*-2-picolyldithiocarbazate (S2PDTC) was synthesized using 2-picolylchloride hydrochloride. Tridentate Schiff bases were prepared by condensation of *S*-2-picolyldithiocarbazate (S2PDTC) with pyridine-2-carboxaldehyde (NNS′), 2-acetylpyrrole (NNS″) and 2-acetylthiophene (NSS), while a bidentate Schiff base (NS) was prepared by condensing the S2PDTC with 2-acetylfuran. Complexes of S2PDTC and its Schiff bases with Ni(II) salts were synthesized and characterized by elemental analyses and various physico-chemical techniques. A square-planar structure has been proposed for the diamagnetic $[Ni(S2PDTC)_2]$ and $[Ni(NNS'')\cdot Cl]$ complexes while $[Ni(NS)\cdot Cl]$ complex was dimeric. Complexes of $[Ni(NNS')_2]$ and $[Ni(NSS)_2]$ were paramagnetic with octahedral stereochemistry. S2PDTC showed activity against bacteria and fungi (inhibitory zones above 15 mm). The NS and NSS Schiff bases showed activity toward a number of the bacteria assayed, while the NS and NSS Schiff bases, and the $[Ni(NNS'')\cdot Cl]$ and $[Ni(NS)\cdot Cl]$ complexes were found to be active only against *C. lypolytica* (2075). S2PDTC proved moderately active against HT-29 and weakly active toward CEM-SS with CD_{50} values of 9.5 and 24.0 μg cm^{-3}, respectively, while among its Schiff bases reported herein, only the NNS′ Schiff base showed strong activity toward CEM-SS (Human cell T-lymphoblastic leukemia) and HT-29 (Human colon adenocarcinoma cells) with CD_{50} values of 2.3 μg cm^{-3}. All of the Ni(II) complexes were inactive against CEM-SS cancer cells.
© 2003 Elsevier Ltd. All rights reserved.

Keywords: *S*-2-picolyldithiocarbazate (Hydrazine carbodithioic acid pyridinium-2-yl methyl ester chloride); Bidentate NS Schiff base; Tridentate NNS and NSS Schiff bases; Ni(II) complexes; Dithiocarbazate derivative

1. Introduction

Dithiocarbazate, NH_2NHCS_2, and its substituted derivatives have been synthesized and investigated over the past few decades [1–28]. Interest remains high in these compounds and the Schiff bases derived from them through condensation with various aldehydes and ketones because of the intriguing observation that they sometimes show different biological properties, although they may differ only slightly in their molecular structures [1–11,15–22]. Transition metal complexes of these ligands are widely studied because of their potential for therapeutic use [2–4,6–20]. They also find applications in health and skin care products and in paint manufacturing [29]. Publications to date have mainly focused on

* Corresponding author: Tel.: +60-3-8946-6788; fax: +60-3-8943-5380.
E-mail address: crouse@pc.jaring.my (K.A. Crouse).
[1] Present address: Department of Chemistry, Rajshahi University, Rajshahi 6205, Bangladesh.
[2] Present address: Malaysian Institute for Nuclear Technology, Bangi, Selangor, Malaysia.

0277-5387/$ - see front matter © 2003 Elsevier Ltd. All rights reserved.
doi:10.1016/j.poly.2003.09.025

S-benzyldithiocarbazate (SBDTC) and *S*-methyldithiocarbazate (SMDTC). Although *S*-benzoyldithiocarbazate (SBODTC) has been synthesized [27], little work has been reported using this ligand. Herein we introduce a new dithiocarbazate derivative, S2PDTC, containing a picolyl group, some of its Schiff bases and their nickel(II) complexes. Isomeric dithiocarbazate derivatives prepared from the 3- and 4-pyridylmethyl halides have also been successfully isolated in our laboratory and will be discussed in later communications. It is anticipated that these compounds will open up many interesting avenues for further research.

2. Experimental

All chemicals were of reagent grade and unless otherwise mentioned, were used as received. The solvents were purified using conventional methods.

2.1. Physical measurements

Carbon, hydrogen, nitrogen and sulfur analyses were carried out using a LECO CHNS-932 instrument. The IR spectra were recorded as KBr pellets, in the 4000–400 cm^{-1} region, on a Perkin–Elmer 1750X FTIR spectrometer. Metal determinations were carried out using a Perkin–Elmer Plasma 1000 Emission Spectrometer. ^1H NMR spectra were recorded on a Jeol JNM 400 MHz NMR spectrometer. The molar conductance of 10^{-3} M solutions of the metal complexes in DMSO were measured at 30 °C using a Jenway 4310 conductivity meter and a dip-type cell with platinised electrode. The UV–Vis spectra were run on a Shimadzu UV-2501 PC spectrophotometer (900–200 nm). Melting points (m.p.) were determined using an Electrothermal digital melting point apparatus. Magnetic susceptibilities were carried out using a Sherwood Auto MSB balance at 298 K. All susceptibilities were corrected for the diamagnetic contribution using Pascal's constants.

2.2. Preparation of S-2-picolyldithiocarbazate (S2PDTC)

The previously reported methods for preparation of substituted dithiocarbazate [12,13] were modified by reaction with 2-picolylchloride hydrochloride.

Potassium hydroxide (11.4 g, 0.2 mol) was dissolved completely in 90% ethanol (70 ml) and the mixture was cooled in ice. To the cold solution, hydrazine hydrate (10 g, 0.2 mol) was added slowly with stirring. Carbon disulfide (15.2 g, 0.2 mol) in ethanol (25 ml) was then added dropwise with vigorous stirring for about 1 h. The temperature of the reaction mixture was kept below 263 K during the addition. During this time two layers formed. The resulting yellow oil (lower layer) was separated using a separatory funnel, dissolved in 40% ethanol (40 ml) and cooled in ice. 2-Picolylchloride hydrochloride (32.8 g, 0.2 mol) was completely dissolved in 100 ml of 80% ethanol and added slowly to the above solution with vigorous mechanical stirring. The resulting light green product was separated by filtration, washed with water and dried. The crude product was recrystallized from absolute ethanol. Yield, 75.1%; melting point, 124 °C.

2.3. General method for preparation of the Schiff bases

The previously reported method for preparation of Schiff bases [12,13] was used to prepare S2PDTC derivatives with pyridine-2-carboxaldehyde, 2-acetylpyrrole, 2-acetylfuran and 2-acetylthiophene.

S2PDTC (4.69 g, 0.02 mol) dissolved in hot absolute ethanol (30–40 ml) was added to the solution of an equimolar amount of carbonyl compound in hot absolute ethanol (20 ml). The mixture was heated for 10 min and then cooled to 0 °C in an ice-bath. The products were filtered, washed with absolute ethanol, recrystallized from absolute ethanol and then dried over silica gel. The yields and melting points are given for each of the Schiff bases in Table 1.

2.4. General method for preparation of metal complexes

The previously reported methods for preparation of metal complexes [12,13] were employed using nickel(II) acetate tetrahydrate or nickel (II) chloride hexahydrate with the prepared ligands. For each preparation 0.1 mol of metal salt was dissolved in absolute ethanol (40 ml) and to the solution was added Schiff base (0.2 mol) in 40 ml of absolute ethanol. The mixture was heated while being stirred. Each precipitate was filtered, washed with ice-cold ethanol and dried over silica gel. The yields and melting points for these metal complexes are given in Table 1.

2.5. X-ray structure determination

The selected crystal of *S*-2-picolyl-β-*N*-(2-acetylpyrrole)dithiocarbazate was mounted on a Bruker SMART 1000 CCD diffractometer. Reflection data were measured at 25 °C using graphite monochromated Mo Kα ($\lambda = 0.71073$ Å) radiation with a detector distance of 4 cm and a swing angle of −35 °C. The data collected were reduced using the program SAINT [30] and an empirical absorption correction was carried out using SADABS [31]. The structure was solved using direct methods and refined using the full-matrix least-square method on F^2_{obs} using the SHELTXL [32] software package. All non-H atoms were anisotropically refined. The hydrogen atom at N4 was located in the difference Fourier map and was refined isotropically, whereas the other H atoms were geographically fixed and treated as riding atoms with C–

Table 1
Analytical data for the ligands, Schiff bases and their complexes

Compound	Colour	Melting point (°C)	Found (calculated)					Yield
			C	H	N	S	M	(%)
(**1**) S2PDTC	light green	124	35.49 (35.66)	3.95 (4.28)	17.46 (17.82)	27.56 (27.20)		75
(**2**) NNS′	yellow	175	54.56 (54.15)	4.39 (4.19)	19.06 (19.43)	21.95 (22.24)		86
(**3**) NNS″	yellow	165	53.01 (53.11)	4.81 (4.86)	19.75 (19.29)	22.70 (22.08)		76
(**4**) NS	orange	174	53.24 (53.58)	4.47 (4.50)	14.35 (14.42)	21.48 (22.01)		86
(**5**) NSS	yellow	155	50.95 (50.78)	4.27 (4.26)	13.55 (13.67)	31.72 (31.29)		79
(**6**) [Ni(S2PDTC)$_2$]	brown	193	36.59 (36.93)	3.96 (3.54)	18.86 (18.46)	28.64 (28.17)	12.67 (12.89)	69
(**7**) [Ni(NNS′)$_2$]	dark brown	225	48.96 (49.28)	3.16 (3.50)	18.10 (17.70)	20.81 (20.26)	8.86 (9.27)	76
(**8**) [Ni(NNS″) · Cl]	brown	205	40.25 (40.80)	3.19 (3.16)	14.12 (14.65)	16.95 (16.77)	15.86 (15.35)	65
(**9**) [Ni(NS) · Cl]	brown	210	40.23 (40.61)	3.50 (3.15)	11.06 (10.93)	16.56 (16.68)	15.21 (15.26)	71
(**10**) [Ni(NSS)$_2$]	dark brown	242	46.56 (46.23)	3.09 (3.58)	12.03 (12.45)	28.65 (29.04)	8.16 (8.70)	69

Note. NNS′ = S2PDTC + pyridine-2-carboxaldehyde; NNS″ = S2PDTC + 2-acetylpyrrole; NS = S2PDTC + 2-acetylfuran; NSS = S2PDTC + 2-acetylthiophene.

H distances = 0.93–0.97 Å, and N–H = 0.86 Å while $U_{iso}(H) = 1.2U_{eq}(C)$ or $1.5U_{eq}(C)$ and $1.2U_{eq}(N)$. The molecular graphics were created using SHELTXL. Crystal data and details on data collection and refinement are summarized in Table 4.

2.6. Bioactivity

2.6.1. Culture of cells and cytotoxic assay

Two types of cell line were used, CEM-SS (Human T-lymphoblastic leukemia) cells and HT-29 (Human colon andenocarcinoma) cells. The CEM-SS cell line was obtained from the National Cancer Institute, USA while the HT-29 cell line was obtained from ATCC (American Type Culture Collection). The cells were cultured in RPMI-1640 (Sigma) medium supplemented with 10% fetal calf serum. Cytotoxicity was determined using the MTT (3-[4,5-dimethylthiozol-2-yl]-2,5-diphenyltetrazolium bromide) assay following Mosmann's report [33]. Cytotoxicity was expressed as CD_{50}, i.e., the concentration that reduced the absorbance of treated cells by 50% with reference to the control (untreated cells). Doxorubicin and tamoxifen were used as cytotoxic standards.

2.6.2. Qualitative antimicrobial assay

Eight pathogenic microbials were used to test the biological potential of the compounds: (i) Methicillin resistant *staphylococcus* (MRSA), (ii) *Bacillus subtilis* wild type (B29), (iii) *B. subtilis* mutant defective DNA repair (B28), (iv) *Pseudomonas aeruginosa* (60 690), (v) *Candida albicans* (C.A.), (vi) *Aspergillus ochraceous* (398), (vii) *Saccharomyces cerevisiae* (20341) and (viii) *Candida lypolytica* (2075). The sources of microbes and culture maintenance were as previously described [33]. The antimicrobial activity of the extracts was qualitatively determined by a modified disc diffusion method as previously reported [34]. Antimicrobial activity was indicated by the presence of clear inhibition zones around the discs. Commercially available streptomycin was used for antibacterial control while nystatin was used as antifungal control.

2.6.3. Quantitative antimicrobial assay

Compounds that showed positive antimicrobial activity with the disc diffusion assay were subjected to the quantitative measurement of microbiostatic (inhibitory) activity as described by Hufford and Clark [35]. The lowest concentration which completely inhibited visible microbial growth was recorded as the minimum inhibitory concentration (MIC, μg cm^{-3}). Streptomycin and nystatin (Sigma) were used as positive controls for the bacteria and fungi, respectively.

3. Results and discussion

As noted above, many studies have been reported on Schiff bases of *S*-methyl- and *S*-benzyl dithiocarbazate and their metal complexes. The successful preparation of a series of *S*-picolyldithiocarbazate derivatives may help in the understanding of the bioactivity of this class

of compounds. We have recently reported the structure of *S*-2-picolyldithiocarbazate [36]. Unlike other dithiocarbazate compounds such as *S*-methyldithiocarbazate [37] and *S*-benzyldithiocarbazate [38], it exists in ionic form with a zwitterionic $^{-}SCNNH_3^{+}$ group and a protonated N on the picolyl ring with Cl^{-} as counter ion [36]. Retention of the protonated character of the picolyl ring has been observed previously [39] and its presence has not seemed to interfere in reaction [40]. It is not surprising that similar behavior is observed in these reactions. Condensation of S2PDTC with pyridine-2-carboxaldehyde, 2-acetylpyrrole, 2-acetylfuran and 2-acetylthiophene produced the expected Schiff bases NNS′ (**2**), NNS″ (**3**), NS (**4**) and NSS (**5**) in high yields. The melting points, elemental analyses and percentage yields are given in Table 1. In the solid phase, all of the Schiff bases exist only in thione (Fig. 1a) tautomeric form as evidenced by their IR spectra (Table 2). However, in solution, they may be expected to exist as an equilibrium mixture of both the thione (Fig. 1a) and thiolo (Fig. 1b) tautomeric forms [34]. None of the solids exhibit ν(S–H) at ca. 2700 cm^{-1}, but strong bands, which can be assigned to the ν(N–H) of the free ligands, are observed at 3241 cm^{-1} and 3064–3093 cm^{-1} in the IR spectra of **1** and its Schiff bases. These bands disappear in the IR spectra of the metal complexes suggesting that the proton attached to the α-nitrogen atom is lost upon complexation. In solution then, tautomerization occurred and through the loss of thiolo proton,

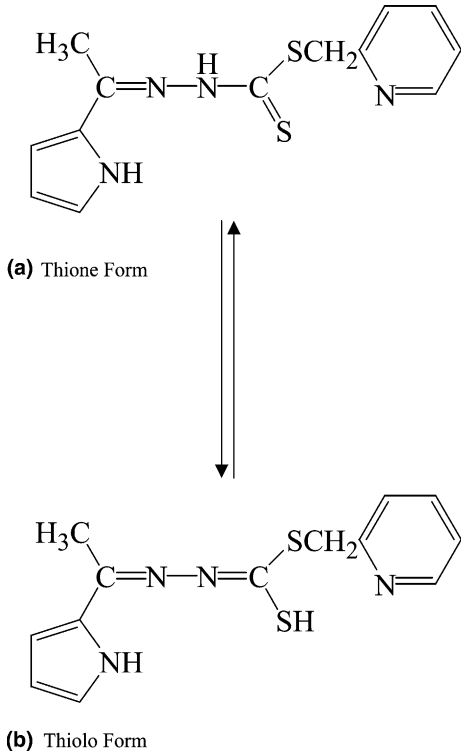

Fig. 1. Tautomeric forms of NNS″ Schiff base.

Schiff bases **2**, **3** and **5** behaved as uninegatively charged tridentate ligands while **1** and **4** behaved as uninegatively charged bidentate ligands. Strong bands at 1041 cm^{-1} and between 1032 and 1054 cm^{-1} for **1** and the Schiff bases, respectively, are assigned to the ν(C=S) mode. This band also disappears in the metal complexes supporting the contention that enethiolization, and consequent deprotonation, gives the thiolate in situ. The **2**, **3**, **4**, and **5** Schiff bases display strong bands at 1470, 1542, 1516 and 1532 cm^{-1}, respectively, which can assigned as the C=N stretching frequency of the aliphatic free ligands [41]. These bands are shifted to lower frequencies in the IR spectra of their complexes. This lowering of the ν(C=N) on complexation may be attributed to a lowering the C=N bond order as a result of the M–N bond formation. The lowering of the frequency of the ν(N–N) band in all the complexes is additional evidence for involvement of azomethine nitrogen in the coordination. The splitting of the ν(CSS) band of the ligands at between 994 and 1010 cm^{-1} in the spectra of the Ni(II) complexes evidences unidentate coordination of aliphatic sulfur [42]. In complex **9**, there was no significant displacement of the frequency of the ring breathing and ν(C–O–C) vibration at 1204 cm^{-1} [43] and there was also no absorption observed at 440–460 cm^{-1} that can be assigned to metal–oxygen bond stretching. It is thus apparent that the furan ring is not coordinated to the metal. In contrast there was significant displacement of the frequency of the pyridine, pyrrole and thiophene ring absorptions in complexes **7**, **9** and **10**, respectively, indicating that the pyridyl-nitrogen, pyrrole-nitrogen and thiophene-sulfur were coordinated to their central metal ion.

The ^{1}H NMR spectra of **1**, **2**, **3**, **4** and **5** in DMSO do show a peak at ca. δ 4.00 ppm attributable to the S–H proton [44], confirming that the thiolo tautomer is present in solution. A signal at ca. δ 8.0–8.5 ppm is attributed to the N–H group on the aliphatic nitrogen atom, and resonance peaks associated with the aromatic groups are observed in the range δ 6.5–7.3 ppm.

The brown complex **6**, resulting from reaction of nickel(II) acetate tetrahydrate with S2PDTC is a non-electrolyte in DMSO (Table 3). Complexes **7** and **10** are also non-electrolytes in DMSO. The non-electrolytic nature of the complexes indicates that these ligands are coordinated to the metal ions as uninegatively charged species. However, complexes **8** and **9** exhibit molar conductances corresponding to 1:1 electrolytes in DMSO [34]. Presumably these complexes undergo solvation releasing Cl^{-} ions as has been previously reported under similar conditions [13].

The magnetic susceptibility data are shown in Table 3. The brown complex **6** was found to be a diamagnetic species consistent with a square-planar stereochemistry. This data provides strong evidence of coordination through the thiolo sulphur, since thiolo

Table 2
Significant IR bands of the ligands, Schiff bases and their complexes

Compound	(N–H)	ν(N–H_2)	ν(C=N)	ν(C=S)	ν(C–O–C)	ν(N–N)	ν(CSS)
1	3241	3095		1041		1065	1000
2	3093		1486	1047		1055	1008
3	3084		1524	1046		1050	996
4	3064		1516	1054	1204	1076	1006
5	3068		1504	1032		1050	1002
6		3193	1468			1036	996
7			1458			1026	1004
8			1478			1026	1002
9			1474		1207	1024	1010
10			1470			1032	994

Table 3
Other physical properties of the metal complexes

Compound	Molar conductance (Ω^{-1} cm^{-2} mol^{-1})	UV–Vis spectra[a] (λ_{max}, nm)	μ_{eff} (BM)
6	4.26	330.5 (4.4), 400.0 (4.2), 570.0 (2.6)	diamagnetic
7	3.62	363.0 (3.2), 430.0 (2.8), 505.0 (1.3)	2.8
8	28.6	330.5 (3.5), 395.5 (3.1), 413.5 (3.1)	diamagnetic
9	33.9	308.5 (3.3), 367.5 (3.2), 462.5 (2.2)	diamagnetic
10	2.31	330.5 (3.2), 370.0 (2.4), 460.5 (2.2)	3.0

[a] log ε (cm^{-1} mol^{-1} L) are given in parentheses.

but not thioethers, cause spin pairing in nickel(II) complexes [2]. The electronic spectra of the complexes recorded in DMSO are summarized in Table 3. An absorption band at approximately 330 nm for complex **6** is attributed to the $n \rightarrow \pi^*$ intra ligand transitions while the band at approximately 400 nm can be assigned to $S \rightarrow Ni(II)$ charge transfer. The appearance of this LMCT band in Ni(II) complexes is also strong evidence that the Ni(II) ion is coordinated to sulfur through the thiolo sulfur atom. The complexes **7** and **10** were dark brown and were found to be paramagnetic at room temperature with magnetic moments of ca. 2.8 and 3.0 BM, respectively, indicating that they are high-spin, six-coordinate complexes. The Schiff bases in complexes **7** and **10** are therefore proposed to be uninegatively charged tridentate ligands. Because the NNS and NSS donors are characteristically planar [45], a meridional disposition of the ligand donor atoms in a distorted octahedral environment is most likely. In all cases, there is no evidence that the picolyl nitrogen is coordinated to the metal ion. Unfortunately, we have not yet been able to grow crystals of the metal complexes suitable for single crystal X-ray analysis.

3.1. X-ray crystal structure

The ORTEP diagram of the *S*-2-picolyl-β-*N*-(2-acetylpyrrole)dithiocarbazate molecule with atomic numbering scheme is shown in Fig. 2. The methyl-pyridine, N1/C4/C3/C2/C1/C5/C6, and (pyrrole-2-yl)ethylamide, N4/C12/C11/C10/C9/C8/C13/N3, groups are at *trans* and *cis* positions with respect to the terminal thione S2 atom about the C7–S1 and C7–N2 bonds, respectively. The bond lengths and angles are in normal ranges typical of dithiocarbazate compounds [37,38,46]. However, the slight shortening of N2–N3 (1.382 (5) Å) and N2–C7 (1.308 (6) Å) bond lengths compared to N1–N2 and N2–C5 of 1.372 (4) and 1.360 (5) Å, respectively, in *S*-methyl-β-*N*-(methylacetyl)methylenedithiocarbazate [46] is due to the conjugation effect in the N4/C12/C11/C10/C9/C8/N3 fragment. The discrete molecule is not planar but with inclination between the methyl-pyridine, N1/C4/C3/C2/C1/C5/C6, group and S2/C7/N2/N3/C8/C9 fragments of 73.43(19)°. Methyl-pyridine, N1/C4/C3/

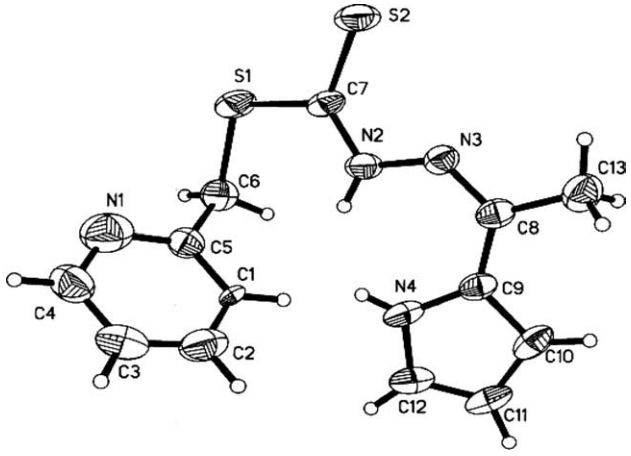

Fig. 2. ORTEP diagram of $C_{13}H_{14}N_4S_2$ (with 50% probability displacement ellipsoids) with atomic numbering scheme.

C2/C1/C5/C6, methyl-pyrrole, N4/C12/C11/C10/C9/C8 and S2/C7/N2/N3/C8/C9 fragments are planar (Table 5).

3.2. Biological activities

3.2.1. Cytotoxic activities

Compounds **3**–**10** were found to be inactive against all cell lines tested (Table 4). Compound **1** was shown to be moderately active against HT-29 with CD_{50} value of 9.5 μg cm^{-3}. This is in contrast to *S*-benzyldithiocarbazate (SBDTC) [28] which was inactive. However, compound **1** showed very weak activity against CEM-SS (CD_{50} value of 24.0 μg cm^{-3}), whereas SBDTC has been shown to be very active with CD_{50} value of 2.6 μg cm^{-3} [28]. Compound **2** was found to be very active against T-lymphoblastic leukemic cells (CEM-SS) and colon adenocarcinoma cells (HT-29) with CD_{50} value of 2.3 μg cm^{-3} for both. That compound **2** is very active towards this cancer cells line compared to compound **1**, is perhaps, due to the presence of two pyridyl nitrogen groups. Complexation with Ni(II) decreases the cytotoxicity (Table 6). The differing activities are currently being investigated in terms of the mechanism of action of these compounds at the cellular level.

3.2.2. Antimicrobial activities

Compounds **2**, **3**, **6**, **7** and **10** were found to be inactive against all bacteria and fungi tested. Whereas the

Table 4
Summary of crystals data, data collection and structure refinement parameters for $C_{13}H_{14}N_4S_2$ Schiff base

Empirical formula	$C_{13}H_{14}N_4S_2$
Formula weight	290.40
Temperature (K)	293 (2)
Wavelength (Å)	0.71073
Crystal system	monoclinic
Space group	$P2_1/n$
Unit cell dimensions	
a (Å)	10.2994 (8)
b (Å)	11.0736 (8)
c (Å)	13.1872 (9)
α (°)	90
β (°)	110.925 (2)
γ (°)	90
Volume (Å^3)	1404.83 (18)
Z, calculated density (Mg m^{-3})	4, 1.373
Absorption coefficient (mm^{-1})	0.370
$F(000)$	608
Crystal size (mm)	$0.22 \times 0.14 \times 0.06$
θ range for data collection (°)	2.17–24.99
Limiting indices	$-10 \leqslant h \leqslant 12$, $-13 \leqslant k \leqslant 11$, $-15 \leqslant l \leqslant 15$
Reflection collected/unique	7450/2445 [$R_{int} = 0.1270$]
Completeness to $\theta = 24.99$ (%)	99.1
Maximum and minimum transmission	0.9781 and 0.9230
Data/restraints/parameters	2445/0/177
Goodness-of-fit on F^2	0.997
Final R indices [$I > 2\sigma(I)$]	$R_1 = 0.0737$, $wR_2 = 0.1713$
R indices (all data)	$R_1 = 0.1279$, $wR_2 = 0.1931$
Extinction coefficient	0.021 (4)
Largest differential peak and hole (e Å^{-3})	0.514 and −0.449

Table 5
Selected bond lengths (Å) and angles (°) for $C_{13}H_{14}N_4S_2$ Schiff base

Bond lengths	
S(1)–C(7)	1.751(5)
S(1)–C(6)	1.815(5)
S(2)–C(7)	1.699(5)
N(1)–C(4)	1.389(8)
N(1)–C(5)	1.422(7)
N(2)–C(7)	1.308(6)
N(2)–N(3)	1.382(5)
N(3)–C(8)	1.314(6)
C(5)–C(6)	1.504(7)
C(8)–C(9)	1.426(7)
C(8)–C(13)	1.474(7)
Bond angles	
C(7)–S(1)–C(6)	104.6(2)
C(8)–N(3)–N(2)	124.3(4)
C(7)–N(2)–N(3)	112.4(4)
N(1)–C(5)–C(6)	120.1(5)
N(2)–C(7)–S(2)	127.5(4)
N(2)–C(7)–S(1)	117.8(4)
S(2)–C(7)–S(1)	114.8(3)
C(5)–C(6)–S(1)	114.0(3)
N(3)–C(8)–C(9)	124.8(4)
N(3)–C(8)–C(13)	115.1(5)
C(9)–C(8)–C(13)	120.1(5)

Table 6
Cytotoxic activities

Compound	CD_{50} (μg cm^{-3})[a]	
	CEM-SS (T-lymphoblastic leukemic cells)	HT-29 (colon cancer cells)
1	24.0	9.5
2	2.3	2.3
3	26.1	na
4	–	na
5	–	na
6	–	na
7	–	na
8	–	na
9	–	na
10	–	na
$NiCl_2 \cdot 6H_2O$	–	–
SBDTC	2.6	–
SMDTC	8.4	7.0
Doxorubicin (standard)	0.10	6.00
Tamoxifen (standard)	36.00	36.00

na, not available; –, inactive.

CD_{50} < 5.0 μg/ml – strongly active; CD_{50} 5.0–<10.0 μg/ml – moderately active; CD_{50} 10.0–25.0 μg/ml – weakly active; CD_{50} >25.0 μg/ml – not active.

[a] CD_{50} (μg cm^{-3}) = cytotoxic dose at 50%, i.e., the concentration to reduce growth of cancer cells by 50%.

Table 7
Qualitative antimicrobial assay (100 mg cm^{-3})[a]

Compound	*Bacillus subtilis* (mutant-defective DNA repair, B28)	*Pseudomonas aeruginosa* (60 690)	Methicillin resistant *Sthaphylococcus* (MRSA)	*Bacillus subtilis*-wild type (B29)	*Saccharomyces cerevisiae* (20341)	*Candida albicans* (C.A.)	*Candida lypolytica* (2075)	*Aspergillus ochraceous* (398)
1	38	34	32	38	36	30	26	24
2	11	9	8	10	8	8	8	8
3	6	6	9	10	6	13	8	6
4	17	17	18	15	10	10	16	na
5	20	6	15	10	8	6	20	na
6	8	9	8	10	9	11	8	9
7	7	6	8	6	6	6	6	7
8	6	6	6	6	8	6	24	na
9	6	6	6	6	6	6	21	na
10	6	6	8	9	6	7	6	6
SBDTC	25	30	19	25	26	26	36	17
SMDTC	38	34	24	40	44	44	38	38
Streptomycin (control)	30	30	31	30				
Nystatin (control)					24	21	27	25

na, not available.
[a] Inhibition diameter in millimeters. Inhibition diameter > 15 mm – strongly active.

Table 8
Quantitative antimicrobial assay (MIC value, μg ml^{-3})[a]

Compound	*Bacillus subtilis* (mutant-defective DNA repair, B28)	*Pseudomonas aeruginosa* (60 690)	Methicillin resistant *Sthaphylococcus* (MRSA)	*Bacillus subtilis*-wild type (B29)	*Saccharomyces cerevisiae* (20341)	*Candida albicans* (C.A.)	*Candida lypolytica* (2075)	*Aspergillus ochraceous* (398)
1	3125	3125	6250	3125	6250	6250	12 500	6250
4	12 500	12 500	6250	6250			6250	na
5	1562		1562				3125	na
8							25 000	na
9							50 000	na
Streptomycin (control)	48.8	12.2	12.2	48.8				
Nystatin (control)					6250	3125	6250	3125

[a] MIC (μg ml^{-3}) = minimum inhibitory concentration, i.e., the lowest concentration to completely inhibit microbial growth.

parent compound **1** showed activity against all the bacteria and fungi assayed (inhibitory zones above 15 mm). Qualitative antimicrobial analyses showed that this compound **1** was more active than SBDTC towards all the bacteria and fungi assayed [28] except for *C. lypolytica* (2075) (Table 7). Compounds **4** and **5** showed activity toward some of the bacteria. Meanwhile, compounds **4**, **5**, **8** and **9** were found to be active against the fungus, *C. lypolytica* (2075). Against bacteria, the MIC values (= 1562.5–12 500 μg cm^{-3}) for compounds **1**, **4**, **5**, **8** and **9** indicate that they are less active than the standard drug, streptomycin, However, the MIC values for compounds **1**, **4** and **5** against fungi were comparable to the drug standard, nystatin (Table 8).

4. Conclusion

The compounds **1** and **4** are uninegatively charged bidentate ligands, whereas **2**, **3** and **5** are uninegatively charged tridentate ligands like their *S*-benzyl analogs [2]. IR spectral analyses have shown that the Schiff bases are in the thione form when in solid state [2]. However, in solution, there occurs an equilibrium between the thione and thiolo isomer forms. The magnetic susceptibility measurements indicate that complexes **7** and **10** are high spin octahedral complexes [2], while complexes **6** and **8** are square-planar in structure. Complex **9** is proposed to be dimeric. The cytotoxic activities have been shown to follow the order S2PDTC < SMDTC < SBDTC for CEM-SS. However, SBDTC was inactive against HT-29 while the SMDTC was shown to be more active than S2PDTC (Table 6). The lower activities of S2PDTC are possibly due to the presence of pyridyl nitrogen group but the actual mechanism of interaction at the cellular level requires further investigation. It was found that SMDTC showed higher activity than SBDTC and S2PDTC for all fungi tested. Comparison studies with *S*-3-picolyldithiocarbazate (S3PDTC) and *S*-4-picolyldithiocarbazate (S4PDTC) are in progress.

5. Supplementary material

Crystallographic data for the structural analysis have been deposited with the Cambridge Crystallographic Data Centre, CCDC no. 186636. A copy of this information may be obtained free of charge from The Director, CCDC, 12 Union Road, Cambridge, CB2 1EZ, UK (fax: +44-1223-336033; email: deposit@ccdc.cam.ac.uk or www: http://www.ccdc.cam.ac.uk).

Acknowledgements

We thank the Department of Chemistry and Laboratory of Molecular and Cell Biology, Institute of Biosciences, University Putra Malaysia, for the provision of laboratory facilities. This research was funded by a grant from the Ministry of Science and Environment, Malaysia, under the Intensification of Research in Priority Areas scheme (IRPA grant No. 09-02-04-0296).

References

[1] M.A. Ali, S.E. Livingstone, Coord. Chem. Rev. 13 (1974) 101.
[2] M.A. Ali, M.T.H. Tarafder, J. Inorg. Nucl. Chem. 39 (1977) 1785.
[3] M.A. Ali, C.M. Haroon, M. Nazimuddin, S.M.M.H. Majumder, M.T.H. Tarafder, M.A. Khair, Transit. Met. Chem. 17 (1992) 133.
[4] M.A. Ali, M.H. Kadir, M. Nazimuddin, S.M.M.H. Majumder, M.T.H. Tarafder, M.A. Khair, Ind. J. Chem. 27A (1988) 1064.
[5] M.A. Ali, S.M.G. Hossain, S.M.M.H. Majumder, M.N. Uddin, M.T.H. Tarafder, Polyhedron 6 (1987) 1653.
[6] M.A. Ali, M. Uddin, M.N. Uddin, D.A. Chowdhury, M.T.H. Tarafder, Ind. J. Chem. 25A (1986) 238.
[7] M.A. Ali, S.M.M.H. Majumder, R.J. Butcher, J.P. Jasinski, J.M. Jasinski, Polyhedron 16 (1997) 2749.
[8] M.T.H. Tarafder, M. Rahim, Ind. J. Chem. 28A (1989) 1105.
[9] Y.P. Tian, C.Y. Duan, X.Z. You, Transit. Met. Chem. 23 (1998) 17.
[10] Y.P. Tian, C.Y. Duan, Z.L. Lu, X.Z. You, Polyhedron 15 (1996) 2263.
[11] X.H. Zhu, S.H. Liu, Y.J. Liu, J. Ma, C.Y. Duan, X.Z. You, Y.P. Tian, F.X. Xie, S.S. Ni, Polyhedron 19 (1998) 181.
[12] M.T.H. Tarafder, M.A. Ali, D.J. Wee, K. Azahari, S. Silong, K.A. Crouse, Transit. Met. Chem. 25 (2000) 456.
[13] M.T.H. Tarafder, M.A. Ali, N. Saravanan, W.Y. Weng, S. Kumar, N. Umar Tsafe, K.A. Crouse, Transit. Met. Chem. 25 (2000) 295.
[14] M.A. Ali, N.E. Ibrahim, R.J. Butcher, J.P. Jasinski, J.M. Jasinski, J.C. Bryan, Polyhedron 17 (1998) 1803.
[15] M.A. Ali, K.K. Dey, M. Nazimuddin, F.E. Smith, R.J. Butcher, J.P. Jasinski, J.M. Jasinski, Polyhedron 5 (1996) 3331.
[16] M.A. Ali, M. Nazimuddin, R. Shaha, R.J. Butcher, J.C. Bryan, Polyhedron 17 (1998) 3955.
[17] M.A. Ali, S.G. Teoh, J. Inorg. Nucl. Chem. 40 (1978) 2013.
[18] S. Bhattacharjee, R. Bhattacharyya, J. Chem. Soc., Dalton Trans. (1992) 1357.
[19] A.G. Bingham, H. Bogge, A. Muller, E.W. Ainscough, A.M. Brodie, J. Chem. Soc., Dalton Trans. (1987) 493.
[20] C.Y. Duan, Y.P. Tian, X.Z. You, T.C.W. Mak, Polyhedron 16 (1997) 4097.
[21] S.M.M.H. Majumder, M.A. Ali, F.E. Smith, M.A.U. Mridha, Polyhedron 7 (1998) 2183.
[22] M.E. Hossain, M.N. Alam, M.A. Ali, M. Nazimuddin, F.E. Smith, R.C. Hynes, Polyhedron 15 (1996) 973.
[23] S. Gou, X. You, Z. Xu, K. Yu, Z. Zhou, Polyhedron 10 (1991) 2659.
[24] M.A. Ali, A.H. Mirza, R.J. Butcher, M.T.H. Tarafder, M.A. Ali, Inorg. Chim. Acta 320 (2001) 1.
[25] M.T.H. Tarafder, M.A. Ali, Can. J. Chem. 56 (1978) 2000.
[26] M.T.H. Tarafder, N. Saravanan, K.A. Crouse, M.A. Ali, Transit. Met. Chem. 26 (2001) 613.
[27] M.T.H. Tarafder, S. Roy, Ind. J. Chem. 27A (1988) 407.
[28] M.T.H. Tarafder, A. Kasbollah, K.A. Crouse, A.M. Ali, B.M. Yamin, H.-K. Fun, Polyhedron 20 (2001) 2363.
[29] M.E. Hossain, M.N. Alam, J. Begum, M.A. Ali, M. Nazimuddin, F.E. Smith, R.C. Hynes, Inorg. Chim. Acta 249 (1996) 207.
[30] G.M. Sheldrick, SAINT V4, Software Reference Manual Siemens Analytical X-ray Systems, Madison, WI, USA, 1996.
[31] G.M. Sheldrick, SADABS, Program for Empirical Absorption Correction of Area Detector Data, University of Göttingen, Germany, 1996.
[32] G.M. Sheldrick, SHELXTL V5.1, Software Reference Manual, Brukel AXS, Inc., Madison, WI, USA, 1997.
[33] T. Mosmann, J. Immunol. Meth. 65 (1983) 55.
[34] M.T.H. Tarafder, Kar-Beng Chew, K.A. Crouse, A.M. Ali, B.M. Yamin, H.-K. Fun, Polyhedron 21 (2002) 2683.
[35] C.D. Hufford, A.M. Clark, Discovery and development in the new drugs for systematic opportunistic infections, in: Atta-ur-Rahman (Ed.), Studies in Natural Product Chemistry, Elsevier, Amsterdam, 1988, p. 421.
[36] K.A. Crouse, Ker-Beng Chew, Bohari M. Yamin, Seik-Weng Ng, M.T.H. Tarafder, Acta Crystallogr. E 59 (2003) 148.
[37] R. Mattes, H. Waber, J. Chem. Soc., Dalton Trans. (1980) 423.
[38] S.S.S. Raj, B.M. Yamin, Y.A. Yussof, M.T.H. Tarafder, H.-K. Fun, K.A. Crouse, Acta Crystallogr. C 56 (2000) 1236.
[39] K.A. Crouse, Lay-Yoong Goh, Inorg. Chim. Acta 99 (1985) 199.
[40] K.A. Crouse, Lay-Yoong Goh, Inorgan. Chem. 25 (1986) 478.
[41] J.E. Kovacic, Spectrochim. Acta 23A (1967) 183.
[42] M.A. Ali, D.J. Philips, S.E. Livingstone, Inorg. Chim. Acta 5 (1971) 119.
[43] M.A. Ali, R.N. Bose, J. Inorg. Nucl. Chem. 39 (1977) 265.
[44] D. Gattegno, A.M. Giuliani, Tetrahedron 30 (1974) 701.
[45] A.B.P. Lever, in: Inorganic Electronic Spectroscopy, 2nd ed., Elsevier, Amsterdam, 1984, p. 553.
[46] M.T.H. Tarafder, N. Saravanan, K.A. Crouse, B.M. Yamin, H.-K. Fun, S.S.S. Raj, I.A. Razak, Z. Kristallogr. 216 (2001) 283.

Available online at www.sciencedirect.com
SCIENCE DIRECT®
Polyhedron 23 (2004) 169–176
POLYHEDRON
www.elsevier.com/locate/poly

Construction of lanthanide(III) coordination polymers with 1,2-bis(4-pyridyl) ethane-N,N'-dioxide and *trans*-1,2-bis(4-pyridyl)ethene-N,N'-dioxide

Lin-Ping Zhang [a], Wen-Jie Lu [a,b], Thomas C.W. Mak [a,*]

[a] *Department of Chemistry, The Chinese University of Hong Kong, Shatin, New Territories, Hong Kong SAR, PR China*
[b] *Department of Chemical and Environmental Engineering, Wuyi University, Jiangmen, Guangdong Province, PR China*

Received 22 July 2003; accepted 29 September 2003

Abstract

Four lanthanide(III) complexes $\{[Ce(L^1)_{1.5}(NO_3)_3](CH_2Cl_2)_{0.25}(H_2O)_{0.25}\}_\infty$ **1**, $[Ln(L^2)_{1.5}(NO_3)_3]_\infty$ (Ln = Ce, **2**; Gd, **3**), and $[Yb(L^2)(CH_3OH)(NO_3)_3]_\infty$ **4** have been synthesized using 1,2-bis(4-pyridyl)ethane-N,N'-dioxide (L^1) and *trans*-1,2-bis(4-pyridyl)ethene-N,N'-dioxide (L^2). Bridged by the flexible L^1 ligand to form binuclear Ce_2O_2 units, compound **1** shows a three-dimensional network with triangular and distorted square channels. The isomorphous pair **2** and **3** composed of rigid L^2 linkers and Ln_2O_2 units (Ln = Ce, Gd) exhibit a layered structure of (4,4) topology. In compound **4**, the mononuclear Yb(III) ions are bridged by L^2 ligands to generate a sinuous chain.
© 2003 Elsevier Ltd. All rights reserved.

Keywords: Lanthanide nitrate; N,N'-dioxide; Self-assembly; Coordination polymer

1. Introduction

The use of transition metal centers and multidentate ligands for directing the assembly of complex structures has developed into one of the most widely used strategies for organizing molecular building blocks into supramolecular arrays in the last decade [1]. An important goal in constructing coordination polymers is to design functional molecular materials, which have potential application as catalytic, conductive, luminescent, magnetic, spin-transition, non-linear optical, and/or nanoporous materials [1–3]. In this context, the most utilized linear spacer for linking the transition metal centers is 4,4′-bipyridine [4]. More recently, other building blocks containing nitrogen donors such as pyrazine [5], 1,2-bis(4-pyridyl)-ethane [6], *trans*-1,2-bis(4-pyridyl)-ethene [7], 1,4-bis(4-pyridyl)benzene [8] and 2,4,6-tri(4-pyridyl)-1,3,5-triazine [9] have been employed in self-assembly reactions with various labile metal moieties. However, few coordination polymers based on bifunctional neutral ligands containing oxygen donors have been explored until recently [10]. 4,4′-Bipyridine-N,N'-dioxide was first employed as a bridging ligand in the construction of coordination networks [11], and a widely applicable strategy using poly(*N*-oxide) ligands as spacer linkers for assembling networks based on f-block metals has been developed [12]. More recently, 1,2-bis(4-pyridyl) ethane-N,N'-dioxide (L^1) and *trans*-1,2-bis(4-pyridyl)ethene-N,N'-dioxide (L^2) have been synthesized in our laboratory (Scheme 1) and used to generate a series of lanthanide(III) coordination polymers: $\{[Ln(L^1)_3]\cdot(ClO_4)_3\cdot(H_2O)\}_\infty$ (Ln = Er, Yb), which comprises two interpenetrating α-polonium nets; $\{[Ln(NO_3)_3(L^1)_{1.5}]\cdot H_2O\}_\infty$ (Ln = Er, Yb), which exhibits a mat-like pattern of three interwoven (6,3) nets; $\{[La(NO_3)_3(L^1)(CH_3OH)]\cdot CH_3OH\cdot CH_2Cl_2\}_\infty$, which is built of an offset stacking of distorted square grids; and $\{[Er(L^2)_{0.5}(H_2O)_3(C_2O_4)](ClO_4)\cdot L^2\cdot 6H_2O\cdot(dioxane)_{0.5}\}_\infty$, which is composed of (6,3) nets [13]. We have extended our investigation and report here three other kinds of lanthanide(III) coordination complexes

* Corresponding author. Tel.: +852-2609-6279; fax: +852-2603-5057.
E-mail address: tcwmak@cuhk.edu.hk (T.C.W. Mak).

0277-5387/$ - see front matter © 2003 Elsevier Ltd. All rights reserved.
doi:10.1016/j.poly.2003.09.023

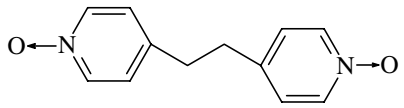

1,2-bis(4-pyridyl)ethane-*N,N'*-dioxide (L^1)

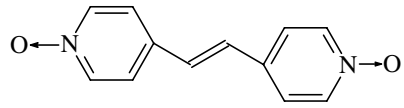

trans-1,2-bis(4-pyridyl)ethene-*N,N'*-dioxide (L^2)

Scheme 1.

constructed with these two ligands, which display new kinds of framework structures, namely $\{[Ce(L^1)_{1.5}(NO_3)_3](CH_2Cl_2)_{0.25}(H_2O)_{0.25}\}_\infty$ **1**, $[Ln(L^2)_{1.5}(NO_3)_3]\}_\infty$ (Ln = Ce, **2**; Gd, **3**) and $[Yb(L^2)(CH_3OH)(NO_3)_3]\}_\infty$, **4**.

2. Experimental

2.1. Materials

The bipyridyl-dioxide ligands 1,2-bis(4-pyridyl)ethane-N,N'-dioxide (L^1) and *trans*-1,2-bis(4-pyridyl)ethene-N,N'-dioxide (L^2) were synthesized as described previously [13]. The lanthanide(III) nitrates were obtained commercially (Aldrich) and used without further purification.

2.2. Synthesis of $\{[Ce(L^1)_{1.5}(NO_3)_3](CH_2Cl_2)_{0.25}(H_2O)_{0.25}\}_\infty$ (*1*)

A solution of L^1 (anhydrous, 50 mg, 0.2 mmol) in MeOH (8 ml) was carefully layered over CH_2Cl_2 (5 ml) in a test tube with solid $Ce(NO_3)_3 \cdot 6H_2O$ (65 mg, 0.15 mmol) placed at the bottom. Several days later, light yellow needle-like crystals gradually appeared on the walls at the bottom of the test tube. Yield ca. 35% (based on L^1). *Anal.* Calc. for $C_{36.5}H_{38}Ce_2ClN_{12}O_{24.5}$: C, 32.42; H, 2.83; N, 12.43. Found: C, 31.94; H, 3.03; N, 12.13%. IR (KBr, cm^{-1}): 3385brs, 3106s, 1656w, 1501m, 1383s, 1339s, 1234s, 1044w, 863m, 789w, 494w.

2.3. Synthesis of $[Ce(L^2)_{1.5}(NO_3)_3]_\infty$ (*2*)

Orange crystals of **2** were obtained by a similar procedure to **1** using L^2 in place of L^1. Yield ca. 40%. *Anal.* Calc. for $C_{18}H_{15}N_6O_{12}Ce$: C, 33.39; H, 2.34; N, 12.98. Found: C, 32.83; H, 2.52; N, 12.56%. IR (KBr, cm^{-1}): 3113w, 1629w, 1486s, 1456s, 1387m, 1315s, 1242s, 1038w, 970w, 863m, 802m, 561w, 500m.

Table 1
Crystallographic data of complexes **1**–**4**

	Complex			
	1	**2**	**3**	**4**
Empirical formula	$C_{36.5}H_{38}Ce_2ClN_{12}O_{24.5}$	$C_{18}H_{15}CeN_6O_{12}$	$C_{18}H_{15}GdlN_6O_{12}$	$C_{13}H_{14}YbN_5O_{12}$
Formula weight	1352.48	647.48	664.61	605.33
Crystal size (mm)	$0.4 \times 0.2 \times 0.2$	$0.4 \times 0.2 \times 0.19$	$0.3 \times 0.2 \times 0.15$	$0.35 \times 0.2 \times 0.15$
Crystal system	monoclinic	triclinic	triclinic	monoclinic
Space group	$P2/n$	$P\bar{1}$	$P\bar{1}$	$P2_1/c$
a (Å)	14.507(2)	10.0921(7)	10.103(1)	11.0890(8)
b (Å)	9.994(1)	10.3318(8)	10.312(1)	7.8615(6)
c (Å)	18.529(3)	11.3161(8)	11.354(1)	21.883(2)
α (°)	90	83.208(1)	83.131(2)	90
β (°)	103.577(3)	82.490(2)	82.398(2)	101.783(2)
γ (°)	90	69.947(1)	70.108(2)	90
V (Å^3)	2611.3(6)	1095.5(1)	1098.9(2)	1867.5(2)
Z	2	2	2	4
D_{calc} (g/cm^3)	1.720	1.963	2.009	2.153
μ(Mo Kα) (mm^{-1})	1.865	2.159	3.098	5.086
F(0 0 0)	1340	638	650	1172
Reflections collected	17323	6343	5956	9765
Independent reflections (R_{int})	6300 (0.0329)	4241 (0.0349)	3829 (0.0394)	3278 (0.0774)
Observed reflections [$I > 2\sigma(I)$]	4880	3865	3235	2527
Parameters	358	334	334	280
Goodness-of-fit	1.035	1.028	1.051	1.018
$R_1[I > 2\sigma(I)]$[a]	0.0322	0.0488	0.0553	0.0447
wR_2 (all data)[b]	0.1043	0.1278	0.1489	0.1173

[a] $R_1 = \sum ||F_0| - |F_c|| / \sum |F_0|$.

[b] $wR_2 = \left[\sum[w(F_0^2 - F_c^2)^2] / \sum[w(F_0^2)^2]\right]^{1/2}$.

Table 2
Selected bond lengths (Å) and angles (°) for compounds **1** to **4**

*Complex **1***			
Bond lengths			
Ce(1)–O(1)	2.445(3)	Ce(1)–O(5)	2.667(4)
Ce(1)–O(2)	2.560(2)	Ce(1)–O(7)	2.690(3)
Ce(1)– O(2a)	2.572(2)	Ce(1)–O(8)	2.554(3)
Ce(1)–O(3)	2.426(3)	Ce(1)–O(10)	2.599(3)
Ce(1)–O(4)	2.659(3)	Ce(1)–O(11)	2.643(3)
Bond angles			
O(1)–Ce(1)–O(2)	73.36(8)	O(3)–Ce(1)–O(2a)	80.69(9)
O(1)–Ce(1)–O(2a)	133.53(8)	O(4)–Ce(1)–O(5)	46.2(1)
O(2)–Ce(1)–O(2a)	61.15(9)	O(8)–Ce(1)–O(7)	48.09(9)
O(3)–Ce(1)–O(1)	145.6(1)	O(10)–Ce(1)–O(11)	48.6(1)
O(3)–Ce(1)–O(2)	140.85(9)		
*Complex **2***			
Bond lengths			
Ce(1)–O(1)	2.370(4)	Ce(1)–O(5)	2.669(4)
Ce(1)–O(2a)	2.462(4)	Ce(1)–O(7)	2.672(4)
Ce(1)–O(3)	2.561(4)	Ce(1)–O(8)	2.671(4)
Ce(1)–O(3b)	2.642(3)	Ce(1)–O(10)	2.643(4)
Ce(1)–O(4)	2.594(4)	Ce(1)–O(11)	2.578(5)
Bond angles			
O(1)–Ce(1)–O(2a)	144.9(2)	O(3)–Ce(1)–O(3b)	59.7(1)
O(1)–Ce(1)–O(3)	85.8(1)	O(4)–Ce(1)–O(5)	48.1(1)
O(1)–Ce(1)–O(3b)	74.0(1)	O(8)–Ce(1)–O(7)	47.4(1)
O(2a)–Ce(1)–O(3b)	71.0(1)	O(11)–Ce(1)–O(10)	48.2(1)
O(2a)–Ce(1)–O(3)	76.1(1)		
*Complex **3***			
Bond lengths			
Gd(1)–O(1)	2.385(5)	Gd(1)–O(5)	2.685(6)
Gd(1)–O(2a)	2.492(6)	Gd(1)–O(7)	2.695(6)
Gd(1)–O(3)	2.586(5)	Gd(1)–O(8)	2.691(6)
Gd(1)–O(3b)	2.655(5)	Gd(1)–O(10)	2.654(6)
Gd(1)–O(4)	2.600(6)	Gd(1)–O(11)	2.594(7)
Bond angles			
O(1)–Gd(1)–O(2a)	145.2(2)	O(3)–Gd(1)–O(3b)	59.8(2)
O(1)–Gd(1)–O(3)	85.6(2)	O(4)–Gd(1)–O(5)	47.4(2)
O(1)–Gd(1)–O(3b)	74.3(2)	O(8)–Gd(1)–O(7)	47.4(2)
O(2a)–Gd(1)–O(3b)	71.0(2)	O(11)–Gd(1)–O(10)	47.8(2)
O(2a)–Gd(1)–O(3)	76.1(2)		
*Complex **4***			
Bond lengths			
Yb(1)–O(1)	2.310(6)	Yb(1)–O(7)	2.433(7)
Yb(1)–O(2)	2.232(6)	Yb(1)–O(9)	2.407(6)
Yb(1)–O(3)	2.430(6)	Yb(1)–O(10)	2.392(7)
Yb(1)–O(4)	2.412(7)	Yb(1)–O(12)	2.343(6)
Yb(1)–O(6)	2.394(7)		
Bond angles			
O(2)–Yb(1)–O(1)	81.1(2)	O(4)–Yb(1)–O(3)	52.6(2)
O(1)–Yb(1)–O(12)	82.9(2)	O(6)–Yb(1)–O(7)	52.5(3)
O(2)–Yb(1)–O(12)	150.5(2)	O(10)–Yb(1)–O(9)	51.9(2)

Symmetry codes: a $-x+1,-y,-z$ for **1**; a $x-1,y+1,z+1$, b $-x+1,-y,-z$ for **2** and **3**.

2.4. Synthesis of $[Gd(L^2)_{1.5}(NO_3)_3]_\infty$ (**3**)

Yellow crystals of **3** were obtained in the same way as **2** using $Gd(NO_3)_3 \cdot 6H_2O$ in place of $Ce(NO_3)_3 \cdot 6H_2O$. Yield ca. 34%. *Anal.* Calc. for $C_{18}H_{15}N_6O_{12}Gd$: C, 32.53; H, 2.27; N, 12.65. Found: C, 32.50; H, 2.51; N, 12.31%. IR (KBr, cm^{-1}): 3113w, 1622w, 1488s, 1458s, 1385w, 1315m, 1239m, 1031w, 970w, 856m, 796m, 554w, 500m.

2.5. Synthesis of $[Yb(L^2)(CH_3OH)(NO_3)_3]_\infty$ (4)

Light yellow crystals of **4** were obtained in a similar way to **2** using $Yb(NO_3)_3 \cdot 5H_2O$ in place of $Ce(NO_3)_3 \cdot 6H_2O$. Yield ca. 30%. *Anal.* Calc. for $C_{13}H_{14}N_5O_{12}Yb$: C, 25.80; H, 2.33; N, 11.57. Found: C, 25.64; H, 2.81; N, 11.07%. IR (KBr, cm^{-1}): 3120w, 1635m, 1495m, 1385s, 1231m, 1185m, 977w, 863w, 802w, 547w, 500w.

2.6. X-ray crystallography

Selected single crystals of **1**–**4** sealed inside Lindemann glass capillaries were used for data collection on a Bruker SMART 1000 CCD diffractometer with graphite monochromated Mo Kα radiation ($\gamma = 0.71073$ Å) at 293 K. An empirical absorption correction was applied using the SADABS program [14]. The structures were solved by direct methods and refined by full-matrix least squares based on F^2 using the SHELXTL program package [15]. The crystallographic data for complexes **1**–**4** are summarized in Table 1.

3. Results and discussion

Pale yellow crystals of **1** were synthesized by slow reaction of $Ce(NO_3)_3$ and L^1 in a MeOH–CH_2Cl_2–H_2O medium. Crystalline compounds **2**, **3** and **4** were prepared in a similar way with $Ln(NO_3) \cdot 6H_2O$ (Ln = Ce and Gd) or $Yb(NO_3)_3 \cdot 5H_2O$ and L^2. Single crystal X-ray analyses confirmed that these materials have polymeric structures. Selected bond lengths and angles are given in Table 2.

In compound **1**, the asymmetric unit contains a Ce(III) ion, three nitrate ions, three independent halves of L^1 ligands that occupy special positions of symmetry

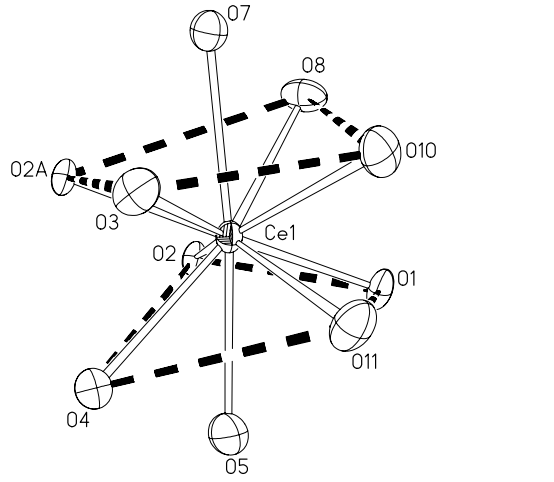

Fig. 1. Bicapped square-antiprismatic coordination environment of the Ce(III) ion in compound **1**.

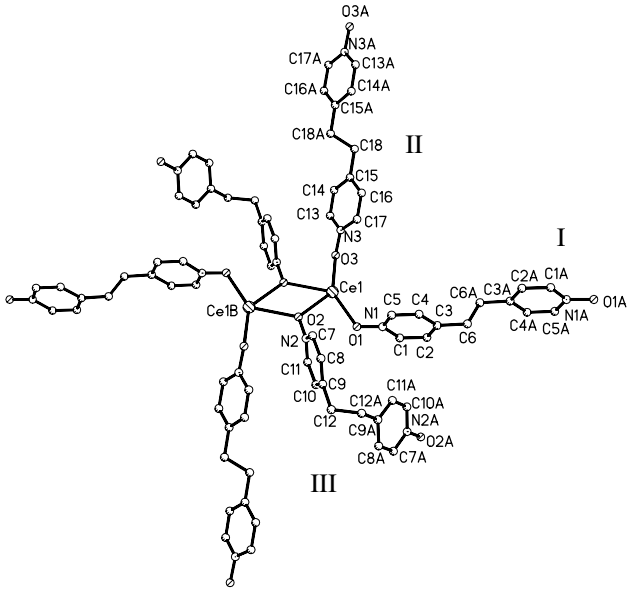

Fig. 2. The centrosymmetric Ce_2O_2 binuclear unit of compound **1**. The nitrate ions, water molecule, CH_2Cl_2 molecule and hydrogen atoms are omitted for clarity.

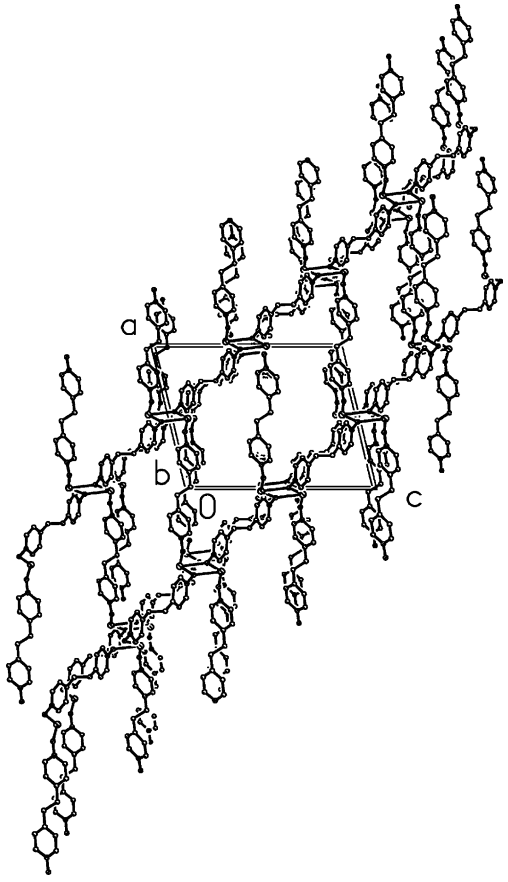

Fig. 3. Three-dimensional framework self-assembled by L^1 ligands of Type II (site symmetry $\bar{1}$) and Type III (site symmetry 2) with large distorted rectangular channels, viewed along the *b* direction.

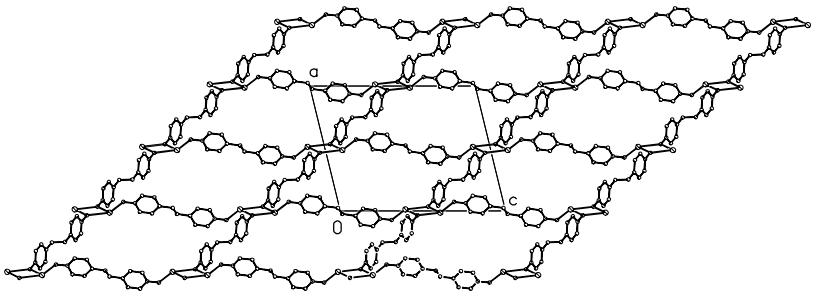

Fig. 4. Layer structure connected by L^1 ligands of Type I (site symmetry $\bar{1}$) and Type III (site symmetry 2), viewed along the *b* direction.

$\bar{1}$ or 2, and lattice water and dichloromethane molecules with only quarter site occupancy. The Ce(III) ions is located inside a bicapped square antiprism [Ce–O, 2.426(3)–2.690(3) Å], being surrounded by three chelating bidentate nitrate and four *N*-oxide groups (Fig. 1). The square antiprism is formed by O1, O2, O3 and O2A from *N*-oxide groups and O4, O8, O10 and O11 from nitrate ions, whereas the caps are formed by O5 and O7 from nitrate ions. Among the three distinguishable L^1 ligands, two located in $\bar{1}$ sites (labeled Type I and II in Fig. 2) act as an end-to-end linkers, whereas the third having site symmetry 2 (labeled Type III in Fig. 2) functions as a μ_4 linker with each *N*-oxide group bridging a pair of Ce(III) ions, leading to a centrosymmetric binuclear Ce_2O_2 subunit with a Ce···Ce distance of 4.42 Å. The dihedral angle of the two pyridine rings of the latter ligand is 57.3° and the torsion angle C9–C12–C12A–C9A is −70.2° (A: $-x+3/2, y, -z+1/2$). The centrosymmetric Ce_2O_2 moieties are bridged by the L^1 ligands of Type II and Type III to generate a three-dimensional network with large distorted rectangular channels (Fig. 3). In addition, the L^1 ligands of Type I

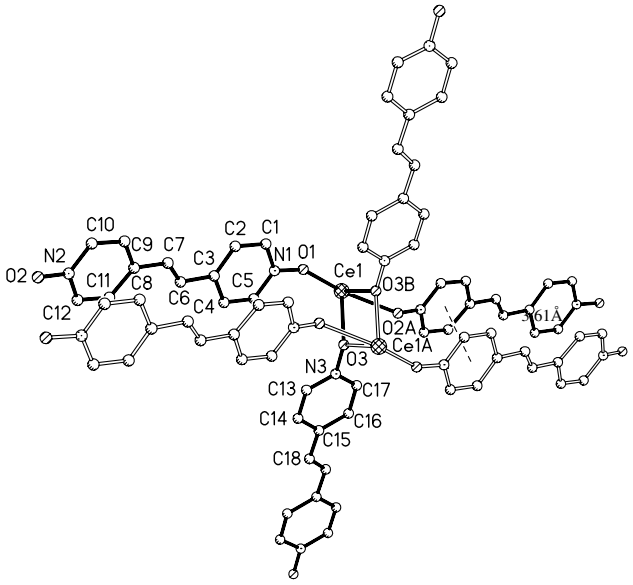

Fig. 6. The centrosymmetric Ce_2O_2 binuclear unit of compound **2**. The nitrate ions and hydrogen atoms are omitted for clarity. Symmetry transformations: A $(x-1, y+1, z+1)$ and B $(-x+1, -y, -z)$.

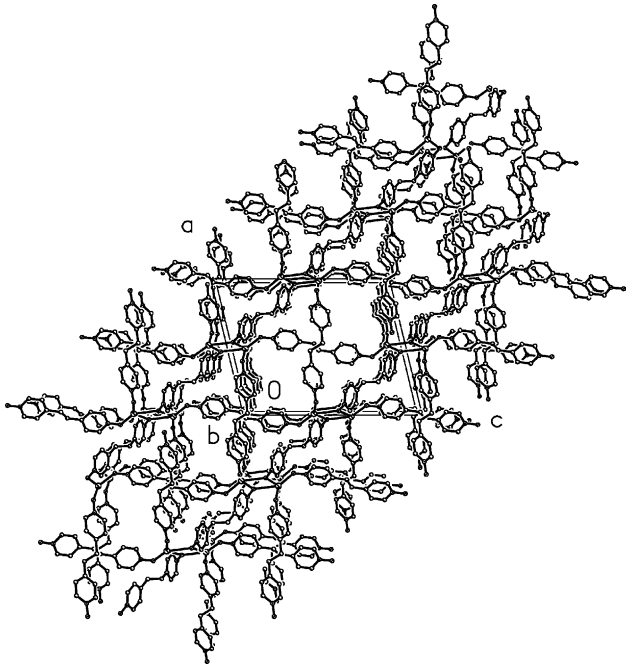

Fig. 5. Three-dimension network of **1** viewed along the *b* direction. This is a combination of the two networks shown in Figs. 3 and 4.

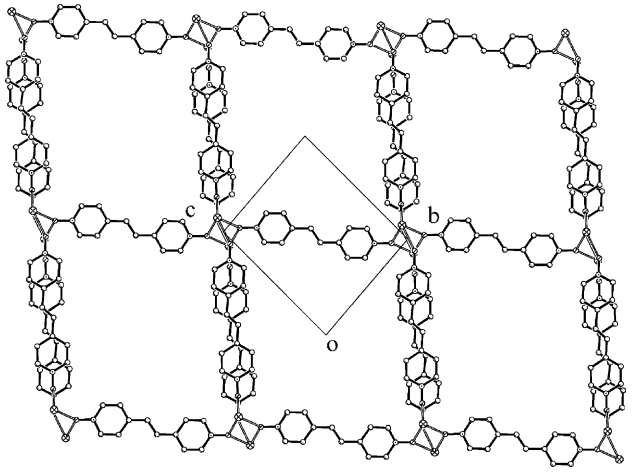

Fig. 7. Two-dimensional framework with large distorted square grids (ca. 12×13.9 Å) in compound **2**.

together with Type III also generate Ce_2O_2 moieties that are connected to form a layer structure normal to *b* axis (Fig. 4). The latter further consolidates the former three-dimensional network into a more complex structure and divides each large distorted rectangular channels into one distorted square and two triangular channels (Fig. 5). The disordered water molecule and CH_2Cl_2 are both located at special positions of site symmetry $\bar{1}$, occupying the larger distorted square channels of the three-dimensional network. In contrast, with the same L^1 ligand, the heavier lanthanide nitrates $Er(NO_3)_3$ and $Yb(NO_3)_3$ give complexes displaying an interpenetrating weave pattern of 3 two-dimensional (6,3) nets [13] that is different from the three-dimensional framework of **1**.

In compound **2**, the asymmetric unit contains a Ce(III) ion, three nitrate ions and one and a half L^2 ligands. The Ce(III) ion is coordinated by four *N*-oxide groups from different rigid L^2 ligands and three chelating bidentate nitrate groups, forming the same bicapped square-antiprismatic CeO_{10} coordination geometry as in **1** [Ce–O 2.370(4)–2.672(4) Å]. In this compound, the oxygen atoms O1, O3 and O2A from *N*-oxide and O5, O7, O8, O10 and O11 from nitrate ions construct the square antiprism, which are capped by O3B and O4 from *N*-oxide and nitrate groups, respectively (A: $x-1, y+1, z+1$; B: $-x+1, -y, -z$). Of the two independent L^2 ligands, one acts as an end-to-end linker, whereas the other occupying a $\bar{1}$ site functions in a μ_4

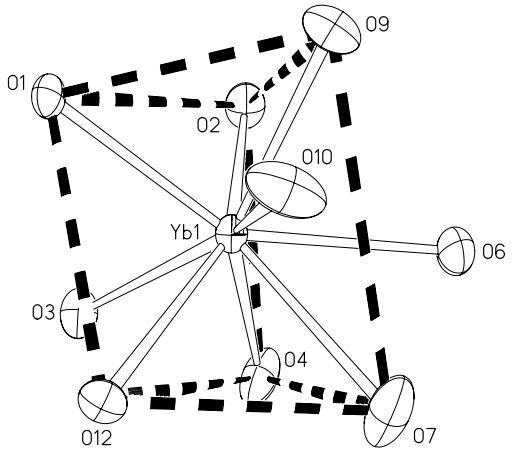

Fig. 8. Tricapped trigonal-prismatic coordination environment of the Yb(III) ion in compound **4**.

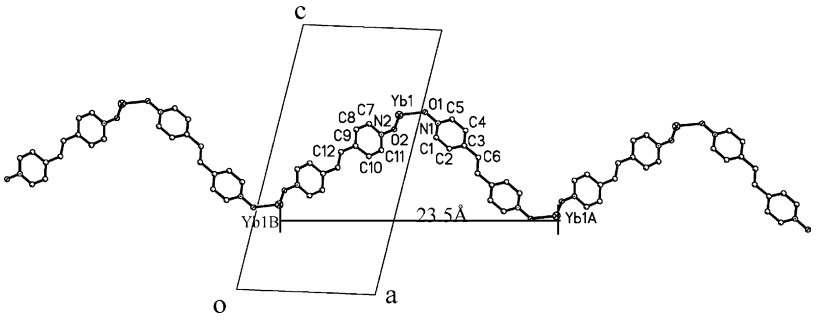

Fig. 9. The wavelike polymeric chain of compound **4**. The nitrate ions, MeOH molecules and hydrogen atoms are omitted for clarity. Symmetry transformations: A $(-x-1, -y+2, -z)$ and B $(-x+1, -y+3, -z)$.

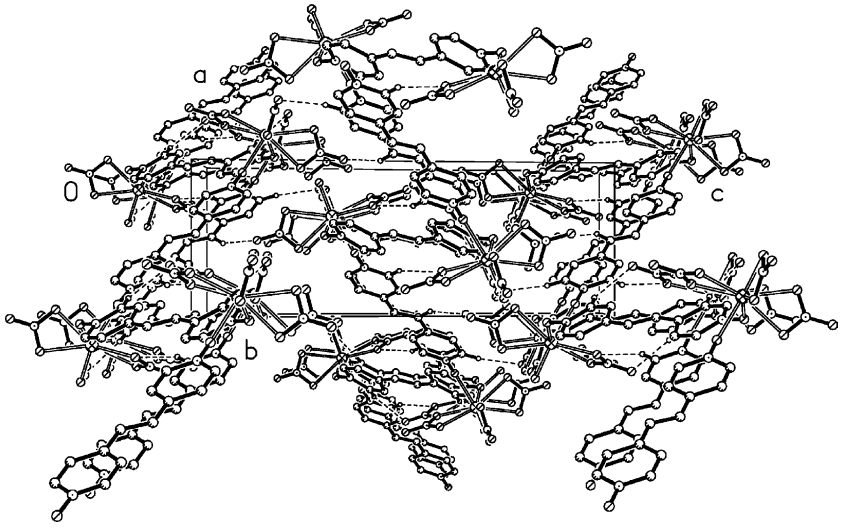

Fig. 10. Hydrogen bonded three-dimensional framework in **4**. The MeOH molecules and hydrogen atoms that have no contribution to the hydrogen bonding are omitted for clarity.

mode with each *N*-oxide group bridging a pair of Ce(III) ions, forming a centrosymmetric Ce_2O_2 binuclear unit with Ce···Ce distance 4.531 Å (Fig. 6). The end-to-end L^2 ligands link the binuclear centers along the [0 1 1] direction, generating an infinite double chain. And these double chains are further cross-linked by the μ_4 L^2 ligands, which bridge the binuclear centers to form an infinite single chain along the [0 1 $\bar{1}$] direction, leading to a layered structure with large distorted square grids (ca. 12×13.9 Å) (Fig. 7). The double chains overlap through π–π interactions between the adjacent pyridyl rings of neighboring L^2 ligands belonging to different chains with the center-to-center distance 3.61 Å and dihedral angel 6.3°. If each Ce_2O_2 unit can be considered as a 4-connected node, this layered structure has the topology of a (4,4) net. Though there are large square grids in this two-dimensional coordination network, the cavities are not filled by solvate molecules.

Compound **3** is isomorphous to compound **2**, with Gd(III) ions replacing Ce(III) ions.

In compound **4**, the asymmetric unit contains a Yb(III) ion, three nitrate ions, two half L^2 ligands and a methanol molecule. The MeOH molecule, three chelating bidentate nitrate ions and two *N*-oxide groups coordinate to Yb(III), leading to a tricapped trigonal prism (Fig. 8). The trigonal prism comprises O1 and O2 from *N*-oxide ligands, O4, O7 and O9 from three nitrate ions, and O12 from the MeOH molecule, whereas the three capping atoms are O3, O6 and O10 from different nitrate ions. The YbO_9 coordination environment [Yb–O 2.232(6)–2.433(7) Å] reflects the reduction in ionic radius from Gd(III) in **2** to Yb(III) in **4**. Both L^2 ligands in consecutive $\bar{1}$ sites act as end-to-end linkers, bridging the Yb(III) centers to generate a sinusoidal chain along the *a* axis with the period $|2\vec{a} + \vec{b}| = 23.5$ Å (Fig. 9). These chains are further connected through weak C–H···O hydrogen bonds: C1–H···O5a 130.7°, C1···O5a 3.11(1) Å; C4–H···O8b 151.0°, C4···O8b 3.38(1) Å; C7–H···O8c 154.9°, C7···O8c 3.40(1) Å; C11–H···O3a 153.6°, C11···O3a 3.27(1) Å; and C12–H···O11c 155.8°, C12···O11c 3.30(1) Å (a: $-x, -y+2, -z$; b: $x-1, y, z$; c: $-x+1, y+1/2, -z+1/2$), generating a three-dimensional framework (Fig. 10). In contrast, with the flexible L^1 ligand, $Yb(NO_3)_3$ forms a complex $\{[Yb(NO_3)_3(L^1)_{1.5}]\cdot H_2O\}_\infty$ showing an interpenetrating weave pattern of three two-dimensional (6,3) nets [13].

4. Conclusion

The building units of the coordination networks in compounds **1**–**3** are all binuclear, whereas that in compound **4** is mononuclear. For the Yb(III) ion of smaller size in **4**, only nine oxygen atoms enter into the coordination sphere, making more space available for the chelating bidentate nitrate groups, which is reflected by the significantly larger O–Ln–O bond angles (51.9°–52.6°) than those in **1**–**3** (46.2°–48.6°). Pair-wise comparison of structure **1** with **2**, and **4** with $\{[Yb(NO_3)_3(L^1)_{1.5}]\cdot H_2O\}_\infty$ [13], demonstrates the versatile coordination behavior of the flexible 1,2-bis(4-pyridyl)ethane-*N*,*N*′-dioxide (L^1), which bridge the Ln(III) ions in different modes, leading to various topological structures. On the other hand, the rigid *trans*-1,2-bis(4-pyridyl)ethene-*N*,*N*′-dioxide (L^2) yields less complex polymeric structures with Ln(III) ions. In all such compounds studied to date, the *N*-oxide group of L^1 and L^2 servers as a donor to one or two Ln(III) centers, and its potential to coordinate three metal centers needs to be further explored. As polypyridines are important ligands for d-block metal ions, poly(pyridine-*N*-oxides) may be expected to become equally versatile for f-block metal ions in coordination network assembly.

5. Supplementary material

Crystallographic data for the structural analysis have been deposited with the Cambridge Crystallographic Data Centre, CCDC Nos. 211536–211539 for compounds **1**–**4**. Copies of this information may be obtained free of charge from the Director, CCDC, 12 Union Road, Cambridge, CB2 1EZ, UK (fax: +44-1233-336033; e-mail: deposit@ccdc.cam.uk or www:http://www.ccdc.cam.ac.uk).

Acknowledgements

This work is supported by Hong Kong Research Grants Council Earmarked Grant CUHK 4268/00P and a Croucher Visiting Scholarship to W.-J. Lu.

References

[1] (a) B.J. Holliday, C.A. Mirkin, Angew. Chem. Int. Ed. Engl. 40 (2001) 2023;
(b) S.R. Batten, R. Robson, Angew. Chem. Int. Ed. Engl. 37 (1998) 1460;
(c) M. Munakata, L.P. Wu, T. Kuroda-Sowa, Adv. Inorg. Chem. 46 (1999) 173;
(d) A.J. Blake, N.R. Champness, P. Hubberstey, W.-S. Li, M.A. Withersby, M. Schröder, Coord. Chem. Rev. 183 (1999) 117;
(e) B. Multon, M.J. Zaworotko, Chem. Rev. 101 (2001) 1629;
(f) O.M. Yagi, H. Li, C. Davis, D. Richardson, T.L. Groy, Acc. Chem. Res. 31 (1998) 474;
(g) G.F. Swiegers, T. Malefetse, Chem. Rev. 100 (2000) 3483;
(h) S. Leininger, B. Olenyuk, P.J. Stang, Chem. Rev. 100 (2000) 853;
(i) D.L. Caulder, K.N. Raymond, Acc. Chem. Res. 32 (1999) 975;
(j) M. Fujita, Acc. Chem. Res. 32 (1999) 53.
[2] C. Janiak, Dalton Trans. (2003) 2781.
[3] C.-T. Chen, K.S. Suslick, Coord. Chem. Rev. 128 (1993) 293.

[4] (a) O.M. Yaghi, H. Li, J. Am. Chem. Soc. 117 (1995) 10401;
(b) P. Losier, M.J. Zaworotko, Angew. Chem. Int. Ed. Engl. 35 (1996) 2779;
(c) M. Fujita, Y.J. Kwon, S. Washizu, K. Ogura, J. Am. Chem. Soc. 116 (1994) 1151;
(d) X.-M. Chen, M.-L. Tong, Y.-J. Luo, Z.-N. Chen, Aust. J. Chem. 49 (1996) 835;
(e) L. Carlucci, G. Ciani, D.M. Proserpio, A. Sironi, J. Chem. Soc., Dalton Trans. (1997) 1801;
(f) Q.-F. Zhang, Y.-Y. Niu, W.-H. Leung, Y.L. Song, I.D. Williams, X.-Q. Xin, Chem. Commun. (2001) 1126.

[5] (a) J.A. Real, G. DeMunno, M.C. Munoz, M. Julve, Inorg. Chem. 30 (1991) 2701;
(b) J.S. Haynes, S.J. Retting, J.R. Sams, R.C. Thompson, J. Trotter, Can. J. Chem. 65 (1987) 420.

[6] (a) M. Fujita, Y.J. Kwon, M. Miyazawa, K. Ogura, Chem. Commun. (1994) 1977;
(b) C.S. Hong, Y. Do, Inorg. Chem. 37 (1998) 4470;
(c) D. Rochon, M. Andruh, R. Melanson, Can. J. Chem. 76 (1998) 1564;
(d) C.V.K. Sharma, R.D. Rogers, Chem. Commun. (1999) 83;
(e) M.L. Hernández, M.G. Barandika, M.K. Urtiaga, R. Cortés, L. Lezama, M.I. Arriortua, T. Rojo, J. Chem. Soc., Dalton Trans. (1999) 1401;
(f) K.N. Power, T.L. Lennigar, M.J. Zaworotko, Chem. Commun. (1998) 595;
(g) T.L. Hennigar, D.C. MacQuarrie, P. Losier, R.D. Rogers, M.J. Zaworotko, Angew. Chem. Int. Ed. Engl. 36 (1997) 972;
(h) Q.-M. Wang, G.-C. Guo, T.C.W. Mak, Chem. Commun. (1999) 1849.

[7] (a) D. Hagrman, R.C. Haushalter, J. Zubieta, Chem. Mater. 10 (1998) 361;
(b) O.S. Jung, S.H. Park, K.M. Kim, H.G. Jang, Inorg. Chem. 37 (1998) 5781;
(c) S.H. Park, K.M. Kim, S. Lee, O.S. Jung, Bull. Korean Chem. Soc. 19 (1998) 79.

[8] M. Fujita, Y.J. Kwon, O. Sasaki, K. Yamaguchi, K. Ogura, J. Am. Chem. Soc. 117 (1995) 7287.

[9] (a) B.F. Abraham, S.R. Batten, H. Hamit, B.F. Hoskins, R. Robson, Angew. Chem. Int. Ed. Engl. 35 (1996) 1690;
(b) S.R. Batten, B.F. Hoskins, R. Robson, J. Am. Chem. Soc. 117 (1995) 5385.

[10] B.-Q. Ma, S. Gao, H.-L. Sun, G.-X. Xu, J. Chem. Soc., Dalton Trans. (2001) 130.

[11] (a) D.-L. Long, A.J. Blake, N.R. Champness, M. Schröder, Chem. Commun. (2000) 1369;
(b) A. Nedelcu, Z. Žak, A.M. Madalan, J. Pinkas, M. Andruh, Polyhedron 22 (2003) 789.

[12] (a) D.-L. Long, A.J. Blake, N.R. Champness, C. Wilson, M. Schröder, J. Am. Chem. Soc. 123 (2001) 3401;
(b) D.-L. Long, A.J. Blake, N.R. Champness, C. Wilson, M. Schröder, Angew. Chem. Int. Ed. Engl. 40 (2001) 2444;
(c) S. Tanase, M. Andruh, A. Müller, M. Schmidtmann, C. Mathonière, G. Rombaut, Chem. Commun. (2001) 1084.

[13] W.-J. Lu, L.-P. Zhang, H.-B. Song, Q.-M. Wang, T.C.W. Mak, New J. Chem. 26 (2002) 775.

[14] G.M. Sheldrick, SADABS: Program for Empirical Absorption Correction of Area Detector Data, University of Göttingen, Germany, 1996.

[15] G.M. Sheldrick, SHELXTL: Structure Determination Software Progarams, Bruker Analytical X-ray System Inc, Madison, WI, 1997.

Available online at www.sciencedirect.com
SCIENCE DIRECT®
Polyhedron 23 (2004) 177–182
POLYHEDRON
www.elsevier.com/locate/poly

Preparation of polystyrene-supported hydrogermanes and their reduction of organic halides

Kunio Mochida [a,*], Kiyoko Amada [a], Hideo Sugimoto [a], Mitsuo Akiba [b], Katsuyuki Sato [b]

[a] Department of Chemistry, Faculty of Science, Gakushuin University, 1-5-1 Mejiro, Toshima-ku, Tokyo 171-8588, Japan
[b] Asai Germanium Research Institute Co., Ltd., 1-1-1 Manpukuji, Asou-ku, Kawasaki 215-0004, Japan

Received 3 September 2003; accepted 30 September 2003

Abstract

Polystyrene-supported hydrogermanes (**1**–**4**) were prepared by functionalization of polystyrenes or functionalization of a styrene followed by polymerization. The hydrogermanes, **1**–**4**, reduced organic halides with or without a catalyst to give alkanes under mild conditions in the order: C–I>C–Br>C–Cl. The hydrogermanes, **1**–**4**, were easily separated after use by filtering and could be regenerated with lithium aluminum hydride after their reactions with organic halides.
© 2003 Elsevier Ltd. All rights reserved.

Keywords: Polystyrene supported; Hydrogermane; Reduction; Recycle

1. Introduction

Reduction of organic halides by hydrostannanes and hydrosilanes in the presence of radical initiators has been investigated extensively and the synthetic utility of these reductions, especially with hydrostannanes, has been widely established [1–9]. The reduction of organic halides involving halogen-abstraction reaction by organostannyl and organosilyl radicals is a radical-chain process described as below [4].

$$R_3E\bullet + R'X \rightarrow R_3EX + R'\bullet$$

$$R'\bullet + R_3EH \rightarrow R'H + R_3E\bullet \quad E = Si, Ge, Sn$$

The radical-chain process by organostannyl radicals is very efficient even at low temperatures [10,11]. However, the tin compounds are toxic and cause disposal problems. Hydrosilanes are possible alternative compounds since organosilyl radicals are better halogen-abstracting reagents than their tin counterparts, and they have no toxic character. However, organosilanes are poor hydrogen atom donors toward organic radicals and do not support radical-chain reactions, except at elevated temperatures [12,13]. Moreover, the isolation of products in the reduction of organic halides by hydrostannanes and hydrosilanes in solutions is difficult. Recently, reduction of organic halides by hydrogermanes has also been of considerable interest from the viewpoint of moderate reactivity combined with selectivity and good hydrogen atom donors as compared with hydrostannanes and hydrosilanes [4,14–20]. In the course of our investigations on the structure and reactivity of organogermyl radicals we have undertaken preparation of polymer-supported hydrogermanes. These hydrogermanes are insoluble in common organic solvents and would easily be separated after use by filtering and would be recyclable. The polymer-supported hydrogermanes would also retain their integrity during chemical reactions. While the organic syntheses, their application and characterization of polymer-supported hydrostannanes have been reported [21–30], there is no report on analogues of germanium so far.

In this paper, we describe the synthesis of several polystyrene-supported hydrogermanes (**1**–**4**) and their reduction of organic halides.

* Corresponding author. Tel.: +81-3-3986-0221; fax: +81-3-5992-1029.
E-mail address: kunio.mochida@gakushuin.ac.jp (K. Mochida).

0277-5387/$ - see front matter © 2003 Elsevier Ltd. All rights reserved.
doi:10.1016/j.poly.2003.09.034

2. Results and discussion

2.1. Preparation of polystyrene-supported hydrogermanes

Polystyrene-supported hydrogermanes were prepared by several methods. Diethyldichlorogermane (Et_2GeCl_2) in THF was treated with one molar amount of poly(4-vinylphenyllithium) at 20 °C for 4 h to afford poly (4-vinylphenyldiethylchlorogermane). The poly(4-vinylphenyllithium) was prepared by the reaction of polystyrene in cyclohexane with a diethylether solution of butyllithium (BuLi) with *N*,*N*,*N*′,*N*′-tetramethylethylenediamine (TMEDA) at 65 °C for 6.5 h. The poly (4-vinylphenyldiethylgermane) (**1**) was obtained by reduction of the polystyrene-supported chlorogermane with lithium aluminum hydride (LAH). The polystyrene-supported chlorogermane and hydrogermane **1** were insoluble in common solvents. The polystyrene-supported hydrogermane **1** was analyzed by FT-IR (νGe–H: 2018 cm^{-1}) and XPS spectra (Ge content: 3.8 $mmol\,g^{-1}$, degree of functionalization = 0.28). The poly(4-vinylbenzyldiethylgermane) (**2**), in which the germyl moiety was separated from the aromatic ring by methylene, was prepared by a similar method to that of **1**. The treatment of Et_2GeCl_2 with one molar amount of poly(4-vinylbenzyllithium), which was prepared by the reaction of poly(4-vinylbenzyl chloride) with a diethylether solution of BuLi/TMEDA at 50 °C for 2 h, gave poly(4-vinylbenzyldiethylchlorogermane). The polystyrene-supported hydrogermane **2** was prepared by reduction of the corresponding chlorogermane with LAH.

The polymer-supported hydrogermane **2** was also insoluble in common solvents and was analyzed with FT-IR (νGe–H: 2015 cm^{-1}) and XPS spectra (Ge content: 3.8 $mmol\,g^{-1}$, degree of functionalization = 0.28). The preparation of polystyrene-supported hydrogermane, **1**–**2** is outlined as Scheme 1.

Poly(4-vinylybenzyl chloride) reacted with trichlorogermane ($HGeCl_3$) and triethylamine (Et_3N) in chloroform under reflux conditions for one day to give poly (4-vinylbenzyltrichlorogermane). The poly(4-vinylbenzyltrichorogermane) was reduced with LAH to give poly(4-vinylbenzylgermane) (**3**). The third polystyrene-supported hydrogermane **3** was analyzed by FT-IR spectra (νGe–H: 2063 cm^{-1}). Flame atomic absorption and oxygen bomb combustion analyses of the polymer-supported hydrogermane **3** revealed that the degree of functionalization with the germane group was 0.55. The preparation of polystyrene-supported germanium hydride **3** is outlined as Scheme 2. The hydrogermane **3** was insoluble in common solvents.

Nefedov and co-workers have reported that benzyl chloride reacts with $HGeCl_3$ in the presence of Et_3N to afford benzyltrichlorogermane [31].

p-Vinylphenethyldiethylchlorogermane was prepared by hydrogermylation of *p*-divinylbenzene with diethylchlorogermane ($Et_2(Cl)GeH$) with a catalytic amount of azobis(isobutyronitrile) (AIBN) at 60 °C for 10 h. Without purification, the crude *p*-vinylphenethyldiethylchlorogermane in octyl alcohol was directly polymerized in water containing methyl cellulose at 30 °C for 18 h to afford poly(4-vinylphenethyldiethylchlorogermane). The poly(4-vinylphenethyldiethylgermane) (**4**) was obtained by reduction of the polystyrene-supported chlorogermane with LAH (see Scheme 3).

The polystyrene-supported hydrogermane **4**, in which the germyl group was separated from the aromatic ring by two methylene units, was identified by FT-IR (νGe–H: 2000 cm^{-1}) and XPS spectra (Ge content: 4.0 $mmol\,g^{-1}$, degree of functionalization = 0.30). The polymer-supported hydrogermane **4** was insoluble in common solvents. The molecular weight of **4** could not be determined by GPC relative to polystyrene standard.

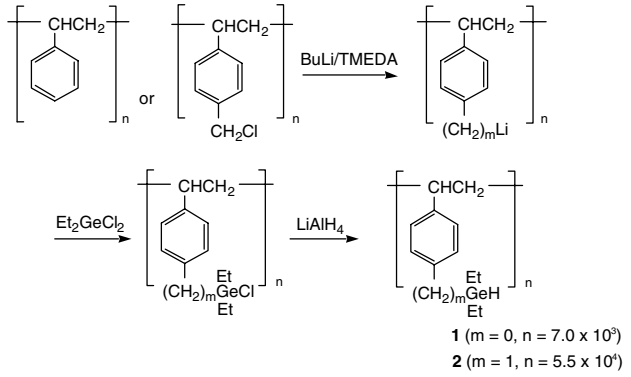

Scheme 1.

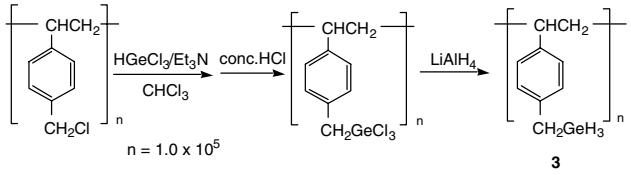

Scheme 2.

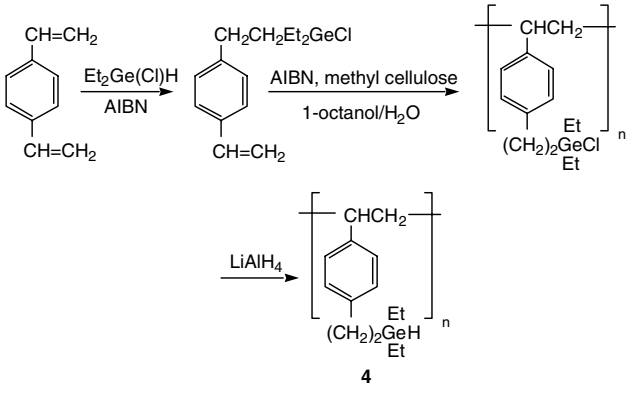

Scheme 3.

The content of germanium atoms in the polystyrene-supported hydrogermanes is low. This is because the carbon–carbon chains of polystyrene are distributed closely to each other and there are few chances of functionalization in polystyrenes.

2.2. Reduction of organic halides with 1–4

The polymer-supported hydrogermanes **1**–**4** and halogermanes are insoluble in common organic solvents. Therefore, the reagents can easily be separated after use simply by filtering after their reactions with organic substrates, and then they can be regenerated by LAH.

Polystyrene-supported germanium hydrides **1**–**4** are capable of reducing organic halides simply by heating without free-radical initiators in contrast to the behavior of hydrosilanes. The uncatalyzed reduction of organic halides with hydrogermanes has been explained in terms of a radical-chain process. The reductions of organic halides with polymer-supported hydrogermanes **1**–**4** were examined in the absence of solvents by heating with di-*tert*-butyl peroxide (DTBP) and without radical initiators. Tables 1–3 summarize the results of the reduction of organic halides. Products analyses were carried out by using GC and GC–MS spectroscopy using authentic samples. The yields of products were determined by GC with an internal standard method taking into account the germanium content of the polystyrene-supported hydrogermanes **1**–**4**.

Tables 1 and 2 show the results of reduction of octyl and aryl halides with polystyrene-supported organogermanium hydrides **1**–**4** catalyzed by DTBP and by only heating. Organic halides were clearly reduced to the corresponding reduction products. No coupling products were detected. The reactivity of the halogen atoms falls in the sequence: I>Br>Cl for **1**–**4**. The ease of reaction decreases in the order: octyl halides > aryl halides. These features are in accord with those found in homolytic reduction of organic halides with trialkylgermanes previously reported [15,16]. The yields of reduction products for octyl and aryl halides are low, except for octyl iodides and the polystyrene-supported hydrogermane **3** system. This is because steric crowding around the germanium atoms in **1**–**4**, in which the germyl group was not well separated from the aromatic ring, will cause a decrease in the reactivity of germanium hydride. The high yield of octane by reduction of octyl iodide with the hydrogermane **3** is attributed to the trihydrogermane (GeH_3). The low yields of reduction products for octyl and aryl bromides and chlorides are explained by the low reactivity of the (halo)dihydrogermanes ($Ge(X)H_2$) produced by reduction of the organic halides with the GeH_3 in **3**, as well as the steric crowding around the germanium atoms. The signals of $Ge(X)H_2$ were confirmed by IR spectroscopy.

Table 1
Reduction of octyl halides with polystyrene-supported hydrogermanes **1**–**4** initiated by DTBP[a]

Run	Polymer	Organic halide	Product (Yield (%))[b]
1	**1**	$C_8H_{17}I$	C_8H_{18}(54)
2	**1**	$C_8H_{17}Br$	C_8H_{18}(17)
3	**1**	$C_8H_{17}Cl$	C_8H_{18}(10)
4	**2**	$C_8H_{17}I$	C_8H_{18}(45)
5	**2**	$C_8H_{17}Br$	C_8H_{18}(20)
6	**2**	$C_8H_{17}Cl$	C_8H_{18}(trace)
7[c]	**3**	$C_8H_{17}I$	C_8H_{18}(260)
8[c]	**3**	$C_8H_{17}Br$	C_8H_{18}(15)
9[c]	**3**	$C_8H_{17}Cl$	C_8H_{18}(1)
10	**4**	$C_8H_{17}I$	C_8H_{18}(54)
12	**4**	$C_8H_{17}Br$	C_8H_{18}(17)
13	**4**	$C_8H_{17}Cl$	C_8H_{18}(10)

[a] At 135 °C for 20 h.
[b] GC yield.
[c] At 130 °C for 20 h without DTBP.

Table 2
Reduction of phenyl halides with polystyrene-supported hydrogermanes **1**–**4** initiated by DTBP[a]

Run	Polymer	Organic halide	Product (Yield (%))[b]
1	**1**	PhI	PhH (38)
2	**1**	PhBr	PhH (13)
3	**1**	PhCl	PhH (0)
4	**2**	PhI	PhH (44)
5	**2**	PhBr	PhH (trace)
6	**2**	PhCl	PhH (0)
7[c]	**3**	*p*-MeC_6H_4I	*p*-MeC_6H_5(60)
8[c]	**3**	*p*-MeC_6H_4Br	*p*-MeC_6H_5(5)
9[c]	**3**	*p*-MeC_6H_4Cl	*p*-MeC_6H_5(1)
10	**4**	PhI	PhH (55)
12	**4**	PhBr	PhH (45)
13	**4**	PhCl	PhH (trace)

[a] At 135 °C for 20 h.
[b] GC yield.
[c] At 130 °C for 20 h without DTBP.

Table 3 summarizes the results of reduction of benzyl halides, phenethyl bromide and polyhalobenzenes with polystyrene-supported hydrogermanes **1**–**4**. The reduction of benzyl bromides and phenethyl bromide with the hydrogermane **3** without free-radical initiators afforded the corresponding hydrocarbon in good yields. The GeH_3 in **3** took part in the reduction of organic halides. The reduction of polyhalobenzenes with polymer-supported hydrogermanes **1**–**4** was also examined. Polyhalobenzenes are reduced by a stepwise method, which makes it possible to carry out the selective reduction of polyhalides. *o*-Bromochlorobenzene and *o*-dibromobenzene were reduced with **1**, **2**, **4** stepwise to afford chlorobenzene and bromobenzene, respectively. The hydrogermane **3** reduced *p*-bromochlorobenzene and *p*-iodochlorobenzene to afford chlorobenzene selectively.

The extent of regeneration of polystyrene-supported hydrogermanes **1**–**4** after several reactions is 90%.

Table 3
Reduction of organic halides with polystyrene-supported hydrogermanes **1**–**4** initiated by DTBP[a]

Run	Polymer	Organic halide	Product (Yield (%))[b]
1[c]	**3**	$PhCH_2Cl$	$PhCH_2$(20)
2[c]	**3**	$PhCH_2Br$	$PhCH_3$(190)
3[c]	**3**	$Ph(CH_3)CHBr$	$PhCH_2CH_3$(300)
4[c]	**3**	$PhCH_2CH_2Br$	$PhCH_2CH_3$(180)
5	**1**	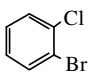	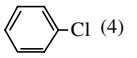 (4)
6	**2**	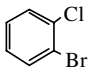	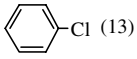 (13)
7	**4**	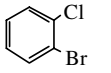	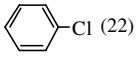 (22)
8	**1**	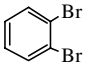	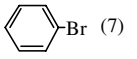 (7)
9	**2**	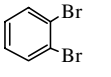	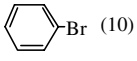 (10)
10	**4**	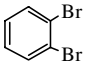	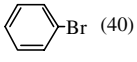 (40)
11[c]	**3**	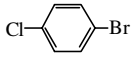	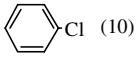 (10)
12[c]	**3**	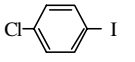	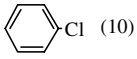 (10)

[a] At 135 °C for 20 h.
[b] GC yield.
[c] At 130 °C for 20 h without DTBP.

In conclusion, we have shown polystyrene-supported hydrogermanes **1**–**4** reduce organic halides under mild conditions. Advantages of the polymer-supported **1**–**4** are easier process, clean and simple work-up of the products and use of recyclable reagents.

3. Experimental

3.1. General methods

The NMR spectra were obtained on a Varin Unity Inova 400 MHz, JEOL JNM-MY 60 MHz, and GX 270 MHz NMR spectrometer. The GC–MS spectra were measured on a JEOL LMS-DX 303 mass spectrometer. The IR spectra were recorded with a Shimadzu FT IR 4200 spectrometer. Gas chromatography was performed on a Shimadzu GC 8A with a 1 m 20% SE column and 1 m 30% Apiezon L column. GPC was performed on a JAL HPLC.

3.2. Materials

Diethyldichlorogermane [32] and diethylchlorogermane [33] were prepared as reported in the literature. Polystyrene, poly(4-vinylbenzyl chloride), *p*-divinylbenzene, trichlorogermane, TMEDA, octyl alcohol, organic halides, AIBN, DTBP, lithium aluminum hydride, methylcellulose and butyllithium were commercially available.

3.3. Preparation of poly(4-vinylphenyldiethylchlorogermane)

To a cyclohexane solution (10 ml) of polystyrene ($M_w = 7.0 \times 10^3$, 1.0 g, 0.01 mol) in a three-necked flask fitted with a condenser, mechanical stirrer and pressure equalizing dropping funnel, TMEDA (1.5 ml) and then butyllithium in diethylether (1.28 N, 11.7 ml, 0.015 mol) were added under an argon atmosphere. The reaction mixture was stirred at 65 °C for 6.5 h. After removal of the liquid phase, the polymer was washed with THF. The washing THF was removed. To the crude poly(4-vinylphenyllithium) in new THF (8 ml), diethyldichlorogermane (Et_2GeCl_2) (2.20 g, 0.01 mol) was added slowly. The resulting mixture was quenched with anhydrous ethanol and then filtered. After drying in vacuo at 60 °C the poly(4-vinylphenyldiethylchlorogermane) weighed 1.2 g.

3.4. Preparation of poly(4-vinylphenyldiethylgermane) (*1*)

To poly(4-vinylphenyldiethylchlorogermane) (1.2 g) in THF (1.5 ml) lithium aluminum hydride (LAH) (0.152 g, 4.0 mmol) suspended in THF (8 ml) was added. The reaction mixture was refluxed with stirring for 1 h. The resulting mixture was quenched with anhydrous ethanol and then filtered. After drying in vacuo at 40 °C the poly(4-vinylphenyldiethylgermane) weighed 1.1 g. Polystyrene bands (cm^{-1}): [34,35] aromatic C–H stretchings, 3010; aliphatic C–H stretchings, 2950, 2920 and 2890; aromatic C–C stretchings, 1490; weak in-plane aromatic C–H bending bands, 1090 and 1020; out-of-plane C–H aromatic bending bands, 830. Other bands (cm^{-1}): Ge–H stretching, 2018. XPS spectra revealed the germanium content in **1** was 3.8 mmol g^{-1}. The degree of functionalization was 0.28.

3.5. Preparation of poly(4-vinylbenzyldiethylchlorogermane)

To a cyclohexane solution (1 ml) of poly(4-vinylbenzyl chloride) ($M_w = 5.5 \times 10^4$, 2.5 g, 0.03 mmol) in a two-necked flask fitted with a condenser, TMEDA (0.1 ml) and then butyllithium in diethylether (1.0 N, 45 μl, 0.045 mmol) were added under an argon atmosphere.

The reaction mixture was stirred at 50 °C for 2 h. After removal of the liquid phase, the polymer was washed with THF. The washing THF was removed. To the crude poly(vinylbenzyllithium) in new THF (1 ml), diethyldichlorogermane (Et_2GeCl_2) (7.0 mg, 0.03 mmol) was added slowly. The resulting mixture was quenched with anhydrous ethanol and then filtered. After drying in vacuo at 60 °C the poly(4-vinylbenzyldiethylchlorogermane) weighed 2.4 g.

3.6. Preparation of poly(4-vinylbenzyldiethylgermane) (**2**)

To poly(4-vinylbenzyldiethylchlorogermane) (2.4 g) in THF (5.0 ml) LAH (0.152 g, 4.0 mmol) suspended in THF (8 ml) was added. The reaction mixture was refluxed with stirring for 1 h. The resulting mixture was quenched with anhydrous ethanol and then filtered. After drying in vacuo at 40 °C the poly(4-vinylbenzyldiethylgermane) weighed 2.1 g. Polystyrene bands (cm^{-1}): [34,35] aromatic C–H stretchings, 3015; aliphatic C–H stretchings, 2872; aromatic C–C stretchings, 1508; weak in-plane aromatic C–H bending bands, 1043 and 984; out-of-plane aromatic C–H bending bands, 762. Other bands (cm^{-1}): Ge–H stretching, 2015. XPS spectra revealed Ge content: 3.8 mmol g^{-1}. The degree of functionalization was 0.28.

3.7. Preparation of poly(4-vinylbenzyltrichlorogermane)

To a chloroform solution (10 ml) of poly(4-vinylbenzyl chloride) ($M_w = 1.0 \times 10^5$, 3.0 g, 0.03 mmol) in a two-necked flask fitted with a condenser, trichlorogermane ($HGeCl_3$) 4.8 ml (0.09 mmol) and then triethylamine (4.8 ml, 0.09 mol) were added under an argon atmosphere. The reaction mixture was refluxed with stirring at 50 °C for one day. The unreacted $HGeCl_3$ was removed by washing with HCl several times. After complete removal of chloroform, the polymer weighed 2.5 g. NMR (δ, THF-d_8) 1.20–2.18 (m, 3H), 3.35–3.84 (m, 2H), 6.23–7.28 (m, 2H).

3.8. Preparation of poly(4-vinylbenzylgermane) (**3**)

To suspended LAH (5.7 g, 0.15 mol) in THF (100 ml) poly(4-vinylbenzyltrichlorogermane) (2.5 g) in THF (20 ml) was added. The reaction mixture was refluxed with stirring for 4 h. The resulting mixture was hydrolyzed with water. The resulting polymer was filtered. After drying in vacuo at 40 °C the poly(4-vinylbenzylgermane) weighed 1.8 g. Polystyrene bands (cm^{-1}): [34,35] aromatic C–H stretchings, 3010; aliphatic C–H strechings, 2920 and 2851; aromatic C–C stretchings, 1508. Other bands (cm^{-1}): Ge–H stretching, 2063. Flame atomic absorption and oxygen bomb combustion analyses of the hydrogermane **3** revealed that the degree of functionalization with the germane group was 0.55.

3.9. Preparation of poly(4-vinylphenethyldiethylgermane) (**4**)

p-Divinylbenzene (55/45 mixture of *p*-isomer/*m*-isomer) (1.3 g, 0.01 mol) and AIBN (0.03 g, 0.2 mmol) were placed in a two-necked flask fitted with a condenser and pressure equalizing dropping funnel. To this mixture diethylchlorogermane ($Et_2(Cl)GeH$) (1.7 g, 0.01 mol) was added. The reaction mixture was stirred at 60 °C. The progress of hydrogermylation was checked by GC. After the disappearance of $Et_2(Cl)GeH$, 1-octyl alcohol (4.5 ml) was added. The octyl alcohol solution of 4-vinylphenethyldiethylchlorogermane was transferred to a water containing methyl cellulose (0.03 g). After stirring at 30 °C for 1 h, the reaction mixture was refluxed with stirring for 18 h. The reaction mixture was collected on a filter and washed with methanol, acetone, and toluene. After drying under vacuum, 1.41 g of poly(4-vinylphenethyldiethylgermane) (**4**) was obtained. Polystyrene bands (cm^{-1}): [34,35] aromatic C–H stretchings, 3005; aliphatic C–H stretchings, 2850 and 2750; aromatic C–C stretchings, 1600, 1510 and 1480; weak in-plane aromatic C–H bending bands, 1020; out-of-plane C–H aromatic bending bands, 700. Other bands (cm^{-1}): Ge–H stretching, 2000. XPS spectra revealed Ge content: 4.0 mmol g^{-1}. The degree of functionalization was 0.30. The molecular weight of **4** could not be determined by GPC relative to polystyrene standard.

3.10. Reactions of organic halides with polystyrene-supported hydrogermanes **1**–**4**

As a representative example, the reaction of octyl iodide with polystyrene-supported hydrogermane **3** is described. A mixture of octyl iodide (0.2 g, 0.8 mmol) and **3** (0.2 g, 0.002 mmol) was heated at 130 °C for 20 h. After washing the reaction mixture with a small amount of benzene, octane was identified by GC and GC–MS spectroscopy using authentic samples. The yield of octane was determined by GC with an internal standard method taking into account the germanium content of the polystyrene-supported hydrogermane **3**.

Acknowledgements

The authors thank Dr. Riichi Nishide of Nissan Auto Co. Ltd., for measuring the XPS of polymer-supported hydrogermanes **1**, **2** and **4**. We also thank Mitsubishi Material Co. Ltd., for a gift of tetrachlorogermane.

References

[1] H.G. Kuivila, Adv. Organomet. Chem. 1 (1964) 47.
[2] H.G. Kuivila, Acc. Chem. Res. 1 (1968) 299.
[3] W.P. Neumann, Angew. Chem. 76 (1964) 849.
[4] H. Sakurai, in: J.K. Kochi (Ed.), Free Radicals, vol. 2, Wiley, New York, 1973 (Ch. 25).
[5] E.J. Kupchik, in: A.K. Sawyer (Ed.), Organotin Compounds, vol. 1, Marcel Dekker, New York, 1971 (Ch. 2).
[6] D.A. Armitage, in: G. Wilkinson, F.G.A. Stone, E.W. Abel (Eds.), Comprehensive Organometallic Chemistry, vol. 2, Pergamon Press, Oxford, 1982 (Ch. 9.1).
[7] A.G. Davies, P.J. Smith, in: G. Wilkinson, F.G.A. Stone, E.W. Abel (Eds.), Comprehensive Organometallic Chemistry, vol. 2, Pergamon Press, Oxford, 1982 (Ch. 9.7).
[8] B. Giese, Radicals in Organic Synthesis: Formation of Carbon–Carbon Bonds, Pergamon, New York, 1986.
[9] C. Chatgilialoglu, D. Griller, M. Lesage, J. Org. Chem. 53 (1988) 3642.
[10] L.K. Kaplan, J. Chem. Soc., Chem. Commun. (1969) 106.
[11] P. Rieviere, M.R. Baudet, J. Sage, in: G. Wilkinson, F.G.A. Stone, E.W. Abel (Eds.), Comprehensive Organometallic Chemistry, vol. 2, Pergamon Press, Oxford, 1982 (Ch. 10.3).
[12] C. Chatgilialoglu, K.U. Ingold, J.C. Scaiano, J. Am. Chem. Soc. 104 (1982) 5123.
[13] J. Lusztyk, B. Maillard, K.U. Ingold, J. Org. Chem. 51 (1986) 2457.
[14] H. Sakurai, K. Mochida, J. Chem. Soc., Chem. Commun. (1971) 151.
[15] H. Sakurai, K. Mochida, A. Hosomi, F. Mita, J. Organomet. Chem. 38 (1972) 275.
[16] H. Sakurai, K. Mochida, J. Organomet. Chem. 42 (1972) 339.
[17] H. Sakurai, K. Mochida, M. Kira, J. Am. Chem. Soc. 94 (1976) 929.
[18] H. Sakurai, K. Mochida, Bull. Chem. Soc. Jpn. 49 (1976) 3703.
[19] H. Sakurai, K. Mochida, M. Kira, J. Organomet. Chem. 124 (1977) 235.
[20] K. Mochida, H. Sugimoto, Y. Yokoyama, Polyhedron 16 (1997) 1767.
[21] H. Schumann, B. Pachaly, Angew. Chem., Int. Ed. 20 (1981) 1043.
[22] Y. Ueno, K. Chino, M. Watanabe, O. Moriya, M. Okawara, J. Am. Chem. Soc. 104 (1982) 5564.
[23] B.L. Miller, J.W. Hershberger, J. Polym. Sci.: Part C: Polym. Lett. 25 (1987) 219.
[24] U. Gergk, M. Gerlach, W.P. Neumann, R. Vieler, V. Weintritt, Synthesis (1990) 448.
[25] M. Gerlach, F. Jordens, H. Kuhn, W.P. Neumann, M. Peterseim, J. Org. Chem. 56 (1991) 5971.
[26] G. Ruel, N.K. The, G. Dumartin, B. Delmond, M. Pereyre, J. Organomet. Chem. 444 (1993) C18.
[27] J.H. Cmeron, in: M. Gielen, R. Willem, B. Wrackmeyer (Eds.), Solid State Organometallic Chemistry: Methods and Applications, Wiley, Chichester, 1999, p. 473, and references cited therein.
[28] F.A.G. Mercier, M. Biesemans, R. Altmann, R. Willem, R. Pintelon, J. Schoukens, B. Delmond, G. Dumartin, Organometallics 20 (2001) 958.
[29] J.C. Martins, F.A.G. Mercier, A. Vandervelden, M. Biesemans, J.-M. Wieruszeski, E. Humpfer, R. Willem, G. Lippens, Chem. Eur. J. 8 (2002) 3431.
[30] H. Dalil, M. Biesemans, R. Willem, L. Angiolini, E. Salatelli, D. Caretti, N.A. Chaniotakis, K. Perdikaki, Helv. Chim. Acta 85 (2002) 852.
[31] O.M. Nefedov, S.P. Kolesnikov, L. Scheinchenko, Angew. Chem. 76 (1964) 498.
[32] L. Horvitz, E.A. Flodd, J. Am. Chem. Soc. 55 (1933) 5055.
[33] M. Lesbre, J. Satge, Compt. Rend. 252 (1961) 1976.
[34] R.M. Silverstein, G.C. Bassler, T.C. Morrill, Spectrometric Identification of Organic Compounds, 5th ed., Wiley, New York, 1991, p. 91.
[35] C.J. Pouchert, The Aldrich Library of Infrared Spectra, 2nd ed., Aldrich Chemical Co., Milwaukee, WI, 1975.

Available online at www.sciencedirect.com
SCIENCE DIRECT®
Polyhedron 23 (2004) 183–187
POLYHEDRON
www.elsevier.com/locate/poly

Synthesis and structure of $LLnBr_2$ ($L = Et_2NCH_2CH_2NC(Me)CHC(Me)NCH_2CH_2NEt_2$; Ln = Y, Sm, and Yb)

Ana Mirela Neculai, Dante Neculai, Herbert W. Roesky *, Jörg Magull

Institut für Anorganische Chemie der Universität Göttingen, Tammannstrasse 4, D-37077, Göttingen, Germany

Received 21 July 2003; accepted 3 October 2003

Abstract

The reaction of the in situ prepared LLi ($L = Et_2NCH_2CH_2NC(Me)CHC(Me)NCH_2CH_2NEt_2$ with $LnBr_3$ (Ln = Y, Sm, and Yb) led to the solvent and alkali salt free dibromoderivative of type $LLnBr_2$ (Ln = Y, **1**, Sm, **2**, and Yb, **3**). Compounds **1**–**3** were characterized by X-ray crystallography, elemental analysis, and NMR (**1**), and their structural features were correlated with those of other compounds bearing the same ligand.
© 2003 Elsevier Ltd. All rights reserved.

Keywords: Lanthanides; Yttrium; Diketiminato

1. Introduction

The efforts of the last years to expand the chemistry of lanthanides beyond the well-known cyclopentadienyl derivatives have brought into the light a large plethora of new complexes [1–10]. In view of the current interest in these compounds as precatalysts [11–13] we have initiated studies in new ligand systems.

Ligands containing the β-diketiminato backbone offer possibilities of stabilisation for unusual bonding situations which have been exploited for various main group and transition metal complexes [14–18]. In comparison with this relatively well developed field, the area of β-diketiminato based complexes of early transition metals and lanthanides remains rather unexplored [19,20].

Previously we reported the synthesis and structural characterization of novel derivatives of scandium $LScX_2$ (X = Cl, Br), praseodymium, $LPrX_2$ (X = Cl, Br, BH_4), $LHoI_2$, $LErI_2$, and of $LTbX_2$ (X = Br, CH_2SiMe_3; $L = Et_2NCH_2CH_2NC(Me)CHC(Me)NCH_2CH_2NEt_2$), that belong to a new class of lanthanide complexes containing a β-diketiminato-based ligand which possesses two pendant arms (Fig. 1) [21–24]. The variety of surprising compounds synthesized involving the derivatives of this ligand [24–27] convinced us to extend the chemistry of the monoanionic precursor to other rare earth metals. Herein we present our recent results in this direction namely complexes with lanthanides and yttrium of the Group 3 elements using ligand L. Moreover, we provide details on structural aspects of β-diketiminato-based complexes of these elements.

2. Experimental

All operations involving air and moisture sensitive compounds were performed using standard Schlenk line and dry box techniques under purified nitrogen atmosphere. $SmBr_3$ and YBr_3 were prepared following the procedures described in the literature [28]. Diethylether, toluene and pentane were dried from appropriate drying agents, Na/benzophenone (diethylether), Na/K alloy (toluene, pentane) and distilled under nitrogen prior to use. C_6D_6 was dried over Na/K alloy and degassed. ^1H and ^{13}C NMR spectra were recorded at ambient temperature on a Bruker AM 200. Chemical shifts are reported in

* Corresponding author. Tel.: +49-551-393001; fax: +49-551-393373.
E-mail address: hroesky@gwdg.de (H.W. Roesky).

0277-5387/$ - see front matter © 2003 Elsevier Ltd. All rights reserved.
doi:10.1016/j.poly.2003.10.009

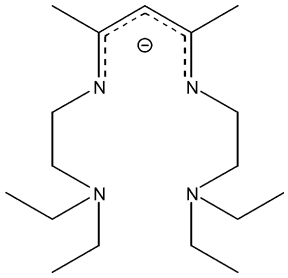

Fig. 1. Monoanionic, β-diketiminato ligand L^- used in this study.

δ units downfield from tetramethylsilane with the solvent as the reference signal. Mass spectra were recorded on a Finnigan MAT 8230 instrument, and elemental analyses were carried out at the Analytical Laboratory of the Institute of Inorganic Chemistry of the University of Göttingen. Melting points were determined in sealed capillary tubes under nitrogen and are uncorrected.

3. Preparation

$LYBr_2$ (**1**). 50 cm^3 of dry diethyl ether were added to 2.85 g (1 mmol) of LH in a 100 cm^3 Schlenk flask. The mixture was cooled to −78 °C and a solution of 6 cm^3 (1.6 M, 9.6 mmol) LiMe in diethylether was added dropwise. The reaction was stirred for 2 h at −78 °C, and then stirred overnight at room temperature until the methane evolution had ceased. The solvent was removed and toluene (50 cm^3) was added. Finally the solution was added dropwise to a suspension of 3.29 g (1 mmol) YBr_3 in toluene (25 cm^3) in a 100 cm^3 Schlenk flask. Then, the reaction mixture was refluxed overnight. The suspension was hot filtered, the solvent removed and the crude product was washed with pentane (50 cm^3) to yield 4.71 g (86.6%) of $LYBr_2$. Large colourless crystals were obtained cooling the mother liquor at −26 °C.

Complexes **2** and **3** can be prepared in a similar manner using $SmBr_3$ and $YbBr_3$, respectively, instead of YBr_3.

1. *Anal.* Calc. for $C_{17}H_{35}Br_2N_4Y$: C, 37.52; H, 6.48; N, 10.20. Found: C, 37.32; H, 6.64; N, 10.06%. ^1H NMR (200 MHz, TMS, C_6D_6): $\delta = 4.80$ (s, 1 H, CH), 3.10 (m, 16 H, $NCH_2CH_2N(CH_2)_2$), 1.59 (s, 6 H, $CHCCH_3$), 0.82 (t, 12H, CH_2CH_3); ^{13}C NMR (125.75 MHz, TMS, C_6D_6): $\delta = 166.25$ (CCHC), 99.91 (CH), 55.07 ($CNCH_2$), 49.43 (NCH_2CH_2), 30.10 (CH_2NCH_2), 23.03 ($CHCCH_3$), 8.23 (NCH_2CH_3); M.p. 150–155 °C; EI-MS: *m/z* (rel. int. %) 544 [M^+, 8], 458 [M^+–$C_5H_{12}N$, 100].
2. *Anal.* Calc. for $C_{17}H_{35}Br_2N_4Sm$: C, 33.71; H, 5.82; N, 9.25. Found: C, 33.51; H, 5.73; N, 8.92%. M.p. 205 °C. EI-MS: *m/z* (rel. int. %): 607 [M^+, 16], 521 [M^+–$C_5H_{12}N$, 100].
3. *Anal.* Calc. for $C_{17}H_{35}Br_2N_4Yb$: C, 32.50; H, 5.61; N, 8.92. Found: C, 32.63; H, 5.65; N, 9.04%. M.p. 177 °C. EI-MS: *m/z* (rel. int. %): 629 [M^+, 45], 573 [M^+–$C_5H_{12}N$, 100].

4. General aspects of X-ray data collection, structure determination, and refinement for complexes 1–3

Crystal, data collection, and refinement parameter are given in Table 1. Data for crystal structures of **1**–**3** were collected on a Stoe Image Plate IPDS II-System.

All structures were solved by direct methods (SHELXS-97) and refined against F^2 using SHELXL-97 [29]. Heavy atoms were refined anisotropically. Hydrogen atoms were included using the riding model with U_{iso} tied to U_{iso} of the parent atoms. Crystal data collection details, and the solution and refinement procedures are summarized in Table 1.

5. Results and discussion

$LLnBr_2$ (Ln = Y: **1**; Ln = Sm: **2**; Ln = Yb: **3**). Reaction of $LnBr_3$ with 1 equiv of LLi at reflux temperature yields tetrahydrofuran, dichloromethane and toluene respectively soluble complexes of general composition $C_{17}H_{35}N_4LnBr_2$ (Ln = Sm: yellow **2**; Ln = Yb: violet **3**) and $C_{17}H_{35}N_4LnBr_2{\cdot}C_7H_8$ (Ln = Y: colourless **1**) in good yields. Crystals of **1**–**3** suitable for X-ray studies were obtained by slow evaporation followed by refrigeration for several h at −26 °C (Fig. 2). It has to be noticed that these compounds do not have in the coordination sphere either solvent molecules or lithium halide which makes them more appropriate for further reactions.

Selected bond distances and angles for compounds **1**–**3** are listed in Table 2. In compounds **1**–**3** both pendant arms of the ligand are coordinated to the metal centre and all four nitrogen atoms and the metal atom are in the same plane. For the complex **3** (see Fig. 3) a local distortion can be observed due to the different orientation of one of the ethyl groups from one of the arms. The coordination number at the metal ion is in every case *six* and the geometry around the metal atom is *pseudooctahedral* which led, as a direct consequence, to the nonequal Ln–Br bond lengths. Nevertheless, these bond lengths are in the range of those for previously reported compounds [30c]. However, in every case the coordination number and the oxidation state of the metal ion centre finely tune the Ln–Br bond lengths. For instance the Y–Br bond length is 2.79 Å (av) [30] in Na_3YBr_6, which is comparable to that in **1** (see Table 2). The Ln–N bond lengths of the pendant arms are longer than those of the backbone, due to the coordinative and covalent character involved in different bonding modes. As far as the Ln–N (β-diketiminato) bond length is

Table 1
Crystallographic data for $LYBr_2$ (**1**), $LSmBr_2$ (**2**), $LYbBr_2$ (**3**)

Complex	**1** · C_7H_8	**2**	**3**
Formula	$C_{17}H_{35}Br_2N_4Y \cdot C_7H_8$	$C_{17}H_{35}Br_2N_4Sm$	$C_{17}H_{35}Br_2N_4Yb$
Formula weight	636.35	605.66	628.35
Space group	$P2_1/n$	$P2_1/c$	$Pca2_1$
Crystal system	monoclinic	monoclinic	orthorhombic
a (Å)	7.829(8)	10.783(9)	20.083(16)
b (Å)	8.379(11)	7.874(4)	8.170(5)
c (Å)	42.04(4)	25.925(2)	13.533(8)
β (°)	94.30(8)	90.28(7)	90
V (Å^3)	2750.3(5)	2201.3(3)	2220.7(3)
Z	4	4	4
D_{calcd} (g/cm^3)	1.537	1.827	1.879
Temperature (K)	133(2)	133(2)	133(2)
2θ range (°)	2.48–24.0984	1.89–24.76	2.03–24.714
Index ranges	$-8 \leqslant h \leqslant 7,\ -8 \leqslant k \leqslant 9,\ -40 \leqslant l \leqslant 48$	$-12 \leqslant h \leqslant 12,\ -9 \leqslant k \leqslant 9,\ -30 \leqslant l \leqslant 30$	$-23 \leqslant h \leqslant 23,\ -8 \leqslant k \leqslant 9,\ -14 \leqslant l \leqslant 15$
Reflections collected/unique	6486/4034 [$R_{int} = 0.0771$]	26141/3761 [$R_{int} = 0.0715$]	19437/3625 [$R_{int} = 0.0462$]
Observed reflections [$I > 2\sigma(I)$]	2820	2462	3472
Completeness to θ_{max} (%)	92.6	99.7	100.0
Data/restraint/parameter	4034/0/288	3761/0/220	3625/3/224
Goodness-of-fit	1.085	1.036	1.061
Final R indices [$I > 2\sigma(I)$]	$R_1 = 0.0551,\ wR_2 = 0.1315$	$R_1 = 0.0215,\ wR_2 = 0.0546$	$R_1 = 0.0164,\ wR_2 = 0.0385$
R indices (all data)	$R_1 = 0.0764,\ wR_2 = 0.1387$	$R_1 = 0.0263,\ wR_2 = 0.0566$	$R_1 = 0.0176,\ wR_2 = 0.0387$
Largest differences in peak and hole (e/A^3)	0.524, −0.760	0.939, −0.537	0.660, −0.410

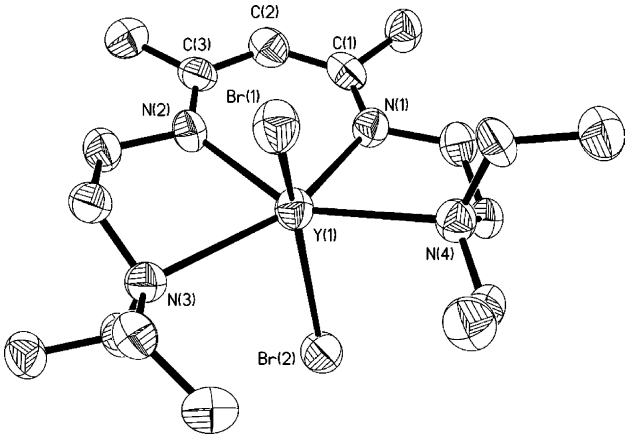

Fig. 2. Molecular structure of $\mathbf{1}\cdot C_7H_8$ showing 50% probability ellipsoids (the hydrogen atoms are omitted for clarity).

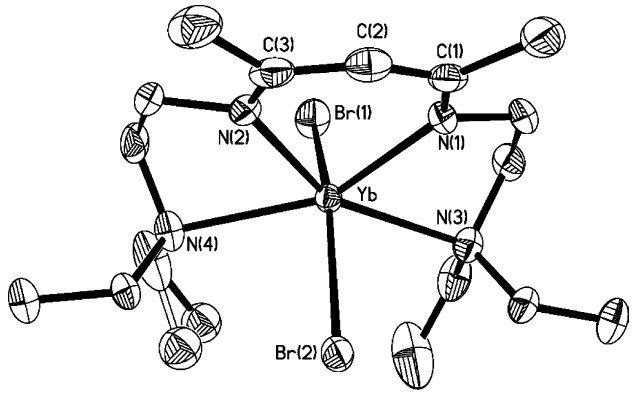

Fig. 3. Molecular structure of **3** showing 50% probability ellipsoids (the hydrogen atoms are omitted for clarity).

concerned it has to be said that only samarium β-diketiminato derivatives are known [20]. The Ln–N bond lengths are similar to those in **2**. In several studies it has been shown that a β-diketiminato ligand can act as either a donor of 4 electrons, in this case the nature of the bonds is σ, or a donor of 6 electrons, in this case the description of the bonds is 2σ–π [19,31]. Information whether there is predominantly 2σ or 2σ–π bonding between the ligand and metal ion can be deduced from the deviation of the metal ion from the NC_3N backbone plane. As it can be seen from Table 3 there is a correlation between the electrophilicity of the metal ion and the deviation from the plane with the exception of the yttrium. It can be rationalized that the deviation from the plane correlates with the electrophilicity of the cation. As a consequence, the smallest deviation is found in the complex **2** (0.07 Å) which correlates with the size of Sm^{3+} that has the biggest ionic radius from this series. Furthermore, the influence on the Ln–Br as well as on Ln–N bond lengths can be observed (see Table 2) and they follow the same tendency as for Ln^{3+} ionic radii. Additionally, it can be pointed out that the 'bite' of a β-diketiminato ligand is big enough to accommodate any metal ion in NC_3N plane, at least the metals from this study. On the other hand, it has also been demonstrated that the bulkiness of the substituents on the β-diketiminato backbone can account for the deviation of the metal ion as well [19] but for the **1**–**3** complexes this is not the case.

Table 3
The distance from the metal ion centre to the backbone plane (NC_3N plane) (Å)

$LScBr_2$ [22b]	$\mathbf{1}\cdot C_7H_8$	**2**	$LTbBr_2$ [24]	**3**
0.467	0.10	0.07	0.79	0.78

Table 2
Selected bond lengths (Å) and angles (°) for the compounds **1**–**3**

	$\mathbf{1}\cdot C_7H_8$	**2**	**3**
Bond lengths			
Ln(1)–N(1)	2.345(6)	2.405(3)	2.285(3)
Ln(1)–N(2)	2.345(6)	2.399(3)	2.282(3)
Ln(1)–N(3)	2.601(6)	2.643(3)	2.567(3)
Ln(1)–N(4)	2.577(6)	2.608(3)	2.560(4)
Ln(1)–Br(1)	2.751(1)	2.828(1)	2.740(1)
Ln(1)–Br(2)	2.776(1)	2.828(1)	2.684(1)
Bond angles			
N(1)–Ln(1)–N(2)	79.9(2)	78.62(9)	81.09(13)
N(1)–Ln(1)–N(4)	72.3(2)	70.74(9)	151.59(12)
N(4)–Ln(1)–N(3)	138.1(2)	142.13(9)	137.72(11)
N(2)–Ln(1)–N(3)	71.9(2)	70.86(10)	151.65(12)
Ln(1)–N(1)–C(1)	130.1(5)	129.9(2)	125.1(3)
N(1)–C(1)–C(2)	125.2(7)	124.7(3)	124.1(4)
C(1)–C(2)–C(3)	130.1(8)	131.8(3)	130.4(4)
C(2)–C(3)–N(2)	124.6(7)	124.6(3)	123.7(4)
C(3)–N(2)–Ln(1)	129.9(5)	130.3(2)	125.0(3)
Br(1)–Ln(1)–Br(2)	145.29(4)	142.615(13)	151.184(16)

6. Conclusions

This study has shown that the ligand L functions as an ancillary system for samarium and ytterbium, as well as yttrium thereby providing an easy access to a novel class of β-diketiminato lanthanide complexes. A subsequent investigation of the reaction chemistry of these systems is currently under way.

7. Supplementary material

Crystallographic data (excluding structure factors) for the structures reported in this paper have been deposited with CCDC Nos.: 175027, 175028 and 175029. Copies of the information may be obtained free of charge from The Director, CCDC, 12 Union Road, Cambridge CB2 1EZ, UK (fax: +44-1223-336033, E-mail: deposit@ccdc.cam.ac.uk or www: http://www.ccdc.cam.ac.uk).

Acknowledgements

We are thankful to the Deutsche Forschungsgemeinschaft for financial support.

References

[1] (a) P.W. Roesky, Eur. J. Inorg. Chem. (2001) 1653;
(b) F. Nief, Eur. J. Inorg. Chem. (2001) 891;
(c) L.H. Gade, Chem. Commun. (2000) 173.
[2] D.D. Graf, W.M. Davis, R.R. Schrock, Organometallics 17 (1998) 5820.
[3] M.D. Fryzuk, T.S. Haddad, S.J. Rettig, Organometallics 11 (1992) 2967.
[4] (a) R. Duchateau, C.T. van Wee, A. Meetsma, J.H. Teuben, J. Am. Chem. Soc. 115 (1993) 4931;
(b) J.R. Hagadorn, J. Arnold, Organometallics 15 (1996) 984.
[5] S. Hajela, W.P. Schaefer, J.E. Bercaw, J. Organomet. Chem. 532 (1997) 45.
[6] A. Maraval, D. Arquier, A. Igau, Y. Coppel, B. Donnadieu, J.-P. Majoral, Organometallics 20 (2001) 1716.
[7] Z. Lu, G.P.A. Yap, D.S. Richeson, Organometallics 20 (2001) 706.
[8] (a) J.A.R. Schmidt, J. Arnold, Chem. Commun. (1999) 2149;
(b) S. Bambirra, M.J.R. Brandsma, E.A.C. Brussee, A. Meetsma, B. Hessen, J.H. Teuben, Organometallics 19 (2000) 3197.
[9] (a) M.R. Bürgstein, H. Berberich, P.W. Roesky, Organometallics 17 (1998) 1452;
(b) P.W. Roesky, M.R. Bürgstein, Inorg. Chem. 38 (1999) 5629;
(c) P.W. Roesky, Inorg. Chem. 37 (1998) 4507.
[10] G.W. Rabe, C.D. Bérubé, G.P.A. Yap, Inorg. Chem. 40 (2001) 2682.
[11] (a) G.R. Giesbrecht, G.D. Whitener, J. Arnold, J. Chem. Soc., Dalton Trans. (2001) 923;
(b) B.J. O'Keefe, M.A. Hillmyer, W.B. Tolman, J. Chem. Soc., Dalton Trans. (2001) 2215.
[12] G.J.P. Britovsek, V.C. Gibson, D.F. Wass, Angew. Chem. 111 (1999) 448.
[13] G.J.P. Britovsek, V.C. Gibson, D.F. Wass, Angew. Chem. Int. Ed. 38 (1999) 428.
[14] (a) L. Bourget-Merle, M. Lappert, J.R. Severn, Chem. Rev. 102 (2002) 3031;
(b) W.E. Piers, D.J.H. Emslie, Coord. Chem. Rev. 233–234 (2002) 131;
(c) F.T. Edelmann, D.M.M. Freckmann, H. Schumann, Chem. Rev. 102 (2002) 1851.
[15] C. Cui, H.W. Roesky, H.-G. Schmidt, M. Noltemeyer, H. Hao, F. Cimpoesu, Angew. Chem. 112 (2000) 4444.
[16] C. Cui, H.W. Roesky, H.-G. Schmidt, M. Noltemeyer, H. Hao, F. Cimpoesu, Angew. Chem. Int. Ed. 39 (2000) 4274.
[17] (a) M.H. Chisholm, J.C. Huffman, K. Phomphrai, J. Chem. Soc., Dalton Trans. (2001) 222;
(b) A. Akkari, J.J. Byrne, I. Saur, G. Rima, H. Gornitzka, J. Barrau, J. Organomet. Chem. 622 (2001) 190.
[18] N.J. Hardman, B.E. Eichler, P.P. Power, Chem. Commun. (2000) 1991.
[19] (a) P.G. Hayes, W.E. Piers, L.W.M. Lee, L.K. Knight, M. Parvez, M.R.J. Elsegood, W. Clegg, Organometallics 20 (2001) 2533;
(b) L.W.M. Lee, W.E. Piers, M.R.J. Elsegood, W. Clegg, M. Parvez, Organometallics 18 (1999) 2947.
[20] D. Drees, J. Magull, Z. Anorg. Allg. Chem. 620 (1994) 814.
[21] D. Neculai, H.W. Roesky, A.M. Neculai, J. Magull, H.-G. Schmidt, M. Noltemeyer, J. Organomet. Chem. 643 (2002) 47.
[22] (a) A.M. Neculai, H.W. Roesky, D. Neculai, J. Magull, Organometallics 20 (2001) 5501;
(b) A.M. Neculai, D. Neculai, G. Nikiforov, H.W. Roesky, J. Magull, C. Schlicker, R. Herbst-Irmer, M. Noltemeyer, Eur. J. Inorg. Chem. (2003) 3120.
[23] G.B. Nikiforov, H.W. Roesky, T. Labahn, D. Vidovic, D. Neculai, Eur. J. Inorg. Chem. (2003) 433.
[24] D. Neculai, H.W. Roesky, A.M. Neculai, J. Magull, R. Herbst-Irmer, B. Walfort, D. Stalke, Organometallics 22 (2003) 2279.
[25] A.M. Neculai, D. Neculai, H.W. Roesky, J. Magull, M. Baldus, O. Andronesi, M. Jansen, Organometallics 21 (2002) 2590.
[26] D. Neculai, H.W. Roesky, A.M. Neculai, J. Magull, B. Walfort, D. Stalke, Angew. Chem. 114 (2002) 4470.
[27] D. Neculai, H.W. Roesky, A.M. Neculai, J. Magull, B. Walfort, D. Stalke, Angew. Chem. Int. Ed. 41 (2002) 4294.
[28] G. Brauer, Handbuch der präparativen Anorganischen Chemie, vol. 20, Ferdinand Enke Verlag, Stuttgart, 1978, p. 1077.
[29] G.M. Sheldrick, SHELXL, Program for Crystal Structure Refinement, University of Göttingen, Göttingen, Germany, 1997.
[30] (a) M.S. Wickleder, G. Meyer, Z. Anorg. Allg. Chem. 621 (1995) 457;
(b) G. Schilling, C. Kunert, T. Schleid, G. Meyer, Z. Anorg. Allg. Chem. 618 (1992) 7;
(c) S. Anfang, M. Karl, N. Faza, W. Massa, J. Magull, K. Dehnicke, Z. Anorg. Allg. Chem. 623 (1997) 1425.
[31] (a) D.W. Randall, S. George DeBeer, P.L. Holland, B. Hedman, K.O. Hodgson, W.B. Tolman, E.L. Solomon, J. Am. Chem. Soc. 122 (2000) 11632;
(b) L. Deng, R. Schmid, T. Ziegler, Organometallics 19 (2000) 3069.

Available online at www.sciencedirect.com
SCIENCE DIRECT®
Polyhedron 23 (2004) 189–194
POLYHEDRON
www.elsevier.com/locate/poly

Synthesis and X-ray crystal structures of hydridotris(3,5-dimethylpyrazolyl)borate (Tp′) molybdenum(VI) bis(imido) complexes

Vernon C. Gibson [a], Carl Redshaw [b,*], William Clegg [c], Mark R.J. Elsegood [d], Ulrich Siemeling [e], Thomas Türk [e]

[a] Department of Chemistry, Imperial College, South Kensington, London SW7 2AY, UK
[b] Wolfson Materials and Catalysis Centre, School of Chemical Sciences and Pharmacy, The University of East Anglia, Norwich NR4 7TJ, UK
[c] School of Natural Sciences (Chemistry), University of Newcastle, Newcastle upon Tyne NE1 7RU, UK
[d] Chemistry Department, Loughborough University, Loughborough, Leicestershire LE11 3TU, UK
[e] Science Department, University of Kassel, Heinrich-Plett-Str. 40, D-34132 Kassel, Germany

Received 5 August 2003; accepted 3 October 2003

Abstract

The reaction between the bridged bis(imido) complexes $\{[(CH_2)_n(2\text{-}C_6H_4N)_2]MoCl_2(dme)\}$ ($n = 1, 2$); dme = 1,2-dimethoxyethane) and one equivalent of potassium hydridotris(3,5-dimethylpyrazolyl)borate (KTp′) in refluxing thf gives $\{[(CH_2)_n(2\text{-}C_6H_4N)_2](Tp')MoCl\}$ ($n = 1$ (**1**), $n = 2$ (**2**)) as red crystalline solids in good yields. Similarly, the reaction between $[Mo(NAr)_2Cl_2(dme)]$ or $[Mo(NAr)(NBu^t)Cl_2(dme)]$ (Ar = 2,6-$Pr^i_2C_6H_3$) and KTp′ gives green [Tp′Mo(NAr)$_2$Cl] (**3**) or brown/black [Tp′Mo(NAr)(NBu^t)Cl] (**4**), respectively. X-ray crystal structures of the compounds **1**, **3** and **4** have been determined. All have octahedral structures with *fac* coordination for the tridentate Tp′ ligands and near-linear imido groups.
© 2003 Elsevier Ltd. All rights reserved.

Keywords: Tris(pyrazolyl)borate; Bis(imido); Molybdenum; Synthesis; Structures

1. Introduction

Bis(imido) molybdenum chemistry is relatively well developed and attracts attention as it provides an entry into well-defined metathesis catalysts [1,2]. We have previously described a number of *ansa*-bis(imido) complexes, containing various sizes (7–9) of molybdacyclic ring, of the form $\{[(CH_2)_n(2\text{-}C_6H_4N)_2]MoCl_2(dme)\}$ ($n = 1, 2$) and $[(NCMe_2CH_2\text{-}2\text{-}C_6H_4N)MoCl_2(dme)]$, isolobal analogues of the *ansa*-zirconocenes [3,4]. In other studies, we and others have been investigating the 'softness' of the angle associated with the imido bond. Near-linear angles in the range 150–180° are frequently observed and can be influenced by interligand steric interactions as well as crystal packing forces [5,6]. These results encouraged us to look at the use of the bulky tris(3,5-dimethylpyrazolyl)hydroborate (Tp′) ligand. Here we report the synthesis, characterisation and crystal structures of several bis(imido) molydenum(VI) complexes containing the Tp′ ligand. A number of transition metal imido species containing hydridotris(pyrazolyl)borate type ligands have previously been reported [7–14].

2. Results and discussion

2.1. Bridged bis(imido) complexes

Interaction of $\{[(CH_2)(2\text{-}C_6H_4N)_2]MoCl_2(dme)\}$ with one equivalent of KTp′ in refluxing thf yields, after work-up, red prisms of $\{[(CH_2)(2\text{-}C_6H_4N)_2](Tp')MoCl\}$ (**1**) in good yield (ca. 65%). In contrast to the Cp de-

* Corresponding author. Tel.: +44-1604-593137; fax: +44-1603-592003.
E-mail address: carl.redshaw@uea.ac.uk (C. Redshaw).

0277-5387/$ - see front matter © 2003 Elsevier Ltd. All rights reserved.
doi:10.1016/j.poly.2003.10.005

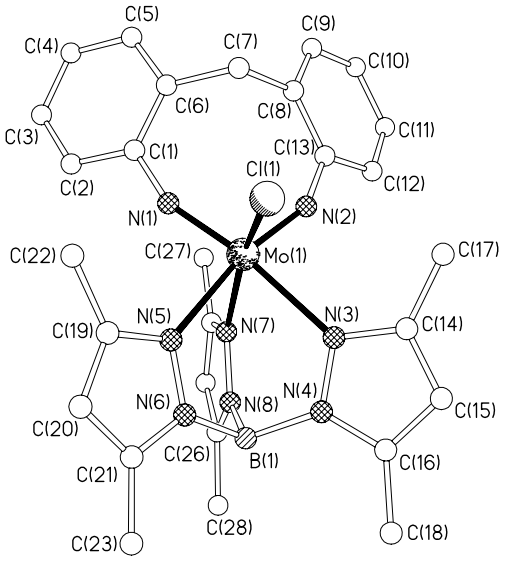

Fig. 1. Molecular structure of **1** without H atoms.

rivative **I** [3,4], where both *endo* and *exo* isomers are observed in solution (^{1}H NMR), for the bulkier Tp′ only the sterically more favourable *endo* isomer is isolated. Hence, the ^{1}H NMR of **1** exhibits signals at 5.65 and 5.87 ppm (ratio 1:2), and four methyl signals at 1.45, 2.40, 2.44 and 2.70 ppm (ratio 3:3:6:6) consistent with two sets of equivalent pyrazole rings. The two protons of the methylene bridge give rise to two doublets centred at 3.63 and 6.10 ppm ($^2J = 12.8$ Hz). The molecular structure of compound **1** · 2MeCN (obtained on recrystallisation of **1** from a saturated acetonitrile solution) was investigated by a single-crystal X-ray diffraction study (Fig. 1, Table 1).

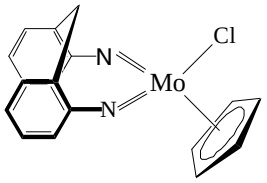

I Endo isomer (for exo isomer Cp and Cl are interchanged)

The molybdenum centre is coordinated by one chloro and five nitrogen atoms in a pseudo-octahedral arrangement. One face of the coordination polyhedron is formed by the three N atoms of the Tp′ ligand; owing to the *trans* influence of the imido ligands, two of the Mo–N bonds formed by the Tp′ group are considerably longer than the third [2.332(2) Å for Mo–N(3) and 2.319(2) Å for Mo–N(5) as opposed to 2.179(2) Å for Mo–N(7)]. Similar behaviour has been described for the complexes [Tp′Mo(N^{t}Bu)$_2$Cl] and [Tp′Mo(NNPh$_2$)$_2$Cl] [7–15]. Compared to the respective values observed for the compound [MoCl$_2$\{[2,2′-(N$_2$)–C$_6$H$_4$]$_2$CH$_2$\}(dme)], the bond parameters of the two imido bonds of **1** seem

Table 1
Selected bond lengths (Å) and angles (°)

	1	**3**	**4** (molecule 1)	**4** (molecule 2)
Bond lengths				
Mo(1)–Cl(1)	2.4200(7)	2.3993(6)	2.4101(10)	2.4103(10)
Mo(1)–N(1)	1.755(2)	1.7740(18)	1.741(3)	1.744(3)
Mo(1)–N(2)	1.765(2)	1.7805(17)	1.765(3)	1.772(3)
Mo(1)–N(3)	2.332(2)	2.3278(18)	2.380(3)	2.375(3)
Mo(1)–N(5)	2.319(2)	2.2880(18)	2.312(3)	2.305(3)
Mo(1)–N(7)	2.179(2)	2.1915(18)	2.183(3)	2.193(3)
N(1)–C	1.392(3)	1.390(3)	1.465(5)	1.451(5)
N(2)–C	1.389(3)	1.396(3)	1.387(5)	1.381(5)
Bond angles				
Cl(1)–Mo(1)–N(1)	98.11(7)	99.77(6)	94.03(10)	93.62(10)
Cl(1)–Mo(1)–N(2)	97.91(7)	94.98(6)	97.42(11)	97.36(10)
Cl(1)–Mo(1)–N(3)	84.47(6)	87.12(5)	82.91(8)	82.44(8)
Cl(1)–Mo(1)–N(5)	84.59(6)	83.80(5)	84.47(8)	84.90(8)
Cl(1)–Mo(1)–N(7)	159.17(6)	163.00(5)	159.36(9)	159.72(9)
N(1)–Mo(1)–N(2)	98.23(11)	105.87(8)	103.23(15)	103.31(14)
N(1)–Mo(1)–N(3)	172.09(9)	164.44(7)	170.37(14)	170.57(13)
N(1)–Mo(1)–N(5)	92.13(9)	89.03(7)	92.70(14)	93.29(13)
N(1)–Mo(1)–N(7)	95.27(9)	88.75(7)	98.14(13)	98.37(13)
N(2)–Mo(1)–N(3)	88.79(9)	87.24(7)	86.25(13)	85.74(13)
N(2)–Mo(1)–N(5)	168.87(9)	165.01(7)	163.75(13)	163.04(13)
N(2)–Mo(1)–N(7)	95.88(9)	96.80(7)	95.94(13)	95.72(13)
N(3)–Mo(1)–N(5)	80.64(8)	77.78(6)	77.95(11)	77.87(10)
N(3)–Mo(1)–N(7)	80.29(8)	81.26(7)	82.34(11)	83.15(12)
N(5)–Mo(1)–N(7)	79.02(8)	81.65(7)	78.39(11)	78.17(11)
Mo(1)–N(1)–C	155.4(2)	173.06(16)	159.9(3)	162.2(3)
Mo(1)–N(2)–C	153.2(2)	168.25(16)	177.2(3)	175.4(3)

to reflect the steric pressure of the bulky Tp′ ligand, leading to a slight compression of the bis(imido) moiety: the N(1)–Mo–N(2) bond angle is 98.23(11)° as opposed to 100.7(5)° for [$MoCl_2${[2,2′-(N_2)–C_6H_4]$_2CH_2$}(dme)], and the Mo–N bonds are marginally elongated [1.755(2) and 1.765(2) Å as opposed to 1.725(7) Å].

Similarly, treatment of {[$(CH_2)_2$(2-$C_6H_4N)_2$]$MoCl_2$(dme)} with KTp′ affords red {[$(CH_2)_2$(2-$C_6H_4N)_2$](Tp′)MoCl} (**2**) in good yield (ca. 60%). As in **1**, solution studies of **2** (^{1}H,^{13}C NMR) are consistent with a 6-coordinate structure containing two sets of equivalent pyrazole rings. The four protons of the ethanediyl bridge appear as an AA′BB′ pattern at δ 3.44 and 3.73 ppm.

2.2. Arylimido complex

The reaction of KTp′ with one equivalent of [Mo(NAr)$_2$Cl$_2$(dme)] (Ar = 2,6-Pr$^i_2$C$_6$H$_3$) gave, after work-up, the green crystalline complex [Tp′Mo(NAr)$_2$Cl] (**3**) in ca. 70% yield. NMR spectra for **3** are consistent with the solid-state structure (Fig. 2, Table 1); the two equivalent pyrazolyl rings are *trans* to the imido ligands with the unique third pyrazolyl ring *trans* to the chloro ligand. The Pr^i groups of the arylimido ligand give rise to two septets (2 × 2H) and four doublets (4 × 6H) reflecting the restricted rotation about the C–N bond and their diastereotopic nature. Within the core geometry the N(1)–Mo–N(2) angle has opened up to 105.87(8)° to accommodate the two bulky arylimido groups. These imido groups are essentially equivalent, with bond lengths of Mo–N 1.7740(18) Å [N(1)] and 1.7805(17) Å [N(2)] and angles Mo–N(1)–C(1) = 173.06(16)° and Mo–N(2)–C(13) = 168.25(16)°; the softness of this angle has been noted previously [5,6]. The Mo–N(pyrazolyl) bonds *trans* to the two imido ligands [2.3278(18) and 2.2880(18) Å are longer than that *trans* to the chloro ligand [Mo–N(5) = 2.1915(18) Å], reflecting the relative *trans* influences of the imido and chloro groups.

2.3. Mixed-imido complex

A similar reaction with the mixed-imido complex [Mo(NAr)(NBu^t)Cl$_2$(dme)] affords brown–black prisms of [Tp′Mo(NAr)(NBu^t)Cl] (**4**). Crystals of **4** suitable for an X-ray determination were grown from acetonitrile at room temperature. The asymmetric unit comprises two independent molecules of the metal complex and two molecules of acetonitrile; the metal complex is a racemic mixture (exactly 50:50%) of *R* and *S* molecules, although the crystal structure itself is non-centrosymmetric. The molecular structure of one of the molecules is shown in Fig. 3, and selected bond lengths and angles in both are given in Table 1. The molybdenum possesses a pseudo-octahedral geometry, coordinated by four different groups. The two imido ligands are considered essentially linear [angles at N 159.9(3)°–177.2(3)°] and exert a *trans* influence on the Mo–N (pyrazolyl) bonds, the longest of which is 2.380(3) Å *trans* to the *tert*-butylimido group.

As in **3**, solution NMR studies indicate steric congestion about the arylimido ligand such that there is restricted rotation.

In conclusion, complexes **1**–**4** described herein are members of a family of pseudo-octahedral complexes having the same structural motif **I**, for which the Tp′ ligand coordinates facially with two elongated Mo–N bonds *trans* to the multiply bonded imido groups and a somewhat shorter bond *trans* to the chloro ligand.

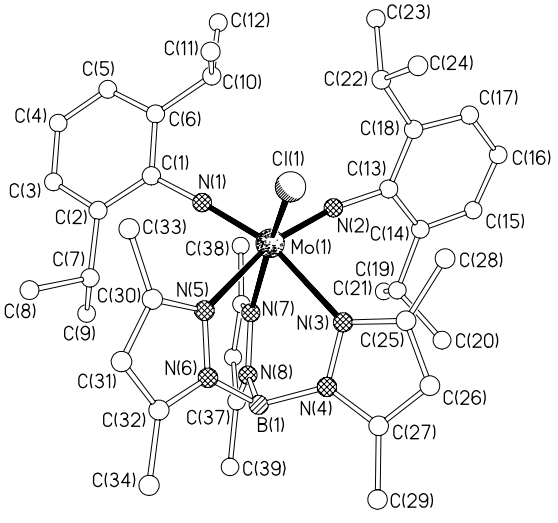

Fig. 2. Molecular structure of **3** without H atoms.

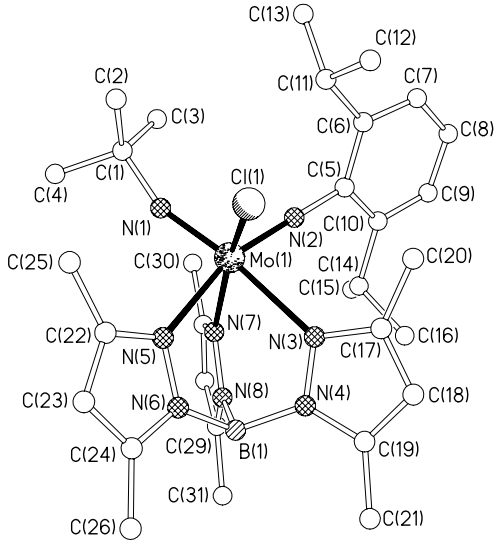

Fig. 3. The structure of one molecule of **4** without H atoms.

3. Experimental

3.1. General

All manipulations were carried out under an atmosphere of nitrogen using standard Schlenk and cannula techniques or in a conventional nitrogen-filled glove-box. Solvents were refluxed over an appropriate drying agent, and distilled and degassed prior to use. Elemental analyses were performed by the microanalytical services of the Department of Chemistry at Durham, Imperial College and Medac Ltd. NMR spectra were recorded on a Varian VXR 400 S spectrometer at 400.0 MHz (^{1}H) and 75.0 MHz (^{13}C); chemical shifts are referenced to the residual protio impurity of the deuterated solvent; IR spectra (nujol mulls, KBr windows), Perkin–Elmer 577 and 457 grating spectrophotometers. The ligand [$(CH_2)(2\text{-}C_6H_4NH_2)_2$] was prepared by the previously published procedure [16,17]. The ligand [$(CH_2)_2(2\text{-}C_6H_4NH_2)_2$] was obtained as its diphosphate salt and extracted from aqueous solution into ethyl acetate, dried ($MgSO_4$) and recrystallized from isopropyl alcohol. 2,6-Diisopropylaniline was distilled prior to use and stored in the dark. [$Mo(NAr)_2Cl_2(dme)$] and [$Mo(NAr)(NBu^t)Cl_2(dme)$] were prepared by literature methods [18,19]. All other chemicals were obtained commercially and used as received unless stated otherwise.

3.2. [$(CH_2)(2\text{-}C_6H_4N)_2$](Tp′)MoCl (1)

THF (20 cm^3) was added to {[$(CH_2)(2\text{-}C_6H_4N)_2$]$MoCl_2(dme)$} (0.5 g, 1.11 mmol) and KTp′ (0.38 g, 1.12 mmol) in a thick-walled 'rotaflo' ampoule. After refluxing for 12 h, the volatiles were removed in vacuo and the residue was extracted with hot MeCN (ca. 25 cm^3), affording on cooling deep red cubes of **1** (0.45 g, 65%). Found: C, 54.7; H, 5.7; N, 19.6%. $MoClN_8C_{28}H_{32}\cdot 2MeCN$ requires C, 54.5; H, 5.4; N, 19.9%. IR: 2254w, 2272w, 1625w, 1587w, 1540s, 1488w, 1463s, 1447s, 1413s, 1377s, 1370s, 1301w, 1279m, 1261m, 1218s, 1197s, 1160w, 1112m, 1074s, 1043, 980w, 969m, 872w, 855s, 812s, 783s, 764s, 748s, 721w, 692m, 673w, 665m, 661m, 655m, 598m, 508m. ^{1}H NMR ($CDCl_3$): δ 1.45, 2.40 (2 s, 2×3 H, pz-CH_3), 2.44, 2.70 (2 s, 2×6 H, pz-CH_3), 3.63 (d, 1 H, $^2J = 12.8$ Hz, CH_aH$_b$), 5.65 (s, 1 H, pz-CH), 5.87 (s, 2 H, pz-CH), 6.10 (d, 1 H, $^2J = 12.8$ Hz, CH$_a$H$_b$), 6.70–6.72 (m, 2 H, Ar–H), 7.03–7.12 (m, 4 H, Ar–H), 7.60–7.62 (m, 2 H, Ar–H); ^{13}C{^{1}H} NMR($CDCl_3$): chemically inequivalent pyrazol rings A and B (ratio 2/1), δ 12.5 (A):13.3 (B) (5-CH_3), 13.4 (B):14.8 (A) (3-CH_3), 35.2 (CH_2), 106.6 (A):106.7 (B) (C-4), 120.5, 126.2, 127.7, 130.0 (aryl = CH), 143.3 (A):145.6 (B) (C-3), 152.8 (A):152.9 (B) (C-5), 153.0 (= CCH_2), 156.1 (aryl = CN).

3.3. [$(CH_2)_2(2\text{-}C_6H_4N)_2$](Tp′)MoCl (2)

By a procedure analogous to that described for **1**, use of {[$(CH_2)_2(2\text{-}C_6H_4N)_2$]$MoCl_2(dme)$} (1.0 g, 2.16 mmol) and KTp′ (0.72 g, 2.14 mmol) afforded **2** as red blocks (0.8 g, 58%). Found: C, 54.7; H, 5.4; N, 18.3%. $MoClBN_8C_{29}H_{34}\cdot\frac{1}{2}MeCN$ requires C, 54.8; N, 5.4; N, 18.1%. IR: 2727w, 2540w, 2246w, 1659w, 1534w, 1544s, 1413s, 1306m, 1279m, 1262m, 1203s, 1155m, 1089m, 1069s, 1041s, 983m, 958m, 872w, 855m, 810s, 786s, 768s, 758m, 744s, 723m, 690m, 648m, 585w, 568w, 555w, 532w, 486m, 473m, 416s. ^{1}H NMR ($CDCl_3$): δ 1.98 (s, 3 H, pz-CH_3), 2.01 (s, 1.5H, 0.5MeCN), 2.42 (s, 6 H, pz-CH_3), 2.46 (s, 3 H, pz-CH_3), 2.57 (s, 6 H, pz-CH_3), 3.44 (AA′BB′, 2H, CH_2), 3.73 (AA′BB′, 2H, CH_2), 5.78 (s, 1 H, pz-CH), 5.84 (s, 2 H, pz-CH), 6.89–6.91 (m, 2 H, Ar–H), 7.07–7.18 (m, 4 H, Ar–H), 7.35–7.37 (m, 2 H, Ar–H). ^{13}C{^{1}H} NMR ($CDCl_3$): chemically inequivalent pyrazol rings A and B (ratio 2/1), δ 12.6 (A):13.3 (B) (5-CH_3), 15.3 (B):15.9 (A) (3-CH_3), 35.9 (CH_2), 106.9 (C-4), 125.3, 125.9, 128.7, 129.6, 143.1, 144.0, 145.9, 151.7, 152.8 (aryl C1), 155.0 (aryl CN).

3.4. [Tp′Mo(NAr)$_2$Cl] (3)

By a procedure analogous to that described for **1**, use of [$Mo(NAr)_2Cl_2(dme)$] (1.0 g, 1.65 mmol) and KTp′ (0.55 g, 1.64 mmol) afforded **3** as deep green prisms. Concentration and cooling of the mother-liquor afforded further crops. Overall yield 70%. Found: C, 60.1; H, 7.0; N, 14.9%. $MoBClN_8C_{39}H_{56}\cdot 1/2MeCN$ requires C, 60.1; H, 7.2; N, 14.9%. IR: 2359w, 2342w, 1543m, 1417m, 1315m, 1258s, 1242m, 1211s, 1174m, 1110m, 1097m, 1078m, 1062m, 1042m, 983w, 954m, 934w, 903w, 876w, 859w, 814m, 793m, 781m, 745m, 724s, 695w, 664w, 651w, 630w, 565w, 541w, 482w, 472w, 439w, 423w, 415w. ^{1}H NMR ($CDCl_3$): δ 0.34 (6H, d, $^3J_{HH}$ 6.4 Hz, CHMe_2), 0.56 (6H, d, $^3J_{HH}$ 6.8 Hz, CHMe_2) 1.41 (6H, d, $^3J_{HH}$ 6.8 Hz, CHMe_2), 1.42 (6H, d, $^3J_{HH}$ 6.8 Hz, CHMe_2), 1.98 (sept, 2H, $^3J_{HH}$ 6.8 Hz, CHMe_2), 2.23 (s, 6H, pz-CH_3), 2.24 (s, 3H, pz-CH_3), 2.35 (s, 6H, pz-CH_3), 2.50 (s, 3H, pz-CH_3), 4.25 (sept, 2H, $^3J_{HH}$ 6.8 Hz, CHMe_2), 5.68 (s, 2H, pz-CH), 5.91 (s, 1H, pz-CH), 6.83–6.89 (m, 4H, aryl H), 7.14 (dd, 2H, ^2J 7.2 Hz, ^3J 2.0 Hz, aryl H). ^{13}C{1H} NMR ($CDCl_3$): chemically inequivalent pyrazol rings A and B (ratio 2/1), δ 12.5 (A):12.7 (B) (5-CH_3), 15.3(A):16.3(B) (3-CH_3), 24.2, 24.7, 24.9, 26.6, 27.2, 28.4, 107.9(A):108.5(B) (C-4), 123.2, 124.9, 142.1, 142.7, 143.3, 144.7, 153.2, 154.7.

3.5. [Tp′Mo(NAr)(NBu^t)Cl] (4)

By a procedure analogous to that described for **1**, use of [$Mo(NAr)(NBu^t)Cl_2(dme)$] (0.75 g, 1.11 mmol) and KTp′ (0.38 g, 1.12 mmol) afforded **4** as brown–black

Table 2
Crystallographic data

Compound	**1** · 2MeCN	**3**	**4** · MeCN
Formula	$C_{28}H_{32}BClMoN_8 \cdot 2CH_3CN$	$C_{39}H_{56}BClMoN_8$	$C_{31}H_{48}BClMoN_8 \cdot CH_3CN$
Formula weight	704.9	779.1	716.0
Crystal system	monoclinic	monoclinic	monoclinic
Space group	$P2_1/c$	$P2_1/c$	$P2_1$
Unit cell dimensions			
a (Å)	10.1652(7)	10.7193(9)	10.5855(4)
b (Å)	16.4685(11)	20.855(2)	22.1065(9)
c (Å)	20.7746(14)	17.9753(14)	15.7718(7)
β (°)	103.740(2)	94.018(2)	97.708(2)
V (Å^3)	3378.3(4)	4008.6(6)	3657.4(3)
Z	4	4	4
Absorption coefficient (mm^{-1})	0.51	0.43	0.47
Crystal size (mm)	$0.66 \times 0.29 \times 0.15$	$0.40 \times 0.20 \times 0.07$	$0.53 \times 0.20 \times 0.05$
θ_{max} (°)	26.4	26.4	28.4
Reflections measured	18122	22650	23032
Unique reflections	6747	8180	12614
Reflections with $F^2 > 2\sigma(F^2)$	5797	6948	10984
Transmission factors	0.785–0.841	0.772–0.860	0.659–0.862
R_{int}	0.0373	0.0377	0.0325
Number of parameters	418	466	839
R^a $[F^2 > 2\sigma(F^2)]$	0.0381	0.0331	0.0370
$R_w{}^b$ (all data)	0.0878	0.0736	0.0804
Goodness-of-fit^c (S)	1.107	1.108	1.026
Largest difference peak and hole (e Å^{-3})	0.52 and −0.93	0.33 and −0.39	0.54 and −0.66

[a] Conventional $R = \sum ||F_o| - |F_c|| / |F_o|$ for 'observed' reflections having $F^2 > 2\sigma(F^2)$.
[b] $R_w = [\sum w(F_o^2 - F_c^2)^2 / \sum w([F_o]^2)^2]^{1/2}$ for all data.
[c] $S = [\sum w(F_o^2 - F_c^2)^2 / (\text{no. of unique reflections} - \text{no. of parameters})]^{1/2}$.

prisms (0.28 g, 37%). Found: C, 54.4; H, 6.8; N, 16.6%. $MoBClN_8C_{31}H_{48}$ requires C, 55.2; H, 7.2; N, 16.6%. IR: 2728w, 2563w, 2359s, 2341m, 1726w, 1711w, 1659w, 1642w, 1544s, 1328m, 1277m, 1219s, 1107m, 1076m, 1042s, 963m, 934w, 873w, 857w, 818m, 796m, 778m, 751m, 723m, 696w, 648m, 581m, 521m, 467m. ^{1}H NMR ($CDCl_3$): δ 0.35 (d, 3H, $^3J_{HH}$ 6.4 Hz, $CHMe_2$), 0.70 (d, 3H, $^3J_{HH}$ 6.8 Hz, $CHMe_2$), 1.26 (d, 3H, $^3J_{HH}$ 6.8 Hz, ^2J 6.4 Hz, $CHMe_2$), 1.45 (d, 3H, $^3J_{HH}$ 6.8 Hz, $CHMe_2$), 1.55 (bs, 6H, 2 × MeCN), 1.58 (s, 9H, $C(CH_3)_3$), 2.00 (s, 1.5H, 0.5MeCN), 2.06 (sept, 1H, $^3J_{HH}$ 6.8 Hz, $CHMe_2$), 2.21, 2.22, 2.35, 2.36, 2.46, 2.75 (6 × s, 6 × 3H, pz-CH_3), 4.40 (sept, 1H, $^3J_{HH}$ 6.8 Hz, $CHMe_2$), 5.62, 5.79, 5.87 (3 × s, 3 × 1H, pz-CH), 6.84–6.90 (m, 2H, aryl H), 7.13–7.15 (m, 1H, aryl H). ^{13}C{^{1}H} NMR ($CDCl_3$): chemically inequivalent pyrazol rings 1:1:1, δ 12.33, 12.80, 13.34 (3 × 5-CH_3), 14.81, 15.97, 17.71 (3 × 3-CH_3), 23.42, 24.01, 24.45, 26.77 (4 × CH*Me*$_2$), 27.41, 28.09 (2 × *C*HMe$_2$), 29.81 (C*Me*$_3$), 75.07 (*C*Me$_3$), 106.82, 107.01, 107.09 (3 × C-4), 122.52, 123.53, 124.81 ($C_m + 2C_o$), 141.38, 141.86, 143.30, 143.86 (3C-3 + C_m), 145.79 (C_p), 151.60, 152.14, 152.33 (C-5), 154.14 (C_i).

3.6. X-ray crystallography

Table 2 gives crystal data and other information on the structure determination and refinement for **1** · 2MeCN, **3** and **4** · MeCN. All measurements were made at 160K on a Siemens SMART CCD diffractometer with graphite-monochromated Mo Kα radiation ($\lambda = 0.71073$ Å) [20]. Cell parameters were refined from the observed ω angles of all strong reflections in each complete data set. Intensities were integrated from several series of narrow-frame exposures (0.3° in ω) covering more than a hemisphere of data in each case. Semi-empirical absorption corrections were applied, based on repeated and symmetry-equivalent reflections. The structures were solved by heavy-atom (**1** and **3**) or direct (**4**) methods, and refined by full-matrix least-squares on F^2 values of all measured data [21]. Non-hydrogen atoms were assigned anisotropic displacement parameters; isotropic hydrogen atoms were included with riding-model constraints. No disorder was detected. For the non-centrosymmetric structure of **4** · MeCN, the absolute structure parameter refined to −0.01(2), confirming the correct assignment [22].

4. Supplementary material

Crystallographic data for the structural analysis of **1** · 2MeCN, **3**, and **4** · MeCN have been deposited with the Cambridge Crystallographic Data Centre, CCDC Nos. 216483, 216484 and 216485, respectively. Copies of this information may be obtained free of charge from The Director, CCDC, 12 Union Road, Cambridge, CB2 1EZ,

UK (fax: +44-1223-336033; e-mail: deposit@ccdc.cam.ac.uk or www: http://www.ccdc.cam.ac.uk).

Acknowledgements

The Engineering and Physical Sciences Research Council, Deutsche Forschungsgemeinschaft and DAAD are thanked for financial support.

References

[1] R.R. Schrock, Acc. Chem. Res. 23 (1990) 158.
[2] A. Bell, W. Clegg, P.W. Dyer, M.R.J. Elsegood, V.C. Gibson, E.L. Marshall, Chem. Commun. (1994) 2547.
[3] V.C. Gibson, C. Redshaw, W. Clegg, M.R.J. Elsegood, U. Siemeling, T. Türk, J. Chem. Soc., Dalton Trans. (1996) 4513.
[4] U. Siemeling, T. Türk, W.W. Schoeller, C. Redshaw, V.C. Gibson, Inorg. Chem. 37 (1998) 4738.
[5] V.C. Gibson, E.L. Marshall, C. Redshaw, W. Clegg, M.R.J. Elsegood, J. Chem. Soc., Dalton Trans. (1996) 4197.
[6] P. Barrie, T.A. Coffey, G.D. Forster, G. Hogarth, J. Chem. Soc., Dalton Trans. (1999) 4519.
[7] A.S. Gamble, J.M. Boncella, Organometallics 12 (1993) 2814.
[8] J. Sundermeyer, J. Putterlik, M. Foth, J.S. Field, N. Ramesar, Chem. Ber. 127 (1994) 1201.
[9] S. Scheuer, J. Fischer, J. Kress, Organometallics 14 (1995) 2627.
[10] W.M. Vaughan, K.A. Abboub, J.M. Boncella, J. Organomet. Chem. 485 (1995) 37.
[11] J.M. Boncella, M.L. Cajigal, A.S. Gamble, K.H. Abboud, Polyhedron 15 (1996) 2071.
[12] A. Galindo, F. Montilla, A. Pastor, E. Carmona, E. Gutierrez-Puebla, A. Monge, C. Ruiz, Inorg. Chem. 36 (1997) 2379.
[13] S.-M. Lee, R. Kowallick, M. Marcaccio, J.A. McCleverty, M.D. Ward, J. Chem. Soc., Dalton Trans. (1998) 3443.
[14] F. Montilla, A. Pastor, A. Galindo, J. Organomet. Chem. 590 (1999) 202.
[15] J.R. Dilworth, V.C. Gibson, N. Davies, C. Redshaw, A.P. White, D.J. Williams, J. Chem. Soc., Dalton Trans. (1999) 2695.
[16] J.H. Clark, J.M. Miller, K.H. So, J. Chem. Soc., Perkin Trans. 1 (1978) 941.
[17] H.J. Teuben, O. Glossauer, Chem. Ber. 98 (1965) 2939.
[18] P.W. Dyer, V.C. Gibson, W. Clegg, J. Chem. Soc., Dalton Trans. (1995) 3313.
[19] A. Bell, W. Clegg, P.W. Dyer, M.R.J. Elsegood, V.C. Gibson, E.L. Marshall, J. Chem. Soc., Chem. Commun. (1994) 2247.
[20] SMART (diffractometer control) and SAINT (integration) software, Siemens Analytical X-Ray Instruments Inc., Madison, WI, USA, 1995.
[21] G.M. Sheldrick, SHELXTL version 5, Siemens Analytical X-Ray Instruments Inc., Madison, WI, USA, 1995.
[22] H.D. Flack, Acta Crystallogr. Sect. A 39 (1983) 876.

Available online at www.sciencedirect.com
SCIENCE DIRECT®
Polyhedron 23 (2004) 195
POLYHEDRON
www.elsevier.com/locate/poly

Foreword

Polyhedron Symposia-In-Print, number 26 Scorpionate and Related Ligands

The correct choice of ligands is of critical importance to the inorganic chemist. This Special Issue of POLYHEDRON is devoted to a particularly important class of ligands – so-called "Scorpionate Ligands" – and is dedicated to their creator, Jerry Trofimenko. Scorpionate ligands have a rather humble origin with the synthesis of simple pyrazolyboron compounds by Trofimenko at DuPont in the 1960s. However, Trofimenko quickly realized that some of these compounds, namely the anionic poly(pyrazolyl)borate derivatives, had the ability to be effective ligands (*via* coordination through the pyrazolyl nitrogen atoms) for a variety of metals while he paved a pathway for others to follow. Applications of poly(pyrazolyl)borate ligands are now very wide spread, covering areas that include bioinorganic chemistry, organometallic chemistry, and materials chemistry. In part, the large success of the poly(pyrazolyl)borate ligand system is due to the ability to tailor the ligands with a multitude of substituents, thereby varying the electronic and steric properties at a metal center. More recent developments of the Scorpionate system have included the incorporation of groups that provide sulfur and phosphorus donors which complement the nitrogen donors of poly(pyrazolyl)borate ligands. This issue of POLYHEDRON presents a compilation of articles that feature the applications of Scorpionate and related ligands as a means of paying due homage to the person that started it all. Thanks Jerry!

G.F. Parkin
Department of Chemistry (Box 3115), Columbia University, New York, NY 10027, USA
E-mail: parkin@chem.columbia.edu

doi:10.1016/S0277-5387(04)00017-8

Available online at www.sciencedirect.com
SCIENCE DIRECT®
Polyhedron 23 (2004) 197–203
POLYHEDRON
www.elsevier.com/locate/poly

Scorpionates: genesis, milestones, prognosis

Swiatoslaw Trofimenko *

Department of Chemistry and Biochemistry, The University of Delaware, Newark, DE 19716, USA

Received 5 May 2003; accepted 6 August 2003

Abstract

The development of the polypyrazolylborate/scorpionate ligand system is traced from its inception, through its early and later stages of development, primarily on the basis of the author's experiences and contributions.
© 2003 Elsevier B.V. All rights reserved.

Keywords: Scorpionates; Polypyrazolylborates; Coordination chemistry; Nitrogen ligands

1. Introduction

Polypyrazolylborate/scorpionate chemistry is a very large, and still growing area. Since its inception until now, there have been about 2000 papers published on polypyrazolylborates, and complexes of seventy elements of the periodic table have been reported. A number of reviews of this area exist covering time-spans, or concentrating on certain elements, or unified by some other feature. However, in this article I would like to recount, on a personal basis, some background and little-known details, as to how this whole field came into being, focusing on my personal experiences and contributions.

2. History

When I joined the Du Pont company at the end of 1959, this was still the heady time of cyanocarbon research, and my initial assignment was to prepare the first percyanoalkane, which I did, synthesizing hexacyanoethane [1]. Shortly thereafter, I developed the first practical synthesis of what was called "cyanoform" [2], and which actually turned out to be dicyanoketeneimine, rather than tricyanomethane [3]. This led to the synthesis of 4-cyanopyrazole, **1**, my first direct experience with this ring system, which I found rather attractive [4]. Other contributions to pyrazole chemistry included 4,4′-bipyrazolyl [5], **2**, made via 1,1,2,2-ethanetetracarboxaldehyde [6], as well as pyrazolo[1,2a]pyrazole, or 3a, 6a-diazapentalene, **3**, an intriguing ligand whose coordination chemistry has not been explored at all [7,8].

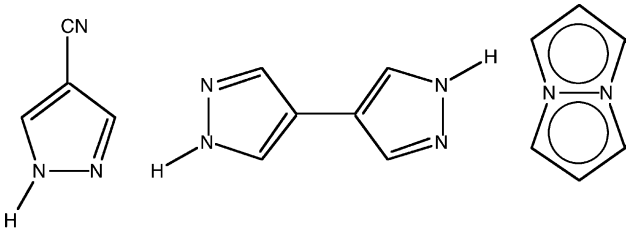

1 **2** **3**

My contact with boron came from working in the group of Earl Muetterties on photochemical nucleophilic substitution reaction in perhalogenated polyhedral boranes, mainly $B_{12}X_{12}^{2-}$ [9,10]. At the time, it was standard policy in the Du Pont Central Research Department that each chemist was absolutely expected, in addition to the assigned project, to explore on a part-time basis some unrelated new area of chemistry. In later years this practice was no longer observed.

3. Earliest developments

It was in this search for something novel, that I decided to work on boron–pyrazole chemistry. What made me

* Tel.: +1-302-831-0716; fax: +1-302-831-6335.
E-mail address: trofimen@udel.edu (S. Trofimenko).

0277-5387/$ - see front matter © 2003 Elsevier B.V. All rights reserved.
doi:10.1016/j.poly.2003.11.013

select this area? Around that time, Fred Hawthorne had published a communication on the reaction of triethylborane with acetylacetone, which yielded a rather stable compound, **4**, in which the diethylboryl group had taken the place of the chelated hydrogen bridge [11]. In other words, the diethylboryl cation took on a metalloid role.

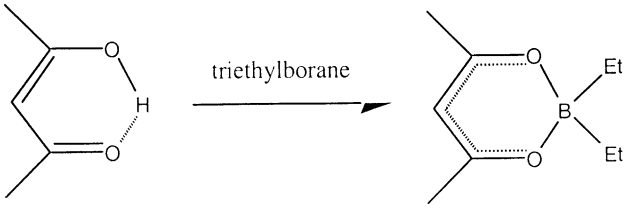

4

I thought that it would be rather interesting to explore such BR_2 bridging in intermolecular context, the hydrogen-bridged pyrazole dimer being the molecule of choice. Considering the three possible bridging moieties: hydrogen, metal and a BR_2 group, one arrives at six different possibilities for the two bridges. If we fix one BR_2 group to act as a hinge, then at the other side one could have another BR_2 group, a metal or a hydrogen. These combinations can be readily recognized now as a pyrazabole, **5**, a scorpionate metal complex, **6**, and a scorpionate free acid, **7**, respectively.

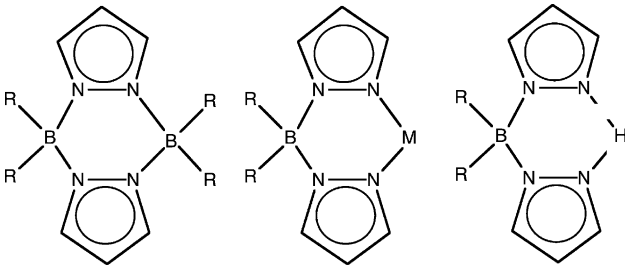

5 **6** **7**

My first attempt in this area was to prepare tris (pyrazolyl)borane which, as a 1,3-dipole, was expected to dimerize to 4,4,8,8-tetrakis(pyrazolyl)pyrazabole, and this just had to be a good difunctional chelating agent.

$$2\,B(pz)_3 \rightarrow (pz)_2B(pz)_2B(pz)_2 \qquad (1)$$

And so I set out to make this compound by bubbling BCl_3 into molten pyrazole. This generated lots of HCl and heat, and when the reaction subsided, I dissolved everything in water, and added to the strongly acidic solution ferric chloride. It was gratifying to see an immediate formation of bright dark red color; moreover the product could be extracted into chloroform, from which red crystals could be obtained. However, elemental analysis was consistent with a species $B(pz)_4FeCl_2$, involving four (rather than the expected three) pyrazolyl groups per boron atom, and so the first assumption was that we had a bidentate chelated $FeCl_2$ species, $(pz)_2B(pz)_2FeCl_2$. Soon, however, I realized hat the red material was the complex ion pair $Fe[B(pz)_4]_2^+$ $[FeCl_4]^-$, involving the $[B(pz)_4]$ ligand chelating in κ^3 fashion, since the $[FeCl_4]^-$ ion could be readily replaced with hexafluorophosphate, maintaining the cation intact. That the iron was octahedrally coordinated followed not only from spectroscopic data, but also from Stuart–Briegleb models, which showed that the $B(pz)_2M$ entity was in a deep boat conformation, and that the third pz group could also readily coordinate to the metal ion. The structure of this very first polypyrazolylborate complex was not determined until very recently (Fig. 1) [12]. It was also quite surprising that the B–N bond was not cleaved in this strongly acidic medium.

As for 4,4,8,8-tetrakis(pyrazolyl)pyrazabole, the original target molecule of this experiment, it was synthesized at a later date by the reaction of pyrazole

$$2\,Me_3N{-}BH_3 + 6\,Hpz \rightarrow (pz)_2B(pz)_2B(pz)_2 + 2\,Me_3N + 6\,H_2 \qquad (2)$$

with trimethylamine–borane and, yes, it was a good bisbidentate chelating agent forming, inter alia, the cationic complex $[(\eta^3\text{-allyl})Pd(pz)_2B(pz)_2B(pz)_2Pd(\eta^3\text{-allyl})]^{2+}$ [13].

But my attention was now directed at the novel ligand system of polypyrazolylborates, which I proceeded to prepare in a much more civilized manner, by the reaction of pyrazole with borohydride ion, making in this fashion via temperature control bis, tris-, and tetrakis-pyrazolylborates, exploring their coordination chemistry with first-row metal ions, isolating via acidification the free acids, and using those to prepare otherwise unavailable tetraalkylammonium salts [14,15]. I also showed that 1,2,4-triazole forms the $HB(trz)_3$ ligand, and that its $Co[HB(trz)_3]_2$ complex is water soluble, in contrast to the hydrophobic $Co[HB(pz)_3]_2$. In studying the reaction of KBH_4 with variously substituted pyrazoles, it turned out that the reaction of 3,5-dimethylpyrazole, and

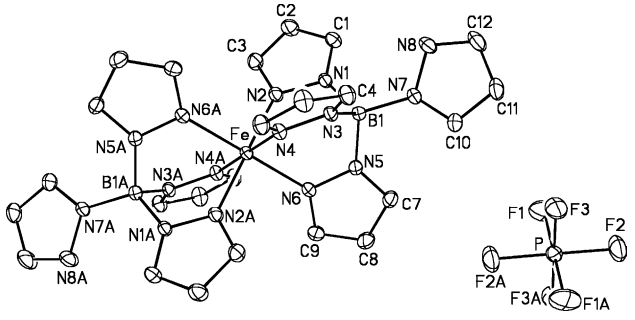

Fig. 1. View of the complex $Fe[B(pz)_4]_2PF_6$.

of other 3,5-disubstituted pyrazoles, stops at the tris-stage [16]. Don Eaton and Peter Jesson joined the effort, studying the physical aspects of the novel compounds, and finding interesting examples of spin equilibria in the iron(II) complexes [17–19]. This early work was featured in the C&E News [20]. Du Pont management was sufficiently impressed by my discovery to let me work on polypyrazolylborates full time, and also providing me with a full-time technician (in those days two chemists normally shared one technician on a half-time basis).

Next came the exploration of polypyrazolylborates in complexes containing additional other ligands: carbonyls, olefins, η^3-allyls [21,22], nitrosyls, arylazo groups [23], in other words the world of half-sandwiches was entered, and it became clear that in many ways the new tris(pyrazolyl)borate ligands, being uninegative tricoordinate six-electron donors, resembled the Cp ligand, while the bis-ligands could be considered analogues of acetylacetonate ion although, unlike M[acac]$_2$ complexes, the M[R$_2$B(pz)$_2$]$_2$ compounds were always monomeric. In an interesting reaction of allyl bromide with the anions {Mo[H$_2$B(3,5-Me$_2$pz)$_2$](CO)$_4$}$^-$ and {Mo[Et$_2$B(pz)$_2$](CO)$_4$}$^-$, there were obtained what appeared to be 16-electron complexes of surprising stability, Mo[H$_2$B(3,5-Me$_2$pz)$_2$](CO)$_2$(η^3-allyl), **8**, and Mo[Et$_2$B(pz)$_2$](CO)$_2$(η^3-allyl), **9**, respectively [24,25]. A structure determination of **8** showed that the pseudo-axial B–H formed a bridge to the metal, thus achieving an 18-electron configuration [26]. This was not entirely unexpected, in view of other known examples of B–H bridging.

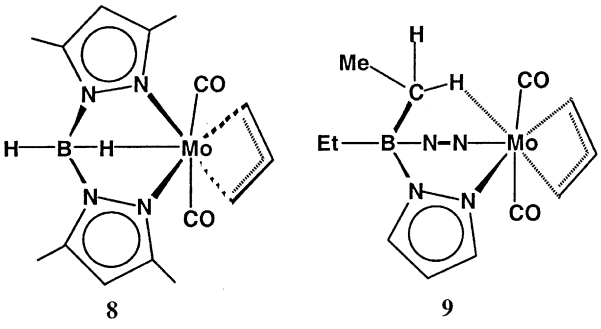

8 9

-N=N- is the hidden pyrazolyl group

More interesting was **9** where the ethyl group should have had no affinity for the metal. Yet in its NMR spectrum one of the ethyl methylenes was shifted into the hydridic range, and unusually low-frequency C–H stretch peaks were observed in the IR. These features disappeared upon coordination of a donor molecule. Stuart–Briegleb models indicated that in **9** the pseudo-axial methylene hydrogens would indeed be sitting on top of the metal. When I gave a seminar at MIT on this new chemistry, I asked if someone would do an X-ray structure to confirm the presence of this unusual bonding. Al Cotton agreed, and later on demonstrated that there is indeed an interaction – now called "agostic" – but between only one of the methylene hydrogens and the metal [27]. In solution, however, the two methylene hydrogens exchanged rapidly on the NMR time scale. So these were not 16-electron complexes after all, and only in the case of Mo[Ph$_2$B(pz)$_2$](CO)$_2$(η^3-allyl) was there a true 16-e structure [28]. The agostic theme was later revisited in the octahedral cobalt complex Co[(cyclooctane-1,5-diyl)B(pz)$_2$]$_2$ which contained two agostic C–H–Co bonds [29].

But apart from the above studies, most of the research in this area by myself and by others, was with the tridentate trispyrazolylborate ligands [HB(pz)$_3$] and, especially, with [HB(3,5-Me$_2$pz)$_3$]. Jon McCleverty and Joe Templeton, each carved out large specialty research areas involving [HB(3,5-Me$_2$pz)$_3$] complexes of low-valent Mo and W, while John Enemark and Charlie Young in Melbourne used the same ligand in high-valent Mo and W chemistry related to various enzymes.

Even at this early stage it became apparent that just modest steric effects played a significant role in the chemistry of polypyrazolylborate ligands. For instance, while the [Mo[HB(pz)$_3$](CO)$_3$]$^-$ anion reacted readily at room temperature with allyl halide, [Mo[HB(3,5-Me$_2$pz)$_3$]CO$_3$]$^-$ was totally inert. In the reaction with diazonium salts, the former gave arylazo derivatives, but the latter only the (η^2-COAr) compounds.

$$[\mathrm{Mo[HB(pz)_3](CO)_3}]^- + \text{allyl bromide} \rightarrow \mathrm{Mo[HB(pz)_3](CO)_2}(\eta^3\text{-allyl}) \quad (3)$$

$$[\mathrm{Mo[HB(3,5\text{-}Me_2pz)_3]CO_3}]^- + \text{allyl bromide} \rightarrow \text{no reaction} \quad (4)$$

$$[\mathrm{Mo[HB(pz)_3](CO)_3}]^- + [\mathrm{ArN_2}]^+ \rightarrow \mathrm{Mo[HB(pz)_3](CO)_2(N{=}NAr)} \quad (5)$$

$$[\mathrm{Mo[HB(3,5\text{-}Me_2pz)_3](CO)_3}]^- + [\mathrm{ArN_2}]^+ \rightarrow \mathrm{Mo[HB(pz)_3](CO)_2}(\eta^2\text{-COAr}) \quad (6)$$

4. Hiatus and second generation of scorpionates

My work on polypyrazolylborates ended in 1973 when I was transferred from Central Research to other departments, working on olefin polymerization catalysis, market development and, finally, to the International Department: overseas, first to Geneva/Switzerland, then to Warsaw/Poland, as manager of the DuPont office. When the Russians invaded Afghanistan, the Du Pont manager of the Moscow office was pulled back to Warsaw, bumping me all the way to Parkersburg, West Virginia. This was a plant site, where my test tube was a

100-gallon nylon autoclave. It was there, that I was soon able to work intermittently on the second generation of trispyrazolylborate ligands, synthesizing those with 3-t-butyl and 3-phenyl substituents. This would have been impossible without the help from my colleagues at Central Research, especially Jeff Thompson. It was truly gratifying to see how steric effects introduced a new dimension in the coordination chemistry of polypyrazolylborates. Finally, in 1985, I was transferred back to Wilmington, and was able to publish the "second generation" ligand work [30,31]. From that point on it was possible to continue a little bit of polypyrazolylborate research, but it was on the margin of other projects in various departments. Under these circumstances I had to reconcile myself with being a gunsmith rather than a hunter, i.e., synthesizing new ligands, but letting others use them to do their exciting research. During this time a fruitful collaboration with Arnie Rheingold commenced and is continuing to this day, despite his departure from Delaware to the West Coast. My move to the University of Delaware after retirement from Du Pont in 1996 enabled me to resume scorpionate work within the group of Klaus Theopold as a Visiting Scholar. It is there that I wrote the book "Scorpionates: The Coordination Chemistry of Polypyrazolylborate Ligands" [32], and developed a number of novel scorpionates. But back to the earlier days.

Dave Curtis came up in 1983 with the very useful abbreviation "Tp" for the trispyrazolylborate ligand, $HB(pz)_3$ [33,34], and I built on this, introducing in my 1993 review a systematic abbreviation system which could be adapted to most types of substitution on the Tp ligand, and which greatly facilitated writing chemical formulas for Tp complexes [35]. In the case of the most commonly used ligand, Tp^{Me2}, an alternative and preferred abbreviation, became Tp*. In that review I also coined the term "scorpionates". It was clear to me that a term for this ligand class was needed which would permit the reader to visualize its coordinative behavior, since no such insight was offered by the cumbersome systematic name "poly(pyrazol-1-yl)borates". In looking for an analogy in nature, the South-American three-toed sloth came to mind first, whose Latin name is "Bradypus tridactylus", and the term "bradypate" did not sound bad at all. Unfortunately, the three claws of this sloth were all curved in the same direction, and thus did not reflect the coordinative behavior of the Tp ligand. Then it occurred to me that the scorpion would be an almost ideal analogue, especially, when taking into account that the sting (the third coordinating site) is not absolutely mandatory, but optional – as happens in the case of complexes where the Tp ligand is only κ^2.

The second generation polypyrazolylborates proved to be quite popular, and accounted for a number of striking new developments in coordination chemistry, such as stabilizing monomeric alkylmagnesium, alkylzinc and alkylberyllium species, novel oxygen complexes, and zinc-based enzyme models, this work being associated with Ged Parkin, Klaus Theopold and Heinrich Vahrenkamp.

A distinctly different family of Tp ligands contained a 3-isopropyl substituent [36,37]. It was intermediate in steric hindrance between the 3-t-butyl and 3-methyl ligands, and had a number of interesting features. On the one hand it permitted isolation of LMX complexes, on the other it also formed octahedral L_2M compounds, although this was always accompanied by ligand rearrangement, which could be borotropic or metallotropic, converting one 3-isopropyl substituent per ligand to the 5-isomer. This, at times bothersome feature, could be circumvented by using a Tp ligand derived from 3,5-diisopropylpyrazole, which precluded such rearrangement, or made it degenerate [38]. The 3,5-diisopropyl Tp ligand was used extensively by the late Nobumasa Kitajima, and is favored today by his successor, Munetaka Akita.

Another unusual feature was the coordination behavior of tetrakis(3-isopropyl)pyrazolylborate, which coordinated only in κ^2 fashion. However, unlike other bispyrazolylborate ligands, which formed square planar complexes with Ni, Cu and Cr, and tetrahedral with Co, Fe and Zn, this ligand gave exclusively tetrahedral complexes **10** across the whole first row of transition metals.

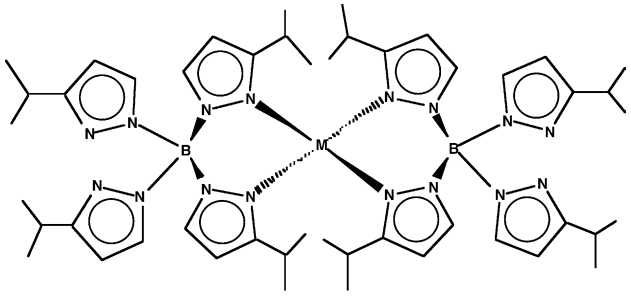

10

We compared this behavior with a series of tetrakis ligands containing 3-cycloalkyl groups ranging from cyclopropyl to cyclohexyl [39–42]. Those with cyclohexyl and cyclopentyl substituents behaved like their isopropyl analogues. The cyclopropyl substituent showed no steric effect, and acted like the parent Tp and pzTp, respectively. Cyclobutyl was special: its tris ligand permitted the isolation of both, tetrahedral LMX complexes, and also of unrearranged octahedral L_2M species. Even the L_2M complexes from its tetrakis ligand were also octahedral.

A long-standing puzzle in the scorpionate area begged to be solved: it appeared, on the basis of some

indirect evidence, that in polyindazolylborates indazole was bonding to boron anomalously through the *more hindered* nitrogen atom, contrary to expectations. We checked this out, and structurally characterized indazolylborate complexes based on a variety of substituted indazoles. It turned out that indazole itself, and indazoles with substituents in the 3, 4, 5, and 6 positions, or any combination thereof, formed the more hindered B–N bond, while indazoles with a 7-substituent formed exclusively the less hindered B–N bond [43–45]. In fact, 7-t-butylindazole formed the most sterically hindered homoscorpionate ligand with a cone angle of over 280°.

In the Tp^{Ph} ligand the phenyl group was freely rotating which was sometimes desirable, and sometimes not. It was, therefore, of interest to modify this ligand so that the phenyl would be in a fixed rotameric disposition. To achieve coplanarity with the pyrazolyl ring, we tethered the phenyl group to the 4-position by a variety of tethers [46]. An ethene tether, **11**, did not provide strict coplanarity, as it zig-zagged across the pyrazolyl ring placing the phenyl group at an angle of about 20°. A methylene tether, **12**, achieved coplanarity, but at the same time pulled back the phenyl group, increasing the "bite" of the ligand. Strict coplanarity without bite change was obtained with an ethyne tether, **13**, making each pyrazolyl arm totally rigid.

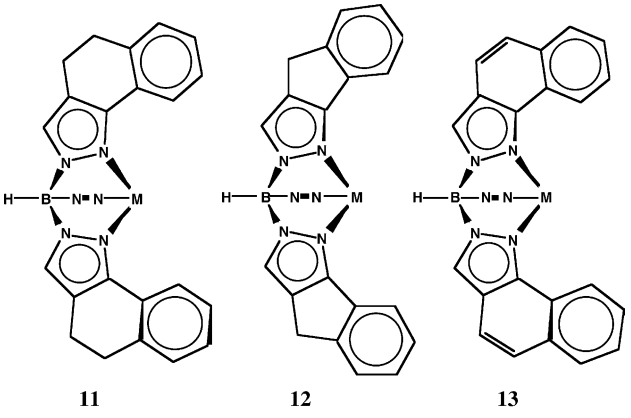

11 **12** **13**

(-N=N- is the third, hidden pyrazolyl group)

This resulted in altered chemistry. While the 3-phenyl Tp ligand permitted the formation of a normal $Mo[Tp^{Ph}](CO)_2(\eta^3$-methallyl) complex, in which the ligand was κ^3, the analogous complex with the ethyne tether did form a similar complex, but in it the ligand was κ^2, with an agostic B–H–Mo bond to achieve an 18-electron structure. Coordination of the third pyrazolyl arm was prevented by the steric interference of the η^3-methallyl group [47].

To make the 3-phenyl group orthogonal to the pyrazolyl plane, I tried to prevent its rotation by using a 3-mesityl [48], or also a 3-(9-anthryl) substituent [49]. The mesityl group was indeed orthogonal in a number of structurally characterized complexes. It was interesting that in the synthesis of this ligand a mixture was obtained containing 85% of the 3,3,5 ligand, and only 15% of the symmetric 3,3,3. However, heating the Tl salt of this mixture above 240 °C, converted everything to the 3,3,3 isomer! In the ligand with the 9-anthryl substituent, the anthryl group deviated from orthogonality, because of non-bonding interference of the peripheral hydrogens of the anthryl groups.

In an attempt to control the rotameric disposition of asymmetric 3-substituents by the presence of bulky 4-substituents, the coordination chemistry of 3-tolyl and 3-isopropyl Tp ligands which also contained a t-butyl group in the 4-position was studied [50]. The effect of the 4-t-butyl group was not major in the case of the 3-tolyl group, as it still could partially swing back-and-forth. However, the 3-isopropyl group became locked into a rigid rotameric conformation with its two methyl groups forking towards the coordinated metal, and thus behaving like a t-butyl group. $Tl[Tp^{iPr,4tBu}]$ also showed the largest Tl^{203}–C^{13} coupling, 218 Hz, surpassing those found in all the known $Tl[Tp^{tBu,R}]$ ligands. Moreover, its reactions did not resemble those of other Tp ligands with a 3-isopropyl substituent, as shown below:

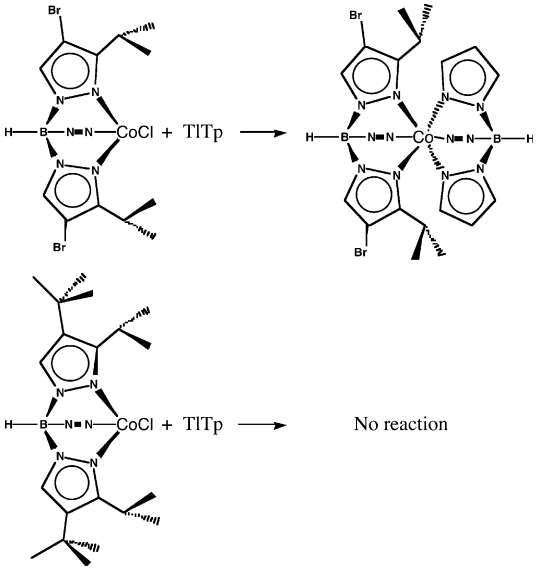

Another interesting new Tp ligand was based on tribromopyrazole [51]. The cone angle of Tp^{Br3} was similar to the popular Tp*, but the ligand was electronically quite different due to the nine electron-withdrawing bromine atoms. It was also the only known Tp ligand devoid of C–H bonds, and thus very suitable for the IR study of coordinated hydrocarbon ligands. Its copper(I) complex was remarkably active in C–H activation catalysis, as was shown by Pedro Pérez [52].

Wishing to extend the dencity of the Tp ligand beyond three by including additional donor atoms on the

3-substituent, we and Jon McCleverty prepared independently the same N6 hexadentate ligand, Tp^{Py} and found it to form beautiful icosahedral $M[Tp^{Py}]_2$ cationic complexes with trivalent lanthanides and actinides [53]. We also synthesized a hexadentate N3O3 ligand, by placing 3-carboxypyrrolidido substituents on Tp [54]. The lanthanide complexes of this ligand showed in solution all pyrazolyl arms NMR-equivalent, but in the crystal one ligand was κ^6, and the other one only κ^4 with an uncoordinated pyrazolyl arm, so that the coordination around the metal ion was 10, as there was no agostic B–H–M bonding. However, when the 3-substituent was carboxy-t-butylamido, both ligands were κ^6 in the crystal [55]. The $Tp^{CONHtBu}$ ligand, while uninegative by itself, has the potential for deprotonation of one, two or even three amido hydrogens, and thus increasing its charge from minus one to minus four. This aspect of its chemistry is still to be explored.

5. Non-classical scorpionates

Although polypyrazolylborates are the oldest and classical examples of the scorpionate ligand system, related scorpionate ligands may be derived from them by replacement of either the central boron, or of pyrazole. A number of such examples have been covered [35], and new ones are appearing ever more frequently. Neutral ligands are best exemplified by geminal polypyrazolylalkanes, which were introduced back in 1970, [56] and are currently being studied in detail by Dan Reger.

In recent years a veritable cornucopia of boron-based scorpionate ligands has emerged. They are generally of the type $[Ph_2B(CH_2Z)_2]^-$ and $[PhB(CH_2Z)_3]^-$, where Z can be a variety of donor functionalities. Examples of Z = SR for $[Ph_2B(CH_2Z)_2]^-$ [57], and for $[PhB(CH_2Z)_3]^-$ [58], of Z = PPh_2 for $[Ph_2B(CH_2Z)_2]$ [59,60], for $[PhB(CH_2Z)_3]^-$ [61,62], and for Z = NMe_2 [63], have already been reported, while those with Z = OR, SeR and AsR_2 are still unknown. Furthermore, one can envisage ligands containing more than one type of donor arms, such as Z_2Z', and Z,Z′,Z″. In addition, coexistence of CH_2Z arms on boron with pyrazolyl or other azolyl groups is also possible, and ligands of the type $[PhB(CH_2SR)_2(pz)]^-$ have also been prepared [64]. The chelate ring size is another adjustable variable, leading to ligands such as $[RB(CH_2Z)_2(ER)]^-$, where E = O, S, Se, or appropriate phosphino or amino functionalities. Related polyrazolylborate examples, containing two pyrazolyl bridges and one dimethylamino [65], or arylmercapto [66], or alkoxy bridge [67], have been reported earlier. While chelates derived from the above ligands involve five- and six-membered rings between boron and the coordinated metal, other similar ligands lead to eight-membered rings. They are hydrotris(mercaptoimidazolyl)borate [68,69], and the related hydrotris(thioxotriazolyl)borate [70]. The former contains twisted eight-membered rings in its complexes, which are always sulfur bonded, while the latter is ambidentate and bonds either through sulfur (with bismuth or tin), or through nitrogen (sodium or manganese). A still different ligand, dihydrobis(thioxotriazolinyl)borate, bonds in tridentate fashion through two sulfurs plus an agostic hydrogen bond [71].

6. Prognosis

So where do we go from here? As someone quipped: ''predictions are difficult, especially about the future''. Nevertheless, I will venture a guess in what areas is further growth likely to occur. First of all, the ''classical'' polypyrazolylborates, while mature ligands, still have room for expansion, especially as heteroscoropionates, containing pyrazolyl arms with additional donor atoms, some of which are shown as homoscorpionates below.

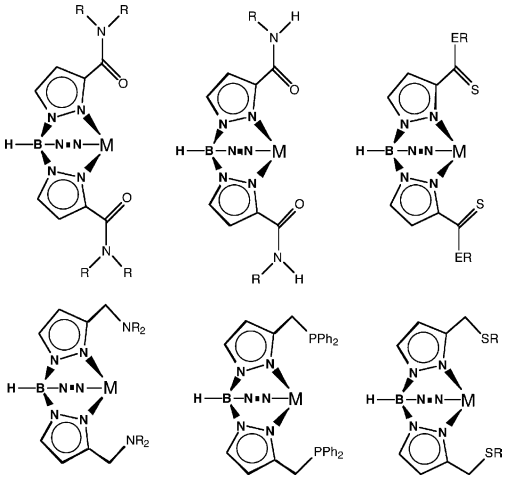

The potential of ligands that can range from tridentate to hexadentate with charges from −1 to −4, i.e. those containing deprotonatable 3-CONHR, or similar substituents, should not be underestimated. The synthesis of Tp ligands with different pyrazoles is another sub-area that may be explored [72].

The area of non-classical scorpionates will surely experience growth, including ligands containing also one or two pz^x groups, in view of the rich portfolio of available diversely substituted pyrazoles. Finally, I am also still hoping that someone will eventually synthesize the dinegative polypyrazolylberyllate ligands, $[R_2Be(pz^x)_2]^{2-}$ and $[RBe(pz^x)_3]^{2-}$, which should yield neutral complexes of tetravalent metals, and other exciting compounds.

All in all, we are dealing with a vast and promising area, the riches of which are yet to be fully exploited by the scorpionate community.

References

[1] S. Trofimenko, B.C. McKusick, J. Am. Chem. Soc. 84 (1962) 3677.
[2] S. Trofimenko, E.L. Little, H.F. Mower, J. Org. Chem. 27 (1962) 433.
[3] S. Trofimenko, J. Org. Chem. 28 (1963) 217.
[4] S. Trofimenko, J. Org. Chem. 28 (1963) 2755.
[5] S. Trofimenko, J. Org. Chem. 29 (1964) 3046.
[6] S. Trofimenko, J. Am. Chem. Soc. 85 (1963) 1357.
[7] S. Trofimenko, J. Am. Chem. Soc. 87 (1965) 4394.
[8] S. Trofimenko, J. Am. Chem. Soc. 88 (1966) 5588.
[9] S. Trofimenko, H.N. Cripps, J. Am. Chem. Soc. 87 (1965) 653.
[10] S. Trofimenko, J. Am. Chem. Soc. 88 (1966) 1899.
[11] M.F. Hawthorne, M. Reintjes, J. Am. Chem. Soc. 86 (1964) 5016.
[12] S. Trofimenko, J.A. Golen, unpublished work.
[13] S. Trofimenko, J. Coord. Chem. 2 (1972) 75.
[14] S. Trofimenko, J. Am. Chem. Soc. 88 (1966) 1842.
[15] S. Trofimenko, J. Am. Chem. Soc. 89 (1967) 3170.
[16] S. Trofimenko, J. Am. Chem. Soc. 89 (1967) 6288.
[17] J.P. Jesson, S. Trofimenko, D.R. Eaton, J. Am. Chem. Soc. 89 (1967) 3148.
[18] J.P. Jesson, S. Trofimenko, D.R. Eaton, J. Am. Chem. Soc. 89 (1967) 3158.
[19] J.P. Jesson, J.F. Weiher, S. Trofimenko, J. Chem. Phys. 48 (1968) 2058.
[20] Chem. Eng. News, August 28 (1967) 71.
[21] S. Trofimenko, J. Am. Chem. Soc. 89 (1967) 3904.
[22] S. Trofimenko, J. Am. Chem. Soc. 91 (1969) 588.
[23] S. Trofimenko, Inorg. Chem. (1969) 2675.
[24] S. Trofimenko, J. Am. Chem. Soc. 90 (1968) 4754.
[25] S. Trofimenko, Inorg. Chem. (1970) 2483.
[26] C.A. Kosky, P. Ganis, G. Avitabile, Acta. Crystallogr. B27 (1971) 1859.
[27] F.A. Cotton, T. LaCour, A.G. Stanislowski, J. Am. Chem. Soc. 96 (1974) 754.
[28] F.A. Cotton, B.A. Frenz, C.A. Murillo, J. Am. Chem. Soc. 97 (1975) 2118.
[29] S. Trofimenko, J.C. Calabrese, J.S. Thompson, Angew. Chem. Int. Ed. Engl. 28 (1989) 205.
[30] J.C. Calabrese, S. Trofimenko, J.S. Thompson, J. Chem. Soc., Chem. Commun. (1986) 1122.
[31] S. Trofimenko, J.C. Calabrese, J.S. Thompson, Inorg. Chem. 26 (1987) 1507.
[32] S. Trofimenko, Scorpionates: The Coordination Chemistry of Polypyrazolylborate Ligands, University College Press, London, 1999.
[33] M.D. Curtis, K.-B. Shiu, W.M. Butler, Organometallics 2 (1983) 1475.
[34] M.D. Curtis, K.-B. Shiu, W.M. Butler, J. Am. Chem. Soc. 108 (1986) 1550.
[35] S. Trofimenko, Chem. Rev. 93 (1993) 943.
[36] S. Trofimenko, J.C. Calabrese, P.J. Domaille, J.S. Thompson, Inorg. Chem. 28 (1989) 1091.
[37] J.C. Calabrese, P.J. Domaille, J.S. Thompson, S. Trofimenko, Inorg. Chem. 29 (1990) 4429.
[38] N. Kitajima, K. Fujisawa, C. Fujimoto, Y. Moro-oka, S. Hashimoto, T. Kitagawa, K. Toriumi, K. Tatsumi, A. Nakamura, J. Am. Chem. Soc. 114 (1992) 1277.
[39] A.L. Rheingold, L.M. Liable-Sands, S. Trofimenko, Chem. Commun. 1 (1997) 691.
[40] A.L. Rheingold, G.P.A. Yap, L.M. Liable-Sands, I.A. Guzei, S. Trofimenko, Inorg. Chem. 36 (1997) 6261.
[41] A.L. Rheingold, G.P.A. Yap, L.N. Zakharov, S. Trofimenko, Eur. J. Inorg. Chem. (2002) 2335.
[42] S. Trofimenko, A.L. Rheingold, L.M. Liable-Sands, Inorg. Chem. 41 (2002) 1889.
[43] A.L. Rheingold, G.P.A. Yap, S. Trofimenko, Inorg. Chem. 34 (1995) 759.
[44] A.L. Rheingold, L.M. Liable-Sands, G.P.A. Yap, S. Trofimenko, Chem. Commun. (1996) 1233.
[45] A.L. Rheingold, B.S. Haggerty, G.P.A. Yap, S. Trofimenko, Inorg. Chem. 36 (1997) 5097.
[46] A.L. Rheingold, R.L. Ostrander, B.S. Haggerty, S. Trofimenko, Inorg. Chem. 33 (1994) 3666.
[47] A.L. Rheingold, B.S. Haggerty, S. Trofimenko, J. Chem. Soc., Chem. Commun. (1994) 1973.
[48] A.L. Rheingold, C.G. White, S. Trofimenko, Inorg. Chem. 32 (1993) 3471.
[49] R. Han, G. Parkin, S. Trofimenko, Polyhedron 14 (1995) 387.
[50] A.L. Rheingold, L.M. Liable-Sands, J.A. Golen, S. Trofimenko, S. Eur, J. Inorg. Chem. (2003) 2767.
[51] A.L. Rheingold, L.M. Liable-Sands, C.L. Incarvito, S. Trofimenko, J. Chem. Soc., Dalton Trans. (2002) 2297.
[52] A. Caballero, M.M. Diaz-Requejo, T.R. Belderrain, M.C. Nicasio, S. Trofimenko, P.J. Pérez, J. Am. Chem. Soc. 125 (2003) 1446.
[53] A.J. Amoroso, J.C. Jeffery, P.L. Jones, J.A. McCleverety, L. Rees, A.L. Rheingold, Y. Sun, J. Takats, S. Trofimenko, M.D. Ward, G.P.A. Yap, J. Chem. Soc., Chem. Commun. (1995) 1881.
[54] A.L. Rheingold, C.D. Incarvito, S. Trofimenko, J. Chem. Soc., Dalton Trans. (2000) 1233.
[55] A.L. Rheingold, S. Trofimenko, unpublished work.
[56] S. Trofimenko, J. Am. Chem. Soc. 92 (1970) 5118.
[57] P. Ge, B.S. Haggerty, A.L. Rheingold, C.G. Riordan, J. Am. Chem. Soc. 116 (1994) 8406.
[58] C. Ohrenberg, P. Ge, P. Schebler, C.G. Riordan, G.P.A. Yap, A.L. Rheingold, Inorg. Chem. 35 (1996) 749.
[59] J.C. Peters, T.D. Feldman, T.D. Tilley, J. Am. Chem. Soc. 121 (1999) 9871.
[60] A.A. Barney, A.F. Heyduk, D.G. Nocera, Chem. Commun. (1999) 2379.
[61] J.C. Thomas, J.C. Peters, J. Am. Chem. Soc. 123 (2001) 5100.
[62] I.R. Shapiro, D.M. Jenkins, J.C. Thomas, M.W. Day, J.C. Peters, Chem. Commun. (2001) 2152.
[63] T.A. Betley, J.C. Peters, Inorg. Chem. 41 (2002) 6541.
[64] S.J. Chiu, P. Ge, C.G. Riordan, L.M. Liable-Sands, A.L. Rheingold, Chem. Commun. (1999) 159.
[65] K. Niedenzu, S. Trofimenko, Inorg. Chem. 24 (1985) 4222.
[66] J.S. Thompson, J.L. Zitzman, T.J. Marks, J.A. Ibers, Inorg. Chim. Acta 46 (1980) L101.
[67] P. Ghosh, G. Parkin, Chem. Commun. (1998) 413.
[68] M. Garner, J. Reglinski, I. Cassidy, M.D. Spicer, A.R. Kennedy, Chem. Commun. (1996) 1975.
[69] J. Reglinski, M. Garner, I.D. Cassidy, P.A. Slavin, D.R. Armstrong, J. Chem. Soc., Dalton Trans. (1999) 2119.
[70] P.J. Bailey, M. Lanfranchi, L. Marchio, S. Parsons, Inorg. Chem. 40 (2001) 5030.
[71] R. Cammi, M. Lanfranchi, L. Marchiò, C. Mora, C. Paiola, M.A. Pellinghelli, Inorg. Chem. 42 (2003) 1769.
[72] T. Ruman, Z. Ciunik, A.M. Trzecial, S. Wolowiec, J.J. Ziólkowski, Organometallics 22 (2002) 1072.

Available online at www.sciencedirect.com
SCIENCE DIRECT®
Polyhedron 23 (2004) 205–209
POLYHEDRON
www.elsevier.com/locate/poly

Potassium tetrakis(2-mercaptothiazolyl)borate; an open-framework material: synthesis and X-ray structure analysis

Luis F. Soares [a], Daniele C. Menezes [a], Rosalice M. Silva [a,*], Antonio C. Doriguetto [b], Javier Ellena [b], Yvonne P. Mascarenhas [b], Eduardo E. Castellano [b]

[a] *Departamento de Quimica, Universidade Federal de Minas Gerais, Belo Horizonte, MG 31270-901, Brazil*
[b] *Instituto de Física de São Carlos, Universidade de São Paulo, São Carlos, SP 13560-970, Brazil*

Received 7 May 2003; accepted 6 August 2003

Abstract

The compound potassium tetrakis(2-mercaptothiazolyl)borate was prepared and characterized in solution and in the solid state. The structure crystallizes in the non-centrosymmetric space group $F\bar{4}3c$ (No. 219) with two independent molecules in the asymmetric unit. In spite of the fact that two molecules are very similar enantiomorphs, the transformation relating the two moieties does not coincide with any of those belonging to the centrosymmetric super space group $Fd\bar{3}c$ (No. 228). The packing gives rise to big holes between the tetrakis(2-mercaptothiazolyl)borate anions, of mean diameter ~9 Å, which are filled by clusters of K^+ and H_2O.
© 2003 Elsevier Ltd. All rights reserved.

Keywords: S,N ambidentate borate ligands; Synthesis; X-ray structure; Open frame material

1. Introduction

Tripodal borate S,N ligands such as hydrotris(thioxoimidazolyl)borate, Tm^-, [1,2] and hydrotris(2-mercaptothiazolyl)borate, Mt^-, [3] are softer than the pyrzolyl analogues [4] and as such are more useful to be used as supporting ligands with soft transition metals. The tetrakis analogue offers the opportunity to bind additional metal ions and accordingly we were able to prepare tetrakis(2-mercaptothiazolyl)borate, Mte^-, as the potassium salt, that was characterized by spectroscopic methods, elemental analysis and by X-ray crystallography. According to the X-ray studies, the diameter of the cavities that are created by the packing of the anions rings, among other data, is in the range normally found for zeolite type of compounds.

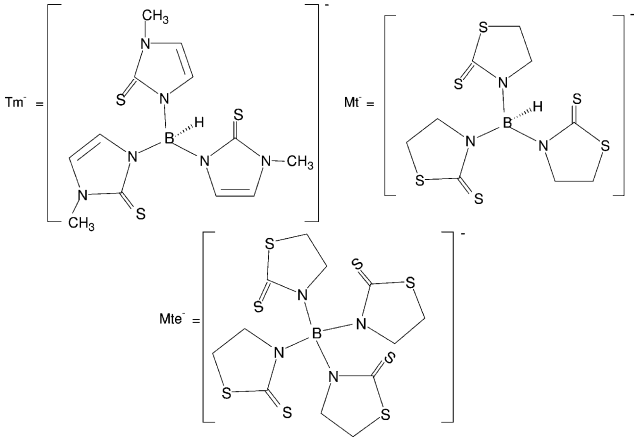

2. Experimental

2.1. General comments

KBH_4 was purchased from Fluka and 2-mercaptothiazoline, from Aldrich. All the reagents were used as received. Elemental analyses (C, H, N) were performed with a Perkin–Elmer mod. PE-2400 CHN instrument.

* Corresponding author. Present address: 1183 North Main St., West Bend, WI 53090, USA.
E-mail address: rosalice@charter.net (R.M. Silva).

0277-5387/$ - see front matter © 2003 Elsevier Ltd. All rights reserved.
doi:10.1016/j.poly.2003.11.012

IR spectra were recorded on a Perkin–Elmer 283B instrument. ^{1}H and ^{13}C spectra were recorded on a Bruker Avance DPX200 spectrometer operating at room temperature, using tetramethylsilane as an internal reference. ^{11}B NMR spectrum was recorded on a Bruker Avance DPX400 spectrometer operating at room temperature, using $BF_3 \cdot Et_2O$ as an internal reference.

2.2. Synthesis

2.2.1. Potassium tetrakis(2-mercaptothiazolyl)borate, KMte

Finely divided KBH_4 (0.10 g, 2.3 mmol) and 2-mercaptothiazoline (1.35 g, 11.5 mmol) were placed, together with a magnetic stirring bar, into a Schlenk flask. The flask was connected to a volumetric device and placed into a bath resting on a heating and stirring plate. The mixture was heated to 100 °C where upon evolution of H_2 commences. The temperature was controlled at 165 °C until 92.0 mmol of H_2 (203.6 mL) had been evolved. Then the mixture was allowed to cool to room temperature and dichloromethane was added. This mixture was stirred for 15 min. The solution was separated and this process was repeated three times. The remaining white solid was dried under vacuum and was washed with three 20-mL portions of THF. The solutions were collected and THF was allowed to evaporate under room temperature. $KMte \cdot 2H_2O$ was obtained in 79.9% yield. ^{1}H NMR (200 MHz, $CDCl_3$): 4.00 (t, NCH_2), 3.58 (t, SCH_2); ^{13}C NMR (200 MHz, $CDCl_3$): δ C=S not observed 51.05 (NCH_2), 33.77 (SCH_2); ^{11}B NMR (δ, $BF_3.Et_2O$): −5.21. *Anal.* Calc. (Found) for $C_{12}H_{20}BKN_4O_2S_8$: C, 25.80 (25.75); H, 3.58 (3.50); N, 10.03 (10.02)%.

2.3. Crystal structure determination

The measurement was made at 120 K on an Enraf–Nonius Kappa-CCD diffractometer (95 mm CCD camera on κ-goniostat) with graphite monochromated Mo Kα ($\lambda = 0.71073$ Å) radiation. The temperature was controlled using an Oxford Cryosystem low temperature device. Data collection (φ scans and ω scans with κ offsets) were made using the COLLECT [5]; integration and scaling of the reflections was performed with the HKL DENZO-SCALEPACK system of programs [6]. The final unit cell parameters were based on all reflections using HKL SCALEPACK [6]. Absorption corrections were carried out using the multi-scan method [7]. The structures were solved using direct methods with SHELXS-97 [8]. The models were refined by full-matrix least-squares procedures on F^2 using SHELXL-97 [9]. The program WINGX was used to analyse and prepare the data for publication [10]. Crystal data, data collection procedures, structure determination methods and refinement results are summarized in Table 1. The ORTEP's were prepared using the ORTEP-3 for Windows [11].

Table 1
Crystal data and structure refinement for KMte

Formula weight	554.68
Temperature (K)	120(2)
Wavelength (Å)	0.71073
Crystal system	cubic
Space group	$F\bar{4}3c$
Unit cell dimensions (Å)	$a = 30.0302(8)$
Volume (Å^3)	27081.6(12)
Z	48
D_{calc} (Mg/m^3)	1.633
Absorption coefficient (mm^{-1})	0.993
$F(000)$	13 632
Crystal size (mm)	$0.10 \times 0.10 \times 0.10$
θ range for data collection	1.36–25.00°
Index ranges	$-35 \leqslant h \leqslant 32$, $-35 \leqslant k \leqslant 32$, $-28 \leqslant l \leqslant 35$
Reflections collected	19 207
Independent reflections	2002 [$R_{int} = 0.0500$]
Completeness to $\theta = 25.00°$	99.7%
Maximum and minimum transmission	0.9072 and 0.9072
Refinement method	Full-matrix least-squares on F^2
Data/parameters	2002/135
Goodness-of-fit on F^2	1.118
Final R indices [$I > 2\sigma(I)$]	$R_1 = 0.0331$, $wR_2 = 0.0916$
R indices (all data)	$R_1 = 0.0424$, $wR_2 = 0.1108$
Absolute structure parameter	0.09(13)
Largest difference peak and hole (e Å^{-3})	0.684 and −0.244

3. Results and discussion

It is very difficult to control the volume of hydrogen evolved in such type of reactions, Eq. (1), in order to obtain the desired compound, since the temperature range where the reaction occurs, for each type of compound, bis, tris and tetrakis, is close and the reactions are done in the solid state.

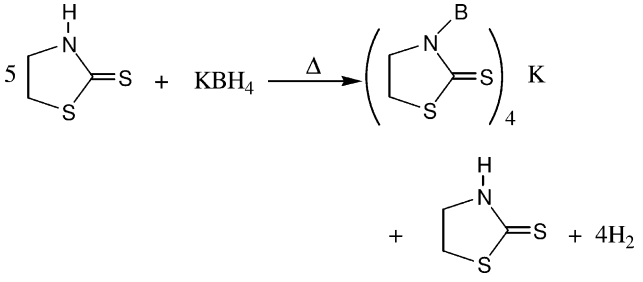

(1)

Indeed, this is especially true in the preparation of the tetrakis compound, as it is always obtained as a mixture with the hydrotris compound. However, as KMte is soluble in THF, it was easily separated. It is a very hygroscopic compound. For this reason it is obtained as

$KMte \cdot 2H_2O$ by allowing a THF solution to evaporate at room temperature. The NMR data indicated that the four rings were equivalent, as just two triplets were observed for the hydrogens next to sulfur and nitrogen, at 3.58 and 4.00δ, respectively, in agreement with literature results [1], and was confirmed by the solid-state structure of the compound, as discussed below.

3.1. Molecular structure of KMte

The structure crystallizes in the non-centrosymmetric space group $F\bar{4}3c$ (No. 219) with two independent molecules in the asymmetric unit, Fig. 1. Comparison of these molecules by the method of Kabsch [12] showed them to be very similar, related by an improper orthogonal transformation and with a root mean square deviation between homologous atoms of 0.047 Å. These facts suggested that the crystal could belong to the centrosymmetric super-group $Fd\bar{3}c$ (No. 228), with just one molecule per asymmetric unit. Closer scrutiny, however, showed this not to be the case because the affin transformation relating the two moieties did not coincide with any of those belonging to the space group. It also turned out that the Flack parameter [0.08(12)] was quite sensitive to structure inversion thus permitting the assigning of the absolute structure in the non-centrosymmetric space group. An interesting crystallographic feature is the highly symmetric space group found for this compound. It is important to emphasize that in the Cambridge Structural Database (CSD) [13], only 25 of the structures deposited crystallize in the $F\bar{4}3c$ space group. This number represent less than 0.01% of the total one.

The mercaptothiazolyl ring geometry, Fig. 1, is very similar to the 1,3-thiazolidine-2-thione structure [14]. The five-member rings A and B present an envelope conformation with C(12) and C(22) in their respective flip point. The C(12), S(11) and B(1) deviate 0.497(6), 0.189(6) and 0.279(4) Å, respectively, from the least-squares plane passing through C(11), C(13), N(1) and S(12). In the same way, the C(22), S(21) and B(2) deviate 0.460(6), 0.131(6) and 0.199(4) Å, respectively, from the equivalent least-square plane passing through molecule B.

The asymmetric unit consists of one mercaptothiazolyl ring for each anion molecule A and B. The whole anions are "generated" by the symmetry $\bar{4}$ passing through the boron atom. Like the asymmetric unit the whole anion geometry of A and B are exactly the same. Fig. 2 is an ORTEP view of molecule A. The rings are bound to the boron through the nitrogen atoms N(1)–B(1) = 1.568(3) Å and N(2)–B(2) = 1.561(3) Å. The geometry around boron is an almost regular tetrahedron with a mean ∠N–B–N = 109(2)°. This value is the same for both molecules. The selected geometric parameters are showed in Table 2.

In each unit the potassium ion is coordinated to six water molecules. Four of these belong to neighbouring $K(H_2O)_6$ units. One of the K–O bond distance is shorter than the sum of the ionic radii of $K^+ + O^{2-}$, 2.73 Å [15]; K(1)–O(11) = 2.453(3) Å in molecule A and K(2)–O(21) = 2.451(3) Å in molecule B. The other K–O bond distances are longer, but still smaller than the sum of the covalent radii of K + O = 2.69 Å [16]; K(1)–O(12) = 2.890(4) Å in molecule A and K(2)–O(22) = 2.909(4) Å in molecule B. Potassium still does interact with the sulfur atoms of the anions rings. These inter-

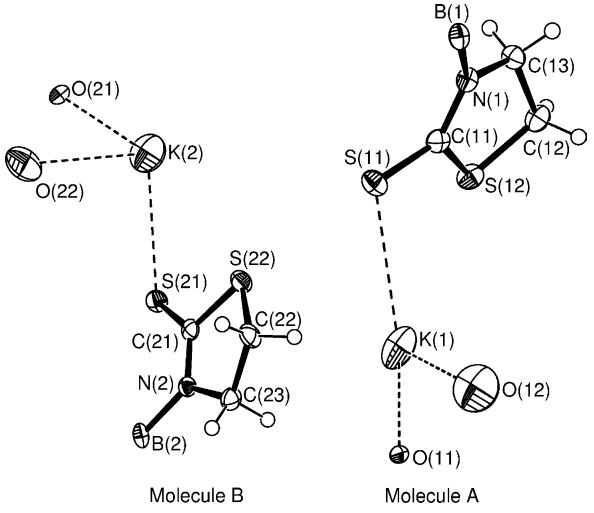

Fig. 1. An ORTEP3 view of $KMte \cdot 2H_2O$ showing the atom-labelling scheme of the two molecules present in the asymmetric unit. Displacement ellipsoids drawn at the 50% probability. H atoms are represented by circles of arbitrary size.

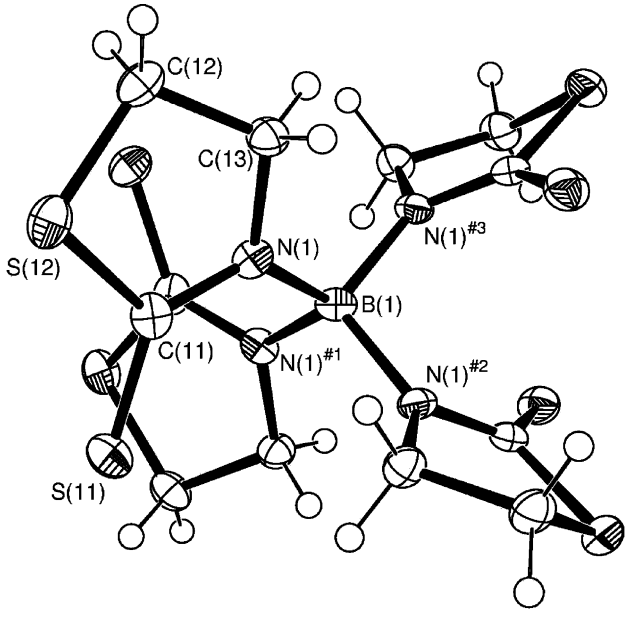

Fig. 2. A ORTEP3 view of the Mte^- anion (molecule A). Displacement ellipsoids drawn at the 50% probability. (*Symmetry codes*: #1, $-x+3/2$, $-y+3/2$, $\mathscr{Z}$; #2, $y+3/2$, x, $-z+2$; #3, y, $x+1/2$, $x+1$, $z+2$).

Table 2
Selected bond distances (Å) and angles (°) for KMte

Molecule A		Molecule B	
Bond distances			
B(1)–N(1)	1.568(3)	B(2)–N(2)	1.561(3)
C(12)–C(13)	1.524(5)	C(22)–C(23)	1.529(5)
N(1)–C(11)	1.342(5)	N(2)–C(21)	1.338(5)
N(1)–C(13)	1.479(4)	N(2)–C(23)	1.480(4)
S(11)–C(11)	1.672(4)	S(21)–C(21)	1.672(4)
S(12)–C(11)	1.763(4)	S(22)–C(21)	1.771(4)
S(12)–C(12)	1.813(4)	S(22)–C(22)	1.804(4)
K(1)–O(11)	2.453(3)	K(2)–O(21)	2.451(3)
K(1)–O(12)	2.890(4)	K(2)–O(22)	2.909(4)
K(1)–S(11)	3.379(2)	K(2)–S(21)	3.388(2)
K(1)–S(12)	3.923(3)	K(2)–S(22)	3.916(3)
K(1)–O(11)	2.453(3)	K(2)–O(21)	2.451(3)
K(1)–O(12)	2.890(4)	K(2)–O(22)	2.909(4)
K(1)–S(11)	3.379(2)	K(2)–S(21)	3.388(2)
K(1)–S(12)	3.923(3)	K(2)–S(22)	3.916(3)
Bond angles			
N(1)–B(1)–$N(1)_{mean}$	109(2)	N(1)–B(1) –$N(1)_{mean}$	109(2)

actions are longer than the sum of the ionic radii of $K^+ + S^{2-} = 3.17$ Å [15], and one of them is much longer than the other; K(1)–S(11) = 3.379(2) and K(1)– S(12) = 3.923(3) Å in molecule A and K(2)– S(21) = 3.388(2) and K921)–S(22) = 3.916(3) Å in molecule B. A view focusing on the potassium solvate sphere is shown in Fig. 3.

The X-ray diffraction analysis of KMt [3] revealed that there is no interaction between the potassium ion and the donor sulfur atoms. For Mte^- the same behaviour was expected. However, as stressed previously, there are interactions between potassium and the sulfur atoms. These interactions can be accounted by crystal packing effects. These effects can lead to structural differences and variations in bond distances and angle parameters for molecules belonging to the same unit cell [17]. Recently, a study that compared geometric data for crystal structures, for which more than one molecule of complex is present per crystallographic asymmetric unit, was performed [18]. This study allowed a quantification of the crystal packing effect on molecular structures. The determined metal–ligand bond distance deviations were found to be in the range 0.01–0.02 Å and for the bond angles the range was 1°–2° (or 3°). In the present work the bond distance differences (mean values), for the longer K–O bonds (K(1)–O(12) and K(2)–O(22)), within the two molecules is 0.019. Bigger deviations were found between the bond angles: e.g., O(11)–K(1)–O(12) and O(21)–K(2)–O(22), 0.28 Å. According to the previously mentioned work, these differences are due to crystal packing effects and we believe that these effects are accounted for the potassium–sulfur interactions in the present work, as they are not expected to exist, like in the Mt^- ligand [3b].

Fig. 4 is a packing of the structure on plane *ab*. In this unit cell fraction the anion generated by molecule B is in the central position. As can be observed there is an alternation between molecules A and B along the unit cell directions. Each anion is octahedrally surrounded by four other anions and two holes. When the central anion is a molecule A, the four neighbour anions are molecules B and vice versa. The big holes observed between the

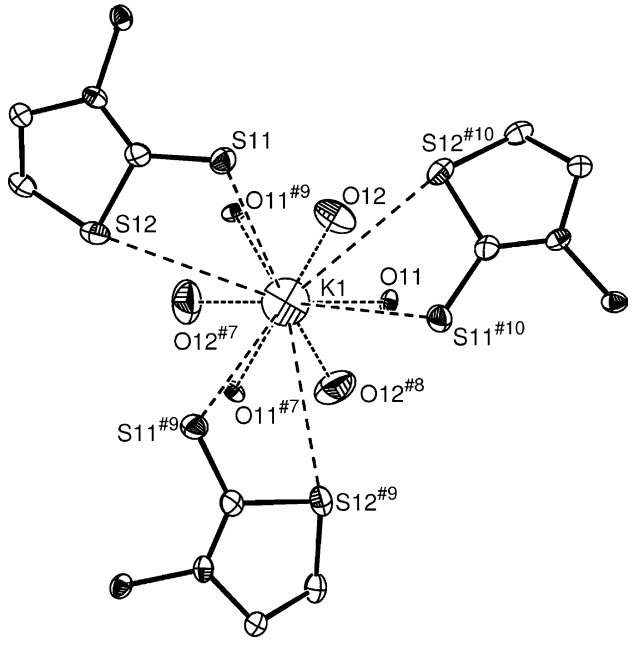

Fig. 3. A ORTEP3 view of potassium coordination environment (molecule A). Displacement ellipsoids drawn at the 50% probability. (*Symmetry codes*: #7, *y*, *z*, *x*; #8, $-z+3/2$, $x+3/2$, *y*; #9, $-z+3/2$, *x*, $-y+3/2$; #10, *y*, $-z+3/2$, $-x+3/2$).

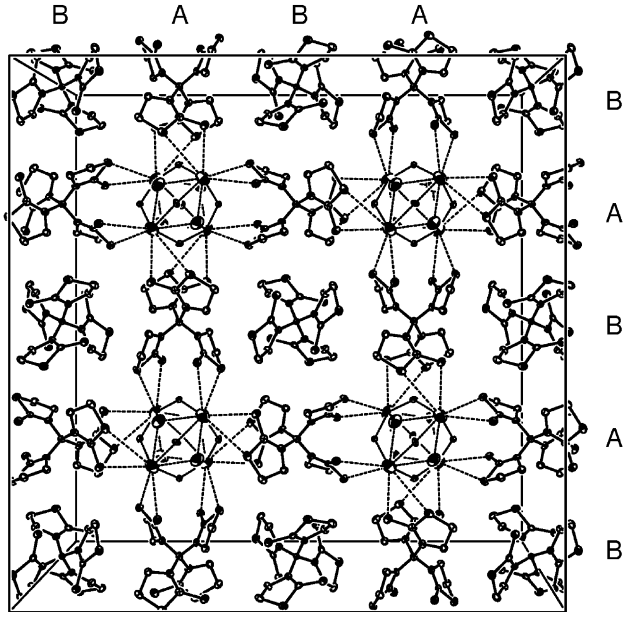

Fig. 4. Packing on plane *ab* ($-1.15 < x < 1.15$; $-1.15 < y < 1.15$; $0.12 < z < 0.38$ is shown). Displacement ellipsoids drawn at the 50% probability.

anions Mte^- have a mean diameter of ~9 Å. Each cavity is filled by a cage-shape cluster constituted by four sites containing K^+ cations and seven sites containing water's oxygens. Cluster with atoms belonged to molecule A is octahedrally surrounded by six Mte^- anions formed by atoms belonged to molecule A and vice versa. Either for molecule A or B, the separation between neighbour hole centres is about 15 Å.

4. Conclusions

The density and size of the cavities of the structure studied in the present work are similar to the ones in zeolite compounds. Also, as these, there are cations and water molecules inside the molecular cavities in order to compensate for the framework negative charge. The potassium and oxygen sites within the holes are not completely occupied. Several models were tested and the best one point to occupancies of 0.75 for K(1) and K(2), 0.5 for O(11) and O(21), and 0.75% for O(12) and O(22) sites. In spite of the non-completeness, if the whole unit cell was considered, the ratio K/Mte^- and K/H_2O are 1/1 and 1/2, respectively. Therefore, the empirical formula obtained from the present X-ray data is $K[BC_{12}H_{12}N_4S_8]\cdot 2H_2O$. The present X-ray data do not permit to find the water's hydrogens.

5. Supplementary material

A table of complete crystallographic data, tables of fractional atomic coordinates for all atoms, complete list of bond distances and angles and tables of anisotropic displacement parameters have been deposit with the Cambridge Crystallographic Data Center, CCDC No. CCDC 206571 for KMte. Copies of this information are available, free of charge, from The Director, CCDC, 12 Union Road, Cambridge, CB2 1EZ, UK (Fax: +441223-336033; e-mail: deposit@ccdc.cam.ac.uk or http://www.ccdc.cam.ac.uk).

References

[1] (a) M. Garner, J. Reglinski, I. Cassidy, M.D. Spicer, A.R. Kennedy, Chem. Commun. (1996) 1975;
(b) J. Reglinski, M. Garner, I.D. Cassidy, P.A. Slavin, M.D. Spicer, D.R. Armstrong, J. Chem. Soc., Dalton Trans. (1999) 2119.
[2] L.F. Soares, R.M. Silva, Inorg. Synth. 33 (2002) 154.
[3] (a) J.F. Ojo, P.A. Slavin, J. Reglinsky, M. Garner, M.D. Spicer, A.R. Kennedy, S.J. Teat, Inorg. Chim. Acta 313 (2001) 15;
(b) L.F. Soares, R.M. Silva, A.C. Doriguetto, J. Ellena, Y.P Mascarenhas, E.E. Castellano, J. Braz. Chem. Soc. (2003), in press.
[4] S. Trofimenko, J. Am. Chem. Soc. 89 (1967) 3170.
[5] Enraf-Nonius, COLLECT, Nonius BV, Delft, The Netherlands, 1997–2000.
[6] Z. Otwinowski, W. Minor, in: C.W. Carter Jr., R.M. Sweet (Eds.), Methods in Enzymology, vol. 276, Academic Press, New York, 1997, p. 307.
[7] R.H. Blessing, Acta Crystallogr., Sect. A 51 (1995) 33.
[8] G.M. Sheldrick, SHELXS-97, Program for Crystal Structure Resolution, University of Göttingen, 1997.
[9] G.M. Sheldrick, SHELXL-97, Program for Crystal Structures Analysis, University of Göttingen, 1997.
[10] L.J. Farrugia, J. Appl. Cryst. 30 (1997) 565.
[11] L.J. Farrugia, J. Appl. Cryst. 32 (1999) 837.
[12] W. Kabsch, Acta Crystallogr., Sect. A 32 (1976) 922.
[13] F.H. Allen, J.E. Davies, J.J. Galloy, O. Johnson, O. Kenard, C.F. Macrae, E.M. Mitchell, G.F. Mitchel, J.M. Smith, D.G. Watson, J. Chem. Inf. Comput Sci. 31 (1999) 187.
[14] E.S. Raper, R.E. Oughtred, I.W. Nowell, Inorg. Chim. Acta 77 (1983) L89.
[15] J.E. Hueey, Inorganic Chemistry, Principles of Structure and Reactivity, Harper International SI Edition, New York, 1983, p. A-37.
[16] J.E. Hueey, Inorganic Chemistry, Principles of Structure and Reactivity, Harper International SI Edition, New York, 1983, p. 258.
[17] (a) M.A.C. Martins, R.M. Silva, J.C. Huffman, Polyhedron 21 (2002) 421;
(b) W. Oberhauser, C. Bachman, P. Brüggler, Inorg. Chim. Acta 238 (1995) 35;
(c) W. Oberhauser, C. Bachman, T. Stamft, P. Brüggler, Inorg. Chim. Acta 256 (1997) 223;
(d) W. Oberhauser, C. Bachman, T. Stamft, P. Brüggler, Inorg. Chim. Acta 274 (1998) 143;
(e) W. Oberhauser, C. Bachman, T. Stamft, P. Brüggler, Polyhedron 16 (1997) 2827.
[18] A. Martin, A.G. Orpen, J. Am. Chem. Soc. 118 (1996) 1464.

Available online at www.sciencedirect.com
SCIENCE DIRECT®
Polyhedron 23 (2004) 211–218
POLYHEDRON
www.elsevier.com/locate/poly

Synthesis, structure and spectroscopic properties of novel half-sandwich nickel(II) complexes with less hindered hydrotris(pyrazolyl)borate ligand

Ying-Ji Sun, Wei-Zheng Shen, Peng Cheng *, Shi-Ping Yan, Dai-Zheng Liao, Zong-Hui Jiang, Pan-Wen Shen

Department of Chemistry, Nankai University, Tianjin 300071, China

Received 9 May 2003; accepted 16 August 2003

Abstract

This paper presents the syntheses, crystal structures and spectroscopic properties of a series of half-sandwich nickel(II) complexes with hydrotris(3,5-dimethylpyrazolyl)borate and azide or thiocyanate, [Tp*Ni(pz*)$_2$(N$_3$)] (**1**), [Tp*Ni(pz*)(SCN)(H$_2$O)] (**2**) and [Tp*Ni(SCN)(CH$_3$OH)$_2$] (**3**) (Tp*: hydrotris(3,5-dimethylpyrazolyl)borate; pz*: 3,5-dimethylpyrazole). Compound **1** crystallizes in the triclinic system, $P\bar{1}$ space group (No. 2), $a = 10.2957(11)$ Å, $b = 11.5080(12)$ Å, $c = 13.6748(15)$ Å, $\alpha = 81.993(2)°$, $\beta = 72.999(2)°$, $\gamma = 74.533(2)°$, $Z = 2$, $R_1 = 0.0454$, $wR_2 = 0.1272$. The nickel(II) ion in **1** is coordinated to six nitrogen atoms of Tp* and azide ion to form a distorted N$_6$ octahedron. The structure of **2** is roughly determined by X-ray crystal diffraction and shown two structurally independent [Tp*Ni(pz)(SCN)(H$_2$O)] units. The nickel(II) ion in **2** is six-coordinated to five nitrogen atoms of Tp*, pz*, thiocyanate and one oxygen atom of water molecule to form a N$_5$O octahedral environment. Compound **3** crystallizes in the monoclinic system, $P2_1/c$ space group, $a = 13.416(4)$ Å, $b = 11.964(3)$ Å, $c = 14.636(4)$ Å, $\beta = 96.195(5)°$, $Z = 4$, $R_1 = 0.0379$, $wR_2 = 0.1079$. The coordination environment of nickel(II) ion in **3** is better to be described as the N$_4$O$_2$ octahedron made up of three nitrogen atoms of Tp*, one nitrogen atom of thiocyanate and two oxygen atoms of coordinated methanol molecules. The half-sandwich compound [Tp*Ni(η_2-O$_2$N)(CH$_3$OH)]$_4$ (**4**), which has been previously reported in a short communication, has the nickel(II) center with N$_3$O$_3$ coordination environment. The influences of N_3^-, SCN^- and NO_2^- in all these half-sandwich nickel(II) complexes were discussed in this paper.
© 2003 Elsevier Ltd. All rights reserved.

Keywords: Nickel(II) complexes; Crystal structures; Hydrotris(pyrazolyl)borate complexes; Coordination environment; Scorpionates

1. Introduction

The scorpionate ligand, hydrotris(pyrazolyl)borate ligand (Tp^R), is widely used in the design of functional molecules, catalysis of chiral induced asymmetric synthesis, liquid crystal materials, molecular ''electronic devices'' and biomimetic chemistry [1–3]. The half-sandwich mononuclear complexes with monohydrotris(pyrazolyl)borate ligand and small molecules or anions can be considered as the model complexes of metalloenzymes such as carbonic anhydrase (CA) [4–8], nitrite reductases (NiR) [9–11], Hemocyanin (Hc) [12,13] and blue copper proteins [14], and as the precursors for synthesis of various multinuclear model complexes [15]. Since the less hindered hydrotris(pyrazolyl)borate ligands Tp and Tp* have strong tendency to form stable and inert full-sandwich complexes [M^{II}Tp$^R_2$], the half-sandwich mononuclear complexes are relatively difficult to obtain [16,17]. However it has been found that the full-sandwich complexes [M^{II}Tp$_2$] and [M^{II}Tp*$_2$] with less hindered hydrotris(pyrazolyl)borate ligands Tp and Tp* have some reactivity under suitable conditions [18,19]. Recently, several methods to synthesize the half-sandwich complexes were summarized [18,20]. We prepared mononuclear half-sandwich nickel(II) complexes with less hindered hydrotris(3,5-dimethylpyrazolyl)borate

* Corresponding author. Tel.: +86-2223509957; Fax: +86-22-23502458.
E-mail address: pcheng@nankai.edu.cn (P. Cheng).

0277-5387/$ - see front matter © 2003 Elsevier Ltd. All rights reserved.
doi:10.1016/j.poly.2003.11.011

and nitrite, [Tp*Ni(η_2-O_2N)(CH_3OH)] (**4**) (Tp*: hydrotris(3,5-dimethylpyrazolyl)borate) by reaction of $Ni(ClO_4)_2 \cdot 6H_2O$ with KTp* and $NaNO_2$ [18]. In the complex, NO_2^- was coordinated in an asymmetric nitrito-O,O′-bidentate coordination mode and the nickel(II) ion was in N_3O_3 octahedral environment. In the present paper, we reported three novel mononuclear half-sandwich nickel(II) complexes with less hindered hydrotris(3,5-dimethylpyrazolyl)borate ligand (Tp) and azide or thiocyanate, [Tp*Ni(pz*)$_2$(N_3)] (**1**), [Tp*Ni(pz*) (SCN)(H_2O)] (**2**) and [Tp*Ni(SCN)(CH_3OH)] (**3**) (pz*: 3,5-dimethylpyrazole). The coordination environments of nickel in these complexes were N_6 (**1**), N_5O (**2**), N_4O_2 (**3**) and N_3O_3 (**4**), respectively.

2. Experimental

2.1. Materials

The scorpionate ligand KTp* was synthesized according to the literature method [19]. The purity was confirmed by IR, MS-FAB and elemental analysis. Other chemicals were reagent grade and used as received.

2.2. Physical measurements

Analyses for C, H and N were carried out on a Perkin–Elmer analyzer at the Institute of Elemental Organic Chemistry, Nankai University. Infrared spectra on KBr pellets were recorded on a Shimadzu IR-408 spectrophotometer in the range of 4000–600 cm^{-1}. UV–Vis spectroscopy in MeOH were recorded on a Shimadzu UV-2401 PC UV–Vis recording spectrophotometer in the range of 200–1000 nm. Mass spectrum analysis was performed at the Central Laboratory of Nankai University on VG ZAB-HS spectrometer.

2.3. Synthesis

2.3.1. [Tp*Ni(pz*)$_2$(N_3)] (*1*)

A solution of NaN_3 (0.6 mmol. 39.1 mg) in 1 ml water is added to 5 ml methanol solution of $Ni(ClO_4)_2 \cdot 6H_2O$ (0.2 mmol, 73.1 mg). The mixture is stirring for 2 h at room temperature. A solution of KTp* (0.2 mmol, 67.3 mg) in 10 ml methanol is added to the mixture and stirred for another 10 h, and the precipitates are filtered. The green crystals suitable for X-ray structure analysis are obtained by slow evaporation of filtrate. The yield is found to be 79% based on the metal salts. *Anal*. Calc. for $C_{25}H_{38}BN_{13}Ni$ (**1**): C, 50.88; H, 6.49; N, 30.85. Found: C, 50.81; H, 6.35; N, 30.53%.

2.3.2. [Tp*Ni(pz*)(SCN)(H_2O)] (*2*)

A solution of KSCN (0.6 mmol, 58.3 mg) in 1 ml water is added to 5 ml methanol solution of $Ni(ClO_4)_2 \cdot 6H_2O$ (0.2 mmol, 73.1 mg). The mixture is stirring for 2 h at room temperature. Then, 10 ml methanol solution of KTp* (0.2 mmol, 67.3 mg) is added to the mixture and stirred for 10 h, and the precipitates are filtered. The blue micro-crystals are obtained by slow evaporation of filtrate. The yield is found to be 73% based on the metal salts. *Anal*. Calc. for $C_{21}H_{32}BN_9NiOS$ (**2**): C, 47.76; H, 6.11; N, 23.87. Found: C, 47.40; H, 5.85; N, 23.60%.

2.3.3. [Tp*Ni(SCN)(CH_3OH)$_2$] (*3*)

The synthetic method of **3** is similar with **2** only the molar ratio ($Ni(ClO_4)_2 \cdot 6H_2O$: KSCN: KTp*) is different (1:1.5:1). An 1 ml aqueous solution of KSCN (0.3 mmol, 30.1 mg) is added to 5 ml methanol solution of $Ni(ClO_4)_2 \cdot 6H_2O$ (0.2 mmol, 73.1 mg). The mixture is stirring for 2 h at room temperature. A solution of KTp*(0.2 mmol, 67.3 mg) in 10 ml methanol is added to the mixture and stirred for 10 h, and the precipitates are filtered. The yield is found to be 58% based on the metal salts. *Anal*. Calc. for $C_{18}H_{30}BNiN_7O_2S$ (**3**): C, 45.22; H, 6.28; N, 20.51. Found: C, 45.26; H, 6.35; N, 20.58%.

2.4. X-ray crystallography

Intensity data for single crystals of complexes **1**, **2** and **3** were collected on a BRUKER SMART 1000 CCD detector with graphite-monochromatized Mo Kα radiation ($\lambda = 0.71073$ Å). The structures were solved by direct methods using the program SHELXS 97 [21] and subsequent Fourier difference techniques, and refined anisotropically by full-matrix least-squares on F^2 using SHELXL-97 [22].

A green single crystal of **1** having the approximate dimensions $0.30 \times 0.20 \times 0.15$ mm was mounted on a glass fiber. Cell parameters were determined from a least-squares refinement on the setting angles from 25 centered reflections in the range from 1.56° to 25.03° at 298(2) K. The intensities of the $\pm hkl$ reflections were measured up to $\theta_{max} = 25.03°$; the ω–2θ scan technique was employed. The index range was $-12 \leqslant h \leqslant 10$, $-11 \leqslant k \leqslant 13$ and $-16 \leqslant l \leqslant 15$. No absorption correction was made during processing. Crystal parameters and structure refinements were summarized in Table 1. All non-hydrogen atoms were refined anisotropically. The hydrogen atoms were set in calculated positions and refined as riding atoms with a common fixed isotropic thermal parameter. The residual maximum and minimum in the final Fourier difference maps were 0.379 and −0.242 e $Å^{-3}$. The value of the goodness-of-fit is 1.040.

The single crystal structure analysis of **2** was carried out. Unfortunately, the single crystals are sensitive to X-ray and the intensity of standard reflections strongly declined. The present results obtained from a crystal having the approximate dimensions $0.40 \times 0.30 \times 0.30$ mm. The intensities of the $\pm hkl$ reflections were

Table 1
Crystal data and structure refinement of complexes **1**, **2** and **3**

Complexes	**1**	**2**	**3**
Chemical formula	$C_{25}H_{38}BN_{13}Ni$	$C_{21}H_{32}BN_9NiOS$	$C_{18}H_{30}BN_7NiO_2S$
Formula weight	590.20	528.14	478.07
Crystal system	triclinic	triclinic	monoclinic
Space group	$P\bar{1}$	$P\bar{1}$	$P2_1/c$
a (Å)	10.2957(11)	10.956(2)	13.416(4)
b (Å)	11.5080(12)	13.044(3)	11.964(3)
c (Å)	13.6748(15)	20.621(4)	14.636(4)
α (°)	81.993(2)	77.820(4)	90
β (°)	72.999(2)	88.178(4)	96.195(5)
γ (°)	74.533(2)	69.858(4)	90
V (Å^3)	1490.0(3)	2701.7(9)	2335.5(11)
Z	2	4	4
D_{calcd} (g cm^{-3})	1.316	1.298	1.360
μ (cm^{-1})	0.690	0.826	0.948
T (K)	298(2)	293(2)	293(2)
$F(000)$	624	1112	1008
θ Range (°)	1.56–25.03	1.01–26.49	1.53–25.03
Maximum and minimum transmission	0.9035, 0.8197	0.7897, 0.7335	0.8152, 0.2805
Number of parameters	365	613	271
R_1, wR_2[a] $[I > 2\sigma(I)]$	0.0454, 0.1272	0.1472, 0.3989	0.0379, 0.1079
Goodness-of-fit (F^2)	1.040	0.961	1.045
$\Delta\rho$, maximum, minimum (e Å^{-3})	0.379, −0.242	2.565, −1.185	0.417, −0.455

[a] $R1 = \sum||F_o| - |F_c||/\sum|F_o|$, $wR_2 = (\sum[w(F_o^2 - F_c^2)^2]/\sum(F_o^2)^2)^{1/2}$, $w = 1/[\sigma^2(F_o^2) + (0.0838P)^2 + 0.0000P]$ and $P = (F_o^2 + 2F_c^2)/3$ for **1**, $w = 1/[\sigma^2(F_o^2) + (0.1005P)^2 + 100.3648P]$ and $P = (F_o^2 + 2F_c^2)/3$ for **2**, and $w = 1/[\sigma^2(F_o^2) + (0.0672P)^2 + 1.3584P]$, where $P = (F_o^2 + 2F_c^2)/3$ for **3**.

measured up to $\theta_{max} = 26.49°$ and the index range was $-13 \leqslant h \leqslant 13$, $-16 \leqslant k \leqslant 15$ and $-22 \leqslant l \leqslant 25$. The poor quality of structure determination resulted in the high standard deviations. In order to compare with the other complexes, some of structural information of **2** were listed in Tables 1–4.

A purple single crystal of **3** having the approximate dimensions $0.20 \times 0.30 \times 0.25$ mm was mounted on a glass fiber. Cell parameters were determined from 1.53° to 25.03° at 293(2) K. The intensities of the $\pm hkl$ reflections were measured up to $\theta_{max} = 25.03°$; the ω–2θ scan technique was employed. The index range was $-15 \leqslant h \leqslant 14$,

Table 2
Selected bond lengths (Å) and angles (°) of **1**, **2** and **3**

1		**2**				**3**	
Bond lengths							
Ni(1)–N(1)	2.121(3)	Ni(1)–N(1)	2.052(12)	Ni(2)–N(2)	2.082(12)	Ni(1)–N(1)	2.054(3)
Ni(1)–N(3)	2.085(2)	Ni(1)–N(11)	2.091(12)	Ni(2)–N(21)	2.113(12)	Ni(1)–N(16)	2.073(2)
Ni(1)–N(5)	2.074(2)	Ni(1)–N(13)	2.106(11)	Ni(2)–N(23)	2.071(11)	Ni(1)–N(14)	2.087(2)
Ni(1)–N(7)	2.173(2)	Ni(1)–N(15)	2.061(11)	Ni(2)–N(25)	2.055(12)	Ni(1)–N(11)	2.090(2)
Ni(1)–N(9)	2.143(3)	Ni(1)–N(18)	2.109(12)	Ni(2)–N(28)	2.082(11)	Ni(1)–O(1)	2.153(2)
Ni(1)–N(11)	2.117(3)	Ni(1)–O(1)	2.159(9)	Ni(2)–O(2)	2.133(10)	Ni(1)–O(2)	2.168(2)
Bond angles							
N(3)–Ni(1)–N(1)	89.87(10)	N(1)–Ni(1)–N(11)	93.5(5)	N(2)–Ni(2)–N(21)	91.6(5)	N(1)–Ni(1)–N(16)	95.35(10)
N(5)–Ni(1)–N(1)	85.56(10)	N(1)–Ni(1)–N(13)	174.3(5)	N(2)–Ni(2)–N(23)	173.8(5)	N(1)–Ni(1)–N(14)	97.02(10)
N(1)–Ni(1)–N(7)	173.16(10)	N(1)–Ni(1)–N(15)	94.6(5)	N(2)–Ni(2)–N(25)	92.6(6)	N(16)–Ni(1)–N(14)	88.18(9)
N(1)–Ni(1)–N(9)	88.66(11)	N(1)–Ni(1)–N(18)	90.6(5)	N(2)–Ni(2)–N(28)	90.2(5)	N(1)–Ni(1)–N(11)	172.42(10)
N(11)–Ni(1)–N(1)	96.04(10)	N(11)–Ni(1)–N(13)	86.1(4)	N(21)–Ni(2)–N(23)	86.4(5)	N(16)–Ni(1)–N(11)	89.58(9)
N(5)–Ni(1)–N(3)	89.10(10)	N(11)–Ni(1)–N(15)	88.6(5)	N(21)–Ni(2)–N(25)	87.9(5)	N(14)–Ni(1)–N(11)	88.87(9)
N(3)–Ni(1)–N(7)	89.39(9)	N(11)–Ni(1)–N(18)	175.9(5)	N(21)–Ni(2)–N(28)	178.1(5)	N(14)–Ni(1)–O(2)	95.91(9)
N(3)–Ni(1)–N(9)	89.33(10)	N(13)–Ni(1)–N(15)	91.1(4)	N(23)–Ni(2)–N(25)	93.2(5)	N(11)–Ni(1)–O(2)	93.39(8)
N(3)–Ni(1)–N(11)	173.35(10)	N(13)–Ni(1)–N(18)	89.8(5)	N(23)–Ni(2)–N(28)	91.8(4)	N(1)–Ni(1)–O(1)	86.47(10)
N(5)–Ni(1)–N(7)	87.63(10)	N(15)–Ni(1)–N(18)	91.0(5)	N(25)–Ni(2)–N(28)	92.1(5)	N(16)–Ni(1)–O(1)	89.53(9)
N(5)–Ni(1)–N(9)	174.02(10)	N(1)–Ni(1)–O(1)	85.7(4)	N(2)–Ni(2)–O(2)	85.8(5)	N(14)–Ni(1)–O(1)	175.99(9)
N(5)–Ni(1)–N(11)	94.40(10)	N(11)–Ni(1)–O(1)	90.5(4)	N(21)–Ni(2)–O(2)	90.7(5)	N(11)–Ni(1)–O(1)	87.82(9)
N(9)–Ni(1)–N(7)	98.13(10)	N(13)–Ni(1)–O(1)	88.6(4)	N(23)–Ni(2)–O(2)	88.4(4)	N(1)–Ni(1)–O(2)	81.30(9)
N(11)–Ni(1)–N(7)	85.11(10)	N(15)–Ni(1)–O(1)	179.1(5)	N(25)–Ni(2)–O(2)	177.9(5)	N(16)–Ni(1)–O(2)	174.99(8)
N(11)–Ni(1)–N(9)	87.75(10)	N(18)–Ni(1)–O(1)	89.8(4)	N(28)–Ni(2)–O(2)	89.3(4)	O(1)–Ni(1)–O(2)	86.55(9)

Table 3
Selected hydrogen bond lengths (Å) and angles (°) for **1**, **3** and **4**

1	2	3	4
N(8)–H(8)···N(13): 2.136 (158.79)	N(17)–H(17)···S(1): 2.624 (154.75)	O(2)–H(2D)···S(1): 2.630	O(3)–H(3)···O(1): 2.197 (163.57)
N(10)–H(10)···N(13): 2.138 (159.66)	N(27)–H(27)···S(2): 2.638 (153.56)	(126.74)	O(3)–H(3)···N(7): 2.307 (163.54)
	O(1)···S(2): 3.195		
	O(2)···S(1): 3.208		

Table 4
Selected structural parameters for **1**, **2**, **3** and **4**

	1	2	3	4
Coordination environment	N_6	N_5O	N_4O_2	N_3O_3
Ni–N(Tp*)	2.094	2.083	2.083	2.051
Ni–N(pz*)	2.158	2.096		
Ni–N(N_3^- or NCS^-)	2.117	2.067	2.054	
Ni–O		2.147	2.161	2.142
Ni···Ni	8.280	7.360	7.420	6.279

$-14 \leqslant k \leqslant 14$ and $-17 \leqslant l \leqslant 14$. Crystal parameters and structure refinements were summarized in Table 1. All non-hydrogen atoms were refined anisotropically. The hydrogen atoms were set in calculated positions and refined as riding atoms with a common fixed isotropic thermal parameter. The residual maximum and minimum in the final Fourier difference maps were 0.417 and −0.455 e $Å^{-3}$. The value of the goodness-of-fit was 1.045.

3. Results and discussion

3.1. Synthesis of the complexes

The scorpionate ligand KTp* can easily form full-sandwich complexes [MTp*$_2$]. The full-sandwich complexes [MTp*$_2$] as well as other substituted complexes [$M^{II}Tp_2^{R1,R2}$] have been considered stable and inert. Although the full-sandwich complexes have the abilities to induce some reactivity in suitable conditions [18,19], it is still the main problem to obtain the half-sandwich mononuclear complexes. Recently, several methods to synthesize the half-sandwich complexes were summarized: (i) the use of bulky substituents (R); (ii) the addition of a Tp^R salt to an excess amount of metal salt; and (iii) the use of salts with a bidentate ligand such nitrate and carboxylate [20]; and (iv) the use of the TpTl salts for the preparation of TpM complexes [3,23]. Combining (ii) and (iii), we prepared **4** by reaction of excess amount of $Ni(ClO_4)_2 \cdot 6H_2O$ with KTp* and $NaNO_2$. In the complex, NO_2^- was in an asymmetric nitrito-O,O′-bidentate coordination mode. For **1**, **2** and **3**, the metal salt $Ni(ClO_4)_2 \cdot 6H_2O$ was firstly added into NaN_3 or KSCN and then reacted with KTp*. The expected mononuclear half-sandwich complexes containing one Tp* ligand and one N_3^- or SCN^- ligand were obtained. For **1** and **2**, one or two pz*, which came from the partly decomposition of KTp* during reaction, were also coordinated to the nickel ion. Similar phenomenon was observed in other complexes with hydrotris(pyrazolyl)borate and hydrotris(pyrazolyl)methane ligands [24–27].

3.2. Structural description

The structures of all complexes have been determined by single-crystal X-ray diffraction. Selected bond lengths and angles of **1**, **2** and **3** were listed in Table 2.

The ORTEP drawing of **1** was shown in Fig. 1. The Ni(II) ion in **1** was coordinated to six nitrogen atoms, three from Tp* ligand, two from two pz* ligands and one from azide ion, to form a distorted octahedron. The average bond lengths of Ni–N(Tp*) and Ni–N(pz*) were 2.094 and 2.158 Å, respectively. The bond length of Ni–N(N_3) is 2.117 Å. In **1**, N(13) of N_3^- was connected by weak intermolecular hydrogen bond with hydrogen atoms of two pyrazole ligands of adjacent complex molecule to form a quasi-dimeric structure. The molecular packing was shown in Fig. 2. The nearest Ni···Ni distances was 8.280 Å. The hydrogen bond lengths of N(8)–H(8)···N(13) and N(10)–H(10)···N(13) were 2.136 and 2.138 Å while the angles of N(8)–H(8)–N(13) and N(10)–H(10)–N(13) were 158.79° and 159.66°, respectively. The hydrogen bond lengths and angles were listed in Table 3.

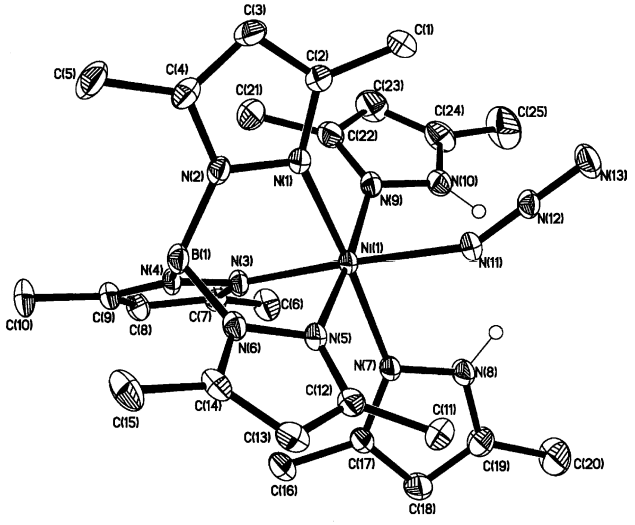

Fig. 1. ORTEP drawing of [Tp*Ni(pz*)$_2$(N_3)] (**1**).

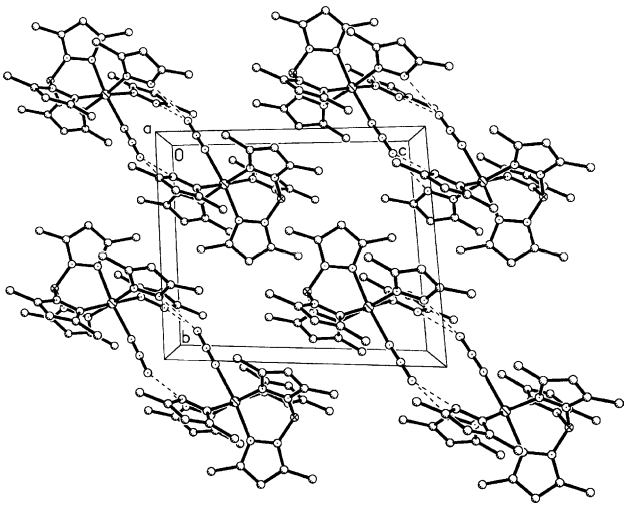

Fig. 2. Molecular packing of $[Tp^*Ni(pz^*)_2(N_3)]$ (**1**).

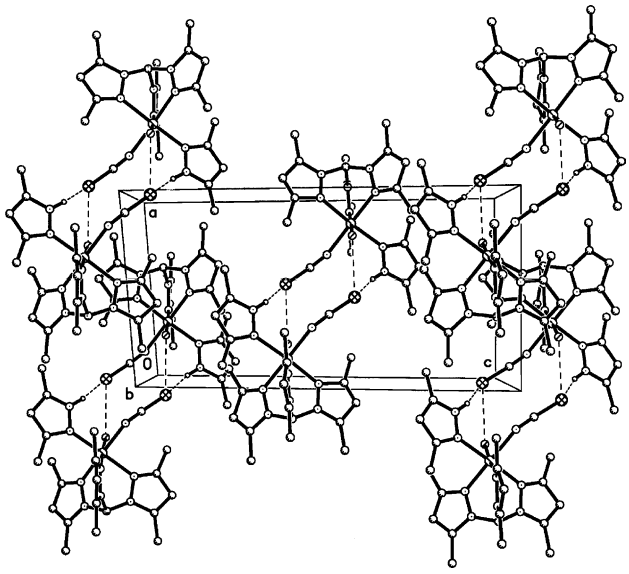

Fig. 4. Molecular packing of $[Tp^*Ni(pz^*)(SCN)(H_2O)]$ (**2**).

The structure of **2** consisted two structurally independent [Tp*Ni(pz*)(SCN)(H_2O)] units and was shown in Fig. 3. The Ni(II) ion in **2** was coordinated to three nitrogen atoms from Tp*, one nitrogen atom from pz*, one nitrogen atom from thiocyanate and one oxygen atom from water molecule to form the N_5O octahedral environment. The average bond lengths of Ni–N(Tp*) and Ni–N(pz*) were 2.083 and 2.096 Å, respectively. The bond length of Ni–N(SCN) and Ni–O(H_2O) were 2.067 and 2.147 Å, respectively. S(1) and S(2) of SCN^- were connected by weak intermolecular hydrogen bonds with hydrogen atoms on pyrazole ring of adjacent complex molecules, and O(1) and O(2) of water molecules were connected by weak intermolecular hydrogen bond with hydrogen atoms of pyrazole to form a quasi-dimeric structure. The molecular packing was shown in Fig. 4. The nearest Ni···Ni distances was 7.360 Å.

The ORTEP drawing of **3** was shown in Fig. 5. The coordination environment of Ni(II) ion in **3** was better to be described as N_4O_2 octahedron. The Ni(II) ion was coordinated with four nitrogen atoms of Tp*, thiocyanate and two oxygen atoms of methanol molecules. The average bond length of Ni–N(Tp) was 2.083 Å. The bond lengths of Ni–N(SCN) and Ni–O(CH_3OH) were 2.054 and 2.161 Å, respectively. S(1) of NCS^- was connected by weak intermolecular hydrogen bond with hydrogen atoms of O(2) in adjacent complex molecule to form a quasi-dimeric structure. The molecular packing was shown in Fig. 6. The nearest Ni···Ni distances

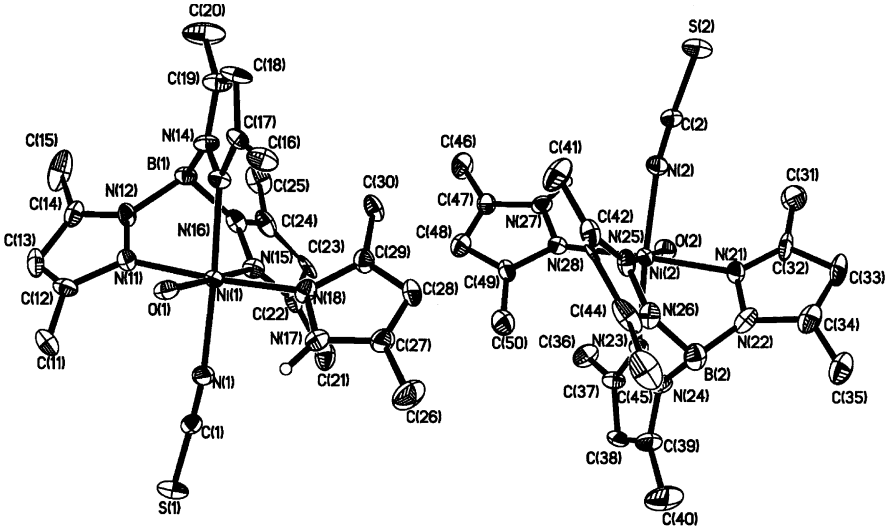

Fig. 3. ORTEP drawing of $[Tp^*Ni(pz^*)(SCN)(H_2O)]$ (**2**).

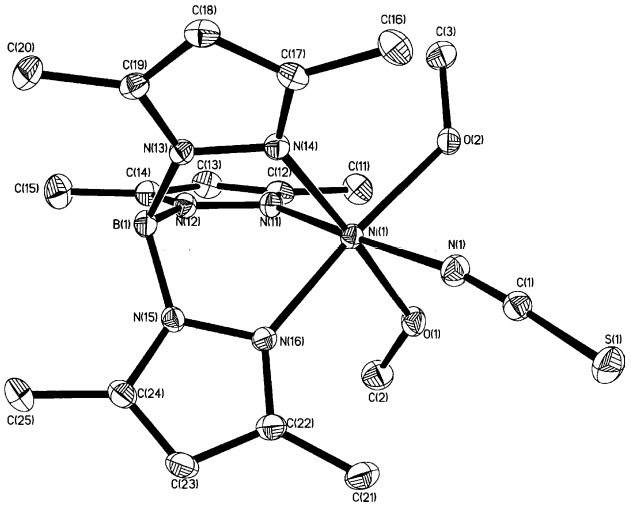

Fig. 5. ORTEP drawing of $[Tp^*Ni(NCS)(CH_3OH)_2]$ (**3**).

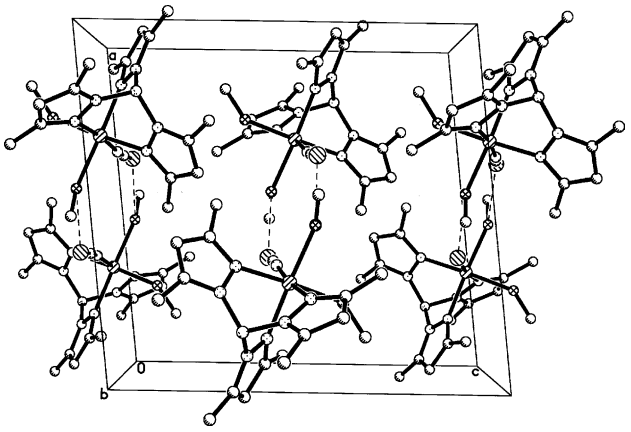

Fig. 6. Molecular packing of $[Tp^*Ni(NCS)(CH_3OH)_2]$ (**3**).

was 7.420 Å. The hydrogen bond length and angle of O(2)–H(2D)···S(1) were 2.630 Å and 126.74°, respectively. The hydrogen bond lengths and angles were also listed in Table 3.

The average bond lengths of Ni–N(Tp*) and Ni–N(pz*) of **2** and **3** were shorter than that of **1**, but longer than that of analogous $[Tp^*Ni(\eta^2\text{-}O_2N)(CH_3OH)]$ (**4**) previously reported [18]. The bond length of Ni–N(N_3) in **1** was longer than Ni–N(SCN) of **2** and **3**. The bond length of Ni–O(H_2O) in **2** was shorter than Ni–O(CH_3OH) in **3** and longer than that of **4**. The average bond lengths of these complexes became shorter with the decreasing numbers of coordinated oxygen atoms. The nickel(II) ions were in N_6-coordinated environment for **1**, N_5O-coordinated environment for **2**, N_4O_2-coordinated environment for **3** and N_3O_3-coordinated environment for **4**, which were shown in Fig. 7. The intermolecular hydrogen bonds were found for all complexes and to form quasi-dimeric structure. Selected structural parameters were listed in Table 4.

3.3. Spectroscopic properties

The IR spectra of complexes **1**–**4** were very similar for the ligand Tp* and the data were listed in Table 5. The typical stretch frequency of ν_{B-H} moved from 2430 cm^{-1} in the free ligand to 2510 cm^{-1} for **1**, 2520 cm^{-1} for **2**, 2485 cm^{-1} for **3** and **4**, respectively. The stretch frequency of $\nu_{N\equiv N}$ of N_3^- and $\nu_{C\equiv N}$ of SCN^- were observed at 2090 cm^{-1} for **1**, 2110 cm^{-1} for **2** and 2085 cm^{-1} for **3**, respectively.

The UV–Vis spectra of complexes **1**–**4** were also similar and the data were listed in Table 5. In the UV range, three strong absorptions appeared. They can be assigned

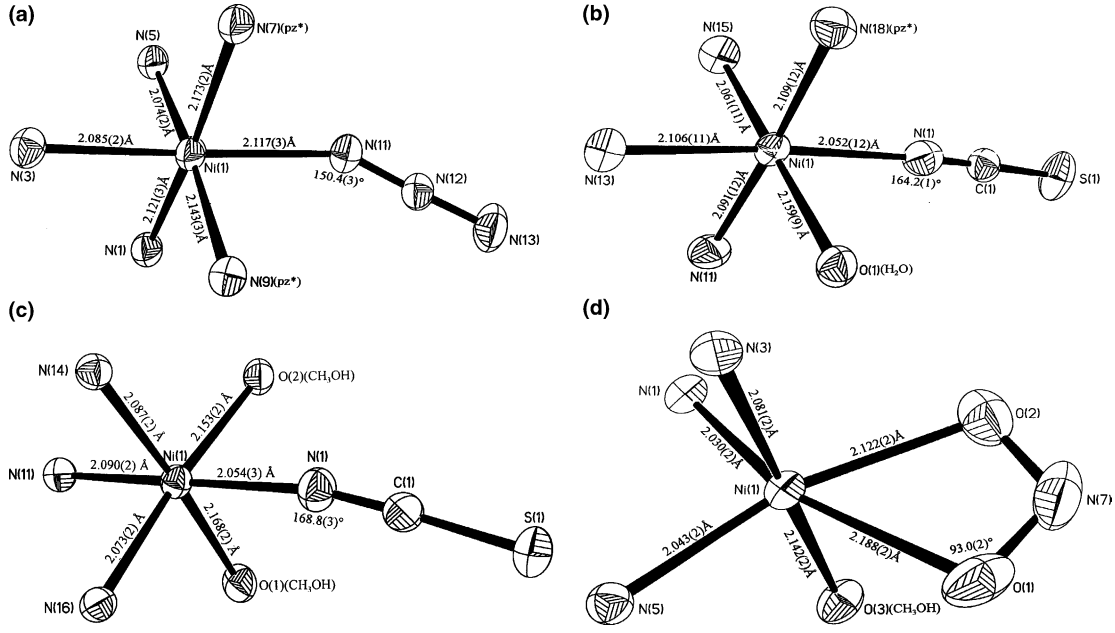

Fig. 7. Coordination environment of **1**, **2**, **3** and **4**: (a) $[Tp^*Ni(pz^*)_2(N_3)]$ (**1**); (b) $Tp^*Ni(pz^*)(SCN)(H_2O)]$ (**2**); (c) $[Tp^*Ni(NCS)(CH_3OH)_2]$ (**3**); (d) $[Tp^*Ni(\eta^2\text{-}O_2N)(CH_3OH)]$ (**4**).

Table 5
Selected spectroscopic data for **1**–**4**

		1	**2**	**3**	**4**
Coordination environment		N_6	N_5O	N_4O_2	N_3O_3
ν (cm^{-1})	ν_{B-H}	2485	2520	2510	2485
	$\nu_{N\equiv N}$	2090			
	$\nu_{C\equiv N}$		2110	2085	
		39 841(4016)	44 444(756.7)	44 444(2242)	40 733(3560)
	CT(L)		36 832(882.5)	36 765(2721)	
			31 348(201.8)	31 596(2937)	
ν (cm^{-1}) (ε/M^{-1} cm^{-1})	$\nu_1(^3T_2 \leftarrow {}^3A_{2g})$	11 033	9813	9804	9311
	$\nu_2(^3T_{1g}(F) \leftarrow A_{2g})$	15 773(68)	15 748(19.6)	15 785(24.5)	15 221(188.5)
	$\nu_3(^3T_{1g}(P) \leftarrow {}^3A_{2g})$	25 907(242)	25 707(43.1)	25 907(48.2)	25 776(441.0)
	$\nu_4(^1E_2 \leftarrow {}^3A_{2g})$	13 289(3)	13 307(4.7)	13 360(6.8)	12 553(4.7)
Dq (cm^{-1})		1103	981	980	931
B' (cm^{-1})		572	801	819	871
β		0.55	0.77	0.79	0.84
$1-\beta$		0.45	0.23	0.21	0.16

to ligand transition bands. In the visible region two relative strong bands can be observed. They can be assigned to spin allowed d–d transition bands of Ni(II)(d^8), $\nu_3(^3T_{1g}(P) \leftarrow {}^3A_{2g})$, $\nu_2(^3T_{1g}(F) \leftarrow {}^3A_{2g})$, respectively. The small band appeared between ν_1 and ν_2 (ca. 13 300 cm^{-1}) can be assigned spin-forbidden d–d transition band of Ni(II)(d^8), $\nu_4(^1E_g \leftarrow {}^3A_{2g})$. The $\nu_1(^3T_2 \leftarrow {}^3A_{2g})$ band was not observed completely in the experimental region (200–1000 nm). The ligands-field constants Dq, B', β and ν_1 were calculated by using observed bands ν_2 and ν_3 [28] and the results were listed in Table 5. The Dq values of all complexes were larger than that of $[Ni^{II}(H_2O)_6]^{2+}$ (850 cm^{-1}). The B' of the complexes were less than that of free Ni(II) ion (1041 cm^{-1}), showing some covalent bonding of Ni(II) in the complexes.

4. Conclusions

Reaction of M(II) with hydrotris(pyrazolyl)borate ligands easily obtained stable full-sandwich complexes $[M^{II}Tp^R_2]$ because of the strong coordination ability of the ligands. These $[M^{II}Tp^R_2]$ complexes have been considered stable and inert. In this paper, we prepared three new half-sandwich nickel(II) complexes with monotris(pyrazdyl)borate ligands and azide or thiocyanate, [Tp*Ni(pz*)$_2$(N_3)] (**1**), [Tp*Ni(pz*)(SCN)(H_2O)] (**2**) and [Tp*Ni(NSC)(CH_3OH)$_2$] (**3**) by reaction of excess amount of $Ni(ClO_4)_2 \cdot 6H_2O$ with KTp* and NaN_3 or KSCN. The synthetic route described here impeded the full-sandwich complexes formation effectively. Compared with [Tp*Ni(η^2-O_2N)(CH_3OH)] **(4)** which was published previously, we can clearly see that the structures of all complexes were six-coordinated octahedral environment, with N_6 for **1**, N_5O for **2**, N_4O_2 for **3** and N_3O_3 for **4**. The different coordination environments made for different results, the bonds in four complexes, so did the intermolecular hydrogen bonds.

Acknowledgements

This work was supported by the National Natural Science Foundation of China (Nos. 29971017 and 90101028), and the TRAPOYT of MOE, PR China.

References

[1] G. Parkin, Adv. Inorg. Chem. 42 (1995) 291.
[2] N. Kitajima, W.B. Tolman, Prog. Inorg. Chem. 43 (1995) 419.
[3] S. Trofimenko, Scorpionates: The Coordination Chemistry of Polypyrazolborate Ligands, Imperial College Press, London, 1999.
[4] K. Weis, H. Vahrenkamp, Inorg. Chem. 36 (1997) 5592.
[5] C. Bergquist, G. Parkin, Inorg. Chem. 38 (1999) 422.
[6] C. Kimblin, V.J. Murphy, T. Hascall, B.M. Bridgewater, J.B. Bonanno, G. Parkin, Inorg. Chem. 39 (2000) 967.
[7] Y.J. Sun, L.Z. Zhang, P. Cheng, H.K. Lin, S.P. Yan, W. Sun, D.Z. Liao, Z.H. Jiang, P.W. Shen, Inorg. Chem. 42 (2003) 508.
[8] Y.J. Sun, W. Sun, L.Z. Zhang, P. Cheng, H.K. Lin, S.P. Yan, D.Z. Liao, Z.H. Jiang, P.W. Shen, J. Mol. Catal. A 198 (2003) 99.
[9] C.E. Ruggiero, S.M. Carrier, W.E. Antholine, J.W. Whittaker, C.J. Cramer, W.B. Tolman, J. Am. Chem. Soc. 115 (1993) 11285.
[10] C.E. Ruggiero, S.M. Carrier, W.B. Tolman, Angew. Chem., Int. Ed. Engl. 33 (1994) 895.
[11] N. Kitajima, Y. Moro-oka, Chem. Rev. 94 (1994) 737.
[12] N. Kitajima, K. Fujisawa, J. Am. Chem. Soc. 115 (1993) 4690.
[13] N. Kitajima, K. Fujisawa, Y. Moro-oka, S. Hashimoto, J. Am. Chem. Soc. 112 (1990) 3210.
[14] N. Kitajima, in: K.D. Karlin, Z. Tyeklar (Eds.), Bioinorganic Chemistry of Copper, Chapman & Hall, New York, 1993, p. 251.
[15] S.H. Cho, D. Whang, K.N. Han, K. Kim, Inorg. Chem. 31 (1992) 519.
[16] S. Trofimenko, Chem. Rev. 93 (1993) 943.
[17] E.W. Abel, F.G.A. Stone, G. Wilkinson (Eds.), Comprehensive Organometallic Chemistry II, Pergamon Press, Oxford, 1995.
[18] Y.J. Sun, P. Cheng, S.P. Yan, D.Z. Liao, Z.H. Jiang, P.W. Shen, Inorg. Chem. Commun. 3 (2000) 289.
[19] D.M. Eichhorn, W.H. Armstrong, Inorg. Chem. 29 (1990) 3607.
[20] M. Akita, D.Q. Ma, S. Hikichi, Y. Moro-oka, J. Chem. Soc., Dolton Trans. (1999) 987.

[21] G.M. Sheldrick, SHELXS 97, Program for the Solution of Crystal Structures, University of Göttingen, 1997.
[22] G.M. Sheldrick, SHELXL-97, Program for the Refinement of Crystal Structures, University of Göttingen, 1997.
[23] R. Han, A. Looney, K. McNeil, G. Parkin, A.L. Rheingold, B.S. Haggerty, J. Inorg. Biochem. 49 (1993) 105.
[24] Y.J. Sun, P. Cheng, S.P. Yan, D.Z. Liao, Z.H. Jiang, P.W. Shen, J. Coord. Chem. 55 (2002) 363.
[25] L.M.L. Chia, S. Radojevic, I.J. Scowen, M. McPartlin, M.A. Halcrow, J. Chem. Soc., Dalton Trans. (2000) 133.
[26] K. Fujita, S. Hikichi, M. Akita, Y. Moro-oka, J. Chem. Soc., Dalton Trans. (2000) 117.
[27] C. Titze, J. Hermann, H. Vahrenkamp, Chem. Ber. 128 (1995) 1095.
[28] A.B.P. Lever, Inorganic Electronic Spectroscopy, 2nd ed., Elsevier, Amsterdam, 1984.

Available online at www.sciencedirect.com
SCIENCE DIRECT®
Polyhedron 23 (2004) 219–223
POLYHEDRON
www.elsevier.com/locate/poly

Complexes of heteroscorpionate trispyrazolylborate ligands. Part XII. Variable hapticity of hydrobis (3-phenyl-5-isopropylpyrazolyl)(3,5-dimethylpyrazolyl) borate in its rhodium(I) complexes with COD and NBD

Tomasz Ruman [a], Zbigniew Ciunik [b], Stanisław Wołowiec [a,*]

[a] *Faculty of Chemistry, Rzeszów University of Technology, 6 Powstańców Warszawy Ave., 35-959 Rzeszów, Poland*
[b] *Faculty of Chemistry, University of Wrocław, 14 Joliot-Curie Str., 50-383 Wrocław, Poland*

Received 11 May 2003; accepted 14 August 2003

Abstract

The structure of Tp″Rh(NBD) complex was determined by X-ray crystallography (Tp″ = hydrobis(3-phenyl-5-isopropylpyrazolyl)(3,5-dimethylpyrazolyl)borate, NBD = 2,5-norbornadiene). The Tp″ was found to be κ^3 coordinated to rhodium(I). Two independent molecules of Tp″Rh(NBD) were found in triclinic crystals with Rh–N(pz) distances in the region of 2.113(3)–2.307(3) Å. On the other hand the same Tp″ ligand was demonstrated to be coordinated in κ^2 fashion in Tp″Rh(COD) (COD = 1,5-cyclooctadiene) by variable temperature 1-D and 2-D ^{1}H NMR measurements. The intramolecular exchange between coordinated and uncoordinated 3-phenyl-5-isopropylpyrazolyl residues occurs with $\Delta G^{\neq} = 42.2$ kJ/mol as it was calculated from the ^{1}H NMR studies.
© 2003 Elsevier Ltd. All rights reserved.

Keywords: Polypyrazolylborate; Rhodium(I); Cyclooctadiene; Norbornadiene; Structure; NMR

1. Introduction

Heteroscorpionate trispyrazolylborates (Tp″) are tripodal anionic ligands of potentially C_s symmetry [1]. The symmetry of the ligands can be preserved in their metal ion complexes, when Tp″s are coordinated in κ^3 fashion. The κ^3 hapticity resulting in effective C_s symmetry of the complexes was observed in the series of high-spin cobalt(II) complexes of the general formula Tp″Co(NCS) [2–8].

In case of Tp″Rh(LL) complexes (where LL = $(CO)_2$ or COD), the Tp″ ligands are coordinated in κ^2 fashion [9]. Fluxional behavior of those complexes was studied in detail by variable-temperature ^{1}H NMR spectroscopy. The homoscorpionate Tp″ ligands are in most cases κ^2-bonded in their Tp″Rh(LL) complexes ([9] and references [6–16] cited therein). However, there are three examples of κ^3 hapticity in rhodium complexes with trispyrazolylborates and ancillary ligands (LL) other than mentioned: Tp^{Me}Rh(NBD) [10], Tp^{Me2}Rh(PEt_3)(C_2H_4) [11], TpRh(PPh_3)[($CCOOCH_3$)$_2$] [12], and Tp^{iPr2}Rh(NBD) [13], in which the N(pz)–Rh bond lengths fall into the region of 2.12–2.27 Å. Here we report on the structure of another complex, in which the Tp″ ligand bearing two sterically demanding 3-phenyl substituents is coordinated in κ^3 fashion in Tp″Rh(NBD), while κ^2 hapticity is found in Tp″Rh(COD) analogue as can be concluded on the basis of variable temperature 1-D and 2-D ^{1}H NMR experiments.

2. Experimental

2.1. Syntheses

The sodium salt of hydrobis(3-phenyl-5-isopropylpyrazolyl)(3,5-dimethylpyrazolyl)borate (NaTp″) was synthesized as before [7]. The Tp″Rh(NBD) (**1**) and Tp″Rh(COD) (**2**) complexes were synthesized upon

* Corresponding author. Tel.: +17-865-1657; fax: +17-854-3655.
E-mail address: sw@prz.rzeszow.pl (S. Wołowiec).

0277-5387/$ - see front matter © 2003 Elsevier Ltd. All rights reserved.
doi:10.1016/j.poly.2003.11.010

addition of 120 mg of NaTp″ dissolved in toluene into the equimolar amounts of $[(COD)RhCl)]_2$ [14] or $[(NBD)RhCl)]_2$ [15] in toluene. The reaction mixtures were stirred at room temperature for 4 h under atmosphere of nitrogen, filtrated by passing through short bed of celite, the solvent was partially removed, the solutions layered with heptane and allowed to stand at 4 °C until formation of yellow crystals of **1** (yield 85%) or **2** (yield 80%).

2.2. Analytical data

1: Elemental analysis: Calc. for $C_{36}H_{42}N_6BRh$ (MW 672.48): C, 64.30; H, 6.29; N, 12.50. Found: C, 64.55; H, 6.16; N, 12.43%.

^{1}H NMR (toluene-d_8, 298 K): 8.01 (4H, m, *o*-H(3-Ph)); 7.25 (4H, m, *m*-H(3-Ph)); 7.16 (2H, m, *p*-H(3-Ph)); 6.31 (2H, s, 4-H(3-Ph,5-*i*Prpz)); 5.58 (1H, s, 4-H(3,5-diMepz)); 3.33 (6H, septet + broad singlet, C*H*(5-*i*Pr) + 2′, 3′, 5′, 6′-H(NBD)); 2.94 (2H, s, 1′, 4′ –H(NBD)); 2.31 (3H, s, 3(5)-CH_3); 2.14 (3H, s, 5(3)-CH_3); 1.29 (6H, d, $J_{(CH_3–CH)} = 6.6$ Hz, 2×CH_3(5-*i*Pr)); 1.21(6H, d, $J_{(CH_3–CH)} = 6.6$ Hz, 2×CH_3(5-*i*Pr)); 0.59 (2H, s, 7′-H(NBD)).

IR (KBr): *ν*(BH) 2534, 2474 cm^{-1}.

2: Elemental analysis: Calc. for $C_{37}H_{46}N_6BRh$ (MW 688.53): C, 64.54; H, 6.73; N, 12.21. Found: C, 64.62; H, 6.86; N, 12.13%.

^{1}H NMR (toluene-d_8, 273 K): 8.10 (4H, m, *o*-H(3-Ph)); 7.25 (4H, m, *m*-H(3-Ph)); 7.10 (2H, m, *p*-H(3-Ph)); 6.45 (2H, s, 4-H(3-Ph,5-*i*Prpz)); 5.56 (1H, s, 4-H(3,5-diMepz)); 4.10 (4H, s, 1′, 2′, 5′, 6′-H(COD)); 3.19 (2H, septet, C*H*(5-*i*Pr)), 2.34 (3H, s, 5-CH_3); 2.22 (3H, s, 3-CH_3); 1.87 (4H, s, 3′, 4′, 7′, 8′-H_{exo} (COD)); 1.39 (6H, d, $J_{(CH_3–CH)}) = 6.6$ Hz, 2×CH_3(5-*i*Pr)); 1.20 (10H, d, $J_{(CH_3–CH)}) = 6.6$ Hz, 2×CH_3(5-*i*Pr) + overlapped s, 3′, 4′, 7′, 8′-H_{endo} (COD)).

IR (KBr): *ν*(BH) 2478 cm^{-1}.

2.3. Methods

The ^{1}H NMR spectra were recorded with Bruker AMX 300 spectrometer. Standard COSY and NOESY experiments were performed with repetition time 1.0 and mixing time 0.3 s (NOESY).

Crystal data are given in Table 1, together with refinement details. All measurements of crystal were performed at low temperature using an Oxford Cryosystem device on a Kuma KM4CCD κ-axis diffractometer with graphite-monochromated Mo Kα radiation. The crystal was positioned 65 mm from the CCD camera. 612 frames were measured at 0.75° intervals with a counting time of 20 s. Accurate cell parameters were determined and refined by least-squares fit of 5950 of the strongest reflections. The data were corrected for Lorentz and polarization effects. No absorption correction was applied. Data reduction and analysis were carried out with the Oxford Diffraction (Poland) Sp. z o.o (formerly Kuma Diffraction Wrocław, Poland) programs. The structure was solved by direct methods (program SHELXS-97 [17]) and refined by the full-matrix least-squares method on all F^2 data using the SHELXL-97 [17] programs. Non-hydrogen atoms were refined with anisotropic displacement parameters; hydrogen atoms were included from geometry of molecules and $\Delta\rho$ maps. During refinement they were fixed.

Table 1
Crystal data and structure refinement

Empirical formula	$C_{36}H_{42}BN_6Rh$
Formula weight	672.48
T (K)	100(2)
λ (Å)	0.71073
Crystal system	triclinic
Space group	$P\bar{1}$
a (Å)	12.197(2)
b (Å)	15.876(3)
c (Å)	17.120(3)
α (°)	102.42(3)
β (°)	102.73(3)
γ (°)	90.88(3)
V (Å^3)	3151.1(10)
Z	4
D_{calc} (Mg m^{-3})	1.418
μ (mm^{-1})	0.578
$F(000)$	1400
Crystal size (mm)	0.17 × 0.15 × 0.15
θ Range for data collection (°)	3.43–28.41
Ranges of h, k, l	−15 to 16, −20 to 20, −22 to 21
Reflections collected	21 925
Independent reflections	13 848 (0.0561)
Data/parameters	13 848/806
Goodness-of-fit (F^2)	0.952
Final R_1/wR_2 indices ($I > 2\sigma(I)$)	0.0549/0.0738
Extinction coefficient	0.00015(10)
Largest diffraction peak/hole (e Å^{-3})	0.569/−0.734

3. Results and discussion

The heteroscorpionate ligand used in these studies, composed of two 3-phenyl-5-isopropylpyrazolyl and 3,5-dimethylpyrazolyl residues ($[HB(3\text{-}Ph,5\text{-}iPrpz)_2(3,5\text{-}diMepz)]^-$) is more sterically demanding in comparison with homoscorpionates Tp^{Me} [10], Tp [11], or Tp^{Me2} [12], which coordinate in κ^3 fashion to the rhodium(I) metal ion in their Tp′Rh(LL) complexes. On the other hand it is probably slightly less demanding than Tp^{iPr2}, which forms Tp″Rh(diene) complexes with κ^3 hapticity, when dien = NBD and κ^2 hapticity in case of diene = COD [13]. Other sterically demanding Tp′ ligands, like Tp^{Ph} [18] and $Tp^{4\text{-}OMePh}$ [19], as well as $[HB(pz)_4]^-$ [20] coordinate in κ^2 fashion in their Tp′Rh(diene) complexes. We have synthesized two compounds: $[HB(3\text{-}Ph,5\text{-}iPrpz)_2(3,5\text{-}diMepz)]Rh(NBD)$ (**1**) and $[HB(3\text{-}Ph,5\text{-}iPrpz)_2(3,5\text{-}$

diMepz)]Rh(COD) (**2**) in which the coordination mode of Tp″ ligand is κ^3 and κ^2, respectively.

The structure of **1** was elucidated crystallographically. There are two independent molecules of **1**. The views of the molecules are shown in Fig. 1 together with relevant bond lengths and angles around metal ion. The Rh–N(pz) distances fall into the region of 2.113(3)–2.307(3) Å (average value 2.24 Å), which is typical for other κ^3-Tp″Rh(NBD) complexes [10–13] and apparently longer in comparison with those for κ^2-Tp″Rh(NBD) ones (average value of Rh–N(pz) is equal 2.08 Å) [18–20].

The ^{1}H NMR spectrum of **1** (Fig. 1(b)) is composed of two 4-H(pz) resonances of relative 2:1 intensity ratio throughout broad range of temperature (down to 193 K) indicating the effective C_s symmetry of the molecule. Thus, the ligand remains coordinated in κ^3 fashion in solution or is in fast exchange between κ^2 and κ^3 mode. The resonances from methyl groups of 5-ispopropyl substituents are diastereotopically split into two doublets due to local chirality in **1**. The mutual rotation of Tp″ and NBD ligands in **1** is fast at the time-scale of the ^{1}H NMR even at the lowest temperature available in toluene-d_8 solvent as can be concluded from the presence of three resonances from NBD throughout the studied temperature range.

The crystals of **2** suitable for X-ray analysis could not be obtained. Therefore, the detailed analysis of the

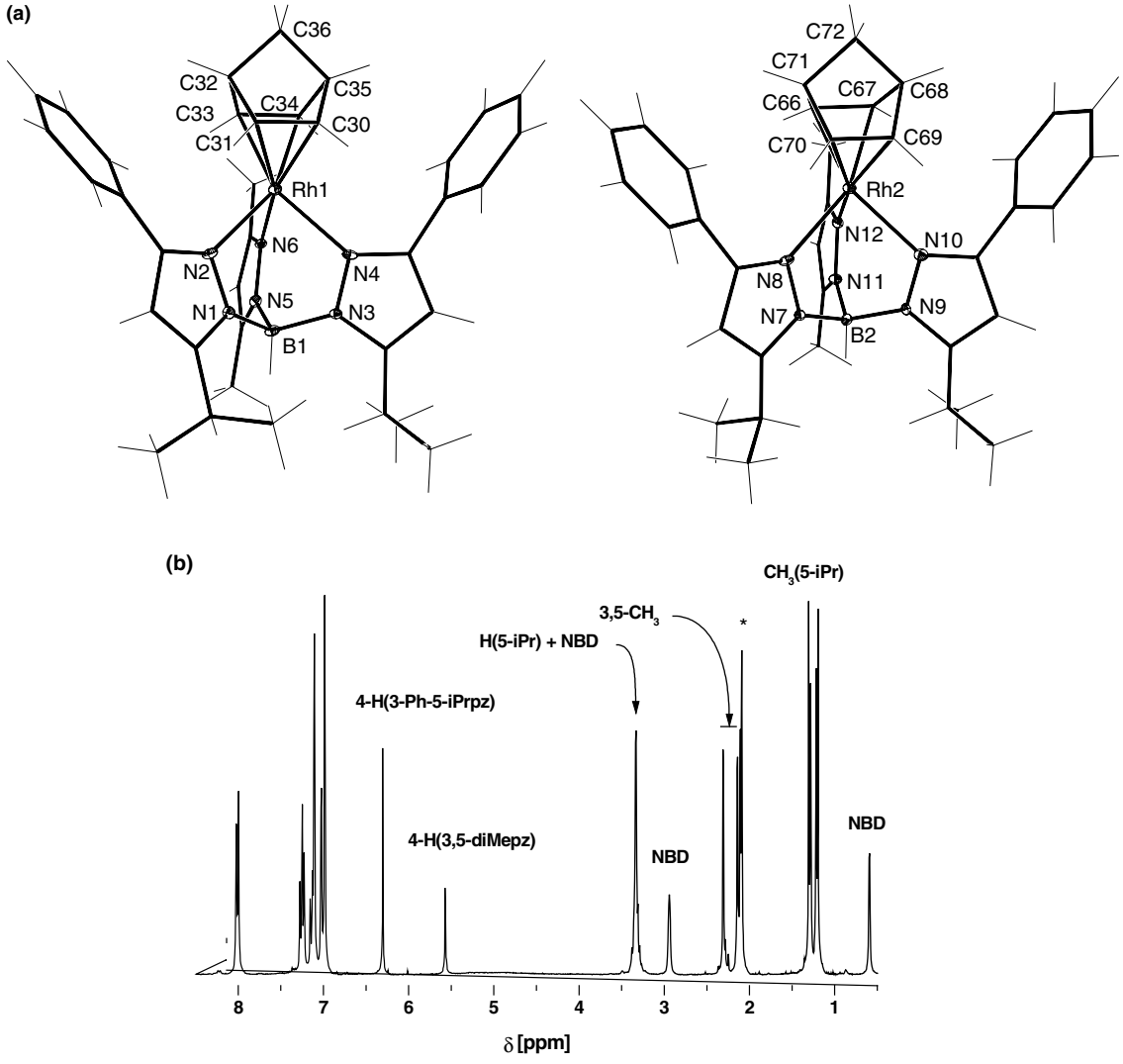

Fig. 1. (a) View of two independent molecules of **1**. Selected bond lengths (Å) and angles (°): Rh(1)–N(2), 2.299(3); Rh(1)–N(4), 2.290(3); Rh(1)–N(6), 2.113(3); Rh(1)–C(30), 2.169(4); Rh(1)–C(31), 2.157(4); Rh(1)–C(33), 2.078(4); Rh(1)–C(34), 2.069(4); N(4)–Rh(1)–N(2), 88.15(12); N(6)–Rh(1)–N(4), 83.26(13); N(6)–Rh(1)–N(2), 83.59(12); C(34)–Rh(1)–C(31), 79.34(16); C(33)–Rh(1)–C(30), 79.55(17) and Rh(2)–N(8), 2.307(3); Rh(2)–N(10), 2.282(4); Rh(2)–N(12), 2.136(3); Rh(2)–C(66), 2.087(4); Rh(2)–C(67), 2.082(4); Rh(2)–C(69), 2.166(4); Rh(2)–C(70), 2.177(4); N(10)–Rh(2)–N(8), 87.26(12); N(12)–Rh(2)–N(8), 85.07(12); N(12)–Rh(2)–N(10), 83.35(13); C(67)–Rh(2)–C(70), 79.44(17); C(66)–Rh(2)–C(69), 79.85(17). (b) ^{1}H NMR spectrum of **1** in toluene-d_8 at 298 K. The residual peak from solvent (q, C*H*D$_2$) is labeled with asterisk. The peaks from norbornadiene are labeled as NBD.

variable temperature ^{1}H NMR experiments was performed for **2** in toluene-d_8. The spectrum of **2** at ambient temperature reflects the effective C_s symmetry of **2**. However, the spectrum changes dramatically upon decrease of temperature; the coalescence point observed at 223 K clearly indicates that a chemical exchange between coordinated and uncoordinated pyrazolyl residues becomes slow at the time-scale of the method. Further decrease of temperature results in decrease of symmetry of the spectrum consistent with slow exchange between coordinated and uncoordinated 3-Ph-5-*i*Prpz residues. Three resonances of 4-H(pz) and four resonances from olefinic COD hydrogens are observed at 193 K (resonances a–d at lower trace at Fig. 2).

These features were already observed in case of other heteroscorpionate complexes: [HB(3-Ph,5-Mepz)$_2$(3-Me,5-Phpz)]Rh(COD) and [HB(3-Ph,5-Mepz)$_2$(3,5-diEtpz)]Rh(COD) [9], in which the Tp″ ligands are coordinated in κ^2 fashion, and attributed to slow exchange between coordinated and uncoordinated 3-Ph,5-Mepz moiety. The ^{1}H-^{1}H COSY and NOESY experiments showed the cross-peaks within a $\Longleftrightarrow$ b and c $\Longleftrightarrow$ d pairs of olefinic protons of COD, similarly as it was found for [HB(3-Ph,5-Mepz)$_2$(3-Me,5-Phpz)]Rh(COD) and [HB(3-Ph,5-Mepz)$_2$(3,5-diEtpz)]Rh(COD) [9]. Thus, the scalar coupling within a $\Longleftrightarrow$ b and c $\Longleftrightarrow$ d pairs of signals in COSY spectrum and concomitant EXSY cross-peaks between the same diagonal peaks in NOESY spectrum clearly confirm that effective C_1 symmetry of the ^{1}H NMR spectrum of **2** at 193 K is consistent with slow exchange between coordinated and uncoordinated 3-Ph,5-*i*Prpz residues. For this interconversion the $\Delta G^{\neq} = 42.2$ kJ/mol has been calculated. The obtained value of energy of activation is very close to those found in other similar systems, in which the coordinated and uncoordinated 3-Ph,5-Mepz residues interchanged with $\Delta G^{\neq} = 41.1$ kJ/mol in case when third, slowly exchanging pyrazolyl residue was 3,5-diEtpz and $\Delta G^{\neq} = 43.2$ kJ/mol in case of 3-Me,5-Phpz as third, coordinated pyrazolyl moiety [9].

The heteroscorpionate [HB(3-Ph,5-*i*Prpz)$_2$(3,5-diMepz)]$^-$ ligand serves a borderline example of steric demand towards the Rh(diene) counterpart, similar to homoscorpionate Tp$^{i\mathrm{Pr}2}$ [13]. The hapticity of Tp″ depends on the rhodium-centered diene cone angle. Tp″ coordinates in κ^2 fashion in case of diene = COD (average value of α for Tp″Rh(COD) complexes is 93.4° [9]), while κ^3 coordination mode occurs for diene = NBD ($\alpha = 79.5°$ in **1**) in solid state at 100 K. However, it should be emphasized that according to the IR spectral criterion proposed by Akita et al. [21] based on the position of ν(BH) the presence of two distinct bands at 2534 and 2474 cm^{-1} (of relative intensity about 2:1 both in KBr and in chloroform solution) for **1** suggests that at ambient temperature the [HB(3-Ph,5-*i*Prpz)$_2$(3,5-diMepz)]$^-$ ligand is coordinated in two ways: κ^3 and κ^2 mode, while in case of **2** (one ν(BH) band at 2478 cm^{-1}) the ligand remains coordinated in κ^2 mode both in solid state and in solution throughout the entire range of temperatures.

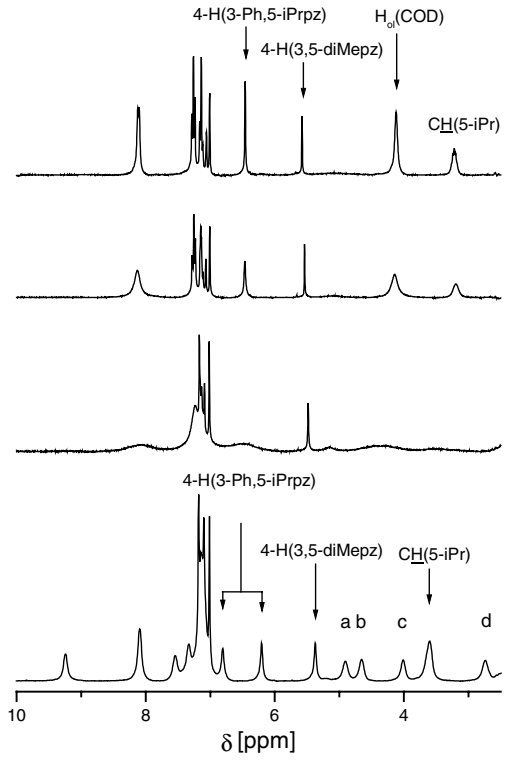

Fig. 2. The relevant fragments of ^{1}H NMR spectra of **2** in toluene-d_8 taken at temperature (from top to bottom): 273, 253, 223, and 193 K, respectively. The resonances labeled with H$_{ol}$(COD) (top trace) and a, b, c, d (bottom trace) belong to 1′, 2′, 5′, and 6′ H(COD).

4. Supplementary data

Crystallographic data for the structures reported in this paper (excluding structure factors) have been deposited with the Cambridge Crystallographic Data Centre, CCDC No. 209564. Copies of this information may be obtained free of charge from The Director, CCDC, 12 Union Road, Cambridge 1EZ, UK (fax: +44-1223-336033; deposit@ccdc.cam.ac.uk or www.ccdc.cam.ac.uk).

Acknowledgements

The authors thank KBN (Poland) for the Grant No. 3 T09A 05219.

References

[1] S. Trofimenko, Scorpionates: The Coordination Chemistry of Polypyrazolylborate Ligands, Imperial College Press, London, UK, 1999.

[2] M. Łukasiewicz, Z. Ciunik, S. Wołowiec, Polyhedron 19 (2000) 2119.
[3] M. Łukasiewicz, Z Ciunik, T. Ruman, M. Skóra, S. Wołowiec, Polyhedron 20 (2001) 237.
[4] T. Ruman, M. Łukasiewicz, Z. Ciunik, S. Wołowiec, Polyhedron 20 (2001) 2551.
[5] T. Ruman, Z. Ciunik, A. Goclan, M. Łukasiewicz, S. Wołowiec, Polyhedron 20 (2001) 2965.
[6] T. Ruman, Z. Ciunik, S. Wołowiec, Eur. J. Inorg. Chem. (2003) 89.
[7] T. Ruman, Z. Ciunik, S. Wołowiec, Eur. J. Inorg. Chem. (2003) 2475.
[8] T. Ruman, Z. Ciunik, S. Wołowiec, Polyhedron 22 (2003) 581.
[9] T. Ruman, Z. Ciunik, A.M. Trzeciak, S. Wołowiec, J.J. Ziółkowski, Organometallics 22 (2003) 1072.
[10] U.E. Bucher, A. Currao, R. Nesper, H. Rüegger, L.M. Venanzi, E. Younger, Inorg. Chem. 34 (1995) 66.
[11] M.C. Nikasio, M. Paneque, P.J. Perez, A. Pizzano, M.L. Poveda, M. Rey, S. Sirol, S. Taboada, M. Trujillo, A. Monge, C. Ruiz, E. Carmona, Inorg. Chem. 39 (2000) 180.
[12] A.F. Hill, A.J.P. White, D.J. Williams, J.D.E.T. Wilton-Ely, Organometallics 17 (1998) 3152.
[13] M. Akita, Y. Takahashi, S. Hikichi, U. Moro-oka, Organometallics 16 (1997) 4121.
[14] G. Giordano, R.H. Crabtree, Inorg. Synth. 28 (1990) 88.
[15] E.W. Abel, M.A. Bennet, G. Wilkinson, J. Chem. Soc. (1959) 3178.
[16] G.M. Sheldrick, Acta Crystallogr., Sect. A 46 (1990) 467.
[17] G.M. Sheldrick, SHELXL-97: Program for Crystal Structure Refinement, University of Göttingen, Göttingen, 1997.
[18] D. Sanz, M.D. Santa Maria, R.M. Claramunt, M. Cano, J.V. Heras, J.A. Campo, F.A. Ruiz, E. Penilla, A. Monge, J. Organomet. Chem. 526 (1996) 341.
[19] M.D. Santa Maria, R.M. Claramunt, J.A. Campo, M. Cano, R. Criado, J.V. Heras, P. Ovejero, E. Pinilla, M.R. Torres, J. Organomet. Chem. 605 (2000) 117.
[20] M. Cocivera, C. Ferguson, B. Kaitner, F.J. Lalor, D.J. O'Sullivan, M. Parvez, B. Ruhl, Organometallics 1 (1982) 1132.
[21] M. Akita, K. Ohta, Y. Takahashi, S. Hikichi, Y. Moro-oka, Organometallics 16 (1997) 4121.

Available online at www.sciencedirect.com
SCIENCE DIRECT®
Polyhedron 23 (2004) 225–234
POLYHEDRON
www.elsevier.com/locate/poly

Oxygenation of a series of cationic aquoruthenium complexes, $Tp^{iPr2}Ru(OH_2)_nL_{3-n}\cdot CF_3SO_3\cdot(THF)_x$, leading to mono- and dinuclear aquo-hydroxo complexes supported by unique hydrogen bonding networks

Yoshiaki Takahashi, Shiro Hikichi [1], Yoshihiko Moro-oka, Munetaka Akita *

Chemical Resources Laboratory, Tokyo Institute of Technology, 4259 Nagatsuta, Midori-ku, Yokohama 226-8503, Japan

Received 13 May 2003; accepted 9 August 2003

Dedicated to Dr. Swiatoslaw Trofimenko in recognition of his important contribution to inorganic chemistry

Abstract

O_2-treatment of the labile cationic aquo-Ru(II) complexes, $Tp^{iPr2}(L)_nRu(OH_2)_{3-n}(OTf)(THF)_x$ [L = bipy (**1d**), py (**2**), THF (**3**)], results in oxidation of the metal center to give the mononuclear hydroxo-Ru(III) complexes, $[Tp^{iPr2}(bipy)Ru^{III}(OH)](OTf)$ (**4**), $Tp^{iPr2}(py)Ru^{III}(OH)(OH_2)(OTf)(THF)_2$ (**5**), and the dinuclear Ru(II)–Ru(III) and Ru(III)–Ru(III) mixed aquo-hydroxo complexes bridged by the Ru–O···H···O–Ru hydrogen-bonding interactions, $Tp^{iPr2}Ru^{II}(OH)_2(OH_2)_4(OTf)Ru^{III}Tp^{iPr2}$ (**6**) and $(Tp^{iPr2}Ru)_2(OH)_2(OH_2)_4(OTf)_2$ (**7**).
© 2003 Elsevier Ltd. All rights reserved.

Keywords: Hydrotris(pyrazolyl)borate; Ruthenium; Hydrogen bond; Oxidation; Aquo complex

1. Introduction

Hydrotrispyrazolylborates (Tp^R), so-called scorpionates, are versatile ligands, which have been used in the wide range of inorganic studies [1]. We have enjoyed the rich chemistry based on the Tp^R ligands, in particular, systematic synthetic study of O_2-complexes bearing the Tp^R ligands [2]. A variety of $Tp^RM–O_2$ complexes containing the first (V, Cr, Mn, Co, Ni) and second row metals (Rh, Pd) were prepared by way of dehydrative condensation of a hydroxo complex with H_2O_2 in addition to the classical O_2-oxidative addition to a low valent precursor, and the unique oxidizing activities of the resultant O_2-adducts were characterized. Our efforts were also devoted to the ruthenium system [3]. In previous papers we reported synthesis of a series of cationic aquo-Ru(II) complexes, $Tp^{iPr2}Ru^{II}(L)_n(OH_2)_{3-n}(OTf)(THF)_x$ **1**–**3**, [2] which were supported by hydrogen-bonding networks (Chart 1) [3a], and diphosphine complexes **1a**–**c** were subjected to oxygenation [3c]. On the basis of the labile nature of the aquo ligands in **1a**–**c** it was anticipated that they were converted into O_2-adducts upon exposure to O_2 atmosphere in a manner similar to the oxygenation of the isoelectronic η^5-C_5Me_5 systems giving the $[(\eta^5\text{-}C_5Me_5)(\text{diphosphine})Ru(\kappa^2\text{-}O_2)]^+$-type adducts [4–6]. Oxygenation of **1a**–**c**, however, did not result in the formation of O_2-adducts but one-electron oxidation of the ruthenium center, and the reaction products were dependent on the structure of the diphosphine ligand. The dppe [1,2-bis(diphenylphosphino)ethane] complex **1c** afforded the corresponding cationic hydroxo-Ru(III) complex, $[Tp^{iPr2}(dppe)Ru–OH]^+$, whereas the dppene [1,2-bis(diphenylphosphino)ethene] complex **1a** and the dppm [bis(diphenylphosphino)

* Corresponding author. Tel./fax: +81-45-924-5230.
E-mail address: makita@res.titech.ac.jp (M. Akita).
[1] Present address: Department of Applied Chemistry, School of Engineering, University of Tokyo, Hongo, Bunkyo-ku, Tokyo 113-8656, Japan.

[2] Abbreviation used in this paper: Tp^{iPr2} = hydrotris(3,5-diisopropylpyrazolyl)borato ligand.

0277-5387/$ - see front matter © 2003 Elsevier Ltd. All rights reserved.
doi:10.1016/j.poly.2003.11.009

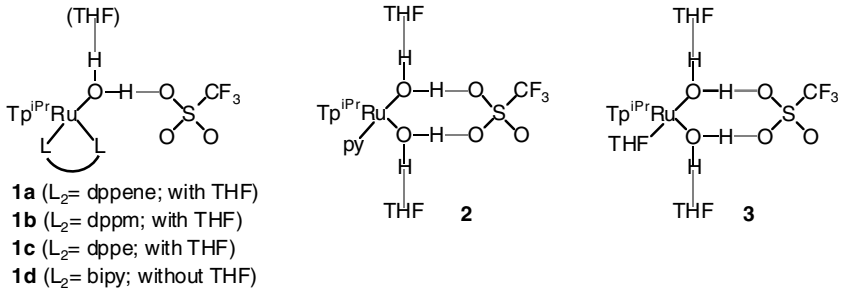

Chart 1.

methane] complex **1b** resulted in oxidative transformations of the ancillary ligands, i.e. **1a** underwent oxidative $C(sp^3)$–$C(sp^3)$ bond cleavage of one of the isopropyl substituents of the Tp^{iPr2} ligand proximal to the metal center and **1b** was converted to the phosphine monooxide-coordinated complex. Herein we wish to report the results of oxygenation of the aquo-ruthenium(II) complexes with N-donors containing the varying number of labile oxygen ligands (OH_2 and THF): 1 (**1d**), 2 (**2**) and 3 (**3**) [Chart 1]. Although O_2-adduct was not obtained, it was revealed that the oxidized products were also supported by unique hydrogen bonding networks as found for **1**–**3**.

2. Results and discussion

2.1. Oxygenation of *1d* and *2* giving cationic mononuclear hydroxo-Ru(III) complexes

When the aquo-bipyridine complex **1d** and the diaquo-pyridine complex **2** dissolved in THF were stirred under O_2 atmosphere (1 atm), red (**4**) and yellow products (**5**) were isolated, respectively, by simple crystallization (Scheme 1). The paramagnetic properties of the products suggested formation of Ru(III) species, which were characterized by X-ray crystallography. Molecular structures of **4** and **5** are shown in Fig. 1 and their selected structural parameters are compared with those of related complexes as summarized in Table 1.

The oxygenation of the bipy complex **1d** resulted in one electron oxidation accompanied by deprotonation to give the mononuclear hydroxo-Ru(III) complex, $[Tp^{iPr2}(bipy)Ru–OH]OTf$ **4**, as observed for the O_2-treatment of the dppe complex **1c** [3c]. Complex **4** adopts an octahedral coordination geometry with the κ^1-OH, κ^2-bipy and κ^3-Tp^{iPr2} ligands as judged by the angles made by adjacent ligands close to the right angle: 85.5(2)–98.6(2)°. The Ru1–O1 length [1.969(3) Å] and the Ru–N(Tp^{iPr2}) distances [2.066(4)–2.085(5) Å] are considerably shorter than those [Ru–O: 2.158(5) Å; Ru–N: 2.157(5)–2.229(3) Å] in the dppe derivative, $[Tp^{iPr2}(dppe)Ru^{III}–OH]PF_6$ (obtained from **1c** [3c]). The shortening of the coordination bonds in **4** may be related to the electron donating ability of the bipy ligand stronger than that of the dppe ligand. In contrast to the other complexes described in this paper, no hydrogen bonding interaction with any other components (even with the TfO anion as in **1d**) is present. This should be also caused by the reduced acidity of the OH proton induced by the electron donation from the bipy ligand. In accord with this consideration, the Ru(II/III) redox potential of **4** (−0.62 eV; reversible) was much lower than that of $[Tp^{iPr2}(dppe)Ru^{III}–OH]PF_6$ (−0.25 V).

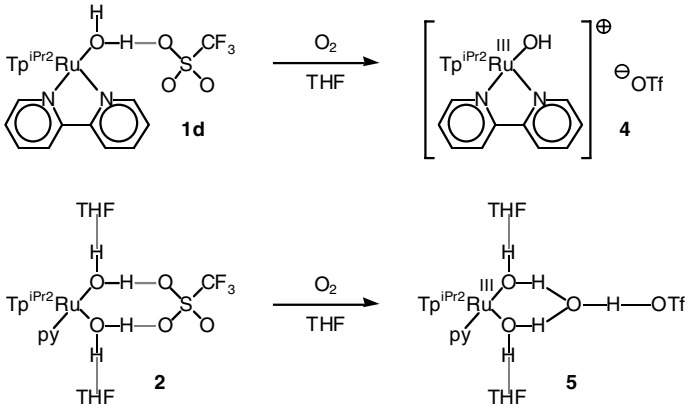

Scheme 1.

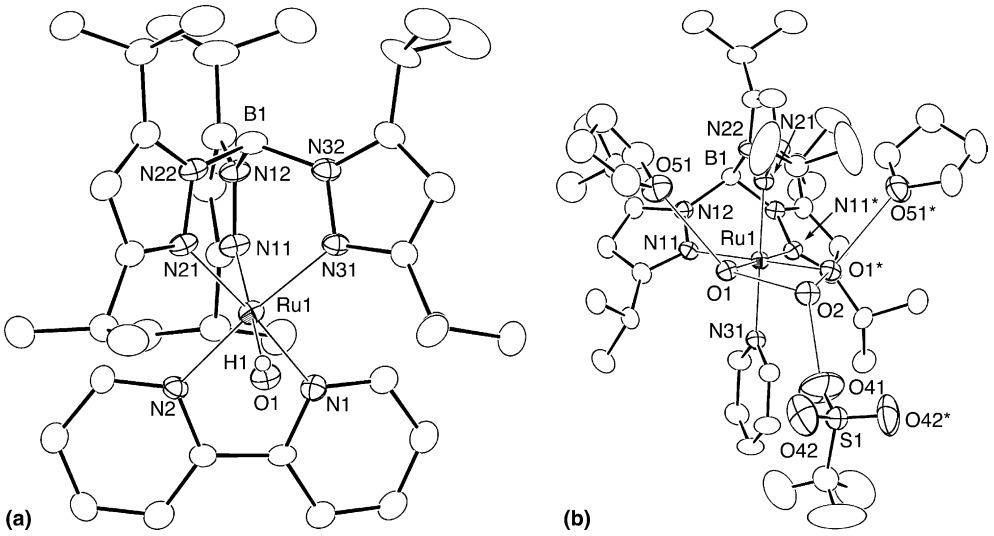

Fig. 1. ORTEP drawings for (a) the cationic part of **4** and (b) **5**. Thermal ellipsoids are drawn at the 30% probability level.

The core structure of the pyridine complex **5** is also an octahedral one sitting on a crystallographic mirror plane. In addition to the κ^1-pyridine and κ^3-Tp^{iPr2} ligands, two oxygen-containing ligands (O1 and O1*) are coordinated to the metal center to complete the octahedral coordination geometry as in the starting complex **2**. The notable structural feature is the hydrogen bonding network associated with the triflate anion and the additional water and THF molecules. The distances between the oxygen ligand (O1 and O1*) and the oxygen atom of the water (O2) and THF molecules (O51, O51*) [2.6–2.8 Å] are in the range of hydrogen bonding interaction, and the water molecule (O2) is further interacted with one of the oxygen atoms of the triflate anion (O41) through hydrogen bond. There is no significant difference in the O···O separations between the Ru(III) species **5** and the aquo-Ru(II) complexes **1**–**3** [3a]. These features are consistent with the structural description as a resonance hybrid of the two canonical aquo-hydroxo-Ru(III) structures **5A** (Scheme 2).

2.2. Oxygenation of *3* leading to cationic dinuclear aquo-hydroxo-Ru(III) complexes

Complex **3** with the three labile oxygen ligands was found to be also susceptible to oxygenation to give two types of products, Ru(II)–Ru(III) species **6** and Ru(III)–Ru(III) species **7**, with the different oxidation states and with complicated hydrogen bonding networks (Scheme 3) as determined by X-ray crystallography (Fig. 2). The two products were isolated in pure forms and never obtained as a mixture but we could not determine the reaction conditions, which led to **6** or **7**, although the oxygenation was repeated many times by varying the reaction time, the amount of O_2, the concentration and so on.

Both of the complexes contain the two $Tp^{iPr2}Ru(OH_x)_3$ units connected by hydrogen bonds but the interaction modes are different as can be seen from the core structures (Fig. 3). The interunit O···O separations between the two $Tp^{iPr2}Ru(OH_x)_3$ units in the Ru(II)–Ru(II) complex **6** can be classified into two categories, those of about 2.5 Å (O11···O21, O12···O22, O13···O23) and those longer than 3.2 Å (the others). As a result, the six oxygen atoms form a trigonal-prismatic framework as can be seen from the core structure and its side view (Fig. 3). The triflate counteranion, which bridges the two oxygen atoms (O11 and O21), should support the prismatic configuration.

The interunit O···O separations for the Ru(III)–Ru(III) complex **7** imposed on a centrosymmetric site are also classified into two groups [2.668(6), 2.680(6)/2.874(6) Å] but the difference is much smaller than that for **6** (see above). Although the distance of 2.87 Å may be in the longer end for the O···O distance of hydrogen bonds and an alternative form **7A** (Chart 2) with the crown-shaped hydrogen-bonding networks may be possible, taking into account the structure of **7′** (another form of **7**; vide infra) it is concluded that (1) **7** is a dimer of the diaquo-hydroxo-Ru(III) species and (2) the three atoms (O13–O11*–O12*/O13*–O11–O12) form the wedge-shaped array through hydrogen bonds. Such ternary 1:2 interactions lead to the twisted trigonal-anitipismatic arrangement of the oxygen atoms in contrast to the trigonal-pismatic configuration observed for **6**. The H_xO···OTf and H_xO···O(THF) separations are comparable to those for the mononuclear hydroxo-aquo-Ru(III) (**5**) and aquo-Ru(II) complexes (**1**–**3**) [3a,3c] and it should be noted that the Ru(III) species **2** and **7** contain the common $Ru(O\cdots H)_2OX$ linkage [X = TfOH (**2**), $RuTp^{iPr2}$ (**7**)].

Table 1
Selected structural parameters for the hydroxoruthenium(III) complexes

4		**5**		**6**				**7**	
Interatomic distances (Å)									
Ru–O									
Ru1–O1	1.969(3)	Ru1–O1	2.029(3)	Ru1–O11	1.991(6)	Ru2–O21	2.046(5)	Ru1–O11	2.062(4)
				Ru1–O12	2.096(3)	Ru2–O22	2.049(6)	Ru1–O12	2.088(5)
				Ru1–O13	2.061(5)	Ru2–O23	2.031(5)	Ru1–O13	2.013(4)
$H_xO\cdots OH_x$									
		O1···O2	2.676(5)	O11···O21	2.511(7)			O11···O12*	2.874(6)
				O12···O22	2.411(7)			O11···O13*	2.680(6)
				O13···O23	2.463(7)			O12···O13*	2.668(6)
				other O···O	>3.2				
$H_xO\cdots OTf$									
		O2···O41	2.66(1)	O11···O31	2.97(1)			O11···O31	2.639(7)
				O21···O32	2.86(1)				
$H_xO\cdots O(THF)$									
		O1···O51	2.843(6)					O12···O41	2.733(7)
Ru–N/Ru–O									
Ru1–N1	2.049(5)	Ru1–O1	2.029(3)	Ru1–O11	1.991(6)	Ru2–O21	2.046(5)	Ru1–O11	2.062(4)
Ru1–N2	2.044(4)	Ru1–N31	2.077(5)	Ru1–O12	2.096(3)	Ru2–O22	2.049(6)	Ru1–O12	2.088(5)
				Ru1–O13	2.061(5)	Ru2–O23	2.031(5)	Ru1–O13	2.013(4)
Ru1–N11	2.066(4)	Ru1–N11	2.041(4)	Ru1–N11	2.077(7)	Ru2–N41	2.050(5)	Ru1–N11	2.039(5)
Ru1–N21	2.085(5)	Ru1–N21	2.085(5)	Ru1–N21	2.051(4)	Ru2–N51	2.069(6)	Ru1–N21	2.041(5)
Ru1–N31	2.080(4)			Ru1–N31	2.048(6)	Ru2–N61	2.050(6)	Ru1–N31	2.046(5)
Bond angles (°)									
N11–Ru1–N21	88.7(2)	N11–Ru1–N21	88.8(1)	N11–Ru1–N21	88.7(2)	N41–Ru2–N51	88.8(2)	N11–Ru1–N21	87.5(2)
N11–Ru1–N31	89.4(2)	N11–Ru1–N31	91.2(1)	N11–Ru1–N31	86.4(2)	N41–Ru2–N61	87.5(2)	N11–Ru1–N31	89.3(2)
N21–Ru1–N31	85.8(2)			N21–Ru1–N31	88.3(2)	N51–Ru2–N61	88.8(2)	N21–Ru1–N31	89.3(2)
O1–Ru1–N1	85.5(2)	O1–Ru1–O1	89.1(2)	O11–Ru1–O12	86.3(2)	O21–Ru2–O22	86.2(2)	O11–Ru1–O12	87.8(2)
O1–Ru1–N2	86.0(2)	O1–Ru1–N11	90.7(1)	O11–Ru1–O13	90.1(2)	O21–Ru2–O23	84.0(2)	O11–Ru1–O13	85.6(2)
O1–Ru1–N11	179.0(2)	O1–Ru1–N11	179.7(1)	O11–Ru1–N11	177.9(2)	O21–Ru2–N41	176.7(2)	O11–Ru1–N11	178.4(2)
O1–Ru1–N21	90.5(2)	O1–Ru1–N21	91.5(1)	O11–Ru1–N21	92.1(2)	O21–Ru2–N51	93.0(2)	O11–Ru1–N21	93.5(2)
O1–Ru1–N31	91.1(2)	O1–Ru1–N31	88.5(1)	O11–Ru1–N31	91.7(2)	O21–Ru2–N61	95.3(2)	O11–Ru1–N31	91.9(2)
N1–Ru1–N2	77.8(2)	N11–Ru1–N11	89.5(2)	O12–Ru1–O13	84.8(2)	O22–Ru2–O23	88.7(2)	O12–Ru1–O13	85.4(2)
N1–Ru1–N11	95.3(2)	N21–Ru1–N31	180.0(2)	O12–Ru1–N11	92.9(2)	O22–Ru2–N41	92.0(2)	O12–Ru1–N11	91.2(2)
N1–Ru1–N21	174.8(2)			O12–Ru1–N21	177.6(2)	O22–Ru2–N51	179.2(2)	O12–Ru1–N21	178.4(2)
N1–Ru1–N31	97.6(2)			O12–Ru1–N31	93.6(2)	O22–Ru2–N61	91.5(2)	O12–Ru1–N31	91.6(2)
N2–Ru1–N11	93.6(2)			O13–Ru1–N11	91.7(2)	O23–Ru2–N41	93.2(2)	O13–Ru1–N11	93.2(2)
N2–Ru1–N21	98.6(2)			O13–Ru1–N21	93.3(2)	O23–Ru2–N51	91.1(2)	O13–Ru1–N21	93.7(2)
N2–Ru1–N31	174.7(2)			O13–Ru1–N31	177.5(2)	O23–Ru2–N61	179.3(2)	O13–Ru1–N31	176.1(2)

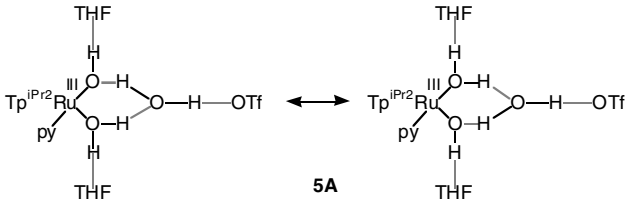

Scheme 2.

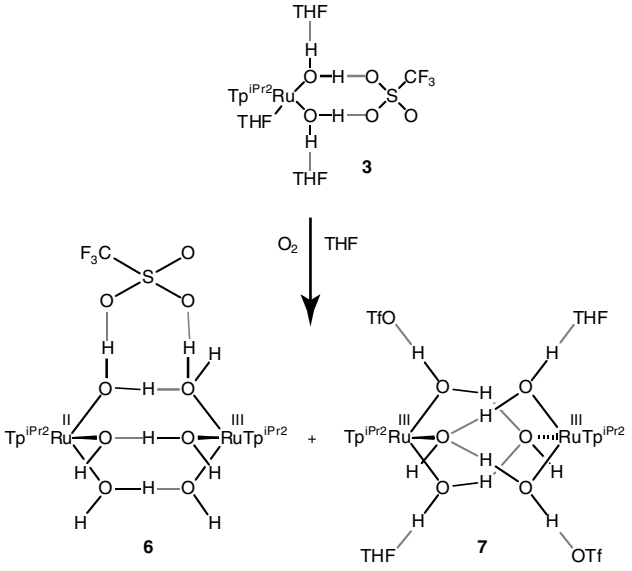

Scheme 3.

The paramagnetic properties of complexes **6** and **7** revealed that these complexes contained a Ru(III) center and in order to determine the oxidation states of the ruthenium centers CV measurements were carried out. Complex **6** showed a reversible oxidation wave at the potential of −0.80 V, which was comparable to that for the Ru(II/III) wave for the bipy derivative **4** (−0.62 V) described above, whereas complex **7** did not exhibit any significant oxidation wave in the range of 0–1.0 V. These CV features indicated that complex **6** contained a Ru(II) center but complex **7** did not; in other words, the oxidation states of the ruthenium centers in the dinuclear complexes were Ru(II)–Ru(III) (**6**) and Ru(III)–Ru(III) (**7**). The distinctive electrochemical behavior observed for **6** and **7** also revealed that the dinuclear structures were integrated in a solution, although the THF and TfO auxiliaries might be dissociated (vide infra; **6′** and **7′**).

On the basis of the above-mentioned data the hydrogen-bonding networks for **6** and **7** are characterized as follows. Taking into account the oxidation states of the central metals of **6** it is formulated as a di(μ-hydroxo)-tetra(μ-aquo)-Ru(II)–Ru(III) species, ($Tp^{iPr2}Ru^{II}$) (Tp^{iPr2}-Ru^{III})$(OH)_2(OH_2)_4(OTf)$, containing 10 protons, of which

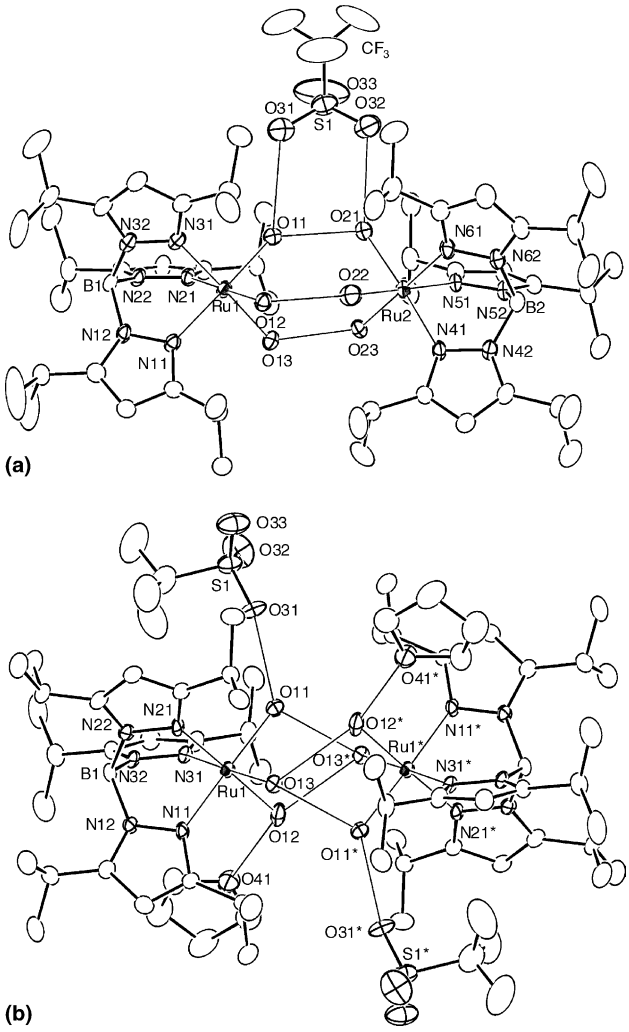

Fig. 2. ORTEP drawings for (a) **6** and (b) **7**. Thermal ellipsoids are drawn at the 30% probability level.

some should be associated with the hydrogen bonding interactions. Each one proton (in total five protons) should be present between the oxygen atoms connected by the hydrogen bonds and four of the remaining five protons should be attached to the oxygen atoms (O12,13, O22,23), which are not interacted with the triflate anion. The nine hydrogen atoms can be located by careful examination of Fourier synthesis, and the 10th proton, which cannot be located by the Fourier synthesis, is tentatively attached to the oxygen atom interacted with the triflate anion as shown in Scheme 3. Because the structural parameters for the two Tp^{iPr2}-$Ru(OH_x)_3$ moieties are essentially the same within the ranges of experimental errors, the oxidation states [Ru(II)/Ru(III)] of the particular ruthenium centers (Ru1 and Ru2) cannot be assigned.

The symmetrical structure of complex **7** as well as the presence of the two triflate conteranions clearly indicates that the oxidation states of the two ruthenium centers are the same and +3. Because each pair of the

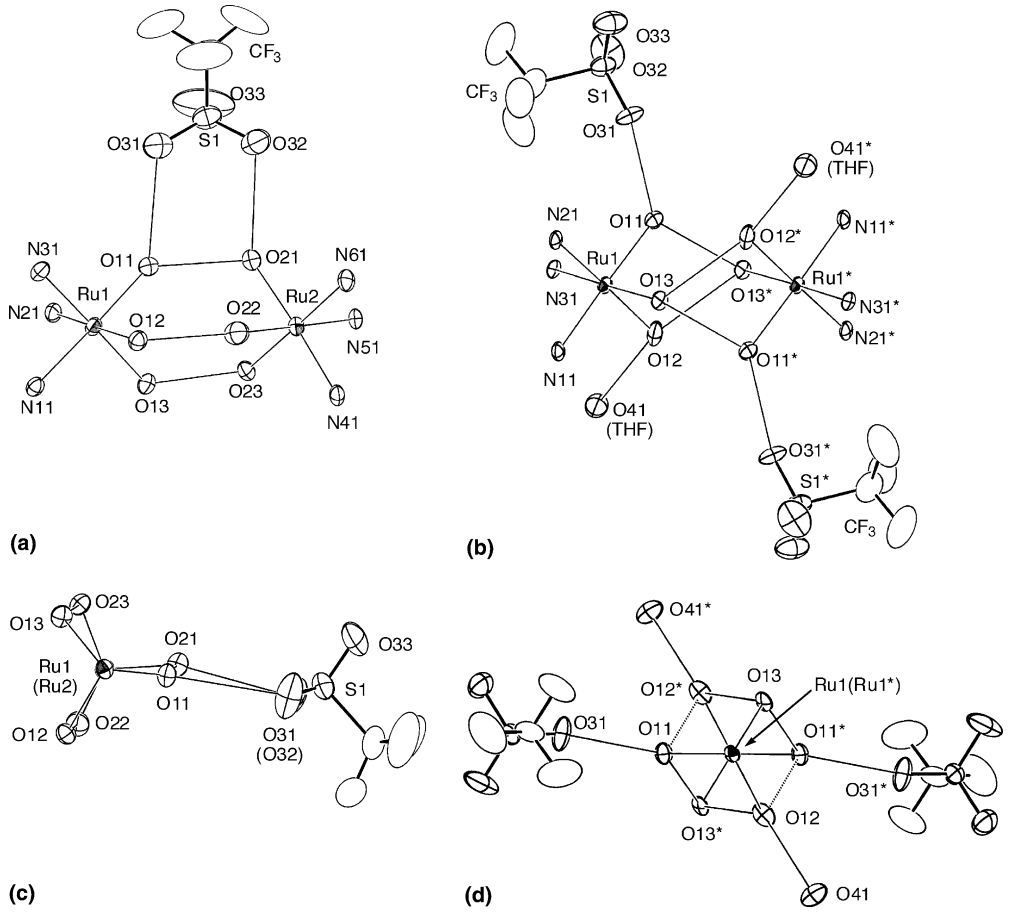

Fig. 3. Core structures of (a) **6** (side view), (b) **7** (side view), (c) **6** (a view along the Ru–Ru axis), and (d) **7** (a view along the Ru–Ru axis). Thermal ellipsoids are drawn at the 30% probability level.

hydrogen-bonded oxygen atoms should be bridged by a proton, the dinuclear system should contain 10 protons. The number of the protons is consistent with the formulation of **7** as a dimer of a hydroxo-diaquo-Ru(III) species, $(Tp^{iPr2}Ru^{III})_2(OH)_2(OH_2)_4(OTf)_2(THF)_2$ [= $\{Tp^{iPr2}Ru^{III}(OH)(OH_2)_2(OTf)(THF)\}_2$].

Let us add a note on the hydrogen bonding interactions. Changing the recrystallization solvent systems caused formation of different types of single crystals **6′** (obtained from THF–hexane) and **7′** (obtained from THF–CH_2Cl_2), which were also characterized by X-ray crystallography. Because, however, the highly disordered THF and TfO moieties hampered satisfactory refinements, the crystallographic results are not included in this paper. [3] The core structures of **6′** and **7′**, however, have been confirmed to be essentially the same as those of **6** and **7**, respectively, as schematically shown in Chart 3. Complex **6′** is formulated as $\mathbf{6}\cdot(THF)_2$ and the additional two THF molecules are found to be hydrogen-bonded to two OH moieties of one of the two $Tp^{iPr2}Ru(OH_x)_3$ fragments. Because the OH_x groups attached to a Ru(III) center should be more acidic than those attached to a Ru(II) center and therefore readily form hydrogen-bonding interactions, the oxidation state of the $Tp^{iPr2}Ru(OH_x)_3$ fragment, with which the THF molecules are interacted, is assigned to Ru(III). No significant difference is observed for the Ru–O distances

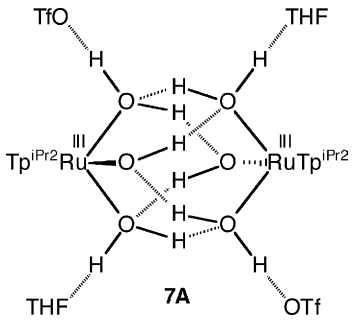

Chart 2.

[3] Crystallographic data for **6′**: $C_{69}H_{122}B_2N_{12}O_{11}F_3SRu_2$, $fw = 1608.6$, temp. −60 °C, monoclinic, space group $P2_1/c$, a = 16.990(3) Å, $b = 24.385(4)$ Å, $c = 21.378(15)$ Å, $\beta = 101.674(3)°$, $V = 8674.0(65)$ Å^3, $Z = 4$. for **7′**: $C_{80}H_{152}B_2N_{12}O_{18}F_6S_2Ru_2$, $fw = 1972.0$, temp. −60 °C, orthorhombic, space group *Pbca*, $a = 31.967(10)$ Å, $b = 17.980(2)$ Å, $c = 17.528(3)$ Å, $V = 10074(2)$ Å^3, $Z = 4$.

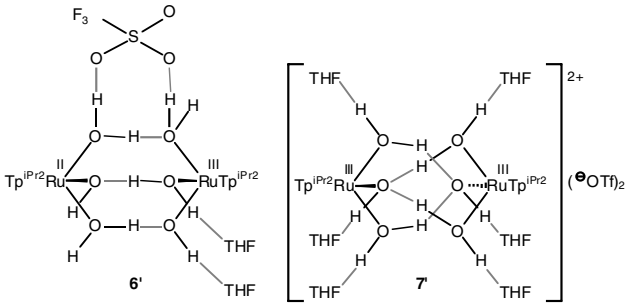

Chart 3.

of the $Tp^{iPr2}Ru^{II}(OH_x)_3$ [2.028(9)–2.06(1) Å] and $Tp^{iPr2}Ru^{III}(OH_x)_3$ fragments [2.020(9)–2.06(1) Å] as observed for **6**. The O···O separations of **6′** [RuO···ORu: 2.47–2.48 Å; RuO···O(THF): 2.81, 2.87 Å] are also similar to those in **6**. On the other hand, the composition of **7′** is found to be [**7**·(THF)$_6$]. In contrast to **7**, the triflate counteranions in **7′** are replaced by THF solvate molecules to give the separated ionic structure and all Ru–O oxygen atoms form hydrogen bonds with the six THF molecules. The features observed for the RuO···ORu separations are similar to those observed for **7**; the shorter ones (2.667, 2.707 Å) and the longer one (2.912 Å). Because six protons form hydrogen bonds with the six THF molecules, the remaining four protons integrate the dinuclear structure. It is therefore concluded that the shorter RuO···ORu linkages are retained by hydrogen bonds, whereas the longer one is not associated with hydrogen bond. This conclusion is the basis for the structural assignment as **7** (not **7A**). The six Ru–O oxygen atoms in **7′** form a trigonal-antiprismatic array similar to that in **7**. The two pairs of structures **6**/**6′** and **7**/**7′** suggest that the hydrogen-bonding interactions of the $[Tp^{iPr2}Ru(OH_X)_3]_2$ core with the THF solvates and the TfO anions may be so weak as to be dissociated in solutions but the dinuclear structure should be retained as discussed above on the basis of the electrochemical data.

The hydrated hydroxo ligand [M-(H)O···H···O(H)-M] is the bridging structural motif unique to polynuclear aquo-hydroxo complexes [7] and, to our knowledge, complexes **6** and **7** are the first examples with the multiple M–(H)O···H···O(H)–M-type hydrogen-bonding bridging interactions. It should be noted that, the O···O separations of **6** (2.4–2.5 Å) are comparable to those found for the previously reported singly or doubly bridging structures such as $[\mu\text{-}H_3O_2]_2\{Cr(bipy)_2\}_2]^{4+}$ and $[(\mu\text{-}H_3O_2)\{Ru^{III}(L)(tacn^{Me3})\}_2]^{3+}$ (L = acac, *o*-benzoquinone diimine) [7], whereas those of **7** with the ternary hydrogen-bonding interactions are substantially longer than them.

3. Conclusions

Oxygenation of a series of the labile cationic aquo-Ru(II) complexes, $Tp^{iPr2}Ru(L)_n(OH_2)_{3-n}(OTf)(THF)_x$ [L/n/x = bipy/2/0 (**1d**), py/1/2(**2**), THF/0/2 (**3**)], which

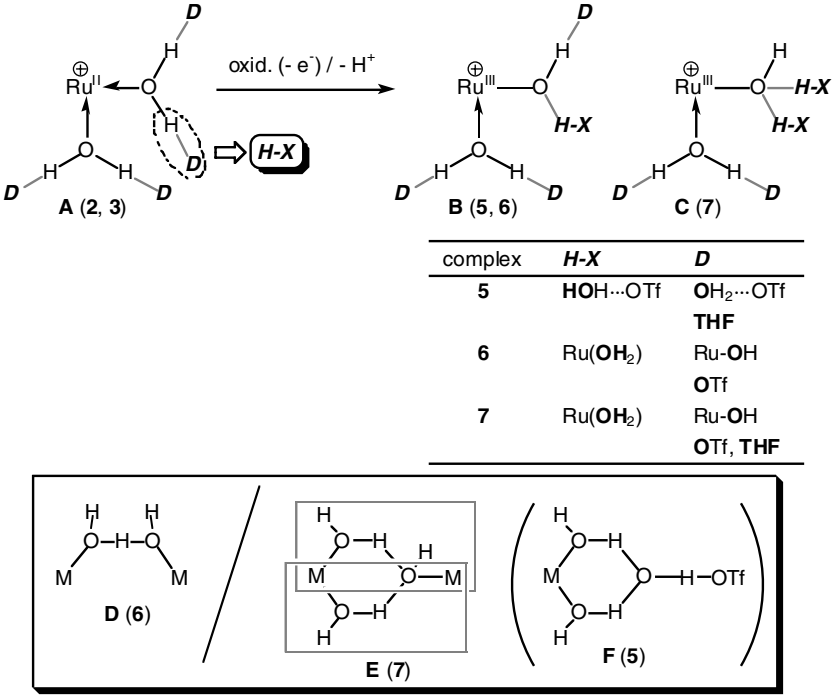

complex	*H-X*	*D*
5	**HO**H···OTf	**O**H$_2$···OTf
		THF
6	Ru(**OH**$_2$)	Ru-**O**H
		OTf
7	Ru(**OH**$_2$)	Ru-**O**H
		OTf, **THF**

Scheme 4.

contain the hydrogen-bonding interactions between the acidic aquo ligand and donor (**D**), results in oxidation of the metal center(s) to give the mono- and dinuclear species **4**–**7** containing a Ru(III) center. The bipy complex **1d** with the only one labile ligand gives the simple hydroxo-Ru(III) complex **4**, whereas complexes **2** and **3** afford **5**–**7** with the unique hydrogen-bonding networks and, in particular, complex **3** with the three labile ligands produce the dinuclear species **6** and **7** with the multiple hydrated aquo bridges, M–(H)O···H···O(H)–M.

A combination of one electron-oxidation and deprotonation causes conversion of the aquo-Ru(II) species **A** into the hydroxo-Ru(III) species **B** and **C** resulting from formal displacement of the H···***D*** moiety by the ***H–X*** fragment (Scheme 4). The ***H–X*** fragment could be an acidic component in the reaction mixture, i.e. H_2O associated with the OTf and $RuTp^{iPr2}$ moieties. When ***H–X*** and/or ***D*** in **B** and **C** are metal components [$Tp^{iPr2}Ru(OH_x)$], the dinuclear structures result from the multiple hydrogen-bonding interactions. In the case of **7**, interaction with the two ***H–X*** fragments leads to the ternary hydrogen-bonding interaction. The bridging interaction found for **7**(**E**) is a unique one as discussed above but can be regarded as a superimposed version of the precedent μ-O_2H_3 motif. The MO_3H_2 six-membered ring structural motifs in **E** and **F** are common for the $Tp^{iPr2}Ru$(III)–OH species.

The electron-donating Tp^{iPr2} ligand renders the Ru(III)-OH moiety basic enough to form hydrogen bonds with the acidic component (***H–X***) and the facial coordination of the Tp^{iPr2} ligand forces *cis*-orientation of the OH_x ligands, which leads to the dimeric structures supported by the hydrogen-bonding networks.

4. Experimental

4.1. General methods

THF and hexane (Na–K alloy), CH_2Cl_2 (P_4O_{10}) and acetone ($KMnO_4$-molecular sieves) were treated with appropriate drying agents, distilled, and stored under argon. IR spectra were obtained on a JASCO FT/IR 5300 spectrometer. CV measurements ($E_{1/2}$ vs. Ag/Ag^+; in THF; NBu_4PF_6) were done with a BAS 100B/W(CV-50W) machine. The starting complexes were prepared according to the reported methods [3a].

4.2. Preparation of *4* (Oxidation of *1d*)

A Schlenk tube containing a THF solution (10 mL) of **1d** (103 mg, 0.12 mmol) was evacuated and then filled with O_2 gas (1 atm). After the mixture was stirred magnetically for 4 h, the solution was concentrated under reduced pressure. Addition of hexane followed by cooling at −20 °C gave **4b** (80 mg, 0.099 mmol, 78% yield) as red needles. IR 3580 (m sh, ν_{OH}), 3488 (m br, ν_{OH}), 3082 (w), 2971 (vs), 2933 (s sh), 2870 (s), 2555 (m, ν_{BH}), 1537 (s), 1473 (s), 1449 (m), 1428 (s), 1392 (s), 1367 (m), 1278 (vs), 1181 (s), 1156 (s), 1058 (s), 1032 (vs), 796 (w), 779 (m), 665 (m), 639 (s), 568 (m). *Anal*. Calc. for $C_{41}H_{61}BN_8O_5F_3SRu$: C, 52.01; H, 6.49; N, 11.83. Found: C, 51.55; H, 6.53; N, 11.83%.

4.3. Preparation of *5* (Oxidation of *2*)

A THF solution (5 mL) of $\mathbf{2}\cdot(THF)_{2.5}$ (72 mg, 0.071 mmol) was stirred under O_2-atmosphere (1 atm) for 30 min. After removal of the volatiles under reduced pressure the residue was dissolved in acetone and then hexane was added. Concentration under reduced pressure followed by cooling at −20 °C gave **5** (44 mg, 0.048 mmol, 67% yield) as yellow plates. IR 3588 (m sh, ν_{OH}), 3384 (m br, ν_{OH}), 2971 (vs), 2933 (s sh), 2871 (s), 2550 (m, ν_{BH}), 1636 (m br, δ_{OH}), 1608 (m), 1537 (s), 1474, (s sh), 1427 (m), 1395 (s), 1366 (m), 1288 (vs), 1225 (s sh), 1179 (vs), 1157 (vs), 1057 (vs), 1032 (vs), 897 (w br), 829 (w), 796 (m), 766 (m), 699 (m), 662 (m), 629 (s), 575 (m). *Anal*. Calc. for $C_{41}H_{72}BN_7O_8F_3SRu$: C, 49.64; H, 7.32; N, 9.88. Found: C, 49.81; H, 7.14; N, 10.17%.

4.4. Oxidation of *3* (Formation of *6*)

A THF solution (10 mL) of **3** (150 mg, 0.14 mmol), was stirred under O_2 atmosphere (1 atm) for 4 h. After filtration through a Celite pad haxane was added and the resulting solution was cooled at −20 °C to give **6** (88 mg, 0.057 mmol, 80% yield) as yellow brown plates. IR 3639 (w, ν_{OH}), 3406 (w br, ν_{OH}), 2968 (vs), 2931 (s sh), 2870 (m), 2546 (m, ν_{BH}), 1630 (w br, δ_{OH}), 1538 (s), 1474 (s), 1395 (s), 1364 (m), 1289 (s), 1253 (s), 1180 (vs), 1156 (s sh), 1056 (s), 1032 (s), 794 (s), 765 (w), 663 (m), 638 (s), 535 (w), 491 (w). *Anal*. Calc. for $C_{55}H_{102}B_2N_{12}O_9F_3SRu_2$: C, 47.58; H, 7.41; N, 12.11. Found: C, 47.71; H, 7.38; N, 12.09%.

4.5. Oxidation of *3* (Formation of *7*)

A THF solution (10 mL) of **3** (75 mg, 0.072 mmol) was stirred under O_2 atmosphere (1 atm) for 4 h. Work up as described for **6** gave **7** (55 mg, 0.033 mmol, 91% yield) as brown crystals. IR 3422 (w, ν_{OH}), 2970 (vs), 2872 (s), 2544 (w, ν_{BH}), 1631 (w br, δ_{OH}), 1538 (s), 1474 (s), 1429 (m), 1394 (s), 1366 (m), 1251 (s), 1180 (vs), 1058 (s), 1034 (vs), 797 (m), 639 (m). *Anal*. Calc. for $C_{64}H_{118}B_2N_{12}O_{14}F_6S_2Ru_2$: C, 45.71; H, 7.07; N, 10.00. Found: C, 46.01; H, 7.39; N, 9.85%.

4.6. X-ray crystallography

Singles crystals of $\mathbf{4}\cdot$acetone (acetone–hexane), $\mathbf{5}\cdot$THF (THF–hexane), $\mathbf{6}\cdot 2CH_2Cl_2\cdot$THF ($CH_2Cl_2$–

Table 2
Crystallographic data

Compound	**5** · THF	**4** · acetone	**6** · $2CH_2Cl_2$ · THF	**7**
Formula	$C_{45}H_{80}BF_3N_7O_9SRu$	$C_{41}H_{61}BN_8O_5F_3SRu$	$C_{61}H_{113}B_2N_{12}O_{10}F_3SCl_4Ru_2$	$C_{64}H_{118}B_2N_{12}O_{14}F_6Ru_2S_2$
Formula weight	1064.1	946.9	1629.3	1681.6
Space group	$P2_1/n$	$P\bar{1}$	$P\bar{1}$	$P2_1/n$
Crystal system	monoclinic	triclinic	triclinic	monoclinic
a (Å)	9.641(4)	12.6833(11)	15.461(5)	13.733(2)
b (Å)	15.187(4)	16.443(2)	19.085(7)	14.124(3)
c (Å)	17.724(5)	11.930(3)	15.443(4)	21.430(7)
α (°)		109.91(2)	116.28(2)	
β (°)	93.04(3)	92.568(17)	97.49(2)	95.30(2)
γ (°)		90.715(10)	95.72(3)	
V (Å^3)	2592(1)	2335.9(7)	3987(2)	4138(1)
Z	2	2	2	2
d_{cald} (g cm^{-3})	1.36	1.35	1.36	1.35
μ (cm^{-1})	4.11	4.42	6.03	4.91
Temperature (°C)	−60	−60	25	−60
Maximum 2θ (°)	54.4	55.1	50.0	40
Number of unique data	5446	9142	14030	3855
Number of parameters refined	327	541	828	472
R_1	0.0788	0.1039	0.0624	0.0508
[for data with $F > 4\sigma(F)$]	[4824 data]	[8850 data]	[8738 data]	[3227 data]
wR_2	0.2314	0.2853	0.1855	0.1640

THF), and **7** (THF–hexane) were obtained by recrystallization from the solvent systems described in the parentheses and mounted on glass fibers. The crystallographic data are summarized in Table 2.

Diffraction measurements of **4** · acetone and **5** · THF were made on a Rigaku RAXIS IV imaging plate area detector with Mo Kα radiation ($\lambda = 0.71069$ Å) at −60 °C. All the data collections were carried out at r.t. Indexing was performed from 3 oscillation images which were exposed for 4 min. The crystal-to-detector distance was 110 mm. Data collection parameters (the detector swing angle/the number of oscillation images/the exposed time) were as follows: 7°/21/45 min (**5** · THF), 6°/24/40 min (**4** · acetone). Readout was performed with the pixel size of 100 μm × 100 μm. Neutral scattering factors were obtained from the standard source [8]. In the reduction of data, Lorentz, polarization, and empirical absorption corrections were made [9].

Diffraction measurements of **6** · $2CH_2Cl_2$ · THF and **7** were made on a Rigaku AFC5S and AFC7R automated four-circle diffractometer, respectively, by using graphite-monochromated Mo Kα radiation ($\lambda = 0.71069$ Å). The unit cell was determined and refined by a least-squares method using 20 independent reflections. Data were collected with an ω-2θ scan technique. If $\sigma(F)/F$ was more than 0.1, a scan was repeated up to three times and the results were added to the first scan. Three standard reflections were monitored at every 100 measurements. All data processing was performed on a FACOM A-70 computer (**6** · $2CH_2Cl_2$ · THF) and a Venturis FX 5133 computer (**7**). Neutral scattering factors were obtained from the standard source [8]. In the reduction of data, Lorentz, polarization, and empirical absorption corrections (Ψ scan) were made.

The structures were solved by a combination of the direct methods (SHELXL 87 [10a]) and Fourier synthesis (DIRDIF [11]). Least-squares refinements were carried out using SCHELEXL97 [10b] linked to TEXSAN [12]. Details of the refinements were as follows. **5** · THF: All the non-hydrogen atoms except for the THF solvate (refined isotropically) were refined anisotropically. The methyl hydrogen atoms were refined by using riding models. Hydrogen atoms attached to the THF solvate were not included in the refinement and the other hydrogen atoms were fixed at the calculated positions. **4b** · acetone and **7**: All the non-hydrogen atoms were refined anisotropically and the hydrogen atoms were fixed at the calculated positions. **6** · $2CH_2Cl_2$ · THF: All the non-hydrogen atoms except for the THF solvate (refined isotropically) were refined anisotropically and the highly disordered oxygen atom (O91) of the THF solvate was fixed at the final stage of the refinement. Hydrogen atoms attached to the THF solvate and one of hydrogen atoms attached to the O11 atom were not included in the refinement and the other hydrogen atoms were fixed at the calculated positions.

5. Supplementary material

Crystallographic data for the structural analysis of compounds **4**–**7**, have been deposited with the Cambridge Crystallographic Data Centre [CCDC Nos. 209824(**4**)–209827(**7**)]. Copies of the information may be

obtained free of charge from The Director, CCDC, 12 Union Road, Cambridge CB2 1EZ, UK (fax: +44-1223-336033; e-mail: deposit@ccdc.cam.ac.uk or www: http://www.ccdc.cam.ac.uk).

Acknowledgements

We are grateful to the Ministry of Education, Culture, Sports, Science and Technology of the Japanese Government for the financial support of this research (Grant-in-Aid for Scientific Research on Priority Areas: No. 11228201).

References

[1] (a) S. Trofimenko, Scorpionates – The Coordination Chemistry of Polypyrazolylborate Ligands, Imperial College Press, London, 1999;
(b) S. Trofimenko, Chem. Rev. 93 (1993) 943;
(c) N. Kitajima, Y. Moro-oka, Chem. Rev. 94 (1994) 737;
(d) N. Kitajima, W.B. Tolman, Prog. Inorg. Chem. 43 (1995) 419.
[2] M. Akita, S. Hikichi, Bull. Chem. Soc. Jpn. 75 (2002) 1657.
[3] (a) Y. Takahashi, M. Akita, S. Hikichi, Y. Moro-oka, Inorg. Chem. 37 (1998) 3186;
(b) Y. Takahashi, M. Akita, S. Hikichi, Y. Moro-oka, Organometallics 17 (1998) 4884;
(c) Y. Takahashi, S. Hikichi, M. Akita, Y. Moro-oka, J. Chem. Soc., Chem. Commun. 1491 (1999);
(d) Y. Takahashi, S. Hikichi, M. Akita, Y. Moro-oka, Organometallics 18 (1999) 2571;
(e) M. Akita, Y. Takahashi, S. Hikichi, Y. Moro-oka, Inorg. Chem. 40 (2001) 169.
[4] K. Kirchner, K. Mauthner, K. Mereiter, R. Schmid, J. Chem. Soc., Chem. Commun. (1993) 892.
[5] I. de los Rios, M.J. Tenorio, J. Padilla, M.P. Puerta, P. Valerga, J. Chem. Soc., Dalton Trans. (1996) 377.
[6] M. Sato, M. Asai, J. Organomet. Chem. 508 (1996) 121.
[7] (a) M. Ardon, A. Bino, Struct. Bond. 65 (1987) 1;
(b) M. Ardon, A. Bino, Inorg. Chem. 24 (1985) 1343;
(c) R. Schneider, T. Weyhermüller, K. Wieghardt, B. Nuber, Inorg. Chem. 32 (1993) 4925;
(d) E.C. Wilkinson, Y. Dong, L. Que, J. Am. Chem. Soc. 116 (1994) 8394;
(e) M. Ruf, K. Weis, H. Vahrenkamp, J. Am. Chem. Soc. 118 (1996) 9288;
(f) A. Llobet, D.J. Hodgson, T.J. Meyer, Inorg. Chem. 29 (1990) 3760;
(g) T. Jüstel, J. Bendix, N. Metzler-Nolte, T. Weyhermüller, B. Nuber, K. Wieghardt, Inorg. Chem. 37 (1998) 35;
(h) M. Kosugi, S. Hikichi, M. Akita, Y. Moro-oka, Inorg. Chem. 38 (1999) 2567.
[8] International Tables for X-ray Crystallography, vol. 4, Kynoch Press, Birmingham, 1975.
[9] T. Higashi, Program for absorption correction, Rigaku Corporation, Tokyo, Japan, 1995.
[10] (a) G.M. Sheldrick, SHELXS-86: Program for Crystal Structure Determination, University of Göttingen, Göttingen, Germany, 1986;
(b) G.M. Sheldrick, SHELXL-97: Program for Crystal Structure Refinement, University of Göttingen, Göttingen, Germany, 1997.
[11] P.T. Beurskens, G. Admiraal, G. Beurskens, W.P. Bosman, S. Garcia-Granda, R.O. Gould, J.M.M. Smits, C. Smykalla, The DIRDIF program system, Technical Report of the Crystallography Laboratory, University of Nijmegen, Nijmegen, The Netherlands, 1992.
[12] teXsan, Crystal Structure Analysis Package, ver. 1.11, Rigaku Corp., Tokyo, Japan, 2000.

Available online at www.sciencedirect.com
SCIENCE DIRECT®
Polyhedron 23 (2004) 235–238
POLYHEDRON
www.elsevier.com/locate/poly

A coordination polymer from a cyanoscorpionate complex

Christopher J. Siemer [a], Michael J. VanStipdonk [a], Pawan K. Kahol [b], David M. Eichhorn [a,*]

[a] Department of Chemistry, Wichita State University, 1845 N. Fairmount, Wichita, KS 67260-0051, USA
[b] Department of Physics, Wichita State University, 1845 N. Fairmount, Wichita, KS 67260-0032, USA

Received 13 May 2003; accepted 16 September 2003

Abstract

Reaction of the copper(II) complex of $Bp^{Ph,4CN}$ with $Rh_2(CF_3COO)_4$ results in coordination of the CN groups of the Bp ligand to Rh and the formation of a coordination polymer. This material has been characterized by IR and EPR spectroscopy and electrospray mass spectrometry.
© 2003 Elsevier Ltd. All rights reserved.

Keywords: Polypyrazolylborate complexes; Copper complexes; Rhodium complexes; Scorpionates; Coordination Polymers; Nitrile coordination

1. Introduction

The past 35 years of research in scorpionates has shown the tremendous versatility of these ligands made possible by virtue of the wide variety of substituents that can be relatively easily attached to the pyrazole carbon atoms. The chemist has, thereby, extraordinary control over the coordination geometry, electronic characteristics, and chemical reactivity of the metal center. This versatility, however, has primarily been achieved using alkyl and aryl substituents, relying largely on steric effects to promote changes in the electronic properties of the coordinated metal. An example is the series of complexes Tp_2Fe, Tp^*_2Fe and Tp^{Ph}_2Fe in which the increasing steric bulk of the substituent in the 3-position results in a progression from a spin-crossover complex that is low-spin at room temperature to a spin-crossover complex that is high-spin at room temperature to a complex that remains high spin at all temperatures [1]. Scorpionate ligands incorporating strongly electron-withdrawing or donating substituents have received comparatively little attention. A few people, most notably Dias and coworkers, have employed bis(3,5-trifluoromethyl)pyrazole, reporting scorpionate complexes that show interesting electronic and reactivity properties [2]. Recently, reports have come out of our group [3] and that of Trofimenko [4] concerning bispyrazolylborate ligands containing the CN substituent in the 4-position of the pyrazole ring.

Aside from its electron-withdrawing character, the cyano group offers a feature that is interesting from a structural standpoint, namely the ability of the cyano group, itself, to coordinate to a metal ion. The cyanoscorpionate complexes are thus candidates to be components of coordination polymers in which two cyanoscorpionate complexes are linked up by binding of the cyano groups on each to a second metal complex. The only examples of scorpionate-based polymers involving the coordination of a functional group on a pyrazole substituent to another metal ion involve the pyridyl-substituted Tp ligands of Vahrenkamp and coworkers [5]. In these ligands, the same metal ion is coordinated both by the pyrazole N atoms of one ligand and the pyridyl N atoms of neighboring ligands.

Our previous work and that of Trofimenko represent two extremes in the continuum of cyanoscorpionate ligands. Trofimenko reported the synthesis of the parent bis(4-cyanopyrazolyl)borate, Bp^{4CN}. The reaction of this ligand with transition metal salts results in an immediate

* Corresponding author. Fax: +316-978-3431.
E-mail address: david.eichhorn@wichita.edu (D.M. Eichhorn).

0277-5387/$ - see front matter © 2003 Elsevier Ltd. All rights reserved.
doi:10.1016/j.poly.2003.11.008

precipitation of intractable solids. These materials show multiple CN stretching bands in the IR spectra. The implication is that, along with coordination of the metal ion to the pyrazole N atoms, the cyano groups also coordinate to the metal ions, resulting in a polymeric material in which a given metal ion is potentially bound to the pyrazole N atoms of one Bp^{4CN} ligand and to the CN group of another. Characterization of these materials was possible only after the addition of ancillary ligands, resulting in the isolation of heteroleptic complexes containing the Bp^{4CN} ligand as well as other ligands. This work clearly demonstrated the feasibility of making cyano-substituted scorpionate ligands and also indicated that the cyano substituent on the pyrazole ring could act as a ligand to another metal ion.

We reported the synthesis of $Bp^{Ph,4CN}$ and its complexes with Co^{2+} and Cu^{2+}. As has been well documented over the last 35 years, the presence of bulky substituents in the 3-position of the pyrazole rings restricts access to the metal [6] and lessens the chance of oligomerization via coordination to the scorpionate-bound metal. The phenyl group has been shown to be a substituent of intermediate steric bulk, allowing for facile isolation of 4- and 5-coordinate complexes with a 1:1 Tp:metal stoichiometry [6a,6d], but also allowing for the preparation of complexes with a 2:1 Tp:metal stoichiometry [1b]. Indeed, the phenyl group in the 3-position of $Bp^{Ph,4CN}$ allowed for the isolation of homoleptic complexes of the form $Bp^{Ph,4CN}{}_2M$ with both Co^{2+} and Cu^{2+} [3]. These complexes showed little structural variations from analogous complexes made with non-cyano-substituted Bp ligands.

2. Results and discussion

With the information from the Trofimenko work confirming the ability of the CN group to serve as a ligand to a transition metal, isolation of the $Bp^{Ph,4CN}{}_2M$ complexes provided a material with which to attempt the rational preparation of a coordination polymer – one in which a metal is bound in the pyrazole pocket and a second metal is bound to CN groups from different $Bp^{Ph,4CN}$ ligands. The first attempt was made using the $Rh_2(CF_3COO)_4$ dimer, which is well known to bind organonitrile ligands [7]. Combination of a yellow methylene chloride solution of $Bp^{Ph,4CN}{}_2Cu$ with a green methylene chloride solution of $Rh_2(CF_3COO)_4$ results in the immediate deposition of a red powder. IR spectroscopy of this powder (Fig. 1) shows peaks attributable to both the scorpionate ligand and the rhodium dimer, including B–H stretches at 2415 and 2480 cm^{-1}, very similar to those apparent in $Bp^{Ph,4CN}{}_2Cu$. Most important, however, is the appearance of a new CN stretch at 2260 cm^{-1} in addition to the stretch at 2229 cm^{-1} seen in both $KBp^{Ph,4CN}$ and $Bp^{Ph,4CN}{}_2Cu$. This

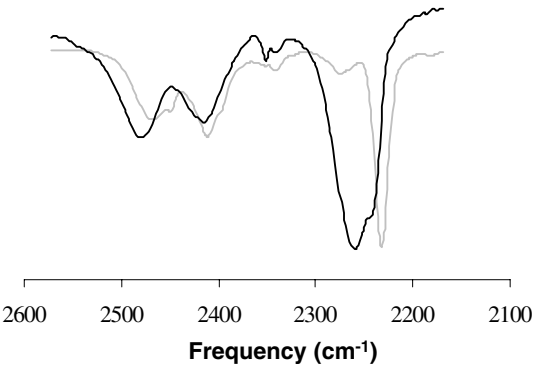

Fig. 1. IR spectra of $Bp^{Ph,4CN}{}_2Cu$ (gray) and the reaction product with $Rh_2(CF_3COO)_4$ (black) showing the B–H and C–N stretching regions.

shifted CN stretch mirrors that seen by Trofimenko at 2262 cm^{-1} in the initial polymeric materials isolated by addition of Bp^{4CN} to divalent metal ions and indicates binding of the CN group to the axial position of the Rh dimer.

Although the red powder is insoluble in methylene chloride, it can be dissolved in more coordinating solvents such as acetonitrile, acetone, and THF to give blue or green solutions. The EPR spectra taken in THF solution and in the solid state are essentially identical with those of the $Bp^{Ph,4CN}{}_2Cu$ starting material, indicating that, not surprisingly, there is no interaction between Cu ions. It is most likely that the solvent breaks up the polymer into smaller, more tractable species by replacing the nitrile coordinated to the Rh atom. ESI-MS characterization of the THF solutions (Fig. 2), however, reveals that some amount of oligomerization remains even after the material is dissolved. The spectra, in negative ion detection mode, show a peak at $m/z = 761$ which corresponds to $Bp^{Ph,4CN}{}_2Cu$. In addition, peaks are observed at $m/z = 1418$ and 2075, which correspond to $Bp^{Ph,4CN}{}_2Cu\text{-}Rh_2(CF_3COO)_4$ and $Bp^{Ph,4CN}{}_2Cu\text{-}(Rh_2(CF_3COO)_4)_2$, respectively [8]. This correlates very well with the elemental analysis performed on the original red powder, which corresponds to a stoichiometry of two rhodium dimers per $Bp^{Ph,4CN}{}_2Cu$ complex. It should be noted that one $Bp^{Ph,4CN}{}_2Cu$ complex contains four CN groups which could potentially coordinate to Rh. MS–MS experiments run on the 1418 peak show fragmentation to give the $Bp^{Ph,4CN}{}_2Cu$ peak at $m/z = 761$.

Although it has not yet been possible to crystallographically characterize either the red powder or the material dissolved in coordinating solvents, the evidence from mass spectrometry and IR spectroscopy as well as the insolubility of the red material in non-coordinating solvents indicate at least oligomerization and possibly polymerization by coordination of the CN substituent on a pyrazole ring to the Rh atom of the $Rh_2(CF_3COO)_4$ dimer, as schematized in Fig. 3.

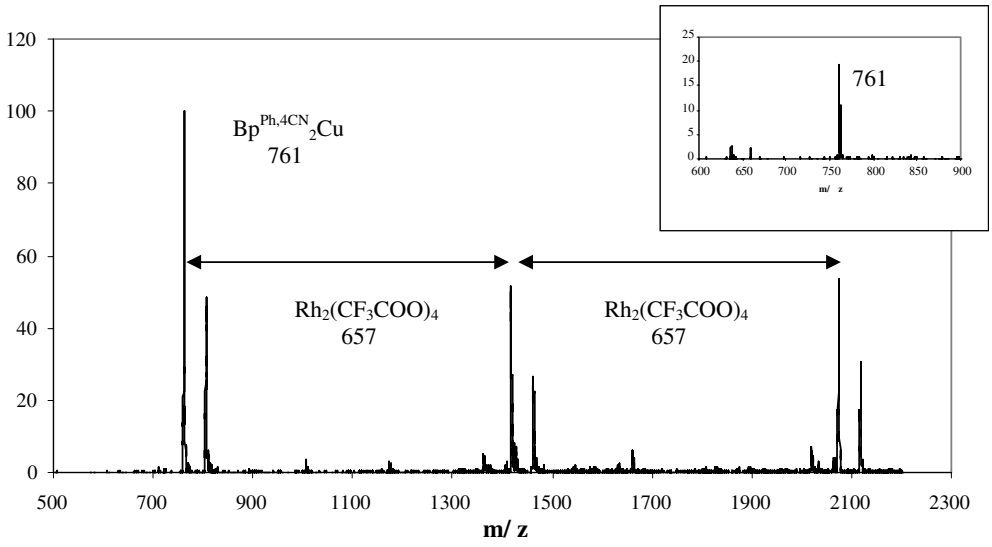

Fig. 2. ESI-MS of the reaction product of $Bp^{Ph,4CN}{}_2Cu$ and $Rh_2(CF_3COO)_4$ dissolved in THF. The inset shows the MS–MS experiment performed on the $m/z = 1418$ peak.

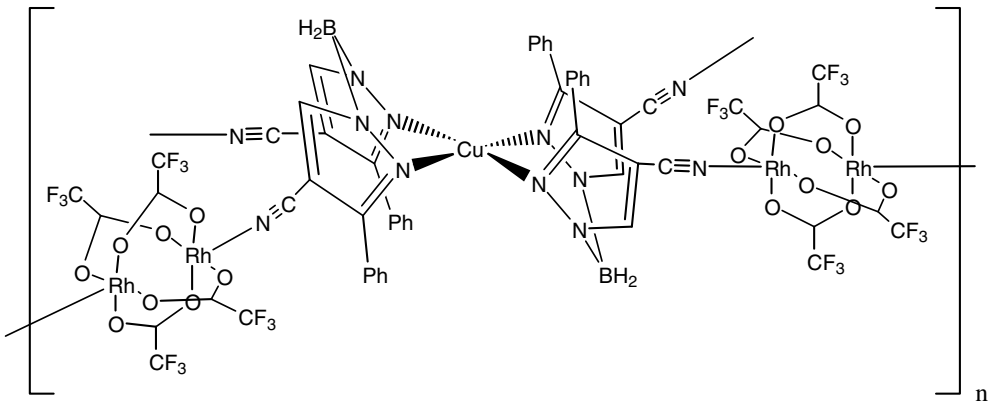

Fig. 3. Proposed structure of the polymer formed by reaction of $Bp^{Ph,4CN}{}_2Cu$ and $Rh_2(CF_3COO)_4$.

3. Conclusions

Using scorpionate ligands substituted by CN at the 4-position and by the relatively bulky phenyl group at the 3-position, it is possible to rationally produce a coordination polymer with coordination of one metal ion in the pyrazole pocket and a second metal ion to the cyano group.

4. Experimental

$KBp^{Ph,4CN}$ and $Bp^{Ph,4CN}{}_2Cu$ were synthesized as previously reported [3]. $Rh_2(CF_3COO)_4$ was purchased from Strem Chemicals and used as received. Solvents were purchased from Fisher Scientific and used as received. IR spectra were obtained on a Nicolet Avatar 360 FTIR. Electrospray Mass Spectrometry was performed on a Finnigan LCQ DECA spectrometer. EPR spectra were obtained on a Bruker EMX 6/1 spectrometer. Elemental Analysis was performed by M-H-W Laboratories, Phoenix, AZ.

To a yellow solution of $Bp^{Ph,4CN}{}_2Cu$ in CH_2Cl_2 is added a green solution containing 2 molar equivalents of $Rh_2(CF_3COO)_4$ in CH_2Cl_2. A red powder is deposited immediately, which is isolated by filtration and washed with CH_2Cl_2. IR (KBr disc, cm^{-1}): 2480 (w, B–H), 2415 (w, B–H), 2260 (m, CN), 1668 (s), 1193 (s), 1156 (s), 859 (m), 786 (m), 738 (m), 697 (w). ESI-MS (THF solution, negative ion detection mode, m/z): 761 $(Bp^{Ph,4CN}{}_2Cu)^-$, 1418 $((Bp^{Ph,4CN}{}_2Cu)\,Rh_2(CF_3COO)_4)^-$, 2074 $((Bp^{Ph,4CN}{}_2Cu)(Rh_2(CF_3COO)_4)_2)^-$. EPR (solid, 298 K, X-band): $g_{||} = 2.23$, $A_{||}^{Cu} = 590$ MHz; EPR (THF solution, 298 K, X-band): $g = 2.15$, $A^{Cu} = 210$ MHz, $A^N = 55$ MHz. Elemental *Anal.* Calc. for $C_{56}H_{28}N_{12}O_{16}F_{24}B_2Cu_1Rh_4$-$((Bp^{Ph,4CN}{}_2Cu)(Rh_2(CF_3COO)_4)_2)$: C, 32.37; H, 1.36; N, 8.09. Found C, 32.16; H, 1.12; N, 7.92%.

Acknowledgements

We would like to acknowledge the National Science Foundation (Grant # EPS-9550 487 to D.M.E. and Grant # EPS-9874 932 to M.J.V.) and matching funds from Wichita State University for funding of this research. We thank Dr. Joshua Telser for helpful discussions.

References

[1] (a) J.D. Oliver, D.F. Mullica, B.B. Hutchinson, W.O. Milligan, Inorg. Chem. 19 (1980) 165;
(b) D.M. Eichhorn, W.H. Armstrong, Inorg. Chem. 29 (1990) 3607;
(c) G.J. Long, B.B. Hutchinson, Inorg. Chem. 27 (1987) 608.

[2] (a) J.L. Schneider, S.M. Carrier, C.E. Ruggiero, V.G. Young, W.B. Tolman, J. Am. Chem. Soc. 120 (1998) 11408;
(b) R. Han, P. Ghosh, P.J. Desrosiers, S. Trofimenko, G. Parkin, J. Chem. Soc., Dalton Trans. (1997) 3713;
(c) V. Rodriguez, J. Full, B. Donnadieu, S. Sabo-Etienne, B. Chaudret, New J. Chem. 21 (1997) 847;
(d) H.V.R. Dias, L. Huai, W. Jin, S.G. Bott, Inorg. Chem. 34 (1995) 1973;
(e) H.V.R. Dias, J.D. Gordon, Inorg. Chem. 35 (1996) 318;
(f) H.V.R. Dias, H.-L. Lu, Inorg. Chem. 39 (2000) 2246;
(g) H.V.R. Dias, W. Jin, Z. Wang, Inorg. Chem. 36 (1997) 6205;
(h) H.V.R. Dias, H. Lu, Inorg. Chem. 34 (1995) 21;
(i) H.V.R. Dias, Z. Wang, Inorg. Chem. 39 (2000) 3724.

[3] C.J. Siemer, N. Goswami, M.J. Van Stipdonk, D.M. Eichhorn, Inorg. Chem. 40 (2001) 4081.

[4] A.R. Rheingold, C.D. Incarvito, S. Trofimenko, Inorg. Chem. 39 (2000) 5569.

[5] K. Weis, H. Vahrenkamp, Inorg. Chem. 36 (1997) 5589.

[6] (a) S. Trofimenko, J.C. Calabrese, J.S. Thompson, Inorg. Chem. 26 (1987) 1507;
(b) S. Trofimenko, J.C. Calabrese, P.J. Domaille, J.S. Thompson, Inorg. Chem. 28 (1989) 1091;
(c) I.B. Gorrell, A. Looney, G. Parkin, J. Chem. Soc. Chem. Commun. 220 (1990);
(d) C.J. Siemer, F.A. Meece, W.H. Armstrong, D.M. Eichhorn, Polyhedron 20 (2001) 2637.

[7] (a) F.A. Cotton, Y. Kim, J. Am. Chem. Soc. 115 (1993) 8511;
(b) H. Miyasaka, C.S. Campos-Fernandez, R. Clerac, K.R. Dunbar, Angew. Chem. IEE 39 (2000) 3831;
(c) H. Miyasaka, C.S. Campos-Fernandez, J.R. Galan-Mascaros, K.R. Dunbar, Inorg. Chem. 39 (2000) 5870.

[8] Each of the peaks in the mass spectrum has a second peak associated with it at M + 46. While we have been unable to determine the identity of this peak, it appears to be associated with the $Bp^{Ph,4CN}{}_2Cu$ starting material, as a peak at $m/z = 807$ is evident in the mass spectrum of this compound.

Available online at www.sciencedirect.com
SCIENCE DIRECT®
Polyhedron 23 (2004) 239–244
POLYHEDRON
www.elsevier.com/locate/poly

New heteroscorpionate ligands with hydrogen bond donor and acceptor groups: synthesis, characterization and reactivity with divalent Co, Zn and Ni ions

Zahida Shirin, Carl J. Carrano *

Department of Chemistry, Southwest Texas State University, San Marcos TX 78666, USA

Received 14 May 2003; accepted 5 September 2003

Abstract

Three new N_2O heteroscorpionate ligands designated L6OH, L7OH and L9OH, containing either appended hydrogen bond donating or accepting residues have been synthesized and characterized. Metal complexes of these ligands with Co(II) and Ni(II) have been characterized by X-ray crystallography. A facile decomposition pathway leading to C–N bond cleavage and isolation of metal pyrazole complexes was also identified.
© 2003 Elsevier Ltd. All rights reserved.

Keywords: Heteroscorpionate ligands; Hydrogen bond; X-ray crystallography; Divalent metals

1. Introduction

Tris(pyrazolyl)borate (Tp) or "scorpionate" ligands have wide application in coordination, organometallic and bioinorganic chemistry [1]. These ligands have become particularly important in the development of biomimetic coordination chemistry of metalloproteins. Despite their advantages, the tris(pyrazolyl)borate ligands are completely symmetric with three nitrogen donors and many metalloproteins active site do not have such monofunctional binding sites. Our major contribution to this field has been the introduction of a family of tripodal N_2X ligands which contain all the biologically relevant donor atoms and are isostructural and isoelectronic with Tp [2,3]. With these we have begun to investigate how donor atom identity affects the properties of the metal center in a series of isostructural and isoelectronic complexes, i.e., *the inorganic chemists equivalent of site-directed mutagenesis*.

However in metalloproteins the structure of the active site has a role beyond just providing the necessary ligands to connect the metal cofactor to protein. It also controls the secondary coordination sphere (microenvironment) around the metal ion. This microenvironment often has a significant role to play in controlling the reactivity of the metal ion. Of the various interactions that proteins use to modify the secondary coordination sphere, perhaps the most important is hydrogen bonding. It is used to control structure, assist in recognition and activation of exogenous substrates or stabilize reactive intermediates. While the use of sterically restricted ligands to control the size and shape of metal binding cavities is well established, it has proven more difficult, despite its importance, to incorporate hydrogen bonding into synthetic small molecule binding site analogs. However, some recent successes in using hydrogen bonding, sterically restricted, metal binding cavities prepared by relatively simple synthetic schemes have become evident [4–7]. Using 5′-ester substituted pyrazoles we have also described a first generation of a simple H-bond accepting Tp ligands that simultaneously provides both steric bulk and hydrogen bonding groups, which can be directed towards the center of a metal binding cavity. The presence of strong intramolecular H-bonding between the ligand carbonyls and water molecules leads to the stabilization of discrete, well

* Corresponding author. Tel.: +1-512-245-2156; fax: +1-512-245-2374.
E-mail address: carrano@sciences.sdsu.edu (C.J. Carrano).

0277-5387/$ - see front matter © 2003 Elsevier Ltd. All rights reserved.
doi:10.1016/j.poly.2003.11.007

characterized, divalent metal aquo complexes of the general type in $[Tp^{CO_2Et,Me}M(L)_x]^+$ where M = Co(II), Ni(II), Mn(II), Zn(II) or Cu(II), L = H_2O, OAc^-, OH^-, or various amino acids, and $x = 2$ or 3 depending on the metal [8,9]. These complexes are both, unprecedented in Tp chemistry, and good structural models for enzymes of the vicinal oxygen chelate (VOC) superfamily [10].

In this work, we describe our initial efforts to combine hydrogen bonding capabilities with the unsymmetrical donor set of our heteroscorpionates to produce a new generation of such ligands.

2. Experimental

All syntheses and crystallizations were carried out under Ar using standard Schlenk or dry box techniques. Solvents dichloromethane and acetonitrile were distilled under argon over CaH_2 while diethyl ether was distilled from Na/benzophenone. 3-Methyl-5-carboxyethylpyrazole was prepared as previously described [8]. All other reagents and solvents were purchased from commercial sources and used as received unless otherwise noted.

2.1. Synthesis of ligands

*L6OH (**1**)*. 3-Methyl-5-carboxyethylpyrazolyl ketone (8.78 g, 26.20 mmol) was dissolved in a minimum amount of anhydrous DMF and placed in a 100 ml round bottom flask which was purged and filled with argon. Salicylaldehyde (3.20 g, 26.20 mmol) and a catalytic amount (0.1 g) of anhydrous $CoCl_2$ were added to the flask. The mixture was then heated at 100 °C for 30 h under Ar. DMF was removed under reduced pressure and the solid mass dissolved in CH_2Cl_2, washed with water thrice, with saturated sodium chloride solution and finally dried over anhydrous $MgSO_4$. CH_2Cl_2 was removed to produce a pale yellow oil. The oil was triturated with pentane and stirred overnight to yield a white microcrystalline solid. This solid was collected by filtration, washed with pentane and dried in vacuo. Yield: 5.4 g (50%) *Anal.* Calc. for $C_{21}H_{24}N_4O_5$: C, 61.16; H, 5.86; N, 13.58. Found: C, 60.84; H, 5.83; N, 13.43%. ^{1}H NMR ($CDCl_3$) δ 8.59 (s, 1H, O*H*), 7.91 (s, 1H, –C*H*–), 7.09 (t, 1H, $J = 7.9$ Hz, Ar*H*), 6.78 (d, 1H, $J = 7.8$ Hz, Ar*H*), 6.74 (t, 1H, $J = 7.6$ Hz, Ar*H*), 6.66 (d, 1H, $J = 8$ Hz, Ar*H*), 6.55 (s, 2H, Pz*H*), 4.26 (q, 4H, $J = 7.2$ Hz, –OCH_2), 2.09 (s, 6H, Pz–CH_3), 1.28 (t, 6H, $J = 7.2$ Hz, –CH_3). ^{13}C NMR ($CDCl_3$) δ 162.29, 154.62, 143.05, 141.90, 130.86, 128.09, 120.34, 119.71, 116.35, 109.41, 72.55, 60.93, 14.13, 11.40.

*L7OH (**2**)*. L6OH (1.0 g, 2.42 mmol) was dissolved in 20 ml of 2.0 M methylamine in THF. To this was added 0.02 g of tetraethylammonium cyanide and the mixture was stirred at 50 °C for 4 days. The white precipitate that separated from the solution was filtered, washed with THF, and dried under vacuo. Yield: 0.58 g (63%) *Anal.* Calc. for $C_{19}H_{22}N_6O_3$: C, 59.68; H, 5.80; N, 21.97. Found: C, 59.51; H, 5.78; N, 21.63%. ^{1}H NMR ($CDCl_3$) δ 9.97 (s, 1H, O*H*), 7.81 (s, 2H, –N*H*–), 7.80 (s, 1H, –C*H*–), 7.24 (t, 1H, $J = 7.4$ Hz, Ar*H*), 6.88 (d, 1H, $J = 7.8$ Hz, Ar*H*), 6.80 (t, 1H, $J = 7.4$ Hz, Ar*H*), 6.75 (d, 1H, $J = 7.2$ Hz, Ar*H*), 6.49 (s, 2H, Pz*H*), 2.71 (s, 3H, NHCH_3), 2.70 (s, 3H, NHCH_3), 2.14 (s, 6H, Pz–CH_3). ^{13}C NMR ($CDCl_3$) δ 163.22, 156.56, 147.57, 142.66, 132.02, 129.89, 122.46, 120.33, 116.83, 108.09, 71.60, 27.11, 12.58. A second, generally minor product was also isolated and identified by ^{1}H and ^{13}C NMR as the mixed ester amide substituted complex and designated L8OH (**3**).

*L9OH (**4**)*. This ligand was synthesized as described previously for L6OH using 3-*tert*-butyl-2-hydroxy-5-methylbenzaldehyde in place of salicylaldehyde. (80% Yield): ^{1}H NMR ($CDCl_3$) δ 8.59 (s, 1H, O*H*), 7.91 (s, 1H, –C*H*–), 7.09 (t, 1H, $J = 7.9$ Hz, Ar*H*), 6.78 (d, 1H, $J = 7.8$ Hz, Ar*H*), 6.74 (t, 1H, $J = 7.6$ Hz, Ar*H*), 6.66 (d, 1H, $J = 8$ Hz, Ar*H*), 6.55 (s, 2H, Pz*H*), 4.30 (q, 4H, $J = 7.2$ Hz, –OCH_2), 2.09 (s, 6H, Pz–CH_3), 1.28 (t, 6H, $J = 7.2$ Hz, –CH_3). ^{13}C NMR ($CDCl_3$) δ 162.29, 154.62, 143.05, 141.90, 130.86, 128.09, 120.34, 119.71, 116.35, 109.41, 72.55, 60.93, 14.13, 11.40.

2.2. Synthesis of Co and Ni complexes

*[L9OHCoBr$_2$]·CH$_2$Cl$_2$ (**5**)*. A solution of L9OH (0.20 g, 0.41 mmol) in 10 ml anhydrous MeOH was treated with solid $NaOCH_3$ (0.02 g, 0.41 mmol) under Ar atmosphere. To the clear solution, solid $CoBr_2$ (0.09 g, 0.41 mmol) was added. The mixture was stirred for 3 h and the MeOH removed under reduced pressure. The solid mass was dissolved in CH_2Cl_2 and filtered. The filtrate was concentrated and layered with hexane whereupon blue crystals separated out. These were filtered, washed and dried under vacuo. Yield: 0.20 g (60%). *Anal.* Calc. (Found) for $C_{27}H_{37}N_4O_6CoBr_2Cl_2$: C, 40.78 (40.16); H, 4.69 (4.80); N, 7.04 (7.33)%.

*[(L7O)Co]$_2$(BF$_4$)$_2$·2DMF (**6**)*. A solution of L7OH (0.20 g, 0.52 mmol) in 10 ml anhydrous DMF was treated with solid KH (0.02 g, 0.52 mmol) under Ar atmosphere. After gas evolution ceased, solid $Co(BF_4)_2 \cdot 6H_2O$ (0.18 g, 0.52 mmol) was added. The resulting purple solution was stirred for 3 h and filtered to remove a small amount of insoluble material. The filtrate was concentrated under reduced pressure. Layering a CH_3CN solution of the complex with diethyl ether caused the separation of purple crystals which were filtered, washed with ether and dried under vacuo. Yield: 0.42 g (68%). *Anal.* Calc. (Found) for $C_{44}H_{56}N_{14}O_8Co_2B_2F_8$: C, 44.03 (43.79); H, 4.70 (4.75); N, 16.33 (16.26)%. ^{1}H NMR (DMF-d_5) 62.52(s), 60.69(s), 38.73(s), 36.09(s), 13.72(s), 8.08(s),

3.56(s), 2.87(dd, $J_1 = 77.8$ Hz, $J_2 = 14$ Hz), −5.23(s), −24.28(s), −27.42(s).

[(L7O)Co]$_2$Br$_2$·2DMF (7). This compound was prepared as described for [(L7O)Co]$_2$(BF$_4$)$_2$·2DMF using $CoBr_2$ as the cobalt precursor (60%). *Anal.* Calc. (Found) for $C_{44}H_{56}N_{14}O_8Co_2Br_2$: C, 44.54 (44.19); H, 4.76 (4.75); N, 16.52 (16.36)%.

[(L7O)Ni]$_2$(ClO$_4$)$_2$·2DMF (8). This complex was synthesized following the same method used for the corresponding Co complexes, using $Ni(ClO_4)_2 \cdot 6H_2O$ as the metal precursor. X-ray quality crystals were grown from DMF/ether, (62%). *Anal.* Calc. (Found) for $C_{44}H_{56}N_{14}O_{16}Ni_2Cl_2$: C, 43.13 (43.38); H, 4.61 (4.78); N, 16.00 (16.09)%.

[pz$^{Me,\,CONHCH_3}$PyCoBr]$_2$·DMF (9). This complex was prepared by gentle warming of a pyridine solution of **7**. Upon cooling blue–green crystals of the title complex appeared which where characterized solely by X-ray crystallography.

2.3. Physical methods

Elemental analyses were obtained from Quantitative Technologies, Inc., White house, NJ. All samples were dried in vacuo prior to analysis. The presence of solvates was corroborated by FTIR, ^{1}H NMR or X-ray crystallography. ^{1}H and ^{13}C NMR spectra were collected on a Varian UNITY INOVA 400 MHz NMR spectrometer. Chemical shifts are reported in ppm relative to an internal standard of TMS. The ^{13}C quaternary carbon peaks that are not observed are a result of either poor solubility and/or overlapping signals. Electrospray mass spectra (ESI-MS) were recorded on a Finnigan LCQ ion-trap mass spectrometer equipped with an ESI source (Finnigan MAT, San Jose, CA). A gateway PC with Navigator software version 1.2 (Finnigan Corp., 1995–1997), was used for data acquisition and plotting. Isotope distribution patterns were simulated using the program IsoPro 3.0. IR spectra were recorded as KBr disks or in solution on a Perkin–Elmer Spectrum One FTIR spectrometer equipped with a Dell Optiplex PC. Electronic spectra were recorded using a Cary 50 spectrophotometer.

2.4. X-ray crystallography

Crystal, data collection, and refinement parameters for **1** and **5**, **6**, **8** and **9** are given in Table 1. Crystals of all complexes were sealed in thin-walled quartz capillaries, mounted on either Siemens P4 diffractometer with a sealed-tube Mo X-ray source ($\lambda = 0.71073$ Å) controlled via PC computer (data collected at 293 K) or a Nonius Kappa CCD diffractometer (data collected at 153 K). For the Siemens system automatic searching (Siemens XSCANS 2.1), centering, indexing, and least-squares routines were carried out for each crystal with at least 25 reflections in the range, $20° \leqslant 2\theta \leqslant 25°$ used to determine the unit cell parameters. During the data collection, the intensities of three representative reflections were measured every 97 reflections, and any decay observed was empirically corrected for by the software during data processing. We thank Dr. Vincent Lynch, Department of Chemistry University of Texas at Austin for data collection on the CCD diffractometer. The structures were all solved using direct methods or via the Patterson function, completed by subsequent difference Fourier syntheses, and refined by full-matrix least-squares procedures on F^2. All non-hydrogen atoms were refined with anisotropic displacement coefficients with hydrogens treated as idealized contributions using a riding model except were noted. All software and sources of the scattering factors are contained in the SHELXTL 5.0 program library (G. Sheldrick, Siemens XRD, Madison WI). Detailed crystallographic data including complete bond distances and angles for **1**, **5**, **6**, **8**, and **9** are on deposit at the CCDC as numbers CCDC 210363–210367.

3. Results and discussion

3.1. Ligand synthesis and characterization

The synthesis, in multigram quantities, of the ester-substituted heteroscorpionate ligands designated L6OH and L9OH (Fig. 1) required only two steps. The initial step involved treatment of two equivalents of 3-methyl-5-carboxyethyl)pyrazole with phosgene in THF in the presence of triethylamine as an acid scavenger to give di(3-methyl-5-carboxyethylpyrazolyl) ketone. Reaction of one equivalent of the ketone with an equivalent of the appropriate salicylaldehyde, either as a solution in dry DMF or as a melt, in the presence of 1% anhydrous $CoCl_2$ gave, after standard workup, the desired heteroscorpionate ligands. Conversion of the ester ligand L6OH to the amide ligand L7OH used a transamidation reaction in THF employing a large excess of methylamine and tetrabutylammonium cyanide as a catalyst. The desired product complex precipitated from solution after 72 h of reaction at 50 °C. A generally minor contaminant, but which in one case was the major product, was the unsymmetrical mixed ester-amide ligand designated L8OH. However as a reliable synthesis for this species was not forthcoming it was not pursued further. Attempts to prepare the corresponding 5-carboxyamido substituted ligand from L9OH were unsuccessful.

In addition to the standard methods for structure verification (elemental analysis, ^{1}H and ^{13}C NMR etc.) ligand L6OH was characterized by X-ray crystallography. The structure of L6OH revealed the presence of a unique and strongly hydrogen bonded water molecule in the crystal lattice. The hydrogen atoms of the water

Table 1
Summary of crystallographic data and parameters for $[L6OH]\cdot H_2O$ (**1**), $[L9OHCoBr_2]\cdot CH_2Cl_2$ (**5**), $[L7OCo]_2(BF_4)_2\cdot 2DMF$ (**6**), $[L7ONi]_2(ClO_4)_2\cdot 2DMF$ (**8**), $[pz^{Me,CONHCH_3}PyCoBr]_2\cdot DMF$ (**9**)

	1	**5**	**6**	**8**	**9**
Molecular formula	$C_{21}H_{26}N_4O_6$	$C_{25}H_{30}Br_2Cl_2N_4O_5Co$	$C_{25}H_{35}BN_8O_5F_4Co$	$C_{25}H_{32}ClN_8O_9Ni$	$C_{25}H_{33}Br_2N_9O_3Co_2$
Formula weight	430.46	756.18	673.33	682.72	785.28
Temperature (K)	293(2)	293(2)	293(2)	293(2)	293(2)
Crystal system	monoclinic	monoclinic	monoclinic	monoclinic	triclinic
Space group cell constants	$P2_1/n$	$P2_1/n$	$P2_1/c$	$P2_1/n$	$P\bar{1}$
a (Å)	8.720(3)	17.498(5)	9.537(2)	9.504(12)	9.434(2)
b (Å)	20.152(2)	11.559(2)	12.675(3)	12.608(2)	12.329(2)
c (Å)	12.936(2)	17.615(3)	26.620(5)	26.666(3)	15.230(3)
α (°)	90	90	90	90	70.68(8)
β (°)	97.04(3)	111.41(2)	97.751(8)	97.477(7)	77.78(2)
γ (°)	90	90	90	90	83.55(2)
Z	4	4	4	4	2
V (Å^3)	2256.1(8)	3317.1(12)	3188.5(12)	3168.4(8)	1632.1(6)
Absorption coefficient μ_{calc} (mm^{-1})	0.094	3.125	0.843	0.725	3.505
δ_{cal} (g/cm^3)	1.267	1.514	1.430	0.865	1.598
$F(0\,0\,0)$	912	1516	1413	880	788
Crystal dimensions (mm)	$0.5\times0.5\times0.6$	$0.6\times0.6\times0.3$	$0.6\times0.6\times0.5$	$0.6\times0.6\times0.6$	$1.0\times0.4\times02$
Radiation	Mo Kα ($\lambda = 0.71073$ Å)	Mo Kα ($\lambda = 0.71073$ Å)	Mo Kα ($\lambda = 0.71073$ Å)	Mo Kα ($\lambda = 0.71073$ Å)	Mo Kα ($\lambda = 0.71073$ Å)
h, k, l ranges collected	$0\to9$, $-21\to0$, $-13\to13$b	$0\to18$, $-12\to0$, $-18\to19$	$-11\to0$, $0\to15$, $-31\to31$	$-10\to0$, $-13\to0$, $-28\to28$	$0\to10$, $-12\to12$, $-16\to16$
Range (°)	1.88–22.49	2.06–23.03	1.78–25.00	3.17–26.30	1.75–22.50
Number of reflections collected	3137	4485	5912	4391	4464
Number of unique reflections	2916	4296	5556	4106	4158
Number of parameters	289	372	397	410	365
Data/parameters ratio	10.08	11.53	13.91	9.92	11.38
Refinement method	full-matrix least-squares of F^2	full-matrix least-squares of F^2	full-matrix least-squares of F^2	full-matrix least-squares of F^2	full-matrix least-squares of F^2
$R(F)$[a]	0.0743	0.0675	0.0591	0.0535	0.0405
$R_w(F^2)$[b]	0.1769	0.1741	0.1611	0.1378	0.0983
Goodness-of-fit w[c]	1.035	1.035	1.062	1.065	1.055
Largest difference peak and hole (e Å^3)	0.237 and −0.288	0.939 and −0.472	0.539 and −0.415	0.382 and −0.769	0.906 and −0.445

[a] $R = [\sum|\Delta F|/\sum|F_o|]$.
[b] $R_w = \left[\sum w(\Delta F)^2/\sum wF_o^2\right]$.
[c] Goodness-of-fit on F^2.

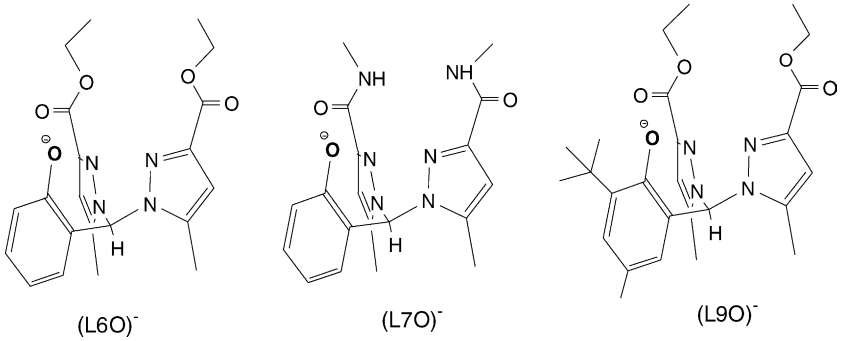

Fig. 1. Ligands used in this study.

molecule (Fig. 2) made a pair of bifurcated hydrogen bonds through O1 and N1 and O2 and N2 on one ligand molecule while the water oxygen atom was H-bonded to the protonated phenolic group on a second. Dissolving the crystals used for X-ray diffraction in $CDCl_3$ revealed the presence of an unexpected sharp peak

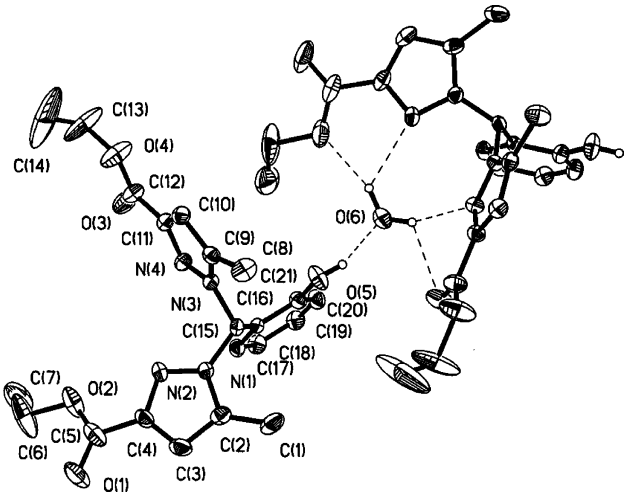

Fig. 2. ORTEP diagram of L6OH · H_2O (**1**), showing complete atomic labeling and hydrogen bonding interactions between the ligand and the water of crystallization. Thermal ellipsoids are at the 30% probability level.

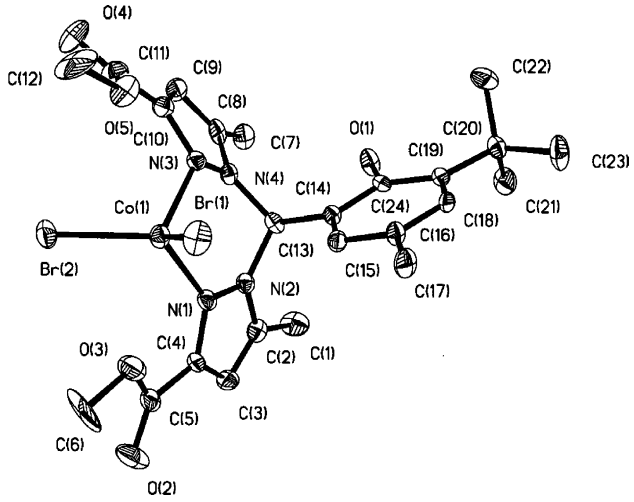

Fig. 3. ORTEP diagram of **5** showing complete atomic labeling. Thermal ellipsoids are at the 30% probability level.

integrating for two protons at 0.055 ppm. This peak was absent in crystals that had been dried under vacuum. If it corresponds to the unique water seen in the X-ray structure remains to be determined.

3.2. Metal complex chemistry

Despite our hopes that the hydrogen bond accepting ester-substituted heteroscorpionate ligands would stabilize interesting new complexes such as those we characterized for the homoscorpionate Tp analogs, such species were not forthcoming. In general the phenolate group proved to be a poor donor for divalent metals such as Ni, Co or Zn and the only species we could structurally characterize even in the presence of base designed to deprotonate the phenolate oxygen, were protonated, tetrahedral, dihalo complexes of which **5** (Fig. 3) is a representative example. No evidence for any hydrogen bonding interactions stabilized by the appended ester groups was evident.

We next turned our attention to the amide containing ligand L7OH. In this case treatment of a solution of the anion of the ligand (prepared by deprotonation of the phenol with KH in DMF) with the bromide, tetrafloroborate or perchlorate salts of Co(II), Ni(II) or Zn(II) produced a series of highly crystalline, isostructural complexes of the type shown in Fig. 4 for **6**. These dinuclear complexes of stoichiometry M_2L_2 have the ligand functioning in an unexpected pentadentate fashion rather than the more usual tridentate mode. In this mode, one pyrazole nitrogen and one amide carbonyl oxygen from each or the two ligands bind to metal with the phenolate oxygens functioning as a bridges to a second metal center. Each metal is thus six coordinate overall with M···M distances on the order of 3.0 Å.

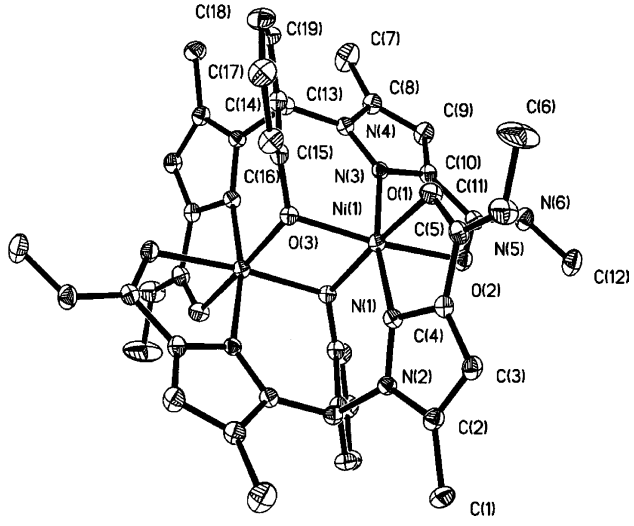

Fig. 4. ORTEP diagram for the cationic portion of **6** showing the atomic labeling for the crystallographically unique half of the molecular dimer. Thermal ellipsoids are at the 30% probability level.

In an initial attempt to grow larger crystals we uneventfully recrystallized both the tetrafloroborate and perchlorate salts of the Co(II) complex from DMF/pyridine. However upon gentle heating of the bromide salt there was a color change from purple to greenish-blue during which time the complex dissolved. Upon slow cooling crystals reappeared which were different from those of the starting complex. X-ray crystallography showed them to be that of the dinuclear 4 + 6 decomposition product **9** (Fig. 5) where the C–N bond between the pyrazole and the bridgehead carbon has been broken. In this structure one Co(II) is tetrahedrally coordinated to two bromides and a pyrazole nitrogen from each of two different 3-methyl-5-carboxamidopyrazole ligands. The second Co(II) is six coordinate with

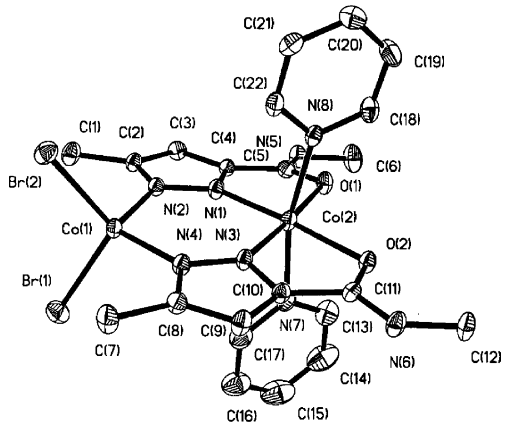

Fig. 5. ORTEP diagram for the decomposition product **9** showing complete atomic labeling. Thermal ellipsoids are at the 30% probability level.

each of the two pyrazoles functioning as bidentate ligand coordinating through a second pyrazole N and the amide carbonyl. The fifth and sixth axial coordination sites are filled by two pyridine nitrogens from the solvent. Bromide clearly plays a part in driving the decomposition reaction as the perchlorate and tetrafloroborate salts do not show this behavior unless bromide is added to the reaction mixture. No reaction takes place (as monitored by paramagnetic NMR spectroscopy) until the reaction mixture is heated. In the absence of pyridine an analogous DMF adduct is obtained showing that its presence is not required for reaction.

4. Conclusions

Several new heteroscorpionate ligands containing either appended hydrogen bond donating or accepting residues have been synthesized and characterized. Although the few metal complexes that we have examined thus far do not show the interesting intra or intermolecular hydrogen bonding interactions we were looking for, our exploration of their potentially rich coordination chemistry continues.

5. Supplementary information

Complete crystallographic data for compounds **1**, **5**, **6**, **8**, and **9**. These data under accession numbers CCDC 210363–210367, can be obtained free of charge from The Director, CCDC, 12 Union Road, Cambridge CB2 1EZ, UK (fax: +44-1223-336033; E-mail: deposit@ccdc.cam.ac.uk or www: http://www.ccdc.cam.ac.uk).

Acknowledgements

This work was supported in part by Grants AI-1157 from the Robert A. Welch Foundation and CHE-0202535 from the NSF. The NSF-ILI program Grant USE-9151286 is acknowledged for partial support of the X-ray diffraction facilities at Southwest Texas State University. We thank Dr. Vincent Lynch, Department of Chemistry, University of Texas at Austin for the data collection of **3–5** on the Nonius Kappa CCD diffractometer.

References

[1] S. Trofimenko, Chem. Rev. 93 (1993) 943.
[2] T.C. Higgs, C.J. Carrano, Inorg. Chem. 36 (1997) 298.
[3] B.S. Hammes, C.J. Carrano, Inorg. Chem. 38 (1999) 4593 (references therein).
[4] Z. Shirin, B.S. Hammes, V.G. Young, A.S. Borovik, J. Am. Chem. Soc. 122 (2000) 1836.
[5] L.M. Berreau, R.A. Allred, M.M. Makowska-Grzyska, A.M. Arif, Chem. Commun. (2000) 1423.
[6] L.E. Cheruzel, J. Wang, M.S. Mashuta, R.M. Buchanan, Chem. Commun. (2002) 2166.
[7] M. Matsu-ura, F. Tani, S. Nakayama, N. Nakamura, Y. Naruta, Angew. Chem. 39 (2000) 1989.
[8] B.S. Hammes, X. Luo, B.S. Chohan, M.W. Carrano, C.J. Carrano, J. Chem. Soc., Dalton Trans. (2002) 3374.
[9] B.S. Hammes, M.W. Carrano, C.J. Carrano, J. Chem. Soc., Dalton Trans. (2001) 1448.
[10] R.N. Armstrong, Biochemistry 39 (2000) 13625.

Available online at www.sciencedirect.com
SCIENCE DIRECT®
Polyhedron 23 (2004) 245–251
POLYHEDRON
www.elsevier.com/locate/poly

Complexes bearing an enantiopure N,N,O scorpionate ligand derived from (−)-menthone

Liv Peters, Nicolai Burzlaff *

Fachbereich Chemie der Universität Konstanz, Universitätsstraße 10, Fach M728, D-78457 Konstanz, Germany

Received 15 May 2003; accepted 12 August 2003

Abstract

Starting from (−)-menthone an enantiopure chiral tripod ligand is obtained via C_2 symmetric bis(menthylpyrazol-1-yl)methane bpm^{4menth} (**2c**) by introducing a carboxylate donor at the bridging carbon atom. A prochiral centre but no additional stereo centre is formed at this carbon atom resulting in a homochiral tripod ligand bpa^{4menth}H (**3**). As first examples, the complexes [Ru(bpa^{4menth})Cl(PPh$_3$)$_2$] (**4**), [Mn(bpa^{4menth})(CO)$_3$] (**5**) and [Re(bpa^{4menth})(CO)$_3$] (**6**) bearing this enantiopure scorpionate ligand were synthesized. Single-crystal X-ray structure analyses of bpm^{4menth} (**2c**), bpa^{4menth}H (**3**) and [Re(bpa^{4menth})(CO)$_3$] (**6**) are reported, too.
© 2003 Elsevier Ltd. All rights reserved.

Keywords: Scorpionate ligands; Tripod ligands; Chirality; Prochirality; Menthone

1. Introduction

Bis(pyrazol-1-yl)acetic acids which represent a new class of "heteroscorpionate" ligands have attracted in recent years an increasing interest. These ligands, which were introduced to coordination chemistry by A. Otero in 1999 [1], are related to the tris(pyrazol-1-yl)methane system, where one of the pyrazolyl groups has been replaced by a carboxylate. Two different synthetic routes for the syntheses of these ligands have been established so far: (a) Deprotonation of bis(pyrazol-1-yl)methanes at the methylene group with *n*-BuLi followed by reaction with carbon dioxide yields lithium salts of the bis(pyrazol-1-yl)acetates. These can either be used directly for further reactions [1] or after acidic workup be isolated as bis(pyrazol-1-yl)acetic acids [2]. This synthetic route is restricted to bis(pyrazol-1-yl)methanes bearing substituents in position 5 of the pyrazol-1-yl groups, since otherwise the deprotonation would take place at this position [3]. (b) In an alternative route dibromoacetic acid reacts under phase transfer conditions with base and unsubstituted pyrazole or 3,5-dimethylpyrazole to the bis(pyrazol-1-yl)acetates. After an acidic workup the targeted bis(pyrazol-1-yl)acetic acids are obtained, namely bis(pyrazol-1-yl)acetic acid (bpzaH) and bis(3,5-dimethylpyrazol-1-yl)acetic acid (bdmpzaH) [2,4].

The coordination chemistry of various bis(pyrazol-1-yl)acetato ligands has been exploited for several transition metals. Examples out of group 4 [5], group 5 [1], group 6 [6], group 7 [4,7], group 8 [2,8,9], group 11 [10] and group 12 [2,11,12] have been published so far. Recent reports focused on chiral though racemic examples out of the class of bis(pyrazol-1-yl)acetato tripod ligands [1c,11]. Usually the chirality originates from two different pyrazolyl donor groups, that are bound to the acetic acid, e.g. (3,5-di-*tert*-butylpyrazol-1-yl)(3′,5′-dimethylpyrazol-1-yl)acetic acid (bpa^{tBu2,Me2}H) (Fig. 1(a)) [11]. [1]

* Corresponding author. Tel.: +49-7531-88-2053; fax: +49-7531-88-3136.
E-mail address: nicolai@chemie.uni-konstanz.de (N. Burzlaff).

[1] To avoid extraordinary long abbreviations the abbreviation system for Tp and benzopyrazolylborates Tp^{Bo} ligands introduced by S. Trofimenko was transferred to this problem. A superscript of 3 or 4 preceding "menth" indicates a 3,4- or 4,5-fusion of the menthyl group to the pyrazole. This resulted in the abbreviations bpa^{tBu2,Me2}H, bpm^{4menth} (2c), bpa^{4menth}H (3) and bpa^{4menth} for the anion of **3**. Following these rules bis(camphorpyrazol-1yl)acetic acid is now abbreviated as bpa^{4cam}H instead of bpa^{cam2}H, as we did in a former publication [9]. For further details see: S. Trofimenko, Scorpionates – The Coordination Chemistry of Polypyrazolylborate Ligands, Imperial College Press, London (1999) pp. 5.

0277-5387/$ - see front matter. © 2003 Elsevier Ltd. All rights reserved.
doi:10.1016/j.poly.2003.11.038

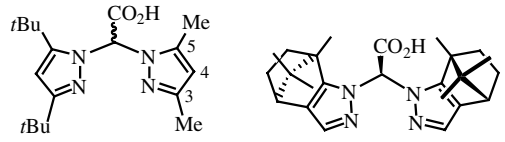

(a) *rac* bpa$^{t\mathrm{Bu2,Me2}}$H **(b)** (+)-bpa$^{4\mathrm{cam}}$H

Fig. 1. Chiral tripod ligands.

For asymmetric induction enantiomers have to be separated, and the enantiomeric purity has to be validated. Such a separation of enantiomers often is an elaborate, low-yield process. In addition a stable configuration of the stereogenic centres has to be assured. If one of the donor groups is chiral and enantiopure or derived from the *chiral pool*, the problem is converted into a separation job of diastereomers, but still elaborate. To overcome these problems, we introduced a general concept to obtain new enantiopure facially binding tripod ligands from C_2 symmetric precursors. Recently we presented a first example for this concept derived from (+)-camphor (Fig. 1(b)) [9]. We now wish to report on a second example derived from (−)-menthone.

2. Results and discussion

Many chiral bidentate ligands exhibit C_2 symmetry as a common feature [13]. If the C_2 axis of such a ligand goes through a tetrahedral bridging atom connecting two identical enantiopure donor groups Y*, any additional group Z at this atom will cause no additional stereo centre, but a prochiral centre (Fig. 2(a)) [14]. (*S*, *S*)-Trihydroxyglutaric acid is an often cited textbook example for such a prochiral compound [14]. Inversion of configuration at C3 in (*S*, *S*)-trihydroxyglutaric acid (Fig. 2(b)) yields the identical compound.

Therefore, enantiopure tripod ligands can be obtained from C_2 symmetric precursors in a direct synthesis by applying this concept. No additional separation of enantiomers or diastereomers is necessary. As a first example for this concept, we recently reported on bis(camphorpyrazol-1-yl)acetic acid (bpa$^{4\mathrm{cam}}$H) (Fig. 1(b)), its direct synthesis in four steps starting from (+)-camphor and its coordination properties as an enantiopure scorpionate ligand [9], 1. In enantiomerically pure C_3 symmetric tripod ligands often pyrazoles derived from (−)-menthone are used instead of camphorpyrazolyl groups [15,16]. Therefore, we took an interest in a C_2 symmetric bis(menthylpyrazol-1-yl)methane reported by Togni and Venanzi [17]. Three structural isomers of bis(menthylpyrazol-1-yl)methane (**2a**, **2b** and **2c**) are formed by coupling of (2*R*, 5*R*)-menthylpyrazole **1** with CH_2Cl_2 in a two-phase system [17]. A reaction with CH_2Cl_2 as reactant and only solvent is higher in yield compared to the two-phase procedure by Togni and Venanzi. All three structural isomers can be separated by column chromatography and additional crystallisation steps. Crystallisation from pentane afforded colourless crystals of bpm$^{4\mathrm{menth}}$ (**2c**). A single-crystal X-ray diffraction experiment proves the desired constitution of **2c** (Fig. 3).

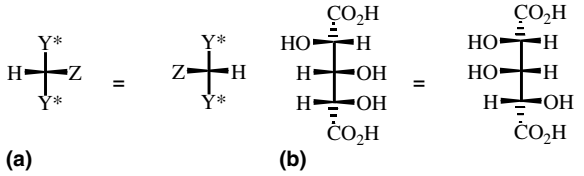

Fig. 2. Prochiral centre of (*S*, *S*)-trihydroxyglutaric acid [14].

By analogy to Otero's synthesis of bis(3,5-dialkylpyrazol-1-yl)acetic acids [1], deprotonation at the bridging carbon atom and subsequent reaction with carbon dioxide introduces a carboxylate group at this position. As mentioned above, the structural isomer bpm$^{3\mathrm{menth}}$ (**2a**) would be deprotonated also at the pyrazolyl C5 by *n*-BuLi, due to missing substituents here [3]. Therefore, only isomer **2c** out of the two C_2 symmetric isomers **2a** and **2c** can be used for this reaction sequence. Acidic workup yields the enantiopure bis(menthylpyrazol-1-yl)acetic acid bpa$^{4\mathrm{menth}}$H (**3**) (Scheme 1).

For the (2*R*, 5*R*)-menthylpyrazolyl groups two sets of signals are found in the ^{1}H and ^{13}C NMR spectra. A strong IR band at 1759 cm^{-1} and a ^{1}H NMR signal at 13.05 ppm indicate the carboxylate group. Crystals of **3** suitable for X-ray structure determination were obtained from CH_3CN (Fig. 4, Tables 1 and 2). Bond distances and bond angles of **3** are in good agreement with those reported earlier for chiral bis(camphorpyrazol-1-yl)acetic acids bpa$^{4\mathrm{cam}}$H [9].

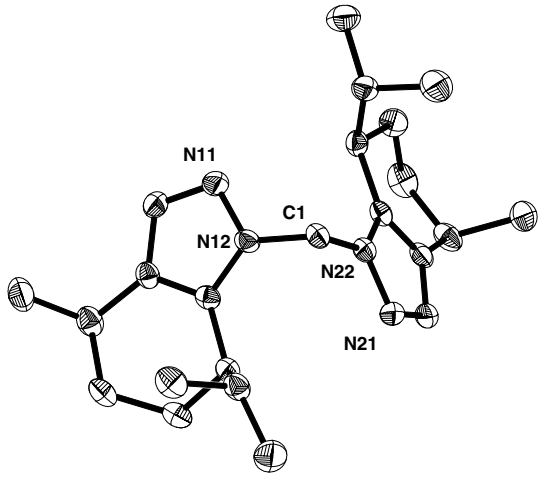

Fig. 3. Molecular structure of bpm$^{4\mathrm{menth}}$ (**2c**); thermal ellipsoids at 50% probability level.

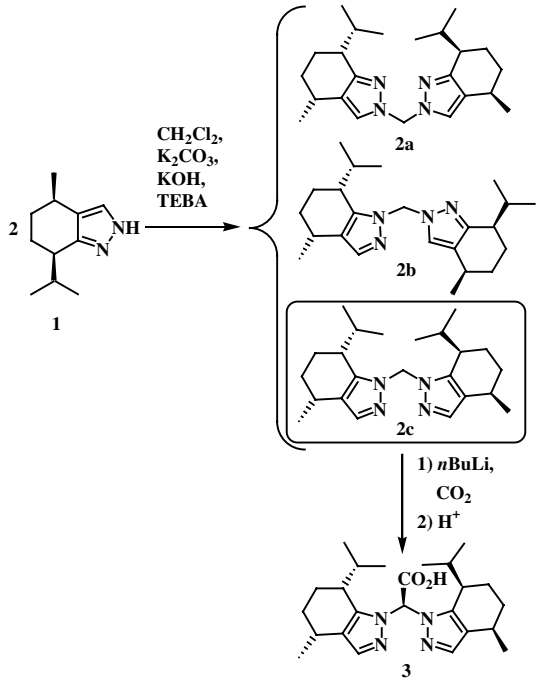

Scheme 1. Synthesis of bis(menthylpyrazol-1-yl)acetic acid.

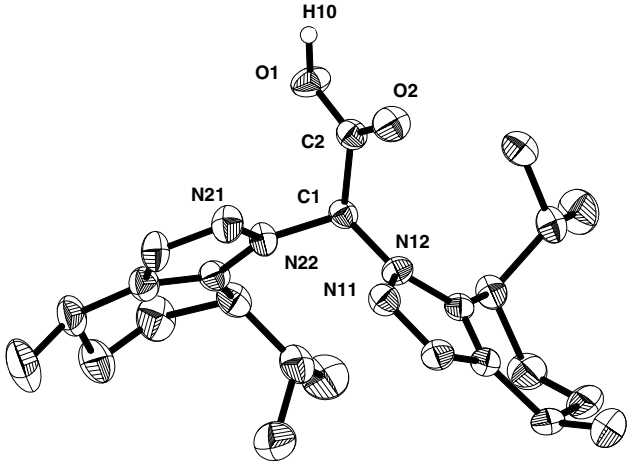

Fig. 4. Molecular structure of bpa^{4menth}H (**3**); thermal ellipsoids at 50% probability level.

Bis(pyrazol-1-yl)acetato ligands are tripodal ligands that are as useful in coordination and organometallic chemistry as hydrido(trispyrazol-1-yl)borate (Tp) and its analogues [4]. As an example we reported recently the formation of the ruthenium complexes [Ru(L)Cl(PPh$_3$)$_2$] (L = bpza, bdmpza, bpa^{4cam}) by reaction of the potassium carboxylates with [RuCl$_2$(PPh$_3$)$_3$] [8,9]. A similar reaction of the potassium salt of bpa^{4menth}H (**3**) with [RuCl$_2$(PPh$_3$)$_3$] yields [Ru(bpa^{4menth})Cl(PPh$_3$)$_2$] (**4**) (Scheme 2). An asymmetric carboxylate IR signal $\nu_{as} = 1670$ cm^{-1} and the MH$^+$ = 1071 peak in the FAB mass spectrum indicate the coordination of the ligand. As in [Ru(bpa^{4cam})Cl(PPh$_3$)$_2$] [9], two sets of signals in the ^{1}H and ^{13}C NMR spectra are observed for the (2*R*, 5*R*)-menthylpyrazolyl groups. Two sets of signals in these spectra and two doublets in the ^{31}P NMR

Table 1
Selected distances of **2c, 3** and **6**

Distance (Å)	2c	3	6
O(2)–C(2)		1.202(4)	1.235(7)
O(1)–C(2)		1.325(4)	1.305(8)
C(1)–C(2)		1.544(4)	1.545(10)
C(1)–N(12)	1.457(4)	1.462(4)	1.463(7)
C(1)–N(22)	1.451(4)	1.459(4)	1.451(8)
Re–N(11)			2.160(5)
Re–N(21)			2.190(5)
Re–O(1)			2.164(5)
Re–C(3)			1.930(6)
Re–C(4)			1.910(7)
Re–C(5)			1.922(7)

Table 2
Selected angles of **2c, 3** and **6**

Angle (°)	2c	3	6
O(1)–C(2)–O(2)		127.1(3)	125.3(7)
C(2)–C(1)–N(12)		111.8(3)	111.2(5)
C(2)–C(1)–N(22)		108.1(2)	109.1(5)
N(12)–C(1)–N(22)	113.4(2)	111.6(3)	111.6(5)
N(11)–Re–N(21)			83.3(2)
O(1)–Re–N(11)			80.5(2)
O(1)–Re–N(21)			80.8(2)
C(3)–Re–C(4)			88.1(3)
C(3)–Re–C(5)			87.0(3)
C(4)–Re–C(5)			89.4(3)
O(1)–Re–C(3)			176.9(2)
N(11)–Re–C(4)			174.8(2)
N(21)–Re–C(5)			174.1(2)

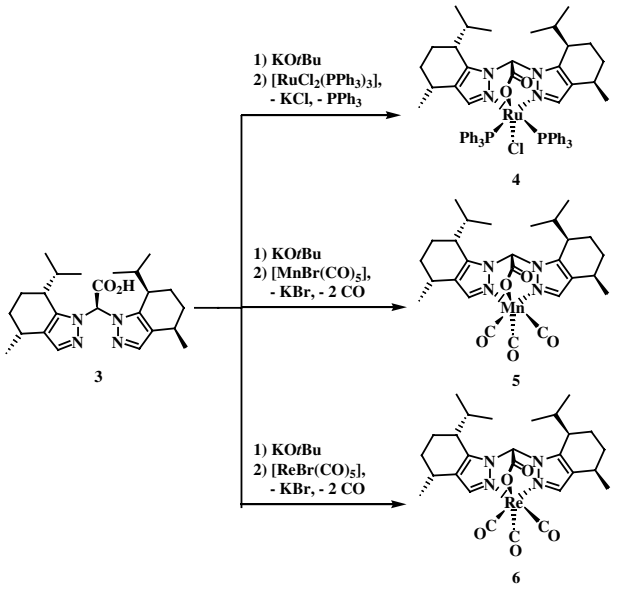

Scheme 2. Syntheses of complexes bearing bis(menthylpyrazol-1-yl)acetato ligands.

spectrum at 38.4 and 42.9 ppm ($^2J_{P,P} = 35.6$ Hz and 32.4 Hz) are reasonable for two PPh_3 ligands in a chiral environment. According to cross coupling observed in the COSY and ROESY spectra, three singlets in the ^1H NMR spectrum are assigned to the two pyrazol C(3)H protons (^1H NMR: 6.78 and 6.95 ppm; ^{13}C NMR: 142.2 and 142.8 ppm) and the bridging CH proton (^1H NMR: 6.32 ppm; ^{13}C NMR: 71.4 ppm). A rather similar distribution of these signals was observed for the symmetric ruthenium complex $[Ru(bpza)Cl(PPh_3)_2]$ [^1H NMR: 6.61 ppm ($C_{bridge}H$), 6.87 ppm ($2 \times C_{pz}(3)H$)], in which both PPh_3 ligands are *trans* to the pyrazolyl groups [8]. Therefore, a geometry with both PPh_3 ligands *trans* to the pyrazolyl groups is assumed for complex **4**.

Another example for the similarity between bis(pyrazol-1-yl)acetato ligands, Tp and Cp ligands, which we reported previously, is the formation of tricarbonyl complexes $[Mn(L)(CO)_3]$ and $[Re(L)(CO)_3]$ (L = bpza, bdmpza) starting from the pentacarbonyl complexes $[MnBr(CO)_5]$ and $[ReBr(CO)_5]$ [4]. By reaction of these pentacarbonyl complexes with potassium bis(menthylpyrazol-1-yl)acetate K[bpa^{4menth}] we were now able to obtain chiral bis(menthylpyrazol-1-yl)acetato tricarbonyl complexes [Mn(bpa^{4menth})$(CO)_3$] (**5**) and [Re(bpa^{4menth})$(CO)_3$] (**6**) (Scheme 2). K[bpa^{4menth}] was produced in situ from the acid and potassium *tert*-butylate. CO evolution was observed during the reactions, and the progress of the reactions was monitored by IR spectroscopy. The complexes **5** and **6** are rather stable and can be stored for days as solids under aerobic conditions. Asymmetric carboxylate IR signals (**5**: $\nu_{as} = 1680$ cm^{-1}, **6**: $\nu_{as} = 1685$ cm^{-1}) and MH^+ peaks in the FAB mass spectra indicate the formation of the targeted complexes. As in **4** two sets of signals in the ^1H and ^{13}C NMR spectra are observed for the (2*R*, 5*R*)-menthylpyrazolyl groups. The NMR signals of **5** are rather broad, some of its ^{13}C NMR signals are covering each other, some are not observed. The IR signals of **5** and **6** are those of unsymmetrical "piano stool" type complexes with single A_1 and two E signals each. These CO absorptions (**5**: $\nu(CO) = 2037$, 1943 and 1920 cm^{-1}, **6**: $\nu(CO) = 2025$, 1918 and 1900 cm^{-1}) are almost identical to those of the previously reported complexes $[Mn(bdmpza)(CO)_3]$ and $[Re(bdmpza)(CO)_3]$ [4]. Therefore, the electron donation properties of the bpa^{4menth} ligand are similar to those of bdmpza, which is a slightly less electron donating ligand compared to the cyclopentadienyl ligand Cp. This implies a future reactivity of **5** and **6** similar to $[MnCp(CO)_3]$ and $[ReCp(CO)_3]$. A strong, broad IR signal at 3570 cm^{-1} indicates a water adduct of **5**. This is supported by the elemental analysis of **5**, which fits to an adduct $\mathbf{5} \times 2\,H_2O$. Crystals of **6** suitable for X-ray structure determination were obtained from acetone (Fig. 5). Selected distances and angles are summarised in Tables 1 and 2

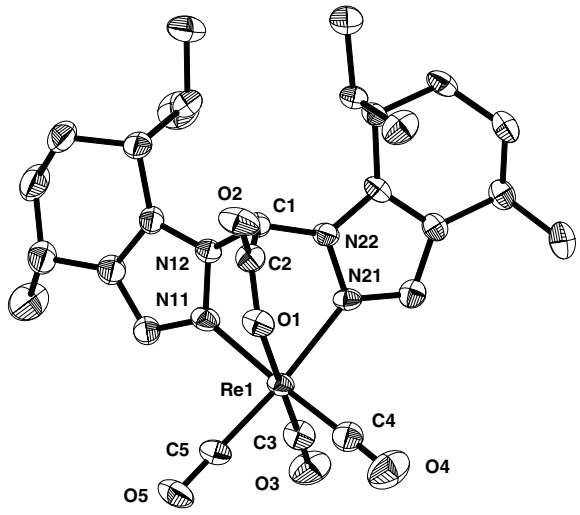

Fig. 5. Molecular structure of [Re(bpa^{4menth})$(CO)_3$] (**6**); thermal ellipsoids at 50% probability level.

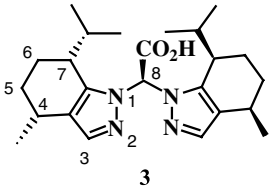

3

Fig. 6. Numbering scheme applied for the assignment of the NMR data.

(see also Fig. 6). A possible *trans* influence of the pyrazolyl acceptors onto the metal-carbonyl bonds is not indicated by the three the Re–C distances. Such a *trans* influence was reported earlier for the complexes [Re(bpza)$(CO)_3$] and [Re(bdmpza)$(CO)_3$] [4]. Nevertheless, the distances and angles of these complexes are in good agreement with those of **6**.

Our results show that new enantiopure facially binding tripod ligands can be obtained from certain C_2 symmetric precursors by adding a third donor, e.g. a carboxylate donor group, onto the bridging carbon atom. No additional stereo centre but a prochiral centre is formed. By applying this concept, a homochiral ligand is obtained by a simple separation of structural isomers (here **2a**, **2b** and **2c**). No additional separation of enantiomers or diastereomers is necessary. Future work to extend this concept will focus on the conversion of other C_2 symmetric ligands derived from the *chiral pool*.

3. Experimental

3.1. Materials

All organometallic experiments were carried out in Schlenk tubes under argon atmosphere. The solvents

were dried by standard procedures, distilled and stored under argon. $[RuCl_2(PPh_3)_3]$, $[MnBr(CO)_5]$ and $[ReBr(CO)_5]$ were prepared according to literature [18–20]. Hydrated ruthenium trichloride (35–40% Ru) was a generous gift of the Degussa AG. (−)-Menthone was used as purchased. Bpm^{4menth} (**2c**) was prepared and isolated in analogy to the procedure reported earlier by A. Togni and L. M. Venanzi [17], but with CH_2Cl_2 as solvent and reagent. **2c** was separated from a crude mixture of **2a**, **2b** and **2c** (60 mmol) via column chromatography with pentane/ethyl acetate (7:2, v/v) on silica (30 cm, ∅ 9 cm). R_f (pentane/ethyl acetate, 7:2, v/v, silica 60 plate, $KMnO_4$ stain) = 0.88 (**2c**), 0.55 (**2b**) and 0.40 (**2a**).

3.2. Instrumentation

Micro crystalline precipitates were separated by filtration or centrifugation with a Hettich Rotina 46 R Schlenk tube centrifuge. IR: Biorad FTS 60, CaF_2 cuvets (0.1 mm). ^1H NMR and ^{13}C NMR: Bruker AC 250, δ values relative to TMS. ^{31}P NMR: JEOL GX 400. Two-dimensional NMR experiments: Bruker DRX 600 (Avance). EI MS and FAB MS: modified Finnigan MAT 312. Elemental analyses: Analytical Laboratory of the Fachbereich Chemie. A modified Siemens P4 diffractometer was used for X-ray structure determinations.

3.3. Ligand synthesis

*$Bpa^{4menth}H$ (**3**).* A solution of bpm^{4menth} (**2c**) (2.13 g, 5.78 mmol) in THF (50 mL) was treated with *n*-BuLi (~1.6 M in hexane, 5.50 mL, 8.80 mmol) at −70 °C. The solution was allowed to warm to −40 °C over a period of 2 h and finally flushed with a flow of CO_2 for 15 min. At ambient temperature the solvent was removed in vacuo and the residue dissolved in water (30 mL). The aqueous solution was acidified with HCl (6 M) to pH 1–2 and extracted with Et_2O (4 × 50 mL). The combined organic layers were dried (Na_2SO_4) and concentrated in vacuo to a residue. Recrystallisation from acetonitrile yielded $bpa^{4menth}H$ **(3)** as a colourless crystal powder. Crystals suitable for X-ray structure determination were obtained from a solution in acetonitrile. Yield 982 mg (41%). m.p. 139–141 °C. $[\alpha]_D^{23} = +162.2$ ($c = 0.1$ g cm^{-3}, CH_2Cl_2). ^1H NMR (400 MHz, $CDCl_3$): $\delta = 0.69$ (d, $^3J_{H,H} = 7.0$ Hz, 3 H, CH_3), 0.86 (d, $^3J_{H,H} = 6.6$ Hz, 3 H, CH_3), 1.03 (d, $^3J_{H,H} = 6.6$ Hz, 3 H, CH_3), 1.06 (d, $^3J_{H,H} = 7.0$ Hz, 3 H, CH_3), 1.17 (d, $^3J_{H,H} = 7.1$ Hz, 3 H, CH_3), 1.23 (d, $^3J_{H,H} = 7.0$ Hz, 3 H, CH_3), 1.30–1.85 (m, 8 H, H5, H5′, H6, H6′), 1.90, 2.25 (m, 2 H, CH*i*Pr, CH*i*Pr′), 2.40–2.90 (m, 4 H, H4, H4′, H7, H7′), 6.77 (s, 1 H, CH), 7.47, 7.59 (s, 2 H, H_{pz}, H_{pz}'), 13.05 (s, br, 1 H, CO_2H). ^{13}C NMR (100.6 MHz, $CDCl_3$): δ = 18.4, 19.5, 21.0, 21.1, 21.3, 21.4 (6 × CH_3), 21.7, 23.3 (C6, C6′), 26.7, 26.8 (C4, C4′), 28.5, 29.6 (C5, C5′), 31.5, 31.8 (CH*i*Pr, CH*i*Pr′), 35.7, 36.6 (C7, C7′), 70.1 (C8), 124.0, 124.7 (C_{pz}, C_{pz}'), 137.6, 139.0 (CH_{pz}, CH_{pz}'), 142.1, 143.4 (C_{pz}, C_{pz}'), 165.3 (CO_2H). EI MS (70 eV, 150 °C): *m/z* (%) = 412 (1) [M^+], 368 (12) [M^+–CO_2], 325 (3) [M^+–CO_2–*i*Pr], 191 (68) [CH_2pz^{menth}], 178 (32) [pz^{menth}], 147 (53) [CH_2pz^{menth}–*i*Pr], 135 (100) [pz^{menth}–*i*Pr]. IR (THF): $\nu = 1759$ (CO_2H) cm^{-1}. *Anal.* Calc. for $C_{24}H_{36}N_4O_2$ (412.58): C, 69.87; H, 8.79; N, 13.58. Found: C, 69.52; H, 8.69; N 13.48%.

3.4. Complex syntheses

*$[Ru(bpa^{4menth})Cl(PPh_3)_2]$ (**4**).* $Bpa^{4menth}H$ (276 mg, 0.668 mmol) in THF (30 mL) with KO*t*Bu (68 mg, 0.606 mmol) was stirred at ambient temperature for 1 h. $[RuCl_2(PPh_3)_3]$ (500 mg, 0.521 mmol) was added, and the solvent was removed in vacuo after 1 h. The residue was washed with H_2O (2 × 10 mL) and pentane (2 × 20 mL) and dried in vacuo. The residue was dissolved in Et_2O (2 mL), precipitated by adding pentane (20 mL) and filtered off to afford $[Ru(bpa^{4menth})Cl(PPh_3)_2]$ (**4**) as yellow-greenish crystal powder. Yield 245 mg (44%). m.p. 210 °C (dec.). $[\alpha]_D^{23} = +10.7$ ($c = 0.1$ g cm^{-3}, CH_2Cl_2). ^1H NMR (600 MHz, $CDCl_3$): $\delta = 0.56$ (d, $^3J_{H,H} = 6.8$ Hz, 3 H, CH_3*i*Pr), 0.79 (d, $^3J_{H,H} = 6.8$ Hz, 3 H, CH_3), 0.90 (d, $^3J_{H,H} = 6.8$ Hz, 3 H, CH_3), 0.92 (d, $^3J_{H,H} = 6.6$ Hz, 3 H, CH_3), 1.07 (d, $^3J_{H,H} = 6.8$ Hz, 3 H, CH_3), 1.09 (d, $^3J_{H,H} = 6.8$ Hz, 3 H, CH_3), 1.20–1.90 (m, 8 H, H5, H5′, H6, H6′), 2.02 (m, 2 H, CH*i*Pr, CH*i*Pr′), 2.10–3.00 (m, 4 H, H4, H4′,H7, H7′), 6.32 (s, 1 H, CH), 6.78, 6.95 (s, 2 H, H_{pz}, H_{pz}'), 7.00–7.50 (m, 30 H, PPh_3). ^{13}C NMR (150.9 MHz, $CDCl_3$): δ = 18.6, 19.2, 20.4, 21.0, 21.1, 21.7 (6 × CH_3), 21.8, 23.0 (C6, C6′), 26.3, 26.5 (C4, C4'), 27.8, 28.9 (C5, C5′), 31.6, 32.0 (CH*i*Pr, CH*i*Pr′), 35.0, 38.5 (C7, C7′), 71.4 (C8), 123.4, 123.7 (C_{pz}, C_{pz}'), 126.8 (d, $^3J_{C,P} = 8.7$ Hz, *m*-PPh_3), 126.9 (d, $^3J_{C,P} = 8.7$ Hz, *m*-PPh_3), 128.3 (s, *p*-PPh_3), 128.4 (d, $^4J_{C,P} = 1.0$ Hz, *p*-PPh_3), 134.5 (d, $^2J_{C,P} = 9.1$ Hz, *o*-PPh_3), 134.9 (d, $^2J_{C,P} = 8.8$ Hz, *o*-PPh_3), 135.2 (d, $^1J_{C,P} = 39.1$ Hz, *i*-PPh_3), 135.7 (d, $^1J_{C,P} = 38.3$ Hz, *i*-PPh_3), 142.2, 142.8 (CH_{pz}, CH_{pz}'), 143.5, 144.8 (C_{pz}, C_{pz}'), 166.2 (CO_2^-). ^{31}P NMR (161.9 MHz, $CDCl_3$): δ = 38.4 (d, $^2J_{P,P} = 35.6$ Hz), 42.9 (d, $^2J_{P,P} = 32.4$ Hz). FAB MS: *m/z* (%) = 1071 (30) [M^+], 1036 (66) [M^+–Cl], 810 (100) [MH^+–PPh_3], 775 (47) [MH^+–PPh_3–Cl]. IR (THF): $\nu = 1670$ (CO_2^-) cm^{-1}; *Anal.* Calc. for $C_{60}H_{65}ClN_4O_2P_2Ru$ (1072.67): C, 67.18; H, 6.11; N, 5.22. Found: C, 67.16; H, 6.30; N, 5.05%.

*$[Mn(bpa^{4menth})(CO)_3]$ (**5**).* $Bpa^{4menth}H$ (447 mg, 1.08 mmol) in THF (50 mL) with KO*t*Bu (121 mg, 1.08 mmol) was stirred at ambient temperature for 30 min. $[MnBr(CO)_5]$ (298 mg, 1.08 mmol) was added, the reaction mixture was heated under reflux and checked by IR on a regular basis. After 4 h the reaction was completed, and the solvent was removed in vacuo. The

residue was washed with H_2O (2×10 mL) and Et_2O (50 mL) and dried in vacuo to afford [Mn(bpa^{4menth})$(CO)_3$] (**5**) as yellow crystal powder. Yield 470 mg (79%). m.p. 235 °C (dec.). $[\alpha]_D^{23} = +88.2$ ($c = 0.1$ g cm^{-3}, CH_2Cl_2). ^{1}H NMR (250 MHz, $CDCl_3$): $\delta = 0.77$ (d, $^3J_{H,H} = 5.8$ Hz, 3 H, CH_3), 0.87 (s, br, 3 H, CH_3), 1.09 (s, br, 6 H, $2 \times CH_3$), 1.22 (d, $^3J_{H,H} = 6.4$ Hz, 3 H, CH_3), 1.29 (d, $^3J_{H,H} = 6.7$ Hz, 3 H, CH_3), 1.35–2.40 (m, 10 H, H5, H5′, H6, H6′, CH*i*Pr, CH*i*Pr′), 2.50–3.10 (m, 4 H, H4, H4′, H7, H7′), 6.32 (s, br, 1 H, CH), 7.81, 7.86 (s, 2 H, H_{pz}, H_{pz}′). ^{13}C NMR (62.9 MHz, $CDCl_3$): $\delta = 18.4$, 18.8, 20.8, 20.9 ($6 \times CH_3$), 21.4, 22.4 (C6, C6′), 26.2, 26.3 (C4,C4′), 28.3, 28.9 (C5, C5′), 31.9, 32.3 (CH*i*Pr, CH*i*Pr′), 35.6, 37.6 (C7, C7′), 69.6 (br, C8), 124.6, 124.9 (C_{pz}, C_{pz}′), 142.2, 142.3 (CH_{pz}, CH_{pz}′), 144.1, 144.3 (C_{pz}, C_{pz}′), 193.6, 194.1, 194.6 ($3 \times CO$). FAB MS (NBOH): *m*/*z* (%) = 551 (15) [MH$^+$], 467 (40) [MH$^+$–3 CO], 423 (100) [MH$^+$–3 CO–CO_2]. IR (THF): $\nu = 3570$ br (H_2O), 2037 s (C═O), 1943 s (C═O), 1920 s (C═O), 1680 (CO_2^-), 1646 w cm^{-1}. *Anal.* Calc. for $C_{27}H_{35}MnN_4O_5 \times 2\ H_2O$ (586.57): C, 55.29; H, 6.70; N, 9.55. Found: C, 55.44; H, 6.48; N, 9.50%.

*[Re(bpa^{4menth})(CO)$_3$] (**6**).* Bpa^{4menth}H (250 mg, 0.606 mmol) in THF (30 mL) with KO*t*Bu (68 mg, 0.606 mmol) was stirred at ambient temperature for 30 min. [ReBr(CO)$_5$] (246 mg, 0.606 mmol) was added, the reaction mixture was heated under reflux and checked by IR on a regular basis. After 24 h the reaction was completed, and the solvent was removed in vacuo. The residue was washed with H_2O (2×10 mL) and Et_2O (30 mL) and dried in vacuo to afford [Re(bpa^{4menth})$(CO)_3$] (**6**) as yellow crystal powder. Re-crystallisation from acetone or acetonitrile yielded pale yellow crystals suitable for X-ray structure determination. Yield 168 mg (41%). m.p. 266 °C (dec.). $[\alpha]_D^{23} = +84.9$ ($c = 0.1$ g cm^{-3}, CH_2Cl_2). ^{1}H NMR (250 MHz, $CDCl_3$): $\delta = 0.77$ (d, $^3J_{H,H} = 6.7$ Hz, 3 H, CH_3), 0.88 (d, $^3J_{H,H} = 6.7$ Hz, 3 H, CH_3), 1.08 (d, $^3J_{H,H} = 6.7$ Hz, 3 H, CH_3), 1.12 (d, $^3J_{H,H} = 7.0$ Hz, 3 H, CH_3), 1.22 (d, $^3J_{H,H} = 6.7$ Hz, 3 H, CH_3), 1.28 (d, $^3J_{H,H} = 6.7$ Hz, 3 H, CH_3), 1.35–2.35 (m, 10 H, H5, H5′, H6, H6′, CH*i*Pr, CH*i*Pr′), 2.50–3.10 (m, 4 H, H4, H4′, H7, H7′), 6.45 (s, 1 H, CH), 7.79, 7.84 (s, 2 H, H_{pz}, H_{pz}′). ^{13}C NMR (62.9 MHz, $CDCl_3$): $\delta = 18.6$, 19.1, 20.9, 21.0, 21.2, 21.5 ($6 \times CH_3$), 21.6, 22.7 (C6,

Table 3
Structure determination details of compounds **2c, 3** and **6**

	2c	**3**	**6**
Empirical formula	$C_{23}H_{36}N_4$	$C_{24}H_{36}N_4O_2 \times CH_3CN$	$C_{27}H_{35}N_4O_5Re$
Formula weight	368.56	453.62	681.79
Crystal colour/habit	colourless cube	colourless block	colourless prism
Crystal system	orthorhombic	monoclinic	orthorhombic
Space group	$P2_12_12_1$	$P2_1$	$P2_12_12_1$
a (Å)	11.127(4)	10.327(5)	9.093(4)
b (Å)	12.144(5)	9.175(4)	14.345(6)
c (Å)	15.876(7)	14.919(7)	22.482(10)
α (°)	90	90	90
β (°)	90	104.759(1)	90
γ (°)	90	90	90
V (Å^3)	2145.3(15)	1366.8(11)	2933(2)
θ (°)	2.11–25.99	2.04–26.00	2.30– 27.99
h	−13 to 0	−12 to 0	0 to 12
k	−14 to 0	−11 to 0	0 to 18
l	−19 to 0	−17 to 18	0 to 29
F(000)	808	492	1360
Z	4	2	4
μ (Mo Kα) (mm^{-1})	0.068	0.071	4.184
Crystal size (mm)	$0.4 \times 0.3 \times 0.3$	$0.5 \times 0.4 \times 0.3$	$0.5 \times 0.4 \times 0.3$
D_c (g cm^{-3})	1.141	1.102	1.544
T (K)	188(2)	188(2)	188(2)
Reflections collected	2388	2955	3964
Independent reflections	2388	2797	3964
Observed reflections ($> 2\sigma I$)	1879	2078	3669
Parameter	244	302	334
Restraints	0	1	0
Weight parameter *a*	0.0524	0.0529	0.0425
Weight parameter *b*	0.3002	0.1293	0.1122
R_1 (obs.)	0.0478	0.0486	0.0297
R_1 (overall)	0.0701	0.0779	0.0345
wR_2 (obs.)	0.1036	0.1017	0. 0719
wR_2 (overall)	0.1139	0.1150	0.0744
Difference peak/hole (e/Å^3)	0.177 and −0.218	0.171 and −0.218	1.227 and −1.135

C6′), 26.3, 26.4 (C4, C4′), 28.2, 28.9 (C5, C5′), 32.1, 32.9 (CH*i*Pr, CH*i*Pr′), 35.8, 37.9 (C7, C7′), 70.8 (C8), 125.1, 125.4 (C_{pz}, C_{pz}'), 143.1, 143.2 (CH_{pz}, CH'_{pz}), 144.3, 144.7 (C_{pz}, C_{pz}'), 163.9 (CO_2^-), 195.5, 195.6, 196.3 (3 CO). FAB MS (NBOH): *m/z* (%) = 1362 (8) [M_2^+], 682 (100) [MH^+], 637 (20) [M^+–CO_2], 609 (37) [M^+–CO_2–CO]. IR (THF): $\nu = 2025$ (C≡O), 1918 (C≡O), 1900 (C≡O), 1685 (CO_2^-) cm^{-1}. *Anal.* Calc. for $C_{27}H_{35}N_4O_5Re$ (681.80): C, 47.56; H, 5.17; N, 8.22. Found: C, 47.12; H, 5.28; N, 8.23%.

3.5. X-ray crystal structure and analysis

Single crystals of **2c**, **3** and **6** were mounted with Paratone N on glass fibres. A modified Siemens P4 diffractometer was used for data collection (graphite monochromator, Mo K_α radiation, $\lambda = 0.71073$ Å, scan rate 4–30° min^{-1} in ω). The structures were solved and refined using the SHELX-97 program package (refined with full-matrix least-squares against F^2) [21]. A weighting scheme was applied in the last steps of the refinement with $w = 1/[\sigma^2(F_o^2) + (aP)^2 + bP]$ and $P = [2F_c^2 + \mathrm{Max}(F_o^2, 0)]/3$. Hydrogen atoms were included in their calculated positions and refined in a *riding model*. One molecule CH_3CN co-crystallised per asymmetric unit in **3**. The carboxylate proton of **3** was found and refined isotropically. All details and parameters of the measurements are summarised in Table 3. Structure pictures were prepared with the program Diamond 2.1e [22].

4. Supplementary data

Crystallographic data (excluding structure factors) for the structures reported in this paper have been deposited with the Cambridge Crystallographic Data Centre as supplementary publication no. CCDC-210441 (bpm^{4menth}) (**2c**), CCDC-210441 ($bpa^{4menth}H \times CH_3CN$) (**3** × CH_3CN), and CCDC-210443 [$Re(bpa^{4menth})(CO)_3$] (**6**). These data can be obtained free of charge via www.ccdc.cam.ac.uk/conts/retrieving.html (or from the Cambridge Crystallographic Data Centre CCDC, 12 Union Road, Cambridge CB2 1EZ, UK; fax: (+44)1223-336-033; or e-mail: deposit@ccdc.cam.ac.uk).

Acknowledgements

This work has been supported by the Fonds der Chemischen Industrie (Liebig-Stipendium to N.B.) and the Deutsche Forschungsgemeinschaft (DFG Project BU 1223/2). Special thanks to Prof. Dr. H. Fischer for support and discussion.

References

[1] (a) A. Otero, J. Fernández-Baeza, J. Tejeda, A. Antiñolo, F. Carrillo-Hermosilla, E. Díez-Barra, A. Lara-Sánchez, M. Fernández-López, M. Lanfranchi, M.A. Pellinghelli, J. Chem. Soc., Dalton Trans. (1999) 3537;
(b) A. Otero, J. Fernández-Baeza, J. Tejeda, A. Antiñolo, F. Carrillo-Hermosilla, E. Díez-Barra, A. Lara-Sánchez, M. Fernández-López, J. Chem. Soc., Dalton Trans. (2000) 2367;
(c) A. Otero, J. Fernández-Baeza, A. Antiñolo, J. Tejeda, A. Lara-Sánchez, L. Sánchez-Barba, M.T. Expósito, A.M. Rodríguez, J. Chem. Soc., Dalton Trans. (2003) 1614.
[2] A. Beck, B. Weibert, N. Burzlaff, Eur. J. Inorg. Chem. (2001) 521.
[3] A. Antiñolo, F. Carrillo-Hermosilla, E. Díez-Barra, J. Fernández-Baeza, M. Fernández-López, A. Lara-Sánchez, A. Moreno, A. Otero, A.M. Rodriguez, J. Tejeda, J. Chem. Soc., Dalton Trans. (1998) 3737.
[4] N. Burzlaff, I. Hegelmann, B. Weibert, J. Organomet. Chem. 626 (2001) 16.
[5] (a) A. Otero, J. Fernández-Baeza, A. Antiñolo, F. Carrillo-Hermosilla, J. Tejeda, E. Díez-Barra, A. Lara-Sánchez, L. Sánchez-Barba, I. López-Solera, M.R. Ribeiro, J.M. Campos, Organometallics 20 (2001) 2428;
(b) A. Otero, J. Fernández-Baeza, A. Antiñolo, F. Carrillo-Hermosilla, J. Tejeda, A. Lara-Sánchez, L. Sánchez-Barba, M. Fernández-López, I. López-Solera, Inorg. Chem. 41 (2002) 5193.
[6] B. Schwenzer, J. Schleu, N. Burzlaff, C. Karl, H. Fischer, J. Organomet. Chem. 641 (2002) 134.
[7] N. Burzlaff, I. Hegelmann, Inorg. Chim. Acta 329 (2002) 147.
[8] A. López-Hernández, R. Müller, H. Kopf, N. Burzlaff, Eur. J. Inorg. Chem. (2002) 671.
[9] I. Hegelmann, N. Burzlaff, Eur. J. Inorg. Chem. (2003) 409.
[10] B. Kozlëar, P. Gamez, R. de Gelder, W.L. Driessen, J. Reedijk, Eur. J. Inorg. Chem. (2003) 47.
[11] I. Hegelmann, A. Beck, C. Eichhorn, B. Weibert, N. Burzlaff, Eur. J. Inorg. Chem. (2003) 339.
[12] (a) J.N. Smith, Z. Shirin, C.J. Carrano, J. Am. Chem. Soc. 125 (2003) 868;
(b) B.S. Hammes, M.T. Kieber-Emmons, J.A. Letizia, Z. Shirin, C.J. Carrano, L.N. Zakharov, A.L. Rheingold, Inorg. Chim. Acta 346 (2003) 227.
[13] Review on C_2 symmetry: J.K. Whitesell, Chem. Rev. 89 (1989) 1581.
[14] H. Hirschmann, K.R. Hanson, Tetrahedron 30 (1974) 3649.
[15] (a) D.D. LeCloux, W.B. Tolman, J. Am. Chem. Soc. 115 (1993) 1153;
(b) D.D. LeCloux, C.J. Tokar, M. Osawa, R.P. Houser, M.C. Keyes, W.B. Tolman, Organometallics 13 (1994) 2855.
[16] C. Moberg, Angew. Chem., Int. Ed. Engl. 37 (1998) 249.
[17] M. Bovens, A. Togni, L.M. Venanzi, J. Organomet. Chem. 451 (1993) C28.
[18] P.S. Hallman, T.A. Stephenson, G. Wilkinson, Inorg. Synth. 12 (1970) 237.
[19] E.W. Abel, G. Wilkinson, J. Chem. Soc. (1959) 1501.
[20] D. Vitali, F. Calderazzo, Gazz. Chim. Ital. 102 (1972) 587.
[21] G.M. Sheldrick, SHELX-97, Programs for Crystal Structure Analysis, University of Göttingen, Germany, 1997.
[22] K. Brandenburg, M. Berndt, Diamond – Visual Crystal Structure Information System, Crystal Impact GbR, Bonn, Germany, 1999, For Software Review see: W.T. Pennington, J. Appl. Cryst. 32 (1999) 1028.

Available online at www.sciencedirect.com
SCIENCE DIRECT®
Polyhedron 23 (2004) 253–262
POLYHEDRON
www.elsevier.com/locate/poly

Tris-pyrazolylborate complexes of redox inactive lanthanides – the structures of $[(Tp^{Me2})_2NdX]$ (X = Cl, NPh_2, dpm, H_2BEt_2) ☆

Jennifer L. Galler [a], Sam Goodchild [a], James Gould [a], Robert McDonald [b], Andrea Sella [a,*]

[a] Christopher Ingold Laboratories, Department of Chemistry, University College London, 20 Gordon Street, London WC1H 0AJ, UK
[b] Department of Chemistry, University of Alberta, Edmonton, Alta. T6G 2G2, Canada

Received 15 May 2003; accepted 22 August 2003

Abstract

A range of complexes of Ce and Nd have been prepared to compare the chemistry of the non-reducible $[(Tp^{Me2})_2LnX]$ (Ln = Ce, Nd) with that reported previously for the redox-active samarium ion. The chloride $[(Tp^{Me2})_2NdCl]$ is a useful starting material for the preparation of the seven coordinate $[Nd(Tp^{Me2})_2OAr]$ (Ar = C_6H_4-4-X; X = H, Bu^t, Br, Ph, OMe, F, Me) and $[Nd(Tp^{Me2})_2NPh_2]$. Crystal structures of $[Nd(Tp^{Me2})_2Cl]$ and $[Nd(Tp^{Me2})_2NPh_2]$ are isostructural with those of the analogous samarium species. The eight coordinate species $[Nd(Tp^{Me2})_2(\beta\text{-dike})]$ (β-dike = $(RC{=}O)_2CH$, R = Me, Ph; Bu^t) and their cerium analogues (R = Ph, Bu^t) have also been prepared. The complexes are fluxional, the extent of this behaviour depending on the steric bulk of the substituents. The structure of $[Nd(Tp^{Me2})_2(Bu^tCO)_2CH]$ has been determined. Finally, in efforts to prepare a neodymium hydride, the unexpected borohydride $[Nd(Tp^{Me2})_2(H_2BEt_2)]$ has been isolated serendipitously and structurally characterized.
© 2003 Elsevier Ltd. All rights reserved.

Keywords: Lanthanides; Neodymium; X-ray structures; Alkoxides; Pyrazolylborates; Borohydrides

1. Introduction

The past few years have witnessed the rapid growth of interest in the lanthanides. This is part driven by a perception of the rare earths as representing a "last frontier" in the periodic table. At the same time the potential applications of the lanthanides in catalysis, diagnostics, and materials chemistry have provided a powerful impetus to this work. A key theme which has underpinned these developments is the observation that kinetic stabilization of the metal centre through the use of bulky ancillaries is critical to the isolation of well-defined species. Although cyclopentadienyls and their derivatives still dominate the field, chemistry using other carbocyclic systems have been developed [1] and nitrogen donor alternatives have been used by a growing number of workers [2]. The pyrazolylborates (Tp) [3] have proved extremely effective in providing a well-defined coordination sphere for the lanthanides. Both first and second-generation Tp ligands [3b,3c] have been explored to generate both sandwich and half-sandwich systems which are resistant to ligand redistribution and which afford mononuclear products. In the case of sandwich complexes, use of the easily accessible Tp^{Me2} ligand has led to a rich divalent reactivity being uncovered for divalent samarium. $[Sm(Tp^{Me2})_2]$ has been shown to react by electron transfer with oxidizers including O_2 [4], azobenzene [5], dichalcogenides [6,7], metal-metal bonds [8,9] etc. to give trivalent species. Hydrides [10] and hydrocarbyls [15] are attractive synthetic targets for catalyst studies. Unfortunately, with Tp^{Me2} ligands no hydrides have been observed and only two complexes containing Sm–C bonds have been prepared: the acetylide, $[Sm(Tp^{Me2})_2CCPh]$, and the cyclopentadienyl, $[Sm(Tp^{Me2})_2(\eta^5\text{-}C_5H_5)]$ by redox transmetallation with mercury phenylacetylide [11] and

☆ Dedicated with admiration and affection to the Great Crawdad of pyrazolylborate chemistry, Jerry Trofimenko – you have been a pioneer, an inspiration, and a friend.

* Corresponding author. Fax: +44-0-20-7679-7463/+44-071-380-7463.
E-mail address: a.sella@ucl.ac.uk (A. Sella).

0277-5387/$ - see front matter © 2003 Elsevier Ltd. All rights reserved.
doi:10.1016/j.poly.2003.11.014

thallium cyclopentadienide [12], respectively. The weak basicity of these ligands, however, precludes many protonolysis reactions. Attempts to use other mercury reagents in analogous reaction have failed and metathesis methods have been equally unsuccessful usually as a result of reduction of the metal to the highly insoluble complex $[Sm(Tp^{Me2})_2]$ [13,14]. Here we present analogous chemistry to that of samarium using the non-reducible lanthanides Ce and Nd together with attempts to prepare hydrides and hydrocarbyls.

2. Results and discussion

Reaction of $NdCl_3$ with either Na or KTp^{Me2} in THF leads to the formation of the pale blue complex $[Nd(Tp^{Me2})_2Cl]$ (**1**) in variable yields although the use of $NdCl_3(THF)_2$ proved to be a rather more reliable.

$$NdCl_3 + 2KTp^{Me2} \rightarrow [Nd(Tp^{Me2})_2Cl] + 2KCl$$

Like its samarium analogue **1** dissolves in THF and aromatic solvents, but not in petroleum ether, and give simple, though paramagnetically shifted ^1H spectra consistent with a fluxional coordination sphere. The Eu analogue **1-Eu** may be prepared analogously, has similar solubility, and is obtained in similar yield. **1-Eu** can be reduced readily to the known insoluble orange divalent complex $[Eu(Tp^{Me2})_2]$ by stirring with sodium chips [14]. Attempts to prepare the analogous complex with yttrium, $[Y(Tp^{Me2})_2Cl]$, was not successful – no significant soluble products were isolated apart from dimethylpyrazole, indicating extensive decomposition.

Compound **1** is a useful starting material for a range of derivatives. Reaction of **1** with NaOAr ($Ar = C_6H_4$-4-R) gives seven coordinate phenoxides, $[Nd(Tp^{Me2})_2OAr]$ ($Ar = C_6H_5$ (**2a**); C_6H_4-4-Bu^t (**2b**); C_6H_4-4-Br (**2c**); C_6H_4-4-Ph (**2d**); C_6H_4-4-OMe (**2e**); C_6H_4-4-F (**2f**); C_6H_4-4-Me (**2g**)) analogous to the samarium complexes some of which have been crystallographically characterized and have been or will be reported elsewhere [13,17].

$$Nd(Tp^{Me2})_2Cl + NaOAr \rightarrow Nd(Tp^{Me2})_2OAr + NaCl$$

Complexes **2a**–**2g** were isolated by pumping down the filtered reaction mixture and were only characterized by their ^1H NMR spectrum. The aryloxides are fluxional in solution giving simple spectra with a 9:9:3 pattern of singlets for the Tp^{Me2} resonances and two broadened and very strongly shifted resonances for the *ortho* and *meta* hydrogens of the phenyl groups, respectively. The ortho protons were particularly striking as they generally appear around +45 ppm as a very broad hump in the baseline only visible after long accumulation times. The spectrum of **2a** ($Ar = C_6H_5$) was invariant down to −90 °C, apart from the typical Curie dependence of the chemical shifts Scheme 1.

Metathesis of **1** with $NaNPh_2$ in THF results in the isolation of $[Nd(Tp^{Me2})_2NPh_2]$ (**3**).

$$[Nd(Tp^{Me2})_2Cl] + NaNPh_2 \rightarrow [Nd(Tp^{Me2})_2NPh_2] + NaCl.$$

In striking contrast to its samarium analogue [13], which is a fairly intense red colour, **3** displays the pale blue/lilac typical of Nd(III) species. This suggests that the red colour in $[Sm(Tp^{Me2})_2NPh_2]$ arises from a LMCT transition from the amide to the more reducible metal centre. Like its samarium analogue, **3** gives a more complex spectrum than **2**, indicating a non-fluxional C_2 symmetric coordination sphere – the phenyl groups of the amide ligand presumably prevent the methyl groups of the Tp^{Me2} ligands from rotating around the Sm-B axis and thereby effectively lock the coordination sphere. The spectra were assigned on the basis of the integrals and the line widths of the methyl groups in the 3-positions which are expected to be significantly broader than those in the 5-position. Curiously, the *ortho* hydrogens of the NPh_2 were quite sharp, showing a normal 6 Hz coupling to their neighbours. The *meta* and *para* protons, on the other hand, were strongly broadened by the neodymium centre.

By contrast to the synthesis of the NPh_2 derivative, attempts to prepare the corresponding $N(SiMe_3)_2$ complex by metathesis of **1** in THF using $KN(SiMe_3)_2$ were not successful and gave greenish mixtures of products indicative of Tp^{Me2} decomposition. Attempts to prepare the corresponding diethylamide complex by metathesis with $LiNEt_2$ resulted in recovery of starting material and significant amounts of $LiTp^{Me2}$. Such transfers of Tp ligands from rare earths to lithium or magnesium have been reported sporadically and presumably reflect the size mismatch between the large lanthanide centre, the rather tight Tp ligand [3,15] and the stronger, more covalent bonding in the latter metals.

Metathesis of **1** with sodium β-diketonates in THF results in the isolation of eight-coordinate complexes $[Nd(Tp^{Me2})_2(\beta\text{-dike})]$ (β-dike = $(RC{=}O)_2CH$, R = Me, **4-Nd**; R = Ph, **5-Nd**; R = Bu^t, **6-Nd**)

$$[Nd(Tp^{Me2})_2Cl] + Na(\beta\text{-dike}) \rightarrow [Nd(Tp^{Me2})_2(\beta\text{-dike})] + NaCl.$$

As with the previous compounds, the diketonates are soluble in THF and aromatic solvents and moderately air stable.

The acac complex, **4-Nd** (R = Me) gave an unreadable ^1H NMR spectrum at room temperature with a mixture of sharp and broad peaks. On cooling to 203 K the spectrum separated into 11 broad peaks, indicating that the eight-coordinate molecule has C_2 symmetry but it is fluxional at room temperature on the NMR time-

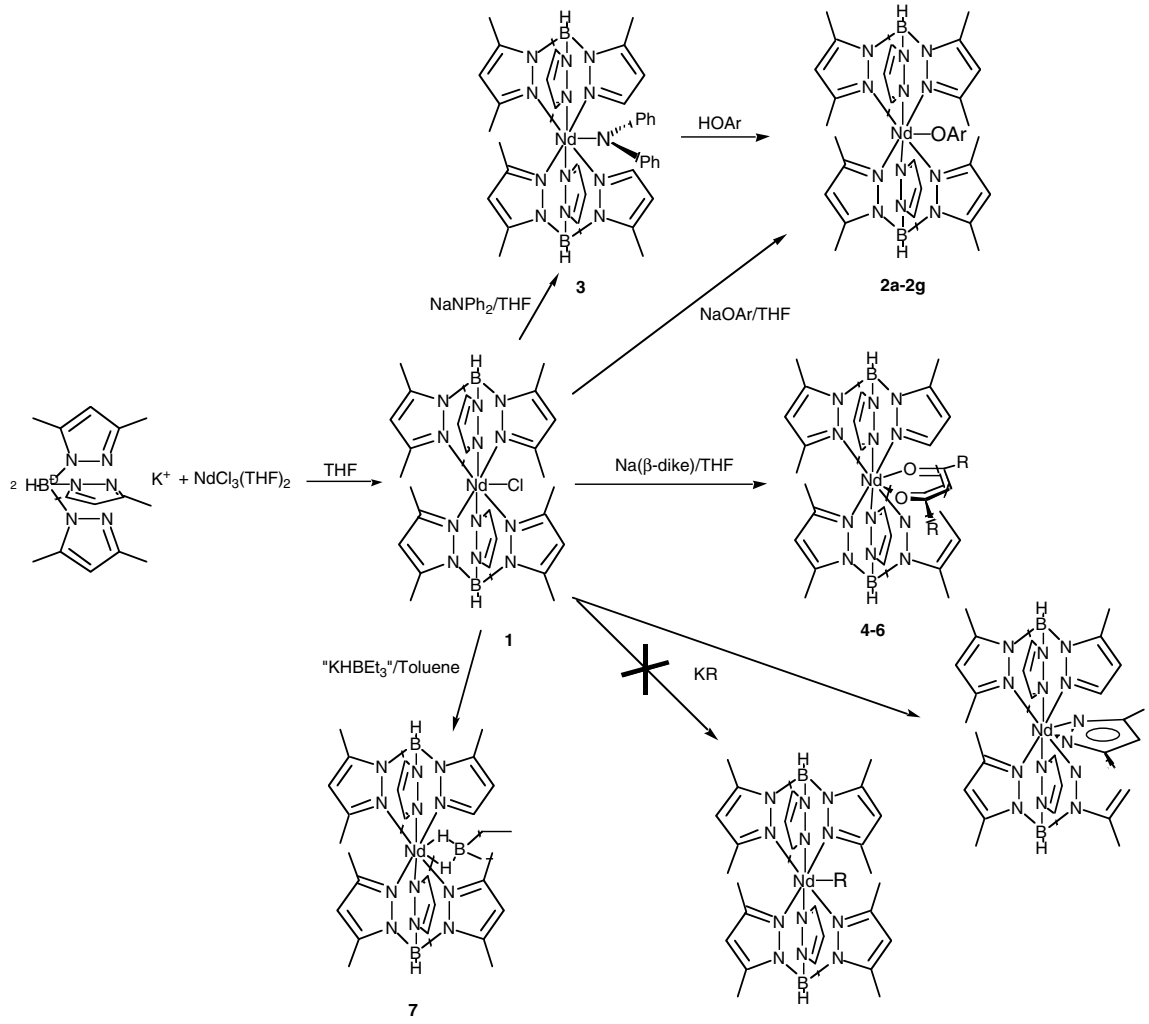

Scheme 1.

scale. The corresponding greenish dbm complex (R = Ph), **5-Nd**, on the other hand, is close to the slow exchange limit at room temperature and gives 13 fairly sharp lines, again consistent with C_2 symmetry. Cooling the sample results in sharper lines. The dpm (R = Bu^t) complex, **6-Nd**, is static at room temperature.

For comparison purposes the corresponding cerium complexes, [(Tp^{Me2})$_2$Ce(β-dike)] (β-dike = (RC=O)$_2$CH; dbm, R = Ph, **5-Ce**; dpm, R = Bu^t, **6-Ce**). were also prepared by metathesis starting, however, from the triflate, [Ce(Tp^{Me2})$_2$OTf] [16], which in our hands is more easily prepared than the chloride.

$$[Ce(Tp^{Me2})_2OTf] + Na(\beta\text{-dike}) \rightarrow [Ce(Tp^{Me2})_2(\beta\text{-dike})] + NaOTf.$$

While the ^{1}H NMR spectrum of **6-Ce** is fairly sharp and readable at room temperature, that of the dbm complex, **5-Ce**, is rather broad and sharpens up on cooling to −40 °C. In both cases the static spectrum indicates a C_2 symmetric molecule. Assignment of these spectra was made with the aid of EXSY spectra which, by correlating the exchange pathways, allowed unambiguous assignment of the methyl peaks to the 3- or 5-positions, respectively. Contrary to what has been observed for the less sterically crowded analogous Tp systems, there is no indication that and of the species **4**, **5**, and **6** exchange by anything other than an intramolecular mechanism [18].

We attempted to convert **1** to the corresponding fluoride, the samarium analogue of which has been prepared previously by redox chemistry [14], and which we hoped might prove an even more useful starting material. Unfortunately, metathesis with both KF and AgF led only to the recovery of the starting material.

A number of attempts were made to introduce a hydride or a hydrocarbyl group into the metal coordination sphere, all of which were unsuccessful. The reaction of **1** with an aged sample of potassium superhydride, "KHBEt$_3$" in toluene, a reagent which has been used

previously by Takats to prepare hydride complexes [15], resulted instead in the isolation of crystals of the unexpected complex $[Nd(Tp^{Me2})_2(H_2BEt_2)]$ which was crystallographically, but not spectroscopically, characterized (vide infra). Examination of the ^{11}B NMR spectrum of the potassium superhydride stock solution used in the reaction showed this to consist of a mixture of $KH_2BEt_2$and $KBEt_4$ as has been observed previously by Fryzuk [19] and Morris [20]. We do not believe that the fact that this behaviour has only ever been observed in Canada is of any great chemical significance. Thus the reaction may be seen as follows:

$$[Nd(Tp^{Me2})_2Cl] + KH_2BEt_2 \rightarrow [Nd(Tp^{Me2})_2(H_2BEt_2)] + KCl.$$

The reaction was repeated several times with an authentic sample of $KHBEt_3$ in THF (the toluene solution being no longer commercially available). Unfortunately such reactions resulted in extensive decomposition and ligand redistribution and only the fluxional pyrazolide complex $[Nd(Tp^{Me2})_2(3,5\text{-dmpz})]$ could be isolated in low yields. While frustrating, this decomposition reaction is intriguing since it may point to the formation of a transient hydride which then attacks one of the Tp^{Me2} ligands, in a manner similar to what we have proposed recently for the hydrolytic decomposition of these ligands at lanthanide centres [21]. Other attempts to prepare this elusive terminal hydride from **1** using KH, by analogy with Baudry's work [22], or by reaction with Ph_2SiH_2 and Ph_3SnH, resulted only in the recovery of the starting material.

Attempts to introduce hydrocarbyl groups into the coordination sphere using potassium reagents (e.g. KCH_2SiMe_3) simply gave greenish solutions from which, again, only small amounts of $[Nd(Tp^{Me2})_2(3,5\text{-dmpz})]$ could be recovered. Reaction of the silver acetylide cluster "$(AgBu^t)_{14}$" [23] with **1**, with a view to preparing $[Nd(Tp^{Me2})_2(C{\equiv}CBu^t)]$ by metathesis gave no detectable reaction apart from the formation of some silver metal. We presume that the stability of the silver acetylide cluster is such as to overcome the driving force provided by the precipitation of AgCl.

Thus the problem of preparing the, presumably highly reactive, hydride and hydrocarbyl species with these ancillaries remains intractable.

3. X-ray crystallography

Single crystals of compounds **1**, **3**, **6-Nd**, and **7** were obtained and their structures have been determined. Selected crystallographic and experimental details for all four structures are given in Table 1. Selected bond lengths and angles are reported in the Figure captions. Compounds **1** and **3** are very similar to their samarium counterparts reported elsewhere, **1** [13,14]. A view of the molecular structures of **1** and **3** are shown in Figs. 1 and 2. Both compounds are seven coordinate adopting a distorted pentagonal bipyramidal metal coordination sphere and show virtually identical metrical parameters as their analogues, allowing for the difference in ionic radius of the metal. We feel it is unnecessary to discuss them further.

The dpm complex, **6-Nd**, is also largely unremarkable, crystallizing with two independent molecules in the asymmetric unit. The differences between the two are insignificant. The eight-coordinate molecule shows the expected tridentate Tp^{Me2} and the bidentate dpm ligands. A view of the molecular structure of **6-Nd** is shown in Fig. 3. Although the complex does not have any crystallographically imposed symmetry, the molecule is effectively C_2 symmetric consistent with the ^1H NMR spectra. The geometry around the metal is dodecahedral, as has been observed previous for other eight-coordinate Tp^{Me2} complexes of the lanthanides [24]. This is in contrast to the Tp complexes which tend to favour square antiprismatic coordination sphere [3a]. Such differences can be attributed to minimization of contacts between the methyl groups of the Tp^{Me2} and dpm ligands. As has become typical in rare earth structures with Tp^{Me2} [3c], twisting of some of the pyrazolyl groups around the B–N bond is observed. For **6-Nd** two pyrazolyl groups on the same ligand and one on the other twist by between 23° and 26° in opposite directions to accommodate the dpm ligand in the wedge between them.

The final molecule, **7**, is rather more interesting as a result of the coordination of the unusual H_2BEt_2 ligand. A view of the molecular structure of **7** is shown in Fig. 4. The compound crystallized in the space group *C2/c* with a somewhat disordered molecule of pentane in the lattice and showed no intermolecular contacts. The molecule lies on a crystallographic C_2 axis. The two tridentate Tp^{Me2} ligands are partnered by a bidentate H_2BEt_2 ligand, a species which has only been characterized once before [20]. Formally, therefore the molecule is eight-coordinate. However, the average Nd–N distance, 2.602(6) Å, is closer to those in **1**, 2.59(1) Å and **3**, 2.582(6) than that seen for **6**, 2.634 Å, and is consistent with the fact that the bite angle of the small bidentate borohydride is fairly tight and the complex may be thought of has having an intermediate coordination number. Nevertheless one pyrazolyl groups of the Tp^{Me2} ligands shows a 35° twist, once more away from the third ligand. The Nd–B distance, 2.883(8) Å is significantly longer than that in $[Nd(C_5H_4CH_2CH_2OMe)_2(BH_4)]$, 2.66(3) Å [25], $[Nd_2(\mu\text{-}C_7H_7)(THF)_4(BH_4)_3]$, 2.68, 2.74 Å. [26] and in $[K(18\text{-crown-}6)\{Nd(C_{13}H_8)CPh_2(C_5H_4)(BH_4)_2\}]_2$, 2.641(8) Å, 2.623(7) Å [27] all of which contain tridentate BH_4 ligands. The longer distance is consistent with the bidentate binding mode

Table 1

Compound	**1**	**3**	**6-Nd**	**7**
A. Crystal data				
Formula	$C_{30}H_{44}B_2ClN_{12}Nd$	$C_{42}H_{54}B_2N_{13}Nd$	$C_{41}H_{63}B_2N_{12}NdO_2$	$C_{36.5}H_{62}B_3N_{12}Nd$
Formula weight	774.08	906.84	921.89	845.65
Crystal dimensions (mm)	$0.30 \times 0.30 \times 0.29$	$0.23 \times 0.18 \times 0.16$	$0.38 \times 0.37 \times 0.32$	$0.50 \times 0.38 \times 0.31$
Crystal color, habit	pale blue, prism	pale blue, prism	pale blue, prism	pale blue, prism
Crystal system	orthorhombic	trigonal	triclinic	monoclinic
Space group	$Pna2_1$ (No. 33)	$R\bar{3}c$ (No. 167)	$P\bar{1}$ (No. 2)	$C2/c$ (No. 15)
Unit cell parameters[a]				
a (Å)	18.6429 (13)	25.4664 (6)	12.6560 (8)	15.7054 (11)
b (Å)	10.2665 (7)		17.7835 (11)	15.9634 (11)
c (Å)	18.4475 (13)	38.2875 (18)	21.1954 (13)	19.5882 (13)
α (°)			81.5820 (12)	
β (°)			84.1022 (12)	112.9030 (11)
γ (°)			80.3489 (11)	
V (Å^3)	3530.8 (4)	21504.2 (12)	4637.2 (5)	4523.8 (5)
Z	4	18	4	4
$\rho_{calc.}$ (g cm^{-3})	1.456	1.260	1.320	1.242
μ (mm^{-1})	1.586	1.129	1.167	1.186
B. Data collection and refinement conditions				
Diffractometer	Bruker PLATFORM/SMART 1000 CCD[b]			
Radiation (λ [Å])	graphite-monochromated Mo Kα (0.71073)			
Temperature (°C)	−80	−80	−80	−80
Scan type	ω scans (0.2°) (25 s exposures)	ω scans (0.2°) (25 s exposures)	ω scans (0.2°) (25 s exposures)	ω scans (0.2°) (20 s exposures)
Data collected 2θ limit (°); completeness	52.78; 100%	52.76; 99.9%	52.74; 97.9%	52.84; 99.4%
Total data collected	18922	34583	26269	11019
Independent reflections (R_{int})	6426 (0.0367)	4899 (0.0543)	18578 (0.0186)	4621 (0.0264)
Observed reflections (NO[$F_o^2 \geqslant \sigma F_o^2$)])	5454	4185	15956	4099
Structure solution method	direct methods (SHELXS-86[c])	Patterson search structure expansion (DIRDIF-96[d])	direct methods (SHELXS-86[c])	Patterson search/ structure expansion (DIRDIF-96[d])
Refinement method	full-matrix least-squares on F^2 (SHELXL-93[e])			
Absorption correction method	multi-scan (SADABS)	multi-scan (SADABS)	Gaussian integration (face-indexed)	multi-scan (SADABS)
Range of transmission factors	0.6563–0.6476	0.8400–0.7813	0.7065–0.6655	0.7100–0.5885
Data [$F_o^2 \geqslant -3\sigma(F_o^2)$]/restraints/ params	6426/0/428	4899/0/269	18578/0/1063	4621/4[f]/241
Flack absolute structure parameter[g]	0.493 (14)			
Goodness-of-fit ($S[F_o^2 \geqslant -3\sigma(F_o^2)]$)[h]	1.038	1.166	1.021	1.160
Final R indices[i]				
$R_1(F)[F_o^2 \geqslant \sigma(F_o^2)]$	0.0304	0.0388	0.0294	0.0420
$wR_2(F^2)[F_o^2 \geqslant -3\sigma(F_o^2)]$	0.0702	0.1430	0.0776	0.1295
Largest difference peak and hole (e Å^{-3})	0.992; −0.334	1.789; −0.321	0.857; −0.430	1.589; −0.576

[a] **1**: obtained from least-squares refinement of 4361 reflections from the data collection with 4.37°<2θ<52.63°; **3**: 5814 reflections with 4.52°<2θ<52.49°; **6-Nd**: 6399 reflections with 4.69°<2θ<52.72°; **7**: 7908 reflections with 4.51°<2θ<52.74°.

[b] Programs for diffractometer operation, data collection, data reduction and absorption correction were those supplied by Bruker.

[c] Sheldrick, G.M. Acta Crystallogr. 1990, A46, 467–473.

[d] Beurskens, P.T., Beurskens, G., Bosman, W.P., de Gelder, R., Garcia Granda, S., Gould, R.O., Israel, R., Smits, J.M.M. (1996). The DIRDIF-96 program system. Crystallography Laboratory, University of Nijmegen, The Netherlands.

[e] Sheldrick, G.M. SHELXL-93. Program for crystal structure determination. University of Göttingen, Germany, 1993.

[f] Distances within the solvent *n*-pentane molecule were given fixed idealized values: d(C1S–C2S) = d(C2S–C3S) = 1.54 Å; d(C1S···C3S) = d(C2S···C2S′) = 2.51 Å (C2S′ is related to C2S via rotation about the crystallographic twofold axis (0, y, 1/4)).

[g] Flack, H.D. Acta Crystallogr. 1983, A39, 876–881. The Flack parameter will refine to a value near zero if the structure is in the correct configuration and will refine to a value near one for the inverted configuration. The value observed for 1 is indicative of racemic twinning, and was accomodated during the refinement (using the SHELXL-93 TWIN instruction [see Ref. *d*]).

[h] $S = [\sum w(F_o^2 - F_c^2)^2/(n-p)]^{1/2}$ (n, number of data; p, number of parameters varied; $w = [\sigma^2(F_o^2) + (A_0P)^2 + A_1P]^{-1}$, where $P = [\text{Max.}(F_o^2, 0) + 2F_c^2]/3$ and A_0 and A_1 are coefficients adjusted as suggested by the refinement program; for **1**, $A_0 = 0.0391$ and $A_1 = 0$; for **3**, $A_0 = 0.0894$ and $A_1 = 49.1609$; for **6-Nd**, $A_0 = 0.0406$ and $A_1 = 2.4216$; for **7**, $A_0 = 0.0747$ and $A_1 = 7.8740$).

[i] $R_1 = \sum ||F_o| - |F_c|| / \sum |F_o|$; $wR_2 = [\sum w(F_o^2 - F_c^2)^2 / \sum w(F_o^4)]^{1/2}$.

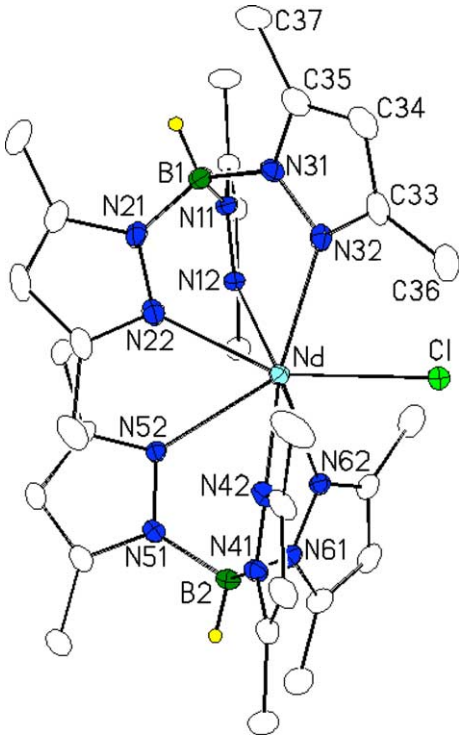

Fig. 1. ORTEP view of the molecular structure of $[Nd(Tp^{Me2})_2Cl]$ (**1**), hydrogens omitted for clarity. Selected bond lengths (Å) and angles (°): Nd–Cl 2.676(1), Nd–N(12) 2.488(3), Nd–N(22) 2.570(4),Nd–N(32) 2.713(4), Nd–N(42) 2.487(4), Nd–N(52) 2.672(4), Nd–N(62) 2.596(4), Nd–B(1) 3.555(1), Nd–B(1) 3.605(1), B1–Nd–B2 144.2(1).

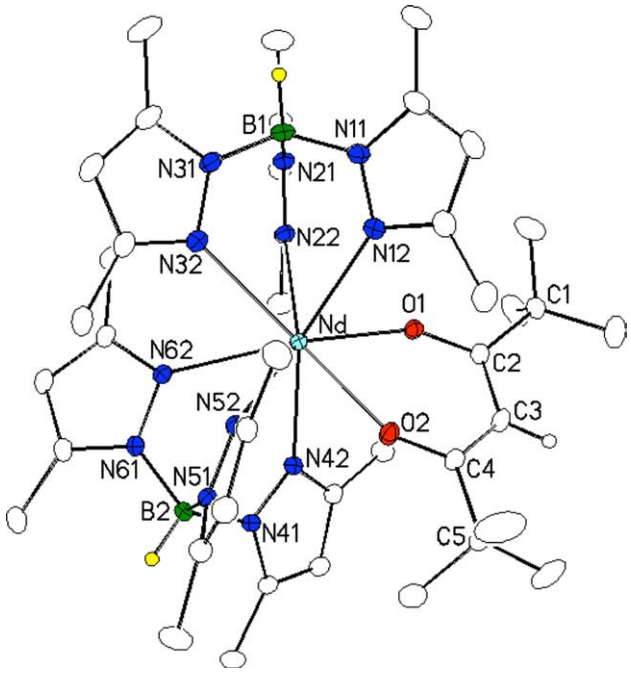

Fig. 3. ORTEP view of the molecular structure of $[Nd(Tp^{Me2})_2(dpm)]$ (**6-Nd**), hydrogens omitted for clarity. Selected bond lengths (Å) and angles (°) for molecule A. Nd–O1 2.257(2), Nd–O2 2.393(2), Nd–N(12) 2.668(2), Nd–N(22) 2.595(2), Nd–N(32) 2.706(2), Nd–N(42) 2.706(2), Nd–N(52) 2.536(2), Nd–N(62) 2.636(2), Nd–B(1) 3.679(2), Nd–B(2) 3.599(2), B1–Nd–B2 141.3(2).

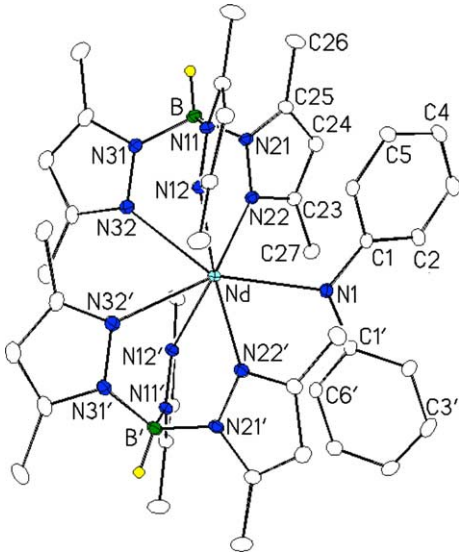

Fig. 2. ORTEP view of the molecular structure of $[Nd(Tp^{Me2})_2NPh_2]$, **3**, hydrogens omitted for clarity. Primed atoms are related to unprimed via the crystallographic twofold axis (0, *y*, 1/4). Selected bond lengths (Å) and angles (°): Nd–N(1) 2.480(5), Nd–N(12) 2.498(3), Nd–N(22) 2.612(3),Nd–N(32) 2.635(4), Nd–B 3.555(5), B–Nd–B′ 151.6(2).

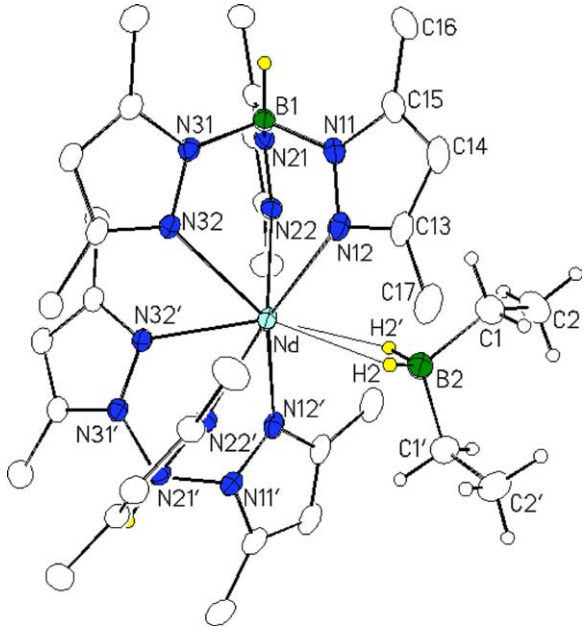

Fig. 4. ORTEP view of the molecular structure of $[Nd(Tp^{Me2})_2(H_2BEt_2)]$ (**7**), non-borohydride hydrogens omitted for clarity. Primed atoms are related to unprimed via the crystallographic twofold axis (0, *y*, 1/4). Selected bond lengths (Å) and angles (°): Nd–B(2) 2.883(8), Nd–N(12) 2.660(4), Nd–N(22) 2.523(4), Nd–N(32) 2.624(3), Nd–B(1) 3.590(5), B(1)–Nd–B(1)′ 144.8(2).

of the BH_2Et_2 ligand and the rather crowded metal centre.

4. Conclusions

A range of simple seven- and eight-coordinate complexes of cerium and neodymium have been prepared by metathesis and the structures of $[Nd(Tp^{Me2})_2Cl]$ (**1**), $[Nd(Tp^{Me2})_2(NPh_2)]$ (**3**), and $[Nd(Tp^{Me2})_2(dpm)]$, **6-Nd**, have been determined. The behaviour of these complexes is broadly similar to that of the analogous samarium complexes. Thus all the complexes are fluxional, and the extent to which the dynamics can be slowed at low temperature depends largely on the steric demand of the substituents on the non-Tp ligand. Attempts to prepare thermally stable hydrides and hydrocarbyls have foundered on the twin rocks of pyrazolyborate fragmentation or of inappropriate solubilities for the products. From one of these attempts, the unusual bis-borohydride complex $[Nd(Tp^{Me2})_2(H_2BEt_2)]$ (**7**) was isolated and its structure determined.

5. Experimental

5.1. General procedures

All preparations and subsequent manipulations were carried out using standard Schlenk line and dry box techniques in an atmosphere of dinitrogen. Oxygen-free nitrogen was further purified by passage over columns containing BASF Cu based catalyst (RE-11) at 100 °C and Aquasorb (Mallinkrodt, P_2O_5 on an inert support) or 3 Å molecular sieves and MnO. Glassware was routinely dried at 250 °C and cooled by a nitrogen atmosphere prior to use. All solvents were pre-dried over 5 Å molecular sieves or sodium wire (UCL). Hexane and pentane were washed with sulfuric acid, dried over $MgSO_4$ prior to distillation (U of A). The solvents were distilled from appropriate drying agents before use; Na (toluene, hexane, HMPA), K (benzene), K/benzophenone ketyl (THF), Na/K alloy (petroleum ether b.p. 4060 °C, pentane, diethyl ether), CaH_2 (CH_2Cl_2). The deuterated solvents for NMR (THF-d_8, benzene-d_6 and toluene-d_8) were vacuum distilled from Na/K alloy (1:3), $CDCl_3$ from P_2O_5. All solvents were degassed prior to use.

$NdCl_3$ was prepared from Nd_2O_3 by the HCl/NH_4Cl method. $NdCl_3(THF)_2$ was prepared by Soxhlet extraction of anhydrous $NdCl_3$ with THF. The THF content was confirmed by elemental analysis. The ligands, potassium and sodium hydrotris(3,5-dimethylpyrazolyl) borate (Na/KTp^{Me2}), were prepared by standard methods [28]. $NaNPh_2$ was prepared by heating $HNPh_2$ with excess NaH in THF, followed by removal of solvent. $[Ce(Tp^{Me2})_2OTf]$ was prepared by literature procedures [16].

Infrared (IR) spectra were recorded as KBr pellets on a Nicolet 205 or BOMEM MB100 FTIR spectrometer. NMR samples were prepared in the dry box and sealed under vacuum. ^1H NMR spectra in solution were recorded on Bruker AM400 FT spectrometers at 400 MHz, respectively. ^{11}B NMR spectra were recorded on the Bruker AM400 instrument at 128 MHz. Spectra were calibrated using residual proton resonances and are reported relative to tetramethylsilane (TMS). ^{11}B chemical shifts are reported relative to external F_3BOEt_2. Elemental analyses were determined by Mr. Alan Stones of the UCL Analytical Services or the Microanalytical Laboratory, Department of Chemistry, University of Alberta.

5.1.1. $[Nd(Tp^{Me2})_2Cl]$ (**1**)

$NdCl_3$ (1.50 g, 3.80 mmol) was suspended in THF (25 cm^3) in a round bottom flask. KTp^{Me2} (2.55 g, 7.58 mmol) was dissolved separately in THF (25 cm^3). The solution of KTp^{Me2} was added to the $NdCl_3(THF)_2$ over 5 minutes. The pale blue solid was seen to dissolve giving a milky pale blue solution. The suspension was stirred for 2 h and then the solvent was removed under reduced pressure. The pale blue residue was extracted with several portions of warm toluene (total volume 50 cm^3), centrifuging each time to remove undissolved salt. Concentrating the solution to 25 cm^3 and cooling to −20 °C) yielded an analytically pure pale blue powder. Yield: 1.66 g (56%). A second crop was obtained. Total yield: 1.94 g (66%). IR (KBr, cm^{-1}): 2563 (BH). ^1H NMR (C_6D_6, 298 K): −6.75 (s, 18H, 3-Me); 2.83 (s, 18H, 5-Me); 7.62 (s, 6H, CH). ^{13}C NMR ($CDCl_3$, 298 K): 11.2 (q, 3 or 5Me); 14.2 (q, 5 or 3Me); 105.4 (d, 4-C); 145.5 (s, 3- or 5-C); 149.4 (s, 5- or 3-C). *Anal.* Calc. for $C_{30}H_{44}N_{12}B_2ClNd$: C, 46.55; H, 5.73; N, 21.79. Found: C, 46.60; H, 5.71; N, 21.40%.

5.1.2. $[Eu(Tp^{Me2})_2Cl]$ (**1-Eu**)

1-Eu was prepared from $EuCl_3$ analogously to **1**. Yield: 69%. IR (KBr, cm^{-1}): 2564 (BH). ^1H NMR (C_6D_6, 298 K): 10.74 (s, 18H, 3-Me); 1.96 (s, 6H, CH); 1.86 (s, 18H, 5-Me). *Anal.* Calc. for $C_{30}H_{44}N_{12}B_2ClNd$: C, 46.55; H, 5.73; N, 21.79. Found: C, 46.60; H, 5.71; N, 21.40%.

5.1.3. $[Nd(Tp^{Me2})_2OPh]$ (**2a**)

1 (200 mg, 0.26 mmol) and NaOPh were each dissolved in THF (10 cm^3) in separate Schlenk flasks. Addition of the NaOPh to the solution of **1** resulted in a pale blue/lilac solution from which a fine white precipitate formed overnight. Removal of solvent was followed by extraction into toluene. Removal of the solvent under reduced pressure gave a pale blue solid. Yield: 110 mg (51%).

IR (KBr) 2553 cm^{-1}. ^1H NMR (C_6D_6, 298 K): −5.66 (s, 18H, 3-Me); 1.24 (s, 18H, 5-Me); 7.41 (s, 6H, 4-CH); 17.48 (br s, 1H, *p*-Ph); 21.88 (br s, 2H, *m*-Ph); 44.89 (v br s, 2H, *o*-Ph). IR (KBr): 2554 (BH) cm^{-1}. *Anal.* Calc. for

$C_{36}H_{49}N_{12}B_2ONd$: C, 51.98; H, 5.94; N, 20.21. Found: C, 50.34; H, 5.86; N 18.95%.

5.1.4. [Nd(Tp^{Me2})$_2$OPh-4-Bu^t] (**2b**)

t-Butyl phenol (39 mg, 0.26 mmol) was dissolved in THF and added dropwise to an excess of NaH suspended in THF and stirred until hydrogen evolution stopped. The filtered supernatant was added dropwise to a stirred solution of **1** (200 mg, 0.26 mmol) in THF (10 cm^3). The mixture was stirred overnight and a fine white precipitate formed. After removal of THF under reduced pressure the residue was extracted with toluene. The resulting solution was filtered and pumped down to give an oily solid. Washing with petroleum ether (b.p. 40/60) gave a pale blue powder. Yield: 100 mg (43%).

^{1}H NMR (C_6D_6, 298 K): −5.31 (s, 18H, 3-Me); 1.40 (s, 18H, 5-Me); 7.35 (s, 9H, Bu^t); 7.50 (s, 6H, 4-CH); 21.93 (br s, 2H, *m*-Ph); 44.33 (v br s, 2H, *o*-Ph). IR (KBr): 2557 (BH) cm^{-1}. *Anal.* Calc. for $C_{40}H_{57}N_{12}B_2ONd$: C, 54.11; H, 6.47; N, 18.93. Found: C, 53.02; H, 6.43; N, 18.19%.

5.1.5. [Nd(Tp^{Me2})$_2$OPh-4-Br] (**2c**)

The procedure was analogous to that of **2a**. Yield: 120 mg (44%) IR (KBr): 2550 cm^{-1}.

^{1}H NMR (400 MHz, C_6D_6, 298 K, δ ppm): −5.44 (s, 18H 3-Me), 1.31 (s, 18H 5-Me), 7.42 (s, 6H 4-CH), 21.86 (2H H_m), 44.15 (2H H_o).

5.1.6. [Nd(Tp^{Me2})$_2$OPh-4-Ph] (**2d**)

The procedure was analogous to that of **2a**. Yield: 92 mg (38%) IR (KBr): 2550, 2524.

^{1}H NMR (400 MHz, C_6D_6, 298K, δ ppm): −5.66 (s, 18H 3-Me), 0.32 (s, 18H 5-Me), 5.88 (s, 6H 4-CH), 9.75 (1H [Ph^2]H_p), 11.39 (2H [Ph^2]H_m), 14.64 (2H [Ph^2]H_o), 24.67 (2H H_m), 45.05 (2H H_o).

5.1.7. [Nd(Tp^{Me2})$_2$OPh-4-OMe] (**2e**)

The procedure was analogous to that of **2a**. Yield: 124 mg (38%) IR (KBr, cm^{-1}): 2554.

^{1}H NMR (400 MHz, C_6D_6, 298K, δ ppm): −5.00 (s, 18H 3-Me), 0.95 (s, 18H 5-Me), 3.65 (s, 3H, CH_3) 10.0 (s, 6H 4-CH), 22.0 (2H H_m), 46.0 (2H H_o).

5.1.8. [Nd(Tp^{Me2})$_2$OPh-4-F] (**2f**)

The procedure was analogous to that of **2a**. Yield: 144 mg (50%). IR (KBr, cm^{-1}): 2553.

^{1}H NMR (400 MHz, C_6D_6, 298K, δ ppm): −5.19 (s, 18H 3-Me), 1.16 (s, 18H 5-Me), 7.42 (s, 6H 4-CH), 21.68 (2H H_m), 47.50 (2H H_o).

5.1.9. [Nd(Tp^{Me2})$_2$OPh-4-Me] (**2g**)

The procedure was analogous to that of **2a**. Yield: 165 mg (51%). IR (KBr, cm^{-1}): 2553.

^{1}H NMR (400 MHz, C_6D_6, 298K, δ ppm): −5.11 (s, 18H 3-Me), 1.00 (s, 18H 5-Me), 7.42 (s, 6H 4-CH), 10.63 (s, 3H 4-CH_3Ph), 22.63 (2H H_m), 46.13 (2H H_o).

5.1.10. [Nd(Tp^{Me2})$_2$NPh$_2$] (**3**)

1 (200 mg, 0.260 mmol) was suspended in THF (6 cm^3) in a round bottom flask. $NaNPh_2$ (54 mg, 0.280 mmol) was dissolved separately in THF (4 cm^3). The solution of $NaNPh_2$ was added to the solution of **1** in four portions. The suspension was stirred for 2 h and then the solvent was removed under reduced pressure. The pale blue residue was extracted with warm toluene (2 cm^3), centrifuging to remove undissolved salt. Concentrating the solution to 2 cm^3 and cooling to −40 °C) yielded an analytically pure pale blue microcrystals of **3**. Yield: 1.66 g (56%). A second crop was obtained. Total yield: 1.94 g (66%). ^{1}H NMR (C_6D_6, 298 K: −26.72 (s, 6H, 3-Me); −6.34 (s, 2H, CH); −5.74 (s, 6H, 5-Me); −5.1 (br s, 2H, *p*-Ph); −1.84 (s, 6H, 5-Me); 2.11 (s, 2H, CH); 3.514 (s, 6H, 5-Me); 5.26 (br s, 6H, 3-Me); 6.05 (br s, 4H, *m*-Ph); 9.55 (d $J_{HH} = 6$ Hz, 4H, *o*-Ph); 19.05 (s, 2H, CH); 23.10 (br s, 6H, 3-Me). *Anal.* Calc. for $C_{42}H_{54}N_{13}B_2Nd$: C, 55.63; H, 6.00; N, 20.08. Found: C, 55.27; H, 5.72; N, 20.35%.

5.1.11. [Nd(Tp^{Me2})$_2$(acac)] (**4-Nd**)

2,4-Pentanedione (26 mg, 0.26 mmol) was added dropwise to excess NaH suspended in THF. After effervescence had subsided, the solution was filtered directly into a solution of **1** (200 mg, 0.26 mmol) in THF (10 cm^3). The resulting yellowish solution was stirred overnight. Workup as for **2a** yielded an oily greenish solid which was pure by NMR but failed to give reliable analyses.

IR (KBr, cm^{-1}): 2515. ^{1}H NMR (C_7D_8, 233 K): −35.0 (br s, 6H, 3-Me); −8.60 (s, 2H, 4-CH); −9.6 (s, 6H, 3-CH_3); −5.5 (s, 6H, 5-Me); 2.32 (s, 6H, 5-Me); 2.38 (s, 6H, 5-Me); 6.02 (s, 2H, 4-CH); 17.0 (s, 2H, 4-CH); 19.0 (s, 6H, acac-Me); 33.0 (s, 6H, 3-Me); 34.5 (s, 1H, dike-CH). *Anal.* Calc. for $C_{35}H_{51}N_{12}B_2O_2Nd$: C, 50.18; H, 6.13; N, 20.06. Found: C, 47.23; H, 6.00; N, 18.19%.

5.1.12. [Nd(Tp^{Me2})$_2$(dbm)] (**5-Nd**)

1 (200 mg, 2.60 mmol) and Na(dbm) (64 mg, 2.6 mmol) were dissolved separately in THF (10 cm^3) in Schlenk flasks under nitrogen. The yellow solution Na(dbm) solution was added dropwise to the solution of **1** with stirring to give a greenish solution. After stirring overnight the solvent was removed under reduced pressure and the residue extracted with warm toluene (2×10 cm^3). Crystallisation at −20 °C afforded a greenish solid. Yield: 0.80 g (33%).

IR (KBr, cm^{-1}): 2500. ^{1}H NMR (C_6D_6, 298 K: −21.30 (s, 6H, 3-Me); −3.09 (s, 6H, 3-CH_3); −2.03 (s, 6H, 5-Me); 0.57 (s, 6H, 5-Me); 1.00 (s, 6H, 5-Me); 3.80 (s, 2H, 4-CH); 5.20 (br s, 2H, 4-CH); 9.17 (s, 2H, *p*-Ph); 9.59 (s, 2H, *m*-Ph); 13.16 (s, 2H, 4-CH); 15.76 (s, 4H, *o*-Ph); 22.35 (br s, 6H, 3-Me); 26.56 (s, 1H, dike-CH).

Anal. Calc. for $C_{45}H_{55}N_{12}B_2O_2Nd$: C, 55.84; H, 5.73; N, 17.36. Found: C, 55.60; H, 5.69; N, 17.06%.

*5.1.13. [Ce(Tp^{Me2})$_2$(dbm)] (**5-Ce**)*

[Ce(Tp^{Me2})$_2$OTf] (500 mg, 5.66 mmol) and Na(dbm) (141 mg, 5.66 mmol) were mixed in a Schlenk flask under nitrogen, and dissolved in 20 ml of THF. The yellow solution was stirred overnight, during which time a fine white precipitate formed. The solution was filtered and the solvent removed under reduced pressure, leaving a bright orange solid. The product was then extracted with toluene. Recrystallisation afforded a bright orange crystalline solid. Yield: 0.35 g (64%).

^{1}H NMR (CD_2Cl_2, 213 K: −33.97 (s, 6H, 3-Me); −4.56 (s, 2H, 4-CH); −2.21 (s, 6H, 5-CH_3); −1.70 (s, 6H, 5-Me); −1.00 (s, 6H, 3-Me); 3.78 (s, 6H, 5-Me); 5.42 (s, 2H, 4-CH); 8.89 (s, 4H, *m*-Ph); 8.96 (s, 2H, *p*-Ph); 12.70 (s, 4H, *o*-Ph); 16.75 (s, 2H, 4-CH); 27.5 (br s, 6H, 3-Me); 35.4 (br s, 1H, dike-CH). *Anal.* Calc. for $C_{45}H_{55}N_{12}B_2O_2Ce_1$: C, 56.43; H, 5.79; N, 17.55. Found: C, 55.88; H, 6.12; N, 17.92%.

*5.1.14. [Nd(Tp^{Me2})$_2$(dpm)] (**6-Nd**)*

The compound was prepared analogously with **4**. Yield: 120 mg (50%). IR (KBr, cm^{-1}): 2527. ^{1}H NMR (C_6D_6, 298 K): −27.94 (s, 6H, 3-Me); −5.58 (s, 6H, 3-CH_3); −1.94 (s, 6H, 5-Me); 1.23 (s, 18H, Bu^t); 2.79 (s, 6H, 5-Me); 5.76 (s, 2H, 4-CH); 7.00 (s, 6H, 5-Me); 14.05 (s, 2H, 4-CH); 16.14 (s, 2H, 4-CH); 20.56 (s, 6H, 3-Me); 25.35 (s, 1H, dike-CH). *Anal.* Calc. for $C_{41}H_{63}N_{12}B_2O_2Nd_1$: C, 53.41; H, 6.88; N, 18.23. Found: C, 53.87; H, 6.23; N, 17.99%.

*5.1.15. [Ce(Tp^{Me2})$_2$(dpm)] (**6-Ce**)*

[Ce(Tp^{Me2})OTf] (0.500 g, 5.66 mmol) and Na(dpm) (0.117 g, 5.66 mmol) were mixed in a Schlenk flask under nitrogen, and dissolved in 20 cm^3 of THF. The yellow solution was stirred overnight, during which time a fine white precipitate formed. The solution was filtered and the solvent removed under reduced pressure, leaving a bright yellow solid. The product was then extracted with toluene. Recrystallisation afforded bright yellow needle crystals. Yield: 0.075 g (15%).

^{1}H NMR ($CDCl_3$, 298 K): −26.42 (s, 6H, 3-Me); 0.80 (br s, 6H, 3-CH_3); 1.46 (s, 2H, 4-CH); 2.90 (s, 6H, 5-Me); 3.30 (s, 6H, 5-Me); 4.50 (s, 2H, 4-CH); 6.54 (s, 6H, 5-Me); 7.26 (s, 18H, Bu^t); 14.80 (s, 2H, 4-CH); 17.49 (br s, 6H, 3-Me); 25.90 (s, 1H, dike-CH). *Anal.* Calc. for $C_{41}H_{63}N_{12}B_2O_2Ce_1$: C, 53.65; H, 6.92; N, 18.31. Found: C, 53.44; H, 6.77; N, 18.50%.

6. Supporting information available

X-ray crystallographic files in CIF format for the structure determinations of [Nd(Tp^{Me2})$_2$Cl] (**1**), [Nd(Tp^{Me2})$_2$(NPh$_2$)] (**3**), [Nd(Tp^{Me2})$_2$(dpm)], (**6-Nd**), and [Nd(Tp^{Me2})$_2$(H$_2$BEt$_2$)] (**7**) have been deposited with the CCDC, 12, Union Road. Cambridge. CB2 1EZ, UK (fax: +44-1223-336033; E-mail: deposit@ccdc.cam.ac.uk or www: http://www.ccdc.cam.ac.uk) with reference numbers CCDC 210687 **1**, CCDC 210689 **3**, CCDC 210688 **6-Nd**, CCDC 210686 **7**, respectively.

Acknowledgements

This work has been supported by EPSRC and NSERC Canada. A.S. is grateful to University of Alberta for a Visiting Professorship and to UCL for leave of absence. We are grateful to Dr. Abil Aliev for assistance with the EXSY spectra. A.S. in particular wishes to acknowledge the contributions of Prof. J. Takats to this work and for his comments during the preparation of this manuscript.

References

[1] (a) F.T. Edelmann, Angew. Chem., Int. Ed. Engl. 34 (1995) 2466; (b) F.T. Edelmann, D.M.M. Freckmann, H. Schumann, Chem. Rev. 102 (2002) 1851; (c) M.N. Bochkarev, Chem. Rev. 102 (2002) 2089.
[2] H.C. Aspinall, Chem. Rev. 102 (2002) 1807.
[3] (a) S. Trofimenko, Scorpionates: The Coordination Chemistry of Polypyrazolylborate Ligands, Imperial College Press, London, 1999; (b) I. Santos, N. Marques, New J. Chem. 19 (1995) 551; (c) N. Marques, A. Sella, J. Takats, Chem. Rev. 102 (2002) 2137.
[4] X.W. Zhang, G.R. Loppnow, R. McDonald, J. Takats, J. Am. Chem. Soc. 117 (1995) 7828.
[5] J. Takats, X.W. Zhang, V.W. Day, T.A. Eberspacher, Organometallics 12 (1993) 4286.
[6] A.C. Hillier, S.Y. Liu, A. Sella, M.R.J. Elsegood, Inorg. Chem. 39 (2000) 2635.
[7] I. Lopes, A.C. Hillier, S.Y. Liu, Â. Domingos, J. Ascenso, A. Galvao, A. Sella, N. Marques, Inorg. Chem. 40 (2001) 1116.
[8] A.C. Hillier, S.Y. Liu, A. Sella, O. Zekria, M.R.J. Elsegood, J. Organomet. Chem. 528 (1997) 209.
[9] A.C. Hillier, A. Sella, M.R.J. Elsegood, J. Organomet. Chem. 664 (2002) 298.
[10] M. Ephritikhine, Chem. Rev. 97 (1997) 2193.
[11] G.Y. Lin, R. McDonald, J. Takats, Organometallics 19 (2000) 1814.
[12] I. Lopes, G. Lin, Â. Domingos, R. McDonald, N. Marques, J. Takats, J. Am. Chem. Soc. 121 (1999) 8110.
[13] I. Lopes, B. Monteiro, G.Y. Lin, A. Domingos, N. Marques, J. Takats, J. Organomet. Chem. 632 (2001) 119.
[14] A.C. Hillier, X.W. Zhang, G.H. Maunder, S.Y. Liu, T.A. Eberspacher, M.V. Metz, R. McDonald, A. Domingos, N. Marques, V.W. Day, A. Sella, J. Takats, Inorg. Chem. 40 (2001) 5106.
[15] L. Hasinoff, J. Takats, X.W. Zhang, P.H. Bond, R.D. Rogers, J. Am. Chem. Soc. 116 (1994) 8833.
[16] S.Y. Liu, G.H. Maunder, A. Sella, M. Stevenson, D.A. Tocher, Inorg. Chem. 35 (1996) 76.
[17] J.L. Galler, A. Sella, D.A. Tocher, unpublished results.
[18] (a) M.A.J. Moss, C.J. Jones, Polyhedron 9 (1990) 697; (b) M.A.J. Moss, C.J. Jones, A.J. Edwards, J. Chem. Soc., Dalton Trans. (1989) 1393.
[19] (a) M.D. Fryzuk, B.R. Lloyd, G.K.B. Clentsmith, S.J. Rettig, J. Am. Chem. Soc. 113 (1991) 4332;

(b) M.D. Fryzuk, B.R. Lloyd, G.K.B. Clentsmith, S.J. Rettig, J. Am. Chem. Soc. 116 (1994) 3804.
[20] G.C. Jia, A.J. Lough, R.H. Morris, J. Organomet. Chem. 461 (1993) 147.
[21] Â. Domingos, G.Y. Lin, S.Y. Liu, N. Marques, G.H. Maunder, R. McDonald, A. Sella, J. Takats, M.R.J. Elsegood, Inorg. Chem. 41 (2002) 6761.
[22] (a) M. Visseaux, D. Baudry, A. Dormond, C. Qian, C.R. Acad. Sci. Paris, Serie II 323 (1996) 415;
(b) M. Visseaux, D. Baudry, A. Dormond, C. Qian, J. Organomet. Chem. 574 (1999) 213.
[23] D. Rais, J. Yau, D.M.P. Mingos, R. Vilar, A.J.P. White, D.J. Williams, Angew. Chem., Int. Ed. Engl. 40 (2001) 3464.
[24] R.J.H. Clark, S.Y. Liu, G.H. Maunder, A. Sella, M.R.J. Elsegood, J. Chem. Soc., Dalton Trans. (1997) 2241.
[25] D. Deng, X. Zheng, C. Qian, J. Sun, L. Zhang, J. Organomet. Chem. 466 (1994) 95.
[26] T. Arliguie, M. Lance, M. Nierlich, M. Ephritikhine, J. Chem. Soc., Dalton Trans. (1997) 2501.
[27] C. Qian, W. Nie, J. Sun, J. Organomet. Chem. 626 (2001) 171.
[28] S. Trofimenko, J. Am. Chem. Soc. 88 (1966) 1842.

Available online at www.sciencedirect.com
SCIENCE DIRECT®
Polyhedron 23 (2004) 263–271
POLYHEDRON
www.elsevier.com/locate/poly

Steric saturation of the ytterbium coordination environment: ($Tp^{tBu,Me}$)Yb(OMes), a four coordinate, monomeric, base-free divalent lanthanide complex, its solvation with tetrahydrofuran, and comparison to the β-diketonate complex, ($Tp^{tBu,Me}$)Yb(dpm)

Martin Morissette [a,1], Stefan Haufe [a,2], Robert McDonald [a], Gregory M. Ferrence [b,*], Josef Takats [a,*]

[a] *Department of Chemistry and Structure Determination Laboratory, University of Alberta, Edmonton, Alta., Canada T6G 2G2*
[b] *Department of Chemistry, Illinois State University, Campus Box 4160, Normal, IL 61790, USA*

Received 15 May 2003; accepted 20 August 2003

Dedicated to Jerry Trofimenko for being a constant inspiration to generations of "scorpionate" chemists, young and old.

Abstract

Reaction of ($Tp^{tBu,Me}$)Yb(I)(THF) with KOMes (Mes = 2,4,6-$C_6H_2Me_3$) in tetrahydrofuran (THF) at −45 °C afforded the monomeric divalent lanthanide aryloxide complex ($Tp^{tBu,Me}$)Yb(OMes)(THF) (**1**). Reaction of [($Tp^{tBu,Me}$)Yb(μ-H)]$_2$ ($Tp^{tBu,Me}$ = hydrotris(3-*tert*-butyl-5-methylpyrazolyl)borate) with HOMes in benzene at ambient temperature gave the monomeric solvent free lanthanide aryloxide complex ($Tp^{tBu,Me}$)Yb(OMes) (**2**). Dissolution of **2** in tetrahydrofuran at ambient temperature resulted in clean transformation to the solvated complex **1**. The coordinated THF ligand is persistent in non-ethereal solvents. Reaction of [($Tp^{tBu,Me}$)Yb(μ-H)]$_2$ with dipivaloylmethane (Hdpm) afforded the related β-diketonate complex ($Tp^{tBu,Me}$)Yb(dpm) (**3**). Complexes **1**–**3** have been fully characterized by spectroscopic methods and their structures were confirmed by X-ray crystallographic studies. Crystal data: $C_{38.5}H_{62.5}BN_6O_2Yb$ (**1**·0.25 C_6H_{14}): monoclinic, $C2/c$, $a = 21.526(4)$ Å, $b = 13.213(2)$ Å, $c = 31.403(7)$ Å, $\beta = 105.80(2)°$, $Z = 8$; $C_{33}H_{51}BN_6OYb$ (**2**): orthorhombic, $Pbcm$, $a = 10.5344(5)$ Å, $b = 20.3495(7)$ Å, $c = 16.3768(6)$ Å, $Z = 4$; $C_{35}H_{59}BN_6O_2Yb$ (**3**): monoclinic, $C2/c$, $a = 13.370(1)$ Å, $b = 21.134(2)$ Å, $c = 28.242(2)$ Å, $\beta = 97.356(2)°$, $Z = 8$.
© 2003 Elsevier Ltd. All rights reserved.

Keywords: Lanthanides; Ytterbium; Aryloxide; Crystal Structures; Tris(pyrazolyl)borate; Divalent

1. Introduction

The organometallic chemistry of divalent lanthanides has witnessed rapid and spectacular development with the introduction of the pentamethylcyclopentadienyl ligand system to this area of chemistry [1–3]. Much of the early work focused on the incorporation of two cyclopentadienyl supporting ligands around the divalent lanthanide, thereby limiting incorporation of additional ligands to neutral donors. Synthesis of a variety of homoleptic 'LnL_2'-type systems has expanded the range of supporting environments, but still limits ligand incorporation [4]. Some of these ancillary ligands have challenged the steric saturation limit around the metal center. In extreme instances such as Sm($Tp^{tBu,Me}$)$_2$ and Yb($Tp^{tBu,Me}$)$_2$, the steric demand of the ligand limits coordination to only 5 of the 6 pyrazolyl arms of the two commonly tridentate tris(pyrazolyl)borate ligands [5]. In order to allow for greater versatility, it was naturally of

* Corresponding author. Tel.: +1-3094387971; fax: +1-3094385538.
E-mail address: ferrence@ilstu.edu (G.M. Ferrence).
[1] Present address: C/D/N Isotopes, Point-Claire, Que., Canada H9R 1H1.
[2] Present address: Sartorius AG, 37079 Göttigen, Germany.

0277-5387/$ - see front matter © 2003 Elsevier Ltd. All rights reserved.
doi:10.1016/j.poly.2003.11.015

interest to investigate extensions of divalent lanthanide species to incorporate mixed anionic ligands.

Heteroleptic divalent lanthanide compounds are rare. Recent examples include some mixed C_5Me_5/ER (ER = OAr, SAr, NR^1R^2) Sm(II) complexes [6,7]. In this context, we and others have initiated an extensive investigation into the synthesis and reactivity of hydrotris(pyrazolyl)borate ($Tp^{R,R'}$) anchored lanthanide(II) complexes [8–10]. We have shown that the very bulky hydrotris(3-*tert*-butyl-5-methylpyrazolyl)borate ($Tp^{tBu,Me}$) ligand is well-suited to stabilize the mono-ligated complexes ($Tp^{tBu,Me}$)LnI(THF)$_x$ (Ln = Yb, $x = 1$; Sm, $x = 2$, 0), which proved to be good starting materials for the synthesis of heteroleptic ($Tp^{tBu,Me}$)LnER (THF)$_x$ (Ln = Sm, Yb; ER = $N(SiMe_3)_2$, CH_2SiMe_3, $CH(SiMe_3)_2$, $HBEt_3$; $x = 1$, 0) [10–12]. The subsequent isolation of solvent free [($Tp^{tBu,Me}$)YbH]$_2$, the first discrete Ln(II) hydride, is providing even greater versatility as illustrated by the recently reported alkynide, ene-diolate, and η^3-propargyl derivatives [13,14]. Here we report the synthesis and structural characterization of solvated and unsolvated heteroleptic ytterbium(II) complexes containing both pyrazolylborate and anionic oxygen donor groups.

2. Results and discussion

2.1. Synthesis and characterization of ($Tp^{tBu,Me}$)Yb(OMes)(THF)$_{1/0}$ (1, 2) and ($Tp^{tBu,Me}$)Yb(dpm) (3) complexes

Reaction of ($Tp^{tBu,Me}$)YbI(THF) [12] with one eq. of KOMes (Mes = 2,4,6-$C_6H_2Me_3$) in THF at −45 °C gave the heteroleptic ($Tp^{tBu,Me}$)Yb(OMes)(THF) (**1**), as a yellow-orange solid in 90% yield (Eq. (1)). The complex is air-sensitive, yet moderately stable in the solid state. Compound **1** is soluble in common aromatic and ethereal solvents. The coordinated THF molecule is retained in the former solvents but exchanges readily with bulk THF (^{1}H NMR spectroscopy). Although the coordinated THF in **1** is labile, simple trituration or heating under vacuum does not reliably produce the unsolvated complex **2**.

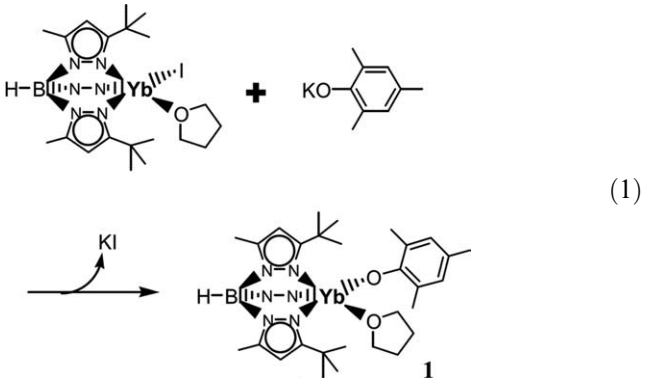

(1)

To prepare **2**, advantage was taken of our recently reported solvent free dinuclear ytterbium hydride, [($Tp^{tBu,Me}$)Yb(μ-H)]$_2$ [13,14]. This compound is proving useful for the high yield synthesis of a variety of solvent free divalent ytterbium complexes. Indeed, reaction of [($Tp^{tBu,Me}$)Yb(μ-H)]$_2$ with two eq. of HOMes (Mes = 2,4,6-$C_6H_2Me_3$) in benzene at room temperature readily gave the solvent free ($Tp^{tBu,Me}$)Yb(OMes) (**2**), as an orange solid in 98% yield (Eq. (2)). Similarly, reaction of [($Tp^{tBu,Me}$)Yb(μ-H)]$_2$ with two eq. of dipivaloylmethane in benzene at room temperature yielded the Yb(II) β-diketonate, ($Tp^{tBu,Me}$)Yb(dpm) (**3**), as a dark green solid in quantitative yield (Eq. (3)). The β-diketonate complex is relevant to the topic at hand since the ligand presents two oxygen donor functionalities and carries one negative charge, much like the aryloxide and THF ligands in **1**, but acting in tandem. Complex **3** is very soluble in a range of solvents. In addition to the common aromatic and ethereal solvents, it also dissolves in aliphatic solvents and dichloromethane. The compound does not appear to react with any of the solvents since its dark green color persists.

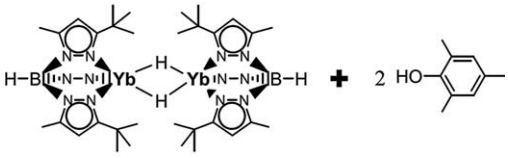

(2)

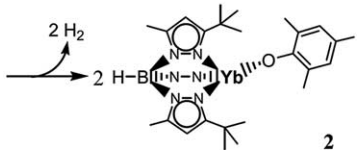

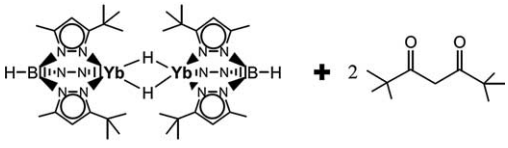

(3)

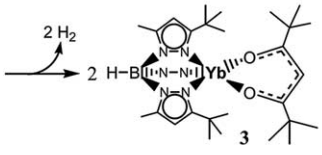

The formulations of the compounds are based on elemental analyses, IR, and multinuclear NMR data. The IR spectra of compounds **1**, **2**, and **3** showed B–H stretching vibrations at 2550, 2553, and 2550 cm^{-1}, respectively. Consistent with the κ^3 bonding of the $Tp^{tBu,Me}$ ligand, the ^{1}H NMR spectrum of **1** showed one set of signals for the $Tp^{tBu,Me}$ and OMes ligands. In C_6D_6, the coordinated THF signals appeared at 3.58 ppm and around 1.3 ppm, overlapped with the 3-^{t}Bu-pz peak. The relative integra-

tions of $Tp^{tBu,Me}$, OMes, and THF signals were in accord with the presence of one of each ligand on the ytterbium. In THF-d_8 the mesityl protons experience a more than 0.4 ppm upfield shift compared to benzene or toluene. The loss of coordinated THF resonances in THF-d_8 indicated rapid exchange between coordinated and bulk THF molecules. The ^{1}H NMR spectrum of the THF free complex **2** is surprisingly similar to that of **1**. In THF-d_8 the spectrum is identical to that observed for **1**, demonstrating rapid reaction of **2** with THF to form **1**. The ^{11}B and ^{171}Yb NMR spectra of **1** and **2**, however, show significant differences. Particularly noteworthy is the 70 ppm upfield shift of the ^{171}Yb resonance position in toluene-d_8, from 670 ppm (**2**) to 600 ppm (**1**). It is also interesting to note that the ^{171}Yb chemical shift of **1** experiences different temperature dependence in THF-d_8 than toluene-d_8. The resonance shifts upfield in THF-d_8 upon lowering the temperature whereas the opposite is seen in toluene-d_8. We have no definite explanation for this, but perhaps the larger temperature effects seen in THF-d_8 are related to the slowing down of exchange between coordinated and bulk THF. Large temperature effects were also seen by Lawless as a result of ligand exchange [15–17].

The ^{1}H and ^{13}C NMR spectra of compound **3** showed one set of resonances for both $Tp^{tBu,Me}$ and dpm ligands in the typical diamagnetic region. This observation confirmed the presence of the divalent Yb center, an important point in light of the unusual green color of complex **3**. The vast majority of Yb(II) complexes, including all $(Tp^{tBu,Me})YbL_n$ compounds reported to date, have colors ranging from red to yellow. Single peaks were also observed in the ^{11}B and ^{171}Yb NMR spectra. The ^{11}B chemical shift is similar to those of **1** and **2** further corroborating the diamagnetic nature of the complex. Surprisingly the ^{171}Yb NMR signal of **3** is highly deshielded and, at 1050 ppm, is more than 400 ppm downfield from its position in **1**. We have no rational to offer for the apparently unusual position of ^{171}Yb chemical shift.

Although leaving no doubt as to the composition of the compounds, the simple spectroscopic signatures did not resolve the details of the structures of the complexes. In particular, it was not clear whether the THF free **2** was a genuine four-coordinate Yb(II) complex and whether **3** was a simple, five-coordinate complex with a chelating dpm ligand or perhaps a dimer with bridging dpm moieties. To obtain unambiguous structures, coordination geometries, and precise metrical parameters, crystals of **1**, **2**, and **3** were subjected to single-crystal X-ray diffraction determinations.

2.2. Molecular structure of *1*, *2*, and *3*

The molecular structure and atom numbering scheme for crystalline **1**, **2**, and **3** are shown in Figs. 1, 2(a), and 3, respectively. The views are so chosen to emphasize the close structural relationship between the complexes.

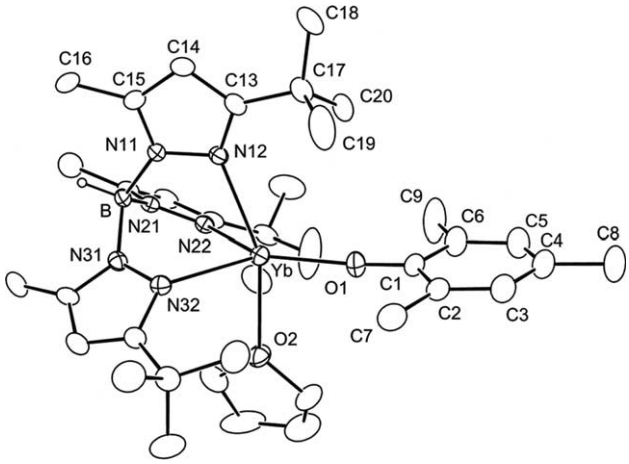

Fig. 1. ORTEP view of **1** showing the atomic numbering scheme. Drawn with 20% ellipsoids and hydrogen atoms omitted for clarity.

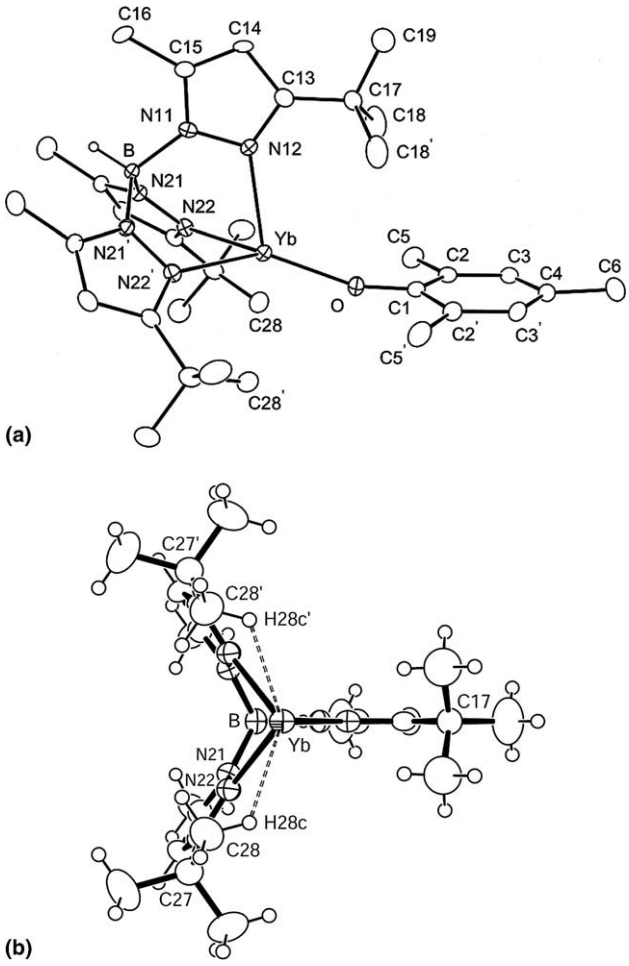

Fig. 2. (a) ORTEP view of **2** showing the atomic numbering scheme. Drawn with 20% ellipsoids and hydrogen atoms omitted for clarity. (b) ORTEP view of **2** depicting agostic Yb–H interactions. View is down Yb–B axis and OMes ligand has been omitted for clarity.

Selected bond lengths and angles are collected in Table 1 such that the corresponding metrical parameters are grouped together for ease of comparison. In this spirit,

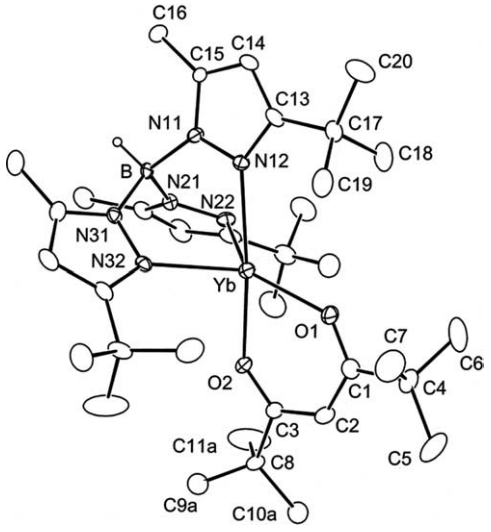

Fig. 3. ORTEP view of **3** showing the atomic numbering scheme. Drawn with 20% ellipsoids and hydrogen atoms omitted for clarity.

Table 1
Selected bond lengths (Å) and angles (°)

Parameter	**1** · $0.25C_6H_{14}$	**2**	**3**
Bond lengths			
Yb–O(1)	2.178(5)	2.168(7)	2.259(5)
Yb–O(2)	2.415(5)		2.308(5)
C(1)–O(1)	1.32(1)	1.32(1)	1.268(9)
C(3)–O(2)			1.256(8)
Yb–N(12)	2.465(5)	2.437(8)	2.504(5)
Yb–N(22)	2.525(6)	2.445(6)	2.452(5)
Yb–N(32)	2.511(6)		2.440(5)
C(1)–C(2)			1.41(1)
C(2)–C(3)			1.41(1)
Bond angles			
Yb–O(1)–C(1)	173.3(6)	162.1(7)	135.3(5)
Yb–O(2)–C(3)			135.2(5)
O(1)–Yb–O(2)	89.5(2)		75.8(2)
N(12)–Yb–O(1)	112.2(2)	117.2(3)	109.4(2)
N(22)–Yb–O(1)	133.5(2)	135.9(2)	135.1(2)
N(32)–Yb–O(1)	135.9(2)		130.9(2)
N(12)–Yb–O(2)	158.1(2)		174.8(2)
N(22)–Yb–O(2)	90.3(2)		98.4(2)
N(32)–Yb–O(2)	83.7(2)		98.8(2)
N(12)–Yb–N(22)	76.9(2)	83.5(2)	78.3(2)
N(22)–Yb–N(32)	90.2(2)	81.4(3)	94.1(2)
N(12)–Yb–N(32)	78.7(2)		77.5(2)
B–Yb–O(1)	161.5(2)	167.3(3)	159.8(3)
C(2)–C(1)–O(1)			123.9(7)
C(2)–C(3)–O(2)			123.0(7)
C(1)–C(2)–C(3)			126.3(8)

the numbering schemes for the three complexes were kept identical as much as possible. The exception is complex **2**, which has a crystallographically imposed mirror plane of symmetry and consequently fewer independent atoms.

The structural study established that each lattice consists of discrete well separated monomeric units with no unusual intermolecular contacts. Although this was the anticipated result, based on the sterically demanding nature of the $Tp^{tBu,Me}$ ligand, alternative dimeric structures for **2** and **3** could not be ruled out on the basis of spectroscopic data.

The Yb centers in **1** and **3** are five coordinate with typical κ^3-$Tp^{tBu,Me}$ ligands and two oxygen donors completing the coordination spheres; OMes and THF in **1**, and a bidentate dpm ligand in **3**. The coordination geometry is best described as a distorted trigonal bipyramid (tbp). Two pyrazolyl nitrogens (N22 and N32) and O1 form the triangular, equatorial plane and the third nitrogen (N12) and O2 occupy the axial positions. The distortions are the result of the constraints imposed by the bite-angles of the tripodal $Tp^{tBu,Me}$ ligand. These distortions are manifest as compression of the equatorial N22–Yb–N32 angle from the ideal 120° in tbp to 90° and 94°, and a corresponding opening of the equatorial angles N22–Yb–O1 and N32–Yb–O1 to 134°/135° and 136°/131° in **1** and **3**, respectively. Similarly, the axial N12–Yb–O2 angle deviates from the ideal tbp of 180°. This value is 158.1(2)° in **1** and the deviation can be traced directly to the $Tp^{tBu,Me}$ ligand, the N12–Yb–O1 angle is 112.2(2)°, some 22° larger than the 90° expected in a rigorous tbp geometry. Indeed the oxygen of the THF ligand, O2 lies nearly orthogonal to the equatorial plane with O2–Yb–O1, O2–Yb–N22 and O2–Yb–N32 angles of 89.5(2)°, 90.3(2)°, and 83.7(2)°, respectively. It is interesting that at first glance the N12–Yb–O2 angle of 174.8(2)° seems to imply a more regular tbp geometry for **3**, but it is in fact, the combined ligand constraints of $Tp^{tBu,Me}$ and dpm that conspire to make this angle close to 180°. Indeed the N12–Yb–O1 angle, 109.4(2)°, is 19.4° larger, whereas the O2–Yb–O1 angle, 75.8(2)°, is 14.2° smaller than the requisite 90° in a regular tbp.

It is instructive to compare the distorted tbp structure of **3** to those of the analogous (Tp^{Ph})M(acac) (M = Zn, Co; acac = pentane-2,4-dionate) complexes, which Kläui and co-workers [18] described as having "a nearly regular trigonal bipyramid" as a coordination geometry. Indeed the axial angle, N12–M–O2 (same numbering as here) is virtually 180° (179.5(1)° and 179.0(1)°), and this is not a consequence of some competing distortions as seen in **3**, since the N12–M–O1 and O2–M–O1 angles are also very close to 90° (90.2(1)°/88.4(1)° and 90.0(1)°/90.7(1)°, respectively). The one distortion that is in common with **3** is in the equatorial plane with one angle about 96° and the other two around 132°. Clearly both the hydrotris(pyrazolyl)borate and the β-diketonate ligands can match the smaller transition metal better than the larger lanthanide ions, and the consequences of the latter mismatch for lanthanides has been noted recently [19,20].

Kläui and co-workers [18] noted that in the above (Tp^{Ph})M(acac) complexes the axial ligand lengths were significantly longer than the equatorial ones. Although

the same trend is seen in **3** the differences are much less pronounced; axial Yb–O2, 2.308(5) Å versus equatorial Yb–O1, 2.259(5) Å and axial Yb–N12, 2.504(5) Å versus equatorial Yb–N22/N32, 2.452(5)/2.440(5) Å, respectively. This, presumably, is the consequence of the more ionic bonding present in the lanthanide complexes compared to their transitional metal analogs. This is also manifest in the solution structure of complex **3**. The unique ligand arrangement is not preserved in solution and the compound undergoes rapid fluxionality as revealed by ^{1}H and ^{13}C NMR spectroscopy.

The coordination environment of **1**, including axial THF and two equatorial pyrazolyl ligands, is very similar to the related $(Tp^{tBu,Me})Yb(CH_2SiMe_3)(THF)$ and $(Tp^{tBu,Me})Yb(\mu\text{-}HBEt_3)(THF)$ complexes [11,12]. The Yb–O2 distance of 2.415(5) Å is significantly shorter than observed in the latter two complexes, 2.482(3) and 2.481(5) Å, respectively. This perhaps indicates that the flat aryloxide ligand simply allows closer approach of the THF or, equally likely, the stronger Yb–O2(THF) interaction is due to the diminished basicity of the aryloxide compared to $Me_3SiCH_2^-/Et_3BH^-$ ligands which gives rise to a more electron deficient metal center in **1**.

The Yb–O1(Mes) distance of 2.178(5) Å is close to the corresponding values, 2.22(1) and 2.20(2) Å, seen in five-coordinate $Yb(OAr)_2(THF)_3$ [21] and is indistinguishable from the corresponding average values, 2.14(2), 2.15(3), and 2.179(9) Å, seen in the four-coordinate complexes $Yb(OAr)_2(THF)_2$ [21], $Yb(OAr)_2(OEt_2)_2$ [21], and $Yb(OAr)_2(HMPA)_2$ [22], respectively; Ar = 2,6-*t*Bu-4-R-C_6H_2 (R = Me) in each of these complexes. The Yb–O1(Mes) distance is ca. 0.22 Å shorter than Yb–O2(THF). This bond length difference is in the 0.2–0.3 Å range observed for other ytterbium aryloxide complexes [23], and the shortening is as expected from the stronger interaction between Yb(II) and the anionic aryloxide ligand.

Turning to the solvent free $(Tp^{tBu,Me})Yb(OMes)$ (**2**) complex, its monomeric nature is in contrast to the dimeric structure of the related divalent samarium complex $[(C_5Me_5)Sm(OAr)]_2$ (Ar = 2,6-*t*Bu-4-R-C_6H_2; R = H, Me, *t*Bu) [6]. Evidently the large cone angle of $Tp^{tBu,Me}$, 243°, compared to 146° for C_5Me_5 is capable of preserving the monomeric structure [24]. Another difference between the two complexes is their reaction with Lewis bases. Although with HMPA $[(C_5Me_5)Sm(OAr)]_2$ yields the monomeric $(C_5Me_5)Sm(OAr)(HMPA)_2$, dissolution in THF led to ligand redistribution and formation of $(C_5Me_5)_2Sm(THF)_2$ and $Sm(OAr)_2(THF)$; whereas, dissolution of **2** in THF simply leads to formation of **1**.

At first glance, the structure of **2** is simply obtained by removal of the coordinated THF ligand and the coordination geometry resembles that of a distorted tbp with an open coordination site. Although subtle differences exist between the "$(Tp^{tBu,Me})Yb(OMes)$" fragment of the five-coordinate **1** and the coordinately unsaturated four-coordinate **2**, the geometry of the latter is definitely not the regular trigonal pyramidal arrangement anticipated for a coordinately unsaturated ML_3L'-type complex. Indeed the three N–Yb–O angles are not the same and neither is the B–Yb–O angle 180° as would be in a regular trigonal pyramid. The N(12)–Yb–O angle of **2**, 117.2(3)°, is somewhat greater than the corresponding angle in **1**, 112.2(2)°, but the other angles, 135.9(2)° (equal by imposed crystal symmetry), are virtually identical to those in **1**, 135.9(2)° and 133.5(2)°. The B–Yb–O angle is 167.3(3)°, some 12.7° away from linearity in a regular trigonal pyramid. Similar distortions were seen in the related "four-coordinate" $(Tp^{tBu,Me})YbN(SiMe_3)_2$ and $(Tp^{tBu,Me})YbCH(SiMe_3)_2$ complexes with L being 18.6° and 15.0° off the B–Yb axis [12]. In the latter two cases the deviations were attributed to a combination of steric and electronic factors; steric repulsion between a ^{t}Bu-Tp substituent and an $SiMe_3$ group, and attractive agostic C–H interactions between the electron deficient ytterbium and the other $SiMe_3$ moiety of the ligands as evidenced by the respective shortest $N(SiMe_3)_2$ and $CH(SiMe_3)_2$ Yb–C_{Me} separations of 3.06 and 3.08 Å. Similar combinations of factors seem to be operating in complex **2** as well. The orientation of the OMes ligand is clearly to reduce steric interactions between the mesityl ring and the 3-^{t}Bu-Tp substituents. And complex **2** displays two 2.61 Å nonbonded interactions between ytterbium and the C28/28′ hydrogen atoms, Fig. 2(b). These agostic C–H interactions serve to reduce the electron deficiency of ytterbium and may be considered as occupying the "vacant fifth" coordination sites. No such interactions are present in the THF solvated complex **1**; the closest Yb–H separation is 2.95 Å.

Comparison of the distance parameters reveals further similarities between **1** and **2**, and indeed **3**. The average Yb–N distance in **2** is 2.44(1) Å, only marginally greater than the related 2.50(2) Å average distance in **1**, and the two bracket the average Yb–N separation of 2.47(2) Å found in **3**. These distances compare favorably with the analogous Yb–N bond lengths in related $(Tp^{tBu,Me})LnL_n$ complexes [8,12,13,25,26]. The Yb–O(Mes) ligand distances for **1** and **2**, 2.178(5) and 2.168(7) Å, are again indistinguishable and further argue for the presence of agostic C–H···Yb interaction and concurrent reduced electron deficiency of Yb in **2**. As mentioned already in discussing the structure of **1**, the distances compare well with the corresponding value in divalent ytterbium aryloxide complexes.

Interestingly, the Yb–O–C1 angle of 162.1(7)° in **2** differs by more than 10° from that in **1**, 173.3(6)°, and, curiously, the mesityl moiety bends further away from the "open" coordination site toward the ^{t}Bu group on C13. Although the angles are different, both values are

in the typical range observed for divalent lanthanide aryloxide complexes. [3] The variation in M–O–R angle in metal–alkoxide complexes was recently discussed by Russo et al. [27], and the near linearity of such bonds in lanthanide complexes was attributed to electrostatic repulsion between the metal and α-carbon of the alkoxide ligand, as compared to the more popularly held view that linearity of M–O–R and shortness of the M–OR bond were due to the π-type interaction between metal and oxygen donor. These authors, and others [28], noted also the softness of the bending potential and, consequently, the role of steric factors influencing the M–O–R angle. On the basis of purely electrostatic arguments, the Yb–O–C1 angle of **2** should in fact be closer to 180° than that of **1**, as the more electron deficient and hence more highly charged ytterbium of the Lewis base free **2** should lead to greater polarization of the O–C1 bond than in complex **1**. The larger charges on Yb and C1 in **2**, and the attendant increase in electrostatic repulsion should result in a more linear Yb–O–C1 angle, contrary to the experimental results. We are thus left with steric effects as being responsible for the more bent Yb–O–C(Mes) moiety in **2**. As mentioned, it is curious that the bending of the mesityl ring in **2** is not toward but away from the "empty" coordination site. It appears that the bending follows the opening up of the N12–Yb–O angle of 112.2(2)° in **1** to 117.2(3)° in **2** and in fact the non-bonding C19/C20···O1 and C18/C18′···O distances in **1** and **2**, respectively, remain fairly constant.

3. Conclusions

By exploiting the solvent free nature of divalent $[(Tp^{tBu,Me})YbH]_2$, preparation of low coordinate, solvent free, divalent lanthanide complexes is possible as illustrated by the isolation of $(Tp^{tBu,Me})Yb(OMes)$ (**2**) and $(Tp^{tBu,Me})Yb(dpm)$ (**3**). The use of the sterically demanding $Tp^{tBu,Me}$ ligand allows isolation and X-ray characterization of the coordinatively unsaturated four-coordinate complex **2**. While bulky, the $Tp^{tBu,Me}$ ligand is barely sufficient to stabilize complex **2**, which in fact features two agostic C–H···Yb interactions. It also readily and irreversibly takes up THF to form **1**. The $Tp^{tBu,Me}$ ligand optimally supports the formation of five-coordinate ytterbium(II) complexes as illustrated by the lack of reactivity complex **3** demonstrates towards polar coordinating solvents.

[3] Cambridge Structural Database Search, 2003 (April), 23 hits for divalent lanthanide aryloxide complexes. Min Ln–O–C = 150.36°; max Ln–O–C = 178.4°; average Ln–O–C = 169.2°. For specific citations see CCDC refcodes: FIDQEO, IBIFAA, JOTSAM10, PEFMUI, PIZBOB10, RIJROR, VATTAL, VATTEP, VATTIT10, RELNAX, RELNEB, WIBVAE, YIKDEB, YIKDIF01, YUGHIR10, NIQTEM, and YURVAI.

4. Experimental

4.1. General

All manipulations were carried out under an inert N_2/He atmosphere in a Vacuum Atmosphere HE-553-2 Dri Lab or MBraun Unilab 2000. Glassware and solvents were treated as described previously [5]. $(Tp^{tBu,Me})YbI(THF)$ and $[(Tp^{tBu,Me})YbH]_2$ were prepared according to published procedures [12,13].

Infrared (IR) spectra were recorded on a Bomem MB/100 or Perkin–Elmer 1600 series FT spectrometer. NMR samples were prepared in a glove box and sealed under vacuum. The spectra were obtained on a Brüker AM-400 or Varian Unity 500 (^{171}Yb) FT spectrometer. Chemical Shifts are reported in ppm relative to TMS (^{1}H, ^{13}C), $F_3B\cdot OEt_2$ (^{11}B) and $Yb(C_5Me_5)_2(THF)_2$ (^{171}Yb). ^{171}Yb spectra were reproducible to within 5 ppm from sample to sample and reproducible to with 2 ppm on a given sample. Variable temperature measurements were collected on a given sample in a single sitting. Elemental analyses were performed by the Microanalytical Laboratory, Department of Chemistry, University of Alberta. Dipivaloylmethane and HO-(2,4,6-$Me_3C_6H_2$) were used as obtained from Aldrich. KO-(2,4,6-$Me_3C_6H_2$) was prepared by reaction of HO-(2,4,6-$Me_3C_6H_2$) with an excess of potassium hydride in THF.

4.2. Preparation of $(Tp^{tBu,Me})Yb(O\text{-}\{2,4,6\text{-}Me_3C_6H_2\})(THF)$ (1)

To a solution of $(Tp^{tBu,Me})YbI(THF)$ (400 mg, 0.50 mmol) in 5 ml THF at −45 °C was added dropwise a solution of KO-(2,4,6-$Me_3C_6H_2$) (88 mg, 0.50 mmol) in 5 ml THF at −45 °C. The mixture was stirred for 1 h while allowing it to warm to room temperature. The color of solution changed from yellow to orange. The mixture was centrifuged to remove KI, then the decanted volume was reduced under vacuum to ca. 2 ml. Cooling this solution to −45 °C followed by isolation of the precipitate gave 364 mg of $(Tp^{tBu,Me})Yb(O\text{-}\{2,4,6\text{-}Me_3C_6H_2\})(THF)$ (**1**) as a yellow/orange solid (Yield: 90%). IR (C_6H_6, cm^{-1}): ν_{B-H} 2550. MS (EI, 70 eV, 270 °C): m/z 735 (M^+–THF). ^{1}H NMR (THF-d_8, 25 °C, ppm): 6.50 (s, 4-OAr–*H*), 5.81 (s, 4-pz-*H*), 3.58 (s, *THF*), 2.32 (s, pz-CH_3), 2.11 (s, 2,6-OAr–CH_3), 2.03 (s, 4-OAr–CH_3), 1.34, 1.30 (s, s C(CH_3)$_3$ in 2:1 with buried *THF*). ^{1}H NMR (C_7D_8, 25 °C, ppm): 5.70 (s, 4-pz-*H*), 3.45 (s, *THF*), 2.54 (s, 2,6-OAr–CH_3), 2.43 (s, 4-OAr–CH_3), 2.20 (s, pz-CH_3), 1.45 (s, C(CH_3)$_3$, buried *THF*). ^{1}H NMR (C_6D_6, 25 °C, ppm): 7.19 (s, 4-OAr–*H*), 5.72 (s, 4-pz-*H*), 3.75 (s, *THF*), 2.61 (s, 2,6-OAr–CH_3), 2.48 (s, 4-OAr–CH_3), 2.20 (s, pz-CH_3), 1.38 (s, C(CH_3)$_3$, buried *THF*). ^{11}B NMR (THF-d_8, 25 °C, ppm): −6.8 (s). ^{171}Yb NMR (THF-d_8, 25 °C, ppm): 600 ($\Delta\nu_{1/2} = 40$ Hz). *Anal.*

Calc. for $C_{37}H_{59}BN_6O_2Yb$: C, 55.29; H, 7.40; N, 10.46. Found: C, 54.05; H, 6.86; N, 10.02%.

4.3. Preparation of $(Tp^{tBu,Me})Yb(O\text{-}\{2,4,6\text{-}Me_3C_6H_2\})$ (2)

To a benzene solution of $[(Tp^{tBu,Me})YbH]_2$ (400 mg, 0.335 mmol) was added a benzene solution of HO-(2,4,6-$Me_3C_6H_2$) (91 mg, 0.668 mmol) at R.T. The color of solution changed from red to orange. After stirring for 30 min, the solvent was removed under vacuum giving 480 mg of $(Tp^{tBu,Me})Yb(O\text{-}\{2,4,6\text{-}Me_3C_6H_2\})$ (**2**) as a orange solid (Yield: 98%). IR (C_6H_6, cm^{-1}): ν_{B-H} 2553. ^1H NMR (C_7D_8, 25 °C, ppm): 7.13 (s, 4-OAr–H), 5.65 (s, 4-pz-*H*), 2.47 (s, 2,6-OAr–CH_3), 2.40 (s, 4-OAr–CH_3), 2.17 (s, pz-CH_3), 1.34 (s, $C(CH_3)_3$). ^1H NMR (C_6D_6, 25 °C, ppm): 5.67 (s, 4-pz-*H*), 2.56 (s, 2,6-OAr–CH_3), 2.45 (s, 4-OAr–CH_3), 2.17 (s, 5-pz-CH_3), 1.35 (s, $C(CH_3)_3$). ^{13}C NMR, APT (C_6D_6, 25 °C, ppm, ^1H cross peaks {x} from HMQC): 163.9 (3-pz-*C*), 145.7 (5-pz-*C*), 129.2 (3,5-C_6), 128, 124.7, 121.2 (1-C_6,2-C_6,4,6-C_6), 102.9 (4-pz-*C*, {× 5.67}), 32.0 ($C(CH_3)_3$), 31.2 ($C(CH_3)_3$, {× 1.35}), 21.2 (4-ArCH_3, {× 2.45}), 19.7 (2,6-ArCH_3, {× 2.56 }), 13.4 (pz-CH_3, {× 2.17}). ^{11}B NMR (THF-d_8, 25 °C, ppm): −7.9 ($\Delta\nu_{1/2} = 240$ Hz). ^{171}Yb NMR (C_7D_8, 25 °C, ppm): 670 ($\Delta\nu_{1/2} = 240$ Hz). *Anal.* Calc. for $C_{33}H_{51}BN_6OYb$: C, 54.17; H, 7.02; N, 11.48. Found: C, 54.18; H, 6.97; N, 10.61%.

4.4. Reaction of $(Tp^{tBu,Me})Yb(O\text{-}\{2,4,6\text{-}Me_3C_6H_2\})$ with THF

Solid **2** (205 mg, 0.335 mmol) was dissolved in 5 ml THF. The orange solution was stirred 30 min, then the solvent was removed under vacuum giving 234 mg of $(Tp^{tBu,Me})Yb(O\text{-}\{2,4,6\text{-}Me_3C_6H_2\})(THF)$ (**1**) as a yellow/orange solid in quantitative yield. Assignment of this product as compound **1** was confirmed by ^1H NMR. ^{171}Yb NMR (THF-d_8, 25 °C, ppm): 590 ($\Delta\nu_{1/2} = 40$ Hz) (−40 °C, 550 ppm) (−80 °C, 460 ppm). ^{171}Yb NMR (C_7D_8, 25 °C, ppm): 600 ($\Delta\nu_{1/2} = 60$ Hz) (−40 °C, 620 ppm) (−80 °C, 630 ppm).

4.5. Preparation of $(Tp^{tBu,Me})Yb\{(CH_3)_3C(O)CHC(O)C(CH_3)_3\}$ (3)

To a slurry of $[(Tp^{tBu,Me})YbH]_2$ (451 mg, 0.377 mmol) in 10 ml benzene was added 158 μl (0.755 mmol) of dipivaloylmethane at R.T. The color of solution instantly changed from red to dark green with evolution of H_2 gas. The solvent was removed under vacuum giving 603 mg of $(Tp^{tBu,Me})Yb(OCC\{CH_3\}_3)_2CH$ (**3**) as a green solid in quantitative yield. IR (C_6H_6, cm^{-1}): ν_{B-H} 2550. ^1H NMR (C_7D_8, 25 °C, ppm): 7.15 (s, small C_6H_6 impurity) 5.89 (s, piv-C*H*), 5.71 (s, 4-pz-*H*), 4.5 (s, vbr, B*H*), 2.17 (s, pz-CH_3), 1.39 (s, pz-$C(CH_3)_3$), 1.25 (s, piv-$C(CH_3)_3$). ^{13}C NMR, APT (C_6D_6, 25 °C, ppm): 198.9 (piv-O-*C*), 163.1 (3-pz-*C*), 145.4 (5-pz-*C*), 102.7 (4-pz-*C*), 91.9 (piv-*C*H), 41.5 (piv-$C(CH_3)_3$), 32.2 (pz-$C(CH_3)_3$), 31.0 ($C(CH_3)_3$), 28.7 (piv-$C(CH_3)_3$), 13.5 (pz-CH_3). ^{11}B NMR (C_7D_8, 25 °C, ppm): −7.6 ($\Delta\nu_{1/2} = 240$ Hz). ^{171}Yb NMR (C_7D_8, 25 °C, ppm): 1050 ($\Delta\nu_{1/2} = 100$ Hz). *Anal.* Calc. for $C_{35}H_{59}BN_6O_2Yb$: C, 53.91; H, 7.63; N, 10.78. Found: C, 54.44; H, 7.74; N, 10.44%.

4.6. X-ray structure determination of $(Tp^{tBu,Me})Yb(O\text{-}\{2,4,6\text{-}Me_3C_6H_2\})(THF)\cdot 0.25C_6H_{14}$ ($\mathbf{1}\cdot 0.25C_6H_{14}$)

Red-orange crystals of $(Tp^{tBu,Me})Yb(O\text{-}\{2,4,6\text{-}Me_3C_6H_2\})(THF)\cdot 0.25C_6H_{14}$ ($\mathbf{1}\cdot 0.25C_6H_{14}$) were obtained from a hexane solution. Data were collected on a Enraf-Nonius CAD4 automated diffractometer using Mo Kα radiation at −50 °C. Unit cell parameters were obtained using the automatic peak search and reflection indexing programs. [4] The systematic absences indicated the space group to be *Cc* (No. 9) [29] or *C*2/*c* (No. 15) [30]; the latter was chosen based on the cell volume and molecular occupancy, and was confirmed by the successful solution and refinement of the structure. The cell constants and orientation matrix were obtained from a least-squares refinement of the setting angles of 24 reflections in the range $19.6° < 2\theta < 25.5°$.

The intensity data were collected with ω scans at 6.7–1.7° min^{-1} (in θ). The scan range and aperture width were varied as a function of θ to compensate for the $\alpha_1 - \alpha_2$ wavelength dispersion: ω scan width $= (0.80 + 0.344\tan\theta)°$ and aperture width $= (3.00 + \tan\theta)$ mm.

The backgrounds for the peaks were measured by extending the scan by 25% on either side of the calculated range; this gave a peak-to-background counting time ratio of 2:1. Intensity measurements were made out to a maximum 2θ of 50.0°. Three reflections were chosen as intensity and orientation standards, and these were remeasured after every 120 min of exposure time to check on crystal and electronic stability over the course of data collection; no appreciable decay was evident.

The positions of most of the non-hydrogen atoms of ($\mathbf{1}\cdot 0.25C_6H_{14}$) were determined using the direct methods program SHELXS-86 [31], and refinement was completed using the program SHELXL-93 [32]. Hydrogen atoms were assigned positions based on the geometries of their attached carbons, and were given thermal parameters of 20% greater than those of the attached carbons. The final model for **2** refined to values of $R_1(F) = 0.0441$ (for 4466 data with $F^2 > 2\sigma(F^2)$) and

[4] Programs for diffractometer operation, data collection, data reduction and absorption correction were those supplied by Enraf-Nonius for the CAD4 diffractometer.

Table 2
Summary of crystallographic data

Compound	$1 \cdot 0.25C_6H_{14}$	2	3
Formula	$C_{38.5}H_{62.5}BN_6O_2Yb$	$C_{33}H_{51}BN_6OYb$	$C_{35}H_{59}BN_6O_2Yb$
Formula weight	825.29	731.65	779.73
Crystal dimensions (mm)	$0.80 \times 0.50 \times 0.30$	$0.34 \times 0.15 \times 0.14$	$0.20 \times 0.13 \times 0.05$
Crystal system	monoclinic	orthorhombic	monoclinic
Space group	$C2/c$ (No. 15)	*Pbcm* (No. 57)	$C2/c$ (No. 15)
Unit cell parameters			
a (Å)	21.526(4)	10.5344(5)	13.370(1)
b (Å)	13.213(2)	20.3495(7)	21.134(2)
c (Å)	31.403(7)	16.3768(6)	28.242(2)
β (°)	105.80(2)		97.356(2)
V (Å^3)	8594(5)	3510.7(2)	7914(1)
Z	8	4	8
ρ_{calcd} (g cm^{-3})	1.276	1.384	1.309
μ (mm^{-1})	2.213	5.171	2.399
Reflection (parameter)	7495(442)	2477(213)	7538(418)
$R_1(F)$	0.0441	0.0546	0.0481
$wR_2(F^2)$	0.1341	0.1409	0.0758
Goodness-of-fit	1.058	1.122	0.774

$wR_2(F^2) = 0.1341$ (for all 7495 independent data). The highest peak in the final difference Fourier map has a density of 1.41 e Å^{-3}, and is without chemical significance.

4.7. X-ray structure determination of ($Tp^{tBu,Me}$)Yb(O-{2,4,6-$Me_3C_6H_2$}) (2)

Orange crystals of ($Tp^{tBu,Me}$)Yb(O-{2,4,6-$Me_3C_6H_2$}) (**2**) were isolated. Data were collected on a Siemens P4/RA diffractometer using Cu Kα radiation at −60 °C. [5] Unit cell parameters were obtained from a least-squares refinement of 46 reflections with $44° < 2\theta < 49.6°$. The systematic absences indicated the space group to be *Pbcm* (No. 57) [33]. The data were corrected for absorption through use of face indexes Gaussian integration. See Table 2 for a summary of crystal data and X-ray collection information.

The structure of **2** was solved using the direct methods program SHELXS-86 [31] and refinement was completed using the program SHELXL-93 [32]. Hydrogen atoms were assigned positions based on the geometries of their attached carbons, and were given thermal parameters of 20% greater than those of the attached carbons. The final model for **2** refined to values of $R_1(F) = 0.0546$ (for 1998 data with $F^2 > 2\sigma(F^2)$) and $wR_2(F^2) = 0.1409$ (for all 2477 independent data). The highest peak in the final difference Fourier map has a density of 2.47 e Å^{-3}, and is without chemical significance.

4.8. X-ray structure determination of ($Tp^{tBu,Me}$)Yb(OCC{CH_3}$_3$)CH (3)

Dark green crystals of ($Tp^{tBu,Me}$)Yb(OCC{CH_3}$_3$)$_2$CH (**3**) were isolated by concentration of a pentane solution by removal of pentane by slow diffusion into toluene at −80 °C in a closed system. Data were collected on a Bruker P4/RA/SMART 1000 CCD diffractometer using Mo Kα radiation at −80 °C. [6] Unit cell parameters were obtained from a least-squares refinement of 5419 centered reflections from the data collection. The systematic absences indicated the space group to be $C2/c$ (No. 15) [30]. The data were corrected for absorption through use of the SADABS procedure. See Table 2 for a summary of crystal data and X-ray collection information.

The structure of **3** was solved using the direct methods program SHELXS-86 [31] and refinement was completed using the program SHELXL-93 [32]. The dpm ^{t}Bu group containing quaternary carbon C8 exhibited a rotational disorder that was dealt with by refining carbon atoms C9A, C10A and C11A with an occupancy factor of 0.7. C9B, C10B, and C11B were refined with an occupancy factor of 0.3, and the pairs of carbon atoms (e.g., C9A and C9B) were rotationally opposed 180° to each other about the C3-C8 bond and were assigned common anisotropic thermal parameters. Hydrogen atoms were assigned positions based on the geometries of their attached carbons, and were given thermal parameters of 20% greater than those of the attached carbons. The final model for **3** refined to values of $R_1(F) = 0.0481$ (for 3744 data with

[5] Programs for diffractometer operation, data collection, data reduction and absorption correction were those supplied by Siemens.

[6] Programs for diffractometer operation, data collection, data reduction and absorption correction were those supplied by Bruker Advanced X-ray Solutions: Madison, WI, 1999.

$F^2 > 2\sigma(F^2)$) and $wR_2(F^2) = 0.0758$ (for all 7538 independent data). The deepest hole in the final difference Fourier map has a density of −0.86 e $Å^{-3}$, and is without chemical significance.

5. Supplementary material

Tables of final atomic coordinates, thermal parameters, and interatomic distances, angles, and torsional angles have been deposited with the Cambridge Crystallographic Data Centre, CCDC Nos. 211165, 211166, and 211167. Copies of this information may be obtained free of charge from The Director, CCDC, 12 Union Road, Cambridge, CB2 1EZ, UK (fax: +44-1223-336-033; e-mail: deposit@ccdc.ca.ac.uk or www: http://www.ccdccam.ac.uk).

Acknowledgements

The authors thank the Natural Sciences and Engineering Research Council of Canada, the University of Alberta, Research Corporation (G.M.F.), and Illinois State University for financial support, and NSF-NATO (USA) for the award of a postdoctoral fellowship (G.M.F.) at Alberta. We would also like to thank Professor M. Cowie of University of Alberta for use of his diffractometer for collection of data used in structure determination of complex **1**, and Dr. X.W. Zhang for advice and technical assistance.

References

[1] W.J. Evans, Polyhedron 6 (1987) 803.
[2] C.J. Schaverien, Adv. Organomet. Chem. 36 (1994) 283.
[3] F.T. Edelmann, in: G. WilkinsonF.G.A. Stone, E.W. Abel (Eds.), Comprehensive Organometallic Chemistry, vol. 4, 2nd ed., Elsevier, Oxford, 1995, p. 11 (Chapter 2).
[4] F.T. Edelmann, Angew. Chem., Int. Ed. Engl. 34 (1995) 2466.
[5] X. Zhang, R. McDonald, J. Takats, New J. Chem. 19 (1995) 573.
[6] Z. Hou, Y. Zhang, T. Yoshimura, Y. Wakatsuki, Organometallics 16 (1997) 2963.
[7] Z. Hou, J. Alloys Compd. 203–204 (2000) 75.
[8] G.H. Maunder, A. Sella, D.A. Tocher, J. Chem. Soc., Chem. Commun. (1994) 885.
[9] A. Domingos, J. Marcalo, N. Marques, A.P. Dematos, A. Galvao, P.C. Isolani, G. Vincenti, K. Zinner, Polyhedron 14 (1995) 3067.
[10] J. Takats, J. Alloys Compd. 249 (1997) 52, and references therein.
[11] X.W. Zhang, Thesis, University of Alberta, 1995.
[12] L. Hasinoff, J. Takats, X.W. Zhang, A.H. Bond, R.D. Rogers, J. Am. Chem. Soc. 116 (1994) 8833.
[13] G.M. Ferrence, R. McDonald, J. Takats, Angew. Chem., Int. Ed. Engl. 38 (1999) 2233.
[14] G.M. Ferrence, J. Takats, J. Organomet. Chem. 647 (2002) 84.
[15] J.M. Keates, G.A. Lawless, in: M. Gielen, R. Willem, B. Wrackmeyer (Eds.), Advanced Application of NMR to Organometallic Chemistry, Wiley, New York, 1996, p. 357.
[16] A.G. Avent, M.A. Edelman, M.F. Lappert, G.A. Lawless, J. Am. Chem. Soc. 111 (1989) 3423.
[17] J.M. Keates, G.A. Lawless, M.P. Waugh, J. Chem. Soc., Chem. Commun. (1996) 1627.
[18] A. Kremer-Aach, W. Kläui, R. Bell, A. Sterath, H. Wunderlich, D. Mootz, Inorg. Chem. 36 (1997) 1552.
[19] N. Marques, A. Sella, J. Takats, Chem. Rev. 102 (2002) 2137.
[20] A. Domingos, M.R.J. Elsegood, A.C. Hillier, G. Lin, S.Y. Liu, I. Lopes, N. Marques, G.H. Maunder, R. McDonald, A. Sella, J.W. Steed, J. Takats, Inorg. Chem. 41 (2002) 6761.
[21] G.B. Deacon, P.B. Hitchcock, S.A. Holmes, M.F. Lappert, P. MacKinnon, R.H. Newnham, J. Chem. Soc., Chem. Commun. (1989) 935.
[22] Z. Hou, H. Yamazaki, K. Kobayashi, Y. Fujiwara, H. Taniguchi, J. Chem. Soc., Chem. Commun. (1992) 722.
[23] G.B. Deacon, T. Feng, P. MacKinnon, R.H. Newnham, S. Nickel, B.W. Skelton, A.H. White, Aust. J. Chem. 46 (1993) 387.
[24] S. Trofimenko, Scorpionates: The Coordination Chemistry of Polypyrazolylborate Ligands, Imperial College Press, London, 1999, p. 105.
[25] A.C. Hillier, A. Sella, M.R.J. Elsegood, J. Chem. Soc., Dalton Trans. (1998) 3871.
[26] G.M. Ferrence, R. McDonald, M. Morissette, J. Takats, J. Organomet. Chem. 596 (2000) 95.
[27] M.R. Russo, N. Kaltsoyannis, A. Sella, J. Chem. Soc., Chem. Commun. (2002) 2458.
[28] W.A. Howard, T.M. Trnka, G. Parkin, Inorg. Chem. 34 (1995) 5900.
[29] T. Hahn (Ed.), International Tables for Crystallography, vol. A, Kluwer Academic Publishers, Boston, MA, 2002, p. 152.
[30] T. Hahn (Ed.), International Tables for Crystallography, vol. A, Kluwer Academic Publishers, Boston, MA, 2002, p. 192.
[31] G.M. Sheldrick, Acta Crystallogr., Sect. A 46 (1990) 467.
[32] G.M. Sheldrick, SHELXL-93: Program for the Refinement of Crystal Structures, Univeristy of Göttingen, Germany, 1993.
[33] T. Hahn (Ed.), International Tables for Crystallography, vol. A, Kluwer Academic Publishers, Boston, MA, 2002, p. 286.

Available online at www.sciencedirect.com
SCIENCE DIRECT®
Polyhedron 23 (2004) 273–282
POLYHEDRON
www.elsevier.com/locate/poly

Fluorinated tris(pyrazolyl)borates. Syntheses and characterization of sodium and copper complexes of $[HB(3\text{-}(CF_3),5\text{-}(Ph)Pz)_3]^-$

H.V. Rasika Dias [a,b,*], Timothy K.H.H. Goh [a]

[a] Department of Chemistry and Biochemistry, The University of Texas at Arlington, Box 19065, Arlington, TX 76019-0065, USA
[b] Institute of Fundamental Studies, Hantana Road, Kandy, Sri Lanka

Received 16 May 2003; accepted 11 August 2003

Abstract

Sodium salt of the fluorinated tris(pyrazolyl)borate ligand $[HB(3\text{-}(CF_3),5\text{-}(Ph)Pz)_3]^-$ has been synthesized from the corresponding pyrazole and $NaBH_4$ in high yield. It forms stable adducts with oxygen-based donors like THF and water. $[HB(3\text{-}(CF_3),5\text{-}(Ph)Pz)_3]Na(THF)$ is monomeric in the solid state whereas $\{[HB(3\text{-}(CF_3),5\text{-}(Ph)Pz)_3]Na(H_2O)\}_n$ forms a polymeric chain structure. These tris(pyrazolyl)boratosodium adducts show intra and/or inter-molecular sodium–fluorine interactions. X-ray crystal structures of $[HB(3,5\text{-}(CF_3)_2Pz)_3]Na(OEt_2)$ and $\{[HB(3\text{-}(CF_3),5\text{-}(CH_3)Pz)_3]Na(H_2O)\}_2$ also display similar CF···Na contacts. The copper carbon monoxide complex $[HB(3\text{-}(CF_3),5\text{-}(Ph)Pz)_3]CuCO$ was prepared by treating $[HB(3\text{-}(CF_3),5\text{-}(Ph)Pz)_3]Na(THF)$ with CuOTf in the presence of CO. The infra-red stretching frequency data show relatively high ν_{CO} value (2103 cm^{-1}) indicating the presence of highly electrophilic copper site on $[HB(3\text{-}(CF_3),5\text{-}(Ph)Pz)_3]CuCO$. Crystal structure of 3-(CF_3),5-(Ph)PzH is also reported. It forms "tub" shaped tetramers in the solid state.
© 2003 Elsevier Ltd. All rights reserved.

Keywords: Sodium; Copper; Tris(pyrazolyl)borate; Fluorinated; Carbonyl

1. Introduction

Fluorinated ligands play an important role in many applications [1–4]. Metal adducts of the fluorinated ligands often show very different physical and chemical properties relative to their nonfluorinated analogs. For example, polyfluorinated ligands commonly improve the volatility, oxidation resistance, thermal stability, and fluorocarbon solubility of their metal adducts. They have also been known to improve the activity and/or selectivity of certain metal-catalyzed reactions. Fluorinated ligands are highly desired for applications in fluorous-biphase and supercritical CO_2 media [5–9]. Weakly coordinating, fluorinated anions also play an important role in chemistry [10]. Consequently, there is a considerable interest in the synthesis and applications of fluorinated ligands.

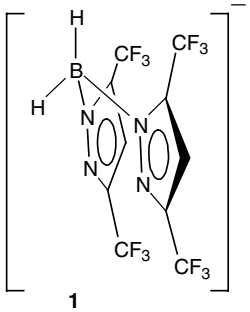

1

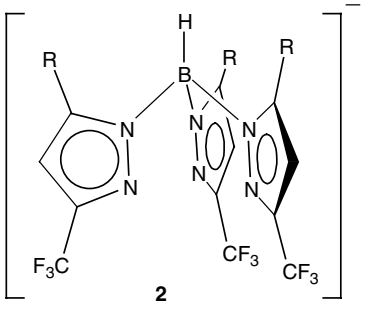

2

Despite the importance and wide utility of poly(pyrazolyl)borate ligands, relatively little is known about their fluorinated versions [11]. Over the past few years, we have reported the synthesis and use of several poly(pyrazolyl)borates containing fluoroalkyl substituents [2,12–16]. These include $[H_2B(3,5\text{-}(CF_3)_2Pz)_2]^-$ (**1**), $[HB(3\text{-}(CF_3)Pz)_3]^-$ (**2**, where R = H), $[HB(3\text{-}(C_2F_5)Pz)_3]^-$, $[HB(3\text{-}(C_3F_7)Pz)_3]^-$, and $[HB(3,5\text{-}(CF_3)_2Pz)_3]^-$ (**2**, where $R = CF_3$). Their metal adducts show very interesting properties. For example, the copper(I) carbonyl and ethylene adducts $[HB(3,5\text{-}(CF_3)_2Pz)_3]CuCO$ [17] and $[HB(3,5\text{-}(CF_3)_2Pz)_3]Cu(\eta^2\text{-}C_2H_4)$ [16] are air

* Corresponding author. Tel.: +817-272-3813.
E-mail address: dias@uta.edu (H.V. Rasika Dias).

0277-5387/$ - see front matter © 2003 Elsevier Ltd. All rights reserved.
doi:10.1016/j.poly.2003.11.016

and thermally stable solids. It is also possible to obtain the corresponding silver(I) complexes [18,19]. The $[HB(3,5\text{-}(CF_3)_2Pz)_3]AgCO$ (**3**) is an example of a metal carbonyl where the bonding between the metal and the CO is essentially of σ-type (with little to no π-backbonding) [20]. Its carbonyl stretching frequency (ν_{CO} = 2178 cm^{-1}) is higher than that of free CO (2143 cm^{-1}). $[HB(3,5\text{-}(CF_3)_2Pz)_3]CuNNN(1\text{-}Ad)$ and $[HB(3,5\text{-}(CF_3)_2Pz)_3]AgN(1\text{-}Ad)NN$ (**4**) represent rare, thermally stable organo azide–metal complexes [21].

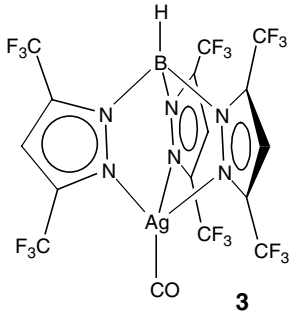

3

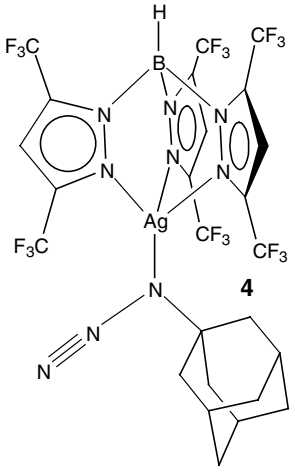

4

The $[HB(3\text{-}(CF_3),5\text{-}(CH_3)Pz)_3]^-$ ligand (**2** where R = CH_3), which was reported by Graham et al, has also shown to be useful in stabilizing rare, reactive and/or labile molecules like the hydrido vinyl species $[HB(3\text{-}(CF_3),5\text{-}(CH_3)Pz)_3]Ir(H)(CO)(CH{=}CH_2)$ [22]. Metal adducts of fluorinated poly(pyrazolyl)borates also catalyze various transformations (e.g., $[HB(3,5\text{-}(CF_3)_2Pz)_3]Cu(\eta^2\text{-}C_2H_4)$ for aziridination; $[HB(3,5\text{-}(CF_3)_2Pz)_3]Ag(THF)$ for C–Cl bond activation; $[HB(3\text{-}(CF_3),5\text{-}(CH_3)Pz)_3]Cu$ for oxidation) [16,23,24]. Overall, fluorinated poly(pyrazolyl)borates are of significant current interest, and are useful for many important applications [2,12,14–19, 21–46].

Here, we describe the synthesis of a new fluorinated tris(pyrazolyl)borate ligand $[HB(3\text{-}(CF_3),5\text{-}(Ph)Pz)_3]^-$ (**2** where R = Ph). Solid state structures of several tris(pyrazolyl)boratosodium complexes featuring oxygen-based donors like THF, Et_2O and H_2O are also reported. The ligand electronic effects were investigated using the IR spectroscopic data of the copper(I) carbonyl complex $[HB(3\text{-}(CF_3),5\text{-}(Ph)Pz)_3]CuCO$.

2. Experimental

2.1. General procedures

All manipulations were carried out under an atmosphere of purified nitrogen using standard Schlenk techniques (unless noted otherwise). Solvents were purchased from commercial sources and distilled from conventional drying agents prior to use. Glassware was oven-dried at 150 °C overnight. NMR spectra were recorded at room temperature on a JEOL Eclipse 500 (^1H, 500.16 MHz; ^{19}F, 470.62 MHz; ^{13}C NMR, 125.78 MHz). Proton and carbon chemical shifts are reported in parts per million versus Me_4Si. ^{19}F NMR chemical shifts were referenced relative to an external $CFCl_3$ standard. Elemental analyses were performed at the University of Texas at Arlington using a Perkin–Elmer Model 2400 CHN analyzer. All the samples gave satisfactory CHN analysis. Benzoyl-1,1,1-trifluoroacetone, $NaBH_4$ hydrazine hydrate (55% N_2H_4 solution), and copper(I) trifluoromethanesulfonate salt $[CF_3SO_3Cu]_2 \cdot C_6H_6$ were purchased from commercial sources and used as received.

2.2. Synthesis of 3-(CF3),5-(Ph)PzH

This was synthesized from $PhCOCH_2COCF_3$ and hydrazine following a procedure slightly different from that described previously [47]. Nitrogen atmosphere is not necessary. Hydrazine hydrate (55% N_2H_4 solution 1.40 g, 24.0 mmol) was added drop wise to a solution of benzoyl-1,1,1-trifluoroacetone (4.32 g, 20.1 mmol) and ethanol in an ice bath. The reaction mixture was stirred for 4 h. Ethanol and water were removed by slow distillation to obtain 3-(CF_3),5-(Ph)PzH, which solidifies when cooled to room temperature. Sublimation under reduced pressure at 140 °C affords analytically pure 3-(CF_3), 5-(Ph)PzH. X-ray quality crystals can be obtained by recrystallization from hexane. Yield: 4.18 g, 95%; m.p. 122–123 °C (Lit. 122–123 °C); ^1H NMR (C_6D_6): δ 10.69 (br, NH), 7.01 (m, Ph), 6.98 (br m, Ph), 6.36 (s, Pz); ^{19}F NMR (C_6D_6): δ −61.6; ^{13}C NMR ($CDCl_3$): δ 145.3, 143.6 (q, $^2J(C,F)$ = 36 Hz), 129.4, 129.3, 127.9, 125.7, 121.2 (q, $^1J(C,F)$ = 270 Hz), 101.0; ^{19}F NMR ($CDCl_3$): δ −61.9.

2.3. Synthesis of [HB(3-(CF3),5-(Ph)Pz)3]Na(THF)

A mixture of 3-(CF_3),5-(Ph)PzH (5.00 g, 23.6 mmol) and $NaBH_4$ (0.288 g, 7.60 mmol) was heated at ca. 180 °C for 4 h. The reaction mixture was allowed to cool to room temperature. The excess 3-(CF_3),5-(Ph)PzH was removed by vacuum sublimation at 140 °C. The remaining solid was dissolved in warm CH_2Cl_2 containing 0.5 mL of THF, filtered over Celite, and the filtrate was collected. The solvent was removed from the filtrate under reduced pressure to obtain $[HB(3\text{-}(CF_3),5\text{-}(Ph)Pz)_3]Na(THF)$ as a colorless solid. Addition of hexane to the filtrate facilitates the precipitation of $[HB(3\text{-}(CF_3),5\text{-}(Ph)Pz)_3]Na(THF)$ as a non-sticky product. This process may also lead to the loss of some coordinated THF. X-ray quality crystals were grown from a hexane/dichloromethane mixture with a few drops of THF at −25 °C; m.p. 187–188 °C. Yield: 4.62 g, 82%. ^1H NMR ($CDCl_3$): δ 7.20 (t, 3H, Ph), 6.91 (t, 6H,

Ph), 6.87 (d, 6H, Ph), 6.43 (s, 3H, Pz), 3.83 (m, 4H, THF), 1.92 (m, 4H, THF); ^{19}F NMR ($CDCl_3$): δ −62.3. IR (KBr), cm^{-1}: 2621 (BH).

2.4. Synthesis of [HB(3-(CF$_3$),5-(Ph)Pz)$_3$]Na(H$_2$O)

A mixture of 3-(CF_3),5-(Ph)PzH (5.00 g, 23.6 mmol) and $NaBH_4$ (0.288 g, 7.60 mmol) was heated at ca. 180 °C for 4 h. The reaction mixture was allowed to cool to room temperature and the excess 3-(CF_3),5-(Ph)PzH was removed by vacuum sublimation at 140 °C. The residue was transferred to a beaker and dissolved in warm petroleum ether. The solution was filtered, and the solvent was allowed to evaporate slowly from the filtrate in open air to obtain colorless crystals of [HB(3-(CF_3),5-(Ph)Pz)$_3$]Na(H_2O); m.p. 200–201 °C. Yield: 3.91 g, 75%. ^{1}H NMR ($CDCl_3$): δ 7.18 (tt, 3H, Ph), 6.89 (br t, 6H, Ph), 6.85 (td, 6H, Ph), 6.41 (s, 3H, Pz), 1.66 (s, 2H, H_2O); ^{19}F NMR ($CDCl_3$): δ −61.6.

2.5. Synthesis of [HB(3-(CF$_3$),5-(Ph)Pz)$_3$]CuCO

$[CF_3SO_3Cu]_2 \cdot C_6H_6$ (0.068 g, 0.135 mmol) was dissolved in THF saturated with CO. [HB(3-(CF_3),5-(Ph)Pz)$_3$]Na(THF) (0.201 g, 0.27 mmol) in THF was added to this mixture at room temperature, and stirred for about 12 h under CO atmosphere. The resulting mixture was filtered and the solvent was removed from the filtrate under reduced pressure to obtain [HB(3-(CF_3),5-(Ph)Pz)$_3$]CuCO as a white solid. It was recrystallized from THF/toluene at −25 °C; m.p: 202 °C (dec.). Yield: 0.145 g, 73%. ^{1}H NMR ($CDCl_3$): δ 7.28 (t, 3H, Ph), 6.94 (t, 6H, Ph), 6.85 (d, 6H, Ph), 6.55 (s, 3H, Pz); ^{19}F NMR ($CDCl_3$): δ −61.2; IR (KBr), cm^{-1}: 2639 (BH), 2103 (CO).

2.6. X-ray structure determination

A suitable crystal covered with a layer of hydrocarbon oil was selected and attached to a glass fiber and immediately placed in the nitrogen stream for low temperature data collections. Room temperature data were collected on crystals attached to glass fibers using epoxy glue. Structures were solved by direct methods followed by successive cycles of full-matrix least-squares refinement on F^2 and difference Fourier analysis. Software programs and the sources of scattering factors are contained in the Bruker SHELXTL 5.1 software package provided by the Bruker Analytical X-ray Instruments, Inc. Some details of data collection and refinements are given in Table 1. Selected bond distances and angles are given in Table 2.

3. Results and discussion

Several methods for the synthesis of 3-(CF_3),5-(Ph)PzH are available in the literature [47–49]. We have used one of those with some minor modifications to obtain 3-(CF_3),5-(Ph)PzH in high yield [47]. The X-ray crystal structure of 3-(CF_3),5-(Ph)PzH is depicted in Fig. 1. It adopts an interesting "tub" shaped, tetrameric structure in the solid state due to N–H···N hydrogen bonding. The (non bonded) N···N distances are 2.844, 2.854, 2.856, and 2.866 Å. The H···N distances range from 1.873 Å to 2.005 Å. N-unsubstituted pyrazoles display structures ranging from dimers, trimers, tetramers, to catemers [50]. Among these, tetrameric form is the least common. The 3,5-(CF_3)$_2$PzH, 3,5-(Ph)$_2$PzH, and 3(5)-phenyl-5(3)-methylpyrazole are examples of related pyrazoles that adopt the tertameric form in the solid state [50–53].

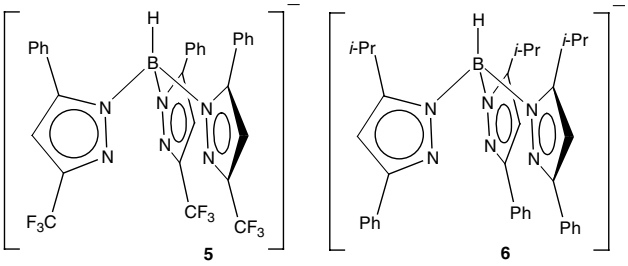

The sodium salt of [HB(3-(CF_3),5-(Ph)Pz)$_3$]$^-$ (**5**) was prepared by heating a mixture of 3-(CF_3),5-(Ph)PzH and $NaBH_4$ to 180 °C. It was isolated as the THF adduct and characterized using NMR and IR spectroscopy and X-ray crystallography. Fig. 2 depicts the X-ray crystal structure of [HB(3-(CF_3),5-(Ph)Pz)$_3$]Na(THF). It confirms the formation of the isomer with trifluoromethyl groups at the pyrazolyl group 3-position (rather than the 3-Ph,5-CF_3 version). [1] The B-H moiety resides in a pocket surrounded by three phenyl groups. The non-fluorinated ligand [HB(3-(Ph),5-(*i*-Pr)Pz)$_3$]$^-$ (**6**) is known [54]. In this system, the phenyl groups occupy the 3-position rather than the 5-position. Considering that the trifluoromethyl group is closer in size to an isopropyl group, these data indicate that (in the absence of adverse steric constraints) the electron rich nitrogen site of the pyrazole preferentially bonds to the boron atom during the ligand formation [55–57]. [2]

[1] We have also synthesized [HB(3-(CF_3),5-(Ph)Pz)$_3$]Tl using [HB(3-(CF_3),5-(Ph)Pz)$_3$]Na(THF) and $TlNO_3$. ^{19}F NMR signal corresponding to CF_3 groups in $CDCl_3$ appear as a doublet at δ −59.3 with $^4J(Tl, F) = 880$ Hz. Comparison of this value to ^{19}F NMR spectroscopic data of [HB(3-(CF_3),5-(thienyl)Pz)$_3$]Tl ([37]: ^{19}F NMR ($CDCl_3$): δ −60.6 with $^4J(Tl, F) = 850$ Hz) further supports the formation of tris(pyrazolyl)borate ligand isomer with CF_3 groups at the pyrazolyl ring 3-position.

[2] Although CF_3 group is larger than a methyl group and somewhat similar in size to an isopropyl group, the "effective steric bulk" of tris(pyrazolyl)borato ligands with CF_3 groups at the pyrazolyl group 3-position is much closer to the 3-methyl analog than the 3-isopropyl analog. This is evident from the cone angle data of tris(pyrazolyl)borates (see [11, p. 105]).

Table 1
Crystal data and summary of data collection and refinement (where $Pz^* = 3\text{-}(CF_3),5\text{-}(Ph)Pz$; $Pz^{\#} = 3\text{-}(CF_3),5\text{-}(CH_3)Pz$)

Compound	Pz^*H	$[HB(Pz^*)_3]Na(THF)$	$[HB(3,5\text{-}(CF_3)_2Pz)_3]Na(OEt_2)$	$[HB(Pz^*)_3]Na(H_2O)$	$[HB(Pz^{\#})_3]Na(H_2O)\cdot Pz^{\#}H$	$[HB(Pz^*)_3]CuCO$
Formula	$C_{10}H_7F_3N_2$	$C_{34}H_{27}BF_9N_6NaO$	$C_{19}H_{14}BF_{18}N_6NaO$	$C_{30}H_{21}BF_9N_6NaO$	$C_{20}H_{20}BF_{12}N_8NaO$	$C_{31}H_{19}BCuF_9N_6O$
F_w	212.18	740.42	718.16	686.33	650.24	736.87
Crystal system	triclinic	monoclinic	triclinic	orthorhombic	triclinic	monoclinic
Space group	$P\bar{1}$	$P2(1)/n$	$P\bar{1}$	Pna2(1)	$P\bar{1}$	$P2(1)/n$
T (K)	208	298	183	100	193	298
λ (Å)	0.71073	0.71073	0.71073	0.71073	0.71073	0.71073
a (Å)	9.8013(17)	14.184(3)	10.648(2)	22.420(3)	11.1226(15)	9.7383(10)
b (Å)	9.8358(16)	12.683(3)	11.934(2)	13.2879(16)	11.6614(17)	23.441(3)
c (Å)	20.903(3)	20.722(4)	13.009(4)	10.1352(13)	12.3654(13)	13.7603(16)
α (°)	80.551(12)	90	101.904(16)	90	73.648(8)	90
β (°)	87.916(13)	108.687(14)	102.256(14)	90	71.769(8)	91.580(9)
γ (°)	89.137(13)	90	113.140(140)	90	71.757(9)	90
V (Å^3)	1986.4(5)	3531.3(11)	1406.1(5)	3019.4(7)	1416.5(3)	3140.0(6)
Z	8	4	2	4	2	4
ρ (calculated) (g/cm^3)	1.419	1.393	1.696	1.510	1.525	1.559
R_1, wR_2 $[I > 2\sigma(I)]$[a]	0.0534, 0.1349	0.0512, 0.1206	0.0524, 0.1298	0.0446, 0.0923	0.0395, 0.0881	0.0453, 0.0923
R_1, wR_2 [all data][a]	0.0703, 0.1474	0.0860, 0.1399	0.0690, 0.1420	0.0499, 0.0944	0.0577, 0.0972	0.0812, 0.1062

[a] $R_1 = \sum \|F_o| - |F_c\| / \sum |F_o|$ and $wR_2 = [\sum[w(F_o^2 - F_c^2)^2] / \sum[w(F_o^2)^2]]^{1/2}$.

The Na–O bond length of 2.261(3) Å in $[HB(3\text{-}(CF_3),5\text{-}(Ph)Pz)_3]Na(THF)$ is slightly shorter than the corresponding distance of 2.303(3) Å observed for dimeric $\{[HB(3\text{-}(CF_3)Pz)_3]Na(THF)\}_2$ [15]. Although it is possible to synthesize $[HB(3,5\text{-}(CF_3)_2Pz)_3]Na(THF)$, we have not been able to obtain suitable crystals for X-ray structure determination. However, the structural data of the related diethyl ether adduct $[HB(3,5\text{-}(CF_3)_2Pz)_3]Na(OEt_2)$ could be obtained (Fig. 3) [15]. It adopts a monomeric structure with a Na–O bond distance of 2.281(3) Å.

The sodium ion in compounds like $[HB(3\text{-}(CF_3),5\text{-}(Ph)Pz)_3]Na(THF)$, $\{[HB(3\text{-}(CF_3)Pz)_3]Na(THF)\}_2$, and $[HB(3,5\text{-}(CF_3)_2Pz)_3]Na(OEt_2)$ lies in a pit surrounded by three trifluoromethyl groups (“Teflon coated cavity”). These molecules show close Lewis acid–base contacts between the sodium ion and fluorine atoms of the CF_3 moieties. For example, $[HB(3\text{-}(CF_3),5\text{-}(Ph)Pz)_3]Na(THF)$ shows several intramolecular Na···FC contacts at 2.915, 3.054, and 3.088 Å. $[HB(3,5\text{-}(CF_3)_2Pz)_3]Na(OEt_2)$ displays similar interactions at 2.874, 3.033, and 3.195 Å. The closest Na···FC contact in $\{[HB(3\text{-}(CF_3)Pz)_3]Na(THF)\}_2$ is of an intermolecular type (2.744(3) Å).

Compounds with CF···M bonding interactions are of significant interest [58,59]. It is, however, difficult to clearly define the upper limit of the inter-atomic distance that points to a bonding interaction between a metal (in particular, hard metal ion like sodium) and fluorine of a fluorocarbon moiety [58]. Continuing revision of radii (ionic, van der Waals, covalent) further complicates this matter [60]. It has been argued that the sum of the van der Waals radii (which is 3.77 Å for Na and F combination) which is commonly used as the upper limit may over estimate the bonding interactions between a *hard metal ion* like sodium and a FC moiety. More appropriate value for the upper limit for Na···FC bonding is considered to be 3.07 Å, which is the sum of van der Waals radius of fluorine and Kollman’s ionic van der Waals radius of sodium [58]. Therefore, in all the sodium adducts illustrated in this paper, only the Na···F contacts lower than 3.07 Å are shown as bonds.

The water adduct $\{[HB(3\text{-}(CF_3),5\text{-}(Ph)Pz)_3]Na(H_2O)\}_n$ could be obtained by allowing a petroleum ether solution of $[HB(3\text{-}(CF_3),5\text{-}(Ph)Pz)_3]Na$ to slowly concentrate in the open atmosphere (or using wet petroleum ether). The X-ray crystal structure (Figs. 4 and 5) shows that it is a polymeric molecule. Short intermolecular Na···FC interactions (2.848 Å) link the $[HB(3\text{-}(CF_3),5\text{-}(Ph)Pz)_3]Na(H_2O)$ units together. In addition, there is an intramolecular Na···FC contact at 3.006 Å (and two other F atoms at a distance of 3.082 and 3.256 Å). $[HB(3,5\text{-}(CF_3)_2Pz)_3]Na(H_2O)$ (Fig. 6) which was reported earlier [15] and $\{[HB(3\text{-}(CF_3),5\text{-}(CH_3)Pz)_3]Na(H_2O)\}_2$ (Fig. 7) are two other examples where the coordination of water molecules to sodium centers of fluorinated tris(pyrazolyl)borates have been observed. $\{[HB(3\text{-}(CF_3),5\text{-}(CH_3)Pz)_3]Na(H_2O)\}_2$ was obtained following a procedure similar to that of $\{[HB(3\text{-}(CF_3),5\text{-}(Ph)Pz)_3]Na(H_2O)\}_n$. It has a dimeric structure. Water molecules and intermolecular Na···FC bonds (2.934 Å) hold the monomers together. In addi-

Table 2
Selected bond lengths [Å] and angles [°]

[HB(3-(CF_3),5-(Ph)Pz)$_3$]Na(THF)			
Bond lengths			
Na–O	2.261(3)	N(11)–B	1.551(4)
Na–N(32)	2.378(3)	N(21)–N(22)	1.350(3)
Na–N(12)	2.384(3)	N(21)–B	1.556(4)
Na–N(22)	2.395(3)	N(31)–N(32)	1.357(3)
Na–F(36D)	2.915(10)	N(31)–B	1.550(4)
N(11)–N(12)	1.357(3)		
Bond angles			
O-Na–N(32)	134.06(13)	N(32)–Na–F(36D)	58.1(2)
O–Na–N(12)	127.28(13)	N(12)–Na–F(36D)	122.5(4)
N(32)–Na–N(12)	79.74(10)	N(22)–Na–F(36D)	120.0(5)
O–Na–N(22)	135.76(12)	N(31)–B–N(11)	111.2(2)
N(32)–Na–N(22)	77.66(10)	N(31)–B–N(21)	109.8(2)
N(12)–Na–N(22)	81.13(10)	N(11)–B–N(21)	110.9(2)
O–Na–F(36D)	76.2(2)		
[HB(3,5-(CF_3)$_2$ Pz)$_3$]Na(Et_2O)			
Bond lengths			
Na–O	2.281(3)	N(11)–B	1.555(4)
Na–N(22)	2.434(3)	N(21)–N(22)	1.356(3)
Na–N(32)	2.443(3)	N(21)–B	1.554(4)
Na–N(12)	2.461(3)	N(31)–N(32)	1.349(4)
Na–F(26B)	2.874(3)	N(31)–B	1.560(4)
N(11)–N(12)	1.353(3)		
Bond angles			
O–Na–N(22)	143.72(13)	N(22)–Na–F(26B)	59.09(7)
O–Na–N(32)	128.97(13)	N(32)–Na–F(26B)	124.56(9)
N(22)–Na–N(32)	78.35(9)	N(12)–Na–F(26B)	118.79(9)
O–Na–N(12)	127.86(12)	N(21)–B–N(11)	108.9(2)
N(22)–Na–N(12)	75.76(9)	N(21)–B–N(31)	109.4(2)
N(32)–Na–N(12)	77.66(9)	N(11)–B–N(31)	109.6(2)
O–Na–F(26B)	84.62(11)		
{[HB(3-(CF_3),5-(Ph)Pz)$_3$]Na(H_2O)}$_n$			
Bond lengths			
Na–O	2.245(2)	N(21)–N(22)	1.355(3)
Na–N(32)	2.386(3)	N(21)–B	1.562(4)
Na–N(22)	2.418(3)	N(31)–N(32)	1.354(3)
Na–N(12)	2.473(3)	N(31)–B	1.547(4)
N(11)–N(12)	1.370(3)	F(16A)–NaB	2.848(2)
N(11)–B	1.567(4)		
Bond angles			
O–Na–N(32)	124.17(10)	N(22)–Na–N(12)	76.64(9)
O–Na–N(22)	151.65(10)	N(31)–B–N(21)	111.7(3)
N(32)–Na–N(22)	80.69(9)	N(31)–B–N(11)	110.7(2)
O–Na–N(12)	118.04(10)	N(21)–B–N(11)	108.6(2)
N(32)–Na–N(12)	79.46(9)		
{[HB(3-(CF_3),5-(CH_3)Pz)$_3$]Na(H_2O)}$_2$			
Bond lengths			
Na–O	2.417(2)	N(11)–N(12)	1.364(3)
Na–N(12)	2.421(3)	N(11)–B	1.540(4)
Na–OA	2.443(2)	N(21)–N(22)	1.358(3)
Na–N(22)	2.505(3)	N(21)–B	1.544(4)
Na–N(32)	2.528(3)	N(31)–N(32)	1.361(3)
Na–F(36K)	2.934(15)	N(31)–B	1.555(4)
Na–NaA	3.670(2)		
Bond angles			
O–Na–N(12)	103.26(8)	N(11)–B–N(31)	110.7(2)
O–Na–OA	81.92(7)	N(21)–B–N(31)	110.8(2)

Table 2 (*continued*)

N(32)–Na–F(36K)	157.65(19)	Na–O–NaA	98.08(7)
N(11)–B–N(21)	110.9(3)		
[HB(3-(CF_3),5-(Ph)Pz_3]CuCO			
Bond lengths			
Cu–C	1.773(5)	N(11)–B	1.545(5)
Cu–N(32)	2.049(3)	N(21)–N(22)	1.362(4)
Cu–N(22)	2.054(3)	N(21)–B	1.562(5)
Cu–N(12)	2.057(3)	N(31)–N(32)	1.363(4)
C–O	1.113(5)	N(31)–B	1.543(5)
N(11)–N(12)	1.366(4)		
Bond angles			
C–Cu–N(32)	128.15(17)	N(22)–Cu–N(12)	91.21(12)
C–Cu–N(22)	123.30(18)	O–C–Cu	177.9(5)
N(32)–Cu–N(22)	88.90(12)	N(31)–B–N(11)	110.7(3)
C–Cu–N(12)	122.87(19)	N(31)–B–N(21)	108.1(3)
N(32)–Cu–N(12)	91.88(12)	N(11)–B–N(21)	108.6(3)

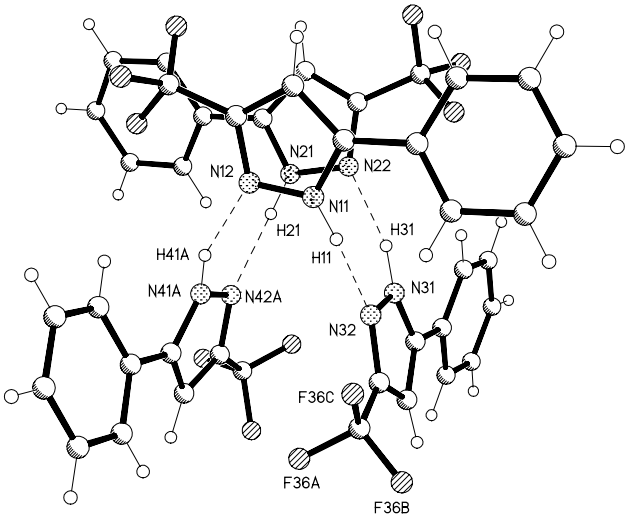

Fig. 1. View of the 3-(CF_3),5-(Ph)PzH showing the tetrameric structure.

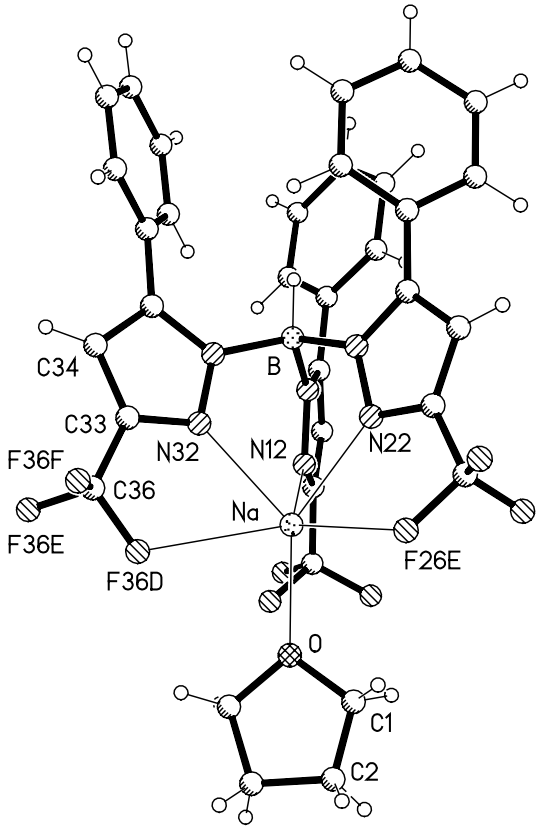

Fig. 2. Molecular structure of [HB(3-(CF_3),5-(Ph)Pz_3]Na(THF).

tion, there is a F–C moiety at 3.094 Å from each sodium site.

Interestingly, despite the wide utility of tris(pyrazolyl)borate salts of alkali metals, only a very few have been characterized using X-ray crystallography. The structurally characterized compounds of this type include {[HB(3,5-(CF_3)$_2$Pz)$_3$]K(DMAC)}$_2$ [12], {[HB(3-(CF_3),5-(CH_3)Pz)$_3$]K(DMAC)}$_2$ [61], {[HB(3-(CF_3),5-(CH_3)Pz)$_3$]K(CH_3CN)}$_2$ [45], [HB(3,5-(CF_3)$_2$Pz)$_3$]Na(H_2O) [15], {[HB(3-(CF_3)Pz)$_3$]Na(THF)}$_2$ [15], {[HB(3-(C_2F_5)Pz)$_3$]Na(3-(C_2F_5)PzH)} [14], [HB(3,4,5-(CH_3)$_3$Pz)$_3$]K [62], [HB(3,5-(*t*-Bu)$_2$Pz)$_3$]K(C_6H_6) [63], [HB(3,5-(*t*-Bu)$_2$Pz)$_3$]Cs [63].

The CO stretching frequency of metal carbonyl adducts serves as a good measure of relative electron density at a metal site (or the electron acceptor/back-donation ability of a metal ion). It also provides information about the donor properties of the auxiliary ligands coordinated to a metal ion. Copper(I) carbonyl adducts have been used in the study of electronic effects of tris(pyrazolyl)borates ligands [2]. ^{63}Cu NMR spectroscopic data [54] and the results from theoretical studies [64] are in good agreement with the conclusions based on CO stretching frequency data.

In order to estimate the relative electronic effects of [HB(3-(CF_3),5-(Ph)Pz_3]$^-$ ligand on metal ions, we have

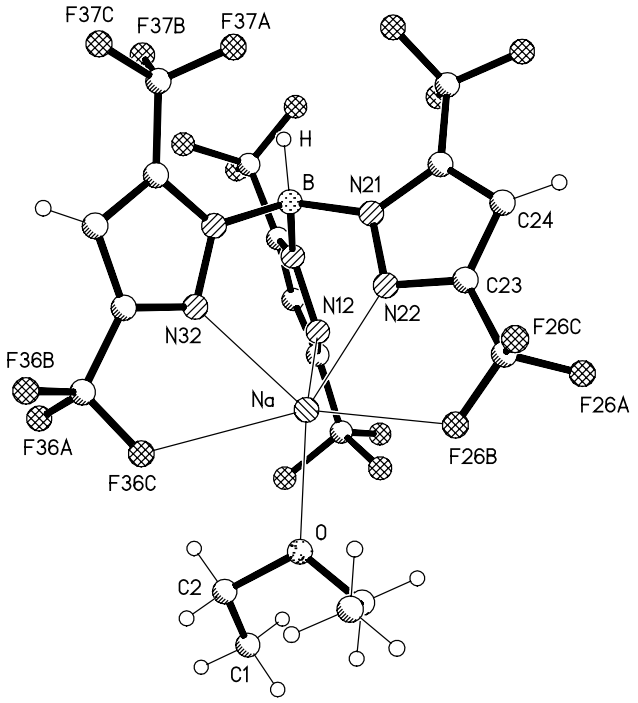

Fig. 3. Molecular structure of $[HB(3,5\text{-}(CF_3)_2Pz)_3]Na(OEt_2)$.

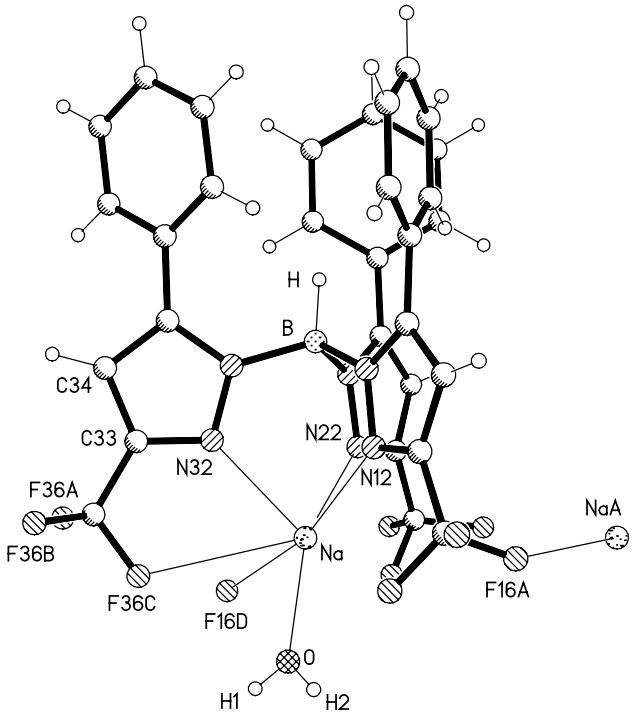

Fig. 4. A view of $\{[HB(3\text{-}(CF_3),5\text{-}(Ph)Pz)_3]Na(H_2O)\}_n$ showing the atom numbering scheme.

synthesized and characterized the copper carbonyl adduct $[HB(3\text{-}(CF_3),5\text{-}(Ph)Pz)_3]CuCO$. The X-ray crystal structure (Fig. 8) shows that it features a typical pseudotetrahedral copper site. The Cu–C–O moiety is essentially linear. The copper–CO bond length of 1.773(5) Å is well within the range reported for tris(pyrazolyl)boratocopper(I) carbonyl complexes (1.752–1.808 Å). The Cu–N bond distances of $[HB(3\text{-}(CF_3),5\text{-}(Ph)Pz)_3]CuCO$ (2.049(3), 2.054(3), 2.057(3) Å) can be compared to the corresponding bond lengths in $[HB(3,5\text{-}(CF_3)_2Pz)_3]CuCO$ (2.035(3), 2.061(2), 2.061(3) Å) [17], $[HB(3,5\text{-}(Ph)_2Pz)_3]CuCO$ (2.059(6), 2.061(2),

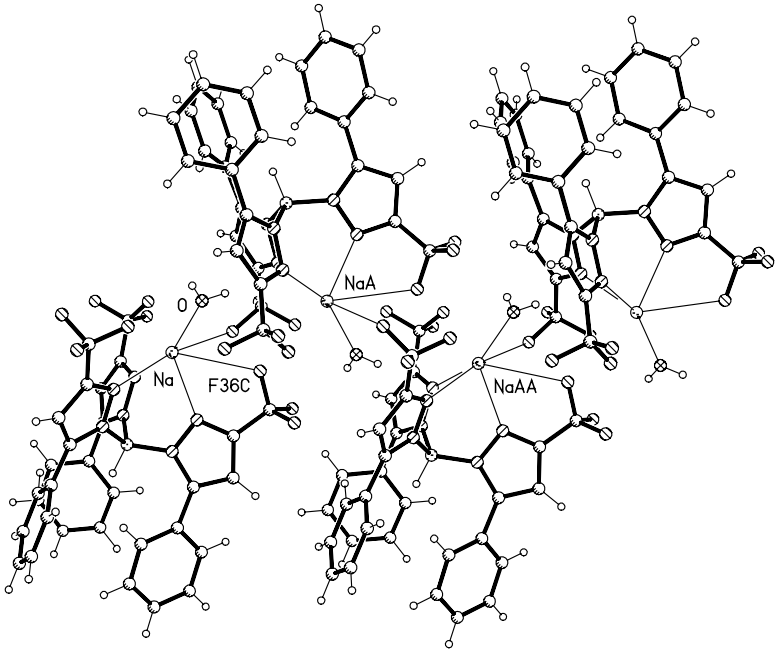

Fig. 5. Molecular structure of $\{[HB(3\text{-}(CF_3),5\text{-}(Ph)Pz)_3]Na(H_2O)\}_n$ showing the polymeric nature.

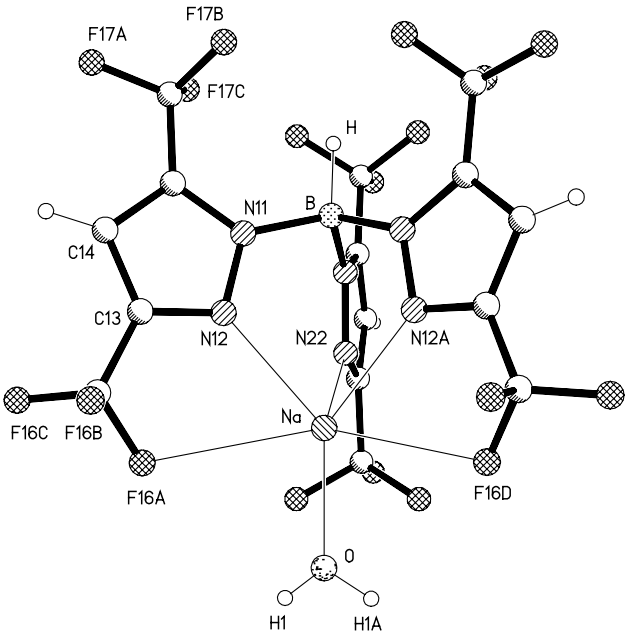

Fig. 6. Molecular structure of $[HB(3,5\text{-}(CF_3)_2Pz)_3]Na(H_2O)$ (from [15]).

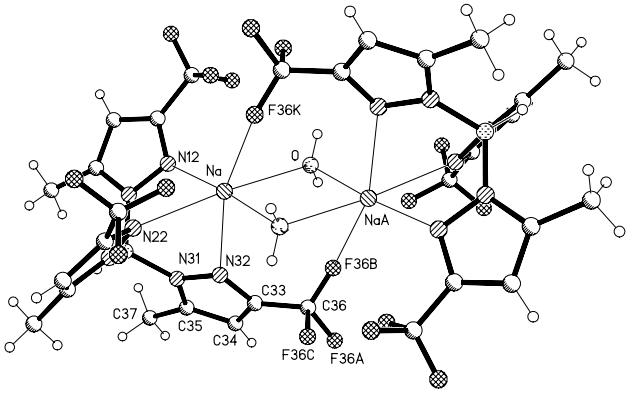

Fig. 7. Molecular structure of $\{[HB(3\text{-}(CF_3),5\text{-}(CH_3)Pz)_3]Na(H_2O)\}_2$.

2.061(3) Å) [54], and $[HB(3,5\text{-}(i\text{-}Pr)_2Pz)_3]CuCO$ (2.019(5), 2.014(6), 2.022(6) Å) [65]. Overall, there is no significant difference in the Cu–N separation between the fluorinated and non-fluorinated tris(pyrazolyl)borate systems of copper(I).

The IR spectrum of $[HB(3\text{-}(CF_3),5\text{-}(Ph)Pz)_3]CuCO$ shows a strong absorption band at 2103 cm^{-1} corresponding to the C–O stretching frequency. This value may be compared to the ν_{CO} data of related copper carbonyl adducts. Fig. 9 summarizes the CO stretching frequency values of closely related tris(pyrazolyl)boratocopper(I) carbonyl adducts [2,14,17,39,54,65–70]. The Cu–CO adducts of the fluorinated tris(pyrazolyl)borates display relatively high ν_{CO} values indicating the presence of fairly acidic copper sites with low back-bonding ability. This is expected based on the highly electron

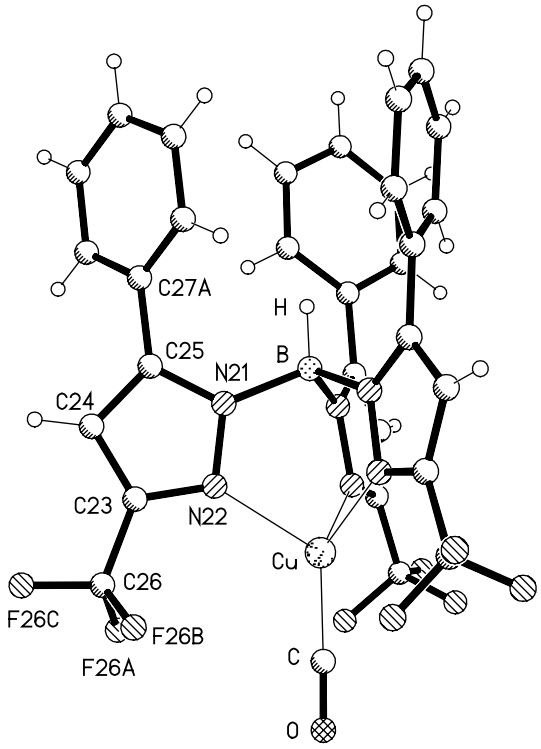

Fig. 8. Molecular structure of $[HB(3\text{-}(CF_3),5\text{-}(Ph)Pz)_3]CuCO$.

withdrawing nature of the fluorocarbon substituents present on the pyrazolyl rings.

Recently, we have reported the synthesis of copper(I) ethylene adduct $[HB(3\text{-}(CF_3),5\text{-}(Ph)Pz)_3]Cu(\eta^2\text{-}C_2H_4)$ [16]. It serves as a good aziridination catalyst. Preliminary data suggest that it may also be possible to synthesize the silver carbonyl adduct $[HB(3\text{-}(CF_3),5\text{-}(Ph)Pz)_3]AgCO$ ($\nu_{CO} = 2149\ cm^{-1}$) [71]. However, so far we have not been able to obtain an analytically pure sample to confirm the identity. Thermally stable, silver carbonyl species are extremely rare [20]. $[HB(3,5\text{-}(CF_3)_2Pz)_3]AgCO$ is the only well authenticated compound of this type in the Scorpionate family [18].

Overall, the synthesis of a new fluorinated ligand is reported along with the crystal structures of several tris(pyrazolyl)boratosodium salts featuring fluorinated Scorpionates. The sodium ion in these systems resides in a pit surrounded by trifluoromethyl groups. Significant Na···FC contacts are present in the solid state as evident from the X-ray crystal structures. The IR data of the copper carbonyl complex $[HB(3\text{-}(CF_3),5\text{-}(Ph)Pz)_3]$-CuCO indicates that $[HB(3\text{-}(CF_3),5\text{-}(Ph)Pz)_3]^-$ is a relatively poor donor to metal ions.

3.1. Supplementary material

Crystallographic data for 3-(CF_3),5-(Ph)PzH, $[HB(3(CF_3),5\text{-}(Ph)Pz)_3]Na(THF)$, $[HB(3,5\text{-}(CF_3)_2Pz)_3]Na(OEt_2)$, $\{[HB(3\text{-}(CF_3),5\text{-}(Ph)Pz)_3]Na(H_2O)\}_n$, $\{[HB(3\text{-}(CF_3),5\text{-}(CH_3)Pz)_3]Na(H_2O)\}_2$, and $[HB(3\text{-}(CF_3),5\text{-}(Ph)$

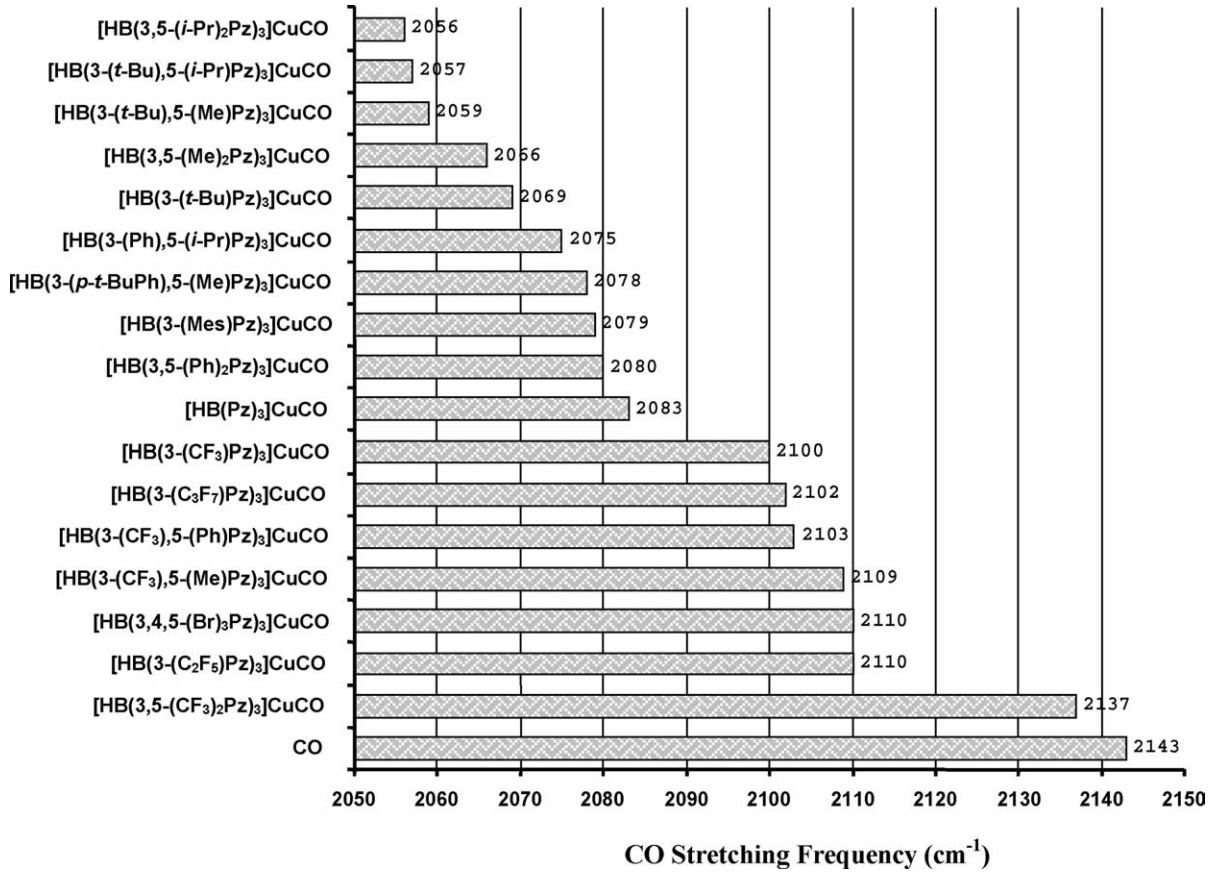

Fig. 9. The C–O stretching frequency data of closely related tris(pyrazolyl)boratocopper(I) carbonyl complexes.

$Pz)_3$]CuCO have been deposited with the Cambridge Crystallographic Data Center, CCDS Nos. 210791–210796. Copies of this information may be obtained free of charge from the Director, Cambridge Crystallographic Data Centre (CCDC), 12 Union Road, Cambridge, CB2 1EZ (fax: +44 1223 336033; deposit@ccdc.cam.ac.uk; or www.ccdc.cam.ac.uk).

Acknowledgements

We thank the Robert A. Welch Foundation and National Science Foundation (CHE-0314666) for support of this work. We also thank the National Science Foundation (CHE-9601771) for providing funds to purchase the 500 MHz NMR spectrometer. We are grateful to Doug Powell (University of Kansas) for collecting X-ray data for $\{[HB(3\text{-}(CF_3),5\text{-}(Ph)Pz)_3]\text{-}Na(H_2O)\}_n$.

References

[1] J.S. Thrasher, S.H. Strauss, Inorganic fluorine chemistry: toward the 21st century. In: ACS Symposium Series, 555, American Chemical Society, Washington, DC, 1994.
[2] H.V.R. Dias, H.-J. Kim, H.-L. Lu, K. Rajeshwar, N.R. de Tacconi, A. Derecskei-Kovacs, D.S. Marynick, Organometallics 15 (1996) 2994, and the references therein.
[3] U. Fekl, R. van Eldik, S. Lovell, K.I. Goldberg, Organometallics 19 (2000) 3535, and the references therein.
[4] M. Witt, H.W. Roesky, Prog. Inorg. Chem. 40 (1992) 353.
[5] R.H. Fish, Chem. Eur. J. 5 (1999) 1677.
[6] I.T. Horvath, Acc. Chem. Res. 31 (1998) 641.
[7] L.P. Barthel-Rosa, J.A. Gladysz, Coord. Chem. Rev. 190–192 (1999) 587.
[8] G. Francio, K. Wittmann, W. Leitner, J. Organomet. Chem. 621 (2001) 130.
[9] P.G. Jessop, W. Leitner, Chemical Synthesis Using Supercritical Fluids, VCH/Wiley, Weinheim, 1999.
[10] S.H. Strauss, Chem. Rev. 93 (1993) 927.
[11] S. Trofimenko, Scorpionates: the Coordination Chemistry of Polypyrazolylborate Ligands, Imperial College, London, 1999.
[12] H.V.R. Dias, H.-L. Lu, R.E. Ratcliff, S.G. Bott, Inorg. Chem. 34 (1995) 1975.
[13] H.V.R. Dias, J.D. Gorden, Inorg. Chem. 35 (1996) 318.
[14] H.V.R. Dias, H.-J. Kim, Organometallics 15 (1996) 5374.
[15] H.V.R. Dias, W. Jin, H.-J. Kim, H.-L. Lu, Inorg. Chem. 35 (1996) 2317;
THF and Et_2O adducts of $[HB(3,5\text{-}(CF_3)_2Pz)_3]Na$ can be obtained by crystallizing the $[HB(3,5\text{-}(CF_3)_2Pz)_3]Na$ complex from toluene/THF or toluene/Et_2O as described for $\{[HB(3\text{-}(CF_3)Pz)_3]Na(THF)\}_2$.
[16] H.V.R. Dias, H.-L. Lu, H.-J. Kim, S.A. Polach, T.K.H.H. Goh, R.G. Browning, C.J. Lovely, Organometallics 21 (2002) 1466.
[17] H.V.R. Dias, H.-L. Lu, Inorg. Chem. 34 (1995) 5380.

[18] H.V.R. Dias, W. Jin, J. Am. Chem. Soc. 117 (1995) 11381.
[19] H.V.R. Dias, Z. Wang, W. Jin, Inorg. Chem. 36 (1997) 6205.
[20] A.J. Lupinetti, S.J. Strauss, G. Frenking, Prog. Inorg. Chem. 49 (2001) 1.
[21] H.V.R. Dias, S.A. Polach, S.-K. Goh, E.F. Archibong, D.S. Marynick, Inorg. Chem. 39 (2000) 3894.
[22] C.K. Ghosh, J.K. Hoyano, R. Krentz, W.A.G. Graham, J. Am. Chem. Soc. 111 (1989) 5480.
[23] H.V.R. Dias, R.G. Browning, S.A. Polach, H.V.K. Diyabalanage, C.J. Lovely, J. Am. Chem. Soc. 125 (2003) 9270.
[24] D. Diaconu, Z. Hu, S.M. Gorun, J. Am. Chem. Soc. 124 (2002) 1564.
[25] H.V.R. Dias, W. Jin, Inorg. Chem. 35 (1996) 3687.
[26] H.V.R. Dias, W. Jin, Inorg. Chem. 35 (1996) 267.
[27] H.V.R. Dias, S.A. Polach, Inorg. Chem. 39 (2000) 4676.
[28] H.V.R. Dias, Z. Wang, Inorg. Chem. 39 (2000) 3890.
[29] H.V.R. Dias, Z. Wang, Inorg. Chem. 39 (2000) 3724.
[30] H.V.R. Dias, W. Jin, Inorg. Chem. 39 (2000) 815.
[31] H.V.R. Dias, A.E. Ayers, Polyhedron 21 (2002) 611.
[32] A.E. Ayers, H.V.R. Dias, Inorg. Chem. 41 (2002) 3259.
[33] U.E. Bucher, A. Currao, R. Nesper, H. Ruegger, L.M. Venanzi, E. Younger, Inorg. Chem. 34 (1995) 66.
[34] E. Del Ministro, O. Renn, H. Ruegger, L.M. Venanzi, U. Burckhardt, V. Gramlich, Inorg. Chim. Acta 240 (1995) 631.
[35] H. Katayama, K. Yamamura, Y. Miyaki, F. Ozawa, Organometallics 16 (1997) 4497.
[36] V. Rodriguez, J. Full, B. Donnadieu, S. Sabo-Etienne, B. Chaudret, New J. Chem. 21 (1997) 847.
[37] R. Han, P. Ghosh, P.J. Desrosiers, S. Trofimenko, G. Parkin, J. Chem. Soc., Dalton Trans. (1997) 3713.
[38] A. Albinati, M. Bovens, H. Ruegger, L.M. Venanzi, Inorg. Chem. 36 (1997) 5991.
[39] J.L. Schneider, S.M. Carrier, C.E. Ruggiero, V.G. Young Jr., W.B. Tolman, J. Am. Chem. Soc. 120 (1998) 11408.
[40] A. Albinati, U.E. Bucher, V. Gramlich, O. Renn, H. Ruegger, L.M. Venanzi, Inorg. Chim. Acta 284 (1999) 191.
[41] S.M. Gorun, Z. Hu, R.T. Stibrany, G. Carpenter, Inorg. Chim. Acta 297 (2000) 383.
[42] Z. Hu, R.D. Williams, D. Tran, T.G. Spiro, S.M. Gorun, J. Am. Chem. Soc. 122 (2000) 3556.
[43] V. Rodriguez, I. Atheaux, B. Donnadieu, S. Sabo-Etienne, B. Chaudret, Organometallics 19 (2000) 2916.
[44] M.H. Chisholm, N.W. Eilerts, J.C. Huffman, S.S. Iyer, M. Pacold, K. Phomphrai, J. Am. Chem. Soc. 122 (2000) 11845.
[45] Z. Hu, S.M. Gorun, Inorg. Chem. 40 (2001) 667.
[46] P. Cecchi, M. Berrettoni, M. Giorgetti, G. Gioia Lobbia, S. Calogero, L. Stievano, Inorg. Chim. Acta 318 (2001) 67.
[47] T. Nishiwaki, Bull. Chem. Soc. Jpn. 42 (1969) 3024.
[48] X.-Q. Tang, C.-M. Hu, J. Fluorine Chem. 73 (1995) 129.
[49] R.J. Linderman, K.S. Kirollos, Tetrahedron Lett. 30 (1989) 2049.
[50] I. Alkorta, J. Elguero, B. Donnadieu, M. Etienne, J. Jaffart, D. Schagen, H.-H. Limbach, New J. Chem. 23 (1999) 1231, and references therein.
[51] R.G. Raptis, R.J. Staples, C. King, J.P. Fackler Jr., Acta Crystallogr. Sect. C: Cryst. Struct. Commun. C49 (1993) 1716.
[52] J. Elguero, N. Jagerovic, C. Foces-Foces, F.H. Cano, M.V. Roux, F. Aguilar-Parrilla, H.-H. Limbach, J. Heter. Chem. 32 (1995) 451.
[53] C. Foces-Foces, I. Alkorta, J. Elguero, Acta Crystallogr., Sect. B: Struct. Sci. B 56 (2000) 1018.
[54] S. Imai, K. Fujisawa, T. Kobayashi, N. Shirasawa, H. Fujii, T. Yoshimura, N. Kitajima, Y. Moro-oka, Inorg. Chem. 37 (1998) 3066.
[55] B.E. Smart, J. Fluorine Chem. 109 (2001) 3.
[56] D. O'Hagan, H.S. Rzepa, Chem. Commun. (1997) 645.
[57] N. Kitajima, W.B. Tolman, Prog. Inorg. Chem. 43 (1995) 419.
[58] H. Plenio, Chem. Rev. 97 (1997) 3363, and the references therein.
[59] J.L. Kiplinger, T.G. Richmond, C.E. Osterberg, Chem. Rev. 94 (1994) 373.
[60] B.P. Hay, Coord. Chem. Rev. 126 (1993) 177.
[61] H.V.R. Dias, W. Jin, R.E. Ratcliff, unpublished results.
[62] G.G. Lobbia, P. Cecchi, R. Spagna, M. Colapietro, A. Pifferi, C. Pettinari, J. Organomet. Chem. 485 (1995) 45.
[63] C.M. Dowling, D. Leslie, M.H. Chisholm, G. Parkin, Main Group Chem. 1 (1995) 29.
[64] P. Deglmann, F. Furche, R. Ahlrichs, Chem. Phys. Lett. 362 (2002) 511.
[65] N. Kitajima, K. Fujisawa, C. Fujimoto, Y. Morooka, S. Hashimoto, T. Kitagawa, K. Toriumi, K. Tatsumi, A. Nakamura, J. Am. Chem. Soc. 114 (1992) 1277.
[66] C. Mealli, C.S. Arcus, J.L. Wilkinson, T.J. Marks, J.A. Ibers, J. Am. Chem. Soc. 98 (1976) 711.
[67] C.E. Ruggiero, S.M. Carrier, W.E. Antholine, J.W. Whittaker, C.J. Cramer, W.B. Tolman, J. Am. Chem. Soc. 115 (1993) 11285.
[68] R.R. Conry, G. Ji, A.A. Tipton, Inorg. Chem. 38 (1999) 906.
[69] M.I. Bruce, A.P.P. Ostazewski, J. Chem. Soc., Dalton Trans. (1973) 2433.
[70] A. Caballero, M.M. Diaz-Requejo, T.R. Belderrain, M.C. Nicasio, S. Trofimenko, P.J. Perez, J. Am. Chem. Soc. 125 (2003) 1446.
[71] H.V.R. Dias, T.K.H.H. Goh, unpublished results.

Available online at www.sciencedirect.com
SCIENCE DIRECT®
Polyhedron 23 (2004) 283–289
POLYHEDRON
www.elsevier.com/locate/poly

Highly selective extraction of Cu(II) and Zn(II) using $[B(3\text{-iPrpz})_4]^-$ (iPrpz = isopropylpyrazolyl)

Tsuyoshi Kitano [a,*], Yoshiki Sohrin [a], Yasuo Hata [a], Hiroshi Mukai [b], Hiroki Wada [c], Kazumasa Ueda [c]

[a] Institute for Chemical Research, Kyoto University, Uji, Kyoto 611-0011, Japan
[b] Department of Chemistry, Kyoto University of Education, Fushimi, Kyoto 612-8522, Japan
[c] Faculty of Technology, Kanazawa University, 2-40-20 Kodatsuno, Kanazawa 920-8667, Japan

Received 21 May 2003; accepted 7 August 2003

Abstract

The solvent extraction of first-series transition metal ions {Mn(II), Fe(II), Co(II), Ni(II), Cu(II) and Zn(II)} with $[B(3\text{-iPrpz})_4]^-$ (iPrpz = isopropylpyrazolyl) is reported. Although the previously reported tetrakis(pyrazolyl)borates, $[B(pz)_4]^-$ and $[B(3\text{-Mepz})_4]^-$, quantitatively extracted all the studied transition metal ions, $[B(3\text{-iPrpz})_4]^-$ extracted only Cu(II) and Zn(II). In order to elucidate the origin of the selectivity, the structures of the extracted species, $[B(3\text{-iPrpz})_4]_2Zn$ (**1**) and $[B(3\text{-iPrpz})_4]Cu(OCOCH_3)$ (**2**), were determined by single-crystal X-ray diffraction. Complex **1** has a tetrahedral geometry with each ligand having bidentate coordination. Complex **2** has a distorted square pyramidal geometry with $[B(3\text{-iPrpz})_4]^-$ having tridentate coordination and the acetate anion having asymmetric bidentate coordination. These structures of the extracted species are different from those of the previously studied tetrakis(pyrazolyl)borates, which are octahedral A_2M with each ligand having tridentate coordination (A^- = tetrakis(pyrazolyl)borate, M^{2+} = first-series transition metal ion). Because the bulky isopropyl groups at the 3-position of the pyrazolyl ring prevent octahedral geometry, the other metal ions cannot form stable and extractable complexes with $[B(3\text{-iPrpz})_4]^-$.
© 2003 Elsevier Ltd. All rights reserved.

Keywords: Tetrakis(3-isopropylpyrazolyl)borate; Solvent extraction; Single-crystal X-ray diffraction; Zinc; Copper

1. Introduction

Poly(pyrazolyl)borates (A^-) are versatile ligands for use as metal centers of transition metal catalysts [1–10] and for mimicking metalloenzyme systems in bioinorganic chemistry [11–14]. In particular, the poly(pyrazolyl)borate incorporated a bulky substituent at the 3-position of the pyrazolyl ring known as a "tetrahedral enforcer" [15], because the bulky substituent prevents a second poly(pyrazolyl)borate ligand from coordinating the metal center and other ancillary ligands (X^-) coordinate with ease. On the other hand, a large number of A_2M complexes of transition metal ions with the poly(pyrazolyl)borates having various bulky substituents were determined by X-ray crystallography. As far as the authors know, as listed in Table 1, there are many examples of the complexes introduced phenyl, cycloalkyl groups, and so on [16–33].

We have been interested in poly(pyrazolyl)borates as extraction reagents for first-series transition metal ions {M^{2+}: Mn(II), Fe(II), Co(II), Ni(II), Cu(II) and Zn(II)} [34–36]. The parent poly(pyrazolyl)borate, $[HB(pz)_3]^-$, extracted all the studied metal ions from very acidic solution at pH <2.1 into an organic phase. $[HB(pz)_3]^-$ forms quite stable A_2M complexes because the unique trigonal structure of $[HB(pz)_3]^-$ is favorable for octahedral coordination. $[B(pz)_4]^-$ and $[B(3\text{-Mepz})_4]^-$ also quantitatively extracted all the metal ions as octahedral A_2M complexes. However, $[B(pz)_4]^-$ extracted large metal ions, such as Mn(II) and Cd(II), at higher pH than $[HB(pz)_3]^-$ due to the intraligand contact between the coordinated and non-coordinated pyrazolyl rings.

* Corresponding author. Tel.: +81-774-38-3098; fax: +81-774-38-3099.
E-mail address: kitano@inter3.kuicr.kyoto-u.ac.jp (T. Kitano).

0277-5387/$ - see front matter © 2003 Elsevier Ltd. All rights reserved.
doi:10.1016/j.poly.2003.11.017

Table 1
Structurally determined A_2M complexes with bulky substituents at 3-position of pyrazolyl ring[a]

Ligand (A^-)	Metal (M^{2+})	Reference
$[HB(3\text{-}CF_3pz)_3]^-$	Fe	[16]
$[HB(3\text{-}Phpz)_3]^-$	Mn	[17]
$[HB(3\text{-}Phpz)_3]^-$	Fe	[17]
$[HB(3\text{-}Phpz)_3]^-$	Co	[18][b]
$[HB(3\text{-}Phpz)_3]^-$	Zn	[19][c]
$[HB(3\text{-}Phpz)_3]^-$	Cd	[20]
$[HB(3\text{-}Ph\text{-}5\text{-}Mepz)_3]^-$	Co	[21]
$[HB(3\text{-}cumyl\text{-}5\text{-}Mepz)_3]^-$	Co	[22]
$[HB(3\text{-}(2\text{-}thienyl)pz)_3]^-$	Co	[23]
$[HB(3\text{-}(3\text{-}pyridyl)\text{-}5\text{-}Mepz)_3]^-$	Zn	[24]
$[H_2B(3\text{-}Phpz)_2]^-$	Co	[25][c]
$[H_2B(3\text{-}Phpz)_2]^-$	Zn	[26][c]
$[H_2B(3\text{-}Ph\text{-}4\text{-}CNpz)_2]^-$	Co	[27][c]
$[H_2B(3\text{-}Ph\text{-}4\text{-}CNpz)_2]^-$	Cu	[27][d]
$[HB(3\text{-}cyclopropylpz)_3]^-$	Fe	[28]
$[B(3\text{-}cyclopropylpz)_4]^-$	Fe	[28]
$[HB(3\text{-}cyclobutylpz)_3]^-$	Co	[29]
$[B(3\text{-}cyclobutylpz)_4]^-$	Co	[29]
$[B(3\text{-}cyclopentylpz)_4]^-$	Co	[29][c]
$[HB(3\text{-}cyclohexylpz)_3]^-$	Cu	[30][d]
$[HB(3\text{-}neopentylpz)_3]^-$	Ni	[31]
$[B(3\text{-}iPrpz)_4]^-$	Co	[32][c]
$[B(3\text{-}iPrpz)_4]^-$	Ni	[33][c]
$[B(3\text{-}iPrpz)_4]^-$	Zn	this work[c]

[a] Complexes of the rearrangement of pyrazolyl rings are omitted.
[b] Square pyramidal geometry.
[c] Tetrahedral geometry.
[d] Square planar geometry.

$[B(3\text{-}Mepz)_4]^-$ extracted all the metal ions at higher pH compared to $[B(pz)_4]^-$ due to the interligand contact caused by the 3-methyl groups. The selectivity of these ligands for the metal ions generally followed the Irving–Williams series in stability constants; the extraction pH increased in the order of Cu(II), Ni(II), Co(II), Fe(II) and Mn(II).

Here, we report on the solvent extraction of the first-series transition metal ions with $[B(3\text{-}iPrpz)_4]^-$. $[B(3\text{-}iPrpz)_4]^-$ extracted only Cu(II) and Zn(II) of all the studied metal ions. In order to examine the steric effects of the isopropyl groups on the extraction, the structures of the extracted species, $[B(3\text{-}iPrpz)_4]_2Zn$ (**1**) and $[B(3\text{-}iPrpz)_4]Cu(OCOCH_3)$ (**2**), were examined by X-ray crystallography.

2. Experimental

2.1. General procedure

$K[B(3\text{-}iPrpz)_4]$ was synthesized as previously reported [32] and recrystallized from hot ethanol–water (1:5). All other chemicals were of reagent grade and distilled water was used throughout. Proton NMR spectra were obtained at 25 ± 1 °C with a JEOL LA-300 spectrometer. Chemical shifts (ppm) are reported downfield from TMS using the solvent chloroform-*d* ($\delta_H = 7.24$) as an internal standard. The reported ^1H coupling constants are $^3J_{HH}$ values. The metal ion concentration was determined with a HITACHI Z-8100 polarized Zeeman atomic absorption spectrometer or a Japan Jarrell Ash ICAP-500 inductively coupled argon plasma emission spectrometer. The pH was measured using a Hitachi-Horiba M-12 pH meter equipped with a glass electrode. The aqueous and organic phases were shaken with a TAITEC Bio-Shaker BR-30L.

2.2. Hydrolysis of the ligand

An aliquot of deuterium oxide (2.0 mL) at various pH was shaken with an equal volume of chloroform-*d* containing 5.0×10^{-3} M $K[B(3\text{-}iPrpz)_4]$ at 25 ± 1 °C for 10–90 min. After the two phases were separated centrifugally, the pH of the aqueous phase was measured. ^1H NMR of the two phases was measured using the JEOL LA-300.

2.3. Extraction of first-series transition metal ions

An aliquot of chloroform (10 mL) containing 1.0×10^{-3} M $K[B(3\text{-}iPrpz)_4]$ was shaken with an equal volume of an aqueous phase containing 1.0×10^{-5} M of a metal ion and 1.0×10^{-2} M of acetic acid, 2-(*N*-morpholino)ethanesulfonic acid (MES), 3-(*N*-morpholino)propanesulfonic acid (MOPS), *N*-tris(hydroxymethyl)methyl-3-aminopropanesulfonic acid (TAPS), 2-(cyclohexylamino)ethanesulfonic acid (CHES) or 3-(cyclohexylamino)propanesulfonic acid (CAPS) at 25 ± 1 °C. After the two phases were separated centrifugally, the pH of the aqueous phase was measured. The metal concentration in the aqueous phase was determined using the Z-8100 or the ICAP-500. The metal concentration in the organic phase was measured after back-extraction into 1.0 M nitric acid.

2.4. Syntheses of the complexes

2.4.1. Preparation of $[B(3\text{-}iPrpz)_4]_2Zn$ (1)

Ten milliliters of chloroform containing 2.0×10^{-3} M $K[B(3\text{-}iPrpz)_4]$ was shaken for 1 h with an aqueous solution (10 mL) at pH 8.0 containing 1.0×10^{-3} M $ZnSO_4$ and 1.0×10^{-2} M acetic acid. After centrifugation, the organic phase was evaporated to precipitate the complex. Recrystallization from a mixture of chloroform and acetonitrile in a 2:1 volume ratio gave colorless crystals suitable for X-ray diffraction. *Anal.* Calc. for $C_{48}H_{72}N_{16}B_2Zn$: C, 60.40; H, 7.52; N, 22.90. Found: C, 60.15; H, 7.64; N, 23.52%; m.p. 263–264 °C. ^1H NMR ($CDC1_3$, δ): 0.74, 1.20 (24, 24, d, d, $J = 6.8$, 7.0 Hz, Me(iPr)), 2.00, 2.95 (4, 4, m, m, CH(iPr)), 5.98, 6.09, 6.42, 7.13 (4, 4, 4, 4, d, d, d, d, $J = 2.2$, 2.6, 2.2, 2.4 Hz, 4-H (pz), 5-H(pz)). Although Trofimenko et al. [32]

prepared and characterized **1**, its X-ray structure has not been reported.

2.4.2. Preparation of $[B(3\text{-}iPrpz)_4]Cu(OCOCH_3)$ (**2**)

Ten milliliters of chloroform containing 1.0×10^{-3} M K[B(3-iPrpz)$_4$] was shaken for 1 h with an aqueous solution (10 mL) at pH 3.0 containing 1.0×10^{-3} M $CuSO_4$ and 1.0×10^{-2} M acetic acid. After centrifugation, the organic phase was evaporated to precipitate the complex. Recrystallization from methanol gave blue crystals suitable for X-ray diffraction. *Anal.* Calc. for $C_{25}H_{39}N_8BO_2Cu$: C, 54.82; H, 6.80; N, 19.67. Found: C, 54.73; H, 7.00; N, 19.71%; m.p. 145–146 °C.

2.5. X-ray crystal structure determination

Crystallographic data are summarized in Table 2. Crystals of **1** and **2** were each mounted onto a fine glass fiber with epoxy cement. The lattice parameters and intensity data were measured on a Rigaku AFC7R four-circle diffractometer with graphite monochromated Cu Kα radiation ($\lambda = 1.54178$ Å) at 20 ± 1 °C. An $\omega - 2\theta$ scan technique to a maximum 2θ value of 140° was used. An empirical absorption correction based on azimuthal scans of several reflections was applied [37]. The data were corrected for Lorentz and polarization effects, and a correction for secondary extinction was applied. The structures were solved by direct methods [38] and expanded using a Fourier technique [39]. The non-hydrogen atoms of **1** were refined anisotropically. For **2**, isotropic temperature factors were used for the nitrogen and carbon atoms of the non-coordinated pyrazolyl ring

Table 2
Crystal data and structure refinement

Compound	**1**	**2**
Empirical formula	$C_{48}H_{72}N_{16}B_2Zn$	$C_{26}H_{39}N_8O_2BCu$
Formula weight	960.20	570.00
Temperature (K)	293	293
Crystal system	monoclinic	orthorhombic
Space group	*C*2/*c*	*Pbca*
a (Å)	19.423(3)	18.867(4)
b (Å)	16.257(3)	20.611(5)
c (Å)	19.160(4)	15.657(2)
α (°)	90	90
β (°)	109.89(1)	90
γ (°)	90	90
V (Å^3)	5689(1)	6088(1)
Z	4	8
D_{calc} (Mg m^{-3})	1.121	1.244
μ (mm^{-1})	0.949	1.296
F(000)	2048	2408
Crystal size (mm)	$0.70 \times 0.40 \times 0.20$	$0.80 \times 0.40 \times 0.30$
Color	colorless	blue
Ranges of *h*, *k*, *l*	−21/23, 0/19, −21/0	0/22, 0/24, −18/0
Reflections collected	5699	6173
Independent reflections (R_{int})	5527 (0.022)	6040 (0.022)
Data/parameters	4336/304	4180/336
Goodness-of-fit on *F*	1.80	2.54
Final R_1/wR_2 indices ($I > 3\sigma(I)$)	0.061/0.094	0.082/0.128
Extinction coefficient	9.9057×10^{-7}	2.0541×10^{-6}
Largest difference peak and hole (e Å^{-3})	0.69 and −0.35	0.73 and −0.37

Table 3
Selected bond distances and angles of $[B(3\text{-}iPrpz)_4]_2Zn$ (**1**) and $[B(3\text{-}iPrpz)_4]Cu(OCOCH_3)$ (**2**)

Compound	Distances (Å)	Angles (°)
1	Zn(1)–N(1) 1.956(2)	N(1)–Zn(1)–N(1) 125.7(1)
	Zn(1)–N(3) 1.956(2)	N(1)–Zn(1)–N(3) 100.03(9)
		N(1)–Zn(1)–N(3) 113.0(1)
		N(1)–Zn(1)–N(3) 103.5(1)
2	Cu(1)–O(1) 2.107(4)	O(1)–Cu(1)–O(2) 63.0(2)
	Cu(1)–O(2) 2.012(4)	O(1)–Cu(1)–N(1) 162.3(2)
	Cu(1)–N(1) 1.996(4)	O(1)–Cu(1)–N(3) 100.2(2)
	Cu(1)–N(3) 1.995(4)	O(1)–Cu(1)–N(5) 104.3(2)
	Cu(1)–N(5) 2.155(4)	O(2)–Cu(1)–N(1) 102.1(2)
		O(2)–Cu(1)–N(3) 155.5(2)
		O(2)–Cu(1)–N(5) 109.6(2)
		N(1)–Cu(1)–N(3) 90.6(2)
		N(1)–Cu(1)–N(5) 89.3(2)
		N(3)–Cu(1)–N(5) 91.2(2)

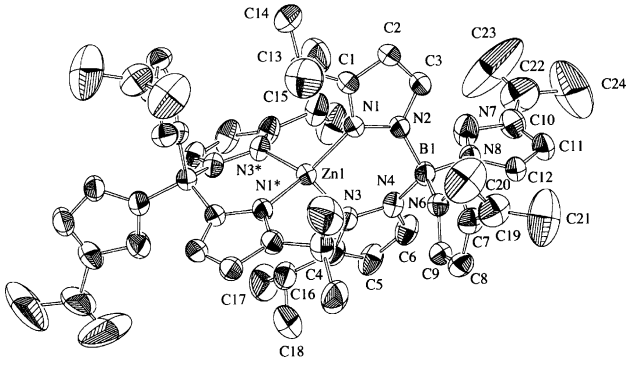

Fig. 1. ORTEP view of $[B(3\text{-}iPrpz)_4]_2Zn$ (**1**) (20% probability). Hydrogen atoms are omitted for clarity.

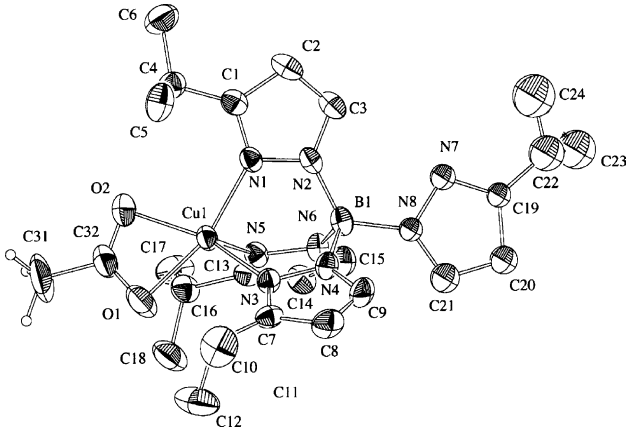

Fig. 2. ORTEP view of $[B(3\text{-}iPrpz)_4]Cu(OCOCH_3)$ (**2**) (20% probability). Hydrogen atoms are omitted for clarity except for the hydrogen atoms bonded to the carbon atom (C31).

because of disorder. Hydrogen atoms were fixed at the positions generated by calculation, while those on the non-coordinated pyrazolyl ring of **2** were not incorporated in the refinement. All calculations were performed using the TEXSAN crystallographic software package developed by Molecular Structure Corporation.

Selected bond distances and angles of **1** and **2** are shown in Table 3. Figs. 1 and 2 show ORTEP drawings of **1** and **2**, respectively.

3. Results and discussion

3.1. Hydrolysis and distribution of the ligands

It was previously reported that poly(pyrazolyl)borates hydrolyzed into pyrazoles and boric acid [34–36]. The chloroform-d solution containing $K[B(3\text{-}iPrpz)_4]$ was shaken with deuterium oxide to study the hydrolysis of $[(3\text{-}iPrpz)_4]^-$. On the basis of ^1H NMR, 5% of $[B(3\text{-}iPrpz)_4]^-$ in chloroform-*d* hydrolyzed into isopropylpyrazole after 10 min of shaking with an aqueous phase at pH 2.5–13. Twenty five percent of $[B(3\text{-}iPrpz)_4]^-$ hydrolyzed after 90 min of shaking. Although no peaks of $[B(3\text{-}iPrpz)_4]^-$ and isopropylpyrazole were observed in deuterium oxide after 10 min of shaking, one set of peaks of isopropylpyrazole was observed after 90 min. We also confirmed that the concentration of K^+ in the aqueous phase does not significantly increase after shaking. These data suggest that $K[B(3\text{-}iPrpz)_4]$ does not distribute into the aqueous phase because of the high hydrophobicity of $[B(3\text{-}iPrpz)_4]^-$, and some isopropylpyrazole distributes into the aqueous phase after hydrolysis of $[B(3\text{-}iPrpz)_4]^-$.

3.2. Extraction of first-series transition metal ions

Fig. 3 shows the relationship between the percent extraction (%*E*) of metal ions and the pH of the aqueous phase using $[B(pz)_4]^-$, $[B(3\text{-}Mepz)_4]^-$ and $[B(3\text{-}iPrpz)_4]^-$ as a ligand. $K[B(pz)_4]$ and $K[B(3\text{-}Mepz)_4]$ were initially dissolved in the aqueous phase, since they were not soluble in chloroform. Ten minutes of shaking was adopted for a comparison with $[B(pz)_4]^-$ and $[B(3\text{-}Mepz)_4]^-$, although they were not sufficient for equilibrium for $[B(3\text{-}iPrpz)_4]^-$. The %*E* values were independent of the metal ion concentrations of 3.0×10^{-5}–3.0×10^{-3} M. $[B(3\text{-}iPrpz)_4]^-$ quantitatively extracted only Cu(II) and Zn(II) ions. It should be noted that the extraction with $[B(3\text{-}iPrpz)_4]^-$ was very different from that with $[B(pz)_4]^-$ and $[B(3\text{-}Mepz)_4]^-$.

The %*E* reached a maximum value after 50 and 90 min of shaking for Cu(II) and Zn(II), respectively. In order to elucidate the extracted species, the distribution ratio (*D*) under these conditions was measured using

$$D = C_{M,o}/C_M \quad (1)$$

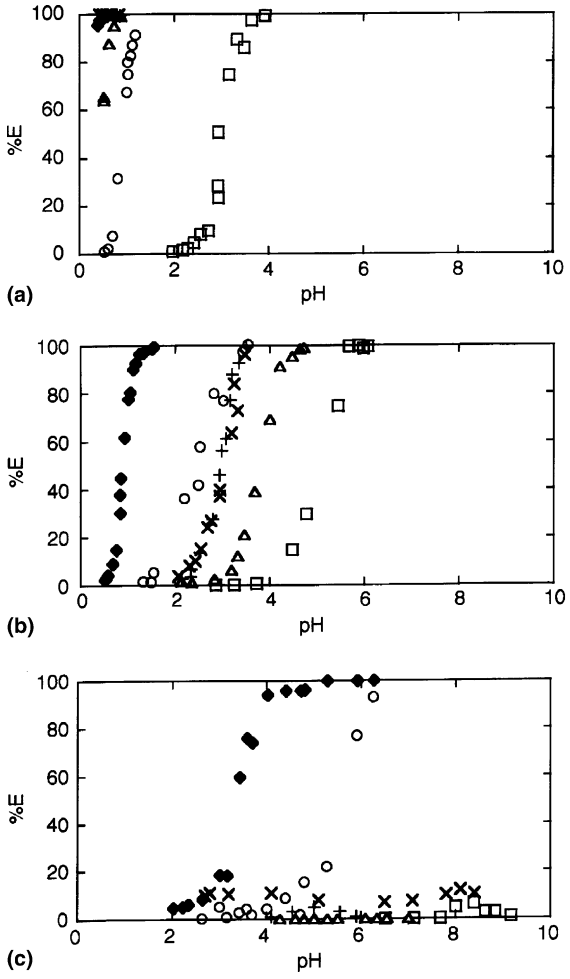

Fig. 3. Effect of pH on the percentage extraction of metal ions. The extraction time was 10 min. Key: □, Mn(II); △, Fe(II); +, Co(II); ×, Ni(II); ◆, Cu(II); ○, Zn(II). (a) $K[B(pz)_4]$; (b) $K[B(3\text{-}Mepz)_4]$; (c) $K[B(3\text{-}iPrpz)_4]$. (a,b) Aqueous phase: 1.0×10^{-2} M buffer, 1.0×10^{-4} M M^{2+}, 1.0×10^{-2} M KA (10 mL). Organic phase: chloroform 10 mL; Data taken from [34,35], respectively. (c) Aqueous phase: 1.0×10^{-2} M buffer, 1.0×10^{-5} M M^{2+} (10 mL). Organic phase: 1.0×10^{-3} M KA (chloroform 10 mL).

where C_M signifies the analytical molar concentration of the metal ion (M^{2+}) and the subscript o denotes the species in the organic phase. When an A_2M complex is formed and extracted, the overall extraction equilibrium and extraction constant (K_{ex}) of M^{2+} are described as follows:

$$M^{2+} + 2KA_o \leftrightarrow A_2M_o + 2K^+ \quad (2)$$

$$K_{ex} = [A_2M]_o[K^+]^2/[M^{2+}][KA]_o^2 \quad (3)$$

$$\log D = \log K_{ex} - 2\log[K^+] + 2\log[KA]_o \quad (4)$$

To analyze the extraction data graphically, the hydrolysis of the ligand must be taken into consideration. $[KA]_o$ is expressed as

$$[KA]_o = C_{KA}a, \quad (5)$$

where C_{KA} and a mean the initial concentration of the ligand in the organic phase and the remaining ratio of the ligand after hydrolysis, respectively. The substitution of Eq. (5) into Eq. (4) and a rearrangement result in

$$\log D - 2\log a + 2\log[K^+] = 2\log C_{KA} + \log K_{ex}. \quad (6)$$

The plot of $\log D - 2\log a + 2\log[K^+]$ versus $\log C_{KA}$ for Zn(II) gave a straight line with a slope close to 2 (Fig. 4). The $\log D$ of Zn(II) did not depend on the initial concentration of Zn(II) [$C(Zn^{2+})$]. These results suggest the validity of Eq. (2) for the extraction of Zn(II). However, the $\log D - 2\log a + 2\log[K^+]$ versus $\log C_{KA}$ plot gave a slope close to 1 for Cu(II) (Fig. 5). The $\log D$ of Cu(II) did not depend on the initial concentration of Cu(II) [$C(Cu^{2+})$]. These results suggest that the extracted species was ACuX, where X^- denotes an ancillary ligand. The extraction equation and constant are expressed as

$$Cu^{2+} + KA_o + X^- \leftrightarrow ACuX_o + K^+ \quad (7)$$

$$K_{ex} = [ACuX]_o[K^+]/[Cu^{2+}][KA]_o[X^-] \quad (8)$$

Since we used acetate as buffer in the pH range where Cu(II) was extracted, acetate is an ancillary ligand candidate.

3.3. Syntheses of the complexes

An aqueous phase containing Zn(II) or Cu(II) and an organic phase containing K[B(3-iPrpz)$_4$] were shaken to form the complexes according to Eq. (2) or Eq. (7). The pH was appropriately adjusted to produce complexes. The complexes, [B(3-iPrpz)$_4$]$_2$Zn (**1**) and [B(3-iPrpz)$_4$] Cu(OCOCH$_3$) (**2**), were obtained after evaporation of the organic phases. They dissolved into chloroform, dichloromethane and benzene, and were stable in air.

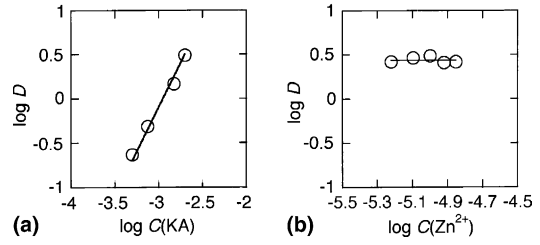

Fig. 4. Effect of $\log C_{KA}$ and $\log C(Zn^{2+})$ on $\log D$ for the extraction of Zn^{2+} with [B(3-iPrpz)$_4$]$^-$. The extraction time was 90 min. (a) pH 4.80, Zn^{2+}; 1.0×10^{-5} M, (b) C_{KA}; 1.0×10^{-3} M, pH 4.85. Solid lines, of which the slopes are 2 and 0, respectively, were obtained by a least-squares fit.

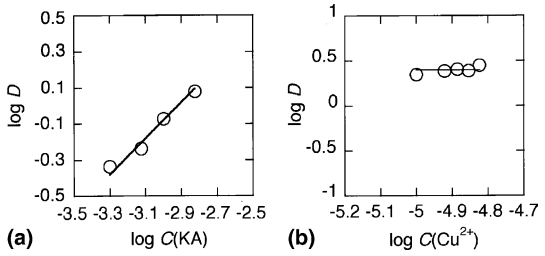

Fig. 5. Effect of $\log C_{KA}$ and $\log C(Cu^{2+})$ on $\log D$ for the extraction of Cu^{2+} with [B(3-iPrpz)$_4$]$^-$. The extraction time was 50 min. (a) pH 3.46, Cu^{2+}; 1.0×10^{-5} M, (b) C_{KA}; 1.0×10^{-3} M, pH 3.51. Solid lines, of which the slopes are 1 and 0, respectively, were obtained by a least-squares fit.

3.4. Structure of the Zn(II) complex

The zinc atom sits on a center of inversion for **1** as seen in Fig. 1. Both ligands are bidentate and the geometry about the zinc atom is a tetrahedron. The ligands coordinate to the zinc atom through the nitrogen atom in the 2-position of two of the 3-isopropylpyrazolyl rings, with the two additional rings of the ligand not coordinated to the metal atom. The metal-coordinated rings have their isopropyl groups bisecting the other chelate ring and the C–H bond oriented toward the metal ion, whereas the isopropyl groups of the non-coordinated groups are in an intermediate position. The structure of **1** resembles that of [B(3-iPrpz)$_4$]$_2$Co [32] and [B(3-iPrpz)$_4$]$_2$Ni [33]. The distances and bond angles between the zinc ion and the nitrogen atoms are nearly identical with those observed for [H$_2$B(pz)$_2$]$_2$Zn [40], which also has the Zn(II) ion coordinated by four pyrazolyl groups from two ligands. These bond distances are also typical of Zn–N distances in poly(pyrazolyl)borate complexes.

[B(pz)$_4$]$_2$Zn (**3**) and [B(3-Mepz)$_4$]$_2$Zn (**4**) are octahedral with [B(pz)$_4$]$^-$ and [B(3-Mepz)$_4$]$^-$ coordinating in a tridentate fashion by X-ray diffraction [34,35]. Only one kind of pyrazolyl ring of **3** and **4** in chloroform-*d* was observed with ^{1}H NMR, because the exchange of the coordinated and non-coordinated pyrazolyl rings in **3** and **4** was fast on the NMR time scale at ambient temperature. However, the structure observed by ^{1}H NMR for **1** indicates that [B(3-iPrpz)$_4$]$^-$ coordinates in a bidentate fashion, probably with tetrahedral geometry around the zinc atom. These facts suggest that the isopropyl group makes the exchange of pyrazolyl rings slower than the hydrogen atom and the methyl group, and that the solution structure of **1** is similar to that in the solid state.

3.5. Structure of the Cu(II) complex

As shown in Fig. 2 the [B(3-iPrpz)$_4$]$^-$ ligand and acetate anion are bonded to the copper atom in a tridentate and an asymmetric bidentate mode, respectively. The non-coordinated pyrazolyl ring stands out in the opposite direction to the copper atom. The geometry about the copper atom is best described as square pyramidal by the structural parameter $\tau = 0.11$; $\tau = (\alpha - \beta)/60°$, where α and β are the largest angles ($\alpha > \beta$) around a five-coordinate metal center, as

reported by Addison et al. [41]. The square plane consists of two nitrogen atoms from the $[B(3\text{-}iPrpz)_4]^-$ ligand and two oxygen atoms from the acetate. This structure is similar to that of $[HB(3,5\text{-}iPr_2pz)_3]Cu(O_2NO)$ [42] and $[HB(3,5\text{-}iPr_2pz)_3]Fe(OCOCH_3)$ [43].

3.6. Steric effects of 3-isopropyl group

When two $[B(3\text{-}iPrpz)_4]^-$ ligands coordinate a metal ion in a trigonal tridentate fashion, the steric repulsion around the metal ion increases by the interligand contact between the isopropyl groups, and the stability of the complexes becomes too low to be extracted into the organic phase. Thus, in order to avoid this steric repulsion, two $[B(3\text{-}iPrpz)_4]^-$ ligands coordinate the Zn(II) ion in a bidentate fashion and one $[B(3\text{-}iPrpz)_4]^-$ coordinates the Cu(II) ion in a tridentate fashion with the acetate anion having a bidentate configuration. Since the stabilities of **1** and **2** are much lower than the octahedral A_2M complexes with $[B(pz)_4]^-$ and $[B(3\text{-}Mepz)_4]^-$, the extraction pH for **1** and **2** are high. Trofimenko et al. prepared the A_2M complexes of Fe(II), Co(II), Ni(II), Cu(II) and Zn(II) with $[B(3\text{-}iPrpz)_4]^-$. They were tetrahedral in the solid state on the basis of infrared spectroscopy. It is likely that the stabilities of the A_2M complexes of Fe(II), Co(II) and Ni(II) are not sufficiently high to be extracted.

4. Conclusion

Selectivity of tetrakis(pyrazolyl)borates for first-series transition metal ions is controlled by the substituents on the 3-position of the pyrazolyl ring. All the studied metal ions form octahedral A_2M complexes with $[B(pz)_4]^-$ and $[B(3\text{-}Mepz)_4]^-$ and their stability follows the common Irving–Williams series. On the other hand, all the metal ions cannot form an octahedral A_2M complex with $[B(3\text{-}iPrpz)_4]^-$ due to the interligand contact between the isopropyl groups. Although only Zn(II) and Cu(II) form tetrahedral A_2M and square pyramidal AMX complexes, respectively, which are extracted into the organic phase, the other metal ions cannot form stable and extractable complexes. Thus, the isopropyl group changes the geometry and stability of the complexes, resulting in the unique selectivity of $[B(3\text{-}iPrpz)_4]^-$.

5. Supplementary data

Crystallographic data for the structures reported in this paper have been deposited with the Cambridge Crystallographic Data Centre, CCDC No. 207207 for **1** and CCDC No. 207208 for **2**. Copies of this information may be obtained free of charge from the Director, CCDC, 12 Union Road, Cambridge, CB2 1EZ, UK (fax: +44-1223-336033; e-mail: deposit@ccdc.cam.ac.uk or www: http://www.ccdc.cam.ac.uk).

Acknowledgements

The authors are grateful to Assistant Professors Yasushi Kawai and Tomomi Fujii (Kyoto University) for their helpful discussion on X-ray crystallography.

References

[1] M.T. Valahovic, T.B. Gunnoe, M. Sabat, W.D. Harman, J. Am. Chem. Soc. 124 (2002) 3309.
[2] L.A. Friedman, M. Sabat, W.D. Harman, J. Am. Chem. Soc. 124 (2002) 7395.
[3] S.H. Meiere, F. Ding, L.A. Friedman, M. Sabat, W.D. Harman, J. Am. Chem. Soc. 124 (2002) 13506.
[4] S.H. Meiere, M.T. Valahovic, W.D. Harman, J. Am. Chem. Soc. 124 (2002) 15099.
[5] K.P. Gable, F.A. Zhuravlev, J. Am. Chem. Soc. 124 (2002) 3970.
[6] A. Dehestani, W. Kaminsky, J.M. Mayer, Inorg. Chem. 42 (2003) 605.
[7] J.S. Wiley, D.M. Heinekey, Inorg. Chem. 41 (2002) 4961.
[8] D. Conner, K.N. Jayaprakash, T.B. Gunnoe, P.D. Boyle, Inorg. Chem. 41 (2002) 3042.
[9] V. Chauby, J.-C. Daran, C.S.-L. Berre, F. Malbosc, P. Kalck, O.D. Gonzalez, C.E. Haslam, A. Haynes, Inorg. Chem. 41 (2002) 3280.
[10] V. Circu, M.A. Fernandes, L. Carlton, Inorg. Chem. 41 (2002) 3859.
[11] D.T. Puerta, S.M. Cohen, Inorg. Chem. 41 (2002) 5075.
[12] D. Badura, H. Vahrenkamp, Inorg. Chem. 41 (2002) 6013.
[13] D. Badura, H. Vahrenkamp, Inorg. Chem. 41 (2002) 6020.
[14] Y.-J. Sun, L.Z. Zhang, P. Cheng, H.-K. Lin, S.-P. Yan, W. Sun, D.-Z. Liao, Z.-H. Jiang, P.-W. Shen, Inorg. Chem. 42 (2003) 508.
[15] S. Trofimenko, Scorpionates: The Coordination Chemistry of Polypyrazolylborate Ligands, Imperial College Press, London, 1999.
[16] P. Cecchi, M. Berrettoni, M. Giorgetti, G.G. Lobbia, S. Calogero, L. Stievano, Inorg. Chim. Acta 318 (2001) 67.
[17] D.M. Eichhorn, W.H. Armstrong, Inorg. Chem. 29 (1990) 3607.
[18] A. Kremer-Aach, W. Klaui, R. Bell, A. Strerath, H. Wunderlich, D. Mootz, Inorg. Chem. 36 (1997) 1552.
[19] F. Hartmann, W. Klaui, A. Kremer-Aach, D. Mootz, A. Strerath, H. Wunderlich, Z. Anorg. Allg. Chem. 619 (1993) 2071.
[20] J.H. Reibenspies, K.K. Klausmeyer, S.A. Niezgoda, M.W. Holtcamp, B. Khandelwal, D.J. Darensbourg, Z. Kristallogr. 210 (1995) 617.
[21] T. Ruman, Z. Ciunik, E. Szklanny, S. Wolowiec, Polyhedron 21 (2002) 2743.
[22] M. Ruf, B.C. Noll, M.D. Groner, G.T. Yee, C.G. Pierpont, Inorg. Chem. 36 (1997) 4860.
[23] J.C. Calabrese, P.J. Domaille, S. Trofimenko, G.J. Long, Inorg. Chem. 30 (1991) 2795.
[24] K. Weis, H. Vahrenkamp, Inorg. Chem. 36 (1997) 5592.
[25] C.J. Siemer, F.A. Meece, W.H. Armstrong, D.M. Eichhorn, Polyhedron 20 (2001) 2637.
[26] D.J. Darensbourg, J.C. Yarbrough, J. Organometallic Chem. 614–615 (2000) 305.
[27] C.J. Siemer, N. Goswami, P.K. Kahol, M.J. Van Stipdonk, D.M. Eichhorn, Inorg. Chem. 40 (2000) 4081.
[28] A.L. Rheingold, G.P.A. Yap, L.M. Liable-Sands, I.A. Guzei, S. Trofimenko, Inorg. Chem. 36 (1997) 6261.

[29] A.L. Rheingold, G.P.A. Yap, L.N. Zakharov, S. Trofimenko, Eur. J. Inorg. Chem. (2002) 2335.
[30] M.A. Halcrow, C.A. Kilner, M. Thornton-Pett, Acta Crystallogr. C 57 (2001) 711.
[31] J.C. Calabrese, S. Trofimenko, Inorg. Chem. 31 (1992) 4810.
[32] S. Trofimenko, J.C. Calabrese, P.J. Domaille, G.S. Thompson, Inorg. Chem. 28 (1989) 1091.
[33] J. Kisala, Z. Ciunik, K. Drabent, T. Ruman, S. Wolowiec, Polyhedron 22 (2003) 1645.
[34] T. Kitano, Y. Sohrin, Y. Hata, H. Kawakami, T. Hori, K. Ueda, J. Chem. Soc., Dalton Trans. (2001) 3564.
[35] T. Kitano, Y. Sohrin, Y. Hata, H. Wada, T. Hori, K. Ueda, Bull. Chem. Soc. Jpn. 76 (2003) 1365.
[36] T. Kitano, H. Wada, H. Mukai, K. Ueda, Y. Sohrin, Anal. Sci. 17 (Suppl.) (2001) 1113.
[37] G.M. Sheldrick, in: G.M. Sheldrick, C. Kruger, R. Goddard (Eds.), Crystallographic Computing, vol. 3, Oxford University Press, London, 1985, p. l75.
[38] A. Altomare, M.C. Burla, M. Camalli, M. Cascarano, C. Gracovazzo, A. Guagliardi, G. Polidori, J. Appl. Cryst. 27 (1994) 435.
[39] P.T. Beurskens, G. Adiniraal, G. Beurskens, W.P. Bosman, R. de Gelder, R. Israel, J.M.M. Smits, The DIRDIF 94 program system, Technical Report of the Crystallography Laboratory, University of Nijmegen, The Netherlands, 1994.
[40] D.L. Reger, T.D. Wright, M.D. Smith, A.L. Rheingold, B. Rhagitan, J. Chem. Crystallogr. 30 (2000) 665.
[41] A.W. Addison, T.N. Rao, J. Reedijk, J. van Rijn, G.C. Verschoor, J. Chem. Soc., Dalton Trans. (1984) 1349.
[42] K. Fujisawa, T. Kobayashi, K. Fujita, N. Kitajima, Y. Moro-oka, Y. Miyashita, Y. Yamada, K. Okamoto, Bull. Chem. Soc. Jpn. 73 (2000) 1797.
[43] N. Kitajima, N. Tamura, H. Amagai, H. Fukui, Y. Moro-oka, Y. Mizutani, T. Kitagawa, R. Mathur, K. Heerwegh, C.A. Reed, C.R. Randall, L. Que Jr., K. Tatsumi, J. Am. Chem. Soc. 116 (1994) 9071.

Available online at www.sciencedirect.com
SCIENCE DIRECT®
Polyhedron 23 (2004) 291–299
POLYHEDRON
www.elsevier.com/locate/poly

Synthesis of *meta*-$C_6H_4[C(1\text{-pyrazolyl})_2(2\text{-pyridyl})]_2$, a fixed geometry bitopic heteroscorpionate and the crystal structure of its unusual square planar silver(I) complex

Daniel L. Reger *, James R. Gardinier, Mark D. Smith

Department of Chemistry and Biochemistry, University of South Carolina, Columbia, SC 29208, USA

Received 21 May 2003; accepted 12 August 2003

Abstract

The reaction between bis(1-pyrazolyl)sulfone (prepared in situ by the reaction between NaH, Hpz, and $SOCl_2$ in THF) and $C_6H_4[C(O)(2\text{-py})]_2$ in THF catalyzed by $CoCl_2$ yields *m*-$C_6H_4[C(pz)_2(2\text{-py})]_2$ (**1**, pz = pyrazolyl, py = pyridyl) in moderate yield, along with 1-$[C(pz)_2(2\text{-py})]$-4-$[C(O)(2\text{-py})]C_6H_4$. The potentially bitopic ligand **1** reacts with $AgPF_6$ to yield $[Ag(\mathbf{1})_2](PF)_6$ (**3**), regardless of the stoichiometry of reagents used in the preparation. X-ray structural analysis of this silver complex shows that two ligands bond to a silver in a κ^2-fashion via the pyrazolyls in one $C(pz)_2(py)$ group in each ligand while the other is non-coordinated. The AgN_4C chelate rings adopt a boat conformation and the silver resides in an unusual square planar coordination environment. Non-covalent forces organize the two-dimensional structure of **3** such that it approaches a layered inorganic–organic hybrid material. Reaction of $C_6H_5[C(pz)_2(2\text{-py})]$ and $AgPF_6$ yields $\{Ag(\kappa^2\text{-}C_6H_5[C(pz)_2(2\text{-py})])_2\}(PF_6)$ (**4**). The structure is disordered but the ligands are bidentate, the nitrogen donor atoms are in a square planar coordination environment about the silver and the overall structure is similar to **3**.
© 2003 Elsevier Ltd. All rights reserved.

Keywords: Bitopic heteroscorpionate ligand; Square planar silver complex

1. Introduction

Current interest in coordination networks is driven in part by the desire to combine the variety in structural, physical, and spectroelectrochemical properties of both the inorganic and organic constituents with the practicality and function of zeolite-type materials [1,2]. Recent work published by Wenbin Lin's group is testament to the potential for the realization of such a goal [3,4]. Advances in the design of polytopic ligands, which serve as organic spacers between two or more metal centers, have been instrumental to this area of research. Over recent years, our group has been interested in exploring the preparation and coordination chemistry of a variety of polytopic poly(pyrazolyl)methane ligands. We have prepared bitopic tetra-(pyrazolyl) compounds that contain two bis(pyrazolyl)methane units linked by either a flexible methylene or a semi-rigid ferrocenyl group, and have explored their coordination chemistry with silver [5,6]. Additionally, we have reported on the preparation of coordination polymers that incorporate semi-rigid organic spacers based on polytopic tris(pyrazolyl)methanes of the type $C_6H_{6-n}[CH_2OCH_2C(pz)_3]_n$ ($n = 2$, 4 [7–9]; pz = pyrazolyl ring). The use of poly(pyrazolyl)methane ligands linked by *rigid* organic spacers would be of interest toward the preparation of either large metallacycles of predefined geometry or the development of coordination networks with a predictable arrangement of metal centers within the material. To this end, we have prepared $\alpha,\alpha,\alpha',\alpha'$-tetrakis(1-pyrazolyl)-$\alpha,\alpha'$-bis(2-pyridyl)-1,3-xylene, *m*-$C_6H_4[C(pz)_2\ (2\text{-py})]_2$ (**1**, py = pyridyl ring), a potentially bitopic heteroscorpionate, that can be envisioned as a 120° rigid organic spacer. In this paper we will detail the preparation of **1** and outline our initial observations regarding its coordination chemistry with silver hexafluorophosphate. For

* Corresponding author. Tel.: +1-803-777-5263; fax: +1-803-777-9521.
E-mail address: reger@mail.chem.sc.edu (D.L. Reger).

0277-5387/$ - see front matter © 2003 Elsevier Ltd. All rights reserved.
doi:10.1016/j.poly.2003.11.018

comparison, the related chemistry involving the monotopic analogue, $C_6H_5[C(pz)_2(2\text{-py})]$ (**2**), will also be described.

2. Experimental

2.1. General

Solvents for synthetic procedures, and spectroscopic studies were dried by conventional methods and distilled under N_2 atmosphere immediately prior to use. The compound $m\text{-}C_6H_4[C(O)(2\text{-py})]_2$ was prepared as described previously [10]. All other reagents were used as received from Aldrich Chemical Co. Silica gel (0.040–0.063 mm, 230–400 mesh) used for chromatographic separations was purchased from Fischer Scientific. Silver hexafluorophosphate was stored and handled under a purified nitrogen atmosphere in a drybox. Robertson Microlit Laboratories performed all elemental analyses. Melting point determinations were made on samples contained in sealed glass capillaries by using an Electrothermal 9100 apparatus and are uncorrected. Mass spectrometric measurements recorded in ESI(+) mode were obtained on a Micromass Q-Tof spectrometer whereas those performed by using direct probe analyses were made on a VG 70S instrument. NMR spectra were recorded by using either a Varian Mercury 400 or a Varian Inova 500 instrument, as noted within the text. Chemical shifts were referenced to solvent resonances at either δ_H 7.27, δ_C 77.2 for $CDCl_3$, or δ_H 2.05, δ_C 29.8 for acetone-d_6.

2.2. Ligand preparation

The preparation of $C_6H_5C(pz)_2(2\text{-py})$ has been described previously [11], however, in this contribution an alternate purification step and additional characterization data are provided. The title bitopic derivative was prepared by using an analogous procedure. Therefore, only the quantity of reagents, solvent, reaction time, and the details of chromatographic separation are described below for each.

2.3. Preparation of $m\text{-}C_6H_4[C(pz)_2(2\text{-py})]_2$, $\alpha,\alpha,\alpha',\alpha'$-tetrakis(1-pyrazolyl)-$\alpha,\alpha'$-bis(2-pyridyl)-1,3-xylene, (*1*)

A mixture of 2.9 mmol $SO(pz)_2$ [from 0.14 g (5.9 mmol) NaH, 0.40 g (5.9 mmol) Hpz and 0.21 ml (2.9 mmol) $SOCl_2$], 0.43 g (1.5 mmol) $C_6H_4[C(O)(2\text{-py})]_2$, and 60 mg (30 mol% of $C_6H_4[C(O)(2\text{-py})]_2$) $CoCl_2$ in 80 ml THF were heated at reflux for four days. After work-up, chromatographic separation of the product mixture on SiO_2 by using Et_2O as the eluent afforded 0.16 g (0.55 mmol) $C_6H_4[C(O)(2\text{-py})]_2$ from the first pale yellow band ($R_f = 0.7$ on TLC plate) and 0.14 g (0.34 mmol) of 1-$[C(pz)_2(2\text{-py})]$-4-$[C(O)(2\text{-py})]C_6H_4$, **1a,** as a colorless solid from the second pale yellow band ($R_f = 0.3$ TLC plate). Mp 113–115 °C. IR (cm^{-1}): ν_{co} 1669 (br, vs). ^1H NMR (400 MHz, $CDCl_3$) 8.68 (d, $J = 4$ Hz, 1H, H_6-py*CO*), 8.62 (d, $J = 4$ Hz, 1H, H_6-py), 8.16 (m, 1H, aryl), 8.00 (d, $J = 8$ Hz, 1H, H_3-py*CO*), 7.98 (s, 1H, aryl), 7.85 (ddd, $J = 8$, 8, 2 Hz, 1H, H_4-py*CO*), 7.73 (ddd, $J = 8$, 8, 2 Hz, 1H, H_4-py, 7.68 (d, $J = 1$ Hz, 2H, H_3-pz), 7.56 (d, $J = 2$ Hz, 2H, H_5-pz), 7.49 (m, 2H, aryl), 7.45 (ddd, $J = 8$, 4, 1 Hz, 1H, H_5-py*CO*), 7.32 (ddd, $J = 8$, 4, 1 Hz, 1H, H_5-py), 7.24 (d, $J = 8$ Hz, 1H, H_3-py), 6.33 (d, $J = 2$ Hz, 2H, H_4-pz). ^{13}C NMR (101.62 MHz, $CDCl_3$) 193.0 (C═O), 158.3 (C_2-py), 154.9 (C_2-py*CO*), 148.9 (C_6-py*CO*), 148.6 (C_6-py), 140.9 (C_5-pz), 139.7 (C_3-aryl), 137.2 (C_4-py*CO*), 137.1 (C_4-py), 136.0 (C_1-aryl), 133.8 (C_4-aryl), 132.6 (C_3-pz), 131.9 ($C_{2,6}$-aryl), 128.1 (C_5-aryl), 126.4 (C_3-py*CO*), 124.9 (C_3-py), 124.6 (C_5-py*CO*), 123.9 (C_5-py), 106.1 (C_4-pz), 87.1 (C_α). Direct probe MS *m/z* (Rel. Int. %) [assgn]: 406(32) $[M]^+$, 338(100) $[M\text{-}Hpz]^+$, 328(21) $[M\text{-}py]^+$, 233(29) $[C(C_6H_4)(pz)py]^+$, 182(12) $[PhC(O)py]^+$, 78(37) $[py]^+$. After complete elution of **1a**, the column was sequentially flushed with acetone, acetonitrile, acetonitrile/methanol (1:4) which after combining these fractions and evaporating the solvents gave 0.27 g (0.51 mmol, 34% based on $C_6H_4[C(O)(2\text{-py})]_2$) of **1** as a pale yellow solid. Mp 223–225 °C dec. ^1H NMR (400 MHz, $CDCl_3$) 8.61 (d, $J = 4$ Hz, 2H, H_6-py), 7.69 (ddd, $J = 8$, 8, 2 Hz, 2H, H_4-py), 7.61 (d, $J = 1$ Hz, 4H, H_3-pz), 7.53 (d, $J = 2$ Hz, 4H, H_5-pz). 7.31 (t, $J = 8$ Hz, 1H, H_5-aryl), 7.29 (ddd, $J = 8$, 4, 2, Hz, 2H, H_5-py), 7.18–7.13 (m, 4H, aryl and H_3-py), 6.28 (d, $J = 2$ Hz, 2H, H_4-pz). ^1H NMR (400 MHz, acetone-d_6) 8.57 (d, $J = 5$ Hz, 2H, H_6-py), 7.82 (ddd, $J = 7$, 7, 2 Hz, 2H, H_4-py), 7.57 (d, $J = 1$ Hz, 4H, H_3-pz), 7.50 (d, $J = 2$ Hz, 4H, H_5-pz). 7.40 (ddd, $J = 7$, 5, 2 Hz, 2H, H_5-py), 7.33 (t, $J = 8$ Hz, 1H, H_5-aryl), 7.25 (s, 1H, aryl), 7.13 (d, $J = 8$ Hz, 2H, aryl), 7.09 (dd, $J = 7$, 2 Hz, 2H, H_3-py), 6.32 (dd, $J = 2$, 1 Hz, 4H, H_4-pz). ^{13}C NMR (101.62 MHz, $CDCl_3$) 158.3 (C_2-py), 148.6 (C_6-py), 140.7 (C_5-pz), 138.8 (C_{ipso}-Ph), 136.9 (C_4-py), 133.7 (aryl), 132.6 (C_3-pz), 129.2 ($C_{4/6}$-aryl), 128.2 (C_2-aryl), 124.8 (C_3-py), 123.8 (C_5-py), 105.9 (C_4-pz), 87.2 (C_α). HRMS-Direct probe (*m/z*): *Anal*. Calc. for $C_{30}H_{24}N_{10}^+$ 524.2185. Found: 524.217. Direct probe MS *m/z* (Rel. Int. %) [assgn]: 524(2) $[M]^+$, 456(100) $[M\text{-}Hpz]^+$, 389(36) $[M\text{-}2pz]^+$, 378(31) $[M\text{-}pz\text{-}py]^+$, 322(19)$[M\text{-}3pz]^+$, 310(18) $[M\text{-}2pz\text{-}py]^+$, 78(12) $[py]^+$.

2.4. Preparation of $C_6H_5[C(pz)_2(2\text{-py})]$, α,α-bis(1-pyrazolyl)-α-(2-pyridyl)toluene (*2*)

A mixture of 21 mmol $SO(pz)_2$ [from 1.0 g (42 mmol) NaH, 2.9 g (42 mmol) Hpz, and 1.5 ml (21 mmol) $SOCl_2$], 3.7 g (20 mmol) 2-benzoylpyridine, and 75 mg (3 mol% of 2-benzoylpyridine) $CoCl_2$ in 20 ml THF were heated at reflux for 15 h. After work-up,

chromatographic separation of the product mixture on SiO_2 with 50% Et_2O/hexanes afforded 2.2 g (37% based on 2-benzoylpyridine) of **2** as a colorless solid from the second colorless band ($R_f = 0.4$ on TLC plate). Mp 138–139 °C (lit. 123–125 °C [11]). ^{1}H NMR (400 MHz, $CDCl_3$) 8.70 (d, $J = 4$ Hz, 1H, H_6-py), 7.73 (ddd, $J = 8$, 8, 2 Hz, 1H, H_4-py), 7.70 (d, $J = 1$ Hz, 2H, H_3-pz), 7.57 (dd, $J = 2$, 1 Hz, 2H, H_5-pz). 7.41–7.35 (m, 3H, *o*- and *p*-H of Ph), 7.31 (ddd, $J = 8$, 4, 1 Hz, 1H, H_5-py), 7.24 (d, $J = 8$ Hz, 1H, H_3-py), 7.20 (dd, $J = 8$, 2 Hz, 2H, *m*-H of Ph), 6.33 (d, $J = 2$ Hz, 2H, H_4-pz). ^{13}C NMR (101.62 MHz, $CDCl_3$) 158.7 (C_2-py), 148.8 (C_6-py), 140.7 (C_5-pz), 139.6 (C_{ipso}-Ph), 137.0 (C_4-py), 132.6 (C_3-pz), 129.4 (*o*- and *p*- of Ph), 128.2 (*m*-C of Ph), 124.3 (C_3-py), 123.7 (C_5-py), 105.8 (C_4-pz), 87.3 (C_α). Direct probe MS *m/z* (Rel. Int. %) [assgn]: 301(62) $[M]^+$, 233(100) $[M\text{-}Hpz]^+$, 223(86) $[M\text{-}py]^+$, 167(99) $[M\text{-}2Hpz]^+$, 77(28) $[Ph]^+$.

2.5. Silver hexafluorophosphate complexes

2.5.1. Preparation of {Ag(κ²-*m*-C₆H₄[C(pz)₂(2-py)]₂)₂}(PF₆), (3)

A mixture of 0.087 g (0.17 mmol) **1** and 0.042 g (0.17 mmol) $AgPF_6$ was dissolved in 15 ml of a 2:1 mixture of CH_3CN/acetone. After a reflux period of 6 h, trace gray solid was observed and solvent was removed by vacuum distillation. The resulting brown solid was washed sequentially with 5 ml each of Et_2O and hexanes. The insoluble residue was then extracted with 10 ml CH_3CN. The filtered extract was layered with 50 ml Et_2O and after allowing the solvents to diffuse overnight, the colorless crystals of $\{Ag(C_6H_4[C(pz)_2(2\text{-}py)]_2)_2\}(PF_6)$ (**3**) were isolated by filtration and were air-dried (84 mg, 78%). Mp, 205–210 °C dec. *Anal.* Calc. for $C_{60}H_{52}N_{20}AgF_6O_2P$, **3**·2 H_2O: C, 53.86 (53.98); H, 3.92 (3.53); N, 20.94 (20.81). ^{1}H NMR (400 MHz, acetone-d_6) 8.60 (d, $J = 4.5$ Hz, 2H, H_6-py), 7.89 (ddd, $J = 8$, 8, 2 Hz, 2H, H_4-py). 7.64 (d, $J = 1$ Hz, 4H, H_3-pz), 7.52 (d, $J = 2$ Hz, 4H, H_5-pz), 7.47–7.40 (m, 3H, aryl), 7.15 (dd, $J = 8$, 2 Hz, 2H, H_5-py), 7.09 (d, $J = 8$ Hz, 2H, H_3-py), 6.95 (s, 1H, aryl), 6.38 (dd, $J = 2$, 1 Hz, 4H, H_4-pz).

2.5.2. Preparation of {Ag(κ²-C₆H₅[C(pz)₂(2-py)])₂}(PF₆) (4)

A solution of 0.333 g (1.10 mmol) $C_6H_5[C(pz)_2(2\text{-}py)]$ in 10 ml THF was added by cannula to a solution of 0.139 g (0.550 mmol) $AgPF_6$ in 10 ml THF under a nitrogen atmosphere. A colorless solid precipitated within a few minutes of mixing and the resulting suspension was stirred 4 h. The product mixture was then separated by cannula filtration. The insoluble colorless solid was washed with two 5 ml portions of Et_2O and dried under vacuum to leave 0.435 g (92% yield) of $\{Ag(C_6H_5[C(pz)_2(2\text{-}py)])_2\}(PF_6)$ as a colorless solid. Crystals suitable for X-ray structural studies were grown by layering an acetone solution with Et_2O and allowing the solvents to diffuse. Mp, 175–178 °C crystals become opaque and shatter; 187–188 °C dec. to green–gray solid. ^{1}H NMR (400 MHz, acetone-d_6) 8.59 (d, $J = 4$ Hz, 1H, H_6-py), 7.98 (ddd, $J = 8$, 8, 2 Hz, 1H H_4-py), 7.62 (d, $J = 1$ Hz, 2H, H_3-pz), 7.59–7.49 (br m, 6H, H_5-pz and aryl), 7.04 (d, $J = 8$ Hz, H_3-py), 6.85–6.83 (br m, H_5-py and aryl), 6.46 (dd, $J = 2$, 1 Hz, H_4-pz). ^{13}C NMR (101.62 MHz, acetone-d_6) 157.5 (C_2-py), 150.4 (C_6-py), 142.8 (C_3-pz), 139.5, 138.9, 135.0, 131.0 (C_5-pz), 129.8, 129.7, 126.1, 125.8, 106.8 (C_4-pz), 88.0 (C_α). HRMS-ESI(+) (*m/z*): *Anal.* Calc. for $[M\text{-}PF_6]^+$, $C_{36}H_{30}N_{10}Ag^+$: 709.1702. Found: 709.1706. ESI(+) MS *m/z* (Rel. Int. %) [assgn]: 709 (100) $[AgL_2]^+$, 449 (29) $[AgL(CH_3CN)]^+$, 408 (2) $[AgL]^+$, 302 (65) $[HL]^+$, 234 (60) $[HL\text{-}pz]^+$.

2.6. Crystallography

2.6.1. X-ray structure determinations of {Ag(κ²-*m*-C₆H₄[C(pz)₂(2-py)]₂)₂}(PF₆), (3) and {Ag(κ²-C₆H₅[C(pz)₂(2-py)])₂}(PF₆)·acetone (4·acetone)

A colorless prism of **3** and a colorless prismatic crystal of **4**·acetone were each mounted onto the end of a thin glass fiber using inert oil. X-ray intensity data were measured in the dark at 190(2) K in the nitrogen cold stream of a Bruker SMART APEX CCD-based diffractometer system (Mo Kα radiation, $\lambda = 0.71073$ Å [12]. A total of 1800 raw data frames of width 0.3° in ω were collected at three different ϕ angles, with an exposure time of 15 and 20 s per frame for **3** and **4**·acetone, respectively. The data collections covered the entire sphere of reciprocal space. The first 50 frames of each were re-collected at the end of the data set to monitor crystal decay. The raw data frames were integrated into reflection intensity files using SAINT+ [12], which also applied corrections for Lorentz and polarization effects. The final unit cell parameters are based on the least-squares refinement of 6425 reflections with $I > 5(\sigma)I$ from the data set for **3** and 3377 reflections with $I > 5(\sigma)I$ from the data set for **4**·acetone. Analysis of the data showed negligible crystal decay during the data collections and no absorption corrections were applied (see Table 1).

2.6.2. Structure refinement of 3

The compound crystallized in the triclinic system; the space group $P\bar{1}$ was confirmed by successful solution and refinement of the structure. The structure was solved by direct methods followed by difference Fourier synthesis, and refined by full-matrix least-squares against F^2, using the SHELXTL software package [13]. The Ag and P atoms both lie on centers of symmetry; all other atoms are on general positions. The asymmetric unit is made up of the Ag ion, one $C_6H_4[C(pz)_2(2\text{-}py)]_2$ ligand, and half a PF_6^- anion. The PF_6^- anion is

Table 1
Experimental and crystal data for $\{Ag(\kappa^2\text{-}m\text{-}C_6H_4[C(pz)_2(2\text{-}py)]_2)_2\}(PF_6)$, (**3**), and $\{Ag(\kappa^2\text{-}C_6H_5[C(pz)_2(2\text{-}py)])_2\}(PF_6)$ (**4**)

	3	**4**·acetone
Formula	$C_{60}H_{48}AgF_6N_{20}P$	$C_{39}H_{36}AgF_6N_{10}OP$
Mw	1302.02	913.62
Crystal system	triclinic	triclinic
Space group	$P\bar{1}$	$P\bar{1}$
a (Å)	8.620(1)	8.316(1)
b (Å)	12.427(2)	10.256(2)
c (Å)	13.683(2)	12.191(2)
α (°)	105.464(2)	73.002(3)
β (°)	91.531(2)	75.898(3)
γ (°)	98.713(2)	79.908(3)
V (Å^3)	1392.8(3)	958.2(3)
Z	1	1
ρ_{calc} (g/cm^3)	1.552	1.583
μ (mm^{-1})	0.473	0.645
θ range (°)	1.56–26.41	1.78–26.48
Index range	$-10 \leqslant h \leqslant 10$	$-10 \leqslant h \leqslant 10$
	$-15 \leqslant k \leqslant 15$	$-12 \leqslant h \leqslant 12$
	$-17 \leqslant l \leqslant 17$	$-15 \leqslant h \leqslant 15$
Total (independent) reflections	12879 (5695)	8836 (3941)
Final R indices [$I > 2\sigma(I)$]	$R_1 = 0.0434$, $wR_2 = 0.0960$	$R_1 = 0.0439$, $wR_2 = 0.0872$
R indices (all data)	$R_1 = 0.0584$, $wR_2 = 0.1012$	$R_1 = 0.0718$, $wR_2 = 0.0964$
Largest different peak/hole (e/Å^3)	0.617/−0.311	0.556/−0.258

disordered over two orientations in an 80/20 ratio. All non-hydrogen atoms were refined with anisotropic displacement parameters; hydrogen atoms were placed in calculated positions and refined as riding atoms.

*2.6.3. Structure refinement of **4**·acetone*

This compound crystallized in the triclinic system where the space group $P\bar{1}$ was confirmed by successful solution and refinement of the structure. The structure was solved by a combination of direct methods and difference Fourier synthesis, and refined by full-matrix least-squares against F^2, using the SHELXTL software package [13]. The Ag and P atoms lie on a centers of symmetry; all other atoms are on general positions. The asymmetric unit is made up of the Ag ion, one $C_6H_5[C(pz)_2(2\text{-}py)]$ ligand, half a PF_6^- anion, and half an acetone molecule of crystallization. All components of the crystal (cation, anion, solvent) are affected by disorder. The ligand bound to Ag is disordered over all three possible κ^2, κ^0 conformations allowed by the combination of two pyrazolyl rings (pz) and one pyridyl ring (py). Only the donor rings are affected; the central methine carbon and the pendant phenyl ring behave normally. Referring to the ring numbering scheme in Figure 5a, the average composition of ring "1n" is 0.75 pz/0.25 py; that of ring "2n" is 0.75 pz/0.25 py, and that of ring "3n" is 0.50/0.50 pz/py. These values were arrived at by initially refining the pz/py composition of each ring with a free variable constrained to sum to unity (SHELX FVAR card), and then fixing the ring occupation factors at reasonable values, such that the overall composition of the ligand would be $PhC(pz)_2py$. The PF_6^- anion is rotationally disordered about one F–P–F axis in a 0.59/0.41 ratio. Finally, the acetone molecule of crystallization is disordered about an inversion center. To achieve a stable refinement, a total of 13 restraints (SHELX EADP and SADI) were employed. Eventually, all non-hydrogen atoms were refined with anisotropic displacement parameters; hydrogen atoms were placed in calculated positions and refined using a riding model. Solution and refinement in the space group $P1$ resulted in the same ligand pz/py ring and PF_6 disorder, as well as unstable ring geometries and large correlations between inversion-related atoms. Therefore, the disorder model in $P\bar{1}$ was retained.

3. Results and discussion

3.1. Syntheses of ligands

The bitopic and monotopic aryl scorpionates **1** and **2**, respectively, were prepared by the $CoCl_2$ catalyzed rearrangement reaction between bis(1-pyrazolyl)sulfone (prepared in situ by the reaction between NaH, Hpz, and $SOCl_2$ in THF) and the appropriate aryl(pyridyl)ketone in THF (Scheme 1). While the reaction to produce the monotopic derivative **2** as described in the literature proceeded smoothly (over the period of about one day), longer reaction times were necessary in order to obtain appreciable quantities of the corresponding bitopic derivative **1**. Even after four days at reflux, the starting material was only 60% consumed and the reaction produces a 1:2 mol ratio of the mono-derivatized compound **1a** and the desired bitopic compound **1**. The two products are easily separable by column

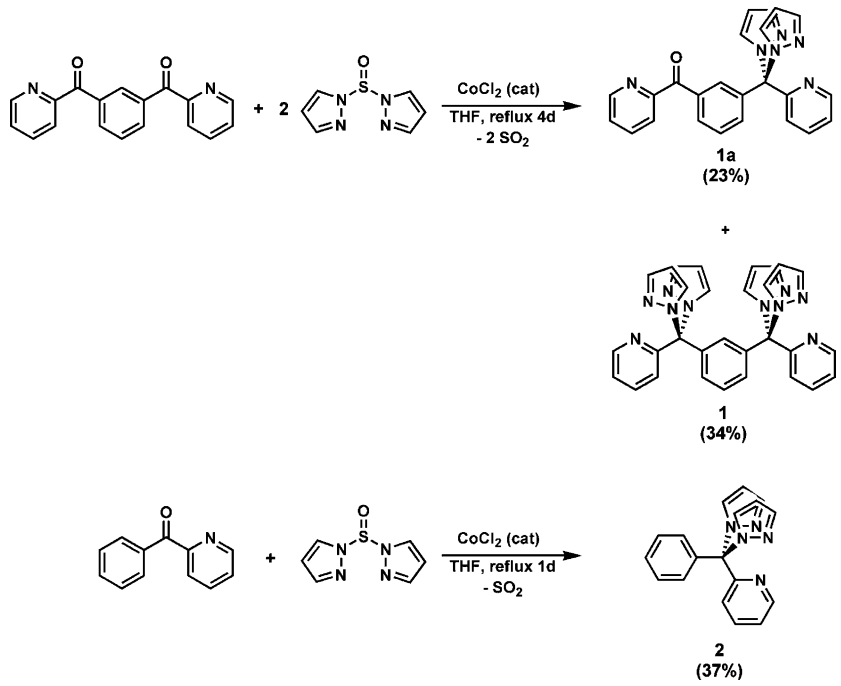

Scheme 1.

chromatography since **1** is strongly retained on silica whereas **1a** is not. It should be noted that yields of either **1** or **2** were not improved by using $CO(pz)_2$ as a replacement for $S(O)(pz)_2$. The low yields and long reaction times for the preparation of **1** and **2** can be contrasted with the preparation of $HC(pz)_2(py)$ by using similar conditions (45%, 4 h) [14]. These observations are consistent with those originally made by Thé and Peterson who indicated that the relative reactivity order for $CoCl_2$ catalyzed rearrangement of aryl carbonyls was: $PhC(O)H > PhC(O)CH_3 \gg Ph_2C(O)$ [15].

Regardless of the stoichiometry of reagents (mol ratios of 2, 1, and 0.5 were investigated), the reactions between silver hexafluorophosphate and either **1** or **2** always produced $[Ag(\mathbf{1})_2](PF)_6$ (**3**), and $[Ag(\mathbf{2})_2][PF_6]$ (**4**), respectively, as indicated from elemental analyses, mass spectral data, and X-ray diffraction studies (vide infra). The insensitivity of the product's metal:ligand mol ratio on the stoichiometry of reactants is fairly common in silver chemistry and has been reported previously for reactions between silver salts and a series of tris(pyrazolyl)methane ligands [16]. Compounds **3** and **4** are hygroscopic but otherwise air stable colorless solids that can be stored for weeks without appreciable decomposition under ambient light. Each is soluble in acetonitrile, moderately soluble in acetone, slightly soluble in methylene chloride, but insoluble in most other common (less polar) solvents. The NMR spectra of each compound in acetone-d_6 show one set of resonances that differ from those of the pure ligand by a downfield shift. This result for **3**, where the stoichiometry and solid state structure (vide infra) indicate the presence of both free and coordinated $C(pz)_2(py)$ groups, can be explained by fast exchange between coordinated and non-coordinated ends of the ligand on the NMR time scale, in accord with the known lability of silver compounds.

The results of single crystal X-ray diffraction study of **3** reveal the monotopic nature of the potentially bitopic ligand **1**. An ORTEP diagram is given in Fig. 1 and important bond distances and angles are provided in Table 2. In the solid state, two ligands are bonded to one silver in a κ^2-fashion via two pyrazolyl groups; the

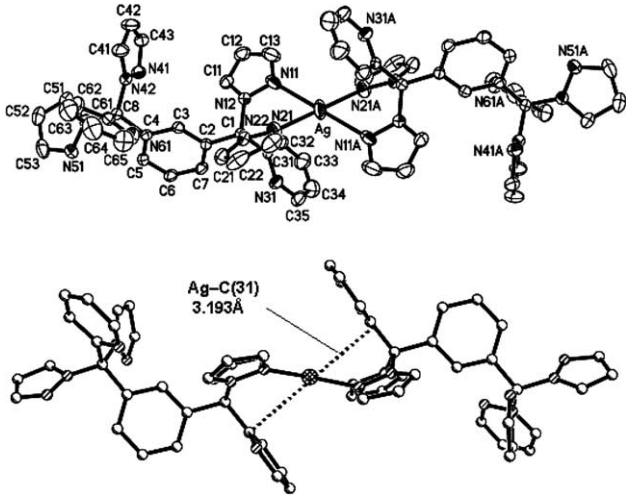

Fig. 1. Two views of the structure of the cation in $Ag(\kappa^2\text{-}m\text{-}C_6H_4[C(pz)_2(2\text{-}py)]_2)_2(PF_6)$ (**3**). Top: ORTEP diagram with 50% thermal ellipsoids. Bottom: ball and stick view emphasizing planar geometry of nitrogens about silver. Hydrogen atoms have been omitted for clarity in each.

Table 2
Selected bond distances and angles in $\{Ag(\kappa^2\text{-}m\text{-}C_6H_4[C(pz)_2(2\text{-}py)]_2)_2\}(PF_6)$, **3**

Bond distances (Å)					
Ag–N(11)	2.398(2)	N(11)–N(12)	1.365(3)	N(12)–C(1)	1.482(3)
Ag–N(21)	2.279(2)	N(11)–N(12)	1.365(3)	N(11)–N(12)	1.365(3)
Bond angles (°)					
N(11)–Ag–N(21)	76.95(8)	N(11)–Ag–N(21a)	103.05(8)	N(11)–Ag–N(11a)	180.00 (0)
N(21a)–Ag–N(11a)	76.95(8)	N(21)–Ag–N(11a)	103.05(8)	N(21)–Ag–N(21a)	180.00 (0)
Ag–N(11)–C(13)	132.46(18)	Ag–N(11)–N(12)	121.56(18)	N(11)–N(12)–C(1)	119.59(18)
C(11)–N(12)–C(1)	127.60(20)	N(12)–C(1)–N(22)	110.62(18)	C(31)–C(1)–C(2)	112.89(18)
C(1)–N(22)–N(21)	119.25(20)	C(21)–N(22)–N(21)	111.60(20)	Ag–N(21)–N(22)	124.55(2)
Ag–N(21)–C(23)	129.20(2)				

Symmetry transformation: $-x+1, -y+1, -z+2$.

pyridyl part of the bonded $C(pz)_2(py)$ group is not coordinated to the silver(I). On each ligand, one of the two $C(pz)_2(py)$ groups is not bonded to a silver(I).

One striking feature of the structure is the planar coordination geometry of the nitrogen donor atoms about silver. There are two short and two longer Ag–N bonds (the silver atom resides on an inversion center) of 2.279 and 2.398 Å involving Ag–N(21) and Ag–N(11), respectfully. These distances are comparable to those found in related systems [5,6,23]. Since the sum of the four N–Ag–N angles is 360°, the coordination geometry about silver can best be described as distorted square planar where the distortion occurs as an elongation along one axis of the plane (rectangular planar coordination). An inspection of Fig. 1 would appear to suggest, using the scorpionate vernacular, that the planar arrangement is forced by the aryl group serving as a 'non-venomous' stinger. While it would be surprising to have C- rather than N-coordination, aryl coordination has been observed in other systems [26,27]. In the case of **3**, the closest contact between silver and the pyridyl ring is associated with the ipso carbon, C(31), (bottom of Fig. 1) where the corresponding Ag–C(31) bond distance of 3.193 Å is outside the 2.4–2.9 Å range found for η^1 silver(I)-arene π complexes [17–19]. As far as we are aware, there are only five other examples of tetracoordinate silver complexes that exhibit square planar coordination geometry as opposed to the more typical tetrahedral or distorted tetrahedral geometries [20,21]. The AgN_4C ring adopts a boat conformation (Fig. 2(a)). If silver is assigned to the bow and C(1) to the stern, the puckering parameters originally defined by Cremer and Pople [22] are $Q = 0.910$, $\theta = 83.1°$, and $\phi = 1.78$. The latter two values may be compared to those for an ideal boat conformation ($\theta = 90°$ and $\phi = 0$) and for an ideal half-boat ($\theta = 54.7°$ and $\phi = 0$); the puckering amplitude Q in these cases would depend on the bond lengths between the ring atoms. It should be noted that the related compound $\{Ag[(pz)_2CMe_2]_2\}(ClO_4)$ [23] contains two different AgN_4C six-member rings and each adopts a slightly distorted half-boat conformation (Fig. 2(b)). The puckering parameters $Q = 0.662$, 0.634; $\theta = 73.2°$, 72.5°; and $\phi = 6.6°$, 5.5° were determined from the data obtained from the Crystallographic Information File extracted from the Cambridge Structural Database after a phase adjustment for consistency in atom labeling and normalization to allow meaningful comparison with **3** (Reference code; SIKYOA). The difference between the boat conformation of the AgN_4C ring in **3** and the half-boat conformation in $\{Ag[(pz)_2CMe_2]_2\}(ClO_4)$ is found in the fold angles involving the respective silver atoms (and to a lesser extent those involving the carbon atoms). The fold angle can be defined as being the deviation from planarity created by the displacement of one atom (at either the bow or stern) from the four (coplanar) atoms that would represent the deck of the boat. In the case of **3**, the fold angles are the complement to those found in Fig. 2(a); that associated with silver is 32.3° whereas that associated with C(1) is 61.4°. The corresponding values in $\{Ag[(pz)_2CMe_2]_2\}(ClO_4)$ are 7.6° and 6.6° for those involving silver and 58.6° and 59.1° for those involving carbon.

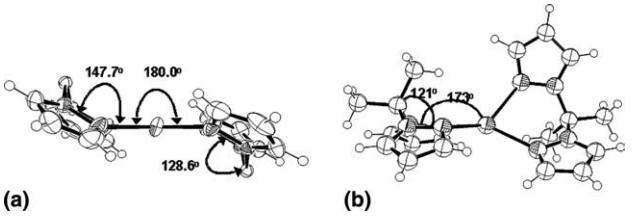

Fig. 2. Comparison of the AgN_4C chelate rings and coordination geometry about silver between (a) square planar compound **3** (with boat conformation) and (b) distorted tetrahedral $Ag[(pz)_2CMe_2]_2(ClO_4)$ (with a half-boat conformation).

Given that there does not to appear to be any significant silver(I)-π interactions in **3**, the unusual coordination environment about silver is likely due to both steric and electronic effects associated with the presence of multiple arene substituents bound to the central methane carbon. The relative orientations of the pyridyl and pyrazolyl groups in the ligands are supported by multiple intracationic CH···π interactions as shown in Fig. 3. The distances and angles associated with the CH···π interactions are given in Table 3 and are in

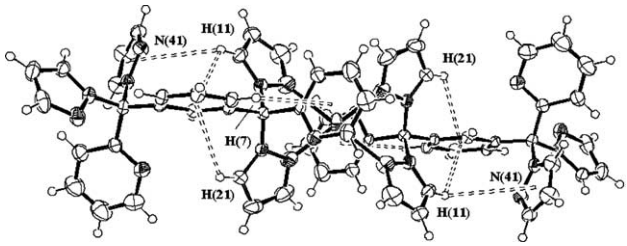

Fig. 3. View of the cation in **3** showing the intracationic CH-π interactions.

Table 3
Summary of non-covalent interactions involving {Ag(κ²-*m*-C_6H_4-[$C(pz)_2(2\text{-}py)]_2$)$_2$}(PF_6), **3**

Donor (D)···Acceptor (Å)	H···A (Å)	C(H)···A (°)
(a) Intramolecular CH···π interactions		
C(11)H(11)···Ct[N(11)][a]	3.546	118.96
C(11)H(11)···Ct[C(7)]	3.032	121.35
C(21)H(21)···Ct[C(7)]	3.148	121.00
C(7)H(7)···Ct[C(33)]	2.961	130.53
(b) Intermolecular interactions		
C(64)H(64)···Ct[N(12)]	3.13	123.7
C(63)H(63)···Ct[N(12)]	3.23	120.1
C(35)H(35)···Ct[N(22)]	3.14	145.8
C(23)H(23)···F(3b)[b]	2.43	142.0
C(23)H(23)···F(2a)[b]	2.46	147.8
C(32)H(32)···F(1a)[b]	2.51	145.6
C(32)H(32)···F(1b)[b]	2.57	143.4
C(33)H(33)···F(2a)[b]	2.40	133.2
C(23)H(23)···F(2b)[b]	2.58	155.5

[a] Ct refers to centroid of the arene ring that contains the element denoted in brackets.
[b] An equivalent interaction is produced through inversion.

accord with accepted values [24]. Since the CH···π interactions occur within each ligand rather than spanning both ligands in the cation, the total number of CH-π bonding interactions would not change if the AgN_4C chelate rings adopted a half-boat conformation similar to those observed in {Ag[$(pz)_2CMe_2]_2$}(ClO_4). Therefore, we attribute the unusual coordination environment about silver to the forces that arrange **3** into its three dimensional supramolecular structure.

The supramolecular structure of **3** approaches that of a inorganic–organic hybrid material where the silver centers and the hexafluourophosphate anions reside in layers in the crystallographinc *ab* planes. The inorganic layers are separated by organic ligands along the *c* axis where the interlayer separation is 13.7 Å as in Fig. 4. Pyridyl rings, located above and below the AgN_4 plane also separate the cation and anions in the 'inorganic layers'. There are two types of non-covalent interactions that assist in organizing **3** in the solid state; CH···π interactions where both pyridyl rings of the ligand act as hydrogen donors and the silver bound pyrazolyl rings act as hydrogen acceptors and CH···F interactions involving the hexafluorophosphate anion and the acidic arene (pyrazolyl and pyridyl) hydrogens. Table 3

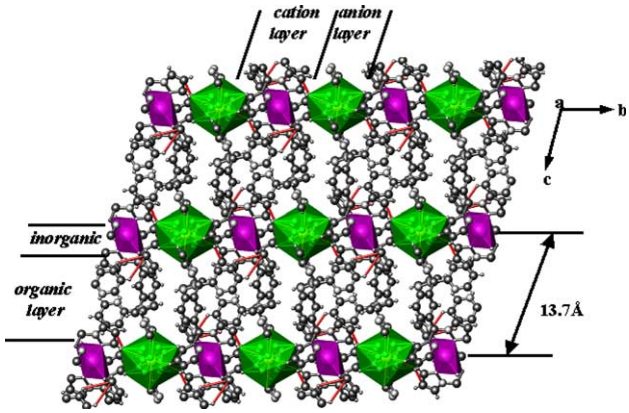

Fig. 4. Supramolecular structure of **3** emphasizing the pseudo inorganic–organic layered structure. Large (green) polyhedra are disordered PF_6^- anions whereas the small (pink) polyhedra represent coordination sphere about silver. The red lines represent intercationic CH···π interactions. The CH···F interactions that associate cationic layers are highlighted and enclosed within the green polyhedra. (For interpretation of the references to color in this figure legend, the reader is referred to the web version of this article.)

provides bond distances and angles for the non-covalent interactions that support the pseudo-layered structure. There are 12 CH···F distances involving a disordered hexafluorophosphate anion and that are shorter than the limit of 2.6 Å suggested to be indicative of weak hydrogen bonding interactions (Table 3) [25]. The result of these interactions is to organize the cationic sheets along the *bc*-plane as in Fig. 4. In particular, within a given cation containing two meta-linked ligands, the hydrogens H(32) and H(33) situated *meta*- and *para*-, respectively, to the nitrogen atom of the pyridyl ring proximal to silver on one ligand and the hydrogen at the 3-position of the silver-bound pyrazolyl rings of the second ligand are each involved in short CH···F bonding interactions with the fluorines of both components of the disordered PF_6 anion. Each hydrogen interacts with a component of the orientationally disordered hexafluorophosphate anion such that the CH···F distances are never greater than 2.6 Å. The CH···π interactions (Table 3) shown as red lines in Fig. 4 afford connectivity in a third dimension (the *a*-axis) such that the sheets depicted in Fig. 4 would stack directly on top of one another into and out of the plane of the paper, forming segregated anion and cation layers. The particular interactions that propagate along the *a*-axis occur between the pyridyl rings proximal to silver of one cation and the silver-bound pyrazolyl groups with the shorter Ag–N distance [Ag–N(21) 2.279(2)]. Those interactions involving the pyridyl rings on the 'silver-free' side of the meta-linked ligand of one cation and the silver-bound pyrazolyl group with the longer Ag–N distance [Ag–N(11) 2.398(2)] of support the overall structure (along the *c*-axis). The boat conformation of the AgN_4C rings is thought to maximize the

total number of CH···F bonding and CH···π interactions, thereby supporting the overall structure. A half-boat arrangement would place the acidic hydrogens of the pyridyl [H(32) and H(33)] and pyrazolyl groups [H(23)] at too great a distance for PF_6^- bridged CH···F interactions and would likely reduce the total number of CH···π interactions. A future report will further address the role of groups bound to the central methine carbon on the intracationic and supramolecular structure of related silver derivatives.

In an effort to determine whether the structural motif found in **3** was unique to the meta-linked ligand or was a more common framework, an X-ray structural study of $\{Ag(\kappa^2\text{-}C_6H_5[C(pz)_2(2\text{-}py)])_2\}(PF_6)$ (**4**), the monotopic derivative of **3** was undertaken and the results are given in Fig. 5. One important feature of the structure is the nature of the disorder that afflicts the nitrogen-containing heterocycles of the ligand (Fig. 5(a)). As described in the experimental, the ligand bound to silver is disordered over all three possible κ^2, κ^0 conformations allowed by the combination of two pyrazolyl and one pyridyl ring. Fig. 5(b) reveals one component of the disordered structure showing that the coordination geometry about silver is square planar, as in compound **3**. The overall structure again has the form of a pseudo-

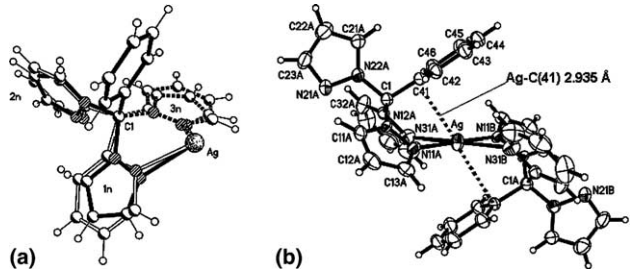

Fig. 5. Results of single crystal X-ray analysis of $Ag(\kappa^2\text{-}C_6H_5[C(pz)_2(2\text{-}py)])_2(PF_6)$ (**4**) showing (a) ligand disorder and (b) one component of the disordered structure emphasizing the square planar geometry about silver and boat conformation of AgN_4C chelate rings.

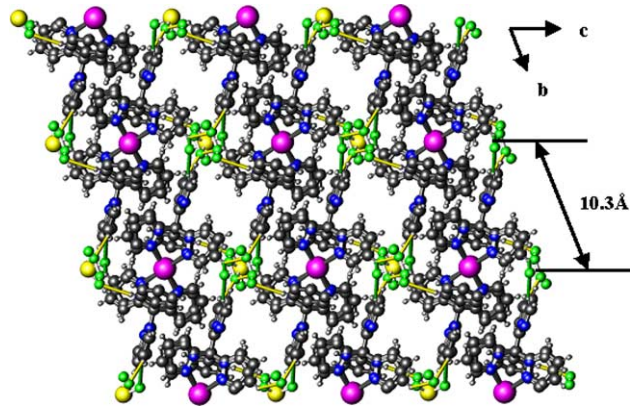

Fig. 6. View of the pseudo-layered structure in the crystal of $Ag(\kappa^2\text{-}C_6H_5[C(pz)_2(2\text{-}py)])_2(PF_6)$ (**4**).

layered inorganic–organic hybrid material (Fig. 6) as in **3**, however in the current case, the separation between layers is 10.3 Å. Unfortunately, detailed analysis of any other bond distances and angles in **4** is precluded since, with the exception of the silver atom, the phenyl ring and the central methine carbon of the cation, disorder affects all components of the structure (cation, anion, and solvent).

4. Conclusions

A potentially bitopic heteroscorpionate, $m\text{-}C_6H_4[C(pz)_2(2\text{-}py)]_2$ (**1**), has been prepared by using the Peterson rearrangement reaction between two equivalents of $SO(pz)_2$ and one equivalent of $m\text{-}C_6H_4[C(O)(2\text{-}py)]_2$. The reactions between this ligand and silver hexafluorophosphate led only to a product with a 2:1 mol ratio of ligand to metal. X-ray structural analysis of this silver complex revealed that the ligand was bound to silver in a κ^2-fashion via the pyrazolyl groups, the silver resided in an unusual square planar coordination environment, and the AgN_4C chelate ring adopted a boat conformation. While a half-boat arrangement is more typical of complexes with a $C(pz)_2Ag$ chelate ring, the unusual boat conformation was proposed to be due to energetics associated with the organization of the two-dimensional structure, specifically, the CH···F interactions between the hexafluorophosphate anion and hydrogen atoms of the ligand. These non-covalent forces, coupled with CH···π interactions, organize the two-dimensional structure of **3** such that it approaches a layered inorganic–organic hybrid material. The structure of the monotopic derivative $\{Ag(\kappa^2\text{-}C_6H_5[C(pz)_2(2\text{-}py)])_2\}(PF_6)$ (**4**) was highly disordered but also revealed the bidentate nature of the $C(pz)_2(2\text{-}py)$ scorpionate moiety towards silver and a square planar arrangement for coordination environment about the metal.

5. Supplementary material

Crystallographic data for the structures reported in this paper have been deposited at the Cambridge Crystallographic Data Centre, 12 Union Road, Cambridge CB2 1EZ, UK (fax: +44-1223-336033; E-mail: deposit@ccdc.cam.ac.uk or www: http://www.ccdc.cam.ac.uk), CCDC 210455 for **3** and 210456 for **4**·acetone.

Acknowledgements

We thank the National Science Foundation (CHE-0110493) for support and a referee for helpful comments. The Bruker CCD Single Crystal Diffractometer

was purchased using funds provided by the NSF Instrumentation for Materials Research Program through Grant DMR:9975623.

References

[1] D. Braga, J. Chem. Soc. Dalton. Trans (2000) 3705.
[2] O.R. Evans, W. Lin, Acc. Chem. Res. 35 (2002) 511.
[3] Y. Cui, H.L. Ngo, P.S. White, W. Lin, Inorg. Chem 42 (2003) 652.
[4] S.J. Lee, A. Hu, W. Lin, J. Am. Chem. Soc. 124 (2002) 12948.
[5] D.L. Reger, J.R. Gardinier, R.F. Semeniuc, M.D. Smith, J. Chem. Soc., Dalton Trans. (2003) 1712.
[6] D.L. Reger, K.J. Brown, J.R. Gardinier, M.D. Smith, Organometallics 22 (2003) 4973.
[7] D.L. Reger, T.D. Wright, R.F. Semeniuc, T.C. Grattan, M.D. Smith, Inorg. Chem. 40 (2001) 6212.
[8] D.L. Reger, R.F. Semeniuc, M.D. Smith, Inorg. Chem. 40 (2001) 6545.
[9] D.L. Reger, R.F. Semeniuc, M.D. Smith, Eur. J. Inorg. Chem. (2002) 543.
[10] D.L. Reger, J.R. Gardinier, M.D. Smith, P.J. Pellechia, Inorg. Chem. 42 (2003) 482.
[11] D.L. Reger, T.C. Grattan, K.J. Brown, C.A. Little, J.J.S. Lamba, A.L. Rheingold, R.D. Sommer, J. Organomet. Chem. 607 (2000) 120.
[12] SAINT+ Version 6.02a, Bruker Analytical X-ray Systems, Inc., Madison, WI, USA, 1998.
[13] G.M. Sheldrick, SHELXTL Version 5.1; Bruker Analytical X-ray Systems, Inc., Madison, WI, USA, 1997.
[14] P.K. Byers, A.J. Canty, R.T. Honeyman, J. Organometal. Chem. 385 (1990) 417.
[15] K.I. Thé, L.K. Peterson, Can. J. Chem. 51 (1973) 422.
[16] A. Cingolani, Effendy, D. Martini, M. Pellei, C. Pettinari, B.W. Skeleton, A.H. White, Inorg. Chim. Acta 328 (2002) 87.
[17] S.V. Lindeman, R. Rathore, J.K. Kochi, Inorg. Chem. 39 (2000) 5707.
[18] M. Munakata, L.P. Wu, G.L. Ning, T. Kuroda-Sowa, M. Maekawa, Y. Suenaga, N. Maeno, J. Am. Chem. Soc. 121 (1999) 4968.
[19] M. Munakata, L.P. Wu, K. Sugimoto, T. Kuroda-Sowa, M. Maekawa, Y. Suenaga, N. Maeno, M. Fujita, Inorg. Chem. 38 (1999) 5674.
[20] D. Carmona, F. Viguri, F.J. Lahoz, L.A. Oro, Inorg. Chem. 41 (2002) 2385, and references.
[21] M. Mascal, J. Hansen, A.J. Blake, W.-S. Li, Chem. Comm. (1998) 355.
[22] D. Cremer, J.A. Pople, J. Am. Chem. Soc. 97 (1975) 1354.
[23] A. Lorenzotti, F. Bonati, A. Cingolani, G.G. Lobbia, D. Leonesi, B. Bovio, Inorg. Chim. Acta 170 (1990) 199.
[24] D. Braga, F. Grepioni, E. Tedesco, Organometallics 17 (1998) 2669.
[25] F. Grepioni, G. Cojazzi, S.M. Draper, N. Scully, D. Braga, Organometallics 17 (1998) 296.
[26] K.-B. Shiu, L.-Y. Yeh, S.-M. Peng, M.-C. Cheng, J. Organomet. Chem. 460 (1993) 203.
[27] K.-B. Shiu, C.-C. Chou, S.-L. Wang, S.-C. Wei, Organometallics 9 (1993) 286.

Available online at www.sciencedirect.com
SCIENCE DIRECT®
Polyhedron 23 (2004) 301–309
POLYHEDRON
www.elsevier.com/locate/poly

Mono and binuclear rhodium dicarbonyl complexes containing the hydridotris(3-*p*-chlorophenylpyrazol-1-yl)borate ligand (Tp^{PhCl}). X-ray structures of the binuclear complex $[(OC)_2Rh(\mu{:}\kappa^2,\kappa^1\text{-}Tp^{PhCl})Rh(Cl)(CO)_2]$ and of three isomers of $[Rh(\kappa^2\text{-}Tp^{PhCl})(CO)_2]$ ☆

Rosario Criado [a], Mercedes Cano [a,*], José A. Campo [a], José V. Heras [a], Elena Pinilla [a,b], M. Rosario Torres [b]

[a] *Departamento de Química Inorgánica I, Facultad de Ciencias Químicas, Universidad Complutense, 28040 Madrid, Spain*
[b] *Laboratorio de Difracción de Rayos-X, Facultad de Ciencias Químicas, Universidad Complutense, 28040 Madrid, Spain*

Received 13 May 2003; accepted 15 September 2003

Dedicated to Dr. S. Trofimenko

Abstract

Two Rh-dicarbonyl complexes $[Rh(\kappa^2\text{-}Tp^{PhCl})(CO)_2]$ (**1**) and $[(OC)_2Rh(\mu{:}\kappa^2,\kappa^1\text{-}Tp^{PhCl})Rh(Cl)(CO)_2]$ (**2**) have been synthesized and structurally characterized by IR and NMR spectroscopies and X-ray crystallography. Three isomeric forms have been isolated for **1**, which showed different environment on the Rh centre related with the uncoordinated third pyrazolyl arm. So, it was rotated to the equatorial position in **1**-A, but occupied the axial position in **1**-B and **1**-B′ with different orientation. As a consequence, two square-planar coordination geometries (one with the third pyrazolyl ring over the square-plane (SP1) and the other inverted with the free pyrazolyl arm away from the square-plane (SP2)) and one square pyramidal geometry (SPy) have been established for **1**-B, **1**-A and **1**-B′, respectively. The X-ray structure of **2** indicates a bridging coordination of the Tp^{PhCl} ligand, being κ^2 to the $[Rh(CO)_2]$ fragment and κ^1 to the $[Rh(Cl)(CO)_2]$ group.
© 2003 Elsevier Ltd. All rights reserved.

Keywords: κ^2-Tp ligands; Bridging Tp ligands; Rhodium dicarbonyl complexes; Isomers; X-ray structure

1. Introduction

The ability of poly(pyrazol-1-yl)borate ligands to modify or control the steric and electronic environment about the metal centre on their coordination compounds has been focus of attention since they were discovered by Trofimenko in 1967 [1–5]. In this context, we were able to demonstrate how, in compounds of the type $[Mo(\kappa^3\text{-}Tp^{An})(NO)(X)(Y)]$ (Tp^{An} = hydridotris(3-*p*-methoxyphenylpyrazol-1-yl)borate; X = Y = CO; X = Cl, Y = NHC_6H_4-*p*-CH_3, NHC_6H_4-*p*-$N(CH_3)_2$, OC_6H_5, NHC_6H_4-*o*-CH_3), the Tp^{An} ligand generated a bowl-shape cavity in which the other co-ligands were included [6–9].

On the other hand, it has been well established the activity of the trispyrazolylborate-complexes $[M(Tp')(L_2)]$ (M = Rh, Ir; Tp′ = hydridotrispyrazol-1-ylborate ligands with substituents on the pyrazolyl rings; L_2 = 2CO, 2CNR, $2CH_2CH_2$, etc.; M = Rh, Ir) towards C–H bond activation reactions [1,10–19], which, from a mechanistic point of view, appear to be depending on the dechelation and rechelation of the Tp′ ligands [20,21]. In turns, it was also proved that denticity of the Tp′ ligands accounts for reactivity of those Rh/Ir complexes and therefore their catalytic applications [1]. Then the knowledge of the coordinative form of the Tp′

☆ The abbreviation system used in this paper in the nomenclature of the trispyrazolylborate ligands is that adopted by Trofimenko [1].

* Corresponding author. Fax: +34-91-3944352.
E-mail address: mmcano@quim.ucm.es (M. Cano).

0277-5387/$ - see front matter © 2003 Elsevier Ltd. All rights reserved.
doi:10.1016/j.poly.2003.11.020

ligands for new $[Rh(Tp')(CO)_2]$ derivatives follows in increasing interest.

In this sense, it is remarkable to note that since Venanzi and co-workers [22] identified three isomeric forms for $[Rh(Tp^{3R,4R,5R})(L_2)]$ (L_2 = NBD (norbornadiene), COD (1,5-cyclooctadiene), 2CO; $Tp^{3R,4R,5R}$ = hydridotrispyrazol-1-ylborate ligands with substituents on the 3, 4 and 5 positions of the pyrazolyl group), two of them four-coordinated κ^2-$Tp^{3R,4R,5R}$ (equatorial, A, or axial, B) and the third pentacoordinated κ^3-$Tp^{3R,4R,5R}$ (C) (Fig. 1), several papers have been reported concerning with the isomerism of those Rh(I) derivatives in solution [19,23–28].

In particular the state of the art on the isomerization of $[Rh(Tp')(CO)_2]$ has been recently reported by Webster and Hall [29]. These authors have developed an excellent work concerning with predictions of structure and energy of $[Rh(Tp^{3R,5R})(CO)_2]$ (R = H, Me) by theoretical functional density calculations. The structural experimental data of different rhodium derivatives compare well with the calculated results.

Despite the variety of Rh(I) compounds studied in previous works, the structural X-ray characterization of different isomers for one determined Tp′-rhodium complex has not been produced yet. It could allow to realize a systematic study avoiding variables as the effect of the substituents on the pyrazolyl rings or the characteristics of the co-ligands.

To this proposal, and by considering our previous results on $[Rh(\kappa^2\text{-}Tp^R)(CO)_2]$ ($Tp^R = Tp^{An}$, Tp^{Ph}) (Tp^{Ph} = hydridotris(3-phenylpyrazol-1-yl)borate) [19,27], we were involved in the isolation and X-ray characterization of potential isomers of dicarbonyl Rh-complexes containing the related hydridotris(3-*p*-chlo- rophenylpyrazol-1-yl)-borate (Tp^{PhCl}) ligand.

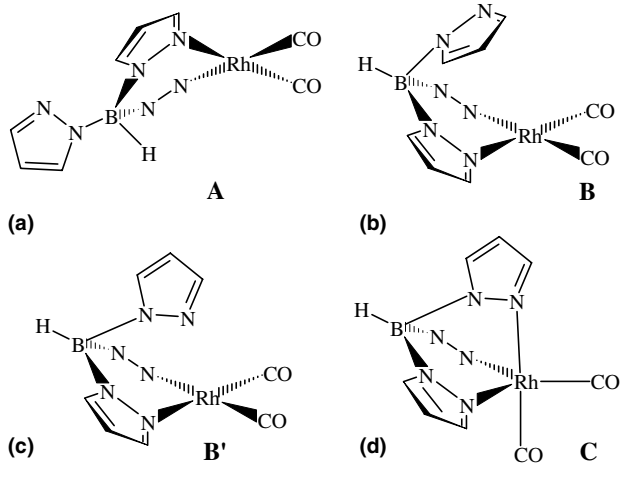

Fig. 1. Schematic representations of different geometric arrangements for $[Rh(Tp')(CO)_2]$: (a) square-planar with the third pyrazolyl arm away from the metal (SP2; isomer A); (b) square-planar with the third pyrazolyl arm over the metal (SP1, isomer B); (c) square pyramidal (SPy, isomer B′); (d) trigonal bipyramidal (TBP, isomer C).

2. Results and discussion

2.1. Previous results

Stimulated for the interest of Tp′-rhodium derivatives in C–H bond activation reactions, and in particular on the knowledge of the isomers which could favour this process, we started to work, some years ago, on Rh(I) chemistry by using bulky Tp′ ligands containing aromatic substituents at the 3 position on the pyrazolyl rings as Tp^{An} and Tp^{Ph} [19,27]. So $[Rh(Tp^R)(L_2)]$ ($Tp^R = Tp^{An}$, Tp^{Ph}; L_2 = NBD, COD, 2CO) were prepared and characterized. In all cases a κ^2-Tp^R axial (B) or equatorial (A) coordination of the ligand was established (Fig. 1). Moreover two different possibilities were also found for the axial compounds. So the X-ray structure of $[Rh(\kappa^2\text{-}Tp^{Ph})(NBD)]$ evidenced a typical axial B shape, while a new axial isomer (B′) was characterized for $[Rh(\kappa^2\text{-}Tp^{An})(CO)_2]$ (Fig. 1). Both forms differ in the spacial orientation of the uncoordinated pyrazolyl arm, which gives rise to an elongated square pyramidal geometry (SPy) [1] in B′, or a square-planar coordination geometry (SP1) in B with the free pyrazolyl ring twisted related to its position in B′ and then separated from the metal. In solution both isomers (B and B′) exhibited the same ^1H NMR pattern consistent with only one set of resonances corresponding to one type of pyrazolyl rings. This feature was attributed to the presence of a very fast equilibrium between the isomeric forms. Photochemical irradiation of $[Rh(\kappa^2\text{-}Tp^{An})(CO)_2]$ resulted in a very clean intramolecular C–H bond activation [19].

During the crystallization process of $[Rh(\kappa^2\text{-}Tp^{An})(CO)_2]$, in addition to the B′ isomer, two new solid products were obtained and assigned on the basis of their IR and NMR spectra to the B isomer and to a mixture of the A and B isomers (which we were not able to separate). Surprisingly the B form containing the nitrogen atom of the uncoordinated third pyrazolyl ring closer to the Rh atom than in the equatorial A isomer exhibited the highest ν(CO) frequencies [19]. Related results were also deduced for $[Rh(\kappa^2\text{-}Tp^{Ph})(CO)_2]$ [27]. These observations, moreover the unexplained values of the ν(CO) absorption bands for the isomers, moved us to prove the identity of those isomers by X-ray determinations. Then we decided to investigate the formation of new Rh(I) carbonyl complexes containing the related Tp^{PhCl} as bulky ligand. The isolation and characterization by X-ray diffraction of three isomers (A, B and B′)

[1] The symbols used for the geometries are those indicated in a recent work published by Webster and Hall [29].

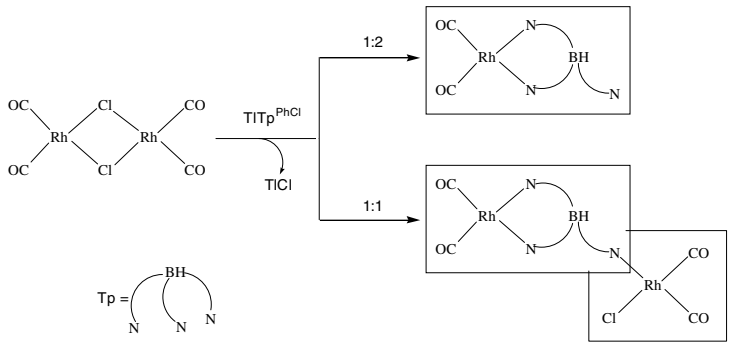

Scheme 1.

as well as a new binuclear compound containing κ^2,κ^1-Tp^{PhCl} are now presented and discussed.

2.2. Synthetic studies

The reaction of the dimer $[Rh(\mu\text{-}Cl)(CO)_2]_2$ and the thalium salt of the Tp^{PhCl} ligand in a 1:2 or 1:1 molar ratio gave rise to the new compounds $[Rh(\kappa^2\text{-}Tp^{PhCl})(CO)_2]$ (**1**) and $[(OC)_2Rh(\mu{:}\kappa^2,\kappa^1\text{-}Tp^{PhCl})Rh(Cl)(CO)_2]$ (**2**), respectively (Scheme 1). Both compounds were air-stable yellow-orange solids and characterized by analytical and spectroscopic (IR and ^1H NMR) techniques.

Complex **1** was crystallized from dichloromethane–hexane solution giving rise to three generations of crystalline solid products characterized as the **1**-A, **1**-B and **1**-B′ isomers, as it is described in the experimental part. They were identified by X-ray crystallography and IR spectroscopy (Table 1). The ^1H NMR spectra of each isomer at room temperature (Table 2) exhibited the same pattern consistent with only one set of signals of the Tp^{PhCl} ligand, which was attributed to the presence of a very fast equilibrium between them on the NMR time-scale. In agreement with these results, the IR spectra in dichloromethane solution showed the same two broad ν(CO) bands for the three isomers (Table 1). However, in solid state, the values of the ν(CO) absorption bands were different each isomer, showing the expected order to their corresponding coordination spheres (Table 1).

Table 1
IR data (cm^{-1}) of compounds **1** and **2**[a]

		1-A	**1**-B	**1**-B′	**2**
KBr discs	ν(CO)	2083vs	2075vs	2063vs	2092vs
		2012vs	2010vs	1993	2076vs
					2028vs
					2003vs
	ν(BH)	2445m	2476m	2476vs	2481m
CH_2Cl_2 solution	ν(CO)	2088br	2088br	2088br	2094vs
		2025br	2025br	2025br	2080vs
					2033vs
					2005vs

[a] vs, very strong; m, medium; br, broad signal.

Table 2
^1H NMR data (δ, ppm; J, Hz) of complexes **1** and **2**, in $CDCl_3$ at room temperature[a]

	Pyrazolyl protons		C_6H_4Cl	
	H4	H5	H*o*	H*m*
1	6.47 (br)	7.70 (br)	7.79 (d, $J = 8.1$)	7.45 (br)
2	6.40	7.11	7.38 (d, $J = 8.7$)	
	(d, $J = 2.4$)	(d, $J = 2.4$)		
	6.59	8.08	7.52 (d, $J = 8.4$)	
	(d, $J = 2.4$)	(d, $J = 2.4$)		
	6.60	8.49	7.56 (d, $J = 8.4$)	
	(d, $J = 2.4$)	(d, $J = 2.4$)		
			7.76 (d, $J = 8.4$)	
			7.82 (d, $J = 8.7$)	
			7.93 (d, $J = 8.4$)	

[a] d, doublet; br, broad signal.

Complex **2** was identified as the binuclear compound $[(OC)_2Rh(\mu{:}\kappa^2,\kappa^1\text{-}Tp^{PhCl})Rh(Cl)(CO)_2]$ which could be considered as the product of coordination of **1** to the $[Rh(Cl)(CO)_2]$ fragment (Scheme 1). Its IR and ^1H NMR spectra were consistent with the proposed formulation. So, the complex exhibited four strong ν(CO) bands both in the solid state and in dichloromethane solution (Table 1). On the other hand the ^1H NMR spectrum showed three different sets of signals for the H4 and H5 pyrazolyl protons as well as for the chlorophenyl substituents (Table 2). These NMR and IR patterns resembled to those of the samples of $[Rh(\kappa^2\text{-}Tp^R)(CO)_2]$ (R = Ph, An) previously considered as mixtures of the A and B isomers [19,27]. These features suggested us that maybe our previous assignment was wrong, the right one being that corresponding to a binuclear tetracarbonyl derivative. Then the reaction of $[Rh(\mu\text{-}Cl)(CO)_2]_2$ and Tp^{An} in a 1:1 molar ratio has now been carried out, giving rise to a solid product whose IR and ^1H NMR data are almost identical to those of the tetracarbonyl compound **2**. We are now involved in its X-ray characterization prior to establish definitive conclusions.

2.3. X-Ray crystal structure of the $[Rh(\kappa^2\text{-}Tp^{PhCl})(CO)_2]$ isomers (1-A, 1-B, 1-B′)

The X-ray structures of the **1**-A, **1**-B and **1**-B′ isomers of $[Rh(\kappa^2\text{-}Tp^{PhCl})(CO)_2]$ have been solved. Figs. 2–4 depict their molecular structures and Table 3 shows selected structural parameters.

For these three isomers, a boat conformation of the metallocycle $Rh(NN)_2B$, defined by the atoms Rh(1)N(12)N(11)B(1)N(21)N(22), was envisaged. The N(11)N(12)N(22)N(21) atoms form a plane with the highest deviation of 0.005(4), 0.020(6) and 0.011(5) Å for **1**-A, **1**-B and **1**-B′, respectively. The Rh(1) and B(1) atoms are out of this plane at distances of 0.912(1) and 0.664(7) Å (**1**-A), 0.968(1) and 0.59(1) Å (**1**-B), and 0.853(1) and 0.605(7) Å (**1**-B′).

The **1**-A and **1**-B isomers can be described as square-planar Rh complexes where the Tp^{PhCl} ligand is coordinated to the Rh atom through two of the three pyrazolyl rings. In **1**-B the uncoordinated third pyrazolyl ring is over the square-plane, but in **1**-A it is located away from the metal plane and inverted at the sp^3 boron of the Tp^{PhCl} ligand, according, respectively, to the SP1 and SP2 geometries proposed by Webster and Hall [29]. The structural core found in **1**-B′ is essentially the same that in **1**-B, but the former exhibits the N atom of the free pyrazolyl arm closer to the metal centre, so generating a square-pyramidal geometry (SPy) (Fig. 1). The dihedral angle between the metal–ligand core and uncoordinated pyrazolyl ring planes is 69.1(2)° and 79.7(2)° for **1**-B and **1**-B′, respectively. The torsion angles defined by N(31), B(1) and the two nitrogens of a single coordinated pyrazolyl ring (N(31)–B(1)–N(11)–N(12) and N(31)–B(1)–N(21)–N(22)) agree with the established geometries (−175.5(4)° and 178.2(4)° (**1**-A); −51.5(9)° and −76.3(9)° (**1**-B); −68.1(7)° and 67.2(7)° (**1**-B′)).

In all cases the sum of the angles around the Rh centre by the coordinated pyrazolic N atoms and the CO ligands was approximately 360°, indicating the planarity of the Rh(1)C(1)C(2)N(12)N(22) moiety. The Rh(1)–N(12), Rh(1)–N(22) and Rh(1)–C(1), Rh(1)–C(2) distances are almost equal suggesting a local mirror symmetry. The N(11)–B(1)–N(21) atoms form an angle of 107.4(4)°, 107.1(6)° and 109.3(5)° for **1**-A, **1**-B and **1**-B′, respectively.

The chlorophenyl substituents are twisted with their own pyrazolyl rings, being more coplanar those of the uncoordinated pyrazolyl arm. So, the corresponding dihedral angles are: 41.4(2)°, 46.9(2)° and 22.7(2)° (**1**-A); 49.0(3)°, 28.9(3)° and 6.0(2)° (**1**-B); and 51.9(2)°, 57.5(2)° and 36.4(2)° (**1**-B′).

The N(12)–Rh(1)–N(22) angles in the equatorial plane are close to 90° in the three isomers. The other two angles involving the axial pyrazolyl group N(12)–Rh(1)···N(32) and N(22)–Rh(1)···N(32) were 72.4(2)°, 91.0(2)° in **1**-B and 79.6(2)°, 82.4(2)° in **1**-B′, respectively, but 45.3(1)° and 48.8(1)° for **1**-A in agreement with the different geometry of the equatorial isomer.

The main differences between the three isomers are related to the spacial orientation of the uncoordinated third pyrazolyl arm, which occupies an axial (B or B′) or

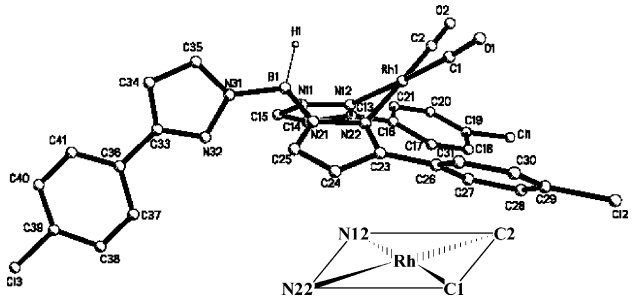

Fig. 2. PLUTO representation of compound **1**-A, showing the atomic numbering scheme. Hydrogen atoms, except that bonded to B(1), have been omitted for clarity. A schematic representation of the coordination sphere around the Rh atom is also included.

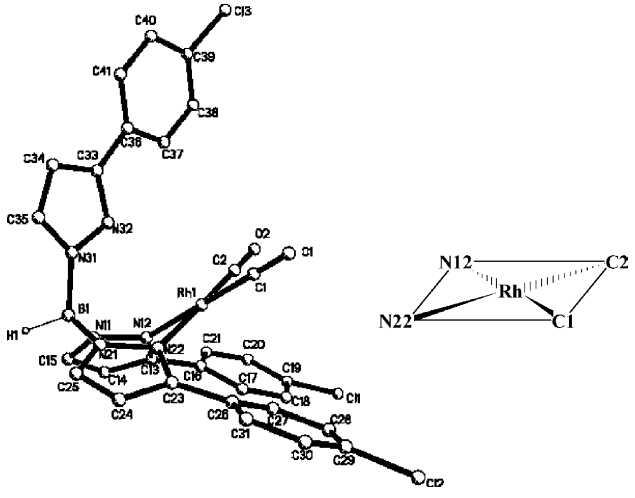

Fig. 3. PLUTO representation of compound **1**-B. Details as in Fig. 2.

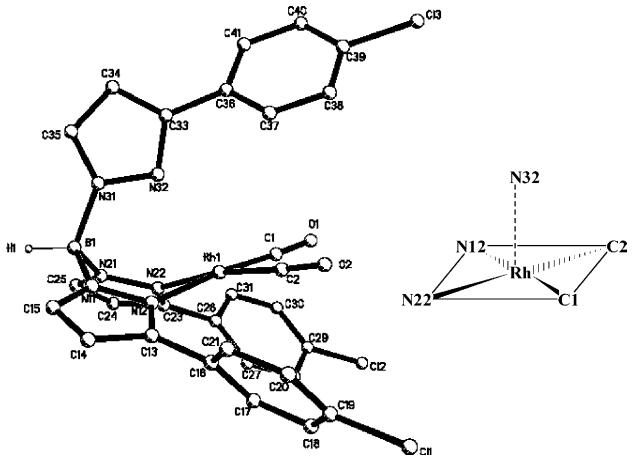

Fig. 4. PLUTO representation of compound **1**-B′. Details as in Fig. 2.

Table 3
Selected distances (Å) and angles (°) with esd's in parentheses

	1-A	**1**-B	**1**-B′	**2**
Bond lengths				
Rh(1)–N(12)	2.072(4)	2.081(6)	2.128(5)	2.09(1)
Rh(1)–N(22)	2.074(5)	2.079(5)	2.128(5)	2.09(1)
Rh(1)–C(1)	1.855(6)	1.844(8)	1.844(8)	1.87(2)
Rh(1)–C(2)	1.813(7)	1.816(7)	1.843(7)	1.87(2)
Rh(2)–N(32)				2.09(1)
Rh(2)–C(4)				1.83(2)
Rh(2)–C(3)				1.81(2)
Rh(2)–Cl(4)				2.334(4)
Rh(1)···N(32)	5.553(4)	3.100(5)	2.599(5)	4.05(1)
Rh(1)···B(1)	3.195(6)	3.269(9)	3.305(7)	3.28(2)
Rh(1)···Rh(2)				5.038(2)
Bond angles				
C(1)–Rh(1)–C(2)	89.4(3)	87.9(3)	85.0(3)	89.0(7)
C(1)–Rh(1)–N(12)	176.5(2)	179.6(3)	175.2(3)	178.5(6)
C(1)–Rh(1)–N(22)	91.3(2)	94.6(3)	93.1(2)	92.2(6)
C(2)–Rh(1)–N(12)	92.2(2)	91.9(3)	94.0(2)	91.9(6)
C(2)–Rh(1)–N(22)	178.5(2)	177.4(3)	171.0(2)	178.8(6)
N(12)–Rh(1)–N(22)	87.0(2)	85.6(2)	87.1(2)	86.9(4)
C(3)–Rh(2)–C(4)				88.7(9)
C(3)–Rh(2)–N(32)				177.0(7)
C(3)–Rh(2)–Cl(4)				91.4(7)
C(4)–Rh(2)–N(32)				90.8(6)
C(4)–Rh(2)–Cl(4)				176.9(5)
N(32)–Rh(2)–Cl(4)				89.3(3)
N(12)–Rh(1)···N(32)	45.3(1)	72.4(2)	79.6(2)	
N(22)–Rh(1)···N(32)	48.8(1)	91.0(2)	82.4(2)	

equatorial (A) position. As a consequence, the Rh(1)···N(32) distances in **1**-A, **1**-B and **1**-B′ were 5.553(4), 3.100(5) and 2.599(5) Å, respectively. This distance is out or in the limit of the range of bonding interactions (sum of the van der Waals radii of Rh and N atoms is 3.15 Å) in **1**-A and **1**-B, but it agrees with a square pyramidal environment (SPy) around the metal centre in **1**-B′. Consistent with this SPy structure, the axial Rh(1)···N(32) distance was 0.468 Å longer than those on the equatorial plane and the metal was above the coordination plane by 0.123(1) Å in **1**-B′. However in **1**-A and **1**-B the metal centre was almost coplanar with the four coordinating atoms of the ligands (0.039(1) and 0.001(1) Å, respectively).

2.4. X-ray structure of $[(OC)_2Rh(\mu{:}\kappa^2,\kappa^1\text{-}Tp^{PhCl})Rh(Cl)(CO)_2]$ (**2**)

The dinuclear molecule, depicted in Fig. 5, was constituted by two metal centres, both exhibiting a square-planar geometry, bridged by a Tp^{PhCl} ligand. The Rh(1) atom has a square-planar coordination comprised by two CO ligands and a pair of pyrazolic N-donor atoms from the Tp^{PhCl} ligand acting as chelate. The third remained pyrazolyl ring coordinates to the Rh(2) atom which complete its square-planar geometry with two carbonyl and one chloride ligands. Selected bond distances and angles are presented in Table 3.

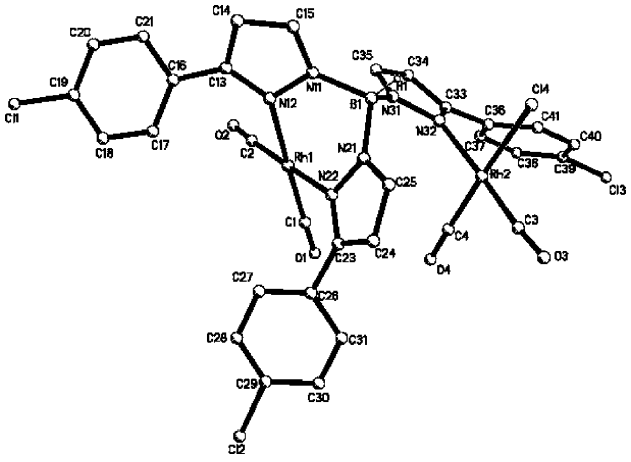

Fig. 5. PLUTO representation of compound **2**. Details as in Fig. 2.

The Rh(1)C(1)C(2)N(12)N(22) and Rh(2)N(32)C(4)C(3)Cl(4) atoms are essentially planar, the Rh(1) and Rh(2) deviating 0.014(1) and 0.012(1) Å, respectively, from the least-squares plane defined by the four corresponding remained atoms.

The observed bond distances and angles for the coordination spheres of the Rh(1) and Rh(2) atoms are almost identical to those found in **1**-A, **1**-B and **1**-B′. The Rh(2)–N(32) distance of 2.09(1) Å was slightly longer than that observed in the related four-coordinated $[Rh(Cl)(CO)_2(Hpz^R)]$ ($R = An$, $C_6H_4OC_{12}H_{25}$)

[30,31], and the Rh(2)–Cl(4) distance is also typical of Rh(I) complexes [30–33].

The chelating part of the Tp^{PhCl} ligand was symmetrically coordinated to the $[Rh(CO)_2]$ fragment. So a local mirror plane which passes through the B(1) and Rh(1) atoms lies orthogonal to the plane formed by the four nitrogen atoms of the two pyrazolyl groups involved in the bidentate coordination. The Rh(1)N(12)N(11)B(1)N(21)N(22) metallocycle adopts a boat conformation, as that observed in the mononuclear species **1**-A, **1**-B and **1**-B′. This metallocycle could be considered symmetrically divided by the above mirror plane, and consequently both carbonyl ligands and the two chlorophenyl groups were also symmetrical. In agreement the dihedral angles between the pyrazolyl rings coordinated to the Rh(1) atom and the N(11)N(12)(21)N(22) plane were almost similar (31.0(4)° and 30.2(5)°).

The dihedral angles formed by the pyrazolyl rings and their own phenyl substituents are similar (37.6(4)°, 45.9(5)° and 40.7(5)°), in contrast to those observed for the mononuclear isomers of **1** (see Section 2.3).

Despite a strict relationship between the solid state structures and the reactivity of structures in solution could not be always considered, we suggest that the **1**-A and **1**-B structures should be the best candidates to the coordination of the second metal centre, in order to accommodate the two metal fragments and at the same time to relieve the strain. In agreement with this proposal the observed Rh(1)···N(32) distance of 4.05(1) Å in **2** was intermediate to that found in **1**-A (5.553(4) Å) and in **1**-B (3.100(5) Å), and the dihedral angle formed by the free pyrazolyl ring and the coordination plane of 75.1(2)° and 69.1(2)° for **1**-A and **1**-B, respectively, was moved to 50.3(5)° in **2**.

2.5. Structural comparison of $[Rh(Tp')(CO)_2]$ complexes

To the best of our knowledge, seven Rh dicarbonyl complexes containing trispyrazol-1-ylborate ligands had been characterized by X-ray crystallography [16,18,19,28,34–36]. In addition, a new related compound containing the asymmetric hydridobis(3-phenyl-5-methylpyrazol-1-yl)(3,5-dimethylpyrazol-1-yl)borate (Tp″) has recently been reported [37], and now we present our results from three isomeric forms containing the Tp^{PhCl} ligand. Table 4 lists relevant results from these structures.

It had been proposed that the hapticity of the Tp ligands was depending on the substitution on the pyrazolyl rings [22]. However for all dicarbonyl complexes, with exception of $[Rh(\kappa^3\text{-}Tp^{3,5iPr})(CO)_2]$ (which showed some decomposition during the X-ray data collection [28,36]), it was evident that the 16-electron square-planar geometry is favoured towards the 18-electron trigonal bipyramidal structure, although the presence of free pyrazolyl arm on the axial position close to a coordinative site may lead to an elongated square pyramidal (SPy) structure, as it has now been considered for complexes $[Rh(\kappa^2\text{-}Tp')(CO)_2]$ ($Tp' = Tp^a$, $Tp^{3CF3,5Me}$, $Tp^{3Ph,5Me}$, Tp^{An}, Tp^{PhCl}).

Moreover from our actual results on $[Rh(\kappa^2\text{-}Tp^{PhCl})(CO)_2]$, we can deduce that an appropriate substitution on the pyrazolyl rings appears to be a requirement to achieve different isomers in solid state (**1**-A, **1**-B and

Table 4
Experimental data for various $[Rh(Tp')(CO)_2]$ complexes

Tp′[a]	Coordinative form of Tp′[b]	Rh–N distance (Å)		Coordination geometry[c]	Isomer[d]	Ref.
Tp^a	κ^2-axial (*)	2.093, 2.091	2.779	SPy (•)	B′	[34]
		2.105, 2.109	2.641			
$Tp^{3CF3,5Me}$	κ^2-axial (*)	2.098, 2.111	2.623	SPy (•)	B′	[16][e]
Tp^{Ph}	κ^2-equatorial	2.06, 2.067		SP2 (•)	A	[16]
$Tp^{3Ph,5Me}$	κ^2-axial (*)	2.098, 2.102	2.835	SPy (•)	B′	[35]
$Tp^{3,5iPr}$	κ^3		2.33	SPy (•)	C	[28,36]
Tp^{Menth}	κ^2-equatorial	2.082, 2.105		SP2 (+)	A	[18]
Tp^{An}	κ^2-axial	2.108, 2.111	2.57	SPy (+)	B′	[19]
Tp″	κ^2-axial	2.086, 2.096	2.84	SPy (+)	B′	[37]
Tp^{PhCl}	κ^2-equatorial	2.072, 2.074	5.553	SP2 (+)	A	this work
Tp^{PhCl}	κ^2-axial	2.079, 2.081	3.099	SP1 (+)	B	this work
Tp^{PhCl}	κ^2-axial	2.127, 2.128	2.598	SPy (+)	B′	this work

[a] Tp^a, hydridotris(2*H*-benz[*g*]-4,5-dihydroindazol-2-yl)borate; $Tp^{3CF3,5Me}$, hydridotris(3-trifluoro-5-methylpyrazol-1-yl)borate; Tp^{Ph}, hydridotris(3-phenylpyrazol-1-yl)borate; $Tp^{3Ph,5Me}$, hydridotris(3-phenyl-5-methylpyrazol-1-yl)borate; $Tp^{3,5iPr}$, hydridotris(3,5-*i*-propylpyrazol-1-yl)borate; Tp^{Menth}, hydridotris(mentho(2,3-*c*)pyrazolyl)borate; Tp^{An}, hydridotris(3-*p*-methoxyphenylpyrazol-1-yl)borate; Tp″, hydridobis(3-phenyl-5-methylpyrazol-1-yl)(3,5-dimethylpyrazol-1-yl)borate; Tp^{PhCl}, hydridotris(3-*p*-chlorophenylpyrazol-1-yl)borate.

[b] Coordination form deduced from the X-ray structures. Asterisks indicate a κ^3 five coordination proposed by Webster and Hall [29].

[c] Coordination sphere geometries: (•) proposed by Webster and Hall [29], (+) proposed in this work according with the criteria of Webster and Hall.

[d] Nomenclature of the isomers according with Venanzi and co-workers [22] and our own previous works [19,27].

[e] This structure has also been solved by other authors with similar data [38].

Table 5
Crystal and refinement data for [Rh(κ²-Tp^{PhCl})(CO)$_2$] (three isomers: **1**-A, **1**-B and **1**-B′) and [(OC)$_2$Rh(μ:κ², κ¹-Tp^{PhCl})Rh(Cl)(CO)$_2$] **2**

	1-A	**1**-B	**1**-B′	**2**
Formula	$C_{29}H_{19}BCl_3N_6O_2Rh$	$C_{29}H_{19}BCl_3N_6O_2Rh$	$C_{29}H_{19}BCl_3N_6O_2Rh$	$C_{31}H_{19}BCl_4N_6O_4Rh_2$
Molecular weight	703.57	703.57	703.57	897.95
Crystal system	monoclinic	orthorhombic	monoclinic	monoclinic
Space group	$C2/c$	$Pca2_1$	$P2_1/n$	$P2_1/c$
a (Å)	41.032(3)	10.607(1)	11.8288(7)	11.123(2)
b (Å)	13.762(1)	21.078(2)	16.626(1)	13.409(2)
c (Å)	10.9170(9)	13.253(2)	15.3878(9)	24.526(4)
β (°)	92.897(2)		95.095(1)	102.553(3)
U (Å^3)	6157.0(8)	2963.2(5)	3014.4(3)	3571(1)
Z	8	4	4	4
$F(000)$	2816	1408	1408	1768
D_c (g cm^{-3})	1.518	1.577	1.550	1.670
Temperature (K)	296(2)	293(2)	296(2)	293(2)
μ (Mo Kα) (mm^{-1})	0.852	0.855	0.870	1.268
Crystal size (mm)	0.50 × 0.50 × 0.06	0.40 × 0.20 × 0.15	0.36 × 0.31 × 0.23	0.20 × 0.16 × 0.16
Scan technique	ϕ and ω	ϕ and ω	ϕ and ω	ϕ and ω
Data collected	(−38, −16, −11) to (48, 16, 12)	(−12, −16, −15) to (11, 25, 7)	(−14, −19, −17) to (7, 19, 18)	(−12, −15, −29) to (13, 15, 23)
θ (°)	1.56–25.00	1.93–24.99	1.81–25.00	1.70–25.00
Reflections collected	15 837	9140	15 417	17 804
Unique reflections	5428 (R_{int} = 0.068)	3649 (R_{int} = 0.077)	5283 (R_{int} = 0.041)	6267 (R_{int} = 0.135)
Data, restraints, parameters	5428, 0, 379	3649, 1, 370	5283, 0, 362	6267, 0, 407
Goodness-of-fit (F^2)	0.859	0.701	1.047	1.032
R [$I > 2\sigma(I)$][a]	0.048 (2657 reflections)	0.038 (2129 reflections)	0.055 (3417 reflections)	0.093 (3054 reflections)
Rw_F[b]	0.114	0.057	0.158	0.261
Largest residual peak (e Å^{-3})	0.643	0.439	1.482	1.776

[a] $\sum[|F_o| - |F_c|]/\sum|F_o|$.
[b] $\{\sum[w(F_o^2 - F_c^2)^2]/\sum[w(F_o^2)^2]\}^{1/2}$.

1-B′). They were isolated in different amounts, which could be related to factors as the kinetics of crystal growth or crystal packing effects as well as their corresponding stability. The theoretical calculations on [Rh(Tp^{3R,5R})(CO)$_2$] (R = H, Me) indicated that the SPy isomer (B′) was the most stable [29]. However, we obtained orange crystals of **1**-B′ (SPy) together with yellow crystals of **1**-B (SP1) at the first stage of the crystallization (1–2 days, T ca. 0 °C), the former being the minor form. By contrast, several days at ca. 0 °C were required to achieve light yellow crystals of **1**-A (SP2), which resulted to be the major isomer. Then it is possible to suggest that the electrowithdrawing character of the chlorophenyl substituents on the pyrazolyl rings does not favour the increasing coordination around the metal centre of the SPy geometry with respect to the square-planar compounds.

3. Concluding remarks

On the [Rh(Tp′)(CO)$_2$] chemistry, the κ² hapticity of the Tp′ ligands has been found to be the most usual feature, specially for those derivatives containing bulky substituents on the pyrazolyl groups. Several examples corresponding to SP2 (square-planar equatorial), SP1 (square-planar axial) or SPy (elongated square-pyramidal) geometries have been described [16,18,19,34,35,37]. The new compound [Rh(κ²-Tp^{PhCl})(CO)$_2$] (**1**), prepared in this work in a 1:1 Tp^{PhCl}/Rh molar ratio, provides the first example in which three isomeric forms containing κ²-Tp^{PhCl} have been isolated and structurally characterized in solid state for a single Tp′ ligand in the [Rh(Tp′)(CO)$_2$] family. Their formation appears to be depending on the crystallization process, and the bidentate κ²-Tp^{PhCl} square-planar coordination is favoured with respect to the SPy geometry, in agreement with the electronic characteristics of the Tp^{PhCl} ligand.

In addition, the coordination of Tp^{PhCl} as bridging ligand to two metal centres has been found for the complex [(OC)$_2$Rh(μ:κ²,κ¹-Tp^{PhCl})Rh(Cl)(CO)$_2$] (**2**), which was obtained when a synthetic 1:2 Tp^{PhCl}/Rh molar ratio was used. Its X-ray crystal structure shows the Tp^{PhCl} ligand bonded to both metal centres in a κ²,κ¹ fashion. It is one of the few examples exhibiting the bridging coordinative form of the Tp′-type ligands [39,40].

4. Experimental

4.1. Materials and equipment

The starting Rh-complex [Rh(μ-Cl)(CO)$_2$]$_2$ was purchased from Sigma–Aldrich and used without further

purification. Commercial reagents were used as supplied. All reaction solvents were dried and degassed according to standard methods prior to use.

Elemental analyses were carried out by the Center for Elemental Microanalysis at the Complutense University. Infrared spectra were recorded on a FTIR Nicolet Magna-550 spectrophotometer with samples as KBr discs or in dichloromethane solutions in the 4000–350 cm^{-1} region. ^1H NMR spectra were performed on a Varian VXR-300 (299.88 MHz) or a Bruker DPX-300 (300.13 MHz) spectrophotometers from $CDCl_3$ solutions. Chemical shifts δ are listed in parts per million relative to tetramethylsilane; coupling constants J are in Hertz. The ^1H chemical shifts and coupling constants are accurate to ±0.01 ppm and ±0.3 Hz, respectively.

4.2. Synthetic methods

4.2.1. Preparation of [Rh(κ²-Tp^{PhCl})(CO)$_2$] (1)

To a solution of $[Rh(\mu\text{-}Cl)(CO)_2]_2$ (0.050 g, 0.13 mmol) in dichloromethane (40 ml) was added $TlTp^{PhCl}$ (0.195 g, 0.26 mmol). The resulting yellow solution was stirred at room temperature for 15 min. The white solid (TlCl) formed is filtered through Celite. Hexane is added over the filtrate and then the solution is kept at ca. 0 °C for 1–2 days giving rise to the formation of a mixture of orange (**1**-B′) and yellow (**1**-B) crystals, which were filtered off, dried and easily separated off under a microscopy. The resulting solution was again kept at ca. 0 °C for several days yielding light yellow (**1**-A) crystals, which were filtered off and dried. *Anal.* Found: C, 49.30; H, 2.65; N, 11.80%; calc. for $C_{29}H_{19}N_6O_2BCl_3Rh$: C, 49.51; H, 2.72; N, 11.94.

4.2.2. Preparation of [(OC)$_2$Rh(μ:κ²,κ¹-Tp^{PhCl})Rh(Cl)(CO)$_2$] (2)

To a solution of $[Rh(\mu\text{-}Cl)(CO)_2]_2$ (0.050 g, 0.13 mmol) in dichloromethane (40 ml) was added $TlTp^{PhCl}$ (0.097 g, 0.13 mmol). The yellow solution was stirred for 15 min, and then filtered over Celite to eliminate TlCl. Addition of hexane led to the precipitation of a yellow solid, which was filtered off. Recrystallization in dichloromethane/diethyl ether gives rise to yellow crystals, which was filtered off, dried in vacuo and characterized as the compound **2**. *Anal.* Found: C, 41.28; H, 2.05; N, 9.10%; calc. for $C_{31}H_{19}N_6O_4BCl_4Rh_2$: C, 41.47; H, 2.13; N, 9.36.

4.3. Crystal structure determinations

Prismatic crystals of [Rh(κ²-Tp^{PhCl})(CO)$_2$] (**1**) (light yellow, **1**-A; yellow, **1**-B; orange, **1**-B′) were obtained from dichloromethane–hexane solutions at low temperature. Yellow prismatic crystals of [(OC)$_2$Rh(μ:κ²,κ¹-Tp^{PhCl})Rh(Cl)(CO)$_2$] (**2**) were obtained from dichloromethane/diethyl ether solutions.

The crystals were mounted on a Smart CCD-Bruker diffractometer with graphite monochromated Mo Kα radiation ($\lambda = 0.71073$ Å). A summary of the fundamental crystal and refinement data for the four structures is given in Table 5. The structures were solved by direct and Fourier methods. The refinement was made by full-matrix least-squares on F^2 [41]. All non-hydrogen atoms were refined anisotropically, except the O(1) and O(2) atoms for **1**-B which were refined two cycles anisotropically and in the subsequent cycle their thermal parameters were fixed. The hydrogen atoms were calculated and refined as riding on bonded carbon atom with a common isotropic displacement parameter, except that bonded to B(1) which was located as one of the first peak in a Fourier difference, and then included with different treatment: its position fixed in **1**-A, refined as riding on the boron atom in **1**-B′ and **2** or its coordinates refined in **1**-B. The largest residual peaks in the final difference map were 0.64, 0.43, 1.48 and 1.78 e $Å^{-3}$ for **1**-A, **1**-B, **1**-B′ and **2**, respectively.

5. Supplementary material

Supplementary data of the structures reported in this paper are available from the Cambridge Crystallographic Data Centre, 12 Union Road, Cambridge CB2 1EZ, UK (fax: +44-1223-336033; E-mail: deposit@ccdc.cam.ac.uk or www: http://www.ccdc.cam.ac.uk) on request, quoting the deposition numbers 211215–211218 for compounds **1**-A, **1**-B, **1**-B′ and **2**, respectively.

Acknowledgements

We are very grateful to Dr. S. Trofimenko for providing a sample of the thalium salt of the Tp^{PhCl} ligand. We also acknowledge to DGI/MCyT for the support of this work.

References

[1] S. Trofimenko, Scorpionates: The Coordination Chemistry of Polypyrazolylborate Ligands, Imperial College Press, London, 1999, and references therein.
[2] S. Trofimenko, Prog. Inorg. Chem. 34 (1986) 115.
[3] S. Trofimenko, Chem. Rev. 93 (1993) 943.
[4] S. Trofimenko, Chem. Rev. 72 (1972) 497.
[5] C. Janiak, Main Group Met. Chem. 21 (1998) 33.
[6] M. Cano, J.V. Heras, A. Monge, E. Gutiérrez, C.J. Jones, S.L.W. McWhinnie, J.A. McCleverty, J. Chem. Soc., Dalton Trans. (1992) 2435.
[7] M. Cano, J.V. Heras, A. Monge, E. Pinilla, C.J. Jones, J.A. McCleverty, J. Chem. Soc., Dalton Trans. (1994) 1555.
[8] J.A. Campo, M. Cano, J.V. Heras, M.C. Lagunas, E. Pinilla, M.R. Torres, Polyhedron 20 (2001) 2997.
[9] J.A. Campo, M. Cano, J.V. Heras, E. Pinilla, A. Monge, J.A. McCleverty, J. Chem. Soc., Dalton Trans. (1998) 3065.

[10] C. Slugovc, I. Padilla-Martínez, S. Sirol, E. Carmona, Coord. Chem. Rev. 213 (2001) 129.
[11] R.H. Crabtree, J. Chem. Soc., Dalton Trans. (2001) 2437, and references therein.
[12] C.K. Ghosh, W.A.G. Graham, J. Am. Chem. Soc. 109 (1987) 4726.
[13] R.G. Ball, C.K. Ghosh, J.K. Hoyano, A.D. McCaster, W.A.G. Graham, J. Chem. Soc., Chem. Commun. (1989) 341.
[14] A.A. Purwoko, S.D. Tibensky, A.J. Lees, Inorg. Chem. 35 (1996) 7049.
[15] J.S. Yetson, B.K. McNamara, R.G. Bergman, C.B. Moore, Organometallics 19 (2000) 3442.
[16] R. Krentz, Ph.D. Thesis, University of Alberta, Edmonton, 1988.
[17] E. Teuma, F. Malbosc, V. Pons, C. Serra-Le Berre, J. Jaud, M. Etienne, P. Kalck, J. Chem. Soc., Dalton Trans. (2001) 2225.
[18] M.C. Keyes, V.G. Young Jr., W.B. Tolman, Organometallics 15 (1996) 4133.
[19] M.D. Santa María, R.M. Claramunt, J.A. Campo, M. Cano, R. Criado, J.V. Heras, P. Ovejero, E. Pinilla, M.R. Torres, J. Organomet. Chem. 605 (2000) 117.
[20] S.E. Brombert, H. Yang, M.C. Asplund, T. Lian, B.K. McNamara, K.T. Kotz, J.S. Yeston, M. Wilkens, H. Frei, R.G. Bergman, C.B. Harris, Science 278 (1997) 260.
[21] S. Zarić, M.B. Hall, J. Phys. Chem. A 102 (1998) 1963.
[22] U.E. Bucher, A. Currao, R. Nesper, H. Rüegger, L.M. Venanzi, E. Younger, Inorg. Chem. 34 (1995) 66.
[23] A. Albinati, M. Bovens, H. Rüegger, L.M. Venanzi, Inorg. Chem. 36 (1997) 5991.
[24] A. Ferrari, M. Merlin, S. Sostero, O. Traverso, H. Rüegger, L.M. Venanzi, Helv. Chim. Acta 81 (1998) 2127.
[25] A. Albinati, U.E. Bucher, V. Gramlich, O. Renn, H. Rüegger, L.M. Venanzi, Inorg. Chim. Acta 284 (1999) 191.
[26] N.G. Connelly, D.J.H. Emslie, B. Metz, A.G. Orpen, M.J. Quayle, Chem. Commun. (1996) 2289.
[27] D. Sanz, M.D. Santa María, R.M. Claramunt, M. Cano, J.V. Heras, J.A. Campo, F.A. Ruíz, E. Pinilla, A. Monge, J. Organomet. Chem. 526 (1996) 341.
[28] K. Ohta, M. Hashimoto, Y. Takahashi, S. Hikichi, M. Akita, Y. Moro-oka, Organometallics 18 (1999) 3234.
[29] C.E. Webster, M.B. Hall, Inorg. Chim. Acta 330 (2002) 268.
[30] M. Cano, J.A. Campo, J.V. Heras, J. Lafuente, C. Rivas, E. Pinilla, Polyhedron 14 (1995) 1139.
[31] M.C. Torralba, M. Cano, J.A. Campo, J.V. Heras, E. Pinilla, M.R. Torres, J. Organomet. Chem. 633 (2001) 91.
[32] M.J. Decker, D.O. Kimberley Fjeldsted, S.R. Stobart, M.J. Zaworotko, J. Chem. Soc., Chem. Commun. (1983) 1525.
[33] F. Bonati, L.A. Oro, M.T. Pinillos, C. Tejel, M.C. Apreda, C. Foces-Foces, F.H. Cano, J. Organomet. Chem. 369 (1989) 253.
[34] A.L. Rheingold, R.L. Ostrader, B.S. Haggerty, S. Trofimenko, Inorg. Chem. 33 (1994) 3666.
[35] M. Moszner, S. Wołowiec, A. Trösch, H. Vahrenkamp, J. Organomet. Chem. 595 (2000) 178.
[36] M. Akita, M. Hashimoto, S. Hikichi, Y. Moro-oka, Organometallics 18 (2000) 3744.
[37] T. Ruman, Z. Ciunik, A.M. Trzeciak, S. Wołowiec, J.J. Ziółkowski, Organometallics 22 (2003) 1072.
[38] E. del Ministro, O. Reun, H. Rüegger, L.M. Venanzi, U. Burckhardt, V. Gramlich, Inorg. Chim. Acta 240 (1995) 631.
[39] J.S. Thompson, R.L. Harlow, J.F. Whitney, J. Am. Chem. Soc. 105 (1983) 3522.
[40] J.S. Thompson, J.F. Whitney, Acta Crystallogr., Sect. C 40 (1984) 756.
[41] G.M. Sheldrick, SHELXL97, Program for Refinement of Crystal Structure, University of Göttingen, Germany, 1997.

Available online at www.sciencedirect.com
SCIENCE DIRECT®
Polyhedron 23 (2004) 311–321
POLYHEDRON
www.elsevier.com/locate/poly

Interconversions of simple monodentate nitrogen donor ligands bound to Tp′ tungsten fragments

Neil J. Vogeley, Joseph L. Templeton *

W.R. Kenan Jr. Laboratories, Department of Chemistry, University of North Carolina, Chapel Hill, NC 27599-3290, USA

Received 2 June 2003; accepted 2 September 2003

Abstract

The dramatic effect of an ancillary alkyne ligand on the regioselectivity of nucleophile and electrophile additions to monodentate nitrogen ligands is illustrated by comparison of ligand based reactions characteristic of nitrogen donor ligands incorporated into $[Tp'(CO)_2W]^+$ and $[Tp'(CO)(PhCCMe)W]^+$ coordination spheres. Nitrogen ligands accessible from free nitriles and amines, including nitrile, azavinylidene, imido, imine, amido, amine, and nitrido, can be interconverted by addition of nucleophiles or electrophiles as well as by hydride abstraction or proton removal. Structural details that reveal important π-bonding interactions for multiply bonded nitrogen ligands are also discussed.
© 2003 Elsevier Ltd. All rights reserved.

Keywords: Acetonitrile reduction; Amine oxidation; Imido; Metal-nitrogen pi bonding; Regioselectivity of nucleophile and electrophile additions

1. Introduction

This paper will compare and contrast the reaction chemistry of nitrogen ligands bound to two superficially similar tungsten(II) d^4 fragments: $[Tp'(CO)_2W]^+$ and $[Tp'(CO)(PhC{\equiv}CMe)W]^+$ (Tp′ = hydridotris(3,5-dimethylpyrazolyl)borate, Fig. 1) [1]. Both of these fragments formally count 14 electrons, but π donation from the second alkyne π orbital, $\pi_\perp$, can effectively increase the electron count to 16 for the alkyne containing metal moiety (Fig. 2) [2,3]. The comparisons here indicate that variable π donation from the alkyne ligand dictates the reaction chemistry available to other ligands coordinated to these fragments.

2. Reactivity patterns for unsaturated ligands with carbon frameworks

Reactions of unsaturated ligands built from carbon skeletons have been extensively studied [4]. Using an iron-acetylide moiety to illustrate the reaction paradigm, the acetylide unit can be reduced to an alkyl ligand by alternating addition of electrophiles and nucleophiles (Scheme 1) [5]. In this and related systems, the metal is able to house electrons pairs or share them with C_α while adhering to the 18-electron rule. It follows naturally that electrophiles will add to C_β, while nucleophiles add to C_α [6].

Addition of an electrophile to C_β of the alkynyl ligand of the starting reagent forms a vinylidene complex [5,7–11]. The vinylidene complex, $L_nM{=}C{=}CRE$, is a unique reagent with both M=C and C=C unsaturation. Two disparate reaction pathways are available to vinylidene complexes: (i) Addition of an electrophile to C_β is possible and forms a carbyne complex [10,12–17]. (ii) Addition of a nucleophile to C_α is possible and forms a vinyl complex [5,9,18]. Carbene complexes can be synthesized either by addition of a nucleophile to C_α of a carbyne complex [19–24], or by addition of an electrophile to C_β of a vinyl complex [7,8,25]. Addition of a nucleophile to the carbene carbon gives an alkyl complex [26,27].

In the iron system reported by Davison and Selegue [5], alternating addition of electrophiles and nucleophiles

* Corresponding author. Fax: +1-919-962-2388.
E-mail address: joetemp@unc.edu (J.L. Templeton).

0277-5387/$ - see front matter © 2003 Elsevier Ltd. All rights reserved.
doi:10.1016/j.poly.2003.11.019

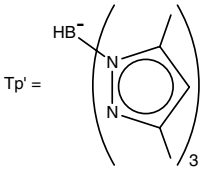

Fig. 1. Tp′ = hydridotris(3,5-dimethylpyrazolyl)borate.

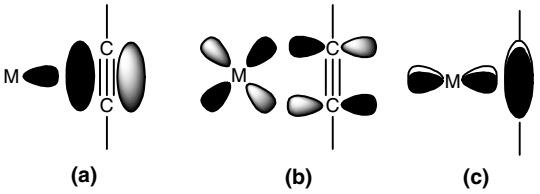

Fig. 2. (a) $\pi_{\|}$ to M(σ) donation; (b) M(dπ) to $\pi^*_{\|}$ backdonation; (c) $\pi_{\perp}$ to M(dπ) donation.

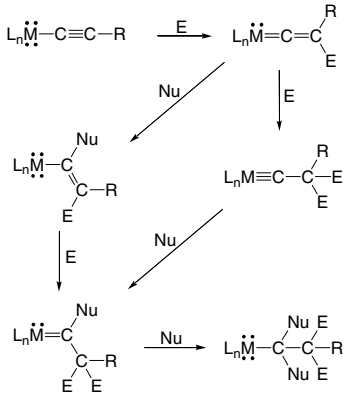

Scheme 1.

leads to the reduced alkyl ligand through a vinyl species; no carbyne is ever present in reduction of the iron-acetylide reagent.

Nitrogen ligands analogous to these carbon ligands are accessible (Fig. 3), but roadmaps for systematic interconversions among the nitrogen based ligand family remain rare. An excellent review of reactions of nitrile ligands has recently appeared [28]. We will return to a reaction scheme, similar to Scheme 1, involving nucleophile and electrophile additions to nitrogen based ligands in the summary.

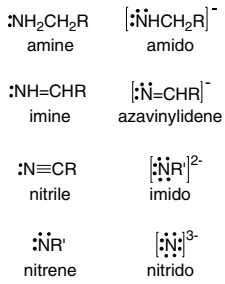

Fig. 3. Nomenclature for monodentate nitrogen donor ligands.

3. Nitrogen donor ligands bound to $[Tp'(CO)_2W]^+$

3.1. Synthesis and reactions of nitrogen ligands bound to $[Tp'(CO)_2W]^+$

Cationic imido complexes, $[Tp'(CO)_2W(\equiv NR)]^+$ (**3**), have been synthesized in two ways: (1) reduction of coordinated nitriles and (2) oxidation of amido complexes. Each of these methods has the advantage of starting from readily available reagents, either nitriles or amines.

In the first method, addition of a nucleophile to the nitrile carbon in $[Tp'(CO)_3W(NCR)]^+$ (**1**) (R = Me (**1a**), ν_{CO} = 2045, 1956 cm^{-1}), which is readily prepared by adding Ag^+ to $Tp'(CO)_3W(I)$ in CH_3CN, leads to loss of one carbonyl ligand during the formation of neutral azavinylidene complex **2** (Eq. (1)) [29]. Azavinylidene complex **2** can also be synthesized by photolysis of $Tp'(CO)_3W(H)$ in the presence of nitriles (Eq. (2)). The two infrared CO stretching frequencies of complex **2,** averaging 1926 and 1814 cm^{-1}, are in the range typical of neutral dicarbonyl tungsten(II) complexes (see Table 1).

The azavinylidene carbon is nucleophilic and electrophiles can be added at the carbon which is α to the nitrogen and β to the metal to form cationic imido complex **3** (Eqs. (1) and (2)) [29]. These imido complexes can be deprotonated to regenerate azavinylidene complex **2** [30]. Both the symmetric and antisymmetric CO stretches absorb above 2000 cm^{-1} for cationic imido complexes (**3**) (averaging 2083 and 2006 cm^{-1}, see Table 1) reflecting a dramatic decrease in electron density at the metal relative to the azavinylidene precursor. This drop in metal electron density is compatible with an increase in formal oxidation state from W(II) to W(IV) upon addition of an electrophile to the azavinylidene carbon to form an imido ligand, formally $[NR]^{2-}$.

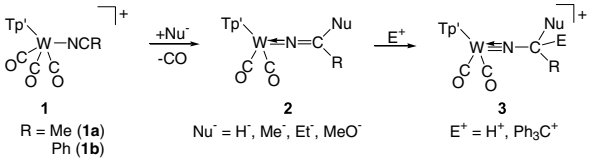

(1)

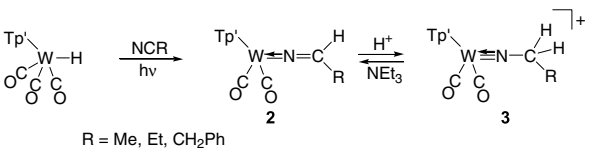

(2)

Table 1
IR and NMR data for $[Tp'W(CO)_2]^+$ complexes

Complex	ν_{CO} (cm^{-1})	^{13}C (ppm): *C*O	^{1}H (ppm): N*H*
$[Tp'(CO)_3W(NCMe)][BF_4]$ (**1a**) [29]	2045, 1956		
$Tp'(CO)_2W(=N=CHMe)$ (**2a**) [29]	1922, 1811	239.5	
$Tp'(CO)_2W(=N=CHEt)$ (**2b**) [29]	1921, 1805	239.3	
$Tp'(CO)_2W(=N=CHCH_2Ph)$ (**2c**) [29]	1928, 1813	239.5	
$Tp'(CO)_2W(=N=CEtPh)$ (**2d**) [29]	1928, 1825	239.5	
$Tp'(CO)_2W(=N=C(OMe)Me)$ (**2e**) [29]	1921, 1800	239.5	
$Tp'(CO)_2W(=N=CHPr)$ (**2f**) [30]	1923, 1815	241.7	
$Tp'(CO)_2W(=N=CHPh)$ (**2g**) [30]	1942, 1830	239.1	
$Tp'(CO)_2W(\equiv NCH_2Me)^+$ (**3a**) [29]	2080, 1997	215.9	
$Tp'(CO)_2W(\equiv NCH_2Et)^+$ (**3b**) [29]	2085, 2002	216.9	
$Tp'(CO)_2W(\equiv NCH_2CH_2Ph)^+$ (**3c**) [29]	2076, 1996	216.9	
$Tp'(CO)_2W(\equiv NCHEtPh)^+$ (**3d**) [29]	2081, 2001	216.6, 216.2	
$Tp'(CO)_2W(\equiv NCHMeCPh_3)^+$ (**3e**) [29]	2081, 2002	220.5, 219.0	
$Tp'(CO)_2W(\equiv NCHEtCPh_3)^+$ (**3f**) [29]	2079, 2002	223.0, 219.5	
$Tp'(CO)_2W(\equiv NCH(CH_2Ph)CPh_3)^+$ (**3g**) [29]	2087, 2010	222.9, 220.5	
$Tp'(CO)_2W(\equiv NtBu)^+$ (**3h**) [31]	2081, 2003	216.6	
$Tp'(CO)_2W(\equiv NPh)^+$ (**3i**) [31]	2079, 2006	216.9	
$[Tp'(CO)_2W(\equiv NBu)][PF_6]$ (**3j**) [30]	2082, 2004	216.8	
$[Tp'(CO)_2W(\equiv NCH_2Ph)][PF_6]$ (**3k**) [30]	2083, 2006	216.0	
$[Tp'(CO)_2W(\equiv NH)][PF_6]$ (**3l**) [35]	2092, 2017	215.6	9.8
$[Tp'(CO)_2W(\equiv NTs)][OTf]$ (**3m**) [32]	2100, 2035	210.5	
$[Tp'(CO)_2W(\equiv NCPh_3)][PF_6]$ (**3n**) [35]	2083, 2008		
$Tp'(CO)(Cl)W(\equiv NC(O)Me)$ (**3o**) [30]	1954	280.6	
$[Tp'(CO)_2W(\equiv NMe)][PF_6]$ (**3p**) [30]	2083, 2006	216.6	
$[Li][Tp'(CO)_2W(\equiv NPh)]$ (**3q**) [30]	1750, 1652		
$[Li][Tp'(CO)_2W(\equiv NCH_2Ph)]$ (**3r**) [30]	1858, 1720		
$[Li][Tp'(CO)_2W(\equiv NH)]$ (**3s**) [30]	1861, 1724		
$[Tp'(CO)(PMe_3)W(\equiv NTs)][X]$ (**3t**) [32]	1996		
$Tp'(CO)W(\equiv NPh)(C(O)H)$ (**5**) [33]	1948, 1680	259, 293	
$Tp'(CO)W(\equiv NPh)(C(O)Ph)$ (**6**) [33]	1937	274, 286	
$Tp'(CO)_2W(NHtBu)$ (**4a**) [31]	1910, 1782	255.6	14.15
$Tp'(CO)_2W(NHPh)$ (**4b**) [31]	1900, 1786	255.6	15.33
$Tp'(CO)_2W(NHBu)$ (**4c**) [30]	1911, 1794	254.6	13.7
$Tp'(CO)_2W(NHCH_2Ph)$ (**4d**) [30]	1910, 1784	254.7	13.57
$Tp'(CO)_2W(NH_2)$ (**4e**) [35]	1915, 1793	254.7	13.50, 11.60
$Tp'(CO)_2W(NHTs)$ (**4f**) [32]	1944, 1828	248.4	14.39
$Tp'(CO)_2W(NMe_2)$ (**4g**) [35]	1904, 1777	254.8	
$Tp'(CO)_2W(NPhCH_2Ph)$ (**4h**) [30]	1914, 1787	254.1	
$Tp'(CO)_2W(NMeCH_2Ph)$ (**4i**) [30]	1904, 1777	254.7	
$Tp'(CO)_2W(\equiv N)$ (**7**) [35]	2035, 1938		
$[Tp'(CO)_2W(PMe_3)_2][X]$ (**8**) [32]	1936, 1840	220.6	

The second method for obtaining an imido complex begins by heating $Tp'(CO)_3W(I)$ in the presence of a primary amine in THF solution to form $Tp'(CO)_2W(=NHR)$ (**4a –e**) with concomitant loss of a carbonyl ligand [31]. The average CO stretching frequencies for these neutral amido complexes are 1912 and 1790 cm^{-1}, significantly lower than for analogous neutral azavinylidene complexes (**2**). The average chemical shift for the amido NH proton is about 14 ppm in the NMR spectrum (see Table 1). These $[NHR]^-$ amido ligands can be oxidized with I_2 or $[Ph_3C]^+$ via net hydride removal from nitrogen to form cationic imido complexes **3h–l** (Eq. (3)).

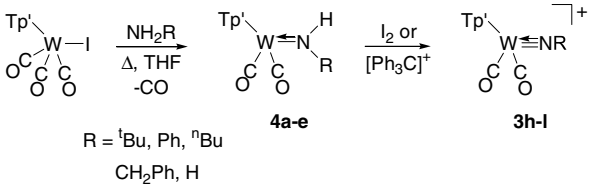

(3)

Tosylamido complex **4f** (tosyl = $SO_2C_6H_4Me$) can be synthesized by refluxing $Tp'(CO)_3W(H)$ in THF with TsN_3. Oxidation by net hydride removal with Ag[OTf] or I_2 gives tosylimido complex **3m** (Eq. (4)) [32].

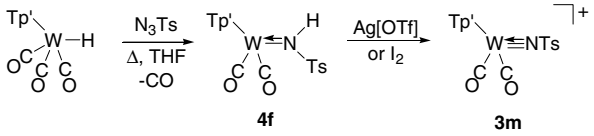

(4)

Tosylimido complex **3m** undergoes two separate reactions in the presence of four equivalents of PMe_3. Three equivalents are involved in transferring the neutral nitrene fragment, NTs, to PMe_3 forming $TsN{=}PMe_3$ and $Tp'(CO)_2W(PMe_3)_2$ (**8**) as the trapped tungsten product. The second tungsten product, $[Tp'(CO)(PMe_3)W(\equiv NTs)]^+$ (**3t**), is formed by displacement of a carbonyl ligand by one equivalent of PMe_3 (Scheme 2) [32].

Hydride reduction of $[Tp'(CO)_2W(\equiv NR)]^+$ imido complexes **3** results in formation of neutral amido complexes **4**. Addition of excess $Li[BH_4]$ to $[Tp'(CO)_2W(\equiv NPh)]^+$ (**3i**) at low temperature adds hydride to a carbonyl ligand leading to formyl complex **5** as an intermediate. Hydride migration from the formyl ligand to the imido ligand to yield phenylamido complex **4b** was monitored by ^1H NMR spectroscopy at −70°C and yielded a k_{obs} of 7.2×10^{-6} s^{-1} ($\Delta G^{\ddagger} = 16.5$ kcal/mol) (Scheme 3) [33].

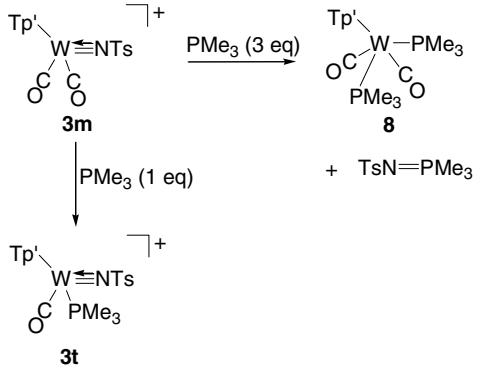

Scheme 2.

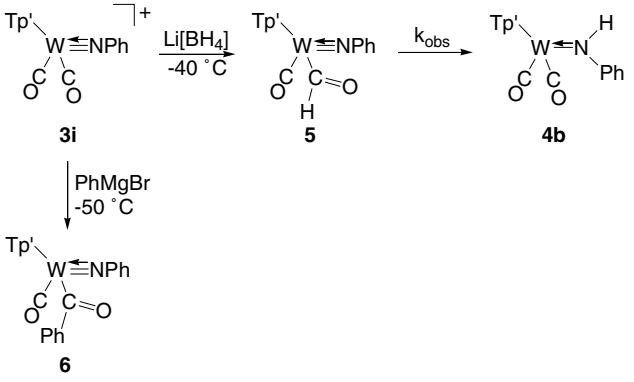

Scheme 3.

Given the high CO stretching frequencies in $[Tp'(CO)_2W(\equiv NPh)]^+$, nucleophilic attack at a carbonyl ligand by the $Li[HBEt_3]$ reagent above is easily rationalized [34]. Another example of nucleophilic addition to a carbonyl ligand is provided by addition of PhMgBr to $[Tp'(CO)_2W(\equiv NPh)]^+$ which gives phenylacyl complex **6** in good yield (Scheme 3).

The parent amido complex, $Tp'(CO)_2W(=NH_2)$ (**4e**), can be synthesized from the 16-electron $Tp'(CO)_2W(I)$ reagent and ammonia. Amido complex **4e** has CO stretches at 1915 and 1793 cm^{-1}; the two distinct NH protons appear at 11.6 and 13.5 ppm in the ^1H NMR spectrum. Dimethylamido complex **4g** can be prepared by deprotonation of the parent amido complex **4e** with LDA (lithium diisopropylamide) followed by quenching with excess MeI. Hydride removal from parent amido complex **4e** using $[Ph_3C]^+$ forms the imido complex $[Tp'(CO)_2W(\equiv NH)]^+$ (**3l**) along with some $[Tp'(CO)_2W(\equiv NCPh_3)]^+$ (**3n**). Parent NH imido complex **3l** has CO stretches at 2092 and 2017 cm^{-1}, and the imido proton resonates at 9.8 ppm in the ^1H NMR spectrum. Deprotonation of parent imido complex **3l** affords neutral nitrido complex **7** with CO stretches at 2035 and 1938 cm^{-1}. These relatively high CO stretches reflect localization of the lone pair on the nitride nitrogen where it is not directly available to enrich the electron density at the metal. The nitrido complex can be reacted with electrophiles to give new imido complexes **3n–p** (Scheme 4) [35].

Neutral amido complexes $Tp'(CO)_2W(NHR)$ (**4b**,**d–e**) can be deprotonated with LDA or ^{t}BuLi to generate reactive anionic imido complexes **3q–s**. These imido intermediates can be trapped by $PhCH_2Br$ or MeI to give new amido complexes **4h**,**i** (Eq. (5)) [30]. The CO stretches for $[Li][Tp'(CO)_2W(\equiv NR)]$ at 1861 and 1724 cm^{-1} in the IR spectrum are much lower than for the cationic imido complexes, as expected for these cationic and anionic complexes with the same ligand set (see Table 1).

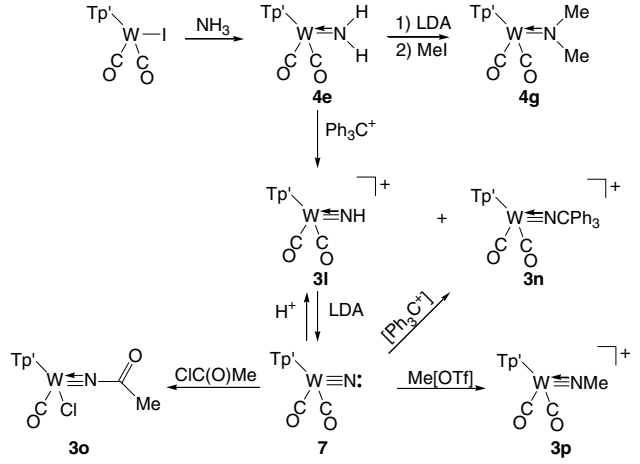

Scheme 4.

The increased π backbonding available to CO ligands in the anionic imido complexes is responsible for lowering the average CO stretching frequency 250 cm^{-1} from the related cationic imido complexes.

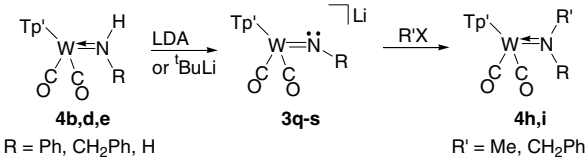

(5)

3.2. Orbital interactions in $[Tp'(CO)_2W]^+$ derivatives

Single-faced π-donor ligands reveal their orbital orientations indirectly but definitively through molecular geometries. X-ray structures in the solid state and NMR data in solution show that the amido fragment in $Tp'(CO)_2W(NHR)$ lies in the mirror plane of the complex. This orientation positions the nitrogen p orbital to donate electrons into the d_{yz} orbital to form the M–N π bond (Fig. 4). The two filled dπ orbitals (d_{xz} and $d_{x^2-y^2}$ in the orientation depicted in Fig. 4) are involved in backbonding to the two carbonyl ligands. In order to maximize constructive orbital overlap, the OC–W–CO angle is less than 90°. This increases the interaction of two CO π^* orbitals with the filled metal d_{xz} orbital and decreases interaction of the same CO π^* orbitals with the empty metal d_{yz} orbital [29,30]. For $Tp'(CO)_2W$ (= NHPh) (**4b**), the barrier for interconversion of the two rotamers has been determined by ^1H NMR spectroscopy at 22 °C to be 24.2 kcal/mol from the thermodynamically favored isomer, and 23.0 kcal/mol from the minor rotamer [31].

The metal–nitrogen orbital interactions in azavinylidene complexes resemble those in amido complexes. Like other cumulenes, the orientation of the pendant XR_2 group rotates by 90° with each additional double bond. The ^1H NMR spectrum of N=CRR′ complexes shows an apparent mirror plane at room temperature, but upon cooling, the spectrum changes. At low temperature, it shows distinct signals for each of the six Tp′ methyl groups indicating that rotation about the W=N=C axis has been effectively stopped on the NMR timescale and that the azavinylidene plane is oriented so that the nitrogen lone pair can donate into the empty d_{yz} orbital with R and R′ breaking the C_s symmetry (Fig. 5). The barrier for W–N–C rotation was determined to be 9.5 kcal/mol at −78°C for $Tp'(CO)_2W(=N=CHMe)$ (**2a**) [29]. The X-ray structure of $Tp'(CO)_2W(=N=C(H)CH_2Ph)$ (**2c**) shows a W=N=C bond angle of 166.6°; the benzyl group is positioned as anticipated [29].

As a cylindrically symmetrical π donor, the $[NR]^{2-}$ ligand has the capability to form a M–N triple bond; there is no rotational preference for linear imido complexes. The two sets of lone pair electrons on nitrogen are able to donate into empty dπ orbitals (d_{yz} and d_{xz}) in this tungsten(IV) d^2 system (Fig. 6). Indeed, the X-ray structure of $[Tp'(CO)_2W(NPh)][PF_6]$ (**3i**) shows an approximately linear W–N–C linkage of 171.6° [30].

Anionic imido complexes, $[Li][Tp'(CO)_2W(=NR)]$ (**3q–s**), would be expected to have a bent imido moiety. These complexes are tungsten(II) with four d-electrons. The imido ligand can form one π bond with tungsten (Fig. 7). This leaves one lone pair of electrons on nitrogen that are not needed for π bonding with tungsten.

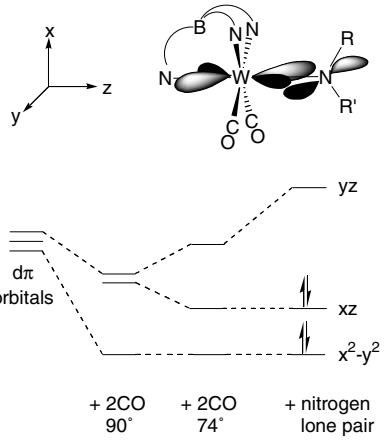

Fig. 4. Orbital interactions in $Tp'(CO)_2W(NRR')$.

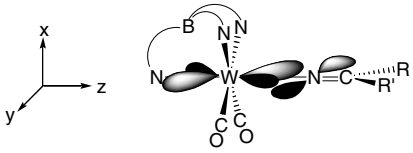

Fig. 5. Orbital interactions in $Tp'(CO)_2W(=N=CRR')$.

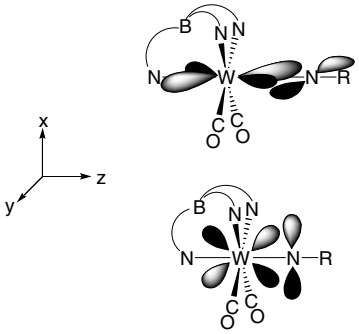

Fig. 6. Orbital interactions in $[Tp'(CO)_2W(\equiv NR)]^+$.

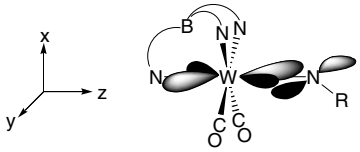

Fig. 7. Orbital interactions in $[Li][Tp'(CO)_2W=NR]$.

It is possible that this lone pair of electrons is available for lithium coordination forming a lithium amido type structure.

4. Nitrogen donor ligands bound to [Tp′(CO)(PhCCMe)W]$^+$

4.1. Synthesis and reactions of nitrogen ligands bound to [Tp′(CO)(PhCCMe)W]$^+$

Addition of a nucleophile to the nitrile carbon in [Tp′(CO)(PhCCMe)W(NCMe)]$^+$ (**9a**) ($\nu_{CO} = 1940\ cm^{-1}$) gives corresponding azavinylidene complexes **10a**,**b** *without the loss of a ligand* (Scheme 5). Recall that nucleophile addition to the nitrile of [Tp′(CO)$_3$W(NCR)]$^+$ promoted loss of one carbonyl ligand, so the reactivity patterns of these two tungsten(II) d^4 nitrile complexes diverge immediately. The azavinylidene complexes can be protonated at nitrogen, thus utilizing the M–N π electrons, to form cationic imine complexes **11a**,**b**. Note that the regiochemistry of electrophile addition is reversed relative to Tp′(CO)$_2$W(=N=CR$_2$) which adds electrophiles to the azavinylidene *carbon*, rather than to the nitrogen. Addition of a nucleophile to the imine carbon in [Tp′(CO)(PhCCMe)W(NH=CRR′)]$^+$ then leads to neutral amido complexes **12a**,**b** which can be protonated at nitrogen to give coordinated amine complexes **13a**,**b** [36,37]. Note that the sites for addition of nucleophiles and electrophiles to this M–N–C linkage are reversed relative to the M–C–C template.

Nucleophilic addition of [CN]$^-$ to [Tp′(CO)(PhCCMe)W(NH=CHMe)][BF$_4$] (**11a**), obtained from reduction of coordinated acetonitrile (Scheme 5), occurs diastereoselectively to form amido complex **12b** (Eq. (6)) [37]. The ability to resolve the enantiomers of the chiral fragment (see below) leads to the possibility for the synthesis of single enantiomer amine products. Diastereoselective addition of nucleophiles to imines coordinated to chiral metal complexes has been observed in other systems [38,39].

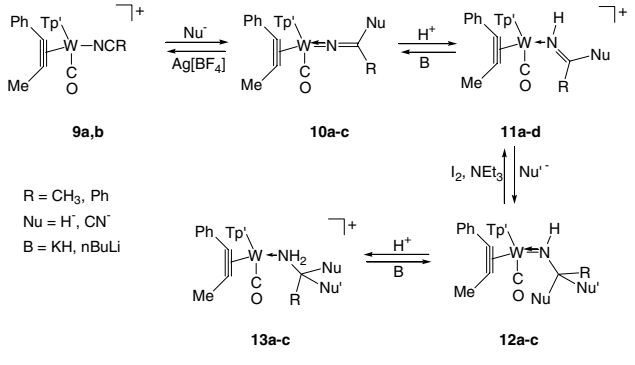

Scheme 5.

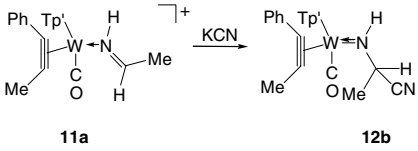

(6)

The reverse scheme, stepwise oxidation of an amine ligand, has been demonstrated with [Tp′(CO)(PhCCMe)W(NH$_2$CH$_2$Ph)]$^+$ (**13c**) as the initial reagent (Scheme 5) [40]. Deprotonation of the benzylamine ligand gives amido complex **12c**. The amido ligand can be oxidized by iodine in the presence of triethylamine to form imine complex **11c**,**d** by net hydride removal from the amido carbon. The imine complex can be deprotonated generating azavinylidene complex **10c,** which can in turn be oxidized by Ag[BF$_4$] to yield benzonitrile complex **9b**.

Amido complexes can also be synthesized directly from the corresponding free amines and [Tp′(CO)$_2$(PhCCMe)W][OTf]. Heating a solution of [Tp′(CO)$_2$(PhCCMe)W][OTf] in THF leads to the loss of one carbonyl ligand and to coordination of the triflate counterion. Addition of a primary amine and continued heating forms amido complexes **12d–i** (Eq. (7)). This method provides convenient access to a wide variety of amido complexes (**12d–i**) ($\nu_{CO} \approx 1850\ cm^{-1}$, ^{1}H NMR: 5.5–7.8 ppm, N*H*) which can then be converted (via Scheme 5) to amine (**13d–i**) ($\nu_{CO} \approx 1917\ cm^{-1}$, ^{1}H NMR: 2.5–5.5 ppm, NH_2), imine (**11e–h**) ($\nu_{CO} \approx 1931\ cm^{-1}$, ^{1}H NMR: 8.9–11 ppm, N*H*), or azavinylidene (**10d–g**) ($\nu_{CO} \approx 1887\ cm^{1}$) complexes (see Table 2) [41,42].

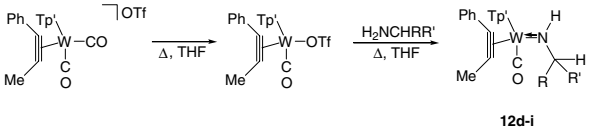

(7)

Enantiomers of chiral derivatives of the [Tp′(CO)(PhCCMe)W]$^+$ fragment have been separated. Synthesis of (*S*)-α-methylbenzylamido complex **12d**,**e** from (*S*)-α-methylbenzylamine allows for fractional recrystallization of the diastereomers. The R_WS_C diastereomer **12d** is recrystallized from CH_2Cl_2/hexanes, while the S_WS_C diastereomer **12e** is left in solution (Eq. (8)) [41].

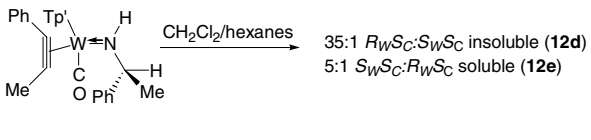

(8)

Cationic amine complexes **13d**,**e** can be obtained by protonation of amido complexes **12d**,**e**, and the amine ligand can be removed as the ammonium salt in the presence of excess acid and acetonitrile to give single

Table 2
IR and NMR data for $[Tp'W(CO)(PhCCMe]^+$ complexes

Complex	ν_{CO} (cm^{-1})	^{13}C (ppm): Ph*C*≡*C*Me	^{13}C (ppm): *C*O	^{1}H (ppm): N*H*
$[Tp'(CO)(PhCCMe)W(NCMe)][BF_4]$ (**9a**) [51]	1940	214.9, 212.8	225.2	
$[Tp'(CO)(PhCCMe)W(NCPh)][BF_4]$ (**9b**) [40]	1928	214.9, 212.4	224.5	
Tp′(CO)(PhCCMe)W(=N=CHMe) (**10a**) [37]	1885	159.7, 158.7	232	
Tp′(CO)(PhCCMe)W(=N=C(CN)Me) (**10b**) [37]	1917	159.4, 158.7	223.5	
Tp′(CO)(PhCCMe)W(=N=CHPh) (**10c**) [40]	1882	157.8, 157.6	228.4	
Tp′(CO)(PhCCMe)W(=N=CMeEt) (**10d**) [42]	1867	158.6, 158.3	234.5	
Tp′(CO)(PhCCMe)W(=N=CMePh) (**10e**) [42]	1886	158.3, 157.1	230.6	
$Tp'(CO)(PhCCMe)W(=N=CPh_2)$ (**10f**) [42]	1894	158.3, 156.3	228.8	
Tp′(CO)(PhCCMe)W(=N=CHCHMePh) (**10g**) [42]	1881			
$[Tp'(CO)(PhCCMe)W(NH=CHMe)][BF_4]$ (**11a**) [37]	1920	214.8, 214.3	228.5	10.86
$[Tp'(CO)(PhCCMe)W(NH=C(CN)Me)][BF_4]$ (**11b**) [37]	1933	217.3, 216.1	224.0	12.12
$[Tp'(CO)(PhCCMe)W(NH=CHPh)][BF_4]$ (**11c**) [40]	1921	215.6, 215.5		
$[Tp'(CO)(PhCCMe)W(NH=CHPh)][BAr'_4]$ (**11d**) [40]	1940	215.2, 212.0	227.5	9.90
$[Tp'(CO)(PhCCMe)W(NH=CMeEt)][BAr'_4]$ (**11e**) [42]	1938	215.9, 213.1	229.2	8.94
$[Tp'(CO)(PhCCMe)W(NH=CMePh)][BAr'_4]$ (**11f**) [42]	1923	216.8, 213.9	228.5	9.42
$[Tp'(CO)(PhCCMe)W(NH=CPh_2)][BAr'_4]$ (**11g**) [42]	1936	217.5, 216.7	227.1	9.81
$[Tp'(CO)(PhCCMe)W(NH=CHCHMePh)][BAr'_4]$ (**11h**) [42]	1936	215.3, 212.0	227.7	9.50
$Tp'(CO)(PhCCMe)W(NHCH_2Me)$ (**12a**) [37]	1854	169.2, 167.1	238.7	6.86
Tp′(CO)(PhCCMe)W(NHCH(CN)Me) (**12b**) [37]	1856	178.6, 175.5	236.2	5.49
$Tp'(CO)(PhCCMe)W(NHCH_2Ph)$ (**12c**) [40]	1840	170.5, 168.2	237.8	6.89
$(-)-(R_W S_C)$-Tp′(CO)(PhCCMe)W(NHCHMePh) (**12d**) [41]	1846	170.4, 167.0	237.4	~6.2–7.2
$(+)-(S_W S_C)$-Tp′(CO)(PhCCMe)W(NHCHMePh) (**12e**) [41]	1852	171.5, 170.2	237.1	~6.2–7.3
Tp′(CO)(PhCCMe)W(NHCHMeEt) (**12f**) [42]	1847	169.2, 166.5	237.8	6.83
$Tp'(CO)(PhCCMe)W(NHCHPh_2)$ (**12g**) [42]	1846	172.4, 170.7	236.9	6.63
$Tp'(CO)(PhCCMe)W(NHCH_2CHMePh)$ (**12h**) [42]	1847	169.6, 167.4	238.3	6.81
Tp′(CO)(PhCCMe)W(NHPh) (**12i**) [43]	1859	181.3, 178.3	238.2	7.83
Tp′(PhCCMe)W(NHPh)(H) (**12j**) [43]		258.8, 240.0		10.8
$[Tp'(CO)(PhCCMe)W(NH_2CH_2Me)][BF_4]$ (**13a**) [37]	1909	214.5, 213.0	230.8	4.10, 3.04
$[Tp'(CO)(PhCCMe)W(NH_2CH(CN)Me)][BF_4]$ (**13b**) [37]	1915	218.4, 215.5	229.8	4.35
$[Tp'(CO)(PhCCMe)W(NH_2CH_2Ph)][BF_4]$ (**13c**) [40]	1907	215.2, 213.7	230.3	4.26, 3.27
$(-)-(R_W S_C)$-$[Tp'(CO)(PhCCMe)W(NH_2CHMePh)[BF_4]$ (**13d**) [41]	1916	216.8, 214.1	229.6	3.95, 3.15
$(+)-(S_W S_C)$-$[Tp'(CO)(PhCCMe)W(NH_2CHMePh)][BF_4]$ (**13e**) [41]	1903	216.4, 214.6	230.5	3.98, 3.40
$[Tp'(CO)(PhCCMe)W(NH_2CHMeEt)][BAr'_4]$ (**13f**) [42]	1928	216.6, 214.4	230.4	3.44, 3.35
$[Tp'(CO)(PhCCMe)W(NH_2CHPh_2)][BAr'_4]$ (**13g**) [42]	1923	217.2, 216.2	229.3	5.53, 4.48
$[Tp'(CO)(PhCCMe)W(NH_2CH_2CHMePh)][BAr'_4]$ (**13h**) [42]	1928	215.3, 213.1	230.3	3.36, 2.45
$[Tp'(CO)(PhCCMe)W(NH_2Ph)][BAr'_4]$ (**13i**) [43]	1927	214.9, 216.4	229.3	5.44, 4.75
$[Tp'(CO)(PhCCMe)W(\equiv NPh)][BAr'_4]$ (**14a**) [43]	2087	138.0, 141.1	205.2	
Tp′(PhCCMe)W(≡NPh)(C(O)H) (**14b**) [43]		156.6, 156.4	291.8	
Tp′(PhCCMe)W(≡NPh)(H) (**14c**) [43]		162.2, 157.7		
Tp′(PhCCMe)W(≡NPh)(C(O)Me) (**14d**) [43]		154.4, 153.2	325.7	
Tp′(PhCCMe)W(≡NPh)(C(O)Ph) (**14e**) [43]		157.9, 155.6	301.3	

enantiomers of nitrile complex **9a**. The enantiomers of Tp′(CO)(PhCCMe)W(I) (**15**) can be obtained by refluxing the resolved amine complexes (**13d**,**e**) in THF with $[NEt_4][I]$ and acid (Scheme 6) [37,41].

Using (+)-**9a** or (−)-**9a** in the stepwise reduction of acetonitrile gives Tp′(CO)(PhCCMe)WNHCH(CN)(CH_3) (**12b**) as a single enantiomer. The amine fragment can then be cleaved by HBF_4 in the presence of acetonitrile to recover one enantiomer of the amine and the same enantiomer of **9a** that was used as the starting reagent. This demonstrates the configurational stability of the $[Tp'(CO)(PhCCMe)W]^+$ fragment.

Aniline is much less basic than alkylamines, and of course the resultant phenylamido complex (**12i**)

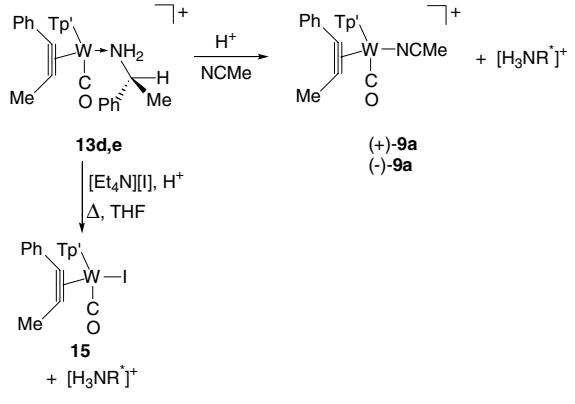

Scheme 6.

(synthesized according to Eq. (7)) has no β hydrogen on the amido ligand. With hydride removal from carbon off the table as an option, oxidation using iodine in the presence of triethylamine does not give an imine complex, but rather cationic phenylimido complex **14a** results from net hydride removal at nitrogen (Eq. (9), BAr'_4 = tetrakis[3,5-bis(trifluoromethyl)phenyl]borate) [43]. The CO stretch for this imido complex is at 2087 cm^{-1} indicating low electron density at the metal which is compatible with oxidation of the metal to tungsten(IV) d^2. In this case, the amido reactivity options are constrained so that the phenylamido ligand relinquishes a hydride just as amido ligands do in the dicarbonyl case of Section 3.

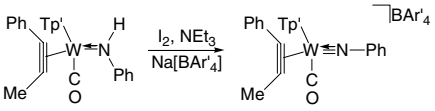

12i **14a** (9)

The imido complex [Tp′(CO)(PhCCMe)W(≡NPh)]$^+$ (**14a**) adds one equivalent of hydride from K[BH_4] to yield amido complex **12i**. Reduction with excess hydride does not generate the amido complex, but rather imido–hydride complex **14c** is obtained instead, reflecting replacement of CO by hydride. The imido ligand is now nucleophilic and can be protonated at nitrogen to give cationic amido-hydride complex **12j** (Scheme 7) [43]. This cationic tungsten(IV) amido complex displays an NH chemical shift of 10.8 ppm which is downfield relative to neutral tungsten(II) amido complexes (Table 2).

Nucleophilic addition of Me^-, Ph^-, or H^- to phenylimido complex **14a** occurs at the carbonyl ligand to generate acyl complexes. Methylacyl complex **14d** inserts the adjacent alkyne into the metal-acyl bond to form metallafuran complex **16**. Formyl complex **14b** deinserts CO to give imido–hydride complex **14c** (Scheme 8) [43].

4.2. Orbital interactions in [Tp′(CO)(PhCCMe)W]$^+$ derivatives

In these tungsten(II) d^4 systems, both of the two filled dπ orbitals, d_{xz} and d_{yz}, are utilized in π backbonding to

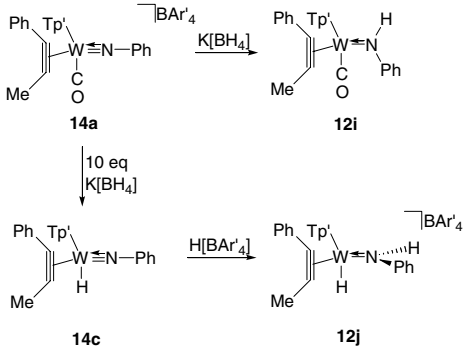

Scheme 7.

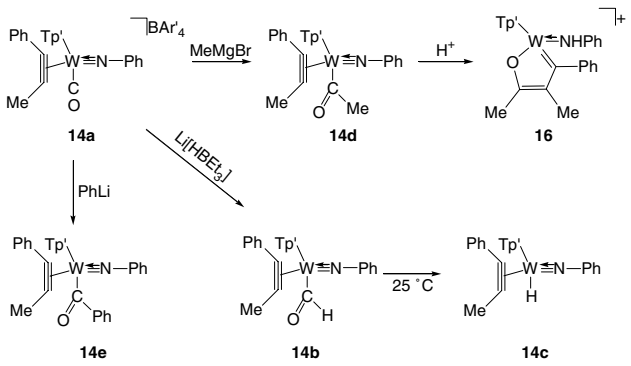

Scheme 8.

CO. The alkyne $\pi^*_{\parallel}$ orbital can further lower the energy of d_{xz}, while $\pi_{\perp}$ is able to donate into the lone empty d_{xy} orbital. These bonding interactions orient the alkyne parallel to the CO axis. Since there is only one empty dπ orbital, the nitrogen lone pair on either an amido or an azavinylidene ligand has to compete with alkyne π donation. Due to π donation into d_{xy} from nitrogen, the plane of the amido ligand is *parallel* to the CO axis. In turn, the cumulene alternation guideline implies that the azavinylidene plane will be *perpendicular* to the CO axis (Fig. 8) [37].

X-ray structures for Tp′(CO)(PhCCMe)W(=N=CMePh) (**11f**) and Tp′(CO)(PhCCMe)W(NHCHMeEt) (**12f**) indeed show the expected alternating orientations for azavinylidene and amido ligands [42]. The W=N=C angle of the azavinylidene fragment is slightly bent at 165.4° [42]. Heating a solution of Tp′(CO)(PhCCMe)W(=N=CMePh) (**11f**) (7:1 ratio of rotamers) to 100 °C in an NMR tube showed no broadening of the signals indicating a barrier for W–N–C rotation in this azavinylidene complex of greater than 19 kcal/mol [42]. The dπ interactions in alkyne complexes are significantly

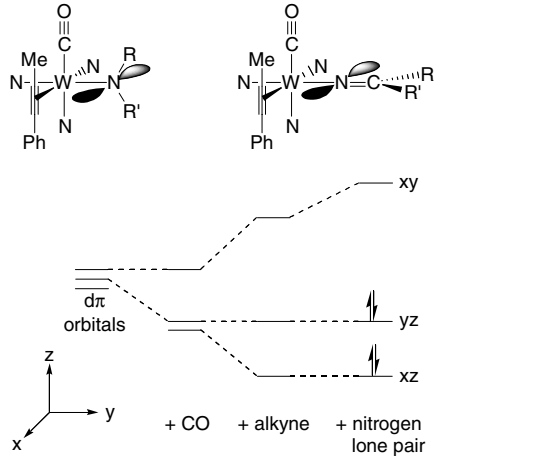

Fig. 8. Orbital interactions in Tp′(CO)(PhCCMe)W(NHR) and Tp′(CO)(PhCCMe)W(=N=CR_2).

restricted relative to the dicarbonyl derivatives, and this is reflected in the difficulty of azavinylidene rotation here which contrasts with the ease of rotation in the analogous $Tp'(CO)_2W(=N=CR_2)$ dicarbonyl complex where a barrier of only 9.5 kcal/mol was observed.

It is noteworthy that in the cationic tungsten(IV) amido-hydride complex **12j** with only two dπ electrons, the alkyne and the amido ligands can find separate vacant dπ orbitals to serve as acceptor sites in order to form two 2-center-2-electron π bonds. Stated differently, both the alkyne and the amido ligands must be net four-electron donor ligands for the metal to adhere to the 18-electron rule. The alkyne and amido ligands do not compete for donation to the metal in this system because there are two empty dπ orbitals. While the geometry was not discussed in the initial report [43], the consequence of this is that the amido ligand would be expected to rotate by 90° relative to the d^4 complexes so that it should be oriented perpendicular to the alkyne triple bond (Fig. 9).

The pivotal factor in the chemistry of the $[Tp'(CO)(PhCCMe)W]^+$ fragment is the ability of the alkyne ligand to donate either two or four electrons which allows chemistry to occur at the nitrogen ligand without the loss of an ancillary ligand. In amido and azavinylidene complexes the lone pair of electrons on the nitrogen donor atom competes with the $\pi_\perp$ electron pair of the adjacent alkyne ligand for the single empty metal dπ orbital. Changes in electron donation from the alkyne ligand are reflected in the ^{13}C NMR spectrum [44,45].

When the alkyne donates four electrons, as in cationic imine and amine complexes, the resonances of the alkyne carbons appear around 215 ppm (see Table 2). When $\pi_\perp$ donation competes with the lone pair on the nitrogen ligand, as in neutral amido and azavinylidene complexes, the alkyne carbon resonances move upfield: alkyne carbons in amido complexes appear around 170 ppm, while alkyne carbons in azavinylidene complexes appear near 160 ppm (see Table 2).

These data indicate that an alkyne ligand in an azavinylidene complex donates less electron density from $\pi_\perp$ than in a similar amido complex, or stated differently, 'an amido ligand is a stronger π donor than an azavinylidene ligand'. The donor ability of amido and azavinylidene ligands is also evident in the CO stretching frequencies of their analogous complexes. The carbonyl ligand in amido complexes absorbs near 1850 cm^{-1}, while those in azavinylidene complexes absorb near 1890 cm^{-1}.

In the cationic amido-hydride complex **12j,** the alkyne carbons appear the farthest downfield (about 250 ppm) indicating that the alkyne is a four-electron donor in this tungsten(IV) d^2 complex. The alkyne carbons of phenylimido complex **14a** appear the farthest upfield (near 140 ppm), suggesting that the alkyne is tending toward two-electron donor behavior in response to strong π donation from the cylindrically symmetrical π-donor ligand $[NPh]^{2-}$.

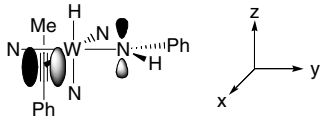

Fig. 9. Orbital interactions in $[Tp'(H)(PhCCMe)W(NHPh)][BAr'_4]$ (**12j**).

5. Summary

Interconversions among monodentate nitrogen donor ligands depend on the ancillary ligands. With classic two-electron donor ligands completing the coordination sphere, nitrogen lone-pair electrons with π character are immutably linked to the metal in a π bond, and they are therefore unavailable for ligand based reactions. Consequently, addition of electrophiles to an azavinylidene complex is directed to C_β leading to the formation of an imido complex. With a variable electron donor alkyne in the coordination sphere, the nitrogen lone pair with M–N π character is not essential for bonding with the metal, and as a result, these electrons are available for reaction with electrophiles. This allows protonation to occur at nitrogen and leads to the synthesis of imine and amine complexes in the stepwise reduction of a coordinated nitrile.

We can now describe a general reaction scheme starting from a metal nitrile complex, comparable to a metal acetylide, with classic two-electron donor ancillary ligands completing the coordination sphere. Addition of a nucleophile to C_β (β with respect to the metal) of the nitrile ligand leads to an azavinylidene complex and allows a second pair of nitrogen electrons to donate to the metal to form an M–N π bond to supplement the original M–N σ bond. Note that adherence to the 18-electron rule will require concomitant loss of a ligand in order to provide an acceptor orbital for N to M π donation in these azavinylidene complexes (Scheme 9). After ligand loss, the second nitrogen lone pair is required in order to maintain an 18-electron count at metal and consequently directs incoming electrophiles to C_β, utilizing the electrons from the N–C double bond [46,47]. A metal lone pair can then replace the π electrons at nitrogen forming an M–N triple bond. The metal is formally oxidized upon formation of an imido complex.

Imido complexes can also be accessed starting from free amines and a metal iodide complex. The first reaction forms an amido complex and is accompanied by loss of a ligand to accommodate π donation from the

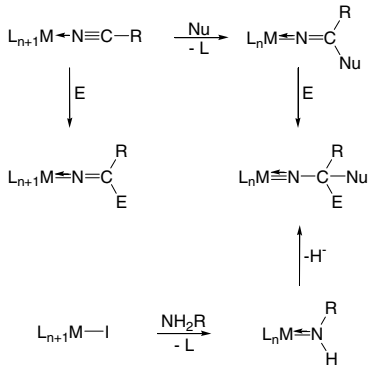

Scheme 9.

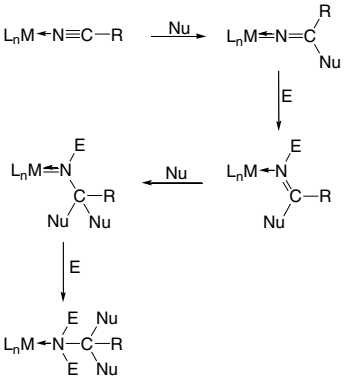

Scheme 10.

amido lone-pair electrons. The amido complex can then be oxidized to the imido complex via net hydride removal from the NHR ligand. In a reaction revealing the dual sites suitable for lone pair electrons in nitrogen based ligand chemistry, addition of electrophiles to C_β of coordinated nitriles has recently been observed to give azavinylidene complexes; no ligand is lost in this reaction (Scheme 9) [48].

If one of the classic two-electron donor ligands in the reagent coordination sphere is replaced with a variable electron donor ligand such as an alkyne [36] or nitrosyl [36,49], the regioselectivity of the electrophile additions can be altered (Scheme 10). Concentrating on the alkyne as the adjacent variable π-donor ligand, the nitrogen can now either house its lone pair or share it with the metal via π donation – no loss of a ligand is required. The alkyne can either act as a lone π donor in a 2-center-2-electron π donor scheme with $\pi_\perp$ or it can act in concert with the nitrogen lone-pair electrons to form a 3-center-4-electron π bond. Flexible donation from the alkyne's $\pi_\perp$ orbital incites competition with the nitrogen lone pair for π donation into a metal dπ orbital. Electrophiles can add directly to nitrogen in such systems and this allows complete reduction of the nitrile ligand to an amine ligand [50].

Acknowledgements

We thank the National Science Foundation, the Petroleum Research Fund, and the Department of Education for generous funding of this research. This article is a small reflection of the dominant role Dr. Swiatoslaw Trofimenko has played in birthing and nurturing the chemistry of scorpionate ligands. Thanks Jerry.

References

[1] S. Trofimenko, Scorpionates: The Coordination Chemistry of Polypyrazolylborate Ligands, Imperial College Press, London, 1999.
[2] S. Otsuka, A. Nakamura, Adv. Organomet. Chem. 14 (1976) 245.
[3] J.L. Templeton, Adv. Organomet. Chem. 29 (1989) 1.
[4] M.I. Bruce, A.G. Swincer, Adv. Organomet. Chem. 22 (1983) 59.
[5] A. Davison, J.P. Selegue, J. Am. Chem. Soc. 102 (1980) 2455.
[6] N.M. Kostić, R.F. Fenske, Organometallics 1 (1982) 974.
[7] A. Davison, J.P. Selegue, J. Am. Chem. Soc. 100 (1978) 7763.
[8] M.I. Bruce, A.G. Swincer, Aust. J. Chem. 33 (1980) 1471.
[9] D.R. Senn, A. Wong, A.T. Patton, M. Marsi, C.E. Strouse, J.A. Gladysz, J. Am. Chem. Soc. 110 (1988) 6096.
[10] A. Mayr, K.C. Schaefer, E.Y. Huang, J. Am. Chem. Soc. 106 (1984) 1517.
[11] M.I. Bruce, M.G. Humphrey, Aust. J. Chem. 42 (1989) 1067.
[12] R.G. Beevor, M. Green, A.G. Orpen, I.D. Williams, J. Chem. Soc., Chem. Commun. 12 (1983) 673.
[13] K.R. Birdwhistell, T.L. Tonker, J.L. Templeton, J. Am. Chem. Soc. 107 (1985) 4474.
[14] A.J.L. Pombeiro, A. Hills, D.L. Hughes, R.L. Richards, J. Organomet. Chem. 352 (1988) C5.
[15] L.N. Lewis, J.C. Huffman, K.G. Caulton, J. Am. Chem. Soc. 102 (1980) 403.
[16] N.E. Kolobova, L.L. Ivanov, O.S. Zhvanko, O.M. Khitrova, A.S. Batsanov, Yu.T. Struchkov, J. Organomet. Chem. 262 (1984) 39.
[17] D.S. Gill, M. Green, J. Chem. Soc., Chem. Commun. 20 (1981) 1037.
[18] D.L. Reger, C.A. Swift, Organometallics 3 (1984) 876.
[19] E.O. Fischer, R.L. Clough, G. Besl, F.R. Kreissl, Angew. Chem., Int. Ed. 15 (1976) 543.
[20] E.O. Fischer, A. Frank, Chem. Ber. 111 (1978) 3740.
[21] H. Fischer, P. Hofmann, F.R. Kreissl, R.R. Schrock, U. Schubert, K. Weiss, Carbyne Complexes, VCH, Weinheim, 1988.
[22] W.R. Roper, in: F.R. Kreissl (Ed.), Transition Metal Carbyne Complexes, Kluwer Academic Publishers, Dordrecht, 1993, p. 155.
[23] M.R. Terry, C. Kelley, N. Lugan, G.L. Geoffroy, B.S. Haggerty, A.L. Rheingold, Organometallics 12 (1993) 3607.
[24] A.E. Enriquez, P.S. White, J.L. Templeton, J. Am. Chem. Soc. 123 (2001) 4992.
[25] R.A. Bell, M.H. Chisholm, D.A. Couch, L.A. Rankel, Inorg. Chem. 16 (1977) 677.
[26] M. Brookhart, Y. Liu, R.C. Buck, J. Am. Chem. Soc. 110 (1988) 2337.
[27] W.A. Kiel, G.-Y. Lin, A.G. Constable, F.B. McCormick, C.E. Strouse, O. Eisenstein, J.A. Gladysz, J. Am. Chem. Soc. 104 (1982) 4865.
[28] V.Yu. Kukushkin, A.J.L. Pombeiro, Chem. Rev. 102 (2002) 1771.
[29] S.G. Feng, P.S. White, J.L. Templeton, J. Am. Chem. Soc. 116 (1994) 8613.
[30] K.R. Powell, P.J. Pérez, L. Luan, S.G. Feng, P.S. White, M. Brookhart, J.L. Templeton, Organometallics 13 (1994) 1851.

[31] L. Luan, P.S. White, M. Brookhart, J.L. Templeton, J. Am. Chem. Soc. 112 (1990) 8190.
[32] P.J. Pérez, P.S. White, M. Brookhart, J.L. Templeton, Inorg. Chem. 33 (1994) 6050.
[33] L. Luan, M. Brookhart, J.L. Templeton, Organometallics 11 (1992) 1433.
[34] R.J. Angelici, Acc. Chem. Res. 5 (1972) 335.
[35] P.J. Pérez, L. Luan, P.S. White, M. Brookhart, J.L. Templeton, J. Am. Chem. Soc. 114 (1992) 7928.
[36] S.G. Feng, J.L. Templeton, J. Am. Chem. Soc. 111 (1989) 6477.
[37] S.G. Feng, J.L. Templeton, Organometallics 11 (1992) 1295.
[38] G.A. Stark, J.A. Gladysz, Inorg. Chim. Acta 269 (1998) 167.
[39] G.C. Martin, J.M. Boncella, E.J. Wucherer, Organometallics 10 (1991) 2804.
[40] T.B. Gunnoe, P.S. White, J.L. Templeton, J. Am. Chem. Soc. 118 (1996) 6916.
[41] J.L. Caldarelli, P.S. White, J.L. Templeton, J. Am. Chem. Soc. 114 (1992) 10097.
[42] L.W. Francisco, P.S. White, J.L. Templeton, Organometallics 15 (1996) 5127.
[43] L.W. Francisco, P.S. White, J.L. Templeton, Organometallics 16 (1997) 2547.
[44] M. Etienne, Coord. Chem. Rev. 156 (1996) 201.
[45] J.L. Templeton, B.C. Ward, J. Am. Chem. Soc. 102 (1980) 3288.
[46] J. Chatt, R.J. Dosser, F. King, G.J. Leigh, J. Chem. Soc., Dalton Trans. 23 (1976) 2435.
[47] P.A. Shapley, J.M. Shusta, J.L. Hunt, Organometallics 15 (1996) 1622.
[48] M.F.C.G. da Silva, J.J.R.F. da Silva, A.J.L. Pombeiro, Inorg. Chem. 41 (2002) 219.
[49] D.A. Knight, M.A. Dewey, G.A. Stark, B.K. Bennett, A.M. Arif, J.A. Gladysz, Organometallics 12 (1993) 4523.
[50] W.-Y. Yeh, C.-S. Ting, S.-M. Peng, G.-H. Lee, Organometallics 14 (1995) 1417.
[51] S.G. Feng, C.C. Philipp, A.S. Gamble, P.S. White, J.L. Templeton, Organometallics 10 (1991) 3504.

Available online at www.sciencedirect.com
SCIENCE DIRECT®
Polyhedron 23 (2004) 323–329
POLYHEDRON
www.elsevier.com/locate/poly

Oxidation of $TpOs^{III}(NH_2Ph)Cl_2$ to $TpOs^{IV}(NHPh)Cl_2$ by O_2

Jake D. Soper, Ian J. Rhile, Antonio G. DiPasquale, James M. Mayer *

Department of Chemistry, University of Washington, Campus Box 351700, Seattle, WA 98195-1700, USA

Received 2 June 2003; accepted 18 August 2003

Abstract

The osmium(III) aniline complex $TpOs(NH_2Ph)Cl_2$ (**$Os^{III}NH_2Ph$**) is formed on heating the triflate complex $[Cp^*_2Fe][TpOs^{III}(OTf)Cl_2]$ in the presence of aniline [Tp = hydrotris(1-pyrazolyl)borate]. It can also be prepared by reduction and protonation of the osmium(IV) anilido complex $TpOs(NHPh)Cl_2$ (**$Os^{IV}NHPh$**). The X-ray structure of **$Os^{III}NH_2Ph$** shows pseudo-octahedral molecules with an Os–N(aniline) bond length of 2.168(7) Å. Unlike most Os(III) coordination complexes, **$Os^{III}NH_2Ph$** is oxidized by O_2, yielding **$Os^{IV}NHPh$**. This reaction occurs readily in the presence of catalytic base. Under these conditions, the reaction proceeds by a stepwise mechanism of pre-equilibrium proton transfer (PT) forming **$Os^{III}NHPh^-$**, which then reacts with O_2 by outer-sphere electron transfer (ET). **$Os^{III}NH_2Ph$** is essentially air stable in the presence of acid, because this PT–ET mechanism is prevented.
© 2003 Elsevier Ltd. All rights reserved.

Keywords: Dioxygen; Osmium; Aniline; Oxidation; Electron transfer self-exchange

1. Introduction

Amine complexes of ruthenium and osmium are one of the classic systems of coordination chemistry, extensively studied by Taube and his students, and others [1]. For osmium complexes, the most stable oxidation state is typically +3. Os(II) complexes without π-acid ligands are quite reducing and air sensitive (e.g., $Os(NH_3)_6^{2+}$), while Os(IV) complexes are usually very oxidizing (cf., $OsCl_6^{2-}$). The hydrotris(1-pyrazolyl)borate (Tp) ligand is a ''hard'' donor, in some ways similar to amines and halides. The osmium(IV) complex $TpOsCl_3$, for instance, is substitution inert and a good outer-sphere oxidant, much like $OsCl_6^{2-}$ [2]. The osmium(III) complex $TpOs(NH_3)Cl_2$ follows this pattern, as it is air stable and difficult to reduce or oxidize ($E_{1/2}$: $Os^{IV/III}$, +0.65 V; $Os^{III/II}$, −1.32 V (irrev.) vs. $Cp_2Fe^{+/0}$ in MeCN [2]).

Described here is the surprising result that the osmium(III) aniline complex $TpOs(NH_2Ph)Cl_2$ (**$Os^{III}NH_2Ph$**) is quite air sensitive in the presence of even trace amounts of base. To our knowledge, this is only the second report of dioxygen-oxidation of an osmium(III) complex to generate osmium(IV), the first being a brief mention by Taube and coworkers that $Cs[Os(NH_3)Cl_5]$ can be prepared using O_2 [3]. Mechanistic studies of this unusual reaction are presented. Oxidations of metal complexes by O_2 (autoxidations) are of particular importance because of the strong interest in using metals to catalyze aerobic oxidations [4]. We have found that O_2 can deliver oxidative equivalents in unusual nucleophilic aromatic substitution reactions of the osmium(IV) anilido complex $TpOs(NHPh)Cl_2$ (**$Os^{IV}NHPh$**) [5,6]. **$Os^{III}NH_2Ph$** was briefly reported in this context [5].

The oxidation of **$Os^{III}NH_2Ph$** to **$Os^{IV}NHPh$** by O_2 is thermodynamically possible because it involves loss of a proton as well as an electron. Such coupling of proton and electron transfers is critical in a wide range of chemical processes, as shown, for instance, by Meyer and coworkers for ruthenium and osmium polypyridyl complexes [7]. Proton, electron, and hydrogen atom self-exchange reactions involving **$Os^{III}NH_2Ph$** and **$Os^{IV}NHPh$** are described elsewhere [8]. In the autoxidation of **$Os^{III}NH_2Ph$**, proton transfer (PT) is critical to the mechanism as well as the thermodynamics, as the preferred pathway involves stepwise proton and then electron transfers.

* Corresponding author.
E-mail address: mayer@chem.washington.edu (J.M. Mayer).

0277-5387/$ - see front matter © 2003 Elsevier Ltd. All rights reserved.
doi:10.1016/j.poly.2003.11.021

2. Experimental

2.1. General considerations

All manipulations were performed under an inert atmosphere using standard vacuum line and nitrogen-filled glove box techniques, unless otherwise noted. NMR spectra were acquired on Bruker DRX-500 spectrometers at 298 K. Temperature calibration of the NMR probes was accomplished by Van Geet's method [9]. Proton NMR chemical shifts were referenced to the residual ^{1}H NMR signals of the deuterated solvents and are reported vs. TMS. IR spectra were obtained as CH_2Cl_2 solutions in a ZnSe solution cell, or as KBr pellets, using a Perkin–Elmer 1720 FTIR spectrophotometer. Elemental analyses were performed by Atlantic Microlab, Inc. in Norcross, Georgia. Absorption spectra were obtained using a HP 8453 UV–Vis spectrophotometer equipped with a temperature-controlled multicell apparatus. Kinetic data were obtained using this HP spectrophotometer or with an OLIS rapid scanning monochromator equipped with an OLIS USA stopped-flow apparatus. Cyclic voltammetry measurements were made with a BAS CV-27. The electrochemical cell typically contained a ~5 mM solution of analyte in acetonitrile (0.1 M $^nBu_4NPF_6$), a $Ag/AgNO_3$ reference electrode, a platinum disk working electrode and a platinum wire auxiliary electrode. Ferrocene was used as an internal standard.

2.2. Materials

All solvents used for the syntheses were degassed and dried according to standard procedures [10]. Acetonitrile was used as obtained from Burdick and Jackson (low-water brand) and stored in an argon-pressurized stainless steel drum plumbed directly into a glove box. Deuterated solvents were purchased from Cambridge Isotope Laboratories, degassed, dried, and distilled by vacuum transfer prior to use. MeCN-d_3 was dried by successively stirring over CaH_2, followed by P_2O_5 and again over CaH_2 to remove trace acids. Reagents were typically purchased from Aldrich and used as received unless otherwise noted. Anilines were distilled from KOH or CaH_2 under reduced pressure and thoroughly degassed prior to use. Sodium naphthalenide was prepared by literature methods [11]. $TpOs(NHPh)Cl_2$ (**$Os^{IV}NHPh$**) [12], $TpOs(OTf)Cl_2$ [2,13], $TpOs(N)Cl_2$ [14] and $[^nBu_4N]^+[TpOs(NHPh)Cl_2]^-$ (**$Os^{III}NHPh^-$**) [8] were prepared according to published procedures. Purity was checked by ^{1}H NMR spectroscopy.

2.3. $TpOs(NH_2Ph)Cl_2$ ($Os^{III}NH_2Ph$)

A glass flask with a Teflon stopcock was charged with $TpOs(OTf)Cl_2$ (20 mg, 32 μmol), Cp^*_2Fe (11 mg, 34 μmol) and CH_2Cl_2 (5 ml). Aniline (15 μl, 160 μmol) was added to the resulting mint-green solution and the reaction mixture was heated at 76 °C for 14 h. CH_2Cl_2 was removed under vacuum and the faint orange product was dissolved in 8 ml C_6H_6 and decanted off the insoluble green $Cp^*_2Fe^+OTf^-$. Following removal of C_6H_6 by sublimation, the solids were washed twice with pentane to remove excess aniline. Small, light orange crystals were obtained by slow diffusion of pentane into a saturated CH_2Cl_2 solution. The crystals were dried in vacuo and quickly washed with minimal MeCN to give **$Os^{III}NH_2Ph$** in moderate yield (10 mg, 17 μmol, 53%). The entire procedure was strictly anaerobic. **$Os^{III}NH_2Ph$** can be purified by silica gel chromatography under argon using 1:1 hexane-CH_2Cl_2 to 10:1 CH_2Cl_2-acetone. ^{1}H NMR (MeCN-d_3): [all resonances are broad, full-width half-maximum (FWHM) 68–1100 Hz; NH_2Ph peaks assigned by comparison with materials prepared from $NH_2C_6D_5$ or $ND_2C_6D_5$] δ 3.3 (1H), 1.7 (2H), −7.7 (2H, NH_2Ph); 64.2 (2H, N<u>H</u>$_2$Ph); 26.4 (1H); 7.6 (1H); 5.1 (2H); −0.8 (2H); −3.4 (1H); −48.2 (2H); −51.1 (1H). IR (CH_2Cl_2): 2504 (m, ν_{B-H}); 1493 (m), 1406 (s), 1309 (m), 1211 (s), 1188 (w), 1118 (s), 1071 (w), 1046 (vs), 987 (w), 654 (w), 615 (m, all Tp); 1602 (w); 1569 (w); 788 (w). *Anal.* Calc. (Found) for $C_{15}H_{17}BCl_2N_7Os$: C, 31.76 (31.76, 31.92); H, 3.02 (2.84, 2.87); N, 17.28 (17.18, 17.35).

2.4. pK_a of $Os^{III}NH_2Ph$

A quartz cuvette with a resealable Teflon valve was charged with 2.8 ml of a MeCN solution containing 91% **$Os^{III}NH_2Ph$** and 9% **$Os^{IV}NHPh$** (by ^{1}H NMR) for a total $[Os] = 3.2 \times 10^{-4}$ M. A 9.9×10^{-2} M solution of quinuclidine ($pK_a = 19.51$ [15]) in MeCN was prepared such that 8 μl corresponded to 1 molar equivalent of base per **$Os^{III}NH_2Ph$**. Absorption spectra were acquired over a range of quinuclidine concentrations, from 1–130 molar equivalents based on **$Os^{III}NH_2Ph$**, yielding K_{eq} and therefore the desired pK_a. Extinction coefficients for **$Os^{III}NHPh^-$** were determined by stoichiometric addition of DBU ($pK_a = 24.32$ [16]) in MeCN to **$Os^{III}NH_2Ph$** solutions under similar conditions and agree with those obtained from isolated samples of **$Os^{III}NHPh^-$**. Addition of >1 equiv DBU results in no further observed spectral changes. **$Os^{IV}NHPh$** is unaffected by quinuclidine under these conditions.

2.5. Stopped flow kinetics of $Os^{III}NHPh^-$ and O_2

A 0.23 mM solution of **$Os^{III}NHPh^-$** in degassed MeCN was loaded into one mixing syringe in the stopped flow apparatus. Oxygen gas was bubbled for 20 min through a separate sample of MeCN, which was subsequently loaded into the other mixing syringe. The data for the obtained runs were fit at 406.7 nm for a rise–fall

(A → B → C) mechanism using the OLIS software. The A → B phase was assigned as consumption of **Os^{III}-NHPh**$^{-}$, based on the spectrum at the end of this phase. B → C apparently is due to further reactions of the initial products.

2.6. Crystal structure of $Os^{III}NH_2Ph$

A red, prism-shaped crystal $0.23 \times 0.08 \times 0.06$ mm was grown by slow evaporation of an acetonitrile-d_3 solution of **Os^{III}NH$_2$Ph** and mounted on a glass capillary with oil. Data were collected at −143 °C with one set of φ scans. Crystal-to-detector distance was 30 mm and exposure time was 40 s per degree for all sets. The scan width was 1.0°. Data collection was 95.2% complete to 28.30° in θ. A total of 12,455 partial and complete reflections were collected of which 3619 reflections were symmetry independent and the $R_{int} = 0.060$ indicated that the quality of data was of better than average quality. The data were integrated and scaled using hkl-2000, a program that applies a multiplicative correction factor (S) to the observed intensities (I). S is calculated from the scale and B factor determined for each frame, which has the form: $S = (e^{-2B(\sin^2\theta)/\lambda^2})$/scale. Solution by direct methods (SIR97) produced a complete heavy atom phasing model consistent with the proposed structure. All hydrogen atoms, except the two on N7 were placed using a riding model. The latter two were located from the Fourier difference map and their locations refined isotropically by full-matrix least-squares (SHELXL-97). All non-hydrogen atoms were refined anisotropically. The one restraint used is a floating origin restraint, which is generated automatically by the SHELXL-97 program. This restraint effectively fixed the X-ray 'center of gravity' of the structure in the polar axis direction.

3. Results

3.1. Synthesis and characterization

The Os(III) aniline complex TpOs(NH$_2$Ph)Cl$_2$ (**Os^{III}NH$_2$Ph**) is obtained from [Cp*$_2$Fe][TpOs^{III}(OTf)-Cl$_2$] and aniline (≈5 equiv.) in CH$_2$Cl$_2$ at 76 °C (Eq. (1); Tp = hydrotris-[1-pyrazolyl]borate). As described earlier in the preparations of

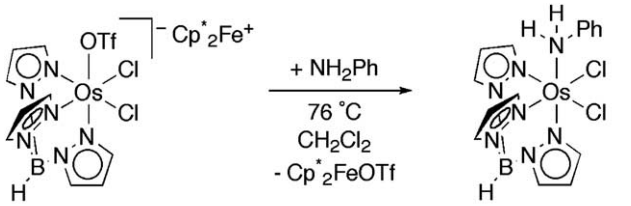

(1)

other TpOs^{III}(L)Cl$_2$ complexes, heating is required to displace triflate from the anionic [TpOs^{III}(OTf)Cl$_2$]$^-$ [2]. This illustrates the remarkable substitution inertness of these TpOs complexes. Kirchner and coworkers have previously shown the strongly substitution inert character of TpRu complexes [17]. **Os^{III}NH$_2$Ph** is also substitution inert, as it is stable to excess triflic acid in MeCN-d_3 solution for at least days at ambient temperatures [8]. **Os^{III}NH$_2$Ph** can be purified by recrystallization or by anaerobic chromatography on silica.

The single crystal X-ray structure of **Os^{III}NH$_2$Ph** contains isolated molecules with pseudo-octahedral coordination (Fig. 1). Crystallographic parameters and selected bond lengths and angles are collected in Tables 1 and 2. The Os–N(7) distance of 2.168 (7) Å is close to those in the *ortho-t*-butylaniline and ethylamine analogues [8,14]. These Os–N(aniline) distances are substantially longer than the ≈1.9 Å Os^{IV}-anilide distances in **Os^{IV}NHPh** and related complexes [8,14]. The orientation of the aniline ligand in **Os^{III}NH$_2$Ph** is such that the osmium atom lies well out of the plane of aromatic ring, as indicated by the Os–N(7)–C(10)–C(11) torsion angle of 103.7(9)°. This contrasts with the structures of Os(IV) anilide derivatives where the osmium, the nitrogen, and the aromatic ring are close to coplanar, with Os–N–C–C dihedral angles near 0° or 180°. The coplanar conformation allows π-conjugation from Os to N to the aromatic ring, and **Os^{IV}NHPh** is probably best described as having an Os=N double bond [5,6,19]. The aniline complex **Os^{III}NH$_2$Ph** simply contains a dative Os←N bond.

The characterization of **Os^{III}NH$_2$Ph** as an Os(III) aniline complex is supported by spectroscopic and analytical data. ^{1}H NMR spectra contain broad, paramagnetically shifted resonances (δ 64 to −51 ppm,

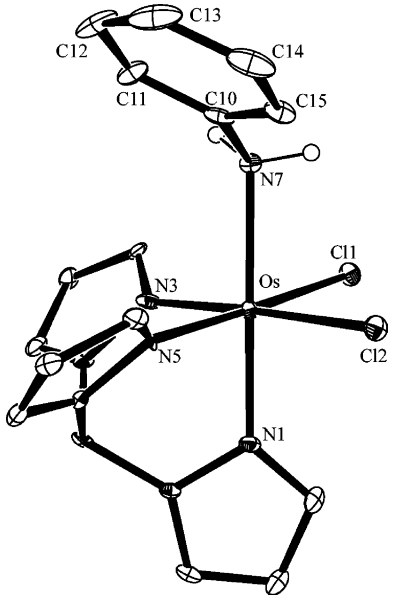

Fig. 1. ORTEP drawing of TpOs(NH$_2$Ph)Cl$_2$ (**Os^{III}NH$_2$Ph**).

Table 1
X-ray diffraction data for **$Os^{III}NH_2Ph$**

Empirical formula	$C_{15}H_{17}BCl_2N_7Os$
Formula weight	567.27
T (K)	130(2)
Wavelength (Å)	0.71073
Crystal system	monoclinic
Space group	$P2_1$ (No. 4)
Unit cell dimensions	
a (Å)	8.4060(3)
b (Å)	12.4150(4)
c (Å)	8.8400(4)
β (°)	97.4120(16)
V (Å^3)	914.84(6)
Z	2
D_{calc} (g cm^{-3})	2.059
Absorption coefficient (mm^{-1})	7.276
Crystal size (mm)	$0.23 \times 0.08 \times 0.06$
θ Range for data (°)	2.94–28.30
Index ranges	$-10 \leqslant h \leqslant 11$, $-16 \leqslant k \leqslant 14$, $-11 \leqslant l \leqslant 11$
Reflections collected/unique	3619/3619
R_{int}	0.060
Restraints/parameters refined	1/241
Goodness-of-fit	1.023
$R_1(I > 2\sigma(I))$	0.0368
wR_2 (all data)	0.0744

Table 2
Selected bond lengths (Å) and angles (°) for **$Os^{III}NH_2Ph$**

Bond lengths			
Os–N(1)	2.052(7)	Os–N(7)	2.168(7)
Os–N(3)	2.047(7)	Os–Cl(1)	2.3595(19)
Os–N(5)	2.061(6)	Os–Cl(2)	2.388(2)
N(7)–C(10)	1.442(12)	C(13)–C(14)	1.396(16)
C(10)–C(11)	1.366(13)	C(14)–C(15)	1.389(13)
C(11)–C(12)	1.403(13)	C(10)–C(15)	1.387(13)
C(12)–C(13)	1.368(16)		
Bond angles			
Cl(1)–Os–Cl(2)	90.47(7)	Os–N(7)–C(10)	121.9(5)
Cl(1)–Os–N(3)	90.65(19)	Os–N(7)–C(10)–C(11)	−103.7(9)
Cl(2)–Os–N(5)	91.26(17)	Os–N(7)–C(10)–C(15)	78.0(9)
N(3)–Os–N(5)	87.7(2)		

FWHM 68–1100 Hz) consistent with a low-spin d^5 configuration. Phenyl resonances for **$Os^{III}NH_2Ph$** were assigned by comparison with deuterium-labeled materials prepared from $[Cp^*_2Fe]^+[TpOs(OTf)Cl_2]^-$ and NH_2Ph-d_5 or ND_2Ph-d_5.

Deprotonation of **$Os^{III}NH_2Ph$** with DBU (1,8-diazabicyclo[5.4.0]undec-7-ene) in acetonitrile ($pK_a = 24.32$ [16]) gives the Os(III) anilide complex $[TpOs(NHPh)Cl_2]^-$ (**$Os^{III}NHPh^-$**). The $^nBu_4N^+$ salt of this anion has previously been prepared by reduction of **Os^{IV}(NHPh)** with sodium naphthalenide and cation exchange [8]. Titrations of **$Os^{III}NH_2Ph$** with quinuclidine in acetonitrile (1–130 molar equiv; $pK_a = 19.51$ [15]) were monitored at 406 and 582 nm (the λ_{max} values for **$Os^{III}NHPh^-$**). Concentrations of each species were calculated from the absorbances and used to determine K_{eq} at each point in the titration. Addition of pK_{eq} to the pK_a of quinuclidine gives pK_a [**$Os^{III}NH_2Ph$**] $= 22.5 \pm 0.1$. The relatively small error reflects the good agreement in calculated pK_a values at each titration point.

The N–H bond dissociation enthalpy in **$Os^{III}NH_2Ph$** is calculated via a thermochemical cycle [18] to be D(N–H) $= 66 \pm 1$ kcal mol^{-1} using the pK_a above and the reported quasi-reversible $Os^{IV/III}$ redox couple for **$Os^{IV}NHPh$** at −1.05 V vs. $Cp_2Fe^{+/0}$ in MeCN (referenced internally) [8,19]. Application of this cycle assumes that the entropy difference between **$Os^{III}NH_2Ph$** and **$Os^{IV}NHPh$** is negligible. The thermochemical cycle mirrors an alternative preparation of **$Os^{III}NH_2Ph$**, by sequential reduction and protonation of **$Os^{IV}NHPh$** using sodium naphthalenide then HCl/Et_2O (Eq. (2)). Cyclic voltammograms of **$Os^{III}NH_2Ph$** show an irreversible oxidation wave at +0.48 V. The irreversibility is presumably due to rapid deprotonation of the highly acidic **$Os^{IV}NH_2Ph^+$** formed [19].

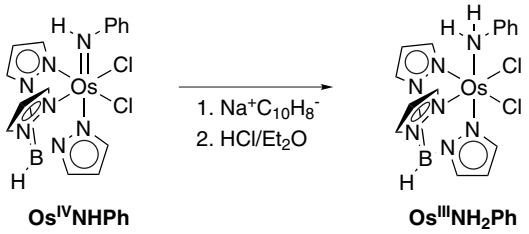

(2)

3.2. Reaction of $Os^{III}NH_2Ph$ with O_2

Exposure of solutions of **$Os^{III}NH_2Ph$** in MeCN-d_3 or chloroform-d to 1 atm O_2 shows complete loss of the characteristic ^{1}H NMR resonances for **$Os^{III}NH_2Ph$** with concomitant growth of resonances for the Os(IV) anilide **$Os^{IV}NHPh$** (Eq. (3)).

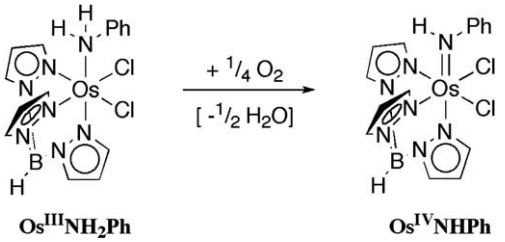

(3)

Concentrations of **$Os^{IV}NHPh$** and **$Os^{III}NH_2Ph$** are determined by integration against an internal standard and the sum of the concentrations is constant throughout the reaction indicating that no other osmium-containing products are formed. (Resonances for **$Os^{IV}NHPh$** and **$Os^{III}NH_2Ph$** are not shifted or broadened significantly during the reaction because H-atom exchange between these species is slow [8].) Quantitative conversion of **$Os^{III}NH_2Ph$** to **$Os^{IV}NHPh$** with O_2 has also been observed by UV–Vis spectroscopy, monitoring the change from light orange **$Os^{III}NH_2Ph$** to dark red

$Os^{IV}NHPh$. To balance Eq. (3) the H-atom removed from **$Os^{III}NH_2Ph$** is presumed converted to H_2O but this has not been observed by NMR.

^1H NMR kinetic data for the disappearance of **$Os^{III}NH_2Ph$** and simultaneous appearance of **Os^{IV}-NHPh** are fit well by an integrated first order rate expression (an example is shown Fig. 2). This indicates that reaction is first order in **$Os^{III}NH_2Ph$**. The derived rate constants, however, are irreproducible between samples of **$Os^{III}NH_2Ph$**. Reactions with O_2 are slow using samples of **$Os^{III}NH_2Ph$** that were purified by recrystallization, and have been scrupulously kept anaerobic. These reactions take weeks to reach completion. In contrast, complete conversion to **$Os^{IV}NHPh$** under 1 atm O_2 in <10 h is observed for samples of **$Os^{III}NH_2Ph$** that have been chromatographed or have briefly been exposed to air. Similar irreproducible rates have also been observed for other reactions of **$Os^{III}NH_2Ph$**, both its self-exchange with **$Os^{IV}NHPh$** and its reaction with TEMPO [8]. In these cases as well, the preparative route to **$Os^{III}NH_2Ph$** is the critical variable [8]. Trace acid impurities appear to be present when strictly anaerobic conditions are maintained during synthesis of **Os^{III}-NH_2Ph**. Samples that are exposed briefly to atmospheric conditions or are isolated from chromatography on silica under argon have trace base impurities.

Experiments with added reagents confirm that the O_2 oxidation is catalyzed by bases and slowed by acid. MeCN solutions of **$Os^{III}NH_2Ph$** containing sub-stoichiometric Et_2NH (0.3–0.5 equiv) react with 1 atm O_2 in seconds, with the color change from orange to dark red indicating conversion to **$Os^{IV}NHPh$**. Complete conversion to **$Os^{IV}NHPh$** is observed upon acquisition of an initial ^1H NMR spectrum (≈12 min). The second order rate constant under these conditions can be estimated as $k_3 \geqslant 10\ M^{-1}\ s^{-1}$, based on a half life of less than ≈10 s ($k_{obs} \geqslant 10^{-1}\ s^{-1}$) and $[O_2] = 8$ mM in MeCN at 1 atm O_2 [20]. Conversely, samples of **$Os^{III}NH_2Ph$** isolated from silica gel, that would normally react quickly with air, are stable for days under 1 atm O_2 when pretreated with acetic acid or sub-stoichiometric HCl/Et_2O.

4. Discussion

Air oxidation of **$Os^{III}NH_2Ph$** to **$Os^{IV}NHPh$** (Eq. (3)) is not typical of Os(III) complexes. It is unexpected given the high redox potential of **$Os^{III}NH_2Ph$** ($E_{p,a} = +0.48$ vs. $Cp_2Fe^{+/0}$ in MeCN) and the oxidizing nature of related Os(IV) complexes [2,13]. This reaction is downhill only because a proton is transferred as well as an electron. Using the N–H bond strength of 66 kcal mol^{-1} in **$Os^{III}NH_2Ph$** and tabulated heats of formation for O_2, H· and H_2O (using ΔH_f° values from [21], the autoxidation of **$Os^{III}NH_2Ph$** is enthalpically favored by 20 kcal mol^{-1} (Eq. (4)).

$$\Delta H^\circ = -20\ \text{kcal mol}^{-1}\ \text{for}$$

$$\textbf{Os}^{\textbf{III}}\textbf{NH}_2\textbf{Ph} + 1/4\ O_2(g) \rightarrow \textbf{Os}^{\textbf{IV}}\textbf{NHPh} + 1/2\ H_2O\ (l) \quad (4)$$

The formal removal of H· from **$Os^{III}NH_2Ph$** by O_2 to form **$Os^{IV}NHPh$** could occur by concerted H· transfer (HAT) or by initial electron transfer (ET) (Scheme 1). Proton-coupled ET processes such as this could, in general, also occur by initial PT. However, O_2 does not act as a base in solution. Scheme 1 (and Scheme 2 below) show only initial mechanistic steps, leading to $O_2^{\cdot-}$ or $HO_2^{\cdot}$, because the subsequent reactions leading to water should be fast. ET from **$Os^{III}NH_2Ph$** to O_2, the vertical line in Scheme 1, is very unfavorable: it is uphill by ≈1.6 V or $\Delta G^\circ \cong +37$ kcal mol^{-1}. This is based on $E_{1/2}$ for $O_2^{0/\cdot-}$ of −1.11 V and the +0.48 V $E_{p,a}$ for **$Os^{III}NH_2Ph$** (both vs. $Cp_2Fe^{+/0}$ in MeCN) [22]. Concerted HAT

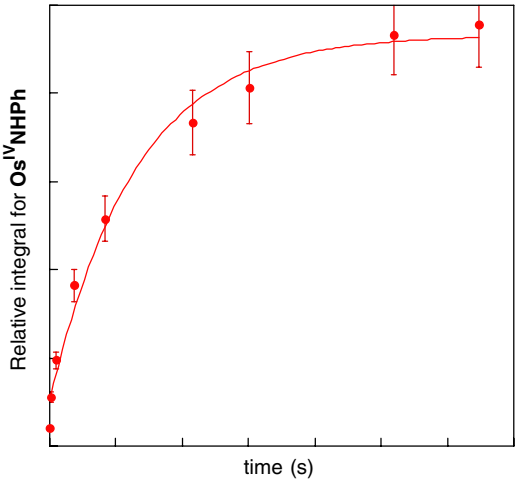

Fig. 2. First order fit for the appearance of **$Os^{IV}NHPh$** as a function of time from reaction of **$Os^{III}NH_2Ph$** with O_2 in chloroform-d at 298 K.

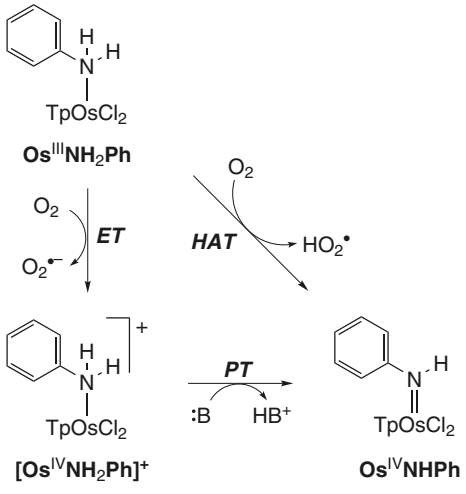

Scheme 1. Possible mechanisms for uncatalyzed net H· transfer from **$Os^{III}NH_2Ph$** to O_2.

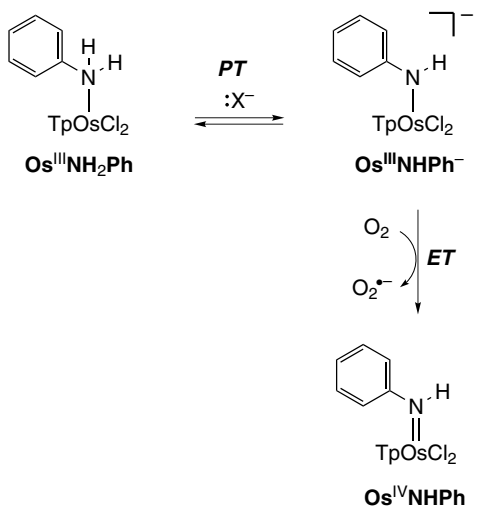

Scheme 2. Mechanism for base-catalyzed oxidation of $\mathbf{Os^{III}NH_2Ph}$ by O_2.

from $\mathbf{Os^{III}NH_2Ph}$ to O_2, the diagonal in Scheme 1, is similarly quite uphill. Addition of H· to O_2 makes a 51.6 kcal mol^{-1} O–H bond in $HO_2^{\cdot}$ [21,23], so HAT from $\mathbf{Os^{III}NH_2Ph}$ to O_2 has $\Delta H^{\cdot}(\cong \Delta G^{\cdot}) = +14$ kcal mol^{-1}. This indicates a very slow rate, since HAT from $\mathbf{Os^{III}NH_2Ph}$ to TEMPO· (2,2,6,6-tetramethyl-1-piperidnyloxyl) is 4 kcal mol^{-1} *downhill* and still occurs fairly slowly, with $k_{HAT} = 4 \times 10^{-2}$ M^{-1} s^{-1}. These arguments explain why the uncatalyzed reaction of $\mathbf{Os^{III}NH_2Ph}$ and O_2 is very slow and $\mathbf{Os^{III}NH_2Ph}$ is stable to air for days in the presence of added acid. Both possible initial steps are very unfavorable.

Addition of a catalytic base to $\mathbf{Os^{III}NH_2Ph}$, however, leads to very rapid reaction with O_2. This is because a new pathway is now accessible: initial PT followed by ET (Scheme 2). The base rapidly generates a small equilibrium amount of $\mathbf{Os^{III}NHPh^-}$, which is much easier to oxidize, with an $Os^{IV/III}$ redox potential couple of −1.05 V (vs. $Cp_2Fe^{+/0}$ in MeCN [19]). This dramatic shift in redox potential results from the $N\ p_\pi - Os\ d_\pi$ antibonding interaction in $\mathbf{Os^{III}NHPh^-}$ and the Os–N π bond that is formed in $\mathbf{Os^{IV}NHPh}$ [8,19]. ET from $\mathbf{Os^{III}NHPh^-}$ to O_2 (Eq. (5)) is roughly isoergic

$$\mathbf{Os^{III}NH_2Ph^-} + O_2 \rightarrow \mathbf{Os^{IV}NH_2Ph} + O_2^- \quad E = +0.06\ \text{V} \tag{5}$$

($\Delta G^\circ = +1.3$ kcal mol^{-1}, $K_5 = 0.1$). Reaction 5 has been examined directly: isolated ^{n}Bu$_4$N[$\mathbf{Os^{III}NHPh}$] [8] reacts very rapidly with O_2 in MeCN solution to give an uncharacterized mixture of products. Monitoring the reaction by stopped-flow gives a tentative rate constant $k_5 = (3.3 \pm 0.5) \times 10^4$ M^{-1} s^{-1} (see Section 2).

In more quantitative terms, Scheme 2 implies the rate law in Eq. (6). As noted above, the reaction of $\mathbf{Os^{III}NH_2Ph}$ (10 mM) with Et_2NH (5 mM) and O_2 (8 mM) gives $\mathbf{Os^{IV}NHPh}$ with $k_3 \geqslant 10$ M^{-1} s^{-1}. Under these conditions, rapid pre-equilibrium PT gives $[\mathbf{Os^{III}NHPh^-}] = [Et_2NH_2^+] = 0.09$ mM based on $K_{eq} = 1.6 \times 10^{-4}$ ($\Delta pK_a = -3.8$ for $\mathbf{Os^{III}NH_2Ph}$ + Et_2NH). Following Eq. (6),

$$-\frac{[\mathbf{Os^{III}NH_2Ph}]}{dt} = K_{eq,PT}k_5[\mathbf{Os^{III}NH_2Ph}][O_2]\frac{[\text{base}]}{[\text{Hbase}^+]} \tag{6}$$

$k_3 = K_{eq,PT}k_5[Et_2NH][Et_2NH_2^+]^{-1}$. If we take, for simplicity, $[Et_2NH_2^+]$ to be constant through the reaction (consistent with the observed pseudo-first order kinetics), the observed k_3 implies that $k_5 \geqslant 10^4$ M^{-1} s^{-1}. This is consistent with the k_5 directly measured by stopped flow, supporting the mechanism in Scheme 2.

The value of k_5 is reasonably close to that estimated using the Marcus cross-relation (Eq. (7)) [24].[1] Electron self-exchange between $\mathbf{Os^{III}NHPh^-}$ and $\mathbf{Os^{IV}NHPh}$ occurs with

$$k_{Os/s.e.} = k_{XY} = \sqrt{k_{XX}\ k_{YY}\ K_{XY}\ f_{XY}} \tag{7}$$

$(5.5 \pm 0.8) \times 10^4$ M^{-1} s^{-1} at 298 K in MeCN-d_3 [8]. To our knowledge, the O_2/O_2^- self-exchange rate constant in acetonitrile has not been reported. The value in water has been established to be $k_{O_2+O_2^-/H_2O} = 450 \pm 160$ M^{-1} s^{-1} [25], after a period of some uncertainty [26]. Using this value, the value K_5 above and $f = 1$, k_5(calculated) $= 1.6 \times 10^3$ M^{-1} s^{-1}, compared to the measured $k_5 \geqslant 10^4$ M^{-1} s^{-1}. Better agreement would require that the O_2/O_2^- self-exchange rate be faster in MeCN than in water, $k_{O_2+O_2^-/MeCN} \cong 10^5$ M^{-1} s^{-1}.

5. Conclusions

The hydrotris(1-pyrazolyl)borate osmium(III) aniline complex $TpOs(NH_2Ph)Cl_2$ ($\mathbf{Os^{III}NH_2Ph}$) has been prepared by substitution of aniline for triflate and by reduction and protonation of the osmium(IV) anilido complex $TpOs(NHPh)Cl_2$ ($\mathbf{Os^{IV}NHPh}$). Surprisingly, $\mathbf{Os^{III}NH_2Ph}$ is air sensitive, reacting with O_2 to give $\mathbf{Os^{IV}NHPh}$. This reaction is catalyzed by bases. In the presence of base, formation of $\mathbf{Os^{IV}NHPh}$ from $\mathbf{Os^{III}NH_2Ph}$ and O_2 proceeds by a stepwise mechanism of initial PT to give $\mathbf{Os^{III}NHPh^-}$, which then reacts with O_2 by outer-sphere ET. In the presence of acid, when the concentration of $\mathbf{Os^{III}NHPh^-}$ is suppressed, the PT–ET mechanism is effectively shut-off. The stepwise mechanism is attractive in this system because the individual PT and ET steps have small intrinsic barriers while HAT is intrinsically slow [8].

[1] $\ln f_{XY} \cong \frac{(\ln K_{XY})^2}{4\ln(\frac{k_{XX}k_{YY}}{Z^2})}$. Corrections to Eq. (7) to account for the energy required to bring together the reactants and products (work terms) are not needed here as both the reactants and products have one uncharged species.

The origin of the unusual air sensitivity of $\mathbf{Os^{III}NH_2Ph}$ vs. Taube-type coordination complexes is not the Tp ligand, but rather the involvement of an aniline ligand. Aniline is much more acidic than ammonia or alkylamines, so a pathway involving deprotonation is much more facile. Deprotonation of the Os(III) complex lowers the redox potential dramatically, because the $\mathbf{Os^{III}NHPh^-}$ is destabilized by a π conflict between the anilide p_π and Os t_{2g} orbitals while $\mathbf{Os^{IV}NHPh}$ is stabilized by d–p π bonding. With this low redox potential, ET to dioxygen is roughly thermoneutral and proceeds rapidly.

6. Supplementary material

Crystallographic data have been deposited with the Cambridge Crystallographic Data Centre, 12 Union Road, Cambridge CB2 1EZ, UK (fax: +44-1223-336033; E-mail: deposit@ccdc.cam.ac.uk or www: http://www.ccdc.cam.ac.uk), as CCDC 211682.

Acknowledgements

We are grateful for financial support from the National Institutes of Health (R01 GM50422) and from the National Science Foundation (under Grant Nos. 9816372 and 0204697).

References

[1] (a) H. Taube, Adv. Chem. Ser. 253 (1997) 1;
(b) W.D. Harman, Chem. Rev. 97 (1997) 1953;
(c) W.P. Griffith, in: G. Wilkinson (Ed.), Comprehensive Coordination Chemistry, vol. 4, Pergamon, New York, 1987, p. 519.
[2] B.K. Bennett, S.J. Pietteri, L. Pilobello, S. Lovell, W. Kaminsky, J.M. Mayer, J. Chem. Soc., Dalton Trans. (2001) 3489.
[3] J.D. Buhr, J.R. Winkler, H. Taube, Inorg. Chem. 19 (1980) 2416.
[4] (a) For leading references, see: D. Sloboda-Rozner, P.L. Alsters, R. Neumann, J. Am. Chem. Soc. 125 (2003) 5280;
(b) A. Mahammed, H.B. Gray, A. Meier-Callahan, Z. Gross, J. Am. Chem. Soc. 125 (2003) 1162;
(c) M.H.V. Huynh, L.M. Witham, J.M. Lasker, M. Wetzler, B. Mort, D.L. Jameson, P.S. White, K.J. Takeuchi, J. Am. Chem. Soc. 125 (2003) 308;
(d) K. Qin, C.D. Incarvito, A.L. Rheingold, K.H. Theopold, J. Am. Chem. Soc. 124 (2002) 14008;
(e) S.S. Stahl, J.L. Thorman, R.C. Nelson, M.A. Kozee, J. Am. Chem. Soc. 123 (2001) 7188;
(f) D.R. Jensen, J.S. Pugsley, M.S. Sigman, J. Am. Chem. Soc. 123 (2001) 7475.
[5] J.D. Soper, W. Kaminsky, J.M. Mayer, J. Am. Chem. Soc. 123 (2001) 5594.
[6] J.D. Soper, E. Saganic, D. Weinberg, D.A. Hrovat, W. Kaminsky, J.M. Mayer, in preparation.
[7] (a) T.J. Meyer, J. Electrochem. Soc. 131 (1984) 221C;
(b) E.L. Lebeau, R.A. Binstead, T.J. Meyer, J. Am. Chem. Soc. 123 (2001) 10535;
(c) T.J. Meyer, M.H.V. Huynh, Inorg. Chem. 42 (2003), ASAP Article.
[8] J.D. Soper, J.M. Mayer, J. Am. Chem. Soc. 125 (2003) 12217.
[9] A.L. Van Geet, Anal. Chem. 40 (1968) 2227.
[10] D.D. Perrin, W.L.F. Armarego, Purification of Laboratory Chemicals, third ed., Pergamon, New York, 1988.
[11] M.K. Cooper, J.M. Downes, P.A. Duckworth, Inorg. Synth. 25 (1989) 129.
[12] (a) T.J. Crevier, J.M. Mayer, Angew. Chemie 110 (1998) 1995;
(b) Angew. Chem. Int. Ed. 37 (1998) 1891.
[13] B.K. Bennett, S. Lovell, J.M. Mayer, J. Am. Chem. Soc. 123 (2001) 4336.
[14] T.J. Crevier, B.K. Bennett, J.D. Soper, J.A. Bowman, A. Dehestani, D.A. Hrovat, S. Lovell, W. Kaminsky, J.M. Mayer, J. Am. Chem. Soc. 123 (2001) 1059.
[15] K. Izutsu, Acid–Base Dissociation Constants in Dipolar Aprotic Solvents, Blackwell Scientific, Boston, MA, 1990.
[16] R. Schwesinger, H. Schlemper, Angew. Chem., Int. Ed. Eng. 26 (1987) 1167.
[17] C. Slugovc, R. Schmid, K. Kirchner, Coord. Chem. Rev. 185–186 (1999) 109.
[18] (a) cf. F.G. Bordwell, J. Cheng, G.Z. Ji, A.V. Satish, X. Zhang, J. Am. Chem. Soc. 113 (1991) 9790;
(b) V.D. Parker, J. Am. Chem. Soc. 114 (1992) 7458;
(c) V. Skagestad, M. Tilset, J. Am. Chem. Soc. 115 (1993) 5077;
(d) R. Ciancanelli, B.C. Noll, D.L. DuBois, M.R. DuBois, J. Am. Chem. Soc. 124 (2002) 2984;
(e) J.M. Mayer, Acc. Chem. Res. 31 (1998) 441;
(f) J.M. Mayer, in: B. Meunier (Ed.), Biomimetic Oxidations Catalyzed by Transition Metal Complexes, Imperial College Press, London, 2000, p. 1.
[19] J.D. Soper, B.K. Bennett, S. Lovell, J.M. Mayer, Inorg. Chem. 40 (2001) 1888.
[20] J.M. Achord, C.L. Hussey, Anal. Chem. 52 (1980) 601.
[21] NIST Chemistry WebBook, http://webbook.nist.gov/, March 2003 Release.
[22] (a) D.L. Maricle, W.G. Hodgson, Anal. Chem. 37 (1965) 1562;
(b) Converted to vs. $Cp_2Fe^{+/0}$ following N.G. Connelly, W.G. Geiger, Chem. Rev. 96 (1996) 877.
[23] S.J. Blanksby, G.B. Ellison, Acc. Chem. Res. 36 (2003) 255.
[24] (a) R.A. Marcus, N. Sutin, Biochim. Biophys. Acta 811 (1985) 265;
(b) N. Sutin, Prog. Inorg. Chem. 30 (1983) 441;
(c) T.J. Meyer, H. Taube, in: G. Wilkinson (Ed.), Comprehensive Coordination Chemistry, vol. 1, Pergamon, New York, 1987, p. 331 (Chapter 7.2).
[25] (a) J. Lind, X. Shen, G. Merenyi, B.Ö. Jonnson, J. Am. Chem. Soc. 111 (1989) 7654;
(b) G. Merenyi, J. Lind, M. Jonsson, J. Am. Chem. Soc. 115 (1993) 4945.
[26] K. Zahir, J.H. Espenson, A. Bakac, J. Am. Chem. Soc. 110 (1988) 5059.

Available online at www.sciencedirect.com
SCIENCE DIRECT®
Polyhedron 23 (2004) 331–360
POLYHEDRON
www.elsevier.com/locate/poly

A short ride on scorpionates: from d- to f-elements

António Paulo, João D.G. Correia, Maria P.C. Campello, Isabel Santos *

Departamento de Química, Instituto Tecnológico e Nuclear, Estrada Nacional 10, P-2686-953 Sacavém Codex, Portugal

Received 3 June 2003; accepted 8 September 2003

Abstract

This paper presents an overview of progress involving group 7 elements and actinides with scorpionate ligands. This includes oxides, polyhydrides and carbonyls of group 7 elements and any type of compounds of actinides (III) and (IV). Synthetic procedures, reactivity and structural data are reviewed.
© 2003 Elsevier Ltd. All rights reserved.

Keywords: Scorpionate ligands; Technetium; Rhenium; Uranium

1. Introduction

All along the periodic table, a rich coordination chemistry has been developed based on the hard scorpionate ligands [1]. Such diversity is due to the easy tunning of the electronic, steric and coordinating properties of scorpionates, achieved by changing the nature of the groups attached to the boron atom (R) and/or by introducing various sterically bulky and/or coordinating groups in the 3- and 5-positions of the pyrazolyl ring (Scheme 1) [1].

Due to their scientific interests, the authors of this manuscript decided to participate in this special issue of Polyhedron with a *short ride on scorpionates*, focused on group 7 elements and actinides. Particular emphasis is given to oxides, polyhydrides and carbonyls of group 7 elements, while for the actinides any type of compound will be reviewed. From group 7, rhenium will be the most extensively described, as oxides, polyhydrides and carbonyls anchored by scorpionates were mainly studied with this element, with a view on stoichiometric or catalytic transformation of substrates [2]. Similar to rhenium, the chemistry of technetium scorpionates is much more limited. This is certainly due to its radioactive nature, although the element is quite relevant to nuclear medicine. Manganese, due to its electronic properties, tends to form mainly homoleptic compounds, which will not be discussed here, but were reviewed elsewhere [1]. Due to accessibility and safety reasons, uranium has been the more extensively studied actinide, and these studies involved mainly U(III) and (IV) compounds anchored by homo- and heteroscorpionates of the first and second generation.

This contribution updates two previous reviews by I. Santos and coworkers [3] one on rhenium poly(pyrazolyl)borates and the other covering both the 4f- and 5f-element chemistry [4]. Special attention will be given to more recent achievements, but to provide some context to the current work, some overlap between this review and its predecessors is unavoidable.

2. Group 7 scorpionate complexes

2.1. M(VII) trioxides

Air-stable M(VII) trioxides [Tp′MO_3] (M = Re, Tp′ = Tp (**1a**), pzTp (**1b**), Tp*(**1c**), PhTp (**1d**); M = Tc, Tp′ = Tp (**1a′**), Tp*(**1c′**)) have been prepared by reacting M_2O_7 (M = Re, Tc) with sodium or potassium salts of the corresponding homoscorpionates [5–9]. Conversion of Re_2O_7 to $ReO_3(O_2CCF_3)$, followed by reaction with KTp*, is an even more efficient alternative for the synthesis of **1c** (Scheme 2) [10].

* Corresponding author. Tel.: +351-219946066; fax: +351-219941455.
E-mail address: isantos@itn.pt (I. Santos).

0277-5387/$ - see front matter © 2003 Elsevier Ltd. All rights reserved.
doi:10.1016/j.poly.2003.11.022

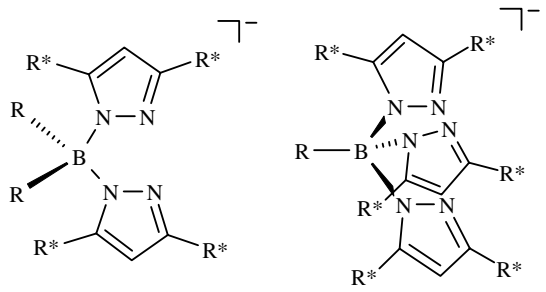

Scheme 1.

Compounds **1a** and **1a′** are also accessible, although in moderate yields, by nitric acid oxidation of $[TpMOCl_2]$ (**3a**) (M = Re, Tc) or by reacting $[MO_4]^-$ (M = Re, Tc) with excess of NaTp in an acidified alcoholic solution [11,12].

The structures of complexes **1a**, **1b** and **1d** were determined by X-ray diffraction analysis, and found to be almost superimposable. The metal center is six-coordinate by three oxygen atoms and the nitrogens of the tridentate homoscorpionate. The coordination geometry around the metal is pseudo-octahedral and within each compound the Re–N distances (mean values: 2.231(3) Å (**1a**), 2.217(6) Å (**1b**) and 2.222(7) Å (**1d**)) are almost identical. The Re–O bond distances of ca. 1.712(2) Å (**1a**), 1.714(6) Å (**1b**) and 1.710(8) Å (**1d**) are consistent with conventional double bonds [5,7,8]. In the IR spectra of the M(VII) trioxides (M = Re, Tc) the stretching vibrations associated with the M=O bonds appear in the range 890–944 and 853–921 cm^{-1} for the Re and Tc complexes, respectively [5–9]. The solution ^1H NMR spectra of **1a**–**d** are consistent with the respective molecular structure indicating a static behavior for these compounds and precluding, in the case of **1b**, the involvement of the fourth uncoordinated pyrazolyl ring in any scrambling process [7].

2.2. M(V) oxides

2.2.1. Key compounds

As would be expected for complexes with the metal in the highest oxidation state, the chemistry of the trioxides **1a**–**d** is dominated by reductive/deoxygenation processes, that led to a certain number of monomeric or dimeric key compounds as entry into Re(V) chemistry, namely $[Tp'ReO(\mu\text{-}O)]_2$ (Tp′ = Tp (**2a**), pzTp (**2b**)), $[Tp'ReOCl_2]$ (Tp′ = Tp (**3a**), pzTp (**3b**), Tp* (**3c**)), [Tp*ReO(OH)Cl] (**4**) and [TpReO(Cl)I] (**5**).

The dimers, $[Tp'ReO(\mu\text{-}O)]_2$ (Tp′ = Tp (**2a**), pzTp (**2b**)), were obtained by reacting $[Tp'ReO_3]$ (Tp′ = Tp (**1a**), pzTp (**1b**)) with PPh_3 in THF (Scheme 3) [13,14]. Interestingly, this type of compound was never identified when the scorpionate involved was Tp*. In this case, Gable et al. [15–17] considered the fragment $\{Tp^*ReO_2\}$ as being the reduced species, which does not dimerize due to the steric bulkiness of the Tp* ligand.

The formulation of **2a**,**b** was mainly based on the spectroscopic properties and reactivity of these compounds. In particular, their IR and mass spectra were consistent with the presence of the $[ReO(\mu\text{-}O)]_2$ unit [13,14]. Compounds **2a**,**b** are rare examples of scorpionate rhenium complexes exhibiting fluxional behavior in solution. Static ^1H NMR spectra could be obtained at low temperature, presenting patterns compatible with the tridentate coordination mode of the scorpionates and with a six-coordination environment around the metal [13,14].

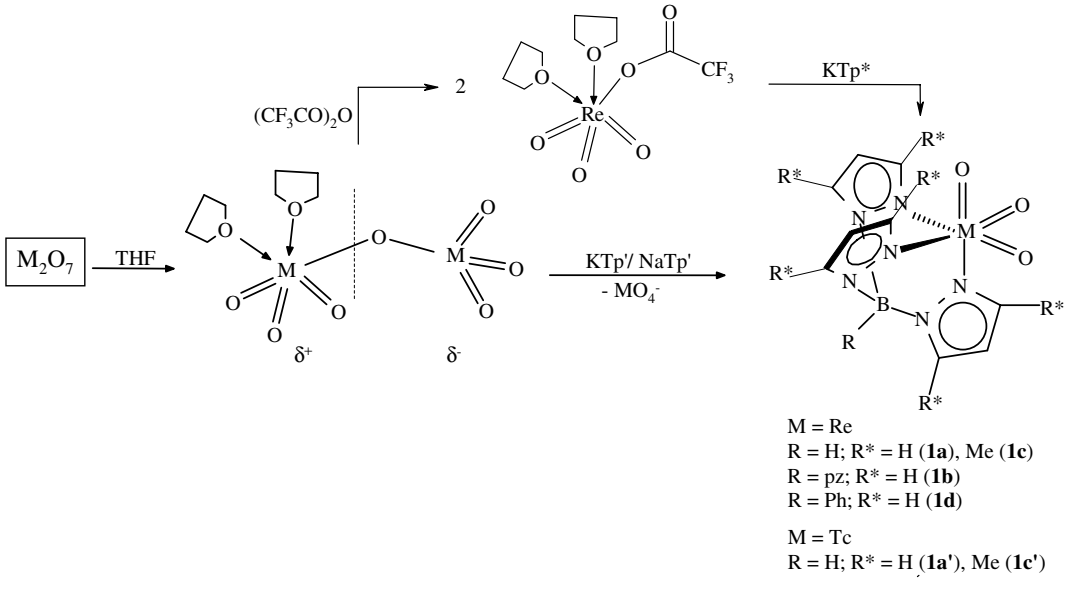

Scheme 2.

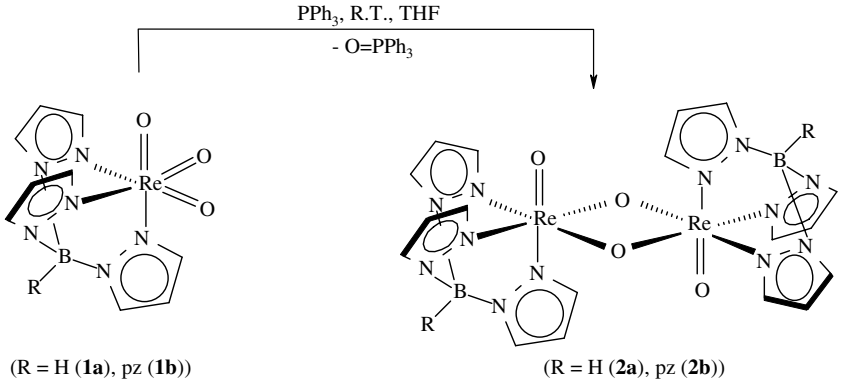

Scheme 3.

As shown in Scheme 4, the oxo-dichlorides [Tp′ReOCl$_2$] (Tp′ = Tp (**3a**), pzTp (**3b**), Tp* (**3c**), PhTp (**3d**)) were synthesized by simultaneous treatment of [Tp′ReO$_3$] (**1a–d**) with PPh$_3$ and chlorotrimethylsilane [6–8,10,18,19]. However, during the formation of **3c** hydrolysis also occurs and compound **3c** is obtained contaminated with [Tp*ReO(OH)Cl] (**4**) [6]. Treatment of this mixture with further Me$_3$SiCl or HCl, in a second reaction step, led to the pure oxodichloride **3c** [10,18]. Moreover, optimal conditions for the synthesis of the hydroxychloride [Tp*ReO(OH)Cl] (**4**), a useful precursor for the synthesis of mixed halide Re(V) derivatives, were also described [10]. Compound [Tp*Re(O)F$_2$] was also prepared by reduction of **1c** with PPh$_3$, followed by

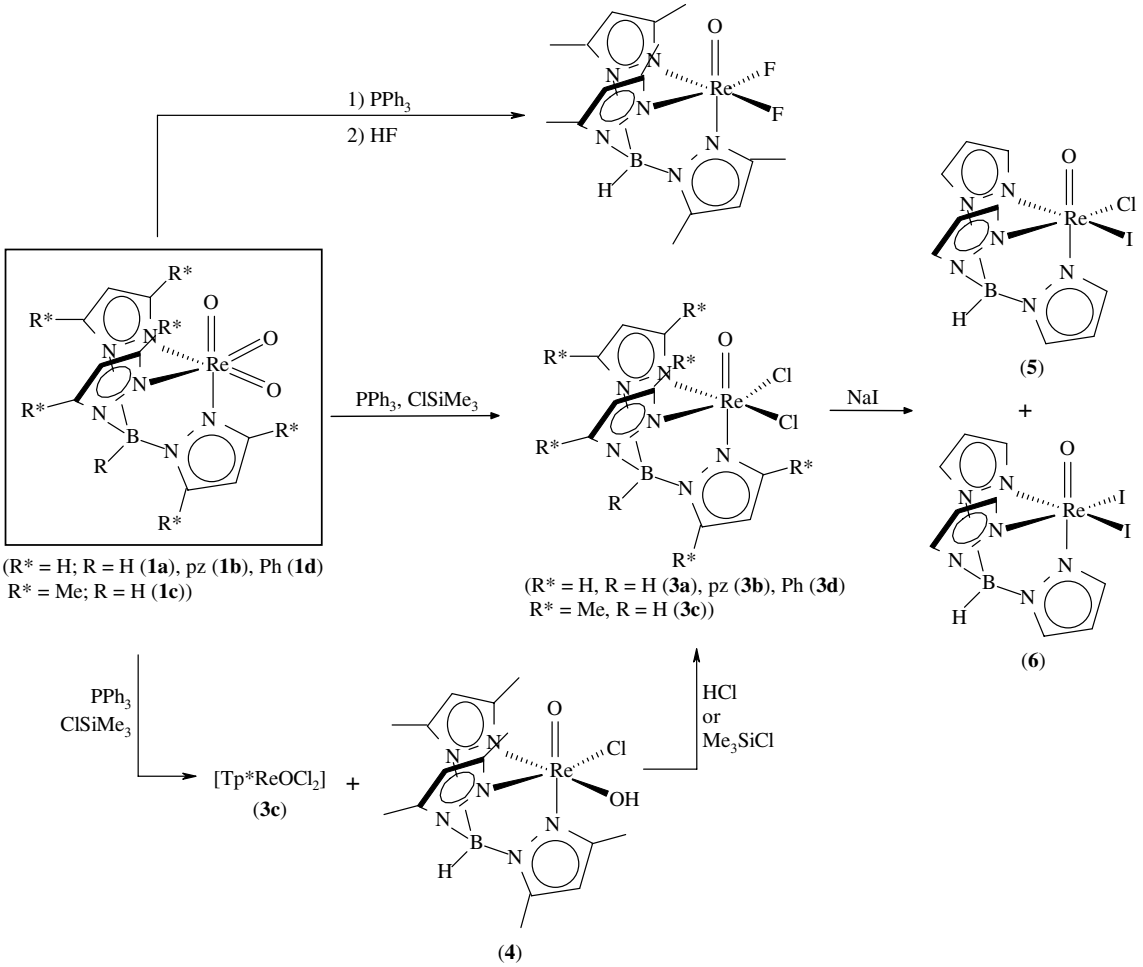

Scheme 4.

addition of aqueous HF. In contrast, all the efforts to prepare oxo-difluorides anchored by Tp have failed [20]. The iodide derivatives [TpReO(Cl)(I)] (**5**) and [TpReOI$_2$] (**6**) were prepared by reacting **3a** with sodium iodide (Scheme 4). Replacement of iodide in compound **5** by triflate gave the mixed halide-triflate [TpReO(Cl)(OTf)] [21,23]. Several mixed halides and triflates of the type [Tp*ReO(X)Cl] (X = Br, I, F) and [Tp*ReO(Y)(OTf)] (Y = OH, F, Cl) were also prepared by reacting, respectively, [Tp*ReO(OH)Cl] (**4**) with HX and [Tp*Re(O)Y(F)] with Me_3SiOTf [10,20].

The original synthesis of the key compounds, [TpMOCl$_2$] (M = Re, **3a**, M = Tc, **3a′**), involved reaction of $[MO_4]^-$ with excess KTp in aqueous HCl solution and took advantage of the reducing properties of the Tp$^-$ ligand [11,24]. By contrast, the reduction of $[ReO_4]^-$ with KTp*, in the presence of HCl, is accompanied by decomposition of the ligand with formation of the dimer [ReOCl$_2$(Hpz^{Me_2})$_2$]$_2$(μ-O) [25]. This symmetric dimer, mixed with the binuclear oxo-bridged asymmetric isomer [{Re(O)Cl(Hpz^{Me_2})$_3$}(μ-O){Re(O)Cl$_3$(Hpz^{Me_2})}] was also identified in the reaction of KTp* with [N^{n}Bu$_4$][ReOCl$_4$] [18]. When the metal is Tc, the precursor [N^{n}Bu$_4$][TcOX$_4$] (X = Br, Cl) reacts with excess Tp yielding [TpTcOX$_2$] as the main product [26]. The isoelectronic sulfido complexes [TpMSCl$_2$] (M = Re, Tc) have been directly prepared from **3a** and **3a′** by atom transfer from B_2S_3, without degradation of the ancillary scorpionate [27–29].

2.2.2. Derivative chemistry of M(V) scorpionate oxides

2.2.2.1. Complexes with oxygen donor co-ligands. Several oxocomplexes with alkoxides, diolates or other oxygen donor co-ligands have been isolated using the dinuclear compounds [Tp′ReO(μ-O)]$_2$ (Tp′ = Tp(**2a**), pzTp (**2b**)) or the in situ generated {Tp*ReO$_2$} fragment as starting materials [13–15]. The reaction of the bis-metoxide [(pzTp)ReO(OMe)$_2$] (**7b**) with diols is also a quite convenient approach for the synthesis of diolates (Scheme 5) [30].

Preparation of this type of compounds was also achieved using the monomeric dichlorides [Tp′ReOCl$_2$] (Tp′ = Tp (**3a**), Tp* (**3c**)) as precursors (Scheme 6) [10,31]. However, comparatively to the synthetic procedures depicted in Scheme 5, this synthetic route is time consuming, demands high temperatures and the use of deprotonating agents.

While the alkoxide derivatives [Tp′ReO(OR′)$_2$] (Tp′ = Tp, pzTp) are somewhat air and moisture sensitive, decomposing mainly to the dimers [Tp′ReO(μ-O)]$_2$ (Tp′ = Tp (**2a**), pzTp (**2b**)), the bisalkoxides anchored by

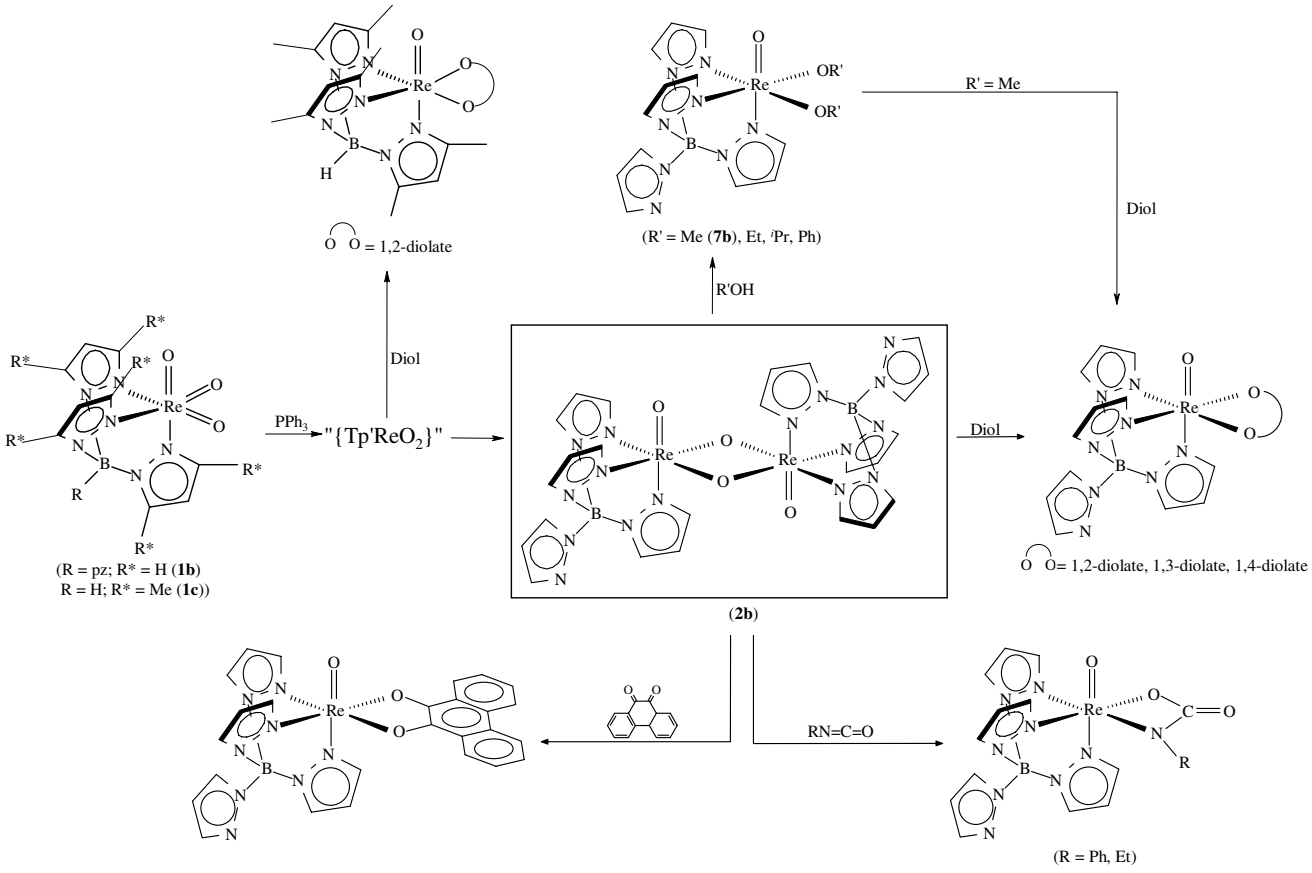

Scheme 5.

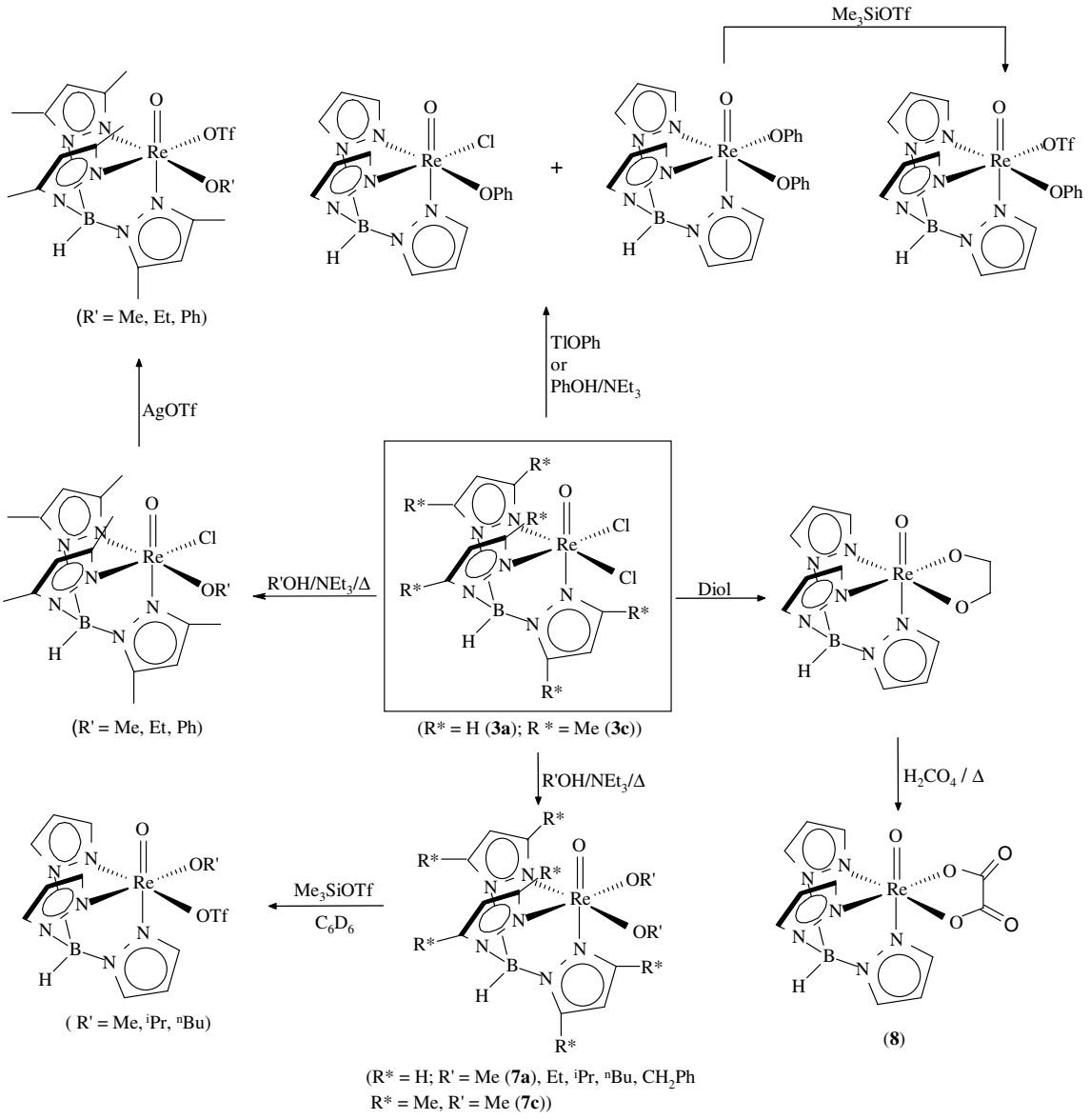

Scheme 6.

Tp* are stable in solution, even after several days [10,13,31]. Vicinal diolates of the type [Tp′ReO(O∩O)] (Tp′ = Tp, pzTp, Tp*) are air and water resistant but their thermolysis regenerates [Tp′ReO$_3$] (Tp′ = Tp (**1a**), pzTp (**1b**), Tp* (**1c**)) and the corresponding alkene [12,15,30,33]. In contrast, the complexes [(pzTp)ReO{O(CH$_2$)$_n$O}] ($n = 3, 4$) hardly eliminate the corresponding olefin under the same conditions [30]. The oxalate [TpReO(C$_2$O$_4$)] (**8**) is also thermally robust [33].

Characterization of this family of compounds, in some cases, also included X-ray structural analysis: [(pzTp)ReO(OPh)$_2$], [(pzTp)ReO(OMe)$_2$] (**7b**), [TpReO(OTf)$_2$], [TpReO(C$_2$O$_4$)] (**8**) and [(pzTp)ReO{O(CH$_2$)$_2$O}]. All are monomeric and the metal is six-coordinate, displaying a distorted octahedral coordination geometry. The homoscorpionate occupies one triangular face of the coordination polyhedron and the oxygen atoms of the two alkoxides or diolate are in the equatorial plane [13,30,32–34].

The nucleophilicity of the Re=O functionality in some of these alkoxide and diolate derivatives allowed the synthesis of the stable Lewis acid–metal complex adducts [TpRe{OB(C$_6$F$_5$)$_3$}(OEt)$_2$], [TpRe{OB(C$_6$F$_5$)$_3$}(OCH$_2$CH$_2$O)], and [TpRe{OB(C$_6$F$_5$)$_3$}(C$_2$O$_4$)], which were prepared by reacting the corresponding monoxocompounds with the strong Lewis acid B(C$_6$F$_5$)$_3$ [35].

Corroborating the versatility of the pzTp systems, reactions of [(pzTp)ReO(OMe)$_2$] (**7b**) with protic oxygen donor substrates, potentially bidentate and uninegative, promoted a haptotropic change of the anchor scorpionate from κ^3-pzTp to κ^2-pzTp (Scheme 7) [36].

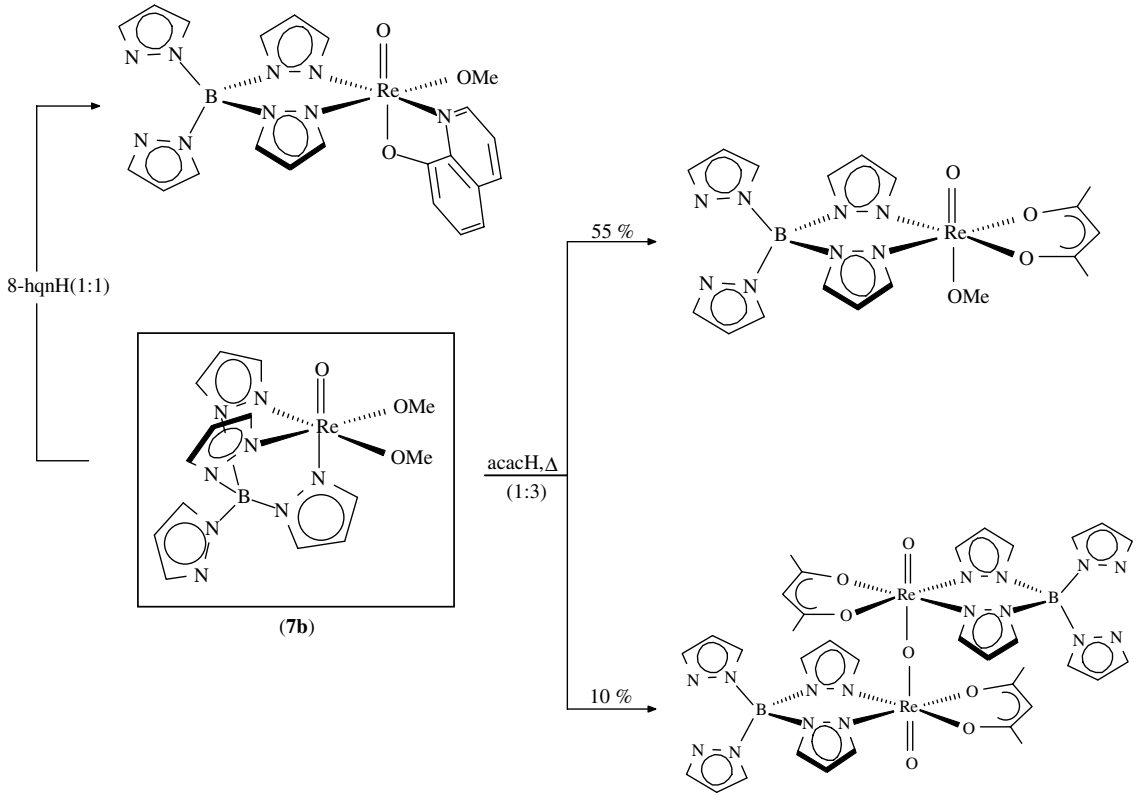

Scheme 7.

The bidentate coordination of pzTp in [(κ^2-pzTp)ReO(acac)(OMe)] and [(κ^2-pzTp)ReO(acac)]$_2$(μ-O) was confirmed by X-ray crystallography. In these six-coordinate octahedral complexes, the oxo groups occupy the axial sites and the κ^2-pzTp and acac ligands lie in the equatorial plane. The dimeric structure of [(κ^2-pzTp)ReO(acac)]$_2$(μ-O) is centrossymmetric, with a quasi linear O=Re–O–Re=O group. The bridging Re–O bond length, 1.910(1) Å, is normal for rhenium complexes containing this type of moiety [36].

2.2.2.2. Complexes with nitrogen-donor co-ligands. Re(V) oxo amido derivatives of the type [TpReOCl(NRR′)] have been isolated by reacting [TpReOCl$_2$] (**3a**) with excess of the corresponding amines (Scheme 8). These oxo-amidos are unstable in solution, decomposing in the presence of air to [TpReO$_3$] (**1a**), and exist in solution as conformational isomers, most likely due to restricted rotation about the Re–N bond [37].

Compound **3a** was also used as precursor in the synthesis of metallacycles of the type [TpReO(κ^2-N–X)] (X = N, O) [38,39]. Some of these compounds contain chiral and bidentate ligands of the type alcoholate or amidate, derived from (1*S*,2*R*)-ephedrine, (1*S*,2*S*)-diphenylethylenediamine, and L-proline (Scheme 8) [38].

Monomeric and dimeric derivatives containing metal–nitrogen bonds were prepared by reacting [(pzTp)ReO(μ-O)]$_2$ (**2b**) or [(pzTp)ReO(OMe)$_2$] (**7b**) with diamines or pyrazoles (Scheme 9) [36]. Diamines react with **2b** or **7b** yielding the monomeric metallacycles [(pzTp)ReO(HN$^\frown$NH)], while reactions of **2b** with pyrazoles afforded dimeric species with bridging pyrazolides. **7b** also reacts with pyrazoles and forms the monomeric **9a**,**b**, which slowly dimerize in solution to **10a**,**b**, releasing pyrazole and methanol (Scheme 9) [36].

The crystal structure of **10a** consists of two independent "{κ^2-(pzTp)ReO}" units triple bridged by an oxygen and two pyrazolide ligands. The O=Re–O–Re=O unit is quite bent (Re–O–Re, 125.4(3)°) due to the steric requirements of the two bridging pyrazolides [36]. This quite unusual structure was also found in the recently described [{κ^2-H(F)Bpz$_2$}Re(O)]$_2$(μ-pz)$_2$(μ-O), obtained by refluxing [TpReOI$_2$] with excess of NaF in acetonitrile [20].

Re(V) imido compounds of general formula [TpRe(NTol)X$_2$] were synthesized by reacting [TpReOX$_2$] (X = Cl (**3a**), I (**6**)) with *p*-toluidine (Scheme 10) [37,40]. Based on [TpRe(NTol)X$_2$] (X = Cl, I) several Re(V) imido alkyl and aryl derivatives have been prepared by methatesis reactions (Scheme 10) [40].

The imido group being isoelectronic with the oxo ligand produces similar types of complexes, as far as general structural patterns are concerned. However, from the electronic point of view the imido derivatives

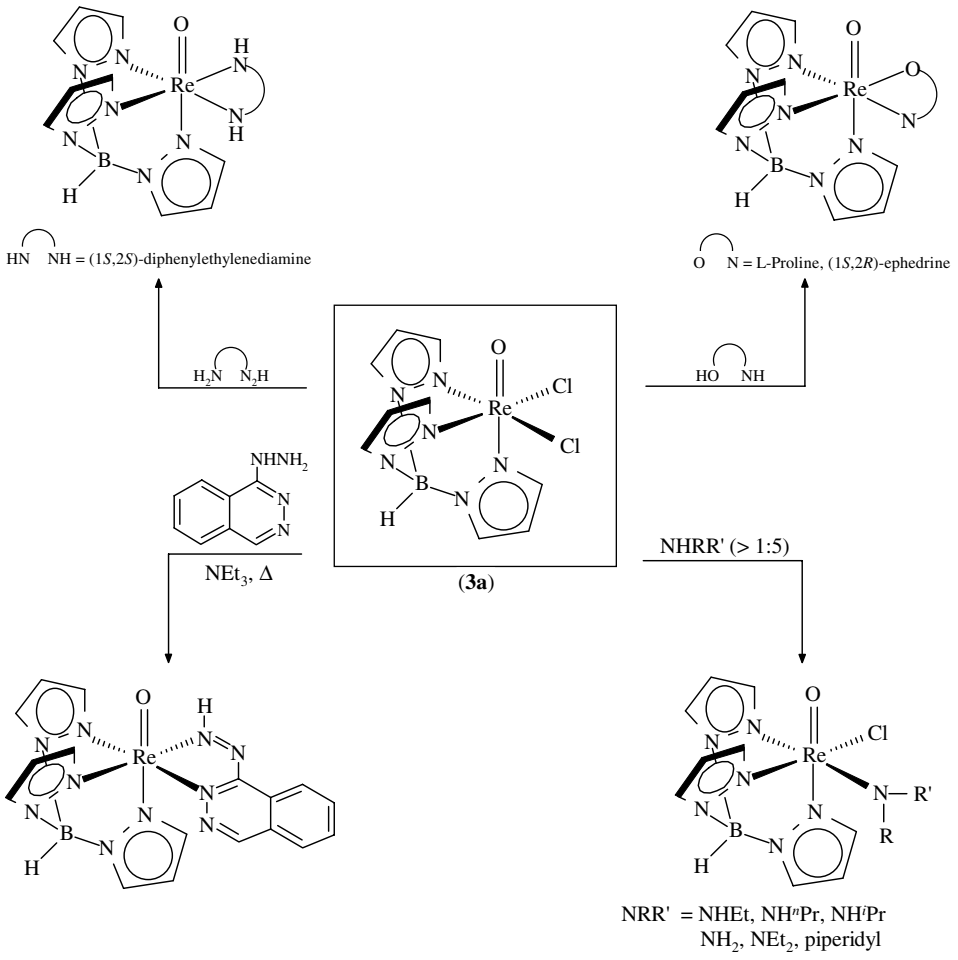

Scheme 8.

are more electron-rich compounds. This trend was confirmed by electrochemical studies performed on a series of imido and oxo-complexes of the type [TpRe(NTol)(X)(Y)] and [TpReO(X)(Y)] (X, Y = triflate, halide, alkyl, aryl). Consistently, the oxo-complexes act as inner-sphere oxidants, reacting as electrophiles towards PPh_3, in contrast with the imido congeners [41].

2.2.2.3. Complexes with sulfur donor-co-ligands. Mono- or bis-thiolates and dithiolates have been synthesized by reacting [TpReOCl$_2$] (**3a**) and the corresponding mono- or bidentate thiols in the presence of deprotonating agents and/or under reflux (Scheme 11) [19,28,39]. Thiophenolates [Tp*ReO(OH)(SPh′)] were also obtained by treatment of [Tp*ReO(Cl)(OH)] (**4**) with the corresponding thiol [6].

A faster and cleaner procedure for the preparation of thiolate derivatives is the reaction of the dinuclear compound [(pzTp)ReO(μ-O)]$_2$ (**2b**), or the in situ generated {Tp*ReO$_2$} unit, with thiols, 2-mercaptopyridine, 2-mercaptoalcohols or dithiol (Scheme 12) [13,17,42,43].

The compounds [TpReOCl(SPh)], [TpReO(SCH$_2$CH$_2$S)], [Tp′ReO(SPh)$_2$] and [Tp′ReO(2-S-py)$_2$] (Tp′ = Tp, pzTp) were structurally characterized. All are six-coordinate by a κ^3-Tp′, an oxo group and two monodentate or one bidentate co-ligand, displaying an octahedral coordination geometry [13,19,28,39,43].

An interesting result, which confirmed the haptotropism of pzTp, was the identification of the complex [(κ^2-pzTp)ReO{κ^2-(C$_5$H$_4$NS)}(OMe)], obtained by reacting [(pzTp)ReO(OMe)$_2$] (**7b**) with 2-mercaptopyridine. As shown by the solid state structural analysis, the metal is six-coordinate by the κ^2-pzTp, the κ^2-pyS and by a metoxide group coordinate *trans* to the oxo (Scheme 12) [43].

2.2.2.4. Complexes with hydrocarbyl co-ligands. Oxo alkyl or aryl derivatives were prepared by reacting [Tp′ReOCl$_2$] (Tp′ = Tp (**3a**), Tp* (**3c**)) with different alkylating agents (Scheme 13) [10,32,44].

The outcome and yield of these reactions depend on the nature of the scorpionate and also on the alkylating agent. It was found that the Tp* system was more resistant to reduction, making possible the use of

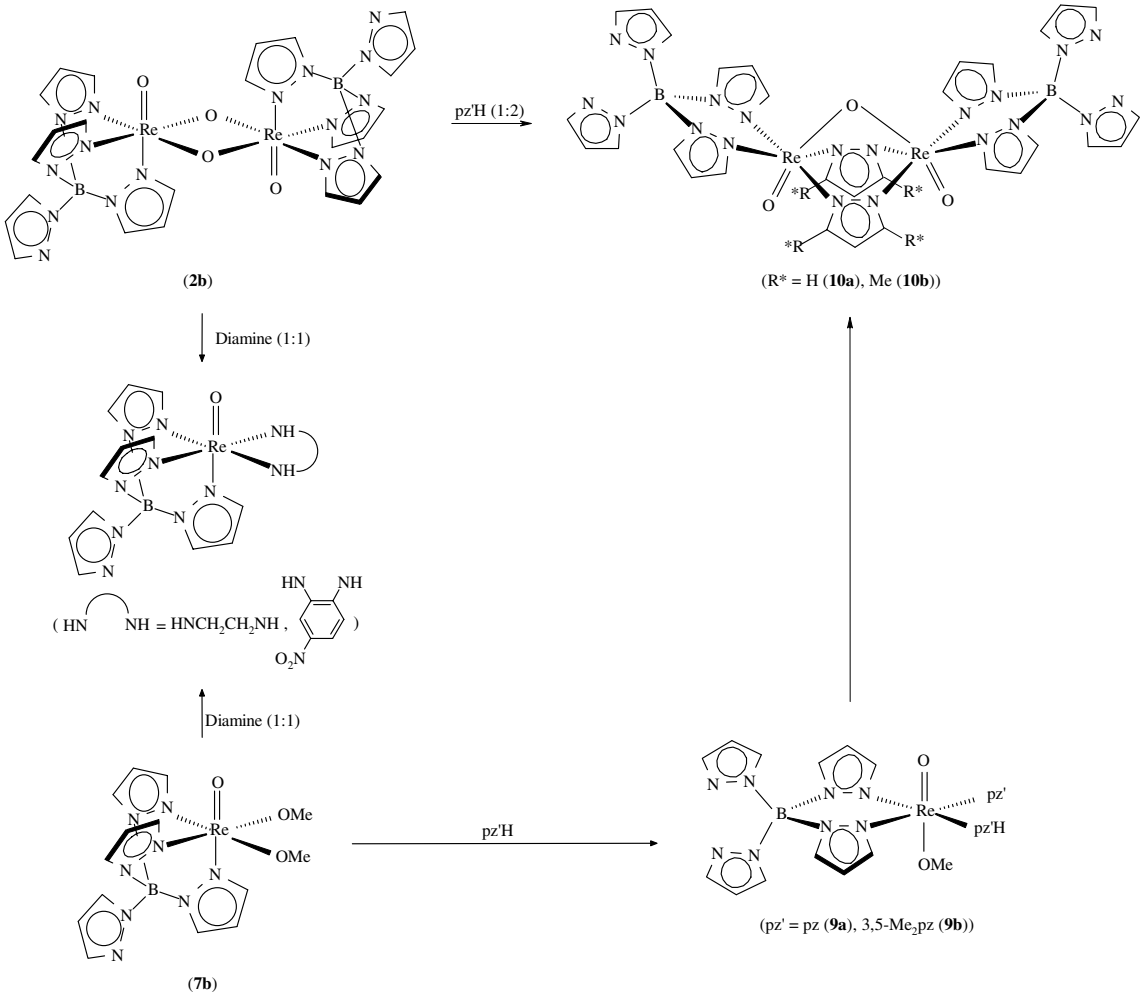

Scheme 9.

Grignard reagents in the arylation. Mayer and co-workers [10] considered that steric factors, more than electronic ones, are responsable for the greater stability of the Tp* organometallic derivatives. Substitution of the halide in [Tp′ReO(X)(R′)] (Tp′ = Tp; X = Cl, R′ = Me, Et, ^{n}Bu, Ph; X = I, R′ = Ph and Tp′ = Tp*, X = Cl, R′ = Et, Ph) by reaction with silver triflate led to [Tp′ReO(OTf)(R′)] [10,32,44]. Unlike the reactions with complexes containing the Tp* ligand, in the case of Tp complexes the reactions require some days for completion, but excess of AgOTf cannot be used due to separation problems.

Some of these organometallic Re(V) oxides were characterized by single crystal X-ray diffraction analysis. The complexes adopt a distorted octahedral geometry with the rhenium atom displaced toward the oxo ligand, similar to other oxo Re(V) scorpionate compounds containing different co-ligands [10,44].

2.2.3. *trans*-Dioxocomplexes

trans-Dioxo derivatives, of general formula *trans*-[(κ^2-Tp′)ReO_2L_2] (**11**–**16**), were obtained by reducing [Tp′ReO_3] (Tp′ = Tp (**1a**), pzTp (**1b**), PhTp (**1d**)) with PPh_3 in the presence of σ donors such as pyridines, imidazoles or diphosphines (L) (Scheme 14) [8,45,46]. The stability of this unusual class of compounds depends on the scorpionate and on the neutral co-ligand. Santos et al. found a higher stability for the pzTp system and identified the dimers [Tp′ReO(μ-O)]$_2$ (**2**) as the major decomposition products.

The synthesis of **11**–**16** was considered to be consistent with the formation of the electronic and coordinatively unsaturated "{Tp′ReO_2}" fragment, which does not dimerize in the presence of neutral σ donor ligands but yields **11**–**16**. The $\kappa^3 \Longleftrightarrow \kappa^2$-haptotropism of the scorpionates facilitates the process [8,45,46].

The structural analysis of some *trans*-dioxocomplexes (**11c**, **13**, **15a**, **15b**) confirmed the κ^2-coordination mode of the scorpionate ligands and the presence of the *trans*-ReO_2 unit. The Re–O bond distances (1.751–1.773) are typical of Re(V) *trans*-dioxocomplexes and are compatible with a certain double character [45,46].

During recrystallization of **15a** a slight decomposition occurred and a pzH molecule of solvation per

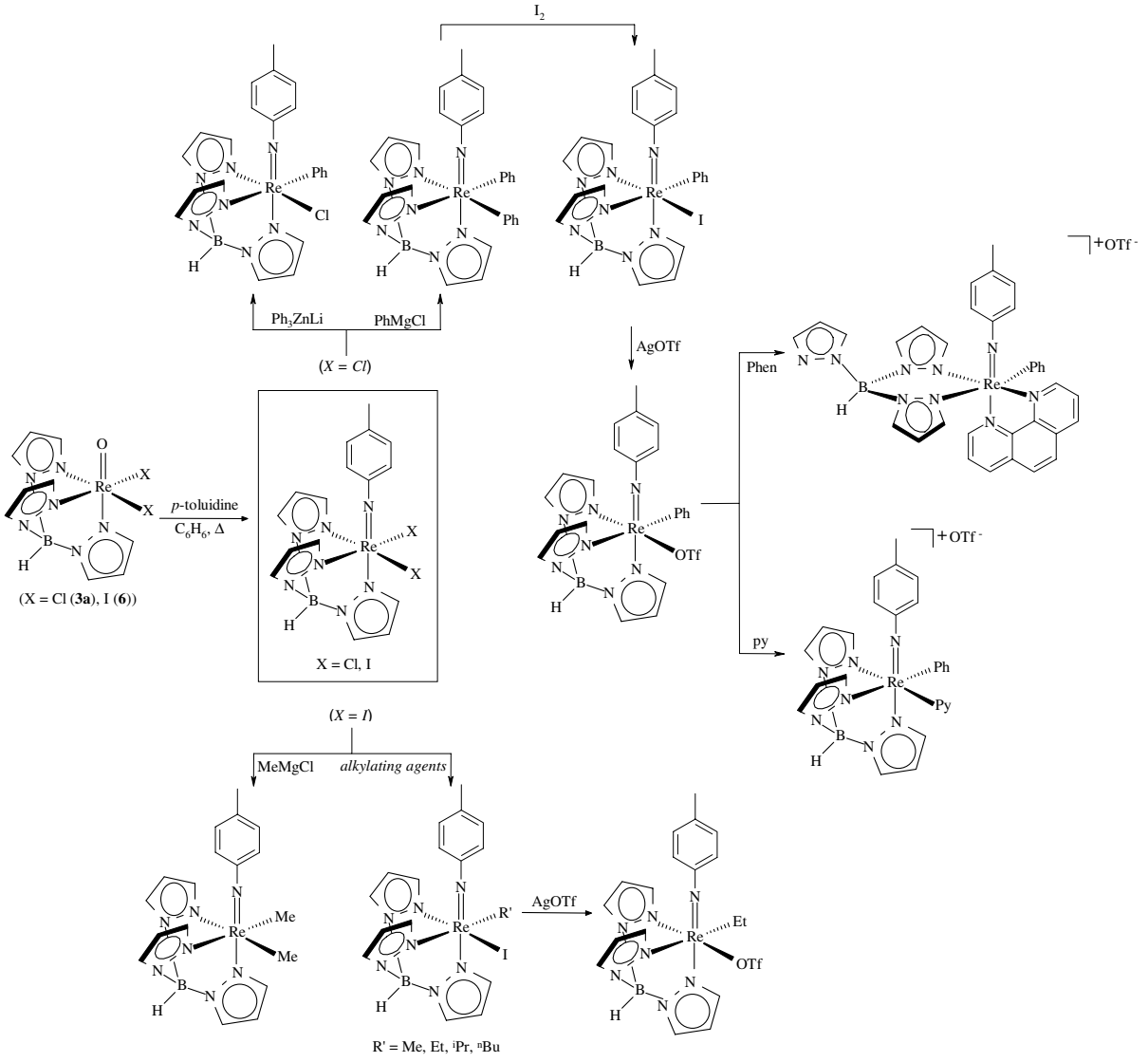

Scheme 10.

asymmetric unit appears in the crystal structure. Another indication for the relative instability of **15a** is the formation of *trans*-$[ReO_2(dmpe)_2]$ [Tp] (**17**), due to the replacement of Tp by dmpe moiety. The crystal structure of **17** consists of *trans*-$[ReO_2(dmpe)_2]^+$ cations and Tp anions, representing a rare example of a d-transition complex with a scorpionate acting as counter-ion [46].

The ^1H NMR spectra of the dioxocomplexes anchored by κ^2-pzTp show abnormally highfield shifted H(3/5) resonances for the two uncoordinated pyrazolyl rings. This behavior is typical of Re(V) oxocomplexes with κ^2-pzTp ligand, and rendered ^1H NMR spectroscopy a powerful tool in assigning the denticity of the pzTp ligand [36,45].

When the synthesis of *trans*-$[(\kappa^2\text{-pzTp})ReO_2(py)_2]$ was tried using *trans*-$[ReO_2(py)_4]Cl$ as starting material, an oxygen attack at the boron atom was observed and a mixture of two compounds anchored by asymmetric κ^2-heteroscorpionates was obtained (Scheme 15) [45].

Reactions of the starting material *trans*-$[ReO_2(py)_4]Cl$ with Bp or Bp* were also studied. No degradation of the scorpionates was observed and the resulting compounds were the anions *trans*-$[(Bp')_2ReO_2]^-$ ($Bp' = Bp$, Bp*), with *trans*-$[ReO_2(py)_4]^+$ as counter ion (Scheme 15). These anionic complexes react readily with the electrophilic substrates $ClXMe_3$ ($X = Si$, Sn), affording $[(Bp')_2ReO(OXMe_3)]$ and providing an easy entry into the chemistry of bis-Bp′ oxocompounds (Scheme 15) [47].

Unusual cationic mono-oxocomplexes of general formula $[(\kappa^2\text{-pzTp})ReO(OSiMe_3)(L)_2]Cl$ were also synthesized by reacting *trans*-$[(\kappa^2\text{-pzTp})ReO_2(L)_2]$ with trimethylsilyl chloride (Scheme 16). In solution, the cationic complexes with monodentate σ-donor ligands

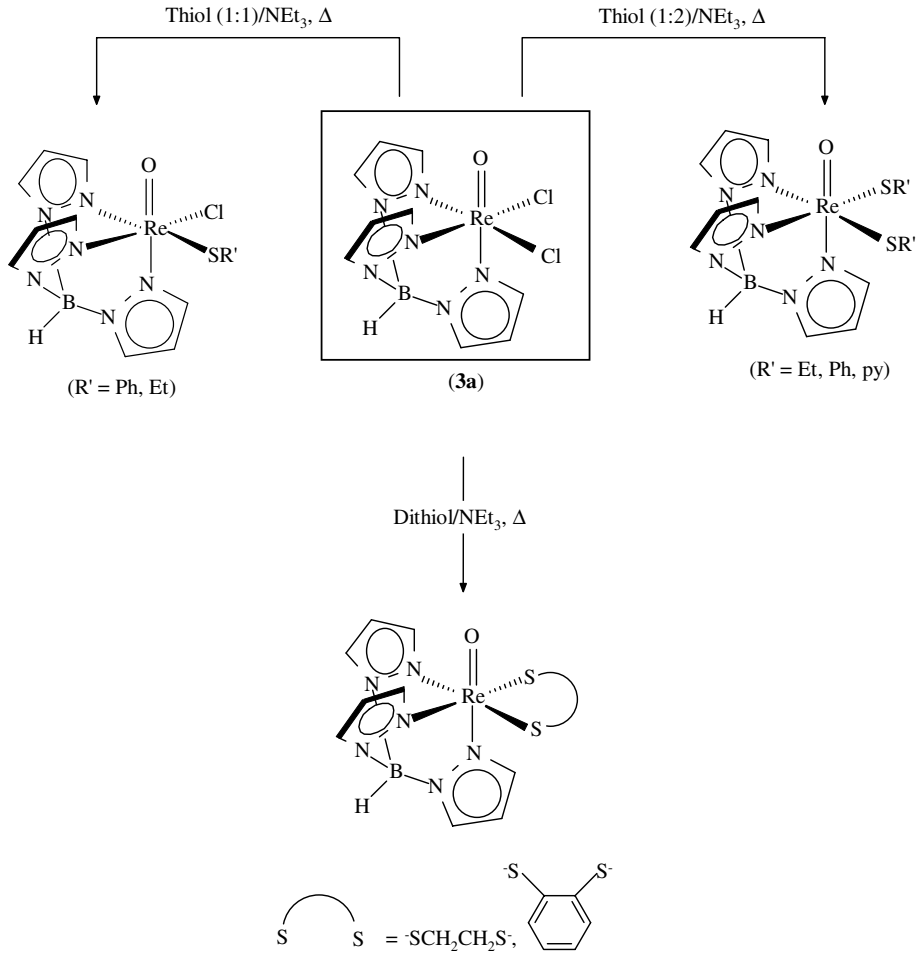

Scheme 11.

rearrange to the neutral compounds [(κ^2-pzTp)ReO(O-$SiMe_3$)Cl(L)]. The use of dmpe improved considerably the stability of the cationic species, preventing such rearrangement (Scheme 16) [48].

2.2.4. Oxygen transfer reactions

Re(III) monomeric adducts of the type [Tp′ReX_2L] (Tp′ = Tp, X = Cl, L = PPh_3, py, 3-hexyne, $OPMe_3$; X = Br, L = py, Meim, $OPEt_3$; Tp′ = pzTp, X = Cl, L = PPh_3, $PEtPh_2$, PEt_2Ph, PEt_3) or the pyridine adducts [TpReCl(X)py] (X = OPh, NEt_2) were obtained by deoxygenation of [Tp′$ReOX_2$] or [TpReOCl(X)] (X = OPh, NEt_2) with tertiary phosphines or phosphites, respectively (Scheme 17) [34,37,49,50].

When oxygen abstraction in [$TpReOCl_2$] (**3a)** is carried out with PMe_3, in the presence of 2,2-bipyridine and thallium triflate, the complex formed is cationic and has been formulated as [TpRe(κ^2-bipy)(Cl)][OTf]. Further reduction of this cationic compound with Zn/Hg in the absence or presence of cyclopentene yields [TpRe(κ^2-bipy)(Cl)] and [TpRe(κ^2-bipy)(η^2-cyclopentene)], respectively [51]. The paramagnetic [(pzTp)$ReCl_3$] has also been identified in the reaction of [$ReOCl_3(PPh_3)_2$] with K(pzTp) in CH_2Cl_2. This compound was considered to be formed through a Re(III) intermediate species, which is unstable and easily oxidized by the solvent (Scheme 18) [30].

The octahedral Re(III) complexes, anchored by Tp or pzTp, and [(pzTp)$ReCl_3$] are all paramagnetic and present relatively sharp but shifted resonances in the ^{1}H NMR spectra [30,34,37,49–51]. As confirmed by X-ray structural analysis, the compounds [$TpReCl_2$(py)], [TpReCl(OPh)(py)] and [(pzTp)$ReCl_2(PEt_2Ph)$] are six-coordinate, displaying an octahedral coordination geometry, with facial and symmetrical coordination of the κ^3-Tp′ ligand. This symmetrical coordination is different from what is observed in the analogous Re(V) oxo complexes, where exists a strong *trans* influence of the oxo group [21,34,49].

Mayer et al. described the first *cis*-[$TpReO_2X$] compounds (X = Cl (**18a**), Br (**18b**), I (**18c**)) obtained by oxidation of oxotriflates with a stoichiometric amount of pyridine *N*-oxide (Scheme 19). On the basis of electronic arguments, the *trans* configuration would be more stable for these d^1-dioxocomplexes, but the facial disposition imposed by the κ^3-Tp is certainly responsible

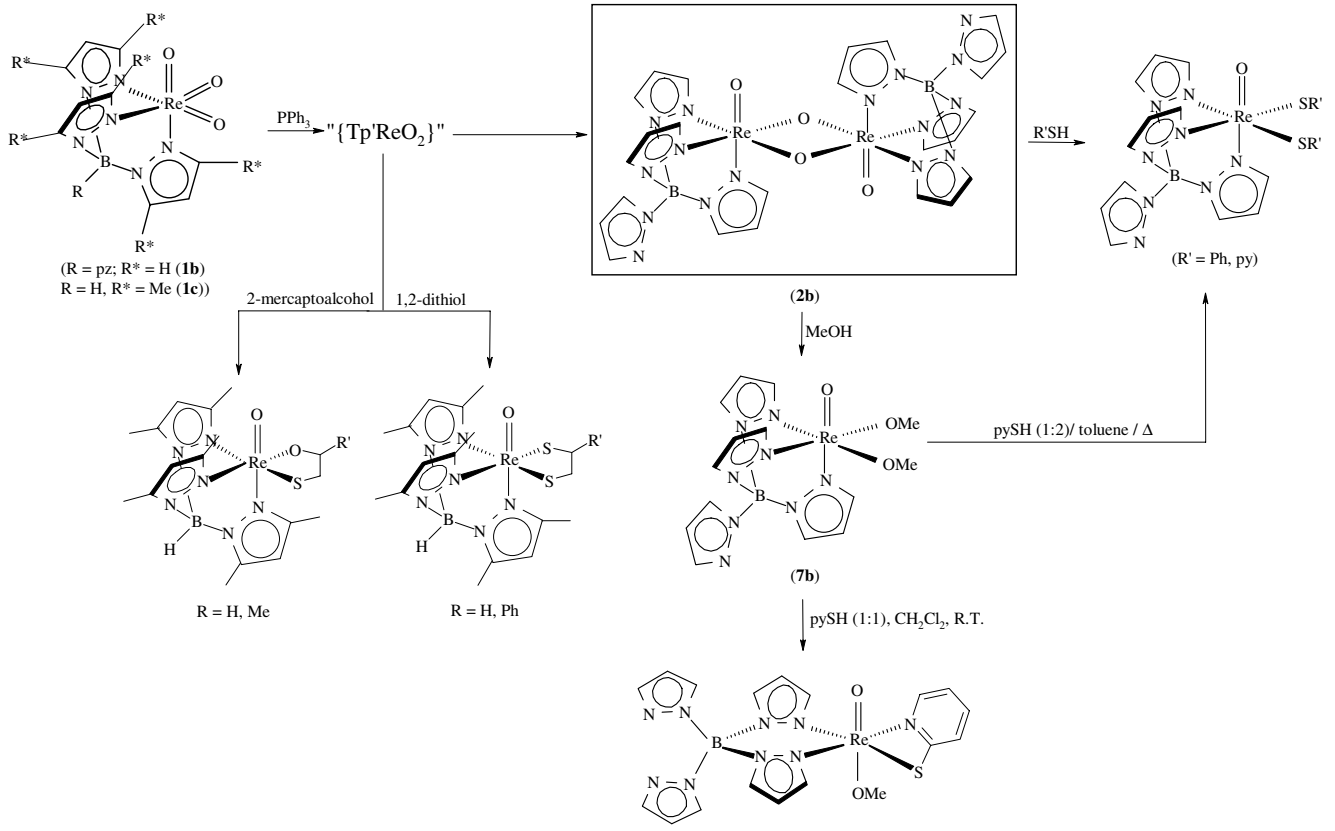

Scheme 12.

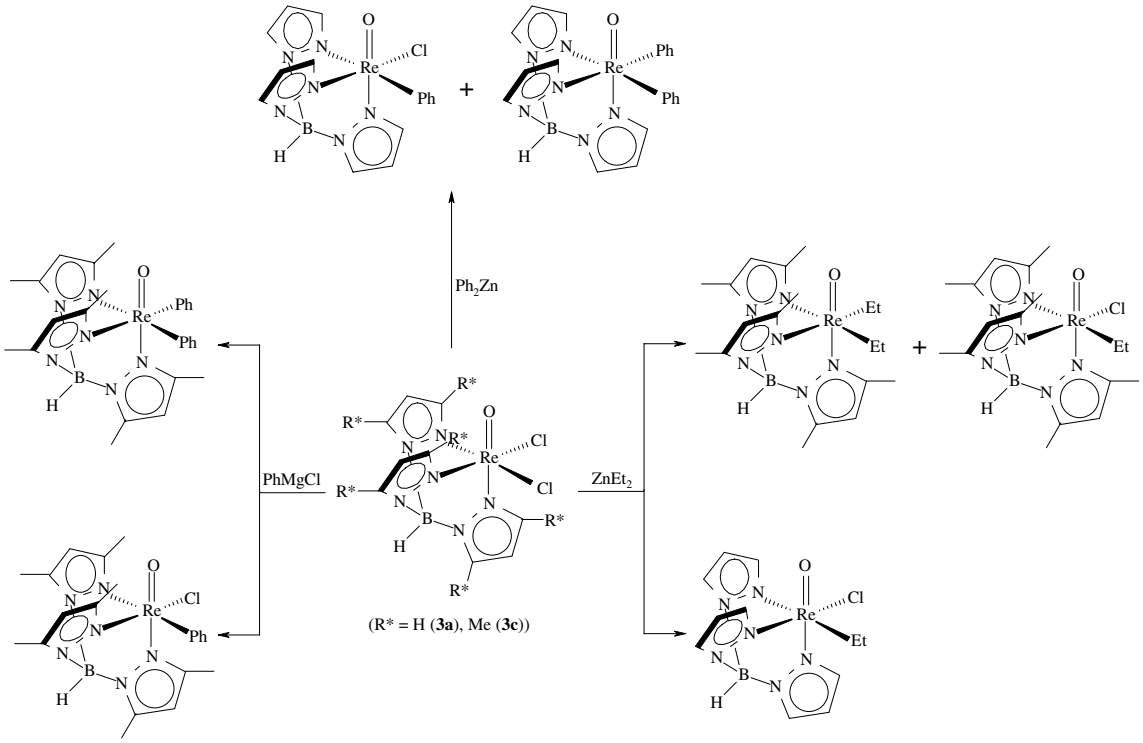

Scheme 13.

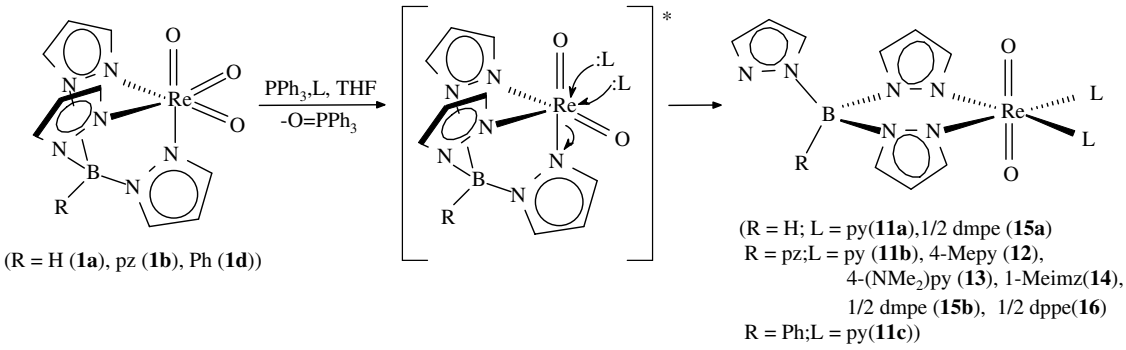

Scheme 14.

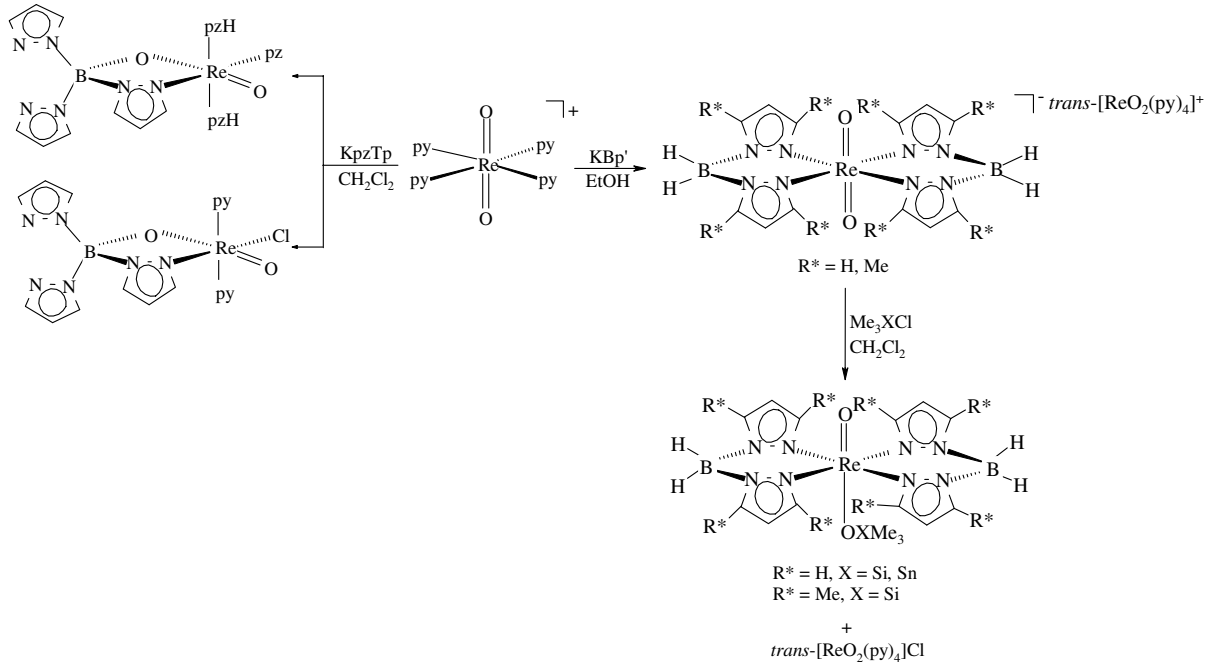

Scheme 15.

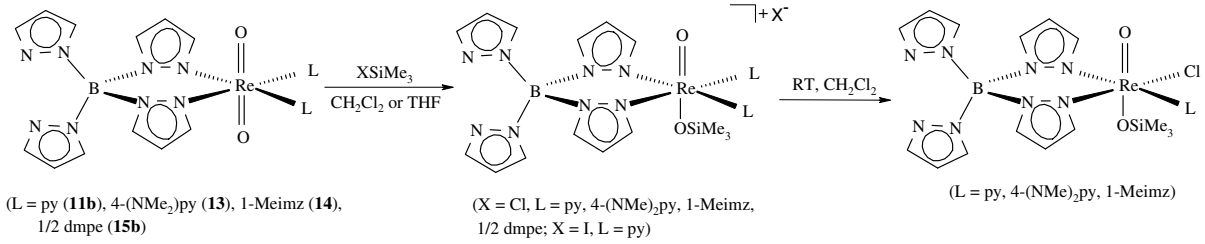

Scheme 16.

for the formation of this unusual Re(VI) *cis*-dioxo complexes [23]. The paramagnetic nature of compounds **18** results in very broad and uninformative ^{1}H NMR resonances, but the X-ray structural analysis of **18a** demonstrated that the two oxo ligands are in a *cis*-arrangement, with the homoscorpionate ligand coordinating in a tridentate and facial way. The Re–O bond lenghts of 1.797(11) and 1.741(10) Å are longer than the typical Re–O triple bonds (1.69(3) Å), but compare well with the Re–O bond distances found in *trans*-dioxo complexes (ca. 1.76(2) Å) [8,45–47]. Compounds **18** are not particularly reactive, being fairly air stable and only slightly water sensitive. As solids or in solution, *cis*-[TpReO$_2$X] (**18**) slowly disproportionate to [TpReO$_3$] (**1a**) and [TpReOX$_2$] [23].

The formation of 18 was considered to go through cationic Re(VII) intermediates [TpReO$_2$X]$^+$ (X = Cl, Br, I), which undergo rapid one electron reduction [23].

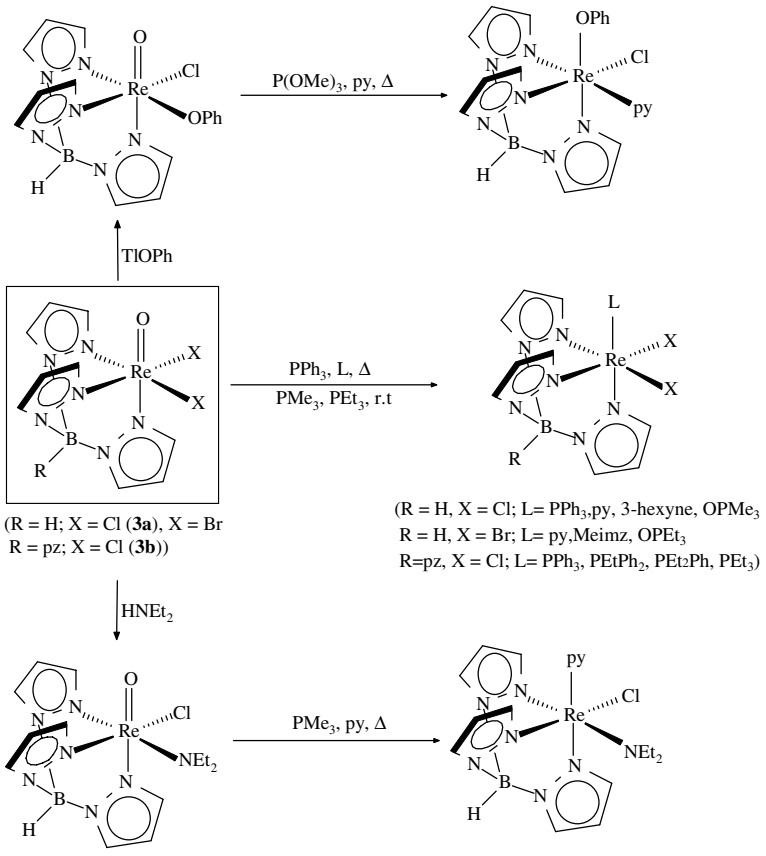

Scheme 17.

Mayer and coworkers [10,31,32,44] also claimed that the related Re(VII) dioxo cations $[Tp'ReO_2Y]^+$ ($Tp' = Tp$, Tp*; Y = aryl, alkyl, hydroxyde, alkoxide) are the key reactive species in the reactions of $[TpReO(OR')_2]$ or $[Tp'ReOY(OTf)]$ with py-O and Me_2SO. The fate of the strongly electrophilic $[Tp'ReO_2Y]^+$ cations, which were never isolated, is quite dependent on the nature of the co-ligands. Alkoxides, alkyl and hydroxy complexes are in general oxidized by py-O or Me_2SO to $[Tp'ReO_3]$ and to the corresponding aldehydes or ketones [10,31,44]. The exception is the oxidation of [Tp*ReO(OTf)(Et)] with Me_2SO, which is not accompanied by release of the expected acetaldehyde [10].

During studies of the oxidation of [Tp′ReO(Ph)OTf] ($Tp' = Tp$, Tp*) with Me_2SO or pyridine *N*-oxide, Mayer and coworkers [10,32] reported the first clear examples of a thermal [1,2]-migration of an aryl group from a metal center to an oxo-ligand (Scheme 20). According to these authors, the phenyl ligand in the Re (VII) intermediates $[Tp'ReO_2(Ph)]^+$ ($Tp' = Tp$, Tp*) migrates to a neighbouring oxo group, forming novel rhenium(V) complexes. However, the nature of the final complexes depends on the scorpionate and on the oxygen atom donor. When Me_2SO is used as oxidant, the reactions proceed with formation of the phenoxide complexes [Tp′ReO(OPh)(OTf)] both for the Tp and Tp* systems. By contrast, the oxidation of [TpReO (Ph)OTf] with py-O led to the formation of a phenoxide and a catecholate, while [Tp*ReO(Ph)OTf] yields a complex mixture of products, which does not include [Tp*ReO(OPh)(OTf)] (Scheme 20) [10,32].

Gable and Brown [16] reduced the compounds $[Tp*ReO_3]$ and $[pzTpReO_3]$ with PPh_3 or $P(OEt)_3$, and evaluated the in situ generated species $\{Tp'ReO_2\}$ ($Tp' = Tp^*$, pzTp) in catalytic oxygen transfer reactions. For the Tp* system, they found efficient catalytic oxygen transfer from epoxides to the stoichiometric phosphorus reductant with consequent deoxygenation of the epoxyde and formation of the corresponding olefin. The catalytic reaction is stereospecific and proceeds more rapidly with *cis*- vs. *trans*-alkenes. These authors also found that the use of Tp* or pzTp has a significant influence on the rate and efficiency of the catalytic cycle, the rate being severely retarded by the presence of pzTp. The higher rate of epoxide deoxygenation achieved with Tp* was considered to be due to the larger steric bulk of Tp*, which disfavor dimerization of the catalytically active $\{Tp*ReO_2\}$ species [16].

2.2.5. Photochemical reactions

Photochemical activation of the complex $[TpReO(C_2O_4)]$ (**8**), by irradiation with UV light, induces reac-

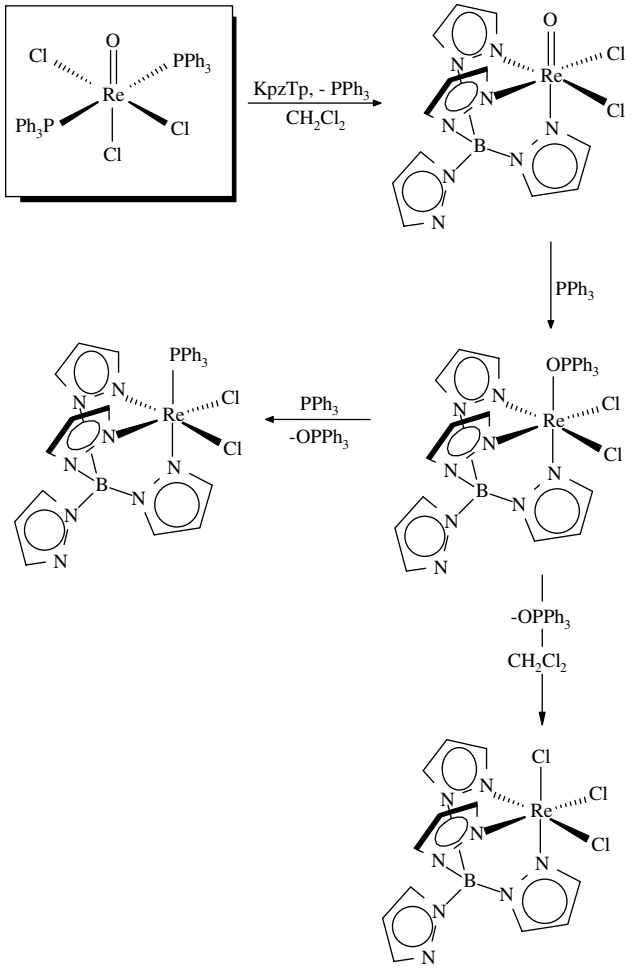

Scheme 18.

tivity towards different substrates (Scheme 21) [33,52]. The authors considered the photochemical process taking place through the reactive transient {TpReO} and with release of CO_2 and CO. The trapping of the intermediate {TpReO} by oxidants like DMSO, $CHCl_3$ and phenanthrenequinone, yielded stable rhenium(V) or rhenium(VII) products (Scheme 21). The starting oxo-oxalate reacts also with the photochemically generated transient yielding the dimer **19**. The reaction with dioxygen was also studied, and the peroxo {TpReO(η^2-O_2)} was formulated as the possible intermediate. This intermediate, which was never isolated, reacts further affording the rhenium(VII) trioxo [$TpReO_3$] [33].

Most of the Re(V) and Re(VII) compounds indicated in Scheme 21 can be obtained either by a photochemical reaction or by a chemical pathway. However, the metallacycle [TpReO($C_9HF_{12}NO_4$)] (**20**) can only be prepared by photolysis of **8**. The formation of **20** results from a condensation of two $(CF_3)_2C{=}O$ molecules and one CH_3CN molecule [52].

Photolysis of [TpReO(Cl)I] (**5**) or [$TpReOI_2$] (**6**) in aromatic hydrocarbons promotes C–H activation of the solvents giving the oxo aryls [TpReOCl(Ph′)] or [$TpReO(Ph')_2$] (Scheme 22). At least one iodide ligand appears to be needed for arylation, as [$TpReOCl_2$] (**3a**) is unreactive [22].

Another interesting result, and a quite rare process in the chemistry of metal transition complexes, is the formation of Re alkoxides by photochemical aryl-to-oxo and alkyl-to-oxo migration in [TpReOCl(Ph)] and [TpReOCl(Et)], respectively. For the phenyl derivative the type of isolated products depends on the reaction conditions (Scheme 23) [22,49]. In the absence of coordinating substrates, photolysis of [TpReOCl(Ph)] in benzene yields two new paramagnetic compounds tentatively assigned as the two diastereomers of the asymmetric [{TpRe(OPh)Cl}(μ-O){TpRe(Ph)(Cl)}] (Scheme 23) [49]. Photolysis in neat CH_3CN or in benzene solutions containing pyridine or Me_3PO produce the paramagnetics adducts [TpReCl(OPh′)(L)] (L = CH_3CN, Me_3PO, py) (Scheme 23), while photolysis in the presence of Me_2SO proceeds with formation of a diamagnetic oxo-phenoxide [TpReOCl(OPh)], due to oxygen atom transfer from Me_2SO. Mechanistic studies showed that the phenyl to oxo migration occurs predominantly via an intramolecular [1,2]-shift. Mayer and coworker [49] also reported that photolysis of the oxo alkyl [TpReOCl(Et)], in the presence of pyridine, gave [TpReCl(OEt)(py)], but the net ethyl migration seems to involve free ethyl radicals.

2.3. Hydrides and oxo-hydrides

Crabtree et al. [53] reported the complexes [$TpReH_6$] and [$TpReH_4(PPh_3)$] which were prepared by reacting $LiAlH_4$ with [$TpReOCl_2$] (**3a**) and

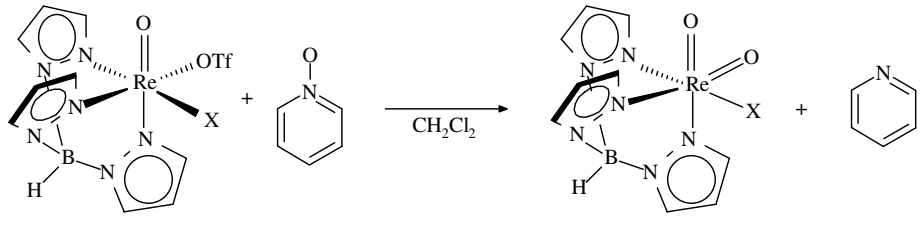

(X = Cl, Br, I) (X = Cl (**18a**), Br (**18b**), I (**18c**))

Scheme 19.

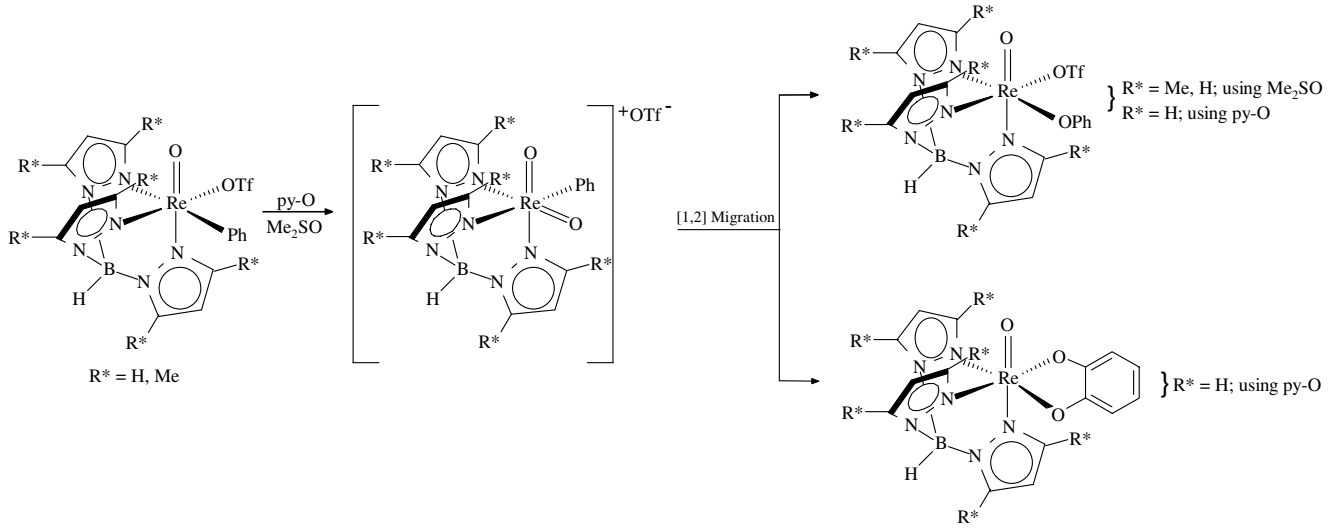

Scheme 20.

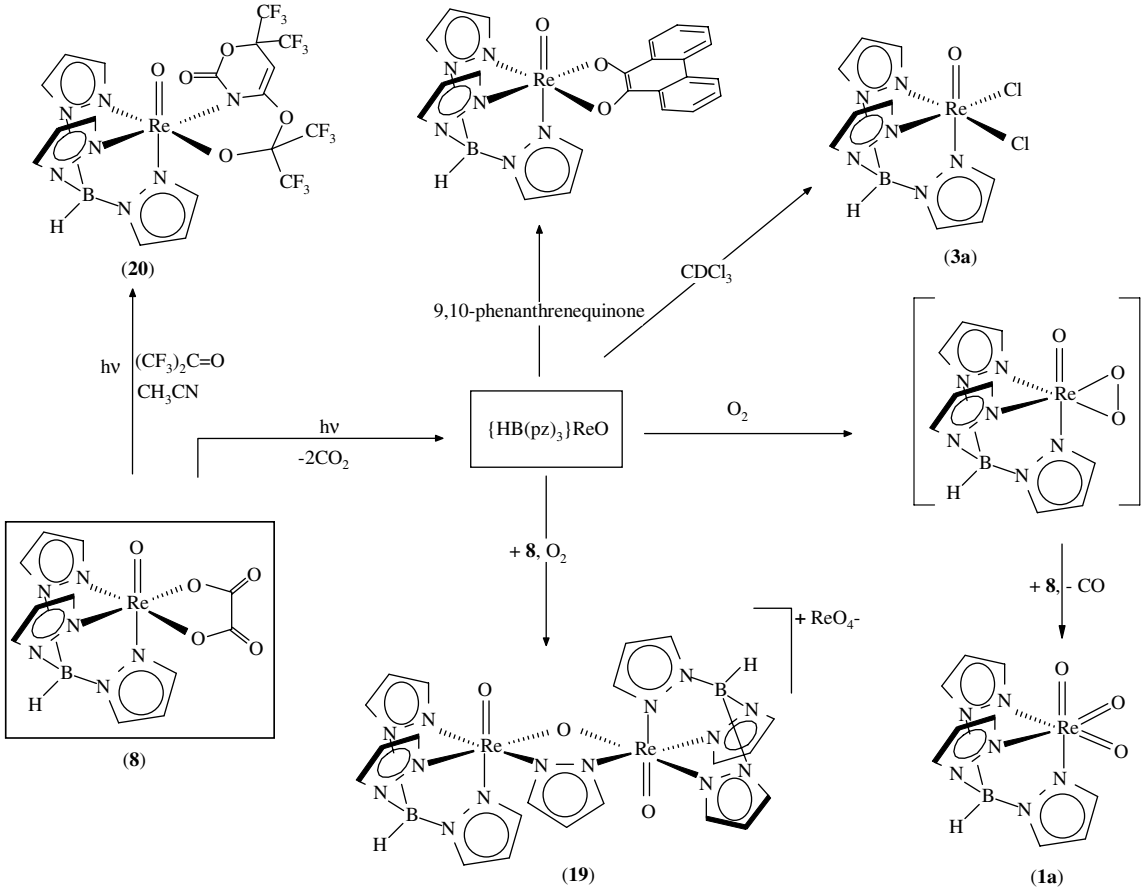

Scheme 21.

[TpReCl$_2$(PPh$_3$)], respectively. Based on T_1 and J_{H-D} measurements, a classical character has been proposed for both hydrides.

Santos et al. described a novel route for preparing Re(III) (**21**) and Re(V) (**22**) hydride complexes, which is based on the reaction of [ReOCl$_3$(PPh$_3$)$_2$] with hetero-scorpionates, using alcohols as the solvent (Scheme 24). These authors also studied the reaction of [ReOCl$_3$(PPh$_3$)$_2$] with Na[Ph$_2$Bp] in methanol. In this case, as expected, no hydrides were formed and, from a mixture of oxocomplexes, it was possible to isolate [ReO(OMe){κ^2-Ph$_2$B(OMe)(pz)}$_2$] [54].

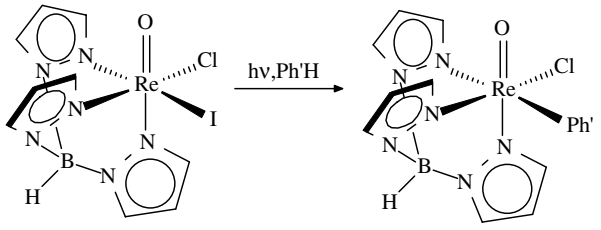

(**5**)

(Ph' = phenyl, p-anisyl, p-phenoxyphenyl, 2,4-dimethylphenyl,2,5-dimethylphenyl)

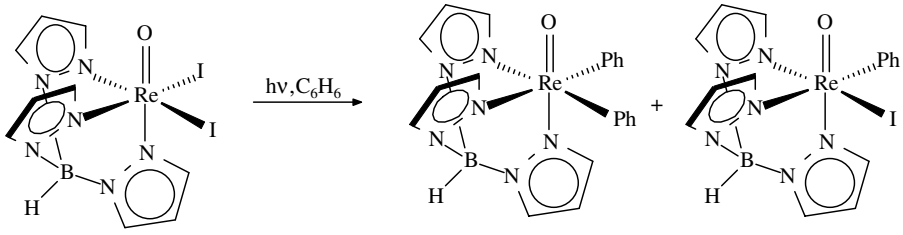

(**6**)

Scheme 22.

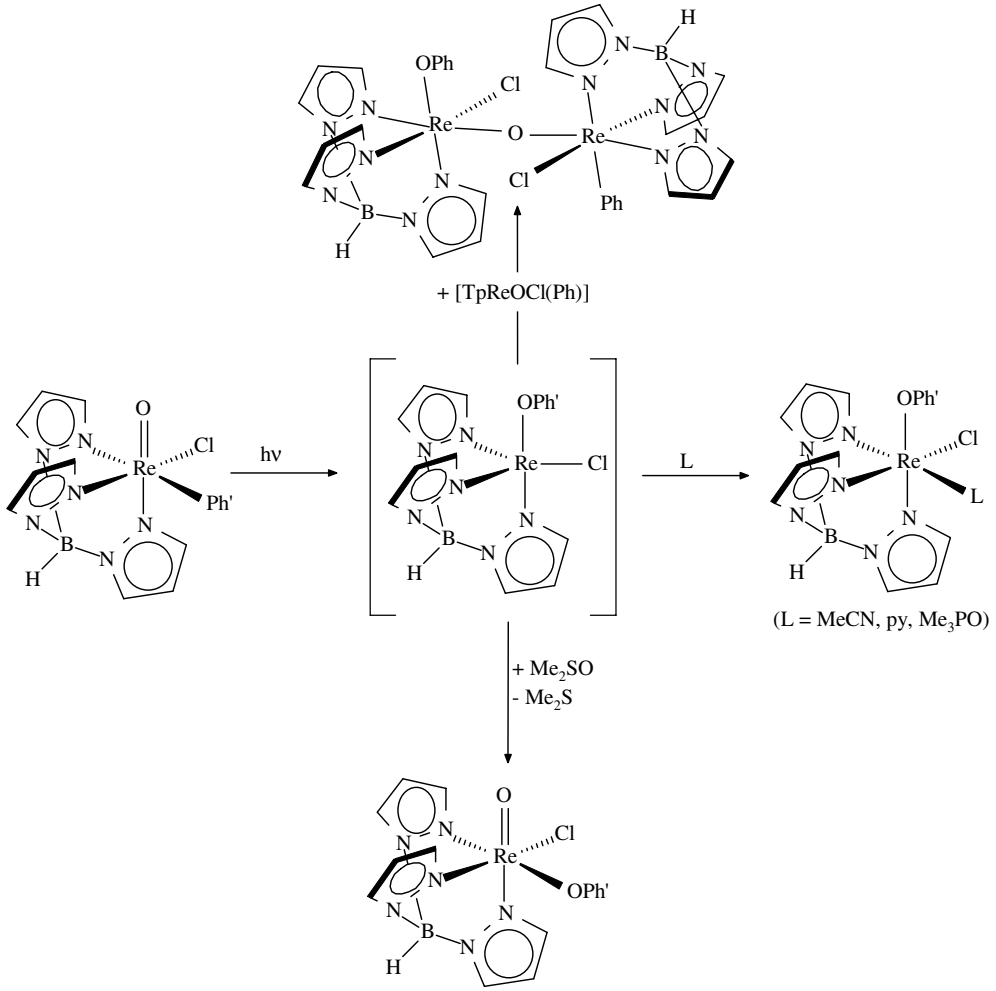

(L = MeCN, py, Me_3PO)

Scheme 23.

The crystal structures of **21a** and **22b** were determined, but the hydride ligands were not located by X-ray. The structural parameters of these hydrides were tentatively assigned by a combination of X-ray diffraction and Molecular Orbital calculations of ab initio and Extended Hückel (EHMO) type [54]. The structures of **21a** and **22b** are the first examples of Re(III) and Re(V) hydrides anchored by asymmetric heteroscorpionates, coordinated in a κ^3-(*N*,*N*,*O*) fashion. The spectroscopic, structural and theoretical studies performed on **21** and **22** indicated a classical character for these hydrides [54].

Recently, Mayer and coworkers [55] reported the quite unusual oxo-hydrides [Tp*ReO(H)Cl] (**23**), [Tp*ReO-$(H)_2$] (**24**) and [TpReO(H)Cl] synthesized by reacting [Tp*ReO(OMe)Cl], [Tp*ReO$(OMe)_2$] or [TpReO(OEt)-Cl] with BH_3·THF in toluene at low temperatures (Scheme 25). Prolonged reactions of [Tp*ReO$(OR')_2$] ($R' = OMe$, OEt) with excess BH_3·THF afford Tp*ReH_6 as the only isolable rhenium product [10].

Complex **23** yields [Tp*ReO(H)(OTf)] (**25**) by metathesis with AgOTf in benzene/CH_2Cl_2 [10,55]. Compound **25** is six-coordinate and displays a distorted octahedral coordination geometry, with the hydride ligand in one of the octahedral sites (Re–H, 1.69 Å) [10].

Compound **25** reacts with $CDCl_3$, acetaldehyde, ethylene and propylene affording [Tp*ReO(Cl)(OTf)], [Tp*ReO(OEt)(OTf)], [Tp*ReO(CH_2CH_3)(OTf)] and [Tp*ReO$(CH_2CH_2CH_3)$(OTf)], respectively [10]. The triflate ligand in **25** is easily displaced by pyridine yielding the cationic compound [Tp*Re(O)H(py)][OTf]. This cation is also formed, together with [Tp*ReO_3] (**1c**), when **25** is treated with pyridine *N*-oxide. Using Me_2SO as the oxygen atom transfer reagents, **25** is oxidized mainly to [Tp*ReO_3]. By analogy with phenyl-to-oxo migrations, the mechanism proposed for these oxidation reactions involves a [1,2]-migration of the hydride to an oxo ligand in [Tp*$ReO_2H]^+$, via the intermediate [Tp*Re(O)(OH)(OTf)], which is further oxidized to **1c**.

2.4. Carbonyl complexes

In the late 1960, the tricarbonyl compounds [Tp′Mn$(CO)_3$] (Tp′ = Tp, pzTp) were the first reported group 7 scorpionate complexes [56,57]. Subsequently, several research groups extended the chemistry of homoscorpionate tricarbonyl complexes to Tc and Re. The structurally characterized [Tp′M$(CO)_3$] (M = Tc, Re; Tp′ = Tp*, Tp) were synthesised by reaction of the starting materials [M$(CO)_5$Br] or [M$(CO)_4$(μ-Cl)]$_2$ with the sodium or potassium salts of the correspondent Tp′ ligands [58–60]. The tridentate and facial coordination of the scorpionates, and the facial arrangement of the CO ligands are common structural features of the [Tp′M$(CO)_3$] (M = Mn, Tc, Re; Tp′ = Tp, Tp*) complexes [60].

By contrast, the chemistry of group 7 heteroscorpionate carbonyl complexes is much more limited, being almost restricted to [BpM$(CO)_3$(pzH)] (M = Mn, Re) [61]. In these compounds, the three CO ligands are facially coordinated and the three remaining coordination sites are occupied by the bidentate dihydrobis(pyrazolyl)borate and a pyrazole, arising from partial fragmentation of the Bp ligand [61]. Interestingly, a similar reaction with Na[H_2B(tim^{Me})$_2$], a soft congener of Bp, yields almost quantitatively a tricarbonyl complex with the heteroscorpionate coordinating through the two thione sulfurs and one robust agostic B–H···Re interaction [62].

Ultraviolet irradiation of complexes [Tp′M$(CO)_3$] (M = Mn, Tc, Re) in THF led to the adducts [Tp′M$(CO)_2$(THF)] [59,63,64]. In these complexes, the THF ligand is quite labile and easily replaced by other donors with formation of compounds of general formula [Tp′M$(CO)_2$(L)] (M = Mn, Tc, Re) (Scheme 26) [59,63,64]. Complexes [Tp′M$(CO)_2$(THF)] (M = Tc, Re) react also with N_2 forming the dinuclear species [Tp′M$(CO)_3]_2$(μ-N_2) (M = Tc, Tp′ = Tp*; M = Re, Tp′ = Tp) (Scheme 26) [66,67]. Complex [Tc(κ^3-

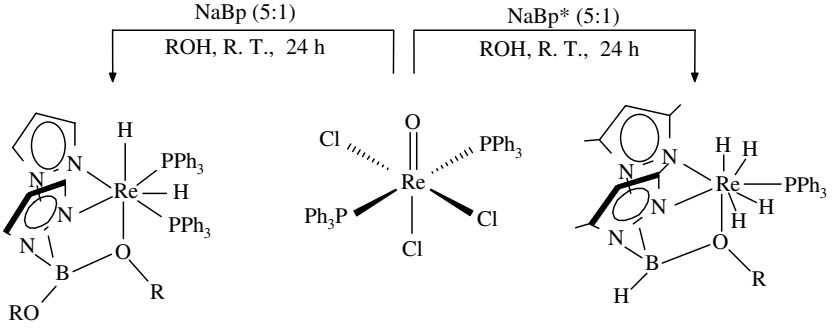

Scheme 24.

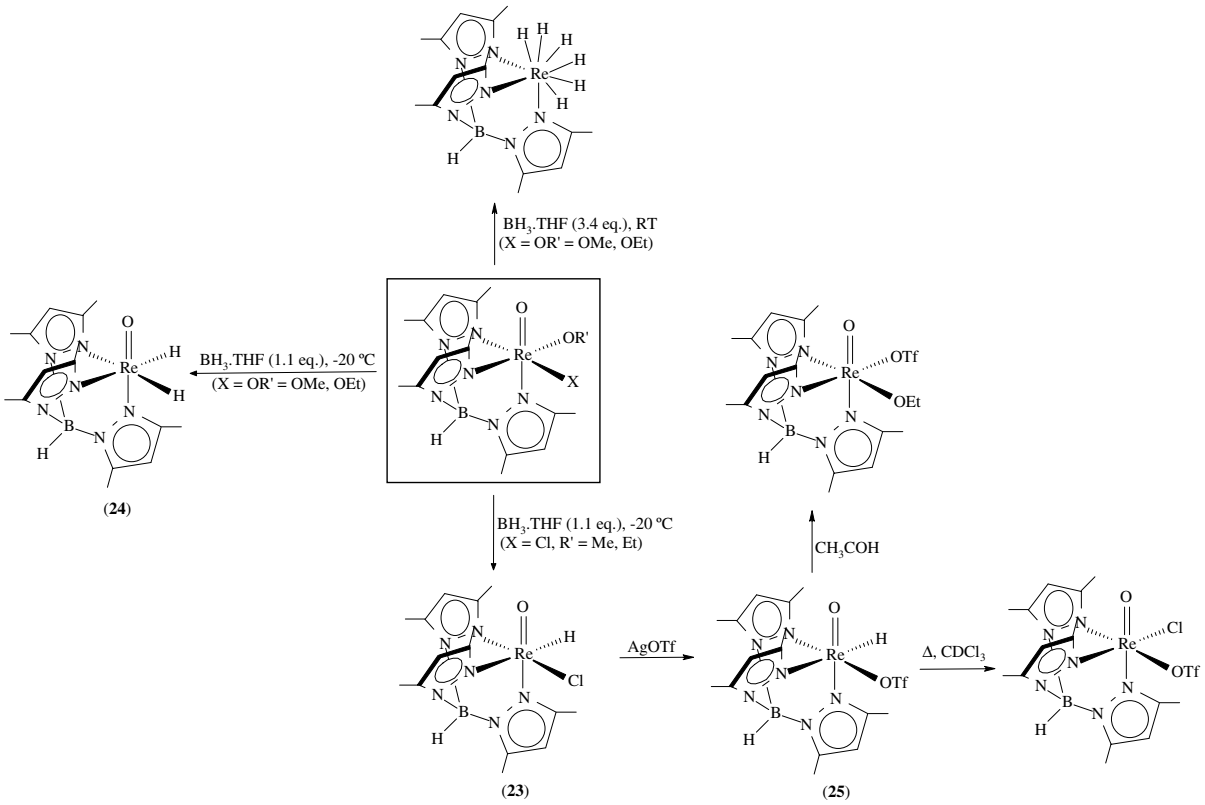

Scheme 25.

Tp)$(CO)_2(PPh_3)$] was alternatively prepared by a metathesis reaction of $[TcCl(CO)_2(PPh_3)_2]$ with KTp [65].

The monomeric di(carbonyl) complexes [Tp′M$(CO)_2$-(L)] (M = Mn, Tc, Re) are six-coordinate, and present an approximately octahedral coordination geometry. The most relevant structural parameter is the shortening of the M–N bond *trans* to the neutral co-ligand (L = THF, PR_3, $P(OR)_3$) [59,64,65]. The dinitrogen-bridged bimetallic complexes [Tp′M$(CO)_3]_2(\mu\text{-}N_2)$ (M = Tc, Tp′ = Tp*; M = Re, Tp′ = Tp) were also structurally characterized, and a different orientation for the scorpionates in the Re and in the Tc compounds was found (Scheme 26). These dimers are unique examples of structurally characterized dinitrogen bridged ditechnetium or dirhenium complexes, and the M(μ-N_2)M moieties are best described as possessing M–N single and N–N triple bonds [66,67].

Recently, Harman and coworkers studied the reactivity of [TpRe$(CO)_2$(THF)] (**26**) towards unsaturated substrates, namely cyclopentene, furan, thiophene, naphthalene and *N*-methylpyrrole, in order to stabilize monomeric complexes containing η^2-bound aromatic ligands (Scheme 27). The postulated monomeric or dimeric structures for the products, and the coordination mode of the unsaturated substrates were based on IR and NMR spectroscopy [67].

To avoid the dimerization process observed in these reactions, Harman and coworkers replaced one of the CO ligands in the fragment {TpRe$(CO)_2$} by a weaker π-acid or stronger σ-donor ligand. Consequently, the resulting fragments, {TpRe(CO)(L)} (L = ^{t}BuNC, PMe_3, NH_3, 1-Meimz), were more π-basic and were able to bind a series of aromatic molecules, without undergoing dimerization or oxidative addition reactions (Schemes 28 and 29) [50,68,69]. Among the more π-basic compounds, [TpRe(CO)(1-Meimz)(η^2-C_6H_6)] (**27**) proved to be remarkably versatile for the direct synthesis of organometallic derivatives with a variety of unsaturated substrates coordinated in a π-fashion to the metal center (Scheme 29). The authors found that, under nitrogen, the rate of dissociation of the dihapto-coordinate aromatic ligand decreases as the fragment becomes more electron-rich, while the stability to air shows a somewhat inverse trend [50,68–73].

X-ray diffraction analysis was performed on the different [TpRe(CO)(L)(η^2-L_π)] (L = ^{t}BuNC, PMe_3, py, NH_3, 1-Meimz) complexes [50,69,70]. In all, the coordinate double bond of the aromatic ligand (L_π) is oriented perpendicular to the rhenium carbonyl bond, in order to optimize π-back-bonding. [50,69,70]. Due to their asymmetric character, the [TpRe(CO)(L)(η^2-L_π)] compounds exist in solution as two diastereomers, which undergo a non-dissociative interconversion (Scheme 30). The author claims that such interconversion occurs via both interfacial and intrafacial migrations. NOE and 2D NMR techniques allowed the

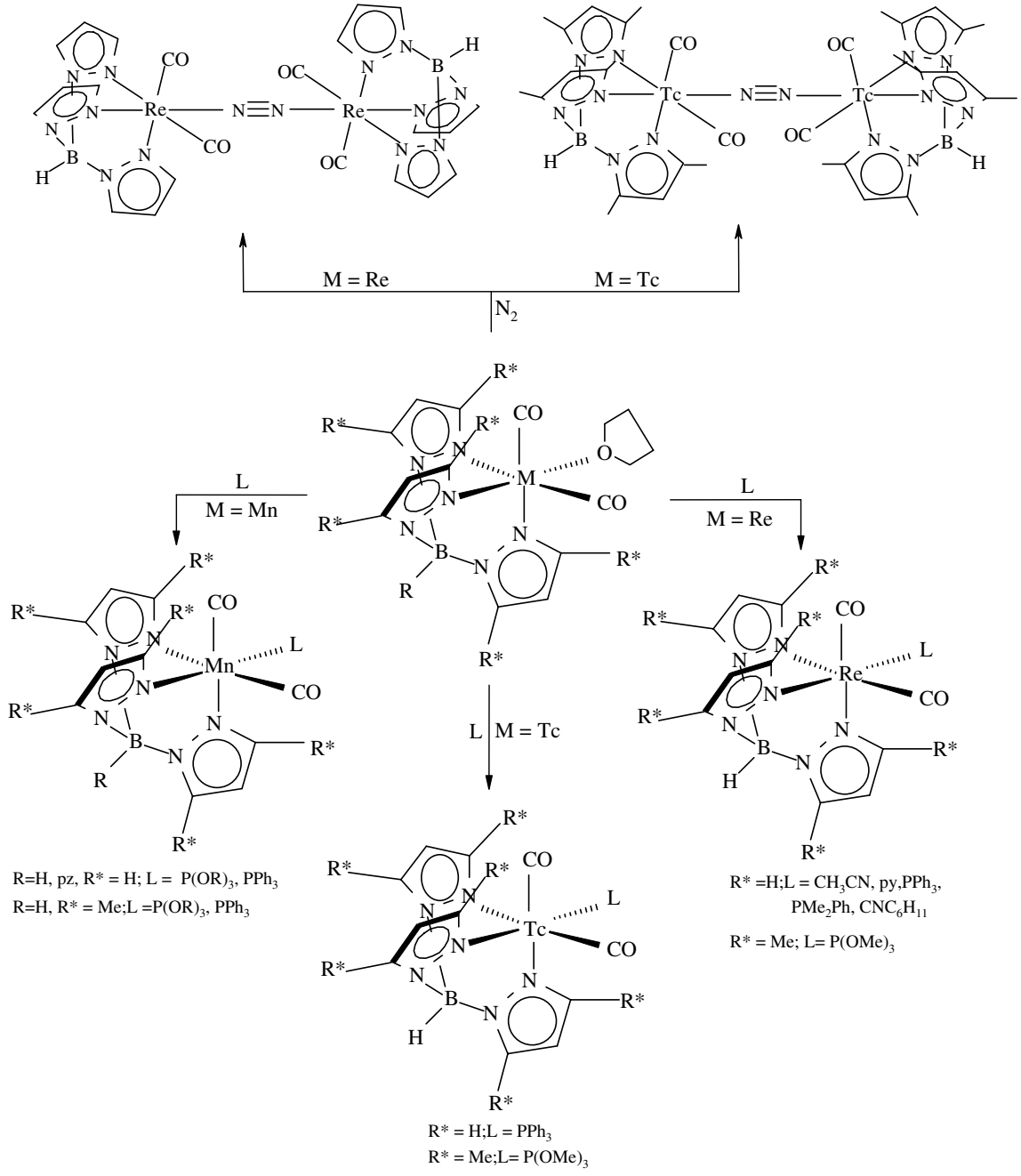

Scheme 26.

identification of each diastereomer and ^{1}H NMR spin transfer experiments were used to calculate the rate and free energy of activation for the isomerization processes [74]. The diastereoselectivity exhibited by these systems is very much dependent on the nature of the L and L_π ligands, being governed by the relative steric interaction of L and *trans* pyrazole ring with the L_π (Scheme 30).

Due to the volume of PMe_3, a single diastereomer predominates in complex [TpRe(CO)(PMe_3)(η^2-naphthalene)] (**A**, Scheme 30) [50,74]. The resolution of racemic [TpRe(CO)(1-Meimz)(η^2-benzene)] into the *R* and *S* enantiomers was achieved using (*R*)-α-pinene as a chiral auxiliary and based on an elaborated series of redox and substitution reactions [75].

The η^2-coordination of the aromatic substrates to the π-basic metal fragments [TpRe(CO)(L)] is accompanied by the disruption of the aromaticity through π-back-bonding. For example, the crystal structure of [TpRe(CO)(1-Meimz)(η^2-benzene)] (**27**) shows dearomatization to such an extent that the uncoordinated portion of the benzene ring closely resembles cyclohexadiene [70]. This dearomatization explains why **27** undergoes a

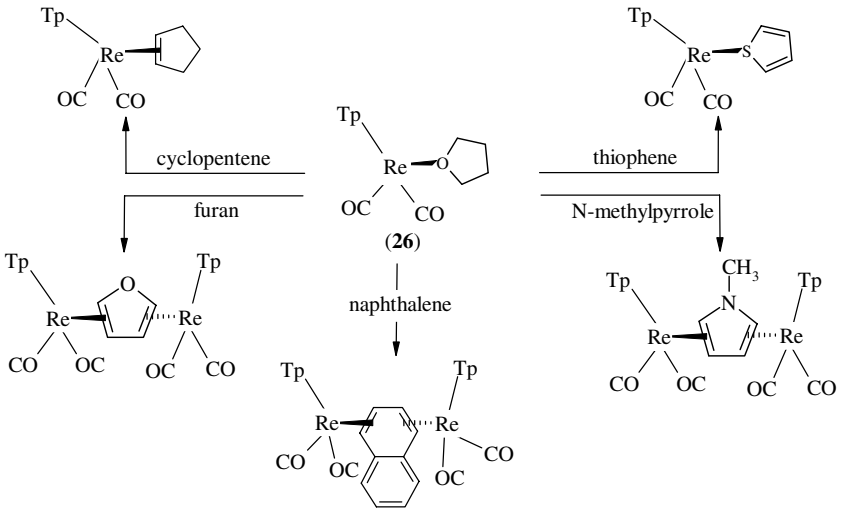

Scheme 27.

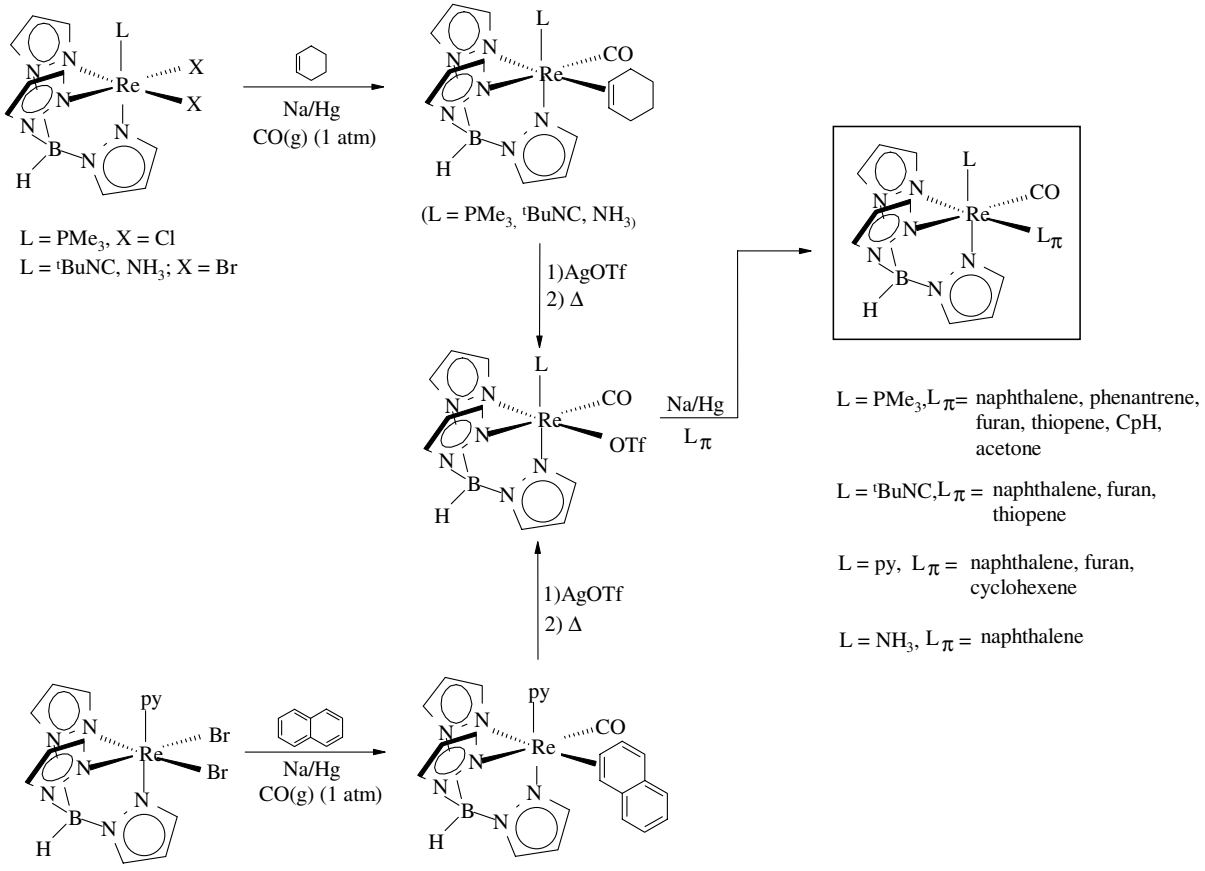

Scheme 28.

Diels-Alder cyclo-addition with *N*-methylmaleimide (NMM) with a specific rate that is 60% faster than that observed for cyclohexadiene (Scheme 31) [76].

X-ray crystallographic analysis of the complex from the cyclo-addition process, **28**, confirmed that the reaction occurs exclusively at the arene face non-coordinated to the metal with exclusive *endo* selectivity. Oxidation of the metal center promotes decomplexation with liberation of bicyclo[2.2.2]-octadiene and/or octenone products, depending on the oxidation conditions (Scheme 31) [76].

Coordination of furans to the fragments {TpRe(CO)(L)} (L = ^{t}BuNC, PMe_3, 1-Meimz) activates these heterocycles towards cycloaddition reactions with dif-

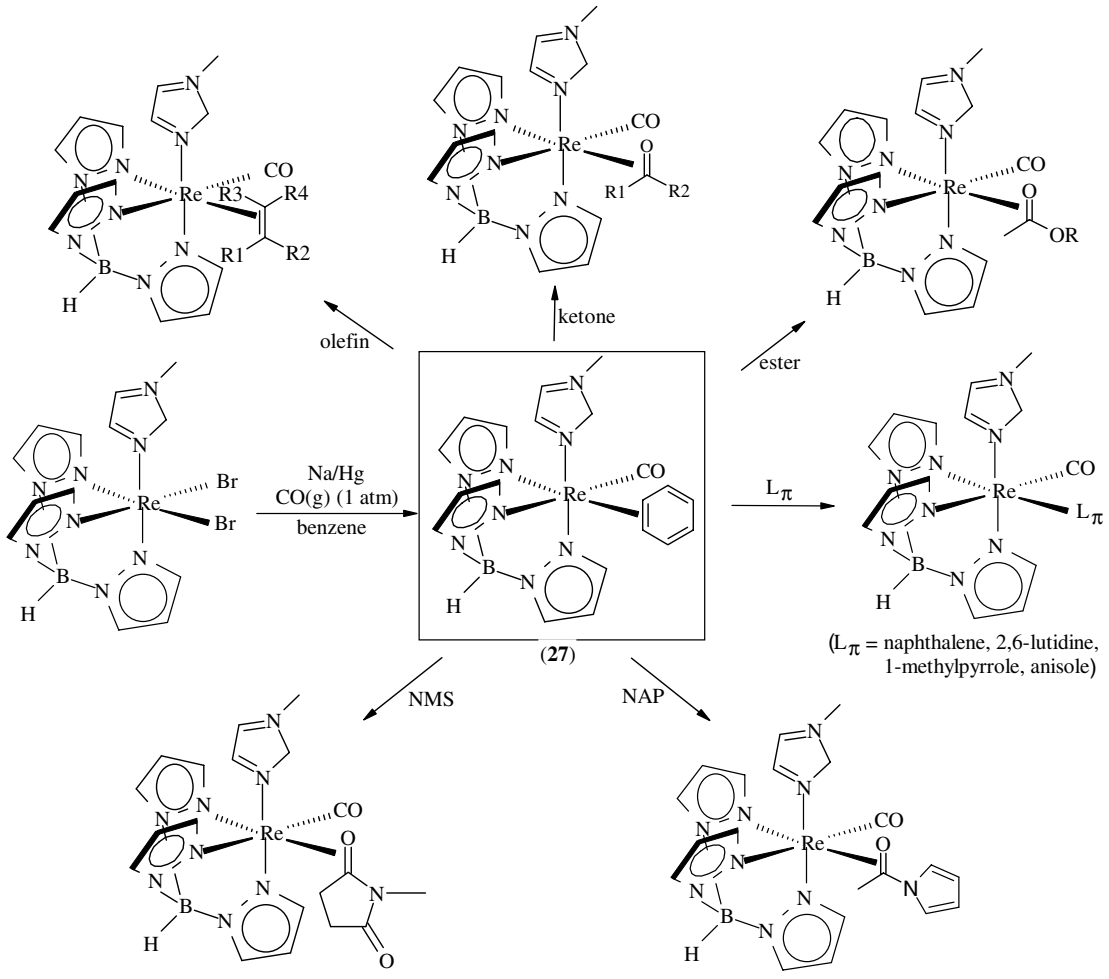

Scheme 29.

ferent dienophiles. When the furan is bound through the 4,5-positions it undergoes [2 + 2] cyclizations, while [3 + 2] cycloaddition reactions occur when the heterocycle is bound through the 3,4-positions [77].

The acid-catalysed addition of methanol to the coordinated furan in complexes [TpRe(CO)(L)(η^2-furan)] (L = ^{t}BuNC, PMe_3, py, 1-Meimz) was also evaluated. In traditional organic reactions methanol attacks at the 3-position of furan, but in these Re(I) systems the reactions occur at the 2-position, and two diastereomers of η^2-coordinated 2-methoxy-2,3-dihydrofurans are formed (Scheme 32) [78].

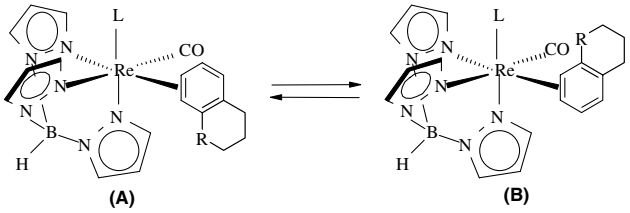

Scheme 30.

The complexes [TpRe(CO)(L)(η^2-naphthalene)] (L = PMe_3, NH_3, py, 1-Meimz) undergo tandem electrophilic/nucleophilic addition reactions, by sequential treatment with triflic acid and a siloxypropene derivative, leading to 1,4- or 1,2-addition products (Scheme 33) [79]. The regioselectivity of these reactions depends on the nature of the co-ligand L. The key for the regiocontrol seems to be the formation of single 1H-naphthalenium intermediates and its orientation relatively to the CO bond, as depicted in Scheme 33. The PMe_3 complex promotes predominantely the 1,4-addition products, while all the other favor the 1,2-addition [79].

3. 5f-Element scorpionate complexes

3.1. Trivalent complexes

3.1.1. Bis- and mono-homoscorpionates

The unique and fully characterized Pu complex is the dimer [PuCl(μ–Cl)(κ^3-Tp*)(Me_2pzH)]$_2$, which has been isolated in good yield by reacting $PuCl_3$ and NaTp*, in

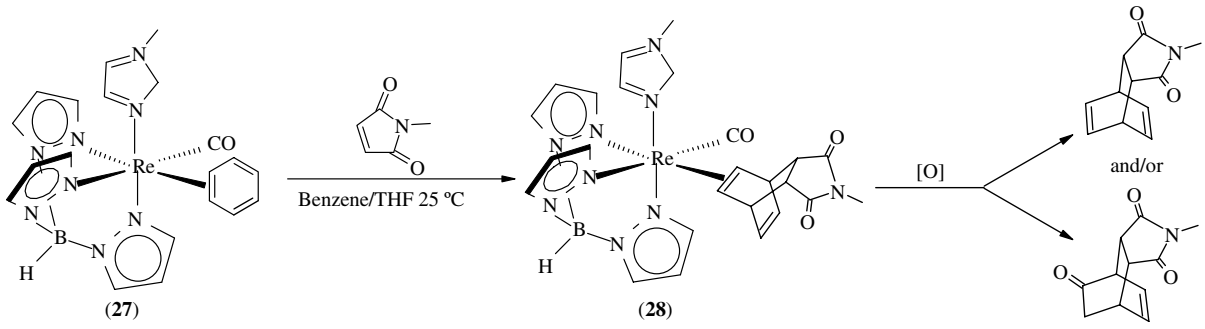

Scheme 31.

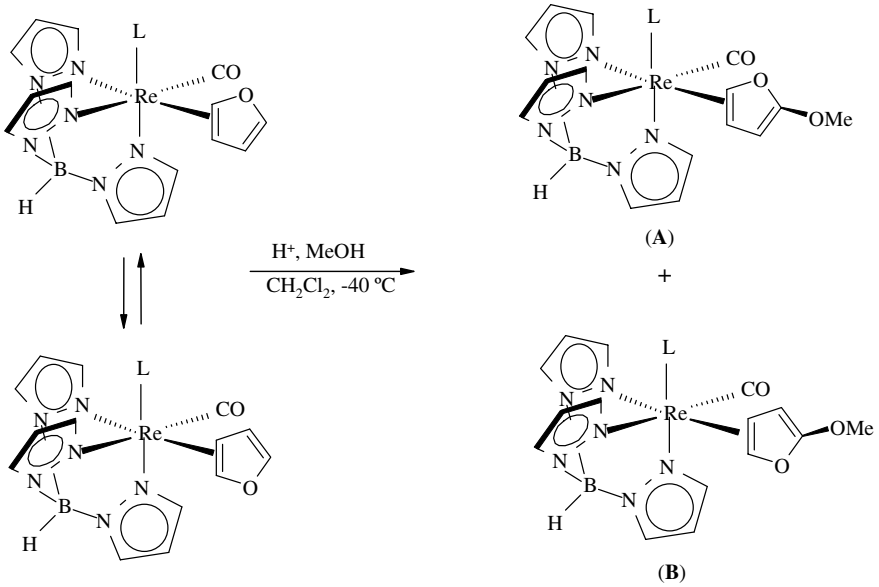

	A:B
L = ^{t}BuNC	1:2
PMe_3	2:1
py	1:1
1-Meimz	1:3

Scheme 32.

refluxing THF during 2 weeks. The synthesis of another plutonium(III) compound, $[PuTp_3]$, was also mentioned, but no details were given [2,80].

Bis- and mono-Tp* U(III) complexes have been synthesized by metathesis of $[UI_3(THF)_4]$ or $[UCl_3(THF)_x]$ in THF (Scheme 34). The iodide derivatives $[(\kappa^3\text{-Tp*})_2UI]$ (**29**) and $[(\kappa^3\text{-Tp*})UI_2(THF)_2]$ (**30**) were fully characterized, including X-ray crystallographic analysis [81,82]. The chloride compound was never characterized in the solid state and its formulation was based on spectroscopic data, as well as on the reactivity towards unsaturated substrates (Scheme 34) [83,84].

Compound **29** readily undergoes iodide abstraction with $TlBPh_4$ to form $[(\kappa^3\text{-Tp*})_2U(THF)]$ $[BPh_4]$ (**31**) [81]. This cation is stable in the solid state but tends to decompose in THF solution. X-ray structural characterization of **29**, **30** and **31** showed that these compounds are seven-coordinate, displaying a distorted capped octahedral coordination geometry. An interesting feature in **29** is the different coordination mode of the two Tp* ligands: one ligand binds normally through three nitrogen atoms, while the other contains one pyrazolyl ring bonded to uranium through both of its nitrogen atoms [82,85].

Takats et al. demonstrated the utility of $[(\kappa^3\text{-Tp*})UI_2(THF)_2]$ as precursor for further derivatization, and by metathesis $[(\kappa^3\text{-Tp*})U\{N(SiMe_3)_2\}I]$, $[(\kappa^3\text{-Tp*})U\{N(SiMe_3)_2\}_2]$, $[(\kappa^3\text{-Tp*})U\{N(SiMe_3)_2\}\{CH(SiMe_3)_2\}]$ and $[(\kappa^3\text{-Tp*})U\{CH(SiMe_3)_2\}_2(THF)]$ were synthesized. The

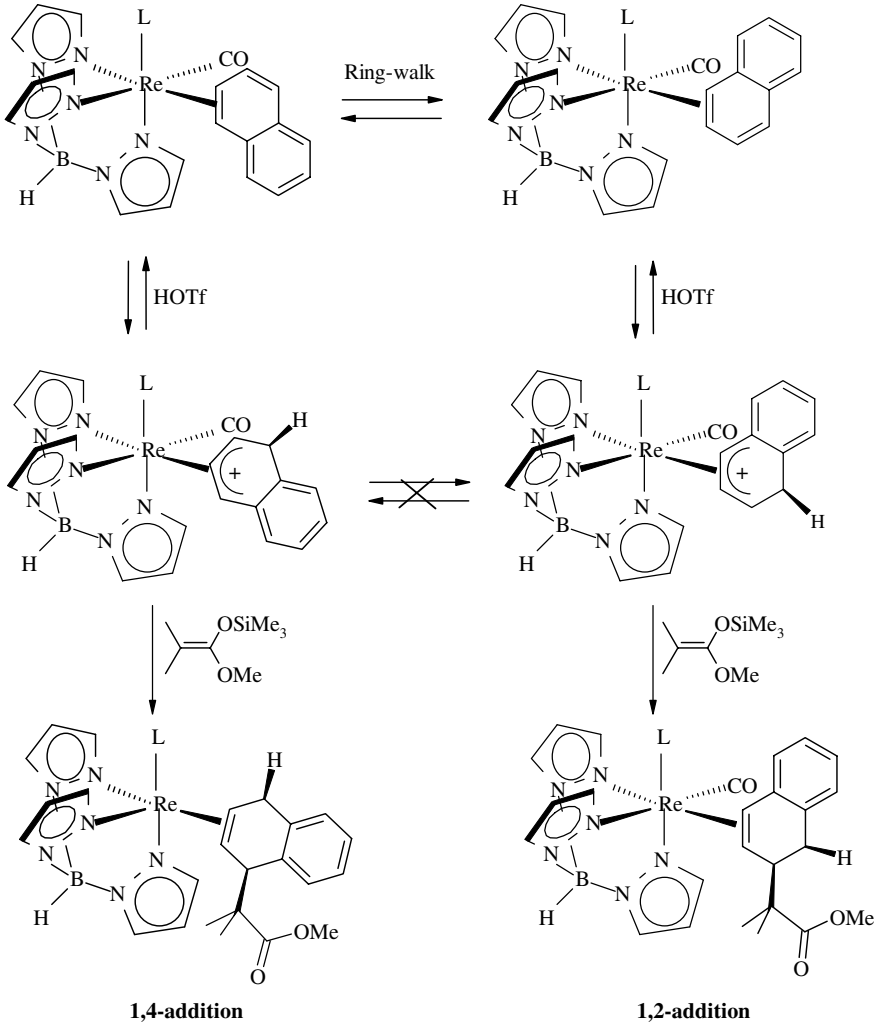

Scheme 33.

bis-amido, bis-alkyl and mixed amido-alkyl derivatives are five- or six-coordinate, displaying trigonal bipyramidal and distorted octahedral coordination geometries [85]. In contrast to $[(\kappa^3\text{-Tp*})U\{N(SiMe_3)_2\}I]$, compounds $[(\kappa^3\text{-Tp*})U\{N(SiMe_3)_2\}_2]$ and $[(\kappa^3\text{-Tp*})U\{CH(SiMe_3)_2\}_2(THF)]$ are thermally unstable in solution and the decomposition process is solvent dependent [85].

Taking advantage of the possibility of introducing different substituents in the 3-position of the pyrazole ring, the podand $Tp^{2\text{-py}}$ ligand has been synthesized. Takats et al. has shown that $[UI_3(THF)_4]$ reacts with $KTp^{2\text{-py}}$ in the 1:2 ratio in THF yielding the homoleptic $[(Tp^{2\text{-py}})_2U]I$. This complex is 12-coordinate by the six nitrogen atoms of the pyrazolyl rings and by the six nitrogen atoms of the pyridyl groups, displaying an unusual icosahedral coordination geometry [86].

Recently, Santos and coworkers [87] have shown that $[UI_3(THF)_4]$ reacts with $KTp^{i\text{Pr}2}$ in THF yielding $(\kappa^3\text{-}Tp^{i\text{Pr}2})UI_2(THF)_{2\text{–}3}]$. This compound is unstable in solution, the main decomposition product being $[(\kappa^3\text{-}Tp^{i\text{Pr}2})UI_2(Hpz^{i\text{Pr}2})]$ (**32**) [87a]. Interestingly, when $[UI_3(THF)_4]$ is treated with $KTp^{i\text{Pr}2}$ in toluene in the presence of other Lewis bases, different from THF, stable mono-$Tp^{i\text{Pr}2}$ complexes can be prepared. These quite robust compounds of general formula $[(\kappa^3\text{-}Tp^{i\text{Pr}2})UI_2(L)_x]$ ($L = OPPh_3$, $x = 1$; L = bipy, $x = 1$; L = py, $x = 2$; $L = Hpz^{t\text{Bu,Me}}$, $x = 2$) were obtained in relatively high yields (65–75%) (Scheme 35). The compounds $[(\kappa^3\text{-}Tp^{i\text{Pr}2})UI_2(OPPh_3)]$, $[(\kappa^3\text{-}Tp^{i\text{Pr}2})UI_2(bipy)]$, $[(\kappa^3\text{-}Tp^{i\text{Pr}2})UI_2(py)_2]$ and $[(\kappa^3\text{-}Tp^{i\text{Pr}2})UI_2(Hpz^{i\text{Pr}2})]$ are six- or seven-coordinate, depending on the steric bulk of the neutral co-ligand.

The six-coordinate compound $[(\kappa^3\text{-}Tp^{i\text{Pr}2})UI_2(OPPh_3)]$ displays an octahedral coordination geometry, while the seven-coordinate $[(\kappa^3\text{-}Tp^{i\text{Pr}2})UI_2(bipy)]$ and $[(\kappa^3\text{-}Tp^{i\text{Pr}2})UI_2(py)_2]$ display, respectively, distorted capped octahedral and pentagonal bipyramidal geometries. Initially, $[(\kappa^3\text{-}Tp^{i\text{Pr}2})UI_2(Hpz^{i\text{Pr}2})]$ (**32**) was considered as six-coordinate, by the three nitrogen atoms of the $\kappa^3\text{-}Tp^{i\text{Pr}2}$, two iodides and one nitrogen of the $Hpz^{i\text{Pr}2}$. However, a careful analysis of the relevant structural parameters has shown an additional interaction between

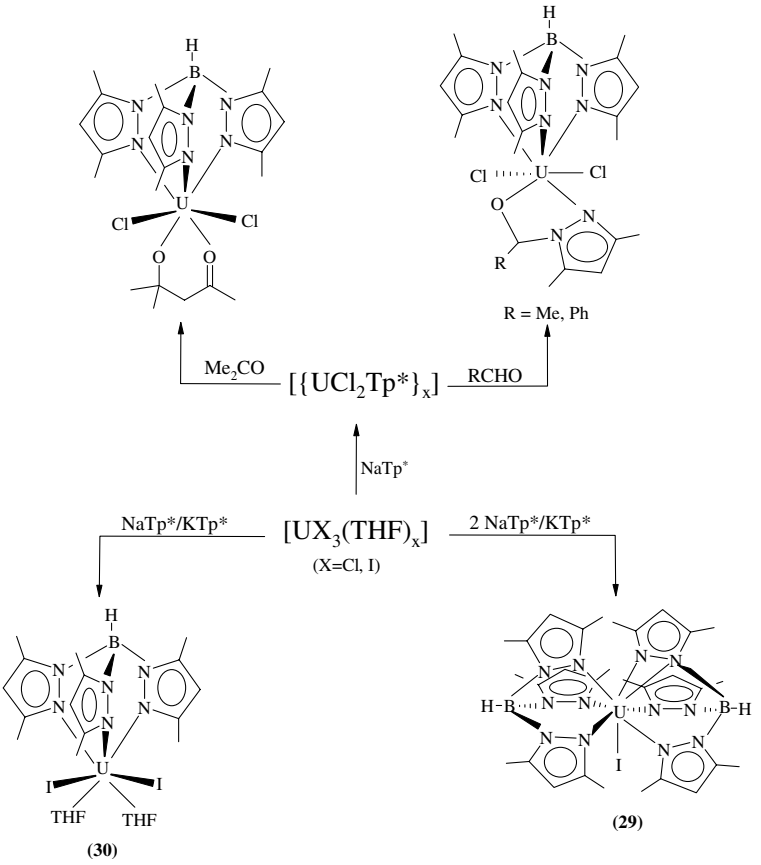

Scheme 34.

the metal and one hydrogen atom of one ^{i}Pr(3) of the Tp$^{i\mathrm{Pr}2}$. This seven-coordinate compound displays a capped octahedral coordination geometry with the axial position defined by the hydrogen atom of the ^{i}Pr group interacting with the metal (U–H, 3.06 Å) and by the nitrogen atom of Hpz$^{i\mathrm{Pr}2}$ [87a].

3.1.2. Tris-, mono- and bis-heteroscorpionates

Uranium tricloride or uranium triiodide react with KBp, KBp*, NaPh$_2$Bp and KBp$^{i\mathrm{Pr}2}$ in a 1:3 ratio yielding [(κ^3-Bp)$_3$U(THF)], [(κ^3-Bp)$_3$U], [(κ^2-Ph$_2$Bp)$_3$U] and [(κ^3-Bp$^{i\mathrm{Pr}2}$)$_3$U, respectively (Scheme 36) [87–90].

These homoleptic and monomeric compounds present high solubility in toluene and *n*-hexane. In all the six nitrogen atoms of the three ligands are arranged in a trigonal prismatic geometry around the U(III) center. For [(κ^3-Bp)$_3$U(THF)], [(κ^3-Bp*)$_3$U] and [(κ^3-Bp$^{i\mathrm{Pr}2}$)$_3$U] each of the three rectangular faces of the trigonal prism is capped by an agostic B–H$\cdots$U interaction, leading in the case of [(κ^3-Bp*)$_3$U] and [(κ^3-Bp$^{i\mathrm{Pr}2}$)$_3$U] to formally nine-coordinate compounds and in the case of [(κ^3-Bp)$_3$U(THF)] to a 10-coordinated compound, due to the presence of the THF molecule. The [(κ^2-Ph$_2$Bp)$_3$U] compound is six-coordinate by the nitrogen atoms of the three κ^2-Ph$_2$Bp ligands, and displays a trigonal prismatic geometry, with a C_{3h} molecular symmetry. The long U$\cdots$B distances observed in [(Ph$_2$Bp)$_3$U] (mean value of 3.817 Å) excludes any interaction of the metal with the phenyl groups [90].

Since the bulky and symmetrical substituents in the 3-position of the Bp ligand can be expected to avoid the formation of homoleptic compounds, Santos et al. studied the chemistry of U(III) with KBp$^{t\mathrm{Bu,Me}}$. In fact, metathesis of [UI$_3$(THF)$_4$] with KBp$^{t\mathrm{Bu,Me}}$ in THF yields the first mono-Bp$^{t\mathrm{Bu,Me}}$ f-element compound [(κ^3-Bp$^{t\mathrm{Bu,Me}}$)UI$_2$(THF)$_2$] (**33**) (Scheme 36) [90]. In **33** the THF is easily replaced by OPPh$_3$, bipy, Hpz$^{t\mathrm{Bu,Me}}$ or Hpz$^{\mathrm{Me}_2}$, and the resulting seven-coordinate compounds all retain the agostic B–H$\cdots$U interaction.

The molecular structure of these ''half-sandwich'' complexes and their dynamic behavior in solution indicated a metal center relatively unprotected from incoming ligands. Therefore, the possibility of preparing bis-Bp$^{t\text{-}\mathrm{Bu,Me}}$ complexes was a challenge and has been studied. It was found that [UI$_3$(THF)$_4$] reacts with KBp$^{t\text{-}\mathrm{Bu,Me}}$ in a 1:2 ratio in toluene yielding the unprecedented [{κ^3-H$_2$B(pz$^{t\text{-}\mathrm{Bu,Me}}$)(pz$^{\mathrm{Me},t\text{-}\mathrm{Bu}}$)}$_2$UI] (**34**). Compound **34** has been formed due to an isomerization of the Bp′ ligand promoted by the metal center [91]. Taking into account that these arrangements are sterically driven processes, this result encouraged the synthesis of the novel asymmetric K[H$_2$B(pz$^{t\text{-}\mathrm{Bu,Me}}$)(pz$^{\mathrm{Me}2}$)]

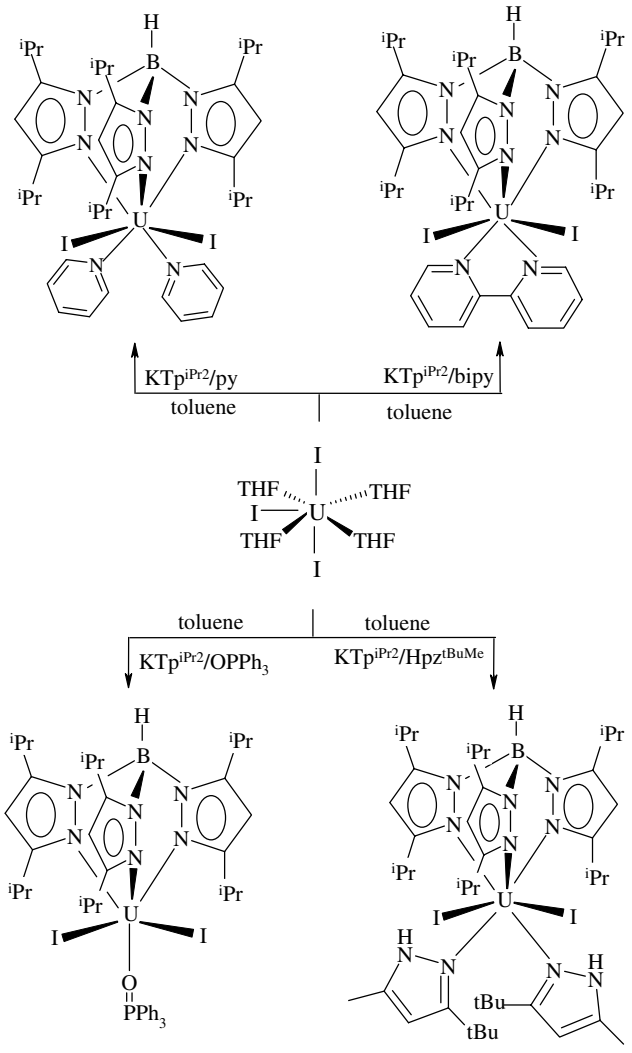

Scheme 35.

ligand, which was expected to have steric properties adequate for the preparation of bis-$Bp^{R,R'}$ U(III) complexes by metathesis. This has been achieved, and the complex $[\{\kappa^3\text{-}H_2B(pz^{tBu,Me})(pz^{Me_2})\}_2UI]$ (**35**) has been synthesized by metathesis [91]. Compounds **34** and **35** are seven-coordinate by two tridentade asymmetric heteroscorpionates (κ^3-N,N,H) and an iodide ligand, both displaying pentagonal bipyramidal coordination geometries [91]. In these studies, the vulnerability of the scorpionates to fragmentation [2,92] led to the formation of the dimeric compound $[(\kappa^3\text{-}Bp^{tBu,Me})UI(Hpz^{t\text{-}Bu,Me})]_2(\mu\text{-}I)_2$ [91].

3.2. Tetravalent complexes

3.2.1. Bis and mono-homoscorpionates

The tetrachlorides, MCl_4 (M = Th, U, Np), react with KTp or KpzTp yielding the bis-Tp′ complexes $[(\kappa^3\text{-}Tp)_2AnX_2]$ (X = Cl and An = U, Th, Np; X = Br, An = Th) and $[(\kappa^3\text{-}pzTp)_2UCl_2]$ [4,93]. However, the same type of reaction with bulkier ligands, such as Tp* or Tp^{Ms}, allowed the stabilization of the mono-complexes $[(\kappa^3\text{-}Tp^*)AnCl_3(THF)]$ (An = U, Th, Np) and $[(\kappa^3\text{-}Tp^{Ms^*})UCl_3]$, respectively (Scheme 37) [4,94].

The utility of compounds $[(\kappa^3\text{-}Tp)_2MX_2]$ (M = U, Th, X = Cl; M = U, X = I) and $[(\kappa^3\text{-}pzTp)_2UCl_2]$ for further derivatization has been demonstrated, and several alkyl, amido, thiolate and alkoxide derivatives have been prepared [4,93,95,96]. The reactivity of some U(IV) hydrocarbyl derivatives towards protic substrates, acetone, acetonitrile and iodide was also studied [95,96]. The outcome of the reactions depends on the nature of the alkyl group, as well as on the nature and stoichiometry of the reactants [95,96]. These studies have shown a less rich derivative chemistry for $[(\kappa^3\text{-}pzTp)_2UCl_2]$ than for $[(\kappa^3\text{-}Tp)_2UCl_2]$. In order to get a better insight on these differences, extended Hückel molecular orbital (EHMO) studies have been performed. The analysis of the frontier orbitals did not show any significant differences between Tp and pzTp ligands. However, the calculations indicated that stereochemical interaction affects the reactivity of the complexes stabilized by Tp or pzTp. It was found that the maximum overlap population between these ligands and the uranium metal center is achieved at a bite distance of 3.05 Å for both ligands. This value is ideal for Tp, but for pzTp this distance is energetically unfavorable due to the repulsive interactions between *ortho* hydrogens of the pyrazolyl rings, that are in the same plane. The most favorable bite distance found for the pzTp ligand is 2.85 Å. This feature on its own makes all complexes anchored by pzTp more unstable than their Tp counterparts [93,96]. EHMO calculations provided also some information on the bonding capabilities of the fragment "$[(\kappa^3\text{-}Tp)_2M]$" compared to "$[M(Cp^*)_2]$" and also on the vulnerability of the scorpionate ligands to nucleophilic attack [95].

A significant amount of structural and solution NMR data exists for compounds containing the $[Tp_2'U]$ moiety. In the solid state all are eight-coordinate by two κ^3-Tp′ ligands (Tp′ = Tp, pzTp) and by two monodentate co-ligands, all displaying square antiprismatic coordination geometries, distorted towards bicapped trigonal prism or dodecahedral [4,93,95,96]. In solution all the compounds are fluxional, but static spectra, in accord with the solid state structure, were obtained for most of them, depending on the bulkiness of the co-ligands and/or the coordination number of the metal [4,93,95,96]. For the uranium compounds anchored by pzTp, variable temperature NMR studies revealed that at high temperatures two distinct dynamic processes exist: one intramolecular dissociative process, which promotes the exchange between coordinated and uncoordinated rings, and a non dissociative process involving interconversion of the common eight-coordinate polyhedra (SAP $\Longleftrightarrow$ DD $\Longleftrightarrow$ BCTP).

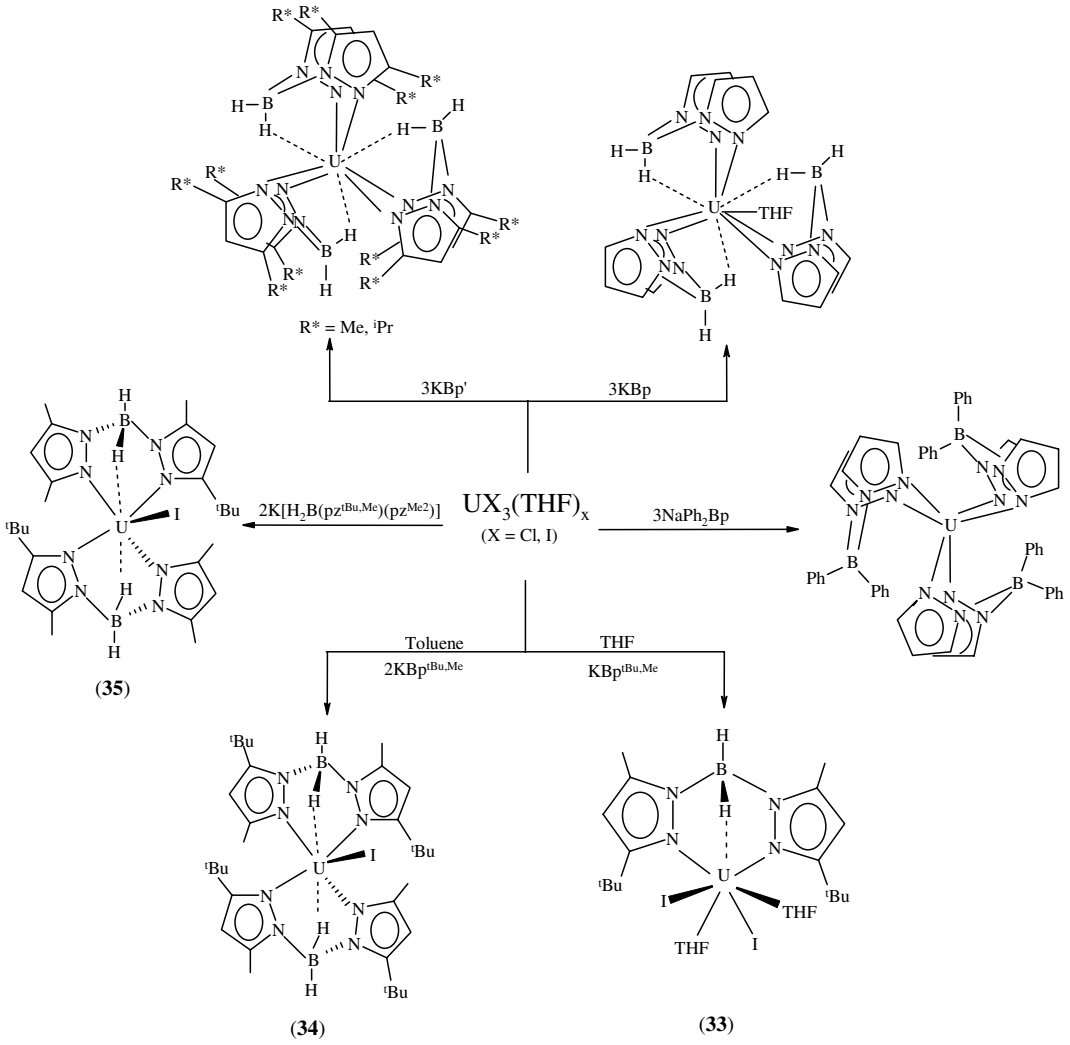

Scheme 36.

The replacement of one, two or three chlorides in $[(\kappa^3\text{-Tp*})AnCl_3(THF)]$ has also been possible, and a large number of alkoxide, amido, thiolate and alkyl derivatives were isolated and characterized The reactivity of some alkyl derivatives towards several unsaturated substrates was also evaluated [4,84,97]. This family of compounds can be six- or seven-coordinate, and presents a static behavior in solution [4,97].

Recently, Marques and coworkers [94] reported the complex $[(\kappa^3\text{-Tp}^{Ms^*})UCl_3]$, as well as some derivative chemistry (Scheme 38).

An interesting result was the characterization of the symmetrical complex $[U(\kappa^3\text{-Tp}^{Ms})Cl_3]$, which has been obtained during the recrystallization of an amido derivative. It has also been found that nitriles, isocyanides and acetone do not insert into the U–C bond of $[(\kappa^3\text{-TpMs*})U(C_6H_4CH_2NMe_2)Cl_2]$, but acetone reacts with this compound yielding the aldolate $[(\kappa^3\text{-TpMs*})U\{\eta^2\text{-}(OC(Me)_2CH_2C(=O)Me\}Cl_2]$ [94]. This reactivity is comparable to the one observed for the analogous $[(\kappa^3\text{-Tp*})UCl_3(THF)]$ [4]. Based on NMR results, the authors considered the Tp^{Ms^*} a poorer electron donor than Tp*, and a less sterically demanding ligand. This last feature being due to the rearrangement of the Tp^{Ms} ligand during formation of the complex. The X-ray analysis of $[(\kappa^3\text{-Tp}^{Ms^*})UCl_3]$, $[(\kappa^3\text{-Tp}^{Ms})UCl_3]$ and $[(\kappa^3\text{-Tp*})U\{N(SiMe_3)_2\}Cl_2]$ revealed that the uranium center has octahedral geometry with the ligand coordinating in its usual κ^3-mode [94].

4. Final remarks

In the last few years a resurgence of interest in the chemistry of rhenium scorpionates is clear from the plethora of contributions and a variety of complexes, mainly anchored by Tp, pzTp and Tp* and with metal in the oxidation states +VII to +I, have been isolated. Using high valent oxides, several oxygen transfer reactions have been studied, allowing the stabilization of unusual neu-

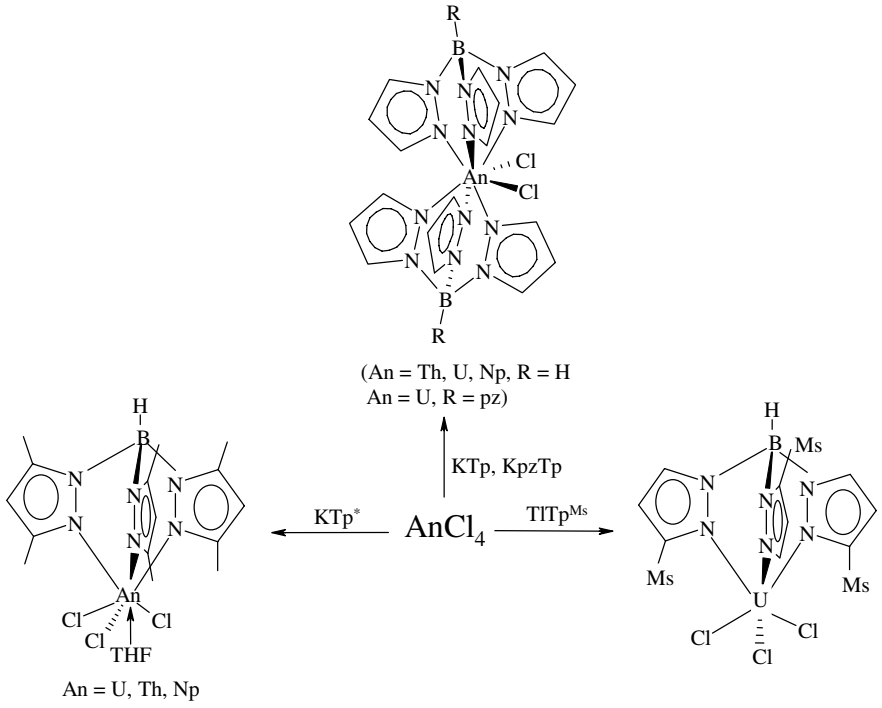

Scheme 37.

tral and anionic Re(V) *trans*-dioxocomplexes anchored by pzTp or Bp′, and Re(VI) cationic *cis*-dioxocompounds anchored by Tp. Thermal and photochemical migration of alkyl or aryl groups from the metal to the oxo ligand have also been reported, for the first time. Catalytic oxygen transfer reactions have been studied using Re(V) oxides anchored by Tp* and pzTp, and a significant effect of the scorpionate ligand on these transfers was found.

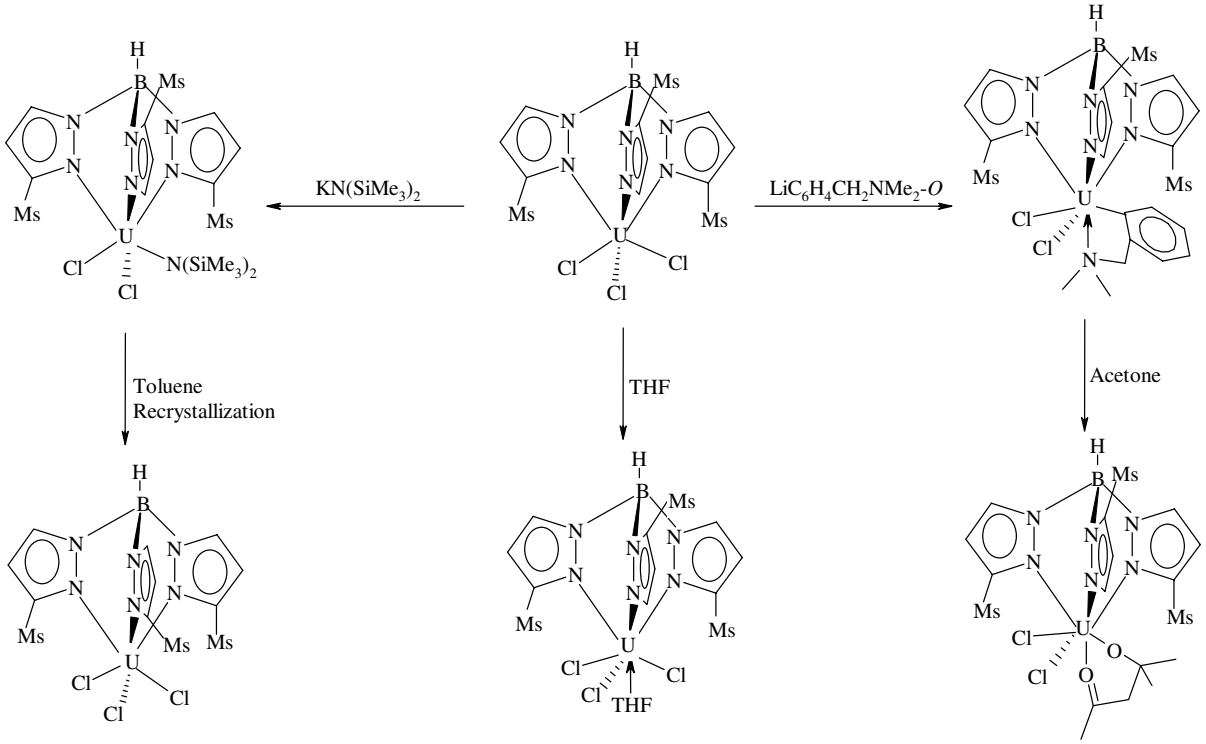

Scheme 38.

A relatively *old compound*, a Re(I) dicarbonyl, has been reinvestigated and an impressive synthetic chemistry around it has been developed. Modulation of the electronic properties of the Re(I) metallic center allowed the stabilizing of rare monomeric η^2-aromatic compounds. A series of reactions involving selective transformation of the organic substrates has been described.

Among the actinides, uranium is still the most studied element and, in the last few years, its chemistry has been extended to the so called second generation of homo and heteroscorpionates. For U(III) it has been clearly shown that the type of compounds formed depends not only on the bulkiness but also on the symmetry of the 3-R substituents. The first mono-heteroscorpionate and bis-asymmetric heteroscorpionate complexes have been described and characterized, confirming the importance of modulating the steric profile of the ligand. This recently described U(III) chemistry certainly has opened a new avenue for heteroscorpionates as ancillary ligands.

5. Abbreviations

acac	acetylacetonate
An	actinides
BCTP	bicapped trigonal prismatic
bipy	bipyridine
Bp	dihydrobis(pyrazolyl)borate
Bp′	substituted dihydrobis(pyrazolyl)borate
Bp*	dihydrobis(3,5-dimethylpyrazolyl)borate
$Bp^{tBu,Me}$	dihydrobis(3-*tert*-butyl-5-methylpyrazolyl)borate
Bu	butyl (superscript n or *t* for normal or tertiary)
Cp*	pentamethylcyclopentadienyl
CpH	cyclopentadiene
DD	dodecahedral
dmpe	1,2-bis(dimethylphosphino)ethane
DMSO	dimethyl sulfoxide
dppe	1,2-bis(diphenylphosphino)ethane
Et	ethyl
$Hpz^{tBu,Me}$	3-*tert*-butyl-5-methylpyrazole
Hpz^{Me_2}	3,5-dimethylpyrazole
8-hqnH	8-hydroxyquinoline
IR	infrared
Me	methyl
1-Meimz	1-methylimydazole
NAP	*N*-acetylpyrrole
NOE	nuclear overhauser effect
NMM	*N*-methylmaleimide
NMR	nuclear magnetic resonance
NTol	*p*-tolylimido
OTf	triflate, OSO_2CF_3
Ph	phenyl
Ph′	substituted pheny
Ph_2Bp	diphenylbis(pyrazolyl)borate
PhTp	phenyltris(pyrazolyl)borate
Pr	propyl (superscript *i* or *n* for iso or normal)
py	pyridine
py-O	pyridine *N*-oxide
pzH	pyrazole
pz′H	substituted pyrazole
pzTp	tetrakis(pyrazolyl)borate
R.T.	room temperature
SAP	square antiprismatic
2-S-py	pyridine-2-thiolate
THF	tetrahydrofuran
tim^{Me}	1-methyl-2-mercaptoimidazole
Tp	hydrotris(pyrazolyl)borate
Tp*	hydrotris(3,5-dimethylpyrazolyl)borate
Tp^{Ms}	hydrotris(3-mesitylpyrazolyl)borate
Tp^{Ms}*	hydrotris(5-mesitylpyrazolyl)borate

Acknowledgements

The authors thank FCT for financial support (PRAXIS XXI, POCTI and Ph.D. and BIC Research Grants). I. Santos also express her gratitude to all the coworkers mentioned in the references and not participating in this review.

References

[1] S. Trofimenko, Scorpionates: The Coordination Chemistry of Polypyrazolylborate Ligands, Imperial College Press, London, 1999.
[2] C.C. Romão, in: R.B. King (Ed.), Encyclopedia of Inorganic Chemistry, vol. 6, Wiley, New York, 1994, p. 3437.
[3] A. Paulo, J.D.G. Correia, I. Santos, Trends Inorg. Chem. 5 (1998) 57.
[4] I. Santos, N. Marques, New J. Chem. 19 (1995) 551.
[5] I.A. Degnan, W.A. Herrmann, E. Herdtweck, Chem. Ber. 123 (1990) 1347.
[6] B.J. Coe, Polyhedron 9 (1992) 1085.
[7] A. Domingos, J. Marçalo, A. Paulo, A. Pires de Matos, I. Santos, Inorg. Chem. 32 (1993) 5114.
[8] R. Garcia, Y.H. Xing, Â. Domingos, A. Paulo, I. Santos, Inorg. Chim. Acta 343 (2003) 27.
[9] J.E. Joachim, C. Apostolidis, B. Kanellakopulos, R. Maier, M.L. Ziegler, Z. Naturforsch. 48b (1993) 227.
[10] Y. Matano, T.O. Northcutt, J. Brugman, B.K. Bennet, S. Lovell, J.M. Mayer, Organometallics 19 (2000) 2781.
[11] M.J. Abrams, A. Davison, A.G. Jones, Inorg. Chim. Acta 82 (1984) 125.
[12] J.A. Thomas, A. Davison, Inorg. Chim. Acta 190 (1991) 231.
[13] A. Paulo, A. Domingos, J. Marçalo, A. Pires de Matos, I. Santos, Inorg. Chem. 34 (1995) 2113.
[14] A. Paulo, J. Marçalo, A. Pires de Matos, I. Santos, in: M. Nicolini, G. Bandoli, U. Mazzi (Eds.), Technetium and Rhenium in Chemistry and Nuclear Medicine, SGEditoriali, Padova, 1995, p. 227.
[15] K.P. Gable, A. Abubaker, K. Zientara, A.M. Wainwright, Organometallics 18 (1999) 173.
[16] K.P. Gable, E.C. Brown, Organometallics 19 (2000) 944.

[17] K.P. Gable, P. Chuawong, A.F.T. Yokochy, Organometallics 21 (2002) 929.
[18] H.A. Hinton, H. Chen, T.A. Hamor, F.S. McQuillan, C.J. Jones, Inorg. Chim. Acta 285 (1999) 55.
[19] I.A. Degnan, J. Behm, M.R. Cook, W.A. Herrmann, Inorg. Chem. 30 (1991) 2165.
[20] D.D. DuMez, T.O. Northcutt, Y. Matano, J.M. Mayer, Inorg. Chem. 38 (1999) 3309.
[21] S.N. Brown, Ph.D. Thesis, University of Washington, 1994.
[22] S.N. Brown, J.M. Mayer, J. Am. Chem. Soc. 116 (1994) 2219.
[23] D.D. DuMez, J.M. Mayer, Inorg. Chem. 37 (1998) 445.
[24] R.W. Thomas, G.W. Estes, R.C. Elder, E. Deutsch, J. Am. Chem. Soc. 101 (1979) 4581.
[25] G.B. Dahmann, J.H. Enemark, Inorg. Chem. 26 (1987) 3960.
[26] R.W. Thomas, A. Davison, H.S. Trop, E. Deutsch, Inorg. Chem. 19 (1980) 2840.
[27] A. Duatti, F. Tisato, F. Refosco, U. Mazzi, M. Nicolini, Inorg. Chem. 28 (1989) 4565.
[28] F. Tisato, C. Bolzati, A. Duatti, G. Bandoli, F. Refosco, Inorg. Chem. 32 (1993) 2042.
[29] A. Duatti, F. Tisato, F. Refosco, A. Moresco, U. Mazzi, G. Bandoli, M. Nicolini, in: M. Nicolini, G. Bandoli, U. Mazzi (Eds.), Technetium and Rhenium in Chemistry and Nuclear Medicine, SGEditoriali, Padova, 1989, p. 129.
[30] D. Nunes, A. Domingos, A. Paulo, L. Patrício, I. Santos, M.F.N.N. Carvalho, A.J.L. Pombeiro, Inorg. Chim. Acta 271 (1998) 65.
[31] D.D. DuMez, J.M. Mayer, Inorg. Chem. 34 (1995) 6396.
[32] S.N. Brown, J.M. Mayer, J. Am. Chem. Soc. 118 (1996) 12119.
[33] S.N. Brown, J.M. Mayer, Inorg. Chem. 31 (1992) 4091.
[34] A. Paulo, A. Domingos, A. Pires de Matos, I. Santos, M.F.N.N. Carvalho, A.J.L. Pombeiro, Inorg. Chem. 33 (1994) 4729.
[35] L.H. Doerrer, J.R. Galsworthy, M.L.H. Green, M.A. Leech, J. Chem. Soc., Dalton Trans. (1998) 2483.
[36] A. Paulo, A. Domingos, I. Santos, Inorg. Chem. 35 (1996) 1798.
[37] C.S. Masui, J.M. Mayer, Inorg. Chim. Acta 251 (1996) 325.
[38] J.W. Faller, A.R. Lavoie, Organometallics 19 (2000) 3957.
[39] P.B. Kettler, Y. Chang, Q. Chen, J. Zubieta, M.J. Abrams, S.K. Larsen, Inorg. Chim. Acta 231 (1995) 13.
[40] W.S. McNeil, D.D. DuMez, Y. Matano, S. Lovell, J.M. Mayer, Organometallics 18 (1999) 3715.
[41] B.K. Bennet, T.J. Crevier, D.D. DuMez, Y. Matano, W.S. McNeil, J.M. Mayer, J. Organomet. Chem. 591 (1999) 96.
[42] A. Paulo, Ph.D. Thesis, Instituto Superior Técnico, Technical University of Lisbon, 1998.
[43] A. Paulo, A. Domingos, I. Santos, J. Chem. Soc., Dalton Trans. (1999) 3735.
[44] D.D. DuMez, J.M. Mayer, J. Am. Chem. Soc. 118 (1996) 12416.
[45] A. Paulo, K.R. Reddy, A. Domingos, I. Santos, Inorg. Chem. 37 (1998) 6807.
[46] A. Paulo, A. Domingos, I. Santos, in: M. Nicolini, G. Bandoli, U. Mazzi (Eds.), Technetium and Rhenium in Chemistry and Nuclear Medicine, SGEditoriali, Padova, 1999, p. 245.
[47] K.R. Reddy, A.. Domingos, A. Paulo, I. Santos, Inorg. Chem. 38 (1999) 4278.
[48] A. Paulo, A. Domingos, R. Garcia, I. Santos, Inorg. Chem. 39 (2000) 5669.
[49] S.N. Brown, J.M. Mayer, Organometallics 14 (1995) 2951.
[50] S.H. Meiere, B.C. Brooks, T.B. Gunnoe, E.H. Carrig, M. Sabat, W.D. Harman, Organometallics 20 (2001) 3661.
[51] T.B. Gunnoe, S.H. Meiere, M. Sabat, W.D. Harman, Inorg. Chem. 39 (2000) 6127.
[52] S.N. Brown, J.M. Mayer, Inorg. Chem. 34 (1995) 3560.
[53] D.G. Hamilton, X.L. Luo, R.H. Crabtree, Inorg. Chem. 28 (1989) 3198.
[54] A. Paulo, J. Ascenso, A. Domingos, A. Galvão, I. Santos, J. Chem. Soc., Dalton Trans. (1999) 1293.
[55] Y. Matano, S.N. Brown, T.O. Northcutt, J.M. Mayer, Organometallics 17 (1998) 2939.
[56] S. Trofimenko, J. Am. Chem. Soc. 89 (1967) 3904.
[57] S. Trofimenko, J. Am. Chem. Soc. 91 (1969) 588.
[58] J.A. McCleverty, I. Wolochowicz, J. Organomet. Chem. 169 (1979) 289.
[59] M. Angaroni, G.A. Ardizzoia, G. D'Alfonso, G. La Monica, J. Chem. Soc., Dalton Trans. (1990) 1895.
[60] J.E. Joachim, C. Apostolidis, B. Kanellakopulos, R. Maier, N. Marques, D. Meyer, J. Müller, A.P. Matos, B. Nuber, J. Rebizant, M.L. Ziegler, J. Organomet. Chem. 448 (1993) 119.
[61] A. Bond, M. Green, J. Chem. Soc. (A) (1971) 682.
[62] R. Garcia, A. Paulo, A. Domingos, I. Santos, K. Ortner, R. Alberto, J. Am. Chem. Soc. 122 (2000) 11240.
[63] A.R. Schoenberg, W.P. Anderson, Inorg. Chem. 11 (1972) 85.
[64] J.E. Joachim, C. Apostolidis, B. Kanellakopulos, D. Meyer, B. Nuber, K. Raptis, J. Rebizant, M.L. Ziegler, J. Organomet. Chem. 492 (1995) 199.
[65] R. Alberto, W.A. Herrmann, P. Kiprof, F. Baumgärtner, Inorg. Chem. 31 (1992) 895.
[66] J.E. Joachim, C. Apostolidis, B. Kanellakopulos, R. Mayer, D. Meyer, J. Rebizant, M.L. Ziegler, J. Organomet. Chem. 455 (1993) 137.
[67] T.B. Gunnoe, M. Sabat, W.D. Harman, J. Am. Chem. Soc. 120 (1998) 8747.
[68] T.B. Gunnoe, M. Sabat, W.D. Harman, J. Am. Chem. Soc. 121 (1999) 6499.
[69] T.B. Gunnoe, M. Sabat, W.D. Harman, Organometallics 19 (2000) 728.
[70] S.H. Meiere, B.C. Brooks, T.B. Gunnoe, M. Sabat, W.D. Harman, Organometallics 20 (2001) 1038.
[71] L.A. Friedman, S.H. Meiere, B.C. Brooks, W.D. Harman, Organometallics 20 (2001) 1699.
[72] S.H. Meiere, W.D. Harman, Organometallics 20 (2001) 3876.
[73] S.H. Meiere, F. Ding, L.A. Friedman, M. Sabat, W.D. Harman, J. Am. Chem. Soc. 124 (2002) 13506.
[74] B.C. Brooks, S.H. Meiere, L.A. Friedman, E.H. Carrig, T.B. Gunnoe, W.D. Harman, J. Am. Chem. Soc. 123 (2001) 3541.
[75] S.H. Meiere, M.T. Valahovic, W.D. Harman, J. Am. Chem. Soc. 124 (2002) 15099.
[76] M.D. Chordia, P.L. Smith, S.H. Meiere, M. Sabat, W.D. Harman, J. Am. Chem. Soc. 123 (2001) 10756.
[77] L.A. Friedman, M. Sabat, W.D. Harman, J. Am. Chem. Soc. 124 (2002) 7395.
[78] L.A. Friedman, W.D. Harman, J. Am. Chem. Soc. 123 (2001) 8967.
[79] M.T. Valahovic, T.B. Gunnoe, M. Sabat, W.D. Harman, J. Am. Chem. Soc. 124 (2002) 3309.
[80] C. Apostolidis, A. Carvalho, A. Domingos, B. Kanellakopulos, R. Maier, N. Marques, A. Pires De Matos, J. Rebizant, Polyhedron 18 (1–2) (1999) 263.
[81] R. McDonald, Y.M. Sun, J. Takats, V.W. Day, T.A. Eberspracher, J. Alloys Compd. 213/214 (1994) 8.
[82] Y.M. Sun, R. McDonald, J. Takats, V.W. Day, T.A. Eberspracher, Inorg. Chem. 33 (1994) 4433.
[83] I. Santos, N. Marques, A. Pires de Matos, J. Less-Common Met. 122 (1986) 215.
[84] A. Domingos, N. Marques, A. Pires de Matos, I. Santos, M. Silva, Organometallics 13 (1994) 654.
[85] Sun Y. Ph.D. Thesis, University of Alberta, 1995.
[86] A.J. Amoroso, J.C. Jeffery, P.L. Jones, J.A. Mccleeverty, L. Rees, A.L. Rheingold, Y.M. Sun, J. Takats, S. Trofimenko, M.D. Ward, G.P.A. Yap, J. Chem. Soc., Chem. Commun. (1995) 1881.

[87] (a) L. Maria, A. Domingos, I. Santos, Inorg. Chem. Commun. 6 (1) (2003) 58;
(b) L. Maria, A. Domingos, I. Santos, Personal communication at ICCC XXXVth International Conference on Coordination chemistry, Heidelberg, 2002;
(c) L. Maria, PhD Thesis, IST, Lisbon, 2003.
[88] Y.M. Sun, J. Takats, W.T. Eberspracher, V. Day, Inorg. Chim. Acta 229 (1-2) (1995) 315.
[89] A. Carvalho, A. Domingos, P. Gaspar, N. Marques, A. Pires de Matos, I. Santos, Polyhedron 11/12 (1992) 1481.
[90] L. Maria, M.P.C. Campello, A. Domingos, I. Santos, R. Andersen, J. Chem. Soc., Dalton Trans. 12 (1999) 2015.
[91] L. Maria, A. Domingos, I. Santos, Inorg. Chem. 42 (2003) 3323.
[92] A. Domingos, M.R.J. Elsegood, A.C. Hiller, G. Lin, S.Y. Liu, I. Lopes, N. Marques, G.H. Maunder, R. McDonald, A. Sella, J.W. Steed, J. Takats, Inorg. Chem. 41 (2002) 6761.
[93] M.P.C. Campello, A. Galvão, A. Domingos, A.P. De Matos, I. Santos, J. Organomet. Chem. 579 (1999) 5.
[94] M. Silva, A. Domingos, A.P. De Matos, N. Marques, S. Trofimemko, J. Chem. Soc., Dalton Trans. 24 (2000) 4628.
[95] M.P.C. Campello, M.J. Calhorda, A. Domingos, A. Galvão, J.P. Leal, A.P. De Matos, I. Santos, J. Organomet. Chem. 538 (1-2) (1997) 223.
[96] M.P.C. Campello, Ph.D. Thesis, FCL, Lisboa, 1998.
[97] M. Silva, N. Marques, A.P. De Matos, J. Organomet. Chem. 493 (1995) 129.

Available online at www.sciencedirect.com
SCIENCE DIRECT®
Polyhedron 23 (2004) 361–371
POLYHEDRON
www.elsevier.com/locate/poly

Ruthenium hydride complexes with a heteroscorpionate ligand derived from methane: 2-phenoxy-bis(pyrazol-1-yl)methane. The hemilabile role of the ligand in substitution and proton transfer reactions

Agustín Caballero [a], M. Carmen Carrión [a], Gustavo Espino [b], Félix A. Jalón [a,*], Blanca R. Manzano [a]

[a] *Departemento de Química Inorgnica, Org. y Bioquim, Facultad de Químicas, Universidad de Castilla-La Mancha, Avda. Camilo J. Cela, 10, E-13071 Ciudad Real, Spain*
[b] *Facultad de Ciencias y de CyTA, Universidad de Burgos, Plaza Misael Bañuelos s/n, E-09001 Burgos, Spain*

Received 3 June 2003; accepted 5 September 2003

Dedicated to Dr. Swiatoslaw Trofimenko in recognition of his outstanding contribution and dedication to Inorganic Chemistry

Abstract

The complex [RuH(κ^3-bpzmPhO)(cod)] (**1**) was synthesized by the reaction of [RuH(cod)(NH_2NMe_2)$_3$][BPh_4] with the potassium salt of 2-phenoxy-bis(pyrazol-1-yl)methane (bpzmPhOK). This ligand adopts a κ^3-*N*, *N*, *O* coordination on the metal center that is reminiscent of the situation usually observed in trispyrazolylborate complexes. Complex **1** exists in solution as a mixture of two diastereoisomers that are in equilibrium. The reaction of **1** with different phosphines (PMe_3, PMe_2Ph, $PMePh_2$ and PPh_3) has been studied. The reaction product depends not only on the nature of the phosphine but also on the complex:L ratio and the temperature. Diphosphine derivatives of stoichiometries [RuH(κ^1-*O*-bpzmPhO)(cod)L_2] (L = PMe_3, PMe_2Ph) and [RuH(κ^3-bpzmPhO)L_2] (L = PMe_3, PMe_2Ph, $PMePh_2$, PPh_3) were prepared. Similarly, tetraphosphine derivatives of formula [*cis*-*O*,*H*-RuH(κ^1-*O*-bpzmPhO)L_4] (L = PMe_3, PMe_2Ph) were obtained. The complex with PMe_2Ph can be transformed into the respective *trans* isomer by heating the solution. The reaction of **1** with five equivalents of PMe_3 gives rise to a pentaphosphine derivative with complete decoordination of the anionic bpzmPhO ligand. This ligand exhibits hemilabile behavior that involve a reversible coordination of the pyrazole fragments. Proton transfer reactions from HBF_4 to **1** have also been studied both in acetone-d_6 and in methanol-d_4. In all of these processes the proton is selectively transferred to the oxygen of the bpzmPhO ligand, which remains coordinated through at least the *N*-donor centers. Three hydride derivatives are formed in these reactions and they differ either in the relative orientation of the ligands or in the coordination of the OH group of the ligand.
© 2003 Elsevier Ltd. All rights reserved.

Keywords: Heteroscorpionates; Ruthenium; Hydrides; Phosphine complexes; Hemilabile ligands

1. Introduction

Homo- and heteroscorpionate borate ligands have been widely used in coordination chemistry [1]. In recent years analogues of the boron-based scorpionates have been prepared and used as ligands. [1] For instance, bis- and tris(pyrazol-1-yl)methane compounds potentially offer analogous coordination modes to those found in the classical scorpionates [2]. In contrast with the classical systems, the methane derivatives are neutral and consequently the metal–ligand interaction is weaker. The introduction of charged groups in the spacer carbon is an interesting possibility in terms of improving the coordination ability of these ligands and, on the other hand, involves the possibility of introducing a hemilabile role for this ligand in the resulting complexes.

* Corresponding author. Fax: +34-926-295318.
E-mail address: felix.jalon@uclm.es (F.A. Jalón).
[1] For an approach, see Chapter 1.9 of [1].

0277-5387/$ - see front matter © 2003 Elsevier Ltd. All rights reserved.
doi:10.1016/j.poly.2003.11.023

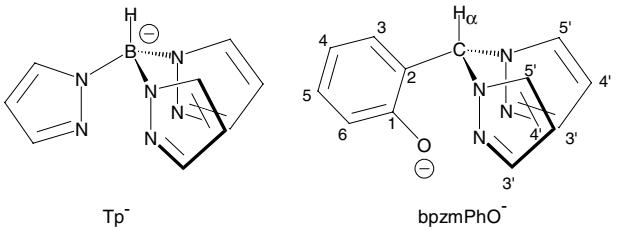

Scheme 1.

In recent years we [3] and others [4] have prepared bis(pyrazol-1-yl)methane derivatives bearing additional functionalized groups in the spacer carbon between the two pyrazoles. The previously described (2-hydroxyphenyl)bis(pyrazol-1-yl)methane is an example of this family of ligands [5]. The ligand is easily prepared by the Peterson method [6] and offers the possibility of deprotonating the phenol group, which transforms it into an anionic compound ($bpzmPhO^-$) that is reminiscent of the original scorpionates (Scheme 1). However, in the anionic form the charge is mainly located at the oxygen, a situation that increases the coordination ability of this atom. In this way, this potentially *NNO*-ligand could stabilize the same complexes as the boron-based scorpionates but the different electronic character of the donor atoms could lead to asymmetrization of the coordination sphere of the metal.

Carrano et al. used the anionic form of this ligand to prepare Co [5,7], Ni [7a,7b,8], V and Fe [7c], Zn, Cu and Mn [7a,7b] complexes. The introduction of substituents in the pyrazole rings or the phenol (or thiol) groups makes the formation of mononuclear species less favorable when bulky ancillary ligands are also coordinated to the metal center. As a consequence, in the work described here we preferred to use the unsubstituted ligand to stabilize mononuclear ruthenium compounds with three main goals in mind: (i) to explore the coordination ability of the three donor atoms of this ligand; (ii) to analyze the potential hemilability of the ligand in substitution processes with different phosphines; (iii) to evaluate the role of the phenoxy group, which is, in principle, in competition with the hydride ligand bonded to the Ru center, in proton transfer reactions.

2. Results and discussion

2.1. Synthesis and characterization of complexes *1a* and *1b*

The new hydride derivative [RuH(bpzmPhO)(cod)] (**1**) which is the starting material for the work described in this paper, can be obtained by reaction of bpzmPhOK with $[RuH(cod)(NH_2NMe_2)_3][BPh_4]$ or [RuClH(bpzm)(cod)] according to Eqs. (1) and (2), respectively. Reaction (2) is slightly less convenient because it requires the separation of the displaced bpzm (see Section 3).

$$[RuH(cod)(NH_2NMe_2)_3][BPh_4] + bpzmPhOK \rightarrow \underset{(\mathbf{1})}{[RuH(bpzmPhO)(cod)]} + KBPh_4 + 3NH_2NMe_2 \quad (1)$$

$$[RuClH(bpzm)(cod)] + bpzmPhOK \rightarrow \mathbf{1} + KCl + bpzm \quad (2)$$

cod = 1,5-cyclooctadiene, bpzm = bis(pyrazol-1-yl)methane.

In the hydride region of the ^1H NMR spectrum of complex **1**, two resonances (−3.64 ppm, d, $J = 2.9$ Hz and −6.84 ppm, s) are observed (see Table 1). This is due to the presence of two isomers whose ratio (**1a**:**1b**) changes with the solvent (acetone-d_6, 1:1; methanol-d_4, 2:1), meaning that the two species are in equilibrium. The assignment of the ^1H NMR resonances of the two isomers (except the aliphatic cod signals) was made on the basis of NOE and ^1H–^1H COSY spectra (acetone-d_6). The ^1H and $^{13}C\{^1H\}$ NMR spectra of isomer **1a** (Tables 1 and 2) show signals for two types of pyrazole ring and four distinct resonances for the olefinic CH groups of the cod ligand (C_1 symmetry). The hydride signal at −3.64 ppm exhibits a NOE with two olefinic protons. Considering all these data, the structure shown in Scheme 2 is proposed for this compound. Two lines are observed for the hydride signal and this is unexpected. However, it was confirmed that the resonance is indeed a doublet after the same coupling constant was observed in spectra acquired using 300, 200 and 80 MHz spectrometers. In addition, the COSY spectra show a correlation between this signal and an aliphatic cod proton (2.21 ppm). The coupling was confirmed when selective irradiation of the cod signal was observed to transform the hydride resonance into a singlet. This coupling can be explained in terms of a distortion of the octahedral geometry, which has been determined by X-ray diffraction for other complexes with the RuH(cod) fragment [9], resulting in the hydride group coming into close proximity with the cod ligand.

The ^1H and $^{13}C\{^1H\}$ NMR spectra of **1b** (Tables 1 and 2) exhibit signals for one type of pyrazole ring and a cod group with C_s symmetry. This data, along with the NOE observed between the hydride resonance (−6.84 ppm) and one type of olefinic cod proton (2H), allowed the structure of this isomer to be determined (see Scheme 2).

The reactivity of **1a/b** with different phosphines and the addition of HBF_4 was explored and the results of these studies will be discussed in the following sections.

2.2. Reaction of *1alb* with phosphines

The reaction of **1a/b** with phosphines of different basicity and, more importantly, different levels of steric

Table 1
^{1}H NMR data for bpzmPhOK and complexes **1**–**3**[a]

Derivative	Ru–H	Pyrazole			H_α	Phenoxy group	cod/Phosphine (Me)	
		$H^{4'}$	$H^{3'}$	$H^{5'}$			cod-H_{olef}	cod-H_{alk}
bpzmPhOK		6.18 (pt)	7.44 (d, $J = 2.2$)	7.52 (d, $J = 2.4$)	8.17 (s)	6.88 (td, $J = 7.6$, 1.9; H^5) 6.83 (dd, $J = 7.6$, 1.9; H^3) 6.43 (dd, $J = 8.3$, 1.2; H^6) 6.08 (td, $J = 7.6$, 1.2; H^4)		
1a	−3.64 (d, $J_{HH} = 2.9$)	6.37 (pt)	8.50 (d, $J = 2.0$)	7.92 (d, $J = 2.4$)	7.57 (s)	6.92 (d, $J = 7.7$, H^3) 6.66 (td, $J = 7.1$,1.5, H^5)	3.51[d] (m) 2.93[d] (m)	2.63 (m); 2.52 (m) 2.32 (m); 2.13 (m)
		6.66 (pt)	7.59 (d, $J = 2.0$)	8.05 (d, $J = 2.4$)		6.16 (d, $J = 8.3$, H^6) 5.95 (t, $J = 7.1$, H^4)	2.83 (m) 1.83 (m)	2.05 (m); 1.96 (m) 1.30 (2H, m)
1b	−6.84 (s)	6.37 (pt)	7.32 (d, $J = 2.3$)	7.96 (dd, $J = 2.6$, $J = 0.8$)	7.47 (s)	6.92 (d, $J = 7.7$, H^3) 6.76 (td, $J = 6.7$,1.6, H^5) 6.56 (d, $J = 8.2$, H^6) 5.90 (t, $J = 6.7$, H^4)	3.59[d] (m,2H) 2.93 (m,2H)	2.72 (m) 2.13 (m) 1.78 (m) 1.64 (m)
2[b]	−1.04 (dd, $J_{HP} = 82.1$, 28.2)	5.90 (pt, $J = 2.1$) 5.96 (pt, $J = 2.1$)	7.54 (bs) 7.11 (bs)	7.02 (d, $J = 2.3$) 7.00 (d, $J = 2.4$)	8.23 (s)	7.65 (d, $J = 8.2$; H^3) 7.44 (pt, $J = 7.4$; H^5) 6.79 (dd, $J = 2.0$, 7.5; H^6) 6.49 (t, $J = 7.2$; H^4)	3.68 (m) 2.84 (m) 2.64 (m)	1.50–2.3
							1.19 (d, $J_{HP} = 6.9$, PMe_3) 0.72 (d, $J_{HP} = 7.9$, PMe_3)	
3[b]	−0.95 (dd, $J_{HP} = 80.5$, 28.7)	5.96 (pt, $J = 1.8$) 6.02 (pt, $J = 1.8$)	[c]	7.13 (d, $J = 2.3$) 7.15 (d, $J = 2.3$)	8.47 (s)	8.09 (d, $J = 8.4$, H^3) 7.33 (m, H^5) 6.69 (m, H^6) 6.57 (pt, $J = 7.5$; H^4)	3.93 (m,2H) 2.93 m 2.77 (m)	2.06–2.66
							1.54 (d, $J_{HP} = 7.3$, PMe) 1.37 (d, $J_{HP} = 7.8$, PMe) 1.20 (d, $J_{HP} = 8.5$, PMe) 1.06 (d, $J_{HP} = 6.8$, PMe)	

[a] Room temperature. H–H coupling if not specified. Solvent, acetone-d_6 if not specified. The phenyl resonances of the phosphines in **3** are in the region 6.8–7.7 ppm.
[b] In benzene-d_6.
[c] Resonances non observed (overlapped).
[d] Signal showing noe with the hydride.

Table 2
$^{13}C\{^1H\}$ NMR data for bpzmPhOK and complex **1**[a]

Derivative	Pyrazole			C_α	Phenoxy group	cod	
	C'_3	C'_4	C'_5			olef	alk
bpzmPhOK	140.62	106.10	129.94	76.31	155.0 (C^1), 131.5 (C^5), 129.6 (C^3) 119.8 (C^4), 118.3 (C^6)		
1a	143.13	106.64 (2C)	131.70	78.48	130.90 (C^5), 130.55 (C^3), 124.03 (C^6), 110.45 (C^4),	61.00; 62.16	26.78; 30.82
	144.25		132.62			69.27; 80.80	32.19; 35.54
1b	141.68	107.04	132.17	79.41	131.28 (C^5), 130.28 (C^3), 125.20 (C^6), 108.84 (C^4)	71.58; 73.24	28.34; 33.20

[a] Room temperature. All signals are singlets. Solvent, acetone-d_6.

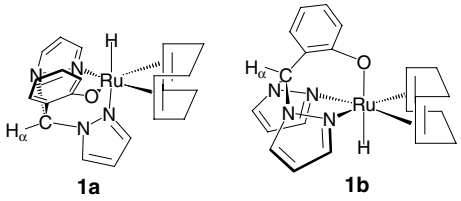

Scheme 2.

hindrance (L = PMe_3, PMe_2Ph, $PMePh_2$, PPh_3) in a range of complex:L ratios and temperatures was studied. Although all possible stoichiometries were not assessed, the preliminary results provide evidence that the most labile functions to be displaced were those on the pyrazole groups and the cod ligand. It was therefore decided that complex:L ratios of 1:2 and 1:4 would be the most suitable for further study. The reactions were carried out in an NMR tube using benzene-d_6 as solvent and reaction progress was monitored by ^1H and $^{31}P\{^1H\}$ NMR spectroscopy. The product was isolated when only one species was detected.

The discussion that follows is based on the processes outlined in Scheme 3 and the nature of the reaction product is essentially dependent on the whole range of factors described above. It must be emphasized that the whole series of steps reflected in Scheme 3 is not complete for any of the phosphines used. However, the scheme is a reasonable general pathway for the reactions observed.

As shown in Scheme 3, reaction of **1a/b** with small phosphines, i.e., PMe_3 and PMe_2Ph, is the most versatile route. A complex:L ratio of 1:2 at room temperature (step i) led to complexes **2** and **3**, which formally can be

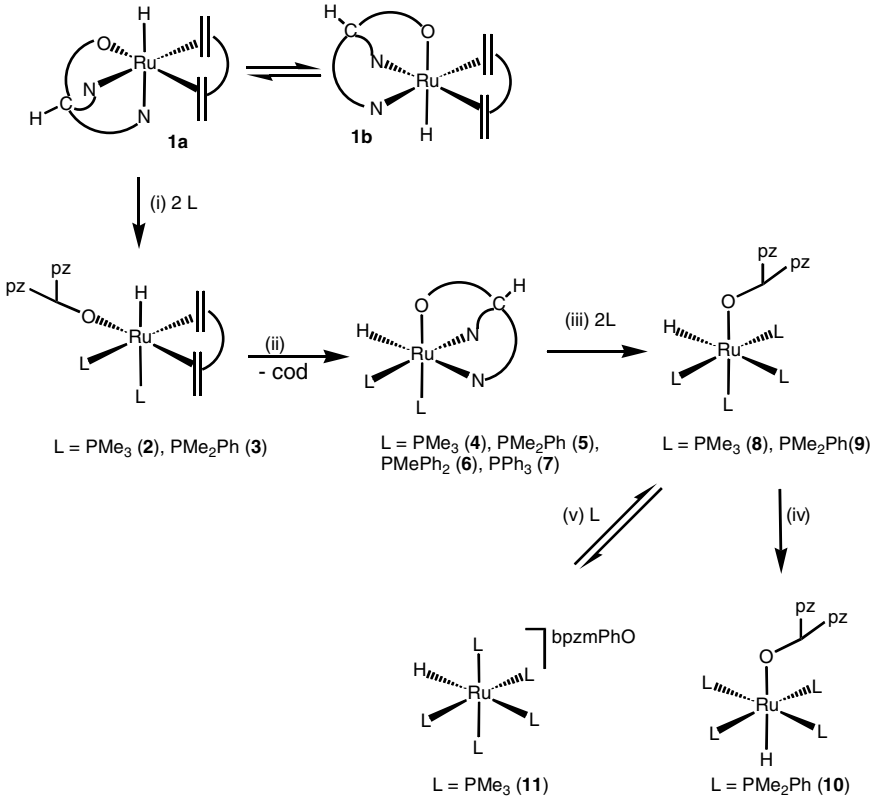

Scheme 3.

considered as the result of the displacement of the pyrazole groups from isomer **1a**, although the possibility of a direct reaction of **1b** with the phosphines followed by rapid rearrangement can not be excluded. Interestingly, when solutions of **2** or **3** were heated at 70 °C, the elimination of cod was observed with the concomitant recoordination of the pyrazole groups to give **4** or **5** (step ii). This behavior implies partial decoordination of the hemilabile ligand, which allows coordination of a second ligand (phosphine, in our case) that can induce the displacement of a third one (cod, in this case) with recoordiantion of the former. To the best of our knowledge, this behavior is very rarely observed [10]. The main conclusion to be drawn from these results is that **2** and **3** can be considered as products of kinetic control while **4** and **5** are the thermodynamically stable species' for this stoichiometry. Complex **5** could be isolated whereas **4** appeared in the solutions as the minor component of a mixture with the tetraphosphine derivative **8** and unidentified compounds with resonances in ^{1}H and ^{31}P NMR.

Bulkier phosphines such as $PMePh_2$ and PPh_3 did not react at room temperature but heating the reaction solutions (70 °C) did give the isolable products **6** and **7**, respectively. These compounds are isostructural with complexes **4** and **5**. The fact that species' of similar structure to **2** or **3** were not obtained with $PMePh_2$ or PPh_3 could be due to the high temperature required for the reactions to occur.

The use of a complex:L ratio of 1:4 with the different phosphines provided the conclusions that only the smallest phosphines (PMe_3 and PMe_2Ph) gave tetraphosphine derivatives and for PMe_2Ph this reaction was only possible above 50 °C (room temperature for PMe_3). Complexes **8** and **9** were initially obtained in these reactions (step iii). Both the cod and the pyrazole groups were displaced, with the bpzmPhO remaining coordinated as a monodentate *O*-donor ligand. When solutions of **9** were heated at 70 °C this complex evolved to give the more symmetrical isomer **10** (step iv), which, despite being the major component of the mixture, could not be isolated as a pure species and was characterized only by NMR.

The smallest phosphine, PMe_3, was even able to remove completely the bpzmPhO ligand from the metallic center when a complex:L ratio of 1:5 was used at room temperature (step v), although in this reaction competition between the two ligands was observed that gave mixtures of **8** and the pentaphosphine derivative **11**. The analogous isomer to **10** was not observed with PMe_3. However, the formation of this derivative as a transient intermediate, with a mutually *trans* disposition of the bpzmPhO and H ligands (hydride has a high *trans* influence), could explain the total displacement of the phenoxy group in **8** to give **11**. Nevertheless, **10** does not react with an excess of PMe_2Ph, even after heating, possibly due to steric factors. The complete decoordination of bpzmPhO by incoming ligands, as observed in the reaction with PMe_3 to give **11**, is an infrequent process but does have a precedent in the chemistry of trispyrazolylborate complexes [11].

It can be concluded that: (i) the displacement reactions from **1a/b** can be controlled by the complex:L ratio and temperature; (ii) the final product also depends on the nature of the phosphine; (iii) the ease of substitution is in the order: pyrazoles > cod > bpzmPhO ligand; (iv) the bpzmPhO ligand shows a hemilabile behavior in these reactions.

The most relevant aspects concerning the characterization of complexes **2**–**11** are discussed below.

The stretching vibrations for the terminal Ru–H bonds were observed in the expected regions of the IR spectra (1973–2025 cm^{-1}).

Complexes **2**–**11** were characterized by ^{1}H (except **4** – which is present as a minor component with **1** and **8**), $^{31}P\{^{1}H\}$ (see Tables 1, 3 and 4) and $^{13}C\{^{1}H\}$ NMR spectroscopy (except **2**–**4**, which are too unstable or could not be isolated) (see Table 4).

The resonances in the ^{1}H and $^{13}C\{^{1}H\}$ NMR spectra for the pyrazole rings provide valuable information about the symmetry of the complexes. For example, the existence of two distinct pyrazoles is deduced for complexes **2**, **3**, **5**–**7** but only one pyrazole is present in **8**–**11**. One of the most noticeable differences between **2** and **3** and the rest of the phosphine complexes is the existence of cod resonances. The cod signals in the ^{1}H NMR spectra of **2** and **3** show the expected pattern for a local C_1 symmetry and more than two different olefinic resonances (in fact three out of the four expected) are observed.

The hydride chemical shifts are very sensitive to the environment, and particularly to the ligand situated in the *trans* position (δ, *trans* to phosphine ca. −1 ppm, **2**–**3**; *trans* to a pyrazole group, between −13 to −15.5 ppm, **4**–**7**). The electronic enrichment of the metallic center induces a corresponding shift to lower frequency of the hydride resonance for the tetra- and pentaphosphine derivatives **8**–**11** and the *trans* effect of the ligand is also observed for this series of complexes (δ, *trans* to phosphine ca. −8 ppm, **8**–**9** or ca. −12 ppm, **11**; *trans* to phenoxy group ca. −18.7 ppm, **10**). The expected multiplicities were observed for the hydride resonances and the coupling constants were in the expected range (*trans* J_{PH}, 70–100 Hz; *cis* J_{PH}, ca. 30 Hz).

The $^{31}P\{^{1}H\}$ NMR spectra of diphosphine derivatives **2**–**7** (see Table 4) show two different resonances with the expected shift to higher frequencies due to the coordination. The J_{PP} coupling constants are indicative of a *cis*-arrangement for both phosphines (J_{PP} = 26–41 Hz). As expected, the tetraphosphine derivatives **8** and **9** give rise to three resonances while only one, although broad, is observed for **10**. A doublet and a quintet, in the corresponding spectrum, are due to the pentaphosphine derivative **11**.

Table 3
^{1}H NMR data for complexes **4**–**11**[a]

Complex	Ru–H	Pyrazole			H_α	Phenoxy group	Phosphine (Me)
		$H^{4'}$	$H^{3'}$	$H^{5'}$			
5	−14.64 (t, $J_{HP} = 32.3$)	5.74 (pt, $J = 2.1$) 5.54 (pt, $J = 2.1$)	6.94[c] (bs) 6.87[c] (bs)	7.09[c] (bs) 7.11[c] (bs)	[d]	6.3–7.6	0.82 (d, $J_{HP} = 7.9$) 1.19 (d, $J_{HP} = 7.6$) 1.62 (d, $J_{HP} = 8.5$) 1.79 (d, $J_{HP} = 8.7$)
6[b]	−14.24 (t, $J_{HP} = 29.9$)	5.84 (bs) 6.32 (bs)	7.82 (d, $J = 2.0$) [d]	8.15 (d, $J = 2.3$) [d]	[d]	6.61 (td, $J = 7.4$, 1.4; H^5) 5.91 (pt, $J = 7.2$; H^4) 5.75 (d, $J = 7.8$; H^6) [d]	1.23 (d, $J_{HP} = 7.4$) 1.42 (d, $J_{HP} = 7.4$)
7	−12.95 (dd, $J_{HP} = 31.0$; 27.9)	5.29 (pt) 5.43 (pt)	6.17 (d, $J = 2.1$) 6.22 (d, $J = 2.1$)	6.71 (d, $J = 2.4$) 7.26 (d, $J = 2.1$)	7.45 (s)	6.66 (dd, $J = 7.4$, 1.7; H^3) 6.25 (td, $J = 7.2$, 1.1; H^4) 5.94 (dd, $J = 8.4$, 1.1; H^6) [d]	
8	−7.76 (ddt, $J_{HPtrans} = 100.1$; $J_{HPcis} = 26.4$, 29.3)	6.00 (pt)	7.26 (d, $J = 2.3$)	7.58 (d, $J = 2.4$)	8.56 (s)	7.74 (dd, $J = 8.4$, 1.0; H^3) 7.35 (td, $J = 7.8$, 2.0; H^5) 7.09 (dd, $J = 7.8$, 1.5; H^6) 6.48 (pt, $J = 8.0$; H^4)	0.88 (d, $J_{HP} = 7.8$, 3Me) 1.02 (pt, 6 Me) 1.11 (d, $J_{HP} = 5.5$, 3Me)
9	−7.91 (ddt, $J_{HP} = 95.8$, 25.6, 25.2)	6.03 (pt)	7.62 (d, $J = 1.8$)	7.29 (d, $J = 2.3$)	8.85 (s)	7.65 (d, $J = 8.2$; H^3) 7.44 (dt, $J = 7.8$, 1.7; H^5) 6.79 (dd, $J = 7.5$, 2.0; H^6) 6.49 (pt, $J = 8.0$; H^4)	0.76 (d, $J_{HP} = 7.8$, 2Me) 1.26 (pt, 4Me) 1.72 (d, $J_{HP} = 5.3$, 2Me)
10	−18.67 (q, $J_{HP} = 20.8$)	5.71 (pt, $J = 1.9$)	7.19 (d, $J = 1.8$)	7.08 (d, $J = 2.3$)	8.26 (s)	6.98 (pt, $J = 8.2$; H^5) 6.32 (pt, $J = 7.4$; H^4) [d]	1.27 (bs, 8Me)
11	−11.83 (dc, $J_{HPtrans} = 72.4$; $J_{HPcis} = 24.8$)	5.97 (pt, $J = 2.1$)	7.32 (d, $J = 2.1$)	7.48 (bs)	8.37 (s)	7.23 (d, $J = 7.5$; $H^{3\text{ or }6}$) 6.58 (pt, $J = 7.3$; $H^{4\text{ or }5}$)	0.96 (d, $J_{HP} = 5.8$, 3Me) [d]

[a] Room temperature. H–H coupling if not specified. All resonances are singlets if not specified . Solvent, benzene-d_6 if not specified. The phenyl resonances of the corresponding phosphines in complexes **5**–**7**, **9** and **10** are in the region 6.8–7.7 ppm. The hydride resonance of **4** appears at −15.46 ppm (t, $J_{HP} = 34.3$, benzene-d_6).

[b] In DMSO-d_6.

[c] The assignment of $H^{3'}$ and $H^{5'}$ resonances may be reversed.

[d] Resonances non observed (overlapped).

Table 4
$^{13}C\{^1H\}$ data for **5**–**11** and $^{31}P\{^1H\}$ NMR data for **2**–**11**[a]

Complex	Pyrazole			C_α	Phenoxy group	Phosphine	
	C'_3	C'_4	C'_5			^{13}C	^{31}P
5	145.71 147.36	105.55 106.31	131.77 [c]	80.54 [c]	171.29 (C^1), 131.20, 125.20,120.79 (C^2), 109.60 [c]	P*Me*$_2$Ph: 21.41, (d, J_{CP} = 26.2) 17.36, (d, J_{CP} = 27.2)	36.40 (d, J_{PP} = 41.5) 41.78 (d)
6[b]	146.07 147.47	108.93 106.58	[c]	79.87	170.55 (C^1), 125.99, 124.43, 121.42 [c]	P*Me*Ph$_2$: 17.99 (d, J_{CP} = 25.7) 19.11, (d, J_{CP} = 28.2) PMe*Ph*$_2$: 127–133.5, m	52.62 (d, J_{PP} = 39.0) 60.40 (d)
7	146.70 148.67	110.27 106.02	132.07 130.06	80.73	171.07 (C^1), 120.5–135.5	134.4–140.7 (m)	78.71 (d, J_{PP} = 34.8) 75.10 (d)
8	140.31	105.45	128.95	75.17	130.63, 128.78, 128.21, 122.32, 111.49	21.37, dt, (J_{CP} = 16.1, 2.3; 3C) 22.59, td (J_{CP} = 3.5; 6C) 26.93, dc (J_{CP} = 25.7, 3.0; 3C)	18.42 (td, J_{PP} = 16.5, 33.6) 2.60 (dd, J_{PP} = 26.8, 33.6) −11.61 (m)
9	140.10	104.93	131.01	75.53	168.74 (C^1), 126.28, 122.07, 111.43 [c]	P*Me*$_2$Ph: 19.01 (d, J_{CP} = 17.1; 2C) 20.16 (m, 4C) 23.65 (d, J_{CP} = 26.2; 2C) PMe$_2$*Ph*: 127–131 (m) c	30.16 (td, J_{PP} = 33.8, 12.8) 16.39 (dd, J_{PP} = 33.8, 21.4) −4.57 (m)
10	139.83	105.34	128.67	75.34	118.49, 114.88 [c]	P*Me*$_2$Ph: 21.30 (bs) 28.43 (d, J_{CP} = 5.8) PMe$_2$*Ph*: 132.67 (bs); 130.78 (d, J_{CP} = 17.8)	10.88 (bs)
11	139.69	104.74	129.61	75.96	130.03, 122.92, 118.69, 116.77	19.27 (d, J_{CP} = 15.1; 3C) 24.45 (m, 12C)	−21.28 (q, J_{PP} = 26.3) −7.76 (d)

[a] Room temperature. All signals are singlets if not specified. Solvent, benzene-d_6 if not specified. $^{13}C\{^1H\}$ NMR for complexes **2**–**4** were not recorded (see text). $^{31}P\{^1H\}$ NMR data for complexes **2**–**4**: **2**, 1.05 (d, J_{PP} = 38.7), −11.24 (d); **3**, 6.52 (d, J_{PP} = 34.8), −1.27 (d); **4**: −0.50 (d, J_{PP} = 26.0), −12.14 (d).
[b] In DMSO-d_6.
[c] Resonances non observed.

2.3. Reaction of *1alb* with HBF_4

This reaction was analyzed in acetone-d_6 and methanol-d_4.

The addition of one equivalent of HBF_4 to **1a/b** (equimolecular amount of HBF_4 and **1a/b**) in acetone-d_6 was carried out at −80 °C and monitored by ^1H NMR from −80 to 50 °C. Two hydride singlets in a 4:1 ratio (**12a**:**12b**) were observed at −80 °C (see Fig. 1). A resonance at 9.83 ppm was observed for the major component **12a**, indicating the protonation of the oxygen atom. A C_s symmetry for the complex was deduced. The following NOEs between different signals (indicated with arrows in Scheme 4) were observed for **12a** (−10 °C): (i) H_α and H'_5; (ii) H_α and OH; (iii) the hydride signal and one olefinic cod resonance; (iv) the hydride signal and H_3 of the phenoxy group. The NOEs of (ii) and (iv) reflect the fact that the OH group is not coordinated to the metal center. The low proportion of **12b** meant that it was not possible to observe and assign all resonances for this species. However, it is worth mentioning that a quartet observed at 4.95 ppm was assigned to a molecule of Et_2O (from the HBF_4 solution) coordinated to the Ru center in this derivative. Considering all these data, the structures proposed for the two derivatives are indicated in Scheme 4. Protonation of the phenoxy group and its decoordination makes possible the formation of these

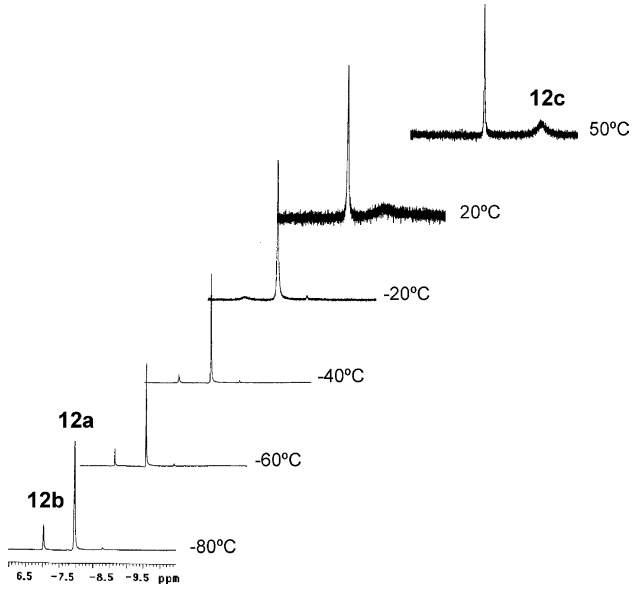

Fig. 1. Variable ^1H NMR spectra of **12a**,**b**,**c** in the hydride region.

two complexes, which mainly differ in the relative disposition of the phenol group with respect to the hydride. We must emphasize that a boat-to-boat inversion of either of these two species' does not lead to the skeleton of the other.

When the temperature of the sample was raised, the resonances of **12b** broadened (clearly observed for the hydride, H_α and Et_2O signals). However, the resonances of **12a** remained sharp. At −10 °C, the resonances of **12b** were not observed. At 10 °C, a new and broad hydride signal appeared (**12c**) (see Fig. 1). At higher temperatures this signal became less broad and at 50 °C the approximate ratio **12a**:**12c** was 1:0.8. A decrease in the temperature to 20 °C indicated that the process is reversible. On the basis of these data it is proposed that **12b** easily interconverts with **12c** in such a way that an increase in temperature favors the latter derivative. A C_s symmetry was deduced for **12c**. We propose the structure indicated in Scheme 4 for this derivative and believe that the equilibrium involves coordination–decoordination of the Et_2O molecule and the OH group. In fact the stated resonances for the Et_2O coordinated on **12b** disappeared when the formation of **12c** was completed. Displacement of the Et_2O molecule must be favored for entropic reasons. In any case, the Ru–O bond must be labilized by the high *trans* influence of the hydride ligand (in both **12b** and **12c**). Considering the stated change of the **12a**:**12b** + **12c** ratio with temperature, the transformation of **12a** into the pair **12b**–**12c** is also possible although less rapid than the transformation between **12b** and **12c**. The ^1H NMR resonances of **12a** (two temperatures) and **12c** (50 °C) are given in Table 5.

The proton transfer evolved in a similar way when carried out in methanol-d_4, with the formation of complexes **13a**,**b**,**c** as depicted in Scheme 4. However, several differences must be pointed out for this system: (i) as expected, a signal for the OH group was not observed in the spectra as a consequence of the rapid proton exchange with the medium; (ii) the three products of the reaction were separately observed in the ^1H NMR spectrum at −90 °C in a 4:1:0.5 ratio (**13a**:**b**:**c**), which implies a relative stabilization of species **13c** in comparison to **12c** in the respective mixtures.

On the other hand, the hydride (also the H_α proton) resonances of **13b** and **c** coalesced (see Fig. 2) as a consequence of the equilibrium that arises due to the competition for the coordination between the OD group of the phenol ring and that of methanol. The free energy of activation calculated at 0 °C is 55.9 kJ mol^{-1}.

The ^1H resonances of **13a** at −90 °C are shown in Table 5.

It can be concluded that the proton transfer from HBF_4 to **1a/b** is selective and occurs on the oxygen atom of the phenoxy group. The previous attack onto the Ru–H bond (kinetic control) with the formation of a dihydrogen compound, acid enough to be transformed onto the final products (thermodynamic control) can not be ruled out, although none evidence of such a pathway can be deduced from the spectra. The acid character of some dihydrogen complexes of Ru [12] and the kinetic control of the proton transfer over the Ru–H bonds of some complexes [13] is well reported.

An isomerization process, at least for isomer **1a**, must take place in these proton transfer processes and gives products with C_s symmetry. Considering the coordination mode of the bpzmPhO ligand, the main reaction products show a κ^2-*NN* coordination (**a** and **b**) with two different configurational dispositions that orientate the phenol group towards (forms **a**) or away from (forms **b**) the hydride ligand. The latter configuration means that the phenol group has an orientation suitable for coordination to the metal center (which leads to isomers of type **c**) but this coordination is in competition with the solvent (methanol or ether, isomers of type **b**). The hydride ligand apparently does not participate in the process.

3. Experimental

3.1. General comments

All manipulations were carried out under an atmosphere of dry oxygen-free nitrogen using standard Schlenk techniques. Solvents were distilled from the

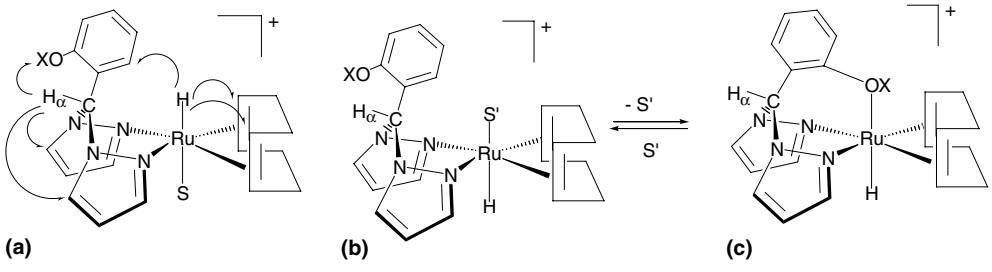

X = H, S = acetone, S' = diethyl ether **12**
X = D, S = S' = methanol-d_4 **13**

Scheme 4.

Table 5
^{1}H NMR data for complexes **12a**,**c** and **13a**[a]

Complex	Ru–H	Pyrazole			H_α	Phenoxy group		cod	
		$H^{3'}$	$H^{4'}$	$H^{5'}$		OH	C_6H_4	H_{olef}	H_{alk}
12a (−80 °C)	−7.96	7.59 (d, $J = 2.2$)	6.61 (pt, $J = 2.2$)	8.46 (d, $J = 2.4$)	8.62	9.83	6.78–7.40	3.54 (m) 3.34[b] (m)	1.78–2.08
12a (−10 °C)	−7.96	7.54 (d, $J = 2.2$)	6.56 (pt, $J = 2.3$)	8.43 (d, $J = 2.4$)	8.61	9.30	6.78–7.40	3.54 (m) 3.34[b] (m)	1.78–2.08
12c (50 °C)	−9.97	7.65 (d, $J = 2.1$)	6.47 (pt, $J = 2.3$)	8.51 (d, $J = 2.4$)	8.87	9.68	6.78–7.40	3.78 (m) 3.69 (m)	1.78–2.08
13a (−90 °C)	−7.54	7.58 (bs)	6.60 (bs)	8.59 (bs)	8.59		6.87–7.76	3.29[b] (m) 3.56 (m)	1.72–2.62

[a] All resonances are singlets if not specified. Solvent, acetone-d_6 for **12** and methanol-d_4 for **13**.
[b] Signal showing noe with the hydride.

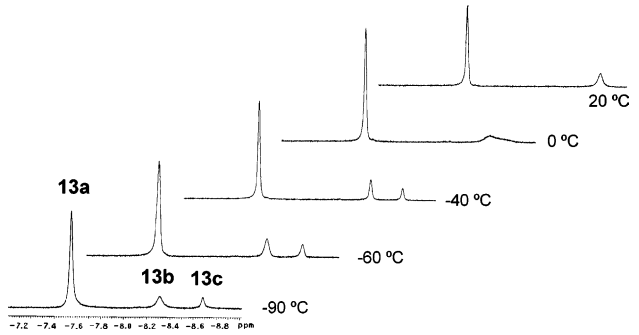

Fig. 2. Variable ^{1}H NMR spectra of **13a**,**b**,**c** in the hydride region. Note the coalescence of the hydride resonances of **13b** and **c** at 0 °C.

appropriate drying agents and degassed before use. $[RuH(cod)(NH_2NMe_2)_3][BPh_4]$ [14], [RuClH(cod)-(bpzm)] [15] and the bpzmPhOH ligand [5] were prepared as described in the literature. PMe_3 (1 M solution in toluene), PMe_2Ph, $PMePh_2$ and PPh_3 were used as purchased from Aldrich. HBF_4 was used as a solution 54 wt% in diethyl ether (Aldrich). Elemental analyses were performed with a Perkin–Elmer 2400 microanalyzer. IR spectra were recorded as KBr pellets with a Perkin–Elmer PE 883 IR spectrometer. ^{1}H, ^{31}P{^{1}H} and ^{13}C{^{1}H} spectra were recorded on a VARIAN UNITY 300 spectrometer. Chemical shifts (ppm) are given relative to TMS. Coupling constants are given in Hz. bs = broad singlet, d = doublet, m = multiplet, pt = pseudo-triplet, q = quintet, t = triplet. COSY spectra: standard pulse sequence with an acquisition time of 0.214 s, pulse width 10 ms, relaxation delay 1 s, number of scans 16, number of increments 512. The NOE difference spectra were recorded with the following acquisition parameters: spectral width 5000 Hz, acquisition time 3.27 s, pulse width 18 ms, relaxation delay 4 s, irradiation power 5–10 dB, number of scans 240. For variable temperature spectra the probe temperature (±1 K) was controlled by a standard unit calibrated with a methanol reference. Free energies of activation were calculated [16] from the coalescence temperature (T_c) and the frequency difference between the coalescing signals (extrapolated at the coalescence temperature) with the formula $\Delta G_c^{\ddagger} = aT\,[9.972 + \log(T/\delta v)]$, $a = 1.914 \times 10^{-2}$. The estimated error in the calculated free energies of activation is ±1.0 kJ mol^{-1}.

3.2. Preparations

3.2.1. bpzmPhOK

This salt was prepared according to a modified method of that described by Carrano and co-workers [7b] for the sodium salt. A solution of bpzmPhOH (111.5 mg, 0.4 mmol) and ^{t}BuOK (56.1 mg, (0.4 mmol) in THF (15 ml) was stirred during 1 h. The solvent was evaporated to dryness and the resulting white solid was washed with diethylether (2 × 8 ml). Yield: 70%.

*3.2.2. [RuH(κ³-bpzmPhO)(cod)] (**1**)*

To a solution of [RuH(cod)(NH_2NMe_2)$_3$][BPh_4] (200 mg, 0.28 mmol) in THF (30 ml) at room temperature one equivalent of the ligand bpzmPhOK (78 mg, 0.28 mmol) was added. The mixture was stirred overnight, and the resulting suspension was filtered off in order to eliminate the $KBPh_4$ formed. The solution was evaporated to dryness, and the resulting white solid was washed with hexane (10 ml). Yield: 65%.

Another way to synthesize this complex is starting from [RuClH(cod)(bpzm)]. To a suspension of [RuClH(bpzm)(cod)] (125 mg, 0.32 mmol) in THF, one equivalent of the ligand bpzmPhOK (88 mg, 0.32 mmol) was added, and the mixture was stirred at room temperature for 10 h. The solution was filtered off in order to eliminate the KCl formed and evaporated to dryness, and the resulting white solid was washed with ether (2 × 10 ml). Yield: 50%. *Anal.* Calc. for $C_{21}H_{24}N_4ORu$: C, 56.11; H, 5.38; N, 12.46. Found: C, 56.11; H, 5.34; N, 12.16%. IR (KBr): 2045 cm^{-1} (*ν* Ru–H).

*3.2.3. [RuH(κ¹-O-bpzmPhO)(cod)(PMe_3)$_2$] (**2**)*

The reaction has been done in an NMR tube. To a solution of [RuH(bpzmPhO)(cod)] (**1**) (18 mg, 0.04 mmol) in 0.5 ml of benzene-d_6 two equivalents of PMe_3 (80 μl, 1 M in toluene, 0.08 mmol) were added. The solution was stirred at 20 °C and the reaction evolution was monitored by ^1H and $^{31}P\{^1H\}$ NMR. After that, the solution was put into a Schlenk and evaporated to dryness, and the resulting yellow solid was washed with hexane (2 × 10 ml). Approximate yield: 70%. *Anal.* Calc. for $C_{27}H_{42}N_4OP_2Ru$: C, 53.90; H, 7.04; N, 9.31. Found: C, 53.90; H, 6.99; N, 9.44%. IR (KBr): 2003 cm^{-1} (*ν* Ru–H).

*3.2.4. [RuH(κ¹-O-bpzmPhO)(cod)(PMe_2Ph)$_2$] (**3**)*

The reaction has been done in an NMR tube. To a solution of [RuH(bpzmPhO)(cod)] (**1**) (20 mg, 0.04 mmol) in 0.5 ml of benzene-d_6 two equivalents of PMe_2Ph (12.7 μl, 0.08 mmol) were added. The yellow solution was stirred at 20 °C and the reaction evolution was monitored over 2 h by ^1H and $^{31}P\{^1H\}$ NMR. After that, the solution was put into a Schlenk and the solvent was evaporated. The resulting yellow solid was washed with 10 ml of hexane. Approximate yield: 69%. *Anal.* Calc. for $C_{37}H_{46}N_4OP_2Ru$: C, 61.23; H, 6.39; N, 7.72. Found: C, 61.45; H, 6.46; N, 7.53%. IR (KBr): 2025 cm^{-1} (*ν* Ru–H).

*3.2.5. [RuH(κ³-bpzmPhO)(PMe_2Ph)$_2$] (**5**)*

When a solution of the complex **3** (15 mg, 0.021 mmol) is heated at 50 °C into an NMR tube in benzene-d_6 for 30 min, complex **5** was obtained. After that, the solution was put into a Schlenk and the solvent was evaporated. The resulting yellow solid was washed with 10 ml of hexane. Yield: 95%. *Anal.* Calc. for $C_{29}H_{34}N_4OP_2Ru$: C, 56.40; H, 5.55; N, 9.07. Found: C, 56.32; H, 5.12; N, 9.05%. IR (KBr): 1948 cm^{-1} (*ν* Ru–H).

*3.2.6. [RuH(κ³-bpzmPhO)($PMePh_2$)$_2$] (**6**)*

To a solution of [RuH(bpzmPhO)(cod)] (**1**) (200 mg, 0.44 mmol) in toluene (15 ml) two equivalents of the ligand $PMePh_2$ (165 μl, 0.88 mmol) were added, and the mixture was heated at 70 °C for 20 min. The pale yellow solution was evaporated to dryness, and the resulting yellow solid was washed with 10 ml of hexane. *Anal.* Calc. for $C_{39}H_{38}N_4OP_2Ru$: C, 63.15; H, 5.16; N, 7.55. Found: C, 63.25; H, 5.99; N, 7.45%. IR (KBr): 2021 cm^{-1} (*ν* Ru–H).

*3.2.7. [RuH(κ³bpzmPhO)(PPh_3)$_2$] (**7**)*

To a solution of [RuH(bpzmPhO)(cod)] (**1**) (125 mg, 0.28 mmol) in acetone (10 ml) two equivalents of PPh_3 (146 mg, 0.56 mmol) were added. The mixture was heated at 70 °C for 1 h and a suspension was formed. A pale yellow solid was obtained after filtration at room temperature and it was washed with hexane (2 × 10 ml). Yield: 80%. *Anal.* Calc. for $C_{39}H_{38}N_4OP_2Ru$: C, 67.97; H, 4.89; N, 6.47. Found: C, 68.16; H, 4.99; N, 6.24%. IR (KBr): 1944 cm^{-1} (*ν* Ru–H).

*3.2.8. [RuH(κ¹-O-bpzmPhO)(PMe_3)$_4$] (**8**)*

The reaction has been done in an NMR tube. To a solution of [RuH(bpzmPhO)(cod)] (**1**) (18 mg, 0.04 mmol) in 0.5 ml of benzene-d_6 four equivalents of PMe_3 (160 μl, 1 M in toluene, 0.16 mmol) were added. The solution was stirred at 20 °C and the reaction evolution was monitored for 1 h by ^1H and $^{31}P\{^1H\}$ NMR. After that, the solution was evaporated to dryness in a Schlenk. The resulting orange solid was washed with 10 ml of hexane. Approximate yield: 73%. *Anal.* Calc. for $C_{25}H_{48}N_4OP_4Ru$: C, 46.51; H, 7.49; N, 8.68. Found: C, 46.32; H, 7.58; N, 8.82%. IR (KBr): 1973 cm^{-1} (*ν* Ru–H).

*3.2.9. [cis-O,H-RuH(κ¹-O-bpzmPhO)(PMe_2Ph)$_4$] (**9**)*

The reaction has been done in an NMR tube. To a solution of [RuH(bpzmPhO)(cod)] (**1**) (20 mg, 0.04 mmol) in 0.5 ml of benzene-d_6 four equivalents of PMe_2Ph (25.4 μl, 0.16 mmol) were added. The solution was stirred and heated at 50 °C for 20 min, and the reaction evolution was monitored by NMR. After that, the solution was put into a Schlenk and evaporated to dryness, and the yellow solid was washed with 10 ml of diethyl ether. Approximate yield: 74%. *Anal.* Calc. for $C_{45}H_{56}N_4OP_4Ru$: C, 60.46; H, 6.31; N, 6.27. Found: C, 60.40; H, 6.27; N, 6.31%. IR (KBr): 1957 cm^{-1} (*ν* Ru–H).

*3.2.10. [trans-O,H-RuH(κ¹-O-bpzmPhO)(PMe_2Ph)$_4$] (**10**)*

A solution of **9** in 0.5 ml of benzene-d_6 in an NMR tube was heated at 70 °C and the reaction evolution was monitored by NMR until complete transformation into **10**. **10** was spectroscopically characterized by NMR.

*3.2.11. [RuH(PMe_3)$_5$] (bpzmPhO) (**11**)*

To a solution of [RuH(bpzmPhO)(cod)] (**1**) (200 mg, 0.44 mmol) in 20 ml of toluene five equivalents of PMe_3 (2.2 ml, 1 M in toluene, 2.2 mmol) were added, and the mixture was stirred at 20 °C for 30 min. The solution was evaporated to dryness, obtaining an orange solid. Complex **11** is not obtained as a single product but only in a mixture with complex **8**. IR (KBr): 1983 cm^{-1} (ν Ru–H).

*3.2.12. General procedure to the formation of complexes **12a–c** and **13a–c***

A solution of [RuH(bpzmPhO)(cod)] (**1**) (18 mg, 0.04 mmol) in 0.5 ml of acetone-d_6 or methanol-d_4 in a NMR tube was cooled to −90 °C. A solution of $HBF_4 \cdot Et_2O$ (54 wt%) was added (3.6 μl, 0.04 mmol). This tube was introduced in the NMR probe previously cooled at −90 °C. The evolution of the reaction was monitored by ^1H NMR with an increasing of temperature up to 50 °C (increments of 10° except in the proximity of the coalescence temperature where the increments were of 1°).

Acknowledgements

We are grateful to the Spanish DGES/MCyT (Project BQU-2002-00286) and the Junta de Comunidades de Castilla-La Mancha (Project PBI-02-002) for financial support.

References

[1] S. Trofimenko, Scorpionates: The Coordination Chemistry of Polypyrazolylbotate Ligand, Imperial College Press, London, 1999.
[2] S. Trofimenko, J. Am. Chem. Soc. 92 (1970) 5118.
[3] (a) N. Arroyo, F. Gómez-de la Torre, F.A. Jalón, B.R. Manzano, B. Moreno-Lara, A.M. Rodríguez, J. Organomet. Chem. 603 (2000) 174;
(b) M.C. Carrión, A. Díaz, A. Guerrero, F.A. Jalón, B.R. Manzano, A. Rodríguez, New J. Chem. 26 (2002) 305;
(c) M.C. Carrión, A. Díaz, A. Guerrero, F.A. Jalón, B.R. Manzano, A. Rodríguez, R.L. Paul, J.C. Jeffery, J. Organomet. Chem. 650 (2002) 210.
[4] P.K. Byers, A.J. Canty, R.T. Honeyman, Adv. Organomet. Chem. 34 (1992) 1.
[5] T.C. Higgs, C.J. Carrano, Inorg. Chem. 36 (1997) 291.
[6] (a) K.I. The, L.K. Peterson, Can. J. Chem. 51 (1973) 422;
(b) K.I. The, L.K. Peterson, E. Kiehlmann, Can. J. Chem. 51 (1973) 2448;
(c) L.K. Peterson, E. Kiehlmann, A.R. Sanger, K.I. The, Can. J. Chem. 52 (1974) 2367.
[7] (a) T.C. Higgs, N.S. Dean, C.J. Carrano, Inorg. Chem. 37 (1998) 1473;
(b) T.C. Higgs, K. Spartalian, C.J. O'Connor, B.E. Matzanke, C.J. Carrano, Inorg. Chem. 37 (1998) 2263;
(c) T.C. Higgs, D. Ji, R.S. Czernuszewicz, B.F. Maizanke, V. Schunemann, A.X. Trautwein, M. Helliwell, W. Ramírez, C.J. Carrano, Inorg. Chem. 37 (1998) 2383.
[8] T.C. Higgs, C.J. Carrano, Inorg. Chem. 36 (1997) 298.
[9] (a) C. Potvin, J.M. Manoli, G. Pannetier, R. Chevalier, J. Organomet. Chem. 146 (1978) 57;
(b) C. Potvin, J.M. Manoli, G. Pannetier, N. Platzer, J. Organomet. Chem. 219 (1981) 115;
(c) F.A. Jalón, A. López-Agenjo, B.R. Manzano, M. Moreno-Lara, A. Rodríguez, T. Sturm, W. Weissensteiner, J. Chem. Soc., Dalton Trans. (1999) 4031.
[10] For one example with decoordination and recoordination of pyrazolylborate ligands see: V. Rodríguez, I. Atheaux, B. Donnadieu, S. Sabo-Etienne, B. Chaudret, Organometallics 19 (2000) 2916.
[11] M. Paneque, S. Sirol, M. Trujillo, E. Gutierrez-Puebla, M.A. Monge, E. Carmona, Angew. Chem., Int. Ed. Engl. 39 (2000) 218.
[12] (a) S.S. Kristjansdottir, J.R. Norton, in: A. Dedieu (Ed.), Transition Metal Hydrides: Recent Advances in Theory and Experiment, VCH, New York, 1991;
(b) G. Jia, R.H. Morris, J. Am. Chem. Soc. 113 (1881) 875;
(c) K. Abdur-Rashid, T.P. Fong, B. Greaves, D.G. Gusev, J.G. Hinman, S.E. Landau, A.J. Luogh, R.H. Morris, J. Am. Chem. Soc. 122 (2000) 9155.
[13] (a) M.S. Chinn, D.M. Heinekey, J. Am. Chem. Soc. 112 (1990) 5166;
(b) G.J. Jia, A.L. Lough, R.H. Morris, Organometallics 11 (1992) 161.
[14] T.V. Ashworth, E. Singleton, J.J. Hough, J. Chem. Soc. (1977) 1809.
[15] M. Fajardo, A. de la Hoz, E. Díez-Barra, F.A. Jalón, A. Otero, A. Rodríguez, J. Tejeda, D. Belletti, M. Lafranchi, M.A. Pellinghelli, J. Chem. Soc., Dalton Trans. (1993) 1935.
[16] J. Sandström, Dynamic NMR Spectroscopy, Academic Press, London, 1982.

Available online at www.sciencedirect.com
SCIENCE DIRECT®
Polyhedron 23 (2004) 373–378
POLYHEDRON
www.elsevier.com/locate/poly

A chromogenic penta-aza scorpionand for nickel(II) and copper(II) ions

Luigi Fabbrizzi *, Maurizio Licchelli, Antonio Poggi, Donatella Sacchi, Cristina Zampa

Dipartimento di Chimica Generale, Università di Pavia, via Taramelli 12, 27100 Pavia, Italy

Received 5 June 2003; accepted 3 September 2003

Abstract

The nickel(II) and copper(II) complexes of a new scorpionand in which the side chain has been functionalized with the powerful chromophore 4-amino-7-nitro-benzo-2-oxa-1,3-diazole have been prepared. The pendant arm of the new ligand undergoes pH-dependent complexation/decomplexation to the metal centre, with simultaneous deprotonation of the aniline nitrogen atom of the pendant arm, thus inducing drastic modifications of the spectral features of the chromophore and a sharp colour change. The pK_a values observed for both complexes change according to the metal promoting the deprotonation, being lower for the Ni complex than for the Cu species, because of the different coordination geometries adopted by the two ions.
© 2003 Elsevier Ltd. All rights reserved.

Keywords: Scorpionands; Chromophores; Copper(II); Macrocycles; Nickel(II)

1. Introduction

There exist two-component ligands which consists of a multidentate macrocycle and of a covalently linked side-chain containing a further donor group. Classical examples are provided by penta-aza ligands **1** [1], and **2** [2]. Each system contains a 14-membered ring which can include a transition metal ion, e.g. Ni^{II}, Cu^{II}. In each complex, the metal centre is firmly incorporated by the tetra-aza-macrocycle, according to a square stereochemical arrangement, in which the four nitrogen atoms of the ring are coplanar with the metal centre. In this situation, the metal is especially resistant to the demetallation due to the so-called *kinetic macrocyclic effect* [3]. In particular, the tetra-aza-macrocyclic complex persists indefinitely in a strongly acidic solution, even if the processes of metal extrusion and protonation of the nitrogen atoms would be very favoured from a thermodynamic point of view. However, the M^{II}–N bond itself (with both amine and pyridine donor atoms) is intrinsically labile: thus, inertness derives from the steric constraints imposed by the cyclic ligand.

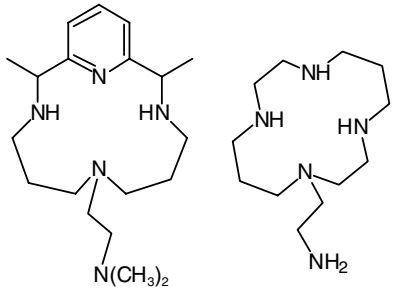

1 **2**

On the other hand, ligands **1** and **2** contain a fifth binding site, the nitrogen atom belonging to the ethylamine side-chain covalently linked to the macrocycle. In particular, the amino group of the side chain binds one of the axial positions of the coordination polyhedron, either an octahedron or a square pyramid. It should be noted that the interaction of the metal ion with the axially bound amine nitrogen atom does not suffer from any steric constraint and is therefore labile. Thus, it should happen that, on acidification, the amino group is protonated and removed from coordination. The change

* Corresponding author. Tel.: +39-0382-507-325; fax: +39-0382-528-544.
E-mail address: fabbrizz@unipv.it (L. Fabbrizzi).

0277-5387/$ - see front matter © 2003 Elsevier Ltd. All rights reserved.
doi:10.1016/j.poly.2003.11.024

is quickly reversible and addition of standard base relocates the pendant arm on the axial position. The complexation/decomplexation of the pendant arm, driven by the protonation/deprotonation of the amino group is illustrated in Scheme 1.

Ligands **1** and **2** have been given the current name of *scorpionands*, by considering that they firmly chelate an individual (the metal ion), which can be stung from the top, at command, by an aggressive tail. Metal scorpionate complexes are interesting systems which consist of a fixed part (the rigid tetra-aza ring) and of a mobile portion (the flexible pendant arm). Taking profit from a chemical input (the addition of either H^+ or OH^-), the pendant arm can be alternatively located between two distinct positions: either axially bound to the metal centre or far away from it in order to minimise the electrostatic repulsions with the ammonium ion. In this sense, scorpionate complexes of the type described are suitable systems for generating controlled molecular motions and, as they convert energy (that of an acid–base reaction) into a repeteable movement, they can be considered the prototypes of elementary molecular machines.

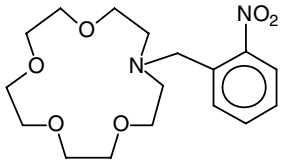

3

Analogous systems exist in the realm of crown ethers. In the ligand **3**, a side chain containing a 2-nitrobenzene fragment is covalently linked to the nitrogen atom of a 15-crown-NO_4 [4]. Under unperturbed conditions, the pendant arm is bound very weakly to the sodium ion encircled by the crown. However, if the nitro group undergoes one-electron electrochemical reduction, the $NO_2^{\bullet -}$ anion radical that forms establishes a rather strong interaction with the alkali metal ion. In this case, alternate reduction/oxidation of the nitro group induces formation-breaking of a coordinative bond, according to a mode reminiscent of that observed with scorpionate complexes. It should be mentioned that Authors gave systems like **3** the name of lariat ethers [5] taking inspiration from the shape of the ligand (a lasso which takes a metal ion). Therefore, the following convention is being currently followed: a multidentate chelate (possibly cyclic) with a pendant arm is called *scorpionand* if the donor atoms are nitrogens, or *lariat* if the donor atoms are oxygens.

In the case of scorpionands, complexation/decomplexation of the pendant arm may induce a variety of effects, which are essentially related to the versatile behaviour of the transition metal centre incorporated by the macrocycle. For instance, complexation–decomplexation may induce a variation of the spin state of a Ni^{II} centre, with a concomitant colour change (blue-to-yellow) [2]. A colour change (red-to-blue) is observed also in the case of Cu^{II} scorpionate complexes [6]. Moreover, the pendant arm can be equipped with a further functionality, whose properties vary depending whether the side-chain is bound or not bound to the metal. For instance, a fluorescent fragment was covalently linked through a $–CH_2–$ fragment to the pendant amine group of **2**: it was observed that coordination of the pendant arm quenched the emission of the fluorophore, which was restored on decomplexation, thus giving rise to an unprecedented mechanical switch of fluorescence [7].

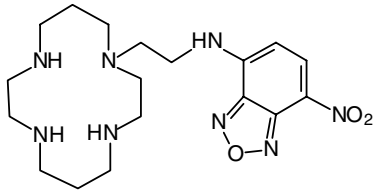

4

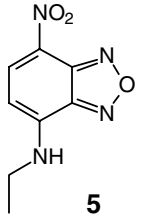

5

We consider now a new type of scorpionand, in which the pendant arm has been equipped with a powerful chromophore: in particular, the 4-amino-7-nitro-benz-2-oxa-1,3-diazole (7-nitrobenzofurazan or NBD) fragment [8] was directly linked to the side-chain of macrocycle **2**, to give **4**. It will be shown that the pendant arm of **4** undergoes pH-dependent complexation–decomplexation to Ni^{II} and Cu^{II}, according to a process which induces a drastic modification of the colour and of the spectral features of the chromophore.

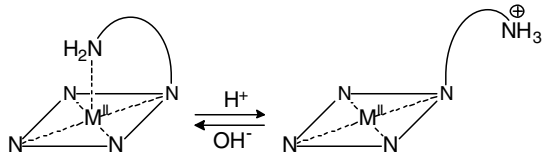

Scheme 1. Protonation–deprotonation equilibrium for the scorpionate complexes of ligand **2**.

2. Experimental

2.1. General remarks

Unless otherwise stated, commercially available reagent grade chemicals (Sigma–Aldrich) were used as received. 1,4,8,11-tetraazacyclotetradecane, cyclam, was prepared according to literature method [9].

UV–Vis spectra were recorded on a Hewlett–Packard 8453 diode array or on a Varian Cary 100 spectrophotometer. NMR spectra were recorded on a Bruker AMX400 spectrometer.

Mass spectra were obtained using an LCQ DECA ion trap mass spectrometer equipped with electrospray ionization (ESI) ion source and controlled by Xcalibur software 1.1 (Thermo-Finnigan).

Potentiometric determinations were performed in a thermostatted cell on aqueous solutions (20 ml, made 0.05 M in $NaClO_4$, 25 °C) containing [Ni(**4**)]$(ClO_4)_2$, [Cu(**4**)]$(ClO_4)_2$ or the reference compound **5** (10^{-4}M) and an excess of standard $HClO_4$, by addition of standard aqueous NaOH (a Radiometer automatic titration apparatus was used). The pH scale was calibrated prior to each experiment according to the Gran method [10]. Refinement of the potentiometric data was made through the Hyperquad package [11].

Spectrophotometric titrations were performed on aqueous solutions (10 ml, made 0.05 M in $NaClO_4$, 25 °C) of the metal complexes or of the reference compound **5** ($1.0–5.0 \times 10^{-5}$ M) adjusted at pH ~2.0 by adding small amounts of a standard solution of $HClO_4$. Subsequently, additions of standard solutions (0.1 or 1.0 M) of NaOH were made until a basic pH (~12.0) was attained. Absorption spectra were taken after each addition of base. In each experiment the overall addition was limited to about 200 μl, so that volume variation was not significant.

Safety note: Perchlorate salts of metal complexes are potentially explosive and should be handled with care. In particular, they should never be heated as solids [12].

2.2. Synthesis of N-ethyl-7-nitrobenzo-2-oxa-1,3-diazol-4-amine (*5*)

A solution of 4-chloro-7-nitrobenzo-2-oxa-1,3-diazole (NBD chloride, 0.5 g, 2.5 mmol) in toluene was added to a refluxing mixture of Cs_2CO_3 (0.48 g, 1.47 mmol) and ethylamine (0.2 ml, 2.5 mmol) in toluene. The reaction was monitored by TLC (Al_2O_3, CH_2Cl_2, $R_f = 0.40$). After 3 h the solvent was removed at the rotary evaporator, the residue treated with MeOH, and the precipitate isolated by filtration; yield 81%. *Anal.* Found: C, 46.01; H, 3.73; N, 27.03. Calc. for $C_8H_8N_4O_3$: C, 46.16; H, 3.87; N, 26.91%. ^{1}H-NMR (400 MHz, CD_3CN): δ(ppm) = 8.6 (d, 1H, *H–Ar*), 7.5 (s, 1H, *NH*), 6.4 (d, 1H, *H–Ar*), 3.6 (m, 2H, CH_2), 1.4 (t, 3H, CH_3).

2.3. Synthesis of N-(2-bromoethyl)-7-nitrobenzo-2-oxa-1,3-diazol-4-amine (*6*)

Bromoethylamine ·HBr (0.27 g, 1.3 mmol) and NaOH (0.12 g, 3 mmol) were dissolved in ethanol (10 ml) and added dropwise to a refluxing solution of NBD chloride (0.26 g, 1.3 mmol) in ethanol (10 ml), under magnetic stirring. The reaction was monitored by TLC (Al_2O_3, CH_2Cl_2). After 5 h the resulting green solution was cooled to room temperature and the solvent was evaporated in vacuo, leaving a red residue. The crude product was purified by liquid chromatography (Al_2O_3, CH_2Cl_2, $R_f = 0.51$); yield 60%. *Anal.* Found: C, 33.31; H, 2.52; N, 19.43. Calc. for $C_8H_7BrN_4O_3$: C, 33.47; H, 2.46; N, 19.52%. ^{1}H-NMR (400 MHz, d_6-DMSO): δ(ppm) = 9.5 (s, 1H; *NH*), 8.5 (d, 1H, *H–Ar*), 6.5 (d, 1H, *H–Ar*), 3.7 (t, 2H, CH_2Br), 3.3 (t, 2H, CH_2N).

2.4. Synthesis of *4*

Cyclam (1.07 g, 5.3 mmol) was dissolved in hot toluene (40 ml) and **6** (0.223 g, 0.78 mmol) was added. The resulting mixture was refluxed for 2 h, then it was cooled at room temperature and the white precipitate (excess cyclam and its hydrobromide salt) was filtered off. The solvent was removed and the residue treated with diethyl ether: an orange product was obtained; yield 73%. *Anal.* Found: C, 52.96; H, 7.56; N, 27.39. Calc. for $C_{18}H_{30}N_8O_3$: C, 53.19; H, 7.44; N, 27.57%. MS (ESI): *m/z*: 407.4 [M+H$^+$].

2.5. Synthesis of metal complexes, [Ni(*4*)]$(ClO_4)_2$ and [Cu(*4*)]$(ClO_4)_2$

Nickel(II) complex: $Ni(ClO_4)_2 \cdot 6H_2O$ (4.5 mg, 0.012 mmol) dissolved in MeOH was added to a solution of **4** (5 mg, 0.012 mmol) in MeOH. A red precipitate formed quickly and was isolated by filtration; yield 93%. *Anal.* Found: C, 32.84; H, 4.32; N, 17.09. Calc. for $C_{18}H_{30}Cl_2NiN_8O_3$: C, 32.56; H, 4.55; N, 16.87%. MS (ESI): *m/z*: 563.2 [M-ClO_4^-]$^+$, 463.3 [M-ClO4$^-$–$HClO_4$]$^+$.

Copper(II) complex: the same procedure but $Cu(ClO_4)_2 \cdot 6H_2O$ (4.6 mg, 0.012 mmol) was used; purple–red product; yield 95%. *Anal.* Found: C, 32.47; H, 4.39; N, 16.88. Calc. for $C_{18}H_{30}Cl_2CuN_8O_3$: C, 32.32; H, 4.52; N, 16.75%. MS (ESI): *m/z*: 568.1 [M-ClO_4^-]$^+$, 468.2 [M-ClO4$^-$–$HClO_4$]$^+$.

3. Results and discussion

3.1. Synthesis of scorpionand *4*

The synthesis of cyclam derivatives containing a substituent group on a nitrogen atom has been recently performed by triprotection of the cyclic tetraamine followed by a specific reaction involving the free amino group [13]. Such a procedure afforded very pure products after the final deprotection step.

However, the protection/deprotection procedure was not necessary in the synthesis of scorpionand **4**, which was prepared, with satisfactory yield and purity, according to a shorter synthetic pathway, as depicted in Scheme 2.

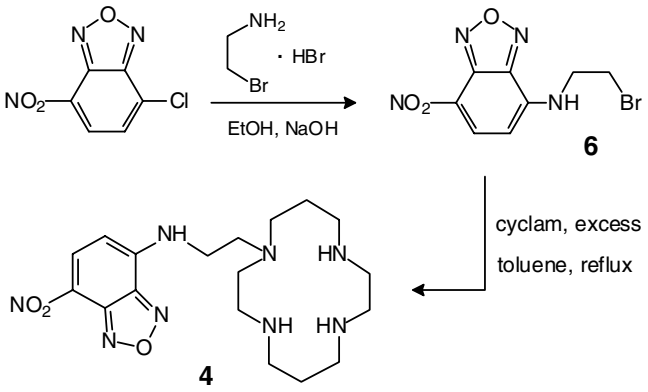

Scheme 2. Synthesis of scorpionand **4**.

In the first step, the commercially available 4-chloro-7-nitro-benzo-2-oxa-1,3-diazole (NBD chloride) was converted into bromoethylamino-NBD (intermediate **6**) by performing an aromatic nucleophilic substitution in boiling ethanol.

The chromophore-containing pendant arm was then appended onto the macrocyclic framework by reaction of **6** with cyclam (fivefold excess) in boiling toluene. The excess of the cyclic tetraamine affords a double advantage: (i) it addresses the reaction toward the formation of the mono-functionalised macrocycle, minimizing the probability of polysubstitution; (ii) it neutralises the hydrobromic acid generated from the reaction, avoiding the addition of a further basic reactant. The scorpionand **4** was easily isolated by cooling the reaction mixture since both excess cyclam and cyclam hydrobromide are insoluble in toluene at room temperature.

Nickel(II) and copper(II) complexes were prepared by addition of stoichiometric amounts of the corresponding perchlorate salts to methanol solutions containing the scorpionand **4**.

3.2. pH-controlled complexation–decomplexation of the pendant arm

A solution of the $[Ni^{II}(\mathbf{4})](ClO_4)_2$ complex, acidified with standard acid to pH 2 and made 0.05 M in $NaClO_4$, was titrated with standard NaOH. The titration curve disclosed a single deprotonation event, with a $pK_a = 7.83 \pm 0.05$, to be ascribed to the acid–base equilibrium: $[Ni^{II}(LH)]^{2+} \rightleftarrows [Ni^{II}(L)]^{+} + H^{+}$, where LH = **4**. Titration with base induces decolorisation of the orange–yellow solution and a drastic change of the absorption spectrum, as shown in Fig. 1.

In particular, the strong band at 475 nm ($\varepsilon = 9100$ $M^{-1}\,cm^{-1}$) decreases, while a new band develops at 394 nm ($\varepsilon = 7180$ $M^{-1}\,cm^{-1}$, limit value at pH 12). Quite interestingly, on increasing pH the molar absorbance of the new band superimposes well with the concentration profile of the $[Ni^{II}(L)]^{+}$ species, as shown in Fig. 2. This indicates that colour and spectral changes are associated

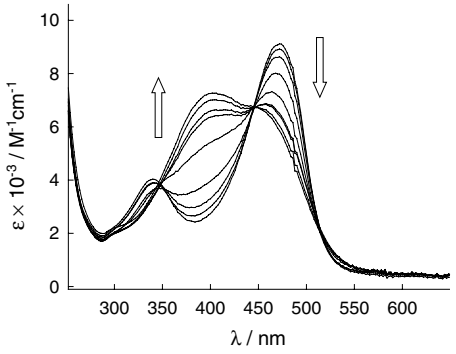

Fig. 1. Absorption spectra of $[Ni^{II}(\mathbf{4})](ClO_4)_2$ in water (1.3×10^{-5} M), measured during a titration with NaOH (pH range: 2–12).

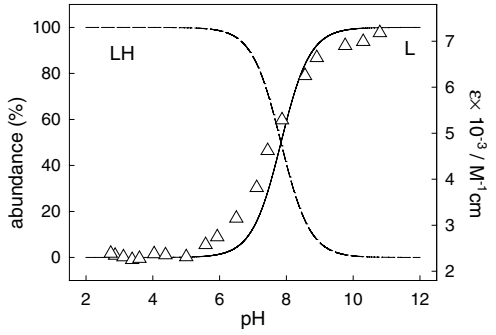

Fig. 2. Right vertical axis, distribution curves of the species present at equilibrium for the nickel(II) complex of scorpionand **4**. Left vertical axis (Δ) molar absorbance measured at 394 during the titration experiment.

to the deprotonation process. It is suggested that deprotonation involves the aniline nitrogen atom of the pendant arm. This hypothesis is supported by the behaviour of the chromogenic fragment **5**, which can be considered as an isolated analogue of the pendant arm, without the appended macrocycle. **5** behaves as a monoprotic acid with $pK_a = 10.75 \pm 0.03$. Moreover, the absorption spectrum shows a pH dependence very similar to that observed with the $[Ni^{II}(\mathbf{4})]^{2+}$ complex (see Fig. 3), with the band at 470 nm ($\varepsilon = 11,150$ $M^{-1}\,cm^{-1}$) which decreases, while a new band forms and develops

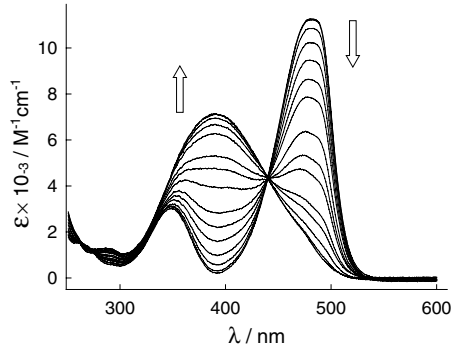

Fig. 3. Absorption spectra of **5** in water (2.4×10^{-5} M) measured during a titration with NaOH (pH range: 2–12).

at 394 nm ($\varepsilon = 7190\ M^{-1}\,cm^{-1}$, limit value at pH 12). Note that in the present case, spectral changes have to be necessarily ascribed to the deprotonation of the amine group.

Therefore, the $[Ni^{II}(L)]^+$ species should be considered as a scorpionate complex, with the deprotonated aniline group coordinated to one of the axial positions of the octahedron. Occurrence of the apical coordination of the pendant arm is demonstrated by the fact that the pK_a value is about three log units lower than that of the reference system **5**. The greater acidity of the aniline group in the $[Ni^{II}(L)]^+$ scorpionate complex has to be ascribed to the exothermic contribution of the metal-deprotonated aniline nitrogen atom. Indeed, this effect is rather moderate. In this connection, it has to be noted that in the case of the Ni^{II} complex with system **2**, the pK_a for the scorpionate (2.8) [2] was 10 orders of magnitude lower than that of the isolated side chain ethylamine (pK_a = 10.8). On the other hand, for system **1**, the difference of pK_a values between the Ni^{II} scorpionate complex (6.2) [1b] and the isolated side chain, *N*,*N*-dimethyl-ethyl-amine (p$K_a \cong 11$) was distinctly lower, probably due to the steric effects exerted by the two methyl groups on the nitrogen atoms that reduced the intensity and the exothermicity of the interaction with the metal. Such a steric repulsive effect must be especially important in the case of the scorpionate complex with **4**, due to the presence of the bulky 7-nitrobenzo[1,2,5]oxadiazole substituent, which is directly bound to the nitrogen atom of the pendant arm. This situation accounts for the low value of ΔpK_a.

An analogous behaviour has been observed in the case of copper(II). Potentiometric titration disclosed the occurrence of an acid–base event with pK_a = 8.78 ± 0.12. Moreover, electronic spectra showed a sharp dependence upon pH. Fig. 4 displays the spectra of an aqueous solution of $[Cu^{II}(\mathbf{4})](CF_3SO_3)_2$, recorded over the 2–12 pH range. It is seen that, on increasing pH, the absorption spectrum changes in the 320–520 nm range and, in particular, the band centred at 475 nm, due to the 4-amino-7-nitro-benz-2-oxa-1,3-diazole chromophore, decreases. Quite interestingly the molar absorbance of this new band superimposes well on the concentration profile of the deprotonated species $[Cu^{II}(L)]^+$. It is therefore suggested that also in the present case the aniline group of the pendant arm deprotonates and simultaneously coordinates the Cu^{II} centre in one of the two available apical positions. Notice that ΔpK_a (about 2) is smaller than that observed for the Ni^{II} complex: this may be due to the fact that the Cu^{II} ion in an octahedral geometry is sensitive to the Jahn–Teller effect and tends to form octahedrally elongated complexes. Thus, the longer distance and the diminished Cu^{II}-deprotonated aniline interaction reduce the exothermic contribution due to the apical metal–ligand interaction, with a consequent lower decrease of pK_a with respect to the isolated side-chain.

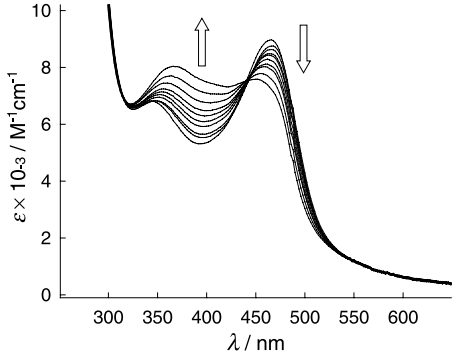

Fig. 4. Absorption spectra of $[Cu^{II}(\mathbf{4})](ClO_4)_2$ in water (2.5×10^{-5} M) measured during a titration with NaOH (pH range: 2–12).

4. Conclusions

This work has introduced a new class of scorpionands, in which the pendant arm has been equipped with a chromophore. In particular, the nitrogen atom of the pendant arm is an essential part of the chosen chromogenic fragment. It may happen that coordination of the metal ion may favour an acid–base event (in the present case deprotonation of the aniline group), with a drastic modification of the spectral features and a sharp colour change. Choice of suitable chromophores and coordinating groups of the pendant arm (amine, aniline, carboxamide, sulphonamide) may give rise to a variety of chromogenic scorpionands, whose activity (complexation–decomplexation of the side-chain) can be displayed over a wide pH range.

Acknowledgements

This work was financially supported by the European Union (RT Network Molecular Level Devices and Machines– Contract HPRN-CT-2000 – 00029), and by MIUR (Progetto 'Dispositivi Supramolecolari').

References

[1] (a) T.J. Lotz, T.A. Kaden, J. Chem. Soc., Chem. Comm. (1977) 15;
(b) T.J. Lotz, T.A. Kaden, Helv. Chim. Acta 61 (1978) 1376.
[2] P. Pallavicini, A. Perotti, B. Seghi, L. Fabbrizzi, J. Am. Chem. Soc. 109 (1987) 5139.
[3] D.K. Cabbiness, D.W. Margerum, J. Am. Chem. Soc. 91 (1969) 6540.
[4] M. Delgado, L. Echegoyen, V.J. Gatto, D.A. Gustowski, G.W. Gokel, J. Am. Chem. Soc. 108 (1986) 4135.
[5] D.M. Dishong, C.J. Diamond, M.I. Cinoman, G.W. Gokel, J. Am. Chem. Soc. 105 (1983) 586.
[6] D. Tschudin, A. Basak, T.A. Kaden, Helv. Chim. Acta 71 (1988) 100.

[7] L. Fabbrizzi, M. Licchelli, P. Pallavicini, L. Parodi, Angew. Chem. Int. Ed. Engl. 37 (1998) 800.
[8] (a) S. Uchiyama, T. Santa, K. Imai, J. Chem. Soc., Perkin Trans. 2 (1999) 2525;
(b) B. Ramachandram, A. Samanta, J. Phys. Chem. A 102 (1998) 10579.
[9] E.K. Barefield, F. Wagner, A.W. Herlinger, A.R. Dahl, Inorg. Synth. 16 (1975) 220.
[10] G. Gran, Analyst 77 (1952) 661.
[11] P. Gans, A. Sabatini, A. Vacca, Talanta 43 (1996) 1739.
[12] W.C. Wolsey, J. Chem. Educ. 50 (1973) A335.
[13] (a) L. Fabbrizzi, F. Foti, M. Licchelli, P.M. Maccarini, D. Sacchi, M. Zema, Chem. Eur. J. 8 (2002) 4965;
(b) L. Fabbrizzi, M. Licchelli, S. Mascheroni, A. Poggi, D. Sacchi, M. Zema, Inorg. Chem. 41 (2002) 6129.

Available online at www.sciencedirect.com
SCIENCE DIRECT®
Polyhedron 23 (2004) 379–383
POLYHEDRON
www.elsevier.com/locate/poly

Mono and dinuclear hydrotris(3,5-dimethylpyrazolyl)borato tantalum complexes

Michel Etienne *, Jean-Cyrille Hierso, Paul J. Daff, Bruno Donnadieu, Françoise Dahan

Laboratoire de Chimie de Coordination du CNRS, UPR 8241, 205 Route de Narbonne, 31077 Toulouse Cedex 4, France

Received 5 June 2003; accepted 18 August 2003

Dedicated to the ever enthusiastic Jerry Trofimenko

Abstract

In an effort to obtain suitable starting materials, the synthesis and crystal structure of hydrotris(3,5-dimethylpyrazolyl)borato (Tp^{Me2}) tantalum(III) complexes are reported. Reaction of KTp^{Me2} with $[TaCl_2(tht)]_2(\mu\text{-}Cl)_2(\mu\text{-}tht)$ (**1**) (tht = tetrahydrothiophene) gives the X-ray characterized unsymmetrical $(Tp^{Me2}Ta)(TaCl_3)(\mu\text{-}Cl_2)(\mu\text{-}tht)$ (**2**) in fair yield. This doubly bonded Ta=Ta complex [2.6791(5) Å, diamagnetic, 18e per Ta] is a rare example of an unsymmetrical $Ta_2X_6L_3$ complex. The X-ray structure of $Tp^{Me2}TaCl_2(PhC{\equiv}CMe)$ (**3**) is also reported. It has the (4e)-alkyne in the symmetry plane of the molecule. The *trans* effects of tht and phenylpropyne are discussed. **1** is inert towards the reaction with a second equivalent of KTp^{Me2}.
© 2003 Elsevier Ltd. All rights reserved.

Keywords: Hydrotris(pyrazolyl)borate; Scorpionate ligands; Tantalum; Metal–metal multiple bond; Alkyne complex; Tetrahydrothiophene complex

1. Introduction

During the last few years, we have been endeavouring a diverse organometallic chemistry of Tp′NbXX′(alkyne) complexes (Tp′ = a susbstituted hydrotris(pyrazolyl)borate, X and/or X′ = Cl, alkyl, CO, etc.) [1], with a particular emphasis on the steric and electronic effects leading to various agostic interactions and on their consequences [2]. However, the development of a rich scorpionate-based chemistry of the heavier group 5 metals (Nb, Ta) has long been hampered by the lack of straightforward, efficient syntheses of suitable starting materials. The early literature in the field pointed to facile in situ decomposition of the compounds by hydrolysis, redox processes, B–N bond cleavage or to the undesired synthesis of ionic complexes [1]. Simple routes to $TpNbCl_4$ or $Tp^{Me2}NbCl_4$ were highly dependent on experimental conditions, and by-products formation precluded the development of these species as useful starting materials [3]. A recent reliable synthesis of the simple niobium(IV) complex $Tp^{Me2}NbCl_3$ [4], which was characterized by an X-ray diffraction, involves Tp^{Me2} exchange between the tin complex $Tp^{Me2}SnCl(n\text{-}Bu)_2$ and $NbCl_4(thf)_2$. The case of tantalum is even more striking. The tin route leads to a cationic Ta(V) complex $[Tp^{Me2}TaCl_3][TaCl_6]$ [4]. Oxo and imido complexes [5] have been prepared but in the case of Tp^{Me2}, $Tp^{Me2}Ta(=NAr)Cl_2$ was formed along with the salt $[HB(Me_2Pz)_3BH][TaCl_4(=NAr)(Me_2PzH)]$ from KTp^{Me2} and $Ta(=NAr)Cl_3(thf)_2$ [6]. The pre-fonctionallized complexes $TaMe_3Cl_2$, $Ta(=CH^tBu)Cl_3(thf)_2$ and $TaCl_3(dme)(PhC{\equiv}CMe)$ reacted quite cleanly with KTp^{Me2} leading to $Tp^{Me2}TaMe_3Cl$ [7], $Tp^{Me2}Ta(=CH^tBu)Cl_2$ [8], and $Tp^{Me2}TaCl_2(PhC{\equiv}CMe)$ [9], respectively. Given our interest in Tp′-based group 5 chemistry, we have been seeking for a convenient route to tantalum derivatives that might lead to simple halo complexes useful for further derivatization. We describe herein some of our observations in this field. The synthesis and X-ray crystal structures of $Tp^{Me2}TaCl_2(PhC{\equiv}CMe)$ [9] and of the new dimer $Tp^{Me2}Ta(\mu\text{-}Cl)_2(\mu\text{-}tht)TaCl_3$, which exhibits a formal Ta=Ta double bond, are reported.

* Corresponding author. Fax: +33-5-61-55-3003.
E-mail address: etienne@lcc-toulouse.fr (M. Etienne).

0277-5387/$ - see front matter © 2003 Elsevier Ltd. All rights reserved.
doi:10.1016/j.poly.2003.11.025

2. Results and discussion

2.1. Syntheses

Given the problems inherent in the use of tantalum(V) derivatives, we looked for a simple Ta(III) starting material akin to the readily available $[NbCl_3(dme)]_n$ (dme = 1,2-dimethoxyethane) [10]. However, such a simple complex does not exist for tantalum. For Ta(III), apart from $TaCl_3(PMe_3)_3$ [11], it appears that among the few useful complexes, all have a dimeric structure of the general type $Ta_2X_6L_3$ or $Ta_2X_6L_4$ [12]. Note that $TaCl_3(PMe_3)_3$ readily converts to $Ta_2Cl_6(PMe_3)_4$ [13]. Thus, one of the simplest and readily available tantalum(III) complex is the dimer $[TaCl_2(tht)]_2(\mu\text{-}Cl)_2(\mu\text{-}tht)$ (**1**) (tht = tetrahydrothiophene) [14]. One equiv of KTp^{Me2} reacted with dark red **1** in dichloromethane to give the new dinuclear species $(Tp^{Me2}Ta)(TaCl_3)(\mu\text{-}Cl_2)(\mu\text{-}tht)$ (**2**) (Eq. (1)) as plum purple crystals in 72% yield.

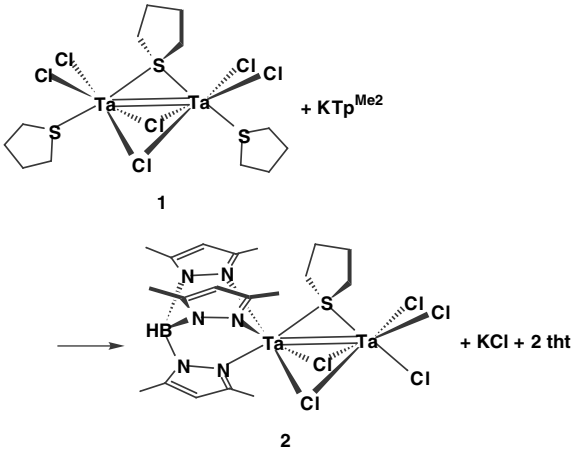

(1)

2 has been characterized by elemental analysis, ^1H NMR spectroscopy and an X-ray diffraction analysis (see below). The ^1H NMR methine and methyl signals of Tp^{Me2} appear as 1:2 and 3:3:6:6 singlets indicating a plane of symmetry in **2**. The tht protons appear as four multiplets, three of them being obscured by Tp^{Me2} methyl signals. During the synthesis of **2**, one chloride is removed as KCl, but also two equivalents of tht are displaced. Thus the bridging core does not change when going from **1** to **2**, but the two ends of the dimer have rearranged. This is due to the fact that Tp^{Me2} is an L_2X ligand that coordinates facially, whereas in **1** the terminal parts of the dimer are identically formed by two X and one L ligand. Indeed, one could describe **2** as having two tantalum(III), a $TaCl_3$ adduct of $Tp^{Me2}TaCl_2(tht)$ with a Ta=Ta double bond to account for diamagnetism. Attempts to use **2** as a source to other $Tp^{Me2}Ta$ complexes have been hampered by its high stability. Refluxing **2** in thf with one equivalent of KTp^{Me2} with or without excess tht did not lead to any reaction. Excess tht was introduced in the hope of forming $Tp^{Me2}TaCl_2(tht)$ since only one tht for two tantalum is present in **2**. $Tp^{Me2}TaCl_2(tht)$ could have been a very promising starting material. It is interesting to note that several vanadium(III) $Tp'VCl_2(L)$ complexes have been synthesized [14]. In all cases, L is indeed a 2e-donor so that the resulting $Tp'VCl_2(L)$ complex is a 14 electron high spin complex, as expected for a first row transition metal. Related complexes with either Nb or Ta have never been formed. Apparently the preference for a low-spin situation with the heavier metals precludes the formation of such species. Similarly, we have not been able to make the low spin vanadium(III) $Tp'VCl_2$(alkyne) akin to the known (4e)-alkyne 16 electron Nb [15] or Ta [9] analogs.

The synthesis and spectroscopic characterization of $Tp^{Me2}TaCl_2(PhC{\equiv}CCH_3)$ (**3**) has been described previously [9]. Just like in the niobium case [15], its starts from $TaCl_3(dme)(PhC{\equiv}CCH_3)$ and KTp^{Me2}, but the formation of $[HB(C_3N_2Me_2H)_3BH][TaCl_6]$ as a by-product limits the yield to ca. 40%. This is in line with previous observations in related systems (see above). The X-ray crystal structure of **3** is described in the following section.

2.2. X-ray structures

A plot of the X-ray molecular structure of **2** is displayed in Fig. 1 and associated metric parameters are collected in Table 1. This ditantalum species, being formally an unsymmetrical $M_2L_3X_6$ i.e., $L_2XM(\mu\text{-}LX_2)MX_3$, exists as a confacial bioctahedron, just like

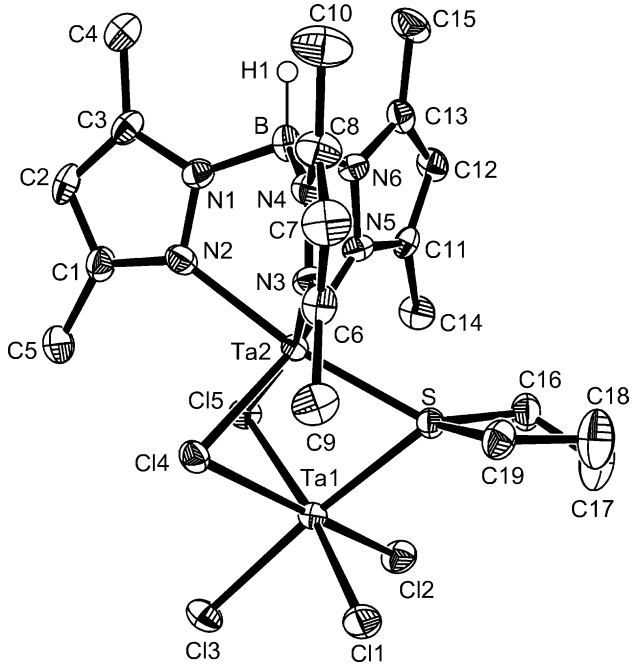

Fig. 1. Plot of the molecular structure of $Tp^{Me2}Ta(\mu\text{-}Cl)_2(\mu\text{-}tht)TaCl_3$ (**2**).

Table 1
Selected bond lengths (Å) and angles (°) for (Tp^{Me2}Ta)($TaCl_3$)(μ-$Cl)_2$(μ-tht) (**2**)

Bond lengths			
Ta(1)–Ta(2)	2.6791(5)	Ta(2)–Cl(5)	2.4662(16)
Ta(1)–Cl(1)	2.3763(14)	Ta(2)–N(2)	2.247(5)
Ta(1)–Cl(2)	2.3700(15)	Ta(2)–N(3)	2.161(5)
Ta(1)–Cl(3)	2.4477(14)	Ta(2)–N(5)	2.165(4)
Ta(1)–Cl(4)	2.5023(14)	Ta(1)–S	2.4293(14)
Ta(1)–Cl(5)	2.5283(14)	Ta(2)–S	2.4098(14)
Ta(2)–Cl(4)	2.4697(13)		
Bond angles			
Ta(1)–Cl(4)–Ta(2)	65.21(3)	Ta(1)–S–Ta(2)	67.23(4)
Ta(1)–Cl(5)–Ta(2)	64.86(4)		

its symmetrical $M_2L_3X_6$ ($LX_2M(\mu\text{-}LX_2)MLX_2$) parent **1**, with X being either Cl or Br [12,16,17]. The shared face consists in all these cases of two X (Cl in **2**) and one L ligand (tht). The Ta–Ta distance of 2.6791(5) in **2** is statistically identical with that (2.681(1) Å) in $[TaCl_2(tht)]_2(\mu\text{-}Cl)_2(\mu\text{-tht})$ **1** [16], consistent with a bond order of 2 (taking into account the diamagnetism of **2** and a formal 18e count for each Ta atom) [12]. The effect of the unsymmetry of the two ends can be probed by examining the bond lengths and angles for key ligands in the bridge and in terminal positions. Indeed in symmetrical **1**, tht ligands are *trans* to one another, whereas in **2**, the bridging tht has a *trans* Cl and a *trans* N. The Ta(1)–Cl(3) distance of 2.4477(14) Å *trans* to tht is 0.075 Å longer than to the two other identical terminal Ta–Cl_t bonds (2.373 Å average). These Ta–Cl_t are fully comparable with those in **1** (2.368 Å average). Similarly, the *trans*-influence of the bridging tht is observed on Ta(2). The Ta(2)–N(2) bond length is 2.247(5) Å, 0.084 Å longer than the two other Ta–N bonds between Ta and Tp^{Me2} nitrogens (2.163 Å average). The bond lengths between the bridging ligands and Ta(1), which bears the three chloro ligands, are all slightly longer than those with Ta(2) which bears Tp^{Me2}. For the chloro bridges, the Ta–Cl bond lengths in **1** (2.503 Å average) are in between those for Ta(1) and Ta(2). For tht, the Ta–S bonds of 2.390 Å (average for **1**) are slightly longer than those in **2**. The angles about the chloro-bridges are marginally larger in **2** than in **1** (64.90(6)°, 64.63(6)°) whereas those about the tht are ca. 1° smaller, consistent with the variations observed for the bond lengths. Overall, the structure of **2** remains very similar to that of **1**, apart from the observed *trans*-influence of the tht ligand.

A plot of the X-ray molecular structure of **3** is displayed in Fig. 2 and associated metric parameters are collected in Table 2. As observed for the niobium analogue [15b], the whole phenylpropyne sits in the molecular mirror plane, with the phenyl ring oriented proximal to the pyrazole rings of Tp^{Me2}. All geometrical parameters for the Nb and Ta compounds are very similar. In **3**, the elongated coordinated C–C bond of the

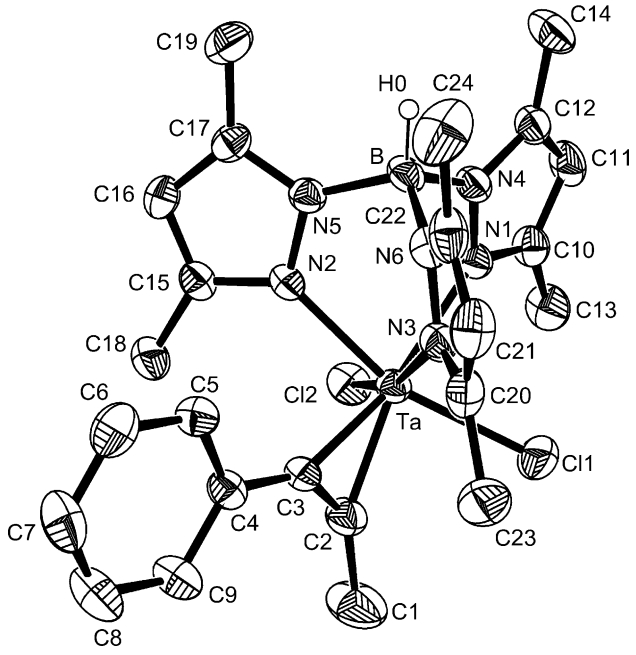

Fig. 2. Plot of the molecular structure of $Tp^{Me2}TaCl_2(PhC{\equiv}CMe)$ (**3**).

Table 2
Selected bond lengths (Å) and angles (°) for $Tp^{Me2}TaCl_2(PhC{\equiv}CMe)$ (**3**)

Bond lengths			
Ta–Cl(1)	2.3993(12)	Ta–N(1)	2.327(3)
Ta–Cl(2)	2.3942(12)	Ta–N(2)	2.211(3)
Ta–C(2)	2.052(4)	Ta–N(3)	2.216(4)
Ta–C(3)	2.069(4)	C(2)–C(3)	1.310(6)
Bond angles			
Cl(1)–Ta–Cl(2)	101.61(5)	C(1)–C(2)–C(3)	142.5(5)
C(2)–Ta–C(3)	37.08(16)	C(2)–C(3)–C(4)	140.6(4)
Ta–C(2)–C(1)	145.1(4)	Cl(1)–Ta–N(2)	161.51(9)
Ta–C(3)–C(4)	148.6(3)	Cl(2)–Ta–N(3)	163.01(9)

alkyne, the short Ta–C bonds and the bent back angles between the alkyne substituents and the coordinated C–C bonds are in accord with a (4e)-donor description [17]. These parameters are typical of other (4e)-donor alkyne Tp^{Me2} [15b], or the numerous examples of Cp′ [18] or non-Cp′ [19] complexes of either Nb or Ta. The orientation of the alkyne has been discussed in Tp′ and Cp′ derivatives. As suggested by Extended Huckel [20,21] or more recent DFT calculations [18], the orientation of the alkyne is mainly due to steric interactions. Whereas steric interactions drive the alkyne in the molecular symmetry plane (perpendicular conformation) in Tp′ complexes [20], orbital interactions have been invoked to explain this same perpendicular orientation in dimethyl derivatives but not in dichloro derivatives of Cp′ [18]. In any instances, the barrier to alkyne rotation remains low unless a bulky Cp′ or Tp′ ligand is used. Finally, one can compare the *trans* influence of tht and alkyne ligands in **2** and **3**. In **3**, the Ta–N bond *trans* to

the alkyne is ca. 0.113 Å longer than the other two, whereas it is 0.084 Å longer *trans* to the tht in **2**.

2.3. Conclusion

In an effort to extend the range of readily available Tp′Ta complexes, we have synthesized and fully characterized one mononuclear alkyne complex and one dinuclear tht complex. The latter was found to be very stable towards further derivatization. Although its reactivity hence its possible use as starting material are quite deceptive, the dinuclear complex exhibits an unprecedented unsymmetrical structure among the $M_2L_3X_6$ complexes.

3. Experimental

All reactions and workup procedures were performed under an atmosphere of dry dinitrogen using conventional vacuum line and schlenk tube techniques. Dichloromethane, *n*-hexane and tht were dried and distilled by refluxing over calcium dihydride under dinitrogen. Tantalum pentachloride was used as received from commercial sources. ^{1}H NMR data were acquired on a Bruker AM 250. Elemental analyses were performed in the Analytical Service of our laboratory. $[TaCl_2(tht)]_2(\mu\text{-}Cl)_2(\mu\text{-}tht)$ (**1**) [14], $Tp^{Me2}TaCl_2(PhC{\equiv}CCH_3)$ (**3**) [9] were prepared according to literature procedures.

3.1. $(Tp^{Me2}Ta)(TaCl_3)(\mu\text{-}Cl)_2(\mu\text{-}tht)$ (2)

Dichloromethane (60 mL) was added to a mixture of solid $[TaCl_2(tht)]_2(\mu\text{-}Cl)_2(\mu\text{-}tht)$ (**1**) (1.00 g, 1.2 mmol) and KTp^{Me2} (0.40 g, 1.2 mmol). The resulting dark red slurry was refluxed for 2 h and then filtered through Celite to give a deep plum purple solution. Hexane (20 mL) was added and solvents were slowly removed under vaccum until incipient crystallization. The solution was left at −30 °C overnight. $(Tp^{Me2}Ta)(TaCl_3)(\mu\text{-}Cl)_2(\mu\text{-}tht)$ (**2**) was then obtained as orange microcrystals that were collected by filtration and washed with hexane. A second batch of crystals was obtained similarly from the

Table 3
Crystal data, data collection and structure refinement

Compound	**2**	**3**
Empirical formula	$C_{19}H_{30}BCl_5N_6STa_2$	$C_{24}H_{30}BCl_2N_6Ta$
Formula weight	924.51	665.20
Temperature (K)	180(2)	293(2)
Wavelength (Å)	0.71073	0.71073
Crystal system	monoclinic	monoclinic
Space group	$P2_1/n$	$C2/c$
Unit cell dimensions		
a (Å)	15.270(3)	19.228(2)
b (Å)	11.686(2)	18.395(2)
c (Å)	20.212(4)	17.490(2)
β (°)	110.81(3)	117.830(11)
Volume (Å^3)	3371.4(11)	5470.8(12)
Z	4	8
Absorption coefficient (mm^{-1})	6.962	4.237
$F(0\,0\,0)$	1752	2624
Crystal size (mm)	$0.35 \times 0.10 \times 0.08$	$0.50 \times 0.35 \times 0.25$
Crystal form	parallelepiped	parallelepiped
Crystal color	dark purple	orange
Diffractometer	STOE IPDS	Enraf Nonius CAD4
Different measured method	ϕ rotation	ω-2θ
θ Range for data collection (°)	2.05–22.46	1.63–25.97
Reflections collected/unique	18006/4381 [$R_{int} = 0.0296$]	5532/5378 [$R_{int} = 0.0233$]
Completeness to 2θ	$2\theta = 44.92$, 99.7%	$2\theta = 25.97$, 50%
Refinement method	full-matrix least-squares on F^2	full-matrix least-squares on F^2
Data/restraints/parameters	4381/0/317	5378/0/307
Weighting scheme	$w = 1/[\sigma^2(F_o^2) + (0.0374P)^2]$ where $P = (F_o^2 + 2F_c^2)/3$	$w = 1/[\sigma^2(F_o^2) + (0.0341P)^2]$ where $P = (F_o^2 + 2F_c^2)/3$
Absorption corrections	semi-empirical[a]	psi-scans[b]
T_{min}–T_{max}	0.372–0.781	0.7177–0.9965
Goodness-of-fit on F^2	0.977	1.004
Final R indices ([$I > 2\sigma(I)$])	$R_1 = 0.0230$, $wR_2 = 0.0543$	$R_1 = 0.0249$, $wR_2 = 0.0588$
R indices (all data)	$R_1 = 0.0283$, $wR_2 = 0.0559$	$R_1 = 0.0565$, $wR_2 = 0.0671$
Largest different peak and hole (e Å^{-3})	0.987 and −0.490	0.921 and −0.689

[a] N. Walker and D. Stuart, Acta Crystallogr. A 39 (1983) 158.
[b] A.C.T. North, D.C. Phillips, F.S. Mathews, Acta Crystallogr. A 24 (1968) 351.

mother liquor. (0.80 g, 0.86 mmol, 72% yield). $C_{19}H_{30}BCl_5N_6STa_2$ Calc.: C 24.7, H 3.25, N 9.1; found: C 24.3, H 2.8, N 8.7%. ^{1}H NMR (CD_2Cl_2, room temperature) δ 2.04, 2.34, 2.37, 2.51 (all s, 6, 3, 3, 6H, $Tp^{Me2}CH_3$), 2.33 (obsc m, 4H, tht), 2.50 (obsc m, 2H, tht), 3.70 (m, 2H, tht), 5.93, 6.19 (both s, 1, 2H, $Tp^{Me2}CH$).

3.2. Crystallographic studies

The acquisition data, solution and refinement of the crystal structure of **2** and **3** proceeded smoothly. Details are provided in Table 3. The CIF data have been deposited with the Cambridge Crystallographic Data Centre, CCDC 211581 and 211582.

References

[1] (a) General reviews: S. Trofimenko, Scorpionates – The Coordination Chemistry of Polypyrazolylborate Ligands, Imperial College Press, London, 1999;
(b) M. Etienne, Coord. Chem. Rev. 156 (1996) 201.

[2] (a) M. Etienne, R. Mathieu, B. Donnadieu, J. Am. Chem. Soc. 119 (1997) 3218;
(b) J. Jaffart, M. Etienne, J.E. McGrady, O. Eisenstein, F. Maseras, J. Am. Chem. Soc. 123 (2001) 6000;
(c) J. Jaffart, M. Etienne, M. Reinhold, J.E. McGrady, F. Maseras, Chem. Commun. (2003) 876;
(d) J. Jaffart, C. Nayral, R. Choukroun, R. Mathieu, M. Etienne, Eur. J. Inorg. Chem. (1998) 425;
(e) M. Etienne, Agostic Interactions in Scorpionate Niobium Complexes, 225th American Chemical Society National Meeting (Symposium: "Scorpionate ligands 35 years later"), INOR 319; New Orleans, LA, 23–027 March 2003.

[3] (a) L.G. Hubert-Pfalzgraf, M. Tsunoda, Polyhedron 2 (1983) 203;
(b) D.C. Bradley, M.B. Hursthouse, J. Newton, N.P.C. Walker, J. Chem. Soc., Chem. Commun. (1984) 188.

[4] (a) K. Mashima, T. Oshiki, K. Tani, Organometallics 16 (1997) 2760;
(b) T. Oshiki, K. Mashima, S. Kawamura, K. Tani, K. Kitaura, Bull. Chem. Soc. Jpn. 73 (2000) 1735.

[5] J. Sundermeyer, J. Putterlik, M. Foth, J.S. Fiel, N. Ramesar, Chem. Ber. 127 (1994) 1201.

[6] J.M. Boncella, M.L. Cajigal, A.S. Gamble, K.A. Abboud, Polyhedron 15 (1996) 2071.

[7] D.L. Reger, C.A. Swift, L. Lebioda, Inorg. Chem. 23 (1984) 349.

[8] J.M. Boncella, M.L. Cajigal, K.A. Abboud, Organometallics 15 (1996) 1905.

[9] J.-C. Hierso, M. Etienne, Eur. J. Inorg. Chem. (2000) 839.

[10] E.J. Roskamp, S.F. Pedersen, J. Am. Chem. Soc. 109 (1987) 3170.

[11] S.M. Rocklage, H.W. Turner, J.D. Fellmann, R.R. Schrock, Organometallics 1 (1982) 703.

[12] (a) F.A. Cotton, R.A. Walton, Multiple Bonds Between Metal Atoms, Wiley, New York, 1982;
(b) L. Messerle, Chem. Rev. 88 (1988) 1229.

[13] (a) A.P. Sattelberger, R.B. Wilson, J.C. Huffman, J. Am. Chem. Soc. 102 (1980) 7111;
(b) A.P. Sattelberger, R.B. Wilson, J.C. Huffman, Inorg. Chem. 21 (1982) 2392.

[14] (a) L.E. Manzer, J. Organomet. Chem. 102 (1975) 167;
(b) M. Mohan, S.M. Holmes, R.J. Butcher, J.P. Jasisnki, C.J. Carrano, Inorg. Chem. 31 (1992) 2029;
(c) M. Herberhold, G. Frohmader, T. Hofman, W. Milius, J. Darkwa, Inorg. Chim. Acta 267 (1998) 19;
(d) D. Rehder, H. Gailus, H. Scmidt, Acta Crystallogr. C C54 (1998) 1590.

[15] (a) M. Etienne, F. Biasotto, R. Mathieu, J.L. Templeton, Organometallics 15 (1996) 1106;
(b) M. Etienne, P.S. White, J.L. Templeton, Organometallics 10 (1991) 3801.

[16] (a) F.A. Cotton, R.C. Najjar, Inorg. Chem. 20 (1981) 2716;
(b) J.L. Templeton, W.C. Dorman, J.C. Clardy, R.E. McCarley, Inorg. Chem. 17 (1978) 1263.

[17] J.L. Templeton, Adv. Organomet. Chem. 29 (1989) 1.

[18] For a recent reference with comprehensive references, see: A. Galindo, M. Gomez, P. Gomez-Sal, A. Martin, D. del Rio, F. Sanchez, Organometallics 21 (2002) 293.

[19] For a recent reference with comprehensive references, see: T. Oshiki, K. Tanaka, J. Yamada, T. Ishiyama, Y. Takaoka, K. Mashima, K. Tani, K. Takai, Organometallics 22 (2003) 464.

[20] M. Etienne, B. Donnadieu, R. Mathieu, J. Fernandez-Baeza, F. Jalon, A. Otero, M.E. Rodrigo-Blanco, Organometallics 15 (1996) 4597.

[21] M.D. Curtis, J. Real, D. Kwon, Organometallics 8 (1989) 1644.

Available online at www.sciencedirect.com
SCIENCE DIRECT®
Polyhedron 23 (2004) 385–394
POLYHEDRON
www.elsevier.com/locate/poly

Sulfur atom transfer reactions of tungsten(VI) and tungsten(IV) chalcogenide complexes

Aston A. Eagle, Robert W. Gable, Simon Thomas, Stephen A. Sproules, Charles G. Young *

School of Chemistry, University of Melbourne, Vic. 3010, Australia

Received 10 June 2003; accepted 22 August 2003

Dedicated to Jerry Trofimenko, whose remarkable contributions to scorpionate chemistry have inspired and sustained our research in Group 6 chemistry

Abstract

The sulfur, oxygen and chlorine atom transfer reactions of thio-W(VI) and -W(IV) complexes containing monodentate and ambidentate dithiophosphinate co-ligands are examined. Systems featuring monodentate ligands are complicated by the instability of the W(IV) species; significantly and in contrast to observations in thio-Mo chemistry, thio-W(VI) complexes such as Tp*WS_2Cl fail to react with cyanide. Dithiophosphinate systems are more tractable and amenable to full description. The oxo-thio and bis(thio) complexes, Tp*$WOS(S_2PPh_2$-*S*) and Tp*$WS_2(S_2PPh_2$-*S*) [Tp* = hydrotris(3,5-dimethylpyrazol-1-yl)borate] undergo sulfur atom transfer to tertiary phosphines to produce Tp*$WO(S_2PPh_2$-*S*,*S*′) and Tp*$WS(S_2PPh_2$-*S*,*S*′), respectively, and phosphine sulfides. The X-ray crystal structures of Tp*$WS_2(S_2PPh_2)\cdot 0.5CH_2Cl_2$ and Tp*$WS(S_2PPh_2)$ have been determined. Both complexes possess six-coordinate, distorted-octahedral tungsten centers ligated by tridentate *fac*-Tp*, terminal thio (W = S = 2.139–2.143 Å) and mono- or bidentate dithiophosphinate ligands, respectively. The W(IV) complexes, Tp*$WE(S_2PPh_2)$ (E = O, S), react with sulfur atom donors to produce thio-W(VI) complexes, Tp*$WES(S_2PPh_2)$ but with oxygen atom donors to yield mixtures of Tp*$WOE(S_2PPh_2)$ and Tp*$WES\{SP(O)Ph_2$-*S*}. The latter result from oxygen atom transfer to phosphorus with concomitant sulfur atom transfer from phosphorus to tungsten. Catalytic sulfur atom transfer by thio-W complexes is demonstrated for the first time.
© 2003 Elsevier Ltd. All rights reserved.

1. Introduction

Group 6 oxo compounds are versatile catalysts in industry and biology. Metal oxides and mixed-oxides have important industrial applications in inter alia hydrogenation, oxidation, condensation, epoxidation, isomerization and polymerization processes [1–3]. In biology, pterin-containing Mo and W enzymes such as sulfite oxidase, nitrate reductase, dimethyl sulfoxide reductase and aldehyde oxidoreductase catalyze a range of net oxygen atom transfer (OAT) reactions crucial to all life and to global bio-geo-chemical cycles [4–7]. For the aforementioned enzymes there is strong evidence for mechanisms involving direct OAT between Mo and substrate [4–7]. Consequently, there has been intense interest in the OAT chemistry of Mo and W; indeed, Mo lies at the epicenter of OAT chemistry and all important enzyme models feature reactions of this type. These reactions have been comprehensively reviewed [6,8]. For kinetic as well as thermodynamic reasons, clean OAT reactions are much less common in W(VI)/W(IV) chemistry [6,8]. Tungsten dithiolene complexes are an exception, as they generally undergo facile OAT inter-converting stable and isolable species [9–13]. The kinetic inertness of W(VI) toward OAT is evident from detailed investigations of the reactions of

* Corresponding author. Tel.: +61-3-8344-6515; fax: +61-3-9347-5180.
E-mail addresses: cgyoung@unimelb.edu.au, c.g.young@chemistry.unimelb.edu.au (C.G. Young).

0277-5387/$ - see front matter © 2003 Elsevier Ltd. All rights reserved.
doi:10.1016/j.poly.2003.11.026

$[MO_2(mnt)_2]^{2-}$ [M = Mo, W; mnt = $S_2C_2(CN)_2^{2-}$] with phosphites, which are characterized by rate constants $k_{Mo}/k_W \sim 10^2$–10^3 [9]. The large bond dissociation enthalpy for W=O moieties (ca. 138–160 kcal mol^{-1}, cf. ca. 98 kcal mol^{-1} for Mo=O units) reduces the thermodynamic driving force for OAT from W(VI) [14].

Certain W-enzymes (or states thereof) are proposed to contain thio- or sulfhydryl-W active sites [15,16]; consequently, the atom transfer chemistry of thio- and oxo-thio-W complexes is fundamental to a complete understanding of these enzymes. This paper examines the sulfur atom transfer (SAT) reactions of thio-W complexes containing the hydrotris(3,5-dimethylpyrazol-1-yl)borate ligand (Tp*). Reactions of this kind are only sparsely represented in the literature [17,18]. Examples of SAT *to* W(II) centers include the reactions of $WCl_2(PMe_3)_4$, $Tp^*W(S_2CNR_2)(CO)_2$ (R = alkyl) and Tp*WX(CO)(MeCN) (X = monoanion) with thiiranes to give $WSCl_2(PMe_3)_3$ [19] (and related mononuclear complexes [20]), $Tp^*WS(S_2CNR_2)$ [21] and Tp*WSX(CO) [22], respectively. Phosphine sulfides also serve as sulfur atom donors to W(II), reacting, for example, with $WCl_2(PMePh_2)_4$ to form $WSCl_2(PMePh_2)_3$ and dinuclear species [23]. We are unaware of any example of SAT *to* mononuclear oxo- or thio-W(IV) complexes. Like OAT [8], SAT *from* thio-W(VI) species is generally not clean or complete. Thus, the reaction of WSX_4 with PPh_3 results in the formation of $W(PPh_3)(SPPh_3)X_4$ (X = Cl, Br) [24] while $Cp^*WS_2(R)$ (R = Me, CH_2SiMe_3) [25], $WS(OBu^t)_4$ [26] and *trans*-$WS_2(PMe_3)_4$ [27] are unreactive toward phosphines. SAT reactions are catalyzed by disulfido species such as $[WO(S_2)(mnt)_2]^{2-}$ [28] and $MoO(S_2)(S_2CNEt_2)_2$ [29,30] but thio-W catalysts for SAT have not been reported.

We have described the synthesis, characterization and electrochemical properties of the complexes Tp^*WO_2X, Tp*WOSX and Tp^*WS_2X (X = monoanion) [31–33]. The thio-W(VI) complexes are reduced at potentials similar to their dioxo-Mo(VI) analogues, which are avid participants in OAT [6]. Moreover, preliminary studies of related oxo-thio-Mo(VI) species have revealed preferential SAT vs. OAT in these systems [34–36]. This paper reports that thio-W(VI) and -W(IV) Tp* complexes participate in stoichiometric as well as catalytic SAT reactions. The stability of the various complexes is dictated by the nature of the co-ligand, complexes containing ambidentate dithiophosphinate ligands being the most stable and tractable. The report includes the X-ray crystal structures of $Tp^*W^{VI}S_2(S_2PPh_2\text{-}S)$ and $Tp^*W^{IV}S(S_2PPh_2\text{-}S,S')$, two complexes that are interconverted by direct SAT reactions. We also describe the first systems for SAT catalysis by high-valent thio-W species. The principal outcomes of the investigation are summarized in Scheme 1.

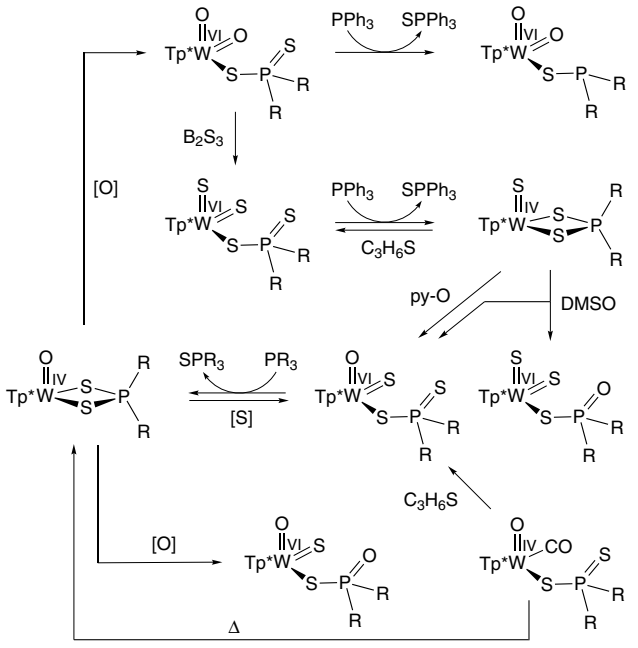

Scheme 1.

2. Experimental

2.1. Materials and methods

The compounds Tp^*WS_2Cl [37], $Tp^*WO_2(S_2PPh_2)$ [31] and $Tp^*WE(S_2PPh_2)(CO)$ (E = O, S) [22] were prepared by literature methods. Unless stated, all reactions were performed under an atmosphere of pure dinitrogen using standard Schlenk techniques and dried, deoxygenated solvents. Infrared spectra were obtained on Jasco A-302 or Perkin–Elmer 983G infrared spectrophotometers using pressed KBr discs. ^1H and $^{31}P\{^1H\}$ NMR spectra were recorded using Varian FT Unity300 or INOVA 400WB spectrometers and were referenced to internal (solvent) chloroform (δ_H 7.26) or benzene (δ_H 7.15) and external H_3PO_4 (δ_P 0), respectively. Electronic spectra were recorded on a Hitachi 150–20 UV spectrophotometer. Electron impact (70 eV) mass spectra were obtained on a Jeol AX 505H mass spectrometer. Column chromatography was performed using Merck Artikel 7734 Kieselgel 60. Microanalyses were performed by Atlantic Microlabs, Norcross, Georgia, USA.

2.2. Syntheses

2.2.1. Tp*WSCl(py)

A mixture of Tp^*WS_2Cl (0.241 g, 0.415 mmol) and PPh_3 (0.120 g, 0.456 mmol) was treated with pyridine (6 ml) and stirred for 30 min. The initial green color changed to deep blue in 2 min. The solvent was removed under vacuum and dry methanol (10 ml) was added to

the sticky residue. The resulting crystals were filtered and washed with methanol and cyclohexane. Yield 0.184 g (71%).

Anal. Unstable. IR (KBr): 2920s, 2845m, *ν*(BH) 2545w, 1625w, 1585w, 1540s, 1475m, 1440s, 1410s, 1380m, 1355s, 1200s, 1150w, 1100w, 1065s, 1040s, 985m, 950w, 935w, 910w, 855m, 810s, 785s, 780m, 755m, 715w, 690s, 640m, 590w,br, 515w, *ν*(W=S) 470m, 440w, 370w, *ν*(W–Cl) 330w cm^{-1}. Mass spectrum, *m/z*: 532 (9%) $[M–Me_2pz]^+$.

2.2.2. Tp*WOS(S_2PPh_2)

Method 1. A deep green solution of Tp*WO(S_2PPh_2) (0.200 g, 0.268 mmol) in benzene (15 ml) was treated with propylene sulfide (100 μl, 1.43 mmol), then refluxed for 2 days. The resulting yellow solution was reduced to dryness, dissolved in CH_2Cl_2 and column chromatographed on silica gel using 3:2 CH_2Cl_2/hexane as eluent. The bright orange band was collected. The compound was recrystallized from CH_2Cl_2/hexane or CH_2Cl_2/methanol, filtered, washed with methanol and dried in vacuo. Yield 0.191 g (92%). A similar reaction between Tp*WO(S_2PPh_2) (0.100 g, 0.134 mmol) and sulfur (0.100 g, 3.12 mmol) in refluxing benzene for 1 h yielded the same compound upon similar work-up (yield 79%).

Method 2. A solution of Tp*WS(S_2PPh_2)(CO) (0.82 g, 1.04 mmol) and pyridine *N*-oxide (0.40 g, 4.21 mmol) in toluene (60 ml) was heated at reflux for 48 h. The reaction mixture was then reduced to dryness and the residue was column chromatographed on silica gel/CH_2Cl_2 and the orange fraction collected. The product was isolated as above. Yield 0.32 g (38%).

Method 3. A solution of Tp*WS(S_2PPh_2) (0.200 g, 0.262 mmol) and pyridine *N*-oxide (0.026 g, 0.275 mmol) was refluxed in 1,2-dichloroethane (15 ml) for 20 h. The brown solution was evaporated to dryness and passed down a silica gel column using 3:2 CH_2Cl_2/hexane as eluent. The first green band yielded Tp*WS_2Cl (0.016 g, 10%) upon concentration and precipitation with MeOH. A slow-moving orange band was then eluted with CH_2Cl_2, concentrated and treated with MeOH to precipitate Tp*WOS(S_2PPh_2). Yield 0.017 g (8%). A similar reaction between Tp*WS(S_2PPh_2) (0.105 g, 0.138 mmol) and dimethyl sulfoxide (0.100 ml, 1.41 mmol) in refluxing benzene (15 ml) for 2 h yielded brown Tp*-WS_2{$SP(O)Ph_2$} (61 mg) and orange Tp*WOS(S_2PPh_2) (0.019 g, 18%) upon work-up. The analytical sample was isolated as the dichloromethane hemisolvate.

Anal. Calc. for $C_{27}H_{32}BN_6OPS_3W \cdot 0.5CH_2Cl_2$: C, 40.24; H, 4.05; N, 10.24; S, 11.72. Found: C, 40.04; H, 4.06; N, 10.15; S, 12.06%. IR (KBr): 2961w, 2853w, *ν*(BH) 2555m, *ν*(CN) 1544s, 1480w, *ν*(Ph) 1450s, 1437s, 1415s, 1384s, 1360s, 1308w, 1211s, 1187m, *ν*(Ph) 1097s, 1074s, 1041s, 999w, *ν*(W=O) 931s, 909w, 876w, 860s, 815m, 792m, 744m, 709s, 690s, *ν*(P=S) 643s, 614m, *ν*(P–S) 525s, *ν*(W=S) 485s, 474s cm^{-1}. ^1H NMR ($CDCl_3$): *δ* 2.35, 2.36, 2.38, 2.51, 2.54, 2.66 (each s, 3H, CH_3), 5.80, 5.85, 5.95 (each s, CH of Tp^*), 7.41, 7.92, 8.13 (m, total 10H, Ph). $^{31}P\{^1H\}$ NMR ($CDCl_3$): *δ* 67.71. Mass Spectrum, *m/z*: 777 (10%) $[M]^+$. Electronic Spectrum (CH_2Cl_2): λ_{max} 475 (40), 395 nm (*ε* 5520 M^{-1} cm^{-1}).

Data for Tp*WS_2{$SP(O)Ph_2$}. *Anal.* Calc. for $C_{27}H_{32}BN_6OPS_3W$: C, 41.66; H, 4.14; N, 10.80; S, 12.34. Found: C, 41.28; H, 4.29; N, 10.57; S, 12.06%. IR (KBr): 3050w, 2955w, 2925w, *ν*(BH) 2560m, 1540s, 1450s, *ν*(Ph) 1435s, 1410s, 1380s, 1355s, 1305w, 1210s, 1185m, 1155w, *ν*(P=O) 1115s, *ν*(Ph) 1100m, 1075s, 1070s, 1035s, 1000w, 895s, 870w, 855s, 815m, 790m, 750m, 725s, 715s, 695s, 655s, 615w, 540m, 510m, *ν*(WS_2) 495m and 475s, 390w cm^{-1}. ^1H NMR ($CDCl_3$): *δ* 2.39, 2.62 (each s, 6H, $2CH_3$), 2.40, 2.71 (each s, 3H, CH_3), 5.86 (s, 2H, 2CH of Tp*), 6.01 (s, 1H, CH of Tp*), 7.41 (m, 6H, Ph), 8.07 (m, 4H, Ph). $^{31}P\{^1H\}$ NMR ($CDCl_3$): *δ* 85.35.

2.2.3. Tp*WS_2(S_2PPh_2)

A red solution of Tp*WS(S_2PPh_2) (0.105 g, 0.138 mmol) and propylene sulfide (100 μl, 0.143 mmol) in benzene (10 ml) was refluxed for 20 h. The resulting brown solution was reduced to dryness and the residue was recrystallized from CH_2Cl_2/hexane, then CH_2Cl_2/MeOH to give brown crystals of product. These were filtered, washed with methanol and dried in vacuo. Yield 0.085 g (78%). The complex was also prepared in the reaction of Tp*WO_2(S_2PPh_2) with boron sulfide [33]. Characterization data are available in the literature [33].

2.2.4. Tp*WO(S_2PPh_2)

Method 1. An orange solution of Tp*WOS(S_2PPh_2) (0.198 g, 0.254 mmol) in benzene (15 ml) was treated with a solution of PMe_2Ph (0.15 g, 1.09 mmol) in toluene (2 ml) and stirred for 20 min at room temperature. The resulting green solution was reduced to dryness and column chromatographed on silica gel using 3:2 CH_2Cl_2/hexane as eluent. The green band was collected and reduced to dryness. The residue was recrystallized from CH_2Cl_2/hexane, then CH_2Cl_2/EtOH to produce green crystals, which were filtered, washed with EtOH and vacuum dried. Yield 0.097 g (51%). A similar reaction between Tp*WOS(S_2PPh_2) and PPh_3 in refluxing benzene for 4 days yielded the same compound upon work-up (yield 57%).

Method 2. A red solution of Tp*WO(S_2PPh_2)(CO) (0.871 g, 1.12 mmol) was refluxed in benzene (15 ml) for 15 min and the resulting deep green solution was reduced to dryness. The residue was recrystallized and the product isolated as above. Yield 0.757 g (90%).

Anal. Calc. for $C_{27}H_{32}BN_6OPS_2W$: C, 43.45; H, 4.32; N, 11.26; S, 8.59. Found: C, 43.40; H, 4.37; N, 11.29; S, 8.49%. IR (KBr): 3050w, 2960w, 2920m, *ν*(BH) 2540m, 1540s, 1445s, *ν*(Ph) 1430s, 1410s, 1375m, 1365s, 1205s, 1160w, *ν*(Ph) 1095s, 1065s, 1035m, 990w, 980w, *ν*(W=O)

945s, 855m, 815m, 780m, 745m, 705s, 695s, 650m, 630m, 605m, $\nu(PS_2)$ 560s, 475m, 420w, 355w cm^{-1}. ^1H NMR ($CDCl_3$): δ 2.16, 2.24 (each s, 3H, CH_3), 2.52, 2.83 (each s, 6H, $2CH_3$), 5.50 (s, 1H, CH of Tp), 5.96 (s, 2H, 2CH of Tp*), 7.57 (m, 6H, Ph), 8.03 (m, 4H, Ph). $^{31}P\{^1H\}$ NMR ($CDCl_3$): δ 85.30. Mass spectrum, *m/z*: 746 (54%) $[M]^+$. Electronic spectrum (CH_2Cl_2): λ_{max} 805 (sh, 30), 630 (400), 438 nm (ε 1830 M^{-1} cm^{-1}).

2.2.5. Tp*WS(S$_2$PPh$_2$)

A benzene (15 ml) solution of $Tp^*WS_2(S_2PPh_2)$ (0.270 g, 0.340 mmol) and PPh_3 (0.107 g, 0.408 mmol) was refluxed for 19 h. The resulting red solution was reduced in vacuo to ca. 1 ml, and dry methanol (8 ml) was added with stirring. The orange solid was filtered in air, and washed with dry MeOH. A second crop of red crystals was obtained by enriching the filtrate in hexane. Yield 0.218 g (84%).

Anal. Calc. for $C_{27}H_{32}BN_6PS_3W$: C, 42.53; H, 4.23; N, 11.03; S, 12.62. Found: C, 42.63; H, 4.23; N, 11.04; S, 12.53%. IR (KBr): 2955w, 2920m, ν(BH) 2545m, 1540s, 1445s, ν(Ph) 1430s, 1415s, 1375m, 1360s, 1300w, 1205s, 1180w, 1155w, ν(Ph) 1095s, 1065s, 1045w, 1035s, 995w, 980w, 870w, 855m, 815m, 785m, 755w, 745m, 705s, 690s, 645w, 630w, 605w, $\nu(PS_2)$ 565s, ν(W=S) 490s, 435w, 345w cm^{-1}. ^1H NMR ($CDCl_3$): δ 2.60 and 2.90 (each br, 9H, $3CH_3$), 5.89 (s, 3H, 3CH of Tp*), 7.40 (m, 2H, Ph), 7.60 (m, 4H, Ph), 8.10 (m, 4H, Ph). Mass spectrum, *m/z*: 762 (4%) $[M]^+$. Electronic spectrum (CH_2Cl_2): λ_{max} 865 (50), 455 nm (ε 1340 M^{-1} cm^{-1}).

2.2.6. Tp*WOS{SP(O)Ph$_2$}

Method 1. A solution of $Tp^*WO(S_2PPh_2)$ (0.100 g, 0.134 mmol) in benzene (8 ml) was prepared in air, then stirred for 6 days in a capped vial. The resulting orange mixture was reduced to dryness, dissolved in CH_2Cl_2 and eluted on a silica gel column with 3:2 CH_2Cl_2/hexane. The first two orange bands were collected and enriched in hexane to precipitate products. The first band yielded $Tp^*WOS(S_2PPh_2)$ (0.012 g, 17% based on S), the second $Tp^*WOS\{SP(O)Ph_2\}$ (0.020 g, 20%). The final light yellow band containing $Tp^*WO_2(S_2PPh_2)$ was eluted with 1:1 THF/hexane, and cream crystals were obtained by hexane enrichment (0.027 g, 27%).

Method 2. A benzene (15 ml) solution of $Tp^*WO(S_2PPh_2)$ (0.100 g, 0.134 mmol), NBu_4NO_3 (0.045 g, 0.147 mmol), and sulfamic acid (0.100 g, 1.03 mmol) was refluxed for 2 h. The resulting solution was worked up as above, to yield $Tp^*WOS\{SP(O)Ph_2\}$ (0.032 g, 31%) and $Tp^*WO_2(S_2PPh_2)$ (0.040 g, 39%).

Method 3. A solution of $Tp^*WO(S_2PPh_2)$ (0.125 g, 0.167 mmol) in benzene (12 ml) was treated with tetramethylene sulfoxide (18.1 μl, 0.201 mmol), then refluxed for 21 h. The resulting orange solution was worked up as above, to yield $Tp^*WOS\{SP(O)Ph_2\}$ (0.097 g, 76%) and $Tp^*WO_2(S_2PPh_2)$ (0.021 g, 16%).

Anal. Calc. for $C_{27}H_{32}BN_6O_2PS_2W$: C, 42.54; H, 4.23; N, 11.02; S, 8.41. Found: C, 42.64; H, 4.24; N, 10.96; S, 8.35%. IR (KBr): 2960w, 2925m, ν(BH) 2555m, 1540s, 1445s, ν(Ph) 1430s, 1415s, 1380s, 1360s, 1305w, 1205s, 1185m, 1155w, ν(P=O) 1110s, 1080s, 1075s, 1040s, ν(W=O) 940s, 890s, 870w, 855s, 815m, 790m, 750m, 725s, 715s, 695s, 655s, 545m, 510m, ν(W=S) 480s, 400w cm^{-1}. ^1H NMR ($CDCl_3$): δ 1.66, 2.20, 2.35, 2.37, 2.38, 2.84 (each s, 3H, CH_3), 5.68, 5.71, 5.99 (each s, 1H, CH of Tp*), 7.35 (m, 5H, Ph), 7.50 (m, 1H, Ph), 7.61 (m, 2H, Ph), 7.81 (m, 2H, Ph). $^{31}P\{^1H\}$ NMR ($CDCl_3$): δ 85.21. Mass spectrum, *m/z*: 667 (4%) $[M–Me_2pz]^+$, 730 (2%) $[M–S]^+$.

2.3. Crystal structures

Yellow-brown crystals of $Tp^*WS_2(S_2PPh_2)\cdot 0.5CH_2Cl_2$ and red crystals of $Tp^*WS(S_2PPh_2)$ were grown by diffusion of hexane into dichloromethane solutions of the complexes. Crystals of dimensions $0.03\times0.18\times0.46$ mm and $0.13\times0.27\times0.27$ mm, respectively, were chosen for examination.

A summary of the crystal data is given in Table 1. In this section, data for $Tp^*WS_2(S_2PPh_2)\cdot 0.5CH_2Cl_2$ are followed in parentheses by the corresponding data for $Tp^*WS(S_2PPh_2)$. Accurate unit cell parameters were obtained by a least squares procedure from the setting angles of 25 reflections, $16.0° < 2\theta < 24.2°$ ($21.2° < 2\theta < 27.6°$). Intensity data were collected using an Enraf-Nonius CAD-4MachS single crystal X-ray diffractometer using the ω:2θ scan method. A total of 3752 (7722) reflections were measured, $4° \leqslant 2\theta \leqslant 50°$ ($4° \leqslant 2\theta \leqslant 52°$), of which 3492 (6011) were unique (R_{int} 0.019; 0.022) with 3113 (4625) having $I \geqslant 2\sigma(I)$. Three intensity control reflections, monitored every 9600 s X-ray exposure time, showed a 2% (no significant) variation in intensity; the data were corrected in accordance with

Table 1
Crystallographic data

Compound	$Tp^*WS_2(S_2PPh_2)\cdot 0.5CH_2Cl_2$	$Tp^*WS(S_2PPh_2)$
Formula	$C_{27.5}H_{33}$ $BClN_6PS_4W$	$C_{27}H_{32}BN_6PS_3W$
Formula weight	836.96	762.42
Crystal system	orthorhombic	monoclinic
Space group	*Fdd*2	$P2_1/n$
a (Å)	32.263(6)	11.627(2)
b (Å)	40.240(7)	10.536(3)
c (Å)	10.357(2)	25.317(4)
β (°)	90	98.385(12)
V (Å^3)	13446(4)	3068.2(11)
Z	16	4
ρ_{calcd} (g cm^{-3})	1.654	1.651
R	0.0282	0.0263
wR	0.0515	0.0621

$R = \sum ||F_o| - |F_c|| / \sum F_o$ and $wR = [\sum w(F_o^2 - F_c^2)^2 / \sum w(F_o^2)^2]^{1/2}$.

these variations as well as for Lorentz and polarization effects, but not for extinction. Absorption corrections, evaluated by Gaussian integration [38], were applied to the data, the maximum and minimum transmission factors being 0.8927 and 0.5115 (0.6751 and 0.5581).

The structures were solved using a combination of Patterson, direct methods and difference synthesis [39,40], and refined with a full-matrix least-squares refinement procedure. All hydrogen atom sites were found on a difference electron-density map; all were included at calculated positions and refined using the riding model. For $Tp^*WS_2(S_2PPh_2)\cdot 0.5CH_2Cl_2$, the dichloromethane molecule was found to be disordered over a site of two-fold symmetry, and was modelled by assigning one component to have the carbon atom lying on the two-fold axis, with the chlorine atoms equally disposed around the two-fold axis, and a second component with one chlorine atom lying on the two-fold axis, with the carbon and chlorine atoms equally disposed around it. Both components were restrained to geometrical estimates with a refinable occupancy factor assigned.

Final refinements, on F^2 and using all data, were carried out with anisotropic displacement factors applied to each of the non-hydrogen atoms and isotropic for the hydrogen atoms and for the atoms of the dichloromethane molecule. A weighting scheme of type $[\sigma^2(F_o^2) + (aP)^2 + bP]^{-1}$, where $P = (F_o^2 + 2F_c^2)/3$ and where a and b were 0.0191 and 13.9650 (0.0254 and 1.8353) was used. At convergence, $R\ [I \geqslant 2\sigma(I)] = 0.0282$ (0.0263) and wR (all data) = 0.0515 (0.0621). For $Tp^*WS_2(S_2PPh_2)\cdot 0.5CH_2Cl_2$, the absolute configuration was determined; the Flack absolute structure factor [41] refined to a value of 0.00(1). In the final difference map the maximum and minimum peak heights were 0.594 and −0.480 (1.021 and −0.810) e $Å^{-3}$, close to the W atom.

The atomic scattering factors for all atoms were those incorporated in the SHELXL-93 program [40]; corrections were made for anomalous dispersion. Calculations were carried out on a Vaxstation 4000 VLC computer system. Distances and angles for the two structures are given in Tables 2 and 3. Figs. 1 and 2 were prepared from the output of ORTEP-II and thermal ellipsoids are drawn at the 50% probability level [42].

Table 2
Distances (Å) and angles (°) for $Tp^*WS_2(S_2PPh_2)$

Distances			
W–S(1)	2.139(2)	W–S(2)	2.137(2)
W–S(3)	2.418(2)	W–N(11)	2.152(6)
W–N(21)	2.298(6)	W–N(31)	2.329(7)
S(3)–P	2.085(3)	S(4)–P	1.953(3)
Angles			
S(1)–W–S(2)	102.38(10)	S(1)–W–S(3)	96.91(8)
S(1)–W–N(11)	97.0(2)	S(1)–W–N(21)	167.4(2)
S(1)–W–N(31)	88.0(2)	S(2)–W–S(3)	99.69(9)
S(2)–W–N(11)	95.3(2)	S(2)–W–N(21)	90.2(2)
S(2)–W–N(31)	169.01(15)	S(3)–W–N(11)	156.8(2)
S(3)–W–N(21)	81.25(14)	S(3)–W–N(31)	82.3(2)
N(11)–W–N(21)	81.1(2)	N(11)–W–N(31)	79.7(2)
N(21)–W–N(31)	79.3(2)	W–S(3)–P	110.55(10)
S(3)–P–S(4)	117.9(2)		

Table 3
Distances (Å) and angles (°) for $Tp^*WS(S_2PPh_2)$

Distances			
W–S(1)	2.1426(12)	W–S(2)	2.4663(11)
W–S(3)	2.4589(11)	W–N(11)	2.174(3)
W–N(21)	2.360(4)	W–N(31)	2.170(3)
S(2)–P	2.020(2)	S(3)–P	2.0321(15)
Angles			
S(1)–W–S(2)	99.70(4)	S(1)–W–S(3)	100.47(4)
S(1)–W–N(11)	94.39(10)	S(1)–W–N(21)	169.65(8)
S(1)–W–N(31)	94.56(11)	S(2)–W–S(3)	80.32(4)
S(2)–W–N(11)	165.48(10)	S(2)–W–N(21)	87.95(9)
S(2)–W–N(31)	93.08(9)	S(3)–W–N(11)	93.73(9)
S(3)–W–N(21)	87.62(9)	S(3)–W–N(31)	164.39(10)
N(11)–W–N(21)	78.53(12)	N(11)–W–N(31)	89.27(12)
N(21)–W–N(31)	77.97(13)	W–S(2)–P	85.71(5)
W–S(3)–P	85.66(5)	S(2)–P–S(3)	103.22(6)

3. Results and discussion

3.1. Sulfur atom transfer from thiotungsten(VI) centers

Oxo-thio- and bis(thio)-W(VI) complexes undergo SAT to tertiary phosphines yielding oxo- and thio-W(IV) complexes, respectively, and phosphine sulfides. Nucleophilic attack by phosphine at the terminal thio ligand is consistent with a sulfur based π^* LUMO [33] and, in the case of oxo-thio species, expectations based on bond dissociation enthalpies (W=S, ca. 82–92 kcal mol^{-1}; W=O, 138–160 kcal mol^{-1}) [14,17]. The observation is also in accord with the outcomes of similar reactions in oxo-thio-Mo chemistry [34–36,43]. The stability of the W-containing products is critically dependent on the conditions of the reaction, particularly the solvent and the nature of the co-ligand (vide infra). While the chemistry observed generally parallels the OAT chemistry of Tp^*MoO_2X complexes [6], the instability of W(IV) species containing monodentate co-ligands limits their clean isolation and full characterization. These difficulties are ameliorated by the presence of stabilizing ambidentate ligands (vide infra).

In pyridine, green Tp^*WS_2Cl reacts rapidly with PPh_3 to produce $SPPh_3$ and blue, air-sensitive Tp*WSCl(py). The instability of the complex toward loss of pyridine, in solution and the solid state, prevented complete characterization. The compound's IR spectrum exhibited medium intensity ν(BH) and ν(W=S) bands at 2545 and 470 cm^{-1}, respectively. The

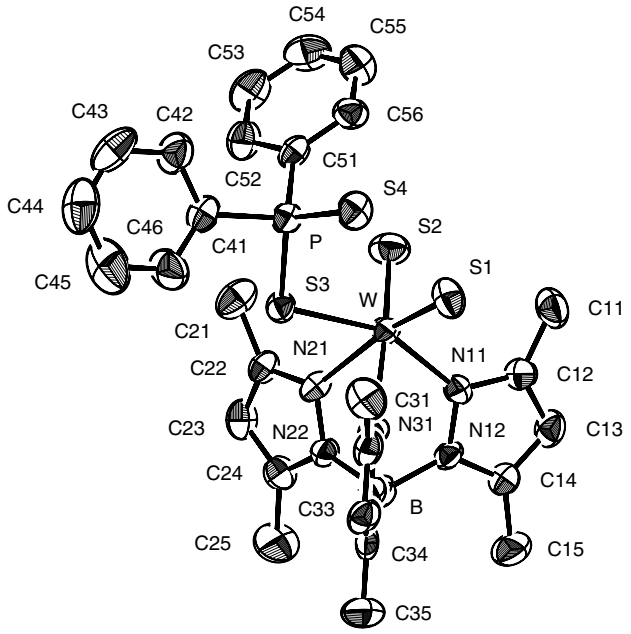

Fig. 1. Molecular structure and atom numbering scheme for $Tp^*WS_2(S_2PPh_2)$. The numbering schemes for the pyrazole ring containing N(31) (unlabelled) parallels those shown for the rings containing N(11) and N(21). Hydrogen atoms have been removed for clarity.

observation of bands at 1625, 1585, 1475, 1150, 755 and 690 cm^{-1} (absent from the spectrum of Tp^*WS_2Cl) were consistent with pyridine ligation. The mass spectrum of

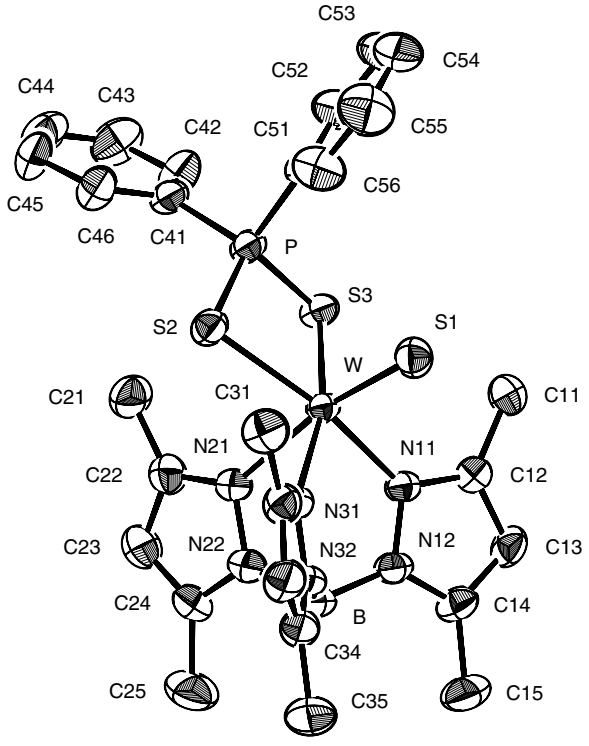

Fig. 2. Molecular structure and atomic numbering scheme for $Tp^*WS(S_2PPh_2)$. Hydrogen atoms have been removed for clarity.

$Tp^*WSCl(py)$ lacked a molecular ion but contained a strong $[M–Me_2pz]^+$ ion at *m/z* 532 (9%); the loss of an Me_2pz is a common fragmentation pattern for complexes of Tp*. The ^1H NMR spectrum of $Tp^*WSCl(py)$ exhibits broad features typical of fluxional oxo- and thio-W(IV) Tp* complexes [21]. The conversion of the compound to Tp^*WOSCl or $Tp^*WS(S_2CNEt_2)$ upon reaction with dimethyl sulfoxide or NaS_2CNEt_2, respectively, supported the proposed formulation. Aspects of this work were previously described [33].

The reactions of Tp^*WS_2X (X = Cl, SPh) with PPh_3 or PMe_2Ph in pyridine or 2,6-lutidine (lut) yielded intensely colored Tp*WSX(solvent). Here, the air-sensitivity of the complexes and persistent contamination by phosphine sulfide prevented full characterization. In light of the isolation of phosphine oxide intermediates in related OAT reactions [44], the generation of phosphine sulfide complexes cannot be excluded nor at this time confirmed. Purple Tp*WS(SPh)(py) and Tp*WS(SPh)(lut) are soluble and moderately stable in CH_2Cl_2 producing dichroic (blue-grey/red) solutions. The former is also solvatochromic, producing green solutions in hexane. Attempts to prepare MeCN complexes such as Tp*WSX(MeCN) by heating Tp^*WS_2X and PPh_3 in MeCN were unsuccessful (cf. clean reactions in oxo-Mo systems [45,46]). The reaction of Tp^*WS_2Cl with PPh_3 in dichloromethane resulted in the generation of orange Tp^*WSCl_2 in 77% yield via consecutive SAT and solvent-based chlorine atom abstraction reactions. The complex was characterized by IR (ν(BH) 2555 cm^{-1}, ν(W=S) 515 cm^{-1}) and EPR ($g = 1.731$) spectroscopy. Chlorine atom abstraction reactions are also observed in related oxo-Mo systems [45].

Green Tp^*WS_2Cl failed to react with NEt_4CN in benzene even after days under reflux. No visible reaction occurred between Tp^*WS_2Cl and NaCN/18-crown-6 in refluxing toluene over two hours but all Tp^*WS_2Cl was consumed after 15 h; numerous products were detected by TLC (silica, 1:1 THF/hexane) but none could be isolated or characterized. Cyanide does not react with $Cp^*WS_2(R)$ (R = Me, CH_2SiMe_3) at room temperature [25]. Tungsten enzymes vary in their response to cyanide. *Pyrococcus furiosus* aldehyde oxidoreductase and *Desulfovibrio gigas* aldehyde dehydrogenase are deactivated by cyanide [47] but, *Thermococcus litoralis* formaldehyde ferredoxin oxidoreductase [16] and *P. acetylenicus* acetylene hydratase [48] are less sensitive to the anion. The formylmethanofuran dehydrogenases from *Methanobacterium thermoautotrophicum* [49] and *M. wolfei* [50] and the aldehyde oxidoreductase from *Thermococcus* sp. ES-1 [51] are unaffected by cyanide. Deactivation of xanthine oxidase [4,5] and $[MoOS]^{2+}$ model complexes [34–36,43] by cyanide is a key indicator of the presence of a terminal thio ligand at Mo. By analogy, it is implicit that, cyanide-stable W enzymes are devoid of W–SH or W=S ligands. However, our results

suggest that, W=S groups can be unusually stable in the presence of cyanide. Hence, the inability of cyanide to deactivate W enzymes cannot be taken as strong evidence for the absence of thio ligands. Aspects of this work were previously described [33].

Tungsten(IV)/(VI) complexes containing dithiophosphinate co-ligands were more stable and amenable to study than the monodentate ligand complexes above. As was the case for Tp*WOSCl (vide supra), orange Tp*WOS(S_2PPh_2) [52] underwent SAT (rather than OAT) to tertiary phosphines, producing air-stable Tp*WO(S_2PPh_2) and SPR_3 according to Eq. (1). Similarly, yellow-brown Tp*WS_2(S_2PPh_2) [33] reacted with one equivalent of PPh_3 in refluxing benzene to yield dark red Tp*WS(S_2PPh_2) and $SPPh_3$ (Eq. (2)).

$$\mathrm{Tp^*WOS(S_2PPh_2\text{-}\mathit{S}) + PR_3 \rightarrow Tp^*WO(S_2PPh_2\text{-}\mathit{S},\mathit{S}') + SPR_3} \quad (1)$$

$$\mathrm{Tp^*WS_2(S_2PPh_2\text{-}\mathit{S}) + PPh_3 \rightarrow Tp^*WS(S_2PPh_2\text{-}\mathit{S},\mathit{S}') + SPPh_3} \quad (2)$$

The oxo-W(IV) complex can also be prepared by thermal decarbonylation of Tp*WO(S_2PPh_2-*S*)(CO) [22] in benzene. The compounds are freely soluble in chlorinated solvents but insoluble in alcohols and alkanes. The oxo-W(IV) complex is moderately air-stable as a solid but air-sensitive in solution, yielding Tp*WO_2(S_2PPh_2) and Tp*WOS{$SP(O)Ph_2$} upon lengthy exposure to air. The thio-W(IV) complex is air-sensitive and decomposes over several days in the solid state, faster in solution. Only Tp*WO(S_2PPh_2) is stable toward column chromatography on silica gel. The IR spectra of Tp*WO(S_2PPh_2) and Tp*WS(S_2PPh_2) exhibit medium intensity ν(BH) bands at 2540–2545 cm^{-1} and strong ν(W=E) (E = O, S) bands at 945 and 490 cm^{-1}, respectively. The bidentate dithiophosphinate ligand gives rise to strong bands at ca. 1430 and 1100 and 560–565 cm^{-1}, which are associated with phenyl [53] and $\nu(PS_2)$ vibrational modes, respectively. The room temperature ^{1}H NMR spectrum of Tp*WS(S_2PPh_2) consisted of broad resonances indicative of (undetermined) fluxional processes; similar behavior is observed for Tp*WO(S_2CNEt_2) and Tp*WS(S_2CNEt_2) [21]. In contrast, the ^{1}H NMR spectrum of Tp*WO(S_2PPh_2) exhibited six sharp methyl and methine Tp* resonances, indicative of a non-fluxional molecule with C_s symmetry.

The sluggish reactions of the dioxo-W(VI) complexes, Tp*WO_2X, with PPh_3 have already been mentioned in the literature [31,54]. Interestingly, Tp*WO_2(S_2PPh_2) reacts with PMe_2Ph in refluxing toluene to produce at least seven species (by thin layer chromatography). One of the major products, an orange compound, has been tentatively characterized as the phosphinothiolate (thiophosphinite) complex, Tp*WO_2($SPPh_2$), on the basis of IR data indicating the presence of oxo ($\nu(WO_2)$ 940 and 905 cm^{-1}) and phenyl groups (1430 and 1100 cm^{-1}) but the absence of PS_2 and P=O units. SAT from P rather than OAT from W is consistent with relative W=O (138–160 kcal mol^{-1}) and P=S (ca. 82–92 kcal mol^{-1}) bond dissociation enthalpies. Mononuclear phosphinothiolate complexes of Ti, Zr and Hf have been reported and the crystal structure of $Cp_2Ti(SPCy_2)$ determined [55]. Full characterization of the W complex is underway.

3.2. Atom transfer to oxo- and thiotungsten(IV) centers

The reactions of Tp*WSCl(py) with dimethyl sulfoxide or Tp*WS(SPh)(py) with dioxygen produced Tp*WOSX via OAT. An alternative but less reliable synthesis of Tp*WOSCl, involving the direct sulfurization of Tp*WO_2Cl, has been reported [32,37].

Green Tp*WO(S_2PPh_2) reacts cleanly with sulfur or propylene sulfide ([S]) in refluxing benzene to produce Tp*WOS(S_2PPh_2) (Eq. (3)); the yields and reaction times are 79% in ca. 30 min and 92% in ca. 3 days, respectively, for the two reagents. The product was identified by IR (ν(W=O) 930s, ν(P=S) 643s, ν(P–S) 525s, ν(W=S) 485m cm^{-1}) and ^{1}H NMR spectroscopy. The reaction contrasts with the formation of $[WO(S_2)(mnt)_2]^{2-}$ rather than $[WOS(mnt)_2]^{2-}$ when $[WO(mnt)_2]^{2-}$ reacts with sulfur [28].

$$\mathrm{Tp^*WO(S_2PPh_2) + [S] \rightarrow Tp^*WOS(S_2PPh_2)} \quad (3)$$

$$\mathrm{Tp^*WS(S_2PPh_2) + MeCH(S)CH_2 \rightarrow Tp^*WS_2(S_2PPh_2) + MeCH{=}CH_2} \quad (4)$$

No reaction was observed between Tp*WO(S_2PPh_2) and excess thiophene over two days in refluxing benzene. The steric bulk of Tp* is likely to prevent the η^5-coordination of thiophene required for desulfurization [56]. SAT to Tp*WS(S_2PPh_2) provides an efficient alternative route to Tp*WS_2(S_2PPh_2) [33] (Eq. (4)) but rather forcing conditions are required for the reaction (benzene reflux). The analogous reaction with elemental sulfur fails to produce Tp*WS_2(S_2PPh_2). These reactions are to our knowledge the first examples of the oxidation of W(IV) by SAT leading to the generation of oxo-thio and bis(thio)-W(VI) centers.

The reactions of Tp*WS(S_2PPh_2) with oxygen atom donors are not as straightforward. Thus, the reaction of Tp*WS(S_2PPh_2) with dimethyl sulfoxide produces two products, orange Tp*WOS(S_2PPh_2) (18%) and brown Tp*WS_2{$SP(O)Ph_2$} (65%). The latter was characterized by IR (ν(BH) 2560m, phenyl modes 1435 and 1100s, ν(P=O) 1035s, $\nu(WS_2)$ 495m and 475s, $\nu(PS_2)$ absent) and ^{1}H NMR spectroscopy (C_s symmetry indicated). The generation of Tp*WS_2{$SP(O)Ph_2$} is consistent with OAT to P with concomitant SAT from P to W. The

reaction of Tp*WS(S_2PPh_2) with pyridine *N*-oxide in refluxing 1,2-dichloroethane (18 h) also gave disappointing yields (8%) of Tp*WOS(S_2PPh_2) (and other intractable products).

The oxygen atom donors dioxygen, tetramethylene sulfoxide (TMSO) and NBu_4NO_3 react with Tp*WO(S_2PPh_2) to give Tp*WO_2(S_2PPh_2) in 27%, 16% and 39% yields, respectively. The unexpectedly low yields are associated with the generation of a second product, orange, air-stable Tp*WOS{$SP(O)Ph_2$}, in 20%, 76% and 31% yield, respectively. The infrared spectrum of this complex contained a medium intensity ν(BH) band at 2555 cm^{-1} and strong phenyl group, ν(W=O) and ν(W=S) bands at 1430, 940 and 480 cm^{-1}, respectively. The strong ν(P–S) band of Tp*WOS(S_2PPh_2) at 525 cm^{-1} was conspicuously absent and new bands were present at 1110, 725, 545, and 510 cm^{-1}. The strong band at 1110 cm^{-1} is assigned to the ν(P=O) mode. The ^1H NMR spectrum was indicative of molecular C_1 symmetry and the retention of both phenyl groups. Mass spectra contained peak clusters at *m*/*z* 528, 730 and 667 (ca. 2–4%) assignable to $[Tp^*WOS]^+$, $[Tp^*WO\{SP(O)Ph_2\}]^+$ and $[M–Me_2pz]^+$ fragments, respectively. Aerial oxidation of Tp*WO(S_2PPh_2) also led to Tp*WOS(S_2PPh_2) (17% based on sulfur). Formation of the dioxo complex is proposed to result from direct OAT to the W center while the generation of oxo-thio species occurs through OAT to P with concomitant SAT from P to W. The distinctly different product distributions observed for the smaller (dioxygen, NO_3^-) vs. larger (TMSO) oxidants are consistent with restricted access of TMSO to the W vs. P centers. Pure Tp*WO(S_2PPh_2) is quite stable in refluxing benzene (for over two days) under nitrogen, and *did not* spontaneously produce *cis*-$[WOS]^{2+}$ complexes.

3.3. Crystal structures

The structures of Tp*WS_2(S_2PPh_2) and Tp*WS(S_2PPh_2) were determined by X-ray diffraction and views of the molecules are shown in Figs. 1 and 2, respectively. Selected bond distances and angles are given in Tables 2 and 3, respectively.

Mononuclear, six-coordinate Tp*WS_2(S_2PPh_2) exhibits a distorted-octahedral coordination geometry comprised of *cis* thio, monodentate $S_2PPh_2^-$ and tridentate *fac*-Tp* ligands. The W=S bond distances of 2.137(2) and 2.139(2) Å are at the short end of the range established for W=S bonds (mean 2.153 Å) [57,58] but similar distances pertain to related complexes, including Tp*WS_2(OPh) (2.130(4) Å) [33] and Cp*WS_2(CH_2SiMe_3) [25]. The W–S(3) distance of 2.418(2) Å is typical of monodentate dithiophosphinate species and close to equivalent bond distances in Tp*WE(S_2PPh_2-*S*)(CO) (E = O, S) [59]. The thio ligands exert a strong *trans* influence on the W–N(21) and W–N(31) bonds, lengthening them significantly with respect to the W–N(11) bond. The S(1)–W–S(2) angle of 102.38(9)° is close to the corresponding angle for Tp*WS_2(OPh) (102.9(1)°) and enhances favorable π-interactions between the thio ligand and metal orbitals [33]. The W–S(3) and W–N(11) vectors are inclined away from the thio ligands producing an S(3)–W–N(11) angle of 156.8(2)°. The W atom lies 1.043(2) Å out of the plane defined by S(1), S(2) and S(3) but 1.509(4) Å out of the plane defined by the N(*n*1) atoms; these parameters highlight the distorted nature of the octahedral geometry.

The monodentate dithiophosphinate ligand adopts a partially extended conformation with S(4)···S(1) and S(4)···S(2) intramolecular contacts of 3.237(3) and 5.013(3) Å, respectively. The former is inside the van der Waals distance of 3.7 Å [60], the latter well outside this distance. A very weak interaction is indicated by the spatial conjunction of the sulfur atoms observed here and in Tp*WOS(S_2PPh_2) [52]. The P–S(4) bond distance is significantly shorter than that of P–S(3) [1.953(3) vs. 2.085(3) Å], a reflection of double bond character in the terminal P=S unit. Similar differences in P–S distances are observed in other monodentate dithiophosph(in)ate ligand complexes, e.g., Tp*MoO_2\{$S_2P(OEt)_2$-*S*\} [61] and Tp*WOS(S_2PPh_2-*S*) [52], as well as $[R_2P(S)]_2S_2$ (R = Me, ^{i}Pr) [62] and the free acid, HS_2PPh_2 [63]. A fully extended structure is observed in the related oxo-Mo species, Tp*MoO_2\{$S_2P(OEt)_2$\} [61]. The other bond distances and angles within the dithiophosphinate and Tp* ligands are unexceptional.

Molecules of Tp*WS(S_2PPh_2) are also mononuclear and six-coordinate, with a distorted octahedral coordination sphere comprised of terminal thio, bidentate $S_2PPh_2^-$ and tridentate *fac*-Tp* ligands. The W–S(1) bond length of 2.1426(12) Å is similar to those found in other mononuclear thio-W(IV) complexes, including Tp*WS(S_2CNEt_2) (2.153(2) Å) [21], WS(S_2CNEt_2)(η^4-C_4Ph_4H) (2.103(4) Å) [64], WS(PhC≡CPh)(S_2CNEt_2)($SCNEt_2$) (2.138(5) Å) [65] and WS(S_2CNEt_2)$_2$(PhC≡CPh) (2.147(2) Å) [66]. The bidentate $S_2PPh_2^-$ ligand is symmetrically bound to tungsten with average W–S and P–S distances of 2.463(1) and 2.026(2) Å, respectively. The S–W–S and S–P–S angles of the dithiophosphinate ligand are 80.32(4)° and 103.22(6)°, respectively. The *trans* influence of the W=S group results in a lengthening of the W–N(21) bond by ca. 0.19 Å compared to the other W–N bonds. The W atom lies 0.288(1) Å out of the plane defined by S(2), S(3), N(11) and N(31) toward the terminal thio ligand. Finally, the P atom is swivelled slightly toward the thio ligand as a result of steric interactions, the dihedral angle between the W, S(2), S(3) and S(2), S(3), P planes being 25.00(5)°. The structure is most closely related to those determined for Tp*MoO\{$S_2P(OEt)_2$\} [61] and Tp*WS(S_2CNEt_2) [21].

3.4. Catalytic SAT reactions

The interconversion of thio-W(IV) and -(VI) complexes by SAT raises the possibility of catalytic SAT. With this aim in mind, we have briefly assessed the capacity of several complexes to catalyze Eq. (5) in dry, deoxygenated benzene.

$$PPh_3 + MeCH(S)CH_2 \rightarrow SPPh_3 + MeCH{=}CH_2 \qquad (5)$$

The reactions were conveniently monitored by ^{31}P NMR spectroscopy, activity being indicated by the replacement of the resonance of PPh_3 (δ 1.3) with that of $SPPh_3$ (δ 46.8). Reactions were performed at room temperature, with a 1:1 mole ratio of PPh_3:C_3H_6S (0.13 mmol each/sample) with 0.1 mole equivalent of W catalyst. A blank reaction was also monitored, giving 85% conversion to products after 43 weeks. The reaction was accelerated by addition of Tp*WS_2X (X = Cl, OPh, SPh). The thiophenolate complex catalyzed 82% conversion to products over a 10 week period but improved catalytic activity, 56% conversion in 16 days, was noted for Tp*WS_2(OPh). The best catalyst was found to be Tp*WS_2Cl, which effected 95% conversion in just 3 days. The active catalyst in this system is unclear as there is in situ ^1H NMR evidence for the presence of a dinuclear species (possibly from the comproportionation of Tp*WS_2Cl and Tp*WSCl(solv)) in this system. Attempts to isolate and characterize the species are underway. Present studies have been hampered by a degree of polymerization in the propylene sulfide used and more effective sulfur atom donor reagents are now under investigation. Future investigations will also examine the use of bulkier trispyrazolylborate ligands to maintain mononuclearity, although this does not appear to be pre-requisite for catalysis. The results to date hold great promise for the development of fully functional SAT catalysts based on terminal thio-W chemistry.

4. Summary

Reduction of oxo-thio- and bis(thio)-W(VI) complexes with phosphines results in the formation of oxo- and thio-W(IV) species, respectively. The products of the reactions of Tp*WS_2Cl or Tp*WOSCl with phosphines are unstable even in the presence of coordinating solvents. In contrast, the ambidentate $S_2PPh_2^-$ ligand stabilizes Tp*WE(S_2PPh_2) (E = O, S), the products of the reactions of Tp*WES(S_2PPh_2) with phosphines, through chelation. The one-electron redox potentials of the thio-W(VI) complexes, as well as the products obtained from reactions with phosphines, are directly comparable with those observed for analogous dioxo-Mo(VI) complexes, and clear parallels exist in the oxygen and sulfur atom transfer capabilities of dioxo-Mo(VI) on one hand and oxo-thio- and bis(thio)-W(VI) centers on the other. If W-enzymes contain thio-W centers and operate by direct atom transfer, then sulfidation rather than oxidation of the substrate would be predicted on the basis of the results reported here. This is at odds with the observed net OAT chemistry of the enzymes (unless an initially formed thio species is hydrolyzed to give the observed product).

The tungsten(IV) complexes Tp*WE(S_2PPh_2) (E = O, S) react cleanly with sulfur atom donors to give the thio-W(VI) complexes, Tp*WES(S_2PPh_2), while reaction with oxygen atom donors gave a mixture of Tp*WOE(S_2PPh_2), through OAT to W, and Tp*WES {$SP(O)Ph_2$}, through OAT to P and concomitant SAT from P to W. In general, reduction of W(VI) to W(IV) was effective through sulfur rather than oxygen atom transfer while oxidation of W(IV) to W(VI) is readily achieved by either oxidant (the complications associated with the phosphorus-containing ligand notwithstanding). Catalysis of SAT has been demonstrated and will be further developed with both thio-W and -Mo systems.

5. Supplementary data

Full details of data collections and structure determinations have been deposited with the Cambridge Crystallographic Data Centre, CCDC Nos. 211 896 [for Tp*$WS_2(S_2PPh_2)\cdot 0.5CH_2Cl_2$] and 211 897 [for Tp*$WS(S_2PPh_2)$]. Copies of this information may be obtained free of charge from: The Director, CCDC, 12 Union Road, Cambridge CB2 1EZ, UK (fax: +44-1223-336033; deposit@ccdc.cam.ac.uk or www.ccdc.cam.ac.uk).

Acknowledgements

We gratefully acknowledge the financial support of the Australian Research Council and the University of Melbourne.

References

[1] J. Haber, in: R.R. Braithwaite, J. Haber (Eds.), Molybdenum: An Outline of its Chemistry and Uses, Elsevier, Amsterdam, 1994.
[2] E.I. Stiefel, Kirk Othmer Encyclopedia of Chemical Technology, Wiley, New York, 1995, p. 940.
[3] B. Cornils, W.A. Herrmann (Eds.), Applied Homogeneous Catalysis with Organometallic Compounds, VCH, Weinheim, 1996.
[4] R. Hille, Chem. Rev. 96 (1996) 2757.
[5] R.S. Pilato, E.I. Stiefel, in: J. Reedijk, E. Bouwman (Eds.), Bioinorganic Catalysis, Marcel Dekker, New York, 1999.
[6] C.G. Young, in: B. Meunier (Ed.), Biomimetic Oxidations Catalyzed by Transition Metal Complexes, Imperial College Press, London, 2000.

[7] A. Sigel, H. Sigel (Eds.), Metal Ions in Biological Systems, Marcel Dekker, New York, 2002.
[8] R.H. Holm, Coord. Chem. Rev. 100 (1990) 183.
[9] G.C. Tucci, J.P. Donahue, R.H. Holm, Inorg. Chem. 37 (1998) 1602.
[10] J.P. Donahue, C. Lorber, E. Nordlander, R.H. Holm, J. Am. Chem. Soc. 120 (1998) 3259.
[11] C. Lorber, J.P. Donahue, C.A. Goddard, E. Nordlander, R.H. Holm, J. Am. Chem. Soc. 120 (1998) 8102.
[12] B.S. Lim, K.-M. Sung, R.H. Holm, J. Am. Chem. Soc. 122 (2000) 7410.
[13] K.-M. Sung, R.H. Holm, J. Am. Chem. Soc. 123 (2001) 1931.
[14] J.C. Bryan, J.M. Mayer, J. Am. Chem. Soc. 112 (1990) 2298.
[15] B.P. Koehler, S. Mukund, R.C. Conover, I.K. Dhawan, R. Roy, M.W.W. Adams, M.K. Johnson, J. Am. Chem. Soc. 118 (1996) 12391.
[16] I.K. Dhawan, R. Roy, B.P. Koehler, S. Mukund, M.W.W. Adams, M.K. Johnson, J. Biol. Inorg. Chem. 5 (2000) 313.
[17] J.M. Mayer, Adv. Transit. Met. Coord. Chem. 1 (1996) 105.
[18] L.K. Woo, Chem. Rev. 93 (1993) 1125.
[19] K.A. Hall, J.M. Mayer, J. Am. Chem. Soc. 114 (1992) 10402.
[20] F.-M. Su, J.C. Bryan, S. Jang, J.M. Mayer, Polyhedron 8 (1989) 1261.
[21] C.G. Young, M.A. Bruck, J.H. Enemark, Inorg. Chem. 31 (1992) 593.
[22] S. Thomas, E.R.T. Tiekink, C.G. Young, Organometallics 15 (1996) 2428.
[23] K.A. Hall, J.M. Mayer, Inorg. Chem. 33 (1994) 3289.
[24] D. Britnell, G.W.A. Fowles, D.A. Rice, J. Chem. Soc., Dalton Trans. (1975) 213.
[25] J.W. Faller, R.R. Kucharczyk, Y. Ma, Inorg. Chem. 29 (1990) 1662.
[26] M.H. Chisholm, J.C. Huffman, J.W. Pasterczyk, Polyhedron 6 (1987) 1551.
[27] D. Rabinovich, G. Parkin, Inorg. Chem. 34 (1995) 6341.
[28] S.K. Das, D. Biswas, R. Maiti, S. Sarkar, J. Am. Chem. Soc. 118 (1996) 1387.
[29] W. Adam, R.M. Bargon, Chem. Commun. (2001) 1910.
[30] W. Adam, R.M. Bargon, W.A. Schenk, J. Am. Chem. Soc. 125 (2003) 3871.
[31] A.A. Eagle, E.R.T. Tiekink, C.G. Young, Inorg. Chem. 36 (1997) 6315.
[32] A.A. Eagle, S. Thomas, C.G. Young, in: E.I. Stiefel, K. Matsumoto (Eds.), Transition Metal Sulfur Chemistry: Biological and Industrial Significance, ACS Symposium Series, No. 653, American Chemical Society, Washington, DC, 1996, pp. 324–335.
[33] A.A. Eagle, E.R.T. Tiekink, G.N. George, C.G. Young, Inorg. Chem. 40 (2001) 4563.
[34] A.A. Eagle, L.J. Laughlin, C.G. Young, E.R.T. Tiekink, J. Am. Chem. Soc. 114 (1992) 9195.
[35] C.G. Young, L.J. Laughlin, S. Colmanet, S.D.B. Scrofani, Inorg. Chem. 35 (1996) 5368.
[36] P.D. Smith, D.A. Slizys, G.N. George, C.G. Young, J. Am. Chem. Soc. 122 (2000) 2946.
[37] A.A. Eagle, E.R.T. Tiekink, C.G. Young, J. Chem. Soc., Chem. Commun. (1991) 1746.
[38] G.M. Sheldrick, SHELX-76, Program for Crystal Structure Determination, University of Cambridge, Cambridge, UK, 1976.
[39] G.M. Sheldrick, Acta Crystallogr. A 46 (1990) 467.
[40] G.M. Sheldrick, SHELXL-93 Program for Crystal Structure Refinement, University of Göttingen, Germany, 1993.
[41] H.D. Flack, Acta Crystallogr. A 39 (1983) 876.
[42] C.K. Johnson, ORTEP-II, Report ORNL-5138, Oak Ridge National Laboratory, Oak Ridge, TN, 1976.
[43] A. Thapper, J.P. Donahue, K.B. Musgrave, M.W. Willer, E. Nordlander, B. Hedman, K.O. Hodgson, R.H. Holm, Inorg. Chem. 38 (1999) 4104.
[44] P.D. Smith, A.J. Millar, C.G. Young, A. Ghosh, P. Basu, J. Am. Chem. Soc. 122 (2000) 9298.
[45] S.A. Roberts, C.G. Young, C.A. Kipke, W.E. Cleland Jr., K. Yamanouchi, M.D. Carducci, J.H. Enemark, Inorg. Chem. 29 (1990) 3650.
[46] Z. Xiao, M.A. Bruck, J.H. Enemark, C.G. Young, A.G. Wedd, Inorg. Chem. 35 (1996) 7508.
[47] S. Mukund, M.W.W. Adams, J. Biol. Chem. 266 (1991) 14208.
[48] B.M. Rosner, B. Schink, J. Bacteriol. 177 (1995) 5767.
[49] P.A. Bertram, R.A. Schmitz, D. Linder, R.K. Thauer, Arch. Microbiol. 161 (1994) 220.
[50] R.A. Schmitz, S.P.J. Albracht, R.K. Thauer, Eur. J. Biochem. 209 (1992) 1013.
[51] J. Heider, K. Ma, M.W.W. Adams, J. Bacteriol. 177 (1995) 4757.
[52] S. Thomas, A.A. Eagle, S.A. Sproules, J.P. Hill, J.M. White, E.R.T. Tiekink, G.N. George, C.G. Young, Inorg. Chem. 42 (2003) 5909.
[53] R.M. Silverstein, C.G. Bassler, T.C. Morrill, Spectrophotometric Identification of Organic Compounds, Wiley, New York, 1981.
[54] A.A. Eagle, R.W. Gable, C.G. Young, Aust. J. Chem. 52 (1999) 827.
[55] L. Gelmini, D.W. Stephan, Organometallics 6 (1987) 1515.
[56] R.J. Angelici, Organometallics 20 (2001) 1259.
[57] A.G. Orpen, L. Brammer, F.H. Allen, O. Kennard, D.G. Watson, R. Taylor, J. Chem. Soc., Dalton Trans. (1989) S1.
[58] G. Parkin, Prog. Inorg. Chem. 47 (1998) 1.
[59] A.A. Eagle, S.M. Harben, E.R.T. Tiekink, C.G. Young, J. Am. Chem. Soc. 116 (1994) 9749.
[60] H.B. Abrahamson, M.L. Freeman, M.B. Hossain, D. van der Helm, Inorg. Chem. 23 (1984) 2286.
[61] S.A. Roberts, C.G. Young, W.E. Cleland Jr., R.B. Ortega, J.H. Enemark, Inorg. Chem. 27 (1988) 3044.
[62] A.C. Gallacher, A.A. Pinkerton, Acta Crystallogr. C48 (1992) 2085.
[63] F.R. Kreißl, W.J. Sieber, M. Wolfgruber, J. Riede, Angew. Chem., Int. Ed. Engl. 23 (1984) 640.
[64] S.G. Feng, A.S. Gamble, J.L. Templeton, Organometallics 8 (1989) 2024.
[65] D.C. Brower, T.L. Tonker, J.R. Morrow, D.S. Rivers, J.L. Templeton, Organometallics 5 (1986) 1093.
[66] J.R. Morrow, T.L. Tonker, J.L. Templeton, Organometallics 4 (1985) 745.

Available online at www.sciencedirect.com
SCIENCE DIRECT®
Polyhedron 23 (2004) 395–403
POLYHEDRON
www.elsevier.com/locate/poly

Poly(mercaptoimidazolyl)borate chemistry and the predominance of κ^3-*S*,*S*,*H* over κ^2-*S*,*S* or κ^3-*S*,*S*,*S* coordination modes: unexpected formation of square pyramidal Ni(II) complexes

Hamsell M. Alvarez [a], Joseph M. Tanski [b], Daniel Rabinovich [a,*]

[a] *Department of Chemistry, The University of North Carolina at Charlotte, 9201 University City Boulevard, Charlotte, NC 28223, USA*
[b] *Department of Chemistry, Columbia University, New York, NY 10027, USA*

Received 10 June 2003; accepted 26 August 2003

Dedicated to Jerry Trofimenko, the true Scorpion King, with our gratitude and admiration.

Abstract

The paramagnetic nickel(II) complexes [(dppe)Ni(L)]X (L = Bm^R or Tm^R) have been readily prepared from the appropriate 1,2-bis(diphenylphosphino)ethane adducts Ni(dppe)X_2 (X = Cl, Br) and the thallium(I) reagents Tl(Bm^R) (R = Me, Bu^t) or Tl(Tm^R) (R = Me, Bu^t, *p*-Tol), and isolated as carmine to deep purple solids in 75–95% yield. X-ray diffraction studies of [(dppe)Ni(Bm^{Me})]Cl and [(dppe)Ni($Tm^{p\text{-Tol}}$)]Cl revealed the presence of a weak pseudo-axial Ni···H–B interaction and an overall square pyramidal geometry in each complex. As such, the cationic complexes $[(dppe)Ni(L)]^+$ are the first structurally characterized species having $[NiP_2S_2H]$ cores and resemble a number of transient species that play a key role in the catalytic cycle of [NiFe] hydrogenases.
© 2003 Elsevier Ltd. All rights reserved.

Keywords: Nickel; Bis(mercaptoimidazolyl)borate complexes; Tris(mercaptoimidazolyl)borate complexes; Diphosphine; Hydrogenases; Crystal structure

1. Introduction

The versatility of the tris(pyrazolyl)borate (scorpionate) ligand system is evident from the nearly 200 members of this family of ligands that have been prepared simply by varying the number and nature of the substituents on either the boron center or the pyrazolyl rings [1–3]. A number of neutral analogues of Tp ligands have also been developed over the years by replacing the boron atom by a different element, e.g., carbon or silicon to produce the corresponding tris(pyrazolyl)methanes [4] or tris(pyrazolyl)silanes [5] (Fig. 1). Interest in the design of more polarizable (i.e., softer) analogues of Tp ligands, prompted by potential applications in bioinorganic and organometallic chemistry, has also arisen within the last decade. In this regard, whereas Riordan introduced the poly(thioether)borates [6,7] and Reglinski originated the tris(mercaptoimidazolyl)borates [8], Peters and Nocera disclosed almost simultaneously the tris(phosphino)borates [9,10] (Fig. 2).

The Tm^R ligands, in conjunction with the related bis(mercaptoimidazolyl)borates (Bm^R) [11], have been particularly appealing for the design of synthetic models for the active centers in the small but conspicuous group of known sulfur-rich metalloenzymes. For example, Parkin and coworkers [12,13] and Vahrenkamp and coworkers [14] have independently prepared several (Tm^R)ZnX complexes (X = halide, alkoxide, thiolate, etc.) in their quest to better understand the structure and function of sulfur-rich zinc enzymes such as liver alcohol dehydrogenase (LADH) and 5-aminolevulinate dehydratase (ALAD). In turn, we have synthesized a series of novel nickel(II) complexes Ni(Bm^R)$_2$ (R = Me, Bz, Bu^t, *p*-Tol) (Fig. 3) [15] as structural models for the nickel center in [NiFe] hydrogenases [16]. The active site in these enzymes consists of a dinuclear nickel–iron

* Corresponding author. Tel.: +1-704-687-4442; fax: +1-704-687-3151.
E-mail address: drabinov@email.uncc.edu (D. Rabinovich).

0277-5387/$ - see front matter © 2003 Elsevier Ltd. All rights reserved.
doi:10.1016/j.poly.2003.11.030

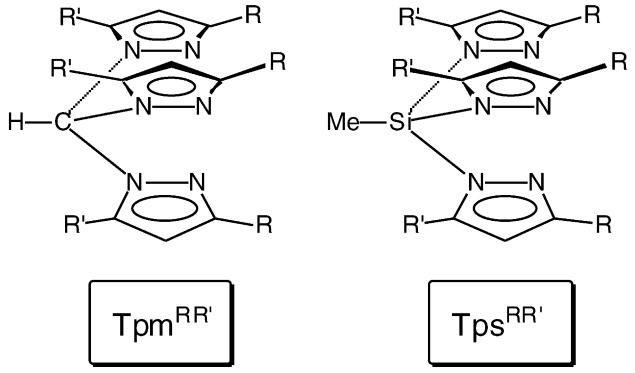

Fig. 1. Neutral analogues of Tp ligands: tris(pyrazolyl)methanes ($Tpm^{RR'}$) and tris(pyrazolyl)silanes ($Tps^{RR'}$).

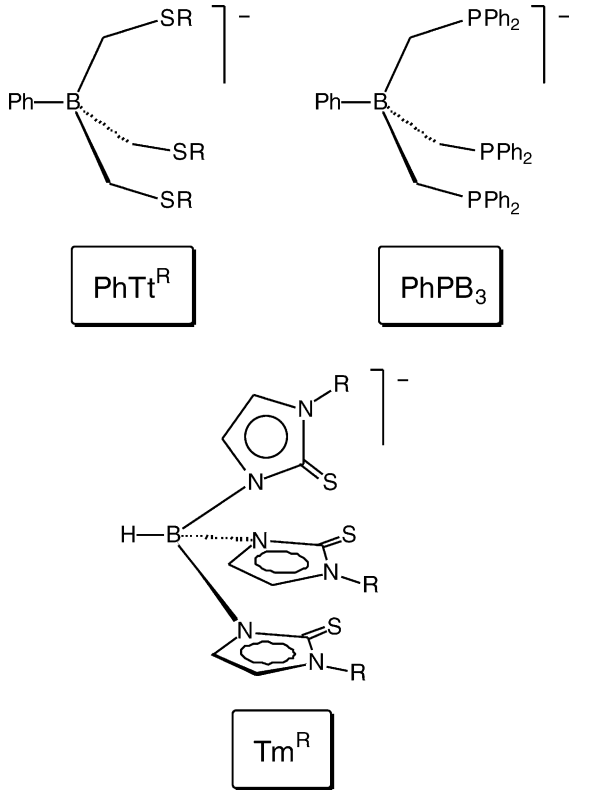

Fig. 2. Soft analogues of Tp ligands: tris(thioether)borates ($PhTt^R$), tris(mercaptoimidazolyl)borates (Tm^R), and tris(phosphino)borates ($PhBP_3$).

complex in which the nickel atom is surrounded by four cysteine groups in a geometry that has been described as either square pyramidal with a missing basal ligand or octahedral with two adjacent coordination vacancies (Fig. 4) [17]. The $Ni(Bm^R)_2$ complexes, having $[NiS_4H_2]$ cores and slightly distorted octahedral geometries resulting from the unexpected presence of two Ni···H–B interactions, constitute unprecedented structural mimics that resemble the nickel coordination environment in the active form of [NiFe] hydrogenases.

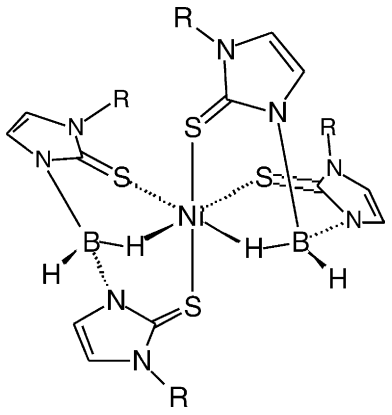

Fig. 3. The bis(mercaptoimidazolyl)borate complexes $Ni(Bm^R)_2$.

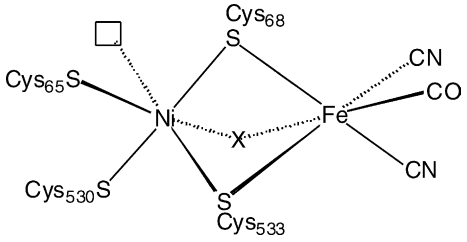

Fig. 4. Representation of the active site in the [NiFe] hydrogenase extracted from *D. gigas* showing the vacant coordination site (open square) and the additional bridging oxo or hydroxo ligand (×) present only in the oxidized (inactive) form of the enzyme.

Seeking to extend our synthetic efforts to the Tm^R ligand system and to investigate the reactivity (i.e., redox chemistry) of a *single* thiolate group bound to nickel in these metalloenzymes, we set out to prepare unusual tetrahedral complexes of the form $(Tm^R)NiSR$. However, the synthesis of such attractive species remains elusive to date since every attempt to access suitable $(Tm^R)NiX$ precursors (X = halide) has yielded instead the homoleptic derivatives $Ni(Tm^R)_2$ as the only isolable nickel products [18,19]. Undeterred by these results, we envisioned that the use of a starting material containing a chelating diphosphine such as 1,2-bis(diphenylphosphino)ethane (dppe) may prevent the addition of a second $[Tm^R]^-$ group to nickel and plausibly generate useful complexes such as $(dppe)Ni(Tm^R)X$, all while preserving the required soft donor ligand set around the metal center. We describe in this paper the synthesis and characterization of the unexpected nickel(II) complexes that are isolated from the reactions of $Ni(dppe)X_2$ (X = Cl, Br) [20] with a variety of poly(mercaptoimidazolyl)borate ligands. These studies will provide insight into the relative affinities of the nickel(II) center for the κ^3-*S*,*S*,*H*, κ^2-*S*,*S*, or κ^3-*S*,*S*,*S* coordination modes that these ligands may exhibit.

2. Results and discussion

2.1. Syntheses of nickel complexes

Nickel(II) products of stoichiometry (dppe)Ni(L)X ($L = Bm^R$ or Tm^R) were readily prepared by reacting equimolar dichloromethane solutions of Ni(dppe)X_2 (X = Cl, Br) and the corresponding thallium(I) reagents Tl(Bm^R) (R = Me, Bu^t) or Tl(Tm^R) (R = Me, Bu^t, *p*-Tol) (Eq. (1)), and isolated as carmine to deep purple solids in ca. 75–95% yield after the appropriate work-up. The use of the sodium reagents Na(Bm^R) or Na(Tm^R) was not nearly as effective and their reactions with Ni(dppe)X_2 produced lower yields of the desired species or, more often, intractable mixtures of unidentified products. All the (dppe)Ni(L)X complexes are air-stable materials, generally soluble in polar solvents such as dichloromethane, chloroform, acetonitrile, acetone, methanol, and dimethyl sulfoxide (DMSO) but insoluble in aliphatic or aromatic hydrocarbons or diethyl ether.

$$\mathrm{Ni(dppe)X_2 + Tl(L) \xrightarrow[\substack{L=Bm^R,Tm^R\\ R=Me,Bu^t,p\text{-}Tol\\ X=Cl,Br}]{CH_2Cl_2} (dppe)Ni(L)X + TlX} \quad (1)$$

The 10 new (dppe)Ni(L)X complexes were characterized by a combination of analytical and spectroscopic techniques, including elemental analyses (CHN) and IR, UV/Vis, and ^{1}H NMR spectroscopies. Their paramagnetism ($\mu_{eff} = 3.0$–$3.2\ \mu_B$) is consistent with $S = 1$ ground states (i.e., two unpaired electrons) and is reflected in solution by broad albeit not significantly contact-shifted signals (relative to the free Bm^R or Tm^R ligands) in their ^{1}H NMR spectra. Electrospray ionization mass spectrometry (ESI-MS) was also used to investigate the nature of the (dppe)Ni(L)X complexes in solution. For example, the positive ion mass spectrum of a dilute acetonitrile solution of (dppe)Ni(Bm^{Me})Cl (Fig. 5) showed only the set of peaks ($m/z = 695$) with the expected isotopic distribution corresponding to the [(dppe)Ni(Bm^{Me})]$^+$ fragment. This observation is in agreement with the fact that loss of a halide is the most common ionization pathway for transition metal complexes containing halide ligands [21]. The complexes were further characterized in acetonitrile solution by UV/Vis spectroscopy. The spectra of (dppe)Ni(L)X ($L = Bm^R$, Tm^R; R = Me, Bu^t; X = Cl, Br) show intense charge-transfer bands at ca. 273 nm ($\varepsilon = 29.4$–$44.7 \times 10^3 M^{-1}\ cm^{-1}$), while those of the $Tm^{p\text{-Tol}}$ derivatives are red-shifted to 302 nm, presumably a consequence of the π influence of the aryl substituents. In addition, all the complexes also exhibit much weaker ($\varepsilon = 1700$–$2700\ M^{-1}\ cm^{-1}$) spin-allowed d–d transitions at ca. 505 nm. Significantly, the overall resemblance in the electronic absorption data for both the Bm^R and Tm^R series of compounds suggests that all the complexes have similar structures in solution (vide infra). The (dppe)Ni(L)X complexes were also characterized in the solid state using FT-IR spectroscopy and their IR spectra, obtained as KBr pellets, typically show several ν_{B-H} bands of medium and weak intensity in the approximate range 2050–2400 cm^{-1}. This situation reflects not only subtle differences in packing effects among similar compounds but also hints at the presence of both terminal and bridging B–H bonds, with the latter likely to be 3-center-2-electron Ni···H–B interactions of the type often seen in other Bm^R and, to a lesser degree, Tm^R complexes [15,22–29].

Despite all the analytical and spectroscopic data described above, the exact nature of the (dppe)Ni(L)X compounds remained uncertain. In particular, the coordination number of nickel and the overall geometry of the complexes could vary depending on the coordination mode of the specific Bm^R and Tm^R ligand (e.g., κ^3-*S*,*S*,*H* versus κ^3-*S*,*S*,*S*). In addition, the potential presence of the halides as counterions, rather than directly bound to nickel, would lead to the formation of cationic complexes. We envisioned that complete and unequivocal structural elucidation would only be derived from X-ray crystallography and therefore we set out to structurally characterize at least one representative for each of the Bm^R and Tm^R series of compounds.

2.2. Molecular structures of [(dppe)Ni(L)]Cl ($L = Bm^{Me}$, $Tm^{p\text{-Tol}}$)

Single crystals suitable for X-ray diffraction studies of [(dppe)Ni(Bm^{Me})]Cl and [(dppe)Ni($Tm^{p\text{-Tol}}$)]Cl were obtained at room temperature by slow diffusion of pentane into dichloromethane solutions of the complexes. Unexpectedly, both [(dppe)Ni(L)]Cl complexes are pentacoordinated and exhibit in the solid state molecular geometries that can be best described as distorted square pyramidal (Figs. 6 and 7), as reflected also in trigonality indexes (τ) of 0.24 and 0.21 for $L = Bm^{Me}$ and $Tm^{p\text{-Tol}}$, respectively. [1] Selected bond lengths and angles are given in Table 1. The nickel atom in [(dppe)Ni(Bm^{Me})]Cl is coordinated to the two phosphino groups of the chelating diphosphine and the two thione sulfurs of the [Bm^{Me}]$^-$ ligand, which also displays a pseudo-axial Ni···H–B interaction towards the metal center (vide infra). The structure of [(dppe)-Ni($Tm^{p\text{-Tol}}$)]Cl is analogous, except that the third mercaptoimidazolyl arm in the [$Tm^{p\text{-Tol}}$]$^-$ ligand is not

[1] The trigonality index $\tau = (\beta - \alpha)/60$, where β and α are the largest and second-largest interligand angles, has been used to estimate the degree of structural distortion from the ideal square pyramidal ($\tau = 0$) and trigonal bipyramidal ($\tau = 1$) geometries in five-coordinate complexes. See A.W. Addison, T.N. Rao, J. Reedijk, J. van Rijn, G.C. Verschoor, J. Chem. Soc., Dalton Trans. (1984) 1349.

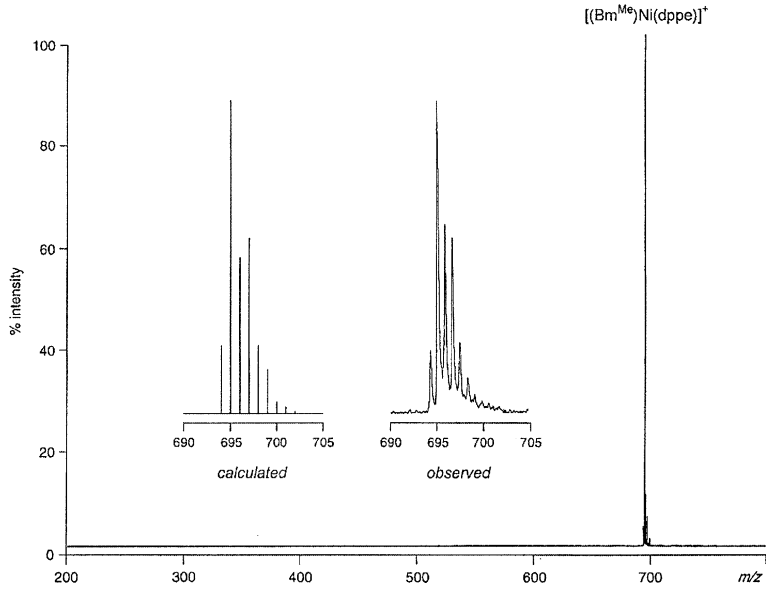

Fig. 5. Positive ion ESI mass spectrum (cone voltage = 90 V) of an acetonitrile solution of [(dppe)Ni(Bm^{Me})]Cl.

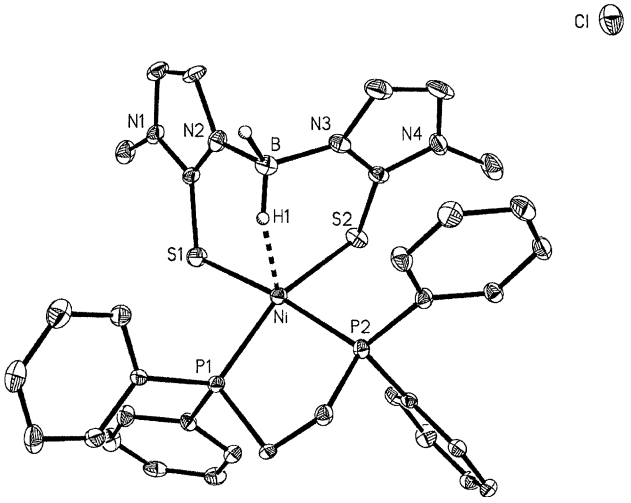

Fig. 6. Molecular structure of [(dppe)Ni(Bm^{Me})]Cl.

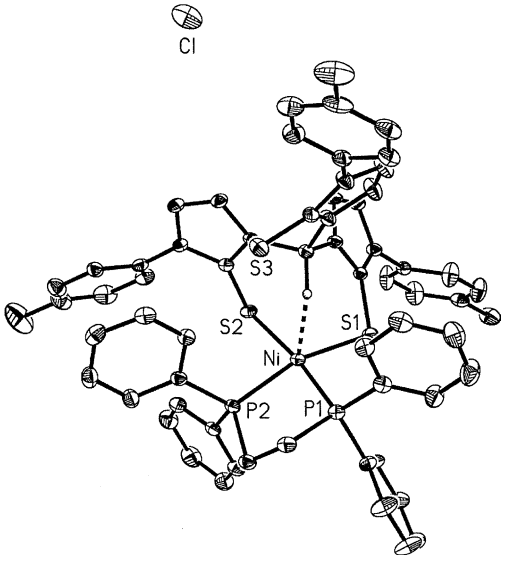

Fig. 7. Molecular structure of [(dppe)Ni($Tm^{p\text{-}Tol}$)]Cl.

bonded to the metal. Significantly, a search of the Cambridge Structural Database (CSD version 5.24, November 2002) [30] revealed that the [(dppe)Ni(L)]Cl complexes are the first structurally characterized five-coordinated nickel compounds having [NiP_2S_2H] cores. As such, they represent coordination environments that bear resemblance to those in certain species proposed to play a key role in the catalytic cycle of [NiFe] hydrogenases (e.g., those having [NiS_4H] cores) [31,32]. It is also worth noting that related examples of distorted square pyramidal Ni(II) complexes displaying [NiP_2S_2X] central moieties (X = Br, I) are known [33,34], as are some elegant dinuclear nickel–iron compounds containing [NiP_2S_2Cl] fragments [35,36] that have been prepared with the same goal in mind.

The Ni–S bond distances in both [(dppe)Ni(L)]Cl complexes, in the range 2.246(2) to 2.296(2) Å, are shorter than those observed in the distorted octahedral complexes Ni(Bm^{Me})$_2$ (2.362(2) and 2.390(2) Å) [15] and Ni(Tm^{Me})$_2$ (2.440(1)–2.483(1) Å) [19] a phenomenon that is likely to be a consequence of the lower coordination number in the square pyramidal derivatives. However, the average Ni–P bond length in the [(dppe)-Ni(L)]Cl complexes (2.168 Å) is virtually identical to the mean value found in the CSD for such bonds in a variety of dppe complexes of nickel (2.174 Å). The Ni···H distances in [(dppe)Ni(L)]Cl, 1.99(4) and 2.15(4) Å for L = Bm^{Me} and $Tm^{p\text{-}Tol}$, respectively, while slightly

Table 1
Selected bond lengths (Å) and bond angles (°) for [(dppe)Ni(L)]Cl

	$L = Bm^{Me}$	$L = Tm^{p\text{-}Tol}$
Bond lengths		
Ni–S(1)	2.246(2)	2.2591(13)
Ni–S(2)	2.270(2)	2.2962(13)
Ni–P(1)	2.166(2)	2.1746(14)
Ni–P(2)	2.156(2)	2.1743(13)
Ni–H(1)	1.99(6)	2.15(4)
Bond angles		
S(1)–Ni–S(2)	96.01(8)	98.20(5)
S(1)–Ni–P(1)	88.46(8)	90.11(5)
S(1)–Ni–P(2)	171.72(9)	158.92(5)
S(1)–Ni–H(1)	87.8(17)	81.6(9)
S(2)–Ni–P(1)	157.37(8)	171.69(5)
S(2)–Ni–P(2)	85.62(8)	85.77(5)
S(2)–Ni–H(1)	89.8(17)	85.3(10)
P(1)–Ni–P(2)	87.01(8)	86.44(5)
P(1)–Ni–H(1)	112.6(17)	96.0(10)
P(2)–Ni–H(1)	100.4(17)	119.4(9)

Table 2
Ni···H–B interactions in nickel(II) complexes

Complex	*d*(Ni···H) (Å)	Reference
$[(tren)Ni(NCBH_3)]_2(BPh_4)_2$	2.145(26)	[37]
$(PCy_3)_2Ni(BH_4)H$	1.73(5), 1.76(6)	[38]
$[(2,7\text{-}Me_2C_2B_9H_9)Ni(CO)]_2$	1.71	[39]
$Ni(Bm^{Me})_2$	1.863(9)	[15]
$Ni(Bm^{Bz})_2$	1.86(3), 1.91(3)	[18]
$Ni(Bp^{t\text{-}Bu})_2$	1.86(5)	[40]
$Ni(Bt^{Et,Me})_2$	1.81(3)–1.89(3)	[41]
$[(dppe)Ni(Bm^{Me})]Cl$	1.99(4)	this work
$[(dppe)Ni(Tm^{p\text{-}Tol})]Cl$	2.15(4)	this work
$(Tp^{Me2})Ni(BH_4)$	1.87(4)–1.94(7)	[42]

longer than those in $Ni(Bm^{Me})_2$ (1.863(9) Å) [15], are still comparable to the values observed in the limited number of structurally authenticated nickel(II) complexes presenting Ni···H–B interactions (Table 2) [37–42]. On the other hand, the latter are all clearly longer than the Ni–H bond lengths (ca. 1.37–1.65 Å) found in bona fide terminal hydride complexes of nickel [38, 43–46].

3. Conclusions

Two series of heteroleptic nickel(II) complexes, $[(dppe)Ni(Bm^R)]X$ and $[(dppe)Ni(Tm^R)]X$ (X = Cl, Br) have been readily prepared in high yield. The successful use of the thallium(I) compounds $Tl(Bm^R)$ and $Tl(Tm^R)$ as clean poly(mercaptoimidazolyl)borate ligand transfer reagents, as opposed to their sodium counterparts, demonstrates their value and applicability under certain reaction conditions. As established by X-ray diffraction studies, the square pyramidal complexes [(dppe)Ni(L)]X exhibit virtually identical coordination environments at the metal centers, including the presence of pseudo-axial Ni···H–B interactions, and they are the first examples of structurally characterized species having $[NiP_2S_2H]$ cores. Since Tm^R ligands, unlike their Bm^R counterparts, are capable of adopting a κ^3-*S*,*S*,*S* coordination mode, it is important to note that the preferred κ^3-*S*,*S*,*H* bonding scheme observed in all of these Ni(II) complexes, independently of the bulk of the R substituents, may stem from electronic rather than steric considerations. Reactivity studies of the cationic $[(dppe)Ni(L)]^+$ complexes towards a variety of nucleophiles and a more detailed investigation of the κ^3-*S*,*S*,*H* versus κ^2-*S*,*S* or κ^3-*S*,*S*,*S* binding modes often seen in poly(mercaptoimidazolyl)borate ligands are currently under way.

4. Experimental

4.1. General considerations

All reactions were performed in the air, solvents were purified and degassed by standard procedures, and all commercially available reagents were used as received. Whereas $Ni(dppe)X_2$ (X = Cl, Br) were synthesized as reported [20], the thallium reagents $Tl(Bm^R)$ and $Tl(Tm^R)$ were prepared following a combination of literature procedures [23,47,48]. ^1H NMR spectra were obtained on General Electric QE 300 or Varian Gemini (300 MHz) FT spectrometers. Chemical shifts (δ) are reported in parts per million relative to $SiMe_4$ ($\delta = 0$ ppm) and were referenced internally with respect to the solvent resonance (δ 2.49 ppm for d_5-DMSO); coupling constants are given in hertz (Hz). IR spectra were recorded as KBr pellets on a Thermo Mattson Satellite 3000 FT-IR spectrophotometer and are reported in cm^{-1}; relative intensities of the absorptions are indicated in parentheses (vs = very strong, s = strong, m = medium, w = weak). UV-Vis spectra were obtained using a Varian Cary 300 Bio spectrophotometer. Electrospray ionization mass spectra were obtained on a PerSeptive Biosystems Mariner ESI-TOF mass spectrometer by direct infusion using dilute acetonitrile solutions and a flow rate of 10 μL/min. Magnetic susceptibility measurements on solid samples were obtained using a Johnson Matthey magnetic susceptibility balance at room temperature and standard diamagnetic correction factors were applied to the data [49]. Elemental analyses were determined by Desert Analytics (Tucson, AZ) or Atlantic Microlab, Inc. (Norcross, GA).

4.2. Synthesis of $[(dppe)Ni(Bm^{Me})]Cl$

A stirred solution of $Ni(dppe)Cl_2$ (0.178 g, 0.337 mmol) in CH_2Cl_2 (10 mL) was treated with a suspension of $Tl(Bm^{Me})$ (0.150 g, 0.338 mmol) in the same solvent (20 mL), resulting in the formation of a purple-brown solution and a white precipitate (TlCl). The suspension was stirred for 15 min and filtered. Concentration of the

filtrate under reduced pressure to ca. 5 mL and addition of pentane (30 mL) resulted in the separation of a purple-brown solid, which was isolated by filtration and dried in vacuo for 18 h (0.178 g, 72%); m.p. = 170 °C (dec). ^{1}H NMR data (in d_6-DMSO): δ 3.16 (s, 6H, CH_3), 6.85 (br s, 4H, imidazole *H*), 7.3–8.3 (m, 20H, C_6H_5), CH_2 and H_2B not located. IR data (cm^{-1}): 2946 (w), 2401 (w), 2266 (w), 2115 (w), 1561 (m), 1551 (m), 1467 (m), 1435 (s), 1407 (w), 1384 (s), 1372 (s), 1323 (w), 1274 (m), 1202 (s), 1157 (w), 1122 (w), 1100 (s), 1027 (w), 998 (w), 815 (w), 747 (m), 715 (w), 691 (s), 530 (vs), 485 (m), 341 (m), 327 (w). UV/Vis [MeCN, λ_{max} (nm), $\varepsilon \times 10^{-3}$ (M^{-1} cm^{-1})]: 273 (43.5), 507 (1.8). *Anal.* Calc. for $C_{34}H_{36}BClN_4NiP_2S_2$: C, 55.8; H, 5.0; N, 7.7. Found: C, 55.4; H, 5.5; N, 6.8%.

4.3. Synthesis of [(dppe)Ni(Bm^{Me})]Br

A stirred solution of Ni(dppe)Br_2 (0.903 g, 1.461 mmol) in CH_2Cl_2 (10 mL) was treated with a suspension of Tl(Bm^{Me}) (0.649 g, 1.463 mmol) in the same solvent (20 mL), resulting in the formation of a purple solution and a white precipitate (TlBr). The suspension was stirred for 15 min and filtered. Concentration of the filtrate under reduced pressure to ca. 5 mL and addition of pentane (30 mL) resulted in the separation of a purple solid, which was isolated by filtration, washed with pentane (10 mL), and dried in vacuo for 18 h (1.126 g, 99%); m.p. = 138 °C (dec). ^{1}H NMR data (in d_6-DMSO): δ 3.16 (s, 6H, CH_3), 6.83 (s, 2H, imidazole *H*), 6.86 (s, 2H, imidazole *H*), 7.2–8.1 (m, 20H, C_6H_5), CH_2 and H_2B not located. IR data (cm^{-1}): 3050 (m), 3014 (w), 2983 (w), 2943 (w), 2400 (m), 2233 (m), 2196 (m), 2046 (w), 1584 (w), 1571 (w), 1555 (m), 1466 (s), 1435 (s), 1419 (w), 1388 (s), 1328 (w), 1306 (w), 1198 (s), 1157 (m), 1102 (s), 1011 (w), 1026 (w), 998 (w), 876 (m), 812 (m), 747 (m), 692 (s), 651 (w), 616 (w), 530 (s), 485 (m), 439 (w). UV/Vis [MeCN, λ_{max} (nm), $\varepsilon \times 10^{-3}$ (M^{-1} cm^{-1})]: 273 (29.4), 506 (2.0). *Anal.* Calc. for $C_{34}H_{36}BBrN_4NiP_2S_2$: C, 52.6; H, 4.7; N, 7.2. Found: C, 51.6; H, 4.8; N, 6.8%.

4.4. Synthesis of [(dppe)Ni(Bm$^{t\text{-}Bu}$)]Cl

A stirred solution of Ni(dppe)Cl_2 (0.150 g, 0.284 mmol) in CH_2Cl_2 (25 mL) was treated with a solution of Tl(Bm$^{t\text{-}Bu}$) (0.150 g, 0.284 mmol) in the same solvent (10 mL), resulting in the formation of a purple solution and a white precipitate (TlCl). The suspension was stirred for 15 min and filtered. Concentration of the filtrate under reduced pressure to ca. 5 mL and addition of pentane (30 mL) resulted in the separation of a purple solid, which was isolated by filtration and dried in vacuo for 3 h (0.214 g, 92%); m.p. = 147 °C (dec). ^{1}H NMR data (in d_6-DMSO): δ 1.37 [s, 18H, C(CH_3)$_3$], 6.97 (s, 2H, imidazole *H*), 7.00 (s, 2H, imidazole *H*), 7.2–8.0 (br s, 20H, C_6H_5), CH_2 and H_2B not located. IR data (cm^{-1}): 2973 (m), 2881 (w), 2408 (w), 2362 (m), 2343 (w), 2224 (m), 2080 (w), 1655 (w), 1561 (w), 1509 (w), 1481 (m), 1434 (m), 1402 (w), 1375 (vs), 1307 (m), 1260 (w), 1231 (w), 1194 (s), 1167 (w), 1149 (m), 1102 (s), 1068 (w), 1028 (w), 998 (w), 931 (w), 879 (w), 811 (w), 749(w), 713 (w), 692 (w), 529 (s), 485 (m), 355 (w). UV/Vis [MeCN, λ_{max} (nm), $\varepsilon \times 10^{-3}$ (M^{-1} cm^{-1})]: 273 (33.3), 295 (35.4), 509 (2.2). $\mu_{eff} = 3.1\ \mu_B$. *Anal.* Calc. for $C_{40}H_{48}BClN_4NiP_2S_2$: C, 58.9; H, 5.9; N, 6.9. Found: C, 58.0; H, 6.1; N, 6.6%.

4.5. Synthesis of [(dppe)Ni(Bm$^{t\text{-}Bu}$)]Br

A stirred solution of Ni(dppe)Br_2 (0.117 g, 0.189 mmol) in CH_2Cl_2 (10 mL) was treated with a solution of Tl(Bm$^{t\text{-}Bu}$) (0.100 g, 0.190 mmol) in the same solvent (20 mL), resulting in the formation of a purple solution and a white precipitate (TlBr). The suspension was stirred for 15 min and filtered. Concentration of the filtrate under reduced pressure to ca. 5 mL and addition of pentane (30 mL) resulted in the separation of a purple solid, which was isolated by filtration and dried in vacuo for 18 h (0.153 g, 94%); m.p. = 169 °C (dec). ^{1}H NMR data (in d_6-DMSO): δ 1.37 [s, 18H, C(CH_3)$_3$], 6.96 (s, 2H, imidazole *H*), 7.00 (s, 2H, imidazole *H*), 7.2–8.0 (br s, 20H, C_6H_5), CH_2 and H_2B not located. IR data (cm^{-1}): 2974 (m), 2934 (w), 2881 (w), 2408 (m), 2345 (w), 2227 (m), 2083 (w), 1561 (w), 1480 (m), 1434 (s), 1418 (w), 1402 (w), 1375 (vs), 1307 (w), 1259 (w), 1231 (w), 1194 (s), 1167 (w), 1102 (s), 1066 (w), 1029 (w), 998 (w), 878 (w), 812 (m), 748 (m), 713 (s), 691(s), 651 (w), 529 (s), 485 (m), 354 (m), 342 (m). UV/Vis [MeCN, λ_{max} (nm), $\varepsilon \times 10^{-3}$ (M^{-1} cm^{-1})]: 272 (44.7), 509 (1.8). *Anal.* Calc. for $C_{40}H_{48}BBrN_4NiP_2S_2$: C, 55.8; H, 5.6; N, 6.5. Found: C, 54.8; H, 5.9; N, 5.9%.

4.6. Synthesis of [(dppe)Ni(Tm^{Me})]Cl

A stirred solution of Ni(dppe)Cl_2 (0.128 g, 0.242 mmol) in CH_2Cl_2 (20 mL) was treated with a suspension of Tl(Tm^{Me}) (0.135 g, 0.243 mmol) in the same solvent (50 mL), resulting in the formation of a carmine solution and a white precipitate (TlCl). The suspension was stirred for 15 min and filtered. Concentration of the filtrate under reduced pressure to ca. 5 mL and addition of pentane (30 mL) resulted in the separation of a carmine solid, which was isolated by filtration and dried in vacuo for 1 h (0.158 g, 77%); m.p. = 165 °C (dec). ^{1}H NMR data (in d_6-DMSO): δ 3.07 (br s, 9H, CH_3), 7.08 (s, 3H, imidazole *H*), 7.2–7.9 (m, 23H, imidazole *H* + C_6H_5), CH_2 and *H*B not located. IR data (cm^{-1}): 3054 (w), 3007 (w), 2981 (w), 2360 (w), 2335 (w), 2271 (w), 1559 (w), 1466 (m), 1436 (s), 1406 (w), 1387 (m), 1372 (m), 1324 (w), 1273 (w), 1204 (s), 1158 (w), 1125 (w), 1100 (s), 1025 (w), 988

(w), 875 (w), 817 (w), 803 (w), 748 (m), 715 (m), 692 (m), 668(w), 614 (w), 530 (vs), 484 (w), 473 (w), 419 (w). UV/Vis [MeCN, λ_{max} (nm), $\varepsilon \times 10^{-3}$ (M^{-1} cm^{-1})]: 266 (29.8), 504 (1.7). $\mu_{eff} = 3.2$ μ_B. *Anal.* Calc. for $C_{38}H_{40}BClN_6NiP_2S_3$: C, 54.1; H, 4.8; N, 10.0. Found: C, 53.3; H, 4.9; N, 9.9%.

4.7. Synthesis of [(dppe)Ni(Tm^{Me})]Br

A stirred solution of Ni(dppe)Br_2 (0.167 g, 0.270 mmol) in CH_2Cl_2 (12 mL) was treated with a suspension of Tl(Tm^{Me}) (0.150 g, 0.270 mmol) in the same solvent (10 mL), resulting in the formation of a carmine solution and a white precipitate (TlBr). The suspension was stirred for 15 min and filtered. Concentration of the filtrate under reduced pressure to ca. 5 mL and addition of pentane (30 mL) resulted in the separation of a carmine solid, which was isolated by filtration and dried in vacuo for 18 h (0.182 g, 76%); m.p. = 169 °C (dec). ^{1}H NMR data (in d_6-DMSO): δ 3.10 (br s, 9H, CH_3), 7.08 (s, 3H, imidazole *H*), 7.36 (s, 3H, imidazole *H*), 7.4–7.9 (m, 20H, C_6H_5), CH_2 and *H*B not located. IR data (cm^{-1}): 3049 (m), 3006 (w), 2367 (w), 2344 (w), 2268 (w), 1560 (w), 1466 (m), 1435 (s), 1407 (w), 1385 (s), 1323 (w), 1273 (m), 1203 (vs), 1157 (w), 1123 (w), 1100 (s), 1027 (w), 997 (w), 816 (w), 747 (m), 715 (w), 702 (w), 691 (s), 530 (vs), 485 (m). UV/Vis [MeCN, λ_{max} (nm), $\varepsilon \times 10^{-3}$ (M^{-1} cm^{-1})]: 273 (34.3), 502 (2.4). *Anal.* Calc. for $C_{38}H_{40}BBrN_6NiP_2S_3$: C, 51.4; H, 4.5; N, 9.5. Found: C, 51.1; H, 4.5; N, 9.1%.

4.8. Synthesis of [(dppe)Ni($Tm^{t\text{-}Bu}$)]Cl

A stirred solution of Ni(dppe)Cl_2 (0.105 g, 0.199 mmol) in CH_2Cl_2 (17 mL) was treated with a solution of Tl($Tm^{t\text{-}Bu}$) (0.135 g, 0.198 mmol) in the same solvent (10 mL), resulting in the formation of a deep purple solution and a white precipitate (TlCl). The suspension was stirred for 15 min and filtered. Concentration of the filtrate under reduced pressure to ca. 5 mL and addition of pentane (30 mL) resulted in the separation of a deep purple solid, which was isolated by filtration and dried in vacuo for 18 h (0.164 g, 85%); m.p. = 134 °C (dec). ^{1}H NMR data (in d_6-DMSO): δ 1.45 [br s, 27H, C(CH_3)$_3$], 7.19 (s, 3H, imidazole *H*), 7.2–7.8 (m, 23H, imidazole $H + C_6H_5$), CH_2 and *H*B not located. IR data (cm^{-1}): 3051 (w), 2965 (m), 2926 (w), 2366 (w), 2222 (w), 1727 (w), 1570 (w), 1482 (w), 1434 (m), 1402 (m), 1363 (s), 1307 (w), 1261 (m), 1192 (m), 1165 (m), 1100 (m), 1028 (w), 998 (w), 930 (w), 879 (w), 820 (w), 794 (w), 746 (m), 714 (m), 691 (m), 617 (w), 598 (w), 562 (w), 529 (m), 483 (m), 440 (w). UV/Vis [MeCN, λ_{max} (nm), $\varepsilon \times 10^{-3}$ (M^{-1} cm^{-1})]: 275 (34.8), 506 (2.0). *Anal.* Calc. for $C_{47}H_{58}BClN_6NiP_2S_3$: C, 58.2; H, 6.0; N, 8.7. Found: C, 57.6; H, 6.2; N, 8.8%.

4.9. Synthesis of [(dppe)Ni($Tm^{t\text{-}Bu}$)]Br

A stirred solution of Ni(dppe)Br_2 (0.122 g, 0.197 mmol) in CH_2Cl_2 (12 mL) was treated with a solution of Tl($Tm^{t\text{-}Bu}$) (0.135 g, 0.198 mmol) in the same solvent (10 mL), resulting in the formation of a deep purple solution and a white precipitate (TlBr). The suspension was stirred for 15 min and filtered. Concentration of the filtrate under reduced pressure to ca. 5 mL and addition of pentane (30 mL) resulted in the separation of a deep purple solid, which was isolated by filtration and dried in vacuo for 18 h (0.191 g, 96%); m.p. = 154 °C (dec). ^{1}H NMR data (in d_6-DMSO): δ 1.46 [s, 27H, C(CH_3)$_3$], 7.20 (s, 3H, imidazole *H*), 7.2–7.8 (m, 23H, imidazole $H + C_6H_5$), CH_2 and *H*B not located. IR data (cm^{-1}): 3050 (w), 2974 (m), 2925 (w), 2368 (w), 2222 (w), 1570 (w), 1482 (w), 1435 (m), 1403 (w), 1364 (s), 1307 (w), 1261 (m), 1227 (w), 1190 (m), 1165 (m), 1100 (m), 1028 (w), 998 (w), 931 (w), 879 (w), 819 (w), 794 (w), 747 (w), 713 (m), 691 (m), 617 (w), 599 (w), 529 (s), 482 (m), 440 (w). UV/Vis [MeCN, λ_{max} (nm), $\varepsilon \times 10^{-3}$ (M^{-1} cm^{-1})]: 275 (33.6), 509 (2.0). *Anal.* Calc. for $C_{47}H_{58}BBrN_6NiP_2S_3$: C, 55.6; H, 5.8; N, 8.3. Found: C, 55.6; H, 5.4; N, 7.1%.

4.10. Synthesis of [(dppe)Ni($Tm^{p\text{-}Tol}$)]Cl

A stirred solution of Ni(dppe)Cl_2 (0.149 g, 0.282 mmol) in CH_2Cl_2 (20 mL) was treated with a suspension of Tl($Tm^{p\text{-}Tol}$) (0.222 g, 0.283 mmol) in the same solvent (15 mL), resulting in the formation of a brown-purple solution and a white precipitate (TlCl). The suspension was stirred for 15 min and filtered. Concentration of the filtrate under reduced pressure to ca. 5 mL and addition of pentane (30 mL) resulted in the separation of a deep purple solid, which was isolated by filtration and dried in vacuo for 2 h (0.241 g, 80%); m.p. = 159 °C (dec). ^{1}H NMR data (in d_6-DMSO): δ 2.35 (s, 9H, CH_3), 6.8–7.9 (m, 38H, imidazole $H + C_6H_5 + C_6H_4$Me), CH_2 and *H*B not located. IR data (cm^{-1}): 3138 (w), 3049 (w), 2919 (m), 2852 (w), 2367 (w), 2345 (w), 1610 (w), 1515 (vs), 1483 (w), 1435 (m), 1413 (m), 1348 (s), 1303 (m), 1245 (w), 1178 (s), 1101 (s), 1023 (w), 998 (w), 955 (w), 878 (w), 818 (m), 747 (m), 713 (s), 7691 (s), 615 (w), 577 (w), 564 (w), 529 (m), 484 (w). UV/Vis [MeCN, λ_{max} (nm), $\varepsilon \times 10^{-3}$ (M^{-1} cm^{-1})]: 302 (36.1), 502 (2.5). $\mu_{eff} = 3.2$ μ_B. *Anal.* Calc. for $C_{56}H_{52}BClN_6NiP_2S_3$: C, 62.7; H, 4.9; N, 7.8. Found: C, 61.5; H, 5.1; N, 7.8%.

4.11. Synthesis of [(dppe)Ni($Tm^{p\text{-}Tol}$)]Br

A stirred solution of Ni(dppe)Br_2 (0.200 g, 0.324 mmol) in CH_2Cl_2 (15 mL) was treated with a suspension of Tl($Tm^{p\text{-}Tol}$) (0.254 g, 0.324 mmol) in the same solvent (15 mL), resulting in the formation of a carmine solution and a white precipitate (TlBr). The suspension was

Table 3
Crystallographic data for [(dppe)Ni(L)]Cl

	$L = Bm^{Me}$	$L = Tm^{p\text{-Tol}}$
Formula	$C_{39}H_{48}BClN_4NiP_2S_2$	$C_{56}H_{52}BClN_6NiP_2S_3 \cdot CH_2Cl_2$
Formula weight	803.84	1157.05
Crystal system	monoclinic	monoclinic
Space group	$C2/c$ (no. 15)	$C2/c$ (no. 15)
Temperature (K)	243(2)	243(2)
Unit cell dimensions		
a (Å)	24.938(6)	32.003(3)
b (Å)	22.684(6)	13.722(1)
c (Å)	13.462(3)	28.730(2)
β (°)	112.346(4)	117.382(1)
V (Å^3)	7043(3)	11203(2)
Z	8	8
ρ (calculated) (g cm^{-3})	1.516	1.372
μ (Mo Kα) (mm^{-1})	0.874	0.702
θ_{max} (°)	28.21	28.33
Number of data	7092	12934
Number of parameters	426	653
R_1 ($I > 2\sigma(I)$)[a]	0.0649	0.0643
wR_2 ($I > 2\sigma(I)$)[a]	0.1173	0.1510

[a] $R_1 = \sum(|F_o| - |F_c|)/\sum F_o|$; $wR_2 = \{\sum[w(F_o^2 - F_c^2)^2]/\sum[w(F_o^2)^2]\}^{1/2}$.

stirred for 15 min and filtered. Concentration of the filtrate under reduced pressure to ca. 5 mL and addition of pentane (30 mL) resulted in the separation of a deep purple solid, which was isolated by filtration and dried in vacuo for 3 h (0.330 g, 91%); m.p. = 159 °C (dec). ^{1}H NMR data (in d_6-DMSO): δ 2.35 (s, 9H, CH_3), 6.8–7.9 (m, 38H, imidazole H + C$_6H_5$ + C$_6H_4$Me), CH_2 and HB not located. IR data (cm^{-1}): 3048 (m), 2361 (m), 2340 (m), 1584 (w), 1560 (w), 1514 (vs), 1483 (w), 1434 (m), 1413 (m), 1348 (m), 1303 (m), 1246 (w), 1177 (m), 1101 (m), 1023 (w), 998 (w), 959 (w), 879 (w), 818 (m), 747 (w), 713 (m), 691 (m), 577 (w), 563 (w), 529 (s), 484 (m). UV/Vis [MeCN, λ_{max} (nm), $\varepsilon \times 10^{-3}$ (M^{-1} cm^{-1})]: 302 (38.4), 504 (2.7). *Anal.* Calc. for $C_{56}H_{52}BBrN_6NiP_2S_3$: C, 60.2; H, 4.7; N, 7.5. Found: C, 60.4; H, 5.0; N, 7.6%.

4.12. X-ray structure determinations

X-ray diffraction data were collected on a Bruker P4 diffractometer using Mo Kα radiation ($\lambda = 0.71073$ Å) and equipped with a SMART CCD detector. A summary of crystal data collection and refinement parameters for [(dppe)Ni(L)]Cl ($L = Bm^{Me}$, $Tm^{p\text{-Tol}}$) is given in Table 3. The structures were solved using direct methods and standard difference map techniques, and were refined by full-matrix least-squares procedures on F^2 using SHELXTL (version 6.10) [50]. Hydrogen atoms on carbon were included in calculated positions.

5. Supplementary data

Crystallographic data (excluding structure factors) for [(dppe)Ni(L)]Cl ($L = Bm^{Me}$, $Tm^{p\text{-Tol}}$) have been deposited with the Cambridge Crystallographic Data Centre with CCDC No. 212127 and 212128, respectively. Copies of this information may be obtained free of charge from The Director, CCDC, 12 Union Road, Cambridge CB2 1EZ, UK (fax: +44-1223-336033; e-mail: deposit@ccdc.cam.ac.uk http://www.ccdc.cam.ac.uk).

Acknowledgements

We thank the Camille and Henry Dreyfus Foundation, Inc. for a Henry Dreyfus Teacher-Scholar Award to D.R., Research Corporation for a Cottrell College Science Award, the donors of the Petroleum Research Fund, administered by the American Chemical Society, and The University of North Carolina at Charlotte for support of this research. H.M.A. is particularly grateful to the Thomas D. Walsh Tuition Fellowship for financial assistance and we also thank Professor Pat Desrochers (University of Central Arkansas) for his communication of results prior to publication.

References

[1] S. Trofimenko, Scorpionates: The Coordination Chemistry of Polypyrazolylborate Ligands, Imperial College Press, London, 1999.
[2] A.P. Sadimenko, Adv. Heterocyclic Chem. 81 (2001) 167.
[3] M. Akita, S. Hikichi, Bull. Chem. Soc. Jpn. 75 (2002) 1657.
[4] D.L. Reger, Comments Inorg. Chem. 21 (1999) 1.
[5] H.W. Yim, L.M. Tran, E.D. Dobbin, D. Rabinovich, L.M. Liable-Sands, C.D. Incarvito, K.-C. Lam, A.L. Rheingold, Inorg. Chem. 38 (1999) 2211.
[6] P. Ge, B.S. Haggerty, A.L. Rheingold, C.G. Riordan, J. Am. Chem. Soc. 116 (1994) 8406.

[7] C. Ohrenberg, P. Ge, P. Schebler, C.G. Riordan, G.P.A. Yap, A.L. Rheingold, Inorg. Chem. 35 (1996) 749.
[8] M. Garner, J. Reglinski, I. Cassidy, M.D. Spicer, A.R. Kennedy, Chem. Commun. (1996) 1975.
[9] J.C. Peters, J.D. Feldman, T.D. Tilley, J. Am. Chem. Soc. 121 (1999) 9871.
[10] A.A. Barney, A.F. Heyduk, D.G. Nocera, Chem. Commun. (1999) 2379.
[11] C. Kimblin, T. Hascall, G. Parkin, Inorg. Chem. 36 (1997) 5680.
[12] C. Kimblin, B.M. Bridgewater, D.G. Churchill, G. Parkin, Chem. Commun. (1999) 2301.
[13] B.M. Bridgewater, G. Parkin, Inorg. Chem. Commun. 4 (2001) 126.
[14] M. Tesmer, M. Shu, H. Vahrenkamp, Inorg. Chem. 40 (2001) 4022.
[15] H.M. Alvarez, M. Krawiec, B.T. Donovan-Merkert, M. Fouzi, D. Rabinovich, Inorg. Chem. 40 (2001) 5736.
[16] M. Frey, Chem. Biochem 3 (2002) 153.
[17] M.A. Halcrow, Angew. Chem. Int. Ed. Engl. 34 (1995) 1193.
[18] H.M. Alvarez, D. Rabinovich, unpublished results.
[19] M. Garner, K. Lewinski, A. Pattek-Janczyk, J. Reglinski, B. Sieklucka, M.D. Spicer, M. Szaleniec, Dalton Trans. (2003) 1181.
[20] G.R. Van Hecke, W.D. Horrocks Jr., Inorg. Chem. 5 (1966) 1968.
[21] W. Henderson, C. Evans, Inorg. Chim. Acta 294 (1999) 183.
[22] C. Santini, G. Gioia Lobbia, C. Pettinari, R. Spagna, M. Pellei, F. Vallorani, Inorg. Chim. Acta 285 (1999) 81.
[23] C. Kimblin, B.M. Bridgewater, G. Parkin, J. Chem. Soc., Dalton Trans. (2000) 891.
[24] R. Garcia, A. Paulo, A. Domingos, I. Santos, K. Ortner, R. Alberto, J. Am. Chem. Soc. 122 (2000) 11240.
[25] G. Gioia Lobbia, C. Pettinari, C. Santini, N. Somers, B.W. Skelton, A.H. White, Inorg. Chim. Acta 319 (2001) 15.
[26] C. Kimblin, D.G. Churchill, B.M. Bridgewater, J.N. Girard, D.A. Quarless, G. Parkin, Polyhedron 20 (2001) 1891.
[27] B.M. Bridgewater, G. Parkin, Inorg. Chem. Commun. 3 (2000) 534.
[28] R. Garcia, Y.-H. Xing, A. Paulo, A. Domingos, I. Santos, J. Chem. Soc., Dalton Trans. (2002) 4236.
[29] H.M. Alvarez, T.B. Tran, M.A. Richter, D.M. Alyounes, D. Rabinovich, J.M. Tanski, M. Krawiec, Inorg. Chem. 42 (2003) 2149.
[30] F.H. Allen, Acta Crystallogr. B 58 (2002) 380.
[31] H.-J. Fan, M.B. Hall, J. Biol. Inorg. Chem. 6 (2001) 467.
[32] A.C. Marr, D.J.E. Spencer, M. Schröder, Coord. Chem. Rev. 219–221 (2001) 1055.
[33] K. Aurivillius, G.-I. Bertinsson, Acta Crystallogr. B 36 (1980) 790.
[34] G.-I. Bertinsson, Acta Crystallogr. C 39 (1983) 698.
[35] S.C. Davies, D.J. Evans, D.L. Hughes, S. Longhurst, J.R. Sanders, Chem. Commun. (1999) 1935.
[36] M.C. Smith, J.E. Barclay, S.P. Cramer, S.C. Davies, W.-W. Gu, D.L. Hughes, S. Longhurst, D.J. Evans, J. Chem. Soc., Dalton Trans. (2002) 2641.
[37] B.G. Segal, S.J. Lippard, Inorg. Chem. 16 (1977) 1623.
[38] T. Saito, M. Nakajima, A. Kobayashi, Y. Sasaki, J. Chem. Soc., Dalton Trans. (1978) 482.
[39] N. Carr, D.F. Mullica, E.L. Sappenfield, F.G.A. Stone, Inorg. Chem. 33 (1994) 1666.
[40] T.R. Belderraín, M. Paneque, E. Carmona, E. Gutiérrez-Puebla, M.A. Monge, C. Ruiz-Valero, Inorg. Chem. 41 (2002) 425.
[41] R. Cammi, M. Lanfranchi, L. Marchiò, C. Mora, C. Paiola, M.A. Pellinghelli, Inorg. Chem. 42 (2003) 1769.
[42] P.J. Desrochers, 2002, personal communication.
[43] L. Sacconi, A. Orlandini, S. Midollini, Inorg. Chem. 13 (1974) 2850.
[44] U. Müller, W. Keim, C. Krüger, P. Betz, Angew. Chem. Int. Ed. Engl. 28 (1989) 1011.
[45] M. Aresta, E. Quaranta, A. Dibenedetto, P. Giannoccaro, I. Tommasi, M. Lanfranchi, A. Tiripicchio, Organometallics 16 (1997) 834.
[46] P.L. Holland, M.E. Smith, R.A. Andersen, R.G. Bergman, J. Am. Chem. Soc. 119 (1997) 12815.
[47] H.M. Alvarez, P.A. Gillespie, C.D. Gause, A.L. Rheingold, J.A. Golen, D. Rabinovich, Polyhedron 23 (2004), in press.
[48] J.F. Ojo, P.A. Slavin, J. Reglinski, M. Garner, M.D. Spicer, A.R. Kennedy, S.J. Teat, Inorg. Chim. Acta 313 (2001) 15.
[49] Z. Szafran, R.M. Pike, M.M. Singh, Microscale Inorganic Chemistry, Wiley, New York, 1991, pp. 49–57.
[50] G.M. Sheldrick, SHELXTL, An Integrated System for Solving, Refining and Displaying Crystal Structures from Diffraction Data, University of Göttingen, Göttingen, Germany, 1981.

Available online at www.sciencedirect.com
SCIENCE DIRECT®
Polyhedron 23 (2004) 405–412
POLYHEDRON
www.elsevier.com/locate/poly

Tris(imidazolyl) cadmium and zinc complexes: structural and spectroscopic characterization of M–OH_2 motifs

Janis K. Voo, Christopher D. Incarvito, Glenn P.A. Yap, Arnold L. Rheingold, Charles G. Riordan *

Department of Chemistry and Biochemistry, University of Delaware, Newark, DE 19716, USA

Received 12 June 2003; accepted 6 September 2003

Dedicated to Jerry Trofimenko, colleague and friend, for his contributions to tripodal coordination chemistry

Abstract

The tris(imidazolyl) cavitand ligand, 1,3,5-triethyl-2,4,6-tris[*N*-methyl-imidazol-2-yl-thiomethyl]benzene, TriMIm, is used to prepare monomeric aqua complexes of cadmium and zinc with the general formula, $[(TriMIm)M(OH_2)]X_2$ ($M = Cd$, $X = BF_4$; $M = Zn$, $X = BF_4$ or NO_3). The molecular structures of each species are characterized by trigonal pyramidal metal ion coordination and hydrogen-bonding between the bound water molecule and the non-coordinating counter ions. The binuclear zinc hydroxo-bridged complex, $[\{(TriMIm)Zn\}_2(\mu\text{-}OH)](BF_4)_3$, has been characterized by X-ray diffraction methods.
© 2003 Elsevier Ltd. All rights reserved.

1. Introduction

The tris(pyrazolyl)hydroborato ligand, $[Tp^{R,R'}]$, developed by Jerry Trofimenko more than 35 years ago [1,2] has found great utility as a scaffold for modeling a number of important metallobiochemistry motifs [2–4]. The tripodal $[N_3]$ donor environment of the ligand mimics the nitrogen-rich ligation sphere found at the active site of numerous non-heme proteins. Leading examples include Kitajima's dicopper peroxo complex [5], $[(Tp^{2iPr})Cu]_2(O_2)$ and Parkin's and Vahenkamp's $[Tp^{R,R'}]Zn(OH)$ species [6]. The former was prepared and authenticated as a structural and spectroscopic precedent of the oxygenated form of the O_2-binding protein hemocyanin in advance of evidence of such $\mu\text{-}\eta^2\text{:}\eta^2\text{-}O_2$ coordination at the protein active site [7]. The mononuclear zinc hydroxide species provided the opportunity to assess the inherent nucleophilicity, and more recently, basicity [8] of a $[N_3]Zn(OH)$ species. Inherent in each of these examples is the utility of systematic variation of the pyrazole substituents in controlling structure and reactivity at the attendant metal complexes, clearly one of the strengths of the [Tp] ligand family.

Recently, we have prepared a new tris(imidazolyl)-based cavitand ligand and reported aspects of its coordination chemistry with copper(I) [9]. The ligand, TriMIm, [1] is preorganized to ligate a single metal ion in a trigonal planar array of imidazoles. The enforced geometry is distinct from the [Tp] ligands where more acute N–M–N angles are observed. Herein, we report the synthesis and structural characterization of cadmium- and zinc-aqua complexes, $[(TriMIm)M(OH_2)]^{2+}$.

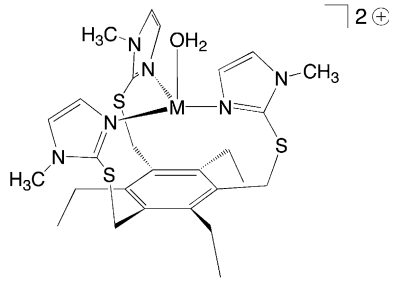

$[(TriMIm)M(OH_2)]^{2+}$

* Corresponding author.
E-mail address: riordan@udel.edu (C.G. Riordan).

[1] *Abbreviation:* TriMIm, 1,3,5-triethyl-2,4,6-tris[*N*-methyl-imidazol-2-yl-thiomethyl]benzene.

0277-5387/$ - see front matter © 2003 Elsevier Ltd. All rights reserved.
doi:10.1016/j.poly.2003.11.006

2. Experimental

2.1. Materials

2-Mercapto-1-methylimidazole, NaH, $MgSO_4$, $Cd(BF_4)_2 \cdot 6H_2O$, $Cd(NO_3)_2 \cdot 4H_2O$, $Zn(BF_4)_2 \cdot xH_2O$, and $Zn(NO_3)_2 \cdot 6H_2O$ were used as supplied by commercial vendors. $[Cu(MeCN)_4]BF_4$ [10], and TriMIm [9] were prepared according to literature procedures. Pentanes, tetrahydrofuran, and diethyl ether were freshly distilled from sodium/benzophenone. Methylene chloride was freshly distilled from calcium hydride. Acetone was freshly distilled over $MgSO_4$. Acetonitrile (UV Grade) was purchased from Burdick and Jackson and stored over 4 Å molecular sieves and stored under N_2. Deuterated solvents were purchased from Cambridge Isotope Laboratories, dried over 4 Å molecular sieves and stored under N_2.

2.2. Physical methods

Proton and carbon NMR spectra were recorded either on a Bruker AC-250, AM-250, or DRX-400 NMR spectrometer. Chemical shifts were referenced to the residual protio solvent signal. Chemical shifts are quoted in δ (ppm) and coupling constants in Hz. Infrared spectra were recorded on a Mattson Genesis Series FT-IR spectrophotometer under dinitrogen purge at ambient temperature, unless stated otherwise. FT-IR samples were prepared as KBr pellets. Melting points were determined with a Melt-Temp melting point determination apparatus and are reported uncorrected. Elemental analyses (C, H, N) were performed by Desert Analytics, Inc., Tucson, AZ.

2.3. Synthesis of [(TriMIm)Cd(OH_2)](BF_4)$_2$ (**1**)

To a stirred solution of $Cd(BF_4)_2 \cdot 6H_2O$ (196 mg, 0.5 mmol) in distilled water, 0.5 ml, was added a solution of TriMIm (272 mg, 0.5 mmol) in acetone, 3 ml, at ambient temperature. The colorless solution was stirred overnight during which time it turned cloudy. Removal of volatiles under reduced pressure followed by extraction into acetonitrile, 1 ml, and filtration through Celite gave a colorless solution. Removal of solvent under reduced pressure yielded a white solid, which was collected on a glass frit and washed with diethyl ether and pentanes. Yield: 200 mg, 48%. Mp (dec.) 296–300 °C. ^{1}H NMR (250 MHz, CD_3CN, 298 K): δ 0.9 (t, 9H, ^3J(HH) 7.5 Hz, CH_2CH_3), 1.1 (m, 3H, CH_2CH_3), 2.1 (m, 3H, CH_2CH_3), 3.7 (d, 3H, ^2J(HH) 15 Hz, SCH_2), 4.0 (s, 9H, NCH_3), 4.2 (d, 3H, ^2J(HH) 15 Hz, SCH_2), 7.1 (d, 3H, ^3J(HH) 1.5 Hz, {CN(Me)C*H*CHN}), 7.6 (d, 3H, ^3J(HH) 1.5 Hz, {CN(Me)CHC*H*N}). ^{13}C{^{1}H} NMR (100 MHz, CD_3CN, 298 K): δ 15.6, 21.9, 34.1, 36.4, 127.5, 131.0, 133.2, 141.4, 143.8. FT-IR (KBr) $\upsilon_{OH} = 3475$ and 3530 cm^{-1}. *Anal.* Calc. for $C_{27}H_{38}N_6S_3OCdB_2F_8$: C, 38.4; H, 4.53; N, 9.95. Found: C, 38.7; H, 4.36; N, 10.0%.

2.4. Synthesis of [(TriMIm)Cd($NCCH_3$)](BF_4)$_2$ (**2**)

To a stirred solution of $Cd(BF_4)_2 \cdot 6H_2O$ (374 mg, 0.95 mmol) in distilled water, 0.8 ml, was added a solution of TriMIm (515 mg, 0.95 mmol) in acetonitrile, 5 ml, at ambient temperature. The colorless solution was stirred overnight. Removal of volatiles under reduced pressure followed by extraction into acetonitrile, 10 ml, and filtration through Celite gave a colorless solution. Removal of solvent under reduced pressure yielded a white solid, which was collected on a glass frit and washed with diethyl ether and pentanes. Yield: 500 mg, 61%. Mp, 252–256 °C. ^{1}H NMR (250 MHz, CD_3CN, 298 K): δ 0.9 (t, 9H, ^3J(HH) 7.5 Hz, CH_2CH_3), 1.1 (m, 3H, CH_2CH_3), 1.9 (s, 3H, $NCCH_3$), 2.1 (m, 3H, CH_2CH_3), 3.7 (d, 3H, ^2J(HH) 15 Hz, SCH_2), 4.0 (s, 9H, NCH_3), 4.2 (d, 3H, ^2J(HH) 14 Hz, SCH_2), 7.1 (d, 3H, ^3J(HH) 2.0 Hz, {CN(Me)C*H*CHN}), 7.6 (d, 3H, ^3J(HH) 2.0 Hz, {CN(Me)CHC*H*N}). ^{13}C{^{1}H} NMR (100 MHz, CD_3CN, 298 K): δ 15.6, 21.9, 34.1, 36.5, 127.5, 131.0, 133.2, 141.4, 143.8. FT-IR (KBr) $\upsilon_{CN} = 2286$ cm^{-1}. *Anal.* Calc. for $C_{29}H_{39}N_7S_3CdB_2F_8$: C, 40.1; H, 4.53; N, 11.3. Found: C, 40.0; H, 4.57; N, 11.4%.

2.5. Synthesis of [(TriMIm)Cd(ONO_2)](NO_3) (**3**)

To a stirred solution of $Cd(NO_3)_2 \cdot 4H_2O$ (118 mg, 0.38 mmol) in acetonitrile, 20 ml, was added a solution of TriMIm (213 mg, 0.39 mmol) in acetonitrile, 5 ml, at ambient temperature. The colorless solution was stirred overnight. Filtration through Celite and removal of volatiles under reduced pressure yielded a white solid, which was collected on a glass frit and washed with diethyl ether and pentanes. Yield: 210 mg, 68%. Mp, 202–206 °C. ^{1}H NMR (250 MHz, CD_3CN, 298 K): δ 0.9 (t, 9H, ^3J(HH) 7.3 Hz, CH_2CH_3), 1.1 (m, 3H, CH_2CH_3), 2.0 (m, 3H, CH_2CH_3), 3.7 (d, 3H, ^2J(HH) 14 Hz, SCH_2), 4.0 (s, 9H, NCH_3), 4.2 (d, 3H, ^2J(HH) 14 Hz, SCH_2), 7.1 (d, 3H, ^3J(HH) 1.5 Hz, {CN(Me)C*H*CHN}), 7.5 (d, 3H, ^3J(HH) 1.5 Hz, {CN(Me)CHC*H*N}). ^{13}C{^{1}H} NMR (62.5 MHz, CD_3CN, 298 K): δ 15.8, 21.6, 34.2, 36.2, 126.8, 131.6, 132.6, 140.8, 142.4. *Anal.* Calc. for $C_{27}H_{36}N_8S_3O_6Cd$: C, 41.7; H, 4.67; N, 14.4. Found: C, 41.1; H, 4.73; N, 13.5%.

2.6. Synthesis of [(TriMIm)Zn(OH_2)](BF_4)$_2$ (**4**)

To a stirred solution of $Zn(BF_4)_2 \cdot xH_2O$ (133 mg, 0.56 mmol) in distilled water, 0.5 ml, was added a solution of TriMIm (300 mg, 0.56 mmol) in methylene chloride, 8 ml, at ambient temperature. The colorless

solution was stirred overnight during which time it turned cloudy gradually. Removal of volatiles under reduced pressure followed by extraction into acetonitrile, 2 ml, and filtration through Celite gave a colorless solution. Removal of solvent under reduced pressure resulted in a white solid, which was collected on a glass frit and washed with diethyl ether and pentanes. Yield: 240 mg, 60%. Mp (dec.) 276–280 °C. ^{1}H NMR (250 MHz, CD_3CN, 298 K): δ 0.9 (t, 9H, ^3J(HH) 7.5 Hz, CH_2CH_3), 1.2 (m, 3H, CH_2CH_3), 2.0 (m, 3H, CH_2CH_3), 3.7 (d, 3H, ^2J(HH) 14 Hz, SCH_2), 4.0 (s, 9H, NCH_3), 4.2 (d, 3H, ^2J(HH) 15 Hz, SCH_2), 7.1 (s, 3H, {CN(Me)C*H*CHN}), 7.5 (s, 3H, {CN(Me)CHC*H*N}). ^{13}C{^{1}H} NMR (62.5 MHz, CD_3CN, 298 K): δ 16.0, 21.7, 34.2, 36.3, 126.9, 131.4, 131.7, 141.2, 143.4. FT-IR (KBr) $\upsilon_{OH} = 3445$ cm^{-1}. *Anal.* Calc. for $C_{27}H_{38}N_6S_3OZnB_2F_8$: C, 40.7; H, 4.80; N, 10.5. Found: C, 40.9; H, 4.87; N, 10.6%.

2.7. Synthesis of [(TriMIm)Zn(OH$_2$)](NO$_3$)$_2$ (5)

To a stirred solution of $Zn(NO_3)_2 \cdot 6H_2O$ (127 mg, 0.43 mmol) in acetonitrile, 50 ml, was added a solution of TriMIm (230 mg, 0.43 mmol) in acetonitrile, 5 ml, at ambient temperature. The colorless solution was stirred overnight. Filtration through Celite and removal of volatiles under reduced pressure yielded a white solid, which was collected on a glass frit and washed with diethyl ether and pentanes. Yield: 230 mg, 72%. Mp, 206–210 °C. ^{1}H NMR (250 MHz, CD_3CN, 298 K): δ 0.9 (t, 9H, ^3J(HH) 7.5 Hz, CH_2CH_3), 1.2 (m, 3H, CH_2CH_3), 2.0 (m, 3H, CH_2CH_3), 3.7 (d, 3H, ^2J(HH) 14 Hz, SCH_2), 4.0 (s, 9H, NCH_3), 4.2 (d, 3H, ^2J(HH) 14 Hz, SCH_2), 7.2 (d, 3H, ^3J(HH) 1.5 Hz, {CN(Me)C*H*CHN}), 7.5 (d, 3H, ^3J(HH) 1.5 Hz, {CN(Me)CHC*H*N}). ^{13}C{^{1}H} NMR (62.5 MHz, CD_3CN, 298 K): δ 16.0, 21.6, 34.3, 36.2, 126.3, 131.5, 132.0, 140.6, 143.3. FT-IR (KBr) $\upsilon_{OH} = 3398$ cm^{-1}. *Anal.* Calc. for $C_{27}H_{38}N_8S_3O_7Zn$: C, 43.3; H, 5.12; N, 15.0. Found: C, 43.8; H, 5.15; N, 14.9%.

2.8. Synthesis of [{(TriMIm)Zn}$_2$(μ-OH)](BF$_4$)$_3$ (6)

To a stirred solution of $Zn(BF_4)_2 \cdot xH_2O$ (440 mg, 1.84 mmol) in distilled water, 2 ml, was added a solution of TriMIm, (1.0 g, 1.85 mmol) in acetone, 50 ml, at ambient temperature. The colorless solution was stirred overnight during which time it turned cloudy. Removal of volatiles under reduced pressure followed by extraction into acetonitrile, 10 ml, and filtration through Celite gave a colorless solution. Removal of solvent under reduced pressure yielded a white solid, which was collected on a glass frit and washed with diethyl ether and pentanes. Yield: 830 mg, 60%. Mp (dec.) 280–284 °C. ^{1}H NMR (250 MHz, CD_3CN, 298 K) δ 0.8 (t, 18H, ^3J(HH) 7.5 Hz, CH_2CH_3), 1.1 (m, 6H, CH_2CH_3), 1.9 (m, 6H, CH_2CH_3), 3.7 (d, 6H, ^2J(HH) 14 Hz, SCH_2), 3.9 (s, 18H, NCH_3), 4.1 (d, 6H, ^2J(HH) 15 Hz, SCH_2), 6.3 (s, 6H, {CN(Me)C*H*CHN}), 7.1 (s, 6H, {CN(Me)CHC*H*N}). ^{13}C{^{1}H} NMR (62.5 MHz, CD_3CN, 298 K): δ 15.9, 21.6, 34.1, 36.0, 126.1, 126.7, 131.1, 139.8, 143.4. FT-IR (KBr) $\upsilon_{OH} = 3450$ cm^{-1}. *Anal.* Calc. for $C_{54}H_{73}N_{12}S_6OZn_2B_3F_{12}$: C, 43.5; H, 4.94; N, 11.3. Found: C, 43.9; H, 5.08; N, 11.2%.

2.9. X-ray structural solution and refinement

Suitable crystals were selected and mounted on glass fibers with epoxy cement. Data were collected on a Siemens P4 diffractometer equipped with a SMART CCD detector with graphite Mo Kα radiation (Kα $\lambda = 0.7107$ Å). The unit cell parameters and orientation matrices were determined by harvesting reflections from three orthogonal sets of 15 frames using 0.3°ω scans. The systematic absences in the diffraction data are uniquely consistent with the reported space group for the compound identified. Crystallographic analysis (direct methods) of the reduced data using the SHELXTL (version 5.1) package of programs located all non-hydrogen atoms, which were refined anisotropically using the conventional full-matrix least-squares method. Hydrogen atoms were treated as idealized contributions, except for the hydrogen atoms on O1 in **1**, which were located in the difference Fourier map. In **2**, the coordinated CH_3CN was found to be disordered over two positions. Attempts to model the disorder were not successful due to insufficient data resolution.

3. Results and discussion

3.1. Synthesis of Cd and Zn aqua complexes

Reaction of equimolar mixtures of TriMIm and a hydrated metal salt in the appropriate solvent yielded the corresponding monomeric metal aqua complex, [(TriMIm)M(OH$_2$)]X$_2$ (M = Cd, X = BF$_4$ (**1**); M = Zn, X = BF$_4$ (**4**), and M = Zn, X = NO$_3$ (**5**)), in moderate to good yields as a white, microcrystalline solid. The materials possess good solubility in acetone, acetonitrile, and methanol but, are only sparingly soluble in hydrocarbons and chlorinated solvents. Spectroscopic (^{1}H, ^{13}C NMR, FT-IR) and combustion analytical data (experimental) support the indicated compositions, which were verified by X-ray diffraction analyses.

Judicious selection of the reaction solvent is required to generate the desired complexes with differing behavior observed between Zn and Cd. TriMIm complexation reactions with Zn favor formation of the aqua complexes, **4** and **5**, even in the donor solvent acetonitrile. However, the analogous reaction in acetone yields the hydroxo-bridged dimer, **6**.

The Cd-aqua complex **1** was prepared in acetone. When the same reaction was conducted in acetonitrile, with BF_4^- as counter ion, the Cd–$NCCH_3$ adduct, **2**, was generated. However, the reaction in acetonitrile with $Cd(NO_3)_2$ as the metal source yielded the O-nitrato complex, **3**. It appears that the fates of the reactions are driven by insolubility of the products.

3.2. Molecular structures

The molecular structures of the aqua complexes **1**, **4** and **5** are depicted in Fig. 1 with crystallographic data collected in Table 1. Relevant, selected metric parameters are contained in Table 2. Each complex consists of a monomeric core, coordinated to three imidazolyl nitrogens of the TriMIm and one water molecule. The geometry at each divalent ion can be described as trigonal pyramidal with the three nitrogens defining the basal plane and the oxygen in the apical position. The imidazolyl rings are all canted in the same direction inducing an asymmetry to the structures that is maintained in solution as evidenced in the ^1H NMR spectra recorded at room temperature. That is, there are two enantiomers that differ in the handedness of the canting (clockwise versus counter clockwise). In contrast, the three coordinate Cu(I), [(TriMIm)Cu]BF_4, exhibited facile interconversion between the two diastereomers with $\Delta G^{\ddagger} = 13$ kcal/mol [9]. The sum of the three N–M–N angles is essentially 360°, thus requiring the metal and three nitrogens to be coplanar. The deviations of the individual N–M–N angles from 120° are small, less than 3.5°. The Cd–OH_2 distance of 2.340(2) Å in **1** is within the range of values reported for the limited number of four coordinate Cd aqua complexes, 2.31–2.38 Å. The distance is somewhat shorter than that of 2.41(1) Å found for [Cd(TPA)(OH_2)(NO_3)]NO_3 [11]. The two zinc aqua complexes, differing only in the identity of the counter anions, show similar molecular structures despite crystallizing in distinct space groups. Further, while the Zn–N distances are all approximately 2.00 Å, the Zn–OH_2 distances differ by 0.10, 2.130(4) Å for **4** and 2.033(1) Å for **5**. The clear difference in Zn–OH_2 distances reflect the variable degrees of hydrogen-bonding between the bound water and the anions. The nitrate ion is a better H-bond acceptor than tetrafluoroborate thus, more effectively polarizing the O–H bond and consequently, shortening the Zn–O distance.

The Zn–O distances in **4** and **5** are significantly longer than those found in two recently characterized [N_3]Zn(OH_2) complexes in which [N_3] is either [$Tp^{tBu,Me}$] [8] or the tris(imidazolyl) calix[6]arene [12,13]. The latter two complexes exhibit Zn–O distances below 2.00 Å, despite Zn–N distances of approximately 2.00 Å, similar to **4** and **5**. In contrast, the Zn–O distances reported for the (presumably) aqua forms of the enzymes carbonic anhydrase II (2.05(2) Å) [14] and adamalysin II (2.35(2) Å) [15] are similar to **4** and **5**. Further, the geometries of these complexes are best described as pseudo-tetrahedral, with more acute N–Zn–N angles.

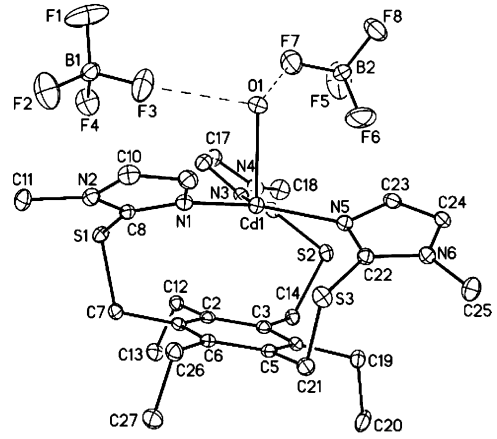

1

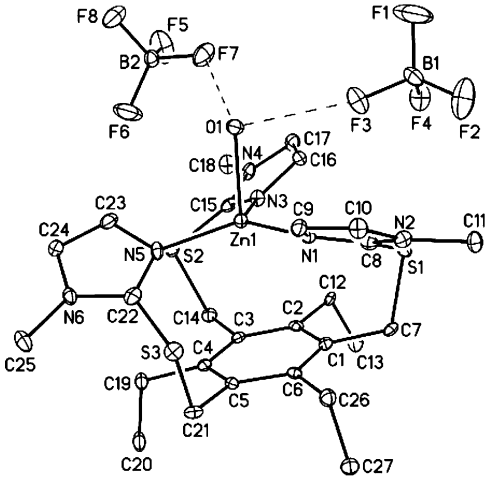

4

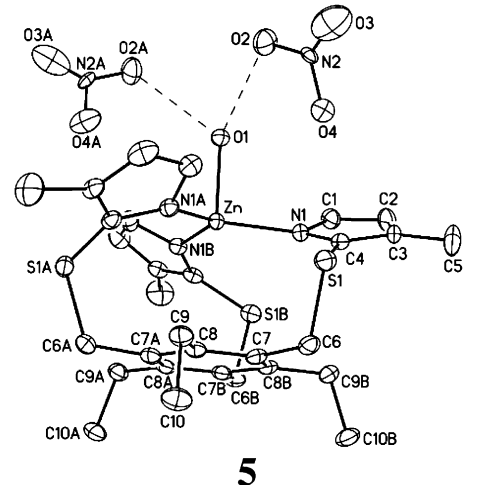

5

Fig. 1. Structures of metal-aqua complexes, **1**, **4** and **5**.

Perhaps the most notable feature in the structures of the metal–aqua complexes is the hydrogen-bonds

Table 1
Crystallographic data for **1–6**

	1	**2**·2CH_3CN	**3**·CH_3CN	**4**	**5**CH_3CN	**6**·7CH_3CN
Lattice	orthorhombic	monoclinic	monoclinic	orthorhombic	rhombohedral	monoclinic
Empirical formula	$C_{27}H_{38}B_2CdF_8N_6OS_3$	$C_{33}H_{45}B_2CdF_8N_9S_3$	$C_{29}H_{39}N_9O_6S_3Cd$	$C_{27}H_{3g}B_2F_8N_6OS_3Zn$	$C_{32}H_{41}N_6O_7S_3Zn$	$C_{68}H_{94}B_3F_{12}N_{19}OS_6Zn_2$
Formula weight	844.83	949.98	818.27	797.80	783.26	1777.15
Color, habit	colorless, rod	colorless, block	colorless, block	colorless, block	colorless, block	colorless, block
Crystal size (mm)	$0.30 \times 0.30 \times 0.20$	$0.30 \times 0.20 \times 0.20$	$0.20 \times 0.20 \times 0.15$	$0.14 \times 0.08 \times 0.08$	$0.10 \times 0.10 \times 0.10$	$0.25 \times 0.25 \times 0.20$
Space group	$P2_12_12_1$	$P2_1/c$	Ia	$P2_12_12_1$	R-3	$P2_1/c$
a (Å)	11.5115(17)	14.2483(11)	19.833(3)	11.5115(17)	12.153(3)	15.1881(14)
b (Å)	15.475(2)	13.3074(10)	15.971(2)	15.475(2)	12.153(3)	25.418(2)
c (Å)	19.060(3)	22.7875(18)	22.557(3)	19.060(3)	12.153(3)	21.487(2)
α (°)	90	90	90	90	84.494(2)	90
β (°)	90	103.574(2)	98.622(2)	90	84.494(2)	102.424(2)
γ (°)	90	90	90	90	84.494(2)	90
V (Å^3)	3395.4(9)	4200.0(6)	7064.2(16)	3395.4(9)	1771.5(9)	8101.1(13)
Z	4	4	8	4	2	4
Density (g/cm^3)	1.653	1.502	1.539	1.561	1.468	1.457
Temperature (K)	173(2)	173(2)	173(2)	173(2)	150(2)	173(2)
2θ range (°)	4.14–56.7	3.68–50.0	3.14–54.0	3.40–56.74	2.28–28.18	3.74–54.0
μ (Mo Kα) (cm^{-1})	9.05	7.41	8.50	9.86	9.25	8.29
$R(F), R_w(F)$	0.0284, 0.0684	0.0529, 0.1566	0.0609, 0.1615	0.0711,0.1249	0.0519,0.1160	0.0647, 0.1507
Goodness of fit on F^2	1.025	1.440	1.100	1.164	1.025	0.924

Quantity minimized: $R(wF^2) = \sum[w(F_o^2 - F_c^2)^2]/\sum[w(F_o^2)^2]^{1/2}$; $R = \sum \Delta/\sum(F_o)$, $\Delta = |(F_o - F_c)|$, $w = 1/[\sigma^2(F_o^2) + (aP)^2 + bP]$, $P = [2F_c^2 + \mathrm{Max}(F_o, 0)]/3$.

formed between the bound water and each of the counter anions. In **1** the H-bonding interactions were established clearly by locating the hydrogen atoms in the difference Fourier maps. In **4** and **5**, the hydrogen atoms were not located, but they were inferred by the characteristically short heavy atom distances, Table 2, and supported by FT-IR spectroscopic data, detailed in the following section. In complexes **1** and **4** the distances between the aqua oxygen and one of the fluorides of the BF_4^- are similar, with each distance below 2.9 Å. For comparison, in the Cu(II) aqua complex, [Cu(pmdien)(OH_2)F]BF_4, the O–FBF_3^- distance is 2.87 Å [16]. In the nitrato complex, **5**, the two nitrates are located at the same distance from the aqua ligand as required by the imposed crystallographic symmetry. The O1---O2 distance is 2.779(2) Å. H-bonding to Zn–OH_2 units is common to the three other structurally authenticated [N_3]Zn(OH_2) species that predate this report. In the Tp supported examples of Vahrenkamp [17] and Parkin [8], novel H-bond acceptors, [$Tp^{Ar,Me}$]Zn(OH) and $(C_6F_5)_3BOH$, respectively are required, with O---O distances in the range of 2.4–2.5 Å. In contrast, Reinaud's calix[6]arene derivative [13] shows the Zn-bound aqua ligand H-bound to a second water molecule in the heart of the calix[6]arene cavity with a O---O distance of 2.539(7) Å. The exceptional stability of this Zn aqua complex has been ascribed to the unique combination of the calixarene cavity and the H-bonding to a second water molecule. Identification of complexes **4** and **5** demonstrates clearly that neither special counter ions nor novel hydrophobic ligand cavity environments are requisite to stabilize [N_3]Zn(OH_2) motifs. It is plausible the enforced trigonal pyramidal geometry in the [(TriMIm)M(OH_2)]$^{2+}$ ions modulates the Lewis acidity of the metals permitting for the isolation of aqua, as opposed to hydroxo, adducts. Deprotonation of the zinc-aqua complexes is elicited facilely by changing the reaction conditions as described later.

The aqua ligand in **1** is replaced with acetonitrile by changing the reaction solvent from acetone to acetonitrile. A thermal ellipsoid representation of [(TriMIm)Cd($NCCH_3$)](BF_4)$_2$, (**2**) is contained in Fig. 2. Selected bond lengths and angles are given in Table 2. The environment of the Cd ion is that of a trigonal pyramid, with the imidazolyl nitrogens lying in the basal plane and an acetonitrile nitrogen in the axial position. The Cd–$NCCH_3$ distance of 2.328(5) Å is within the range of distances for the limited number of crystallographically defined Cd–$NCCH_3$ derivatives. The three imidazolyl donors and the Cd constitute a trigonal plane with the sum of the three N–Cd–N angles of 359.9°. The Cu–N_{Im} average distance in **2** at 2.190(7) Å is similar to that observed in the aqua derivative **1** at 2.184(3) Å. The acetonitrile ligand is positioned on the three-fold axis as indicated in the narrow range of N(7)–Cd–N_{Im} angles, 87.5(2)°–94.2(2)°.

The nitrato complex **3** prepared by reaction of $Cd(NO_3)_2 \cdot 6H_2O$ and TriMIm in acetonitrile indicates that the nitrato ligand binds to Cd preferentially over H_2O and CH_3CN, the latter two ligands binding only

Table 2
Selected distances (Å) and angles (°) for complexes **1**–**6**

*Complex **1***	
Bond lengths	
Cd1–N1	2.183(2)
Cd1–N3	2.185(2)
Cd1–N5	2.184(2)
Cd1–O1	2.340(2)
O1–F3	2.717(3)
O1–F7	2.894(3)
Bond angles	
N1–Cd1–N3	122.10(8)
N1–Cd1–N5	117.82(9
N3–Cd1–N5	120.02(8)
N1–Cd1–O1	87.50(9)
N3–Cd1–O1	86.13(9)
N5–Cd1–O1	99.19(9)
*Complex **2***	
Bond lengths	
Cd1–N1	2.197(4)
Cd1–N3	2.196(4)
Cd1–N5	2.177(4)
Cd1–N7	2.328(5)
Bond angles	
N1–Cd1–N3	119.1(2)
N1–Cd1–N5	119.4(2)
N3–Cd1–N5	121.2(2)
N1–Cd1–N7	87.5 (2)
N3–Cd1–N7	93.1(2)
N5–Cd1–N7	94.2(2)
Cd1–N7–C28	173.4(8)
N7–C28–C29	159.5(14)
*Complex **3***	
Bond lengths	
Cd1–N1	2.188(7)
Cd1–N3	2.213(9)
Cd1–N5	2.205(10)
Cd1–O1	2.342(9)
Cd1–O2	2.731(9)
Bond angles	
N1–Cd1–N3	115.2(4)
N1–Cd1–N5	120.4(4)
N3–Cd1–N5	122.4(3)
N1–Cd1–O1	110.9(4)
N3–Cd1–O1	79.6(3)
N5–Cd1–O1	93.9(3)
*Complex **4***	
Bond lengths	
Zn1–N1	2.00(1)
Zn1–N3	2.01(1)
Zn1–N5	2.00(1)
Zn1–O1	2.13(1)
O1–F3	2.735(3)
O1–F7	2.805(3)
Bond angles	
N1–Zn1–N3	123.1(2)
N1–Zn1–N5	116.5(2)
N3–Zn1–N5	118.3(2)
N1–Zn1–O1	91.2(2)
N3–Zn1–1	90.1(3)
N5–Zn1–O1	101.5(3)

Table 2 (*continued*)

*Complex **5***	
Bond lengths	
Zn–N1	1.983(1)
Zn–O1	2.033(1)
O1–O2	2.779(2)
Bond angles	
N1–Zn–N1A	119.033(8)
N1–Zn–O1	95.68(2)
*Complex **6***	
Bond lengths	
Zn1–N1	1.98(1)
Zn1–N3	1.99(1)
Zn1–N5	1.99(1)
Zn2–N7	1.99(1)
Zn2–N9	1.98(1)
Zn2–N11	2.01(1)
Zn1–O1	1.95(1)
Zn2–O1	1.94(1)
Zn1–Zn2	3.84(2)
Bond angles	
Zn1–O1–Zn2	160.0(2)

when BF_4^- is the counter ion. The structure of [(TriMIm)Cd(NO_3)](NO_3), (**3**) is depicted in Fig. 2 with selected metric parameters contained in Table 2. Of interest is the coordination mode of the nitrato group as such ligands can coordinate via unidentate, bidentate and anisobidentate modes. The Cd–O distances are 2.342(9) and 2.731 (9) Å while the Cd–O–N angles are 87.7(8)° and 107.4(8)°.

Parkin and coworkers proposed that the nature of the interaction between the bicarbonate intermediate and the metal ion influences the efficiency of carbonic anhydrase enzymes [18–23]. Accordingly, metals showing greater tendency to form bidentate bicarbonate intermediates are anticipated to be slow catalysts. As there are significant synthetic challenges in isolating mononuclear bicarbonate adducts, metal nitrates have been pursued as structural analogs due to the similar coordination modes available to nitrates and bicarbonates. The criteria established to classify the nitrato coordination mode rely on the differences in M–O interaction as defined by the differences in the two M–O distances and M–O–N angles [24]. The values determined for **3** are in accord with anisobidentate nitrato coordination. Comparison with a number of Cd(NO_3) complexes, Table 3, reveals **3** shows the greatest degree of asymmetry in nitrato binding. The trigonal planar coordination defined by the TriMIm accounts for this observation, as it is not sufficiently flexible to accommodate neither the trigonal bipyramidal nor square pyramidal geometries required for (more) symmetric nitrato coordination.

The zinc hydroxo dimer, **6**, was produced via the simple change of reaction solvent from acetone to acetonitrile. While a similar change in the synthesis of the

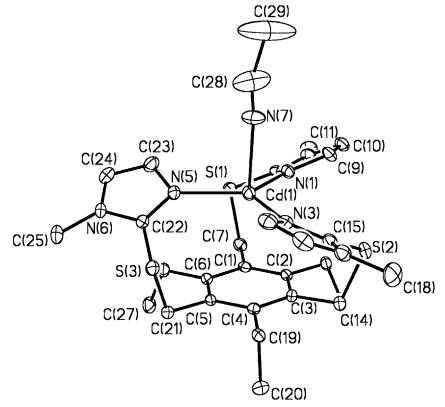

2

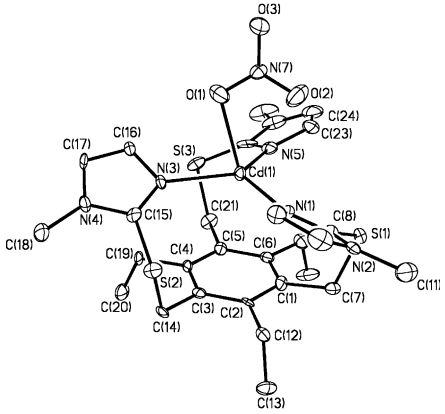

3

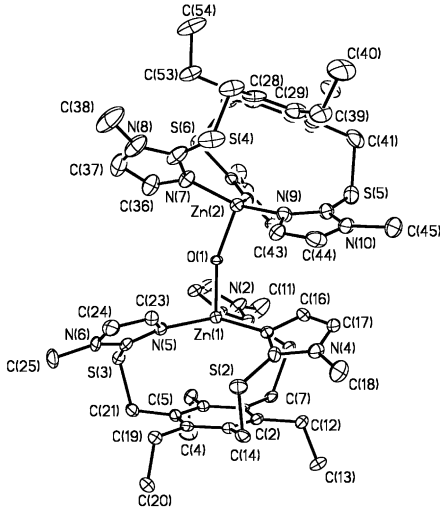

6

Fig. 2. Structures of the cations of **2**, **3** and **6**.

corresponding Cd complexes resulted in isolation of **2**, such a solvento species was not evident for Zn. Presumably, the higher polarity of the acetonitrile permits for generation of **6**. X–ray structural analysis provided unequivocal evidence for the hydroxo-bridged dimer, **6**, Fig. 2. Selected bond angles and distances are listed in Table 2. Each Zn ion lies in the basal plane defined by the three imidazolyl nitrogens, where the sums of N–Zn(1)–N′ and N–Zn(2)–N′ angles are 355.8(4)° and 355.1(3)°, respectively. Both zinc atoms are bridged by a hydroxo group with a substantially linear Zn(1)–O(1)–Zn(2) angle of 160.0(2)°. The steric demands of the TriMIm ligand require that the single atom bridge forms with the wide M–O–M angle. The bridging hydroxide is symmetric with Zn–O distances of Zn(1)–O(1), 1.95(1) Å and Zn(2)–O(1), 1.94(1) Å. The Zn–O distances support assignment of the bridging group as hydroxide. Although the hydrogen atom of the bridging unit was not located in the difference Fourier map, its presence was supported further by the identification of three BF_4^- per cation as required for charge balance and by infrared analysis, ν(OH) at 3450 cm^{-1}. Unlike the aqua complexes, the hydroxide does not appear to participate in hydrogen bonding with a BF_4^- anion as the closest O- - - F distance is 4.19(1) Å.

As the Zn-aqua complex is formed exclusively in acetone, it is likely the first species generated in acetonitrile. However, due to the higher polarity of the latter solvent, the aqua complex then ionizes to a mononuclear Zn–OH. While the identity of the base has not been established, TriMIm could serve this role. Under acidic conditions the free acid form, $[H_3TriMIm]^{3+}$, is accessible. The $[(TriMIm)Zn(OH)]^+$, reacts subsequently with a second Zn-aqua complex to generate the binuclear product. The presence of a $[N_3Zn]_2$–OH unit serves as a model compound for the hydrolytic function of hydroxo bridging zinc enzymes such as aminopeptidase and phospholipase C [25].

3.3. Spectroscopic data for metal aqua complexes

Proton and C-13 NMR spectroscopic data were consistent with the indicated formulations for **1**, **4** and **5**. However, even in aprotic solvents proton signals for the bound water were not evident. Infrared spectra of solid samples prepared as KBr pellets revealed broad features ascribed to the ν(OH) modes above 3400 cm^{-1}. Similar features were absent from the spectra of **2** and **3** further supporting the assignment. In **1** the band is split due to solid state effects with values of 3530 and 3475 cm^{-1}. The single broad ν(OH) bands for **4** and **5** occur at 3445 and 3398 cm^{-1}, respectively. The relative ordering for the Zn aqua species is consistent with stronger H-bonding between the bound water and the nitrato anion in **5**, as stronger H-bonds exhibit shifts to lower energy.

Despite the apparent acidity of the metal aqua complexes, attempts to generate the conjugate metal hydroxo species via deprotonation have failed. Addition of a range of bases including NEt_3, $LiNEt_2$, KOH, KOEt, and BuLi, resulted in either direct replacement of the aqua ligand or other, more catastrophic degradation to ill-defined species. Alternatively, efforts to generate **4** via

Table 3
Comparison of metric parameters for Cd-nitrato complexes

Compound	d_1/Å	d_2/Å	θ_1/°	θ_2/°	Δd/Å	$\Delta\theta$/°	Classification
[TriMIm]Cd(NO_3)]$^+$	2.34	2.73	107.4	87.7	0.39	19.7	anisobidentate
[Pim$^{i\mathrm{Pr}t\mathrm{Bu}}$]Cd($NO_3$)]$^+$ [23]	2.25	2.38	97.8	90.4	0.13	7.4	bidentate
[Tp$'^{\mathrm{Bu,Me}}$]Cd(NO_3)] [23]	2.27	2.29	102.9	101.1	0.02	1.8	bidentate
[Tp$^{\mathrm{Ph,Me}}$]Cd(NO_3)] [26]	2.33	2.35	95.2	95.0	0.02	0.2	bidentate
[16aneN_4]Cd(NO_3)]$^+$ [27]	2.40	2.46	95.2	96.9	0.06	1.7	bidentate

$\Delta d = |d_2 - d_1|$, $\Delta\theta = |\theta_2 - \theta_1|$.
Pim$^{i\mathrm{Pr}t\mathrm{Bu}}$, tris(1-isopropyl-4-tert-butylimidazolyl)phosphine.
16aneN_4, 1,5,9,13-tetramethyl-1,5,9,13-tetra-azacyclohexadecane.

protonation of **6** have yet to be successful. Efforts to verify that species **4** and **6** are a conjugate acid/base pair continue in this laboratory.

Acknowledgements

We thank the National Institutes of Health (GM-59191) for support of this work.

References

[1] S. Trofimenko, J. Am. Chem. Soc. 88 (1966) 1842.
[2] S. Trofimenko, Scorpionates – The Coordination Chemistry of Polypyrazolylborate Ligands, Imperial College Press, London, 1999.
[3] N. Kitajima, W.B. Tolman, Prog. Inorg. Chem. 43 (1995) 419.
[4] G. Parkin, Chem. Commun. (2000) 1971.
[5] N. Kitajima, K. Fujisawa, C. Fujimoto, Y. Moro-oka, S. Hashimoto, T. Kitagawa, K. Toriumi, K. Tatsumi, A. Nakamura, J. Am. Chem. Soc. 114 (1992) 1277.
[6] R. Alsfasser, S. Trofimenko, A. Looney, G. Parkin, H. Vahrenkamp, Inorg. Chem. 30 (1991) 4098.
[7] K.A. Magnus, B. Hazes, H. Tonthat, C. Bonaventura, J. Bonaventura, W.G.J. Hol, Proteins 19 (1994) 302.
[8] C. Bergquist, G. Parkin, J. Am. Chem. Soc. 121 (1999) 6322.
[9] J.K. Voo, K.C. Lam, A.L. Rheingold, C.G. Riordan, J. Chem. Soc., Dalton Trans. (2001) 1803.
[10] G.J. Kubas, Inorg. Synth. 19 (1979) 90.
[11] C.S. Allen, C.L. Chuang, M. Cornebise, J.W. Canary, Inorg. Chim. Acta 239 (1995) 29.
[12] O. Séneque, M.N. Rager, M. Giorgi, O. Reinaud, J. Am. Chem. Soc. 122 (2000) 6183.
[13] O. Séneque, M.N. Rager, M. Giorgi, O. Reinaud, J. Am. Chem. Soc. 123 (2001) 8442.
[14] K. Håkansson, M. Carlsson, L.A. Svensson, A. Liljas, J. Mol. Biol. 227 (1992) 1192.
[15] F.X. Gomisruth, L.F. Kress, J. Kellermann, I. Mayr, X. Lee, R. Huber, W. Bode, J. Mol. Biol. 239 (1994) 513.
[16] S.J. Barlow, S.J. Hill, J.E. Hocking, P. Hubberstey, W.S. Li, J. Chem. Soc., Dalton Trans. (1997) 4701.
[17] M. Ruf, K. Weis, H. Vahrenkamp, J. Am. Chem. Soc. 118 (1996) 9288.
[18] R. Han, G. Parkin, J. Am. Chem. Soc. 113 (1991) 9707.
[19] R. Han, A. Looney, K. McNeill, G. Parkin, A.L. Rheingold, B.S. Haggerty, J. Inorg. Biochem. 49 (1993) 105.
[20] A. Looney, R.Y. Han, K. McNeill, G. Parkin, J. Am. Chem. Soc. 115 (1993) 4690.
[21] A. Looney, A. Saleh, Y.H. Zhang, G. Parkin, Inorg. Chem. 33 (1994) 1158.
[22] A. Looney, G. Parkin, Inorg. Chem. 33 (1994) 1234.
[23] C. Kimblin, V.J. Murphy, T. Hascall, B.M. Bridgewater, J.B. Bonanno, G. Parkin, Inorg. Chem. 39 (2000) 967.
[24] G.J. Kleywegt, W.G.R. Wiesmeijer, G.J. Vandriel, W.L. Driessen, J. Reedijk, J.H. Noordik, J. Chem. Soc., Dalton Trans. (1985) 2177.
[25] W.N. Lipscomb, N. Sträter, Chem. Rev. 96 (1996) 2375.
[26] S.L. Guo, E. Ding, Y.Q. Yin, K.B. Yu, Polyhedron 33 (1998) 3841.
[27] N.W. Alcock, E.H. Curzon, P. Moore, C. Pierpoint, J. Chem. Soc., Dalton Trans. (1984) 605.

Available online at www.sciencedirect.com
SCIENCE DIRECT®
Polyhedron 23 (2004) 413–417
POLYHEDRON
www.elsevier.com/locate/poly

Carbon–hydrogen bond activation of chloroalkanes by a rhodium trispyrazolylborate complex

Andrew J. Vetter, William D. Jones *

Department of Chemistry, University of Rochester, Rochester, NY 14627, USA

Received 20 June 2003; accepted 28 August 2003

Abstract

The trispyrazolylborate complex fragment [Tp′Rh(CNneopentyl)], generated photochemically from the carbodiimide complex, reacts with chloro-substituted alkanes to give primary C–H oxidative addition products. Little reactivity is seen of the carbon–chlorine bond except when chlorine is in the β-position of the alkyl group.
© 2003 Elsevier Ltd. All rights reserved.

Keywords: Trispyrazolylborate; C–H activation; Rhodium

1. Introduction

The activation of C–H bonds of alkanes and arenes by coordinatively unsaturated metal complexes is a well-studied area of organometallic chemistry [1]. A number of complexes shown to be successful in alkane activation are Cp or Cp* metal complexes [2–4]. More recently, however, the analogous trispyrazolylborate complexes [5] have been shown to also activate a variety of C–H bonds in aliphatic and aromatic hydrocarbons [6–11]. Despite these many investigations, there are only a few examples that look at the activation of hydrocarbons that already contain reactive functional groups ([12], for examples of C–H activation in aryl halides, see [13]), perhaps because of a belief that the functional group would prove more reactive than the C–H bond. In this report, the reactions of a number of monochloroalkanes with the reactive fragment [Tp′Rh(CNneopentyl)] are investigated.

2. Experimental

2.1. General

All operations were performed under a nitrogen atmosphere, either in a Vacuum Atmospheres Corporation Glove Box or on a high vacuum line using modified Schlenk techniques. Benzene-d_6 was purchased from the Cambridge Isotope Labs and distilled under vacuum from dark purple solutions of benzophenone ketyl and stored in ampules with Teflon-sealed vacuum line adaptors. 1-Chloropentane, 2-chloropentane, and 2-chloropropane were purchased from Aldrich Chemical Co., distilled and dried over 4A molecular sieves. 3-chloropentane was prepared according to a published procedure [14]. Preparation of Tp′Rh(L)(η^2-PhN=C=NCH$_2$C(CH$_3$)$_3$) (**1**), Tp′Rh(L)Cl$_2$ (**2**), and neopentylisocyanide (L), have been previously reported [15–17]. All NMR spectra were recorded on a Bruker AMX400 or Bruker AVANCE 400 spectrometer. Chemical shifts are reported in ppm relative to tetramethylsilane and referenced using chemical shifts of residual solvent resonances (C_6D_5H, δ 7.15).

2.2. Preparation of Tp′Rh(L)HCl (3)

5.7 mg (0.010 mmol) of Tp′Rh(CNCH$_2$C(CH$_3$)$_3$)Cl$_2$ was dissolved in 0.75 ml of C_6D_6. To this solution was added 1.7 mg (0.0076 mmol) of Cp_2ZrH_2 in increments of 3 equal amounts with stirring for 20 min in between additions. Intermediate ^{1}H NMR spectra showed the conversion of **2** into **3**. The reaction mixture was stirred an additional 30 min, after which a ^{1}H NMR spectrum showed the formation of **3**. For **3**, ^{1}H NMR

* Corresponding author. Tel.: +1-716-275-5493; fax: +1-716-473-6889.
E-mail address: jones@chem.rochester.edu (W.D. Jones).

0277-5387/$ - see front matter © 2003 Elsevier Ltd. All rights reserved.
doi:10.1016/j.poly.2003.11.029

(C_6D_6): δ Rh–H: −13.40 (d, $J = 11.5$ Hz, 1H); Tp′Me: 2.074 (s, 3H), 2.120 (s, 3H), 2.207 (s, 3H), 2.286 (s, 3H), 2.862 (s, 3H), 2.869 (s, 3H); TpCH: 5.499 (s, 2H), 5.803 (s, 1H); CNR: 0.655 (s, 9H), 2.554 (s, 2H). For Tp′Rh(L)Cl_2 (**2**), ^{1}H NMR (C_6D_6): 2.033 (s, 6H), 2.106 (s, 3H), 2.735 (s, 6H), 3.241 (s, 3H), 5.491 (s, 2H), 5.522 (s, 1H), 2.688 (s, 2H), 0.793 (s, 9H).

2.3. Activation of 1-chloropentane: Tp′Rh(L)(H)($CH_2CH_2CH_2CH_2CH_2Cl$) (*4*)

A bright yellow solution of 9.7 mg of **1** in 0.75 ml of 1-chloropentane was irradiated with $\lambda > 345$ nm for 20 min at −20 °C. The solution changes to a tan color upon photolysis. The volatiles were removed under vacuum at 0 °C, leaving a brown oily solid. The resulting solid was dissolved in C_6D_6 and a ^{1}H NMR spectrum was taken immediately showing a single C–H bond activated product, **4**. ^{1}H NMR (C_6D_6): δ Rh–H: −14.92 (d, $J = 24.5$ Hz, 1H); Tp′Me: 2.197 (s, 3H), 2.211 (s, 3H), 2.295 (s, 3H), 2.374 (s, 3H), 2.544 (s, 3H), 2.566 (s, 3H); Tp′CH: 5.656 (s, 1H), 5.661 (s, 1H), 5.843 (s, 1H); CNR: 0.653 (s, 9H), 2.647 (s, 2H); CH_2Cl: δ 3.219 (t, $J = 6.8$ Hz, CH_2Cl). The remaining CH_2 resonances for the alkyl group were highly split and obscured, δ 1.0–2.3.

2.4. Activation of 3-chloropentane: Tp′Rh(L)(H)($CH_2CH_2CHClCH_2CH_3$) (*5*)

The activation of 3-chloropentane was identical to that of 1-chloropentane except that 7.1 mg of **1** was dissolved in 0.75 ml of 3-chloropentane. The ^{1}H NMR spectrum in C_6D_6 shows evidence for two products assigned as diastereomers in a 1:1 ratio. For Tp′Rh(L) (H)(CH_2CH_2-$CHClCH_2CH_3$) (**5**) (two diastereomers present), ^{1}H NMR (C_6D_6): δ Rh–H: 14.92 (d, $J = 24$ Hz, 2H); Tp′Me: 2.184 (s, 3H), 2.197 (s, 6H), 2.203 (s, 3H), 2.282 (s, 3H), 2.287 (s, 3H), 2.364 (s, 6H), 2.519 (s, 3H), 2.532 (s, 3H), 2.606 (s, 6H); Tp′CH: 5.626 (s, 1H), 5.645 (s, 1H), 5.654 (s, 2H), 5.821 (s, 1H), 5.839 (s, 1H); CNR: 0.652 (s, 9H), 0.667 (s, 9H), 2.638 (s, 2H), 2.651 (s, 2H); CH_2CH_3: 1.010 (t, $J = 7.3$ Hz, 3H), 1.017 (t, $J = 7.3$ Hz, 3H); CHCl: 3.93 (m, 1H), 4.00 (m, 1H); the remaining CH_2 resonances for the alkyl group were highly split and obscured.

2.5. Activation of 2-chloropentane: Tp′Rh(L)(H)($CH_2CH_2CH_2CHClCH_3$) (*6*) and Tp′Rh(L)HCl (*3*)

The procedure was identical to that for activation of 1-chloropentane except that 10.5 mg of **1** was dissolved in 0.75 ml of 2-chloropentane and irradiated at −20 °C. The volatiles were removed under vacuum, and examination by GC showed the presence of 1-pentene. The non-volatiles were dissolved in C_6D_6. Both Tp′Rh(L) HCl (**3**) and a CH activated product **6** were observed by ^{1}H NMR spectroscopy in a 1:2.5 ratio. The C–H activation product **6** was assigned as the terminal 4-chloropentyl derivative (two diastereomers present). For **6** (two diastereomers present), ^{1}H NMR (C_6D_6): δ Rh–H: 14.915 (d, $J = 24.8$ Hz, 1H), −14.909 (d, $J = 24.8$ Hz, 1H), Tp′Me: 2.194 (s, 3H), 2.201 (s, 3H), 2.208 (s, 6H), 2.286 (s, 3H), 2.293 (s, 3H), 2.378 (s, 6H), 2.537 (s, 3H), 2.560 (s, 3H), 2.578 (s, 3H), 2.611 (s, 3H); Tp′CH: 5.659 (s, 4H), 5.835 (s, 1H), 5.845 (s, 1H); CNR: 2.691 (s, 2H), 2.731 (s, 2H), 0.677 (s, 9H), 0.680 (s, 9H); $CHClCH_3$: 1.082 (d, $J = 6.1$ Hz, 3H), 1.031 (d, $J = 6.1$ Hz, 3H), 3.98 (m, 1H), 4.06 (m, 1H); the remaining CH_2 resonances for the alkyl group were highly split and obscured.

2.6. Activation of 2-chloropropane

The photolysis of 2-chloropropane was identical to that of 1-chloropentane except that 5.1 mg of **1** was dissolved in 0.75 ml of 2-chloropropane and irradiated at −20 °C for 20 min. Hydridochloride **3** was observed as well as the dichloride **2** in roughly a 3:1 ratio.

2.7. Activation of 1,1,1-trichloroethane

The photolysis of 1,1,1-trichloroethane was identical to that of 1-chloropentane except that 4.9 mg of **1** was dissolved in 0.75 ml of 1,1,1-trichloroethane and irradiated at −20 °C for 20 min. The only product observed was the dichloride **2**. A control experiment demonstrated that hydridochloride **3** reacts rapidly with 1,1,1-trichloroethane to give **2**.

2.8. Activation and quench of 1-chloropentane: Tp′Rh(L)(Cl)($CH_2CH_2CH_2CH_2CH_2Cl$) (*4-Cl*)

A bright yellow solution of 10 mg of **1** was dissolved in 0.75 ml of 1-chloropentane. The solution was cooled to −20 °C and photolyzed for 20 min. The resulting tan solution was quenched in vacuo with CCl_4 and kept at −20 °C for 2 h. Solvent was removed yielding a yellow-brown solid. A ^{1}H NMR spectrum shows Tp′Rh(L)(Cl)($CH_2CH_2CH_2CH_2CH_2Cl$) (**4-Cl**) and **2** in a 4:1 ratio, respectively. For **4-Cl**, ^{1}H NMR (C_6D_6): δ Tp′Me: 2.092 (s, 3H), 2.156 (s, 3H), 2.220 (s, 3H), 2.345 (s, 3H), 2.775 (s, 3H), 2.949 (s, 3H); Tp′CH: 5.574 (s, 1H,), 5.627 (s, 1H), 5.704 (s, 1H); CNR: 0.712 (s, 9H), 2.632 ('d' of AB quartet, $J = 3.8$ Hz, 2H); $RhCH_2$: 3.34 (m, 1H), 3.16 (m, 1H); CH_2Cl: 3.157 (t, $J = 6.8$ Hz, 2H), the three remaining CH_2 resonances for the alkyl group were highly split and obscured, δ 1.3–2.0.

2.9. Activation and quench of 3-chloropentane: Tp′Rh(L)(Cl)($CH_2CH_2CHClCH_2CH_3$) (*5-Cl*)

Activation and quench was identical to that of 1-chloropentane except that 9.7 mg of **1** was photolyzed in 0.75 ml of 3-chloropentane. Quenching in vacuo with

CCl_4 and removal of volatiles afforded a yellow-brown solid. A ^{1}H NMR spectrum shows two products assigned as diastereomers in a 1:1 ratio and about 20% **2**. For **5-Cl**, ^{1}H NMR (C_6D_6): δ Tp′Me: 2.057 (s, 3H), 2.080 (s, 3H), 2.152 (s, 3H), 2.165 (s, 3H), 2.206 (s, 3H), 2.210 (s, 3H), 2.442 (s, 3H), 2.493 (s, 3H), 2.770 (s, 3H), 2.775 (s, 3H), 2.879 (s, 3H), 2.954 (s, 3H); Tp′CH: 5.550 (s, 1H), 5.559 (s, 1H), 5.586 (s, 1H), 5.619 (s, 1H), 5.695 (s, 2H), CNR: 0.703 (s, 9H), 0.710 (s, 9H), 2.601 (s, 2H), 2.628 (s, 2H). CH_2CH_3: 1.063 (t, $J = 7.3$ Hz, 3H), 0.874 (t, $J = 7.5$ Hz, 3H); CHCl: 4.12 (br m, 2H); Rh–CH_2: 3.2–3.5 (br m, 4H), the remaining CH_2 resonances for the alkyl group were highly split and obscured.

2.10. Activation and quench of 2-chloropentane

The exact procedure was followed as for 1-chloropentane except that 8.0 mg of **1** was dissolved in 0.75 ml of 2-chloropentane. Removal of the solvent leaves a yellow-brown solid. ^{1}H NMR spectroscopy shows three products: Tp′Rh(L)(Cl)($CH_2CH_2CH_2CHClCH_3$) (**6-Cl**) (two isomers), and Tp′(L)Cl_2 (**2**) in a 1:1:1 ratio. For **6-Cl** (two diastereomers present), ^{1}H NMR (C_6D_6): δ Tp′Me: 2.068 (s, 3H), 2.080 (s, 3H), 2.155 (s, 3H), 2.167 (s, 3H), 2.218 (s, 6H), 2.407 (s, 3H), 2.426 (s, 3H), 2.779 (s, 3H), 2.785 (s, 3H), 2.946 (s, 3H), 2.980 (s, 3H); Tp′CH: 5.703 (s, 2H), 5.644 (s, 1H), 5.611 (s, 1H), 5.579 (s, 2H); CNR: 0.726 (s, 9H), 0.755 (s, 9H), 2.654 (s, 2H), 2.675 (s, 2H); $CHClCH_3$: 1.270 (d, $J = 6.6$ Hz, 3H), 1.248 (d, $J = 6.5$ Hz, 3H), 2.86 (m, 1H), 3.92 (m, 1H); $RhCH_2$: 3.29 (m, 2H). The remaining CH_2 resonances for the alkyl group were highly split and obscured.

3. Results and discussion

The fragment [Tp′Rh(L)] (L = neopentyl isocyanide), generated cleanly by irradiation of the carbodiimide complex Tp′Rh(L)(PhN=C=Nneopentyl) (**1**), is known to react selectively with the terminal C–H bonds of linear alkanes [15–17]. Importantly, activation of the internal secondary C–H bonds has been demonstrated *not* to occur. In looking at the reaction of this fragment with chloroalkanes, it was expected that the reactive C–Cl bond would undergo oxidative addition to the Rh^I fragment to give Tp′Rh(L)(*n*-alkyl)Cl in light of the ubiquitous reactivity of four-coordinate d^8 Rh(I) and Ir(I) complexes with alkyl halides. It was found, however, that irradiation of **1** in neat 1-chloropentane gives a single product that displays a hydride resonance in the ^{1}H NMR spectrum at δ −14.92 (d, $J = 24.5$ Hz), indicating that a selective C–H bond activation had occurred (Eq. (1)). The presence of six Tp′ methyl and three Tp′ methine resonances was diagnostic for an asymmetric Tp′Rh(L)XY product. The observation of a triplet at δ 3.219 ($J = 6.8$ Hz) indicated the presence of a terminal CH_2CH_2Cl group, and the product was assigned as Tp′Rh(L)($CH_2CH_2CH_2CH_2CH_2Cl$)H (**4**). No evidence for activation of the C–Cl bond or other positions on the hydrocarbon was seen. The hydride product could be converted to its stable chloride derivative (**4-Cl**) by treatment with CCl_4. **4-Cl** displayed a similar set of resonances in the ^{1}H NMR spectrum. Neither **4** nor **4-Cl** could be crystallized suitably for structure determination. **4Cl** displays characteristic multiplet resonances for the α-CH_2Rh protons at δ 3.2 [18]. The alkyl hydride **4** appears to have a stability towards reductive elimination of chloropentane comparable to that of the *n*-pentyl hydride complex studied earlier ($\tau_{1/2} = 2$ h at 22 °C) [15–17].

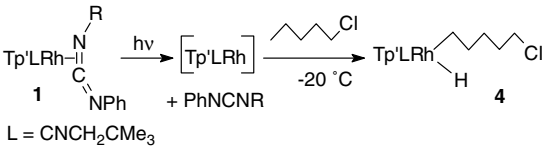

(1)

The irradiation of a solution of **1** in 3-chloropentane also leads to a C–H bond activation product, **5**. A single hydride resonance is observed just as for **4** at δ −14.92 (d, $J = 25$ Hz). However, examination of the Tp′ region of the spectrum shows evidence for *two* products. It was recognized that terminal activation of 3-chloropentane should yield two diastereomers of **5** due to the presence of chiral centers both at rhodium and at the γ-carbon of the pentyl chain (Eq. (2)). Confirmation of this possibility was obtained by the observation of two distinct triplets ($J = 7.3$ Hz) at δ 1.017 and 1.010 for the terminal methyl groups and two multiplets at δ 3.93 and 4.00 for the CHCl groups. Distinct *t*-butyl resonances for the isocyanide ligands were also observed. Once again, no activation of the C–Cl or other C–H bonds is seen. The hydride **5** could be converted to the stable chloride derivative **5-Cl**, but once again the product resisted attempts to produce X-ray quality crystals. Hydride complex **5** undergoes reductive elimination of 3-chloropentane over a period of several hours, similar to other alkyl hydrides of the type [15–17].

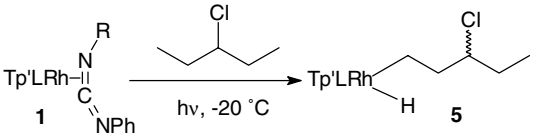

(2)

The photochemical reaction of **1** with 2-chloropentane was examined next. It was anticipated that two products would form resulting from the activation of either terminal methyl group, with each regioisomer existing as a pair of diastereomers. Upon irradiation of **1** in 2-chloropentane, two hydride resonances are seen inthe ^{1}H NMR spectrum in a 2.5:1 ratio. The minor resonance is

for the compound, Tp′Rh(L)HCl (**3**), not previously reported, but easily prepared by the titration of **2** with Cp_2ZrH_2. **3** displays a doublet at −13.40 with an unusually small Rh–H coupling constant ($J = 11.5$ Hz), along with characteristic Tp′ resonances. The second hydride belongs to a C–H bond activation product assigned as diasteriomers of $Tp'Rh(L)(CH_2CH_2CH_2CHClCH_3)H$ (**6**) (Eq. (3)). Two sets of Tp′ resonances are observed in a 1:1 ratio and two doublets are seen for the terminal methyl groups at δ 1.082 and 1.031. The CHCl methines appear as multiplets at δ 3.98 and 4.06. While no activation of the opposite end of the 2-pentylchloride is seen (position 1), it is proposed that this isomer did indeed form in the reaction, but that rapid β-chloride elimination leads to the formation of **3** and 1-pentene. 1-Pentene could be identified by GC examination of the volatiles removed from the initial solution. Treatment of **6** with CCl_4 leads to the formation of the chloro derivative, **6-Cl**. The observation of a 2.5:1 ratio of **6**:**3** therefore implies that a CH_3-CH_2-methyl group is 2.5× more reactive than a CH_3–CHCl–methyl group.

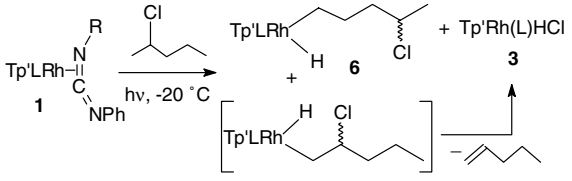

(3)

As further evidence for the occurrence of β-chloride elimination in β-chloro substituted alkyl hydrides, a solution of **1** in 2-chloropropane was irradiated. The ^1H NMR spectrum of this reaction shows the formation of **3** and **2** in a 3:1 ratio, but no C–H activation products (Eq. (4)). Propene was identified in the GC of the solution. Similarly, irradiation of a solution of **1** in 1,1,1-trichloroethane yields only **2**. In both of these reactions, the formation of **2** is believed to occur by reaction of **3** with chloroalkane, as confirmed by control experiments. In comparison, the earlier described reaction of **1** with 2-chloropentane showed formation of **3**, but not **2**, implying that **3** is less reactive with 2-chloropentane than 2-chloropropane.

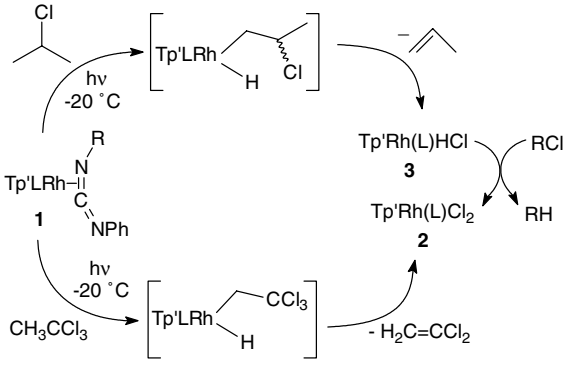

(4)

One issue that remains to be addressed is the mechanism of β-chloride elimination to generate **3**. The intermediate alkyl hydride complexes in these reactions are formally d^6 octahedral Rh(III) species, which should be inert towards ligand loss. Yet β-elimination of the chloro group would be expected to require an adjacent vacant site, by analogy to the well-established need for a vacant site in β-hydride elimination from an alkyl group [19]. Either these intermediates are indeed labile (η^3-Tp′ → η^2-Tp′), which seems unlikely, or β-chloride elimination does not require an adjacent vacant site. Perhaps the presence of a pair of electrons on the chlorine permits this elimination by way of a direct attack at the metal to displace the incipient olefin that is formed, as indicated in Eq. (5). Such β-chloroalkyl compounds may indeed be inherently unstable towards elimination. A search of the literature showed *no examples* of stable rhodium compounds containing simple β-chloroalkyl ligands (for rhodium, β-chlorofluoroalkyls and β-chloroacetyls are known. For Rh and $IrCl_2(CF_2CF_2Cl)(CO)(PEt_3)_2$, see [20]; for $Rh(COCH_2Cl)Cl_2(CO)(PEt_3)_2$, see [21]; for $RhCl_2(PPh_3)_2$(COCHClMe), see [22]. For iridium, β-chloroalkyls are known. For $IrHCl(CO)(PPh_3)_2(CH_2CCl_2Ph)$, see [23]; for $Ir(PEt_2Ph)_2(CO)Cl_2(CH_2CHClMe)$, see [24]; for $[Re_7C(CO)_{21}Ir(C_8H_{14})(CO)(CH_2CH_2Cl)Cl]^{2-}$, see [25]), yet examples with α-chloroalkyl [26–28] and γ-chloroalkyl ligands were found [29,30]. Indeed the β-chloroalkyl group represents the 'missing link' in the polymerization of vinyl chloride to polyvinylchloride (PVC). Most attempts to polymerize vinylchloride via olefin insertion into a metal-alkyl have failed due to the tendency for β-chloride elimination to occur faster than insertion [31–33].

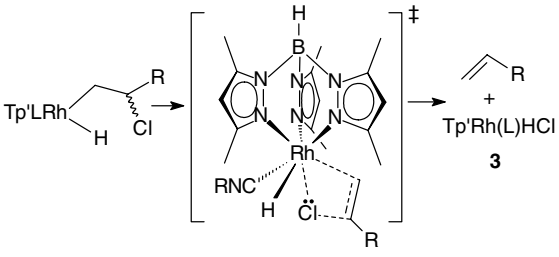

(5)

4. Conclusions

The reactive fragment [Tp′Rh(CNR)] is found to react with chlorinated alkanes to give terminal methyl group C–H activation products exclusively. If the alkane has chlorine substitution β to the methyl group, then activation is followed by rapid β-elimination to give Tp′Rh(L)HCl and the corresponding olefin. In no case is C–Cl oxidative addition observed.

Acknowledgements

This work was supported in full by a grant from the US Department of Energy, Grant FG02-86ER13569.

References

[1] S. Murai (Ed.), Topics Organometallic Chemistry, vol. 3, Springer, New York, 1999.
[2] For example, A.H. Janowicz, R.G. Bergman, J. Am. Chem. Soc. 104 (1982) 352.
[3] J.K. Hoyano, W.A.G. Graham, J. Am. Chem. Soc. 104 (1982) 3723.
[4] W.D. Jones, F.J. Feher, J. Am. Chem. Soc. 106 (1984) 1650.
[5] S. Trofimenko, Scorpionates: The Coordination Chemistry of Polypyrazolylborate Ligands, Imperial College Press, London, 1999.
[6] C.K. Ghosh, W.A.G. Graham, J. Am. Chem. Soc. 109 (1987) 4726.
[7] C.K. Ghosh, W.A.G. Graham, J. Am. Chem. Soc. 111 (1989) 375.
[8] A.A. Purwoko, A.J. Lees, Inorg. Chem. 34 (1995) 424.
[9] R.S. Tanke, R.H. Crabtree, Inorg. Chem. 28 (1989) 3444.
[10] M.J. Fernández, M.J. Rodriguez, L.A. Oro, F.J. Lahoz, J. Chem. Soc., Dalton Trans. (1989) 2073.
[11] P. Pérez, M.L. Poveda, E. Carmona, J. Chem. Soc., Chem. Commun. (1992) 8.
[12] F. Kakiuchi, S. Murai, Acc. Chem. Res. 35 (2002) 826.
[13] (a) E. Ben-Ari, M. Gandelman, H. Rozenberg, L.J.W. Shimon, D. Milstein, J. Am. Chem. Soc. 125 (2003) 4714;
(b) J.-Y. Cho, M.K. Tse, D. Holmes, R.E. Maleczka Jr., M.R. Smith, Science 295 (2002) 305;
(c) D.T. Tellers, C.M. Yung, B.A. Arndtsen, D.R. Adamson, R.G. Bergman, J. Am. Chem. Soc. 124 (2002) 1400;
(d) T. Ishiyama, J. Takagi, K. Ishida, N. Miyaura, N.R. Anastasi, J.F. Hartwig, J. Am. Chem. Soc. 124 (2002) 390;
(e) Y. Fuchita, Y. Utsunomiya, M. Yasutake, J. Chem. Soc., Dalton Trans. (2001) 2330;
(f) A.D. Selmeczy, W.D. Jones, M.G. Partridge, R.N. Perutz, Organometallics 13 (1994) 522;
(g) P.L. Alsters, P.F. Engel, M.P. Hogerheide, M. Copijn, A.L. Spek, G. van Koten, Organometallics 12 (1993) 1831.
[14] F.C. Whitmore, F.A. Karnatz, J. Am. Chem. Soc. 60 (1938) 2536.
[15] W.D. Jones, E.T. Hessell, J. Am. Chem. Soc. 115 (1993) 554.
[16] W.D. Jones, D.D. Wick, Organometallics 18 (1999) 495.
[17] T.O. Northcutt, D.D. Wick, A.J. Vetter, W.D. Jones, J. Am. Chem. Soc. 123 (2001) 7257.
[18] D.D. Wick, W.D. Jones, Inorg. Chem. 36 (1997) 2723.
[19] J.P. Collman, L.S. Hegedus, J.R. Norton, R.G. Finke, Principles and Applications of Organotransition Metal Chemistry, University Science Books, Sausalito, CA, 1987, p. 386.
[20] A.K. Burrell, G.R. Clark, C.E.F. Rickard, W.R. Roper, J. Organomet. Chem. 482 (1994) 261.
[21] W.S. Weston, D.J. Cole-Hamilton, Inorg. Chim. Acta 280 (1998) 99.
[22] J.Y. Shie, Y.C. Lin, Y. Wang, J. Organomet. Chem. 371 (1989) 383.
[23] R.H. Walter, B.F.G. Johnson, J. Chem. Soc., Dalton Trans. (1978) 381.
[24] J.M. Duff, B.E. Mann, E.M. Miller, B.L. Shaw, J. Chem. Soc., Dalton Trans. (1972) 2337.
[25] L. Ma, J.R. Shapley, Inorg. Chim. Acta 212 (1993) 303.
[26] J. Wolf, H. Werner, J. Organomet. Chem. 336 (1987) 413.
[27] R.D.W. Kemmitt, D.I. Nichols, J. Chem. Soc. A (1969) 1577.
[28] R.D.W. Kemmitt, D.I. Nichols, Inorg. Nucl. Chem. Lett. 4 (1968) 739.
[29] D. Steinborn, M. Rausch, C. Bruhn, H. Schmidt, D. Strohl, J. Chem. Soc., Dalton Trans. 2 (1998) 221.
[30] R.H. Hill, J. Chem. Soc., Chem. Commun. (1989) 293.
[31] R.A. Stockland Jr., R.F. Jordan, J. Am. Chem. Soc. 122 (2000) 6315.
[32] S.A. Strazisar, P.T. Wolczanski, J. Am. Chem. Soc. 123 (2001) 4728.
[33] M. Kang, A. Sen, L. Zakharov, A.L. Rheingold, J. Am. Chem. Soc. 124 (2002) 12080.

Available online at www.sciencedirect.com
SCIENCE DIRECT®
Polyhedron 23 (2004) 419–428
POLYHEDRON
www.elsevier.com/locate/poly

Synthesis and characterization of cyclometalated Ir(III) complexes with pyrazolyl ancillary ligands

Jian Li, Peter I. Djurovich, Bert D. Alleyne, Irina Tsyba, Nam N. Ho, Robert Bau, Mark E. Thompson *

Department of Chemistry, University of Southern California, Los Angeles, CA 90089-0744, USA

Received 24 June 2003; accepted 11 September 2003

Abstract

The syntheses and structures of a series of $(N,C^{2\prime}$-(2-*para*-tolylpyridine))$_2$Ir(LX) [$(tpy)_2$Ir(LX)] and $(N,C^{2\prime}$-(4′,6′-difluorophenylpyridine))$_2$Ir(LX) [$(dfppy)_2$Ir(LX)] are reported, where LX are pyrazolyl and pyrazolyl-borate ligands. Reaction of the dichloro-bridged dimer [$(tpy)_2$Ir(μ-Cl)]$_2$ with excess pyrazolyl-borate ligands forms a protonated-dipyrazolyl Ir complex, $(tpy)_2$Ir(pz_2H). The Ir bound chloride in [$(tpy)_2$Ir(μ-Cl)]$_2$ presumably facilitates the hydrolysis of pyrazolyl-borate. Thus, the syntheses of Ir complexes with bis(pyrazolyl)borates, e.g., $(tpy)_2$Ir(pz_2Bpz$_2$) and $(tpy)_2$Ir(pz_2BEt$_2$) require the chloride abstraction by CF_3SO_3Ag before pyrazolyl-borate is added to the reaction solution. $(tpy)_2$Ir(pz_2H), $(tpy)_2$Ir(pzH)$_2$(CF_3SO_3), $(tpy)_2$Ir(pz_2Bpz$_2$) and $(tpy)_2$Ir(pz_2BEt$_2$) have been structurally characterized by X-ray crystallography. The two pyrazolyl rings of $(tpy)_2$Ir(pz_2H) are nearly coplanar (dihedral angle, 12°), due to the presence of N–H···N hydrogen bond (N···N distance of 2.56 Å), while the two pyrazolyl rings of $(tpy)_2$Ir(pzH)$_2$(CF_3SO_3) are not coplanar (pz–pz dihedral angle, 47°). Unlike other η^2-pyrazolyl-borate complexes, the $(tpy)_2$Ir(pz_2BEt$_2$) exhibits a rare *quasi*-chair conformation adopted by $\overline{\text{Ir–N–N–B–N–N}}$ the ring, rather than the more common boat conformations which have been observed previously. Similarly, the $\overline{\text{Ir–N–N–B–N–N}}$ cycle of $(tpy)_2$Ir(pz_2Bpz$_2$) adopts a *half*-chair conformation, more flattened than the typical boat conformation. While the choice of pyrazolyl-borate ligand does not change the structural properties of the "$(tpy)_2$Ir" fragment, it markedly affects the photophysical properties of both $(tpy)_2$Ir(pz_2BR$_2$) and $(dfppy)_2$Ir(pz_2BR$_2$) complexes. The pyrazolyl-borate ancillary ligands affect the absorption and emission energies of these complexes by tuning the HOMO (highest occupied molecular orbital) energies. The electron-withdrawing ancillary ligands, e.g., $pz_2Bpz_2^-$, decrease the electron density on the iridium, stabilizing the metal-centered HOMOs.
© 2003 Elsevier Ltd. All rights reserved.

Keywords: Iridium; Cyclometalated Ir(II) complexes; Pyrazolyl ancillary ligands; Boat conformations; Luminescent; Electroluminescence

1. Introduction

Since their introduction in 1967, poly(pyrazolyl)borate ligands have been widely used as auxiliary ligands in coordination, organometallic, and bioinorganic chemistry [1–4]. Due to their relative ease of synthesis, complexes with pyrazolyl-borates of almost all metals of the periodic table have been synthesized. The ligating properties of pyrazolyl-borates and substituted pyrazolyl-borates have therefore been well established and extensively explored [2–17]. The poly(pyrazolyl)borate complexes have been used to investigate a wide range of topics including catalysis for C–H bond activation [13], models for enzymatic reactions [6,17], metal extraction [2,12], and biomedical applications [6], to name but a few [2–7]. There has been little reported, however, on the use of these ligands to influence the photophysical properties of metal complexes [15].

During the last two decades cyclometalated Ir(III) complexes, because of their interesting photophysical properties, have attracted attention for a potential range of applications [8–22]. These applications include sensitizers for outer-sphere electron-transfer reactions [23,24], photocatalysts for CO_2 reduction [24,25], photooxidants and singlet oxygen sensitizers [26]. We have

* Corresponding author.
E-mail address: met@usc.edu (M.E. Thompson).

0277-5387/$ - see front matter © 2003 Elsevier Ltd. All rights reserved.
doi:10.1016/j.poly.2003.11.028

recently found that the high luminescent quantum yields and comparatively short phosphorescent lifetimes of these Ir complexes make them ideal emissive dopants in organic light emitting devices (OLEDs) [27–29]. OLEDs prepared with these phosphors have the highest efficiency to date, giving internal quantum efficiencies approaching 100% [30]. Both homoleptic Ir tris cyclometalates, $(CN_2)Ir$, and heteroleptic Ir complexes, $(CN)_2Ir(LX)$, have been incorporated into highly efficient OLEDs [19,27,28,31], where CN is a general abbreviation used hereafter for a cyclometalating ligand and LX is an anionic ancillary ligand, such as β-diketonate, 2-picolinic acid and *N*-alkylsalicylimine. In this paper, we expand the list of ancillary ligands to include a series of pyrazolyl and pyrazolyl-borates, with the ultimate goal of investigating their influence on the photophysics of these cyclometalated complexes. This report provides syntheses, structures and gives a preliminary account of the photophysical properties of a series of cyclometalated Ir(III) complexes with pyrazolyl and pyrazolyl-borates ancillary ligands. Two different cyclometalating ligands were used to prepare the $(CN)_2Ir$ (pyrazolylborate) complexes, i.e., $N,C^{2\prime}$-(2′-*para*-tolylpyridyl) (abbreviated as *tpy*) and $N,C^{2\prime}$-(4′,6′-difluorophenyl-pyridyl) (abbreviated as *dfppy*) (Fig. 1). The types of products formed in reactions between pyrazolyl-borate anions and the Ir chloride precursors were found to depend strongly on the presence of chloride ligand. The X-ray structures, as well as some photophysical properties of these Ir complexes, are discussed. The η^2-pyrazolyl-borate ligands adopt conformations that differ from orientations more commonly observed for these ligands. Comparisons of selected $(tpy)_2Ir(LX)$ complexes, in their absorption spectra and room temperature emission spectra, demonstrate that the new Ir complexes with pyrazolyl ancillary ligands can have different photophysical properties, e.g., absorption energies of the lowest-energy transition and emission energies, than $(tpy)_2Ir(acac)$ having the same "$(tpy)_2Ir$" fragment. A similar trend is also observed for $(dfppy)_2Ir$ (LX) complexes.

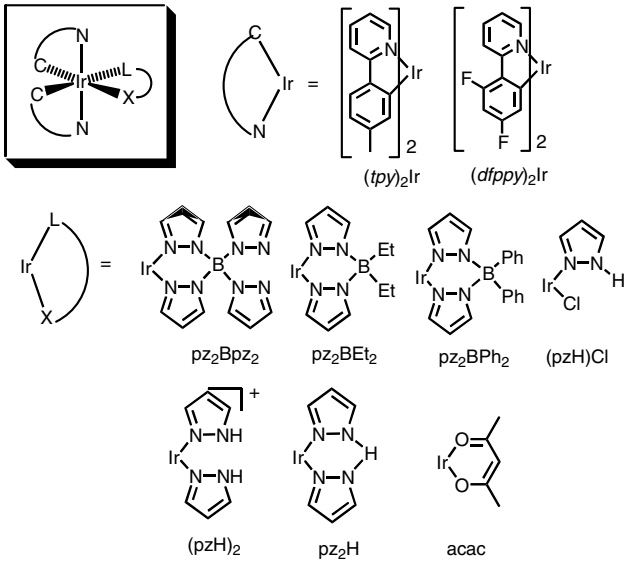

Fig. 1. Abbreviations of iridium complexes used through out the paper.

2. Experimental

2.1. Equipment

Photoluminescent spectra were measured using a Photon Technology International fluorometer. NMR spectra were recorded on Bruker AC 250 MHz, AM 360 MHz, AMX 500 MHz instruments. The Microanalysis Laboratory at the University of Illinois, Urbana-Champaign, performed all elemental analysis.

2.2. X-ray crystallography

The crystallographic data for the four structures reported here have been deposited in the Cambridge Database [$(tpy)_2Ir(pz_2BEt_2)$, CCDC #213343; $(tpy)_2Ir(pz_2H)$, CCDC #213345; $(tpy)_2Ir(pzH)_2(CF_3SO_3)$, CCDC #213346 and $(tpy)_2Ir(pz_2Bpz_2)$, CCDC #213344)]. X-ray diffraction data for $(tpy)_2Ir(pz_2BEt_2)$, $(tpy)_2Ir(pz_2H)\cdot CHCl_3$ and $(tpy)_2Ir(pzH)_2(CF_3SO_3)$ were collected at room temperature, 296(2) K on a Bruker SMART APEX CCD diffractometer with graphite-monochromated Mo Kα radiation ($\lambda = 0.71073$Å) while the data of $(tpy)_2Ir(pz_2Bpz_2)$ were collected at 273(2) K. The cell parameters for the Ir complexes were obtained from the least-squares refinement of spots (from 60 collected frames) using the SMART program. A hemisphere of the crystal data was collected up to a resolution of 0.75 Å and the intensity data was processed using the SAINT PLUS program. All calculations for the structure determination were carried out using the SHELXTL package (version 5.1) [32]. Initial atomic positions were located by Patterson methods using XS, and the structures of $(tpy)_2Ir(pz_2BEt_2)$ were refined by least-squares methods using SHELX 93 with 6983 independent reflections and within the range of $\Phi = 1.57°$ to 27.51° (completeness 95.9%). For $(tpy)_2Ir(pz_2H)$, $(tpy)_2Ir(pzH)_2(CF_3SO_3)$ and $(tpy)_2Ir(pz_2Bpz_2)$, the data are $\Phi = 1.61°$ to 24.71° (completeness 99.9%), $\Phi = 1.68°$ to 23.25° (completeness 100.0%) and $\Phi = 1.45°$ to 27.63° (completeness 91.8%), respectively. Absorption corrections were applied by using SADABS [33]. Calculated hydrogen positions were input and refined in a riding manner along with the attached carbons. A summary of the refinement details and resulting factors are given in Table 1.

Table 1
Crystal data and summary of intensity data collection and structure refinement

	$(tpy)_2Ir(pz_2H)\cdot CHCl_3$	$(tpy)_2Ir(pzH)_2(CF_3SO_3)$	$(tpy)_2Ir(pz_2BEt_2)$	$(tpy)_2Ir(pz_2Bpz_2)$
Empirical formula	$C_{31}H_{28}Cl_3IrN_6$	$C_{31}H_{28}F_3IrN_6O_3S$	$C_{34}H_{36}BIrN_6$	$C_{36}H_{32}BIrN_{10}$
Formula weight	782.14	811.84	731.7	807.73
Temperature (K)	296(2)	296(2)	296(2)	273(2)
Wavelength (Å)	0.71073	0.71073	0.71073	0.71073
Crystal system	monoclinic	orthorhombic	monoclinic	triclinic
Space group	$P2_1/n$	*Cmca*	$P2_1/n$	$P\bar{1}$
Unit cell dimensions				
a (Å)	9.194(3)	24.234(3)	8.9981(4)	9.4357(9)
b (Å)	21.049(6)	15.805(2)	21.9447(11)	13.044(1)
c (Å)	15.862(4)	17.593(2)	16.0326(8)	14.991(1)
α (°)	90	90	90	70.224(2)
β (°)	90.284(5)	90	90.8240(10)	78.844(2)
γ (°)	90	90	90	70.547(2)
Volume (Å^3)	3069.7(15)	6738.2(15)	3165.5(3)	1630.3(3)
Z	4	8	4	2
$d_{calc.}$ (g/cm^3)	1.692	1.601	1.535	1.645
Absorption coefficient (mm^{-1})	4.642	4.081	4.251	4.139
$F(000)$	1532	3184	1456	800
θ range for data collection (°)	1.61–24.71	1.68–23.25	1.57–27.51	1.45–27.63
Reflections collected	15 497	14 655	19 216	10 070
Independent reflections	5219 [$R_{int} = 0.0678$]	2490 [$R_{int} = 0.0709$]	6982 [$R_{int} = 0.0328$]	6970 [$R_{int} = 0.0259$]
Refinement method	full-matrix least-squares on F^2	full-matrix least-squares on F^2	full-matrix least-squares on F^2	full-matrix least-squares on F^2
Data/restraints/parameters	5219/0/353	2490/0/190	6982/0/384	6970/0/436
Goodness-of-fit on F^2	1.013	1.147	0.98	1.001
Final R indices [$I > 2\sigma(I)$]	0.0646	0.0588	0.0327	0.0408
R indices (all data)	0.0982	0.093	0.0447	0.0513

2.3. Synthetic section

2′,4′-Difluorophenylpyridine was prepared by Suzuki coupling reaction with commercially available 2,4-difluorophenyl boronic acid and 2-bromopyridine [34]. The compounds sodium diethylbis(1-pyrazolyl)borate [35,36], potassium tetrakis(1-pyrazolyl)borate [1] and the cyclometalated Ir(III) μ-chloro-bridged dimers $[(tpy)_2Ir(\mu\text{-}Cl)]_2$ and $[(dfppy)_2Ir(\mu\text{-}Cl)]_2$ [37] were prepared following published procedures. Potassium diphenylbis(1-pyrazolyl)borate was purchased from STREM Chemical Co. Silver trifluoromethylsulfonate (AgOTf) and all other materials were purchased from Aldrich Chemical Co. and used without further purification.

2.3.1. Synthesis of $(tpy)_2Ir(pz_2BX_2)$ (X=pz, Et, Ph) complexes

2.3.1.1. General procedure. $[(tpy)_2Ir(\mu\text{-}Cl)]_2$ (1.0 g, 0.89 mmol) was dissolved in 50 ml of CH_2Cl_2 and a solution of 2.1 equiv. AgOTf (0.48 g, 1.9 mmol) in 50 ml of MeOH was added to yield a cream-colored slurry. After stirring for 2 h at room temperature, the slurry was centrifuged to precipitate the AgCl. The clear decantate was evaporated to dryness to yield a yellow oily residue. The residue was dissolved in 50 ml CH_3CN and was treated with 3–4 equiv. of either $K(pz_2BX_2)$ (X = Ph, pz) or $NaBEt_2pz_2$. The solution was refluxed under N_2 for 18 h, and then cooled to room temperature. The colored precipitate was filtered, dissolved in 50 ml CH_2Cl_2 and refiltered. The filtrate was collected and evaporated to dryness to yield a crude product. The yellow $(tpy)_2Ir(pz_2Bpz_2)$ product was purified by recrystallization in $MeOH/CH_2Cl_2$ while the yellow $(tpy)_2Ir(pz_2BPh_2)$ or $(tpy)_2Ir(pz_2BEt_2)$ products were purified by chromatography on a silica/CH_2Cl_2 column.

2.3.1.2. $(tpy)_2Ir(pz_2Bpz_2)$: iridium(III) bis(2′-para-tolylpyridinato-N,C$^{2\prime}$)η^2-tetrakis(1-pyrazolyl)borate (yield 73%). ^{1}H NMR (360 MHz, CD_2Cl_2), ppm: 7.75 (d, $J = 7.9$ Hz, 2H), 7.68 (s, 2H), 7.58 (ddd, $J = 7.8$, 7.8, 1.5 Hz, 2H), 7.51 (d, $J = 7.8$ Hz, 2H), 7.28 (d, $J = 4.4$ Hz, 2H), 7.06 (d, $J = 2.4$ Hz, 2H), 6.93 (s, 2H), 6.80 (d, $J = 7.8$ Hz, 2H), 6.71 (ddd, $J = 6.3$, 6.3, 1 Hz, 2H), 6.24 (d, $J = 1.5$ Hz, 2H), 6.17 (s, 2H), 6.07 (s, 2H), 5.99 (s, 2H), 2.08 (s, 6H). *Anal.* Calc. for $(tpy)_2Ir(pz_2Bpz_2)\cdot 0.5CH_2Cl_2$: C, 51.56; H, 3.91; N, 16.47. Found: C, 51.76: H, 3.76; N, 16.16%.

2.3.1.3. $(tpy)_2Ir(pz_2BEt_2)$: iridium(III) bis(2′-para-tolylpyridinato-N,C$^{2\prime}$)diethylbis(1-pyrazolyl)borate (yield 41%). ^{1}H NMR (360 MHz, $CDCl_3$), ppm: 7.73 (d,

$J = 7.8$ Hz, 2H), 7.70 (dd, $J = 2.4$, 1.0 Hz, 2H), 7.57 (ddd, $J = 7.8$, 7.8, 1.5 Hz, 2H), 7.46 (d, $J = 7.8$ Hz, 2H), 7.06 (dd, $J = 5.8$, 1.0 Hz, 2H), 6.81 (ddd, $J = 5.8$, 5.8, 1.5 Hz, 2H), 6.72 (m, 4H), 6.03 (m, 4H), 2.07 (s, 6H) 0.51 (t, $J = 5.4$ Hz, 6H), 0.61–0.45 (m, 4H). *Anal*. Calc. for $(tpy)_2Ir(pz_2BEt_2)$: C, 55.81; H, 4.96; N, 11.49. Found: C, 55.48; H, 4.67; N, 11.34%.

2.3.1.4. $(tpy)_2Ir(pz_2BPh_2)$: iridium(III) bis(2′-para-tolylpyridinato-N,$C^{2'}$)diphenylbis(1-pyrazolyl)borate (yield 51%). ^{1}H NMR (360 MHz, CD_2Cl_2), ppm: 7.72 (d, $J = 8.2$ Hz, 2H), 7.56–7.47 (m, 4H), 7.24–7.00 (m, 10H), 6.83 (dd, $J = 1.9$, 1 Hz, 2H), 6.77 (dd, $J = 8.2$, 1.9 Hz, 2H), 6.60 (dd, $J = 8.2$, 1.5 Hz, 2H), 6.51 (m, 2H), 6.02 (dd, $J = 2.4$, 2.4 Hz, 2H), 5.99 (d, $J = 1.9$ Hz, 2H), 2.07 (s, 6H). *Anal*. Calc. for $(tpy)_2Ir(pz_2BPh_2)$ $0.5CH_2Cl_2$: C, 58.65; H, 4.29; N, 9.66. Found: C, 58.23; H, 4.29; N, 9.32%.

2.3.2. Synthesis of $(tpy)_2Ir(pzH)Cl$: (chloro)bis(2′-para-tolylpyridinato-N,$C^{2'}$)(pyrazole)iridium(III)

$[(tpy)_2Ir(\mu\text{-}Cl)]_2$ (0.1 g, 0.09 mmol) was dissolved in 10 ml of CH_2Cl_2 and 8 equiv. pyrazole (0.05 g, 0.74 mmol) was added to yield a cream-colored slurry. After the slurry was stirred for overnight at room temperature, the colored precipitate was filtered off. The crude product was washed with 2×10 ml CH_2Cl_2, followed by ether and hexane, then dried under the vacuum to yield yellow $(tpy)_2Ir(pzH)Cl$ (0.09 g, 80%). ^{1}H NMR (360 MHz, acetone-d_6), ppm: 13.2 (s, 1H), 9.77 (d, $J = 6.5$ Hz, 1H), 8.01 (d, $J = 8.3$ Hz, 1H), 7.98 (d, $J = 8.3$ Hz, 1H), 7.94 (d, $J = 1.8$ Hz, 1H), 7.83 (m, 2H), 7.73 (d, $J = 5.5$ Hz, 1H), 7.60 (d, $J = 7.4$ Hz, 1H), 7.53 (d, $J = 8.3$ Hz, 1H), 7.25 (ddd, $J = 6.5$, 6.5, 1.8 Hz, 1H), 7.14 (ddd, $J = 6.5$, 6.5, 1.8 Hz, 1H), 6.71 (s, 1H), 6.70 (d, $J = 5.5$ Hz, 1H), 6.57 (d, $J = 8.3$ Hz, 1H), 6.30 (s, 1H), 6.15 (s, 1H), 6.01 (s, 1H), 2.84 (s, 3H), 2.80 (s, 3H). *Anal*. Calc. for $(tpy)_2Ir(pzH)Cl$: C, 51.30; H, 3.83; N, 8.86. Found: C, 50.69; H, 3.45; N, 8.51%.

2.3.3. Synthesis of $(tpy)_2Ir(pzH)_2(CF_3SO_3)$: bis(2′-para-tolylpyridinato-N,$C^{2'}$)bis(pyrazole)iridium(III) trifluoromethylsulfate

$[(tpy)_2Ir(\mu\text{-}Cl)]_2$ (0.1 g, 0.09 mmol) and 2.1 equiv. AgOTf (0.05 g, 1.9 mmol) was dissolved in 10 ml of CH_2Cl_2 followed by 8 equiv. pyrazole (0.05 g, 0.74 mmol) to yield a cream-colored slurry. The slurry was stirred for 2 h at room temperature and the colored precipitate collected by filtration and dissolved in 30 ml acetone and refiltered. The acetone filtrate was evaporated to dryness to yield yellow $(tpy)_2Ir(pzH)_2(CF_3SO_3)$ (0.1 g, 70%). ^{1}H NMR (360 MHz, acetone-d_6), ppm: 12.26 (s, 2H), 8.84 (d, $J = 6.5$ Hz, 2H), 8.05 (d, $J = 8.0$ Hz, 2H), 7.97 (ddd, $J = 7.1$, 7.1, 1.8 Hz, 2H), 7.86 (s, 2H), 7.63 (s, 2H), 7.56 (d, $J = 8.0$ Hz, 2H), 7.38 (ddd, $J = 6.0$, 6.0, 1.8 Hz, 2H), 6.70 (d, $J = 8.0$ Hz, 2H), 6.42 (s, 2H), 6.24 (s, 2H), 2.84 (s, 6H). *Anal*. Calc. for $(tpy)_2Ir(pzH)_2CF_3SO_3$: C, 45.75; H, 3.47; N, 10.33. Found: C, 45.47; H, 3.15; N, 10.01%.

2.3.4. Synthesis of $(tpy)_2Ir(pz_2H)$: bis(2′-para-tolylpyridinato-N,$C^{2'}$)(pyrazolato)(pyrazole) iridium(III)

This complex can be prepared by four different methods.

Method A. $[(tpy)_2Ir(\mu\text{-}Cl)]_2$ (0.2 g, 0.18 mmol) was dissolved in 25 ml of CH_2Cl_2 followed by 4 equiv. $NaBEt_2pz_2$ (0.16 g, 7.2 mmol) and the solution was stirred for overnight at room temperature. The resultant slurry was filtered and the filtrate was collected and evaporated to dryness. The crude product was washed with 3×10 ml methanol. Recrystallization in CH_2Cl_2/MeOH gave a yellow product (0.07 g, yield 30%). ^{1}H NMR (500 MHz, $CDCl_3$), ppm: 19.9 (s, 1H), 7.76 (d, $J = 5.5$ Hz, 2H), 7.72 (d, $J = 7.4$ Hz, 2H), 7.66 (d, $J = 1.8$ Hz, 2H), 7.55 (ddd, $J = 7.4$, 7.4, 1.8 Hz, 2H), 7.46 (d, $J = 7.4$ Hz, 2H), 6.83 (ddd, $J = 6.5$, 6.5, 1.8 Hz, 2H), 6.71 (d, $J = 7.4$ Hz, 2H), 6.64 (d, $J = 1.8$ Hz, 2H), 6.12 (s, 2H), 6.07 (dd, $J = 1.8$, 1.8 Hz, 2H), 2.08 (s, 6H). *Anal*. Calc. for $(tpy)_2Ir(pz_2H)$: C, 54.28; H, 4.10; N, 12.66. Found: C, 53.62; H, 3.85; N, 12.28%.

Method B. $[(tpy)_2Ir(\mu\text{-}Cl)]_2$ (0.1 g, 0.09 mmol) was dissolved in 20 ml of CH_3CN followed by 4 equiv. $KBpz_4$ (0.14 g, 4 mmol). The solution was refluxed for 2 days under N_2 and was then evaporated to dryness under reduced pressure. The crude product was recrystallized in CH_2Cl_2/MeOH to give $(tpy)_2Ir(pz_2H)$ in 80% yield.

Method C. $(tpy)_2Ir(pzH)_2(CF_3SO_3)$ (0.2 g, 0.25 mmol) was added to 30 ml $CHCl_3$. After addition of 0.2 g MeONa, the solution was heated up to 70 °C for 2 h. The cooled solution was filtered and the filtrate was collected and evaporated to dryness. Recrystallization in CH_2Cl_2/MeOH gave $(tpy)_2Ir(pz_2H)$ (0.13 g, 80%).

Method D. $[(tpy)_2Ir(\mu\text{-}Cl)]_2$ (0.2 g, 0.18 mmol) was dissolved in 25 ml of CH_2Cl_2 followed by 4.4 equiv. pyrazole (0.05 g, 0.8 mmol) and 0.05 g MeONa. The solution was stirred for overnight at room temperature and the crude product was collected by filtration. The crude product was recrystallized in CH_2Cl_2/MeOH to give $(tpy)_2Ir(pz_2H)$ in 90% yield.

2.3.5. Synthesis of $(dfppy)_2Ir(acac)$: iridium(III) bis(4′,6′-difluorophenylpyridinato-N, $C^{2'}$) acetylacetonate

The compound was prepared according to a previously reported method [19], $[(dfppy)_2Ir(\mu\text{-}Cl)]_2$ (0.1 mmol), 0.3 mmol of 2,4-pentanedione, and 0.1 g sodium carbonate were refluxed under N_2 atmosphere in 1,2-dichloroethane for 12 h. After cooling to room temperature, the reaction mixture was evaporated to dryness. The pure yellow product (yield 80%) was obtained by chromatography in a silica/CH_2Cl_2 column.

^{1}H NMR (500 MHz, $CDCl_3$), ppm: 8.42 (d, $J = 5.6$ Hz, 2H), 8.23 (d, $J = 8.4$ Hz, 2H), 7.78 (ddd, $J = 7.4$, 7.4 Hz, 1.4 Hz, 2H), 7.17 (ddd, $J = 6.5$, 6.5, 1.4 Hz, 2H), 6.31 (ddd, $J = 8.4$, 8.4, 2.4 Hz, 2H), 5.63 (dd, $J = 3.7$, 2.4 Hz, 2H), 5.23 (s, 1H), 1.79 (s, 6H). *Anal.* Calc. for (*dfppy*)$_2$Ir(acac): C, 48.28; H, 2.85; N, 4.17. Found: C, 48.20; H, 2.61; N, 3.90%.

2.3.6. Synthesis of (dfppy)$_2$Ir(pz$_2$H): bis(4′,6′-difluorophenylpyridinato-N,C$^{2'}$)(pyrazolato)(pyrazole)iridium(III)

This yellow compound was prepared analogous to the synthesis of (*tpy*)$_2$Ir(pz$_2$H) (method D), and was obtained after recrystallization from MeOH/CH_2Cl_2 in 70% yield. ^{1}H NMR (360 MHz, $CDCl_3$), ppm: 20.01 (s, 1H), 8.19 (d, $J = 8.3$ Hz, 2H), 7.76 (dd, $J = 5.8$, 1.0 Hz, 2H), 7.68 (d, $J = 1.9$ Hz, 2H), 7.65 (dd, $J = 8.3$, 8.3Hz, 2H), 6.92 (vt, $J = 6.3$ Hz, 2H), 6.67 (d, $J = 1.9$ Hz, 2H), 6.41 (m, 2H), 6.12 (dd, $J = 1.9$, 1.9 Hz, 2H), 5.71 (dd, $J = 8.3$, 2.4 Hz, 2H). *Anal.* Calc. for (*dfppy*)$_2$Ir(pz$_2$H): C, 47.52; H, 2.71; N, 11.88. Found: C, 47.40; H, 2.49; N, 11.54%.

2.3.7. Synthesis of (dfppy)$_2$Ir(pz$_2$Bpz$_2$): iridium(III) bis(4′,6′-difluorophenylpyridinato-N,C$^{2'}$)η^2-tetrakis(1-pyrazolyl)borate

This yellow-greenish compound was prepared analogous to the synthesis of (*tpy*)$_2$Ir(pz$_2$Bpz$_2$), and was obtained after recrystallization from MeOH/CH_2Cl_2 in 60% yield. ^{1}H NMR (360 MHz, $CDCl_3$), ppm: 8.15 (d, $J = 8.3$ Hz, 2H), 7.72 (s, 2H), 7.60 (vt, $J = 7.8$ Hz, 2H), 7.28 (s, 2H), 7.13 (d, $J = 2.4$ Hz, 2H), 6.92 (d, $J = 1.5$ Hz, 2H), 6.74 (d, $J = 6.3$ Hz, 2H), 6.44 (m, 2H), 6.23 (vt, $J = 2.4$ Hz, 2H), 6.18 (s, 2H), 6.03 (s, 2H), 5.55 (dd, $J = 8.8$, 2.4 Hz, 2H). *Anal.* Calc. for (*dfppy*)$_2$Ir(pz$_2$Bpz$_2$): C, 47.95; H, 2.84; N, 16.45. Found: C, 47.65; H, 2.40; N, 16.05%.

3. Results and discussion

3.1. Synthesis and structure

Cyclometalated chloride-bridged Ir(III) dimers, [(CN)$_2$Ir(μ-Cl)]$_2$, can be readily converted to emissive, monomeric complexes by treating the dimer with acetylacetone and base [Eq. (1)] [19]. However, the related reaction, treating [(*tpy*)$_2$Ir(μ-Cl)]$_2$ with an excess of $Na^+pz_2BEt_2^-$, does not lead to the desired product, i.e. (*tpy*)$_2$Ir(pz$_2$BEt$_2$), but rather a protonated dipyrazolyl complex, (*tpy*)$_2$Ir(pz$_2$H), is formed in good yield (30%, Eq. (2)). This unexpected reaction product was characterized by a proton NMR spectrum that displays a sharp low-field singlet ($\delta = 19.9$ ppm) that is consistent with the presence of a strong N–H···N hydrogen bond. This chemical shift for the bridging proton is similar to those observed for iridium [38], osmium [39] and rhodium complexes [40], having the "pz$_2$H" ligand. In addition to spectroscopic and analytical characterization, the identity of (*tpy*)$_2$Ir(pz$_2$H) was confirmed by an X-ray crystal structure analysis, vide infra. A similar transformation was observed when [(*tpy*)$_2$Ir(μ-Cl)]$_2$ was treated with an excess of KBpz$_4$ in acetonitrile [Eq. (3)], giving (*tpy*)$_2$Ir(pz$_2$H) in high yield (80%). While we have not carried out a complete survey of pyrazolyl-borate ligands and solvents, it appears that the decomposition of the pyrazole borate ligand, and reaction to give (*tpy*)$_2$Ir(pz$_2$H), is not related to a solvent specific process

$$[(tpy)_2\mathrm{Ir}(\mu\text{-Cl})]_2 + \text{excess acacH} \xrightarrow[C_2H_4Cl_2,\text{reflux}]{Na_2CO_3} (tpy)_2\mathrm{Ir}(\text{acac}) \quad (1)$$

$$[(tpy)_2\mathrm{Ir}(\mu\text{-Cl})]_2 + \text{excess } Napz_2BEt_2 \xrightarrow[CH_2Cl_2,\mathrm{RT}]{} (tpy)_2\mathrm{Ir}(pz_2H) \quad (2)$$

$$[(tpy)_2\mathrm{Ir}(\mu\text{-Cl})]_2 + \text{excess } KBpz_4 \xrightarrow[CH_3CN,\text{reflux}]{} (tpy)_2\mathrm{Ir}(pz_2H) \quad (3)$$

Once the identity of (*tpy*)$_2$Ir(pz$_2$H) was established, efforts were made to prepare the complex by direct reaction between [(*tpy*)$_2$Ir(μ-Cl)]$_2$ and pyrazole. However, when [(*tpy*)$_2$Ir(μ-Cl)]$_2$ is treated with excess pyrazole in CH_2Cl_2 solution, the only observable product is (*tpy*)$_2$Ir(pzH)Cl. The proton NMR spectrum of (*tpy*)$_2$Ir(pzH)Cl shows a sharp low-field singlet ($\delta = 13.2$ ppm), suggesting the presence of a strong hydrogen bond (N–H···Cl) which stabilizes the complex against further substitution. A [OsCl(pzH)(H)(≡CCH$_2$Ph) (P^{i}Pr$_3$)$_2$]BF$_4$ complex was found to have a similar hydrogen bond between the pzH and Cl ligands and displays a similar proton resonance for the pyrazole bound proton ($\delta = 12.4$ ppm) [39]. Although pyrazole does not displace the bound chloride, addition of CF_3SO_3Ag to the reaction mixture abstracts the Ir bound chloride and leads to the formation of (*tpy*)$_2$Ir(pzH)$_2$(CF_3SO_3). Subsequent treatment of this dipyrazole cation with sodium methoxide yields the desired (*tpy*)$_2$Ir(pz$_2$H). Alternately, (*tpy*)$_2$Ir(pz$_2$H) can be prepared directly by reacting the dimer, [(*tpy*)$_2$Ir(μ-Cl)]$_2$, with excess pyrazole and NaOMe, without the need for the silver salt [Eq. (4)]. A similar synthetic method was reported for the synthesis of [Os(pz$_2$H)(H)(=C=CHPh) (P^{i}Pr$_3$)$_2$ [39]

$$[(tpy)_2\mathrm{Ir}(\mu\text{-Cl})]_2 + \text{excess pzH} \xrightarrow[CH_2Cl_2,\mathrm{RT}]{NaOMe} (tpy)_2\mathrm{Ir}(pz_2H) \quad (4)$$

It was initially suspected that the mere presence of chloride ion was responsible for the decomposition of pyrazolyl-borate, giving the protonated-dipyrazolyl ligand. Experiments showed that Na(pz$_2$BEt$_2$) partially

decomposes when heated with excess NMe_4Cl in either CD_2Cl_2 or CD_3CN. However, the rate of this decomposition reaction is markedly lower than the rate of $(tpy)_2Ir(pz_2H)$ formation [Eq. (2)]. Moreover, although we see chloride-mediated decomposition of the pyrazolyl-borate ligands, this is not commonly observed reaction. A wide range of metal complexes with poly (pyrazolyl)borate ligands have been prepared through the direct reaction between a metal chloride and the pyrazolyl-borate ligand [2,12,15,35]. For example, metal chlorides of first-row of transition metals react with $KBpz_4$ in aqueous solution, efficiently forming metal pyrazolyl-borate complexes [1,2,12]. For these complexes, however, the halide ligands are rapidly lost by solvolysis, leading to a metal-solvento complex, analogous to $(tpy)_2Ir(H_2O)_2^+$, which react cleanly, without pyrazolyl-borate decomposition. In light of that fact, we postulate that the presence of an Ir bound chloride ligand promotes the decomposition of the pyrazolyl-borate. Based on the previous reports that the ligating solvents, i.e., acetonitrile and DMF, do not dissociate the chloride from the Ir complex [18,24], it is plausible that the Ir dimer reacts with $pz_2BEt_2^-$ via a $(tpy)_2IrCl[\eta^1\text{-}pzB(pz)Et_2]^-$ intermediate, in a manner analogous to the formation of $(tpy)_2Ir(pzH)Cl$. Intramolecular attack of chloride at the pyrazolyl-borate ligand could then lead to cleavage of the pz-B bond.

It was found possible to prepare the desired pyrazolyl-borate complexes in good yields provided that the complex is chloride-free prior to the addition of the pyrazolyl-borate ligand. The removal of chloride can be accomplished by treating the dimer with CF_3SO_3Ag to first produce $(tpy)_2Ir(H_2O)_2(CF_3SO_3)$ [24]. This chloride-free Ir complex reacts with $K(pz_2BX_2)$ (X = pz, Ph) or $Na(pz_2BEt_2)$ in acetonitrile solution, forming the corresponding $(tpy)_2Ir(pz_2BX_2)$ complexes with yields of 40% to 70%

$$[(tpy)_2Ir(\mu\text{-}Cl)]_2 \xrightarrow[CH_2Cl_2/MeOH]{AgOTf} (tpy)_2Ir(H_2O)_2(CF_3SO_3) \xrightarrow[CH_3CN,\ reflux]{excess\ KBpz_4} (tpy)_2Ir(pz_2Bpz_2) \quad (5)$$

The same synthetic method can be applied to other cyclometalated complexes. For example, $(dfppy)_2Ir(pz_2H)$ and $(dfppy)_2Ir(pz_2Bpz_2)$ are prepared in a similar manner as given in Eqs. (4) and (5), respectively, in high yield.

3.2. Crystal structures

Single crystals of $(tpy)_2Ir(pz_2H)$, $(tpy)_2Ir(pz_2Bpz_2)$ and $(tpy)_2Ir(pz_2BEt_2)$ were prepared by slow evaporation of chloroform, while single crystals of a fourth compound, $(tpy)_2Ir(pzH)_2(CF_3SO_3)$, were prepared via slow evaporation of acetone. Molecular plots of $(tpy)_2Ir(pz_2H)$, $(tpy)_2Ir(pzH)_2(CF_3SO_3)$, $(tpy)_2Ir(pz_2Bpz_2)$ and $(tpy)_2Ir(pz_2BEt_2)$ are shown in Figs. 2 and 3. Crystallographic data are given in Table 1. Selected bond lengths for six Ir complexes with the same "tpy_2Ir" fragment, including *mer*–$Ir(tpy)_3$ [42] and $(tpy)_2Ir(acac)$ [19], are reported in Table 2. All of these complexes have an octahedral coordination geometry around Ir, retaining the *cis*-C,C *trans*-N,N chelate disposition of the chloride-bridged precursor complex, $[(tpy)_2Ir(\mu\text{-}Cl)]_2$. For the two *trans*-N,N atoms, the N–Ir–N angles in these complexes are between 172° and 175°. The Ir–C and Ir–N bond lengths among these $(tpy)_2Ir(LX)$ (LX = pyrazolyl and pyrazolyl-borate ligands) complexes are not significantly different from those reported for the "$(tpy)_2Ir$" fragment of $(tpy)_2Ir(acac)$.

In the structure of $(tpy)_2Ir(pz_2H)$, the two pyrazolyl rings are nearly coplanar, with a dihedral angle between the two pyrazolyl rings of 15°. Although we were unable to refine the position of bridging hydrogen atom of N–

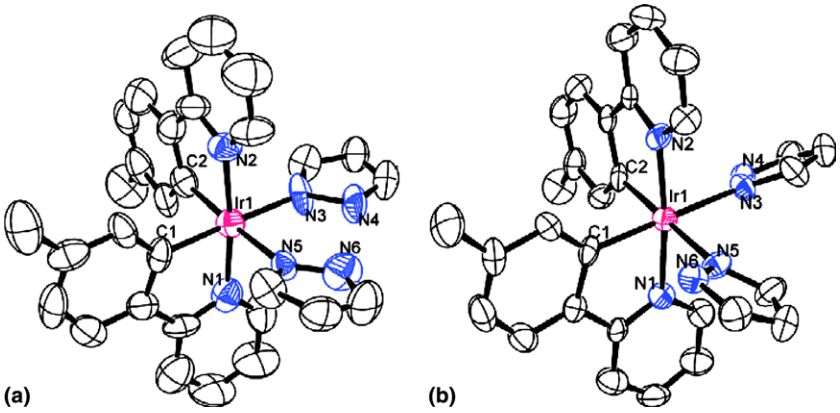

Fig. 2. ORTEP drawings of $(tpy)_2Ir(pz_2H)\cdot CHCl_3$ (a) and $(tpy)_2Ir(pzH)_2(CF_3SO_3)$ (b). The thermal ellipsoids for the image represent 50% probability limit. The hydrogen atoms, solvent, and counter anion are omitted for clarity.

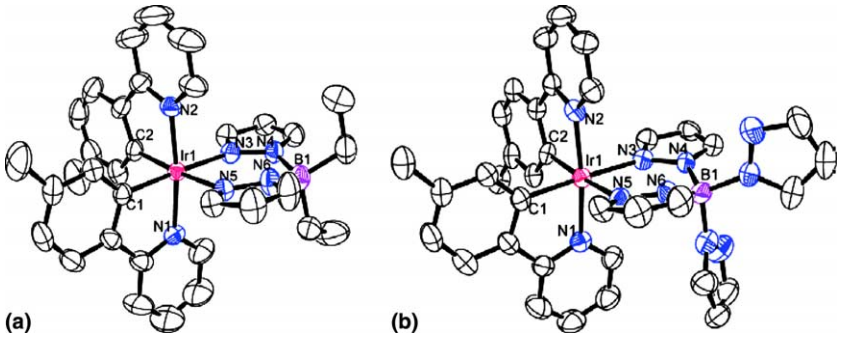

Fig. 3. ORTEP drawings of $(tpy)_2Ir(pz_2BEt_2)$ (a) and $(tpy)_2Ir(pz_2Bpz_2)$ (b). The thermal ellipsoids for the image represent 50% probability limit. The hydrogen atoms are omitted for clarity.

Table 2
Selected bond distance (Å) for $(tpy)_2Ir(X_1X_2)$

$(tpy)_2Ir(X_1X_2)$	Ir–C_1	Ir–C_2	Ir–N_1	Ir–N_2	Ir–X_1/N_3	Ir–X_2/N_5
mer-Ir(tpy_3)	2.020(8)	2.086(12)	2.065(8)	2.044(8)	2.076(10)	2.151(9)
$(tpy)_2Ir(acac)$	1.982(6)	1.985(7)	2.023(5)	2.040(5)	2.161(4)	2.136(4)
$(tpy)_2Ir(pz_2H)$	2.005(12)	2.020(13)	2.031(10)	2.042(9)	2.155(9)	2.181(10)
$(tpy)_2Ir(pzH)_2(CF_3SO_3)$	1.995(12)	1.995(12)	2.045(10)	2.045(10)	2.180(9)	2.180(10)
$(tpy)_2Ir(pz_2BEt_2)$	2.005(4)	2.007(4)	2.030(3)	2.033(3)	2.141(3)	2.137(3)
$(tpy)_2Ir(pz_2Bpz_2)$	2.009(5)	2.007(5)	2.044(4)	2.039(4)	2.147(4)	2.137(4)

H···N by X-ray crystallography, the existence of the bridging hydrogen atom could be inferred from the short $N_4\cdots N_6$ distance of 2.56 Å, consistent with a strong hydrogen bonding interaction [43]. The $Os(pz_2H)(H)(=C=CHPh)(P^iPr_3)_2$ [39], and $Rh((3,5\text{-}Me_2\text{-}4\text{-}NO_2\text{-}pz)_2H)(PPh_3)_2(H)_2$ [40] complexes have similar coordination geometries for the pz_2H ligand, with pz–pz dihedral angles of 4° and 12°, and N···N distances of 2.58 Å and 2.55 Å, respectively. In contrast to $(tpy)_2Ir(pz_2H)$, the two pyrazolyl rings of $(tpy)_2Ir(pzH)_2(CF_3SO_3)$ (Fig. 2(b)) are far from coplanar, with a 47° dihedral angle between the two pyrazoles. The two protonated nitrogen atoms of the pyrazolyl rings (N_4 and N_6) adopt an anti conformation.

The crystal structure of $(tpy)_2Ir(pz_2BEt_2)$ is presented in Fig. 3(a). The two pyrazolyl rings of this complex are nearly coplanar, with a dihedral angle (11°) similar to that found for the pyrazolyl ligands of $(tpy)_2Ir(pz_2H)$. The Ir–N–N–B–N–N ring of $(tpy)_2Ir(pz_2BEt_2)$ exhibits a *quasi*-chair conformation. The iridium atom lies 0.12(2) Å above the plane formed by the four pyrazolyl N atoms, while the boron atom is 0.43(2) Å below the same plane.

The *quasi*-chair conformation adopted by the Ir–N–N–B–N–N ring of $(tpy)_2Ir(pz_2BEt_2)$ is not common for metal complexes of diethyl-bis(pyrazolyl)borate. All of the other crystallographically characterized pz_2BEt_2 metal complexes show boat like conformations of the M–N–N–B–N–N ring, where M is a metal atom [44–47]. In some cases the boat conformation has been cited as evidence for a possible agostic interaction between the metal ion and the methylene proton from the pz_2BEt_2 ligand nearby [44]. However, boat conformations have also been observed for complexes where agostic interactions are not likely [45–47]. The other reported metal complexes of $pz_2BEt_2^-$ also show more marked deviations from the N_4 plane than those observed for $(tpy)_2Ir(pz_2BEt_2)$, i.e., boron atoms of the reported complexes lie 0.67–0.76 Å above the four nitrogen plane and the metal atoms range from 0.58 to 1.11 Å above the same plane. The complexes in which the metal shows the largest deviation from the N_4 plane (0.97 and 1.11 Å) have strong agostic interactions, stabilizing the boat conformation [45]. The two pyrazolyl rings of the agostic $pz_2BEt_2^-$ complexes have dihedral angles >70°, whereas the two pyrazolyl rings of $(tpy)_2Ir(pz_2BEt_2)$ are nearly coplanar. The relatively high dihedral angle for the agostic interactions is necessary to maximize the metal–pyrazolyl bonding interaction in the boat conformer. It therefore appears that the steric constraints of octahedral coordination sphere around the Ir atom, along with the absence of any agostic interaction to stabilize the boat conformation, leads to the rare *quasi*-chair conformation in $(tpy)_2Ir(pz_2BEt_2)$, with nearly coplanar pyrazolyl rings.

Fig. 3(b) shows the crystal structure of $(tpy)_2Ir(pz_2Bpz_2)$. Similar to $(tpy)_2Ir(pz_2BEt_2)$, the dihedral angle between the two coordinated pyrazolyl rings is relatively small, 17°. The Ir–N–N–B–N–N ring of $(tpy)_2Ir(pz_2Bpz_2)$ is in a *half*-chair conformation, where the iridium atom is in the least square plane of four

nitrogen atoms (Ir is 0.04(3) Å below the plane), while the boron atom lies 0.48(3) Å above the same plane. As expected, the two non-coordinated pyrazolyl rings of the η^2-pz_2Bpz_2 ligand are not coplanar, having a dihedral angle of 81°. The *half*-chair conformation is also more flattened than the typical boat conformation of the M–N–N–B–N–N ring [2]. The heights of boron atoms above the four nitrogen planes of η^2-pz_2Bpz_2 complexes fall within a fairly narrow range, i.e., in a range 0.56–0.67(6) Å, greater than is observed for $(tpy)_2Ir(pz_2Bpz_2)$ [17,48–51].

3.3. Photophysical properties

Fig. 4 shows absorption spectra of three different $(tpy)_2Ir(LX)$ complexes, i.e. $(tpy)_2Ir(pz_2Bpz_2)$, $(tpy)_2Ir(pz_2H)$ and $(tpy)_2Ir(acac)$, and the room temperature emission spectra of $(tpy)_2Ir(pz_2Bpz_2)$, $(tpy)_2Ir(pz_2H)$, $(tpy)_2Ir(pzH)Cl$, and $(tpy)_2Ir(acac)$ are shown in Fig. 5. Although all of them have the same "$(tpy)_2Ir$" fragment, there is a clear blue shift in the lowest energy absorption band as well as the maximum emission wavelength (λ_{max}), as the ancillary ligand is changed. Figs. 4 and 5 demonstrate that different ancillary ligands clearly influence the photophysical properties of $(tpy)_2Ir(LX)$ complexes. For example, $(tpy)_2Ir(pz_2Bpz_2)$ has the highest emission energy among all of $(tpy)_2Ir(LX)$ complexes, and its absorption band, ascribed to an MLCT transition [19], is the highest in energy among all of $(tpy)_2Ir(LX)$ complexes. Previous investigations have shown that the HOMOs (highest occupied molecular orbitals) of these Ir complexes are largely metal-centered, while the LUMOs (lowest unoccupied molecular orbitals), are primarily localized on the pyridyl rings of the cyclometalating ligands [52–54], thus the ancillary ligand is not directly involved in the lowest energy excited state. However, the ancillary ligand can alter the excited state energy by modifying the electron density at the metal center. A net electron-withdrawing ancillary ligand will pull electron density away from the iridium atom, thereby stabilizing the metal orbitals and lowering the HOMO energy, whereas the LUMO of the $(tpy)_2Ir(LX)$ complexes, localized on the pyridyl rings, is expected to be largely unaffected in energy. Consequently, the HOMO-LUMO gap should increase for stronger electron-withdrawing ancillary ligands, leading to a blue shift in both absorption and emission. [1] Substituting fluorine in the 4′, 6′-positions of the phenyl-

[1] Electrochemical studies of $(tpy)_2Ir(LX)$ complexes showed that the reduction potentials of $(tpy)_2Ir(LX)$ are largely unaffected, i.e., the reduction potentials of $(tpy)_2Ir(LX)$ stay in a narrow range between −2.62 and −2.68 V, while the oxidation potentials vary by as much as 400 mV between two different LX ligands, i.e., the oxidation potential of $(tpy)_2Ir(pz_2Bpz_2)$ is 310 mV higher than that of $(tpy)_2Ir(acac)$. The electrochemical properties of $(tpy)_2Ir(LX)$ complexes will be discussed in detail in a subsequent publication.

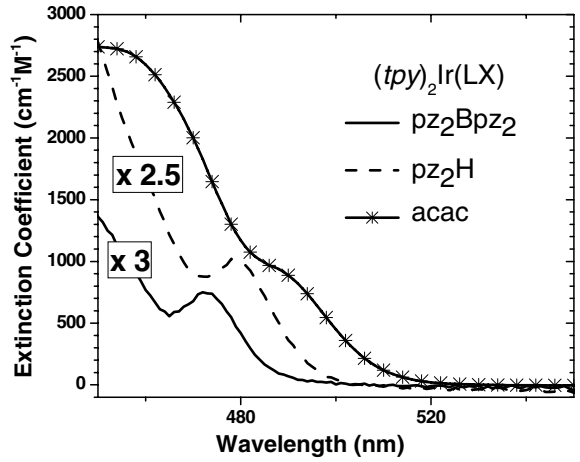

Fig. 4. Absorption spectra of $(tpy)_2Ir(pz_2Bpz_2)$, $(tpy)_2Ir(pz_2H)$ and $(tpy)_2Ir(acac)$ complexes in CH_2Cl_2.

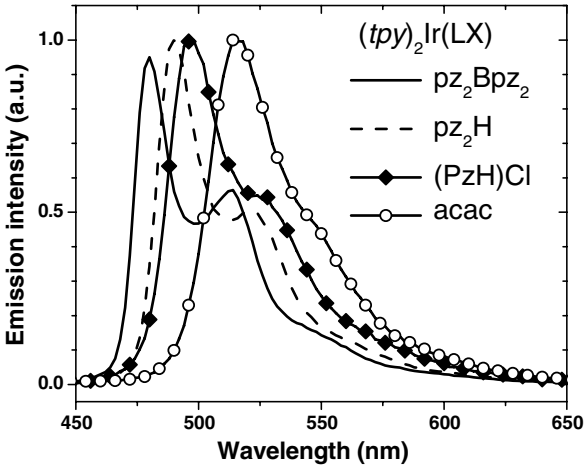

Fig. 5. Room temperature emission spectra of $(tpy)_2Ir(pz_2Bpz_2)$, $(tpy)_2Ir(pz_2H)$, $(tpy)_2Ir(pzH)Cl$, and $(tpy)_2Ir(acac)$ complexes in 2-MeTHF.

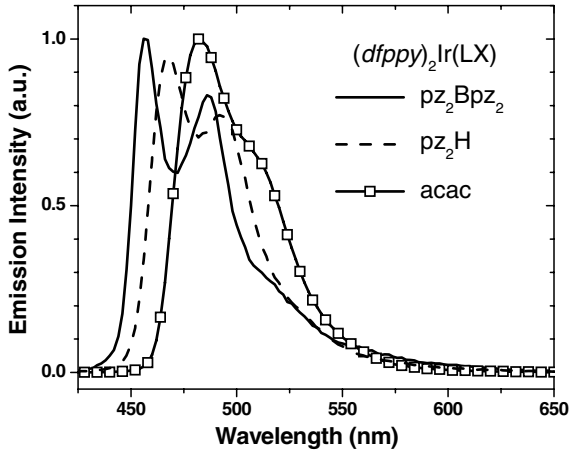

Fig. 6. Room temperature emission spectra of $(dfppy)_2Ir(pz_2Bpz_2)$, $(dfppy)_2Ir(pz_2H)$, and $(dfppy)_2Ir(acac)$ complexes in 2-MeTHF.

pyridyl ligand leads to a further blue shift in the emission energy, as expected from the luminescent properties of related tris-cyclometalated complexes [22,42,54]. The room temperature emission spectra of $(dfppy)_2$Ir(pz_2Bpz_2), $(dfppy)_2$Ir(pz_2H), and $(dfppy)_2$Ir (acac) are shown in Fig. 6. As observed for the *tpy* complexes, the $pz_2Bpz_2^-$ ligand blue shifts the emission spectra of $(dfppy)_2$Ir(LX) complexes relative to the other pyrazolyl ligands.

4. Conclusion

We have reported the synthesis and characterization of a family of organometallic Ir pyrazolyl and pyrazolylborate complexes. The pyrazolyl-borate complexes were prepared from dimer of chloride-bridged complexes [i.e., $((tpy)_2Ir(\mu\text{-}Cl))_2$] by first extracting the chloride ion with Ag^+ followed by treatment with the desired pyrazolylborate ligand, to give $(tpy)_2Ir(pz_2BR_2)$, R = Et, Ph, pz. The same synthesis can be applied to other cyclometalated complexes, e.g., $(dfppy)_2$Ir(LX). If the chloride is not removed by silver ion prior to treatment with the pyrazolyl-borate ligand, extensive ligand decomposition is observed. Crystallographic studies showed that the organometallic fragments of these complexes are not significantly affected by the choice of pyrazolyl ancillary ligands. Unlike other reported η^2-pyrazolyl-borate complexes, the $(tpy)_2Ir(pz_2BR_2)$ complexes show rare *half*-chair or *quasi*-chair conformations for the Ir–N–N–B–N–N ring, rather than the most common boat conformations that have been observed previously. While the choice of pyrazolyl-borate ligand does not change the structural properties of the "$(tpy)_2$Ir" fragment, it does markedly affect the photophysical properties of both $(tpy)_2Ir(pz_2BR_2)$ and $(dfppy)_2$Ir (pz_2BR_2) complexes. The pyrazolyl-borate ancillary ligands affect the absorption and emission energies of these complexes by tuning the metal (HOMO) orbital energies.

Many of the Ir complexes reported here are highly emissive at room temperature. For example, $(dfppy)_2$Ir (pz_2Bpz_2) is very useful as emissive dopant in blue phosphorescent OLEDs. Devices have been fabricated with $(dfppy)_2Ir(pz_2Bpz_2)$ doped films which have external efficiencies of >8%, and spectra that closely match the emission spectrum shown in Fig. 6 [55]. The tetrakis(pyrazolyl)borate ligand also offers the possibility of expanded coordination. The non-coordinated pyrazoles of $(tpy)_2Ir(pz_2Bpz_2)$ can be used to bind a second metal center [15,41]. Related dinuclear organometallic complexes have been reported for Pd and Ru complexes, but not, thus far, for photoactive metal fragments such as the Ir complexes reported here. The ability to make homo-metallic and hetero-metallic complexes of this type may lead to further applications of cyclometalated Ir complexes, such as photosensitizers [56] and donor–acceptor dyads [57].

5. Supporting information available

Tables of crystal data, atomic coordinates, bond distances, bond angles, and anisotropic displacement parameters for $(tpy)_2Ir(pz_2H)$, $(tpy)_2$ $Ir(pzH)_2(CF_3SO_3)$, $(tpy)_2Ir(pz_2BEt_2)$, and $(tpy)_2Ir(pz_2Bpz_2)$, as well as the corresponding CIF files are available on request from the authors.

Acknowledgements

The authors thank Universal Display Corporation and the Defense Advanced Research Projects Agency for financial support of this work.

References

[1] S. Trofimenko, J. Am. Chem. Soc. 89 (1967) 3170.
[2] (a) S. Trofimenko, Chem. Rev. 93 (1993) 943;
(b) S. Trofimenko, Scorpionates: The Coordination Chemistry of Polypyrazolylborate Ligands, Imperial College Press, London, 1999, p. 943;
(c) S. Trofimenko, Prog. Inorg. Chem. 34 (1986) 115.
[3] A. Shaver, Comprehensive Coordination Chemistry, vol 2, Pergamon, New York, 1987.
[4] S.K. Ritter, CE & EN News 81 (17) (2003) 40.
[5] F.A. Cotton, G. Wilkinson, M. Bochman, C.A. Murillo, Advanced Inorganic Chemistry, Wiley-Interscience, New York, 1999.
[6] N. Kitajima, W.B. Tolman, Prog. Inorg. Chem. 43 (1995) 419.
[7] G. Parkin, Adv. Inorg. Chem. 42 (1995) 291.
[8] M. Onishi, S. Kumagae, K. Asai, H. Kawano, Y. Shigemitsu, Chem. Lett. (2001) 96.
[9] M. Paneque, S. Sirol, M. Trujillo, E. Gutierrez-Puebla, M.A. Monge, E. Carmona, Angew. Chem., Int. Ed. 39 (2000) 218.
[10] J. Vicente, M.T. Chicote, R. Guerrero, U. Herber, D. Bautista, Inorg. Chem. 41 (2002) 1870.
[11] G.G.L. Effendi, G.G. Lobbia, C. Pettinari, C. Santini, B.W. Skelton, A.H. White, J. Chem. Soc., Dalton Trans. (1998) 2739.
[12] T. Kitano, Y. Sohrin, Y. Hata, H. Kawakami, T. Hori, K. Ueda, J. Chem. Soc., Dalton Trans. (2001) 3564.
[13] (a) D.M. Tellers, R.G. Bergman, J. Am. Chem. Soc. 123 (2001) 11508;
(b) D.M. Tellers, R.G. Bergman, J. Am. Chem. Soc. 122 (2000) 954;
(c) J.S. Wiley, D.M. Heinekey, Inorg. Chem. 41 (2002) 4961;
(d) E. Gutierrez-Puebla, A. Monge, M. Paneque, M.L. Poveda, V. Salazar, E. Carmona, J. Am. Chem. Soc. 121 (1999) 248;
(e) D.M. Tellers, R.G. Bergman, Organometallics 20 (2001) 4819.
[14] A.A. Bowden, R.P. Hughes, D.C. Lindner, C.D. Incarvito, L.M. Liable-Sands, A.L. Rheingold, J. Chem. Soc., Dalton Trans. (2002) 3245.
[15] L. Huang, K.J. Seward, B.P. Sullivan, W.E. Jones, J.J. Mecholsky, W.J. Dressick, Inorg. Chim. Acta 310 (2000) 227.

[16] (a) N. Moliner, L. Salmon, L. Capes, M.C. Munoz, J.-F. Letard, A. Bousseksou, J.-P. Tuchagues, J.J. McGarvey, A.C. Dennis, M. Castro, R. Burriel, J.A. Real, J. Phys. Chem. B 106 (2002) 4276;
(b) N. Armaroli, G. Accorsi, F. Barigelletti, S.M. Couchman, J.S. Fleming, N.C. Harden, J.C. Jeffrey, K.L.V. Mann, J.A. McCleverty, L.H. Rees, S.R. Starling, M.D. Ward, Inorg. Chem. 38 (1999) 5769;
(c) Z.R. Reeves, K.L.V. Mann, J.C. Jeffrey, J.A. McCleverty, M.D. Ward, F. Barigelletti, N. Armaroli, J. Chem. Soc., Dalton Trans. (1999) 349.
[17] P. Cecchi, B. Bovio, G.G. Lobbia, C. Pettinari, D. Leonesi, Polyhedron 14 (17) (1995) 2441.
[18] S. Sprouse, K.A. King, P.J. Spellane, R.J. Watts, J. Am. Chem. Soc. 106 (1984) 6647.
[19] S. Lamansky, P. Djurovich, D. Murphy, F. Abdel-Razzaq, R. Kwong, I. Tsyba, M. Bortz, B. Mui, R. Bau, M.E. Thompson, Inorg. Chem. 40 (2001) 1704.
[20] (a) V.V. Grushin, N. Herron, D.D. LeCloux, W.J. Marshall, V.A. Petrov, Y. Wang, Chem. Commun. (2001) 1494;
(b) Y. Wang, N. Herron, V.V. Grushin, D. LeCloux, V. Petrov, Appl. Phys. Lett. 79 (2001) 449.
[21] J.C. Ostrowski, M.R. Robinson, A.J. Heeger, G.C. Bazan, Chem. Commun. (2002) 784.
[22] C. Adachi, R.C. Kwong, P. Djurovich, V. Adamovich, M.A. Baldo, M.E. Thompson, S.R. Forrest, Appl. Phys. Lett. 79 (2001) 2082.
[23] (a) N. Sutin, Acc. Chem. Res. 1 (1968) 225;
(b) T.J. Meyer, Acc. Chem. Res. 11 (1978) 94.
[24] B. Schmid, F.O. Garces, R.J. Watts, Inorg. Chem. 33 (1994) 9.
[25] (a) K.A. Belmore, R.A. Vanderpool, J.-C. Tsai, M.A. Khan, K.M. Nicholas, J. Am. Chem. Soc. 110 (1988) 2004;
(b) N.D. Silavwe, A.S. Goldman, R. Ritter, D.R. Tyler, Inorg. Chem. 28 (1989) 1231.
[26] (a) J.N. Demas, E.W. Harris, R.P. McBride, J. Am. Chem. Soc. 99 (1977) 3547;
(b) J.N. Demas, E.W. Harris, C.M. Flynn, J.D. Diemente, J. Am. Chem. Soc. 97 (1975) 3838;
(c) R. Gao, D.G. Ho, B. Hernandez, M. Selke, D. Murphy, P.I. Djurovich, M.E. Thompson, J. Am. Chem. Soc. 124 (2002) 14828.
[27] (a) M.A. Baldo, D.F. O'Brien, Y. You, A. Shoustikov, S. Sibley, M.E. Thompson, S.R. Forrest, Nature 395 (1998) 151;
(b) M.A. Baldo, S. Lamansky, P.E. Burrows, M.E. Thompson, S.R. Forrest, Appl. Phys. Lett. 75 (1999) 4;
(c) M.E. Thompson, P.E. Burrows, S.R. Forrest, Curr. Opin. Solid State Mater. Sci. 4 (1999) 369;
(d) M.A. Baldo, M.E. Thompson, S.R. Forrest, Nature 403 (2000) 750.
[28] (a) S. Lamansky, P.I. Djurovich, F. Abdel-Razzaq, S. Garon, D.L. Murphy, M.E. Thompson, J. Appl. Phys. 92 (2002) 1570;
(b) F.C. Chen, Y. Yang, M.E. Thompson, J. Kido, Appl. Phys. Lett. 80 (2002) 2308;
(c) J.P.J. Markham, S.-C. Lo, S.W. Magennis, P.L. Burn, I.D.W. Samuel, Appl. Phys. Lett. 80 (2002) 2645;
(d) W. Zhu, Y. Mo, W. Yuan, Y. Cao, Appl. Phys. Lett. 80 (2002) 2045.
[29] P.A. Lane, L.C. Palilis, D.F. O'Brien, C. Giebeler, A.J. Cadby, D.G. Lidzey, A.J. Campbell, W. Blau, D.D.C. Bradley, Phys. Rev. B 63 (2001) 235206.
[30] C. Adachi, M.A. Baldo, S.R. Forrest, M.E. Thompson, Appl. Phys. Lett. 77 (2000) 904.
[31] M.G. Colombo, T.C. Brunold, T. Riendener, H.U. Gudel, M. Fortsch, H.-B. Burgi, Inorg. Chem. 33 (1994) 545.
[32] G.M. Sheldrick, SHELXTL, version 5.1, Bruker Analytical X-ray System, Inc., Madison, WI, 1997.
[33] R.H. Blessing, Acta Crystallogr., A 51 (1995) 33.
[34] O. Lohse, P. Thevenin, E. Waldvogel, Synlett. 1 (1999) 45.
[35] K.R. Breakell, D.J. Patmore, A. Storr, J. Chem. Soc., Dalton Trans. (1975) 749.
[36] L. Komorowski, W. Maringgele, A. Meller, K. Niedenzu, J. Serwatowski, Inorg. Chem. 29 (1990) 3845.
[37] M. Nonoyama, Bull. Chem. Soc. Jpn. 47 (1974) 767.
[38] D. Carmona, L.A. Oro, M.P. Lamata, J. Elguero, M.C. Apreda, C. Foces, F.H. Cano, Angew. Chem., Int. Ed. Engl. 25 (1986) 1114.
[39] M.A. Esteruelas, M. Olivan, E. Onate, N. Ruiz, M.A. Tajada, Organometallics 18 (1999) 2953.
[40] G.A. Ardizzoia, S. Brenna, G. LaMonica, A. Maspero, N. Masciocchi, M. Moret, Inorg. Chem. 41 (2002) 610.
[41] J. Ruiz, F. Florenciano, V. Rodriguez, C.D. Haro, G. Lopez, J. Perez, Eur. J. Inorg. Chem. 10 (2002) 2736.
[42] A.B. Tamayo, B.D. Alleyne, P.I. Djurovich, S. Lamansky, I. Tsyba, N.H. Ho, R. Bau, M.E. Thompson, J. Am. Chem. Soc. 125 (2003) 7377.
[43] (a) The N···N distance of a proton sponge, i.e., protonated *N*,*N*-9-bis(benzylmethyl)-1,8-diaminonaphthalene iodide, is 2.65 Å, while the N···N distance of neutral compound, i.e., *N*,*N*-9-bis(benzylmethyl)-1,8-diaminonaphthalene, is 2.81 Å. Ref: J.P.H. Charmant, G.C. Lloyd-Jones, T.M. Peakman, R.L. Woodward, Tetrahedron Lett. 39 (1998) 4733;
(b) J.P.H. Charmant, G.C. Lloyd-Jones, T.M. Peakman, R.L. Woodward, Eur. J. Org. Chem. 10 (1999) 2501.
[44] (a) F.A. Cotton, R.L. Luck, Inorg. Chem. 28 (1989) 3210;
(b) F.A. Cotton, T. LaCour, A.G. Stanislowski, J. Am. Chem. Soc. 96 (1974) 754;
(c) F.A. Cotton, Inorg. Chem. 41 (2002) 643.
[45] F.A. Cotton, G.N. Mott, Inorg. Chem. 22 (1983) 1136.
[46] B.W. Davies, N.C. Payne, J. Organomet. Chem. 102 (1975) 245.
[47] H.M. Echols, D. Dennis, Acta Crystallogr., B 30 (1974) 2173.
[48] A. Paulo, A. Domingos, I. Santos, Inorg. Chem. 35 (1996) 1798.
[49] G.G. Lobbia, P. Cecchi, F. Giordano, C. Santini, J. Organomet. Chem. 515 (1996) 213.
[50] G.G.L. Effendi, G.G. Lobbia, M. Pellei, C. Pettinari, C. Santini, B.W. Skelton, A.H. White, Inorg. Chim. Acta 315 (2001) 153.
[51] C.H. Dungan, W. Maringgele, A. Meller, K. Niedenzu, H. Noth, J. Serwatowska, J. Serwatowski, Inorg. Chem. 30 (1991) 4799.
[52] Y. Ohsawa, S. Sprouse, K.A. King, M.K. DeArmond, K.W. Hanck, R.J. Watts, J. Phys. Chem. 91 (1987) 1047.
[53] P.J. Hay, J. Phys. Chem. A 106 (2002) 1634.
[54] J. Brooks, Y. Babayan, S. Lamansky, P.I. Djurovich, I. Tsyba, R. Bau, M.E. Thompson, Inorg. Chem. 41 (2002) 3055.
[55] R.J. Holmes, B.W. D'Andrade, S.R. Forrest, X. Ren, J. Li, M.E. Thompson, Appl. Phys. Lett. 83 (2003) 3818.
[56] (a) M.A. Subhan, T. Suzuki, S. Kaizaki, J. Chem. Soc., Dalton Trans. (2002) 1416;
(b) T. Sanada, T. Suzuki, T. Yoshida, S. Kaizaki, Inorg. Chem. 37 (1998) 4712;
(c) S.I. Klink, H. Keizer, F.C.J.M. van Veggel, Angew. Chem., Int. Ed. 39 (23) (2000) 4319.
[57] M. Kercher, B. Konig, H. Zieg, L. DeCola, J. Am. Chem. Soc. 124 (2002) 11541.

Available online at www.sciencedirect.com
SCIENCE DIRECT®
Polyhedron 23 (2004) 429–438
POLYHEDRON
www.elsevier.com/locate/poly

Photoelectron spectra of potassium salts of hydrotris(pyrazol-1-yl)borates: electronic structure of the electron withdrawing scorpionates $Tp^{(CF_3)_2}$, Tp^{*Cl} and comparison to Tp* and Tp

Hemant K. Joshi, Michael E. Arvin, Jason C. Durivage, Nadine E. Gruhn, Michael D. Carducci, Barry L. Westcott [1], Dennis L. Lichtenberger, John H. Enemark [*,2]

Department of Chemistry, The University of Arizona, Tucson, AZ 85721, USA

Received 25 June 2003; accepted 8 October 2003

Abstract

The electronic structures of the potassium salts of the homoscorpionates hydrotris(3,5-dimethylpyrazol-1-yl)borate (Tp*, **1**), hydrotris(4-chloro-3,5-dimethylpyrazol-1-yl)borate (Tp^{*Cl}, **2**) and hydrotris(3,5-bis(trifluoromethyl)pyrazol-1-yl)borate ($Tp^{(CF_3)_2}$, **3**) are compared using gas-phase photoelectron spectroscopy and density functional theory (DFT). DFT calculations also are reported for the generic scorpionate potassium (hydrotris(pyrazol-1-yl)borate) (KTp). This is the first such experimental probe of the electronic structure of halogen containing scorpionate ligands and subtle differences in the ionizations from the frontier orbitals in the photoelectron spectra of **1** and **3** are observed that give insight into the influence of substituents upon metal–scorpionate bonding. Distinct assignments of the ionizations from the nitrogen σ-donor orbitals (σ_N) and σ_{BH} molecular orbitals are possible experimentally by the use of variable (He I and He II) excitation energies. The experimentally observed first ionization energy of **3** is stabilized by ~2.0 eV relative to **1** due to the strong electron withdrawing effect of the trifluoromethyl groups. The photoelectron spectroscopic studies of $NaTp^{(CF_3)_2}$ further confirm the assignments of ionizations from σ_N orbitals for **3** associated with the *a* and *e* sets in C_3 symmetry. The X-ray crystal structure of **2** as the (μ-aqua)$_3$(potassium hydrotris(4-chloro-3,5-dimethylpyrazol-1-yl)borate)$_2$ dimer is also reported.
© 2003 Elsevier Ltd. All rights reserved.

Keywords: Hydrotris(pyrazol-1-yl)borates; Scorpionates; Polypyrazolylborates; Photoelectron spectra

1. Introduction

Scorpionates based on polypyrazolylborates are a well-known class of ligands with very rich coordination chemistry [1–3]. One of the most symmetric (C_{3v}) of these, hydrotris(pyrazol-1-yl)borate (Tp), is a generic tridentate monoanionic ligand (Fig. 1). Symmetrically substituted Tp ligands (Fig. 1) that conserve pseudo-C_3 symmetry and coordinate to a metal center in a tridentate fashion are called homoscorpionates. Complexes of the Tp-based ligands are known for most of the metals in the periodic table. Substitutions at the 3, 4 and 5 positions of the pyrazole in the Tp framework allow both steric and electronic control of metal centers by restricting the number and the positions of vacant coordination sites [4–6], the size and/or shape of the substrates [7] and by stabilizing electron rich [8,9] or electron poor [6,10] metal centers. One example of such substitution at the 3 and 5 positions of the pyrazole ring is the trifluoromethyl (CF_3) group. The resulting

* Corresponding author. Tel.: +1-520-621-2245; fax: +1-520-626-8065.
E-mail address: jenemark@u.arizona.edu (J.H. Enemark).
[1] Present address: Department of Chemistry, Central Connecticut State University, New Britain, CT 06050, USA.
[2] Contribution for the Special Feature Issue on Scorpionate Chemistry. Dedicated to Swiatoslaw (Jerry) Trofimenko in recognition of his landmark contributions to the development of scorpionate compounds and his enthusiastic encouragement of others to pursue their fascinating chemistry.

0277-5387/$ - see front matter © 2003 Elsevier Ltd. All rights reserved.
doi:10.1016/j.poly.2003.11.027

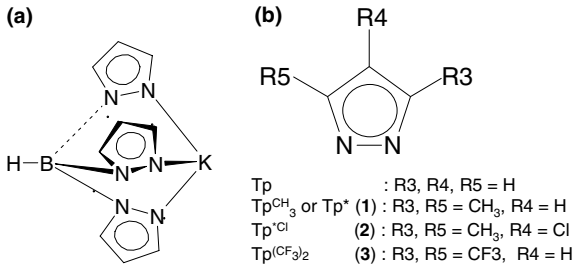

Fig. 1. (a) A generic tripodal scorpionate ligand hydrotris(pyrazol-1-yl)borate; KTp. (b) Examples of substitutions at 3 and 4 positions of the pyrazole ring. These substitutions retain the C_3 symmetry of the adducts.

hydrotris(3,5-bis(trifluoromethyl)pyrazol-1-yl)borate ($Tp^{(CF_3)_2}$) ligand is structurally similar to its methylated analogue hydrotris(3,5-dimethylpyrazol-1-yl)borate (Tp*), and therefore, allows perturbations of ligand electronic effects without significant perturbations in steric factors. Polyfluorinated ligands such as $Tp^{(CF_3)_2}$ commonly improve the volatility and oxidation resistance of their metal complexes [11,12]. They have very electrophilic metal centers relative to their hydrocarbon analogues (Tp*) [11,12].

Another widely accepted family of ligands in organometallic chemistry is the derivatives of the cyclopentadienyl (η^5-$C_5H_5^-$, Cp) ligands. The Tp and the Cp ligands are both monoanionic and formally six-electron donors, but one notable difference lies in the mode of their ligation to metals. The Cp-based ligands involve a π-type interaction with the metal centers whereas the Tp-based ligands are primarily σ-donors, with the exception of the recent report of a η^5-$Tp^{CF3,CH3}$ potassium π-bonding interaction by Gorun et al. [13]. Bergman and co-workers [14] have compared the relative electron-donating abilities of Tp and Cp and found a lack of generalization as any comparison varies with the identity of the metal, its oxidation state and other ligands present. Pioneering research work in the area of C–H bond activation by Jones and Feher [15] and Tellers and Bergman [16] has compared the differences in reactivity of related Tp and Cp transition metal complexes. A recent theoretical study of methane activation by $TpRe(CO)_2$ and $CpRe(CO)_2$ compounds reported by Cundari and co-workers [17] reveals that the Tp framework is more stereoelectronically flexible than Cp.

Previous photoelectron spectroscopic studies have been reported on the metal complexes of the Cp-based ligands and their electronic structure perturbation due to direct halogen (F, Cl) substitutions on the Cp rings [18]. However, the Cp ligands involving CF_3 substitutions are very difficult to synthesize and their metal adducts are rare in the literature. The analogous $Tp^{(CF_3)_2}$ ligands are well known [11,12] and they form stable metal adducts.

Na^+ or K^+ salts of the Tp-based ligands are used in almost all ligand transfer reactions for the synthesis of the transition metal adducts of these scorpionates. Previous structural characterization and computational work have been applied to these salts. Reglinski et al. have compared the Tp and the trismethylimazolyl borate (Tm) ligands by X-ray crystallography and ab initio calculations and found a clear difference in behavior on going from hard nitrogen donor atoms in Tp to soft sulfur donor atoms in Tm [19]. The X-ray crystal structures of the Na^+ or K^+ salts of several Tp-based ligands are known and have provided the starting geometry for our computational studies. The molecular structure of hydrotris(4-chloro-3,5-dimethylpyrazol-1-yl)borate (Tp^{*Cl}) is presented here. Fewer than 15 structures of metal adducts of Tp^{*Cl} are included in more than four hundred complexes containing scorpionate ligands that are reported in the Cambridge Structural Database (CSD).

Sterically demanding bulky ligands like the scorpionates discussed here are used to facially coordinate a metal and prevent the polynucleation of metal complexes. Several complexes of these ligands have been used in bioinorganic model chemistry [1,10]. One of the questions in this ligand chemistry is whether the ligand itself is chemically innocent. For example, Tp* ligands have been used to stabilize the oxo-molybdenum complexes that are minimum molecular models for the pyranopterin molybdenum and tungsten enzymes. EPR studies of the paramagnetic molybdenum center in these complexes [4,5] show very small ^{14}N superhyperfine interactions from the trispyrazolylborate nitrogen atoms. The Tp-based ligands are also silent for electronic absorption and MCD spectroscopies [20–22] and thus allow spectroscopic investigations of other coordinated biologically relevant functional groups/ligands and of the metals in the model complexes. A technique capable of assessing the metal and ligand characters of orbitals and studying the electronic structure of small molecules is gas-phase photoelectron spectroscopy using multiple energy ionization sources [23]. Photoelectron spectroscopic studies of the Mo adducts of the homoscorpionate Tp* have been reported earlier by our group [24,25] and others [26]. All of these studies found that the Tp* ligand has a very prominent signature in the 8–11 eV region of the photoelectron spectra of these Mo complexes, which could allow electronic structure studies of scorpionate ligands. However, these previous studies were focused on metal–sulfur ionizations that are located at lower ionization energies than the Tp*-based ionizations, and no attempts were made to explore the origin of the Tp* signatures (referred to as the "forest region" in these earlier studies). A series of photoelectron spectroscopic and computation studies using density functional theory were done to understand metal–halide interactions in $(Tp^*)MoO(X)_2$ (X = F, Cl, Cr, I) [27]. The importance of

understanding of the electronic structure of Tp* is illustrated by photoelectron spectroscopic studies of (Tp*)MoO(qdt) (qdt = quinoxaline dithiolate), where the Tp*-based ionizations overshadow the metal and sulfur-based ionizations [26]. Previous related photoelectron spectroscopy studies have investigated the electronic structure of pyrazole [28], several compounds containing the BH_4^- group [29a], poly(triazolyl)borato ligands [29b], and the parent Tp ligand [30,31]. Fragalà and coworkers [30,31] utilized a combination of semi-empirical theoretical calculations (complete neglect of differential overlap; CNDO) and photoelectron spectroscopy and found that in the scorpionate–metal adducts, the ionizations of the ligand-based molecular orbitals are generally unaffected by the nature of the central metal [31]. However, a detailed comparison among homoscorpionates using high-level density functional theory (DFT) and experimental gas-phase photoelectron spectroscopy has not been described. This report is the first gas-phase photoelectron spectroscopic investigation of the electronic structures of halogen containing scorpionates. The reported experimental and computational findings quantitates the electron withdrawing effects of CF_3 and Cl substituents on the Tp and Tp* ligand.

2. Experimental

2.1. General

All reactions were carried out under an inert atmosphere of argon using standard Schlenk techniques and a high-vacuum/gas double line setup. All glassware was dried in an oven at 150 °C and Schlenkware was further purged by repeated evacuation and inert gas flushes prior to use. Benzene and toluene were distilled from Na/benzophenone; triethylamine was distilled from Na/K amalgam [32]. The prepurified solvents were subsequently transferred and stored under N_2 over fresh drying agents. These solvents were freshly distilled under nitrogen prior to use, thoroughly degassed by repeated freeze–thaw–pump cycles, and transferred to reaction vessels via steel cannulae under a positive pressure of inert gas. Compounds **1**–**3** were prepared according to the literature procedures [2,3,11,12,33]. All of these compounds were purified by Soxhlet extraction and by sublimation as required. Mass spectra were recorded on a JEOL HX110 high-resolution sector instrument utilizing fast atom bombardment (FAB) ionization in a matrix of 3-nitrobenzyl alcohol (NBA). IR spectra (4000–400 cm^{-1}) were collected on a Nicolet Avatar ESP 360 FT-IR spectrophotometer in KBr disks or as dichloromethane solutions (between NaCl plates) at room temperature. Solvent background corrections were made in all cases. ^1H NMR ($CDCl_3$) spectra were acquired on a Bruker DRX-500 spectrometer operating at a ^1H frequency of 500.13 MHz using a 5 mm Nalorac triple-resonance 3-axis gradient probe. Chemical shifts were referenced to residual $CHCl_3$ at 7.24 ppm.

2.2. X-ray crystallography

2.2.1. Crystal structure of 2

A colorless block of **2** was mounted on a glass fiber for structure determination using a Bruker SMART 1000 CCD detector X-ray diffractometer. The X-ray quality crystals were obtained from hexanes. Key parameters for the structure determination are also summarized in Table 1. The structure was solved by direct methods using SHELXS in the Bruker SHELXTL (Version 5.0) software package. Refinements were performed on F^2 by full-matrix least squares with anisotropic displacement parameters for all the non-hydrogen atoms (using SHELXL and illustrations were made using XP). Hydrogen atoms were added at idealized positions, constrained to ride on the atom to which they are bonded and given thermal parameters equal to 1.2 or 1.5 times U_{iso} of that bonded atom. Scattering factors and anomalous dispersion were taken from International Tables vol. C, Tables 4.2.6.8 and 6.1.1.4 [34,35].

2.3. Photoelectron spectroscopy

Photoelectron spectra were recorded using an instrument that features a 36-cm radius, 8-cm gap hemispherical analyzer [36] and custom-designed excitation source, sample cells, and detection and control electronics that have been described in more detail [24]. The difference between the argon $^2P_{3/2}$ ionization at 15.759 eV and the methyl iodide $^2E_{1/2}$ ionization at 9.538 eV was used to calibrate the ionization energy scale. The argon $^2P_{3/2}$ ionization also was used as an internal calibration lock of the absolute ionization energy throughout data collection. During data collection the instrument resolution (measured using fwhm of the argon $^2P_{3/2}$ peak) was 0.020–0.035 eV. All data are intensity corrected with an experimentally determined instrument analyzer sensitivity function.

All samples sublimed cleanly with no detectable evidence of decomposition products in the gas phase or as a solid residue. The potassium and sodium salts of these ligands are hygroscopic and usually crystallize as a dimer with bridging water molecules. Contamination from the water of crystallization was observed in the photoelectron spectrum, but disappeared with time. Therefore, upon sublimation only the monomer is likely to be present in the gas phase. The sublimation temperatures were (°C, 10^{-4} Torr, monitored using a "K" type thermocouple passed through a vacuum feedthrough and attached directly to the sample cell) 210–225° for compound **1,** 195–230° for compound **2** and 50–60° for compound **3**.

Table 1
Crystal data and structure refinement for KTp^{*Cl}

Empirical formula	$C_{60}H_{86}B_2C_{l12}K_2N_{24}O_3$
Formula weight	429.19
Temperature (K)	170(2)
Wavelength (Å)	0.71073
Crystal system	rhombohedral
Space group	$R\bar{3}c$
Unit cell dimensions	
a (Å)	17.9560(4)
b (Å)	17.9560(4)
c (Å)	43.828(2)
α (°)	90
β (°)	90
γ (°)	120
Volume (Å^3)	12237.7(7)
Z	24
Density (calculated) (Mg/m^3)	1.398
Absorption coefficient (mm^{-1})	0.567
$F(000)$	5340
Crystal size (mm)	$0.44 \times 0.34 \times 0.21$
θ range for utilized data (°)	1.61–26.04
Limiting indices	$-21 \leqslant h \leqslant 22,\ -22 \leqslant k \leqslant 22,\ -54 \leqslant l \leqslant 54$
Reflections utilized	40 006
Independent reflections	2692 [$R_{int} = 0.0629$]
Completeness to $\theta = 26.04°$ (%)	99.9
Absorption correction	none
Maximum and minimum transmission	0.8902 and 0.7886
Refinement method	full-matrix least-squares on F^2
Data/restraints/parameters	2692/0/170
Goodness-of-fit on F^2	1.067
Final R indices [$I > 2\sigma(I)$]	$R_1 = 0.0384$, $wR_2 = 0.0883$
R indices (all data)	$R_1 = 0.0625$, $wR_2 = 0.1055$
Largest difference peak and hole (e Å^{-3})	0.334 and −0.252
RMS difference density (e Å^{-3})	0.063

For the photoelectron spectroscopy data presented in Figs. 3–7, the vertical length of each data mark represents the experimental variance of that point. The valence ionization bands are represented analytically with the best fit of asymmetric Gaussian peaks as described in more detail elsewhere [37]. The bands are defined with the position, amplitude, halfwidth for the high binding energy side of the peak, and the halfwidth for the low binding energy side of the peak. The number of peaks used in a fit was based solely on the features of a given band profile. The peak positions and halfwidths are reproducible to about ± 0.02 eV $\sim 3\sigma$. The parameters describing an individual Gaussian peak are less certain when two or more peaks are close in energy and overlap.

2.4. Theoretical methods

Calculations were performed on NaTp, KTp and **1**–**3** using the ADF (Amsterdam Density Functional theory calculations) package (release 2000.02). Starting geometries were obtained from crystal structures of NaTp [19] and **3** [11]. A generalized gradient approximation, with the exchange correction of Becke [38] and the correlation correction of Lee et al. [39], was used for all density functional calculations. All core levels (up to 2s for K, up to 1s for C, N, B and Na) were treated as frozen orbitals. The calculations employed triple-zeta basis sets with Slater type orbitals and a polarization function for all elements. Calculations on the ground-state molecules were performed in the spin-restricted mode. Spin-unrestricted ΔSCF (self-consistent field) calculations were performed on the proposed ion states formed by photoionization by removing one electron from the relevant orbital and comparing the total energy of the ion with that of the ground state molecule. The calculated ΔSCF energies and orbital energies were shifted by the difference between experimentally obtained and calculated energies of the highest occupied molecular orbital (HOMO) for comparison of the calculated ionization energies with the experimental ionization energies.

3. Results and discussions

3.1. Molecular structure of KTp^{*Cl}

The potassium salt of **2** was isolated as its H_2O adduct and characterized using X-ray crystallography. The

final refinement revealed that the (μ-aqua)$_3$ (potassium hydrotris(4-chloro-3,5-dimethylpyrazol-1-yl) borate)$_2$ dimer cocrystallized with unreacted 4-chloro-3,5-dimethylpyrazole. A perspective drawing of **2** is given in Fig. 2. The potassium atom is coordinated to three nitrogen atoms from pyrazole rings (Tp*^{Cl}) and three oxygen atoms of the three coordinated μ-aqua ligands. Crystal packing analysis reveals that the space group $R\bar{3}c$ imposes 32 (D_3) site symmetry on the molecule with a threefold axis passing through the two potassium atoms of the dimer and a twofold axis passing through the bridging oxygen atoms. The key bond lengths, angles and torsion angles are reported in Table 2.

The striking difference in the crystal structures of NaTp [19] and compounds **2** and **3** is the relative orientation of the pyrazole rings. The molecular structures of NaTp [19] and compound **3** feature pseudo-C_{3v} symmetry, whereas in **2** the propeller-shaped pyrazole rings reduce its symmetry to pseudo-C_3. The B–N–N–metal torsion angle containing nitrogen atoms of the same pyrazole ring is a sensitive parameter for this deviation and should be 0.0° for ideal C_{3v} symmetry. This torsion angle in **2** is −28.7°. This value is in contrast with the published structures of the Mo ([40] torsion angles of 3.72°, −4.68° and −15.83°) and Rh ([41], torsion angles of 4.07°, −0.94° and −2.72°) complexes of Tp*^{Cl}, and indicates that a large deviation from C_{3v} symmetry might be occurring due to the larger size of the potassium ion. The reported (Tp*^{Cl})$_2$Cu structure [42] also has a propeller-shaped arrangement of pyrazole rings (torsion angles of 17.15°, 24.92°, −15.54° and 17.54°, 25.60°, 19.07°). The Cl–C bond length of 1.728(2) in **2** is comparable to those of 1.724, 1.720 and 1.721 Å in the (Tp*^{Cl})Rh adduct and 1.697, 1.714 and 1.719 Å in the (Tp*^{Cl})Mo adduct.

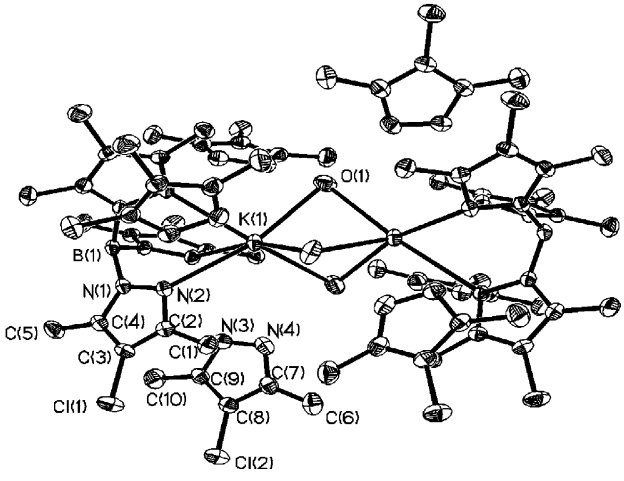

Fig. 2. The ORTEP drawings of (μ-aqua)$_3$(potassium hydrotris(4-chloro-3,5-dimethylpyrazol-1-yl)borate)$_2$dimer. The thermal ellipsoids are drawn at 50% probability level, and H atoms are not shown.

Table 2
Key bond lengths (Å), bond angles (°) and torsion angles (°) of KTp*^{Cl}

Bond lengths	
K(1)–N(2)	2.915(2)
N(1)–N(2)	1.382(2)
N(1)–B(1)	1.545(2)
N(1)–C(4)	1.359(3)
C(4)–C(3)	1.376(3)
C(2)–C(3)	1.393(3)
N(2)–C(2)	1.330(3)
C(4)–C(5)	1.491(3)
Cl(1)–C(3)	1.728(2)
C(2)–C(1)	1.495(3)
K(1)–O(1)	2.732(2)
Bond angles	
N(1)–N(2)–K(1)	120.39(13)
N(2)–N(1)–B(1)	122.5(2)
C(2)–N(2)–K(1)	122.26(15)
C(4)–N(1)–B(1)	126.8(2)
B(1)–N(1)–N(2)–K(1)	−28.7(2)

3.2. Gas-phase photoelectron spectroscopy

The gas-phase photoelectron spectra of **1**–**3** recorded with a He I photon source (21.2 eV) are shown in Fig. 3. There are several differences among these spectra that result from the changes in substituents on the pyrazole rings. In the ionization energy region greater than ∼12 eV the main differences among these three spectra are due to the addition or removal of ionizations associated with the C–Hσ bonds of the CH_3 substituents, the C–Fσ bonds of the CF_3 substituents, or the halogen lone pair ionizations of the Cl and CF_3 substituents. For example, the spectrum of **2** has one moderate and one sharp feature between 10.7 and 12 eV, which is the energy region expected for Cl lone pair ionizations (X) [18], while the spectrum of **3** contains much intensity in the region of 15–18 eV due to F lone pair ionizations. In general, however, the region of the photoelectron spectra greater than ∼12 eV gives very little information for these molecules due to the large number of overlapping ionizations present.

The region of the photoelectron spectra with ionization energies below ∼12 eV contains the most information that can be used to analyze the electronic differences between these scorpionate ligands. This region of the spectra is shown in more detail in Fig. 4. The features in this region and our assignments in general agree with those of NaTp and TlTp previously reported by Fragalà and co-workers [30,31]. Each of these spectra contain at lowest ionization energy an envelope of ionizations labeled A that is fairly well separated from all other ionizations. The ionizations under bands A can be assigned to the total of six possible linear combinations of the pyrazole π-orbitals, two from each pyrazole ring, each of which has one node. In the deconvolutions shown in Fig. 4 (positions of the Gaussians used in the

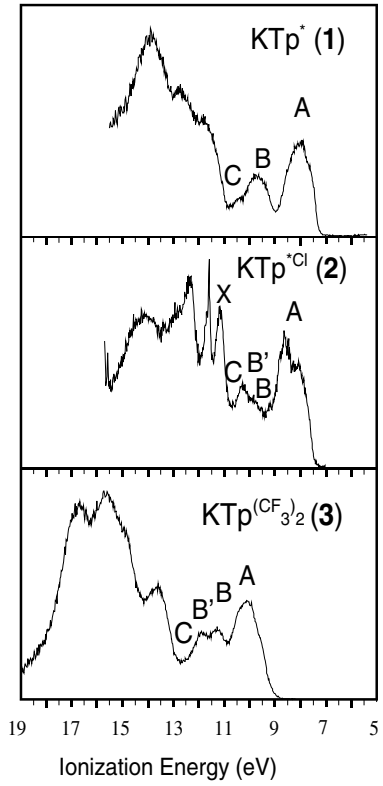

Fig. 3. The He I full photoelectron spectra of the potassium salts of: hydrotris(3,5-dimethylpyrazol-1-yl)borate, Tp* (**1**); hydrotris(4-chloro-3,5-dimethylpyrazol-1-yl)borate, Tp^{*Cl} (**2**); and hydrotris(3,5-bis(trifluoromethyl)pyrazol-1-yl)borate, $Tp^{(CF_3)_2}$ (**3**). All of the spectra have three general features labeled as bands A, B and C in the lower energy region. These bands are assigned as A: pyrazole-π ; B, B′: σ_N of the pyrazole nitrogen orbitals; C: σ_{BH} of the trispyrazole borate ligands; X: The chlorine lone pair based orbital.

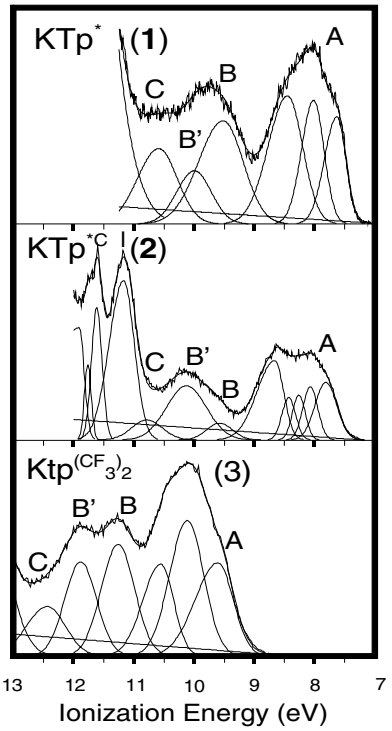

Fig. 4. The He I close up photoelectron spectra of KTp* (**1**); KTp^{*Cl} (**2**); and $KTp^{(CF_3)_2}$ (**3**). Bands A, B and C are assigned as in Fig. 3.

deconvolutions are listed in Table 3), bands A can be modeled with three Gaussians for **1** and **3**, but the shape of band A for **2** is different and deconvolution requires at least five Gaussians to fully describe the shape of the band. This extra structure is typical for π ionizations with halide substituents due to the sharpening of the ionizations with an admixture of lone pair character and also the presence of additional vibrational fine structure on the ionizations [18]. As the substituents are varied the ionizations under band A shift in energy but the spread of the ionizations does not change dramatically, indicating that all the ionizations under band A are approximately shifting by the same amount. If the position of the lowest energy Gaussian that is used to model the band is used as a measure of the shift, the total stabilization of band A from **1** to **3** is 1.98 eV, indicative of a very strong electron withdrawing effect of the trifluoromethyl substitutions.

In each of the photoelectron spectra the ionizations labeled as bands B and C are due to the σ_N and σ_{BH} molecular orbitals. Band C is not observed clearly because of proximity to other ionizations. According to group theory, for scorpionate ligands in C_3 symmetry the σ_N orbitals transform as *e* and *a* sets. The *a*-symmetry σ_N orbitals have the proper symmetry to overlap with the empty s orbital on K and therefore will be expected to be stabilized relative to the *e*-symmetry σ_N orbitals. In Fragalà and co-workers [30] previous study on NaTp there were two distinct bands in this energy region, and they assigned the *e*-symmetry σ_N ionization at lower ionization energy followed by the overlapping *a*-symmetry σ_N and σ_{BH} ionizations. In contrast, the spectra of **1**–**3** reported here all require three Gaussians to model the shape of the ionization envelope in this region.

To aid in the assignment of these ionizations, data were also collected on **1** and **2** with a He II excitation source (40.8 eV), which will change the relative intensity of ionizations depending upon the atomic character of the molecular orbitals with which they are associated [23,43,44]. A comparison of the He I and He II spectra of **1** is shown in Fig. 5. The most distinct difference between the spectra collected with different ionization sources is that the band labeled C decreases in intensity dramatically in the He II spectrum, as would be expected for the σ_{BH} ionization. The assignment of these ionizations of **1** is then that band B is the *e*-symmetry σ_N ionization, band B′ is the *a*-symmetry σ_N ionization and band C is the σ_{BH} ionization. Some splitting of the *e*-symmetry σ_N ionizations would be expected if the symmetry is lower than C_3, but any such splitting is not large enough to be experimentally observed. The He I

Table 3
Experimental ionization energies (I.E.), calculated absolute orbital eigenvalues ($-\varepsilon_i$) and calculated ΔSCF first ionization energies of compounds **1**–**3** (all values in eV)

Experimental I.E.	Calculated $-\varepsilon_i$ (shifted)[b]	$(-\varepsilon_i)$ HOMO	ΔSCF	Label and assignment
K(Tp*) (**1**)				
7.63–8.45[a]	7.63–8.08	4.66	6.66	band A, pyrazole-π
9.51, 9.99	8.93–9.31			band B, σ_N
10.58	9.88			band C, σ_{BH}
K(Tp*^{Cl}) (**2**)				
7.81–8.67[a]	7.81–9.41	4.87	6.64	band A, pyrazole-π
9.58, 10.13	9.66, 10.25			band B, σ_N
10.78	10.41			band C, σ_{BH}
K(Tp$^{(CF_3)_2}$) (**3**)				
9.61–10.55[a]	9.61–10.13	6.93	8.78	band A, pyrazole-π
11.26, 11.88	10.66–11.23			band B and B′, σ_N
12.44	11.88			band C, σ_{BH}

[a] Range of experiment I.E. values for Band A are taken from the positions of Gaussians used to deconvolute the data. This does not imply that these values are vertical ionization energies.
[b] Eigenvalues were shifted so the HOMO eigenvalue matches the position of the lowest energy Gaussian used to deconvolute the experimental data.

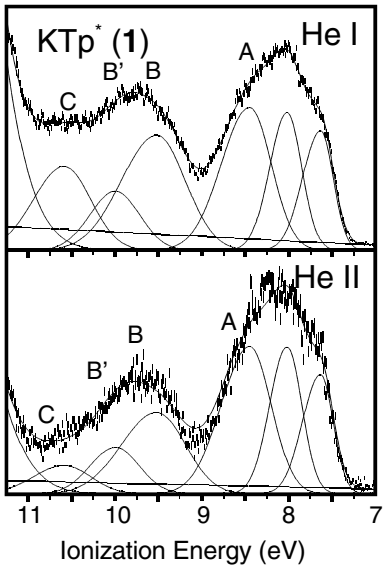

Fig. 5. The He I and He II close up spectra of KTp*. Ionizations associated with molecular orbitals with hydrogen contributions decrease in relative intensity with the He II source.

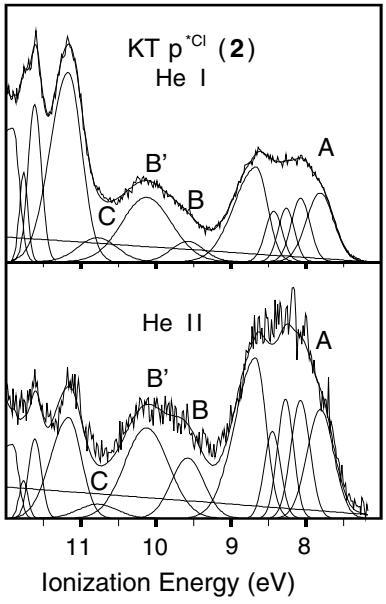

Fig. 6. The He I and He II close up spectra of K(Tp*^{Cl}). Ionizations associated with molecular orbitals with chlorine contribution decrease in relative intensity with the He II source.

and He II spectra of **2** shown in Fig. 6 can be assigned in a similar fashion, with the σ_{BH} ionization (C) assigned as the small shoulder on the high energy side of the band from 9.5 to 11 eV.

The σ_N and σ_{BH} ionizations also shift as the substituents on the pyrazole rings are varied. All three ionizations are stabilized for **2** as compared to **1**, and only slightly more than the pyrazole π ionizations under band A. In **3**, band C (σ_{BH}) shifts to higher ionization energy due to the electron withdrawing effect of the trifluoromethyl groups on the pyrazole rings.

Fragalà and co-workers [30] have reported changes in the position and the intensity of the σ_N ionizations for unsubstituted MTp as M is changed from Na to Tl. They have observed that the *a*-symmetry σ_N ionization is stabilized in the Tl complex due to the more covalent interaction of the nitrogen σ-donors orbitals with the softer Tl atom than with the relatively harder Na atom. The ionization of the nitrogen σ-donor orbitals (bands B and B′) for Tp* is shifted to higher ionization energy in the photoelectron spectra of molybdenum complexes [24,25] than for **1**, consistent with a more covalent nature of the interaction with the Mo metal center with the nitrogen-donor orbitals as compared to the K^+ cation. To further evaluate the effect that differences in metals have on the σ-donor abilities of more electron withdrawing scorpionate ligands, a photoelectron spectrum

was collected of $Na(Tp^{(CF_3)_2})$ for comparison to $K(Tp^{(CF_3)_2})$. Fig. 7 shows a stack plot of the close-up spectra of these Na and K adducts of $Tp^{(CF_3)_2}$. A slight shift to higher energy of bands B and B′ is observed in $Na(Tp^{(CF_3)_2})$ in comparison to $K(Tp^{(CF_3)_2})$, which is counterintuitive to the expectation that K^+ complexes should be more covalent than complexes containing the harder Na^+, but is consistent with the fact that Na^+ is more electronegative than K^+. These shifts might be due to the strong electron withdrawing effect of CF_3 in $Tp^{(CF_3)_2}$ resulting in electron deficient nitrogen atoms σ-bonded to the metal. These electron deficient (harder) σ-donor nitrogen atoms can interact better with hard Na^+ relative to K^+. The bands A, B and B′ are destabilized by 0.1, 0.28 and 0.62 eV, respectively, in the photoelectron spectrum of $K(Tp^{(CF_3)_2})$ in comparison to $Na(Tp^{(CF_3)_2})$. A significant destabilization of B′ from the Na to the K adduct is further evidence of its assignment to the *a* set of symmetric σ-donor nitrogen orbitals, which is the right symmetry to have overlap bonding with the unfilled symmetric metal s orbitals and hence is affected the most by metal substitution.

3.3. Computational results

Geometry optimization of NaTp beginning from the reported crystal structure [19] converged without significant changes in the geometry. We used this ligand geometry as a starting point for the geometry optimization of the KTp, **1** and **2**. Geometry optimization of **3** started with the crystal structure coordinates [11]. A similar pattern of molecular orbitals was calculated for KTp and for compounds **1**–**3**. The results for KTp are generalized and discussed below in detail, with representative molecular orbitals plotted in Fig. 8. The lowest unoccupied molecular orbital (LUMO), has primarily metal s character (Fig. 8(a)), and is well isolated (4.216 eV in KTp) from the filled ligand-based molecular orbitals. The highest occupied and several lower energy molecular orbitals that are closely spaced in energy (HOMO to HOMO-5) are primarily pyrazole-π in character, as shown by the molecular orbital plots for the HOMO and HOMO-1 in Figs. 8(b) and (c). These orbitals correspond to the ionizations under band A of the photoelectron spectra for **1**–**3** (Fig. 3).

These pyrazole-π orbitals are separated by 0.68 eV from the next group of molecular orbitals that comprise mainly the σ-donor nitrogen orbitals of the pyrazole rings. These σ-donor nitrogen orbitals are *e* and *a*-symmetry orbitals in C_3 symmetry. The orbital with the correct symmetry to interact with the metal-s orbital (K 4s) is plotted in Fig. 8(d). A third type of calculated molecular orbital is 0.68 eV more stable than the σ-donor combination of the nitrogen orbitals discussed above. This molecular orbital is σ_{BH} in character (Fig. 8(e)) and corresponds to the ionization occurring under band C in Figs. 3–6 for **1**–**3**.

The computed molecular orbital energies and ΔSCF estimate of calculated ionization energies for removal of an electron from **1** to **3** are reported in Table 3, and plots of the HOMO of each of these molecules are shown in Fig. 9. The calculated HOMO for **2** (Fig. 9) has significant chlorine character (~20%). This corroborates well with the experimental finding of the halogen character in frontier molecular orbitals of **2** discussed earlier. The substitution of CF_3 in **3** results in a very strong electron

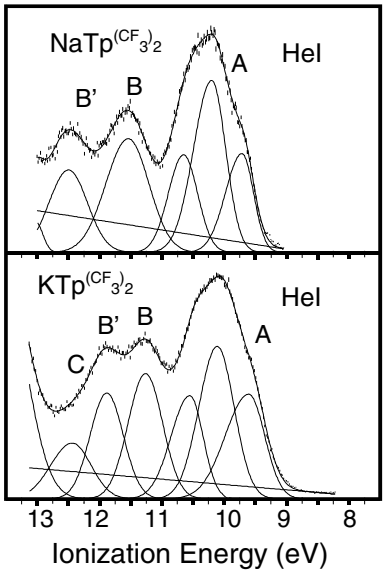

Fig. 7. He I close-up photoelectron spectra of $Na(Tp^{(CF_3)_2})$ (top) and $K(Tp^{(CF_3)_2})$ (bottom). The bands are assigned as A: pyrazole-π; B, B′: σ_N (*e*-symmetric and *a* symmetric combinations, respectively) of the pyrazole nitrogen orbitals; C: σ_{BH} of the trispyrazole borate ligand.

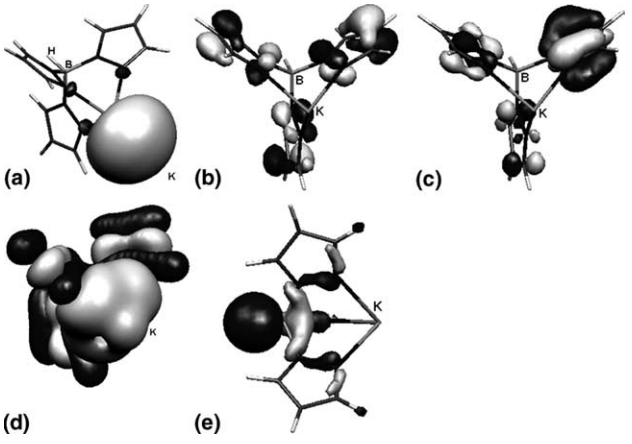

Fig. 8. Molecular orbital plots (at 0.05 cutoff levels unless stated) of KTp. (a) Lowest unoccupied molecular orbital (LUMO) is primarily metal in character (at 0.03 cutoff levels). (b) The highest occupied molecular orbital (HOMO) is primarily pyrazole-π in character. (c) HOMO-1 is again pyrazole-π in character. (d) An example of the pyrazole σ-donor (σ_N) molecular orbital (at 0.008 cutoff levels). (e) The hydrotris(pyrazol-1-yl)borate σ_{BH} molecular orbital.

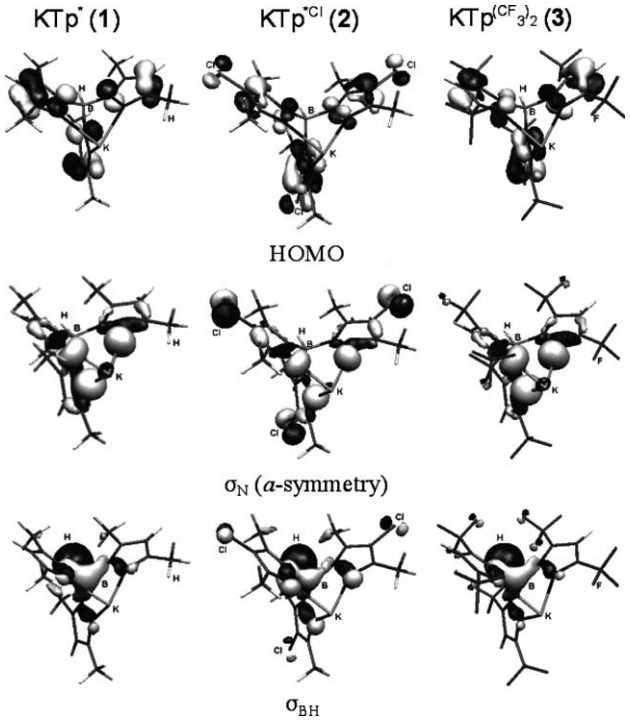

Fig. 9. Comparison of the highest occupied molecular orbitals (HOMO), σ_N (*a*-symmetric) and σ_{BH} orbitals of compounds **1**–**3** (at 0.05 cutoff levels).

withdrawing effect and stabilizes the pyrazole-π based molecular orbitals (HOMO) by 2.27 eV relative to **1**. This calculated shift compares very well with the corresponding experimentally obtained value of ~2.0 eV. The σ_{BH} and σ_N (*a*-symmetry) orbitals for **1**–**3** also are plotted in Fig. 9 for comparison. The methyl or trifluoromethyl substitutions, for **1** and **3**, at the 3 and 5 positions of pyrazole ring do not significantly change the nature of the σ_{BH} and σ_N orbitals.

Finally, we note that the Mulliken charges at the potassium atom for compounds **1**, KTp, **2**, **3** (0.88, 0.91, 0.89 and 0.99, respectively) correspond very well to the electron withdrawing properties of the substitutions in these compounds. The Mulliken charge at the metal center in compound **3** (0.99) contrasts with that of 0.88 in **1** and confirms the experimental findings of us and others [11] of a very electropositive metal center in the metal adducts of $Tp^{(CF_3)_2}$. Thus, the homoscorpionates discussed here offer a variety of possibilities for the modification of the steric and the electronic properties by variations of the substitution at the 3, 4 and 5 positions of the pyrazole rings.

4. Conclusions

The general shape of the low energy ionizations bands A, B, and C in the photoelectron spectra of **1**–**3**, is not greatly affected by the nature of the metal ions as reported here and by others [31]. However, substitutions at the 3, 4 and 5 positions of the pyrazole ring can shift the ionization energies of the bands significantly, as especially shown by the CF_3 substitutions, and can perturb the distributions of the orbitals, as shown most clearly by the Cl substitutions.

The scorpionates discussed in this work are coordinated to the metal through the nitrogen atoms of the pyrazole rings and this σ-bonding is modulated by electron density at the metal center or vice versa. The electronic structure of scorpionate ligands presented here includes distinct assignments of σ_{BH} and σ_N (*a* and *e*-symmetry) orbitals confirmed experimentally for the first time. This will help in understanding the electronic structure of scorpionate-based transition metal complexes utilized in bioinorganic modeling and organometallic catalysis. The shift in the positions of band B might be an indicator of the extent of σ-bonding of these scorpionate ligands upon coordination with transition metals and will be a topic of discussion in later studies [45].

5. Supporting information

Crystallographic data for the structural analysis have been deposited with the Cambridge Crystallographic Data Center, 12 Union Road, Cambridge CB2 1EZ, UK (fax: +44-1223-336033; E-mail: deposit@ccdc.cam.ac.uk or www: http://www.ccdc.cam.ac.uk), CCDC No. 213807 for compound **2**.

Acknowledgements

Authors thank Dr. P.J. Desrochers, at University of Central Arkansas for a sample of $K(Tp^{*Cl})$. Support by the National Institutes of Health (Grant GM-37773 to JHE) and the National Science Foundation (Grant CHE-0078457 to DLL and Grant CHE 9610374 for the X-ray diffractometer) is gratefully acknowledged. The determination of the structure of $K(Tp^{*Cl})$ was a special class project of MEA in Chemistry 517.

References

[1] S. Trofimenko, Scorpionates – The Coordination Chemistry of Polypyrazolylborate Ligands, Imperial College Press, London, 1999.
[2] S. Trofimenko, J. Am. Chem. Soc. 89 (13) (1967) 3170.
[3] S. Trofimenko, J. Am. Chem. Soc. 89 (24) (1967) 6288.
[4] I.K. Dhawan, A. Pacheco, J.H. Enemark, J. Am. Chem. Soc. 116 (1994) 7911.
[5] I.K. Dhawan, J.H. Enemark, Inorg. Chem. 35 (1996) 4873.
[6] F.E. Inscore, N. Rubie, H.K. Joshi, M.L. Kirk, J.H. Enemark, Inorg. Chem., submitted.

[7] S. Trofimenko, Abstracts of Papers, 225th ACS National Meeting, New Orleans, LA, USA, March 23–27, 2003, 2003, INOR-008.
[8] H.K. Joshi, F.E. Inscore, J.T. Schirlin, I.K. Dhawan, M.D. Carducci, T.G. Bill, J.H. Enemark, Inorg. Chim. Acta 337 (2002) 275.
[9] J.T. Schirilin, F.E. Inscore, H.K. Joshi, I.K. Dhawan, J.H. Enemark, Abstracts of Papers – American Chemical Society 221st, 2001, INOR-505.
[10] H.K. Joshi, J.J.A. Cooney, F.E. Inscore, N.E. Gruhn, D.L. Lichtenberger, J.H. Enemark, Proc. Natl. Acad. Sci. USA 100 (7) (2003) 3719.
[11] H.R. Dias, W. Jin, H.J. Kim, H.L. Lu, Inorg. Chem. 35 (8) (1996) 2317.
[12] H.R. Dias, H.J. Kim, Organometallics 15 (25) (1996) 5374.
[13] Z. Hu, S.M. Gorun, Inorg. Chem. 40 (4) (2001) 667.
[14] D.M. Tellers, S.J. Skoog, R.G. Bergman, T.B. Gunnoe, W.D. Harman, Organometallics 19 (13) (2000) 2428.
[15] W.D. Jones, F.J. Feher, J. Am. Chem. Soc. 104 (15) (1982) 4240.
[16] D.M. Tellers, R.G. Bergman, J. Am. Chem. Soc. 123 (46) (2001) 11508.
[17] R.G. Bergman, T.R. Cundari, A.M. Gillespie, T.B. Gunnoe, W.D. Harman, T.R. Klinckman, M.D. Temple, D.P. White, Organometallics 22 (11) (2003) 2331.
[18] K. Kimura, S. Katsumata, Y. Achiba, T. Yamazaki, S. Iwata, Handbook of HeI Photoelectron Spectra of Fundamental Organic Molecules, Halsted Press, New York, 1981.
[19] J. Reglinski, M. Garner, I.D. Cassidy, P.A. Slavin, M.D. Spicer, D.R. Armstrong, J. Chem. Soc., Dalton Trans. (1999) 2119.
[20] F.E. Inscore, R. McNaughton, B. Westcott, M.E. Helton, R. Jones, I.K. Dhawan, J.H. Enemark, M.L. Kirk, Inorg. Chem. 38 (1999) 1401.
[21] M.D. Carducci, C. Brown, E.I. Solomon, J.H. Enemark, J. Am. Chem. Soc. 116 (1994) 11856.
[22] J. McMaster, M.D. Carducci, Y.-S. Yang, E.I. Solomon, J.H. Enemark, Inorg. Chem. 40 (2001) 687.
[23] J.C. Green, Acc. Chem. Res. 27 (5) (1994) 131.
[24] B.L. Westcott, N.E. Gruhn, J.H. Enemark, J. Am. Chem. Soc. 120 (1998) 3382.
[25] H.K. Joshi, F.E. Inscore, J.T. Schirlin, I.K. Dhawan, M.D. Carducci, T.G. Bill, J.H. Enemark, Inorg. Chim. Acta 337 (2002) 275.
[26] M.E. Helton, N.E. Gruhn, R.L. McNaughton, M.L. Kirk, Inorg. Chem. 39 (11) (2000) 2273.
[27] H.K. Joshi, A.E. McElhaney, N.E. Gruhn, D.L. Lichtenberger, J.H. Enemark, manuscript in preparation.
[28] S. Cradock, R. Findlay, M. Palmer, Tetrahedron 29 (14) (1973) 2173.
[29] (a) A.J. Downs, R.G. Egdell, A.F. Orchard, P.D. Thomas, J. Chem. Soc., Dalton Trans. (1978) 1755;
(b) C. Janiak, T.G. Scharmann, J.C. Green, R.P.G. Parkin, M.J. Kolm, E. Riedel, W. Mickler, J. Elguero, R.M. Claramunt, D. Sanz, Chem. Eur. J. 2 (8) (1996) 992.
[30] G. Bruno, E. Ciliberto, I. Fragalà, G. Granozzi, Inorg. Chim. Acta 48 (1) (1981) 61.
[31] G. Bruno, G. Centineo, E. Ciliberto, S. Di Bella, I. Fragalà, Inorg. Chem. 23 (13) (1984) 1832.
[32] W. Armarego, D. Perrin, Purification of Laboratory Chemicals, 4th Ed., Butterworth Heinemann, Boston, MA, 1997, p. 512.
[33] O. Renn, L.M. Vananzi, A. Marteletti, V. Gramlich, Helv. Chim. Acta 78 (4) (1995) 993.
[34] D.T. Cromer, J. Waber, Int. Tables X-Ray Crystallogr. 4 (1974) 71.
[35] D.T. Cromer, J.A. Ibers, Int. Tables X-Ray Crystallogr. 4 (1974) 148.
[36] K. Siegbahn, C. Nordling, A. Fahlman, R. Nordberg, K. Hamrin, J. Hedman, G. Johansson, T. Bergmark, S.-E. Karlsson, I. Lindgren, B. Lindberg, ESCA: Atomic, Molecular and Solid State Structure Studied by Means of Electron Spectroscopy, Almqvist and Wiksells, Uppsala, 1967.
[37] D.L. Lichtenberger, A.S. Copenhaver, J. Electron Spectrosc. Relat. Phenom. 50 (4) (1990) 335.
[38] A.D. Becke, Phys. Rev. A 38 (1988) 3098.
[39] C. Lee, W. Yang, R.G. Parr, Phys. Rev. B 37 (1988) 785.
[40] J.A. McCleverty, D. Seddon, N.A. Bailey, N.J. Walker, J. Chem. Soc., Dalton Trans. (1976) 898.
[41] E. Teuma, F. Malbosc, V. Pons, C. Serra Le Berre, J. Jaud, M. Etienne, P. Kalck, J. Chem. Soc., Dalton Trans. (2001) 2225.
[42] C. Santini, C. Pettinari, M. Pellei, G.G. Lobbia, A. Pifferi, M. Camalli, A. Mele, Polyhedron 18 (17) (1999) 2255.
[43] J. Yeh, I. Lindau, At. Data Nucl. Data Tables 32 (1) (1985) 1.
[44] R.S. Glass, N.E. Gruhn, D.L. Lichtenberger, E. Lorance, J.R. Pollard, M. Birringer, E. Block, R. DeOrazio, C. He, Z. Shan, X. Zhang, J. Am. Chem. Soc. 122 (21) (2000) 5065.
[45] H.K. Joshi, F.E. Inscore, N.E. Gruhn, J.H. Enemark, manuscript in preparation.

Available online at www.sciencedirect.com
SCIENCE DIRECT®
Polyhedron 23 (2004) 439–444
POLYHEDRON
www.elsevier.com/locate/poly

Preparation and ligand substitution reactions of $Tp^{Ms}Ru(COD)H$ including intramolecular ligand metalation

Chandi Pariya, Christopher D. Incarvito, Arnold L. Rheingold, Klaus H. Theopold *

Department of Chemistry and Biochemistry, Center for Catalytic Science and Technology, University of Delaware, Newark, DE 19716-2522, USA

Received 25 June 2003; accepted 30 August 2003

Dedicated to S. Trofimenko, inventor of scorpionates and esteemed colleague

Abstract

Reaction of $[RuH(COD)(NH_2N(CH_3)_2)_3]BPh_4$ (COD = 1,5-cyclooctadiene) with $Tp^{Ms}Tl$ (Tp^{Ms} = hydrotris(3-mesitylpyrazolyl)borate) yielded $Tp^{Ms}Ru(COD)H$ (**1**). Treatment of **1** with CO afforded acyl complex $Tp^{Ms}Ru(CO)_2C(O)C_8H_{13}$ (**2**) via intramolecular olefin insertion followed by CO addition and insertion. In contrast, reaction of **1** with acetonitrile was accompanied by C–H activation of a ligand methyl group and H_2 elimination, ultimately producing $Tp^{Ms@}Ru(NCCH_3)_2$ (**3**) as the final product. The molecular structures of complexes **1**–**3** have been determined by single crystal X-ray diffraction methods.
© 2003 Elsevier Ltd. All rights reserved.

Keywords: Ruthenium; Scorpionate; Tris(pyrazolyl)borate; Hydride; C–H activation

1. Introduction

Tris(pyrazolyl)borate ligands with bulky substituents in the 3-position of the pyrazolyl rings – i.e. homoscorpionates of the second generation – have provided a plethora of interesting organometallic and coordination compounds [1,2]. For example, we have used the $Tp^{R,Me}$ ligands (R = ^{t}Bu, ^{i}Pr) in our exploration of the dioxygen chemistry of cobalt and chromium [3–12], and Moro-Oka et al. [13–20] have extensively used the Tp^{iPr2} ligand. In an attempt to extend our work to second row metals, we encountered unexpected difficulties in preparing ruthenium complexes of the $Tp^{tBu,Me}$ ligand, and were thus forced to pursue alternatives. A consideration guiding our choice was the desire to exclude C–H bonds from the immediate vicinity of any metal bound oxygen atom. We reasoned that the sterically enforced orthogonality between the pyrazolyl rings and mesityl ring planes of Tp^{Ms} (Tp^{Ms} = hydrotris(3-mesitylpyrazolyl)-borate) [21,22] would keep the vulnerable benzylic C–H bonds out of harm's way and present the aromatic π-system to any reactive groups bound to ruthenium. Herein we describe the facile preparation of a starting material for $Tp^{Ms}Ru$ chemistry and some observations bearing on our working hypothesis.

2. Results and discussion

We have found that the reaction of $[RuH(COD)(NH_2\text{-}N(CH_3)_2)_3]BPh_4$ (COD = 1,5-cyclooctadiene) [23] with $Tp^{Ms}Tl$ is an efficient method for the synthesis of $Tp^{Ms}Ru(COD)H$ (**1**, see Scheme 1). The use of the ruthenium dimethylhydrazine complex was first reported by Kirchner and co-workers [24] for the synthesis of TpRuCl(COD) (Tp = hydrotris(pyrazolyl)borate), but it has not been widely employed. Complex **1** can also be made by the reaction of RuH(COD)(bpm)Cl (bpm = *bis* (pyrazolyl)methane) [25] with $Tp^{Ms}Tl$, as described earlier for the synthesis of Tp*RuH(COD) (Tp* = hydrotris(3,5-dimethylpyrazolyl)borate) and $Tp^{iPr,4Br}RuH$ (COD) ($Tp^{iPr,4Br}$ = hydrotris(3-isopropyl-4-bromopyrazolyl)borate) [26–29]. The formulation of complex **1** is based on spectroscopic and analytical data and it has been confirmed by an X-ray crystal structure determination.

* Corresponding author. Fax: +302-831-6335.
E-mail address: theopold@udel.edu (K.H. Theopold).

0277-5387/$ - see front matter © 2003 Elsevier Ltd. All rights reserved.
doi:10.1016/j.poly.2003.11.031

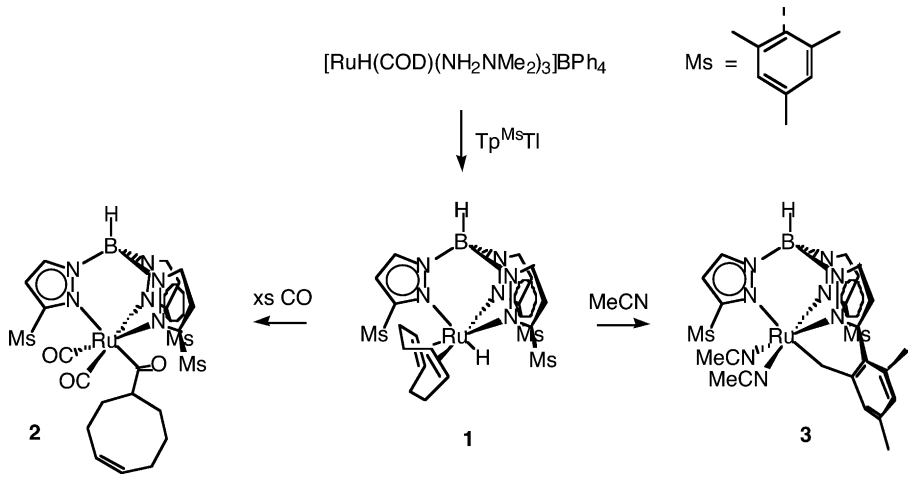

Scheme 1.

The result of the structure determination is shown in Fig. 1, and selected interatomic distances and angles are listed in Table 1. The complex features six-coordinate ruthenium in roughly octahedral coordination geometry. The hydride ligand was located, but the structural parameters associated with it must of course be viewed with some suspicion. However, the effect of the hydride is clearly seen in its *trans* influence upon one of the pyrazolyl groups. Thus the Ru(1)–N(1) bond distance (2.450(5) Å) is considerably longer than the other two Ru–N bonds (2.215(5) and 2.252(5) Å). The latter are more typical of TpRu(II) complexes. Other notable features of the structure include the significant lengthening of the olefinic C=C double bonds (1.421(9) and 1.400(10) Å) due to π-backbonding from the electron rich metal, and the near orthogonality of the mesityl planes and the pyrazolyl rings. The latter gives the $Tp^{Ms}Ru$ fragment its characteristic bowl shape.

The solid state IR spectrum of **1** showed the ν_{Ru-H} and ν_{B-H} vibrations at 2087 and 2444 cm^{-1}, respectively. The ^1H NMR spectrum (in C_6D_6) shows the presence of a Tp^{Ms} ligand, a COD and a signal at $\delta = -6.88$ ppm with an integrated intensity of one hydrogen per Tp^{Ms} ligand; the latter was assigned to the hydrido ligand. These data are in agreement with the solid state structure. **1** is soluble in most common organic solvents and its solutions decompose upon exposure to air.

As our interest in **1** was chiefly its utility as precursor for other complexes, we subjected it to reactions aimed at removing the COD ligand. Unfortunately, **1** did not react directly with either N_2O or O_2 at room temperature, and prolonged heating of these reactions led to decomposition. By contrast, exposure to an excess of carbon monoxide at room temperature resulted in the quantitative conversion of **1** to a new organometallic compound (**2**). The IR spectrum of **2** exhibited three

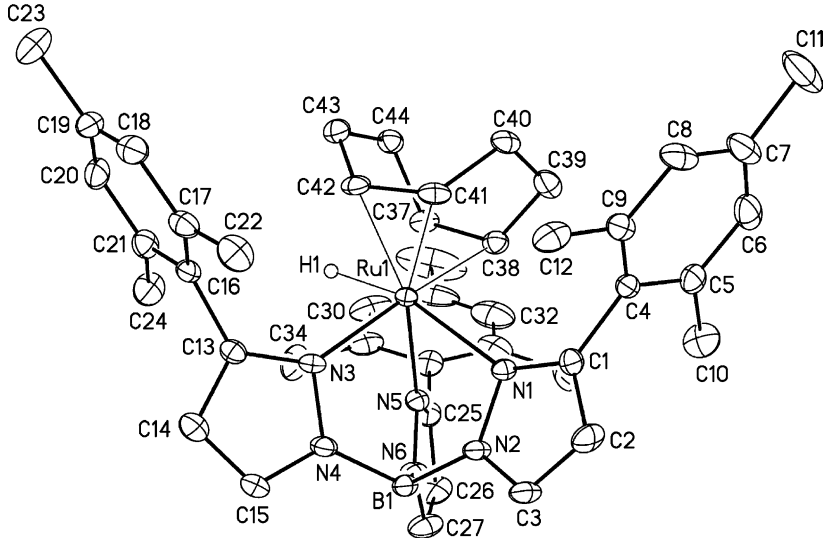

Fig. 1. The molecular structure of $Tp^{Ms}Ru(COD)H$ (**1**).

Table 1
Selected interatomic distances and angles for $Tp^{Ms}Ru(COD)H$ (**1**)

Distances (Å)			
Ru(1)–N(1)	2.450(5)	Ru(1)–N(3)	2.252(5)
Ru(1)–N(5)	2.215	Ru(1)–C(37)	2.191(6)
Ru(1)–C(38)	2.147(7)	Ru(1)–C(41)	2.167(6)
Ru(1)–C(42)	2.177(6)	Ru(1)–H(1)	1.66(4)
C(37)–C(38)	1.421(9)	C(41)–C(42)	1.400(10)
Angles (°)			
N(1)–Ru(1)–N(3)	83.72(17)	N(1)–Ru(1)–N(5)	83.18(19)
N(3)–Ru(1)–N(5)	88.17(18)	N(1)–Ru(1)–H(1)	165(4)
N(3)–Ru(1)–H(1)	84(2)	N(5)–Ru(1)–H(1)	89(2)
C(38)–C(37)–C(44)	122.8(6)	C(37)–C(38)–C(39)	121.8(6)
C(40)–C(41)–C(42)	122.7(6)	C(41)–C(42)–C(43)	123.3(6)

resonances in the carbonyl stretching frequency range; two of these (at 2040 and 1970 cm^{-1}) were consistent with terminal carbonyls, whereas the third (at 1661 cm^{-1}) indicated the presence of an acyl moiety. Furthermore, the ^1H NMR spectrum of **2** indicated the loss of the metal hydride functionality, but showed resonances of the eight-membered ring. A proposed structure of **2** that is entirely consistent with the spectroscopic data, namely $TpMsRu(CO)_2C(O)C_8H_{13}$, is shown in Scheme 1. This assignment was also confirmed by a crystal structure determination by X-ray diffraction. The molecular structure of **2** is shown in Fig. 2, while selected interatomic distances and angles are listed in Table 2. Once again, the ruthenium exhibits octahedral coordination, with the angles between *cis*-ligands ranging from 84.0(2)° to 96.1(2)°. This time, however, the Ru–N distances are much more similar (2-197(5)–2.252(5) Å); they as well as the Ru–C bonds are entirely unexceptional. It should be noted that the cyclooctenyl group is disordered over two positions; this has been modeled and Fig. 2 only shows one of the two arrangements. Accordingly, the bond distances in the ring are of low accuracy, but there can be no doubt that one of them is a double bond.

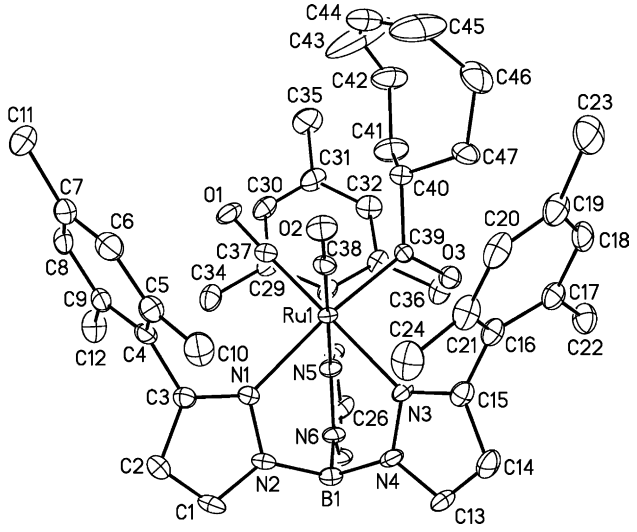

Fig. 2. The molecular structure of $Tp^{Ms}Ru(CO)_2C(O)C_8H_{13}$ (**2**); only one of the two disordered conformers is shown.

Table 2
Selected interatomic distances and angles for $Tp^{Ms}Ru(CO)_2C(O)C_8H_{13}$ (**2**)

Distances (Å)			
Ru(1)–N(1)	2.252(5)	Ru(1)–N(3)	2.197(5)
Ru(1)–N(5)	2.206(5)	Ru(1)–C(37)	1.855(7)
Ru(1)–C(38)	1.868(6)	Ru(1)–C(39)	2.062(6)
C(37)–O(1)	1.145(8)	C(38)–O(2)	1.147(8)
C(39)–O(3)	1.203(7)	C(39)–C(40)	1.564(8)
Angles (°)			
N(1)–Ru(1)–N(3)	84.0(2)	N(1)–Ru(1)–N(5)	84.3(2)
N(3)–Ru(1)–N(5)	87.5(2)	C(37)–Ru(1)–C(38)	85.1(3)
C(37)–Ru(1)–C(39)	89.3(3)	C(38)–Ru(1)–C(39)	89.0(2)
C(37)–Ru(1)–N(1)	95.2(2)	C(37)–Ru(1)–N(3)	178.0(2)
C(37)–Ru(1)–N(5)	94.2(2)	C(38)–Ru(1)–N(1)	96.1(2)
C(38)–Ru(1)–N(3)	93.2(2)	C(38)–Ru(1)–N(5)	179.2(2)
C(39)–Ru(1)–N(1)	173.4(2)	C(39)–Ru(1)–N(3)	91.6(2)
C(39)–Ru(1)–N(5)	90.7(2)	Ru(1)–C(39)–C(40)	121.9(4)
Ru(1)–C(39)–O(3)	119.5(4)	O(3)–C(39)–C(40)	118.5(5)
Ru(1)–C(37)–O(1)	176.6(6)	Ru(1)–C(38)–O(2)	175.5(6)

The formation of **2** implies an insertion of one of the double bonds of COD into the ruthenium hydride to form an alkyl complex. Trapping of this coordinatively unsaturated species with CO, followed by a migratory CO-insertion and trapping again delivers **2**. While the exact sequence of these individual mechanistic steps remains uncertain, they are clearly implicated in their aggregate by the final product. Based on these observations it seemed reasonable to suggest a rate determining equilibration between **1** and its less stable alkyl olefin complex isomer. Evidence for such a mechanism might be gathered from a reaction with a trapping reagent less likely to undergo insertion into the metal–carbon σ-bond. This was our intent when we reacted **1** with an excess of acetonitrile. However, this reaction took an entirely different path.

1 is very poorly soluble in acetonitrile. However, on refluxing a suspension of **1** in acetonitrile under argon the starting material dissolved and within a few minutes the solution changed color from yellow to green and finally a green microcrystalline powder of **3** precipitated. The ^1H NMR spectrum of **3** was consistent with a molecule lacking any symmetry, as indicated by the large number of proton resonances; furthermore, it no longer showed a resonance attributable to a hydride. The IR spectrum showed two bands at 2255 and 2238 cm^{-1}, which indicated the presence of coordinated acetonitrile. The nature of **3** was ultimately revealed by a crystal structure determination; its result is depicted in Fig. 3 and selected interatomic distances and angles are listed in Table 3. **3** is the apparent product of a C–H activation of one of the ortho-methyl groups of a mesityl substituent. Elimination of H_2 and replacement of the COD ligand with two coordinated acetonitrile molecules complete the transformation of **1**–**3** (abbreviated $Tp^{Ms@}Ru(NCMe)_2$ to indicated the functionalized

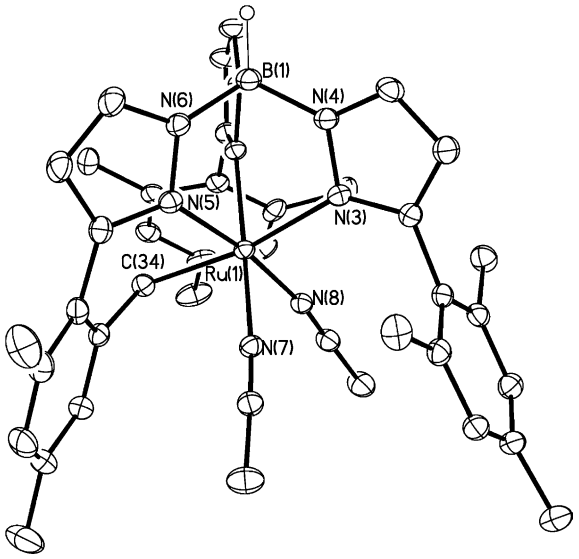

Fig. 3. The molecular structure of $Tp^{Ms@}Ru(NCMe)_2$ (**3**).

Table 3
Selected interatomic distances and angles of $Tp^{Ms@}Ru(NCMe)_2$ (**3**)

Distances (Å)			
Ru(1)–N(1)	2.1100(19)	Ru(1)–N(3)	2.205(2)
Ru(1)–N(5)	2.023(2)	Ru(1)–N(7)	1.992(2)
Ru(1)–N(8)	2.005(2)	Ru(1)–C(34)	2.113(3)
N(7)–C(37)	1.134(3)	N(8)–C(39)	1.137(4)
Angles (°)			
N(1)–Ru(1)–N(3)	87.16(8)	N(1)–Ru(1)–N(5)	86.49(8)
N(1)–Ru(1)–N(7)	176.57(9)	N(1)–Ru(1)–N(8)	96.80(9)
N(1)–Ru(1)–C(34)	89.96(9)	N(3)–Ru(1)–N(5)	86.43(9)
N(3)–Ru(1)–N(7)	91.29(8)	N(3)–Ru(1)–N(8)	100.37(9)
N(3)–Ru(1)–C(34)	167.37(10)	N(5)–Ru(1)–N(7)	90.36(9)
N(5)–Ru(1)–N(8)	172.55(9)	N(5)–Ru(1)–C(34)	81.12(10)
N(7)–Ru(1)–N(8)	86.50(9)	N(7)–Ru(1)–C(34)	90.90(9)
N(8)–Ru(1)–C(34)	92.17(10)	Ru(1)–C(34)–C(29)	109.82(18)
Ru(1)–N(7)–C(37)	175.5(2)	Ru(1)–N(8)–C(39)	170.6(2)

ligand). The coordination geometry about ruthenium is once again close to octahedral, with the angles between *cis*-ligands spanning the range of 81.12(10)°–100.37(9)°. The metalation of the mesityl methyl does not appear to create any unusual strain; thus, the Ru(1)–C(34) bond is of normal length (2.113(3) Å) and the bond angle at C(34) (Ru(1)–C(34)–C(29), 109.82(18)°) approximates the ideal tetrahedral angle. Naturally, the mesityl plane is turned somewhat from the perpendicular position with respect to the pyrazole ring. The nitriles are coordinated in the common 'end-on' fashion. The solid state structure is in complete accord with the complicated solution spectrum, which indicates that the molecule is static on the NMR time scale in solution. Most importantly, the formation of **3** suggests that the mesityl substituents of the Tp^{Ms}-ligand are subject to facile attack by metal bound ligands. This does not bode well for the stabilization of highly oxidizing intermediates containing $Tp^{Ms}M$ fragments.

3. Conclusions

With the synthesis of TpMsRu(COD)H (**1**) we have devised a convenient entry into the chemistry of the $Tp^{Ms}Ru(II)$ fragment. Ligand substitution reactions of **1** are facile and mechanistically diverse. Depending on the entering group, the COD ligand may be retained in some form (as in **2**) or completely lost (as in **3**). The causes for this mechanistic divergence are not clear at this juncture. A novel and unexpected feature of this chemistry was the ready metalation of the Tp^{Ms}-ligand at an ortho-methyl group. This observation would seem to disqualify this particular scorpionate from consideration as an 'oxidation resistant' ligand. However, we have reason to believe that it is useful for less severe chemistry.

4. Experimental

4.1. General procedures

The preparation and handling of all compounds was performed in oven-dried glassware with exclusion of air and moisture under nitrogen or argon atmosphere, using standard vacuum line and Schlenk techniques. All solvents were dried and distilled under a nitrogen atmosphere prior to use. C_6D_6 was predried with Na and stored under vacuum over Na/K (1:3) alloy. $RuCl_3 \cdot x H_2O$ was purchased from Strem Chemical Co. 1,5-cyclooctadiene (COD) and *N*,*N*-dimethyl hydrazine were purchased from Aldrich Chemical Co and Fisher Scientific Co, respectively. $Ru(COD)Cl_2$ [30] and $[RuH(COD)(NH_2\text{-}N(CH_3)_2)_3]BPh_4$ [23] were synthesized by literature procedures. NMR spectra were recorded on Bruker AM 250 and AC250 spectrometers. FT-IR spectra were run using a Mattson Alpha Centauri spectrometer. Combustion analyses were obtained from Oneida Research Services, Whitesboro, NY or Schwarzkopf Microanalytical Laboratory, Woodside, NY.

4.2. Preparation of $Tp^{Ms}Ru(COD)H$ (*1*)

Solid $[RuH(COD)(NH_2N(CH_3)_2)_3]BPh_4$ (2.32 g, 3.27 mmol) was added to a suspension of $Tp^{Ms}Tl$ (2.54 g, 3.29 mmol) in 100 ml of THF. The reaction mixture was stirred for 12 h at room temperature, over which time a white precipitate separated. The color of the solution changed from colorless to yellow. The resulting yellow solution was filtered and evaporated to dryness. The product was extracted with pentane and filtered. Removal of solvent under reduced pressure gave 1.67 g (66%) of **1** after drying. Recrystallization of **1** from pentane gave crystals suitable for X-ray analysis. ^1H NMR (250 MHz, C_6D_6): $\delta = 7.86$ (s, 1H, 5-H), 7.59 (s, 2H, 5-H), 6.93 (s, 2H, 3′,5′-H), 6.80 (s, 2H, 3′,5′-H), 6.70

(s, 2H, 3′,5′-H), 6.04 (s, 1H, 4-H), 5.79 (s, 2H, 4-H), 3.40 (s, 4H, olefin H of COD), 2.58 (s, 6H, 2′-CH_3), 2.22 (d, 6H, 6′-CH_3), 2.13 (d, 9H, 4′-CH_3), 1.92 (s, 6H, 2′, 6′-CH_3), 1.55 (m, 4H, H of COD), 1.12–1.04 (m, 4H, H of COD) and −6.88 (s, 1H); IR (KBr): $\nu_{B-H} = 2444$ cm^{-1}, $\nu_{Ru-H} = 2087$ cm^{-1}. Elemental analysis Calc. for $C_{44}H_{53}N_6BRu$ ($M = 777.83$): C, 67.94; H, 6.87; N, 10.80. Found: C, 67.74; H, 6.81; N, 10.94%.

4.3. Preparation of $Tp^{Ms}Ru(CO)_2C(O)C_8H_{13}$ (2)

A pentane (20 ml) solution of Tp^{Ms}RuH(COD) (**1**) (350 mg, 0.45 mmol) was prepared in the glovebox. The reaction flask attached with needle valve was set up in the high vacuum line. The solution was frozen in liquid N_2 and flask was evacuated. Repeated freezing and evacuation was performed to make sure the solution is completely free from N_2. Then the solution was placed under 1 atm of CO at ambient temperature for 10 h. During this time light yellow crystals appears. After a brief evacuation to remove excess CO the flask and contents were transferred to a glovebox. It was filtered and the solvent was removed in vacuo. The combined amount of product shows the reaction is virtually quantitative. The product was recrystallized from ether: yield 374 mg (96%). ^{1}H NMR (250 MHz, C_6D_6): $\delta = 7.54$ (s, 1H, 5-H), 7.51 (s, 2H, 5-H), 6.96 (s, 2H, 3′,5′-H), 6.75 (d, 4H, 3′,5′-H), 5.93 (s, 1H, 4-H), 5.78 (m, 2H,4-H), 5.58 (m, 1H, olefin H of cyclooctene), 5.35 (m, 1H, olefin H of cyclooctene), 2.36 (s, 3H, 2′-CH3), 2.28 (s, 3H, 6′-CH3), 2.21 (d, 6H, 2′-CH3), 2.11 (d, 6′-CH3), 2.06 (d, 9H, 4′-CH3), 1.74 (m, 4H, H of cyclooctene), 1.17 (m, 2H, H of cyclooctene), 0.95 (m, 2H, H of cyclooctene), 0.75 (m, 2H, H of cyclooctene), 0.05 (m, 1H (H of cyclooctene); IR (KBr disk): $\nu_{B-H} = 2458$, $\nu_{C\cong O} = 2040$, 1970; $\nu_{C\cong O} = 1661$ cm^{-1}. *Anal.* Calc. for $C_{47}H_{53}N_6BO_3Ru$ ($M = 861.36$): C, 65.48; H, 6.20; N, 9.80. Found: C, 65.38; H, 6.37; N, 9.86%.

4.4. Preparation of $Tp^{Ms}@Ru(CH_3CN)_2$ (3)

A suspension of Tp^{Ms}Ru(COD)H (**1**, 200 mg, 0.26 mmol) in 15 ml of acetonitrile was refluxed for 4 h. Within half an hour all starting material dissolved and the clear yellow solution turned green. A green solid precipitated out from the homogeneous solution. The reaction mixture was cooled to room temperature and filtered. The product was dried under vacuum to give pure **3** (93 mg, yield: 48%). A small amount was recrystallized from CH_3CN and diethyl ether to get crystals suitable for the X-ray crystal structure determination. ^{1}H NMR (250 MHz, C_6D_6): $\delta = 7.99$ (m, 1H), 7.80 (m, 1H), 7.65 (m, 1H), 7.12 (s, 1H), 6.84 (s, 1H), 6.71 (s, 1H), 6.62 (s, 1H), 6.57 (s, 2H), 6.42 (m, 1H), 6.14 (m, 1H), 5.90 (m, 1H), 3.53 (d, 1H, $J_{HH} = 10$ Hz) 2.38 (s, 3H), 2.26 (s, 6H), 2.13 (m, 9H), 2.00 (s and d, 4H), 1.80 (s, 3H) 1.30 (s, 3H), 0.80 (s, 3H). IR (KBr disk): $\nu_{B-H} = 2473$, $\nu_{C=N} = 2255$, 2238 cm^{-1}. *Anal.* Calc. for $C_{40}H_{45}N_8BRu$ ($M = 749.74$): C, 64.08; H, 6.05; N, 14.95. Found: C, 63.62; H, 5.75; N, 14.93%.

4.5. Crystallographic structure determinations

Crystal, data collection, and refinement parameters are given in Table 4. Suitable crystals for data collection were selected, mounted with Paratone oil and flash cooled to the data collection temperature. All data were collected at 173 K with a Siemens P4/CCD diffractometer

Table 4
Crystallographic data for **1**–**3**

	1	**2**	**3**
Formula	$C_{44}H_{53}BN_6Ru$	$C_{47}H_{53}BN_6O_3Ru$	$C_{40}H_{45}BN_8Ru$
Formula weight	777.80	861.83	749.72
Temperature (K)	173(2)	173(2)	173(2)
Crystal system	orthorhombic	monoclinic	monoclinic
Space group	*Pbca*	$P2_1/n$	$P2_1/c$
a (Å)	13.4924(2)	12.4642(3)	11.4887(6)
b (Å)	20.3670(2)	25.8090(5)	19.6077(12)
c (Å)	29.1887(5)	13.6875(3)	16.8230(10)
α (°)	90	90	90
β (°)	909	97.0090(10)	100.9590(10)
γ (°)	90	90	90
V (Å^3)	8021.05(19)	4370.21(17)	3720.6(4)
Z	8	4	4
D_{calcd} (g cm^{-3})	1.288	1.310	1.338
μ (Mo Kα) (cm^{-1})	4.29	4.06	4.61
Data/parameters	7520/477	9239/545	8277/457
Radiation	Mo Kα ($\lambda = 0.71073$ Å)		
Goodness-of-fit (F^2)	1.539	1.095	1.076
$R(F)$ (%)	8.26	8.18	3.79
$R_w(F^2)$ (%)	20.89	19.22	9.35

with graphite-monochromated Mo Kα X-radiation ($\lambda = 0.71073$ Å). The structures were solved by direct methods and were completed by subsequent difference Fourier syntheses and refined by full-matrix least-squares procedures. The cyclooctene moiety in **2** was found to be severely disordered and was modeled using two contributing structures having a 50/50 site occupancy distribution, with restrained 1,2 and 1,3 C–C distances and with common displacement parameters for chemically equivalent carbon atoms. The hydride ligand, H(1), was located in the difference map of **1**; all other hydrogen atoms were treated as idealized contributions excepting those on the disordered cyclooctene moiety which were ignored. All non-hydrogen atoms were refined with anisotropic displacement coefficients. All software and sources of the scattering factors are contained in the SHELXTL (5.1) program library (G. Sheldrick, Siemens XRD, Madison, WI).

5. Supplementary material

Crystallographic data for the structural analyses have been deposited with the Cambridge Crystallographic Data Centre, CCDC No. 212260 for compound **1**, CCDC No. 212259 for compound **2**, and CCDC No. 212261 for compound **3**. Copies of this information may be obtained free of charge from The Director, CCDC, 12 Union Road, Cambridge CB2 1EZ, UK (fax: +44-1223-336033; e-mail: deposit@ccdc.cam.ac.uk or www: http://www.ccdc.cam.ac.uk).

Acknowledgements

Support of this work by a grant from the United States Department of Energy is gratefully acknowledged.

References

[1] S. Trofimenko (Ed.), Scorpionates, Imperial College Press, London, 1999.
[2] N. Kitajima, W.B. Tolman, Coordination Chemistry with Sterically Hindered Hydrotris(Pyrazolyl)Borate Ligands – Organometallic and Bioinorganic Perspectives, Progress in Inorganic Chemistry, vol. 43, Wiley, New York, 1995, p. 419.
[3] J.W.J. Egan, B.S. Haggerty, A.L. Rheingold, S.C. Sendlinger, K.H. Theopold, J. Am. Chem. Soc. 112 (1990) 2445.
[4] O.M. Reinaud, K.H. Theopold, J. Am. Chem. Soc. 116 (1994) 6979.
[5] O.M. Reinaud, G.P.A. Yap, A.L. Rheingold, K.H. Theopold, Angew. Chem. Int. Ed. 34 (1995) 2051.
[6] K.H. Theopold, O.M. Reinaud, D. Doren, R. Konecny, in: R.K. Grasselli, S.T. Oyama, A.M. Gaffney, J.E. Lyons (Eds.), 3rd World Congress on Oxidation Catalysis, Elsevier, Amsterdam, 1997, p. 1081.
[7] D.J. Doren, R. Konecny, K.H. Theopold, Catal. Today 50 (1999) 669.
[8] A. Hess, M.R. Hörz, L.M. Liable-Sands, D.C. Lindner, A.L. Rheingold, K.H. Theopold, Angew. Chem. Int. Ed. 38 (1999) 166.
[9] S. Thyagarajan, C.D. Incarvito, A.L. Rheingold, K.H. Theopold, Chem. Commun. (2001) 2198.
[10] K. Qin, C.D. Incarvito, A.L. Rheingold, K.H. Theopold, Angew. Chem. Int. Ed. 41 (2002) 2333.
[11] K. Qin, C.D. Incarvito, A.L. Rheingold, K.H. Theopold, J. Am. Chem. Soc. 124 (2002) 14008.
[12] C.J. Cramer, W.B. Tolman, K.H. Theopold, A.L. Rheingold, Proc. Natl. Acad. Sci. USA 100 (2003) 3635.
[13] N. Kitajima, K. Fujisawa, Y. Moro-oka, J. Mol. Catal. 74 (1992) 143.
[14] S. Hikichi, M. Akita, Y. Moro-oka, Coord. Chem. Rev. 198 (2000) 61.
[15] Y. Moro-oka, Catal. Today 45 (1998) 3.
[16] Y. Moro-oka, M. Akita, Catal. Today 41 (1998) 327.
[17] M. Akita, K. Fujisawa, S. Hikichi, Y. Moro-Oka, Res. Chem. Intermediates 24 (1998) 291.
[18] M. Ito, K. Fujisawa, N. Kitajima, Y. Moro-Oka, Catal. Metal Complexes 19 (1997) 345.
[19] M. Akita, Y. Moro-oka, Studies Surf. Sci. Catal. 92 (1995) 137.
[20] N. Kitajima, Y. Moro-oka, Chem. Rev. (Washington, DC) 94 (1994) 737.
[21] M. Silva, A. Domingos, A.P. de Matos, N. Marques, S. Trofimenko, J. Chem. Soc., Dalton Trans. (2000) 4628.
[22] A.L. Rheingold, C.B. White, S. Trofimenko, Inorg. Chem. 32 (1993) 3471.
[23] T.V. Ashworth, E. Singleton, J.J. Hough, J. Chem. Soc., Dalton Trans. (1977) 1809.
[24] C. Gemel, G. Trimmel, C. Slugovc, S. Kremel, K. Mereiter, R. Schmid, K. Kirchner, Organometallics 15 (1996) 3998.
[25] M. Fajardo, A. Delahoz, E. Diezbarra, F.A. Jalon, A. Otero, A. Rodriguez, J. Tejeda, D. Belletti, M. Lanfranchi, M.A. Pellinghelli, J. Chem. Soc., Dalton Trans. (1993) 1935.
[26] B. Moreno, S. Saboetienne, B. Chaudret, A. Rodriguez, F. Jalon, S. Trofimenko, J. Am. Chem. Soc. 117 (1995) 7441.
[27] C. Vicente, G.B. Shulpin, B. Moreno, S. Saboetienne, B. Chaudret, J. Mol. Catal. A 98 (1995) L5.
[28] B. Moreno, S. Saboetienne, B. Chaudret, A. Rodriguezfernandez, F. Jalon, S. Trofimenko, J. Am. Chem. Soc. 116 (1994) 2635.
[29] M.A. Halcrow, B. Chaudret, S. Trofimenko, J. Chem. Soc., Chem. Commun. (1993) 465.
[30] E.W. Abel, M.A. Bennett, G. Wilkinson, J. Chem. Soc. (1959) 3178.

Available online at www.sciencedirect.com
SCIENCE DIRECT®
Polyhedron 23 (2004) 445–450
POLYHEDRON
www.elsevier.com/locate/poly

Soft scorpionate complexes of the fourth and fifth period elements arsenic and tin

Christopher A. Dodds, Małgorzata Jagoda, John Reglinski *, Mark D. Spicer *

Department of Pure and Applied Chemistry, University of Strathclyde, Glasgow G1 1XL, UK

Received 27 June 2003; accepted 8 August 2003

Abstract

We report the synthesis and structure of arsenic (III) and tin(IV) adducts of the hydrotris(methimazolyl)borate anion (Tm^{Me}). Both species are found to be $[E(\kappa^3Tm^{Me})_2]^{n+}$ anions (E = As, $n = 1$; E = Sn, $n = 2$). Comparisons are made between each of these species and the compounds formed with their heavier and larger group partners bismuth and lead. Due to the remarkable flexibility in the soft scorpionate ligand we were unable to form a charge-separated species analogous to that reported by Parkin for the phenyl analogue (Tm^{Ph}). Attempts to prepare the tin(II) adduct curiously produced the tin(IV) product $[Sn(\kappa^3Tm^{Me})_2][Tm^{Me}]_2$ even when the reaction was carried out under inert atmospheres.
© 2003 Elsevier Ltd. All rights reserved.

1. Introduction

The hydrotris(pyrazolyl)borate anion (Tp), first reported in 1966 [1,2], has found great favour with synthetic inorganic chemists, and since the initial reports an extensive family of poly(pyrazolyl)borate ligands has been gradually developed. Concurrent with these developments, the synthetic community have generated examples of poly(pyrazolyl)borate complexes of every d-block element [3]. With few exceptions these ligands are easy to prepare and they readily support transition metals during changes in their oxidation state and co-ordination sphere. They have thus been found to be highly versatile ligands, which repeatedly appear as a chemical component of new materials, reagents and catalysts [3].

While the chemistry of the poly(pyrazolyl)borates with transition metals is extensive and continues to expand, reports of their complexes with the softer, lower main group elements are few [3] principally due to the hard donor character of the Tp ligand. However, the more recent syntheses of soft hydrotris(thiaimidazolyl)borate (Tm^R) analogues of Tp has enabled workers to study the co-ordination chemistry of the lower main group in a C_3 environment relatively simply. Thus far compounds of thallium(I/III) [4–7], tin(IV) [8,9], lead(II) [10,11] and bismuth(III) [8,12] have been reported and a number of structural motifs have been observed (Fig. 1). The (thiaimidazolyl)borate anions would seem to have a distinct preference for the κ^3 co-ordination mode. Examples of the simple 1:1 Tm^R:E species include those of thallium(I), lead(II) (**1a**) and tin(IV) (**1b**) [5–8,10], with the 2:1 Tm^R:E (**2**) complexes being represented by bismuth(III) [8,12]. However, alternative structural motifs may be isolated if the conditions are carefully manipulated. Where non-exchangeable bulky alkyl groups are present at the central atom (e.g., triscyclohexyl-tin(IV)) it was found [9] that the ligand is restricted to a simple monodentate co-ordination mode (**3**). A similar contrast in motifs is observed in the chemistry of lead(II), which has been shown to adopt two distinct structural types [10,11]. In the presence of non-co-ordinating anions simple salts such as $[Pb(\kappa^3\text{-}Tm^{Ph})][ClO_4]$ (**1a**) are obtained [10]. However, when the ratio of ligand to metal is increased to 2:1 an intriguing bis-thiaimidazolylborate adduct (**4**) is obtained [11] where one ligand is κ^3, typical of the 1:1 adducts, but the second ligand is inverted, weakly associating with the metal fragment through three thione donors and the hydrogen atom on the

* Corresponding authors. Tel.: +141-548-2349; fax: 0141-552-0876 (J. Reglinski), Tel.: +141-548-2800 (M.D. Spicer).
E-mail addresses: j.reglinski@strath.ac.uk (J. Reglinski), m.d.spicer@strath.ac.uk (M.D. Spicer).

0277-5387/$ - see front matter © 2003 Elsevier Ltd. All rights reserved.
doi:10.1016/j.poly.2003.11.032

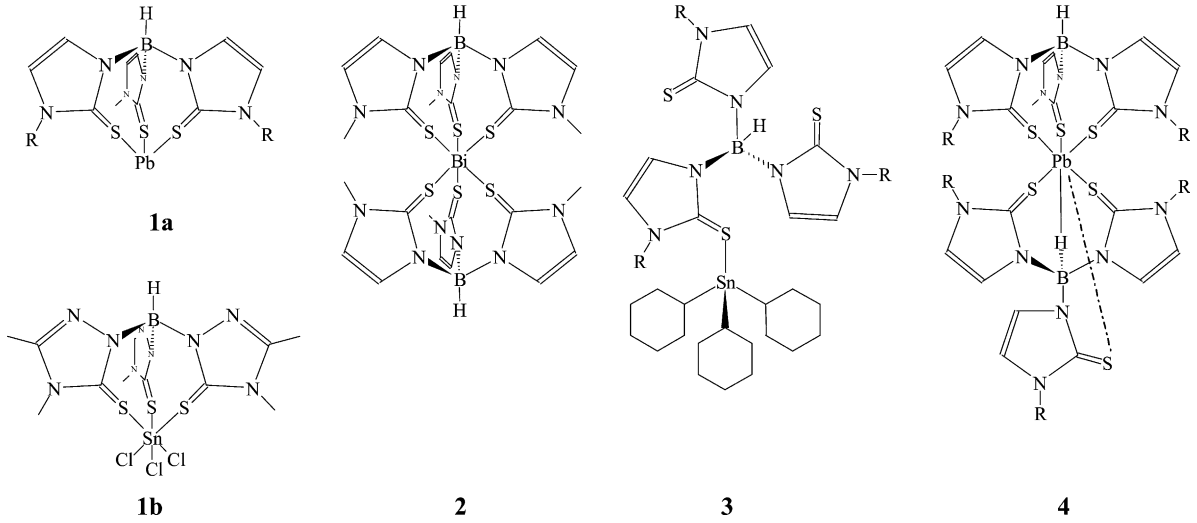

Fig. 1. The reported structural motifs of the thiaimidazolylborates with the elements from groups 13–15.

boron. That lead adopts this fascinating structure has been ascribed to the increased steric bulk of the Tm^R ligand (R = phenyl) which prevents the close approach of the two scorpionate ligands in a facial mode. The metal hydrogen interaction displayed by **4** has subsequently been observed in a number of other structures [13,14] and its has been the subject of some discussion. It has been described variously as an inverse hydrogen bond ($H^- \rightarrow M$), as an agostic interaction and as an electrostatic interaction, but as yet no consensus has been reached.

The contrast in the structures of "$[Pb(Tm^{Ph})_2]$" [10,11] and $[Bi(Tm^{Me})_2]$ [8,12] is very evident and is presumably driven by the steric effect of the phenyl substituents. In almost all of the bis-κ^3-Tm^{Me} adducts with metals the S–M–S angles between the two coordinated scorpionates is found to be less than 90°. This effect is seen also in six coordinate thiourea complexes of lead [15] and bismuth [16] and is thus not unique to soft scorpionates. However, this observation further supports the hypothesis that the motif displayed by **4** may result from steric hindrance. Although Parkin et al have been successful in structurally characterising two Tm^{Ph} lead species [10,11] we remain unsuccessful in our attempts to fully characterise the parent Tm^{Me} lead species [12] and an argument based on steric effects cannot conclusively be made. As such, it was postulated that by decreasing the size of the central atom we could increase the steric interactions between the Tm^{Me} ligands. The implications are that moving from the sixth period elements into the fourth period (namely arsenic) we should increase the preference of the complexes formed to adopt structures analogous to those reported for lead (**1a** and **4**) over those reported for bismuth (**2**). The comparison between bismuth and tin and lead would be best served if the structural aspects of tin chemistry were expanded further and we have thus included these species in this report.

2. Experimental

Unless otherwise stated, all chemicals were commercially obtained. Sodium hydrotris(methimazolyl)borate (NaTm) was prepared by published methods [17]. No precautions were taken to exclude air or moisture.

2.1. Reaction of AsI_3 with NaTm

Arsenic(III) iodide (0.110 g, 0.24 mmol) was dissolved in chloroform (5 ml) and a solution of $NaTm^{Me}$ (0.181 g, 0.48 mmol) in chloroform (15 ml) was added. After stirring for 24 h the resulting orange solid was filtered off. Recrystallisation from DMF by vapour diffusion with diethyl ether yielded red-orange crystals. Yield: 90 mg; 41%. Found: C, 31.78; H, 3.66; N, 17.34. Expected for $C_{24}H_{32}AsB_2IN_{12}S_6$: C, 31.89; H, 3.54; N, 18.59. ^1H NMR (400.1 MHz; δ DMSO-d_6): 7.4 (s, 1H, –CH=), 7.1 (s, 1H, –CH=), 3.6 (s, 3H, $-CH_3$). IR (KBr disc) $\nu_{(B-H)}$ 2433 cm^{-1}.

2.2. Reaction of $SnBr_2$ with NaTm

Tin(II) bromide (0.14 g, 0.5 mmol) was suspended in acetone (50 ml) to which was added NaTm (0.375 g, 1.0 mmol). The mixture was allowed to stir for 1 h after which time the solvent was removed at reduced pressure (16 mmHg) to help nucleate the sodium bromide. The solid obtained was recrystallised from DMF/ether using vapour diffusion to produce orange crystals. Yield: 50% based on $[Sn(Tm^{Me})_2]_2[Tm^{Me}]_2 \cdot DMF \cdot H_2O$. Found: C, 38.17; H, 4.70; N, 21.25. Expected for

$C_{51}H_{73}N_{25}S_{12}B_2O_2Sn$: C, 37.93; H, 4.56; N, 21.68. ^{1}H NMR (400.1 MHz;δ d_6-dmso): 7.8 (d, 1H, –CH=, $J_{H–H}$ 2 Hz, $J_{Sn–H}$ 8.8 Hz), 7.6 (d, 1H, –CH=, $J_{H–H}$ 2 Hz, $J_{Sn–H}$ 8.8 Hz), 6.8 (d, 1H, –CH=, $J_{H–H}$ 2 Hz), 6.4 (d, 1H, –CH=, $J_{H–H}$ 2 Hz), 3.65 (s, 3H, $–CH_3$), 3.4 (s, 3H, $–CH_3$), 2.91 (s, 3H, DMF), 2.75 (s, 3H, DMF). IR (KBr disc) $\nu_{(B–H)}$ 2468 cm^{-1}.

2.3. Reaction of SnI_4 with NaTm

Tin(IV) iodide (0.31 g, 0.5 mmol) dissolved in dichloromethane (15 ml) was added drop-wise to a suspension of NaTm (0.375 g, 1.0 mmol) in dichloromethane (10 ml). The mixture was allowed to stir for 1 h after which time the solvent was removed at reduced pressure (16 mmHg) to help nucleate the sodium iodide. The orange solid was extracted with warm dichloromethane (2×50 ml), filtered and the solvent volume reduced to 25 ml. The yellow solid obtained was recrystallised from DMF by vapour diffusion with diethyl ether.

The orange solid remaining in the filter funnel was extracted with DMF (5 ml), filtered through celite and placed in a vapour diffusion chamber with diethyl ether. Yellow crystals suitable for X-ray diffraction were obtained overnight. Yield: 200 mg; 36%. Found: C, 27.08; H, 3.34; N, 15.32. Expected for $C_{24}H_{32}N_{12}S_6B_2SnI_2$: C, 26.81; H, 3.00; N, 15.63. ^{1}H NMR (400.1 MHz; δ $CDCl_3$): 7.8 (d, 1H, –CH=, $J_{H–H}$ 2 Hz, $J_{Sn–H}$ 8.8 Hz), 7.6 (d, 1H, –CH=, $J_{H–H}$ 2 Hz, $J_{Sn–H}$ 8.8 Hz), 3.6 (s, 3H, $–CH_3$). IR (KBr disc) $\nu_{(B–H)}$ 2468 cm^{-1}.

2.4. X-ray crystallography

Crystals were coated in mineral oil and mounted on glass fibres. Data were collected at 123 K on a Nonius Kappa CCD diffractometer using graphite monochromated Mo Kα radiation. The heavy atom positions were determined by Patterson methods and the remaining atoms located in difference electron density maps. Full matrix least-squares refinement was based on F^2, with all non-hydrogen atoms anisotropic. While hydrogen atoms were mostly observed in the difference maps, they were placed in calculated positions riding on the parent atoms. *Notes*. $[As(Tm^{Me})_2]I \cdot 2DMF \cdot Et_2O$: the diethyl ether molecule is disordered over two sites. $[Sn(Tm^{Me})_2]I_2 \cdot Et_2O$: the diethyl ether molecule site is only partially occupied and not particularly well defined. The molecule is set at 50% occupation and refined isotropically. $[Sn(Tm^{Me})_2]_2[Tm^{Me}]_2 \cdot DMF \cdot \frac{1}{2}H_2O$: the free Tm^{Me} ligand is disordered over two equally occupied sites and both the DMF and water molecule sites are partially occupied (set at 50% and 25%, respectively). The structure solution and refinement used the program SHELX 97 [18] and the graphical interface WinGX [19]. A summary of the crystallographic parameters is given in Table 1. Selected metrical parameters are reported in Table 2.

Table 1
Crystallographic data

Complex	$[As(Tm^{Me})_2]I \cdot 2DMF \cdot Et_2O$	$[Sn(Tm^{Me})_2]I_2.Et_2O$	$[Sn(Tm^{Me})_2]_2[Tm^{Me}]_2 \cdot DMF \cdot \frac{1}{2}H_2O$
Empirical formula	$C_{34}H_{56}AsB_2IN_{14}O_3S_6$	$C_{28}H_{42}B_2I_2N_{12}OS_6Sn$	$C_{51}H_{72}B_4N_{25}O_{1.5}S_{12}Sn$
F_w	1124.73	1149.21	1605.99
T (K)	123	123	123
Crystal system	monoclinic	triclinic	triclinic
Space group	$C2/c$	$P\bar{1}$	$P\bar{1}$
a (Å)	29.4062(7)	9.6007(2)	8.9287(5)
b (Å)	17.5719(6)	10.0553(2)	11.0643(7)
c (Å)	9.9250(4)	12.0758(3)	19.4871(11)
α (°)	90	112.142(1)	95.668(4)
β (°)	107.715(1)	92.229(1)	97.863(4)
γ (°)	90	91.841(1)	99.118(3)
Z	4	1	1
V (Å^3)	4885.29(17)	1077.60(5)	1868.60(19)
μ_{calc} (mm^{-1})	1.633	2.356	0.734
$F(000)$	2256	564	832
Crystal dimensions (mm)	$0.6 \times 0.4 \times 0.08$	$0.280.22 \times 0.12$	$0.88 \times 0.60 \times 0.09$
Radiation	Mo Kα	Mo Kα	Mo Kα
Number of reflections measured	16 742	8759	9118
Number of unique reflections (R_{int})	5762 (0.0779)	4864 (0.0229)	5564 (0.0372)
Number of parameters	277	242	604
R ($I > 2\sigma(I)$)[a]	0.0507	0.0325	0.0605
R_w (all reflections)[b]	0.1407	0.0843	0.1721
Goodness-of-fit	1.096	1.055	1.109

[a] $R = \sum ||F_o| - |F_c|| / \sum |F_o|$.
[b] $R_w = \{\sum[w(F_o^2 - F_c^2)^2] / \sum[w(F_o^2)^2]\}^{1/2}$.

Table 2
A comparison of selected bond angles, bond distances, torsion angles and non-bonded distances for $[E(Tm^{Me})_2]^{n+}$, E = As, Bi; $n = 1$; E = Sn; $n = 2$

	∠S–E–S (°)	∠S–E–S′ (°)	*d*(E–S) (Å)	∠H–B–N–C (°)	B···E (Å)	S···S (Å)
$[As(Tm)_2]^+$	92.3, 93.5, 94.4	86.5, 87.7 85.6, 180.0	2.570(x4) 2.590(x2)	37.5, 34.9, 46.4	4.12	3.50–3.57
$[Bi(Tm)_2]^+$ [12]	89.8, 90.7, 91.3	76.2, 88.7 (x2) 89.3 (x2), 90.2, 180.0 (x3)	2.80	37.8, 41.7, 50.0	4.26	3.92–3.97
$(Mo_3S_4)_2$ As [22]	80.6, 81.1, 82.8	98.9, 97.2 99.3, 180.0 (x3)	2.445, 2.434 2.489	N/A		3.66
$[Sn(Tm)_2]^{2+}$	93.4, 93.0, 93.1	86.7, 87.1, 86.9	2.549, 2.550, 2.555	37.9, 37.9, 45.6	4.10	3.50

3. Results and discussion

The reactions of the halides of the main group elements arsenic and tin with NaTm are effected with ease. In each case the initial reactions were conducted using excess ligand to allow the species to adopt their favoured configuration. From the reaction of arsenic triiodide we obtained the $[As(\kappa^3\text{-}Tm^{Me})_2]^+$ cation, i.e., a sandwich motif (Fig. 1), iso-structural with the cation previously reported [12] for its heavier group 15 partner viz. $[Bi(\kappa^3\text{-}Tm^{Me})_2]^+$, (Table 2). The arsenic atom is situated within an almost regular S_6 octahedral environment. Consistent with other bis κ^3 motifs the intra ligand ∠S–E–S angles are slightly more obtuse than the inter ligand ∠S–E–S angles. The non-bonded distance between the bridgehead boron and chelated main group cation is shorter for arsenic than for bismuth by a distance commensurate with the difference in their covalent radii (1.20 versus 1.42 Å) indicating that the eight membered rings ($BN_2C_2S_2E$) are flexing to accommodate smaller and larger cations, respectively. This is exemplified in the ∠H–B–N–C torsion angles, which are a measure of the twist of the heterocycle plane from the H–B…E plane. The torsion angles, and thus the twist. are found to be lower for the smaller central arsenic cation.

Although the interaction of sulphur with arsenic(III) has an established importance in biological chemistry [20], the range of structurally characterised compounds are limited especially those which have a high coordination number AsL_xS_n $(n = 2-6, \times + n > 3)$. Although a range of tris–dithiocarbamate adducts have been reported [21] they provide a poor comparison with the cation generated here as they form three highly constrained four membered rings, with significant asymmetry in the As–S distances (i.e., 2.35–2.82 Å) and ∠S–As–S angles. Perhaps the best comparison is with the arsenic adduct of the bis-molybdosulfido cubane of Hernandez-Molina [22] (Table 2). Considering the disparate nature of these two ''ligands'' the bond distances are similar but with the cubane As–S distances being slightly shorter due to the greater charge on the sulphur in the vertices of the cubes. The cubane motif constrains the angles to such an extent that the inter ligand angles are now smaller than 90° whereas the intra ligand angles rise to values greater than 90°.

Our attempt to change the structural motif of the group 15 Tm adducts by simply moving to a smaller cation has been thwarted by the Tm ligand system. The impressive flexibility of the eight membered chelates would seem to be able prevent the pendant methyl groups from a adopting sterically compromising positions which would prevent the formation of the the bis κ^3-Tm^{Me} species and could possibly lead to the formation of charge a separated anion similar to that reported for lead [11]. There is no evidence in the NMR to suggest that there is any fluxionality in this system in solution as is found with the pyrazolylborato adducts of arsenic [23]. Thus the integrity of the bis κ^3-Tm motif would seem to be assured in solution also.

A simple rationalisation of the chemistry of observed for arsenic and bismuth would be that the charge on the central atom may preclude the inversion of one of the Tm ligands and thus the formation of the charge separated species. Thus since we have had little success in retrieving a structure of lead (II) with Tm [12], we turned our attention to tin(IV) and tin(II) again in a further attempt to increase the influence of steric bulk around a smaller central atom (Sn versus Pb).

In contrast to the structures observed by Bailey et al. [8] (**1b**) and Santini et al. [9] (**3**), our reaction with stannic iodide produced yet another bis κ^3-Tm motif in formation of the $[Sn(\kappa^3\text{-}Tm^{Me})_2]^{2+}$ cation (Fig. 2). Unlike arsenic, tin has a greater propensity to adopt an S_6 coordination environment. Examples exist for the ubiquitous dithiocarbamates [24] and dithiolenes [25]. It is thus curious that this motif has not been reported previously by other workers. On comparison with the structure of $[As(\kappa^3\text{-}Tm^{Me})_2]^+$ above (Fig. 1, Table 1) the ∠S–Sn–S angles are found to follow a similar pattern, with the intra ligand angles being larger than the inter ligand angles by a substantial amount (6°). Considering the similarities in the covalent radii for the two ions, the similarity in the E–S distances, the E…B distance, the S…S distances and torsion angles (∠HBNC) is again not surprising.

Although Bailey et al. [8] and Santini et al. [9] have looked at the high oxidation state complexes of tin, the compounds of tin(II) remain unexplored. From our initial reactions in acetone we retrieved a curious tin(IV) product $[Sn(Tm^{Me})_2]_2[Tm^{Me}]_2$ in good yield. Crystal-

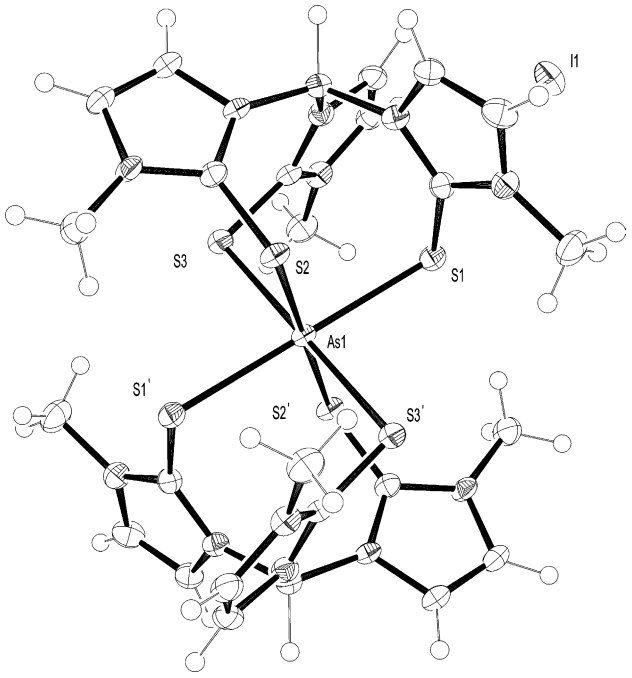

Fig. 2. The X-ray crystal structure of $[As(\kappa^3\text{-}Tm^{Me})_2]^+$ cation. The key bond distances are given in Table 2.

lography reveals that the structure of the $[Sn(\kappa^3\text{-}Tm^{Me})_2]^{2+}$ motif is isostructural with that obtained from the reaction with stannic iodide (Fig. 3) and confirms the presence of a non coordinated ligand. The facile oxidation of tin(II) was surprising. However, on repeating the reaction under anaerobic conditions we continued to isolate the Tin(IV) adduct. NMR/IR analysis provided no evidence for the presence of a tin(II) complex, but again confirmed the presence of the $[Sn(Tm^{Me})_2]^{2+}$ cation (with $^{117/119}Sn$ satellites) and of the non-coordinated ligand. In general one would expect the soft scorpionate

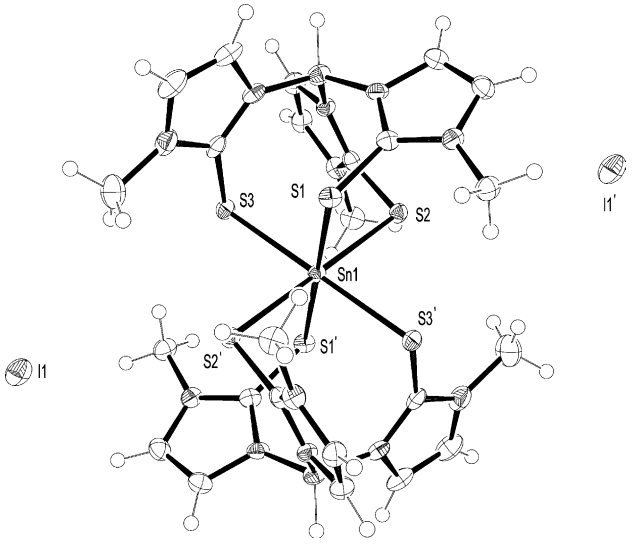

Fig. 3. The X-ray crystal structure of the $[Sn(Tm^{Me})_2]^{2+}$ cation.

ligand to support tin(II) in preference to tin (IV) and consequently it is curious that the Tin(II) adducts of the pyrazolylborates (viz. $\kappa^3Tp\kappa^2TpSn(II)$, $\kappa^3TpSnCl$) have been reported [26,27]. Similarly although a range of unstable six coordinate $TpSnX_3$ (X = Cl, Me, pz_3) species [23,28,29] are isostructural with **1b**, a motif similar to that shown in Fig. 2 remains absent. Thus it seems that our understanding of the structural preferences and redox properties of tin in a hard and soft coordination environment is not yet complete.

4. Supplementary data

Crystallographic data have been deposited with the Cambridge Crystallographic Data Centre, CCDC Nos. 215615–215617. Copies of this information may be obtained free of charge from The Director, CCDC, 12 Union Road, Cambridge, CB2 1EZ, UK (fax: +44-1223-336033; e-mail: deposit@ccdc.cam.ac.uk or http://www.ccdc.cam.ac.uk).

Acknowledgements

C.A.D. thanks the EPSRC for financial support.

References

[1] S. Trofimenko, J. Am. Chem. Soc. 88 (1966) 1842.
[2] S. Trofimenko, Chem. Rev. 93 (1993) 943.
[3] S. Trofimenko, Scorpionates: The Coordination Chemistry of Polypyrazolylborate Ligand, Imperial College Press, London, 1999.
[4] P.A. Slavin, J. Reglinski, M.D. Spicer, A.R. Kennedy, J. Chem. Soc., Dalton Trans. (2000) 239.
[5] J.F. Ojo, P.A. Slavin, J. Reglinski, M. Garner, M.D. Spicer, A.R. Kennedy, S.J. Teat, Inorg. Chim. Acta 313 (2001) 15.
[6] C. Kimblin, B.M. Bridgewater, T. Hascall, G. Parkin, Dalton Trans. (2000) 891.
[7] C. Kimblin, B.M. Bridgewater, T. Hascall, G. Parkin, Dalton Trans. (2000) 1267.
[8] P.J. Bailey, M. Lanfranchi, L. Marchio, S. Parsons, Inorg. Chem. 40 (2001) 5030.
[9] C. Santini, M. Pellei, G.G. Lobbia, C. Pettinari, A. Drozdov, S. Troyanov, Inorg. Chim. Acta 325 (2001) 20.
[10] B.M. Bridgewater, G. Parkin, J. Am. Chem. Soc. 122 (2000) 7140.
[11] B.M. Bridgewater, G. Parkin, Inorg. Chem. Commun. 3 (2000) 534.
[12] J. Reglinski, M.D. Spicer, M. Garner, A.R. Kennedy, J. Am. Chem. Soc. 121 (1999) 2317.
[13] C. Kimblin, D.G. Churchill, B.M. Bridgewater, J.N. Girard, D.A. Quarless, G. Parkin, Polyhedron 20 (2001) 1891.
[14] R. Garcia, A. Paulo, A. Domingos, I. Santos, K. Ortner, R. Alberto, J. Am. Chem. Soc. 122 (2000) 11240.
[15] I. Goldberg, F.H. Herbstein, Acta Crystallogr.: Sect. B 28 (1972) 400.
[16] L.P. Battaglia, A.B. Corradi, G. Pelizzi, M.E.V. Tani, J. Chem. Soc., Dalton Trans. (1977) 1141.

[17] J. Reglinski, M. Garner, I.D. Cassidy, P.A. Slavin, M.D. Spicer, D.R. Armstrong, J. Chem. Soc., Dalton Trans. (1999) 2119.
[18] G.M. Sheldrick, SHELX 97 Programs for Crystal Structure Analysis (Release 97-2), Institüt für Anorganische Chemie der Universität, Tammanstrasse 4, D-3400 Göttingen, Germany, 1998.
[19] L.J. Farrugia, J. Appl. Crystallogr. 32 (1999) 837.
[20] B.P. Rosen, FEBS Lett. 529 (2002) 86.
[21] C.L. Raston, A.H. White, J. Chem. Soc., Dalton Trans. (1975) 2425.
[22] R. Hernandez-Molina, A.J. Edwards, W. Clegg, A.G. Sykes, Inorg. Chem. 37 (1998) 2989.
[23] H. Dugan, W. Maringgle, A. Meller, K. Niedenzu, H. Noth, J. Serwatowska, J. Seratowski, Inorg. Chem. 30 (1991) 4799.
[24] D. Dakternieks, H.-J. Zhu, D. Masi, C. Mealli, Inorg. Chim. Acta 211 (1993) 155.
[25] R.O. Day, J.M. Holmes, S. Shafieezad, V. Chandrasekhar, R.R. Holmes, J. Am. Chem. Soc. 110 (1988) 5377.
[26] A.H. Cowley, R.L. Geerts, C.M. Nunn, C.J. Carrano, J. Organomet. Chem. 341 (1988) C27.
[27] D.L. Reger, Y. Ding, Polyhedron 13 (1994) 869.
[28] B.K. Nicholson, J. Organomet. Chem. 265 (1984) 153.
[29] G.G. Lobbia, P. Cecchi, C. Santini, S. Calogero, G. Valle, F.E. Wagner, J. Organomet. Chem. 513 (1996) 139.

Available online at www.sciencedirect.com
SCIENCE DIRECT®
Polyhedron 23 (2004) 451–469
POLYHEDRON
www.elsevier.com/locate/poly

Copper and silver derivatives of scorpionates and related ligands

Claudio Pettinari *, Augusto Cingolani, Giancarlo Gioia Lobbia, Fabio Marchetti, Domenico Martini, Maura Pellei, Riccardo Pettinari, Carlo Santini

Dipartimento di Scienze Chimiche, Università degli Studi di Camerino, Via S. Agostino 1, 62032 Camerino MC, Italy

Received 30 June 2003; accepted 3 September 2003

Abstract

A comprehensive survey of the syntheses and of spectroscopic, analytical and structural data of silver(I), copper(I), and copper(II) complexes containing scorpionate and related ligands and prepared by this group has been reported. This review outlines the possible strategies that can be used in this field for the synthesis of analogous complexes. Statistical analyses of structural features are reported as a function of (1) the steric and electronic properties of the scorpionate ligand, (2) the steric and electronic properties of eventual ancillary ligands, and (3) the nature of the counter-ion. The most important results obtained in this field have been also summarized.
© 2003 Elsevier Ltd. All rights reserved.

Abbreviations

We have employed the method of representing the tris(pyrazolyl)borate ligands proposed by Curtis [1,2] and the rules recently described by Trofimenko for the "second generation" scorpionates [3]. However a more detailed list of abbreviations employed is below.

HAz	azole
Bn	benzyl
Bp^x	dihydrobis(pyrazolyl)borate
cy	cyclohexyl
dppm	bis(diphenylphosphino)methane
dppe	1,2-bis(diphenylphosphino)ethane
dppp	1,3-bis(diphenylphosphino)propane
dppb	1,4-bis(diphenylphosphino)butane
dppf	4,4′-bis(diphenylphosphino)ferrocene
Hbtz	1,2,3-benzotriazole
Him	imidazole
Hmimt	1-methy-2-mercaptoimidazole
Hpz^x	pyrazole
Htz	1,2,4-triazole
Me	methyl
Mes	2,4,6-trimethylphenyl
Ph	phenyl
pz^oTp^x	tetrakis(pyrazolyl)borate
Tm	hydrotris(3-methyl-2-thioxo-1-imidazolyl)borate
Tp^x	tris(pyrazolyl)borate
Tpms	tris(pyrazolyl)methanesulfonate

1. Introduction

Since the first report of Trofimenko [4], poly(pyrazolyl)borates (Fig. 1) and in particular tris(pyrazolyl)borates (Tp^x), have been extensively employed as anionic σ-donor ligands in a wide variety of metal complexes [3]. They form stable complexes in which they often act as tridentate, facial, five-electron donors (covalent formalism for electron counting [5]). These ligands are extremely versatile because the number of pyrazolate groups and the substituents thereon or at the B center can be easily modified in order to obtain ligands with different steric and electronic profiles. They have been extensively used to prepare complexes of main and transition group metals and are particularly useful for the synthesis of monomeric derivatives in which the coordination sphere about the metal can be carefully controlled.

Modifications of poly(pyrazolyl)borates can be made by changing the substituents on the hererocyclic ring or also by replacement of the pyrazolyl with triazolyl [6,7], imidazolyl [8], methimazolyl [9,10], thioether [11,12], thiazolyl and benzothiazolyl [13] and mercaptotriazolyl

* Corresponding author. Tel.: +39-737-402234; fax: +39-737-637345.
E-mail address: claudio.pettinari@unicam.it (C. Pettinari).

0277-5387/$ - see front matter © 2003 Elsevier Ltd. All rights reserved.
doi:10.1016/j.poly.2003.11.033

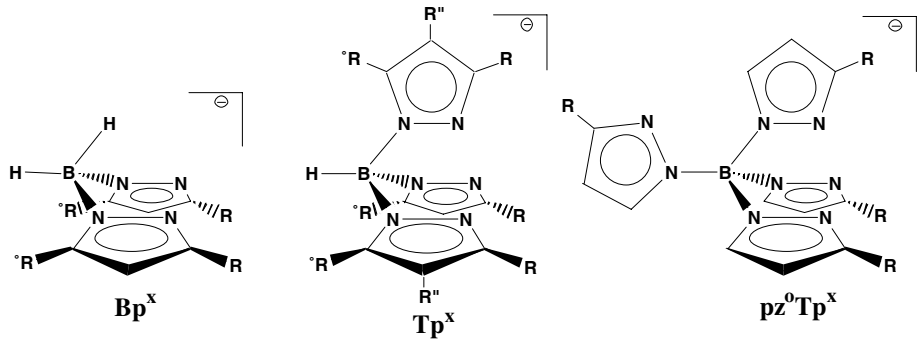

Fig. 1.

moieties [14,15]. Another important variation can be effected by replacement of the boron bridging atom with carbon [16], silicon [17], or phosphorus [18,19].

Poly(pyrazolyl)alkanes (Fig. 2) $[R^*_nC(pz^x)_{4-n}]$ ($n = 0$, 1 or 2, $R^* = H$ or a generic substituent), for example, are stable and flexible polydentate ligands isoelectronic and isosteric with poly(pyrazolyl)borate. They can be prepared readily and in good yields by the procedures reported by Reger [20] and Elguero [21]. Various substituents may replace each hydrogen atom, so that electronic and steric effects can be varied nearly at will. These molecules are generally very stable towards chemical attack, for example, against both oxidizing and reducing agents.

Copper is the center of active sites of many metalloenzymes and metalloproteins, such as hemocyanin and nitrite reductase. In such metalloenzymes and metalloproteins, each copper atom is coordinated by the three nitrogen atoms of three imidazoles or histidine groups of proteins. In 1973 the use of the Tp anion has permitted isolation of the first copper carbonyl complex TpCu(-CO) [22]. Recently, interest in copper poly(pyrazolyl)borate complexes has been aroused by their resemblance to the active sites in some copper-containing metalloproteins, Tp^{iPr2} and Tp^{Ph2} being useful in the revealing the mode of dioxygen binding at the copper site of hemocyanin [23,24], while Tp^{tBu} and Tp^{Ph2} have assisted the development of models for nitric oxide adducts of mononuclear copper in nitrite reductase [25–28]. $[Cu(Tp^*)(C_2H_4)]$ has also been reported as a catalyst for carbene and nitrene transfer to form cyclopropanes, cyclopropenes, and aziridines [29]. Very recently a series of $[Cu(Tp^x)]$ derivatives, generated in situ, has been reported to catalyze the cyclopropanation of terminal olefins as well as the industrially important 2,5-dimethyl-2,4-hexadiene [30,31].

Dias and coworkers in 1996 reported some group 11 metal complexes of fluorinated tris(pyrazolyl)borates [32] and very recently has described the synthesis of $[Ag(Tp^{(CF3)2})\{OC(OCH_3)\}_2CN_2]$ which features a diazoalkane moiety with Ag–O (rather than Ag–N) interactions [33]. The stability of this compound suggests that the metal–oxygen bonded species may also play an important role in metal-mediated activation of diazoketones.

On the basis of the increasing interest in this field and on the potential applications of silver and copper scorpionate complexes we have started a systematic investigation concerning the reactivity of scorpionate-like ligands towards silver(I), copper(I) and copper(II), in the presence of auxiliary ligands such as phosphines, isonitriles or neutral monodentate azoles. Here we report a survey of the results obtained by us in the last decade. A summary of the most relevant molecular pa-

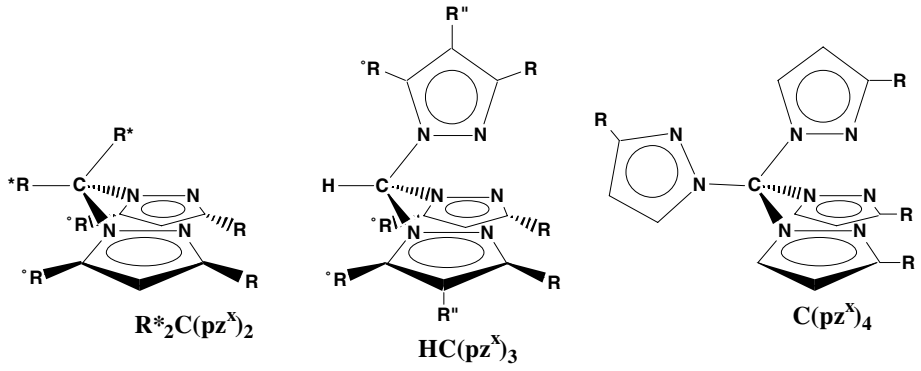

Fig. 2.

Table 1
Comparison of relevant structural and molecular parameters in copper and silver scorpionate derivatives[a]

Compound	Geometry	NC (nuclearity)	M–X	M–Y	Bite angles Y–M–Y	Reference
$Cu(Bp)(PMePh_2)_2$[b]	Td	4 (1)	2.2480(5)	2.045(1)	90.47(5)	[39]
			2.2730(5)	2.073(1)		
$Cu(Bp^{(CF3)2})(PPh_3)_2$[bc]	Td	4 (1)	2.2388(7)	2.057(2)		[40]
			2.2690(7)			
$Cu(Tp)(PPh_3)$[b]	Td	4 (1)	2.153(2)	2.081(5)	91.0(2)	[42]
				2.065(5)	88.4(2)	
				2.083(5)	91.8(2)	
$Cu(Tp)(Pcy_3)$[b]	Td	4 (1)	2.170(1)	2.104(2)	90.8(1)	[43]
				2.095(2)	87.5(1)	
				2.093(2)	90.6(1)	
$Cu(Tp^*)(Pcy_3)$[b]	Td	4 (1)	2.207(1)	2.133(2)	90.2(1)	[43]
					89.5(1)	
					89.5(1)	
$Cu(Tp^*)(PPh_3)$[b]	Td	4 (1)	2.166(6)	2.106(14)	90.1(5)	[47]
				2.101(10)	91.7(5)	
				2.086(13)	90.0(4)	
$Cu(Tp)(PMePh_2)$[b]	Td	4 (1)	2.1472(5)	2.065(1)	89.39(5)	[39]
				2.100(1)	92.01(5)	
				2.051(1)	90.02(5)	
$Cu(Tp^*)(PMePh_2)$[b]	Td	4 (1)	2.164(6)	2.090(2)	92.94(6)	[39]
				2.069(2)	88.81(6)	
				2.093(2)	91.22(6)	
$Cu(Tp)(P(o\text{-tolyl})_3)$[b]	Td	4 (1)	2.158(1)	2.070(3)	90.3(1)	[39]
$Cu(Tp^{(CF3)2})(PPh_3)$[b]	Td	4 (1)	2.219(1)	2.168(3)	89.4(1)	[32]
				2.243(3)	86.8(1)	
				2.108(3)	86.4(1)	
$Cu(pzTp)(PPh_3)_2$[b]	Td	4 (1)	2.273(1)	2.087(3)	92.6(1)	[38]
			2.359(1)	2.051(3)		
$Cu(pz^oTp^{Me})(PPh_3)$[b]	Td	4 (1)	2.165(1)	2.091(2)	90.12(9)	[39]
				2.099(2)	89.47(9)	
				2.068(2)	90.9(1)	
$Cu(pz^oTp^{Me})(P(p\text{-tolyl})_3)$[b]	Td	4 (1)	2.1611(7)	2.134(2)	89.76(7)	[39]
				2.038(2)	90.89(8)	
				2.083(2)	89.85(7)	
$Cu(pz^oTp^{Me})(Pcy_3)$[b]	Tg	3 (1)	2.1874(6)	2.044(2)	93.43(7)	[39]
				2.005(2)		
$Cu(Tp^{4Me})_2$[d]	Oh	6 (1)		2.055(7)	86.9(3)	[51]
				2.107(8)	84.6(3)	
				2.274(8)	84.8(3)	
				2.025(8)	87.8(3)	
				2.000(6)	83.8(3)	
				2.469(6)	84.8(2)	
$Cu(Tp^{Me})_2$[d]	Oh	6 (1)		2.112(4)	87.8(1)	[51]
				2.342(4)	87.7(1)	
				2.024(3)	86.6(1)	
				2.057(4)	86.5(2)	
				2.392(4)	86.1(2)	
				2.063(4)	85.9(1)	
$Cu(Tp^{*Cl})_2$[d]	Oh	6 (1)		2.126(8)	88.3(3)	[51]
				2.255(8)	86.0(3)	
				2.108(()	87.1(3)	
				2.124(8)	86.0(3)	
				2.263(7)	87.0(3)	
				2.086/8)	87.7(3)	
$Cu(pz^oTp^{Me})_2$[d]	Oh	6 (1)		2.361(3)		[51]
				2.055(3)		
				2.036(2)		
$Cu(Tm)(P(m\text{-tolyl})_3)$[e]	Td	4 (1)	2.217(3)	2.357(2)	104.59(6)	[57]
$Cu(Tm)(P(p\text{-tolyl})_3)$[e]	Td	4 (1)	2.226(1)	2.3323(9)	107.10(4)	[57]
$Cu(HB(Btz)_3)(PBn_3)_2$	Tg	3 (1)	2.2380(5)	2.021(2)		[55]
			2.2463(6)			
$Cu(HB(Btz)_3)(P(m\text{-tolyl})_3)$[b]	Td	4 (1)	2.1760(7)	2.103(2)	89.15(8)	[55]
				2.089(2)	88.12(9)	
				2.108(2)	89.11(8)	

Table 1 (*continued*)

Compound	Geometry	NC (nuclearity)	M–X	M–Y	Bite angles Y–M–Y	Reference
$Cu(H_2B(tz)_2)(PPh_3)_2$[b]	Td	4 (1)	2.2686(4) 2.2697(4)	2.050(1) 2.110(1)	93.17(5)	[54]
$Cu(H_2B(tz)_2)(Pcy_3)$[b]	Td	4 (∞)	2.231(1)	2.091(3) 2.175(3) 2.101(3)	88.7(1)	[54]
$Cu(H_2B(tz)_2)(PBn_3)_2$[b]	Td	4 (1)	2.2642(4) 2.2647(4)	2.106(1) 2.138(1)	90.01(4)	[54]
$Cu(HB(tz)_3)(Pcy_3)$[b]	Td	4 (1)	2.1817(3)	2.1433(8)	88.20(3) 88.37(3) 90.49(3)	[54]
$Cu(HB(tz)_3)(P(o\text{-tolyl})_3)$[b]	Td	4 (1)	2.1662(4)	2.096(6) 2.093(5) 2.075(7)	88.6(2) 90.3(3) 88.6(2)	[54]
$Cu(HB(tz)_3)(P(p\text{-tolyl})_3)$[b]	Td	4 (1)	2.1562(4)	2.071(1) 2.100(1) 2.097(1)	90.04(5) 91.05(5) 88.48(4)	[54]
$Cu(HB(tz)_3)(P(m\text{-tolyl})_3)_2$[b]	Td	4 (∞)	2.263(1) 2.279(1)	2.096(3) 2.079(3)		[54]
$Cu(NO_3)_2$:$(pz^*_3)CH$[d] 1:2	Oh	6 (1)		2.044(1) 2.347(2) 2.025(2)	86.06(8) 85.71(6) 83.33(6)	[62]
$Cu(NO_3)_2$:$(pz^{*Me})_3CH$[d] 1:2	Oh	6 (1)		2.0202(9) 2.150(1) 2.220(2)	84.39(4) 85.02(5) 85.98(6)	[62]
$Cu(ClO_4)_2$:$(pz^{*Me})_3CH$[d] 1:2	Oh	6 (1)		2.035(3) 2.353(3) 2.024(4) 2.033(3) 2.384(3) 2.026(3)	86.2(1) 85.7(1) 83.3(1) 83.0(1) 84.9(1) 86.5(1)	[62]
$CuBr_2$:$(pz^{4Me})_3CH$[d] 1:2 Molecule a	Oh	6 (1)		1.970(4) 2.378(3) 2.020(3)	82.1(1) 87.9(1) 84.6(1)	[62]
$CuBr_2$:$(pz^{4Me})_3CH$[d] 1:2 Molecule b	Oh	6 (1)		2.003(3) 2.355(4) 1.996(4)	83.3(1) 85.9(1) 84.2(1)	[62]
$CuBr_2$:$(pz^{4Me})_3CH$[d] 1:2 Molecule c	Oh	6 (1)		1.986(4) 2.373(4) 2.019(3) 1.987(4) 2.439(4) 2.026(3)	83.3(1) 85.9(1) 84.2(1)	[62]
$Ag(Bp)(PPh_3)_2$[b]	Td	4 (1)	2.4256(9) 2.5049(9)	2.326(3) 2.360(3)	89.3(1)	[63]
$Ag(Bp^*)(Pcy_3)$[b]	Tg	3 (1)	2.3538(6)	2.250(1) 2.299(2)	86.71(7)	[63]
$Ag(Bp^*)(PEtPh_2)$[b] Molecule a	Tg	3 (1)	2.358(1)	2.251(4) 2.260(4)	86.2(1)	[63]
$Ag(Bp^*)(PEtPh_2)$[b] Molecule b	Tg	3 (1)	2.349(1)	2.249(4) 2.245(3)	87.1(1)	[63]
$Ag(Tp^*)(PMePh_2)$[b]	Td	4 (1)	2.336(2)	2.336(5) 2.329(6) 2.316(6)	82.1(2) 84.8(2) 83.0(2)	[68]
$Ag(Tp^*)(P(o\text{-tolyl})_3)$[b]	Td	4 (1)	2.375(2)	2.361(4)	83.9(9)	[68]
$Ag(Tp)(PPh_3)$[b] Molecule a	Td	4 (1)	2.336(3)	2.325(4) 2.351(3) 2.355(3)	83.5(2) 86.2(2) 79.7(2)	[67]

Table 1 (*continued*)

Compound	Geometry	NC (nuclearity)	M–X	M–Y	Bite angles Y–M–Y	Reference
Ag(Tp)(PPh_3) Molecule b	Td	4 (1)	2.337(2)	2.321(3)	80.9(2)	[67]
				2.374(3)	83.7(2)	
				2.340(4)	83.8(2)	
Ag(Tp)(PBn_3)	Td	4 (1)	2.328(2)	2.343(4)	81.4(2)	[67]
				2.383(4)	82.0(2)	
				2.357(4)	83.8(1)	
Ag(Tp)(P(*o*-tolyl)$_3$)[b]	Td	4 (1)	2.368(1)	2.357(3)	81.70(1)	[67]
Ag(Tp^{4Br})(PPh_3)[b]	Td	4 (1)	2.345(3)	2.446(8)	83.3(3)	[67]
				2.383(9)	84.1(3)	
				2.304(8)	79.9(3)	
Ag(Tp^*)(P(*p*-tolyl)$_3$)[b]	Td	4 (1)	2.332(2)	2.348(4)	83.8(1)	[67]
				2.292(3)	84.9(1)	
				2.356(4)	82.5(2)	
Ag(Tp^{Ph2})(PPh_3)[b]	Td	4 (1)	2.360(1)	2.390(3)	80.9(1)	[69]
				2.336(3)	85.3(1)	
				2.383(3)	80.6(1)	
Ag(Tp^{Ph2})(PBn_3)[b] Molecule a	Td	4 (1)	2.394(6)	2.46(1)	81.1(4)	[69]
Ag(Tp^{Ph2})(PBn_3)[b] Molecule b	Td	4 (1)	2.387(6)	2.405(9)	82.9(3)	[69]
Ag($Tp^{(CF3)2}$)(PPh_3)[b]	Td	4 (1)	2.376(1)	2.401(4)	80.4(1)	[32]
				2.469(4)	80.9(1)	
				2.427(3)	78.0(1)	
Ag(pzTp)(P(*o*-tolyl)$_3$)[b]	Td	4 (1)	2.368(2)	2.358(7)	80.7(2)	[77]
Ag(pzTp)(PPh_3)[b] Molecule a	Tg	3 (1)	2.331(2)	2.205(6)	86.6(2)	[77]
				2.296(7)		
Ag(pzTp)(PPh_3)[b] Molecule b	Tg	3 (1)	2.335(2)	2.217(7)	85.9(3)	[77]
				2.314(7)		
Ag(pzTp)(P(*m*-tolyl)$_3$)[b]	Tg	3 (1)	2.352(1)	2.248(3)	85.4(1)	[77]
				2.289(3)		
Ag(pzTp)($PMePh_2$)[b]	Tg	3 (1)	2.341(2)	2.217(5)	85.1(2)	[77]
				2.301(4)		
Ag(pzTp)($PEtPh_2$)[b]	Tg	3 (1)	2.347(1)	2.220(3)	85.5(1)	[77]
				2.322(3)		
Ag(pzTp)(Pcy_3)[b]	Tg	3 (1)	2.351(1)	2.261(4)	84.9(1)	[77]
				2.297(3)		
Ag(pz^oTp^{Me})($PMePh_2$)[b]	Tg	3 (1)	2.328(2)	2.228(4)	88.0(2)	[77]
				2.257(5)		
Ag(pz^oTp^{Me})(PBn_3)[b]	Tg	3 (1)	2.333(2)	2.276(7)	84.2(2)	[77]
				2.244(6)		
Ag(pz^oTp^{Me})(P(*p*-tolyl)$_3$)[b]	Tg	3 (1)	2.358(1)	2.225(3)	86.4(1)	[77]
				2.281(4)		
Ag(pz^oTp^{Me})(Pcy_3)[b]	Tg	3 (1)	2.333(1)	2.206(1)	84.9(3)	[77]
				2.332(7)		
Ag(pz^oTp^{Me})(PPh_3)[b]	Td	4 (1)	2.328(2)	2.325(3)	82.0(1)	[77]
Ag(pz^oTp^{Me})(P(*o*-tolyl)$_3$)[b]	Td	4 (1)	2.384(2)	2.363(5)	82.1(2)	[77]
Ag(pz^oTp^{Me})(P(*m*-tolyl)$_3$)[b]	Td	4 (1)	2.353(3)	2.297(4)	81.2(4)	[77]
				2.347(9)	80.1(3)	
				2.334(8)	82.9(3)	
Ag(Tm)(Pcy_3)[e]	Tg[f]	3 (1)	2.420(1)	2.602(1)	107.35(3)	[78]
				2.580(1)		
Ag(Tp^*)(CN^tBu)[g]	Td	4 (1)	2.05(1)	2.271(9)	83.5(3)	[76]
				2.36(1)	82.9(4)	
				2.38(1)	80.8(3)	
Ag(Tp^{Ph2})(CN^tBu)[g]	Td	4 (1)	2.063(5)	2.289(4)	81.4(1)	[76]
				2.352(3)	81.7(1)	
Ag(Tp^{Ph2})(CNcy)[g]	Td	4 (1)	2.08(1)	2.319(7)	84.4(3)	[76]
				2.363(7)	81.5(2)	
				2.321(7)	82.1(3)	
$[Ag(Tm)]_2$[h]	Td	4 (2)		2.857(2)	107.30(6)	[65]
				2.552(2)		

Table 1 (*continued*)

Compound	Geometry	NC (nuclearity)	M–X	M–Y	Bite angles Y–M–Y	Reference
$[Ag(Tp^*)]_2$[d] Molecule 1	Td	4 (2)		2.234(2)	85.85(8)	[66]
				2.233(2)	84.66(8)	
				2.434(2)		
				2.443(2)		
				2.144(2)		
				2.147(2)		
				2.700(2)		
				2.704(2)		
$Ag(im_2BH_2)(Pcy_3)$[b]	Tg	3 (1)	2.367(7)	2.189(2)		[79]
				2.349(2)		
$Ag(im_2BH_2)(P(m\text{-tolyl})_3)_2$[b]	Td	4 (1)	2.4594(8)	2.327(2)		[79]
			2.4597(9)	2.380(2)		
$Ag(im_4B)(Pcy_3)_2$[b]	Td	4 (1)	2.479(1)	2.523(4)		[79]
			2.480(1)	2.449(3)		
Ag(Bp)(dppf)[b]	Td	4 (1)	2.4608(8)	2.295(3)	87.5(1)	[64]
			2.4550(8)	2.337(3)		
Ag(pzTp)(dppf)[b] Molecule a	Td	4 (1)	2.477(3)	2.294(9)	83.6(4)	[64]
			2.453(3)	2.33(1)		
Ag(pzTp)(dppf)[b] Molecule b	Td	4 (1)	2.476(3)	2.294(9)	84.6(4)	[64]
			2.465(3)	2.33(1)		
$AgClO_4$:$(pz)_2CMe_2$ (1:2)[d]	Td	4 (1)		2.289(4)	82.6(1)	[80]
			2.324(4)	83.8(1)		
			2.432(4)			
			2.247(4)			
$AgNO_3$:pz_3CH (1:1)[i] Ag(2)	Distorted Sp	5 (∞)	2.38(1)	2.24(1)		[82]
			2.506(9)	2.28(1)		
			2.90(1)			
$AgNO_3$:pz_3CH (1:1)[i] Ag(1)	Distorted Oh	6 (∞)	2.738(9)	2.32(1)	75.9(3)	[82]
			2.82(1)	2.59(1)	82.5(3)	
				2.38(1)	80.9(4)	
				2.38(1)		
$AgNO_3$:$(pz^*)_3CH$ (1:2)[d]	Oh	6 (1)		2.434(1)	75.25(4)	[82]
				2.455(1)	74.96(4)	
				2.594(1)	79.00(4)	
AgO_3SCF_3:$(pz^*)_3CH$[d] (1:2)	Oh	6 (1)		2.461(7)	75.6(2)	[83]
				2.487(7)	75.8(2)	
				2.596(7)	78.6(2)	
$AgNO_2$:tz_2CH_2 (1:1)[i] Ag(1)	Sp	5 (∞)	2.314(4)	2.519(5)		[84]
				2.670(5)		
				2.420(5)		
				2.536(7)		
$AgNO_2$:tz_2CH_2 (1:1)[i] Ag(2)	Td	4 (∞)	2.217(4)	2.572(5)		[84]
			2.194(4)			
			2.499(4)			
$AgNO_3$:tz_2CH_2 (1:1)[i]	Td	4 (∞)	2.645(2)	2.163(2)		[84]
			2.802(2)	2.164(2)		
$Ag(O_3SCF_3)$:tz_2CH_2 (3:4)[d] Ag(1)	Sp	5 (∞)		2.356(9)	96.8(3)	[84]
				2.371(8)		
				2.385(8)		
				2.517(8)		
				2.635(9)		
$Ag(O_3SCF_3)$:tz_2CH_2 (3:4)[d] Ag(2)	Td	4 (∞)		2.272(9)	96.8(3)	[84]
				2.301(9)		
				2.371(8)		
				2.351(8)		

Table 1 (*continued*)

Compound	Geometry	NC (nuclearity)	M–X	M–Y	Bite angles Y–M–Y	Reference
$Ag(O_3SCF_3):tz_2CH_2$ (3:4)[d] Ag(3)	Sp	5 (∞)		2.334(9)	75.7(3)	[84]
				2.549(10)		
				2.705(10)		
				2.317(9)		
				2.390(10)		

[a] NC: coordination number, Td: tetrahedron, Sp: square pyramidal, Oh: octahedron, Tg: trigonal.
[b] X = P, Y = N.
[c] Cu–H: 2.01(2) Å.
[d] Y = N.
[e] X = P, Y = S.
[f] Additional Ag–H interaction.
[g] X = C, Y = N.
[h] Y = S.
[i] X = O, Y = N.

rameters, coordination numbers and environments for those compounds structurally characterized is reported in Table 1.

2. Results

2.1. Copper poly(pyrazol-1-yl)borates

2.1.1. Bis(pyrazol-1-yl)borates (Bp^x) derivatives

Dihydrobis(pyrazolyl)borate and other scorpionate copper(I) (triaryl)phosphino complexes $[Cu(Bp^x)(PR'_3)_2]$ were firstly reported by Bruce and coworkers [34–37], and further spectroscopically investigated by us in 1995 [38]. These compounds have been only recently structurally characterized [39]. Monophosphine $[Cu(Bp^x)(PR'_3)]$ adducts may be obtained with sterically hindered donors such as P(*o*-tolyl)$_3$, the copper centre in these cases achieving three-coordination by way of bidentate chelation of the ligand (κ^2-hapticity), whereas less sterically hindered phosphines such as $PMePh_2$ and PPh_3 allow the attainment of 1:2 $[Cu(Bp^x)(PR'_3)_2]$ adducts (Scheme 1). Dias has recently reported that fluorinated Bp^x ligands yield compounds of similar stoichiometry but with the scorpionate acting as N,H-donor [40].

It has been previously reported that $[M(Bp^x)(L)_2]$ may be subject to boat inversion [41]. In the ^{31}P NMR spectrum of our $[Cu(Bp^x)(PR'_3)_2]$ complexes only one sharp peak is observed, indicating that, unless there is fortuitous synchronicity, the boat inversion is operating at room temperature.

2.1.2. Tris(pyrazol-1-yl)borates (Tp^x) derivatives

The first systematic investigation of triaryl- [42] and tricyclohexylphosphine [43] copper(I) complexes containing anionic tris(pyrazol-1-yl)borates, prepared from the metathetic and displacement reaction (1) in chlorinated solvents, was reported seven years ago.

$$[Cu(NO_3)(PR'_3)_2] + MTp^x \rightarrow [Cu(Tp^x)(PR'_3)] + PR'_3 + MNO_3 \quad (M = Na \text{ or } K, R = cy \text{ or aryl}) \quad (1)$$

Four-coordinate Cu(I) species, in a tetrahedral configuration strongly distorted because of the bulky PR'_3 and Tp^x ligands, were always obtained (Fig. 3). We have

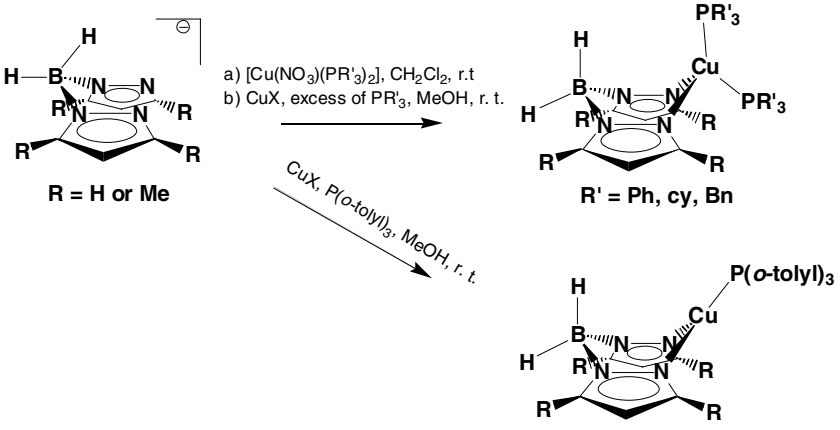

Scheme 1.

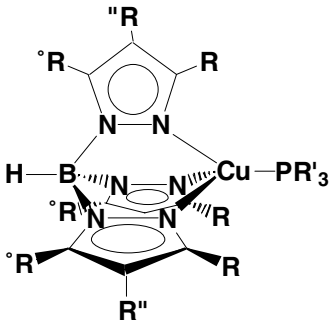

R = H, Me or Ph; R° = H or Me, R" = H or Br
R' = Ph, Bn, cy, *o*-tolyl, *m*-tolyl, *p*-tolyl, Mes

Fig. 3.

found that these compounds can be prepared more efficiently by using a Cu(I) starting material such as [CuBr(Me_2S)] or [$Cu(C_6H_6)_{0.5}(O_3SCF_3)$]$_2$ [39]. The [$Cu(Tp^x)(PR'_3)$] complexes are generally soluble in chlorinated solvents, acetone and DMSO in which they are non-electrolytes. They are air-stable but decompose in solution in accordance with non-ionic equilibria such as (2), followed by disproportionation of the well known polynuclear complexes [44–46] to copper metal and copper(II) species (3). Attempted reactions of [$Cu(Tp^x)(PR'_3)$] with imidazole, pyrazole, bipyridyl or phenanthroline were unsuccessful, the starting materials always being recovered.

$$n[Cu(Tp^x)(PR'_3)] \rightarrow [Cu(Tp^x)]_n + nPR'_3 \quad (2)$$

$$2[Cu(Tp^x)]_n \rightarrow n[Cu(Tp^x)_2] + nCu \quad (3)$$

Kitajima reported that displacement of the carbonyl group in a mononuclear copper complex [$Cu(Tp^*)(CO)$] with PPh_3 can afford [$Cu(Tp^*)(PPh_3)$] quantitatively. The reaction of [$Cu(Tp^*)(PPh_3)$] with an excess amount of PhIO results in the formation of a μ-oxo dinuclear copper(II) complex [$Cu(Tp)]_2O$ which immediately converts to a bis(μ-hydroxo) dinuclear species [$Cu(Tp)]_2(\mu\text{-}OH)_2$ [47].

Volatility studies, electrospray mass spectra and IR in vapour phase have been carried out for selected [$Cu(Tp^x)(PR'_3)$] complexes [48,49]. The volatility has been related to structural features and molecular parameters of the copper(I) complexes. These compounds are much more volatile than copper(I) pyrazolonates [48] and seem to be promising precursors for thin film deposition as the heterocyclic rings in the ligand are not involved in the conjugation and do not contain additional donor centres. XRD data of films obtained from metal organic chemical vapor deposition MOCVD on [$Cu(Tp^x)(PR'_3)$] [48] and [$Cu(Bp^x)(PR'_3)_n$] ($n = 1$ or 2) complexes [49] have been also reported.

By using the water-soluble P-donor ligand 4-(diphenylphosphane)benzoic acid, some water-soluble copper(I) complexes [$Cu(Tp^x)\{PPh_2(4\text{-}C_6H_4COOH)\}$] have recently been obtained [50] which have been investigated by chemiluminescence techniques in order to evaluate their superoxide scavenging activity.

A series of $Cu(Tp^x)_2$ derivatives ($Tp^x = Tp^{Me3}$, Tp^{4Me}, Tp^{*Cl}, Tp^{3Me}) were synthesised and spectroscopically characterized in 1999 [51]. These complexes, with the metal in a strongly distorted octahedral environment (Fig. 4) (X-ray studies), have been also characterized by fast atom bombardment spectrometry and magnetic susceptibility measurements.

2.1.3. Tetrakis(pyrazol-1-yl)borate (pz^oTp^x) derivatives

Tetrakis(pyrazolyl)borate copper(I) bis(triaryl)phosphino species [$Cu(pz^oTp^x)(PR'_3)_2$] (Fig. 5(a)) were reported in 1995 [38] and characterized by way of IR, ^1H, ^{13}C and ^{31}P NMR measurements. These compounds are more stable in solution with respect to the analogous Tp^x and Bp^x derivatives. They are fluxional in solution, all pyrazolyl groups being equivalent down to −60 °C. Selected [$Cu(pz^oTp^x)(PR'_3)_2$] derivatives have been characterized by IR in the gas phase across a wide temperature range, confirming the stability of these species and suggesting the molecular structure in vapour to be similar to that previously determined by single crystal X-ray studies. The dependence of the volatility on the number of the pyrazolyl moieties has been discussed, the pz^oTp^x derivatives being more volatile with respect to Bp^x and Tp^x derivatives containing the same phosphine.

More recently monophosphine [$Cu(pz^oTp^x)(PR'_3)$] (Fig. 5(b)–(c)) species have been reported as well [39] with two different structurally authenticated arrays: (i) [$Cu(pz^oTp^{Me})(Pcy_3)$], with a three coordinate $PCu(N)_2$ coordination environment and the donor with κ^2-hapticity and (ii) [Cu(pzTp)(P(*p*-tolyl)$_3$)], with a four coordinate $PCu(N)_3$ metal core and the scorpionate with κ^3-hapticity.

The strongly distorted octahedral $Cu(pz^oTp^{Me})_2$ and $Cu(pz^oTp^{4Me})_2$ have been also described. In these compounds the ligands act as tripodal N_3-donors; complexation of the fourth pyrazole ring and formation of

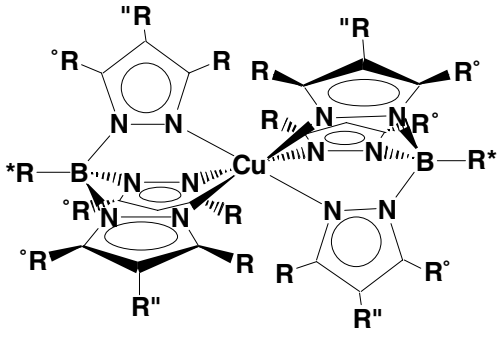

Fig. 4.

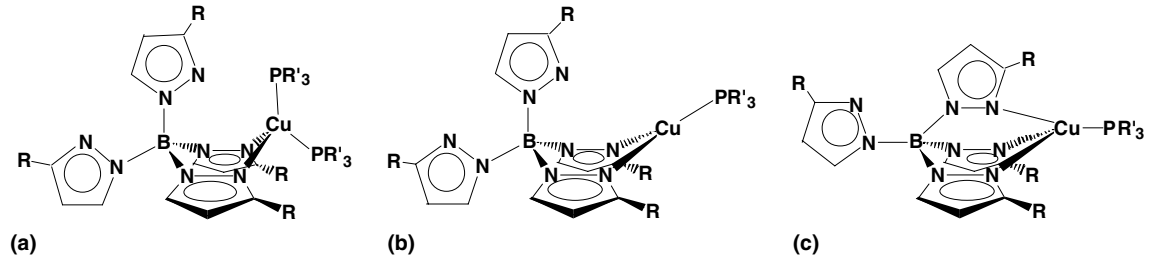

Fig. 5.

polynuclear or oligonuclear species has never been observed [51].

2.2. Copper poly(triazol-1-yl)borates

Although a cobalt complex of hydrotris(1,2,4-triazolyl)borate was reported by Trofimenko in 1967 [52], the chemistry of poly(triazolyl)borate ($H_nB(tz)_{4-n}$) species (Fig. 6) has remained undeveloped. Two features make them attractive candidates for further examination: they should be electron-withdrawing relative to their pyrazole-based counterparts, and the properties of metal complexes should differ accordingly; the exo ring nitrogen atoms of triazole-based ligands may bridge between metal centers, thereby creating coordination polymers with interesting solid state structural and optical properties as recently shown by Janiak [53]. We have recently reported several copper(I) coordination polymers as well as mononuclear copper complexes derived from poly(1,2,4-triazolyl)borate ligands and triorganophosphines [54]. The structurally authenticated arrays fall into four different types (Fig. 7): (a) discrete mononuclear bis(triazolyl)boratebis(triorganophosphine) copper(I) species; (b) discrete mononuclear tris(triazolyl)borate-(triorganophosphine)copper(I) species, with CuN_3P coordination spheres; (c) one dimensional polynuclear species containing bis(triazolyl)borate wherein the triazolyl groups are coordinated throughout both N2 and N4 within CuN_3P coordination spheres; (d) one-dimensional polynuclear species containing tris(triazolyl)borate, wherein one of the triazolyl rings is uncoordinated and the other two bridge through the N to successive copper atoms. Two $[Cu(H_nB(tz)_{4-n})\{PPh_2(4\text{-}C_6H_4COOH)\}]$ ($n = 1$ or 2) have been also reported [50].

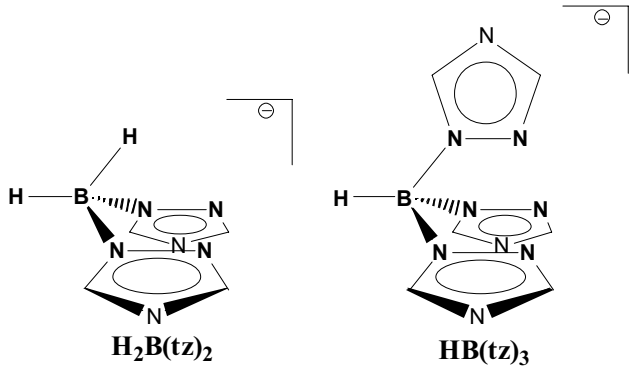

Fig. 6.

2.3. Copper poly(benzotriazol-1)borates

A series of copper(I)$(PR'_3)_n$ ($n = 1$ or 2) complexes of $\{H_xB(btz)_{4-x}\}$ (Fig. 8) ($x = 1$ or 2) has been synthesised and characterized by X-ray studies, and by IR and NMR spectroscopy [55]. 1:1:1 and 1:2:1 Cu:PR'_3:$\{H_xB(btz)_{4-x}\}$ species were afforded, depending on the

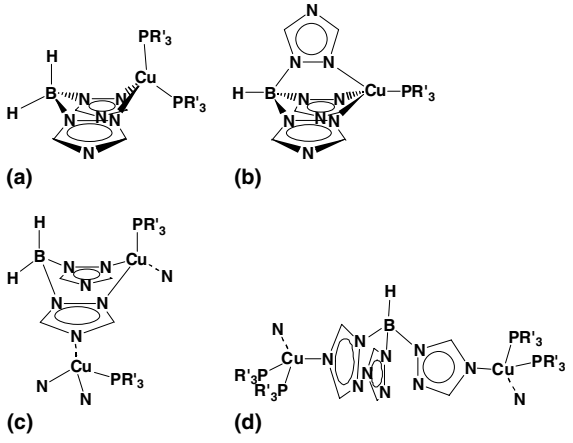

Fig. 7.

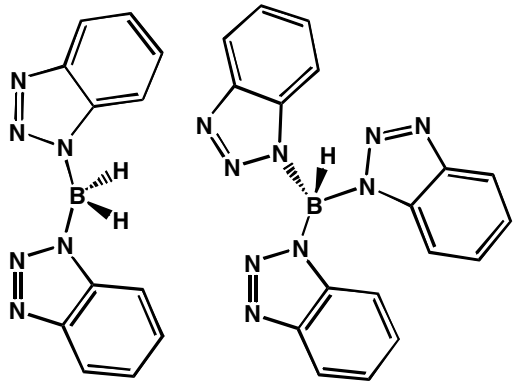

Fig. 8.

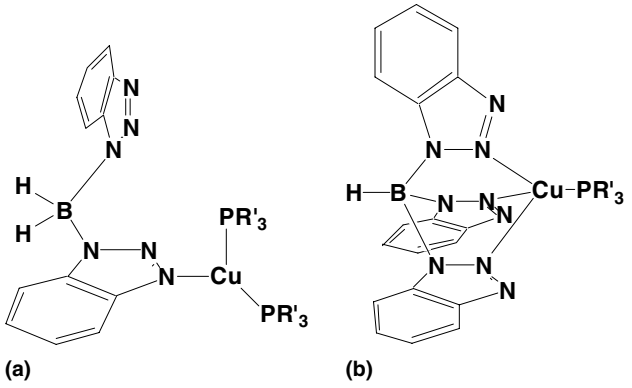

Fig. 9.

nature of the P-donor, and in some cases, on the reaction conditions employed. All species are of limited stability in solution and fluxional at room temperature. The $\{H_xB(btz)_{4-x}\}$ ligand is able to coordinate in uni-, bi- or tri-dentate fashion, coordination occurring not only through the three N2 atoms, but also through one N3 atom. Two structurally authenticated arrays were found: (i) $[Cu\{H_2B(btz)_2\}(PBn_3)_2]$ with a three coordinate P_2CuN coordination sphere and the donor coordinated throughout only one N3 atom (Fig. 9(a)); (ii) $[Cu\{HB(btz)_3\}\{P(m\text{-tolyl})_3\}]$ with a four coordinate $PCuN_3$ coordination sphere, and the $\{HB(btz)_3\}$ acting as tripodal donor by way of all N2 atoms (Fig. 9(b)).

A copper(II) derivative, $[Cu\{HB(btz)_3\}_2]$, has also been reported and characterized by IR and EI MS spectra [56].

2.4. Copper(I) hydrotris(3-methyl-2-thioxo-1-imidazolyl)borates

1:1:1 $[Cu(Tm)(PR'_3)]$ triorganophosphine copper(I) complexes containing the anionic, potential S_3-donor face-capping ligand hydrotris(3-methyl-2-thioxo-1-imidazolyl)borate Tm^- [9] (Fig. 10) were synthesised from

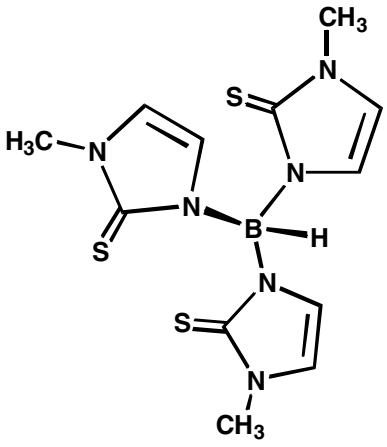

Fig. 10.

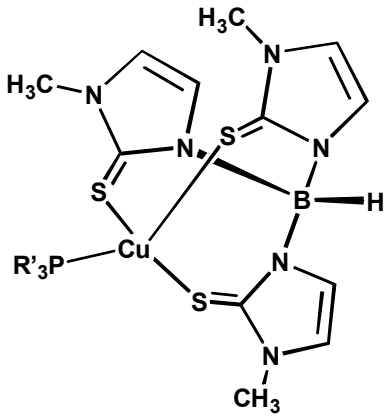

Fig. 11.

K(Tm), CuCl and the corresponding P-donor [57]. The copper atoms are tetracoordinated, the Tm^- behaving as a tripodal donor (Fig. 11). In the absence of P-donors Cu(I) salts react with K(Tm) yielding a possibly polynuclear $[Cu(Tm)]_n$ species which is unreactive toward NH_3, CS_2, H_2O and CO, but reacts with pyridine yielding [Cu(Tm)(py)]. $[Cu(Tm)]_n$ reacts with H_2O_2 yielding the poorly soluble $[Cu(mimt)]_n$ (Hmimt = 3-methyl-1-imidazoline-2-thione) upon breaking of the B–N bond in the mercaptoimidazolylborate ligand.

2.5. Copper(I) heteroscorpionate derivatives

Interest in the coordination chemistry of new heteroscorpionates monoanionic ligands, N-, O- or S-donor is increasing. Some recent papers report the synthesis of the tris(pyrazol-1-yl)methane sulfonate ligand (Tpms) [58] which is highly water soluble and stable over a wide pH range ligand. Its interaction with CuCl in the presence of PR'_3 has provided a series of new copper(I) coordination compounds of formula $[Cu(Tpms)(PR'_3)]$ (Scheme 2) and also a copper(II) species $[Cu(Tpms)_2]$ when R is cyclohexyl. [Cu(Tpms)(PPh_3)] is the first example of structurally characterised complex containing Tpms coordinated to a metal ion in an unusual κ^3-N,N′,O fashion [59].

2.6. Copper poly(azol-1-yl)alkanes

2.6.1. Bis(azolyl)alkane derivatives $\{(Az)_2CH_2\}$

The interaction of a bis(azol-1-yl)alkane $(Az)_2CH_2$ (Az = pyrazole or triazole) with $[CuX(PR'_3)_2]$ (X = NO_3, BF_4, ClO_4, halide) [60,61] can yield ionic $[Cu\{(Az)_2CH_2\}(PR'_3)_2]^+X^-$ or neutral $[CuX\{(Az)_2CH_2\}(PR'_3)]$ derivatives upon displacement of X^- or PR'_3, respectively, from the copper coordination sphere. The stoichiometry and structure of the complexes are dependent on the nature of the substituent on the azolyl group and also on the nature of the counter-ion X. As an example in the Scheme 3 [60] the reaction of $[CuNO_3(PR'_3)_2]$

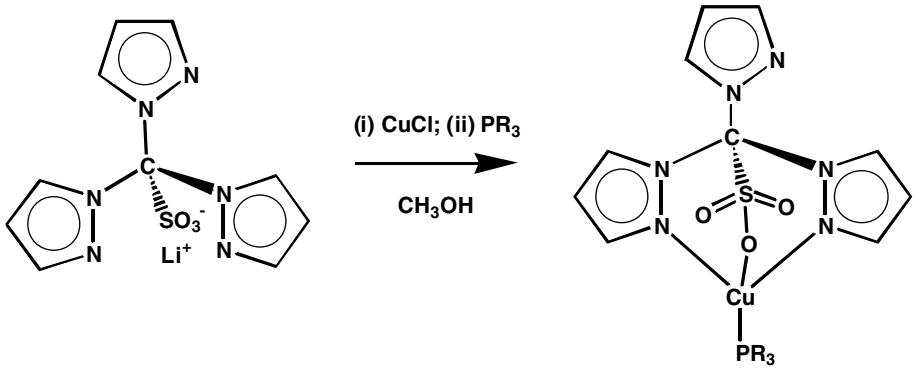

Scheme 2.

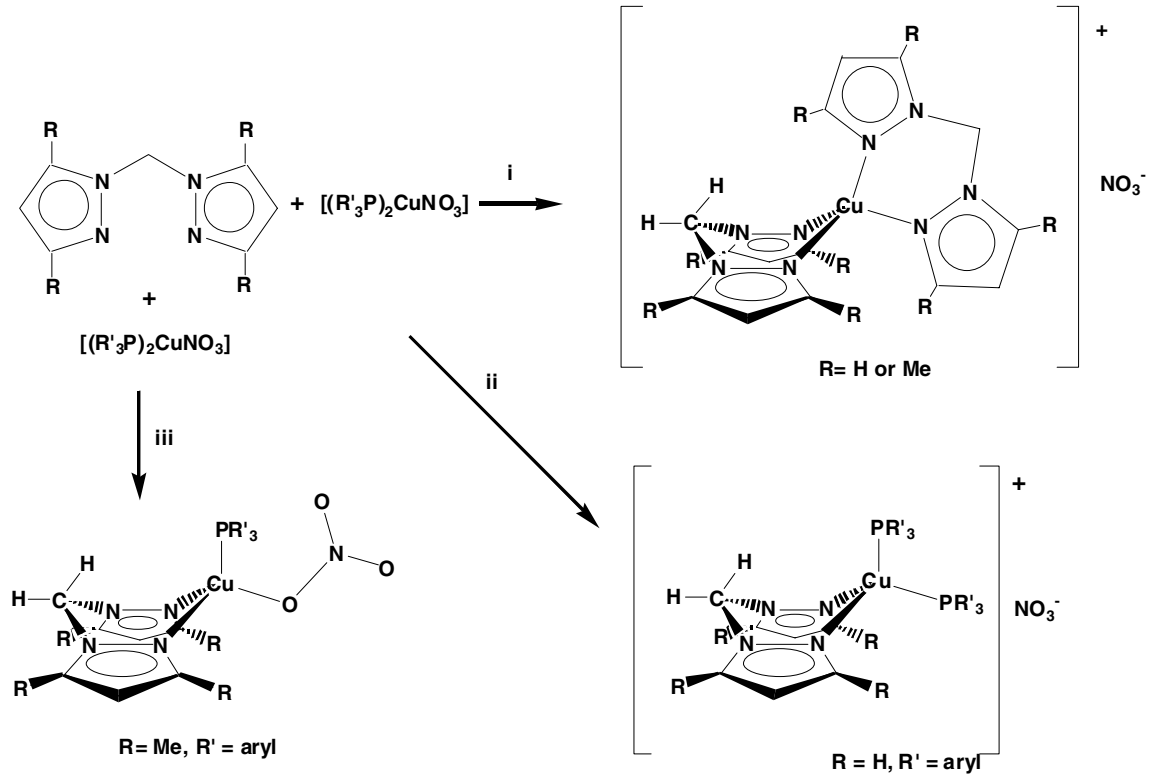

Scheme 3.

with several $(pz^x)_2CH_2$ is described. Displacement of the nitrate is observed with the less hindered and less basic ligands of the family such as pz_2CH_2. Nevertheless, one PR'_3 may be displaced from $[CuNO_3(PR'_3)_2]$ by the more bulky and more basic $(pz^*)_2CH_2$. By contrast, no difference in behaviour has been observed with the arsine and stybine derivatives $[CuNO_3(AsPh_3)_3]$ and $[CuNO_3(SbPh_3)_3]$ which always yield $[CuNO_3\{(pz^x)_2CH_2\}(EPh_3)]$ derivatives. Displacement of all the phosphine ligands to yield $[Cu\{(pz^x)_2CH_2\}_2]^+X^-$ is possible although forcing conditions are required, i.e. strong excess of the N_2-donor ligand in refluxing benzene. The compounds $[Cu\{(Az)_2CH_2\}_2]^+X^-$ can be more efficiently prepared from $[CuNO_3(SbPh_3)_3]$ taking advantage of the decreasing strength of the metal-E bond in the sequence P, As and Sb. The reactivity of the bis(azol-1-yl)alkanes towards $[Cu(PR'_3)_4]ClO_4$ [61] is summarized (Scheme 4).

2.6.2. Tris(pyrazol-1-yl)methanes derivatives $\{HC(pz^x)_3\}$

The interaction of CuX_2 ($X = ClO_4$, NO_3, Cl, Br, O_2CCH_3) with excess of tris(pyrazol-1-yl)methane

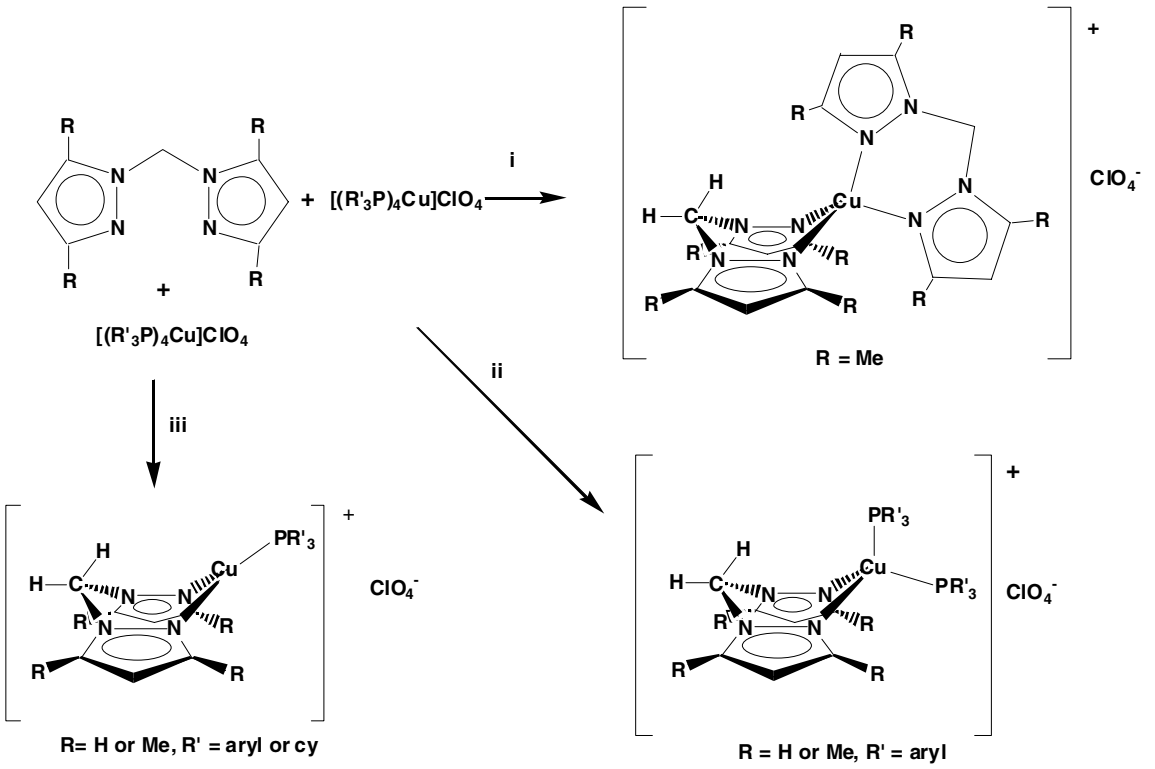

Scheme 4.

$HC(pz^x)_3$ yielded $[CuX_2\{(pz)_3CH\}]$, $[\{CuX_2\}_3\{(pz)_3CH\}_2]$ or $[\{Cu\{(pz)_3CH\}_2\}]X_2$ depending on the substituents on the azolyl moiety and, more particularly, on the nature of the counter-ion [62]. All complexes have been characterized by analytical and spectroscopic measurements (IR, UV, and conductivity measurements) and also in the case of the strongly distorted octahedral $[\{Cu\{(pz)_3CH\}_2\}]X_2$ species, by X-ray diffraction studies.

2.7. Silver(I) poly(pyrazol-1-yl)borate

2.7.1. Bis(pyrazol-1-yl)borates derivatives

Silver(I) derivatives containing triorganophosphine and bis(pyrazolyl)borates were synthesised in 2000 by the reaction of $AgNO_3$ with K(Bp) and K(Bp*) in the presence of PR'_3 in methanol [63]. They have been characterized both in the solid and solution state through analytical and spectroscopic measurements. They are air- but not solution-stable. The structures of $[Ag(Bp)(PPh_3)_2]$, $[Ag(Bp^*)(Pcy_3)]$ and $[Ag(Bp^*)(PEtPh_2)]$ have been determined by X-ray crystallographic studies. In these compounds Bp and Bp* are bidentate, with their silver(I) centres adopting tetrahedral (a) or trigonal geometries (b) (Fig. 12). The ^{31}P NMR data show that the bis(triorganophosphino)derivatives are more stable than the mono-organophosphino species and that the stability decreases with increasing cone angle of the P-donor.

We have also investigated the reactivity of K(Bp) and K(Bp*) toward $AgNO_3$ in the presence of bidentate diphosphines such as dppm, dppe, dppp, dppb and dppf. The ^1H and ^{31}P NMR spectra have been interpreted

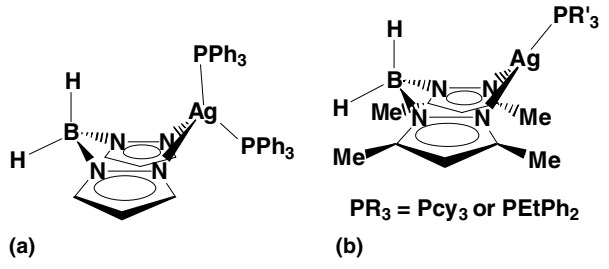

Fig. 12.

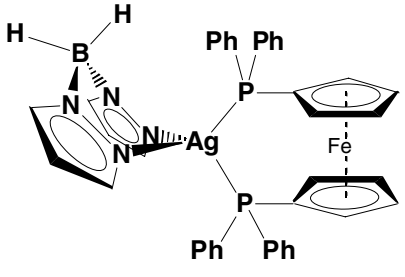

Fig. 13.

with equilibria that involve mono- and di-nuclear species, or the presence of 1:1 and 1:2 silver:diphosphine adducts. The structure of [Ag(Bp)(dppf)] as determined by single crystal X-ray studies indicates the Bp to be bidentate, with the silver centre in a distorted tetrahedral geometry (Fig. 13) [64].

No derivative containing Bp^x and CNR ligands simultaneously coordinated to silver(I) has been to date reported.

2.7.2. Tris(pyrazol-1-yl)borates derivatives

The silver derivatives $[Ag(Tp^*)]_2$, $[Ag(Tp^{4Br})]_2$, and $[Ag(Tp)_2]$ [65], have been synthesised and characterized by IR and NMR spectroscopy. The complexes $[Ag(Tp^*)]_2$ and $[Ag(Tp^{4Br})]_2$ are fluxional with a pyrazolyl ring exchange process occurring rapidly at 293 K, but not at 193 K, whereas $[(Ag(Tp)_2]$ and the crystalline form of $[Ag(Tp^*)]_2$ are not fluxional even at room temperature. The structure of $[Ag(Tp^*)]_2$ as described by McCleverty and coworkers [66] and substantiated by our own work, despite substitution, is not that of its copper(I) homologue, with no bridging pyrazolate units, but rather, that of the unsubstituted parent $[Cu(Tp)]_2$ [44–46] with $N_2M(\mu\text{-}N)$ metal atom environments (Fig. 14), presumably a consequence of greater flexibility contingent upon the incorporation of the larger (silver) metal atom.

Trialkyl- and triaryl-phosphine silver(I) derivatives containing anionic tris(1*H*-pyrazolyl)borates $[Ag(Tp^x)(PR'_3)]$ were prepared from AgX (X = OTf or NO_3), PR'_3 (R′ = Ph, Bn, cy, *o*-, *m*-, *p*-tolyl, Mes) and MTp^x, Tp^x = Tp [67], Tp^{4Br}, Tp^* [68], Tp^{Ph2} [69]; M = Na or K). These air-stable, light sensitive complexes, are non-electrolytes in dichloromethane and acetone, and have been characterized through analytical and spectral measurements. The X-ray diffraction studies show that the silver atom adopts a distorted tetrahedral geometry. $[Ag(Tp^x)(PR'_3)]$ (Fig. 15(a)) generally decompose in acetone solution, even with strict exclusion of oxygen and light. Comparison of the Ag–N bond lengths suggests the bonding of Tp^x to the $Ag(PR'_3)^+$ fragment to be similar despite the steric and electronic differences of the supporting ligand PR'_3. The magnitude

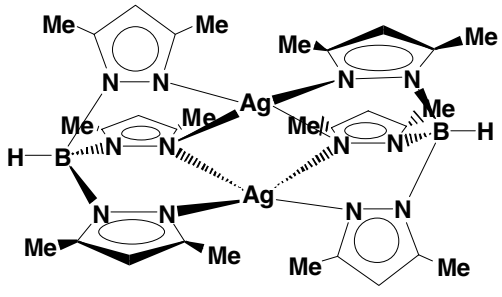

Fig. 14.

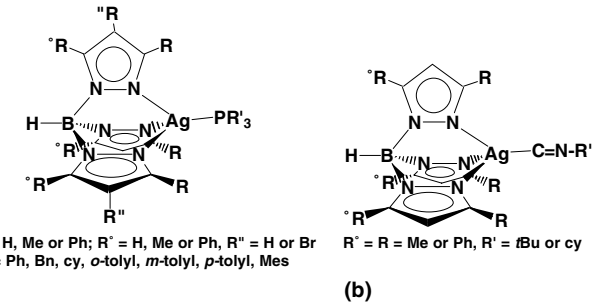

Fig. 15.

of the silver–phosphorus coupling constant and the ^{31}P chemical shift indicate that the structure and the stability of complexes in solution is strongly dependent on the Tolman cone angle and pK_a of PR'_3. We have also found that, in $[Ag(Tp^x)(PR'_3)]$, it is possible to displace the PR'_3 donor from the Ag(I) center with a more basic triorganophosphine, but not with a neutral N-donor mono or bidentate, such as imidazoles, pyrazoles or phenanthroline.

Despite the large number of papers describing Group 11 poly(pyrazol-1-yl)borate derivatives, relatively little attention has been devoted to systems which also contain small unsaturated molecules such as CO and CNR [70–75]. Complexes of the formula $[Ag(Tp^x)CNR]$ ($Tp^x = Tp^*$ or Tp^{Ph2}; R = cy or *t*Bu) (Fig. 15(b)) have been generally obtained independently under the reaction conditions employed when the reaction between Tp^* and silver salts was carried out in the presence of isonitrile ligands [76], no derivatives being obtained when the unsubstituted Tp was used. Those $[Ag(Tp^x)CNR]$ structurally characterized are all unsolvated mononuclear arrays with tripodal Tp^x and unidentate CNR making up the four coordinate environment of the silver atom.

2.7.3. Tetrakis(pyrazol-1)borate derivatives

A systematic investigation of the interaction between silver(I) and the anionic tetrakis(pyrazol-1-yl)borates pzTp and pz^oTp^{Me} was reported in 1998 [77]. These complexes are generally more stable in solution than the analogous derivatives obtained with Bp and Tp ligands. At room temperature, in $CDCl_3$ solution the six-membered AgN_4B rings formed by pzTp and pz^oTp^{Me} are fluxional, probably undergoing a rapid dissociation-reassociation mechanism (boat–boat flip), whereas at low temperature a process which equilibrates only three pyrazolyl rings, with the fourth remaining uncoordinated, is likely. Room-temperature single crystal structural characterizations showed that the scorpionate ligand may be bidentate or tridentate, with a three- or four-coordinate array about the silver. The variation in the silver(I) coordination number and environment in various combinations of various degrees of steric inter-

action among the above entities has been explored and structures similar to those described for Cu(I) have been found [77]. The interaction of pzTp and pz^oTp^{Me} with silver(I) in the presence of chelating bidentate diphosphines was also investigated [64].

The silver(I) tetrakis(pyrazol-1-yl)borates $[Ag(pzTp)]_n$ and $[Ag(pz^oTp^{Me})]_n$ have been also reported and their spectroscopic features and reactivity toward imidazole described [65].

The silver isonitrile derivatives [Ag(pzTp)CNR] and $[Ag(pz^oTp^{Me})(CNR)_x]$ ($x = 1$ or 2) have been successfully synthesised. They exhibit a fluxional behaviour in solution with a pyrazolyl ring exchange process occurring rapidly even at 218 K. Reaction of $[Ag(pz^oTp^{Me})(CNcy)_2]$ with Hmimt and ImH yield $[Ag(mimt)]_n$ and $[Ag(pz^oTp^{Me})(CNcy)(ImH)]$, respectively, whereas reaction of [Ag(pzTp)(CN^{t}Bu)] with ImH yields [Ag(pzTp)(ImH)] [76].

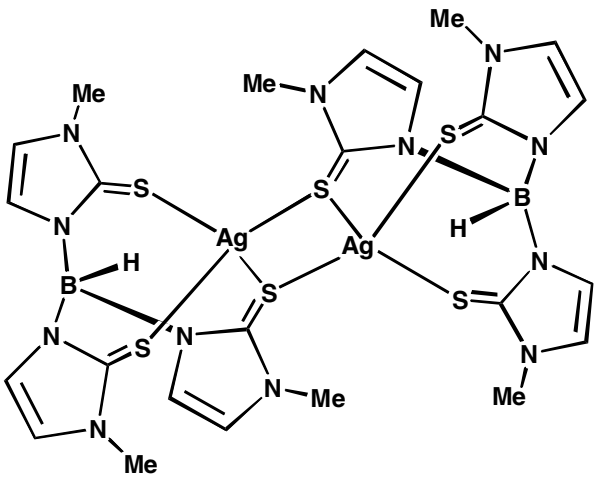

Fig. 17.

2.8. Silver(I) hydrotris(3-methyl-2-thioxo-1-imidazolyl)borates

1:1:1 $[Ag(Tm)(PR'_3)]$ triorganophosphine silver(I) complexes were synthesised in methanol from K(Tm), $AgNO_3$, and the corresponding PR'_3 donor [78]. In [Ag(Tm)(Pcy_3)] (Fig. 16) the silver atom are tricoordinated, with the donor Tm behaving as an S_2-donor. A short Ag···B distance suggests the existence of a two-electron B–H···Ag agostic interaction. The syntheses of the 1:1:2 $[Ag(Tm)(PEtPh_2)_2]$ and the 2:2:1 $[Ag_2(Tm)_2P(m\text{-tolyl})_3]$ were also reported. The complex $[Ag(Tm)]_2$, obtained in methanol from the methathesis reaction of $AgNO_3$ with K(Tm), in the chloroform solvate form $[Ag(Tm)]_2 \cdot 2CHCl_3$ [65], has been shown to be dinuclear, the core of the dimer (Fig. 17) being a four-membered $Ag(\mu\text{-}S)_2Ag$ ring, the two sulfur atoms of the bridging mercaptoimidazolyl rings coordinating two silver atoms in somewhat unsymmetrically mode. The B–H groups of the Tm ligand is disposed with the hydrogen atom projecting into the Ag_2S_2 ring. The silver coordination environment is completed by two sulfur atoms from the remaining mimt rings.

2.9. Silver(I) poly(imidazolyl)borates

The anionic dihydrobis(imidazolyl)borates $[H_2B(im)_2]^-$ and tetrakis(imidazolyl)borate $[B(im)_4]^-$ (Fig. 18) react with $AgNO_3$ in the presence of PR'_3 yielding binuclear $[Ag(PR'_3)_2\{(im)BX_2(im)\}]_2$ (X = H or im) (Fig. 19(a)) or polymeric compounds $[Ag(PR'_3)\{(im)BX_2(im)\}]_n$ compounds (Fig. 19(b)) [79]. Solution data are consistent with a partial dissociation of complexes, occurring through breaking of both Ag–N and Ag–P bonds. In particular the ^{31}P NMR data indicate that the structure and stability are strongly dependent on the stoichiometry and on the Tolman cone angle of the phosphorus donor ligand. $[Ag\{(im)BH_2(im)\}(Pcy_3)]_n$ is a single stranded polymer containing three-coordinate silver atoms ($PAgN_2$ core), while in $[Ag\{(im)B(im)_2(im)\}(Pcy_3)_2]_2$ the silver atoms are four-coordinate with P_2AgN_2 cores.

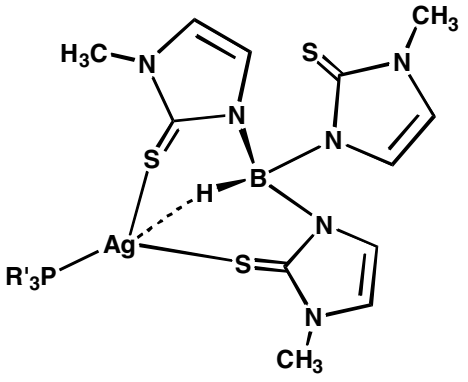

Fig. 16.

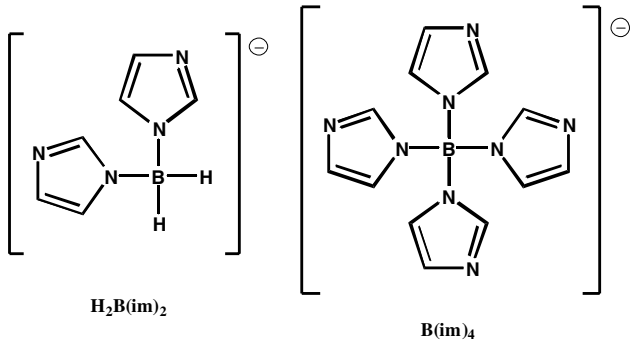

Fig. 18.

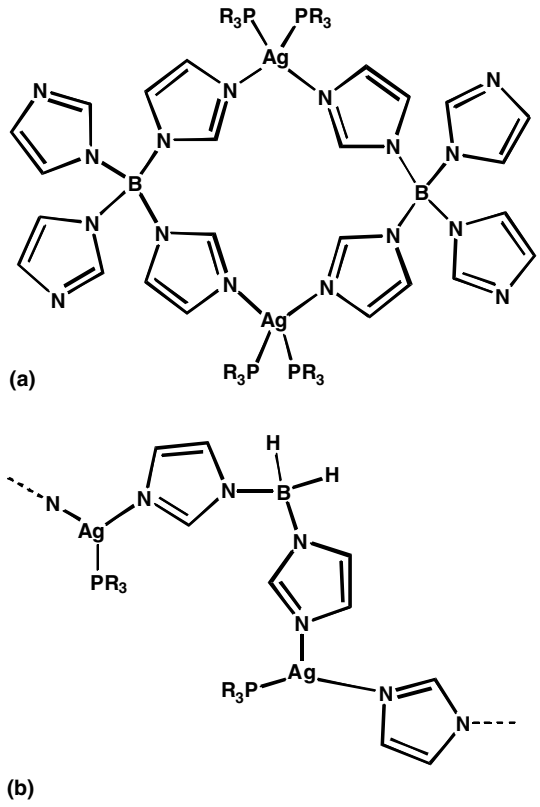

Fig. 19.

2.10. Silver poly(azolyl)alkanes

2.10.1. Bis(pyrazolyl)alkanes

Bis(pyrazolyl)-methanes and -ethanes react with AgX species ($X = NO_3$, ClO_4, O_3SCF_3, O_3SCH_3, O_2CCH_3, BF_4) yielding complexes of different stoichiometry dependent on the nature of X [80,81]. The bis(pyrazolyl)alkane/silver ratio rises from 0.5 in $[(Ag(O_3SCH_3))_2\{(pz^{4NO2})_2(1,2\text{-}C_2H_4)\}]$ [81] to 2 in the distorted tetrahedral $[Ag\{(pz)_2CMe_2\}_2]ClO_4$ (Fig. 20) [80]. The $(pz)_2CH_2$ ligand reacts with $AgNO_3$ yielding a 1:1 neutral species whereas with $Ag(O_2CCH_3)$ a polynuclear $[Ag(pz)]_n$ species is formed, presumably following hydrolysis of the acetate and breaking of the bridging C-N bond in the organic ligand.

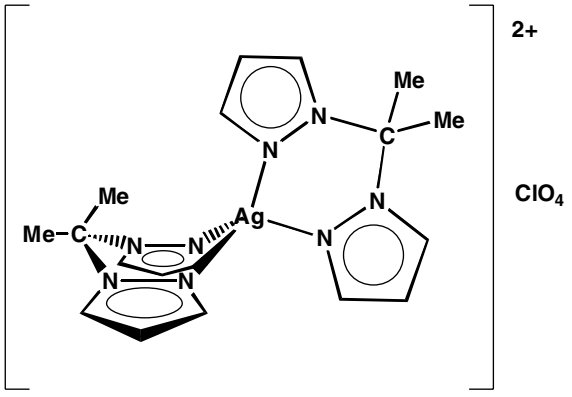

Fig. 20.

2.10.2. Tris(pyrazolyl)alkanes

The reaction of AgX ($X = ClO_4$, NO_3, O_3SCH_3) with excess of tris(pyrazolyl)methane ligand $(pz^x)_3CH$ ($Hpz^x = Hpz$, Hpz^{4Me}, Hpz*, Hpz^{Me3}) yields 1:1, 2:1 or 3:2 complexes. The ligand to metal ratio is dependent on the number and disposition of the methyls on the azole ring and primarily on the nature of the counter-ion X. IR, NMR and conductivity measurements have been reported for all complexes. $Ag(NO_3):(pz)_3CH$ 1:1 crystallizes with two formula units devoid of crystallographic symmetry as the asymmetric unit of the complex which is an infinite, unsolvated, two dimensional polymer, lying parallel to the *ac* plane. The Ag(2) atom in Fig. 21 has a tris(bidentate) environment due to a pairs of pyrazolate N from each of the independent $(pz)_3CH$ ligands and approximately bidentate nitrate, whereas Ag(1) is five-coordinated by three pyrazolate from three independent pz_3H and one bidentate nitrate [82]. In $Ag(NO_3):(pz)_3CH$ 1:2, each ligand behaves as a tripod, the silver atom being in a strongly distorted octahedral environment (Fig. 22) [82,83].

2.10.3. Bis(triazol-1-yl)methanes

Only few examples of triazolylalkane complexes have been to date reported, because of the ready formation of polymeric insoluble species. We have had success in the synthesis of a series of soluble silver complexes containing the tz_2CH_2 ligand [84]. The structure of $AgNO_3:tz_2CH_2$ 1:1 is based on a silver atom essentially linearly coordinated from different rings of different

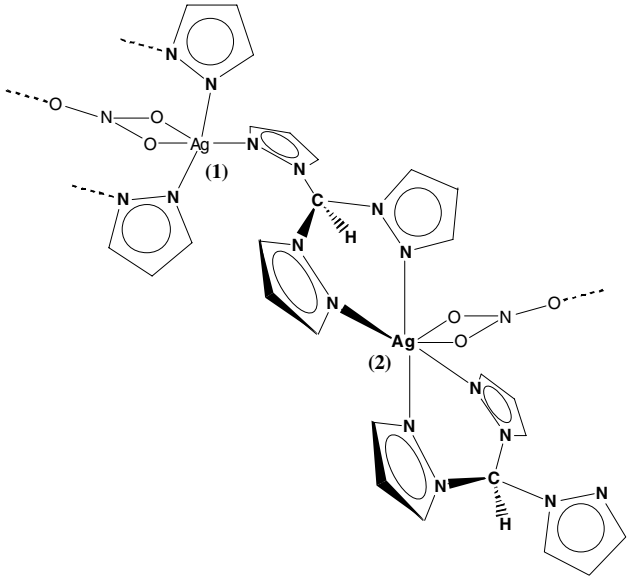

Fig. 21.

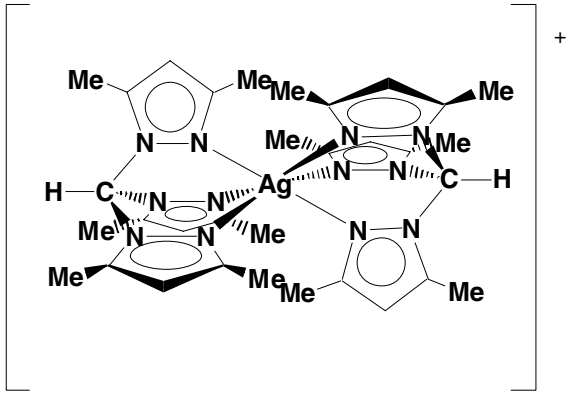

Fig. 22.

ligands. Polymer strands overlaid with juxtaposed silver atoms have the latter weakly bridged by only one of the nitrate oxygen atoms which interacts significantly, further feeble cross-linking in the third dimension occurring by way of another nitrogen atom (Fig. 23(a)). The character of the silver(I) nitrite:tz_2CH_2 (1:1) adduct is quite different, two formula units comprising the asymmetric unit of the structure. The coordination of the first silver is quasi linear as in the nitrate counterpart. Perturbation of the coordination occurs through the approach of a nitrogen of another triazolyl group and a nitrite nitrogen, but the remainder of the coordination sphere of the latter is made up of a pair of nitrite chelates (Fig. 23(b)). The 4:3 adduct between tz_2CH_2 and silver(I) triflate is devoid of metal-anion interactions, with concomitant increase in salt ligand stoichiometry. One AgO_3SCF_3:(tz_2CH_2) (3:4). MeCN formula unit comprises the asymmetric unit of the structure with the $(Ag_3(tz_2CH_2)_4)^{3+}$ cation array polymeric (Fig. 23(c)).

3. Conclusions

A summary of the most important results obtained in this field by other researchers was reported in Table 2. From the reaction of scorpionate-like ligands with Cu and Ag more than five hundred new derivatives have

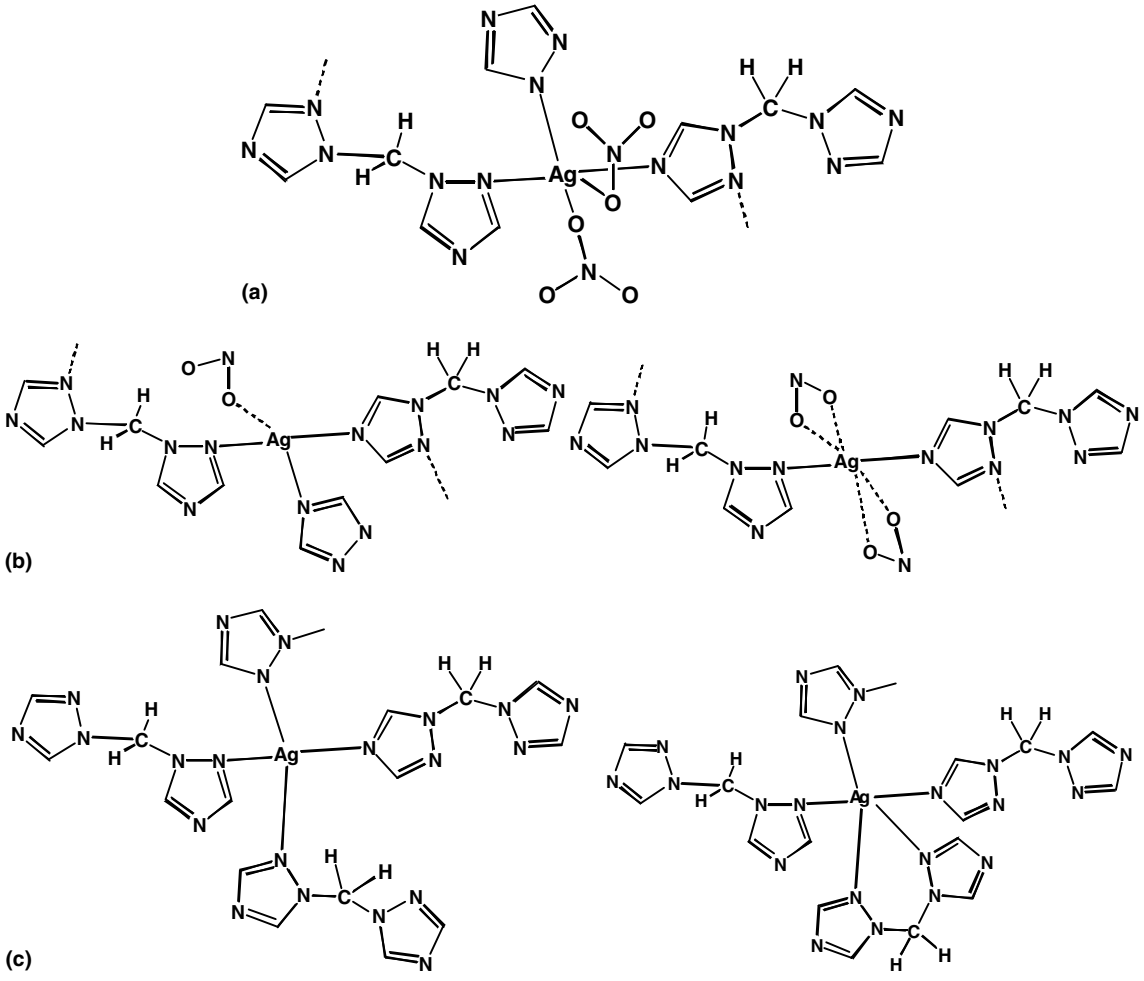

Fig. 23.

Table 2
The most important results in the field of Cu and Ag scorpionates

Results	Author	Reference
First homoscorpionate $(Tp^x)_2Cu$	Trofimenko	[85,86]
First X-ray crystal structure determination of $(Tp^x)_2Cu$	Kitajiima	[87]
First stable Cu^I carbonyl complex TpCu(CO)	Bruce	[10,34–37]
Synthesis of the dimer $[Tp^xCu]_2$	Bruce	[88]
X-ray crystal structure determination of $[Tp^xCu]_2$	Marks	[44,45]
Synthesis and investigation of the chloro-bridged dimer $[Tp^xCuCl]_2$	Roundhill	[89]
TpCu(L) as models for the blue copper proteins	Marks/Kitajima	[90–92]
Tp^{Ph}Cu(pterin) as model for the active metal site in phenylalanine hydroxylase	Perkinson	[93]
Dinuclear TpCu(II) peroxo complexes	Kitajima	[23,24,47,94]
Tp^xCu derivatives as models for the active site of the plastocyanin	Marks	[95]
Copper complexes of optically active Tp	Tolman	[96]
Theoretical characterisation of TpCuCl complexes	LLedós	[97]
Tp copper nitrosyl derivatives as models for nitric oxide adducts	Tolman	[25–28]
Copper(I) ethylene adducts of fluorinated Tp^x a aziridinanation catalysts	Dias	[98]
Tp- and Bp-Cu complexes as catalysts for the olefin cyclopronation	Pérez	[29,99,100]
$TpCu(PR_3)$ as precursor for the metal organic vapor deposition	Dahmen	[101]
A TpCu(L) complex as model for the copper center of galactose oxidase	Pierpont	[102]
TpCu(Nitronyl Nitroxide-Semiquinone) complexes	Shultz	[103]
$[Tp^{Ph}]$CuX-catalyzed dehydration of HCO_3	Cheng	[104]
TpCu-catalyzed carbene insertion into OH-bonds: conversion of alcohols into ethers	Pérez	[105]
Ternary TpCu(II) complexes containing N–N-donor heterocyclics	Chakravarty	[106]
TpCuX as catalyst for the insertion of diazo compounds into nitrogen-hydrogen bonds of amines and amides	Pérez	[107]
Cu...H interactions in hindered TpCu(I) complexes	Stavropoulos	[108]
Homoleptic copper complexes with cyano substituted scorpionate ligands	Eichhorn	[109]
Design of enzyme-like active site with fluorinated Tp ligands	Gorun	[110–112]
Reactivity of Cu-$HC(pz^x)_3$ derivatives toward O_2	Murray	[113]
First silver complexes of structure $(Tp^x)Ag(L)$ (L = P-donor or isonitrile)	Bruce	[114–116]
Fluorinated $(Tp^x)Ag$ derivatives as ligand transfer agent.	Dias	[117]
Activation of alkyl halides via a Ag–Tp catalyzed carbene insertion process	Dias	[118]
A sandwich six-coordinate derivative of silver(I) with $HC(3,5\text{-}Me_2pz)_3$	Reger	[83]
Synthesis and characterization of Cu and Ag complexes of $HC(pz^x)_3$	Reger	[119]
Synthesis of coordination polymers by using $HC(pz^x)_3$	Reger	[120]
Structure of the first binary complex $(Tp^x)Ag$	Ward	[66]
Encapsulation of a trinuclear silver(I) cluster by a hexadentate podand scorpionate	McCleverty	[121]
Ethyelene oxide and Propylene sulfid complexes of AgTpx	Dias	[122]
A coordination polymers derived from Ag and $HB(tz)_3$	Janiak	[48]

been synthesised. The coordination number ranges from 3, in sterically hindered complexes, to 6 in polynuclear species containing coordinating O-donor counter-ions as nitrate. The most common geometries observed are the trigonal planar and the tetrahedral (Table 1). The following cores for the metal coordination environment have been structurally characterized: MN_3P, MN_2P, MNP_2, MN_2P_2, MN_6, MN_4, MS_4, MS_2P, MS_3P, MN_4O_2, MN_4O, MN_2O_3, MN_2O_2, MN_5, MN_2O_3, MN_3C, $MNHP_2$.

Our work also demonstrated that from the reaction of copper(I) or silver(I) salts with anionic poly(pyrazolyl)borates neutral mononuclear complexes have been generally obtained in the presence of auxiliary ligands, such as phosphines and isonitriles. On the other hand poly(pyrazolyl)borates interact with silver(I) and copper(I) yielding dinuclear species where the metal obtains its classical maximum coordination number (4) through bridging coordination of the nitrogen ligands. The hapticity of the donor is strongly dependent on the number of pyrazolyl groups, Tp^x being generally tridentate, Bp^x uni- or bidentate, pz^oTp^x, bi- or tri-dentate. The coordination environment can be determined by a careful choice of the substituents on the azolyl ring and on the nature and steric hindrance of the auxiliary ligands. Finally poly(pyrazolyl)borates interacts with copper(II) yielding sandwich-type $Cu(Tp^x)_2$ and $Cu(pz^oTp^x)_2$ complexes.

Ionic mononuclear compounds can be generally synthesised by using poly(pyrazolyl)alkane ligands. The metal complexes formed by $R^*C(pz^x)_3$ and $R^*_2C(pz^x)_2$ are generally less stable than those obtained with the analogous anionic counterparts Bp^x and Tp^x. In the presence of coordinating counterions such as NO_3 poly(azolyl)alkanes seems able to form neutral polynuclear silver species. In these compounds the metal expands its classical coordination number (4) until to six, whereas derivatives containing non-coordinating anions such as ClO_4 or triflate, are generally cationic mononuclear or polynuclear species.

Polynuclear species can be also readily produced by using ligands such as $HB(tz)_3$ and $H_2C(tz)_2$ characterized by an exo-ring nitrogen able to bridge between metal centers, whereas $H_2B(im)_2$ and $B(im)_4$ seem efficient molecules for the synthesis of both dinuclear and polynuclear complexes depending on the reaction conditions, and on the steric properties (cone angle) of the auxiliary ligands. S-donor ligands such as Tm stabilize Cu and Ag complexes in the low oxidation state also through supplementary M–H interaction, but their reaction with Cu(II) yields, upon reduction of the metal by the S-donor, insoluble Cu(I) species.

Acknowledgements

We thank the University of Camerino (FAR and Progetto Strategico di Ateneo), MIUR, Fondazione CARIMA for funds and Prof. Allan H. White for the helpful discussion.

References

[1] M.D. Curtis, K.B. Shiu, W.M. Butler, Organometallics 2 (1983) 1475.
[2] M.D. Curtis, K.B. Shiu, W.M. Butler, J. Am. Chem. Soc. 108 (1986) 1550.
[3] See for example S. Trofimenko, Scorpionates, The Coordination Chemistry of Polypyrazolylborate Ligands, Imperial College Press, Singapore, 1999.
[4] S. Trofimenko, J. Am. Chem. Soc. 88 (1966) 1842.
[5] R.H. Crabtree, The Organometallics Chemistry of the Transition Metals, 2nd Ed., Wiley, New York, 1994.
[6] C. Janiak, J. Chem. Soc., Chem. Commun. (1994) 545.
[7] C. Janiak, Chem. Ber. 127 (1994) 1379.
[8] C. Janiak, S. Temizdemir, C. Röhr, Z. Anorg. Allg. Chem. 626 (2000) 1265.
[9] J. Reglinski, M. Garner, I.D. Cassidy, P.A. Slavin, D.R. Armstrong, J. Chem. Soc., Dalton Trans. (1999) 2119.
[10] M. Shu, R. Walz, B. Wu, J. Seebacher, H. Vahrenkamp, Eur. J. Inorg. Chem. (2003) 2502.
[11] S.J. Chiou, P.H. Ge, C.G. Riordan, L.M. Liable-Sands, A.L. Rheingold, J. Inorg. Biochem. 74 (1999) 98.
[12] S.J. Chiou, P.H. Ge, C.G. Riordan, L.M. Liable-Sands, A.L. Rheingold, J. Chem. Soc., Chem. Commun. (1999) 159.
[13] J.F. Ojo, P.A. Slavin, J. Reglinski, M. Garner, M.D. Spicer, A.R. Kennedy, S.J. Teat, Inorg. Chim. Acta 313 (2001) 15.
[14] M. Careri, L. Elviri, M. Lanfranchi, L. Marchiò, C. Mora, M. Pellinghelli, Inorg. Chem. 42 (2003) 2109.
[15] P.J. Bailey, M. Lanfranchi, L. Marchiò, S. Parsons, Inorg. Chem. 40 (2001) 5030.
[16] S. Trofimenko, J. Am. Chem. Soc. 92 (1970) 5118.
[17] L.M. Richburg, J.A. Farouq, C.D. Incarvito, A.L. Rheingold, D. Rabinovich, Polyhedron 19 (2000) 1815.
[18] C. Kimblin, V.J. Murphy, G. Parkin, J. Chem. Soc., Chem. Commun. (1996) 235.
[19] V.S. Joshi, V.K. Kale, K.M. Sathe, A. Sarkar, S.S. Tavale, C.G. Suresh, Organometallics 10 (1991) 2898.
[20] D.L. Reger, T.C. Grattan, K.J. Brown, C.A. Little, J.J.S. Lamba, A.L. Rheingold, R.D. Sommer, J. Organomet. Chem. 607 (2000) 120.
[21] S. Julia, J. Ma del Mazo, L. Avila, J. Elguero, Org. Prep. Proc. Int. 16 (1984) 299.
[22] M.J. Bruce, A.P.P. Ostazewski, J. Chem. Soc., Dalton Trans. (1973) 2433.
[23] N. Kitajima, K. Fujisawa, C. Fujimoto, Y. Moro-oka, S. Hashimoto, T. Kitagawa, K. Toriumi, K. Tatsumi, A. Nakamura, J. Am. Chem. Soc. 114 (1992) 1277.
[24] N. Kitajima, in: K.D. Karlin, Z. Tyeklár (Eds.), Bioinorganic Chemistry of Copper, Chapman and Hall, New York, 1993, p. 251.
[25] C.E. Ruggiero, S.M. Carrier, W.E. Antholine, J.W. Whittaker, C.J. Cramer, W.B. Tolman, J. Am. Chem. Soc. 115 (1993) 11285.
[26] W.B. Tolman, S.M. Carrier, C.E. Ruggiero, W.E. Antholine, J.W. Whittaker, in: K.D. Karlin, Z. Tyeklár (Eds.), Bioinorganic Chemistry of Copper, Chapman and Hall, New York, 1993, p. 406.
[27] C.E. Ruggiero, S.M. Carrier, W.B. Tolman, Angew. Chem., Int. Ed. Engl. 33 (1994) 895.
[28] R.P. Houser, W.B. Tolman, Inorg. Chem. 34 (1995) 1632.
[29] P.J. Pérez, M. Brookhart, J.L. Templeton, Organometallics 12 (1993) 261.
[30] M.M. Díaz-Requejo, T. Belderraín, S. Trofimenko, P.J. Pérez, J. Am. Chem. Soc. 123 (2001) 3167.
[31] M.M. Díaz-Requejo, T. Belderraín, M.C. Nicasio, S. Trofimenko, P.J. Pérez, J. Am. Chem. Soc. 124 (2002) 896.
[32] H.V.R. Dias, W. Jin, H.-J. Kim, H.-L. Lu, Inorg. Chem. 35 (1996) 2317.
[33] H.V.R. Dias, S.A. Polach, Inorg. Chem. 39 (2000) 4676.
[34] M.I. Bruce, A.P.P. Ostazewski, J. Chem. Soc., Chem. Commun. (1972) 1124.
[35] M.R. Churchill, B.G. DeBoer, F.J. Rotella, O.M. Abu Salah, M.I. Bruce, Inorg. Chem. 14 (1975) 2051.
[36] O.M. Abu Salah, M.I. Bruce, J.D. Walsh, Aust. J. Chem. 32 (1979) 1209.
[37] O.M. Abu Salah, M.I. Bruce, C. Hameister, Inorg. Synth. 21 (1982) 107.
[38] P. Cecchi, B. Bovio, G. Gioia Lobbia, C. Pettinari, D. Leonesi, Polyhedron 14 (1995) 2441.
[39] M. Pellei, C. Pettinari, C. Santini, B.W. Skelton, N. Somers, A.H. White, J. Chem. Soc., Dalton Trans. (2000) 3416.
[40] H.V.R. Dias, H.-L. Lu, Inorg. Chem. 39 (2000) 2246.
[41] F.G. Herring, D.J. Patmore, A. Storr, J. Chem. Soc., Dalton Trans. (1975) 711.
[42] G. Gioia Lobbia, C. Pettinari, F. Marchetti, B. Bovio, P. Cecchi, Polyhedron 15 (1996) 881.
[43] G. Gioia Lobbia, C. Pettinari, C. Santini, M. Colapietro, P. Cecchi, Polyhedron 16 (1997) 207.
[44] C. Mealli, C.S. Arcus, J.L. Wilkinson, T.J. Marks, J.A. Ibers, J. Am. Chem. Soc. 98 (1976) 711.
[45] S.M. Carrier, C.E. Ruggiero, R.P. Houser, W.B. Tolman, Inorg. Chem. 32 (1993) 4889.
[46] C.S. Arcus, J.L. Wilkinson, C. Mealli, T.J. Marks, J.A. Ibers, J. Am. Chem. Soc. 96 (1974) 7564.
[47] N. Kitajima, T. Koda, S. Hashimoto, T. Kitagawa, Y. Moro-oka, J. Am. Chem. Soc. 113 (1991) 5664.
[48] C. Pettinari, F. Marchetti, C. Santini, R. Pettinari, A. Drozdov, S. Troyanov, G.A. Battiston, R. Gerbasi, Inorg. Chim. Acta 315 (2001) 88.
[49] A. Drozdov, S.I. Troyanov, C. Pettinari, F. Marchetti, C. Santini, R. Pettinari, G.A. Battiston, R. Gerbasi, J. Phys. IV France 11 (2001) Pr3-585.
[50] C. Santini, M. Pellei, G. Gioia Lobbia, D. Fedeli, G. Falcioni, J. Inorg. Biochem. 94 (2003) 348.
[51] C. Santini, C. Pettinari, M. Pellei, G. Gioia Lobbia, A. Pifferi, M. Camalli, A. Mele, Polyhedron 18 (1999) 2255.
[52] S. Trofimenko, J. Am. Chem. Soc. 89 (1967) 3903.

[53] C. Janiak, T.G. Scharmann, P. Albrecht, F. Marlow, R. MacDonald, J. Am. Chem. Soc. 118 (1996) 6307, and references therein.
[54] G. Gioia Lobbia, M. Pellei, C. Pettinari, C. Santini, B.W. Skelton, N. Somers, A.H. White, J. Chem. Soc., Dalton Trans. (2002) 2333.
[55] G. Gioia Lobbia, M. Pellei, C. Pettinari, C. Santini, N. Somers, A.H. White, Inorg. Chim. Acta 333 (2002) 100.
[56] P. Cecchi, G. Gioia Lobbia, D. Leonesi, C. Pettinari, C. Sepe, V. Vincinguerra, Gazz. Chim. Ital. 123 (1993) 560.
[57] G. Gioia Lobbia, C. Pettinari, C. Santini, N. Somers, B.W. Skelton, A.H. White, Inorg. Chim. Acta 319 (2001) 15.
[58] W. Kläui, M. Berghahn, G. Rheinwald, H. Lang, Angew Chem., Int. Ed. 39 (2000) 2464.
[59] C. Santini, M. Pellei, G. Gioia Lobbia, A. Cingolani, R. Spagna, M. Camalli, Inorg. Chem. Commun. 5 (2002) 430.
[60] F. Bonati, A. Cingolani, G. Gioia Lobbia, D. Leonesi, A. Lorenzotti, C. Pettinari, Gazz. Chim. Ital. 120 (1990) 341.
[61] C. Pettinari, F. Marchetti, R. Polimante, A. Cingolani, G. Portalone, M. Colapietro, Inorg. Chim. Acta 249 (1996) 215.
[62] D. Martini, M. Pellei, C. Pettinari, B.W. Skelton, A.H. White, Inorg. Chim. Acta 333 (2002) 72.
[63] Effendy, G. Gioia Lobbia, M. Pellei, C. Pettinari, C. Santini, B.W. Skelton, A.H. White, J. Chem. Soc., Dalton Trans. (2000) 2123.
[64] Effendy, G. Gioia Lobbia, M. Pellei, C. Pettinari, C. Santini, B.W. Skelton, A.H. White, Inorg. Chim. Acta 315 (2001) 153.
[65] Effendy, G. Gioia Lobbia, C. Pettinari, C. Santini, B.W. Skelton, A.H. White, Inorg. Chim. Acta 308 (2000) 65.
[66] E.R. Humphrey, Z. Reeves, J.C. Jeffery, J.A. McCleverty, M.D. Ward, Polyhedron 18 (1999) 1335.
[67] C. Santini, G. Gioia Lobbia, C. Pettinari, M. Pellei, G. Valle, S. Calogero, Inorg. Chem. 37 (1998) 890.
[68] C. Santini, C. Pettinari, G. Gioia Lobbia, D. Leonesi, G. Valle, S. Calogero, Polyhedron 17 (1998) 3201.
[69] C. Santini, G. Gioia Lobbia, M. Pellei, C. Pettinari, G. Valle, S. Calogero, Inorg. Chim. Acta 282 (1998) 1.
[70] H.V.R. Dias, W. Jin, Inorg. Chem. 35 (1996) 267.
[71] H.V.R. Dias, Z. Wang, W. Jin, Inorg. Chem. 36 (1997) 6205.
[72] H.V.R. Dias, W. Jin, J. Am. Chem. Soc. 117 (1995) 11381.
[73] H.V.R. Dias, W. Jin, Inorg. Chem. 35 (1996) 3687.
[74] H.V.R. Dias, H.-L. Lu, Inorg. Chem. 34 (1995) 5380.
[75] H.V.R. Dias, H.-L. Lu, J.D. Gorden, W. Jin, Inorg. Chem. 35 (1996) 2149.
[76] Effendy, G. Gioia Lobbia, C. Pettinari, C. Santini, B.W. Skelton, A.H. White, Inorg. Chim. Acta 298 (2000) 146.
[77] Effendy, G. Gioia Lobbia, C. Pettinari, C. Santini, B.W. Skelton, A.H. White, J. Chem. Soc., Dalton Trans. (1998) 2739.
[78] C. Santini, C. Pettinari, G. Gioia Lobbia, R. Spagna, M. Pellei, F. Vallorani, Inorg. Chim. Acta 285 (1999) 81.
[79] Effendy, G. Gioia Lobbia, M. Pellei, C. Pettinari, C. Santini, B.W. Skelton, A.H. White, J. Chem. Soc., Dalton Trans. (2001) 528.
[80] A. Lorenzotti, B. Bovio, F. Bonati, A. Cingolani, G. Gioia Lobbia, D. Leonesi, Inorg. Chim. Acta 170 (1990) 199.
[81] C. Pettinari, A. Lorenzotti, A. Cingolani, D. Leonesi, M. Marra, F. Marchetti, Gazz. Chim. Ital. 123 (1993) 481.
[82] A. Cingolani, Effendy, D. Martini, M. Pellei, C. Pettinari, B.W. Skelton, A.H. White, Inorg. Chim. Acta 328 (2002) 87.
[83] D.L. Reger, J.E. Collins, A.L. Rheingold, L.M. Liable-Sands, G.P.A. Yap, Organometallics 16 (1997) 349.
[84] Effendy, F. Marchetti, C. Pettinari, R. Pettinari, B.W. Skelton, A.H. White, Inorg. Chem. 42 (2003) 112.
[85] S. Trofimenko, J. Am. Chem. Soc. 89 (1967) 3170.
[86] S. Trofimenko, J. Am. Chem. Soc. 89 (1967) 6288.
[87] N. Kitajima, Y. Moro-oka, A. Uchida, Y. Sasada, Y. Ohashi, Acta Cryst. C 44 (1988) 1876.
[88] O.M. Abu Salah, M.I. Bruce, J. Organomet. Chem. 87 (1975) C15.
[89] S.G.N. Roundhill, D.M. Roundhill, D.R. Bloomquist, C. Landee, R.D. Willett, D.M. Dooley, H.B. Gray, Inorg. Chem. 18 (1979) 831.
[90] J.S. Thompson, T.J. Marks, J.A. Ibers, J. Am. Chem. Soc. 101 (1979) 4180.
[91] N. Kitajima, K. Fujisawa, Y. Moro-oka, J. Am. Chem. Soc. 112 (1990) 3210.
[92] D. Qiu, L. Kilpatrick, N. Kitajima, T.G. Spiro, J. Am. Chem. Soc. 116 (1994) 2585.
[93] J. Perkinson, S. Brodie, K. Yoon, K. Mosny, P.J. Carroll, T.V. Morgan, S.J.N. Burgmayer, Inorg. Chem. 30 (1991) 719.
[94] N. Kitajima, Y. Moro-oka, Chem. Rev. 94 (1994) 737.
[95] J.S. Thompson, J.L. Zitzman, T.J. Marks, J.A. Ibers, Inorg. Chim. Acta 46 (1980) L101.
[96] D.D. LeCloux, M.C. Keyes, M. Osawa, V. Reynolds, W.B. Tolman, Inorg. Chem. 33 (1994) 6361.
[97] L. Cucurull-Sánchez, F. Maseras, A. Lledós, Inor. Chem. Commun. 3 (2000) 590.
[98] H.V.R. Dias, H.-L. Lu, H.-J. Kim, S.H. Polach, T.K.H.H. Goth, R.G. Browning, C.J. Lovely, Organometallics 21 (2002) 1466.
[99] M.M. Díaz-Requejo, M.C. Nicasio, P.J. Pérez, Organometallics 17 (1998) 3051.
[100] M.M. Díaz-Requejo, T.R. Belderrain, M.C. Nicasio, P.J. Pérez, Organometallics 19 (2000) 285.
[101] E.C. Plappert, T. Stumm, H. van den Bergh, R. Hauert, K.H. Dahmen, Chem. Vap. Dep. 3 (1997) 37.
[102] M. Ruf, C.G. Pierpont, Angew. Chem., Int. Ed. 37 (1998) 1736.
[103] D.A. Shultz, K.E. Vostrikova, S.H. Bodnar, H.-J. Koo, M.-H. Whangboo, M.L. Kirk, E.C. Depperman, J.W. Kampf, J. Am. Chem. Soc. 125 (2003) 1607.
[104] Y.J. Sun, L.Z. Zhang, P. Cheng, H.K. Lin, S.-P. Yan, W. Sun, D.-Z. Liao, Z.-H. Jiang, P.-W. Shen, Inorg. Chem. 42 (2003) 508.
[105] M.E. Morilla, M.J. Molina, M.M. Díaz-Requejo, T.R. Belderrain, M.C. Nicasio, S. Trofimenko, P.J. Pérez, Organometallics 22 (2003) 2914.
[106] S. Dhar, P.A.N. Reddy, M. Nethaji, S. Mahadevan, M.K. Saha, A.R. Chakravarty, Inorg. Chem. 41 (2002) 3469.
[107] M.E. Morilla, M.M. Díaz-Requejo, T.R. Belderrain, M.C. Nicasio, P.J. Pérez, J. Chem. Soc., Chem. Commun. (2002) 2998.
[108] S. Kiani, J.R. Long, P. Stavropoulos, Inorg. Chim. Acta 263 (1997) 357.
[109] C.J. Siemer, N. Goswami, P.K. Kahol, M.J. Van Stipdonk, D.M. Eichhorn, Inorg. Chem. 40 (2001) 4081.
[110] Z. Hu, G.N. George, S.M. Gorun, Inorg. Chem. 40 (2001) 4812.
[111] Z. Hu, R.D. Williams, D. Tran, T.G. Spiro, S.M. Gorun, J. Am. Chem. Soc. 122 (2000) 3556.
[112] D. Diaconu, Z. Hu, S.M. Gorun, J. Am. Chem. Soc. 124 (2002) 1564.
[113] M. Cvetokovic, S.R. Batten, B. Moubaraki, K.S. Murray, L. Spiccia, Inorg. Chim. Acta 324 (2001) 131.
[114] O.M. Abu Salah, M.I. Bruce, J. Organomet. Chem. 87 (1974) C15.
[115] O.M. Abu Salah, G.S. Ashby, M.I. Bruce, E.A. Pederzolli, J.D. Walsh, Aust. J. Chem. 32 (1979) 1613.
[116] M.I. Bruce, J.D. Walsh, Aust. J. Chem. 32 (1979) 2753.
[117] H.V.R. Dias, W. Jin, Inorg. Chem. 42 (2003) 5034.
[118] H.V.R. Dias, R.G. Browning, S.A. Polach, H.V.K. Diyabalanage, C.J. Lovely, J. Am. Chem. Soc. 125 (2003) 9270.
[119] D.L. Reger, Comments Inorg. Chem. 21 (1999) 1.
[120] D.L. Reger, R.F. Semeniuc, M.D. Smith, Inorg. Chem. 40 (2001) 6545.
[121] A.J. Amoroso, J.C. Jeffery, P.L. Jones, J.A. McCleverty, E. Psillakis, M.D. Ward, J. Chem. Soc., Chem. Commun. (1995) 1175.
[122] H.V.R. Dias, Z. Wang, Inorg. Chem. 39 (2000) 3724.

Available online at www.sciencedirect.com
SCIENCE DIRECT®
Polyhedron 23 (2004) 471–480
POLYHEDRON
www.elsevier.com/locate/poly

Multiple bonding modes exhibited by heteroscorpionate N_2S(alkylthiolate) ligands with Zn(II) and Fe(II)

Vivek V. Karambelkar [a], Robert C. diTargiani [a], Christopher D. Incarvito [b], Lev N. Zakharov [c], Arnold L. Rheingold [c], Charlotte L. Stern [d], David P. Goldberg [a,*]

[a] *Department of Chemistry, Johns Hopkins University, Baltimore, MD 21218, USA*
[b] *Department of Chemistry, Yale University, New Haven, CT 06520-8107, USA*
[c] *Department of Chemistry and Biochemistry, University of California, San Diego, CA 92093, USA*
[d] *X-ray Crystallography Facility, Northwestern University, Evanston, IL 60208, USA*

Received 9 July 2003; accepted 20 August 2003

Abstract

Two related heteroscorpionate N_2S(thiolate) ligands L^1 and L^2 have been employed in the synthesis of new zinc(II) and iron(II) complexes. These ligands contain two imidazolyl donors and one alkylthiolate donor connected by a central carbon atom. The ligand L^1 was reacted with $ZnBr_2$ to give the trinuclear zinc complex $[(L^1)_3Zn_3Br_2]Br$ (**1**). The X-ray structure of **1** reveals one of the zinc ions to be coordinated by two L^1 ligands in a tripodal arrangement resulting in a distorted octahedral geometry, while the other two zinc ions are both held in a distorted tetrahedral geometry and are coordinated to another molecule of L^1 in an unusual tridentate, multibridging coordination mode. Modification of L^1 to include phenyl substituents on the imidazole groups leads to L^2, and these substituents cause quite a different result to be obtained in the reaction with $ZnBr_2$. The combination of L^2 and $ZnBr_2$ leads to the dimeric zinc complex $(L^2)_2Zn_2Br_2$, (**2**). Characterization of **2** by X-ray diffraction shows this complex to be a dimer with a central $Zn_2(\mu\text{-}SR)_2$ rhomb. Each zinc ion is found in a distorted tetrahedral geometry coordinated by L^2 in a bidentate, N,S fashion. The ^1H NMR spectrum of **2** provides strong evidence this structure is retained in solution. In comparison, reaction of L^2 with $FeCl_2$ leads to the monomeric complex $(L^2)_2Fe^{II}$ (**3**), which has each ligand coordinated in the same bidentate, N,S bonding mode. Interestingly, the methoxy groups of the two ligands in **3** are close enough to the iron center for a possible bonding interaction, suggesting an unexpected N_2O coordination mode.
© 2003 Elsevier Ltd. All rights reserved.

Keywords: Heteroscorpionate; Tripodal; Alkylthiolate; Imidazole; Iron; Zinc

1. Introduction

A variety of metalloproteins rely on a single metal ion cofactor bound to the protein by a combination of His_xCys_y amino acid ligands. Examples include zinc proteins such as the matrix metalloproteinases [1], zinc fingers [2], alcohol dehydrogenase [3], farnesyl transferase [4] and spinach carbonic anhydrase [5], as well as the blue copper proteins [6] and the non-heme iron enzymes nitrile hydratase [7] and peptide deformylase (PDF) [8]. We have specifically targeted the metal active site of the latter enzyme for synthetic modeling because we find it especially intriguing from an inorganic point of view; it utilizes an iron(II) center in vivo yet belongs to the mononuclear zinc(II) enzyme family in terms of both structure and function [8b]. In order to mimic the active site of PDF, which has a His_2Cys donor set coordinated to an M(II) ion in all of its known derivatives (M(II) = Fe(II), Zn(II), Co(II), Ni(II)), we have made efforts to synthesize ligands with mixed nitrogen/alkylthiolate donor sets. Accordingly, we recently prepared a simple linearly disposed N_2S(thiolate) ligand called PATH, which has led to the synthesis of a novel series of

* Corresponding author.
E-mail address: dpg@jhu.edu (D.P. Goldberg).

0277-5387/$ - see front matter © 2003 Elsevier Ltd. All rights reserved.
doi:10.1016/j.poly.2003.11.034

monomeric, pseudotetrahedral N_2S(thiolate) complexes ((PATH)$M^{II}L$; M = Zn, Co) [9–11]. These complexes have served as structural models for the generalized $(His)_2(Cys)M^{II}L$ active site of PDF, and recently we have shown that a PATH-Zn(II) complex generated in water acts as a functional model complex by catalyzing the hydrolysis of an ester substrate [12].

At the same time, we have also pursued the construction of scorpionate ligands bearing an N_2S(thiolate) donor set. The tris(pyrazolyl)borate (Tp) family of scorpionate ligands has proven remarkably useful for the construction of many enzyme model complexes, especially models of the zinc enzyme family [13–16]. Their incredible success has spurred the development of many variations, including systems in which the pyrazolyl N groups have been replaced by sulfur donors. Such systems include thioether [17] and methimazolyl-containing [18–20] ligands. However, to our knowledge there are as yet no boron-based scorpionate ligands bearing a sulfur donor derived from an alkylthiolate group, most likely because of the synthetic difficulties of installing an alkylthiolate appendage. We have turned to a carbon-centered framework as a synthetically feasible alternative to the boron-centered systems. Herein we describe the coordination behavior of the scorpionate ligands L^1H and L^2H (Fig. 1). Both of these ligands rely on a central carbon atom in place of boron to link the imidazolyl and alkylthiolate donors into a tripodal framework [21]. The ligand L^1H was originally synthesized by Bosnich over 20 years ago for use in the preparation of models of blue copper proteins [22]. Still, little is known about its coordination chemistry, and to our knowledge no X-ray structures of complexes containing L^1 have been reported to date. The synthesis of the ligand L^2H was previously communicated by some of us [23].

We report here the first X-ray structure of any transition metal complex of the scorpionate ligand L^1. In addition, the first iron(II) complex of L^2 has been synthesized and crystallographically characterized, and a new dinuclear zinc(II) complex of L^2 has been characterized by both ^1H NMR spectroscopy and X-ray crystallography, allowing for a comparison between solution and solid-state structures. These different structures reveal that the L^1/L^2 framework can adopt three different coordination modes, including the expected tripodal N_2S bonding mode.

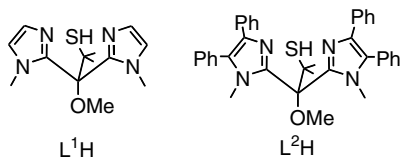

L^1H L^2H

Fig. 1. Schematic presentation of the ligands.

2. Experimental

2.1. Materials and general methods

No special precautions were taken for the synthesis of **1**. All synthetic procedures for complexes **2** and **3** were carried out by using a dry-box or Schlenk techniques. For the synthesis of complex **3**, MeOH and CH_2Cl_2 were dried by refluxing over CaH_2 for 18 h and then distilled. Traces of oxygen were removed from these solvents by 3 cycles of freeze–pump–thaw. Ligands L^1H [22] and L^2H [23] were prepared as described in the literature. All other chemicals used in the experiments were of analytical grade from commercial sources and used without further purifications.

2.1.1. Synthesis of $[(L^1)_3Zn_3Br_2]Br$ (**1**)

Methanol (15 mL) was added to L^1H (0.050 g, 0.178 mmol), NaOMe (0.011 g, 0.196 mmol) and $ZnBr_2$ (0.044 g, 0.196 mmol) to yield a clear yellow solution. Overnight a white precipitate formed and the solution was filtered. This precipitate was dissolved by addition of 2 mL of hot CH_3CN. Crystals suitable for X-ray diffraction were obtained by diffusion of Et_2O into a CH_3CN solution of **1**. Yield <2%.

2.1.2. Synthesis of $[(L^2)_2Zn_2Br_2]$ (**2**)

To a solution of L^2H (0.1 g, 0.17 mmol) in CH_2Cl_2 (10 mL) was added NaOH (0.008 g, 0.19 mmol) in MeOH, and then the mixture was bubbled with argon for 30 minutes to make sure that the solution was oxygen-free. An amount of $ZnBr_2$ (0.039 g, 0.17 mmol) was dissolved in MeOH (5 mL) and bubbled with argon for 30 minutes. The methanolic solution of $ZnBr_2$ was added dropwise to the solution of deprotonated ligand and the reaction mixture was stirred for 18 h under argon. The complex **2** precipitated from the reaction mixture as a white powder, which was filtered, washed with Et_2O and dried under vacuum. Yield: 0.07 g, 56%. Crystals suitable for X-ray diffraction were obtained by diffusion of Et_2O into a CH_2Cl_2 solution of **2**. *Anal.* Calc. for $C_{74.5}H_{71}N_8O_2S_2Zn_2Br_2Cl$ [**2** · $(CH_2Cl_2)_{0.5}$]: C, 59.63; H, 4.77; N, 7.47. Found: C, 59.40; H, 4.91; N, 7.29%. ^1H NMR ($CDCl_3$, ppm): 7.56–7.11 (m, 40H, C_6H_5); 3.51 (s, 6H, N–CH_3); 3.26 (s, 6H, N–CH_3); 2.74 (s, 6H, O–CH_3); 1.93 (s, 12H, C–CH_3).

2.1.3. Synthesis of $(L^2)_2Fe$ (**3**)

A 2 mL solution of NaOH (0.009 g, 0.23 mmol) in MeOH was added to L^2H (0.06 g, 0.1 mmol) dissolved in CH_2Cl_2 (3 mL) and the mixture was stirred for 30 minutes. The solution of deprotonated ligand was then added to a solution of $FeCl_2$ (0.014 g, 0.11 mmol) in 3 mL MeOH, which was then stirred for 18 h to get a green precipitate. This precipitate was dissolved by addition of 2 mL CH_2Cl_2 to the reaction mixture. To the

resulting clear green solution, 3 mL of MeOH was added and colorless crystals were obtained by storing this solution at −20 °C for four days. Yield 0.03 g, 45%. IR of $\mathbf{3}\cdot(CH_3OH)_2$ (KBr, cm^{-1}): 3479, 3051, 2975, 2915, 1603, 1504, 1463, 1443, 1367, 1262, 1229, 1179, 1125, 1075, 1027, 1001, 966, 930, 775, 697, 671, 648, 569, 530. For comparison the IR of L^2H is as follows (KBr, cm^{-1}): 3062, 2925, 1602, 1504, 1443, 1375, 1303, 1240, 1178, 1128, 1080, 1026, 964, 776, 698, 666, 627, 528. *Anal.* Calc. for $C_{76}H_{78}N_8O_4S_2Fe[\mathbf{3}\cdot(CH_3OH)_2]$: C, 70.90; H, 6.11; N, 8.70. Found: C, 71.35; H, 5.79; N, 8.97%.

2.2. Physical measurements

Elemental analyses were performed at Atlantic Microlab, Inc. (Norcross, GA). ^1H NMR spectrum in $CDCl_3$ was recorded on a Varian Unity Plus 400 spectrometer (400 MHz) at ambient probe temperature with tetramethylsilane as the internal reference. IR spectra were recorded on a Bruker Vector 22 IR spectrometer as KBr disks.

2.3. X-ray crystallography

Diffraction intensity data were collected with a Bruker Smart Apex CCD (**1** and **3**) and a SMART-1000 CCD (**2**) diffractometer with graphite monochromated Mo Kα radiation. Crystal data, data collection, and refinement parameters for all structures are given in Table 1. The structures were solved using direct methods, completed by subsequent difference Fourier syntheses, and refined by full matrix least-squares procedures on F^2. SADABS absorption corrections were applied to **1** and **3** (T_{min}, $T_{max} = 0.390$, 0.699 (**1**) and 0.898, 0.924 (**3**)). In the case of **2**, an analytical absorption correction was applied. Minimum and maximum transmission factors were 0.746 and 0.932, respectively. All non-hydrogen atoms were refined with anisotropic displacement coefficients, and hydrogen atoms were treated as idealized contributions in a riding group model.

In the crystal structure of **2** there is a disordered CH_2Cl_2 molecule. It was refined isotropically with occupancy factors of 0.125 for four chlorine atoms, 0.25

Table 1
Crystal data, data collection, and refinement parameters for **1–3**

Empirical formula	$C_{41}H_{60}Br_3N_{13}O_3S_3Zn_3(\mathbf{1}\cdot CH_3CN)$	$C_{74.5}H_{69}Br_2ClN_8O_2S_2Zn_2[\mathbf{2}\cdot(CH_2Cl_2)_{0.5}]$	$C_{80}H_{94}FeN_8O_8S_2[\mathbf{3}\cdot(CH_3OH)_6]$
Formula weight	1315.4	1498.56	1415.60
Temperature (K)	173(2)	153(2)	150(2)
Wavelength (Å)	0.71073	0.71073	0.71073
Crystal system	monoclinic	triclinic	triclinic
Space group	$P2_1/c$	$P(\bar{1})$	$P(\bar{1})$
Unit cell dimensions			
a (Å)	11.7069(7)	10.784(2)	11.0038(14)
b (Å)	22.4018(13)	11.371(2)	16.164(2)
c (Å)	20.4328(13)	29.455(4)	21.639(3)
α (°)	90	97.326(3)	78.800(2)
β (°)	104.721(1)	97.564(2)	88.549(2)
γ (°)	90	96.209(3)	89.858(2)
Volume (Å^3)	5182.7(5)	3522.3(8)	3774.3(8)
Z	4	2	2
Density (calculated) (g cm^{-3})	1.685	1.413	1.246
Absorption coefficient (mm^{-1})	3.862	1.967	0.315
$F(000)$	2656	1534	1504
Crystal size (mm)	$0.30\times0.20\times0.10$	$0.17\times0.15\times0.04$	$0.35\times0.30\times0.25$
θ Range for data collection (°)	1.80–27.00	1.41–28.31	1.45–28.30
Index ranges	$-14\leqslant h\leqslant14$	$-13\leqslant h\leqslant13$	$-12\leqslant h\leqslant14$
	$-28\leqslant k\leqslant26$	$-14\leqslant k\leqslant14$	$-21\leqslant k\leqslant19$
	$-15\leqslant l\leqslant26$	$-37\leqslant l\leqslant39$	$-28\leqslant l\leqslant26$
Reflections collected	23055	32478	22764
Independent reflections	10738 [$R_{int}=0.0467$]	16280 [$R_{int}=0.044$]	16247 [$R_{int}=0.0390$]
Absorption correction	SADABS	Analytical	SADABS
Refinement method	full-matrix least-squares on F^2	full-matrix least-squares on F^2	full-matrix least-squares on F^2
Data/restraints/parameters	10738/0/595	8660/0/839	16247/0/820
Goodness-of-fit on F^2	1.004	1.60	1.060
Final R indices [$I>2\sigma(I)$][a]	$R_1=0.0426$ $wR_2=0.1018$	$R_1=0.041$ $wR_2=0.088$	$R_1=0.1071$ $wR_2=0.3003$
R indices (all data)[a]	$R_1=0.0723$, $wR_2=0.1158$	$R_1=0.066$, $wR_2=0.097$	$R_1=0.1428$, $wR_2=0.3186$
Largest difference peak and hole (e Å^{-3})	0.96 and −0.89	0.91 and −0.57	2.58 and −0.76

[a] $R_1=\sum||F_o|-|F_c||/\sum|F_o|$; $wR_2=\left\{\sum[w(F_o^2-F_c^2)^2]\Big/\sum[w(F_o^2)^2]\right\}^{1/2}$; $w=1/[s^2(F_o^2)+(aP)^2+bP]$; $P=[2F_c^2+\max(F_o,0)]/3$.

for two chlorine atoms and the occupancy factor of 0.5 for the carbon atom to give half a CH_2Cl_2 molecule per dimer unit while the remaining non-hydrogen atoms were refined anisotropically. Hydrogen atoms were included in idealized positions but not refined.

In the crystal structure of **3**, there are six MeOH solvent molecules. Two of those MeOH molecules are involved in weak hydrogen bonding with the thiolate sulfur atoms. The other four highly disordered MeOH molecules were treated as diffuse contributions with the SQUEEZE program (A. Spek, Platon software package). Corrections of the X-ray data by SQUEEZE found 159 e^-/unit cell which is close to the required value of 144 e^-/unit cell for four MeOH molecules. All samples of **3** examined diffracted weakly and diffusely, almost certainly a result of the loosely fixed solvent molecules, resulting in a rather high final *R* factor.

All software and sources of scattering factors for **1** and **3** are contained in the SHELXTL (5.10) program package (G. Sheldrick, Bruker XRD, Madison, WI). For **2** all calculations were performed using the TEXSAN crystallographic software package of Molecular Structure Corporation (TEXSAN *for Windows version 1.05*: Crystal Structure Analysis Package, Molecular Structure Corporation (1997–1998)).

3. Results and discussion

3.1. Synthesis of $[(L^1)_3Zn_3Br_2]Br$ (1)

The heteroscorpionate N_2S(thiolate) ligand L^1H, shown in Fig. 1, was originally prepared over 20 years ago for use in the synthesis of "blue copper" protein model complexes [22]. We recognized L^1 to be an intriguing example of a tripodal ligand with an alkylthiolate donor, which also had the added advantage of containing biomimetic imidazole donors. To our knowledge the blue copper modeling work was the only published account discussing L^1, and there were as yet no crystallographically characterized compounds containing L^1. As pointed out in the Introduction, heteroscorpionate ligands bearing an alkylthiolate donor are extremely rare, and thus we were compelled to see if we could develop the coordination chemistry of this system. We reacted L^1 with a Zn(II) source to determine its coordination behavior with this ion, and obtained a trinuclear zinc complex in which L^1 displays two distinct bonding modes.

For the synthesis of $[(L^1)_3Zn_3Br_2]Br$ (**1**), the three starting materials L^1H, NaOMe, and $ZnBr_2$ are dissolved together in MeOH, as shown in Scheme 1. The ligand L^1H is freely soluble in MeOH, unlike L^2H, and therefore the use of CH_2Cl_2 can be avoided, in contrast to the synthesis of **2** and **3** (vide infra). Initially a clear solution is obtained, but after 18 h a small amount of white precipitate is formed and isolated by filtration. This solid has limited solubility, but can be redissolved in hot CH_3CN. From Et_2O/CH_3CN a very small amount of **1** can be obtained as X-ray quality crystals. Attempts to scale up the reaction or obtain subsequent crops of **1** led to the formation of yellow oils or solids which could not be re-crystallized to give more **1**. Thus the yield of **1** is extremely low, and sometimes no crystals of **1** form, but the few crystals that were obtained by this method were utilized for X-ray crystallography. The low yield of **1** precluded us from obtaining other characterization data on **1**.

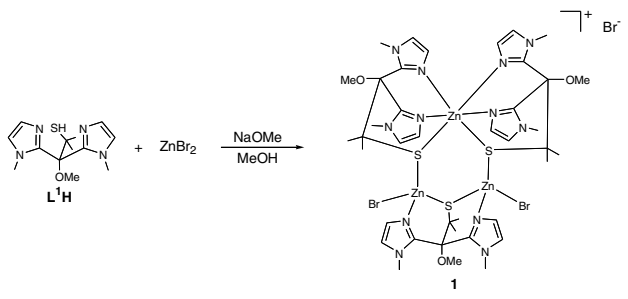

Scheme 1.

3.2. Crystal structure of $[(L^1)_3Zn_3Br_2]Br$ (1)

An ORTEP view of **1** is shown in Fig. 2. Crystallographic data are summarized in Table 1. Selected bond distances and angles are given in Table 2. Structural characterization of **1** has revealed a trinuclear zinc complex that crystallizes in the monoclinic space group $P2_1/c$. The metal:ligand ratio is 1:1, but the overall structure is much less symmetric than the simple formula

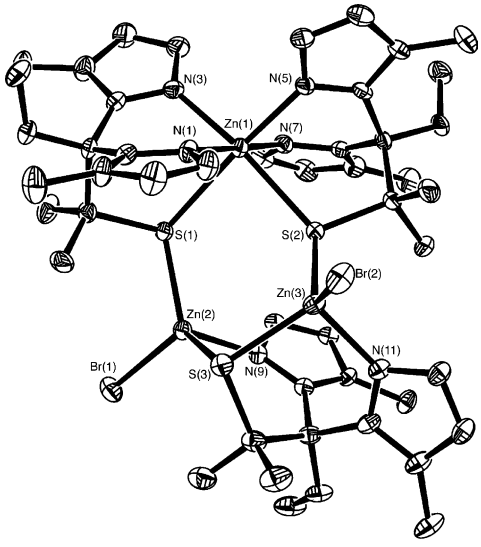

Fig. 2. Thermal ellipsoid plot of the cation of **1** at 40% probability. Hydrogen atoms are omitted for clarity.

Table 2
Bond lengths (Å) and angles (°) for **1**

Bond lengths	
Zn(1)–S(1)	2.6697(11)
Zn(1)–S(2)	2.5110(12)
Zn(1)–N(1)	2.091(3)
Zn(1)–N(3)	2.068(4)
Zn(1)–N(5)	2.055(3)
Zn(1)–N(7)	2.141(3)
Zn(2)–Br(1)	2.4371(7)
Zn(2)–S(1)	2.3115(12)
Zn(2)–S(3)	2.3575(12)
Zn(2)–N(9)	2.026(3)
Zn(3)–Br(2)	2.3931(6)
Zn(3)–S(2)	2.2843(11)
Zn(3)–S(3)	2.3715(12)
Zn(3)–N(11)	2.034(4)
Bond angles	
N(5)–Zn(1)–N(3)	99.28(14)
N(5)–Zn(1)–N(1)	98.94(14)
N(3)–Zn(1)–N(1)	84.15(14)
N(5)–Zn(1)–N(7)	83.42(13)
N(3)–Zn(1)–N(7)	93.26(14)
N(1)–Zn(1)–N(7)	176.73(14)
N(5)–Zn(1)–S(2)	88.92(10)
N(3)–Zn(1)–S(2)	169.75(10)
N(1)–Zn(1)–S(2)	100.75(10)
N(7)–Zn(1)–S(2)	81.50(10)
N(5)–Zn(1)–S(1)	175.56(11)
N(3)–Zn(1)–S(1)	84.21(10)
N(1)–Zn(1)–S(1)	84.11(10)
N(7)–Zn(1)–S(1)	93.66(9)
S(2)–Zn(1)–S(1)	87.33(4)
N(9)–Zn(2)–S(1)	108.76(10)
N(9)–Zn(2)–S(3)	90.86(10)
S(1)–Zn(2)–S(3)	123.06(4)
N(9)–Zn(2)–Br(1)	100.78(9)
S(1)–Zn(2)–Br(1)	108.29(4)
S(3)–Zn(2)–Br(1)	119.96(3)
N(11)–Zn(3)–S(2)	107.90(10)
N(11)–Zn(3)–S(3)	99.86(11)
S(2)–Zn(3)–S(3)	109.06(4)
N(11)–Zn(3)–Br(2)	103.06(10)
S(2)–Zn(3)–Br(2)	121.46(4)
S(3)–Zn(3)–Br(2)	112.93(3)

implies. The ligands exhibit two distinct coordination modes. One of the zinc centers, Zn(1), is bound by two ligands each through the expected tripodal N_2S coordination. The geometry at this zinc center is best described as distorted octahedral with *cis* angles ranging from 83° to 101° and *trans* angles ranging from 170° to 177°. The two sulfur atoms are in a *cis* arrangement. The Zn(1)–N(im) distances range from 2.055(3) to 2.141(3) Å. In the case of the longer Zn(1)–N(im) distances (Zn(1)–N(7) = 2.141(3) Å and Zn(1)–N(1) = 2.091(3) Å), the imidazoles are *trans* to one another, while the imidazoles with shorter bond distances (Zn(1)–N(5) = 2.055(3) Å and Zn(1)–N(3) = 2.068(4) Å) are *trans* to the sulfur atoms. From these distances it is reasonable to conclude that N(7) and N(1) lie on axial positions while N(5) and N(3) lie on equatorial positions in the distorted octahedral geometry. All of these Zn–N(im) distances are reasonable compared to other octahedral zinc complexes containing imidazole donors [24,25]. Interestingly, the Zn(1)–S distances of Zn(1)–S(1) = 2.6697(11) Å and Zn(1)–S(2) = 2.5110(12) Å are quite long for a typical Zn–S bond, and considerably longer than the distances from the thiolate sulfur atoms to the respective tetrahedral zinc(II) ions: Zn(2)–S(1) 2.3115(12) Å and Zn(3)–S(2) 2.2843(11) Å. This observation is counterintuitive to the expectation that the Zn–S bonds of the chelate ring should be shorter than the bridging Zn–S bonds. However, this same trend is observed for two other trinuclear zinc complexes, $[(MBPA)_4Zn_3]I_2$ (MBPAH = *N*-(2-mercaptoisobutyl)-(picolyl)amine)[26] and $[Zn\{Zn(L^3)_2\}_2](ClO_4)_2$ (L^3 = 2-[(2-pyridylmethyl)amino]ethanethiolate) [27], both of which have 6-coordinate and 4-coordinate zinc(II) ions bridged by thiolate ligands. In these compounds the sulfur distance to the six-coordinate zinc ion is significantly longer than the sulfur distance to the four-coordinate zinc center ($[(MBPA)_4Zn_3]I_2$: $Zn_{octahedral}$–S = 2.545(3) Å, $Zn_{tetrahedral}$–S = 2.365(3) Å; $[Zn\{Zn(L^3)_2\}_2](ClO_4)_2$: $Zn_{octahedral}$–S = 2.538(3)–2.596(3) Å, $Zn_{tetrahedral}$–S = 2.346(3)–2.363(3) Å). In both of the latter complexes the thiolate donor is also part of a chelate ring that includes the octahedral zinc ion. The considerably longer $Zn_{octahedral}$–S distances are likely a consequence of the increase in coordination number compared to a tetrahedral zinc site.

The tetrahedral zinc centers Zn(2) and Zn(3) are not only bridged by sulfur atoms to the octahedral zinc ion, but are also connected to each other by the thiolate arm of a third ligand. Each of these four-coordinate zinc ions is also bound by a separate imidazole donor from the same ligand. Thus the imidazolyl groups together with the bridgehead carbon atom also participate in bridging the dinuclear zinc fragment. This (im)-C-(im)-type bridge has been observed previously for the related N_3 scorpionate ligand tris[2-(1-methylimidazolyl)methoxymethane (timm), which has three imidazolyl donors connected by a central C_3 symmetric carbon atom. The dimeric complexes of formula $[Cu(timm)]_2[BF_4]_2$ [28] and $[Pd_2Cl_2(timm)_2]Cl_2$ [29] have structures which show the ligand bound to one metal ion through two imidazole rings while the third imidazole group coordinates to the other metal ion of the dimer. Interestingly, the unusual "1 + 2" assembly of an octahedral zinc ion bridged to a dinuclear fragment of two tetrahedral zinc ions has been seen before for another N_2S(thiolate) scorpionate ligand, but in this case the tetrahedral zinc ions are bridged by a $(PhO)_2PO_2^-$ ligand [21b]. The fourth site of each distorted tetrahedral zinc center in **1** is occupied by a bromide ion. The Zn–N(im) distances for the four-coordinate zinc sites are 2.026(3) and 2.034(4) Å. These Zn–N lengths are slightly shorter than those found for the octahedral zinc site, as to be expected from the lower coordination number of the

tetrahedral centers. The angles around the two four-coordinate zinc ions are distinct, ranging from 90.9°–123.1° for Zn(2) to 99.9°–121.5° for Zn(3), making them both rather distorted from ideal tetrahedral geometry.

3.3. Coordination behavior of L^2

Although L^1 exhibited the desired tripodal bonding mode in complex **1**, it also demonstrated a propensity to form both 2:1 octahedral complexes as well as thiolate-bridged oligomers. Given these results, we sought methods for synthetically modifying L^1 to incorporate steric bulk near the metal center during tripodal coordination, thereby favoring monomeric $(N_2S)ZnL$ complexes. Modification of the imidazole groups was the most synthetically feasible method of achieving this goal given the stepwise synthesis of L^1H [22], and thus we targeted the diphenyl-substituted analog L^2H, shown in Fig. 1. The synthesis of L^2H has been communicated previously, and in the same work L^2 was shown to react with $Zn(CH_3)_2$ to give the neutral, monomeric zinc alkyl complex $(L^2)ZnCH_3$, as seen in Scheme 2 [23]. The synthesis of this complex demonstrated that L^2 coordinates in the desired tridentate facial mode to give a tetrahedral $(N_2S)ZnL$ complex. This complex was prepared as a possible starting material for the formation of $(L^2)ZnOH$ by reaction with water. However, upon reaction of $(L^2)ZnCH_3$ with water in toluene, a redistribution of ligand:metal stoichiometry took place along with a rearrangement of the N_2S bonding mode of L^2 to a bidentate N,S mode, resulting in the formation of a four-coordinate N_2S_2–Zn complex. Alternatively, if $(L^2)ZnCH_3$ was reacted under acidic conditions (HBF_4 or CF_3SO_3H in CH_3CN), the rearranged $Zn–N_2S_2$ product was not obtained, but instead the dinuclear complexes $[(L^2)_2Zn_2(CH_3CN)_2(\mu\text{-}OH)](X)_3$ ($X = BF_4^-$, $CF_3SO_3^-$) were isolated and crystallographically characterized [23]. During the formation of these dimers an undesirable intramolecular disulfide linkage had formed. These synthetic observations are summarized in Scheme 2.

In continuing our efforts to determine the coordination behavior of L^2, we have reacted L^2 with the metal salts $ZnBr_2$ and $FeCl_2$, as shown in Scheme 2. The syntheses of **2** and **3** were carried out under the strict exclusion of air to prevent the possible oxidation of the thiolate ligand to a disulfide and in the case of **3**, to prevent oxidation of the Fe(II) product. The ligand L^2H is freely soluble in CH_2Cl_2 but only sparingly soluble in MeOH. Thus, L^2H was first dissolved in CH_2Cl_2 and then deprotonated by the addition of NaOH in MeOH in the synthesis of both **2** and **3**. For **2**, a solution of $ZnBr_2$ in MeOH was added dropwise to the solution of L^2 whereas for **3** the addition was reversed and ligand was added to metal. Complex **2** precipitates from the reaction mixture as a white powder. After workup this powder was shown to be pure **2** by its ^1H NMR spectrum. Complex **2** is freely soluble in CH_2Cl_2, and recrystallization of **2** from vapor diffusion of Et_2O into CH_2Cl_2 gave the crystals that were used for the structural determination. In the case of **3**, a precipitate also forms in the reaction mixture, but this precipitate is not isolated and instead is simply recrystallized directly by the addition of CH_2Cl_2 to the reaction mixture to redissolve the solid. X-ray quality crystals of **3** are obtained after storage of this mixture at −20 °C.

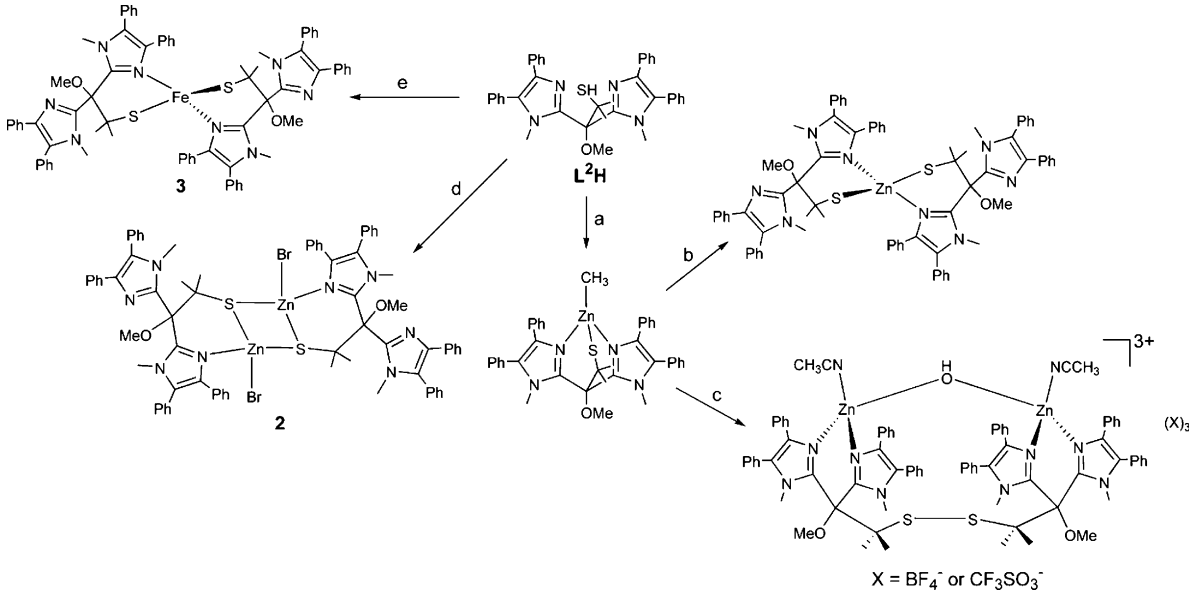

Scheme 2. Conditions: (a) 1.4 $Zn(CH_3)_2$, toluene, rt, 3 h. (b) 30 H_2O, toluene, rt, 6 d. (c) 2 HBF_4 (aq.) or 2 CF_3SO_3H, CH_3CN, rt, 24 h. (d) 1.1 NaOH, MeOH; 1 $ZnBr_2$, MeOH; 18 h. (e) 2.2 NaOH, MeOH; 1.1 $FeCl_2$, MeOH; 18 h.

3.4. Crystal structure of $[(L^2)_2Zn_2Br_2]$ (2)

An ORTEP view of **2** is shown in Fig. 3. Crystallographic data are summarized in Table 1. Selected bond distances and angles are given in Table 3. Complex **2** crystallizes in the triclinic $P(\bar{1})$ space group. The dimer does not sit on an inversion center, and therefore all bonds and angles are crystallographically unique. A CH_2Cl_2 molecule of 1/2 occupancy was located per dimeric unit. Both zinc centers have a distorted tetrahedral geometry and are bridged by two sulfur atoms from two ligand molecules to give a Zn_2S_2 rhomb. In addition to the bridging thiolates, a nitrogen atom from one of the *N*-methyl-4,5-diphenylimidazole rings coordinates each zinc atom. A bromide ion completes the coordination sphere of each zinc atom. Each ligand has one imidazole moiety that is free and not coordinated to a zinc atom, and thus each ligand binds in a bidentate N,S fashion through one nitrogen atom and one μ-sulfur atom. As pointed out in Section 3.3, evidence for this type of bonding mode has been obtained previously for L^2. In comparison, the dimeric complexes of the N_3 scorpionate ligand timm, $[Cu(timm)]_2[BF_4]_2$ [28] and $[Pd_2Cl_2(timm)_2]Cl_2$ [29], described previously in Section 3.2, have structures which show a bidentate N,N bonding mode. Thus, the bidentate bonding mode of these carbon-centered scorpionate ligands is not unique to mixed N/S systems, and is seen for the homoleptic N_3 systems as well.

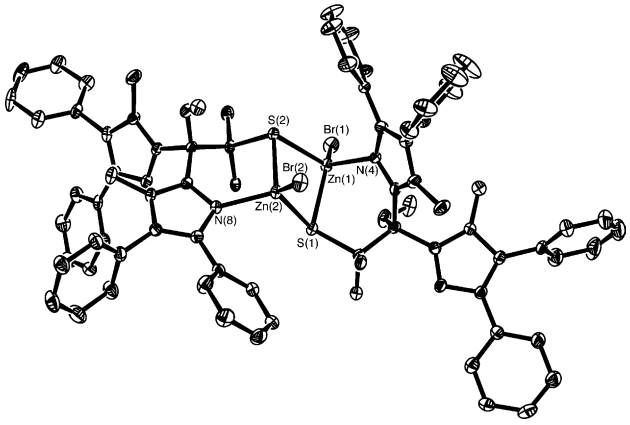

Fig. 3. Thermal ellipsoid plot of **2** at 40% probability. Hydrogen atoms are omitted for clarity.

Table 3
Bond lengths (Å) and angles (°) for **2**

Bond lengths	
Br(1)–Zn(1)	2.3706(9)
Br(2)–Zn(2)	2.3573(9)
Zn(1)–S(1)	2.3400(13)
Zn(1)–S(2)	2.3807(13)
Zn(1)–N(4)	2.061(3)
Zn(2)–S(1)	2.4034(13)
Zn(2)–S(2)	2.3787(13)
Zn(2)–N(8)	2.050(4)
Bond angles	
Br(1)–Zn(1)–S(1)	114.89(4)
Br(1)–Zn(1)–S(2)	122.77(4)
Br(1)–Zn(1)–N(4)	111.00(9)
S(1)–Zn(1)–S(2)	94.84(4)
S(1)–Zn(1)–N(4)	99.19(10)
S(2)–Zn(1)–N(4)	110.77(10)
Br(2)–Zn(2)–S(1)	113.12(4)
Br(2)–Zn(2)–S(2)	129.23(4)
Br(2)–Zn(2)–N(8)	117.78(10)
S(1)–Zn(2)–S(2)	93.25(4)
S(1)–Zn(2)–N(8)	104.66(10)
S(2)–Zn(2)–N(8)	94.06(10)
Zn(1)–S(1)–Zn2	82.92(4)
Zn(1)–S(2)–Zn(2)	82.59(4)

The Zn–S distances of **2** range between 2.3400(13) and 2.4034(13) Å, which is within the range of other $Zn_2(\mu\text{-}SR)_2$ complexes [30–34], such as the homoleptic complex $[(Et_4N)_2Zn_2(SEt)_6]$ [33] where d(Zn–S) = 2.394(1) and 2.456(1) Å, or $[Zn_2(CH_3)_2(\{SC_6H_4(R)\text{-}CH(Me)NMe_2\}\text{-}2\})_2$, where the zinc ions are bound by an N,S chelate ring and d(Zn–S) ranges between 2.389(1) and 2.453(2) Å [34]. The carbon atoms attached to each thiolate bridge are on opposite sides of the Zn_2S_2 plane, as are the bromine atoms, and thus **2** can be classified in the *anti* form [33]. The Zn(1)–N(4) and Zn(2)–N(8) distances of 2.061(3) and 2.050(4) Å, respectively, are close to other $Zn_{tetrahedral}$–$N_{imidazole}$ distances [35–37]. The Zn–Br distances of 2.3573(9) and 2.3706(9) Å are also unexceptional [9,35,38]. The angles around the zinc centers range from 82.59(4)°–129.23(4)°, which indicates a significant distortion from tetrahedral geometry. The dihedral angle between the two planes defined by $Zn(1)S_2$ and $Zn(2)S_2$ is 19.3°, giving a slight V shape to the Zn_2S_2 unit. In the literature this dihedral angle is found to vary from 0° for $[(Et_4N)_2Zn_2(SEt)_6]$ [33] to 29.18° for $[(Me)Zn(SBu^t)(cis\text{-}C_6H_{15}N_3)]_2$ where $(cis\text{-}C_6H_{15}N_3)$ = 1,3,5-trimethylhexahydro-1,3,5-triazine [39]. The reasons for the variance in this fold angle are not clear. The distance between the two zinc atoms in **2** is 3.141 Å which is also in the normal range for $Zn_2(\mu\text{-}SR)_2$ complexes [33].

3.5. ^1H NMR spectrum of $[(L^2)_2Zn_2Br_2]$ (2)

The ^1H NMR spectrum for **2** in $CDCl_3$ provides good evidence that the dinuclear structure obtained from X-ray crystallography remains intact in solution. The resonances for the phenyl protons of **2** appear as a complex multiplet in the region δ 7.11–7.56 ppm, and do not provide much structural information. However, for the N–CH_3 substituents, two distinct singlets are observed at 3.51 and 3.26 ppm, consistent with the two different types of imidazole groups in the dimer. We assign the upfield peak at 3.26 ppm to the non-coordinated imidazole group, whereas the peak at 3.51 ppm is assigned to

the imidazole group bound to the zinc(II) ion. The latter assignment is based on the ^{1}H NMR spectra for $(L^2)ZnCH_3$ and $[(L^2)_2Zn_2(CH_3CN)_2(\mu\text{-}OH)](X)_3$ ($X = BF_4^-$, $CF_3SO_3^-$), both of which have only the coordinated type of imidazolyl group (Scheme 2) and exhibit downfield-shifted N–CH_3 resonances of δ 3.87 and 3.95 ppm, respectively [23]. A similar pattern to that of **2** was seen for $(L^2)_2Zn$, which exhibited two peaks at 2.95 and 3.87 ppm, presumed to be the free and bound imidazole groups, respectively [23]. Curiously, the free ligand itself, L^2H, gives rise to a relatively downfield N–CH_3 resonance of 3.53 ppm. However, the precedent for a coordinated N–CH_3 peak being significantly downfield-shifted is clear from the former data. The singlet at 2.74 ppm in the spectrum of **2** is assigned to the O–CH_3 resonance, which is close to the same peak found for $(L^2)_2Zn$ (O–CH_3: δ 2.57 ppm), yet quite distinct from that of $(L^2)ZnCH_3$ (3.57 ppm) or $[(L^2)Zn\text{–}(\mu\text{-}OH)\text{–}Zn(L^2)]^{3+}$ (3.56 ppm). Finally, the gem-dimethyl protons for **2** appear as a singlet at δ 1.93 ppm, which is downfield of the same resonance found for the free ligand L^2H (1.60 ppm) or for $(L^2)ZnCH_3$ (1.64 ppm), in which L^2 is bound in a tripodal mode. Thus the ^{1}H NMR spectrum of **2** appears to be quite characteristic of the bonding mode of L^2 (N,S versus N,N,S for $(L^2)ZnCH_3$ and N,N for $[(L^2)Zn\text{–}(\mu\text{-}OH)\text{–}Zn(L^2)]^{3+}$).

3.6. Crystal structure of $(L^2)_2Fe$ (3)

An ORTEP view of **3** is shown in Fig. 4. Crystallographic data are summarized in Table 1. Selected bond distances and angles are given in Table 4. This complex crystallizes in the triclinic space group $P(\bar{1})$. The ferrous ion adopts a distorted tetrahedral geometry and is coordinated by two ligand molecules through one imidazole and one thiolate donor, which makes the complex neutral in charge. As observed in the case of **2**, the other imidazole donor from each ligand molecule remains uncoordinated, demonstrating the preference for an N,S binding mode over an N_2S mode for L^2. The two MeOH molecules found in the lattice appear to be involved in hydrogen bonding with separate thiolate sulfur atoms.

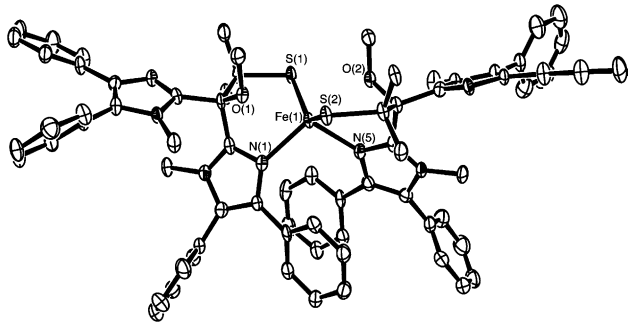

Fig. 4. Thermal ellipsoid plot of **3** at 40% probability. Hydrogen atoms are omitted for clarity.

Table 4
Bond lengths (Å) and angles (°) for **3**

Bond lengths	
Fe(1)–N(1)	2.157(4)
Fe(1)–N(5)	2.157(4)
Fe(1)–S(2)	2.3363(14)
Fe(1)–S(1)	2.3480(14)
Bond angles	
N(1)–Fe(1)–N(5)	102.77(15)
N(1)–Fe(1)–S(2)	107.65(11)
N(5)–Fe(1)–S(2)	99.65(11)
N(1)–Fe(1)–S(1)	98.68(10)
N(5)–Fe(1)–S(1)	109.78(11)
S(2)–Fe(1)–S(1)	134.72(6)

The hydrogen atoms on the MeOH molecules could not be located by X-ray diffraction, but the distances between the oxygen and sulfur atoms, O(1S)–S(1) = 3.183 Å and O(2S)–S(2) = 3.167 Å, indicate an H-bonding interaction [40]. Despite these putative hydrogen bonds, the Fe–S distances of Fe–S(1) = 2.3480(14) Å and Fe–S(2) = 2.3363(14) Å, are quite normal. Interestingly, both the methoxy oxygen atoms of the ligands are oriented towards the iron(II) ion, with distances of Fe–O(1) = 2.462 and Fe–O(2) = 2.473 Å. These distances are comparable to other Fe–O(ether) distances for compounds in which an Fe–O(ether) bond has been assigned. For example, a mean Fe–O distance of 2.40 Å is found for the crown ether complex {[Fe([12]-crown-4)$_2$](PF$_6$)$_2$}[41], and $(Fe\text{–}O)_{ave} = 2.386(3)$ Å for the calixarene complex [Fe(II–H)](FeCl$_4$)$_2$ [42] [(II–H) = 5,11,17,23-tetra-*tert*-butyl-24-hydroxy-26,27,28-tris (diethyl-carbamoylmethoxy)calix-[4]arene]. These data suggest that there is a bonding interaction between the Fe^{2+} ion and the methoxy oxygen atoms, and the ligand has adopted the unexpected tripodal N_2O bonding mode. However, the angles do not support an assignment of octahedral geometry in preference to a distorted tetrahedral geometry, and therefore we conclude that this O(ether)–Fe^{II} interaction is weak at best. The Fe–N distances of 2.157(4) Å are slightly longer than the bond length of 2.095(4) Å for the related $Fe^{II}(N_2S_2)$ complex Fe(S-2,6-*i*-Pr$_2$C$_6$H$_3$)$_2$(1-MeIm)$_2$ [43]. The X-ray structures of complexes **2** and **3** together with the synthesis and spectroscopic characterization of $(L^2)_2Zn$ (Scheme 2) make it clear that L^2 has a particular preference for coordination via a bidentate N,S bonding mode.

4. Conclusions

We have succeeded in obtaining the first X-ray structure of a transition metal complex of the N_2S(thiolate) ligand L^1. This trinuclear zinc complex **1** showed that L^1 does bind in the designed tripodal mode, but also exhibits another multibridging bonding mode involving bridging imidazole and thiolate groups. The

ligand L^2 is a modified version of L^1 bearing phenyl substituents, and exhibits a third type of bidentate N,S bonding mode evidenced by the X-ray structures of the dinuclear zinc(II) complex **2** and the mononuclear iron(II) complex **3**. This bonding mode is likely favored in the case of L^2 because of a combination of strain around the central carbon atom and the weakened donor power of the imidazole groups caused by the electron-withdrawing phenyl substituents. In addition, yet another type of bonding mode may be operative in **3**; there is some evidence for a weak bond between the methoxy oxygen atom of L^2 and Fe(II), giving rise to tripodal NSO(ether)-type coordination. Clearly, further modifications to these heteroscorpionate N_2S(thiolate) ligands are necessary before they can rival the tris(pyrazolyl)borates in terms of their ability to enforce a biologically relevant monomeric, tetrahedral geometry at the metal center. The results obtained here suggest that replacing the phenyl substituents with electron-donating groups (e.g. alkyl groups), as well as increasing the steric encumbrance near the sulfur atom to discourage thiolate bridges from forming, should favor complexes of the desired nuclearity and geometry.

5. Supplementary material

The X-ray crystallographic files, in CIF format, have been deposited with the Cambridge Crystallographic Data Center, CCDC Nos. 213062, 213475 and 211497 for **1**, **2**, and **3**, respectively. Copies of this information may be obtained from The Director, CCDC, 12 Union Road, Cambridge, CB2 1EZ, UK, (fax: +44-1223-336033; email: deposit@ccdc.cam.ac.uk or www: http://www.ccdc.cam.ac.uk/conts/retrieving.html) on request, quoting the deposition number.

Acknowledgements

The authors wish to acknowledge the National Institutes of Health (GM 62309) for financial support. D.P.G. is also grateful for an Alfred P. Sloan, Jr. Research Fellowship.

References

[1] N. Borkakoti, J. Mol. Med. 78 (2000) 261.
[2] C.O. Pabo, E. Peisach, R.A. Grant, Annu. Rev. Biochem. 70 (2001) 313.
[3] R. Meijers, R.J. Morris, H.W. Adolph, A. Merli, V.S. Lamzin, E.S. Cedergren-Zeppezauer, J. Biol. Chem. 276 (2001) 9316.
[4] H.W. Park, S.R. Boduluri, J.F. Moomaw, P.J. Casey, L.S. Beese, Science 275 (1997) 1800, and references therein.
[5] M.H. Bracey, J. Christiansen, P. Tovar, S.P. Cramer, S.G. Bartlett, Biochemistry 33 (1994) 13126, and references therein.
[6] D.W. Randall, D.R. Gamelin, L.B. LaCroix, E.I. Solomon, J. Biol. Inorg. Chem. 5 (2000) 16.
[7] W. Huang, J. Jia, J. Cummings, M. Nelson, G. Schneider, Y. Lindqvist, Structure 5 (1997) 691.
[8] (a) P.T.R. Rajagopalan, S. Grimme, D. Pei, Biochemistry 39 (2000) 779;
(b) T. Meinnel, C. Lazennec, S. Blanquet, J. Mol. Biol. 254 (1995) 175.
[9] S. Chang, V.V. Karambelkar, R.C. diTargiani, D.P. Goldberg, Inorg. Chem. 40 (2001) 194.
[10] S. Chang, V.V. Karambelkar, R.D. Sommer, A.L. Rheingold, D.P. Goldberg, Inorg. Chem. 41 (2002) 239.
[11] S. Chang, R.D. Sommer, A.L. Rheingold, D.P. Goldberg, Chem. Commun. (2001) 2396.
[12] R.C. diTargiani, S. Chang, M.H. Salter Jr., R.D. Hancock, D.P. Goldberg, Inorg. Chem. 42 (2003) 5825.
[13] S. Trofimenko, Scorpionates – The Coordination Chemistry of Polypyrazolylborate Ligands, Imperial College Press, River Edge, NJ, 1999.
[14] G. Parkin, Chem. Commun. (2000) 1971.
[15] R. Alsfasser, S. Trofimenko, A. Looney, G. Parkin, H. Vahrenkamp, Inorg. Chem. 30 (1991) 4098.
[16] N. Kitajima, S. Hikichi, M. Tanaka, Y. Moro-oka, J. Am. Chem. Soc. 115 (1993) 5496.
[17] S.J. Chiou, J. Innocent, C.G. Riordan, K.C. Lam, L. Liable-Sands, A.L. Rheingold, Inorg. Chem. 39 (2000) 4347.
[18] M. Garner, J. Reglinski, I. Cassidy, M.D. Spicer, A.R. Kennedy, Chem. Commun. (1996) 1975.
[19] J. Reglinski, M. Garner, I.D. Cassidy, P.A. Slavin, M.D. Spicer, D.R. Armstrong, J. Chem. Soc., Dalton Trans. (1999) 2119.
[20] C. Kimblin, T. Hascall, G. Parkin, Inorg. Chem. 36 (1997) 5680.
[21] (a) For a related heteroscorpionate $N_2S_{thiolate}$ ligand see B.S. Hammes, C.J. Carrano, Inorg. Chem. 40 (2001) 919;
(b) B.S. Hammes, C.J. Carrano, J. Chem. Soc., Dalton Trans. (2000) 3304;
(c) B.S. Hammes, C.J. Carrano, Chem. Commun. (2000) 1635.
[22] J.M. Downes, J. Whelan, B. Bosnich, Inorg. Chem. 20 (1981) 1081.
[23] V.V. Karambelkar, D. Krishnamurthy, C.L. Stern, L.N. Zakharov, A.L. Rheingold, D.P. Goldberg, Chem. Commun. (2002) 2772.
[24] T.A. Zevaco, H. Görls, E. Dinjus, Inorg. Chim. Acta 269 (1998) 283.
[25] N. Niklas, O. Walter, F. Hampel, R. Alsfasser, J. Chem. Soc., Dalton Trans. (2002) 3367.
[26] U. Brand, H. Vahrenkamp, Inorg. Chim. Acta 308 (2000) 97.
[27] M. Mikuriya, X. Jian, S.I. Ikemi, T. Kawahashi, H. Tsutsumi, Bull. Chem. Soc. Jpn. 71 (1998) 2161.
[28] T.N. Sorrell, A.S. Borovik, J. Am. Chem. Soc. 109 (1987) 4255.
[29] T. Rüther, M.C. Done, K.J. Cavell, E.J. Peacock, B.W. Skelton, A.H. White, Organometallics 20 (2001) 5522.
[30] W.P. Chung, J.C. Dewan, M.A. Walters, Inorg. Chem. 30 (1991) 4280.
[31] B. Kaptein, L. Wang-Griffin, G. Barf, R.M. Kellogg, Chem. Commun. (1987) 1457.
[32] K.S. Anjali, J.J. Vittal, Main Group Metal Chemistry 24 (2001) 129.
[33] A.D. Watson, C.P. Rao, J.R. Dorfman, R.H. Holm, Inorg. Chem. 24 (1985) 2820.
[34] D.M. Knotter, M.D. Janssen, D.M. Grove, W.J.J. Smeets, E. Horn, A.L. Spek, G. van Koten, Inorg. Chem. 30 (1991) 4361.
[35] R.J. Read, M.N.G. James, Acta Cryst. B36 (1980) 3100.
[36] B. Müller, A. Schneider, M. Tesmer, H. Vahrenkamp, Inorg. Chem. 38 (1999) 1900.
[37] W. Kläui, C. Piefer, G. Rheinwald, H.R. Lang, Eur. J. Inorg. Chem. (2000) 1549.

[38] N. Galván-Tejada, S. Bernès, S.E. Castillo-Blum, H. Nöth, R. Vicente, N. Barba-Behrens, J. Inorg. Biochem. 91 (2002) 339.
[39] M.A. Malik, M. Motevalli, J.R. Walsh, P. O'Brien, A.C. Jones, J. Mater. Chem. 5 (1995) 731.
[40] M. Rombach, H. Vahrenkamp, Inorg. Chem. 40 (2001) 6144.
[41] K. Meier, G. Rihs, Angew. Chem. Intl. Ed. Engl. 24 (1985) 858.
[42] M.I. Ogden, B.W. Skelton, A.H. White, J. Chem. Soc., Dalton Trans. (2001) 3073.
[43] C.E. Forde, A.J. Lough, R.H. Morris, R. Ramachandran, Inorg. Chem. 35 (1996) 2747.

Available online at www.sciencedirect.com
SCIENCE DIRECT®
Polyhedron 23 (2004) 481–488
POLYHEDRON
www.elsevier.com/locate/poly

N–H···O hydrogen bonding interactions in tetrahedral [ZnS_4] complexes of relevance to zinc enzymes: the synthesis, structures and reactivity of *tris*(2-mercapto-1-arylimidazolyl)hydroborato zinc(2-mercapto-1-arylimidazole) complexes, {[Tm^{Ar}]Zn(mim^{Ar})}[ClO_4] (Ar = Ph, *p*-Tol)

Arefa Docrat, Melissa M. Morlok, Brian M. Bridgewater, David G. Churchill, Gerard Parkin *

Department of Chemistry, Columbia University, New York, NY 10027, USA

Received 12 July 2003; accepted 2 October 2003

Dedicated to Jerry Trofimenko for creating the *poly*(pyrazolyl) borate ligand system that has provided inspiration for so many other chemists, and especially myself (G.P.)!

Abstract

The tris(2-mercapto-1-arylimidazolyl)hydroborato complexes {[Tm^{Ar}]Zn(mim^{Ar})}[ClO_4], which feature tetrahedrally coordinated zinc centers in a sulfur rich environment, may be prepared by the reaction of [Tm^{Ar}]Li with $Zn(ClO_4)_2$ in the presence of 2-mercapto-1-arylimidazole (mim^{Ar}; Ar = Ph, *p*-Tol). X-ray diffraction studies demonstrate that the mim^{Ar} ligands are almost orthogonal to the Zn–S–C plane, in contrast to the almost planar arrangement that is calculated for {[Tm^{H}]Zn(mim^{H})}$^+$ and {[Tm^{H}]Zn(mim^{Me})}$^+$. The orthogonal arrangement observed experimentally for both {[Tm^{Ph}]Zn(mim^{Ph})}$^+$ and {[$Tm^{p\text{-}Tol}$]Zn($mim^{p\text{-}Tol}$)}$^+$ is a consequence of the existence of a N–H···O hydrogen bond between the N–H group of the mim^{Ar} ligand and a molecule of methanol. Evidently, the hydrogen bonding interactions in {[Tm^{Ar}]Zn(mim^{Ar})···(HOMe)}$^+$ are sufficiently strong to counter the electronic destabilization resulting from rotation of the mim^{Ar} ligand from the Zn–S–C plane. The mim^{Ph} ligand of {[Tm^{Ph}]Zn(mim^{Ph})}$^+$ may be immediately displaced by I^- to give [Tm^{Ar}]ZnI; however, {[Tm^{Ph}]Zn(mim^{Ph})}$^+$ does not react rapidly with MeI, thereby demonstrating that the zinc coordinated mim^{Ph} ligand is less susceptible to electrophilic attack than is a zinc thiolate ligand.
© 2003 Published by Elsevier Ltd.

Keywords: Zinc; Enzyme; Thiolate; Alkylation

1. Introduction

Tetrahedrally coordinated zinc in a sulfur-ligated environment, i.e. [S_4Zn^{II}], is a prominent feature of structural and functional sites of zinc enzymes and proteins, as exemplified by the structural site of liver alcohol dehydrogenase and the functional site of the Ada DNA repair protein [1,2]. While considerable insight into the chemistry of zinc enzymes has been achieved by studying synthetic analogues that feature nitrogen rich active sites (for example, see [3]), comparatively few studies have been devoted to the chemistry of synthetic analogues with [S_4Zn^{II}] coordination environments. In this paper, we describe the synthesis, structures and reactivity of tetrahedral zinc complexes [S_4Zn^{II}] that employ tripodal tris(2-mercapto-1-arylimidazolyl)hydroborato ligands.

* Corresponding author. Tel.: +212-932-1289; fax: +212-854-2202.
E-mail address: parkin@chem.columbia.edu (G. Parkin).

0277-5387/$ - see front matter © 2003 Published by Elsevier Ltd.
doi:10.1016/j.poly.2003.11.035

2. Results and discussion

We have previously reported the application of tris (2-mercapto-1-arylimidazolyl)hydroborato ligands, i.e. [Tm^{Ar}] for providing a [S_3] donor array to model aspects of the chemistry of zinc enzymes with sulfur-rich active sites [4]. For example, we have described the synthesis of [Tm^{Ph}]ZnSPh and have demonstrated that the phenylthiolate ligand is readily alkylated by MeI to give PhSMe and [Tm^{Ph}]ZnI ([4d], for other examples of alkylation of zinc thiolate derivatives, see [5]). Such reactivity mimics aspects of the mechanism of action of the Ada DNA repair protein which also possesses a [S_4Zn^{II}] active site [6]. A notable feature of the reaction between [Tm^{Ph}]ZnSPh and MeI is that the reaction occurs specifically at the sulfur atom of the phenylthiolate ligand, with the sulfur atoms of the [Tm^{Ph}] ligand being inert to alkylation. To address the issue of whether the inertness of the sulfur atoms of the [Tm^{Ph}] ligand is a consequence of constraints associated with the three mercaptoimidazole groups being attached to a common boron center, we sought to investigate the reactivity of {[Tm^{Ph}]Zn(mim^{Ar})}$^+$, in which the phenylthiolate ligand has been replaced by a 2-mercapto-1-arylimidazole ligand (mim^{Ar}; Ar = Ph, *p*-Tol).

2.1. Synthesis and structural characterization of {[Tm^{Ar}]Zn(mim^{Ar})}$^+$

{[Tm^{Ph}]Zn(mim^{Ph})}[ClO_4] may be prepared by the reaction of [Tm^{Ph}]Li with $Zn(ClO_4)_2$ in the presence of mim^{Ph} (Scheme 1). The *para*-tolyl derivative {[$Tm^{p\text{-Tol}}$]Zn($mim^{p\text{-Tol}}$)}[ClO_4] has likewise been synthesized (Scheme 1). Both {[Tm^{Ph}]Zn(mim^{Ph})}$^+$ and {[$Tm^{p\text{-Tol}}$]Zn($mim^{p\text{-Tol}}$)}$^+$ feature zinc centers that are coordinated to four mim^{Ar} groups, of which three are components of the [Tm^{Ar}] ligand. As such, {[Tm^{Ph}]-Zn(mim^{Ph})}$^+$ provides a means to determine whether the inertness of the sulfur atoms of the [Tm^{Ph}] ligand of [Tm^{Ph}]ZnSPh is associated with constraints imposed by attachment to the boron center.

The molecular structures of both {[Tm^{Ph}]Zn(mim^{Ph})} [ClO_4] and {[$Tm^{p\text{-Tol}}$]Zn($mim^{p\text{-Tol}}$)} [ClO_4] have been determined by X-ray diffraction (Figs. 1 and 2) and display several noteworthy features. First, the coordination geometry of the zinc is close to regular tetrahedral, with S–Zn–S bond angles in the range 103°–115° for {[Tm^{Ph}]-Zn(mim^{Ph})}$^+$ and 103°–120° for {[$Tm^{p\text{-Tol}}$]Zn ($mim^{p\text{-Tol}}$)}$^+$ (Table 1). In this regard, it is pertinent to compare the structures of {[Tm^{Ph}]- Zn(mim^{Ph})}$^+$ and {[$Tm^{p\text{-Tol}}$]-Zn($mim^{p\text{-Tol}}$)}$^+$ with that of [$Zn(SPh)_4$]$^{2-}$, a complex that may be expected to have an idealized tetrahedral zinc coordination environment. However, it has been noted by Koch and Millar that [$M(SPh)_4$]$^{2-}$ derivatives exist with two conformations that differ according to the positions of the phenyl groups; the two conformations have

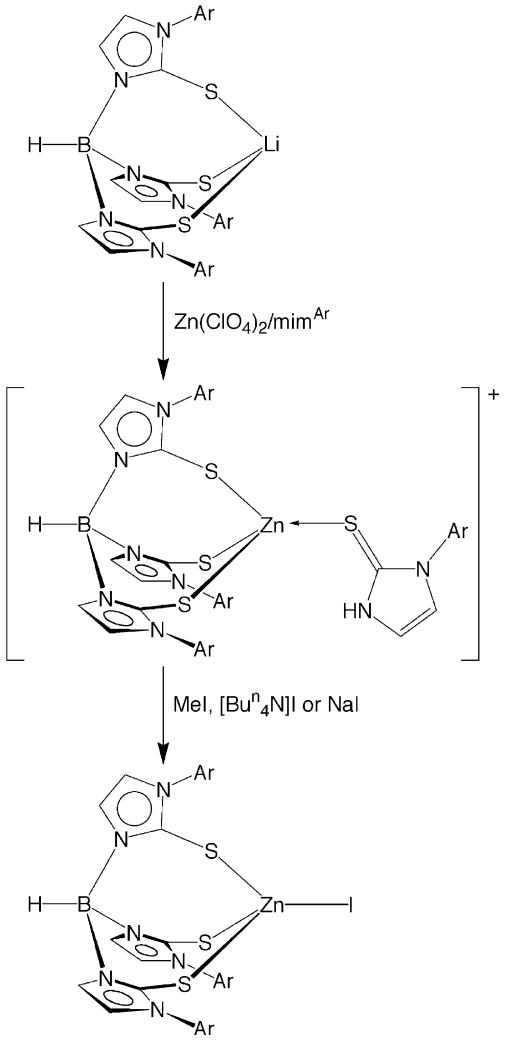

Scheme 1.

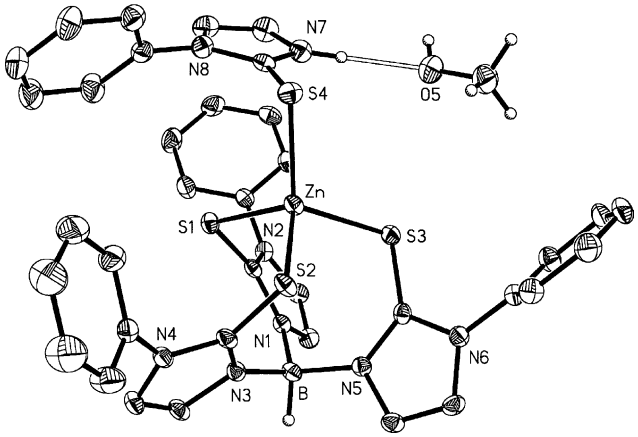

Fig. 1. Molecular structure of {[Tm^{Ph}]Zn(mim^{Ph})···(HOMe)}$^+$.

idealized S_4 and D_{2d} symmetry [7]. Steric interactions cause a distortion of the MS_4 core from tetrahedral geometry [8] such that the S_4 isomer is tetragonally compressed along the S_4 axis, while the D_{2d} isomer is tetragonally elongated.

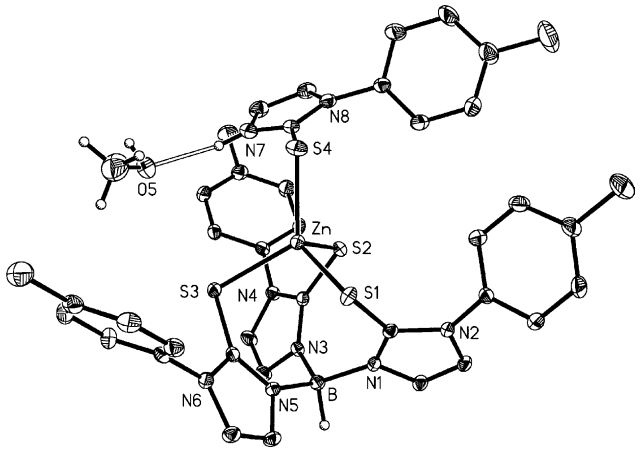

Fig. 2. Molecular structure of $\{[Tm^{p\text{-}Tol}]Zn(mim^{p\text{-}Tol})\cdots(HOMe)\}^+$.

Table 1
Selected bond lengths (Å) and angles (°) for $\{[Tm^{Ph}]Zn(mim^{Ph})\}^+$ and $\{[Tm^{p\text{-}Tol}]Zn(mim^{p\text{-}Tol})\}^+$

	$\{[Tm^{Ph}]Zn(mim^{Ph})\}^+$	$\{[Tm^{p\text{-}Tol}]Zn(mim^{p\text{-}Tol})\}^+$
Bond lengths		
Zn–S(1)	2.348(1)	2.350(1)
Zn–S(2)	2.347(1)	2.359(1)
Zn–S(3)	2.354(1)	2.344(1)
Zn–S(4)	2.326(1)	2.324(1)
S(1)–C(11)	1.724(4)	1.722(4)
S(2)–C(21)	1.728(4)	1.724(4)
S(3)–C(31)	1.720(4)	1.735(4)
S(4)–C(41)	1.720(5)	1.709(4)
Bond angles		
Zn–S(4)–C(41)	97.8(1)	97.90(1)
S(1)–Zn–S(2)	109.32(4)	109.69(4)
S(1)–Zn–S(3)	107.23(4)	103.17(4)
S(1)–Zn–S(4)	109.62(5)	111.32(4)
S(2)–Zn–S(3)	102.92(5)	106.05(4)
S(2)–Zn–S(4)	112.45(4)	106.46(4)
S(3)–Zn–S(4)	114.94(5)	119.83(4)

Due to increased steric interactions, distortions from idealized tetrahedral coordination (109.5°) are expected to be greater for the D_{2d} isomer. Thus, the S–Zn–S bond angles in $[Ph_4P]_2[Zn(SPh)_4]$ with D_{2d} geometry spread the substantial range of 97°–121° [9], while those in $[Me_4N]_2$-$[Zn(SPh)_4]$ with S_4 geometry span the range 100°–117° [10]. It is, therefore, evident that $\{[Tm^{Ph}]Zn(mim^{Ph})\}^+$ (with S–Zn–S bond angles in the range 103°–115°) and $[Tm^{Ph}]ZnSPh$ (with S–Zn–S bond angles in the range 105°–115°) are better models for a tetrahedral zinc site than simple $[Zn(SPh)_4]^{2-}$. However, it should be noted that incorporation of different aryl groups can have a profound effect; thus, $[Et_4N]_2$-$[Zn(SAr)_4]$ (Ar = *o*-C_6H_4Ph) exhibits rigorous S_4 symmetry and the S–Zn–S angles are close to tetrahedral (106°–116°) [7a], whereas $[Et_3NH]_2[Zn(SAr)_4]$ (Ar = *o*-$C_6H_4pyr^{Me_2}$) deviates substantially from tetrahedral coordination (95°–119°) [11,12].

Second, the N–H protons of the mim^{Ar} ligands participate in a hydrogen bonding interaction with a molecule of methanol; the N···O distances are 2.80 Å (Ar = Ph) and 2.77 Å (Ar = *p*-Tol). Furthermore, it is noteworthy that the intermolecular N–H···O hydrogen bonding interaction with methanol is favored over an intramolecular N–H···S to one of the sulfur ligands attached to zinc. In this regard, it is worth noting that intramolecular N–H···S hydrogen bonding interactions involving Zn–S linkages have been previously observed [13], and that in one case, namely $[HC(pz^{Bu^t,\,Me})_2$-$(CO_2)]ZnS[C_6H_4$-*o*-NHC(O)Me], an intramolecular N–H···O hydrogen bond is favored over an intramolecular N–H···S hydrogen bond [13d].

Third, and of most interest to the present study, the coordination of the mim^{Ar} ligands is very similar to that of the analogous groups of the $[Tm^{Ar}]$ ligand. Specifically, not only are the Zn–S bond lengths comparable, but so are the C–S bond lengths and Zn–S–C bond angles, as summarized in Table 1. It is, therefore, evident that the attachment of the three mim^{Ar} groups to boron exerts very little perturbation on the ability of the mim^{Ar} groups to bind to zinc.

For further comparison, we have also determined the structure of $mim^{p\text{-}Tol}$, as illustrated in Fig. 3. The structure of $mim^{p\text{-}Tol}$ is analogous to that of mim^{Me} [14], consisting of a centrosymmetric N–H···S hydrogen bonded dimer, with a N···S separation (3.30 Å) that is comparable to that of mim^{Me} (3.35 Å). The diffraction study also indicates that the protons involved in the hydrogen bond interaction are attached primarily to the nitrogen [d(N–H) = 0.87 Å] and so $mim^{p\text{-}Tol}$ exists as the imidazole thione tautomer, as does mim^{Me}. Examination of the bond length data demonstrates that coordination of the $mim^{p\text{-}Tol}$ ligand is accompanied by little structural perturbation; as expected, the most significant change is associated with the C=S thione linkage, but this only increases from 1.690(2) to 1.720(5) Å upon coordination.

2.2. Reactivity of $\{[Tm^{Ph}]Zn(mim^{Ph})\}^+$

As previously noted, methyl iodide reacts with $[Tm^{Ph}]ZnSPh$ selectively at the sulfur atom of the phenylthiolate ligand and not with the sulfur atoms of the $[Tm^{Ph}]$ ligand [4d]. Since $\{[Tm^{Ph}]Zn(mim^{Ph})\}^+$ features

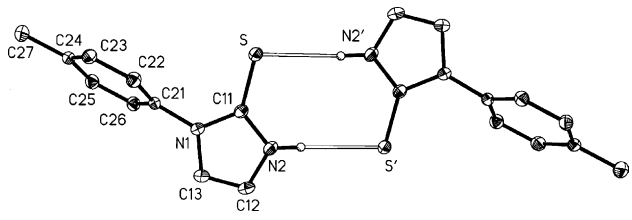

Fig. 3. Molecular structure of mim^{Ph}. Selected bond lengths (Å): S–C(11) 1.690(2), C(11)–N(1) 1.368(3), N(1)–C(13) 1.389(3), C(13)–C(12) 1.337(3), C(12)–N(2) 1.373(3), N(2)–C(11) 1.347(3), S···N(2′) 3.30 Å.

a zinc center that is coordinated to four mim^{Ph} groups, of which three are components of the $[Tm^{Ph}]$ ligand, it provides a means to determine whether the inertness of the sulfur atoms of the $[Tm^{Ph}]$ ligand of $[Tm^{Ph}]ZnSPh$ is associated with constraints imposed by attachment to the boron center. It is, therefore, notable that whereas $[Tm^{Ph}]ZnSPh$ reacts immediately with MeI to give $[Tm^{Ph}]ZnI$, the corresponding reaction of $\{[Tm^{Ph}]Zn(mim^{Ph})\}^+$ occurs over a period of days (Scheme 1). The iodide complex $[Tm^{Ph}]ZnI$ is, nevertheless, obtained immediately upon treatment of $\{[Tm^{Ph}]Zn(mim^{Ph})\}^+$ with either $[Bu^n_4N]I$ or NaI (Scheme 1). The reduced reactivity of $\{[Tm^{Ph}]Zn(mim^{Ph})\}^+$ towards MeI, as compared to that for $[Tm^{Ph}]ZnSPh$, clearly demonstrates that the coordinated mim^{Ph} ligand is less susceptible to electrophilic attack than is a zinc thiolate ligand, presumably a reflection the ''thione'' versus ''thiolate'' nature of the sulfur atoms [15].

2.3. DFT Calculations concerned with mim^R orientation and intermolecular N–H···O hydrogen bonding interactions

To address the issue pertaining to the intermolecular N–H···O hydrogen bond between the mim^{Ar} ligand and methanol, we have performed a series of DFT (B3LYP) calculations in which the aryl group of the $[Tm^{Ar}]$ ligand is replaced by hydrogen. Interestingly, the calculations indicate that while the geometry optimized structure of $\{[Tm^H]Zn(mim^H)\}^+$ is comparable to the experimental structures of $\{[Tm^{Ar}]Zn(mim^{Ar})\}^+$ in terms of the Zn–S and S–Zn–S bond lengths and angles, as illustrated in Fig. 4 and Table 2, a notable difference is concerned with the orientation of the mim^H ligand. Specifically, the mim^H ligand of $\{[Tm^H]Zn(mim^H)\}^+$ lies close to the plane defined by Zn–S–C, whereas the mim^{Ar} ligands of the experimentally determined structures of $\{[Tm^{Ar}]Zn(mim^{Ar})\cdots(HOMe)\}^+$ are almost orthogonal (Figs. 1 and 2). The ''in–plane'' Zn–mim^H geometry calculated for $\{[Tm^H]Zn(mim^H)\}^+$ is in accord with the orientations of the lone pairs in the imidazole thione mim^H. As a result of the orientation of the mim^H ligand in $\{[Tm^H]Zn(mim^H)\}^+$, the N–H hydrogen comes into proximity with one of the sulfur atoms of the $[Tm^H]$ ligand, with H···S and N···S separations of 2.37 and 3.34 Å, respectively. The N···S separation is very similar to the value of 3.30 Å described above for the hydrogen bonded dimeric structure of $mim^{p\text{-Tol}}$ (Fig. 3). It is, therefore, possible that this represents a N–H···S hydrogen bonding interaction. However, the N···S separation of 3.34 Å is longer than the separations that have been previously reported for zinc complexes with N–H···S hydrogen bonds, e.g., $[Ph(pz^{Bu^t})Bt^{Bu^t}]ZnS[C_6H_4\text{-}o\text{-}NHC(O)Bu^t]$ (2.94 Å) [5i], $[Tm^{Ph}]ZnSCH_2C(O)N(H)Ph$ (2.99 and 3.05 Å) [13c], and $Zn[S\text{–}2\text{–}C_6H_4N(H)C(O)Ph]_2(1\text{-}MeImH)_2$ (2.96 Å) [13b], such that the hydrogen bonding interaction in $\{[Tm^H]Zn(mim^H)\}^+$ must be regarded as weak. There are two principal reasons that may account for the longer N···S hydrogen bond separation in $\{[Tm^H]Zn(mim^H)\}^+$: (i) the N–H···S hydrogen bond interaction is part of a six-membered ring, whereas the hydrogen bonds in the other complexes that have been reported are components of a five-membered ring; and (ii) the sulfur of the $[Tm^H]$ ligand has thione character, whereas the other complexes have thiolate sulfurs that are likely to be more amenable to participating in a hydrogen bonding interaction. Thus, for these two reasons, the intramolecular N–H···S hydrogen bonding interaction would be expected to be weaker

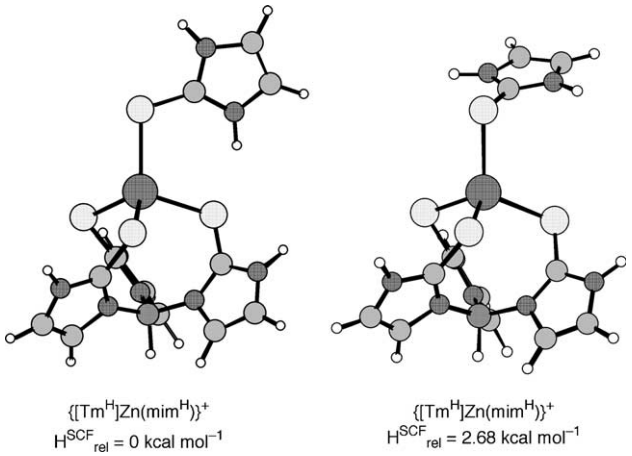

Fig. 4. Geometry optimized structure of $\{[Tm^H]Zn(mim^H)\}^+$ and that with the mim^H ligand constrained to be orthogonal to the Zn–S–C group by imposing a Zn–S–C–N torsion angle of 90°.

Table 2
Comparison of the geometries of the calculated structures of $\{[T]Zn(mim^H)\}^+$, $\{[Tm]Zn(mim^{Me})\}^+$, and $\{[Tm]Zn(mim^{Me})\cdots(HOMe)\}^+$ with those of the experimental structures for $\{[Tm^{Ph}]Zn(mim^{Ph})\cdots(HOMe)\}^+$ and $\{[Tm^{p\text{-Tol}}]Zn(mim^{p\text{-Tol}})\cdots(HOMe)\}^+$

	$\{[Tm^{Ph}]Zn(mim^{Ph})\cdots(HOMe)\}^+$ experiment	$\{[Tm^{Tol}]Zn(mim^{Tol})\cdots(HOMe)\}^+$ experiment	$\{[Tm]Zn(mim^H)\}^+$ calculated	$\{[Tm]Zn(mim^{Me})\}^+$ calculated	$\{[Tm]Zn(mim^{Me})\cdots(HOMe)\}^+$ calculated
Zn–S(Tm^R)$_{av}$ (Å)	2.35	2.35	2.45	2.45	2.45
Zn–S(mim^R) (Å)	2.33	2.32	2.46	2.45	2.44
O···N (Å)	2.80	2.77			2.76
S···N (Å)			3.34	3.32	
Zn–S–C(mim^R) (°)	97.9(1)	97.9	109.0	108.3	104.6
S(mim^R)–Zn–S(Tm^R) (°)	109.6–114.9	106.5–119.8	109.6–115.0	110.0–114.8	107.7–118.3

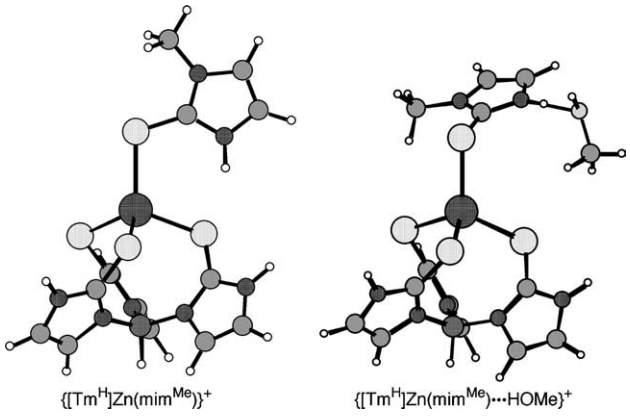

Fig. 5. Geometry optimized structure of $\{[Tm^H]Zn(mim^{Me})\}^+$ and the methanol adduct $\{[Tm^H]Zn(mim^{Me})\cdots(HOMe)\}^+$.

than in the aforementioned thiolate complexes. Nevertheless, evidence which suggests that the N–H···S interaction is not insignificant is provided by the observation that the mim^H ligand does not adopt a position that bisects the S–Zn–S angle (which would minimize steric interactions), but is rather located such that one of the sulfur atoms of the $[Tm^H]$ ligand lies close to the plane of the mim^H ligand. Calculations on $\{[Tm^H]Zn(mim^H)\}^+$ with an orthogonal position for the mim^H ligand (i.e., a fixed Zn–S–C–N torsion angle of 90°) indicate that the preference for the "in-plane" position is 2.68 kcal mol^{-1} (Fig. 4).

To emulate the intermolecular N–H···O hydrogen bonding interaction with methanol, geometry optimization calculations were performed on $\{[Tm^H]Zn(mim^{Me})\}^+$ and $\{[Tm^H]Zn(mim^{Me})\cdots(HOMe)\}^+$ (Fig. 5), the methyl group on the imidazole thione ligand being present to prevent an additional N–H···S hydrogen bonding interaction with the $[Tm^H]$ ligand. Significantly, while the mim^{Me} ligand of $\{[Tm^H]Zn(mim^{Me})\}^+$ adopts a similar conformation to that of mim^H in $\{[Tm^H]Zn(mim^H)\}^+$, coordination of MeOH results in rotation of the mim^{Me} ligand in $\{[Tm^H]Zn(mim^{Me})\cdots(HOMe)\}^+$ to a position that closely reflects the experimentally observed geometry of $\{[Tm^{Ph}]Zn(mim^{Ph})\cdots(HOMe)\}^+$ (Fig. 5). Furthermore, the calculated N···O hydrogen bonding separation for $\{[Tm^H]Zn(mim^{Me})\cdots(HOMe)\}^+$ (2.76 Å) compares favorably with the experimental values for $\{[Tm^{Ph}]Zn(mim^{Ph})\cdots(HOMe)\}^+$ (2.80 Å) and $\{[Tm^{p\text{-}Tol}]Zn(mim^{p\text{-}Tol})\cdots(HOMe)\}^+$ (2.77 Å). Thus, the N–H···O hydrogen bonding interaction in $\{[Tm^H]Zn(mim^{Me})\cdots(HOMe)\}^+$ is sufficient (5.55 kcal mol^{-1}) to counter the electronically favored "in-plane" location of the mim^{Me} ligand.[1]

[1] The difference in energy between geometry optimized $\{[Tm^H]Zn(mim^{Me})\}^+$ and that of the same fragment in geometry optimized $\{[Tm^H]Zn(mim^{Me})\cdots(HOMe)\}^+$ is 3.44 kcal mol^{-1}. Thus, the magnitude of the hydrogen bonding interaction in the absence of rotation of the mim^{Me} ligand is 8.99 kcal mol^{-1}.

3. Experimental

3.1. General considerations

All manipulations were performed using a combination of glovebox, high-vacuum or Schlenk techniques [16]. Solvents were purified and degassed by standard procedures. ^1H NMR chemical shifts are reported in ppm relative to $SiMe_4$ ($\delta = 0$) and were referenced internally with respect to the protio solvent impurity. All coupling constants are reported in Hz. IR spectra were recorded as KBr pellets and are reported in cm^{-1}. C, H, and N elemental analyses were measured using a Perkin–Elmer 2400 CHN Elemental Analyzer. $[Tm^{Ph}]Li$ [4a] and mim^{Ar} [17] were synthesized as previously reported, and $[Tm^{p\text{-}Tol}]Li$ was prepared analogously to $[Tm^{Ph}]Li$.

3.2. Synthesis of $\{[Tm^{Ph}]Zn(mim^{Ph})\}[ClO_4]$

A mixture of $[Tm^{Ph}]Li$ (100 mg, 0.18 mmol), $Zn(ClO_4)_2\cdot 6H_2O$ (69 mg, 0.19 mmol) and mim^{Ph} (33 mg, 0.19 mmol) in MeOH (50 mL) was stirred overnight at room temperature. After this period, the mixture was filtered and the volatile components were removed from the filtrate. The resultant white product was washed with pentane (2×5 mL) and dried in vacuo to give $\{[Tm^{Ph}]Zn(mim^{Ph})\}[ClO_4]$ as a white solid (99 mg, 62%). *Anal.* Calc. for $C_{36}H_{30}N_8S_4BZnClO_4$: C, 49.2; H, 3.4; N, 12.8. Found: C, 49.0; H, 3.3; N, 12.5%. IR data (KBr disk, cm^{-1}): 2423 (ν_{B-H}). ^1H NMR (CD_3CN): 6.82 [br, $HB\{C_3N_2H_2(C_6H_5)S\}_3ZnS\{CN(C_6H_5)C_2H_2NH\}$], 7.02 [br, $HB\{C_3N_2H_2(C_6H_5)S\}_3ZnS\{CN(C_6H_5)C_2H_2NH\}$], 7.24–7.58 [m, $HB\{C_3N_2H_2(C_6H_5)S\}_3ZnS\{CN(C_6H_5)C_2H_2NH\}$], 10.62 [br,$HB\{C_3N_2H_2(C_6H_5)S\}_3ZnS\{CN(C_6H_5)C_2H_2NH\}$]. Crystals for X-ray diffraction were obtained from methanol.

3.3. Synthesis of $\{[Tm^{p\text{-}Tol}]Zn(mim^{p\text{-}Tol})\}[ClO_4]$

A mixture of $Zn(ClO_4)_2\cdot 6H_2O$ (98 mg, 0.26 mmol), $mim^{p\text{-}Tol}$ (50 mg, 0.26 mmol), and $[Tm^{tol}]Li$ (154 mg, 0.26 mmol) in CH_3CN (10 mL) was stirred for four days at room temperature. After this period, the mixture was filtered and the volatile components removed in vacuo from the filtrate. The resultant white product was washed with pentane (2×5 mL) and dried in vacuo to give $\{[Tm^{p\text{-}Tol}]Zn(mim^{p\text{-}Tol})\}[ClO_4]\cdot 3CH_3CN$ as a white solid (158 mg, 57%). *Anal.* Calc. for $C_{46}H_{47}BClN_{11}O_4S_4Zn$: C, 52.2; H, 4.5; N, 14.6. Found: C, 51.8; H, 4.0; N, 14.1%. IR data (KBr disk, cm^{-1}) = 2438 (ν_{B-H}). ^1H NMR (CD_3CN): 2.37 [s, $HB\{C_3N_2H_2(C_6H_4CH_3)S\}_3ZnS\{CN(C_6H_4CH_3)C_2H_2NH\}$], 2.40 [s, $HB\{C_3N_2H_2(C_6H_4CH_3)S\}_3ZnS\{CN(C_6H_4CH_3)C_2H_2NH\}$], 6.63 [d, $^3J_{H-H} = 2$ [3H], $HB\{C_3N_2H_2(C_6H_4CH_3)S\}_3ZnS$-

Table 3
Crystal, intensity collection and refinement data

	$\{[Tm^{Ph}]Zn(mim^{Ph})\}^{-}[ClO_4]\cdot MeOH$	$\{[Tm^{p\text{-}Tol}]Zn\text{-}(mim^{p\text{-}Tol})\}^{+}[ClO_4]\cdot MeOH$	mim^{Ph}
Lattice	triclinic	triclinic	monoclinic
Formula	$C_{37}H_{34}BClN_8O_5S_4Zn$	$C_{41}H_{42}BClN_8O_5S_4Zn$	$C_{10}H_{10}N_2S$
Formula weight	910.59	966.70	190.26
Space group	$P\bar{1}$	$P\bar{1}$	$C2/c$
a (Å)	13.161(3)	13.204(2)	15.851(7)
b (Å)	13.403(3)	13.611(2)	9.656(5)
c (Å)	15.075(4)	15.284(2)	13.026(6)
α (°)	96.273(4)	67.088(3)	90
β (°)	110.776(3)	88.942(3)	97.14(1)
γ (°)	116.257(4)	65.799(3)	90
V (Å^3)	2114.4(8)	2274.9(6)	1978(1)
Z	2	2	8
Temperature (K)	233	233	233
Radiation (λ, Å)	0.71073	0.71073	0.71073
ρ (calcd.) (g cm^{-3})	1.430	1.411	1.278
μ (Mo Kα) (mm^{-1})	0.893	0.834	0.280
θ_{max} (°)	28.2	28.3	28.3
Number of data	9106	10092	2294
Number of parameters	524	564	120
R_1	0.0591	0.0554	0.0482
wR_2	0.1003	0.1113	0.1207
Goodness-of-fit	1.085	1.015	1.029

$\{CN(C_6H_4CH_3)C_2H_2NH\}$], 6.94 [d, $^3J_{H-H} = 2$ [3H], $HB\{C_3N_2H_2(C_6H_4CH_3)S\}_3ZnS\{CN(C_6H_4CH_3)C_2H_2$-NH}], 7.11–7.32 [m, $HB\{C_3N_2H_2(C_6H_4CH_3)S\}_3ZnS$-$\{CN(C_6H_4CH_3)C_2H_2NH\}$], 10.62 [br,$HB\{C_3N_2H_2(C_6H_4CH_3)S\}_3ZnS\{CN(C_6H_4CH_3)C_2H_2NH\}$]. Crystals suitable for X-ray diffraction were obtained from methanol.

3.4. Reaction of $\{[Tm^{Ph}]Zn(mim^{Ph})\}[ClO_4]$ with MeI

A solution of $\{[Tm^{Ph}]Zn(mim^{Ph})\}[ClO_4]$ (ca. 3 mg) in $CDCl_3$ (0.5 mL) was treated with MeI (ca. 2 μl). The reaction was monitored by ^1H NMR spectroscopy, thereby demonstrating the formation of $Tm^{Ph}ZnI$ over a period of 2 days at room temperature.

3.5. Reaction of $\{[Tm^{Ph}]Zn(mim^{Ph})\}[ClO_4]$ with NaI

A solution of $\{[Tn^{Ph}]Zn(mim^{Ph})\}[ClO_4]$ (ca. 3 mg) in $CDCl_3$ (0.5 mL) was treated with NaI (ca. 5 mg). The reaction was monitored by ^1H NMR spectroscopy, thereby demonstrating the immediate formation of $Tm^{Ph}ZnI$.

3.6. Reaction of $\{[Tm^{Ph}]Zn(mim^{Ph})\}[ClO_4]$ with $[Bu_4N]I$

A solution of $\{[Tm^{Ph}]Zn(mim^{Ph})\}[ClO_4]$ (ca. 3 mg) in $CDCl_3$ (0.5 mL) was treated with $[Bu_4N]I$ (ca. 5 mg). The reaction was monitored by ^1H NMR spectroscopy, thereby demonstrating the immediate formation of $Tm^{Ph}ZnI$.

3.7. X-ray structure determination

X-ray diffraction data were collected on a Bruker P4 diffractometer equipped with a SMART CCD detector and crystal data, data collection and refinement parameters are summarized in Table 3. The structures were solved using direct methods and standard difference map techniques, and were refined by full-matrix least-squares procedures on F^2 with SHELXTL (Version 5.03) [18].

3.8. Computational details

All calculations were carried out using DFT as implemented in the Jaguar 4.1 suite of ab initio quantum chemistry programs [19]. Geometry optimization was performed with the B3LYP [20] functional employing 6-31G** (H, B, C, N, O, S) and LAV3P** (Zn) basis sets [21]. The energies of the optimized structures were reevaluated by additional single point calculations on each optimized geometry using the cc-pVTZ(-f) [22] (H, B, C, N, O, S) and LAV3P** (Zn) basis sets [21].

4. Summary

In conclusion, $\{[Tm^{Ph}]Zn(mim^{Ph})\}^{+}$ and $\{[Tm^{p\text{-}Tol}]$-$Zn(mim^{p\text{-}Tol})\}^{+}$ provide examples of tetrahedrally coordinated zinc in a sulfur-ligated environment and, as such, represent models for the structural and functional sites of zinc enzymes and proteins, such as the Ada

DNA repair protein. X-ray diffraction studies demonstrate that the mim^{Ar} ligands are almost orthogonal to the Zn–S–C plane, in contrast to the almost planar arrangement that is calculated for $\{[Tm^{H}]Zn(mim^{H})\}^{+}$ and $\{[Tm^{H}]Zn(mim^{Me})\}^{+}$. The orthogonal arrangement observed experimentally is a consequence of the existence of N–H···O hydrogen bonds between the N–H group of the mim^{Ar} ligand and a molecule of methanol. Evidently, the hydrogen bonding interactions in $\{[Tm^{Ar}]Zn(mim^{Ar})\cdots(HOMe)\}^{+}$ are sufficiently strong to counter the electronic destabilization resulting from rotation of the mim^{Ar} ligand from out of the Zn–S–C plane. The mim^{Ph} ligand of $\{[Tm^{Ph}]Zn(mim^{Ph})\}^{+}$ may be immediately displaced by I^{-} to give $[Tm^{Ar}]ZnI$; however, $\{[Tm^{Ph}]Zn(mim^{Ph})\}^{+}$ does not react rapidly with MeI, thereby demonstrating that the zinc coordinated mim^{Ph} ligand is less susceptible to electrophilic attack than is a zinc thiolate ligand.

5. Supplemental material

The crystallographic data for $\{[Tm^{Ph}]Zn(mim^{Ph})\cdots(HOMe)\}$ $[ClO_4]$ (CCDC #215019), $\{[Tm^{p\text{-}Tol}]Zn(mim^{p\text{-}Tol})\cdots(HOMe)\}[ClO_4]$ (CCDC #215018), and mim^{Ph} (CCDC #215020) have been deposited with the Cambridge Crystallographic Data Centre. Copies of the information may be obtained free of charge from The Director, CCDC, 12 Union Road, Cambridge CB2 1EZ, UK (fax: +44-1223-336033; E-mail: deposit@ccdc.cam.ac.uk or www: http://www.ccdc.cam.ac.uk).

Acknowledgements

We thank the National Institutes of Health (Grant GM46502) for support of this research.

References

[1] (a) B.L. Vallee, D.S. Auld, Acc. Chem. Res. 26 (1993) 543;
(b) D.S. Auld, Struct. Bond. 89 (1997) 29;
(c) J.E. Coleman, Curr. Opin. Chem. Biol. 2 (1998) 222;
(d) S. Rahuel-Clermont, M.F. Dunn, Copper Zinc Inflamm. Degener. Dis. (1998) 47;
(e) R.H. Holm, P. Kennepohl, E.I. Solomon, Chem. Rev. 96 (1996) 2239;
(f) W.N. Lipscomb, N. Sträter, Chem. Rev. 96 (1996) 2375;
(g) S. Lindskog, Pharmacol. Ther. 74 (1997) 1.

[2] (a) S. Iuchi, Cell. Mol. Life Sci. 258 (2001) 625;
(b) J.M. Berg, Y. Shi, Science 271 (1996) 1081;
(c) J.H. Laity, B.M. Lee, P.E. Wright, Curr. Opin. Struct. Biol. 11 (2001) 39;
(d) J.M. Berg, H.A. Godwin, Annu. Rev. Biophys. Biomol. Struct. 26 (1997) 357.

[3] (a) G. Parkin, in: A. Sigel, H. Sigel (Eds.), Met. Ions Biol. Syst., vol. 38, Marcel Dekker, New York, 2001, p. 411 (Ch. 14);
(b) G. Parkin, Chem. Commun. (2000) 1971;
(c) H. Vahrenkamp, Acc. Chem. Res. 32 (1999) 589;
(d) H. Vahrenkamp, Bioinorganic Chemistry – Transition Metals in Biology and their Coordination Chemistry, Wiley–VCH, Weinheim, 1997, pp. 540–551;
(e) E. Kimura, E. Kikuta, J. Biol. Inorg. Chem. 5 (2000) 139.

[4] (a) C. Kimblin, B.M. Bridgewater, D.G. Churchill, G. Parkin, Chem. Commun. (1999) 2301;
(b) B.M. Bridgewater, G. Parkin, J. Am. Chem. Soc. 122 (2000) 7140;
(c) B.M. Bridgewater, G. Parkin, Inorg. Chem. Commun. 4 (2001) 126;
(d) B.M. Bridgewater, T. Fillebeen, R.A. Friesner, G. Parkin, J. Chem. Soc., Dalton Trans. (2000) 4494.

[5] (a) J.J. Wilker, S.J. Lippard, Inorg. Chem. 36 (1997) 969;
(b) J.J. Wilker, S.J. Lippard, J. Am. Chem. Soc. 117 (1995) 8682;
(c) U. Brand, M. Rombach, H. Vahrenkamp, Chem. Commun. (1998) 2717;
(d) R. Burth, H. Vahrenkamp, Z. Anorg. Allg. Chem. 624 (1998) 381;
(e) C.A. Grapperhaus, T. Tuntulani, J.H. Reibenspies, M.Y. Darensbourg, Inorg. Chem. 37 (1998) 4052;
(f) B.S. Hammes, C.J. Carrano, Chem. Commun. (2000) 1635;
(g) C.R. Warthen, B.S. Hammes, C.J. Carrano, D.C. Crans, J. Biol. Inorg. Chem. 6 (2001) 82;
(h) J.N. Smith, Z. Shirin, C.J. Carrano, J. Am. Chem. Soc. 125 (2003) 868;
(i) S.J. Chiou, C.G. Riordan, A.L. Rheingold, Proc. Natl. Acad. Sci. USA 100 (2003) 3695.

[6] (a) L.C. Myers, M.P. Terranova, A.E. Ferentz, G. Wagner, G.L. Verdine, Science 261 (1993) 1164;
(b) L.C. Myers, F. Jackow, G.L. Verdine, J. Biol. Chem. 270 (1995) 6664.

[7] (a) A. Silver, S.A. Koch, M. Millar, Inorg. Chim. Acta 205 (1993) 9;
(b) L.E. Maelia, M. Millar, S.A. Koch, Inorg. Chem. 31 (1992) 4594;
(c) S.A. Koch, L.E. Maelia, M. Millar, J. Am. Chem. Soc. 105 (1983) 5944.

[8] D. Coucouvanis, D. Swenson, N.C. Baenziger, C. Murphy, D.G. Holah, N. Sfarnas, A. Simopoulos, A. Kostikas, J. Am. Chem. Soc. 103 (1981) 3350.

[9] D. Swenson, N.C. Baenziger, D. Coucouvanis, J. Am. Chem. Soc. 100 (1978) 1932.

[10] N. Ueyama, T. Sugawara, K. Sasaki, A. Nakamura, S. Yamashita, Y. Wakatsnki, H. Yamazaki, N. Yasuoka, Inorg. Chem. 27 (1988) 741.

[11] J. Otto, I. Jolk, T. Viland, R. Wonnemann, B. Krebs, Inorg. Chim. Acta 285 (1999) 262.

[12] (a) Other comparisons include $[Zn\{SC(NH_2)_2\}_4]^{2+}$ (100°–122°)[a] and $[Zn(N\text{-methyl-2-thioxopyrrolidine})_4]^{2+}$ (106°–115°)[b] R. Vega, A. Lopezcastro, R. Marquez, Acta Crystallogr. Sect. B: Struct. Commun. 34 (1978) 2297;
(b) A. Wilk, M.A. Hitchman, W. Massa, D. Reinen, Inorg. Chem. 32 (1993) 2483.

[13] (a) Examples of zinc complexes with intramolecular N–H···S interactions include $[Ph(pz^{Bu^t})Bt^{Bu^t}]ZnS[C_6H_4\text{-}o\text{-}NHC(O)Bu^t]$,[a] $Zn[S\text{–}2\text{–}C_6H_4N(H)C(O)Ph]_2(1\text{–}MeImH)_2$,[b] $[Tm^{Ph}]ZnSCH_2C(O)N(H)Ph$,[c] $[HC(pz^{Me_2})_2(C_6H_2MePr^iO)]ZnS[C_6H_4\text{-}o\text{-}NHC(O)Me]$,[d] and $[HC(pz^{Me_2})_2(Me_2CS)]ZnS$ $[C_6H_4\text{-}o\text{-}NHC(O)Me]$.[d]
(a) Ref. [5i];
(b) W.Y. Sun, L. Zhang, K.B. Yu, J. Chem. Soc., Dalton Trans. (1999) 795;
(c) D. Quarless, M.M. Morlok, K.E. Janak, G. Zhu, G. Parkin, unpublished results;
(d) Ref. [5h].

[14] (a) H.T. Flakus, A. Miros, P.G. Jones, Spectrochim. Acta Part A 58 (2002) 225;
(b) G. Vampa, S. Benvenuti, F. Severi, L. Malmusi, L. Antolini, J. Heterocyclic Chem. 32 (1995) 227.
[15] Uncoordinated imidazole-2-thiones are known to be alkylated at sulfur by alkyl halides. See [14b] and S. Laufer, G. Wagner, D. Kotschenreuther, Angew. Chem., Int. Ed. Engl. 41 (2002) 2290.
[16] (a) J.P. McNally, V.S. Leong, N.J. Cooper, in: A.L. Wayda, M.Y. Darensbourg (Eds.), Experimental Organometallic Chemistry, American Chemical Society, Washington, DC, 1987, p. 6 (Ch. 2);
(b) B.J. Burger, J.E. Bercaw, in: A.L. Wayda, M.Y. Darensbourg (Eds.), Experimental Organometallic Chemistry, American Chemical Society, Washington, DC, 1987, p. 79 (Ch. 4);
(c) D.F. Shriver, M.A. Drezdzon, The Manipulation of Air-sensitive Compounds, 2nd ed., Wiley–Interscience, New York, 1986.
[17] K. Matsuda, I. Yanagisawa, Y. Isomura, T. Mase, T. Shibanuma, Synth. Commun. 2 (1997) 3565.
[18] G.M. Sheldrick, SHELXTL, An Integrated System for Solving, Refining and Displaying Crystal Structures from Diffraction Data, University of Göttingen, Göttingen, Germany, 1981.
[19] Jaguar 4.1 Schrödinger, Inc., Portland, OR, 2001.
[20] (a) J.C. Slater, Quantum Theory of Molecules and Solids, The Self-consistent Field for Molecules and Solids, vol. 4, McGraw-Hill, New York, 1974;
(b) S.H. Vosko, L. Wilk, M. Nusair, Can. J. Phys. 58 (1980) 1200;
(c) C.T. Lee, W.T. Yang, R.G. Parr, Phys. Rev. B 37 (1988) 785;
(d) A.D. Becke, Phys. Rev. A 38 (1988) 3098;
(e) A.D. Becke, J. Chem. Phys. 98 (1993) 5648.
[21] (a) P.J. Hay, W.R. Wadt, J. Chem. Phys. 82 (1985) 299;
(b) W.R. Wadt, P.J. Hay, J. Chem. Phys. 82 (1985) 284;
(c) P.J. Hay, W.R. Wadt, J. Chem. Phys. 82 (1985) 270.
[22] T.H. Dunning, J. Chem. Phys. 90 (1989) 1007.

Available online at www.sciencedirect.com
SCIENCE DIRECT®
Polyhedron 23 (2004) 489–497
POLYHEDRON
www.elsevier.com/locate/poly

Platinum-alkyl and hydride complexes supported by a tris(phosphino)borate ligand: structural and spectroscopic studies

J. Christopher Thomas, Jonas C. Peters *

Division of Chemistry and Chemical Engineering, Arnold and Mabel Beckman Laboratories of Chemical Synthesis, California Institute of Technology, Pasadena, CA 91125, USA

Received 30 July 2003; accepted 8 October 2003

Abstract

The synthesis and characterization of platinum-methyl and hydride complexes containing the ligand [$PhBP_3$] ([$PhBP_3$] = [$PhB(CH_2PPh_2)_3]^-$) are described. Metalation of [$PhBP_3$][TBA] (**1[TBA]**, [TBA] = [$^nBu_4N]^+$) with platinum methyl precursors provided the corresponding phosphine methyl platinum species [$PhBP_3$]$PtMe_3$ (**2**) and [[κ^2-$PhBP_3$]$PtMe_2$][TBA] (**3**). The reactivity of octahedral **2** and square planar **3** are discussed, and their X-ray diffraction structures are reported. Octahedral Pt(IV) **2** was found to be very thermally and chemically robust. In contrast, the square planar Pt(II) complex **3** demonstrated reactivity at both the platinum center and the unbound phosphine. The reaction of **3** with one equivalent of elemental sulfur provided the corresponding phosphine-sulfide [[κ^2-$PhB(CH_2P(S)Ph_2)(CH_2PPh_2)_2$]$PtMe_2$][TBA] (**4**). Similarly, the reaction of **3** with one equivalent of $BH_3 \cdot SMe_2$ generated the borane-protected complex [[κ^2-$PhB(CH_2P(BH_3)Ph_2)(CH_2PPh_2)_2$]$PtMe_2$][TBA] (**5**). Complex **5** was significantly less reactive than **3** to a variety of substrates under similar conditions; however, the reaction of **5** with additional $BH_3 \cdot SMe_2$ resulted in the formation of the platinum(I) bridged hydride species [[κ^2-$PhB(CH_2P(BH_3)Ph_2)(CH_2PPh_2)_2$]Pt($\mu$-H)]$_2$[TBA]$_2$ (**6**).
© 2003 Elsevier Ltd. All rights reserved.

Keywords: Zwitterions; Monoanionic ligands; Syntheses; Structures; Methyl; Hydrides

1. Introduction

Trofimenko's tris(pyrazolyl)borate ligands [1] have been widely used in mechanistic C–H activation studies. Several studies of the noble group 9 metals (Rh and Ir) have exploited the scorpionates, such as the recent works of Bergman and Harris [2], as well as that of Jones [3]. Important advances in [Tp]-supported platinum C–H activation chemistry have also emerged ([Tp] = hydrotris(pyrazolyl)borate, $[HB(pz)_3]^-$). For example, in an elegant experiment, Goldberg's group showed that the anionic complex K[[κ^2-Tp_2^{Me}]$PtMe_2$] ([Tp_2^{Me}] = hydrotris(3,5-dimethylpyrazolyl)borate) reacts with $B(C_6F_5)_3$ to generate an unobserved, presumed 3-coordinate species, "[κ^2-Tp_2^{Me}]PtMe", that then undergoes oxidative C–H bond addition to afford octahedral platinum(IV) alkyl hydride products, [κ^3-Tp_2^{Me}]Pt(Me)(R)H [4]. A number of interesting studies have followed this early report, including the isolation of a well-defined five-coordinate Pt(IV) species [5], a rare η^2-benzene adduct of platinum(II) [6], and mechanistic investigations of reductive elimination from platinum(IV) [7,8]. Given the considerable momentum behind [Tp]-supported C–H activation studies, it seemed prudent to us to begin examining other tripodal borate ligands for comparison [9]. We have therefore begun to develop the platinum chemistry of a related class of tris(phosphino)borate ligands. These latter ligands resemble the classic scorpionates by virtue of having three donor arms anchored by a borate unit so that they bind most typically in a tripodal fashion. Despite these similarities, the (phosphino)borates appear to be electronically, as well as sterically, quite distinct from [Tp]-type ligands. For example, the monoanionic (phosphino)borate complexes of platinum feature an anionic borate unit that is more spacially separated from the coordinated platinum center in both κ^3- and κ^2-binding modes

* Corresponding author.
E-mail address: jpeters@caltech.edu (J.C. Peters).

0277-5387/$ - see front matter © 2003 Elsevier Ltd. All rights reserved.
doi:10.1016/j.poly.2003.11.036

by comparison to structurally related [Tp] complexes (vide infra). Moreover, the absence of simple resonance contributors that would efficiently distribute the anionic borate charge in these (phosphino)borate complexes suggests that they can be reasonably regarded as molecular "zwitterions" [10]. Such a descriptor is not typically attributed to [Tp]-supported complexes, where resonance delocalization of the borate charge is normally presumed [11].

In the present study, we describe for the first time aspects of the platinum coordination chemistry of the tris(phosphino)borate ligand $[PhB(CH_2PPh_2)_3]^-$ (**1**, $[PhBP_3]$). We report on the synthesis and characterization of several methyl and hydride complexes of platinum supported by **1** and emphasize the electronic contribution that the anionic phosphine ligand provides.

2. Experimental

2.1. General

Unless otherwise noted, all syntheses were carried out under a dinitrogen atmosphere in the absence of water and dioxygen, using standard Schlenk or glovebox techniques. Acetonitrile, tetrahydrofuran, diethyl ether, dichloromethane, toluene, benzene, and petroleum ether were deoxygenated and dried by thorough sparging with N_2 gas followed by passage through an activated alumina column. Pentane and hexanes were deoxygenated by repeated evacuation under reduced pressure followed by introduction of dinitrogen and were dried by storing over 3-Å molecular sieves. Hydrocarbon and ethereal solvents were typically tested with a standard purple solution of sodium benzophenone ketyl in tetrahydrofuran in order to confirm effective oxygen and moisture removal. Ethanol and acetone were dried and distilled over calcium sulfate under dinitrogen. Morpholine and TMEDA were dried and distilled from CaH_2 under dinitrogen. Deuterated chloroform, benzene, dichloromethane, THF, acetonitrile, and acetone were purchased from Cambridge Isotope Laboratories, Inc. and were degassed by repeated freeze–pump–thaw cycles and dried over activated 3-Å molecular sieves prior to use. $[PhBP_3][Li(TMEDA)]$ [9a] and $(COD)PtMe_2$ [12] were prepared by literature methods. All other chemicals were purchased from commercial vendors and used without further purification. NMR spectra were recorded on Varian Mercury 300 MHz and Inova 500 MHz, and Joel 400 MHz spectrometers at ambient temperature, unless otherwise noted. ^1H and $^{13}C\{^1H\}$ chemical shifts were referenced to residual solvent as determined relative to Me_4Si (0 ppm). $^{31}P\{^1H\}$ NMR, $^{11}B\{^1H\}$ NMR, and $^{19}F\{^1H\}$ NMR chemical shifts are reported relative to an external standard (0 ppm) of 85% H_3PO_4, neat $BF_3 \cdot Et_2O$, and neat $CFCl_3$ respectively. Abbreviations for reported signal multiplicities are as follows: s, singlet; d, doublet; t, triplet; q, quartet; m, multiplet; br, broad. IR spectra were recorded at 4 cm^{-1} resolution on a Bio-Rad Excalibur FTS 3000 spectrometer controlled by Win-IR Pro software using either a KBr solution cell or KBr plates. Elemental analyses were performed by Desert Analytics, Tucson, AZ. X-ray diffraction experiments were carried out by the Beckman Institute Crystallographic Facility on a Bruker SMART 1000 CCD diffractometer.

2.2. Syntheses of complexes

2.2.1. $[PhB(CH_2PPh_2)_3][^nBu_4N]$ (**1[TBA]**, $[PhBP_3][TBA]$)

The previously reported compound $[PhBP_3][Li(TMEDA)]$ [9] (20.987 g, 25.952 mmol) was dissolved in MeOH in air (50 mL). The methanolic solution was quickly filtered through diatomaceous earth and added slowly to tetra-*n*-butyl ammonium bromide (9.603 g, 28.55 mmol) dissolved in water (300 mL), yielding a white gelatinous solid which dispersed into a coarse chunky powder upon addition of Et_2O (40 mL). The mixture was stirred for 5 min, and then the solids were collected by filtration and washed sequentially with water (30 mL), Et_2O (30 mL), water (30 mL), and Et_2O (30 mL). The resulting white solids were dissolved in acetonitrile (100 mL), yielding a somewhat cloudy yellowish solution which was dried by stirring the reaction mixture over sodium sulfate for 10 min. The solution was then filtered over diatomaceous earth affording a clear yellow solution, which was concentrated by rotary evaporation and triturated with Et_2O, yielding white solid **1[TBA]** (16.453 g, 67.3%). This compound is not air or moisture stable and should be stored under inert atmosphere. ^1H NMR (400 MHz, CD_3CN): δ 7.48 (br, 2H, [*ortho*-$C_6H_5BP_3$]), 7.22 (m, 12H, aryl protons), 7.13 (m, 18H, aryl protons), 6.86 (t, 2H, [*meta*-$C_6H_5BP_3$]), 6.74 (t, 1H, [*para*-$C_6H_5BP_3$]), 3.04 (m, 8H, $[(CH_3CH_2CH_2CH_2)_4N]$), 1.57 (m, 8H, $[(CH_3CH_2CH_2CH_2)_4N]$), 1.33 (m, 8H, $[(CH_3CH_2CH_2CH_2)_4N]$), 1.08 (br, 6H, $[PhB(CH_2PPh_2)_3]$), 0.96 (t, 12H, $[(CH_3CH_2CH_2CH_2)_4N]$). $^{31}P\{^1H\}$ NMR (161.9 MHz, CD_3CN): δ −11.31. *Anal.* Calc. for $C_{62}H_{79}BNP_3$: C, 79.05; H, 8.45; N, 1.49. Found: C, 79.36; H, 8.52; N, 1.37%.

2.2.2. $[PhBP_3]PtMe_3$ (**2**)

Solid off-white $[PhBP_3][TBA]$ (263.6 mg, 0.2840 mmol) and $IPtMe_3$ (104.5 mg, 0.2847 mmol) were dissolved in THF (7 mL). The reaction mixture was stirred for 2 h and then concentrated to 4 mL. Upon standing, white solids precipitated. The supernatant was decanted, and the solids were dried under reduced pressure. Benzene (6 mL) was added, and the reaction mixture was stirred for 10 min. The cloudy solution was filtered, and volatiles were removed under reduced pressure from the

resulting solution, providing white solid **2** (193.2 mg, 73.5%). Clear, colorless block crystals suitable for X-ray diffraction were obtained from pentane diffusion into a THF solution of **2**. ^{1}H NMR (300 MHz, C_6D_6): δ 7.90 (d, 2H, [*ortho*-$C_6H_5BP_3$]), 7.54 (t, 2H, [*meta*-$C_6H_5BP_3$]), 7.36 (m, 13H, aryl protons), 6.85 (m, 18H, aryl protons), 2.01 (br, 6H, [PhB(CH_2PPh_2)$_3$]), 1.35 (d, 9H, Pt(CH_3)$_3$, $^2J_{Pt-H} = 55.5$ Hz, $^3J_{P-H} = 7.2$ Hz). ^{13}C{^{1}H} NMR (125.7 MHz, C_6D_6): δ 136.9, 133.9, 132.4, 129.5, 128.9, 124.9, 15.8 (br, [PhB(CH_2PPh_2)$_3$]), 6.5 (dd, Pt(CH_3)$_3$, $^1J_{Pt-C} = 497$ Hz, $^2J_{P-C} = 11$, 111 Hz). ^{31}P{^{1}H} NMR (121.4 MHz, C_6D_6): δ −26.01 ($^1J_{Pt-P} = 1094$ Hz). ^{11}B{^{1}H} NMR (128.3 MHz, C_6D_6): δ −11.9. *Anal.* Calc. for $C_{48}H_{50}BP_3Pt$: C, 62.28; H, 5.44. Found: C, 62.44; H, 5.67%.

2.2.3. [[κ^2-PhBP$_3$]PtMe$_2$][TBA] (3)

Solid off-white [PhBP$_3$][TBA] (1.6076 g, 1.732 mmol) was dissolved in THF (8 mL). A solution of (COD)PtMe$_2$ (577.0 mg, 1.731 mmol) dissolved in THF (1 mL) was added to the stirring [PhBP$_3$][TBA] solution, forming a colorless to pale yellow solution. After stirring the reaction mixture for 4 h, the volume of the reaction was reduced by removal of volatiles under reduced pressure. Precipitation with pentane produced off-white to pale yellow solids which were repeatedly triturated with pentane. Drying the solids under reduced pressure resulted in off-white to pale yellow solid **3** (1.8024 g, 90.3%). Clear, colorless rectangular prism crystals suitable for X-ray diffraction were grown by slow evaporation of a saturated toluene solution of **3**. ^{1}H NMR (300 MHz, acetone-d$_6$): δ 7.64 (br, 4H), 7.44 (br, 4H), 6.86–7.28 (m, 24H), 6.63 (m, 3H), 3.36 (m, 8H, [($CH_3CH_2CH_2CH_2$)$_4$N]), 1.76 (m, 8H, [($CH_3CH_2CH_2CH_2$)$_4$N]), 1.55 (br, 4H, [[PhB(CH_2PPh_2)(CH_2PPh_2)$_2$]PtMe$_2$]), 1.39 (m, 8H, [($CH_3CH_2CH_2CH_2$)$_4$N]), 0.96 (t, 12H, [($CH_3CH_2CH_2CH_2$)$_4$N]), 0.65 (br, 2H, [[PhB(CH_2PPh_2)(CH_2PPh_2)$_2$]PtMe$_2$]), 0.08 (t, 6H, Pt(CH_3)$_2$, $^2J_{Pt-H} = 67$ Hz, $^3J_{P-H} = 5$ Hz). ^{13}C{^{1}H} NMR (125.7 MHz, acetone-d$_6$): δ 122–148 (aryl carbons), 59.9 ([($CH_3CH_2CH_2CH_2$)$_4$N]), 25.0 ([($CH_3CH_2CH_2CH_2$)$_4$N]), 24 (br), 21.0 ([($CH_3CH_2CH_2CH_2$)$_4$N]), 14.6 ([($CH_3CH_2CH_2CH_2$)$_4$N]), 6.7 (Pt(CH_3)$_2$, $^1J_{Pt-C} = 616$ Hz, $^2J_{P-C} = 8.8$, 103 Hz). ^{31}P{^{1}H} NMR (121.4 MHz, acetone-d$_6$): δ 18.96 (s, 2P, $^1J_{Pt-P} = 1888$ Hz), −9.61 (s, 0.12P), −12.60 (s, 0.88P). ^{11}B{^{1}H} NMR (160.4 MHz, acetone-d$_6$): δ −14.10. *Anal.* Calc. for $C_{63}H_{83}BNP_3Pt$: C, 65.86; H, 7.34; N, 1.20. Found: C, 65.51; H, 7.29; N, 1.06%.

2.2.4. [[κ^2-PhB($CH_2P(S)Ph_2$)(CH_2PPh_2)$_2$]PtMe$_2$][TBA] (4)

Solid **3** (159.0 mg, 0.1379 mmol) was dissolved in THF (2 mL). While stirring the reaction mixture, a suspension of elemental sulfur (4.6 mg, 0.14 mmol of S atoms) in THF (1 mL) was added to the reaction. After 1h, the sulfur had been visibly consumed and the reaction changed color from colorless to yellow. The reaction mixture was filtered, and volatiles were removed under reduced pressure, providing pale yellow solid **4** (160.7 mg, 97.2%) in > 95% purity. Analytically pure **4** has not yet been isolated. ^{1}H NMR (300 MHz, acetone-d$_6$): δ 7.62 (br, 4H), 7.46 (br, 4H), 6.8–7.3 (m, 24H), 6.62 (m, 3H), 3.36 (m, 8H, [($CH_3CH_2CH_2CH_2$)$_4$N]), 1.76 (m, 8H, [($CH_3CH_2CH_2CH_2$)$_4$N]), 1.6 (br, 4H, [[PhB($CH_2P(S)Ph_2$)(CH_2PPh_2)$_2$]PtMe$_2$]), 1.39 (m, 8H, [($CH_3CH_2CH_2CH_2$)$_4$N]), 0.96 (t, 12H, [($CH_3CH_2CH_2CH_2$)$_4$N]), 0.73 (br, 2H, [[PhB($CH_2P(S)Ph_2$)(CH_2PPh_2)$_2$]PtMe$_2$]), 0.07 (t, 6H, Pt(CH_3)$_2$, $^2J_{Pt-H} = 68$ Hz, $^3J_{P-H} = 5$ Hz). ^{31}P{^{1}H} NMR (121.4 MHz, acetone-d$_6$): δ 44.44 (s, 1P), 18.37 (s, 2P, $^1J_{Pt-P} = 1875$ Hz).

2.2.5. [[κ^2-PhB($CH_2P(BH_3)Ph_2$)(CH_2PPh_2)$_2$]PtMe$_2$][TBA] (5)

Solid **3** (241.2 mg, 0.2092 mmol) was added to a fresh 2 M solution of $BH_3 \cdot SMe_2$ (104.6 μL, 0.2092 mmol) in toluene/THF. After 5 min, concentration of the reaction mixture under reduced pressure followed by addition of petroleum ether precipitated solid **5**. Analytically pure **5** was obtained from repeated washing of the solids with petroleum ether (237.6 mg, 97.3%). ^{1}H NMR (500 MHz, CD_2Cl_2): δ 7.72, 7.49, 7.0–7.4, 6.95, 6.54 (m, 35H, aryl protons), 2.96 (m, 8H, [($CH_3CH_2CH_2CH_2$)$_4$N]), 1.50 (m, 8H, [($CH_3CH_2CH_2CH_2$)$_4$N]), 1.35 (m, 8H, [($CH_3CH_2CH_2CH_2$)$_4$N]), 0.99 (t, 12H, [($CH_3CH_2CH_2CH_2$)$_4$N]), 0.04 (t, 6H, Pt(CH_3)$_2$, $^2J_{Pt-H} = 67$ Hz, $^3J_{P-H} = 5.5$ Hz). ^{13}C{^{1}H} NMR (125.7 MHz, CD_2Cl_2): δ 161 (br), 140.1 (m), 137.5 (d), 137.2 (d), 134.7 (m), 133.9 (m), 133.3, 132.4 (d), 129.0, 128.4, 128.0, 127.8 (d), 127.5, 127.1, 125.5, 122.3, 59.3 ([($CH_3CH_2CH_2CH_2$)$_4$N]), 24.3 ([($CH_3CH_2CH_2CH_2$)$_4$N]), 23.5 (br), 22.5 (br), 20.2 ([($CH_3CH_2CH_2CH_2$)$_4$N]), 13.9 ([($CH_3CH_2CH_2CH_2$)$_4$N]), 5.1 (dd, Pt(CH_3)$_2$, $^1J_{Pt-C} = 602$ Hz, $^2J_{P-C} = 9.1$, 102 Hz). ^{31}P{^{1}H} NMR (121.4 MHz, CD_2Cl_2): δ 18.01 (s, 2P, $^1J_{Pt-P} = 1878$ Hz), 15.30 (br, 1P). ^{11}B{^{1}H} NMR (160.4 MHz, CD_2Cl_2): δ −14.8, −30.3. *Anal.* Calc. for $C_{63}H_{86}B_2NP_3Pt$: C, 65.09; H, 7.51; N, 1.19. Found: C, 64.69; H, 7.53; N, 1.02%.

2.2.6. [[κ^2-PhB($CH_2P(BH_3)Ph_2$)(CH_2PPh_2)$_2$]Pt(μ-H)]$_2$[TBA]$_2$ (6)

Solid **3** (277.4 mg, 0.2377 mmol) was dissolved in THF (2 mL). While stirring the reaction mixture, a fresh 2 M solution of $BH_3 \cdot SMe_2$ in toluene/THF was added (250 μL, 0.500 mmol). After 15 min, the solution was concentrated to dryness under reduced pressure. The resulting solids were washed with petroleum ether [5 × 2 mL] and dried under reduced pressure, providing analytically pure **6** (268.4 mg, 99.2%). ^{1}H NMR (500 MHz, C_6D_6): δ 7.97 (br), 7.83 (m), 7.76 (br), 7.54 (br), 7.45 (d), 7.04 (br), 6.93 (m), (m, 35H, aryl protons), 2.66 (m, 8H, [($CH_3CH_2CH_2CH_2$)$_4$N]), 2.10 (br, 4H), 1.61 (br, 2H),

1.15 (m, 16H, [($CH_3CH_2CH_2CH_2$)$_4$N] and [(CH_3CH_2 CH_2CH_2)$_4$N]), 0.84 (t, 12H, [($CH_3CH_2CH_2CH_2$)$_4$N]), −3.17 (“quintet of quintets”, 2H, $[Pt(\mu-H)]_2$, $^1J_{Pt-H} = 464$ Hz, $^2J_{P-H} = 40$ Hz). $^{13}C\{^1H\}$ NMR (125.7 MHz, C_6D_6): δ 161 (br), 142.5 (br d), 141.3 (br d), 138.2 (d), 137.5 (d), 134.6 (br m), 134.2 (d), 134.0, 133.2 (d), 133.0 (d), 129.4, 128.9 (m), 127.9 (m), 126.5, 123.1, 58.8 ([($CH_3CH_2CH_2CH_2$)$_4$N]), 24.4 ([($CH_3CH_2CH_2$ CH_2)$_4$N]), 20.2 ([($CH_3CH_2CH_2CH_2$)$_4$N]), 20 (br), 14.3 ([($CH_3CH_2CH_2CH_2$)$_4$N]). $^{31}P\{^1H\}$ NMR (121.4 MHz, C_6D_6): δ 25.69 (s, 2P, $^1J_{Pt-P} = 2959$ Hz, $^2J_{Pt-P} = 168$ Hz), 16.06 (br, 1P). $^{11}B\{^1H\}$ NMR (160.4 MHz, C_6D_6): δ −15.3, −31.1. ES–MS (CH_3CN, anion observe): Calc. for $[C_{90}H_{90}B_4P_6Pt_2]^{2-}$: 1790.5, found: 1790.9 [$M^{2-} + H^+$], 1777.1 [$M^{2-} + H^+ - BH_3$], 1763.3 [$M^{2-} + H^+ - 2BH_3$]. IR (Nujol, cm^{-1}): ν 2368 ($R_3P{:}BH_3$), 2003 (Pt-*H*), 1966 (Pt-*H*). IR (THF, cm^{-1}): ν 2378 ($R_3P{:}BH_3$), 2010 (Pt-*H*), 1969 (Pt-*H*). *Anal.* Calc. for $C_{122}H_{162}B_4N_2P_6Pt_2$: C, 64.64; H, 7.26; N, 1.22. Found: C, 64.26; H, 7.26; N, 1.46%.

2.3. X-ray crystallography

Single crystals of **2** and **3** were grown as described and were mounted on a glass fiber with Paratone N (Exxon) and transferred to the 98 K cold stream of a Bruker CCD X-ray diffraction system controlled by the SMART (v5.060) software package. Collected data were processed using SAINT+ (v6.02). No empirical absorption corrections were calculated. Structures were solved either by direct or Patterson methods using the XS program, followed by difference Fourier methods and refinements carried out with SHELXTL, both part of the SHELXTL software package (v5.1). Non-hydrogen atoms were refined anisotropically by a series of least-squares cycles. All hydrogen atoms were assigned idealized positions and refined isotropically. Crystallographic information is provided in Table 1, and interatomic distances and angles are contained in Table 2.

3. Results and discussion

3.1. Synthesis of a platinum(IV) trimethyl complex

The tridentate phosphine ligand **1** was initially reported as the lithium(TMEDA) salt, [$PhB(CH_2PPh_2)_3$][Li(TMEDA)] (**1[Li(TMEDA)]**) [9a]. Salt metathesis protocols developed in our laboratories have resulted in the useful thallium adduct, [$PhB(CH_2PPh_2)_3$]Tl (**1[Tl]**) [13] and the tetra(*n*-butyl)ammonium salt, [$PhB(CH_2$ $PPh_2)_3$][TBA] (**1[TBA]**) [14]. For the ensuing discussion of platinum chemistry supported by **1**, it was found that **1[TBA]** resulted in clean substitution onto platinum starting materials.

Table 1
Crystal data and refinement parameters of **2 · THF** and **3**

Compound	[$PhBP_3$]$PtMe_3 \cdot THF$ (**2 · THF**)	[[κ^2-$PhBP_3$]$PtMe_2$][TBA] (**3**)
Empirical formula	$C_{48}H_{41}BP_3Pt \cdot C_4H_8O$	$C_{63}H_{83}BNP_3Pt$
Formula weight	925.72 · 72.11	1153.15
Crystal description	colorless block	colorless fragment
Crystal size (mm)	0.19 × 0.15 × 0.15	0.33 × 0.11 × 0.07
Crystal system	triclinic	monoclinic
Space group	$P\bar{1}$ (#2)	$P2_1/n$ (#14)
Unit cell dimensions		
a (Å)	12.1517(8)	10.656(3)
b (Å)	13.4760(9)	26.546(6)
c (Å)	15.218(1)	20.462(5)
α (°)	88.345(1)	90
β (°)	67.998(1)	95.821(4)
γ (°)	71.325(1)	90
V (Å^3)	2177.1(2)	5758(2)
Z	2	4
D_{calc} (g cm^{-3})	1.522	1.330
Absorption coefficient (mm^{-1})	3.372	2.559
T (K)	98	98
Radiation λ (Å)	0.71073	0.71073
Reflections collected	40 405	90 893
Unique data/parameters	10 339/526	13 924/628
R_1, wR_2, [$I > 2\sigma(I)$]	0.0263, 0.0557	0.0695, 0.1258
Goodness-of-fit	1.065	1.209
Largest difference peak and hole (e Å^{-3})	1.597 and −0.718	4.398 and −4.510

$R_1 = \sum ||F_o| - |F_c|| / \sum |F_o|$, $wR_2 = \{\sum[w(F_o^2 - F_c^2)^2] / \sum[w(F_o^2)^2]\}^{1/2}$.

Table 2
Selected interatomic distances (Å) and angles (°) for **2**·**THF** and **3**

2·**THF**		**3**	
Interatomic distances (Å)			
Pt1–C46	2.114(3)	Pt–C46	2.082(8)
Pt1–C47	2.112(3)	Pt–C47	2.096(6)
Pt1–C48	2.107(3)	Pt–P1	2.271(2)
Pt1–P1	2.4044(7)	Pt–P2	2.282(2)
Pt1–P2	2.3976(7)	Pt–B	4.058(8)
Pt1–P3	2.4307(7)		
Pt1–B	3.640(3)		
Bond angles (°)			
P–Pt–P (average)	88.33	P2–Pt–P3	90.28(6)
C–Pt–C (average)	82.98	C46–Pt–C47	85.5(3)
C–Pt–P (average)	94.29	C46–Pt–P1	90.9(2)
		C47–Pt–P2	93.2(2)

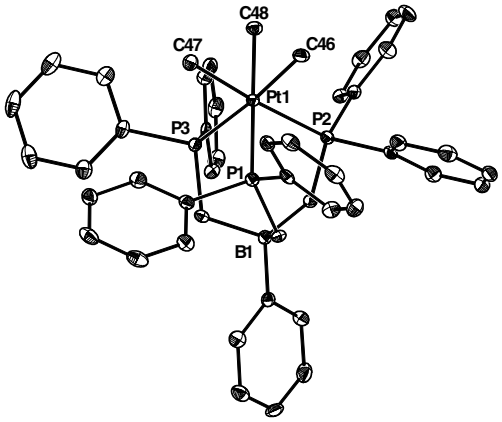

Fig. 1. A 50% displacement ellipsoid representation of **2**·**THF**. Hydrogen atoms and THF molecule are omitted for clarity.

Reaction of **1[TBA]** in THF with $IPtMe_3$ led to the formation of a single product, $[PhBP_3]PtMe_3$ (**2**), as a colorless, neutral, octahedral Pt(IV) complex Eq. (1). In solution, **2** exhibited C_{3v} symmetry. Protons on the platinum-methyl groups showed coupling to both platinum ($^2J_{Pt-H} = 55.5$ Hz) and phosphorus ($^3J_{P-H} = 7.2$ Hz) in the ^1H NMR spectrum. Similarly, platinum coupling was seen for the ligand phosphines in the $^{31}P\{^1H\}$ NMR spectrum ($^1J_{Pt-P} = 1094$ Hz). Interestingly, the only other *fac*-platinum trimethyl complex supported by trialkyl phosphines that has been reported in the literature is $[(Me_2PhP)_3PtMe_3][PF_6]$ [15].

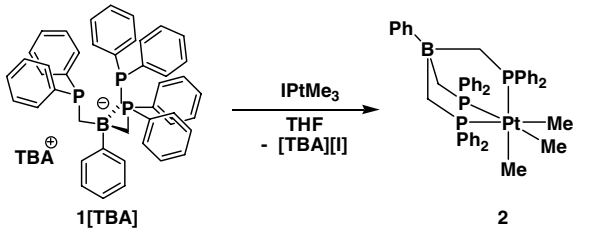

1[TBA] 2 (1)

An X-ray diffraction study carried out on a single crystal of **2** verified the structure (Fig. 1). The X-ray structure of **2** shows the tridentate *fac* coordination of ligand **1**, with P–Pt–P bond angles being very close to 90°. Space-filling models of **2** derived from the crystallographic data show that the phosphino-phenyl groups provide sufficient steric bulk to force the platinum-methyl groups slightly away from octahedral, as evidenced by the average C–Pt–C bond angle of 83.0°. Complex **2** is very robust, being stable to air, moisture, aqueous mineral acids (e.g., 12M HCl (aq)), strong Lewis acids (e.g., $B(C_6F_5)_3$, $[Ph_3C][BF_4]$), and reductants such as methyl lithium and sodium borohydride. Thermolysis of **2** in 1,3-dichlorobenzene showed that the complex was stable for several hours even at 170 °C; however, thermal decomposition occurred relatively quickly (hours) at 180 °C to provide a complex mixture of uncharacterized products. The marked stability of **2** is comparable to that observed for $[(Me_2PhP)_3PtMe_3][PF_6]$ by Clark and Manzer [15].[1] Compared to the recently structurally characterized $[Tp_2^{Me}]PtMe_3$, the Pt–C bond lengths of **2** are longer, presumably due to the greater *trans* influence of the phosphine ligands. More importantly, the Pt–B distance (3.640 Å) in **2** is much larger than for its [Tp] analogue (3.184 Å), likely providing a better through space separation of charge for **2**.

3.2. Synthesis and reactivity of platinum(II) complexes

Formation of the platinum(II)-methyl compound $[[\kappa^2\text{-}PhBP_3]PtMe_2][TBA]$ (**3**) proceeded cleanly at room temperature by the reaction of **1[TBA]** and $(COD)PtMe_2$ in THF solution (Eq. (2)). The ability to use $(COD)PtMe_2$ as a reagent is consistent with previous results using phosphine donor ligands and stands in contrast to (pyrazolyl)borate ligands which require more labile starting materials to achieve substitution [16,17].

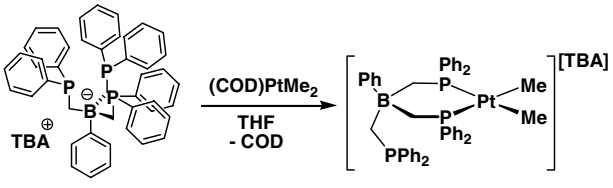

1[TBA] 3 (2)

Examination of the ^1H and $^{31}P\{^1H\}$ NMR spectra of **3** shows the C_s symmetry of the platinum complex: the platinum-methyl protons are equivalent, with readily apparent coupling to platinum ($^2J_{Pt-H} = 67$ Hz) and phosphorus ($^3J_{P-H} = 5$ Hz). The coordinated phosphines in **3** have a very different chemical shift and platinum coupling constant ($\delta = 18.96$, $^1J_{Pt-P} = 1885$

[1] Interestingly, the authors observed high stability for $[Pt(CH_3)_3(OH_2)_3]^+$ and $[Pt(CH_3)_3(NC_2H_5)_3]^+$ as well, noting that the complexes "are quite stable and exhibit no tendency towards reductive decomposition" [15]. We presume that this is due to the electronic nature of the threefold symmetric octahedral molecules.

Hz) from those in **2** ($\delta = -26.01$, $^1J_{Pt-P} = 1093$ Hz), demonstrating a substantial change in the electronic character of the ligated phosphines between Pt(II) and Pt(IV) states. In contrast to two related $[[\kappa^2\text{-Tp}]PtMe_2]^-$ complexes, **3** exhibits smaller methyl $^2J_{Pt-H}$ values ($[[\kappa^2\text{-Tp}]PtMe_2]^-$, $^2J_{Pt-H} = 86$ Hz [16b]; $[[\kappa^2\text{-Tp}_2^{Me}]PtMe_2]^-$, $^2J_{Pt-H} = 83$ Hz [4]), consistent with stronger trans influencing phosphine donors. Relative to a series of previously prepared bidentate phosphine platinum-dimethyl compounds [18], $[E(CH_2PPh_2)_2]Pt(CH_3)_2$ (E $= Ph_2B^-$, Ph_2Si, H_2C), the phosphorus-platinum coupling constant of **3** is comparable to the anionic bis(phosphino)borate complex $[[Ph_2BP_2]PtMe_2][ASN]$ ($^1J_{Pt-P} = 1892$ Hz), and both anionic complexes have larger platinum phosphorus coupling constants than similar neutral compounds. A structurally analogous neutral Pt(II) compound, $(\kappa^2\text{-tripod})Pt(CH_3)_2$, has been previously prepared [19], though it was not thoroughly characterized nor explored further.

Examination of the $^{31}P\{^1H\}$ NMR spectrum of **3** showed two phosphine environments consistent with two phosphines ligated to a square planar platinum(II) center and one unligated phosphine. The pendant arm of the (phosphino)borate ligand in an analytically pure sample of **3** demonstrated unusual behavior. Two peaks were observed at −9.61 and −12.60 ppm whose integrated intensity corresponded to one phosphine relative to the two phosphines coordinated to platinum in the $^{31}P\{^1H\}$ NMR spectrum. Both of these signals are similar to the chemical shift of the uncoordinated ligand **1[TBA]** ($^{31}P\{^1H\}$ NMR (CD_3CN): δ −11.3). The two distinct signals suggest that there is a barrier to rotation about the phosphine-methylene (or the boron-methylene) carbon bond. The difference in chemical shifts between the two signals also suggests that a there is a modest change in the magnetic environment on the pendant phosphine depending on whether the phosphine lone pair is directed toward the metal or away from it. Two possible orientations are depicted in Fig. 2.

An X-ray diffraction experiment confirmed the structure of **3** (Fig. 3), showing that two arms of the tridentate ligand bind to platinum in a *cis* fashion to form a square planar dimethyl platinum complex while one arm of the ligand remains uncoordinated. The uncoordinated arm in the crystal lattice is oriented so that the phosphine lone pair is directed away from the metal. Examination of the bond angles around the platinum center reveals a square planar motif which has been slightly altered due to the steric demands of the aryl rings and the twisted conformation of the chelating ligand. Comparison of the bond lengths and angles observed for **3** with those observed for the related bis(phosphino)borate platinum(II) dimethyl anion $[[\kappa^2\text{-Ph}_2BP_2]PtMe_2][ASN]$ demonstrate that no significant structural changes occur by replacing the uncoordinated phosphine arm for a more innocent phenyl group pendant to boron [18]. Fortunately, the crystal structure of the related $[[\kappa^2\text{-Tp}_2^{Me}]PtMe_2]^-$ has been reported [4]. Similar to **2**, the Pt–C bond lengths (2.09 Å) are longer than for the Tp analogue (2.03 Å). The Pt–B distance in **3** is significantly longer (4.06 Å) than for its Tp analogue (3.37 Å), again suggesting a greater degree of spacial charge separation for $[PhBP_3]$-ligated complexes. It is interesting to note that for both **3** and $[[\kappa^2\text{-Tp}_2^{Me}]PtMe_2]^-$ the pendant donor is directed away from the metal center in the solid state structure. Presumably, interactions between the donor lone pair and the occupied d_z^2-type orbital results in electron-electron repulsion.

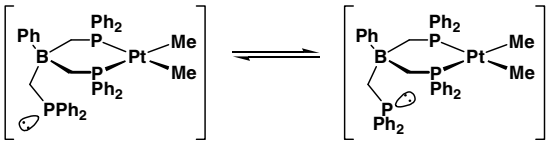

Fig. 2. Possible orientations for the pendant phosphine arm in **3**.

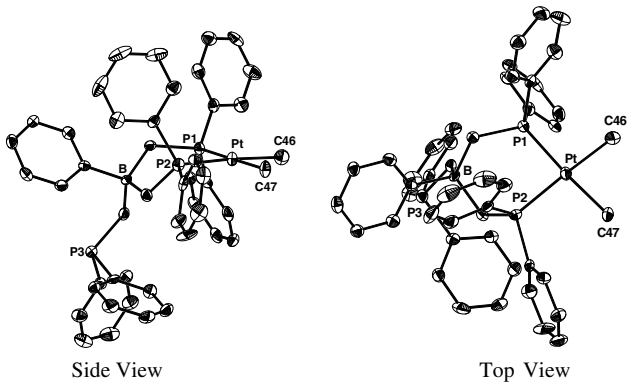

Fig. 3. A 50% displacement ellipsoid representation of **3**. Hydrogen atoms and the TBA cation are omitted for clarity.

Complex **3** exhibited reactivity with dioxygen, water, protic and Lewis acids (e.g., HCl in Et_2O, HOTf, $[Et_3NH][BPh_4]$, $B(C_6F_5)_3$), and small alkyl halides such as CH_3I, CH_2Cl_2, and $CHCl_3$. In most cases, complex product mixtures were formed, as determined by $^{31}P\{^1H\}$ NMR spectroscopy. In particular, reactivity at the pendant phosphine arm was frequently observed, as evinced by new $^{31}P\{^1H\}$ NMR signals without platinum satellites. Related $[[\kappa^2\text{-Tp}]PtMe_2]^-$ species also show a wide variety of reactivity, including well-characterized reactions with H_2O, and protic and Lewis acids [4,16,20]. Reactivity at the uncoordinated pyrazolyl donor has been primarily limited to protonation [21]. The apparent contrast in reactivity of the uncoordinated donor in **3** is most likely attributed to its greater basicity and lower oxidation potential.

3.3. Protection of the unchelated phosphine

In order to sidestep undesirable reactivity at the pendant phosphine arm, phosphine protection strategies

were considered. The pendant arm of the ligand reacted with one equivalent of elemental sulfur to provide a single major product Eq. (3), assigned by NMR spectroscopy as $[[\kappa^2\text{-PhB}(CH_2P(S)Ph_2)(CH_2PPh_2)_2]PtMe_2][TBA]$ (**4**). The chemical shift of a singlet at 44.4 ppm ($^{31}P\{^1H\}$ NMR) suggests an oxidized trialkylphosphine and is consistent with the $^{31}P\{^1H\}$ NMR chemical shifts of known $R_3P=S$ compounds [22]. Additionally, the $^{31}P\{^1H\}$ NMR chemical shift (18.4 ppm) and coupling ($^1J_{Pt-P} = 1875$ Hz) of the coordinated phosphines do not change significantly upon modification of the pendant arm. ^1H NMR spectra of **4** showed no significant changes as compared to **3**. Due to the difficulty in stoichiometric control of the sulfur addition, **4** was typically isolated in >95% purity. The addition of excess sulfur provides uncharacterized products.

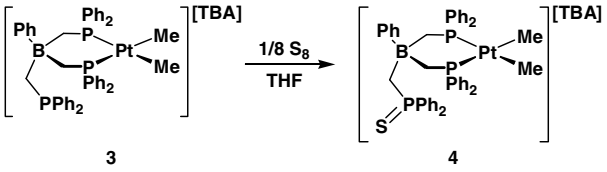

3 4

(3)

A second protection strategy involved addition of the Lewis acid, $BH_3 \cdot SMe_2$. Using one equivalent of a 2.0 M solution of $BH_3 \cdot SMe_2$ in toluene ($BH_3 \cdot THF$ can also be used), clean formation of the BH_3-phosphine adduct **5** can be observed by $^{31}P\{^1H\}$ NMR spectroscopy Eq. (4). $^{31}P\{^1H\}$ NMR spectra show the disappearance of the peaks at −9 and −12 ppm (vide supra) and the growth of a broad peak at ca. 15 ppm. This downfield shift is expected for the formation of a phosphine-borane adduct due to the decreased shielding of the phosphorus nucleus upon borane complexation, and the broadness of the new peak results from unresolved coupling to the boron nucleus. Examination of **5** by ^{11}B NMR spectroscopy confirmed the formation of the phosphine-borane adduct with the presence of a new upfield signal (−30.3 ppm) consistent with known phosphine-borane complexes. The resonances from the platinum-bound phosphines demonstrate virtually no change in their $^{31}P\{^1H\}$ NMR chemical shift and register only a slight change in their coupling to platinum ($^1J_{Pt-P}(\mathbf{5}) = 1870$ Hz versus $^1J_{Pt-P}(\mathbf{3}) = 1885$ Hz).

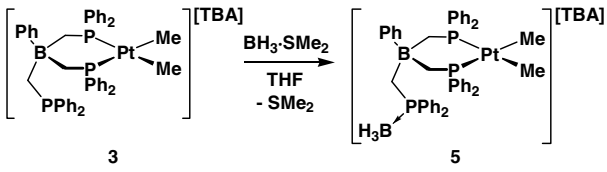

3 5

(4)

Protection of the pendant phosphine arm with BH_3 provides altered reactivity with various substrates relative to the reactivity found in **3**. For example, **3** begins to react immediately when dissolved in dichloromethane, providing a mixture of products over a period of hours [10].[2] In contrast, **5** shows no spectroscopic change over 2.5 hours when dissolved in dichloromethane. Additionally, **5** shows no reaction with air and water in THF solution over several hours. These examples show that the reactivity of complex **3** is dependent upon the pendant phosphine arm, either as a site of reactivity or as a neutral donor facilitating reactivity at the platinum center. Deprotection of the pendant phosphine $\cdot BH_3$ adduct of **5** can be accomplished by heating **5** to 55 °C for several hours in the presence of excess (~200 equiv.) morpholine, a common deprotection method [23].

3.4. Reactivity of protected platinum(II) species

If **5** is allowed to react with an additional equivalent of $BH_3 \cdot SMe_2$ (or $BH_3 \cdot THF$), then clean formation of a new product is observed Eq. (5). Spectroscopic (NMR), mass spectrometric, and combustion analyses are consistent with the formation of the reduced platinum(I) dimeric species, $[[\kappa^2\text{-PhB}(CH_2P(BH_3)Ph_2)(CH_2PPh_2)_2]Pt(\mu\text{-H})]_2[TBA]_2$ (**6**). BH_3 reagents are widely known to act as reducing agents, and, in this case, it appears that BH_3 is serving as a reductant and H-atom donor. The fate of the methyl groups on platinum is unknown at this point: possible methyl containing products are methane or methylborane species, neither of which has been spectroscopically observed.

Bridging platinum(I) hydride dimers have been previously described in detail by Schwarz and Andersen [24]. The NMR spectra of **6** are consistent with their observations and those of others [24–26], including the unusual "quintet of quintets" signal for the hydrides (Table 3). The observed trends of the ^1H NMR spectroscopic data for several bisphosphine platinum(I) bridged hydrides suggest that the hydrides in **6** are *trans* to a more electron-rich bisphosphine ligand as compared to other neutral bisphosphine platinum(I) hydride dimers, based on the reduced Pt–H coupling constant. The IR data (Nujol) for **6** contain a broad peak at 2368 cm^{-1}, and two peaks at 2003 and 1966 cm^{-1}. The first of these peaks is consistent with previously observed BH_3-phosphine adducts, typically observed between 2450 and 2350 cm^{-1} [27]. The two peaks at 2003 and 1966 cm^{-1} are assigned as the Pt–H stretching modes.

[2] The unligated tris(phosphino)borate $[PhBP_3][TBA]$ also demonstrates reactivity with halide-containing solvents such as CH_2Cl_2 and $CHCl_3$.

Table 3
^{1}H NMR and IR data for bisphosphine platinum(I) dimers

Compound	δ (Pt–H) (ppm)	$^1J_{Pt-H}$ (Hz)	$^2J_{P-H}$ (Hz)	ν (Pt–H) (cm^{-1})Nujol	Ref.
6	−3.17	464	40	2003, 1966	
[(dppe)PtH]$_2$	0.30	564	42	[a]	[25b]
[(dippe)PtH]$_2$	0.49	516	40	1939, 1926	[24]
[(dcype)PtH]$_2$	0.49	512	40	1965, 1937	[24]
[(dtbpe)PtH]$_2$	0.05	570	42	1975, 1951	[24]
[(dfepe)PtH]$_2$	3.55	737	47	[b]	[26]

[a] IR data were not reported.
[b] The authors did not observe Pt–H stretching bands in the IR spectrum (see footnote 7 of [26]).

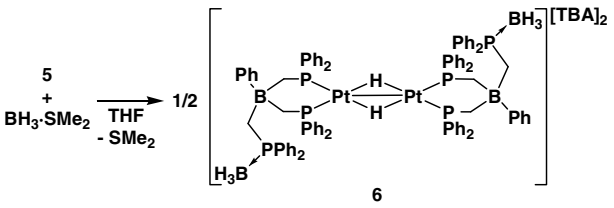

(5)

4. Conclusions

Several platinum methyl and hydride complexes containing the monoanionic tris(phosphino)borate ligand **1** have been synthesized, and preliminary investigations into their chemistry has begun. In general, a zwitterionic description for complexes ligated by **1** seems more appropriate than for related [Tp]-containing systems, given that comparative structural data often shows similar binding modes for the two ligands but greater separation between the metal center and the anionic borate for [PhBP$_3$] systems. Although the binding modes are similar between [Tp] and [PhBP$_3$], particularly notable for **3** and its [Tp] congener, we have found that much of the reactivity of the anionic dimethyl complex **3** is attributable to the unligated phosphine arm of the trisphosphine ligand. In comparison to related [Tp]-ligated platinum systems, the free phosphine donor readily participates in reactivity due to its greater basicity. Protection of the pendant phosphine arm can be achieved using either BH_3 or sulfur. The sulfur-protected complex **4** promises to be an interesting candidate for further reactivity studies based on its donor potential. Studies of the reactivity of the BH_3-protected compound **5** have shown it to be significantly less reactive than **3** under comparable conditions, demonstrating the role of the unbound phosphine in reactivity. Future studies of [PhBP$_3$]Pt systems will aim at further understanding the structural and electronic differences between analogous [Tp]- and [PhBP$_3$]-ligated complexes.

5. Supplementary material

Crystallographic data for the structural analyses have been deposited at the Cambridge Crystallographic Data Center, CCDC Numbers 216189 (**2·THF**) and 216190 (**3**). Copies of this information may be obtained free of charge from the Director, CCDC, 12 Union Road, Cambridge, CB2 1EZ, UK (fax: +44-1223-336033; e-mail: deposit@ccdc.cam.ac.uk or http://www.ccdc.cam.ac.uk).

Acknowledgements

Larry Henling is acknowledged for his assistance with X-ray crystallography. Joseph Duimestra is acknowledged for assistance with the protocol for [PhBP$_3$][TBA]. J.C.T. is grateful to the NSF and to the Moore Foundation for graduate research fellowships. The authors acknowledge financial support from the NSF (CHE-0132216) and the DOE (PECASE).

References

[1] S. Trofimenko, Scorpionates. The Coordination Chemistry of Polypyrazolylborate Ligands, Imperial College Press, London, 1999.
[2] (a) S.E. Bromberg, H. Yang, M.C. Asplund, T. Lian, B.K. McNamara, K.T. Kotz, J.S. Yeston, M. Wilkens, H. Frei, R.G. Bergman, C.B. Harris, Science 278 (1997) 260;
(b) D.M. Tellers, R.G.J. Bergman, J. Am. Chem. Soc. 122 (2000) 954;
(c) J.S. Yeston, R.G. Bergman, Organometallics 19 (2000) 2947;
(d) J.S. Yeston, B.K. McNamara, R.G. Bergman, C.B. Moore, Organometallics 19 (2000) 3442;
(e) D.M. Tellers, R.G. Bergman, Organometallics 20 (2001) 4819;
(f) M.C. Asplund, P.T. Snee, J.S. Yeston, M.J. Wilkens, C.K. Payne, H. Yang, K.T. Kotz, H. Frei, R.G. Bergman, C.B. Harris, J. Am. Chem. Soc. 124 (2002) 10605.
[3] (a) D.D. Wick, T.O. Northcutt, R.J. Lachicotte, W.D. Jones, Organometallics 17 (1998) 4484;
(b) D.D. Wick, W.D. Jones, Organometallics 18 (1999) 495;
(c) D.D. Wick, K.A. Reynolds, W.D. Jones, J. Am. Chem. Soc. 121 (1999) 3974;
(d) T.O. Northcutt, D.D. Wick, A.J. Vetter, W.D. Jones, J. Am. Chem. Soc. 123 (2001) 7257.
[4] D.D. Wick, K.I. Goldberg, J. Am. Chem. Soc. 119 (1997) 10235.
[5] S. Reinartz, P.S. White, M. Brookhart, J.L. Templeton, J. Am. Chem. Soc. 123 (2001) 6425.
[6] S. Reinartz, P.S. White, M. Brookhart, J.L. Templeton, J. Am. Chem. Soc. 123 (2001) 12724.

[7] M.P. Jensen, D.D. Wick, S. Reinartz, P.S. White, J.L. Templeton, K.I. Goldberg, J. Am. Chem. Soc. 125 (2003) 8614.
[8] M.A. Iron, H.C. Lo, J.M.L. Martin, E. Keinan, J. Am. Chem. Soc. 124 (2002) 7041.
[9] (a) J.C. Peters, J.D. Feldman, T.D. Tilley, J. Am. Chem. Soc. 121 (1999) 9871;
(b) J.D. Feldman, J.C. Peters, T.D. Tilley, Organometallics 21 (2002) 4050;
(c) A.A. Barney, A.F. Heyduk, D.G. Nocera, Chem. Commun. (1999) 2379.
[10] J.C. Thomas, J.C. Peters, Inorg. Chem. 42 (2003) 5055.
[11] S.J. Trofimenko, J. Am. Chem. Soc. 89 (1967) 3170.
[12] E. Costa, P.G. Pringle, M. Ravetz, Inorg. Synth. 31 (1995) 284.
[13] I.A. Shapiro, D.M. Jenkins, J.C. Thomas, M.W. Day, J.C. Peters, Chem. Commun. (2001) 2152.
[14] J.C. Peters, J.C. Thomas, Inorg. Synth., in press.
[15] H.C. Clark, L.E. Manzer, Inorg. Chem. 12 (1973) 362.
[16] (a) A.J. Canty, S.D. Fritsche, H. Jin, B.W. Skelton, A.H. White, J. Organomet. Chem. 490 (1995) C18;
(b) A.J. Canty, S.D. Fritsche, H. Jin, J. Patel, B.W. Skelton, A.H. White, Organometallics 16 (1997) 2175.
[17] S.A. O'Reilly, P.S. White, J.L. Templeton, J. Am. Chem. Soc. 118 (1996) 5684.
[18] J.C. Thomas, J.C. Peters, J. Am. Chem. Soc. 125 (2003) 8870.
[19] R.M. Kirchner, R.G. Little, K.D. Tau, D.W. Meek, J. Organomet. Chem. 149 (1978) C15.
[20] A.J. Canty, A. Dedieu, A. Milet, M.K. Richmond, Organometallics 15 (1996) 2845.
[21] S. Reinartz, P.S. White, M. Brookhart, J.L. Templeton, Organometallics 19 (2000) 3854.
[22] V. Mark, C.H. Dungan, M.M. Crutchfield, J.R. Van Wazer, Top. Phosphorus Chem. 5 (1967) 227 (Note: referenced ^{31}P NMR chemical shifts are reported as $-\delta$ being downfield and $+\delta$ being upfield of H_3PO_4, contrary to current standards..
[23] R.M. Stoop, A. Mezzetti, F. Spindler, Organometallics 17 (1998) 668.
[24] D.J. Schwartz, R.A. Andersen, J. Am. Chem. Soc. 117 (1995) 4014.
[25] (a) T.H. Tulip, T. Yamagata, T. Yoshida, R.D. Wilson, J.A. Ibers, S. Otsuka, Inorg. Chem. 18 (1979) 2239;
(b) D. Carmichael, P.B. Hitchcock, J.F. Nixon, A.J. Pidcock, J. Chem. Soc., Chem. Commun. (1988) 1554.
[26] B.L. Bennett, D.M. Roddick, Inorg. Chem. 35 (1996) 4703.
[27] J.M. Brunel, B. Faure, M. Maffei, Coord. Chem. Rev. (1998) 178, pp. 665–698 and references therein.

Available online at www.sciencedirect.com
SCIENCE DIRECT®
Polyhedron 23 (2004) 499–506
POLYHEDRON
www.elsevier.com/locate/poly

Ground and excited state spectral comparisons of models for sulfite oxidase

Martin L. Kirk *, Katrina Peariso

Department of Chemistry, The University of New Mexico, MSC03 2060, 1 University of New Mexico, Albuquerque, NM 87131-0001, USA

Received 1 August 2003; accepted 7 October 2003

Abstract

Determining the contributions of thiolate and ene-1,2-dithiolate donors to the underlying electronic structure of the Mo site in sulfite oxidase (SO) has been a goal pursued by inorganic chemists for almost twenty years. The use of the hydrotris(3,5-dimethyl-1-pyrazolyl)borate ligand provided the framework for the first low-symmetry oxo-molybdenum(V) models in which the oxo donor was *cis* to the dithiolene moiety of benzene-1,2-dithiolate. Recent work from the Carrano and Kirk laboratories has produced a second-generation model of the SO active site based upon the (2-dimethylethanethiol)bis(3,5-dimethylpyrazolyl)methane heteroscorpionate ligand. Use of this heteroscorpionate framework provides for an oxo-molybdenum(V) complex with both a thiolate and an ene-1,2-dithiolate in the equatorial plane. In addition to providing a good structural model, the heteroscorpionate thiolate offers a constrained O–Mo–$S_{thiolate}$–C torsion angle of ~115°, closer to that of the ~90° O–Mo–S_{Cys}–C torsion angle observed in the chicken liver SO active site than can be obtained with thiophenolate ligands. This constrained torsion angle allows for the examination of how second-coordination sphere effects influence the electronic structure of the Mo site. Here we compare and contrast the molecular and electronic structures of these first- and second-generation models of the SO active site. Additionally, the electron paramagnetic resonance (EPR) parameters for both of these models are compared with those measured for the Mo(V) form of both low pH (*lpH*) and high pH (*hpH*) forms of SO in order to determine what insight these structural models can offer about the electronic structure of the active site of SO.
© 2003 Published by Elsevier Ltd.

Keywords: Sulfite oxidase; Pyranopterin molybdenum enzymes; Electronic structure; Molybdenum complexes; MCD (Magnetic Circular Dichroism); EPR (Electron Paramagnetic Resonance)

1. Introduction

Pyranopterin molybdenum enzymes are ubiquitous in biology, performing such essential functions as the degradation of amino acids, nucleobases and various drugs in addition to their involvement in pro-drug activation [1]. These enzymes have previously been categorized into three families, two of which are represented in mammalian systems; the xanthine oxidase (XO) and sulfite oxidase (SO) families [1]. Members of the XO family are involved in the oxidation of simple aldehydes and the hydroxylation of purines while mammalian SO converts sulfite to sulfate, presumably via an inner sphere oxygen atom transfer process. The consensus active site structures for oxidized (SO_{ox}) and reduced (SO_{red}) SO are given in Scheme 1. Both sites are pentacoordinate, possessing an apical oxo donor and equatorial ene-1,2-dithiolate and cysteine sulfur (S_{Cys}) coordination [2–6]. The 5-coordinate site in SO_{ox} is completed by a second terminal oxo donor, which is replaced by water or hydroxide in reduced forms of the enzyme [2,3,5]. Catalysis is initiated in the reductive half-reaction, where the sulfite lone pair is proposed to attack the *equatorial* oxo donor (O_{eq}) resulting in a $2e^-$ reduction of the Mo center and a subsequent transfer of O_{eq} to the substrate to form sulfate [1,7]. The oxidative half reaction formally consists of sequential coupled electron–proton transfer steps which regenerate the oxidized active site, and the ene-1,2-dithiolene chelate has been hypothesized to play a key role in this process by modulating the reduction potential of the Mo and/or

* Corresponding author. Fax: +1-505-277-2609.
E-mail address: mkirk@unm.edu (M.L. Kirk).

0277-5387/$ - see front matter © 2003 Published by Elsevier Ltd.
doi:10.1016/j.poly.2003.11.037

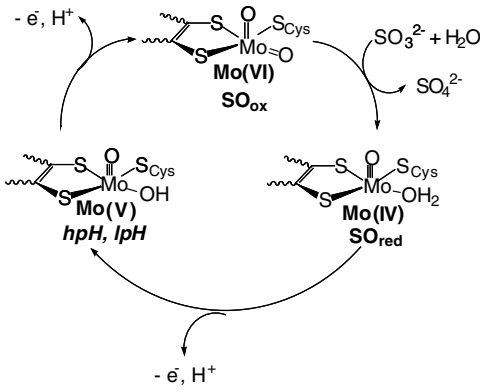

Scheme 1.

coupling the active site into hole superexchange pathways for electron transfer regeneration of SO_{ox} [8,9]. As the coordinated cysteine is essential for catalytic activity, these same roles may also be ascribed to the S_{Cys} donor as well. Charge density maps of the chicken liver enzyme indicate that electrons may be sequentially transferred out of the Mo active site following docking of the b-type heme domain [1] at the surface of the substrate access channel [10,11]. It has therefore been suggested that the S_{Cys}, which is directed toward this substrate access channel, could act as an electron transfer conduit between Mo and the b-type heme and facilitate the electron transfer regeneration process. As such, understanding the roles of the S_{Cys} and ene-1,2-dithiolate donors in reduced forms of SO has been a fundamental goal of researchers in this field.

Deconvoluting the different contributions of thiolate and ene-1,2-dithiolate donors to the underlying electronic structure of the Mo site in SO has proven to be a difficult task. Very accurate synthetic models of SO_{ox} and SO_{red} have recently been synthesized and structurally characterized. Holm and coworkers [12] have reported the synthesis and structural characterization of $(Et_4N)[MoOCl(bdt)(2,4,6\text{-}Pr^i_3\text{–}SC_6H_2)]$, however, the use of synthetic models to probe structure-property relationships that directly relate to the reduced SO active site has been hampered by the dearth of structural models that possess both ene-1,2-dithiolate and thiolate donors to molybdenum.

The synthesis and structures of new oxo-Mo(V) complexes as effective models for the one electron reduced active site of SO have also been recently reported. In these complexes, the tridentate heteroscorpionate ligand (2-dimethylethanethiol)bis(3,5-dimethylpyrazolyl)methane (L3SH) [13–15] was used to model the constrained cysteinyl sulfur (S_{Cys}) ligand environment observed in the crystal structure of the enzyme. In addition, an equatorial benzene-1,2-dithiol (bdt) provides a mimic of the ene-1,2-dithiolate chelate. As such, [(L3S)MoO(bdt)] is only the second known model compound that closely approximates the active site structure of reduced forms of SO. The incorporation of the $L3S^-$ chelate allows the O–Mo–S–C torsion angle to be effectively constrained in these new models. This is important, as bond torsions about this angle have been shown to be critical in modulating the degree of Mo–$S_{thiolate}$ covalency in oxomolybdenum thiolate complexes, affecting the overlap between the S^v p orbital [2] and the Mo $d_{x^2-y^2}$ redox orbital. The crystallographically determined O–Mo–S'_{Cys}–C torsion angle in SO is ~90° [5], which is markedly different from that found in small molecule complexes such as $[MoO(SPh)_4]^{1-}$ [16].

In this paper, we compare the structure and spectroscopic characterization of first and second generation models of the SO active site, [Tp*MoO(bdt)] and [(L3S)MoO(bdt)], respectively. These complexes allow for probing the effects of thiolate and ene-1,2-dithiolate coordination on the electronic structure of *hpH* and *lpH* SO and the respective abilities of these sulfur donor ligands to facilitate catalytically crucial ET processes.

2. Experimental

2.1. Preparation of compounds

Both [(L3S)MoO(bdt)] [17] and [Tp*MoO(bdt)] [18,19] were synthesized by literature methods.

2.2. Abbreviations

Tp* = hydrotris(3,5-dimethyl-1-pyrazolyl)borate; L3SH = (2-dimethylethane-thiol)bis(3,5-dimethylpyrazolyl)-methane; bdt = 1,2-benzenedithiolate; $S_{op}^{a',a''}$ = out-of-plane dithiolene S orbital; = $S_{ip}^{a',a''}$ in-plane dithiolene S orbital.

2.3. Electronic absorption spectroscopy

Solution electronic absorption spectra were collected using a Hitachi-3501 UV–Vis–NIR dual-beam spectrophotometer. The electronic absorption spectra were measured in 1-cm path length, black-masked, Wilmad quartz cuvettes with a Teflon stopper to prevent the introduction of O_2. The spectra for [(L3S)MoO(bdt)] was measured using dry, degassed dichloromethane as the solvent, and the spectrum for [Tp*MoO(bdt)] was measured in 1,2-dichloroethane. The measurements

[1] Vertebrate SO is a homodimer. Each half of the dimer consists of a molybdenum binding domain and a heme domain that are connected by a flexible loop region.

[2] S^v is the S p orbital that is orthogonal to the Mo–S bond and not involved in S–C σ bonding.

were repeated at a number of time points to ensure the structural stability and integrity of the complex in solution during the measurements.

2.4. Magnetic circular dichroism spectroscopy

Low temperature MCD spectra were collected on a system consisting of a Jasco J600 CD spectropolarimeter employing Hamamatsu photomultiplier tubes of either S-1 or S-20 response, an Oxford Instruments SM4000-7T superconducting magneto-optical cryostat (0–7 T, 1.4–300 K), and an ITC503 Oxford Instruments temperature controller. The spectrometer was calibrated for circular dichroism intensity with camphorsulfonic acid and the wavelength was calibrated using Nd-doped glass. All spectra were collected at 2.0 nm resolution at a temperature of 5 K in an applied magnetic field of 7 T. Samples were prepared by dispersing the solids in poly(dimethylsiloxane) and placing the mull between quartz disks. Depolarization of the incident radiation by the sample was determined by comparing the intrinsic circular dichroism of a standard Ni (+)-tartrate solution positioned in front of and then in back of each sample.

2.5. Electron paramagnetic resonance spectroscopy

Solution and frozen glass EPR spectra were measured at X-band (~9.3 GHz) using a Bruker EMX spectrometer. The room-temperature solution spectra were measured in dichloromethane. For the low temperature measurements, a 1:1 toluene–dichloromethane mixture was used as a glassing solvent, and the temperature was held at 4 K in an Oxford liquid helium flow cryostat. Simulations of the EPR spectra were performed using the program QPOW [20–22]. The enzyme and [Tp*MoO(bdt)] spectra were simulated using previously published parameters [18]. The proton hyperfine coupling has been removed in the enzyme spectral simulations for clarity and to aid in making direct comparisons with the model spectra.

3. Results and discussion

3.1. Comparing the solid state structures of [Tp*MoO(bdt)] and [(L3S)MoO(bdt)]

The structure of [Tp*MoO(bdt)] has been determined previously by Dhawan and Enemark [18]. The coordination geometry is that of a six-coordinate oxo-molybdenum complex with the sulfur atoms of the coordinated dithiolene oriented *cis* to the terminal oxo ligand. The effective symmetry of the molecule is C_s, with the mirror plane bisecting the two sulfur donors of the bdt ligand and containing the oxo-molybdenum unit. As is typical for mono oxo-molybdenum complexes, the Mo(V) ion was found to lie out of the N_2S_2 equatorial plane toward the apical oxo.

The crystal structure of [(L3S)MoO(bdt)] shows that the two pyrazolyl nitrogens and the alkyl thiolate sulfur donor of the $(L3S)^-$ ligand are facially coordinated to the Mo center [17]. An appreciable lengthening of the Mo–N(3) bond in [(L3S)MoO(bdt)] results from a strong structural *trans* effect due to the presence of the terminal oxo group, and this is reflected in the shorter Mo-oxo distance for [(L3S)MoO(bdt)] (1.657 Å) when compared to [Tp*MoO(bdt)] (1.678 Å). Thus, while the Mo–N(1) bonds average 2.178(5) Å in [(L3S)MoO(bdt)], and [Tp*MoO(bdt)] [18,23], the *trans* Mo(V)–N_{pz} bond lengths are 2.521, and 2.372 Å, respectively. Of particular interest is the very long distance recorded for the Mo–N(3) bond in the [(L3S)MoO(bdt)] derivative which is ~0.3 Å longer than the *cis* Mo–N bond. As was the case for [Tp*MoO(bdt)], the Mo atom lies above the center of a square plane consisting of atoms N(1), S(1), S(2) and S(3). Again, the oxo oxygen O(1) is orthogonal to this plane and the Mo ion lies approximately 0.3–0.4 Å out of the plane toward the oxo ligand. As anticipated, addition of a third sulfur in the equatorial plane of [(L3S)MoO(bdt)] results in Mo–$S_{dithiolene}$ bond distances that are somewhat longer, at an average of 2.405 Å, than those of [Tp*MoO(bdt)] which average 2.375 Å. This 2.40 Å Mo–S distance observed for [(L3S)MoO(bdt)] is completely consistent with the crystallographically and XAS determined Mo–S distances in the models of the SO active site published by Holm and coworkers [12,24]. Despite the increase in Mo–$S_{dithiolene}$ distance, the sulfur fold angles (the angle between the plane containing the Mo and the dithiolene sulfurs and that containing the dithiolene sulfurs and the S-bonded C atoms of the benzene-1,2-dithiolate ring) are very similar, at 23.6° in [(L3S)MoO(bdt)] and 21.3° in [Tp*MoO(bdt)] [18]. The O–Mo–S(1)–C dihedral angle in [(L3S)MoO(bdt)], which involves the alkyl thiolate donor from the L3S ligand, is 115° [17]. This angle is constrained by the chelate ring, and may be compared to the ~90° dihedral angle found in the structure of SO. The very close similarity in first coordination sphere sulfur donor atoms that exists between [(L3S)MoO(bdt)] and the enzyme is clearly evident in Fig. 1.

Fig. 1. Schematic representation of (left to right) the SO active site [5], [Tp*MoO(bdt)] [18], and [(L3S)MoO(bdt)] [17].

3.2. Electronic absorption spectra

A detailed electronic structure study of the first generation model compound [Tp*MoO(bdt)] has been previously undertaken and complete band assignments have been made [8]. The Gaussian resolved solution absorption spectrum of [Tp*MoO(bdt)] is shown in Fig. 2, and the band assignments are as follows: Bands 1 and 2, $S_{op}^{a',a''} \rightarrow d_{x^2-y^2}$; Band 3, $d_{x^2-y^2} \rightarrow d_{xz,yz}$; Band 4, $S_{ip}^{a'} \rightarrow d_{x^2-y^2}$; Band 5, $S_{op}^{a''} \rightarrow d_{xz,yz}$; Band 6, $S_{op}^{a'} \rightarrow d_{xz,yz}$. The intensities of the lowest energy charge transfer transitions are weak, which is indicative of the poor orbital overlap between out-of-plane dithiolene S orbitals and the in-plane Mo $d_{x^2-y^2}$ orbital. Band 3 is the lowest energy ligand field transition and reflects the splitting of the metal t_{2g} orbital set under the influence of a strong π^* interaction with the terminal oxo ligand. The intensity of band 4 reflects the degree of overlap between the in-plane dithiolene S orbital of a' symmetry and the Mo d_{xy} redox orbital. This overlap is of fundamental importance to hole transfer superexchange mechanisms for electron transfer regeneration involving the dithiolene chelate in pyranopterin molybdenum enzymes [8]. The intensity of bands 5 and 6 reflect dithiolene charge transfer to the higher energy, vacant, Mo $d_{xz,yz}$ orbitals and has been postulated to play a key role in modulating the reduction potential of [(Tp*)MoO(dithiolene)] [9] complexes as well as the SO_{red} site.

The electronic absorption spectra of [Tp*MoO(bdt)] and [(L3S)MoO(bdt)] are overlayed in Fig. 3 for comparative purposes. There are three distinct, lower intensity features that are clearly resolvable in the [(L3S)MoO(bdt)] spectrum, and these are observed at 9750 cm^{-1} ($\varepsilon = 400$ M^{-1} cm^{-1}), 14,792 cm^{-1} ($\varepsilon = 1020$ M^{-1} cm^{-1}) and 17,908 cm^{-1} ($\varepsilon = 630$ M^{-1} cm^{-1}) [17]. As stated earlier, three $S_{dithiolene} \rightarrow$ Mo charge transfer bands were assigned in a relatively similar energy region for [Tp*MoO(bdt)] [8]. The weak $d_{x^2-y^2} \rightarrow d_{xz,yz}$ ligand field transition cannot be assigned at this time and is almost certainly obscured beneath the ~14,800 cm^{-1} band in the [(L3S)MoO(bdt)] spectrum. By analogy with the [Tp*MoO(bdt)] spectrum, the 9750 cm^{-1} band is easily assignable as the lowest energy component of the $S_{op}^{a',a''} \rightarrow d_{x^2-y^2}$ charge transfer. A precise assignment of the 14,792 and 17,980 cm^{-1} bands is more difficult, however. Interestingly, the relative intensity of the transitions observed at 14,792 and 17,980 cm^{-1} in [(L3S)MoO(bdt)] are reversed from those observed in [Tp*MoO(bdt)]. This may be due, in part, to a dominant $L3S \rightarrow d_{x^2-y^2}$ LMCT contribution to the intensity of the 14,792 cm^{-1} band in the [(L3S)MoO(bdt)] model that is not present in the [Tp*MoO(bdt)] complex due to the fact it lacks an alkyl thiolate donor. The 17,980 cm^{-1} band is tentatively assigned as the $S_{ip}^{a'} \rightarrow d_{x^2-y^2}$ charge transfer transition. Provided that this is the correct assignment, it indicates a considerable reduction in the degree of overlap between the key in-plane dithiolene S orbital and the Mo $d_{x^2-y^2}$ redox orbital. A fundamental question that remains regarding the oxidative half reaction of SO is which S donor functions to assist in the electron transfer process whereby two electrons are shuttled sequentially from the SO_{red} site to the endogenous b-type heme. To the extent that the overlap between the dithiolene S p orbitals and Mo $d_{x^2-y^2}$ is attenuated in SO, this may result in a reduced capability for the dithiolene to effectively couple the Mo site into hole transfer superexchange pathways for electron transfer regeneration.

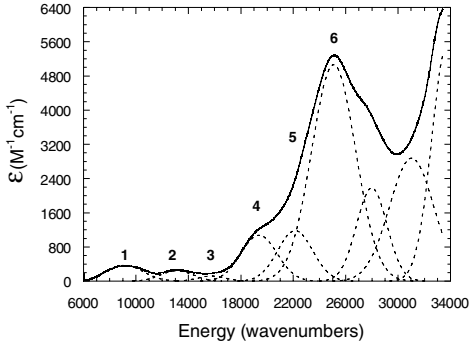

Fig. 2. Gaussian resolved electronic absorption spectrum of [Tp*MoO(bdt)]. Adapted from [8].

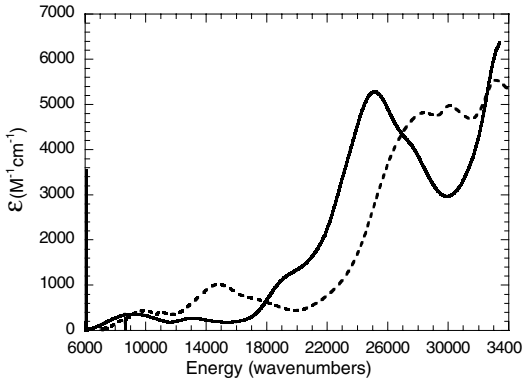

Fig. 3. Electronic absorption overlay of [Tp*MoO(bdt)] (solid line) and [(L3S)MoO(bdt)] (dashed line).

3.3. Magnetic circular dichroism spectroscopy

Given the discrepancy observed in the peak intensities in the low-energy region of the electronic absorption spectra for [(L3S)MoO(bdt)] and [Tp*MoO(bdt)], it is not surprising that there are significant differences in both the number and the intensity of the low-energy MCD features (relative to that of the high energy region of the spectrum) (Fig. 4). As discussed in the previous section, the region below 20 000 cm^{-1} is dominated by LMCT transitions from the sulfur donors to the Mo $d_{x^2-y^2}$ orbital. The increased MCD intensity in this re-

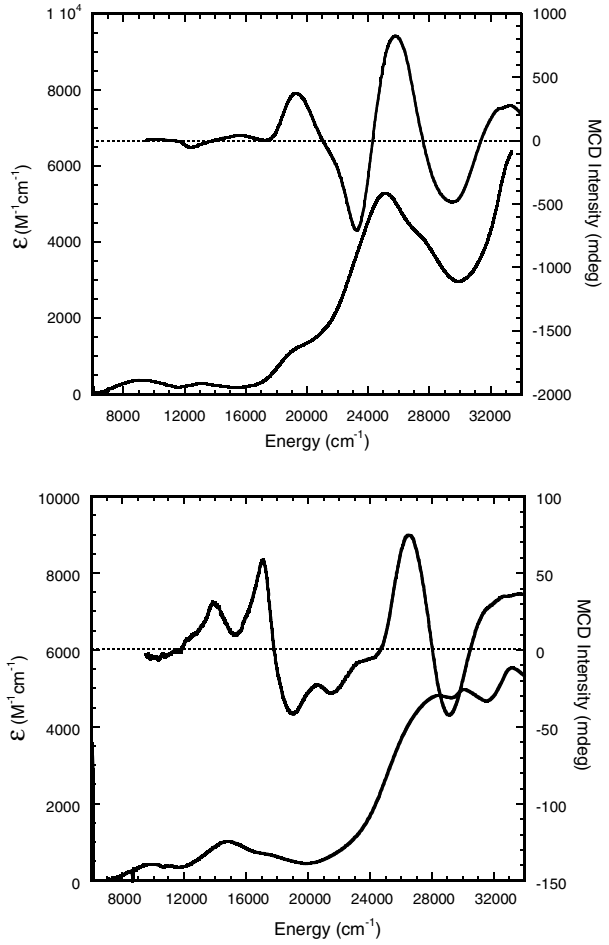

Fig. 4. Solution absorption and solid MCD overlay for [Tp*MoO(bdt)] (top) and [(L3S)MoO(bdt)] (bottom).

gion for [(L3S)MoO(bdt)] suggests an increase in out-of-state spin–orbit mixing between the $L3S \rightarrow d_{x^2-y^2}$, $S_{dithiolene} \rightarrow d_{x^2-y^2}$, and $d_{x^2-y^2} \rightarrow d_{xz,yz}$, states relative to that observed for [Tp*MoO(bdt)], especially for the transitions between 14 000 and 18 000 cm^{-1}. While the band assignments for the spectrum of [(L3S)MoO(bdt)] are not yet complete, the decreased symmetry of the [(L3S)MoO(bdt)] complex and the observed intensity increase in the low-energy MCD features indicates that the CT transitions likely arise from a linear combination of $L3S \rightarrow d_{x^2-y^2}$ and $S_{dithiolene} \rightarrow d_{x^2-y^2}$ one-electron promotions.

Despite these differences in the low-energy regions of the absorption and MCD spectra for [(L3S)MoO(bdt)] and [Tp*MoO(bdt)], the spectra above 24 300 cm^{-1} are strikingly similar. This is not entirely unexpected, since this region of the spectrum is dominated by CT transitions from the sulfur donors to the Mo $d_{xz,yz}$ orbitals. The planar geometry of the benzenedithiolate ligand allows for a large $S_{op}\pi$–Mo $d_{xy,yz}$ orbital overlap. If the constrained O_{ax}–Mo–$S_{thiolate}$–C torsion angle in [(L3S)MoO(bdt)] were closer to the ~90° O_{ax}–Mo–S_{Cys}–C torsion angle observed in SO, an increase in $S_{thiolate}$–Mo $d_{xy,yz}$ orbital overlap would be anticipated. However, the strong MCD spectral similarity between [(L3S)MoO(bdt)] and [Tp*MoO(bdt)] in the high energy region suggests that the $S_{thiolate} \rightarrow$ Mo $d_{xy,yz}$ CT transition is attenuated in [(L3S)MoO(bdt)], and this likely results from the larger 115° O_{ax}–Mo–$S_{thiolate}$–C torsion angle in [(L3S)MoO(bdt)] relative to that of the enzyme.

Understanding the electronic origin of CT contributions to the absorption and MCD spectra of [Tp*MoO(bdt)] and [(L3S)MoO(bdt)] has provided insight into the requirement of both thiolate and dithiolene donors in the first coordination sphere of SO_{red}. Interestingly, MCD spectra of the [Mo(V):Fe(II)] form of chicken liver SO show a distinct lack of low-energy CT bands [25]. While this may be due, in part, to the subtraction method employed to remove the heme signatures in the spectrum, it does suggest that, if these bands are present, they have very low intensity. This would suggest that despite the similarity in the first coordination sphere between [(L3S)MoO(bdt)] and SO_{red}, the electronic structure of the high pH MCD active SO_{red} active site is such that there is little S_{Cys}–Mo $d_{x^2-y^2}$ mixing, indicative of an ~90° O–Mo–S_{Cys}–C torsion angle also being present in the [Mo(V):Fe(II)] form of chicken liver SO. Studies are currently underway to investigate the electronic structure of SO in the absence of the heme cofactor, so that the S→Mo CT transitions may be more easily observed.

3.4. EPR spectroscopy

The EPR spectra of [(L3S)MoO(bdt)] and [Tp*MoO(bdt)], in addition to the enzyme spectra, have been analyzed using the spin-Hamiltonian given in Eq. (1), where the parameters and symbols have their usual meaning.

$$H = \beta H(g_{xx}\hat{S}_x + g_{yy}\hat{S}_y + g_{zz}\hat{S}_z) + A_{xx}\hat{S}_x\hat{I}_x + A_{yy}\hat{S}_y\hat{I}_y + A_{zz}\hat{S}_z\hat{I}_z. \quad (1)$$

We assign the *molecular* axes for [(L3S)MoO(bdt)] and [Tp*MoO(bdt)] using an orthogonal right hand coordinate frame with the molecular z along the terminal oxo and y bisecting the two sulfur donors of the dithiolene. Thus, for [Tp*MoO(bdt)] the x axis is orthogonal to the mirror plane. The anisotropic ^{95,97}Mo ($I = 5/2$; 25.38% abundance) hyperfine parameters (A_{ii}) are often difficult to determine from spectral simulations. Thus, the expression $\langle A \rangle = (A_{xx} + A_{yy} + A_{zz})/3$ has been used, which relates the isotropic solution hyperfine parameter, $\langle A \rangle$, to A_{ave}. A further complication often arises in the simulation of low-symmetry oxo-molybdenum complexes, namely the noncoincidence of the **g** and **A**(^{95,97}Mo) tensors. Thus, the Euler angles α, β, and γ are commonly used to transform the **A**(^{95,97}Mo) hyperfine

tensor onto that of the **g** frame. Metal complexes such as [(L3S)MoO(bdt)] that have very low or no symmetry (C_i or C_l) are not required to possess coincident **g** and **A**(^{95,97}Mo) tensors, while higher symmetry sites (C_s, C_2, or C_{2h}), such as the one present in [Tp*MoO(bdt)] are required to possess one coincident set of principal **g** and **A**(^{95,97}Mo) axes [26]. Understanding the electronic origin of **g** and **A** (^{95,97}Mo) tensor noncoincidence is important, as this relates directly to the degree of d orbital and charge transfer excited state mixing in low symmetry oxomolybdenum sites.

Single crystal EPR studies of oxomolybdenum complexes are quite rare and, to our knowledge, no such measurements have been performed on oxomolybdenum dithiolene complexes. However, the natural mixed isotope EPR spectra for [Tp*MoO(bdt)] [18] and [(L3S)MoO(bdt)] [17] in frozen glass matrices have recently been simulated and the spin-Hamiltonian parameters determined. These data are collected in Table 1 along with the analogous parameters for *hpH* and *lpH* SO. A comparison of these results shows that g_1 is greater than 2.00 for both of the model complexes, with [(L3S)MoO(bdt)] possessing the larger g_1 value and markedly less rhombicity in the **g** tensor. The **A**(^{95,97}Mo) tensors for both complexes are essentially axial. However, the [Tp*MoO(bdt)] complex possesses a rather unusual **A**(^{95,97}Mo) tensor with large and approximately equal A_1 and A_3 components, and coincident **g** and **A**(^{95,97}Mo) tensors. In marked contrast, [(L3S)MoO(bdt)] possesses only one large hyperfine component, A_1, and noncoincident **g** and **A**(^{95,97}Mo) tensors with $\beta = 40°$, the latter likely being a reflection of the lower point symmetry for this complex.

The values of the principal components for the **g** and **A**(^{95,97}Mo) tensors are directly related to the electronic structure of the complexes [27]. According to Eqs. (2)–(4), one may observe g_i values greater than the free electron value (2.0023) with large contributions from Δ_{gi}^{CT}, the charge transfer terms.

$$g_x = g_e - \Delta_{g_x}^{LF} + \Delta_{g_x}^{CT}, \quad (2)$$

$$g_y = g_e - \Delta_{g_y}^{LF} + \Delta_{g_y}^{CT}, \quad (3)$$

$$g_z = g_e - \Delta_{g_z}^{LF} + \Delta_{g_z}^{CT}. \quad (4)$$

The principal factors that affect **g** tensor anisotropy and, in particular, result in g_i values greater than 2.0023 for oxomolybdenum complexes are metal–ligand covalency, ligand spin–orbit coupling, and the presence of low energy L → Mo charge transfer states that mix into the ground state by the spin–orbit operator [27]. It has been empirically observed that g_1, the largest g_i component, is the one that is most affected by the $\Delta_{g_i}^{CT}$ term while the charge transfer contributions to g_2 and g_3 are minimal. Furthermore, for high symmetry oxomolybdenum halide complexes, both ground state and excited state covalency has been determined to be the dominant contributor to **g** tensor anisotropy and g_1 values greater the free electron value.

While spin–orbit mixing of charge transfer and ligand field excited states into the ground state wavefunction are important in determining **g** tensor anisotropy [27–29], the principal components of **A**(^{95,97}Mo) primarily reflect contributions from the isotropic Fermi contact and spin dipolar terms. Therefore, the ground state orbital wavefunction plays an important role in defining the principal directions of the **A**(^{95,97}Mo) tensor. Detailed electronic absorption, magnetic circular dichroism, and resonance Raman spectroscopic studies have shown that the singly occupied orbital in oxomolybdenum thiolates and dithiolenes is always orthogonal to the Mo≡O bond (i.e. the $d_{x^2-y^2}$ orbital in our coordinate frame) and A_{zz} should be oriented along this bond. The analysis of the [Tp*MoO(bdt)] frozen glass EPR spectra was based on previous studies of high symmetry oxomolybdenum complexes and single crystal experiments on a series of [(Tp*)(MoEX$_2$)] complexes (E = O, S; X = Cl, NCS) [30]. The analysis resulted in g_1 and A_1 being colinear and tentatively assigned as g_z and A_z. Both tensor components were found to be closely aligned with the Mo≡O bond. Since [Tp*MoO(bdt)] possesses effective C_s symmetry, g_2 and A_2 are fixed by symmetry, corresponding to g_x and A_{xx} and aligned perpendicular to the mirror plane. This leaves $g_3(g_y)$ and $A_3(A_y)$ bisecting the dithiolene sulfur donors in the equatorial plane of the molecule.

The unusual EPR spectral parameters for [Tp*MoO(bdt)] are all the more unique in light of a recent single crystal EPR study on the homologous series of complexes, [(Tp*)(MoOX$_2$)] (X = F, Cl, Br) [29]. This work revealed that A_{zz} is indeed oriented along

Table 1
EPR parameters for high and low pH SO and the oxo-molybdenum(V) models of the SO active site[a]

Sample	g_1	g_2	g_3	$\langle g \rangle$	A_1	A_2	A_3	$\langle A \rangle$	α	β	γ	Refs.
HpH SO	1.990	1.966	1.954	1.970	54.4	21.0	11.3	28.9	0	14	22	[18]
LpH SO	2.007	1.974	1.968	1.983	56.7	25.0	16.7	32.8	0	18	0	[18]
[Tp*MoO(bdt)]	2.004	1.972	1.934	1.971	50.0	11.4	49.7	37.0	0	0	0	[18]
[(L3S)MoO(bdt)]	2.016	1.972	1.949	1.979	52	26	24	34	8	40	0	[17]

[a] **A**(^{95,97}Mo) are reported $\times 10^{-4}$ cm^{-1}.

the Mo≡O bond for [(Tp*)($MoOF_2$)] and [(Tp*)($MoOBr_2$)]. However, β increases dramatically across the series ($\beta(F) = 17°$, $\beta(Cl) = 31°$, and $\beta(Br) = 57°$) indicating that M–L covalency, in concert with low energy charge transfer excited states, results in the rotation of g_{zz} off the molecular z axis. Drawing upon these studies, some preliminary tentative spectral assignments may be made for [(L3S)MoO(bdt)]. The A_{zz} hyperfine component is likely oriented along the Mo≡O bond (the molecular z axis) and g_1, assigned as g_z, is rotated away from A_{zz} by ~40° [17]. The orientations of g_2, g_3, A_2, and A_3 relative to the molecular coordinate frame have yet to be determined for this complex. Regardless, it appears that a fundamental difference in electronic structure exists between [Tp*MoO(bdt)] and [(L3S)MoO(bdt)]. One explanation for these observations is that the low energy S → Mo charge transfer states of [(L3S)MoO(bdt)] spin–orbit mix more efficiently into the ground state compared to [Tp*MoO(bdt)], and this is supported by the key differences observed in the electronic absorption spectra of these two complexes.

The EPR spectral parameters obtained for [(L3S)MoO(bdt)] and [Tp*MoO(bdt)] reflect the inherent differences in their geometric structures, ultimately influencing ground and excited state electronic structural differences as well. As the first coordination sphere of [(L3S)MoO(bdt)] is remarkably similar to that of chicken SO (Fig. 1) it might be expected that these similarities extend to their EPR spectra as well. Simulations of previously reported spectra for *hpH* and *lpH* SO clearly show that g_1 for *lpH* SO is greater than g_e [18], and quite similar to that observed for [Tp*MoO(bdt)] and [(L3S)MoO(bdt)] [17] (Fig. 5), while g_1 for *hpH* SO is significantly lowered, yielding $g_1 < g_e$ [18]. Furthermore, the hyperfine anisotropy pattern observed for [(L3S)MoO(bdt)], *hpH* SO, and *lpH* SO is similar with one large hyperfine component oriented along the Mo≡O bond and two smaller hyperfine components. Additionally, the simulations of the [(L3S)MoO(bdt)] and *lpH* SO spectra yield a similar noncoincidence of the **A**(^{95,97}Mo) hyperfine and **g** tensor components. In brief,

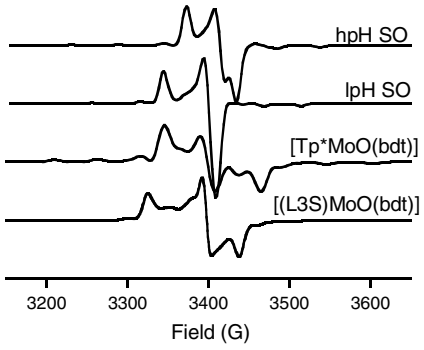

Fig. 5. EPR spectral simulations of hpH and lpH SO, and [Tp*MoO(bdt)] with the experimental spectrum of [(L3S)MoO(bdt)].

the EPR spectral parameters for [(L3S)MoO(bdt)] appear to be more closely related to those determined for SO than those for [Tp*MoO(bdt)], indicating that [(L3S)MoO(bdt)] is not only a good structural model for SO_{red} but a good electronic structural model as well. Although much can be gleaned from this type of combined analysis, the inherent ambiguities associated with spectral fitting of frozen glass EPR spectra underscore the need for detailed single crystal studies on accurate models for the one-electron reduced from of SO.

4. Summary

A geometric and electronic structural comparison of [(L3S)MoO(bdt)] and [Tp*MoO(bdt)], models for the one electron reduced site of sulfite oxidase, has been presented and discussed. EPR spectroscopy has been the technique of choice for probing the electronic structure of SO_{red}, since it is impossible to isolate 100% Mo(V) SO for electronic absorption spectroscopic studies. Thus, the relevant spin-Hamiltonian parameters have been determined for the models and directly compared with enzyme spectra.

The inherent electronic structure differences between [Tp*MoO(bdt)], and [(L3S)MoO(bdt)] are readily apparent in the EPR spectra of these complexes. Appreciable differences in g-tensor anisotropy are observed in the low temperature EPR spectra of [Tp*MoO(bdt)], and [(L3S)MoO(bdt)]. This is consistent with the fact that these complexes possess noticeably different electronic absorption spectra, which indicates that the charge transfer manifolds of these two complexes are different. Since g-tensor anisotropy is a function of both the energy of these LMCT states and their ability to spin–orbit couple with the ground state, the spectroscopic data presented for [Tp*MoO(bdt)] and [(L3S)MoO(bdt)], provide an initial basis for the interpretation of the enzyme EPR spectra. Indeed, specific spectral differences are observed between the models and the enzymes. Of particular importance is the fact that $g_1 > g_e$ for *both* [Tp*MoO(bdt)] and [(L3S)MoO(bdt)], in contrast to the fact that $g_1 < g_e$ for *hpH* SO. For [(L3S)MoO(bdt)] this is likely due to the fact that the O–Mo–$S_{thiolate}$–C dihedral angle is more obtuse than that observed in the structure of SO, where this angle was found to be ~90°. Bond torsions about this angle have been shown to be critical in modulating the degree of Mo–$S_{thiolate}$ covalency in oxomolybdenum thiolate complexes, affecting the overlap between a $S_{thiolate}$ p orbital and the Mo $d_{x^2-y^2}$ redox orbital [31].

The ability to directly examine the interplay between thiolate and dithiolene donors in [(L3S)MoO(bdt)] allows insight into possible hole superexchange mechanisms for electron transfer regeneration of the SO_{ox} site. Since the O–Mo–$S_{thiolate}$–C dihedral angle in [(L3S)MoO(bdt)] is more obtuse than that observed in

the structure of SO, akyl thiolate covalency contribution to the Mo $d_{x^2-y^2}$ orbital is increased in the model. This is evident in the intensity of the L3S $\rightarrow d_{x^2-y^2}$ LMCT band, which is of greater intensity than many of the $S_{dithiolene} \rightarrow d_{x^2-y^2}$ LMCT transitions in [Tp*MoO(bdt)]. The key point here is that the O–Mo–$S_{thiolate}$–C dihedral angle in reduced forms of SO may play a key role in the electron transfer regeneration process by acting as a switch, with dominant covalency contributions to the $d_{x^2-y^2}$ redox orbital involving the dithiolene and cysteine sulfurs being a direct function of this angle.

The results presented here demonstrate the importance of d^1 oxo-molybdenum thiolate/dithiolene electronic structure to the analysis of magnetic resonance data, since both metal–ligand covalency and the energy of low-lying LMCT states contribute significantly to the observed **g**-tensor anisotropy [27,28]. A more detailed spectroscopic and electronic structure study on these and related model complexes is currently underway in our laboratories with the primary focus of addressing specific issues regarding Mo–S bond covalency as they relate to SO mediated catalysis.

Acknowledgements

This work was supported by the NIH (GM-057378) to M.L.K. K.P. is supported by an NRSA fellowship (DK59724) from the NIH.

References

[1] R. Hille, Chem. Rev. 96 (1996) 2757.
[2] G.N. George, R.M. Garrett, R.C. Prince, K.V. Rajagopalan, J. Am. Chem. Soc. 118 (1996) 8588.
[3] S.P. Cramer, R. Wahl, K.V. Rajagopalan, J. Am. Chem. Soc. 103 (1981) 7721.
[4] R. Huber, P. Hof, R.O. Duarte, J.J.G. Moura, I. Moura, M.-Y. Liu, J. LeGall, R. Hille, M. Archer, M.J. Romao, Proc. Natl. Acad. Sci. USA 93 (1996) 8846.
[5] C. Kisker, H. Schindelin, A. Pacheco, W.A. Wehbi, R.M. Garrett, K.V. Rajagopalan, J.H. Enemark, D.C. Rees, Cell 91 (1997) 973.
[6] C. Enroth, B.T. Eger, K. Okamoto, T. Nishino, T. Nishino, E.F. Pai, Proc. Natl. Acad. Sci. USA 97 (2000) 10723.
[7] K. Peariso, R.L. McNaughton, M.L. Kirk, J. Am. Chem. Soc. 124 (2002) 9006.
[8] F.E. Inscore, R.L. McNaughton, B.L. Westcott, M.E. Helton, R. Jones, I.K. Dhawan, J.H. Enemark, M.L. Kirk, Inorg. Chem. 38 (1999) 1401.
[9] M.E. Helton, N.E. Gruhn, R.L. McNaughton, M.L. Kirk, Inorg. Chem. 39 (2000) 2273.
[10] A. Pacheco, J.T. Hazzard, G. Tollin, J.H. Enemark, J. Bioinorg. Chem. 4 (1999) 390.
[11] S.J. Elliott, A.E. McEhaney, C. Feng, J.H. Enemark, F.A. Armstrong, J. Am. Chem. Soc. 124 (2002) 11612.
[12] B.S. Lim, M.W. Willer, M. Miao, R.H. Holm, J. Am. Chem. Soc. 123 (2001) 8343.
[13] B.S. Hammes, C.J. Carrano, Inorg. Chem. 38 (1999) 4593.
[14] B.S. Hammes, C.J. Carrano, Chem. Commun. (2000) 1635.
[15] B.S. Hammes, C.J. Carrano, Inorg. Chem. 40 (2001) 919.
[16] G.R. Hanson, A.A. Brunette, A.C. McDonell, K.S. Murray, A.G. Wedd, J. Am. Chem. Soc. 103 (1981) 1953.
[17] K. Peariso, B.S. Chohan, C.J. Carrano, M.L. Kirk, Inorg. Chem. 42 (2003) 6194.
[18] I. Dhawan, J.H. Enemark, Inorg. Chem. 35 (1996) 4873.
[19] W.E. Cleland Jr., K.M. Barnhart, K. Yamanouchi, D. Collison, F.E. Mabbs, R.B. Ortega, J.H. Enemark, Inorg. Chem. 26 (1987) 1017.
[20] M.J. Nilges, Ph.D. Dissertation, University of Illinois, Urbana, IL, 1979.
[21] R.L. Belford, M.J. Nilges, in: . In: 21st Rocky Mountain Conference, Denver, CO, 1979.
[22] A.M. Maurice, Ph.D. Dissertation, University of Illinois, Urbana, 1980.
[23] I.K. Dhawan, A. Pacheco, J.H. Enemark, J. Am. Chem. Soc. 116 (1994) 7911.
[24] F. Jalilehvand, B.S. Lim, R.H. Holm, B. Hedman, K.O. Hodgson, Inorg. Chem. 42 (2003) 5531.
[25] M.E. Helton, A. Pacheco, J. McMaster, J.H. Enemark, M.L. Kirk, J. Inorg. Biochem. 80 (2000) 227.
[26] F.E. Mabbs, D. Collison, Electron Paramagnetic Resonance of d Transition Metal Compounds, Elsevier, Amsterdam, 1992.
[27] C. Balagopalakrishna, J.T. Kimbrough, T.D. Westmoreland, Inorg. Chem. 35 (1996) 7758.
[28] J. Swann, T.D. Westmoreland, Inorg. Chem. 36 (1997) 5348.
[29] N.S. Niaples, T.D. Westmoreland, Inorg. Chem. 36 (1997) 756.
[30] D. Collison, D.R. Eardley, F.E. Mabbs, K. Rigby, M.A. Bruck, J.H. Enemark, P.A. Wexler, J. Chem. Soc., Dalton Trans. (1994) 1003.
[31] R.L. McNaughton, A.A. Tipton, N.D. Rubie, R.R. Conry, M.L. Kirk, Inorg. Chem. 39 (2000) 5697.

Available online at www.sciencedirect.com
SCIENCE DIRECT®
Polyhedron 23 (2004) 507–508
POLYHEDRON
www.elsevier.com/locate/poly

Author Index of Symposia-In-Print number 26

Akita, M., see Takahashi, Y., 225
Alleyne, B.D., see Li, J., 419
Alvarez, H.M., Tanski, J.M. and Rabinovich, D., Poly(mercaptoimidazolyl)borate chemistry and the predominance of κ^3-*S*,*S*,*H* over κ^2-*S*,*S* or κ^3-*S*,*S*,*S* coordination modes: unexpected formation of square pyramidal Ni(II) complexes, 395
Arvin, M.E., see Joshi, H.K., 429

Bau, R., see Li, J., 419
Bridgewater, B.M., see Docrat, A., 481
Burzlaff, N., see Peters, L., 245

Caballero, A., Carmen Carrión, M., Espino, G., Jalón, F.A. and Manzano, B.R., Ruthenium hydride complexes with a heteroscorpionate ligand derived from methane: 2-phenoxy-bis(pyrazol-1-yl)methane. The hemilabile role of the ligand in substitution and proton transfer reactions, 361
Campello, M.P.C., see Paulo, A., 331
Campo, J.A., see Criado, R., 301
Cano, M., see Criado, R., 301
Carducci, M.D., see Joshi, H.K., 429
Carmen Carrión, M., see Caballero, A., 361
Carrano, C.J., see Shirin, Z., 239
Castellano, E.E., see Soares, L.F., 205
Cheng, P., see Sun, Y.-J., 211
Churchill, D.G., see Docrat, A., 481
Cingolani, A., see Pettinari, C., 451
Ciunik, Z., see Ruman, T., 219
Correia, J.D.G., see Paulo, A., 331
Criado, R., Cano, M., Campo, J.A., Heras, J.V., Pinilla, E. and Torres, M.R., Mono and binuclear rhodium dicarbonyl complexes containing the hydridotris(3-p-chlorophenylpyrazol-1-yl)borate ligand (Tp^{PhCl}). X-ray structures of the binuclear complex $[(OC)_2Rh(\mu{:}\kappa^2,\kappa^1\text{-}Tp^{PhCl})Rh(Cl)(CO)_2]$ and of three isomers of $[Rh(\kappa^2\text{-}Tp^{PhCl})(CO)_2]$, 301

Daff, P.J., see Etienne, M., 379
Dahan, F., see Etienne, M., 379
DiPasquale, A.G., see Soper, J.D., 323
diTargiani, R.C., see Karambelkar, V.V., 471
Djurovich, P.I., see Li, J., 419
Docrat, A., Morlok, M.M., Bridgewater, B.M., Churchill, D.G. and Parkin, G., N–H···O hydrogen bonding interactions in tetrahedral $[ZnS_4]$ complexes of relevance to zinc enzymes: the synthesis, structures and reactivity of *tris*(2-mercapto-1-arylimidazolyl)hydroborato zinc(2-mercapto-1-arylimidazole) complexes, $\{[Tm^{Ar}]Zn(mim^{Ar})\}[ClO_4]$ (Ar=Ph, p-Tol), 481
Dodds, C.A., Jagoda, M., Reglinski, J. and Spicer, M.D., Soft scorpionate complexes of the fourth and fifth period elements arsenic and tin, 445
Donnadieu, B., see Etienne, M., 379
Doriguetto, A.C., see Soares, L.F., 205
Durivage, J.C., see Joshi, H.K., 429

Eagle, A.A., Gable, R.W., Thomas, S., Sproules, S.A. and Young, C.G., Sulfur atom transfer reactions of tungsten(VI) and tungsten(IV) chalcogenide complexes, 385
Eichhorn, D.M., see Siemer, C.J., 235
Ellena, J., see Soares, L.F., 205
Enemark, J.H., see Joshi, H.K., 429
Espino, G., see Caballero, A., 361
Etienne, M., Hierso, J.-C., Daff, P.J., Donnadieu, B. and Dahan, F., Mono and dinuclear hydrotris(3,5-dimethylpyrazolyl)borato tantalum complexes, 379

Fabbrizzi, L., Licchelli, M., Poggi, A., Sacchi, D. and Zampa, C., A chromogenic penta-aza scorpionand for nickel(II) and copper(II) ions, 373
Ferrence, G.M., see Morissette, M., 263

Gable, R.W., see Eagle, A.A., 385
Galler, J.L., Goodchild, S., Gould, J., McDonald, R. and Sella, A., Tris-pyrazolylborate complexes of redox inactive lanthanides – the structures of $[(Tp^{Me2})_2NdX]$ (X=Cl, NPh_2, dpm, H_2BEt_2), 253
Gardinier, J.R., see Reger, D.L., 291
Goh, T.K.H.H., see Rasika Dias, H.V., 273
Goldberg, D.P., see Karambelkar, V.V., 471
Goodchild, S., see Galler, J.L., 253
Gould, J., see Galler, J.L., 253
Gruhn, N.E., see Joshi, H.K., 429

Hata, Y., see Kitano, T., 283
Haufe, S., see Morissette, M., 263
Heras, J.V., see Criado, R., 301
Hierso, J.-C., see Etienne, M., 379
Hikichi, S., see Takahashi, Y., 225
Ho, N.N., see Li, J., 419

Incarvito, C.D., see Karambelkar, V.V., 471
Incarvito, C.D., see Voo, J.K., 405
Incarvito, C.D., see Pariya, C., 439

Jagoda, M., see Dodds, C.A., 445
Jalón, F.A., see Caballero, A., 361
Jiang, Z.-H., see Sun, Y.-J., 211
Jones, W.D., see Vetter, A.J., 413
Joshi, H.K., Arvin, M.E., Durivage, J.C., Gruhn, N.E., Carducci, M.D., Westcott, B.L., Lichtenberger, D.L. and Enemark, J.H., Photoelectron spectra of potassium salts of hydrotris(pyrazol-1-yl)borates: electronic structure of the electron withdrawing scorpionates $Tp^{(CF_3)_2}$, Tp^{*Cl} and comparison to Tp* and Tp, 429

Kahol, P.K., see Siemer, C.J., 235
Karambelkar, V.V., diTargiani, R.C., Incarvito, C.D., Zakharov, L.N., Rheingold, A.L., Stern, C.L. and Goldberg, D.P., Multiple bonding modes exhibited by heteroscorpionate N_2S(alkylthiolate) ligands with Zn(II) and Fe(II), 471
Kirk, M.L. and Peariso, K., Ground and excited state spectral comparisons of models for sulfite oxidase, 499
Kitano, T., Sohrin, Y., Hata, Y., Mukai, H., Wada, H. and Ueda, K., Highly selective extraction of Cu(II) and Zn(II) using $[B(3\text{-iPrpz})_4]^-$ (iPrpz=isopropylpyrazolyl), 283

doi:10.1016/S0277-5387(04)00018-X

Li, J., Djurovich, P.I., Alleyne, B.D., Tsyba, I., Ho, N.N., Bau, R. and Thompson, M.E., Synthesis and characterization of cyclometalated Ir(III) complexes with pyrazolyl ancillary ligands, 419
Liao, D.-Z., see Sun, Y.-J., 211
Licchelli, M., see Fabbrizzi, L., 373
Lichtenberger, D.L., see Joshi, H.K., 429
Lobbia, G.G., see Pettinari, C., 451

Manzano, B.R., see Caballero, A., 361
Marchetti, F., see Pettinari, C., 451
Martini, D., see Pettinari, C., 451
Mascarenhas, Y.P., see Soares, L.F., 205
Mayer, J.M., see Soper, J.D., 323
McDonald, R., see Morissette, M., 263
McDonald, R., see Galler, J.L., 253
Menezes, D.C., see Soares, L.F., 205
Morissette, M., Haufe, S., McDonald, R., Ferrence, G.M. and Takats, J., Steric saturation of the ytterbium coordination environment: $(Tp^{tBu,Me})Yb(OMes)$, a four coordinate, monomeric, base-free divalent lanthanide complex, its solvation with tetrahydrofuran, and comparison to the β-diketonate complex, $(Tp^{tBu,Me})Yb(dpm)$, 263
Morlok, M.M., see Docrat, A., 481
Moro-oka, Y., see Takahashi, Y., 225
Mukai, H., see Kitano, T., 283

Pariya, C., Incarvito, C.D., Rheingold, A.L. and Theopold, K.H., Preparation and ligand substitution reactions of $Tp^{Ms}Ru(COD)H$ including intramolecular ligand metalation, 439
Parkin, G., see Docrat, A., 481
Paulo, A., Correia, J.D.G., Campello, M.P.C. and Santos, I., A short ride on scorpionates: from d- to f-elements, 331
Peariso, K., see Kirk, M.L., 499
Pellei, M., see Pettinari, C., 451
Peters, J.C., see Thomas, J.C., 489
Peters, L. and Burzlaff, N., Complexes bearing an enantiopure N,N,O scorpionate ligand derived from (−)-menthone, 245
Pettinari, R., see Pettinari, C., 451
Pettinari, C., Cingolani, A., Lobbia, G.G., Marchetti, F., Martini, D., Pellei, M., Pettinari, R. and Santini, C., Copper and silver derivatives of scorpionates and related ligands, 451
Pinilla, E., see Criado, R., 301
Poggi, A., see Fabbrizzi, L., 373

Rabinovich, D., see Alvarez, H.M., 395
Rasika Dias, H.V. and Goh, T.K.H.H., Fluorinated tris(pyrazolyl)-borates. Syntheses and characterization of sodium and copper complexes of $[HB(3\text{-}(CF_3),5\text{-}(Ph)Pz)_3]^-$, 273
Reger, D.L., Gardinier, J.R. and Smith, M.D., Synthesis of *meta*-$C_6H_4[C(1\text{-pyrazolyl})_2(2\text{-pyridyl})]_2$, a fixed geometry bitopic hetero-scorpionate and the crystal structure of its unusual square planar silver(I) complex, 291
Reglinski, J., see Dodds, C.A., 445
Rheingold, A.L., see Karambelkar, V.V., 471
Rheingold, A.L., see Voo, J.K., 405
Rheingold, A.L., see Pariya, C., 439
Rhile, I.J., see Soper, J.D., 323
Riordan, C.G., see Voo, J.K., 405
Ruman, T., Ciunik, Z. and Wolowiec, S., Complexes of heteroscorpionate trispyrazolylborate ligands. Part XII. Variable hapticity of hydrobis(3-phenyl-5-isopropylpyrazolyl)(3,5-dimethylpyrazolyl) borate in its rhodium(I) complexes with COD and NBD, 219

Sacchi, D., see Fabbrizzi, L., 373
Santini, C., see Pettinari, C., 451
Santos, I., see Paulo, A., 331
Sella, A., see Galler, J.L., 253
Shen, P.-W., see Sun, Y.-J., 211
Shen, W.-Z., see Sun, Y.-J., 211
Shirin, Z. and Carrano, C.J., New heteroscorpionate ligands with hydrogen bond donor and acceptor groups: synthesis, characterization and reactivity with divalent Co, Zn and Ni ions, 239
Siemer, C.J., VanStipdonk, M.J., Kahol, P.K. and Eichhorn, D.M., A coordination polymer from a cyanoscorpionate complex, 235
Silva, R.M., see Soares, L.F., 205
Smith, M.D., see Reger, D.L., 291
Soares, L.F., Menezes, D.C., Silva, R.M., Doriguetto, A.C., Ellena, J., Mascarenhas, Y.P. and Castellano, E.E., Potassium tetrakis(2-mercaptothiazolyl)borate; an open-framework material: synthesis and X-ray structure analysis, 205
Sohrin, Y., see Kitano, T., 283
Soper, J.D., Rhile, I.J., DiPasquale, A.G. and Mayer, J.M., Oxidation of $TpOs^{III}(NH_2Ph)Cl_2$ to $TpOs^{IV}(NHPh)Cl_2$ by O_2, 323
Spicer, M.D., see Dodds, C.A., 445
Sproules, S.A., see Eagle, A.A., 385
Stern, C.L., see Karambelkar, V.V., 471
Sun, Y.-J., Shen, W.-Z., Cheng, P., Yan, S.-P., Liao, D.-Z., Jiang, Z.-H. and Shen, P.-W., Synthesis, structure and spectroscopic properties of novel half-sandwich nickel(II) complexes with less hindered hydrotris(pyrazolyl)borate ligand, 211

Takahashi, Y., Hikichi, S., Moro-oka, Y. and Akita, M., Oxygenation of a series of cationic aquoruthenium complexes, Tp^{iPr2}-$Ru(OH_2)_nL_{3-n}{\cdot}CF_3SO_3{\cdot}(THF)_x$, leading to mono- and dinuclear aquo-hydroxo complexes supported by unique hydrogen bonding networks, 225
Takats, J., see Morissette, M., 263
Tanski, J.M., see Alvarez, H.M., 395
Templeton, J.L., see Vogeley, N.J., 311
Theopold, K.H., see Pariya, C., 439
Thomas, S., see Eagle, A.A., 385
Thomas, J.C. and Peters, J.C., Platinum-alkyl and hydride complexes supported by a tris(phosphino)borate ligand: structural and spectroscopic studies, 489
Thompson, M.E., see Li, J., 419
Torres, M.R., see Criado, R., 301
Trofimenko, S., Scorpionates: genesis, milestones, prognosis, 197
Tsyba, I., see Li, J., 419

Ueda, K., see Kitano, T., 283

VanStipdonk, M.J., see Siemer, C.J., 235
Vetter, A.J. and Jones, W.D., Carbon–hydrogen bond activation of chloroalkanes by a rhodium trispyrazolylborate complex, 413
Vogeley, N.J. and Templeton, J.L., Interconversions of simple monodentate nitrogen donor ligands bound to Tp' tungsten fragments, 311
Voo, J.K., Incarvito, C.D., Yap, G.P.A., Rheingold, A.L. and Riordan, C.G., Tris(imidazolyl) cadmium and zinc complexes: structural and spectroscopic characterization of $M\text{–}OH_2$ motifs, 405

Wada, H., see Kitano, T., 283
Westcott, B.L., see Joshi, H.K., 429
Wolowiec, S., see Ruman, T., 219

Yan, S.-P., see Sun, Y.-J., 211
Yap, G.P.A., see Voo, J.K., 405
Young, C.G., see Eagle, A.A., 385

Zakharov, L.N., see Karambelkar, V.V., 471
Zampa, C., see Fabbrizzi, L., 373

Available online at www.sciencedirect.com
SCIENCE DIRECT®
Polyhedron 23 (2004) 511–518
POLYHEDRON
www.elsevier.com/locate/poly

A structural model for oxidized type II copper nitrite reductase with a polyimidazole tripodal ligand

Marciela Scarpellini [a], Ademir Neves [b], Eduardo E. Castellano [c], Eduardo F. de Almeida Neves [d], Douglas W. Franco [a,*]

[a] *Departamento de Química e Fisica Molecular de São Carlos, Universidade de São Paulo, Av. Trabalhador San Carlense 400, São Carlos, SP 13560-970, Brazil*
[b] *Departamento de Química, Universidade Federal de Santa Catarina, Florianópolis, SC 88040-900, Brazil*
[c] *Instituto de Física, Universidade de São Paulo, São Carlos, SP 13560-970, Brazil*
[d] *Departamento de Química, Universidade Federal de São Carlos, São Carlos, SP 13565-905, Brazil*

Received 29 July 2003; accepted 26 August 2003

Abstract

The new copper(II)–nitrite complex $[Cu^{II}(L)(ONO)]ClO_4$ (**2**), L = [(bis(1-methylimidazol-2-yl)methyl)(2-(pyridyl-2-yl)ethyl)amine] was synthesized and characterized by cyclic voltammetry, UV–Vis spectroscopy, X-band EPR and X-ray crystallography. Complex **2** crystallizes in the monoclinic system, space group $P2_1/n$ and has the metal center in a somewhat distorted square pyramidal geometry, with three nitrogen atoms from the chelate ligand and one nitrite ion outlining the basal plane. One imidazole nitrogen from the tripodal molecule is at the apical position at 2.158(2) Å from the metal. Spectrophotometric and electrochemical experiments in water solution reveal that complex **2** readily releases the nitrite ligand in this medium ($t_{1/2} < 10$ s at 25 °C) yielding the precursor complex **1**, $[Cu^{II}(L)(S)]^{2+}$. The affinity of complex **1** for nitrite was evaluated by spectrophotometric titration, following the appearance of the Cu(II)–nitrite band at 376 nm, and by the cyclic voltammetric peak potential data. Both experiments were carried out in methanolic solution ($\mu = 0.1$ mol L^{-1}, $TBAPF_6$, $T = 25 \pm 1$ °C). The formation constant value obtained from the voltammetric experiments ($1.2 \pm 0.1 \times 10^3$ M^{-1}) agrees quite well with that from the spectrophotometric titration ($1.4 \pm 0.2 \times 10^3$ M^{-1}) and is within the range of values observed for other Cu(II)–nitrite complexes. The geometrical arrangements of the tripodal ligand and the nitrite ion coordination allows considering complex **2** a potential biomimetic structural model for type II copper in nitrite reductases.
© 2003 Elsevier Ltd. All rights reserved.

Keywords: Cu-NIRs; Model complex; Crystalline structure; Tripodal ligand; Polyimidazole ligand

1. Introduction

Copper-containing nitrite reductases (Cu-NIRs) are a class of enzymes related to the reduction of nitrite (NO_2^-) to nitric oxide in one electron pathway [1,2]. This is one of the four classes of enzymes involved in the denitrification process, in which nitrate is gradually reduced to nitrite, gaseous nitric oxide, nitrous oxide and finally dinitrogen [1–3]. This is an anaerobic respiratory process achieved by anaerobic denitrifying which returns fixed nitrogen from the soil to the atmosphere [4]. There are two types of denitrification-associated nitrite reductases, one containing copper (Cu-NIRs) and the other an iron-heme core (Fe-NIRs) in the active site. Although the iron-containing nitrite reductases (Fe-NIRs) are the most abundant NIRs in nature, the Cu-NIRs ones show more physiological diversity, as they are found in a greater variety of ecological systems [5,6]. Cu-NIRs have been isolated from a large number of bacteria and are spectroscopically [7–10] and structurally [11–14] well characterized. Recently [15], two new mutant forms of NIRs from *Alcaligenes faecalis* (AfNIRs), D98N[NO_2^-] and H255[NO_2^-], have been structurally characterized. The D98N[NO_2^-] is a mutant AfNIR, in which Asp98 is displaced at ca. 1.00 Å in relation to the wild AfNIR. H255[NO_2^-] is another mutant AfNIR, in which His255 is replaced by Asn255,

* Corresponding author. Tel.: +55-16-2739970; fax: +55-16-2739976.
E-mail address: douglas@iqsc.usp.br (D.W. Franco).

0277-5387/$ - see front matter © 2003 Elsevier Ltd. All rights reserved.
doi:10.1016/j.poly.2003.09.036

providing significant insight in the understanding of the catalytic mechanism involved in this important environmental process [15]. The native AfNIR [13] is a green 110 kDa homotrimer, with each monomer containing one type I and one type II copper centers. Type I is coordinated to four chain amino acids (His95, Cys136, His45 and Met150) in distorted trigonal bipyramidal geometry. Type II presents a tetrahedral coordination and is bound to three histidine ligands (His100, His135 and His306) and one water molecule. In the oxidized D98N[NO_2^-] structure [8], nitrite is coordinated to the type II copper as a bidentate ligand via the oxygen atoms [Cu502–O1: 2.42 (0.05) and Cu502–O2: 2.21 (0.08) Å]. This coordination form is the same as that observed in the wild enzyme [13], in which the nitrite ion replaces the water molecule. In contrast, the structure [15] of the oxidized H255N[NO_2^-] features the binding of the nitrite through a single oxygen atom O2 [Cu502–O1: 3.60 (0.15) and Cu502–O2: 2.16 (0.05)] without the displacement of the water ligand [Cu502–503OH_2: 2.15 (0.09)]. Type II copper is therefore pentacoordinated and adopts a distorted square pyramidal geometry, in which the histidine HIS306 is at the apical position. The reduced forms of the D98[NO_2^-] and H255[NO_2^-] were also studied and in both structures nitrite adopts a similar position in the active site to that of the oxidized forms. Based on these studies, Boulanger and Murphy [15] suggested that the nitrite form mimics the electronic and structural properties of a proposed catalytic intermediate [12] in native AfNIR and that this stage is energetically accessible. In the catalytic mechanism, a protonated nitrite molecule [12] displaces the water ligand and coordinates to the type II copper prior to the electron transfer from the type I copper. Then, after the reduction of the type II copper, a pentacoordinated copper(II) transient complex is formed, which is coordinated to one hydroxyl and one nitric oxide. The protonation of the active site, the release of the NO molecule and the rebinding of the water ligand to the type II copper complete the catalytic process.

Aiming to mimic the arrangement of the histidine and the nitrite groups in the type II Cu-NIRS, we describe here a new copper(II)–nitrite complex (**2**) with a polyimidazole moiety. The copper(II)–chloride precursor complex (**1**) is only briefly discussed here, as it will be fully reported in a later paper [16]. Complex **2** presents structural features that allow us to consider it as a model for the active site of the oxidized type II copper nitrite reductases.

2. Experimental

2.1. Abbreviations

L, [(bis(1-methylimidazol-2-yl)methyl)(2-(pyridyl-2-yl)ethyl)amine]; $TBAPF_6$, tetrabutylammonium hexafluorophosphate; TEPA, tris[2-(2-pyridyl)ethyl] amine; TMBA, tris((benzimidazol-2-yl)methyl)amine; BIAP, *N*,*N*-bis(2-ethyl-5-methyl-imidazol-4-ylmethyl)aminopropane; L^{py}, 1,4-diisopropyl-7-R″-1,4,7-triazacyclononane (R″ = 6-methyl-2-pyridylmethyl); 1-BB, bis[(1-methylbenzimidazol-2-yl)methyl]amine; bdmppy, 2,6-bis[(3,5-dimethyl)pyrazol-1-yl]pyridine; dpyam, di-2-pyridylamine.

2.2. Materials

2-Methyl-2-imidazolecarboxaldehyde [17] and the [(bis(2-methylimidazol-2-yl)methyl)(2-(pyridyl-2-yl)ethyl) amine] (**L**) tripodal ligand [18] were synthesized as previously described. All reagents for syntheses and analyses were of analytical and/or spectroscopic grade and were used without further purification. In aqueous studies, deionized (Millipore) distilled water was used.

2.3. Instrumentation

Infrared spectra (KBr pellet) were taken with an FTIR Bomen MB-102 spectrometer. Elemental analysis was performed on a Perkin–Elmer elemental analyzer 2400 CHN. UV–Vis spectra were recorded on a Carry 5G UV–Vis spectrometer. Cyclic voltammograms were recorded using a Princeton Applied Research (PAR) 264A at room temperature (25 ± 1) °C and under argon atmosphere. A standard three-electrode cell was used, composed of the following electrodes: a glass carbon working, a platinum auxiliary and calomel or Ag/AgCl reference, for use in aqueous or methanolic measurements, respectively. Aqueous cyclic voltammograms (+1.2 to −0.5 V) of complexes **2** and **1** (1.0×10^{-3} mol L^{-1}) were recorded in CF_3COOH solutions (0.2 mol L^{-1}) in the pH range 4.5–8.5 (pH values were adjusted with NaOH solution, 0.1 mol L^{-1}). In the methanolic experiments, cyclic voltammograms were recorded in the +1.0 to −0.7 V range using $TBAPF_6$ [0.1 mol L^{-3}] as the supporting electrolyte and the ferrocenium–ferrocene [19] couple (Fc^+/Fc = 197 mV versus SCE, $\Delta E_p = 126$ mV) to monitor the reference electrode potential. EPR spectra were recorded on a Bruker ESP300E spectrometer at room and liquid N_2 temperatures.

2.4. Equilibrium constant determination

Spectrophotometric measurements were taken in methanol as follows: A methanolic solution of complex **1** (1.5×10^{-3} mol L^{-1}, $\mu = 0.1$ mol L^{-1} $TBAPF_6$) and a standard methanolic solution of sodium nitrite (1.8×10^{-2} mol L^{-1}) were previously prepared and pre-equilibrated at 25 ± 1 °C. A fixed volume of 2 mL complex **1** solution was placed in a cuvette, into which aliquots of the nitrite solution were added and spectrophotometric

measurements were taken after each addition until the relation [complex]:[nitrite] = 1 was reached. The equilibrium constant (K_{eq}) for the $[Cu^{II}(L)(ONO)]^+$ species was determined by the measurement of solutions containing the same concentration of complex **1**, C_x, and variable concentrations of the nitrite ligand (C'_L and C''_L). Eqs. (1) and (2) [20] were applied to calculate the K_{eq} constant, in which C'_z and C''_z are the concentration of the complex with absorbance values A_1 and A_2, respectively, at 376 nm. The absorbance values were corrected with respect to the absorbance of the precursor $[Cu^{II}(L)(S)]^+$ complex and the dilution.

$$K_{eq} = \frac{(C_x - pC'_z)C''_z}{pC'_z}, \tag{1}$$

where

$$C'_z = \frac{C_z(C''_L - pC'_L)}{p(C''_L - C'_L)} \quad \text{and} \quad C''_z : C'_z = A_2 : A_1 = p. \tag{2}$$

Potentiometric experimental data were also used to estimate the relative power of the nitrite ligand to complex with the $[Cu^{II}(L)(S)]^{2+}$ and $[Cu^{I}(L)(S)]^+$ species, since the electrochemical data correspond to the Cu(II)/Cu(I) redox system. This estimate can be achieved by means of the Leden "complexity" function, $F_0(x)_{ox,red}$ (Eq. (3)), in the presence of a defined concentration of the complexing agent [21]. In addition, estimation of the average ligand number $\bar{n}_{ox,red}$ (Bjerrum's function, Eq. (4)) [22] is also possible. These functions are readily evaluated from electrochemical data [23,24] at 25 °C.

$$F_0(x)_{ox,red} \cong \text{anti}\log\left\{ -\frac{n[(E_{1/2})_x - (E_{1/2})_s]}{0.05915} \right\} \cong 1 + (\beta_1)_{ox,red}[NO_2^-] + (\beta_2)_{ox,red}[NO_2^-]^2 + \cdots, \tag{3}$$

$$\Delta\frac{(E_{1/2})_{x',x}}{\log[X]} = \bar{n}_{ox,red}\frac{0.05915}{n}, \tag{4}$$

where the $(E_{1/2})_x$ and $(E_{1/2})_s$ are, respectively, the half-wave potentials in the complexing and non-complexing medium; n is the number of electrons involved in the Cu(II)/Cu(I) reduction process, [X] is the concentration of the complexing agent and ox,red is the Cu(II),Cu(I) oxidation states of the metal center.

From a plot $F_1(x)_{ox,red}$ versus [nitrite], the K_{ox}/K_{red} ratio can be graphically calculated [23,24] according to the following equations:

$$F_1(x)_{ox,red} = (\beta_1)_{ox,red} + (\beta_2)_{ox,red}[NO_2^-] + \cdots \tag{5}$$

$$F_1(x)_{ox,red} = \frac{F_0(x)_{ox,red} - 1}{[NO_2^-]}. \tag{6}$$

2.5. Synthesis

2.5.1. [Cu^II(L)Cl]ClO4 (1)

A solution of $CuCl_2 \cdot 2H_2O$ (0.17 g, 1 mmol, in 10 mL of ethanol) was added to an ethanolic solution of **L** (0.31 g, 1 mmol, in 10 mL) while stirring and heating. After 15 min, $NaClO_4 \cdot H_2O$ (0.12 g, 1 mmol, in 10 mL) was added resulting in a deep blue solution, from which a blue power was obtained. Monocrystals suitable for X-ray analysis were obtained from recrystallization in methanol/diisopropyl ether (5:1) solution. Yield: 0.28 g (56%). *Anal.* Calc. for $CuC_{17}H_{22}N_6O_4Cl_2$: C, 40.13; H, 4.36; N, 16.52. Found: C, 39.74; H, 4.33; N, 16.12%. $\Lambda_M = 194\ \Omega^{-1}\,cm^2\,mol^{-1}$ in CH_3CN. IR(KBr): ν(OH) 3445; $\nu(CH_{Ar}/CH_{Alif})$ 3158–2945; ν(C=N/C=C) 1602–1442; $\nu(ClO_4)$ 1096; $\delta(CH_{Ar})$ 753 in cm^{-1}.

2.5.2. [Cu^II(L)(ONO)]ClO4 (2)

Approximately 0.28 g of $NaNO_2$ (40 mmol) was added to a round-bottom flask containing a solution of the precursor complex $[Cu^{II}(L)Cl]ClO_4$ (**1**) (0.20 g, 0.40 mmol, in 30 mL of HBF_4, 0.10 mol L^{-1}). The reaction flask was sealed, stirred for 20 min and kept at 4 °C for 1 day, after which monocrystals suitable for X-ray analysis were collected. Yield: 60%. *Anal.* Calc. for $CuC_{17}H_{22}N_7O_6Cl$: C, 39.3; H, 4.27; N, 18.9. Found C, 39.3; H, 4.17; N, 18.8%. IR(KBr): $\nu(CH_{Ar}/CH_{Alif})$ 3151–2905; ν(C=N/C=C) 1603–1441; ν(N=O) 1383; ν(N–O) 1270; $\nu(ClO_4)$ 1092; $\delta(CH_{Ar})$ 761 in cm^{-1}.

Caution! Perchlorate salts with organic ligands are potentially explosive and should be carefully handled.

2.6. X-ray crystallography

Data collection, structure solution and refinement. The crystal was measured on an Enraf–Nonius Kappa-CCD diffractometer with graphite monochromated Mo Kα ($\lambda = 0.71073$ Å) radiation. Data were collected up to 50° in 2θ, with a redundancy of 4. The final unit cell parameters were based on all reflections. Data collection was made using the COLLECT program [25]; integration and scaling of the reflections were performed with the HKL Denzo-Scalepack system of programs [26]. Absorption corrections were carried out using the multi-scan method [27]. The structure was solved by direct methods with SHELXS 97 [28]. The model was refined by full-matrix least-squares on F^2 with SHELXL 97 [29]. All hydrogen atoms were stereochemically positioned and refined with the riding model [29]. Hydrogen atoms of the aromatic rings and CH_2 were set isotropic with a thermal parameter 20% greater than the equivalent isotropic displacement parameter of the atom to which each one is bonded; this percentage was set to 50% for the hydrogen atoms of the methyl groups. Data collection and experimental

details for the complex are summarized in Table 1 and relevant bond lengths and angles are listed in Table 2.

Table 1
Crystal data and structure refinement for the complex $[Cu^{II}(L)(ONO)]ClO_4$ (**2**)

Empirical formula	$C_{17}H_{22}ClCuN_7O_6$
Formula weight	519.41
Temperature (K)	120(2)
Wavelength (Å)	0.71073
Crystal system, space group	monoclinic, $P2_1/n$
Unit cell dimensions	
a (Å)	10.9419(4)
b (Å)	12.2950(5)
c (Å)	16.7661(6)
β (°)	107.614(2)
Volume (Å^3)	2149.81(14)
Z, D_{calc} (Mg m^{-3})	4, 1.605
Absorption coefficient (mm^{-1})	1.191
$F(000)$	1068
Crystal size (mm)	$0.16 \times 0.08 \times 0.06$
θ range for data collection (°)	3.04–25.00
Index ranges	$-13 \leqslant h \leqslant 11$, $-14 \leqslant k \leqslant 14$, $-19 \leqslant l \leqslant 19$
Reflections collected/unique	13098/3760 [$R_{int} = 0.0461$]
Completeness to $2\theta = 25.00$ (%)	94.8
Maximum and minimum transmission	0.9320 and 0.8323
Refinement method	full-matrix least-squares on F^2
Data/restraints/parameters	3760/0/291
Goodness-of-fit on F^2	1.105
Reflections with $I > 2\sigma(I)$	3227
Final R indices [$I > 2\sigma(I)$]	$R_1 = 0.0389$, $wR_2 = 0.0951$
R indices (all data)	$R_1 = 0.0476$, $wR_2 = 0.1003$
Largest difference peak and hole (e Å^{-3})	0.356 and −0.713

Table 2
Selected bond distances (Å) and angles (°) for the complex $[Cu^{II}(L)(ONO)]ClO_4$ (**2**)

Bond distances	
Cu–N(5)	1.963(3)
Cu–O(1)	1.973(2)
Cu–N(2)	2.030(2)
Cu–N(3)	2.132(2)
Cu–N(7)	2.158(2)
O(1)–N(1)	1.262(4)
O(2)–N(1)	1.215(4)
Bond angles	
N(5)–Cu–O(1)	93.18(11)
N(5)–Cu–N(2)	153.89(10)
O(1)–Cu–N(2)	93.23(10)
N(5)–Cu–N(3)	79.89(11)
O(1)–Cu–N(3)	170.30(10)
N(2)–Cu–N(3)	95.96(10)
N(5)–Cu–N(7)	110.44(10)
O(1)–Cu–N(7)	95.60(9)
N(2)–Cu–N(7)	94.07(9)
N(3)–Cu–N(7)	80.65(9)
N(1)–O(1)–Cu	116.6(2)
O(2)–N(1)–O(1)	116.0(3)

3. Results and discussion

3.1. Synthesis and general characterization

The synthesis of **2** was achieved by the reaction of the precursor complex $[Cu^{II}(L)Cl]ClO_4$ (**1**) with $NaNO_2$ in a 1:1 ratio to give green single-crystals. The elemental analysis agrees quite well with the proposed $CuC_{17}H_{22}N_7O_6Cl$ formula. The infrared spectrum of **2** is mainly characterized by the skeletal ligand vibrations, the ν(N=O)/ν(N–O) stretching of the nitrite ligand and the ClO_4^- counter-ion. Although nitrite ligand vibrations can only be assigned with certainty by isotopic substitution, they are tentatively attributed here through the spectra differences between complexes **1** and **2**.

3.2. X-ray analysis

A ZORTEP [30] view of complex **2** is presented in Fig. 1. Complex **2** is a nitrite compound five-coordinated in a distorted square pyramidal stereochemistry, as the O(2) atom of the nitrite ligand is far from the metal center [Cu–O(2) = 2.76(2) Å]. This square pyramidal distortion is evidenced by the structural Addison [31] parameter ($\tau = 0.27$), which is zero for a perfectly square pyramidal geometry. As seen in Fig. 1, the tripodal ligand is coordinated in such a way that the ethylpyridine group (N2) lies in the basal plane and is *trans* to an imidazole nitrogen (N5) and mutually *cis* to the amine nitrogen (N3) and to one oxygen atom (O1) from the nitrite group. The coordination sphere is completed by the other imidazole nitrogen (N7) coordinated apically at 2.158(2) Å. The small bite angle resulting from the five-membered ring of the apical coordination, N(3)–Cu(1)–N(7) = 80.66(9)° deviates significantly from orthogonality. Consequently, the Cu^{II} ion is 0.1761(1) Å

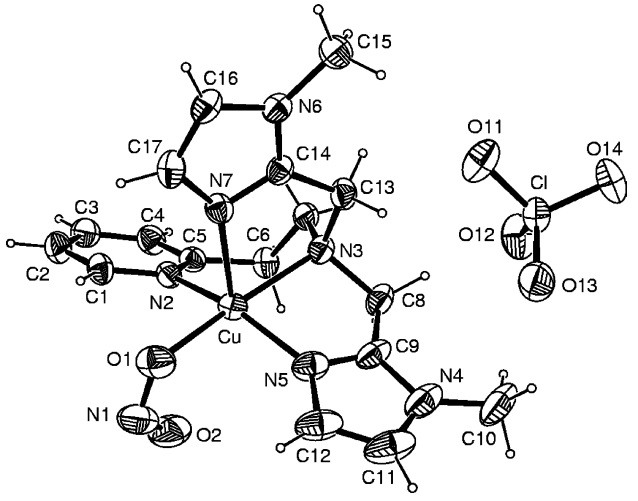

Fig. 1. The ZORTEP view of complex $[Cu(L)(ONO)]ClO_4$ (**2**), showing the atom labeling and the 50% probability ellipsoids.

above the least-square plane through N(2), N(3), O(1) and N(5). The coordination mode in complex **2** shows that the ligand undergoes a geometrical rearrangement when the nitrite group replaces the chloride ligand present in the precursor complex $[Cu^{II}(L)Cl]ClO_4$ (**1**). As in **1**, the ethylpyridine group coordinates at the apical position of the square pyramidal geometry ($\tau = 0.14$). The Cu^{II}–N_{amine} bond distance in complex **2** (Table 3) is smaller than that observed in $[Cu^{II}(L)Cl]ClO_4$ (**1**) (Table 3) and is within the range observed for other complexes given in Table 3. In complex **2**, the Cu–O(1) bond length [1.973(2) Å] is in the middle range observed (Table 3) for other copper(II)–nitrite complexes [32–38]. This bond length is a little shorter than those reported for the oxidized D98N[NO_2] and for the H255N[NO_2] enzymes (Table 3). The basal Cu–$N_{imidazole}$ bond length in complex **2** [Cu(1)–N(5): 1.963(3) Å] is the shortest of the coordination sphere and is similar to those observed for $[Cu^{II}(L)Cl]ClO_4$ (**1**) (Table 3), in which both imidazole groups also lie in the basal plane. On the other hand, the apical Cu–$N_{imidazole}$ bond length [Cu(1)–N(7): 2.158(2) Å] is the longest of the coordination sphere in complex **2**. In addition to the similarities of these bond lengths with those observed (Table 3) in complexes with imidazole ligands [33,34,36], the Cu–$N_{imidazole}$ bond length is close to the Cu–His distances reported [15] for the oxidized form of D98N[NO_2] and the oxidized form of H255N[NO_2]. As observed in Table 3, the Cu–$N_{pyridine}$ bond distance in **2** is slightly different to that in $[Cu^{II}(L)Cl]ClO_4$ (**1**), probably due to the coordination of this group in the basal plane and in the apical positions, respectively. However, the Cu–$N_{pyridine}$ bond length in $[Cu^{II}(L)Cl]ClO_4$ (**1**) is longer than those reported [32] for the $[Cu^{II}(TEPA)(NO_2)]^+$ complex, where two pyridine groups are coordinated in the basal plane (Table 3). Although the nitrite ligand in the wild copper-containing NIRs exhibits an asymmetric η^2-*O*,*O* coordination, and that in complex **2** a η^2-*O* coordination, the similarities of the Cu–$O(1)_{nitrite}$ and the Cu–$N_{imidazole}$ bond lengths with the analogous groups in the enzymes discussed above allow us to consider complex **2** as a

Table 3
Structural parameters for some copper(II) complexes and for the enzymes D98N[NO_2] and H255N[NO_2]

Complex	Cu–N_{amine}	Basal Cu–N_{ring}	Apical Cu–N_{ring}	Cu–O_{bonded}	Cu–$O_{interacting}$	Reference
$[Cu^{II}(L)Cl]ClO_4$ (**1**)	2.148(3)	1.951(3)[a]	2.185(3)[b]			[16]
		1.943(3)[a]				
$[Cu^{II}(L)(ONO)]ClO_4$ (**2**)	2.133(2)	1.963(3)[a]	2.158(2)[a]	1.973(2)	2.76(2)	this work
		2.133(2)[b]				
		2.00(0.01)				
Oxidized D98N[NO2]		2.08(0.04)		2.21(0.08)	2.42(0.05)	[15]
		2.06(0.03)				
Oxidized H255N[NO2]		2.04(0.06)				
		2.19(0.02)		2.26(0.05)	3.60(0.15)	[15]
		2.19(0.01)				
$[Cu^{II}(TEPA)(NO_2)]^+$	2.083(5)	2.039(5)	2.253 (5)	2.012(5)	2.633(6)	[32]
		2.049(5)				
$[Cu(TMBA)(NO_2)]^+$		1.951(6)				
	2.405(6)	1.964(6)		1.988(6)		[33]
		2.056(6)				
$[Cu(biap)(NO_2)_2]$	2.143(5)	1.958(6)		2.012(5)	2.648 (6)	[34]
		1.964(6)		2.348(6)		
$[LpyCu(NO_2)]^+$	2.050(2)					
	2.061(2)	2.001(2)		1.982(1)	2.779	[35]
	2.292(2)					
[Cu(1-BB)(DMSO-O) $(NO_2)_2$]		1.970(5)				
	2.049(6)	1.978(5)		1.962(6)	2.678(8)	[36]
		1.997(3)				
		1.964(3)		1.962(3)	2.577(3)	
$[Cu(bdmppy)(NO_2)]_2$		2.010(3)				[37]
(μ-NO_2-κO: κN)]$^+$						
		1.968(3)				
		2.006(4)		1.957(3)	2.576(3)	
		2.011(4)				
		1.979(2)				
$[Cu(dpyam)_2(NO_2)]^+$		2.038(3)		2.179(3)	2.459(3)	[38]
		2.001(3)				
		2.117(3)				

[a] Imidazole nitrogen.
[b] Pyridine nitrogen.

structural model complex for the oxidized type II copper-containing nitrite reductases.

3.3. Electronic and EPR spectroscopies

The electronic spectrum of **2** recorded in acetonitrile solution (1.03×10^{-3} mol L^{-1}) presents two bands at 650 nm ($\varepsilon = 1.4 \times 10^2$ mol^{-1} L cm^{-1}) and 385 nm ($\varepsilon = 1.3 \times 10^3$ mol^{-1} L cm^{-1}), which are ascribed as a ligand field and a charge transfer transition, respectively, based on their molar absorption coefficients. As complex **2** presents only a broad ligand field band near 600–700 nm, it could be suggested that [39], in solution, the complex is in an octahedral coordination with a solvent molecule (S) occupying the vacant position in the first metal coordination sphere, affording the $[Cu^{II}(L)(S)ONO]^+$ species. The blue shift of the d–d transition from 687 nm ($\varepsilon = 1.2 \times 10^2$ mol^{-1} L cm^{-1}) in $[Cu^{II}(L)Cl]ClO_4$ (**1**) to 650 nm ($\varepsilon = 1.4 \times 10^2$ mol^{-1} L cm^{-1}) in **2** shows, as expected, that the nitrite ligand exhibits a stronger ligand field than the neutral acetonitrile molecule, which displaces the chloride ligand in **1** when it is dissolved [16]. As mentioned above, complex **2** also presents a charge transfer band in the near-UV region (385 nm, $\varepsilon = 1.3 \times 10^3$ mol^{-1} L cm^{-1}), with a molar extinction coefficient similar to that reported for the $[Cu(1\text{-}BB)(NO_2)]^+$ complex [36] (364 nm, $\varepsilon = 1.4 \times 10^3$ mol^{-1} L cm^{-1}). Such a result strongly suggests that the nature of this band is a nitrite–Cu^{II} charge transfer transition in copper(II)–nitrite complexes.

Spectra of **2** were also recorded in water (CF_3COOH, 0.2 mol L^{-1}, pH 7, adjusted with NaOH) and in methanolic (1.5×10^{-3} mol L^{-1}, $\mu = 0.1$ mol L^{-1} with $TBAPF_6$) solutions. In water, the spectrum presents only the d–d band at 682 nm ($\varepsilon = 1.0 \times 10^2$ mol^{-1} L cm^{-1}), which is within the same range observed for complex **1** under the same conditions (676 nm, $\varepsilon = 1.1 \times 10^2$ mol^{-1} L cm^{-1}). This fact may be indicative that the nitrite ligand is released in this medium. In methanolic solution, complex **2** exhibits spectral characteristics similar to those observed in acetonitrile (376 nm, $\varepsilon = 1.3 \times 10^3$ mol^{-1} L cm^{-1} and 648 nm, $\varepsilon = 1.7 \times 10^2$ mol^{-1} L cm^{-1}), indicating the coordination of nitrite in this medium.

The X-band EPR spectra of complex **2** in the polycrystalline state show only isotropic signals in the range of $g \cong 4.3$ (room temperature: $g_{iso} \cong 4.148$ and liquid N_2: $g_{iso} \cong 4.261$) and $g \cong 2$ (room temperature: $g_{iso} \cong 2.079$ and liquid N_2: $g_{iso} \cong 2.104$). This behavior is typical of a copper–copper interaction among close molecules [40], which may arise from the packing of the molecules in the crystalline cell. The first signal is large and not very intense corresponding to the forbidden transition $\Delta M_s = 2$. The second one is due to the allowed transition $\Delta M_s = \pm 1$ [40]. For comparison purposes, EPR spectra were also recorded in ethanol/water (1:1) solution at liquid N_2 temperature (Fig. 3) and reveals a typical spectrum of tetragonal distorted stereochemistry ($g_\parallel > g_\perp > g_e$ and high hyperfine constant $A_\parallel$) and the fitted parameters [41] for complex **2** ($g_\parallel = 2.261$, $g_\perp = 2.084$ and $A_\parallel = 163.0 \times 10^{-4}$ cm^{-1}) show a decrease in the $g_\parallel$ and an increase in the $A_\parallel$ values with respect to the precursor complex $[Cu^{II}(L)Cl]ClO_4$ (**1**) ($g_\parallel = 2.267$, $g_\perp = 2.096$ and $A_\parallel = 148.0 \times 10^{-4}$ cm^{-1}). This fact has been interpreted [42] as an increase in the delocalization of the unpaired electron, which moves away from the metal center as a consequence of the increase in the covalence of the metal–ligand bond. This agrees with the replacement of the neutral solvent molecule by the nitrite group. Comparison of EPR data for complex **2** with copper(II)–nitrite complexes is difficult as their parameters were recorded in very different media.

3.4. Electrochemical studies

The redox behavior of complex **2** was investigated in water and in methanolic solutions. In water (1.0×10^{-3} mol L^{-1}, CF_3COOH 0.2 mol L^{-1}, pH range 4.5–8.5, potential range of +1.2 to −0.7 V) complex **2** presents two redox processes: one reversible at $E_{1/2} = -235$ mV versus SCE ($\Delta E_p \approx 80$ mV, $i_{pa}/i_{pc} \approx 1.0$) and one irreversible at $E_{pc} = +970$ mV versus SCE. Both processes do not undergo significant changes (less than 5 mV) in the studied pH range. For complex **1**, the reversible Cu(II)/Cu(I) couple process, under the same experimental conditions, is observed at $E_{1/2} = -234$ mV versus SCE ($\Delta E_p \approx 82$ mV, $i_{pa}/i_{pc} \approx 1.0$), which is attributed to the presence of the $[Cu^{II}(L)(S)]^{2+}$ species in

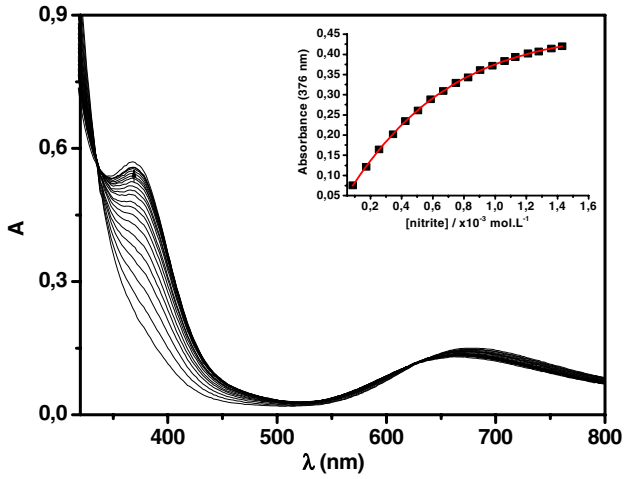

Fig. 2. Difference spectra recorded during the titration of complex **1** (1.5×10^{-3} mol L^{-1}, $\mu = 0.1$ mol L^{-1} $TBAPF_6$) with nitrite (8.0×10^{-5}–1.8×10^{-3} mol L^{-1}) in methanolic solution at 25 ± 1 °C and best fit plot (inset) of absorbance at 376 nm against nitrite concentration.

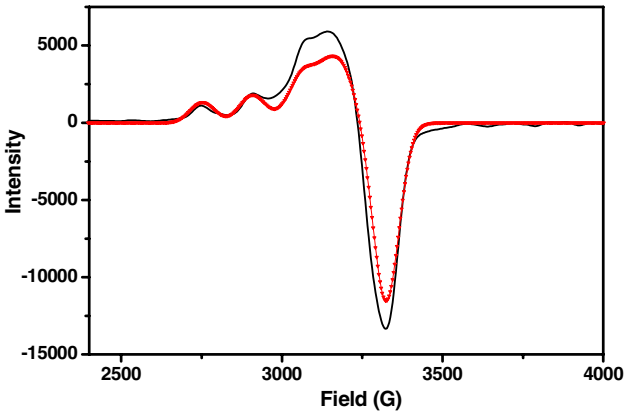

Fig. 3. X-band EPR spectrum of complex **2** in ethanol/water (1:1) at liquid N_2 temperature [solid line (experimental)/line + symbol (simulated)], recorded under the following experimental conditions: microwave frequency: 9.443669 GHz, microwave power: 16.0 mW, modulation frequency: 100.00 kHz, modulation amplitude: 1.02 G, receiver gain: 1.00×10^4 and conversion time: 81.92 ms. Fitted parameters: $g_{\|} = 2.261$, $g_{\perp} = 2.084$ and $A_{\|} = 163.0 \times 10^{-4}$ cm^{-1}.

solution. The similarity between the $E_{1/2}$ values observed for complexes **1** and **2** strongly corroborates the proposal of the releasing of the nitrite ligand by complex **2** in water solution, as discussed above for the spectrophotometric data. In view of this, the irreversible process at $E_{pc} = +970$ mV versus SCE can be attributed to the two electron oxidation process of free nitrite to nitrate in solution [43], which is upheld by the fact that the addition of $NaNO_2$ to the electrochemical solution results in an increased peak current.

Cyclic voltammograms of **2** recorded in methanolic solution show only the Cu(II)/Cu(I) redox process (Fig. 4) in the +1.0 to −0.7 V potential range ($E_{1/2} = -335$ mV versus SCE, $\Delta E_p \approx 112$ mV, $i_{pa}/i_{pc} = 0.94$). The $E_{1/2} = -335$ mV versus SCE observed in methanol for complex **2** is cathodically shifted

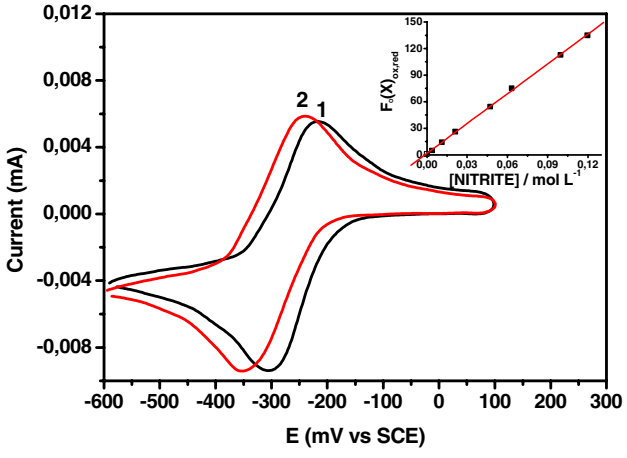

Fig. 4. Cyclic voltammogram of complexes **1** and **2**, in methanolic solution, at 25 ± 1 °C, scan rate of 20 mV s^{-1}, and the best fit plot of $F_0(x)_{ox,red}$ against nitrite concentration (inset).

with regard to the value observed for complex **1** ($E_{1/2} = -300$ mV versus SCE, $\Delta E_p \approx 87$ mV, $i_{pa}/i_{pc} = 0.82$), in which the substitution of the chloride by a solvent molecule has been proposed in pure methanol [16]. This shift of the $E_{1/2}$ value to a more negative potential is consistent with the replacement of a neutral molecule by a nitrite anion as shown by Monzani and coworkers [44] through a lowering of the Cu(II)/Cu(I) reduction potential to ca. 30 mV.

3.5. Equilibrium studies

As mentioned before, since the electrochemical data relate to the Cu(II)/Cu(I) redox process, the evaluation of the relative power of the nitrite ligand to complex with the $[Cu^{II}(L)(S)]^{2+}$ and $[Cu^{I}(L)(S)]^{+}$ species may be inferred from potentiometric experimental data. The average number of $\bar{n}_{ox,red}$ ligands for the Cu(II) and Cu(I) species was calculated as 1.06–1.04 in the 5.0×10^{-3}–1.9×10^{-1} mol L^{-1} nitrite concentration range, suggesting that no change in the coordination sphere of the copper center occurs during the one-electron transfer process. From the electrochemical data, it was also possible to calculate the K_{ox}/K_{red} ratio by plotting $F_0(x)_{Cu(II)/Cu(I)}$ against the corresponding nitrite concentration [21]. A straight line was obtained suggesting that Eq. (3) takes the form of Eq. (7) and that only the $[Cu^{II}(L)ONO]^{+}$ and $[Cu^{I}(L)ONO]$ species are present at the electrode. Thus, the K_{ox}/K_{red} ratio was calculated as equal to $(1.16 \pm 0.04) \times 10^3$ M^{-1}.

$$F_0(x)_{ox,red} \cong 1 + (\beta_1)_{ox,red}[NO_2^-] \quad (7)$$

The affinity of the nitrite ligand for complex **1**, $[Cu^{II}(L)(S)]^{2+}$, was also estimated by spectrophotometric titration of the anion with the $[Cu^{II}(L)(S)]^{2+}$complex, in methanolic solution (1.5×10^{-3} mol L^{-1}, $\mu = 0.1$ mol L^{-1} $TBAPF_6$), following the development of the near-UV charge transfer band at 376 nm (Fig. 2). Spectra recorded in the presence of variable concentrations of nitrite allowed us to utilize of the different absorption spectra of reagents and products to calculate the equilibrium constant for the following reaction:

$$[Cu(L)(S)]^{2+} + NO_2^- \rightleftharpoons [Cu(L)(ONO)]^{+} + S$$

Applying Eqs. (1) and (2) to the data of Fig. 2, the $K_{eq} = 1.4 \pm 0.5 \times 10^3$ M^{-1} value was obtained.

Combining the spectrophotometrical (K_{ox}) and the cyclic voltammetric data with K_{eq} for the reaction above, and since $K_{eq(ox,red)} = K_{ox}/K_{red}$, the value of K_{red} for the following reaction was estimated as 1.2 M^{-1}, which is consistent with the known low affinity of Cu(I) centers for nitrite ligands.

$$[Cu(L)(S)]^{+} + NO_2^- \rightleftharpoons [Cu(L)(ONO)] + S$$

Similar equilibrium study has been performed for the formation of the $[Cu(1\text{-}BB)(NO_2)]^{+}$ complex [34], being

the value of $K_{eq} = 7.5 \times 10^4$ M^{-1}. This higher affinity can be attributed to the tridentated character of the 1-BB ligand. The tetradentated ligand in 1, occupy one more coordinated site, which would decrease the metal center affinity for the nitrite ligand.

4. Conclusions

A new imidazole–copper(II) complex, of potential interest in the context of type II copper nitrite reductase biomimetic model chemistry, is reported. The tripodal ligand **L** closely reproduces the presence of three histidine residues in the active site of copper nitrite reductase. In addition, the O-nitrite coordination, the similarities of the Cu–O(1) nitrite distance, as well as the $Cu–N_{imidazole}$ bond lengths allow us to consider complex **2** as a good structural model complex for the oxidized type II copper-containing nitrite reductases.

5. Supplementary material

Crystallographic data for the structure reported here have been deposited with the Cambridge Crystallographic Data Center, 12 Union Road, Cambridge CB2 1EZ, UK (fax: +44-1223-336033; E-mail: deposit@ccdc.cam.ac.uk or www: http://www.ccdc.cam.ac.uk), as supplementary publication number CCDC 216312.

Acknowledgements

The authors are grateful for the grants provided by FAPESP (processes numbers 1999/07109-9 and 01/08563-7), CNPq and Pronex.

References

[1] B.A. Averill, Chem. Rev. 96 (1996) 2951.
[2] I.M. Wasser, S. de Vries, P. Moënne-Loccoz, I. Schröder, K.D. Karlin, Chem. Rev. 102 (2002) 1201.
[3] W.B. Tolman, S.M. Carrier, C.E. Ruggiero, et al., in: K.D. Karline, Z. Tyeklár (Eds.), Bioinorganic Chemistry of Copper, Chapman & Hall, New York, 1993, p. 406.
[4] T.C. Hollocher, in: J. Lancaster Jr. (Ed.), Nitric Oxide: Principles and Actions, Academic Press, San Diego, CA, 1996, p. 289.
[5] I. Moura, J.J.G. Moura, Curr. Opin. Chem. Biol. 5 (2001) 168.
[6] F. Cutruzzola, Biochim. Biophys. Acta 1411 (1999) 231.
[7] J. Han, T.M. Loehr, Y. Lu, J.S. Valentine, B.A. Averill, J. Sanders-Loehr, J. Am. Chem. Soc. 115 (1993) 4256.
[8] B.D. Howes, Z.H.L. Abraham, D.J. Lowe, T. Brüser, R.R. Eady, B.E. Smith, Biochemistry 33 (1994) 3171.
[9] K. Olesen, A. Veselov, Y. Zhao, Y. Wang, B. Danner, C.P. Scholes, J.P. Shapleigh, Biochemistry 37 (1998) 6086.
[10] A. Veselov, K. Olesen, A. Sienkiewicz, J.P. Shapleigh, C.P. Scholes, Biochemistry 37 (1998) 6095.
[11] M. Kukimoto, M. Nishiyama, M.E.P. Murphy, S. Turley, E.T. Adman, S. Horinouchi, T. Beppu, Biochemistry 33 (1994) 5246.
[12] E.T. Adman, J.W. Godden, S. Turley, J. Biol. Chem. 270 (1995) 27458.
[13] M.E.P. Murphy, S. Turley, E.T. Adman, J. Biol. Chem. 272 (1997) 28455.
[14] M.J. Boulanger, M. Kukimoto, M. Nishiyama, S. Horinouchi, M.E.P. Murphy, J. Biol. Chem. 275 (2000) 23957.
[15] M.J. Boulanger, M.E.P. Murphy, Biochemistry 40 (2001) 9132.
[16] M. Scarpellini, A. Neves, A.J. Bortoluzzi, B. Szpoganicz, R. Hörner, H. Terenzi, manuscript in preparation.
[17] K.J. Oberhausen, J.F. Richardson, R.M. Buchanan, W. Pierce, Polyhedron 8 (1989) 659.
[18] M. Scarpellini, J.C. Toledo Jr, A. Neves, J. Ellena, E.E. Castellano, D.W. Franco, Inorg. Chim. Acta (in press).
[19] R.R. Gagné;, C.A. Koval, G.C. Lisensky, Inorg. Chem. 19 (1980) 2854.
[20] A. Babko, A. Pilipenko, Photometric Analysis: General Principles and Working Tools, MIR Publishers, Moscow, 1971.
[21] E.A. Neves, D.W. Francol, J. Inorg. Nucl. Chem. 37 (1975) 277, and references therein.
[22] J.B. Bjerrum, Chem. Rev. 46 (1950) 381.
[23] D.D. Deford, D.N. Hume, J. Am. Chem. Soc. 73 (1951) 5321.
[24] D.N. Hume, D.D. Deford, G.C.B. Cave, J. Am. Chem. Soc. 73 (1951) 5323.
[25] Enraf-Nonius (1997–2000), COLLECT, Nonius BV, Delft, The Netherlands.
[26] Z. Otwinowski, W. Minor, in: C.W. Carter Jr., R.M. Sweet (Eds.), Methods in Enzymology, vol. 276, Academic Press, New York, 1997, p. 307.
[27] R.H. Blessing, Acta Cryst. A 51 (1995) 33.
[28] G.M. Sheldrick, SHELXS 97. Program for Crystal Structure Resolution, University of Göttingen, Göttingen, Germany, 1997.
[29] G.M. Sheldrick, SHELXL 97. Program for Crystal Structures Analysis, University of Göttingen, Göttingen, Germany, 1997.
[30] L. Zsolnai, ZORTEP, An Interactive ORTEP Program, University of Heidelberg, Heidelberg, Germany, 1997.
[31] A.W. Addison, T.N. Rao, J. Reedijk, J. Van Rijn, G.C. Verschoor, J. Chem. Soc., Dalton Trans. (1984) 1349.
[32] F. Jiang, R.R. Conry, L. Bubacco, Z. Tyeklár, R.R. Jacobson, K.D. Karlin, J. Peisach, J. Am. Chem. Soc. 115 (1993) 2093.
[33] A.R. Oki, A. Tandilashvili, D. Patel, M. Macillo, E. Wolfe, J. Coord. Chem. 52 (2001) 305.
[34] M. Beretta, E. Bouwman, L. Casella, B. Douziech, W.L. Driessen, L. Gutierrez-Soto, E. Monzani, J. Reedijk, Inorg. Chim. Acta 310 (2000) 41.
[35] L.M. Berreau, J.A. Halfen, V.G. Young Jr., W.B. Tolman, Inorg. Chim. Acta 297 (2000) 115.
[36] L. Casella, O. Carugo, M. Gullotti, S. Doldi, M. Frassoni, Inorg. Chem. 35 (1996) 1101.
[37] A.J. Blake, S.J. Hill, P. Hubberstey, Chem. Commun. (1998) 1587.
[38] S. Youngme, N. Chaichit, N. Koonsaeng, Inorg. Chim. Acta 335 (2002) 36.
[39] A.B. P Lever, in: . In: Inorganic Electronic Spectroscopy, 2nd ed., Elsevier Science, Amsterdam, 1984, p. 553.
[40] J.W. Orton, Electron Paramagnetic Resonance, London Life Books Ltd, London, 1968.
[41] Bruker EPR, WIN-EPR and SimFonia: post-processing program and simulation software for PC-Windows or CD-rom, version 1.0, 1997.
[42] U. Auerbach, U. Eckert, K. Wieghardt, B. Nuber, J. Weiss, Inorg. Chem. 29 (1990) 938.
[43] M. Bertotti, D. Pletcher, J. Braz. Chem. Soc. 8 (1997) 391.
[44] E. Monzani, G.J. Anthony, A. Koolhaas, A. Spandre, E. Leggieri, L. Casella, M. Gullotti, G. Nardin, L. Randaccio, M. Fontani, P. Zanello, J. Reedijk, J. Biol. Inorg. Chem. 5 (2000) 251.

Available online at www.sciencedirect.com
SCIENCE DIRECT®
Polyhedron 23 (2004) 519–527
POLYHEDRON
www.elsevier.com/locate/poly

Compartmental unsymmetrical lateral macrobicyclic ligands with an aromatic backbone providing a phenoxo bridge: synthetic, spectral, magnetic, electrochemical and kinetic features of mono and binuclear copper(II) complexes

M. Thirumavalavan, P. Akilan, P. Amudha, M. Kandaswamy *

Department of Inorganic Chemistry, School of Chemical Sciences, University of Madras, Guindy Campus, Chennai 600 025, India

Received 10 July 2003; accepted 19 September 2003

Abstract

From macrobicyclic ligands having different compartments originated from their corresponding precursor compounds (PC-1: 3,4:9,10-dibenzo-1,12[*N*,*N*′-bis{(3-formyl-2-hydroxy-5-methyl)benzyl}diaza]-5,8-dioxacyclotetradecane and PC-2: 3,4:9,10-dibenzo-1,12[*N*,*N*′-bis{(3-formyl-2-hydroxy-5-methyl)benzyl}diaza]-5,8-dioxacyclopentadecane) several mono and binuclear copper(II) complexes denoted as $[CuL](ClO)_4$ and $[Cu_2L(ClO_4)](ClO_4)$ have been synthesized. Electrochemical studies vindicate that one quasireversible reduction wave ($E_{pc} = -0.80$ to -0.88 V) for the mononuclear complexes and two quasireversible one electron transfer reduction waves ($E^1_{pc} = -0.84$ to -0.94 V, $E^2_{pc} = -1.25$ to -1.40 V) for the binuclear complexes are obtained in the cathodic region. The probe of room temperature magnetic moment studies depicts the presence of an antiferromagnetic interaction in the binuclear complexes (μ_{eff} of 1.35–1.42 B.M.), which is also observed from the broad ESR spectra with a *g* value of 2.10 or 2.11. Whereas, hyperfine splitting in ESR spectra is observed for mononuclear complexes and the magnetic moment value is found to be close to the spin only value (μ_{eff} of 1.69–1.71 B.M.). A variable temperature magnetic susceptibility study of the complex was carried out and the calculated $-2J$ values for the binuclear complexes $[Cu_2L^{1a}(ClO_4)](ClO_4)$ and $[Cu_2L^{1b}(ClO_4)](ClO_4)$ are 240 and 219 cm^{-1}, respectively. The initial rate constant values of catechol oxidation using the complexes as catalysts have been found to span a domain ranging from 5.06×10^{-3} to 2.56×10^{-2} min^{-1} and the values are found to be higher for binuclear complexes than the corresponding mononuclear complexes. Spectral, electrochemical and catalytic studies support the distortion of the copper ion geometry that arises as the macrocyclic ring size increases.
© 2003 Elsevier Ltd. All rights reserved.

Keywords: Macrobicylic ligands; Compartmental; Copper(II) complexes; Electrochemistry; Antiferromagnetic interaction; Catalytic study

1. Introduction

The rich chemistry of complexes of compartmental ligands binding two metals has been applied to the investigation of magnetic exchange interaction between the two metal ions, the stabilization of mixed-valent species and the activation of small molecules [1–5]. The success in molecular recognition promoting selective binding, transformation and transfer of large varieties of substrates has been enhanced by the development of highly preorganized macrocyclic and macropolycyclic ligands [6]. In particular, azamacrocyclic receptors are able to bind different kinds of substrates [7]. Structural factors have been shown to play a significant role to determine the strength of the interaction between the polyaza receptor and the guest molecule [8–10]. In this connection to introduce into the molecular framework a structural feature that imparts high selectivity in the recognition of different guests is one of the goals in the design of synthetic receptors. Aromatic subunits are often introduced as an integral part of the host molecules. Cyclic ligands containing aromatic rings in their backbone have received much attention [11]. Fewer efforts have been devoted to the study of macrocylic

* Corresponding author. Tel.: +91-44-2230-0488 (dir), +91-44-2235-1269/1137x220/227; fax: +91-44-2230-0488/2235-2494.
E-mail address: mkands@yahoo.com (M. Kandaswamy).

0277-5387/$ - see front matter © 2003 Elsevier Ltd. All rights reserved.
doi:10.1016/j.poly.2003.09.032

systems containing two metal binding sites within the same macrocyclic framework mainly due to synthetic difficulties. The present work tries to rationalize the study of various macrobicyclic compartmental mono and binuclear copper(II) complexes containing aromatic subunits in the imine compartment which is associated with an electrochemical translocation process. In our previous works [12–14] we have reported the distinct properties of mono and binuclear copper(II) complexes containing aliphatic diimines.

2. Experimental

Elemental analysis was carried out on a Carlo Erba Model 1106 elemental analyzer. ^{1}H NMR spectra were recorded using a FX-80-Q Fourier transition NMR spectrometer. Electronic spectral studies were carried out on a Hitachi 320 spectrophotometer in the range 200–800 nm. IR spectra were recorded on a Hitachi 270–50 spectrophotometer on KBr disks in the range 4000–250 cm^{-1}. Mass spectra were obtained on a JEOL DX-303 mass spectrometer. Molar conductivity was measured by using an Elico model SX 80 conductivity bridge using a freshly prepared solution of the complex in CH_3CN. Cyclic voltammograms were obtained on a CHI600A electrochemical analyzer. The measurements were carried out under oxygen free conditions using a three electrode cell in which a glassy carbon electrode was the working electrode, a saturated Ag/AgCl electrode was the reference electrode and a platinum wire was used as the auxiliary electrode. The ferrocene/ferrocenium (1+) couple was used as an internal standard and $E_{1/2}$ of the ferrocene/ferrocenium (Fc/Fc^+) couple under the experimental conditions is 470 mV in DMF and ΔE_p for Fc/Fc^+ is 70 mV. Tetra(*n*-butyl)ammonium perchlorate was used as the supporting electrolyte. The room temperature magnetic moment was measured on a PAR vibrating sample magnetometer Model-155. X-band ESR spectra were recorded at 25 °C on a Varian EPR-E 112 spectrometer using diphenylpicrylhydrazine (DPPH) as the reference. The catalytic oxidation of catechol to *o*-quinone by the complexes was studied in a 10^{-3} M acetonitrile solution. The reaction was followed spectrophotometrically by choosing the strongest absorbance at 390 nm and monitoring the increase in the absorbance at this wavelength as a function of time. A plot of $\log(A_\infty/A_\infty - A_t)$ versus time was made for each complex and the initial rate constant for the catalytic oxidation was calculated.

2.1. Materials

5-Methylsalicylaldehyde [15], 3-chloromethyl-5-methylsalicylaldehyde [16] and 3,4:9,10-dibenzo-1,12-diaza-5,8-dioxacyclohexadecane [17,18] were prepared from the literature methods. TBAP used as supporting electrolyte in the electrochemical measurements was purchased from Fluka and recrystallised from hot methanol. (*Caution*! TBAP is potentially explosive; hence care should be taken in handling the compound). DMF and CH_3CN were obtained from E. MERCK. All other chemicals and solvents were of analytical grade and were used as received without any further purification.

2.2. Synthesis of precursor compounds

2.2.1. 3,4:9,10-Dibenzo-1,12[*N*,*N*′-bis{(3-formyl-2-hydroxy-5-methyl}benzyl)diaza]-5,8-dioxacyclotetradecane (PC-1)

A mixture of 3,4:9,10-dibenzo-1,12-diaza-5,8-dioxacyclotetradecane (0.95 g, 3.2 mmol) and triethylamine (1.32 g, 6.4 mmol) in THF was added slowly to a stirred solution of 3-chloromethyl-5-methyl salicylaldehyde (1.16 g, 6.4 mmol) in THF. After the addition was over the stirring was continued further for one more hour. The whole solution was then refluxed over a water bath for 3 h and was allowed to cool on standing at room temperature. Copious water was added to this solution to dissolve any salt obtained. Then the required compound was extracted in organic medium using chloroform. The extraction was repeated for two to three times. A pale yellow compound was obtained on evaporation of solvent at room temperature (25 °C). Light yellow crystals were obtained on recrystallization from chloroform. Yield: 1.82 g (80%), m.p.: 100 °C. Analytical data for $C_{36}H_{38}O_6N_2 \cdot CHCl_3$: Calc.: C, 60.50; H, 5.32; N, 3.92. Found: C, 60.72; H, 5.36; N, 3.98%. IR data (ν cm^{-1}): 1678 (νC=O, s), 3448 (νOH, br). ^{1}H NMR (δ ppm in $CDCl_3$): 10.0 (s, 2H, CHO protons), 7.0 (m, 12H, aromatic protons), 4.7 (m, 4H, methylene protons attached to oxygen atom), 3.8 (m, 4H, methylene protons attached to nitrogen atom), 3.5 (s, 8H, benzylic protons), 2.3 (s, 6H, aromatic CH_3 protons). Mass (EI) m/z: 594 (m^+).

2.2.2. 3,4:9,10-Dibenzo-1,12[*N*,*N*′-bis{(3-formyl-2-hydroxy-5-methyl}benzyl)diaza]-5,8-dioxacyclopentadecane (PC-2)

The compound PC-2 can be prepared from the procedure mentioned above by using 3,4:9,10-dibenzo-1,12-diaza-5,8-dioxacyclopentadecane instead of 3,4:9,10-dibenzo-1,12-diaza-5,8-dioxacyclotetradecane. Yield: 1.98 g (85%), m.p.: 112 °C. Analytical data for $C_{37}H_{40}O_6N_2 \cdot CHCl_3$: Calc.: C, 60.98; H, 5.49; N, 3.84. Found: C, 61.02; H, 5.58; N, 3.88%. IR data (ν cm^{-1}): 1677 (νC=O, s), 3435 (νOH, br). ^{1}H NMR (δ ppm in $CDCl_3$): 10.0 (s, 2H, CHO protons), 7.0 (m, 12H, aromatic protons), 4.5 (m, 4H, methylene protons attached to oxygen atom), 3.7 (m, 4H, methylene protons attached to nitrogen atom), 3.5 (s, 8H, benzylic protons),

2.5 (s, 6H, aromatic CH_3 protons), 2.0 (s, 2H, CH_2 protons). Mass (EI) m/z: 608 (m^+).

2.3. Synthesis of macrobicyclic mononuclear copper(II) complexes

[CuL^{1a}](ClO$_4$): A methanolic solution of copper(II)perchlorate hexahydrate (0.676 g, 1.8 mmol) was added to the hot solution of PC-1 (1.085 g, 1.8 mmol) in $CHCl_3$ followed by the addition of *o*-phenylenediamine (0.195 g, 1.8 mmol) in methanol. The solution was refluxed on a water bath for 24 h. After the reaction was over, the solution was filtered hot and allowed to stand at room temperature. After slow evaporation of the solvent at 25 °C, a dark green compound was obtained, washed with methanol and dried in vacuum. Attempts to obtain crystals were unsuccessful. Yield: 1.21 g (77%). Analytical data for $C_{44}H_{44}O_8N_5ClCu$: Calc.: C, 60.68; H, 5.05; N, 8.04. Found: C, 60.75; H, 5.11; N, 8.13%. Selected IR (KBr): 1626 (s), 1099 (s), 625 (s) cm^{-1}. Conductance (Λ_m/S cm^2 mol^{-1}) in CH_3CN: 129. λ_{max} (nm) (ε/M^{-1} cm^{-1}) in CH_3CN: 590 (181), 428 (20,500), 360 (34,200), 308 (39,700), 270 (34,200). $g_{\|} = 2.21$, $g_{\perp} = 2.06$; μ_{eff}: 1.69 B.M.

[CuL^{1b}](ClO$_4$): [CuL^{1b}](ClO$_4$) was synthesized by following the previously described procedure for [CuL^{1a}](ClO$_4$), using 1,8-diaminonaphthelene instead of *o*-phenylenediamine. The compound obtained was dark green. Yield: 1.32 g (79%). Analytical data for $C_{48}H_{46}O_8N_5ClCu$: Calc.: C, 62.60; H, 5.00; N, 7.60. Found: C, 62.69; H, 5.09; N, 7.68%. Selected IR (KBr): 1625 (s), 1098 (s), 625 (s) cm^{-1}. Conductance (Λ_m/S cm^2 mol^{-1}) in CH_3CN: 151. λ_{max} (nm) (ε/M^{-1} cm^{-1}) in CH_3CN: 620 (135), 350 (13,500), 308 (38,700), 275 (33,200). $g_{\|}$: 2.19, $g_{\perp}$: 2.03; μ_{eff}: 1.70 B.M.

[CuL^{2a}](ClO$_4$): [CuL^{2a}](ClO$_4$) was synthesized by following the previously described procedure for [CuL^{1a}](ClO$_4$), using PC-2 instead of PC-1. The compound obtained was dark green. Yield: 1.21 g (76%). Analytical data for $C_{45}H_{46}O_8N_5ClCu$: Calc.: C, 61.08; H, 5.20; N, 7.91. Found: C, 61.16; H, 5.31; N, 8.01%. Selected IR (KBr): 1620 (s), 1100 (s), 623 (s) cm^{-1}. Conductance (Λ_m/S cm^2 mol^{-1}) in CH_3CN: 133. λ_{max} (nm) (ε/M^{-1} cm^{-1}) in CH_3CN: 610 (179), 420 (29,700), 355 (13,100), 274 (33,300). $g_{\|}$: 2.23, $g_{\perp}$: 2.04; μ_{eff}: 1.70 B.M.

[CuL^{2b}](ClO$_4$): [CuL^{2b}](ClO$_4$) was synthesized by following the previously described procedure for [CuL^{1b}](ClO$_4$), using PC-2 instead of PC-1. The compound obtained was dark green. Yield: 1.29 g (76%). Analytical data for $C_{49}H_{48}O_8N_5ClCu$: Calc.: C, 62.95; H, 5.13; N, 7.49. Found: C, 63.01; H, 5.20; N, 7.56%. Selected IR (KBr): 1626 (s), 1100 (s), 625 (s) cm^{-1}. Conductance (Λ_m/S cm^2 mol^{-1}) in CH_3CN: 149. λ_{max} (nm) (ε/M^{-1} cm^{-1}) in CH_3CN: 625 (141), 362 (12,200), 330 (38,600), 272 (32,200). $g_{\|}$: 2.18, $g_{\perp}$: 2.03; μ_{eff}: 1.71 B.M.

2.4. Synthesis of macrobicyclic binuclear copper(II) complexes

[Cu$_2$L^{1a}(ClO$_4$)](ClO$_4$): A methanolic solution of copper(II)perchlorate hexahydrate (0.676 g, 1.8 mmol) was added to the hot solution of PC-1 (1.085 g, 1.8 mmol) in $CHCl_3$ followed by the addition of *o*-phenylenediamine (0.195 g, 1.8 mmol) and triethylamine (0.251 g, 1.8 mmol) in methanol. After one hour copper(II) perchlorate (0.676 g, 1.8 mmol) was added and the whole reaction mixture was refluxed on a water bath for 24 h. After the reaction was over, the reaction mixture was filtered and allowed to stand at room temperature (25 °C). After slow evaporation of the solvent at 25 °C, the dark green compound obtained was washed with methanol and dried in vacuum. Attempts to obtain crystals were unsuccessful. Yield: 1.49 g (77%). Analytical data for $C_{46}H_{46}O_{12}N_6Cl_2Cu_2$: Calc.: C, 51.54; H, 4.29; N, 7.84. Found: C, 51.62; H, 4.36; N, 7.98%. Selected IR (KBr): 1621 (s), 1089, 1096, 1100 (w), 628 (s) cm^{-1}. Conductance (Λ_m/S cm^2 mol^{-1}) in CH_3CN: 148. λ_{max} (nm) (ε/M^{-1} cm^{-1}) in CH_3CN: 610 (255), 420 (20,500), 365 (12,300), 308 (39,600), 275 (32,500). $g = 2.11$; μ_{eff}: 1.35 B.M.

[Cu$_2$L^{1b}(ClO$_4$)](ClO$_4$): [Cu$_2$L^{1b}(ClO$_4$)](ClO$_4$) was synthesized by following the previously described procedure for [Cu$_2$L^{1a}(ClO$_4$)](ClO$_4$), using 1,8-diaminonaphthelene instead of *o*-phenylenediamine. The compound obtained was dark green. Yield: 1.62 g (80%). Analytical data for $C_{50}H_{48}O_{12}N_6Cl_2Cu_2$: Calc.: C, 53.52; H, 4.28; N, 7.49. Found: C, 53.59; H, 4.37; N, 7.59%. Selected IR (KBr): 1624 (s), 1087, 1096, 1101 (w), 625 (s) cm^{-1}. Conductance (Λ_m/S cm^2 mol^{-1}) in CH_3CN: 138. λ_{max} (nm) (ε/M^{-1} cm^{-1}) in CH_3CN: 630 (245), 360 (12,300), 305 (37,300), 272 (32,500). $g = 2.10$; μ_{eff}: 1.39 B.M.

[Cu$_2$L^{2a}(ClO$_4$)](ClO$_4$): [Cu$_2$L^{2a}(ClO$_4$)](ClO$_4$) was synthesized by following the previously described procedure for [Cu$_2$L^{1a}(ClO$_4$)](ClO$_4$), using PC-2 instead of PC-1. The compound obtained was dark green. Yield: 1.51 g (77%). Analytical data for $C_{47}H_{48}O_{12}N_6Cl_2Cu_2$: Calc.: C, 51.98; H, 4.42; N, 7.74. Found: C, 52.07; H, 4.53; N, 7.88%. Selected IR (KBr): 1627 (s), 1084, 1099, 1106 (w), 625 (s) cm^{-1}. Conductance (Λ_m/S cm^2 mol^{-1}) in CH_3CN: 139. λ_{max} (nm) (ε/M^{-1} cm^{-1}) in CH_3CN: 620 (280), 420 (29,400), 355 (12,400), 320 (36,600), 278 (34,900). $g = 2.10$; μ_{eff}: 1.36 B.M.

[Cu$_2$L^{2b}(ClO$_4$)](ClO$_4$): [Cu$_2$L^{2b}(ClO$_4$)](ClO$_4$) was synthesized by following the previously described procedure for [Cu$_2$L^{1b}(ClO$_4$)](ClO$_4$), using PC-2 instead of PC-1. The compound obtained was dark green. Yield: 1.52 g (74%). Analytical data for $C_{51}H_{50}O_{12}N_6Cl_2Cu_2$: Calc.: C, 53.92; H, 4.40; N, 7.40. Found: C, 54.11; H,

4.54; N, 7.60%. Selected IR (KBr): 1625 (s), 1086, 1098, 1102 (w), 624 (s) cm^{-1}. Conductance (Λ_m/S cm^2 mol^{-1}) in CH_3CN: 137. λ_{max} (nm) (ε/M^{-1} cm^{-1}) in CH_3CN: 640 (253), 360 (12,070), 310 (38,600), 277 (33,200). $g = 2.11$; μ_{eff}: 1.42 B.M.

3. Results and discussion

Using the template method various macrobicyclic mono and binuclear copper(II) complexes were synthesized by Schiff's base condensation of the precursor compounds with diamines in the presence of the metal ion. The synthetic pathway of mono and binuclear complexes is shown in Scheme 1. The structure of the ligand can be represented graphically as follows:

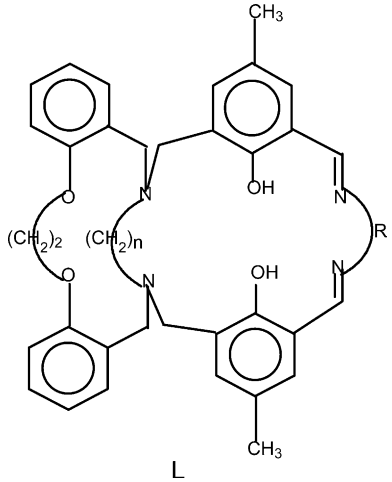

L

Our previous studies [12] rationalize the crystal structure of a similar type of mono and binuclear copper(II) complexes. Hence, in accordance with this, it is proposed that the geometry around the copper(II) ion in the mononuclear complex is distorted square planar and one of the tertiary nitrogen atoms is protonated. In the binuclear copper(II) complex one copper(II) ion is four coordinated and another copper(II) ion is five coordinated. Conductivity measurements also vindicate that both mono and binuclear copper(II) complexes are 1:1 electrolytes. Spectral, magnetic, electrochemical and catalytic studies of the complexes were carried out.

3.1. Spectral studies

In the IR spectra of the complexes a ν(C=N) peak [19] is observed at 1620–1626 cm^{-1}. The effective schiff base condensation is indicated by the formation of this new peak and the disappearance of the ν(C=O) peak at 1678 cm^{-1} in the complexes. The mononuclear complexes show peaks near 1100 and 620 cm^{-1} characteristic of the uncoordinated perchlorate ion. The binuclear complexes show two peaks near 1100 cm^{-1} and one peak near 620 cm^{-1}. Among the two peaks, one peak shows splittings [20], which is due to the presence of coordinated perchlorate ion, and the other peak due to the presence of uncoordinated perchlorate ion does not show any splitting. The electronic spectra of the complexes were observed as three main transitions. A weak band observed in the range 590–640 nm is due to a d–d transition of the metal ion. An increase in λ_{max} (red shift) [21] of the d–d transition of the Cu(II) ion in the complexes from L^{1a} to L^{1b} and L^{2a} to L^{2b} was observed for both mono and binuclear copper(II) complexes. A moderately intense band observed in the range 350–365 nm is due to a ligand to metal charge transfer transition and the strong band observed in the range 270–274 nm is due to an intraligand charge transfer transition [22]. Apart from these, additional peaks are observed due to the presence of the aromatic ring in the imine nitrogen compartment.

Hyperfine splittings of the solid state ESR spectra of the mononuclear copper(II) complexes show four lines with nuclear hyperfine spin 3/2. For mononuclear complexes the observed $g_{\|}$ values range from 2.19 to 2.22 and $g_{\perp}$ values vary from 2.03 to 2.06. The binuclear copper(II) complexes show a broad spectra centred at g; 2.10–2.11, which testifies the presence of an antiferromagnetic interaction between the two copper ions. Fig. 1 shows the ESR spectra of the mono and binuclear copper(II) complexes of ligand L^{1b}.

3.2. Magnetic studies

It is worth noting to infer that the probe of room temperature magnetic studies of the mononuclear copper(II) complexes resulted in the magnetic moment values range 1.69–1.71 B.M., which is very close to that of the spin only value (1.73 B.M.) expected for complexes having one copper(II) ion [23] with a single unpaired electron sited in an essentially $d_{x^2-y^2}$ orbital. The observed room temperature magnetic moment values for the binuclear copper(II) complexes ranges from 1.35 to 1.42 B.M. conveying the presence of an antiferromagnetic interaction between the two copper(II) ions. To evaluate the singlet–triplet energy separation ($-2J$), a variable-temperature magnetic study of the binuclear complexes was carried out in the temperature range 77–300 K and the experimental magnetic susceptibility values were fitted to the modified Bleany–Bowers equation [24].

$$\chi_m = (Ng^2\beta^2/3kT)[3 + \exp(-2J/kT)]^{-1}(1 - P) + 0.45P/T + N_\alpha.$$

In which N_α and g have been fixed as 60×10^{-6} cm^3 M^{-1} and 2.20, respectively. χ_m is the molar magnetic susceptibility corrected for diamagnetism, P is the percentage of monomeric impurities and other symbols

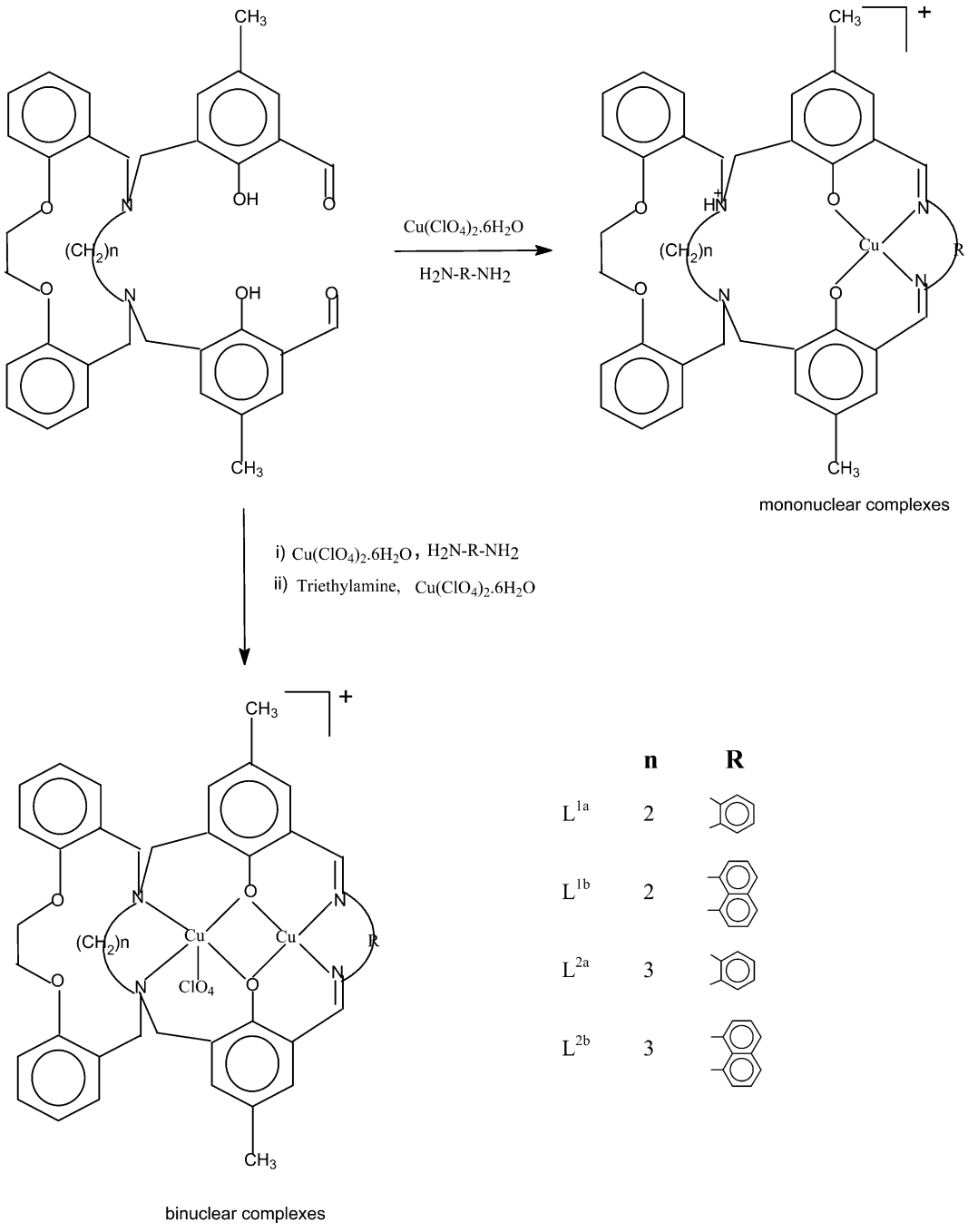

Scheme 1. Synthesis of macrobicyclic mono and binuclear copper(II) complexes.

have their usual meaning. The $-2J$ values were evaluated by a nonlinear regression analysis in which $-2J$, P and g are variables. Fig. 2 depicts the temperature dependent magnetic properties of complexes $[Cu_2L^{1a}(ClO_4)](ClO_4)$ and $[Cu_2L^{1b}(ClO_4)](ClO_4)$.

Magneto-structural correlations for several phenoxo bridged [25] dicopper complexes show that the major factor controlling the exchange interactions is the Cu–O–Cu bridge angle; however other factors [26] such as degree of distortion from planarity [27] and the dihedral angle [28] between the two copper planes also have an influence on the extent of spin–spin interaction. Generally phenoxo-bridged planar dicopper complexes with $Cu–O_{ph}–Cu$ bridge angles greater than 99° show exchange coupling values greater than 420 cm^{-1} and for the complexes with bridge angles less than 99° the exchange interaction is less (<70 cm^{-1}) [22]. Thompson et al. [25] reported that for symmetrical planar complexes with a bridge angle greater than 99° the $-2J$ values are ≈500–700 cm^{-1}. But Okawa et al. [27]

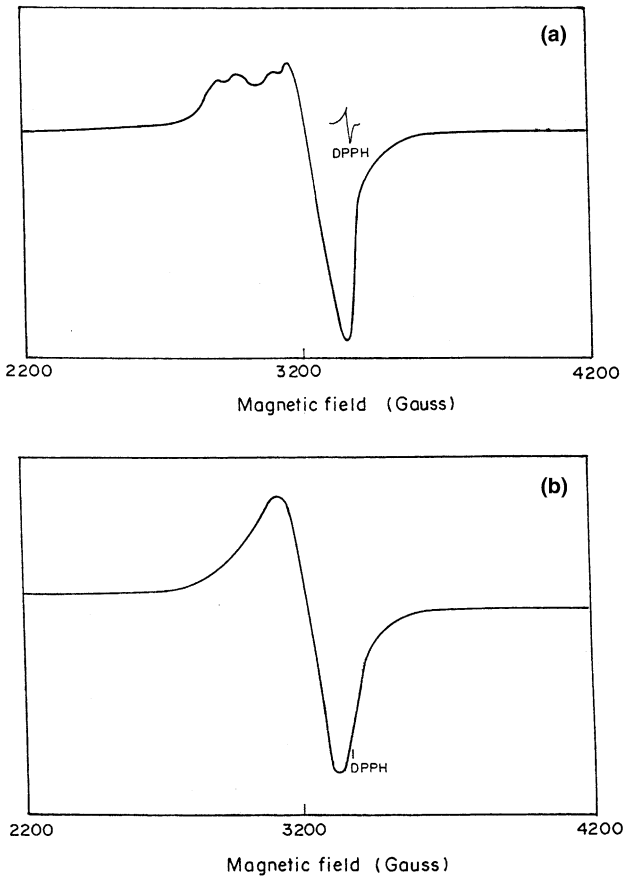

Fig. 1. ESR spectra of (a) $[CuL^{1b}]ClO_4$, (b) $[Cu_2L^{1b}(ClO_4)](ClO_4)$.

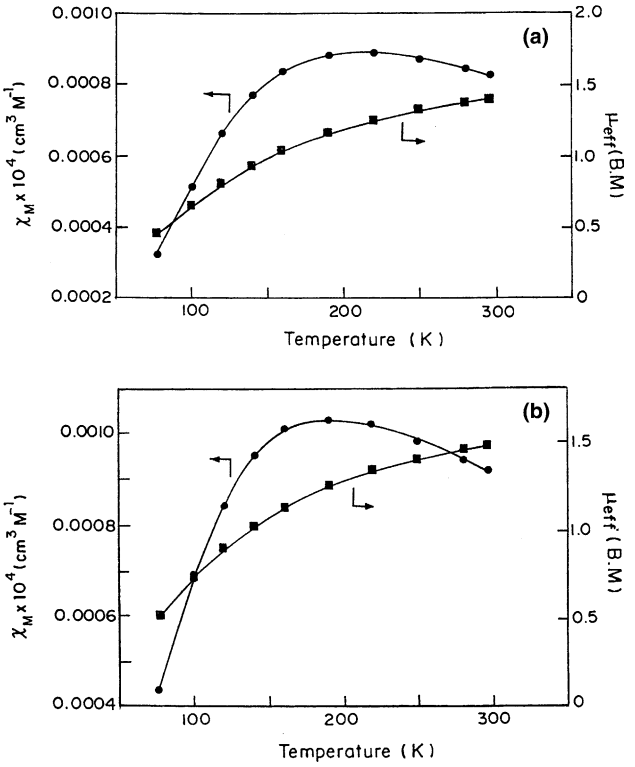

Fig. 2. Temperature dependent magnetic properties of complex (a) $[Cu_2L^{1a}(ClO_4)](ClO_4)$, (b) $[Cu_2L^{1b}(ClO_4)](ClO_4)$.

reported for distorted copper(II) complexes the $-2J$ values are 220 cm^{-1}. This low value is due to the distortion of the geometry of one of the Cu(II) ions, which causes deviation from co-planarity. For the complexes $[Cu_2L^{1a}(ClO_4)](ClO_4)$ and $[Cu_2L^{1b}(ClO_4)](ClO_4)$ the observed exchange interaction values ($-2J$) are 240 and 219 cm^{-1}, respectively. The distortion of the geometry [27] and the deviation from co-planarity [26] may be the possible reasons for this low exchange interaction value. The observed room temperature magnetic moment value of the binuclear copper(II) complex of L^{1a} is lower than that of L^{1b}. This is mainly because of the reason that the planarity of N_2O_2 of the imine nitrogen compartment is more in the case of L^{1a}. In the case of L^{1b} the planarity is lowered due to the presence of a bulky group, which makes L^{1b} comparatively flexible and hence the exchange interaction is lowered to some extent. Thus the greater planarity causes the higher exchange interaction and hence the low magnetic moment values.

3.3. Electrochemistry

The range of conductance values from 129 to 151 Λ_m/S cm^2 mol^{-1} of mono and binuclear copper(II) complexes in acetonitrile resulted from the conductivity measurements [20] implies that the complexes are of 1:1 electrolyte type. Usually phenoxo copper complexes undergo reduction at negative potentials due to the electronegativity and hard nature of the phenoxide atoms in the ligands [29,30]. Electrochemical properties of the complexes reported in the present work were studied by cyclic voltammetry in the potential range 0 to −1.5 V in dimethylformamide containing 10^{-1} M tetra(*n*-butyl)ammonium perchlorate and the data are summarized in Table 1. The cyclic voltammograms for the mononuclear complexes are shown in Fig. 3. Each voltammogram shows one quasireversible reduction wave at negative potential in the range −0.80 to −0.88 V. Controlled potential electrolysis carried out at 100 mV more negative than the reduction wave ratifies the consumption of one electron per molecule ($n = 0.96$) and the experiment reports the couple corresponding to the one electron transfer process. Fig. 4 represents the cyclic voltammograms of the binuclear complexes. Binuclear complexes are acquainted with two quasireversible reduction waves. The first reduction potential ranges from −0.84 to −0.94 V and the second reduction potential lies in the range −1.25 to −1.40 V. Controlled potential electrolysis was also carried out and the experiment reports that each couple corresponds to a one electron transfer process. So, the two redox processes are assigned as follows,

Table 1
Electrochemical data[a] of mono and binuclear copper(II) complexes in DMF medium

Complexes	E^1_{pc} (V)	E^1_{pa} (V)	$E^1_{1/2}$ (V)	ΔE (mV)	E^2_{pc} (V)	E^2_{pa} (V)	$E^2_{1/2}$ (V)	ΔE (mV)	K_{con}
$[CuL^{1a}](ClO_4)$	−0.88	−0.72	−0.80	160					
$[CuL^{1b}](ClO_4)$	−0.85	−0.75	−0.78	150					
$[CuL^{2a}](ClO_4)$	−0.86	−0.71	−0.79	150					
$[CuL^{2b}](ClO_4)$	−0.80	−0.65	−0.73	140					
$[Cu_2L^{1a}(ClO_4)](ClO_4)$	−0.94	−0.81	−0.88	130	−1.40	−1.28	−1.34	120	6.07×10^7
$[Cu_2L^{1b}(ClO_4)](ClO_4)$	−0.88	−0.76	−0.82	120	−1.30	−1.19	−1.25	110	1.89×10^7
$[Cu_2L^{2a}(ClO_4)](ClO_4)$	−0.91	−0.79	−0.85	120	−1.35	−1.24	−1.30	110	4.11×10^7
$[Cu_2L^{2b}(ClO_4)](ClO_4)$	−0.84	−0.73	−0.79	110	−1.25	−1.15	−1.20	100	1.28×10^6

[a] Measured by CV at 50 mV/s. E versus Ag/AgCl conditions: GC working and Ag/AgCl reference electrodes; supporting electrolyte TBAP; concentration of complex 1×10^{-3} M, concentration of TBAP 1×10^{-1} M.

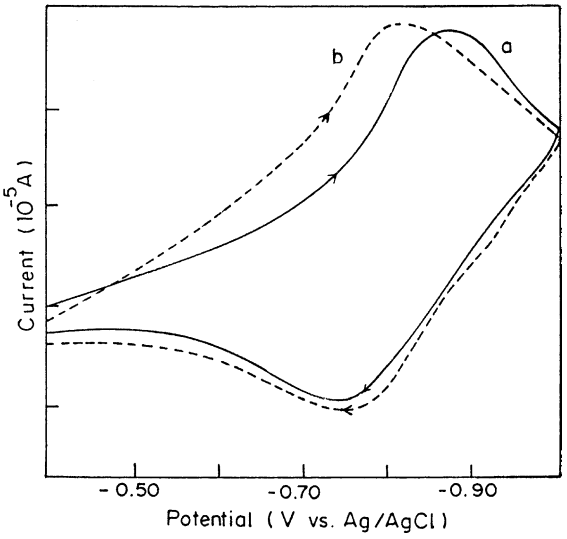

Fig. 3. Cyclic voltammograms of the mononuclear copper(II) complexes (1×10^{-3} M) (a) $[CuL^{1a}](ClO_4)$, (b) $[CuL^{1b}](ClO_4)$.

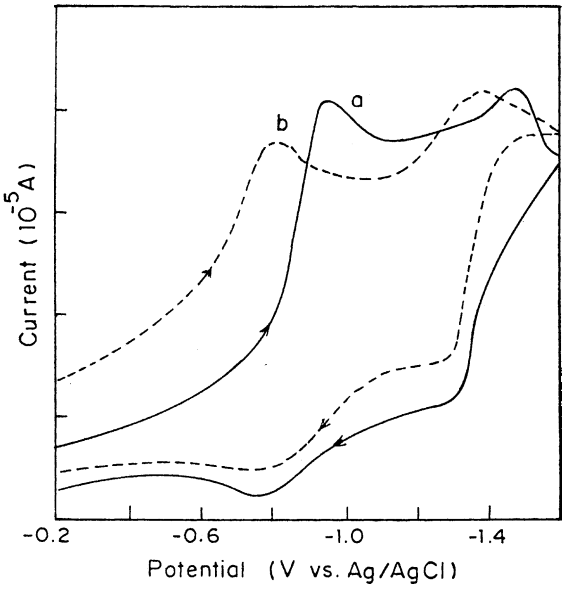

Fig. 4. Cyclic voltammograms of the binuclear copper(II) complexes (1×10^{-3} M) (a) $[Cu_2L^{1a}(ClO_4)](ClO_4)$, (b)$[Cu_2L^{1b}(ClO_4)](ClO_4)$.

$$Cu^{II}Cu^{II} \rightleftharpoons Cu^{II}Cu^{I} \rightleftharpoons Cu^{I}Cu^{I}$$

The conproportionation constant for the equilibrium

$$Cu^{II}Cu^{II} + Cu^{I}Cu^{I} \overset{K_{con}}{\rightleftharpoons} 2Cu^{II}Cu^{I}$$

was calculated using the relationship $\log K_{con} = \Delta E/0.0591$.

It is of interest to compare the electrochemical behaviour of the complexes heedfully. The reduction potential of the mononuclear copper(II) complexes of ligands L^{1a} to L^{1b} and L^{2a} to L^{2b} shifts anodically from −0.88 to −0.85 V and from −0.86 to −0.80 V, respectively, as the macrocyclic ring size increases due to the presence of the bulky group. This imparts more flexibility to the macrocycle [31–34] and tries to stabilize the copper(I) complex. The observed ΔE values for mononuclear complexes are found to be larger than the corresponding binuclear complexes and the reason may be attributed to the occurrence of electrochemical interconversion (translocation) [35] of the reduced cation Cu(I) from the rigid imine nitrogen compartment (N_2O_2) to the flexible tertiary nitrogen compartment (N_2O_2), which favours the tetrahedral geometry. The larger ΔE values also indicate that the reduction process is associated with an ECE mechanism. It is also noticed that the decrease in ΔE value as the chain length between two imine nitrogens increases, eases the translocation process and favours the tetrahedral geometry [12–14] moving from the complexes of ligands L^{1a} to L^{1b} and L^{2a} to L^{2b}. The interesting feature connoted for the binuclear complexes is anodic shifting of both first and second reduction potentials as the size of the macrocycle is increased. For example the complex $[Cu_2L^{1a}(ClO_4)](ClO_4)$ has $E^1_{pc} = -0.94$ V and $E^2_{pc} = -1.40$ V, which is more negative compared to the complex $[Cu_2L^{1b}(ClO_4)](ClO_4)$ ($E^1_{pc} = -0.88$ V, $E^2_{pc} = -1.30$ V) and the same observation is inferred for the complexes of L^2 also. Thus due to the presence of a bulky group in the imine compartment, the whole macrocyclic ring becomes more flexible and hence undergoes easy reduction. Thus the large size of cavity easily holds the reduced cation and stabilizes the formation of Cu(I) in

the compartment. Concern in the calculation of K_{con} values of binuclear copper(II) complexes leads to another interesting feature. The decrease in K_{con} values for the complexes of ligands L^{1a} to L^{1b} (6.07×10^7, 1.89×10^7) and of ligands L^{2a} to L^{2b} (4.11×10^7, 8.66×10^6) explains that as the ring size increases the stability of the mixed-valent species, formed as a result of the one electron reduction of complexes, decreases. This is because of the reason that the increase in ring size produces more distortion of the geometry around the metal center and the added electron is localized in the first metal ion itself and its impact on the other metal ion is negligible. Thus the lowered interaction between the two metal ions in the distorted geometry makes the reduction of the second metal ion easier.

An intensive speculation can be made concerning the comparison of reduction potentials of copper(II) complexes of ligands L^1 and L^2, which leads to the observation that the complexes of ligand L^2 get reduced at less negative potentials than the complexes of ligand L^1, because of the flexibility due to increase in the ring size of the macrocycle.

3.4. Kinetic studies of oxidation of catechol

Emphasis has been indeed made to carry out kinetic studies of the complexes. All the complexes synthesized were subjected for catecholase activity. The product *o*-quinone is considerably stable and has a strong absorbance at 390 nm. For this purpose, 10^{-3} mol dm^{-3} solutions of the complexes in acetonitrile were treated with 50 equivalents of 3,5-ditertiarybutylcatechol in the presence of air.

The course of the reaction was followed at 390 nm for nearly 45 min at regular time intervals. The slope was determined by the method of initial rates by monitoring the growth of the 390 nm band of the product *o*-quinone. A linear relationship for initial rate and the complex concentration obtained for all the complexes shows a first order dependence on the complex concentration for the systems.

A plot of $\log(A_\infty/A_\infty - A_t)$ versus time for catecholase activity of the mono and binuclear complexes are obtained and shown in Figs. 5 and 6, respectively. The rate constant values are also reported in Table 2. The first apparent result was that the reactivities of the complexes differ significantly, as the size of the macrocycle increases. The binuclear complexes have higher activities than the mononuclear complexes [36–40]. For example the binuclear complexes $[Cu_2L^{1a}(ClO_4)](ClO_4)$, $[Cu_2L^{1b}(ClO_4)](ClO_4)$, $[Cu_2L^{2a}(ClO_4)](ClO_4)$, and $[Cu_2L^{2b}(ClO_4)](ClO_4)$ have the rate constant values 1.24×10^{-2}, 2.17×10^{-2}, 1.56×10^{-2}, and 2.56×10^{-2} min^{-1}, respectively, whereas the mononuclear complexes $[CuL^{1a}](ClO_4)$, $[CuL^{1b}](ClO_4)$, $[CuL^{2a}](ClO_4)$ and $[CuL^{2b}](ClO_4)$ have the rate constant values 5.06×10^{-3}, 5.84×10^{-3}, 5.53×10^{-3} and 6.67×10^{-3} min^{-1}, respectively. The oxidation of catechol to *o*-quinone requires the presence of two metal ions in close proximity and

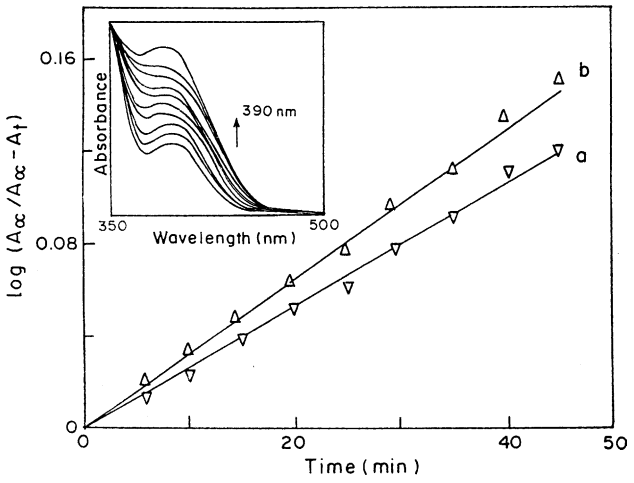

Fig. 5. Catecholase activity of mononuclear copper(II) complexes (a) $[CuL^{2a}](ClO_4)$, (b) $[CuL^{2b}](ClO_4)$.

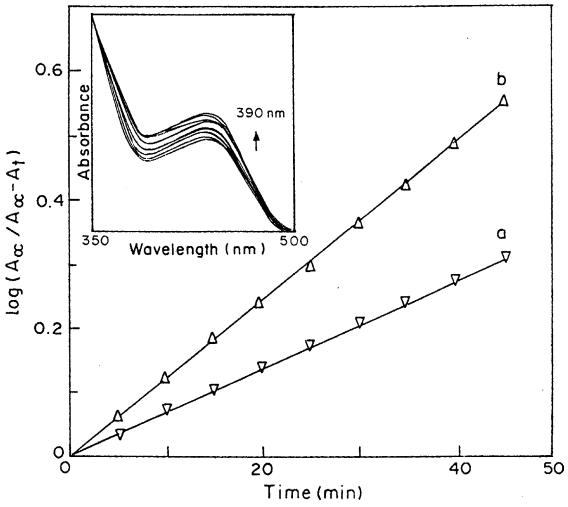

Fig. 6. Catecholase activity of the binuclear copper(II) complexes (a) $[Cu_2L^{2a}(ClO_4)](ClO_4)$, (b) $[Cu_2L^{2b}(ClO_4)](ClO_4)$.

Table 2
Catecholase activity[a] of mono and binuclear copper(II) complexes

Complexes	Rate constant (min^{-1})
$[CuL^{1a}](ClO_4)$	5.06×10^{-3}
$[CuL^{1b}](ClO_4)$	5.84×10^{-3}
$[CuL^{2a}](ClO_4)$	5.53×10^{-3}
$[CuL^{2b}](ClO_4)$	6.67×10^{-3}
$[Cu_2L^{1a}(ClO_4)](ClO_4)$	1.24×10^{-2}
$[Cu_2L^{1b}(ClO_4)](ClO_4)$	2.17×10^{-2}
$[Cu_2L^{2a}(ClO_4)](ClO_4)$	1.56×10^{-2}
$[Cu_2L^{2b}(ClO_4)](ClO_4)$	2.56×10^{-2}

[a] Measured spectrophotometrically in CH_3CN medium. Concentration of the complexes: 1×10^{-3} M, concentration of 3,5-ditertiarybutylcatechol: 1×10^{-1} M.

hence the rate constant values of binuclear complexes are comparatively high. The catalytic activities of both mono and binuclear complexes are found to increase as the macrocyclic ring size increases due to the intrinsic flexibility because of which the metal ion easily gets reduced and binds with the substrate and the same was supported by both spectral and electrochemical studies. The study implies that for mononuclear complexes the observed variation in the value of rate constant is very small when compared to the binuclear complexes. It can be stated that the planarity that is associated with the aromatic ring imparts the lesser catalytic efficiency due to the rigidity of the systems as observed in the case of electrochemical reduction of the complexes.

The observation on the comparison of catalytic activities of the complexes of ligands L^1 and L^2 unambiguously evinces that the complexes of ligand L^2 are accomplished with enhanced catalytic activity. It is indeed noteworthy to say that the increase in flexibility due to increase in the ring size of macrocycle is the possible reason for the observed higher rate constant value of the complexes of ligand L^2.

4. Conclusion

Various mono and binuclear copper(II) complexes of tricompartmental ligands containing aromatic units in the imine nitrogen compartment have been synthesized and spectral, magnetic, electrochemical and catalytic studies were carried out. These studies vividly indicate that a small variation in the ligand framework influences the spectral, magnetic, electrochemical and catalytic properties of the complexes.

Acknowledgements

The author M.T. gratefully acknowledges the financial support received from CSIR and UGC major project sanctioned to M.K., New Delhi.

References

[1] P. Guerriero, S. Tamburini, P.A. Vigato, Coord. Chem. Rev. 139 (1995) 17.
[2] C. Fraser, R. Ostrander, A.L. Rheingold, C. White, B. Bosnich, Inorg. Chem. 33 (1994) 324.
[3] C.J. Cairns, D.H. Busch, Coord. Chem. Rev. 69 (1986) 1.
[4] P.A. Vigato, S. Tamburini, D.E. Fenton, Coord. Chem. Rev. 106 (1990) 25.
[5] A.J. Atkins, D. Black, A.J. Blake, A.M. Becerra, S. Parsons, L.R. Ramirez, M. Schroder, Chem. Commun. (1996) 457.
[6] J.S. Bradshaw, K. Krakowiak, R.M. EnIzher, Tetrahedron 48 (1992) 4475.
[7] R.M. Izatt, K. Pawlak, J.S. Bradshaw, R.L. Bruening, Chem. Rev. 91 (1991) 1721.
[8] S. Claude, J.M. Lehn, F. Schmidt, J.P. Vingeron, J. Chem. Soc., Chem. Commun. (1991) 1182.
[9] E. Kimura, Y. Kuramoto, T. Koike, M. Kodama, J. Org. Chem. 55 (1990) 42.
[10] A. Bencini, A. Bianchi, M.I. Burguette, E.G. Espara, S.V. Luis, J.A. Ramirez, J. Am. Chem. Soc. 114 (1992) 1919.
[11] Y. Murakami, J. Kikuchi, T. Ohno, T. Hirayama, Y. Hisaeda, Y. Nishimura, J.P. Snyder, K. Steliov, J. Am. Chem. Soc. 113 (1991) 8229.
[12] M. Thirumavalavan, P. Akilan, M. Kandaswamy, K. Chinnakali, G. Senthil Kumar, H.K. Fun, Inorg. Chem. 42 (2003) 3308.
[13] M. Thirumavalavan, P. Akilan, M. Kandaswamy, Inorg. Chem. Commun. 5 (2002) 422.
[14] P. Akilan, M. Thirumavalavan, M. Kandaswamy, Polyhedron 22 (2003) 1407.
[15] J.C. Duff, J. Chem. Soc. (1941) 547.
[16] J.D. Crane, D.E. Fenton, J.M. Latour, A.J. Smith, J. Chem. Soc., Dalton Trans. (1991) 2279.
[17] L.G. Armstrong, L.F. Lindoy, Inorg. Chem. 14 (1975) 1322.
[18] P.G. Grimsley, L.F. Lindoy, H.C. Lip, R.J. Smith, J.T. Baker, Aust. J. Chem. 30 (1977) 2095.
[19] G. Das, R. Shukala, S. Mandal, R. Singh, P.K. Bharadwaj, J.V. Singh, K.U. Whitmire, Inorg. Chem. 36 (1997) 323.
[20] K.R. Adam, G. Andergee, L.F. Lindoy, H.C. Lip, M. Mcpartlin, J.H. Rea, R.J. Smith, P.A. Tasker, Inorg. Chem. 19 (1980) 2956.
[21] R. Bhalla, M. Helliwell, C.D. Garner, Inorg. Chem. 36 (1997) 2944.
[22] P. Amudha, M. Kandaswamy, L. Govindaswamy, D. Velmurugan, Inorg. Chem. 37 (1998) 4490.
[23] A. Bottcher, H. Elias, E. Jager, H. Lanffelderova, M. Mazur, L. Mullor, H. Paulus, P. Pelikan, M. Rudolph, M. Valko, Inorg. Chem. 32 (1993) 4131.
[24] B. Bleaney, K.D. Bowers, Proc. R. Soc. London, Ser. A 214 (1952) 451.
[25] L.K. Thompson, S.K. Mandal, S.S. Tandon, J.N. Bridson, M.K. Park, Inorg. Chem. 35 (1996) 3117.
[26] E.V.R. Akimova, D.H. Bush, P.K. Kahol, N. Pinto, N.W. Alcock, H.J. Clase, Inorg. Chem. 36 (1997) 510.
[27] H. Okawa, J. Nishio, M. Ohba, M. Tadakoro, N. Matsumoto, M. Koikawa, S. Kida, D.E. Fenton, Inorg. Chem. 32 (1993) 2949.
[28] S.L. Lambert, D.N. Hendrickson, J. Am. Chem. Soc. 105 (1983) 1513.
[29] Y. Guitnech, K.D. Karlin, Inorg. Chem. 35 (1987) 219.
[30] A. Benzekeri, P. Dubourdeaux, J.M. Latour, P. Rey, J. Laugier, J. Chem. Soc., Dalton Trans. (1991) 3359.
[31] J. Manonmani, R. Thirumurugan, M. Kandaswamy, V. Narayanan, S.S. Raj, M.N. Ponnuswamy, G. Shanmugam, H.K. Fun, Polyhedron 20 (2001) 3039.
[32] H. Okawa, M. Tadakora, T.Y. Aretake, M. Ohba, K. Shindo, M. Mitsumi, M. Koikawa, M. Tomono, D.E. Fenton, J. Chem. Soc., Dalton Trans. (1993) 253.
[33] E. Gao, W. Bu, G. Yang, D. Liao, Z. Jiang, S. Yan, G. Wang, J. Chem. Soc., Dalton Trans. (2000) 1431.
[34] P.A. Connick, K.A. Macor, Inorg. Chem. 30 (1991) 4654.
[35] V. Amendola, L. Fabbrizzi, C. Mangano, P. Pallavicini, Acc. Chem. Res. 43 (2001) 488.
[36] S. Parimala, S.N. Gita, M. Kandaswamy, Polyhedron 17 (1998) 3445.
[37] K. Moore, G.S. Vigee, Inorg. Chim. Acta. 66 (1982) 125.
[38] G.S. Vigee, E.E. Eduok, J. Inorg. Nucl. Chem. 43 (1981) 2171.
[39] N. Oishi, Y. Nishida, K. Ida, Bull. Chem. Soc. Jpn. 53 (1980) 2847.
[40] J. Reim, B. Krebs, J. Chem. Soc., Dalton Trans. (1997) 3793.

Available online at www.sciencedirect.com
SCIENCE DIRECT®
Polyhedron 23 (2004) 529–536
POLYHEDRON
www.elsevier.com/locate/poly

Synthesis, structure and luminescence properties of europium and zinc ionic complexes

Ming-Cai Yin *, Liang-Jie Yuan, Chang-Chun Ai, Chi-Wei Wang, E-Ting Yuan, Ju-Tang Sun *,[1]

Department of Chemistry, Wuhan University, Wuhan 430072, PR China

Received 3 September 2003; accepted 26 September 2003

Abstract

Two europium and zinc ionic complexes $[Eu_2(Hsal)_8][Zn(phen)_3]\cdot(H_2sal)(H_2O)$ (**1**) and $[Eu_2(TPA)_8][Zn(TPA)(Phen)_2]_2\cdot(H_2O)_2$ (**2**) (where H_2sal = salicylic acid, TPA = α-thiophene carboxylic acid, phen = 1,10-phenanthroline) have been synthesized by the rheological phase reaction method and structurally characterized by IR spectra and X-ray crystallography. The results show that in both complexes the carboxylate groups adopt three modes: bidentate bridging, bidentate chelating and tridentate chelating-bridging. Complex **1** consists of a discrete dinuclear $[Eu_2(Hsal)_8]^{2-}$ anion, $[Zn(phen)_3]^{2+}$ cation, free salicylic acid and a lattice water molecule. Interestingly, in the unit cell there are two types of dimeric $[Eu_2(Hsal)_8]^{2-}$ anions with inversion centers. The hydrogen bonds between the chelating carboxylate groups and the lattice water molecules link the dimeric Eu1 units into 1-D chains. Complex **2** comprises of a dimeric $[Eu_2(TPA)_8]^{2-}$ anion, two $[Zn(TPA)(Phen)_2]^{+}$ cations and two lattice water molecules. One obvious difference from complex **1** is that besides phen ligands, the TPA^- group also coordinates to the Zn^{2+} ion. The C–H···O, O–H···O hydrogen bonds and π–π stacking interactions play an important role in the crystal structure. These two complexes emit strong red light when irradiated by UV light. The emission bands at about 590, 610 nm correspond to the characteristic $^5D_0 \rightarrow {}^7F_1$,$^5D_0 \rightarrow {}^7F_2$ transitions of Eu^{3+} ions. The large intensity ratio of $^5D_0 \rightarrow {}^7F_2/{}^5D_0 \rightarrow {}^7F_1$ indicates the low symmetry of Eu^{3+} ion sites in both complexes, consistent with the results of the structure determination.
© 2003 Elsevier Ltd. All rights reserved.

Keywords: Ionic complex; Rheological phase reaction; Crystal structure; Photoluminescence; Europium; Zinc

1. Introduction

Lanthanide ions, especially Eu^{3+}, Tb^{3+} and Sm^{3+}, are very attractive luminescent centers owing to the high color purity and high luminescence efficiency. However, because of their low ultraviolet absorption ability, the luminescence intensity is very weak. The remedial method is to chelate the lanthanide ions with appropriate ligands, which have broad intense absorption bands and can enhance the emission intensity greatly [1–6]. Aromatic carboxylic acids, which commonly possess a large conjugated π-electron system and multiple coordination modes, are good activators of lanthanide ions luminescence. A large number of lanthanide aromatic carboxylates have been reported [7–10]. They often exhibit fascinating structures and strong luminescence, e.g., the luminescence of the Tb^{3+} ion is enhanced 10^4-fold by dipicolinic acid [7]. Studies have also shown that luminescent lanthanide aromatic carboxylates have potential applications as emitters in electroluminescence (EL) devices [11–13].

In order to further enhance the luminescence intensity of lanthanide ions, new approaches have also been developed. Some investigations have shown that the introduction of an auxiliary ligand or a second metal ion can alter not only the architectures but also the photoluminescence properties [14,15]. Numerous ternary

* Corresponding authors. Tel: +86-27-87218264; fax: +86-27-87647617.
E-mail addresses: mingcaiy@163.com (M.-C. Yin), jtsun@whu.edu.cn (J.-T. Sun).
[1] Tel: +86-27-87218494.

0277-5387/$ - see front matter © 2003 Elsevier Ltd. All rights reserved.
doi:10.1016/j.poly.2003.10.006

aromatic carboxylates of europium and terbium have been studied, which usually occur in dimeric forms and display intense luminescence [16–19]. However, they are commonly prepared by conventional solution reaction methods. In this paper, a rheological phase reaction method [20] was used for the synthesis of two europium and zinc ionic complexes, $[Eu_2(Hsal)_8][Zn(phen)_3]\cdot(H_2sal)(H_2O)$ (**1**) and $[Eu_2(TPA)_8][Zn(TPA)(Phen)_2]_2\cdot(H_2O)_2$ (**2**) (where H_2sal = salicylic acid, TPA = α-thiophene carboxylic acid, phen = 1,10-phenanthroline). The crystal structures and luminescence properties of these two complexes are reported here.

2. Experimental

2.1. Materials and methods

$EuCl_3\cdot 5H_2O$ was prepared by dissolving Eu_2O_3 in hydrochloric acid and then drying. All other chemicals were analytical reagent grade and used without further purification. The IR spectra were recorded on a Thermo Nicolet Avatar 360 FT-IR spectrophotometer as KBr pellets. Elemental analyses were carried out with a Perkin–Elmer 240B elemental analyzer. The excitation and emission spectra of the solid sample were measured on a Shimadzu RF-5301PC spectrofluorophotometer from 220 to 750 nm at room temperature.

2.2. Synthesis of complexes

2.2.1. Synthesis of $[Eu_2(Hsal)_8][Zn(phen)_3]\cdot(H_2sal)(H_2O)$ (**1**)

0.08 g (1.0 mmol) ZnO, 0.35 g (1.0 mmol) $EuCl_3\cdot 5H_2O$, 0.70 g (5.0 mmol) H_2sal, 0.39 g (2.0 mmol) phen·H_2O and 1.8 ml distilled water were placed in a closed container to get a rheological body [20]. It was kept at 80 °C for 3 days and then cooled to room temperature slowly. The product was washed with acetone and dried at ambient temperature. Block-shaped light red crystals were obtained (0.36 g, yield 33.3% based on Eu). *Anal*. Calc. for **1**: C, 54.95; H, 3.37; N, 3.88. Found: C, 54.61; H, 3.57; N, 3.69%. IR (KBr, cm^{-1}): 3424 (w), 3062 (w), 1626 (s), 1598 (vs), 1519 (s), 1484 (s), 1462 (vs), 1425 (s), 1391 (vs), 1252 (s), 1144 (w), 1030 (w), 850 (m), 760 (s), 726 (s), 534 (w), 456 (w).

2.2.2. Synthesis of $[Eu_2(TPA)_8][Zn(TPA)(Phen)_2]_2\cdot(H_2O)_2$ (**2**)

0.08 g (1.0 mmol) ZnO, 0.17 g (0.5 mmol) Eu_2O_3, 0.63 g (5.0 mmol) α-thiophene carboxylic acid, 0.39 g (2.0 mmol) phen·H_2O and 2.2 ml distilled water were placed in a closed container to get a rheological body. Reacted at 80 °C for 3 days and then cooled to room temperature slowly, colorless crystals were formed (0.43 g, yield 32.5% based on Eu). *Anal*. Calc. for **2**: C, 47.79; H, 2.70; N, 4.55. Found: C, 47.76; H, 2.66; N, 4.50%. IR (KBr, cm^{-1}): 3061 (w), 1601 (s), 1570 (s), 1518 (s), 1428

Table 1
Crystal data and structure refinement for **1** and **2**

Compound	**1**	**2**
Empirical formula	$C_{99}H_{72}Eu_2N_6O_{28}Zn$	$C_{49}H_{33}EuN_4O_{11}S_5Zn$
Molecular weight	2162.92	1231.42
Crystal system	triclinic	triclinic
Space group	$P\bar{1}$	$P\bar{1}$
Unit cell dimensions		
a (Å)	15.470(3)	13.536(3)
b (Å)	22.814(5)	15.563(3)
c (Å)	14.945(3)	13.103(3)
α (°)	94.06(3)	114.55(3)
β (°)	114.46(3)	90.90(3)
γ (Å^3)	70.94(3)	71.79(3)
V (Å^3)	4525.0(16)	2364.3(8)
Z, D_{calc} (g/cm^3)	2, 1.587	2, 1.730
μ (mm^{-1})	1.718	2.110
$F(000)$	2176	1232
Crystal size (mm)	$0.24\times0.20\times0.20$	$0.24\times0.20\times0.20$
θ range (°)	0.95–25.00	1.53–27.55
Index ranges (°)	$0\leqslant h\leqslant 18$, $-25\leqslant k\leqslant 27$, $-17\leqslant l\leqslant 16$	$0\leqslant h\leqslant 17$, $-18\leqslant k\leqslant 20$, $-17\leqslant l\leqslant 17$
Reflections collected	12 032	8326
Reflections unique	12 032	7461
Parameters	1221	616
Goodness-of-fit on F^2	0.965	1.069
Final R indices [$I>2\sigma(I)$]	$R_1=0.0401$, $wR_2=0.0734$	$R_1=0.0667$, $wR_2=0.1827$
R indices (all data)	$R_1=0.0674$, $wR_2=0.0781$	$R_1=0.0767$, $wR_2=0.1885$
Extinction coefficient	0.00056(6)	0.0041(7)
Largest diffraction peak and hole (e Å^{-3})	0.736 and −0.667	3.439 and −1.373

Table 2
Selected bond lengths (Å) for **1** and **2**

Compound	Bond	Length	Bond	Length
Complex **1**	Eu(1)–O(2)	2.528(4)	Eu(2)–O(18)	2.544(4)
	Eu(1)–O(3)	2.448(4)	Eu(2)–O(20)	2.342(4)
	Eu(1)–O(5)	2.448(4)	Eu(2)–O(21)#2	2.337(5)
	Eu(1)–O(6)	2.492(4)	Eu(2)–O(23)	2.399(4)
	Eu(1)–O(8)	2.383(4)	Eu(2)–O(24)#2	2.347(5)
	Eu(1)–O(9)#1	2.369(5)	Eu(2)–O(24)	3.102(5)
	Eu(1)–O(11)	2.316(4)	Zn(1)–N(1)	2.186(6)
	Eu(1)–O(12)#1	2.367(4)	Zn(1)–N(2)	2.137(5)
	Eu(1)-Eu(1)#1	4.3385(12)	Zn(1)–N(3)	2.161(5)
	Eu(2)–O(14)	2.463(4)	Zn(1)–N(4)	2.158(6)
	Eu(2)–O(15)	2.450(4)	Zn(1)–N(5)	2.168(5)
	Eu(2)–O(17)	2.460(5)	Zn(1)–N(6)	2.191(5)
Complex **2**	Eu(1)–O(1)	2.397(6)	Eu(1)–O(8)	2.537(6)
	Eu(1)–O(2)#1	2.372(6)	Zn(1)–N(1)	2.150(8)
	Eu(1)–O(3)	2.331(5)	Zn(1)–N(2)	2.136(7)
	Eu(1)–O(3)#1	2.902(6)	Zn(1)–N(3)	2.125(7)
	Eu(1)–O(4)#1	2.442(6)	Zn(1)–N(4)	2.150(7)
	Eu(1)–O(5)	2.637(8)	Zn(1)–O(9)	2.348(8)
	Eu(1)–O(6)	2.412(7)	Zn(1)–O(10)	2.142(7)
	Eu(1)–O(7)	2.455(6)		

Symmetry transformations used to generate equivalent atoms. For **1**: #1 $-x,-y,-z+1$; #2 $-x+2,-y+1,-z+2$; for **2**: #1 x,y,z, #2 $-x,-y,-z$.

(vs), 1389 (vs), 1225 (w), 1118 (w), 1033 (w), 856 (m), 809 (m), 775 (s), 719 (s), 654 (w), 509 (w), 419 (m).

2.3. X-ray crystallographic analyses

The diffraction data of complexes **1** and **2** were collected at 291(2) K on a RIGAKU R-AXIS IV imaging plate diffractionmeter with graphite-monochromatized Mo Kα radiation ($\lambda = 0.71073$ Å). The structures were solved by direct methods and refined by a full-matrix least-squares technique based on F^2 using the SHELXL-97 and SHELXS-97 programs [21]. All non-hydrogen atoms were refined with anisotropic thermal parameters. The hydrogen atoms were generated geometrically and treated by a mixture of independent and constrained refinement. A summary of the crystallographic data of complexes **1** and **2** is given in Table 1. The selected bond lengths are listed in Table 2.

3. Results and discussions

3.1. Synthesis

In this paper, two ionic complexes were obtained by the rheological phase reaction method. Since the reaction speed is essentially dictated by the starting materials, an appropriate selection of the latter is key to the successful synthesis of the product. In the experiment, ZnO and $EuCl_3 \cdot 5H_2O$ were used to prepare **1**, while ZnO and Eu_2O_3 were used for **2**. When $EuCl_3 \cdot 5H_2O$ was replaced by Eu_2O_3 in the preparation of **1**, only a polycrystalline powder was obtained. This is probably due to the fact that salicylic acid ($pK_a = 3.00$) is stronger than HTPA ($pK_a = 3.53$), and when two metal oxides were used, the reaction is too fast for the formation of a crystalline product. In contrast, the use of $EuCl_3 \cdot 5H_2O$ lowers the pH value of the reaction system, which can suppress the deprotonation of salicylic acid and weaken the coordination ability of phen since its N atoms are liable to be protonated, so as to decrease the reaction speed.

These two complexes are very stable in air, soluble in methanol, CH_3CN, DMF and DMSO, but almost insoluble in acetone, chloroform and benzene.

3.2. Infrared spectra

The IR spectra of complexes **1** and **2** both show the characteristic bands of carboxylate and phen ligands (see Section 2). The δ_{C-H} (out-of-plane bending vibration) bands of the phen ligand appear at 850, 726 cm^{-1} for **1** and 856, 719 cm^{-1} for **2**. The stretching vibration band of C=N at 1588 cm^{-1} for the free phen is shifted to 1519 cm^{-1} for these two complexes, indicating that the N atoms coordinate to the metal ions. The asymmetric and symmetric stretching vibration bands of carboxylate groups emerge at 1626, 1462, 1391 cm^{-1} for **1** and 1570, 1428, 1389 cm^{-1} for **2**, suggesting the presence of two or more coordination modes. The vibration bands of the Eu(Zn)–O bond and Zn–N bonds are seen at 534, 456 cm^{-1} in **1** and 509, 419 in **2** [22].

3.3. Crystal structure

X-ray single-crystal analyses indicate that both complexes **1** and **2** are ionic complexes containing

europium and zinc. Interestingly, in complex **1** the harder O donors only bind to Eu atoms and the softer N donors only bind to Zn atoms, while in complex **2** the O donors of TPA^- also coordinate to Zn atoms. This is probably due to the pH difference in the two reaction systems. For complex **1**, the stronger acidity in the reaction system decreases the deprotonation rate of salicylic acid and the Zn^{2+} ion is prone to be coordinated by three phen ligands. However, in the preparation of complex **2**, the reaction rate of Eu_2O_3 may be comparable with that of ZnO, so the two ligands, α-thiophene carboxylic acid and phen, coordinate to Eu and Zn atoms, respectively. Since the molar ratio of Zn:phen in the starting material is only 1:2, the other coordination sites of Zn^{2+} ion are completed by a TPA^- group.

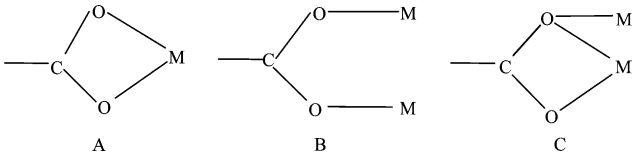

Scheme 1. Coordination modes of carboxylate groups in complexes **1** and **2**.

In complexes **1** and **2**, the carboxylate groups both adopt three coordination modes: bidentate chelating (A), bidentate bridging (B) and tridentate chelating-bridging (C) (as shown in Scheme 1).

3.3.1. Structure of complex *1*

The molecular structure of complex **1** is shown in Fig. 1. It is composed of a discrete dinuclear $[Eu_2(Hsal)_8]^{2-}$ anion, $[Zn(phen)_3]^{2+}$ cation, free salicylic acid and a lattice water molecule. It is worth noting that in a unit cell there are two types of $[Eu_2(Hsal)_8]^{2-}$ anions. Eu1 is in an eight-coordinate environment and Eu2 is in a nine-coordinate one.

The dimeric Eu1 and Eu2 units are both located on inversion centers. Eu1 is coordinated by eight oxygen atoms: four from two chelating salicylate groups and four from bidentate bridging ones. The Eu–O distances range from 2.316(4) to 2.528(4) Å. Two Eu^{3+} ions are linked together by the four bridging salicylate groups with an Eu1···Eu(1A) separation of 4.3385(12) Å.

Eu2 is coordinated by four oxygen atoms from two chelating salicylate groups, two oxygen atoms from two bidentate bridging salicylate groups and three oxygen

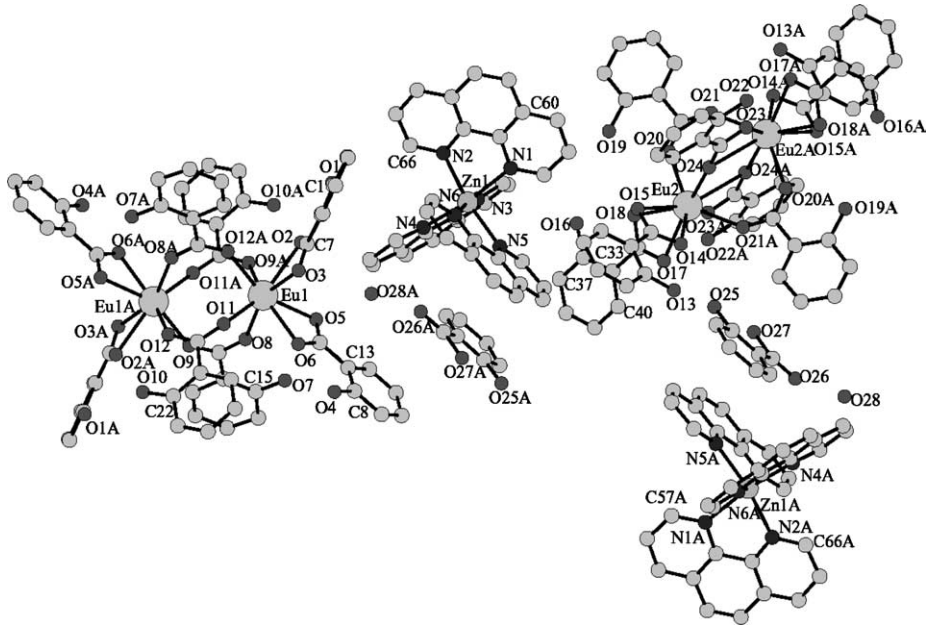

Fig. 1. Molecular structure of complex **1** with atom numbering scheme. Hydrogen atoms are omitted for clarity.

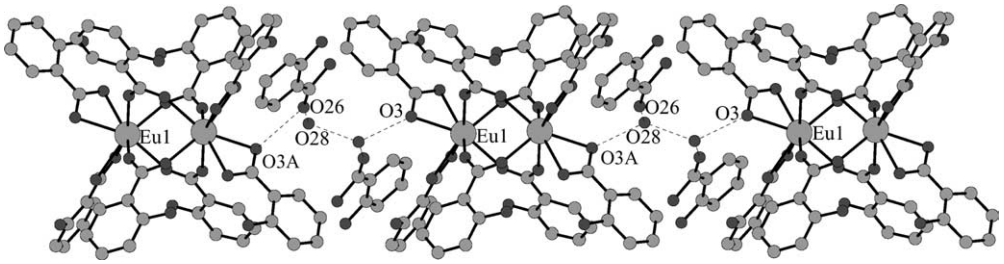

Fig. 2. Fractional structure showing the hydrogen bonds linking the dimeric Eu1 units into a 1-D chain.

atoms from two tridentate chelating-bridging salicylate groups to furnish a ninefold coordination. The Eu–O distances lie in the range from 2.337(5) to 2.544(4) Å, similar to that for Eu1, whereas the bond length of Eu2–O24 (the oxygen atom of the tridentate chelating-bridging salicylate group) is 3.102 Å, much longer than the other Eu2–O bonds and the literature value, which is only 2.549(3) or 2.800(4) Å [16,19]. Two Eu2 ions are connected together by two bidentate bridging and two tridentate chelating-bridging salicylate groups. The Eu2···Eu(2A) distance is 4.14 Å, shorter than Eu1···Eu(1A) owing to the existence of the tridentate chelating-bridging coordination mode.

In the $[Zn(phen)_3]^{2+}$ cation, the Zn atom is in a distorted octahedral geometry, surrounded by six nitrogen atoms from three chelating phen ligands. The Zn–N bonds are slightly different, ranging from 2.137(5) to 2.191(5) Å.

Weak intermolecular hydrogen bonds are formed between the lattice water molecules and the oxygen atoms of chelating salicylate groups [$O28_w\cdots O(3A)_{carboxylate} = 3.07$ Å, $O28_w\cdots O(28A)_w = 3.00$ Å, $O(28A)_w\cdots O3_{carboxylate} = 3.07$ Å]. These hydrogen bonds link the Eu1 units into 1-D chains along the *a*-axis. Further hydrogen bonds also exists between the free salicylic acid and the lattice water molecule ($O26_{salicylic\ acid}\cdots O28_w = 2.76$ Å) (Fig. 2). The $[Zn(phen)_3]^{2+}$ cations lie between these 1-D chains and the discrete dimeric Eu2 anions.

In the crystal, each anion is surrounded by six $[Zn(phen)_3]^{2+}$ cations and simultaneously each cation is surrounded by six $[Eu_2(Hsal)_8]^{2-}$ anions, three dimeric Eu1 units and three Eu2 ones. The hydrogen bonds and

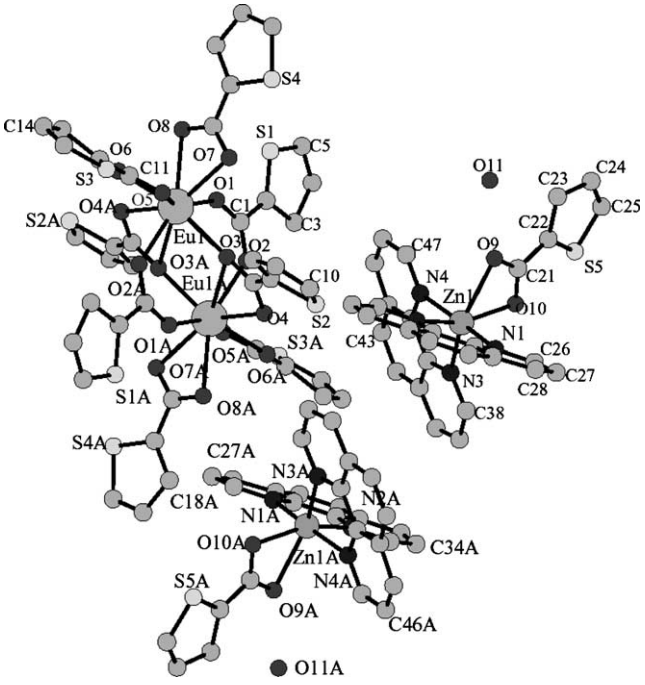

Fig. 3. Molecular structure of complex **2** with atom numbering scheme. Hydrogen atoms are omitted for clarity.

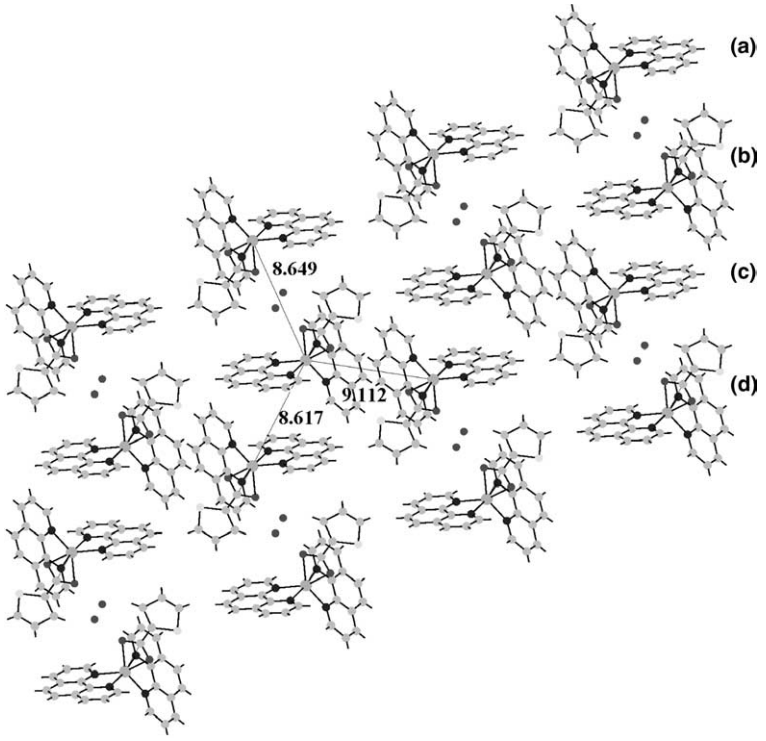

Fig. 4. The arrangment of $[Zn(TPA)(phen)_2]^+$ cations in **2**.

eletrostatic attractions existing among them result in stabilization of the crystal structure.

3.3.2. Structure of complex 2

Complex **2** consists of a discrete dimeric $[Eu_2(TPA)_8]^{2-}$ anion, two $[Zn(TPA)(phen)_2]^+$ cations and two lattice water molecules (Fig. 3).

The dimeric $[Eu_2(TPA)_8]^{2-}$ anion resembles the dimeric Eu2 anion in **1**. Each Eu^{3+} ion is coordinated by four oxygen atoms from two chelating TPA^- groups, two oxygen atoms from two bidentate bridging TPA^- groups and three oxygen atoms from two tridentate chelating-bridging TPA^- groups to complete a ninefold coordination. The Eu–O distances vary from 2.331 to 2.902 Å, similar to the Eu2–O bonds in complex **1**. The Eu–O bonds of the chelating TPA^- groups (2.455–2.637 Å are a little longer than those of the bridging TPA^- groups (2.331–2.442 Å) as expected, except for Eu–O(3A) (2.902 Å).

In the $[Zn(TPA)(phen)_2]^+$ cation, the Zn^{2+} center is six-coordinated by four nitrogen atoms from two chelating phen ligands and two oxygen atoms from a chelating TPA^- group. The Zn–N bonds are in the range from 2.125 to 2.150 Å, much shorter than the Zn–N bonds in complex **1**, which has a larger steric effect than complex **2**. The Zn–O bonds are 2.142 Å (Zn–O9) and 2.348 Å (Zn–O10). The Zn–O10 bond is much longer than Zn–O9 because of hydrogen bond formation between O9 and the lattice water molecule (O9···O11 = 2.645 Å).

In the crystal, the $[Zn(TPA)(phen)_2]^+$ cations are arranged in the manner shown in Fig. 4. The shortest Zn···Zn distances between the layers A, B, C and D are 8.649, 8.617 and 9.112 Å, respectively.

The two neighboring $[Zn(TPA)(phen)_2]^+$ cations separated by 8.649 Å are linked through hydrogen bonds (O9···O11 = 2.645 Å mentioned above and C23–H(23A)···O11 = 2.175 Å), as shown in Fig. 5(a). Two adjacent Zn cations with a separation of 9.112 Å are held together by the π–π stacking interactions existing between the two parallel phen(N3, N4) ligands (Fig. 5(b)). The average distance between the ring C(41A)–C(44A) and the ring C38–C41 is 3.708 Å. Through the hydrogen bonds between TPA^- and phen ligands (C34–H(34A)···O6 = 2.650 Å; C38–H(38A)···O6 = 2.574 Å), two adjacent Zn cations separated by

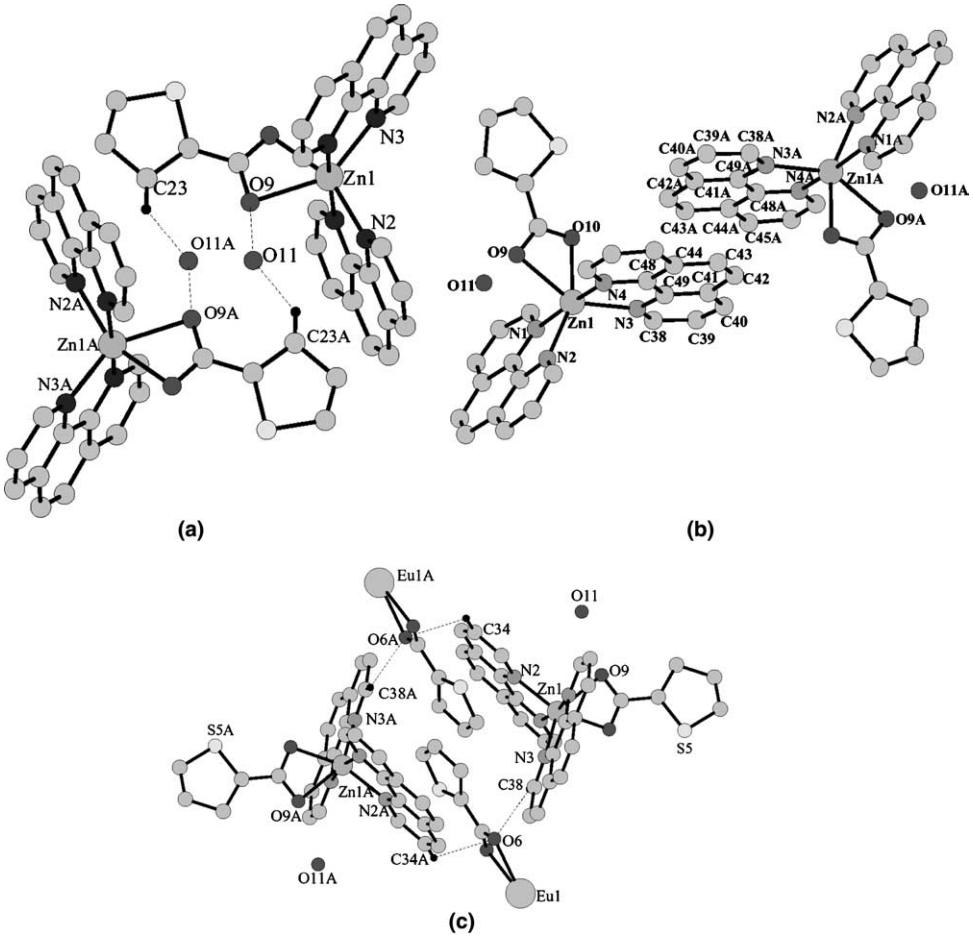

Fig. 5. The interactions linking the Zn cations and the dimeric Eu units in **2**. Hydrogen bonds are represented by the dotted lines and the hydrogen atoms not involved in the hydrogen bonds are omitted for clarity.

8.617 Å are linked (Fig. 5(c)). These hydrogen bonds and the electrostatic attractions between the dimeric Eu anions and Zn cations connect them to form a network.

Notably, the Zn and Eu centers in the ionic compounds **1** and **2** are both discrete, different from heterometallic complexes in which the two metal centers are linked together via bridging groups [23–25].

3.4. Photoluminescence

Under the excitation of UV light, complexes **1** and **2** emit strong red light. The luminescent properties of the solid-state samples at room temperature are shown in Fig. 6.

The broad excitation bands at 280, 335 nm for **1** and 345 nm for **2** are attributed to the $n\pi^*$ or $\pi\pi^*$ states of the aromatic carboxylate groups. The sharp bands at 383, 393, 414, 463, 534 nm are assigned to the Eu^{3+}-centred $^7F_1 \rightarrow {}^5L_7$, $^7F_0 \rightarrow {}^5L_6$, $^7F_1 \rightarrow {}^5D_3$, $^7F_0 \rightarrow {}^5D_2$, $^7F_1 \rightarrow {}^5D_1$ transitions, respectively [26]. One obvious difference between them is that for complex **1**, the excitation bands of the Eu^{3+} ion are much more strong than those of the $Hsal^-$ group, whereas for complex **2** the contrary is true. It indicates a more efficient energy transfer from the TPA^- ligand to the Eu^{3+} ions occurs in **2**.

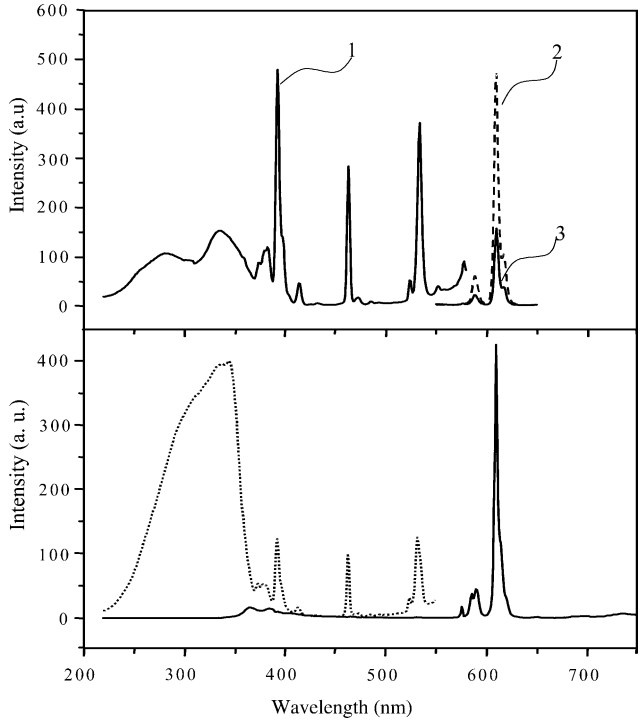

Fig. 6. The excitation and emission spectra of complex **1** (top) and complex **2** (bottom). (top: 1, $\lambda_{em} = 610$ nm; 2, $\lambda_{em} = 393$ nm; 3, $\lambda_{em} = 335$ nm) bottom: left, $\lambda_{em} = 610$ nm; right, $\lambda_{em} = 345$ nm).

The emission bands of **1** and **2** are essentially identical. The peaks at about 590 and 610 nm correspond to the characteristic $^5D_0 \rightarrow {}^7F_1$ and $^5D_0 \rightarrow {}^7F_2$ transitions of Eu^{3+} ions. The large intensity ratios of $^5D_0 \rightarrow {}^7F_2$/$^5D_0 \rightarrow {}^7F_1$ show the low symmetry of Eu^{3+} ion sites in both complexes [27], in agreement with the structure analyses.

It is well known that pure europium salicylate $Eu(Hsal)_3 \cdot H_2O$ has no luminescence (both salicylate and Eu^{3+} ion) under the excitation of UV light, possibly owing to the energy mismatch between the lowest triplet state of the salicylate group and the first excited state of the Eu^{3+} ion [28]. However, complex **1** emits the characteristic luminescence of Eu^{3+} ion when excited by UV light although the phen ligands are not directly coordinated to the Eu^{3+} ion. Furthermore, in the experiment no excitation and emission bands of phen ligands were observed. The specific luminescence mechanism is not clear now and further studies are underway.

4. Supplementary materials

X-ray crystallographic files in CIF format for complexes **1** and **2** have been deposited at the Cambridge Crystallographic Data Center, CCDC No. 210827 for **1**, 214067 for complex **2**. Copies of this information may be obtained free of charge from The Director, CCDC, 12 Union Road, Cambridge, CB2 IEZ, UK (fax: +44-1223-336033; e-mail: deposit@ccdc.cam.ac.uk or www: http://www.ccdc.cam.ac.uk).

References

[1] R.C. Ropp, Luminescence and the Solid State, Elservier, Amsterdam, 1991.
[2] R.G. Charles, E.P. Riedel, J. Inorg. Nucl. Chem. 29 (1967) 715.
[3] E.J. Nassar, P.S. Calefi, I.L.V. Rosa, O.A. Serra, J. Alloys Comp. 275-285 (1998) 838.
[4] J.-C.G. Bünzli, F. Ihringer, Inorg. Chim. Acta 246 (1996) 195.
[5] J.B. Lamture, Z.H. Zhou, A.S. Kumar, T.G. Wensel, Inorg. Chem. 34 (1995) 864.
[6] S. Petoud, J.-C.G. Bünzli, K.J. Schenk, C. Piguet, Inorg. Chem. 36 (1997) 1345.
[7] A.W.H. Lam, W.T. Wong, S. Gao, G.H. Wen, X.X. Zhang, Eur. J. Inorg. Chem. (2003) 149.
[8] C. Seward, N.X. Hu, S. Wang, J. Chem. Soc., Dalton Trans. (2001) 134.
[9] X. Li, X. Zheng, L. Jin, S. Lu, W. Qin, J. Mol. Struct. 519 (2000) 85.
[10] B. Barja, R. Baggio, M.T. Garland, P.F. Aramendia, O. Peña, M. Perec, Inorg. Chim. Acta 346 (2003) 187.
[11] C. Seward, N.X. Hu, S. Wang, J. Chem. Soc., Dalton Trans. (2001) 134.
[12] Y.X. Zheng, C.Y. Shi, Y.J. Liang, Q. Lin, C. Guo, H.J. Zhang, Synth. Methods 114 (2000) 321.
[13] A. Edward, C. Claude, I. Sokolic, T.Y. Chu, Y. Okamoto, R. Dorsinville, J. Appl. Phys. 82 (1997) 1841.

[14] G.F. Liu, Z.P. Qiao, H.Z. Wang, X.M. Chen, G. Yang, New J. Chem. 26 (2002) 791.
[15] M. Latva, H. Takalo, K. Simberg, J. Kankare, J. Chem. Soc., Perkin Trans. 2 (1995) 995.
[16] X. Li, L. Jin, S. Lu, J. Zhang, J. Mol. Struct. 604 (2002) 65.
[17] X. Li, L. Jin, X. Zhang, S. Lu, J. Zhang, J. Mol. Struct. 607 (2002) 59.
[18] R. Wang, S. Wang, J. Zhang, J. Mol. Struct. 648 (2003) 151.
[19] X.J. Zhang, L.P. Jin, Z.M. Wang, C.H. Yan, S.Z. Lu, Q. Li, Polyhedron 22 (2003) 323.
[20] J.T. Sun, K.L. Zhang, L.J. Yuan, D.L. Wang, Thermochim. Acta 343 (2000) 105.
[21] G.M. Sheldrick, SHELX-97: Program for X-ray Crystal Structure Solution and Refinement, Göttingen University, Germany, 1997.
[22] J.G. Mao, L. Song, X.Y. Huang, J.S. Huang, Polyhedron 16 (1997) 963.
[23] Y.C. Liang, M.C. Hong, R. Cao, W.P. Su, Y.J. Zhao, J.B. Weng, R.G. Xiong, Bull. Chem. Soc. Jpn. 75 (2002) 1521.
[24] W.K. Wong, H.Z. Liang, W.Y. Wong, Z.W. Cai, K.F. Li, K-W. Cheah, New J. Chem. 26 (2002) 275.
[25] Y. Cui, Y.T. Qian, J.S. Huang, Polyhedron 20 (2000) 1795.
[26] W.T. Carnall, P.R. Fields, K. Rajnak, J. Chem. Phys. 49 (1968) 4450.
[27] J.C.G. Bünzli, G.R. Choppin (Eds.), Lanthanide Probes in Life, Chemical and Earth Sciences, Theory and Practices, Elsevier, Amsterdam, 1989 (Ch. 7).
[28] H.Y. Zeng, Y.S. Yang, S.H. Huang, Chin. J. Lumin. 16 (4) (1995) 354.

Available online at www.sciencedirect.com
SCIENCE DIRECT®
Polyhedron 23 (2004) 537–543
POLYHEDRON
www.elsevier.com/locate/poly

Dioxomolybdenum(VI) thionates: molecular structure of dioxobis(pyridine-2-thiolate-*N*,*S*)molybdenum(VI) ☆

Francisco J. Arnáiz [a,*], Rafael Aguado [a], María R. Pedrosa [a], Miguel A. Maestro [b]

[a] *Laboratorio de Química Inorgánica, Universidad de Burgos, Pz Misael Bañuelos s/n, 09001 Burgos, Spain*
[b] *Servicios Xerais de Apoio á Investigación, Universidade da Coruña, E-15071 A Coruña, Spain*

Received 5 August 2003; accepted 7 October 2003

Abstract

Dioxomolybdenum(VI) thionates were readily isolated from the reactions of MoO_2Cl_2 with thallium salts of representative thiones [2-mercaptopyridine (Py-SH), 2-mercaptopyrimidine (Pym-SH), 2-mercapto-4-methylpyrimidine (MePym-SH), 2-mercaptobenzothiazol (BzTz-SH), 2-mercaptobenzoxazol (BzOx-SH) and 2-mercaptonicotinic acid methyl ester (MeNic-SH)]. They behave as Lewis acids and addition compounds with pyridines could be readily prepared. The molecular structure of dioxobis(pyridine-2-thiolate-*N*,*S*)molybdenum(VI), $MoO_2(Py\text{-}S)_2$, has been established by X-ray diffraction analysis. It displays catalytic activity in oxotransfer reactions from dimethyl sulfoxide (DMSO) to phosphines and phosphites in mild conditions.
© 2003 Elsevier Ltd. All rights reserved.

Keywords: Dioxomolybdenum(VI) thionates; Oxotransfer catalysts

1. Introduction

Heterocyclic thiones, characterized by thione–thiol tautomerism, have a coordination chemistry that makes extensive use of the exocyclic thione sulfur atom [1–5]. Thiones and thionates, the latter readily obtained by deprotonating the parent thiones, are electron-rich and polyfunctional ligands that lie on the borderline of stability between the +5 and +6 oxidation states of molybdenum. Thus, although a number of derivatives of thiones with molybdenum in oxidation states ranging from +2 to +5 have been prepared and characterized [6–13], there are only a few reports on Mo(VI) complexes. Zubieta and his co-workers [14,15] prepared and structurally characterized the Mo(VI) species $MoCl_2(2\text{-}SC_5H_3N\text{-}3\text{-}SiMe_3)_2(NNMePh)$ and $Mo(NNMePh)_2(2\text{-}SC_5H_3N\text{-}3\text{-}SiMe_3)_2$ and soon after a couple of dioxomolybdenum(VI) complexes, those derived from Py-SH and Pym-SH, were reported [16]. More recently a series of complexes with esters of 2-mercaptonicotinic acid has been isolated in low yield (below 15%) and structurally characterized [17].

As part of an ongoing study on oxomolybdenum complexes we have undertaken the preparation of dioxomolybdenum(VI) derivatives of a number of common thiones. To this purpose, we tested the behavior of sodium molybdate and $MoO_2(acac)_2$ with the thiones; and that of MoO_2Cl_2 as well as that of the readily available $MoO_2Cl_2(DMF)_2$ [18,19] with thallium thionates. Previously, we found that a number of addition compounds of MoO_2Cl_2 and MoO_2Br_2 with O-donor ligands oxidize a variety of thiols in mild conditions [20–22]. In this paper, we report the synthesis of representative dioxomolybdenum(VI) thionates along with the crystal structure of $MoO_2(Py\text{-}S)_2$.

2. Experimental

2.1. General procedures and measurements

Unless otherwise specified all operations were carried out in air. Diethyl ether and tetrahydrofuran (THF) were distilled over Na-benzophenone ketyl prior to use.

☆ Supplementary data associated with this article can be found, in the online version, at doi:10.1016/j.poly.2003.10.007

* Corresponding author.
E-mail address: farnaiz@ubu.es (F.J. Arnáiz).

0277-5387/$ - see front matter © 2003 Elsevier Ltd. All rights reserved.
doi:10.1016/j.poly.2003.10.007

Acetone was distilled immediately prior to use from $KMnO_4$. Acetonitrile was purified by distillation from $KMnO_4$ and then from CaH_2. 2-Mercaptonicotinic acid methyl ester was prepared by reacting 2-mercaptonicotinic acid with methanol and sulfuric acid and purified by crystallization. Thallium thionates were prepared by adding solutions of the thiones in ethanol (methanol for 2-mercaptonicotinic acid methyl ester) over aqueous TlOH; the precipitates were washed (water and then acetone) and dried under vacuum. $MoO_2(acac)_2$ was prepared as previously reported [23]. All other reagents were commercial products and were used without further purification. Elemental analyses (C, H, N, S) were performed on a LECO CHNS-932 analyzer (Module VTF-900 for O). Molybdenum was eventually determined by titration with lead(II) nitrate [24]. IR spectra (KBr dispersion, 4000–400 cm^{-1} range) were recorded on a Nicolet Impact 410 (Software Omnic for Windows) spectrometer. NMR spectra were recorded on a Varian Unity Inova-400 spectrometer (400 MHz for ^1H and 161.92 MHz for ^{31}P) at 20 °C. Chemical shifts are relative to TMS (^1H), or external 85% H_3PO_4 (^{31}P), with downfield values reported as positive. Coupling constants J are given in Hertz.

2.2. Preparation of thionates

2.2.1. Preparation of MoO_2(L-N,S)$_2$ (L-N,S = Py-S, Pym-S, MePym-S, MeNic-S)

A mixture of 0.100 g (0.5 mmol) of MoO_2Cl_2, 1 mmol of thallium thionate and 25 ml of acetonitrile was stirred for 2 h at r.t. The solid was filtered off and the filtrate was concentrated to approximately 5 ml. Then 20 ml of diethyl ether was added and the precipitate formed was collected by filtration, washed with diethyl ether (3 × 2 ml) and dried under vacuum.

MoO_2(Py-S)$_2$: Yield 0.156 g (89.6%). IR(cm^{-1}): ν(Mo=O) 897(s), 928(s). ^1H NMR(acetone-d_6): 8.52 ppm (dq, $^3J_{H-H} = 4.5$ Hz, 2H, for protons on C_6); 7.83 ppm (dt, $^3J_{H-H} = 7.5$ Hz, $^4J_{H-H} = 1.8$ Hz, 2H, for protons on C_4); 7.37 ppm (dd, $^3J_{H-H} = 7.5$ Hz, $^4J_{H-H} = 1.5$ Hz, 2H, for protons on C_3); 7.19 ppm (ddd, $^3J_{H-H} = 7.5$ Hz, $^3J_{H-H} = 4.5$ Hz, $^4J_{H-H} = 1.3$ Hz, 2H, for protons on C_5). *Anal.* Calc. for $C_{10}H_8MoN_2O_2S_2$: C, 34.49; H, 2.32; N, 8.04; S, 18.41. Found: C, 34.61; H, 2.22; N, 8.11; S, 18.10%.

MoO_2(Pym-S)$_2$: Yield 0.157 g (89.7%). IR(cm^{-1}): ν(Mo=O) 901(s), 934(s). ^1H NMR (acetone-d_6): 8.78 ppm (d, $^3J_{H-H} = 5$ Hz, 4H, for protons on C_4 and C_6); 7.30 ppm (t, $^3J_{H-H} = 5$ Hz, 2H, for protons on C_5). *Anal.* Calc. for $C_8H_6MoN_4O_2S_2$: C, 27.44; H, 1.73; N, 16.00; S, 18.31. Found: C, 27.20; H, 1.68; N, 15.72; S, 18.02%.

MoO_2(MePym-S)$_2$: Yield 0.163 g (86.2%). IR(cm^{-1}): ν(Mo=O) 911(s), 937(s). ^1H NMR (acetone-d_6): 8.56 ppm (d, $^3J_{H-H} = 5$ Hz, 2H, for protons on C_6); 7.20 ppm (d, $^3J_{H-H} = 5$ Hz, 2H, for protons on C_5); 1.27 ppm (s, 6H, CH_3). *Anal.* Calc. for $C_{10}H_{10}MoN_4O_2S_2$: C, 31.75; H, 2.66; N, 14.81; S, 16.95. Found: C, 31.50; H, 2.85; N, 14.58; S, 16.66%.

MoO_2(MeNic-S)$_2$: Yield 0.198 g (85.3%). IR(cm^{-1}): ν(Mo=O) 903(s), 932(s). ^1H NMR (acetone-d_6): 8.73 ppm (dd, $^3J_{H-H} = 5.3$ Hz, $^4J_{H-H} = 1.7$ Hz, 2H, for protons on C_6); 7.33 ppm (dd, $^3J_{H-H} = 8.0$ Hz, $^3J_{H-H} = 5.3$ Hz, 2H, for protons on C_5); 8.42 ppm (dd, $^3J_{H-H} = 8.0$ Hz, $^4J_{H-H} = 1.7$ Hz, 2H, for protons on C_4); 3.92 ppm (s, 6H, CH_3). *Anal.* Calc. for $C_{14}H_{12}MoN_2O_6S_2$: C, 36.22; H, 2.61; N, 6.06; S, 13.81. Found: C, 34.53; H, 2.69; N, 5.56; S, 13.20%.

2.2.2. Preparation of MoO_2(L-N,S)$_2$ (L-N,S = BzTz-S, BzOx-S)

A mixture of 0.100 g (0.5 mmol) of MoO_2Cl_2, 1 mmol of thallium thionate and 25 ml of THF was stirred for 2 h at r.t. The solid was filtered off and the filtrate was concentrated to approximately 5 ml. Then 20 ml of diethyl ether was added and the precipitate was collected by filtration, washed with diethyl ether (3 × 2 ml) and dried under vacuum. All operations were carried out under dry nitrogen.

MoO_2(BzTz-S)$_2$: Yield 0.195 g (84.7%). ν(Mo=O) 903(s), 932(s). *Anal.* Calc. for $C_{14}H_8MoN_2O_2S_4$: C, 36.52; H, 1.75; N, 6.08; S, 27.85. Found: C, 35.96; H, 1.42; N, 5.74; S, 26.40%.

MoO_2(BzOx-S)$_2$: Yield 0.186 g (86.9%). ν(Mo=O) 909(s), 952(s). *Anal.* Calc. for $C_{14}H_8MoN_2O_4S_2$: C, 39.26; H, 1.88; N, 6.54; S, 14.97. Found: C, 38.41; H, 1.35; N, 6.17; S, 13.95%.

2.2.3. Preparation of Mo_2O_3(L-N,S)$_4$ (L-N,S = Py-S, Pym-S, MePym-S, MeNic-S)

To a solution of 0.3 mmol of dioxomolybdenum(VI) thionate in 10 ml of acetonitrile, 0.2 mmol of triphenyl phosphine (PPh_3) was added. The mixture was stirred under nitrogen for 2 h and then 20 ml of diethyl ether was added. The precipitate was filtered, washed with diethyl ether (3 × 2 ml) and dried under vacuum.

Mo_2O_3(Py-S)$_4$: Yield 0.087 g (85.2%). IR(cm^{-1}): ν(Mo=O) 945(s). ^1H NMR (acetone-d_6): 8.41 ppm (dq, $^3J_{H-H} = 4.5$ Hz, 4H, for protons on C_6); 7.82 ppm (dt, $^3J_{H-H} = 7.5$ Hz, $^4J_{H-H} = 1.8$ Hz, 4H, for protons on C_4); 7.37 ppm (dd, $^3J_{H-H} = 7.5$ Hz, $^4J_{H-H} = 1.5$ Hz, 4H, for protons on C_3); 7.19 ppm (ddd, $^3J_{H-H} = 7.5$ Hz, $^3J_{H-H} = 4.5$ Hz, $^4J_{H-H} = 1.3$ Hz, 4H, for protons on C_5). *Anal.* Calc. for $C_{20}H_{16}Mo_2N_4O_3S_4$: C, 35.30; H, 2.37; N, 8.23; S, 18.85. Found: C, 34.96: H, 2.51; N, 8,21; S, 18.63%.

Mo_2O_3(Pym-S)$_4$: Yield 0.078 g (76.0%). IR(cm^{-1}): ν(Mo=O) 958(s). ^1H NMR (acetone-d_6): 8.77 ppm (d, $^3J_{H-H} = 5$ Hz, 8H, for protons on C_4 and C_6); 7.35 ppm (t, $^3J_{H-H} = 5$ Hz, 4H, for protons on C_5). *Anal.* Calc. for $C_{16}H_{12}Mo_2N_8O_3S_4$: C, 28.08; H, 1.77; N, 16.74; S, 18.74. Found: C, 27.74, H, 2.12; N, 15.98; S, 18.24%.

Mo_2O_3(MePym-S)$_4$: Yield 0.082 g (73.8%). IR(cm^{-1}): ν(Mo=O) 950(s). ^{1}H NMR (acetone-d$_6$): 8.45 ppm (d, $^3J_{H-H} = 5$ Hz, 4H, for protons on C_6); 7.15 ppm (d, $^3J_{H-H} = 5$ Hz, 4H, for protons on C_5); 1.27 ppm (s, 12H, CH_3). *Anal*. Calc. for $C_{20}H_{20}Mo_2N_8O_3S_4$: C, 32.44; H, 2.72; N, 15.13; S, 17.32. Found: C, 31.85; H, 3.10; N, 14.61; S, 16.80%.

Mo_2O_3(MeNic-S)$_4$: Yield 0.115 g (84.0%). IR(cm^{-1}): ν(Mo=O) 956(s). ^{1}H NMR (acetone-d$_6$): 8.36 ppm (dd, $^3J_{H-H} = 5.2$ Hz, $^4J_{H-H} = 1.7$ Hz, 4H, for protons on C_6); 7.33 ppm (dd, $^3J_{H-H} = 8.0$ Hz, $^3J_{H-H} = 5.2$ Hz, 4H, for protons on C_5); 8.42 ppm (dd, $^3J_{H-H} = 8.0$ Hz, $^4J_{H-H} = 1.7$ Hz, 4H, for protons on C_4); 3.92 ppm (s, 12H, CH_3). *Anal*. Calc. for $C_{28}H_{24}Mo_2N_4O_{11}S_4$: C, 36.85; H, 2.65; N, 6.14; S, 14.05. Found: C, 36.96; H, 2.99; N, 6.08; S, 14.03%.

2.2.4. Preparation of MoO_2(Py-S)$_2L_2$ (L = pyridine (Py), 4-methylpyridine (MePy), 1/2 2,2′-bipyridine (Bipy))

To a solution of 0.100 g (0.29 mmol) of MoO_2(Py-S)$_2$ in 10 ml of acetonitrile 1 mmol of Py or MePy, or 0.5 mmol of Bipy, dissolved in 2 ml of acetonitrile, was added. After stirring the mixture for 15 min the precipitate was filtered, washed with acetonitrile (3 × 2 ml) and dried under vacuum.

MoO_2(Py-S)$_2$Py$_2$: Yield 0.128 g (84.3%). IR(cm^{-1}): ν(Mo=O) 908(s), 941(s). ^{1}H NMR (DMSO-d$_6$): 8.58 ppm (dt, $^3J_{H-H} = 4.5$ Hz, $^4J_{H-H} = 1.5$ Hz, 6H, for Py protons on C_2 and C_6 and thionate protons on C_6); 7.86 ppm (tt, $^3J_{H-H} = 7.6$ Hz, $^4J_{H-H} = 1.5$ Hz, 4H, for Py protons on C_4 and and thionate protons on C_4); 7.44 ppm (ddd, $^3J_{H-H} = 7.6$ Hz, $^3J_{H-H} = 7.5$ Hz, $^4J_{H-H} = 1.5$ Hz, 8H, for Py protons on C_3 and C_5 and thionate protons on C_3 and C_5). *Anal*. Calc. for $C_{20}H_{18}MoN_4O_2S_2$: C, 47.43; H, 3.58; N, 11.06; S, 12.66. Found: C, 48.01; H, 3.23; N, 10.21; S, 12.86%.

MoO_2(Py-S)$_2$(MePy)$_2$: Yield 0.131 g (81.7%). IR(cm^{-1}): ν(Mo=O) 902(s), 932(s). ^{1}H NMR (DMSO-d$_6$): 8.46 ppm (dq, $^3J_{H-H} = 4.5$ Hz, 2H, for thionate protons on C_6); 7.26 ppm (ddd, $^3J_{H-H} = 7.5$ Hz, $^3J_{H-H} = 4.5$ Hz, $^4J_{H-H} = 1.3$ Hz, 2H, for thionate protons on C_5); 7.78 ppm (td, $^3J_{H-H} = 7.5$ Hz, $^4J_{H-H} = 1.8$ Hz, 2H, for thionate protons on C_4); 7.60 ppm (dd, $^3J_{H-H} = 7.5$ Hz, $^4J_{H-H} = 1.3$ Hz, 2H, for thionate protons on C_3); 8.50 ppm (d, $^3J_{H-H} = 6.0$ Hz, 4H, for MePy protons on C_2 and C_6); 7.40 ppm (d, $^3J_{H-H} = 6.0$ Hz, 4H, for MePy protons on C_3 and C_5); 2.37 ppm (s, 6H, CH_3]. *Anal*. Calc. for $C_{22}H_{22}MoN_4O_2S_2$: C, 49.44; H, 4.15; N, 10.48; S, 12.00. Found: C, 48.71; H, 3.89; N, 9.98; S, 12.04%.

MoO_2(Py-S)$_2$(Bipy): Yield 0.127 g (83.9%). IR(cm^{-1}): ν(Mo=O) 883(s), 914(s). ^{1}H NMR (DMSO-d$_6$): 8.50 ppm (dq, $^3J_{H-H} = 4.5$ Hz, 2H, for thionate protons on C_6); 7.30 ppm (ddd, $^3J_{H-H} = 7.5$ Hz, $^3J_{H-H} = 4.5$ Hz, $^4J_{H-H} = 1.3$ Hz, 2H, for thionate protons on C_5); 7.82 ppm (td, $^3J_{H-H} = 7.5$ Hz, $^3J_{H-H} = 7.5$ Hz, $^4J_{H-H} = 1.8$ Hz, 2H, for thionate protons on C_4); 7.66 ppm (dd, $^3J_{H-H} = 7.5$ Hz, $^4J_{H-H} = 1.3$ Hz, 2H, for thionate protons on C_3); 8.66 ppm (dd, $^3J_{H-H} = 4.5$ Hz, $^4J_{H-H} = 1.4$ Hz, 2H, for Bipy protons on C_6 and $C_{6'}$); 7.42 ppm (ddd, $^3J_{H-H} = 7.5$ Hz, $^3J_{H-H} = 4.5$ Hz, 2H, for Bipy protons on C_5 and $C_{5'}$); 7.92 ppm (td, $^3J_{H-H} = 7.5$ Hz, $^4J_{H-H} = 1.4$ Hz, 2H, for Bipy protons on C_4 and $C_{4'}$); 8.36 ppm (dd, $^3J_{H-H} = 7.5$ Hz, $^4J_{H-H} = 1.3$ Hz, 2H, for Bipy protons on C_3 and $C_{3'}$). *Anal*. Calc. for $C_{20}H_{16}MoN_4O_2S_2$: C, 47.62; H, 3.20; N, 11.11; S, 12.71. Found: C, 48.01; H, 3.27; N, 11.08; S, 12.33%.

2.2.5. Preparation of MoO_2(BzTz-S)$_2L_2$ (L = Py, MePy, 1/2Bipy)

To a solution of 0.140 g (0.3 mmol) of MoO_2(BzTz-S)$_2$ in 20 ml of THF 1 mmol of Py or MePy, or 0.5 mmol of Bipy, dissolved in 5 ml of THF, was added. After stirring the mixture for 15 min the precipitate was filtered, washed with THF (3 × 2 ml) and dried under vacuum. All operations were carried out under dry nitrogen.

MoO_2(BzTz-S)$_2$Py$_2$: Yield 0.163 g (87.8%). IR(cm^{-1}): ν(Mo=O) 917(s), 932(s). ^{1}H NMR (DMSO-d$_6$): 7.36 ppm (dd, $^3J_{H-H} = 7.5$ Hz, $^4J_{H-H} = 1.5$ Hz, 2H, for thionate protons on C_7); 7.27 ppm (t, $^3J_{H-H} = 8.0$ Hz, $^3J_{H-H} = 7.5$–8.0 Hz, 2H, for thionate protons on C_6); 7.26 ppm (t, $^3J_{H-H} = 8.0$ Hz, 2H, for thionate protons on C_5); 7.66 ppm (dd, $^3J_{H-H} = 8.0$ Hz, $^4J_{H-H} = 1.5$ Hz, 2H, for thionate protons on C_4); 8.59 ppm (dt, $^3J_{H-H} = 4.5$ Hz, $^4J_{H-H} = 1.5$ Hz, 4H, for Py protons on C_2 and C_6); 7.44 ppm (ddd, $^3J_{H-H} = 7.6$ Hz, $^3J_{H-H} = 4.5$ Hz, $^4J_{H-H} = 1.5$ Hz, 4H, for Py protons on C_3 and C_5); 7.85 ppm (tt, $^3J_{H-H} = 7.5$ Hz, $^4J_{H-H} = 1.5$ Hz, 2H, for Py protons C_4). *Anal*. Calc. for $C_{24}H_{18}MoN_4O_2S_4$: C, 46.60; H, 2.93; N, 9.06; S, 20.73. Found: C, 46.81; H, 2.74; N, 9.15, S, 19.99%.

MoO_2(BzTz-S)$_2$(MePy)$_2$: Yield 0.178 g (91.8%). IR(cm^{-1}): ν(Mo=O) 915(s), 935(s). ^{1}H NMR (DMSO-d$_6$): 7.36 ppm (dd, $^3J_{H-H} = 7.5$ to 8.0 Hz, $^4J_{H-H} = 1.5$ Hz, 2H, for thionate protons on C_7); 7.27 ppm (t, $^3J_{H-H} = 8.0$ Hz, $^3J_{H-H} = 7.5$ to 8.0 Hz, 2H, for thionate protons on C_6); 7.26 ppm (t, $^3J_{H-H} = 8.0$ Hz, 2H, for thionate protons on C_5); 7.66 ppm (dd, $^3J_{H-H} = 8.0$ Hz, $^4J_{H-H} = 1.5$ Hz, 2H, for thionate protons on C_4); 8.50 ppm (d, $^3J_{H-H} = 6.0$ Hz, 4H, for MePy protons on C_2 and C_6); 7.40 ppm (d, $^3J_{H-H} = 6.0$ Hz, 4H, for MePy protons on C_3 and C_5); 2.38 ppm (s, 6H, CH_3). *Anal*. Calc. for $C_{26}H_{22}MoN_4O_2S_4$: C, 48.29; H, 3.43; N, 8.66; S, 19.83. Found: C, 48.41; H, 3.28; N, 8.57; S, 19.63%.

MoO_2(BzTz-S)$_2$(Bipy): Yield 0.167 g (90.3%). IR(cm^{-1}): ν(Mo=O) 897(s), 917(s). ^{1}H NMR (DMSO-d$_6$): 7.36 ppm (dd, $^3J_{H-H} = 7.5$ to 8.0 Hz, $^4J_{H-H} = 1.5$ Hz, 2H, for thionate protons on C_7); 7.27 ppm (t, $^3J_{H-H} = 8.0$ Hz, $^3J_{H-H} = 7.5$ to 8.0 Hz, 2H, for thionate

protons on C_6); 7.26 ppm (t, $^3J_{H-H} = 8.0$ Hz, 2H, for thionate protons on C_5); 7.66 ppm (dd, $^3J_{H-H} = 8.0$ Hz, $^4J_{H-H} = 1.5$ Hz, 2H, for thionate protons on C_4); 8.66 ppm (dd, $^3J_{H-H} = 4.5$ Hz, $^4J_{H-H} = 1.4$ Hz, 2H, for Bipy protons on C_6 and $C_{6'}$); 7.42 ppm (ddd, $^3J_{H-H} = 7.5$ Hz, $^3J_{H-H} = 4.5$ Hz, 2H, for Bipy protons on C_5 and $C_{5'}$); 7.92 ppm (td, $^3J_{H-H} = 7.5$ Hz, $^4J_{H-H} = 1.4$ Hz, 2H, for Bipy protons on C_4 and $C_{4'}$); 8.36 ppm (dd, $^3J_{H-H} = 7.5$ Hz, $^4J_{H-H} = 1.3$ Hz, 2H, for Bipy protons on C_3 and $C_{3'}$). *Anal.* Calc. for $C_{24}H_{16}MoN_4O_2S_4$: C, 46.75; H, 2.62; N, 9.09; S, 20.80. Found: C, 45.74; H, 2.54; N, 9.06; S, 19.91%.

2.3. Crystal-structure determinations

Suitable single crystals were grown at r.t. by diffusion of diethyl ether on acetone solutions of the complex in a dry atmosphere. Crystal data for MoO_2(Py-S)$_2$: monoclinic, $P2_1/c$, $a = 6.8605(4)$ Å, $b = 15.2004(9)$ Å, $c = 12.1751(8)$ Å, $\alpha = \gamma = 90°$, $\beta = 98.491(1)°$, $V = 1255.73(13)^3$ Å^3, $Z = 4$, $R = 0.0246$, $R_w = 0.0636$.

Crystals of MoO_2(Py-S)$_2$ (block, yellow, dimensions $0.50 \times 0.15 \times 0.15$ mm) were used for the structure determination. X-ray data were collected using a Bruker SMART CCD area detector single-crystal diffractometer with graphite monochromatized Mo Kα radiation ($\lambda = 0.71073$ Å) by the $\phi - \omega$ scan method. 2171 Frames of intensity data were collected. The first 50 frames were recollected at the end of data collection to monitor for decay. The crystal used for the diffraction study showed little decomposition during data collection (0.4%). The integration processes yield a total 7404 reflections, of which 2476 were independent [$R_{int} = 0.0262$]. Absorption corrections were applied using SADABS [25] program (maximum and minimum transmission coefficients, 1.000 and 0.6458) for MoO_2(Py-S)$_2$. The structure was solved using the Bruker SHELXTL-PC [26] software by direct methods and refined by full-matrix least-squares methods on F^2. Hydrogen atoms were included in calculated positions and refined in the riding mode. For MoO_2(Py-S)$_2$ convergence was reached at a final $R_1 = 0.0246$ [for $I > 2\sigma(I)$], $wR_2 = 0.0661$ [for all data], 186 parameters, 0 restraints, with allowance for the thermal anisotropy for all non-hydrogen atoms. The weighting scheme employed was $w = [\sum^2(F_o^2 + (0.112P)^2 + 0.1345P]$ and $P = (|F_o|^2 + 2|F_c|^2)/3$. Residual electron densities extremes were 0.301 and −0.559 e Å^{-3} and the goodness-of-fit on F^2 was 1.073 for all observed reflections. Crystal data and details on the data collection and refinement are given in the supplementary material.

2.4. Catalytic activity

The measurement of the catalytic activity of MoO_2(Py-S)$_2$ in the oxidation of PPh_3 with DMSO was followed by ^{31}P NMR spectroscopy as previously reported [27].

3. Results and discussion

3.1. Synthesis and characterization of dioxomolybdenum(VI) thionates

It is well known that a variety of dioxomolybdenum(VI) chelatocomplexes – such as oxinates, diketonates and dialkyl dithiocarbamates – are readily isolated from aqueous media by treating acidic solutions of molybdates with the corresponding ligands or their soluble salts [28]. So we tested the reactions of hydrochloric solutions of sodium molybdate with solutions of the thiones in the acid. In general the reactions are immediate at r.t. as evidenced by changes in the coloration of the resulting solutions and/or formation of precipitates. The analytical data (C, H, N, S) for the products were not in agreement with those expected for dioxomolybdenum(VI) thionates. Also, the characteristic couple of bands for dioxomolybdenum(VI) species, around 900 cm^{-1}, was absent in the IR spectra of the products. In view that the preparation of compounds such as dialkyl dithiocarbamates by this procedure require a fine control of pH to avoid redox processes leading to formation of dinuclear oxomolybdenum(V) complexes [29], we examined these reactions in a wide range of conditions (pH, temperature and concentration). Despite our efforts, we have been unable to establish the conditions, if any, to obtain dioxomolybdenum(VI) thionates as primary products.

Since the reported dioxomolybdenum(VI) thionates [16,17] were prepared by reacting MoO_2(acac)$_2$ with the thiones we also attempted to extend this procedure to the synthesis of other related thionates. To this respect it should be noted that the complexes derived from the esters of mercaptonicotinic acid were prepared in warm alcohols with yields below 15%, and that important amounts of both oxomolybdenum(V) thionates and disulphides were simultaneously produced. To minimize redox processes we conducted the reactions in acetone at r.t. Under these conditions acetone thioketals did not form and after 48 h stirring a significant amount of solid separated from the solutions. Analytical data and IR spectra for these solids were consistent with those expected for dinuclear oxomolybdenum(V) thionates, such as the prototypical Mo_2O_3(Py-S)$_4$ [6]. The mother liquors from which the solids separated were treated with diethyl ether and the precipitates formed were analyzed (C, H, N, S and IR spectroscopy). The results were consistent with those expected for mixtures of dioxomolybdenum(VI) thionates and the corresponding disulfides. Thus, the behavior of these thiones towards

$MoO_2(acac)_2$ is closely related to that of the esters of 2-mercaptonicotinic acid previously reported [17].

The air-stable, readily available $MoO_2Cl_2(DMF)_2$ [19] reacted with thallium thionates at r.t. in acetone or acetonitrile. The soluble products of the reactions showed characteristic patterns for new dioxomolybdenum(VI) compounds in the IR spectra. However, unsatisfactory analytical results were obtained assuming they were the foreseen thionates. We also found evidence of DMF in some of the products. For example, the ^1H NMR spectrum of the product derived from 2-thiolpyridine in acetone-d_6 showed, in addition to the signals for the thionate ligand, three singlets at 3.07, 3.14 and 8.25 ppm, close to those of DMF in the parent $MoO_2Cl_2(DMF)_2$. In general the composition of the products is in agreement with the formulation $MoO_2(thionate)_2(DMF)_x$ ($x < 2$). It should be noted that we did not find evidences for redox processes under these conditions.

These results suggest that metathesis involving dioxomolybdenum(VI) halides and thionates in aprotic media may be a convenient way to prepare the corresponding dioxomolybdenum(VI) thionates, but also that the reactions should be conducted in low coordinating solvents to allow coordination of the thionate ligands in a N–S bidentate manner. According to this assumption, when we treated MoO_2Cl_2 with thallium thionates in solvents such as acetonitrile, acetone or THF at r.t. we were able to obtain the expected dioxomolybdenum(VI) thionates in good yield without evidences of competitive redox reactions.

All compounds are yellow-brown. To this respect it should be noted that the purple color associated to the dioxomolybdenum(VI) thionates previously reported [16,17] is very probably due to contamination with dinuclear oxomolybdenum(V) species. Indeed, the products we obtained by reaction of $MoO_2(acac)_2$ with the thiones, while having essentially the same IR spectra and in occasions the same elemental composition than those prepared from MoO_2Cl_2 and thallium thionates, are considerable darker.

A significant difference toward moisture could be appreciated among the dioxomolybdenum(VI) thionates. Those having the nitrogen atom(s) into a six-membered ring, MoO_2(L-*N*,*S*)$_2$ (L-*N*,*S* = Py-S, Pym-S, MePym-S, MeNic-S), are considerably more stable than those having it into a five-membered ring, MoO_2(L-*N*,*S*)$_2$ (L-*N*,*S* = BzTz-S, BzOx-S). The former could be prepared and handled in air without special precautions while the latter required the use of a dry atmosphere, especially during the preparation.

The compounds are insoluble in hexane and diethyl ether; moderately soluble in THF, acetone and acetonitrile, solvents from which they could be crystallized; and very soluble in DMF and DMSO, solvents from which they could not be recovered. They have a low thermal stability and decompose before melting. However, they can be stored for weeks at r.t. in the dark and in a dry atmosphere without noticeable decomposition.

Dioxomolybdenum(VI) thionates react with common organophosphines and phosphites at r.t. leading to purple, sometimes green solutions. However, only the dinuclear oxomolybdenum(V) complexes derived from the thiones having the nitrogen atom(s) into a six-membered ring, Mo_2O_3(L-*N*,*S*)$_4$ (L-*N*,*S* = Py-S, Pym-S, MePym-S, MeNic-S), could be isolated.

The results obtained from the reactions of $MoO_2Cl_2(DMF)_2$ with thallium thionates suggest that the thionate ligands may also behave as monodentate. So we tested the behavior of two representative thionates, $MoO_2(Py\text{-}S)_2$ and $MoO_2(BzTz\text{-}S)_2$, toward a variety of N- and O-donor ligands. As a result we could isolate addition compounds with Py, MePy and Bipy. Although at present we have been unable to obtain crystals for X-ray structural characterization of these compounds we believe that the strained chelating thionate ligand, in the presence of strong bases, becomes monodentate S-coordinated. These addition compounds are noticeably less soluble in common organic solvents, and less intense colored (from white to pale yellow) than the parent thionates.

The IR spectra of dioxomolybdenum(VI) thionates are characterized by two strong bands in the region 880–950 cm^{-1} which indicates that, as usual for dioxomolybdenum(VI) species, all of them contain the *cis*-MoO_2 moiety [30]. We find it difficult to establish correlations between the position of these bands and the nature of the ligands. Thus, from the fact that pyridines coordinate to molybdenum, presumably displacing the coordinated nitrogen atoms in MoO_2(L-*N*,*S*)$_2$, we could expect lower values for ν(Mo=O) in the addition compounds than in the parent thionates (the π-donation from the oxo ligands to molybdenum should be influenced by the electronic density on the metal). However, this is only applicable to adducts of Bipy.

No special features are observed in the ^1H NMR spectra of the complexes. In the addition compounds with pyridine and its derivatives the signals characteristic for the free ligands are shifted, as usual, to lower fields upon coordination, though competition of DMSO-d_6 with the neutral ligands for the coordination sphere of molybdenum could be appreciated.

3.2. Molecular structure

Based on the stoichiometry and structure for similar complexes it is probable that all compounds be closely related. The molecular structure for $MoO_2(Py\text{-}S)_2$ was determined from single-crystal X-ray diffraction analysis. A view of $MoO_2(Py\text{-}S)_2$ is shown in Fig. 1. Selected bond lengths and angles are listed in Table 1.

The molybdenum is coordinated in a pseudo-octahedral fashion by two *cis* oxo functions and two che-

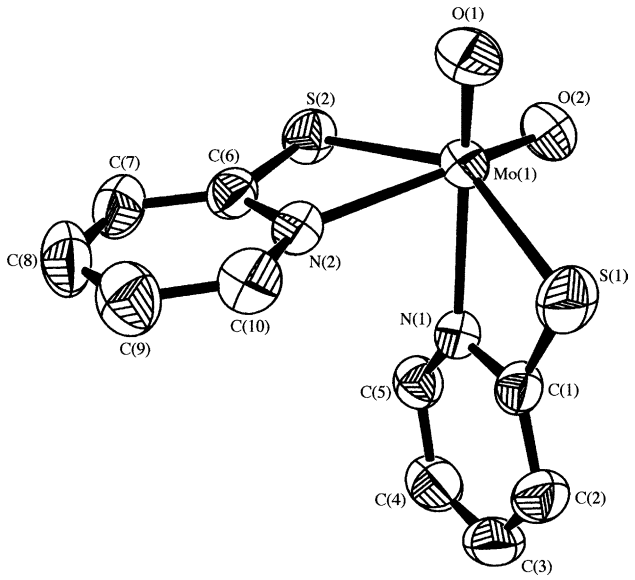

Fig. 1. Molecular structure and atom-labeling scheme for $MoO_2(Py\text{-}S)_2$ with thermal ellipsoids at the 50% probability level; hydrogen atoms are omitted.

Table 1
Selected bond lengths (Å) and angles (°) for $MoO_2(Py\text{-}S)_2$

Bond lengths			
Mo(1)–O(1)	1.7012(19)	Mo(1)–O(2)	1.7047(18)
Mo(1)–N(2)	2.3011(19)	Mo(1)–N(1)	2.3089(19)
Mo(1)–S(1)	2.4395(7)	Mo(1)–S(2)	2.4492(7)
Bond angles			
O(1)–Mo(1)–O(2)	106.91(10)	N(2)–Mo(1)–S(1)	86.47(5)
O(1)–Mo(1)–N(2)	91.31(8)	N(1)–Mo(1)–S(1)	65.11(5)
O(2)–Mo(1)–N(2)	156.35(9)	O(1)–Mo(1)–S(2)	106.27(7)
O(1)–Mo(1)–N(1)	156.44(8)	O(2)–Mo(1)–S(2)	94.81(7)
O(2)–Mo(1)–N(1)	90.18(8)	N(2)–Mo(1)–S(2)	65.04(5)
N(2)–Mo(1)–N(1)	77.39(7)	N(1)–Mo(1)–S(2)	87.82(5)
O(1)–Mo(1)–S(1)	93.93(7)	S(1)–Mo(1)–S(2)	144.84(3)
O(2)–Mo(1)–S(1)	106.66(7)		

lating Py–S ligands. Distortions from the ideal octahedral geometry (see Table 1) mainly arise from the disparate donor atom set and the restricted bite of the Py–S ligands, which subtend angles at the molybdenum center of approximately 65°. The Py–S ligands are arranged so that the two sulfur atoms are approximately *trans* to each other [S–Mo–S 144.84(3)°] compelling the nitrogen atoms to occupy approximate *cis*-positions [N–Mo–N 77.39(7)°]. The two equivalent Mo=O bond distances, and the *cis*-MoO_2 angle, are within the range usually found in dioxomolybdenum(VI) compounds (1.65–1.75 Å and 95°–110°, respectively) [31]. The two Mo–S bond distances are not equivalent and the same is applicable to the Mo–N distances. However, an intraligand compensation of distances can be perceived so that the shortest M–N and the largest M–S distances occur in the same ligand. The cause of the disparity in the mode of coordination of the Py–S ligands can be traced, more than to the *trans* influence of the oxo ligands (both N-donor atoms occupy positions *trans* to an oxo function with identical O–Mo–N angles), to packing forces. As could be expected, all distances and angles are in the range of those reported for dioxomolybdenum(VI) complexes with the esters of 2-mercaptonicotinic acid [17].

3.3. Catalytic tests in oxotransfer reactions

The behavior of dioxomolybdenum(VI) thionates toward phosphines and phosphites is indicative of oxotransfer processes from the dioxomolybdenum center to

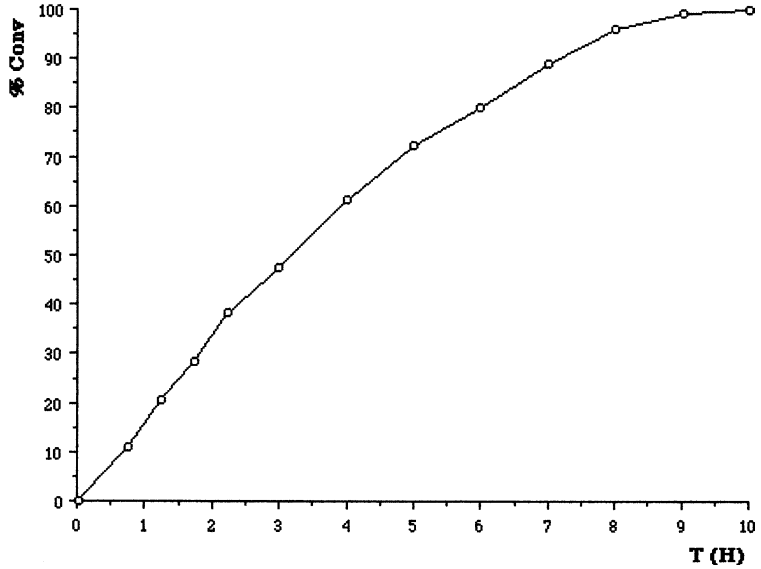

Fig. 2. Oxidation of PPh_3 to $OPPh_3$ by DMSO-d_6 at 60 °C as a function of time for [Mo] = 0.02 mol dm^{-3} and $[PPh_3]_0/[Mo] = 20$.

the P-oxoaceptor. Evolution of the foul-smelling dimethyl sulphide was detected when DMSO was added to the resulting mixtures oxoaceptor-MoO_2(L-*N*,*S*)$_2$, suggesting the potential of the thionatocomplexes to work as oxotransfer catalysts from sulfoxides to phosphorus(III) compounds. In the vicinity of r.t. the catalytic activity of MoO_2(Py-S)$_2$ for the conversion of PPh_3 into $OPPh_3$ by DMSO is very low, presumably due to the stability of the dinuclear species Mo_2O_3(Py-S)$_4$. However the activity dramatically increases with the temperature. Thus, while only 10% conversion was produced after 24 h at 20 °C, complete oxidation to $OPPh_3$ was observed in 10 h at 60 °C (see Fig. 2).

4. Supplementary material

Crystallographic data for the structural analysis have been deposited with the Cambridge Crystallographic Data Centre, CCDC No. 213716. Copies of this information may be obtained free of charge from The Director, CCDC, 12 Union Road, Cambridge, CB2 1EZ, UK (Fax: + 44-1223-336033; e-mail: deposit@ccdc.cam.ac.uk or www: http://www.ccdc.cam.ac.uk).

Acknowledgements

This work was supported by the Ministerio de Ciencia y Tecnología (Grant BQU2002-00435) and Junta de Castilla y Leon (Grant BU 15/03).

References

[1] E.S. Raper, Coord. Chem. Rev. 61 (1985) 115.
[2] E.S. Raper, Coord. Chem. Rev. 129 (1994) 91.
[3] E.S. Raper, Coord. Chem. Rev. 153 (1996) 199.
[4] E.S. Raper, Coord. Chem. Rev. 165 (1997) 475.
[5] P.D. Akrivos, Coord. Chem. Rev. 213 (2001) 181.
[6] F.A. Cotton, P.E. Fanwick, J.W. Fitch III, Inorg. Chem. 17 (1978) 3254.
[7] F.A. Cotton, W.H. Isley, Inorg. Chem. 20 (1981) 614.
[8] J.L. Templeton, Adv. Organomet. Chem. 29 (1989) 1.
[9] A.J. Deeming, M. Karim, N. Powell, J. Chem. Soc., Dalton Trans. (1990) 2321.
[10] E. Block, G. Ofori-Okai, H. Kang, J. Zubieta, Inorg. Chim. Acta 190 (1991) 179.
[11] P.K. Baker, P.D. Jackson, M.E. Harman, M.B. Hursthouse, J. Organomet. Chem. 468 (1994) 171.
[12] P.K. Baker, P.D. Jackson, M.G.B. Drew, J. Chem. Soc., Dalton Trans. (1994) 37.
[13] I.A. Latham, G.J. Leigh, C.J. Picket, G. Huttner, I. Jibrill, J. Zubieta, J. Chem. Soc. Dalton Trans. (1986) 1181.
[14] E. Block, M. Gernon, G. Ofori-Okai, J. Zubieta, Inorg. Chem. 30 (1990) 1736.
[15] E. Block, H. Kang, J. Zubieta, Inorg. Chim. Acta 181 (1991) 227.
[16] P.R. Traill, A.G. Wedd, E.R.T. Tiekink, Aust. J. Chem. 45 (1992) 1933.
[17] M. Cindric, N. Strukan, T. Kajfez, G. Giester, B. Kamenar, Z. Anorg. Allg. Chem. 627 (2001) 2604.
[18] M.L. Larson, F.W. Moore, Inorg. Chem. 5 (1966) 801.
[19] F.J. Arnáiz, R. Aguado, J. Sanz-Aparicio, M. Martínez-Ripoll, Polyhedron 13 (1994) 2745.
[20] R. Sanz, R. Aguado, M.R. Pedrosa, F.J. Arnáiz, Synthesis 7 (2002) 856.
[21] F.J. Arnáiz, R. Aguado, M.R. Pedrosa, J. Mahía, M.A. Maestro, Polyhedron 21 (2002) 1635.
[22] F.J. Arnáiz, R. Aguado, M.R. Pedrosa, A. De Cian, Inorg. Chim. Acta 347 (2003) 33.
[23] F.J. Arnáiz, J. Chem. Educ. 72 (1995) A7.
[24] R. Pürschel, E. Lassner, R. Scharf, Zeitschr. Anal. Chem. 163 (1958) 104.
[25] G.M. Sheldrick, SADABS. A Program for Empirical Absorption Correction of Area Detector Data, University of Göttingen, Germany, 1996.
[26] G.M. Sheldrick, SHELXS-97, A Program for Solving Crystal Structures and Crystal Structure Refinement, University of Göttingen, Germany, 1997.
[27] F.J. Arnáiz, R. Aguado, J.M. Martínez-Ilarduya, Polyhedron 13 (1994) 3257.
[28] See, e.g.: W.C. Fernelius, K. Terada, B.E. Bryant, Inorg. Synth. 6 (1960) 147.
[29] R.N. Jowit, P.C.H. Mitchell, J. Chem. Soc. A (1970) 1702.
[30] J.H. Enemark, C.G. Young, Adv. Inorg. Chem. 40 (1994) 2.
[31] W.A. Nugent, J.M. Mayer, Metal-Ligand Multiple Bonds, Wiley, New York, 1988.

Available online at www.sciencedirect.com
SCIENCE DIRECT®
Polyhedron 23 (2004) 545–552
POLYHEDRON
www.elsevier.com/locate/poly

Synthesis, structure and properties of $[Zn(dpa)(N_3)_2]$ and $[Zn(dpa)(N_3)(NO_3)]_2$ (dpa = 2,2′-dipyridylamine): composition tailored architectures

Doyel Bose [a], Sk Hafijur Rahaman [a], Golam Mostafa [b], Rosa D. Bailey Walsh [c], Michael J. Zaworotko [c], Barindra K. Ghosh [a,*]

[a] Department of Chemistry, The University of Burdwan, Burdwan 713104, India
[b] Department of Physics, Jadavpur University, Kolkata 700032, India
[c] Department of Chemistry, The University of South Florida, 4202 East Fowler Avenue, Tampa, FL 33620-5250, USA

Received 26 June 2003; accepted 8 October 2003

Abstract

The synthetic details, characterization data and single crystal X-ray structural analyses of $[Zn(dpa)(N_3)_2]$ (**1**) and $[Zn(dpa)(N_3)(NO_3)]_2$ (**2**) (dpa = 2,2′-dipyridylamine) are described. Structural study reveals that the zinc(II) centre in **1** is in a pseudotetrahedral ZnN_4 environment ligated by two terminal azide N atoms and two pyridine N atoms of the chelator. The coordination polyhedron around each metal ion in dinuclear **2** is best described as a ZnN_4O_2 distorted octahedron linked by two end-on azido bridges. The mononuclear units in **1** are engaged in bifurcated intermolecular hydrogen bonding (N–H...N) between amine N of dpa and coordinated N of azide along with aromatic π–π stacking leading to a 2D sheet. In **2**, the dinuclear units participate in intermolecular N–H...O hydrogen bonding between amine N of dpa and bound O of bidentate nitrate in combination with π–π interactions resulting to a 3D supramolecular continuum. **1** and **2** display high energy intraligand $^1(\pi–\pi^*)$ fluorescence and intraligand $^3(\pi–\pi^*)$ phosphorescence in glassy solutions (DMF at 77 K). A band (372 nm) observed for both **1** and **2** in their solid-state emission spectra is an excimeric emission arising due to aromatic π–π interaction. The role of dpa, a tailored diimine (–N=C–NH–C=N–) in **1** and **2** is discussed towards functionalisation on crystal engineering and luminescence behaviour.
© 2003 Elsevier Ltd. All rights reserved.

Keywords: Zinc(II)azide; Mononuclear; Dinuclear; 2,2′-Dipyridylamine; Luminescence; Crystal engineering

1. Introduction

The development of supramolecular architectures [1–4] of inorganic organic hybrid molecules with various shapes and sizes [5] formed through control and manipulation of weak interaction [6,7] via non-covalent forces is an exciting area of research that has implications for the rational design of functional materials [8–17]. The fascinating structures of these compounds, coupled with their specific functionality, have made them highly promising to be used as catalysts [8], electrical conducting materials [9,10], molecular magnetic materials [11,12], non-linear optical materials [13,14], liquid crystals (mesogens) [15], sensor materials [16] and molecular recognitions [17]. Self-assembly [18] of suitable molecular components is an efficient way for facile tuning of structural and electronic functions on materials research [8–17] and in the interpretation of electron/energy transport in the bio-active molecules [19] as well. Exploiting the veracity of coordination geometry around metal centres, diverse network topologies can be accessed with the use of ligand building blocks. The purpose is to tailor the composition, structure and function of materials, which may lead to new properties for well-known standard materials and hence to new applications. We are interested in this approach for the construction of metallo-organic supramolecule through variation of ligand backbone and metal ion coordination environment. 2,2′-Dipyridylamine (dpa), a

* Corresponding author. Tel.: +91-342-255-8545; fax: +91-342-253-0452.
E-mail address: barin_1@yahoo.co.uk (B.K. Ghosh).

0277-5387/$ - see front matter © 2003 Elsevier Ltd. All rights reserved.
doi:10.1016/j.poly.2003.10.012

tailored diimine (–N=C–NH–C=N–) is important in this regard because of its ability to form hydrogen bonded network through active amine (–NH–) hydrogen [20–23] and to luminescence through π–π^* transitions [24]. Zinc is well suited [25–27] as its d^{10} configuration permitting a wide variety of symmetries and coordination numbers and it has drawn special attention for its importance in bioinorganic chemistry [28,29]. Azide is a versatile [30–32] ligand and may bind to metal ion through terminal or bridges with end-on or end-to-end motif. Report on blue photoluminescence [26,27] of some zinc(II) complexes of dpa by Che et al. has prompted us to develop new luminous materials with polymeric supramolecular structures. Successfully we have synthesized and X-ray crystallographically characterized one mononuclear [Zn(dpa)$(N_3)_2$] (**1**) and one dinuclear [Zn(dpa)$(N_3)(NO_3)]_2$ (**2**) complexes. **1** and **2** show self-assembled superstructures in solid state via cooperative hydrogen bonds and aromatic π–π interactions [33]. In this paper an emphasis has been made to show how use of such non-covalent forces may be effectively harnessed to synthesize non-molecular solids of varied architectures. The individual zero-dimensional (0D) unit in **1** is engaged in N–H. . .N hydrogen bonding resulting 1D chains, which thereby yield a sheet-like supramolecular architecture via π–π interactions. In **2**, a two-dimensional (2D) sheet is the result through N–H. . .O hydrogen bonds followed by π–π stackings to yield a 3D continuum.

2. Experimental

2.1. Materials

High purity 2,2′-dipyridylamine (Fluka, Germany), zinc nitrate hexahydrate (E. Merck, India) and sodium azide (E. Merck, India) were purchased from respective concerns and used as received. Zinc perchlorate hexahydrate was prepared on treatment of zinc carbonate (E. Merck, India) with perchloric acid (E. Merck, India) followed by slow evaporation on steam-bath, filtration through a fine glass-frit, and preservation in a desiccator containing concentrated sulphuric acid for subsequent use. All other chemicals and solvents were AR grade and were used as received.

Caution! Azido compounds and perchlorate salts of metal ions are potentially explosive. Only a small amount of material should be prepared and handled with care.

2.2. Physical measurements

Elemental analyses (carbon, hydrogen and nitrogen) were performed on a Perkin-Elmer 2400 CHNS/O elemental analyzer. IR spectra (KBr discs, 4000–300 cm^{-1}) were recorded using a JASCO FTIR model 420 spectrometer. Molar conductances were measured using a Systronics conductivity meter where the cell constant was calibrated with 0.01 M KCl solution and dry DMF was used as solvent. Ground state absorption and steady-state fluorescence measurements were made with a JASCO model V-530 UV–Vis spectrophotometer and Hitachi model F-4010 spectrofluorimeter, respectively. Time-resolved fluorescence measurements were carried out using a time-correlated single photon counting (TCSPC) spectrometer Edinburgh Instruments, model 199; a hydrogen filled coaxial flash lamp with a pulse width of 1.2 ns at FWHM and a Philips XP-2020Q Photomultiplier tube were respectively used as the excitation source and the fluorescence detector.

2.3. Preparation of the complexes

Mononuclear **1** was prepared from both nitrate and perchlorate salts of zinc(II) using the same (1:1:2) mole ratio of the metal, dpa and azide. **2** was prepared using a 1:1:1 ratio of zinc(II) nitrate, dpa and azide; the corresponding ratio with perchlorate salt resulted mononuclear **1** but with low yield. The typical syntheses are described below.

2.3.1. *[Zn(dpa)$(N_3)_2$] (**1**)*

An acetonitrile solution (5 cm^3) of dpa (0.056 g, 0.324 mmol) was added to a solution of $Zn(ClO_4)_2 \cdot 6H_2O$ (0.121 g, 0.324 mmol) in the same solvent (10 cm^3) followed by NaN_3 (0.043 g, 0.656 mmol) in water (5 cm^3). The mixture was filtered and the supernatant liquid was kept in air for slow evaporation. After a few days ***1*** was separated, washed with toluene and dried in vacuo over silica gel indicator. Yield, 0.068 g (80%). *Anal*. Found: C, 37.75; H, 2.96; N, 39.85. Calc. for $C_{10}H_9N_9Zn$ (**1**): C, 37.46; H, 2.83; N, 39.32%. IR (KBr, cm^{-1}): ν(N–H) 3304 (br); ν(N=N=N) 2073; ν(C=N) 1590. Λ_M (DMF, $ohm^{-1}\,cm^2\,mol^{-1}$): 5; UV–Vis (λ, nm): 255, 315.

2.3.2. *[Zn(dpa)$(N_3)(NO_3)]_2$ (**2**)*

To an acetonitrile solution (10 cm^3) of $Zn(NO_3)_2 \cdot 6H_2O$ (0.096 g, 0.324 mmol) were added dpa (0.056 g, 0.324 mmol) in the same solvent (5 cm^3) and NaN_3 (0.021 g, 0.328 mmol) in water (5 cm^3). The colourless solution was filtered and was kept for slow evaporation. After 7 days ***2*** was separated and was processed as in ***1***. Yield, 0.172 g (75%). *Anal*. Found: C, 35.65; H, 2.84; N, 28.95. Calc. for $C_{20}H_{18}N_{14}O_6Zn_2$ (**2**): C, 35.26; H, 2.66; N, 28.79%. IR (KBr, cm^{-1}): ν(N–H) 3324 (br); ν(N=N=N) 2071; ν(C=N) 1592; $\nu(NO_3)$ 1384. Λ_M (DMF, $ohm^{-1}\,cm^2\,mol^{-1}$): 10; UV–Vis (λ, nm): 257, 315.

2.4. X-ray crystallographic analyses

Single crystals were obtained by slow evaporation of 3:1 MeCN–H_2O solution of the reaction mixtures.

Table 1
Crystal data and structure refinement parameters for **1** and **2**

	1	**2**
Empirical formula	$C_{10}H_9N_9Zn$	$C_{20}H_{18}N_{14}O_6Zn_2$
Formula weight	320.63	681.22
Colour	colourless	colourless
Temperature (K)	200(2)	200(2)
Wavelength (Å)	0.71073	0.71073
Crystal system	monoclinic	monoclinic
Space group	$C2/c$	$P2(1)/n$
a (Å)	15.024(2)	7.6902(9)
b (Å)	7.3603(10)	15.4993(18)
c (Å)	13.6117(19)	11.0722(13)
β (Å)	122.514(2)	102.344(2)
V (Å^3)	1269.3(3)	1289.2(3)
Z	4	2
D_c (Mg m^{-3})	1.678	1.755
μ (mm^{-1})	1.940	1.928
$F(0\,0\,0)$	648	688
Crystal size (mm)	$0.20 \times 0.20 \times 0.10$	$0.35 \times 0.15 \times 0.15$
θ ranges (°)	3.20 to 28.22	2.30 to 28.26
$h/k/l$	−15,19/−8,9/−16,17	−6,10/−20,19/−14,12
Reflections collected	3669	7573
Independent reflections	1463 ($R_{int} = 0.0247$)	2987 ($R_{int} = 0.0263$)
Completeness to θ (%)	93.4	93.4
T_{max} and T_{min}	1.000 and 0.536	1.000 and 0.693
Data/restraints/parameters	1463/0/92	2987/0/191
Goodness-of-fit on F^2	1.105	1.100
Final R indices [$I > 2\sigma(I)$]	$R_1 = 0.0509$, $wR_2 = 0.1296$	$R_1 = 0.0360$, $wR_2 = 0.0825$
R indices (all data)	$R_1 = 0.0580$, $wR_2 = 0.1336$	$R_1 = 0.0467$, $wR_2 = 0.0861$
Largest peak and hole (e Å^{-3})	2.700, −0.295	0.468, −0.286

Colourless crystals suitable for X-ray crystallographic analyses were selected following examination under a microscope. Diffraction data were collected on a Bruker-AXS SMART APEX/CCD diffractometer using Mo Kα radiation, which were corrected for Lorentz and polarization effects and for absorption using the SADABS [34] program. The structure was solved by direct methods and the structure solution and refinement were based on $|F^2|$. All non-hydrogen atoms were refined with anisotropic displacement parameters whereas hydrogen atoms were placed in calculated positions when possible and given isotropic U values 1.2 times that of the atom to which they are bonded. The crystallographic calculations were conducted with the SHELXTL v. 6.1 [35] program package. The crystal data and data collection parameters of **1** and **2** are listed in Table 1.

3. Results and discussion

3.1. Synthesis and formulation

The tetracoordinated mononuclear complex $[Zn(dpa)(N_3)_2]$ (**1**) was prepared as a colourless powder through one-pot reactions of a 1:1:2 molar ratio of the metal perchlorate/nitrate, organic blocker and the pseudohalide from an aqueous acetonitrile solution. The hexacoordinated dinuclear $[Zn(dpa)(N_3)(NO_3)]_2$ (**2**) was obtained with a 1:1:1 molar ratio of metal nitrate, dpa and azide; however, use of a similar ratio but a change to perchlorate salt instead of nitrate leads to mononuclear **1** with albeit lower yield which again increases if the required ratio (1:1:2) is employed. Attempts to prepare hexacoordinated mononuclear compound of the composition $[Zn(dpa)_2(N_3)_2]$ with a ratio of 1:2:2 of the metal nitrate/perchlorate, dpa and azide resulted **1**. Similarly, started with 1:2:1 ratio of Zn(II) salt, dpa and azide to have hexacoordinated dinuclear compound of the type $[Zn(dpa)_2(N_3)]_2(Y)_2$ ($Y = ClO_4$ or NO_3) resulted **2** with metal nitrate and **1** with perchlorate. This shows inherent tendency towards formation of compounds **1** and **2** due to some kind of stability associated with themselves. Microanalytical (C, H and N) results and spectroscopic data (see Section 2) are useful in this regard to formulate the products. The air-stable moisture-insensitive complexes **1** and **2** are insoluble in common solvents like, methanol, ethanol, dichloromethane, acetonitrile, but has poor solubility in warm dimethylformamide and dimethylsulfoxide. In dimethylformamide the compounds behave as non-electrolytes as are evident [36] from their low conductivity values (5–10 ohm^{-1} cm^2 mol^{-1}); however **2** shows an increase in conductance value if it is left in solution, which is expected from dissociation of the nitrate ion from the coordination zone due to its weak coordinating property.

In IR spectra the point of interest is the band due to azide in **1** and both azide and nitrate, in **2**. The asymmetric stretch, $\nu_{as}(N_3)$ appears [37] as a strong band at 2073 cm^{-1} in **1** and at 2071 cm^{-1} in **2**. The azido symmetric stretch, $\nu_s(N_3)$ corresponding to the end-on (EO) bridging mode is observable as a band of medium intensity at about 1330 cm^{-1}. The inactiveness of this band for symmetrical end-to-end (EE) coordination supports the presence of EO motif in **2**. The presence of $\nu(NO_3)$ band at 1384 cm^{-1} in **2** is noticed. The splitting in the nitrate stretch indicates the presence of some kind of hydrogen bonding in **2**. Furthermore, the IR spectra of **1** and **2** feature the bands characteristic [38] of dpa molecule, seen in the stretching and bending modes of C–C and C–N bands in the ranges between 1645–1390 and 1270–750 cm^{-1}. The –NH– band is noticeable at ~3300 cm^{-1}. Reflectance spectra [**1**: λ, 257, 315 nm; **2**: λ, 259, 315 nm] in nujol and electronic spectra [**1**: λ, 255, 315 nm; **2**: λ, 257, 315 nm] in DMF solutions are akin in both complexes reflecting gross structure and electronic structure in solid state and in solution.

3.2. Structure

The structural analyses show that mononuclear **1** and dinuclear **2** consist of 2D sheet and 3D supramolecular continuum respectively formed by cooperative hydrogen bonds and π–π interactions. The ORTEP diagram of mononuclear unit, perspective view of the 2D sheet and arrangement of these sheets in **1** are shown in Figs. 1–3, respectively. Figs. 4–6 show the structure of the dimeric unit, hydrogen bonded 2D sheet with one kind of π–π interaction and 3D continuum with further π–π inter-

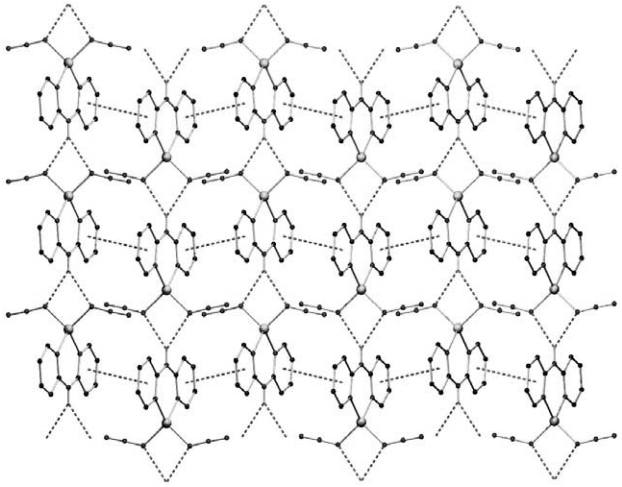

Fig. 2. Packing view of 2D supramolecular sheet formed by bifurcated H-bonding and π–π interaction in **1**.

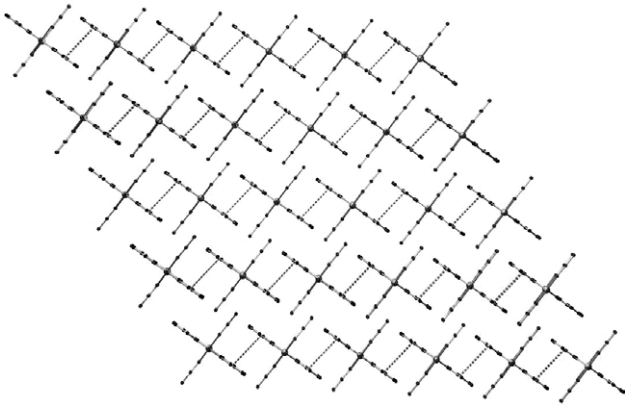

Fig. 3. The arrangement of sheets in **1**.

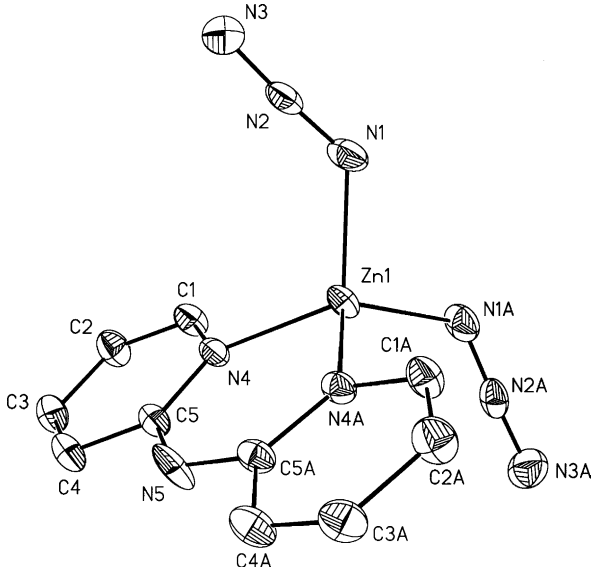

Fig. 1. ORTEP representation of the monomeric $[Zn(dpa)(N_3)_2]$ (**1**) with atom numbering scheme and 50% probability ellipsoids for all non-hydrogen atoms.

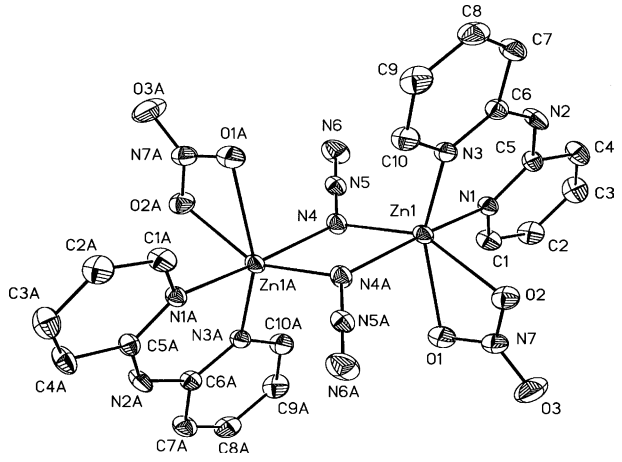

Fig. 4. ORTEP diagram of the dimeric $[Zn(dpa)(N_3)(NO_3)]_2$ (**2**) with atom numbering scheme and 50% probability ellipsoids for all non-hydrogen atoms.

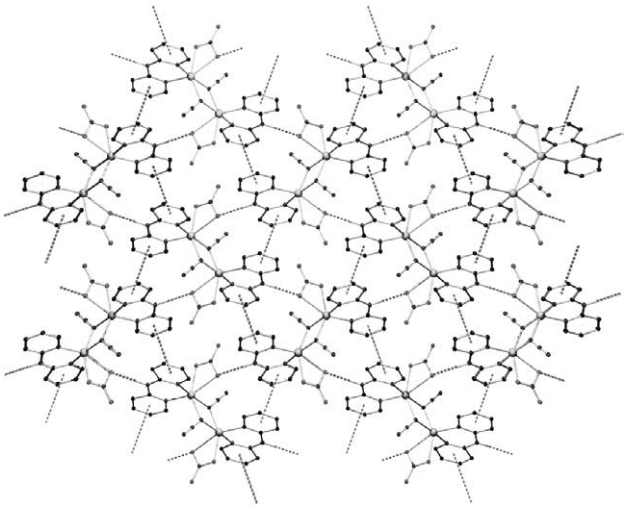

Fig. 5. Packing diagram of 2D supramolecular sheet formed by H-bonding and π–π interaction in **2**.

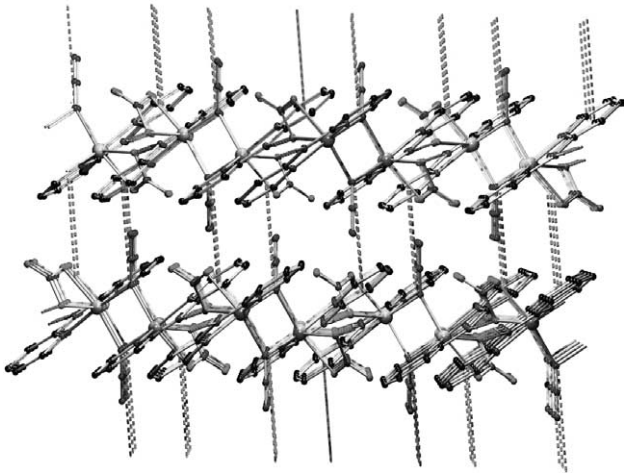

Fig. 6. 3D continuum in **2** formed by π–π interactions within the supramolecular sheets.

action in **2**. Selected bond distances and bond angles relevant to the Zn coordination spheres in **1** and **2** are given in Tables 2 and 3, respectively. The significant hydrogen bonding and π–π interaction parameters are set in Table 4.

The coordination polyhedron around Zn in **1** is best described as distorted tetrahedron with ZnN_4 chromophore. The coordination includes (Fig. 1) the chelated tailored diimine (–N=C–NH–C=N–) ligated by two pyridine N atoms (N4, N4A) and two terminal azide N atoms (N1, N1A). All the four Zn–N bond lengths lie within a close range [1.943(3)–1.997(3) Å]. The N1–N2 distance [1.187(5) Å] is greater than N2–N3 distance [1.165(5) Å] as expected, and the values are very similar to different transition metal azido complexes [31]. The bite [N4–Zn1–N4A, 94.94(18)°] is less than the angle [N1–Zn1–N1A, 98.9(2)°] between the two bound azides (Table 2), and both are substantially less than the ideal tetrahedral value [109.5°]. Interestingly, in $[Zn(dpa)(CN)_2]$ the bite is very close [92.3(2)°] to this one but non-bite C–Zn–C angle is 118.3(2)° which is significantly greater [26]. In **1** the low dihedral angle [0.4(2)°] between the two planar pyridine rings in dpa reflects almost planarity of the organic ligand.

The NH group in **1** acts as a hydrogen-bond donor to N1 and symmetry related N1A [H5...N1, 2.500 Å; N5...N1, 3.248(5) Å; <N5–H5...N1, 144.0° (Table 4)] forming 1D chain through bifurcated hydrogen bonds. The N–H...N bonds generate a cyclic motif $R_2^1(4)$ in Etter's graph notation [39]. The chains running in anti-parallel fashion in *bc*-plane form 2D sheet (Fig. 2) through face-to-face π–π interaction. The dihedral angle between the interacting pyridyl rings is within 0.0°–5.83° and the perpendicular distance between baricentres of these planes is in range 3.587 Å. The arrangement of the sheets is shown in Fig. 3.

The structure (Fig. 4) of **2** is made up of a centro-symmetric binuclear $[Zn(dpa)(N_3)(NO_3)]_2$ unit. Each metal centre is linked by two pyridine N atoms of organic blocker, two bridging azide N atoms and two O atoms of the bidentate chelating nitrate. The geometry around each zinc centre is distorted octahedral with a ZnN_4O_2 chromophore. The nitrogens (N4, N4A) of doubly bridging end-on azido, one pyridine nitrogen (N1) of dpa, and oxygen (O2) from nitrate define the equatorial plane around Zn1, whereas axial positions are occupied by N3 from the other pyridine ring of the same dpa unit and O1, the second coordinated oxygen of the nitrate. The maximum deviation of Zn atom from

Table 2
Selected bond distances (Å) and angles (°) for **1**

Bond distances			
Zn(1)–N(1)	1.943(3)	Zn(1)–N(4A)	1.997(3)
Zn(1)–N(1A)	1.943(3)	Zn(1)–N(4)	1.997(3)
N(1)–N(2)	1.187(5)	N(2)–N(3)	1.165(5)
Bond angles			
N(1)–Zn(1)–N(1A)	98.9(2)	N(1A)–Zn(1)–N(4)	119.11(14)
N(1)–Zn(1)–N(4A)	119.11(14)	N(4A)–Zn(1)–N(4)	94.94(18)
N(1A)–Zn(1)–N(4A)	113.08(14)	N(2)–N(1)–Zn(1)	126.5(3)
N(1)–Zn(1)–N(4)	113.08(14)	N(3)–N(2)–N(1)	176.5(4)

Table 3
Selected bond distances (Å) and angles (°) for **2**

Bond distances			
Zn(1)–N(3)	2.062(2)	O(1)–Zn(1)	2.423(2)
Zn(1)–N(1)	2.094(2)	O(2)–Zn(1)	2.155(2)
Zn(1)–N(4A)	2.130(2)	O(3)–N(7)	1.197(3)
Zn(1)–N(4)	2.090(2)	O(2)–N(7)	1.256(3)
O(1)–N(7)	1.289(3)		
Bond angles			
N(3)–Zn(1)–N(4)	111.55(9)	N(4)–Zn(1)–O(2)	147.64(8)
N(3)–Zn(1)–N(1)	90.61(8)	N(1)–Zn(1)–O(2)	90.51(8)
N(4)–Zn(1)–N(1)	93.27(8)	N(4A)–Zn(1)–O(2)	92.28(8)
N(3)–Zn(1)–N(4A)	99.86(8)	N(3)–Zn(1)–O(1)	155.94(8)
N(4)–Zn(1)–N(4A)	78.47(10)	N(4)–Zn(1)–O(1)	92.51(8)
N(1)–Zn(1)–N(4A)	168.47(8)	N(1)–Zn(1)–O(1)	87.27(8)
N(3)–Zn(1)–O(2)	100.52(8)	N(4A)–Zn(1)–O(1)	85.10(8)
O(2)–Zn(1)–O(1)	55.57(7)	N(7)–O(1)–Zn(1)	87.85(14)
N(7)–O(2)–Zn(1)	101.45(17)	Zn(1)–N(4)–Zn(1A)	101.53(10)

the mean plane passing through the equatorial plane is 0.20 Å. The Zn–N distances are in the range [2.062(2)–2.130(2) Å] which are consistent with corresponding values of analogous octahedrally coordinated zinc(II) complexes [25]. The Zn–O lengths [Zn1–O1, 2.423(2) Å, Zn1–O2, 2.155(2) Å] reflect asymmetric and weak coordination of a nitrate. The three N–O distances [N7–O1, 1.289(3); N7–O2, 1.256(3) and N7–O3, 1.197(3) Å] and O1–N7–O2 angle of 115.0(2)° consistent with an asymmetric bidentate coordination [40]. The *cisoid* [55.57(7)°–111.55(9)°] and *transoid* [147.64(8)°–168.47(8)°] angles (Table 3) around Zn are in line with strong distortion from an idealised octahedron. The Zn1–N4–Zn1A bridging angle is 101.53(10)° – an usual feature of azide bridges in most metal complexes [30–32]. The Zn...Zn separation is 3.269(3) Å. The dpa ligand is slightly folded as the value of the dihedral angle between the planar pyridine rings is 5.80(4)°. The dpa bite [90.61(8)°] is less than that in **1** as expected for crowded octahedral environment compared to open coordination sphere in a tetrahedron.

In **2**, each NH group acts as a hydrogen-bond donor to one metal bound oxygen, O1 of the chelating nitrate [H11...O1, 2.040 Å; N2...O1, 2.939(3) Å; <N2–H11...O1, 175.0° (Table 4)]. The nitrates are so oriented around the metal centre that they point to two quite opposite directions and at the same time come very close to the vicinity of amine hydrogen of the next unit thereby facilitating hydrogen bonding in two directions. The sheet structure is further strengthened by a face-to-face π–π interaction (dihedral angles = 5.80°, perpendicular distance between baricentres = 3.60 Å) (Fig. 5). These sheets are linked by another face-to-face π–π interaction (dihedral angles = 16.4°, perpendicular distance between baricentres = 3.40 Å) to form a 3D continuum in solid state (Fig. 6).

3.3. Luminescence spectra

The spectroscopic data are listed in Table 5. Complexes with dpa, feature [27] two intense absorptions at 257 and 315 nm which are assigned to intraligand π–π* transitions. The emission energy of **1** and **2** in DMF solutions at 298 K is almost same ($\lambda_{max} \approx 350$ nm) and is assignable to intraligand fluorescence [26,27]. The lifetimes of the fluorescence of **1** and **2** are 2.63 and 2.59

Table 4
Hydrogen bond distances (Å) and angles (°) for **1** and **2**

D–H...A	D–H	H...A	D...A	D–H...A
N(5)–H(5)...N(1)[a] (**1**)	0.88	2.500	3.248(5)	144.00
N(5)–H(5)...N(1A)[b](**1**)	0.88	2.500	3.248(5)	144.00
N(2)–H(11)...O(1)[c] (**2**)	0.91	2.040	2.939(3)	175.00
π–π interaction				
Ring(*i*) → Ring(*j*)	Dihedral angle (*i*, *j*)	⊥ Distance between baricentres (*i*, *j*)		
N4–C5 → N4–C5[i] (**1**)	0.0	3.587		
N1–C5 → N3–C10[ii] (**2**)	5.8	3.600		
N1–C5 → N3–C10[iii] (**2**)	16.4	3.400		

Symmetry code: [a] $x, -1+y, z$; [b] $1-x, -1+y, 3/2-z$; [c] $3/2-x, 1/2+y, 1/2-z$; [i] $1-x, -y, 2-z$; [ii] $-1+x, y, z$; [iii] $-1/2+x, 1/2-y, -1/2-z$.

Table 5
Photophysical data for **1** and **2**

Sample	Absorption (λ/nm)	Emission (λ/nm)			Lifetime (ns)
		Fluorescence[a]	Phosphorescence[b]	Solid state[c]	
Dpa	314	349	425	366	2.58
1	315	350	425	372	2.63
2	315	350	425	372	2.59

[a] In DMF at room temperature (298 K).
[b] In DMF at 77 K.
[c] At room temperature.

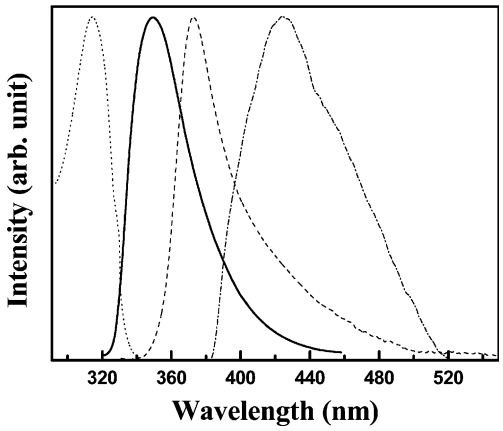

Fig. 7. Emission spectra of **1**: UV in DMF solution at 298 K (···), fluorescence in DMF solution at 298 K (—), phosphorescence in DMF glassy solution (-·-·-·-), fluorescence in solid state at 298 K (- - -).

ns, respectively. In glassy solutions (DMF at 77 K) both fluoresce and $^3(\pi–\pi^*)$ phosphorescence is observed at 425 nm. In solid state they show distinct emission band at 372 nm differing from their fluorescence spectra in DMF. This emission is expected to be due to excimer formation arising from the π–π aromatic stacking in solid state (Fig. 7).

4. Conclusion

To the best of our knowledge, **2** is the first example of hexacoordinated zinc compound and **1**, the second [26] tetracoordinated one containing tailored diimine (dpa) where cooperative hydrogen bonds and π–π interaction lead to network and sheet structures, respectively. The advantage of amine group with active hydrogen in dpa over polypyridines like 2,2′-bipyridine, 1,10-phenanthroline [41] with no such tailoring, afford superstructures. The difference in long-range structures in **1** and **2** above show how composition may tailor topology with different architectures through malleable coordination interaction and using strong and weak non-covalent forces in coordination polymers behaving as luminous materials. The preparation of these compounds illustrates a potentially versatile approach to the construction of uncharged inorganic organic hybrid [42] coordination network which is an exciting area of research for the rational design [43] of functional materials. The long range structural motif through use of tailored organic spacer, dpa, ensures us further study of it in combination with different pseudohalides like NCS^-, NCO^-, $NCSe^-$ and carboxylates in different 3d and 4d metal ions environments towards extended structures [2,3].

5. Supplementary data

These have been deposited with the Cambridge Crystallographic Data Centre nos. 203075 (**1**) and 203076 (**2**). Copies of this information can be had free of charge from The Director, CCDC, 12 Union Road, Cambridge, CB2 IEZ, UK (fax: +44-1223-336033; e-mail: deposit@ccdc.cam.ac.uk or www.ccdc.cam.ac.uk).

Acknowledgements

Financial support from the Department of Science and Technology (DST), Council of Scientific and Industrial Research (CSIR) and the University Grants Commission (UGC), New Delhi, India is gratefully acknowledged. D.B. and H.R. are respectively thankful to the CSIR and UGC for fellowships. M.J.Z. and R.D.B.W. acknowledge grant to NSF (DMR 101641).

References

[1] J.W. Steed, J.L. Atwood, Supramolecular Chemistry, Wiley, New York, 2000.
[2] D. Braga, F. Grepioni, A.G. Orpen, Crystal Engineering: From Molecules and Crystals to Materials, Kluwer, Dordrecht, 1999.
[3] M.J. Zaworotko, Chem. Commun. (2001) 1.
[4] G.R. Desiraju, Nature (London) 412 (2001) 397.
[5] S.T. Hyde, B. Ninham, S. Anderson, Z. Blum, T. Landh, K. Larsson, S. Liddin, The Language of Shape, Elsevier, Amsterdam, 1997.
[6] G.R. Desiraju, T. Steiner, The Weak Hydrogen Bond in Structural Chemistry and Biology, Oxford University Press, Oxford, 1999.

[7] T. Steiner, Angew. Chem. Int. Ed. 41 (2002) 48.
[8] B. Cornils, W.A. Herrmann, R. Schlogl (Eds.), Catalysis from A to Z: A Concise Encyclopedia, Wiley, New York, 2000.
[9] J.R. Farraro, J.M. Williams, Introduction to Synthetic Electrical Conductors, Academic Press, New York, 1987.
[10] G.W. Gokel, A. Mukhopadhyay, Chem. Soc. Rev. 30 (2001) 274.
[11] O. Kahn, Molecular Magnetism, VCH, New York, 1993.
[12] J.S. Miller, M. Drillon (Eds.), Magnetism: Molecules to Materials IV, Wiley-VCH, Weinheim, 2003.
[13] S.R. Marder, in: D.W. Bruce, D. O'Hare (Eds.), Metal Containing Materials for Nonlinear Optics in Inorganic Materials, 2nd ed., Wiley, Chichester, 1996, pp. 121–169.
[14] O.R. Evans, W. Lin, Acc. Chem. Res. 35 (2002) 511.
[15] D. Demus, J.W. Goodby, G.W. Gray, H.-W. Spiess, V. Vill (Eds.), Handbook of Liquid Crystals, Wiley-VCH, Weinheim, 1998.
[16] Special issue on Chemical Sensors, Chem. Rev. 100 (2000) Number 7.
[17] M. Kondo, T. Yoshitomi, K. Seki, H. Matsuzaka, S. Kitagawa, Angew. Chem. Int. Ed. Engl. 36 (1997) 1725.
[18] Special issue on Focus on Self-Assembly, Acc. Chem. Res. 32 (1999) Number 4.
[19] W. Kaim, B. Schwederski, Bioinorganic Chemistry: Inorganic Elements in the Chemistry of Life, Wiley, New York, 1994.
[20] A. Camus, N. Marsich, A.M.M. Lanfredi, F. Ugozzoli, C. Massera, Inorg. Chim. Acta 309 (2000) 1, and references therein.
[21] F.A. Cotton, L.M. Daniels, G.T. Jordan IV, C.A. Murillo, J. Am. Chem. Soc. 119 (1997) 10377, and references therein.
[22] E.-C. Yang, M.-C. Cheng, M.-S. Tsai, S.-M. Peng, J. Chem. Soc., Chem. Commun. (1994) 2377.
[23] L.-P. Wu, P. Field, T. Morrissey, C. Murphy, P. Nagle, B. Hathaway, C. Simmons, P. Thornton, J. Chem. Soc., Dalton Trans. (1990) 3835, and references therein.
[24] W. Liu, A. Hassan, S. Wang, Organometallics 16 (1997) 4257.
[25] F.A. Cotton, G. Wilkinson, C.A. Murillo, M. Bochmann, Advanced Inorganic Chemistry, 6th ed., Wiley, New York, 1999, p. 598.
[26] K.-Y. Ho, W.-Y. Yu, K.-K. Cheung, C.-M. Che, Chem. Commun. (1998) 2101.
[27] K.-Y. Ho, W.-Y. Yu, K.-K. Cheung, C.-M. Che, J. Chem. Soc., Dalton Trans. (1999) 1581.
[28] A.S. Prasad, Biochemistry of Zinc, Plenum, New York, 1993.
[29] S.J. Lippard, J.M. Berg, Bioinorganic Chemistry, University Science Books, Mill Valley, CA, 1994.
[30] A.M. Golub, H. Kohler, V.V. Skopenko (Eds.), Chemistry of Pseudohalides, Elsevier, Amsterdam, 1986.
[31] J. Ribas, A. Escuer, M. Monfort, R. Vicente, R. Cortes, L. Lezama, T. Rojo, Coord. Chem. Rev. 193 (1999) 1027.
[32] T.K. Karmakar, S.K. Chandra, J. Ribas, G. Mostafa, T.-H. Lu, B.K. Ghosh, Chem. Commun. (2002) 2364, and references therein.
[33] C.A. Hunter, Chem. Soc. Rev. 23 (1994) 101.
[34] SADABS v. 2.02: Area-Detector Absorption Correction, Siemens Industrial Automation, Inc., Madison, WI, 1996.
[35] SHELXTL 6.1, Bruker AXS Inc., Madison, WI, 2001.
[36] W.J. Geary, Coord. Chem. Rev. 7 (1971) 81.
[37] K. Nakamoto, Infrared and Raman Spectra of Inorganic and Coordination Compounds, Part B, 5th ed., Wiley, New York, 1997, p. 125.
[38] M. Villanueva, J.L. Mesa, M.K. Urtiaga, R. Cortés, L. Lezama, M.I. Arriortua, T. Rojo, Eur. J. Inorg. Chem. (2001) 1581.
[39] M.C. Etter, J. Phys. Chem. (1991) 4601.
[40] S. Youngme, S. Tonpho, K. Chinnakali, S. Chantraproma, H.-K. Fun, Polyhedron 18 (1999) 851.
[41] Z.-W. Mao, F.W. Heinemann, G. Liehr, R. van Eldik, J. Chem. Soc., Dalton Trans. (2001) 3652.
[42] B. Moulton, M.J. Zaworotko, Chem. Rev. 101 (2001) 1629.
[43] W. Gans, A. Amann, J.C.A. Boeyens (Eds.), Fundamental Principles of Molecular Modeling, Plenum Press, New York, 1996.

Available online at www.sciencedirect.com
SCIENCE DIRECT®
Polyhedron 23 (2004) 553–559
POLYHEDRON
www.elsevier.com/locate/poly

Four new coordination polymers of Cu(II) with 1,1′-(1,4-butanediyl)bis(imidazole)

Jian-Fang Ma *, Jin Yang, Guo-Li Zheng, Li Li, Yong-Mei Zhang, Fang-Fang Li, Jing-Fu Liu

Department of Chemistry, Northeast Normal University, No. 138 Renmin Street, Changchun 130024, PR China

Received 31 July 2003; accepted 8 October 2003

Abstract

Four new complexes, namely $[CuL(IN)_2(H_2O)_2]\cdot 4H_2O$ (**1**), $[CuL_2(H_2O)]Cl_2\cdot 5H_2O$ (**2**), $[CuL_2(H_2O)](NO_3)_2\cdot H_2O$ (**3**) and $[CuL_2]SO_4\cdot 8H_2O$ (**4**), where IN = isonicotinate anion, were obtained from self-assembly of the corresponding copper(II) salts with 1,1′-(1,4-butanediyl)bis(imidazole) (**L**), and their structures were determined by X-ray diffraction method. In complex **1**, each copper(II) cation is six-coordinated by two water molecules and four nitrogen atoms from two L molecules and two isonicotinate anions. Each L molecule coordinates to two copper(II) cations, acting as a bridging ligand. The copper(II) cations are bridged by L to form an infinite zigzag chain structure. In complexes **2** and **3**, the copper(II) cation is five-coordinated by one water molecule and four nitrogen atoms from four L molecules. In **4** the copper(II) cation is four-coordinated by four nitrogen atoms from four L molecules. Copper(II) cations are bridged by L ligands to form infinite $(4,4)$ networks that contain 44-membered rings in **2**, **3** and **4**. No interpenetration occurs in **2** and **3**, while in **4** two $(4,4)$ networks are interpenetrated in parallel fashion to form a layer.
© 2003 Elsevier Ltd. All rights reserved.

Keywords: Coordination polymer; Crystal structure; Hydrogen bonds; Copper(II)

1. Introduction

The synthesis and characterization of coordination polymers with infinite two- and three-dimensional networks have been an area of rapid growth in recent years because of the potential of these polymers in various applications, such as catalysis, electrical conductivity, host–guest chemistry and magnetism [1–4]. Much of the work has so far been focused on coordination polymers with rigid ligands, such as 4,4′-bipyridine and pyrazine [5,6]. The linear and bifunctional ligand 4,4′-bipyridine and its analogs upon reaction with transition metals are known to form several types of coordination networks that include one-dimensional networks (ladders, linear chains and railroads) [7–12], two-dimensional networks (square and rectangular grids, brick-wall and bilayers) [13,14] and three-dimensional networks (octahedral and diamondoid) [15]. Most of these structures have relatively large voids and potential interest for host–guest interaction and molecular recognition. Some transition metal complexes with flexible ligands have been investigated [16] and we are interested in coordination polymers containing flexible ligands. Based on its structure, 1,1′-(1,4-butanediyl)bis(imidazole) (**L**) can be used as a flexible divergent ligand to fabricate coordination polymer materials [17]. In this paper, we present the preparation and crystal structures of four coordination polymers of L with copper(II) salts, namely $[CuL(IN)_2(H_2O)_2]\cdot 4H_2O$ (**1**), $[CuL_2(H_2O)]Cl_2\cdot 5H_2O$ (**2**), $[CuL_2(H_2O)](NO_3)_2\cdot H_2O$ (**3**) and $[CuL_2]SO_4\cdot 8H_2O$ (**4**).

2. Experimental

All materials were commercially available and used as received. The FT-IR spectra were recorded from KBr pellets in range 4000–400 cm^{-1} on a Mattson Alpha-Centauri spectrometer. Elemental analyses were carried out with a Carlo Erba 1106 elemental analyzer.

* Corresponding author. Tel.: +86-431-5268620; fax: +86-431-5684009.
E-mail address: jfma@public.cc.jl.cn (J.-F. Ma).

0277-5387/$ - see front matter © 2003 Elsevier Ltd. All rights reserved.
doi:10.1016/j.poly.2003.10.002

2.1. Synthesis of 1,1′-(1,4-butanediyl)bis(imidazole) (*L*)

A mixture of imidazole (3.4 g, 50 mmol) and NaOH (2.0 g, 50 mmol) in DMSO (10 ml) was stirred at 60 °C for 1 h, then 1,4-dichlorobutane (3.2 g, 25 mmol) was added. The mixture was cooled to room temperature after stirring at 60 °C for 2 h, then poured into 200 ml of water and a white solid formed immediately which weighted 4.1 g after drying in air. *Anal.* Calc. for $C_5H_7N_2$: C, 63.16; H, 7.37, N, 29.47. Found: C, 63.11; H, 7.42; N, 29.31%.

2.2. Synthesis of $[CuL(IN)_2(H_2O)_2]\cdot 4H_2O$ (*1*)

A mixture of $CuCl_2\cdot 2H_2O$ (0.171 g, 1 mmol) and NaOH (0.08 g, 2 mmol) in water was stirring for 10 min at room temperature, then the $Cu(OH)_2$ solid was filtered. Isonicotinic acid (0.246 g, 2 mmol) was added to the $Cu(OH)_2$ suspension in water with constant stirring and give blue precipitation. Then L (0.380 g, 2 mmol) was added to the precipitation with stirring for 1 h and blue solution was obtained. Blue crystals were obtained from the filtrate after standing at room temperature for several days (68% yield based on Cu). *Anal.* Calc. for $C_{22}H_{34}CuN_6O_{10}$: C, 43.56; H, 5.61; N, 13.86. Found: C, 43.67; H, 5.52; N, 13.93%. IR (cm^{-1}, KBr): 3431(s), 3130(m), 2344(w), 1610(vs), 1551(s), 1450(m), 1382(vs), 1234(w), 1110(m), 1057(w), 951(w), 846(w), 779(w), 688(w), 669(m).

2.3. Synthesis of $[CuL_2(H_2O)]Cl_2\cdot 5H_2O$ (*2*)

A mixture of $CuCl_2\cdot 2H_2O$ (0.171 g, 1 mmol) and L (0.380 g, 2 mmol) in water (20 ml) was refluxed for 30 min, then filtered whilst hot. Blue crystals were obtained from the filtrate after standing at room temperature for several days (73% yield based on Cu). *Anal.* Calc. for $C_{20}H_{40}Cl_2CuN_8O_6$: C, 38.52; H, 6.42; N, 17.98. Found: C, 38.67; H, 6.31; N, 18.08%. IR (cm^{-1}, KBr): 3449(s), 3125(m), 2950(w), 1640(m), 1526(m), 1451(m), 1285(w), 1238(s), 1107(vs), 1099(vs), 948(w), 849(w), 771(w), 756(m), 664(s), 627(w).

2.4. Synthesis of $[CuL_2(H_2O)](NO_3)_2\cdot H_2O$ (*3*)

A mixture of $Cu(NO_3)_2$ (0.126 g, 1 mmol) and L (0.380 g, 2 mmol) in water (20 ml) was refluxed for 30 min and blue precipitate was obtained. It was filtered

Table 1
Crystal data for compounds **1**–**4**

	1	**2**	**3**	**4**
Formula	$C_{22}H_{34}CuN_6O_{10}$	$C_{20}H_{40}Cl_2CuN_8O_6$	$C_{20}H_{32}CuN_{10}O_8$	$C_{20}H_{44}CuN_8O_{12}S$
Formula weight	606.09	623.04	604.10	684.23
Crystal size	$0.288\times 0.214\times 0.179$	$0.304\times 0.249\times 0.044$	$0.439\times 0.173\times 0.090$	$0.322\times 0.308\times 0.146$
Crystal system	monoclinic	triclinic	monoclinic	triclinic
Space group	$C2/c$	$P\bar{1}$	$C2/c$	$P\bar{1}$
Unit cell dimensions				
a (Å)	12.205(2)	10.919(2)	20.509(4)	8.1383(16)
b (Å)	13.448(3)	11.844(2)	9.3405(19)	11.648(2)
c (Å)	17.308(4)	12.724(3)	15.239(3)	16.780(3)
α (°)	90	82.09(3)	90	73.49(3)
β (°)	106.93(3)	68.51(3)	101.27(3)	88.78(3)
γ (°)	90	73.85(3)	90	82.06(3)
V (Å^3)	2717.7(9)	1469.6(5)	2863.0(10)	1510.1(5)
Z	4	2	4	2
D_c ($g\,cm^{-3}$)	1.481	1.408	1.401	1.505
$F(000)$	1268	654	1260	722
μ (mm^{-1})	0.868	0.972	0.822	0.863
Wavelength (Å)	0.71073	0.71073	0.71073	0.71073
Temperature (K)	293(2)	293(2)	293(2)	293(2)
θ Range for data collection (°)	2.31–27.48	1.72–27.48	2.02–27.40	1.27–27.42
Index ranges	$0<h<15$, $0<k<17$, $-22<l<21$;	$0<h<14$, $-14<k<15$, $-15<l<16$;	$0<h<26$, $0<k<12$, $-19<l<19$;	$0<h<10$, $-14<k<15$, $-21<l<21$
R_{int}	0.0360	0.0288	0.0287	0.0228
GOF on F^2	0.962	0.968	1.006	1.047
Largest difference peak and hole (e Å^{-3})	0.317 and −0.446	1.351 and −0.627	0.798 and −0.463	1.089 and −0.455
Reflections collected	12 396	13 631	13 530	14 122
Unique reflections	3125	6631	3251	6823
Observed reflections ($I>2\sigma(I)$)	2393	4883	2540	5143
$R_1(I>2\sigma(I))$	0.0329	0.0368	0.0420	0.0335
$wR_2(I>2\sigma(I))$	0.0811	0.0940	0.1213	0.0917

off, washed with water and dissolved in a minimum amount of ammonia (14 M). Blue single crystals were obtained by slow evaporation of the ammoniacal solution of the solid at room temperature (64% yield based on Cu). *Anal.* Calc. for $C_{20}H_{32}CuN_{10}O_8$: C, 39.73; H, 5.30; N, 23.17. Found: C, 39.81; H, 5.22; N, 23.21%. IR (cm^{-1}, KBr): 3436(s), 3121(w), 2943(w), 2340(w), 1641(w), 1529(m), 1458(w), 1382(vs), 1240(w), 1103(s), 1038(w), 948(w), 837(w), 757(w), 622(m).

2.5. Synthesis of $[CuL_2]SO_4 \cdot 8H_2O$ (4)

A mixture of $CuSO_4 \cdot 5H_2O$ (0.250 g, 1 mmol) and L (0.380 g, 2 mmol) in water (20 ml) was refluxed for 30 min, then filtered whilst hot. Blue crystals were obtained from the filtrate after standing at room temperature for several days (77% yield based on Cu). *Anal.* Calc. for $C_{20}H_{44}CuN_8O_{12}S$: C, 35.08; H, 6.43; N, 16.37. Found: C, 35.11; H, 6.32; N, 16.53%. IR (cm^{-1}, KBr): 3431(s), 3119(w), 2945(w), 2342(w), 1631(m), 1524(w), 1452(s), 1384(w), 1239(m), 1114(vs), 949(w), 880(w), 753(w), 668(m), 622(m).

2.6. X-ray crystallography studies

Experimental details of the X-ray analyses are provided in Table 1. Diffraction intensities for the compounds **1**–**4** were collected on a Rigaku RAXIS-RAPID image plate diffractometer using ω scan technique with Mo Kα radiation ($\lambda = 0.71069$ Å). Absorption corrections were applied using multi-scan technique [18]. The structures were solved with the direct method of SHELXS-97 [19] and refined with full-matrix least-squares techniques using the SHELXL-97 program [20] within WINGX [21]. Non-hydrogen atoms were refined anisotropically. Analytical expression of neutral-atom scattering factors were employed, and anomalous dispersion corrections incorporated [22]. Drawings were produced with SHELXTL PLUS [23].

Table 2
Selected bond distances (Å) and angles (°) for complexes **1**–**4**

$[CuL(IN)_2(H_2O)_2]\cdot 4H_2O$ (**1**)			
Bond distances			
Cu(1)–N(1)	2.0554(15)	Cu(1)–N(2)	2.0067(15)
Cu(1)–Ow1	2.4163(14)		
Bond angles			
N(1)–Cu(1)–Ow_1	92.63(6)	N(1)–Cu(1)–Ow_1^{i}	87.37(6)
N(2)–Cu(1)–Ow1^{i}	88.91(6)	N(2)–Cu(1)–N(1)	90.11(6)
N(2)–Cu(1)–Ow1	91.09(6)	N(2)–Cu(1)–N(1)^{i}	89.89(6)
$[CuL_2(H_2O)]Cl_2\cdot 5H_2O$ (**2**)			
Bond distances			
Cu(1)–N(11)	2.015(2)	Cu(1)–Ow_1	2.393(2)
Cu(1)–N(21)	2.014(2)	Cu(1)–N(31)	2.017(2)
Cu(1)–N(14)^{i}	2.015(2)		
Bond angles			
N(21)–Cu(1)–N(11)	88.72(8)	N(11)–Cu(1)–N(14)^{i}	176.80(8)
N(11)–Cu(1)–N(31)	88.21(8)	N(21)–Cu(1)–Ow_1	91.11(8)
N(14)^{i}–Cu(1)–Ow_1	90.53(9)	N(21)–Cu(1)–N(14)^{i}	91.08(7)
N(21)–Cu(1)–N(31)	176.78(7)	N(14)^{i}–Cu(1)–N(31)	91.93(8)
N(11)–Cu(1)–Ow_1	92.67(9)	N(31)–Cu(1)–Ow_1	90.01(8)
$[CuL_2(H_2O)](NO_3)_2\cdot H_2O$ (**3**)			
Bond distances			
Cu(1)–N(1)	1.980(2)	Cu(1)–N(3)	2.014(2)
Cu(1)–Ow_1	2.210(3)		
Bond angles			
N(1)^{i}–Cu(1)–N(1)	161.43(14)	N(1)–Cu(1)–N(3)	87.55(9)
N(1)–Cu(1)–N(3)^{i}	91.47(9)	N(3)–Cu(1)–N(3)^{i}	173.90(13)
N(1)–Cu(1)–Ow_1	99.29(7)	N(3)–Cu(1)–Ow_1	93.05(7)
$[CuL_2]SO_4\cdot 8H_2O$ (**4**)			
Bond distances			
Cu(1)–N(11)	2.00(2)	Cu(1)–N(21)	2.04(2)
Cu(2)–N(14)	2.00(2)	Cu(2)–N(24)^{i}	2.00(2)
Bond angles			
N(11)–Cu(1)–N(21)^{ii}	88.8(7)	N(11)–Cu(1)–N(21)	91.2(7)
N(14)–Cu(2)–N(24)^{i}	87.9(7)	N(14)–Cu(2)–N(24)^{iii}	92.1(7)

Symmetry codes for **1**: i, $-x+1, -y, -z+1$. Symmetry codes for **2**: i, $x, y, z-1$. Symmetry codes for **3**: i, $-x+2.5, -y+0.5, -z+2$. Symmetry codes for **4**: i, $x, y, z+1$; ii, $-x+2, -y+1, -z+2$ and iii, $-x+4, -y+1, -z+2$.

3. Results and discussion

Selected bond distances and angles for complexes **1**–**4** are listed in Table 2. Fig. 1(a) shows the coordination environments of the copper(II) cations in $[CuL(IN)_2(H_2O)_2]\cdot 4H_2O$ **1**. The copper(II) cation lies at an inversion center. Each copper(II) cation is six-coordinated by two water molecules and four nitrogen atoms from two L molecules and two isonicotinate anions. The presence of an un-coordinated carboxylate group is somewhat unexpected because the carboxylate group of isonicotinate anion is a better coordinating group than water oxygen atom for copper(II) cation. In the related compound, $\{[Cu_2(IN)_4\cdot 3H_2O]\cdot[Cu_2(IN)_4\cdot 2H_2O]\}\cdot 3H_2O$ [24], the carboxylate oxygen atom coordinated to the copper(II) cation. The Cu–N (isonicotinate) distance of 2.0554(15) Å is similar to that of copper(II) isonicotinate complex [25]. The distance between the copper(II) cation and the nitrogen atom from L molecule is 2.0067(15) Å. The Cu–O (water) distance of 2.4163(14) Å is near to those of other copper(II) complexes [26,27]. Due to Jahn–Teller effects the axial Cu–O (water) distance is much longer than those of Cu–N (IN and L). The distance between the neighboring copper(II) cations is 8.654 Å. Each L molecule coordinates to two copper(II) cations, acting as a bridging ligand to form an infinite zigzag chain structure [Fig. 1(b)]. In **1**, one carboxylate oxygen atom H-bonds to one lattice water molecule and one coordinated water molecule of the neighboring Cu(II) cation within the same polymeric chain while the other carboxylate oxygen atom H-bonds to one lattice water molecule and one coordinated water molecule from adjacent polymeric chain. The extended structure was formed through H-bonds interactions between adjacent chains as illustrated in Fig. 1(c).

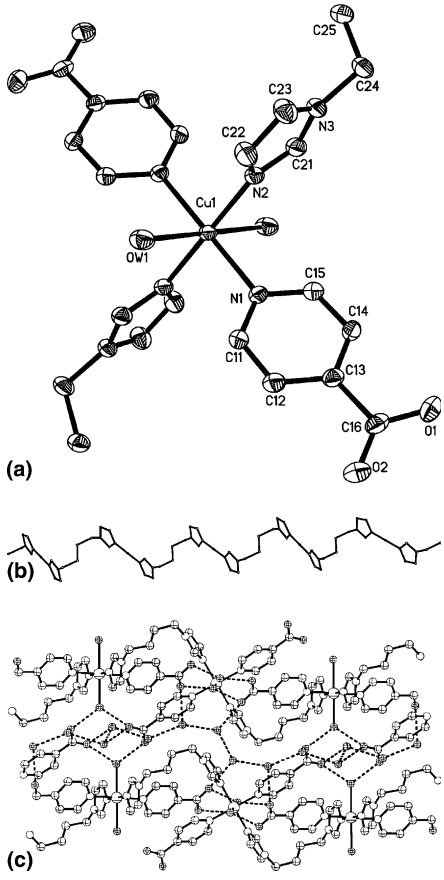

Fig. 1. (a) An ORTEP drawing of the local coordination of Cu(II) cation in complex **1**. Atoms are shown 50% probability ellipsoids. (b) The infinite zigzag polymeric chain of **1** (The water molecules and isonicotinate anions are omitted for clarity). (c) The extended structure of **1** through H-bonds interactions between adjacent chains.

Part of the structure of $[CuL_2(H_2O)]Cl_2\cdot 5H_2O$ (**2**) and $[CuL_2(H_2O)](NO_3)_2\cdot H_2O$ (**3**) are shown in Figs. 2(a) and 3(a), respectively. The coordination geometries of the copper(II) cation are all completed by four nitrogen atoms from four L molecules and by one water molecule. Both the chloride anions and nitrate anions only play a role of un-coordinating counter-anions. In **2**, there exist inversion centers at the mid-points of the C_{24}–C_{24}* and C_{34}–C_{34}# bonds. In **3**, Cu_1 cation and Ow_1 lie on a twofold axis, and there are inversion centers at the mid-points of C_{15}–C_{15}* and C_{25}–C_{25}# bonds. The average Cu–N distance and the Cu–O (water) distance in **2** and **3** are quite near to those of **1**. Each L molecule coordinates to two copper(II) cations, bridging the copper(II) cations to form infinite $(4,4)$ networks [Figs. 2(b) and (c), 3(b) and (c)]. In **2**, chloride ions and some lattice water molecules are encapsulated in the 44-membered rings of the $(4,4)$ network, one chloride ion H-bonds to one coordinated water molecule and three lattice water molecules while the other chloride ion H-bonds to three lattice water molecules. The adjacent $(4,4)$ networks are interconnected through hydrogen bonds as shown in Fig. 2(d). In **3**, nitrate ions are encapsulated in the 44-membered rings of the $(4,4)$ network, and each nitrate ion H-bonds to one coordinated water molecule from the adjacent $(4,4)$ networks as shown in Fig. 3(d). The uncoordinating counter-anions and water molecules filled in the networks may be the main reason for the non-interpenetrating structures of **2** and **3**.

As shown in Fig. 4(a), **4** consists of two crystallographically unique Cu(II) ions in the asymmetric unit. Both of them lie at the inversion center and have the similar coordination environment. The copper(II) cation of **4** is coordinated by four nitrogen atoms from four L molecules. In the related compound, $[ZnL_{1.5}(H_2O)(SO_4)]\cdot 6H_2O$ complex with infinite $(6,3)$ networks, the sulfate anion coordinates to the central zinc(II) cation [17a]. But in the present complex the sulfate anions play a role of counter-anion. The Cu–N (L) distances of 2.00(2) and 2.04(2) Å are similar to those in complex **1**, **2** and **3**. In complex **4**, copper(II) ions are bridged by L to form infinite $(4,4)$ networks [Fig. 4(b)], and two $(4,4)$ networks are interpenetrated in parallel mode to form a layer [Fig. 4(c)]. The sulfate anions and water molecules

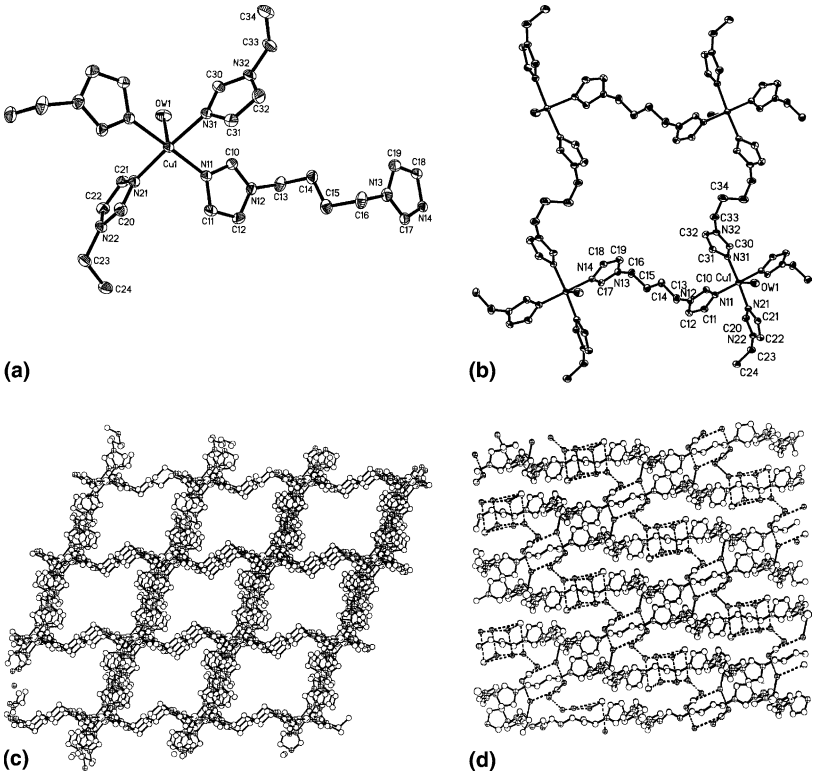

Fig. 2. (a) An ORTEP drawing of the local coordination of Cu(II) cation in complex **2**. Atoms are shown 50% probability ellipsoids. (b) The large ring of the (4, 4) network in **2**. (c) Extended structure of **2** (water and chloride anions are omitted for clarity). (d) The H-bonds interactions between adjacent layers.

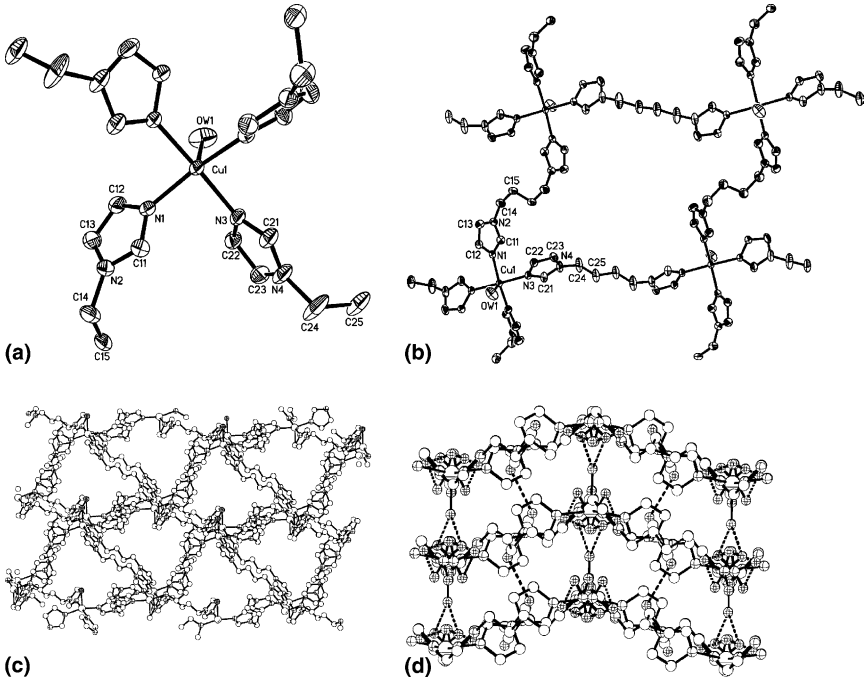

Fig. 3. (a) An ORTEP drawing of the local coordination of Cu(II) cation in complex **3**. Atoms are shown 50% probability ellipsoids. (b) The large ring of the (4, 4) network in **3**. (c) Extended structure of **3** (water and nitrate anions are omitted for clarity). (d) The H-bonds interactions between adjacent layers.

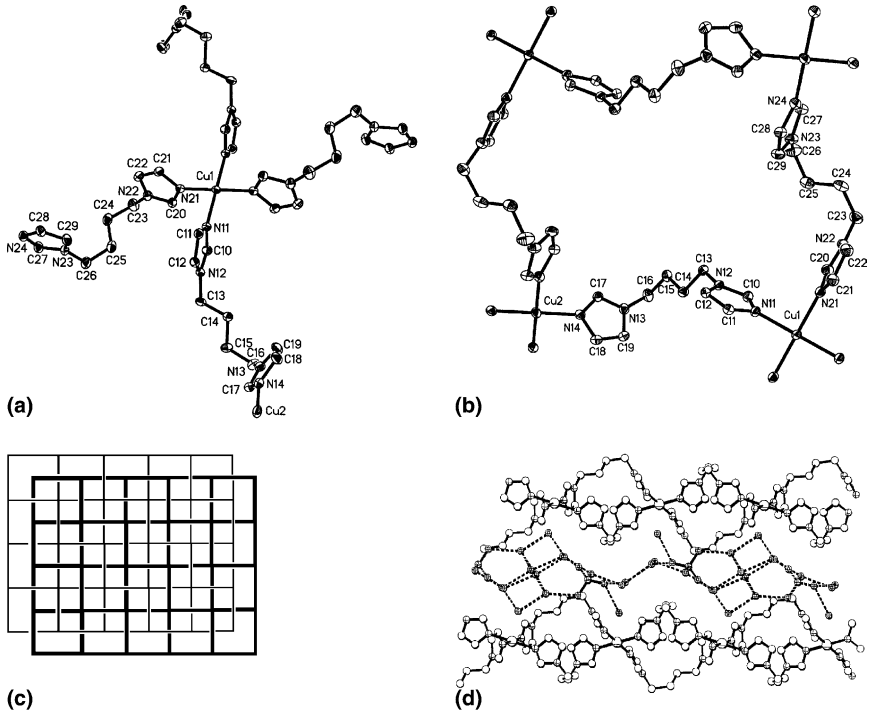

Fig. 4. (a) An ORTEP drawing of the local coordination of Cu(II) in complex **4**. Atoms are shown 50% probability ellipsoids. (b) The large ring of the $(4,4)$ network in **4.** (c) Schematic representation of the mode of interpenetration. (d) The alternative H-bonding layers and $[CuL_2]^{2+}$ layers.

are intercalated into the layers, and each sulfate ion H-bonds to six lattice water molecules. The extended structure was formed by stacking the layer of hydrogen-bonded water molecules and sulfate ions and the layer of polymeric $[CuL_2]^{2+}$ alternatively [Fig. 4(d)]. The number of different ways two $(4,4)$ nets could theoretically interpenetrate in the parallel fashion may be given by systematic study of the topology of interpenetration [28]. The interpenetrating structures of related complexes, $[MnL_3(BF_4)_2]$ [29] and $[ZnL_{1.5}(H_2O)(SO_4)]\cdot 6H_2O$ [17a] have been reported. The reported $[MnL_3(BF_4)_2]$ complexes are composed of two equivalent, mutually interpenetrating three-dimensional networks, while in complex $[ZnL_{1.5}(H_2O)(SO_4)]\cdot 6H_2O$, the networks are interpenetrated in an inclined mode by symmetry related, identical networks to give an interlocked three-dimensional structure.

In complexes **1**, **2**, **3** and **4** each L molecule coordinates to two copper(II) cations through its two aromatic nitrogen atoms acting as a bridging bidentate ligand. Copper(II) cations are bridged by L molecules to form one-dimensional chain in **1**, $(4,4)$ networks in **2**, **3** and **4**. The networks contain square grids (44-membered) with a copper(II) cation at each corner and a molecule of L at each edge connecting two copper(II) cations. The lengths of the opposite edges are equal in **2**, **3** and **4**. The edge lengths are 12.317 and 12.724 Å for **2**, 11.886 and 14.225 Å for **3**, 11.812 and 11.564 Å for **4**.

The structures of these complexes imply a role of counter-anions in the fabrication of the framework. Since isonicotinate anion is a better ligand for Cu(II) than other three anions, isonicotinate anions are coordinated to copper(II) ion in **1** while in other complexes the anions are non-coordinating. In each compound the anions are connected to water molecules through H-bonding interactions, and it can be seen that the polymeric networks can be tailored by using different anions.

4. Supplementary material

CCDC-198614 (for **1**), 198615 (for **2**), 198616 (for **3**) and 198617 (for **4**) contain the supplementary crystallographic data for this paper. These data can be obtained free of charge from the Cambridge Crystallographic Data Centre, 12, Union Road, Cambridge CB2 1EZ, UK (fax: +44-1223-336-033; E-mail: deposit@ccdc.cam.ac.uk or http://www.ccdc.cam.ac.uk).

Acknowledgements

We thank the Fok Ying Tung Education Foundation and the Ministry of Education of China for support.

References

[1] M. Fujita, Y.J. Kwon, S. Washizu, K. Ogura, J. Am. Chem. Soc. 116 (1994) 1151.
[2] O. Ermer, Adv. Mater. 3 (1991) 608, and references therein.

[3] T. Kitazawa, S. Nishikiori, R. Kuroda, T. Iwamoto, J. Chem. Soc., Dalton Trans. (1994) 1029, and references therein.
[4] K. Inoue, T. Hayamizu, H. Iwamura, D. Hashizume, Y. Ohashi, J. Am. Chem. Soc. 118 (1996) 1803.
[5] (a) J. Lu, T. Paliwala, S.C. Lim, C. Yu, T. Niu, A.J. Jacobson, Inorg. Chem. 36 (1997) 923;
(b) R.W. Gable, B.F. Hoskins, R. Robson, Chem. Commun. (1990) 1677;
(c) N. Masciocchi, P. Cairati, L. Carlucci, G. Mezza, G. Ciani, A. Sironi, J. Chem. Soc., Daton Trans. (1996) 2739;
(d) S.D. Huang, R. Xiong, Polyhedron 16 (1997) 3929;
(e) L. Carlucci, G. Ciani, D.M. Proserpio, A. Sironi, Chem. Commun. (1994) 2755;
(f) F. Robinson, M.J. Zaworotko, Chem. Commun. (1995) 2413;
(g) M. Kondo, T. Yoshitomi, K. Seki, H. Matsuzaka, S. Kitagawa, Angew. Chem., Int. Ed. Engl. 36 (1997) 1725.
[6] (a) S. Kawata, S. Kitagawa, H. Kumagai, S. Iwabuchi, M. Katada, Inorg. Chim. Acta 267 (1998) 143;
(b) L. Carlucci, G. Ciani, D.M. Proserpio, A. Sironi, Angew. Chem., Int. Ed. Engl. 34 (1995) 1895;
(c) F. Lloret, G.D. Munno, M. Julve, J. Cano, R. Ruiz, A. Caneschi, Angew. Chem., Int. Ed. Engl. 37 (1998) 135.
[7] P. Losier, M.J. Zaworotko, Angew. Chem., Int. Ed. Engl. 35 (1996) 2779.
[8] M. Fujita, Y.J. Kwon, O. Sasaki, K. Yamaguchi, K. Ogura, J. Am. Chem. Soc. 117 (1995) 7287.
[9] O.M. Yaghi, H. Li, T.L. Groy, Inorg. Chem. 36 (1997) 4292.
[10] A.J. Blake, N.R. Champness, M. Crew, S. Parsons, New J. Chem. 23 (1999) 13.
[11] K. Biradha, C. Seward, M.J. Zaworotko, Angew. Chem., Int. Ed. Engl. 38 (1999) 492.
[12] L. Carlucci, G. Ciani, D.M. Proserpio, Chem. Commun. (1999) 449.
[13] (a) X.-M. Ouyang, B.-L. Fei, T.-A. Okamura, H.-W. Bu, W.-Y. Sun, W.-X. Tang, N. Ueyama, Eur. J. Inorg. Chem. (2003) 618;
(b) L.R. MacGillivray, R.H. Groeneman, J.L. Atwood, J. Am. Chem. Soc. 120 (1998) 2676;
(c) K. Biradha, M. Fujita, Chem. Commun. (2001) 15.
[14] M.J. Zaworotko, Chem. Commun. (2001) 1, and references therein.
[15] (a) Comprehensive Supramolecular Chemistry, vol. 6, Solid-state Supramolecular Chemistry: Crystal Engineering, Pergamon, Oxford, 1996;
(b) S. Subramanian, M.J. Zaworotko, Angew. Chem., Int. Ed. Engl. 34 (1995) 2127;
(c) L.R. MacGillivray, S. Subramanian, M.J. Zaworotko, Chem. Commun. (1994) 1325.
[16] (a) T.L. Hennigar, D.C. MacQuaarrie, P. Losier, R.D. Rogers, M.J. Zaworotko, Angew. Chem., Int. Ed. Engl. 36 (1997) 972;
(b) O.-S. Jung, S.H. Park, D.C. Kim, K.M. Kim, Inorg. Chem. 37 (1998) 610;
(c) B.F. Hoskins, R. Robson, D.A. Slizys, J. Am. Chem. Soc. 119 (1997) 2952;
(d) B.F. Hoskins, R. Robson, D.A. Slizys, Angew. Chem., Int. Ed. Engl. 36 (1997) 2336.
[17] (a) J.-F. Ma, J.-F. Liu, Y. Xing, H.-Q. Jia, Y.-H. Lin, J. Chem. Soc., Dalton Trans. (2000) 2403;
(b) J.-F. Ma, J.-F. Liu, Y.-C. Liu, Y. Xing, H.-Q. Jia, Y.-H. Lin, New J. Chem. 24 (2000) 759.
[18] T. Higashi, Program for Absorption Correction, Rigaku Corporation, Tokyo, 1995.
[19] G.M. Sheldrick, SHELXS-97, A Program for Automatic Solution of Crystal Structure, University of Goettingen, Germany, 1997.
[20] G.M. Sheldrick, SHELXL-97, A Programs for Crystal Structure Refinement, University of Goettingen, Germany, 1997.
[21] L.J. Farrugia, WINGX, A Windows Program for Crystal Structure Analysis, University of Glasgow, Glasgow, 1988.
[22] International Tables for X-ray Crystallography, vol. C, Kluwer Academic Publishers, Dordrecht, 1992.
[23] G.M. Sheldrick, SHELXTL PLUS, Structure Determination Program, Siemens Analytical X-ray Instruments Inc, Madison, WI, 1990.
[24] J.Y. Lu, A.M. Babb, Chem. Commun. (2001) 821.
[25] M.A.S. Goher, T.C.W. Mak, Inorg. Chim. Acta 101 (1985) 27.
[26] J.W. Cai, C.-H. Chen, C.-Z. Liao, J.-H. Yao, X.-P. Hu, X.-M. Chen, J. Chem. Soc., Dalton Trans. (2001) 1137.
[27] D. Riou, F. Belier, C. Serre, M. Nogues, D. Vichard, G. Ferey, Int. J. Inorg. Mater. 2 (2000) 29.
[28] (a) S.R. Batten, R. Robson, Angew. Chem., Int. Ed. Engl. 37 (1998) 1460;
(b) S.R. Batten, A.R. Harris, P. Jensen, K.S. Murray, A. Ziebell, J. Chem. Soc., Dalton Trans. (2000) 3829;
(c) M.J. Plater, M.R.St.J. Foreman, T. Gelbrich, S.J. Coles, M.B. Hursthouse, J. Chem. Soc., Dalton Trans. (2000) 3065;
(d) M.J. Plater, M.R.St.J. Foreman, R.A. Howie, J.M.S. Skakle, Inorg. Chim. Acta 318 (2000) 175;
(e) H. Hou, Y. Wei, Y. Song, Y. Zhu, L. Li, Y. Fan, J. Mater. Chem. 12 (2002) 838;
(f) O.R. Evans, W. Lin, Chem. Mater. 13 (2001) 3009.
[29] P.C.M. Duncan, D.M.L. Goodgame, S. Menzer, D.J. Williams, Chem. Commun. (1996) 2127.

Available online at www.sciencedirect.com
SCIENCE DIRECT®
Polyhedron 23 (2004) 561–566
POLYHEDRON
www.elsevier.com/locate/poly

Reactivity of $Ti(bipy)_3$ and preparation of the $Li(THF)_4[Al(bipy)_2]$ complex with the dinegative bipy ligand

Grigori B. Nikiforov, Herbert W. Roesky *, Mathias Noltemeyer, Hans-Georg Schmidt

Institut für Anorganische Chemie, Universität Göttingen, Tammannstrasse 4, D-37077 Göttingen, Germany

Received 14 August 2003; accepted 8 October 2003

Abstract

The reaction of $Ti(bipy)_3$ with BF_3 resulted in the formation of $[Ti(bipy)_3]BF_4$ (**1**), whereas the interaction of $Ti(bipy)_3$ with the $LiAlH_4$ yielded the unforeseen aluminum complex $Li(THF)_4[Al(bipy)_2]$ (**2**). The complexes **1** and **2** were characterized by NMR, mass spectra and elemental analysis. Complex **2** was investigated by X-ray structural analysis and consists of cationic $[Li(THF)_4]^+$ and anionic $[Al(bipy)_2]^-$ units containing the coordinated dinegatively charged [bipy] ligand.
© 2003 Elsevier Ltd. All rights reserved.

Keywords: Bipyridine; Titanium; Aluminum; Coordination compound; Crystal structure

1. Introduction

Various complexes of transition and non-transition metals with bipyridyl $[bipy]^-$ and $[bipy]^{2-}$ anions have been synthesized (for selected references, see [1]). The formation of $[bipy]^-$ and $[bipy]^{2-}$ anions from bipy and lithium metal was briefly described in 1968 [1b]. The complex $Ti(bipy)_3$ was first prepared by Herzog and Taube [2] and later it has been studied by several authors in connection with the metal oxidation state [1g,4b,3]. Analysis of the EPR, NMR, electronic spectra and chemical behavior of the complex led to the conclusion that the ligands in $Ti(bipy)_3$ carries a considerable negative charge and a formulation employing integral oxidation numbers of the metal and the ligands is not recommended [3b,3c,3f]. To the best of our knowledge complexes of non-transition metals with the negatively charged 2,2′-bipyridyl ligands were structurally characterized only for sodium in 1999 [1c,1d]. The complexes containing bipy anions were extensively studied for decades due to their interesting chemical and physical properties. A number of reactions of bipy complexes have been reported involving electron and proton transfer processes. In these reactions the bipy ligand is suggested to act as a kind of an electron reservoir [4].

Herein we report the reaction of the $Ti(bipy)_3$ complex with the Lewis acid BF_3, interaction of $Ti(bipy)_3$ with the reducing agent $LiAlH_4$ and synthesis and characterization of the monomeric aluminum complex $Li(THF)_4[Al(bipy)_2]$ with the negatively charged bipy ligand.

2. Experimental

2.1. General procedures and starting materials

All operations were performed using standard Schlenk line and dry box techniques under purified nitrogen and argon atmosphere. Water-free titanium trichloride used was of commercial reagent quality (Aldrich, purity 99.99%); the titanium tetrachloride of commercial reagent quality (Aldrich, purity 99%) was refluxed with $SOCl_2$ prior to use. The 2,2′-dipyridyl of commercial reagent quality (Aldrich, purity 99%) was sublimed in vacuum. The lithium aluminum hydride

* Corresponding author. Tel.: +49-551-39-3001; fax: +49-551-39-3373.
E-mail address: hroesky@gwdg.de (H.W. Roesky).

0277-5387/$ - see front matter © 2003 Elsevier Ltd. All rights reserved.
doi:10.1016/j.poly.2003.10.008

powder (Aldrich, purity 97%) and the boron trifluoride (Aldrich, purity 99.5%) were used as received. The titanium complex $Ti(bipy)_3$ was prepared by the reaction of $TiCl_3$ or $TiCl_4$ with three equivalents of bipy and excess of Li metal in THF. The purity of $Ti(bipy)_3$ was checked by elemental analysis, ^1H and ^{13}C NMR spectra. The proton NMR spectrum for $Ti(bipy)_3$ is consistent with those previously reported for this substance [4b]. THF, Et_2O were dried over Na/benzophenone and distilled under nitrogen prior to use, C_6D_6 and [D_8] THF were dried over Na and degassed. CD_2Cl_2 and CH_2Cl_2 were dried over CaH_2 and degassed. Proton NMR spectra were recorded using Bruker AM 500 NMR spectrometer. Chemical shifts are reported in δ units downfield from Me_4Si with the solvent as the reference resonance. Mass spectra were recorded using a Finnigan MAT 8230 mass spectrometer, and elemental analysis were carried out at the Analytical Laboratories of the Institute of Inorganic Chemistry at the University of Göttingen. Melting points were measured in sealed capillary tubes under nitrogen and are not corrected.

2.2. Reaction between $Ti(bipy)_3$ with excess of BF_3 in CH_2Cl_2

Gaseous BF_3 (22 mmol) was condensed in trap I by cooling with liquid nitrogen. The solid BF_3 in trap I was kept 15 min under dynamic vacuum. Then the liquid nitrogen was removed from trap I and the content of trap I is allowed to warm slowly. The volatile BF_3 was passed through the stirred solution of $Ti(bipy)_3$ (0.85 g, 1.6 mmol) in CH_2Cl_2 at −79 °C (solid CO_2 in acetone) (Schlenk flask) under dynamic vacuum and condensed into a second trap with the help of liquid nitrogen. Finally, the Schlenk flask with the reaction mixture was closed and the remaining BF_3 condensed into the second trap neutralized while passing through the aqueous solution of $CaCl_2$. The reaction mixture was stirred at −79 °C for 30 min, allowed to warm to −20 °C and stirred for additional 30 min. The solution was filtered, concentrated and left undisturbed at −24 °C. After 4 days, violet solid (0.41 g) was deposited from the CH_2Cl_2 solution and separated by filtration. Yield of compound **1** 0.41 g (43 %). M.p.: 170–172 °C. EI-MS: m/z (%) = 503(1) [$TiC_{29}H_{23}N_6^+$], 474 (1) [$TiC_{29}H_{22}N_4^+$], 429 (2) [$Ti(bipy)_2BF_3^+$], 401 (1) [$TiC_{18}H_{13}N_4BF_3^+$], 373 (3) [$TiF_4C_{15}H_{12}N_4^+$], 354 (3) [$TiF_3C_{15}H_{12}N_4^+$], 340 (3) [$TiF_3C_{15}H_{12}N_3^+$], 300 (5) [$TiN_2(bipy)BF_3^+$], 281 (6) [$TiN_2BF_2(bipy)^+$], 267 (3) [$TiNBF_2(bipy)^+$], 232 (2) [$Ti(bipy)N_2^+$], 225 (6) [$Ti(bipy)F^+$], 207 (8) [$Ti(bipy)^+$], 156 (100) [$bipy^+$], 128 (25) [$(bipy)^+$–C_3H_3N]. ^{11}B MAS NMR(15 KHz, BF_3OEt_2 r.t.) $\delta = 0$ ppm, satellites 117, −117 ppm. ^1H NMR (500 MHz, C_6D_6, r.t.), $\delta = -26.50$, −25.20, −8.39, −3.96, 1.76, 2.30, 3.67, 7.19, 7.41, 8.10, 8.71, 9.63, 10.09, 17.80 ppm.

2.3. Reaction of $Ti(bipy)_3$ with $LiAlH_4$

A mixture of $Ti(bipy)_3$ (1.2 g, 2.3 mmol) and $LiAlH_4$ (0.35 g, 9.2 mmol) in a 100 ml Schlenk flask in THF (40 ml) was stirred for 36 h. The supernatant solution was filtered and all volatiles were removed in vacuum, the residue was extracted with Et_2O (50 ml). The resulting solution was filtered and concentrated, while two liquid layers were observed. The heavy violet liquid on the bottom of the flask slowly crystallized at r.t. to afford black crystals of **2**. The crystals of **2** are extremely air sensitive and start immediately burning when contacted to air. Yield of $Li(THF)_4[Al(bipy)_2]$ **2** (0.58 g, 40%). M.p.: 123–125 °C. EI-MS: m/z (%) = 281(0.2) [$Al(bipy)_2^+$–C_3H_5N], 207 (0.5) [$Li(THF)_3^+$–CH_4], 182 (1) [$Al(bipy)^+$], 156 (100) [$bipy^+$], 128 (25) [$(bipy)^+$–C_3H_3N], 106 (15) [$(bipy)^+$–C_5H_4N], 79 (18) [$Li(THF)^+$], 72 (22) [THF^+]. ^1H NMR (500 MHz, C_6D_6, r.t.), $\delta = 1,11$ (t, 4H, $J = 6.1$ Hz, CH_2, THF), 1.42 (t, 4H, $J = 6.2$ Hz, CH_2, THF), 2.1, 3.0, 3.3 (q, 4H, $J = 7.0$ Hz, CH_2, THF), 3.4, 3.6 (t, 4H, $J = 6.1$ Hz, CH_2, THF), 4.9, 5.5, 6.4, 6.7 ppm.

2.4. Computational detail

All computations were done with program GAUSSIAN 98, Revision A.6 [5]. The geometry of $[Al(bipy)_2]^-$ was optimized at the UHF/3-21G* level followed by UMPW1PW91/6-31G* and at the HF/6-31++G** level followed by B3LYP/6-31++G**, gas phase, C_1 symmetry and singlet ground state. The calculations were performed starting from the experimental structural data. Frequency calculations were performed at the UMPW1PW91/6-31G* level and the structure represents true minima without imaginary frequencies on the respective hypersurface. For the anionic species Mulliken population analysis has been performed using the B3LYP/6-31++G** or UMPW1PW91/6-31G* electron densities. Proton chemical shifts were calculated at the B3LYP/6-31++G** and UMPW1PW91/6-31G* level. For the calculation of chemical shifts CH_2Cl_2 was used as a reference. The geometry of CH_2Cl_2 was optimized at the UHF/3-21G* followed by UMPW1PW91/6-31G* level and at the HF/6-31++G** followed by B3LYP/6-31++G** level (gas phase). The proton chemical shift of CH_2Cl_2 was calculated at the B3LYP/6-31++G** and UMPW1PW91/6-31G* level.

2.5. Crystallography

Intensity data for the crystal structure of **2** was collected on a Stoe-Siemens four-circle diffractometer. The structure was solved by direct methods (SHELXS-97) and refined against F^2 using SHELXS-97 [6]. The heavy atoms were refined anisotropically. Hydrogen atoms were

included using the riding model with U_{iso} tied to U_{iso} of the parent atoms.

Crystal data: empirical formula: $C_{36}H_{48}AlLiN_4O_4$; $M = 634.70$, crystal size $1.00 \times 0.80 \times 0.20$ mm, black block, triclinic, space group $P\bar{1}$, $a = 9.108(2)$ Å, $b = 10.311(2)$ Å, $c = 11.040(2)$ Å, $\alpha = 114.94(3)°$, $\beta = 97.46(3)°$, $\gamma = 107.14(3)°$, $V = 858.7(3)$ Å^3, $Z = 1$, $D_c = 1.227$ g cm^3, μ (Mo Kα, $\lambda = 0.71073$ Å) $= 0.103$ mm^{-1}, $T = 203(2)$ K, 3544 reflections measured, 3544 unique. Scan range $\theta = 3.56°$–$25.03°$, completeness to $\theta_{max}(25.03°) = 99.4\%$, $F(000) = 340$, index ranges: $-10 \leqslant h \leqslant 10$, $-12 \leqslant k \leqslant 11$, $-11 \leqslant l \leqslant 13$; data/restrains/parameters 3544/3/415. Refinement on all F^2, final $R_1 = 0.0553$ (for reflections with $I > 2\sigma(I)$) $R_1 = 0.0567$ (for all data), $wR_2 = 0.1513$ (for all data), goodness-of-fit on $F^2 = 1.043$, maximum/minimum electron density 0.396/−0.377 (e Å^{-3}). Program: SHELXS-97 [6].

3. Results and discussion

3.1. Reaction of Ti(bipy)$_3$ with BF$_3$

The titanium complex Ti(bipy)$_3$ treated with an excess of gaseous BF_3 in CH_2Cl_2 at −79 °C yielded a violet air sensitive polycrystalline solid **1** that was crystallized from CH_2Cl_2 at −24 °C (Scheme 1). The same reaction in the presence of the electron donor solvents THF and Et_2O led to a colourless oil, whereas reaction of Ti(bipy)$_3$ and BF_3 in MeCN afforded a grey insoluble solid.

The resulting solid **1** is soluble in CH_2Cl_2 and $CHCl_3$. The ^{19}F NMR spectrum of **1** in CD_2Cl_2 exhibits a resonance at 11.2 ppm. It was found that the chemical shift of this resonance is close to that of the BF_4^- anion ($(Ph_3C)BF_4$ δ 11.0 ppm in CD_2Cl_2). In the solid state ^{11}B MAS NMR spectrum of **1** is observed one strong resonance with two weak satellites, which suggests tetrahedral symmetric environment for the ^{11}B nucleus. This observation is in agreement with a BF_4^- anion. The proton NMR spectrum of **1** in CD_2Cl_2 exhibits a set of resonances in the range from −26.6 to 19.6 ppm, connected with the paramagnetic nature of **1**. While the neutral Ti(bipy)$_3$ complex is diamagnetic, the anionic complex [Ti(bipy)$_3$]$^-$ was shown to be paramagnetic and electronic spectra of it suggested the presence of the negatively charged bipy$^-$ and bipy^{2-} ligands [3b]. Similar features have been observed in the electronic and IR spectra of the tris(2,2′-bipyridyl) complexes [M(bipy)$_3$]$^-$, [M(bipy)$_3$], [M(bipy)$_3$]$^{n+}$ ($n = 1, 2$), M = Ti, V, Cr, Fe [3b,3c,3f] and these complexes are considered containing negatively charged bipy ligands. Therefore, complex **1** can be formally described containing bipy^0, bipy$^-$ and bipy^{2-} ligands. The presence of bipy$^-$ ligand might be responsible for the paramagnetism of **1**. However, an estimate of the actual composition of the ground state of **1** in terms of metal and the various ligand orbital contributions will be possible on the basis of detailed MO calculations using experimentally determined bond lengths and angles.

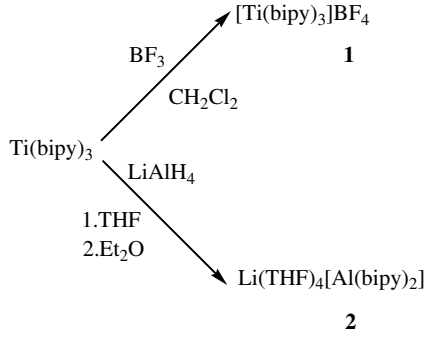

Scheme 1. Synthesis of complexes **1** and **2**.

Solid **1** was investigated by means of mass spectrometry. The fragment with the largest m/z corresponds to the [(Ti(bipy)$_3$–CH)$^+$] cation. In addition several fragments of [Ti(bipy)$_3$]BF$_4$ were observed including a strong signal for [bipy$^+$]. The elemental analysis of **1** is close to the [Ti(bipy)$_3$]BF$_4$ composition, however, it does not correspond exactly to this composition possibly due to the high reactivity of **1** toward air.

Thus, the soluble reaction product **1**, obtained by interaction of Ti(bipy)$_3$ with an excess of BF_3 in CH_2Cl_2, was confirmed. The conversion of complex Ti(bipy)$_3$ to the [Ti(bipy)$_3$]$^+$ cation can be promoted with the strong Lewis acid BF_3, that acts under the reported reaction conditions as an electron acceptor under formation of the BF_4^- anion. It should be pointed out, that oxidation of Ti(bipy)$_3$ with iodine was studied by Herzog and Taube [2] but they did not find experimental evidence for the oxidation of Ti(bipy)$_3$ to [Ti(bipy)$_3$]$^+$. In general, the molecular low valent titanium complexes can be oxidized and form the corresponding cationic complexes [7].

3.2. Reaction of Ti(bipy)$_3$ with LiAlH$_4$

Reaction of Ti(bipy)$_3$ with $LiAlH_4$ in THF followed by crystallization from Et_2O affords the unforeseen complex Li(THF)$_4$[Al(bipy)$_2$] **2** (Scheme 1). Complex **2** is extremely air and moisture sensitive and starts immediately to burn when exposed to air. All attempts to accomplish elemental analysis were unsuccessful due to the high reactivity of **2**. The melting point of **2** is in the range from 123 to 125 °C. Complex **2** exhibits a signal for the [Al(bipy)$^+$] ion as well as [bipy$^+$] and [LiTHF$^+$] cations in the EI-MS spectrum.

Complex **2** is soluble in THF, Et_2O and toluene. The ^{1}H NMR spectrum of **2** in C_6D_6 showed a strong THF resonance and four weak and broadened resonances in

the range from 6.7 to 4.9 ppm that can be assigned to the coordinated bipy. The intensive colour change observed upon complexation with bipy suggests the presence of a considerable negative charge on the coordinated ligand. The negative charge on the bipy ligand in **2** seems to be even larger compared to the titanium complex $Ti(bipy)_3$, since the proton resonances of $[Al(bipy)_2]^-$ are shifted upfield by ca. 0.5–1 ppm relative to the resonances of $Ti(bipy)_3$ [4b].

To assign the resonances in the ^1H NMR spectrum, the anionic complex $[Al(bipy)_2]^-$ was optimized at the B3LYP/6-31++G** and UMPW1PW91/6-31G* DFT levels (C_1 symmetry, singlet ground state) (Fig. 1). The calculation is in qualitatively good agreement with the available experimental data. The C–C and C–N bond lengths of the coordinated bipyridyl ligand (Table 2) and the Al–N distances 1.84 Å (exp.) vs. 1.87 Å (calcd.) within the calculated anion of **2** have acceptable deviations. The calculated bond lengths are overestimated of about 0.03–0.05 Å which is common for DFT calculations. The calculated partial charge residing on the Al atom is 2.48 at the B3LYP/6-31++G** level, that is in agreement with the formal approach, where the formal charge on the aluminum atom should be +3. The calculated partial charge on the Al atom is only 0.88 using the open shell method UMPW1PW91. The chemical shift of the proton resonances for $[Al(bipy)_2]^-$ calculated with the B3LYP/6-31++G** level differs (1.4–1.2 ppm) substantially from the experimental values. The open shell method UMPW1PW91/6-31G* gives, however, smaller deviations and the calculated resonances are shifted by 0.9–0.4 ppm upfield. The calculated chemical shifts can be rescaled. Adding the 1.2 ppm to the chemical shifts of the proton resonances calculated with the B3LYP/6-31++G** level and the 0.7 ppm to the chemical shifts of the proton resonances calculated with the UMPW1PW91/6-31G* afford deviations less than 0.5 ppm (Table 1).

Table 1
Calculated ^1H chemical shifts for the $[Al(bipy)_2]^-$ anion

Number of protons	δ (# B3LYP/6-31++G**) + 1.2 ppm	δ (#UMPW1PW91/6-31G*) + 0.7 ppm	δ (exp.), ppm
26	4.7	4.7	4.9
27	7.1	7.0	6.7
28	6.5	6.4	6.4
29	5.5	5.4	5.5
30	5.5	5.4	5.5
31	6.5	6.4	6.4
32	7.1	7.0	6.7
33	4.7	4.7	4.9
34	4.7	4.7	4.9
35	7.1	7.0	6.7
36	6.5	6.4	6.4
37	5.5	5.4	5.5
38	5.5	5.4	5.5
39	6.5	6.4	6.4
40	7.1	7.0	6.7
41	4.7	4.7	4.9

Complex **2** crystallizes in the triclinic space group $P\bar{1}$. The X-ray structural analysis revealed that compound **2** is monomeric and contains separated $[Li(THF)_4]^+$ cations and $[Al(bipy)_2]^-$ anions (Fig. 2). The two bipy ligands coordinate to the Al1 atom through the nitrogen atoms. The coordination number at the aluminum atom in **2** is four and the geometry around the metal atom is distorted tetrahedral. The empirical bond-valence-method [8] can be applied for the description of the coordination sphere around the Al1 atom. Since the $[Al(bipy)_2]^-$ can formally be described as an Al(III) complex, the sum of the aluminum bond valency is expected to be 3. The sum of four Al–N bond valency is 3.45 indicating that the aluminum coordination sphere in **2** can be represented as AlN_4. The deviation from 3 might be connected with the non-integral oxidation number of the metal center in $[Al(bipy)_2]^-$, similarly to those in complexes $[M(bipy)_3]^n$ ($n = -1$ to -3), (M = Ti, V, Cr) [3].

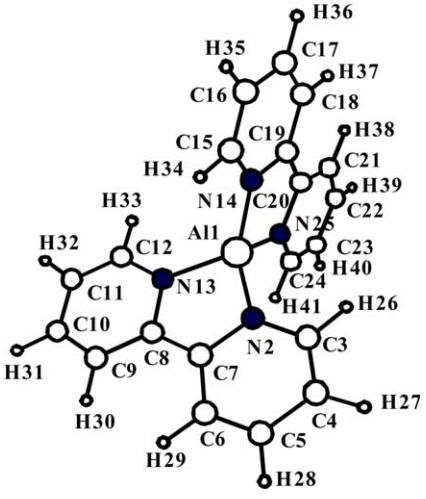

Fig. 1. Calculated geometry of $[Al(bipy)_2]^-$ at the UMPW1PW91/6-31G* level.

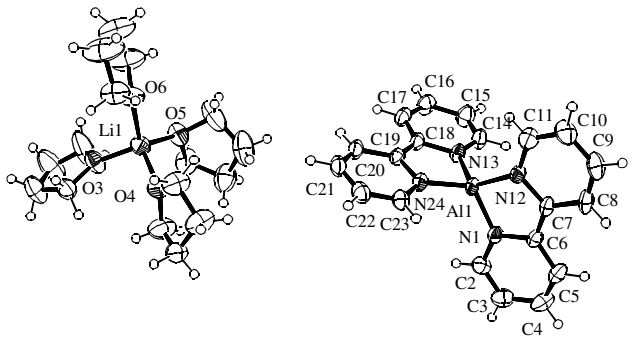

Fig. 2. Molecular structure of $Li(THF)_4[Al(bipy)_2]$ **2**.

Table 2
Comparison of averaged C–C and C–N bond lengths (Å) of coordinated $bipy^{2-}$ in different complexes: (a) $[Na_2(bipy)(dme)_2]$, (b) $[Yb(\mu\text{-}N_2C_{10}H_8)(THF)_2]_3$, (c) $[Al(bipy)_2]^-$ **2** (N1C2C3C4C5C6C7C8C9C10C11N12 unit), (d) **2** (N13C14C15C16C17C18C19C20C21C22C23N24 unit), (e) calculated distances at the UMPW1PW91/6-31G* level, (f) B3LYP/6-31++G** level

	A	*B*	*C*	*D*	*E*	*F*	*G*
(a)	1.44	1.34	1.37	1.41	1.34	1.45	1.38
(b)	1.44	1.39	1.36	1.43	1.36	1.46	1.41
(c)	1.44 (1.43)	1.38	1.35	1.44	1.34 (1.35)	1.42 (1.44)	1.36
(d)	1.44 (1.43)	1.38 (1.37)	1.33 (1.36)	1.44 (1.42)	1.36 (1.34)	1.42 (1.44)	1.37
(e)	1.43	1.37	1.36	1.44	1.36	1.43	1.38
(f)	1.44	1.37	1.36	1.45	1.37	1.43	1.39

See text for references, labeling see Scheme 2.

The bipy ligands are nearly planar, the first one with the N4 and N12 atoms has deviation of 0.03 Å from planarity, the second one with the N13 and N24 atoms has a deviation of 0.02 Å (aluminum atoms are 0.05 and 0.02 Å out of the plane). The two bipy ligands are rotated by 88.9° to each other. The C–C and C–N bond lengths in the two bipy ligands are close to those in the known complexes $[Na_2(bipy)(DME)_2]$ (DME = dimethoxyethane) [1c,1d], $[Yb(\mu\text{-}N_2C_{10}H_8)(THF)_2]_3$ [1e,1f] where the bipy ligands were formally described as dianionic (Table 2; Scheme 2).

The Al–N distances in **2** (Table 3) are considerably shorter than those in the aluminum complex $[AlCl_2(bipy)_2]Cl \cdot MeCN$ (Al–N 2.020(3)–2.042(3) Å) [9] between aluminum and coordinated neutral bipy ligand and are comparable with the Al–N single bond length in $(2,6\text{-}iPr_2C_6H_3)N(SiMe_3)AlMe_2$, (Al–N 1.823(2) Å) [10], $[K \cdot THF(2,6\text{-}iPr_2C_6H_3N(SiMe_3)Al(C{\equiv}CPh)_3)]_2$ (Al–N 1.836(2) Å) [11].

Finally, a comparison of the Al–N bond lengths, C–C and C–N distances in the anionic complex $[Al(bipy)_2]^-$ (c), (d) (Table 2) and the distances of a coordinated $bipy^{2-}$ in known complexes (a) and (b) (Table 2) [1c–1f] reveals that complex $[Al(bipy)_2]^-$ formally can be described as an Al(III) complex with two $bipy^{2-}$ dianionic antiaromatic ligands. On the other side essential electron density can be located on the aluminum atom. Calculation of chemical shifts with the open shell method UMPW1PW91 giving the partial charge on the Al atom (0.88) leads to reasonable small deviations from experimental values (Table 1). Therefore the bipy ligands in the anionic form of **2** are essentially carrying the negative charge, corresponding to a successive filling of the LUMO of the neutral bipy. It is possible to conclude that the oxidation number of the aluminum and the bipy ligands is likely to be non-integral, this is in agreement with the previous assumption for the oxidation state of the metals and bipy in $[M(bipy)_3]^n$ ($n = -1$ to -3), (M = Ti, V, Cr) complexes [3].

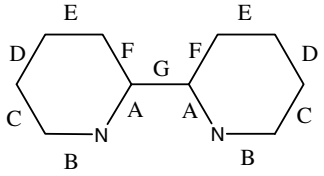

Scheme 2. Labeling scheme of the bipy ligand.

Table 3
Selected bond lengths (Å) and angles (°) for **2**

Al(1)–N(1)	1.839(3)	N(1)–Al(1)–N(12)	87.80(13)
Al(1)–N(12)	1.844(3)	N(1)–Al(1)–N(24)	121.40(13)
Al(1)–N(24)	1.844(3)	N(12)–Al(1)–N(24)	123.84(14)
Al(1)–N(13)	1.846(3)	N(1)–Al(1)–N(13)	120.74(14)
Li(1)–O(3)	1.923(7)	N(12)–Al(1)–N(13)	119.19(14)
Li(1)–O(5)	1.953(7)	N(24)–Al(1)–N(13)	87.70(14)
		O(3)–Li(1)–O(4)	109.8(3)
		O(3)–Li(1)–O(5)	104.6(3)
		O(4)–Li(1)–O(5)	110.1(4)

4. Conclusions

The reaction between $Ti(bipy)_3$ and BF_3 leads to the conversion of the titanium complex to the corresponding cationic complex $[Ti(bipy)_3]^+$. The strong Lewis acid BF_3 acts as an electron acceptor under the reaction conditions given and promotes the electron transfer process. A transfer of a negatively charged bipy ligand was observed from the titanium to the aluminum center in the $Ti(bipy)_3$–$LiAlH_4$ system. The resulting anionic complex $[Al(bipy)_2]^-$ carries the bipy ligands with a considerable negative charge.

5. Supplementary material

Crystallographic data have been deposited with the Cambridge Crystallographic Data Centre as supplementary publication no. CCDC 214500. Copies of the data can be obtained free of charge on application to the CCDC, 12 Union Road, Cambridge CB2 1EZ, UK [fax: +44-1223-336033; e-mail: deposit@ccdc.cam.ac.uk or www: http://www.ccdc.cam.ac.uk].

Acknowledgements

Support of this work by the Deutsche Forschungsgemeinschaft is highly acknowledged.

References

[1] (a) J.-M. Lehn, Supramolecular Chemistry: Concepts and Perspectives, VCH, Weinheim, 1995;
(b) S. Herzog, U. Grimm, Z. Chem. 8 (1968) 186;
(c) H. Bock, J.-M. Lehn, J. Pauls, S. Holl, V. Krenzel, Angew. Chem. 111 (1999) 1004;
(d) H. Bock, J.-M. Lehn, J. Pauls, S. Holl, V. Krenzel, Angew. Chem. Int. Ed. 38 (1999) 952;
(e) I.L. Fedushkin, T.V. Petrovskaya, F. Girgsdies, R.D. Köhn, M.N. Bochkarev, H. Schumann, Angew. Chem. 111 (1999) 2407;
(f) I.L. Fedushkin, T.V. Petrovskaya, F. Girgsdies, R.D. Köhn, M.N. Bochkarev, H. Schumann, Angew. Chem. Int. Ed. 38 (1999) 2262;
(g) J. Quirk, G. Wilkinson, Polyhedron 1 (1982) 209;
(h) W.J. Evans, D.K. Drummond, J. Am. Chem. Soc. 111 (1989) 3329;
(i) W.J. Evans, S.L. Gonzales, J.W. Ziller, J. Am. Chem. Soc. 116 (1994) 2600;
(j) M.N. Bochkarev, I.L. Fedushkin, V.I. Nevodchikov, V.K. Cherkasov, H. Schumann, H. Hemling, R. Weimann, J. Organomet. Chem. 524 (1996) 125;
(k) T.V. Petrovskaya, I.L. Fedushkin, M.N. Bochkarev, H. Schumann, R. Weimann, Russ. Chem. Bull. 46 (1997) 1766;
(l) G.R. Feistel, T.P. Mathai, J. Am. Chem. Soc. 90 (1968) 2988;
(m) M.N. Bochkarev, A.A. Trifonov, F.G.N. Cloke, C.I. Dalby, P.T. Matsunaga, R.A. Andersen, H. Schumann, J. Loebel, H. Hemling, J. Organomet. Chem. 486 (1995) 177.

[2] S. Herzog, R. Taube, Z. Anorg. Allg. Chem. 306 (1960) 159.

[3] (a) R. Pappalardo, Inorg. Chim. Acta 2 (1968) 209;
(b) E. König, S. Herzog, J. Inorg. Nucl. Chem. 32 (1970) 613;
(c) E. König, S. Herzog, J. Inorg. Nucl. Chem. 32 (1970) 601;
(d) Y. Kaizu, T. Yazaki, Y. Torii, H. Kobayashi, Bull. Chem. Soc. Jpn. 43 (1970) 2068;
(e) I. Hanazaki, S. Nagakura, Bull. Chem. Soc. Jpn. 44 (1971) 2312;
(f) E. König, E. Lindner, Spectrochim. Acta 28A (1972) 1393.

[4] (a) W. Kaim, R. Reinhardt, E. Waldhör, J. Fiedler, J. Organomet. Chem. 524 (1996) 195;
(b) A. Flamini, A.M. Giuliani, Inorg. Chim. Acta 112 (1986) L7.

[5] M. J. Frisch, G.W. Trucks, H.B. Schlegel, G.E. Scuseria, M.A. Robb, J.R. Cheeseman, V.G. Zakrzewski, J.A. Montgomery Jr., R.E. Stratmann, J.C. Burant, S. Dapprich, J.M. Millam, A.D. Daniels, K.N. Kudin, M.C. Strain, O. Farkas, J. Tomasi, V. Barone, M. Cossi, R. Cammi, B. Mennucci, C. Pomelli, C. Adamo, S. Clifford, J. Ochterski, G.A. Petersson, P.Y. Ayala, Q. Cui, K. Morokuma, D.K. Malick, A.D. Rabuck, K. Raghavachari, J.B. Foresman, J. Cioslowski, J.V. Ortiz, B.B. Stefanov, G. Liu, A. Liashenko, P. Piskorz, I. Komaromi, R. Gomperts, R.L. Martin, D.J. Fox, T. Keith, M.A. Al-Laham, C.Y. Peng, A. Nanayakkara, C. Gonzalez, M. Challacombe, P.M.W. Gill, B. Johnson, W. Chen, M.W. Wong, J.L. Andres, C. Gonzalez, M. Head-Gordon, E.S. Replogle, J.A. Pople, Gaussian, Inc., Pittsburgh, PA, 1998.

[6] G.M. Sheldrick, SHELXL: Program for Crystal Structure Refinement, University of Göttingen, Göttingen, Germany, 1997.

[7] A. Kayal, J. Kuncheria, S.C. Lee, Chem. Commun. 23 (2001) 2482.

[8] I.D. Brown, in: M. O'Keefe, A. Navrotsky (Eds.), Structure and Bonding in Crystals, Academic Press, London, 1981.

[9] P.L. Bellavance, E.R. Corey, J.Y. Corey, G.W. Hey, Inorg. Chem. 16 (1977) 462.

[10] S.D. Waezsada, F.-Q. Liu, E.F. Murphy, H.W. Roesky, M. Teichert, I. Usón, H.-G. Schmidt, T. Albers, E. Parisini, M. Noltemeyer, Organometallics 16 (1997) 1260.

[11] M. Schiefer, H. Hatop, H.W. Roesky, H.-G. Schmidt, M. Noltemeyer, Organometallics 21 (2002) 1300.

Available online at www.sciencedirect.com
SCIENCE DIRECT®
Polyhedron 23 (2004) 567–573
POLYHEDRON
www.elsevier.com/locate/poly

Syntheses and crystal structures of the potential tridentate ligand formed from condensation of ferrocenoylacetone and S-benzyldithiocarbazate and its bivalent metal complexes

Yao-Cheng Shi [a,*], Hua-Mei Yang [a], Hai-Bin Song [b], Chao-Guo Yan [a], Xiao-Ya Hu [a]

[a] School of Chemistry and Chemical Engineering, Yangzhou University, Yangzhou 225002, PR China
[b] State Key Laboratory of Elemento-Organic Chemistry, Nankai University, Tianjin 300071, PR China

Received 2 August 2003; accepted 14 October 2003

Abstract

A new potential tridentate ligand (**H_2L**) was synthesized from condensation of ferrocenoylacetone ($C_5H_5FeC_5H_4C(O)CH_2C(O)CH_3$) with S-benzyldithiocarbazate in refluxing benzene. Reaction of the ligand (**H_2L**) with a bivalent metal salt ($M(OAc)_2 \cdot xH_2O$, M = Cu, Ni, Mn, Hg, Zn; $SnCl_2 \cdot 2H_2O$) afforded the corresponding bivalent metal complexes M(**HL**)$_2$ (**I**, M = Cu; **II**, M = Ni; **III**, M = Mn; **IV**, M = Hg; **V**, M = Zn; **VI**, M = Sn). All the new compounds have been characterized by elemental analyses, ^{1}H NMR, IR and UV spectroscopies. A single-crystal X-ray analysis indicates that the ligand exists as a single iminone and not a tautomeric mixture of the iminone and enaminone. Crystallography of complex **VI** shows that the ligand acts as monoanionic tridentate coordinated to the tin atom via the carbonyl oxygen, deprotonated enamine nitrogen and thione sulfur atoms and the coordination geometry of the central metal is a distorted octahedron.
© 2003 Elsevier Ltd. All rights reserved.

Keywords: Ferrocene; Dithiocarbazate; Ligand; Complex; Tin; Crystal structure

1. Introduction

N-substituted acid hydrazides are well-known to act as chelating agents [1–4]. Furthermore, these compounds and their metal complexes exhibit a broad spectrum of biological, bactericidal and fungicidal activities [5–7]. Since the discovery of ferrocene in 1951, it has played an important role in developing a knowledge of electronic structures of organometallic compounds and materials chemistry. A considerable number of ferrocene derivatives have been prepared directly or indirectly from ferrocene and their properties have been extensively studied. Among them, some have been reported to display biological activity and act as β-lactamase inhibitors [8,9]. In view of relatively few studies on reactions of 1,3-diketones and acylhydrazides, here we report the syntheses and crystal structures of the potential tridentate ligand [$C_5H_5FeC_5H_4C(O)CH_2C(CH_3)=NNHCSSCH_2C_6H_5$] (**$H_2L$**) formed from condensation of ferrocenoylacetone and S-benzyldithiocarbazate and its bivalent metal complexes [10,11].

2. Experimental

2.1. Reagents and general procedures

All chemicals were of analytical grade and used without further purification. S-benzyldithiocarbazate and ferrocenoylacetone were synthesized according to the literature methods [12–14]. Progress of the reaction was monitored by TLC (silica gel H). The ^{1}H NMR spectra were determined with a Bruker Avance 500 spectrometer using TMS as an external standard in $CDCl_3$. IR spectra were recorded on a Perkin–Elmer 402 as KBr disks in the range of 400–4000 cm^{-1}. UV spectra were measured with a Shimadzu UV-240 spectrometer using a solution in DMF. Analyses for C, H

* Corresponding author. Tel/fax: +865147857939.
E-mail address: yzssyc@yzcn.net (Y.-C. Shi).

0277-5387/$ - see front matter © 2003 Elsevier Ltd. All rights reserved.
doi:10.1016/j.poly.2003.10.003

and N were performed on an Elementa Vario EL III microanalytical instrument. Melting points were measured on a Yanagimoto apparatus and uncorrected.

2.2. Synthesis of ligand

S-benzyldithiocarbazate (1.98 g, 10 mmol) was added to a solution of ferrocenoylacetone ($C_5H_5FeC_5H_4C(O)CH_2C(O)CH_3$) (2.7 g, 10 mmol) in 30 ml of benzene, the mixture was refluxed for 5 h and then evaporated to dryness and finally isolated by vacuum liquid chromatography (VLC), using a mixed solvent of CH_2Cl_2 and petroleum ether (v/v, 5:1) to afford the ligand. **H_2L** as orange red crystals, yield: 3.51 g (78%). M.p. 141–142 °C. *Anal.* Found: C, 58.48; H, 4.58; N, 5.89. Calc. for $C_{22}H_{22}FeN_2OS_2$: C, 58.66; H, 4.93; N, 6.22%. ^{1}H NMR (500 Mz, δ, in $CDCl_3$): iminone A isomer (shown in Scheme 1), 2.18 (s, CH_3), 3.73 (s, SCH_2), 3.94 (s, CH_2), 4.23 (s, C_5H_5), 4.55, 4.82 (s, s, ^{3}H/^{4}H and ^{2}H/^{5}H of C_5H_4 ring), 7.22–7.41 (m, C_6H_5), 6.54 (s, br, NH); enaminone B isomer (shown in Scheme 1), 2.07 (s, CH_3), 3.54, 3.58, 3.83, 3.86 (q, $^2J_{HH}$ = 18.6 Hz, SCH_2), 4.21 (s, C_5H_5), 4.68, 4.78 (s, s, ^{3}H/^{4}H and ^{2}H/^{5}H of C_5H_4 ring), 5.73 (s, CH), 7.22–7.41 (m, C_6H_5), 9.82 (s, $NHCS_2$), 11.67 ppm (s, NH). IR (KBr disk): ν(NH) 3431(w, br), ν(C=O) 1665 (vs), ν(C=N) 1637 (m), ν(C=S) 1068 (vs), ν(C–S) 1035 (m), ν(N–N) 984 (m) cm^{-1}. UV (nm, in DMF): λ_{max} ($\varepsilon \times 10^4$, in dm^3 mol^{-1} cm^{-1}) 405 (1.8) (K-band), 553 (0.053) (R-band). Single crystals of the ligand for X-ray determination were obtained by slow evaporation of its solution in dichloromethane and petroleum ether.

2.3. Syntheses of complexes

A solution of an appropriate metal acetate or $SnCl_2 \cdot 2H_2O$ (0.5 mmol) in 5 ml of absolute ethanol was added dropwise to a stirred solution of the ligand (**H_2L**) (0.45 g, 1 mmol) in 20 ml of absolute ethanol. The mixture was stirred for 6 h at room temperature and then filtered to afford the crude product. The resulting solid recrystallized from dichloromethane and petroleum ether gave the corresponding complex (**I** to **VI**).

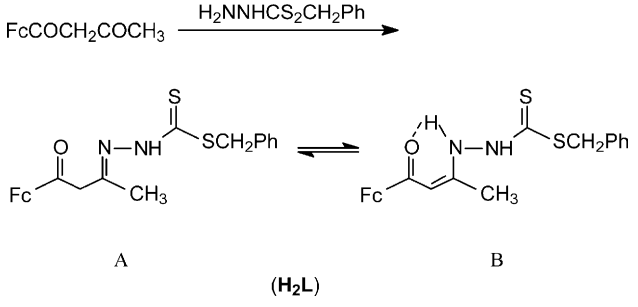

Scheme 1. Synthesis of ligand.

Complex **I** as a black solid, yield: 0.847 g (88%). M.p. 131–132 °C. *Anal.* Found: C, 54.54; H, 3.95; N, 5.42. Calc. for $C_{44}H_{42}Fe_2N_4O_2S_4Cu$: C, 54.92; H, 4.40; N, 5.82%. IR (KBr disk): ν(NH) 3435 (w, br), ν(C=O) 1664 (vs), ν(C=C) 1614 (m), ν(C=S) 1070(s), ν(C–S) 1019 (s), ν(N–N) 951 (m) cm^{-1}. UV (nm, in DMF): λ_{max} ($\varepsilon \times 10^4$, in dm^3 mol^{-1} cm^{-1}) 265 (3.4) (B-band), 404 (4.5) (K-band).

Complex **II** as a dark red solid, yield: 0.536 g (56%). M.p. 158–158.5 °C. *Anal.* Found: C, 55.48; H, 4.08; N, 5.58. Calc. for $C_{44}H_{42}Fe_2N_4O_2S_4Ni$: C, 55.19; H, 4.42; N, 5.83%. ^{1}H NMR (500 Mz, δ, in $CDCl_3$): 1.83 (s, 6H, $2CH_3$), 4.37 (s, 4H, $2SCH_2$), 4.13 (s, 10H, $2C_5H_5$), 4.19–4.30, 4.63–4.69 (d, d, 4H, 4H, ^{3}H/^{4}H and ^{2}H/^{5}H of two C_5H_4 rings), 5.28 (s, 2H, 2CH), 7.22–7.40 (m, 10H, $2C_6H_5$), 8.28 ppm (s, 2H, 2NH). IR (KBr disk): ν(NH) 3434 (m), ν(C=O) 1663 (vs), ν(C=C) 1534 (m), ν(C=S) 1068 (s), ν(C–S) 1028 (m), ν(N–N) 966 (s) cm^{-1}. UV (nm, in DMF): λ_{max} ($\varepsilon \times 10^4$, in dm^3 mol^{-1} cm^{-1}) 398 (2.0) (K-band), 624 (0.047) (R-band).

Complex **III** as a black purple solid, yield: 0.801 g (84%). M.p. 192–193 °C. *Anal.* Found: C, 54.90; H, 3.97; N, 5.50. Calc. for $C_{44}H_{42}Fe_2N_4O_2S_4Mn$: C, 55.41; H, 4.41; N, 5.87%. IR (KBr disk): ν(NH) 3427 (w, br), ν(C=O) 1529 (vs), ν(C=C) 1519 (vs), ν(C=S) 1062 (m), ν(C–S) 1020 (m), ν(N–N) 965 (m) cm^{-1}. UV (nm, in DMF): λ_{max} ($\varepsilon \times 10^4$, in dm^3 mol^{-1} cm^{-1}) 387 (1.64) (K-band), 507 (0.052) (R-band).

Complex **IV** as a brown yellow solid, yield: 0.858 g (78%). M.p. 137 °C (dec.). *Anal.* Found: C, 47.77; H, 3.57; N, 4.77. Calc. for $C_{44}H_{42}Fe_2N_4O_2S_4Hg$: C, 48.05; H, 3.85; N, 5.10%. IR (KBr disk): ν(NH) 3434 (w), ν(C=O) 1666 (vs), ν(C=C) 1614 (m), ν(C=S) 1070 (m), ν(C–S) 1026 (m), ν(N–N) 944 (s) cm^{-1}. UV (nm, in DMF): λ_{max} ($\varepsilon \times 10^4$, in dm^3 mol^{-1} cm^{-1}) 328 (1.74), 360 (1.72) (K-band).

Complex **V** as an orange yellow solid, yield: 0.868 g (90%). M.p. 192 °C (dec.). *Anal.* Found: C, 54.80; H, 4.09; N, 5.54. Calc. for $C_{44}H_{42}Fe_2N_4O_2S_4Zn$: C, 54.81; H, 4.39; N, 5.81%. IR (KBr disk): ν(NH) 3434 (w), ν(C=O) 1666 (vs), ν(C=C) 1622 (m), ν(C=S) 1071 (m), ν(C–S) 1024 (m), ν(N–N) 951 (m) cm^{-1}. UV (nm, in DMF): λ_{max} ($\varepsilon \times 10^4$, in dm^3 mol^{-1} cm^{-1}) 265 (4.79), 277 (2.43) (B-band), 404 (3.74) (K-band).

Complex **VI** as an orange solid, yield: 0.916 g (90%). M.p. 238–239 °C. *Anal.* Found: C, 51.72; H, 4.22; N, 5.41. Calc. for $C_{44}H_{42}Fe_2N_4O_2S_4Sn$: C, 51.94; H, 4.16; N, 5.51%. ^{1}H NMR (500 Mz, δ, in $CDCl_3$): 2.45 (s, 6H, $2CH_3$), 4.31, 4.34, 4.53. 4.56 (q, 4H, $^2J_{HH}$ = 13.5 Hz, $2SCH_2$), 4.21 (s, 10H, $2C_5H_5$), 4.37–4.39, 4.62–4.64 (d, d, 4H, 4H, ^{3}H/^{4}H and ^{2}H/^{5}H of two C_5H_4 rings), 5.39 (s, 2H, 2CH), 7.31–7.43 (2m, 10H, $2C_6H_5$), 7.28 ppm (s, 2H, 2NH). IR (KBr disk): ν(NH) 3439(w, br), ν(C=O) 1550 (s), ν(C=C) 1515 (vs), ν(C=S) 1051 (m), ν(C–S) 1018 (m), ν(N–N) 966 (m) cm^{-1}. UV (nm, in DMF): λ_{max} ($\varepsilon \times 10^4$, in dm^3 mol^{-1} cm^{-1}) 400 (1.90) (K-band).

Table 1
Crystallographic data for ligand and complex **VI**

Formula	$C_{22}H_{22}FeN_2OS_2$	$C_{44}H_{42}Fe_2N_4O_2S_4Sn$
Formula weight	450.39	1017.45
Crystal size (mm)	$0.30 \times 0.25 \times 0.20$	$0.16 \times 0.14 \times 0.08$
Crystal system	triclinic	monoclinic
Space group	$P\bar{1}$	$P2_1/n$
Unit cell dimensions		
a (Å)	7.993(3)	16.452(7)
b (Å)	10.503(4)	10.819(5)
c (Å)	13.770(5)	23.932(10)
α (°)	108.573(6)	90.00
β (°)	90.576(6)	101.065(8)
γ (°)	102.356(6)	90.00
V (Å^3)	1066.6(6)	4180(3)
Z	2	4
D_c (g cm^{-1})	1.402	1.617
F (0 0 0)	468	2064
T (K)	293(2)	293(2)
μ(Mo Kα) (mm^{-1})	0.917	1.521
Scan mode	ϕ and ω scans	ϕ and ω scans
θ Range (°)	1.57–26.44	1.39–26.44
Limiting indices	$-9 \leqslant h \leqslant 8$, $-9 \leqslant k \leqslant 13$, $-17 \leqslant l \leqslant 16$	$-20 \leqslant h \leqslant 20$, $-13 \leqslant k \leqslant 13$, $-15 \leqslant l \leqslant 29$
Reflections collected	6149	19,253
Independent reflections	4318	8582
Number of parameters refined	279	516
Absorption correction	multi-scan	multi-scan
Final R indices [$I > 2.0\sigma(I)$]	$R = 0.0496$, $Rw = 0.1074$	$R = 0.0562$, $Rw = 0.1057$
R indices (all data)	$R = 0.0923$, $Rw = 0.1346$	$R = 0.1452$, $Rw = 0.1399$
Goodness-of-fitF	1.011	0.990
Largest peak and hole (e Å^{-3})	0.445 and −0.291	0.830 and −0.691

Single crystals of complex **VI** for X-ray determination were obtained by slow evaporation of its solution in dichloromethane and petroleum ether.

2.4. Crystal structure determination

For each of compounds (**H_2L** and **VI**), a selected single crystal was mounted on a Bruker SMART 1000 CCD diffractometer using graphite-monochromated Mo Kα radiation ($\lambda = 0.71073$ Å) at 293 K. Data collection and reduction were performed using the SMART and SAINT software [15]. An empirical absorption correction was applied using the SADABS program [16]. The structures were solved by direct methods and refined by full-matrix least-squares methods, based on F^2 with anisotropic thermal parameters for all non-hydrogen

Table 2
Selected bond distances (Å) and angles (°) for ligand

Bond distances			
Fe(1)–C(1)	2.027(3)	N(1)–C(13)	1.271(5)
Fe(1)–C(2)	2.047(4)	N(2)–C(14)	1.335(4)
Fe(1)–C(3)	2.056(4)	N(1)–N(2)	1.395(4)
Fe(1)–C(4)	2.047(4)	O(1)–C(11)	1.221(4)
Fe(1)–C(5)	2.033(4)	C(1)–C(11)	1.472(5)
Fe(1)–C(6)	2.044(4)	C(11)–C(12)	1.515(5)
Fe(1)–C(7)	2.029(5)	C(12)–C(13)	1.508(5)
Fe(1)–C(8)	2.041(5)	S(1)–C(14)	1.749(4)
Fe(1)–C(9)	2.051(4)	S(1)–C(15)	1.820(4)
Fe(1)–C(10)	2.044(4)	S(2)–C(14)	1.667(4)
Bond angles			
C(1)–C(11)–C(12)	116.8(3)	N(1)–C(13)–C(22)	126.9(3)
O(1)–C(11)–C(1)	121.4(3)	N(2)–C(14)–S(1)	113.9(2)
O(1)–C(11)–C(12)	121.8(3)	N(2)–C(14)–S(2)	121.4(3)
C(11)–C(12)–C(13)	112.9(3)	S(2)–C(14)–S(1)	124.7(2)
C(12)–C(13)–C(22)	117.5(3)	C(13)–N(1)–N(2)	117.4(3)
N(1)–C(13)–C(12)	115.6(3)	C(14)–N(2)–N(1)	119.4(3)

Table 3
Selected bond distances (Å) and angles (°) for complex **VI**

Bond distances			
Fe(1)–C(1)	2.010(7)	Fe(2)ndash;C(23)	2.026(7)
Fe(1)–C(2)	2.024(7)	Fe(2)–C(24)	2.016(8)
Fe(1)–C(3)	2.027(7)	Fe(2)–C(25)	2.045(8)
Fe(1)–C(4)	2.052(8)	Fe(2)–C(26)	2.025(8)
Fe(1)–C(5)	2.022(8)	Fe(2)–C(27)	2.019(7)
Fe(1)–C(6)	2.022(8)	Fe(2)–C(28)	2.012(9)
Fe(1)–C(7)	2.021(10)	Fe(2)–C(29)	2.054(9)
Fe(1)–C(8)	2.023(8)	Fe(2)–C(30)	2.059(9)
Fe(1)–C(9)	2.027(8)	Fe(2)–C(31)	2.032(9)
Fe(1)–C(10)	2.022(9)	Fe(2)–C(32)	1.989(9)
Sn(1)–O(1)	2.069(5))	Sn(1)–O(2)	2.061(5)
Sn(1)–N(1)	2.141(6)	Sn(1)–N(3)	2.137(6)
Sn(1)–S(1)	2.481(2)	Sn(2)–S(3)	2.487(2)
N(1)–C(13)	1.348(8)	N(3)–C(35)	1.333(9)
N(2)–C(15)	1.280(8)	N(4)–C(37)	1.262(9)
N(1)–N(2)	1.376(8)	N(3)–N(4)	1.382(8)
O(1)–C(11)	1.310(8)	O(2)–C(33)	1.311(8)
C(11)–C(12)	1.379(10)	C(33)–C(34)	1.371(9)
C(12)–C(13)	1.379(9)	C(34)–C(35)	1.407(10)
C(13)–C(14)	1.496(10)	C(35)–C(36)	1.502(9)
S(1)–C(15)	1.736(7)	S(3)–C(37)	1.745(8)
S(2)–C(15)	1.752(7)	S(4)–C(37)	1.744(8)
S(2)–C(16)	1.816(8)	S(4)–C(38)	1.801(8)
Bond angles			
N(1)–Sn(1)–N(3)	172.5(2)	Sn(1)–N(1)–N(2)	118.3(4)
O(1)–Sn(1)–O(2)	86.6(2)	S(1)–Sn(1)–S(3)	97.06(8)
O(1)–Sn(1)–N(1)	85.8(2)	S(1)–Sn(1)–N(1)	80.81(17)
O(1)–Sn(1)–N(3)	92.6(2)	S(1)–Sn(1)–N(3)	100.50(16)
O(1)–Sn(1)–S(1)	166.58(14)	S(1)–Sn(1)–O(2)	91.44(15)
O(2)–Sn(1)–N(1)	86.9(2)	S(3)–Sn(1)–N(1)	106.88(16)
O(2)–Sn(1)–N(3)	85.7(2)	S(3)–Sn(1)–N(3)	80.41(17)
O(2)–Sn(1)–S(3)	164.80(15)	S(3)–Sn(1)–O(1)	87.98(15)

atoms and hydrogen atoms were included in the model at their calculated positions and refined isotropically using the SHELXTL program package [17]. Crystal structure data and refinement details for both compounds are summarized in Table 1. Selected bond distances and angles are given in Tables 2 (**H_2L**) and 3 (**VI**).

3. Results and discussion

3.1. Syntheses of ligand and its complexes

Syntheses of ligand and its complexes are shown in Schemes 1 and 2. Reaction of ferrocenoylacetone ($C_5H_5FeC_5H_4C(O)CH_2C(O)CH_3$) and S-benzyldithiocarbazate in refluxing benzene via removal of water affords a new ligand (**H_2L**) as orange-red crystals. The ligand (**H_2L**) reacts with bivalent metal ions forming neutral complexes M(**HL**)$_2$ (**I,** M = Cu; **II,** M = Ni; **III,** M = Mn; **IV,** M = Hg; **V,** M = Zn; **VI,** M = Sn). TLC analysis of **H_2L** shows, that it exists as an equilibrium mixture of two isomers (major orange–red and minor brown spots) in solution. However, it can crystallize in an orange–red isomer. All complexes listed in Section 2 are soluble in polar organic solvents such as DMF, THF and dichloromethane and insoluble in non-polar organic solvents such as benzene, toluene and petroleum ether.

$$2\mathbf{H_2L} + M(OAc)_2 \xrightarrow{\text{Ethanol}} (\mathbf{HL})_2M + 2\mathbf{H}OAc \quad (M = Cu,Ni,Mn,Hg,Zn)$$

$$2\mathbf{H_2L} + SnCl_2 \xrightarrow{\text{Ethanol}} (\mathbf{HL})_2Sn + 2\mathbf{H}Cl$$

Scheme 2. Syntheses of complexes **I**–**VI**.

3.2. ^1H NMR Spectra

The ^{1}H NMR spectral data of ligand (**H_2L**) and complexes **II** and **VI** are listed in Section 2. Although **H_2L** contains the thioamide $NHCS_2$ functional group, in principle, it can exhibit thione–thiol tautomerism. However, its ^{1}H NMR spectrum does not display any signal at approximately 4.00 ppm due to the H–S proton, indicating even in solution it exists as the thione tautomers (iminone A and enaminone B isomers) as shown in Scheme 1 [12], which is in agreement with the above TLC

analysis of $\mathbf{H_2L}$. Two methyl groups of tautomers A and B exhibit two well-resolved singlets at δ 2.18 and 2.07 ppm. According to relative intensities of both singlets, two tautomers A and B exist in a 3:2 ratio in solution at room temperature. For tautomer A, the protons of SCH_2 and $COCH_2C$ moieties display two singlets at δ 3.73 and 3.94 ppm. The substituted cyclopentadienyl ring shows two singlets at δ 4.55 and 4.82 ppm which are due to protons of 3, 4- and 2, 5-positions, whereas a singlet at δ 4.23 ppm is due to protons on the unsubstituted cyclopentadienyl ring. The NH absorption appears at δ 6.54 ppm as a broad peak [11,19]. For tautomer B, the protons of COCH=C moiety displays a singlet at δ 5.73 ppm while the protons of SCH_2 moiety exhibits a typical doublet–doublet quartet ($^2J_{HH} = 18.55$ Hz) [14,18]. The substituted cyclopentadienyl ring shows two singlets at δ 4.68 and 4.78 ppm which are due to protons of 3, 4- and 2, 5-positions, whereas a singlet at δ 4.21 ppm is due to protons on the unsubstituted cyclopentadienyl ring. The $NHCS_2$ (thioamide) and HN (enamine) absorptions appear at δ 9.82 and 11.67 ppm, respectively [14,19]. For both tautomers, benzene rings show three slightly-resolved multiplets at δ 7.22–7.41 ppm.

The ^{1}H NMR spectral data of complexes **II** and **VI** are characterized by the absence of the δ 3.94 ppm signal of $COCH_2C$ in the tautomer A or the δ 11.67 ppm signal of HN (enamine) in the tautomer B and the appearance of the methine (CH) at δ 5.28 and 5.39 ppm in complexes **II** and **VI** [14]. Therefore, the above evidence indicates that the ligand is deprotonated and bonded to the metal ion, which is also supported by the crystal structure of complex **VI** as described below. In addition, all the signals of protons in complex **II** display high-field shifts compared with those in the tautomer B, which may be due to the increase of electron density resulting from deprotonation and nickel-to-ligand feedback after forming the planar–square complex [2,14].

3.3. Crystal structures of ligand and complex VI

3.3.1. Crystal structure of ligand

The crystal structure of the ligand together with the atomic numbering scheme is shown in Fig. 1. The O(1)–C(11) (1.221(4) Å) and N(1)–C(13) (1.271(5) Å) bond distances indicate that these correspond to typical double bonds [20,21], so the ligand in the solid state exists in the form of the tautomeric iminone A. The N(1)–N(2) bond distance is 1.395(4) Å, which is slightly shorter than the single bond distance of 1.411(7) Å [11,21]. The C–S bond distances are 1.749(4) (S(1)–C(14)) and 1.820(4) Å (S(1)–C(15)). Of the two distances, one is close to the C–S distance of 1.81 Å, while the other shows an intermediate value between the single and double bond distances, indicating partial double bond character. The S(2)–C(14) distance (1.667(4) Å) is close to the C=S distance of 1.69 Å, suggesting that this is a

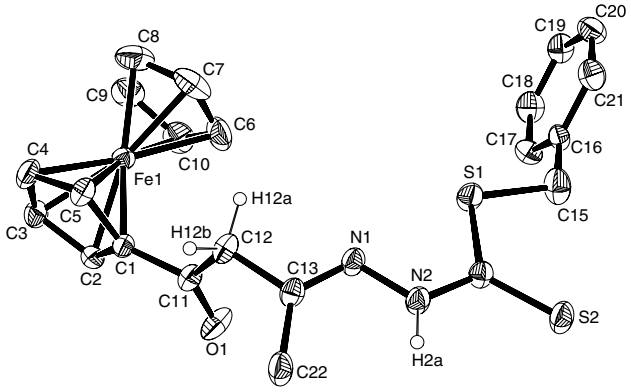

Fig. 1. Crystal structure of ligand.

double bond. Therefore, the above data indicate, that the bonding mode in the $NNCS_2CH_2Ph$ moiety is very similar to that in the S-benzyldithiocarbazate [22]. The average distance of iron to carbon in the ferrocenyl group is 2.042(4) Å and very close to 2.045 Å in ferrocene [23]. The mean C–C distances in the cyclopentadienyl rings with and without the side-chain are 1.422(5) and 1.403(7) Å and also close to 1.41 Å in ferrocene [23]. The distances of N(1)···S(1) (2.756(3) Å) and S(1)···S(2) (3.027 Å) fall in the range of the sum of van der waals radii of the corresponding two atoms (3.35 and 3.6 Å), which indicates that there is a weak interaction between the two atoms. Similarly, the distances of S(2)···H(2A) and S(2)···H(22A) show the existence of N(2)–H(2A)···S(2) and C(22)–H(22A)···S(2) intramolecular hydrogen bondings, whereas the O(1)···H(4) distance displays an O(1)···H(4)–C(4) intermolecular hydrogen bonding [24].

3.3.2. Crystal structure of complex VI

The crystal structure of the new tin complex **VI** together with the atomic numbering scheme is shown in Fig. 2. The complex consists of two monoanionic tridentate ligands ($\mathbf{HL^-}$), each of which coordinates to the Sn(II) ion via carbonyl oxygen, deprotonation enamine

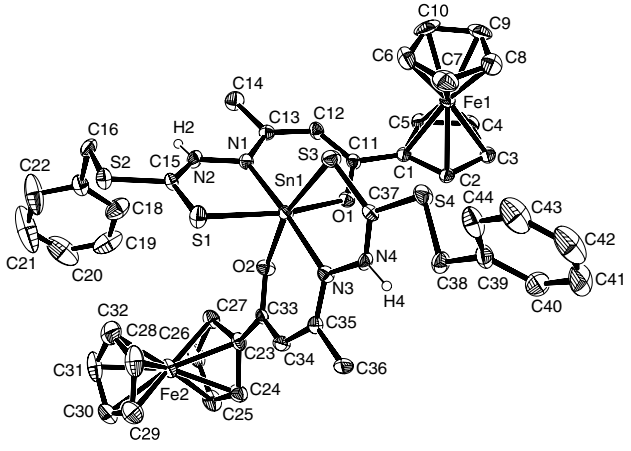

Fig. 2. Crystal structure of complex **VI**.

nitrogen and thione sulfur (ONS donor set), viz., through the deprotonated tautomer B. The coordination geometry of the central metal ion is a distorted octahedron, the bond angle of N(1)–Sn–N(3) being 172.5(2)°. The Sn–S, Sn–O and Sn–N bond distances are larger than values reported for a related complex (2.458(3), 2.396(3) and 2.187(4) Å) [25].

A comparison of the bond distances within the coordinated $\mathbf{HL}^-$ ligands shows extensive delocalization to be present. The N–N bond at mean 1.379(8) Å, which is singnificantly shorter than the single bond distance of 1.411(7) Å, is observed to have some double bond character [12,21]. More double bond character is present in the C–N bond of the $HNCS_2$ moiety as judged from its bond distance of mean 1.271(8) Å. This very clearly indicates a pronounced lone pair delocalization between carbon and nitrogen, namely the p–π conjugation. More interestingly, formal C=S and C–S bonds in the $HNCS_2$ moiety also display marked electron delocalization [12,21]. The C–N bond distances (1.348(8) and 1.333(9) Å) in the $CH{=}C(CH_3)N$ moiety are close to the value of the C–N single bond (1.335(4) Å) of the $HNCS_2$ moiety in the free ligand while the C=O bonds are longer than the corresponding bond in the free ligand [20,21]. In addition, delocalization evidence is further supported by the fact that the hybridized states of C (attached to N and O atoms) and N atoms are all sp^2. Although that the protons of thioamide $NHCS_2$ functional groups are not removed on complexation are unusual, similar cases also appear in two metal complexes of thiosemicarbazone and dithiocarbazate ligands [26,27]. The average distance of iron to carbon (2.026(7) Å) and mean C–C distances with and without side-chains (1.42(1) and 1.39(1) Å) in the ferrocenyl groups are all shorter than those in the free ligand [2]. The distance of N(2)···H(16B) (2.43 Å) indicates that there is the C(16)–H(16B)···N(2) intramolecular hydrogen bonding in complex **VI**. It is more noted that although it contains the NH group no intermolecular hydrogen bonding about the NH group in complex **VI** is observed because of the steric hindrance from the methyl and benzyl groups. However, the S(2)···H(36A) distance (2.85 Å) may display a weak S(2)···H(36A)–C(36) intermolecular hydrogen bonding [24].

3.4. IR spectra

The important IR absorptions of the ligand ($\mathbf{H_2L}$) and its complexes are given in Section 2. The ligand shows bands at ca. 3169, 1665, 1637, 1068, 1035 and 983 cm^{-1} which are assignable to ν(NH), ν(C=O), ν(C=N), ν(C=S), ν(C–S) and ν(N–N), respectively. The ν(C=N) band disappears and new bands at 1513–1622 and 1220–1287 cm^{-1}, which can be assigned to ν(C=C) and ν(C–N), are observed. For complexes **I, II, IV** and **V,** the ν(C=O) band remains nearly unchanged, whereas for complexes **III** and **VI** the corresponding band shows a significant red-shift compared with the free ligand. These facts indicate that the ligand possesses two bonding modes: as an NS bidentate bonded to Cu, Ni, Hg and Zn ions and as an ONS tridentate coordinated to Mn and Sn ions (N, deprotonation enamine nitrogen and S, thione sulfur) [12,14]. The ONS bonding mode has confirmed by the above crystal structure of complex **VI,** however efforts to grow single crystals of complex **I, II, IV** or **V** in order to further support the NS bonding mode were unsuccessful.

3.5. UV spectra

The UV spectral data of the ligand ($\mathbf{H_2L}$) and its complexes are listed in Section 2. The UV spectrum of the ligand shows two absorptions at 405 and 553 nm, which are attributable to the K-band of the skelton $[C(O)CH{=}C(CH_3)N]$ and the R-band ($n \rightarrow \pi^*$ transition) [12,18,21]. For complex **I,** the shortest wavelength absorption which is assigned as the B-band of the benzene and cyclopentadienyl rings. However, complex **V** exhibits two B-bands of the benzene and cyclopentadienyl rings. Interestingly, the K-bands in all complexes show hypsochromic shifts compared with that of the free ligand [2].

4. Summary and conclusions

Reaction of ferrocenoylacetone and S-benzyldithiocarbazate yields a new ligand ($\mathbf{H_2L}$). The ligand exists as a single iminone in the solid state while as a tautomeric mixture of the iminone and enaminone (3:2) in solution.

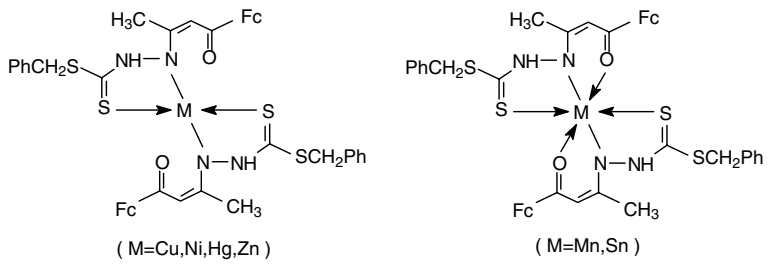

Fig. 3. Proposed structures of complexes.

Upon coordinating to the bivalent metal ion, the ligand exhibits two bonding modes (NS and ONS donor sets). In complexes **I, II, IV** and **V** (**I,** M = Cu; **II,** M = Ni; **IV,** M = Hg; **V,** M = Zn), the ligand acts as a monoanionic bidentate coordinated to the metal ion via the deprotonated enamine nitrogen and thione sulfur atoms (NS donor set) whereas in complexes **III** and **VI** (**III,** M = Mn; **VI,** M = Sn) as a monoanionic tridentate via the carbonyl oxygen, deprotonated enamine nitrogen and thione sulfur atoms (ONS donor set). Suggested structures for new complexes are shown in Fig. 3.

5. Supplementary material

Full crystallographic data (CCDC No. 213725 for ligand and CCDC No. 211558 for complex **VI**) have been deposited at the Cambridge Crystallographic Database Centre and are available on request from the Director, CCDC, 12 Union Road, Cambridge, CB2 1EZ, UK (fax: +44-1223-336033; e-mail: deposit@ccdc.cam.ac.uk or http//www.ccdc.cam.ac.uk).

Acknowledgements

Y.C. Shi thanks the National Nature Science Foundation of China (No. 20175023) and Yangzhou University (No. D0009107) for financial support of this work.

References

[1] Y.M. Temerk, A.A.M. Aly, M.M. Kamal, S.A. Ibrahim, J. Prakt. Chemie 328 (1986) 285.
[2] Y.C. Shi, Q.B. Song, X.L. Wu, Y.X. Ma, Polyhedron 13 (1994) 2101.
[3] Q.B. Song, X.L. Wu, Y.M. Liang, G.S. Huang, Y.X. Ma, Polyhedron 15 (1996) 1303.
[4] D.X. West, M.M. Salberg, G.A. Bain, A.E. Liberta, Transition Met. Chem. 22 (1997) 180.
[5] Z. Huszti, G. Szilayi, E. Kasztreiner, Biochem. Pharmacol. 32 (1983) 627.
[6] D.K. Johnson, T.B. Murphy, N.J. Rose, W.H. Goodwin, L. Pickart, Inorg. Chim. Acta 67 (1982) 259.
[7] N.K. Singh, S.K. Kushawaha, A. Srivastava, A. Sodhi, Synth. React. Inorg. Met.-Org. Chem. 32 (2002) 1743.
[8] E.I. Edwards, R. Epton, G. Marr, J. Organometal. Chem. 85 (1975) C23.
[9] M. Cais, Nature 270 (1977) 534.
[10] K.N. Zelenin, I.P. Bezhan, B.A. Brshov, A.K. Zelenin, Tetrahedron 50 (1994) 11447.
[11] W. Wang, F.L. Zeng, X. Wang, M.Y. Tan, Polyhedron 15 (1996) 1699.
[12] M.T.H. Tarafder, A. Kasbollah, K.A. Crouse, A.M. Ali, B.M. Yamin, H.-K. Fun, Polyhedron 20 (2001) 2363.
[13] C.E. Cain, T.A. Mashburn, C.R. Hauser, J. Org. Chem. 26 (1960) 1030.
[14] Y.C. Shi, H.M. Yang, W.B. Shen, C.G. Yan, X.Y. Hu, Polyhedron 22 (2003) Xref: S0277-5387(03)00608-9.
[15] G.M. Sheldrick, SMART 5.0 and SAINT 4.0 for Windows NT, Area Detector Control and Integration Software, Bruker Analytical X-ray Systems, Inc., Madison, WI, 1998.
[16] G.M. Sheldrick, SADABS Program for Empirical Absorption Correction of Area Detector Data, University of Gottingen, University of Gottingen, Germany, 1996.
[17] G.M. Sheldrick, SHLXTL 5.10 for Windows NT, Structure Determination Software, Bruker Analytical X-ray Systems, Inc., Madison, WI, 1998.
[18] Z.L. Liu, Y.Q. Tu, Synth. React. Inorg. Met.-Org. Chem. 32 (2002) 265.
[19] S. Jayasree, K.K. Aravindakshan, Polyhedron 12 (1993) 1187.
[20] E.W. Ainscough, A.M. Brodie, A.J. Dobbs, J.M. Waters, Inorg. Chim. Acta 267 (1998) 27.
[21] M. Akbar Ali, A.H. Mirza, R.J. Butcher, M.T.H. Tarafder, M.A. Ali, Inorg. Chim. Acta 320 (2001) 1.
[22] S. Shanmuga Sundara Raj, B.M. Yamin, Y.A. Yussof, M.T.H. Tarafder, H.-K. Fun, K.A. Grouse, Acta Cryst. C 56 (2000) 1236.
[23] J.D. Dunitz, L.E. Orgel, A. Rich, Acta Cryst. 9 (1956) 373.
[24] B.E. Douglas, D.H. McDaniel, J.J. Alexander, Concepts and Models of Inorganic Chemistry, Wiley, New York, 1983.
[25] L.J. Tian, B. Zhao, Q.S. Yu, Z.C. Shang, Synth. React. Inorg. Met.-Org. Chem. 32 (2002) 1177.
[26] M.D. Timken, S.R. Wilson, D.N. Hendrickson, Inorg. Chem. 24 (1985) 3450.
[27] Y.C. Shi, J. Coord. Chem., submitted.

Available online at www.sciencedirect.com
SCIENCE DIRECT®
Polyhedron 23 (2004) 575–581
POLYHEDRON
www.elsevier.com/locate/poly

Spectral characterization, X-ray structure and biological investigations of copper(II) ternary complexes of 2-hydroxyacetophenone 4-hydroxybenzoic acid hydrazone and heterocyclic bases

P.B. Sreeja [a], M.R. Prathapachandra Kurup [a,*], Archana Kishore [b], C. Jasmin [b]

[a] Department of Applied Chemistry, Cochin University of Science and Technology, Kochi 682022, India
[b] Department of Biotechnology, Cochin University of Science and Technology, Kochi 682022, India

Received 14 August 2003; accepted 14 October 2003

Abstract

Two new heterocyclic base adducts of copper(II) complexes of the general formula CuLB, where L is the dianion of 2-hydroxyacetophenone 4-hydroxybenzoic acid hydrazone and B is the heterocyclic base, 2,2′-bipyridine (bipy) or 1,10-phenanthroline (phen), have been synthesized and characterized by different physicochemical methods. The molar conductivity measurements in DMF solution indicate the non-electrolyte nature of both complexes. The electronic and IR spectroscopic data indicate that the complexes have square pyramidal geometry with one dibasic tridentate ligand L^{2-} and one bidentate heterocyclic base. The coordination takes place through the deprotonated hydroxyl group, azomethine nitrogen and oxygen from the hydrazide moiety. The magnetic susceptibility values at room temperature are consistent with the spin only value for monomeric copper(II) species. EPR studies of all compounds gave axial spectra. Simulation EPR spectra gave the best values for g and A for each compound. The g values indicate that the unpaired electron resides in the $d_{x^2-y^2}$ orbital. The crystal and molecular structure of CuLphen was determined by the single crystal X-ray diffraction method. Investigations on antimicrobial activities showed that the compounds are moderately active against *Gram negative* bacteria.
© 2003 Elsevier Ltd. All rights reserved.

Keywords: Hydrazones; Copper(II) hydrazonate complexes; 1,10- Phenanthroline; 2,2′-Bipyridine; X-ray single crystal structure; EPR

1. Introduction

The chemical properties of hydrazones have been intensively investigated in several research areas because of their chelating capability and their pharmacological applications. The antibacterial and antifungal properties of bis acyl hydrazone and their complexes with some first transition metal ions was studied and reported by Carcelli et al. [1]. They have noted good activity against *Gram positive* bacteria in vitro for some of the complexes. The copper(II) complex of salicylaldehyde benzoylhydrazone was shown to be a potent inhibitor of DNA synthesis and cell growth. This hydrazone also has mild bacteriostatic activity and a range of analogues has been investigated as potential oral iron chelating drugs for genetic disorders such as thalassemia [2–4]. Intriguingly, the copper(II) complexes were shown to be significantly more potent than the metal free chelate, leading to the suggestion that the metal complex was the biologically active species. Prior to this, the ligand was found to possess mild bacteriostatic activity [5]. Because of the biological interest in these types of chelate systems, several structural studies have been carried out on its copper(II) complexes [6,7] with salicylaldehyde and its analogues. This type of diprotic ligand typically acts as a tridentate planar chelating agent coordinating through the phenolic and amide oxygens and imine nitrogen.

* Corresponding author. Tel.: +91-484-2575804; fax: +91-484-2577595.
E-mail address: mrp@cusat.ac.in (M.R. Prathapachandra Kurup).

0277-5387/$ - see front matter © 2003 Elsevier Ltd. All rights reserved.
doi:10.1016/j.poly.2003.11.005

Acyl hydrazones of salicylaldehyde also display radioprotective properties [8], and a range of acyl hydrazones have been shown to be cytotoxic, the copper(II) complexes again showing enhanced activity.

2. Experimental

2.1. Materials

2-Hydroxyacetophenone (BDH), 4-hydroxybenzoic acid hydrazide (Fluka), 2,2′-bipyridine (S.D. Fine. Chem. Ltd), 1,10-phenanthroline (Merk) and copper(II) chloride dihydrate (BDH) were of Analar grade and used without further purification. All the solvents were dried using standard methods before use.

2.2. Preparation of ligand

4-Hydroxybenzoic acid hydrazide (1 mmol) dissolved in methanol was refluxed with a methanolic solution of 2-hydroxyacetophenone (1 mmol), in the presence of a few drops of glacial acetic acid for 6 h. On cooling the reactant media, crystals of hydrazone were separated out. The compound was recrystallised from methanol and characterized by analytical and different spectral methods (see Fig. 1).

2.3. Preparation of complexes

Mixed ligand complexes CuLB, where L is the dianion of 2-hydroxyacetophenone 4-hydroxybenzoic acid hydrazone and B is the heterocyclic base, 2,2′-bipyridine or 1,10-phenanthroline, were prepared as follows. To a hot ethanolic solution of 1 mmol of the appropriate heterocyclic base, H_2L (0.27 g, 1 mmol) a filtered solution of copper(II) chloride dihydrate (0.2 g, 1 mmol) in ethanol was added. Resultant homogeneous green solution was stirred for 2 h. The green product formed was filtered and washed with hot ethanol, followed by ether, and dried in vacuo over P_4O_{10}. The X-ray quality single crystal of CuLphen was obtained from DMF solution by slow evaporation over a period of 2 weeks.

2.4. Physical measurements and instrumentation

Elemental analyses were carried out using a Heraeus Elemental Analyzer at the Regional Sophisticated Instrumentation Center, Central Drug Research Institute, Lucknow, India. IR spectra, in the range of 4000–400 cm^{-1} were recorded on a Shimadzu DR 8001 series FTIR instrument as KBr pellets at the Regional Sophisticated Instrumentation Center, Central Drug Research Institute, Lucknow, India. Far-IR spectra were recorded in a polyethylene matrix on an IFS 66 V FT-IR spectrometer in the range 500–50 cm^{-1}. Magnetic susceptibility measurements at room temperature were made using a Vibrating Sample Magnetometer at the Indian Institute of Technology, Roorkee, India. EPR spectra were recorded in a Varian E-112 spectrometer at X-band, using TCNE as the standard at the Regional Sophisticated Instrumentation Center, Indian Institute of Technology, Bombay, India. Solid state reflectance was measured using an Ocean Optics, Inc. SD-2000 Fiber Optic Spectrometer.

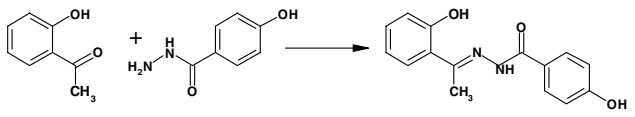

Fig. 1. Scheme of the synthesis of H_2L.

2.5. X-ray data collection, structure solution and refinement

A dark green monoclinic crystal of CuLphen having approximate dimensions $0.275 \times 0.225 \times 0.175$ mm was sealed in a glass capillary, and intensity data were measured at 212 K on an Enraf–Nonius CAD-4 diffractometer equipped with graphite-monochromated Mo Kα ($\lambda = 0.70930$ Å) radiation. The crystallographic data along with details of the structure solution refinements are given in Table 5. Unit cell dimensions were obtained using 25 centered reflections in the θ range 5.54–12.20°. The intensity data were collected by the ω-scan mode within $1.75° < \theta < 24.92°$ for *hkl* ($0 \leqslant h \leqslant 10, 0 \leqslant k \leqslant 18, -21 \leqslant l \leqslant 21$) in the monoclinic system. The trial structure was obtained by direct methods using SHELXS-97 [9], and refinement by full matrix least square on F_2 (SHELXL-97) [10]. The non-hydrogen atoms were refined with anisotropic thermal parameters. All hydrogen atoms were geometrically fixed and allowed to refine using a riding model. Absorption corrections were employed using ψ-scan ($T_{max} = 1.000$ and $T_{min} = 0.982$).

3. Results and discussion

The ^1H NMR spectrum of H_2L shows four singlets corresponding to $-^1OH$, –NH, $-^2OH$ and $-CH_3$ (see Fig. 2). The singlet at $\delta = 13.3$ ppm and $\delta = 11.1$ ppm represent $-^1OH$ and $-^3NH$, respectively. The signal for $-^1OH$ is obtained downfield due to the possibility of the formation of intramolecular hydrogen bonding with the azomethine nitrogen. Upon addition of D_2O the intensities of both OH and NH protons significantly decrease. This supports the assignment. The peak at $\delta = 10.2$ ppm is assigned to the $-^2OH$ which is also an exchangeable proton. Another singlet is at $\delta = 2.5$ ppm which represents the aliphatic $-CH_3$. The aromatic protons appear as multiplets at 6.9–7.9 ppm.

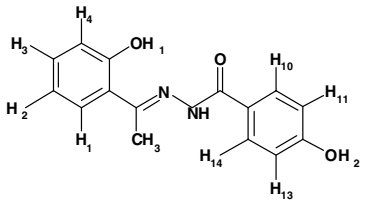

Fig. 2. Formula of H_2L.

The colors, elemental analyses, stoichiometries of H_2L and its complexes are presented in Table 1. The elemental analyses data are consistent with a 1:1:1 ratio of the metal ion:hydrazone:heterocyclic base for the complexes prepared. The complexes are insoluble in most common polar and non-polar solvents. They are soluble in DMF and DMSO. The conductivity measurements in DMF showed that the complexes are non-electrolytes.

The magnetic moment in the polycrystalline state at 300 K of the complexes were found to be 1.85–1.93 BM, which are consistent with the spin only values for mononuclear d^9 copper(II) systems [11].

3.1. EPR spectra

The EPR parameters obtained for the complexes in frozen DMF solution are presented in Table 2.

The EPR spectra of the Cu(II) complexes in frozen DMF solution (77 K) gave axial spectra (see Fig. 4). The spectra of the complexes consist of four well defined hyperfine lines due to copper nuclei in the parallel region. However, for CuLphen the four line hyperfine splitting due to the copper nucleus is observed in the perpendicular region also. The super hyperfine splitting due to coordinated nitrogen is not visible for both the complexes. The $g_{\|} > g_{\perp}$ value suggest a distorted square pyramidal structure and rules out the possibility of a trigonal bipyramidal structure which would be expected to have $g_{\perp} > g_{\|}$. Thus, the polyhedron consists of one phenanthroline/bipyridine nitrogen, azomethine nitrogen, phenolate oxygen and enolate oxygen of hydrazone which form the base of the pyramid, and the remaining nitrogen of the heterocyclic base occupies the apical position of the square pyramid [12,13]. EPR spectra are simulated to get accurate values of various magnetic parameters. The energies of d–d transitions were used to evaluate the bonding parameters α^2, β^2 and γ^2 which

Table 2
EPR and bonding parameters of copper(II) complexes

	CuLphen	CuLbipy
$g_{\|}$	2.2402	2.2194
$g_{\perp}$	2.0586	2.0481
$g_{av/iso}$	2.1193	2.1052
$A_{\|}$ (cm^{-1})	186.2×10^{-4}	175.1×10^{-4}
$A_{\perp}$ (cm^{-1})	13.6×10^{-4}	13.5×10^{-4}
$A_{av/iso}$ (cm^{-1})	68.1×10^{-4}	64.9×10^{-4}
G	4.09	4.562
α^2	0.818	0.764
β^2	0.936	0.955
γ^2	0.911	0.882
K_0	0.313	0.297
$K_{\|}$	0.767	0.731
$K_{\perp}$	0.74	0.674
f (cm)	120.24	126.70

may be regarded as measures of covalency of in-plane σ bonds, in-plane π bonds and out-of-plane π bonds, respectively (see Fig. 3).

The geometric parameter, $G = (g_{\|} - 2/g_{\perp} - 2)$, for axial spectra measures the exchange interaction between copper(II) centers in the polycrystalline state. If $G > 4.0$, the exchange interaction is negligible and if it is less than 4.0 considerable exchange interaction is indicated. In this complex $G = 4.09$ to 4.56 indicating the exchange interaction is negligible. The observed g values in the complex lie above 2.040 with $G > 4.0$, which are consistent with a $d_{x^2-y^2}$ ground state and with square base pyramidal stereochemistry [14,15]. The relatively high

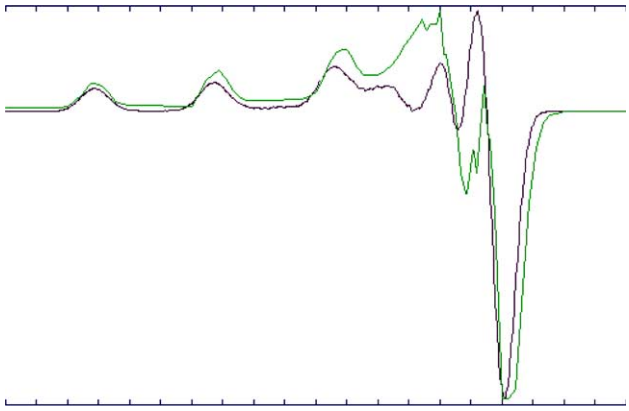

Fig. 3. Simulated best fits of CuLphen (simulated – pink and experimental –green).

Table 1
Colors, elemental analyses and magnetic susceptibilities of the copper(II) complexes

Compound	Formulae	Color	Found (Calc.) (%)			μ_{eff} (BM)
			C	H	N	
H_2L	$C_{15}H_{14}N_2O_3$	yellow	66.70 (66.66)	5.26 (5.22)	10.43 (10.36)	
CuLbip	$CuC_{25}H_{20}N_4O_3$	green	61.92 (61.53)	3.98 (4.13)	11.59 (11.48)	1.85
CuLphen	$CuC_{27}H_{20}N_4O_3$	green	62.87 (63.34)	4.04 (3.94)	10.86 (10.94)	1.93

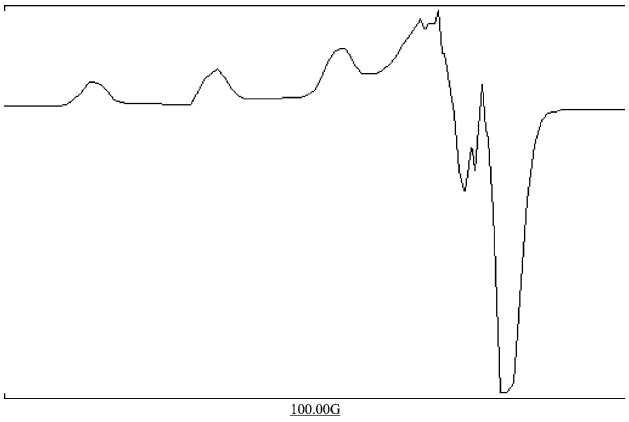

Fig. 4. Solution EPR spectra of CuLphen at 77 K.

values of $A_{\parallel}$ ($>150 \times 10^{-4}$ cm^{-1}) suggests small axial interaction [16].

The value of the in-plane π bonding parameter α^2 can be estimated from the expression and is found to be ~0.78:

$$\alpha^2 = -A_{\parallel}/0.036 + (g_{\parallel} - 2.0023) + 3/7(g_{\perp} - 2.0023) + 0.04.$$

The orbital reduction factors $K_{\parallel} = \alpha^2\beta^2$ and $K_{\perp} = \alpha^2\gamma^2$ were calculated using the following expressions:

$$K_{\parallel}^2 = (g_{\parallel} - 2.0023)\Delta E(d_{xy} \rightarrow d_{x^2-y^2})/8\lambda_0,$$

$$K_{\perp}^2 = (g_{\perp} - 2.0023)\Delta E(d_{xz,yz} \rightarrow d_{x^2-y^2})/2\lambda_0,$$

where λ_0 is the spin–orbit coupling constant and is of the value −828 cm^{-1} for a copper(II) d^9 system.

According to Hathaway for pure σ bonding $K_{\parallel} \approx K_{\perp} \approx 0.75$, for in-plane π bonding $K_{\parallel} < K_{\perp}$, while for out-of-plane π bonding $K_{\parallel} > K_{\perp}$. In this complex, $K_{\parallel} > K_{\perp}$ indicates stronger out-of-plane π bonding. The metal–ligand in-plane σ bond is purely ionic if α^2 is unity. The trend of the β^2 value is opposite to that observed for α^2, indicating the competitive mechanism of in-plane σ and π bonding. The value of γ^2 shows there is appreciable out-of-plane π bonding, which is further supported by $K_{\parallel} > K_{\perp}$.

The Fermi contact hyperfine interaction term, which is the measure of contribution of the s electron to the hyperfine interaction, can be estimated from the expression:

$$K_0 = A_{iso}/P\beta^2 + (g_{av} - 2.0023)/\beta^2,$$

where P is the free ion dipolar term and its value is 0.036. K_0 is a dimensionless quantity and is generally found to have a value of 0.30. The K_0 value obtained is in good agreement with the theoretical one, indicating the mixing of the 4s orbital with the d orbital possessing an unpaired electron.

The empirical factor $f = g_{\parallel}/A_{\parallel}$ is an index of tetragonal distortion, and is calculated as 120.24 cm for CuLphen and 126.70 cm for CuLbipy. The value may vary from 105 to 135 for small to extreme distortion. The f values for the compounds indicate a medium distortion from the square pyramidal geometry. The greater tetrahedral distortion may be due to the flexible structure or the in vivo environment in which the complex is located in the solvent system. Recent studies have shown that the biological activity is related to the geometry at the metal site in terms of SOD like activity. The compounds with more tetrahedral distortion are reported to display higher activity [17–19].

3.2. Electronic spectra

The significant electronic absorption bands in the spectra of the complexes recorded in the solid state are presented in Table 3. The hydrazone ligands have $\pi \rightarrow \pi^*$ at 42 553 and $n \rightarrow \pi^*$ at 31 746 cm^{-1}. A second $n \rightarrow \pi^*$ band is found at 27 778 cm^{-1}. There is a slight shift in these bands during complexation. The charge transfer maxima range from 21 978 to 28 736 cm^{-1} for the complexes and may be assigned to an $O \rightarrow Cu$ charge transfer transition, LMCT [20]. The d–d absorption maxima range from 16 394 to 11 560 cm^{-1} and tend to be indicative of tetragonal geometries [21,22].

3.3. IR spectra

The tentative assignment of H_2L, CuLphen and CuLbipy are presented in Table 4. The peak at 1610 cm^{-1} corresponding to ν(C=N) in the IR spectrum of uncomplexed hydrazone shifts to ~1592 cm^{-1} upon complexation indicating azomethine nitrogen coordination [12,13,23]. Further proof for the complexation for azomethine nitrogen is obtained from the appearance of a new band ~423 cm^{-1} which is assignable for the ν(Cu–N) for the complexes. The increase in ν(N–N) in the spectra of the complexes from 1001 to ~1020 cm^{-1}, is due to the increase in the double bond character offsetting the loss of electron density via donation to metal and is a further confirmation of coordination of the ligand through the azomethine atom. The spectral band of ν(N–

Table 3
Electronic spectral assignments (cm^{-1})

Compound	d → d	LMCT	n → π*	π → π*
H_2L			31 746 27 778	42 553
CuLphen	18 149 16 393 14 066	21 978	30 675 28 248	42 545
CuLbipy	16 394 15 385 13 889	22 875	31 746 28 736	36 364

Table 4
Selected IR frequencies of H_2L and CuLphen (cm^{-1})

Compound	C=N	N=C	Cu–N	Cu–N (heterocyclic base)	N–N	Heterocyclic breathing	Cu–O	C–O
H_2L	1610				1001			1279
CuLPhen	1593	1499	423	419, 304	1018	1430, 727	400	1243
CuLBip	1598	1503	420	422, 310	1022	1432, 861	391	1237

H) of hydrazone disappears in the complexes indicating the deprotonation of the N–H proton and coordination via the enol oxygen. The IR spectra show a sharp band at ~1500 cm^{-1} which indicates the newly formed uncomplexed N=C by enolisation, confirming the coordination of hydrazone takes place in the form of the enol rather than the keto form. The loss of the OH proton is indicated by the absence of a band at ~3400 cm^{-1} in the complexes. The ν(C–O) also decrease from 1279 to ~1240 cm^{-1} when compared to the uncomplexed ligand. The fourth and fifth positions are occupy by the nitrogen atoms of the heterocyclic bases, these ν(Cu–N) bands are assigned to the 400–291 cm^{-1} region, indicated by the heterocyclic ring breathing in the fingerprint region of 1400–600 cm^{-1}. The second OH group in the aromatic ring remains uncomplexed indicated by a band at ~3057 cm^{-1} in the complexes (see Fig. 5).

3.4. Crystal structure of CuLphen

The molecular structure of the complex along with selected bond angles and bond lengths are summarized in Tables 5 and 6. The compound crystallized in a monoclinic lattice with a space group $P2_1/c$. The unit cell volume contains four molecules. The copper in the

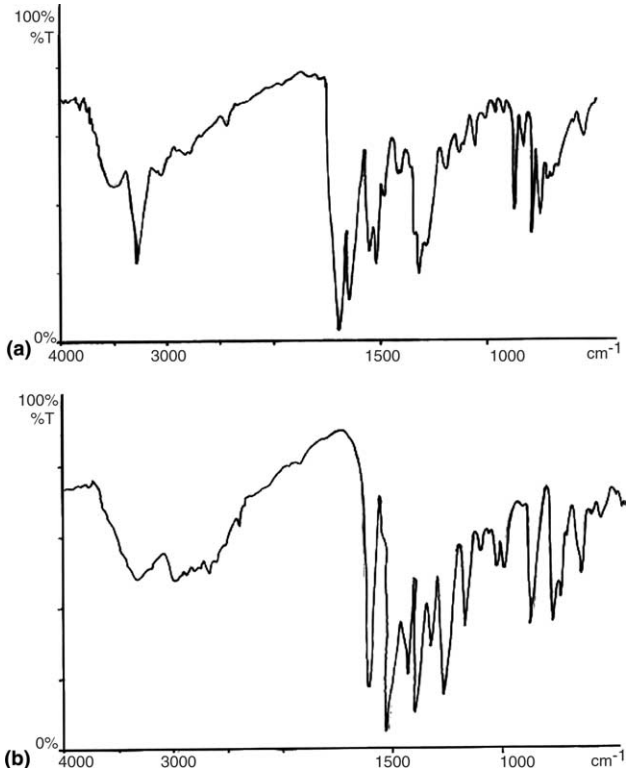

Fig. 5. IR spectra of H_2L (a) and CuLphen (b) (cm^{-1}).

Table 5
Crystal data and structure refinement for CuLphen

Empirical formula	$C_{27}H_{20}CuN_4O_3$
Formula weight	512.01
Temperature (K)	212(2)
Wavelength (Å)	0.70930
Crystal system	monoclinic
Space group	$P2_1/c$
Unit cell dimensions	
a (Å)	8.4240(9)
b (Å)	15.4330(14)
c (Å)	17.8140(11)
α (Å)	90.000(7)
β (Å)	95.190(7)
γ (Å)	90.000(8)
Volume (Å ^{3})	2306.5(4)
Z, Calculated density (Mg/m^3)	4, 1.474
Absorption coefficient (mm^{-1})	0.985
$F(000)$	1052
Crystal size (mm)	$0.275 \times 0.225 \times 0.175$
θ range for data collection (°)	1.75 to 24.92
Index range	$0 \leqslant h \leqslant 10, 0 \leqslant k \leqslant 18, -21 \leqslant l \leqslant 21$
Reflections collected/unique	3139/3139 [$R_{int} = 0.0000$]
Completeness to 2θ	24.92 (74.8%)
Absorption correction	ψ-scan
Maximum and minimum transmission	1.000 and 0.982
Refinement method	full-matrix least-squares on F^2
Data/restraints/parameters	3139/0/396
Goodness-of-fit on F	1.050
Final R indices [$I > 2\sigma(I)$]	$R_1 = 0.0410$, $wR_2 = 0.0882$
R indices (all data)	$R_1 = 0.0628$, $wR_2 = 0.0985$
Largest difference peak and hole (e A^{-3})	0.383 and −0.276

Table 6
Selected bond lengths (Å) and bond angles (°) for the compound CuLphen

Cu(1)–O(1)	1.926(3)	O(1)–Cu(1)–N(3)	91.90(13)
Cu(1)–N(3)	1.938(3)	O(1)–Cu(1)–O(2)	162.76(12)
Cu(1)–O(2)	1.954(3)	N(3)–Cu(1)–O(2)	82.39(13)
Cu(1)–N(1)	2.047(3)	O(1)–Cu(1)–N(1)	91.63(12)
Cu(1)–N(2)	2.241(3)	N(3)–Cu(1)–N(1)	176.31(14)
		O(2)–Cu(1)–N(1)	93.92(11)
		O(1)–Cu(1)–N(2)	101.34(12)
		N(3)–Cu(1)–N(2)	102.55(12)
		O(2)–Cu(1)–N(2)	95.79(12)
		N(1)–Cu(1)–N(2)	77.81(12)
		C(13)–O(1)–Cu(1)	124.3(3)
		C(21)–O(2)–Cu(1)	108.5(3)

mononuclear complex is five coordinate and has approximate square pyramidal geometry. The basal coordination positions (see Fig. 6) are occupied by the phenolato oxygen O(1), azomethine nitrogen N(3), enolate oxygen O(2) of the hydrazone, and phen nitrogen N(1). The apical position occupied by the second nitrogen of phen N(2) is at a larger distance than compared to N(1). The four basal atoms are coplanar showing a significant distortion from square geometry indicated by the O(1)–Cu(1)–O(2) bond angle. The central copper atom is displaced from the basal plane in the direction of the axial nitrogen, which is evident from the bond angles of N(1)–Cu(1)–N(3) and O(1)–Cu(1)–N(3). The bond angles O(1)–Cu(1)–N(2), N(1)–Cu(1)–N(2) and N(3)–Cu(1)–N2 indicate the distortion from the perfect square pyramidal geometry. One of the reasons for the deviation from an ideal stereochemistry is the restricted bite angle imposed by both the L and phen ligands. The O(1)–Cu(1)–N(2) bond angle is 101.34° and the O(2)–Cu(1)–N(2) bond angle is 95.79° indicating a slight tilting of the axial Cu(1)–N(2) bond in the direction of the O(2)–Cu(1) bond, away from the O(1)–Cu(1) bond. The variation in Cu(1)–N(1), Cu(1)–N(2), and Cu(1)–N(3) bond lengths indicate the different strength of the bond formed by each of the coordination nitrogen atoms. The difference in bond lengths can be attributed the difference in extent of π back donating between the phen and hydrazone moieties [13]. The packing of the complex is stabilized by intermolecular hydrogen bonding interactions and C–H π interaction between the atoms (see Fig. 7). The H-bonding parameters are listed in Tables 7 and 8.

3.5. Biological activities

The synthesized chemical ligands and complexes were tested for their antimicrobial activity. The antimicrobial agent may be either bacteriostatic or bactericidal. The effectiveness of an antimicrobial agent in sensitivity testing is based on the size of the zones of inhibition when the test substances are introduced onto a lawn of bacterial culture by the disc diffusion method.

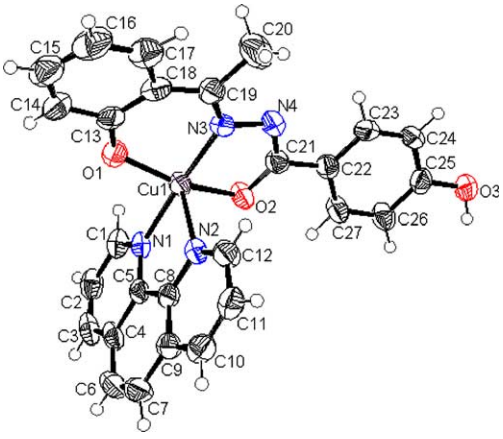

Fig. 6. A view of the compound CuLphen with the atom numbering scheme. Displacement ellipsoids are drawn at the 50% probability level and hydrogen atoms are shown as small spheres of arbitrary radii.

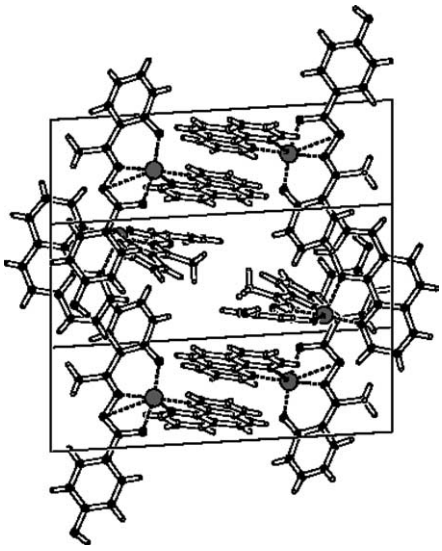

Fig. 7. Packing diagram for the compound CuLPhen.

Table 7
π–π interaction

D–A	Cg–Cg (Å)	α (°)	β (°)
Cg(6)–Cg(6)[1]	3.6243	0	25.48
Cg(6)–Cg(8)[1]	3.5232	1.6	23.02
Cg(7)–Cg(8)[2]	3.5479	2.12	19.89
Cg(8)–Cg(8)[2]	3.7596	0	28.18

1: $1-x,-y,1-z$ and 2: $2-x,-y,1-z$.

3.5.1. Test organisms

The microorganisms used as test organisms were bacteria isolated from clinical samples. Two Gram positive bacteria and three Gram negative bacteria were used as test organisms.

(A) Gram positive	(B) Gram negative
1. *Staphylococcus aureus*	3. *Escherichia coli*
2. *Bacillus* sp.	4. *Salmonella paratyphi*
	5. *Vibrio cholerae O1*

The disc diffusion method was used for screening for the antimicrobial property of the test samples.

The free ligand showed no or little activity against both the Gram positive and Gram negative bacteria. CuLbipy was found to be active against Gram positive *Bacillus* sp. and active against Gram negative *V. cholerae O1*. CuLphen is found to be active against *S. aureus*. The results of the antimicrobial studies are given in Table 9.

Table 8
C–H···π interactions

X–H···Cg	H–Cg (Å)	∠X–H–Cg (°)	X–Cg (Å)
C(3)–H(3)–Cg(4)[2]	3.257	101.54	3.5370
C(15)–H(15)–Cg(10)[3]	3.120	177.88	4.0012
C(20)–H(20)–Cg(10)[4]	3.245	160.89	4.1621
Cg(6)	N(1)C(1)C(2)C(3)C(4)C(5)	1: $1-x,-y,1-z$	
Cg(7)	N(2)C(8)C(9)C(C(11)C(12)	2: $2-x,-y,1-z$	
Cg(8)	C(4)C(5)C(8)C(9)C(7)C(6)	3: $1-x,1/2+y,1/2-z$	
Cg	(10)C(22)C(23)C(24) C(25)C(26)C(27)	4: $-1+x,y,z$	

Table 9
The antimicrobial activities of H_2L and the complexes

Compound	Microbial activity inhibition zone				
	Bacillus sp.	*Vibrio cholerae O1*	*Escherichia coli*	*Staphylococcus aureus*	*Salmonella paratyphi*
H_2L					
CuLbipy	+9 mm	+11 mm		−8 mm	−8 mm
CuLphen	−8 mm	+10 mm		+9 mm	

4. Supplementary data

Crystallographic data for the structural analysis has been deposited with the Cambridge Crystallographic Data Center, CCDC 216912 for compound CuLphen. Copies of the information may be obtained free of charge from the director, CCDC, 12 Union Road, Cambridge, CB2, IEZ, UK, (fax: +44-1223-336-033; E-mail: deposit@ccdc.cam.ac.uk or http://www.ccdc.cam.ac.uk).

Acknowledgements

One of the authors S.P.B. is thankful to Cochin University of Science and Technology, Kochi 22, India, for the financial assistance in the form of a Junior Research Fellowship. The authors are thankful to Professor P. Mathur, National Single X-ray Diffraction Facility, IIT, Mumbai, India for X-ray crystallographic data, sophisticated instruments facility, Indian institute of science, Bangalore, India for NMR data and Regional Sophisticated Instrumentation Center, Central Drug Research Institute, Lucknow for elemental analysis and M.R.P.K is thankful to STED, Government of Kerala, India for financial support.

References

[1] M. Carcelli, P. Mazza, C. Pelizzi, G. Pelizzi, Zani, J. Inorg. Biochem. 57 (1995) 43.
[2] D.K. Johnson, T.B. Murphy, N.J. Rose, W.H. Goodwin, L. Pickart, Inorg. Chim. Acta 67 (1982) 159.
[3] J.D Ranford, J.J. Vittal, Yu.M. Wang, Inorg. Chem. 37 (1998) 1226.
[4] L. Pickart, W.H. Goodwin, W. Burgua, T.B. Murphy, D.K. Johnson, Biochem. Pharmacol. 32 (1983) 3868.
[5] H.A. Offe, W. Siefken, G. Domagk, Naturforsch 7B (1952) 462.
[6] E.W. Ainscough, A.M. Brodie, A.J. Dobbs, J.D. Ranford, Inorg. Chim. Acta 267 (1998) 27.
[7] C. Chan, L.L. Koh, P-H. Leung, J.D. Ranford, K.Y. Sim, Inorg. Chim. Acta 236 (1995) 101.
[8] O.V. Arapov, O.F. Alferva, E.I. Levocheskaya, I. Krasil'nikov, Radiobiologiya 27 (1987) 843.
[9] G.M. Sheldrick, SHELXS-97, Program for Solution of Crystal Structures, University of Göttingen, Germany, 1997.
[10] G.M. Sheldrick, SHELXL-97, Program for Solution of Crystal Structures, University of Göttingen, Germany, 1997.
[11] F.A. Cotton, G. Wilkinson, C.A. Murillo, M. Bochmann, Advanced Inorganic Chemistry, 6th Ed., Wiley, New York, 1999, p. 867.
[12] P. Bindu, M.R.P. Kurup, T.R. Satyakeerthy, Polyhedron 18 (1999) 321.
[13] R.P. John, A. Sreekanth, M.R.P. Kurup, Anwar Usman, Abdul Razak Ibrahim, H.K. Fun, Spectrochim. Acta, Part A 59 (2003) 1349.
[14] B.J. Hathaway, A.A.G. Tomlison, Coord. Chem. Rev. 5 (1970) 1.
[15] C.R.K. Rao, P.S. Zacharias, Polyhedron 16 (1997) 1201.
[16] B.S. Garg, M.R.P. Kurup, S.K. Jain, Y.K. Bhoon, Trans. Met. Chem. 13 (1988) 309.
[17] A. Diaz, R. Pogni, R. Cao, R. Basosi, Inorg. Chim. Acta 275–276 (1998) 552.
[18] W.A. Alves, I.A. Bagatin, Ana Maria Da Costa Ferreira, Inorg. Chim. Acta 321 (2001) 11.
[19] U. Sakaguchi, A.W. Addison, J. Chem. Soc., Dalton Trans. (1979) 600.
[20] M. Mikuriya, H. Okawa, S. Kida, Bull. Chem. Soc. Jpn. 53 (1980) 3717.
[21] A.B.P Lever, Inorganic Electronic Spectroscopy, Elsevier, Amsterdam, 1968.
[22] E.W. Ainscough, A.M. Brodie, A.J. Dobbs, J.D. Ranford, Inorg. Chim. Acta 267 (1998) 27.
[23] P. Bindu, M.R.P. Kurup, Trans. Met. Chem. 22 (1997) 578.

Available online at www.sciencedirect.com
SCIENCE DIRECT®
Polyhedron 23 (2004) 583–588
POLYHEDRON
www.elsevier.com/locate/poly

Kinetics and mechanism of reduction of 3,9-diethyl-4,8-diaza-3,8-undeca-2,10-dionedioximatocopper(III) complex by *p*-methoxyphenol, 1,2-dihydroxybenzene, 1,4-dihydroxybenzene and some of its derivatives in aqueous acidic solutions ☆

Yousif Sulfab [a,*], Fawziyah M. Al-Sogair [b]

[a] *Department of Chemistry, University of Qatar, P.O. Box 2713, Doha, Qatar*
[b] *Department of Chemistry, Faculty of Medicine, King Faisal University, Dammam, Saudi Arabia*

Received 19 June 2003; accepted 21 October 2003

Abstract

The kinetics of the reduction a copper(III)–imine–oxime complex $[Cu^{III}L]^+$ ($H_2L = 3,9$-diethyl-4,8-diaza-3,8-undecadiene-2,10-dione dioxime) by catechol (H_2Cat), *p*-methoxyphenol (*p*MHP), hydroquinone (H_2Q), 2-methylhydroquinone (MH_2Q), and 2-chlorohydroquinone (ClH_2Q), have been studied in aqueous acidic solutions. The rate law showed a first order dependence on both the oxidant and the reductant. The second-order rate constant, k_2, for H_2Q, MH_2Q and *p*MHP decreased with increasing pH over the entire range studied. Both H_2Cat and ClH_2Q showed complex behavior, and in theses cases k_2 decreases then increases with increasing pH. The complex pH dependence is interpreted in terms of the involvement of protonated and deprotonated reactants in the rate determining step. In the case of H_2Cat not only one, but two protons are lost from the diol in the rate-determining step in the high pH range. It is very unlikely that the doubly deprotonated species Cat^{2-} is formed to an appreciable extent at pH < 5 ($pK_{a2} = 13$). It was therefore necessary to invoke an interaction between $[Cu^{III}L]^+$ and $HCat^-$ in which the high charge on Cu^{III} facilitates the loss of the second proton. It seems that the proximity of the OH in the ortho position is important as none of the other diols showed an inverse second-order dependence on $[H^+]$. The oxidation of deprotonated H_2Cat is believed to proceed by an inner-sphere mechanism. Observed rate constants for the pathway showing a first-order dependence on $[H^+]$ correlate well with those calculated from the Marcus equation.
© 2003 Elsevier Ltd. All rights reserved.

Keywords: Copper(III); Imine-oxime ligand; Diols; Kinetics; Mechanism; Electron transfer

1. Introduction

The oxidation of 1,2- and 1,4-dihydroxybenzene and their derivatives has been the subject of many reports. These compounds are well characterized as two-electron reducing agents and are important in biological transport systems [1]. The availability of varying substituent groups on the benzene ring provides a wide range of reduction potentials [2]. This has facilitated the examination of Marcus theory [3] for outer-sphere electron transfer over several orders of magnitude of rate constants. Outer-sphere electron transfer mechanisms were proposed in the reduction of the substitution inert complexes $[Fe^{III}(NN)_3]^{3+}$ (NN = 1,10-phenanthroline or 2,2′-bipyridine), $[Ir^{IV}Cl_6]^{2-}$, $[Co^{III}(H_2O)_6]^{3+}$, $[Mo^{V}(CN)_8]^{3-}$, $[Fe(CN)_6]^{3-}$, $[Ni^{III}cyclam]^{3+}$ (cyclam = 1,4,8,11-tetraazacyclotetradecane) and $[Ni^{IV}N_6]^{2+}$ (N_6 = 3,14,-dimethyl-4,7,10,13-tetraazahexadeca-3,13-diene-2,15-dione dioxime) [4–9]. The aqua metal ions Fe^{III}, Mn^{III}, and Tl^{III}, were also used to oxidize 1,2- and 1,4-dihydroxybenzene and their derivatives [10–13]. A number of kinetic studies involving monomeric and mixed-valent manganese complexes have

☆ Abstracted from the Ph.D. thesis of F.M.A.
* Corresponding author. Fax: +794-485-1049.
E-mail address: yousifsulfab@yahoo.com (Y. Sulfab).

0277-5387/$ - see front matter © 2003 Elsevier Ltd. All rights reserved.
doi:10.1016/j.poly.2003.10.011

been reported using H_2Q and H_2Cat [14–16]. Both outer- and inner-sphere mechanisms seem to be operative depending on the nature of the oxidant. It was not always possible to assign definitively either an outer- or an inner-sphere mechanism for some of the systems despite the fact that linear free energy relationships were obtained between $\Delta G^{\#}$ and ΔG^0. Marcus theory for outer-sphere electron transfer was reported to be applicable to weak inner-sphere electron transfer as well as for hydrogen atom transfer reactions [17,18].

Margerum and coworkers initially proposed that Cu^{III}–peptide complexes undergo electron transfer via an outer-sphere mechanism [19]. Applying Marcus's theory for outer-sphere electron transfer, the self-exchange rate constant for $Cu^{III/II}$–peptide couples was estimated as 7×10^7 M^{-1} s^{-1}. Direct measurement of the self-exchange rate constant of $Cu^{III/II}$–peptide couples using ^1H NMR broadening gave a value of $\sim 5.5 \times 10^5$ M^{-1} s^{-1}, which is below that calculated using the Marcus theory by about two orders of magnitude. It was, therefore, concluded that in reactions where a bridging ligand is available, as in the cases of $[Ir^{III}Cl_6]^{3-}$ and $[Fe^{II}(CN)_6]^{4-}$, electron transfer proceeds via a weak inner-sphere pathway [20,21].

We have previously reported that Cu^{III} is stabilized by tetradentate imine–oxime ligands [22].

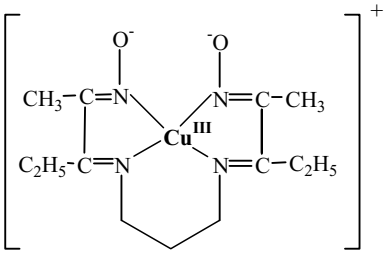

(I)

In this work we report the results of the kinetic study of the reduction of Cu^{III}–imine–oxime complex (**I**) by 1,2-dihydroxybenzene (H_2Cat), 1,4-dihydroxybenzene (H_2Q), 2-chloro-1,4-dihydroxybenzene (ClH_2Q), 2-methy-1,4-dihydroxybenzene (MH_2Q) and *p*MHP in weakly acidic solutions.

Cyclic voltammetry has shown that complex (**I**) undergoes a reversible one-electron transfer according to Eq. (1).

$$[Cu^{III}L]^+ + H^+ + e \rightleftharpoons [Cu^{II}HL]^+ \quad (1)$$

The reduction potential E^0 obtained from a linear plot of E against pH was found to be 1.16 V at 25 °C (versus n.h.e., normal hydrogen electrode). The reduction potential E^0 of (**I**) in the region where E is independent of pH (Eq. (2)) was determined as 0.51 V [22].

$$[Cu^{III}L]^+ + e \rightleftharpoons [Cu^{II}L] \quad (2)$$

2. Experimental

2.1. Materials

The syntheses of the imine–oxime ligand and Cu^{II}–imine–oxime complex have been reported previously [22]. Stock solutions of the Cu^{II} complexes were prepared by weight. The Cu^{III} complex was generated by chemical oxidation of buffered solutions of the Cu^{II} complex by PbO_2 immediately before each kinetic run. 1,2-Dihydroxybenzene (BDH) was recrystallized from toluene and washed with ether. 1,4-Dihydroxybenzene (BDH), and 2-methy-1,4-dihydroxybenzene (Aldrich Gold label) were used as received. 2-Chloro-1,4-dihydroxybenzene (BDH) and *p*MHP were recrystallized from petroleum ether. Stock solutions of the reductants were prepared by weight in oxygen-free distilled water and were used in the same day. Buffer solutions were prepared using $CH_3CO_2H/NaCH_3CO_2$ or $HNO_3/NaCH_3CO_2$. The ionic strength was maintained at 0.10 M using $NaNO_3$. The concentration of the $CH_3CO_2^-$ ion was always maintained at 0.01 M. The UV–Vis absorption spectrum of the Cu^{III} complex showed no noticeable change when recorded using 0.09 M $NaNO_3$ and 0.01 M acetate buffer; the typical concentrations used in maintaining ionic strength. The pH of the reaction mixture was measured using a Radiometer digital pH meter Model PHM 62.

The stoichiometry of each reaction was determined spectrophotometrically by the addition, at pH 4.60, of known amounts of the reductant to excess Cu^{III}. The unreacted Cu^{III} was then determined spectrophotometrically. Kinetic measurements were carried out under pseudo-first order conditions with the reductant concentrations being at least $\geqslant$10-fold excess over that of the Cu^{III} complex. The reactions were followed by monitoring the disappearance of Cu^{III} at λ_{max} (518 nm) using a thermostated Hi-Tech stopped-flow spectrophotometer Model SF.3L. The signal and trigger pulse from the stopped-flow were fed into a DL-901 transient recorder, where the information was stored in the memory in digital form and displayed continuously on an oscilloscope. The transient recorder was interfaced with a Hewlett–Packard 9825 B desktop calculator that was used to analyze the absorbance data. At all pH values, plots of $\ln(A_t - A_\infty)$ against time were linear for at least three half-lives.

3. Results and discussion

The stoichiometry of the reduction the Cu^{III}–imine-oxime complex (**I**), by each of the four benzene diols and *p*-methoxyphenol, in mildly acidic solutions indicates that 1.95 ± 0.06 mol of each Cu^{III} is consumed by 1 mol of the reductant. This is consistent with the reduction of

Cu^{III} complex to the corresponding Cu^{II}–imine–oxime complex and the formation of the dehydro-derivatives of the diols and *p*-methoxyphenol. The formation of the product quinones was confirmed spectrophotometrically. The overall reactions may be represented by Eq. (3) where H_2A represents any of the reductants and A the corresponding quinone.

$$2[Cu^{III}L]^+ + H_2A \rightarrow 2[Cu^{II}HL]^+ + A \quad (3)$$

Pseudo-first order plots, using excess of reductant, were linear to beyond three half-lives. The magnitudes of the pseudo-first order rate constants at fixed pH, ionic strength and temperature, are independent of the initial concentration of Cu^{III} complex (Table 1). Fig. 1 shows the linear dependence of k_{obs} on the reductant concentration. The rate law for the reduction of the Cu^{III} complex at constant reaction conditions obeyed Eq. (4).

$$-d[Cu^{III}L^+]/dt = 2k_2[Cu^{III}L^+][H_2A]_T \quad (4)$$

The overall second order rate constant k_2 ($k_2 = k_{obs}/2[H_2A]_T$) was measured at 25.0 ± 0.1 °C over a wide pH range. The effect of pH on k_2 is complex and depends on both the reductant and Cu^{III} complex. In the reduction of complex (**I**) by H_2Q, MH_2Q and *p*MPH, k_2 decreases with increasing pH over the entire range studied for each reductant, 2.07–4.82, 2.68–5.25 and 1.19–4.83 respectively. In the reduction of (**I**) by both ClH_2Q and H_2Cat, k_2 increases with decreasing pH below 3.94 and 3.73, respectively. Above these pH values, k_2 increases with increasing pH. This behavior is consistent with the lower pK_{a1} values of ClH_2Q and H_2Cat and it seems that deprotonated species of these reductants are involved in the redox reactions (Table 3).

Fig. 2 shows a variation of k_2 with $[H^+]$ for the reduction of (**I**) by H_2Q and MH_2Q in the lower pH range. Similar plots were obtained for the reduction of (**I**) by the other three reductants. The dependence k_2 on $[H^+]$, in the lower pH range for the reduction of (**I**) obeys Eq. (5).

$$k_2 = k_3 + k_4[H^+] \quad (5)$$

Values of k_3 and k_4, obtained from the intercepts and slopes respectively of plots of k_2 against $[H^+]$, are collected in Table 2. The values of k_3 showed high degree of uncertainty. The dependence of k_2 on $[H^+]$, in the higher pH range for the oxidation of ClH_2Q by (**I**) obeys Eq. (6), and a plot of k_2 against $[H]^{-1}$ is shown in Fig. 3. Values of k_5 and k_6 obtained from the intercept and slope of Fig. 3, respectively are collected in Table 2.

$$k_2 = k_5 + k_6[H^+]^{-1} \quad (6)$$

The oxidation of H_2Cat by (**I**) showed a more complex behavior over the high pH range. The dependence of k_2 on $[H^+]$ obeys Eq. (7) and a polynomial fit of the results is shown in Fig. 4. Values of k_7, k_8 and k_9 obtained from the polynomial plot are collected in Table 2.

$$k_2 = k_7 + k_8[H^+]^{-1} + k_9[H^+]^{-2} \quad (7)$$

A full reaction sequence for the reduction of complex (**I**) by the reductants H_2Q, MH_2Q, Cl_2H_2Q and *p*MHP may be described by Eqs. (8)–(13).

$$[Cu^{III}L]^+ + H^+ \rightleftharpoons [Cu^{III}HL]^{2+} \quad K_1 \quad (8)$$

Table 1
Dependence of k_{obs} on the initial concentration of complex (**I**) at $[H_2Q] = 1.26 \times 10^{-3}$, pH 4.08, $\mu = 0.10$ M ($NaNO_3$), $T = 25.0 \pm 0.1$ °C

10^5 [Cu^{III}] (M)	k_{obs} (s^{-1})
2.50	6.32 ± 0.26
5.00	6.35 ± 0.05
7.50	6.29 ± 0.04
8.00	6.32 ± 0.06
12.0	6.33 ± 0.05

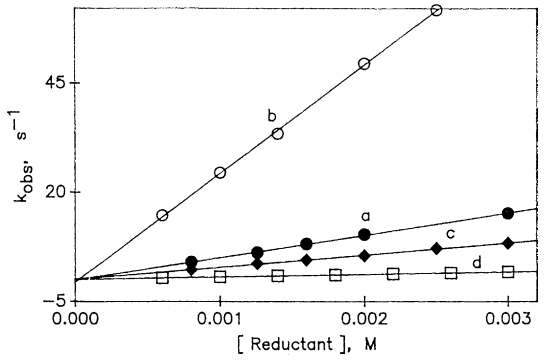

Fig. 1. Dependence of k_{obs} on reductant concentration at fixed pH, ionic strength at 25.0 ± 0.1 °C.

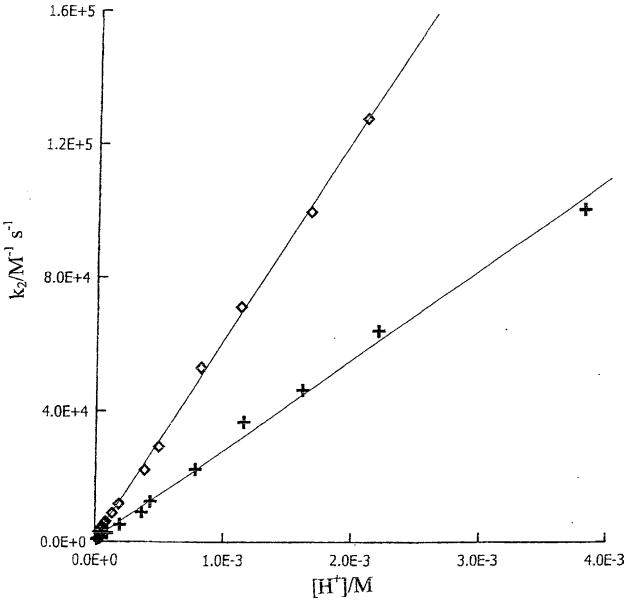

Fig. 2. Dependence of k_2 on $[H^+]$ for H_2Q (+) and MH_2Q (•) at $\mu = 0.10$ M ($NaNO_3$), $T = 25.0 \pm 0.1$ °C.

Table 2
Rate constants for the reduction of complex (**I**) at low and high pH ranges at $T = 25.0 \pm 0.1$ °C, $\mu = 0.10$ M ($NaNO_3$)

Reductant	$10^{-2}\ k_3$ ($M^{-1}\ s^{-1}$)	$10^{-6}\ k_4$ ($M^{-2}\ s^{-1}$)	$10^{-2}\ k_5$ ($M^{-1}\ s^{-1}$)	$10^{2}\ k_6$ (s^{-1})	$10^{-2}\ k_7$ ($M^{-1}\ s^{-1}$)	$10^{2}\ k_8$ (s^{-1})	$10^{6}\ k_9$ ($M\ s^{-1}$)
MH_2Q	11.5	60					
H_2Q	9.3	27.3					
*p*MHP	1.6	2.61					
ClH_2Q	4.7	5.21	5.8	3.14			
H_2Cat	16.0	1.85			4.6	4.21	2.87

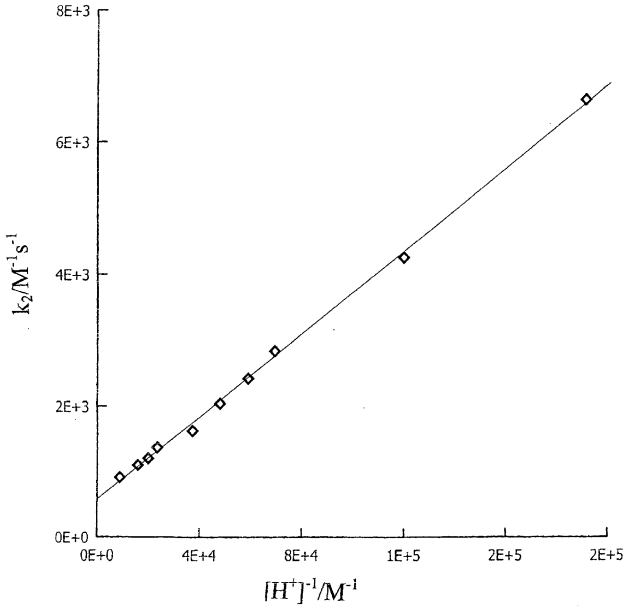

Fig. 3. Dependence of k_2 on $[H^+]^{-1}$ for the oxidation of ClH_2Q in the high pH range at $\mu = 0.10$ M ($NaNO_3$), $T = 25.0 \pm 0.1$ °C.

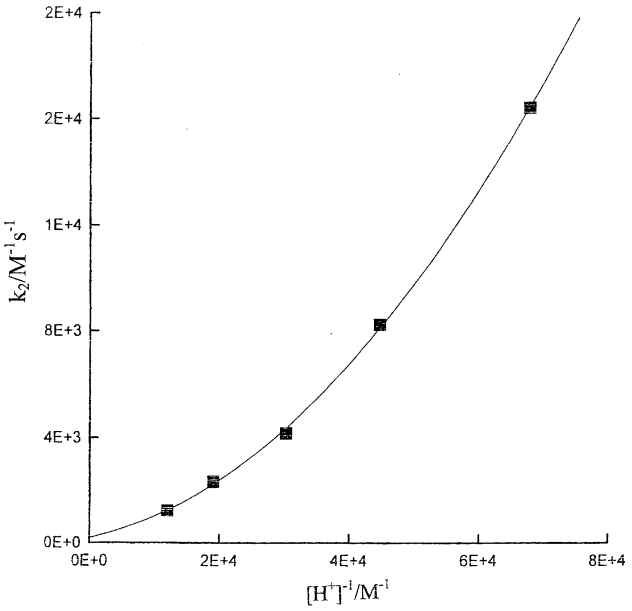

Fig. 4. A plot of k_2 versus $[H^+]^{-1}$ using a polynomial fit of the second degree at $\mu = 0.10$ M ($NaNO_3$), $T = 25.0 \pm 0.1$ °C.

$$H_2A \rightleftharpoons HA^- + H^+ \quad K_a \tag{9}$$

$$[Cu^{III}HL]^{2+} + H_2A \xrightarrow{k_a} [Cu^{II}HL]^+ + H_2A^{\cdot +} \tag{10}$$

$$[Cu^{III}HL]^{2+} + HA^- \xrightarrow{k_b} [Cu^{II}HL]^+ + HA^{\cdot} \tag{11}$$

$$[Cu^{III}L]^+ + H_2A \xrightarrow{k_c} [Cu^{II}L] + H_2A^{\cdot +} \tag{12}$$

$$[Cu^{III}L]^+ + HA^- \xrightarrow{k_d} [Cu^{II}L] + HA^{\cdot} \tag{13}$$

The semiquinone radicals produced in Eqs. (10)–(13) react rapidly with another Cu^{III} complex species to produce the corresponding quinones. The rate law for the disappearance of complex (**I**) is given by Eq. (14).

$$\frac{-d[Cu^{III}L^+]}{dt} = \frac{2\{k_aK_1[H^+] + k_bK_1K_a + k_c + k_dK_a[H^+]^{-1}\}[Cu^{III}L^+]_T[H_2A]_T}{(1 + K_1[H^+])(1 + K_a/[H^+])} \tag{14}$$

In the low pH range, where the reductants are undissociated, $1 \gg K_a/[H^+]$; and if $1 \gg K_1[H^+]$ and only reactions (10) and (12) are important, the dependence of k_2 on $[H^+]$ is given by Eq. (15) which has the same form as that of Eq. (5). From Eqs. (5) and (15) it can be seen that $k_3 = k_c$ and $k_4 = k_aK_1$

$$k_2 = k_c + k_aK_1[H^+] \tag{15}$$

In the higher pH range reactions (11) and (13) are expected to dominate. The lower reduction potentials of deprotonated HA^- would facilitate the oxidation of these substrates and their rates of oxidation were observed to be several orders of magnitude higher than those of H_2A by the same oxidant [9]. The condition that $1 \gg K_a/[H^+]$ and $1 \gg K_1[H^+]$ seems to hold also at the higher pH range for the oxidation of ClH_2Q. The dependence of k_2 on $[H^+]$, given by Eq. (16), is similar to that shown in Eq. (6), with $k_5 = k_bK_1K_a$ and $k_6 = k_dK_a$. The value of K_{a_1} has been estimated as 4.6×10^{-9} M, using the approach of Perrin et al. [23]. Values of pK_a obtained using this approach are in fairly good agreement with experimental results. The lower pK_a values calculated for ClH_2Q are consistent with the known electron withdrawing property of the Cl substituent. The value of k_d can be obtained from the relation $k_d = k_6/K_a$

Table 3
Proton equilibrium constants and reduction potentials for the benzene diols and *p*-methoxyphenol

Reductant	pK_{a1}	pK_{a2}	E_1 (V)	E_2 (V)
MH_2Q	10.05	11.6	1.02	0.38
H_2Q	9.85	11.4	1.06	0.45
*p*MHP[a]	10.21		1.11	
ClH_2Q	8.34[b]	10.57[b]	1.09	0.41[c]
H_2Cat	9.24	13.00	1.12	0.49

Unless otherwise mentioned the values are taken from [9].
[a] Ref. [26].
[b] pK_{a1} and pK_{a2} calculated using [23] (agreement with experimental values is within ±10%).
[c] E_2 calculated using Marcus equation.

$$\frac{-d[Cu^{III+}]}{dt} = \frac{2\{k_aK_1[H^+] + k_bK_1K_a + k_c + k_eK_aK_2[H^+]^{-1} + k_fK_aK_2K_3[H^+]^{-2}\}[Cu^{III}L^+]_T[H_2A]_T}{(1 + K_1[H^+])(1 + K_a/[H^+])} \quad (21)$$

as 6.8×10^6 M^{-1} s^{-1}. The reduction potential of $ClHQ^-$/$ClHQ^{\cdot}$ couple is not known and has been estimated using the value of k_d and $k_{22} = 2 \times 10^6$ M^{-1} s^{-1} as 0.41 V. This value seems to be in fairly good agreement with the values obtained for the other HA/HA$^{\cdot}$ couples (Table 3).

$$k_2 = k_bK_1K_a + k_dK_1[H^+]^{-1} \quad (16)$$

Reactions of the protonated Cu^{III} complex are much more rapid than those of the unprotonated form. This in agreement with reactions involving the protonated and unprotonated Ni^{III} complex ($[Ni^{III}HL]^{2+}$) and $[Ni^{III}L]^+$) with H_2Q, H_2MQ and H_2Cat, where the former was found to be more reactive than the latter [9]. It is to be noted that both ClH_2Q and H_2Cat because of their lower first pK_a values dissociate more readily than the other reactants and show an increase in reaction rate with increasing pH.

The oxidation of H_2Cat in the lower pH range can be described by Eqs. (8)–(12). However, over the high pH range the oxidation of H_2Cat by complex (**I**) can be described by Eqs. (17)–(20).

$$[Cu^{III}L]^+ + HA^- \rightleftharpoons [Cu^{III}LHA] \quad K_2 \quad (17)$$

$$[Cu^{III}LHA] \rightleftharpoons [Cu^{III}LA]^- + H^+ \quad K_3 \quad (18)$$

$$[Cu^{III}LHA] \xrightarrow{k_e} [Cu^{II}L] + HA^{\cdot} \quad (19)$$

$$[Cu^{III}LA]^- \xrightarrow{k_f} [Cu^{II}L] + A^{\cdot -} \quad (20)$$

The mechanism represented by reactions (11) and (13) does not explain the inverse second order dependence on $[H^+]$. This may arise from the involvement of completely deprotonated H_2Cat. It is very unlikely that H_2Cat loses both protons in the pH range investigated. For the second proton to be lost, it is necessary to invoke an interaction with the Cu^{III} complex. An increase in the acidity of the proton of the second OH group may be due to coordination the monodeprotonated $HCat^-$ to the positively charged Cu^{III} complex. It is very likely that these processes involve an inner-sphere mechanism in which the oxygen of the deprotonated hydroxyl group coordinates axially to the Cu^{III} complex. The formation of a five-coordinate species in the transition state is plausible as low-spin d^8 square planar complexes are known to undergo substitution reactions by an associative mechanism [24].

The rate law given by Eq. (21) is obtained by considering the scheme (8)–(12) together with (17)–(20).

From Eq. (21) it can be seen that in the high pH range, where reactions (11), (12), (19) and (20) are important, the variation of the second-order rate constant varies with $[H^+]$ according to Eq. (22). Under conditions where $1 > K_1[H^+]$ and $1 > K_a/[H^+]$.

$$k_2 = \{k_bK_1K_a + k_c + k_eK_aK_2[H^+]^{-1} + k_fK_aK_2K_3[H^+]^{-2}\} \quad (22)$$

Eq. (22) is of the same form as Eq. (7), with $k_7 = k_bK_1K_a + k_c$, $k_8 = k_eK_aK_2$, and $k_9 = k_fK_aK_2K_3$. The values of k_7, k_8 and k_9, obtained from the polynomial fit shown in Fig. 4 are: 464 M^{-1} s^{-1}, 4.21×10^{-2} s^{-1} and 2.87×10^{-6} M s^{-1}, respectively. The values of K_2 and K_3 are not known and it was not possible to calculate the values of k_e and k_f.

The rate constants are observed to increase with the decrease in the reduction potentials of the semiquinone radicals. Such observations have previously been used as an indication for the operation of an outer-sphere electron transfer mechanism in the rate-determining step [2]. Marcus theory for outer-sphere electron transfer has been utilized to rationalize the relationship between the rate constant for a cross-reaction, k_{12}, and the self-exchange rate constants for the oxidant (k_{11}) and reductant (k_{22}) reactions, and the equilibrium constant for the cross-reaction K_{12}. In its simplest form Marcus relationship is given by Eqs. (23) and (24) and Z is the collision frequency in solution, usually taken as 10^{11} s^{-1}.

$$k_{12} = (K_{12}k_{11}k_{22}f)^{1/2}, \quad (23)$$

$$\log f = (\log K_{12}/4\log(k_{11}k_{22}/Z^2). \quad (24)$$

The self-exchange rate constant k_{11} for complex (**I**) has previously been estimated as $\sim 5 \times 10^5$ M^{-1} s^{-1} [25]. Reported estimates of the self-exchange rate constants

Table 4
Calculated and observed rate constants for the reaction $[Cu^{III}HL]^{2+} + H_2A \rightarrow [Cu^{II}HL]+H_2A^{\cdot +}$

H_2A	k_{obs}[a] ($M^{-2}\,s^{-1}$)	k_{calc} ($M^{-1}\,s^{-1}$)
MH_2Q	6.00×10^7	6.38×10^{7b}
H_2Q	2.73×10^7	3.18×10^{7c}
ClH_2Q	5.21×10^6	3.80×10^{6d}
pMPH	2.61×10^6	2.60×10^{6d}
H_2Cat	1.85×10^6	2.13×10^{6d}

[a] k_{obs} is k_4 (k_2 at $[H^+] = 1.0$ M).
[b] $f = 0.7$.
[c] $f = 0.8$.
[d] $f = 0.9$.

of the hydroquinone/semiquinone couples (k_{22}), for both neutral and anionic species, vary over the 2×10^6–5×10^7 $M^{-1}\,s^{-1}$ range [2]. The value of K_{12} for each cross-reaction was calculated from the known reduction potentials of $Cu^{III/II}$ and the hydroquinone/semiquinone couples [9,26] and these are collected in Table 4. It is to be noted that the reduction potentials reported for $H_2A/H_2A^{\cdot +}$ show some variation and are not known with certainty. Thus for $H_2Q/H_2Q^{\cdot +}$, the reported reduction potential covers the range 1.02–1.09 V [9,26]. It was found that using the average value of 1.06 V for H_2Q gives a better result for the reaction reported here. In the application of Marcus theory the value of k_2 at $[H^+] = 1.0$ M (k_4 in Eq. (5)) was used. The values of the cross-reaction rate constants were calculated using $k_{22} = 5 \times 10^7$ $M^{-1}\,s^{-1}$. This value gave reasonably good results with MH_2Q and H_2Q as shown in Table 4. However, using this value for H_2Cat, ClH_2Q and *p*MPH, the calculated value for each reductant is much higher than the experimental value. Good agreement was obtained between the calculated and the experimental values as shown in Table 4 by using $k_{22} = 2 \times 10^6$ $M^{-1}\,s^{-1}$. It thus seems that 1,4-dihydroxybenzene and its derivatives with electron donating substituents have an exchange rate constant $k_{22} \sim 5 \times 10^7$. The exchange rate constant $k_{22} \sim 2 \times 10^6$ seems to be applicable to derivatives of 1,4-dihydroxybenzene with electron withdrawing substituents, as well as for 1,2-dihydroxybenzene and its derivatives [2a].

The rate constants obtained from the slope of Eq. (5) only were used in testing Marcus equation as the values obtained from the intercepts are less reliable. The agreement between the calculated and experimental values does not completely rule out an inner-sphere mechanism as the OH of the diol can form a weak bond with Cu^{III} in the axial position.

References

[1] P.R. Rich, Faraday Discuss. Chem. Soc. 74 (1982) 349.
[2] (a) J.W. Herbert, D.H. Macartney, J. Chem. Soc., Dalton Trans. (1986) 1931;
(b) J.C. Brodovitch, A. McAuley, T. Oswald, Inorg. Chem. 21 (1982) 3442.
[3] R.A. Marcus, Ann. Rev. Phys. Chem. 15 (1964) 155.
[4] (a) E. Pelizzetti, E. Mentasti, Z. Phys. Chem. 105 (1977) 21;
(b) E. Mentasti, E. Pelizzetti, Int. J. Chem. Kinet. 9 (1977) 215.
[5] (a) E. Pelizzetti, E. Mentasti, C. Baiocchi, J. Phys. Chem. 80 (1976) 2979;
(b) E. Mentasti, E. Pelizzetti, C. Biaocchi, J. Chem. Soc., Dalton Trans. (1977) 132.
[6] E. Pelizzetti, E. Mentasti, J. Chem. Soc., Dalton Trans. (1976) 2222.
[7] E. Pelizzetti, E. Mentasti, E. Pramauro, Inorg. Chem. 17 (1978) 1688.
[8] J.C. Brodovitch, A. McAuley, T. Oswald, Inorg. Chem. 21 (1982) 3442.
[9] (a) D.H. Macartney, A. McAuley, J. Chem. Soc., Dalton Trans. (1984) 103;
(b) S.F. Munn, A.M. Lannon, M.C.M. Laranjera, A.G. Lappin, J. Chem. Soc., Dalton Trans. (1984) 1317.
[10] E. Mentasti, E. Pelizzetti, G. Saini, J. Chem. Soc., Dalton Trans. (1973) 2609.
[11] E. Mentasti, E. Pelizzetti, E. Pramauro, G. Giraudi, Inorg. Chim. Acta 12 (1975) 61.
[12] E. Pelizzetti, E. Mentasti, G. Giraudi, Inorg. Chim. Acta 15 (1975) L1.
[13] E. Pelizzetti, E. Mentasti, J. Inorg. Nucl. Chem. 38 (1976) 2005.
[14] N. Shaikh, M. Ali, P. Banerjee, Inorg. Chim. Acta 339 (2002) 341.
[15] M.C. Gosh, J.W. Reed, R.N. Bose, E.S. Gould, Inorg. Chem. 33 (1994) 73.
[16] M.M. Monzyk, R.A. Holwerda, Inorg. Chem. 31 (1992) 1969.
[17] W.H. Woodruff, D.W. Margerum, Inorg. Chem. 13 (1974) 2578.
[18] A. Haim, N.J. Sutin, J. Am. Chem. Soc. 88 (1966) 434.
[19] G.D. Owens, K.L. Chellappa, D.W. Margerum, Inorg. Chem. 18 (1979) 960.
[20] C.A. Koval, D.W. Margerum, Inorg. Chem. 20 (1981) 2311.
[21] J.M. Anast, D.W. Margerum, Inorg. Chem. 21 (1982) 3494.
[22] Y. Sulfab, F.M. Al-Sogair, Trans. Met. Chem. 27 (2002) 299, and references there in.
[23] D.D. Perrin, B. Dempsey, E.P. Serjeant, pK_a Prediction for Organic Acids and Bases, Chapman and Hall, New York, 1981, p. 44.
[24] F. Basolo, R.G. Pearson, Mechanisms of Inorganic Reactions. A Study of Metal Complexes in Solution, Wiley, New York, 1967 (Ch. 4).
[25] A. Hussein, Y. Sulfab, M. Nasreldin, Inorg. Chem. 28 (1989) 157.
[26] M. Kimura, Y. Kaneko, J. Chem. Soc., Dalton Trans. (1984) 341.

Available online at www.sciencedirect.com
SCIENCE DIRECT®
Polyhedron 23 (2004) 589–598
POLYHEDRON
www.elsevier.com/locate/poly

Electropolymerisable bipyridine ruthenium(II) complexes: synthesis, spectroscopic and electrochemical characterisation of 4-((2-thienyl) ethenyl)- and 4,4′-di((2-thienyl) ethenyl)-2,2′-bipyridine ruthenium complexes

Viviane Aranyos [a], Anders Hagfeldt [a], Helena Grennberg [b], Egbert Figgemeier [a,*]

[a] Department of Physical Chemistry, University of Uppsala, P.O. Box 579, Uppsala S-75123, Sweden
[b] Department of Organic Chemistry, University of Uppsala, P.O. Box 599, Uppsala S-75124, Sweden

Received 16 July 2003; accepted 21 October 2003

Abstract

Four new ruthenium polypyridyl complexes with mono- or di-((2-thienyl) ethenyl) substituted bipyridines have been synthesized. The complexes were characterized by NMR, elemental analysis, UV–Vis absorption and electrochemistry (differential pulse and cyclic voltammetry). Electroactive polymer films of these complexes have been prepared by oxidative electropolymerisation and characterized by UV–Vis absorption spectroscopy and electrochemistry. The electrochemically induced polymerisation of the complexes resulted in a significant shift of the oxidation potential of the Ru(II)–Ru(III) process towards more positive potentials. Also, MLCT absorption band of the polymeric complexes is shifted towards shorter wavelengths. These results are interpreted in terms of an interruption of the conjugated system of the (2-thienyl)ethenyl-substituted bipyridine ligands due to a radical polymerisation mechanism affecting rather the ethenyl part of the ligand than the thienyl.
© 2003 Elsevier Ltd. All rights reserved.

Keywords: Electropolymerisation; Ru-complexes; Thiophene; Differential pulse voltammetry; 4-((2-Thienyl)-ethenyl)-2,2′-bipyridine; Redox-polymers

1. Introduction

Nano-structured dye-sensitized photoelectrochemical solar cells (NSCs) and solar cells based on conjugated polymers are considered as promising routes to decrease significantly the price of electricity by means of solar power in the future [1,2]. Moreover, these types of solar cells have features like flexibility and lightweight, which give them an even higher market potential. Nevertheless, polymer-based solar cells are currently using either Buckminsterfullerenes or polymers as electron acceptors which is costly or triggers stability problems. On the other side, the highly efficient nano-structured solar cells based on TiO_2 as electron acceptor are incorporating liquid electrolytes for the transport of charge, which is problematic in terms of stability and production. With this background it can be very beneficial to combine the advantages of conducting polymers and nano-structured TiO_2 in the design of a solar cell. In this context we are currently investigating Ru-complexes, which can act as dye sensitizers in NSCs, which are modified with thiophene substituents on the bipyridine ligands. These thienyl groups are thought to be used as starting points for a covalent link between the dye and a solid electrolyte as, e.g., polythiophene. Also, an extension of the absorbtion spectrum together with an increased hydrophobicity improving stability of the NSC towards water penetration gives these substituents a bright future in the field of photoelectrochemical solar cells. However, in order to apply this type of dyes in a complex system such

* Corresponding author. Present address: Departement Chemie, Universität Basel, Spitalstrasse 51, Basel CH-4056, Switzerland. Tel.: +46-18-471-3661; Fax: +46-18-471-3654.
E-mail address: egbert.figgemeier@fki.uu.se (E. Figgemeier).

0277-5387/$ - see front matter © 2003 Elsevier Ltd. All rights reserved.
doi:10.1016/j.poly.2003.10.004

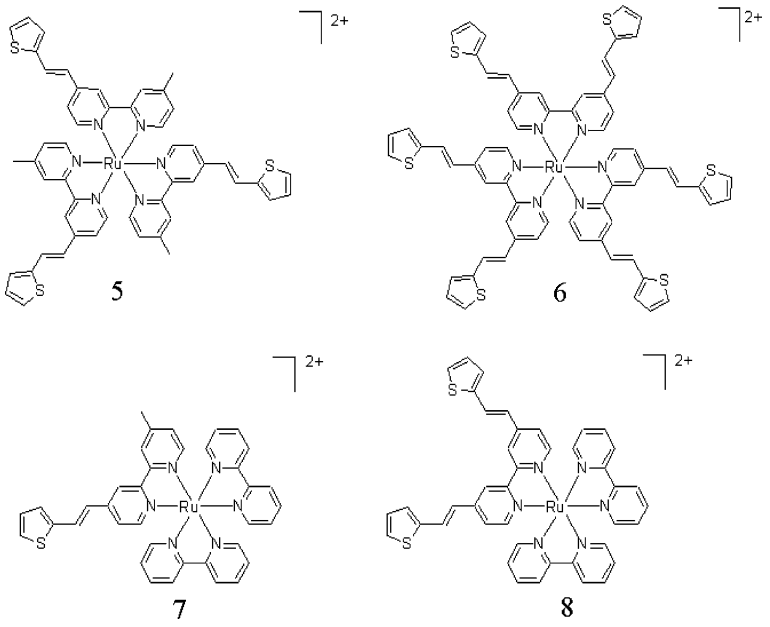

Scheme 1.

as the NSC, the study of models compounds **5–8** (Scheme 1) is a necessity.

In the past we have presented the synthesis and properties of ruthenium *tris*-bipyridyl complexes with methoxystyryl substituents and the characteristics of electrochemically produced polymers [3]. Following up this investigation, we here report the synthesis and the study of some ruthenium polypyridyl complexes with hydrophobic polymer precursors as ethylene-thiophene. Electroactive polymers of these complexes have been prepared by oxidative electropolymerisation. The resulting materials have been characterized with UV–Vis spectroscopy and by means of electrochemistry.

2. Experimental

2.1. Materials

All reagents were from commercial sources and were used without further purification. Solvents were HPLC grade and were used without further purification with the following exceptions: Tetrahydrofuran (THF) was distilled from sodium, diisopropylamine (DIPA) and triethylamine (Et_3N), which were distilled from CaH_2. For electrochemical experiments, acetonitrile (Fluka, $H_2O \leqslant 0.001\%$) stored over molecular sieves was used. Butyl lithium (BuLi) was stored in a desiccator under nitrogen and used as fresh (no precipitate) 1.6 M solutions in hexane. Trifluoroacetic acid (TFA) and trifluoroacetic acid anhydride (TFAA) were stored at −18 °C and used as received. Tetrabutylammonium hexafluorophosphate ((TBA)PF_6) (Aldrich, 98%) was dried under vacuum at 120 °C for 48 h before performing electrochemistry. Syntheses were performed under a nitrogen atmosphere. Transparent conducting oxide electrodes of fluorine-doped tin oxide (FTO) on a 3-mm glass support (sheet resistance 8 Ω/square) were purchased from Liffey–Owens–Ford. Elemental analyses were performed by the Analytische Laboratorien, Lindlar, Germany.

2.2. Physical characterisation

NMR spectra (^{1}H NMR at 400 MHz and ^{13}C NMR at 100 MHz) were recorded on a Varian Unity 400 spectrometer for $CDCl_3$ and CD_3COCD_3 solutions unless otherwise stated. The chloroform signals at 7.26 ppm (for ^{1}H) or 77.0 ppm (for ^{13}C) and the acetone signals at 2.04 ppm (for ^{1}H) or 29.8 ppm (for ^{13}C) were used as indirect reference to TMS.

UV–Vis absorption spectra were recorded using a Hewlett-Packard 8453 diode-array spectrophotometer and referenced against a solvent blank (CH_3CN). The fluorine-doped tin oxide (FTO) electrodes with polymer films deposited on the surface were positioned against the wall of a 1-cm quartz cuvette containing CH_3CN. The absorption of the FTO glass substrates was substracted from the measured spectra of the compound.

Electrochemistry was performed using a CH Instruments Model 660. Electrochemical workstation and a conventional three electrode cell with a silver wire as pseudo-reference electrode. After the experiments ferrocene was added as an internal reference and all potentials given are quoted against the ferrocene–ferrocenium redox couple.

2.3. Synthesis

2.3.1. Ligands

*2.3.1.1. 4-Methyl-4′-(2-hydroxy-2-(2-thienyl) ethyl)-2,2′-bipyridine (**1**).* LDA was formed by mixing 1.54 mL BuLi (1.6 M in hexane) with 0.39 mL of DIPA in 10 mL THF at −60 °C under N_2. The mixture was then stirred at room temperature for 1/2 h. Thereafter, 4,4′-dimethyl-2,2′-bipyridine (0.50 g, 2.48×10^{-3} mol) dissolved in 15 mL THF was added through a double tipped needle after the temperature was cooled to −40 °C. The black reaction mixture was then stirred at room temperature during 1 h. The aldehyde (0.25 mL, 2.72×10^{-3} mol) was diluted in 10 mL THF and added the same fashion to the reaction mixture to form a yellow precipitate. After stirring for 1 h, the reaction was stirred into water and extracted with dichloromethane. The organic phase was then washed with brine and dried over $MgSO_4$. The dried solution was then concentrated. NMR of the crude product showed more than 85% of conversion compared to the aldehyde and complete conversion compared to the bipyridine. The crude product was used in the next step without further purification. ^{1}H NMR (400 MHz) ($CDCl_3$) δ 8.54 (1H, d, $J = 4.8$ Hz, aromatic pyridine), 8.50 (1H, $J = 4.8$ Hz, d, aromatic pyridine), 8.30 (1H, broad s, aromatic pyridine), 8.21 (1H, broad s, aromatic pyridine), 7.26 (1H, multiplet, thiophene), 7.13 (2H, multiplet, aromatic pyridine), 6.96 (2H, multiplet, thiophene), 5.29 (1H, dd, $J = 7.6$ Hz, $J = 6$ Hz, benzylic alcohol), 3.21 (1H, d, $J = 7.6$ Hz, benzylic), 3.21 (1H, d, $J = 6$ Hz, benzylic), 2.43 (3H, s).

*2.3.1.2. 4,4′-(2-hydroxy-2-(2-thienyl) ethyl)-2,2′-bipyridine (**2**).* LDA was formed by mixing 3.72 mL BuLi (1.6 M in hexane) with 0.83 mL of DIPA in 20 mL THF at −60 °C under N_2. The mixture was then stirred at room temperature for 1/2 h. Thereafter, 4,4′-dimethyl-2,2′-bipyridine (0.50 g, 2.48×10^{-3} mol) dissolved in 15 mL THF was added through a double-tipped needle after the temperature was cooled to −40 °C. The black reaction mixture was then stirred at room temperature during 1 h. The aldehyde (0.52 mL, 5.96×10^{-3} mol) was diluted in 10 mL THF and added in the same fashion to the reaction mixture to form a yellow precipitate. After stirring for 1 h, the reaction was stirred into water and extracted with dichloromethane. The organic phase was then washed with saturated aq. NaCl and dried over $MgSO_4$. The dried solution was then concentrated yielding 0.836 g (2.04×10^{-3}, 75%) of the product.^{1}H NMR (400 MHz) ($CDCl_3$) δ 8.58 (2H, m, aromatic pyridine), 8.30 (2H, broad s, aromatic pyridine), 7.26 (2H, multiplet, thiophene), 7.15 (2H, multiplet, aromatic pyridine), 6.99 (4H, multiplet, thiophene), 5.29 (2H, m, benzylic alcohol), 3.21 (2H, m, benzylic).

*2.3.1.3. 4-Methyl-4′-(2-(2-thiophene) ethenyl)-2,2′-bipyridine (**3**).* 4-Methyl-4′-(2-hydroxy-2-(2-thienyl) ethyl)-2,2′-bipyridine (2.30 mmol) was dissolved in 10 mL of CH_2Cl_2 under nitrogen. As trifluoroacetic anhydride (TFA) (3.90 mL, 27.6 mmol) was added dropwise, the reaction mixture became orange. The mixture was stirred overnight and then concentrated to dryness, dissolved into EtOAc (50 mL), washed with water (2×50 mL), dried over $MgSO_4$ and concentrated to dryness. The product was afforded as yellow crystals in 96% yield (0.616 g, 2.21 mmol). ^{1}H NMR (400 MHz) ($CDCl_3$) δ 8.85 (1H, d, $J = 5.6$ Hz, aromatic pyridine), 8.78 (1H, $J = 5.2$ Hz, d, aromatic pyridine), 8.55 (1H, broad s, aromatic pyridine), 8.35 (1H, broad s, aromatic pyridine), 7.81 (1H, d, $J = 16$ Hz, alkene), 7.60 (1H, dd, $J = 5.6$ Hz, $J = 1.2$ Hz, pyridine), 7.52 (1H, d, $J = 5.2$ Hz, pyridine), 7.42 (1H, d, $J = 5.6$ Hz, thiophene), 7.33 (1H, d, $J = 3.6$ Hz, thiophene), 7.11 (1H, dd, $J = 3.6$ Hz, $J = 5.2$ Hz, thiophene), 6.93 (1H, d, $J = 16$ Hz, alkene), 2.63 (3H, s, Methyl). ^{13}C NMR, 154.7, 151.2, 148.3, 147.9, 146.2, 146.0, 140.6, 131.6, 131.7, 130.9, 128.5, 128.4, 127.3, 124.4, 122.7, 122.4, 119.6, 21.8.

*2.3.1.4. 4,4′-(2-(2-thiophene) ethenyl)-2,2′-bipyridine (**4**).* Crude **2** (2.04×10^{-3} mol) was dissolved in 15 mL of CH_2Cl_2 under nitrogen. As trifluoroacetic anhydride (TFAA) (3.90 mL, 27.6×10^{-3} mol) was added dropwise, the reaction mixture turned orange. The mixture was stirred overnight and then concentrated to dryness, dissolved into EtOAc (50 mL), washed with water (2×50 mL), dried over $MgSO_4$ and concentrated to dryness. The product was afforded as a yellow powder in 37% yield (0.281 g, 7.54×10^{-3} mol). ^{1}H NMR (400 MHz) ($CDCl_3$) δ 8.73 (1H, d, $J = 5.2$ Hz, aromatic pyridine), 8.65 (1H, broad s, aromatic pyridine), 7.70 (1H, d, $J = 16$ Hz, alkene), 7.41 (1H, d, $J = 4.8$ Hz, pyridine), 7.32 (1H, d, $J = 4.8$ Hz, thiophene), 7.24 (1H, m, thiophene), 7.06 (1H, dd, $J = 3.6$ Hz, $J = 4.8$ Hz, thiophene), 6.94 (1H, d, $J = 16$ Hz, alkene). ^{13}C NMR, 148.1, 141.5, 131.1, 129.7, 129.4, 129.0, 128.4, 127.4, 124.2, 122.3, 119.3.

2.3.2. Homoleptic complexes

*2.3.2.1. Tris-(4-methyl-4′-(2-thienylethenyl)-2,2′-bipyridine) ruthenium dihexafluorophosphate (**5**).* $RuCl_3 \cdot xH_2O$ (0.079 g, 0.38 mmol) and **L** (0.321 g, 1.15 mmol) were stirred at reflux in a 20 mL mixture of EtOH and H_2O (1:1), under nitrogen during 24 h. The solution turned dark red. NH_4PF_6 (1.24 g, 7.66 mmol) dissolved in water was added to the reaction mixture, after which a brown precipitate appeared. The precipitate was filtered off, washed with water and ether. The product was dried under reduced pressure during 24 h and was afforded in 24% yield (0.115 g, 0.095 mmol). *Anal.* Calc. for $Ru(Bpy\text{-}Th_1)_3(PF_6)_2 + 4H_2O$ (Mol Form.: $C_{51}H_{42}$

$F_{12}N_6P_2RuS_3 \cdot 4H_2O$): C, 47.19; H, 3.88; N, 6.47. Found: C, 46.82; H, 3.89; N, 5.85%.

*2.3.2.2. Tris-(4,4′-(2-thienylethenyl)-2,2′-bipyridine) ruthenium dihexafluorophosphate (**6**).* $RuCl_3 \cdot xH_2O$ (0.079 g, 0.89 mmol) and **L** (0.100 g, 0.268 mmol) were stirred at reflux in a 20 mL mixture of EtOH and H_2O (1:1), under nitrogen during 24 h. The solution turned dark red. NH_4PF_6 (0.145 g, 0.89 mmol) dissolved in water was added to the reaction mixture, after which a brown precipitate appeared. The precipitate was filtered off, washed with water and ether. The product was dried under reduced pressure during 24 h and was afforded in 68% yield (0.092 g, 0.45 mmol). *Anal.* Calc. for Ru(Bpy-$Th_2)_3(PF_6)_2 + 5H_2O$ (Mol Form.: $C_{66}H_{48}F_{12}N_6P_2RuS_6 \cdot 5H_2O$): C, 49.59; H, 3.66; N, 5.26; Found: C, 49.23; H, 3.83; N, 4.50%.

2.3.3. Heteroleptic complexes

2.3.3.1. Bis-2,2′-bipyridyl ruthenium dichloride [4]. $RuCl_3 \cdot xH_2O$ (0.200 g, 0.96 mmol), 2,2′-bipyridyine (0.316 g, 2.02 mmol) and LiCl (0.173 g, 4.08 mmol) were stirred at reflux in 20 mL reagent grade DMF under argon for 8 h. After the reaction had cooled to room temperature, 100 mL of reagent grade acetone was added. The solution was then refrigerated overnight at 0 °C. Filtration gave a red violet solution and dark green crystals. Those were washed with water (3 × 15 mL) and with ether (3 × 15 mL). The product was then dried at room temperature under reduced pressure for 24 h. ^{1}H NMR ($CDCl_3$) δ 10.07 (d, $J = 5.6$ Hz, 2H, aromatic), 8.15 (d, $J = 8$ Hz, 2H, aromatic), 7.99 (d, $J = 8$ Hz, 2H, aromatic), 7.84 (t, $J = 8$ Hz, 2H, aromatic), 7.55 (m, 4H, aromatic), 7.46 (t, $J = 8$ Hz, 2H, aromatic), 6.87 (t, $J = 5.6$ Hz, 2H, aromatic). ^{13}C NMR, 160.4, 157.9, 153.9, 152.6, 134.5, 133.4, 125.5, 124.7, 121.9, 121.7.

*2.3.3.2. Bis-2,2′-bipyridyl-(4-methyl-4′-(2-thienylethenyl)-2,2′-bipyridine) ruthenium dihexafluorophosphate (**7**).* *Bis*-2,2′-bipyridyl ruthenium dichloride (0.050 g, 0.10 mmol) and 4,4′-(2-thienylethenyl)-2,2′-bipyridine (0.027 g, 0.10 mmol) were stirred at reflux in a 20 mL mixture of EtOH and H_2O (1:1), under argon for 1 h. The solution turned red. $NaPF_6$ (0.250 g, ~20 eq) was added to the reaction mixture, which was stirred overnight (18 h), resulting in an orange precipitate. The precipitate was filtered and dried under reduced pressure during 24 h to give 0.043 g (0.044 mmol, 42% yield) of *bis*-2,2′-bipyridyl-(4-methyl-4′-(2-thienylethenyl)-2,2′-bipyridine) ruthenium dihexafluorophosphate. ^{1}H NMR (CD_3COCD_3) δ 8.95 (substituted bipyridine, d, $J = 1.2$ Hz, 1H), 8.81 (non-substituted bipyridine, d, $J = 7.2$ Hz, 4H), 8.76 (substituted bipyridine, s, 1H), 8.23-8.18 (non-substituted bipyridine, m, 4H), 8.16 (substituted bipyridine, d, $J = 0.8$ Hz, 1H), 8.15–8.04 (non-substituted bipyridine, m, 4H), 7.98 (–C*H*=C*H*–, d, $J = 16$ Hz, 1H), 7.91 (substituted bipyridine, d, $J = 6$ Hz, 1H), 7.86 (substituted bipyridine, d, $J = 5.4$ Hz, 1H), 7.64 (substituted bipyridine, dd, $J_1 = 6.4$ Hz, $J_2 = 2$ Hz, 1H), 7.62–7.55 (non-substituted bipyridine, m, 4H), 7.42 (substituted bipyridine, unresolved dd, 1H), 7.38 (substituted bipyridine, d, $J = 3.2$ Hz, 1H), 7.13 (substituted bipyridine, dd, $J_1 = 5.2$ Hz, $J_2 = 4$ Hz, 1H), 2.59 (–CH_3, s, 3H). *Anal.* Calc. for $C_{37}H_{30}F_{12}N_6P_2RuS \cdot 2H_2O$: C, 43.66; H, 3.37; N, 8.26; Found: C, 43.82; H, 3.21; N, 8.09%.

*2.3.3.3. Bis-2,2′-bipyridyl-(4,4′-(2-thienylethenyl)-2,2′-bipyridine) ruthenium dihexafluorophosphate (**8**).* *Bis* 2,2′-bipyridyl ruthenium dichloride (0.050 g, 0.10 mmol) and 4,4′-(2-thienylethenyl)-2,2′-bipyridine (0.038 g, 0.10 mmol) were stirred at reflux in a 20 mL mixture of EtOH and H_2O (1:1), under argon for 1 h. The solution turned red. $NaPF_6$ (0.250 g, ~20 eq) was added to the reaction mixture, which was stirred overnight (18 h), resulting in an orange precipitate. The precipitate was filtered and dried under reduced pressure during 24 h to give 0.065 g (0.6 mmol, 60% yield) of *bis*-2,2′-bipyridyl-(4,4′-(2-thienylethenyl)-2,2′-bipyridine) ruthenium dihexafluorophosphate. ^{1}H NMR (CD_3COCD_3) δ 8.98 (substituted bipyridine, s, 2H), 8.81 (non-substituted bipyridine, d, $J = 8$ Hz, 4H), 8.21 (non-substituted bipyridine, t, $J = 8$ Hz, 4H), 8.16 (substituted bipyridine, d, $J = 5.6$ Hz, 2H), 8.05 (substituted bipyridine, d, $J = 5.2$ Hz, 2H), 7.97 (–C*H*=C*H*–, d, $J = 16$ Hz, 2H), 7.91 (substituted bipyridine, d, $J = 8$ Hz, 2H), 7.68 (dd, $J_1 = 6.4$ Hz, $J_2 = 2$ Hz, 2H), 7.62–7.55 (non-substituted bipyridine + substituted bipyridine, m, 4 + 2H), 7.40 (substituted bipyridine, broad d, $J = 3.8$ Hz, 2H), 7.68 (substituted bipyridine + –C*H*=C*H*–, dd + d, $J_1 = 5.2$ Hz, $J_2 = 3.8$ Hz, $J_3 = 16$ Hz, 4H). ^{13}C NMR, 157.7, 157.5, 152.0, 151.6, 146.8, 141.37, 138.2, 130.1, 129.8, 128.6, 128.1, 124.6, 124.1, 123.4, 122.6, 121.1. *Anal.* Calc. for $C_{42}H_{32}F_{12}N_6P_2RuS_2 \cdot 8H_2O$: C, 41.35; H, 3.97; N, 6.89; Found: C, 40.94; H, 3.41; N, 7.10%.

3. Results and discussion

3.1. Synthesis

A two-step synthesis was used to afford 4-methyl-4′-(2-(2-thiophene) ethenyl)-2,2′-bipyridine (ligand **3**), or 4,4′-(2-(2-thiophene) ethenyl)-2,2′-bipyridine (ligand **4**) as pictured in Scheme 2.

First, a nucleophilic addition of the mono- or di-anion of 4,4′-dimethyl-2,2′-bipyridine to 2-thiophenecarboxaldehyde (one or two equivalents) gave the corresponding alcohol (**1** or **2**) [4]. Dehydration was achieved using trifluoroacetic anhydride (TFAA) followed by precipitation. The preparation of the homo-

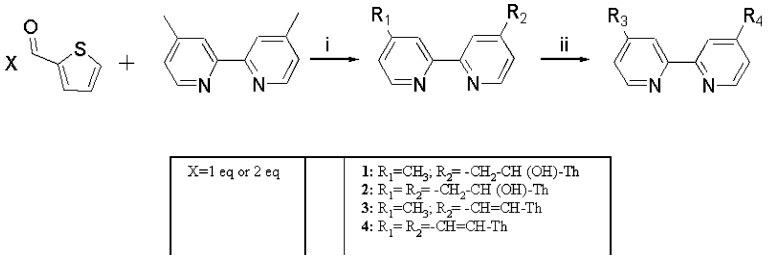

Scheme 2.

leptic complexes **5** and **6** was done in methoxyethanol (MeOEtOH) by mixing one equivalent of the ruthenium salt with three equivalents of the desired ligand (**1** or **2**). After the reaction mixture became dark red, the solution was cooled and the complex precipitated out of the solution by addition of (NH_4PF_6)-saturated water. The complex was filtered and dried under vacuum.

The heteroleptic complexes were prepared using a two-step synthesis. The dichloro bis-bipyridyl ruthenium complex was prepared according to a literature procedure [5]. The third ligand was introduced by mixing the dichloro bis-bipyridyl ruthenium salt to one equivalent of the mono- or di-substituted ligands followed by an exchange of the counter ion by addition of (NH_4PF_6)-saturated water.

3.2. Absorption properties

The absorption spectra for the ligands **2** and **4** were compared and clearly showed the substituent influence (see Fig. 1): [1] The very typical Ligand Centered Charge Transfer (LCCT/π–π^*) for bipyridine ligands is represented around 280 nm in both cases, and the conjugated thiophene gives an extra LCCT at ~340 nm [6].

The absorption properties of the different complexes have been recorded in acetonitrile and are shown in Fig. 2. [1]

The metal to ligand charge transfer (MLCT) correlates very well with the number of substituents on the molecules (see Table 1).

The more extended conjugated system is expected to have a smaller energy difference between its HOMO and its LUMO, which corresponds to a shift of the MLCT towards longer wavelengths.

The extinction coefficients reflect as well the structures of the complexes: The more extended conjugation on the complex leads to a shift of the MLCT towards longer wavelengths and a higher ε-value, although the variation between ε_{MLCT} for **7** and **8** is not significant, showing the little difference between the presence of one or two thiophene groups as substituents.

[1] The symbols are for orientation purposes only and the spectra were measured with a 1 nm resolution.

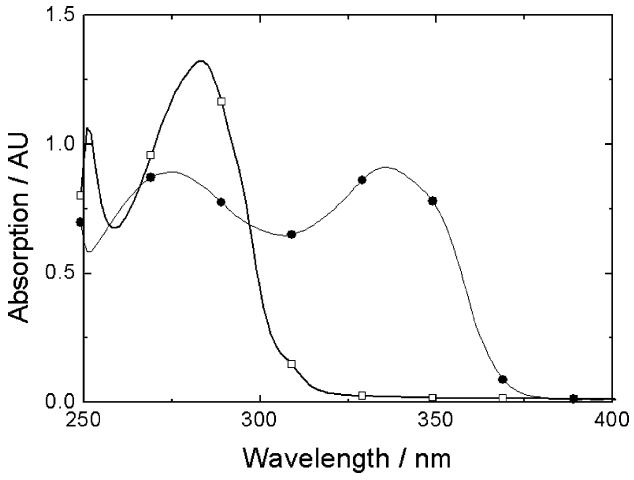

Fig. 1. Absorption spectra for both the conjugated and the non-conjugated thiophene substituted ligands 2 (-○-) and 4 (-●-) [7].

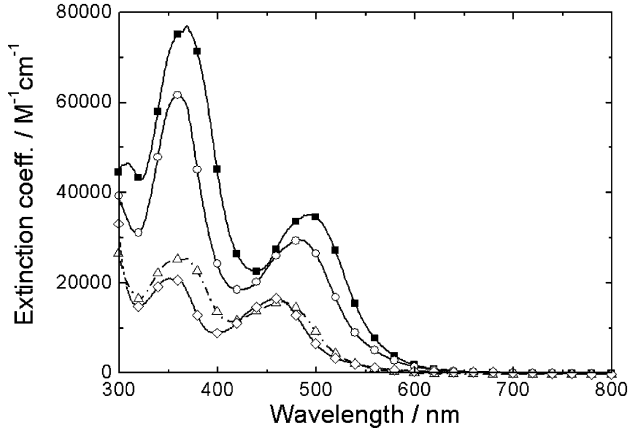

Fig. 2. Absorption spectra for the different complexes **5**–**8** (complex **5**: -○-; complex **6**: -■-; complex **7**: -◇-; complex **8**: -△-) (Footnote 1).

Table 1
Absorption properties of complexes **5**–**8** in acetonitrile

Complex	LCCT (nm)	ε_{LCCT}[a] (mol^{-1} cm^{-1})	MLCT (nm)	ε_{MLCT}[a] (mol^{-1} cm^{-1})
5	362	61 700	483	29 500
6	368	76 950	493	35 000
7	350	20 900	458	16 600
8	369[b]	25 200	463	15 700

[a] Extinction coefficient for the absorption maximum in the visible region.

[b] The relatively high value is due to an artefact from the absorption spectrum. The average would be around 358.

Table 2
Electrochemical data for complexes **5**–**8** as determined by differential pulse voltammetry[a,b]

Complex	Oxidation (V)		Reduction (V)		
3	1.08		−1.24		
4	1.08		−1.24		
	(1.05)				
5	1.12	(0.75)	−1.61	−1.80	−1.99
	(0.98)	0.72			
6	1.14	(0.74)	−1.58	−1.70	−1.92
	(1.21)	0.74			
7	1.35	(0.90)	−1.71	−1.91	−2.14
	(1.20)	0.85			
8	1.51	(0.90)	−1.62	−1.89	−2.12
		0.85			
$[Ru(bpy)_3]^{2+}$		0.93	−1.69	−1.90	−2.14
$[Ru(4,4'dsty\text{-}bpy)_3]^{2+}$		0.83			
$[Ru(Me2bpy)_3]^{2+}$		0.82	−1.75	−1.93	−2.17

[a] In Volts. A glassy carbon electrode was used as working electrode, the redox couple Fc/Fc^+ was used as internal reference and (TBA), PF_6 as electrolyte. The scan rate was 100 mV s^{-1}. The solvent was acetonitrile.

[b] The values given in brackets are measured in dichloromethane

3.3. Electrochemical properties

The electrochemistry of complexes **5**–**8** was measured. All complexes were electrochemically active in CH_2CL_2 and acetonitrile solution with 0.1 M (TBA)PF_6 as supporting electrolyte. [2] For comparison purposes also the ligands **3** and **4** were electrochemically investigated. The results are summarized in Table 2.

The redox potentials listed were measured by differential pulse voltammetry (DPV). A significant difference to numbers determined by cyclic voltammetry (CV) was not observed.

3.3.1. Oxidation

All complexes **5**–**8** showed in CV experiments at least one fully reversible peak in the oxidative region of the potential window, which can be assigned to the oxidation of Ru(II)–Ru(III). The position of the signal depends on the substitution of the bipyridine ligands. This oxidation characteristic is illustrated in Fig. 3.

As can be seen from Table 1, the Ru(II)–Ru(III) redox process of the homoleptic complexes **5** and **6** is shifted by slightly more than 100 mV towards less positive potentials in comparison to the heteroleptic complexes **7** and **8** and 200 mV relative to $[Ru(bpy)_3]^{2+}$. This experimental result can be interpreted as a stabilisation of the Ru(III)-ion in these complexes relative to $[Ru(bpy)_3]^{3+}$. Having two chemically very different substituents on the bpy-ligands (–CH_3 and –CH=CH–Th), the separation of the effects on the electronic structure within the complexes is difficult, but literature data of related compounds point out that both substituents are electron donating, which is stabilizing the oxidized state of the complex (Table 2) [7,8].

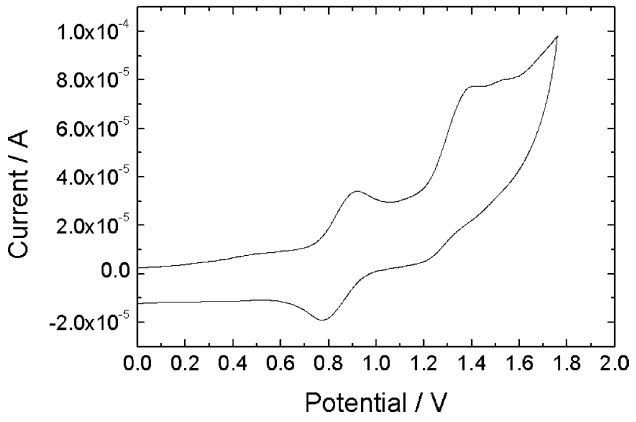

Fig. 3. Cyclic voltammogram of complex **7**. A glassy carbon electrode was used and the voltammogram was measured in acetonitrile with (TBA)PF_6 as supporting electrolyte at a scan speed of 0.1 V s^{-1}.

Beside the Ru(II)–(III) transition another – irreversible – oxidation process was observed for all complexes **5**–**8**. We assign these signals to a ligand-centred oxidation of the ethylene–thiophene substituent. A comparison with the electrochemistry of the uncoordinated ligand supports this assumption (see Table 2). Also in the literature, an oxidation of thiophene substituted polypyridine complexes was described at similar potentials [9,10].

Besides the influence of the different ligands on the oxidation potentials, an effect of the solvent was observed: Whereas the Ru(II)–Ru(III) transition remains at the same position when switching the solvent, the peaks assigned to the ethylene–thiophene oxidation were shifted by more than 100 mV to less positive potentials when changing the solvent from acetonitrile to CH_2Cl_2. To a smaller extent, such an effect was observed for thiophene oligomers for which the authors found a shift of 50 mV to less positive potentials when switching the solvent from acetonitrile to dichloromethane [11]. In the same contribution it was pointed out that the radical produced due to electrochemical oxidation is strongly stabilized by dichloromethane, which also was described generally before [12]. Therefore, we assign the shift of the second oxidation of the complexes to a solvent induced energetic stabilisation of the produced radical.

3.3.2. Reduction

Beside the electrochemical characteristics in the oxidative region of the potential window, the reduction of complexes **5**–**8** and the ligands **3** and **4** were investigated. The results are summarized in Table 2.

[2] The complexes **5** and **6** showed only poor solubility in acetonitrile and dichloromethane ($<0.5 \times 10^{-4}$ mol/l), which is reflected in the low intensity of the electrochemistry shown in Fig. 3.

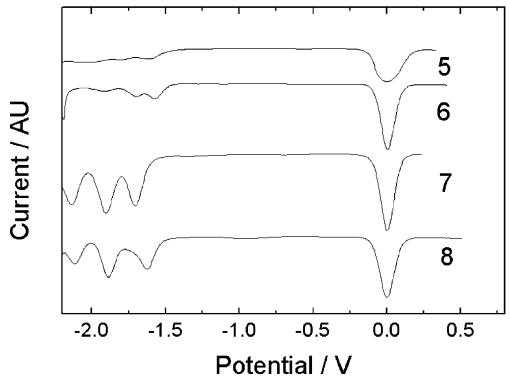

Fig. 4. DPV for compounds **5**–**8** (reductive region of the potential window). A glassy carbon electrode was used as working electrode, the redox couple Fc/Fc^{+} was employed as internal reference and $(TBA)PF_6$ (0.1 M in acetonitrile) as electrolyte.

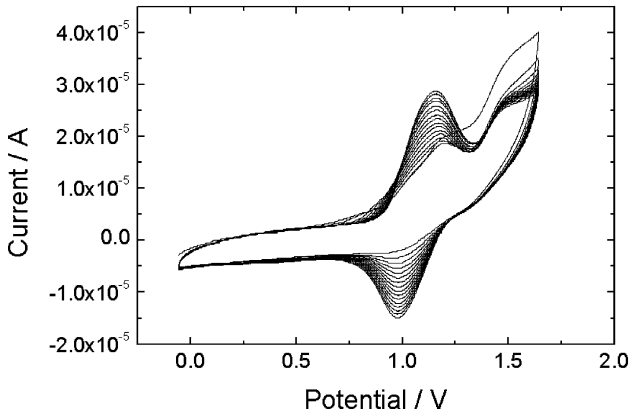

Fig. 5. Cyclic voltammogram for complex **6**. A glassy carbon electrode was used as working electrode, the redox couple Fc/Fc^{+} was employed as internal reference and $(TBA)PF_6$ (0.1 M in dichloromethane) as electrolyte at a scan rate of 100 $mV\,s^{-1}$.

For all complexes at least three signals were detected in CV and DPV (see Fig. 4) experiments at negative potentials within the potential window of acetonitrile and CH_2Cl_2 with $(TBA)PF_6$ as the supporting electrolyte, which correspond to the successive reduction of the three bipyridine ligands [13].

As expected from this type of complexes, the difference in potential between the processes is close to 200 mV. A further reduction of the bpy-ligands was also observed as expected but not analysed [3] [13].

Relative to the reduction potentials of $[Ru(bpy)_3]^{2+}$, the values for the homoleptic complexes **5** and **6** are significantly shifted to less negative potentials for all three ligand centred processes. It can be assumed that the expansion of the conjugated system by the substitution of the bpy ligand with ethylene–thiophene groups is responsible for the lowering of the LUMO. On the other side, the methyl substituents seem to have a smaller or even opposite effect since the reductions of complex **5** are located at more negative potentials than for complex **6**. For the heteroleptic complex **7**, no significant shift of the reduction potentials relative to $[Ru(bpy)_3]^{2+}$ were observed pointing out that methyl groups are rather lifting the LUMO level. This can be confirmed by a comparison with $[Ru(bpyMe_2)_3]^{2+}$ (Table 2). For complex **8**, we measured a less negative reduction process only for one ligand whereas the other two reductions are taking place at the same potentials as the equivalent processes in $[Ru(bpy)_3]^{2+}$. This allows us to attribute the first reduction of complex **8** to a localisation on the ethylene-thiophene substituted bpy-ligand.

[3] Differential pulse voltammetry had to be deployed for the determination of redox potentials since the cyclic voltammograms were dominated for the compounds **5**, **6** and **8** by polymerisation processes as discussed in the following section.

3.3.3. Electrochemical polymerisation at positive potentials

For complexes **5**, **6** and **8**, an increase in intensity of the oxidation waves in the CV experiments were observed from one cycle to the next (see Fig. 5): The first scan gives an oxidation wave for the ruthenium center as well as a strong oxidation corresponding to the irreversible oxidation of the thiophene groups [14].

The oxidation waves merge together after the first scan in combination with a substantial growth of the peaks. One can also see a red-orange film deposited on the working electrode after the experiment. These effects was only seen when the potential window of the voltammetry experiments reached the oxidation of the complexes associated with the oxidation of the ethylene-thiophene ligand substituents. We assign these observations to a radical induced polymerisation as other authors described it for similar complexes leading to three-dimensional networks with the Ru in the backbone [15–21]. This polymerisation process was mainly observed in dichloromethane, whereas a stable effect in acetonitrile could only be seen for complex **6**. As discussed earlier, a stabilisation of radical cations was observed in dichloromethane relative to acetonitrile. It seems likely that besides the shift of the oxidation potential, the stabilisation of radicals favours a successful polymerisation, since the longer lifetime increases the probability of finding a thiophene counterpart for polymerisation. Also, the shift of the ligand centred oxidation towards less positive potential in dichloromethane increased the accessibility of the process within the potential window, decreasing the interferences with traces of water or solvent related processes. A typical example for the electrochemically induced polymerisation is given in Fig. 5 for complex **6**.

By cyclic voltammetry and DPV, one can see a tremendous shift (over 100 mV) of the oxidation potential of the Ru(II)–Ru(III) redox wave, indicating a change of

Table 3
Absorption and electrochemical properties of the complexes **5**–**8** (non-polymerized and oxidatively polymerized on FTO-glass support)

Complex	λ_{max}, MLCT (nm)		E_0 (V) (vs. Fc/Fc^+)[a]	
	Monomer	Polymer	Monomer	Polymer
5	483	472	0.72	0.85
6	493	475	0.74	1.07
7	485		0.85	
8	463	450	0.85	1.02

[a] E_0 was determined in dichloromethane. The electrodes modified with a polymer were removed from the complex solution after polymerisation, rinsed with dichloromethane and then measured in dichloromethane/$(TBA)PF_6$ without the corresponding complex.

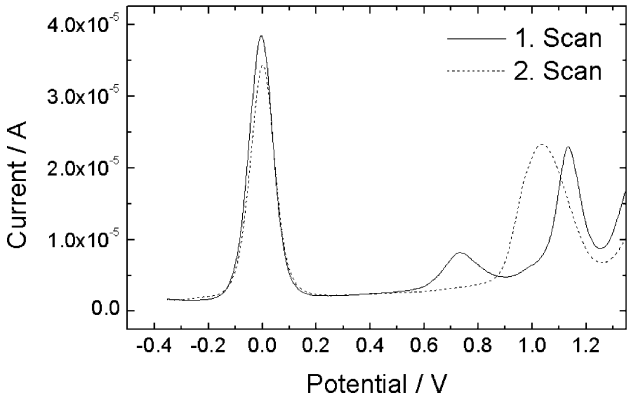

Fig. 6. DPV for complex **6**. A glassy carbon electrode was used as working electrode, the redox couple Fc/Fc^+ was used as internal reference and $(TBA),PF_6$ (0.1 M in acetonitrile) as electrolyte. First scan – solid line and second scan - - - - dashed line.

the ligand's substituents polarity (see also Table 3). This effect can be seen most clearly for the polymerisation of complex **6** in acetonitrile. [4] In Fig. 6 two successive DPVs are shown: The first scan shows two distinct peaks for the Ru(II)–Ru(III) and the ligand centred process, whereas the second scan only shows one strong peak – presumably the oxidation of the polymeric material on the electrode surface.

As discussed previously, the low oxidation potentials of complexes **5**–**8** relative to $[Ru(bpy)_3]^{2+}$ has its origin in the increased size of the conjugated system of the bpy-ligand, therefore the strong shift of the oxidation potential is indicative of a loss of this conjugation. At the same time, the disappearance of the strong oxidation peak at 1.42 V is indicative of either a consumption or a cut of the thiophene groups from the conjugated system moving the oxidation potential of the group outside the potential window due to the polymerisation.

[4] The same effect was also observed for complexes **5**, **6** and **8** in dichloromethane, but due to the close vicinity of the ligand and metal centred oxidations, the shift of oxidation due to polymerisation is less obvious than for the electrochemistry of **6** in acetonitrile.

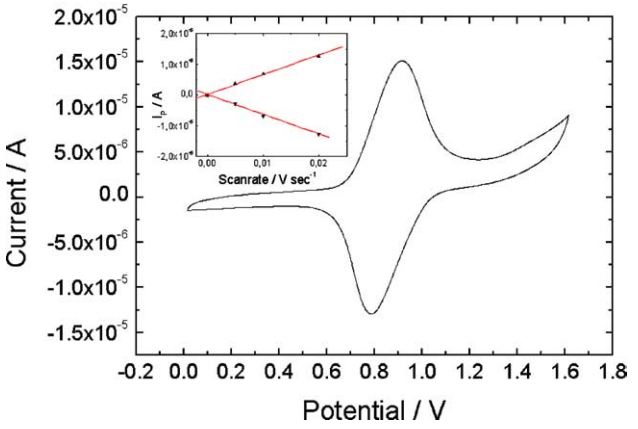

Fig. 7. Cyclic voltammogram of the polymer of complex **5** in CH_2Cl_2 with $(TBA)PF_6$ as supporting electrolyte and scan rate dependency of the peak current (inset).

The electrochemistry of the polymers was also measured in monomer-free electrolyte. A typical cyclic voltammogram is presented in Fig. 7, and the values for the oxidation potentials are given in Table 3.

In all cases we find only one oxidation peak, which we relate to the Ru(II)–Ru(III) redox couple, whereas no further ligand-located oxidation as for the monomer was detected within the potential window. For a surface bound species, the separation between the oxidation and reduction peak is even at moderate scan rates rather high for a surface bound species. For the given example it is 130 mV at a scan rate of only 20 mV s^{-1}, which is an indication of slow electron transport and transfer processes [15]. On the other side, the scan rate dependency of the peak current shows the linear behaviour expected for surface bound electro-active material, where the scan rate dependency is not influenced by its diffusion to and from the electrode (see Fig. 7, inset). [5]

Two possible mechanisms for the polymerisation can be taken into account and are pictured in Scheme 3.

Thiophenes are known to dimerize via a radical cation mechanism through the 2- and 5-positions (Scheme 3A) [22], which eventually leads for complexes with multiple thiophene substituents on the ligands to polythiophene type polymers with metal complexes in the backbone. However, in the present case the positive

[5] From the area under the redox signals, the charge and therefore the absolute number of complex entities deposited on the electrode and incorporated into the polymer network can be calculated. For example, the evaluation of the redox peaks shown in Fig. 7 gives a total charge of 3.5×10^{-5} C, which corresponds to 3.6×10^{-10} mol of complex **5** deposited on the electrode. Taking into account the surface of the electrode and that a monolayer of these complexes includes about 7.7×10^{-11} mol cm^{-2} (J. Am. Chem. Soc. 116 (1994) 5444), the thickness of the polymer is equivalent to 66 monolayers and therefore the thickness of the polymer layer is in the order of 50–100 nm after 16 deposition cycles, assuming an average Ru–Ru distance of 15–20 Å.

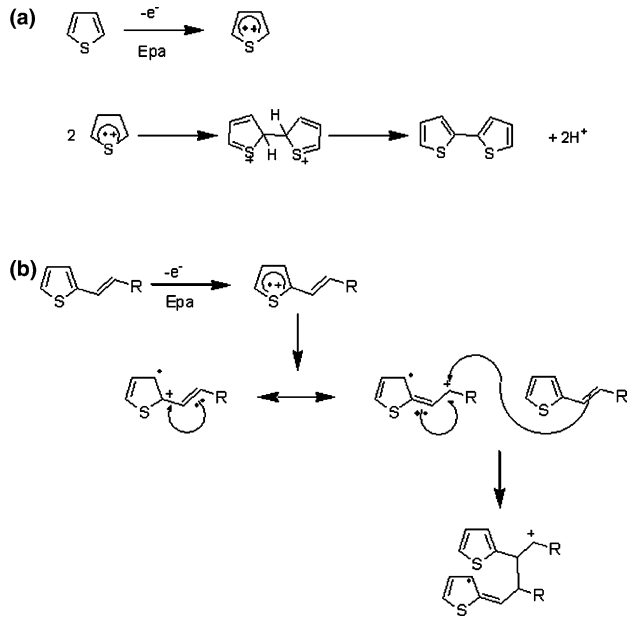

Scheme 3.

charge can delocalize towards the olefinic double bond, which will eventually dimerize (Scheme 3B) and therefore offers a alternative pathway for reaction of the oxidized species [22–26].

Absorption spectra of the polymers on FTO-glass have been recorded, and the influence of the polymerisation method is clearly seen, as exemplified for **6** (see Fig. 8) and listed in Table 3.

The blue shift of the MLCT, which we find for all oxidatively produced polymers, points towards a loss of conjugation as it is depicted in Fig. 8. The disappearance of the LC-transition for the substituted ligand at 360 nm confirms the loss of conjugation in the ligand structure (see Fig. 8).

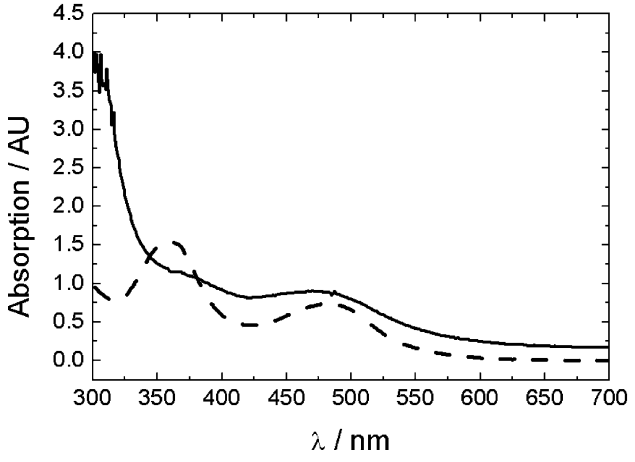

Fig. 8. Absorption spectra of polymer films of 5, deposited on glass with a conducting layer of fluorine doped tin oxide (FTO) (solid line), and of the monomer 5 in solution (dashed line).

4. Conclusions

We have reported the synthesis, characterisation and polymerisation behaviour of four thiophene substituted ruthenium complexes. The polymerisation behaviour of the complexes at positive potentials showed the behaviour of a redox active film. No polymerisation was observed at negative potentials showing the low reactivity of the vinyl functionality in these complexes. The shift of the MLCT band of the absorption spectra towards shorter wavelengths in combination with an oxidation potential at less positive potentials implied a loss of conjugation within the ligands **3** and **4** due to a radical polymerisation through the vinyl functionality after delocalisation instead of the expected thiophene–thiophene coupling. Nevertheless, an interesting feature for an application in the NSC is the broader absorption spectrum of the dye compared to a ruthenium *tris*-bipyridyl complex. Also, the introduction of a thiophene-group makes this type of dye a possible base to form a solid-state solar cell by polymerisation. These compounds, used as a model, lay the ground for the development of new dyes possessing broader absorption properties and better water tolerance for solar cell application.

Acknowledgements

The authors thank the University of Uppsala and the Ångström Solar Center for support. E.F. acknowledges the European Community for the financial support (Marie-Curie Fellowship contract no. MCFI-2001-01264).

References

[1] C.J. Brabec, N.S. Sariciftci, J.C. Hummelen, Adv. Funct. Mater. 11 (2001) 15.
[2] A. Hagfeldt, M. Grätzel, Acc. Chem. Res. 33 (2000) 269.
[3] V. Aranyos, J. Hjelm, A. Hagfeldt, H. Grennberg, J. Chem. Soc. Dalton Trans. (2001) 1319.
[4] B.P. Sullivan, D.J. Salmon, T.J. Meyer, Inorg. Chem. 17 (1978) 3334.
[5] T.A. Heimer, S.T. D'Arcangelis, F. Farzad, J.M. Stipkala, Inorg. Chem. 35 (1996) 5319.
[6] A. Juris, V. Balzani, F. Barigilletti, S. Campagna, P. Belser, A. von Zelewsky, Coord. Chem. Rev. 84 (1988) 85.
[7] V. Skarda, M.J. Cook, A.P. Lewis, G.S.G. McAuli, A.J. Thomson, D.J. Robbins, J. Chem. Soc., Perkin Trans. 2 (1984) 1293.
[8] P.A. Mabrouk, M.S. Wrighton, Inorg. Chem. 25 (1986) 526.
[9] J. Hjelm, E.C. Constable, E. Figgemeier, A. Hagfeldt, R. Handel, C.E. Housecroft, E. Mukhtar, E. Schofield, Chem. Commun. (2002) 284.
[10] T.M. Pappenfus, K.R. Mann, Inorg. Chem. 40 (2001) 6301.
[11] P. Hapiot, L. Gaillon, P. Audebert, J.J.E. Moreau, J.-P. Lère-Porte, M. Wong Chi Man, Synth. Met. 72 (1995) 129.

[12] H Lund, in: H Lund, M.M. Baizer (Eds.), Organic Electrochemistry, 3rd ed., Marcel Dekker, New York, 1991, p. 301.
[13] A. Juris, V. Balzani, F. Barigelletti, S. Campagna, P. Belser, A. von Zelewsky, Coord. Chem. Rev. 84 (1988) 85.
[14] B.J. MacLean, P.G. Pickup, J. Chem. Soc. Chem. Commun. (1999) 2471.
[15] M.O. Wolf, Adv. Mater. 13 (2001) 545.
[16] A.J. Bard, L.R. Faulkner, Electrochemical Methods: Fundamentals and Applications, Wiley, New York, 1980.
[17] R.C. Leidner, B.P. Sullivan, R.A. Reed, B.A. White, M.T. Crimmins, R.W. Murray, T.J. Meyer, Inorg. Chem. 26 (1987) 882.
[18] P.D. Beer, O. Kocian, R.J. Mortimer, C. Ridgeway, J. Chem. Soc. Faraday Trans. 89 (1993) 333.
[19] H. Segawa, F.P. Wu, N. Nakayama, H. Maruyama, S. Nagisaka, N. Higuchi, M. Fujitsuka, T. Shimidzu, Synth. Met. 71 (1995) 2151.
[20] T. Shimidzu, H. Segawa, F. Wu, N. Nakayama, J. Photochem. Photobiol. A: Chem. 92 (1995) 121.
[21] R.P. Kingsborough, T.M. Swager, J. Mater. Chem. 9 (1999) 2123.
[22] J. Roncali, Chem. Rev. 92 (1992) 711.
[23] V. Ruiz, A. Colina, A. Heras, J. Lopez-Palacios, R. Seeber, Helv. Chim. Acta 84 (2001) 3628.
[24] Refs. [29] and [30] from previous reference: J. Heinze, P. Tschuncky, A. Smie, J. Solid State Electrochem. 2 (1998) 102.
[25] Refs. [29] and [30] from previous reference: J.R. Lenhard, R.L. Parton, J. Am. Chem. Soc. 109 (1987) 5808.
[26] M. Pagels, J. Heinze, B. Geschke, V. Rang, Electrochim. Acta 46 (2001) 3943, Citation: 'Recent studies of the oxidation of radical ions containing olefinic double bonds have shown that such radicalic species dimerises at one of the olefinic carbon atoms, forming dimers. The dimerisation process may be reversible.'.

Available online at www.sciencedirect.com
SCIENCE DIRECT®
Polyhedron 23 (2004) 599–603
POLYHEDRON
www.elsevier.com/locate/poly

Synthesis and structures of new octahedral water-soluble heterometal rhenium–molybdenum clusters

Nikolai G. Naumov [a,b], Konstantin A. Brylev [b], Yuri V. Mironov [b], Alexander V. Virovets [b], Dieter Fenske [c,1], Vladimir E. Fedorov [a,b,*]

[a] Novosibirsk State University, 2 Pirogova st., 630090 Novosibirsk, Russia
[b] Nikolaev Institute of Inorganic Chemistry, Siberian Branch of the Russian Academy of Sciences, 3 prosp. Akad. Lavrentieva, 630090 Novosibirsk, Russia
[c] Institut für Anorganische Chemie, Universität Karlsruhe, Engesserstrasse 30.45, D-76128 Karlsruhe, Germany

Received 9 July 2003; accepted 22 October 2003

Abstract

The interaction of polymeric $Re_3MoS_4Te_4$ with molten KCN at 850 °C results in rearrangement of the tetrahedral $\{Re_3MoS_4\}$ cluster core to an octahedral one, $\{Re_{6-x}Mo_xS_8\}$, and formation of two new molecular octahedral heterometal rhenium–molybdenum thiocyanide cluster complexes, $[Re_5MoS_8(CN)_6]^{5-}$ and $[Re_4Mo_2S_8(CN)_6]^{5-}$, co-existing in the crystals $Cs_5[Re_{4.5}Mo_{1.5}(\mu_3\text{-}S)_8(CN)_6]\cdot 2H_2O$. The EDAX analyses and magnetic measurements data confirm the presence of a mixture of cluster anions with $x = 1$ and 2.
© 2003 Elsevier Ltd. All rights reserved.

Keywords: EDAX analyses; Anisotropic approximation; Cluster anions; Heterometal cluster complexes

1. Introduction

Among a variety of octahedral chalcogenide cluster compounds of transition metals (1–4 and references herein) there are few examples containing mixed-metal cluster cores $Mo_{6-x}M_xQ_8$ (M = Re, Q = S, Se, Te, $x = 4$; M = Ru, Q = Se, Te, $0 \leqslant x \leqslant 2$; M = Rh, Q = Te, $x = 0.5$, 1.33) [5], $Nb_{6-x}Ru_xTe_8$ ($2.50 \leqslant x \leqslant 3.17$) [6], $Cs_3Re_5OsS_{11}$ [7]. These compounds have been prepared by routine solid state synthesis and are insoluble in water and common organic media. The only soluble heterometal cluster complexes $Cs_3Re_{6-x}Os_xSe_8Cl_6$ ($x = 1$, 2) and $K_2[Re_3Os_3Se_8Cl_6][Re_4Os_2Se_7Cl_7]$ were reported very recently [8].

In the present work we report the synthesis and crystal structure of the first soluble mixed metal rhenium–molybdenum cluster complexes with terminal cyano-ligands $[Re_{6-x}Mo_x(\mu_3\text{-}S)_8(CN)_6]^{5-}$. The compound was prepared with moderate yield by the reaction of polymeric solid $Re_3MoS_4Te_4$ containing a tetrahedral cluster core with molten KCN at 850 °C.

2. Experimental

2.1. Materials and methods

X-ray powder diffraction patterns were collected on a Philips APD 1700 diffractometer (Cu Kα radiation, graphite monochromator) in the 2θ range 5°–80°. UV–Vis spectra were recorded on an Ultrospec 3300 pro spectrophotometer in the range of 200–1100 nm. IR spectra were recorded on a Bruker IFS-85 spectrometer in KBr pellets. KCN, CsCl were used as purchased. $Re_{4-x}Mo_xS_4Te_4$ ($x = 0.67$, 1, 1.33 and 2) were prepared as described in [9]. X-ray diffractometry revealed the identity of these phases. The $Re_2Mo_2S_4Te_4$ sample contained traces of MoS_2, other samples were single phase.

* Corresponding author. Tel.: +7-3832-344253; fax: +7-3832-344489.
E-mail addresses: dieter.fenske@chemie.uni-karlsruhe.de (D. Fenske), fed@che.nsk.su (V.E. Fedorov).
[1] Fax: +49(0721)-661921.

0277-5387/$ - see front matter © 2003 Elsevier Ltd. All rights reserved.
doi:10.1016/j.poly.2003.10.017

A mixture of $Re_3MoS_4Te_4$ (1 g, 0.773 mmol) and KCN (0.5 g, 7.678 mmol) was placed in a quartz tube. The tube was evacuated, sealed and kept at 850 °C for 48 h. The products of the reaction were put in 50 ml of water, boiled until potassium polytelluride decomposed and was filtered off. CsCl (0.5 g, 2.970 mmol) was added to the solution. The dark-brown solution was reduced to 2 ml and slowly cooled. The well shaped dark-brown crystals were separated by filtration and dried in air. The yield of the crystals of **1** was 0.612 g (56.67%). Chemical analysis, %: found (calcd.) Cs 31.50 (31.72), Re 39.90 (40.00), Mo 6.92 (6.87), S 12.10 (12.25). EDAX for different crystals: energy dispersive spectrometry (EDS) analyses performed on two selected single-crystals led to the following average atomic percentage, Cs/Re/Mo/S: 5.05/4.20/1.80/7.90 for crystal **1** and Cs/Re/Mo/S: 4.95/4.40/1.60/8.05 for crystal **2**. IR, cm^{-1}: 1605 (δ_{HOH}), 2106 (ν_{CN}), 3574 (ν_{OH}), UV–Vis [λ/nm (ε/M^{-1} cm^{-1} per cluster)] 455 (747), 472 (720), 490 (651) and 526 (276). $\mu_{eff} = 1.08$ μ_B (300 K).

2.1.1. Crystallography

X-ray structural analysis was carried out for two crystals on a STOE Stadi4 four-circle diffractometer (Mo K_α, $\lambda = 0.7107$ Å, graphite monochromator, standard techniques). Both crystals of $Cs_5[Re_{6-x}Mo_x(\mu_3\text{-}S)_8(CN)_6]\cdot 2H_2O$ in the form of dark brown hexagonal prisms were manually selected from the bulk sample.

2.1.2. Crystal data for the first crystal (data were collected at 211 K, size: 0.15 × 0.14 × 0.10 mm)

$C_6H_4Cs_5Mo_{1.79}N_6O_2Re_{4.21}S_8$, $M = 2068.82$, trigonal crystal system, space group $P\bar{3}c1$, $a = 9.792(3)$ Å, $c = 19.14(2)$ Å, $V = 1589.7(18)$ Å^3, $Z = 2$, $D_c = 4.322$ g cm^{-3}. A total of 2116 reflections were collected up to $2\theta_{max} = 50°$, of which 946 were unique ($R_{int} = 0.0598$). Absorption corrections ($\mu = 22.835$ mm^{-1}) were applied by integration from the crystal shape, transmission factors ranging from 0.0614 to 0.0190. The crystal is merohedry twin with law of (1 0 0/0 1 0/0 0 −1). The structure was solved by direct methods and refined by full-matrix least-squares on F^2 with an anisotropic approximation using SHELX-97 [10]. Hydrogen atoms were not located. Metal atom positions correspond to the mixture of Mo and Re atoms. The relative occupancy factors were refined together with the rest parameters without constrains. Final R values: $R_1 = 0.0378$, $wR_2 = 0.0903$ for 808 $F_o \geqslant 4\sigma(F)$, $R_1 = 0.0527$, $wR_2 = 0.0967$, GOF = 1.100 for all unique data, relative weights of twin components are 0.313(3) and 0.687(3).

2.1.3. Crystal data for the second crystal (data were collected at room temperature, size: 0.19 × 0.18 × 0.12 mm)

$C_6H_4Cs_5Mo_{1.64}N_6O_2Re_{4.36}S_8$, $M = 2082.81$, trigonal crystal system, space group $P\bar{3}c1$, $a = 9.838(3)$ Å, $c = 19.195(6)$ Å, $V = 1608.9(9)$ Å^3, $Z = 2$, $D_c = 4.299$ g cm^{-3}. A total of 4051 reflections were collected up to $2\theta_{max} = 50°$, of which 1240 were unique ($R_{int} = 0.0954$). Absorption corrections ($\mu = 23.084$ mm^{-1}) were applied by integration from the crystal shape, transmission factors ranging from 0.9952 to 0.5312. The crystal is merohedry twin with law of (1 0 0/0 1 0/0 0 −1). The structure was solved by direct methods and refined by full-matrix least-squares on F^2 with an anisotropic approximation using SHELX-97 [10]. As in the first crystal, metal atom positions correspond to the mixture of Mo and Re atoms. The relative occupancy factors also were refined together with the rest parameters without constrains. Hydrogen atoms were not located. Final R values: $R_1 = 0.0406$, $wR_2 = 0.0765$ for 808 $F_o \geqslant 4\sigma(F)$, $R_1 = 0.0678$, $wR_2 = 0.0905$, GOF = 1.125 for all unique data. Relative weights of twin components are 0.408(3) and 0.592(3).

Crystal data and selected bond lengths for the two crystals are given in the Tables 1 and 2, respectively.

Table 1
Crystal data and structure refinements for $Cs_5[Re_{4.21}Mo_{1.79}S_8(CN)_6]\cdot 2H_2O$ (**1**) and $Cs_5[Re_{4.36}Mo_{1.64}S_8(CN)_6]\cdot 2H_2O$ (**2**)

Compound	**1**	**2**
Chemical Formula	$C_6H_4Cs_5Mo_{1.79}N_6O_2Re_{4.21}S_8$	$C_6H_4Cs_5Mo_{1.63}N_6O_2Re_{4.36}S_8$
Formula weight	2068.82	2082.81
Space group	$P\bar{3}c1$	$P\bar{3}c1$
a (Å)	9.792(3)	9.838(3)
c (Å)	19.14(2)	19.195(6)
V (Å^3)	1589.7(18)	1608.9(9)
Z	2	2
λ (Å)	0.71073	0.71073
T (K)	211	293
ρ_{calc} (g/cm^3)	4.322	4.299
μ (cm^{-1})	228.35	230.84
$R(F)$[a]	0.0378	0.0406
$R_w(F^2)$	0.0967[b]	0.0905[c]

[a] $R(F) = \sum ||F_o| - |F_c|| / \sum |F_o|$ for $F_o^2 > 2\sigma(F_o^2)$.
[b] $R_w(F_o^2) = \{\sum [w(F_o^2 - F_c^2)^2] / \sum wF_o^4\} \cdot w^{-1} = \sigma^2(F_o^2) + (0.053F_o^2)^2$ for $F_o^2 \geqslant 0$ and $w^{-1} = \sigma^2(F_o^2)$ for $F_o^2 < 0$.
[c] $R_w(F_o^2) = \{\sum [w(F_o^2 - F_c^2)^2] / \sum wF_o^4\} \cdot w^{-1} = \sigma^2(F_o^2) + (0.028F_o^2)^2$ for $F_o^2 \geqslant 0$ and $w^{-1} = \sigma^2(F_o^2)$ for $F_o^2 < 0$.

Table 2
Selected bond lengths (Å) for $Cs_5[Re_{4.21}Mo_{1.79}S_8(CN)_6]\cdot 2H_2O$ (**1**) and $Cs_5[Re_{4.36}Mo_{1.64}S_8(CN)_6]\cdot 2H_2O$ (**2**)[a]

Compound	**1**	**2**
Re,Mo(1)–Re,Mo(1)#1	2.619(2)	2.6244(13)
Re,Mo(1)–Re,Mo(1)#2	2.6201(14)	2.6268(13)
Re,Mo(1)–S(1)	2.444(6)	2.443(5)
Re,Mo(1)–S(2)	2.449(4)	2.458(4)
Re,Mo(1)–S(2)#1	2.458(4)	2.463(4)
Re,Mo(1)–S(2)#2	2.459(4)	2.4588(4)
Re,Mo(1)–C(1)	2.151(17)	2.139(16)
C(1)–N(1)	1.14(2)	1.14(2)

#1: $-x, -y+1, -z$; #2: $-x+y-1, -x+1, z$.
[a] Symmetry transformation used to generate equivalent atoms.

3. Discussion

The concurrent formation of Re_4 and Re_6 clusters realized in high temperature reactions is known. The study of Re–Te–Cl and Re–Se–Cl systems showed that Re_4 clusters are stable below 400 °C, while above this temperature Re_6 ones are stable [11]. Up to now $Re_4S_4Te_4$ [12] found in the ternary Re–S–Te system is the only tetrahedral cluster compound stable at 900 °C.

Our preliminary study of the interaction of the $Re_4S_4Te_4$ with molten KCN at 850 °C showed that the reaction resulted in rearrangement from a Re_4 to Re_6 cluster core and formation of a compound isostructural to the known cubic phase $Cs_3K[Re_6(\mu_3\text{-}S)_6(\mu_3\text{-}Te_{0.66}S_{0.34})_2(CN)_6]$ [13] with cell parameters $a = 17.80(1)$ Å, $V = 5640$ Å^3. Therefore we could expect that heterometallic $Re_{4-x}Mo_xS_4Te_4$ [9] clusters can be used as starting materials for preparation of new compounds with an octahedral $\{Re_{6-x}Mo_x\}$ cluster core.

The interaction of the tetrahedral heterometallic cluster compound $Re_3MoS_4Te_4$ under the conditions reported in Section 2 leads to the formation of a compound with an average composition $Cs_5[Re_{4.5}Mo_{1.5}(\mu_3\text{-}S)_8(CN)_6]\cdot 2H_2O$. EDAX for a set of single crystals showed that the Re/Mo ratio for them vary in the range $Re_{4.2}Mo_{1.8}$–$Re_{4.5}Mo_{1.5}$, while the Cs/(Re,Mo) ratio is nearly constant. No remarkable amount of tellurium presents in the tested crystals. All crystals in the synthesis have the same shape, hexagonal prisms. It should mean that all of them have the same structure, which was confirmed by measuring the powder diffraction pattern. The X-ray powder diffraction and EDAX data show that we have a typical solid solution with variable

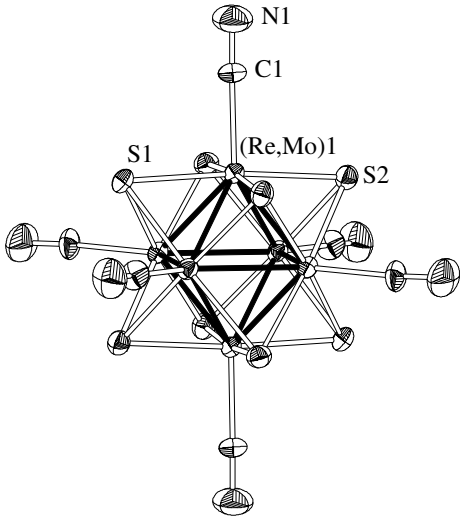

Fig. 1. Anion in **2** (a.d.p. ellipsoids at 50% probability level). Some geometrical parameters (Å): (Re,Mo)–(Re,Mo), 2.624(1)–2.627(1), av. 2.626[2]; (Re,Mo)-μ_3-S, 2.443(5)–2.463(4), av. 2.455[7]; (Re,Mo)–C, 2.139(16); C–N, 1.14(2).

Table 3
Interatomic distances (Å) in the octahedral cluster cores $\{M_6Q_8\}$

Compounds	M–M	Δ(M–M)	Mean (M–M)	M–Q	Δ(M–Q)	Mean (M–Q)	Ref.
$KCs_3Re_6S_8(CN)_6$	2.598–2.608	0.01	2.603	2.399–2.590	0.191	2.454	[13]
$NaCs_3Re_6S_8(CN)_6$	2.597–2.607	0.01	2.602	2.398–2.429	0.031	2.411	[18]
$K_7[Mo_6S_8(CN)_6]\cdot 8H_2O$	2.666(1)	0	2.666(1)	2.457(1)	0	2.457(1)	[16]
$[Mo_6S_8(PEt_3)_6]$	2.662–2.664	0.002	2.663	2.438–2.449	0.011	2.444	[19]
$Cs_5[Re_{4.21}Mo_{1.79}S_8(CN)_6]\cdot 2H_2O$	2.619(2)–2.620(1)	0.001	2.620	2.444(6)–2.459(4)	0.013	2.452(7)	this work
$Cs_5[Re_{4.36}Mo_{1.64}S_8(CN)_6]\cdot 2H_2O$	2.624(1)–2.627(1)	0.003	2.626(2)	2.443(5)–2.463(4)	0.020	2.455(7)	this work
$Mo_6S_8(py)_6\cdot 2py$	2.641(2)–2.647(2)	0.006	2.644(2)	2.455(3)–2.467(3)	0.012	2.462(3)	[20]
$Mo_6S_8(pyrr)_6\cdot pyrr$	2.635(2)–2.672(2)	0.037	2.649(2)	2.435(4)–2.463(3)	0.028	2.447(4)	[20]
$Mo_6S_8(pip)_6\cdot 7pip$	2.637(1)–2.658(1)	0.021	2.649(1)	2.431(2)–2.465(2)	0.034	2.452(2)	[20]
$K_6W_6S_8(CN)_6\cdot 10H_2O$	2.6772(7)	0	2.6772(7)	2.452(2)	0	2.452(2)	[17]
$Na_6W_6S_8(CN)_6\cdot 18DMSO$	2.6818(4)–2.6875(4)	0.006	2.685(3)	2.452(2)–2.467(1)	0.015	2.459	[17]
$Cs_5Re_5OsS_{11}$	2.614(2)–2.619(2)	0.005	2.617	2.398(4)–2.422(3)	0.024	2.415	[7]

composition, namely, different crystals belonging to the same structural type have variable Re/Mo ratio. To investigate this phenomenon we have selected two crystals for X-ray structural analysis. Both of them appeared to be merohedry twins which is typical for trigonal crystals with hexagonal shape. As expected the structures of both crystals were the same but relative Re/Mo occupancies are different.

The cluster anion in the structure of the reported compounds (Fig. 1) has a structure which is similar to well-known $[M_6Q_8(CN)_6]^{n-}$ octahedral chalcocyanide cluster complexes (M = Re, Q = S, Se, Te, $n = 3$, 4 [13,14]; M = Mo, Q = S, Se, $n = 6$, 7 [15,16]; M = W, Q = S, $n = 6$ [17]). As usual, the metal octahedron is surrounded by eight μ_3-S ligands forming a S_8 cube. Additionally each metal atom is coordinated by the linear CN ligand through the C atom. Average bond lengths are given in Table 3 together with the data for other related compounds. We can see that Re–Re bond distances in $[Re_6S_8(CN)_6]^{4-}$ (2.603 Å) are significantly shorter than Mo–Mo bond distances in $[Mo_6S_8(CN)_6]^{7-}$ (2.666 Å). X-ray structural analysis shows that the metal–metal bond distances in our heterometallic phase, $[Re_{6-x}Mo_x(\mu_3\text{-}S)_8(CN)_6]^{5-}$, depend on the value of x (2.619(2)–2.620(1) and 2.624(1)–2.627(1) for $x = 1.79$ and $x = 1.63$, respectively, Table 3), lying in the range between Re–Re and Mo–Mo. The M–S distances for all $[M_6S_8(CN)_6]^{n-}$ (M = Mo, W, Re; $n = 4$, 5, 6, 7) anions are almost the same and therefore are not sensitive to the nature of the metal atoms. The crystal packing is shown in Fig. 2.

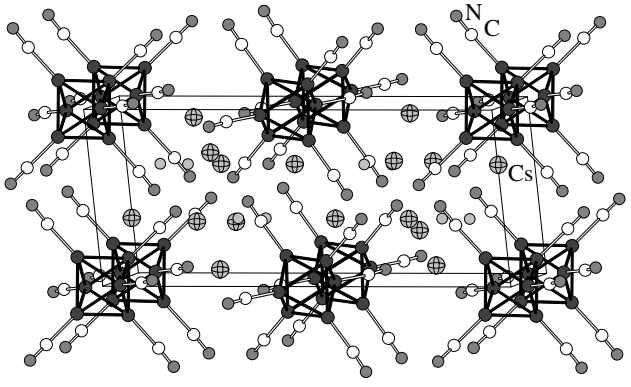

Fig. 2. Crystal packing in **2**. Sulfur atoms are omitted for clarity.

All the experimental data show that the prepared phase is the solid solution of cesium salts of different $[Re_{6-x}Mo_xS_8(CN)_6]^{5-}$ anions. Because the average value of x is close to 1.5 we can expect that we have mixture of $[Re_5MoS_8(CN)_6]^{5-}$ and $[Re_4Mo_2S_8(CN)_6]^{5-}$ clusters. The structural and EDAX data show that the Cs/(Re,Mo) ratio is constant. It means that both anions have the same charge, −5. From this it is possible to conclude that the valence electron concentration (VEC) for the $[Re_5MoS_8(CN)_6]^{5-}$ anion is equal to 24 electrons and this anion is diamagnetic, while $[Re_4Mo_2S_8(CN)_6]^{5-}$ has a VEC = 23 and is paramagnetic. The measured value of effective magnetic moment, 1.08 MB, is in good agreement with the suggestion that only half of the cluster units contain an unpaired electron.

We also have investigated the reaction of other phases in the $Re_{4-x}Mo_xS_4Te_4$ series [9] with molten KCN and found that under similar experimental conditions similar phases with different Re/Mo ratio were formed. The crystallization with CsCl resulted in phases isostructural to crystals **1** and **2**. EDAX analysis made on several crystals gave compositions summarized in Table 4. We can suppose that these phases contain {Re_5Mo}, {Re_4Mo_2} and {Re_3Mo_3} octahedral clusters.

In conclusion, interaction of tetrahedral $Re_{4-x}Mo_xS_4Te_4$ cluster compounds with molten KCN leads to the formation of octahedral heterometallic $[Re_{6-x}Mo_xS_8(CN)_6]^{5-}$ cluster anions, $x = 1$, 2 co-existing in the crystals $Cs_5[Re_{6-x}Mo_x(\mu_3\text{-}S)_8(CN)_6]\cdot 2H_2O$. The solubility of these salts opens the way for further study of the chemical properties of Re–Mo heterometallic cluster complexes.

4. Supplementary data

Supplementary data are available from the CCDC, 12 Union Road, Cambridge CB2 1EZ, UK (fax: +44-1223-336033; E-mail: deposit@ccdc.cam.ac.uk or www: http://www.ccdc.cam.ac.uk) on request, quoting the deposition Nos. 391226 and 391227.

Table 4
Expected and found Re/Mo ratios in $Cs_5[Re_{6-x}Mo_xS_8(CN)_6]\cdot 2H_2O$ series

Starting polymeric solid	Expected Re/Mo ratio in octahedral cluster	Experimental Re/Mo ratio averaged by several crystals	Yield of salt, %
$Re_{3.33}Mo_{0.67}S_4Te_4$	Re_5Mo	$Re_{4.9}Mo_{1.1}$	40
$Re_3MoS_4Te_4$	$Re_{4.5}Mo_{1.5}$	$Re_{4.4}Mo_{1.6}$	56.7
$Re_{2.7}Mo_{1.3}S_4Te_4$	Re_4Mo_2	$Re_{4.1}Mo_{1.9}$	45
$Re_2Mo_2S_4Te_4$	Re_3Mo_3	$Re_{3.8}Mo_{2.2}$	15

Acknowledgements

This work was supported by the Program "Universities of Russia" of the Education Ministry of Russian Federation, Grant UR.05.01.038.

References

[1] T. Saito, Adv. Inorg. Chem. 44 (1997) 45.
[2] J.R. Long, L.S. McCarty, R.H. Holm, J. Am. Chem. Soc. 118 (1996) 4603.
[3] J.C.P. Gabriel, K. Boubekeur, S. Uriel, P. Batail, Chem. Rev. 101 (2001) 2037.
[4] N.G. Naumov, A.V. Virovets, V.E. Fedorov, J. Struct. Chem. (Engl. Transl.) 41 (2000) 499.
[5] (a) A. Perrin, M. Sergent, Ø. Fischer, Mater. Res. Bull. 13 (1978) 259;
(b) A. Perrin, R. Chevrel, M. Sergent, Ø. Fischer, J. Solid State Chem. 33 (1980) 43;
(c) W. Hönle, H.D. Flack, K. Yvon, J. Solid State Chem. 49 (1983) 157;
(d) F.J. Berry, C.D. Gibbs, J. Chem. Soc., Dalton Trans. (1991) 57;
(e) F.J. Berry, C.D. Gibbs, C. Greaves, J. Solid State Chem. 92 (1991) 148.
[6] J. Neuhausen, E.W. Finckh, W. Tremel, Inorg. Chem. 35 (1996) 5622.
[7] W. Bronger, C. Koppe, M. Loevenich, D. Schmitz, T. Schuster, Z. Anorg. Allg. Chem. 623 (1997) 695.
[8] E.G. Tulsky, J.R. Long, Inorg. Chem. 40 (2001) 6990.
[9] G.F. Khudorozhko, E.A. Kravtsova, L.N. Mazalov, V.E. Fedorov, L.G. Bulusheva, I.P. Asanov, G.K. Parygina, Y.V. Mironov, J. Struct. Chem. (Engl. Transl.) 37 (1996) 767.
[10] G.M. Sheldrick, SHELX-97 Release 97-2, Göttingen University, Göttingen, Germany, 1997.
[11] Y.V. Mironov, V.E. Fedorov, J. Struct. Chem. (Engl. Transl.) 40 (1999) 959.
[12] V.E. Fedorov, Y.V. Mironov, V.P. Fedin, H. Imoto, T. Saito, Acta Cryst. C 52 (1996) 1065.
[13] (a) Y.V. Mironov, A.V. Virovets, V.E. Fedorov, N.V. Podberezskaya, O.V. Shishkin, Y.T. Struchkov, Polyhedron 14 (1995) 3171;
(b) A. Slougui, Y.V. Mironov, A. Perrin, V.E. Fedorov, Croat. Chem. Acta 68 (1995) 885.
[14] (a) Y.V. Mironov, J.A. Cody, T.A. Albrecht-Schmitt, J.A. Ibers, J. Am. Chem. Soc. 119 (1997) 493;
(b) N.G. Naumov, A.V. Virovets, N.V. Podberezskaya, V.E. Fedorov, J. Struct. Chem. (Engl. Transl.) 38 (1997) 857;
(c) H. Imoto, N.G. Naumov, A.V. Virovets, T. Saito, V.E. Fedorov, J. Struct. Chem. (Engl. Transl.) 39 (1998) 720;
(d) N.G. Naumov, E.V. Ostanina, A.V. Virovets, M. Schmidtmann, A. Muller, V.E. Fedorov, Russ. Chem. Bull. 51 (2002) 866.
[15] Y.V. Mironov, A.V. Virovets, N.G. Naumov, V.N. Ikorskii, V.E. Fedorov, Chem. Eur. J. 8 (2000) 1361.
[16] K.A. Brylev, A.V. Virovets, N.G. Naumov, Y.V. Mironov, D. Fenske, V.E. Fedorov, Russ. Chem. Bull. 50 (2001) 1140.
[17] S. Jin, F.J. DiSalvo, Chem. Commun. (2001) 1586.
[18] L.G. Beauvais, M.P. Shores, J.R. Long, Chem. Mater. 10 (1998) 3783.
[19] T. Saito, N. Yamamoto, T. Yamagata, H. Imoto, J. Am. Chem. Soc. 110 (1988) 1646.
[20] S.J. Hilsenbeck, V.G. Young Jr., R.E. McCarley, Inorg. Chem. 33 (1994) 1822.

Available online at www.sciencedirect.com
SCIENCE DIRECT®
Polyhedron 23 (2004) 605–609
POLYHEDRON
www.elsevier.com/locate/poly

Titanium(IV) iodide complexes with phosphine and arsine donor ligands and the crystal structures of the iron(II)/(III) redox pair $[FeI_2\{o\text{-}C_6H_4(AsMe_2)_2\}_2]^{0/+}$

William Levason *, Melissa L. Matthews, Bhavesh Patel, Gillian Reid, Michael Webster

Department of Chemistry, University of Southampton, Highfield, Southampton SO17 1BJ, UK

Received 19 September 2003; accepted 24 October 2003

Abstract

Red-brown $[TiI_4\{o\text{-}C_6H_4(PMe_2)_2\}]$ and $[TiI_4\{o\text{-}C_6H_4(AsMe_2)_2\}]$ have been prepared from the ligands and TiI_4 in a 1:1 molar ratio in anhydrous CH_2Cl_2. They have been characterised by analysis, IR, ^1H and $^{31}P\{^1H\}$ NMR and UV–Visible spectroscopy as appropriate and have six-coordinate (*cis*) octahedral geometries. Investigation of the yellow or fawn products from reactions of TiI_4 and the ligands in a 1:2 molar ratio, and suggested in the literature to be bis(ligand)-Ti(IV) complexes, have shown that these are mixtures containing iodinated and oxidised ligands, but do not contain Ti(IV)–iodide complexes. The crystal structures of two iron–diarsine complexes $[FeI_2\{o\text{-}C_6H_4(AsMe_2)_2\}_2]$ and $[FeI_2\{o\text{-}C_6H_4(AsMe_2)_2\}_2]I_3 \cdot 2CH_2Cl_2$ arising from iron iodide impurities in one commercial sample of TiI_4 are reported. The complexes constitute a redox pair and the iron(III) complex is the first *pseudo*-octahedral iron(III) iodide complex to be structurally characterised.
© 2003 Elsevier Ltd. All rights reserved.

Keywords: Titanium iodide; Phosphine; Arsine; Iron iodide; Crystal structures

1. Introduction

Titanium(IV) chloride is a strong Lewis acid and forms many complexes with neutral ligands with Groups 15 or 16 donor atoms [1,2]. The majority are six-coordinate $[TiCl_4L_2]$ or $[TiCl_4(L–L)]$ (L = monodentate, L–L = bidentate ligand), but with a very limited number of diphosphine or diarsine ligands, including $o\text{-}C_6H_4(PMe_2)_2$, $Me_2PCH_2CH_2PMe_2$ and $o\text{-}C_6H_4(AsMe_2)_2$, both six-coordinate $[TiCl_4(L–L)]$ and eight-coordinate $[TiCl_4(L–L)_2]$ can be isolated [3,4]. Titanium(IV) bromide generally forms similar complexes, although its Lewis acidity is weaker than the chloride and the complexes are more extensively dissociated in solution. In marked contrast, very little is known about the complexes of titanium(IV) iodide, which is a weak Lewis acid. Early studies reported the formation of dark coloured oils or solids on reaction with ethers or amines [5,6], none of which has been thoroughly characterised. With $o\text{-}C_6H_4(AsMe_2)_2$ a yellow product, suggested to be $[TiI_2\{o\text{-}C_6H_4(AsMe_2)_2\}_2]I_2$ has been reported [7], but with little data and its nature is unclear. A weakly paramagnetic yellow $[TiI_4L_3]$ (L_3 = the triarsine $MeAs(CH_2CH_2CH_2AsMe_2)_2$) has also been mentioned, but is similarly ill-defined [8]. We have reported two red-brown diselenoether complexes $[TiI_4(L–L)]$ (L–L = $MeSeCH_2CH_2SeMe$, $o\text{-}C_6H_4(SeMe)_2$) [9].

We recently re-examined the complexes formed by $TiCl_4$ and $TiBr_4$with a variety of diphosphines and diarsines and obtained detailed characterisations of six- ($[TiX_4(L–L)]$) and eight-coordinate ($[TiX_4(L–L)_2]$) (X = Cl or Br) complexes [4], including multinuclear NMR studies of their solution behaviour and crystallographic studies of several examples. The most stable complexes were produced by L–L = $o\text{-}C_6H_4(PMe_2)_2$ and $o\text{-}C_6H_4(AsMe_2)_2$ and these also offer the possibility of obtaining

* Corresponding author. Tel.: +44-2380-593792; fax: +44-2380-593781.
E-mail address: wxl@soton.ac.uk (W. Levason).

0277-5387/$ - see front matter © 2003 Elsevier Ltd. All rights reserved.
doi:10.1016/j.poly.2003.10.010

both six- and eight-coordinate examples [4]. In view of the paucity of titanium(IV) iodide complexes, we have examined the reactions of these two ligands with TiI_4 under a variety of conditions, and show that whilst six-coordinate $[TiI_4(L–L)]$ can be isolated, there is no evidence for eight-coordination, and that the yellow products described in the literature are not titanium(IV) complexes.

2. Results and discussion

2.1. $[TiI_4\{o\text{-}C_6H_4(PMe_2)_2\}]$ and $[TiI_4\{o\text{-}C_6H_4(AsMe_2)_2\}]$

The reaction of TiI_4 in rigorously anhydrous CH_2Cl_2 with one equivalent of $o\text{-}C_6H_4(PMe_2)_2$ gave a red-brown solid identified as $[TiI_4\{o\text{-}C_6H_4(PMe_2)_2\}]$ by analysis. The solid is stable under dry dinitrogen, but is rapidly hydrolysed on exposure to air, and instantly decomposed in solution by trace moisture with loss of the colour. The complex is less soluble in chlorocarbons than the corresponding chloride or bromide and these initially red-brown solutions pale over several days, indicative of decomposition. Repeated attempts to obtain crystals for an X-ray study have been unsuccessful. The dark red-brown $[TiI_4\{o\text{-}C_6H_4(AsMe_2)_2\}]$ was made analogously and has very similar properties. The Nujol mull IR spectra of both complexes are similar to those of the corresponding chloro- or bromo-complexes except for the absence of Ti–halogen stretches, which are expected to lie <200 cm^{-1} in the iodides, outside the range of the spectrometer. The UV–Visible spectra show broad features >20 000 cm^{-1} which are attributed to $\sigma(P, As) \rightarrow Ti(t_{2g})$ charge transfer bands [4], and notably, very broad intense features centred at ca. 17 500 cm^{-1} which tail down to ca. 13 000 cm^{-1}, assigned as $\pi(I) \rightarrow Ti(t_{2g})$ and which are responsible for the dark red-brown colours. The assignment of the latter bands as $\pi(I) \rightarrow Ti(t_{2g})$ follows the expected bathochromic shifts in $\pi(X) \rightarrow Ti(t_{2g})$ as X changes $Cl \rightarrow Br \rightarrow I$ [10], and is clear evidence for the presence of Ti(IV)–iodide bonds.

The ^1H NMR spectrum of $[TiI_4\{o\text{-}C_6H_4(PMe_2)_2\}]$ in dry CD_2Cl_2 solution showed a single second order multiplet δ(Me) resonance, which was unchanged on cooling the solution to 190 K, showing that dissociation of the diphosphine is negligible. The $^{31}P\{^1H\}$ NMR spectrum was a singlet at $\delta = 18$, which compares with the values in the "free" ligand (δ −55), and in $[TiCl_4\{o\text{-}C_6H_4(PMe_2)_2\}]$ (δ 29.5) and $[TiBr_4\{o\text{-}C_6H_4(PMe_2)_2\}]$ (δ 24.5) [4], showing a stepwise decrease in coordination shift along the series Cl > Br > I, consistent with the reduced Lewis acidity in the same order. The ^1H NMR spectrum of $[TiI_4\{o\text{-}C_6H_4(AsMe_2)_2\}]$ in dry CD_2Cl_2 solution shows partial dissociation of the ligand with a singlet (Me) at 2.11 attributed to the coordinated $AsMe_2$ groups, and one at 1.20 due to "free" $AsMe_2$ groups, with approximately equal intensities (and corresponding aromatic resonances). This continues the pattern found with the lighter halides [4] – whilst $[TiCl_4\{o\text{-}C_6H_4(AsMe_2)_2\}]$ shows only a singlet δ(Me) due to coordinated ligand, in solutions of $[TiBr_4\{o\text{-}C_6H_4(AsMe_2)_2\}]$ resonances due to both "free" and coordinated diarsine groups are present. It was also noted that in rigorously dry CH_2Cl_2 solutions, neither $[TiCl_4\{o\text{-}C_6H_4(PMe_2)_2\}]$ or $[TiBr_4\{o\text{-}C_6H_4(PMe_2)_2\}_2]$ underwent halogen exchange with $^nBu_4NI$ (on the basis of their $^{31}P\{^1H\}$ NMR spectra recorded 30 min after mixing), showing the expected preference of hard Ti(IV) for the lighter halide. Although we have been unable to obtain crystallographic confirmation of the structure, the spectroscopic properties of these two complexes are entirely consistent with their formulation as *cis pseudo*-octahedral monomers.

2.2. The "$TiI_4(L–L)_2$" complexes

The addition of a second equivalent of $o\text{-}C_6H_4(AsMe_2)_2$ to a solution of $[TiI_4\{o\text{-}C_6H_4(AsMe_2)_2\}]$ in dry CH_2Cl_2, or direct reaction of two equivalents of $o\text{-}C_6H_4(AsMe_2)_2$ with TiI_4 in dry CH_2Cl_2, produces yellow solutions which precipitate (in poor yield) yellow or fawn powders on concentration. The products hydrolyse rapidly in air and contain Ti, As and I (EDX study). [1] However the UV–Vis spectrum of the solid shows only intense, ill-defined features >26 000 cm^{-1} and no significant absorption <20 000 cm^{-1}. Crucially this rules out the presence of Ti(IV)–I bonds, compare $[TiI_4\{o\text{-}C_6H_4(AsMe_2)_2\}]$ (above). Notably, in the $[TiX_4\{o\text{-}C_6H_4(AsMe_2)_2\}_n]$ (X = Cl or Br, $n = 1$ or 2) the $\pi(X) \rightarrow Ti(t_{2g})$ differ little in energy between the six- and eight-coordinate centres [4]. The ^1H NMR spectra in anhydrous $CDCl_3$ of different samples of the yellow substance show a mixture of species present, with Me resonances in two groups ca. δ 1.2 (corresponding to "free" $AsMe_2$ groups) and ca. 1.85–2.2. The latter resonances could be due to coordinated $AsMe_2$ groups but are similar to those found in solutions of the diarsine in $CDCl_3$ treated with diiodine. The relative intensities of the resonances differ between samples. Significantly, none of the resonances are attributable to $[TiI_4\{o\text{-}C_6H_4(AsMe_2)_2\}]$, which would have been expected to be formed by dissociation of a 1:2 complex [4]. On this basis the products are formulated as mixtures of partially iodinated diarsine, e.g., $o\text{-}C_6H_4(AsMe_2)(AsMe_2I_2)$, possibly arsine oxide (formed by hydrolysis), and lower oxidation state titanium species. Studies of the reaction of tertiary

[1] C, H analysis is not helpful. We found values for our samples C, 22 ± 1%; H, ca. 3 ± 0.5%. Calculated for $[TiI_4(\{o\text{-}C_6H_4(AsMe_2)_2\}_2]$: C, 21.3; H, 2.9%. $[TiI_3(\{o\text{-}C_6H_4(AsMe_2)_2\}_2]$: C, 24.0; H, 3.2%. $o\text{-}C_6H_4(AsMe_2)(AsMe_2I_2)$: C, 22.3; H, 3.0%.

arsines with diiodine have shown that a variety of R_3AsI_2, R_3AsI_4 and more complex materials form [11,12]. Little is known about complexes of titanium iodides in lower oxidation states, although a brown $[Ti_2I_6(PMe_3)_4]$ has been structurally characterised [13], and the presence of Ti(III) would account for the paramagnetism reported for some titanium iodide–arsine complexes in the older literature [8].

The reaction of TiI_4 with o-$C_6H_4(PMe_2)_2$ in a 1:2 ratio also gives a fawn-yellow solid with generally similar properties. The $^{31}P\{^1H\}$ NMR spectrum of this material in dry CH_2Cl_2 shows resonances at δ −47 (v br), −26, +33 and +38 along with some other much weaker features; species with δ −47 (v br), +37, +38 are formed by treating o-$C_6H_4(PMe_2)_2$ in CH_2Cl_2 with I_2, and no resonance at δ 18, which would indicate some $[TiI_4\{o\text{-}C_6H_4(PMe_2)_2\}]$, was found. It seems clear that the product of reacting TiI_4 with two equivalents of o-$C_6H_4(PMe_2)_2$ is also a mixture containing substantial amounts of iodinated diphosphine and no Ti(IV). We note that Cotton and Kibala [12] reported isolation of $[(Ph_3PI)_2I_3]I_3$ as a by-product of the reactions of ZrI_4 with Ph_3P – reduction of Zr(IV) is considerably harder than of Ti(IV). It is probable that eight-coordination (as in $[TiI_4\{o\text{-}C_6H_4(EMe_2)_2\}_2]$) is sterically precluded for the larger iodide ligands, and instead Ti(IV) is reduced by the excess phosphine or arsine present.

2.3. Diarsine complexes of Fe(II) and Fe(III) Iodide

Many attempts were made to obtain crystals from the samples of "$[TiI_4\{o\text{-}C_6H_4(AsMe_2)_2\}_2]$" by slow evaporation of solutions in rigorously dry chlorocarbons or by layering chlorocarbon solutions with dry hexane. Most failed, producing only pale yellow powders. However, from two independently prepared solutions containing TiI_4 and o-$C_6H_4(AsMe_2)_2$ in a 1:2 ratio in CH_2Cl_2, allowed to evaporate slowly in a dry glove-box, a few brown and red-purple crystals were isolated (along with much decomposed material). X-ray data were collected on both, and initial solution and refinement proceeded to yield structures which appeared to be $[TiI_2\{o\text{-}C_6H_4(AsMe_2)_2\}_2]$ and $[TiI_2\{o\text{-}C_6H_4(AsMe_2)_2\}_2]I_3$. The apparent formation of Ti(II) was very unexpected, and more detailed examination of the "Ti–As" and "Ti–I" bond lengths showed these were unreasonably short, and it was also apparent that the thermal parameters associated with the metal centres were unusually large. Comparison of the parameters with published collected bond length tables [14], suggested that the "Ti" atom might in fact be Fe, and refinement of the data using iron gave a much better model with sensible bond lengths (Table 1) and thermal parameters. Examination of the crystals using EDX (energy dispersive X-ray spectroscopy) confirmed the presence of iron, arsenic and iodine, with no detectable titanium, and thus is it clear that the crystals were actually $[FeI_2\{o\text{-}C_6H_4(AsMe_2)_2\}_2]$ and $[FeI_2\{o\text{-}C_6H_4(AsMe_2)_2\}_2]I_3$. EDX examination of the TiI_4 sample used in these syntheses showed significant amounts of iron (ca. 5%) whereas other samples of TiI_4 used in this study, including the synthesis of the 1:1 complexes in Section 2.2, showed no iron present. The $[FeI_2\{o\text{-}C_6H_4(AsMe_2)_2\}_2]$ is easily made from $[FeCl_2\{o\text{-}C_6H_4(AsMe_2)_2\}_2]$ and LiI [15,16], but iron(III) iodide itself is unstable at ambient temperatures [17] and very few complexes have been described [18–20]. Some years ago we [16] described the synthesis of $[FeI_2\{o\text{-}C_6H_4(EMe_2)_2\}_2]BF_4$ (E = P or As) by HNO_3 oxidation of $[FeI_2\{o\text{-}C_6H_4(EMe_2)_2\}_2]$ suspended in HBF_4 at 0 °C. Their instability in solution prevented growth of crystals for an X-ray study, but Fe–I and Fe–P(As) bond lengths were obtained via Fe K-edge EXAFS data. The X-ray determined bond lengths in the present study are in generally good agreement with the EXAFS data within the usual precision of the latter (±0.02 Å) (Table 1). The two iron complexes constitute a redox pair $[FeI_2\{o\text{-}C_6H_4(AsMe_2)_2\}_2]^{0/+}$ with both the Fe species being centrosymmetric (Figs. 1 and 2) and comparison of the heavy atom bond lengths show that on oxidation from Fe(II) to Fe(III) the Fe–I

Table 1
Selected bond lengths (Å) and angles (°) for $[FeI_2\{o\text{-}C_6H_4(AsMe_2)_2\}_2]$ and $[FeI_2\{o\text{-}C_6H_4(AsMe_2)_2\}_2]I_3 \cdot 2CH_2Cl_2$

	$[FeI_2\{o\text{-}C_6H_4(AsMe_2)_2\}]$[a]	$[FeI_2\{o\text{-}C_6H_4(AsMe_2)_2\}]I_3 \cdot 2CH_2Cl_2$[b]
Bond lengths		
Fe(1)–As(1)	2.3372(5)	2.3792(4)
Fe(1)–As(2)	2.3388(5)	2.3822(5)
Fe(1)–I(1)	2.6823(4)	2.6009(3)
Bond angles		
As(1)–Fe(1)–As(2)	86.34(2)	84.53(2)
As(1)–Fe(1)–I(1)	92.03(2)	87.47(1)
As(2)–Fe(1)–I(1)	92.22(2)	87.34(1)
Bond lengths		
I(2)–I(3)		2.9343(4)

EXAFS determined parameters for comparison [16].
[a] Fe–I 2.70, Fe–As 2.34 Å.
[b] Fe–I 2.55, Fe–As 2.37 Å (as BF_4^- salt).

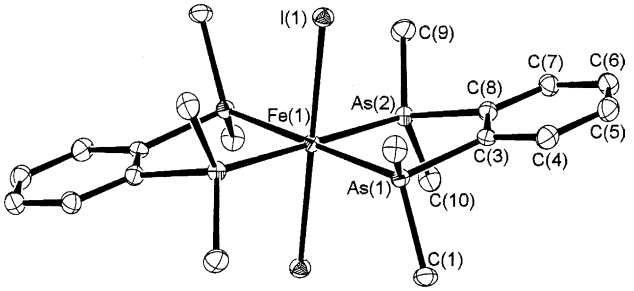

Fig. 1. Structure of $[FeI_2\{o\text{-}C_6H_4(AsMe_2)_2\}_2]$ showing the atom numbering scheme. Thermal ellipsoids are drawn at the 40% probability level and the H atoms omitted for clarity. There is a centre of symmetry at the Fe(1) atom.

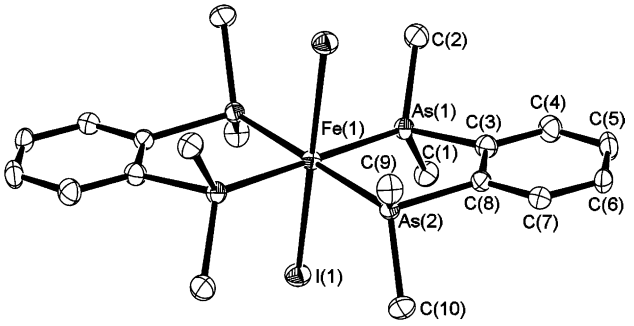

Fig. 2. Structure of the cation in $[FeI_2\{o\text{-}C_6H_4(AsMe_2)_2\}_2]I_3 \cdot 2CH_2Cl_2$ showing the atom numbering scheme. Thermal ellipsoids are drawn at the 40% probability level and the H atoms omitted for clarity. There is a centre of symmetry at the Fe(1) atom.

bonds shorten and the Fe–As bonds lengthen. The metal centres are both low-spin (d^6 and d^5, respectively) and thus the contraction in Fe–I bond length on oxidation is consistent both with the slightly smaller radius of Fe(III) over Fe(II), and with stronger interaction between the charged iodide and the harder metal centre. The lengthening of the Fe–As bonds on oxidation can be attributed to weaker interaction between the soft neutral arsenic ligand and the harder metal centre. The trends are also compatible with the Orpen–Connelly model [21] of metal–phosphine/arsine bonding, which would predict a reduced π-backbonding component when the metal has a higher oxidation state and hence a longer Fe–As bond. This latter model also predicts that π-backbonding Fe → As uses the C–As σ* as acceptor orbitals and should be accompanied by a lengthening of the C–As bonds. However, the differences in the C–As bond lengths between the structures are not significant and, as is often the case, this test cannot be applied. The origin of the iron in this particular TiI_4 sample is unknown, possibly it arises from ilmenite ($FeTiO_3$) which may have been the original ore source for the titanium. It is possible that similar impurities could go some way to accounting for the poor reproducibility of titanium iodide species described in the older literature.

3. Experimental

All reactions were carried out using Schlenk techniques and samples were handled in a glove-box (<5 ppm water). Solvents were dried as described [4,9] and freshly distilled before use. Physical measurements were made as described elsewhere [4,9]. The ligands were made by literature methods [22,23]. Titanium(IV) iodide was obtained from Strem or Aldrich and checked for impurities by EDX (see Discussion). EDX measurements were obtained on a Philips XL30 ESEM fitted with an EDAX Phoenix detector.

Table 2
Crystallographic data[a]

Compound	$[FeI_2\{o\text{-}C_6H_4(AsMe_2)_2\}_2]$	$[FeI_2\{o\text{-}C_6H_4(AsMe_2)_2\}_2]I_3 \cdot 2CH_2Cl_2$
Formula	$C_{20}H_{32}As_4FeI_2$	$C_{22}H_{36}As_4Cl_4FeI_5$
Formula weight	881.79	1432.34
Crystal system	orthorhombic	triclinic
Space group	*Pbca* (no. 61)	$P\bar{1}$ (no. 2)
a (Å)	9.229(1)	9.3985(5)
b (Å)	16.328(2)	9.5346(5)
c (Å)	17.374(2)	11.7627(5)
α (°)	90	78.137(3)
β (°)	90	86.560(3)
γ (°)	90	70.568(3)
U (Å^3)	2618.0(5)	972.75(8)
Z	4	1
μ(Mo Kα) (mm^{-1})	7.957	8.019
Total number of observations	15421	16043
Number of unique observations (R_{int})	2667 (0.061)	3956 (0.097)
Number of parameters	126	169
$R(I > 2\sigma(I))$	0.0352	0.0440
R (all data)	0.0416	0.0456
$wR_2(I > 2\sigma(I))$	0.0859	0.1173
wR_2 (all data)	0.0897	0.1186

[a] Common data: Temperature, 150 K; Mo-Kα ($\lambda = 0.71073$ Å). $R = \sum ||F_o| - |F_c|| / \sum |F_o|$; $wR_2 = [\sum w(F_o^2 - F_c^2)^2 / \sum wF_o^4]^{1/2}$.

3.1. [$TiI_4\{o\text{-}C_6H_4(PMe_2)_2\}$]

TiI_4 (0.20 g, 0.36 mmol) was dissolved in gently refluxing dry CH_2Cl_2 (80 ml), the solution filtered to remove any residual solid, cooled, and the deep purple solution treated with o-$C_6H_4(PMe_2)_2$ (0.07 g, 0.36 mmol) in CH_2Cl_2 (10 ml). The dark red solution produced, was stirred at ambient temperature for 30 min, then concentrated in vacuum to 5 ml. Dry hexane (20 ml) was added dropwise with stirring to form a purple precipitate, which was filtered off and dried in vacuo. Yield 0.08 g, 31%. *Anal*. Found: C, 15.8; H, 2.2. Calc. for $C_{10}H_{16}I_4P_2Ti$: C, 15.9; H, 2.1%. ^{1}H NMR (300 K, CD_2Cl_2): 7.60–7.75 (m), 2.28 (m). $^{31}P\{^1H\}$ NMR (300 K, CD_2Cl_2): 18.0. UV–Visible (diffuse reflectance (DR) in $BaSO_4$)/cm^{-1}: 34 200, 27 500, 22 700(sh), 17 800.

3.2. [$TiI_4\{o\text{-}C_6H_4(AsMe_2)_2\}$]

Was made similarly to the above using o-$C_6H_4(AsMe_2)_2$ (0.103 g, 0.36 mmol). Dark red-brown solid. Yield 26%. *Anal.* Found: C, 14.5; H, 2.1. Calc. for $C_{10}H_{16}As_2I_4Ti$: C, 14.3; H, 1.9%. ^{1}H NMR (300 K, CD_2Cl_2): 7.70–7.55 (m), 7.50–7.30 (m), 2.11 (s), 1.20 (s). UV–Visible (DR in $BaSO_4$)/cm^{-1}: 28 300, 22 200, 17 500.

3.3. X-ray studies

Brief details of the crystallographic data collection and refinement are given in Table 2. The crystals of the iron complexes were obtained as described in the text. Data collection used a Nonius Kappa CCD diffractometer equipped with an Oxford Cryosystems low temperature device operating at 150 K, and with graphite monochromated Mo-Kα radiation ($\lambda =$ 0.71073 Å). Data solution [24] and refinement [25] were routine, except for the initial modelling of the iron centres as titanium (see text).

4. Conclusions

We have shown that TiI_4 forms six-coordinate 1:1 complexes with o-$C_6H_4(AsMe_2)_2$ and o-$C_6H_4(PMe_2)_2$ which are analogous to the complexes formed by $TiCl_4$ and $TiBr_4$, although rather less stable and more prone to dissociation in solution. The reported 1:2 complexes do not appear to exist, the products suggested to be such in previous work, appear to be mixtures containing partially oxidised or iodinated ligands, and probably lower oxidation states of titanium, which would account for the paramagnetism of some samples. The absence of any intense UV–Visible absorptions <20 000 cm^{-1} rules out the presence of Ti(IV)–I bonds. Structures of two unusual iron complexes arising from iron impurity in the titanium(IV) iodide have also been determined.

5. Supplementary data

Crystallographic data for the structures have been deposited with the Cambridge Crystallographic Data Centre (CCDC) and given number 219522 (Fe(II)) and 219523 (Fe(III)). Copies of the data can be obtained free of charge from The Director, CCDC, 12 Union Road, Cambridge CB2 1EZ, UK (fax: +44-1223-336033; e-mail: deposit@ccdc.cam.ac.uk or www: http://www.ccdc.cam.ac.uk).

Acknowledgements

We thank EPSRC for support.

References

[1] R.J.H. Clark, in: J.C. Bailar, H.J. Emeleus, R.S. Nyholm, A.F. Trotman-Dickenson (Eds.), Comprehensive Inorganic Chemistry, vol. 3, Pergamon, Oxford, 1973 (Ch. 3).
[2] C.A. McAuliffe, D.S. Barratt, in: G. Wilkinson, R.D. Gillard, J.A. McCleverty (Eds.), Comprehensive Coordination Chemistry I, vol. 3, Pergamon, Oxford, 1987 (Ch. 31).
[3] F.A. Cotton, J.H. Matonic, C.A. Murillo, M.A. Petrukhina, Inorg. Chim. Acta 267 (1998) 173.
[4] R. Hart, W. Levason, B. Patel, G. Reid, Eur. J. Inorg. Chem. (2001) 2927.
[5] R.F. Rolsten, H.H. Sisler, J. Am. Chem. Soc. 79 (1957) 1068.
[6] R.T. Cowdell, G.W.A. Fowles, R.A. Walton, J. Less Common Met. 5 (1963) 386.
[7] R.J.H. Clark, W. Errington, J. Lewis, R.S. Nyholm, J Chem. Soc. (A) (1966) 989.
[8] G.A. Barclay, I.K. Gregor, M.J. Lambert, S.B. Wild, Aust. J. Chem. 20 (1967) 1571.
[9] W. Levason, B. Patel, G. Reid, V.-A. Tolhurst, M. Webster, J. Chem. Soc., Dalton Trans. (2000) 3001.
[10] A.B.P. Lever, Inorganic Electronic Spectroscopy, Elsevier, Amsterdam, 1984.
[11] N. Bricklebank, S.M. Godfrey, H.P. Lane, C.A. McAuliffe, R.G. Pritchard, J.-M. Moreno, J. Chem. Soc., Dalton Trans. (1995) 3873.
[12] F.A. Cotton, P.A. Kibala, J. Am. Chem. Soc. 109 (1987) 3308.
[13] S.I. Troyanov, A. Meetsma, J.H. Teuben, Inorg. Chim. Acta 271 (1998) 180.
[14] F.H. Allen, L. Brammer, O. Kennard, A.G. Orpen, R. Taylor, D.G. Watson, J. Chem. Soc., Dalton Trans. (1989) S1.
[15] R.S. Nyholm, J. Chem. Soc. (1950) 851.
[16] N.R. Champness, W. Levason, R.D. Oldroyd, S.R. Preece, Inorg. Chem. 33 (1994) 2060.
[17] K.B. Yoon, J.K. Kochi, Inorg. Chem. 29 (1990) 869.
[18] S. Pohl, W. Saak, Z. Anorg. Allgem. Chem. 523 (1985) 25.
[19] S. Pohl, W. Saak, Z. Naturforsch., Teil B 39 (1984) 1236.
[20] S. Pohl, U. Bierbach, W. Saak, Angew. Chem. Int. Ed. Eng. 28 (1989) 776.
[21] A.G. Orpen, N.G. Connelly, Chem. Commun. (1985) 1310.
[22] R.D. Feltham, A. Kasenally, R.S. Nyholm, J. Organometal. Chem. 7 (1967) 285.
[23] E.P. Kyba, S.-T. Liu, R.L. Harris, Organometallics 2 (1983) 1877.
[24] G.M. Sheldrick, SHELXS 97, Program for crystal structure solution, University of Göttingen, 1997.
[25] G.M. Sheldrick, SHELXL 97, Program for crystal structure refinement, University of Göttingen, 1997.

Available online at www.sciencedirect.com
SCIENCE DIRECT®
Polyhedron 23 (2004) 611–616
POLYHEDRON
www.elsevier.com/locate/poly

Novel ferrocenyl-oxazoline ligands: first preparation of non-symmetrical bis(oxazoline) ☆

Montserrat Gómez [a,*], Eduardo Peris [b,*], Helena Teruel [c,*], Ingrid Arevalo [c], José A. Mata [b], Guillermo Muller [a]

[a] *Departament de Química Inorgànica, Universitat de Barcelona, Martí i Franquès, 1-11, E-08028 Barcelona, Spain*
[b] *Departamento de Química Inorgánica y Orgánica, Universitat Jaume I, E-12080 Castellón, Spain*
[c] *Universidad Simón Bolivar, Baruta 6000, Caracas 1081, Venezuela*

Received 22 September 2003; accepted 24 October 2003

Abstract

New ferrocenyl-arenylethenyl-oxazoline derivatives have been prepared (**5**–**10**) from the mono- and (1,1′)-disubstituted (nitrile-ethenylaryl)ferrocene compounds (**1** and **2**) and the appropriated β-aminoalcohol (**3** and **4**) in one step synthesis. The X-ray crystal structure of one of the ferrocenyl-ethenylaryl-oxazoline (**5**) is described, revealing the unusual quasi-planarity of the oxazoline ring with the phenyl and cyclopentadienyl cycles. Two compounds end-capped (**9** and **10**) with both, nitrile and oxazoline groups, are the key intermediates to obtain the non-symmetrical bis(oxazoline) **11**, containing two different substituted heterocycles.
© 2003 Elsevier Ltd. All rights reserved.

Keywords: Ferrocenes; Oxazolines; Non-symmetrical ligands; X-ray diffraction

1. Introduction

During the last three decades, much attention has been devoted to the chemistry of ferrocenyl complexes because ferrocene combines chemical versatility with high thermal stability. These properties, together with the exceptional electrochemical properties of ferrocene, make ferrocene-based complexes good candidates for the preparation of new materials with applications in organic synthesis, catalysis and materials science [1,2].

In the search of new materials with electronic communication between terminal subunits, we have focused our interest on the preparation of new conjugated ferrocenyl complexes with end capped nitro [3], pyridine [4] and nitrile [5] groups. End-capping ferrocene with pyridine and nitrile, allowed the ferrocenyl subunit to link to different metallic fragments, affording interesting bimetallic complexes, in which the terminal metallic fragments are connected by a conjugated bridge. In all cases, our compounds showed excellent coordination capabilities which made them appropriate to obtain highly stable heterometallic complexes [5c,6]. In the last decade, an increasing eager effort to the introduction of ferrocene fragments in the design of new homogeneous catalysts has been done [1,7]. Since one of the most useful tools in organic synthesis is asymmetric catalysis, a great effort has been devoted to the synthesis of chiral ferrocenyl ligands, some of which show the planar chirality in the ferrocenyl moiety [8], and some others also in the ancillary ligands [9]. Among the latter ones, oxazoline-type ligands have shown excellent coordination properties [10], which make them good candidates to the synthesis of a large variety of chiral catalysts [11].

Despite the number of ferrocene-oxazoline compounds reported so far is large, most of the examples that we can find in the literature are phosphine based [12]. In this work, we report the synthesis and characterization of new phosphine-free ferrocenyl-oxazoline ligands from our previously reported ferrocenyl-ethenylaryl-nitrile ligands [5a,5b]. The introduction of the ethenylaryl bridge between the ferrocene and the

☆ Supplementary data associated with this article can be found, in the online version, at doi:10.1016/j.poly.2003.10.013

* Corresponding author. Tel.: +34-934-021271; fax: +34-934-907725.
E-mail address: montserrat.gomez@qi.ub.es (M. Gómez).

0277-5387/$ - see front matter © 2003 Elsevier Ltd. All rights reserved.
doi:10.1016/j.poly.2003.10.013

terminal oxazoline unit introduces a new dimension to this new type of complexes, since all of the ferrocene-oxazoline compounds reported so far have the oxazoline fragment directly bound to ferrocene, because of the ortho directing behaviour of this functional group which leads to the synthesis of planar chiral ferrocenes [7,13]. In this exploratory work, racemic amino alcohols have been used. Preliminary attempts to coordinate these compounds to Pd and Au failed.

2. Experimental

2.1. General data

All compounds were prepared under a purified nitrogen atmosphere using standard Schlenk and vacuum-line techniques. The solvents were purified by standard procedures [14] and distilled under nitrogen. Ethenyl-ferrocene derivatives **1** and **2** were prepared as previously described [5a,5b]. 2-aminobutanol (Fluka) and leucinol (Aldrich) were used without previous purification. NMR spectra were recorded on JEOL Eclipse 400, Bruker DRX 500 (^{1}H, standard $SiMe_4$) and Varian Gemini 200 (^{13}C, 50 MHz, standard $SiMe_4$) in $CDCl_3$. Chemical shifts were reported downfield from standards. IR spectra were recorded on a Nicolet 520 FT-IR and FTIR Nicolet Impact 400 spectrometers. FAB mass chromatograms were obtained on a Fisons V6-Quattro instrument. Optical rotations were measured on a Perkin Elmer 241MC spectropolarimeter. Elemental analyses were carried out by the *Serveis Científico-Tècnics de la Universitat de Barcelona* in an Eager 1108 microanalyzer.

2.2. 1-Ethenyl-(4-(4′-ethyl-3′,4′-dihydrooxazol-2′-yl)phenyl)ferrocene, **5**

0.100 g (0.227 mmol) of 1-(ethenyl-4-cianophenyl)ferrocene, 0.155 g (1.74 mmol) of 2-aminobutanol and a catalytic amount of zinc chloride were dissolved in 10 cm^3 of toluene at room temperature. The mixture was refluxed for 8 days (monitored by TLC). The mixture was filtered off and the solvent was removed under reduced pressure, affording an oil, which was chromatographied over SiO_2 using ethyl acetate/hexane (1/1) as eluent. After removing the solvent, **5** was obtained as a red solid. Yield: 0.045 g (52%). ^{1}H NMR (400 MHz, $CDCl_3$) δ 1.01 (t, 7.0 Hz, 3H), 1.72 (m, 2H), 4.05 (m, 2H), 4.28 (m, 1H), 4.32 (2, 5H), 4.46 (m, 4H), 6.65 (d, 16.0 Hz, 1H), 6.76 (d, 16.0 Hz, 1H), 7.69 (d, 8.0 Hz, 2H), 7.81 (d, 8.0 Hz, 2H) ppm. ^{13}C NMR (50 MHz, $CDCl_3$) δ 12.00, 22.00, 25.20, 44.35, 64.00, 65.40, 68.00, 68.10, 71.50, 82.00, 123.90, 124.30, 127.40, 127.70, 164.00 ppm. IR (KBr) 1650 (C=N) cm^{-1}. *Anal.* Calc. for $C_{23}H_{23}NOFe$: C, 71.70; H, 6.02; N, 3.64. Found C, 70.50; H, 6.00; N, 3.50%. MS (FAB positive) m/z 385 ([M]$^+$).

2.3. 1-Ethenyl-(4-(4′-isobutyl-3′,4′-dihydrooxazol-2′-yl)-phenyl)ferrocene, **6**

Compound prepared following the methodology described for **5**. Starting materials: 0.100 g (0.227 mmol) of 1-(ethenyl-4-cianophenyl)ferrocene, 0.204 g (1.74 mmol) of leucinol and a catalytic amount of zinc chloride. Yield: 0.068 g (73%). ^{1}H NMR (400 MHz, $CDCl_3$) δ 0.95 (m, 3H), 0.97 (m, 3H), 1.40 (m, 1H), 1.80 (m, 2H), 3.98 (t, 8.0 Hz, 1H), 4.13 (s, 5H), 4.29 (m, 2H), 4.47 (m, 2H), 6.69 (d, 16.0 Hz, 1H), 6.94 (d, 16.0 Hz, 1H), 7.42 (d, 8.0 Hz, 2H), 7.88 (d, 8.0 Hz, 2H) ppm. ^{13}C NMR (50 MHz, $CDCl_3$) δ 21.62, 21.93, 24.46, 44.54, 64.06, 65.97, 68.17, 68.24, 71.93, 81.69, 124.13, 124.35, 127.43, 127.86, 163.0 ppm. IR (KBr) 1640 (C=N) cm^{-1}. *Anal.* Calc. for $C_{25}H_{27}NOFe$: C, 72.65; H, 6.58; N, 3.39. Found C, 71.90; H, 6.80; N, 3.10%. MS (FAB positive) m/z 413 ([M]$^+$).

2.4. 1,1′-Bis(ethenyl-(4-(4′-ethyl-3′,4′-dihydrooxazol-2′-yl)phenyl))ferrocene, **7**

0.200 g (0.454 mmol) of 1,1′-bis(ethenyl-4-cianophenyl)ferrocene, 0.624 g (7.0 mmol) of 2-aminobutanol and a catalytic amount of zinc chloride. The mixture was filtered off and the solvent was removed under reduced pressure, affording an oil, which was chromatographied over SiO_2 using dichloromethane/hexane (1/1) as eluent. The product corresponded to the fractions with $R_f = 0.4$ on the TLC sheet. After removing the solvent, **7** was obtained as a red solid. Yield (based on **2**): 0.053 g (20%). ^{1}H NMR (400 MHz, $CDCl_3$) δ 0.98 (t, 7.5 Hz, 6H), 1.63 (m, 2H), 1.77 (m, 2H), 4.05 (t, 8.0 Hz, 2H), 4.28 (m, 2H), 4.29 (m, 4H), 4.42 (m, 4H), 4.44 (dd, 11.8 Hz, 8.0 Hz, 2H), 6.61 (d, 16.5 Hz, 2H), 6.85 (d, 16.5 Hz, 2H), 7.31 (d, 8.4 Hz, 4H), 7.81 (d, 8.4 Hz, 4H) ppm. IR (KBr) 1645 (C=N) cm^{-1}. *Anal.* Calc. for $C_{36}H_{36}N_2O_2Fe$: C, 73.97; H, 6.21; N, 4.79. Found C, 74.30; H, 6.40; N, 4.55%. MS (FAB positive) m/z 585 ([M]$^+$).

2.5. 1,1′-Bis(ethenyl-(4-(4′-isobutyl-3′,4′-dihydrooxazol-2′-yl)phenyl))ferrocene, **8**

0.200 g (0.454 mmol) of 1,1′-bis(ethenyl-4-cianophenyl)ferrocene, 0.820 g (7.0 mmol) of leucinol and a catalytic amount of zinc chloride. The mixture was filtered off and the solvent was removed under reduced pressure, affording an oil, which was chromatographied over SiO_2 using dichloromethane/hexane (1/1) as eluent. The product corresponded to the fractions with $R_f = 0.4$ on the TLC sheet. After removing the solvent, **8** was obtained as a red solid. Yield (based on **2**): 0.047 g (16%). ^{1}H NMR (400 MHz, $CDCl_3$) δ 0.98 (m, 12H), 1.39 (m, 2H), 1.73 (m, 2H), 1.76 (m, 2H), 3.98 (t, 8.0 Hz, 2H), 4.14 (m, 8H), 4.29 (m, 4H), 4.46 (m, 4H), 6.52 (dd,

11.8 Hz, 8.0 Hz, 2H), 6.69 (d, 16.0 Hz, 2H), 6.96 (d, 16.0 Hz, 4H), 7.43 (d, 8.0 Hz, 4H), 7.88 (d, 8.0 Hz, 4H) ppm. *Anal*. Calc. for $C_{40}H_{44}N_2O_2Fe$: C, 74.95; H, 6.92; N, 4.37. Found C, 74.40; H, 7.05; N, 4.40%. MS (FAB positive) m/z 641 ($[M]^+$).

2.6. 1-Ethenyl-(4-(4′-ethyl-3′,4′-dihydrooxazol-2′-yl)phenyl)-1′-ethenyl-(4-cianophenyl)ferrocene, 9

Co-product obtained with **7** (see preparation of **7**) by condensation of **2** with **3**. The compound **9** corresponded to the eluted fractions with $R_f = 0.6$ on the TLC sheet, on the column chromatography over SiO_2 using dichloromethane/hexane (1/1) as eluent. Yield (based on **2**): 0.082 g (41%). ^{1}H NMR (400 MHz, $CDCl_3$) δ 1.01 (t, 7.2 Hz, 3H), 1.65 (m, 1H), 1.80 (m, 1H), 4.09 (t, 8.1 Hz, 1H), 4.20 (m, 1H), 4.29 (m, 2H), 4.32 (m, 2H), 4.45 (m, 4H), 4.55 (dd, 8.0 Hz, 9.5 Hz, 2H), 6.45 (d, 16.1 Hz, 1H), 6.52 (d, 16.5 Hz, 1H), 6.65 (d, 16.1 Hz, 1H), 6.67 (d, 16.5 Hz, 1H), 7.14 (d, 8.5 Hz, 2H), 7.16 (d, 8.5 Hz, 2H), 7.33 (d, 8.5 Hz, 2H), 7.69 (d, 8.5 Hz, 2H) ppm. *Anal*. Calc. for $C_{32}H_{28}N_2OFe$: C, 75.01; H, 5.51; N, 5.47. Found C, 75.30; H, 5.60; N, 5.30%. MS (FAB positive) m/z 512 ($[M]^+$).

2.7. 1-Ethenyl-(4-(4′-isobutyl-3′,4′-dihydrooxazol-2′-yl)-phenyl)-1′-ethenyl-(4-cianophenyl)ferrocene, 10

Co-product obtained with **8** (see preparation of **8**) by condensation of **2** with **4**. The compound **10** corresponded to the eluted fractions with $R_f = 0.6$ on the TLC sheet, on the column chromatography over SiO_2 using dichloromethane/hexane (1/1) as eluent. Yield (based on **2**): 0.076 g (31%). ^{1}H NMR (500 MHz, $CDCl_3$) δ 0.98 (m, 6H), 1.42 (m, 2H), 1.75 (m, 2H), 1.82 (m, 2H), 4.02 (t, 8.0 Hz, 2H), 4.28 (m, 2H), 4.31 (m, 2H), 4.35 (m, 2H), 4.44 (m, 4H), 4.55 (dd, 8.0 Hz, 9.5 Hz, 2H), 6.45 (d, 16.0 Hz, 1H), 6.51 (d, 16.0 Hz, 1H), 6.66 (pt, 16.8 Hz, 2H), 7.13 (d, 7.0 Hz, 2H), 7.15 (d, 8.5 Hz, 2H), 7.32 (d, 8.5 Hz, 2H), 7.68 (d, 8.5 Hz, 2H) ppm. ^{13}C NMR (50 MHz, $CDCl_3$) δ 22.68, 22.99, 25.57, 45.59, 65.26, 68.10, 68.14, 68.30, 70.21, 70.48, 73.11, 77.20, 83.21, 84.07, 109.28, 119.22, 124.81, 125.19, 125.68, 126.11, 127.34, 128.47, 130.01, 132.27, 140.18, 141.86, 163.03 ppm. *Anal*. Calc. for $C_{34}H_{32}N_2OFe$: C, 75.56; H, 5.97; N, 5.18. Found C, 75.00; H, 6.05; N, 5.25%. MS (FAB positive) m/z 540 ($[M]^+$).

2.8. 1-Ethenyl-(4-(4′-isobutyl-3′,4′-dihydrooxazol-2′-yl)-phenyl)-1′-ethenyl-(4-(4′-ethyl-3′,4′-dihydrooxazol-2′-yl)-phenyl)ferrocene, 11

0.100 g (0.220 mmol) of **9**, 0.400 ml (2.386 mmol) of leucinol and a catalytic amount of zinc chloride. The mixture was filtered off and the solvent was removed under reduced pressure, affording an oil, which was chromatographied over SiO_2 using dichloromethane/hexane (1/1) as eluent. After removing the solvent, **11** was obtained as a red solid. Yield: 0.015 g (11%). ^{1}H NMR (400 MHz, $CDCl_3$) δ 0.91 (t, 3H), 0.99 (7, 6H), 1.30 (m, 2H), 1.41 (m, 2H), 1.82 (m, 1H), 4.17 (t, 8.0 Hz, 1H), 4.22 (m, 1H), 4.29(m, 1H), 4.32 (m, 2H), 4.45 (m, 2H), 4.48 (m, 1H), 6.43 (d, 16.3 Hz, 1H), 6.53 (d, 16.0 Hz, 1H), 6.63 (d, 16.0 Hz, 1H), 6.68 (d, 16.3Hz, 1H), 7.05–7.15 (m, 4H), 7.15 (d, 8.5 Hz, 2H), 7.32 (d, 8.5 Hz, 2H), 7.68 (d, 8.5 Hz, 2H) ppm. *Anal*. Calc. for $C_{38}H_{40}N_2O_2Fe$: C, 74.50; H, 6.58; N, 4.57. Found C, 75.00; H, 6.40; N, 4.55%.

2.9. Crystallography

Single crystals were grown by slow diffusion of hexane into concentrated CH_2Cl_2 solution of **5** and mounted on a glass fiber in a random orientation. Data collection was performed at room temperature on a Siemens Smart CCD diffractometer using graphite

Table 1
Crystal data and structure refinement for compound **5**

Empirical formula	$C_{23}H_{23}FeNO$
Formula weight	385.27
Temperature (K)	293(2)
Wavelength (Å)	0.71073
Crystal system	monoclinic
Space group	$P2(1)/n$
Unit cell dimensions	
a (Å)	7.9462(18)
b (Å)	22.897(5)
c (Å)	10.922(3)
α (°)	90
β (°)	106.222(5)
γ (°)	90
Volume (Å^3)	1908.0(8)
Z	4
Density (calculated) (Mg/m^3)	1.341
Absorption coefficient (mm^{-1})	0.801
$F(000)$	808
Crystal size (mm)	$0.19 \times 0.15 \times 0.14$
θ range for data collection	1.78–20.81°
Index ranges	$-7 \leqslant h \leqslant 7$, $-22 \leqslant k \leqslant 22$, $-8 \leqslant l \leqslant 10$
Reflections collected	7111
Independent reflections	1992 [$R_{int} = 0.0340$]
Completeness to $\theta = 20.81°$	100.0%
Absorption correction	Bruker SADABS
Maximum and minimum transmission	1.955654 and 1.409375
Refinement method	Full-matrix least-squares on F^2
Data/restraints/parameters	1992/0/253
Goodness-of-fit on F^2	1.164
Final R indices [$I > 2\sigma(I)$]	$R_1 = 0.0492$, $wR_2 = 0.1152$
R indices (all data)	$R_1 = 0.0626$, $wR_2 = 0.1203$
Largest diffraction peak and hole (e Å^{-3})	0.319 and −0.329

monochromated Mo Kα radiation ($\lambda = 0.71073$ Å) with a nominal crystal to detector distance of 4.0 cm. An hemisphere of data was collected based on three ω-scans runs (starting $\omega = -28°$) at values $\phi = 0°$, 90° and 180° with the detector at $2\theta = 28°$. At each of these runs, frames (606, 435 and 230, respectively) were collected at 0.3° intervals and 40 s per frame. Space group assignments are based on systematic absences, E statistics and successful refinement of the structures. Structure was solved by direct methods with the aid of successive difference Fourier maps and were refined using the SHELXTL 5.1 software package [15]. All non-hydrogen were refined anisotropically. Hydrogen atoms were assigned to ideal positions and refined using a riding model. Details of the data collection and cell dimensions are given in Table 1 and structure refinement. The diffraction frames were integrated using the SAINT package and corrected for absorption with SADABS [16].

3. Synthesis and characterization

Ferrocenyl-ethenylphenyl-oxazoline compounds **5**–**10** have been obtained (Scheme 1), by zinc-catalyzed reaction of the corresponding nitrile derivative (**1** or **2**) [5b,5c] with the appropriate β-aminoalcohol (*rac*-**3** or *rac*-**4**), as described in the literature for related compounds [17]. The products were obtained in moderate to good yields (up to ca. 70% on the pure product) and fully characterized by usual techniques (IR and NMR spectroscopies, FAB-mass spectra, elemental analysis and X-ray diffraction).

Monoxazolines **5** and **6** were obtained in one-step synthesis from **1** and the aminoalcohol **3** and **4**, respectively (see Scheme 1). Suitable monocrystals for **5** were obtained by slow evaporation from dichloromethane/hexane solution.

Reaction of the ferrocenyl-dinitrile **2** with the aminoalcohols **3** or **4** gave a mixture of the bis(oxazoline) (**7** or **8**) and nitrile-oxazoline (**9** or **10**) compounds (Scheme 1), after one week in refluxing toluene. The nitrile-oxazoline compounds (**8** and **10**) were the major products obtained, with a bis(oxazoline):nitrile-oxazoline molar ratio of ca. 1:2. Further silica column chromatography (dichloromethane/hexane (1/1) used as eluent) of crude led to the separation of both compounds: nitrile-oxazoline ligands (**9** and **10**) and bis(oxazoline) compounds (**7** and **8**), as described in the experimental section. Starting material **2**, was also recovered (ca. 50–60%).

One of the main goals of our work is that the synthesis of pure **9** and **10** allowed the synthesis of non-symmetrical bis(oxazoline) compounds, containing different substituents in the oxazoline ring. Therefore, **11** was obtained by reaction of **9** with the aminoalcohol **4** in low yield (11%), following the same methodology described above.

3.1. Molecular structure of 5

Slow diffusion of a CH_2Cl_2 solution of a racemic mixture of **5** in hexane afforded orange crystals suitable for X-ray diffraction. Compound **5** crystallizes in the centrosymmetric space group $P2(1)/n$. The unit cell contains four molecules, two corresponding to each of the enantiomeric forms because racemic mixture of aminoalcohol was used in the synthesis of the product. As seen in Fig. 1, the molecule displays a quasiplanar arrangement between the ferrocenyl, the phenyl and the oxazoline groups, which facilitates conjugation. The distances from iron to cyclopentadienyl rings, and the C–C distances within the rings lie in the expected range.

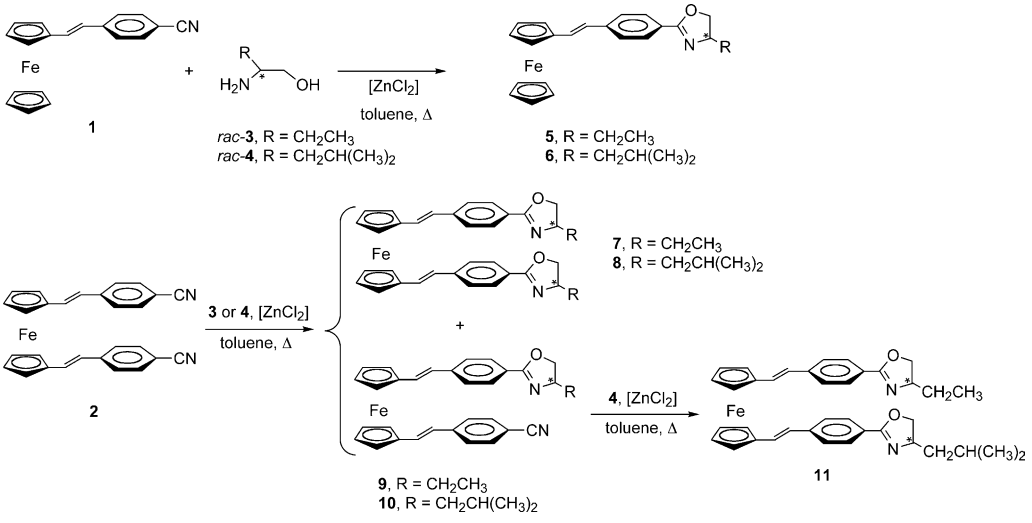

Scheme 1. Synthesis of compounds **5**–**11**.

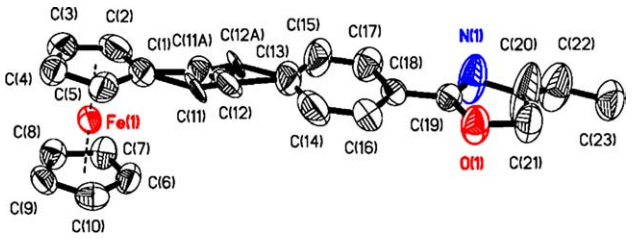

Fig. 1. Molecular structure and atomic labelling scheme for **5**. All hydrogens and double bond disorder have been omitted for clarity. Anisotropic displacement ellipsoids at 50%. Selected bond distances (Å) and angles (°). Fe-Cp(centr.) = 1.65; Fe–C (Cp) = 2.04; C(18)–C(19) = 1.480(8); C(19)–N(1) = 1.237(7); C(19)–O(1) = 1.342(6); O(1)–C(21) = 1.457(7); N(1)–C(20) = 1.493(9); C(20)–C(21) = 1.429(10); N(1)– C(19)–O(1) = 118.7(5); C(19)–O(1)–O(21) = 104.4(4); C(19)–N(1)–C(20) = 105.7(6); N(1)–C(20)–C(21) = 105.2(6). Planes: Cp_{subs}–Cp = 1.03(0.43); Cp_{subs}–Ph = 8.31(0.40); Ph–Oxazoline ring = 2.82(0.49).

The molecular structure presents a disorder in a 1:1 ratio with regard to the orientation of the *trans* olefinic moieties. This kind of disorder has been observed in similar molecules [4,18].

3.2. NMR studies

^{1}H NMR spectra of bis(oxazoline) products (**7**, **8**, **11**) do not exhibit the evidence of isomers in solution (^{1}H NMR spectra were recorded in the temperature range 223–323 K), in spite of the formation of diastereomers due to the racemic aminoalcohols employed in their syntheses. We can establish that average structures are observed, because polarimetry results (for **7** and **8**) indicate that no optically enriched compounds are obtained.

Preliminary coordination tests of these ligands towards gold, [AuCl(PPh$_3$)], and palladium, [PdCl$_2$-(PhCN)$_2$], precursors led to decomposition products, using several solvents (chloroform, dichloromethane, toluene) at different temperatures (253–298 K).

In conclusion, we have prepared new oxazoline compounds from ferrocene ethenylaryl conjugated bridge derivatives, describing for the first time a non-symmetrical bis(oxazoline). Unfortunately, these ligands are not good candidates to stabilize coordination compounds with transition metals.

4. Supplementary material

^{1}H NMR spectra of compounds **8**, **9** and **11**.

The crystal structure of **5** has been deposited at the Cambridge Crystallographic Data Centre and allocated the deposition number CCDC 215315. Copies of the information may be obtained free of charge from The Director, CCDC, 12 Union Road, Cambridge CB2 1EZ, UK (fax: +44-1223-336033; E-mail: deposit@ccdc.cam.ac.uk or www: http://www.ccdc.cam.ac.uk).

Acknowledgements

The authors thank the *Ministerio de Ciencia y Tecnología* (BQU 2001-3358), the *Generalitat de Catalunya*, DGESIC (MAT2002-04421-C02-01) and the *Decanato de Investigación y Desarrollo de la Universidad Simón Bolívar* (S1-CB-005) for financial support. The authors thanks Miss G. Noguera and Miss Y. Gorrín for their help in the preparation of the ferrocenyl precursors.

References

[1] (a) A. Togni, T. Hayshi (Eds.), Ferrocenes: Homogenous Catalysis. Organic Synthesis. Materials Science, VCH, Weinheim, Germany, 1995;
(b) O.B. Sutcliffe, M.R. Bryce, Tetrahedron: Asymmetry 14 (2003) 2297.
[2] N.J. Long, Metallocenes, 1st ed., Blackwell Science, London, 1997.
[3] J.A. Mata, E. Peris, I. Asselberghs, R. Van Boxel, A. Persoons, New. J. Chem. 25 (2001) 299.
[4] J.A. Mata, S. Uriel, R. Llusar, E. Peris, Organometallics 19 (2000) 3797.
[5] (a) J.A. Mata, E. Peris, R. Llusar, S. Uriel, M.P. Cifuentes, M.G. Humphrey, M. Samoc, B. Luther-Davies, Eur. J. Inorg. Chem. (2001) 2113;
(b) J.A. Mata, E. Falomir, R. Llusar, E. Peris, J. Organomet. Chem. 616 (2000) 80;
(c) J. Mata, S. Uriel, E. Peris, R. Llusar, S. Houbrechts, A. Persoons, J. Organomet. Chem. 562 (1998) 197.
[6] J.A. Mata, E. Peris, S. Uriel, R. Llusar, I. Asselberghs, A. Persoons, Polyhedron 20 (2001) 2083.
[7] C.J. Richards, A.J. Locke, Tetrahedron: Asymmetry 9 (1998) 2377.
[8] (a)
See, for example: J. Chiffre, Y. Coppel, G.G.A. Balavoine, J.C. Daran, E. Manoury, Organometallics 21 (2002) 4552;
(b) C. Bolm, K. Muniz-Fernandez, A. Seger, G. Raabe, K. Gunther, J. Org. Chem. 63 (1998) 7860;
(c) T. Tu, Y.G. Zhou, X.L. Hou, L.X. Dai, X.C. Dong, Y.H. Yu, J. Sun, Organometallics 22 (2003) 1255;
(d) S. Shirakami, T. Itoh, Tetrahedron: Asymmetry 11 (2000) 2823.
[9] (a) C.O. Turrin, J. Chiffre, D. de Montauzon, G. Balavoine, E. Manoury, A.M. Caminade, J.P. Majoral, Organometallics 21 (2002) 1891;
(b) M. Catasus, A. Bueno, A. Moyano, M.A. Maestro, J. Mahia, J. Organomet. Chem. 642 (2002) 212;
(c) A. Hess, J. Sehnert, T. Weyhermuller, N. Metzler-Nolte, Inorg. Chem. 39 (2000) 5437;
(d) M. Takeuchi, T. Mizuno, S. Shinkai, S. Shirakami, T. Itoh, Tetrahedron: Asymmetry 11 (2000) 3311;
(e) M. Widhalm, U. Nettekoven, K. Mereiter, Tetrahedron: Asymmetry 10 (1999) 4369;
(f) A. Togni, T. Hayashi (Eds.), Ferrocenes: Homogenous Catalysis. Organic Synthesis. Materials Science, VCH, Weinheim, Germany, 1995, pp. 279–316.
[10] M. Gómez, G. Muller, M. Rocamora, Coord. Chem. Rev. 193–195 (1999) 769.
[11] (a) A.K. Ghosh, P. Mathivanan, J. Cappiello, Tetrahedron: Asymmetry 9 (1998) 1;
(b) G. Helmchen, A. Pfaltz, Acc. Chem. Res. 33 (2000) 336.
[12] A. Togni, Angew. Chem., Int. Ed. Engl. 35 (1996) 1475.

[13] (a) First works published simultaneously by: C.J. Richards, T. Damalidis, D.E. Hibbs, M.B. Hursthouse, Synlett (1995) 74;
(b) T. Sammakia, H.A. Latham, D.R. Schaad, J. Org. Chem. 60 (1995) 10;
(c) Y. Nishibayashi, S. Uemura, Synlett (1995) 79.
[14] D.D. Perrin, W.L.F. Armarego, D.R. Perrin, Purification of Laboratory Chemicals, third ed., Pergamon Press, Oxford, UK, 1988.
[15] SAINT version 5.0 Bruker Analytical X-ray Systems, Madison, WI.
[16] G.M. Sheldrick, SADABS empirical absorption program, University of Göttingen, 1996.
[17] (a) C. Bolm, K. Weickhardt, M. Zehnder, T. Ranff, Chem. Ber. 124 (1991) 1173;
(b) A. El Hatimi, M. Gómez, S. Jansat, G. Muller, M. Font-Bardía, X. Solans, J. Chem. Soc., Dalton Trans. (1998) 4229, and references therein.
[18] (a) S. Sakanishi, D.A. Bardwell, S. Couchman, J.C. Jeffrey, J.A. McCleverty, M.D. Ward, J. Organomet. Chem. 528 (1997) 35;
(b) A. Hradsky, B. Bildstein, N. Schuler, H. Schottenberger, P. Jaitner, K.-H. Ongania, K. Wurst, J.-P. Launay, Organometallics 16 (1997) 392.

Available online at www.sciencedirect.com
SCIENCE DIRECT®
Polyhedron 23 (2004) 617–622
POLYHEDRON
www.elsevier.com/locate/poly

Thallium(I) bis(mercaptoimidazolyl)borates

Hamsell M. Alvarez [a], Patricia A. Gillespie [b], Cornelius D. Gause [a], Arnold L. Rheingold [c,*], James A. Golen [c,1], Daniel Rabinovich [a,*]

[a] Department of Chemistry, The University of North Carolina at Charlotte, 9201 University City Boulevard, Charlotte, NC 28223, USA
[b] Department of Natural Sciences and Mathematics, Johnson C. Smith University, Charlotte, NC 28216, USA
[c] Department of Chemistry and Biochemistry, The University of Delaware, Newark, DE 19716, USA

Received 12 June 2003; accepted 27 October 2003

Abstract

Thallium(I) bis(mercaptoimidazolyl)borates Tl(Bm^R) (R = Me, Bz, Bu^t, *p*-Tol) have been conveniently obtained in a one-pot reaction by metathesis of thallium(I) acetate and the corresponding sodium derivatives Na(Bm^R), in turn generated in high yield from $NaBH_4$ and the appropriate 2-mercapto-1-alkylimidazoles. In contrast to polymeric Tl(Bm^{Me}), the *tert*-butyl-substituted complex Tl(Bm^{tBu}) consists of discrete dimeric molecules in the solid state, as determined by single-crystal X-ray diffraction, and is highly soluble in aromatic hydrocarbons.
© 2003 Elsevier Ltd. All rights reserved.

Keywords: Thallium; Bis(mercaptoimidazolyl)borate complexes; Crystal structure

1. Introduction

Despite their contemporary genesis, progress in the chemistry of bis(mercaptoimidazolyl)borates has lagged behind that experienced by the closely related tris(mercaptoimidazolyl)borates (Fig. 1), for which literally dozens of compounds have now been prepared [1–26]. Relatively few complexes of Bm^R ligands have been isolated since the synthesis of Li(Bm^{Me}) was first reported by Parkin in 1997 [27]. Together with the mesityl-substituted analogue Li(Bm^{Mes}), these lithium species were used to obtain the corresponding thallium compounds Tl(Bm^R) (R = Me, Mes) and some zinc derivatives thereof, including (Bm^{Me})ZnX (X = I, Me), Zn(Bm^{Me})$_2$, and (Bm^{Mes})$ZnNO_3$ [28]. Subsequently, a number of $[Bm^R]^-$ complexes of technetium, rhenium, and uranium have been isolated by Santos [29–32] and we have synthesized the homoleptic nickel(II) complexes Ni(Bm^R)$_2$ (R = Me, Bz, Bu^t, *p*-Tol) as structural models for the nickel center in the active site of [NiFe] hydrogenases [33]. More recently, the X-ray structure of (Bm^{Me})Au(PPh_3) has been disclosed [34] and several group 12 derivatives M(Bm^R)$_2$ (M = Zn, Cd, Hg), including the first complete series of Bm^R complexes to be structurally characterized, have been obtained [35].

Interested in further developing Bm^R coordination chemistry, we envisioned that a systematic investigation of thallium complexes Tl(Bm^R) may produce valuable species for ensuing reactivity studies. In this regard, thallium reagents, despite their inherent toxicity and cost, have played a conspicuous role in the development of modern inorganic and organometallic chemistry. For example, thallium(I) cyclopentadienyls and tris(pyrazolyl)borates, usually regarded as milder (less reducing) transfer reagents than their alkali metal counterparts, have been extensively used to introduce these ubiquitous ligands to the coordination sphere of both main group and transition metals [36–38]. In addition, effective driving forces in their metathesis reactions with metal halide or metal alkyl complexes are the formation of insoluble thallium(I) halides or the decomposition of

* Corresponding authors. Present address: Department of Chemistry and Biochemistry, University of California – San Diego, 9500 Gilman Drive, La Jolla, CA 92093, USA (A.L. Rheingold). Tel.: +1-704-687-4442; fax: +1-704-687-3151 (D. Rabinovich).
E-mail addresses: arheingold@ucsd.edu (A.L. Rheingold), drabinov@email.uncc.edu (D. Rabinovich).
[1] Permanent address: Department of Chemistry and Biochemistry, University of Massachusetts – Dartmouth, North Dartmouth, MA 02747, USA.

0277-5387/$ - see front matter © 2003 Elsevier Ltd. All rights reserved.
doi:10.1016/j.poly.2003.10.015

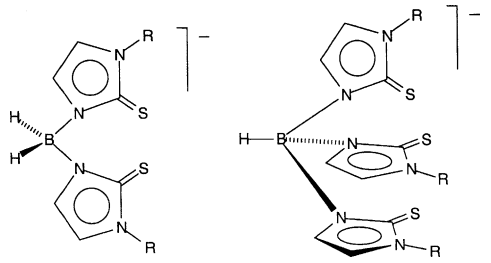

Fig. 1. The bis(mercaptoimidazolyl)borate (Bm^R) and tris(mercaptoimidazolyl)borate (Tm^R) ligand systems.

thermodynamically unstable thallium(I) alkyl by-products, respectively. We report in this paper an improved synthesis of $Tl(Bm^{Me})$ and the preparation and characterization of the hitherto unknown benzyl, *tert*-butyl, and *para*-tolyl derivatives $Tl(Bm^R)$ (R = Bz, Bu^t, *p*-Tol).

2. Results and discussion

2.1. Thallium bis(mercaptoimidazolyl)borates

The thallium(I) complexes $Tl(Bm^R)$ (R = Me, Mes) were originally obtained in ca. 70% yield by the metathetical reactions of thallium(I) acetate with the corresponding lithium precursors $Li(Bm^R)$ in methanol [28]. Following an analogous strategy, but taking advantage of our almost quantitative protocol for generating $Na(Bm^{Me})$ [35], $Tl(Bm^{Me})$ was prepared by reacting a methanolic solution of $Na(Bm^{Me})$ with an aqueous solution of TlOAc, as illustrated in Eq. (1), and typically isolated in 90–95% yield.

$$Na(Bm^{ME}) + TlOAc \overset{MeOH/H_2O}{\rightarrow} Tl(Bm^{Me}) + NaOAc \quad (1)$$

The new thallium(I) bis(mercaptoimidazolyl)borates $Tl(Bm^R)$ (R = Bz, Bu^t, *p*-Tol) were similarly synthesized in 75–80% yield from the corresponding $Na(Bm^R)$ derivatives, accessed in turn by reacting $NaBH_4$ with 2 molar equiv. of the appropriate mercaptoimidazoles in tetrahydrofuran (THF) [35]. The four $Tl(Bm^R)$ complexes described above are white (R = Me, Bz, *p*-Tol) or pale yellow (R = Bu^t) air-stable solids, very soluble in chloroform, dichloromethane, and dimethyl sulfoxide (DMSO) but insoluble in diethyl ether, methanol, or water. In addition, some of the compounds are also soluble in acetone (R = *p*-Tol), acetonitrile (R = Me, *p*-Tol), benzene or toluene (R = Me, Bu^t, *p*-Tol), and THF (R = Bz, *p*-Tol).

The thallium complexes $Tl(Bm^R)$ (R = Me, Bz, Bu^t, *p*-Tol) were characterized by a combination of analytical and spectroscopic techniques, including elemental analyses (CHN) and IR and NMR spectroscopies. For example, the IR spectra of $Tl(Bm^R)$, obtained as KBr pellets, show the expected medium-intensity ν_{B-H} bands between 2350 and 2440 cm^{-1}. ^{1}H and ^{13}C NMR data for all the complexes are similar to those of the corresponding $Na(Bm^R)$ species [35], with only modest downfield chemical shifts observed for both the imidazolyl hydrogen and carbon atoms upon complexation to thallium. However, unlike the $Na(Bm^R)$ derivatives, small broad singlet peaks assigned to the H_2B groups (δ = 3.89–4.06 ppm) are readily observed in the case of the thallium complexes.

2.2. Molecular structure of $Tl(Bm^{tBu})$

Single crystals of $Tl(Bm^{tBu})$ suitable for an X-ray diffraction study were obtained by slow evaporation at room temperature of a saturated benzene solution of the complex. There are two chemically similar but crystallographically independent half molecules in the asymmetric unit, with selected bond lengths and angles for both summarized in Table 1. As shown in Fig. 2, each of the two thallium atoms in the centrosymmetric dinuclear molecules is coordinated to a single thione group from one $[Bm^{tBu}]^-$ ligand and both from the other. In addition, each H_2B moiety also partakes in a weak Tl···H–B interaction of the type prevalent in Bm^R chemistry [28,29,32,33,35]. A similar coordination environment about each metal has been observed for $Li(Bm^{Mes})$, which is dimeric in the solid state as well [28]. The S–Tl–S angles subtended at each metal center in $Tl(Bm^{tBu})$ are in the approximate range 91–131° and the almost rectangular $[Tl_2S_2]$ core [Tl(1)–S(2)–Tl(1A) = 88.91(4)°, S(2)–Tl(1)–S(2A) = 91.09(4)°] is thus virtually identical to that present within polynuclear $Tl(Bm^{Me})$ [28]. However, there are no non-bonded (i.e., intermolecular) Tl–S distances shorter than 3.6 Å in $Tl(Bm^{tBu})$, a phenomenon that effectively precludes the formation of the extended structure observed for $Tl(Bm^{Me})$.

The Tl–S bond lengths in $Tl(Bm^{tBu})$, varying from 2.928(2) to 3.228(2) Å, are comparable to the corre-

Table 1
Selected bond lengths (Å) and bond angles (°) for the two crystallographically independent molecules of $Tl(Bm^{tBu})$

	Molecule 1	Molecule 2
Bond lengths		
Tl(1)–S(1)	2.973(2)	2.961(2)
Tl(1)–S(2)	2.928(2)	2.903(2)
Tl(1)–S(2A)	3.058(2)	3.228(2)
Tl(1)···B(1)	3.835(7)	3.517(6)
Tl(1)···B(1A)	3.525(6)	4.087(6)
Tl(1)···Tl(1A)	4.193(1)	4.199(1)
S(2)···S(2A)	4.273(3)	4.480(3)
Bond angles		
S(1)–Tl(1)–S(2)	101.12(4)	92.98(4)
S(1)–Tl(1)–S(2A)	102.59(4)	131.39(4)
S(2)–Tl(1)–S(2A)	91.09(4)	93.73(4)
Tl(1)–S(2)–Tl(1A)	88.91(4)	86.27(4)
Tl(1)–S(1)–C(1)	123.4(2)	114.6(2)
Tl(1)–S(2)–C(8)	100.6(2)	113.0(2)

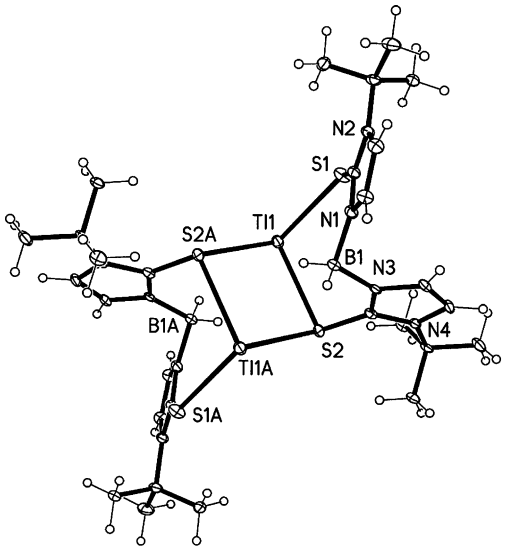

Fig. 2. Molecular structure of Tl(Bm^{tBu}) with thermal ellipsoids at the 30% probability level (only one of the two crystallographically independent molecules in the unit cell is shown).

sponding values found in Tl(Bm^{Me}), in the range 3.043(2)–3.206(2) Å [28]. Similarly, the closest Tl···H–B interactions in the former [d(Tl···B) = 3.52 and 3.53 Å for the two crystallographically independent molecules] are only marginally longer than those in the latter [d(Tl···B) = 3.50 Å]. Predictably, the S–C bond distances for the terminal thione groups (i.e., those bound to a single thallium) in Tl(Bm^{tBu}), 1.693(6) and 1.710(5) Å, are slightly shorter than the corresponding values found in the bridging mercaptoimidazolyl moieties [1.725(5) and 1.733(5) Å]. This situation was also verified in Tl(Bm^{Me}), for which the difference between such terminal and bridging interactions, 1.707(5) and 1.712(5) Å, respectively, is nevertheless less noticeable. More significantly, the Tl···Tl separations in the two crystallographically independent molecules of Tl(Bm^{tBu}), 4.193(1) and 4.199(1) Å, suggest that neither compound [nor Tl(Bm^{Me}), where [d(Tl···Tl) = 4.37 Å] exhibits any discernible thallium–thallium bonding, the very nature of which has been under intense scrutiny in recent years [39,40].

3. Conclusions

The new thallium(I) complexes Tl(Bm^{R}) (R = Bz, Bu^t, *p*-Tol), together with the known methyl-substituted derivative Tl(Bm^{Me}), have been readily prepared in ca. 75–95% yield. The *tert*-butyl derivative displays in the solid state a discrete dinuclear structure that results in an enhanced solubility in organic solvents relative to that of polymeric Tl(Bm^{Me}). The Tl(Bm^{R}) compounds described herein constitute a potentially useful family of reagents for the transfer of bis(mercaptoimidazolyl)borate ligands to transition metals. In this regard, it is worth noting that the Tl(Bm^{R}) reagents, unlike their sodium counterparts, cleanly react with the nickel(II) diphosphine complexes (dppe)NiX_2 (X = Cl, Br) to produce derivatives of general formula (dppe)Ni(Bm^{R})X, the syntheses and characterization of which will be reported separately [41].

4. Experimental

4.1. General considerations

All reactions were performed in the air except for the syntheses of the Na(Bm^{R}) intermediates, which were carried out under dry oxygen-free nitrogen in an Innovative Technology System One-M-DC glovebox or under argon using high-vacuum techniques [42–44]. Solvents were purified and degassed by standard procedures and all commercially available reagents, including methimazole (Acros or Aldrich), were used as received. The 2-mercapto-1-alkylimidazoles $Hmim^{R}$ (R = Bz, Bu^t, *p*-Tol) were prepared by the acid-catalyzed cyclization of aminoacetaldehyde diethyl acetal [$H_2NCH_2CH(OEt)_2$] and the appropriate alkylisothiocyanates (RNCS) following literature procedures [45,46]. ^{1}H and ^{13}C NMR spectra were obtained on General Electric QE 300 or Varian Gemini (300 MHz) FT spectrometers. Chemical shifts (δ) are reported in parts per million relative to $SiMe_4$ (δ = 0 ppm) and were referenced internally with respect to the solvent resonances (^{1}H δ: 2.49 for d_5-DMSO; ^{13}C δ: 39.5 for d_6-DMSO); coupling constants are given in hertz (Hz). IR spectra were recorded as KBr pellets on a Thermo Mattson Satellite 3000 FT-IR spectrophotometer and are reported in cm^{-1}; relative intensities of the absorptions are indicated in parentheses (vs, very strong; s, strong; m, medium; w, weak). Elemental analyses were determined by Atlantic Microlab, Inc. (Norcross, GA).

4.2. Synthesis of Tl(Bm^{Me})

A suspension of $NaBH_4$ (0.500 g, 13.22 mmol) and 2-mercapto-1-methylimidazole (3.000 g, 26.28 mmol) in tetrahydrofuran (55 mL) was heated to reflux for 15 h under an atmosphere of argon. The resulting clear colorless solution was allowed to cool to room temperature and the solvent was removed under reduced pressure to give crude Na(Bm^{Me}) as a white solid residue. The solid was dissolved in methanol (55 mL) and the slightly cloudy solution was treated with a solution of thallium(I) acetate (3.460 g, 13.13 mmol) in water (50 mL), resulting in the formation of an off-white precipitate. After stirring the suspension for 15 min, the product was isolated by filtration, washed with water (2 × 15 mL), and dried in vacuo for 2.5 h (5.649 g, 97%); m.p. = 218

°C (dec). NMR data (in d_6-DMSO): ^{1}H δ: 3.42 (s, 6H, CH_3), 3.92 (br s, 2H, H_2B), 6.74 (s, 2H, imidazole *H*), 7.01 (s, 2H, imidazole *H*); ^{13}C δ: 34.3 (q, $^1J_{C-H} = 140$, 2C, *C*H$_3$), 118.7 (dd, $^1J_{C-H} = 195$, $^2J_{C-H} = 12$, 2C, imidazole *C*), 122.6 (dd, $^1J_{C-H} = 194$, $^2J_{C-H} = 10$, 2C, imidazole *C*), 160.1 (s, 2C, *C*=S). IR data (cm^{-1}): 3144 (w), 3114 (m), 3077 (w), 2963 (w), 2935 (w), 2404 (w), 2360 (m), 2345 (m), 2262 (w), 2211 (w), 1655 (w), 1554 (w), 1452 (m), 1410 (w), 1372 (s), 1299 (w), 1261 (w), 1201 (m), 1186 (m), 1166 (w), 1151 (w), 1109 (s), 889 (w), 801 (w), 750 (m), 729 (s), 696 (w), 680 (w), 519 (w), 500 (w), 459 (w). *Anal.* Calc. for $C_8H_{12}BN_4S_2Tl$: C, 21.7; H, 2.7; N, 12.6. Found: C, 22.0; H, 2.8; N, 12.2%.

4.3. Synthesis of Tl(Bm^{Bz})

A suspension of $NaBH_4$ (0.050 g, 1.32 mmol) and 2-mercapto-1-benzylimidazole (0.500 g, 2.63 mmol) in tetrahydrofuran (40 mL) was heated to reflux for 18 h under an atmosphere of argon. The resulting clear colorless solution was allowed to cool to room temperature and the solvent was removed under reduced pressure to give crude Na(Bm^{Bz}) as a white solid residue. The solid was dissolved in methanol (40 mL) and the slightly cloudy solution was treated with a solution of thallium(I) acetate (0.345 g, 1.31 mmol) in water (25 mL), resulting in the formation of an off-white precipitate. After stirring the suspension for 15 min, the product was isolated by filtration, washed with water (2×10 mL), and dried in vacuo for 20 h (0.623 g, 80%); m.p. = 200 °C (dec). NMR data (in d_6-DMSO): ^{1}H δ: 3.93 (br s, 2H, H_2B), 5.20 (s, 4H, CH_2C$_6$H$_5$), 6.84 (s, 2H, imidazole *H*), 7.02 (s, 2H, imidazole *H*), 7.2–7.4 (m, 10H, CH$_2$C$_6H_5$); ^{13}C δ: 49.4 (t, $^1J_{C-H} = 140$, 2C, *C*H$_2$C$_6$H$_5$), 117.3 (dd, $^1J_{C-H} = 195$, $^2J_{C-H} = 12$, 2C, imidazole *C*), 123.2 (dd, $^1J_{C-H} = 193$, $^2J_{C-H} = 10$, 2C, imidazole *C*), 127.2 (d, $^1J_{C-H} = 160$, 2C, C_p in Bz), 127.6 (d, $^1J_{C-H} = 159$, 4C, C_o or C_m in Bz), 128.3 (dd, $^1J_{C-H} = 160$, $^2J_{C-H} = 6$, 4C, C_o or C_m in Bz), 137.6 (s, 2C C_{ipso} in Bz), 160.7 (s, 2C, *C*=S). IR data (cm^{-1}): 2920 (w), 2437 (m), 2391 (w), 1495 (w), 1442 (w), 1418 (w), 1390 (m), 1361 (w), 1327 (m), 1223 (w), 1172 (w), 1147 (m), 1115 (w), 1057 (w), 724 (m), 695 (m), 674 (w), 334 (vs), 321 (w), 313 (w). *Anal.* Calc. for $C_{20}H_{20}BN_4S_2Tl$: C, 40.3; H, 3.4; N, 9.4. Found: C, 40.0; H, 3.3; N, 9.1%.

4.4. Synthesis of Tl(Bm^{tBu})

A suspension of $NaBH_4$ (0.061 g, 1.60 mmol) and 2-mercapto-1-*tert*-butylimidazole (0.501 g, 3.21 mmol) in tetrahydrofuran (35 mL) was heated to reflux for 20 h under an atmosphere of argon. The resulting clear colorless solution was allowed to cool to room temperature and the solvent was removed under reduced pressure to give crude Na(Bm^{tBu}) as a white solid residue. The solid was dissolved in methanol (30 mL) and the slightly cloudy solution was treated with a solution of thallium(I) acetate (0.421 g, 1.60 mmol) in water (25 mL), resulting in the formation of a pale yellow precipitate. After stirring the suspension for 15 min, the product was isolated by filtration, washed with water (2×10 mL), and dried in vacuo for 20 h (0.660 g, 78%); m.p. = 208 °C (dec). NMR data (in d_6-DMSO): ^{1}H δ: 1.69 [s, 18H, C(CH_3)$_3$], 4.06 (br s, 2H, H_2B), 6.64 (d, $^3J_{H-H} = 2.3$, 2H, imidazole *H*), 7.08 (d, $^3J_{H-H} = 2.3$, 2H, imidazole *H*); ^{13}C δ: 28.3 [q, $^1J_{C-H} = 127$, 6C, C(*C*H$_3$)$_3$], 57.5 [s, 2C, *C*(CH$_3$)$_3$], 115.7 (dd, $^1J_{C-H} = 194$, $^2J_{C-H} = 13$, 2C, imidazole *C*), 121.6 (dd, $^1J_{C-H} = 193$, $^2J_{C-H} = 9$, 2C, imidazole *C*), 158.6 (s, 2C, *C*=S). IR data (cm^{-1}): 3176 (w), 3132 (m), 3094 (w), 2970 (s), 2927 (s), 2372 (vs), 2211 (w), 1710 (w), 1686 (w), 1562 (m), 1481 (m), 1468 (w), 1449 (w), 1421 (m), 1404 (m), 1395 (m), 1354 (vs), 1298 (w), 1281 (w), 1253 (w), 1224 (w), 1199 (w), 1162 (w), 1111 (w), 1088 (w), 1026 (w), 978 (w), 966 (w), 929 (w), 875 (w), 819 (w), 735 (s), 723 (s), 704 (s), 681 (s), 627 (w), 583 (w), 554 (w), 482 (m). *Anal.* Calc. for $C_{14}H_{24}BN_4S_2Tl$: C, 31.9; H, 4.6; N, 10.6. Found: C, 32.1; H, 4.6; N, 10.5%.

4.5. Synthesis of Tl(Bm$^{p\text{-}Tol}$)

A suspension of $NaBH_4$ (0.050 g, 1.32 mmol) and 2-mercapto-1-*p*-tolylimidazole (0.501 g, 2.63 mmol) in tetrahydrofuran (40 mL) was heated to reflux for 19 h under an atmosphere of argon. The resulting clear colorless solution was allowed to cool to room temperature and the solvent was removed under reduced pressure to give crude Na(Bm$^{p\text{-Tol}}$) as a white solid residue. The solid was dissolved in methanol (40 mL) and the slightly cloudy solution was treated with a solution of thallium(I) acetate (0.348 g, 1.32 mmol) in water (25 mL), resulting in the formation of a pale yellow precipitate. After stirring the suspension for 15 min, the product was isolated by filtration, washed with water (3×10 mL), and dried in vacuo for 18 h (0.598 g, 76%). Melting point = 114 °C (dec). NMR data (in d_6-DMSO): ^{1}H δ: 2.33 (s, 6H, CH_3), 3.89 (br s, 2H, H_2B), 7.04 (s, 2H, imidazole *H*), 7.12 (s, 2H, imidazole *H*), 7.24 (d, $^3J_{H-H} = 8.1$, 4H, H_o or H_m in *p*-Tol), 7.43 (d, $^3J_{H-H} = 8.1$, 4H, H_o or H_m in *p*-Tol); ^{13}C δ: 20.6 (q, $^1J_{C-H} = 126$, 2C, *C*H$_3$), 118.7 (dd, $^1J_{C-H} = 197$, $^2J_{C-H} = 13$, 2C, imidazole *C*), 123.9 (dd, $^1J_{C-H} = 193$, $^2J_{C-H} = 9$, 2C, imidazole *C*), 126.1 (dd, $^1J_{C-H} = 163$, $^2J_{C-H} = 5$, 4C, C_o or C_m in *p*-Tol), 129.0 (d, $^1J_{C-H} = 160$, 4C, C_o or C_m in *p*-Tol), 136.2 (s, 2C, C_{ipso} or C_p in *p*-Tol), 136.8 (s, 2C, C_{ipso} or C_p in *p*-Tol), 160.6 (s, 2C, *C*=S). IR data (cm^{-1}): 3130 (w), 3032 (w), 2918 (w), 2380 (m), 1555 (w), 1584 (w), 1560 (w), 1515 (s), 1419 (m), 1354 (vs), 1308 (w), 1263 (w), 1156 (m), 1179 (w), 1104 (m), 1020 (w), 818 (m), 711 (w), 680 (w), 602 (w), 563 (w). *Anal.* Calc. for $C_{20}H_{20}BN_4S_2Tl$: C, 40.3; H, 3.4; N, 9.4. Found: C, 41.1; H, 3.5; N, 9.6%.

Table 2
Crystallographic data for $Tl(Bm^{tBu})$

Formula	$C_{28}H_{48}B_2N_8S_4Tl_2$
Formula weight	1055.34
Crystal system	monoclinic
Space group	$P2_1/c$ (no. 14)
Temperature (K)	100(2)
Unit cell dimensions	
a (Å)	15.925(3)
b (Å)	13.295(3)
c (Å)	17.543(4)
β (°)	91.324(4)
V (Å^3)	3713.5(13)
Z	4
ρ_{calc} (g cm^{-3})	1.888
μ(Mo Kα) (mm^{-1})	8.924
θ_{max} (°)	26.00
Number of data	7195
Number of parameters	397
$R_1(I > 2\sigma(I))$[a]	0.0419
$wR_2(I > 2\sigma(I))$[a]	0.1060

[a] $R_1 = \sum(|F_o| - |F_c|)/\sum|F_o|$; $wR_2 = \{\sum[w(F_o^2 - F_c^2)^2]/\sum[w(F_o^2)^2]\}^{1/2}$.

4.6. X-ray structure determination

A summary of crystal data collection and refinement parameters for $Tl(Bm^{tBu})$ is given in Table 2. A colorless crystal suitable for data collection was selected and mounted on a glass fiber using Paratone-N oil and then placed in the cold nitrogen stream of a Siemens/Bruker P4 diffractometer using Mo Kα radiation ($\lambda = 0.71073$ Å) and equipped with a SMART CCD detector. The data were corrected for absorption using the program SADABS and the space group was uniquely determined as $P2_1/c$. The structure was solved by direct methods and all non-hydrogen atoms were refined anisotropically by least-squares Fourier analysis. Hydrogen atoms were placed in idealized positions and fitted to their attached atoms with U_{eq} of 1.2 or 1.5. High residual electron densities greater than 1 e Å^{-3} found for 10 peaks which were less than 1 Å from neighboring thallium atoms suggests a relatively poor correlation with the SADABS absorption model. All software used is contained in the SMART, SAINT, SADABS, and SHELXTL program libraries [47].

5. Supplementary data

Crystallographic data (excluding structure factors) for $Tl(Bm^{Me})$ have been deposited with the Cambridge Crystallographic Data Centre with CCDC No. 210721. Copies of this information may be obtained free of charge from The Director, CCDC, 12 Union Road, Cambridge CB2 1EZ, UK (fax: +44-1223-336033; e-mail: deposit@ccdc.cam.ac.uk; www: http://www.ccdc.cam.ac.uk).

Acknowledgements

We thank the Camille and Henry Dreyfus Foundation, Inc. for a Henry Dreyfus Teacher-Scholar Award to D.R., Research Corporation for a Cottrell College Science Award, the donors of the Petroleum Research Fund, administered by the American Chemical Society, and The University of North Carolina at Charlotte for support of this research. P.A.G. also acknowledges the National Institute of General Medical Sciences and its MBRS/RISE program at Johnson C. Smith University (Grant No. GM58042) for financial support and C.D.G. is also grateful to the American Chemical Society's Project SEED program for financial assistance during the summer of 2002. H.M.A. also acknowledges financial assistance from the Thomas D. Walsh Tuition Fellowship Fund at UNC Charlotte.

References

[1] M. Garner, J. Reglinski, I. Cassidy, M.D. Spicer, A.R. Kennedy, Chem. Commun. (1996) 1975.
[2] C. Santini, G. Gioia Lobbia, C. Pettinari, M. Pellei, G. Valle, S. Calogero, Inorg. Chem. 37 (1998) 890.
[3] C. Santini, C. Pettinari, G. Gioia Lobbia, R. Spagna, M. Pellei, F. Vallorani, Inorg. Chim. Acta 285 (1999) 81.
[4] J. Reglinski, M.D. Spicer, M. Garner, A.R. Kennedy, J. Am. Chem. Soc. 121 (1999) 2317.
[5] J. Reglinski, M. Garner, I. Cassidy, P.A. Slavin, M.D. Spicer, D.R. Armstrong, J. Chem. Soc., Dalton Trans. (1999) 2119.
[6] A.F. Hill, G.R. Owen, A.J.P. White, D.J. Williams, Angew. Chem., Int. Ed. 38 (1999) 2759.
[7] C. Kimblin, B.M. Bridgewater, D.G. Churchill, G. Parkin, Chem. Commun. (1999) 2301.
[8] P.A. Slavin, J. Reglinski, M.D. Spicer, A.R. Kennedy, J. Chem. Soc., Dalton Trans. (2000) 239.
[9] C. Kimblin, B.M. Bridgewater, T. Hascall, G. Parkin, J. Chem. Soc., Dalton Trans. (2000) 1267.
[10] B.M. Bridgewater, G. Parkin, J. Am. Chem. Soc. 122 (2000) 7140.
[11] Effendy, G. Gioia Lobbia, C. Pettinari, C. Santini, B.W. Skelton, A.H. White, Inorg. Chim. Acta 308 (2000) 65.
[12] B.M. Bridgewater, G. Parkin, Inorg. Chem. Commun. 3 (2000) 534.
[13] B.M. Bridgewater, T. Fillebeen, R.A. Friesner, G. Parkin, J. Chem. Soc., Dalton Trans. (2000) 4494.
[14] B.M. Bridgewater, G. Parkin, Inorg. Chem. Commun. 4 (2001) 126.
[15] G. Gioia Lobbia, C. Pettinari, C. Santini, N. Somers, B.W. Skelton, A.H. White, Inorg. Chim. Acta 319 (2001) 15.
[16] C. Kimblin, D.G. Churchill, B.M. Bridgewater, J.N. Girard, D.A. Quarless, G. Parkin, Polyhedron 20 (2001) 1891.
[17] R. Garcia, A. Paulo, A. Domingos, I. Santos, J. Organomet. Chem. 632 (2001) 41.
[18] M. Tesmer, M. Shu, H. Vahrenkamp, Inorg. Chem. 40 (2001) 4022.
[19] C. Santini, M. Pellei, G. Gioia Lobbia, C. Pettinari, A. Drozdov, S. Troyanov, Inorg. Chim. Acta 40 (2001) 4022.
[20] S. Bakbak, V.K. Bhatia, C.D. Incarvito, A.L. Rheingold, D. Rabinovich, Polyhedron 20 (2001) 3343.
[21] M. Garner, M.-A. Lehmann, J. Reglinski, M.D. Spicer, Organometallics 20 (2001) 5233.

[22] I. Cassidy, M. Garner, A.R. Kennedy, G.B.S. Potts, J. Reglinski, P.A. Slavin, M.D. Spicer, Eur. J. Inorg. Chem. (2002) 1235.
[23] S. Bakbak, C.D. Incarvito, A.L. Rheingold, D. Rabinovich, Inorg. Chem. 41 (2002) 998.
[24] J.L. White, J.M. Tanski, D. Rabinovich, J. Chem. Soc., Dalton Trans. (2002) 2987.
[25] M. Garner, K. Lewinski, A. Pattek-Janczyk, J. Reglinski, B. Sieklucka, M.D. Spicer, M. Szaleniec, Dalton Trans. (2003) 1181.
[26] M.R.St.-J. Foreman, A.F. Hill, A.J.P. White, D.J. Williams, Organometallics 22 (2003) 3831.
[27] C. Kimblin, T. Hascall, G. Parkin, Inorg. Chem. 36 (1997) 5680.
[28] C. Kimblin, B.M. Bridgewater, T. Hascall, G. Parkin, J. Chem. Soc., Dalton Trans. (2000) 891.
[29] R. Garcia, A. Paulo, A. Domingos, I. Santos, K. Ortner, R. Alberto, J. Am. Chem. Soc. 122 (2000) 11240.
[30] L. Maria, A. Domingos, I. Santos, Inorg. Chem. 40 (2001) 6863.
[31] R. Garcia, A. Domingos, A. Paulo, I. Santos, R. Alberto, Inorg. Chem. 41 (2002) 2422.
[32] R. Garcia, Y.-H. Xing, A. Paulo, A. Domingos, I. Santos, J. Chem. Soc., Dalton Trans. (2002) 4236.
[33] H.M. Alvarez, M. Krawiec, B.T. Donovan-Merkert, M. Fouzi, D. Rabinovich, Inorg. Chem. 40 (2001) 5736.
[34] A.A. Mohamed, D. Rabinovich, J.P. Fackler, Acta Crsytallogr. E 58 (2002) m726.
[35] H.M. Alvarez, T.B. Tran, M.A. Richter, D.M. Alyounes, D. Rabinovich, J.M. Tanski, M. Krawiec, Inorg. Chem. 42 (2003) 2149.
[36] C. Janiak, Coord. Chem. Rev. 163 (1997) 107.
[37] C. Janiak, Main Group Met. Chem. 21 (1998) 33.
[38] E. Craven, E. Mutlu, D. Lundberg, S. Temizdemir, S. Dechert, H. Brombacher, C. Janiak, Polyhedron 21 (2002) 553.
[39] C. Janiak, R. Hoffmann, J. Am. Chem. Soc. 112 (1990) 5924.
[40] P. Schwerdtfeger, Inorg. Chem. 30 (1990) 1660.
[41] H.M. Alvarez, J.M. Tanski, D. Rabinovich, Polyhedron 23 (2004) 395.
[42] R.J. Errington, Advanced Practical Inorganic and Metalorganic Chemistry, Blackie, London, 1997.
[43] A.L. Wayda, M.Y. Darensbourg (Eds.), Experimental Organometallic Chemistry, American Chemical Society, Washington, DC, 1987.
[44] D.F. Shriver, M.A. Drezdzon, The Manipulation of Air-sensitive Compounds, second ed., Wiley-Interscience, New York, 1986.
[45] K. Matsuda, I. Yanagisawa, Y. Isomura, T. Mase, T. Shibanuma, Synth. Commun. 27 (1997) 3565.
[46] C.S. Cassidy, L.A. Reinhardt, W.W. Cleland, P.A. Frey, J. Chem. Soc., Perkin Trans. 2 (1999) 635.
[47] Bruker-AXS, Inc., 5465 East Cheryl Parkway, Madison, WI 53711-5373, USA.

Available online at www.sciencedirect.com
SCIENCE DIRECT®
Polyhedron 23 (2004) 623–627
POLYHEDRON
www.elsevier.com/locate/poly

Crystal structure of the first octanuclear uranium(IV) complex with compartmental Schiff base ligands

Lionel Salmon *, Pierre Thuéry *, Michel Ephritikhine *

Service de Chimie Moléculaire, DSM, DRECAM, CNRS URA 331, CEA Saclay, Bât. 125, 91191 Gif-sur-Yvette, France

Received 22 September 2003; accepted 27 October 2003

Abstract

The crystal structure of the dianionic $[U_8L_4Cl_{10}O_4]^{2-}$ cluster [$H_4L = N,N'$-*bis*(3-hydroxysalicylidene)-1,2-phenylenediamine] is built up of four U_2LCl_2O subunits which are held together by eight μ_2-phenoxo bridges, four μ_4-oxo bridges and two additional μ_2-chloro bridges. The four U atoms in the external cavities of the bicompartmental hexadentate Schiff base ligands and the four μ_4-oxo ions form an unprecedented U_4O_4 cubane arrangement. The U_8O_4 core consists of four distorted uranium tetrahedra, each of them sharing a common edge with its three neighbours and containing a μ_4-oxo ion at its centre. This complex is one of the highest nuclearity assemblages in the chemistry of uranium compounds.
© 2003 Elsevier Ltd. All rights reserved.

Keywords: Uranium; Schiff base; Cluster; Crystal structure

1. Introduction

The design of polynuclear, nanometer-sized metal complexes has received a new impulse in recent years due to the use of methods of self-assembly in an attempt to model the structural and functional aspects of multimetal active sites in biological processes or to prepare nanometric materials and single molecule magnets [1–3]. In the particular case of uranium, which has been the subject of relatively little attention up to now, discrete polynuclear species including up to six [4] and even eight [5,6] uranyl [dioxouranium(VI)] ions are known, as well as two clusters comprising six uranium(V) [7] or six uranium(III,IV) [8] centres. We have reported previously the crystal structure of an octanuclear uranium(IV) compound with the cp*py ligand [tetramethyl-5-(2-pyridyl)cyclopentadiene], which is the assemblage of highest nuclearity in the molecular chemistry of uranium (uranyl excluded) [9]. In order to investigate the magnetic behaviour of heterobi- and heterotrimetallic complexes containing paramagnetic 5f (U^{IV}) and 3d metal ions, we turned recently to the use of hexadentate Schiff bases as associating ligands [10–12]. In these compounds, the internal N_2O_2 cavity of the Schiff base is adequate for the complexation of the 3d ion and the external O_4 cavity is well suited for the f ion. However, several crystal structures reported in the literature show that the U^{IV} ion can also be located in the inner N_2O_2 coordination site [13,14]. In the course of this study, we serendipitously synthesized bi- and tetranuclear uranyl/3d metal ions complexes [15] and the title compound containing an octanuclear uranium(IV) cluster. The crystal structure of the latter, which is described herein, gives a new example of a high nuclearity uranium complex and it also evidences the ability of Schiff base ligands to build polynuclear assemblies.

2. Results and discussion

The crystal structure of $(Hpy)_2[U_8L_4Cl_{10}O_4]\cdot 10py$ shows the presence of a dianionic octanuclear cluster, represented in Fig. 1, and two pyridinium ions which are hydrogen bonded to two pyridine molecules [N5···N6 2.67(2) Å]; additionally, the crystal contains 10

* Corresponding authors. Tel.: +33-1-69-08-6329; fax: +33-1-69-086640.
E-mail addresses: salmon@drecam.cea.fr (L. Salmon), thuery@drecam.cea.fr (P. Thuéry), ephri@drecam.cea.fr (M. Ephritikhine).

0277-5387/$ - see front matter © 2003 Elsevier Ltd. All rights reserved.
doi:10.1016/j.poly.2003.10.014

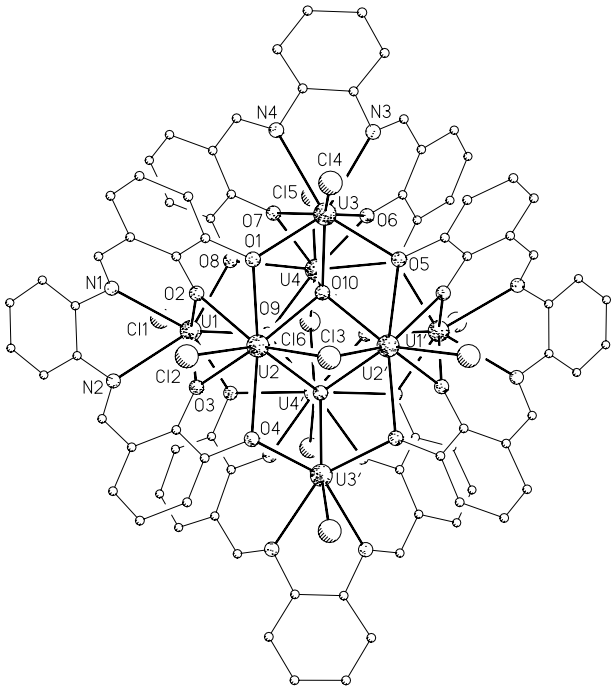

Fig. 1. View of the $[U_8L_4Cl_{10}O_4]^{2-}$ cluster. Hydrogen atoms, counter-ions and solvent molecules are omitted for clarity. Atoms are represented as spheres, the carbon ones being arbitrarily reduced. Symmetry code: $' = -x, y, 0.5 - z$.

encapsulated molecules of pyridine. The axis defined by the two bridging chlorine atoms Cl3 and Cl6 is a crystallographic twofold symmetry axis and, apart from the counter-ions and solvent molecules, the asymmetric unit contains four uranium atoms and two Schiff base ligands (Fig. 2). The C_2 axis, which is also a pseudo-S_4 symmetry axis, is perpendicular to two pseudo binary axes; one of those associates U1 to U3, U2 to U4 and O9 to O10, as can be seen in Fig. 2, and the other associates U1 to U3′, U2 to U4′ and O9 to O10′. Two non-crystallographic dihedral symmetry planes σ_d intersect along C_2, one of them containing U1, U2, U1′ and U2′ and the other U3, U4, U3′ and U4′. The cluster thus exhibits a pseudo-D_{2d} symmetry and can be viewed as four binuclear U_2LCl_2O subunits which are held together by eight μ_2-phenoxo bridges from the L ligand (O1, O4, O5, O8 and their symmetric counterparts), four μ_4-oxo bridges, (O9, O10, O9′, O10′), in addition to the two μ_2-chloro bridges (Cl3 and Cl6). In each U_2LCl_2O subunit, the two uranium, two chlorine and the μ_4-oxygen atoms are lying in the σ_d pseudo-symmetry plane; the U1U2 and U3U4 vectors making angles of $\sim$30° with the C_2 axis and 41.2° one with the other. As observed in the mononuclear $UL'(acac)_2 \cdot thf$ compound [14] [$L' = N,N'$-*bis*(3-hydroxysalicylidene)-2-methyl-1,2-propanediamine] and the series of heterobi-, tri- and tetranuclear complexes in which uranium ions are associated to d transition metal ions [10–12,15], the Schiff base ligands in the present complex are in an *umbrella* conformation but the dihedral angles between the two external aromatic rings, with values of 74.7(4)° and 75.4(4)°, are much larger than those in the above compounds, which vary from 7° to 27°. When viewed along the C_2 axis, the four Schiff bases have their concave sides alternately up and down, and the dihedral angles between the N_2O_2 planes defining the inner bonding sites and the symmetry axis are 32.6° and 31.8° for the two Schiff bases in the repeat unit. Overall, the four ligands assume a rather flat saddle shape. The complex itself is

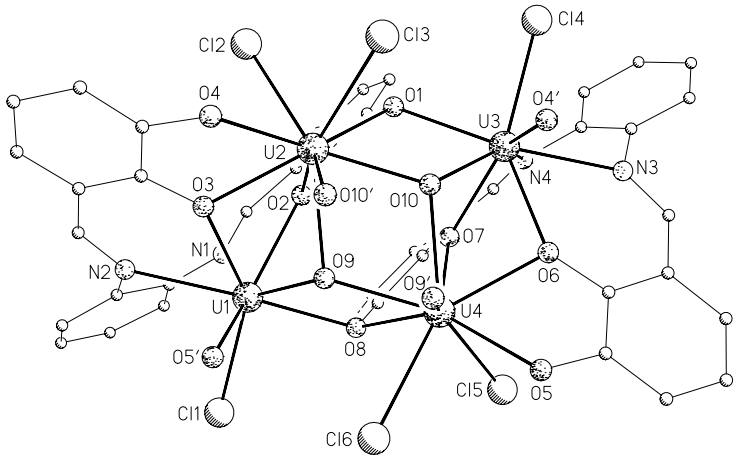

Fig. 2. View of the environment of the uranium atoms in the repeat unit. Atoms are represented as spheres, the carbon ones being arbitrarily reduced. Selected distances (Å): U1–O2 2.367(9), U1–O3 2.346(9), U1–O5′ 2.366(9), U1–O8 2.359(8), U1–O9 2.264(8), U1–N1 2.598(12), U1–N2 2.612(11), U1–Cl1 2.679(4), U2–O1 2.510(8), U2–O2 2.378(9), U2–O3 2.406(8), U2–O4 2.525(8), U2–O9 2.473(8), U2–O10 2.329(8), U2–O10′ 2.311(8), U2–Cl2 2.708(3), U2–Cl3 2.810(4), U3–O1 2.368(8), U3–O4′ 2.348(9), U3–O6 2.358(8), U3–O7 2.335(8), U3–O10 2.261(8), U3–N3 2.596(11), U3–N4 2.604(11), U3–Cl4 2.662(4), U4–O5 2.525(8), U4–O6 2.399(8), U4–O7 2.405(8), U4–O8 2.516(8), U4–O9 2.341(8), U4–O9′ 2.343(8), U4–O10 2.528(9), U4–Cl5 2.709(4), U4–Cl6 2.819(4), U1···U2 3.5907(7), U1···U3 5.9222(7), U1···U4 3.9646(7), U1···U4′ 3.9714(7), U2···U2′ 3.5236(9), U2···U3′ 3.9661(7), U3···U4 3.5885(7), U4···U4′ 3.5299(9). Symmetry code: $' = -x, y, 0.5 - z$.

roughly cylinder-shaped, with a diameter of about 18 Å and a height of about 9 Å (along the binary axis).

The U1, U3 and U2, U4 atoms occupy respectively the inner N_2O_2 and outer O_4 cavities of the Schiff bases. The two metal atoms in each subunit are bridged by the oxygen atoms of the salicylidene fragments (O2, O3 or O6, O7), as are the d transition metal and uranium ions in the bi- and trinuclear complexes $CuLUCl_2(py)_2$ and $(ZnL)_2U$ [16] and other CuU and M_2U compounds (M = Cu, Zn) associated with Schiff base ligands [10–12]. The four oxygen atoms of the O_4 cavity define a mean plane with a small maximum deviation of 0.009(5) and 0.023(5) Å for the planes associated with U2 and U4, respectively, and the uranium atoms are at 0.573(5) and 0.583(5) Å from these planes, with mean U–O bond lengths of 2.45(7) and 2.46(7) Å. The atoms U2 and U4 are much more displaced out of the external cavity of the L ligand than in the aforementioned hetero bi- and trinuclear complexes [16], in which the uranium atom is located at 0.184(3) and 0.091(6) Å (mean value) from the O_4 plane, with mean U–O distances of 2.37(6) and 2.35(6) Å. However, in the octanuclear cluster, the phenoxide oxygen atoms at the 3-position of the ligand L (O1, O4 or O5, O8) are also in bridging positions, between U2 and U3 or U1 and U4 or their symmetry equivalents; the corresponding U–O distances range from 2.348(9) to 2.368(8) Å, with an average value of 2.360(9) Å. Thus, the external U atom of each binuclear subunit is linked to the internal U atoms of the two adjacent subunits. The U atoms in the external cavities of the four binuclear subunits are also linked via the four μ_4-oxo ions which ensure the unusually high nuclearity of the cluster. The metal atoms U2, U4, U2′, U4′ and the oxo atoms O9, O10, O9′ and O10′ display a much distorted cubane-type arrangement located at the very centre of the complex (Fig. 3). While the cubane

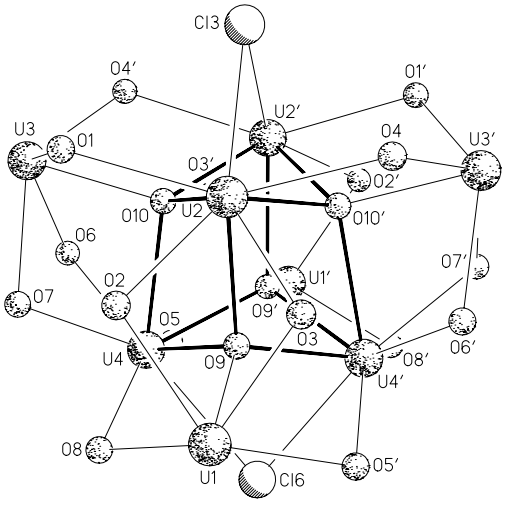

Fig. 3. View of the U_8 cluster with the bridging chlorine and oxygen atoms. The U_4O_4 cubane-type central motif is highlighted.

assemblage is commonly observed in structures of metal-oxo compounds [17–19], this edifice is, to the best of our knowledge, unprecedented in the molecular chemistry of uranium. The U–O bond lengths in the cubane moiety vary from 2.311(8) to 2.528(9) Å, with an average value of 2.39(9) Å. The U2 and U4 atoms are further bound to one terminal Cl atom [U2–Cl2 2.708(3), U4–Cl5 2.709(4) Å] and one μ_2-chloro ion [U2–Cl3 2.810(4) Å, U2–Cl3–U2′ 77.66(12)° and U4–Cl6 2.819(4) Å, U4–Cl6–U4′ 77.53(12)°] showing the expected bond lengthening for the bridging species. The coordination geometry of the nine-coordinate U2 and U4 ions may perhaps best be viewed as a very distorted tricapped trigonal prism, with respectively O9, Cl2 and Cl3 and O10, Cl5 and Cl6 in the capping positions [20].

The four atoms (O2, O3, N1 and N2) and (O6, O7, N3 and N4) of the internal coordination site of the Schiff bases define a mean plane with a maximum deviation of 0.009(5) and 0.007(5) Å, respectively, and the uranium atoms U1 and U3 are strongly displaced from these planes, by 1.566(5) and 1.579(5) Å. This large displacement differs from the distance measured in the mononuclear $UL'(acac)_2 \cdot thf$ compound, which is 0.088(3) Å [14]. This feature is likely due to the coordination of U1 and U3 to the 3-phenoxide atoms of the Schiff bases of the adjacent binuclear subunits (O1, O4 and O5, O8), and to the μ_4-oxygens O9 and O10, respectively; the U1–O9 and U3–O10 distances are equal to 2.264(8) and 2.261(8) Å. The U1 and U3 atoms are also bound to one terminal Cl atom, Cl1 and Cl4, with bond lengths of 2.679(4) and 2.662(4) Å, respectively. The coordination geometry of the eight-coordinate atoms U1 and U3 can be viewed as that of a slightly distorted square antiprism. If the eight uranium and the μ_4-oxo atoms only are considered, the central octa-metallic core can be viewed as an assemblage of four very distorted uranium tetrahedra, each of them sharing a common edge with its three neighbours and containing a μ_4-oxo ion located at its centre, surrounding a central, empty tetrahedron built from the four uranium atoms of the cubane moiety (Fig. 4). A search of the Cambridge Structural Database [21] gives our previous complex $U_8Cl_{24}O_4(cp^*py)_2^{2-}$ as the only other compound containing such μ_4-oxo ions [9]. In the latter, the U–O bond lengths involving the μ_4-oxo group are in the range 2.303(7)–2.493(8) Å, with a mean value of 2.40(9) Å, larger than the present value, which is closer to the mean value of 2.24(7) Å for the μ_3-oxo bridges reported in the Database. The mean U–O–U angle is 110(5)° in the previous compound and it is 110(9)° for both O9 and O10 in the present case. It may be noted that a μ_6-oxo group is present in the U(V) hexanuclear isopolyoxometalate complex reported by Duval et al. [7], with a mean U–O bond length of 2.6(1) Å.

This structure of the octanuclear $[U_8L_4Cl_{10}O_4]^{2-}$ cluster evidences the assembling ability of hexadentate

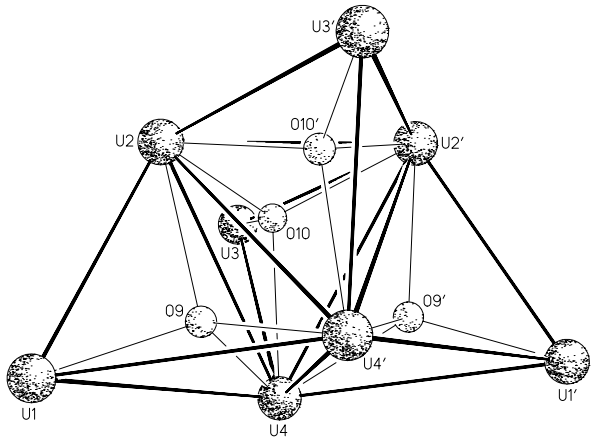

Fig. 4. View of the central U_8O_4 core showing the four assembled distorted tetrahedra in bold lines.

Schiff bases, which has recently been demonstrated in the case of a cluster of eight zinc atoms [22,23]. In this compound, the flexible ligand *N*,*N*′-*bis*(3-hydroxysalicylidene)-1,4-butanediamine leads to an octanuclear assemblage involving four Schiff bases with, as in the present case, extended μ-phenoxide bridging, but with no other bridging species. The high bridging ability, versatility and flexibility of the Schiff base have been considered to play a crucial role in the building of this polynuclear zinc complex. The high bridging ability is also involved in the present case, albeit in a somewhat lesser degree, but, considering the increased rigidity of the phenylene diamino chain, it appears that a high flexibility is not a prerequisite for such polynuclear assembling. However, even if the overall metal/Schiff base stoichiometry is identical in both compounds, the much different geometrical requirements of uranium and zinc atoms clearly result in different detailed coordination and assembling features. An assemblage of eight Cu(II) ions, four pentadentate, trianionic Schiff bases [*N*,*N*′-(2-hydroxypropane-1,3diyl)*bis*(salicylaldimine)] and four bridging hydroxy groups has also been described very recently [24]. All these results evidence the potential of Schiff bases as associating ligands for the design of supramolecular, polynuclear complexes, either with 3d transition metal ions or, as exemplified here for the first time, with larger 5f metal ions.

3. Experimental

3.1. Synthesis

UCl_4 was synthesized as reported in the literature [25]. The zinc complex ZnH_2L was synthesized by reaction of H_4L with one equivalent of $Zn(acac)_2$ in thf. The mononuclear metal complex was mixed in a 1:1 ratio with UCl_4 in pyridine. Adventitious traces of oxygen and/or water probably entered the reaction flask during prolonged heating at 80 °C, which resulted in the formation of orange crystals of the octanuclear compound $(Hpy)_2[U_8L_4Cl_{10}O_4]\cdot 10py$ following the substitution of Zn for U. Attempts to prepare this complex in a controlled way, by introducing measured quantities of water into the reaction mixture, were unsuccessful.

3.2. Crystallography

Data were collected at 100(2) K on a Nonius Kappa-CCD area detector diffractometer [26] using graphite monochromated Mo Kα radiation ($\lambda = 0.71073$ Å) and processed with DENZO-SMN [27]. The structure was solved by direct methods with SHELXS-97 and refined by full-matrix least-squares on F^2 with SHELXL-97 [28]. Absorption effects were empirically corrected with the program DELABS from PLATON [29]. All non-hydrogen atoms were refined with anisotropic displacement parameters. One solvent pyridine molecule has been found disordered over two positions related by a symmetry centre and sharing two atoms, which have been refined with 0.5 occupancy factors. Another pyridine is disordered over a binary axis. Some restraints on bond lengths, angles and displacement parameters have been applied to all solvent pyridine molecules. The hydrogen atoms were introduced at calculated positions (except in the disordered parts) as riding atoms with an isotropic displacement parameter equal to 1.2 times that of the parent atom. Some short H···H contacts involving protons from the pyridine molecules are likely due to the low resolution and resulting imperfect location of these molecules. The molecular plots were drawn with SHELXTL [30].

Crystal data and structure refinement details. $(Hpy)_2[U_8L_4Cl_{10}O_4]\cdot 10py$: $C_{140}H_{110}Cl_{10}N_{20}O_{20}U_8$, $M = 4651.22$, monoclinic, space group $C2/c$, $a = 34.9432(12)$, $b = 14.4932(9)$, $c = 31.8143(18)$ Å, $\beta = 120.339(3)°$, $V = 13905.5(13)$ Å^3, $Z = 4$, $D_c = 2.222$ g cm^{-3}, $\mu = 9.547$ mm^{-1}, $F(000) = 8624$. $R_1 = 0.055$, $wR_2 = 0.119$, $S = 1.022$, $\Delta\rho_{max} = 1.17$ e Å^{-3} for 12 366 independent reflections out of 43 999 measured reflections ($R_{int} = 0.096$) and 851 parameters.

4. Supplementary material

Crystallographic data for the structural analysis have been deposited with the Cambridge Crystallographic Data Centre, CCDC No. 215918. Copies of this information may be obtained free of charge from The Director, CCDC, 12 Union Road, Cambridge CB2 1EZ, UK (fax: +44-1223-336033; e-mail: deposit@ccdc.cam.ac.uk or http://www.ccdc.cam.ac.uk).

References

[1] J.M. Lehn, Supramolecular Chemistry, VCH, Weinheim, 1995.
[2] J.W. Steed, J.L. Atwood, Supramolecular Chemistry, Wiley, Chichester, UK, 2000.
[3] R.E.P. Winpenny, Adv. Inorg. Chem. 52 (2001) 1.
[4] P. Thuéry, M. Nierlich, B. Souley, Z. Asfari, J. Vicens, J. Chem. Soc., Dalton Trans. (1999) 2589.
[5] P. Thuéry, M. Nierlich, B.W. Baldwin, N. Komatsuzaki, T. Hirose, J. Chem. Soc., Dalton Trans. (1999) 1047.
[6] P. Thuéry, B. Masci, Supramol. Chem. 15 (2003) 95.
[7] P.B. Duval, C.J. Burns, D.L. Clark, D.E. Morris, B.L. Scott, J.D. Thompson, E.L. Werkema, L. Jia, R.A. Andersen, Angew. Chem. Int. Ed. 40 (2001) 3358.
[8] L.M. Mokry, N.S. Dean, C.J. Carrano, Angew. Chem. Int. Ed. 35 (1996) 1497.
[9] L. Moisan, T. Le Borgne, P. Thuéry, M. Ephritikhine, Acta Crystallogr., Sect. C 58 (2002) 98.
[10] T. Le Borgne, E. Rivière, J. Marrot, P. Thuéry, J.J. Girerd, M. Ephritikhine, Chem. Eur. J. 8 (2002) 774.
[11] L. Salmon, P. Thuéry, E. Rivière, J.J. Girerd, M. Ephritikhine, Chem. Commun. (2003) 762.
[12] L. Salmon, P. Thuéry, E. Rivière, J.J. Girerd, M. Ephritikhine, J. Chem. Soc., Dalton Trans. (2003) 2872.
[13] F. Calderazzo, C. Floriani, M. Pasquali, M. Cerasi, G. Perego, Gazz. Chim. Ital. 106 (1976) 127.
[14] L. Salmon, P. Thuéry, M. Ephritikhine, Acta Crystallogr., Sect. C 59 (2003) m246.
[15] L. Salmon, P. Thuéry, M. Ephritikhine, Polyhedron 22 (2003) 2683.
[16] L. Salmon, P. Thuéry, M. Ephritikhine, to be published.
[17] S. Parsons, A.A. Smith, R.E.P. Winpenny, Chem. Commun. (2000) 579.
[18] V. Artero, A. Proust, P. Herson, R. Thouvenot, P. Gouzerh, Chem. Commun. (2000) 883.
[19] W.J. Evans, M.A. Ansari, J.D. Feldman, R.J. Doedens, J.W. Ziller, J. Organomet. Chem. 545 (1997) 157.
[20] D.L. Kepert, Inorganic Stereochemistry, Springer, Heidelberg, 1982, pp. 179–187.
[21] F.H. Allen, Acta Crystallogr., Sect. B 58 (2002) 380.
[22] J. Sanmartín, M.R. Bermejo, A.M. García-Deibe, A.L. Llamas-Saiz, Chem. Commun. (2000) 795.
[23] J. Sanmartín, M.R. Bermejo, A.M. García-Deibe, I.M. Rivas, A.R. Fernández, J. Chem. Soc., Dalton Trans. (2000) 4174, and references therein.
[24] A. Mukherjee, I. Rudra, M. Nethaji, S. Ramasesha, A.R. Chakravarty, Inorg. Chem. 42 (2003) 463, and references therein.
[25] J.A. Hermann, J.F. Suttle, Inorg. Synth. 5 (1957) 143.
[26] Kappa-CCD Software, Nonius BV, Delft, 1998.
[27] Z. Otwinowski, W. Minor, Methods Enzymol. 276 (1997) 307.
[28] G.M. Sheldrick, SHELXS-97 and SHELXL-97, University of Göttingen, Germany, 1997.
[29] A.L. Spek, PLATON, University of Utrecht, 2000.
[30] G.M. Sheldrick, SHELXTL, Version 5.1, Bruker AXS Inc., Madison, WI, 1999.

Available online at www.sciencedirect.com
SCIENCE DIRECT®
Polyhedron 23 (2004) 629–636
POLYHEDRON
www.elsevier.com/locate/poly

The synthesis and molecular and crystal structures of 1-methyl-2-carboxy-1,2-dicarba-*closo*-dodecaborane(12), 1-phenyl-2-carboxy-1,2-dicarba-*closo*-dodecaborane(12) and 1-phenyl-2-benzoyl-1,2-dicarba-*closo*-dodecaborane(12)

Ulaganathan Venkatasubramanian [a], David J. Donohoe [a], David Ellis [a], Barry T. Giles [a], Stuart A. Macgregor [a], Susan Robertson [a], Georgina M. Rosair [a], Alan J. Welch [a,*], Andrei S. Batsanov [b], Lynn A. Boyd [b], Royston C.B. Copley [b], Mark A. Fox [b,*], Judith A.K. Howard [b], Kenneth Wade [b]

[a] *School of Engineering and Physical Sciences, Heriot-Watt University, Edinburgh EH14 4AS, UK*
[b] *Department of Chemistry, University of Durham, South Road, Durham DH1 3LE, UK*

Received 29 July 2003; accepted 30 October 2003

Abstract

The structures of 1-Me-2-COOH-1,2-*closo*-$C_2B_{10}H_{10}$ (**1**), 1-Ph-2-COOH-1,2-*closo*-$C_2B_{10}H_{10}$ (**2**) and 1-Ph-2-COPh-1,2-*closo*-$C_2B_{10}H_{10}$ (**3**) have been determined by X-ray crystallography. In **1** the orientation of the COOH group is defined by $\theta_{COOH} = 65.0(2)_{syn}°$, and this group H-bonds to that in a second molecule via a centrosymmetric eight-membered ring, $R_2^2(8)$. DFT calculations on the parent species 1-COOH-1,2-*closo*-$C_2B_{10}H_{11}$ reveal that the structure with $\theta_{COOH} = 90_{syn}°$ is preferred, with a barrier to COOH rotation of $\approx$17 kJ mol^{-1}. Similar calculations on **1** yield a lower rotational barrier, $\approx$7 kJ mol^{-1}, because internal H-bonding is now denied. In compound **2** the COOH group is twisted to lower θ values [5.0(3)° and 39.7(3)°] but both crystallographically independent molecules exist as dimers in the solid state by virtue of $R_2^2(8)$ rings. Compound **2** crystallises from wet solvent as a monohydrate, the structure of which reveals a non-planar centrosymmetric $R_4^4(12)$ ring and near-orthogonal Ph and COOH substituents [$\theta_{Ph} = 6.7(2)$ and $\theta_{COOH} = 78.0(2)_{syn}°$]. In compound **3** molecular association by H-bonding is blocked, so **3** serves as a useful comparative structure for **2**.
© 2003 Elsevier Ltd. All rights reserved.

Keywords: Carborane; Spectroscopy; DFT calculations; X-ray crystallography

1. Introduction

Over the last few years the field of crystal engineering, part of which involves the development of rational strategies for the design of new crystalline materials, has emerged as an area of significant research activity [1]. Although the use of heteroboranes in studies of crystal engineering has begun to be exploited only fairly recently [2] the potential is vast. Heteroboranes are generally chemically and thermally stable species, existing as polyhedra or fragments of polyhedra of differing size and shape, but having architectures that are well-understood [3]. Isomeric possibilities mean that C-substituted (hetero)carboranes have the potential to function as supramolecular building blocks with differing directionalities in two-dimensions, which can further be expanded into three-dimensions via additional B-atom substitution [4]. Moreover, heteroboranes are usually neutral or anionic, but can also be cationic [5], thus further extending their potential applications as building block units.

* Corresponding authors. Tel.: +44-131-451-3217; fax: +44-131-451-3180 (A.J. Welch), Tel.: +44-191-334-2038; fax: +44-191-384-4737 (M.A. Fox).
E-mail addresses: a.j.welch@hw.ac.uk (A.J. Welch), m.a.fox@durham.ac.uk (M.A. Fox).

0277-5387/$ - see front matter © 2003 Elsevier Ltd. All rights reserved.
doi:10.1016/j.poly.2003.10.016

There are currently two main strategies for crystal engineering, based on the use of either co-ordinate bonds or weaker intermolecular interactions. Within the latter area, H-bonding has attracted most interest due to its relative strength and directionality [6]. Carboxylic acid groups are frequently used in the field of crystal engineering because they are capable of forming various types of hydrogen bonds between themselves and/or with other species such as solvents [7]. Accordingly, we have begun a systematic study of the crystal structures of carboxylic acid carboranes, their derivatives, and related species, in order further to increase our understanding of the effect of the carboxy group on the cage and any other substituents. We have already described 1-COOH-1,2-*closo*-$C_2B_{10}H_{11}$ [2m] (a dimer), 1,2-$(COOH)_2$-1,2-*closo*-$C_2B_{10}H_{10}\cdot 1/2C_2H_5OH$ [2p] and 1-CH_2OMe-2-COOH-1,2-*closo*-$C_2B_{10}H_{10}$ [2q] (both tetramers). Herein we report the structures of the methyl and phenyl derivatives 1-Me-2-COOH-1,2-*closo*-$C_2B_{10}H_{10}$ and 1-Ph-2-COOH-1,2-*closo*-$C_2B_{10}H_{10}$, as well as that of the related species 1-Ph-2-COPh-1,2-*closo*-$C_2B_{10}H_{10}$. Although the compounds described in this paper do not themselves give rise to extended arrays via H-bonding they do afford us a greater understanding of substituent effects in carborane structures that will be important if carboranes are to be used for crystal engineering in the future.

2. Experimental

2.1. Synthetic and spectroscopic studies

Experiments were performed under dry, oxygen-free N_2 using standard Schlenk techniques, with some subsequent manipulation in the open laboratory. Toluene, diethylether and 40–60° petroleum ether were freshly distilled over Na. IR spectra were recorded as a CH_2Cl_2 solution or a KBr disk on a Perkin–Elmer Spectrum RX or 337 FTIR spectrophotometer. NMR spectra were recorded on a Varian Unity 300 or Bruker DPX 400 spectrometer as $CDCl_3$ solutions at ambient temperature, chemical shifts being recorded relative to $SiMe_4$ or $CHCl_3$ (^{1}H), $BF_3\cdot OEt_2$ (^{11}B) and $CDCl_3$ (^{13}C). Some ^{11}B NMR peak assignments were determined with the aid of ^{1}H–{^{11}B} (selective) spectra. ^{13}C NMR peak assignments corresponding to the aromatic carbons were determined with the benefit of ^{13}C coupled spectra. Mass spectra were recorded on a VG Micromass 7070E instrument operating in the EI mode at 70 eV. Elemental analyses were determined by the departmental services at Heriot–Watt and Durham. The starting materials 1-Me-1,2-*closo*-$C_2B_{10}H_{11}$ [8] and 1-Ph-1,2-*closo*-$C_2B_{10}H_{11}$ [9] were prepared by literature methods or slight variants thereof. All other reagents were used as supplied.

2.1.1. Synthesis of 1-Me-2-COOH-1,2-closo-$C_2B_{10}H_{10}$ (**1**)

To a stirred solution of 1-Me-1,2-*closo*-$C_2B_{10}H_{11}$ (0.8 g, 5 mmol) in diethylether (25 ml) at 0 °C was added dropwise 1.1 equivalents of MeLi (as an ether solution). The solution was allowed to warm to room temperature, at which point gaseous CO_2 was bubbled through the solution for about 20–30 min. The milky solution thus formed was hydrolysed with 2 M HCl and transferred to a separating funnel. The ethereal layer plus ethereal washings of the aqueous layer were dried over $MgSO_4$ overnight. Removal of solvent afforded 1-Me-2-COOH-1,2-*closo*-$C_2B_{10}H_{10}$ (**1**) as an off-white microcrystalline solid. Yield: 0.69 g, 67%. *Anal*. Found: C, 23.7; H, 7.3. Calc. for $C_4H_{14}B_{10}O_2$: C, 23.8; H, 7.0%. IR ν(cm^{-1}): 2630–2560 (s, BH), 1724 (s, CO). ^{1}H NMR, δ(ppm): 2.22 (s, CH_3). ^{11}B–{^{11}H} NMR, δ(ppm): 2.7 (1B), −2.4 (1B), −6.3 (8B).

2.1.2. Synthesis of 1-Ph-2-COOH-1,2-closo-$C_2B_{10}H_{10}$ (**2**)

Starting from 1-Ph-1,2-*closo*-$C_2B_{10}H_{11}$ (2.2 g, 10 mmol) in toluene (40 ml) and using one equivalent of *n*-butyllithium as deprotonating reagent, was similarly prepared 1-Ph-2-COOH-1,2-*closo*-$C_2B_{10}H_{10}$ (**2**) as a white solid, recrystallised from 40–60° petroleum ether. Yield: 1.48 g, 56%. *Anal*. Found: C, 40.6; H, 6.1; M_r (EI mass spectrum) 264 with typical carborane isotope pattern 258–268. Calc. for $C_9H_{16}B_{10}O_2$: C, 40.9; H, 6.1%; M_r 264. IR ν(cm^{-1}): 3200–2800 (OH), 2651–2570 (s, BH), 1724 (s, CO). ^{1}H NMR, δ(ppm): 7.53 (d, 2H, *o*-C_6H_5), 7.36 (t, 1H, *p*-C_6H_5), 7.25 (t, 2H, *m*-C_6H_5), 3.05 (2H, B3,6*H*), 2.58 (1H, B9*H*), 2.49 (2H), 2.43 (3H, inc. B12*H*), 2.35 (2H). ^{11}B–{^{11}H} NMR, δ(ppm): −0.2 (1B, B9), −3.2 (1B, B12), −9.4 (4B), −10.3 (2B), −11.3 (2B, B3,6). ^{13}C NMR, δ(ppm): 162.8 (CO), 130.7 (*i*, *o*-C_6H_5), 130.5 (*p*-C_6H_5), 128.6 (*m*-C_6H_5), 83.6 (C1), 75.3 (C2). Compound **2** can be recrystallised pure from dry 40–60° petroleum ether, or recrystallised from wet solvents as the 1:1 water solvate, **2**·**H$_2$O**. *Anal*. Found: C, 38.3; H, 6.6; Calc. for $C_9H_{16}B_{10}O_2\cdot H_2O$: C, 38.3; H 6.4%.

2.1.3. Synthesis of 1-Ph-2-COPh-1,2-closo-$C_2B_{10}H_{10}$ (**3**)

The compound 1-Ph-1,2-*closo*-$C_2B_{10}H_{11}$ (1.2 g, 5 mmol) in toluene (40 ml) was treated with *n*-butyllithium (2 ml of 2.5 M solution = 5 mmol). After heating to reflux for 30 min and cooling, PhCOCl (0.7 g, 5 mmol) was added. After further heating to reflux for 2 h, solvents were removed in vacuo and the residue dissolved in Et_2O and washed successively with $NaHCO_3$ (3 × 20 ml) and H_2O (4 × 30 ml). The ethereal layer was separated and dried over $MgSO_4$ overnight. Removal of solvent and recrystallisation from 40–60° petroleum ether afforded 1 Ph-2-COPh-1,2-*closo*-$C_2B_{10}H_{10}$ (**3**) as large white crystals. Yield: 1.00 g, 62%. *Anal*. Found: C, 55.6; H, 6.0; M_r (EI mass spectrum) 324, typical carborane isotope

pattern 318–327. Calc. for $C_{15}H_{20}B_{10}O$: C, 55.5; H, 6.2%; M_r 324. IR ν(cm^{-1}): 2621–2562 (s, BH), 1701 (s, CO). ^1H NMR, δ(ppm): 7.48 (d, 2H, *o*-C_6H_5), 7.40 (t, 1H, *p*-C_6H_5), 7.28–7.23 (m, 7H, C_6H_5), 3.15 (2H, B3,6*H*), 2.55 (3H, inc. B9*H*), 2.39 (3H, inc. B12*H*), 2.33 (2H). ^{11}B–$\{^1H\}$ NMR, δ(ppm): 0.2 (1B, B9), −3.0 (1B, B12), −9.3 (4B), −10.5 (4B, inc. B3,6). ^{13}C NMR, δ(ppm): 185.5 (CO), 136.3 (*i*-COC_6H_5), 132.5 (*p*-COC_6H_5), 130.8 (*o*-C_6H_5), 130.6 (*i*,*p*-C_6H_5), 128.5 (*o*-COC_6H_5, *m*-C_6H_5), 127.9 (*m*-COC_6H_5), 85.0 (C1), 82.6 (C2).

2.2. Crystallographic studies

Single crystals of compounds **1**, **2**, **2 · H₂O** and **3** were grown from MeCN, dry 40–60° petroleum ether, CH_2Cl_2/40–60° petroleum ether, and hexane, respectively. Compounds **1** and **2** were studied at 160(2) K on a Bruker P4 diffractometer (Heriot-Watt University) with graphite-monochromated Mo Kα radiation ($\lambda = 0.71069$ Å) using ω scans. Compounds **2 · H₂O** and **3** were studied at 293(2) and 150(2) K, respectively, on a Rigaku AFC6S diffractometer (University of Durham) with graphite-monochromated Cu Kα radiation ($\lambda = 1.54178$ Å) using ω scans. All structures were solved by direct and difference Fourier methods and refined by full-matrix least-squares against F^2, with non-hydrogen atoms assigned anisotropic displacement parameters [10]. For **1**, all H atoms were refined positionally and thermally. For **2**, only the hydroxy H atoms were allowed such refinement, all other H atoms being treated as riding. For **2 · H₂O** and **3** non-phenyl H atoms were refined independently and phenyl H atoms treated as riding. Table 1 lists details of unit cell data, intensity data collection and structure refinement.

2.3. Computational studies

DFT calculations on 1-COOH-1,2-*closo*-$C_2B_{10}H_{11}$ and 1-Me-2-COOH-1,2-*closo*-$C_2B_{10}H_{10}$ were performed using the ADF1999 programme [11] with the BP86 functional [12] and incorporating the quasi-relativistic corrections of Snijders and co-workers [13]. A double-ζ plus polarisation STO basis set was employed for all atoms and the frozen core approximation was applied (C, B: 1s). The C2–C1–C=O torsion angle, τ, was varied in nine steps of 22.5° from 0° to 180°, with full optimisation of the structure at every step. Within the COOH group the H–O–C=O torsion angle was originally set at 0° and did not deviate significantly from this during optimisation.

3. Results and discussion

3.1. Syntheses and spectroscopy

The carboxycarboranes 1-Me-2-COOH-1,2-*closo*-$C_2B_{10}H_{10}$ (**1**) and 1-Ph-2-COOH-1,2-*closo*-$C_2B_{10}H_{10}$ (**2**)

Table 1
Crystallographic data[a]

	1	2	2·H₂O	3
Colour and habit	colourless plate	colourless block	colourless block	colourless block
Crystal size (mm)	0.14 × 0.80 × 0.98	0.20 × 0.20 × 0.33	0.24 × 0.30 × 0.54	0.15 × 0.30 × 0.30
Formula	$C_4H_{14}B_{10}O_2$	$C_9H_{16}B_{10}O_2$	$C_9H_{16}B_{10}O_2 \cdot H_2O$	$C_{15}H_{20}B_{10}O$
M	202.25	264.32	282.33	324.41
System	monoclinic	monoclinic	monoclinic	monoclinic
Space group	$P2_1/c$	$P2_1/n$	$P2_1/c$	$P2_1/n$
T (K)	160(2)	293(2)	160(2)	150(2)
a (Å)	12.073(2)	12.3493(13)	10.330(2)	10.469(8)
b (Å)	7.0945(8)	13.2722(12)	22.151(4)	15.154(7)
c (Å)	13.4283(12)	18.4075(16)	7.0260(10)	11.945(8)
β (°)	102.235(12)	90.632(8)	106.240(10)	106.57(5)
U (Å^3)	1124.0(3)	3016.9(5)	1543.5(5)	1816(2)
Z	4	8	4	4
D_{calc} (Mg m^{-3})	1.195	1.164	1.215	1.186
μ (mm^{-1})	0.066 (Mo Kα)	0.489 (Cu Kα)	0.072 (Mo Kα)	0.458 (Cu Kα)
F(0 0 0)	416	1088	584	672
$\theta_{datacollection}$ (°)	3.10–24.99	4.11–60.00	2.05–25.01	4.84–75.09
Data measured	2663	7262	5279	5320
Unique data, R_{int}	1970, 0.0336	3951, 0.0343	2726, 0.0499	3491, 0.0794
Data $I > 2\sigma(I)$	1775	2479	2000	2481
R, wR_2 , (all data)	0.0446, 0.1195	0.0923, 0.1390	0.0730, 0.1133	0.1068, 0.2462
S (all data)	1.058	1.021	1.015	0.880
a, *b*	0.0728, 0.2098	0.0770, 0.3147	0.0461, 0.4911	0.1860, 0
Variables	201	387	251	276
ρ_{max}, ρ_{min} (e Å^{-3})	0.2610, −0.278	0.160, −0.156	0.223, −0.207	0.300, −0.275

[a] $R = \sum ||F_o| - |F_c|| / \sum |F_o|$, $wR_2 = [\sum[w(F_o^2 - F_c^2)^2] / \sum w(F_o^2)^2]^{1/2}$, (where $w^{-1} = [\sigma^2(F_o)^2 + (aP)^2 + bP]$ and $P = [0.333(F_o)^2 + 0.667(F_c)^2]$), $S = [\sum[w(F_o^2 - F_c^2)^2]/(n-p)]^{1/2}$, (where *n* is the number of data and *p* the number of parameters).

were prepared in good yields by the established [14,15] method of deprotonation of the corresponding 1-R-1,2-*closo*-$C_2B_{10}H_{11}$ species with LiR′, addition of CO_2, and protonation during aqueous work-up. Although **1** and **2** are known species [14,15], spectroscopic characterisation has not previously been reported.

Spectroscopically, both **1** and **2** are consistent with time-averaged C_s molecular symmetry (or, of course, simple coincidence), arising from C(O)OH/C(OH)O exchange and/or rotation of the COOH group about the C_{cage}–C bond. The ^{11}B–$\{^1H\}$ NMR spectrum of **1** at 128 MHz is fairly uninformative, with only three resonances of relative integrals 1:1:8 (high frequency to low frequency), each appearing as doublets ($^1J_{BH}$ ≈140 Hz) in the proton-coupled spectrum. In contrast, the ^{11}B–$\{^1H\}$ spectrum of **2** is somewhat more informative. The presumed 2+2+2+2 low-frequency co-incidence of **1** (assuming time-averaged C_s symmetry) is partially resolved (appearing as a 4[2+2]:2:2 set of three peaks). Moreover, the highest and lowest frequency resonances have been assigned. Given that we assign the highest-frequency B*H* resonance in the ^1H spectrum (3.05 ppm) of **2** to B3,6*H* on the basis of several precedents [16], then by ^1H–$\{^{11}B\}$ (selective) spectroscopy the lowest-frequency ^{11}B resonance (–11.3 ppm) is due to B3,6. It is well established that B atoms antipodal to C in closo carboranes occur at high frequency [17], and therefore the two resonances at –0.2 and –3.2 ppm are due to B9 and B12. Of these we assign the resonance at –0.2 ppm to B9 and that at –3.2 ppm to B12 by analogy with the B9,12 chemical shifts in the disubstituted analogues 1,2-$(COOH)_2$-1,2-*closo*-$C_2B_{10}H_{10}$ (0.3 ppm) [2p] and 1,2-Ph_2-1,2-*closo*-$C_2B_{10}H_{10}$ (–2.7 ppm), [1] respectively. In the ^1H NMR spectra of **1** and **2** the OH peak shift varies with concentration and the presence of water. The ^{13}C NMR spectrum of **2** is fully assigned, albeit with overlapping resonances at 130.7 ppm.

We have also prepared 1-Ph-2-COPh-1,2-*closo*-$C_2B_{10}H_{10}$ (**3**), a further known compound [18,19] not previously characterised spectroscopically. Both the ^1H and ^{11}B spectra are only partially assigned, but reveal clear evidence for time-averaged C_s molecular symmetry (which must involve rotation of the COPh group about the C_{cage}–C bond that is rapid on the NMR timescale at 293 K). Thus H3 and H6 are equivalent (3.15 ppm) and the ^{11}B spectrum appears as a 1:1:2+2:2+2 pattern (high to low frequency). Again the two highest-frequency ^{11}B resonances are due to the B atoms antipodal to C [17], with that at higher frequency (δ 0.2, B9) opposite the carboxy substituent. The ^{13}C NMR spectrum of **3** is fully assigned, albeit with overlapping resonances at 130.6 and 128.5 ppm.

[1] 128.38 MHz, $CDCl_3$, δ relative to neat $BF_3 \cdot OEt_2$ at 0 ppm: –2.6 (2B, B9,12), –9.3 (4B, B4,5,7,11), –10.6 (2B, B8,10), –11.6 (2B, B3,6).

3.2. Structural and computational studies

We performed crystallographic analyses of compounds **1** and **2** to investigate the influence (if any) of adjacent Me and Ph substituents on the ability of the COOH group to participate in intermolecular H-bonding. A structural study of **3** was undertaken for comparison with that of **2**, since in **3** H-bonding is blocked by the OH unit of **2** having been replaced by Ph.

In broad terms, compound **1** forms a double H-bonded dimer in the solid state (Fig. 1) via the mutual association of two carboxylic acid groups in an eight-membered ring about a crystallographic inversion centre, denoted $R_2^2(8)$ in graph-set terminology [20]. Essentially the same situation is seen in both crystallographically independent molecules of **2**, Fig. 2 showing the dimer of molecule **A**. In the water solvate **2 · H₂O** two molecules of H_2O are incorporated into the H-bonded ring to give a 12-membered ring, $R_4^4(12)$, shown in Fig. 3.

3.2.1. Intramolecular parameters in 1 and 2

Since we have previously reported crystallographic studies of 1-COOH-1,2-*closo*-$C_2B_{10}H_{11}$ (**I**) [2m] and 1,2-$(COOH)_2$-1,2-*closo*-$C_2B_{10}H_{10} \cdot 1/2C_2H_5OH$ (**II**) [2p] it is instructive, on more detailed analysis, to consider first the influence of the Me and Ph groups of **1** and **2** on intramolecular parameters involving the COOH group. Table 2 summarises C1–C2, C–COOH, and θ_{COOH} (the modulus of the average C_{cage}–C_{cage}–C–O torsion angle) for **1**, **2** (two independent molecules) and **2 · H₂O**, as well as for the mono- and dicarboxycarboranes referred to above. For completeness, θ_{Ph} [21] (the modulus of the average C_{cage}–C_{cage}–C_{Ph}–C_{Ph} torsion angle) is also given for **2** and **2 · H₂O**. Our definition of θ_{COOH} here [2p,2q]

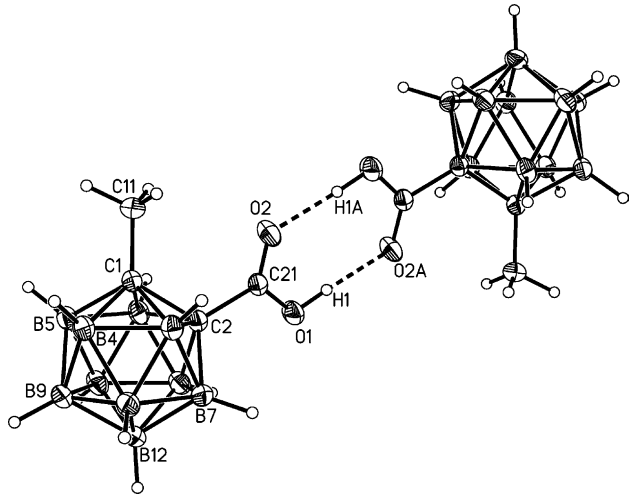

Fig. 1. Perspective view of the H-bonded dimer of compound **1**. Thermal ellipsoids are drawn at the 50% probability level, except for H atoms.

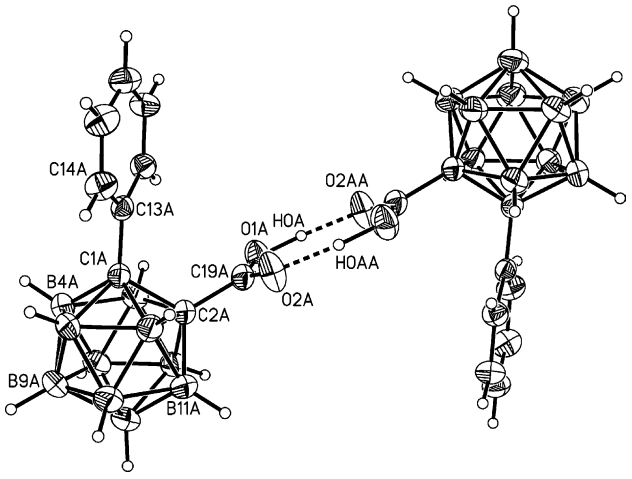

Fig. 2. Perspective view of the H-bonded dimer of compound **2** (molecule A only). Thermal ellipsoids are drawn at the 30% probability level, except for H atoms.

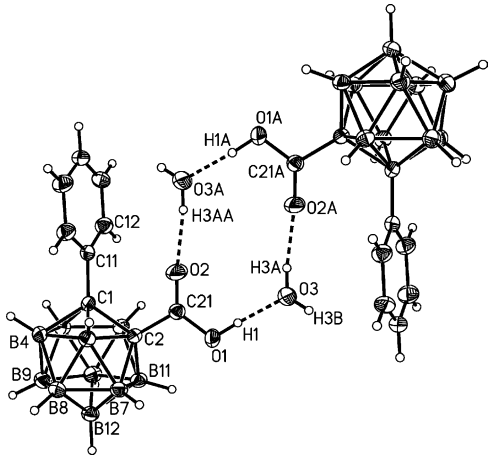

Fig. 3. Perspective view of the H-bonded dimeric unit of compound **2·H₂O**. Thermal ellipsoids are drawn at the 50% probability level, except for H atoms.

differs from that originally used [2m] for 1-COOH-1,2-*closo*-$C_2B_{10}H_{11}$ and 1,2-$(COOH)_2$-1,2-*closo*-$C_2B_{10}H_{10}$ but is preferred as it is now calculated in an analogous way to θ_{Ph}. Complete listings of derived molecular parameters for **1**, **2** and **2·H₂O** have been deposited as supplementary material.

In compound **1** the orientation of the COOH group with respect to C1 is specified by $\theta_{COOH} = 65.0(2)_{syn}°$, the subscript [necessary for large θ_{COOH} ($\geqslant 45°$) values] identifying that the C=O moiety is roughly syn to C1. The C1–C2 distance, 1.6694(17) Å and C2–C21 distance, 1.5172(16) Å, are 0.04 and 0.01 Å longer, and the C1–C2–C21 angle, 118.75(10)°, is 4° wider, than the corresponding parameters in **I**, collectively suggesting a degree of intramolecular steric crowding between the Me and COOH substituents in **1**. [2] Since such crowding could have been relieved by re-orientation of the COOH group, we were prompted to investigate the preferred orientation of the carboxy group in carboxycarboranes **I** and **1** by DFT calculations. Fig. 4 shows (upper plot) the energy of **I** as a function of fixed C_{cage}–C_{cage}–C=O torsion angle, τ, varied in 22.5° steps from 0° to 180°, with full structural optimisation at each stage; $\tau = 0°$ corresponds to $\theta_{COOH} = 90_{syn}°$, $\tau = 90°$ corresponds to $\theta_{COOH} = 0°$, and $\tau = 180°$ corresponds to $\theta_{COOH} = 90_{anti}°$. The orientation $\theta_{COOH} = 90_{syn}°$ is preferred to $\theta_{COOH} = 90_{anti}°$ by $\approx$6 kJ mol^{-1}, and the barrier to rotation is $\approx$17 kJ mol^{-1}. In **I** the observed [2m] orientation, $87.5(2)_{syn}°$, is close to the optimal one predicted.

The lower plot in Fig. 4 shows the result of a similar DFT calculation on **1** drawn on the same scale as the upper plot. This time the energy profile is flatter (barrier to rotation $\approx$7 kJ mol^{-1}) which we ascribe to the $\theta_{COOH} = 90_{anti}°$ and (particularly) the $\theta_{COOH} = 90_{syn}°$ orientations no longer being stabilised by intramolecular H-bonding, as was the case with **I**. Such intramolecular H-bonding, involving the relatively acidic proton on C2, has recently been noted [22] in 1-(C_5H_4N-2′)-1,2-*closo*-$C_2B_{10}H_{11}$ and its 4′-Br analogue, both of which have a C_{cage}–C_{cage}–C–N torsion angle close to 0°. In **1** the observed 25° twist about the C–COOH bond [$\theta_{COOH} = 65.0(2)_{syn}°$], presumably due to the steric influence of the adjacent Me group, is accurately reproduced in the calculations, which show a minimum energy when τ is $\approx$30°.

The 1,2-dicarboxycarborane crystallises as the $\cdot 1/2C_2H_5OH$ solvate, **II** [2p]. In **II** there are four crystallographically independent carborane molecules arranged in two centrosymmetric tetrameric units held together by H-bonding that incorporates the solvate. Every carborane has one COOH in a low and one COOH in a high θ orientation (half the high θ orientations are syn, half are anti). The experimental data in Table 2 reveal a definite pattern – high θ (whether syn or anti) is associated with a C–COOH bond length of $\approx$1.51 Å and low θ is associated with a measurably longer C–COOH bond, $\approx$1.52–1.53 Å. This pattern is reproduced in the DFT calculations on **I**, which give C–COOH 1.515 ($\theta = 90_{syn}°$), 1.514 ($\theta = 90_{anti}°$) and 1.525 Å ($\theta = 0°$).

Compound **2** crystallised from dry solvent has two crystallographically independent molecules (**A** and **B**) per asymmetric unit. In both **A** and **B** the orientations of Ph and COOH substituents are characterised by low θ

[2] Further evidence for intramolecular crowding in **1** is demonstrated from fully optimised MP2/6-31G* geometries of 1-Me-1,2-*closo*-1,2-$C_2B_{10}H_{11}$ and **1** where the C–C–C(Me) angle widens from 118.4° to 120.6°, respectively. The crystallographic structure of the carborane 1-Me-1,2-*closo*-1,2-$C_2B_{10}H_{11}$ remains unreported (search of the Cambridge Crystallographic Database, version 5.24, July 2003).

Table 2
Summary of C1–C2 and C–COOH distances (Å) and Ph and COOH orientations (°) for carboxycarboranes

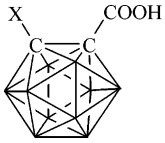

Compound	X	C1–C2	C–COOH	θ_{Ph}[a]	θ_{COOH}[b]	Reference
I	H	1.631(2)	1.507(2)	–	$87.5(2)_{syn}$	[2m]
II (A)[c]	COOH	1.660(2)	1.527(3)	–	5.3(2)	[2p]
			1.515(3)		$74.5(2)_{anti}$	
II (B)	COOH	1.651(2)	1.523(3)	–	0.6(2)	[2p]
			1.510(3)		$87.9(2)_{syn}$	
II (C)	COOH	1.652(2)	1.525(2)	–	4.9(2)	[2p]
			1.510(3)		$89.2(2)_{syn}$	
II (D)	COOH	1.653(2)	1.522(3)	–	14.1(2)	[2p]
			1.514(3)		$60.2(2)_{anti}$	
1	Me	1.6694(17)	1.5172(16)	–	$65.0(2)_{syn}$	this work
2(A)[d]	Ph	1.678(3)	1.509(4)	26.6(3)	5.0(3)	this work
2(B)	Ph	1.691(3)	1.504(4)	16.2(3)	39.7(3)	this work
2 · H₂O	Ph	1.705(2)	1.517(2)	6.7(2)	$78.0(2)_{syn}$	this work

[a] θ_{Ph} defined [21] as the modulus of the average C_{cage}–C_{cage}–C_{Ph}–C_{Ph} torsion angle.
[b] θ_{COOH} defined as the modulus of the average C_{cage}–C_{cage}–C–O torsion angle. For high values of θ_{COOH} it is instructive also to specify the conformation of the C = O moiety of the COOH group relative to the C_{cage} atom to which COOH is *not* bound as either syn or anti. These terms correspond to τ values of 0° and 180° respectively (Fig. 4).
[c] Four crystallographically independent molecules.
[d] Two crystallographically independent molecules.

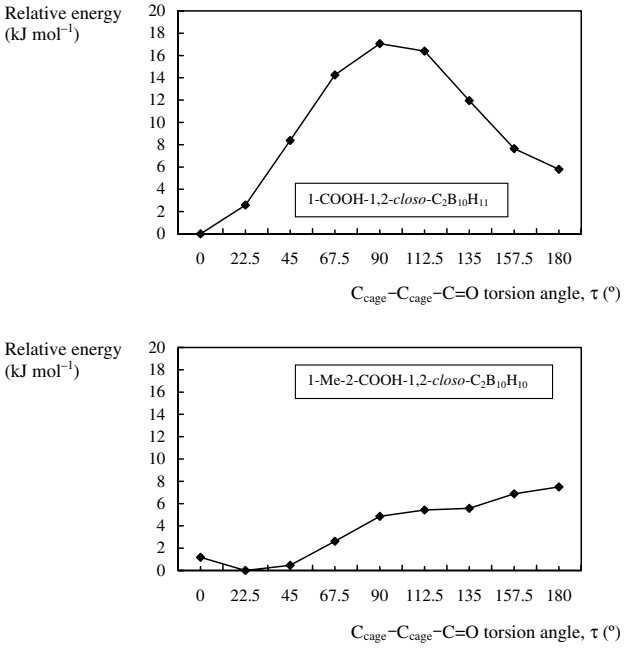

Fig. 4. Plot of relative energy of 1-COOH-1,2-*closo*-$C_2B_{10}H_{11}$ (**I**) and 1-Me-2-COOH-1,2-*closo*-$C_2B_{10}H_{10}$ (**1**) as a function of the C_{cage}–C_{cage}–C=O torsion angle, τ, by DFT calculation.

values (broadly similar to the situation observed in 1,2-diaryl-1,2-*closo*-C_2B_{10} species [23]), but in **2(A)** the Ph group is the more twisted [$\theta_{Ph} = 26.6(3)°$, $\theta_{COOH} = 5.0(3)°$] whilst in **2(B)** θ_{COOH} is the greater [$\theta_{Ph} = 16.2(3)°$, $\theta_{COOH} = 39.7(3)°$]. In **2** C1–C2 distances are marginally larger, and C–COOH distances marginally shorter, than those in **1**.

When crystallised from wet solvent, 1-Ph-2-COOH-1,2-*closo*-$C_2B_{10}H_{10}$ crystallises as the monohydrate **2 · H₂O** and incorporates two molecules of H_2O in an extended (12-membered) H-bonded ring system. In **2 · H₂O** the COOH group stands effectively perpendicular to the Ph ring, $\theta_{COOH} = 78.0(2)_{syn}°$, reminiscent of its relative orientation in **1**. The C–COOH distance in **2 · H₂O** is identical to that in **1**, but C1–C2 is the longest of all the structures described herein.

3.2.2. Intermolecular parameters in *1* and *2*

As previously noted, both **1** and **2** form centrosymmetric eight-membered H-bonded rings in the solid state [$R_2^2(8)$] whilst **2·H₂O** forms a centrosymmetric 12-membered ring that incorporates water [$R_4^4(12)$]. Parameters involved in these H-bonding rings are summarised in Table 3.

According to current conventions [24], all the H-bonds observed in this study are classified as "strong", with H···O distances (d) < 2 Å and O–H··· O angles (δ) close to 180°. The planar eight-membered cyclic H-bonded homodimer of two COOH groups observed in **1** and **2** is ubiquitous [7] for this well-known supramolecular synthon [1] and dimensions within it are quite standard. The 12-membered H-bonded ring of **2·H₂O** is of approximate chair conformation. Within it, H3A···O2$^{\#}$, $d = 1.87(4)$ Å, appears somewhat weaker than H1···O3, $d = 1.65(3)$ Å, and the former is accompanied by an angle ϕ at the COOH acceptor that is close to 180° (c.f. ϕ in **1** and **2** near 120°). A search of the Cambridge Crystallographic Database (version 5.24,

Table 3
Hydrogen bonding distances (Å) and angles (°) in the carboxycarborane compounds **1** and **2**

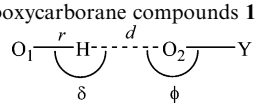

Compound	O_1	H	O_2	*Y*	*r*	*d*	*δ*	*ϕ*
1	O1	H1	O2[a]	C21[a]	0.90(2)	1.75(2)	175(2)	122(2)
2(A)	O1A	HOA	O2A[a]	C19A[a]	1.11(6)	1.55(6)	171(4)	128(4)
2(B)	O1B	HOB	O2B[a]	C19B[a]	1.02(5)	1.61(5)	176(4)	124(4)
2·H$_2$O	O1	H1	O3	H3A	0.90(3)	1.65(3)	173(3)	120(3)
	O1	H1	O3	H3B				120(3)
2·H$_2$O	O3	H3A	O2[a]	C21[a]	0.85(4)	1.87(4)	172(3)	174(3)

[a] Atom generated by inversion in centre of H-bonding ring.

July 2003) reveals 57 similar 12-membered rings involving two COOH groups and two H_2O molecules in the current literature, of which 42 do not involve charged species. In only 15 cases are all four H···O distances <2 Å, with the shortest distances [$H_{COOH}\cdots O_{H2O}$ 1.43; $H_{H2O}\cdots O_{COOH}$ 1.61 Å] recorded for 1,3,5-cyclohexanetricarboxylic acid monohydrate [25]. The H-bonded distances observed in **2·H$_2$O** are most clearly mirrored in 2,3-dihydroxysuccinic acid monohydrate [26] [$H_{COOH}\cdots O_{H2O}$ 1.64; $H_{H2O}\cdots O_{COOH}$ 1.90 Å].

3.2.3. The structure of *3*

As a complement to the crystallographic study of **2** we have also determined the structure of the phenylbenzoylcarborane **3**. Fig. 5 shows a perspective view of a single molecule and Table 4 hosts selected intramolecular parameters.

Compound **3** crystallises as discrete molecules with no significant intermolecular contacts – replacing the carboxy group of **2** with the benzoyl group prevents association via H-bonding. As far as we are aware this structural study is the first reported of a simple carborane ketone, i.e. carborane-C(O)–R. The C1–C2 distance, 1.695(3) Å, identical to that in related acetato compound [{1-Ph-2-COO(Sn^{n}Bu$_2$)-1,2-*closo*-$C_2B_{10}H_{10}$}$_2$O]$_2$ [27]

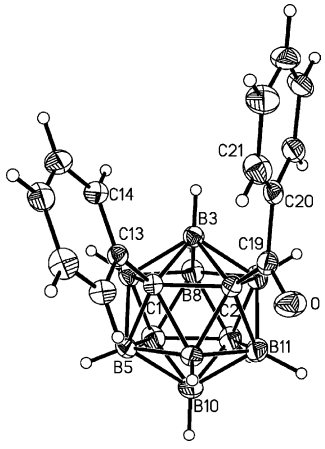

Fig. 5. Perspective view of compound **3**. Thermal ellipsoids are drawn at the 50% probability level, except for H atoms.

Table 4
Selected interatomic distances (Å) and interbond angles (°) for **3**

Bond distances			
C(1)–C(2)	1.695(3)	C(19)–O	1.210(3)
C(1)–C(13)	1.507(3)	C(19)–C(20)	1.485(3)
C(2)–C(19)	1.547(3)		
Bond angles			
C(2)–C(19)–C(20)	124.2(9)	O–C(19)–C(20)	93.48(9)
C(2)–C(19)–O	117.2(9)		

and similar to those in **2**, is shorter than that in 1,2-Ph$_2$-1,2-*closo*-$C_2B_{10}H_{10}$ [23a] [1.727(6) Å, averaged over the two crystallographically independent molecules]. The cage-bound Ph group is oriented with $\theta_{Ph} = 6.9(2)°$. The primary benzoyl orientation θ_{benz} (the modulus of the average C1–C2–C19–O and C1–C2–C19–C20 torsion angles) is 12.3(2)°, and there is a twist of 48.8(2)° about the C19–C20 bond, as is clearly evident from Fig. 5.

4. Conclusions

In the solid state the substituted carboxy carboranes 1-R-2-COOH-1,2-*closo*-$C_2B_{10}H_{10}$ give rise to homodimers with eight-membered H-bonded rings (R = Me, **1**; R = Ph, **2**). The monohydrate **2·H$_2$O** crystallises with a 12-membered H-bonded ring incorporating two carboxylic acid groups and one water molecule. In **1** the orientation of the COOH group is close to that shown computationally to be preferred and a similar orientation persists in **2·H$_2$O**, whilst in **2** it is twisted to a much lower θ_{COOH} value. In the context of the relative orientations of cage substituents, **2** is similar to 1-Ph-2-COPh-1,2-*closo*-$C_2B_{10}H_{10}$ (**3**), which crystallises as discrete monomers.

5. Supplementary material

Crystallographic data for the structural analyses have been deposited with the Cambridge Crystallographic Data Centre, CCDC Nos. 214908 (**1**), 214909 (**2**), 214910 (**2·H$_2$O**) and 214911 (**3**). Copies of this infor-

mation may be obtained free of charge from The Director, CCDC, 12 Union Road, Cambridge CB2 1EZ, UK (fax: +44-1233-336-033; e-mail: deposit@ccdc.cam.ac.uk or www: http//www.ccdc.cam.ac.uk).

Acknowledgements

We thank the ORS Award Scheme, UK, (U.V.), Heriot-Watt University (U.V., S.R.), the EPSRC (D.J.D., B.T.G.) for studentships, and the Leverhulme Trust (D.E.) for support. M.A.F. thanks the EPSRC for an Advanced Research Fellowship. A.J.W. acknowledges the award of a Royal Society Leverhulme Trust Senior Research Fellowship 2003-03.

References

[1] G.R. Desiraju, Angew. Chem. Int. Ed. 34 (1995) 2311.
[2] (a) R. Centore, M.R. Ciajolo, A. Tuzi, L.G. Komarova, A.L. Rusanov, V.A. Vasnev, Acta Crystallogr. C 50 (1994) 905;
(b) M.G. Davidson, T.G. Hibbert, J.A.K. Howard, A. Mackinnon, K. Wade, Chem. Commun. (1996) 2285;
(c) N.S. Hosmane, T. Demissie, H. Zhang, J.A. Maguire, W.N. Lipscomb, F. Baumann, W. Kaim, Organometallics 17 (1998) 293;
(d) M.J. Hardie, C.L. Raston, Eur. J. Inorg. Chem. 1 (1999) 195;
(e) M.J. Hardie, C.L. Raston, Co-ord. Chem. Rev. 189 (1999) 169;
(f) H. Lee, C.B. Knobler, M.F. Hawthorne, Chem. Commun. (2000) 2485;
(g) M.J. Hardie, C.L. Raston, B. Wells, Chem. Eur. J. 6 (2000) 3293;
(h) M.J. Hardie, C.L. Raston, Angew. Chem. Int. Ed. 39 (2000) 3835;
(i) M.J. Hardie, C.L. Raston, Cryst. Growth Des. 1 (2001) 53;
(j) M.J. Hardie, N. Malic, C.L. Raston, B.A. Roberts, Chem. Commun. (2001) 865;
(k) M.J. Hardie, C.L. Raston, Chem. Commun. (2001) 905;
(l) M.J. Hardie, C.L. Raston, Cryst. Eng. Commun. (2001) 39;
(m) A.J. Welch, U. Venkatasubramanian, G.M. Rosair, D. Ellis, D.J. Donohoe, Acta Crystallogr. C 57 (2001) 1295;
(n) C. O'Dowd, J.D. Kennedy, M. Thornton-Pett, J. Organometal. Chem. 657 (2002) 20;
(o) G. Barberà, C. Viñas, F. Teixidor, G.M. Rosair, A.J. Welch, J. Chem. Soc., Dalton Trans. (2002) 3647;
(p) U. Venkatasubramanian, D. Ellis, G.M. Rosair, A.J. Welch, Acta Crystallogr. C 59 (2003) o559;
(q) U. Venkatasubramanian, D. Ellis, G.M. Rosair, A.J. Welch, Acta Crystallogr. C 59 (2003) o586.
[3] K. Wade, Adv. Inorg. Chem. Radiochem. 18 (1976) 1.
[4] (a) e.g. W. Jiang, C.B. Knobler, M.F. Hawthorne, Angew. Chem. Int. Ed. 35 (1996) 2536;
(b) G. Barberà, F. Teixidor, C. Viñas, R. Sillanpää, R. Kivekäs, Eur. J. Inorg. Chem. 8 (2003) 1511, and references therein.
[5] e.g. N.L. Douek, A.J. Welch, J. Chem. Soc., Dalton Trans. (1993) 2147.
[6] G.A. Jeffrey, An Introduction to Hydrogen Bonding, Oxford University Press, New York, 1997.
[7] L. Leiserowitz, Acta Crystallogr. B 32 (1976) 775.
[8] M.M. Fein, J. Bobinski, N. Mayes, N. Schwartz, M.S. Cohen, Inorg. Chem. 2 (1963) 1111.
[9] M.M. Fein, D. Grafstein, J.E. Paustian, J. Bobinski, B.M. Lichstein, N. Mayes, N.N. Schwartz, M.S. Cohen, Inorg. Chem. 2 (1963) 1115.
[10] G.M. Sheldrick, SHELXTL Version 5.1. Bruker AXS Inc., Madison, WI, USA, 1999.
[11] (a) E.J. Baerends, D.E. Ellis, P. Ros, Chem. Phys. 2 (1973) 41;
(b) G. te Velde, E.J. Baerends, J. Comput. Phys. 99 (1992) 84;
(c) C. Fonseca Guerra, J.G. Snijders, G. te Velde, E.J. Baerends, Theor. Chem. Acc. 99 (1998) 391.
[12] (a) A.D. Becke, Phys. Rev. A. 38 (1988) 3098;
(b) J.P. Perdew, Phys. Rev. B. 33 (1986) 8822.
[13] (a) J.G. Snijders, E.J. Baerends, P. Ros, Mol. Phys. 38 (1979) 1909;
(b) T. Ziegler, V. Tschinke, E.J. Baerends, J.G. Snijders, W. Ravenek, J. Phys. Chem. 93 (1989) 3050;
(c) E. van Lenthe, E.J. Baerends, J.G. Snijders, J. Chem. Phys. 99 (1993) 4597.
[14] D. Grafstein, J. Dvorak, Inorg. Chem. 2 (1963) 1128.
[15] L.I. Zakharkin, V.I. Stanko, A.I. Klimova, Yu.A. Chapovskii, Bull. Acad. Sci. USSR, Div. Chem. Sci. (Engl. Transl.) (1963) 2072.
[16] (a) P.T. Brain, J. Cowie, D.J. Donohoe, D. Hnyk, D.W.H. Rankin, D. Reed, B.D. Reid, H.E. Robertson, A.J. Welch, M. Hofmann, P.v.R. Schleyer, Inorg. Chem. 35 (1996) 1701;
(b) M.A. Fox, J.A.H. MacBride, K. Wade, Polyhedron 16 (1997) 2499;
(c) M.A. Fox, K. Wade, Polyhedron 16 (1997) 2517.
[17] S. Heřmánek, Chem. Rev. 92 (1992) 325, and references therein.
[18] L.I. Zakharkin, A.I. L'vov, Bull. Acad. Sci. USSR, Div. Chem. Sci. (Engl. Transl.) (1966) 128.
[19] D.A. Brown, H.M. Colquhoun, J.A. Daniels, J.A.H. MacBride, I.R. Stephenson, K. Wade, J. Mater. Chem. 2 (1992) 793.
[20] (a) M.C. Etter, J.C. MacDonald, J. Bernstein, Acta Cryst. B 46 (1990) 256;
(b) M.C. Etter, Acc. Chem. Res. 23 (1990) 120.
[21] J. Cowie, B.D. Reid, J.M.S. Watmough, A.J. Welch, J. Organometal. Chem. 481 (1994) 283.
[22] E.S. Alekseyeva, A.S. Batsanov, L.A. Boyd, M.A. Fox, T.H. Hibbert, J.A.K. Howard, J.A.H. MacBride, A. Mackinnon, K. Wade, J. Chem. Soc., Dalton Trans. (2003) 475.
[23] (a) Z.G. Lewis, A.J. Welch, Acta Crystallogr. C 49 (1993) 705;
(b) T.D. McGrath, M.A. Fox, A.J. Welch, Acta Crystallogr. C 56 (2000) 487;
(c) E.S. Alekseyeva, M.A. Fox, J.A.K. Howard, J.A.H. MacBride, K. Wade, Appl. Organometal. Chem. 17 (2003) 499, and references therein.
[24] G.R. Desiraju, T. Steiner, The Weak Hydrogen Bond in Structural Chemistry and Biology, Oxford University Press, Oxford, 1999, Ch 1.
[25] CCDC Refcode BANGONB.R. Bhogala, P. Vishweshwar, A. Nangia, Cryst. Growth Des. 2 (2002) 325.
[26] CCDC Refcode TARTDL01J.-J. Nie, D.-J. Xu, J.-Y. Wu, M.Y. Chang, Acta Crystallogr. E 57 (2001) o428.
[27] E.R.T. Tiekink, M. Gielen, A. Bouhdid, R. Willem, V.I. Bregadze, L.V. Ermanson, S.A. Glazun, Met.-Based Drugs 4 (1997) 75.

Available online at www.sciencedirect.com
SCIENCE DIRECT®
Polyhedron 23 (2004) 637–641
POLYHEDRON
www.elsevier.com/locate/poly

Synthesis and characterization of two pentanuclear complexes $(NEt_4)_2[MS_4(CuBp)_4]$ (M = Mo, W; Bp = H_2B(pyrazolyl)$_2$) and crystal structure determination of $(NEt_4)_2[WS_4(CuBp)_4]$

Moayad Hossaini Sadr [a,*], William Clegg [b,*], Hamid Reza Bijhanzade [c]

[a] Department of Chemistry, Faculty of Science, Azarbaijan University of Tarbiat Moallem, Tabriz, Iran
[b] School of Natural Sciences (Chemistry), University of Newcastle, Newcastle upon Tyne NE1 7RU, UK
[c] Department of Chemistry, Faculty of Science, Tarbiat Modarres University, Tehran, Iran

Received 22 July 2003; accepted 4 November 2003

Abstract

Two new copper(I) complexes containing the $[MS_4]^{2-}$ core (M = Mo or W) and anionic bis(pyrazolyl)borate (Bp) ligands have been prepared from the reactions of $(Et_4N)_2[MS_4]$, CuCl and KBp. In addition to elemental analysis, their IR, UV–Vis, ^1H and ^{13}C NMR spectra have been studied. The structure of $(NEt_4)_2[WS_4(CuBp)_4]$ has been determined by single-crystal X-ray diffraction. In the pentanuclear dianion, $[WS_4(CuBp)_4]^{2-}$, which has crystallographic S_4 symmetry, the coordination environment around each copper atom is distorted tetrahedral, with two N donors of the bidentate Bp ligands and two S donors of the WS_4 core, representing a structural model for some copper proteins. The W atom retains the tetrahedral geometry of the free $[WS_4]^{2-}$ anion.
© 2003 Elsevier Ltd. All rights reserved.

Keywords: Tetrathiomolybdate; Tetrathiotungstate; Dihydridobis(pyrazolyl)borate; Copper(I) complexes; Crystal structure; Model compounds

1. Introduction

The synthesis and characterization of clusters containing tetrathiometallate anions of tungsten and molybdenum, $[MS_4]^{2-}$ (M = Mo, W), has been a fertile area of research with respect to their physico-chemical, bioinorganic, and structurally oriented coordination chemistry [1–8]. In particular, the chemistry of these multidentate chelating ligands with copper(I), because of their high tendency to form Cu–S bonds, has continued to attract attention [8–13]. The first biological function of Mo/S/Cu clusters was recognized in ruminants [14]. Tetrathiomolybdates, which are formed in the complex stomach of ruminants from molybdate and electron-rich sulfide, can act as efficient chelating ligands for positively charged, albeit π electron-rich ('soft'), metal ions such as Cu^+ and cause copper deficiency in them [15]. Recently, some medicinal applications of tetrathiomolybdate have been reported [16,17].

Poly(pyrazolyl)borates, $[H_nB(Pz)_{4-n}]^-$, are anionic nitrogen-donor ligands, which form a wide variety of stable inorganic and organometallic compounds with structural and functional importance [18–23]. Because of the close similarity between the imidazole of the amino acid histidine and pyrazole, copper complexes with these ligands are also of interest from the bioinorganic point of view and can be considered as model compounds of several copper proteins such as plastocyanin [24,25].

Recently we have reported some Mo–S–Cu–N systems which were the first complexes containing both Bp′ (= H_2B(3,5-Me_2Pz)$_2$) and $[MS_4]^{2-}$ ligands [26,27], offering potential models of copper proteins [28]. Continuing this interest, we report here two pentanuclear complexes of this type, the first ones containing four chelating Bp (= H_2BPz_2) ligands and four Cu(I) atoms around the $[MS_4]^{2-}$ core.

* Corresponding authors. Tel.: +98-411-6577864; fax: +98-412-452-4991 (M. Hossaini Sadr); Tel.: +44-191-222-6649; fax: +44-191-222-6929 (W. Clegg).
E-mail addresses: hosainisadr@azaruniv.edu (M. Hossaini Sadr), w.clegg@ncl.ac.uk (W. Clegg).

0277-5387/$ - see front matter © 2003 Elsevier Ltd. All rights reserved.
doi:10.1016/j.poly.2003.11.039

2. Experimental

2.1. General procedures

Starting materials were purchased from commercial sources and purified by standard procedures [29]. Literature methods were used for the preparation of KBp [30], $(NH_4)_2[MS_4]$ and $(NEt_4)_2[MS_4]$ [31]. CuCl (reagent grade) was washed with acetic acid on a filter several times and with absolute ethanol three times, and the white product was treated with dry diethyl ether and dried under vacuum. The complexes were initially prepared under a dry nitrogen atmosphere, but crystallization and other manipulations were performed in air. Solvents were dried and distilled before use [29].

2.2. Physical measurements

UV–Vis spectra of the ligands and complexes were recorded on a JASCO model 7850 spectrophotometer. IR spectra were obtained on FT BRUKER or SHIMADZU IR-470 infrared spectrophotometers using pressed KBr disks with polystyrene as reference. ^1H and ^{13}C NMR spectra were obtained using a BRUKER DRX500 AVANCE spectrometer.

2.3. Synthesis of $(NEt_4)_2[WS_4(CuBp)_4]$ (1)

To a dichloromethane solution (70 ml) of $(NEt_4)_2[WS_4]$ (0.29 g, 0.5 mmol), solid CuCl (0.21g, 2.1 mmol) was added. After vigorous stirring for 10 h, the resulting yellow solution was filtered. KBp (0.37 g, 2 mmol) and THF (10 ml) were added to the filtrate and the mixture was stirred for 40 h at room temperature and filtered. The yellow–orange precipitate was collected, triturated with THF (2×20 ml) and toluene (2×20 ml) to remove the excess KBp, washed with *n*-hexane (2×25 ml) and diethyl ether (2×25 ml) and dried in vacuo. Dissolving the crude product in CH_3CN and drying the filtrate removed the co-precipitated KCl. Suitable crystals for X-ray crystallography were obtained by diffusing diethyl ether into a saturated CH_3CN solution of **1** and leaving it for 5–6 days in a refrigerator. The crystals were washed with diethyl ether several times. Yield: 80%. IR (KBr, cm^{-1}): ν(W–S) 448 (s); ν(B–H) 2258 and 2365 (doublet). Electronic spectrum (DMF, λ nm, absorbance): 494 (0.198), 367 (0.490), 309 (0.904), 304 (0.893), 266 (1.186). ^1H NMR (CH_3CN-d_3, δ): 1.106 (t, 3H, CH_3), 3.127 (q, 2H, CH_2), 5.998 (s, 1H, ^{4}HPz), 7.118 (s, 1H, ^{3,5}HPz), 7.551 (s, 1H, ^{3,5}HPz). ^{13}C NMR (CH_3CN-d_3, δ): 8.752 (CH_3, Et_4N), 52.855 (t,CH_2, Et_4N), 104.783 (^{4}CPz), 135.824 (^{3,5}CPz), 141.137 (^{3,5}CPz). *Anal.* Calc. for $C_{40}H_{72}B_4Cu_4N_{18}S_4W$: C, 33.93; H, 5.08; N, 17.81; S, 9.05; Cu, 17.95. Found: C, 33.91; H, 5.03; N, 17.94; S, 9.09; Cu, 18.01%.

2.4. Synthesis of $(NEt_4)_2[MoS_4(CuBp)_4]$ (2)

$(NEt_4)_2[MoS_4]$ (0.25 g, 0.5 mmol) was dissolved in acetone (100 ml) and CuCl (0.21 g, 2.1 mmol) was added to the pink solution. After vigorous stirring for 4 h, the solution was filtered. KBp (0.37 g, 2 mmol) was added to the filtrate and the mixture was stirred for 8 h at room temperature. Precipitated KCl was removed by filtration and the deep violet filtrate evaporated on a vacuum pump. The resultant solid was triturated in toluene (2×30 ml) to remove the excess of KBp, washed with *n*-hexane (2×30 ml) and diethyl ether (3×25 ml) and dried in vacuo. Yield: 75%. IR (KBr, cm^{-1}): ν(Mo–S) 442(s); ν(B–H) 2255 and 2365 (doublet). Electronic spectrum (DMF, λ nm, absorbance): 524 (0.263), 392 (sh), 313 (1.204), 304 (0.893), 287 (1.823), 266 (1.299). ^1H NMR (acetone-d_6, δ): 1.166 (t, 3H, CH_3), 3.185 (q, 2H, CH_2), 5.954 (s, 1H, ^{4}HPz), 6.973 (s, 1H, ^{3,5}HPz), 7.521 (s, 1H, ^{3,5}HPz). ^{13}C NMR (acetone-d_6, δ): 6.824 (CH_3, Et_4N), 51.190 (t, CH_2, Et_4N), 102.785 (^{4}CPz), 134.149 (^{3,5}CPz), 139.078 (^{3,5}CPz). *Anal.* Calc. for $C_{40}H_{72}B_4Cu_4N_{18}S_4Mo$: C, 36.18; H, 5.43; N, 18.99; S, 9.65; Cu, 19.14. Found: C, 36.14; H, 5.39; N, 19.07; S, 9.67; Cu, 19.19%.

2.5. X-ray crystallography

Crystal data for **1**: $C_{40}H_{72}B_4Cu_4N_{18}S_4W$, $M = 1414.7$, tetragonal, space group $I4_1/a$, $a = 13.3299(3)$, $c = 32.4399(15)$ Å, $V = 5764.1(3)$ Å^3, $Z = 4$, $D_{calc} = 1.630$ g cm^{-3}, $\mu = 3.63$ mm^{-1} (Mo Kα, $\lambda = 0.71073$ Å), $T = 160$ K, crystal size $0.20 \times 0.18 \times 0.15$ mm; 25 818 reflections measured, 3615 unique, $R_{int} = 0.0649$; transmission factors 0.53–0.61; $R(F, F^2 > 2\sigma) = 0.0291$, R_w (F^2, all data) = 0.0635, goodness of fit = 1.093 for all F^2 values and 165 refined parameters; final difference map extremes +1.28 and −0.79 e Å^{-3}.

Data were collected on a Bruker AXS SMART CCD diffractometer with narrow frames (0.3° in ω). Absorption corrections were semi-empirical from symmetry-equivalent and repeated reflections. The structure was solved by direct methods and refined by full-matrix least-squares on all unique F^2. Non-hydrogen atoms were refined with anisotropic displacement parameters. Hydrogen atoms were included in calculated positions and refined with isotropic displacement parameters riding on those of the parent atoms. Programs were standard Bruker AXS control and integration software, and SHELXTL [32].

3. Result and discussion

3.1. Synthesis

Generally, MCuS complexes can be prepared by self-assembly (reaction (1)), or ligand substitution (reaction (2)) [8d,31]:

$$(Et_4N)_2[MS_4] + 4CuCl \rightarrow (Et_4N)_2[MS_4(CuCl)_4] \quad (1)$$

$$(Et_4N)_2[MS_4(CuCl)_4] + 4KBp \rightarrow (Et_4N)_2[MS_4(CuBp)_4] + 4KCl \quad (2)$$

The $(Et_4N)_2[MS_4(CuCl)_4]$ precursor complexes were prepared simply through one-pot reaction by direct mixing of the reagents; nevertheless, our attempt to synthesize **1** and **2** by the self-assembly method via direct mixing of reactants led to oily or unwanted compounds. It seems that the ligand substitution process is a more reliable route for preparing complexes of the type **1** and **2**, according to our previous experiences also [26,27]. It is likely that the steric crowding of the chelating Bp ligands makes self-assembly more difficult. We have found that the order of addition of reactants, the stoichiometric ratios, and the counterion can affect the final product [8,27]. The compounds **1** and **2** are air-stable and can be stored for months in desiccators.

3.2. Infrared spectra

The 400–500 cm^{-1} region of the IR spectra of heterothiometallic cluster compounds containing the $[MXS_3]^{2-}$ (X = O, S; M = V, Mo, W, Re) moiety has proven valuable in arguments concerning their electronic and structural characteristics [1,9]. A single sharp band in this region indicates symmetrical coordination around the MS_4^{2-} core [33] and ν(M–S) decreases on increasing the number of coordinated hetero-metal atoms [9,34]. The spectra of **1** and **2** exhibit a single strong band at 443 and 441 cm^{-1}, respectively, which can be attributed to the ν(M–S) stretching vibrations. Comparing these values with corresponding ones for $(NEt_4)_2[WS_4]$ (458 cm^{-1}) and $(NEt_4)_2[MoS_4]$ (470 cm^{-1}) reveals some red shift to lower frequencies, indicating weakening of the M–S bonds as a result of coordination. As expected, the ν(B–H) frequencies are observed as doublet bands at 2365 and 2258 cm^{-1} and at 2360 and 2255 cm^{-1} for **1** and **2**, respectively, verifying the presence of Bp ligands in the complexes. The simultaneous presence of absorption bands arising from B–H and M–S stretching in IR spectra can be used as a facile and distinctive criterion for the formation of these complexes.

3.3. Description of the crystal structure of $(NEt_4)_2[WS_4(CuBp)_4]$ (1)

The structure of **1** is constructed from four CuBp and one WS_4 fragment through bridging sulfur atoms, similar to those of other monomeric compounds $[MS_4(CuX)_4]^{2-}$ (M = Mo, W; X = Cl, Br) [35,36]. There is no significant interaction among the dianion $[MS_4(CuBp)_4]^{2-}$ and the two Et_4N^+ counterions other than normal coulombic and van der Waals forces. A view of the dianion of complex **1**, with the atomic labelling scheme for the unique atoms, is shown in Fig. 1 and selected bonding parameters are presented in Table 1. The symmetrical coordination of four copper atoms does not lower the symmetry of the WS_4 core essentially; the anion has S_4 symmetry overall, and the two independent S–W–S angles are very similar. The W–S distance of 2.2413(8) Å is slightly longer than those of the bis-coordinated analogue $(NEt_4)_2[WS_4(CuBp')_2]$ (2.210 Å) [27] and rather longer than in the free $[WS_4]^{2-}$ anion (2.165 Å in the ammonium salt) [37,38]. This elongation of W–S and reduction of its double bond character as a result of coordination is in agreement with the decrease of the ν(W–S) frequency in the IR spectrum. The very acute angles about the sulfur atoms bridging Cu and W [72.13(3)° and 72.75(3)°], together with the short W···Cu distance (2.688 Å) are suggestive of direct tungsten-copper bonding interactions within the $Cu(S_b)_2W$ rings. Although no definitive statement can be made about the existence of a metal–metal bond, the observed distances are consistent with a strong attractive interaction between Cu and W atoms, as expected when placing two metals with greatly different formal oxidation states, d^{10} Cu(I) and d^0 W(VI), in close proximity, as they are in this pentanuclear cluster.

The coordination environment of each copper atom is highly distorted tetrahedral, with angles about Cu ranging from 122.21(11)° for S–Cu–N(21) to 92.54(13)° for N(11)–Cu–N(21), and each Cu atom is coordinated by two sulfur atoms from WS_4 and two nitrogen atoms of Bp ligands. The bond distances in CuS_2N_2 units are 2.3224(13) and 2.2896(12) Å for Cu–S and 2.021(3) and 2.093(3) Å for Cu–N. These values are in agreement

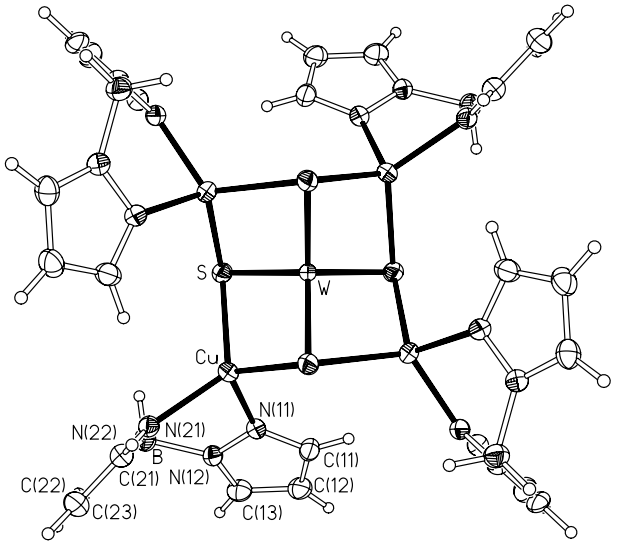

Fig. 1. Structure of the $[WS_4(CuBp)_4]^{2-}$ anion in **1**, showing 50% probability displacement ellipsoids and the numbering scheme for atoms of the asymmetric unit.

Table 1
Selected bond lengths (Å) and angles (°) for (**1**)

Bond lengths			
W–S	2.2413(8)	Cu–S	2.3224(13)
W···Cu	2.6875(5)	Cu–S(B)	2.2896(12)
Cu–N(11)	2.093 (3)	Cu–N(21)	2.021(3)
N(11)–N(12)	1.361(4)	N(21)–N(22)	1.362(4)
N(12)–B	1.548(6)	N(22)–B	1.556(5)
Bond angles			
S–W–S(A)	108.91(2)	S–W–S(C)	110.59(4)
S–Cu–S(B)	104.53(4)	N(11)–Cu–N(21)	92.54(13)
N(11)–Cu–S	105.49(9)	N(11)–Cu–S(B)	111.87(9)
N(21)–Cu–S	122.21(11)	N(21)–Cu–S(B)	118.76(9)
W–S–Cu	72.13(3)	W–S–Cu(A)	72.75(3)
Cu–S–Cu(A)	111.80(4)		

Symmetry operations for equivalent atoms: A $y-1/4, -x+5/4, -z+1/4$; B $-y+5/4, x+1/4, -z+1/4$; C $-x+1, -y+3/2, z$.

with previously reported ones for compounds of this type [26,27] or for similar compounds {e.g. 2.290(5) Å for Cu–S and 2.02(1) Å for Cu–N in $[WS_4Cu_3Cl(bpy)_2]$ [39]}.

In addition to the similarity between pyrazole (as N-donor in **1** and **2**) and imidazole of amino acids of living systems, the arrangement and coordination environment of Cu atoms in **1** are comparable to those found in the active sites of some copper proteins such as poplar plastocyanin, cuperedoxin, cytochrome *c* oxides, etc. [28,40,41], leading to the possibility of using these complexes **1** and **2** as models for copper proteins. It is also noeworthy that, as far as we know, the compounds **1** and **2** are the first ones containing four chelate ligands around the MS_4Cu_4 core except for a dithiocarbamate complex [42], and **1** is the first crystallographically characterized complex containing the Bp ligand.

4. Supplementary material

Crystallographic data, excluding structure factors, have been deposited at the Cambridge Crystallographic Data Centre, CCDC No. 215465. Copies of this information may be obtained free of charge from the Director, CCDC, 12 Union Road, Cambridge, CB2 1EZ, UK (fax: +44-1223-336-033; e-mail: deposit@ccdc.cam.ac.uk or http://www.ccdc.cam.ac.uk).

Acknowledgements

We thank EPSRC (UK) for equipment funding and the Research Office of Azarbaijan University of Tarbiat Moallem for financial support.

References

[1] (a) A. Müller, E. Diemann, R. Jostes, H. Bögge, Angew. Chem., Int. Ed. Engl. 20 (1981) 934;
(b) E. Diemann, A. Müller, Coord. Chem. Rev. 10 (1973) 79.
[2] (a) R.H. Holm, Chem. Soc. Rev. 10 (1981) 455, and references therein;
(b) J. Sola, Y. Do, J.M. Berg, R.H. Holm, J. Am. Chem. Soc. 105 (1983) 105;
(c) Y. Do, E.D. Simhon, R.H. Holm, Inorg. Chem. 24 (1985) 4635.
[3] (a) D. Coucouvanis, Acc. Chem. Res. 14 (1981) 201;
(b) D. Diaz, J. Robles, T. Ni, S.E. Castillo-Blum, D. Nagesha, O.J.A. Fergoso, N.A. Kotov, J. Phys. Chem. B 103 (1999) 9859;
(c) C.A. McConnachie, E.I. Stiefel, Inorg. Chem. 38 (1999) 964.
[4] (a) I. Bezverkhyy, P. Afanasiev, M. Lacriox, Mater. Res. Bull. 37 (2002) 161;
(b) S. Shi, Z. Lin, Y. Mo, X.Q. Xin, J. Phys. Chem. 100 (1996) 10696;
(c) Y. Liu, J. Chen, M.D. Ryan, Inorg. Chem. 37 (1998) 425.
[5] (a) S.P. Cramer, K.O. Hodgson, L.E. Mortenson, J. Am. Chem. Soc. 100 (1978) 339;
(b) S.P. Cramer, W.O. Gillum, K.O. Hodgson, L.E. Mortenson, E.I. Stiefel, J.R. Brill, V.K. Shah, J. Am. Chem. Soc. 100 (1978) 3814.
[6] (a) J.P. Lang, K. Tatsumi, Inorg. Chem. 37 (1998) 6308, and references 2–8 therein;
(b) T. Ecclestone, I. Harvy, S.H. Laurie, M.C.R. Symons, F.A. Taiwo, Inorg. Chem. Commun. 1 (1998) 460;
(c) R. Dessapt, C. Simonnet-Jegat, J. Marroy, F. Sécheresse, Inorg. Chem. 40 (2001) 4072.
[7] (a) K.E. Howard, J.R. Lockemeyer, M.A. Massa, T.B. Rauchfuss, S.R. Wilson, X. Yahg, Inorg. Chem. 29 (1990) 4385;
(b) H.G. Zheng, W. Tan, C. Jin, W. Ji, Q. Jin, X. Huang, X.Q. Xin, Inorg. Chim. Acta 305 (2000) 14.
[8] (a) D. Shaow, Z. Nianyong, C. Pengcheng, W. Xintao, L. Jiaxi, Polyhedron 11 (1992) 109;
(b) D.L. Long, J.T. Chen, J.S. Huang, Inorg. Chim. Acta 285 (1999) 241;
(c) M. Hong, D. Wu, R. Cao, X. Lei, H. Liu, J. Lu, Inorg. Chim. Acta 258 (1997) 25;
(d) Y. Jeannin, F. Sécheresse, S. Bernès, F. Robert, Inorg. Chim. Acta 198–200 (1992) 493.
[9] (a) C. Zhang, G.C. Jin, J.X. Chen, X.Q. Xin, K.P. Qian, Coord. Chem. Rev. 213 (2001) 51;
(b) H.W. Hou, X.Q. Xin, S. Shi, Coord. Chem. Rev. 153 (1996) 25;
(c) R. Colton, Coord. Chem. Rev. 62 (1985) 145.
[10] (a) G.N. George, I.J. Pickering, H.H. Harris, J. Gailer, D. Klein, J. Lichtmannegger, K.-H. Summer, J. Am. Chem. Soc. 125 (2003) 1704;
(b) R.J. Salm, A. Misetic, J.A. Ibers, Inorg. Chim. Acta 240 (1995) 239.
[11] H.G. Zheng, W. Ji, M.L.K. Low, G. Sakane, T. Shibahara, X.Q. Xin, J. Chem. Soc., Dalton Trans. (1997) 2537.
[12] (a) H. Hou, D. Long, X. Xin, X. Huang, B. Kang, P. Ge, W. Ji, S. Shi, Inorg. Chem. 35 (1996) 5363;
(b) J.M. Manoli, C. Potvin, Inorg. Chim. Acta 150 (1988) 257.
[13] (a) W. Clegg, A. Beheshti, M. Hosaini Sadr, Acta Crystallogr., Sect. E 58 (2002) m349;
(b) A. Beheshti, W. Clegg, H. Fallah, Inorg. Chim. Acta 322 (2001) 1.
[14] W.S. Ferguson, A.H. Lewis, S.J. Walson, Nature 141 (1943) 553.
[15] W. Kaim, B. Schwederski, Bioinorganic Chemistry: Inorganic Elements in the Chemistry of Life, Wiley, New York, 1996 (Chs. 10 and 11).
[16] Q. Pan, C.G. Kleer, L.V. Golden, J. Irani, M. Bottema, C. Bias, M.D. Carvalho, E.A. Mesri, D.M. Robin, R.D. Dick, J. Brewer, S.D. Merajver, Cancer Res. 62 (2002) 4854, and refs. 5–7 therein.

[17] K.D. Bissig, T.C. Voegelin, M. Solioz, FEBS Lett. 507 (2001) 367.
[18] S. Trofimenko, Scorpionates: The Coordination Chemistry of Polypyrazolylborate Ligands, Imperial College Press, London, 1999.
[19] (a) S. Trofimenko, Chem. Rev. 93 (1993) 943;
(b) S. Trofimenko, Prog. Inorg. Chem. 34 (1986) 115;
(c) S. Trofimenko, Acc. Chem. Res. 4 (1971) 17;
(d) S. Trofimenko, Inorg. Chem. 1 (1970) 99;
(e) S. Trofimenko, J. Am. Chem. Soc. 88 (1966) 1842;
(f) S. Trofimenko, J. Am. Chem. Soc. 89 (1967) 3170.
[20] D.T. Puerta, S.M. Cohen, Inorg. Chem. 41 (2002) 5075, and references 3–5 therein.
[21] (a) C. Slugovc, I.P. Martinez, S. Sirol, E. Carmona, Coord. Chem. Rev. 213 (2001) 129;
(b) M.D. Ward, J.A. McCleverty, J.C. Jeffery, Coord. Chem. Rev. 222 (2001) 251;
(c) D. Reger, Coord. Chem. Rev. 147 (1996) 571;
(d) C. Slugovc, R. Schmid, K. Krichner, Coord. Chem. Rev. 185–186 (1999) 109;
(e) S. Hikichi, Munetaka, Y. Moro-oka, Coord. Chem. Rev. 198 (2000) 61;
(f) N. Marques, A. Sella, J. Takats, Chem. Rev. 102 (2002) 2159.
[22] N. Kitajima, W.B. Tolman, Prog. Inorg. Chem. 43 (1995) 419.
[23] S. Dhar, P.A.N. Reddy, M. Nethaji, S. Mahadevan, M.K. Saha, A.R. Chakravarty, Inorg. Chem. 41 (2002) 3469.
[24] (a) J.S. Thompson, T.J. Marks, J.A. Ibers, J. Am. Chem. Soc. 101 (1979) 4180;
(b) R.E. Davis, T.A. Dodds, T.H. Hseu, J.C. Wagnon, T. Devon, J. Tancrede, J.S. McKennis, R. Pettit, J. Am. Chem. Soc. 96 (1974) 7565;
(c) T.C. Higgs, D.J. Roman, S. Czernuszewicz, C.J. Carrano, Inorg. Chim. Acta 273 (1998) 14.
[25] (a) N. Kitajima, K. Fujisawa, C. Fujimoto, Y. Moro-oka, S. Hashimoto, T. Kitagawa, K. Toriumi, K. Tatsumi, A. Nakamura, J. Am. Chem. Soc. 114 (1992) 1277;
(b) N. Kitajima, K. Fujisawa, Y. Moro-oka, J. Am. Chem. Soc. 111 (1989) 8975;
(c) N. Kitajima, T. Koda, S. Hashimoto, T. Kitagawa, Y. Moro-oka, J. Am. Chem. Soc. 113 (1991) 5664;
(d) R. Osterberg, Coord. Chem. Rev. 12 (1974) 309.
[26] A. Beheshti, W. Clegg, M. Hosaini Sadr, Polyhedron 20 (2001) 179.
[27] A. Beheshti, W. Clegg, M. Hosaini Sadr, Inorg. Chim. Acta 335 (2002) 21.
[28] (a) A.G. Sykes, Adv. Inorg. Chem. 36 (1991) 377;
(b) E.I. Solomon, K.W. Penfeild, D.E.W. lcox, Struct. Bonding 53 (1983) 1.
[29] D.D. Perrin, W.L.F. Armarego, Purification of Laboratory Chemicals, third ed., Pergamon Press, Oxford, 1988.
[30] S. Trofimenko, Inorg. Synth. 12 (1970) 99.
[31] J.W. McDonald, G.D. Friesen, L.D. Rosenhei, W.E. Newton, Inorg. Chim. Acta 72 (1983) 205.
[32] G.M. Sheldrick, SHELXTL User Manual, Bruker AXS Inc., Madison, WI, 1997.
[33] G. Alonso, G. Berhault, R.R. Chianlli, Inorg. Chim. Acta 316 (2001) 105.
[34] A. Müller, W. Jaegermann, W. Hellman, J. Mol. Struct. 100 (1983) 559.
[35] F. Sécheresse, S. Bernès, F. Robert, Y. Jeannin, J. Chem. Soc., Dalton Trans. (1991) 2875.
[36] J.R. Nicholson, A.C. Flood, C.D. Garner, W. Clegg, J. Chem. Soc., Chem. Commun. (1983) 1179.
[37] S.R. Acott, C.D. Garner, J.R. Nichsolson, W. Clegg, J. Chem. Soc., Dalton Trans. (1983) 713.
[38] J.C. Huffman, R.S. Roth, A.R. Siedle, J. Am. Chem. Soc. Commun. 98 (1976) 4340.
[39] S. Bernès, F. Sécheresse, Y. Jeannin, Inorg. Chim. Acta 194 (1992) 105.
[40] S. Mandal, G. Das, R. Singh, R. Shukla, P.K. Bharadwaj, Coord. Chem. Rev. 160 (1997) 191.
[41] (a) N. Kitajima, Adv. Inorg. Chem. 39 (1992) 18;
(b) N. Kitajima, K. Fujisawa, C. Fujimoto, Y. Moro-Oka, Chem. Lett. (1989) 421.
[42] R. Cao, Q. Zhang, W. Su, M. Bao, Y. Zheng, M. Hong, Polyhedron 18 (1999) 333.

Available online at www.sciencedirect.com
SCIENCE DIRECT®
Polyhedron 23 (2004) 643–647
POLYHEDRON
www.elsevier.com/locate/poly

An angular trinuclear copper(II) complex as a model for the active site of multicopper oxidases ☆

Sunita Gupta, Arindam Mukherjee, Munirathinam Nethaji, Akhil R. Chakravarty *

Department of Inorganic and Physical Chemistry, Indian Institute of Science, Sir C.V. Raman Avenue, Bangalore 560012, India

Received 13 September 2003; accepted 4 November 2003

Abstract

A new angular trinuclear copper(II) complex $[Cu_3L^1L^2(1\text{-MeIm})(H_2O)](ClO_4)$ (**1**), where H_3L^1 and H_2L^2 are penta and tetradentate Schiff base ligands, is prepared from a reaction of $[CuL^2]$ and $[Cu_2L^1(\mu\text{-Br})]$ in the presence of 1-methylimidazole (1-MeIm) and isolated as a perchlorate salt. The complex which crystallizes in the monoclinic space group $P2_1/n$ shows the presence of a discrete angular trinuclear copper(II) core in which the monomeric precursor is linked with the dimeric precursor through phenoxo bridges. The core structure resembles well with the active site structure of blue multicopper oxidases. The Cu···Cu separations of ca. 3.3 Å in the angular unit is 0.4 Å shorter than those observed in the active site of the oxidized form of ascorbate oxidase. The complex displays a visible band at 620 nm ($\varepsilon = 500\ M^{-1}\ cm^{-1}$) in DMSO. It shows magnetic moment values of 3.07 and 2.18 μ_B at 300 and 18 K, respectively, for the Cu_3 cluster. The complex models the structural and magnetic properties of the trinuclear active site of blue copper oxidases.
© 2003 Elsevier Ltd. All rights reserved.

Keywords: Tricopper(II) complex; Schiff bases; Ascorbate oxidase model; Crystal structure; Magnetic properties

1. Introduction

Blue multi-copper oxidases are copper containing metalloproteins that catalyze the four-electron reduction of dioxygen to water [1–6]. The active site of such oxidases has an angular trinuclear copper unit that consists of a putative type-2 (mononuclear) and type-3 (dinuclear) copper centers. The trinuclear core is located ~12 Å from a type-1 copper center in ascorbate oxidase [7]. Within the active site, the type-2 (or normal) copper center is bonded to two histidines and an aqua ligand, while the dicopper type-3 unit which is strongly antiferromagnetically (AF) coupled unit, has each copper bonded to three histidines and one bridging hydroxide giving a four-coordinate structure in its oxidized form (Chart 1). The average Cu···Cu distance is 3.74 Å. The reduced form of the oxidase shows an increase of the Cu···Cu distance in absence of any hydroxide bridge. The role of type-1 copper is to transfer electron to the trinuclear unit via His506–Cys507–His508 amino acid sequence in ascorbate oxidase to effect simultaneous four-electron reduction of dioxygen. The trinuclear active site has generated lot of interest in modeling the structural, magnetic and functional properties of the blue multicopper oxidases [8].

The majority of the reported trinuclear copper(II) complexes have either a linear arrangement of the metal centers or a $Cu_3(\mu_3\text{-X})$ unit (X = Cl, OH) [9–11]. Some angular tricopper(II) complexes are also known in the literature [12–19] but the model complexes resembling well to the active site structure are rare [12,15]. We have been interested to model the active site by following a new synthetic methodology involving the formation of the trinuclear core by linking of a type-2 mimic monomeric copper(II) complex with a type-3 mimic dinuclear copper(II) complex. We have recently reported trinuclear copper(II) complexes of formulation $[Cu_3(HL^1)L^1L'](ClO_4)$ by reacting $[Cu(HL^1)]$ and $[Cu_2L^1(\mu\text{-Br})]$ in the presence of imidazole bases like 1-methylimidazole or imidazole (L′), where H_3L^1 is a pentadentate Schiff base, *N*,*N*′-(2-hydroxypropane-1,3-diyl)bis(salicylaldi-

☆ Supplementary data associated with this article can be found, in the online version, at doi:10.1016/j.poly.2003.11.001.

* Corresponding author. Tel.: +91802932533; fax: +91803600683.
E-mail address: arc@ipc.iisc.ernet.in (A.R. Chakravarty).

0277-5387/$ - see front matter © 2003 Elsevier Ltd. All rights reserved.
doi:10.1016/j.poly.2003.11.001

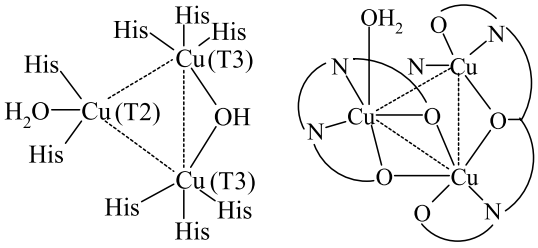

Chart 1. Trinuclear active site of ascorbate oxidase and the core structure of the model complex **1**.

mine) [20]. While these complexes model the structural and magnetic properties of the active site of ascorbate oxidase, they, however, show the formation of network structures involving the hydrogen atom of the uncoordinated hydroxypropane unit of the Schiff base. The present work stems from our interest to improve the synthetic methodology for the preparation of a discrete angular trinuclear copper(II) complex. For that purpose we have chosen a new type-2 mimic using a tetradentate Schiff base, *N*,*N*′-(propane-1,3-diyl)bis(salicylaldimine) (H_2L^2) for the monomeric precursor, and [Cu_2L^1(μ-Br)] as a type-3 mimic dimeric precursor having a pentadentate Schiff base (H_3L^1). The reaction of [CuL^2] with [Cu_2L^1(μ-Br)] in presence of 1-methylimidazole forms a trinuclear complex that has been isolated as a perchlorate salt of composition [$Cu_3L^1L^2$(1-MeIm)(H_2O)](ClO_4) (**1**). The significant result is the observation of discrete molecular nature of the complex which shows structural resemblance to the active site structure of ascorbate oxidase (Chart 1).

2. Experimental

2.1. Materials and measurements

Chemicals and reagents were purchased from commercial sources. Solvents were purified by standard procedures. The Schiff bases *N*,*N*′-(2-hydroxypropane-1,3-diyl)bis(salicylaldimine) (H_3L^1), *N*,*N*′-(propane-1,3-diyl) bis(salicylaldimine) (H_2L^2) and the precursor complexes [Cu_2L^1(μ-Br)] and [CuL^2] were prepared by literature procedures [21]. The elemental analysis was done using a Heraeus CHN–O Rapid instrument. The infrared and electronic spectra were recorded on a Bruker Equinox 55 and Hitachi U3000 spectrometers, respectively. Variable temperature magnetic susceptibility data for the polycrystalline sample of **1** were obtained in the temperature range 18–300 K using Model 300 Lewis Coil Force magnetometer (George Associates Inc., Berkeley, CA), equipped with a closed cycle cryostat (Air Products) and a Cahn balance. Hg[$Co(NCS)_4$] was used as a standard. Experimental susceptibility data were corrected for diamagnetic contributions and for temperature-independent paramagnetism [22]. Electrochemical measurements were made at 25 °C under dinitrogen atmosphere using a EG&G PAR Model 253 Versastat Potentiostat/Galvanostat with an electrochemical analysis software 270 for the cyclic voltammetric work using a three-electrode setup consisting of a glassy carbon working, a platinum wire auxiliary and a saturated calomel reference electrode (SCE). The electrochemical data were uncorrected for junction potentials. A 0.1 M tetrabutylammonium perchlorate (TBAP) was used as a supporting electrolyte in MeCN. Ferrocene was used as a standard to monitor the reference electrode showing the Fe(III)/Fe(II) couple at 0.38 V (vs. SCE) under similar experimental conditions in MeCN–0.1 M TBAP. Conductivity measurement was made at 25 °C using a Control Dynamics conductivity meter with a 10^{-3} M MeCN solution of complex **1**.

2.2. Synthesis

Complex **1** was prepared by reacting a 0.22 g (0.59 mmol) quantity of [CuL^2] taken in 15 ml of chloroform with 0.3 g (0.59 mmol) of [Cu_2L^1(μ-Br)] in a 20 ml MeCN–MeOH mixture (1:1 v/v) whilst stirring for 15 min. The reaction mixture was initially refluxed for 30 min followed by addition of 0.048 g 1-methylimidazole (0.59 mmol) and the reflux was continued for a further period of 1 h. The solution was then cooled to an ambient temperature and 0.073 g sodium perchlorate (0.59 mmol) was added to the reaction mixture. The solution was filtered and the solid product was isolated on slow evaporation of the solvent. It was washed with petroleum ether and water, and finally dried in vacuum over P_4O_{10} (yield: ~60%). Single crystals suitable for X-ray diffraction and other analytical studies were obtained from the mother liquor on slow evaporation. *Anal.* Calc. for $C_{38}H_{39}N_6O_{10}ClCu_3$ (**1**): C, 47.25; H, 4.07; N, 8.70. Found: C, 47.34; H, 4.06; N, 8.79%. FT-IR (KBr phase), cm^{-1}: 3413 br, 3133 w, 2922 w, 2359 w, 1634 s, 1447 s, 1303 s, 1194 m, 1093 vs, 903 m, 754 s, 626 m (br, broad; vs, very strong; s, strong; m, medium; w, weak). Electronic spectral data in DMSO [λ_{max}, nm (ε, M^{-1} cm^{-1})]: 620 (500), 370 (21 400), 273 (39 000). Magnetic susceptibility data [χ_M^{corr} (per copper), cm^3 M^{-1}]: 1.32×10^{-3} at 300 K; 1.21×10^{-2} at 18 K. Magnetic moment (μ_{eff}) per copper (per cluster): 1.78 μ_B (3.07 μ_B) at 300 K; 1.28 μ_B (2.18 μ_B) at 18 K. Complex **1** is air stable and soluble in common organic solvents other than hydrocarbons and water. *It contains perchlorate anion and as perchlorate salts of metal complexes with organic ligands are potentially explosive, only small quantity of the complex was handled with caution.*

2.3. Crystallographic studies

The intensity data were collected using a Bruker SMART APEX CCD diffractometer, equipped with a

Table 1
Selected crystallographic data for $[Cu_3L^1L^2(1\text{-}MeIm)(H_2O)](ClO_4)$ (**1**)

	1
Empirical formula	$C_{38}H_{39}ClCu_3N_6O_{10}$
Crystal size (mm)	$0.16 \times 0.14 \times 0.08$
Crystal morphology	cuboid
Crystal system	monoclinic
Space group	$P2_1/n$
Formula weight	965.82
Unit cell dimensions	
a (Å)	10.992(2)
b (Å)	13.606(2)
c (Å)	26.380(5)
$\alpha = \gamma$ (°)	90
β (°)	100.163(3)
V (Å^3)	3883.6(12)
Z	4
D_{calc} (g cm^{-3})	1.652
μ(Mo) (mm^{-1})	1.764
$F(000)$	1972
λ(Mo Kα) (Å)	0.71073
T (K)	293(2)
Reflections collected	8583
Reflections observed [$I > 2\sigma(I)$]	6892
Parameters	523
R (observed data) [R (all data)]	0.0401 [0.0526]
R_w (observed data) [R_w (all data)]	0.1128 [0.1214]
Goodness-of-fit on F^2	1.051
Shift/e.s.d. (maximum)	0.001
Largest differential peak and hole (e Å^{-3})	0.839; −0.396

fine focus 1.75 kW sealed tube Mo Kα X-ray source, with increasing ω (width of 0.3°/frame) at a scan speed of 12 s/frame. The SMART software was used for data acquisition and SAINT software was used for data extraction. Empirical absorption corrections were made on the intensity data using SADABS program [23]. The structure was solved and refined with SHELX programs [24]. Perspective view of the complex was obtained by ORTEP [25]. All non-hydrogen atoms were refined anisotropically. The hydrogen atoms were generated in their calculated positions and refined using a riding model. The hydrogen atoms were used for structure factor calculation only. Selected crystallographic data are given in Table 1.

3. Results and discussion

3.1. Synthesis and general aspects

Complex **1** has been prepared in high yield using a modified synthetic method to the one reported by us for analogous trinuclear copper(II) complexes [20]. In this synthetic methodology, a monomeric copper(II) complex (**I**) which is a structural mimic for type-2 copper centers has been linked to a dinuclear type-3 structural mimic (**II**) to form a trinuclear core (Scheme 1). The formation of this trinuclear core is facile in the presence of a unidentate ligand that is 1-methylimidazole in the

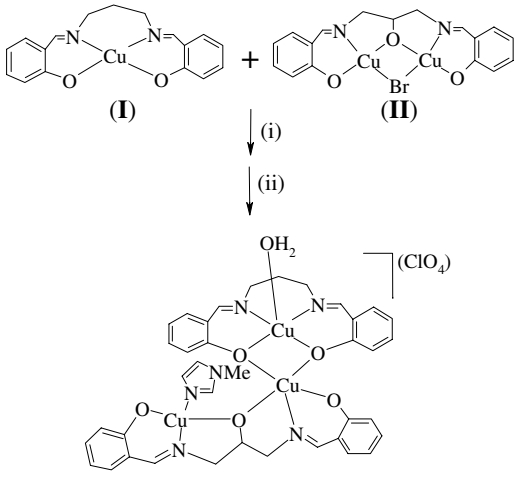

Scheme 1. Reaction conditions: (i) $CHCl_3$–MeCN–MeOH, reflux, followed by addition of 1-methylimidazole; (ii) $NaClO_4$.

Table 2
Physicochemical data for complex **1**

1. IR in KBr phase [$\nu(ClO_4^-)$, cm^{-1}]	1093
2. UV–Vis in DMSO [λ_{max} nm	620 (500); 370
(ε, M^{-1} cm^{-1})]	(21 400); 273 (39 000)
3. μ_{eff}/Cu (μ_B)	
300 K	1.78
18 K	1.28
4. CV in MeCN −0.1 M TBAP at 50 mV s^{-1}	
$E_{1/2}$ (V) [ΔE_p (mV), i_{pa}/i_{pc}]	−1.0 [98, 0.94]

present synthesis. The monomeric precursor complex has a tetradentate Schiff base ligand. The dinuclear precursor, on the other hand, has a pentadentate Schiff base. A linkage of **I** and **II** has formed a trinuclear complex which is found to be a discrete molecular species.

The complex has been characterized from analytical and spectral data (Table 2). Complex **1** is 1:1 electrolytic in nature and shows an IR band at 1093 cm^{-1} assignable to the perchlorate anion. It displays a d–d band at 620 nm in its electronic spectrum in dimethylsulfoxide (DMSO). The complex exhibits a cathodic peak at −1.05 V with an anodic response at −0.95 V for the Cu(II)/Cu(I) couple in the cyclic voltammogram at 50 mV s^{-1} in MeCN–0.1 M TBAP. The ΔE_p value of 100 mV suggests quasireversible nature of the redox process.

3.2. Magnetic properties

The variable temperature magnetic susceptibility data for **1** in the temperature range 300–18 K show an overall antiferromagnetic behavior of the complex (Fig. 1). The complex has a magnetic moment value of 1.78 μ_B at 300 K per copper(II) center. This suggests near paramagnetic behavior of the complex at room temperature. At lower temperatures, the complex exhibits antiferromagnetic interaction giving a magnetic moment value of

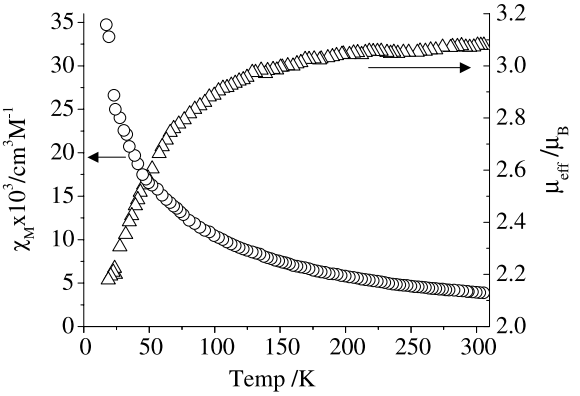

Fig. 1. Temperature dependence of magnetic susceptibility (o, per cluster) and the magnetic moment (Δ, per cluster) for $[Cu_3L^1L^2(1\text{-MeIm})(H_2O)](ClO_4)$ (**1**).

1.28 μ_B per copper at 18 K. The μ_{eff} value per cluster at 18 K is 2.18 μ_B which is close to the value of a core having a single paramagnetic copper(II) center and one strongly AF coupled dicopper(II) unit. The magnetic behavior of **1** thus models the magnetic property of the trinuclear active site of the ascorbate oxidase at the low temperature limit.

3.3. Crystal structure

The complex crystallizes in the monoclinic space group $P2_1/n$ with four molecules in the unit cell. The asymmetric unit consists of a trinuclear complex and a perchlorate anion. An ORTEP view of the cationic complex is shown in Fig. 2. Selected bond distances and angles are given in Table 3. The structure shows binding of the monomeric precursor to one copper center of the dinuclear precursor through the phenoxo oxygen atom O(3). The Cu(1) atom has a four coordinate geometry in a CuN_2O_2 coordination environment. This metal atom is bonded to the terminal phenoxo O(1), imine N(1), 1-methylimidazole N(5) and the bridging alkoxo O(2)

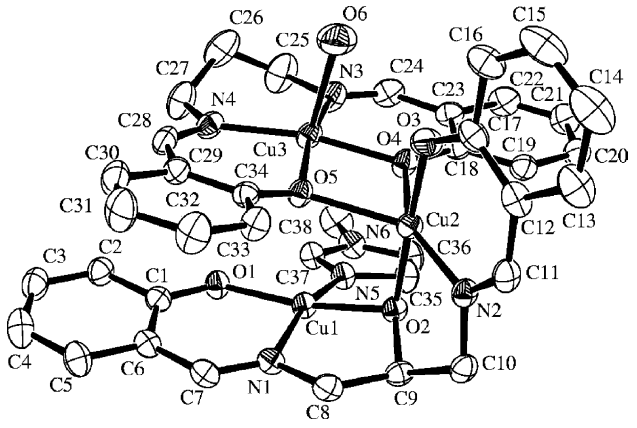

Fig. 2. An ORTEP view of the cationic complex in $[Cu_3L^1L^2(1\text{-MeIm})(H_2O)](ClO_4)$ (**1**) showing 50% probability thermal ellipsoids and the atom labeling scheme.

Table 3
Selected bond distances (Å) and angles (°) for **1**

Bond lengths			
Cu(1)···Cu(2)	3.239(1)	Cu(2)–O(4)	2.061(2)
Cu(2)···Cu(3)	3.206(1)	Cu(2)–O(5)	2.153(2)
Cu(1)–O(1)	1.897(2)	Cu(2)–N(2)	1.932(2)
Cu(1)–O(2)	1.975(2)	Cu(3)–O(4)	1.950(2)
Cu(1)–N(1)	1.920(2)	Cu(3)–O(5)	1.944(2)
Cu(1)–N(5)	1.970(2)	Cu(3)–O(6)	2.440(3)
Cu(2)–O(2)	1.961(2)	Cu(3)–N(3)	1.980(3)
Cu(2)–O(3)	1.912(2)	Cu(3)–N(4)	1.967(3)
Bond angles			
Cu(1)–O(2)–Cu(2)	110.79(9)	O(3)–Cu(2)–N(2)	93.24(10)
Cu(2)–O(4)–Cu(3)	106.11(9)	O(4)–Cu(2)–O(5)	71.96(7)
Cu(2)–O(5)–Cu(3)	102.91(8)	O(4)–Cu(2)–N(2)	150.30(9)
O(1)–Cu(1)–O(2)	166.82(9)	O(5)–Cu(2)–N(2)	137.31(9)
O(1)–Cu(1)–N(1)	94.59(10)	O(4)–Cu(3)–O(5)	78.99(8)
O(1)–Cu(1)–N(5)	90.99(9)	O(4)–Cu(3)–O(6)	84.93(10)
O(2)–Cu(1)–N(1)	84.01(9)	O(4)–Cu(3)–N(3)	91.19(10)
O(2)–Cu(1)–N(5)	93.75(9)	O(4)–Cu(3)–N(4)	168.37(10)
N(1)–Cu(1)–N(5)	164.56(10)	O(5)–Cu(3)–O(6)	84.04(10)
O(2)–Cu(2)–O(3)	177.11(8)	O(5)–Cu(3)–N(3)	167.26(10)
O(2)–Cu(2)–O(4)	91.42(8)	O(5)–Cu(3)–N(4)	90.80(10)
O(2)–Cu(2)–O(5)	91.60(8)	O(6)–Cu(3)–N(3)	103.33(12)
O(2)–Cu(2)–N(2)	83.99(9)	O(6)–Cu(3)–N(4)	99.67(11)
O(3)–Cu(2)–O(4)	91.39(9)	N(3)–Cu(3)–N(4)	98.07(12)
O(3)–Cu(2)–O(5)	89.91(9)		

atom. The copper atom is essentially in the basal plane showing a deviation of 0.025(1) Å from the plane. The Cu(2) atom has a five coordinate structure in a $CuNO_4$ environment. In this axially elongated structure, the metal is displaced by 0.235(1) Å from the plane formed by O(2), N(2), O(3) and O(4) atoms. The O(5) atom occupies the axial site showing a Cu(2)–O(5) distance of 2.153(2) Å. The Cu(2) atom belonging to the dinuclear precursor is linked to two other copper atoms through alkoxo O(2) and phenoxo O(4) atoms. The Cu(3) atom has the dianionic Schiff base ligand L^2 showing chelating tetradentate bonding mode. The metal has a square pyramidal geometry with the Schiff base at the basal plane and an aqua ligand occupying the axial site. The Cu(3) atom is 0.126(1) Å displaced from the basal plane.

Complex **1** has an angular trinuclear copper(II) core. A structural comparison to the active site of ascorbate oxidase is made in Chart 1. The Cu···Cu distances in the trinuclear unit is ~3.25 Å which is shorter than that observed in the active site (3.74 Å) of the oxidized form of the enzyme [7]. The av. Cu···Cu···Cu angle in **1** is 60°. The basal planes in **1** are not coplanar. The angle between two basal planes containing Cu(1) and Cu(2) atoms is 80.43(6)°. The angle between Cu(2) and Cu(3) planes is 89.02(7)°. Such a structural feature of **1** in which the dihedral angles between the basal planes are ~90° is expected to make the Cu(3) center paramagnetic by retaining its type-2 mimic properties while the alkoxo bridged Cu(1) and Cu(2) atoms form an AF coupled dicopper(II) unit. As a consequence, the complex models the magnetic and structural properties of the active site.

While AF coupling between Cu(2) and Cu(3) atoms are possible through O(4) atom located at the basal planes of two units, the dihedral angle of ~90° could reduce the extent of magnetic interaction significantly. Again, the interaction between two metal atoms through O(5) atom should be negligible considering the involvement of $d_{x^2-y^2}$ of Cu(3) and d_{z^2} of Cu(2) atom. The interaction between Cu(1) and Cu(2) atoms involving the alkoxo bridge is expected to be antiferromagnetic in nature considering the Cu(1)–O(2)–Cu(2) angle of 110.8° [26] The structural and magnetic results of **1** are of significance as the majority of known model complexes do not resemble to the active site structure. Another significant structural aspect of **1** is the discrete molecular nature of the complex. The aqua ligand bound to Cu(3) atom shows hydrogen bonding interaction only with the perchlorate anion [O(6)···O(12), 2.979(6) Å] and there is no other non-covalent interaction observed in the crystal structure of the complex. This makes complex **1** significantly different from its analogues with a pendant hydroxy group in the monomeric precursor that forms the hydrogen bonded network structure [20].

In summary, a new angular trinuclear copper(II) complex has been prepared from the reaction of a mononuclear copper(II) complex with a dinuclear copper(II) precursor in presence of 1-methylimidazole. The complex models the active site structure of ascorbate oxidase. It also models the magnetic properties of the active site but at a lower temperature giving one-electron magnetic moment for the trinuclear cluster at 18 K indicating the presence of a strong antiferromagnetically coupled dicopper(II) unit (type-3 mimic) and a copper(II) center (type-2 mimic). The synthetic methodology has been found to be useful for the preparation of discrete molecular angular trinuclear copper(II) complexes.

4. Supplementary data

Crystallographic data for the structural analysis of **1** have been deposited with the Cambridge Crystallographic Data Center, CCDC No. 218816. Copies of this information may be obtained free of charge from The Director, CCDC, 12 Union Road, Cambridge, CB2 1EZ, UK (fax: +44-1223-366-033; e-mail: deposit@ccdc.ac.uk or http://www.ccdc.cam.ac.uk).

Acknowledgements

We thank the Department of Science and Technology, Government of India, for the financial support and for the CCD diffractometer facility. We also thank the Alexander von Humboldt Foundation (Germany) for donation of an electroanalytical system. S.G. thanks CSIR for a fellowship.

References

[1] A. Messerschmidt, Struct. Bond. 90 (1998) 37.
[2] (a) E.I. Solomon, U.M. Sundaram, T.E. Machonkin, Chem. Rev. 96 (1996) 2563;
(b) T.E. Machonkin, E.I. Solomon, J. Am. Chem. Soc. 122 (2000) 12547;
(c) S.-K. Lee, G.S. DeBeer, W.E. Antholine, B. Hedman, K.O. Hodgson, E.I. Solomon, J. Am. Chem. Soc. 124 (2002) 6180;
(d) A.E. Palmer, L. Quintanar, S. Severance, T.-P. Wang, D.J. Kosman, E.I. Solomon, Biochemistry 41 (2002) 6438.
[3] R. Malkin, B.G. Malmström, Adv. Enzymol. 33 (1970) 177.
[4] J.P. Klinman, Chem. Rev. 96 (1996) 2541.
[5] P. Vachette, E. Dainese, V.B. Vasyliev, P. Di Muro, M. Beltramini, D.I. Svergun, V. De Filippis, B. Salvato, J. Biol. Chem. 277 (2002) 40823.
[6] H.-W. Huang, T. Sakurai, S. Maritano, A. Marchesini, S. Suzuki, J. Inorg. Biochem. 75 (1999) 19.
[7] A. Messerschmidt, R. Ladenstein, R. Huber, M. Bolognesi, L. Avigliano, R. Petruzzelli, A. Rossi, A. Finazzi-Agró, J. Mol. Biol. 224 (1992) 179.
[8] (a) D.E. Fenton, H. Okawa, J. Chem. Soc., Dalton Trans. (1993) 1349;
(b) A.P. Cole, D.E. Root, P. Mukherjee, E.I. Solomon, T.D.P. Stack, Science 273 (1996) 1848.
[9] E. Colacio, M. Ghazi, R. Kivekas, J.M. Moreno, Inorg. Chem. 39 (2000) 2882.
[10] A. Pasini, F. Demartin, O. Pioveseena, B. Chiari, A. Cinti, O. Crispu, J. Chem. Soc., Dalton Trans. (2000) 3467.
[11] C. Fernandes, A. Neves, A.J. Bortolussi, B. Szpoganics, E. Schwingel, Inorg. Chem. Commun. 4 (2001) 354.
[12] H. Adams, N.A. Bailey, M.J.S. Dwyer, D.E. Fenton, P.C. Hellier, P.D. Hempstead, J.-M. Latour, J. Chem. Soc., Dalton Trans. (1993) 1207.
[13] P. Chaudhuri, I. Karpenstein, M. Winter, C. Butzlaff, E. Bill, A.X. Trautwein, U. Flörke, H.-J. Haupt, J. Chem. Soc., Chem. Commun. (1992) 321.
[14] S. Meenakumari, S.K. Tiwary, A.R. Chakravarty, Inorg. Chem. 33 (1994) 2085.
[15] B. Graham, L. Spiccia, G.D. Fallon, M.T.W. Hearn, F.E. Mabbs, B. Moubaraki, K.S. Murray, J. Chem. Soc., Dalton Trans. (2001) 1226.
[16] P.V. Bernhardt, E.J. Hayes, J. Chem. Soc., Dalton Trans. (1998) 3539.
[17] E. Colacio, J.M. Dominguez-vera, A. Escuer, M. Klinga, R. Kivekas, A. Romerosa, J. Chem. Soc., Dalton Trans. (1995) 343.
[18] S.J. Frey, H.H.J. Sun, N.N. Murthy, K.D. Karlin, Inorg. Chim. Acta 242 (1996) 329.
[19] J. Sanmartin, M.R. Bermejo, A.M. Garcia-Deibe, O. Piro, E.E. Castellano, Chem. Commun. (1999) 1953.
[20] A. Mukherjee, I. Rudra, S.G. Naik, M. Nethaji, S. Ramasesha, A.R. Chakravarty, Inorg. Chem. 42 (2003) 5660.
[21] (a) N. Kitajima, K. Whang, Y. Moro-oka, A. Uchida, Y. Sasada, J. Chem. Soc., Chem. Commun. (1986) 1504;
(b) W. Mazurek, K.J. Berry, K.S. Murray, M.J. O'Connor, M.R. Snow, A.G. Wedd, Inorg. Chem. 21 (1982) 3071.
[22] O. Kahn, Molecular Magnetism, VCH, Weinheim, Germany, 1993.
[23] R.H. Blessing, Acta Crystallogr. A 51 (1995) 33.
[24] G.M. Sheldrick, SHELX 97, Programs for Crystal Structure Solution and Refinement, University of Göttingen, Göttingen, Germany, 1997.
[25] M.N. Burnett, C.K. Johnson, ORTEP-III, Report ORNL-6895, Oak Ridge National Laboratory, Oak Ridge, TN, 1996.
[26] M. Handa, N. Koga, S. Kida, Bull. Chem. Soc. Jpn. 61 (1988) 6853.

Available online at www.sciencedirect.com
SCIENCE DIRECT®
Polyhedron 23 (2004) 649–654
POLYHEDRON
www.elsevier.com/locate/poly

Hetero(tri- and tetra-)nuclear complexes of uranyl and alkali metal (Li^+, K^+) ions with *p-tert*-butylhexahomotrioxacalix[6]arene

Pierre Thuéry [a,*], Bernardo Masci [b]

[a] *CEA/Saclay, DSM/DRECAM/SCM (CNRS URA 331), Bât. 125, F-91191 Gif-sur-Yvette, France*
[b] *Dipartimento di Chimica and IMC-CNR Sezione Meccanismi di Reazione, Università "La Sapienza", P.O. Box 34, Roma 62, P.le Aldo Moro 5, 00185 Rome, Italy*

Received 29 September 2003; accepted 7 November 2003

Abstract

In the presence of lithium or potassium hydroxides, *p-tert*-butylhexahomotrioxacalix[6]arene (LH_6) gives uranyl complexes different from those obtained with amine bases. The dianionic trinuclear complex $[(UO_2)_2Li(OH)L(py)]$ is a monomeric species containing two tri-phenoxide-coordinated and hydroxo-bridged uranyl ions and a lithium ion bound to two phenoxide and one ether groups and a pyridine molecule. In the neutral $[UO_2K(LH_3)(H_2O)_2]_2$ complex, each macrocycle contains a tri-phenoxide-coordinated uranyl ion. The potassium ion is bound to two phenolic and one ether groups, to one of the uranyl oxo groups, to two bridging water molecules and to a phenoxide atom of a neighboring molecule. The latter bonds give rise to a centrosymmetrical, tetranuclear dimer.
© 2003 Elsevier Ltd. All rights reserved.

Keywords: Uranyl ion; Alkali metal ions; Calixarenes; Homooxacalixarenes; Crystal structures

1. Introduction

In spite of their suitable size and versatility, calixarenes have been little used in the design of heteropolymetallic complexes with transition metal ions and only recently a Re/Pd complex of *p-tert*-butylcalix[4]arene has been described [1]. However, several heteropolymetallic species involving alkali metal ions as one of the components were reported [2] and, following our previous work on uranyl ion complexes with calixarenes and homooxacalixarenes [3], we published recently the synthesis and crystal structures of mixed uranyl/alkali metal ions complexes with homooxacalixarenes [4,5]. We began this work with the rather simple case of *p-tert*-butyltetrahomodioxacalix[4]arene, which is perfectly suited for tetra-phenoxide complexation of a single uranyl ion. When deprotonation is carried out with alkali metal hydroxides in place of the usual amines, the uranyl complex core does not change, but oxo(uranyl)-coordination of the alkali metals ensues as a general trend [4]. Depending on the size and predominantly 'hard' or 'soft' character of the alkali metal, different arrangements are obtained, monomeric with Li^+, dimeric with Na^+ and polymeric with K^+ and Cs^+, 'endo' coordination associated with cation–π interactions being favoured for the larger cations. The much larger and versatile *p-tert*-butyloctahomotetraoxacalix[8]arene, when deprotonated with rubidium hydroxide, does not give the tetra-uranate internal complex obtained in the presence of triethylamine [6], but a dimeric capsule in which two calixarenes are held by $[(UO_2)_2(OH)_2]$ links and which contains the disordered Rb^+ ions [5]. We report herein the results of a similar investigation involving *p-tert*-butylhexahomotrioxacalix[6]arene, which is intermediate in size between the two previous ones (Scheme 1). This ligand has been shown to be of a convenient size to complex a $[(UO_2)_3(OH)_3]$ core in the presence of 1,4-diazabicyclo[2.2.2]octane (DABCO) [7]. The difficulties encountered in growing single crystals of suitable quality prevented the complete series

* Corresponding author. Tel.: +33-1-69-08-63-29; fax: +33-1-69-08-66-40.
E-mail address: thuery@drecam.cea.fr (P. Thuéry).

0277-5387/$ - see front matter © 2003 Elsevier Ltd. All rights reserved.
doi:10.1016/j.poly.2003.11.002

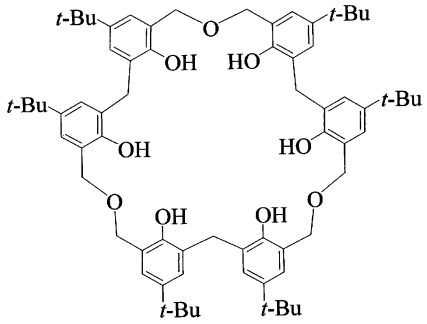

Scheme 1. *p-tert*-Butylhexahomotrioxacalix[6]arene, LH_6.

of alkali metal ions to be investigated, but crystal structures of complexes with two cations very different in size, Li^+ and K^+, are herein described and discussed.

2. Experimental

2.1. Synthesis

The ligand *p-tert*-butylhexahomotrioxacalix[6]arene LH_6 was synthesized as previously reported [8].

2.1.1. $[(UO_2)_2Li(OH)L(py)][Li(H_2O)_3(py)]\cdot(Hpy)\cdot H_2O\cdot 4.5py$ (**1**)

LH_6 (17 mg, 0.016 mmol) and an excess of $LiOH\cdot H_2O$ (9 mg, 0.21 mmol) were heated to reflux in $CHCl_3/CH_3OH$ (70/10 ml). A solution of $UO_2(NO_3)_2\cdot 6H_2O$ (26 mg, 0.052 mmol) in CH_3OH (10 ml) was then added dropwise, resulting in a bright orange solution which was stirred for 15 min. The powder obtained after complete evaporation of the solution was dissolved in pyridine and yielded orange single crystals, mixed with powder, on slow evaporation. No chemical or spectroscopic analysis could be performed due to the heterogeneous nature of the sample.

2.1.2. $[UO_2K(LH_3)(H_2O)_2]_2\cdot 14py$ (**2**)

LH_6 (20 mg, 0.019 mmol) was dissolved in $CHCl_3$ (70 ml) in the presence of an excess of KOH (10 mg, 0.18 mmol) in CH_3OH (10 ml). $UO_2(NO_3)_2\cdot 6H_2O$ (30 mg, 0.060 mmol) in CH_3OH (25 ml) was added dropwise at room temperature, giving a dark orange solution. Recrystallization in pyridine afforded dark orange single crystals mixed with an orange powder. No chemical or spectroscopic analysis could be performed due to the heterogeneous nature of the sample.

2.2. Crystallography

The data were collected on a Nonius Kappa-CCD area detector diffractometer [9] using graphite-monochromated Mo Kα radiation ($\lambda = 0.71073$ Å). The crystals were introduced in glass capillaries with a

Table 1
Crystal data and structure refinement details

	1	**2**
Empirical formula	$C_{106.5}H_{131.5}Li_2N_{7.5}O_{18}U_2$	$C_{208}H_{252}K_2N_{14}O_{26}U_2$
M (g mol^{-1})	2294.63	3918.50
Crystal system	triclinic	triclinic
Space group	$P\bar{1}$	$P\bar{1}$
a (Å)	16.0751(14)	17.1499(14)
b (Å)	18.6552(18)	17.3484(13)
c (Å)	20.7758(17)	18.1032(10)
α (°)	95.703(4)	79.098(4)
β (°)	106.162(5)	69.862(4)
γ (°)	112.630(4)	88.739(3)
V (Å^3)	5371.5(8)	4960.2(6)
Z	2	1
D_{calc} (g cm^{-3})	1.419	1.312
μ (mm^{-1})	3.077	1.741
Crystal size (mm)	$0.12\times 0.12\times 0.05$	$0.18\times 0.10\times 0.05$
$F(000)$	2314	2028
θ range (°)	2.7–25.7	2.8–25.7
T (K)	100(2)	100(2)
Number of data collected	36 960	34 284
Number of unique data	18 853	17 368
Number of 'observed' data [$I > 2\sigma(I)$]	10 430	11 928
R_{int}	0.083	0.081
Number of parameters	1249	1075
R_1	0.073	0.068
wR_2	0.153	0.149
S	1.004	1.010
$\Delta\rho_{min}$ (e Å^{-3})	−1.56	−1.04
$\Delta\rho_{max}$ (e Å^{-3})	1.45	1.44

Table 2
Environment of the uranium and alkali metal atoms in compounds **1** and **2**: selected bond lengths (Å) and angles (°)

1	U1–O1	2.318(8)	U2–O5	2.275(8)	Li1–O1	2.10(2)	Li2–O15	1.85(3)
	U1–O2	2.264(8)	U2–O7	2.202(8)	Li1–O8	1.97(2)	Li2–O16	1.93(3)
	U1–O4	2.272(8)	U2–O8	2.331(7)	Li1–O9	2.05(2)	Li2–O17	1.96(3)
	U1–O10	1.803(8)	U2–O12	1.788(7)	Li1–N1	2.07(2)	Li2–N4A	2.21(3)
	U1–O11	1.799(8)	U2–O13	1.779(7)	O1–Li1–O8	143.0(10)	O15–Li2–O16	100.5(14)
	U1–O14	2.336(8)	U2–O14	2.328(8)	O1–Li1–O9	94.3(8)	O15–Li2–O17	121.9(17)
	O1–U1–O2	90.9(3)	O5–U2–O7	97.5(3)	O1–Li1–N1	104.4(10)	O15–Li2–N4A	90.5(13)
	O2–U1–O4	95.0(3)	O7–U2–O8	82.5(3)	O8–Li1–O9	93.4(9)	O16–Li2–O17	111.1(15)
	O4–U1–O14	91.7(3)	O8–U2–O14	80.3(3)	O8–Li1–N1	106.5(9)	O16–Li2–N4A	126.7(17)
	O14–U1–O1	82.2(3)	O14–U2–O5	99.5(3)	O9–Li1–N1	110.5(9)	O17–Li2–N4A	106.0(13)
	O10–U1–O11	177.7(4)	O12–U2–O13	177.3(4)				
2	U–O1	2.248(6)	K–O5	2.694(6)	O2′–K–O13	81.38(19)		
	U–O2	2.225(5)	K–O6	2.733(6)	O2′–K–O13′	94.0(2)		
	U–O4	2.334(5)	K–O7	2.791(6)	O10–K–O13	76.76(19)		
	U–O10	1.786(5)	K–O10	2.757(5)	O10–K–O13′	75.29(19)		
	U–O11	1.772(5)	K–O13	2.695(7)	O13–K–O13′	88.6(2)		
	U–O12	2.371(5)	K–O13′	2.779(7)	U–O10–K	149.0(3)		
	O1–U–O2	90.5(2)	K–O2′	2.727(5)	K–O13–K′	91.4(2)		
	O2–U–O4	98.36(19)	O5–K–O6	66.58(16)				
	O4–U–O12	87.62(19)	O6–K–O7	63.45(16)				
	O12–U–O1	84.11(19)	O7–K–O10	67.43(16)				
	O10–U–O11	178.0(3)	O10–K–O5	70.11(17)				

Symmetry code: $' = 2 - x, 2 - y, 1 - z$.

protecting 'Paratone-N' oil (Hampton Research) coating. The unit cell parameters were determined from ten frames, then refined on all data. A 180° φ-range was scanned with 2° steps during data collection, with a crystal-to-detector distance fixed to 28 mm. The data were processed with DENZO-SMN [10]. The structures were solved by Patterson map interpretation with SHELXS-97 and subsequent Fourier-difference synthesis and refined by full-matrix least-squares on F^2 with SHELXL-97 [11]. Absorption effects were corrected empirically with the program DELABS from PLATON [12]. In compound **1**, one *tert*-butyl group was found to be rotationally disordered over two positions and three pyridine molecules were found to be disordered over two sites each. These positions were refined with occupancy parameters constrained to sum to unity. The pyridinium ion (as indicated by possible hydrogen bonds) is also disordered over two positions, corresponding to N2 and N3, which cannot be occupied simultaneously and have been affected with a 0.5 occupancy parameter. In compound **2**, one pyridine molecule was found disordered over two sites which were refined with occupancy parameters constrained to sum to unity, and the nitrogen atom was not located in another, badly resolved, pyridine molecule. In both **1** and **2**, some pyridine molecules have been refined as idealized hexagons. In both compounds, all non-hydrogen atoms were refined with anisotropic displacement parameters (except some of the disordered ones) with some restraints for some badly behaving atoms. The hydrogen atoms bound to oxygen and nitrogen atoms in **1** were not found, nor introduced, whereas those bound to oxygen atoms in **2** (except those of the water oxygen atom O13) were found on a Fourier-difference map. The other hydrogen atoms were introduced at calculated positions, except in the disordered parts. All hydrogen atoms were treated as riding atoms with a displacement parameter equal to 1.2 (OH, CH, CH_2) or 1.5 (CH_3) times that of the parent atom. Crystal data and structure refinement details are given in Table 1 and selected bond lengths and angles in Table 2. The molecular plots were drawn with SHELXTL [13]. All calculations were performed on a Silicon Graphics workstation.

3. Results and discussion

The uranyl complex obtained in the presence of lithium hydroxide, $[(UO_2)_2Li(OH)L(py)][Li(H_2O)_3(py)] \cdot (Hpy) \cdot H_2O \cdot$ 4.5py (**1**) contains the trimetallic dianionic species $[(UO_2)_2Li(OH)L(py)]$ in which the three cations are complexed in 'internal' fashion (Fig. 1). The two uranyl ions are bound to three phenoxide groups and a central hydroxide ion, which results in a distorted square bipyramidal environment for the uranium atoms, and the lithium ion is bound to two phenoxide and one ether oxygen atoms and a pyridine molecule. This arrangement is different from the pseudo-trigonal geometry of the previously reported tri-uranate complex with the same ligand [7], in which the trianionic complex core $[(UO_2)_3(OH)_3L]$ contains three cations, each of them bound to two phenoxide groups (separated by a methylene link) and two hydroxide ions in their equatorial plane. The mean U–O(phenoxide) bond length in **1** is

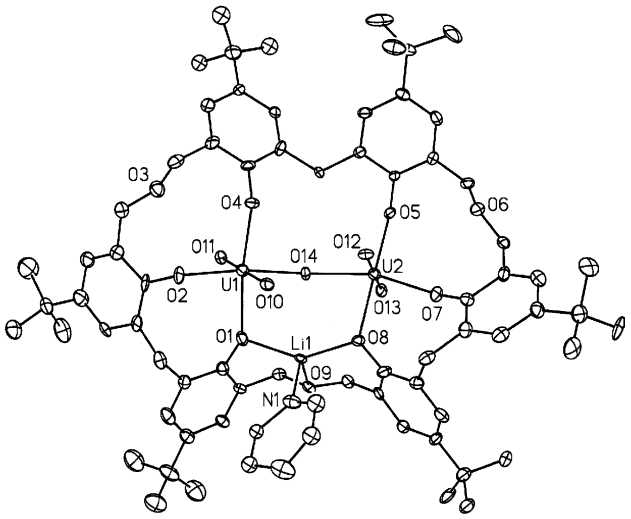

Fig. 1. View of the complex $[(UO_2)_2Li(OH)L(py)][Li(H_2O)_3(py)] \cdot (Hpy) \cdot H_2O \cdot 4.5py$ (**1**). Hydrogen atoms, counter-ions and solvent molecules have been omitted for clarity. Displacement ellipsoids are drawn at the 30% probability level.

2.28(5) Å, in agreement with usual values. However, the bond lengths involving the atoms O1 and O8, which are also bound to Li^+, are significantly larger than the other ones [mean values 2.325(9) versus 2.25(3) Å]. The mean U–O(hydroxide) bond length, 2.332(6) Å, as well as the U1–O14–U2 angle, 139.7(4)°, are comparable to the values in similar cases [7]. The four donor atoms around each uranyl ion define a mean plane with a maximum deviation of 0.042(4) Å, the uranium atoms being separated by 0.067(4) and 0.076(4) Å from these planes, which define a dihedral angle of 52.1(2)°. The space left in the macrocycle cavity by the absence of the third uranyl ion is occupied by the lithium ion, which is chelated by two phenoxide groups (not bound to the same uranium atom) and the ether atom O9. The mean Li1–O(phenoxide) bond length, 2.04(9) Å is in the range 1.87–2.09 Å reported for the literature values [14] and the Li1–N1 bond length, 2.07(2) Å, agrees well with the mean Li–N(pyridine) bond length value of 2.07(7) Å for the structures reported in the Cambridge Structural Database [15]. The environment of Li^+ is a very distorted tetrahedron, with the O1–Li1–O8 angle much larger than the other ones, due to geometrical constraints. Li^+ is located at 0.568(18) Å above the plane defined by the three atoms O1, O8 and O9 from the calixarene and can thus be considered to be complexed in an 'internal' mode.

Whereas the conformation of the macrocycle in the previous, tri-uranate complex was that of a rather regular trigonal cone, it is rather flat and very distorted in the present case. All three ether links define two *anti* torsion angles, which, in the case of O9, brings this atom closer to Li1. However, the phenolic rings orientation is such that the complex possesses no pseudo-symmetry, even approximate. If we adopt the notation of Kanamathareddy and Gutsche [16] and introduce the ether bridges as (b), the conformation of L in **1** can be represented by the sequence [uu(b)ud(b)du(b)]. As a result, Li1 has a different position with respect to the two mean equatorial planes corresponding to U1 and U2, being at 1.51(2) Å from the first and 0.03(2) Å from the second and thus located in the plane corresponding to U2.

The repeat unit contains also two counter-cations and several solvent molecules. The second Li^+ cation is bound to three water molecules and one disordered pyridine molecule and it is thus isolated from the uranyl complex moiety. The presence of a pyridinium ion, disordered over two positions, can be inferred from N···O(phenoxide, ether) distances indicative of hydrogen bonds [N2···O4 3.17(2), N3···O6 3.12(2) Å]. Among the solvent pyridine molecules, one is hydrogen bonded to the hydroxide group [O14···N5 2.77(1) Å], and two others to lithium-bound water molecules.

The complex obtained in the presence of potassium hydroxide, $[UO_2K(LH_3)(H_2O)_2]_2 \cdot 14py$ (**2**), is dimeric in nature and different from **1** as well as from the tri-uranate species. The asymmetric unit contains the heterobinuclear unit $[UO_2K(LH_3)(H_2O)_2]$, represented in Fig. 2, and pyridine solvent molecules. As in complex **1**, the uranyl ion is bound to three phenoxide groups and the potassium ion to two phenol and one ether groups. However, at variance with **1**, the macrocycle is not completely deprotonated and contains two cations only. The uranyl ion completes its coordination sphere with a water molecule (O12) to give the usual square bipyra-

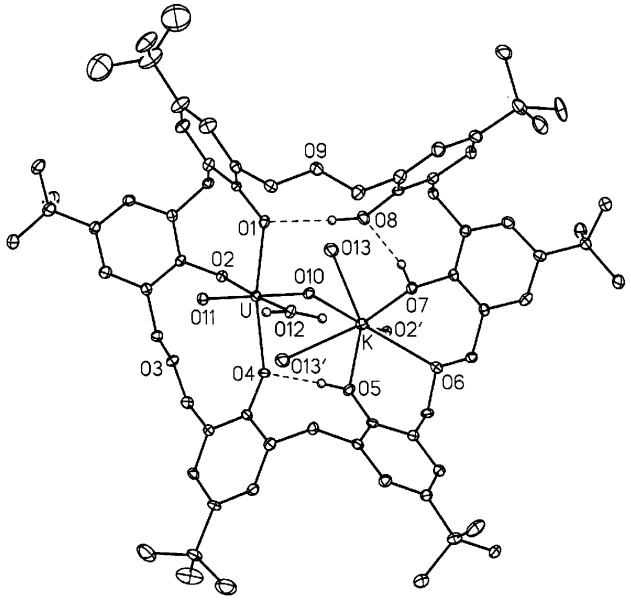

Fig. 2. View of one unit in the dimeric complex $[UO_2K(LH_3)(H_2O)_2]_2 \cdot 14py$ (**2**). Hydrogen atoms (except for the hydrogen bonded ones) and solvent molecules have been omitted for clarity. Intramolecular hydrogen bonds are represented as dashed lines. Displacement ellipsoids are drawn at the 20% probability level. Symmetry code: $' = 2 - x, 2 - y, 1 - z$.

midal geometry around the uranium atom, with a mean U–O(phenoxide) bond length of 2.27(6) Å. The four donor atoms define a mean equatorial plane with a maximum deviation of 0.141(3) Å, which contains also the uranium atom [deviation of 0.058(3) Å]. The mean K–O(phenol) bond length is 2.74(7) Å, which is in the range 2.544–3.160 Å for the literature values [14] and agrees also with the value 2.731(6) Å in the uranyl/potassium complex of *p-tert*-butyltetrahomodioxacalix[4]arene [4]. The K–O(ether) bond length, 2.733(6) Å, is slightly shorter than the mean value in the latter complex, 2.808(5) Å, which is likely due to the different geometrical constraints arising from much different potassium locations. It is noticeable that, considering the macrocycle only, K^+ in **2** is bonded in a similar way as Li^+ in **1**, the bridging phenoxide groups being replaced by hydrogen bonded phenolic ones. Apart from the three oxygen atoms from the macrocycle, the potassium ion is bound to the oxo group of the uranyl ion, with a K–O10 bond length of 2.757(5) Å which perfectly matches the mean value of 2.8(3) Å in the *p-tert*-butyltetrahomodioxacalix[4]arene complex (in which, however, each oxo atom is bound to two potassium ions), two water molecules (O13 and its symmetry-related equivalent) and the phenoxide atom O2 from a neighboring molecule. The potassium is thus hepta-coordinated, and the environment geometry can best be viewed as a much distorted capped octahedron with the oxo atom O10 in capping position [17]. K^+ is located at a distance of 2.016(4) Å from the plane defined by the three atoms O5, O6 and O7 from the calixarene and, in contrast with Li^+ in **1**, it can thus be considered to be complexed in an 'external' mode. It is noteworthy that, at variance with the previous UO_2/K complex [4] and several other calixarene complexes [14,18,19], the potassium cation in **2** is not involved in obvious cation–π interactions. The only possibly significant K···C(arom) interaction involves the carbon atom bound to O2 in the second calixarene, but the corresponding K···C distance, 3.423(7) Å, is larger than the shortest contact in the previous complex, 3.180(8) Å [4]. The three phenolic protons are involved in intramolecular hydrogen bonds [O5···O4 2.653(7), O7···O8 2.839(7) and O8···O1 2.894(8) Å]. The bonding of the potassium atom to a phenoxide of a neighboring molecule as well as the bridging character of the water molecules (O13 and its symmetry-related equivalent) ensure the formation of a centrosymmetrical, tetranuclear dimer, represented in Fig. 3. This dimeric species can be viewed as a capsule built from two uranyl-containing macrocycles facing each other, with a $K_2(H_2O)_2$ group occupying the central cavity and ensuring the cohesion of the whole assembly.

The macrocycle adopts a conformation which can be described as a double partial cone, with the three phenoxide units bound to the uranyl ion building one subunit and the two bound to the potassium ion and the non-coordinated one the second subunit (it may be noted that a similar conformation is adopted by calix[6]arene in its di-potassium complexes [19]). The overall appearance is somewhat analogous to a saddle shape. The two partial cones are connected by one methylene and one ether-containing bridges and they are also linked by two intramolecular hydrogen bonds. The dihedral angle between the planes defined by O1, O2, O4 in the first part and O5, O7, O8 in the second is 77.5(2)°. The water molecules bound to the uranium atoms are located in each homooxacalixarene cavity and are hydrogen bonded to two pyridine molecules [O12···N2 2.709(9), O12···N3 2.631(8) Å]. Two other pyridine molecules are hydrogen bonded to the bridging water molecules [O13···N1 2.801(10) Å].

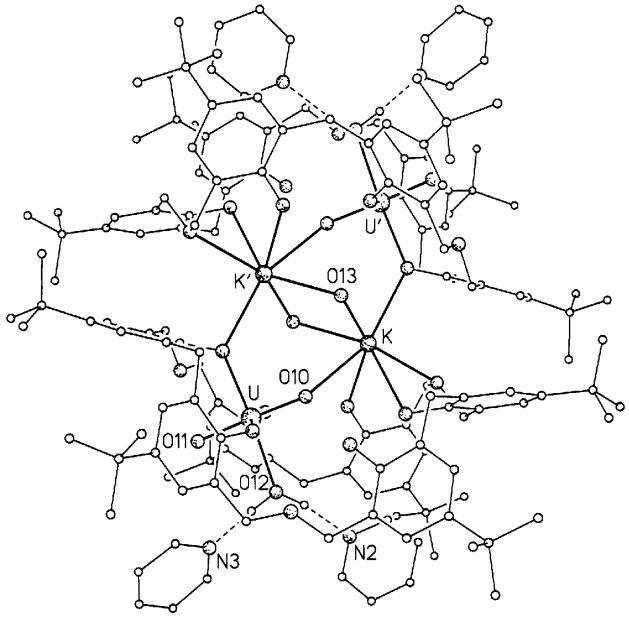

Fig. 3. View of the complex $[UO_2K(LH_3)(H_2O)_2]_2 \cdot 14py$ (**2**). The hydrogen atoms (except those of the water oxygen atom O12) and some solvent molecules have been omitted for clarity. Intermolecular hydrogen bonds are represented as dashed lines. Carbon atoms have been arbitrarily reduced for clarity. Symmetry code: $' = 2 - x, 2 - y, 1 - z$.

4. Conclusion

In spite of the characterization of uranyl/alkali metal ions complexes with the ligand LH_6 having been performed for Li^+ and K^+ only, the large difference in size, and hence in behavior, between these two cations permits some conclusions to be drawn. In the previously investigated case of *p-tert*-butyltetrahomodioxacalix[4]arene, these two cations give much different complexes, both of them including the same uranyl complex core. Li^+ leads to a monomeric complex in which each of the two lithium ions is bound to an oxo(uranyl) atom, one in the macrocycle cavity and the other outside, and to three water/methanol molecules. With K^+, a polymeric species is formed (as with Cs^+), the two potassium ions being

located in the cavity and bound both to the oxo atom directed inside and to the oxo atom of a neighboring molecule, and also to an ether oxygen atom and water and pyridine molecules. In the present case, we observe the same tendency for Li^+ to give rise to monomeric species by completing its coordination sphere with solvent molecules rather than with an oxygen atom of a neighboring macrocycle (complete dissociation of the lithium counterion has also been observed in the case of the uranyl complex of an homoazacalixarene [20]). As mentioned above, the potassium ion in **2** is not involved in cation–π interactions as it was the case in the previous complex, but the K^+—oxo bonding is still present. Furthermore, the larger size of this cation, with respect to that of Li^+, enables its bonding to a phenoxide unit of a neighboring complex, which results in dimerization. As noticed above, Li^+ and K^+ are similarly chelated by two phenol/phenoxide and one ether groups of the homooxacalixarene. The differences between the two complexes arise from the larger coordination sphere and resulting higher bridging ability of potassium.

With respect to the nuclearity of complexes **1** and **2**, it can be noted that in none of them is the available space so efficiently occupied than in the tri-uranate complex [4]. **1** is also a trinuclear species, but one uranyl ion and two hydroxide bridges of the tri-uranate complex are replaced by one Li^+ cation only, whereas the macrocycle in **2** contains two cations only, with furthermore, K^+ located largely outside the macrocycle. We have shown previously that the highest uranyl nuclearity which can be expected on the basis of the calixarene/homooxacalixarene size alone [6] can be reduced in the case of less optimal homooxacalixarene positional isomers [21] or in the presence of coordinating solvents which prevent oxo/hydroxo bridging of the uranyl units [22]. As illustrated here, replacement of amine bases by alkali metal hydroxides can also be a source of global nuclearity reduction, in the case of macrocycles sufficiently large to complex more than one cation and for which uranyl and alkali metal ions compete for the bonding sites.

5. Supplementary material

Crystallographic data for the structural analysis have been deposited with the Cambridge Crystallographic Data Centre, CCDC Nos. 220661 and 220662. Copies of this information may be obtained free of charge from The Director, CCDC, 12 Union Road, Cambridge CB2 1EZ, UK (fax: +44-1223-336033; e-mail: deposit@ccdc.cam.ac.uk or www: http://www.ccdc.cam.ac.uk).

References

[1] K. Iwasa, T. Kochi, Y. Ishii, Angew. Chem. Int. Ed. 42 (2003) 3658.
[2] (a) C. Floriani, R. Floriani-Moro, in: Z. Asfari, V. Böhmer, J. Harrowfield, J. Vicens (Eds.), Calixarenes 2001, Kluwer Academic Publishers, Dordrecht, 2001, pp. 536–560 (Ch. 29) and references therein;
(b) V.C. Gibson, C. Redshaw, W. Clegg, M.R.J. Elsegood, Chem. Commun. (1997) 1605.
[3] P. Thuéry, M. Nierlich, J. Harrowfield, M. Ogden, in: Z. Asfari, V. Böhmer, J. Harrowfield, J. Vicens (Eds.), Calixarenes 2001, Kluwer Academic Publishers, Dordrecht, 2001, pp. 561–582 (Ch. 30) and references therein.
[4] P. Thuéry, B. Masci, Dalton Trans. (2003) 2411.
[5] P. Thuéry, B. Masci, Supramol. Chem., in the press.
[6] P. Thuéry, M. Nierlich, J. Vicens, B. Masci, J. Chem. Soc., Dalton Trans. (2001) 867.
[7] P. Thuéry, M. Nierlich, J. Vicens, B. Masci, J. Chem. Soc., Dalton Trans. (2001) 3410.
[8] B. Masci, Tetrahedron 57 (2001) 2841.
[9] Kappa-CCD Software, Nonius BV, Delft, 1998.
[10] Z. Otwinowski, W. Minor, Methods Enzymol. 276 (1997) 307.
[11] G.M. Sheldrick, SHELXS-97 and SHELXL-97, University of Göttingen, 1997.
[12] A.L. Spek, PLATON, University of Utrecht, 2000.
[13] G.M. Sheldrick, SHELXTL: Version 5.1, Bruker AXS Inc., Madison, WI, 1999.
[14] T.A. Hanna, L. Liu, A.M. Angeles-Boza, X. Kou, C.D. Gutsche, K. Ejsmont, W.H. Watson, L.N. Zakharov, C.D. Incarvito, A.L. Rheingold, J. Am. Chem. Soc. 125 (2003) 6228, and references therein.
[15] F.H. Allen, Acta Crystallogr., Sect. B 58 (2002) 380.
[16] S. Kanamathareddy, C.D. Gutsche, J. Am. Chem. Soc. 115 (1993) 6572.
[17] D.L. Kepert, Inorganic Stereochemistry, Springer, Heidelberg, 1982.
[18] T.A. Hanna, L. Liu, L.N. Zakharov, A.L. Rheingold, W.H. Watson, C.D. Gutsche, Tetrahedron 58 (2002) 9751.
[19] K. Murayama, K. Aoki, Inorg. Chim. Acta 281 (1998) 36.
[20] P. Thuéry, H. Takemura, Acta Crystallogr., Sect. C 59 (2003) m384.
[21] B. Masci, P. Thuéry, Supramol. Chem. 15 (2003) 101.
[22] P. Thuéry, B. Masci, Polyhedron 22 (2003) 3499.

Available online at www.sciencedirect.com
SCIENCE DIRECT®
Polyhedron 23 (2004) 655–663
POLYHEDRON
www.elsevier.com/locate/poly

Synthesis, solution and crystal structures of dinuclear vanadium(V) oxo monoperoxo complexes with mandelic acid: $(NR_4)_2[V_2O_2(O_2)_2(mand)_2]\cdot xH_2O$ [R = H, Me, Et; mand = mandelato(2−) = $C_8H_6O_3^{2-}$]

M. Ahmed [a], P. Schwendt [a,*], J. Marek [b], M. Sivák [a]

[a] Department of Inorganic Chemistry, Faculty of Natural Sciences, Comenius University, Mlynská dolina, SK-84215 Bratislava 4, Slovak Republic
[b] Laboratory of Functional Genomics and Proteomics, Faculty of Natural Sciences, Masaryk University, Kotlářská 2, Brno CZ-61137, Czech Republic

Received 26 September 2003; accepted 10 November 2003

Abstract

Vanadium(V) oxo peroxo mandelato complexes were prepared from aqueous solution and characterized by elemental analysis, IR, UV–Vis and ^{51}V NMR spectroscopies. The single crystal X-ray studies of $(NMe_4)_2[V_2O_2(O_2)_2(R,S\text{-mand})_2]\cdot 6.5H_2O$ (**3**), $(NMe_4)(NH_4)[V_2O_2(O_2)_2(R,S\text{-mand})_2]\cdot 2H_2O$ (**4**) and $(NEt_4)_2[V_2O_2(O_2)_2(R\text{-mand})_2]$ (**8**) revealed that the mandelato ligand behaves as a bidentate chelator adopting the (O^-, COO^-) donor set. The complex anions in structures of **3** and **8** contain a dinuclear V_2O_2 core with cyclic arrangement of two vanadium atoms and two hydroxyl oxygen atoms from the bridging mand ligands. Each vanadium atom is coordinated by six oxygen atoms arising from two hydroxyl and one carboxyl groups, η^2-peroxo ligand and one end-bonded oxo ligand. The coordination polyhedron can be described as distorted pentagonal pyramid. The structure of **4** is unique as it contains in the unit cell differently coordinated water molecules in two types of dinuclear anions: $[V_2O_2(O_2)_2(R\text{-mand})_2(H_2O)]^{2-}$, with nearly symmetrically bonded bridging water molecule and pentagonal bipyramidal arrangement arround both vanadium atoms, and $[V_2O_2(O_2)_2(S\text{-mand})_2(H_2O)]^{2-}$, with the water molecule coordinated only to one vanadium atom. The vanadium atoms thus have different coordination geometries: pentagonal pyramidal and pentagonal bipyramidal, the latter exhibiting a better planarity of the fitted atoms of the pentagonal plane and a smaller deviation of the vanadium atom from this plane.
© 2003 Elsevier Ltd. All rights reserved.

Keywords: Crystal structure; Vanadium(V) peroxo mandelato complex; IR spectra; ^{51}V NMR spectra

1. Introduction

Over the past years, an increased attention has been paid to the chemistry of peroxovanadium(V) complexes, due to their important role in biological systems and application in oxidation reactions. Vanadium is thought to be a trace metal in most of the higher animals and it is known to be essential to some organisms, including tunicates and mushrooms. The best evidence for the biological role of this element comes from bacteria and plants (vanadium containing nitrogenase and haloperoxidases) [1].

Vanadium, both in cationic and anionic forms and in its several oxidation states, has an exceptional ability to interact with biomolecules. Among the biological functions of vanadium, many important therapeutic effects have been described, including hormonal, cardiovascular, anticarcinogenic and insulin mimetic activities [2]. Vanadium and hydrogen peroxide were shown to act synergistically to mimic insulin activity [3] and such mimetic ability has also been found for several peroxovanadium complexes [2,4–6]. These complexes are also known to have antitumour activity [7], and have been studied as functional models for the vanadium haloperoxidase enzymes [8–10] which are involved in catalysis

* Corresponding author. Tel.: +421-7-6029-63-46; fax: +421-7-6029-62-73.
E-mail address: schwendt@fns.uniba.sk (P. Schwendt).

0277-5387/$ - see front matter © 2003 Elsevier Ltd. All rights reserved.
doi:10.1016/j.poly.2003.11.040

of the oxidation of halides by hydrogen peroxide, and probably also in the biosynthesis of a large number of natural marine products, many of them with potent antifungal, antibacterial or antiviral (e.g., HIV) properties [11].

As the coordination compounds of vanadium and their reactivity play a predominant role in physiological effects, the complexation behaviour of vanadium with organic ligands is of great interest. The anions of α-hydroxycarboxylic acids are involved in many basic biochemical processes and represent thus an important group of biogenic ligands. That is the reason why peroxovanadium complexes with α-hydroxycarboxylato ligands are currently investigated. In particular, the monoperoxo complexes of citric, malic, tartaric, glycolic and mandelic acids were isolated and characterized [7,12–17].

The solid state structures have been determined for a large number of mono- and diperoxovanadium(V) complexes by X-ray diffraction. The studies showed that the most common geometry for the monomeric oxo peroxo complexes is the pentagonal bipyramid and that the peroxo group is always bound in the equatorial plane relative to the axial oxo ligand [3]. The remaining equatorial and one apical positions in the coordination polyhedron are occupied by the heteroligand/s.

For the α-hydroxycarboxylato oxo peroxo complexes of vanadium, an interesting coordination number ambiguity has been observed. If we consider the value d(V–L) ≈ 2.5 Å as limiting for the apical covalent V–L bond [18], then some of the complexes (glycolato- or lactato-) exhibit pentagonal pyramidal geometry, while others (tartrato-, citrato- or malato-) are pentagonal bipyramidal. In the mandelato complex, $(NBu_4)_2[V_2O_2(O_2)_2(R,S\text{-mand})_2]\cdot R,S\text{-}H_2$mand ($H_2$mand is mandelic acid) [14], the coordination number of the vanadium atom can be considered to be six. However, there is a weak interaction ($d \approx 2.55$ Å) between the vanadium atom and carboxyl oxygen from the neutral molecule of mandelic acid, which indicates a certain tendency of the vanadium atom to complete the coordination polyhedron to the pentagonal bipyramid. We have also described the stereospecific formation and different structures of the lactato oxo peroxo complexes of vanadium(V) as a consequence of different combinations of the ligand enantiomers in the dinuclear anion [15].

This paper is focused on the synthesis and characterization of peroxovanadium(V) complexes with mandelic acid. We have tried to address both actual problems of the stereochemistry of the α-hydroxycarboxylato oxo peroxo complexes of vanadium(V): the stereospecifity of formation and the ambiguity of the coordination number of vanadium.

2. Experimental

2.1. Synthesis of complexes

All chemicals were of analytical grade and used as supplied by Aldrich. The crystallization of all complexes proceeded in refrigerator at 278 K.

2.1.1. $(NH_4)_2[V_2O_2(O_2)_2(R,S\text{-mand})_2]\cdot R,S\text{-}H_2mand\cdot 2H_2O$ (**1**)

NH_4VO_3 (0.585 g, 5 mmol) was dissolved in a diluted H_2O_2 solution (1 ml 30% H_2O_2 and 10 ml H_2O) under stirring and under cooling in ice bath. Racemic H_2mand (0.76 g, 5 mmol) was dissolved in 5 ml H_2O and added under continuous stirring to the solution of peroxovanadate. The red crystals of **1** were isolated from mother solution after 5 days. Calc. for $C_{24}H_{32}N_2O_{17}V_2$: C, 39.9; H, 4.5; N, 3.9; O_2^{2-}, 8.8; V, 14.0. Found: C, 39.7; H, 4.4; N, 3.3; O_2^{2-}, 9.3; V, 13.5%.

2.1.2. $(NEt_4)_2[V_2O_2(O_2)_2(R,S\text{-mand})_2]$ (**2**)

NEt_4OH (2.1 ml, 5 mmol; 35%) was added to a solution of NH_4VO_3(0.585 g, 5 mmol) in 5 ml H_2O. The ammonia was removed from the resulting solution by brief boiling. The solution was cooled and added to a solution of R,S-H_2mand (0.76 g, 5 mmol) in 10 ml H_2O. A solution of H_2O_2 (30%, 1 ml) was then added under vigorous stirring. The obtained solution was allowed to crystallize, and the product formed within few days was isolated. The red crystals of **2** were obtained by recrystallization from acetonitrile. Calc. for $C_{32}H_{52}N_2O_{12}V_2$: C, 50.6; H, 6.9; N, 3.7; O_2^{2-}, 8.4; V, 13.4. Found: C, 50.2; H, 7.3; N, 3.6; O_2^{2-}, 8.9; V, 13.2%.

2.1.3. $(NMe_4)_2[V_2O_2(O_2)_2(R,S\text{-mand})_2]\cdot 6.5H_2O$ (**3**)

V_2O_5 (0.2 g, 1.1 mmol) was dissolved in a solution of 25% NMe_4OH (0.8 ml, 2.2 mmol). To the vanadate solution, a solution of R,S-H_2mand (0.334 g, 2.2 mmol) in 10 ml H_2O and H_2O_2 (30%, 0.4 ml) were then added under stirring. The resulting solution was allowed to crystallize. The red crystal of **3** were isolated after 5 days. Calc. for $C_{24}H_{49}N_2O_{18.5}V_2$: C, 37.7; H, 6.5; N, 3.7; O_2^{2-}, 8.3; V, 13.3. Found: C, 39.7; H, 6.0; N, 3.7; O_2^{2-}, 9.3; V, 13.9%.

2.1.4. $(NMe_4)(NH_4)[V_2O_2(O_2)_2(R,S\text{-mand})_2]\cdot 2H_2O$ (**4**)

To a solution of NH_4VO_3 (0.585 g, 5 mmol) in 5 ml H_2O, 25% NMe_4OH (1.8 ml, 5 mmol) was added. The solution was heated for a short time, then cooled and added to a solution of R,S-H_2mand (0.76 g, 5 mmol) in 10 ml H_2O. Finally, 0.8 ml H_2O_2 (30%) was added under vigorous stirring. The obtained solution was allowed to crystallize, the red crystals of **4** were isolated after few days. Calc. for $C_{20}H_{34}N_2O_{15}V_2$: C, 37.3; H, 5.3; N, 4.3;

O_2^{2-}, 9.9; V, 15.8. Found: C, 36.1; H, 4.6; N, 3.9; O_2^{2-}, 9.7; V. 14.9%.

*2.1.5. $(NMe_4)_2[V_2O_2(O_2)_2(S\text{-}mand)_2]\cdot 0.5S\text{-}H_2mand\cdot 7H_2O$ (**5**)*

V_2O_5 (0.2 g, 1.1 mmol) was dissolved in a solution of 5 ml H_2O and 25% NMe_4OH (0.8 ml, 2.2 mmol). The solution was then mixed under stirring with a solution of *S*-H_2mand (0.334 g, 2.2 mmol) in 10 ml H_2O and H_2O_2 (30%, 0.4 ml). The obtained solution was allowed to crystallize, and the red-orange crystals of **5** were isolated after 4 days. Calc. for $C_{28}H_{54}N_2O_{20.5}V_2$: C, 39.6; H, 6.4; N, 3.3; O_2^{2-}, 7.5; V, 12.0. Found: C, 39.4; H, 4.8; N, 3.2; O_2^{2-}, 6.9; V, 10.7%.

*2.1.6. $(NEt_4)_2[V_2O_2(O_2)_2(S\text{-}mand)_2]$ (**6**)*

V_2O_5 (0.2 g, 1.1 mmol) was dissolved in aqueous 35% NEt_4OH (0.92 ml, 2.2 mmol). A solution of *S*-H_2mand (0.334 g, 2.2 mmol) in 10 ml H_2O and a solution of H_2O_2 (30%, 0.4 ml) were then added under continuous stirring. The obtained solution was allowed to crystallize, the red crystals of **6** were isolated after few days. Calc. for $C_{32}H_{52}N_2O_{12}V_2$: C, 50.7; H, 6.9; N, 3.7; O_2^{2-}, 8.4; V, 13.4. Found: C, 48.9; H, 7.2; N, 3.4; O_2^{2-}, 8.4; V, 13.1%.

*2.1.7. $(NH_4)_2[V_2O_2(O_2)_2(S\text{-}mand)_2]\cdot S\text{-}H_2mand\cdot 2H_2O$ (**7**)*

NH_4VO_3 (0.585 g, 5 mmol) was dissolved in a diluted H_2O_2 solution (0.7 ml 30% in 10 ml H_2O) under cooling in ice bath. *S*-H_2mand (0.76 g, 5 mmol) was dissolved in 5 ml H_2O and added under continuous stirring to the solution of peroxovanadate. The light red crystals of **7** were isolated from mother solution after 4 days. Calc. for $C_{24}H_{32}N_2O_{17}V_2$: C, 39.9; H, 4.5; N, 3.9; O_2^{2-}, 8.8; V, 14.1. Found: C, 39.6; H, 4.7; N, 3.4; O_2^{2-}, 9.0; V, 13.9%.

*2.1.8. $(NEt_4)_2[V_2O_2(O_2)_2(R\text{-}mand)_2]$ (**8**)*

NH_4VO_3 (0.585 g, 5 mmol) was dissolved in a stirred solution of NEt_4OH (2.1 ml 35%, 5 mmol) in 5 ml H_2O. The ammonia was removed from the solution by brief boiling. The solution was cooled and 10 ml H_2O, *R*-H_2mand (0.76 g, 5 mmol) and H_2O_2 (30%, 1 ml) were added under vigorous stirring. The red solution obtained was allowed to stand at 278 K, and 5 ml acetonitrile were added after 2 days. The red crystals of **8** were isolated after few days. Calc. for $C_{32}H_{52}N_2O_{12}V_2$: C, 50.7; H, 6.9; N, 3.7; O_2^{2-}, 8.4; V, 13.4. Found: C, 46.7; H, 6.6; N, 3.2; O_2^{2-}, 8.4; V, 13.2%.

*2.1.9. $(NMe_4)_2[V_2O_2(O_2)_2(R\text{-}mand)_2]\cdot H_2O$ (**9**)*

NH_4VO_3 (0.234 g, 2 mmol) was dissolved in a solution of 5 ml H_2O and 25% NMe_4OH (0.73 ml, 2 mmol). Ammonia was removed from the vanadate solution by brief boiling. After cooling, a solution of *R*-H_2mand (0.304 g, 2 mmol) in 5 ml H_2O and H_2O_2 (30%, 0.3 ml) were added under stirring. The red complex crystallized within few days. Calc. for $C_{24}H_{38}N_2O_{13}V_2$: C, 43.4; H, 5.8; N, 4.2; O_2^{2-}, 9.6; V, 15.3. Found: C, 43.1; H, 6.0; N, 5.4; O_2^{2-}, 9.9; V, 14.9%.

*2.1.10. $(NH_4)_2[V_2O_2(O_2)_2(S\text{-}mand)_2]\cdot 5H_2O$ (**10**)*

NH_4VO_3 (0.292 g, 2.5 mmol) was dissolved in diluted H_2O_2 (0.5 ml 30% in 10 ml H_2O) under cooling in ice bath. *R*-H_2mand (0.38 g, 2.5 mmol) was dissolved in 5 ml H_2O and added under stirring to the solution of peroxovanadate. The light red crystals of **10** crystallized within 3 days. Calc. for $C_{16}H_{30}N_2O_{17}V_2$: C, 30.8; H, 4.8; N, 4.5; O_2^{2-}, 10.2; V, 16.3. Found: C, 30.2; H, 4.0; N, 4.5; O_2^{2-}, 9.8; V, 16.6%.

2.2. Measurements and analysis

Infrared spectra in KBr pellets or in nujol mulls were measured on Nicolet 750 Magna FT IR spectrometer. UV–Vis spectra were measured on a Hewlett–Packard 84-52 A spectrophotometer. ^{51}V NMR spectra were recorded on a Varian Gemini 2000 spectrometer operating at 78.94 MHz, the chemical shifts were referenced to $VOCl_3$ as external standard. Peroxidic oxygen was determined by titration with $KMnO_4$. Vanadium(V) was determined by titrating with $FeSO_4$. C, H, N were determined on a CHN-analyzer (Carlo Erba). The results of elemental analysis were not always satisfactory because of the instability of the compounds.

2.3. X-ray structure determination

Low-temperature X-ray measurements were made on a KUMA KM4 + CCD diffractometer with monochromated (monochromator Enhance, Oxford Diffraction, UK) Mo Kα radiation using rotation method with ω-scan technique. Cell parameters and an orientation matrix for data reduction were obtained from all strong reflections. For data collection, cell refinement and data reduction we used the CrysAlis (Oxford Diffraction, 2002) software package. Data were not corrected for absorption effects. All calculations for data reduction, structure solution and refinement were done using the SHELX 97 program [19].

In the structure of **8**, there is a disorder involving alternative positions of the peroxo (O2–O3) and oxo (O1) ligands (alternative donor atoms are O2N–O3N and O1N). The sum of s.o.f.s. was constrained to be unity during refinement which converged to the occupation factor 0.7(1). Fig. 2 depicts the major arrangement. The structure of **3** could be refined only to $R_1 = 0.0817$, because of rapid decomposition of the complex after removing it from the mother liquor.

3. Results and discussion

The red or orange-red peroxo complexes of vanadium(V) of composition $(NR_4)_2[V_2O_2(O_2)_2(mand)_2]\cdot xH_2O\cdot yH_2mand$ (R = H, Me or Et, $x = 0$, 1, 2, 5, 6.5 or 7, and $y = 0$, 0.5 or 1) were obtained by crystallization from the aqueous NH_4VO_3–H_2mand–H_2O_2, V_2O_5–H_2mand–NMe_4OH/NEt_4OH–H_2O_2 or NH_4VO_3–H_2mand–NMe_4OH/NEt_4OH–H_2O_2 reaction solutions. The complexes decompose at room temperature, both in the solid state and in aqueous solution. The release of peroxidic oxygen is followed by reduction of vanadium(V) to vanadium(IV) which manifests itself by colour change from red, through brown and green, to black.

3.1. IR spectra

The IR spectra of complexes prepared are listed in Table 1. The bands at 1708, 1709 and 1732 cm^{-1} in the spectra of complexes **1**, **5** and **7** containing neutral ligand molecules, H_2mand, prove the presence of protonated and uncoordinated carboxylic groups [13]. The monodentate coordination of the deprotonated carboxylate groups in mand is apparent from the band positions corresponding to asymmetric $\nu_{as}(COO^-)$ and symmetric $\nu_s(COO^-)$ vibrations in the regions 1601–1656 and 1386–1349 cm^{-1}, respectively. The above mentioned coordination mode is substantiated by the difference value, $\Delta = \nu_{as}(COO^-) - \nu_s(COO^-)$, which is in all cases larger than 200 cm^{-1} [20]. The characteristic bands of the $VO(O_2)$ group were observed in the expected region [21,22] at 969 to 984 cm^{-1} for $\nu(V{=}O)$, 914 to 938 cm^{-1} for $\nu(O_p–O_p)$, and at 539–585 cm^{-1} for $\nu(V–O_p)$.

3.2. Crystal and molecular structures

The crystal parameters and details for data collection for the complexes **3**, **4** and **8** are given in Table 2, and the selected interatomic distances and bond angles are listed in Tables 3–5, respectively. The ORTEP diagrams of the complex anions in structures of **3** and **8** are shown in Figs. 1 and 2. Two vanadium atoms of the anion are doubly bridged by two deprotonated hydroxyl oxygen atoms, O6 and O12, of two mand ligands to give a central V_2O_2 core. Moreover, each mand ligand coordinates to one vanadium atom via the carboxyl oxygen atom to form five-membered chelate. The coordination geometry of each vanadium atom can be described as

Table 1
Characteristic IR bands (cm^{-1}) for the vanadium(V) oxo peroxo mandelato complexes **1**–**10**

Complex	$\nu(H_2O)$ or $\nu(NH)$	$\nu(C{=}O)$[a]	$\nu_{as}(COO^-)$	$\nu_s(COO^-)$	$\nu(V{=}O)$	$\nu(O_p–O_p)$	$\nu(V–O_p)$
1	3632 m 3542 w 3334 m	1732 m	1616 vs	1355 s	984 s	926 vs	563 m
2			1655 vs	1377 s	973 vs	914 vs	585 m
3	3396 m 3263 sh		1624 vs	1371 vs	982 vs	922 vs	539 m
4	3474 m 3212 m		1646 sh 1617 m	1376 m	979 sh 969 s	938 s	561 w 540 m
5	3579 w 3542 w 3343 sh	1709 vs	1612 s	1386 s	984 vs	925 s	563 m
6			1656 s	1376 s	981 s	935 m 927 m	573 m
7	3577 w 3543 w 3331 sh	1708 vs	1630 sh 1611 m	1378 s	978 vs	925 vs	563 m 542 m
8			1656 vs	1377 s	982 s	936 s 927 w	573 s
9	3576 w 3479 sh 3400 w		1652 s	1377 m 1349 m	981 s	926 s	568 m
10	3624 w 3585 w 3313 sh		1641 m 1601 m	1377 s	975 s	919 s	571 m 542 m

[a] Protonated uncoordinated carboxylic group.

Table 2
Crystal data and structure refinement for $(NMe_4)_2[V_2O_2(O_2)_2(R,S\text{-mand})_2]\cdot 6.5H_2O$ (**3**), $(NMe_4)(NH_4)[V_2O_2(O_2)_2(R,S\text{-mand})_2(H_2O)]\cdot 2H_2O$ (**4**) and $(NEt_4)_2[V_2O_2(O_2)_2(R\text{-mand})_2]$ (**8**)

	3	**4**	**8**
Formula	$C_{24}H_{49}N_2O_{18.50}V_2$	$C_{40}H_{68}N_4O_{30}V_4$	$C_{32}H_{52}N_2O_{12}V_2$
Crystal system	monoclinic	monoclinic	orthorhombic
Space group	$C2/c$	$P2_1/c$	$P2_12_12_1$
T (K)	120(2)	120(2)	120(2)
a (Å)	22.676(3)	15.6808(6)	13.4851(6)
b (Å)	23.504(5)	11.5513(5)	14.2140(6)
c (Å)	16.348(3)	31.7383(8)	18.8756(9)
α (°)	90	90	90
β (°)	127.13(2)	103.71(3)	90
γ (°)	90	90	90
V (Å^3)	6947(2)	5585.1(4)	3618.0(3)
Z	8	4	4
D_c (g/cm^3)	1.385	1.533	1.393
λ (Å)	0.71073	0.71073	0.71073
Crystal size (mm)	$0.50\times0.40\times0.35$	$0.45\times0.35\times0.20$	$0.50\times0.35\times0.20$
θ range (°)	3.06–25.00	2.65–25.00	3.34–25.00
Index ranges	$-25\leqslant h\leqslant 26$, $-27\leqslant k\leqslant 19$, $-19\leqslant l\leqslant 19$	$-18\leqslant h\leqslant 18$, $-13\leqslant k\leqslant 12$, $-37\leqslant l\leqslant 37$	$-16\leqslant h\leqslant 15$, $-16\leqslant k\leqslant 16$, $-19\leqslant l\leqslant 22$
Reflections collected	12 428	25 429	13 869
Independent reflections	5836 ($R_{int}=0.0627$)	9787 ($R_{int}=0.0361$)	5984 ($R_{int}=0.0367$)
Goodness-of-fit on F^2	0.987	1.007	1.083
Final R indices ($I>2\sigma_I$)	$R_1=0.0817$, $R_{w2}=0.2230$	$R_1=0.0396$, $R_{w2}=0.1131$	$R_1=0.0376$, $R_{w2}=0.0966$
R indices (all data)	$R_1=0.0982$, $R_{w2}=0.2382$	$R_1=0.0455$, $R_{w2}=0.1167$	$R_1=0.0402$, $R_{w2}=0.0979$
Largest differential peak and hole (e Å^{-3})	0.914 and −0.799	0.401 and −0.431	1.103 and −0.392
Refinement method	full-matrix least-squares on F^2	full-matrix least-squares on F^2	full-matrix least-squares on F^2
Data/restraints/parameters	5836/0/452	9787/0/970	5984/0/496

Table 3
Selected bond lengths (Å) for $(NMe_4)_2[V_2O_2(O_2)_2(R,S\text{-mand})_2]\cdot 6.5H_2O$ (**3**)

V(1)–O(1)	1.585(4)
V(1)–O(3)	1.876(4)
V(1)–O(2)	1.888(4)
V(1)–O(6)	1.975(4)
V(1)–O(4)	2.031(4)
V(1)–O(12)	2.035(3)
V(2)–O(7)	1.580(5)
V(2)–O(8)	1.867(4)
V(2)–O(9)	1.869(4)
V(2)–O(12)	1.967(3)
V(2)–O(6)	1.990(4)
V(2)–O(10)	2.007(4)
O(2)–O(3)	1.435(5)
O(8)–O(9)	1.434(6)

Table 4
Selected bond lengths (Å) for $(NEt_4)_2[V_2O_2(O_2)_2(R\text{-mand})_2]$ (**8**)

V(1)–O(1)	1.611(4)
V(1)–O(2)	1.828(4)
V(1)–O(3)	1.850(3)
V(1)–O(6)	1.975(2)
V(1)–O(4)	2.004(2)
V(1)–O(12)	2.018(19)
V(2)–O(7)	1.584(3)
V(2)–O(8)	1.830(3)
V(2)–O(9)	1.859(3)
V(2)–O(12)	1.954(2)
V(2)–O(10)	2.013(2)
V(2)–O(6)	2.042(2)
O(2)–O(3)	1.442(5)
O(8)–O(9)	1.376(4)

distorted pentagonal pyramid formed by two hydroxyl and one carboxyl oxygen atoms, the oxo ligand and two peroxo oxygen atoms. All interatomic distances and bond angles for **3** and **8** are in expected ranges (Tables 3 and 4). The molecular structures of both complexes are typical for vanadium(V) oxo peroxo complexes with two identical enantiomers of the α-hydroxycarboxylato ligands in the dinuclear unit: the V_2O_2 core is non-planar and the oxygen atoms of the terminal V=O groups are *cis* oriented with respect to the vanadium atoms of the core [15].

The unit cell of **8** contains four $[V_2O_2(O_2)_2(R\text{-mand})_2]^{2-}$ anions and eight NEt_4^+ cations, whereas that of **3** eight $[V_2O_2(O_2)_2(R,S\text{-mand})_2]^{2-}$ anions (four with *R*-mand and four with *S*-mand ligands) and 16 NMe_4^+ cations.

An interesting feature of the crystal structure of **4** is the different coordination mode of water molecules in two types of dinuclear ions present: $[V_2O_2(O_2)_2(R\text{-mand})_2(H_2O)]^{2-}$ with almost symmetrically bonded bridging water molecule and pentagonal bipyramidal surroundings of both vanadium atoms (Fig. 3), and the asymmetric $[V_2O_2(O_2)_2(S\text{-mand})_2(H_2O)]^{2-}$ ion, in which

Table 5
Selected bond lengths (Å) for $(NMe_4)(NH_4)[V_2O_2(O_2)_2(R,S\text{-mand})_2(H_2O)]\cdot 2H_2O$ (**4**)

V(1)–O(1)	1.593(2)
V(1)–O(3)	1.864(2)
V(1)–O(2)	1.884(2)
V(1)–O(6)	1.9747(19)
V(1)–O(12)	2.0004(19)
V(1)–O(4)	2.015(2)
V(2)–O(7)	1.602(2)
V(2)–O(9)	1.882(2)
V(2)–O(8)	1.888(2)
V(2)–O(12)	1.9871(19)
V(2)–O(6)	2.0211(19)
V(2)–O(10)	2.0588(19)
V(2)–O(93)	2.395(2)
V(3)–O(13)	1.597(2)
V(3)–O(14)	1.879(2)
V(3)–O(15)	1.892(2)
V(3)–O(24)	1.9979(19)
V(3)–O(18)	2.006(2)
V(3)–O(16)	2.0295(19)
V(3)–O(92)	2.469(2)
V(4)–O(19)	1.594(2)
V(4)–O(21)	1.869(2)
V(4)–O(20)	1.882(2)
V(4)–O(24)	1.9977(19)
V(4)–O(18)	2.0056(19)
V(4)–O(22)	2.0368(19)
V(4)–O(92)	2.475(2)
O(2)–O(3)	1.445(3)
O(8)–O(9)	1.439(3)
O(14)–O(15)	1.441(3)
O(20)–O(21)	1.438(3)

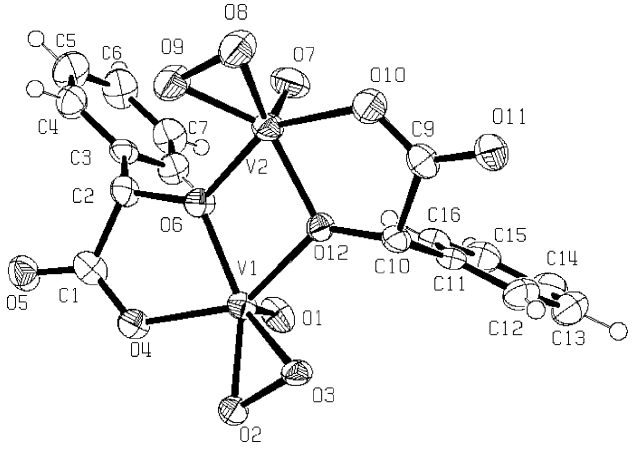

Fig. 1. ORTEP presentation of the $[V_2O_2(O_2)_2(S\text{-mand})_2]^{2-}$ anion in **3** at the 50% probability level.

the water molecule is coordinated only to one vanadium atom (Fig. 4). In the latter anion, one vanadium atom has the coordination number six while the other one is seven-coordinated. This situation, when the coordination spheres of two vanadium atoms of the core differ just by the presence/absence of the coordinated water molecule, provides a rare possibility to ascertain how the structural parameters are influenced by the change of

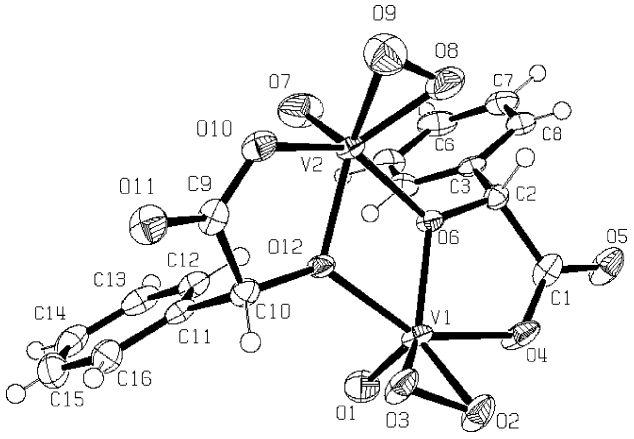

Fig. 2. ORTEP presentation of the $[V_2O_2(O_2)_2(R\text{-mand})_2]^{2-}$ anion in **8** at the 50% probability level.

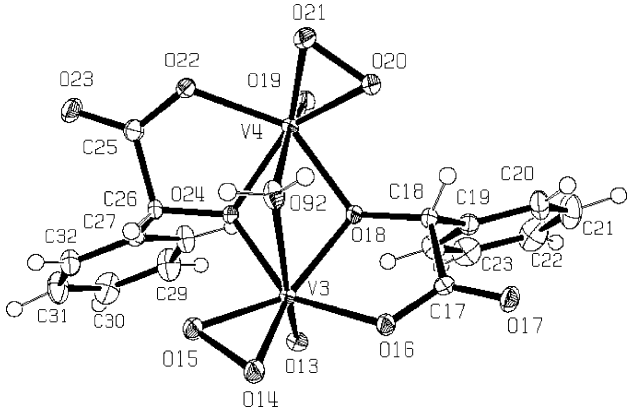

Fig. 3. ORTEP presentation of the $[V_2O_2(O_2)_2(R\text{-mand})_2(H_2O)]^{2-}$ anion in **4** at the 50% probability level.

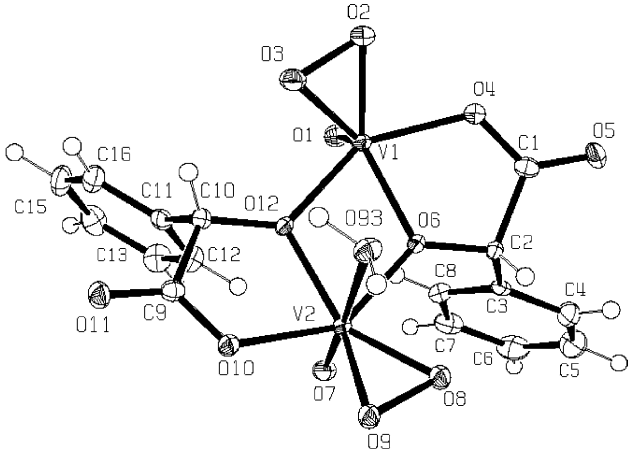

Fig. 4. ORTEP presentation of the $[V_2O_2(O_2)_2(S\text{-mand})_2(H_2O)]^{2-}$ anion in **4** at the 50% probability level.

geometry from pentagonal pyramidal to pentagonal bipyramidal. Thus, the comparison of the interatomic distances in the coordination polyhedra of V_1–V_4 with

the literature data enables estimation of the extend of structural *trans* influence. For the compounds $M_2[V_2O_2(O_2)_4H_2O]\cdot nH_2O$ [23–25], where the coordinated water molecule is in the *cis* position to the double bonded oxygen atom, the V–OH_2 bond lengths are significantly shorter (1.998–2.030 Å) than the d(V–OH_2) distances in structure of **4** with *trans* positioned water molecules: 2.395–2.475 Å. The deviations of the vanadium atoms from the least squares pentagonal plane are: 0.4588 Å for the six-coordinated V1 atom and 0.3166–0.3464 Å for the seven-coordinated V2, V3 and V4 atoms. As expected, both V_2O_2 cores in the above described different molecular structures in **4** are non-planar, nevertheless, the bridging water molecule induces larger deviations of atoms in the V_2O_2 core from the planarity when compared with asymmetric anion (the sums of internal angles are 347.55° and 358.54°, respectively). The unit cell of **4** contains eight $[V_2O_2(O_2)_2(mand)_2]^{2-}$ anions (four with *R*- and four with *S*-mand ligands) and 16 cations (eight NH_4^+ and eight NMe_4^+).

In structures of **3**, **4** and **8**, the dinuclear anions contain the same enantiomers of the heteroligand: $[V_2O_2(O_2)_2(S\text{-mand})_2]^{2-}$ or $[V_2O_2(O_2)_2(R\text{-mand})_2]^{2-}$. The formation of the $[V_2O_2(O_2)_2(S\text{-mand})(R\text{-mand})]^{2-}$ stereoisomer was not observed. The complexes crystallize either as pure enantiomers **8** or as racemic compounds **3** and **4**.

3.3. ^{51}V NMR spectral measurements

The ^{51}V NMR spectra of α-hydroxycarboxylato oxo peroxo complexes of vanadium(V) have been currently studied [17,26–30] and the chemical shifts for the 2:2 (vanadium:α-hydroxycarboxylate) species were observed at about −580 ppm. The ^{51}V NMR spectrum of the aqueous solution of $(NH_4)_2[V_2O_2(O_2)_2(R,S\text{-mand})_2]\cdot R,S\text{-}H_2mand\cdot 2H_2O$ (Fig. 5, spectrum 1) exhibits two peaks at −555 and −570 ppm of very low intensity, and thus almost undistinguishable in the figure, and two major species at −524 (**A**) and −588 (**B**). While the origin of the signals of low integral intensity is unclear, the species **A** can be attributed to a decomposition product and **B** is obviously the species with the same structure as found in the solid state structure. The chemical shift assignment for **A** we have based on the measurements of in situ formation and decomposition of the mandelato peroxo complexes in aqueous vanadate–H_2mand–H_2O_2 solutions. As can be seen from the time course of the ^{51}V NMR spectra (Fig. 5, spectra 2–6), the concentration of **B** decreases with time, but the concentration of **A** increases and then decreases after reaching a maximum. The final decomposition product is the non-peroxo complex **C** with $\delta_V = -535$ ppm, which we consider, based on the ^{51}V NMR spectrum of the aqueous vanadate–H_2mand solution (Fig. 5, spectrum 7) and the literature data [30], to be the dinuclear dioxo mandelato complex, $[V_2O_4(mand)_2]^{2-}$. The spectra 2–6 in Fig. 5 also exhibit peaks of $H_xV_{10}O_{28}^{(6-x)-}$ (**D**) or $[VO(O_2)_2(H_2O)_x]^-$ (**E**) at −507 and −698 ppm, respectively.

As the decomposition process of $[V_2O_2(O_2)_2(R,S\text{-mand})_2]^{2-}$ in solution seems to be analogous to that of the glycolato and lactato complexes [17,27,30], we propose the species **A** to be the asymmetric monoperoxodivanadate with two non-equivalent vanadium atoms, $[V_2O_3(O_2)(mand)_2]^{2-}$, formed by release of oxygen atom from one of two peroxo ligands in **B**. For the

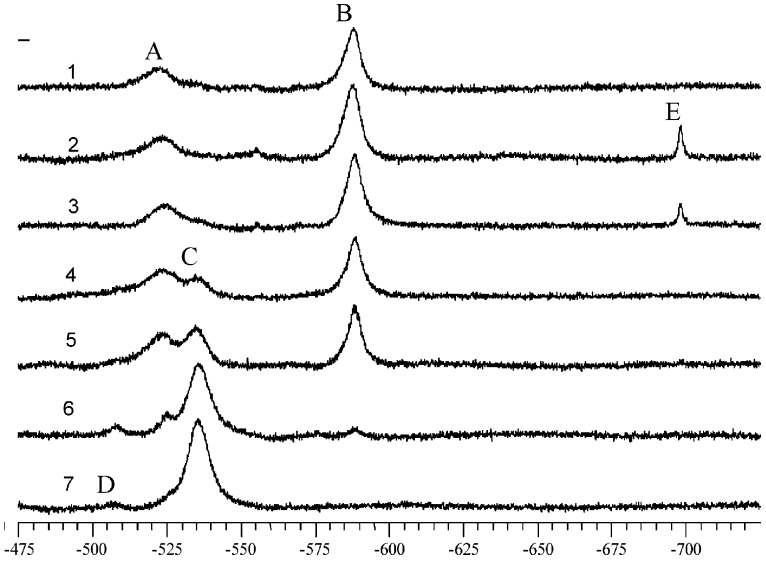

Fig. 5. The ^{51}V NMR spectra of aqueous solution of vanadium(V) peroxo mandelato complexes. (**1**) 0.02 M solution of $(NH_4)_2[V_2O_2(O_2)_2(R,S\text{-mand})_2]\cdot R,S\text{-}H_2mand\cdot 2H_2O$. (**2**)–(**6**) Solutions prepared by mixing of aqueous NH_4VO_3 (final concentration 0.02 mol/dm^3), mandelic acid (0.02 mol/dm^3) and H_2O_2 (0.02 mol/dm^3), $T = 278$ K: **2**, 15 min; **3**, 79 min; **4**, 198 min; **5**, 315 min; **6**, 25 h after preparation. (**7**) Solution prepared by mixing of aqueous NH_4VO_3 (final concentration 0.02 mol/dm^3) and mandelic acid (0.02 mol/dm^3), $T = 278$ K, 45 min after preparation.

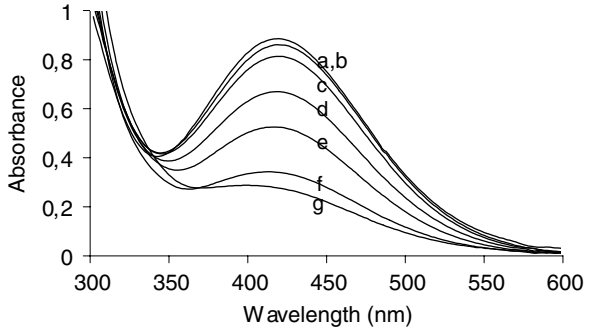

Fig. 6. UV–Vis spectra of 10^{-3} M $(NMe_4)_2[V_2O_2(O_2)_2(R,S\text{-mand})_2]\cdot 6.5H_2O$ in CH_3CN at $T = 278$ K and: 50 min (a), 24 h (b), 3 days (c), 4 days (d), 5 days (e), 7 days (f), 9 days (g) after dissolution.

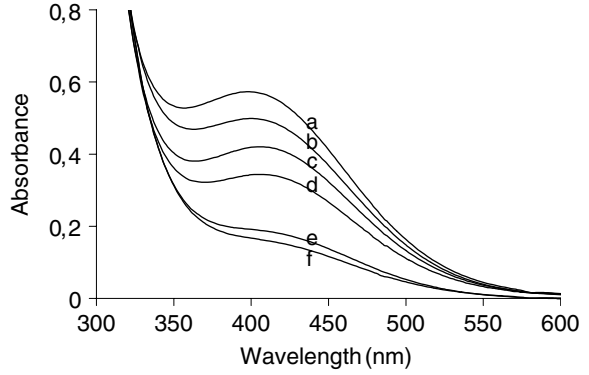

Fig. 7. UV–Vis spectra of 10^{-3} M $(NMe_4)_2[V_2O_2(O_2)_2(S\text{-mand})_2]\cdot 0.5S\text{-}H_2mand\cdot 7H_2O$ in H_2O at $T = 278$ K and: 11 min (a), 19 min (b), 33 min (c), 47 min (d), 81 min (e), 90 min (f) after dissolution.

$[V_2O_3(O_2)(mand)_2]^{2-}$ ion we should expect two ^{51}V NMR signals: one for the vanadium atom without coordinated peroxo group ($\delta_V = -524$ ppm), and the second one in the region observed for the α-hydroxycarboxylato monoperoxo complexes of vanadium(V). This second signal is lacking in the spectra but it might be hidden in the signal at −588 ppm.

3.4. UV–Vis spectroscopy

The UV–Vis spectra of the complexes in CH_3CN and water exhibit a LMCT band (O_2^{2-}–V) with maximum at 420 and 400 nm, respectively; which is characteristic of the monoperoxovanadium(V) complexes [31,32]. In solution, the peroxo oxygen release from the complex can be monitored on the basis of decreasing absorbance at λ_{max}. As follows from Figs. 6 and 7, the decomposition of the complexes is much faster in the protic then in the aprotic solvent.

4. Conclusions

Dinuclear mandelato bridged oxo peroxo complexes of vanadium(V) were synthesized. Besides the coordinated mandelato(2−) ligand, the structures of some of these complexes also contain uncoordinated molecules of mandelic acid. Stereospecifity of the formation, i.e., dependence of the molecular structure of the dinuclear complex anions on combination of the ligand enantiomers, was not observed. The reaction with *R*-mandelic acid gave a complex in form of a pure enantiomer, while the products of synthesis with racemic mandelic acid were racemic compounds. The vanadium atoms in dinuclear complexes have different coordination numbers. This seems to be a characteristic property of α-hydroxycarboxylatooxoperoxovanadates. The usual pentagonal pyramidal arrangement arround the vanadium atom may be, in some complexes, completed by water molecule or by a very weak bond with neutral acid molecule to form a pentagonal bipyramid. The decomposition of the complexes in aqueous solution proceeds through an intermediate, which is probably a dinuclear complex with the $n(O_2^{2-})/n(V)$ molar ratio equal to 0.5.

5. Supplementary material

Supplementary data are available from CCDC, 12 Union Road, Cambridge, CB2 1EZ, UK (fax: +44-1223-336033; E-mail: deposit@ccdc.cam.ac.uk or www: http://www.ccdc.cam.ac.uk) on request, quoting the deposition numbers 219616, 219617, 219618.

Acknowledgements

This work was supported by the Ministry of Education of the Slovak Republic (Grant 1/8201/01) and the Ministry of Education of the Czech Republic (MSMT CR MSM 143100008).

References

[1] D. Rehder, Coord. Chem. Rev. 182 (1999) 297.
[2] K.H. Thompson, J.H. McNeill, C. Orvig, Chem. Rev. 99 (1999) 2561.
[3] A. Butler, M.J. Clague, G.E. Hall, B.S. Meister, Chem. Rev. 94 (1994) 625.
[4] A. Shaver, J.B. Ng, D.A. Hall, B.S. Lum, B.I. Posner, Inorg. Chem. 32 (1993) 3109.
[5] B.I. Posner, R. Faure, J.W. Burgess, A.P. Bevan, D. Lachance, G. Zhang-Sun, I.G. Fantus, J.B. Ng, D.A. Hall, B.S. Lum, A. Shaver, J. Biol. Chem. 269 (1994) 4596.
[6] A.P. Bevan, J.W. Burgess, J.F. Yale, P.G. Drake, D. Lachance, G. Baquiran, A. Shaver, B.I. Posner, Am. J. Physiol. 268 (1995) E60.
[7] C. Djordjevic, M. Lee, F. Sinn, Inorg. Chem. 28 (1989) 719, and references cited therein.
[8] G.J. Colpas, B.J. Hamstra, J.W. Kampf, V.L. Pecoraro, J. Am. Chem. Soc. 116 (1994) 3627.
[9] G.J. Colpas, B.J. Hamstra, J.W. Kampf, V.L. Pecoraro, J. Am. Chem. Soc. 118 (1996) 3469.
[10] K. Kanamori, K. Nishida, N. Miyata, K. Okamoto, Chem. Lett. (1998) 1267.

[11] A. Butler, J.V. Walker, Chem. Rev. 93 (1993) 1937.
[12] C. Djordjevic, M. Lee-Renslo, E. Sinn, Inorg. Chim. Acta 233 (1995) 97.
[13] P. Schwendt, P. Švančárek, L'. Kuchta, J. Marek, Polyhedron 17 (1998) 2161.
[14] I. Kutá-Smatanová, J. Marek, P. Švančárek, P. Schwendt, Acta Crystallogr.: C 56 (2000) 154.
[15] P. Schwendt, P. Švančárek, I. Smatanová, J. Marek, J. Inorg. Biochem. 80 (2000) 59.
[16] F. Demartin, M. Biagioli, L. Strinna-Erre, A. Panzanelli, G. Micera, Inorg. Chim. Acta 299 (2000) 123.
[17] P. Švančárek, P. Schwendt, J. Tatiersky, I. Smatanová, J. Marek, Monatsh. Chem. 131 (2000) 145.
[18] P. Schwendt, J. Tyršelová, F. Pavelčík, Inorg. Chem. 34 (1995) 1964.
[19] G.M. Sheldrick, SHELX 97 Program, Department of Inorganic Chemistry, University of Göttingen, Germany.
[20] K. Nakamoto, Infrared and Raman Spectra of Inorganic and Coordination Compounds, 4th ed., Wiley, New York, 1990, p. 253.
[21] H. Mimoun, L. Saussine, E. Daire, M. Postel, J. Fischer, R. Weiss, J. Am. Chem. Soc. 105 (1983) 3101.
[22] P. Schwendt, Coll. Czech. Chem. Commun. 48 (1983) 248.
[23] A.E. Lapshin, Y.I. Smolin, Y.F. Shepelev, D. Gyepesová, P. Schwendt, Acta Crystallogr.: C 45 (1989) 1477.
[24] A.E. Lapshin, Y.I. Smolin, Y.F. Shepelev, P. Schwendt, D. Gyepesová, Acta Crystallogr.: C 46 (1990) 738.
[25] V. Suchá, M. Sivák, J. Tyršelová, J. Marek, Polyhedron 16 (1997) 2837.
[26] V. Conte, F. Di Furia, S. Moro, J. Mol. Catal. 104 (1995) 159.
[27] S. Hati, R.J. Batchelor, F.W.B. Einstein, A.S. Tracey, Inorg. Chem. 40 (2001) 6258.
[28] L.L.G. Justino, M.L. Ramos, M.M. Caldeira, V.S. Gil, Inorg. Chim. Acta 311 (2000) 119.
[29] L.L.G. Justino, M.L. Ramos, M.M. Caldeira, V.M.S. Gil, Eur. J. Inorg. Chem. (2000) 1617.
[30] A. Gorzsás, I. Andersson, L. Pettersson, Dalton Trans. (2003) 2503.
[31] M. Orhanovic, R.G. Wilkins, J. Am. Chem. Soc. 89 (1967) 278.
[32] M. Sivák, Chem. Papers 41 (1987) 311.

Available online at www.sciencedirect.com
SCIENCE DIRECT®
Polyhedron 23 (2004) 665–672
POLYHEDRON
www.elsevier.com/locate/poly

Synthesis of unsymmetrical 'end-off' phenoxo and oximinato di bridged copper(II) and nickel(II) complexes: spectral, electrochemical and magnetic properties

D. Saravanakumar [a,*], N. Sengottuvelan [a], G. Priyadarshni [a], M. Kandaswamy [a,*], H. Okawa [b]

[a] *Department of Inorganic Chemistry, School of Chemical Sciences, University of Madras, Guindy Campus, Chennai 600 025, India*
[b] *Department of Chemistry, Faculty of Science, Kyushu University, Hakozaki, Fukuoka 812-81, Japan*

Received 8 September 2003; accepted 11 November 2003

Abstract

New mononuclear and unsymmetrical binuclear copper(II) and nickel(II) complexes of the general formula $[ML^1](ClO_4)\cdot H_2O$, $[M_2L^1](ClO_4)_2\cdot 2H_2O$, $[ML^2](ClO_4)\cdot H_2O$ and $[M_2L^2](ClO_4)_2\cdot 2H_2O$ have been prepared by the condensation of 2-formyl-4-methyl-6-[(4-methylpiperazine-1yl)methyl]phenol (**1**) with *N*-β-aminoethyl isonitrosoethyl methyl ketimine(PCI) or *N*-β-aminomethylethyl isonitrosoethyl methyl ketimine(PCII) in the presence of M(II) salts (where M = Cu and Ni). The complexes were characterized by elemental and spectral analysis. Cyclic voltammetric studies evidenced one quasireversible reduction wave for all mononuclear complexes in the cathodic region. Two quasireversible one electron reduction waves are obtained for all binuclear complexes in the cathodic region. The binuclear copper(II) complexes illustrate an antiferromagnetic interaction (μ_{eff}: 1.55–1.58 BM) at 298 K with a broad EPR signal ($g = 2.1$). Variable temperature magnetic susceptibility study of the binuclear copper(II) complex $[Cu_2L^1](ClO_4)_2\cdot 2H_2O$ (**5**) shows the observed $-2J$ value is 283 cm^{-1}. The mononuclear copper(II) complexes have a magnetic moment value close to the spin only value with four hyperfine EPR signals.
© 2003 Elsevier Ltd. All rights reserved.

Keywords: Electrochemistry; Magnetic properties; Oximinato monocopper(II) and mononickel(II) complexes; Unsymmetrical oximinato dicopper(II) complexes and unsymmetrical oximinato dinickel(II) complexes

1. Introduction

Several types of ligand system, which can bind two metal ions in close proximity, have been used as biomimetic studies of binuclear metalloenzyme and metallo proteins due to their interesting catalytic properties, their ability to stabilize unusual oxidation states and possibilities for magnetic interaction between two metal ions [1–4]. From a bioinorganic viewpoint, oximes are known to be present as ligands in metalloproteins, although oxime-containing tetrapeptides with antibacterial, cytotoxic or anti-inflammatory activity have been found in marine sponges [5]. Also, the enzyme ammonia monooxygenase produces hydroxylamine [6], which forms oximes upon reaction with aldehydes or ketones. The asymmetric nature of a number of homodinuclear or heterodinuclear transition metal-derived metallobiosites and the ability of the individual metal ions (Cu, Ni, Mn, Co and Fe) has quite distinct roles in the functioning of the metalloenzyme [7–9]. Synthesis of unsymmetrical binucleating ligands and their copper(II) complexes has gained attention in recent years with the establishment of the unsymmetrical nature of the active site of hemocyanin and tyrosinase and also in multinuclear proteins like laccase, ceruloplasmin, catechol oxidase and ascorbate oxidase [10–14]. The enzymes that depend on nickel are urease, carbon monoxide dehydrogenase, hydrogenase and methyl-*S*-coenzyme-M-methyl reductase [15–17]. Most of the work is concerned

* Corresponding authors. Tel.: +91-44-22351269; fax: +91-44-22300488.
E-mail addresses: dsarav2003@yahoo.com (D. Saravanakumar), mkands@yahoo.com (M. Kandaswamy).

0277-5387/$ - see front matter © 2003 Elsevier Ltd. All rights reserved.
doi:10.1016/j.poly.2003.11.004

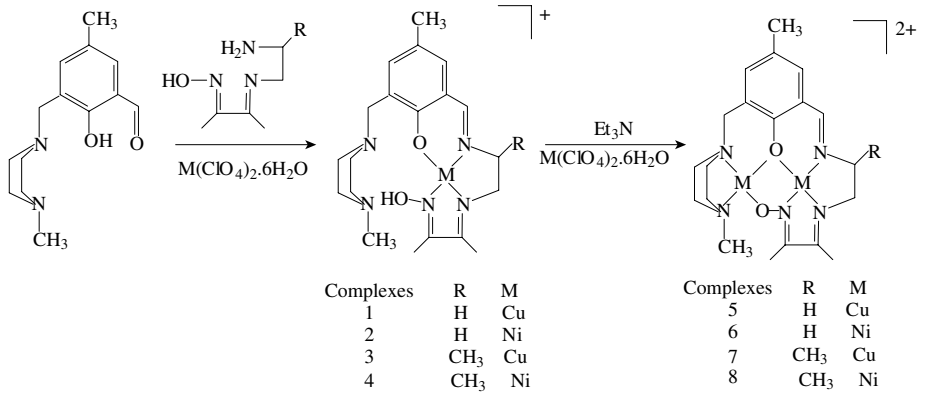

Complexes	R	M
1	H	Cu
2	H	Ni
3	CH_3	Cu
4	CH_3	Ni

Complexes	R	M
5	H	Cu
6	H	Ni
7	CH_3	Cu
8	CH_3	Ni

Scheme 1.

with the studies of symmetrical dinuclear complexes, and the study of unsymmetrical dinuclear complexes is sparse. Until now only a limited number of unsymmetrical dicopper and dinickel complexes were available [18–22]. In physiochemical aspects these dicopper complexes have significance as new inorganic materials capable of showing peculiar magnetic and redox properties and hence these model complexes have a wealth of application in magneto chemistry [23,24]. With the continuation of our previous work [25–27], the present work deals with the synthesis of unsymmetrical end-off mono and binuclear copper and nickel complexes and their spectral, electrochemical and magnetic behavior were studied. The synthetic pathway is shown in Scheme 1.

2. Experimental

2.1. Physical measurements

Elemental analysis of the complexes was obtained in a Heraeus CHN rapid analyzer. Electronic spectral studies were carried out on a Hitachi 320-model double beam spectrophotometer in the range 200–800 nm in acetonitrile. IR spectra were recorded on a Perkin–Elmer model 598 spectrophotometer on KBr disks in the range 4000–400 cm^{-1}. The electrochemical measurements were performed at room temperature in DMF by using a CH instrument electrochemical analyzer. Three electrode cell assembly was used in which the working electrode is glassy carbon, the counter electrode is a platinum wire and the saturated Ag/AgCl electrode is the reference electrode. The ferrocene/ferrocenium(1+) couple was used as an internal standard. All potentials are reported relative to the Ag/AgCl reference electrode. The $E_{1/2}$ of the ferrocene/ferrocenium (Fc/Fc^+) couple under the experimental conditions is 470 mV in DMF and ΔE_p for Fc/Fc^+ is 70 mV. Tetra(*n*-butyl)ammonium perchlorate was used as the supporting electrolyte. All electrochemical measurements were carried out in solutions purged with pure nitrogen for 30 min in advance. The conductivity measurements were carried out on an Elico digital conductivity bridge model CM-88 using freshly prepared solutions of the complexes in acetonitrile. Room temperature magnetic moment was measured on a PAR vibrating sample magnetometer Model-155. Variable-temperature magnetic studies were performed on a PAR model 155 vibrating-sample magnetometer in the temperature range 77–300 K, and the instrument was calibrated using metallic nickel. X-band ESR spectra were recorded at 25 °C on a Varian EPR-E 112 spectrometer using diphenylpicrylhydrazine (DPPH) as the reference. The Atomic absorption spectral data were recorded using Varian spectra AA-200 model atomic absorption spectrophotometer.

2.2. Materials

5-Methylsalicylaldehyde [28], 2-formyl-4-methyl-6-[(4-methylpiperazine-1-yl)methyl] phenol [18] (I) and *N*-β-aminoethyl isonitrosoethyl methyl ketimine [29] (PCI) were prepared by following the literature procedure. Tetrabutyl ammoniumperchlorate (TBAP) was obtained from Fluka and recrystallized from methanol. (*Caution*! All perchlorate salts are explosive and hence care should be taken while handling.) DMF and acetonitrile (HPLC) were obtained from Qualigens and used as such for spectral analysis. All other chemicals and solvents were of reagent grade. Solvents methanol, diisopropyl ether and acetonitrile were purified according to standard procedure.

2.3. Synthesis of N-β-aminomethylethyl isonitrosoethyl methyl ketimine (PC II)

This compound was synthesized by following the procedure [29] used for the synthesis of PC I. 1,2-Diaminopropane (3.7 g, 0.05 m) was added to a solution of biacetyl monoxime (5.055 g, 0.05 m) in dry isopropyl ether. The mixture was heated to reflux for 30 min and

then cooled to room temperature in a stoppered flask. After 5 h a yellowish crystalline product was obtained, filtered off and washed with diisopropyl ether and dried over calcium chloride. Yield: 6.4 g (80%), m.p.: 100 °C. *Anal.* Calc. for $C_7H_{15}N_3O$: C, 53.50; N, 26.53; H, 9.37. Found: C, 53.34; N, 26.72; H, 9.61%. ^{1}H NMR ($CDCl_3$, δ): 1.24 (d, 3H, 2-methyl protons), 2.1 (s, 6H, isonitroso ethyl methyl protons), 3.2 (m, 1H, proton of –CH– between amino and 2-methyl), 3.4 (d, 2H, $-CH_2$ between ketimine N and amino substituted carbon), 4.49 (bs, 3H, protons of –OH and NH_2). Selected IR (KBr disc, ν/cm^{-1}): 3213 (m), 3134 (m), 2750 (br), 1633 (sh).

2.4. Synthesis of complexes

2.4.1. $[CuL^1]ClO_4 \cdot H_2O$ (**1**)

A methanolic solution of compound I (2-formyl-4-methyl-6-[(4-methylpiperazine-1-yl)methyl] phenol) (0.5 g, 0.002 mol) was slowly added to a stirred solution of PC I (*N*-β-aminoethyl isonitrosoethyl methyl ketimine) (0.286 g, 0.002 mol) in methanol (20 ml) and refluxed for 1 h. To this solution, a methanolic solution of $Cu(ClO_4)_2 \cdot 6H_2O$ (0.74 g, 0.002 mol) was added and refluxed for 5 h. Then the green solution was filtered off. The green coloured product obtained on evaporation at room temperature was recrystallized from acetonitrile. Yield: 1.0 g (69%). *Anal.* Calc. for $C_{20}H_{30}N_5O_2Cu(ClO_4) \cdot H_2O$: C, 43.4; N, 12.6; H, 5.8; Cu, 11.5. Found: C, 43.3; N, 12.6; H, 5.7; Cu, 11.4%. Selected IR (KBr disc, ν/cm^{-1}): 3439 (br), 2760 (br), 1633 (sh), 1230 (m), 1091 (br), 624 (m). Conductance (Λ_m/S cm^2 mol^{-1}) in acetonitrile 168. UV–Vis [λ_{max}(nm) (ε, M^{-1} cm^{-1})] in acetonitrile: 581 (148), 365 (1090), 275 (2380).

2.4.2. $[NiL^1]ClO_4 \cdot H_2O$ (**2**)

This complex was prepared by following the above procedure used for $[CuL^1]ClO_4 \cdot H_2O$ using $Ni(ClO_4)_2 \cdot 6H_2O$ (0.73 g, 0.002 mol) instead of $Cu(ClO_4)_2 \cdot 6H_2O$. A brick red compound was obtained by recrystallization from acetonitrile. Yield: 2.0 g (83%). *Anal.* Calc. for $C_{20}H_{30}N_5O_2Ni(ClO_4) \cdot H_2O$: C, 43.8; N, 12.8; H, 5.8; Ni, 11.1. Found: C, 43.7; N, 12.7; H, 5.8; Ni, 11.2%. Selected IR (KBr disc, ν/cm^{-1}): 3446 (br), 2756 (br), 1627 (sh), 1236 (m), 1093 (br), 622 (m). Conductance (Λ_m/S cm^2 mol^{-1}) in acetonitrile 165. UV–Vis [λ_{max}(nm) (ε, M^{-1} cm^{-1})] in acetonitrile: 524 (138), 407 (2780), 326 (8040).

2.4.3. $[CuL^2]ClO_4 \cdot H_2O$ (**3**)

This complex was prepared by following the above procedure used for $[CuL^1]ClO_4 \cdot H_2O$ using PC II (*N*-β-aminomethylethyl isonitrosoethyl methyl ketimine) (0.32 g, 0.002 mol) instead of PC I (*N*-β-aminoethyl isonitrosoethyl methyl ketimine). A green coloured compound was obtained by recrystallization from acetonitrile. Yield: 0.83 g (74%). *Anal.* Calc. for $C_{21}H_{32}N_5O_2Cu(ClO_4) \cdot H_2O$: C, 44.4; N, 12.3; H, 6.1; Cu, 11.2. Found: C, 44.4; N, 12.7; H, 6.0; Cu, 11.3%. Selected IR (KBr disc, ν/cm^{-1}): 3437 (br), 2762 (br), 1630 (sh), 1230 (m), 1094 (str), 628 (m). Conductance (Λ_m/S cm^2 mol^{-1}) in acetonitrile 161. UV–Vis [λ_{max}(nm) (ε, M^{-1} cm^{-1})] in acetonitrile: 590 (147), 363 (1080), 275 (2380).

2.4.4. $[NiL^2]ClO_4 \cdot H_2O$ (**4**)

This complex was prepared by following the above procedure used for $[NiL^1]ClO_4 \cdot H_2O$ using PC II (*N*-β-aminomethylethyl isonitrosoethyl methyl ketimine) (0.32 g, 0.002 mol) instead of PC I (*N*-β-aminoethyl isonitrosoethyl methyl ketimine). A brick red compound was obtained by recrystallization from acetonitrile. Yield: 0.89 g (79%). *Anal.* Calc. for $C_{21}H_{32}N_5O_2Ni(ClO_4) \cdot H_2O$: C, 44.8; N, 12.4; H, 6.1; Ni, 10.4. Found: C, 44.8; N, 12.4; H, 6.0; Ni, 10.5%. Selected IR (KBr disc, ν/cm^{-1}): 3444 (br), 2758 (br), 1630 (sh), 1236 (m), 1094 (br), 624 (m). Conductance (Λ_m/S cm^2 mol^{-1}) in acetonitrile 163. UV–Vis [λ_{max}(nm) (ε, M^{-1} cm^{-1})] in acetonitrile: 553 (148), 403 (2760), 319 (2040).

2.4.5. $[Cu_2L^1](ClO_4)_2 \cdot 2H_2O$ (**5**)

A methanolic solution of compound I (2-formyl-4-methyl-6-[(4-methylpiperazine-1-yl)methyl] phenol) (0.5 g, 0.002 mol) was added to a stirred solution of PC I (*N*-β-aminoethyl isonitrosoethyl methyl ketimine) (0.286 g, 0.002 mol) in methanol (20 ml) and refluxed for 1 h. To this, one mole of $Cu(ClO_4)_2 \cdot 6H_2O$ (0.74 g, 0.002 mol) in methanol (20 ml) was added and the solution was refluxed for 1 h, then triethylamine (0.27 ml, 0.002 mol) and another mole of $Cu(ClO_4)_2 \cdot 6H_2O$ (0.74 g, 0.002 mol) in methanol (15 ml) were added and refluxed for a further 6 h. The resulting green solution yielded dark green crystals on slow evaporation. Yield: 1.2 g (80%). *Anal.* Calc. for $C_{20}H_{29}N_5O_2Cu_2(ClO_4)_2 \cdot 2H_2O$: C, 32.7; N, 9.6; H, 4.5; Cu, 17.1. Found: C, 32.7; N, 9.5; H, 4.4; Cu, 17.2%. Selected IR (KBr disc, ν/cm^{-1}): 3437 (br), 1633 (sh), 1228 (m), 1085 (br), 628(m). Conductance (Λ_m/S cm^2 mol^{-1}) in acetonitrile 202. UV–Vis [λ_{max}(nm) (ε, M^{-1} cm^{-1})] in acetonitrile: 600 (306), 380 (3420), 270 (4940).

2.4.6. $[Ni_2L^1](ClO_4)_2 \cdot 2H_2O$ (**6**)

This complex was prepared by following the above procedure used for $[Cu_2L^1](ClO_4)_2 \cdot 2H_2O$, using nickel(II) perchlorate hexahydrate (1.46 g, 0.004 mol) instead of copper(II) perchlorate. Brown coloured compound. Yield: 1.46 g (76%). *Anal.* Calc. for $C_{20}H_{29}N_5O_2Ni_2(ClO_4)_2 \cdot 2H_2O$: C, 33.2; N, 9.7; H, 4.6; Ni, 16.2. Found: C, 33.1; N, 9.6; H, 4.5; Ni, 16.1%. Selected IR (KBr disc, ν/cm^{-1}): 3440 (br), 1624 (sh), 1248 (m), 1083 (br), 632 (m) Conductance (Λ_m/S cm^2

mol^{-1}) in acetonitrile 209. UV–Vis [λ_{max}(nm) (ε, M^{-1} cm^{-1})] in acetonitrile: 550 (280), 408 (4200), 322 (6380).

2.4.7. $[Cu_2L^2](ClO_4)_2 \cdot 2H_2O$ (7)

This complex was prepared by following the procedure used for the synthesis of $[Cu_2L^1](ClO_4)_2 \cdot 2H_2O$ using PC II (0.32 g, 0.002 mol) instead of PC I. Dark green coloured compound. Yield: 1.98 g (70%). *Anal.* Calc. for $C_{21}H_{31}N_5O_2Cu_2(ClO_4)_2 \cdot 2H_2O$: C, 33.7; N, 9.4; H, 4.7; Cu, 17.0. Found: C, 33.7; N, 9.3; H, 4.6; Cu, 16.9%. Selected IR (KBr disc, ν/cm^{-1}): 3440 (br), 1635 (sh), 1247 (m), 1083 (br), 628 (m). Conductance (Λ_m/S cm^2 mol^{-1}) in acetonitrile 217. UV–Vis [λ_{max}(nm) (ε, M^{-1} cm^{-1})] in acetonitrile: 625 (290), 350 (3800), 275 (5600).

2.4.8. $[Ni_2L^2](ClO_4)_2 \cdot 2H_2O$ (8)

This complex was synthesised by following the procedure used for the synthesis of $[Ni_2L^1](ClO_4)_2 \cdot 2H_2O$ using PC II (0.32 g, 0.002 mol) instead of PC I. Brick red compound. Yield: 2.2 g (87%). *Anal.* Calc. for $C_{21}H_{31}N_5O_2Ni_2(ClO_4)_2 \cdot 2H_2O$: C, 34.2; N, 9.5; H, 4.7; Ni, 16.8. Found: C, 34.1; N, 9.4; H, 4.7; Ni, 16.7%. Selected IR (KBr disc, ν/cm^{-1}): 3513 (br), 1625 (sh), 1250 (m), 1087 (br), 631 (m). Conductance (Λ_m/S cm^2 mol^{-1}) in acetonitrile 225. UV–Vis [λ_{max}(nm) (ε, M^{-1} cm^{-1})] in acetonitrile: 580 (304), 408 (3420), 328 (4530).

3. Results and discussion

3.1. Spectral studies

The IR spectrum of the precursor compound II shows characteristic NH_2 (3213 and 3134 cm^{-1}), OH (2750 cm^{-1}) and C=N (1633 cm^{-1}) stretching frequencies. The low frequency and broadness of the OH band suggest that the system is hydrogen bonded. This is consistent with the earlier report [29]. The IR spectra of mononuclear complexes **1**–**4** show bands in the range 1627–1633 and 1230–1236 cm^{-1} due to ν(C=N) and ν(N–O), respectively, and a broad band observed at about 2760 cm^{-1} due to ν(OH) of the oxime group. The binuclear complexes **4**–**8** show bands at 1624 and 1248 cm^{-1} due to ν(C=N) and ν(N–O), respectively, and the absence of a peak around 2750 cm^{-1} indicates the absence of ν(OH) due to complexation. A broad band in the region around 3450 cm^{-1} indicates the presence of ν(OH) of water molecules for all the complexes. The presence of uncoordinated perchlorate anions in all complexes **1**–**8** are inferred from single broad bands at 1100 cm^{-1} (ν_3-antisymmetric stretching) which are not split and at 650 cm^{-1} (ν_4-antisymmetric bending). The intense band around 930 cm^{-1} (ν_2-symmetric stretching) due to coordinated perchlorate is not observed and this vividly indicates that no perchlorate ions are coordinated in the complexes [30–32]. The absorption spectra of the complexes exhibit three main features: one or two intense peaks below 300 nm assigned to the intraligand charge transfer transition, a peak or shoulder in the range 390–430 nm due to phenolate to copper charge transfer transitions and a weak band in the visible region (580–600 nm) is due to d–d transitions. Even though the metal ions are present in two different compartments (N_2O_2 and N_3O), we observed a broad d–d band which could not be further resolved. The broad band was observed for all mono and dinuclear Cu(II) complexes **1**, **3**, **5** and **7** in the region 580–625 nm which are assigned to the d–d transition of the Cu(II) ions [33]. The mono and homo dinuclear Ni(II) complexes **2**, **4**, **6** and **8** show a single weak d–d band in the region 524–580 nm due to an $^1A_{1g} \rightarrow {}^1A_{2g}$ transition and this indicates that the Ni(II) complexes have a square planar structure [33,34].

3.2. Electrochemical studies

The conductance measurement of all the complexes was carried out in acetonitrile. For the mononuclear complexes, the conductance value was found to be in the range 160–170 (Λ_m/S cm^2mol^{-1}) suggesting that the mononuclear complexes belong to 1:1 electrolytes. Conductance values of the binuclear complexes are in the range 200–225 (Λ_m/S cm^2 mol^{-1}) indicating that the complexes are 1:2 electrolytes [35].

3.3. Cyclic voltammetric studies

3.3.1. Reduction process

Electrochemical properties of the complexes were studied by cyclic voltammetry in the potential range 0 to −2.0 V in DMF containing 0.1 M tetrabutylammonium perchlorate and the data are summarized in Table 1. The cyclic voltammograms for mononuclear complexes **2** and **4** are depicted in Fig. 1. The mononuclear copper(II) and nickel(II) complexes **1**–**4** show quasireversible one electron transfer reduction in the cathodic region. The reduction potential of $Cu[L^2](ClO_4) \cdot H_2O$ (**3**) and $Ni[L^2](ClO_4) \cdot H_2O$ (**4**) complexes are reduced at lesser negative potential than $Cu[L^1](ClO_4) \cdot H_2O$ (**1**) and $Ni[L^1](ClO_4) \cdot H_2O$ (**2**). This may be due to the substitution of the CH_3 group on the ligand periphery (i.e. CH_3 substituted on *N*-β-amino ethyl carbon), which causes a distortion in the geometry of the complex. When compared with tertiary amine nitrogen, azomethine nitrogen coordination is stronger [36] and the oxime compartment has more chelation than the piperazine compartment. Hence the metal ion may be coordinated with the oxime compartment. The dicopper(II) complexes **5** and **7** show two quasireversible one electron reduction processes in the cathodic region. The first process corresponds to the $Cu^{II}Cu^{II}/Cu^{II}Cu^{I}$ couple and the second process to the $Cu^{II}Cu^{I}/Cu^{I}Cu^{I}$ couple.

Table 1
Electrochemical data of copper(II) and nickel(II) complexes (reduction at cathodic potential)

Number	Complex	E^1_{pc} (V)	E^1_{pa} (V)	$E^1_{1/2}$ (V)	ΔE (mV)	E^2_{pc} (V)	E^2_{pa} (V)	$E^2_{1/2}$ (V)	ΔE (mV)	K_{con}
1	$[CuL^1](ClO_4)\cdot H_2O$	−0.74	−0.67	−0.70	70					
2	$[NiL^1](ClO_4)\cdot H_2O$	−0.88	−0.72	−0.80	160					
3	$[CuL^2](ClO_4)\cdot H_2O$	−0.63	−0.52	−0.57	110					
4	$[NiL^2](ClO_4)\cdot H_2O$	−0.76	−0.63	−0.69	130					
5	$[Cu_2L^1](ClO_4)_2\cdot 2H_2O$	−0.76	−0.41	−0.58	350	−1.35	−1.20	−1.27	150	4.73×10^{11}
6	$[Ni_2L^1](ClO_4)_2\cdot 2H_2O$	−0.92	−0.76	−0.84	160	−1.82	−1.65	−1.73	170	1.14×10^{15}
7	$[Cu_2L^2](ClO_4)_2\cdot 2H_2O$	−0.65	−0.32	−0.49	330	−1.20	−1.08	−1.14	120	9.96×10^{10}
8	$[Ni_2L^2](ClO_4)_2\cdot 2H_2O$	−0.85	−0.71	−0.78	140	−1.72	−1.60	−1.66	120	7.76×10^{14}

Measured by CV at 25 mV/s. *E* vs Ag/AgCl conditions: GC working and Ag/AgCl reference electrode; supporting electrolyte TBAP; concentration of complex, 1×10^{-3} M; concentration of TBAP, 1×10^{-1} M.

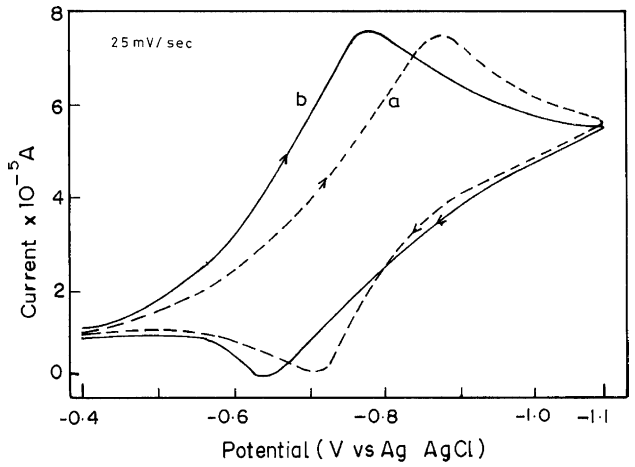

Fig. 1. Cyclic voltammograms of the mononuclear complex: (a) $Ni[L^1](ClO_4)\cdot H_2O$ (**2**); (b) $Ni[L^2](ClO_4)\cdot H_2O$ (**4**) (reduction process).

The copper(II) ion present in the oxime compartment reduces at a lesser potential compared to the other copper(II) ion present in the piperazine compartment, because the oxime compartment has three imino nitrogen coordinating sites [37]. The Cu(II) ion present in the piperazine compartment reduces at −1.2 to −1.3 V. The higher reduction potential is due to the influence of the electron density on the Cu(I) in the oxime compartment through exchange interaction between the two copper ions through bridging sites. Complex **7** reduces at a lesser negative potential (−1.20 V) than complex **5** (−1.35 V). This may be due to the distortion in geometry of the metal center by CH_3 substitution in the ligand periphery, which minimizes the exchange interaction between the two copper(II) ions in complex **7** when compared to the unsubstituted complex **5**. The difference between the half-wave potential of the two redox processes is a measure of the relative stability of the mixed valent $Cu^{II}Cu^{I}$ species. This approach obviously cannot be applied to asymmetrical complexes with two copper ions in different coordination environments. However K_{con} still characterizes the stability of mixed valent species [15]. The differences in half-wave potentials are sometimes very high for complexes with ligands possessing significantly different coordination sites [38,39]. The K_{con} value for complexes **5** and **7** are 4.73×10^{11} and 9.96×10^{10}. Binuclear nickel(II) complexes **6** and **8** show two quasireversible reduction waves. The first process corresponds to the $Ni^{II}Ni^{II}/Ni^{II}Ni^{I}$ couple and the second process to the $Ni^{II}Ni^{I}/Ni^{I}Ni^{I}$ couple. As observed in the binuclear Cu(II) complexes, the methyl substituted complex **8** reduces at lower potential than the unsubstituted complex **6**. The K_{con} value for complexes **6** and **8** are 1.14×10^{15} and 7.76×10^{14}. Cyclic voltammograms of the complexes **6** and **8** are shown in Fig. 2. The two reduction processes are assigned generally as follows,

$$M^{II}M^{II} \rightleftharpoons M^{II}M^{I} \rightleftharpoons M^{I}M^{I}.$$

The conproportionation constant for the equilibrium

$$M^{II}M^{II} + M^{I}M^{I} \overset{K_{con}}{\rightleftharpoons} 2M^{II}M^{I}$$

was calculated using the relationship $\log K_{con} = \Delta E/0.0591$.

3.3.2. Oxidation process

The electrochemical data for the complexes at the positive potential region is given in Table 2. The cyclic

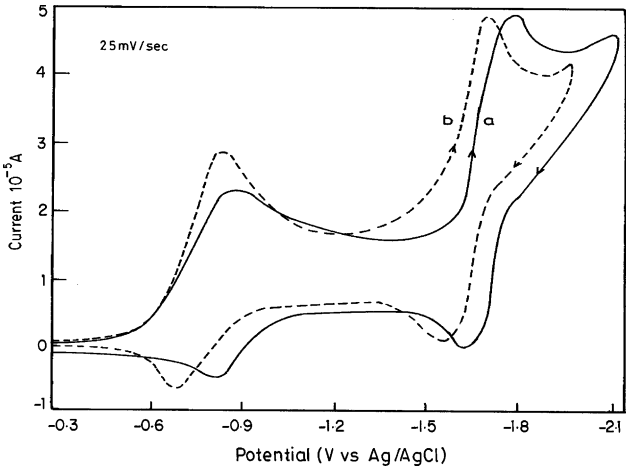

Fig. 2. Cyclic voltammograms of the binuclear complex: (a) $Ni^2[L^1](ClO_4)_2\cdot 2H_2O$ (**6**); (b) $Ni_2[L^2](ClO_4)_2\cdot 2H_2O$ (**8**) (reduction process).

Table 2
Electrochemical data of the nickel(II) complexes (oxidation at anodic potential)

Number	Complex	E^1_{pa} (V)	E^1_{pc} (V)	$E^1_{1/2}$ (mV)	ΔE^1_p (V)	E^2_{pa} (V)	E^2_{pc} (V)	$E^2_{1/2}$ (mV)	ΔE^2_p (V)	K_{con}
2	$[NiL^1](ClO_4)\cdot H_2O$	0.85	0.68	0.76	170					
4	$[NiL^2](ClO_4)\cdot H_2O$	0.93	0.75	0.84	180					
6	$[Ni_2L^1](ClO_4)_2\cdot 2H_2O$	0.83	0.69	0.76	140	1.20	1.02	1.11	180	8.55×10^5
8	$[Ni_2L^2](ClO_4)_2\cdot 2H_2O$	0.88	0.77	0.82	110	1.38	1.22	1.30	160	1.36×10^8

Measured by CV at 25 mV/s. *E* vs Ag/AgCl conditions: GC working and Ag/AgCl reference electrode; supporting electrolyte TBAP; concentration of complex, 1×10^{-3} M; concentration of TBAP, 1×10^{-1} M.

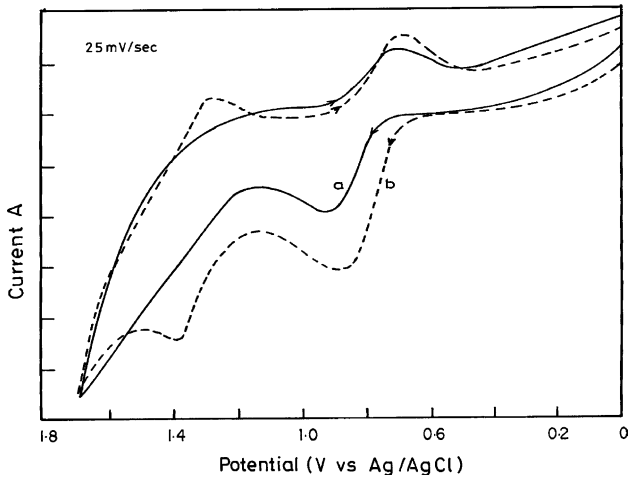

Fig. 3. Cyclic voltammograms of the binuclear nickel complex: (a) $Ni[L^2](ClO_4)\cdot H_2O$ (**4**); (b) $Ni_2[L^2](ClO_4)_2\cdot 2H_2O$ (**8**) (oxidation process).

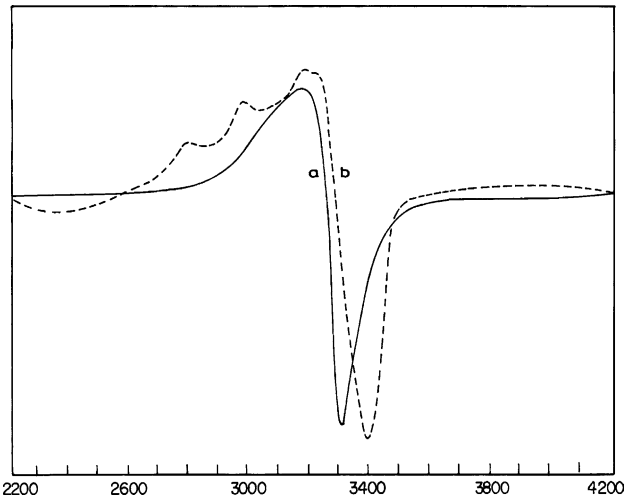

Fig. 4. ESR spectra of binuclear: (a) $Cu_2[L^1]$ $(ClO_4)_2\cdot 2H_2O$ (**5**) and mononuclear; (b) $Cu[L^1](ClO_4)\cdot H_2O$ (**1**) complexes.

voltammogram of the nickel complexes **4** and **8** in the anodic potential region is given in Fig. 3. The mononuclear nickel(II) complexes show one quasireversible oxidation and dinuclear nickel(II) complexes show two quasireversible single electron oxidation waves in the anodic region. The methyl substituted (on the oxime compartment) complex **4** has the higher oxidation potential than the unsubstituted complex **2**. This is because as the substitution on the oxime compartment increases, the distortion of the geometry around the metal ion increases. Similarly, for dinuclear nickel(II) complex **8** oxidation waves are observed at higher positive potential than unsubstituted binuclear nickel(II) complex **6**. The K_{con} value for complexes **6** and **8** are $8.55\times10^5$and 1.36×10^8, respectively. The two oxidation processes are assigned generally as follows,

$$M^{II}M^{II} \rightleftharpoons M^{III}M^{II} \rightleftharpoons M^{III}M^{III}.$$

3.4. Electron spin resonance

The solution ESR spectra of the complexes were recorded in the X-band region. The ESR spectra of mononuclear complex $Cu[L^1](ClO_4)\cdot H_2O$ (**1**) and binuclear complex $Cu_2[L^1](ClO_4)_2\cdot 2H_2O$ (**5**) are shown in Fig. 4. ESR spectra of the mononuclear copper(II) complexes show four lines [40] with a nuclear hyperfine spin 3/2, having $g_{\|}$ values in the range 2.21–2.29 and a $g_{\perp}$ value of 2.09. A broad [41] spectrum with no hyperfine splitting of the parallel component was obtained for both the dicopper complexes **3** and **5** with $g = 2.1$ centered at 3200 G indicating the presence of an antiferromagnetic interaction between the two copper ions. Owing to the favorable relative orientation of the magnetic orbitals and in spite of the Cu–Cu separation, an antiferromagnetic interaction is observed. All the nickel(II) complexes are diamagnetic in nature (see Table 3).

3.5. Magnetic studies

The measured magnetic susceptibility of the mononuclear copper(II) complex $[CuL^1](ClO_4)\cdot H_2O$ at room temperature (298 K) is 1.73 BM and that is equal to the spin only value. Room temperature magnetic susceptibilities of the binuclear copper(II) complexes $[Cu_2L^1](ClO_4)_2\cdot 2H_2O$ and $[Cu_2L^2](ClO_4)_2\cdot 2H_2O$ are 1.55 and 1.58 BM which are lower than the spin only value. In order to find out the magnetic exchange interaction, the magnetic moment of the complex $[Cu_2L^1](ClO_4)_2\cdot 2H_2O$ was measured in the temperature range 77–300 K. The temperature dependence of the magnetic property of the complex was interpreted using the modified Bleaney–Bowers equation [42]

Table 3
ESR spectral data of the copper(II) complexes

Number	Complex	$g_{\parallel}$	$g_{\perp}$	$A_{\parallel}$ (G)	g	μ_{eff} (BM) (RT)	$-2J$ cm^{-1}
1	$[CuL^1](ClO_4)\cdot H_2O$	2.27	2.02	172		1.73	
3	$[CuL^2](ClO_4)\cdot H_2O$	2.28	2.08	202		1.75	
5	$[Cu_2L^1](ClO_4)_2\cdot 2H_2O$				2.10	1.55	283
7	$[Cu_2L^2](ClO_4)_2\cdot 2H_2O$				2.15	1.58	

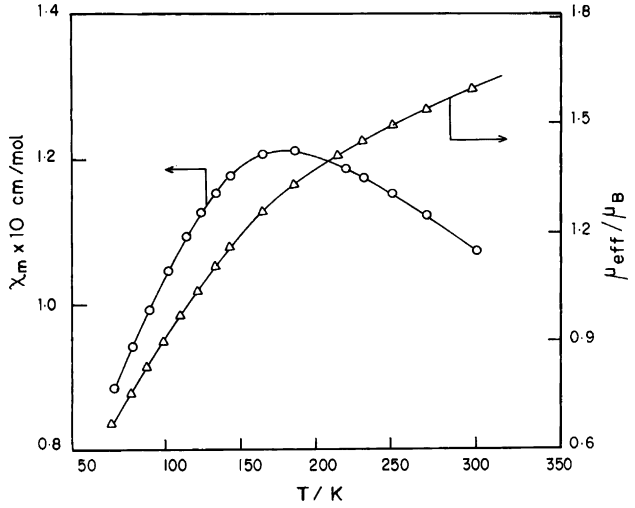

Fig. 5. Temperature dependence of the magnetic properties for complex $Cu_2[L^1](ClO_4)_2\cdot 2H_2O$ (**5**).

$$\chi_m = (Ng^2\beta^2)/(3kT)[3+\exp(-2J/kT)]^{-1}(1-P) + (0.45P/T) + N_\alpha,$$

where χ_m is the molar magnetic susceptibility of the complex, P is the percentage of monomeric impurities, N is Avagadro's number, β is the Boltzman constant, g is the average gyromagnetic ratio, $-J$ is the singlet–triplet separation and N_α is the temperature independent paramagnetism (120×10^6 cgs units). A nonlinear least-square fitting program was employed to calculate $-2J$, g and P. The temperature dependence of the magnetic properties for complex $[Cu_2L^1](ClO_4)_2\cdot 2H_2O$ is given in Fig. 5. The antiferromagnetic exchange interaction $-2J$ value 283 cm^{-1} observed with $g = 2.12$ and $p = 0.03$ for the complex $[Cu_2L^1](ClO_4)_2\cdot 2H_2O$ is similar to that of the analogous unsymmetrical complexes reported by Kandaswamy and coworkers [25]. Magneto structural correlation in phenoxo-bridged dicopper(II) complexes reveal that the dominant pathway for super exchange interaction through the oxygen atom involves interaction of the two copper ($d_{x^2-y^2}$) orbitals and the p orbitals on the oxygen.

4. Summary

New unsymmetrical binucleating copper(II) and nickel(II) complexes have been prepared and characterized. Both the variable temperature magnetic and ESR spectral studies of the binuclear copper(II) complexes ratify the presence of magnetic exchange interaction between the two copper atoms. The cyclic voltammetric study of the complexes in the cathodic as well as anodic region implies that the substitution on the ligand periphery affects the redox potentials.

Acknowledgements

Financial support received by one of the authors, D.S., from ISRO, Bangalore is gratefully acknowledged.

References

[1] C.J. Cairns, D.H. Busch, Coord. Chem. Rev. 69 (1986) 1.
[2] A.J. Atkins, D. Black, A.J. Blake, A. Marin-Bacerra, S. Parsons, L. Ruiz-Ramirez, M. Schroder, Chem. Commun. (1996) 457.
[3] O. Kahn, Struct. Bond. (Berlin) 68 (1987) 89.
[4] P. Guerriero, S. Tamburini, P.A. Vigato, Coord. Chem. Rev. 139 (1995) 17.
[5] M.A. Franklin, S.G. Penn, C.B. Lebrilla, T.H. Lam, I.N. Pessah, T.F. Molinski, J. Nat. Prod. 59 (1996) 1121.
[6] T.C. Hollocher, M.E. Tate, D.J.D. Nicholas, J. Biol. Chem. 256 (1981) 10834.
[7] J.A. Ibers, R.H. Holm, Science 209 (1980) 223.
[8] E. Bouwman, J. Reedijk, Bioinorganic Catalysis, 2nd ed., Marcel Dekker, New York, 1999.
[9] S. Ito, S.E.V. Stevens, S.B. Ogel, M.J. McPherson, M.N. Keen, K.D.S. Yadav, P.F. Knowles, Nature 350 (1991) 87.
[10] K.D. Karlin, J. Zubieta, Biological and Inorganic Copper Chemistry, Academic Press, New York, 1996.
[11] H. Adams, D.E. Fenton, S.R. Haque, S.L. Heath, M. Ohba, H. Okawa, S.E. Spey, J. Chem. Soc., Dalton Trans. (2000) 1849.
[12] M. Maekawa, S. Kitagawa, M. Munakata, H. Masuda, Inorg. Chem. 28 (1989) 1904.
[13] E.V. Rybak-Akimova, D.H. Busch, P.K. Kahol, N. Pinto, N.W. Alcock, H.J. Clase, Inorg. Chem. 36 (1997) 510.
[14] F. Birkelbach, M. Winter, V. Florke, H.J. Haupt, C. Butzlaff, M. Lengen, E. Bill, A.X. Trautwein, K. Wieghardt, P. Chaudhuri, Inorg. Chem. 33 (1994) 3990.
[15] J.P. Lancaster, The Bioinorganic Chemistry of Nickel, VCH, New York, 1998.
[16] B. Zerner, Biol. Org. Chem. 19 (1991) 116.
[17] M.D. Bond, B. Holmqust, B.L. Valle, J. Inorg. Biochem. 28 (1986) 97.
[18] M. Lubben, R. Hage, A. Meetsma, K. Byma, B.L. Feringa, Inorg. Chem. 34 (1995) 2217.
[19] M. Mahroof-Tahir, N.N. Murthy, K.D. Karlin, N.J. Blackburn, S.N. Shaikh, J. Zubieta, Inorg. Chem. 31 (1992) 3001.

[20] J.D. Crane, D.E. Fenton, J.M. Latour, A.J. Smith, J. Chem. Soc., Dalton Trans. (1991) 2979.
[21] M. Lubben, B.L. Feringa, J. Org. Chem. 59 (1994) 2227.
[22] N.A. Bailey, D.E. Fenton, G. Papageorgiou, C.O. Rodriguez de Barbarin, Synth. Lett. (1994) 79.
[23] D. Willett, G. Gatteschi, O. Khan, Magneto-structural correlations in exchange coupled systems; NATO-ASI Series C 140, Reidel, Dordrecht, The Netherlands, 1985.
[24] O. Khan, Molecular Magnetism, VCH, New York, 1993.
[25] P. Amudha, M. Thirumavalavan, M. Kandaswamy, Polyhedron 18 (1999) 1371.
[26] P. Amudha, P. Akilan, M. Kandaswamy, Polyhedron 18 (1999) 1355.
[27] P. Amudha, M. Kandaswamy, L. Govindaswamy, D. Velmurugan, Inorg. Chem. 37 (1998) 4486.
[28] J.C. Duff, J. Chem. Soc. (1941) 547.
[29] A.N. Singh, R.P. Singh, J.G. Mohanty, A. Chakravorty, Inorg. Chem. 16 (1977) 2597.
[30] K. Nakamoto, Infrared and Raman Spectra of Inorganic and Coordination Compounds, Wiley-Interscience, New York, 1978.
[31] M. Lachkar, R. Guilard, A. Atmani, A. DeCian, J. Fischer, R. Weiss, 37 (1998) 1575.
[32] B.J. Hathaway, A.E. Underhill, J. Chem. Soc. (1961) 3091.
[33] A.B.P. Lever, Inorganic Electronic Spectroscopy, 2nd ed., Elsevier, Amsterdam, 1984.
[34] S. Bhattacharyya, T.J.R. Weakley, M. Chaudhury, Inorg. Chem. 38 (1999) 633.
[35] W.J. Geary, Coord. Chem. Rev. 7 (1971) 81.
[36] J. Manonmani, R. Thirumurugan, M. Kandaswamy, M. Kuppayee, S. Shanmuga sundararaj, M.N. Ponnuswamy, G. Shanmugam, H.K. Fun, Polyhedron 19 (2001) 2011.
[37] S.K. Mandal, B. Adhikary, K. Nag, J. Chem. Soc., Dalton. Trans. (1986) 1175.
[38] C. Fraser, B. Bosnich, Inorg. Chem. 33 (1994) 338.
[39] S. Karunakaran, M. Kandaswamy, J. Chem. Soc., Dalton Trans. (1994) 1595.
[40] A. Bottcher, H. Elias, E.G. Jager, H. Langfelderova, M. Mazur, L. Muller, H. Paulus, P. Pelikan, M. Rudolph, M. Valko, Inorg. Chem. 32 (1993) 4131.
[41] M. Thirumavalavan, P. Akilan, M. Kandaswamy, K. Chinnakali, G. Senthilkumar, H.K. Fun, Inorg. Chem. 42 (2003) 3308.
[42] B. Bleaney, K.D. Bowers, Prog. R. Soc. Lond., Ser. A 214 (1952) 451.

Available online at www.sciencedirect.com
SCIENCE DIRECT®
Polyhedron 23 (2004) 673–678
POLYHEDRON
www.elsevier.com/locate/poly

Binuclear coordination compounds as building-blocks in designing polynuclear complexes

Mirela Pascu [a], Marius Andruh [a,*], Achim Müller [b], Marc Schmidtmann [b]

[a] *Inorganic Chemistry Laboratory, Faculty of Chemistry, University of Bucharest, Str. Dumbrava Rosie nr. 23, 020464 Bucharest, Romania*
[b] *Fakultät für Chemie der Universität, D-33501 Bielefeld, Germany*

Received 18 October 2003; accepted 12 November 2003

Dedicated to Professor Pedro Aymonino on the occasion of his 75th anniversary

Abstract

The syntheses and crystal structures of two new polynuclear complexes are reported: $_{\infty}^{1}[Cu_2L^1(acdca)]\cdot CH_3OH\cdot 4H_2O$ (**1**) and $[(CuZnL^2)_2(bpete)_2](ClO_4)_4\cdot 4.5CH_3OH$ (**2**) (H_2L^1 is the Schiff-base proligand resulted from the condensation reaction of 2,6-diformyl-4-methyl-phenol with 1,3-diamino-propane; H_2L^2 is a dissymmetric macrocyclic Robson proligand resulted from 2,6-diformyl-4-methyl-phenol, ethylenediamine and diethylenetriamine). The two compounds have been obtained by reacting binuclear [Cu_2] and [CuZn] complexes with the dianion of the of the acetylene-dicarboxylic acid ($acdca^{2-}$), and, respectively, bis(4-pyridyl)ethylene, bpete. The structure of **1** consists of linear chains resulted by connecting the $\{Cu_2L^1\}$ moieties through $acdca^{2-}$ linkers. The copper(II) ions within the chains exhibit an elongated octahedral geometry. Compound **2** contains cationic $[Cu_2Zn_2]$ rectangles, with the copper(II) ions, as well as the zinc(II) ions, diagonally disposed.
© 2003 Elsevier Ltd. All rights reserved.

Keywords: Crystal structures; Copper complexes; Zinc complexes; Molecular rectangles

1. Introduction

The self-assembly processes of coordination compounds into well-defined architectures is of current interest in supramolecular chemistry [1]. The synthetic effort is oriented towards discrete species with predetermined nuclearities and topologies of the metallic centers (molecular squares and rectangles, boxes, grids, ladders, racks, helicates) [2], and towards compounds exhibiting extended structures, 1D, 2D, 3D, with a large variety of solid-state architectures [3].

In a series of papers we have shown that homo- and heterobinuclear complexes can be successfully used as starting materials for the synthesis of either discrete high-nuclearity species, or of high-dimensionality systems [4–6]. We are currently using the following types of coordination compounds as building-blocks in designing supramolecular polymetallic architectures: (i) binuclear copper(II) species with end-off compartmental Schiff-base ligands [4]; (ii) alkoxo-bridged copper(II) species [5]; (iii) heterobinuclear 3d–4f species with side-off Schiff-base ligands [6]. In the first case, we have shown that the reaction between $[L(\mu\text{-}OH)Cu_2](ClO_4)_2$ (L stands for a compartmental end-off ligand, 2,6-bis[*N*-2-pyridylethyl)formimidoyl]-phenolato), and *exo*-dentate ligands [bis-(4-pyridyl)-derivatives, the fumarate anion, fum^{2-}, and the isonicotinato anion, IN^{-}] represents a straightforward synthetic route toward tetranuclear copper(II) complexes with both short and long distances between the metallic centers. The second case represents an extension of the classical 'node-and-spacer' approach (see, for example [7]). It also broadens the synthetic concept proposed by Cotton et al. [8], which is based on binuclear metal–metal bonded cationic entities as building units. Finally, the heterobinuclear nodes are very attractive, since they afford extended structures with interesting magnetic properties, emerging from those pre-existing within the nodes.

* Corresponding author. Tel.: +40744870656; fax: +40213159249.
E-mail address: marius.andruh@dnt.ro (M. Andruh).

0277-5387/$ - see front matter © 2003 Elsevier Ltd. All rights reserved.
doi:10.1016/j.poly.2003.11.041

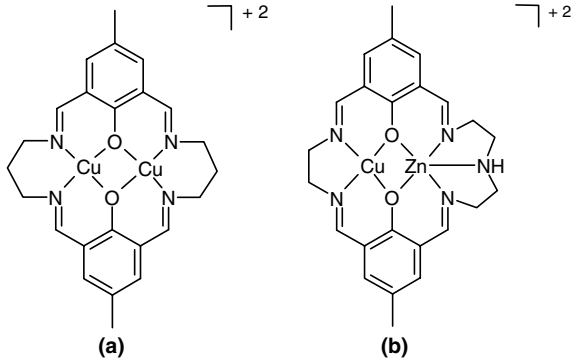

Scheme 1.

We are now developing this synthetic approach by using: (a) binuclear copper(II) complexes with macrocyclic Robson-type ligands; (b) heterobinuclear complexes with dissymmetric macrocyclic Robson-type ligands. In this paper, we report on two such complexes, a 1D coordination polymer with macrocyclic platforms, and a $[Cu_2Zn_2]$ molecular rectangle, which have been constructed starting from the binuclear complexes depicted in Scheme 1.

Table 1
Crystal data and details of the structure determination for complexes **1** and **2**

	1	**2**
Empirical formula	$Cu_2C_{29}H_{38}N_4O_{11}$	$Cu_2Zn_2C_{76.50}H_{90}Cl_4N_{14}O_{24.50}$
Formula weight	745.71	1997.24
Crystal system	trigonal	monoclinic
Space group	$P3(2)21$	$C2/c$
Unit cell dimensions		
a (Å)	16.2653(4)	35.7656(15)
b (Å)	16.2653(4)	13.7680(6)
c (Å)	10.2173(3)	25.5661(10)
α (°)	90	90
β (°)	90	132.9210(10)
γ (°)	120	90
Volume (Å)	2340.94(11)	9219.0(7)
D_{calc} (mg m^{-3})	1.587	1.439
Z	3	4
μ (mm^{-1})	1.429	1.163
$F(000)$	1158	4116
θ range (°)	2.46–26.99	1.55–22.49
R_1, $wR_2[I > 2\sigma(I)]$	0.0439, 0.1219	0.0779, 0.2145
Goodness-of-fit on F^2	1.039	1.063
$\Delta\rho$, maximum, minimum (e Å^{-3})	0.661 and −0.269	1.208 and −0.669

2. Experimental

The chemicals were purchased from commercial sources and all manipulations were performed using materials as received. The starting materials, $[Cu_2L^1]Cl_2 \cdot 6H_2O$ and $CuZnL^2](ClO_4)_2 \cdot CH_3OH \cdot H_2O$ were prepared as outlined in literature [9,10].

2.1. $_\infty{}^1[Cu_2L^1(acdca)] \cdot CH_3OH \cdot 4H_2O$ (1)

To the methanolic solution (20 ml) of the binuclear precursor, $[Cu_2L^1]Cl_2 \cdot 6H_2O$ (0.05 mmol) has been added a methanolic solution (10 ml) of acetylenedicarboxylic acid (0.05 mmol) and triethylamine (0.05 mmol). The slow evaporation of the resulting mixture gave after several days green single crystals suitable for X-ray analysis. Yield: 80%. IR bands (KBr, cm^{-1}): 3209br, 2927w, 2861w, 1637vs, 1592s, 1570s, 1441m, 1419m, 1328s, 1242w, 1197w, 1121m, 1073w, 976m, 945w, 821m, 784m, 761m, 675m. Diffuse reflectance spectrum: 700 nm, 480 nm (shoulder), 400 nm (shoulder). Elem. *Anal*. Calc.: C, 46.71; H, 5.13; N, 7.51. Found: C, 45.9; H, 5.3; N, 7.5%.

2.2. $[(CuZnL^2)_2(bpete)_2](ClO_4)_4 \cdot 4.5CH_3OH$ (2)

To the acetonitrile solution (20 ml) of the binuclear precursor $[CuZnL^2](ClO_4)_2 \cdot CH_3OH \cdot H_2O$ (0.05 mmol), an acetonitrile solution (10 ml) of *trans*-1,2-bis(4-pyridyl)-ethylene (0.05 mmol) has been added. The slow evaporation of the resulting solution gave, after several days, light blue–green rectangular crystals suitable for X-ray analysis. Yield: 60%. IR bands (KBr, cm^{-1}): 3407br, 2925m, 2857m, 1640vs, 1553m, 1435m, 1419m, 1327m, 1261s, 1092vs, 804s, 690w, 622m, 548w. Diffuse reflectance spectrum: 390 nm, 570 nm). Elem. *Anal*. Calc. C, 46.00; H, 4.54; N, 9.82. Found: C, 45.7; H, 4.3; N, 9.8%. The 1:1 Zn:Cu molar ratio was determined by electron microscopy.

Caution! Perchlorate salts are potentially explosive and should be handled in small quatities.

The IR spectra (KBr pellets) were recorded with a BIO-RAD FTS 135 spectrophotometer. UV–Vis spectra (diffuse reflectance technique) were recorded with a UV4 (Unicam) spectrophotometer, using MgO as a standard.

The crystals were measured on a Bruker AXS SMART diffractometer (Mo Kα radiation monochromator). The structures were solved by direct methods and refined by full-matrix least-squares techniques based on F^2. The non-H atoms were refined with anisotropic displacement parameters. Calculations were performed using SHELX-97 crystallographic software package [11]. The crystallographic data and other pertinent information are collected in Table 1.

3. Results and discussion

The first step of our study was to emphasize the role of the compartmental ligand, holding the two copper(II) ions, on the nature of the polynuclear species resulting from the self-assembly process. The reaction between

$[L(\mu\text{-}OH)Cu_2](ClO_4)_2$ (H_2L is the end-off compartmental proligand resulted from the reaction of 2,6-diformyl-4-methyl-phenol and 2-(2-aminoethyl-pyridine) and the dianion of a dicarboxylic acid (fumarate, acetylenedicarboxylate) led to tetranuclear complexes [4b,4c]. By replacing now the end-off compartmental ligand with a macrocyclic one, L^1 (H_2L^1 is the Schiff-base proligand resulted from the condensation reaction of 2,6-diformyl-4-methyl-phenol with 1,3-diamino-propane), the process involving the corresponding binuclear copper(II) complex (Scheme 1(a)) and the anion of the acetylenedicarboxylic acid leads to a linear coordination polymer, **1**, the binuclear nodes being connected through the dicarboxylato linkers (Fig. 1). The copper atoms are quadruply bridged: two preexisting phenoxo oxygen atoms arising from the macrocyclic ligand, and two carboxylato groups, exhibiting the classical *syn–syn* bridging mode (Fig. 2). Selected bond distances and angles are gathered in Table 2. Each copper(II) ion is hexacoordinated, with an elongated octahedral geometry. The apical positions are occupied by the carboxylato oxygen atoms [Cu(1)–O(2) = 2.536(2) Å; Cu(2)–O(3) = 2.610(2) Å]. The basal plane distances are very close: Cu(1)–N(1) = 1.963(4) Å, Cu(2)–N(2) = 1.976(4) Å; Cu(1)–O(1) = 1.971(3) Å, Cu(2)–O(1) = 1.974(2) Å. The distance between the quadruply bridged copper(II) ions is 3.052 Å, while the distance between the copper(II) ions belonging to two neighboring platforms is 10.21 Å. A similar 1D coordination polymer, namely an infinite ladder with macrocyclic platforms, has been obtained by reacting the analogous $[Zn_2]$ derivative with 4,4′-bipyridine [12].

The packing diagram of crystal **1** reveals interesting features. First of all we notice that the phenyl rings from the macrocyclic ligands arising from three coordination polymers interact through graphite-like π–π staking (Fig. 3). The distances between the phenyl rings range between 3.37 and 3.74 Å. The infinite chains run along the crystallographic *c* axis. The solid-state architecture is expanded through such interactions involving both phenyl rings of each macrocyclic ligand. This particular

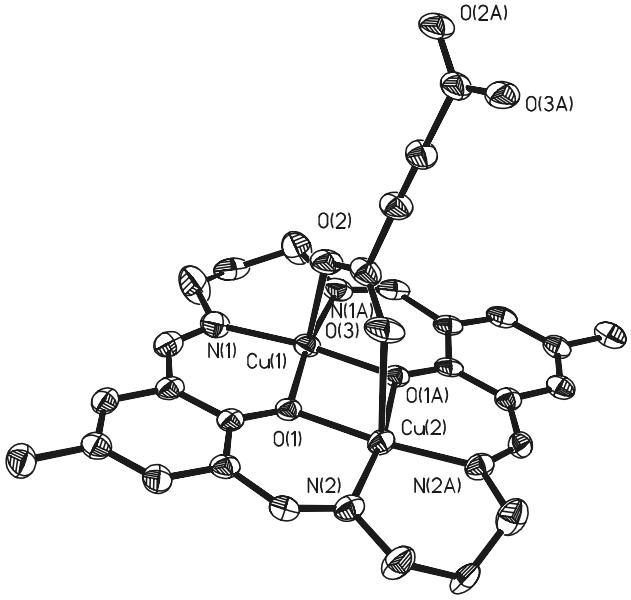

Fig. 2. Perspective view of the repeating unit in **1**, along with the labeling scheme.

packing generates channels, which parallel the polynuclear chains (Fig. 4). The channels are filled by the solvent molecules, which are interconnected through hydrogen bonds.

The electronic spectrum of compound **1** consists of three bands with maxima located at 400, 480, and 700 nm. The last two bands arise from d-d transitions from the lower d orbitals to the $d_{x^2-y^2}$ orbital, in an elongated octahedral stereochemistry [13]. The first band is most probably due to a charge transfer transition.

By employing a heterobinuclear [CuZn] complex as a starting material (Scheme 1(b)), and bis(4-pyridyl)-ethylene (bpete) as a linker, we obtained a heterotetranuclear complex, $[(CuZnL^2)_2(bpete)_2](ClO_4)_4 \cdot 4.5CH_3OH$ (**2**), with the metal ions located in the corners of a rectangle (Fig. 5). Selected bond distances and angles are given in Table 2. To the best of our knowledge, this compound is the first molecular heterometal rectangle obtained by using Werner-type complexes as building

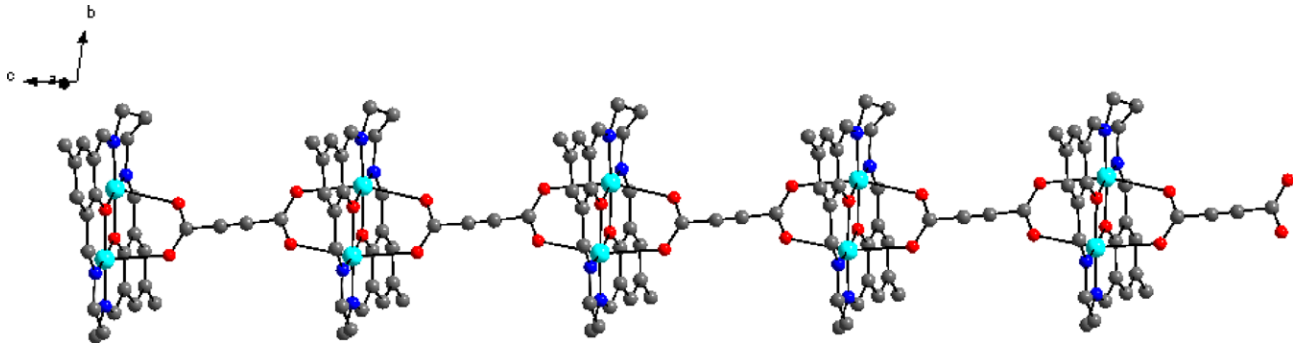

Fig. 1. View of the polymeric chain $_\infty{}^1[Cu_2L^1(acdca)]$.

Table 2
Selected bond distances and angles for compounds **1** and **2**

1		**2**	
Bond lengths			
Cu(1)–O(1)	1.971(3)	Cu(1)–O(1)	1.919(5)
Cu(1)–O(1)#1	1.971(3)	Cu(1)–N(3)	1.924(8)
Cu(1)–N(1)	1.963(4)	Cu(1)–N(1)	1.929(7)
Cu(1)–N(1)#1	1.963(4)	Cu(1)–O(2)	1.949(5)
Cu(1)–O(2)	2.536(2)	Cu(1)–N(6)	2.297(6)
Cu(1)–O(2)#1	2.536(2)	Zn(1)–N(2)	2.032(7)
Cu(2)–O(1)	1.974(2)	Zn(1)–N(7)#2	2.059(6)
Cu(2)–O(1)#1	1.974(2)	Zn(1)–N(4)	2.080(9)
Cu(2)–N(2)	1.976(4)	Zn(1)–O(2)	2.168(5)
Cu(2)–N(2)#1	1.976(4)	Zn(1)–O(1)	2.220(5)
Cu(2)–O(3)	2.610(2)	Zn(1)–N(5)	2.650(2)
Cu(2)–O(3)#1	2.610(2)		
Bond angles			
N(1)–Cu(1)–N(1)#1	95.9(3)	O(1)–Cu(1)–N(3)	159.4(3)
N(1)#1–Cu(1)–O(1)#1	92.69(14)	O(1)–Cu(1)–N(1)	93.8(3)
N(1)–Cu(1)–O(1)#1	171.38(15)	N(3)–Cu(1)–N(1)	84.5(4)
O(1)–Cu(1)–N(1)#1	171.38(15)	O(1)–Cu(1)–O(2)	82.9(2)
N(1)–Cu(1)–O(1)	92.69(14)	N(3)–Cu(1)–O(2)	94.5(3)
O(1)–Cu(1)–O(1)#1	78.70(14)	N(1)–Cu(1)–O(2)	168.0(2)
N(1)–Cu(1)–O(2)#1	95.50(12)	O(1)–Cu(1)–N(6)	102.1(2)
O(2)#1–Cu(1)–N(1)#1	95.18(0)	N(3)–Cu(1)–N(6)	98.4(3)
O(1)–Cu(1)–O(2)#1	84.22(6)	N(1)–Cu(1)–N(6)	90.6(3)
O(2)#1–Cu(1)–O(1)#1	83.39(1)	O(2)–Cu(1)–N(6)	101.4(2)
O(2)–Cu(1)–N(1)	95.20(14)	N(2)–Zn(1)–N(7)#2	125.7(3)
O(2)–Cu(1)–N(1)#1	95.53(8)	N(2)–Zn(1)–N(4)	107.8(3)
O(2)–Cu(1)–O(1)	83.41(10)	N(7)#2–Zn(1)–N(4)	101.8(3)
O(2)–Cu(1)–O(1)#1	84.24(7)	N(2)–Zn(1)–O(2)	131.4(2)
		N(7)#2–Zn(1)–O(2)	95.6(2)
		N(4)–Zn(1)–O(2)	84.0(3)
		N(2)–Zn(1)–O(1)	81.8(2)
		N(7)#2–Zn(1)–O(1)	91.7(2)
		N(4)–Zn(1)–O(1)	153.0(3)
		O(2)–Zn(1)–O(1)	71.4(2)

Symmetry transformations used to generate equivalent atoms: #1 $-x+2, -x+y+1, -z+5/3$.
Symmetry transformations used to generate equivalent atoms: #2 $-x+1/2, -y+5/2, -z+2$.

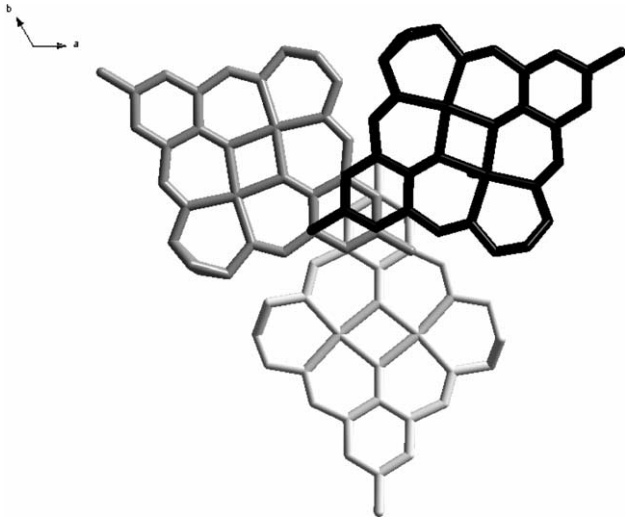

Fig. 3. Stacking interactions of the phenyl rings belonging to different chains.

blocks. The starting heterobinuclear complex has been obtained by employing a dissymmetric macrocyclic compartmental ligand $(L^2)^{2-}$ [7]. The copper(II) and, respectively, the zinc(II) ions are diagonally disposed. The copper(II) ions are pentacoordinated with a square planar geometry, in which the apical position is occupied by the nitrogen atom arising from the bpete linker [Cu(1)–N(6) = 2.297(6) Å]. The basal plane is formed by two nitrogen atoms arising from the Schiff-base ligand, and two phenoxo oxygen atoms, with the Cu–O and Cu–N distances falling in the range 1.919(5)–1.949(5) Å. The zinc ions are coordinated by two imino nitrogen atoms arising from the Schiff-base [Zn(1)–N(4) = 2.080(9) Å; Zn(1)–N(2) = 2.032(7) Å], two phenoxo oxygens [Zn(1)–O(1) = 2.220(5) Å; Zn(1)–O(2) = 2.168(5) Å] and one nitrogen atom from the bpete bridge [Zn(1)–N(7) = 2.059(6) Å]. The secondary amine nitrogen, N(5), can be considered as being semi-coordinated [Zn(1)–N(5) = 2.650(2) Å]. The values of the Cu–O–Zn angles

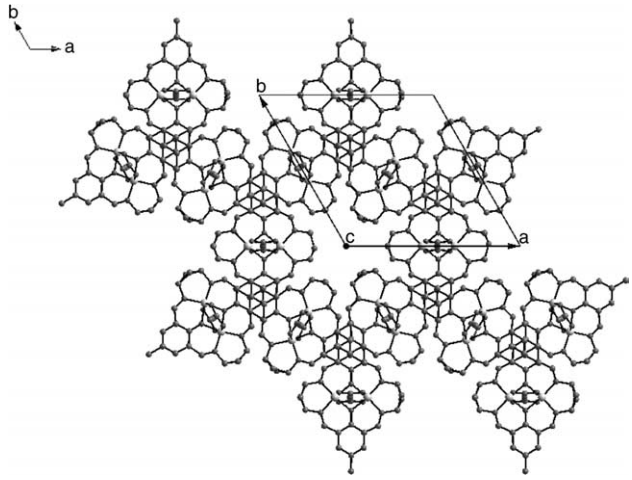

Fig. 4. Detail of the packing diagram for crystal **1** (view along the crystallographic *c* axis).

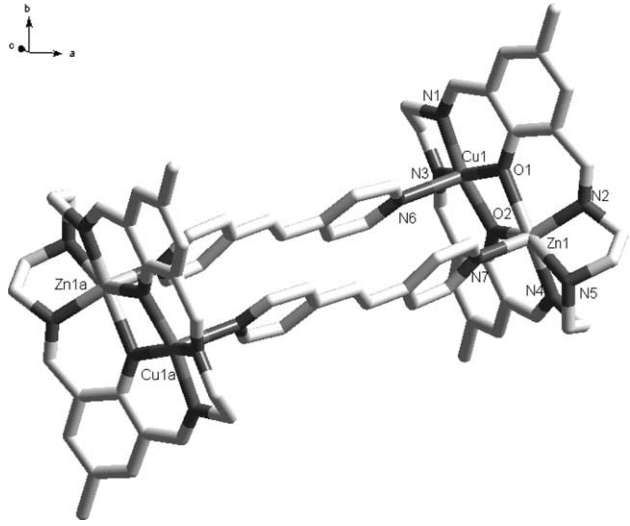

Fig. 5. Perspective view of the $[Cu_2Zn_2]$ molecular rectangle, **2**, along with the atom numbering scheme.

are: Cu(1)–O(1)–Zn(1) = 100.90(22)° and Cu(1)–O(2)–Zn(1) = 101.81(26)°. The Cu(1)···Zn(1) distance is 3.198 Å. The distance between the diagonally disposed metal ions are: Cu(1)···Cu(1a) = 13.84 Å and Zn(1)···Zn(1a) = 14.28 Å.

The packing of the tetranuclear entities in the crystal generates channels, which are occupied by the perchlorate ions as well as by the solvent molecules (Fig. 6).

The solid-state electronic spectrum of compound **2** exhibits one band with maximum at 390 nm, and a large unsymmetrical band with maximum at 570 nm and a tail on its low-energy side. This last band is characteristic for copper(II) chromophores with a square pyramidal geometry [14]. The band with the maximum located at 390 nm can be ascribed to a charge transfer transition.

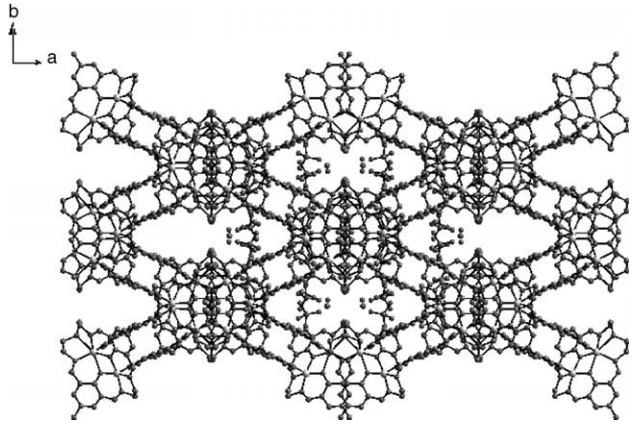

Fig. 6. Packing diagram for crystal **2** (view along the crystallographic *c* axis).

The room temperature value of the $\chi_M T$ product (χ_M is the paramagnetic susceptibility) is in line with the presence of two isolated, uncoupled copper(II) ions: 0.90 $cm^3\ mol^{-1}\ K$ (the calculated value, assuming $g = 2.2$, is 0.91 $cm^3\ mol^{-1}\ K$).

The examples discussed here in, together with those already published by us, illustrate that homo- and heterobinuclear complexes are useful and attractive building-blocks for the design of polynuclear complexes with various nuclearities or dimensionalities.

4. Supplementary material

Crystallographic data for the structural analysis have been deposited with the Cambridge Crystallographic Data Centre, CCDC Nos. 221213 and 221214. Copies of this information may be obtained free of charge from The Director, CCDC, 12 Union Road, Cambridge, CB2 1EZ, UK (fax: +44-1223-336-033; deposit@ccdc.cam.ac.uk or www.ccdc.cam.ac.uk).

References

[1] (a) B.J. Holliday, C.A. Mirkin, Angew. Chem. Int. Ed. 40 (2001) 2022;
(b) P.J. Stang, B. Olenyuk, Acc. Chem. Res. 30 (1997) 502.
[2] P.N.W. Baxter, in: J.L. Atwood, J.E.D. Davies, D.D. MacNicol, F. Vögtle (Eds.), Comprehensive Supramolecular Chemistry, vol. 9, Pergamon Press, Oxford, 1996, p. 165.
[3] B. Moulton, M. Zaworotko, Chem. Rev. 101 (2001) 1629.
[4] (a) D. Visinescu, M. Andruh, A. Müller, M. Schmidtmann, Y. Journaux, Inorg. Chem. Commun. 5 (2002) 42;
(b) D. Visinescu, G.I. Pascu, M. Andruh, J. Magull, H.W. Roesky, Inorg. Chim. Acta 340 (2002) 201;
(c) D. Visinescu, A.M. Madalan, V. Kravtsov, Y.A. Simonov, M. Schmidtmann, A. Müller, M. Andruh, Polyhedron 22 (2003) 1385.
[5] V. Tudor, G. Marin, V. Kravtsov, Y.A. Simonov, J. Lipkowski, M. Brezeanu, M. Andruh, Inorg. Chim. Acta 353 (2003) 35.

[6] (a) R. Gheorghe, M. Andruh, A. Müller, M. Schmidtmann, Inorg. Chem. 41 (2002) 5314;
(b) R. Gheorghe, M. Andruh, J.-P. Costes, B. Donnadieu, Chem. Commun. (2003) 2778.
[7] (a) O.M. Yaghi, H. Li, C. Davis, D. Richardson, T.L. Groy, Acc. Chem. Res. 31 (1998) 474;
(b) S. Kitagawa, M. Kondo, Bull. Chem. Soc. Jpn. 71 (1998) 1739;
(c) S.R. Batten, R. Robson, Angew. Chem. Int. Ed. 37 (1998) 1460;
(d) P.J. Hagram, D. Hagram, J. Zubieta, Angew. Chem. Int. Ed. 38 (1999) 2638;
(e) M.J. Zaworotko, Chem. Commun. (2001) 1;
(f) R. Robson, J. Chem. Soc., Dalton Trans. (2000) 3735;
(g) A.N. Khlobystov, A.J. Blake, N.R. Champness, D.A. Lemenovskii, A.G. Majouga, N.V. Zyk, M. Schröder, Coord. Chem. Rev. 222 (2001) 155.
[8] F.A. Cotton, C. Lin, C.A. Murillo, Acc. Chem. Res. 34 (2001) 759.
[9] N.H. Pilkington, R. Robson, Aust. J. Chem. 23 (1970) 2225.
[10] H. Okawa, J. Nishio, M. Ohba, M. Tadakoro, N. Matsumoto, M. Koikawa, S. Kida, D.E. Fenton, Inorg. Chem. 32 (1993) 2949.
[11] G.M. Sheldrick, SHELXS-97, Program for the Refinement of Crystal Structures, University of Göttingen, Göttingen, Germany, 1997.
[12] W. Huang, S. Gou, D. Hu, S. Chantrapromma, H.-K. Fun, Q. Meng, Inorg. Chem. 40 (2001) 1712.
[13] A.B.P. Lever, Inorganic Electronic Spectroscopy, second ed., Elsevier, Amsterdam, 19884, pp. 557–567.
[14] B.J. Hathaway, in: G. Wilkinson, R.D. Gillard, J.A. McCleverty (Eds.), Comprehensive Coordination Chemistry, vol. 5, Pergamon Press, Oxford, 1987, p. 674.

Available online at www.sciencedirect.com
SCIENCE DIRECT®
Polyhedron 23 (2004) 679–686
POLYHEDRON
www.elsevier.com/locate/poly

Dianionic silicate derivatives of transition metals: synthesis by a facile ion exchange route, characterization and thermolysis studies

P. Bindu, J.V. Kingston, M.N. Sudheendra Rao *

Department of Chemistry, Indian Institute of Technology – Madras, Chennai 600 036, India

Received 2 October 2003; accepted 13 November 2003

Abstract

A new series of transition metal complexes [M = Cr(III) (**1**), Mn(II) (**2**), Co(III) (**3**), Ni(II) (**4a–d**), and Cu(II) (**5a–b**)] with the dianionic hypervalent, tris(catecholato)silicate, $[Si(C_6H_4O_2)_3]^{2-}$, have been synthesized by an ion exchange method under both aqueous and non-aqueous conditions using bis(triethylammonium) tris(catecholato)silicate and a cationic transition metal complex, $[ML_n]X$ [L = ethylenediamine (en), diethylenetriamine (dien), ammonia or water and X = Cl^-, SO_4^{2-}]. Different ammonium tris(catecholato)silicates [viz. morpholinium, diisopropylammonium and diethylammonium] also serve as appropriate for the ion exchange reaction. Ligands like H_2O and NH_3 afford less stable complexes compared to the ligands en and dien. The powdered form of Ni(II) complexes, $[NiL_6][Si(C_6H_4O_2)_3]$ (L = H_2O, NH_3), readily convert to $[Ni(en)_3][Si(C_6H_4O_2)_3]$ quantitatively when treated with en. The new derivatives have been characterized on the basis of analytical, spectroscopic (IR, UV–Vis, solid state NMR, EPR and MS) and magnetic data. The results of TG and EG analysis of the complexes **1**–**5** reveal (i) different decomposition behaviour compared to ammonium catecholatosilicates and (ii) the influence of the bulky tris(catecholato)silicate anion on the thermal stability of these complexes. The bulk pyrolysis study of the above complexes provides a stoichiometric mixture of the corresponding metal oxide and silica except in case of Co(III) which gave the orthosilicate, Co_2SiO_4. Variable temperature magnetic susceptibility measurements indicate a weak antiferromagnetic interaction in case of $[Ni(en)_3][Si(C_6H_4O_2)_3]$ and $[Cu(en)_2][Si(C_6H_4O_2)_3]$.
© 2003 Elsevier Ltd. All rights reserved.

Keywords: Six coordinate silicates; Ion exchange; Transition metals; Ligand environment; Thermal studies; Magnetism

1. Introduction

Studies on six coordinate silicates, which are also known as examples of hypervalent silicon systems, have afforded many novel findings with regard to their structural and reactivity behaviour [1–3]. Kost and co-workers [4,5] have also designed neutral six coordinate silicon systems and unraveled their structural dynamics behaviour. Very recently, Tacke and co-workers [6,7] have synthesized six coordinate silicates of many new chelating ligands and observed interesting structural details arising due to inter ionic interactions assisted by hydrogen bonding. Studies from our laboratory have also revealed similar findings [8–10]. Further, these studies have proved relevant to both catalysis [11,12] and biology [13–17]. Tris(catecholato)silicates have been reported in the literature with different alkali metal cations (Li, Na, K) as well [18,19]. However, the use of transition metals as counter cations in their synthesis have not been considered so far, excepting a brief report on this in 1977 [20]. Of late, synthesis of silicon compounds containing transition metals have proved advantageous for the development of new types of catalysts [21] and materials especially as precursors to metal silicides [1,22]. Interestingly, salt elimination strategy has been made use of in some of their syntheses [23]. This scenario and our continued interest in search of new reaction behaviour for ammonium tris(catecholato)silicates [9] has prompted us to verify an ion exchange approach for obtaining transition metal incorporated six coordinate silicate systems of $[Si(C_6H_4O_2)_3]^{2-}$. We report here a simple and high yield synthesis of several such compounds of chromium,

* Corresponding author. Tel.: +91-44-2257-8253; fax: +91-44-2257-8241.
E-mail addresses: mns_rao@yahoo.com, mnsrao@iitm.ac.in (M.N. Sudheendra Rao).

0277-5387/$ - see front matter © 2003 Elsevier Ltd. All rights reserved.
doi:10.1016/j.poly.2003.11.003

manganese, cobalt, nickel and copper, and their characterization. A study on their thermal behaviour (TG, DT, EG and bulk pyrolysis) and a comparison of the same with ammonium tris(catecholato)silicate precursors is also described. For the first time, a facile ion exchange reaction of general applicability for obtaining transition metal containing tris(catecholato)silicate has been demonstrated.

2. Experimental

2.1. Instrumentation

Elemental analyses (C, H, N) were performed with a Heraeus CHN rapid microanalyser. Metal estimations were done by using a Varian Spectr AA – 20 Atomic Absorption Spectrometer as well as standard wet chemical analysis procedures [24]. IR (Nujol mull, 4000–400 cm^{-1}), UV–Vis (Nujol mull, 180–800 nm) and ^1H, ^{13}C NMR (400 MHz; D_3-acetonitrile as solvent, TMS as internal standard) spectra were recorded on Perkin Elmer 1430, Shimadzu UV-240 (and/or Shimadzu NIR 3100) and JEOL JNM JGX-400 instruments, respectively. The Cross-Polarization Magic Angle Spinning (CP-MAS) ^{29}Si NMR spectra were recorded on a JEOL JNM GSX-400 FT NMR spectrometer at the Larmour frequency of 79.464 MHz as reported previously [9]. Mass spectral analyses were carried out on Finnigan MAT 8230 and Hewlett Packard 6890 GC attached to a micromass GC time of flight mass spectrometer. Perkin Elmer TGA-7 and Balzers GAM 440 were used for TG and EG analysis, respectively. Powder XRD patterns were obtained by the Rigaku Miniflex table top model with Co Kα radiation source ($\lambda = 1.7902$ Å). EPR spectra were recorded on Varian E-112 and Bruker Win EPR spectrometers. The room temperature magnetic susceptibility measurements were done on a Par model 155 vibrating sample magnetometer (5000 Oe) and variable temperature magnetic susceptibility (SQUID) measurements were carried out on a George Associates model 300 Lewis Coil force magnetometer at a field of 1.0 T in the temperature range 2–290 K.

2.2. Synthesis

All syntheses and subsequent manipulations performed in non-aqueous media were carried out under argon atmosphere by conventional Schlenk techniques. Solvents (CH_3CN, CH_3OH, Et_2O), catechol and amines [Et_3N, Et_2NH, OC_4H_8NH, $(C_3H_7)_2NH$] were purified by standard procedures [25]. Tetraethoxysilane, TEOS (Metkem silicon, 99% pure) was used as such.

All the precursors needed for the present study, namely ammonium tris(catecholato)silicates, $R_2[Si(C_6H_4O_2)_3]$ (amsicats) [R = (i) Et_3NH, (ii) Et_2NH_2, (iii) $OC_4H_8NH_2$ and (iv) $(C_3H_7)_2NH_2$] and transition metal complexes, $[Cr(en)_3]Cl_3$, $[Mn(en)_3]Cl_2$, $[Co(en)_3]Cl_3$, $[Co(en)_3]Cl(SO_4)$, $[Co(en)_3]Cl$(*d*-tartarate), $[Ni(en)_3]Cl_2$, $[Ni(dien)_2]Cl_2$, $[Ni(NH_3)_6]Cl_2$, $[Ni(H_2O)_6]Cl_2$, $[Cu(en)_3]SO_4$ and $[Cu(en)_2]SO_4$ were synthesized according to reported procedures [26,27] and their identities established on the basis of their IR, UV–Vis and NMR (^1H, ^{13}C) spectra [9] before use.

2.3. Synthesis of tris(catecholato)silicate complexes of transition metals

2.3.1. $[Cr(en)_3][Si(C_6H_4O_2)_3]Cl$ (1)

To a stirred solution of bis(triethylammonium) tris(catecholato)silicate (1.39 g, 2.50 mmol) in acetonitrile (25 mL), a fine powder of $[Cr(en)_3]Cl_3$ (0.86 g, 2.50 mmol) was added at RT in small quantities over 15 min and stirred for 8 h. The dull yellow precipitate formed was filtered, washed with methanol (3×5 mL), ether (3×5 mL) and dried in vacuo.

Other silicate complexes viz. $[Mn(en)_3][Si(C_6H_4O_2)_3]$ (**2**), $[Co(en)_3][Si(C_6H_4O_2)_3]Cl$ (**3**), $[Ni(en)_3][Si(C_6H_4O_2)_3]$ (**4a**), $[Cu(en)_2][Si(C_6H_4O_2)_3]$ (**5a**) and $[Cu(en)_3][Si(C_6H_4O_2)_3]$ (**5b**) were synthesized in a similar way.

Table 1
Analytical data of transition metal HV silicates, **1**–**5**

Complex	Colour	Yield (%)	Elemental analysis found (Calc.) (%)				
			C	H	N	M[a]	Si[b]
1	dull yellow	90	46.57(46.48)	5.93(5.85)	13.64(13.55)	8.68(8.38)	4.59(4.53)
2	dull white	92	49.20(49.05)	6.25(6.18)	14.46(14.30)	9.67(9.35)	4.72(4.78)
3	dull yellow	95	45.81(45.97)	5.68(5.78)	13.48(13.40)	9.02(9.39)	4.55(4.47)
4a	pale purple	99	48.81(48.73)	6.20(6.14)	14.00(14.21)	9.66(9.92)	4.60(4.74)
4b	pale purple	97	50.71(50.58)	6.12(6.20)	13.50(13.61)	9.20(9.50)	4.44(4.55)
4c	pale green	96	41.55(41.68)	4.51(4.63)		10.95(11.32)	5.35(5.40)
4d	bluish grey	97	42.24(42.17)	6.01(5.85)	16.47(16.38)	11.53(11.45)	5.53(5.46)
5a	pale purple	96	49.13(49.28)	5.38(5.26)	10.50(10.45)	11.57(11.85)	5.33(5.23)
5b	pale purple	96	48.23(48.35)	6.13(6.08)	14.18(14.09)	10.78(10.66)	4.84(4.71)

[a] AA data are reported. It was in good agreement with the data obtained from wet analysis.
[b] Values are deduced from the amount of silica obtained.

Table 2
IR, UV–Vis, EPR spectral and magnetic moment data of complexes **1**–**5**

Complex	UV–Vis (λ_{max} nm)	EPR g_{iso} (300 K)	μ_{eff} BM (300 K)	IR (cm^{-1})[a]
1	470, 330, 265	1.999	3.38	3340, 3280, 1571, 1488, 1376, 1277, 1248, 1214, 1152, 1100, 1052, 1019, 882, 860, 810, 739, 672
2	440, 335, 280	1.998	5.03	3325, 3243, 1591, 1488, 1376, 1280, 1248, 1222, 1148, 1094, 1016, 952, 885, 870, 815, 738, 681
3	465, 335, 280		dia magnetism	3360, 3173, 1582, 1488, 1455, 1376, 1347, 1310, 1289, 1248, 1210, 1172, 1102, 1056, 1021, 882, 868, 810, 741, 682
4a	525, 330, 275		2.93	3328, 3259, 1593, 1577, 1489, 1458, 1376, 1321, 1272, 1249, 1224, 1150, 1096, 1033, 958, 903, 885, 869, 815, 738, 681
4b	520, 335, 275			3320, 3240, 1620, 1500, 1460, 1380, 1260, 1180, 1096, 1020, 970, 890, 820, 760, 740, 680
4c	635[b], 390, 307, 222			3152, 1628, 1587, 1494, 1459, 1376, 1344, 1248,1100, 1021, 867, 822, 739, 682
4d	555[b], 392, 304, 223			3328, 3168, 1619, 1590, 1484, 1450, 1373, 1344, 1283, 1248, 1101, 1018, 880, 871, 816, 742, 680
5a	530, 320, 290	2.055	1.65	3295, 3220, 1591, 1488, 1456, 1376, 1282, 1252, 1150, 1098, 1049, 1018, 971, 912, 883, 870
5b	585, 350, 240	2.056	1.98	3319, 3202, 1593, 1488, 1456, 1376, 1282, 1252, 1150,1098, 1049, 1018, 971, 912, 883, 870

[a] Strong bands are given.
[b] Broad with a shoulder.

2.3.2. *[Ni(dien)$_2$][Si(C$_6$H$_4$O$_2$)$_3$] (**4b**)*

To a stirred solution of bis(diethylammonium) tris(catecholato)silicate (1.00 g, 2.00 mmol) in acetonitrile (20 mL), a solution of [Ni(dien)$_2$]Cl$_2$ (0.67 g, 2.00 mmol) in acetonitrile (10 mL) was added dropwise over 15 min and stirred for 1 h. The pale purple precipitate was filtered and washed quickly with methanol (3×5 mL), ether (3×5 mL) and dried in vacuo.

2.3.3. *[Ni(H$_2$O)$_6$][Si(C$_6$H$_4$O$_2$)$_3$] (**4c**)*

To a stirred solution of bis(diethylammonium) tris(catecholato)silicate (1.00 g, 2.00 mmol) in acetonitrile (20 mL), a solution of $NiCl_2 \cdot 6H_2O$ (0.48 g, 2.0 mmol) in methanol (15 mL) was added and stirred for 30 min to isolate a pale green precipitate. The precipitate was washed quickly with methanol (3×5 mL), ether (3×5 mL) and dried in vacuo.

In a similar way, a bluish grey precipitate of [Ni(NH$_3$)$_6$][Si(C$_6$H$_4$O$_2$)$_3$] (**4d**) was also isolated. In selected cases, the exchange reaction was repeated with other 'amsicats' mentioned above to isolate the same complexes. Additional preparative details and characterization data of the above complexes are given in Tables 1 and 2.

3. Results and discussion

Bis(triethylammonium) tris(catecholato)silicate, TEASICAT readily participates in an ion exchange reaction with cationic transition metal complexes to afford the corresponding metal derivatives having the six coordinate silicate ion (Eq. (1))

$$[(C_2H_5)_3NH]_2[Si(C_6H_4O_2)_3] + [ML_n]X_2 \rightarrow [ML_n][Si(C_6H_4O_2)_3] + 2[(C_2H_5)_3NH]X. \quad (1)$$

Reactions proceed smoothly in non-aqueous media (CH_3CN, CH_3OH) and at room temperature to afford the complexes in very good yield (Table 1). Exchanges were also effective for different choice of the 'amsicats' and different anions of the transition metal complexes (experimental). Interestingly, complexes having both the silicate and chloride ions were isolated when trivalent metal complexes were considered for the reaction (2)

$$[M(en)_3]Cl_3 + (TEA)_2SICAT \rightarrow [M(en)_3]SICAT(Cl) + 2TEACl, \quad [M = Cr \text{ and } Co]. \quad (2)$$

Further, in case of cobalt, different anions employed namely chloride, sulfate and tartrate got exchanged with the tris(catecholato)silicate ion with equal ease. However, reactions with nickel complexes comprising of different ligands afforded the silicate derivatives having different stabilities. Powdered samples of complexes, **4c** and **4d**, are found to slowly change their colour even in a sealed tube while **4a** and **4b** posed no problem of stability, indicating the importance of the ligand environment around the metal ion for obtaining stable complexes of six coordinate silicates. This was further substantiated by the observation that **4c** and **4d** readily convert to **4a** in the solid state itself, upon addition of a slight excess of ethylenediamine (Scheme 1). This indicates that chelating ligands impart greater stability and thus facilitate their isolation in much higher yields.

Prior to this study, the only work in the literature on such complexes was by Sackerer and Nagorsen [20] who reported the isolation and structural characterization of a copper derivative, [Cu(en)$_2$][Si(C$_6$H$_4$O$_2$)$_3$] (**5a**). This complex was obtained by treating aqueous solutions of silicic acid and Cu(en)$_2$SO$_4$ with an excess of catechol in

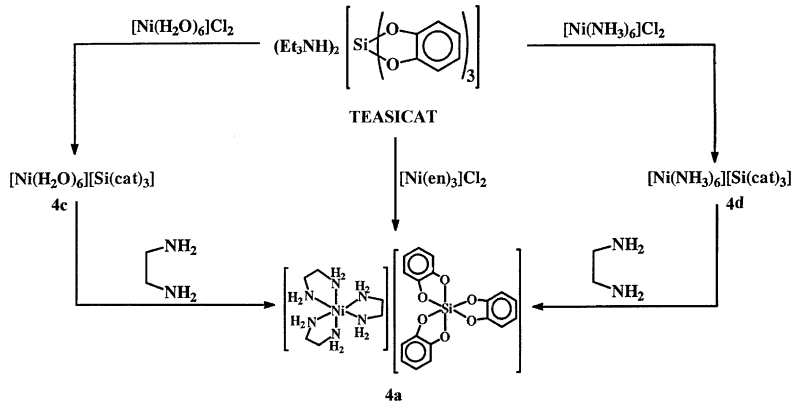

Scheme 1. Facile interconversion reactions of **4c** and **4d** to **4a**.

the presence of concentrated ammonia and keeping the mixture in an ampule at 50 °C for 24 h. The role of $[NH_4]_2[Si(C_6H_4O_2)_3]$ in the formation of the copper derivative was also mentioned which implies an ion exchange step.

For the first time in this study, several complexes of different transition metals having a hexacoordinate silicate ion have been prepared from an ion exchange reaction involving ammonium tris(catecholato)silicate. An interesting observation made with the transition metal 'sicat' derivatives, **1**–**5** is that in all cases the colour of the exchanged product was found to be less intense than the precursors. In addition, excepting **4c** and **4d**, all are found to be air and thermally stable and highly insoluble in nature.

3.1. Characterization

The important IR and UV–Vis spectral assignments of **1**–**5** are given in Tables 1 and 2, respectively. Infrared spectra of **1**–**5** are very similar and provide an unambiguous clue to the presence of tris(catecholato)silicate ion by showing all the strong peaks of the $[Si(C_6H_4O_2)_3]^{2-}$ ion of the precursor approximately at the same positions (Table 2). The presence of the transition metal ion is revealed by observing the expected NH/OH stretching frequencies due to the ligand part in the region 3360–3150 cm^{-1}. Electronic spectra of **1**–**5** (recorded as Nujol mulls) also provide useful clues to their characterization. The visible absorption bands indicate the presence of the metal ion and the UV bands found at approximately the same positions in all of them was characteristic of the hypervalent silicate ion. A millimolar solution of Teasicat in CH_3CN gave absorption maxima at 248 and 310 nm. A small shift observed in the absorption band positions and intensity is suggestive of interaction between the oppositely charged ions (Table 2).

Mass spectra of complexes **1**, **2**, **3**, **4a** and **5** (**a** and **b**) recorded in EI mode, gave peaks corresponding to m/z 110 (catechol$^+$) and 61 (enH$^+$) providing evidence for the presence of both metal ion and the $[Si(C_6H_4O_2)_3]$

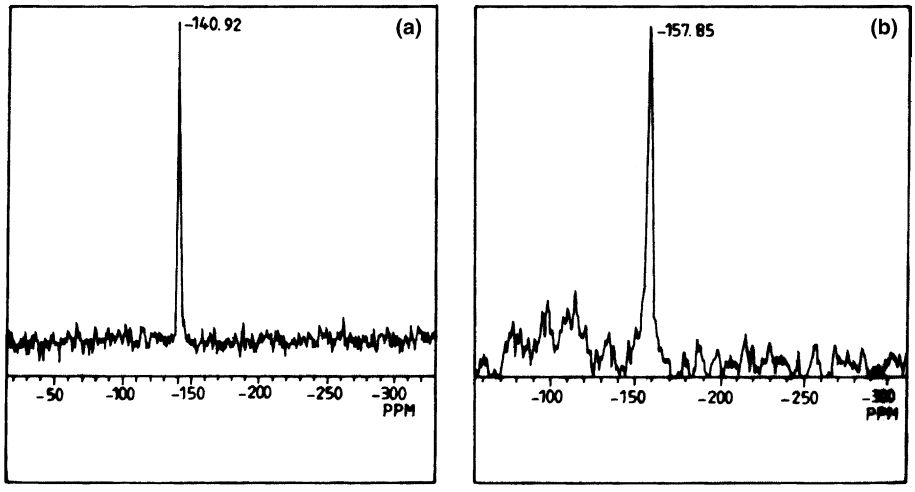

Fig. 1. CPMAS ^{29}Si NMR spectra of (a) **3** and (b) **5a**.

Table 3
Thermoanalytical data of metal complexes **1**–**5**[a]

Complex	First decomposition[b]			Second decomposition[c]			Percentage of SiO_2 + MO	
	Temperature range (°C)	Weight loss (%)		Temperature range (°C)	Weight loss (%)		Calc.	Found
		Calc.	Found		Calc.	Found		
1	51–528	52.21	52.37	528–724	27.07	27.63	20.65	20.00
2	52–431	49.06	49.09	431–600	28.58	30.91	22.29	20.00
3	52–500	51.63	50.96	500–709	26.78	28.13	21.53	20.17
4a	78–437	48.74	48.67	437–600	28.39	26.03	22.78	25.30
5a	55–343	42.58	42.09	343–562	31.32	30.50	26.04	27.41
5b	60–337	43.34	43.31	337–600	33.19	33.33	23.42	23.33

[a] End residues are either a mixture of silica and the corresponding metal oxide or the metal silicate.
[b] Expulsion of 'en', catechol (and HCl in the case of **1** and **3**).
[c] Decomposition of $M[Si(cat)_2]$.

ion. Several low mass fragments were common to all and the base peak was due to ethylenediamine, in most of the cases. A comparison with those of ammonium tris(catecholato)silicates revealed some important differences [9]. Contrary to the peak due to spirosilane, $[Si(C_6H_4O_2)_2]$ (m/z = 244) observed in the case of $[RR'R''NH]_2[Si(C_6H_4O_2)_3]$, none of the metal derivatives, **1–5** gave this peak thereby suggesting that their decomposition pathway may be entirely different. Besides, some fragments of low intensity which are assignable to those formed with exchange of ligands between the metal and silicon [eg., Si(cat)(en) (m/z = 196); $Si(cat)(en)_2$ (m/z = 256); $Ni(cat)(en)_2$ (m/z = 286)] were found in some cases.

NMR studies of **1–5** posed difficulty for two reasons. They are highly insoluble and except **3**, all others have paramagnetic metal centres. However, in two cases, namely **3** (diamagnetic cobalt) and **5a** (paramagnetic copper), solid state CPMAS-^{29}Si NMR spectra could be recorded which is shown in Fig. 1. Both of them gave a sharp signal at −140.9 and −157.9 ppm, respectively, in evidence for the presence of the tris(catecholato)silicate ion [8,9]. A slightly broad and more shielded signal observed in the case of **5a** could possibly be due to the paramagnetic influence of copper.

X-band polycrystalline EPR spectra of **1**, **2**, **4a**, **5a** and **5b** were recorded both at 300 and 77 K. All of them gave a single broad signal. The g_{iso} observed (Table 2) were well within the range reported for similar examples [28–33]. All the complexes did not exhibit any appreciable change in the EPR signal pattern when the temperature was lowered. The broad nature of the signal is presumably due to the dipolar broadening caused by the presence of the bulky anionic tris(catecholato) silicate moiety.

Magnetic susceptibility measurements at 300 K were carried out for **1**, **2**, **4a**, **5a** and **5b** and the corresponding magnetic moments are given in Table 2. In all cases, the anticipated value for the corresponding oxidation state and geometry of each of the metal ion was observed

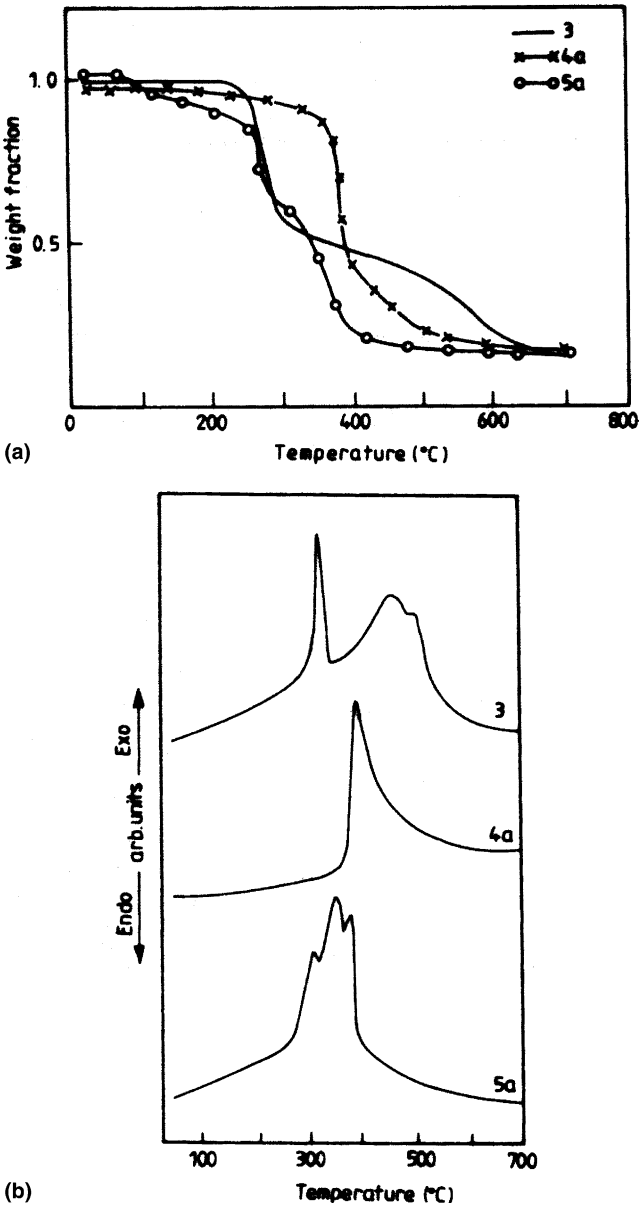

Fig. 2. (a) TGA and (b) DTA plots of **3**, **4a** and **5a**.

[28–33]. However, the trend in some cases presented an interesting variation. A comparison of the observed value reveals that **4a** and **5a** are in good agreement with the reported values, which may be due to the prevailing intermolecular antiferromagnetic exchange interaction.

Variable temperature magnetic susceptibility measurements (SQUID) were also carried out over the temperature 290–2 K in case of **4a** and **5a**. The plots of effective magnetic moments per molecule (μ_{eff}) versus T are given in Fig. 4. Over the temperature range 290–2 K, the magnetic moment values for **4a** and **5a** are found to lie in the range 2.93–2.59 and 1.77–1.52 BM, respectively [34,35].

3.2. Thermal studies

Thermogravimetric (TG) analysis of compounds **1**–**5** was carried out to understand the influence of the bulky hypervalent silicate anionic moiety on the thermal behaviour of these complexes and the results are given in Table 3. The thermograms of **1**–**5** recorded in the temperature range, RT to 800 °C (in air), indicate that the decomposition temperature is different for various complexes and their observed order of thermal stability is **4a** > **5b** > **2**–**3** > **5a** > **1**. A comparison of TGA and DTA plots of **3**, **4a** and **5a** (Fig. 2) show that complex **4a** is the most stable and **5a** is the least stable. A noteworthy feature is that the ligand 'en' coordinated to Ni(II) in **4a** does not get expelled even at high temperature (~200 °C) and its onset of decomposition temperature is found to be well above 200 °C. Similar to the mass spectral behaviour, the TGA plots also revealed that these complexes do not undergo 'spirosilane' formation, unlike ammonium tris(catecholato)silicates [9]. Further, the exothermic nature of these processes (DTA plots) is also in contrast to the endothermic nature of the process observed for the formation of the spirosilane. Evolved gas analysis profiles of **1**–**5** (Fig. 3) clearly show evidence for the expulsion of both catechol ($m/z = 110$) and ethylenediamine ($m/z = 60$) from these complexes upon heating. It is seen from both TG and EG data that the expulsion of ethylenediamine ligand gets completed only around 330 °C.

3.3. Pyrolysis studies

Bulk scale pyrolysis of **1**–**5** were carried out by heating a known weight of the complex in an electrical furnace at 800 °C in static air for 4 h. Excepting cobalt complex **3**, which gave the corresponding orthosilicate, Co_2SiO_4, all other complexes gave the oxide mixtures as products of pyrolysis. These products were identified by IR spectra and powder XRD data [36].

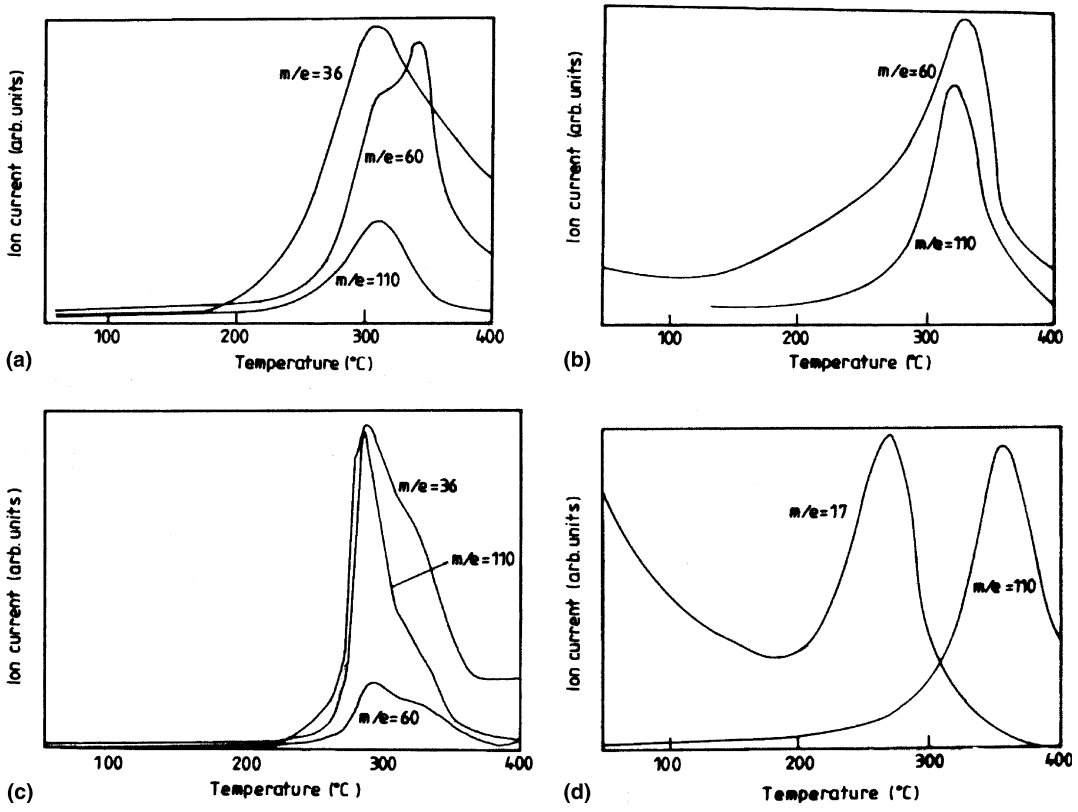

Fig. 3. EGA profiles for (a) **1**, (b) **2**, (c) **3** and (d) **4d**.

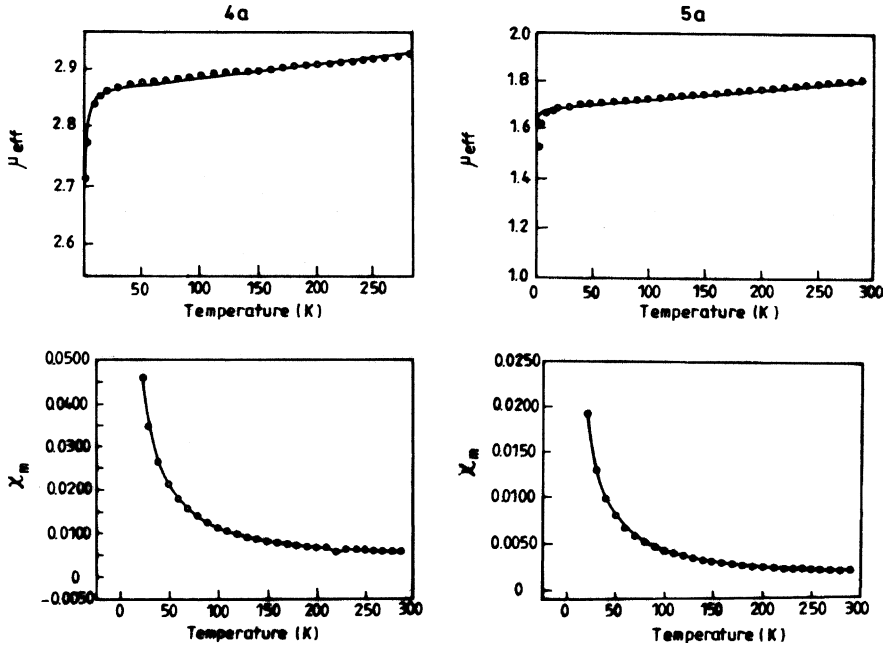

Fig. 4. Plots of (a) magnetic moment and (b) magnetic susceptibility data as a function of temperature for **4a** and **5a**.

Acknowledgements

This work was financially supported by the Council of Scientific and Industrial Research (CSIR), New Delhi, India by a Grant No. (01/1577/99), awarded to M.N.S. Rao. We profusely thank Professor Dr. Phalguni Chaudhuri, Max-Plank-Institut fuer Bioanorganische Chemie, Muelheim, Germany for recording variable temperature magnetic susceptibility data of **4a** and **5a** and for valuable discussions on EPR and magnetism. Regional Sophisticated Instrumentation Centre (RSIC) and Catalysis Division of Department of Chemistry, IIT Madras are gratefully acknowledged for spectral, analytical and powder XRD facilities.

References

[1] (a) C. Chuit, R.J.P. Corriu, C. Reye, C. Young, Chem. Rev. 93 (1993) 1371;
(b) C.Y. Wong, J.D. Woollins, Coord. Chem. Rev. 130 (1994) 175.
[2] M.J. Caulfield, T. Russo, D.H. Solomon, Aust. J. Chem. 54 (2001) 375.
[3] M.J. Caulfield, D.J. McAllister, T. Russo, D.H. Solomon, Aust. J. Chem. 54 (2001) 383.
[4] V. Kingston, B. Gostevskii, I. Kalikhman, D. Kost, Chem. Commun. 14 (2001) 1272.
[5] I. Kalikhman, V. Kingston, O. Girshberg, D. Kost, Organometallics 20 (2001) 4713.
[6] A. Biller, C. Burschka, M. Penka, R. Tacke, Inorg. Chem. 41 (2002) 3901.
[7] I. Richter, M. Penka, R. Tacke, Inorg. Chem. 41 (2002) 3950.
[8] J.V. Kingston, M.N. Sudheendra Rao, Tetrahedron Lett. 38 (1997) 4841.
[9] J.V. Kingston, Babu Varghese, M.N. Sudheendra Rao, Main Group Chem. 3 (2000) 79.
[10] P. Bindu, Babu Varghese, M.N. Sudheendra Rao, Phosphorus, Sulphur and Silicon 178 (2003) 1.
[11] D.E. Soil, S.A. Monoso, M. Patterson, P. Deshong, A.D. Favor, R. Hirschmann, B.A. Smith, J. Org. Chem. 64 (1999) 6526.
[12] K. Shu, N. Koichi, J. Org. Chem. 59 (1994) 6620.
[13] B. Delord, M.C. Guillorit, J. Lafay, M.L. Andreola, D. Tharaud, L. Tarrago-Litvak, H.J.A. Fleury, G. Deleris, Eur. J. Med. Chem. 31 (1996) 111.
[14] R.R. LeVier, M.L. Chandler, S.R. Wendel, The Biochemistry of Silicon and Related Problems, Plenum Press, New York, 1978.
[15] R.R. LeVier, Actual Chim. 3 (1986) 89.
[16] C.Y. Anderson, K. Freye, K.A. Tubesing, Y.S. Li, M.E. Kenney, H. Muktar, C.A. Elmets, Photochem. Photobiol. 67 (1998) 332.
[17] J. He, H.E. Larkin, Y.S. Li, B.D. Rihter, S.I.A. Zaidi, M.A.J. Rodgers, H. Mukhtar, M.E. Kenney, N.L. Oleinick, Photochem. Photobiol. 65 (1997) 581.
[18] F.E. Hahn, M. Keck, K.N. Raymond, Inorg. Chem. 34 (1995) 1402.
[19] D.W. Barnum, Inorg. Chem. 9 (1970) 1942.
[20] V.D. Sackerer, G. Nagorsen, Z. Anorg. Allg. Chem. 437 (1977) 188.
[21] W. Palitzsch, U. Bohme, G. Roewer, J. Organomet. Chem. 540 (1997) 83.
[22] M.A. Brook, Silicon in Organic, Organometallic and Polymer Chemistry, Wiley, New York, 2000.
[23] A.J. Wiseman, R.G. Jones, M.J. Went, J. Organomet. Chem. 544 (1997) 129.
[24] G.H. Jeffery, J. Bassett, J. Mendham, R.C. Denney, Vogel's Text Book of Quantitative Chemical Analysis, ELBS and Longman, London, 1989.
[25] D.D. Perrin, W.L. Armarego, D.R. Perrin, Purification of Laboratory Chemicals, Pergamon Press, Oxford, 1980.
[26] A.I. Vogel, A Text Book of Practical Organic Chemistry, ELBS and Longman, London, 1975.
[27] C.L. Rollinson, J.C. Bailer, J. Am. Chem. Soc. 65 (1943) 250.
[28] B.R. Mc Garvey, in: Transition Metal Chemistry – A Series of Advances, vol. 3, Marcel Dekker, New York, 1966.

[29] R.L. Carlin, A.J. van Duyneveldt, Magnetic Properties of Transition Metal Compounds, Springer, New York, 1977.
[30] L. Sacconi, F. Mani, A. Bencini, Comprehensive Coordination Chemistry, vol. 5, Pergamon Press, Oxford, New York, 1987.
[31] B.J. Hathaway, Comprehensive Coordination Chemistry, vol. 5, Pergamon Press, Oxford, New York, 1987.
[32] G.W.A. Fowles, W.R. Mc Gregor, J. Am. Chem. Soc. (1958) 136.
[33] B. Chiswell, E.D. Mc Kenzie, L.F. Lindoy, Comprehensive Coordination Chemistry, vol. 4, Pergamon, Oxford, New York, 1987.
[34] A. Earnshaw, An Introduction to Magnetochemistry, Academic Press, London, 1968.
[35] F.E. Mabbs, D.J. Machin, Magnetism and Transition Metal Complexes, Chapman&Hill, London, 1973.
[36] (a) Luz, Anorg. Allg. Chem. 8 (1948) 2540;
(b) Cowley, Walkley, Nature (London) 4 (1948) 326;
(c) Swanson, Tatge, Natl. Bur. Stand. (US) Circ. 5 (1953) 661i;
(d) Toussaint, C. Euraton, Ispra, Italia, Private Commun. 22 (1969) 1189i.

Available online at www.sciencedirect.com
SCIENCE DIRECT®
Polyhedron 23 (2004) 687–691
POLYHEDRON
www.elsevier.com/locate/poly

2,3,4,7-Tetrahydro-1*H*-inden-2-ol: synthesis, molecular structure and coordination chemistry

Ludovic Vieille-Petit, Bruno Therrien *, Georg Süss-Fink *

Institut de Chimie, Université de Neuchâtel, Case postale 2, CH-2007 Neuchâtel, Switzerland

Received 23 October 2003; accepted 13 November 2003

Abstract

2,3,4,7-Tetrahydro-1*H*-inden-2-ol (**1**) has been synthesised by Birch reduction of indan-2-ol. A single-crystal X-ray structure analysis of **1** shows the compound to exist as hydrogen-bonded polymers along the *c*-axis due to the presence of a series of hydrogen-bonds between hydroxo functions. The ferrocene ester derivatives, ferrocene carboxylic acid 2,3,4,7-tetrahydro-1*H*-inden-2-yl ester (**2**) and ferrocene carboxylic acid indan-2-yl ester (**3**) have been prepared by peptidic coupling of ferrocene carboxylic acid with **1** and with indan-2-ol, respectively. The single-crystal X-ray structure analyses of **2** and **3** reveal in both cases the cyclopentadienyl rings to adopt an eclipsed conformation with the indenyl substituent being rotated out of the Cp ester plane by almost 90°, allowing no efficient interaction between the π-system of the Cp ring and the indene moiety. The dienyl derivative **2** reacts with $RuCl_3 \cdot nH_2O$ in refluxing ethanol to afford $[Ru(arene)Cl_2]_2$ (**4**) (arene = ferrocene carboxylic acid indan-2-yl ester) as a mixture of isomers.
© 2003 Elsevier Ltd. All rights reserved.

Keywords: Arene ligand; Ferrocene carboxylic acid; Ferrocene derivative; Ruthenium

1. Introduction

A wide variety of methods for the synthesis of ferrocenoyl ester derivatives are found in the literature, among them reaction of $FeCl_2$ with cyclopentadienyl ester derivatives [1], condensation of chlorocarbonylferrocene with hydroxo derivatives [2], oxazoline ring-opening reaction of ferrocenoyloxazole derivatives [3], reaction of ferrocene carboxylic acid with diazomethane [4], reaction of ferrocenoyl imidazolide with hydroxo derivatives [5], haloferrocene with acids [6], reaction of ferrocene carboxylic acid with hydroxo derivatives [7], and reaction of 2-(*N*,*N*-dimethylaminoethylferrocene)carboxylic acid with sodium bicarbonate and methyl iodide [8].

Recently, we reported the synthesis of ferrocene ester derivatives by standard peptidic coupling conditions [9]. The method has been proven to be an efficient synthetic route for the synthesis of ferrocene ester derivatives [10]. Herein, we report the synthesis of two new ferrocenoyl ester derivatives by coupling of ferrocene carboxylic acid with 2,3,4,7-tetrahydro-1*H*-inden-2-ol and indan-2-ol. The dienyl-ester derivative reacts with $RuCl_3 \cdot nH_2O$ to form a dinuclear arene–ruthenium complex incorporating ferrocenoyl groups. The single-crystal structure analyses of ferrocene carboxylic acid 2,3,4,7-tetrahydro-1*H*-inden-2-yl ester, ferrocene carboxylic acid indan-2-yl ester and the new 2,3,4,7-tetrahydro-1*H*-inden-2-ol are presented.

2. Experimental

2.1. General

All manipulations were carried out using routine procedures, under a nitrogen atmosphere. Organic solvents were distilled under nitrogen prior to use. NMR spectra were recorded using a Varian Gemini 200 MHz spectrometer and a Bruker 400 MHz spectrometer. IR spectra were recorded on a Perkin–Elmer Spectrum One

* Corresponding authors. Tel.: +41-32-718-2499; fax: +41-32-718-2511 (B. Therrien).
E-mail addresses: bruno.therrien@unine.ch (B. Therrien), georg.suess-fink@unine.ch (G. Süss-Fink).

0277-5387/$ - see front matter © 2003 Elsevier Ltd. All rights reserved.
doi:10.1016/j.poly.2003.11.042

FT-IR spectrometer (4000–400 cm^{-1}). Microanalyses were performed by the Laboratory of Pharmaceutical Chemistry, University of Geneva (Switzerland). Electrospray mass spectra were obtained in positive-ion mode with an LCQ Finnigan mass spectrometer. All reagents were purchased (Fluka or Aldrich) and used as received.

2.2. Syntheses

2.2.1. 2,3,4,7-Tetrahydro-1H-inden-2-ol (1)

1 was synthesised by sodium reduction of indan-2-ol in liquid ammonia by analogy to published methods [11]. Crystals suitable for X-ray analysis were obtained by slow evaporation of a dichloromethane solution of **1**.

Spectroscopic data for **1**: ^{1}H NMR (400 MHz, $CDCl_3$): $\delta = 5.75$ (m, 2H, ethylenic *H*), 4.50 (m, 1H, –C*H*OH), 2.66 (m, 4H, –C=C–CH_2–), 2.62 (m, 2H, –CH_2CHOH), 2.34 (s, 1H, –CHO*H*), 2.22 (dd, 2H, $^2J = 17.02$ Hz, $^3J = 1.02$ Hz, –CH_2CHOH). $^{13}C\{^1H\}$ NMR (100 MHz, $CDCl_3$): $\delta = 129.91$, 124.89, 70.90, 46.08, 27.70. MS (EI, acetone): *m*/*z*: 136 $[M]^+$. *Anal.* Calc. for $C_9H_{12}O$: C, 79.37; H, 8.88. Found: C, 79.41; H, 8.82%.

2.2.2. Ferrocene carboxylic acid 2,3,4,7-tetrahydro-1H-inden-2-yl ester (2)

A solution of ferrocene carboxylic acid (3.30 g, 14.34 mmol), *N*,*N*-dicyclohexylcarbodiimide (4.54 g, 22.06 mmol), 4-(dimethylamino)pyridine (1.35 g, 11.03 mmol), 4-pyrrolidinopyridine (1.63 g, 11.03 mmol), and 2,3,4,7-tetrahydro-1*H*-inden-2-ol (1.50 g, 11.03 mmol) in CH_2Cl_2 (150 mL) was stirred under nitrogen at room temperature for 3 days. The resulting solution was filtered through celite to remove *N*,*N*-dicyclohexylurea, and the filtrate concentrated under reduce pressure. The residue was separated by column chromatography on silica gel eluting with hexane/acetone (20:1). The pure product was isolated from the first fraction, giving **2** as red-orange solid. Yield: 3.50 g (91%). Crystals suitable for X-ray analysis were grown by slow evaporation of an acetone/hexane solution of **2**.

Spectroscopic data for **2**: IR (KBr, cm^{-1}): $\nu = 1709$ vs (C=O ester), 1460m, 1277s, 1134s. ^{1}H NMR (400 MHz, $CDCl_3$): $\delta = 5.80$ (m, 2H, ethylenic *H*), 5.53 (m, 1H, –C*H*O–), 4.84 (m, 2H, Cp*H*), 4.42 (m, 2H, Cp*H*), 4.24 (s, 5H, Cp*H*), 2.81 (dd, 2H, $^2J = 16.38$ Hz, $^3J = 6.14$ Hz, –CH_2CHO–), 2.71 (m, 4H, –C=C–CH_2–), 2.42 (dd, 2H, $^2J = 16.38$ Hz, $^3J = 2.36$ Hz, –CH_2CHO). $^{13}C\{^1H\}$ NMR (50 MHz, $CDCl_3$): $\delta = 171.84$, 129.84, 129.77, 71.96, 71.46, 71.68, 70.09, 70.00, 43.01, 27.47. MS (EI, acetone): *m*/*z*: 348 $[M]^+$. *Anal.* Calc. for $C_{20}H_{20}Fe_1O_2$: C, 68.98; H, 5.79. Found: C, 68.93; H, 5.82%.

2.2.3. Ferrocene carboxylic acid indan-2-yl ester (3)

A solution of ferrocene carboxylic acid (2.00 g, 8.70 mmol), *N*,*N*-dicyclohexylcarbodiimide (2.75 g, 13.38 mmol), 4-(dimethylamino)pyridine (0.82 g, 6.69 mmol), 4-pyrrolidinopyridine (0.99 g, 6.69 mmol), and indan-2-ol (0.90 g, 6.72 mmol) in CH_2Cl_2 (80 mL) was stirred under nitrogen at room temperature for 3 days. The resulting solution was filtered through celite to remove *N*,*N*-dicyclohexylurea, and the filtrate concentrated under reduce pressure. The residue was separated by column chromatography on silica gel eluting with hexane/acetone (20:1). The pure product was isolated from the first fraction, giving **3** as red-orange solid. Yield: 1.72 g (81%). Crystals suitable for X-ray analysis were grown by slow evaporation of an acetone/hexane solution of **3**.

Spectroscopic data for **3**: IR (KBr, cm^{-1}): $\nu = 1692$vs (C=O ester), 1459m, 1277s, 1141s. ^{1}H NMR (200 MHz, $CDCl_3$): $\delta = 7.26$ (m, 4H, H_{arom}), 5.70 (m, 1H, –C*H*O–), 4.81 (m, 2H, Cp*H*), 4.41 (m, 2H, Cp*H*), 4.20 (s, 5H, Cp*H*), 3.44 (dd, 2H, $^2J = 16.66$ Hz, $^3J = 6.22$ Hz, –CH_2CHO–), 3.15 (dd, 2H, $^2J = 16.66$ Hz, $^3J = 2.19$ Hz, –CH_2CHO–). $^{13}C\{^1H\}$ NMR (50 MHz, $CDCl_3$): $\delta = 171.93$, 140.87, 128.14, 126.05, 75.23, 73.45, 71.68, 70.92, 70.09, 40.05. MS (EI, acetone): *m*/*z*: 346 $[M]^+$. *Anal.* Calc. for $C_{20}H_{18}Fe_1O_2$: C, 69.39; H, 5.24. Found: C, 69.37; H, 5.23%.

2.2.4. [Ru(arene)Cl$_2$]$_2$ (4) (arene = ferrocene carboxylic acid indan-2-yl ester)

To a solution of ruthenium trichloride hydrate (470 mg, 1.80 mmol) in ethanol (50 mL) was added **2** (2.50 g, 7.18 mmol), and the mixture was refluxed for 4 h. After cooling to room temperature, half of the volume was evaporated in vacuo, the orange-brown precipitate was filtered, washed with ether and acetone, dissolved in $CHCl_3$ and filtered through celite to eliminate insoluble particles. After evaporation to dryness, **4** was obtained as orange powder. Yield: 495 mg (53%).

Spectroscopic data for **4**: IR (KBr, cm^{-1}): $\nu = 1709$ vs (C=O ester), 1458m, 1276s, 1137s. ^{1}H NMR for **4a** (400 MHz, dmso-d_6): $\delta = 5.88$ (m, 8H, Ru–H_{arom}), 5.55 (m, 2H, –C*H*O–), 4.79 (m, 4H, Cp*H*), 4.53 (m, 4H, Cp*H*), 4.26 (s, 10H, Cp*H*), 3.36 (dd, 4H, $^2J = 16.18$ Hz, $^3J = 5.56$ Hz, –CH_2CHO–), 2.87 (dd, 4H, $^2J = 16.18$ Hz, $^3J = 2.03$ Hz, –CH_2CHO–). ^{1}H NMR for **4b** (400 MHz, dmso-d_6): $\delta = 6.03$ (m, 8H, Ru–H_{arom}), 5.63 (m, 2H, –C*H*O–), 4.90 (m, 4H, Cp*H*), 4.46 (m, 4H, Cp*H*), 4.29 (s, 10H, Cp*H*), 3.27 (dd, 4H, $^2J = 16.22$ Hz, $^3J = 5.60$ Hz, –CH_2CHO–), 3.15 (dd, 4H, $^2J = 16.22$ Hz, $^3J = 2.07$ Hz, –CH_2CHO–). MS (EI, acetone): *m*/*z*: 1000.5 $[M - Cl]^+$. *Anal.* Calc. for $C_{20}H_{18}Fe_1O_2$: C, 46.36; H, 3.50. Found: C, 46.33; H, 3.52%.

2.3. X-ray crystallography

Crystals of **1** and **2** were mounted on a Stoe Image Plate Diffraction system equipped with a ϕ circle goniometer, using Mo Kα graphite monochromated radiation ($\lambda = 0.71073$ Å) with ϕ range 0–200°, increment of

Table 1
Crystallographic and selected experimental data of **1**–**3**

	1	**2**	**3**
Chemical formula	$C_9H_{12}O$	$C_{20}H_{20}FeO_2$	$C_{20}H_{18}FeO_2$
Formula weight	136.19	348.21	346.19
Crystal system	tetragonal	monoclinic	triclinic
Space group	$I4_1/a$	$P2_1/a$	$P\bar{1}$
Crystal colour and shape	colourless block	orange block	orange block
Crystal size	$0.50 \times 0.50 \times 0.50$	$0.40 \times 0.40 \times 0.25$	$0.38 \times 0.23 \times 0.19$
a (Å)	21.9204(14)	17.315(1)	8.078(2)
b (Å)	21.9204(14)	10.7738(8)	9.886(2)
c (Å)	6.2552(4)	19.478(1)	11.171(2)
α (°)	90	90	64.66(3)
β (°)	90	116.360(6)	77.44(3)
γ (°)	90	90	78.53(3)
V (Å^3)	3005.7(3)	3255.8(4)	781.3(4)
Z	16	8	2
T (K)	153(2)	153(2)	293(2)
D_c (g cm^{-3})	1.204	1.421	1.472
μ (mm^{-1})	0.076	0.933	0.972
Scan range (°)	$5.26 < 2\theta < 51.92$	$4.20 < 2\theta < 51.92$	$4.08 < 2\theta < 50.24$
Unique reflections	1432	6328	2712
Reflections used [$I > 2\sigma(I)$]	1150	4580	2410
R_{int}	0.0274	0.0435	0.0719
Final R indices [$I > 2\sigma(I)$]	0.0353, wR_2 0.0914	0.1102, wR_2 0.2591	0.0628, wR_2 0.1646
R indices (all data)	0.0449, wR_2 0.0948	0.1295, wR_2 0.2645	0.0698, wR_2 0.1695
Goodness-of-fit	1.054	1.184	1.212
Maximum and minimum $\Delta\rho$ (e Å^{-3})	0.164 and −0.117	1.522 and −1.126	0.737 and −0.843

1.1° and 1.2°, $D_{max} - D_{min} = 12.45 - 0.81$ Å. Crystal of **3** was mounted on a Stoe AED2 4-circle diffractometer using Mo Kα graphite monochromated radiation with $\omega/2\theta$ scans in the 2θ range 4–135°. The structures were solved by direct methods using the program SHELXS-97 [12]. The refinement and all further calculations were carried out using SHELXL-97 [13]. In **1**–**3**, the hydrogen atoms have been included in calculated positions and treated as riding atoms using the SHELXL default parameters, except for the hydroxo H-atom in **1** which was located from difference Fourier maps and refined isotropically. All non-H atoms were refined anisotropically, using weighted full-matrix least-square on F^2. Crystallographic details are summarised in Table 1. Figs. 1 and 3 were drawn with ORTEP [14] and Fig. 2 with the program POV-RAY [15].

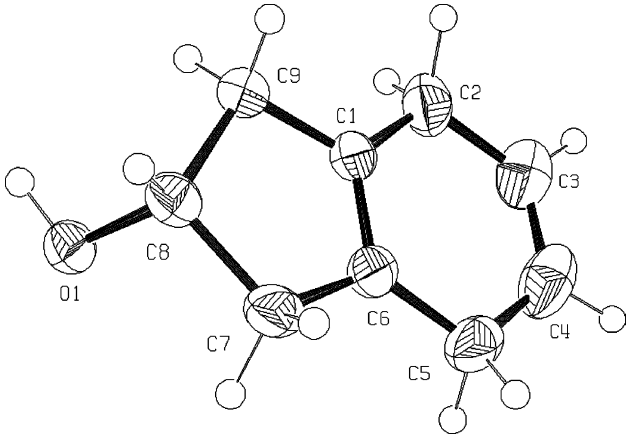

Fig. 1. ORTEP view of **1**, displacement ellipsoids are drawn at the 50% probability level. Selected bond lengths (Å) and angles (°): O(1)–C(8) 1.4321(14), C(1)–C(6) 1.3521(18); O(1)–C(8)–C(7) 107.67(10), O(1)–C(8)–C(9) 111.64(10).

3. Results and discussion

Indan-2-ol as well as 2,3,4,7-tetrahydro-1*H*-inden-2-ol (**1**), accessible by standard Birch reduction of indan-2-ol, react with ferrocenyl carboxylic acid in dichloromethane in the presence of condensation agents (*N*,*N*-dicyclohexylcarbodiimine, 4-(dimethylamino)pyridine, 4-pyrrolidinopyridine) to give the corresponding ferrocenoyl ester derivatives, ferrocene carboxylic acid 2,3,4,7-tetrahydro-1*H*-inden-2-yl ester (**2**) and ferrocene carboxylic acid indan-2-yl ester (**3**), see Scheme 1. Compound **1** can be recrystallised from a slow evaporation of a dichloromethane solution to give colourless crystals, while **2** and **3** can be recrystallised from an acetone–hexane solution to give orange, air-stable crystals.

The molecular structure of **1** is shown in Fig. 1. The indenyl moiety [C(1)–C(9)] is almost planar with a maximum deviation from the mean plane of −0.114(1) Å for C(8), with the oxygen lying out of the plane by 1.446(1) Å.

The hydrogen atom of the hydroxo function, which was located from difference Fourier maps, is involved in a hydrogen bond with the oxygen of a neighbouring

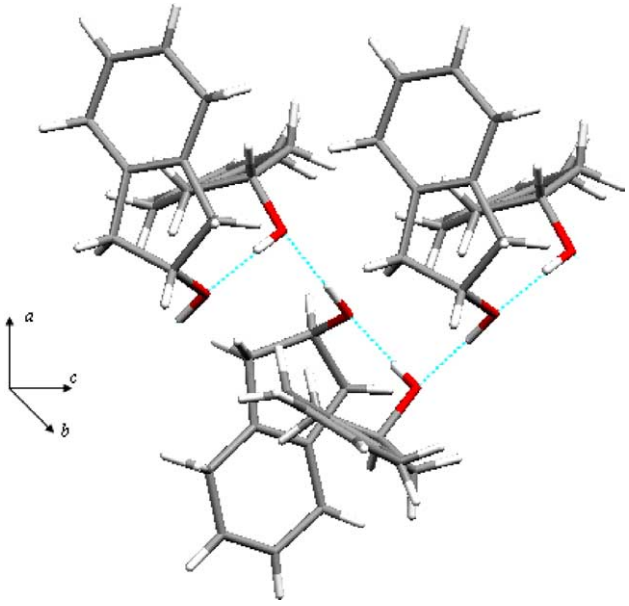

Fig. 2. Hydrogen bonded arrangement of **1** along the *c*-axis.

molecule, distance O···O being 2.7376(9) Å with a O–H···O angle of 175.5(15)°. They form one-dimensional hydrogen-bonded chains along the *c*-axis of the crystal, see Fig. 2.

The infrared spectra of **2** and **3** exhibit the characteristic ν_{CO} absorption at 1709 cm^{-1} for **2** and 1692 cm^{-1} for **3** of the ester function and the bands at 1460, 1277 and 1134 cm^{-1} for **2** and 1459, 1277 and 1141 cm^{-1} for **3** due to the presence of a ferrocene moiety. Single-crystal structure analyses of **2** and **3** have been performed, see Fig. 3. The molecular structure of **2** comprises two independent molecules per asymmetric unit. Fig. 3 shows only one independent molecule of **2**. Selected bond lengths (Å) and angles (°) are given in Table 2.

In both cases, the ferrocene moiety is in the eclipsed conformation. The Cp rings are almost parallel to each other, the angle between the two Cp planes are 2.1(1)°, 3.4(1)° and 2.1(3)°, respectively. The indenyl substituents are rotated out of the Cp-ester plane by 79.7(2)°, 80.6(3)° and 84.5(1)°, respectively, allowing no efficient interaction between the π-system of the Cp ring and the indene moiety. A similar behavior has been observed for

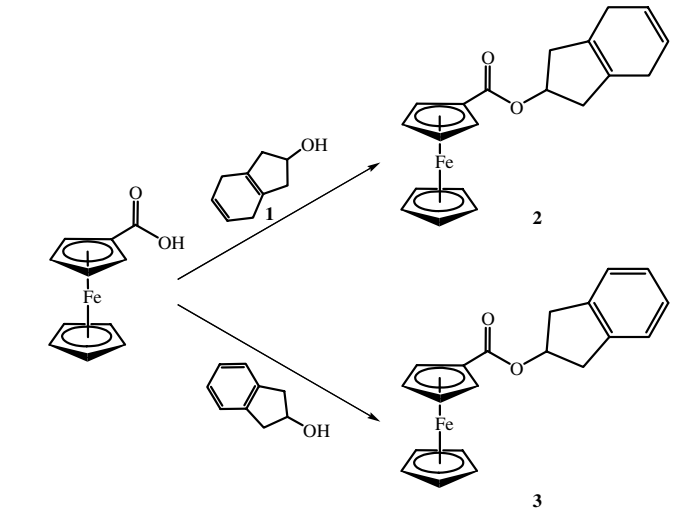

Scheme 1.

Table 2
Selected bond lengths (Å) and angles (°) for compounds **2** and **3**

	2	**2**[a]	**3**
Interatomic distances			
O(1)–C(10)	1.370(12)	1.342(11)	1.355(5)
O(2)–C(10)	1.194(12)	1.212(12)	1.204(6)
C(10)–C(11)	1.454(13)	1.459(13)	1.466(6)
O(1)–C(8)	1.459(11)	1.466(11)	1.466(5)
C(1)–C(2)	1.483(16)	1.480(13)	1.399(7)
Bond angles			
O(1)–C(10)–C(11)	111.0(8)	112.0(8)	111.8(4)
O(2)–C(10)–C(11)	125.9(10)	124.8(9)	125.3(4)
O(2)–C(10)–O(1)	123.0(9)	123.2(9)	122.8(4)
C(8)–O(1)–C(10)	116.0(8)	116.2(8)	116.3(3)

[a] Values for the second independent molecule of **2**.

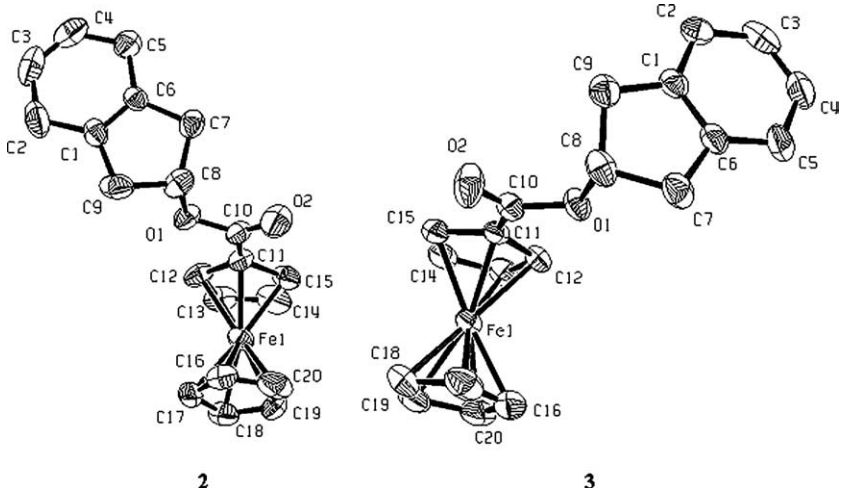

2 **3**

Fig. 3. ORTEP view of **2** and **3**, displacement ellipsoids are drawn at the 50% probability level, hydrogen atoms are omitted for clarity.

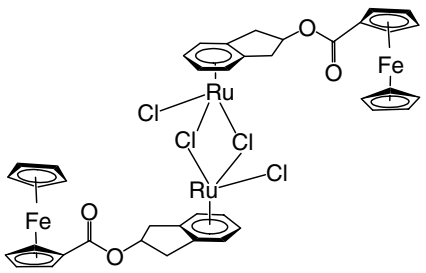

4

Scheme 2.

benzoylferrocene [16] and for methylenebenzotriazolylferrocene derivatives [10a]. The C(10)–O(1) distance [1.355(5) Å] is shorter than that of ferrocene carboxylic acid benzotriazole ester [1.427(2) Å], which is known to have a weak and reactive ester bond [7a].

The dienyl function of **2** reacts with $RuCl_3 \cdot nH_2O$, in refluxing ethanol to afford in moderate yield $[Ru(arene)Cl_2]_2$ (**4**) (arene = ferrocene carboxylic acid indan-2-yl ester), see Scheme 2.

In **4**, as observed for related complexes $[Ru(trindane)Cl_2]_2$ [17] and $[Ru(indane)Cl_2]_2$ [18], the complexation of the indane to the ruthenium atoms generates diastereotopic methylene protons, the two faces of the arene being non-equivalent. The *endo* and *exo* benzylic protons integrate for two whereas the central methylene proton for one. In principle, the central methylene proton can be folded toward (*endo*) or away (*exo*) from the metal, giving rise to three possible isomers in a 2:1:1 ratio (*exo–endo*:*exo–exo*:*endo–endo*). In fact, only two isomers have been observed by ^1H NMR in a 2:1 ratio (**4a**:**4b**). We believed that the *endo–endo* isomer, where the central methylene protons are folded away from the metals, is sterically disfavoured.

4. Supplementary material

Full tables of atomic parameters, bond lengths and angles are deposited at the Cambridge Crystallographic Data Centre, 12 Union Road, Cambridge CB2 1EZ, UK (fax: +44-1223-336033; E-mail: deposit@ccdc.cam.ac.uk or www: http://www.ccdc.cam.ac.uk). Deposition numbers: (**1**) 218893, (**2**) 220073, (**3**) 218892.

Acknowledgements

The authors are grateful to the Fonds National Suisse de la Recherche Scientifique for financial support. A generous loan of ruthenium chloride hydrate from the Johnson Matthey Technology Centre is gratefully acknowledged.

References

[1] (a) M. Hobi, O. Ruppert, V. Gramlich, A. Togni, Organometallics 16 (1997) 1384;
(b) M. Costa, E. Dalcanale, F. Santos Dias, C. Graiff, A. Tiripicchio, L. Bigliardi, J. Organomet. Chem. 619 (2001) 179.
[2] (a) P.D. Beer, A.D. Keefe, A.M.Z. Slawin, D.J. Williams, J. Chem. Soc., Dalton Trans. (1990) 3675;
(b) A.C. Benniston, A. Harriman, Angew. Chem., Int. Ed. Engl. 32 (1993) 1459;
(c) M. Buda, J.-C. Moutet, E. Saint-Aman, A. De Cian, J. Fischer, R. Ziessel, Inorg. Chem. 37 (1998) 4146;
(d) S. Shirakami, T. Itoh, Tetrahedron: Asymmetry 11 (2000) 2823;
(e) A. Ion, J.-C. Moutet, E. Saint-Aman, G. Royal, S. Tingry, J. Pecaut, S. Menage, R. Ziessel, Inorg. Chem. 40 (2001) 3632;
(f) N. Godbert, A.S. Batsanov, M.R. Bryce, J.A.K. Howard, J. Org. Chem. 66 (2001) 713;
(g) C.G. Hartinger, A.A. Nazarov, V.B. Arion, G. Giester, M. Jakupec, M. Galanski, B.K. Keppler, New J. Chem. 27 (2002) 671.
[3] (a) A.A. Nazarov, C.G. Hartinger, V.B. Arion, G. Giester, B.K. Keppler, Tetrahedron 58 (2002) 8489;
(b) P. Štěpnička, New J. Chem. 26 (2002) 567.
[4] J. Podlaha, P. Štěpnička, J. Ludvik, I. Císařová, Organometallics 15 (1996) 543.
[5] C. Imrie, L. Cook, D.C. Levendis, J. Organomet. Chem. 637–639 (2001) 266.
[6] Akabori, M. Sato, S. Ebine, Synthesis (1981) 278.
[7] (a) H.-B. Kraatz, J. Lusztyk, G.D. Enright, Inorg. Chem. 36 (1997) 2400;
(b) Q. Wang, R. Huang, J. Chem. Research(S) (2001) 246;
(c) C. Imrie, E.R.T. Elago, C.W. McCleland, N. Williams, Green Chem. 4 (2002) 159.
[8] Y. Luo, R.J. Barton, B.E. Robertson, Acta Crystallogr., Sect. C 46 (1990) 1388.
[9] A. Hassner, V. Alexanian, Tetrahedron Lett. 19 (1978) 4475.
[10] (a) C.M. Thomas, B. Therrien, A. Neels, H. Stoeckli-Evans, G. Süss-Fink, J. Organomet. Chem. 658 (2002) 251;
(b) L. Vieille-Petit, S. Unternährer, B. Therrien, G. Süss-Fink, Inorg. Chim. Acta 355 (2003) 335.
[11] M.E. Kuehne, B.F. Lambert, Organic Synth. 5 (1973) 400.
[12] G.M. Sheldrick, Acta Crystallogr., Sect. A 46 (1990) 467.
[13] G.M. Sheldrick, SHELXL-97, University of Göttingen, Göttingen, Germany, 1999.
[14] L.J. Farrugia, J. Appl. Cryst. 30 (1997) 565.
[15] S. Anger, D. Bayer, C. Cason, C. Dayley, S. Demlow, A. Enzmann, D. Farmer, T. Wegner, C. Young, POV-RAY software version 3.1, Indianapolis, IN, USA, 1991.
[16] I.R. Butler, W.R. Cullen, S.J. Rettig, J. Trotter, Acta Crystallogr., Sect. C 44 (1988) 1666.
[17] H.K. Gupta, P.E. Lock, D.W. Hughes, M.J. McGlinchey, Organometallics 16 (1997) 4355.
[18] L. Vieille-Petit, B. Therrien, G. Süss-Fink, Acta Crystallogr., Sect. E 58 (2002) m656.

Available online at www.sciencedirect.com
SCIENCE DIRECT®
Polyhedron 23 (2004) 693–699
POLYHEDRON
www.elsevier.com/locate/poly

Bis(phosphine) derivatives of diamines

Mireia Rodriguez I. Zubiri, Heather L. Milton, David J. Cole-Hamilton, Alexandra M.Z. Slawin, J. Derek Woollins *

School of Chemistry, University of St. Andrews, St. Andrews, Fife KY16 9ST, UK

Received 11 October 2003; accepted 19 November 2003

Abstract

The synthesis, oxidation and coordination chemistry of new bis(aminophosphines) based on diamines is demonstrated. $Ph_2PN(CH_2Ph)CH_2CH_2(CH_2Ph)NPPh_2$, $^iPr_2PN(CH_2Ph)CH_2CH_2(CH_2Ph)NP^iPr_2$, $Ph_2PNH(C_{10}H_6)_2NHPPh_2$, $Ph_2PNH(C_{10}H_6)(C_6H_4)NHPPh_2$ were prepared and tested in the hydroformylation of hex-1-to give aldehydes with poor selectivity (up to l:b = 2.5:1) to the desired linear products. Modelling calculations were performed for all ligands. R_2 groups enlarge the natural bite angle when going from $R_2 = Ph_2$ to $R_2 = {}^iPr_2$ which are more bulky. Most of the ligands seem to be rigid (with flexibility ranges of 25°–46°). Four demonstrative X-ray structures are reported.
© 2003 Elsevier Ltd. All rights reserved.

Keywords: Ligand; Catalysis; X-ray structure; Complex

1. Introduction

Hydroformylation of alkenes is a very important catalytic reaction in industry and great effort has been devoted to obtaining highly active and selective catalysts [1–6]. This is a very important area of investigation since it has been extensively reported that selective catalytic processes are affected by many factors such as the configuration that the ligand may have, i.e., its bite angle and its range of flexibility and the electronic properties of the ligands when binding the precursor metal species [7–12]. These factors influence the direction of approach of the substrate to the active catalyst and therefore the selectivity of the reaction.

By altering the substituents on the phosphorus atoms and keeping the same diamine backbone (piperazine and homopiperazine) [13,14] we were able to conduct a systematic study on the electronic and steric effects of a wide range of the bis(aminophosphines) derivatives of piperazine and homopiperazine. In recent work [13–22], we studied synthesis of new P–N containing ligands and the effect of the electronic properties of different ligands on the regioselectivity of rhodium catalysed hydroformylation of alkenes. Continuing our studies on the preparation of potentially active ligands for homogeneous catalysis, we investigated the synthesis, oxidation and coordination chemistry of new bis(aminophosphines) based on simple diamines in anticipation that the resulting phosphines will have different steric and electronic properties. Here, we report the synthesis of two new phosphines together with hydroformylation studies and four demonstrative X-ray structures.

2. Results and discussion

Reaction of *N*,*N*′-dibenzylethylenediamine with two equivalents of R_2PCl gives **1** and **2** (Eq. (1)). **1** was first prepared by Payne and Stephan [23] and later by Balakrishna et al. [24]. However, they did not report IR or FAB^+ mass spectrometry data and neither did they study its oxidation chemistry nor its activity in homogeneous catalysis. Therefore, we considered it to be of interest to study this compound further, including the preparation of its diselenide derivative and the study of its activity in rhodium catalysed hydroformylation of alkenes whilst **2** offers a steric and electronic variant in this regard.

* Corresponding author. Tel.: +44-1334-463869; fax: +44-1334-463384.
E-mail address: jdw3@st-andrews.ac.uk (J. Derek Woollins).

0277-5387/$ - see front matter © 2003 Elsevier Ltd. All rights reserved.
doi:10.1016/j.poly.2003.11.048

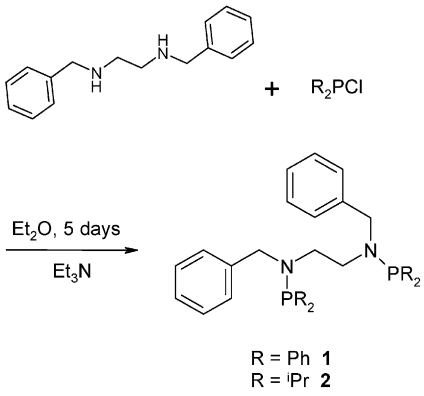

(1)

FAB$^+$ mass spectrometry confirms the proposed identity of the ligands by showing the expected parent-ion peaks and elemental analysis data is in agreement with calculated values.

The $^{31}P\{^1H\}$ NMR spectrum of **2** displays a singlet at δ (P) 89.1 ppm, the large downfield shift when compared to **1** (δ (P) 66.5 ppm) reflecting the close proximity of the phosphorus centres to the isopropyl substituents in **2** instead of the phenyl groups in **1**.

Crystals of compound **2** (Fig. 1) suitable for X-ray analysis were obtained by recrystallisation of the compound from hot toluene. The molecular structure shows that the P–N bonds adopt a *trans* orientation relative to one another. The molecule has a centre of symmetry and, thus, the bond lengths and angles are equal for the two halves of the molecule. P–N bond lengths are typical for this type of compound. The phosphorus atoms adopt a flattened tetrahedral geometry with C–P–N angles somewhat less than 109°, whilst the nitrogen centres have trigonal character (P–N–C angles are closer to 120° than 109°) though the P–N bond is quite long.

Reaction of (S)-(−)-1,1′-binaphthyl-2,2′-diamine and 1-(2-aminophenyl)-2-naphthalene with two equivalents of Ph_2PCl, after deprotonation by *n*BuLi, proceeds in thf to give $Ph_2PNH(C_{10}H_6)_2NHPPh_2$ (**3**) (BDPAB) and $Ph_2PNH(C_{10}H_6)(C_6H_4)NHPPh_2$ (**4**), respectively (Eq. (2))

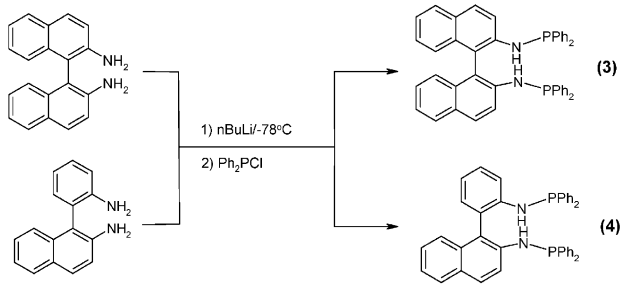

(2)

The $^{31}P\{^1H\}$ NMR spectrum of **3** comprises a singlet at δ (P) 27.7 ppm. The identity of this compound is supported by FAB$^+$ mass spectrometry (m/z 652 [M$^+$]) and the IR spectrum, because a band associated with a ν(N–H) stretch (3330 cm^{-1}) is observed. ^1H NMR and elemental analysis data are in agreement with the literature. It presents interesting characteristics such as its structural rigidity and chirality and, although it is not a new bis(aminophosphine) [25,26], we considered it important to study it because its, the ligand had not been tested in the rhodium catalysed hydroformylation of alkenes. Recrystallisation from hot toluene gives **3** as colourless crystals. The X-ray structure (Fig. 2) reveals

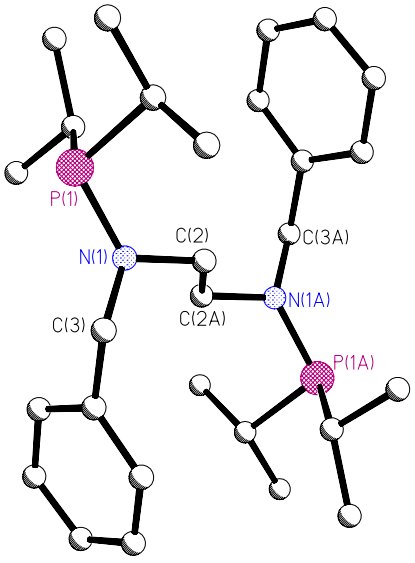

Fig. 1. Solid state structure of $^iPr_2PN(CH_2Ph)CH_2CH_2(CH_2Ph)NP^iPr_2$ **2**. Selected bond lengths (Å) and angles (°) N(1)–P(1) 1.704(2), P(1)–C(13) 1.850(3), P(1)–C(10) 1.856(3), N(1)–C(3) 1.466(3), C(3)–N(1)–C(2) 114.9(2), C(3)–N(1)–P(1) 116.26(17), C(2)–N(1)–P(1) 123.11(17), N(1)–P(1)–C(13) 100.49(13), N(1)–P(1)–C(10) 105.72(12), C(13)–P(1)–C(10) 102.85(17).

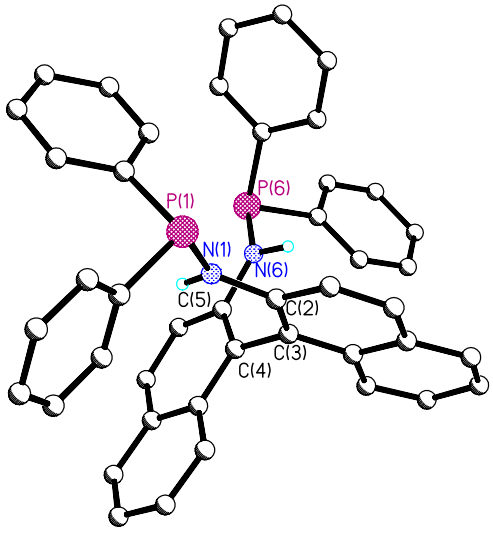

Fig. 2. Solid state structure of $Ph_2PNH(C_{10}H_6)_2NHPPh_2$ **3**. Selected bond lengths (Å) and angles (°) P(1)–N(1) 1.7043(19), P(1)–C(25) 1.836(2), P(1)–C(19) 1.835(2), N(1)–C(2) 1.402(3), C(5)–N(6) 1.403(3), N(6)–C(6) 1.7115(18), N(1)–P(1)–C(25) 103.32(10), N(1)–P(1)–C(19) 99.54(10), C(25)–P(1)–C(19) 101.25(10), C(2)–N(1)–P(1) 125.33(16) C(5)–N(6)–P(6) 126.38(15), N(6)–P(6)–C(7) 99.73(9), N(6)–P(6)-C(13) 102.33(10), C(7)–P(6)–C(13) 99.68(10).

an interesting orientation of the naphthyl rings of the amine backbone relative to one another with a dihedral angle of 98° P–N bond lengths are typical for this type of compound. The two nitrogen atoms in the molecule adopt a geometry close to trigonal whilst, like **2** the phosphorus centres are flattened from tetrahedral.

The magnitude of P–Se J values can be used to assess the donor ability of phosphines [32,33] with better donors having lower $^1J\{^{77}Se–^{31}P\}$ values, as a consequence of the degree of s character in the phosphorus lone pair, etc., i.e., larger coupling constants imply more s character and a poorer donor. Reaction of **1** and **2** with two equivalents of elemental selenium in toluene proceeds smoothly to give $Ph_2P(Se)N(CH_2Ph)CH_2CH_2(CH_2Ph)NP(Se)Ph_2$ (**5**) and $^iPr_2P(Se)N(CH_2Ph)CH_2CH_2(CH_2Ph)NP(Se)^iPr_2$ (**6**). The $^{31}P\{^1H\}$ NMR spectra of **5** and **6** consist of singlets at δ (P) 70.8 and δ (P) 104.1 ppm, respectively, shifted-downfield from the free ligand in both cases, with $^1J(^{77}Se–^{31}P)$ coupling constants of 777 and 741 Hz, respectively, which are in accord with values previously reported for similar selenides [27–31] and suggest that as expected **2**, with electron donating alkyl groups, is the better donor system.

5 and **6** show, in their IR spectra, bands that can be assigned to ν(P–N) [943 cm^{-1} for **5** and 936 cm^{-1} for **6**] and ν(P–Se) at 557 cm^{-1} for **5** and 594 cm^{-1} for **6**.

Slow diffusion of diethyl ether into a dichloromethane solution of **6** gives the product as colourless crystals suitable for X-ray analysis (Fig. 3). The molecular structure shows that the P=Se bonds adopt a *trans* orientation relative to one another. The P–N bond is significantly shorter in this P(V) compound compared to the parent P(III) system which is somewhat counter-intuitive and suggests that in **2** there may be some antibonding π character in the P–N linkage. The P=Se bond lengths are typical for this type of compound. The phosphorus atoms are close to tetrahedral – implying that the selenium atom in **6** is less stereochemically active than the lone pair in **2**.

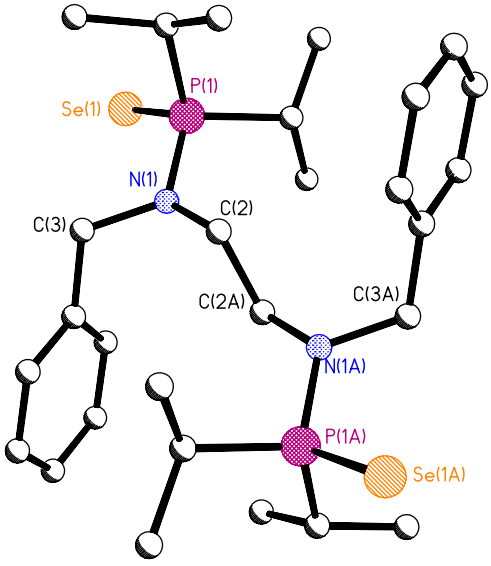

Fig. 3. Solid state structure of $^iPr_2P(Se)N(CH_2Ph)CH_2CH_2(CH_2Ph)NP(Se)^iPr_2$ **6.** Selected bond lengths (Å) and angles (°): Se(1)–P(1) 2.1115(10), P(1)–N(1) 1.679(3), P(1)–C(10) 1.822(4), P(1)–C(13) 1.853(4), N(1)–C(3) 1.477(4), N(1)–C(2) 1.475(4), N(1)–P(1)–C(10) 105.63(18), N(1)–P(1)–C(13) 109.80(17), C(10)–P(1)–C(13) 107.1(2), N(1)–P(1)–Se(1) 111.94(11), C(10)–P(1)–Se(1)111.31(15), C(13)–P(1)–Se(1) 110.86(13), C(3)–N(1)–C(2) 114.3(3), C(3)–N(1)–P(1) 118.9(2), C(2)–N(1)–P(1) 121.2(2).

Reaction of **2** with equimolar quantities of $[PtCl_2(cod)]$ in dichloromethane gives the seven-membered, *P P′* chelate *cis*-$[PtCl_2\{^iPr_2PN(CH_2Ph)CH_2CH_2N(CH_2Ph)P^iPr_2\}]$ **7**.

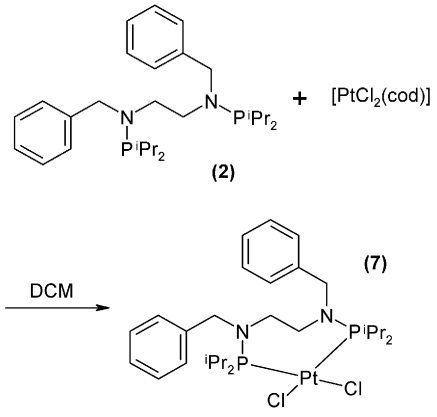

as a colourless solid in good yield (82%).

The $^{31}P\{^1H\}$ NMR spectrum of **7** consists of a singlet (δ (P) 86.7 ppm) with a $^1J(^{195}Pt–^{31}P)$ coupling constants of 4106 Hz. The analogous platinum complex with ligand **1** shows a very similar $^1J(^{195}Pt–^{31}P)$ (4048 Hz) and a singlet (δ (P) 59.1 ppm) at almost 27 ppm upfield because of the presence of phenyl groups on the phosphorus atoms instead of the more electron donating isopropyl groups present in **7**.

FAB^+ mass spectrometry does not show the parent-ion peak and shows instead fragmentation patterns consistent with the loss of one or two chloride ions (m/z) 702/3 [M–Cl^-] and 666/8 [M–$2Cl^-$] and the IR spectrum of **7** shows bands for ν(P–N) (887 cm^{-1}) and ν(Pt–Cl) (337 and 326 cm^{-1}) which supports the *cis* geometry of **7**.

Recrystallisation from hot toluene gives **7** as colourless crystals suitable for X-ray analysis. The X-ray structure of **7** (Fig. 4 and Table 2) reveal that the ligand is bound in a bidentate coordination mode to the platinum centre with *cis* geometry. The complex forms a seven-membered Pt–P–N–C–C–N–P ring and the metal has distorted square planar geometry because the bite angle of the ligand is larger than the ideal 90° and Cl–Pt–Cl is smaller than 90°. The P–N distances are typical of a single bond and are, as was the case for **6**, shorter than that in **2** (see Fig. 4).

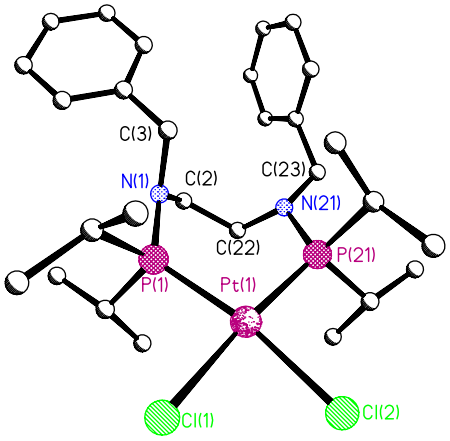

Fig. 4. Solid state structure of *cis*-[$PtCl_2\{^iPr_2PN(CH_2Ph)CH_2CH_2N(CH_2Ph)P^iPr_2\}$] **7**. Selected bond lengths (Å) and angles (°): Pt(1)–P(21) 2.2531(8), Pt(1)–P(1) 2.2594(8), Pt(1)–Cl(1) 2.3724(8), Pt(1)–Cl(2) 2.3777(8), P(1)–N(1) 1.6843(19), P(1)–C(10) 1.844(3), P(1)–C(13) 1.888(2), N(1)–C(3) 1.467(3), N(1)–C(2) 1.489(3), P(21)–Pt(1)–P(1) 100.64(3), P(21)–Pt(1)–Cl(1) 174.60(3), P(1)–Pt(1)-Cl(1) 84.74(3), P(21)–Pt(1)–Cl(2) 88.64(3), P(1)–Pt(1)–Cl(2) 170.44(2), Cl(1)–Pt(1)–Cl(2) 86.01(3), N(1)–P(1)–C(10) 103.84(12), N(1)–P(1)–C(13) 101.26(11), C(10)–P(1)–C(13) 106.58(12), N(1)–P(1)–Pt(1) 123.57(8), C(10)–P(1)–Pt(1) 107.82(9), C(13)–P(1)–Pt(1) 112.42(9), C(3)–N(1)–C(2) 112.06(19), C(3)–N(1)–P(1) 122.52(16),C(2)–N(1)–P(1) 119.13(17).

Ligands **1–4** were tested in the rhodium catalysed hydroformylation of hex-1-ene using a simple batch autoclave (Table 1) Generally the linear:branched selectivity is not particular impressive. We conducted simple molecular modelling calculations (Spartan Pro) of the natural bite angle (β_n) according to the method of Casey and co-workers [34,35] as well as the flexibility range of the ligand (Table 1) since van Leeuwen has proposed that ligands with a natural bite angle of 112°–120° favour equatorial–equatorial coordination during the catalytic cycle and thus give better l:b ratios. We have found a relatively poor correlation between natural bite angle (which specifically ignores metal orbital electronic effects) and the real bite angles, although generally the so-called natural bite angle is somewhat larger than either calculated or measured 'real' bite angle [36,37]. The results obtained with the ligands **1–4** which have natural bite angles in the range 108.9°–127.7° do not support the hypothesis that there is a correlation between bite angle and selectivity (see Table 2).

This work illustrates the usefulness of P–N containing ligands in hydroformylation, in particular the ease of the simple P–N bond forming reaction enables rapid screening of different ligand bite angles and electronic properties. Further work is in progress.

Table 1
Hydroformylation of oct-1-ene catalysed by rhodium complexes with batch autoclave test unit at 100 °C and 20 bar CO/H_2 (1:1); all reactions gave 100% conversion

Compound	Formula	Time (h)	Selectivity to aldehyde %	l:b	β_n	Flexibility range
1	$Ph_2PN(CH_2Ph)CH_2CH_2(CH_2Ph)NPPh_2$	22.2	79.8	1.9:1	108.9	28
2	$^iPr_2PN(CH_2Ph)CH_2CH_2(CH_2Ph)NP^iPr_2$	5	78.4	1.2:1	127.7	25
3	$Ph_2PNH(C_{10}H_6)_2NHPPh_2$	13.9	94.5	1.8:1	120	46
4	$Ph_2PNH(C_{10}H_6)(C_6H_4)NHPPh_2$	13.9	86.1	2.3:1	115.5	33

β is the natural bite angle [35].

Table 2
Details of the X-ray data collections and refinements

Compound (local ID number)	**2**	**3**	**6**	**7**
Empirical formula	$C_{28}H_{46}N_2P_2$	$C_{44}H_{34}N_2P_2$	$C_{28}H_{46}N_2P_2Se_2$	$C_{28}H_{46}N_2P_2Cl_2Pt$
M	472.6	652.7	630.5	738.6
Crystal system	triclinic	triclinic	orthorhombic	monoclinic
Space group	$P\bar{1}$	$P\bar{1}$	*Pbca*	$P2(1)/n$
a (Å)	8.392(2)	10.4672(19)	16.1838(7)	10.308(2)
b (Å)	9.344(4)	11.128(2)	13.6979(6)	22.822(4)
c (Å)	11.192(5)	15.555(3)	14.2025(7)	13.710(3)
α (°)	87.53(4)	89.499(3)		
β (°)	76.43(3)	85.136(3)		110.145(2)
γ (°)	61.64(2)	71.093(3)		
U (Å^3)	748	1708	3148	3028
Z	1	2	4	4
D_c (g cm^{-3})	1.049	1.269	1.330	1.620
μ (mm^{-1})	0.162	0.162	2.468	4.936
T (K)	293	125	293	125
Reflections measured	2263	8538	12,551	13,700
Independent reflections (R_{int})	1561(0.0174)	4776(0.0245)	2229(0.1166)	3924(0.1381)
Final R_1, wR_2 [$I > 2\sigma(I)$]	0.0464, 0.1174	0.0389, 0.0951	0.0352, 0.0841	0.0531, 0.1147

3. Experimental

General conditions for the syntheses and catalytic studies were as previously described [13,14].

$Ph_2PN(CH_2Ph)CH_2CH_2(CH_2Ph)NPPh_2$ ***1*** was prepared following the procedure of Balakrishna et al. [24].

A dry and degassed Et_2O (20 ml) solution of chlorodiphenylphosphine (3.2 ml, 3.95 g, 17.95 mmol) was added dropwise over a period of 30 min to a stirred solution of *N*,*N*′-dibenzylethylenediamine (2.050 g, 8.51 mmol) and triethylamine (2.4 ml, 1.72 g, 16.99 mmol) in dry and degassed Et_2O (20 ml) at 0 °C. Stirring was continued overnight, during which time a white precipitate separated from the colourless solution. This precipitate was isolated by suction filtration and consecutively washed with water, methanol and diethyl ether. The product was dried under *vacuum* to give a white solid which was crystallised from CH_2Cl_2–hexane. Yield: 4.25 g, 82%; Microanalysis: Found: (*Anal.* Calc.) C, 78.6 (78.9); H, 6.7 (6.3); N, 4.7 (4.6)%; $^{31}P\{H\}$ NMR ($CDCl_3$): 66.5 (s) ppm; Selected IR data (KBr): *v*(PN) 916 cm^{-1}; FAB^+ MS: *m*/*z* 610 $[M+H]^+$, 632 $[M+Na^+]$.

$(^iPr)_2PN(CH_2Ph)CH_2CH_2(CH_2Ph)NP(^iPr)_2$ ***2***. A dry and degassed Et_2O (10 ml) solution of chlorodiisopropylphosphine (3.5 ml, 3.386 g, 22.00 mmol) was added dropwise over a period of 30 min to a stirred solution of *N*,*N*′-dibenzylethylenediamine (2.5 ml, 2.644 g, 11.00 mmol) and triethylamine (3.1 ml, 2.23 g, 22.00 mmol) in dry and degassed Et_2O (40 ml). Stirring was continued for 5 days. The solution was evaporated to dryness in vacuo and thf (30 ml) was added. Triethylammonium hydrochloride separated from the colourless solution. This precipitate was removed by suction filtration under nitrogen. The filtrate was evaporated to dryness in vacuo to give a yellowish oil. Crystallisation from hot toluene gave white crystals.: Yield: 2.391 g, 46%; Microanalysis: Found: (*Anal.* Calc.) C, 70.7 (71.2); H, 10.3 (9.8); N 5.8 (5.9)%; $^{31}P\{H\}$ NMR ($CDCl_3$): 89.1 (s) ppm; FAB^+ MS: *m*/*z* 473 $[M+H^+]$.

$Ph_2PNH(C_{10}H_6)_2NHPPh_2$ ***3*** was prepared following the method of Miyano et al. [25,26].

A dry and degassed thf (10 ml) solution of (S)-(−)-1,1′-binaphthyl-2,2′-diamine (0.446 g, 1.57 mmol) was cooled to −78 °C in an acetone–dry Ice bath. To the cooled solution was added dropwise a hexane solution of BuLi (1.3 ml, 2.5 mol dm^{-3}, 3.28 mmol) over 30 min. After the addition the mixture was stirred at −78 °C for 1 h and another 30 additional min at room temperature. The reaction solution was cooled to −78 °C again and to it was added dropwise a solution of diphenylchlorophosphine (0.6 ml, 0.709 g, 3.21 mmol) in thf (10 ml) over 1 h. Stirring was continued for another 1 h at −78 °C. Then the cooling bath was removed and the mixture was stirred overnight at room temperature. The solution was evaporated to dryness in vacuo and dichloromethane (30 ml) was added. Lithium chloride, which precipitated, was removed by filtration under nitrogen and then the volatiles were evaporated in vacuo to leave a white solid. Recrystallisation from ethanol–benzene gave white crystals. $^{31}P\{H\}$ NMR ($CDCl_3$): 27.7 (s) ppm. IR, Mass Spectroscopy, ^1H NMR and elemental analysis are in agreement with literature data.

$Ph_2PNH(C_{10}H_6)(C_6H_4)NHPPh_2$ ***4***. A dry and degassed thf (25 ml) solution of 1-(2-aminophenyl)-2-naphthylamine (0.998 g, 4.26 mmol) was cooled to −78 °C in an acetone–dry Ice bath. To the cooled solution was added dropwise a hexane solution of BuLi (3.6 ml, 2.5 mol dm^{-3}, 8.91 mmol) over 50 min. After the addition, the mixture was stirred at −78 °C for 1 h and another 30 additional min at room temperature. The reaction solution was cooled to −78 °C again and to it was added dropwise a solution of diphenylchlorophosphine (1.6 ml, 1.928 g, 8.74 mmol) dissolved in thf (10 ml) over 1 h. Stirring was continued for another 1 h at −78 °C. Then the cooling bath was removed and the mixture was stirred overnight at room temperature. The solution was evaporated to dryness in vacuo and dichloromethane (30 ml) was added. Lithium chloride, which precipitated, was removed by filtration under nitrogen and then the volatiles were evaporated in vacuo to leave a white solid. Yield: 2.362 g, 92%; Microanalysis: Found: (*Anal.* Calc.) C, 79.4 (79.7); H, 5.2 (5.4); N, 4.6 (4.7)%; ^1H NMR: δ 7.86–6.86 ppm (m, 20 H, aromatic), 4.3 ppm (d, 1 H, $^2J(PH) = 78.3$ Hz, NH), 4.7 ppm (d, 1 H, $^2J(PH) = 78.3$ Hz, NH); $^{31}P\{H\}$ NMR ($CDCl_3$): 28.8 (s), 28.1 (s) ppm; Selected IR data (KBr): *v*(NH) 3367 and 3322 cm^{-1}, *v*(PN) 891 and 889 cm^{-1}; FAB^+ MS: *m*/*z* 603 $[M+H^+]$.

$Ph_2P(Se)N(CH_2Ph)CH_2CH_2(CH_2Ph)NP(Se)Ph_2$ ***5***. To a dry and degassed toluene (10 ml) solution of selenium (0.026 g, 0.33 mmol) was added solid $Ph_2PN(CH_2Ph)$ $CH_2CH_2(CH_2Ph)NPPh_2$ (0.100 g, 0.16 mmol). The solution was heated to reflux for ca. 2–3 h and allowed to cool to room temperature. The solution was evaporated to dryness in vacuo and the solid was dissolved in dichloromethane (2 ml). The dichloromethane solution was filtered through Celite and diethyl ether (20 ml) was added. The white product was collected by suction filtration and washed with diethyl ether (2×10 ml). Yield: 0.108 g, 88%; Microanalysis: Found: (Anal. Calc.) C, 62.9 (62.7); H, 4.6 (5.0); N, 3.6 (3.6)%; $^{31}P\{H\}$ NMR ($CDCl_3$): 70.8 (s) ppm, $^1J(^{77}Se–^{31}P)$ 777 Hz; Selected IR data (KBr): *v*(PN) 943 cm^{-1}, *v*(PSe) 557 cm^{-1}; FAB^+ MS: *m*/*z* 768 $[M+H^+]$.

$(^iPr)_2P(Se)N(CH_2Ph)CH_2CH_2$ $(CH_2Ph)NP(Se)(^iPr)_2$ ***6***. To a dry and degassed toluene (5 ml) solution of selenium (0.055 g, 0.70 mmol) was added $(^iPr)_2PN(CH_2Ph)CH_2CH_2(CH_2Ph)NP(^iPr)_2$ (0.165 g, 0.35 mmol) in toluene (5 ml). The solution was heated to reflux for ca. 2–3 h and allowed to cool to room temperature. The solution was evaporated to dryness in vacuo and the solid was dissolved in dichloromethane

(2 ml). The dichloromethane solution was filtered through Celite and diethyl ether (20 ml) was added. The white product was collected by suction filtration and washed with diethyl ether (2 × 10 ml). Recrystallisation from Toluene–hexane gave crystals. Yield: 0.159 g, 72%; Microanalysis: Found: (*Anal*. Calc.) C, 53.8 (53.3); H, 7.7 (7.4); N, 4.4 (4.4)%; $^{31}P\{H\}$ NMR ($CDCl_3$): 104.1 (s) ppm, $^{1}J(^{77}Se–^{31}P)$ 741 Hz; Selected IR data (KBr): ν(PN) 936 cm^{-1}, ν(PSe) 594 cm^{-1}; FAB^+ MS: *m/z* 630/2 [M], 655 [M+Na^+].

cis-[PtCl$_2${(^{i}Pr)$_2$PN(CH$_2$Ph)CH$_2$ CH$_2$(CH$_2$Ph)NP(^{i}Pr)$_2$}] 7. To a dichloromethane (10 ml) solution of [$PtCl_2$(cod)] (0.195 g, 0.52 mmol) was added (^{i}Pr)$_2$PN(CH$_2$Ph)CH$_2$CH$_2$(CH$_2$Ph)NP(^{i}Pr)$_2$ (0.246 g, 0.52 mmol) in dichloromethane (5 ml) and the colourless solution stirred for ca. 2–3 h. The solution was concentrated under reduced pressure to ca. 1 ml and diethyl ether (10 ml) added. The white product was collected by suction filtration and washed with diethyl ether (2 × 10 ml). Yield: 0.315 g, 82%; $^{31}P\{H\}$ NMR ($CDCl_3$): 86.7 (s) ppm, $^{1}J(^{195}Pt–^{31}P)$ 4106 Hz; Selected IR data (KBr): ν(PN) 887 cm^{-1}, ν(PtCl) 337 and 326 cm^{-1}; FAB^+MS: *m/z* 702/3 [M–Cl^-], 666/8 [M–2Cl^-].

Catalytic studies [Rh(acac)(CO)$_2$] (0.01 mol dm^{-3}), phosphine (0.023 mol dm^{-3}), hex-1-ene(1 cm^3) were reacted in toluene (4 cm^3) at 100 °C and 20 bar CO/H_2 (1:1) for time stated in Table 1. The rhodium complex, phosphine and toluene were heated at 100 °C and 14 bar CO/H2 (1:1) for 45 min, to allow the active catalyst to form before injection of the hex-1-ene and pressurising to 20 bar.

Crystallography was performed using a Bruker SMART diffractometer; full hemisphere of data with 0.3° 'slices', room temperature, Mo Kα radiation and empirical absorption corrections. All of the non-H atoms were refined anisotropically with the hydrogen atoms being refined in idealised geometries. All calculations employed the SHELXTL program system [38].

4. Supplementary materials

Crystallographic data for the structural analyses has been deposited with the Cambridge Crystallographic data centre, CCDC Nos. 221581–221584 Copies of this information may be obtained free of charge from The Director CCDC, 12 Union Road, Cambridge, CB2 1EZ UK (Fax +44 1223 336-033 or E-mail deposit@ccdc.cam.ac.uk or www: http://www.ccdc.cam.ac.uk).

Acknowledgements

We are grateful to the EPSRC for support, to Johnson Matthey for loans of precious metals and to the JREI for an equipment grant.

References

[1] S. Miyano, M. Nawa, A. Mori, H. Hashimoto, Bull. Chem. Soc. Jpn. 57 (1984) 2171.
[2] (a) P.W.N.M. van Leeuwen, C.P. Casey, G.T. Whiteker, Rhodium Catalysed Hydroformylation, in: P.W.N.M. van Leeuwen, C. Claver, Kluber Academic Publishers, Dordrecht, The Netherlands, 2000 (Ch. 4);
(b) F. Agbossou, J.F. Carpentier, A. Mortreux, Chem. Rev. 95 (1995) 2485;
(c) M. Beller, B. Cornils, C.D. Frohning, C.W. Kohlpaintner, J. Mol. Catal. A 104 (1995) 17.
[3] C.P. Casey, E.L. Paulsen, E.W. Beuttenmueller, B.R. Proft, B.A. Matter, D.R. Powell, J. Am. Chem. Soc. 121 (1999) 63.
[4] C.P. Casey, G.T. Whiteker, M.G. Melville, L.M. Petrovich, J.A. Gavney Jr., D.R. Powell, J. Am. Chem. Soc. 114 (1992) 5535.
[5] L.A. Van der Veen, M.D.K. Boele, F.R. Bregman, P.C.J. Kamer, P.W.N.M. van Leeuwen, K. Goubitz, J. Fraanje, H. Schenk, C. Bo, J. Am. Chem. Soc. 120 (1998) 11616.
[6] (a) P.W.N.M. van Leeuwen, C.F. Roobeek, J. Organomet. Chem. 258 (1983) 343;
(b) T. Jongsma, G. Challa, P.W.N.M. van Leeuwen, J. Organomet. Chem. 421 (1991) 121;
(c) A. van Rooy, E.N. Orij, P.C.J. Kamer, F. Van den Aardweg, P.W.N.M. van Leeuwen, J. Chem. Soc., Chem. Commun. (1991) 1096;
(d) A. van Rooy, E.N. Orij, P.C.J. Kamer, P.W.N.M. van Leeuwen, Organometallics 14 (1995) 34;
(e) M.P. Magee, W. Luo, W.H. Hersh, Organometallics 21 (2002) 362;
(f) B. Breit, R. Winde, T. Mackewitz, R. Paciello, K. Harms, Chem. Eur. J. 7 (2001) 3106;
(g) R. Jackstell, H. Klein, M. Beller, K.-D. Wiese, D. Rottger, Eur. J. Org. Chem. 20 (2001) 3871.
[7] J.D. Unruh, J.R. Christenson, J. Mol. Catal. 14 (1982) 19.
[8] W.R. Moser, C.J. Papile, D.A. Brannon, R.A. Duwell, J. Mol. Catal. 41 (1987) 271.
[9] L.A. van der Veen, P.C.J. Kamer, P.W.N.M. van Leeuwen, Organometallics 18 (1999) 4765.
[10] D.J. Wink, T.J. Kwok, A. Yee, Inorg. Chem. 29 (1990) 5006.
[11] E. Billing, A.G. Abatjoglou, D.R. Bryant, U.S. Patent 4,668,651, European Patent Application 213,639, 1987 (to Union Carbide), Chem. Abstr., 107 (1987) 7392.
[12] E. Billing, A.G. Abatjoglou, D.R. Bryant, R.E. Murray, J.M. Maher, U.S. Patent 4,599,206, 1986 (to Union Carbide), Chem. Abstr., 109 (1988) 233177.
[13] M. Rodriguez i Zubiri, M.L. Clarke, D.F. Foster, D.J. Cole-Hamilton, A.M.Z. Slawin, J.D. Woollins, J. Chem. Soc., Dalton Trans. (2001) 969.
[14] M. Rodriguez i Zubiri, A.M.Z. Slawin, M. Wainwright, J.D. Woollins, Polyhedron 21 (2002) 1729.
[15] M.L. Clarke, A.M.Z. Slawin, M.V. Wheatley, J.D. Woollins, JCS Dalton (2001) 3421.
[16] S.M. Aucott, A.M.Z. Slawin, J.D. Woollins, JCS Dalton (2001) 2279.
[17] M. Wainwright, J.D. Woollins, JCS Dalton (2001) 2724.
[18] M.L. Clarke, D.J. Cole-Hamilton, J.D. Woollins, JCS Dalton (2001) 2721.
[19] M.L. Clarke, G. Holliday, A.M.Z. Slawin, J.D. Woollins, JCS Dalton (2002) 1093.
[20] Q. Zhang, S.M. Aucott, A.M.Z. Slawin, J.D. Woollins, Eur. J. Inorg. Chem., Cover (2002) 1635.
[21] M.L. Clarke, A.M.Z. Slawin, J.D. Woollins, Polyhedron 22 (2003) 22.
[22] Q. Zhang, G. Hua, P. Bhattacharyya, A.M.Z. Slawin, J.D. Woollins, Eur. J. Inorg. Chem. (2003) 2426.

[23] N.C. Payne, D.W. Stephan, J. Organomet. Chem. 221 (1981) 203.
[24] M.S. Balakrishna, R.M. Abhyankar, J.T. Mague, J. Chem. Soc., Dalton Trans. (1999) 1407.
[25] S. Miyano, M. Nawa, H. Hashimoto, Chem. Lett. (1980) 729.
[26] S. Miyano, M. Nawa, A. Mori, H. Hashimoto, Bull. Chem. Soc. Jpn. 57 (1984) 2171.
[27] P. Bhattacharyya, A.M.Z. Slawin, M.B. Smith, D.J. Williams, J.D. Woollins, J. Chem. Soc., Dalton Trans. (1996) 3647.
[28] A. Sen, Acc. Chem. Res. 26 (1993) 303.
[29] V.S. Reddy, K.V. Katti, C.L. Barnes, Chem. Ber. 127 (1994) 1355.
[30] P. Bhattacharyya, J. Novosad, J. Phillips, A.M.Z. Slawin, D.J. Williams, J.D. Woollins, J. Chem. Soc., Dalton Trans. (1995) 1607.
[31] P.A.W. Dean, Can. J. Chem. 57 (1979) 754.
[32] P.W. Dyer, J. Fawcett, M.J. Hanton, R.D.W. Kemmitt, R. Padda, N. Singh, Dalton Trans. (2003) 104.
[33] N.G. Anderson, B.A. Keay, Chem. Rev. 101 (2001) 997.
[34] C.P. Casey, G.T. Whiteker, M.G. Melville, L.M. Petrovich, J.A. Gavney Jr., D.R. Powell, J. Am. Chem. Soc 114 (1992) 5535.
[35] P.C.J. Kamer, P.W.N.M. van Leeuwen, J.N.H. Reek, Acc. Chem. Res. 34 (2001) 895, and references therein.
[36] M. Rodriguez i Zubiri, PhD Thesis, University of St. Andrews, 2002.
[37] S.C. van der Slot, J. Duran, J. Luten, P.C.J. Kamer, P.W.N.M. van Leeuwen, Organometallics 21 (2002) 3873.
[38] SHELXTL, Bruker AXS, Madison, WI, 1999.

Available online at www.sciencedirect.com
SCIENCE DIRECT®
Polyhedron 23 (2004) 701–707
POLYHEDRON
www.elsevier.com/locate/poly

Characterization of the mixed-valent intermediate ($n = 3$) of the complex series $\{(\mu, \eta^3{:}\eta^3\text{-L})[(Ru(terpy)]_2\}^{n+}$ with the unsaturated bridging ligand N,N'-bis (α-picolinoyl)hydrazido(2−) = L^{2-}

Axel Knödler [a], Jan Fiedler [b], Wolfgang Kaim [a,*]

[a] Institut für Anorganische Chemie, Universität Stuttgart, Pfaffenwaldring 55, D-70550 Stuttgart, Germany
[b] J. Heyrovsky Institute of Physical Chemistry, Academy of Sciences of the Czech Republic, Dolejškova 3, CZ-18223 Prague, Czech Republic

Received 1 September 2003; accepted 25 November 2003

Abstract

N,N'-Bis(α-picolinoyl)hydrazine H_2L, a potentially bis-tridentate conjugated ligand in its doubly deprotonated form L^{2-}, has been used to synthesize the diruthenium(II) complex $\{(\mu\text{-L})[Ru(terpy)]_2\}(PF_6)_2$. Its electrochemical and spectroelectrochemical (UV–Vis–NIR, EPR) investigation reveals a mixed-valent ($Ru^{III}Ru^{II}$) intermediate with electrochemical and spectroscopic characteristics related to those of the $\{(\mu\text{-adc-R})[Ru(bpy)_2]_2\}^{3+}$ ions (adc-R^{2-} = bis-bidentate C-substituted diacylhydrazido(2−) ligands): comproportionation constant $K_c = 10^{9.0}$ (CH_2Cl_2), intervalence charge transfer band at 1000 nm ($\varepsilon = 3800\ M^{-1}\ cm^{-1}$), EPR signal at $g_\perp = 2.14$, $g_\parallel = 1.953$. The non-innocent nature of L^{n-} is inferred from comparative analysis of the spectroscopic data.
© 2003 Elsevier Ltd. All rights reserved.

Keywords: EPR spectroscopy; Hydrazido ligand; Mixed-valence; Ruthenium complexes; Spectroelectrochemistry

1. Introduction

Non-innocent bridging ligands such as azo-containing compounds [1,2] are of interest in coordination chemistry because they can strongly modify the metal–metal interaction. The remarkable properties of the bis-bidentate N,N'-diacylhydrazido(2−) ligands (adc-R^{2-}) [1,3,4] such as facile two-step electron transfer involving radical-bridged [4] or mixed-valent intermediates [3] with rather short metal–metal distances of less than 5 Å [4] have motivated our interest in the potentially *bis-tridentate* conjugated bridging ligand N,N'-bis(α-picolinoyl)hydrazido(2−) (L^{2-} = adc-R^{2-} with R = 2-pyridyl). The adc-R/adc-$R^{\cdot-}$/adc-R^{2-} two-step redox system has been shown to exhibit quinonoid characteristics [3,4] with a typically stable radical intermediate, an oxidized (azodicarbonyl) form, and two conceivable resonance structures for the two-electron reduced (dianionic) state (Scheme 1). While the "S frame" conformation of Scheme 1 ensures a relatively short metal–metal distance <5 Å in dinuclear complexes [4], the group R allows for an electronic [3] and, as will be shown here, geometrical tuning. The protonated form [5,6] H_2L of the ligand has been studied before in connection with its anti-HIV and antitumor potential [7].

In this report we describe the synthesis of the bis-terpyridineruthenium complex as prepared from (terpy)(DMSO)Cl_2Ru [8] and H_2L [6], including studies of the $Ru_2^{II,II}$, $Ru_2^{III,II}$ and $Ru_2^{III,III}$ oxidation states. In contrast to bis(N,O)-coordinated complexes [3,4] such as $\{(\mu\text{-adc-R})[Ru(bpy)_2]_2\}^{n+}$ (Scheme 2A) the system $\{(\mu\text{-L})[Ru(terpy)]_2\}^{n+}$ was expected to exhibit a bis(N,N',O)-coordination of the bridging ligand (Scheme 2B).

Conjugated ligands with $\mu, \eta^3{:}\eta^3$ coordination are not very common, examples used in mixed valence chemistry include the π accepting polypyridyl systems 2,3,4,5-tetrakis(2-pyridyl)pyrazine [9] and spacer-linked bis-terpy compounds [10].

* Corresponding author. Tel.: +49-711-685-4170; fax: +49-711685-4165.
E-mail address: kaim@iac.uni-stuttgart.de (W. Kaim).

0277-5387/$ - see front matter © 2003 Elsevier Ltd. All rights reserved.
doi:10.1016/j.poly.2003.11.043

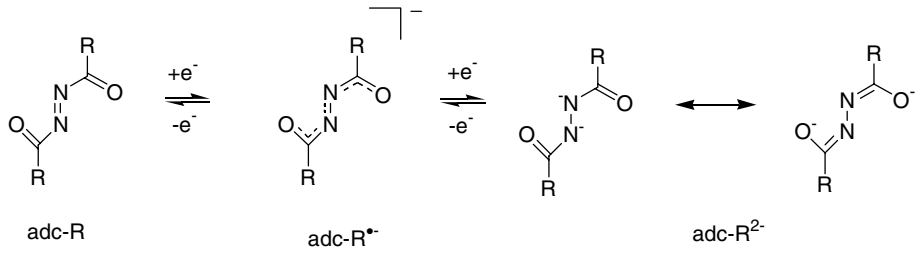

Scheme 1.

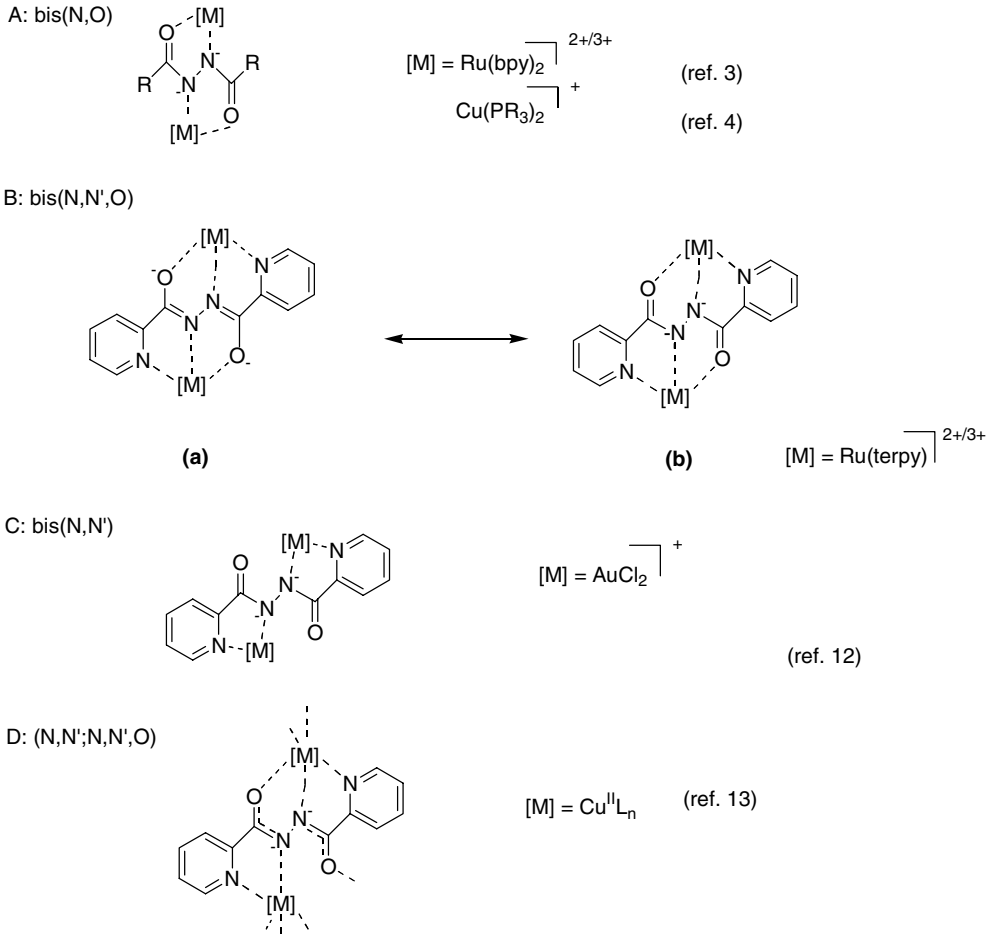

Scheme 2.

Considering the continued interest in diruthenum mixed-valent systems [11a], our interest was to study the effect of this different coordination on the properties of the $Ru_2^{II,III}$ intermediate state.

Complexes of L^{2-} have been observed to result from ring-opening reactions of 3,6-bis(2-pyridyl)-1,2,4,5-tetrazine, e.g. with $KAuCl_4$ in aqueous medium to produce a bis(N,N')-coordinated bis(dichlorogold(III)) species (Scheme 2C) [12]; in a similar recent report [13] it was described that the use of copper(II) complexes leads to tetranuclear species with (N,N',O) and (N,N') coordination of L^{2-} (Scheme 2D).

2. Experimental

2.1. Instrumentation

EPR spectra were recorded in the X band on a Bruker System ESP 300 equipped with a Bruker ER035M gaussmeter and a HP 5350B microwave counter. ^{1}H NMR spectra were taken on a Bruker AC 250 spectrometer. UV–Vis–NIR absorption spectra were recorded on a Bruins Instruments Omega 10 spectrophotometer. IR spectra were measured on a Paragon 1000 PC FTIR instrument from Perkin–Elmer. Cyclic

voltammetry was carried out at 100 mV/s scan rate in 0.1 M Bu_4NPF_6 containing solutions using a three-electrode configuration (glassy carbon working electrode, Pt counter electrode, Ag/AgCl reference) and a PAR 273 potentiostat and function generator. The ferrocene/ferrocenium couple served as internal reference. Spectroelectrochemical measurements were performed using an optically transparent thin-layer electrode (OTTLE) cell [14] for UV–Vis spectra and a two-electrode capillary for EPR studies [15].

2.2. Syntheses

N,*N*′-Bis(α-picolinoyl)hydrazine H_2L was prepared from hydrazinium sulfate and α-picolinoyl chloride in aqueous medium according to a general procedure [16]. Its identity was confirmed by comparison with reported spectroscopic and structural characteristics [5,6]. The precursor complex (terpy)(DMSO)Cl_2Ru was obtained as described [8a].

*{(**μ**-L)[Ru(terpy)]$_2$}(PF$_6$)$_2$*. A mixture of 130.2 mg (0.269 mmol) (terpy)(DMSO)Cl_2Ru, 32.6 mg (0.135 mmol) H_2L and 30 mg NaOH, dissolved in 40 ml H_2O and 8 ml CH_3OH, was heated to reflux for 40 h. After cooling to room temperature 0.50 g KPF_6, dissolved in 20 ml water, were added to produce a reddish-brown precipitate which was collected, washed with water and dried to yield 70 mg (43%). *Anal*. Calc. for $C_{42}H_{30}F_{12}N_{10}O_2P_2$ $Ru_2 \cdot 4H_2O$ (1279.90): C, 39.41; H, 3.07; N, 10.95. Found: C, 39.46; H, 2.71; N, 10.56%. ^{1}H NMR (acetone-d_6): 6.86–6.99 (m, 3H), 7.30–7.38 (m, 3H), 7.66 (ddd, 2H), 7.77 (m, 2H), 7.92 (m, 4H), 8.11–8.33 (m, 6H), 8.70 (m, 2H), 8.76–8.95 (m, 7H), 9.16 (ddd, 1H). IR (KBr): 1600br, 1550w, 1487s, 1448m, 1432m, 1376s.

3. Results and discussion

3.1. Synthesis and characterization of {(μ-L)[Ru(terpy)]$_2$}$^{2+}$

The hydrazine form H_2L of the ligand[5] was obtained according to Scheme 3, its identity was established *inter alia* through a confirmation of the reported crystal structure analysis [6]. The well-known precursor complex (terpy)(DMSO)Cl_2Ru was also characterized crystallographically [8b], exhibiting *trans*-positioned chloride ligands, S-bonded DMSO with the S–O bond in the (terpy)Ru plane and a symmetrically coordinated 2,2′:6′,2″-terpyridine ligand.

Reaction of H_2L with two equivalents of (terpy)(DMSO)Cl_2Ru in basic H_2O/MeOH yielded {(μ-L)[Ru(terpy)]$_2$}$(PF_6)_2$. The complex was found to be well behaved but only moderately soluble in non-coordinating dichloromethane, studies in coordinating solvents such as CH_3CN produced unsatisfactory, variable results which we attribute to a competition between the solvent molecules and the presumably weakly bonded carbonyl groups for the metal coordination. In less coordinating acetone-d_6 where the compound is well soluble the NMR data suggest a lower symmetry that C_{2h}, possibly due to nonsymmetrical coordination of the tridentate ligands. The IR spectra in KBr confirm the η^3:η^3 coordination pattern of L: The intense bands at 1709 and 1675 cm^{-1} in the free ligand H_2L are shifted to much lower values of 1487 and 1376 cm^{-1}, in agreement with deprotonation and metal coordination at the carbonyl oxygen atoms. Similar observations were made for $[(bpy)_2Ru(adc\text{-}R)Ru(bpy)_2](PF_6)_2$ [3].

3.2. Cyclic voltammetry

As illustrated in Fig. 1, the diruthenium(II) complex is oxidized in CH_2Cl_2 via two one-electron steps with a separation of 530 mV between the half-wave potentials. The comproportionation constant $K_c = 10^{9.0}$ calculated according to Eq. (2) is similar to the one observed for the related complex $\{(\mu\text{-adc-R})[Ru(bpy)_2]_2\}^{3+}$, R = Ph, with $K_c = 10^{9.7}$ [3]. This similarity reflects a comparable charge and distance situation for both systems.

$$\underset{\text{Red}}{M^n\text{-L-}M^n} \underset{+e^-}{\overset{-e^-}{\rightleftharpoons}} \underset{\text{Int}}{M^n\text{-L-}M^{n+1}} \underset{+e^-}{\overset{-e^-}{\rightleftharpoons}} \underset{\text{Ox}}{M^{n+1}\text{-L-}M^{n+1}} \qquad (1)$$

$$\text{Comproportionation constant } K_c = \frac{[\text{Int}]^2}{[\text{Red}][\text{Ox}]} = 10^{\Delta E/59mV} \quad \Delta E = E_2 - E_1 \qquad (2)$$

The electrochemical data for the phenyl and 2-pyridyl substituted complexes are compared in Table 1.

The absolute potentials are slightly higher for {(μ-adc-Ph)[Ru(bpy)$_2$]$_2$}$^{n+}$ although the substitution of

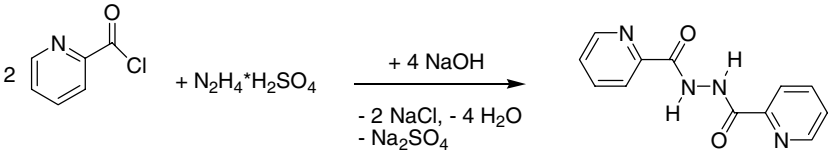

Scheme 3.

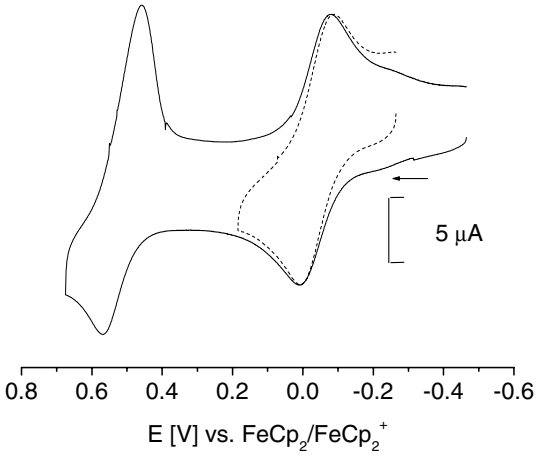

Fig. 1. Cyclic voltammogram of $\{(\mu\text{-L})[Ru(terpy)]_2\}(PF_6)_2$ in CH_2Cl_2/0.1 M Bu_4NPF_6 at 100 mV scan rate (adsorption on re-reduction).

Table 1
Cyclovoltammetric data of adc-R-bridged diruthenium complexes[a]

	[(terpy)Ru(μ-adc-py) Ru(terpy)]$^{2+}$[c]	[(bpy)$_2$Ru(μ-adc-Ph) Ru(bpy)$_2$]$^{2+}$[b]
E^{4+}/E^{3+}	0.49	0.73
E^{3+}/E^{2+}	−0.04	0.16
E^{2+}/E^{+}	−1.78[d]	−1.91
E^{+}/E^{0}	−1.88[d]	−1.91
ΔE^{3+}[e]	0.53	0.57
K_c(3+)	$10^{9.0}$	$10^{9.7}$

[a] Potentials in V vs ferrocene$^{0/+}$.
[b] 0.1 M Bu_4NPF_6/DCE (Ref. [3]).
[c] 0.1 M Bu_4NPF_6/CH_2Cl_2.
[d] E_{pc} for irreversible process (terpy reduction).
[e] $\Delta E^{3+} = E^{4+/3+} - E^{3+/2+}$.

phenyl by the better accepting 2-pyridyl in $\{(\mu\text{-L})[Ru(terpy)]_2\}^{n+}$ should cause an anodic shift. However, the different coordination arrangements have to be considered (Scheme 4) when formally shifting one 2-pyridyl substituent from each of the $[Ru(bpy)_2]$ fragments to the bridging ligand in L^{2-}. Obviously, interaction between the π ligands in their probably close to perpendicular situation is expected to be smaller for the (terpy)Ru complex.

Reduction occurs irreversibly at two closely spaced peak potentials (Table 1). It is not uncommon that terpy exhibits irreversible reduction because of enhanced reactivity at the 4′ position [17]. Cyclic voltammetry of $(\mu\text{-L})[Ru(terpy)]_2\}(PF_6)_2$ in acetonitrile did not yield straightforward results, additional waves point to partial replacement of donor functions of L^{2-} by the potentially coordinating solvent.

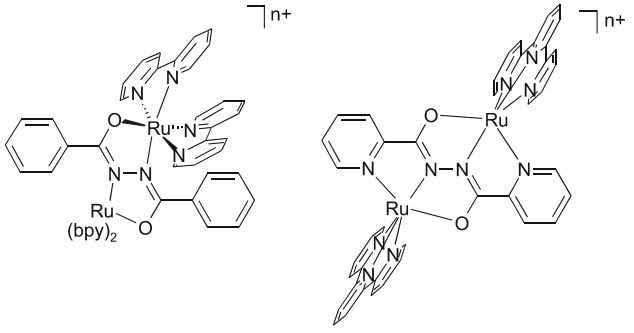

Scheme 4.

3.3. UV–Vis–NIR spectroelectrochemistry

Spectroelectrochemistry in the UV–Vis–NIR region using an OTTLE cell [14] produced characteristic reversible changes (Fig. 2, Table 2). Whereas the $Ru^{II}Ru^{II}$(2+) state exhibits a long-wavelength ligand(L^{2-})-to-ligand(terpy) charge transfer (LLCT) transition and typical [10] metal-to-(terpy-)ligand MLCT absorption bands, the (3+) intermediate is dis-

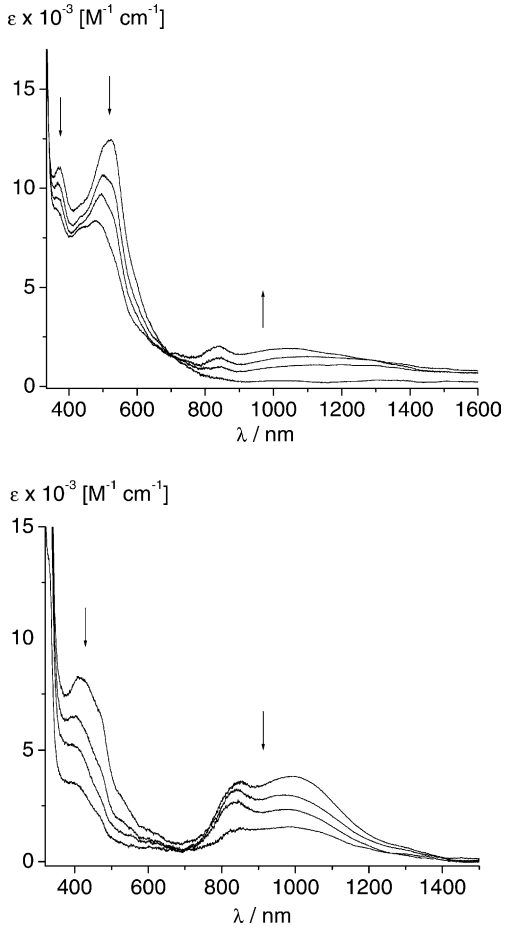

Fig. 2. Spectroelectrochemical response of $\{(\mu\text{-L})[Ru(terpy)]_2\}(PF_6)_2$ in CH_2Cl_2/0.1 M Bu_4NPF_6 on oxidation, starting from the (2+) form (top) and the electrogenerated (3+) state (bottom) of the complex cation, respectively.

Table 2
UV–Vis–NIR data of adc-R-bridged diruthenium complexes[a]

n+	[(terpy)Ru(μ-adc-py)Ru(terpy)]$^{n+}$[b]		[(bpy)$_2$Ru(μ-adc-Ph)Ru(bpy)$_2$]$^{n+}$[c]	
2+	314 (50 900)	$\pi \rightarrow \pi^*$		
	369 (11 900)	MLCT	358 (27 900)	MLCT
	500sh			
	525 (12 400)	MLCT	524 (19 100)	MLCT
	590sh	LLCT		
3+	314 (41 200)	$\pi \rightarrow \pi^*$		
	430 (8200)	MLCT	430 (23 300)	MLCT
	470sh			
	530sh			
	615sh			
	840 (3600)[d]	LMCT		
	1000 (3800)[e]	IVCT	1603 (6200)	IVCT
4+	311 (17 600)	$\pi \rightarrow \pi^*$		
	332sh	MLCT		
	405sh (3000)	MLCT		
	480sh	MLCT	893[f]	MLCT/LMCT

[a] Wavelengths λ_{max} in nm, molar extinction coefficients ε in M^{-1} cm^{-1} in parentheses.
[b] Measurements in 0.1 M Bu_4NPF_6/CH_2Cl_2.
[c] Measurements in DCE [3].
[d] $\Delta\nu_{1/2} = 1850$ cm^{-1}.
[e] $\Delta\nu_{1/2} = 2650$ cm^{-1}.
[f] For [(bpy)$_2$Ru(μ-adc-OEt)Ru(bpy)$_2$]$^{4+}$ (Ref. [3]).

tinguished by two discernible bands in the near infrared region at about 1000 and 840 nm. At least one such band would be typical for the intervalence charge transfer (IVCT) transition of a mixed-valent compound [11] as has been similarly observed [3] albeit at distinctly longer wavelengths for the bis(2,2′-bipyridine) ruthenium complexes of the adc-R ligands (Table 2). The presence of two low-energy CT bands would be in agreement with recent calculations employing a three-state model, including a mediating LMCT or MLCT state, for ligand-bridged mixed-valent systems [11d]. The higher energy for $\{(\mu, \eta^3{:}\eta^3\text{-L})[Ru(terpy)]_2\}^{3+}$ suggests stronger electronic coupling through the bis-tridentate conjugated bridge. If class III behavior [11,18] (valence averaging) is assumed as supported by the large K_c and by the rather small band width (Table 2), the interaction energy can be estimated [11] at $\nu(IVCT)/2 = 5000$ cm^{-1}, a rather high value. For a class II situation, however, the electronic interaction would be calculated [19] at 1307 cm^{-1} according to $H_{AB} = 2.06 \times 10^{-2} R^{-1} \sqrt{\varepsilon \nu_{max} \Delta\nu_{1/2}}$ (ν in cm^{-1}, R estimated at 5 Å [4]). The hypsochromic shifts of the $Ru \rightarrow \pi^*$(terpy) MLCT band on oxidation are as expected [3], reflecting a decreasing relative donor effect of the bridge.

The absence of an intense long-wavelength absorption band for the (4+) form is conspicuous (Table 2). Such band was observed for all dinuclear bis(bipyridine)ruthenium complexes and was assigned to a mixed MLCT/LMCT transition originating from the possible resonance structures (3): LMCT for formulation (3A), MLCT for formulation (3C).

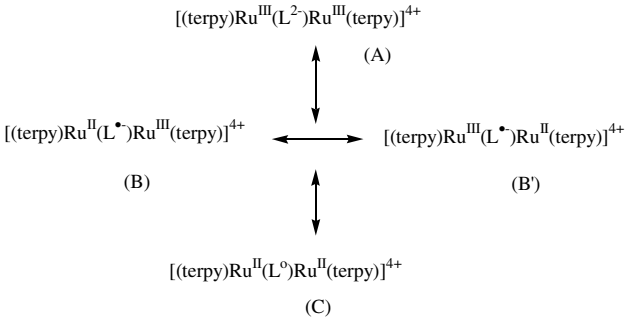

(3)

We interpret the absence of a long-wavelength band to an interrupted π conjugation of μ-adc-py [12], made possibly by the dissociation of the Ru–O coordinative bonds. This would be facilitated especially in formulation (3C) through the absence of negative charge on the bridging ligand which would render the carbonyl oxygen atoms as very weak donors. Although the spectroelectrochemical experiments show fully reversible spectral changes, this does not rule out specific reversible dissociation processes, especially in the presence of a polydentate ligand with rather different donor atoms.

3.4. EPR spectroscopy

The EPR spectrum of the (3+) intermediate should help to clarify whether this is an L^{2-} bridged $Ru^{III}Ru^{II}$ system or a radical complex $Ru^{II}(\mu\text{-}L^{\cdot-})Ru^{II}$ (4).

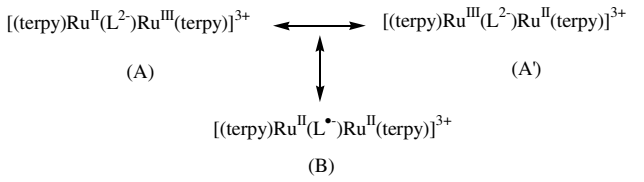

(4)

The spectrum (Fig. 3) and the data in Table 3 clearly point to the mixed-valent formulation although contributions from the bridging ligand to the singly occupied MO can be expected in a donor-bridged (''hole-transfer'') situation [3,11].

While both the g_{av} value and the sizeable g anisotropy $g_1 - g_3$ rule out a predominant diruthenium(II)-radical situation for which $1.99 < g_{av} < 2.02$ and $g_1 - g_3 < 0.1$ [3,20,21], the distinctly smaller axial g anisotropy for $\{(\mu, \eta^3{:}\eta^3\text{-L})[\mathrm{Ru(terpy)}]_2\}^{3+}$ suggests higher contributions from the more conjugated adc-py ligand to the singly occupied MO (SOMO). In agreement with this interpretation the EPR signal is still observable at 77 K at which temperature the dinuclear bis(bipyridine)ruthenium species are already EPR silent [3]. We thus assume a more delocalized metal/ligand/metal situation for $\{(\mu, \eta^3{:}\eta^3\text{-L})[\mathrm{Ru(terpy)}]_2\}^{3+}$ supported by the conjugated pyridyl rings.

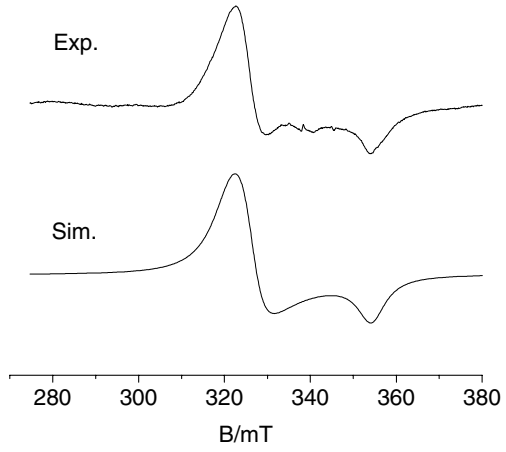

Fig. 3. EPR spectrum of $\{(\mu\text{-L})[\mathrm{Ru(terpy)}]_2\}^{3+}$ in CH_2Cl_2/0.1 M Bu_4NPF_6 at 3.4 K with computer simulation.

Table 3
EPR data of paramagnetic intermediates

	[(terpy)Ru(μ-adc-py)Ru(terpy)]$^{3+}$	[(bpy)$_2$Ru(μ-adc-Ph)Ru(bpy)$_2$]$^{3+}$
g_1	2.150	2.344
g_2	2.120	2.003
g_3	1.953	1.895
g_{av}[a]	2.076	2.089
$g_1 - g_3$	0.197	0.449
Solvent (temperature)	CH_2Cl_2 (3.4 K)	Acetone (3.8 K)

[a] $g_{av} = [(g_1^2 + g_2^2 + g_3^2)/3]^{1/2}$.

3.5. Conclusions

Apparently, the formal transfer of one pyridyl group in $\{(\mu\text{-adc-R})[\mathrm{Ru(bpy)_2}]_2\}^{n+}$ from one bpy to the bridging ligand in $\{(\mu\text{-L})[\mathrm{Ru(terpy)}]_2\}^{n+}$ while converting the polypyridyl set to terpy with its constraint to meridional coordination affects the electronic structure but does not significantly influence the electrochemical coupling.

The N,N'-bis(α-picolinoyl)hydrazido(2−) ligand L^{2-} can act as bis-bidentate, bidentate/tridentate or bis-tridentate ligand due to the very different nature of the donor atoms N_{py}, N_{azo} and O. Whereas the bis(N,N')-coordination in the digold(III) compound (Scheme 2C) allows for a complete twist around the central N–N bond to produce orthogonal and thus non-conjugated molecular halves [12], the bis(N,N',O)-coordination achieved for $\{(\mu\text{-L})[\mathrm{Ru(terpy)}]_2\}^{n+}$ ensures ligand-mediated metal–metal communication, as evident most strikingly from the properties of the mixed-valent intermediate ($n = 3$).

Acknowledgements

Support from the Deutsche Forschungsgemeinschaft, the Fonds der Chemischen Industrie, the Grant Agency of the Czech Republic (Grant No. 203/03/082) and the Ministry of Education of the Czech Republic (Grant COST OC D15.10) is gratefully acknowledged.

References

[1] W. Kaim, Coord. Chem. Rev. 291–221 (2001) 463.
[2] W. Kaim, Coord. Chem. Rev. 230 (2002) 127.
[3] V. Kasack, W. Kaim, H. Binder, J. Jordanov, E. Roth, Inorg. Chem. 34 (1995) 1924.
[4] M. Moscherosch, J.S. Field, W. Kaim, S. Kohlmann, M. Krejcik, J. Chem. Soc., Dalton Trans. (1993) 211.
[5] H. Zhao, T.R. Burke Jr., Tetrahedron 53 (1997) 4219.
[6] S. Shao, D. Zhu, Y. Song, X.Z. You, S.S.S. Raj, H.-K. Fun, Acta Crystallogr., Sect. C 55 (1999) 1841.
[7] (a) H. Zhao, N. Neamati, S. Sunder, H. Hong, S. Wang, G.W.A. Milne, Y. Pommier, T.R. Burke Jr., J. Med. Chem. 40 (1997) 937; (b) H. Rutner, N. Lewin, E.C. Woodbury, T.J. McBride, K.V. Rao, Cancer Chemother. Rep., Part 1 58 (1974) 803.
[8] (a) T. Norrby, A. Börje, B. Åkermark, L. Hammarström, J. Alsins, K. Lashgari, R. Norrestam, J. Mårtensson, G. Stenhagen, Inorg. Chem. 36 (1997) 5850; (b) A. Knödler, W. Kaim, unpublished results.
[9] (a) N. Chanda, R.H. Laye, S. Chakraborty, R.L. Paul, J.C. Jeffery, M.D. Ward, G.K. Lahiri, J. Chem. Soc., Dalton Trans. (2002) 3496; (b) J.P. Collin, P. Laine, J.P. Launay, J.P. Sauvage, A. Sour, J. Chem. Soc., Chem. Commun. (1993) 434;

(c) C.R. Arana, D.H. Abruna, Inorg. Chem. 32 (1993) 194;
(d) R.P. Thummel, S. Chirayil, Inorg. Chim. Acta 154 (1988) 77;
(e) L.M. Vogler, B. Scott, K.J. Brewer, Inorg. Chem. 32 (1993) 898;
(f) J.-D. Lee, L.M. Vrana, E.R. Bullock, K.J. Brewer, Inorg. Chem. 37 (1998) 3575;
(g) T.S. Akasheh, D. Marji, Z.M. Al Ahmed, Inorg. Chim. Acta 141 (1988) 125;
(h) C.M. Hartshorn, N. Daire, V. Tondreau, B. Loeb, T.J. Meyer, P.S. White, Inorg. Chem. 38 (1999) 3200;
(i) L.M. Vogler, K.J. Brewer, Inorg. Chem. 35 (1996) 818;
(j) R. Ruminski, J. Kiplinger, T. Cockroft, C. Chase, Inorg. Chem. 28 (1989) 370;
(k) D.M. Dattelbaum, C.M. Hartshorn, T.J. Meyer, J. Am. Chem. Soc. 124 (2002) 4938.

[10] (a) M. Beley, J.-P. Collin, R. Louis, B. Metz, J.-P. Sauvage, J. Am. Chem. Soc. 113 (1991) 8521;
(b) J.-P. Sutter, D.M. Grove, M. Beley, J.-P. Collin, N. Veldman, A.L. Spek, J.-P. Sauvage, G. van Koten, Angew. Chem., Int. Ed. Engl. 33 (1994) 1282;
(c) M. Beley, S. Chodorowski-Kimmes, J.-P. Collin, P. Lainé, J.-P. Launay, J.-P. Sauvage, Angew. Chem., Int. Ed. Engl. 33 (1994) 1775.

[11] (a) W. Kaim, A. Klein, M. Glöckle, Acc. Chem. Res. 33 (2000) 755;
(b) R.J. Crutchley, Adv. Inorg. Chem. 41 (1994) 273;
(c) K.D. Demadis, C.M. Hartshorn, T.J. Meyer, Chem. Rev. 101 (2001) 2655;
(d) B.S. Brunschwig, C. Creutz, N. Sutin, Chem. Soc. Rev. 31 (2002) 168.

[12] A. Dogan, B. Schwederski, T. Schleid, F. Lissner, J. Fiedler, W. Kaim, Inorg. Chem. Commun., in press.

[13] (a) X.H. Bu, H. Liu, M. Du, L. Zhang, Y.-M. Guo, M. Shionoya, J. Ribas, Inorg. Chem. 41 (2002) 1855, 5634;
(b) See also J.P. Wignacourt, S. Sueur, M. Lagrenée, Acta Crystallogr., Sect. C 46 (1990) 394;
(c) M. Lagrenée, S. Sueur, J.P. Wignacourt, Acta Crystallogr., Sect. C 47 (1991) 1158.

[14] M. Krejcik, M. Danek, F. Hartl, J. Electroanal. Chem. 317 (1987) 179.

[15] W. Kaim, S. Ernst, V. Kasack, J. Am. Chem. Soc. 112 (1990) 173.

[16] H.H. Watt, Org. Synth. Coll. II (1943) 208.

[17] M. Ziegler, V. Monney, H. Stoeckli-Evans, A. von Zelewsky, I. Sasaki, G. Dupic, J.-C. Daran, G.G.A. Balavoine, J. Chem. Soc., Dalton Trans. (1999) 667.

[18] M.B. Robin, P. Day, Adv. Inorg. Chem. Radiochem. 10 (1967) 247.

[19] N.S. Hush, Prog. Inorg. Chem. 8 (1967) 391.

[20] M. Haga, E.S. Dodsworth, A.B.P. Lever, Inorg. Chem. 25 (1986) 447.

[21] (a) S. Ernst, P. Hänel, J. Jordanov, W. Kaim, V. Kasack, E. Roth, J. Am. Chem. Soc. 111 (1989) 1733;
(b) E. Waldhör, B. Schwederski, W. Kaim, J. Chem. Soc., Perkin Trans. (1993) 2109.

Available online at www.sciencedirect.com
SCIENCE DIRECT®
Polyhedron 23 (2004) 709
POLYHEDRON
www.elsevier.com/locate/poly

Corrigendum

Corrigendum to: Silver(I) and mercury(II) complexes of $Me_3N(+)–N(-)X$ ylides: synthesis and structure [Polyhedron 22 (2003) 3345–3535] ☆,☆☆

David G. Morris, Kenneth W. Muir *, Cindy Ong Woei Chii

Chemistry Department, University of Glasgow, Scotland G12 8QQ, UK

Received 10 December 2003

The bond key to Table 3 on page 3351 is incorrect. The correct formula is:

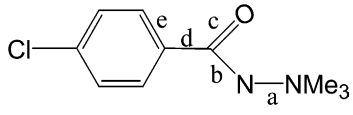

☆ PII of original article: S0277-5387(03)00488-1.
☆☆ DOI of original article: 10.1016/j.poly.2003.08.001.
* Corresponding author. Tel.: +44-0141-330-5345; fax: +44-0141-330-4888.
E-mail address: ken@chem.gla.ac.uk (K.W. Muir).

0277-5387/$ - see front matter © 2003 Elsevier Ltd. All rights reserved.
doi:10.1016/j.poly.2003.08.019

Available online at www.sciencedirect.com
SCIENCE DIRECT®
Polyhedron 23 (2004) 711–717
POLYHEDRON
www.elsevier.com/locate/poly

Syntheses and solid state structures of europium and terbium complexes of N,N'-bis(2-pyridylmethyl)urea and N,N'-bis(3-pyridylmethyl)oxalamide

Daniel L. Reger *, Delia M. Ciurtin Smith, Ken D. Shimizu *, Mark D. Smith

Department of Chemistry and Biochemistry, The University of South Carolina, Columbia, SC 29208, USA

Received 3 May 2003; accepted 23 September 2003

Abstract

Two organic ligands, N,N'-bis(2-pyridylmethyl)urea, "**2u**", and N,N'-bis(3-pyridylmethyl)oxalamide, "**3o**", were employed in the synthesis of three new extended structures. The reaction between $EuCl_3 \cdot 6H_2O$ (**1**) and **2u** afforded a molecular species, Eu(**2u**H_2)Cl_5, which assembled in one-dimensional chains by hydrogen bonding. When $EuCl_3 \cdot 6H_2O$ was replaced by $TbCl_3 \cdot 6H_2O$, the reaction with **2u** yielded another molecular compound, Tb(**2u**H_2)Cl_5, having the same structural features as **1**. **3o** reacted with $EuCl_3 \cdot 6H_2O$ and formed compound **3**, [Eu(**3o**H)$(H_2O)_2Cl_3$]Cl, in which the **3o** ligand acts as a bridge between the metal centers to form an infinite one-dimensional chain structure. The chains are further linked in three dimensions by hydrogen bonds and π–π stacking. Luminescence data for all three compounds are presented.
© 2003 Elsevier Ltd. All rights reserved.

Keywords: Coordination polymer; Europium; Hydrogen bonds; Luminescence; Supramolecular; Terbium

1. Introduction

Substantial progress has been made recently in the areas of crystal engineering and the rational design of extended frameworks based on multitopic organic ligands for the formation of coordination polymers. The characteristics of the organic ligand (length, flexibility, shape) and the coordination preferences of the metal centers are the primary factors that determine the resultant extended structures [1–6]. Careful management of these factors can lead to a certain predictability and control over the architecture of the products. In this context, control of strong, coordinative covalent forces as well as of weaker non-covalent interactions involving hydrogen bonding and π–π stacking can be envisioned.

Our target was to synthesize new mixed organic–inorganic materials in which covalent interactions would coexist with hydrogen bonds and/or π–π stacking and would lead to the formation of supramolecular assemblies. The approach was to employ a flexible organic ligand capable of multiple hydrogen bonding interactions, hence we decided to employ N,N'-bis(2-pyridylmethyl)urea (**2u**) and N,N'-bis(3-pyridylmethyl)oxalamide (**3o**) (Scheme 1). The organic cores that connect the pyridine rings in **2u** and **3o** have a great potential for participating in non-covalent interactions through the acceptor oxygen atoms and the N–H donor groups [7–14]. The oxygen and the nitrogen atoms, as well as the ortho- and meta-nitrogen atoms on the pyridine rings can be involved in coordinative covalent bonds with metal centers. Our choices for the inorganic components were the lanthanides $EuCl_3 \cdot 6H_2O$ and $TbCl_3 \cdot 6H_2O$. The main interest in these lanthanides resides in their luminescence properties and in the possibility of modulating them by incorporation into organic–inorganic hybrid materials [15–20].

In this paper, we report the synthesis, crystal structures and luminescence properties of three new compounds: two isostructural molecular species,

* Corresponding authors. Tel.: +1-803-777-0455; fax: +1-803-777-9521.
E-mail addresses: reger@mail.chem.sc.edu (D.L. Reger), shimizu@mail.chem.sc.edu (K.D. Shimizu).

0277-5387/$ - see front matter © 2003 Elsevier Ltd. All rights reserved.
doi:10.1016/j.poly.2003.09.037

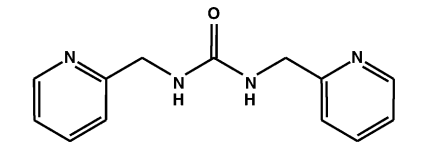

2u

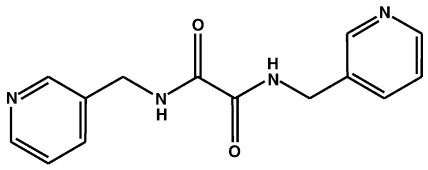

3o

Scheme 1.

Eu(**2u**H_2)Cl_5, (**1**) and Tb(**2u**H_2)Cl_5, (**2**) and [Eu(**3o**H)$(H_2O)_2Cl_3$]Cl (**3**), a one-dimensional polymeric chain. Hydrogen bonds and, in the case of **3**, π–π stacking, assemble all the structures into higher dimensionality.

2. Experimental

2.1. Materials

$EuCl_3 \cdot 6H_2O$ (Alfa Aesar, 99.9%), $TbCl_3 \cdot 6H_2O$ (Alfa Aesar, 99.99%), 2-(aminomethyl)pyridine (Aldrich, 98%), 3-(aminomethyl)pyridine (Aldrich, 99+%), diphenyl carbonate (Aldrich, 99%) and diethyl oxalate (Matheson Coleman & Bell) were used without further purification.

2.2. Synthesis of *2u* and *3o*

N,*N*′-bis(2-pyridylmethyl)urea (**2u**) and *N*,*N*′-bis(3-pyridylmethyl)oxalamide (**3o**) were prepared according to the literature [7].

2.3. Synthesis of Eu(*2u*H_2)Cl_5, (*1*)

$EuCl_3 \cdot 6H_2O$ (0.2 mmol, 0.073 g) was dissolved in ethanol (5 ml) and carefully layered onto a solution of **2u** (0.1 mmol, 0.024 g) in chloroform (5 ml). Colorless crystals formed within four days.

2.4. Synthesis of Tb(*2u*H_2)Cl_5, (*2*)

The procedure is identical to that used for the preparation of **1**, except that $TbCl_3 \cdot 6H_2O$ (0.2 mmol, 0.053 g) was used instead of $EuCl_3 \cdot 6H_2O$. Colorless crystals formed.

2.5. Synthesis of [Eu(*3o*H)$(H_2O)_2Cl_3$]Cl (*3*)

The procedure is identical to that used for the preparation of **1**, except that **2u** was replaced by **3o** (0.1 mmol, 0.027 g) and $CHCl_3$ by CH_2Cl_2 (7 ml). Colorless crystals formed.

2.6. Physical measurements

The luminescent emission spectra for all three compounds were carried out on a Jasco FP-6500 spectrometer. Crystalline powders of **1**, **2** and **3** were mounted on the top of a plastic pin and placed in the path of the excitation source. The excitation wavelength for **1** and **2** was 300 nm and for **3** was 275 nm.

2.7. Crystallography

X-ray intensity data for **1**–**3** were measured at 150(1) K on a Bruker SMART APEX diffractometer (Mo Kα radiation, $\lambda = 0.71073$ Å) [21]. Raw data frame integration and Lp corrections were performed with SAINT+ [21]. Final unit cell parameters were determined by least-squares refinement of all reflections with $I > 5(\sigma)I$ from each data set (6654 for **1**, 5124 for **2**, 7373 for **3**). An empirical absorption correction was applied to each data set with SADABS [21]. All structures were solved by a combination of direct methods and subsequent difference Fourier syntheses and refined by full-matrix least squares against F^2, using all data, with SHELXTL [22].

Compounds **1** and **2** crystallize in the monoclinic crystal system; the space group $P2_1/n$ was determined in each case by examination of the pattern of systematic absences in the intensity data. Compound **3** crystallizes in the triclinic system; the space group $P\bar{1}$ was assumed and confirmed by the successful solution and refinement of the structure. All non-hydrogen atoms in each structure were refined anisotropically; hydrogen atoms attached to carbon were placed in geometrically idealized positions and included as riding atoms. Hydrogens bound to nitrogen atoms were located in the difference maps and refined freely with isotropic displacement parameters. The water hydrogens in **3** were located in the difference map and refined isotropically with O–H distances restrained to be similar to one another. Further details of the crystallographic refinements are given in Table 1.

3. Results and discussion

3.1. Synthesis

The starting materials *N*,*N*′-bis(2-pyridylmethyl)urea (**2u**) and *N*,*N*′-bis(3-pyridylmethyl)oxalamide (**3o**), were

Table 1
Crystallographic data for **1**, **2**, and **3**

	1	**2**	**3**
Empirical formula	$C_{13}H_{16}Cl_5EuN_4O$	$C_{13}H_{16}Cl_5N_4OTb$	$C_{14}H_{19}Cl_4EuN_4O_4$
Formula weight	573.51	580.47	601.09
Crystal system	monoclinic	monoclinic	triclinic
a (Å)	7.8358(4)	7.8143(4)	7.7323(4)
b (Å)	19.8638(11)	19.8751(11)	11.3366(6)
c (Å)	12.9644(7)	12.9455(7)	12.2080(7)
α (°)	90	90	94.8340(10)
β (°)	104.0180(10)	104.1560(10)	101.6270(10)
γ (°)	90	90	102.3810(10)
V (Å^3)	1957.80(18)	1949.51(18)	1014.66(9)
Space group	$P2_1/n$	$P2_1/n$	$P\bar{1}$
Z value	4	4	2
ρ_{calc} (g/cm^3)	1.946	1.978	1.967
μ (Mo Kα) (mm^{-1})	3.894	4.321	3.645
Temperature (°C)	−123	−123	−123
Residuals: R_1; wR_2[a]			
$I > 2\sigma(I)$	0.0214; 0.0482	0.0290; 0.0617	0.0299; 0.0615
All data	0.0244; 0.0491	0.0346; 0.0637	0.0345; 0.0626
GOF	0.993	1.057	1.009

GOF $= \left\{\sum[w(F_o^2 - F_c^2)^2]/(n-p)\right\}^{1/2}$ (n = number of reflections; p = number of refined parameters). $w = 1/[\sigma^2(F_o^2) + (aP)^2 + bP]$, where P is $[2F_c^2 + \max(F_o^2, 0)]/3$.
[a] $R_1 = \sum ||F_o| - |F_c|| / \sum |F_o|$. $wR_2 = \left\{\sum[wF_o^2 - F_c^2)^2] / \sum[w(F_o^2)^2]\right\}^{1/2}$.

synthesized by reaction of 2-aminomethylpyridine with diphenylcarbonate and 3-aminomethylpyridine with diethyloxalate, according to synthetic methods previously reported [7]. N,N'-bis(3-pyridylmethyl)urea (**3u**) and N,N'-bis(2-pyridylmethyl)oxalamide (**2o**) have been similarly prepared, but no new compounds have been isolated with these ligands. Layering an ethanolic solution of $EuCl_3 \cdot 6H_2O$ with **2u** dissolved in chloroform in a 1:1 molar ratio yielded colorless crystals of a new molecular complex, Eu(**2u**H_2)Cl_5 (**1**). When $EuCl_3 \cdot 6H_2O$ is replaced by $TbCl_3$, in the same reaction conditions and molar ratio, another complex, Tb(**2u**H_2)Cl_5 (**2**) forms, displaying the same structural characteristics as **1**. In both of these reactions the ligand has been doubly protonated and the metal has gained two chloride ligands, leading to a neutral complex. The reaction between $EuCl_3 \cdot 6H_2O$ and **3o** generated colorless crystals of [Eu(**3o**H)$(H_2O)_2Cl_3$]Cl (**3**). In this case, the ligand has been singly protonated, leading to a complex with an overall +1 charge, balanced by an uncoordinated chloride ion. All of the resulting compounds are luminescent, and their luminescence properties will be discussed further below.

Table 2
Interatomic distances (Å) and bond angles (°) with esds ( ) for **1**, **2**, and **3**

*$C_{13}H_{16}Cl_5EuN_4O$ (**1**)*			
Eu–O(1)	2.2988(19)	O(1)–Eu–Cl(2)	94.49(5)
Eu–Cl(1)	2.7115(7)	O(1)–Eu–Cl(3)	88.02(5)
Eu–Cl(2)	2.6258(7)	Cl(2)–Eu–Cl(3)	94.20(3)
Eu–Cl(3)	2.6302(7)	Cl(2)–Eu–Cl(4)	178.05(3)
Eu–Cl(4)	2.6804(7)	Cl(3)–Eu–Cl(4)	87.45(2)
Eu–Cl(5)	2.7215(7)	Cl(2)–Eu–Cl(1)	91.25(2)
*$C_{13}H_{16}Cl_5N_4OTb$ (**2**)*			
Tb–O(1)	2.271(3)	O(1)–Tb–Cl(2)	94.40(7)
Tb–Cl(1)	2.6842(9)	O(1)–Tb–Cl(3)	8.31(7)
Tb–Cl(2)	2.6053(10)	Cl(2)–Tb–Cl(3)	94.15(4)
Tb–Cl(3)	2.6110(11)	Cl(2)–Tb–Cl(4)	178.07(4)
Tb–Cl(4)	2.6582(9)	Cl(3)–Tb–Cl(4)	87.47(3)
Tb–Cl(5)	2.6985(10)	Cl(2)–Tb–Cl(1)	90.98(3)
*$C_{14}H_{19}Cl_4EuN_4O_4$ (**3**)*			
Eu–O(1)	2.341(3)	O(1)–Eu–O(3)	69.82(11)
Eu–O(2)#1	2.380(3)	O(1)–Eu–O(4)	71.37(10)
Eu–O(3)	2.368(3)	O(1)–Eu–Cl(2)	82.98(7)
Eu–O(4)	2.431(3)	Cl(2)–Eu–Cl(1)	94.26(3)
Eu–Cl(1)	2.6950(11)	O(1)–Eu–Cl(3)	89.35(7)
Eu–Cl(2)	2.6735(10)	Cl(1)–Eu–Cl(3)	97.86(3)
Eu–Cl(3)	2.6981(10)	O(1)–Eu–O(2)#1	138.73(10)

3.2. Crystal structure of *1*

Compound **1** is a molecular species, of composition Eu(**2u**H_2)Cl_5. Relevant bond distances and angles are compiled in Table 2. The coordination sphere around the europium center is comprised of five chlorine atoms (the Eu–Cl bond length ranges from 2.6258(7) to 2.7215(7) Å) and an oxygen atom from a **2u** ligand (Eu–O = 2.2988(19) Å) (Fig. 1). Although both nitrogen atoms on the pyridine rings of the ligand are protonated, the complex is neutral due to the presence of two additional chloride ligands coordinated to europium. Two different types of hydrogen bonding interactions assemble the molecules into one-dimensional chains

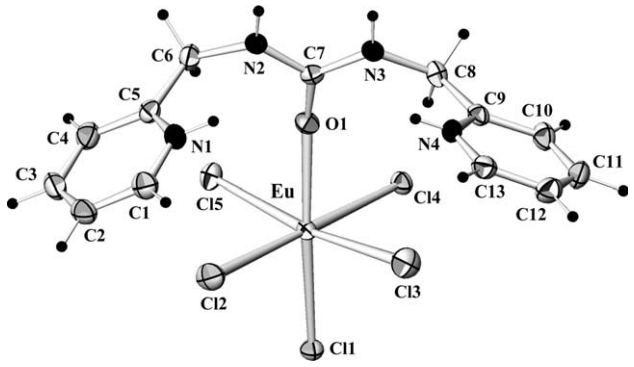

Fig. 1. Drawing of Eu(**2u**H_2)Cl_5 (**1**), shown with 50% probability displacement ellipsoids.

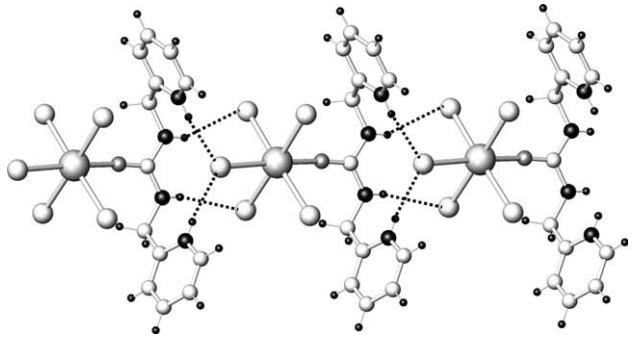

Fig. 2. Molecules of **1** assembled into one-dimensional chains by hydrogen bonding interactions. Eu atoms are shown as large gray circles; Cl, large shaded circles; N, small black circles; O, small gray circles; C, small shaded circles; H, smaller black circles.

(Fig. 2). Both hydrogens on the urea nitrogen atoms are involved in hydrogen bonding with two chlorines coordinated to the adjacent lanthanide (N(2)–H(2N)···Cl(5)#1; D···A = 3.296(3) Å, H···A = 2.60(3) Å, D–H···A = 143(3)°; N(3)–H(3N)···Cl(4)#1; D···A = 3.246(3) Å, H···A = 2.55(3) Å, D–H···A = 144(3)°). The two protons attached to the nitrogens in the pyridine rings of the ligand form hydrogen bond with a third chlorine atom of the same adjacent molecule (N(1)–H(1N)···Cl(1)#1; D···A = 3.123(3) Å, H···A = 2.35(3) Å, D–H···A = 150(3)°; N(4)–H(4N)···Cl(1)#1; D···A = 3.175(3) Å, H···A = 2.47(3) Å, D–H···A = 151(3)°), thus enhancing the intermolecular interactions that lead to the formation of the chains. (Symmetry code #1 is $x-1, y, z$). As shown in Fig. 3(a), sets of interdigitated one-dimensional chains assemble in "layers" in the *bc* plane, which then stack on top of each other (Fig. 3(b)) to form the overall extended structure.

Compound **2**, Tb(**2u**H_2)Cl_5, also a molecular species, is isostructural to compound **1**. The same atom labeling scheme was used for **2** as for **1**, and analogous bond distances and angles are given in Table 2.

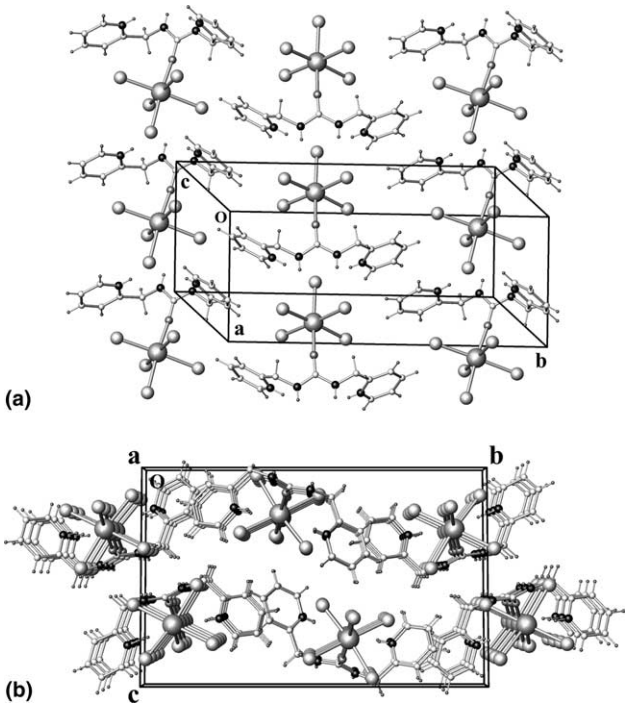

Fig. 3. (a) Schematic view of a "layer" of interdigitated chains in **1**. (b) Packing of two such "layers" of interdigitated chains (the view is rotated 90°).

3.3. Crystal structure of *3*

Single crystal analysis of **3** revealed an infinite one-dimensional structure consisting of chains running along the [1 0 0] direction. As shown in Fig. 4, the europium atoms are hepta-coordinated and are surrounded by three chlorines (Eu–Cl = 2.6735(10), 2.6950(11), 2.6981(10) Å), two molecules of water (Eu–O = 2.368(3), 2.431(3) Å) and two carbonyl oxygens provided by two different **3o** ligands (Eu–O = 2.341(3), 2.380(3) Å, see Table 2). One of the nitrogens on the pyridine rings is protonated, hence the chains are positively charged. The structure is supported by an intricate network of hydrogen bonds. Two types of hydrogen bonds can be distinguished in the overall network of compound **3**. The first type are intrachain hydrogen bonds (Fig. 4) and do not participate in building the extended network. These bonds involve a chlorine atom on the metal center and the hydrogen on one of the oxalamide nitrogen atoms (N(3)–H(3N)···Cl(2); D···A = 3.311(3) Å, H···A = 2.51(4) Å, D–H···A = 163(4)°), as well as a bifurcated hydrogen bond between the hydrogen on the other core nitrogen and two acceptors: the carbonylic oxygen (N(2)–H(2N)···O(2); D···A = 2.715(4) Å, H···A = 2.28(5) Å, D–H···A = 111(4)°) and a chlorine coordinated to the europium (N(2)–H(2N)···Cl(3)#2; D···A = 3.290(3) Å, H···A = 2.47(5) Å, D–H···A = 159(4)°). (Symmetry code #2 is $x+1, y, z$.)

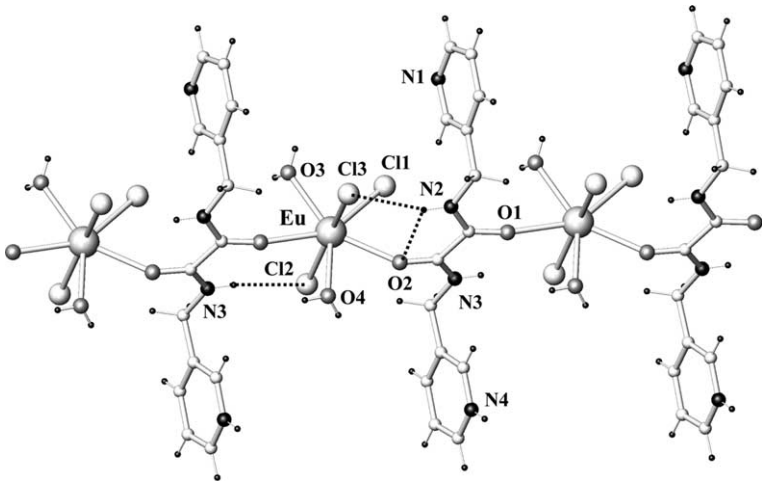

Fig. 4. One-dimensional chains in [Eu(**3o**H)$(H_2O)_2Cl_3$]Cl (**3**), showing intrachain hydrogen bonding. Eu atoms are shown as large gray circles; Cl, large shaded circles; N, small black circles; O, small gray circles; C, small shaded circles; H, smaller black circles.

The second type of hydrogen bond is interchain and organizes the structure into a 2D arrangement. Five such hydrogen bonds are present in the overall network. Adjacent, interdigitated chains are linked in the *ac* plane by one of the europium-coordinated waters, which forms two hydrogen bonding interactions with the free nitrogen on the pyridine ring (O(3)–H(3A)$\cdots$N(1)#4; D$\cdots$A = 2.658(5) Å, H$\cdots$A = 1.90(3) Å, D–H$\cdots$A = 168(5)°) and one chlorine atom (O(3)–H(3B)$\cdots$Cl(1)#5; D$\cdots$A = 3.228(4) Å, H$\cdots$A = 2.49(3) Å, D–H$\cdots$A = 111(4)°), both acceptors being located in the same adjacent chain. (Symmetry code #4 is $-x+1, -y, -z$; symmetry code #5 is $-x, -y, -z$.) The chains are also linked by π–π interactions between the pyridine rings. The ring centroid–centroid distance is 3.725(2) Å, with short contacts in the range 3.443–3.601 Å [23]. Overall, these interactions organize the one-dimensional chains in two-dimensional layers in the *ac* plane (a fragment of a layer is shown in Fig. 5(a)). Further, the layers are linked in three dimensions by another water molecule, O(4), involved in hydrogen bonding. It acts as an acceptor to the proton attached to the nitrogen on the pyridine ring (N(4)–H(4N)$\cdots$O(4); D$\cdots$A = 2.916(5) Å, H$\cdots$A = 2.21(3) Å, D–H$\cdots$A = 148(4)°) (Fig. 5(b)).

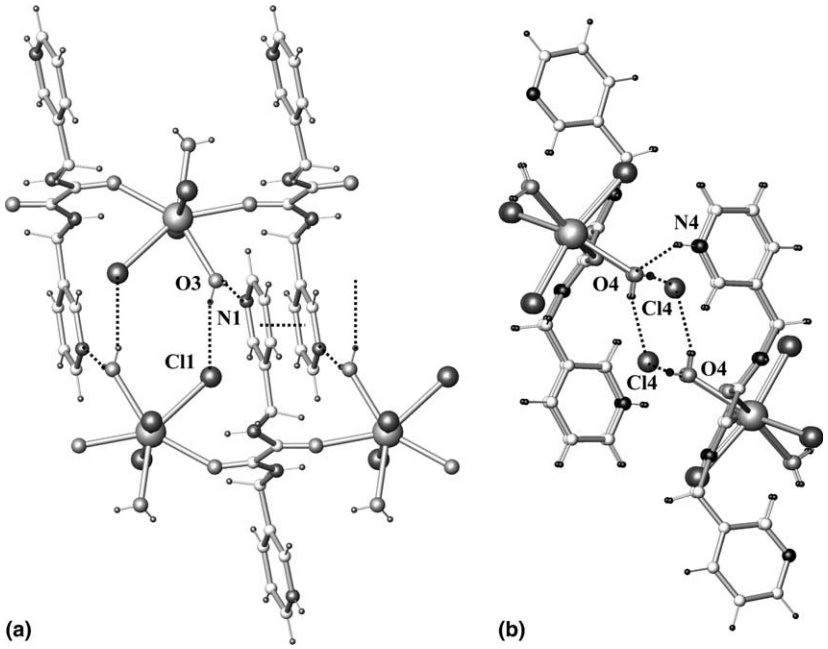

Fig. 5. (a) Fragment of two adjacent chains in **3**, showing interchain hydrogen bond and π–π stacking. (b) Additional interchain hydrogen bonding interactions as viewed down the crystallographic *a*-axis.

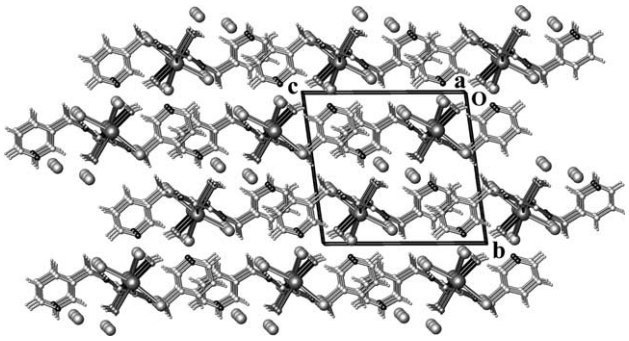

Fig. 6. Packing diagram of **3**, with chlorine anions between chains (hydrogen bonds omitted for clarity).

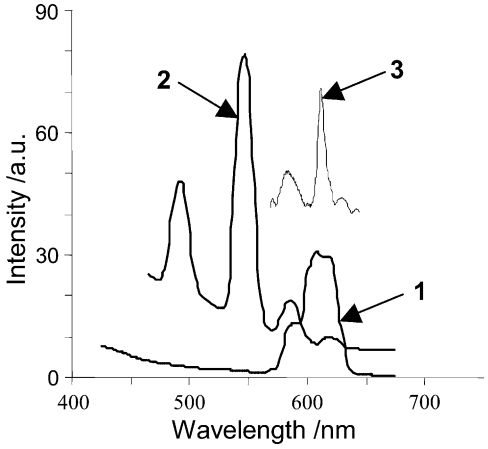

Fig. 7. Luminescence data for **1**, **2** and **3**.

The interstitial chlorine anions support the three-dimensional structure by acting as acceptors in two extra hydrogen bonds. As shown in Fig. 5(b), each chlorine is connected to two hydrogen atoms contained in two O(4) waters from two adjacent chains (O(4)–H(4A)···Cl(4); D···A = 3.050(3) Å, H···A = 2.32(3) Å, D–H···A = 159(5)°; O(4)–H(4B)···Cl(4)#3; D···A =3.052(3) Å, H···A = 2.31(3) Å, D–H···A = 164(4)°). (Symmetry code #3 is $-x+1, -y+1, -z+1$.)

In conclusion, hydrogen bonding and π–π interactions assemble the chains into two-dimensional layers, while additional hydrogen bonding with the interstitial chlorine anions and the proton on the pyridine rings expands the structure into three dimensions (Fig. 6).

3.4. Luminescence measurements

We have measured the luminescence spectra of crystalline powders of **1**, **2** and **3** at room temperature (Fig. 7). **1** and **2** were excited at 300 nm and **3** was excited at 275 nm. Compound **1** emitted red. It has two emission peaks at 589 and 607 nm and they can be assigned to $^5D_0 \rightarrow {}^7F_n$ ($n = 1, 2$) transitions. The first emission corresponds to the $^5D_0 \rightarrow {}^7F_1$ transition and is less intense than the second one, corresponding to $^5D_0 \rightarrow {}^7F_2$, which agrees with the fact that europium centers do not lie on an inversion center [24]. Compound **2** emits green light and shows four maxima at 495, 549, 591, 627 nm. The peaks can be assigned to $^5D_4 \rightarrow {}^7F_n$ ($n = 6, 5, 4, 3$) transitions. In the case of compound **3**, although a different ligand has been incorporated in the structure resulting in a one-dimensional infinite polymeric chain, the emission spectra has not changed very much. It emitted in red, showing two peaks at 583 and 609 nm, corresponding to $^5D_0 \rightarrow {}^7F_n$ ($n = 1, 2$) transitions.

4. Conclusions

In summary, the synthesis, the luminescence properties and the structural characterization of three new compounds have been presented. Compounds **1** and **2** feature the same organic ligand, *N*,*N*′-bis(2-pyridylmethyl)urea, **2u**, in its diprotonated form and are molecular. The molecules are assembled into one-dimensional chains by hydrogen bonding and are isostructural. Compound **3** contains the monoprotonated *N*,*N*′-bis(3-pyridylmethyl)oxalamide ligand, resulting in a markedly different architecture, a polymeric one-dimensional chain. The chains are held in three dimensions by an intricate array of hydrogen bonds. As anticipated, these ligands form complexes that have new supramolecular structures mainly organized by using the hydrogen bonding features built into them. The new complexes exhibit luminescence.

5. Supplementary material

Crystallographic data (excluding structure factors) for the structures in this paper have been deposited with the Cambridge Crystallographic Data Centre as supplementary publication nos. CCDC 213924–213926. Copies of the data can be obtained, free of charge, on application to CCDC, 12 Union Road, Cambridge CB2 1EZ, UK (fax: +44 1223 336033 or e-mail: deposit@ccdc.cam.ac.uk or www: http://www.ccdc.cam.ac.uk).

Acknowledgements

The authors thank the National Science Foundation (CHE-0110493) and the University of South Carolina for support. The Bruker CCD Single Crystal Diffractometer was purchased using funds provided by the NSF Instrumentation for Materials Research Program through Grant DMR: 9975623.

References

[1] P.J. Hagrman, D. Hagrman, J. Zubieta, Angew. Chem. Int. Ed. 38 (1999) 2638.
[2] S.R. Batten, Curr. Opinion Solid State Mater. Sci. 5 (2001) 107.
[3] B.J. Holliday, C.A. Mirkin, Angew. Chem. Int. Ed. 40 (2001) 2022.
[4] S.R. Batten, R. Robson, Angew. Chem. Int. Ed. 37 (1998) 1460.
[5] A.J. Blake, N.R. Champness, P. Hubberstey, W.-S. Li, M.A. Withersby, M. Schröder, Coord. Chem. Rev. 183 (1999) 117.
[6] B. Moulton, M.J. Zaworotko, Curr. Opinion Solid State Mater. Sci. 6 (2002) 117.
[7] C.L. Schauer, E. Matwey, F.W. Fowler, J.W. Lauher, Cryst. Eng. 1 (1998) 213.
[8] T.L. Nguyen, F.W. Fowler, J.W. Lauher, J. Am. Chem. Soc. 123 (2001) 11057.
[9] S. Coe, J.J. Kane, T.L. Nguyen, L.M. Toledo, E. Wininger, F.W. Fowler, J.W. Lauher, J. Am. Chem. Soc. 119 (1997) 86.
[10] F. Lloret, M. Julve, J. Faus, Y. Journaux, M. Philoche-Levisalles, Y. Jeannin, Inorg. Chem. 28 (1989) 3702.
[11] C.S.A. Fraser, D.J. Eisler, M.C. Jennings, R.J. Puddephatt, Chem. Commun. (2002) 1224.
[12] H.-X. Zhang, B.-S. Kang, Z.-Y. Zhou, A.S.C. Chan, C. Ren, J. Chem. Soc., Dalton Trans. (2001) 1664.
[13] D.L. Reger, D.M. Ciurtin Smith, K.D. Shimizu, M.D. Smith, Acta Cryst. E 59 (2003) 652.
[14] M.J. Plater, B.M. de Silva, J.M.S. Skakle, R.A. Howie, A. Riffat, T. Gelbrich, M.B. Hursthouse, Inorg. Chim. Acta 325 (2001) 141.
[15] H.-S. He, Z.-X. Zhao, W.-K. Wong, K.-F. Li, J.-X. Meng, K.-W. Cheah, J. Chem. Soc., Dalton Trans. (2003) 980.
[16] N.M. Shavaleev, S.J.A. Pope, Z.R. Bell, S. Faulkner, M.D. Ward, J. Chem. Soc., Dalton Trans. (2003) 808.
[17] L. Ma, O.R. Evans, B.M. Foxman, W. Lin, Inorg. Chem. 38 (1999) 5837.
[18] B. Barja, R. Baggio, M.T. Garland, P.F. Aramendia, O. Peña, M. Perec, Inorg. Chim. Acta 346 (2003) 187.
[19] B.S. Panigrahi, J. Alloys Compd. 334 (2002) 228.
[20] X. Wang, Y. Guo, Y. Li, E. Wang, C. Hu, N. Hu, Inorg. Chem. 42 (2003) 4135.
[21] SMART version 5.619, SAINT+ version 6.02a and SADABS. Bruker Analytical X-ray Systems, Inc., Madison, WI, 1998.
[22] G.M. Sheldrick, SHELXTL version 5.1; Bruker Analytical X-ray Systems, Inc., Madison, WI, 1997.
[23] C. Janiak, J. Chem. Soc., Dalton Trans. (2000) 3885.
[24] G. Blasse, B.C. Grabmaier, Luminescent Materials, Springer-Verlag, New York, 1994.

Available online at www.sciencedirect.com
SCIENCE DIRECT®
Polyhedron 23 (2004) 719–725
POLYHEDRON
www.elsevier.com/locate/poly

Attachment of 2-aminomethylpyridine molecule onto grafted silica gel surface and its ability in chelating cations

Jose A.A. Sales [a], Flavia P. Faria [a], Alexandre G.S. Prado [b], Claudio Airoldi [a,*]

[a] *Instituto de Química, Universidade Estadual de Campinas, Caixa Postal 6154, Campinas, São Paulo 13084-971, Brazil*
[b] *Instituto de Química, Universidade de Brasília, Caixa Postal 4478, 70919-970 Brasília, Brazil*

Received 3 May 2003; accepted 23 September 2003

Abstract

A route for incorporating the chelate molecule, AMP, onto silica gel was established. In the first stage a precursor silylant agent, 3-chloropropyltrimethoxysilane, is reacted with the support. The chelate molecule was then covalently bonded to the precursor surface to give 0.76 mmol of chelate per gram of silica. The immobilization reaction was confirmed through infrared spectroscopy and thermogravimetry. The anchored surface showed ability for adsorbing cations from water solution, presenting the maximum adsorption, calculated from the Langmuir equation, of: 0.84, 0.67, 0.40 and 0.22 mmol g^{-1} for the divalent cations copper, cobalt, nickel and zinc, respectively. All cation/surface interactions showed favorable enthalpic and entropic values, reflected in a thermodynamic stability of the complex formed.
© 2003 Elsevier Ltd. All rights reserved.

Keywords: Silica gel; Immobilization; 2-Aminomethylpyridine; Epoxide; Adsorption; Thermodynamic

1. Introduction

Heavy metal ion removal from waste-waters has been the subject of extensively technological research and recovering processes can often result in considerable cost saving [1]. Such analytical procedure developments are widely encouraged because many metals attain toxicity at distinct levels [2] or can show either vital or toxic effects in a series of biological systems as a function of concentration [2,3]. Therefore, increasing pressure from environmental authorities forces the establishment of discharge limits, which in turn, require an effective use of decontamination and purification methods [4].

A series of approaches can be applied to metal ion removal from waters, based on precipitation, exchange resins, membrane filtration and adsorbent methods. Among a diversity of adsorptive compounds that are capable of adsorbing metal ions from water, activated charcoal and clays are applied on a large scale [1,5,6]. However, some disadvantages such as heterogeneous pore structure and low selectivity are detected for these materials. Bearing in mind this proposal, new adsorbent materials are now being employed for removal of toxic and valuable compounds from water and other solvents [7–10].

Covalent immobilization onto solid supports of a desired chelate moiety, with the specific purpose of obtaining selectively adsorbent materials, is one of the most important procedures to develop highly selective matrices [11]. Therefore, considering such a proposal, many organic polymers and inorganic oxides have been chemically modified by attaching chelate groups onto the backbone chain, in order to increase their technological and scientific capabilities [12–19]. Among a series of these important supports, silica gel presents a high thermal, chemical and mechanical stability [20] and enables chemical modifications with functional compounds through the available silanol groups dispersed on its surface [21]. Thus, the ability of such a support to be modified leads to the acquisition of new materials, which can be used in many applications, such as chromatography [22], in sensors [23], pesticides removal [24], as well as in catalysis [25].

* Corresponding author. Fax: +55-19-37883023.
E-mail address: airoldi@iqm.unicamp.br (C. Airoldi).

0277-5387/$ - see front matter © 2003 Elsevier Ltd. All rights reserved.
doi:10.1016/j.poly.2003.11.051

Designed applications to improve environmental quality through metal removal have recently been emerged. Moreover, the versatility of the inorganic silica support to be chemically modified induces its application to produce new materials available to remove contaminants from water and other solvents [26].

The aim of the present investigation is to report the incorporation of the 2-aminomethylpyridine (AMP) molecule onto a previously modified silica gel surface and the ability of this new chelating moiety on this anchored surface for cation removal from water.

2. Experimental

2.1. Chemicals

Reagent grade solvents were used. The compounds 2-aminomethylpyridine (AMP) and 3-chloropropyltrimethoxysilane (CTS) were used without purification. Silica gel with a particle size of 70–230 mesh and average pore diameter of 60 Å was activated in a stream of dry nitrogen by heating at 423 K for 10 h and used immediately [7]. The triethylamine was distilled under reduced pressure before use.

2.2. Organofunctionalization

A sample of 20.0 g of activated silica gel was suspended in 100 cm^3 of dry toluene and 20.0 cm^3 (108.0 mmol) of CTS was added to this suspension. The mixture was mechanically stirred under reflux of the solvent in an inert atmosphere for 72 h. The suspension was filtered and the solid was washed with toluene and dried under vacuum at 230 K for several hours, to give the modified silica, named SiCl [27].

2.3. Incorporation of 2-aminomethylpyridine

A sample of 5.0 g of SiCl reacted with 3.50 cm^3 (0.034 mmol) of the compound AMP in 50 cm^3 of toluene, containing 5.0 cm^3 of triethylamine in order to favor the reaction equilibrium [28]. The suspension was kept under reflux and mechanically stirred for 72 h at 363 K. The final product, SiAMP, was filtered, washed with toluene and ethanol, and dried under vacuum at 230 K for 24 h.

2.4. Characterization

The amounts of the organic pendant chains CTS and 2-aminomethylpyridine, immobilized onto the surfaces were calculated based on the carbon and nitrogen contents, determined through elemental analysis on a Perkin–Elmer PE-2400 elemental analyzer. Samples of the precursor modified silica (SiCl) of ca. 0.10 g was reacted with a large excess of pyridine during 2 h at 380 K. The mixture was treated with nitric acid and filtered. The amount of chlorine was determined by titration with standard silver nitrate solution [29]. The mass loss was followed on a DuPont Model 951 instrument, using approximately 10.0 mg of the sample under nitrogen at a heating rate of 0.17 $K\,s^{-1}$. The surface area of hexagonal mesoporous materials was obtained using the BET equation on a Flowsorb 2300 analyzer. The infrared spectra of solid samples in KBr pellets were performed by diffuse reflectance by accumulating 250 scans on a MB-Bomem FTIR spectrophotometer. Nuclear magnetic resonance spectra of the solid samples were obtained on a Bruker AC 300/P spectrometer at room temperature. For each run, approximately 1 g of modified silica was compacted into a 7-mm zirconium oxide rotor. The measurements were obtained at frequencies of 75.47 and 59.61 MHz, for carbon and silicon, respectively, with a magic-angle spinning speed of 4 Hz. In order to increase the signal-to-noise ratio of the solid-state spectra, the CP/MAS technique was used. ^{29}Si and ^{13}C CP/MAS spectra were obtained with pulse repetitions of 1 and 3 s and contact times of 1 and 5 ms, respectively [30].

2.5. Isotherms of adsorption

The isotherms of adsorption were obtained by using the batchwise method, in which a series of samples of 50.0 mg of SiAMP were suspended in 20.0 cm^3 of aqueous solution with the desired cations at several concentrations, varying from 1.0 to 15.0 $mmol\,dm^{-3}$. The samples were mechanically stirred for 8 h at 298 ± 1 K and the solid was separated by centrifugation and filtration. The adsorbed content was determined by difference by sampling the filtered supernatant, using a Perkin–Elmer 3000 DV ICP-OES instrument [31–33].

2.6. Calorimetry

The calorimetric titrations were followed on a differential isothermal LKB 2277 microcalorimetric system. The titration consisted in suspending a sample of approximately 20.0 mg in 2.0 cm^3 of water inside a steel ampoule, which was vigorously stirred at 298.15 ± 0.02 K. After equilibrium, the cation solution was incrementally added through a microsyringe coupled to the calorimetric vessel. For each increment, the thermal effect ($\Delta_{tit}Q$) was recorded and the end if the titration was indicated by a constant thermal effect. The same procedure was employed to monitor the thermal effect of cation dilution ($\Delta_{dil}Q$) without the solid and also of adding water to the surface, which gave a null value. By combining these two heat outputs, the net value ($\sum \Delta_r Q$) can be determined by the expression $\sum \Delta_r Q = \sum[(\Delta_{tit}Q) - (\Delta_{dil}Q)]$ [34,35].

3. Results and discussion

The attachment of the 2-aminomethylpyridine onto silica gel followed a sequence of two distinct steps. The first one consisted in grafting 3-chloropropyltrimethoxysilane (CTS) onto silica gel to yield the new surface, SiCl, as represented in Eq. (1). In the next stage, this precursor was reacted with 2-aminomethylpyridine (AMP) to give the product SiAMP, presented in Eq. (2).

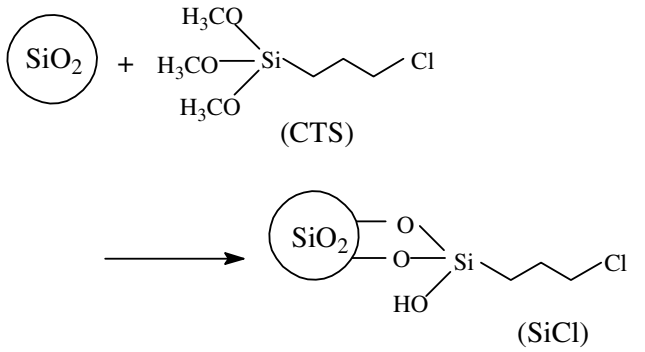

(1)

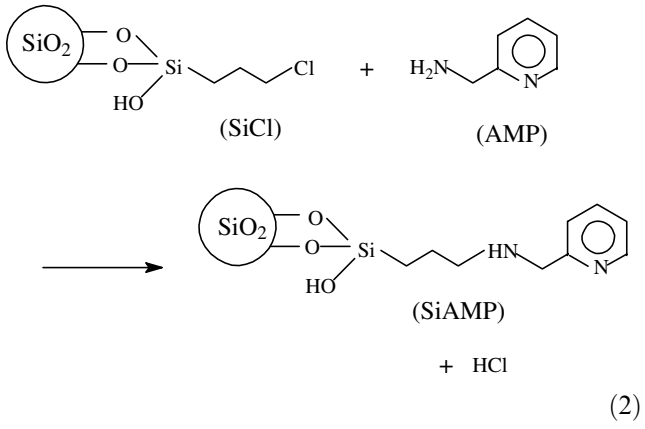

(2)

The degree of immobilization on the surface was determined by considering the elemental analysis data. From the percentage amount of carbon, 4.73 ± 0.02 and 8.17 ± 0.36 for SiCl and SiAMP, and the percentage of nitrogen 1.88 ± 0.01 for SiAMP, the number of moles of the compounds attached onto surface were calculated as 1.31 ± 0.01 and 0.76 ± 0.04 mmol g^{-1} for the SiCl and SiAMP surfaces, respectively. By considering the existence of two nitrogen atoms on final AMP anchored molecule surface, the 0.66 mmol of the available chlorine atoms bonded on the ends of the organic chain on the SiCl surface was required to react with the basic amino group to attach the desired molecule. In such condition, an excess of 13% of this anchored precursor remaining on surface without reacting.

The immobilization onto the surfaces can be confirmed through infrared spectra for the crude, the modified surface SiCl and the anchored SiAMP final surface. A small difference in spectra is observed in relation to the number and intensities of the displayed bands for activated silica and the immobilized compounds. The main features of the silica spectra are connected to the similarity of bands associated with the inorganic backbone such as (i) a large broad band between 3400 and 3200 cm^{-1}, which is attributed to the presence of the O–H stretching frequency of silanol groups and also to the remaining adsorbed water, (ii) the intense band related to siloxane stretching ν(Si–O–Si) of these groups at 1100 cm^{-1}, (iii) a band assigned to Si–OH stretching frequency for silanol groups at 900 cm^{-1} and (iv) the band around 1650 cm^{-1}, assigned to angular vibration of water molecules. However, the modified silicas, SiCl and SiAMP, presented a characteristic peak at 2950 cm^{-1}, assigned to C–H stretching of the tetrahedral carbon, which confirms the anchoring of the organic molecule onto the silica surface [28].

The surface areas for SiCl and SiAMP silicas were determined through the BET method, gave the results 420.8 ± 3.4, 347.2 ± 9.8 and 121.4 ± 8.6 $m^2\,g^{-1}$, respectively. The decrease in surface area after incorporation of organic groups can be easily interpreted due to the fact that the presence of pendant group partially blocks the adsorption of nitrogen molecules on surface and consequently causes a decrease in the surface area. As shown, this hindrance is more pronounced for the largest organic moiety, originating from the AMP molecule.

The thermogravimetric curves for all surfaces enable the establishing of information on thermal stability and also to confirm the amount of the compounds immobilized, as shown in Fig. 1. The profiles indicate that the SiAMP has more thermal stability than the SiCl surface. The curves also showed distinct mass losses, reflecting the molar mass of the pendant groups covalently bonded to inorganic phase.

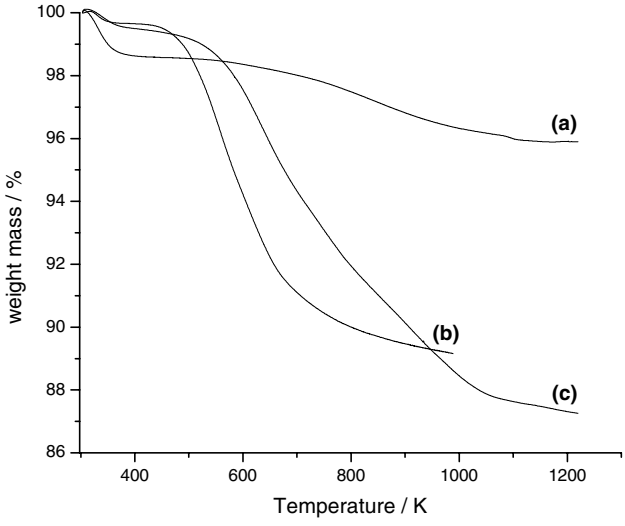

Fig. 1. Thermogravimetric curves of activated silica gel (a), and the chemically modified SiCl (b) and SiAMP (c) samples.

The activated silica gel present a first mass loss stage of 1.52% from 320 to 380 K, assigned to physically adsorbed water. A following stage of 2.56% is attributed to condensation of the silanols, to yield siloxane groups, resulting in water loss, from 670 to 1080 K [36]. Again two distinct mass loss steps were detected for SiCl sample. Thus, for the first one, a small mass loss of 0.35% in the 320–353 K range is attributed to the remaining silanol hydration water, as a consequence of the use of these groups on immobilization process. On the other hand, a pronounced increase of 10.52% in mass loss was observed for the second step, between 550 and 780 K, which corresponds to the organic matter added onto surface during immobilization. As expected, the immobilized SiAMP surface also presented two distinct stages of mass loss. Following the preceding interpretation, the first mass loss of 0.59% in the 320–360 K range is assigned to adsorbed water, and the other mass loss of 13.32%, between 560 and 865 K, was attributed to the organic groups immobilized on surface. The increase in mass loss is in agreement with the increase of the organic chain covalently attached to the inorganic backbone. For both anchored surfaces, the expected small degree of silanol condensation is hidden by the organic matter loss in the second step of decomposition.

Important features related to the immobilization of pendant group on the inorganic structure of the hybrid formed can be obtained through ^{13}C NMR spectra in solid state, as shown for SiAMP in Fig. 2. The proposed attachment of 2-aminomethylpyridine molecule to the precursor spacer modified agent is presented with carbon numbered. The three carbon atoms related to the spacer, numbered 1, 2 and 3 gave signals at 10, 26 and 46 ppm [30]. The ethylene carbon 4 gave a signal at 60 ppm and the aromatic carbons labeled 5–9 were assigned in the 120–160 ppm range, in good agreement with previous report [37]. These peaks corroborate to the expected immobilization of both materials, taking into account that the sequence of peaks are related to pendant carbon atoms of the organic part of these groups, results which support the success of the preparation of this new material.

The ^{29}Si NMR spectra in the solid state for both silicas confirm the covalent bond formed between the silylant agents and the silanol groups dispersed onto silica gel surface, as presented in Fig. 3. These spectra present four peaks located at −59, −69, −100 and −110 ppm. The first one is assigned to the silicon atom of the silylant agent bonded to one OH group and forming two siloxane bonds with silicon of the silica structure, $RSi(OSi)(OH)_2$, usually named as the T^2 signal. The peak at −69 ppm is assigned to $RSi(OSi)_3$, the T^3 signal. Both these signals confirm that organic groups were covalently bonded onto the silica surface. The other two peaks are attributed to pure surface signals described as: $Si(OSi)_4$, Q^4 at −110 ppm and $Si(OSi)_3OH$, Q^3 at −100 ppm [38–40].

The ability of the SiAMP surface in adsorbing cations from water is based on the free pair of electrons present on nitrogen atoms, represented as good Lewis bases of amine the and pyridine centers. Such disposition of pendant chains attached to the inorganic surface can chelate cations from aqueous solution. This adsorption ability was evaluated by measuring the sorption isotherms for a series of divalent cations, copper, nickel, zinc and cobalt. Under equilibrium conditions, the

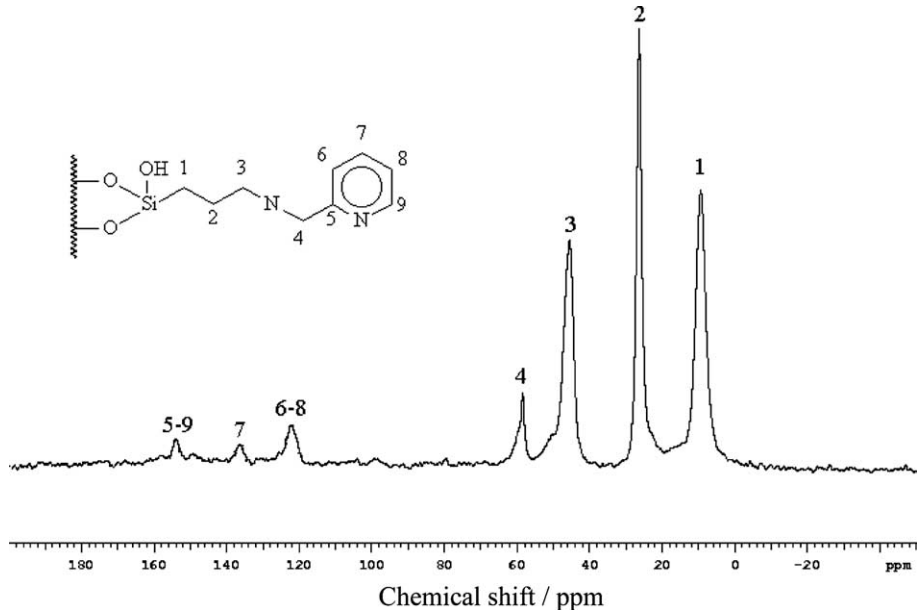

Fig. 2. ^{13}C NMR solid-state spectrum of anchored SiAMP silica.

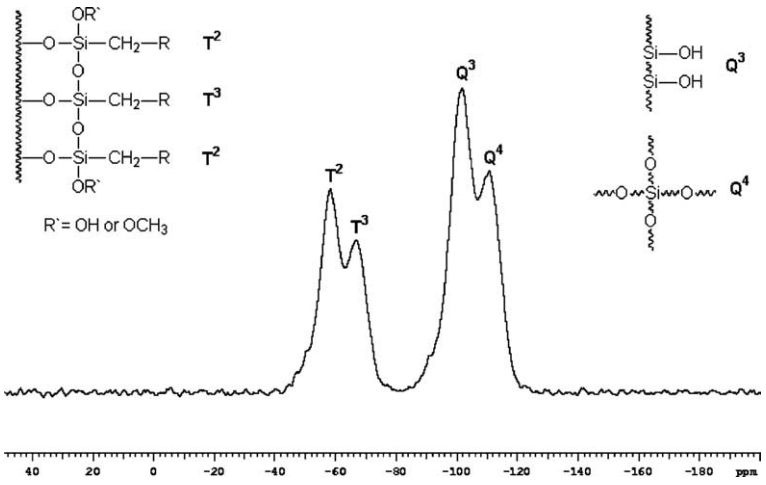

Fig. 3. ^{29}Si NMR solid-state spectrum of anchored SiAMP silica.

original solvent molecules that act as weakly bonded basic species are exchanged with the cations at the solid/liquid interface. The amount involved in this process characterizes the number of moles adsorbed (N_f), for 1 g of the solid. From the experimental point of view, this value was obtained from the initial number of moles of cation (n_i) added to the system and those at equilibrium (n_s) for a mass (m) of the support in grams, by applying the expression: $N_f = (n_i - n_s)/m$.

Profiles of the adsorption isotherms for all cations in water are represented in Fig. 4, in which the number of moles adsorbed versus the concentration at equilibrium condition is illustrated. Taking into account the maximum adsorption values, the isotherms obtained are distinguishable from each selected cation dissolved in water.

The established behavior in this adsorption process at a solid/liquid interface resembles those previously obtained for similar systems [31,32]. Therefore, the present data can be applied to a general equation, based on the Langmuir model, for such kinds of interaction:

$$\frac{C_s}{N_f} = \frac{C_s}{N_s} + \frac{1}{N_s b}.$$

From this expression, C_s is the concentration in solution at equilibrium (mol dm^{-3}), N_f as defined before (mol g^{-1}), N_s the maximum amount of solute adsorbed per gram of surface (mol g^{-1}), which depends on the number of adsorption sites and b is a constant. All these adsorption studies were based on the linearized form of the adsorption isotherm derived from a C_s/N_f as a function of C_s plot, as shown in Fig. 5. From these data, the maximum retention capacity (N_s) was determined for each cation–surface interaction. Thus, N_s and b were obtained from the angular and linear coefficients of the linearized form of the isotherms. These determinations from the obtained data showed that the adsorption followed the sequence Cu > Co > Ni > Zn. The N_s values are listed in Table 1.

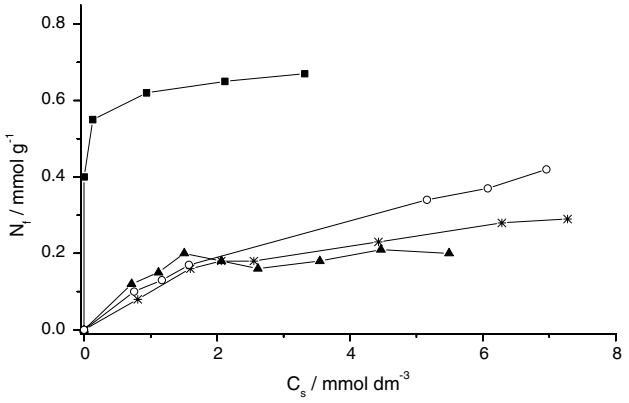

Fig. 4. Adsorption isotherms through batch method of divalent cations: Cu (■), Ni (●), Co (○) Zn (◆) on the SiAMP surface at 298 ± 1 K.

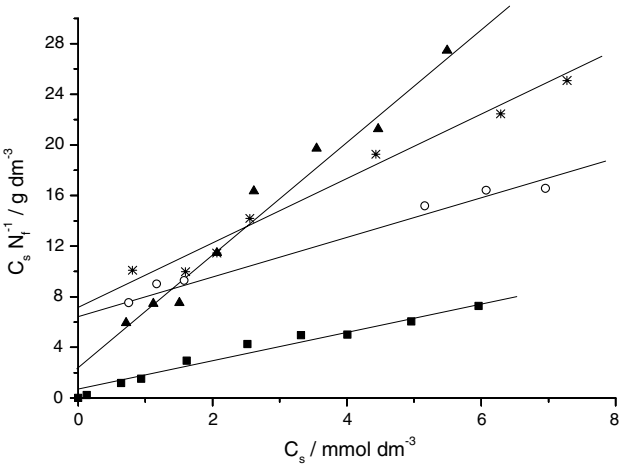

Fig. 5. Linearized Langmuir form of adsorption isotherms from calorimetric data for divalent cations: Cu (■), Ni (●), Co (○) Zn (◆) for SiAMP surface at 298 ± 1 K.

Table 1
The maximum retention capacity (N_s) and thermodynamic data for the interaction between divalent cations M^{2+} (Cu, Ni, Co and Zn) with the SiAMP surface at 298.15 ± 0.02 K

M^{2+}	$-\Delta H$ (kJ mol^{-1})	$-\Delta G$ (kJ mol^{-1})	ΔS (J mol^{-1} K^{-1})	N_s (mmol g^{-1})
Cu	4.09 ± 0.21	8.16 ± 0.30	14 ± 1	0.75 ± 0.04
Ni	1.95 ± 0.11	14.48 ± 0.40	42 ± 1	0.40 ± 0.10
Zn	1.27 ± 0.66	15.49 ± 0.40	48 ± 1	0.22 ± 0.40
Co	0.50 ± 0.01	13.36 ± 0.30	43 ± 1	0.67 ± 0.40

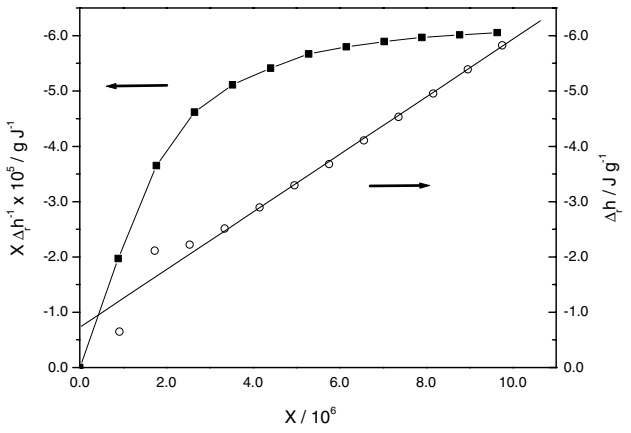

Fig. 6. Isotherm for the integral enthalpy of adsorption ($\sum \Delta h_r$) vs. molar fraction ($\sum X$) obtained from a calorimetric titration of a suspension of 0.020 g of SiAMP, in 2.0 cm^3 of water, with 0.015 mol dm^{-3} $Cu(NO_3)_2$ in the same solvent at 298.15 ± 0.02 K. The straight line is the isotherm.

Cation solutions were incrementally added to SiAMP samples suspended in water and the thermal effects produced were calorimetrically followed, in order to obtain more information about the basic centers/cation interactions at the surface. The thermal effect outputs from the net reactions can be calculated by the expression by $\sum \Delta_r Q = \sum[(\Delta_{tit} Q) - (\Delta_{dil} Q)]$.

The net resultant thermal effect outputs from the reactions were adjusted to a modified Langmuir equation [34,35,41] and were used to obtain the integral enthalpies involved in the formation of a monolayer per unit mass of adsorbate $\Delta_{mono} H$, by applying the expression:

$$\frac{\sum X}{\sum \Delta_r H} = \frac{1}{(K-1)\Delta_{mono} H} + \frac{\sum X}{\Delta_{mono} H}.$$

In this equation, $\sum X$ is the total mole fraction of the cation in solution after adsorption, X values are obtained for each addition of titrand, by using the modified Langmuir equation, whose behavior was shown to be a good adjustable model for such heterogeneous systems [40]. $\Delta_r H$ is the integral enthalpy of adsorption (J g^{-1}) obtained through the net thermal effect of adsorption and the number of moles of the adsorbate, K is a constant of proportionality that also includes the equilibrium constant. By using the angular and linear values from the $\sum X/\Delta_r H$ versus $\sum X$ plot, as illustrated for copper adsorption in Fig. 6, $\Delta_{mono} H$ and the enthalpy of adsorption, $\Delta_{ads} H$, values can be calculated by means of the expression: $\Delta_{ads} H = \Delta_{mono} H / N_s$. From K values, Gibbs free energies were calculated by the expression: $\Delta G = -RT \ln K$, and the entropy values are calculated through $\Delta G = \Delta H - \Delta TS$. All thermodynamic data are listed in Table 1.

For all determinations the cation-basic center interactions on SiAMP samples demonstrated spontaneity for the proposed reactions, as shown by the negative G values. Furthermore, in all cases, the exothermic enthalpic and positive entropic values are favorable conditions for the chelation of the cations by SiAMP, with stable complexes being formed. This anchored silica thus showed to be a good chelating agent to remove heavy metal ions from water. The success of AMP molecule incorporation on grafted silica with high thermal stability, significant adsorption ability and favorable thermodynamic interaction data suggest that this surface can be applied to remove contaminant cations from water.

4. Conclusion

The success of the 2-aminomethylpyridine chelate molecule attachment onto a silica gel surface and the ability of this material in easily adsorbing metal ions from water have been demonstrated. This proposal is confirmed through stable complexes formed between cations and free electron pairs on the nitrogen atoms disposed on the pendant groups, whose behavior was proven by the thermodynamic results. Thus, this new surface is a promising material to be applied to cation removal from aqueous solutions.

Acknowledgements

The authors are indebted to FAPESP for financial support and for a fellowship to AGSP, and to CNPq for fellowships to F.P.F., J.A.A.S. and C.A.

References

[1] B. Lee, Y. Kim, H. Lee, J. Yi, Microp. Mesop. Mater. 50 (2001) 77.
[2] S. Samal, S. Acharya, R.K. Dey, A.R. Ray, Talanta 57 (2002) 1075.
[3] J.W. Moore, S. Ramamoorthy, Heavy Metals in Natural Waters, Springer Verlag, New York, 1984.
[4] A.A. Mozeto, W.F. Jardim, Quim. Nova 25 (2002) 7.
[5] J.S. Kim, J. Yi, Sep. Sci. Technol. 34 (1999) 2957.
[6] J.S. Kim, J. Yi, J. Chem. Technol. Biotechnol. 74 (1999) 544.

[7] A.G.S. Prado, L.N.H. Arakaki, C. Airoldi, J. Chem. Soc., Dalton Trans. (2001) 2206.
[8] M.A. Zolfigol, T. Madrakian, E. Ghaemi, A. Afkhami, S. Aziziam, S. Afshar, Green Chem. 4 (2002) 611.
[9] O.A. Zaporozhets, T.E. Keda, L.E. Seletskaya, V.V. Sukhan, J. Anal. Chem. 55 (2000) 635.
[10] O.A. Zaporozhets, L.S. Ivan'ko, I.V. Marchenko, V.V. Sukhan, J. Anal. Chem. 55 (2000) 640.
[11] R.E. Morrid, E.L. Chang, Petrol. Sci. Technol. 18 (2000) 1147.
[12] C. Borgo, Y. Gushikem, J. Colloid. Interface Sci. 246 (2002) 343.
[13] L. Mercier, T.J. Pinnavaia, Microp. Mesop. Mater. 20 (1998) 101.
[14] J. Brown, L. Mercier, T.J. Pinnavaia, Chem. Commun. (1999) 69.
[15] A.M. Lazarin, Y. Gushikem, J. Braz. Chem. Soc. 13 (2002) 88.
[16] A.G.S. Prado, C. Airoldi, Anal. Chim. Acta 432 (2001) 401.
[17] A. Seifert, S. Spange, H. Muller, S. Hesse, C. Jager, J. Sol–Gel Sci. Technol. 26 (2003) 77.
[18] S. Spange, A. Seifert, H. Muller, S. Hesse, C. Jager, Angew. Chem., Int. Ed. 41 (2002) 1729.
[19] O.A. Zaporozhets, L.Y. Tsyukalo, Talanta 58 (2002) 861.
[20] A. Goswani, A.K. Singh, Anal. Chim. Acta 454 (2002) 229.
[21] A.G.S. Prado, C. Airoldi, Pest Manag. Sci. 56 (2000) 419.
[22] C.R. Silva, I.C.S.F. Jardim, C. Airoldi, J. Chromatogr. A 987 (2003) 139.
[23] S.T. Fujiwara, C.A. Pessoa, Y. Gushikem, Anal. Lett. 35 (2002) 1117.
[24] A.G.S. Prado, C. Airoldi, Fresenius J. Anal. Chem. 371 (2001) 1028.
[25] M.H. Valkenberg, W.F. Holderich, Catal. Rev. 44 (2002) 321.
[26] P.M. Price, J.H. Clark, D.J. Macquairre, J. Chem. Soc., Dalton Trans. (2001) 101.
[27] A.G.S. Prado, L.N.H. Arakaki, C. Airoldi, Green Chem. 4 (2002) 42.
[28] A.G.S. Prado, C. Airoldi, J. Colloid. Interface Sci. 236 (2001) 161.
[29] C. Airoldi, M.R.M.C. Santos, J. Mater. Chem. 4 (1994) 1479.
[30] J.A.A. Sales, A.G.S. Prado, C. Airoldi, Polyhedron 21 (2002) 2647.
[31] L.N.H. Arakaki, A.N. Sousa, J.G.P. Espinola, S.F. Oliveira, C. Airoldi, J. Colloid. Interface Sci. 249 (2002) 290.
[32] C. Airoldi, L.N.H. Arakaki, J. Colloid. Interface Sci. 249 (2002) 1.
[33] J.A.A. Sales, A.G. Souza, J.G.P. Espinola, E.E.S. Teotonio, C.D. Pinheiro, An. Ass. Bras. Quim. 47 (1998) 342.
[34] C. Airoldi, L.N.H. Arakaki, Polyhedron 20 (2001) 929.
[35] L.N.H. Arakaki, L.M. Nunes, J.A. Simoni, C. Airoldi, J. Colloid Interface Sci. 228 (2000) 46.
[36] A.G.S. Prado, J.A.A. Sales, C. Airoldi, J. Therm. Anal. Calorim. 70 (2002) 191.
[37] H.J. Hoorn, P. Joode, W.L. Driessen, J. Reedjk, Recl. Trav. Chim. Pays-Bas. 115 (1996) 191.
[38] K. Kosuge, P.S. Singh, Chem. Mater. 13 (2001) 2476.
[39] K. Albert, E. Bayer, J. Chromatogr. 544 (1991) 345.
[40] A.G.S. Prado, C. Airoldi, J. Mater. Chem. 12 (2002) 3823.
[41] J.A.A. Sales, A.G.S. Prado, C. Airoldi, J. Therm. Anal. Calorim. 70 (2002) 135.

Available online at www.sciencedirect.com
SCIENCE DIRECT®
Polyhedron 23 (2004) 727–733
POLYHEDRON
www.elsevier.com/locate/poly

Synthesis, spectral studies, crystal structure and redox properties of homoleptic tris-chelated ruthenium(II)-arylazoimidazoles

Sk. Jasimuddin [a], P. Byabartta [a], G. Mostafa [b], T.-H. Lu [b], C. Sinha [a,*]

[a] *Department of Chemistry, The University of Burdwan, Burdwan 713 104, India*
[b] *Department of Physics, National Tsing Hua University, Hsinchu, 300 Taiwan, ROC*

Received 19 June 2003; accepted 7 October 2003

Abstract

Tris-chelated $[Ru(o/p\text{-}RaaiR')_3]Cl_2$ (where RaaiR′ = 1-alkyl-(2-arylazo)imidazole, R = H (**5**), *p*-Me (**6**) *p*-OMe (**7**) *o*-OMe (**8**), R′ = Me (**a**), Et (**b**), CH_2Ph (**c**)) were prepared by the microwave technique. Complexes have been characterized by IR, UV–Vis and ^1H NMR spectral data. The structural confirmation has been done in one case, $[Ru(o\text{-}OMeaaiCH_2Ph)_3]Cl_2$. The UV–Vis spectra of the complexes show an intense peak in the visible region (510–570 nm) and it has been assigned to a MLCT transition. Cyclic voltammetry of the complexes shows one metal oxidation Ru(II)/Ru(III) at 1.2–1.5 V and three successive ligand reduction couples negative to SCE as the reference electrode.
© 2003 Elsevier Ltd. All rights reserved.

Keywords: Ruthenium(II)-tris-chelates; Azoimidazoles; X-ray structure; Electrochemistry

1. Introduction

It is without a doubt that bipyridine and its derivatives have been extensively used to develop the field of ruthenium–diimine chemistry [1–6]. In search of new ligands having similar or higher π-acidity to α-diimines based on pyridine heterocycle a series of arylazopyridines have been used successfully to synthesise ruthenium complexes [7–24]. We have been associated with the exploration of the chemistry of arylazoheterocycles for the last several years and have succeeded in modifying the organic molecule by using imidazole and pyrimidine, and substituting the aryl group by a naphthyl group. We have studied the coordination chemistry of 2-(arylazo)imidazoles [25–28], 2-(naphthylazo)imidazoles [29] and 2-(arylazo)pyrimidines [30]. The ligands are unsymmetric *N*,*N*′-chelators. Dihalo-bis-chelated-{2-(arylazo)heterocycle}ruthenium(II) may exist in five isomeric forms; three of them have *cis*-$RuCl_2$ and two isomers carry a *trans*-$RuCl_2$ configuration [7–9,25]. Complexes with a *trans*-$RuCl_2$ fragment cannot be used for the synthesis of tris chelates. The complexes with *cis*-$RuCl_2$ configuration may act as a precursor to synthesise tris-chelated derivatives [8,9,26].

Usually halide free ruthenium starting material $[Ru(dmf)_6](OTf)_3$ (Otf = trifluoromethane sulfonate) is used [31] or synthetic manipulation has been carried out to phase out halide from the reaction process [26] during preparation of tris-chelates. In the microwave assisted synthetic technique halide is removed forcibly and tris-chelates are isolated. This technique has saved time, energy and minimizes the cost of the reaction. Microwave accelerating chemical transformations is a part of cost benefit green chemical development process and has successfully been employed in organic reactions and synthesis of metal complexes [32].

Metal d^6 tris-complexes with asymmetric chelating ligands can have either facial (*fac*) or meridional (*mer*) configuration. The photophysical and electrochemical properties of facial and meridional isomers have been investigated for a number of Ru(II) complexes having diimine ligands [33,34]. However, for these complexes it

* Corresponding author. Tel.: +91-342-557683; fax: +91-342-2530452.
E-mail address: c_r_sinha@yahoo.com (C. Sinha).

0277-5387/$ - see front matter © 2003 Elsevier Ltd. All rights reserved.
doi:10.1016/j.poly.2003.10.018

has been difficult to achieve control over the synthesis of a specific isomer. Using the present technique of microwave assisted synthesis we have been able to isolate only the meridional isomer. In this article, we report the one pot synthesis of tris-chelated ruthenium(II)-1-alkyl-2-(arylazo)imidazole complexes which have been characterized by their spectra, and electrochemistry. A confirmatory structural study has been done in one case using the single crystal X-ray diffraction technique.

2. Experimental

2.1. Materials

$RuCl_3 \cdot nH_2O$ was obtained from Arrora Matthey, Calcutta and was digested three times with concentrated HCl before use. 1-Alkyl-2-(arylazo)imidazoles were synthesized by the reported procedure [25]. Commercially available silica gel (60–120 mesh) from SRL was used for chromatographic separation. The purification of solvents for electrochemical and spectral work and [*n*-Bu_4N][ClO_4] (TBAP) were prepared as described earlier [28]. Super dry EtOH was obtained from ordinary alcohol following the drying procedure reported elsewhere [35]. All other solvents and chemicals were of reagent grade and were used without further purification.

2.2. Physical measurements

Microanalytical data (C, H, N) were collected using a Perkin–Elmer 2400 CHN Elemental analyzer. Solution electronic spectra were recorded on a JASCO UV–Vis–NIR V-570 spectrophotometer. Infrared (IR) spectra were obtained using a JASCO 420 spectrophotometer (using KBr disks, 4000–200 cm^{-1}). The ^1H NMR spectra in $CDCl_3$ were obtained on a Bruker 500 MHz FT NMR spectrometer using $SiMe_4$ as the internal reference. Solution electrical conductivities were measured using a Systronics 304 conductivity meter with solute concentration $\sim 10^{-3}$ M in acetonitrile. Electrochemical work was carried out using a PAR model 250 Versastat potentiostat/galvanostat with EG and G 270 electrochemistry software. All experiments were performed under a N_2 atmosphere at 298 K using a Pt-disk milli working electrode and Pt-wire auxiliary electrode. All results were referenced to a saturated calomel electrode (SCE). Reported potentials are uncorrected for junction potential. $K_4[Fe(CN)_6]$ was used as a standard showing the Fe(III)/Fe(II) couple at 0.19 V versus SCE in MeCN–0.1(M) TBAP and 50 mV/s scan rate. Molecular orbital calculations have been performed with the use of the ICON software package originally developed by Hoffmann. The crystallographic parameters of **8c** have been used for the calculation.

2.3. Preparation of complexes: tris-{1-benzyl-2-(o-methoxy-phenylazo)imidazole}ruthenium(II) chloride [Ru(o-OMeaaiCH$_2$Ph)$_3$]Cl$_2$(**8c**)

$RuCl_3 \cdot 3H_2O$ (0.25 g, 0.95 mmol) was dissolved in super dry EtOH (20 ml) in a Teflon reactor (100 ml capacity) and dry N_2 gas flushed for a few minutes. The reactor was corked and placed in the microwave oven 450 W for three lots of 5 min with 5 min interval between each step. The solution was cooled and 1-benzyl-2-(*o*-methoxyphenylazo)imidazole (*o*-O-MeaaiCH$_2$Ph) (0.95 g, 3.25 mmol) in degassed warm ethanol (30 ml) was added into it. The reactor was then placed in the microwave oven for another three lots of 5 min with 5 min interval between each step. The red-greenish solution was then evaporated slowly in air and washed with cold water. The dark solid was dried and dissolved in a minimum volume of CH_2Cl_2 and chromatographed over a wet silica gel column prepared in toluene. A light green-blue band was eluted by toluene-MeCN (1:1, v/v) and rejected. The desired red-brown band was eluted with MeOH (2 drops of HCl/100 ml MeOH) and collected. The eluent was slowly evaporated in air, and crystals were filtered and washed with cold water. They were then dried over P_4O_{10}. Yield: 0.63 g, 63%.

Other complexes were prepared under identical conditions; the yields varied in the 55–70% range.

2.4. X-ray structure determination

A crystal suitable for X-ray diffraction study of [Ru(*o*-OMeaaiCH$_2$Ph)$_3$]$Cl_2 \cdot H_2O$ (**8c**) was grown by slow diffusion of hexane into a dichloromethane solution of the complex. X-ray diffraction data were collected at 295 K with the Siemens SMART CCD using graphite-monochromatized Mo Kα radiation (λ =0.71073 Å). Crystal data are summarized in Table 1. The unit cell parameters were determined by least square refinements of all reflections. The intensity data were corrected for Lorentz and polarization effects and an empirical absorption correction was also employed using the SAINT program. The structure was solved by direct methods using SHELXS 97 and followed by successive Fourier and difference Fourier syntheses. Full matrix least-squares refinements on F^2 were carried out using SHELXL 97 with anisotropic displacement parameters for all non hydrogen atoms in all cases. Hydrogen atoms were constrained to ride on the respective carbon atoms with an isotropic displacement parameter equal to 1.2 times the equivalent isotropic displacement parameter of their parent atom. The final difference Fourier map showed the maximum and minimum peak heights at 0.73 and −0.74 e Å^{-3}, respectively, having no chemical significance. Complex neutral atom scattering factors were used throughout. All calculations were carried out using SHELXS 97, SHELXL 97, PLATON 99 and ORTEP 3.

Table 1
Crystallographic data of $[Ru(o\text{-}OMeaaiCH_2Ph)_3]Cl_2 \cdot H_2O$ (**8c**)

Chemical formula	$C_{51}H_{48}Cl_2N_{12}O_3Ru \cdot H_2O$
Crystal size (mm)	$0.30 \times 0.25 \times 0.13$
Crystal system	triclinic
Formula weight	1067
Space group	$P\bar{1}$
a (Å)	12.4174(6)
b (Å)	14.1775(7)
c (Å)	17.2745(9)
α (°)	91.7620(10)
β (°)	107.2810(10)
γ (°)	106.1740(10)
V (Å^3)	2767.5(2)
Z	2
T (K)	295
ρ_{calc} (g cm^{-3})	1.280
λ (Å)	0.71073
2θ range (°)	$3.0 < 2\theta < 56.6$
μ(Mo Kα) (mm^{-1})	0.432
Reflection collected	28 904
Unique reflection, R_{int}	12 989, 0.022
Observed data [$I > 2\sigma(I)$]	9560
R[a]	0.0594
wR_2[b]	0.1290
Goodness-of-fit[c]	1.08

[a] $R = \sum ||F_o| - |F_c|| / \sum |F_o|$.
[b] $wR_2 = [\sum w(F_o^2 - F_c^2)^2 / \sum w(F_o^2)^2]^{1/2}$, $w = 1/[\sigma^2(F_o^2) + (0.0472P)^2 + 2.0068P]$, $P = (F_o^2 + 2F_c^2)/3$.
[c] Goodness-of-fit is defined as $[w(F_o - F_c)/(n_o - n_v)]^{1/2}$, where n_o and n_v denote the number of data and variables, respectively.

3. Results and discussion

3.1. Synthesis and spectroscopic properties

1-Alkyl-2-(*o*/*p*-alkyl-phenylazo)imidazole complexes (*o*-RaaiR′ or *p*-RaaiR′, Scheme 1) of ruthenium(II) have been prepared in super dry EtOH using microwave frequency 450 W in a Teflon reactor. Time and power have been optimized to maximize the yield of $[Ru(RaaiR')_3]Cl_2$. The complexes are purified by chromatography and isolated in 55–70% yield.

The ligands are an unsymmetric *N*,*N*′-chelator. *o*-OMe/OH substituted arylazo ligands exhibit flexidenticity: bidentate or ter-dentate [36,37]. However, in the present reaction *o*-OMeaaiR′ behaves as a bis-chelating *N*,*N*′ system. The composition of the complexes are formulated by elemental analyses and by the structural study of $Ru(o\text{-}OMeaaiCH_2Ph)_3Cl_2$. The complexes show 1:2 conductivity (Λ_M: 210–225 Ω^{-1} cm^2 mol^{-1}) and are diamagnetic (d^6, $S = 0$) in nature.

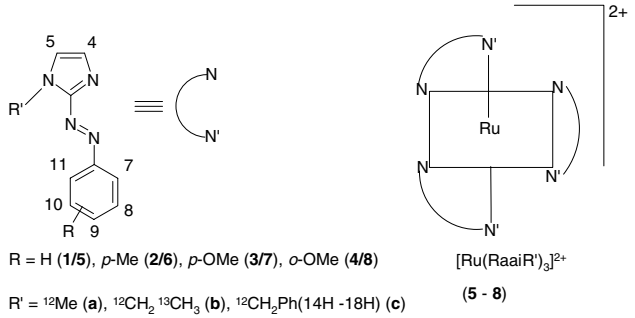

Scheme 1. Ligands used and their atom numbering scheme.

Assignment of the infrared spectral bands has been made on comparison with the spectra of RaaiR′, *ctc*-$RuCl_2(RaaiR')_2$ [25] (*ctc* refers to *cis–trans–cis* orientation of donor centers around Ru(II) in the sequence of coordination pairs of Cl, N(imidazole), N(azo), respectively) and $[Ru(bpy)(RaaiR')_2](ClO_4)_2$ [26]. Infra-red stretchings at 1370–1375 and 1590–1610 cm^{-1} have been assigned to ν(N=N) and ν(C=N), respectively. High intense transitions in the solution spectra (MeCN) below <400 nm are ligand centered charge transfer transition ($n \rightarrow \pi^*$ and $\pi \rightarrow \pi^*$). The visible region of the spectra exhibit high intense transitions at 515–570 along with two high energy transitions below 400 nm (Table 2, Fig. 1). Three transitions are well defined in $[Ru(o\text{-}OMeaaiR')_3]Cl_2$ (**8**) while in $[Ru(p\text{-}OMeaaiR')_3]Cl_2$ two transitions are overlapped (Fig. 1). The extended Huckel molecular orbital calculation (EHMO) using crystallographic parameters of **8c** has shown that the HOMO constitutes 60% metal dπ and the LUMO is 80% ligand character. The high intense transition in the visible region is thus a MLCT transition. Besides, the transition is shifted to the higher energy side in the case of *ortho* substitution, $[Ru(o\text{-}OMeaaiR')_3]Cl_2$ (**8**). Steric crowding may be the reason to destabilize the LUMO (which is ligand dominated as per the EHMO calculation, vide infra) and thus shift the main MLCT band to higher energy (Table 2).

The assignment of ^{1}H NMR signals has been done on considering spin–spin interactions, effect of substituents and on comparing with spectra of free ligands and *ctc*-$RuCl_2(RaaiR')_2$[25]. The proton numbering pattern is shown in Scheme 1 and data for the aliphatic region (1–6 ppm) only are set out in Table 3. The 9-R and 1-R′ groups are useful to support the structure of the compounds. Three ligands in the tris chelates give three sets of separate signals of 9-R and 1-R′. $Ru(RaaiMe)_3Cl_2$ (**5a**–**8a**) show three resonances at av. 4.20, 4.27 and 4.31 ppm. The methylene signals (–CH_2–) of $Ru(RaaiCH_2CH_3)_3Cl_2$ (**5b**–**8b**) exhibit multiplets at 4.65, 4.70 and 4.78 ppm suggesting three unsymmetrical groups. The –CH_3 of –(CH_2)–CH_3 exist as triplets at av. 1.45, 1.50 and 1.54 ppm. $Ru(RaaiCH_2Ph)_3Cl_2$ (**5c**–**8c**) show methylene (–CH_2–) resonances as three pairs of doublets. This suggests that the ligands chelated around Ru(II) are unsymmetrically disposed.

3.2. Structural characterization of $[Ru(o\text{-}OMeaaiCH_2Ph)_3]Cl_2 \cdot H_2O$ (**8c**)

The crystal structure of $[Ru(o\text{-}OMeaaiCH_2Ph)_3]Cl_2 \cdot H_2O$ (**8c**) is shown in Fig. 2. Selected bond distances and

Table 2
Elemental analyses[a], UV–Vis spectral[b] and cyclic voltammetric[c] data of $[Ru(RaaiR')_3]Cl_2 \cdot H_2O$

Compounds	Elemental analyses (%)			UV–Vis data	Cyclic voltammetric data			
	C	H	N	λ_{max}, nm (ε, dm^3 mol^{-1} cm^{-1})	$E_{1/2}$, V (ΔE_p, mV)			
					$Ru^{III/II}$	Ligand reductions		
$[Ru(HaaiMe)_3]Cl_2 \cdot H_2O$ (**5a**)	48.27 (48.13)	4.20 (4.28)	22.58 (22.46)	524 (14.01), 488 (13.04)[d], 422 (23.04), 382 (41.22), 338(17.81)	1.50 (140)	−0.52 (100)	−0.77 (110)	−1.27 (90)
$[Ru(HaaiEt)_3]Cl_2 \cdot H_2O$ (**5b**)	50.03 (50.13)	4.72 (4.81)	21.35 (21.27)	520 (10.44), 486 (10.11)[d], 420 (18.08), 397 (28.11), 358(24.75)	1.52 (130)	−0.51 (80)	−0.75 (110)	−1.24 (120)
$[Ru(HaaiCH_2Ph)_3]Cl_2 \cdot H_2O$ (**5c**)	59.11 (59.02)	4.42 (4.51)	17.30 (17.21)	538 (13.85), 489 (13.21)[d], 411 (24.58), 401 (27.73), 358(25.34)	1.53 (140)	−0.52 (120)	−0.77 (120)	−1.26 (130)
$[Ru(p\text{-}MeaaiMe)_3]Cl_2 \cdot H_2O$ (**6a**)	50.00 (50.13)	4.95 (4.81)	21.10 (21.27)	516 (11.64), 480 (10.65)[d], 420 (32.25), 384 (39.63), 358 (26.02)	1.40 (130)	−0.57 (90)	−0.80 (110)	−1.35 (165)
$[Ru(p\text{-}MeaaiEt)_3]Cl_2 \cdot H_2O$ (**6b**)	52.08 (51.92)	5.36 (5.29)	20.00 (20.19)	524 (14.17), 426 (33.6), 386 (33.64), 340 (13.75)	1.39 (120)	−0.55 (90)	−0.78 (104)	−1.25 (120)
$[Ru(p\text{-}MeaaiCH_2Ph)_3]Cl_2 \cdot H_2O$ (**6c**)	60.23 (60.12)	5.00 (4.91)	16.42 (16.50)	540 (14.19), 428 (31.38), 401 (43.67), 367(25.89)	1.37 (100)	−0.56 (80)	−0.78 (100)	−1.30 (160)
$[Ru(p\text{-}OMeaaiMe)_3]Cl_2 \cdot H_2O$ (**7a**)	47.18 (47.26)	4.44 (4.53)	20.18 (20.05)	532 (11.67), 436 (27.54), 404 (24.13)[d], 314 (13.07)	1.39 (110)	−0.56 (80)	−0.75 (120)	−1.24 (130)
$[Ru(p\text{-}OMeaaiEt)_3]Cl_2 \cdot H_2O$ (**7b**)	49.20 (49.09)	4.88 (5.00)	18.88 (19.09)	540 (13.11), 438 (21.26), 316 (12.07)[d]	1.37 (100)	−0.55 (90)	−0.79 (120)	−1.26 (140)
$[Ru(p\text{-}OMeaaiCH_2Ph)_3]Cl_2 \cdot H_2O$ (**7c**)	57.66 (57.41)	4.57 (4.69)	15.85 (15.76)	568 (11.68), 414 (36.55), 370 (19.58)[d]	1.36 (100)	−0.55 (110)	−0.72 (110)	−1.29 (150)
$[Ru(o\text{-}OMeaaiMe)_3]Cl_2 \cdot H_2O$ (**8a**)	47.03 (47.26)	4.44 (4.53)	20.18 (20.05)	526 (5.05), 440 (9.57), 362 (14.18),	1.45 (120)	−0.51 (80)	−0.73 (160)	−1.21 (170)
$[Ru(o\text{-}OMeaaiEt)_3]Cl_2 \cdot H_2O$ (**8b**)	48.88 (49.09)	5.09 (5.00)	19.21 (19.09)	532 (9.03), 420 (16.73), 372 (22.22), 346 (27.18), 320 (22.74)	1.47 (140)	−0.52 (110)	−0.77 (100)	−1.22 (170)
$[Ru(o\text{-}OMeaaiCH_2Ph)_3]Cl_2 \cdot H_2O$ (**8c**)	57.28 (57.41)	4.56 (4.69)	15.68 (15.76)	540 (15.23), 442 (15.23), 442 (17.38), 346 (20.53)	1.47 (110)	−0.52 (90)	−0.70 (100)	−1.25 (140)

[a] Calculated values are in parentheses.
[b] In MeCN.
[c] Solvent MeCN, Pt-disk milli working electrode, SCE reference and Pt-wire auxiliary electrodes, $[NBu_4][ClO_4]$ supporting electrolyte, 50 mV s^{-1}, potentials are in V vs. SCE, $E_{1/2} = 0.5(E_{pc} + E_{pa})$ where E_{pc} and E_{pa} are cathodic and anodic peak potentials, $\Delta E_p = |E_{pc} - E_{pa}|$.
[d] Shoulder.

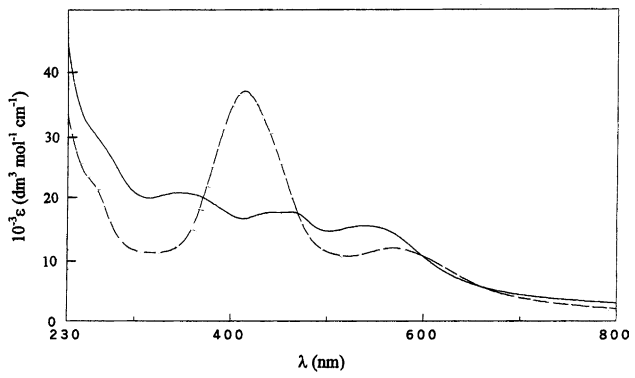

Fig. 1. UV–Vis Spectra of Ru(*o*-OMeaaiCH$_2$Ph)$_3$Cl$_2$ (—) and Ru(*p*-OMeaaiCH$_2$Ph)$_3$Cl$_2$ (---) in MeCN at 298 K.

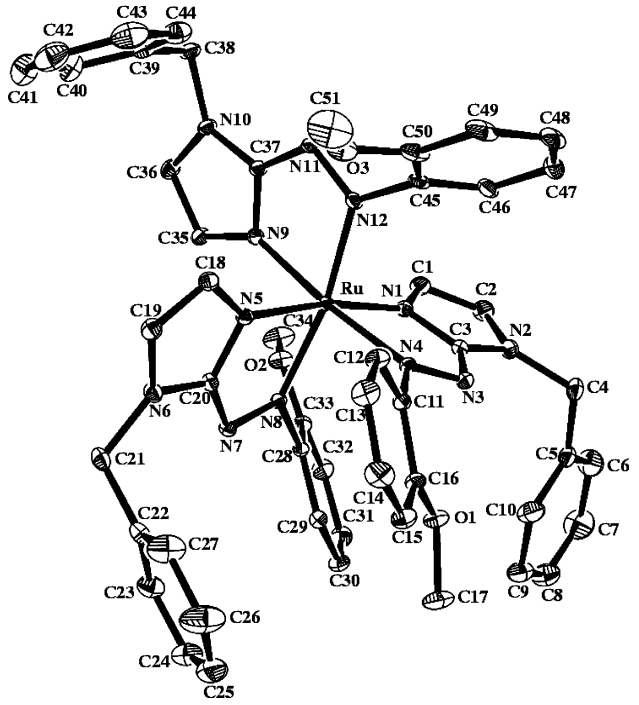

Fig. 2. Perspective view of Ru(*o*-OMeaaiCH$_2$Ph)$_3^{2+}$ showing atom labelling pattern. For clarity, all hydrogen atoms have been omitted.

angles are listed in Table 4. The constraints imposed on the RuN_6 meridional configuration are reflected from the planarity, bond angles and bond length data. The atomic arrangement Ru, N1, C3, N3, N4; Ru, N5, C20, N7, N8 and Ru, N9, C37, N11, N12 constitute three good chelate planes (mean deviation <0.06 Å). The planes are orthogonal to each other and the dihedral angle lie 82°–96°. The pendent *o*-OMeC$_6$H$_4$ group attached to metalated-azoimine chelate plane is no longer planar and is twisted by an acute angle (52°–68°). The atomic arrangements Ru, N1, N4, N5, N9 (plane 1) and Ru, N1, N12, N5, N8 (plane 2) constitute two molecular planes (mean deviation <0.08 Å). Maximum perturbation is observed to N4 in plane 1 which is deviated by 0.11 Å from the mean plane. These two planes make a dihedral angle of ~80°. The groups Ru, N4, N8, N9, N12 (plane 3) exhibit maximum perturbation and suffers deviation from the mean plane by ~0.11 Å. The azo-Ns exhibit maximum perturbation and the deviations from the mean plane are N12, −0.12; N4, 0.12 and N8, −0.15 Å. Thus, plane 3 is not a good plane. The plane 3 makes dihedral angles of 96° and 100° with planes 1 and 2, respectively. No bond lengths and angles are identical. The chelate angles are N9–Ru–N12, 76.42(12)°, N1–Ru–N4, 76.03(11)° and N5–Ru–N8, 76.21(10)°. Bond angle data in Table 2 reflect that N4a is *cis*-oriented with N1 (94.95 (12)°), N4 (99.10 (11)°) and N5 (93.00(12)°) and *trans* oriented with N8 (168.35 (11)°). We may assign *cis* and *trans*-orientation for other N-centres also. Other *trans* angles are N9–Ru–N4, 174.15 (11)° and N1–Ru–N5, 170.53 (10)°.

Table 3
^{1}H NMR spectral data (only aliphatic region) of the complexes in CDCl$_3$

Compound	δ, ppm (J, Hz)			
	N(1)–CH$_2$	N(1)–Me	(N(1)–CH$_2$)CH$_3$(t)	9-R
5a		4.01, 4.09, 4.14		
5b	4.44, 4.65, 4.80 (m)		1.42 (7.0), 1.49 (7.0), 1.54 (7.0)	
5c	5.41, 5.63 (18.0); 5.49, 5.75 (17.0); 5.58, 5.92 (18.0) (q)			
6a		4.07, 4.15, 4.22		2.30, 2.32, 2.42
6b	4.49, 4.60, 4.83 (m)		1.46 (7.0), 1.53 (7.0), 1.59 (7.0)	2.31, 2.33, 2.37
6c	5.41, 5.60 (20.0); 5.48, 5.72 (20.0); 5.56, 5.902 (18.0) (q)			2.27, 2.32, 2.35
7a		4.00, 4.05, 4.11		3.48, 3.70, 3.83
7b	4.45, 4.61, 4.79 (m)		1.50 (7.0), 1.54 (7.0), 1.61 (7.0)	3.57, 3.65, 3.86
7c	5.36, 5.66 (15.0); 5.47, 5.80 (17.0); 5.55, 5.92 (18.0) (q)			3.55, 3.68, 3.84
8a		4.20,4.27, 4.31		3.52, 3.64, 3.80
8b	4.64, 4.70, 4.78 (m)		1.46 (7.0), 1.50 (7.0), 1.54 (7.0)	3.52, 3.66, 3.83
8c	5.36, 5.66 (15.0); 5.45, 5.80 (17.0); 5.49, 5.92 (15.0) (q)			3.50, 3.63, 3.86

(m), (t) and (q) refer to multiplet, triplet and quartets, respectively.

Table 4
Selected bond distances (Å) and angles (°) for [Ru(*o*-OMeaaiCH$_2$Ph)$_3$]Cl$_2$ · H$_2$O (**8c**)

Bond distances			
Ru–N1	2.039(3)	N1–C3	1.339(4)
Ru–N4	2.070(3)	N3–C3	1.358(5)
Ru–N5	2.051(3)	N4–C11	1.450(5)
Ru–N8	2.062(3)	N5–C20	1.339(4)
Ru–N9	2.056(3)	N7–C20	1.348(4)
Ru–N12	2.032(3)	N8–C28	1.454(4)
N3–N4	1.282(4)	N9–C37	1.353(4)
N7–N8	1.287(4)	N11–C37	1.362(5)
N11–N12	1.297(4)	N12–C45	1.409(9)
Bond angles			
N9–Ru–N12	76.42(12)	N9–Ru–N4	174.15(11)
N1–Ru–N4	76.03(11)	N9–Ru–N5	86.42(11)
N5–Ru–N8	76.21(10)	N9–Ru–N8	98.20(10)
N12–Ru–N5	93.00(12)	N1–Ru–N8	96.20(11)
N12–Ru–N1	94.95(12)	N1–Ru–N5	170.53(10)
N12–Ru–N4	99.10(11)	N4–Ru–N8	86.87(10)
N12–Ru–N8	168.35(11)	N4–Ru–N5	97.65(11)
N9–Ru–N1	100.43(11)		

There are two types of N donor centres: N (imidazole) – N1, N5, N9 and N (azo) – N4, N8, N12. The Ru–N (imidazole) bond lengths are in general less than those of Ru–N(azo) distances. Ru–N(imidazole): Ru–N9/N1/N5: 2.056(3), 2.039(3), 2.051(3) Å; Ru–N(azo): Ru–N12/N4/N8: 2.032(3), 2.070(3), 2.062(3) Å. The Ru–N distances in this complex do not follow any sequence. In an individual chelate ring the Ru–N(imidazole) and Ru–N(azo) distances differ significantly. The Ru–N9 bond is longer ($\Delta d \approx 0.03$ Å) than the Ru–N12 bond while the Ru–N5 bond length is shortened by 0.01 Å from that of the Ru–N8 bond distance. Most significant distortion is observed in the chelate ring constituted by Ru, N1, C3, N3, N4; the Ru–N4 bond is elongated by ~0.03 Å from that of the Ru–N1 bond. The N3–N4 bond length is the shortest in the series, (1.282(4) chelated) and N11–N12 is the longest one (1.297(4) Å). The N7–N8 bond distance is 1.287(4) Å. The N–N length in this complex is longer than the free ligand value (1.250(1) Å) [37,38]. This may be due to the π-back bonding dπ (Ru) → π* (azo) charge transferences.

The molecular packing shows a 1D polymer (Fig. 3) which has been observed due to hydrogen bonding and π–π interaction. The Cl$^-$ forms a hydrogen bonding interaction with the imidazole-H (5-H as per the atom numbering pattern in Scheme 1) and bridges via N(1)–CH(Ph)–H–Cl of the neighbouring molecule (C(19)–H(19)–Cl(1): C(19)–H(19), 0.93; H(19)–Cl(1), 2.71; C(19)–Cl(1), 3.526(4) Å; ∠C(19)–H(19)–Cl(1), 147.0°. C(38)–H(38a)–Cl(1): C(38)–H(38a), 0.97; H(38a)–Cl(1), 2.76; C(38)–Cl(1), 3.661(5) Å; ∠C(38)–H(38a)–Cl(1), 154.0°). The second Cl$^-$ also acts similarly forming a hydrogen bonded cyclic dimer. Each dimer repeats along the *c*-axis and they are under face-to-face π–π interactions of two pendant anicidine rings of two different dimeric units (Cg(12)–Cg(12): 3.530 Å).

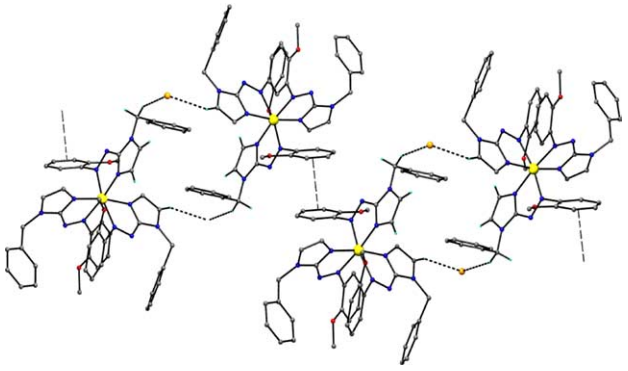

Fig. 3. Packing diagram showing C–H–Cl hydrogen bonded cyclic dimer and π–π interaction between anicidine rings to form a 1D polymer. (Yellow, Ru; blue, N; red, O; black C; orange, Cl; Hs are omitted except hydrogen bonded H for clarity).

3.3. Redox studies

A quasireversible couple at >1.30 V versus SCE reference electrode in MeCN (0.1 M TBAP) has been assigned to the Ru(II)/Ru(III) couple (Table 2, Fig. 4). Two closely spaced reversible to quasireversible redox couples ($\Delta E_p > 70$ mV) at −0.5 to −0.6 and −0.7 to −0.8 V are observed. A third couple, irreversible in nature ($\Delta E_p > 120$ mV), is observed at a potential of >−1.2 V. The one electron nature of the couple is supported from the i_d value in CV and DPV. Three couples at negative to reference potential are assigned to the ligand reduction centered at the azo group. The reduction is electron accommodation in the LUMO. LUMOs are ligand dominated (80%) so voltammograms negative to SCE are correctly assigned to ligand reductions. Since the HOMO possesses 60% metal dπ character; the oxidation may be described as electron extraction from the Ru(II) centre. During coulometric oxidation at a potential of 1.6 V for **6c** we found a continuous current count which may be due to solvent oxidation; one electron stoichiometric reduction becomes difficult because of closely

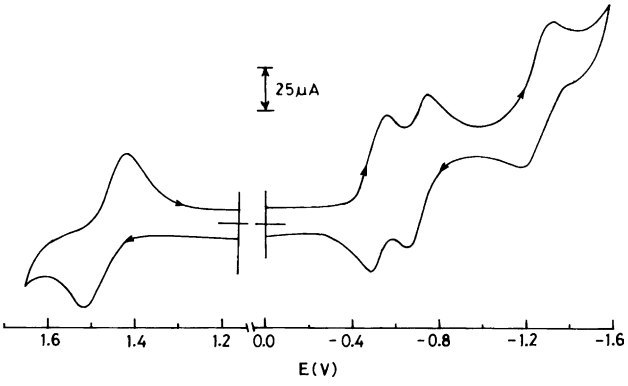

Fig. 4. Cyclic voltammogram of Ru(*o*-OMeaaiCH$_2$Ph)$_3$Cl$_2$ (**8c**) in MeCN using Pt-disk milli electrode, Pt-wire auxiliary, SCE reference electrodes.

spaced reduction couples. Further reduction of the co-ordinated ligand was not observed within the potential window +2.0 to −2.0 V.

4. Conclusion

The work describes microwave assisted one pot synthesis of tris-(1-alkyl-2-(arylazo)imidazole)ruthenium(II) chloride. The complexes have been characterised by spectroscopic data. The X-ray structure shows a bidentate *N*,*N*′-donation mode. The redox properties exhibit a Ru(III)/Ru(II) couple at very high positive potential and ligand reductions.

5. Supplementary data

Supplementary data are available from the Cambridge Crystallographic Data Centre, 12 Union Road, Cambridge CB2 1EZ. UK [fax: (internet.) +44-1223/336-033; e-mail: deposit@ccdc.cam.ac.uk or www: http://www.ccdc.cam.ac.uk] on request. The deposition number is 212243. These data can be obtained free of charge at www.ccdc.cam.ac.uk/conts/retrieving.html.

Acknowledgements

Financial assistance from the Council of Scientific and Industrial Research (CSIR), New Delhi, is gratefully acknowledged. One of us (S.J.) is thankful to CSIR for a fellowship. T.-H.L. and G.M. thank the National Science Council, ROC, for support.

References

[1] F.A. Cotton, G. Wilkinson, Advanced Inorganic Chemistry, 5th ed., 1998.
[2] A. Juris, V. Balzani, F. Bargelletti, S. Campagna, P. Belser, A. von Zelewsky, Coord. Chem. Rev. 84 (1988) 85.
[3] M.D. Ward, A. McCleverty, J. Chem. Soc., Dalton Trans. (2002) 275.
[4] H.E. Toma, K. Araki, Coord. Chem. Rev. 196 (2000) 307.
[5] D.S. Senevirante, Md.J. Uddin, V. Swayambhunathan, H.B. Schlegel, J.F. Endicott, Inorg. Chem. 41 (2002) 1502.
[6] V. Balzani, L. de Cola (Eds.), Supramolecular Chemistry, Kluwer, Dordrecht, 1992.
[7] B.K. Ghosh, A. Chakravorty, Coord. Chem. Rev. 95 (1989) 239.
[8] S. Goswami, A.R. Chakravarty, A. Chakravorty, Inorg. Chem. 20 (1981) 2246.
[9] S. Goswami, R.N. Mukherjee, A. Chakravorty, Inorg. Chem. 22 (1983) 2825.
[10] A.H. Velders, H. Kooijman, A.L. Spek, J.G. Haasnoot, D. de Vos, J. Reedijk, Inorg. Chem. 39 (2001) 2966.
[11] M. Kakoti, A.K. Deb, S. Goswami, Inorg. Chem. 31 (1992) 1302.
[12] S. Sengupta, I. Chakraborty, A. Chakravorty, Eur. J. Inorg. Chem. (2003) 1157, and references therein.
[13] I. Chakraborty, S. Sengupta, S. Das, S. Banerjee, A. Chakravorty, J. Chem. Soc., Dalton Trans. (2003) 134.
[14] C. Das, A. Saha, C.-H. Hung, G.-H. Lee, S.-M. Peng, S. Goswami, Inorg. Chem. 42 (2003) 198.
[15] N. Chanda, R.H. Laye, S. Chakraborty, R.L. Paul, J.C. Jeffery, M.D. ward, G.K. Lahiri, J. Chem. Soc., Dalton Trans. (2002) 3496.
[16] B.K. Santra, G.K. Lahiri, Proc. Indian Acad. Sci. (Chem. Sci.) 111 (1999) 509.
[17] A. Das, S.-M. Peng, S. Bhattacharya, Polyhedron 19 (2000) 1227.
[18] J. Otsuki, N. Omokawa, K. Yoshiba, I. Yoshikawa, T. Akasaka, T. Suenobu, T. Takidi, K. Araki, S. Fukuzumi, Inorg. Chem. 42 (2003) 3057, and references therein.
[19] G.A. Berf, R.A. Sheldon, J. Mol. Catal. A (Chem.) 98 (1995) 143.
[20] K. Akoi, M. Nakagawa, T. Seki, K. Ichimura, Bull. Chem. Soc. Jpn. 75 (2002) 2533.
[21] K.L.-Y. Sze, Y. Li, Inorg. Chem. Commun. 2 (1999) 599.
[22] V.V.W.-W. Yam, Y.C.-Y. Lan, L.-X. Wu, J. Chem. Soc., Dalton Trans. (1998) 1461.
[23] M.N. Ackermann, J.W. Naylor, E.J. Smith, G.A. Mines, N.S. Amin, M.L. Kerns, C. Woods, Organometallics 11 (1992) 1919.
[24] W. Kaim, S. Kohlmann, J. Jordanov, D. Fenske, Z. Anorg. Alleg. Chem. 217 (1991) 598–599.
[25] T.K. Misra, D. Das, C. Sinha, P.K. Ghosh, C.K. Pal, Inorg. Chem. 37 (1998) 1672.
[26] P. Byabartta, J. Dinda, P.K. Santra, C. Sinha, K. Panneerselvam, F.-L. Liao, T.-H. Lu, J. Chem. Soc., Dalton Trans. (2001) 2825.
[27] P. Byabartta, S. Pal, C. Sinha, F.-L. Liao, K. Panneerselvam, T.-H. Lu, J. Coord. Chem. 55 (2002) 479.
[28] P. Byabartta, Sk. Jasimuddin, B.K. Ghosh, C. Sinha, A.M.Z. Slawin, J.D. Woollins, New J. Chem. 26 (2002) 1415.
[29] J. Dinda, S. Pal, B.K. Ghosh, J. Cheng, F.-L. Liao, T.-H. Lu, C. Sinha, J. Coord. Chem. 55 (2002) 1271.
[30] S. Senapati, U.S. Ray, P.K. Santra, C. Sinha, A.M.Z. Slawin, J.D. Woollins, Polyhedron 21 (2002) 753.
[31] A.A. La Pensee, J. Bickley, S.J. Higgis, M. Marcaccio, F. Paolucci, S. Roffia, J.M. Charnock, J. Chem. Soc., Dalton Trans. (2002) 4095.
[32] I.M. Larhed, C. Moberg, A. Hallberg, Acc. Chem. Rev. 35 (2002) 717.
[33] N.C. Fletcher, M. Neiuwenhuyzen, S. Rainey, J. Chem. Soc., Dalton Trans. (2001) 2641.
[34] P.J. Steel, E.C. Constable, J. Chem. Soc., Dalton Trans. (1990) 1383.
[35] A.I. Vogel, A Text Book of Practical Organic Chemistry, third ed., Longmans, 1958, p. 167.
[36] G.K. Lahiri, S. Bhattacharya, M. Mukherjee, A.K. Mukherjee, A. Chakravorty, Inorg. Chem. 26 (1987) 3359.
[37] R.C. Khulbe, R.P. Singh, Y.K. Bhoon, Indian J. Chem. 22A (1983) 214.
[38] J. Dinda, K. Bag, C. Sinha, G. Mostafa, T.-H. Lu, Polyhedron 22 (2003) 1367.

Available online at www.sciencedirect.com
SCIENCE DIRECT®
Polyhedron 23 (2004) 735–741
POLYHEDRON
www.elsevier.com/locate/poly

Synthesis and molecular structures of cobalt(II) β-diketonate complexes as new MOCVD precursors for cobalt oxide films

Sergej Pasko [a,b], Liliane G. Hubert-Pfalzgraf [a,*], Adulfas Abrutis [b,*], Jacqueline Vaissermann [c]

[a] Université Lyon 1, IRC-CNRS, 2 av. A. Einstein, 69626 Villeurbanne cedex, France
[b] Department of Chemistry, Vilnius University, Naugarduko 24, LT2006 Vilnius, Lithuania
[c] Laboratoire de Chimie des Métaux de transition, UMR-CNRS, 4 place Jussieu, Paris, France

Received 17 September 2003; accepted 18 October 2003

Abstract

Adducts of cobalt(II) 2,4-pentanedionate (acac) and 2,2,6,6-tetramethyl-3,5-heptanedionate (thd) with TMEDA (N,N,N',N'-tetramethyl-1,2-diaminoethane) and aminoalcohols, namely 1-dimethylamino-2-propanol (DMAPH) and 2-dimethylaminoethanol (DMAEH), have been synthesized and characterized by elemental analyses, FT-IR, ^{1}H NMR, mass spectrometry and TGA. The molecular structures of $Co(acac)_2$(TMEDA) (**1**) and $[Co(acac)_2(DMAPH)]_2$ (**2**) have been determined by single-crystal X-ray diffraction. **1** is monomeric while **2** is dimeric with two molecules linked by hydrogen bonds (O–H–O distance 2.708 Å av.). The most volatile and stable new adducts $Co(acac)_2$(TMEDA) and $Co(thd)_2$(TMEDA) have been studied as precursors for cobalt oxide deposition by liquid injection MOCVD in DME on monocrystalline $LaAlO_3$ and Si substrates. Films were characterized by XRD and XPS. These preliminary MOCVD experiments showed that epitaxial Co_3O_4 films can be obtained by using both new precursors.
© 2003 Elsevier Ltd. All rights reserved.

Keywords: Cobalt; Oxide; β-diketonates; Adducts; Structures; MOCVDf

1. Introduction

Cobalt oxides are of great interest due to useful properties, such as high catalytic activity at low cost [1], antiferromagnetism [1], electrochromism [2]. Cobalt oxide films have been considered for uses as magnetic detectors, membranes for oxidation of hydrocarbons, counter electrodes, humidity or oxygen optical sensors [3,4], solar-selective absorbers and protective layers [1,5,6]. Cobalt oxide films have been deposited by a variety of methods including conventional MOCVD [1,2,5–8]. However, despite the interest of MOCVD of Co_3O_4, reports are scarce. $[Co(acac)_2]_4$ was generally used as a precursor [1,5,7,8], although the use of $Co(acac)_3$ [8], $Co(OAc)_2$ [9] and more recently of $Co(thd)_2$ [10] or $Co(NO_3)_3$ [11] has been reported. Another use of cobalt β-diketonates is for the CVD of Co films [12]. A number of cobalt(II) acetylacetonate adducts with N-donors have been described [13–18]. Although some of them such as $Co(acac)_2$(LL) [LL = 2,2′-bipyridyl (130 °C/10^{-2} Torr), 1,10-phenantroline (190 °C/10^{-2} Torr)] [19] and $Co_2(acac)_4$(piperidine) (80 °C/10^{-4} Torr) [20] were volatile, no adduct was used so far for MOCVD applications. Cobalt β-diketonate adducts are also good catalysts for a number of reactions, such as polymerisation, enantioselective Michael addition, etc. [21–23].

We report here the synthesis and structural characterization of some new adducts of cobalt(II) 2,4-pentanedionate and 2,2,6,6-tetramethylheptane-3,5-dionate and the preliminary study of the most volatile and stable new adducts as precursors for the deposition of cobalt oxide films by liquid injection MOCVD.

* Corresponding authors. Tel.: +37052331004; fax: +37052330987.
E-mail address: adulfas.abrutis@chf.vu.lt (A. Abrutis).

0277-5387/$ - see front matter © 2003 Elsevier Ltd. All rights reserved.
doi:10.1016/j.poly.2003.11.044

2. Experimental

2.1. Syntheses

Syntheses of air-sensitive complexes were performed under argon using Schlenk tubes and vacuum line techniques. Solvents were purified by standard methods. TMEDA (N,N,N',N'-tetramethylethylenediamine), DMAEH (2-dimethylaminoethanol), DMAPH (1-dimethylamino-2-propanol), thdH (2,2,6,6-tetramethyl-3,5-heptanedione) and acacH (acetylacetone, 2,4-pentanedione) were distilled and stored over molecular sieves. $Co(thd)_2$ and $Co(acac)_2(H_2O)_2$ were prepared as reported [10,24]. $[Co(acac)_2]_4$ was obtained by sublimation of $Co(acac)_2(H_2O)_2$ at 100–120 °C/2×10^{-4} Torr (67%). It is slightly hygroscopic. FT-IR spectra were recorded with a Perkin–Elmer Paragon 500 Spectrometer as Nujol mulls. Mass spectra were obtained using a Thermofinnigan Mat95XL spectrometer under standard electron ionization conditions ($E_1 = 70$ eV). TGA experiments were performed under air with a Setaram 62 system using a thermal ramp of 10 °C/min. Proton NMR spectra were recorded in the range −130 to +130 ppm using the solvent peak as a reference on an AM250 Bruker spectrometer. Elemental analyses were done at the Centre de microanalyses du CNRS and at Vilnius University.

*$Co(acac)_2(TMEDA)$ (**1**)* was previously reported [15], it was prepared by a modified procedure. TMEDA (10% excess) was added to $Co(acac)_2(H_2O)_2$, the reaction medium was evaporated after 2 h and sublimed at 70 °C/2×10^{-4} Torr (90%). MS (m/z^+, %): M (5), M-acac (26), M-TMEDA (43), M-CH_3-TMEDA (76), M-acac-TMEDA (84), M-acac-CH_3-TMEDA (7), TMEDA (7), acacH (4), $Me_2N{=}CH_2$ (100). ^{1}H NMR ($CDCl_3$, 20 °C): −13.19 broad (Me(acac) + CH, 8H), 10.51 s (6H, Me acac), 38.69 s (2H, CH_2), 47 s (6H, Me_2N), 67 s (2H, CH_2), 78.08 s (6H, Me_2N).

*$[Co(acac)_2(DMAPH)]_2$ (**2**)*. 0.70 g (0.68 mmol) of $[Co(acac)_2]_4$ were dissolved in 20 ml of toluene and 0.37 ml (3.02 mmol) of DMAPH were added. The color of the solution changed from dark violet to red. After stirring for 2 h and concentration, **2** crystallized at −30 °C (0.72 g, 73%). *Anal.* Calc. for $C_{15}H_{27}CoNO_5$: C, 50.00; H, 7.55, N, 3.89. Found: C, 49.50; H, 7.49, N, 3.85%. IR, cm^{-1}: 3390 w (*ν*OH); 1599 vs, 1519 vs (*ν*C=O, *ν*C=C); 558 m, 505 w (*ν*Co–O, *ν*Co–N). ^{1}H NMR ($CDCl_3$, 20 °C): −14.52 s (2H, CH), 12.28 broad [15H, Me(acac) + Me(CH)], 32.85 broad (8H, $Me_2N + CH_2$), 71.93 s (1H, CHO).

*$[Co(acac)_2(DMAEH)]$ (**3**)*. 0.88 g (0.85 mmol) of $[Co(acac)_2]_4$ were dissolved in 25 ml of toluene. Addition of 0.38 ml (3.75 mmol) of DMAEH gave a red precipitate which was filtered after 16 h. A second crop of **3** was obtained by concentration at −30 °C (0.74 g, 72%). *Anal.* Calc. for $C_{14}H_{25}CoNO_5$: C, 48.56; H, 7.28; N, 4.04. Found: C, 48.00; H, 7.30; N, 3.92%. IR, cm^{-1}: 3109 w (*ν*OH); 1595 vs, 1520 vs (*ν*C=O, *ν*C=C); 554 w (*ν*Co–O, *ν*Co–N). ^{1}H NMR ($CDCl_3$, 20 °C): −14.10 s (2H, CH), 12.13 s (12H, Me, acac), 32.85 broad ($Me_2N + CH_2$, 8H), 71.93 s (2H, CH_2O).

*$Co(thd)_2(TMEDA)$ (**4**)*. Same procedure as for **2** applied to 0.32 g (0.75 mmol) of $Co(thd)_2$ in 10 ml of toluene and 0.12 ml (0.83 mmol) of TMEDA. The reaction mixture was evaporated after 2 h and sublimed at 125 °C/2.3×10^{-2} Torr (80%). *Anal.* Calc. for $C_{28}H_{54}CoO_4N_2$: C, 62.09; H, 10.05, N, 5.17. Found: C, 62.73; H, 10.16, N, 5.40%. IR, cm^{-1}: 1594 vs, 1582 vs, 1570 vs; 1531 s, 1504 vs (*ν*C=O, *ν*C=C); 609 w, 586 w, 478 m (*ν*Co–O, *ν*Co–N). MS (m/z^+, %): M (19), M-TMEDA (35), M-^{t}Bu-TMEDA (100), M-$C_{11}H_{19}O_2$ (10), M-$C_{11}H_{19}O_2$-TMEDA (15). thdH (2.8), ^{t}BuCOCH$_2$CO (15), TMEDA (10). ^{1}H NMR ($CDCl_3$, 20 °C): −17.53 s (2H, CH), −5.09 s (18H, ^{t}Bu), 8.06 s (4H, Me_2N), 32.24 (18H, ^{t}Bu), 46.80 (2H, CH_2), 67.82 (2H, CH_2), 78.87 (12H, Me_2N).

All compounds were soluble in usual organic solvents, except for **2** and **3,** insoluble in aliphatic hydrocarbons. Solubility was generally lower in polar solvents (N,N-dimethylformamide, CH_3CN, alcohols). All complexes but **1** are slightly air-sensitive, their colour changed to green on storage for over six months in air, oxidation to Co(III) was faster in solutions especially polar ones.

2.2. Crystallography of *1* and *2*

Crystals of **1** and **2** were obtained by sublimation at 80–85 °C/2.3×10^{-2} Torr and by recrystallisation in toluene at −20 °C, respectively. Data were collected with an Enraf–Nonius MACH3 diffractometer. Unit cell dimensions with estimated standard deviations were obtained from least squares refinements of the setting angles of 25 well-centred reflections. Corrections were made for Lorentz and polarization effects. Empirical absorption correction (Difabs) was applied. Crystallographic data and other pertinent information are summarized in Table 1. Computations were performed using CRYSTALS [25]. Atomic form factors for neutral Co, O, N and C were taken from [26]. Anomalous dispersion was taken in account. All atoms were anisotropically refined. Hydrogen atoms were introduced in calculated positions. Least-squares refinements (full matrix) were carried out by minimizing the function $\sum w(|F_o| - |F_c|)^2$, where F_o and F_c are the observed and calculated structure factors. Models reached convergence with $R = \sum(||F_o| - |F_c||)/\sum|F_o|$ and $R_w = [\sum(|F_o| - |F_c|)^2/\sum w(F_o)^2]^{1/2}$ having values listed in Table 1. A weighting scheme [27] was applied. Criteria for a satisfactory complete analysis were the ratios of rms shift to standard deviation being less than 0.1 and no significant features in the final map.

Table 1
Crystal data for $Co(acac)_2(TMEDA)$ and $[Co(acac)_2(DMAPH)]_2$

Formula	$C_{16}H_{30}CoN_2O_4$ (**1**)	$C_{15}H_{27}CoNO_5$ (**2**)
Formula weight	373.36	360.3
a (Å)	8.500(4)	10.674(2)
b (Å)	10.193(3)	12.083(1)
c (Å)	11.565(6)	14.452(2)
α (°)	90	93.11(1)
β (°)	92.35(4)	91.96(2)
γ (°)	90	92.01(1)
V (Å^3)	1001.0(7)	1858.8
Z	2	4
Crystal system	monoclinic	triclinic
Space group	Pn	$P\bar{1}$
Linear absorption coefficient μ (cm^{-1})	8.71	9.39
Density ρ (g cm^{-3})	1.24	1.29
Radiation	Mo Kα ($\lambda = 0.71069$ Å)	Mo Kα ($\lambda = 0.71069$ Å)
θ Limits (°)	1–28	1–26
Temperature of measurement (K)	295	251
Number of data collected	2720	7700
Number of unique data collected	2422 ($R_{int} = 0.03$)	7288 ($R_{int} = 0.01$)
Number of unique data used for refinement (on F)	1764 $(F_o)^2 > 3\sigma(F_o)^2$	4884 $(F_o)^2 > 3\sigma(F_o)^2$
$R = \sum \|\|F_o\| - \|F_c\|\| / \sum \|F_o\|$	0.0476	0.0399
$R_w^* = \left[\sum w(\|F_o\| - \|F_c\|)^2 / \sum wF_o^2\right]^{1/2}$	0.0525	0.0496
Extinction parameter	691	122
Number of variables	210	398
Largest difference peak and hole (e Å^{-3})	0.40	0.50

2.3. CVD experiments and films characterisation

Deposition of Co_3O_4 films was carried out by innovative pulsed liquid injection MOCVD (PI-MOCVD) [28]. Detailed description of this technique and of the reactor is given elsewhere [29,30]. Solutions (0.05 M) of precursors in 1,2-dimethoxyethane (monoglyme) were used for the depositions (injection frequency 2 Hz, microdose mass ~4 mg). The carrier gas was a mixture of Ar (54 l/h) and O_2 (36 l/h). Depositions were performed on monocrystalline $LaAlO_3$(1 0 0) and Si(1 0 0) substrates under 5 Torr total pressure. Substrates were cleaned in boiling toluene and its vapour before use. After deposition, films were cooled down to RT in an O_2 atmosphere (~1 atm).

Films crystallization and texture were studied by X-ray diffraction (XRD) with a Siemens D500 diffractometer (Cu Kα radiation). The film in-plane orientation was studied by XRD in Schultz geometry. X-ray photoelectron spectroscopy (XPS, VG ESCALAB 200R, Al Kα radiation) was also used. The in-depth film purity was evaluated after Ar^+ sputtering at 4 keV, 3.75×10^{-7} Torr argon pressure. A non-linear least-squares program (Eclipse V2.0) adopting Gaussian–Lorentzian peak shapes was used for the raw spectra fitting and for the evaluation of atomic compositions. Thickness of the films on Si(1 0 0) substrates was determined by profilometry (Taylor–Hobson) on a step formed by lithography. The thickness value was used for the calculation of the film growth rate.

3. Results and discussion

3.1. Synthesis and characterization

Adducts of cobalt(II) acetylacetonate with TMEDA, DMAEH and DMAPH were easily obtained either by ligand exchange reaction from $Co(acac)_2(H_2O)_2$ or by decomplexation of $[Co(acac)_2]_4$ at RT. It is noticeable that the decomplexation of $[Co(acac)_2]_4$ by aminoalcohols was more effective than that of $[Ni(acac)_2]_3$ [31]. $[Co(acac)_2]_4$ by contrast did not react with O-donors such as DME, triglyme and tetraglyme even in refluxing toluene for 24 h. These observations account for the absence of decomplexation and/or ligand exchange reactions in DME solutions, the solvent used for the CVD experiments. $Co(thd)_2$ and $Co(thd)_2(TMEDA)$, the first adduct of $Co(thd)_2$ reported, are also stable in DME. The complexes were characterized by elemental analyses, FT-IR, ^{1}H NMR, mass spectrometry and TGA. Their FT-IR spectra display the νC=O and νC=C absorption bands of the β-diketonate ligands in the 1504–1600 cm^{-1} range as well as those of the Lewis base. The spectra of **2** and **3**, the complexes with aminoalcohols, showed also absorptions at 3390 and 3109 cm^{-1}, respectively, due to νOH stretching. Their frequency is lower than that of the corresponding free alcohol – 3433 and 3385 cm^{-1} – respectively suggesting thus coordination. All compounds were volatile, the order of their sublimation rate under vacuum in identical conditions was as follows: $Co(acac)_2(TMEDA) >$

$Co(thd)_2 > Co(thd)_2(TMEDA) > [Co(acac)_2]_4 > [Co(acac)_2(DMAPH)]_2 \gg [Co(acac)_2(DMAEH)]_2$. The two latter adducts sublimed at 80 and 90 °C/10^{-4} Torr, respectively, but with partial loss of the aminoalcohol ligand especially for **3**, the DMAEH adduct. Due to this behaviour, adducts **2** and **3** were not investigated as MOCVD precursors for cobalt oxide films. The complexes with TMEDA were totally recovered as adducts by sublimation under vacuum thus reflecting the higher thermal stability of the N,N-donor Co β-diketonate adducts as compared to those with the O,N-donors. The volatility of the tetramethylheptanedionate derivatives, is, as expected higher than that of the acetylacetonate ones except **1** [32]. TGA-DTA analyses were performed in air. Fig. 1 illustrates the data for **1**. The amount of residue of black Co_3O_4 (18.3%), lower than the theoretical amount (21.5%) and the almost horizontal DTA curve part show that 1 sublimed partially (~15%) in the 130–230 °C temperature range. Subsequent events are the loss of TMEDA and acacH which occurred at temperatures lower than 260 °C and the oxidation of the residue as evidenced by the strong exothermic peak at 370 °C.

The mass spectra of $Co(acac)_2(TMEDA)$ (**1**) and of $Co(thd)_2(TMEDA)$ (**4**) show the molecular ions, the stability being in the favour of **4**. The main decomposition pathways of the molecular ions are the loss of TMEDA then of the methyl groups and acac for **1**, of both TMEDA and butyl groups for **4**. These patterns are in agreement with the literature. [10]. A peak at $m/z = 608$ (25%) attributed to $Co(thd)_3$ was observed for samples of **4** stored in air for ~6 months. The oxidation rate to Co(III) species by air was **1** < **4** < **2** < $[Co(acac)_2]_4$ < $Co(thd)_2$ < **3** according to ^{1}H NMR data. Thus, an advantage of the Co(II)-TMEDA adducts **1** and **4** by comparison to ligand free Co(II) β-diketonates is a higher resistance to oxidation.

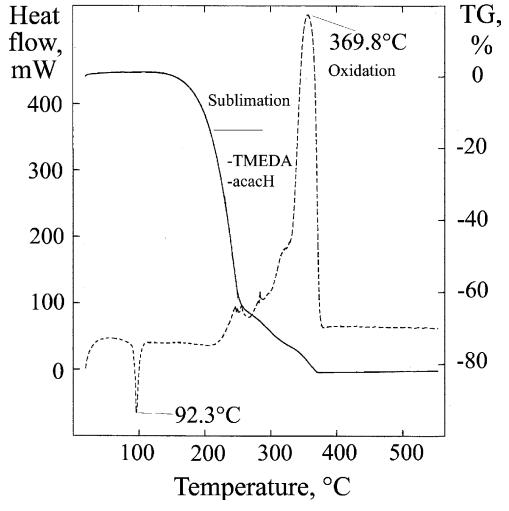

Fig. 1. TGA curve of $Co(acac)_2(TMEDA)$.

Despite the paramagnetic nature of the complexes, proton NMR spectra could be obtained. The NMR signals spread over the range −20 to +90 ppm. The signals are relatively narrow and, for complexes **1** and **4** account for the two types of magnetically non-equivalent substituents on the β-diketonate ring, *cis* and *trans* to the nitrogen donor sites of the TMEDA ligand. The complexes with the aminoalcohols are more stereolabile and only one signal was observed at RT for the substituents of the β-diketonate ring.

3.2. Molecular structures of *1* and *2*

The molecular structures of **1** and **2** were established by single crystal X-ray diffraction. **1** is monomeric (Fig. 2), while **2** contains two different dimeric molecules, **2a** and **2b**, in the asymmetric unit cell (Fig. 3). One molecule corresponds to the association of two monomeric units with chelating η^2-aminoalcohol ligands having an R configuration whereas the other involves chelating aminoalcohol ligands with an S configuration. The dimeric nature of **2** is due to assembly via hydrogen bonds from O(H) on one molecule to an O(acac) of another unit. The O–O distances have values of 2.684(3) and 2.733(3) Å for O(10)H–O′(8) and O(5)H–O′(4),

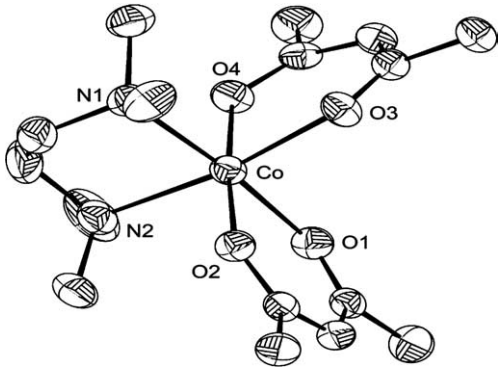

Fig. 2. Molecular structure of $Co(acac)_2(TMEDA)$ showing the atom numbering scheme (thermal ellipsoids at 20% probability).

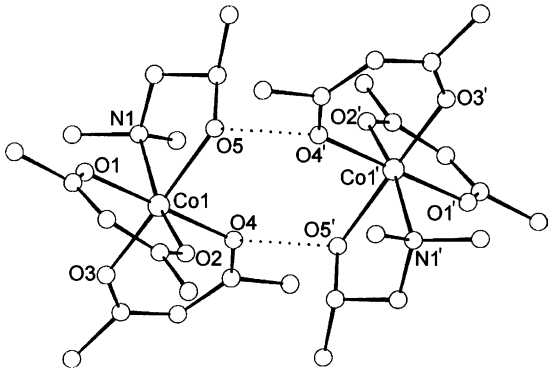

Fig. 3. Molecular structure of $[Co(acac)_2(DMAPH)]_2$ showing the atom numbering scheme (dotted line indicate H bonding).

respectively. Intramolecular hydrogen bonding in complexes with a β-diketonate ligand has been observed previously for instance for $[Ba_2Cu(\mu_3,\eta^2\text{–}OCH\text{-}MeCH_2NMe_2)_2(\mu,\eta^2\text{-thd})_2(\eta^2\text{-thd})(^i PrOH)_2]$ (O–H–O 2.58 Å av.) [33]. The structure of **2** is similar to that of $[Ni(acac)_2(DMAEH)]_2$ [31] or $[Ni(acac)_2(DMAPH)]_2$ [34] (O–H–O 2.54 Å av.). Selected bond distances and angles are collected in Table 2.

All adducts adopt a *cis* geometry, and the metals lie in a distorted octahedral CoO_4N_2 or CoO_5N cores. The Co–O(η^2-acac) bond distances in **1** [2.043(4)–2.076(4) Å] and **2** [2.023(3)–2.079(2) Å], are similar to the literature body as illustrated by $Co(acac)_2$(6-methylquinoline) [35] or $[Co(acac)_2(H_2O)]_2$ [36] for instance. The Co–O bonds in **1** *trans* to the nitrogen atoms [2.076(4)–2.090(4) Å] are longer than those *trans* to the oxygen's [2.044(4) Å av.]. A similar *trans* effect was observed for $Co(acac)_2$(TEEDA) [15] and $Co(thtf)_2$(TMEDA), thtf = 1-(2-thienyl)-4,4,4-trifluoro-1,3-butanedionate [37] but not for $Co(acac)_2$(bipy) [38,39]. The Co–O(H) coordination bonds are as expected longer (2.112(2)–2.125(2) Å) than the Co–O(η^2-acac) ones and similar to those observed in *trans*-$Co(acac)_2(MeOH)_2$ [40]. The Co–N distances [2.227(6) Å av. and 2.257(2) Å av. for **1** and **2**, respectively] are comparable for both compounds. They are in agreement with the values on adducts N-donors such as *N*,*N*,*N*′,*N*′-tetraethyl-1,2-diaminoethane [15], 6-methylquinoline [35] and pyridine [41], but longer than for instance for $Co(thtf)_2$(TMEDA) [37] or $Co(acac)_2$(bipy) [38,39] [2.161(3) and 2.147(5) Å for the α and β forms, respectively]. The major distortions are related to the neutral ligands as observed for the bite angles N–Co–N [82.3(2)°] in **1** or the even smaller N–Co–O ones [78.10(9)° and 78.66(9)°] in **2** and to those related to the ligands in *trans* positions [<O(6)–Co(2)–N(2) 167.5(1)°] and/or involved in H-bonding [<O(3)–Co(1)–O(5) 169.44(9)°].

3.3. MOCVD growth of Co_3O_4 films and film characterization

Deposition of cobalt oxide films was carried out by innovative pulsed liquid injection MOCVD technique (PI-MOCVD) [28]. This technique is based on repetitive injections of microdoses (several microliters) of solution of a volatile precursor, flash evaporation, vapour transport by a carrier gas and decomposition on a hot substrate. One advantage of liquid injection CVD over classical CVD is that it places less demands on the precursor in terms of volatility and stability [28,31,42]. Cobalt oxide films were deposited using the two most volatile and stable new adducts namely $Co(acac)_2$-(TMEDA) and $Co(thd)_2$(TMEDA). The main objective was to evaluate the possibility to apply these new adducts for cobalt oxide deposition. Films were deposited on monocrystalline $LaAlO_3$(1 0 0), and Si(1 0 0) substrates at two different substrate temperatures (450 and 600 °C) and were characterized in order to compare the

Table 2
Selected bond lengths (Å) and angles (°) of $Co(acac)_2$(TMEDA) and $[Co(acac)_2(DMAPH)]_2$

$Co(acac)_2$(TMEDA)		$[Co(acac)_2(DMAPH)]_2$			
		Molecule a		Molecule b	
Bond lengths					
Co–O(1)	2.076(4)	Co(1)–O(1)	2.024(2)	Co(2)–O(7)	2.032(2)
Co–O(2)	2.043(4)	Co(1)–O(2)	2.039(2)	Co(2)–O(6)	2.058(2)
Co–O(3)	2.090(4)	Co(1)–O(3)	2.041(2)	Co(2)–O(9)	2.023(3)
Co–O(4)	2.046(4)	Co(1)–O(4)	2.079(2)	Co(2)–O(8)	2.060(2)
Co–N(1)	2.237(5)	Co(1)–O(5)	2.125(2)	Co(2)–O(10)	2.112(2)
Co–N(2)	2.218(6)	Co(1)–N(1)	2.252(2)	Co(2)–N(2)	2.262(3)
Bond angles					
O(1)–Co–O(2)	88.1(1)	O(1)–Co(1)–O(2)	90.12(8)	O(6)–Co(2)–O(7)	89.8(1)
O(1)–Co–O(3)	93.6(2)	O(1)–Co(1)–O(3)	96.2(1)	O(7)–Co(2)–O(9)	91.2(1)
O(2)–Co–O(3)	90.8(2)	O(2)–Co(1)–O(3)	95.3(1)	O(6)–Co(2)–O(9)	95.2(1)
O(1)–Co–O(4)	87.9(2)	O(1)–Co(1)–O(4)	176.23(9)	O(7)–Co(2)–O(8)	178.9(1)
O(2)–Co–O(4)	175.2(2)	O(2)–Co(1)–O(4)	88.78(9)	O(6)–Co(2)–O(8)	89.58(9)
O(3)–Co–O(4)	86.7(2)	O(3)–Co(1)–O(4)	87.44(9)	O(8)–Co(2)–O(9)	88.0(1)
O(1)–Co–N(1)	174.6(2)	O(1)–Co(1)–O(5)	89.21(9)	O(7)–Co(2)–O(10)	90.7(1)
O(2)–Co–N(1)	89.3(2)	O(2)–Co(1)–O(5)	93.68(9)	O(6)–Co(2)–O(10)	89.14(9)
O(3)–Co–N(1)	91.2(2)	O(3)–Co(1)–O(5)	169.44(9)	O(9)–Co(2)–O(10)	175.3(1)
O(4)–Co–N(1)	94.9(2)	O(4)–Co(1)–O(5)	87.27(9)	O(8)–Co(2)–O(10)	90.21(9)
O(1)–Co–N(2)	93.3(2)	O(1)–Co(1)–N(1)	86.55(9)	O(7)–Co(2)–N(2)	87.8(1)
O(2)–Co–N(2)	94.9(2)	O(2)–Co(1)–N(1)	171.16(9)	O(6)–Co(2)–N(2)	167.5(1)
O(3)–Co–N(2)	171.2(2)	O(3)–Co(1)–N(1)	93.16(9)	O(9)–Co(2)–N(2)	97.1(1)
O(4)–Co–N(2)	88.0(2)	O(4)–Co(1)–N(1)	94.02(9)	O(8)–Co(2)–N(2)	93.0(1)
N(1)–Co–N(2)	82.3(2)	O(5)–Co(1)–N(1)	78.10(9)	O(10)–Co(2)–N(2)	78.66(9)

behaviour of the precursors at lower and higher deposition temperature.

Films of cubic Co_3O_4 were deposited in all cases due to sufficient excess of oxygen during deposition and cooling (film thickness 100–400 nm). XRD study of Co_3O_4 films deposited on $LaAlO_3$ show that both precursors **1** and **4** give (1 1 0) textured films on $LaAlO_3$ substrates (Fig. 4). Moreover, additional XRD study in Schultz geometry showed that films were grown epitaxially with "cube-on-cube" in-plane orientation of Co_3O_4 crystallites. The formation of (1 1 0) texture during film growth can be explained by a better lattice match between the (0 0 1) plane of the pseudo-cubic substrates and the (1 1 0) plane of cubic Co_3O_4 (mismatch ~0.5%) compared to the (0 0 1) plane of Co_3O_4 (~6% mismatch).

All Co_3O_4 films deposited on Si(1 0 0) substrates were polycrystalline independently of the precursor and deposition temperature used. Films on Si were etched with HF in order to form a step for the determination of film thickness and growth rate. The use of $Co(acac)_2$(TMEDA) lead to higher growth rate (0.7 μm/h at 450 °C and 1.6 μm/h at 600 °C) compared to $Co(thd)_2$(TMEDA) (0.5 μm/h at 450 °C and 1.3 μm/h at 600 °C). Growth of Co_3O_4 films from both precursors was kinetically limited in the temperature range 450–600 °C investigated.

XPS studies of the deposited films were performed in the Co 2p, O 1s region. Fig. 5 shows an Al Kα XPS spectrum in the Co 2p, O 1s region of a film deposited at 600 °C using **1**. The position of the Co $2p_{3/2}$ peak (780.5 eV), the presence of a weak shake up satellite at 790.5 eV and the value of the Auger α parameter (1553.5 eV) confirmed that the film surface consisted of Co_3O_4 [10]. Contamination with carbon (23%) could be reduced to 5.3% after sputtering of the surface by Ar^+ ions.

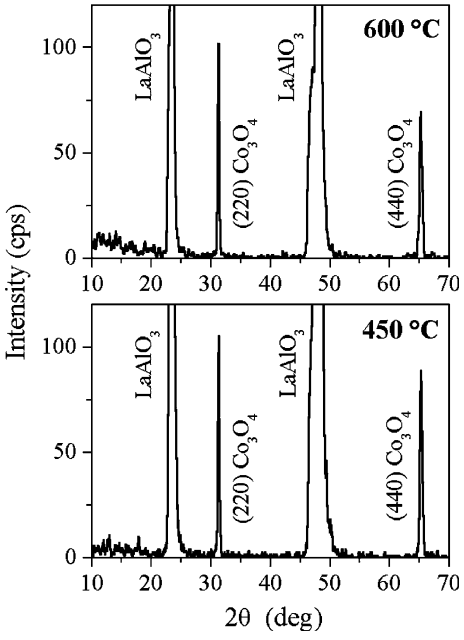

Fig. 4. XRD for Co_3O_4 films deposited on $LaAlO_3$ substrates from $Co(acac)_2$(TMEDA) at 450 and 600 °C. Similar scans were obtained in the case of $Co(thd)_2$(TMEDA).

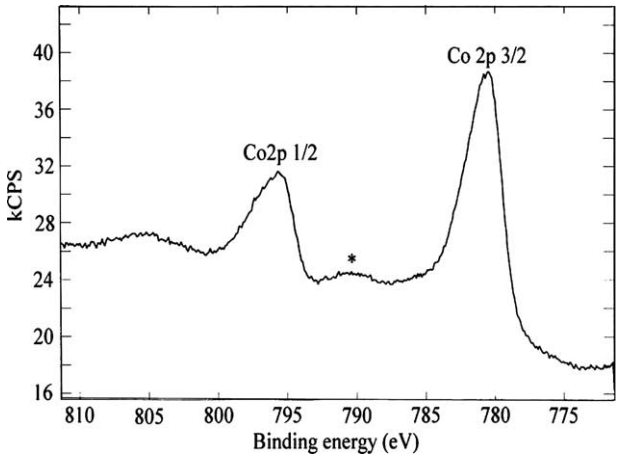

Fig. 5. Part of an XPS spectrum showing the peaks of Co in Co_3O_4 films deposited from $Co(acac)_2$(TMEDA) at 600 °C, the asterisk (*) indicates the weak shake up satellite.

These preliminary MOCVD experiments show that both new Co(II) β-diketonate adducts **1** and **4** can be applied for the deposition of pure, epitaxial Co_3O_4 films by liquid injection MOCVD. They outperform the existing CVD precursors in terms of volatility and oxidation stability; the quite cheap, air stable $Co(acac)_2$ (TMEDA) adduct is most attractive.

4. Supplementary material

Crystallographic data (atomic coordinates, thermal parameters, full lists of bond distances and angles) have been deposited at the Cambridge Crystallographic Data Centre, CCDC No. 186320 and 171430 for **1** and **2**, respectively. Copies of the data can be obtained free of charge from CCDC, 12 Union Road, Cambridge CB2 1EZ, UK (fax: +44-1223-336033; e-mail: deposit@ccdc.com.ac.uk or www: http://www.ccdc.cam.ac.uk).

Acknowledgements

The authors acknowledge partial financial support from European Community (FP5, MULTIMETOX network, contract C5RT-CT-1999-05001). S. Pasko is grateful to CNOUS (Centre National des Oeuvres Universitaires et Scolaires) for a fellowship.

References

[1] E. Fischer Rivera, B. Atakan, K. Kohse-Höinghaus, J. Phys. IV 11 (2001) Pr3-629.

[2] C.G. Granquist, Handbook of Inorganic Electrochromic Materials, Elsevier, Amsterdam, 1995.
[3] M. Ando, T. Kobayashi, S. Iijima, M.J. Haruta, Mater. Chem. 7 (1997) 1779.
[4] E. Barrera, I. Gonzalez, T. Viveros, Sol. Energy Mater. Solar Cells 51 (1998) 69.
[5] A.U. Mane, K. Shalini, S.A. Shivashankar, J. Phys. IV 11 (2001) Pr3-63.
[6] P.S. Patil, L.D. Kadam, C.D. Lokhande, Thin Solid Films 144 (1996) 29.
[7] E. Fujii, H. Torii, A. Tomozawa, R. Takayama, T. Hirao, J. Mater. Sci. 30 (1995) 6013.
[8] E. Fujii, Eur. Patent No EP0733 721A1, 1996.
[9] T. Maruyama, T. Nakai, Sol. Energy Mater. 22 (1991) 107.
[10] D. Barreca, C. Massignan, S. Daolio, M. Fabrizio, C. Piccirillo, L. Armelao, E. Tondello, Chem. Mater. 13 (2001) 588.
[11] D.G. Colombo, D.C. Gilmer, V.G. Young, S.A. Campbell, W.I. Gladfelter, Chem. Vap. Dep. 4 (1998) 220.
[12] T. Maruyama, Jpn. J. Appl. Phys., Part 2 36 (1997) 705L.
[13] P.O. Dunstan, Thermochim. Acta 303 (1997) 209.
[14] R.C. Aggarwal, D.S. Surya Narayana, Indian J. Chem. 21A (1982) 318.
[15] R.E. Colborn, M.F. Garbauskas, C.I. Hejna, Inorg. Chem. 27 (1988) 3661.
[16] G.C. Pellacani, R. Battistuzzi, G. Marcotrigliano, J. Inorg. Nucl. Chem. 35 (1973) 2243.
[17] W. Ludwig, M. Döring, R. Fischer, A. Friedrich, W. Seidel, E. Uhlig, D. Walther, J. Therm. Anal. 38 (1992) 239.
[18] D.S. Sankhla, R.C. Mathur, S.N. Misra, J. Inorg. Nucl. Chem. 42 (1980) 489.
[19] A.Yu. Steblyanko, A.N. Grigor'ev, L.I. Martynenko, Russ. J. Inorg. Chem. 42 (1997) 215.
[20] M.A. Laffey, P. Thornton, J. Chem. Soc., Dalton Trans. (1982) 313.
[21] V.J. Eddy, J.L. Hallgreen, E. Robert, J. Polym. Sci. 28A (1990) 2417.
[22] K. Kaeriyama, Makromol. Chem. 175 (1974) 2285.
[23] H. Brunner, B. Hammer, Angew. Chem. 96 (1984) 305.
[24] J.B. Ellern, R.O. Ragsdale, Inorg. Syn. 11 (1968) 89.
[25] D.J. Watkin, C.K. Prout, J.R. Carruthers, P.W. Betteridge, In: Crystal Issue 10; Chemical Crystallography Laboratory, University of Oxford, UK, 1996.
[26] D.T. Cromer, in: International Tables for X-ray crystallography, vol. 4, Kynoch Press, Birmingham, 1974.
[27] J.R. Carruthers, D.J. Watkin, Acta Cryst. A35 (1979) 698.
[28] J.P. Senateur, C. Dubourdieu, V. Galindo, F. Weiss, A. Abrutis, in: Kwang-Leong Choy (Ed.), Innovative Processing of Films and Nanocrystalline Powders, Imperial College Press, London, 2002, p. 71.
[29] A. Abrutis, V. Plausinaitiene, V. Kubilius, A. Teiserskis, Z. Saltyte, R. Butkute, J.P. Senateur, Thin Solid Films 413 (2002) 32.
[30] A. Abrutis, V. Kubilius, V. Bigelyte, A. Teiserskis, Z. Saltyte, J.P. Senateur, F. Weiss, Mater. Lett. 31 (1997) 201.
[31] P.A. Williams, A.C. Jones, J.F. Bickley, A. Steiner, H.O. Davies, T.J. Leedham, S.A. Impey, J. Garcia, S. Allen, A. Rougier, A. Blyr, J. Mater. Chem. 11 (2001) 2329.
[32] H. Guillon, L.G. Hubert-Pfalzgraf, Appl. Organometal. Chem. 12 (1998) 231.
[33] F. Labrize, L.G. Hubert-Pfalzgraf, J. Vaissermann, C.B. Knobler, Polyhedron 15 (1996) 577.
[34] L.G. Hubert-Pfalzgraf, J. Vaissermann, unpublished results.
[35] M.B. Hursthouse, K.M.A. Malik, J.E. Davies, J.H. Harding, Acta Cryst. B34 (1978) 1355.
[36] F.A. Cotton, R.C. Elder, Inorg. Chem. 5 (1996) 423.
[37] L.C. Tzavellas, C. Tsianis, C.A. Kavounis, C.J. Cardin, Inorg. Chim. Acta 262 (1997) 53.
[38] A.N. Grigor'ev, A.Yu. Steblyanko, A.V. Goncharov, K.A. Potekhin, A.S. Batsanov, Yu.T. Struchkov, Russ. J. Inorg. Chem. 32 (1987) 396.
[39] A.Yu. Steblyanko, A.N. Grigor'ev, L.I. Martynenko, M.V. Reshetnyak, A.S. Batsanov, Yu.T. Struchkov, Russ. J. Inorg. Chem. 33 (1988) 857.
[40] P. Werndrup, V.G. Kessler, J. Chem. Soc., Dalton Trans. (2001) 574.
[41] R.C. Elder, Inorg. Chem. 7 (1968) 1117.
[42] L.G. Hubert-Pfalzgraf, Inorg. Chem. Commun. 6 (2003) 102.

Available online at www.sciencedirect.com
SCIENCE DIRECT®
Polyhedron 23 (2004) 743–747
POLYHEDRON
www.elsevier.com/locate/poly

Divalent transition metal complexes of the anionic form of 4,7-dihydro-1,2,4-triazolo[1,5-*a*]pyrimidine-7-one: crystal structure of the zinc(II) compound

Mohammad Abul-Haj [a], Miguel Quirós [b,*], Juan M. Salas [b]

[a] *Department of Chemistry and Chemical Technology, Al-Quds University, P.O. Box 20002 Abu Dis, Jerusalem, Palestine*
[b] *Departamento de Química Inorgánica, Facultad de Ciencias, Universidad de Granada, 18071 Granada, Spain*

Received 24 September 2003; accepted 24 October 2003

Abstract

Several complexes of the ligand 4,7-dihydro-1,2,4-triazolo[1,5-*a*]pyrimidine-7-one (7HtpO) in its anionic form ($7tpO^-$) with divalent metals (the complete first series from Mn to Zn plus Cd) have been synthesized and characterized by means of analytical techniques (elemental analysis, thermogravimetry and differential scanning calorimetry), spectral methods (IR and electronic spectroscopy), magnetic measurements (77–290 K) and EPR in the case of the Cu compound. All compounds display a $M(7tpO)_2 \cdot nH_2O$ stoichiometry. The crystal structure of $[Zn(7tpO)_2(H_2O)_4]$. $2H_2O$ has been solved by single crystal X-ray diffraction. In this compound, the ligand $7tpO^-$ binds the metal ion through the N atom in position 3 and four water molecules complete the slightly distorted octahedral environment with the Zn atom occupying an inversion center. For all other compounds except Cu, infrared data suggest that the ligand binds in a similar fashion whereas visible spectroscopy and magnetic measurements point to octahedral geometry. On the other hand, magnetic and EPR measurements of the copper compound indicate that it is dinuclear with an antiferromagnetic coupling constant $2J = -87.8$ cm^{-1} and a zero-field splitting parameter $D = 0.168$ cm^{-1}.
© 2003 Elsevier Ltd. All rights reserved.

Keywords: Triazolopyrimidine; Zn complexes; Copper dimers; EPR

1. Introduction

The 1,2,4-triazolo[1,5-*a*]pyrimidine ring has a chemical structure similar to purine, differing from it by the presence of a pyrimidime nitrogen atom in a bridgehead position with the disappearance of the acidic H-proton of the five-membered ring [1]. Metal complexes of these heterocycles may be considered as model systems for some naturally occurring metal coordination compounds. The study of the interaction of metal cations with 1,2,4-triazolo[1,5-*a*]pyrimidine derivatives has been carried out by a few research groups including one at the State University of Leiden [2] and more recently another one at the Nicholas Copernicus University at Torun [3], apart from our group at the University of Granada. The work in this field previous to 1999 was reviewed by us [4].

Single crystal X-ray diffraction studies of these metal complexes display an appreciable variability in their molecular structures. There are examples of mononuclear compounds, usually with the ligand monodentately bound through the nitrogen atom at position 3 [5], but with a few cases showing chelating behaviour through an endocyclic N atom and an exocyclic O atom [6] There are also many examples of binuclear or polynuclear compounds in which the metal atoms are bridged either by the triazolopyrimidine derivative [7] or by other auxiliary ligands [8]. The biological activity of a number of these complexes have been tested, finding that some of them inhibit the growth of Gram(+) and Gram(−) bacteria [9,10] as well as other parasites [11]. Antitumour activity has also been detected for several platinum group metals with triazolo[1,5-*a*]pyrimidine derivatives [12].

* Corresponding author. Tel.: +34958240441; fax: +34958248526.
E-mail address: mquiros@ugr.es (M. Quirós).

0277-5387/$ - see front matter © 2003 Elsevier Ltd. All rights reserved.
doi:10.1016/j.poly.2003.11.052

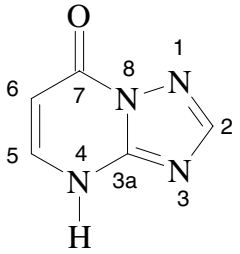

Scheme 1.

Most of the work in this field has been mainly focused on a few metal ions, namely platinum group metals [13], silver(I) [14] and copper(II) [15] with few examples of other divalent cations [16]. Following this research line, we present in this paper the synthesis, spectroscopic characterization, thermal and magnetic behaviour of a series of divalent metal complexes (Mn to Zn plus Cd) bearing the anionic form of 4,7-dihydro-1,2,4-triazolo[1,5-*a*]pyrimidine-7-one (7HtpO), which is an isomer and mimic of the purine base hypoxanthine. The crystal structure of the zinc compound is described. The molecular structure of the ligand and the numbering scheme for its atoms are shown in Scheme 1.

2. Experimental

2.1. Synthesis of the complexes

The compound 4,7-dihydro-1,2,4-triazolo[1,5-*a*]pyrimidine-7-one (7HtpO) was prepared according to published method from 3-amino-1,2,4-triazole and malic acid in strong acidic medium [17]. Other reagents were obtained from commercial sources.

Metal complexes were obtained by mixing two aqueous solutions, 10 mL each, one containing 0.1 g of 7HtpO and the other containing 0.1 g of the appropriate salt (sulfate for Mn and Fe, and acetate for Ni, Co, Cu, Zn and Cd). A small pH adjustment was necessary in the case of Mn and Ni, five drops of 1 M NaOH were added in the first case and one drop of concentrated acetic acid was added in the second. From the solution containing 7HtpO and zinc acetate, colorless crystals of the complex suitable for X-ray analysis were isolated after 24 h. The other complexes were obtained as powders from their corresponding solution after 24 h except for Cd for which the compound precipitated immediately. In all cases, the solids were washed with water and ethanol and dried with ether.

From elemental analyses, the following formulae were deduced for the isolated compounds:

$Mn(7tpO)_2 \cdot 6H_2O$ (**1**), white powder. *Anal.* Calc. for $C_{10}N_8O_8H_{18}Mn$: C, 27.72; H, 4.19; N, 25.86. Found: C, 27.4; H, 4.2; N, 25.4%. $Fe(7tpO)_2 \cdot 6H_2O$ (**2**), light brown microcrystals. *Anal.* Calc. for $C_{10}N_8O_8H_{18}Fe$: C, 27.67; H, 4.18; N, 25.81. Found: C, 27.5; H, 4.1; N, 25.4%. $Co(7tpO)_2 \cdot 6H_2O$ (**3**), orange powder. *Anal.* Calc. for $C_{10}N_8O_8H_{18}Co$: C, 27.49; H, 4.15; N, 25.64. Found: C, 27.7; H, 4.1; N, 25.5%. $Ni(7tpO)_2 \cdot 6H_2O$ (**4**), blue powder. *Anal.* Calc. for $C_{10}N_8O_8H_{18}Ni$: C, 27.49; H, 4.15; N, 25.64. Found: C, 27.7; H, 4.5; N, 26.1%. $Cu(7tpO)_2 \cdot 5H_2O$ (**5**), dark green powder. *Anal.* Calc. for $C_{10}N_8O_7H_{16}Cu$: C, 28.34; H, 3.81; N, 26.44. Found: C, 28.8; H, 3.8; N, 26.2%. $Zn(7tpO)_2 \cdot 6H_2O$ (**6**), colourless crystals. *Anal.* Calc. for $C_{10}N_8O_8H_{18}Zn$: C, 27.07; H, 4.09; N, 25.26. Found: C, 27.0; H, 4.1; N, 24.9%. $Cd(7tpO)_2 \cdot 4H_2O$ (**7**), white powder. *Anal.* Calc. for $C_{10}N_8O_6H_{14}Cd$: C, 26.42; H, 3.10; N, 24.06. Found: C, 26.4; H, 3.1; N, 24.1%.

2.2. Instrumentation

Microanalysis of C, H and N were performed in a Fisons Instruments EA-1008 analyzer. Thermal behaviour was studied under an air flow in Shimadzu TGA-50 and Shimadzu DSC-50 equipment. Reflectance diffuse spectra were recorded in a Cary-5 spectrophotometer. Magnetic susceptibility was measured in a Manics DSM-8 Faraday balance. An electron paramagnetic resonance spectrum was obtained in a X-band Bruker ESP-300E apparatus (all this equipment was sited at the Centre of Scientific Instrumentation of the University of Granada). IR spectra were obtained using a FT MIDAC Prospect 1 spectrophotometer with samples dispersed in KBr pellets.

2.3. Crystallography

Data were collected at room temperature for a brick-shaped colourless crystal (dimensions $0.20 \times 0.24 \times 0.32$ mm) in a Stoe Stadi4 diffractometer with Mo Kα radiation ($\lambda = 0.7107$ Å). Data were corrected for absorption (ψ-scans, transmission range, 0.6309–0.7119). The structure was solved by the heavy atom method and refined in F^2 using SHELXL-97 [18]. Hydrogen atoms of the heterocycle were placed in ideal positions and those of water molecules were located and refined with fixed (0.86 Å) O–H distances. Isotropic thermal parameters of all H atoms were fixed to 1.2 times the equivalent isotropic thermal parameter of their parent atoms.

Crystal data for $[Zn(C_5H_3N_4O)_2(H_2O)_4] \cdot 2H_2O$, orthorrombic, space group *Pbca*, $a = 7.5430(8)$, $b = 13.1384(12)$, $c = 17.2599(10)$ Å, $V = 1710.5(3)$ Å^3, $Z = 4$, $D_{calc.} = 1.723$ Mg m^{-3}, $\mu = 1.497$ mm^{-1}, 2487 unique reflections collected (θ range, 2.36°–30°), $wR_2 = 0.2760$, R (for 1389 data with $I > 2\sigma(I)$) $= 0.0872$.

3. Results and discussion

3.1. X-ray structural study of the zinc compound

Fig. 1 displays the molecular structure of compound **6**. The crystal structure comprises separate molecules of $[Zn(7tpO)_2(H_2O)_4]$ in which the metal atom lies in a crystallographic inversion center. Its environment is a slightly distorted octahedron defined by two symmetry related $7tpO^-$ ligands in *trans* disposition, and four water molecules. The two $7tpO^-$ ligands are coordinated in a monodentate manner through the N atom in position 3, which is the most frequent binding site for this type of ligand [4] This behaviour is also found in the analogous 5-methylated derivative, although an example of N1–O7 chelation has also been described for this compound with copper [15] as well as for the 5,7-dioxo derivative with Mn [6]. Two interstitial water molecules complete the structure. Distances and angles in the coordination sphere are listed in Table 1.

The Zn–N3 bond distance is within the range found for similar Zn(II) complexes [19,20]. Comparing bond distances and angles within the ligand with those in free 7HtpO [17], we found noticeable changes in the angles involving the atom C3A (3–4°) and the distances C7–O7 (0.040 Å longer) and C6–C7 (0.042 Å shorter). These changes are probably more attributable to the deprotonation of the ligand rather than to coordination. The plane of the ligand is almost perpendicular to the $Zn(H_2O)_4$ plane (dihedral angle 93.5(2)°) and the projection of the first plane over the second bisects the O1W–Zn–O2W angle (torsion angle C3a–N3–Zn–O1W, – 44.3(5)°) which minimizes steric repulsions.

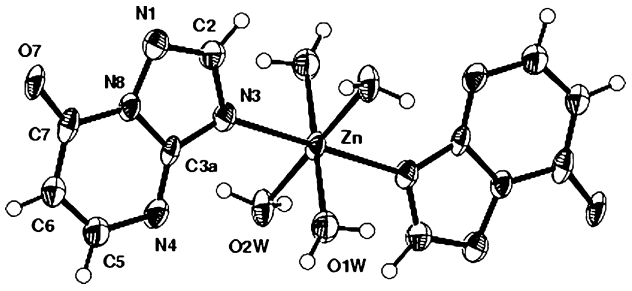

Fig. 1. Molecular structure of compound **6** as deduced from X-ray diffraction data. Nonhydrogen atoms are represented by ellipsoids at the 50% probability level.

Table 1
Selected interatomic distances (Å) and angles (°)

Coordination sphere		
Zn–N3 2.125(5)	N3–Zn–O1W	92.0(2)
Zn–O1W 2.113(4)	N3–Zn–O2W	89.4(2)
Zn–O2W 2.143(5)	O1W–Zn–O2W	89.3(2)
Hydrogen bonds		
O1W···O3W	2.697(6)	
O1W···O3W $(-1/2+x, 1/2-y, 1-z)$	2.765(7)	
O2W···O7 $(1/2-x, 1-y, -1/2+z)$	2.740(6)	
O2W···O7 $(-1/2+x, y, 3/2-z)$	2.892(6)	
O3W···N4 $(1/2+x, 1/2-y, 1-z)$	2.791(6)	
O3W···O7 $(3/2+x, 1-y, -1/2+z)$	2.772(7)	

All hydrogen atoms of both coordinated and non-coordinated water molecules are involved in hydrogen bonds stabilizing the structure (see Table 1). The main acceptor of these bonds is the exocyclic oxygen atom of $7tpO^-$.

3.2. Spectral, thermal, magnetic and EPR studies

The thermal study of these compounds in air has been carried out from their TG and DSC plots. All compounds are hydrated and loss of water is the first step of their thermal decomposition. For compound **5** (Cu), the corresponding effects are very broad showing the unspecific nature of water, the percentage of which is not reproducible. The remaining complexes display well defined weight losses in the range 50–180 °C which agree well with the number of water molecules indicated by their elemental analysis. Dehydration takes place in a single step (endothermic peaks in the range 98–110 °C) except for **4** (Ni) for which two well-defined stages are observed (peaks at 92.2 and 121.4 °C). Dehydration energy is very similar for all the compounds, ranging from 45.5 to 48.8 kJ/mol of water. The anhydrous complexes are stable up to ~350 °C, when pyrolitic decomposition starts.

The infrared spectra of the complexes **1**–**4**, **6** and **7** are virtually identical, differing from that of the free ligand [17] by the presence of a broad band at 3400 cm^{-1} due to ν(O–H) of water molecules, the absence of the intense ν(N–H) band and the batochromic shift of ν(C=O) which appears at 1625–1630 cm^{-1}. On the other hand, the spectrum of **5** (Cu) is noticeably different from the other: thus, the bathochromic shift of the ν(C=O) vibration is smaller (band at 1674 cm^{-1}), which may indicate a different coordination mode of the ligand. Such different behaviour of copper(II) if compared with the rest of the divalent transition ions has also been observed for the complexes of the analogous ligand that contains a second oxygen atom at position 5 [6].

The diffuse reflectance spectra of **2, 3** and **4** are typical of octahedral species [21]. Thus, the spectrum of **2** shows two overlapped bands even if only one is expected ($^5E_g \leftarrow {}^5T_{2g}$) for a d^6 high spin configuration, which can be due to a strong Jahn–Teller distortion of the excited state. The splitting energy between the t_{2g} and e_g levels has been calculated as the average of the two bands, the corresponding value being $\Delta_o = 10\,160$ cm^{-1}. The cobalt complex **3** exhibits a spectrum with two main absorptions: a broad one centered at 8420 cm^{-1}, assigned to the $^4T_{2g}(F) \leftarrow {}^4T_{1g}(F)$ (ν_1) transition and another at 20 325 cm^{-1}, assigned to $^4T_{1g}(P) \leftarrow {}^4T_{1g}(F)$ (ν_3). This band presents a shoulder at higher wavenumber that could be

Table 2
Magnetic susceptibility data for compounds **1**–**4**

Compound	μ_{eff} (100 K)	μ_{eff} (298 K)	μ_{eff} $(T \rightarrow \infty)$	θ (K)
1 (Mn)	6.08	6.03	6.00	+2.6
2 (Fe)	5.37	5.42	5.42	−1.9
3 (Co)	4.90	4.98	5.03	−5.1
4 (Ni)	3.24	3.24	3.24	+1.2

μ_{eff} values are in BM.

due to the proximity of the $^2A_{2g}$ level or to spin–orbit coupling, which would also be responsible for the asymmetry of the ν_1 band. Ligand field parameters were calculated by Dou equations [22] on the basis of octahedral geometry giving $\Delta_o = 9580$ and $B = 872$ cm^{-1}. The transition $^4A_{2g}(F) \leftarrow {}^4T_{1g}(F)$ (ν_2) may be assigned to the weak shoulder at 18 000 cm^{-1}. The spectrum of **4** shows the typical three bands expected for octahedral Ni(II) complexes at 9530 $(^3T_{2g} \leftarrow {}^3A_{2g})$, 15 600 $(^3T_{1g} \leftarrow {}^3A_{2g})$ and 26 385 cm^{-1} $(^3T_{1g}(P) \leftarrow {}^3A_{2g})$, from which the parameters $\Delta_o = 9530$ cm^{-1} and $B = 982$ cm^{-1} were calculated. Finally, the spectrum of the copper complex **5** presents a very broad band with a shoulder, with a maximum at 17 150 cm^{-1} that can be assigned for a d–d transition in a d^9 configuration with distorted octahedral geometry (this may include tetragonal pyramidal or square planar). An additional band at 25 100 cm^{-1} may be attributed to a ligand–metal charge transfer transition.

The magnetic susceptibility of the paramagnetic compounds has been measured as a function of temperature and corrected for diamagnetism [23]. The values for compounds **1**–**4** have been adjusted by least squares to the Curie–Weiss law yielding the values of θ and μ_{eff} $(T \rightarrow \infty)$ indicated in Table 2, which also collects the values of μ_{eff} at 100 and 298 K. These are normal values for octahedral complexes and the variation with T for **2** and **3** (reflected in the negative values of θ) is attributable to the orbital contribution in a T ground state.

Compound **5** presents a quite different behaviour, the representation of the magnetic susceptibility versus T in the range 5–300 K shows a maximum at 70 K (Fig. 2), which is indicative of an antiferromagnetic interaction between the copper centers. Data have been fitted to the Bleany–Bowers equation for Cu(II) dimers [24] including the correction due to the presence of a small amount of the mononuclear species (indicated by the points at very low T). From this fitting the following values were obtained: $g = 2.17$, $2J = -87.82$ cm^{-1}, $\rho = 0.12$.

The X-band EPR spectrum of a powdered sample of this compound at room temperature also suggest its dinuclear nature. The main features of this spectrum have been assigned to $(S = 1,\ \Delta M_S = 1)$ transitions with axial symmetry. By means of computer simulations with the XEMR program [25], the values $g_{\parallel} = 2.25$, $g_{\perp} = 2.00$, $D = 0.168$ cm^{-1} have been obtained. Fig. 3 represents the experimental and the simulated spectra. The differences are attributable to the signal of the $S = 1/2$ transition (mononuclear species, around 3200–3300 G), not included in the simulation and the possible existence of a $\Delta M_S = 2$ (half-field) transition which should overlap with the strong signal at 1300–1500 G.

The magnetic susceptibility and EPR data are very similar to those found for the dimeric copper complex

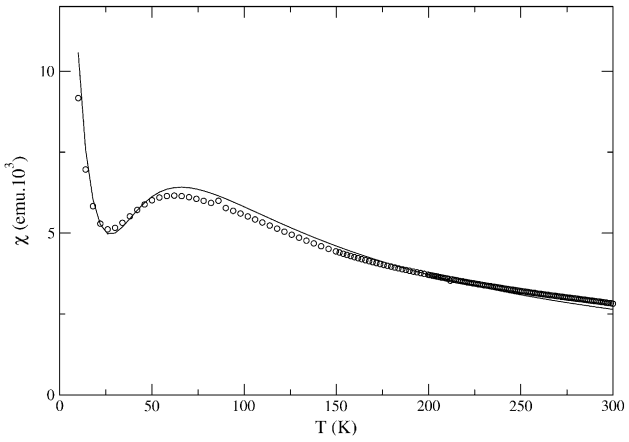

Fig. 2. Magnetic susceptibility of compound **5** as a function of temperature. Experimental data are represented by small circles which have been fitted to the Bleany–Bowers equation (solid line) with the parameters indicated in the text.

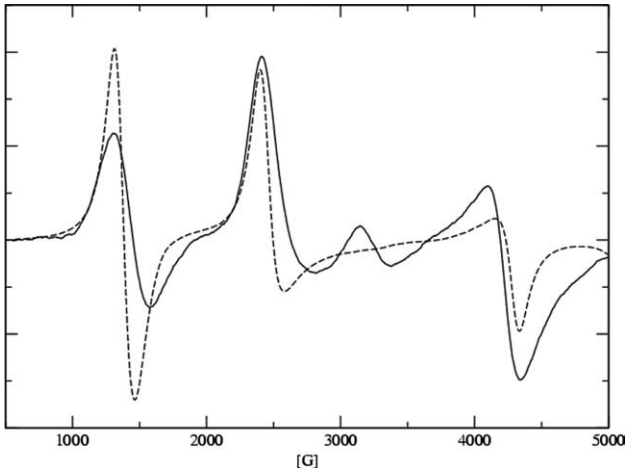

Fig. 3. Experimental (continuous line) and simulated (dashed line) X-band EPR spectra of compound **5**. Parameters for the simulation are indicated in the text.

with the isomeric ligand 4,5-dihydro-1,2,4-triazolo[1,5-*a*]pyrimidine-5-one (5HtpO) [26], which let us propose for compound **5** a dinuclear structure with two metal atoms bridged by four $7tpO^-$ moieties linked through the N atoms at positions 3 and 4. Copper(II) complexes of purine bases with this kind of structure and strong antiferromagnetic coupling have been described [27] including one of hypoxanthine [28], the purine base for which 7HtpO is a mimic.

4. Supplementary data

The supplementary crystallographic data for this paper have been deposited in the CCDC (Deposition No. CCDC 220311). These data can be obtained free of charge via www.ccdc.cam.ac.uk/conts/retrieving.html (or from the CCDC, 12 Union Road, Cambridge CB2 1EZ, UK; fax: +44 1223 336033; e-mail: deposit@ccdc.cam.ac.uk or www: http://www.ccdc.cam.ac.uk).

Acknowledgements

This work was supported by a project of the Ministry of Science and Technology of Spain (BQU 2001-2955-CO2). M. Abul Haj acknowledges the TEMPUS program of the European Community for an individual mobility grant.

References

[1] G. Fischer, Adv. Heterocycl. Chem. 57 (1993) 81.
[2] A.H. Velders, F. Ugozzoli, M. Biagini-Cingi, A.M. Manotti-Lanfredi, J.G. Haasnoot, J. Reedijk, Eur. J. Inorg. Chem. 2 (1999) 213.
[3] E. Szlyk, I. Lakomska, A. Surdykowski, T. Glowiak, L. Pazderski, J. Sitkowski, L. Kozerski, Inorg. Chim. Acta 333 (2002) 93.
[4] J.M. Salas, M.A. Romero, M.P. Sánchez, M. Quirós, Coord. Chem. Rev. 193 (1999) 1119.
[5] M. Abul Haj, M. Quirós, J.M. Salas, Acta Cryst. E 59 (2003) m903.
[6] S. Orihuela, M.P. Sánchez, M. Quirós, D. Martin, R. Faure, Polyhedron 17 (1998) 2477.
[7] M.A. Romero, J.M. Salas, M. Quirós, M.P. Sánchez, J. Molina, J. El Bahraoui, R. Faure, J. Mol. Struct. 354 (1995) 189.
[8] A. Grodzicki, E. Szlyk, A. Wojtczak, G. Wrzeszcz, L. Pazderski, T. Muziol, Polyhedron 18 (1999) 519.
[9] M.A. Romero, J.M. Salas, M. Quirós, D.J. Williams, J. Molina, Trans. Met. Chem. 18 (1993) 595.
[10] A. Rahmani, M.A. Romero, J.M. Salas, M. Quirós, G. Álvarez de Cienfuegos, Inorg. Chim. Acta 247 (1996) 51.
[11] J.M. Salas, M. Quirós, M. Abul Haj, R. Magán, C. Marin, M. Sánchez-Moreno, R. Faure, Metal Based Drugs 8 (2001) 119.
[12] K. Akdi, R.A. Vilaplana, S. Kamah, J.A.R. Navarro, J.M. Salas, F. González-Vílchez, J. Inorg. Biochem. 90 (2002) 51.
[13] J.A.R. Navarro, M.A. Romero, J.M. Salas, M. Quirós, Inorg. Chem. 36 (1997) 3277.
[14] J.M. Salas, M.A. Romero, A. Rahmani, M. Quirós, Anal. Quím. Int. Ed. 92 (1996) 249.
[15] J.A.R. Navarro, M.A. Romero, J.M. Salas, J. Molina, E.R.T. Tiekink, Inorg. Chim. Acta 274 (1998) 53.
[16] J.M. Salas, C. Enrique, M.A. Romero, K. Tagaki, K. Aoki, Y. Miyashita, I. Suh, Polyhedron 11 (1992) 2903.
[17] M. Abul Haj, J.M. Salas, M. Quirós, J. Molina, R. Faure, J. Mol. Struct. 519 (2000) 165.
[18] G.M. Sheldrick, SHELXL-97, University of Göttingen, Germany, 1997.
[19] E. Szlyk, A. Grodzicki, L. Pazderski, J. Sitkowski, Pol. J. Chem. 72 (1998) 55.
[20] J.M. Salas, M.A. Romero, A. Rahmani, R. Faure, Acta Cryst. C 50 (1994) 510.
[21] A.B.P. Lever, Inorganic Electronic Spectroscopy, Elsevier, Amsterdam, 1986.
[22] Y. Dou, J. Chem. Ed. 67 (1990) 134.
[23] K. Burger, Coordination Chemistry: Experimental Methods, Butterworths, London, 1973.
[24] B. Bleany, K.D. Bowers, Proc. R. Soc. Lond. Ser. A (1952) 451.
[25] J. Eloranta, Xemr 0.7-7. University of Jyväskylä, Finland, 1999. Available from http://epr.chem.jyu.fi/xemr.
[26] M. Abul Haj, M. Quirós, J.M. Salas, J. Dobado, J. Molina, M.G. Basallote, M.Á. Máñez, Eur. J. Inorg. Chem. (2002) 811.
[27] D. Sonnenfroh, R.W. Kreilick, Inorg. Chem. 19 (1980) 1259.
[28] E. Sletten, Acta Cryst. B 26 (1970) 1609.

Available online at www.sciencedirect.com
SCIENCE DIRECT®
Polyhedron 23 (2004) 749–754
POLYHEDRON
www.elsevier.com/locate/poly

Copper and nickel complexes of the tetradentate ligand derived from the condensation of ferrocenoylacetone with 1,2-diaminoethane

Yao-Cheng Shi [a,*], Wen-Bin Shen [b], Hua-Mei Yang [a], Hai-Bin Song [c], Xiao-Ya Hu [a,*]

[a] School of Chemistry, Yangzhou University, Yangzhou 225002, PR China
[b] Analytical Center, China Pharmaceutical University, Nanjin 210009, PR China
[c] State Key Laboratory of Elemento-Organic Chemistry, Nankai University, Tianjin 300071, PR China

Received 30 June 2003; accepted 27 October 2003

Abstract

Ferrocenoylacetone [$C_5H_5FeC_5H_4C(O)CH_2C(O)CH_3$] reacts with 1,2-diaminoethane in refluxing ethanol to yield three isolated isomers $\mathbf{H_2L}$, $\mathbf{H_2L}^1$ and $\mathbf{H_2L}^2$. In solution, $\mathbf{H_2L}^1$ and $\mathbf{H_2L}^2$ can change into $\mathbf{H_2L}$ on standing over two days. Reaction of the tetradentate enaminone ligand [$C_5H_5FeC_5H_4C(O)CH{=}C(CH_3)NHCH_2]_2$ ($\mathbf{H_2L}$) with hydrated copper acetate and nickel acetate affords complexes **I** (**L**Cu) and **II** (**L**Ni). All compounds have been characterized by elemental analyses, ^{1}HNMR, IR and UV spectroscopies. The X-ray crystallography of complexes **I** and **II** reveals that the enaminone dianion coordinates to the central metal ion (copper and nickel) via two oxygen and two nitrogen atoms, and complex **I** exists as a mixture of the *anti* and *syn* isomers in a molar ratio of 1:1 while the complex **II** exists as a single *syn* isomer.
© 2003 Elsevier Ltd. All rights reserved.

Keywords: Ferrocene; Enaminone; Ligands; Complexes; X-ray crystallography

1. Introduction

Recently cyclic and acyclic multidentate ligands with varying combinations of donor atoms and charges have become increasingly popular for bonding transition metals, lanthanides and main group elements [1–3]. Among them, Group IV metal complexes of enaminones have attracted much attention because such complexes act as possible alternatives to catalysts containing the bent metallocene fragment Cp_2M, and anions generated from the enaminones are another potential isoelectronic alternatives to cyclopentadienyl-based anions [4–7]. Enaminones are easily prepared from inexpensive and readily available starting materials. Moreover, through a judicious choice of primary amine and β-diketone used in their syntheses, the steric and electronic properties of this ligand type can be tuned, and chirality and further functionalization readily introduced [8–10]. Although the reaction of ferrocenoylacetone and 1,2-diaminoethane, and transition metal complexes of the thus formed tetradentate ligand, have been studied, recently we have researched the above reaction in more detail in order to further develop the chemistry of organometallic enaminones [11,12]. Here we report the related results: syntheses and crystal structures of copper and nickel complexes with the tetradentate enaminone ligand [$C_5H_5FeC_5H_4C(O)CH{=}C(CH_3)NHCH_2]_2$ ($\mathbf{H_2L}$).

2. Experimental

2.1. Reagents and general procedures

All chemicals were of reagent grade and used without further purification. Ferrocenoylacetone [$C_5H_5FeC_5H_4C(O)CH_2C(O)CH_3$] was synthesized by acylation of acetylferrocene on the substituted cyclopentadienyl ring using ethyl acetate in THF in the presence of sodium

* Corresponding authors. Tel.: +86-514-785-7939; fax: +86-514-785-7939.
E-mail address: yzssyc@yzcn.net (Y.-C. Shi).

0277-5387/$ - see front matter © 2003 Elsevier Ltd. All rights reserved.
doi:10.1016/j.poly.2003.10.019

ethoxide [13–15]. Progress of the reactions was monitored by TLC (silica gel H). ^{1}H NMR spectra were determined on a Bruker Avance 300 spectrometer using TMS as an external standard in $CDCl_3$. IR spectra were recorded on a Perkin–Elmer 402 spectrometer as KBr disks in the range of 400–4000 cm^{-1}. UV spectra were measured with a Shimadzu UV-240 spectrometer using a solution in DMF. Analyses for C, H and N were performed on an Elementa Vario EL III instrument. Melting points were measured on a Yanagimoto apparatus and are uncorrected.

2.2. Reaction of ferrocenoylacetone and 1,2-diaminoethane

1,2-Diaminoethane (0.305 g, 5 mmol) was added to a solution of ferrocenoylacetone [$C_5H_5FeC_5H_4C(O)CH_2C(O)CH_3$] (1.35 g, 5 mmol) in 30 ml of absolute ethanol and then the mixture was refluxed for 10 h, during which time the product $\mathbf{H_2L}$ (0.305 g) was precipitated. The filtrate was evaporated to dryness and isolated by TLC using a mixed solvent of CH_2Cl_2 and ethanol (v/v, 5:2). The first orange band gives 0.282 g of acetylferrocene. The following three orange-yellow bands in the decreasing order of R_f values furnish 0.052 g of $\mathbf{H_2L}$, 0.40 g of $\mathbf{H_2L}^1$ and 0.122 g of $\mathbf{H_2L}^2$. $\mathbf{H_2L}$ (26.4%), D.p. 174 °C. *Anal.* Calc. for $C_{30}H_{32}N_2Fe_2O_2$: C, 63.86; H, 5.72; N, 4.96. Found: C, 63.51; H, 5.73; N, 4.96%. IR (KBr disk): ν(NH) 3096 (w), ν(C=O) and ν(C=C) 1601 (vs), 1558 (vs) and 1520 (vs) cm^{-1}. UV (nm, in DMF): λ_{max} ($\varepsilon \times 10^4$) 271 (2.05) (B-band); 342 (5.77) (K-band); 450 (0.31) (CT-band of ferrocenyl groups). ^{1}H NMR ($CDCl_3$): δ 2.20 (s, 6H, $2CH_3$), 3.49 (t, 4H, $J_{HH} = 11.2$ Hz, $2CH_2$), 4.17 (s, 10H, $2C_5H_5$), 4.37 (s, 4H, 2 (H^3, H^4) of C_5H_4 rings), 4.72 (s, 4H, 2 (H^2, H^5) of C_5H_4 rings), 5.29 (s, 1H, CH), 11.10 (s, br, 2H, 2NH). $\mathbf{H_2L}^1$ (28.4%), D.p. 180 °C. *Anal.* Calc. for $C_{30}H_{32}N_2Fe_2O_2$: C, 63.86; H, 5.72; N, 4.96. Found: C, 63.44; H, 5.82; N, 4.88%. IR (KBr disk): ν(OH) 3429 (w), ν(NH) 3096 (w), ν(C=O) 1600 (vs), ν(C=N) 1557 (vs), ν(C=C) 1520 (vs) cm^{-1}. UV (nm, in DMF): λ_{max} ($\varepsilon \times 10^4$) 265 (2.09) (B-band); 346 (5.69) (K-band); 453 (0.31) (CT-band of ferrocenyl groups). ^{1}H NMR ($CDCl_3$): δ 2.01 (s, 6H, $2CH_3$), 3.49 (t, 4H, $J_{HH} = 12.7$ Hz, $2CH_2$), 4.17 (s, 10H, $2C_5H_5$), 4.36 (t, 4H, 2 (H^3, H^4) of C_5H_4 rings), 4.72 (t, 4H, 2 (H^2, H^5) of C_5H_4 rings), 5.30 (s, 1H, CH), 11.10 (s, br, 2H, (OH, NH)). $\mathbf{H_2L}^2$ (9%), D.p. 166 °C. *Anal.* Calc. for $C_{30}H_{32}N_2Fe_2O_2$: C, 63.86; H, 5.72; N, 4.96. Found: C, 64.10; H, 5.81; N, 5.34%. IR (KBr disk): ν(OH) 3417 (w), ν(C=N) and ν(C=C) 1599 (vs), 1557 (s) and 1523 (s) cm^{-1}. UV (nm, in DMF): λ_{max} ($\varepsilon \times 10^4$) 271 (2.35) (B-band); 347 (8.06) (K-band); 446 (0.36) (CT-band of ferrocenyl groups). ^{1}H NMR ($CDCl_3$): δ 2.03 (s, 6H, $2CH_3$), 3.50 (t, 4H, $J_{HH} = 12.7$ Hz, $2CH_2$), 4.17 (s, 10H, $2C_5H_5$), 4.37 (t, 4H, 2 (H^3, H^4) of C_5H_4 rings), 4.72 (t, 4H, 2 (H^2, H^5) of C_5H_4 rings), 5.30 (s, 1H, CH), 11.11 (s, br, 2H, 2OH).

2.3. Syntheses of complexes

A solution of the ligand ($\mathbf{H_2L}$) (0.564 g, 1 mmol) in 15 ml of dichloromethane was added dropwise to a stirred solution of copper acetate monohydrate (0.1997g, 1 mmol) or nickel acetate tetrahydrate (0.2489 g, 1 mmol) in 15 ml of absolute ethanol. The mixture was stirred for 12 h at room temperature and then filtered to afford the crude product. The resulting solid recrystallized from ethanol and dichloromethane gave the corresponding complex. **I**, 0.563 g (90%) as black crystals. M.p. 201–202 °C (dry sample). *Anal.* Calc. for $C_{30}H_{30}N_2Fe_2O_2Cu$: C, 57.58; H, 4.84; N, 4.48. Found: C, 57.69; H, 4.88; N, 4.42%. IR (KBr disk): ν(C=O) 1578 (m), ν(C=C) 1511 (vs) cm^{-1}. UV (nm, in DMF): λ_{max} ($\varepsilon \times 10^4$) 265 (3.52) (B-band); 344 (6.04) (K-band); 446 (0.48) (CT-band of ferrocenyl groups). **II**, 0.497 g (80%) as brown crystals.

Table 1
Crystallographic data for complexes **I** and **II**

	Complex **I** [(**L**Cu)$_2 \cdot H_2O \cdot CH_3OH \cdot C_2H_5OH$][a]	Complex **II** [**L**Ni]
Formula	$C_{63}H_{64}Fe_4N_4O_7Cu_2$	$C_{30}H_{30}Fe_2N_2O_2Ni$
Formula weight	1341.66	620.97
Crystal size (mm)	$0.40 \times 0.30 \times 0.30$	$0.30 \times 0.12 \times 0.08$
Crystal system	triclinic	monoclinic
Space group	$P\bar{1}$	$P2_1/c$
Unit cell dimensions		
a (Å)	13.470(3)	6.516(2)
b (Å)	14.860(3)	22.295(6)
c (Å)	15.770(3)	17.964(5)
α (°)	97.96(3)	90.00
β (°)	96.72(3)	92.005(5)
γ (°)	106.12(3)	90.00
V (Å^3)	2963(1)	2608(1)
Z	2	4
$D_{(calc)}$ (g cm^{-1})	1.502	1.581
$F(0\,0\,0)$	1376	1280
T (K)	293(2)	293(2)
λ (Mo Kα) (mm^{-1})	1.714	1.843
θ Range (°)	1.32; 24.99	1.46; 26.42
Limiting indices	$0 \leqslant h \leqslant 16$, $-17 \leqslant k \leqslant 16$, $-18 \leqslant l \leqslant 18$	$-8 \leqslant h \leqslant 5$, $-17 \leqslant k \leqslant 27$, $-22 \leqslant l \leqslant 18$
Reflections collected	10 868	12276
Independent reflections ($I > 2.0/\sigma(I)$)	10 383	5299
Number of parameters refined	721	382
R_1	0.0778	0.0500
wR_2	0.2269	0.0918
Goodness-of-fit	1.230	1.032
Largest difference peak and hole (e Å^{-3})	1.822 and −0.578	0.404 and −0.331

[a] Water and methanol are from commercial ethanol.

M.p. 209.5–210.5 °C. *Anal.* Calc. for $C_{30}H_{30}N_2Fe_2O_2Ni$: C, 58.03; H, 4.87; N, 4.51. Found: C, 58.48; H, 4.77; N, 4.36%. IR (KBr disk): ν(C=O) 1577 (m), ν(C=C) 1513 (vs) cm^{-1}. UV (nm, in DMF): λ_{max} ($\varepsilon \times 10^4$) 262 (2.06) (B-band); 295 (2.18) (K-band). ^1H NMR ($CDCl_3$): δ 1.92 (s, 6H, $2CH_3$), 3.03 (s, 4H, $2CH_2$), 4.19 (s, 10H, $2C_5H_5$), 4.22 (t, 4H, 2 (H^3, H^4) of C_5H_4 rings), 4.61 (t, 4H, 2 (H^2, H^5) of C_5H_4 rings), 5.24 (s, 2H, 2CH).

2.4. Crystal structure determination

Single crystals of complex **I** were obtained by slow evaporation of its solution of CH_2Cl_2 and ethanol. Single crystals of complex **II** were obtained by slow evaporation of its solution of CH_2Cl_2 and petroleum ether. X-ray data were collected on an Enraf-Nonius CAD4 diffractometer for complex **I** and a Bruker SMART CCD area detector diffractometer for complex **II** using graphite-monochromated Mo Kα radiation ($\lambda = 0.71073$ Å) at 293 K. The intensity data were corrected using PSI-scan for complex **I** and Multi-scan for complex **II**. The structure was solved by direct methods and refined by full-matrix least-squares methods based on F^2 with anisotropic thermal parameters for all non-hydrogen atoms. Hydrogen atoms were placed in their calculated positions, assigned fixed isotropic thermal parameters and allowed to ride on their respective parent atoms. All computations were carried out using SHELXS-97 and SHELXL-97 programs [16,17]. ORTEP drawings were made with ORTEP-3 for Windows [18]. The unsubstituted cyclopentadienyl rings of complex **II** are highly disordered. A summary of the data collection and structure refinement parameters for the two complexes is given in Table 1. Selected bond distances (Å) and angles (°) are listed in Tables 2 (complex **I**) and 3 (complex **II**).

Table 2
Selected bond distances (Å) and angles (°) for complex **I**

Syn isomer		*Anti* isomer	
Bond distances			
Cu(1)–O(1)	1.901(7)	Cu(2)–O(3)	1.929(7)
Cu(1)–O(2)	1.925(6)	Cu(2)–O(4)	1.919(6)
Cu(1)–N(1)	1.931(8)	Cu(2)–N(3)	1.941(8)
Cu(1)–N(2)	1.917(8)	Cu(2)–N(4)	1.914(8)
N(1)–C(3)	1.47(1)	N(3)–C(32)	1.47(1)
N(2)–C(4)	1.48(1)	N(4)–C(33)	1.48(1)
N(1)–C(8)	1.30(1)	N(3)–C(39)	1.30(1)
N(2)–C(6)	1.33(1)	N(4)–C(35)	1.32(1)
C(3)–C(4)	1.46(2)	C(32)–C(33)	1.48(2)
C(6)–C(9)	1.41(1)	C(34)–C(35)	1.40(1)
C(5)–C(7)	1.39(1)	C(34)–C(38)	1.38(1)
C(7)–C(8)	1.41(1)	C(37)–C(39)	1.43(1)
C(9)–C(10)	1.39(1)	C(37)–C(40)	1.37(1)
O(1)–C(10)	1.29(1)	O(3)–C(40)	1.27(1)
O(2)–C(5)	1.28(1)	O(4)–C(38)	1.29(1)
Bond angles			
O(1)–Cu(1)–O(2)	89.3(3)	O(3)–Cu(2)–O(4)	88.9(3)
O(1)–Cu(1)–N(1)	171.4(3)	O(3)–Cu(2)–N(4)	176.2(3)
O(1)–Cu(1)–N(2)	93.3(3)	O(3)–Cu(2)–N(3)	92.7(3)
O(2)–Cu(1)–N(1)	93.3(3)	O(4)–Cu(2)–N(4)	93.7(3)
O(2)–Cu(1)–N(2)	172.8(3)	O(4)–Cu(2)–N(3)	172.7(3)
N(1)–Cu(1)–N(2)	85.1(3)	N(3)–Cu(2)–N(4)	85.1(4)

Table 3
Selected bond distances (Å) and angles (°) for complex **II**

Bond distances			
Ni(1)–O(1)	1.839(3)	O(1)–C(1)	1.292(5)
Ni(1)–O(2)	1.845(3)	O(2)–C(8)	1.294(5)
Ni(1)–N(1)	1.852(4)	C(1)–C(2)	1.365(6)
Ni(1)–N(2)	1.850(4)	C(2)–C(3)	1.405(6)
N(1)–C(3)	1.324(6)	C(4)–C(5)	1.503(7)
N(2)–C(6)	1.312(6)	C(3)–C(9)	1.508(6)
N(1)–C(4)	1.472(5)	C(6)–C(7)	1.412(6)
N(2)–C(5)	1.474(6)	C(7)–C(8)	1.371(6)
Bond angles			
O(1)–Ni(1)–O(2)	82.5(1)	O(2)–Ni(1)–N(1)	177.1(1)
O(1)–Ni(1)–N(1)	95.1(2)	O(2)–Ni(1)–N(2)	94.4(2)
O(1)–Ni(1)–N(2)	176.3(2)	N(1)–Ni(1)–N(2)	88.1(2)

3. Results and discussion

3.1. Reaction of ferrocenoylacetone and 1,2-diaminoethane, and syntheses of complexes

Reaction of ferrocenoylacetone and 1,2-diaminoethane, and the syntheses of complexes are shown in Schemes 1 and 2 respectively. Reaction of ferrocenoylacetone [$C_5H_5FeC_5H_4C(O)CH_2C(O)CH_3$] and 1,2-diaminoethane in refluxing ethanol for 10 h followed by TLC separation affords three isolated isomers $\mathbf{H_2L}$, $\mathbf{H_2L^1}$ and $\mathbf{H_2L^2}$ as orange-yellow crystals in yields of 26.4%, 28.4% and 9%, respectively. In addition, acetylferrocene resulting from heated decomposition of ferrocenoylacetone is also isolated. More interestingly, in the solid state the three isomers cannot interchange whereas in solution either $\mathbf{H_2L^1}$ or $\mathbf{H_2L^2}$ can change into the more stable $\mathbf{H_2L}$ on standing over two days. For this reason, reactions of $\mathbf{H_2L}$ with copper(II) and nickel(II) ions at room temperature have been investigated. TLC analyses of complexes **I** (**L**Cu) and **II** (**L**Ni) show that the former

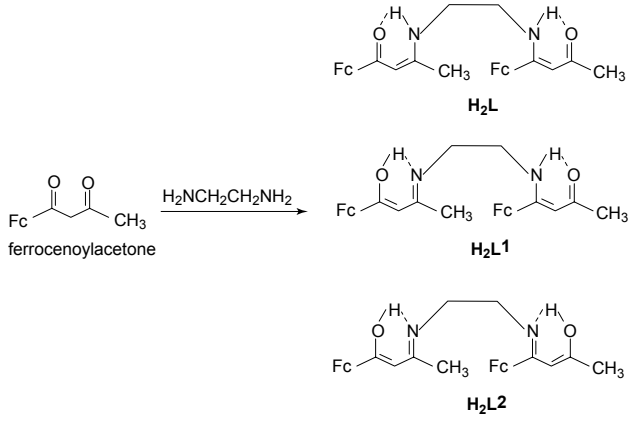

Scheme 1. Reaction of ferrocenoylacetone and 1,2-diaminoethane.

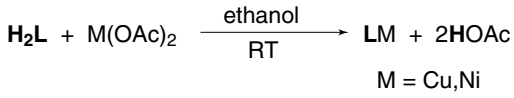

Scheme 2. Syntheses of complexes.

is a mixture of two isomers whereas the latter is a single isomer. However attempts to isolate any isomer of complex **I** have proven to be unsuccessful. In contrast, the same reaction of ferrocenoylacetone and 1,2-diaminoethane in refluxing methanol for 1.5 h furnished a ligand (H_2bfe) in a yield of 84% [11,12]. An analytical data comparison of the three isolated isomers $\mathbf{H_2L}$, $\mathbf{H_2L^1}$ and $\mathbf{H_2L^2}$ with H_2bfe reveals that $\mathbf{H_2L}$ seems to be H_2bfe [11]. However, none of the three isomers is fully consistent with H_2bfe. Therefore, perhaps H_2bfe is a mixture of the above isomers [13]. Complexes **I** and **II** were prepared in refluxing methanol and dichloromethane for 17 h [12]. In fact, at room temperature, $\mathbf{H_2L}$ can react with copper(II) and nickel(II) ions in ethanol and dichloromethane for 12 h to produce complexes **I** and **II**.

3.2. Spectra

The ^{1}H NMR spectrum of the free ligand ($\mathbf{H_2L}$) shows clearly that it exists entirely in the bis(ketoenamine) form (both acidic protons on enamine nitrogen atoms), namely $[C_5H_5FeC_5H_4COCH{=}C(CH_3)NHCH_2]_2$ [13,19–21]. The protons of the substituted cyclopentadienyl rings display two singlets at δ4.37 and 4.72 ppm, whereas a singlet at δ4.17 ppm is due to protons on the unsubstituted cyclopentadienyl rings. Moreover, methylene protons of the NCH_2 moiety exhibit a triplet at δ3.50 ppm. In contrast, the methyl protons show a singlet at δ2.02 ppm. A singlet at δ5.30 ppm may be assigned to two methine protons. A singlet signal attributed to the enamino NH appears at δ11.10 ppm and disappears in the presence of D_2O. The very downfield position of this signal may be mainly resulted from the intramolecular hydrogen bonding [13,22]. It is obvious that the above evidence is consistent with the proposed structure of the ligand [13,22]. Similarly, two other isomers $\mathbf{H_2L^1}$ and $\mathbf{H_2L^2}$ display corresponding absorptions [13,22]. For example, those of methyl, methylene, methine, unsubstituted cyclopentadienyl and substituted cyclopentadienyl (two triplets) groups appear at δ2.01, 2.03; 3.49, 3.50; 5.30, 5.30; 4.17, 4.19 and 4.36, 4.37 as well as 4.72, 4.72 ppm whereas signals of labile hydrogens are observed at δ11.1 and 11.11 ppm. For complex **II**, the signal corresponding to the enamino NH at ca. 11.1 ppm disappears and the absorption of methylene protons is present as a singlet, indicating that the ligand is deprotonated and bonded to the nickel ion which is also supported by the crystal structure as described below. In addition, all the signals of protons shift highfield in complex **II**, which may be due to the increase of electron density resulting from deprotonation and nickel-to-ligand feedback after forming the complex [12,23].

In the IR spectrum of the ligand, the band at ca. 3100 cm^{-1} due to ν(NH) appears. However, no band assignable to ν(NH) is present in the spectra of the complexes. This fact indicates that the ligand is bonded to copper and nickel ions in the dianionic form. Moreover, the strong bands attributed to the stretching vibrations of the skeleton C=O and C=C groups, which are observed at 1601, 1557 and 1520 cm^{-1} in the ligand, are red-shifted to the region 1576–1578 and 1511–1513 cm^{-1} in the complexes [3,13,19]. This is because the doubly deprotonated ligand ($\mathbf{L^{2-}}$) has a stronger conjugate effect which results in the decrease of the double bond character of C=O and C=C groups [13]. It is noted that $\mathbf{H_2L^1}$ and $\mathbf{H_2L^2}$ display the following absorptions at 3429, 3096, 1600, 1557, 1520 and 3417, 3090, 1599, 1561, 1523 cm^{-1}, respectively. Among the three isomers, the most marked differences result from the relative intensities of the four last characteristic absorptions.

The UV spectrum of the ligand shows three absorptions at 271, 342 and 450 nm, which are attributable to the B-band of the cyclopentadienyl ring, K-band of the skeleton and an intraligand charge transfer transition band [13,23]. Similarly, $\mathbf{H_2L^1}$ and $\mathbf{H_2L^2}$ display three absorptions at 265, 346, 453 and 271, 347, 446 nm, respectively. Because the three isomers have similar curves of UV absorptions, they should have similar conjugated systems. This further supports the proposed structures for the three isomers as described in Scheme 1. For complex **I**, the shortest wavelength absorption which is assigned as the B-band of the cyclopentadienyl ring displays a hypsochromic shift compared with that of the ligand [12,23]. However, the K-band at 344 nm shows a red shift. In addition, complex **I** exhibits an intense absorption band at 446 nm which may be due to a ligand-to-metal charge transfer transition. For complex **II**, interestingly, compared with those absorptions of the ligand, the B-band and K-band show hypsochromic shifts. It is noteworthy that as expected, tetrahedral complex **I** does not show a d–d absorption, however, the theoretically planar nickel complex **II** should exhibit a d–d absorption, in fact, the ligand field band of complex **II** is not observed because the weak d–d transition is obscured by other intense absorptions [13,23].

3.3. Crystal structures

In principle, in view of the planar or tetrahedral coordination geometry of the central metal ion (copper or nickel) and *anti* or *syn* arrangement of the ferrocenyl groups with respect to the mean plane with the central metal ion (copper or nickel) and donor atoms, four-coordinate copper or nickel complexes may have four stereoisomers: planar-*anti*, planar-*syn*, tetrahedral-*anti* and tetrahedral-*syn* [13].

3.3.1. Crystal structure of complex *I*

Complex **I** with solvent molecules belongs to the triclinic space group of $P\bar{1}$. In addition to one water molecule, one methanol molecule and one ethanol molecule, two independent molecules are contained in the asymmetric unit. ORTEP plots of the two independent molecules are shown in Figs. 1 and 2. Each of the two independent copper atoms displays a tetrahedral coordination by two nitrogen atoms and two oxygen atoms of the doubly deprotonated ligand ($\mathbf{L}^{2-}$), and complex **I** exists as a mixture of tetrahedral-*anti* and tetrahedral-*syn* isomers. In the former both ferrocenyl groups are *anti* and the two Fe atoms have a separation of 9.508 Å, while in the other both ferrocenyl groups are *syn* and the two Fe atoms are separated by 8.875 Å. As expected, the two six-membered chelate rings for each isomer are planar. The five-membered rings defined by the copper atom and diaminoethane moiety are definitely nonplanar, the ethylene bridges have a gauche conformation as usually observed, with torsion angles of 37.22° and 38.91° for N(3)–C(32)–C(33)–N(4) (*anti* isomer) and N(1)–C(3)–C(4)–N(2) (*syn* isomer), respectively. The angles O(3)–Cu(2)–N(4) and O(4)–Cu(2)–N(3) (mean 174.4(3)°) for the *anti* isomer and O(1)–Cu(1)–N(1) and O(2)–Cu(1)–N(2) (mean 172.1(3)°) for the *syn* isomer indicate that each coordination geometry of the two independent copper atoms is tetrahedral as described above. The measured N–Cu–N and O–Cu–O angles (Table 2) are close to the corresponding values observed in related structures [24–27]. A comparison of the Cu–O and Cu–N bond lengths (mean 1.924(6) and 1.927(8) Å for the *anti* isomer and 1.913(6) and 1.924(8) Å for the *syn* isomer) reveals them to be considerably shorter than those reported for *N*,*N*′-ethylenebis(acetylacetoneiminato)copper (mean 1.94 and 1.98 Å) [24]. Also, these are slightly smaller than the reported values of the complex bfeCu [11,12]. The bond length pattern within the six-membered ring system suggests partial delocalization of bonding electron density. For example, the C–O bond lengths of 1.27(1) and 1.29(1) Å for the *anti* isomer and 1.28(1) and 1.29(1) Å for the *syn* isomer are between a normal single bond (1.43 Å) and a normal double bond (1.23 Å). It is interesting that the ethylene bond lengths of 1.48(1) (C(32)–C(33)) for the *anti* isomer and 1.46(1) (C(3)–C(4)) for the *syn* isomer are significantly shorter than that for the related complex mentioned above (1.55 Å) and the complex bfeCu (1.514(6) and 1.510(7) Å) [12,24].

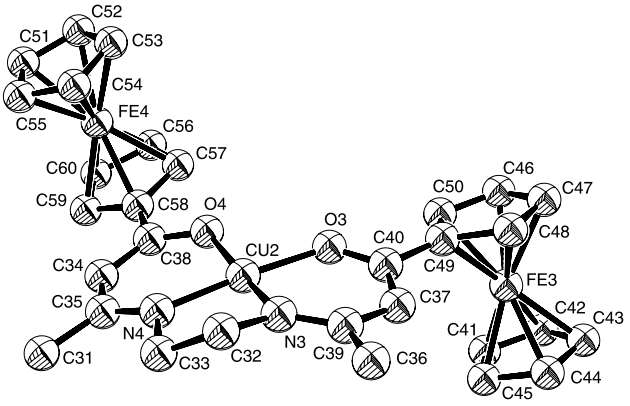

Fig. 1. An ORTEP plot of the *anti* isomer in the asymmetric unit of complex **I**. The atoms are drawn with 50% probability ellipsoids. Hydrogen atoms and solvent molecules are omitted for clarity.

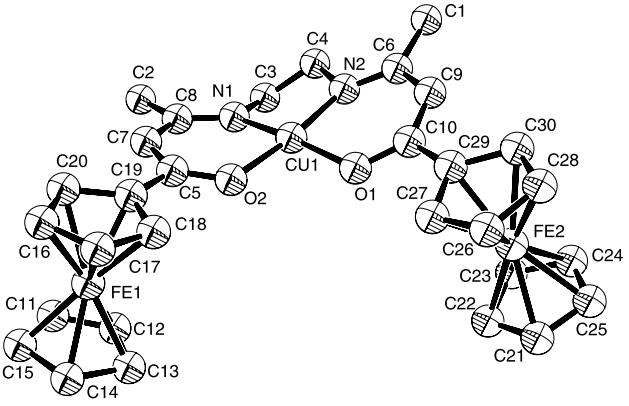

Fig. 2. An ORTEP plot of the *syn* isomer in the asymmetric unit of complex **I**. The atoms are drawn with 50% probability ellipsoids. Hydrogen atoms and solvent molecules are omitted for clarity.

3.3.2. Crystal structure of complex *II*

Complex **II** crystallizes in the monoclinic space group $P2_1/c$. Fig. 3 is its crystal structure. In the molecule of complex **II**, both ferrocenyl groups (the

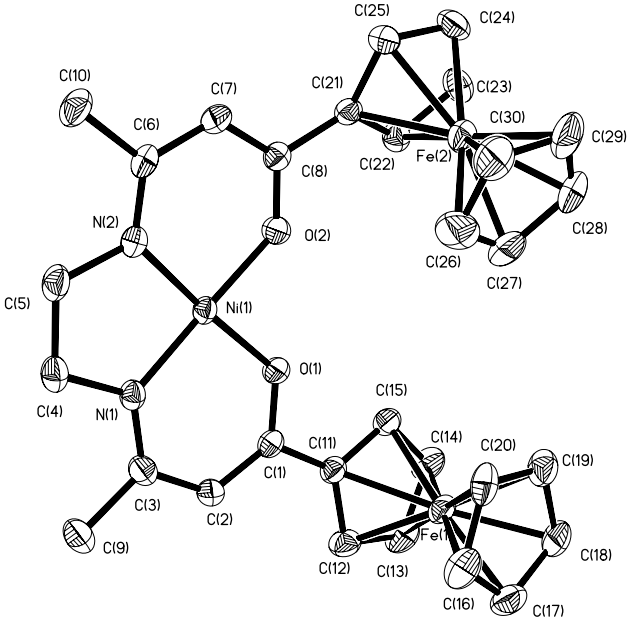

Fig. 3. An ORTEP plot of complex **II**. The atoms are drawn with 40% probability ellipsoids. Hydrogen atoms are omitted for clarity.

distance of the two Fe atoms is 6.604 Å) are *syn* to each other; in other words, complex **II** exists in the planar-*syn* form. The angles O(1)–Ni(1)–N(2) and O(2)–Ni(1)–N(1) (mean 176.7(1)°) indicate that the coordination geometry of the nickel atom is planar as described above, which is in agreement with a measured standard and beautiful ^{1}H NMR spectrum and diamagnetism of complex **II** [12]. The Ni–O distances of 1.839(3) and 1.845(3) Å for Ni(1)–O(1) and Ni(1)–O(2) are very close to the corresponding values in related structures [21]. However, the Ni–N distances of 1.852(4) and 1.850(4) Å for Ni(1)–N(1) and Ni(1)–N(2) are significantly shorter than that for a related complex (1.910(4) Å) [21,28]. It is notable that to our knowledge examples of very close distances of Ni–N and Ni–O bonds are very scarce. The measured N–C, C–C and C–O bond distances in the six-membered rings of complex **II** are very close to the values 1.306(5), 1.361(6), 1.413(7) and 1.297(4) Å reported for a related nickel(II) complex, showing that the enaminoketonate ion is partially delocalized [21,28].

4. Supplementary data

Crystallographic data (CCDC 208967 for complex **I** and CCDC 208966 for complex **II**) have been deposited at the Cambridge Crystallographic Database Centre and is available on request from the Director, CCDC, 12 Union Road, Cambridge, CB2 1EZ, UK (Fax: +44-1223-336033; e-mail: deposit@ccdc.cam.ac.uk or www: http//www.ccdc.cam.ac.uk).

Acknowledgements

Yao-Cheng Shi thanks the National Nature Science Foundation of China (No. 20175023) and Yangzhou University (No. D0009107) for financial support of this work.

References

[1] J.P. Costes, F. Dahan, J.P. Laurent, Inorg. Chem. 24 (1985) 1018.
[2] T. Dubé, S. Gambarotta, G. Yap, Organometallics 19 (2000) 121.
[3] T. Sato, H. Takeda, K. Sakai, T. Tsubomuram, Inorg. Chim. Acta 246 (1996) 413.
[4] M. Mazzanti, J.M. Rosset, C. Floriani, J. Chem. Soc., Dalton Trans. (1989) 953.
[5] M.J. Bochmann, J. Chem. Soc., Dalton Trans. (1996) 255.
[6] D. Jones, A. Roberts, K. Cavell, W. Keim, U. Englert, B.W. Skelton, A.H. White, J. Chem. Soc., Dalton Trans. (1998) 255.
[7] J. Kim, J.W. Hwang, Y. Kim, M.H. Lee, Y. Han, Y. Do, J. Organomet. Chem. 620 (2001) 1.
[8] S.G. McGeachin, Can J. Chem. Soc. 46 (1968) 1903.
[9] G.W. Everett, R.H. Holm, J. Am. Chem. Soc. 88 (1965) 2117.
[10] J.P. Costes, Inorg. Chim. Acta 130 (1987) 17.
[11] Y.X. Ma, H.S. Sun, P.S. Jing, G.S. Huang, Transit. Met. Chem. 16 (1991) 308.
[12] Y. Zhu, H.S. Sun, G.S. Huang, Y.X. Ma, Transit. Met. Chem. 18 (1993) 635.
[13] Y.C. Shi, H.M. Yang, W.B. Shen, C.G. Yan, X.Y. Hu, Polyhedron 23 (2004) 15.
[14] C.E. Cain, T.A. Mashburn, C.R. Hauser, J. Org. Chem. 26 (1960) 1030.
[15] P.J. Graham, R.V. Lindsey, G.W. Parshall, M.L. Peterson, G.M. Whitman, J. Am. Chem. Soc. 79 (1957) 3416.
[16] G.M. Sheldrick, SHELXS-97, Program for the Solution of Crystal Structures, University of Göttingen, Germany, 1997.
[17] G.M. Sheldrick, SHELXL-97, Program for the Refinement of Crystal Structures, University of Göttingen, Germany, 1997.
[18] L.J. Farrugia, ORTEP-3 for Windows, Version 1.076, University of Glasgow, UK, 2003.
[19] H. Iida, Y. Yuasa, C. Kibayashi, Y. Iitaka, J. Chem. Soc., Dalton Trans. (1981) 2212.
[20] J.V. Greenhill, Chem. Soc. Rev. 6 (1977) 277.
[21] M. Kwiatkowski, E. Kwiatkowski, A. Olechnowicz, J. Chem. Soc., Dalton Trans. (1990) 2497.
[22] Y.C. Shi, H.M. Yang, H.B. Song, C.G. Yan, X.Y. Hu, Polyhedron 23 (2004) in press.
[23] Y.C. Shi, Q.B. Song, X.L. Wu, Y.X. Ma, Polyhedron 13 (1994) 2101.
[24] D. Hall, A.D. Rae, T.N. Waters, J. Chem. Soc. (1963) 5897.
[25] G.E. Gurr, Inorg. Chem. 3 (1964) 614.
[26] J.P. Costes, J.F. Serra, F. Dahan, J.P. Laurent, Inorg. Chem. 25 (1986) 2790.
[27] M.B. Cingi, A.C. Villa, A.G. Manfredotti, C. Guastini, M. Nardelli, Acta Crystallogr., Sect. B 28 (1972) 1075.
[28] M. Kwiatkowski, G. Bandoli, J. Chem. Soc., Dalton Trans. (1992) 379.

Available online at www.sciencedirect.com
SCIENCE DIRECT®
Polyhedron 23 (2004) 755–761
POLYHEDRON
www.elsevier.com/locate/poly

Syntheses, structures and third-order nonlinear optical properties of heterometal and homometal clusters containing iron

Jing Lu [a], Chang-Hai Lü [a], Jie-Hui Yu [a], Ji-Qing Xu [a,*], Yong Li [a], Xiao Zhang [a], Tie-Gang Wang [a], Qing-Xin Yang [b]

[a] College of Chemistry and State Key Laboratory of Inorganic Synthesis and Preparative Chemistry, Jilin University, No. 119 JieFang Road, Changchun, Jilin 130023, PR China
[b] College of Physics, Jilin University, Changchun, Jilin 130023, PR China

Received 22 September 2003; accepted 31 October 2003

Abstract

Both the heterometal cluster $\{[FeMo_2O_{10}(FRA)_4(DMF)_4]\cdot 2DMF\}$ (**1**) (FRA = α-furoic acid) and the homometal cluster $\{Fe[DTC]_4\}$ (**2**) (DTC = diethyl-dithiocarbamate) were successfully synthesized by low-temperature solid-state reactions. X-ray single-crystal diffraction studies suggest that compound **1** is a hexanuclear cluster including two solvent DMF molecules, with α-furoic acid and DMF as auxiliary ligands, and compound **2** is a dinuclear neutral cluster. The two compounds were characterized by elemental analyses, IR spectra and UV–Vis spectra. The third-order nonlinear optical (NLO) properties of the clusters were also investigated and all exhibited nice nonlinear absorption and self-defocusing performance with moduli of the hyperpolarizabilities 1.21×10^{-31} esu for **1** and 5.123×10^{-31} esu for **2**.
© 2003 Elsevier Ltd. All rights reserved.

Keywords: Iron clusters; Solid-state reactions; Third-order nonlinear optical properties

1. Introduction

It has been found that iron plays a very important role in the biological system [1–6]. For example, the iron protein, one of the essential metalloproteins of nitrogenase, is a very specific ATP-activated electron donor to the other, the molybdenum–iron protein [1]. In iron protein, iron is present with the form of a [4Fe4S] subunit [2]. Some other metalloproteins such as methane monooxygenase (MMO) [3], ribonucleotide reductase (RR) [4], hemerythrin (Hr) [5] and purpleacid phosphatase (PAPs) [6] all belong to the class of non-heme diiron enzymes, which are capable of binding and activating dioxygen [7,8]. Their active sites contain either an Fe(II)-Fe(II)center (MMO, RR, Hr) or a mixed-valent Fe(II)-Fe(III) core (PAPs) which is directly involved in the reaction with dioxygen [9]. During studying the intricate mechanistic and structural details of these metalloproteins, the coordination chemistry of iron has been further developed, and a number of iron complexes have been synthesized in different models. For example, cubane-like clusters $Fe_4S_4(^tBu_3P)_3Cl$ [10], $(Et_3N)_3[(Meida)VFe_3S_4Cl_3]$ [11] (Meida = *N*-methylimidodiacetate(2−)), lineshape cluster $(Bu_4N)_3[(edt)_2M_2Fe_2S_6]$ [12] (M = Mo,W; edt = ethane-1,2-dithiolate) were synthesized to simulate nitrogenase. Several diiron peroxo complexes, such as $[Fe_2(N\text{-}Et\text{-}HPTB)(O_2)(Ph_3PO)_2](BF_4)_3\cdot 3CH_3CN$ (HPTB = *N*,*N*,*N*′,*N*′-tetrabis (2-benzimidazdylmethyl)-2-hydroxo-1,3-diaminopropane) [13] and $[Fe_2(ph\text{-}bimp)(O_2)(C_6H_5COO)](BF_4)_2\cdot 2CH_3CN\cdot C_2H_5OC_2H_5\cdot H_2O$ [14], have been prepared by the reaction of the corresponding diferrous precursor complex with dioxygen, which have been researched in more detail [14,15]. Their spectroscopy characteristics and structures have been studied. However, the third-order nonlinear optical (NLO) properties of them have been less well mentioned. In this paper, we not only describe the syntheses and structures of one heterometal cluster and one homometal cluster but also study their NLO properties.

* Corresponding author. Tel.: +86-431-894-3977; fax: +86-431-892-3907.
E-mail address: xjq@mail.jlu.edu.cn (J.-Q. Xu).

0277-5387/$ - see front matter © 2003 Elsevier Ltd. All rights reserved.
doi:10.1016/j.poly.2003.11.046

2. Experimental

2.1. Materials and physical measurements

$(NH_4)_2MoS_4$ was prepared by a modified published procedure [16]. Other reagents were used as received from commercial suppliers without further purification. Infrared spectra of the title clusters were recorded as KBr pellets on a Perkin–Elmer Spectrum One FT-IR spectrometer in the 225–4000 cm^{-1} region. Element analyses were performed on a Perkin–Elmer 2400LSII element analyzer. Electronic spectra were measured on a Shimadzu UV-3100 spectrophotometer.

2.2. Synthesis of compounds

2.2.1. $[Fe_4Mo_2O_{10}(FRA)_4(DMF)_4]\cdot 2DMF$ (1)

A mixture of $(NH_4)_2MoS_4$ (0.3 g, 1 mmol), $FeCl_2\cdot 4H_2O$ (0.4 g, 2 mmol), α-furoic acid (0.5 g, 4.5 mmol) and $(CH_3)_4NBr$ (0.4 g, 2.5 mmol) was pestled for 30 min. After being sealed in a reaction tube, it was heated at 95 °C for 18 h. Then, the mixture was cooled to room temperature and extracted with 10 ml *N*,*N*′-dimethylformamide (DMF). Isopropyl alcohol (30 ml) was added slowly to the filtered extract. After the dark solution had stood without disturbance for one month, dark-red crystals were found (0.15 g, yield 61.4%, based on Mo). IR (KBr pellet, cm^{-1}): $\nu_{(asym,C=O)}$ 1657 (vs), $\nu_{(sym,C=O)}$ 1472 (s), 1427 (s), $\nu_{(Mo=O)}$ 1014 (m), 929 (m), $\nu_{(Mo–O–Fe)}$ 786 (s), $\nu_{(Fe–O)}$ 365 (w). *Anal*. Calc. for $C_{19}H_{27}Fe_2MoN_3O_{14}$: Mo, 26.32; Fe, 30.64; C, 31.29; H, 3.83; N, 5.76. Found: Mo, 26.26; Fe, 30.51; C, 31.20; H, 3.82; N, 5.51%.

2.2.2. $Fe_2[(DTC)_4]$ (2)

A mixture of $(NH_4)_2MoS_4$ (0.2 g, 0.67 mmol), $FeCl_2\cdot 4H_2O$ (0.1 g, 0.5 mmol), cupric tartrate (0.1 g, 0.3 mmol) and sodium diethyl-dithiocarbamate (0.2 g, 1 mmol) was pestled for 30 min. It was heated at 90 °C for 24 h after being sealed in a reaction tube. Then the mixture was cooled to room temperature and extracted with 10 ml CH_2Cl_2. Isopropyl alcohol (10 ml) was added slowly to the filtered extract. After the brown solution had stood without disturbance for one month, black crystals were found (0.069 g, yield 78.3%, based on Fe). IR (KBr pellet, cm^{-1}): $\nu_{(Fe\text{-}S)}$ 327 (s), 359 (s). *Anal*. Calc. for $C_{10}H_{20}FeS_4N_2$: Fe, 15.84; C, 34.09; H, 2.84; N, 7.95. Found: Fe, 16.01; C, 35.1; H, 2.9; N, 7.8%.

2.3. X-ray crystal structure determination

Crystal data and structure refinement for the title compounds are given in Table 1. Selected bond lengths and angles are given in Table 2. Data were collected with Mo Kα radiation ($\lambda = 0.71073$ Å) using a Siemens SMART CCD diffractometer. The structures were solved using direct methods with the SHELXTL program

Table 1
Crystal data and structure refinement for the title compounds

	1	2
Empirical formula	$C_{19}H_{27}Fe_2MoN_3O_{14}$	$C_{10}H_{20}FeS_4N_2$
Formula weight	729.08	352.37
Temperature (K)	293(2)	293(2)
Wavelength (Å)	0.71073	0.71073
Crystal system	monoclinic	monoclinic
Space group	$C2/c$	$P2_1/n$
Unit cell dimensions		
a (Å)	24.669(5)	9.751(2)
b (Å)	15.005(3)	10.573(2)
c (Å)	16.366(3)	15.494(3)
β (°)	108.97(3)	101.80(3)
Volume (Å^3)	5729(2)	1563.6(5)
Z	8	4
Calculated density (g/cm^3)	1.691	1.497
Absorption coefficient (mm^{-1})	1.498	1.480
$F(000)$	2944	736
Crystal size (mm)	$0.473\times 0.264\times 0.230$	$0.665\times 0.497\times 0.100$
θ Range for data collection	1.61–27.48°	2.28–27.48°
Limiting indices	$0\leqslant h\leqslant 32, 0\leqslant k\leqslant 19, -21\leqslant l\leqslant 20$	$0\leqslant h\leqslant 12, 0\leqslant k\leqslant 13, -20\leqslant l\leqslant 19$
Reflections collected/unique	6556/6556 [$R_{int} = 0.0487$]	3527/3527 [$R_{int} = 0.0168$]
Refinement method	full-matrix least-squares on F^2	full-matrix least-squares on F^2
Data/restraints/parameters	6556/0/342	3527/0/154
Goodness-of-fit on F^2	0.906	1.095
Final R indices [$I > 2\sigma(I)$]	$R_1 = 0.0511$, $wR_2 = 0.1407$	$R_1 = 0.0378$, $wR_2 = 0.1136$
R indices (all data)	$R_1 = 0.0857$ $wR_2 = 0.1614$	$R_1 = 0.0407$ $wR_2 = 0.1153$
Largest diffraction peak and hole (e Å^{-3})	1.021 and −1.145	0.554 and −0.822

Table 2
Selected bonds lengths (Å) and angles (°) for the title compounds

1			
Bond lengths			
Mo(1)–O(9)	1.694(4)	Fe(1)–O(12)#1	2.065(4)
Mo(1)–O(11)	1.777(4)	Fe(2)–O(10)	1.883(3)
Mo(1)–O(13)	1.782(3)	Fe(2)–O(11)	1.992(4)
Mo(1)–O(12)	1.810(4)	Fe(2)–O(3)	2.013(4)
Fe(1)–O(10)#1	1.972(4)	Fe(2)–O(5)	2.036(4)
Fe(1)–O(10)	1.985(3)	Fe(2)–O(2)	2.044(4)
Fe(1)–O(4)#1	2.022(3)	Fe(2)–O(1)	2.062(3)
Fe(1)–O(6)	2.026(4)	Fe(1)–Fe(1)#1	2.9610(14)
Fe(1)–O(13)	2.025(4)		
Bond angles			
O(9)–Mo(1)–O(11)	107.2(2)	O(10)–Fe(2)–O(1)	90.25(14)
O(9)–Mo(1)–O(13)	109.0(2)	O(10)–Fe(2)–O(3)	96.60(14)
O(11)–Mo(1)–O(13)	110.71(17)	O(11)–Fe(2)–O(3)	93.01(16)
O(9)–Mo(1)–O(12)	107.3(2)	O(10)–Fe(2)–O(5)	94.23(14)
O(11)–Mo(1)–O(12)	112.50(17)	O(11)–Fe(2)–O(5)	90.64(18)
O(13)–Mo(1)–O(12)	109.82(16)	O(3)–Fe(2)–O(5)	168.55(15)
O(10)#1–Fe(1)–O(10)	83.12(13)	O(10)–Fe(2)–O(2)	95.72(15)
O(10)#1–Fe(1)–O(4)#1	94.46(13)	O(11)–Fe(2)–O(2)	172.76(16)
O(10)–Fe(1)–O(4)#1	175.61(15)	O(3)–Fe(2)–O(2)	90.38(17)
O(10)#1–Fe(1)–O(6)	174.75(16)	O(5)–Fe(2)–O(2)	84.84(19)
O(10)–Fe(1)–O(6)	95.44(13)	O(10)–Fe(2)–O(1)	177.13(16)
O(4)#1–Fe(1)–O(6)	87.29(14)	O(11)–Fe(2)–O(1)	87.45(15)
O(10)#1–Fe(1)–O(13)	93.79(14)	O(3)–Fe(2)–O(1)	85.24(14)
O(10)–Fe(1)–O(13)	85.66(14)	O(5)–Fe(2)–O(1)	84.08(14)
O(4)#1–Fe(1)–O(13)	90.86(15)	O(2)–Fe(2)–O(1)	86.46(16)
O(6)–Fe(1)–O(13)	91.14(17)	Fe(2)–O(10)–Fe(1)#1	130.08(16)
O(10)#1–Fe(1)–O(12)#1	87.04(14)	Fe(2)–O(10)–Fe(1)	130.65(17)
O(10)–Fe(1)–O(12)#1	92.57(14)	Fe(1)#1–O(10)–Fe(1)	96.88(13)
O(4)#1–Fe(1)–O(12)#1	90.96(16)	Mo(1)–O(11)–Fe(2)	113.13(17)
O(6)–Fe(1)–O(12)#1	87.98(16)	Mo(1)–O(12)–Fe(1)#1	112.61(18)
O(13)–Fe(1)–O(12)#1	177.94(14)	Mo(1)–O(13)–Fe(1)	115.39(18)
2			
Bond lengths			
Fe(1)–S(4)	2.3047(11)	Fe(1)–S(3)	2.3338(8)
Fe(1)–S(1)	2.3088(10)	Fe(1)–S(3A)	2.801(6)
Fe(1)–S(2)	2.3202(8)		
Bond angles			
S(4)–Fe(1)–S(1)	160.77(3)	S(2)–Fe(1)–S(3)	171.71(3)
S(4)–Fe(1)–S(2)	101.61(3)	C(9)–S(1)–Fe(1)	84.57(9)
S(1)–Fe(1)–S(2)	77.10(3)	C(9)–S(2)–Fe(1)	84.30(9)
S(4)–Fe(1)–S(3)	76.65(3)	C(10)–S(3)–Fe(1)	84.52(9)
S(1)–Fe(1)–S(3)	101.81(3)	C(10)–S(4)–Fe(1)	85.55(9)

Symmetry transformation used to generate equivalent atoms: # $1-x+1/2,-y+1/2,-z$.

and refined by full-matrix least-squares techniques. The non-hydrogen atoms were assigned anisotropic displacement parameters in the refinement. The hydrogen atoms were treated using a riding model. The structure was then refined on F^2 using SHELXTL-97.

3. Results and discussion

3.1. Syntheses

Low-temperature solid-state reaction is a very ideal method to synthesize clusters containing sulfur atoms, for example $[MS_4(Cu(P\text{-}MeOC_6H_4)_3P_2)]\cdot 0.5C_6H_{12}$ (M = Mo,W) [17] and $[(n\text{-}Bu)_4N]_3[WS_4Cu_3Cl_3Br]$ [18] were both obtained by this method, with $(NH_4)MS_4$ (M = Mo,W) as a precursor. Mo–Fe–S clusters including auxiliary ligands would have been designed based on this method. Unluckily, in the reaction of compound **1**, there is no sulfur atom in the product, and many light-yellow crystals were found at the bottom of the flask, which were identified as S_8 by its IR spectrum. From these facts it is supposed that all of the sulfur atoms of $(NH_4)_2MoS_4$ were substituted by oxygen atoms from the atmosphere. The reaction can be demonstrated by the following equation:

$$4FeCl_2 \cdot 4H_2O + 2(NH_4)_2MoS_4 + 4C_4H_3OCOOH + 6DMF + 5O_2 \rightarrow [Fe_4Mo_2O_{10}(FRA)_4(DMF)_4] \cdot 2DMF + S_8 + 4HCl + 4NH_4Cl + 16H_2O$$

While in the reaction of compound **2**, only the iron atoms were coordinated by sulfur atoms coming from DTC molecules. So we can conclude that the iron atom is easier to coordinate by DTC than the molybdenum atom.

3.2. Crystal structures

3.2.1. $[Fe_4Mo_2O_{10}(FRA)_4(DMF)_4]\cdot 2DMF$ (1)

The molecular structure of compound **1** is shown in Fig. 1. It is a hexanuclear $[Mo_2Fe_4O_{10}]$ cluster including two solvent DMF molecules, with α-furoic acid and DMF as auxiliary ligands. In each molecule unit there exist crystallographically one unique Mo atom and two Fe atoms. The Mo atom, coordinated by the terminal oxygen atom [O(9)] and three μ_2-oxygen atoms [O(11), O(12), O(13)], is in a tetrahedral coordination circumstance, with a distance to the terminal O(9) of 1.694(4) Å, which is shorter than the ones of Mo–(μ_2-O) [1.777(4)–1.810(4) Å] as expected. The O–Mo–O angles 107.2(2)°–112.50(17)° suggest that the tetrahedron is distorted. Although the two iron atoms are both in octahedrons, they have different coordination circumstances. Fe(1) is coordinated by two μ_3-oxygen atoms [O(10) and O(10A)], two μ_2-oxygen atoms [O(13) and O(12A)] and two oxygen atoms from two carboxyl of α-furoic acid molecules [O(4A) and O(6)]; while μ_3-O(10), μ_2-O(11), two oxygen atoms from DMF molecules [O(1) and O(2)] and two oxygen atoms from carboxyl of α-furoic acid molecules [O(3) and O(5)] coordinate to Fe(2). In the two kinds of octahedrons $[Fe(1)O_6]$ and $[Fe(2)O_6]$, the mean distance of Fe–(μ_2-O) (2.027 Å) is longer than that of Fe(2)–(μ_3-O) (1.883(3) Å) and Fe(1)–(μ_3-O) (1.972(3), 1.985(3) Å), and shorter than the mean length between the iron atom and the oxygen atoms from ligands 2.034 Å. The range of *cis*-angles and *trans*-angles are 83.12(13)°–96.60(14)° and 168.55(15)°–177.94(14)°, respectively, which suggests that the octahedrons are strongly distorted. As shown in Fig. 2, the two octahedrons $[Fe(1)O_6]$ and $[Fe(1A)O_6]$ share an edge O(10)–O(10A) with each other, and also share a corner with $[Fe(2)O_6]$ (or $[Fe(2A)O_6]$) by μ_3-O [O(10) or O(10A)]. Moreover, the tetrahedral $[MoO_4]$ share the corners with its adjacent octahedrons by three μ_2-O atoms [O(11), O(12) and O(13)]. There is a hydrogen bond, C(15)–H···O(13) [3.320Å, 144.5°], between the μ_2-O atom [O(13)] and the C(15) of α-furoic acid in the adjacent iron–molybdate cluster, which connect the cluster units $[Fe_4Mo_2O_{10}]^{4+}$ into a one-dimensional supramolecular chain.

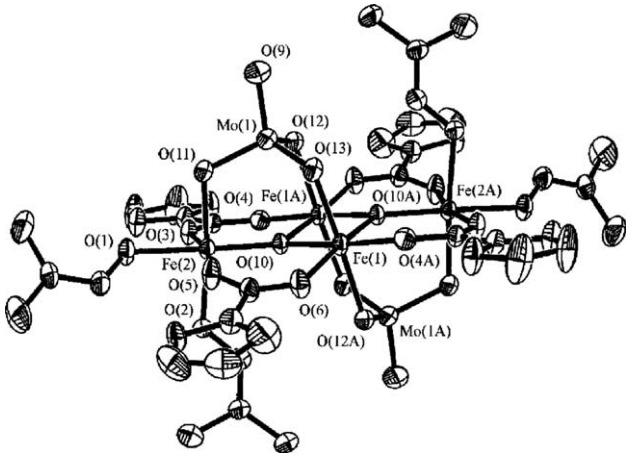

Fig. 1. The view of the structure of $\{Fe_4^{III}Mo_2^{VI}O_{10}(FRA)_4(DMF)_4\}$.

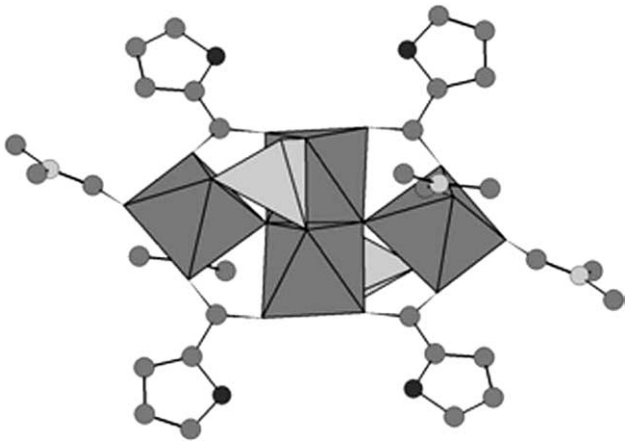

Fig. 2. The polyhedron represents of the structure of compound **1**. The deep grey polyhedrons represent the FeO_6 octahedron, the light ones represent MoO_4 tetrahedron.

3.2.2. $Fe_2[(Dtc)_4]$ (2)

As shown in Fig. 3(a), compound **2** is a dinuclear neutral cluster. The dimer can be described as two distorted square pyramids doubly bridged by the sulfur atoms occupying the axial sites. In the square pyramid, four sulfur atoms coming from two DTC molecules, composing the equatorial plane, meanly deviate 0.1088 Å from the least-squares plane, above which the iron atom is displaced by 0.2774 Å. In the equatorial plane, as S3 is a μ_2 atom, the Fe–S (2.3047(11)–2.3202(8) Å) distance is shorter than Fe(1)–(μ_2-S3) 2.3338(8) Å, while all of them are longer than Fe–SR in Cubane type MFe_3S_4 (M = Mo,W,V) 2.232 Å [19]. The axial direction distance of Fe(1)–(μ_2-S3A) 2.801(26) Å is shorter than the van der Waals 2.965 Å. There are two types of weaker intermolecular interactions (shown in Fig. 3(b)). One exists between the iron atom and the hydrogen atom attached to C4A coming from another dinuclear cluster, and the Fe···H–C distance 3.761 Å and angle 143.5° both can be comparable to those of M···H–C

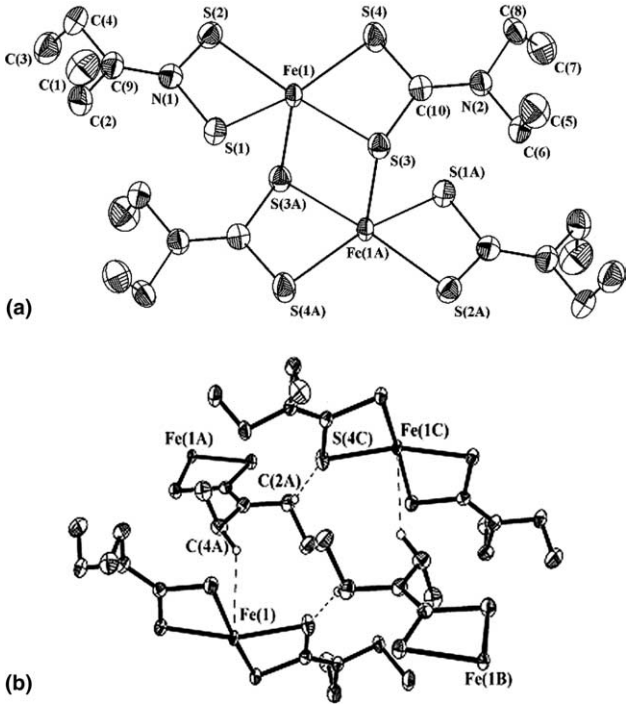

Fig. 3. (a) The perspective view of the molecule of **2**. (b) A view of the intermolecular interactions of **2**.

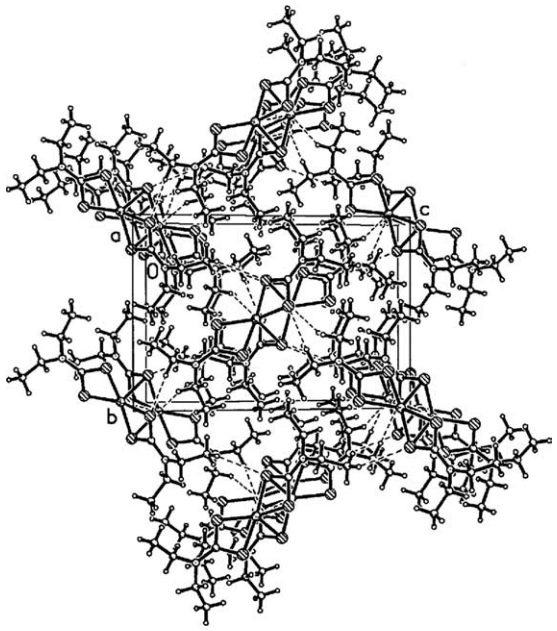

Fig. 4. A view of the packing diagram of compound **2**.

hydrogen bonds reported previously [20], although the ligand, coordinated to the metal center, does not contain electronegative atoms (chiefly oxygen and nitrogen but also sulfur and chlorine). The other is between the C2A atom as the hydrogen-donor and S4C as the acceptor, and the S(4C)···H–C(2A) distance 3.753 Å is longer than that of S···H–C hydrogen bonds (3.44–3.53 Å), which contains electronegative atoms (chlorine) [21]. Because of the intermolecular interactions, a two-dimensional network structure of compound **2** is formed. Fig. 4 shows the packing view of compound **2**.

3.3. Nonlinear optical properties

The electronic spectra of the title compounds were given in Fig. 5 and the absorption band and attribution were listed in Table 3. (The molar extinction coefficient is in the bracket, $cm^{-1}\,mol^{-1}\,dm^3$.) The electronic spectra of the title clusters show relatively low linear absorption in the visible and near-infrared regions, promising low-intensity loss, and little temperature change caused by photon absorption when pulsed light propagates in the materials both show that the clusters have potential as optical limiters have potential as optical limiters [22].

So the NLO properties of the title clusters were evaluated by a Z-scan technique with a Q-switched frequency-doubled Nd:YAG laser at 532 nm with 7 ns pluses. The DMF solution was contained on a 5-mm thick quartz cell with a concentration of 1.71×10^{-4} and 7.804×10^{-4} M

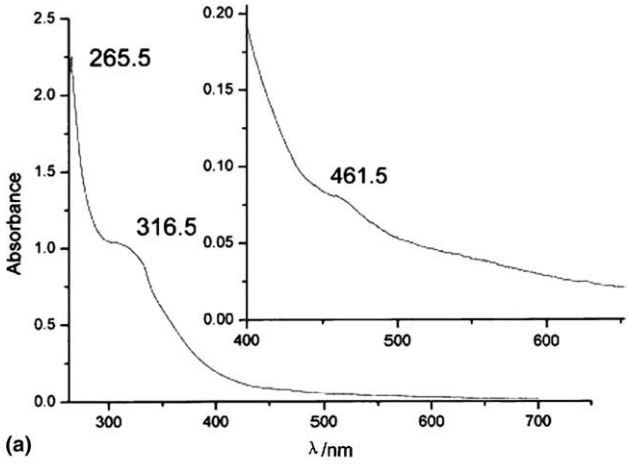

Fig. 5. (a) The UV–Vis spectra of complex **1**. (b) The UV–Vis spectra of complex **2**.

Table 3
The UV-spectra absorption (nm) and attribution

1		2	
Absorption	Attribution	Absorption	Attribution
265.5 nm (5.3×10^5)	(d)Mo ← (π)O	272.4 nm (1.91×10^4)	(d)Fe ← (π)S
316.5 nm (2.4×10^4)	(d)Fe ← (π)O	291.8 nm (1.03×10^4)	(d)Fe ← (π)S
461.5 nm	d ← d	433.5 nm (1.37×10^3)	d ← d
		628.5 nm (1.98×10^3)	d ← d

for **1** and **2**, respectively. The Z-scan data of the cluster **1** and **2** are given in Figs. 6 and 7, respectively, where the open circles represent the experimental data and the solid curves represent the theoretical data based on Z-scan theoretical calculations [23,24]. From the effective third-order NLO absorption coefficient α_2, the effective nonlinear refractive index n_2 (given in Table 4) and the figures, we can conclude that both of the two clusters exhibit strong reverse saturable absorption (RAS) and effective self-defocusing performance. In accordance with the observed α_2 and n_2 values, the modulus of the effective third-order susceptibility $\chi^{(3)}$ can be calculated by the following equation:

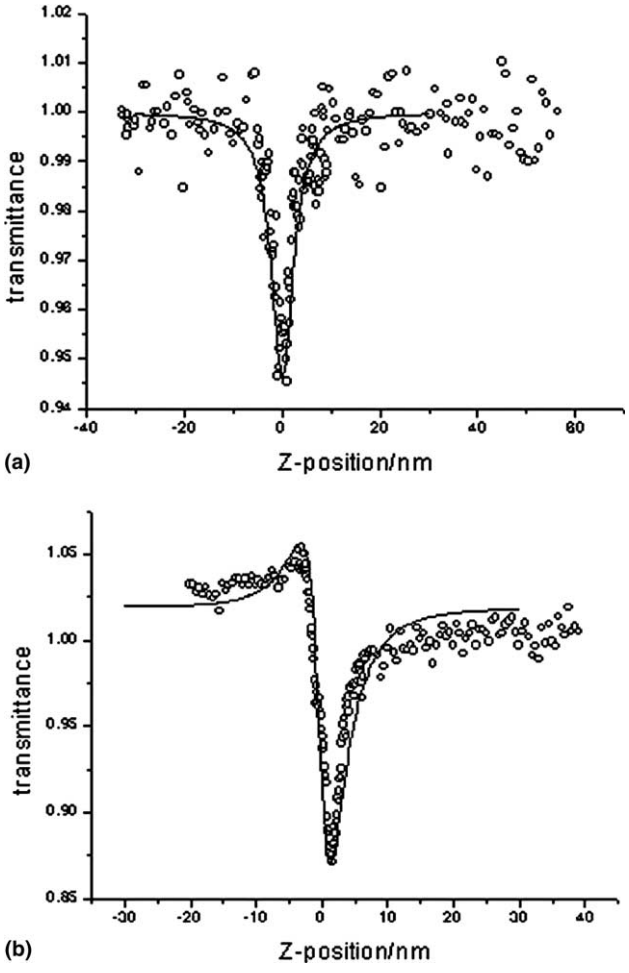

Fig. 6. Open-aperture (a) and close-aperture (b) of Z-scan data (the solid curve is a theoretical fit) of compound **1**.

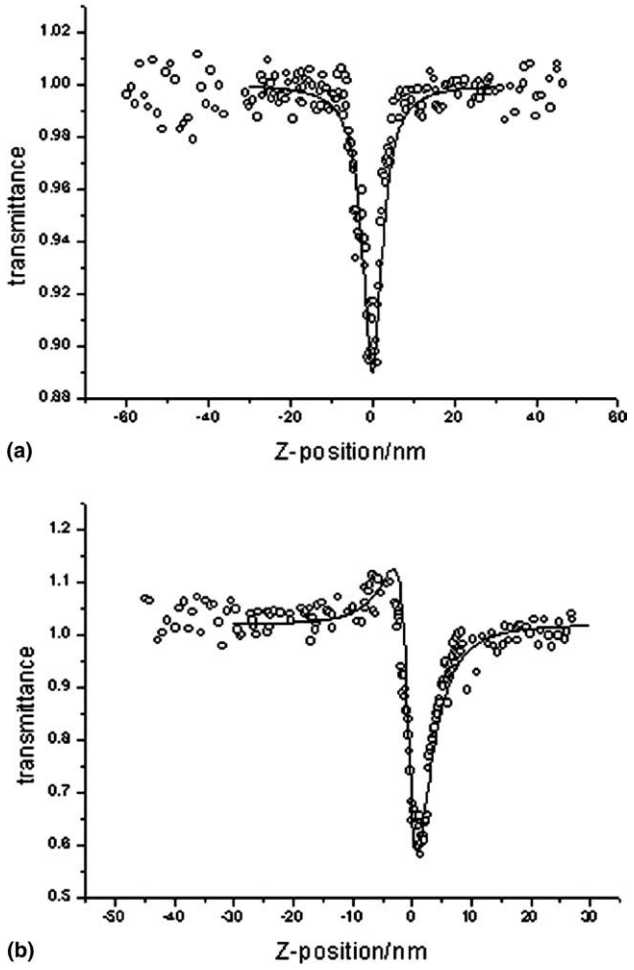

Fig. 7. Open-aperture (a) and close-aperture (b) of Z-scan data (the solid curve is a theoretical fit) of compound **2**.

$$|\chi^{(3)}| = [(9 \times 10^8 \varepsilon_0 n_0^2 c\lambda\alpha_2/8\pi^2)^2 + (n_0^2 c n_2/80\pi^2)^2]^{1/2}.$$

Here, λ is the wavelength of the laser light, n_0 is the linear refractive index of the sample, ε_0 and c are the permittivity and the speed of light in a vacuum, respectively. The corresponding moduli of the hyperpolarizabilities γ was obtained from $|\gamma| = |\chi^{(3)}|/NF^4$, where N is the number density of the clusters in the samples, and $F^4 = [(n^2+2)/3]^4$ (n is the linear refractive index of the solvent, 1.43 for DMF). All the calculated results and some literature data on the NLO properties are listed in Table 4, from which we can see that the NLO

Table 4
Third-order nonlinear optical properties of some clusters

Compound	α_2 (m/w)	n_2 (m^2/w)	$\lvert\chi^{(3)}\rvert$ (esu)	γ (esu)	Ref.
$[Fe_4Mo_2O_{10}(FRA)_4(DMF)_4]\cdot 2DMF$[a]	0.085×10^{-11}	-1.550×10^{-19}	1.238×10^{-13}	1.210×10^{-31}	this work
$Fe_2[DTC]_4$[b]	0.5×10^{-11}	-1.000×10^{-18}	7.953×10^{-13}	5.123×10^{-31}	this work
$[WAg_3OS_3(Pph_3)_3\{S_2P(OP^r_i)_2\}]$[c]	2.9×10^{-10}	-1.74×10^{-17}		7.8×10^{-30}	[25]
$[WCu_3S_4(Pph_3)_3\{S_2P(OCH_2ph)_2\}]$[d]	2.53×10^{-10}	-6.03×10^{-17}		3.0×10^{-29}	[25]

Concentrations of samples (mol dm^{-3}): (a) 1.71×10^{-4}, (b) 7.084×10^{-4}, (c) 1.16×10^{-3}, (d) 8.74×10^{-4}.

performances of the clusters containing sulfur atoms are better than those of the cluster containing no sulfur atom, and the more sulfur atoms, the stronger the NLO performances. It also has been proved that both the cluster skeletons and the heavy atoms are responsible for the NLO effects [26], but which one plays the more important role is still not clear and needs to be further explored.

4. Supplementary material

Additional details of the two compounds structure determinations and data tables have been deposited at the Cambridge Crystallographic Data Centre (CCDC No. 200991 for **1**, No. 215548 for **2**). Copies of these information may be obtained free of charge from the Director, CCDC 12 Union Road, Cambridge, CB12 1EZ, UK (fax: +44-1223-336033; E-mail: deposit@ccdc.cam.ac.uk or www: http://www.ccdc.cam.ac.uk).

Acknowledgements

This work was supported by the State Key Basic Research Project of China (No. 2001CB108906) and National Nature Science Foundation of China (No. 20271021).

References

[1] J.B. Howard, D.C. Ress, Annu. Rev. Biochem. 63 (1994) 235.
[2] M.M. Georgiadis, H. Komiya, P. Chakrabarti, D. Woo, J.J. Kornuc, Science 257 (1992) 1653.
[3] A. Mohamed, F. Marc, W.C. Patricia, D. Howard, Eur. J. Biochem. (1993) 217.
[4] N. Par, E. Hans, J. Mol. Biol. 232 (1993) 123.
[5] H. Thomann, M. Bernadro, J.M. McCornick, S. Pulver, K.K. Andersson, J. Am. Soc. 115 (1993) 6661.
[6] G. Morten, M.J. Christine, M. Anke, P. Annie, K.U. Jens, W. Sigrid, J. Chem. Soc., Dalton Trans. (1997) 4011.
[7] B.J. Milla, J.D. Lipscomb, Chem. Rev. 96 (1996) 2625.
[8] H. Suerbaum, M. Körner, H. Witzel, E. Althaus, B.M. Mosel, W. Müller-Warmuth, Eur. J. Biochem. 214 (1993) 313.
[9] L. Westerheide, F.K. Miiller, R. Than, B. Krebs, Inorg. Chem. 40 (2001) 1951.
[10] M.A. Tyson, K.D. Demadis, D. Coucouvanis, Inorg. Chem. 34 (1995) 4519.
[11] J. Huang, S. Mukerjee, B.M. Segal, H. Akashi, J. Zhou, R.H. Holm, J. Am. Chem. Soc. 119 (1997) 8662.
[12] H.C. Zhou, W.P. Su, C. Achim, P.V. Rao, R.H. Holm, Inorg. Chem. 41 (2002) 3191.
[13] T. Ookubo, F. Sugimoto, T. Nagayama, H. Masuda, T. Sato, K. Tanaka, Y. Maeda, H. Okawa, Y. Hayashi, A. Uehara, M. Suzuki, J. Am. Chem. Soc. 118 (1996) 701.
[14] Y.H. Dong, S.P. Yan, V.G. Young, L. Que, Angew. Chem., Int. Ed. Engl. 35 (1996) 618.
[15] A.L. Feig, M. Becker, S. Schindler, R.V. Eldik, S.J. Lippard, Inorg. Chem. 35 (1996) 2590.
[16] J.M. Donald, G.D. Frieser, L.D. Rosenhein, J.M. Donald, G.D. Frieser, L.D. Rosenhein, W.E. Newton, Inorg. Chim. Acta 72 (1983) 205.
[17] H.G. Zheng, J.L. Zhou, W.L. Tan, Y.Y. Niu, W. Ji, X.Q. Xin, Inorg. Chim. Acta 340 (2002) 29.
[18] J.P. Lang, G.Q. Bian, J.H. Cai, B.S. Kang, X.Q. Xin, Transition Met. Chem. 20 (1995) 376.
[19] D.V. Fomitchev, C.C. Mclauchlan, R.H. Holm, Inorg. Chem. 41 (2002) 958.
[20] D. Braga, F. Grepioni, E. Tedesco, Organometallics 16 (1997) 1846.
[21] T. Steiner, J. Mol. Struct. 447 (1998) 39.
[22] C. Zhang, Y.L. Song, F.E. Kuhn, Y. Xu, X.Q. Xin, H.K. Fun, W.A. Herrmann, Eur. J. Inorg. Chem. (2002) 55.
[23] M. Sherk-Bahae, A.A. Said, T.H. Wei, D.J. Hagan, E.W.V. Stryland, IEEE J. Quantum Electron. (1990) 26.
[24] A.A. Said, M. Sherk-Bahae, D.J. Hagan, T.H. Wei, J. Wang, J. Young, E.W.V. Stryland, J. Opt. Soc. Am. B 9 (1992) 405.
[25] H.G. Zheng, W.L. Tan, M.K.L. Low, W. Ji, D.L. Long, W.T. Wong, K.B. Yu, X.Q. Xin, Polyhedron 18 (1999) 3115.
[26] C. Zhang, Y.L. Song, B.M. Fung, Z.L. Xue, X.Q. Xin, Chem. Commun. (2001) 843.

Available online at www.sciencedirect.com
SCIENCE DIRECT®
Polyhedron 23 (2004) 763–772
POLYHEDRON
www.elsevier.com/locate/poly

Synthesis, structure and magnetism of $M(hfac)_2$ complexes with spin labelled amides

Eugene V. Tretyakov [a], Olga V. Koreneva [b], Galina V. Romanenko [a], Yu G. Shvedenkov [c], Victor I. Ovcharenko [a,*]

[a] International Tomography Center, Siberian Branch, Russian Academy of Sciences, Institutskaya Str., 3a, RU-630090 Novosibirsk, Russia
[b] Novosibirsk State University, Pirogova Str., 2, RU-630090 Novosibirsk, Russia
[c] Institute of Inorganic Chemistry, Siberian Branch, Russian Academy of Sciences, Lavrentjev Ave., 3, RU-630090 Novosibirsk, Russia

Received 18 August 2003; accepted 4 November 2003

Abstract

An effective method for the synthesis of 4,4,5,5-tetramethyl-3-oxide-1-oxyl-4,5-dihydro-1*H*-imidazole-2-carbonitrile (**1**) has been found. 4,4,5,5-Tetramethyl-3-oxide-1-oxyl-4,5-dihydro-1*H*-imidazole-2-carboxylic (**8**) and 4,4,5,5-tetramethyl-1-oxyl-4,5-dihydro-1*H*-imidazole-2-carboxylic (**9**) acid amides have been synthesized and structurally characterized using **1** as the starting compound. Reactions of $Mn(hfac)_2$, $Cu(hfac)_2$ and $Co(hfac)_2$ with **8** and **9** lead to heterospin compounds tending to form in solid bi- or tetranuclear complexes due to intermolecular H-bonding between the peripheral NH_2 groups and the coordinated carbonyl oxygen atoms.
© 2003 Elsevier Ltd. All rights reserved.

Keywords: Nitronyl nitroxide; Imino nitroxide; Amide; Manganese complexes; Copper complexes; Cobalt complexes

1. Introduction

Nitronyl and imino nitroxides are valuable building blocks for design of heterospin exchange clusters and highly dimensional systems with high energies of exchange between the odd electrons of the paramagnetic centers. This is the reason for sustained interest in these compounds from researchers engaged in molecular magnet design [1–4]. Importantly, the structure of heterospin systems formed by coordination of nitronyl and imino nitroxides to metal ions largely depends on the spatial and electronic characteristics of substituents in the radical molecule. Variation of these substituents is an effective tool for selective control over the magnitude and sign of exchange interaction energies within heterospin exchange clusters [5]. Furthermore, in addition to the substituent effect on the character of exchange interactions between the odd electrons of the paramagnetic centers, introduction of donor groups in the structure of the substituent becomes a significant factor which opens up an opportunity of coordination to the donor atoms of the substituent, drastically enhancing the potential of the given nitroxide in design of magnetically active systems. Multifunctional nitronyl and imino nitroxides, therefore, continuously grow in number. The basic procedure giving new nitronyl and imino nitroxides to be applied to design of heterospin systems and molecular magnets is Ullman's classical method for the synthesis of nitronyl and imino nitroxides [6,7]. In this procedure, 2,3-bis(hydroxylamino)-2,3-dimethylbutane reacts with a specially designed aldehyde or its synthetic equivalent with subsequent oxidation of 1,3-dihydroxyimidazolidine into nitroxide. In view of some essential limitations of this method such as inaccessibility of the aldehyde, an alternative synthetic approach is modification of the substituent itself in the structure of the nitroxide. Using this approach, we have developed syntheses of new compounds – 4,4,5,5-tetramethyl-4,5-dihydro-1*H*-imidazole-3-oxide-1-oxyl-2-carboxylic (**8**) and 4,4,5,5-tetramethyl-1-oxyl-4,5-dihydro-1*H*-imidazole-2-carboxylic (**9**) acid amides using 4,4,5,5-tetramethyl-3-oxide-1-oxyl-4,

* Corresponding author. Tel.: +7-3832-331945; fax: +7-3832-331399.
E-mail address: ovchar@tomo.nsc.ru (V.I. Ovcharenko).

0277-5387/$ - see front matter © 2003 Elsevier Ltd. All rights reserved.
doi:10.1016/j.poly.2003.11.054

5-dihydro-1*H*-imidazole-2-carbonitrile (**1**) as a substrate. Spin-labelled amides **8** and **9** were subsequently employed in syntheses of heterospin complexes based on metal hexafluoroacetylacetonates. Crystallization of these complexes from solution leads to specific bi- or tetranuclear multispin molecules whose synthesis, structure and magnetic properties are discussed in the present paper.

2. Experimental

2.1. Materials and instruments

The reactions were monitored by TLC on Silica gel 60 F_{254} aluminum sheets (Merck). IR spectra were recorded for KBr pellets on a Vector 22 (Bruker) spectrometer. 2-Bromo-4,4,5,5-tetramethyl-4,5-dihydro-1*H*-imidazole-3-oxide-1-oxyl (**3**) was prepared by the procedure described in [8] except that the bromo derivative was recrystallized from ethyl acetate containing ~5% Et_3N. $M(hfac)_2 \cdot nH_2O$, where M = Cu [9], Mn [10], Co [10], was prepared by known procedures. Prior to its use in the synthesis, $Cu(hfac)_2$ was purified by sublimation. All reagents and organic solvents were analytical quality and used as purchased. All solvents were removed at reduced pressures.

2.2. Syntheses of nitroxides

2.2.1. 4,4,5,5-Tetramethyl-3-oxide-1-oxyl-4,5-dihydro-1H-imidazole-2-carbonitrile (*1*)

A mixture of **3** (1.20 g, 5.08 mmol) and Et_3N (0.3 ml) in DMF (7 ml) was stirred in an argon atmosphere for 20 min. Then NaCN (1.0 g, 20 mmol) was added, and the flask was immediately placed on a water bath at ~60 °C. The reaction mixture was stirred for 40 min, diluted with $CHCl_3$ (20 ml) and filtered on a glass filter funnel (porosity 1, ∅ 60 mm) at a pressure of ~300–400 Torr. The filtrate was diluted with benzene (20 ml) and hexane (20 ml) and kept overnight in a refrigerator at ~0 °C. The resulting precipitate was filtered off and recrystallized with filtration from THF (20 ml) to give 0.40 g (43%) of **1** [11].

The filtrates were combined; the solvents were removed on a water bath at a temperature not higher than 60 °C. The residue was dissolved with heating in benzene (15 ml) and chromatographed on a SiO_2 column (1.5 × 22 cm, the product eluted with benzene). The orange fraction was collected, the solvent removed, and the residue recrystallized from hexane to give 0.13 g (15%) of **4**. The greenish-blue fraction additionally gave 0.16 g (18%) of **1**.

2.2.2. 4,4,5,5-Tetramethyl-1-oxyl-4,5-dihydro-1H-imidazole-2-carbonitrile (*4*)

A mixture of **1** (0.50 g, 2.75 mmol), $NaNO_2$ (0.50 g, 7.25 mmol), AcOH (0.8 ml), H_2O (0.8 ml) and $CHCl_3$ (15 ml) was stirred at 40–50 °C for 2 h. The mixture was filtered through an Al_2O_3 column (1.5 × 10 cm); the column was washed with $CHCl_3$. The solvent was removed, and the residue recrystallized from hexane to give 0.35 g (77%) of **4** [6], $\mu_{eff}/\beta = 1.73$ (295 K).

2.2.3. 4,4,5,5-Tetramethyl-4,5-dihydro-1H-imidazole-3-oxide-1-oxyl-2-carboxylic acid amide (*8*)

A mixture of nitrile **1** (50 mg, 0.27 mmol), Et_3N (0.1 ml) and water (2 ml) was stirred for 1 h at room temperature and poured to $CHCl_3$ (30 ml). The resulting mixture was dried with Na_2SO_4 and chromatographed on a SiO_2 column (1.5 × 10 cm, by-products eluted with $CHCl_3$; the product eluted with AcOEt). The solvent was distilled off, the residue was ground with petroleum ether, the solvent was decanted, and the resulting crystals were dissolved in CH_2Cl_2 (2 ml). Then *n*-heptane (2 ml) was added carefully, and the mixture was kept in an open flask at 25 °C to give blue-violet crystals suitable for an X-ray investigation. Yield: 29 mg (53%); m.p. 166–167 °C with decomp. IR (KBr, ν/cm^{-1}): 575, 656, 866, 1140, 1171, 1224, 1308, 1376, 1415, 1460, 1591, 1704, 2989, 3218, 3328. Calc. for $C_8H_{14}N_3O_3$: C, 48.0; H, 7.1; N, 21.0. Found: C, 47.9; H, 7.0; N, 21.0%.

2.2.4. 4,4,5,5-Tetramethyl-1-oxyl-4,5-dihydro-1H-imidazole-2-carboxylic acid amide (*9*)

Procedure 1. A mixture of nitrile **4** (85 mg, 0.51 mmol), Et_3N (0.05 ml) and water (2 ml) was stirred for 6 h at room temperature. The solvent was distilled off and the residue was dissolved in $CHCl_3$ (15 ml). The resulting solution was dried with Na_2SO_4 and chromatographed on a SiO_2 column (1.5 × 5 cm, the product eluted with AcOEt). Then the product was purified as described for **8**. Yield: 52 mg (55%); m.p. 100–101 °C. IR (KBr, ν/cm^{-1}): 580, 651, 816, 883, 957, 1131, 1231, 1371, 1427, 1447, 1587, 1690, 1722, 2986, 3145, 3395. Calc. for $C_8H_{14}N_3O_2$: C, 52.2; H, 7.7; N, 22.8. Found: C, 52.3; H, 7.9; N, 22.9%.

Procedure 2. A mixture of **8** (0.10 mg, 0.50 mmol) and $NaNO_2$ (40 mg, 0.58 mmol) in DMF (3 ml) was stirred at 40–50 °C for 2.5 h. The solvent was distilled off, and the residue extracted with hot hexane (3 × 5 ml). The solution was concentrated to 5 ml and cooled to give 36 mg (39%) of **9**.

2.3. Syntheses of complexes

2.3.1. [Cu(hfac)$_2$*8*] (*10*)

Hexane (10 ml) was added to a solution of $Cu(hfac)_2$ (45 mg, 1 mmol) and **8** (20 mg, 1 mmol) in CH_2Cl_2 (2 ml). The reaction mixture was kept for 1 day in an open flask at room temperature. The perfect red-green dichroic crystals were filtered off, washed with cold hexane, and air dried. Yield: 45 mg (66%). IR (KBr, ν/cm^{-1}): 546, 592, 621, 677, 803, 1087, 1143, 1206, 1258,

1326, 1374, 1403, 1472, 1530, 1552, 1603, 1645, 1699, 3175, 3325. Calc. for $C_{18}H_{16}N_3CuF_{12}O_7$: C, 31.9; H, 2.4; N, 6.2. Found: C, 31.7; H, 2.2; N, 6.0%.

2.3.2. *[Mn(hfac)$_2$**8**] (**11**)*

Hexane (10 ml) was added to a solution of $Mn(hfac)_2 \cdot 2H_2O$ (50.5 mg, 1 mmol) and **8** (20 mg, 1 mmol) in CH_2Cl_2 (2 ml). The reaction mixture was kept for 1 day in a refrigerator. The perfect red-brown crystals were filtered off, washed with cold hexane, and air dried. Yield: 48 mg (74%). IR (KBr, ν/cm^{-1}): 584, 629, 666, 741, 799, 1145, 1210, 1258, 1379, 1397, 1418, 1498, 1532, 1557, 1595, 1648, 1697, 3249, 3295, 3400. Calc. for $C_{18}H_{16}N_3F_{12}MnO_7$: C, 32.3, H,2.4; N, 6.3. Found: C, 32.1; H, 2.7; N, 6.2%.

2.3.3. *[Cu(hfac)$_2$**9**] · C$_6$H$_6$ (**12a**); [Cu(hfac)$_2$**9**] · C$_6$H$_5$CH$_3$ (**12b**)*

Heptane (15 ml) was added to a solution of $Cu(hfac)_2$ (45 mg, 1 mmol) and **9** (20 mg, 1 mmol) in CH_2Cl_2 (5 ml). The reaction mixture was kept for 1 day in an open flask at room temperature. The yellow-brown fine powder precipitate was filtered off, washed with cold heptane, and air dried. According to elemental analysis data, the product had the formula *[Cu(hfac)$_2$**9**]*. Calc. for $C_{18}H_{16}N_3CuF_{12}O_6$: C, 32.7; H, 2.4; N, 6.4. Found: C, 33.1; H, 2.5; N, 6.1%. Yield: 40 mg (62%). Recrystallization from benzene or toluene gave unstable (after separation from the mother solution) solvate single crystals **12a** and **12b** suitable for an X-ray diffraction study. The crystals of *[Cu(hfac)$_2$**9**]* (**12c**) containing no solvate molecules were prepared as follows. A mixture of solid $Cu(hfac)_2$ (45 mg, 1 mmol) and **9** (20 mg, 1 mmol) was dissolved in ethyl acetate (15 ml); the resulting solution was filtered, and the mother solution was kept for five days in an open flask at room temperature. The light brown crystalline precipitate was filtered off, washed with cold heptane, and air dried. Yield: 48 mg (74%). IR (KBr, ν/cm^{-1}): 591, 671, 744, 767, 799, 1091, 1146, 1203, 1258, 1379, 1415, 1457, 1494, 1530, 1557, 1606, 1645, 1712, 3231, 3383. Calc. for $C_{18}H_{16}N_3CuF_{12}O_6$: C, 32.7; H, 2.4; N, 6.4. Found: C, 32.2; H, 2.3; N, 6.1%.

2.3.4. *[Mn(hfac)$_2$**9**] · C$_6$H$_6$ (**13**)*

A mixture of $Mn(hfac)_2 \cdot 2H_2O$ (50.5 mg, 1 mmol) and **9** (20 mg, 1 mmol) was dissolved in benzene (10 ml) and kept for five days in a refrigerator. The brown crystalline precipitate was filtered off and washed with cold hexane. Yield: 55 mg (78%). For an X-ray study, crystals **13** were immediately sealed, because they lost crystallization benzene molecules faster than **12a**. Magnetic measurements were also fulfilled for freshly prepared samples of **13**. Before elemental analysis, compound **13**, which is unstable under normal conditions, was desolvated by thermal storage at 50 °C in a vacuum chamber for 6 h until constant weight. Calc. for $C_{18}H_{16}MnF_{12}N_3O_6$: C, 33.1; H, 2.5; N, 6.4. Found: C, 33.4; H, 2.3; N, 6.1%.

2.3.5. *[Co(hfac)$_2$**9**] (**14**)*

Heptane (15 ml) was added to a solution of $Co(hfac)_2 \cdot 2H_2O$ (51 mg, 1 mmol) and **9** (20 mg, 1 mmol) in CH_2Cl_2 (5 ml). The reaction mixture was kept

Table 1
Crystal data and details of experiment for nitroxides **4**, **8**, **9**

Compound	**4**	**8**	**9**
Formula	$C_8H_{12}N_3O$	$C_8H_{14}N_3O_3$	$C_8H_{14}N_3O_2$
FW	166.21	200.22	184.22
Crystal system	tetragonal	orthorhombic	monoclinic
Space group	$P\bar{4}2_1m$	$Pna2_1$	Cc
a (Å)	7.415(5)	13.604(3)	9.206(2)
b (Å)	7.415(5)	11.310(2)	11.125(2)
c (Å)	8.718(5)	6.6130(1) Å	10.091(2)
β (°)			97.327(4)
V (Å^3)	479.3(5)	1017.5(4)	1025.1(3)
Z	2	4	4
d_{calc} (g cm^{-3})	1.152	1.307	1.194
μ(Mo Kα) (cm^{-1})	0.08	1.01	0.88
θ range (°)	$3.89 < \theta < 22.47$	$2.34 < \theta < 25.00$	$2.89 < \theta < 23.24$
I_{hkl} collected/unique	389/218	980/980	2170/1284
R_{int}	0.0445	0.0000	0.1012
Data/N	218/53	980/184	1284/175
Goodness-of-fit	1.148	0.990	0.774
R_1 for $I > 2\sigma_I$	0.0566	0.0447	0.0479
wR_2	0.1572	0.1173	0.0942
R_1 for all data	0.0760	0.0675	0.0851
wR_2	0.1715	0.1436	0.1121

Table 2
Crystal data and details of experiment for complexes **10**–**14**

Compound	**10**	**11**	**12a**	**12b**	**12c**	**13**	**14**
Formula	$C_{18}H_{16}CuF_{12}N_3O_7$	$C_{18}H_{16}MnF_{12}N_3O_7$	$C_{24}H_{22}CuF_{12}N_3O_6$	$C_{25}H_{24}CuF_{12}N_3O_6$	$C_{18}H_{16}CuF_{12}N_3O_6$	$C_{24}H_{22}F_{12}MnN_3O_6$	$C_{18}H_{16}CoF_{12}N_3O_6$
FW	677.88	669.28	739.99	754.01	661.88	731.39	657.27
Crystal system	monoclinic	triclinic	triclinic	triclinic	triclinic	triclinic	triclinic
Space group	$P2_1/c$	$P\bar{1}$	$P\bar{1}$	$P\bar{1}$	$P\bar{1}$	$P\bar{1}$	$P\bar{1}$
a (Å)	11.467(1)	10.541(1)	10.0197(9)	10.085(1)	16.113(1)	10.162(1)	9.748(1)
b (Å)	13.256(1)	10.669(1)	12.567(1)	12.995(2)	16.496(1)	13.158(1)	10.656(1)
c (Å)	17.440(1)	12.684(1)	14.199(1)	14.523(2)	23.052(2)	14.517(1)	13.093(2)
α (°)		108.10(1)	113.121(2)	66.349(2)	76.256(1)	113.698(2)	113.035(2)
β (°)	98.92(1)	90.87(1)	91.901(2)	89.965(2)	77.456(2)	91.856(2)	90.366(3)
γ (°)		104.27(1)	111.345(2)	67.615(2)	64.980(2)	111.325(2)	99.953(3)
V (Å^3)	2618.9(3)	1307.5(2)	1498.8(2)	1585.8(3)	5345.7(7)	1619.0(1)	1228.5(3)
Z	4	2	2	2	8	2	2
d_{calc} (g cm^{-3})	1.719	1.700	1.640	1.579	1.645	1.500	1.777
μ(Mo Kα) (cm^{-1})	9.62	6.33	8.46	8.01	9.83	5.17	8.30
θ range (°)	$1.80 < \theta < 25.00$	$2.00 < \theta < 25.00$	$2.23 < \theta < 23.27$	$1.85 < \theta < 23.30$	$1.56 < \theta < 23.36$	$1.82 < \theta < 23.34$	$2.12 < \theta < 23.29$
I_{hkl} collected/unique	4107/3862	4739/4468	6518/4263	6950/4545	23 437/15 358	6996/4615	5328/3477
R_{int}	0.0280	0.0242	0.1392	0.0496	0.0626	0.1047	0.0692
Data/N	3862/543	4468/543	4263/492	4545/494	15 358/1842	4615/420	3477/426
Goodness-of-fit	0.905	0.893	0.717	0.808	0.870	0.759	0.796
R_1 for $I > 2\sigma_I$	0.0429	0.0542	0.0741	0.0534	0.0590	0.0697	0.0598
wR_2	0.1176	0.1447	0.1598	0.1198	0.1422	0.1383	0.1179
R_1 for all data	0.0648	0.0841	0.1699	0.0986	0.0937	0.2151	0.1227
wR_2	0.1350	0.1700	0.2067	0.1376	0.1605	0.1805	0.1424

for a week in an open flask at room temperature. The dark red crystalline precipitate was filtered off, washed with cold heptane, and air dried. Yield: 52 mg (73%). IR (KBr, ν/cm^{-1}): 586, 605, 625, 670, 798, 1101, 1146, 1210, 1261, 1377, 1397, 1462, 1481, 1531, 1558, 1593, 1640, 1704, 3310, 3414. Calc. for $C_{18}H_{16}N_3CoF_{12}O_6$: C, 32.9; H, 2.5; N, 6.4. Found: C, 32.9; H, 2.2; N, 5.9%.

2.4. X-ray structure determination

For **8**, **10**, **11** (P4 Bruker AXS) and **4**, **9**, **12**–**15** (Smart APEX Bruker AXS), data were collected on an automatic diffractometer. The structures were solved by direct methods and refined by the full-matrix least-squares technique on F^2 in an anisotropic approximation for all non-hydrogen atoms. Hydrogen atoms were located from the difference Fourier maps and refined in an isotropic approximation. All calculations were performed using SHELX 97 on an IBM PC AT (Tables 1 and 2).

2.5. Magnetic measurements

All measurements were carried out on an MPMS-5S (''Quantum Design'') SQUID magnetometer at temperatures from 2 to 300 K in an external magnetic field of up to 5 kOe. The molar magnetic susceptibility (χ) of the compounds was calculated using Pascal's additive scheme including diamagnetic corrections and temperature-independent paramagnetism of Cu(II) ions taken to be 60×10^{-6} cm^3/mol. The effective magnetic moment was determined by the formula $\mu_{\text{eff}} = [(3k/N_A\beta^2)\chi T]^{1/2} \approx (8\chi T)^{1/2}$, where k is Boltzmann's constant, N_A is the Avogadro number and β is the Bohr magneton.

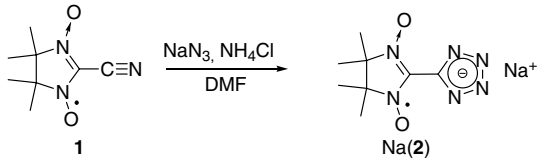

Scheme 1.

3. Results and discussion

3.1. Synthesis of spin-labelled nitriles

As stated in the Introduction, the increasingly wide use of multifunctional nitronyl and imino nitroxides has stimulated the development of new synthetic approaches. One of these is modification of a substituent in the structure of nitroxide not affecting the free valence. This approach was reported in [8,12]. We have concentrated on the nitrile derivative **1**, because the presence of a –C≡N group opens up an opportunity of nitroxide multifunctionalization in the vicinity of the radical fragment. Thus, recently, we have reported on the synthesis of a new spin-labelled Na(**2**) tetrazole (Scheme 1) and highly dimensional heterospin complexes with this ligand [13], obtained by using **1** as a starting compound.

Compound **1** was first described by Boocock and Ullman [14]; it was noted that the nitroxide is highly reactive. Details of this synthesis were not discussed [14]. A recently suggested procedure for the synthesis of **1** [11] affords this compound in sufficient quantities for further experiments, but is very sensitive to the purity of the bromine-substituted precursor **3**, and also to the reaction temperature and time (Scheme 2). This limitation precludes the use of **1** as a synthon for planning retro syntheses of many new chelate-forming nitronyl and imino nitroxides possessing favorable structures for the preparation of highly dimensional heterospin systems.

Attempts to synthesize **1** face the following difficulty. The reaction of **3** with NaCN in DMF forms a mixture of products among which we identified (by TLC and comparison with authentic samples) nitroxides **1**, **4**, **5**, **6** and zwitterion **7** (Scheme 2). When the reaction is carried out at temperatures above or below the optimal temperature (~65 °C), **7** is the major reaction product. We have found that introduction of Et_3N in the reaction system stabilizes **3**, decreasing the number of by-products. In the presence of Et_3N, **7** is not formed at all. The reaction of **3** with NaCN in DMF in the presence of Et_3N occurs smoothly and does not demand careful preliminary purification of **3**, which is rather labile. The synthetic procedure suggested above in the

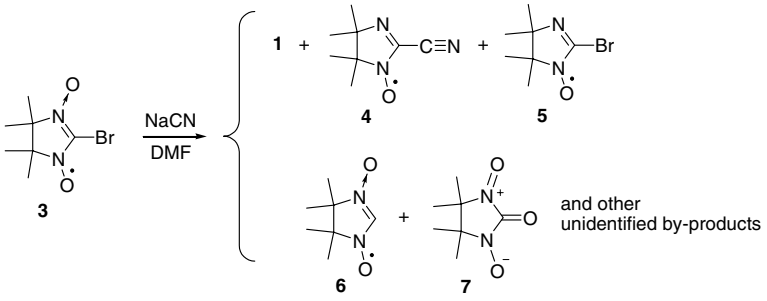

Scheme 2.

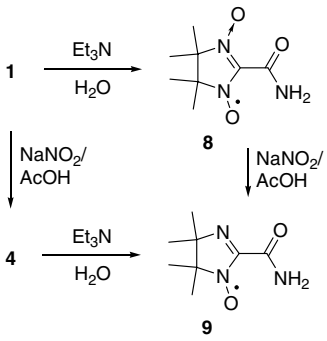

Scheme 3.

Experimental section simultaneously affords **1** and **4** with yields of the order of 60% and 15%, respectively. Imino nitroxide **4** may be obtained in a high yield (~75%) by reduction of **1** with $NaNO_2$ (Scheme 3).

Structure **1** was described previously [11,15]. An X-ray diffraction study of **4** indicated that the crystal structure of nitroxide **4** is identical to that of **1**. The molecule also has 2mm symmetry suggestive of a planar structure of the imidazoline ring (Fig. 1), and the oxygen atom is also disordered over two positions with weight 0.5. The N–O and C–N distances in the cycle are typical for nitronyl nitroxides (Table 3).

3.2. Syntheses and structures of spin-labelled amides and their complexes

Among the numerous derivatives of imino and nitronyl nitroxides actively employed in design of molecular magnets, amide derivatives **8** and **9** are new compounds. They were synthesized by base-catalyzed hydration of the corresponding nitriles **1** and **4**. Compound **9** may also be prepared by reduction of nitronyl nitroxide **8** (Scheme 3). In contrast to the corresponding acids, amides **8** and **9** are stable under normal conditions. They were isolated as high-quality crystals, whose crystal and molecular structure was completely solved.

Solid compounds **8** and **9** have a polymer chain structure formed from bifurcated intermolecular hydrogen bonds between the amide H atom of one nitroxide molecule and the N–O and amide O atoms (for **8**) or the amide H atoms and the imine N atom (for **9**) of a neighboring nitroxide molecule (Figs. 2 and 3). The other H atom of the amide group forms an intramolecular hydrogen bond with the O atom of the N–O group. All atoms of the nitronyl or imino nitroxide fragments are nearly coplanar with the atoms of the $-C(O)NH_2$ fragments. Selected bond lengths for **8** and **9**, as well as hydrogen bond parameters, are listed in Tables 3 and 4.

All heterospin complexes **10**–**15** were prepared by reaction between the appropriate metal hexafluoroacetylacetonates and **8** or **9**, in which the ratio $M(hfac)_2 \cdot nH_2O$/paramagnetic ligand is 1:1. Compounds **10**, **11** and **14** were isolated as perfect $M(hfac)_2L$ crystals when the reaction was fulfilled in a hexane (or heptane)/CH_2Cl_2 mixture. Under similar conditions, complex **12c** formed as a finely disperse powder. The crystals of this compound suitable for an X-ray diffraction study were obtained by recrystallization of the complex from benzene and toluene in the form of the corresponding solvates **12a** and **12b**. Desolvation of **12a** gave a powder whose IR spectra and magnetic properties were identical to those of **12c** prepared as single crystals in the reaction of $Cu(hfac)_2$ with **9** in ethyl acetate. A crystalline complex of $Mn(hfac)_2$ with **9** could only be isolated in the form of a solvate with benzene (**13**).

All solid complexes except **12c** are packings of centrosymmetric dimer molecules formed by hydrogen bonding between the atoms of the two amide groups (Figs. 4 and 5). The structure of **8** and **9** (Figs. 2(a) and 3(a)) does not change on complexation except that the angle between the planes of the CN_2 fragment of the

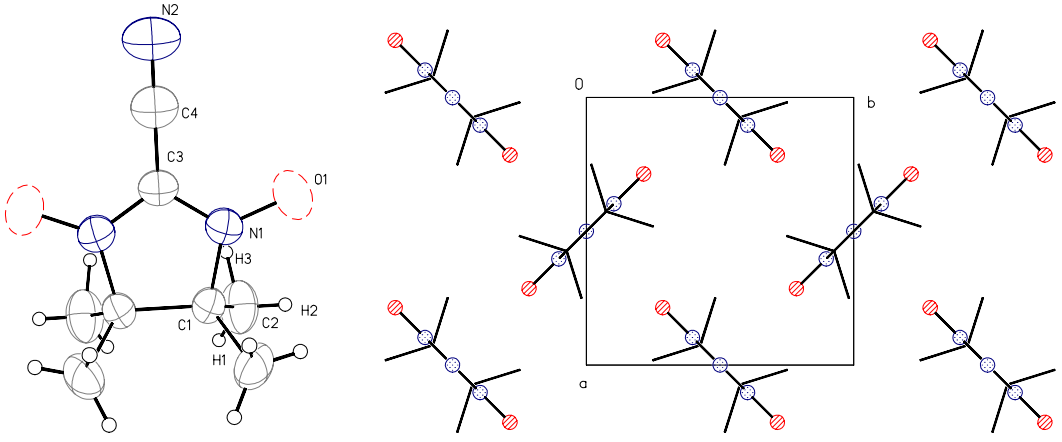

Fig. 1. General view of **4** and a layer in the crystal structure of **4** projected on the (0 0 1) plane.

Table 3
Selected bond lengths (Å) and angles (°)

	4	8	9	10	11	12a	12b	12c	13	14
Bond lengths										
M–O_{hfac}				1.932(3)–1.956(3) 2.248(4)	2.115(2)–2.158(2)	1.966(4)–1.984(4) 2.210(5)	1.949(3)–1.966(4) 2.201(4)	1.921(4)–1.996(4) 2.215(4)–2.256(4)	2.095(4)–2.139(4)	2.035(5)–2.080(5)
M–O(01)				1.973(3)	2.181(2)					
M–O(03)				2.416(3)	2.170(3)	2.371(5)	2.376(3)	2.390(5)–2.482(4)	2.214(3)	2.120(4)
M–N(1)						2.041(5)	2.021(4)	2.020(4)–2.047(4)	2.224(4)	2.131(5)
N(1)–O(01)	1.266(3)	1.271(4)		1.287(4)	1.280(3)					
N(2)–O(02)		1.294(5)	1.277(6)	1.269(4)	1.268(4)	1.273(7)	1.262(5)	1. 255(6)–1.268(6)	1.263(5)	1.264(6)
N(1)–C(07)	1.313(3)	1.351(6)	1.263(6)	1.331(5)	1.341(4)	1.284(8)	1. 275(5)	1.272(6)–1.285(7)	1.272(6)	1.273(7)
N(2)–C(07)		1.345(5)	1.374(7)	1.345(6)	1.343(4)	1.387(9)	1.368(6)	1. 344(6)–1.389(7)	1.361(6)	1.371(7)
C(07)–C(08)	1.385(5)	1.488(7)	1.511(7)	1.489(5)	1.491(4)	1.500(8)	1. 508(6)	1.491(8)–1.513(9)	1.497(5)	1.497(8)
C(08)–O(03)		1.227(5)	1.222(6)	1.223(5)	1.230(4)	1.220(8)	1.207(5)	1. 214(6)–1.229(9)	1.228(6)	1.226(7)
C(08)–N(3)		1.319(7)	1.319(6)	1.304(6)	1.299(5)	1.322(9)	1.313(6)	1.288(9)–1.314(8)	1.302(6)	1.286(9)
Bond angles										
N(1)–O(01)–M				119.4(2)	124.4(2)					

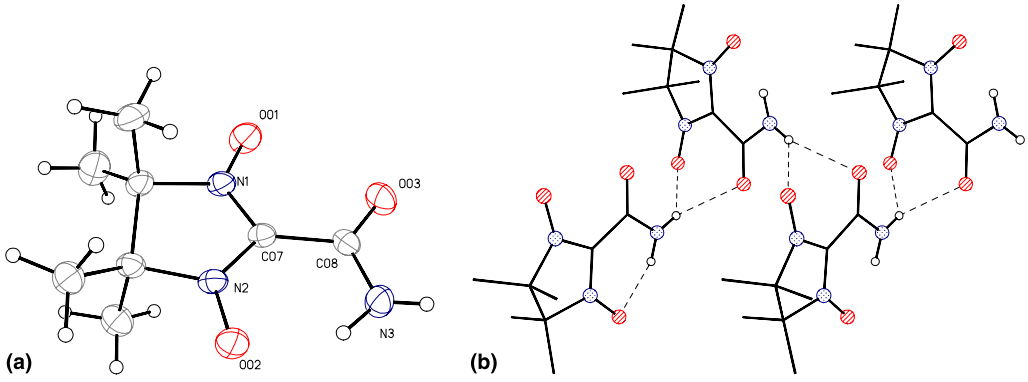

Fig. 2. General view (a) and chain (b) of **8**.

imidazoline ring and the amide group slightly increases, reaching 12° in **10**. The coordination number of the central atom is 6. In complexes with **8**, the CuO_6 coordination unit is formed from four O atoms of the cis-coordinated hfac anions and the O atoms of the amide group and the N–O fragment of the paramagnetic ligand. In complexes with **9**, the CuO_5N coordination unit involves the imine N atom of the heterocycle. The chelate rings in **10** and **11** are nonplanar and folded along the $O_{NO}\ldots O_{amide}$ line at an angle of 40.0° in **10**. The angle between the planes of the amide group and the NCN fragment of the imidazoline ring is up to 5.5° in **11**–**14** and 12° in **10**. In the Cu complexes, the coordinated octahedron is tetragonally distorted. The axial Cu–O_{hfac} distances are 2.210–2.257, and the Cu–O_{amide} distances are 2.371–2.482 Å. The equatorial Cu–O_{hfac} distances equal 1.921–1.996, Cu–O_{NO} = 1.973 and Cu–N = 2.022–2.046 Å. In Mn(II) and Co(II) complexes **13** and **14**, respectively, the coordination polyhedra of the metal atoms are isometric. Note, however, that the Mn–O and Mn–N bonds to the donor atoms of the paramagnetic ligand in **13** are longer than those in **11**. Selected bond lengths and hydrogen bond parameters are given in Tables 3 and 4.

The structure of solid **12c** is slightly different from the structure of all other complexes. As in other complexes, $\{Cu(hfac)_2\mathbf{9}\}_4$ tetramer molecules (Fig. 6) are formed with the aid of the bridging N–H…O

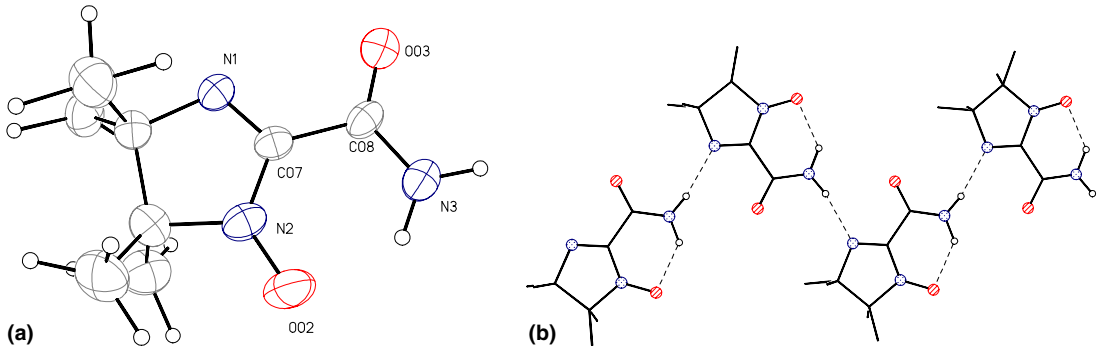

Fig. 3. General view (a) and chain (b) of **9**.

Table 4
Hydrogen bond parameters

Compound	N–H…O or N–H…N	*d*(N–H)	*d*(H…O) or *d*(H…N)	*d*(N…O) or *d*(N…N)	∠NHO or ∠NHN
8	N(3)–H…O(02)	0.88(6)	1.91(6)	2.688(6)	146(5)
	N(3)–H…O(03′)	0.80(8)	2.21(9)	2.949(7)	153(7)
	N(3)–H…O(01′)	0.80(8)	2.52(7)	3.120(6)	134(7)
9	N(3)–H…N(2′)	0.94(7)	2.08(7)	3.010(7)	167(6)
	N(3)–H…O(2′)	0.94(7)	2.61(8)	3.185(6)	120(5)
	N(3)–H…O(1)	1.00(6)	1.96(5)	2.756(8)	135(5)
10	N(3)–H…O(03′)	0.77(5)	2.16(5)	2.924(5)	171(5)
	N(3)–H…O(02)	0.87(5)	2.07(5)	2.699(6)	128(4)
11	N(3)–H…O(3′)	0.79(4)	2.16(4)	2.940(4)	170(4)
	N(3)–H…O(02)	0.81(3)	2.08(4)	2.719(4)	135(4)
12a	N(3)–H…O(03′)	0.83(5)	2.07(5)	2.899(7)	178(6)
	N(3)–H…O(02)	0.73(5)	2.26(4)	2.779(7)	129(5)
12b	N(3)–H…O(02)	0.75	2.08	2.753(7)	150.4
	N(3)–H…O(03′)	0.71(4)	2.24(4)	2.941(6)	166(5)
12c	N(3a)–H…O(03d)	0.70(11)	2.17(11)	2.851(9)	167(11)
	N(3a)–H…O(02a)	0.81(8)	2.21(8)	2.775(11)	127(6)
	N(3b)–H…O(03a)	0.73(8)	2.13(8)	2.862(10)	175(7)
	N(3b)–H…O(02b)	0.90(8)	2.01(8)	2.739(11)	137(7)
	N(3c)–H…O(03b)	0.82(7)	2.18(7)	2.995(7)	176(6)
	N(3c)–H…O(02c)	0.69(7)	2.18(7)	2.778(9)	146(7)
	N(3d)–H…O(03c)	0.75(7)	2.18(7)	2.923(8)	169(6)
	N(3d)–H…O(02d)	0.85(7)	2.23(7)	2.782(9)	122(6)
13	N(3)–H…O(03′)	0.86	2.18	3.004(5)	160.4
	N(3)–H…O(02)	0.86	2.09	2.758(5)	134.3
14	N(3)–H…O(4′)	0.69(6)	2.45(7)	3.106(9)	160(8)
	N(3)–H…O(03′)	0.69(6)	2.65(7)	3.091(9)	125(7)
	N(3)–H…O(02)	0.82(5)	2.23(5)	2.796(10)	126(5)

intermolecular hydrogen bonds. The difference lies in the fact that in **12c** the NH_2 fragment of the amide group of one $Cu(hfac)_2$**9** molecule is bonded to the O_{amide} atom of another molecule, and NH_{amide} of the latter is bonded to O_{amide} of the third molecule, etc., thus linking four crystallographically independent molecules into a cycle. The coordination polyhedra inside the {$Cu(hfac)_2$**9**} fragments do not differ in structure between **12c** and **12a** (or **12b**). Note that a heterospin tetramer complex could only be obtained for the Cu(II) complex by crystallization from ethyl acetate. For other $M(hfac)_2$ complexes, slow removal of ethyl acetate from the reaction mixture led to a viscous mass solidifying into lacquer-film.

3.3. Magnetic properties of the compounds

In the temperature range 20–300 K, μ_{eff} is the same for radicals **8** and **9** and close to 1.73β. Below 20 K, $\mu_{eff}(T)$ gradually decreases in magnitude for **8** and **9**,

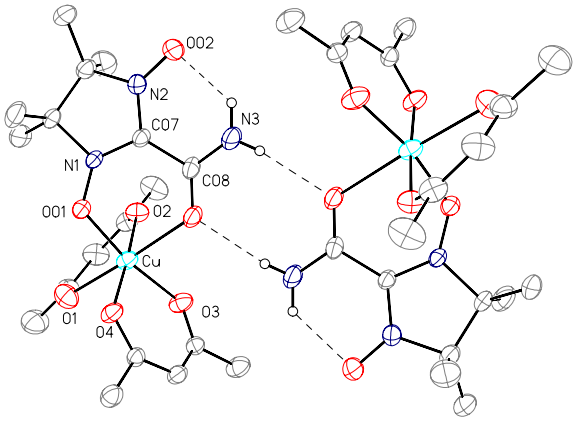

Fig. 4. General view of dimer molecule **10**. Centrosymmetric dimer **11** has a similar structure.

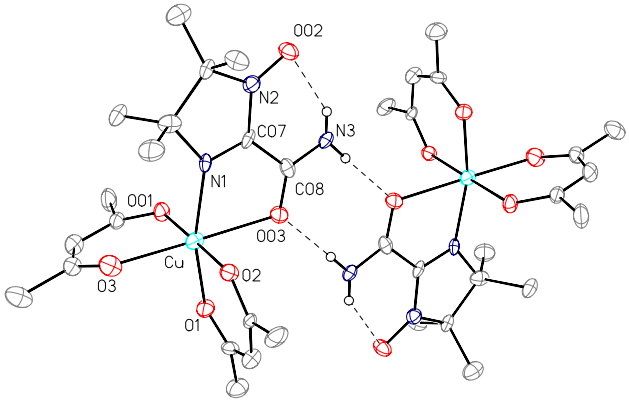

Fig. 5. General view of dimer molecule **12a**. Dimer molecules **12b**, **13**, and **14** have a similar structure.

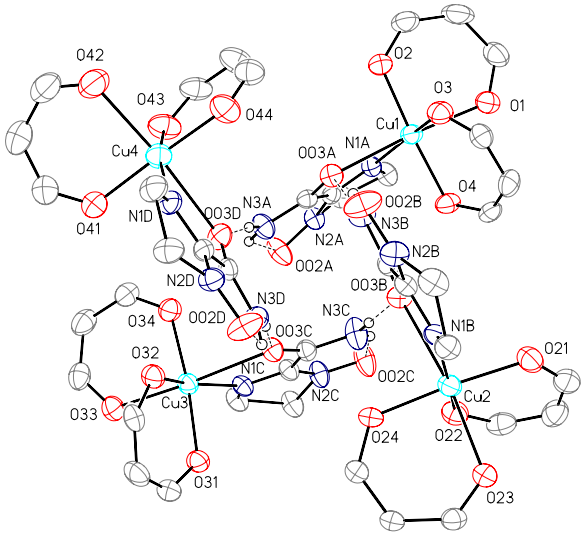

Fig. 6. General view of $[Cu(hfac)_2\mathbf{9}]_4$ tetramer molecule (**12c**).

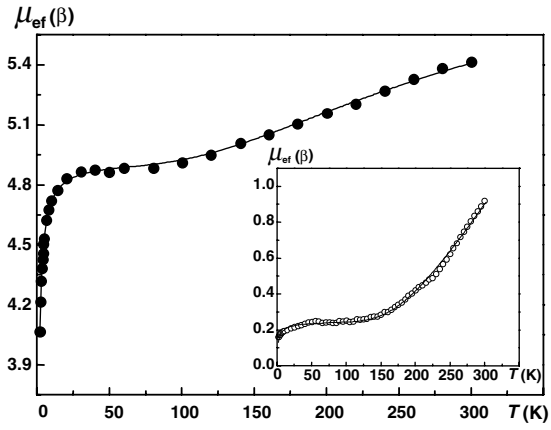

Fig. 7. Dependences $\mu_{eff}(T)$ for **10** (○) and **11** (●).

indicating that the solid nitroxides have only weak antiferromagnetic intermolecular exchange interactions.

The dependences $\mu_{eff}(T)$ for the complexes are presented in Figs. 7 and 8.

The magnetic behavior of complexes **10**, **11** and **13** (Figs. 7 and 8) suggests full spin coupling between the metal and the coordinated radical at temperatures of the order of 120 K due to strong antiferromagnetic exchange interactions. In the region of the plateau, the value of μ_{eff} for **11** and **13** is close to the theoretical value 4.9β for the residual spin $s = 2$ with g-factor 2. In **14**, μ_{eff} increases oppositely with temperature (Fig. 8), indicating that ferromagnetic exchange interactions between the spins of Co(II) and the radical inside the bischelate fragments are dominant.

At 300 K for **12c**, μ_{eff} is 2.85β, which is close to the theoretical value 2.83β for $s = 1$. That is, due to the strong ferromagnetic interaction of spins inside the molecular exchange cluster, the triplet state is the occupied ground state even at room temperature. The decrease in μ_{eff} with temperature, as well as the maximum at 20 K on the $\chi(T)$ curve, point to negative exchange interactions between $\{Cu(hfac)_2\mathbf{9}\}$ exchange clusters in solid **12c**.

For **10**, **11** and **13**, theoretical treatment of experimental data was fulfilled using the isotropic spin Hamiltonian in the framework of an approach suggested earlier [16]. For approximation, we employed two-center exchange clusters. The resulting optimal parameters: the effective g-factor of the metal (g_M), exchange interaction energies (J) inside the exchange cluster and intermolecular interaction energies (nJ') of the complexes are presented in Table 5. The calculated curves are shown as solid lines in Figs. 7 and 8. As is known, antiferromagnetic exchange interactions dominate in the {M–O·–N<} exchange cluster of paramagnetic metal complexes with coordinated nitronyl nitroxides, whereas ferromagnetic exchange interactions prevail in the {M–N=C–N–·O} exchange clusters of complexes with imino nitroxides [17]. The data obtained for **10**–**14** follow this general tendency. However, it is worthwhile to note that

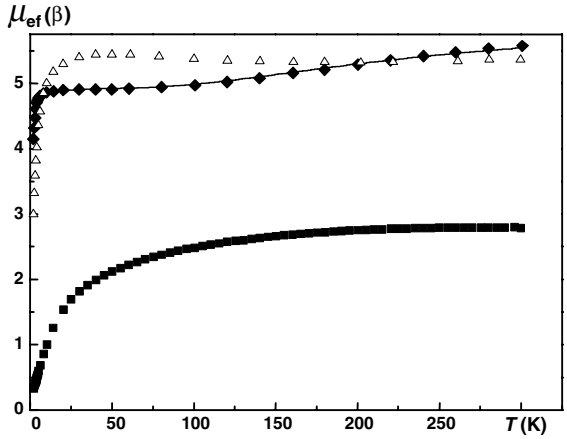

Fig. 8. Dependences $\mu_{eff}(T)$ for **12c** (■), **13** (◆) and **14** (Δ).

Table 5
Exchange parameters for complexes

Compound	g_M	J (cm^{-1})	nJ' (cm^{-1})	σ
10	2.11 ± 0.05	-380 ± 30		0.01428
11	2.008 ± 0.002	-57.2 ± 0.6	-0.15 ± 0.01	0.00016
13	2.02 ± 0.01	-47 ± 2	-0.07 ± 0.01	0.00052

in the {Mn–N=C–N–·O} exchange clusters of complexes with imino nitroxides (**12c**, **13** and **14**), the antiferromagnetic exchange channels are much more effective than those in {Cu–N=C–N–·O} and {Co–N=C–N–·O} clusters.

4. Conclusions

The development of an effective procedure for the synthesis of nitrile **1** has made this compound an easily accessible nitroxide that may be used as a starting compound for syntheses of spin-labelled amides **8** and **9**. Interaction of $M(hfac)_2$ with **8** and **9** affords compounds with $\{M(hfac)_2L\}$ fragments H-bonded into bi- or tetranuclear multispin complexes in the solid state. Exchange interactions in these complexes are concentrated inside the $\{M(hfac)_2L\}$ fragments. In Cu(II) and Mn(II) complexes with nitronyl nitroxide **8**, strong antiferromagnetic exchange interactions take place. In complexes with imino nitroxide **9**, the antiferromagnetic exchange interaction channels in the {Mn–N=C–N–·O} exchange cluster also proved to be much more effective, whereas in {Cu–N=C–N–·O} and {Co–N=C–N–·O} exchange clusters, ferromagnetic exchange interactions prevail.

5. Supplementary material

Crystal data for the structural analysis of investigated compounds have been deposited with the Cambridge Crystallographic Data Centre, CCDC Nos. 217536 (**9**), 217537 (**11**), 217538 (**12a**), 217539 (**12b**), 217540 (**12c**), 217541 (**13**), 217542 (**14**), 217543 (**8**), 217544 (**10**), 217584 (**4**). Copies of this information may be obtained free of charge from The Director, CCDC, 12 Union Road, Cambridge, CB2 1EZ, UK (fax: +44-1233-336033; e-mail: deposit@ccdc.cam.ac.uk or www: http://www.ccdc.cam.ak.uk).

Acknowledgements

The work was supported by RFBR (02-03-33112, 03-03-32518), Minobr (E02-5.0-188), CRDF (NO-008-X1), Integration grants, and young scientists grant of SB RAS.

References

[1] K. Inoue, T. Hayamizu, H. Iwamura, D. Hashizumi, Y. Ohashi, J. Am. Chem. Soc. 118 (1996) 1803.
[2] K. Fegy, D. Luneau, T. Ohm, C. Paulsen, P. Rey, Angew. Chem., Int. Ed. Engl. 37 (1998) 1270.
[3] K. Fegy, N. Sanz, D. Luneau, E. Belorizky, P. Rey, Inorg. Chem. 37 (1998) 4518.
[4] V.I. Ovcharenko, R.Z. Sagdeev, Russ. Chem. Rev. 68 (1999) 345.
[5] A. Caneschi, D. Gatteschi, R. Sessoli, P. Rey, Acc. Chem. Res. 22 (1989) 392.
[6] E.F. Ullman, L. Call, J.H. Osiecki, J. Org. Chem. 35 (1970) 3623.
[7] E.F. Ullman, J.H. Osiecki, D.G.B. Boocock, R. Darcy, J. Am. Chem. Soc. 94 (1972) 7049.
[8] H. Sakurai, A. Izuoka, T. Sugawara, J. Am. Chem. Soc. 122 (2000) 9723.
[9] J.A. Bertrand, R.I. Kaplan, Inorg. Chem. 5 (1966) 489.
[10] F.A. Cotton, R.H. Holm, J. Am. Chem. Soc. 82 (1960) 2979.
[11] O.V. Koreneva, G.V. Romanenko, V.N. Ikorsky, S.V. Fokin, V.I. Ovcharenko, Russ. J. Struct. Chem. 42 (2001) 977.
[12] R. Weiss, N. Kraut, F. Hampel, J. Organomet. Chem. 617–618 (2001) 473.
[13] E.V. Tretyakov, S.V. Fokin, G.V. Romanenko, V.I. Ovcharenko, Polyhedron 22/14–17 (2003) 1965.
[14] D.G.B. Boocock, E.F. Ullman, J. Am. Chem. Soc. 90 (1968) 6873.
[15] C. Hirel, D. Luneau, J. Pécaut, L. Öhrström, G. Bussière, C. Reber, Chem. Eur. J. 8 (2002) 3157.
[16] V.I. Ovcharenko, Y.G. Shvedenkov, R.N. Musin, V.N. Ikorskii, Russ. J. Struct. Chem. 40 (1999) 29.
[17] F. Lanfranc de Panthou, D. Luneau, R. Musin, L. Öhrström, A. Grand, P. Turek, P. Rey, Inorg. Chem. 35 (1996) 3484.

Available online at www.sciencedirect.com
SCIENCE DIRECT®
Polyhedron 23 (2004) 773–777
POLYHEDRON
www.elsevier.com/locate/poly

Hydrothermal synthesis and structure characterization of a Keggin tungstocobaltate $[Co(2,2'\text{-bipy})_3]_2H_2[CoW_{12}O_{40}]\cdot 9.5H_2O$

Jing-Yang Niu *, Zi-Liang Wang, Jing-Ping Wang

Chemistry Department, School of Chemistry and Chemical Engineering, Henan University, Minlun Street, Kaifeng 475001, PR China

Received 24 September 2003; accepted 4 November 2003

Abstract

A Keggin-type tungstocobaltate $[Co(2,2'\text{-bipy})_3]_2H_2[CoW_{12}O_{40}]\cdot 9.5H_2O$ was prepared by the hydrothermal method for the first time and characterized by elemental analyses, IR, UV, EPR spectra, TG-DTA analyses and X-ray single crystal diffraction, showing that the complex consists of a Keggin anion $[CoW_{12}O_{40}]^{6-}$ and two isolated chiral ions $[Co(2,2'\text{-bipy})_2]^{2+}$. The characteristic band of Keggin anion $[CoW_{12}O_{40}]^{6-}$ appears at 298 nm in the UV spectrum. EPR spectra reveal two Co^{2+} coordination environments in the title compound, high spin state ($g = 5.1$, 4.2) and low spin state ($g = 2.0$). Furthermore, when the temperature increases from 110 K to room temperature, the signal $g = 5.1$ of high spin Co^{2+} disappears, caused by the negative zero-field splitting. Thermal analysis indicates that the Keggin anion skeleton begins to decompose at 560.4 °C.
© 2003 Elsevier Ltd. All rights reserved.

Keywords: Polyoxometalates; Hydrothermal synthesis; Crystal structure; Keggin; Cobalt

1. Introduction

Polyoxometalates (POMS), because of having discrete structures of definite sizes, shapes [1] and potential applications in catalysis, medicine, materials science, geochemistry and nuclear waste processing [2–6], have been attracting chemists' interests. As well known, the Keggin POMS continue to have an important place at the forefront of the polyoxometalate field. In recent decades, Keggin polyoxometalates associated with organic donors like ET and TTF construct a series of compounds [7–9] coupling magnetic and conducting properties or with metal coordination cations form a series of novel compounds [10–17]. Among previously reported literature, few of their heteroatoms are transition metals [8,9,13]. Furthermore, most of them are prepared by conventional aqueous solution syntheses. So we attempted to explore hydrothermal routes for preparation of such solid-states materials based on Keggin heteropolyanions using simple reactants, and we succeeded in doing so. This paper describes the hydrothermal synthesis, structure and properties of a new Keggin tungstocobaltate $[Co(2,2'\text{-bipy})_3]_2H_2[CoW_{12}O_{40}]\cdot 9.5H_2O$.

2. Experimental

2.1. Materials and measurements

All chemicals were of reagent grade as received from commercial sources and used without further purification. C, H, N elemental analyses were performed on a Perkin–Elmer 240C elemental analyzer. The infrared spectrum was recorded as a KBr pellet on a Nicolet 170SXFT-IR spectrometer in the range 400–4000 cm^{-1}. The UV spectrum was obtained on a Shimzu UV-250 spectrometer in the range 190–350 nm. The EPR spectrum was recorded with a Bruker ER-2000-DSRC10 spectrometer at the X-band, at a temperature of 300 and 110 K. TG-DTA measurements were performed on a Perkin–Elmer7 thermal analyzer in flowing nitrogen gas with a heating rate of 10 °C/min.

* Corresponding author. Tel.: +86-378-219-2443; fax: +86-378-285-3650.
E-mail address: jyniu@henu.edu.cn (J.-Y. Niu).

0277-5387/$ - see front matter © 2003 Elsevier Ltd. All rights reserved.
doi:10.1016/j.poly.2003.11.050

2.2. Synthesis of $[Co(2,2'\text{-bipy})_3]_2H_2[CoW_{12}O_{40}]\cdot 9.5H_2O$

The title compound was prepared by the hydrothermal method from a mixture of $Na_2WO_4\cdot 2H_2O$ (1.0 g, 3.2 mmol), $CoCl_2\cdot 6H_2O$ (0.076 g, 0.32 mmol), $Co(Ac)_2\cdot 4H_2O$ (0.08 g, 0.32 mmol), 2,2′-bipyridine (0.1 g, 0.64 mmol) and H_2O (15 ml) in the mole ratio 1:0.1:0.1:0.2:260, heated in a Teflon-lined steel autoclave inside a programmable electric furnace at 160 °C for 96 h with a starting pH of 4, adjusted with hydrochloric acid (4 mol/l). After cooling the autoclave to room temperature for 48 h, green crystals were obtained, filtered, washed several times with distilled water and dried in air (yield 25% based on W). *Anal.* Calc. for $C_{60}H_{67}N_{12}O_{49.5}W_{12}Co_3$: C, 17.42; H, 1.62; N, 4.06. Found: C, 17.21; H, 1.66; N, 3.96%.

2.3. X-ray single crystal diffraction analysis

A green single crystal of $[Co(2,2'\text{-bipy})_3]_2H_2[CoW_{12}O_{40}]\cdot 9.5H_2O$ with dimensions $0.26\times 0.23\times 0.11$ mm was used for X-ray work. Data collections were made on a Rigaku RAXIS-IV image plate area detector using graphite mono-chromated Mo Kα diffraction ($\lambda = 0.71073$ Å) at 293(2) K. A total of 13 362 independent reflections ($R_{int} = 0.0562$) were measured in the range of $4.42^\circ \leqslant 2\theta \leqslant 50.00^\circ$ with $-16 \leqslant h \leqslant +17$, $-19 \leqslant k \leqslant +20$, $-22 \leqslant l \leqslant +22$. The intensities were corrected by Lorentz-polarization factors and empirical absorption. The structures were solved by direct methods and refined by a full-matrix least-squares technique based on F^2 using the SHELXTL-97 program [18]. All non-hydrogen atoms were refined anisotropically. Hydrogen atoms were added according to theoretical models. The maximum and minimum peaks on the final difference Fourier map correspond to 2.722 and −3.896 e Å^{-3}, respectively.

The crystallographic data and structure determination parameters for $[Co(2,2'\text{-bipy})_3]_2H_2[CoW_{12}O_{40}]\cdot 9.5H_2O$ are summarized in Table 1. Selected bond distances and angles are given in Table 2.

Table 1
Summary of crystallographic data for $[Co(2,2'\text{-bipy})_3]_2H_2[CoW_{12}O_{40}]\cdot 9.5H_2O$

Molecular formula	$C_{60}H_{67}N_{12}O_{49.5}W_{12}Co_3$
Molecular weight	4131.25
Temperature (K)	293(2)
Wavelength (Å)	0.71073
Colour	green
Crystal system	triclinic
Space group	$P\bar{1}$
a (Å)	14.482(3)
b (Å)	17.520(4)
c (Å)	19.177(4)
α (°)	80.98(3)
β (°)	69.67(3)
γ (°)	71.31(3)
V (Å^3)	4316.2(15)
Z	2
D_{calc} (Mg m^{-3})	3.179
Absorption coefficient (mm^{-1})	16.580
$F(000)$	3752
$R_1,\ wR_2[I > 2\sigma(I)]$	0.0513, 0.1205
$R_1,\ wR_2$ (all data)	0.0771, 0.1270

$w^{-1} = [\sigma^2(F_o^2) + (0.0860P)^2]$, $P = (F_o^2 + 2F_c^2)/3$.

3. Results and discussion

3.1. Structure description

As shown in Fig. 1, the complex consists of one α-Keggin anion $[CoW_{12}O_{40}]^{6-}$, two discrete $[Co(2,2'\text{-bipy})_3]^{2+}$ cations and nine point five crystallization water molecules. As other Keggin anions [1], the $[CoW_{12}O_{40}]^{6-}$ anion includes a CoO_4 tetrahedron surrounded by 12 WO_6 octahedrons, present in the four W_3O_{13} groups. According to the different coordination environments of oxygen atoms in the polyanion, these oxygen atoms can be divided into four groups: O_t (terminal oxygen atoms connecting to one W atom), O_b (atoms located in the shared corners between two W_3O_{13} units), O_c (oxygen atoms connecting edge-sharing WO_6 octahedra in the W_3O_{13} unit) and O_a (oxygen atoms connecting the Zn and W atoms). Relevant W–O bonds can be classified into three categories: (1) W–O_t, 1.694(10)–1.740(12) Å with an average bond length 1.716 Å ; (2) W–$O_{b,c}$, 1.818(11)–2.065(12) Å with a mean bond distance 1.934 Å; (3) W–O_a, 2.123(11)–2.201(10) Å with an average bond distance 2.162 Å. Comparing the W–O bonds with that of the potassium salt $K_6[CoW_{12}O_{40}]$ [19], the W–O_t and W–O_a lengths in the title compound show an obvious increase except for the W–$O_{b,c}$ distances which have no evident change. The results indicate that the static electric interaction between the $[CoW_{12}O_{40}]^{6-}$ anion and discrete $[Co(2,2'\text{-bipy})_3]^{2+}$ cations are relatively weak. For the CoO4 tetrahedron, the Co–O distances are 1.875(10)–1.908(12) Å with an average bond length 1.890 Å, while the O–Co–O angles vary from 108.6(5)° to 110.4(5)°, which are consistent with the literature [19]. The results show that the central CoO_4 tetrahedron, depended upon by the surrounding WO_6 octahedrons, was more regular. Comparing W–O bonds with that of $[Me_4N]_7[VW_{12}O_{40}]\cdot 15H_2O$ [20], the average W–O_t and W–$O_{b,c}$ distances in the title compound elongate 0.008 and 0.021 Å, respectively, while the average W–O_a distance decreases 0.163 Å, which proved that the average W–O_t and W–$O_{b,c}$ distances increase and mean W–O_a length decreases with increase of the heteroatom radius. It should be pointed out that the two discrete Co^{2+} coordination cations have chirality, each Co^{2+} site is defined by six nitrogen atoms from three 2,2′-bipyridine molecules and formed a distorted CoN_6 octahedron with Co(2)–N and

Table 2
Selected bond lengths (Å) and angles (°) for $[Co(2,2'\text{-bipy})_3]_2H_2[CoW_{12}O_{40}]\cdot 9.5H_2O$

Bond lengths			
Co(1)–O(37)	1.875(10)	Co(1)–O(39)	1.891(12)
Co(1)–O(38)	1.884(11)	Co(1)–O(40)	1.908(11)
Co(2)–N(2′)	1.925(13)	Co(2)–N(1′)	1.928(16)
Co(2)–N(3′)	1.924(14)	Co(2)–N(2)	1.938(12)
Co(2)–N(3)	1.936(12)	Co(2)–N(1)	1.947(13)
Co(3)–N(4)	1.915(14)	Co(3)–N(5′)	1.934(13)
Co(3)–N(5)	1.927(13)	Co(3)–N(4′)	1.939(14)
Co(3)–N(6′)	1.932(14)	Co(3)–N(6)	1.947(14)
W(1)–O(1)	1.716(11)	W(1)–O(37)	2.175(10)
W(2)–O(2)	1.714(11)	W(2)–O(37)	2.168(11)
W(3)–O(3)	1.697(11)	W(3)–O(37)	2.166(10)
W(4)–O(4)	1.740(12)	W(4)–O(38)	2.165(12)
W(5)–O(5)	1.700(10)	W(5)–O(38)	2.182(10)
W(6)–O(6)	1.714(10)	W(6)–O(38)	2.140(10)
W(7)–O(7)	1.739(11)	W(7)–O(39)	2.152(11)
W(8)–O(8)	1.694(10)	W(8)–O(39)	2.132(12)
W(9)–O(9)	1.714(11)	W(9)–O(39)	2.201(10)
W(10)–O(10)	1.695(14)	W(10)–O(40)	2.164(12)
W(11)–O(11)	1.740(10)	W(11)–O(40)	2.123(11)
W(12)–O(12)	1.728(10)	W(12)–O(40)	2.171(11)
Bond angles			
O(37)–Co(1)–O(38)	109.8(4)	O(37)–Co(1)–O(40)	109.8(5)
O(37)–Co(1)–O(39)	109.1(5)	O(38)–Co(1)–O(40)	108.6(5)
O(38)–Co(1)–O(39)	110.4(5)	O(39)–Co(1)–O(40)	109.1(5)
N(3′)–Co(2)–N(3)	82.6(6)	N(2)–Co(2)–N(3)	178.3(6)
N(5)–Co(3)–N(5′)	83.3(6)	N(5′)–Co(3)–N(4′)	177.7(6)

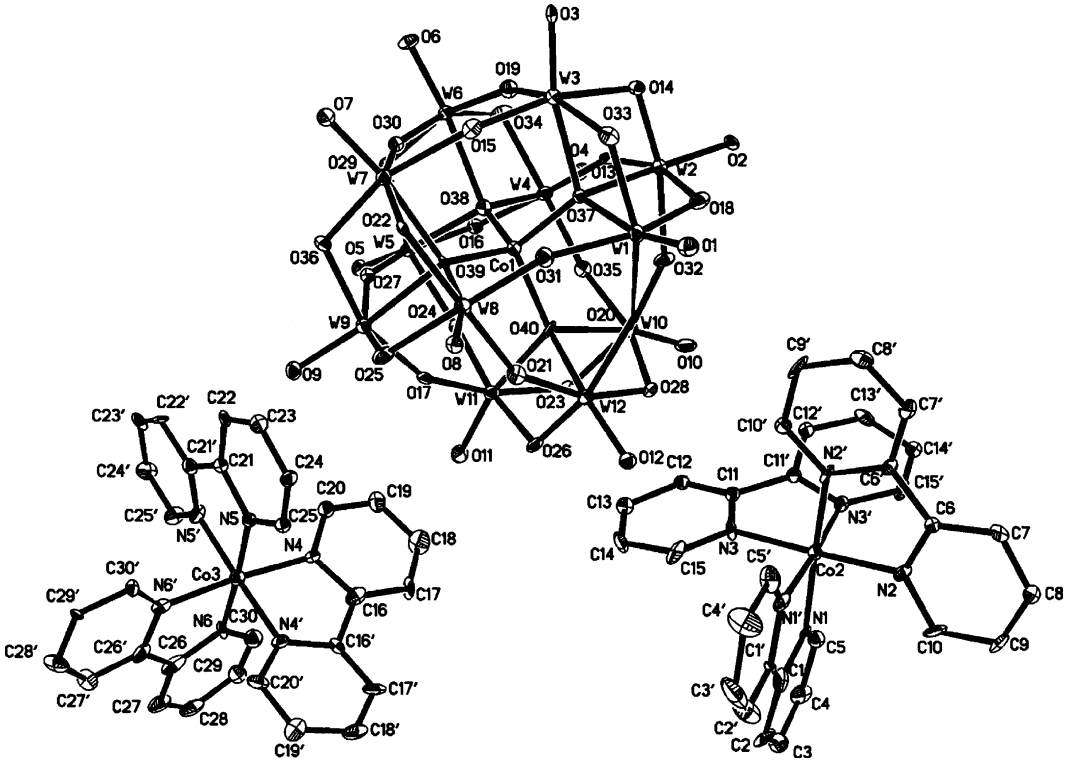

Fig. 1. Molecular structure of the title compound. Water molecules and all hydrogen atoms are omitted for clarity.

Co(3)–N bond lengths in the range of 1.924(13)–1.947(13) Å and 1.915(14)–1.947(14) Å, corresponding to their mean Co(3)–N length 1.933 and 1.932 Å, respectively. While bond angles in the Co(2) and Co(3) are 82.6(6)°–176.8(6)° and 83.3(6)°–95.6(6)°. Furthermore, the dihedral angles among the three ideal 2,2′-bipyridine planes in

$[Co(2)(2,2'\text{-bipy})_3]^{2+}$ are 93.6°, 78.7° and 89.6°. For $[Co(3)(2,2'\text{-bipy})_3]^{2+}$, the three dihedral angles among the three ideal 2,2′-bipyridine planes are 94.6°, 78.7° and 89.6°. The results indicate that the three ideal planes in each $[Co(2,2'\text{-bipy})_3]^{2+}$ ion are not vertical to each other.

3.2. IR spectrum

The IR spectrum of the title compound has some characteristic bands for the cations at 1635, 1448, 1168 and 1106 cm^{-1}. Features at 1635 and 1448 cm^{-1} are attributed to stretching vibrations of C=N and C–N bonds. Features at 1168 and 1106 cm^{-1} are ascribed to ring stretching of 2,2′-bipyridine. In addition, the IR spectrum of the title compound exhibits prominent bands for the anion at 931, 869, 757 and 455 cm^{-1}, attributed to $\nu(W{=}O_t)$, $\nu(W{-}O_b)$, $\nu(W{-}O_c)$ and $\nu(Co{-}O)$, respectively.

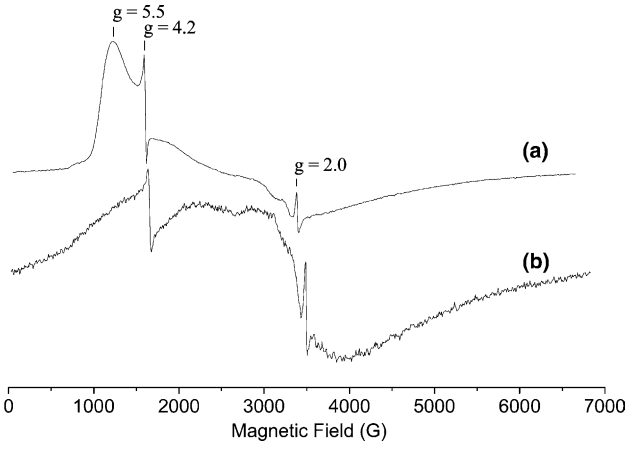

Fig. 2. EPR spectra of $[Co(2,2'\text{-bipy})_3]_2H_2[CoW_{12}O_{40}]\cdot 9.5H_2O$: (a) 100 K, 9.4841 GHz; (b) 300 K, 9.7747 GHz.

3.3. UV and EPR spectra

The UV spectrum of the title compound in distilled water solution exhibits two absorption peaks at 194 and 298 nm (characteristic of Keggin anion), ascribed to the charge-transition absorption of $O_t \rightarrow W$ and $O_{b,c} \rightarrow W$, respectively. The EPR spectra (Fig. 2) reveal obviously that there are two kinds of cobalt: high spin state and low spin state in the complex. At 110 K, the EPR spectra display a broad signal $g = 5.5$ and two narrow symmetric bands centered at $g = 4.2$ and 2.0. The signals $g = 5.5$, 4.2 and $g = 2.0$ are attributed to high spin and low spin Co^{2+}, respectively. However, when the temperature increases to room temperature, the EPR signal $g = 5.5$ disappears and at the same time the signal $g = 4.2$ decreases and the signal $g = 2.00$ increases. In addition the noise signals become stronger. The disappearance of the broad signal $g = 5.5$ is caused by the zero-field splitting, which can be explained by the ligand field energy-level diagram of the ground state $^4A_2$ of high spin Co^{2+} [21]. Distortion of the tetrahedron will split the ground state into two Kramers doublets ($Ms = \pm 1/2$ and $Ms = \pm 3/2$). When the temperature increases from 110 K to room temperature, the negative zero-field splitting between $Ms = \pm 1/2$ and $Ms = \pm 3/2$ emerges so that the Co^{2+} ions tend to populate the $Ms = \pm 3/2$ level which is not ESR-active. Thus the ESR signal $g = 5.5$ disappears at room temperature.

3.4. Thermal properties

The thermal decomposition profile (Fig. 3) of the title compound gives a total weight loss of 24.63% in the range 24.5–809.3 °C. The thermal analysis curve can be divided into two stages. In the first stage, the weight loss of 3.03% (< calculated 4.14%, attributed to the loss of

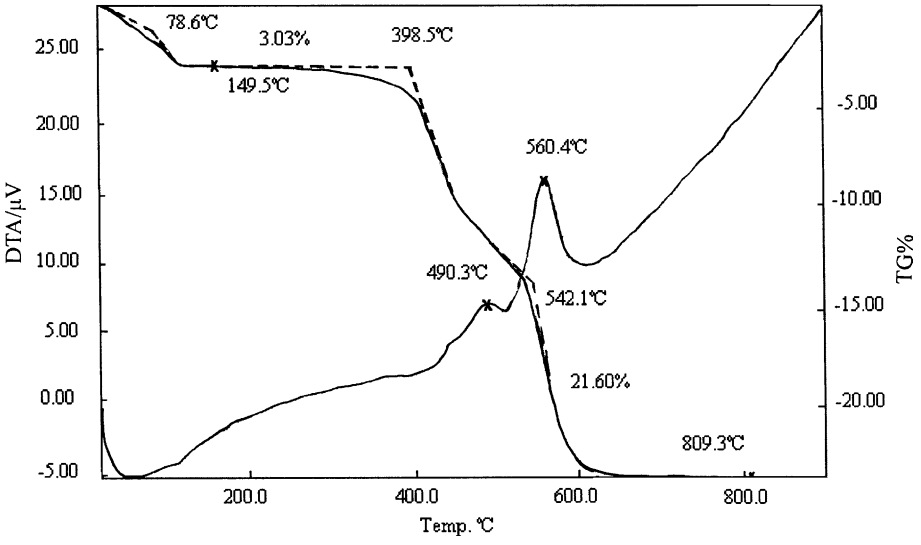

Fig. 3. TG/DTA traces for the $[Co(2,2'\text{-bipy})_3]_2H_2[CoW_{12}O_{40}]\cdot 9.5H_2O$ complex.

surface water of the single crystal) in the range of 24.5–149.5 °C is due to the loss of seven crystallization water molecules. In the second stage, the weight loss of 21.60% in the range 149.5–809.3 °C corresponds to the decomposition of six 2,2′-bipyridine ligands and one structural water, adjoining combustion of the organic ligands in that there is a little exothermal peak at 490.3 °C in the DTA curve. In addition, the other exothermal peak at 560.4 °C shows that the Keggin anion $[CoW_{12}O_{40}]^{6-}$ begins to decompose.

4. Supplementary material

Crystallographic data for the structural analysis of the title compound have been deposited with the Cambridge Crystallographic Data Centre, CCDC No. 204618. Copies of this information may be obtained free of charge from The Director, CCDC, 12 Union Road, Cambridge, CB2 1EZ, UK (fax: +44-1223-336033; e-mail: deposit@ccdc.cam.ac.uk or www:http://www.ccdc.cam.ac.uk).

Acknowledgements

This work was supported by the Natural Science Foundation of Henan Province and the Outstanding Youth Foundation of Henan Province of China.

References

[1] M.T. Pope, Heteropoly and Isopoly Oxometalates, Springer, Berlin, 1983.
[2] N. Mizuno, M. Misono, Chem. Rev. 98 (1998) 199.
[3] J.T. Rhule, C.L. Hill, D.A. Judd, Chem. Rev. 98 (1998) 327.
[4] E. Coronado, C.J. Gomez-Garcia, Chem. Rev. 98 (1998) 273.
[5] W.H. Casey, B.L. Phillips, Geochim. Cosmochim. Acta 65 (2001) 705.
[6] A.V. Besserguenev, M.H. Dickman, M.T. Pope, Inorg. Chem. 40 (2001) 2582.
[7] J.R. Galán-Mascarós, C. Giménez-Saiz, S. Triki, C.J. Gómez-García, E. Coronado, L. Ouahab, Angew. Chem., Int. Ed. Engl. 34 (1995) 1460.
[8] C.J. Gómez-García, C. Giménez-Saiz, S. Triki, E. Coronado, L. Ducasse, P. Le Magueres, L. Ouahab, P. Delhaès, Synth. Met. 70 (1995) 783.
[9] C.J. Gómez-García, L. Ouahab, C. Giménez-Saiz, S. Triki, E. Coronado, P. Delhaès, Angew. Chem., Int. Ed. Engl. 33 (1994) 223.
[10] Y. Xu, J.-Q. Xu, K.-L. Zhang, Y. Zhang, X.-Z. You, Chem. Commun. (2000) 153.
[11] B.B. Yan, Y. Xu, X.H. Bu, N.K. Goh, L.S. Chia, G.D. Stucky, J. Chem. Soc., Dalton Trans. (2001) 2009.
[12] J.Y. Niu, Q. Wu, J.P. Wang, J. Chem. Soc., Dalton Trans. (2002) 2512.
[13] J.Y. Niu, Z.L. Wang, J.P. Wang, Inorg. Chem. Commun. 6 (2003) 1272.
[14] P.J. Wang, Q. Wu, J.Y. Niu, Sci. China B 45 (2002) 647.
[15] M. Nyman, F. Bonhomme, T.M. Alam, M.A. Rodriguez, B.R. Cherry, J.L. Krumhansl, T.M. Nenoff, A.M. Sattler, Science 297 (2002) 996.
[16] J.Y. Niu, M.L. Wei, J.P. Wang, D.B. Dang, J. Mol. Struct. 655 (2003) 171.
[17] A. Dolbecq, P. Mialane, L. Lisnard, J. Marrot, F. Sécheresse, Chem. Eur. J. 9 (2003) 2914.
[18] G.M. Sheldrick, SHELXTL-97: Program for Crystal Structure Refinement, University of Göttingen, Germany, 1997.
[19] N. Casañ-Pastor, P. Gomez-Romero, G.B. Jameson, L.C.W. Baker, J. Am. Chem. Soc. 113 (1991) 5658.
[20] M. Ishaque, S. Cevik, R. Hayashi, J. Chem. Soc., Dalton Trans. (1999) 1651.
[21] El-M. El-Malki, D. Werst, P.E. Doan, W.M.H. Sachtler, J. Phys. Chem. B 104 (2000) 5924.

Available online at www.sciencedirect.com
SCIENCE DIRECT®
Polyhedron 23 (2004) 779–786
POLYHEDRON
www.elsevier.com/locate/poly

Syntheses, characterizations and crystal structures of new organotin complexes with 2-mercapto-6-nitrobenzothiazole

Chunlin Ma [a,b,*], Qin Jiang [a], Rufen Zhang [a]

[a] Department of Chemistry, Liaocheng University, Liaocheng 252059, PR China
[b] Taishan University, Taian 271021, PR China

Received 24 September 2003; accepted 4 November 2003

Abstract

A series of organotin(IV) complexes with 2-mercapto-6-nitrobenzothiazole (HMNBT) of the type, $[R_nSn(MNBT)_{4-n}]$ ($n = 2$, R = Me, **4**; $n = 3$, R = Me, **5**; *n*-Bu, **6**; Ph, **7**; $PhCH_2$, **8**) were synthesized. All the complexes **4**–**8** have been characterized by elemental, IR and ^1H NMR analyses. Among them, complexes **4**, **7** and **8** were also characterized by X-ray crystallography diffraction analyses, which revealed that the structures of both complexes **7** and **8** are penta-coordinated with R_3Sn coordinated to the thiol S and heterocyclic N atoms, and the structural distortion for each is a displacement from tetragonal towards trigonal bipyramidal geometry. For complex **4**, the geometry of the center tin atom is a distorted trapezoidal bipyramid. Besides, intermolecular S···S and Sn···S non-bonded interactions were recognized in crystal structures of complexes **4** and **7**, respectively. The IR and ^1H NMR spectral data indicate such an inclination that those structures of trialkyltin derivatives are apt to be penta-coordinated and those dialkyltin derivatives are likely in six-coordination.
© 2003 Elsevier Ltd. All rights reserved.

Keywords: 2-Mercapto-6-nitrobenzothiazole; Organotin(IV); Non-bonded interaction; Crystal structure; X-ray crystallography diffraction

1. Introduction

Organotin compounds have been the subjects of interest for some time because of their biometrical and commercial applications [1,2]. To aid in understanding their biochemical action, it was felt that the coordination chemistry of tin(IV) toward O-, S- and N-containing ligands requires further exploration. Solid state structures of several simple triorganotin thiolates, R_3SnSR', where the R′ groups contain no donor atoms, have been reported before [3,4], and all of them were found to have four-coordinate geometry. However, if the R′ group contains a donor atom (N or O), then the coordination number of tin will increase [5].

Our interest in the structures of organotin(IV) complexes containing {N, S} donor sites has prompted us to embark on a study of the ligand 2-mercapto-6-nitrobenzothiazole (HMNBT). This ligand is interesting because of its potential bidentate coordination possibilities, so that bonding may take place either by the heterocyclic N or the thiol S. In our previous work, we have reported three diorganotin derivatives from the ligand (see Scheme 1): the complexes **1**, **2** and **3**, which take on versatile structures due to the existence of π–π stacking interaction or non-bonded interactions in the crystals [6,7].

To continue our studies in this field, we carried out more experiments with the ligand and obtained another five organotin complexes of the type $[R_nSn(MNBT)_{4-n}]$ ($n = 2$, R = Me, **4**; $n = 3$, R = Me, **5**; *n*-Bu, **6**; Ph, **7**; $PhCH_2$, **8**). All complexes **4**–**8** were characterized by elemental, IR, ^1H NMR analyses. Among them, complexes **4**, **7** and **8** were also characterized by X-ray crystallography diffraction analyses, which reveal that the structures of complexes **7** and **8** are penta-coordinated with R_3Sn coordinated to the thiol S and

* Corresponding author. Tel.: +866358238121; fax: +866358238274.
E-mail address: macl@lctu.edu.cn (C. Ma).

0277-5387/$ - see front matter © 2003 Elsevier Ltd. All rights reserved.
doi:10.1016/j.poly.2003.11.045

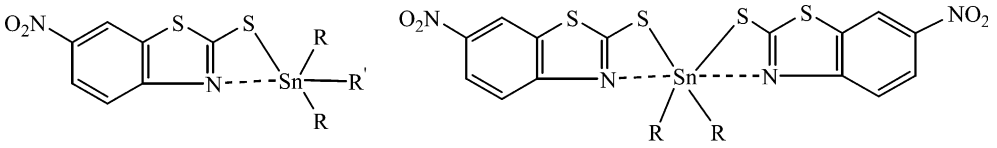

(a) R=R'=Me, **5**; *n*-Bu, **6**; Ph, **7**; $PhCH_2$, **8**; R=Ph, R'=Cl, **1** **(b)** R=$PhCH_2$, **2**, *n*-Bu, **3**; Me, **4**

Scheme 1.

heterocyclic N atoms and the structural distortion for each is a displacement from tetragonal towards trigonal bipyramidal geometry. For complex **4**, the geometry of the center tin atom is a distorted trapezoidal bipyramid. It is worth to note that intermolecular S···S and Sn···S non-bonded interactions were recognized in the crystal structures of complexes **4** and **7**, respectively.

2. Experimental

2.1. Materials and measurements

All reagents and solvents were purchased commercially and used without further purification unless otherwise noted. The melting points were obtained on a Kofler micro melting point apparatus and are uncorrected. Infrared spectra were recorded on a Nicolet-460 spectrophotometer using KBr discs and sodium chloride optics. ^{1}H NMR spectra were obtained on a Jeol-FX-90Q NMR spectrometer. Chemical shifts are given in ppm relative to Me_4Si in $CDCl_3$ as solvent. Elemental analyses were performed with a PE-2400 II elemental analyser.

2.2. Syntheses of the complexes *4–8*

2.2.1. *[$Me_2Sn(MNBT)_2$] (4)*

The 2-mercapto-6-nitrobenzothiazole (0.424 g, 2 mmol), sodium ethoxide (0.136 g, 2 mmol) and dimethyltin dichloride (0.220 g, 1 mmol) were added to benzene (20 ml) in turn, stirred for 12 h at 40 °C and then filtered. After removing the solvent, the solid was recrystallized from diethylether–petroleumether. Salmon pink crystals of complex **4** were formed. Yield: 89%; m.p. >200 °C (dec.). *Anal*. Calc. for $C_{16}H_{12}N_4O_4S_4Sn$: C, 33.65; H, 2.12; N, 9.81. Found: C, 33.24; H, 2.33; N, 9.67%. ^{1}H NMR ($CDCl_3$): 7.33–7.86 (m, 3H), 1.42 (s, 6H).

2.2.2. *[$Me_3Sn(MNBT)$] (5)*

The reaction was carried out under dry nitrogen atmosphere. 2-Mercapto-6-nitrobenzothiazole (0.212 g, 1 mmol) and sodium ethoxide (0.068 g, 1 mmol) were added to benzene (20 ml) in a Schlenk flask and stirred for about half an hour. Trimethyltin chloride (0.199 g, 1 mmol) was added to the reactor subsequently. The reaction mixture was stirred for 12 h at 40 °C and then filtered. The filtrate was gradually evaporated under vacuum until a solid product was obtained. The solid was then recrystallized and yellow crystals of complex **5** were obtained. Yield: 88%; m.p.108–110 °C. *Anal*. Calc. for $C_{10}H_{12}N_2O_2S_2Sn$: C, 32.03; H, 3.23; N, 7.47. Found: C, 31.86; H, 3.54; N, 7.65%. ^{1}H NMR ($CDCl_3$): 7.36–7.87 (m, 3H), 0.73 (s, 9H).

2.2.3. *[$(n\text{-}Bu)_3Sn(MNBT)$] (6)*

The solid of complex **6** is made in the same way as complex **5**. Yield: 91%; m.p. 82–84 °C. *Anal*. Calc. for $C_{19}H_{30}N_2O_2S_2Sn$: C, 45.53; H, 6.03; N, 5.59. Found: C, 45.31; H, 6.33; N, 5.74%. ^{1}H NMR ($CDCl_3$): 7.23–7.80 (m, 3H), 0.75–1.22m (t, 9H), 1.22–1.45 (m, 18H).

2.2.4. *[$Ph_3Sn(MNBT)$] (7)*

The procedure is the same as that of complex **5** and yellow crystalline complex **7** was formed in diethylether–dichloromethane (1:3). Yield: 0.50 g (89%); m.p. 189–191 °C. *Anal*. Calc. for $C_{25}H_{18}N_2O_2S_2Sn$: C, 53.50; H, 3.23; N, 4.99. Found: C, 53.13; H, 3.53; N, 4.64%. ^{1}H NMR ($CDCl_3$): 7.39–7.85 (m, 18H).

2.2.5. *[$(PhCH_2)_3Sn(MNBT)$] (8)*

The procedure is the same as that of complex **5** and in diethyl ether yellow crystals of complex **8** were obtained. Yield: 93%; m.p. 100–102 °C. *Anal*. Calc. for $C_{28}H_{24}N_2O_2S_2Sn$: C, 55.74; H, 4.01; N, 4.64. Found: C, 55.36; H, 4.52; N, 4.29%. ^{1}H NMR ($CDCl_3$): 7.24–7.90 (m, 18H), 2.63 (s, 6H).

2.3. X-ray crystallographic studies of complexes *4, 7 and 8*

All X-ray crystallographic data were collected on a Bruker SMART CCD 1000 diffractometer. Correction for semi-empirical from equivalents was applied, and the structures were solved by direct methods and refined by a full-matrix least squares procedure based on F^2 using the SHELXL 97 program system. All data were collected with graphite-monochromated Mo Kα radiation ($\lambda = 0.71073$ Å) at 298(2) K. The positions of hydrogen atoms were calculated, and their contributions were included in structural factor calculations.

3. Results and discussion

3.1. Syntheses of the complexes 4–8

The synthesis procedure was as in Scheme 2:

3.2. IR spectroscopic studies of the complexes 4–8

The characteristic IR frequencies (cm^{-1}) of HMNBT and its di- and triorganotin(IV) derivatives **1**–**8** are listed in Table 2.

The explicit feature in the infrared spectra of all complexes **4**–**8** is the absence of the band in the region 2550–2430 cm^{-1}, which appears in the free ligand as the ν(S–H) vibration, indicating metal-ligand bond formation through this site. While in the far-infrared spectra, a strong absorption appears in the range 280–346 cm^{-1} in the spectra of complexes **4**–**8**, which is absent in the spectrum of the ligand, is assigned to the Sn–S stretching mode of vibration. All these values are consistent with that detected in a number of organotin(IV)–sulfur derivatives [8].

The ν(C=N) band, occurring at about 1586 cm^{-1}, is considerably shifted towards lower frequencies with respect to that of the free ligand (1616 cm^{-1}), confirming the coordination of the heterocyclic N atom to tin. The stretching frequency is lowered owing to the displacement of electron density from N to the Sn atom, thus resulting in a weakening of the C=N bond as reported in the literature [9]. Thus, the weak or medium-intensity band appearing at 453, 460, 475, 488 and 480 cm^{-1} for the respective spectra of complexes **4**–**8** may be assigned to Sn–N stretching vibrations.

Besides, in organotin complexes, the IR spectra can provide useful information concerning the geometry of the SnC_n moiety [10]. In the cases of our complexes, for both di- and triorganotin derivatives, two bands were assigned to asymmetric and symmetric Sn–C vibrations, thus suggesting non-linear C–Sn–C units for the dimethyltin derivative **4** and no-planar SnC_3 fragments for the trialkyltin derivatives **5**–**8**, respectively. Thus the bands at 556 and 523 cm^{-1} for complex **4**, 532 and 497 cm^{-1} for **5**, 562 and 544 cm^{-1} for **6**, 570 and 520 cm^{-1} for **7** and 447 and 424 cm^{-1} for **8** can be assigned to ν_{as}(Sn–C) and ν_s(Sn–C), respectively.

3.3. ^1H NMR data of the complexes 4–8

^1H NMR data showed that the signal of the –SH proton in the spectrum of the ligand is absent in all the complexes **4**–**8**, indicating the removal of the –SH proton and the formation of Sn–S bonds. This information agrees with what the IR data have revealed.

3.4. Crystal structures of complexes 4, 7 and 8

The crystal structures or unit cells of complexes **4**, **7** and **8** are shown in Figs. 1–4. All H atoms have been omitted for the purpose of clarity. Table 1 lists the crystal data and structure refinement parameters for complexes **4**, **7** and **8** and their selected bond lengths and angles are shown in Tables 4–6, respectively.

3.4.1. Structure of complex 4

Complex **4** contains a six-coordinated tin atom as its analogous dialkyltin derivatives from the ligand (see

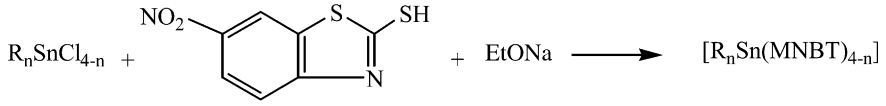

(n=2, R=Me, **4**; n=3, R=Me, **5**; n-Bu, **6**; Ph, **7**; $PhCH_2$, 8)

Scheme 2.

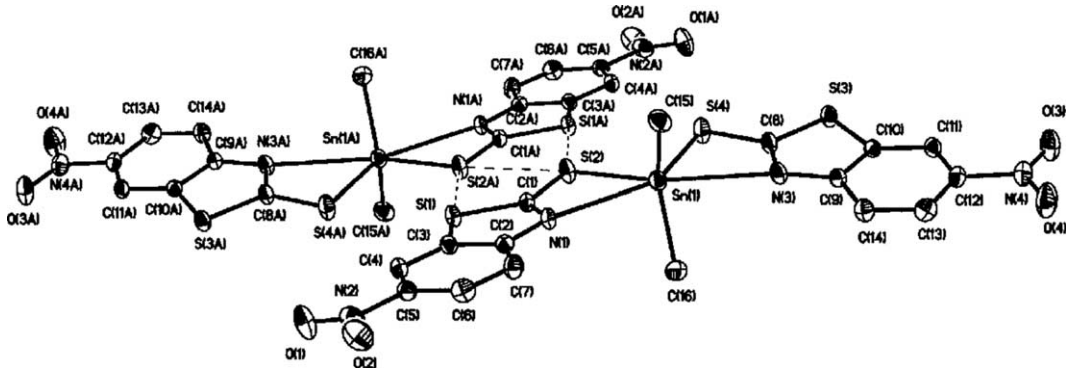

Fig. 1. Crystal structure of complex **4**.

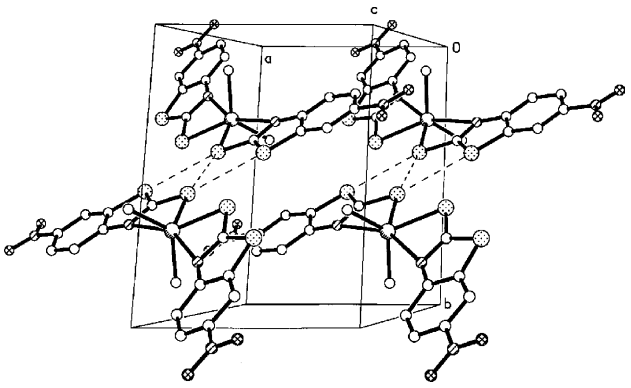

Fig. 2. Unit cell of complex **4**.

Scheme 2(b)) [6]. In this case, the crystal structure of **4** consists of a dimer unit in which tin atoms are coordinated to two methyl carbons and to two sulfur and nitrogen atoms from the two deprotonated ligands. The valence extension is performed via two nitrogen atoms and they occupy *trans* positions with the angle, N(1)–Sn(1)–N(3), 155.68(12)°, while the case for the sulfur bonding vary and they occupy *cis* positions (S(2)–Sn(1)–S(4), 85.82(7)°). On each side of the tin atom, the S and N equatorial ligating atoms belong to the same moiety (S(2)–Sn(1)–N(1): 59.08(11)° and S(4)–Sn(1)–N(3): 59.51(11)°, which are reconcilable with skew-trapezoidal bipyramid geometry), so their positions are fixed and the S–Sn–N angles can only admit very little deformation.

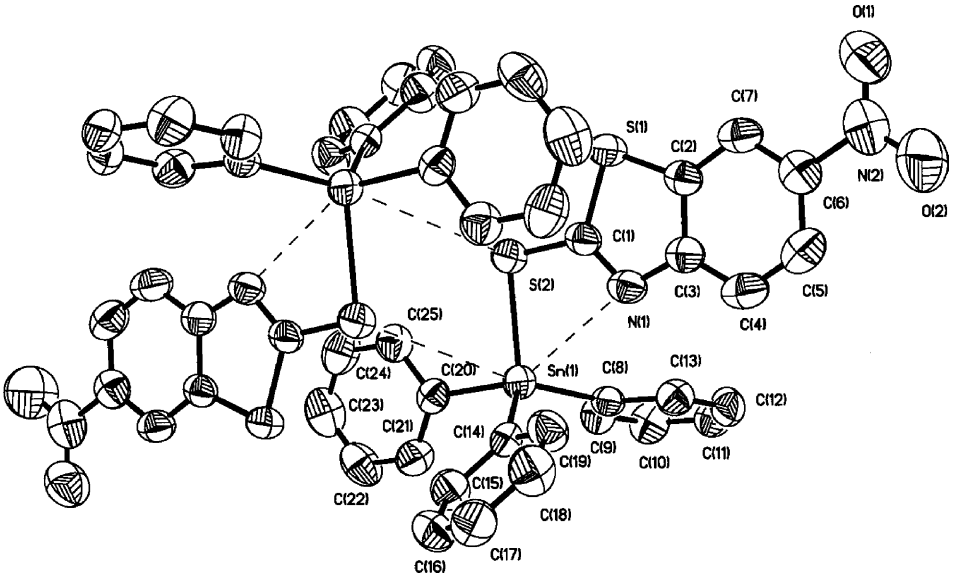

Fig. 3. Crystal structure of complex **7**.

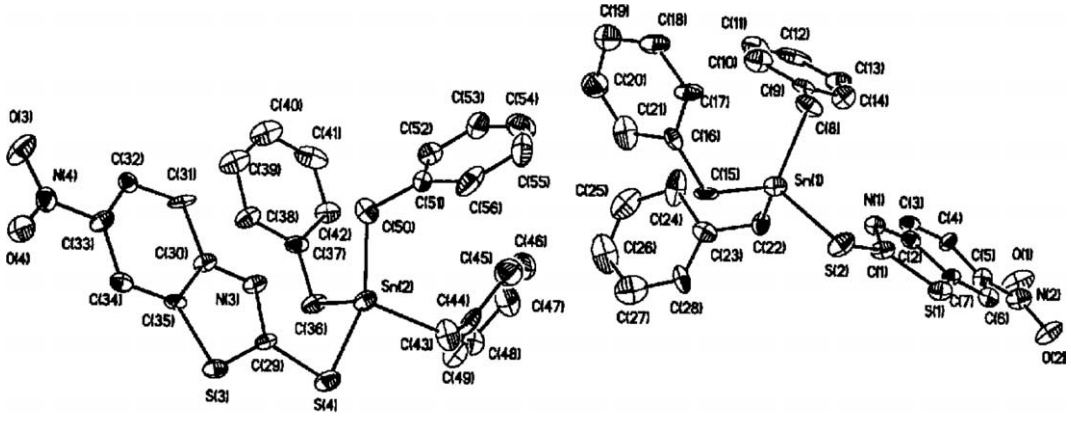

Fig. 4. Crystal structure of complex **8**.

Table 1
Crystal data and structure refinement parameters for complexes **4**, **7** and **8**

	Complex **4**	Complex **7**	Complex **8**
Empirical formula	$C_{16}H_{12}N_4O_4S_4Sn$	$C_{25}H_{18}N_2O_2S_2Sn$	$C_{28}H_{24}N_2O_2S_2Sn$
Formula weight	571.23	561.22	603.30
Crystal system	triclinic	triclinic	triclinic
Space group	$P\bar{1}$	$P\bar{1}$	$P\bar{1}$
Unit cell dimensions			
a (Å)	8.324(12)	9.895(5)	7.680(2)
b (Å)	11.704(17)	10.707(5)	7.814(3)
c (Å)	11.993(17)	11.735(6)	44.722(14)
α (°)	72.88(2)	68.476(7)	93.138(6)
β (°)	71.572(19)	89.032(7)	92.035(6)
γ (°)	87.22(2)	80.859(7)	93.773(6)
V (Å^3)	1058(3)	1140.7(9)	2672.0(15)
Z	2	2	4
D_c (g cm^{-3})	1.793	1.634	1.500
Crystal size (mm)	$0.30 \times 0.17 \times 0.13$	$0.15 \times 0.10 \times 0.04$	$0.20 \times 0.10 \times 0.06$
$F(000)$	564	560	1216
Total reflections	5598	4980	12775
Independent reflections	3693	3235	8666
Data/restraints/parameters	3693/0/262	3235/0/361	8666/0/631
Final R indices [$I > 2\sigma(I)$]	$R_1 = 0.0385$	$R_1 = 0.0315$	$R_1 = 0.0616$
	$wR_2 = 0.0901$	$wR_2 = 0.0558$	$wR_2 = 0.0669$
R indices (all data)	$R_1 = 0.0553$	$R_1 = 0.0455$	$R_1 = 0.2408$
	$wR_2 = 0.1103$	$wR_2 = 0.0608$	$wR_2 = 0.1029$
Goodness-of-fit	0.993	0.972	0.741
Θ range for data colletion (°)	1.82–25.02	1.87–23.42	2.28–24.86
Absorption coefficient (mm^{-1})	1.633	1.328	1.140
Largest differential peak and hole (e Å^{-3})	0.645 and −0.752	0.509 and −0.391	0.393 and −0.497

Table 2
Characteristic IR frequencies (cm^{-1}) of HMNBT and its di- and triorganotin(IV) derivatives **1**–**8**

Number	Ligand/complex	ν(Sn–C)	ν(Sn–S)	ν(Sn–N)	ν(C=N)	Reference
1	$[Ph_2SnCl(MNBT)]$	278, 232	290	448	1599	[6]
2	$[(PhCH_2)_2Sn(MNBT)_2]$	468, 426	265	455	1598	[6]
3	$[(n\text{-}Bu)_2Sn(MNBT)_2]$	529, 461	270	457	1597	[6]
4	$[Me_2Sn(MNBT)_2]$	556, 523	280	453	1590	this work
5	$[Me_3Sn(MNBT)]$	532, 497	317	460	1586	this work
6	$[(n\text{-}Bu)_3Sn(MNBT)]$	562, 544	346	475	1585	this work
7	$[Ph_3Sn(MNBT)]$	570, 520	289	488	1586	this work
8	$[(PhCH_2)_3Sn(MNBT)]$	447, 424	306	480	1587	this work
9	HMNBT		2550–2430 ν(S–H)		1616	this work

The geometry around the metal may thus be viewed as a distorted trapezoidal bipyramid with the two methyl carbons in bent axial positions and the trapezoidal plane being defined by the two Sn–S covalent bonds and the two Sn–N secondary interactions. The five equatorial atoms are nearly coplanar, and the sum of angles between the tin atom and the equatorial ligating atoms (i.e., two N and two S in each case) is 360.1°, almost equal to the ideal octahedral value of 360°. It should be mentioned that notably similar *trans*-$R_2SnS_2N_2$ coordination geometries are found in analogous systems of 2-pyridinethiolate and tetrazole-thione ligands [11,12].

As shown in Table 3, the Sn–C distances (2.114(6) and 2.122(6) Å) and Sn–S distances (2.491(3) and 2.524(4) Å) are similar to those found in other dialkyltin derivatives from the ligand (2.13–2.16 and 2.49–2.55 Å, respectively) [6]. The Sn–N distances, 2.815(5) and 2.882(5) Å, are similar to that found in dimethyldi(pyrimidine-2-thiolato)tin (2.83(2) Å) but shorter than that of dimethylbis(1-phenyl-1H-tetrazole-5-thiolate)tin (2.947(4) Å) [11,12], which though less than the sum of the van der Waals radii, 3.75 Å, is one of the largest reported for analogue dialkyltin derivatives from the ligand (2.60–2.86 Å) [6].

Furthermore, intra-molecular non-bonded S···S interactions were recognized in the crystallographic analysis of complex **4,** which help the construction of the dimer. Comparing with other dialkyltin derivatives, the consequence of the formation of non-bond interactions between molecules is $[Me_2Sn(MNBT)_2] \sim [Bu_2Sn(MNBT)_2] > [Ph_2Sn(MNBT)_2]$ (Table 3), which are partly

Table 3
Bond lengths (Å) and angles (°) for some di- and triorganotin(IV) derivatives from HMNBT

Number	Sn–S	Sn–N	Sn···S/S···X	N–Sn–S	Axial–Sn–axial	Geometry	Reference
1	2.444(2), 2.446(3)	2.595(7), 2.580(6)	3.42–3.56 (Cl···S)	62.90(16), 63.06(17)	153.96(16), 154.78(18)	*cis*-trigonal bipyramid	[6]
2	2.5358(12), 2.5239(11)	2.82, 2.596 (3)		62.17(8), 59.5	133.96 (18)	trapezoidal bipyramid	[6]
3	2.494(3), 2.498(3)	2.82, 2.86	3.51 (S···S)	58.8, 59.4	131.0(5)	trapezoidal bipyramid	[6]
4	2.491(3), 2.524(4)	2.882(5), 2.815(5)	3.43, 3.42 (S···S)	59.08(11), 59.51(11)	125.0(3)	trapezoidal bipyramid	this work
7	2.453(16)	3.137(4)	3.97 (Sn···S)	55.85(7)	152.75(13)	*cis*-trigonal bipyramid	this work
8	2.480(3), 2.501(3)	2.968(9), 2.949(10)		58.61(17), 57.81(19)	155.2(3), 155.8(3)	*cis*-trigonal bipyramid	this work

Table 4
Selected bond lengths (Å) and angles (°) of complex **4**

Bond lengths			
Sn(1)–C(15)	2.122(6)	Sn(1)–C(16)	2.114(6)
Sn(1)–S(2)	2.491(3)	Sn(1)–S(4)	2.524(4)
Sn(1)–N(1)	2.882(5)	Sn(1)–N(3)	2.815(5)
N(1)–C(1)	1.304(6)	N(3)–C(8)	1.304(6)
S(1)–C(1)	1.761(5)	S(3)–C(8)	1.753(5)
S(2)···S(1)#	3.43	S(2)···S(2)#	3.42
Bond angles			
C(16)–Sn(1)–C(15)	125.0(3)	S(2)–Sn(1)–S(4)	85.82(7)
S(2)–Sn(1)–N(1)	59.08(11)	S(4)–Sn(1)–N(3)	59.51(11)
N(3)–Sn(2)–N(1)	155.68(12)		

Table 5
Selected bond lengths (Å) and angles (°) of complex **7**

Bond lengths			
Sn(1)–C(20)	2.130(4)	Sn(1)–C(14)	2.131(4)
Sn(1)–C(8)	2.134(4)	Sn(1)–S(2)	2.453(16)
N(1)–C(1)	1.309(5)	N(1)–C(3)	1.378(5)
S(1)–C(2)	1.720(4)	S(1)–C(1)	1.744(4)
S(2)–C(1)	1.705(4)	C(2)–C(3)	1.404(5)
Sn(1)···N(1)	3.137(4)	Sn(1)···S(4)	3.97
Bond angles			
C(20)–Sn(1)–C(14)	109.56(15)	C(20)–Sn(1)–C(8)	108.83(16)
C(14)–Sn(1)–C(8)	118.40(14)	C(20)–Sn(1)–S(2)	96.90(11)
C(8)–Sn(1)–S(2)	107.25(10)	C(14)–Sn(1)–S(2)	113.71(11)
N(1)–Sn(1)–S(2)	55.85(7)	N(1)–Sn(1)–C(8)	82.40(13)
N(1)–Sn(1)–C(14)	84.64(13)	N(1)–Sn(1)–C(20)	152.75(13)

Table 6
Selected bond lengths (Å) and angles (°) of complex **8**

Molecule A		Molecule B	
Bond lengths			
Sn(2)–C(36)	2.149(11)	Sn(1)–C(8)	2.102(10)
Sn(2)–C(43)	2.122(11)	Sn(1)–C(15)	2.118(11)
Sn(2)–C(50)	2.153(12)	Sn(1)–C(22)	2.109(11)
Sn(2)–S(4)	2.480(3)	Sn(1)–S(2)	2.501(3)
Sn(2)–N(3)	2.965(9)	Sn(1)–N(1)	2.949(10)
N(3)–C(30)	1.354(11)	N(1)–C(1)	1.351(11)
N(3)–C(29)	1.371(11)	N(1)–C(2)	1.388(12)
S(3)–C(35)	1.685(10)	S(1)–C(1)	1.741(11)
S(3)–C(29)	1.724(10)	S(1)–C(7)	1.747(11)
S(4)–C(29)	1.709(10)	S(2)–C(1)	1.662(10)
Bond angles			
C(43)–Sn(2)–C(36)	113.7(4)	C(8)–Sn(1)–C(22)	113.4(4)
C(36)–Sn(2)–C(50)	113.6(4)	C(22)–Sn(1)–C(15)	108.9(5)
C(36)–Sn(2)–S(4)	106.7(3)	C(8)–Sn(1)–C(15)	114.7(5)
C(43)–Sn(2)–C(50)	109.8(5)	C(8)–Sn(1)–S(2)	107.1(3)
C(43)–Sn(2)–S(4)	99.2(3)	C(22)–Sn(1)–S(2)	110.4(3)
C(50)–Sn(2)–S(4)	113.0(3)	C(15)–Sn(1)–S(2)	101.7(3)
N(3)–Sn(2)–C(36)	85.4(3)	N(1)–Sn(1)–C(8)	85.7(4)
N(3)–Sn(2)–C(50)	73.7(4)	N(1)–Sn(1)–C(22)	71.4(4)
N(3)–Sn(2)–C(43)	155.2(3)	N(1)–Sn(1)–C(15)	155.8(3)
S(4)–Sn(2)–N(3)	58.61(17)	S(2)–Sn(1)–N(1)	57.81(19)

due to the constraints from R groups (R = Me, Bu and Ph). The non-bonded S···S distances (S(2)···S(1)#, 3.43 and S(2)···S(2)#, 3.42 Å) are longer than those reported in the literature [13,14], shorter than the sum of the van

der Waals radii (S and S) (3.70 Å) [15], but well consistent with those in [(*n*-Bu)$_2$Sn(MNBT)$_2$] [6].

3.4.2. Structures of complexes 7 and 8

The structures of both complexes **7** and **8** are penta-coordinated with R_3Sn coordinated to the thiol S and heterocyclic N atoms of the same ligand and the structural distortion for each is a displacement from tetragonal towards trigonal bipyramidal geometry.

For complex **7**, the central tin atom forms four primary bonds: three to the phenyl groups and one to the sulfur atom. In addition, there is a weak intramolecular Sn–N interaction, the Sn(1)–N(1) bond length (3.14 Å) is longer than the sum of covalent radii (2.15 Å), but is considerably shorter than the sum of van der Waals radii of Sn and N atoms (3.75 Å) [5]. This bond length is almost equal to that in Ph_3Sn(MTS) (3.16 Å) [8], slightly shorter than that of triphenyl-(5-mercapto-1-phenyl-1,2,3,4-tetrazolato)tin(IV) (3.28 Å) [16], but a little longer than that reported in Ph_3Sn(MBZ) (3.07 Å) [8]. Thus complex **7** has a distorted *cis*-trigonal-bipyramidal geometry with the sulfur (S(2)) atom and two carbon atoms (C(14) and C(8)) occupying the equatorial plane, whereas the nitrogen (N(1)) and another carbon atom (C(20)) are in axial positions. The sum of the equatorial angles around the tin atom, (C(14)–Sn(1)–C(8), C(14)–Sn(1)–S(2) and C(8)–Sn(1)–S(2)), is 339.0° and the axial–Sn–axial angle, C(20)–Sn(1)–N(1), is 152.8°. The significant distortion is mainly due to the rigidity of the chelate ring (N(1)–Sn(1)–S(2): 55.8°), together with the large covalent radius of tin(IV). The Sn(1)–S(2) bond length (2.453 (2) Å) is just outside the range (2.39–2.44 Å) found in four-coordinate R_3SnSR' [3] but similar to that reported in the penta-coordinated organotin complex Ph_3Sn(MTS) (2.47 Å) [8].

Besides, intra-molecular non-bonded Sn···S interactions were recognized in the crystallographic analysis of complex **7**. The Sn···S bond length (3.97 Å) is longer than that reported in [2-(Me_2NCH_2)C_6H_4]$SnPh_2$ [S(S)PPh_2] (3.63 Å) and $Ph_2Sn(SCH_2CH_2S)$ (3.89 Å) but shorter than that of tribenzyl(2-thiolatopyridine-N-oxide)tin(IV) (4.15 Å) [17–19]. Due to the very weak intramolecular interaction, complex **7** can be thought of as a dimer.

For complex **8**, there exist two monomers in the asymmetric unit (see Fig. 3), which are different from a crystallographic point of view. Conformations of the two independent molecules are almost the same, with only little differences in bond lengths and bond angles (see Table 5). Each monomer has a distorted *cis*-tigonal-bipyramidal geometry with a tin–nitrogen intramolecular interaction similar to complex **7**. The two chelate bite angles, N(1)–Sn(1)–S(2) and N(3)–Sn(2)–S(4) are 57.81(19)° and 58.61(17)°, respectively. The axial–Sn–axial angles (C(15)–Sn(1)–N(1) = 155.8(3)° and C(43)–Sn(2)–N(3) = 155.2(3)°), strongly affected by the small bite angle, are well removed from the ideal trigonal-bipyramidal angle. The Sn–S bond length is around 2.49 Å (2.501(3) for Sn(1)–S(2) and 2.480(3) Å for Sn(2)–S(4)), which lies in the normal range for those higher-than-four-coordinated organotin structures and is slightly shorter than that reported in tribenzyl(2-thiolatopyridine-*N*-oxide)tin(IV) (2.58 Å) [19]. Concerning the Sn–N bonds, the bond lengths (Sn(1)–N(1): 2.949(10) Å and Sn(2)–N(3): 2.965(9) Å) are just between the sum of the van der Waals and covalent radii of Sn and N (3.74 and 2.15 Å, respectively) but shorter than that in complex **7** (3.14 Å), which evidences the influence of stereo-constraints, the larger the stereo-constraint of R groups, the more difficult the substituent for the nitrogen atom. In this situation, the stereo-constraint of Ph– is larger than that of $PhCH_2$–, so that the Sn–N bonds of complex **8** are stronger than that of complex **7**. Moreover, it is worth to note that both the Sn–N bond lengths of complexes **7** and **8** are consistent with the average Sn–N bond length (>2.39 Å) of active Sn complexes having antitumour activity [20].

The most significant difference between complexes **7** and **8** is that no Sn···S interactions between the molecules were found in the crystals of complex **8**. The possible reason is that in complex **8** three benzyl groups are bigger than the three phenyl groups in complex **7** so that there are more stereo-constraint coming from the $PhCH_2$– than that from Ph– to prevent the heterocyclic sulfur from bonding to the central tin. The drawings of the unit cells for complexes **7** and **8** support our reasoning quite well.

4. Conclusions

A series of organotin complexes based on 2-mercapto-6-nitrobenzothiazole have been synthesized and characterized. Detailed studies on the structures and spectra of these complexes indicate that there exist such an inclination that the structures of those dialkyltin complexes are likely to construct distorted trapezoidal bipyramidal geometry and those trialkyltin complexes are apt to have distorted trigonal bipyramidal geometry. Besides, the stereo-constraints from the R groups of trialkyltin chloride were found to have great influence to the final coordination mode and crystal structures. As for as the stereo-constraint of coordination from the nitrogen atom to the tin atom is concerned, the consequence is $PhCH_2$<Ph, but as to that of construction of a dimer, it is Ph<$PhCH_2$.

5. Supplementary material

Crystallographic data for the structural analysis have been deposited with the Cambridge Crystallographic Data Center, CCDC Nos. 220043, 192488 and 192499 for complexes **4**, **7** and **8**, respectively. Copies of these

information may be obtained free of charge from the Director, CCDC, 12 Union Road, Cambridge, CB2 1EZ, UK (fax: +44-1223-336033; deposit@ccdc.cam.ac.uk or http://www.ccdc.cam.ac.uk).

Acknowledgements

We thank the National Natural Foundation, PR China (20271025), the Key Teachers Foundation from the State Education Ministry of China and the National Natural Foundation of Shandong Province, PR China for financial support of this work.

References

[1] T.S.B. Baul, S. Dhar, S.M. Pyke, E.R.T. Tiekink, E. Rivarola, R. Butcher, F.E. Smith, J. Organomet. Chem. 633 (2001) 7.
[2] M. Kemmer, H. Dalil, M. Biesemans, J.C. Martins, B. Mahieu, E. Horn, D. de Vos, E.R.T. Tiekink, R. Willem, M. Gielen, J. Organomet. Chem. 608 (2000) 63.
[3] N. Speziali, B.G. Guimarães, R.M. Silva, P.H. Duarte, S.R. Aguiar, Acta Crystallogr. C50 (1994) 1059.
[4] G.D. Andreeti, G. Bocelli, G. Calestani, P. Sgarabotto, J. Organomet. Chem. 273 (1984) 31.
[5] J.S. Casas, A. Castiñeiras, E.G. Martínez, A.S. González, A. Sánchez, J. Sordo, Polyhedron 16 (1997) 795.
[6] C. Ma, Q. Jiang, R.F. Zhang, Appl. Organomet. Chem. 17 (2003) 623.
[7] C. Ma, Q. Jiang, R.F. Zhang, Can. J. Chem. 81 (2003) 825.
[8] C.V. Rodarte de Moura, A.P.G. de Sousa, R.M. Silva, A. Abras, M. Hörner, A.J. Bortoluzzi, C.A.L. Filgueiras, J.L. Wardell, Polyhedron 18 (1999) 2961.
[9] C. Pettinari, F. Marchetti, R. Pettinari, D. Martini, A. Drozdov, S. Troyanov, Inorg. Chim. Acta 325 (2001) 103, and references therein.
[10] R.C. Poller, The Chemistry of Organotin Compounds, Logos Press, London, 1970, p. 221.
[11] S.K. Hadjikakou, M.A. Demertzis, M. Kubicki, D. Kovala-Demertzi, Appl. Organomet. Chem. 14 (2000) 727.
[12] O. Jiménez-Sandoval, R. Cea-Olivares, S. Hernández-Ortega, Polyhedorn 16 (1997) 4129.
[13] Y. Nagao, H. Nishijima, H. Iimori, H. Ushirogochi, S. Sano, M. Shiro, J. Organomet. Chem. 611 (2000) 172.
[14] H.D. Yin, C.H. Wang, C.L. Ma, Y. Wang, Chin. J. Chem. 20 (2002) 913.
[15] J. Dai, M. Munakata, L.P. Wu, T. Kuroda-Sowa, Y. Suenaga, Inorg. Chim. Acta 258 (1997) 65.
[16] J. Bravo, M.B. Cordero, J.S. Casas, A. Sánchez, J. Sado, E.E. Castellano, J. Zakerman-Schpector, J. Organomet. Chem. 482 (1994) 147.
[17] R.A. Varga, M. Schuermann, C. Silvestru, J. Organomet. Chem. 623 (2001) 161.
[18] A.P.G. de Sousa, R.M. Silva, A. Cesar, J.L. Wardell, J.C. Huffmna, A. Abras, J. Organomet. Chem. 605 (2002) 82.
[19] S.W. Ng, C. Wei, K.V.G. Das, T.C.W. Mak, J. Organmet. Chem. 334 (1987) 283.
[20] L. Pellerito, L. Nagy, Coord. Chem. Rev. 224 (2002) 111.

Available online at www.sciencedirect.com
SCIENCE DIRECT®
Polyhedron 23 (2004) 787–791
POLYHEDRON
www.elsevier.com/locate/poly

Synthesis and characterization of metal-free and metallo phthalocyanines with four pendant naphthoxy-substituents

H. Yasemin Yenilmez, İbrahim Özçeşmeci, Ali İhsan Okur, Ahmet Gül *

Department of Chemistry, Technical University of Istanbul, Fen-Edebiyat Fakltesi, TR34469 Maslak, Istanbul, Turkey

Received 30 September 2003; accepted 10 November 2003

Abstract

Phthalocyanines with four naphthoxy pendant groups on the periphery were prepared by cyclotetramerization of 4-(1-naphthoxy)phthalonitrile and 4-(2-naphthoxy)phthalonitrile. The new compounds were characterized by elemental analyses, ^{1}H NMR, IR and UV–Vis spectral data. The electronic spectra exhibit an intense $\pi \rightarrow \pi^*$ transition of naphthyl identity together with characteristic Q and B bands of the phthalocyanine core.
© 2003 Elsevier Ltd. All rights reserved.

Keywords: Phthalocyanine; Cobalt; Zinc; Nickel; Naphthalene

1. Introduction

The use of tetrapyrrol derivatives and related compounds as advanced materials has shown a rapid increase in recent decades owing to their special features which make them extremely interesting products in new technological applications such as PDT, eletrochromism and chemical sensors, in addition to their traditional use as dyes and pigments [1–5]. Tailoring of the properties of these compounds by either addition of various groups on the periphery or by insertion of different metal ions brings an outstanding architectural flexibility [6,7]. Long chain alkyl, alkoxy or alkylthio substituents have been often added on the periphery of phthalocyanines to improve solubility in nonpolar solvents; the presence of crown ethers or tetraazamacrocycles at the same position, on the other hand, results in products capable of selectively binding alkali or transtion metal ions, respectively [8–15].

Condensed multicyclic aromatic compounds (e.g., naphthalene derivatives) are functional groups effective in photoemission studies [16]. Naphthalocyanines which might be considered among these compounds are essentially porphyrazine derivatives in which naphthalenyl groups are fused to the tetrapyrrol core. These compounds are discriminated as 1,2-naphthalocyanines or 2,3-naphthalocyanines depending on whether the starting material is a 1,2- or 2,3-naphthalonitrile derivative [17–20]. As bulky electron rich units, the presence of naphthalenyl groups on the periphery of phthalocyanines is also expected to change the ordering of molecules in the solid state. However, in the case of naphthalocyanines, the physical and chemical identity of naphthalene units is no longer distinct. In contrast to the extensive number of studies on naphthalocyanines, the description of phthalocyanines with naphthalenyl substituents are unprecedented, except a recent paper giving the crystal structure of the phthalonitrile derivative with 1-naphthoxy substituents [21] and another recent one giving the synthesis of a phthalocyanine carrying nitro groups together with α-naphthoxy substituents on a peripheral position [22].

2. Experimental

IR spectra were recorded on a Mattison 1000 FTIR spectrophotometer using KBr pellets, electronic spectra on a Unicam UV2 spectrophotometer. Elemental analyses were performed by the Instrumental Analysis Laboratory of the TUBITAK Marmara Research Centre. ^{1}H NMR spectra were recorded on a Bruker

* Corresponding author. Tel.: +90-212-285-6827; fax: +90-212-285-6386.
E-mail address: ahmetg@itu.edu.tr (A. Gül).

0277-5387/$ - see front matter © 2003 Elsevier Ltd. All rights reserved.
doi:10.1016/j.poly.2003.12.003

250 MHz spectrometer using TMS as internal reference. 4-Nitro-phthalonitrile (**1**) was prepared as given in the literature [23].

2.1. Synthesis of phthalonitrile derivatives

2.1.1. 4-(1-naphthoxy)Phthalonitrile (**2**)

4-Nitro-phthalonitrile (**1**) (1.73 g, 0.01 mol) and 1-naphthol (1.44 g, 0.01 mol) were added successively with stirring to dry DMSO (15 ml). After they were dissolved, anhydrous K_2CO_3 (2.0 g, 0.014 mol) was added portionwise over 2 h and the mixture was stirred vigorously at room temperature for a further 28 h. Then, the reaction mass was poured into water (100 ml) and the precipitate formed was filtered off, washed with water, and crystallized from EtOH–water to give the product as a yellow, crystalline powder. Yield: 2.05 g, 76%. Melting point 101–102 °C. IR (KBr), $\nu(cm^{-1})$: 3080 (H–Ar), 2238 (C=N), 1574 (Ar C=C), 1268 (Ar–O–Ar), 782; ^{1}H NMR (d-chloroform 250 MHz): 7.17–7.96 (m, H–Ar). UV–Vis λ_{max}(nm) (log ε) in $CHCl_3$: 285 (4.4).

2.1.2. 4-(2-naphthoxy)Phthalonitrile (**3**)

Compound **3** was prepared according to the same procedure as described for the preparation of **2** by starting from 2-naphthol (1.44 g, 0.01 mol) Yield: 2.0 g, 74.3%. Melting point 119–120 °C. IR (KBr), $\nu(cm^{-1})$: 3080 (H–Ar), 2238 (C=N), 1570 (Ar C=C), 1268, 1242 (Ar–O–Ar), 782; ^{1}H NMR (d-chloroform 250 MHz): 7.17–7.97 (m, H–Ar). UV–Vis λ_{max}(nm) (log ε) in $CHCl_3$: 290 (4.0) (sh).

2.2. General procedures for phthalocyanine derivatives (**4a–d**, **5a–c**)

A mixture 0.5 mmol (0.135 g) of phthalonitrile derivative (**2** or **3**), 0.125 mmol of anhydrous metal salt [$CoCl_2$ (0.016 g), $Zn(OAc)_2$ (0.016 g) or $NiCl_2$ (0,016 g)] and 0.04 mmol of 1.8-diazabicyclo [5.4.0] undec-7-ene (DBU) (0.07 ml) in 1.5 ml of hexanol was heated and stirred at 160 °C for 24 h under N_2. For cobalt derivatives (**4a** and **5a**) no DBU and for metal-free phthalocyanines no metal salt was required. The resulting green suspension was cooled to ambient temperature and then filtered off. The precipitate was washed first with water, then with ethanol and then dried in vacuo. Finally, pure phthalocyanine derivatives were obtained by chromatography on silica gel using chloroform or chloroform/hexane (100:1) mixture as eluent.

2.2.1. 2,9,16,23-Tetrakis(1-naphthoxy)-phthalocyaninatocobalt (II) (**4a**)

Yield: 58 mg, 40.9%. Melting point >200 °C IR (KBr), $\nu(cm^{-1})$: 3080 (H–Ar), 1574 (Ar C=C), 1268, 1242 (Ar–O–Ar), 782.

2.2.2. 2,9,16,23-Tetrakis(1-naphthoxy)-phthalocyanine (**4b**)

Yield: 38 mg, 28%. Melting point >200 °C IR (KBr), $\nu(cm^{-1})$: 3080 (H–Ar), 3310 (N-H), 1574 (Ar C=C), 1268, 1242 (Ar–O–Ar), 782. ^{1}H NMR (d-chloroform 250 MHz): 6.56–8.81 (m, H–Ar), −7.12 (br s, N–H).

2.2.3. 2,9,16,23-Tetrakis(1-naphthoxy)-phthalocyaninatonickel (II) (**4c**)

Yield: 22 mg, 15.5%. Melting point >200 °C IR (KBr), $\nu(cm^{-1})$: 3080 (H–Ar), 1574 (Ar C=C), 1268, 1242 (Ar–O–Ar), 782.

2.2.4. 2,9,16,23-Tetrakis(1-naphthoxy)-phthalocyaninatozinc (II) (**4d**)

Yield: 30 mg, 21%. Melting point >200 °C IR (KBr), $\nu(cm^{-1})$: 3080 (H–Ar), 1574 (Ar C=C), 1268, 1242 (Ar–O–Ar), 782. ^{1}H NMR (d-chloroform 250 MHz): 6.87–8.00 (m, H–Ar).

2.2.5. 2,9,16,23-Tetrakis(2-naphthoxy)-phthalocyaninatocobalt (II) (**5a**)

Yield: 14 mg, 9.82%. Melting point >200 °C IR (KBr), $\nu(cm^{-1})$: 3055 (H–Ar), 1620, 1470 (Ar C=C), 1268, 1242 (Ar–O–Ar), 782.

2.2.6. 2,9,16,23-Tetrakis(2-naphthoxy)-phthalocyanine (**5b**)

Yield: 19 mg, 14%. Melting point >200 °C IR (KBr), $\nu(cm^{-1})$: 3080 (H–Ar), 3310 (N–H), 1500–1470 (Ar C=C), 1268, 1242 (Ar–O–Ar), 782. ^{1}H NMR (d-chloroform 250 MHz): 6.8–7.8 (m, H–Ar), −4.83 (br s, N–H).

2.2.7. 2,9,16,23-Tetrakis(2-naphthoxy)-phthalocyaninatonickel (**5c**)

Yield: 16 mg, 11.25%. Melting point >200 °C IR (KBr), $\nu(cm^{-1})$: 3055 (H–Ar), 1600–1570 (Ar C=C), 1268, 1242 (Ar–O–Ar), 782. ^{1}H NMR (d-chloroform 250 MHz): 6.4–7.35 (m, H–Ar).

3. Results and discussion

The phthalonitrile derivatives **2** and **3** were obtained through displacement reaction of 4-nitrophthalonitrile **1** with 1-naphthol and 2-naphthol, respectively [24] (Fig. 1). Conversion of **2** and **3** into the corresponding metal-free and metallo-phthalocyanines (**4a–d**, **5a–c**) was accomplished in high-boiling solvents in the presence of 1,8-diazabicyclo[5.4.0]undec-7-ene and/or metal salts. All of these new compounds were characterized by elemental analysis, IR, UV–Vis and NMR spectroscopic techniques (Table 1).

The spectroscopic data of the new compounds were in accordance with the structures [7–15]. Naturally, the

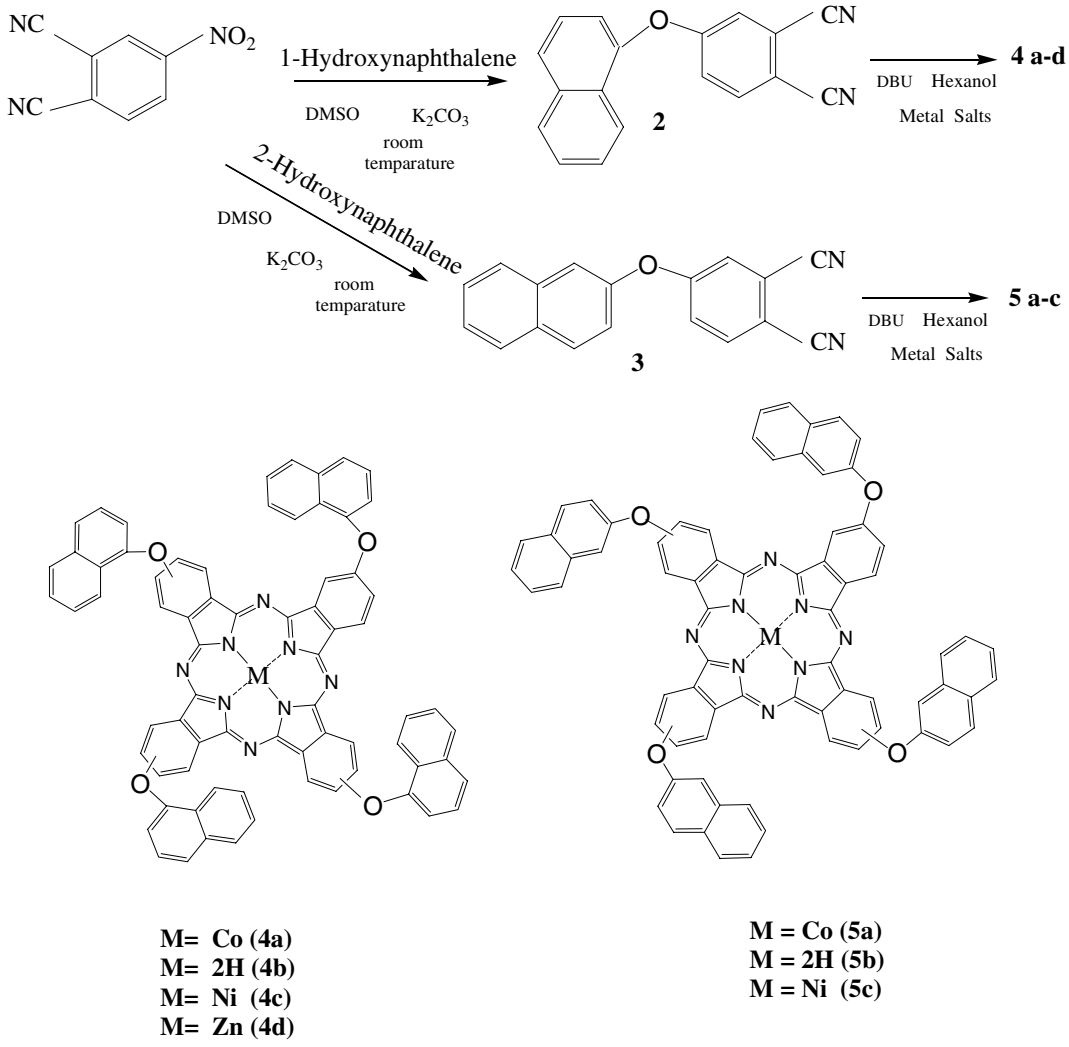

Fig. 1. Napthoxyphthalonitrile derivatives and the phthalocyanines derived from them.

phthalocyanine products synthesized during this work are a mixture of positional isomers while both of the phthalonitrile precursor **2** and **3** carry a single substituent [2,25].

There is only a very slight difference between the chemical shift values of aromatic protons for **2** (7.13–7.96 ppm) and for **3** (7.17–7.97 ppm). In addition, when compared with the IR spectrum of **1**, those of **2** and **3** confirmed the proposed structures by the disappearance of the aromatic $-NO_2$ band at 1548 cm^{-1} and the appearance of an intense new absorption at 1268 cm^{-1} attributable to aromatic C–O–C [24]. After conversion of dinitrile derivatives **2** and **3** to phthalocyanines, the sharp C≡N vibration around 2238 cm^{-1} disappeared. The NH stretching absorption of the inner core of the metal-free phthalocyanines **4b** and **5b** was observed around 3310 cm^{-1}. The N–H protons of the metal-free phthalocyanine **4b** and **5b** were also identified in the ^1H NMR spectrum with a broad peak at $\delta = -7.12$, $\delta = -4.83$ ppm, presenting the typical shielding of inner core protons, which is a common feature of the ^1H NMR spectra of metal-free phthalocyanines [9,15] (Fig. 2). The difference between the chemical shift values of the inner core protons in **4b** and **5b** is a consequence of differences in the concentration of these compounds when taking the spectra. It should be noted that the

Table 1
Elemental analyses results of the phthalocyanines[a]

Compound	C	H	N
2	79.47 (79.99)	3.68 (3.79)	10.12 (10.36)
3	79.67 (79.99)	3.97 (3.79)	9.91 (10.36)
4a	75.91 (75.86)	3.20 (3.54)	9.31 (9.83)
4b	79.60 (79.84)	4.12 (3.91)	10.52 (10.35)
4c	75.32 (75.87)	3.10 (3.54)	9.85 (9.83)
4d	75.05 (75.43)	3.81 (3.52)	10.12 (9.77)
5a	76.05 (75.86)	3.38 (3.54)	10.15 (9.83)
5b	79.62 (79.84)	3.87 (3.91)	9.97 (10.35)
5c	75.95 (75.87)	3.89 (3.54)	9.64 (9.83)

[a] Required values are given in parentheses.

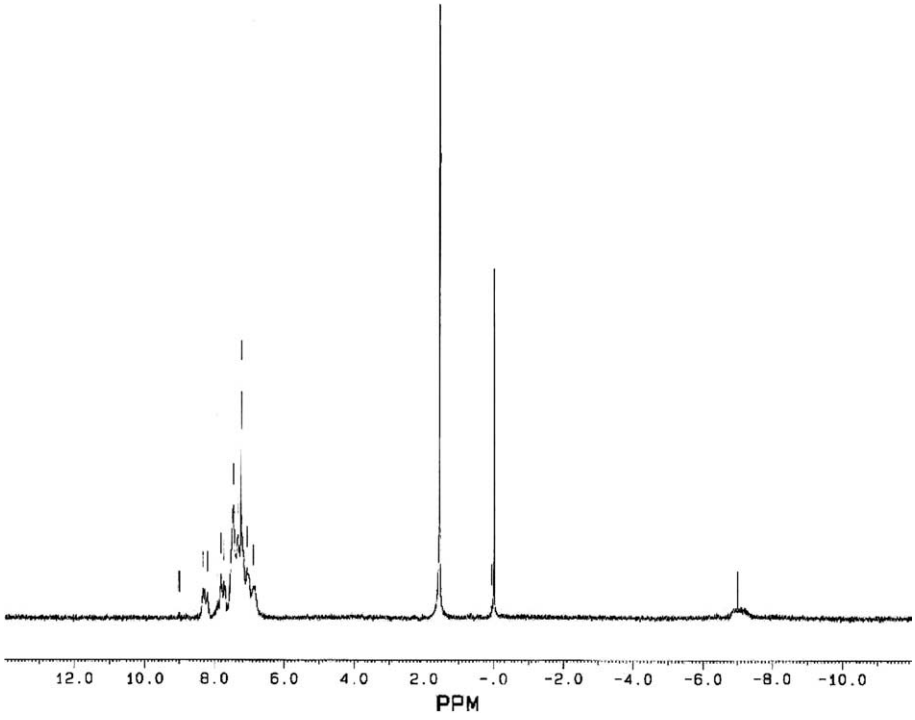

Fig. 2. H^1 NMR spectra of metal-free phthalocyanine **4b**.

chemical shifts of α-protons of the Pc core could not be observed in the case of **5b** and **5c** probably due to aggregation. IR spectra of all phthalocyanine derivatives **4a**–**d**, **5a**–**c** showed aromatic C–O–C peaks at 1268 and 1242 cm^{-1} and a characteristic substituted naphthalene peak at 782 cm^{-1}.

Electronic spectra are especially fruitful to establish the structure of all the phthalocyanines **4a**–**d**, **5a**–**c**. The UV–Vis spectra of the phthalocyanine core is dominated by two intense bands, the Q band around 680 nm and the B band in the near UV region, around 330 nm, both correlate to $\pi \rightarrow \pi^*$ transitions [7–15]. UV–Vis spectra of metallo phthalocyanines (**4a** in THF, **4b**–**d**, **5a**–**c** in $CHCl_3$) exhibited an intense single Q band absorption of the $\pi \rightarrow \pi^*$ transitions around 660–680 nm and B bands in the UV region around 327–343 nm (Fig. 3). For metal-free derivatives **4b** and **5b** (in $CHCl_3$) split Q bands appeared at 702–667 nm, while the B band remained at 339 nm (Table 2). In the case of naphthalocyanines, the naphtho groups are fused to the planar phthalocyanine core and their π-electrons are integrated into the aromatic system of the main core [17–20]. The consequence of this structure is some bathochromic shift to the near IR region, especially in the Q band, while the B band remains almost the same as in the case of the parent phthalocyanine molecules. Here, in the case of the phthalocyanines with appending naphthoxy substituents the electronic spectra appear very similar to those of tetra-substituted phthalocyanines, but additionally an intense absorption due to the $\pi \rightarrow \pi^*$ tran-

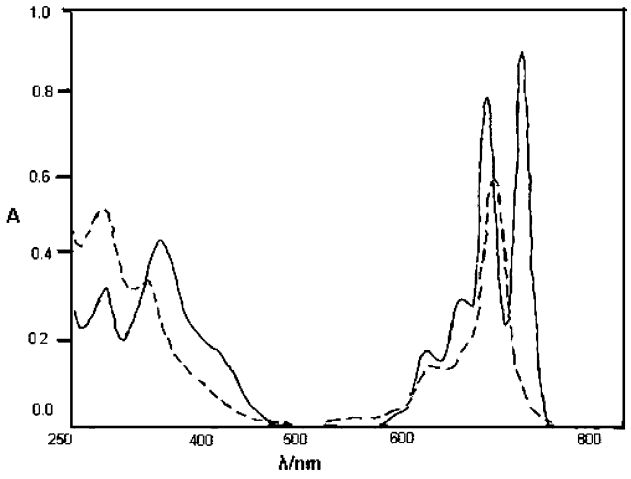

Fig. 3. UV–Vis spectra of metal-free phthalocyanine **5b** (——) and its Co complex **5a** (– – –).

Table 2
UV–Vis data for the phthalocyanines in chloroform

Compound	λ/nm (log ε/dm^3 mol^{-1} cm^{-1})			
4a[a]	327 (4.86)	601 (4.37)	664 (5.03)	
4b	290 (4.63)	339 (4.73)	667 (4.90)	702 (4.95)
4c	299 (4.92)	343 (4.42)	664 (5.04)	
4d	287 (4.24)	343 (4.42)	680 (4.88)	
5a	288 (3.76)	328 (4.59)	664 (4.82)	
5b	287 (4.52)	343 (4.46)	668 (4.67)	703 (4.73)
5c	281 (4.18)	329 (4.04).	671 (5.16)	

[a] In THF.

sition of naphthalene groups appeared for all these phthalocyanine derivatives **4a**–**d**, **5a**–**c** in the UV region at about 290 nm (Table 2).

In conclusion, we have described the synthesis and spectral characterization of seven new phthalocyanines with 1-naphthoxy and 2-naphthoxy substituents on the periphery; the distinctive property of these compounds is a second absortion in the ultraviolet region of comparable intensity to the intense B band of phthalocyanines.

Acknowledgements

This work was supported by the Research Fund of the Technical University of Istanbul.

References

[1] C.G. Claessens, W.J. Blau, M. Cook, M. Hanack, R.J.M. Nolte, T. Torres, D. Wöhrle, Monatsh. Chem. 132 (2001) 3.
[2] N.B. Mc Keown, Phthalocyanine Materials: Synthesis, Structure and Function, Cambridge University Press, Cambridge, 1998.
[3] D. Wöhrle, Macromol. Rapid. Commun. 22 (2001) 68.
[4] H.S. Nalwa, Handbook of Organic Conductive Molecules and Polymers, Wiley, Chichester, 1997, p. 741.
[5] E.A. Lukyanets, J. Porphyrins Phthalocyanines 3 (1999) 424.
[6] C.C. Leznoff, A.B.P. Lever, Phthalocyanines Properties and Applications, VCH, Weinheim, 1989.
[7] Ö. Bekaroğlu, Appl. Organomet. Chem. 10 (1996) 605.
[8] M. Hanack, A. Gül, A. Hirsch, B.K. Mandal, L.R. Subramanian, E. Witke, Mol. Cryst. Liq. Cryst. 187 (1990) 365.
[9] İ. Gürol, V. Ahsen, Ö. Bekaroğlu, J. Chem. Soc., Dalton Trans. (1994) 497.
[10] Z.A. Bayír, E. Hamuryudan, A.G. Gürek, Ö. Bekaroğlu, J. Porphyrins Phthalocyanines 1 (1997) 349.
[11] G. Gümüş, A. Gül, V. Ahsen, New J. Chem. 21 (1997) 589.
[12] M. Koçak, A. Cihan, A.İ. Okur, A. Gül, Ö. Bekaroğlu, Dyes Pig. 45 (2000) 9.
[13] M. Koçak, A.İ. Okur, Ö. Bekaroğlu, J. Chem. Soc., Dalton Trans. (1994) 323.
[14] M. Koçak, A. Gürek, A. Gül, Ö. Bekaroğlu, Chem. Ber. 127 (1994) 355.
[15] V. Ahsen, E. Yílmazer, M. Ertas, J. Chem. Soc., Dalton Trans. (1988) 401.
[16] V.V. Rozhkov, M. Khajehpour, S.A. Inogradov, Inorg. Chem. 42 (2003) 14.
[17] G.Y. Yang, M. Hanack, Y.W. Lee, Y. Chen, M.K.Y. Lee, D. Dini, Chem. A Eur. J. 9 (12) (2003) 2758.
[18] M.T.M. Choi, P.P.S. Li, D.K.P. Ng, Tetrahedron 56 (2000) 3881.
[19] C. Penglei, W. Xiaobing, T. Daihua, Z. Zhen, Z. Jiancheng, L. Xinhou, Dyes Pig. 48 (2001) 85.
[20] Y. Chen, S. O'Flaherty, M. Fujitsuka, M. Hanack, L.R. Subramanian, O. Ito, W.J. Blau, Chem. Mater. 14 (12) (2002) 5163.
[21] N. Karadayí, N. Akdemir, E. Ağar, I.E. Gümrükçüoğlu, O. Büyükgüngör, Acta Crystallogr., Sect. E 59 (2003) 945.
[22] O.V. Shishkina, B.E. Maizlish, G.P. Shaposhnikov, R.P. Smirnov, Russ. J. Gen. Chem. 70 (6) (2002) 937.
[23] J.G. Young, W. Onyebuagu, J. Org. Chem. 55 (1990) 2155.
[24] T.M. Keller, T.R. Price, J.R. Grhinh, Synthesis (1980) 613.
[25] M. Hanack, G. Schmid, M.. Sommeraner, Angew. Chem. Int., Ed. Eng. 32 (1993) 1422.

Available online at www.sciencedirect.com
SCIENCE DIRECT®
Polyhedron 23 (2004) 793–800
POLYHEDRON
www.elsevier.com/locate/poly

Silver(I) complexes of the naphthyl-azoimine function: single crystal X-ray structure of bis-[1-ethyl-2-(naphthyl-α-azo)imidazole]silver(I) perchlorate

Joydev Dinda [a], Sk. Jasimuddin [a], G. Mostafa [b], C.-H. Hung [c], Chittaranjan Sinha [a,*]

[a] Department of Chemistry, The University of Burdwan, Burdwan 713104, India
[b] Department of Physics, National Tsing-Hua University, 101 Sec2, Kuang Fu Road, 300, Taiwan, ROC
[c] Department of Chemistry, National Changhua University of Education, Changhua 50058, Taiwan, ROC

Received 24 July 2003; accepted 11 November 2003

Abstract

Reaction of $AgNO_3$ and 1-alkyl-2-(naphthyl-(α/β)-azo)imidazole (α-/β-NaiR) in MeOH followed by the addition of $NaClO_4$ has isolated $[Ag(\alpha\text{-/}\beta\text{-NaiR})_2](ClO_4)$ (**3/4**). The complexes are characterized by microanalytical and spectral data. Single crystal X-ray diffraction study of bis-[1-ethyl-2-(naphthyl-α-azo)imidazole]silver(I) perchlorate confirms the structure of the complex. Argentophilicity of imidazole-N and steric crowding by naphthyl groups have forced a {2+2} distorted linear geometry. The structure shows intramolecular and intermolecular H-bonding in a 1D helical framework along with face-to-face π–π interactions.
© 2003 Elsevier Ltd. All rights reserved.

Keywords: Naphthylazoimidazole; Silver(I) complexes; Helical structure; EHMO

1. Introduction

Imidazole is ubiquitous in chemistry and biology [1]. In this respect, the chemical modification of imidazole to synthesize polydentate ligands is of current interest [2–4]. We are also engaged to synthesize imidazole containing ligands, arylazoimidazoles by anchoring an arylazo (Ar–N=N$^+$) group to the imidazole backbone. As a part of our continuing program of research in the field of azohetereocyclic molecules we have designed arylazoheterocycles of pyridine, pyrimidine and imidazole [5–7]. They differ in their π-acidity in the order of imidazole < pyridine < pyrimidine [8]. Arylazoheterocycles bear the functional group azoimine, –N=N–C=N–, which is an efficient group to stabilize the low valent metal redox state [9–12].

Imidazole, being a five-membered heterocycle, is less π-acidic and a better π-donor than six-membered pyridine/pyrimidine rings. The electronic property of the molecule may be finely adjusted by changing substituents in the aryl group or complete replacement of the aryl group by an α- and/or β-naphthyl group [9–12]. The α- and β-naphthyl moieties also exhibit different thermodynamic stability [13] which may indirectly perturb the electronic levels of the metal complexes.

We have recently reported the coordination chemistry of platinum(II) [9], ruthenium(II) [10], osmium(II) [11] and palladium(II) [12] naphthylazoimidazoles. In recent years the coordination chemistry of coinage metals came into the field for their (i) biological and medicinal importance [14–16], (ii) metal–metal interaction between closed shell (d^{10}–d^{10}) cations or the aurophilic interaction [17–20] and (iii) supramolecular assemblies with particular reference to helicity in silver(I) complexes [21–25]. Several single and double stranded helical polymers of silver(I) and their photophysical and spectrochemical properties are topics of developing interest. Because of the flexibility in coordination number in Ag(I) [26, 27], covalent interaction may lead to the synthesis of coordination polymers [28]. The assembly of coordination networks through H-bonding and π–π stacking

* Corresponding author. Tel.: +91-342-57683; fax: +91-342-64452/2530452.
E-mail addresses: buclib@satyam.net.in, c_r_sinha@yahoo.com (C. Sinha).

0277-5387/$ - see front matter © 2003 Elsevier Ltd. All rights reserved.
doi:10.1016/j.poly.2003.11.056

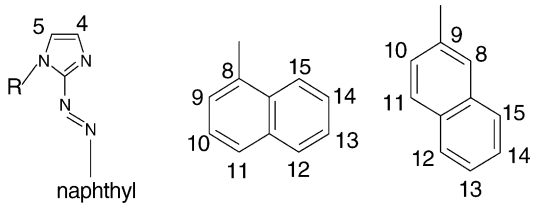

1-alkyl-2-(naphthylazo)imidazole (α-NaiR) (β-NaiR)

R = Me (**a**), Et (**b**), CH_2Ph (**c**)

Scheme 1.

interactions has been of great interest in recent years [29,30]. Presence of suitable oxo counter ions (e.g. NO_3^-, ClO_4^-, $CF_3SO_3^-$, etc) in the complexes may result in secondary interactions, C–H···O and act as a determining factor for crystal packing and helicity [31].

Ag(I)-azoimidazole complexes have been reported by a different researcher [32–36]. In this work, we have selected closely related ligands, 2-(naphthyl-(α/β)-azo)imidazole (α/β-NaiR) (Scheme 1) which provide larger steric crowding and better electron donating ability than a conventional aryl group. In this work we have explored the coordination chemistry of Ag(I)-naphthylazoimidazoles. Synthesis, spectral, electrochemical studies have been carried out and a single crystal X-ray structure of Ag(I)-naphthylazoimidazoles are described.

2. Experimental

2.1. Materials

1-Alkyl-2-(naphthyl-(α/β)-azo)imidazoles (α-NaiR (**1**), β-NaiR (**2**)) were synthesized by a reported procedure [10,12]. $AgNO_3$ and α-/β-naphthylamines were obtained from E. Merck, Germany and $NaClO_4$ was obtained from Fluka, USA. Purification of solvents was performed as in the reported procedure [12]. All other solvents and chemicals were of reagent grade and were used without further purification.

2.2. Physical measurements

Microanalytical (C, H, N) data were collected using a Perkin–Elmer 2400 elemental analyzer. UV–Vis spectra were recorded by a JASCO V-570 UV/Vis/NIR spectrophotometer. IR data were collected from a JASCO-420 FTIR (KBr disk, 4000–200 cm^{-1}). ^1H NMR spectra were collected in $CDCl_3$ using a 500 MHz FT-NMR spectrometer. Electrical conductivity was measured using a Systronics 305 digital conductivity meter with a solution concentration of $\sim 10^{-3}$ M cm^{-3}. Silver was analyzed gravimetrically [37]. Electrochemical measurements were carried out under dinitrogen conditions with the help of an EG&G PARC 270 computer controlled Versastat using a Pt-disk milli working electrode. All results were collected at 298 K with the saturated calomel electrode (SCE) as reference. Reported potentials are uncorrected for junction effects.

Caution! Perchlorate salts of metal complexes are explosive in nature and should be handled carefully.

2.3. Preparation of bis-[1-ethyl-2-(naphthyl-α-azo)imidazole]silver(I) perchlorate, $[Ag(\alpha\text{-NaiEt})_2](ClO_4)$ (**3b**)

The ligand α-NaiEt (0.50 g, 2 mmol) in dry MeOH (20 ml) was added to a methanolic solution of $AgNO_3$ (0.17 g, 1 mmol). The red-brown solution was stirred for 4 h in a dark environment and covered with carbon paper. The solution volume was reduced to half of its original volume by bubbling nitrogen gas. The compound was collected as the perchlorate salt by adding $NaClO_4$(1 g in 2 ml aqueous solution). The brown-red mass was recrystalized from diffusion of a CH_2Cl_2 solution of the complex into hexane. Yield was 0.60 gm (90%). *Anal.* Calc. for $C_{30}H_{28}N_8ClO_4Ag$ (**3b**): C, 50.78; H, 3.87; N, 15.90; Ag, 15.03. Found: C, 50.89; H, 3.96; N, 15.83; Ag, 15.24%. IR (KBr, cm^{-1}): 1384 (N=N), 1582 (C=N).

All other complexes were prepared following an identical procedure and yields were 75–90%. *Anal.* Calc. for $C_{28}H_{24}N_8ClO_4$ Ag (**3a**): C, 49.35; H, 3.91; N, 15.78; Ag, 16.15. Found: C, 49.46; H, 3.59; N, 16.49; Ag, 15.87%. IR (KBr, cm^{-1}): 1386 (N=N), 1585 (C=N). *Anal.* Calc. For $C_{40}H_{32}N_8ClO_4Ag$ (**3c**): C, 57.60; H, 3.78; N, 13.39; Ag, 13.11. Found: C, 57.74; H, 3.85; N, 13.47; Ag, 13.25%. IR (KBr, cm^{-1}): 1381 (N=N), 1590 (C=N). *Anal.* Calc. For $C_{28}H_{24}N_8ClO_4$ Ag (**4a**): C, 49.39; H, 3.51; N, 16.43; Ag, 15.69. Found: C, 49.46; H, 3.59; N, 16.49; Ag, 15.87%. IR (KBr, cm^{-1}): 1382 (N=N), 1587 (C=N). *Anal.* Calc. for $C_{30}H_{28}N_8ClO_4Ag$ (**4b**): C, 50.80; H, 3.90; N, 15.73; Ag, 15.84. Found: C, 50.89; H, 3.96; N, 15.83; Ag, 15.24%. IR (KBr, cm^{-1}): 1384 (N=N), 1582 (C=N). *Anal.* Calc. for $C_{40}H_{32}N_8ClO_4Ag$ (**4c**): C, 57.69; H, 3.80; N, 13.43; Ag, 13.02. Found: C, 57.74; H, 3.85; N, 13.47; Ag, 13.25%. IR (KBr, cm^{-1}): 1381 (N=N), 1585 (C=N).

2.4. Crystallographic data collection and refinement

A crystal suitable for X-ray diffraction study was obtained after several trials by slow diffusion of a CH_2Cl_2 solution of the complex into a hexane layer. A suitable single crystal of complex $[Ag(\alpha\text{-NaiEt})_2](ClO_4)$ (**3b**) was mounted on a Siemens CCD diffractometer equipped with graphite monochromated Mo Kα ($\lambda = 0.71073$ Å) radiation. The intensity data were corrected for Lorentz and polarization effects. Details of data collection and structure solution are given in Table 1. The structure was solved by Patterson syntheses and

Table 1
Summarized crystallography data for [Ag(α-NaiEt)$_2$][ClO$_4$] (**3b**)

Crystal parameters	
Empirical formula	$C_{30}H_{28}N_8ClO_4Ag$
Formula weight	707.9
Crystal system	tetragonal
Space group	*P*-4*n*2
a (Å)	16.376(4)
b (Å)	16.376(4)
c (Å)	22.971(8)
α (°)	90
β (°)	90
γ (°)	90
V (Å^3)	6160(3)
λ (Å)	0.71073
ρ_{calc} (Mg m^{-3})	1.52
Z	8
T (K)	293(2)
μ(Mo Kα) (mm^{-1})	0.791
Total data	37,885
Unique data	7091
Observed data ($I > 2\sigma(I)$)	2938
Refined parameters	397
R	0.0394
wR_2	0.0920
Goodnees-of-fit	1.00

$R = \sum||F_o| - |F_c||/\sum|F_o|$. $wR_2 = [\sum w(|F_o|^2 - |F_c|^2)^2/\sum w(|F_o|^2)^2]^{1/2}$, $w = 1/[\sigma^2(F_o^2) + (0.0299P)^2]$, $P = (F_o^2 + 2F_c^2)/3$. Goodness-of-fit (GOF) is defined as $[w(F_o - F_c)/(n_0 - n_v)]^{1/2}$ where n_0 and n_v denote the number of data and variables, respectively.

followed by successive Fourier and difference Fourier syntheses. Full-matrix least-squares refinements on F^2 were carried out using SHELXL-97 with anisotropic displacement parameters for all non-hydrogen atoms. Hydrogen atoms were constrained to ride on the respective carbon atoms with an isotropic displacement parameter equal to 1.2 times the equivalent isotropic displacement parameter of their parent atom. Since the complex was crystallized in a non-centrosymmetric space group, the absolute configuration was determined (Flack × parameter $= -0.00(3)$) [38]. Complex neutral atom scattering factors were used throughout this program. All calculations were carried out using SHELXS 86 [39] SHELXL 97 [40], PLATON 99 and ORTEP-3 [41,42] programs.

3. Results and discussion

3.1. Synthesis

The two classes of ligands used in the present study belong to the azoimine (–N=N–C=N–) family. 1-Alkyl-2-(naphthyl-α-azo)imidazoles are abbreviated as α-NaiMe (**1a**), α-NaiEt (**1b**), α-NaiBz (**1c**); 1-alkyl-2-(naphthyl-β-azo)imidazoles are abbreviated as β-NaiMe (**2a**), β-NaiEt (**2b**) and β-NaiBz (**2c**). They are synthesized by the reported procedure [10–12]. The ligands are an unsymmetric bidentate N,N′ chelating type.

These ligands in MeOH–$CHCl_3$ mixture react with $AgNO_3$in MeOH and the complexes have been isolated as their perchlorate salts. They were purified by crystallization by diffusion of CH_2Cl_2 solution of the complex into hexane. The complexes are highly photosensitive and decomposed with separation of black metallic silver from solution upon exposure to light. The complexes are characterized by elemental analyses, IR, UV–Vis (Table 2), ^{1}H NMR (Table 3) data and support the formulation [Ag(α-/β-NaiR)$_2$][ClO$_4$] (**3**, **4**). The complexes are diamagnetic and 1:1 electrolytes in nitromethane. The structural configuration has been determined by a single crystal X-ray diffraction study of [Ag (α-NaiEt)$_2$][ClO$_4$] (**3b**).

3.2. Spectral properties

The complexes [Ag(NaiR)$_2$]$^+$ exhibit characteristic IR transmissions for *ν*(N=N) and *ν*(C=N) at around 1382 and 1485 cm^{-1}. The free ligand values are 1410 and 1600 cm^{-1}, respectively. The observation is interesting. The *ν*(C=N) is red-shifted by >100 cm^{-1}. This supports very strong interaction of Ag^+ with imidazolic-N compared to azo-N. This is also confirmed by bond length data (Table 4). The perchlorate (ClO_4^-) exhibits bands at 1147, 1108 and 1090 cm^{-1} along with a weak band at 620–625 cm^{-1}. The splitting of *ν*(ClO_4^-) supports reduction in symmetry, which may be due to some hydrogen bonding interaction. This is observed, indeed (vide infra).

Solution electronic spectra of the complexes were recorded in dichloromethane in the range of 600–200 nm. Bathochromic shift relative to the free ligand indicates interaction between Ag^+ and the ligand (Table 2). The silver(I) complexes exhibit the absorption at ca. 400 nm and are assigned to intraligand charge transitions.

The ligands and complexes show highly resolved ^{1}H NMR spectra in $CDCl_3$ at 298 K. 1-Alkyl-2-(naphthylazo)imidazoles (NaiR) have been characterized previously [10,12] and serve as guides to determine the structure of the silver(I) complexes. The spectral data are collected in Table 3. The 1-alkyl groups in [Ag(NaiR)$_2$]$^+$ show significant shifting downfield by 0.1– 0.2 ppm from that of the free ligand values [10–12]. A significant difference is observed in the resonance signal of imidazole protons 4- and 5-H from that of naphthyl protons. Imidazole protons 4- and 5-H appear upfield (6.9–7.2 ppm) and naphthyl protons (8-H–15-H) resonate downfield, 7.5–8.0 ppm. In [Ag(NaiR)$_2$]$^+$ the signal pattern shows that imidazole protons are shifted to the downfield side by 0.4–0.5 ppm and naphthyl protons are shifted to upfield side except 9-H in α-NaiR and 8, 10-H in β-NaiR compared to the free ligand values.

Table 2
Electronic spectroscopic[a] and cyclic voltammetric[b,c] data

Compound	UV–Vis spectral data λ_{max}, nm (10^{-3} ε, M^{-1} cm^{-1})	Redox data		Ligand reductions [c] azo/azo$^-$
		E_0[d] (V)	E_s[e] (V)	
3a	480 (1555)[f], 434 (2011), 418 (9305), 384 (10,043)	−0.087	0.503	−0.551
3b	472 (1240)[f], 436 (1665), 354 (7450)	−0.093	0.495	−0.569
3c	484 (1465)[f], 436 (1911), 354 (8940)	−0.088	0.505	−0.578
4a	414 (1675)[f], 400 (2430), 378 (9450)	−0.081	0.462	−0.679
4b	416 (2248)[f], 400 (3260), 384 (10,936)	−0.085	0.449	−0.761
4c	414 (1765)[f], 402 (2050), 384 (9467), 378 (9840)	−0.091	0.476	−0.881

[a] Solvent CH_2Cl_2.
[b] Solvent MeCN, working electrode Pt-disk, reference SCE, supporting electrolyte [nBu$_4$N][ClO$_4$] (0.1 M), solute concentration $\sim10^{-3}$ M, scan rate 50 mV, potential is expressed in V, E_{pa} stands for anodic peak potential.
[c] E_{pc} cathodic peak potential in V and i_{pa}/i_{pc} lies between 0.5 and 0.6.
[d] Threshold potential to reduction of Ag(I) → Ag(0) on the electrode surface.
[e] Anodic stripping potential for Ag(0) → Ag(I).
[f] Shoulder.

Table 3
^{1}H NMR data recorded in $CDCl_3$ at 298K

Compound	δ (ppm (J, Hz))										
	4-H[a]	5-H[a]	8-H[a]	9-H[b]	10-H [c]	11-H[c]	12-H [d]	13-H[d]	14-H[c]	15-H[b]	N-R
(**3a**)	7.58	7.52		8.44 (7.10)	7.77 (7.0)	7.46 (7.0)	7.08	7.08	7.19 (7.2)	7.04 (7.5)	4.13[e]
(**3b**)	7.61	7.59		8.44 (8.1)	7.80 (7.5)	7.44 (7.2)	7.04	7.04	7.15 (7.2)	6.91 (7.5)	4.44[f](12.0)
(**3c**)	7.65	7.63		8.45 (8.4)	7.82 (7.5)	7.46 (7.2)	7.12	7.12	7.23 (7.5)	7.06 (7.8)	5.67[g]
(**4a**)	7.55	7.45	8.03		7.78 (8.1)	7.67 (7.5)	7.50	7.42	7.42 (7.5)	7.62 (7.5)	4.11[e]
(**4b**)	7.58	7.50	8.04		7.75 (8.1)	7.65 (7.5)	7.49	7.41	7.41 (7.2)	7.60 (7.8)	4.35[f] (12.0)
(**4c**)	7.63	7.55	8.08		7.83 (8.4)	7.71 (8.1)	7.5	7.47	7.47 (8.1)	7.69 (7.8)	5.74 [g]

[a] Singlet broad.
[b] Doublet.
[c] Triplet.
[d] Multiplet.
[e] 1-CH_3.
[f] Quartet for –CH_2– and δ(CH_2)–CH_3: **5b**, 1.51(7.0)[b]; **6b**, 1.47(7.0)[b] ppm.
[g] 1-CH_2(Ph) and δ(Ph): 7.4–7.5 ppm.

Table 4
Selected bond distances (Å) and angles (°) for [Ag(α-NaiEt)$_2$](ClO$_4$) (**3b**) along with their esd in parentheses

Bond distances (Å)		Bond angles (°)	
Ag–N(1)	2.124(5)	N(1)–Ag–N(4)	65.45(2)
Ag–N(5)	2.128(5)	N(5)–Ag–N(8)	64.86(2)
Ag–N(4)	2.851(5)	N(1)–Ag–N(5)	174.54(2)
Ag–N(8)	2.859(5)	N(4)–Ag–N(8)	74.88(1)
N(3)–N(4)	1.266(5)	N(3)–N(4)–Ag	106.6(3)
N(7)–N(8)	1.265(5)	N(7)–N(8)–Ag	106.6(4)
C (3)–N(3)	1.360(7)	C(3)–N(1)–Ag	122.8(4)
C (3)–N(1)	1.333(7)	C(18)–N(5)–Ag	123.8(5)
C (18)–N(5)	1.310(7)		
C (18)–N(7)	1.369(7)		

3.3. Molecular structure

A molecular view of the complex [Ag(α-NaiEt)$_2$][ClO$_4$] (**3b**) is shown in Fig. 1 and the bond parameters are given in Table 4. A review of the bond lengths and angles shows that the complex is essentially linear with a further two weak interactions to azo-N of the azoimine group. The N=N distances are equivalent in the two azoimine chelates (1.266(5), 1.265(5) Å). Free ligand bond parameters are available for 1-ethyl-2-(naphthyl-azo)imidazolium hexafluorophosphate, [α-NaiEtH]$^+$[PF_6^-] [43] and the N–N distance is 1.267(3) Å. The N–N distance in 1-methyl-2-(phenylazo)imidazolium perchlorate is 1.250(1) Å [44]. The elongation is likely to be a result of a high steric crowding provided by the naphthyl group relative to the phenyl group. This may be due to better σ-donor character of the ligand compared to the aryl group. The Ag–N distances are as follows: Ag–N (imidazole) [Ag–N(1), 2.124(5); Ag–N(5), 2.128(5) Å]. The distance is shortened by >0.7 Å than that of the proposed Ag–N(azo) distance [Ag–N(4), 2.851(5); Ag–N(8), 2.859(5) Å]. This accounts for the argentophilicity [17,18] of imidazole-N compared to azo-N donor centers. On considering the weak interaction of Ag(I) with the azo-N leading to the chelated structure, the proposed chelate angles are: N(1)–Ag–

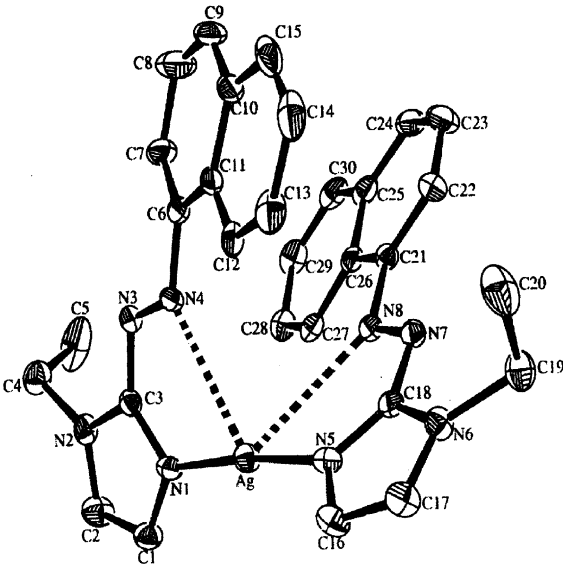

Fig. 1. X-ray crystal structure of $[Ag(\alpha\text{-NaiEt})_2]$ (ClO_4) (**3b**).

N(4), 65.45(2)° and N(5)–Ag–N(8), 64.86(2)°. This example bears the lowest chelate bite angles so far reported in the azoimine family [9–12]. This smallest chelate angle may lead to distortion in the tetrahedral geometry. The naphthyl ring is no longer planar with the chelate plane. The plane-1 (Ag–N(1)–C(3)–N(3)–N(4)) inclines at an angle of 23.4(2)° with the α-naphthyl group whereas plane-2 (Ag–N(5)–C(18)–N(7)–N(8)) makes an angle of 49.89(2)°. Thus, the two naphthyl groups are skewed by 18.9(2)°. The bulky size of the naphthyl groups may provide high steric interaction and may be responsible for the unusual distortion in geometry. The strain is manifested in stereochemical change from tetrahedral to linear symmetry. This has led us to conclude that the structure may be described as a {2+2} distorted linear geometry tending to tetrahedral symmetry. Usually macrocycles are described by [m+n] nomenclature. For brevity we use the {2+2} symbol to designate bi-coordinated linear geometry with some distortion towards tetrahedral symmetry.

1-Ethyl-2-(naphthyl-α-azo)imidazoles (α-NaiEt) and 2-(phenylazo)pyrimidines (papm) [45] have an azoimine, –N=N–C=N–, chelating function with an inbuilt imine (–C=N–) group in a heterocyclic back bone. Imidazole is a five-membered *meta* related two-N heterocycle while pyrimidine is a six-membered two-N heterocycle system. The replacement of a six-membered heterocycle by a five membered one reduces both the σ-donor and π-acceptor character of the system [8] and also introduces angular strain in the chelate ring [2]. This is reflected in the comparison of chelate ring structures of Ag(I)-naphthylazoimidazole and Ag(I)-2-(phenylazo)pyrimidine (Ag(papm) system [28]) molecules (Fig. 2). The elongation of the Ag–N (azo) [Ag–N(4)] distance by ~0.3 Å in Ag(-NaiEt) compared to Ag(papm) is a support of the

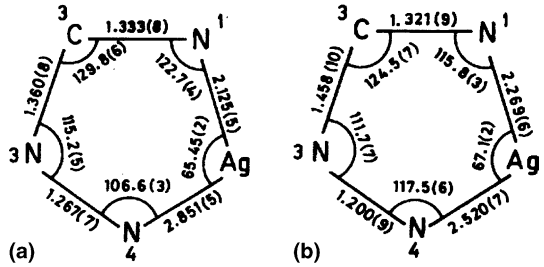

Fig. 2. Dimensions of chelate rings of (a) $Ag(\alpha\text{-NaiEt})_2^+$ and (b) $Ag(papm)^+$.

reduction in σ-donation capacity of α-NaiEt with respect to papm. The naphthyl group is a better electron donor, and provides higher steric strain relative to the phenyl ring and that plays a crucial role to monitor the σ-/π-acidity of the azo function [46]. The π-acidity of naphthyl < phenyl as well as imidazole < pyrimidine [8]. This may support the shortening of the Ag–N(4) bond in Ag-(papm) [28] compared to the present silver(I) complex. The same argument cannot explain the shortening of bond length (by ~0.15 Å) of Ag–N(1) (Ag–N (heterocycle)) in $Ag(\alpha\text{-NaiEt})_2^+$ relative to that of Ag-(papm). The strain that is developed due to replacement of pyrimidine by imidazole has been released by the elongation of the Ag–N(azo) bond length in the $Ag(\alpha\text{-NaiEt})_2^+$ system compared to that of the Ag-(papm) complex. However, the –N=N– bond length is unusually shortened in Ag-papm, which may be due to the helical network and triangular $Ag(N)_3$ coordination in the complex. The phenomena is more likely to be a result of bond alteration in Ag(papm) vs. a bond delocalization in Ag(α-NaiEt) in C3–N3–N4 bond lengths, probably caused by electronic effects.

The packing view of the crystal structure shows (Fig. 3) that $Ag(\alpha\text{-NaiEt})_2^+$ contains an intramolecular and intermolecular H-bonded 1D helical framework. Intramolecular H-bonding is playing between the azo-N and α-H of the naphthyl group [N(4)···H(12), 2.477(8); N(8)···H(27), 2.531(3) Å]. This enhances the acidity of the C(12)–H(12)/C(27)–H(27) group leading to activation of this bond. This is observed by adding $PdCl_4^{2-}$ to the solution of this complex and the cyclopalladated complex has been synthesized by a transmetallation reaction followed by the C–H activation process [12]. Intermolecular H-bonds operate between the two

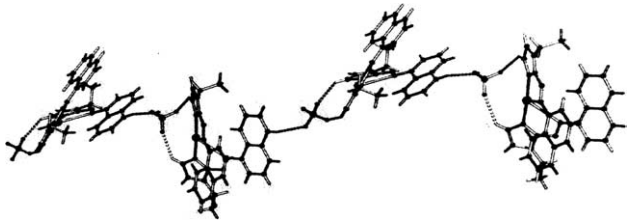

Fig. 3. Helical 1D polymer showing intramolecular and intermolecular H-bonding.

Table 5
Hydrogen bonding and weak interaction geometry (Å, °), H-bonding interaction

D–H···A	D–H (Å)	H···A (Å)	D···A (Å)	∠D-H···A (°)
C12–H12···N4	0.93	2.478	2.812(9)	101.3
C27–H27···N8	0.93	2.521	2.835(8)	100.1
C15–H15···O1	0.93	2.554	3.461(14)	165.5
C1–H1···O3	0.93	2.440	3.199(13)	138.7
C16–H16···O4	0.93	2.568	3.314(12)	137.8
C–H···π interaction				
X–H···Cg(J)	H···Cg	H-Perp	∠X–H···Cg	X···Cg
C14–H14···Cg(1)	3.365	3.332	81.97	3.363(13)
π–π Interaction				
Cg(I)–Cg(J)	Cg–Cg	Dihedral (I,J ring)	Perp. From CgI to J	
Cg(1)–Cg(4)	3.8404(52)	0.71	3.307	
Cg(2)–Cg(6)	3.7900(40)	2.40	3.261	
Cg(3)–Cg(5)	3.9209(44)	19.38	3.842	

Cg(I) → centroid of ring I. Ring(1) → N1–C1–C2–N2–C3; Ring(2) → N5–C16–C17–N6–C18; Ring(3) → C6–C7–C8–C9–C10–C11; Ring(4) →C10–C11–C12–C13–C14–C15; Ring(5) → C21–C22–C23–C24–C25–C26; Ring(6) → C25–C26–C27–C28–C29–C30.

fragments around the azo group. The C–H group of the imidazole moiety *ortho* to metal coordinated-N (imidazole) [C(1)–H(1)/C(16)–H(16)] develops an electrostatic interaction with perchlorate-O(1)/O(4) while naphthyl C(15)–H(15) gives a H-bonding interaction with the second perchlorate ion. In addition to these, the complex experiences C–H–O as well as face-to-face π–π interactions (Table 5).

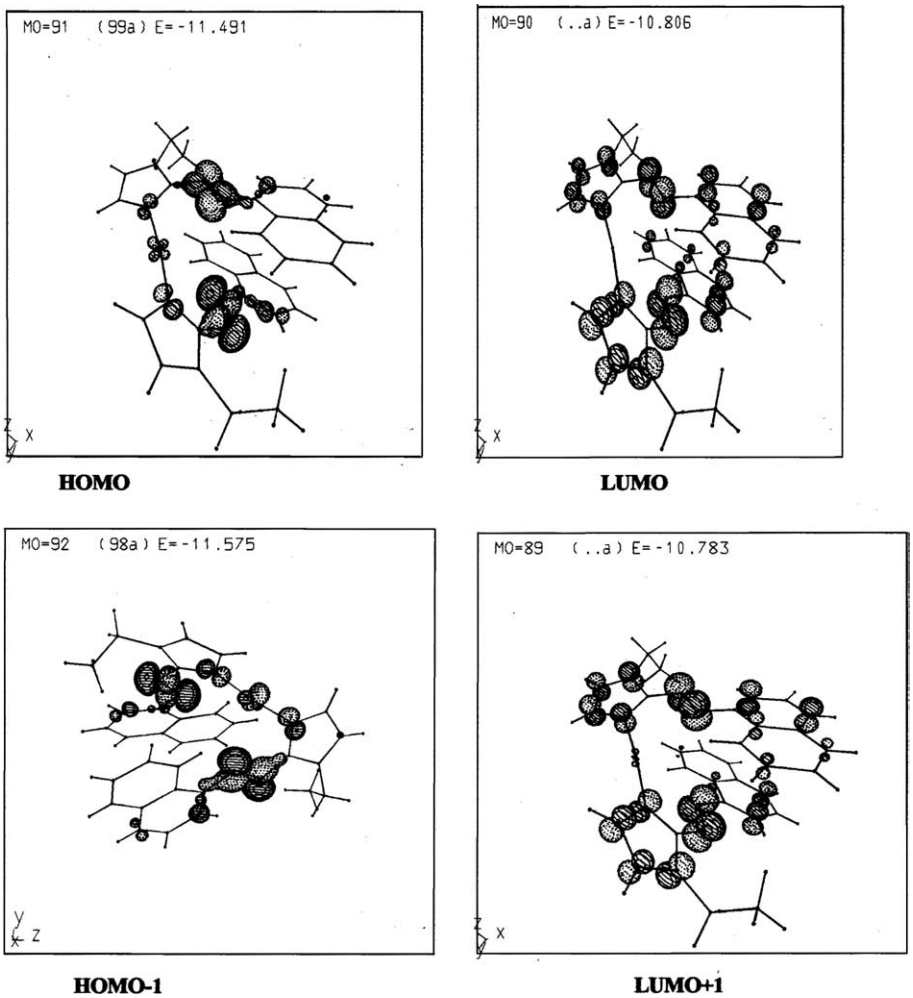

Fig. 4. HOMO, LUMO, HOMO-1 and LUMO+1 of $Ag(\alpha\text{-NaiEt})_2^+$.

Table 6
Relative percent atomic contribution to MOs of the complex $Ag[\alpha\text{-NaiEt}]_2^+$

MO	Energy (eV)	Ag	N(imidazole)	Azo(N=N)	Naphthyl ring
Percentage of contribution					
92 (HOMO-1)	−11.575	5.5	6.6	78.9	6.6
91 (HOMO)	−11.491	2	3.3	77	7.7
90 (LUMO)	−10.806	0	21.4	52.5	25.5
89 (LUMO+1)	−10.783	0	24.5	55.31	20.2

3.4. Redox studies

The electrochemical properties of the complexes were examined by cyclic voltammetry in MeCN using $[n\text{Bu}_4\text{N}][\text{ClO}_4]$ as supporting electrolyte at the scan rate 50 mV s^{-1}. The complexes of silver exhibit an irreversible oxidation–reduction response with the Pt-disk working electrode and saturated calomel electrode (SCE) as reference electrode. The complexes undergo reduction processes, which, given the redox non-innocence of the azoimine group [10], are assigned to ligand-centred-processes. The quasireversibility of the reductive process is observed from the peak separation ($\Delta E > 130$ mV) and the reduction is referred to the accommodation of an electron to the azo function dominated orbital of the bound ligand. Such processes, coupled to chemical complications for the reduction of Ag(I) on the electrode surface, result in that the current ratio i_{pa}/i_{pc} is always less than unity (i_{pa}/i_{pc} lies between 0.5 and 0.6). In this connection, the presence of anodic stripping peaks in the backscan ($E_{pa} \sim +0.5$ V, Table 2) looks likely to testify for reoxidation of electro-deposed silver metal. This means that the reduction processes more than likely trigger release of silver ion with its consequent reduction to silver metal [47]. The reoxidation of $Ag(0) \rightarrow Ag(I)$ is associated with very high anodic current at positive to SCE (stripping potential ~+0.5 V) which on repeat scan progressively increases the current. Besides, the approach to more negative potential followed by backscan increases the peak current height. The increase in potential gradient enhances the reaction rate which may cause deposition of larger amounts of Ag on the surface.

3.5. EHMO calculation and correlation with spectral and electrochemical properties

In order to highlight the electronic properties of silver(I)-naphthylazoimidazoles, an MO calculation has been performed in the framework of extended Huckel formalism. Crystallographic data of **3b** are used for the EHMO calculation. The MO pictures are shown in Fig. 4 and the percentage contribution of participating fragment/atomic functions to the MOs are given in Table 6. The HOMO(91) is contributed from 2% silver and 88% [77% azo (N=N), 7.7% naphthyl group and 3.3% N(imidazole)] ligand orbital. The LUMO has no metal contribution, it is mainly ligand orbital, 99.4% [52.5% azo (N=N), 25.5% naphthyl group and 21.4% N(imidazole)]. Other low-lying orbitals (HOMO-1, HOMO-2) show a greater metal contribution but other higher energy orbitals (UMOs) show no metal contribution. It can be concluded that there should be no M → Ligand charge transfer and this happens indeed. The complexes show only the interligand (between imidazole and naphthyl group) charge transition in the lower wavelength region. Because of the weak M–L interaction, Ag^+ is quickly separated from the ligands claw under the electrode field potential and has been deposited on the electrode surface. However, Cu(I)-complexes show somewhat different results because of the higher contribution of copper(I) to the HOMO and other occupied MOs [48].

4. Supplementary material

Crystallographic data for the structural analysis have been deposited with the Cambridge Crystallographic Data Centre, CCDC No. 172833 for bis-[1-ethyl-2-(naphthyl-α-azo)imidazole]silver(I) perchlorate. Copies of this information may be obtained free of charge from the Director, CCDC, 12 Union Road, Cambridge, CB2 1EZ, UK (fax: +44-1223-336033; E-mail: deposit@ccdc.cam.ac.uk or www: http://www.ccdc.cam.ac.uk).

Acknowledgements

Financial support from the Department of Science and Technology is gratefully acknowledged. One of us (GM) is thankful to the National Science Council, ROC for support under grants NSC 89-2811-M-007-0086 and NSC 89-2112-M-007-083. We are also thankful to Prof. T. -H. Lu, Department of Physics, National Tsing Hua University, Taiwan, ROC for his help.

References

[1] H. Sigel (Ed.), Metal Ions in Biological System, vol. 13, Marcel Dekker, New York, 1981.
[2] C. Place, J.-L. Zimmermann, E. Mulliez, G. Guillot, C. Bois, J.-C. Chottard, Inorg. Chem. 37 (1998) 4030.

[3] J.M. Dominguez-Vera, A. Rodriguez, R. Cuesta, R. Kivekas, E. Colacio, J. Chem. Soc., Dalton Trans. 561 (2002).
[4] S. Nagasato, Y. Sunatsuki, S. Ohsato, T. Kido, N. Matsumoto, M. Kojima, Chem. Commun. 14 (2002).
[5] G.K. Rauth, S. Pal, D. Das, C. Sinha, A.M.Z. Slawin, J.D. Woollins, Polyhedron 20 (2001) 1825.
[6] P.K. Santra, P. Byabartta, S. Ckattopadhyay, L.R. Falvello, C. Sinha, Eur. J. Inorg. Chem. 1124 (2002), and references therein.
[7] P. Byabartta, J. Dinda, P.K. Santra, C. Sinha, K. Paneerselvam, F.-L. Liao, T.-H. Lu, J. Chem. Soc., Dalton Trans. 2825 (2001).
[8] E.C. Constable, Coord. Chem. Rev. 93 (1989) 205.
[9] S. Pal, D. Das, P. Chattopadhyay, C. Sinha, K. Pannerselvam, T.-H. Lu, Polyhedron 19 (2000) 1263.
[10] P. Byabartta, P.K. Santra, T.K. Misra, C. Sinha, C.H.L. Kennard, Polyhedron 20 (2001) 905.
[11] J. Dinda, S. Pal, B.K. Ghosh, C. Sinha, J. Cheng, F.-L. Liao, T.-H. Lu, J. Coord. Chem. 55 (11) (2002) 1271.
[12] J. Dinda, D. Das, P.K. Santra, C. Sinha, L.R. Falvello, J. Organomet. Chem. 629 (2001) 28.
[13] I. Torok, T. Gajda, B. Gyurcscik, G.K. Toth, A. Peter, J. Chem. Soc., Dalton Trans. 1205 (1998).
[14] W. Kaim, B. Schwederski, Bioinorganic Chemistry: Inorganic Elements in the Chemistry of Life, Wiley, New York, 1994, p. 373.
[15] D. de Vos, P. Clements, S.M. Pyke, D.R. Smyth, E.R.T. Tiekink, Metal-Based Drugs 631 (1999).
[16] K. Nomiya, K. Tsuda, Y. Tanabe, H. Nagano, J. Inorg. Biochem. 699 (1998).
[17] A.J. Blake, G. Baum, N.R. Champness, S.S.M. Chung, P.A. Cooke, D. Fenske, A.N. Khlobystov, D.A. Lemenovskii, W.-S. Li, M. Schroder, J. Chem. Soc., Dalton Trans. 4285 (2000).
[18] S. Ganguly, S. Chattopadhyay, C. Sinha, A. Chakravorty, Inorg. Chem. 39 (2000) 2954.
[19] D. Braga, F. Grepioni, G.R. Desiraju, Chem. Rev. 98 (1998) 1375.
[20] H. Schmidbaur, Chem. Soc. Rev. 24 (1995) 391.
[21] K. Nomiya, S. Takahashi, R. Noguchi, J. Chem. Soc., Dalton Trans. 1343 (2000), and reference therein.
[22] P.L. Caradoc- Davies, L.R. Hanton, Chem. Commun. 1098 (2001).
[23] Y.-P. Cai, H.-X. Zhang, A.-W. Xu, C.-Y. Su, C.-L. Chen, H.-Q. Liu, L. Zhang, B.-S. Kang, J. Chem. Soc., Dalton Trans. 2429 (2001).
[24] R.H. Wang, M.C. Hong, W.P. Su, Y.C. Liang, R. Cao, Y.J. Zhao, J.B. Weng, Inorg. Chim. Acta 323 (2001) 139.
[25] D.L. Reger, R.F. Semenive, M.D. Smith, Eur. J. Inorg. Chem. 543 (2002).
[26] F.A. Cotton, G. Wilkinson, Advanced Inorganic Chemistry, 5th ed., Wiley, New York, 1998.
[27] E.T. Bell-Loncella, C.A. Bessel, Inorg. Chim. Acta 303 (2000) 799.
[28] P.K. Santra, U.S. Ray, S. Pal, C. Sinha, Inorg. Chem. Commun. 4 (2001) 269.
[29] J. Chem. Soc., Dalton Trans. (3) (2000).
[30] D. Braga, F. Grepioni, G.R. Desiraju, Acc. Chem. Res. 33 (2000) 601.
[31] X.-Z. Li, L. Yu, S.-F. Si, D.-Z. Liao, Z.-H. Jiang, S.-P. Yen, Inorg. Chem. Commun. 5 (2002) 478.
[32] A.K. Deb, S. Choudhury, S. Goswami, Polyhedron 9 (1990) 2251.
[33] T.K. Misra, D. Das, C. Sinha, Polyhedron 16 (1997) 4163.
[34] S.S.S. Raj, H.-K. Fun, X.-F. Chen, X.-H. Zhu, X.-Z. You, Acta Crystallogr., Sect. C 55 (1999) 1644.
[35] S.P. Yang, H.-L. Zhu, X.-H. Yin, X.-M. Chen, J.-N. Li, Polyhedron 19 (2000) 2237.
[36] H. Oshio, T. Yaginuma, T. Ito, Inorg. Chem. 38 (1999) 2750.
[37] A.I. Vogel, A Text Book of Quantitative Inorganic Analysis, ELBS & Longmans, London, 1962.
[38] International Tables for Crystallography, Vol. C, Tables 4.2.6.8 and 6.1.1.4.
[39] G.M. Sheldrick, SHELXS 86, Program for the Solution of Crystal Structure, University of Göttingen, Germany, 1985.
[40] G.M. Sheldrick, SHELXL 97, Program for the Solution of Crystal Structure, University of Göttingen, Germany, 1997.
[41] A.L. Spek, PLATON, Molecular Geometry Program, University of Utrecht, The Netherlands, 1999.
[42] J. Farrugia, ORTEP-3 for Windows version 1.07, J. Appl. Cryst. 30 (1997) 565.
[43] J. Dinda, K. Bag, C. Sinha, G. Mostafa, T.-H. Lu, Polyhedron 22 (2003) 1367.
[44] D. Das, Ph.D. Thesis, Burdwan University, 1998.
[45] P.K. Santra, T.K. Misra, D. Das, C. Sinha, A.M.Z. Slawin, J.D. Woolins, Polyhedron 18 (1999) 2869.
[46] I.L. Finar, Organic Chemistry, vol. I, sixth ed., Longmans, New York, 1971 (Chapter 29).
[47] G. Matsubayashi, T. Maikawa, H. Tamura, M. Nakano, R. Arakowa, J. Chem. Soc., Dalton Trans. 1539 (1996).
[48] J. Dinda, U.S. Ray, G. Mostafa, T.-H. Lu, A. Usman, I.A. Razak, S. Chantrapromma, H.-K. Fun, C. Sinha, Polyhedron 22 (2002) 247.

Available online at www.sciencedirect.com
SCIENCE DIRECT®
Polyhedron 23 (2004) 801–807
POLYHEDRON
www.elsevier.com/locate/poly

Routes to titanium tetrazole complexes ☆

Michael S. Hill [a,*], Peter B. Hitchcock [b], Nikki Smith [b]

[a] Department of Chemistry, Imperial College London, Exhibition Road, South Kensington, London SW7 2AZ, UK
[b] The Chemistry Laboratory, University of Sussex, Falmer, Brighton, East Sussex BN1 9QJ, UK

Received 15 October 2003; accepted 12 November 2003

Abstract

The titanium tetrazole coordination complex $[TiCl_4 \cdot (PhCN_4H)_2]$ has been prepared by treatment of $TiCl_4$ with two equivalents of 5-phenyltetrazole in dichloromethane and spectroscopically and crystallographically characterised. The solid-state structure of this compound consists of six-coordinate titanium centres with *cis* ligated tetrazoles. The individual $[TiCl_4 \cdot (PhCN_4H)_2]$ dimerise via intermolecular N···H–N hydrogen bonding interactions and are further organised into 2D supramolecular arrays. Mass spectral evidence indicates that the individual tetrazole ligands are only weakly bound, limiting the potential of this complex as a titanium nitride precursor. 3 + 2 cycloaddition of tributyltin azide with 2-toluinitrile at 200 °C has afforded the tributylstannyl tetrazole $[SnBu_3\{5\text{-}(2\text{-}MeC_6H_4)CN_4\}]_n$. Crystallographic analysis shows that this compound exists as a supramolecular coordination polymer propagated via trigonal bipyramidal tin centres linked by N^1–Sn–N^3 interactions. Preliminary reactivity studies of this tin complex with titanium tetrachloride in an effort to synthesise a covalently bound titanium tetrazolyl complex have thus far yielded incomplete elimination of the expected Bu_3SnCl by-product and intractable titanium-containing products.
© 2003 Elsevier Ltd. All rights reserved.

Keywords: Titanium; Tin; Tetrazole; Nitride precursor; Cycloaddition

1. Introduction

The combination of a better conductivity (4698 $kS\,cm^{-1}$) than titanium metal (2381 $kS\,cm^{-1}$), extreme hardness (9–10 Moh) and a refractory nature dictate that titanium nitride (TiN) is perhaps the most extensively applied transition metal nitride in both microelectronic (metal/semiconductor interconnects) and architectural applications (protective coatings) [1,2]. High quality thin films of cubic TiN may be produced by atmospheric pressure chemical vapour deposition (APCVD) in a process which conventionally employs ammonia gas and gaseous titanium tetrachloride transported in an inert carrier [3]. Although efficient, this process suffers problems of pre-reaction and requires removal of the corrosive HCl by-product. These qualities, coupled to inconveniently high substrate temperatures of 600–900 °C required by this process, have prompted a search for alternative 'designed' or 'single source' molecular precursors with more amenable reaction/decomposition characteristics. Although successfully attenuating undesirable prereactions, alternative dual source systems which apply volatile tetrakis(dialkyl)amido titanium precursors such as $Ti(NMe_2)_4$ and $Ti(NEt_2)_4$ and ammonia and mixed $TiCl_4$/alkyl amine feedstocks have provided their own additional problems of carbon contamination and poor step coverage [4–7]. Initial efforts to address these difficulties by design of suitable single source precursors containing a preprogrammed combination of titanium and nitrogen were prompted by speculation about the nature of intermediate products formed by these systems prior to film growth. Accordingly, a number of titanium amido and imido species, such as $[CpTiCl_2\{N(SiMe_3)_2\}]$ and $[\{Ti(\mu\text{-}N^tBu)(NMe_2)_2\}_2]$, have been prepared and examined in this context [8–12]. Neither these nor more recent studies of mono- or bis-azido complexes [for example $[\{Ti(N^tBu)Cl(N_3)(py)_2\}_2]$ and $[\{Ti(NCy)(N_3)_2(py)_2\}_2]$ (py = pyridine)] have, however, yielded effective TiN precursors. Film growth in these latter cases is hampered either by a lack of volatility or unacceptably

☆ Supplementary data associated with this article can be found, in the online version, at doi:10.1016/j.poly.2003.11.047.

* Corresponding author. Tel.: +44-207-594-5709; fax: +44-207-594-5804.
E-mail address: mike.hill@imperial.ac.uk (M.S. Hill).

0277-5387/$ - see front matter © 2003 Elsevier Ltd. All rights reserved.
doi:10.1016/j.poly.2003.11.047

high levels of carbon contamination approaching 35% [13,14].

Pyrazolate anions derived by deprotonation of parent pyrazole heterocycles have been shown to provide a flexible N-donor ligand set in titanium chemistry [15–17]. The use of titanium pyrazolyl derivatives as molecular precursors to TiN is likely to be hampered, however, by similar problems of carbon contamination to those outlined above due to the presence of direct carbon to nitrogen bonds in the delocalised heterocycle. We have turned our attention therefore to the synthesis of titanium tetrazolato derivatives in the hope that the high nitrogen content of this latter ligand type will encourage clean elimination of thermodynamically stable small molecule (N_2 and nitrile) side products and retention of Ti–N linkages at relatively low temperatures.

Although a number of inorganic and organometallic tetrazolyl derivatives have been cystallographically characterised in recent years [18–34], structurally authenticated titanium derivatives are restricted to the seven coordinate tris(3,5-di-*tert*-butylpyrazolato)(5-phenyltetrazolato)titanium (**I**) [31]. Although the subject of a low precision X-ray structural determination and not reported in detail, η_1-N^2 coordination of the tetrazolyl anion to titanium was confirmed. Due to the multiplicity of potential nitrogen donors, many metal-coordinated tetrazoles are prone to coordination polymerisation. The monodenticity of the tetrazolyl ligand of **I** is, most likely, therefore enforced by the η^2-coordination of the three bulky pyrazolato co-ligands. As such co-ligands were reasoned to be of likely detriment to clean precursor decomposition, our initial studies have targeted titanium tetrazole complexes with simple chloride ligands sets. We now report our studies which have resulted in the high yield synthesis of a simple Ti(IV) tetrazole coordination complex along with our initial exploration of an organotin-based strategy that attempts to effect both clean formation of titanium tetrazolyl derivatives and a means by which the steric demands at the C^5 position of the tetrazole ring may be readily modulated.

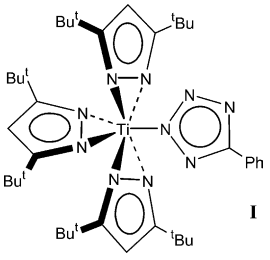

I

2. Experimental

2.1. General

All reactions were conducted under an atmosphere of dry argon and manipulated either on a double manifold vacuum line or in a dinitrogen-filled drybox operating at less than 1 ppm of O_2. Solvents were purified by distillation from an appropriate drying agent (THF from potassium, CH_2Cl_2 from CaH_2 and hexane from Na/K alloy). NMR spectra were recorded at 300.13 (^{1}H), 125.8 (^{13}C) and 186.4 MHz (^{119}Sn) from samples in $CDCl_3$ or d_8-THF; Chemical shifts are relative to $SiMe_4$ for ^{1}H and ^{13}C NMR. ^{119}Sn NMR were referenced externally to Me_4Sn. Mass spectra were obtained at 70 eV. Tributyltin azide was synthesised by a literature procedure [35].

Caution! All reactions of azides and tetrazole compounds must be treated as potentially explosive and conducted behind a rigid safety screen.

2.2. $[TiCl_4 \cdot (PhCN_4H)_2]$ (**1**)

A solution of titanium tetrachloride (1.97 g, 10.4 mmol) in dichloromethane (30 cm^3) was added at room temperature to a stirred slurry of $PhCN_4H$ (3.04 g, 20.8 mmol) in dichloromethane (40 cm^3). This resulted in the formation of a dense pale yellow precipitate and a yellow solution. The yellow solid, **1** (4.70 g, 94%), was isolated by filtration and dried under vacuum. Cooling of the filtrate to −30 °C resulted in the formation of a small number of yellow crystals suitable for X-ray diffraction after 3 days. Elemental and spectroscopic analysis of the bulk powder was consistent with an unsolvated form. *Anal.* Calc. for $C_{14}H_{12}Cl_4N_8Ti$: C, 34.87; H, 2.51; N, 23.25. Found: C, 34.71; H, 2.36; N, 23.00%. ^{1}H NMR [d^8-THF, 298 K] δ: 7.49 (m, 6H, m, *p*-C_6H_5), 8.01 (m, 4H, *o*-C_6H_5), 15.1 (br.s, 2H, N–H). ^{13}C{^{1}H} NMR [d^8-THF, 298 K] δ: 126.3 (*i*-C_6H_5), 127.4 (*o*-C_6H_5), 129.3 (*m*-C_6H_5), 131.2 (*p*-C_6H_5). MS (EI$^+$, 70 eV), 190 (55%, $TiCl_4$), 153 (100, $TiCl_3$), 118 (70, $TiCl_2$), 103 (25, PhCN), 83 (45, TiCl).

2.3. $[SnBu_3\{5\text{-}(2\text{-}MeC_6H_4)CN_4\}]_n$ (**2**)

Bu_3SnN_3 (3.17 g, 9.75 mmol) and 2-toluinitrile (1.25 g, 9.75 mmol) were heated at 200 °C for 2 h under nitrogen to yield a pale amber glass. This was washed with hexane (30 cm^3) and dried in vacuo. Storage of the resultant colourless glass at room temperature for 3 days induced crystallisation to produce compound **2** in effectively stoichiometric yield. *Anal.* Calc. for $C_{20}H_{34}N_4Sn$: C, 53.47; H, 7.64; N, 12.48. Found: C, 53.56; H, 7.64; N, 12.48%. ^{1}H NMR [$CDCl_3$, 298 K] δ: 0.71 (t, 9H, $(CH_2)_3CH_3$), 1.05–1.34 (m, 18H, $(CH_2)_3CH_3$), 2.17 (s, 3H, Ar–Me), 7.15–7.29 (m, 4H, Ar–H). ^{13}C{^{1}H} NMR [$CDCl_3$, 298 K] δ: 13.6 $(CH_2)_3CH_3$, 18.2 ($CH_2(CH_2)_2CH_3$, $^1J_{117,119\ Sn/C} = 457$ Hz), 20.2 (Ar–Me), 27.0 ($(CH_2)_2CH_2CH_3$, $^3J_{117,119\ Sn/C} = 70.9$ Hz), 28.0 ($CH_2CH_2CH_2CH_3$ $^2J_{117,119\ Sn/C} = 27.9$ Hz), 125.6, 128.6, 129.8, 130.5, 137.7 (Ar–C), 161.5 (CN_4). ^{119}Sn{^{1}H} NMR [$CDCl_3$, 298 K] δ: −17.9 ($\Delta\nu_{1/2}$ −2 kHz).

2.4. Attempted reaction of **2** and $TiCl_4$

To a solution of compound **2** (2.37 g, 5.26 mmol) in dichloromethane (120 cm^3) was added a solution of titanium tetrachloride (1.0 g, 5.26 mmol) in dichloromethane (20 cm^3). This resulted in the immediate formation of an orange solution which darkened to a vivid red over the subsequent 48 h. In vacuo removal of the solvent produced a dark red sticky solid, which was washed with hexane (2×30 cm^3) to produce a yellow solid. The ^1H NMR spectrum of this material in d^8-THF displayed resonances corresponding to both Bu_3Sn and the tetrazole ligand. Crystals which formed in the NMR tube were suitable for X-ray analysis and proved to be a hydrolysis product, the oxo-bridged species $(THF)_2Cl_3Ti–O–TiCl_3(THF)_2$.

3. Results and discussion

Winter [36] has studied the treatment of titanium tetrachloride with two equivalents of a variety of substituted pyrazoles. Reaction with 3,5-di-*tert*-butylpyrazole resulted in HCl elimination and the formation of a mixture of molecular L_2TiCl_4 and ionic $[LH^+]_2[TiCl_6^{2-}]$ (where L = 3,5-di-*tert*-butylpyrazole) products. Conversely, reaction with less sterically demanding heterocycles produced a series of six-coordinate $TiCl_4$. L'_2 adducts (where L′ = 3,5-dimethylpyrazole, 3-methylpyrazole, 4-iodopyrazole), where the adoption of either a *cis* or *trans* coordination geometry was reasoned to be largely dependent upon the steric profile of the pyrazole ligand. Prompted by these observations, and intrigued by the possible divergent reactivity that may be induced by the increased acidity of the tetrazole heterocycle [37], we carried out the analogous reaction between two equivalents of commercially available 5-phenyltetrazole and $TiCl_4$ in dichloromethane. This resulted in the immediate precipitation of compound **1** as a pale yellow powder, which was isolated by filtration. Elemental analysis indicated that a 2:1 adduct had been formed, while the presence of a tetrazole N–H functionality was confirmed by the observation of weak absorptions at 3340 and 3390 cm^{-1} in the infra-red spectrum. Although **1** was not soluble in non-donor solvents, ^1H NMR data collected in THF-d_8 displayed resonances similar to those of the free neutral tetrazole. Although these data do not preclude the presence of compound **1** in solution, we tentatively conclude that the tetrazole ligands are displaced from the titanium coordination sphere by the donor solvent. Despite this problematic insolubility, storage of the pale yellow, dilute but saturated supernatant dichloromethane solution from the original reaction at −30 °C for one week produced a small number of yellow single crystals of **1** as a bis-dichloromethane solvate suitable for an X-ray diffraction analysis. The asymmetric unit resulting from this analysis is illustrated in Fig. 1. Selected bond lengths and angles are provided in Table 1, while details of the X-ray analysis are listed in Table 2.

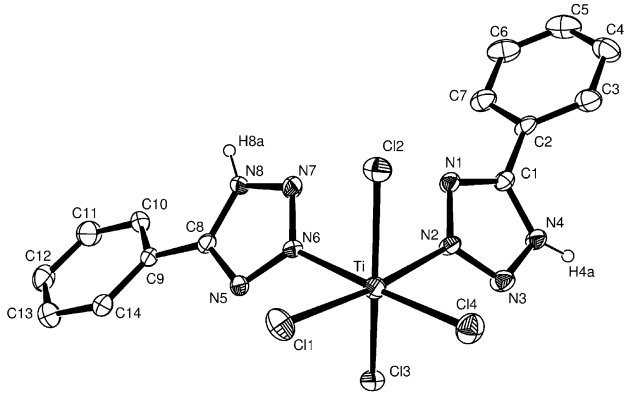

Fig. 1. The asymmetric unit of **1** with thermal ellipsoids drawn at the 30% probability level. All hydrogen atoms apart from H4a, H4b removed for clarity.

Complex **1** is revealed to exist as a six-coordinate adduct with *cis* tetrazole ligands. The coordination sphere exhibits significant deviations from ideal octahedral geometry, with *cis* angles ranging from 81.94(14)° [N(6)–TiCl(3)] to 99.30(8)° [Cl(4)–Ti–Cl(1)] and the *trans* angles between 160.92(8)° [Cl(3)–TiCl(2)] and 174.06(14)° [Cl(4)–Ti–N(6)]. The Ti–Cl(1) [2.231(2) Å] and Ti–Cl(4) [2.216(2) Å] bonds that are *trans* to the tetrazole N-donor atoms are significantly shorter than the mutually *trans* Ti–Cl(2) [2.275(2) Å] and Ti–Cl(3)

Table 1
Selected bond lengths (Å) and angles (°) for compound **1**

Bond lengths			
Ti–Cl(4)	2.216(2)	Ti–Cl(1)	2.231(2)
Ti–N(6)	2.265(5)	Ti–Cl(3)	2.271(2)
Ti–Cl(2)	2.275(2)	Ti–N(2)	2.279(5)
N(1)–C(1)	1.326(7)	N(1)–N(2)	1.357(6)
N(2)–N(3)	1.294(6)	N(3)–N(4)	1.344(7)
N(4)–C(1)	1.340(7)	N(5)–C(8)	1.324(7)
N(5)–N(6)	1.365(7)	N(6)–N(7)	1.290(6)
N(7)–N(8)	1.329(7)	N(8)–C(8)	1.336(8)
Bond angles			
Cl(4)–Ti–Cl(1)	99.30(8)	Cl(4)–Ti–N(6)	174.06(14)
Cl(1)–Ti–N(6)	86.43(14)	Cl(4)–Ti–Cl(3)	95.71(8)
Cl(1)–Ti–Cl(3)	96.86(8)	N(6)–Ti–Cl(3)	81.94(14)
Cl(4)–Ti–Cl(2)	96.32(8)	Cl(1)–Ti–Cl(2)	95.72(8)
N(6)–Ti–Cl(2)	84.62(14)	Cl(3)–Ti–Cl(2)	160.93(8)
Cl(4)–Ti–N(2)	89.82(14)	Cl(1)–Ti–N(2)	170.84(15)
N(6)–Ti–N(2)	84.48(18)	Cl(3)–Ti–N(2)	82.93(14)
Cl(2)–Ti–N(2)	82.37(14)	C(1)–N(1)–N(2)	105.4(5)
N(3)–N(2)–N(1)	112.0(5)	N(3)–N(2)–Ti	120.5(4)
N(1)–N(2)–Ti	127.0(4)	N(2)–N(3)–N(4)	105.1(5)
C(1)–N(4)–N(3)	109.9(5)	C(8)–N(5)–N(6)	105.8(5)
N(7)–N(6)–N(5)	111.1(5)	N(7)–N(6)–Ti	123.0(4)
N(5)–N(6)–Ti	125.9(4)	N(6)–N(7)–N(8)	105.5(5)
N(7)–N(8)–C(8)	110.6(5)	N(1)–C(1)–N(4)	107.6(5)

Table 2
Selected crystallographic and data collection parameters for compounds **1** and **2**

	1	**2**
Chemical formula	$C_{14}H_{12}Cl_4N_8Ti \cdot 2(CH_2Cl_2)$	$C_{20}H_{34}N_4Sn$
Formula weight	651.87	449.20
T (K)	173(2)	173(2)
Crystal size (mm)	$0.2 \times 0.2 \times 0.1$	$0.4 \times 0.2 \times 0.4$
Crystal system	monoclinic	orthorhombic
Space group	$P2_1/n$ (No. 14)	$Fdd2$ (No. 43)
a (Å)	12.4934(14)	21.2292(10)
b (Å)	14.1217(19)	33.379(3)
c (Å)	16.0886(17)	12.8979(11)
α (°)	90	90
β (°)	105.519(5)	90
γ (°)	90	90
Z	4	16
V (Å^3)	2735.0(6)	9140(1)
D_{calc} (Mg m^{-3})	1.58	1.31
μ (mm^{-1})	1.12	1.13
θ range (°)	3.76–21.96	3.76–25.04
R_1; $wR_2[I > 2\sigma(I)]$	0.059; 0.108	0.050, 0.101
R_1; wR_2 all data	0.100; 0.122	0.073; 0.110
Measured/independent reflections/R_{int}	10 987/3310/0.092	10 141/3559/0.068
Reflections with $I > 2\sigma(I)$	2277	2755

[2.271(2) Å] bonds. These observations and bond lengths are similar to those in other $TiCl_4 \cdot L_2$ *cis* adducted structures including the bis-pyrazole adduct $[TiCl_4(4\text{-}IC_3H_2N_2)_2]$ [36]. The Ti–N bond distances [2.279(5), 2.265(5) Å] of **1** are, however, significantly longer than those reported for this analogous pyrazole adduct [2.235(7) Å] and possibly result from the reduced basicity of the tetrazole moiety [37].

Mass spectral analysis of compound **1** displayed a highest mass fragment at 190 corresponding to the molecular ion $[TiCl_4]^+$. This is an indication that the tetrazole ligands are only weakly bound and most likely inhibits the practical potential of **1** as a nitride precursor. For this reason, we turned our attention to the synthesis of titanium tetrazolyl derivatives containing more robust covalent Ti–N bonds. Winter [31] has reported previously that reactions of the 5-phenyltetrazolyl anion with titanium tetrahalides resulted in intractable mixtures of products, an observation that was confirmed by the present study. Ab initio calculations undertaken as part of the same study highlighted the small energy difference (ca. 5 kcal/mol) that exists between η^1- and η^2-ligated titanium tetrazolyl derivatives while older quantum mechanical calculations have shown that N^1 and N^2 binding are energetically equivalent [38]. The mixture of species that likely results from such facile isomer interconversion, as well as the potential for the formation of complex extended network structures, mitigates therefore against the isolation of simple homo- and heteroleptic titanium tetrazolyl complexes unless the reaction conditions are very carefully controlled. In an attempt to address this issue, we reasoned that enhanced product solubility may result by variation of the tetrazole C^5 substituent steric demands. A very wide range of tetrazole derivatives may be accessed by the straightforward 3 + 2 cycloaddition reaction of organotin azides and RCN dipolarophiles (Scheme 1) [22–27,39]. The ready availability of a great number of substituted nitriles allows facile variation of the resultant tetrazole substituent and provides the heterocycle in a synthetically convenient deprotonated form for subsequent metathesis with $TiCl_4$ (Scheme 1). A similar strategy involving Me_3SiCl elimination has previously been successfully applied to the synthesis of sterically encumbered pyrazolatotrichlotitanium derivatives [16], while R_3SnX elimination from reaction between triorganostannyltetrazoles and alkyl halides has been demonstrated as a straightforward means to tetrazole N-alkylation [40]. Although a great number of potential nitrile precursors are available, our initial

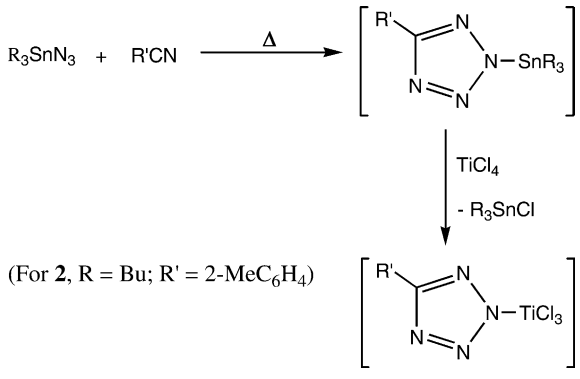

Scheme 1.

efforts identified 2-toluinitrile as a suitable candidate due to the small incremental increase in steric demands over 5-phenyltetrazole and the spectroscopic simplicity of the *ortho*-substituted aryl tetrazolyl product.

Tributyltin azide was synthesised by literature methods [35] while $[SnBu_3\{5\text{-}(2\text{-}MeC_6H_4)CN_4\}]$ (**2**) was synthesised using the well established methodology in which the neat triorganotin azide is heated with a slight excess of the chosen nitrile [39]. The reaction was monitored by the disappearance of the IR bands due to ν(CN) at ca. 2250 cm^{-1} and $\nu_{asym}(N_3)$ at ca. 2060 cm^{-1}. The glassy, crude solid product that was produced upon cooling was washed with hexane to remove excess nitrile and crystallised upon standing at room temperature for three days to produce analytically pure compound **2**.

Compound **2** was sufficiently soluble in $CDCl_3$ to enable the collection of good quality NMR data. The ^1H and ^{13}C NMR spectra were consistent with the proposed structure. The $^1J(^{13}C–^{119}Sn)$ coupling constant of 457 Hz implied a coordination number of >4 about tin, while use of the semiempirical relationship derived by Holecek and Lycka for correlating ^1J data and coordination geometry yielded a value of 123.2° for the C–Sn–C bond angles, consistent with a *trans*-trigonal bipyramidal N_2SnC_3 geometry about tin [41]. These observations are similar to those of previous solution NMR studies of triorganostannyl tetrazoles that have deduced the formation of concentration- and temperature-dependent *N*,*N*′-bridged oligomeric species in solution [22,23,42]. The fluxionality of these systems and similar dynamic behaviour deduced for certain platinum and cobalt tetrazoles [43,44] may also be used to rationalise the broad $^{119}Sn\{^1H\}$ NMR signal ($\Delta\nu_{1/2}$, ca. 2 kHz) observed at −17.9 ppm.

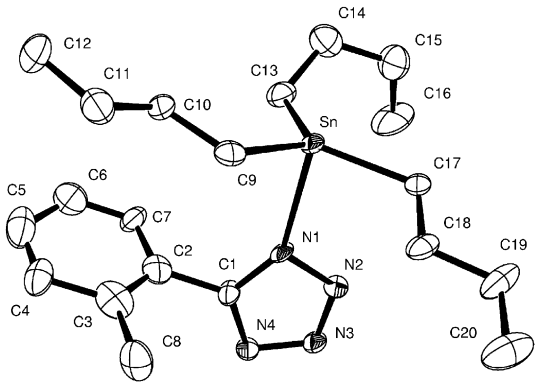

Fig. 2. The asymmetric unit of **2** with thermal ellipsoids drawn at the 50% probability level. All hydrogen atoms removed for clarity.

The solid-state structure of **2** has been crystallographically confirmed. Details of the analysis are listed in Table 2, while selected bond lengths and angles are produced in Table 3. Although the asymmetric unit (Fig. 2) contains only one nitrogen donor, the geometry at tin is best described as trigonal bipyramidal and is defined by *trans*-N_2SnC_3 coordination. The additional tetrazole coordination is provided by a nitrogen atom of an adjacent tetrazole unit. This structural feature is similar to that found in all previously characterised organotin tetrazoles, while both inter- and intramolecular bonding parameters are typical of molecules of this type [22–24]. Within the accuracy of the data, the two Sn–N bonds are identical and serve to propagate a 1D, helical polymeric array along 2_1 screw axes parallel to *c*. This occurs via the $N^1 + N^3$ (N(1)/N(3)) bridging mode, which has previously been observed in a number of related triorganostannyl tetrazole derivatives (Fig. 3)

Table 3
Selected bond lengths (Å) and angles (°) for compound **2**

Bond lengths			
Sn–C(13)	2.131(9)	Sn–C(17)	2.134(8)
Sn–C(9)	2.138(9)	Sn–N(3)′	2.368(7)
Sn–N(1)	2.406(7)	N(1)–C(1)	1.336(9)
N(1)–N(2)	1.354(16)	N(2)–N(3)	1.294(19)
N(3)–N(4)	1.365(8)	N(4)–C(1)	1.315(9)
C(1)–C(2)	1.492(12)		
Bond angles			
C(13)–Sn–C(17)	125.8(4)	C(13)–Sn–C(9)	115.9(3)
C(17)–Sn–C(9)	118.3(3)	C(13)–Sn–N(3)′	89.0(3)
C(17)–Sn–N(3)′	89.9(3)	C(9)–Sn–N(3)′	89.6(3)
C(13)–Sn–N(1)	89.5(3)	C(17)–Sn–N(1)	89.4(3)
C(9)–Sn–N(1)	92.9(3)	N(3)′–Sn–N(1)	177.5(3)
C(1)–N(1)–N(2)	104.6(8)	C(1)–N(1)–Sn	141.5(5)
N(2)–N(1)–Sn	113.7(7)	N(3)–N(2)–N(1)	108.5(7)
N(2)–N(3)–N(4)	110.7(8)	N(2)–N(3)–Sn″	125.1(6)
N(4)–N(3)–Sn″	123.7(5)	C(1)–N(4)–N(3)	103.4(6)
N(4)–C(1)–N(1)	112.8(6)	N(4)–C(1)–C(2)	124.9(7)
N(1)–C(1)–C(2)	121.8(7)		

Symmetry elements: ′, $-x,\ 0.5-y,\ -0.5+z$; ″, $-x,\ 0.5-y,\ 0.5+z$.

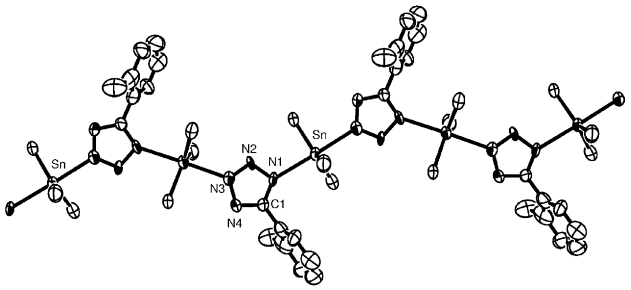

Fig. 3. The 1D polymeric structure of **2**. All hydrogen atoms and butyl carbon atoms except Sn-αC removed for clarity.

[22–24]. Although the thermal parameters of for several of the carbon atoms after refinement were large relative to the rest of the structure, this in no way negates our analysis of the overall lattice structure. The thermal parameters of the C_4H_9 units are ascribed to disorder inherent in the packing of the flexible butyl chains. This feature is common to many structures containing the Bu_3Sn fragment and has been commented upon previously with specific reference to organotin tetrazole compounds [22a].

Although attempts to apply **2** to the synthesis of titanium tetrazolyl derivatives have, thus far, met with only limited success, our initial observations are sufficiently encouraging to prompt further study and also serve to illustrate the difficulties inherent in the application of this class of ligand. Reaction of equimolar quantities of **2** and $TiCl_4$ in dichloromethane at room temperature produced a deep red solution which, upon removal of solvent, yielded a sticky red solid. This material was washed with dry hexane to remove eliminated Bu_3SnCl (confirmed by NMR analysis of the hexane filtrate) and the yellow solid produced by this procedure was analysed by ^1H NMR and 70 eV mass spectrometry. This analysis revealed the presence of both the tetrazole ligand and residual Bu_3Sn-, which persisted even upon repeated hexane washing. This observation is suggestive of either incomplete reaction or inclusion of Bu_3SnCl by adduct formation with the Lewis basic tetrazole nitrogen atoms. Indirect evidence for the formation of a titanium tetrazolyl linkage were provided by an X-ray study of a small quantity of yellow crystals obtained from the NMR tube prepared for the analysis of these reaction products in d_8-THF. These were identified as the known μ-oxo complex $(THF)_2Cl_3Ti–O–TiCl_3(THF)_2$ (**II**) [45], and are tentatively suggested as a result of preferential hydrolysis of the Ti–N bond of the target trichloroamido species.

We are continuing to study related reactivity of more sterically encumbered triorganostannyl-substituted tetrazoles in the hope of obtaining more tractable titanium-containing products. These studies and related work on the synthesis of group 5 and 6 metal complexes will be reported in due course.

4. Crystallography

Crystals of **1** and **2** were covered in oil and suitable single crystals were selected under a microscope and mounted on a KappaCCD diffractometer. Data were collected at 173 K; $\lambda(\text{Mo K}\alpha) = 0.71073$ Å; details are given in Table 2. The structures were solved by direct methods (SHELXS 97) [46] and refined by full matrix least squares (SHELXL 97) [47] with non-H atoms anisotropic and H atoms included in riding mode. No absorption correction was applied.

5. Crystal structure data

Crystallographic data for the structural analyses have been deposited with the Cambridge Crystallographic Data Centre, CCDC Nos. 221843 and 221844 for compounds **1** and **2**, respectively. Copies may be obtained free of charge from the director, CCDC, 12 Union Road, Cambridge, CB2 1EZ, UK (fax: +44-1223-336033; email: deposit@ccdc.cam.ac.uk or http://www.ccdc.cam.ac.uk).

Acknowledgements

The Royal Society is thanked for the provision of a University Research Fellowship (M.S.H.).

References

[1] S.T. Oyama, The Chemistry of Transition Metal Carbides and Nitrides, Blackie Academic & Professional, Glasgow, 1996.
[2] H.B. Pogger, Electonic Materials Chemistry, Marcel Dekker, New York, 1996.
[3] S.R. Kurtz, R.G. Gordon, Thin Solid Films 140 (1986) 277.
[4] K. Sugiyama, S. Pac, Y. Takahashi, S. Motojima, J. Electrochem. Soc. 12 (1975) 1545.
[5] R.M. Fix, R.G. Gordon, D.M. Hoffman, J. Am. Chem. Soc. 112 (1990) 7833.
[6] R.M. Fix, R.G. Gordon, D.M. Hoffman, Chem. Mater. 3 (1991) 1138.
[7] D.M. Hoffman, Polyhedron 13 (1994) 1169.
[8] C.H. Winter, P.H. Sheridan, T.S. Lewkebandara, M.J. Heeg, J.W. Proscia, J. Am. Chem. Soc. 114 (1992) 1095.
[9] T.S. Lewkebandara, P.H. Sheridan, M.J. Heeg, A.L. Rheingold, C.H. Winter, Inorg. Chem. 33 (1994) 5879.
[10] P.J. Mckarns, G.P.A. Yap, A.L. Rheingold, C.H. Winter, Inorg. Chem. 35 (1996) 5968.
[11] R.M. Fix, R.G. Gordon, D.M. Hoffman, Chem. Mater. 2 (1990) 235.
[12] C.H. Winter, T.S. Lewkebandara, J.W. Proscia, A.L. Rheingold, Inorg. Chem. 33 (1994) 1227.
[13] C.J. Carmalt, A.H. Cowley, R.D. Culp, R.A. Jones, Y.-M. Sun, B. Fitts, S. Whaley, H.W. Roesky, Inorg. Chem. 36 (1997) 3108.
[14] C.J. Carmalt, S.R. Whaley, P.S. Lall, A.H. Cowley, R.A. Jones, D.G. McBurnett, J.G. Eckert, J. Chem. Soc., Dalton Trans. (1998) 553.

[15] I.A. Guzei, A.G. Baboul, G.P.A. Yap, A.L. Rheingold, H.B. Schlegel, C.H. Winter, J. Am. Chem. Soc. 119 (1997) 3387.
[16] C. Yélamos, M.J. Heeg, C.H. Winter, Inorg. Chem. 38 (1999) 1871.
[17] C. Yélamos, M.J. Heeg, C.H. Winter, Organometallics 18 (1999) 1168.
[18] K.D. Demadis, E.–S. El Samanody, T.J. Meyer, P.S. White, Inorg. Chem. 37 (1998) 838.
[19] B. Morosin, R.G. Dunn, R. Assink, T.J. Massis, J. Fronaberger, E.N. Duesler, Acta Crystallogr., Sect. C: Cryst. Stuct. Commun. 53 (1997) 1609.
[20] R. Guillard, I. Perrot, A. Tabard, P. Richard, C. Lecomte, Y.H. Liu, K.M. Kadish, Inorg. Chem. 30 (1991) 27.
[21] R. Das, P. Paul, K. Nag, K. Venkatsubramanian, Inorg. Chim. Acta 185 (1991) 221.
[22] (a) M. Hill, M.F. Mahon, J. McGinley, K.C. Molloy, J. Chem. Soc., Dalton Trans. (1996) 835;
(b) A. Goodger, M. Hill, M.F. Mahon, J. McGinley, K.C. Molloy, J. Chem. Soc., Dalton Trans. (1996) 847.
[23] M. Hill, M.F. Mahon, K.C. Molloy, J. Chem. Soc., Dalton Trans. (1996) 1857.
[24] S. Bhandari, M.F. Mahon, K.C. Molloy, J. Chem. Soc., Dalton Trans. (1999) 1951.
[25] M. Barret, S. Bhandari, M.F. Mahon, K.C. Molloy, J. Organomet. Chem. 587 (1999) 101.
[26] S. Bhandari, C.G. Frost, C.E. Hague, M.F. Mahon, K.C. Molloy, J. Chem. Soc., Dalton Trans. (2000) 663.
[27] S. Bhandari, M.F. Mahon, K.C. Molloy, J.S. Palmer, S.F. Sayers, J. Chem. Soc., Dalton Trans. (2000) 1053.
[28] M.–A. Munoz-Hernandez, M.S. Hill, D.A. Atwood, Polyhedron 17 (1998) 2237.
[29] X.-G. Zhou, Z.-E. Hwang, R.-F. Cai, L.-X. Zhang, X.-F. Hou, X.-J. Feng, X.-Y. Hwang, J. Organomet. Chem. 563 (1998) 101.
[30] H.P.H. Arp, A. Decken, J. Passmore, D.J. Wood, Inorg. Chem. 39 (2000) 1840.
[31] C. Yélamos, K.R. Gust, A.G. Baboul, M.J. Heeg, H.B. Schlegel, C.H. Winter, Inorg. Chem. 40 (2001) 6451.
[32] M. Hill, J. Jegier, M.A. Munoz-Hernandez, D. Rutherford, A. Singer, D.A. Atwood, Phosphorus, Sulfur, Silicon Relat. Elem. 125 (1997) 183.
[33] L. Carlucci, G. Ciani, D.M. Prosperio, Angew. Chem., Int. Ed. 38 (1999) 3488.
[34] W. Zheng, M.J. Heeg, C.H. Winter, Angew. Chem., Int. Ed. 42 (2003) 2761.
[35] W.T. Reichle, Inorg. Chem. 3 (1964) 237.
[36] C. Yélamos, M.J. Heeg, C.H. Winter, Inorg. Chem. 36 (1997) 4415.
[37] R.N. Butler, in: A.R. Karitsky (Ed.), Comprehensive Heterocyclic Chemistry, Pergamon, Oxford, 1984.
[38] J.H. Nelson, D.L. Schmitt, R.A. Henry, D.W. Moore, H.B. Jonassen, Inorg. Chem. 9 (1970) 2678.
[39] S. Kozima, T. Hiomi, T. Akiyama, T. Ishida, J. Organomet. Chem. 92 (1975) 303.
[40] P.A. Bethel, M.S. Hill, M.F. Mahon, K.C. Molloy, J. Chem. Soc., Perkin Trans 1 (1999) 3507.
[41] J. Holecek, A. Lycka, Inorg. Chim. Acta 118 (1986) L15.
[42] S.J. Blunden, M.F. Mahon, K.C. Molloy, P.C. Waterfield, J. Chem. Soc., Dalton Trans. (1994) 2135.
[43] W. Beck, K. Schorpp, Chem. Ber. 108 (1975) 3317.
[44] W.G. Jackson, S. Cortez, Inorg. Chem. 23 (1994) 1921.
[45] R. Mahrwald, B. Ziemer, S. Troyanov, Tetrahedron Lett. 42 (2001) 6843.
[46] G.M. Sheldrick, SHELXS 97, Program for the Solution of Crystal Structures, Göttingen, 1997.
[47] G.M. Sheldrick, SHELXL 97, Program for the Refinement of Crystal Structures, Göttingen, 1997.

Available online at www.sciencedirect.com
SCIENCE DIRECT®
Polyhedron 23 (2004) 809–813
POLYHEDRON
www.elsevier.com/locate/poly

Homobinuclear copper(I) hexafluoroacetylacetonate complexes with non-cyclic diene ligands ☆

Vladislav V. Krisyuk, Assia E. Turgambaeva *, Shi-Woo Rhee *

Laboratory for Advanced Molecular Processing (LAMP), Electrical and Computer Engineering Division, Department of Chemical Engineering, Pohang University of Science and Technology (POSTECH), Pohang 790-784, Republic of Korea

Received 16 September 2003; accepted 13 November 2003

Abstract

Binuclear copper(I) hexafluoroacetylacetonate (hfac) complexes with non-cyclic divinyl ligands of $[Cu^{I}(hfac)]_2L$ composition (**1**) L = 1,5-hexadiene (HD), (**2**) L = allyl ether, (**3**) L = diallyldimethylsilane, (**4**) L = 1,3-divinyltetramethyldisiloxane were prepared. Sublimation tests showed that the complexes **1** and **4** are most thermally stable and can be sublimated at 50–70 °C in a vacuum (5×10^{-4} Torr) with good yield (>80%). The new yellow crystalline complex **4** is air stable at room temperature and **1** is stable under an inert atmosphere. These complexes were characterized by NMR spectroscopy, TG-DSC analysis and single crystal X-ray diffraction. The $[Cu(hfac)]_2L$ composition for both complexes is realized by copper atom coordination to one vinyl and one hexafluoroacetylacetonate group. The main reason of volatility and thermal stability of compounds **1** and **4** is high symmetry and hence low polarity of their molecules resulting in a relatively low energy of the lattice. Higher thermal stability of **4** in comparison with **1** is due to the stronger metal–ligand bonding due to the presence of dimethylsilyl groups.
© 2003 Elsevier Ltd. All rights reserved.

Keywords: Copper(I) complexes; Hexafluorocetylacetonate; Olefin complexes; Divinyl organics; Crystal structure; Thermal analysis

1. Introduction

A great number of Lewis base stabilized copper(I) β-diketonates have been prepared to date. For the most part, they are homonuclear hexafluoroacetylacetonate complexes of the formula $(hfac)Cu^{I}L$. Interest in these compounds was provoked by the fact that they form a pure copper film through the reaction of disproportionation [1–3]:

$$2(hfac)Cu^{I}L \rightarrow Cu^{0} + Cu^{II}(hfac)_2 + 2L$$

To take advantage of these compounds for copper deposition, they should be volatile, thermally stable at room temperature and susceptible to thermally induced disproportionation at elevated temperatures. As a L ligand, organic compounds like alkenes and alkynes have shown the greatest potential [4–13]. The above-mentioned reaction of disproportionation is bimolecular and occurs on a surface. Due to this reason, the use of a binuclear copper(I) complex towards facilitating the disproptionation of two Cu^{I} centers on a heated surface is desirable. Usually attempts to utilize this approach are faced with the decreased volatility and the decreased thermal stability of binuclear $[Cu^{I}(hfac)]_2L$ complexes [5,8,12]. Formation of air-sensitive products of $[Cu(hfac)]_2L$ composition was observed after heating the monometallic complexes of potentially bidentate donor ligands: hex-3-yn-1-ene, 2-methyl-1-hexen-3-yne [8] and bis(trimethylsilyl)acetylene [12]. Application of tetraalkenesilanes allowed the isolation of low-volatile mono-, bis-, tris- and tetrakis-$Cu^{I}(hfac)$ containing compounds [11]. $[Cu(hfac)]_2L$ type compounds have also been prepared for alkynes [9,14] and 1,3,5,7-cyclooctatetraene [5] mainly by changing the reaction mixture stoichiometry. Stable complex with norbornadiene of composition 2:2:1 was reported to have been prepared

☆ Supplementary data associated with this article can be found, in the online version, at doi:10.1016/j.poly.2003.12.001.

* Corresponding authors. Tel.: +82-54-279-2265/82-54-279-8614; fax: +82-54-279-8619.

E-mail addresses: taetae@postech.ac.kr (A.E. Turgambaeva), srhee@postech.ac.kr (S.-W. Rhee).

0277-5387/$ - see front matter © 2003 Elsevier Ltd. All rights reserved.
doi:10.1016/j.poly.2003.12.001

independently of the reactant ratio whereas isoprene and 1,3-butadiene complexes appeared to be unstable [5].

Our idea was to find an approach to prepare volatile and stable complexes containing two atoms of copper. As the L ligand, we tried divinyl organics, which represent a doubled variant of known olefin ligands used to prepare monometallic (hfac)Cu^{I}L complexes. In our opinion, non-cyclic ligands with terminal double bonds bridged by different linkers provide more flexibility for metal coordination (Fig. 1). In this report, we focused mainly on the relation between structure and thermal properties of these new compounds. Compounds **1** and **4** were used for copper film deposition and preliminary results have been reported [15].

2. Results and discussion

2.1. Synthesis and properties

We obtained yellow crystalline complexes of $[Cu^{I}(hfac)]_2L$ composition: (**1**) with L = 1,5-hexadiene (HD), (**2**) with allyl ether, (**3**) with diallyldimethylsilane, (**4**) with 1,3-divinyltetramethyldisiloxane (DVTMSO) (Fig. 1). These copper complexes were prepared by a slightly modified technique described elsewhere [10]. Independent of the reaction stoichiometry, and even at a Cu:hfac:L ratio of 1:1:2, we separated products $[Cu(hfac)]_2L$ with a 2:2:1 ratio as confirmed from elemental analysis. As sublimation tests showed, among this series of complexes (Fig. 1), only two compounds appeared to be volatile and thermally stable: **1** is formed with the HD ligand and **4** with the DVTMSO ligand. Therefore, detailed investigation was carried out for these two compounds and the discussion is focused mainly on them. Complex **4** is air stable at room temperature and **1** is stable under inert atmosphere mostly. Both of them have been purified by sublimation at 50–70 °C in a 10^{-4} Torr vacuum with good yield (>80%). Thermogravimetric analysis (TGA) and differential scanning calorimetry (DSC) were performed in a dynamic inert atmosphere (Fig. 2). The first peak in the DSC curve indicates a melting point of 71 °C for $[Cu^{I}(hfac)]_2$(DVTMSO) and 101 °C for $[Cu^{I}(hfac)]_2$-(HD). The endothermic peak at around 220 °C for **4** and 160 °C for **1** indicates maximum weight loss rate detected at these temperatures. The percentage of non-volatile residue for both compounds is much below the Cu content in the complex indicating that the complex was not decomposed below the melting point. At the same time the residue amount for compound $[Cu^{I}(hfac)]_2$(DVTMSO) is almost half of that for $[Cu^{I}(hfac)]_2$(HD). A noticeable exothermic peak at 310 °C for $[Cu^{I}(hfac)]_2$(HD) is assigned to a copper crystallization process. Thus, $[Cu^{I}(hfac)]_2$(DVTMSO) is believed to be more stable than $[Cu^{I}(hfac)]_2$(HD). Comparison of volatility was carried out by vapor pressure measurement for compounds **1**, **4** and well-known mononuclear complex (hfac)Cu^{I}(1,5-cyclooctadiene) results has been previously reported [15].

2.2. Structure consideration

To understand the thermal stability of these two complexes with such different donor ligands, we studied their structure and nature of chemical bonding. The crystal structure determination confirmed the new compounds to be bimetal molecules in which the copper(I) ions are tricoordinated by a chelate-bound β-diketonate and η^2-coordinated vinyl unit (Figs. 3 and 4). Here, we concentrate the attention on structural features of both compounds omitting routine description of each structural element in the molecules. Table 1 shows selected structural data that characterize the main differences in these two complexes.

(hfac)Cu^{I}(vinyl) groups in the molecule of compound **1** are oriented in an opposite manner in parallel planes so the molecule has minimum dipole moment (Fig. 3). The hexadiene ligand in the molecule takes the conformation with minimum energy that stabilizes the complex molecule despite of the relatively simple ligand composition, whereas $[Cu^{I}(hfac)]_2L$ complexes with the simplest alkadienes, 1,3-butadiene and isoprene, are known to be very unstable [5].

The complex with DVTMSO **4** has a structure that is more complicated because it is formed by a ligand containing heteroatoms (Fig. 4). Metal-carbon(vinyl) distances in **1** and **4** are distributed in the same manner (Table 1), while in metal-oxygen(hfac) and C=O distances in the chelate cycle, there is a difference. In

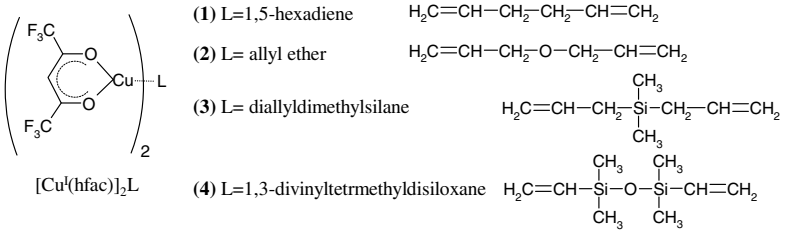

Fig. 1. Copper(I) complexes reported in this work.

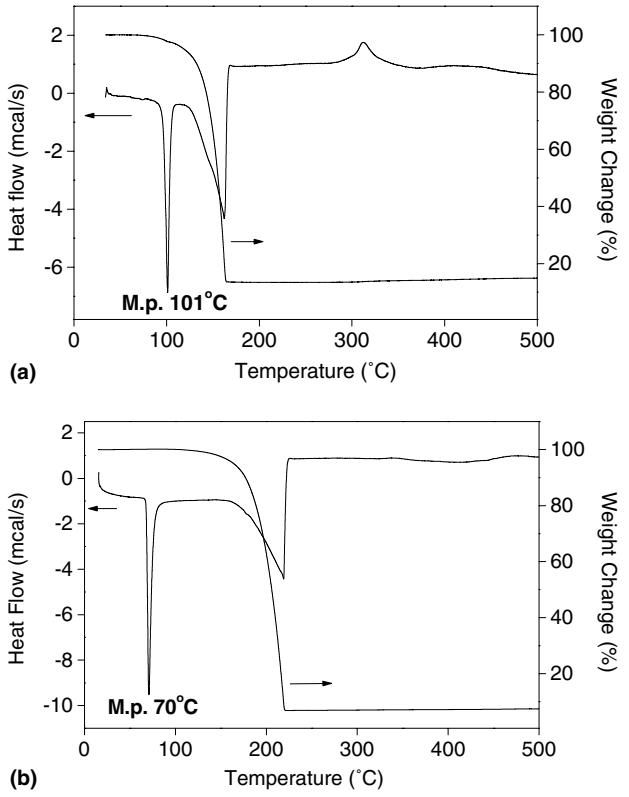

Fig. 2. Thermogravimetric analysis and differential scanning calorimetry of compounds (a) $[Cu^{I}(hfac)]_2(HD)$ (**1**) and (b) $[Cu^{I}(hfac)]_2(DVTMSO)$ (**4**) at 10 °C/min of heating rate in dynamic inert atmosphere.

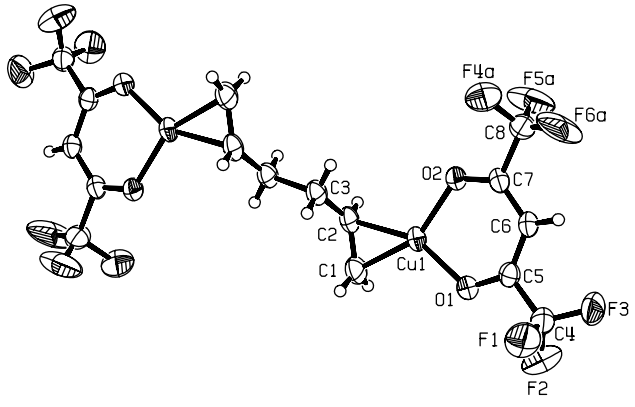

Fig. 3. ORTEP view of the binuclear complex $[Cu^{I}(hfac)]_2(HD)$ (**1**).

contrast to **1**, the following is observed in **4**: if Cu–O(2) is shorter than Cu–O(3), then Cu–C(3) is longer than Cu–C(4). If Cu–O is longer, the adjacent C=O bond is also longer. Such a disordering can be explained by the presence of an intermolecular short contact between O(3) and the copper atom of the nearest molecule. This distance is equal to 2.85 Å. Nevertheless, the molecule as a whole has rotational symmetry, a center of inversion and seems to be non-polar. The angle Si–O–Si is equal

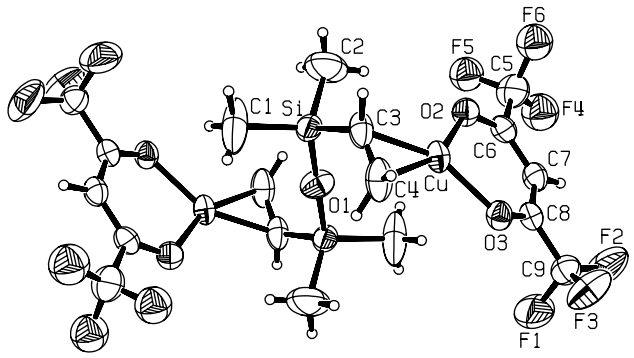

Fig. 4. ORTEP view of the binuclear complex $[Cu^{I}(hfac)]_2(DVTMSO)$ (**4**).

Table 1
Selected bond distances (Å) and angles (°) for complexes **1** and **4**

$[Cu^{I}(hfac)]_2(HD)$ (**1**)		$[Cu^{I}(hfac)]_2(DVTMSO)$ (**4**)	
Bond distances			
Cu(1)–O(1)	1.959(2)	Cu–O(3)	1.972(5)
Cu(1)–O(2)	1.965(2)	Cu–O(2)	1.961(5)
Cu(1)–C(1)	1.993(3)	Cu–C(4)	1.987(9)
Cu(1)–C(2)	2.018(3)	Cu–C(3)	2.000(7)
O(2)–C(7)	1.247(4)	O(2)–C(6)	1.254(8)
O(1)–C(5)	1.255(4)	O(3)–C(8)	1.264(8)
C(1)–C(2)	1.366(5)	C(3)–C(4)	1.355(13)
C(2)–C(3)	1.495(5)	Si–O(1)	1.5968(19)
C(3)–C(3)#1	1.538(6)	Si–C(1)	1.832(10)
		Si–C(2)	1.853(13)
		Si–C(3)	1.868(8)
		Cu–O(1)	3.292(2)
		Cu–Si	3.149(9)
Bond angles			
		Si–O(1)–Si#1	180.00(14)
		O(1)–Si–C(3)	107.8(3)
C(1)–C(2)–C(3)	123.8(4)	Si–C(3)–Cu	109.0(4)
C(2)–C(3)–C(3)#1	111.2(4)	C(4)–C(3)–Si	125.5(7)
O(1)–Cu(1)–O(2)	94.05(9)	O(2)–Cu–O(3)	93.2(2)

For **1**:#1 $1-x, 2-y, z$; for **2**:#1 $2-x, -y, 1-z'$.

to 180 °C due to a typical $\pi(d_{Si}–p_O)$ interaction between oxygen and silicon in the siloxanes. At the same time, Cu(hfac) groups are oriented in the way of possible $\pi(d_{Cu} \rightarrow d_{Si})$ or even $\pi(d_{Cu} \rightarrow \pi(d_{Si}–p_O))$ interaction. It is noteworthy that the Cu–Si distance is less than the sum of the Van der Waals radii. This interaction seems to be weak but stabilizes the molecule with this structure. The coordinated C=C bond in **4** is a little bit shorter than that in **1** (Table 1) and shorter than that in (hfac)-Cu^{I}(VTMS) (1.38 Å) [4]. Hence, the structural data obtained are indicative of different character in the chemical bonding between metal and donor ligand.

To explore the metal–ligand bonding in detail, we have used NMR. Coordination of olefins to Cu^{+} is thought to be composed of two components: one is σ donation from the π orbitals of the olefin into empty σ 4s orbitals of the metal. The other one is the bonding of filled d orbitals of the metal into empty π^* orbitals of the olefin. For a series of copper olefin complexes, the

relative contribution of each bonding component can be assessed from its ^1H or better from ^{13}C NMR [13]. Typically, the σ component produces a chemical shift in the signals of coordinated olefin protons to weaker field (deshielding) while the back bonding gives the opposite result (shielding). The combination of these two effects results in the absolute chemical shift. The predominant role of $d \rightarrow \pi^*$ back bonding has been shown for alkylsilyl derivatives of olefins and alkynes [4,12]. Data from ^1H and ^{13}C NMR spectra for complexes **1**, **4** and free ligands are presented in Table 2. Comparing chemical shifts, we conclude that the contribution of back bonding from the metal to vinyl group in **1** and **4** is almost equal. But in **4**, there are intermolecular contacts in the crystal between the copper atom and the oxygen atom in the diketonate of the nearest molecule. This indicates that the electron density on the copper atom in **4** is decreased in comparison with **1**, where such contacts are absent. Summarizing all these facts, we believe that in $[Cu^I(hfac)]_2$(DVTMSO), there is donation from filled d-orbitals of copper to silicon in addition to the typical back bonding to the vinyl group. This leads to the higher stability of compound **4** in comparison with **1** and particularly with the monomer analogue, (hfac)-Cu^I(VTMS).

Thus, we believe that the main reason for the volatility of compounds **1** and **4** is high symmetry and hence low polarity of their molecules resulting in relatively low energy of the lattice. Higher thermal stability of **4** in comparison with **1** is from the stronger metal–ligand bonding due to the presence of dimethylsilyl groups.

As to compounds **2** and **3** from the series, we could not obtain good crystal by sublimation owing to their low thermal stability. In the absence of favorable substituents in donor ligand, the minimal dipole moment seems to be one of the dominant factors for increased volatility and thermal stability of the molecule. We believe that low stability and volatility of complex **2** is due to the donor ligand (Fig. 1) that cannot take a suitable conformation to reduce the polarity of the complex. Note that compensation of the dipole moment due to mutual orientation (coupling) of molecules has been observed for monometallic complexes of (hfac)Cu^IL in the solid state [16].

In compound **3**, the electronic effect of the alkylsilyl group upon vinyl is minimized by the presence of the intermediate –CH_2– groups in the ligand reducing the complex stability. In support of this interpretation, the comparison of the properties of copper(I) hexafluoroacetylacetonate complexes with vinyltrimethylsilane and allyltrimethylsilane can be taken into consideration [7].

Table 2
Experimentally determined chemical shift changes for protons and carbons by comparing the chemical shifts of L and $[Cu^I(hfac)]_2L$[a]

Group	δ ^1H[b]	$\Delta\delta$ ^1H	δ ^{13}C	$\Delta\delta$ ^{13}C
Complex **1**/L				
=CH–	4.3/5.7	−1.4	90.3/138.2	−47.9
CH_2=	3.6/5.0	−1.4	81.0/114.9	−33.9
Complex **4**/L				
=CH–	4.0/6.3–5.8	∼2	102.0/139.7	−37.7
CH_2=			90.8/131.9	−41.1

[a] The NMR data are obtained in C_6D_6 solvent, the chemical shifts are in ppm.
[b] At peak maximum.

3. Conclusion

The possibility of the preparation of stable and volatile binuclear copper(I) hexafluoroacetylacetonate complexes with non-cyclic ligands having terminal double bonds bridged by different linkers was demonstrated. A simple synthetic technique allowed the isolation of complexes with exact $[Cu^I(hfac)]_2L$ composition. A thermo-analytical study showed that from the series of similar compounds, the most thermally stable and volatile binuclear copper(I) hexafluoroacetylacetonate complexes have been obtained with donor ligands 1,5-hexadiene (HD) and 1,3-divinyltetramethyldisiloxane (DVTMSO). Crystal structure determination confirmed that the $[Cu(hfac)]_2L$ composition is realized by copper atom coordination to one vinyl group in the donor ligand and one hexafluoroacetylacetonate. In spite of the essential distinction in composition, the common feature of HD and DVTMSO ligands is the fact that their conformation provides non-polarity of the complex molecules. Such a structure determines high storage and thermal stability and volatility of these compounds. Higher thermal stability of $[Cu^I(hfac)]_2$(DVTMSO) in comparison with $[Cu^I(hfac)]_2$(HD) is from the stronger metal–ligand bonding due to the presence of dimethylsilyl groups.

4. Experimental

4.1. Measurements

The CHN elemental analyses were carried out with an Elementar Analysensysteme GmbH VarioEL. ^1H and ^{13}C NMR spectra were recorded with DRX300 Bruker instruments at frequencies of 300 and 75 MHz, respectively. Thermal analysis was performed in N_2 atmosphere at a heating rate of 10 °C/min using a SDT 2960 TA Instruments device. Single crystals for X-ray analysis were obtained by sublimation. The intensity data were collected with a Siemens diffractometer equipped with a graphite-monochromated Mo Kα (λ = 0.71073 Å) radiation source and CCD detector. SHELXS 97 and SHELXL 97 implemented with the SHELXTL program package were used to solve and refine the

structure. Experimental details of the structure determination as well as bond lengths, bond angles and thermal parameters are available as supplementary material. (see the online version.)

4.2. Syntheses

All manipulations were carried out under dry nitrogen atmosphere using standard Schlenk techniques. To synthesize $[Cu^{I}(hfac)]_2(HD)$ (**1**), hexafluoroacetylacetone (Hhfac) (5 ml in 10 ml of ether) was added slowly dropwise to the mixture of Cu_2O (5 g), 1,5-hexadiene (5 ml) in 40 ml of ether with stirring under 0 °C. After completing the addition of Hhfac, stirring was maintained for 10 min and then the material was filtered to another flask through a PTFE capillary filter. Solvent was removed under dynamic vacuum. The product consists of yellow crystals (10 g, yield: 90%). *Anal.* Found/Calc. for $C_{16}H_{12}F_{12}O_4Cu_2$: C, 30.21/30.83; H, 1.87/1.94%. ^{1}H NMR (C_6D_6) δ ppm versus TMS: 6.2 (s, 2H, –*CH*– on hfac), 4.3 (m, 2H, –*CH*═), 3.6 (d, $^2J_{H-H} = 12.5$ Hz, 4H, ═*CH*$_2$), 1.4 (q, $^2J_{H-H} = 6.1$ Hz, 4H, –*CH*$_2$–). ^{13}C NMR (C_6D_6) δ ppm versus TMS: 178.0 (q, $^2J_{C-F} = 34.4$ Hz, *C*═*O*), 124.2, 120.4, 116.6, 112.8 (q, $J_{C-F} = 286.8$ Hz, –*CF*$_3$), 104.7 (s, –*CH*– on hfac), 90.3 (s, –*CH*═), 81.0 (s, ═*CH*$_2$), 33.0 (s, –*CH*$_2$–).

To synthesize $[Cu^{I}(hfac)]_2$(DVTMSO) (**4**), Hhfac (5 ml in 10 ml of ether) was added slowly dropwise to the mixture of Cu_2O (5 g), DVTMSO (5.5 ml) and Na_2SO_4 (10 g) in 40 ml of ether with stirring under 0 °C. After completing the addition of Hhfac, stirring was maintained for 10 min and then the material was filtered and transferred to another flask. Solvent was removed under dynamic vacuum. The product consists of yellow crystals (11 g, yield: 86%). *Anal.* Found/Calc. for $C_{18}H_{20}F_{12}O_5Si_2Cu_2$: C, 29.72/29.71; H, 2.82/2.77%. ^{1}H NMR (C_6D_6) δ ppm versus TMS: 6.2 (s, 2H, –*CH*– on hfac), 4.0 (m, 6H, –*CH*═*CH*$_2$), 0.0 (s, 12H, –*Si*(*CH*$_3$)$_2$). ^{13}C NMR (C_6D_6) δ ppm versus TMS: 179.0 (q, $^2J_{C-F} = 34.6$ Hz, *C*═*O*), 124.6, 120.9, 117.1, 113.3 (q, $J_{C-F} = 285.7$ Hz, –*CF*$_3$), 110.0 (s, –*CH*– on hfac), 102.0 (s, –*CH*═), 90.8 (s, ═*CH*$_2$), 1.2 (s, –*Si*(*CH*$_3$)$_2$).

Compounds **2** and **3** have been prepared by the same procedure. *Anal.* Found/Calc. for $C_{16}H_{12}F_{12}O_5Cu_2$ **2**: C, 29.62/30.05; H, 2.12/1.89%, ^{1}H NMR (C_6D_6) δ ppm versus TMS: 6.1 (s, 2H, –*CH*– on hfac), 4.4 (m, 2H, –*CH*═), 3.9–3.5 (q, 4H, ═*CH*$_2$), 3.2 (d, 4H, –*CH*$_2$–); *Anal.* Found/Calc. for $C_{18}H_{18}F_{12}O_4SiCu_2$ **3**: C, 31.12/31.72; H, 2.54/2.66%. ^{1}H NMR (C_6D_6) δ ppm versus TMS: 6.2 (s, 2H, –*CH*– on hfac), 4.4 (m, 2H, –*CH*═), 3.5 (q, 4H, ═*CH*$_2$), 0.8 (d, 4H, –*CH*$_2$–), −0.4 (s, 6H, –*Si*(*CH*$_3$)$_2$).

5. Supplementary material

Crystallographic data for the structures reported in this paper have been deposited with the Cambridge Crystallographic Data Centre as supplementary publication CCDC Nos. 212772 and 212771 for compounds **1** and **4**, respectively. Copies of the data can be obtained free of charge on application to The Director, CCDC, 12 Union Road, Cambridge, CB2 1EZ, UK (fax:/44-1223-336033; e-mail: deposit@ccdc.cam.ac.uk or www.ccdc.cam.ac.uk).

References

[1] M.J. Hampden-Smith, T.T. Kodas, Polyhedron 14 (1995) 699.
[2] P. Doppelt, Coord. Chem. Rev. 178 (1998) 1785.
[3] J.A.T. Norman, J. Phys. IV France 11 (2001) Pr3-497.
[4] J.A.T. Norman, B.A. Muratore, P.N. Dyer, D.A. Roberts, A.K. Hochberg, Mater. Sci. Engrg. B7 (1993) 87.
[5] G. Doyle, K.A. Eriksen, D. Van Engon, Organometallics 4 (1985) 830.
[6] K.M. Chi, H.-K. Shin, M.J. Hampden-Smith, E.N. Duesler, T.T. Kodas, Polyhedron 10 (1991) 2293.
[7] K.-K. Choi, S.-W. Rhee, Thin Solid Films 409 (2002) 147.
[8] T.-Y. Chen, J. Vaissermann, P. Doppelt, Inorg. Chem. 40 (2001) 6167.
[9] T.-Y. Chen, J. Vaissermann, E. Ruiz, J.P. Senateur, P. Doppelt, Chem. Mater. 13 (2001) 3993.
[10] W. Zhuang, L.J. Charneski, D.R. Evans, S.T. Hsu, Z. Tang, A.M. Guloy, J. Phys. IV France 11 (2001) Pr3-553.
[11] G.G. Rozenberg, J.H.G. Steinke, T. Gelbrich, M.B. Hursthouse, Organometallics 20 (2001) 4001.
[12] P. Doppelt, T. Baum, J. Organomet. Chem. 517 (1996) 53.
[13] T. Baum, C.E. Larson, G. May, J. Organomet. Chem. 425 (1992) 189.
[14] G. Schmidt, U. Behrens, J. Organomet. Chem. 503 (1995) 101.
[15] S.-W. Kang, J.-H. Yun, S.-W. Rhee, V.V. Krisyuk, A.E. Turgambaeva, in: M. Allendorf, F. Maury, F. Teyssandier (Eds.), ECS Proceedings Volume 2003-08, CVD XVI and EUROCVD 14, p. 1305.
[16] M. Joulaud, L. Omnes, T. Mourier, D. Mayer, P. Doppelt, in: M. Allendorf, F. Maury, F. Teyssandier (Eds.), ECS Proceedings Volume 2003-08, CVD XVI and EUROCVD 14, p. 1268.

Available online at www.sciencedirect.com
SCIENCE DIRECT®
Polyhedron 23 (2004) 815–821
POLYHEDRON
www.elsevier.com/locate/poly

Synthesis, characterization, electrochemistry and solvatochromic studies of $[Ru(dppt)(dien)]^{2+}$ and $[Ru(pta)(dien)]^{2+}$

Xian-Lan Hong [a,b], Hui Chao [a,*], Jun-Hua Yao [c], Hong Li [d], Liang-Nian Ji [a,e,*]

[a] Department of Chemistry, Sun Yat-Sen University, Guangzhou 510275, PR China
[b] Department of Chemistry, Shaoguan University, Shaoguan, Guangdong 512005, PR China
[c] Center of Analysis and Determination, Sun Yat-Sen University, Guangzhou 510275, PR China
[d] Department of Chemistry, Southern China Normal University, Guangzhou 510631, PR China
[e] State Key Laboratory of Gene Engineering of Ministry of Education, Sun Yat-Sen University, Guangzhou 510275, PR China

Received 10 September 2003; accepted 17 November 2003

Abstract

Two novel Ru(II) complexes $[Ru(dppt)(dien)](ClO_4)_2$ (**1**) and $[Ru(pta)(dien)](ClO_4)_2$ (**2**) (dppt, pta and dien stand for 3-(1,10-phenanthrolin-2-yl)-5,6-diphenyl-as-triazine, 3-(1,10-phenanthrolin-2-yl)-5,6-diphenyl-as-triazino[5,6-f]acenaphthylene and diethylenetriamine, respectively) were synthesized and characterized by elemental analysis, ES-MS and ^1H NMR spectroscopy. Due to the strong electron donor ability of dien, the oxidation potentials of complexes **1** and **2** are less positive and their MLCT bands significantly shift to lower energies in comparison with those of the homoleptic complexes $[Ru(dppt)_2](ClO_4)_2$ and $[Ru(pta)_2](ClO_4)_2$. The solvatochromic behaviors of the two complexes were also investigated.
© 2003 Elsevier Ltd. All rights reserved.

Keywords: Ruthenium(II) complexes; Polypyridine ligands; Diethylenetriamine

1. Introduction

Ruthenium(II) polypyridine complexes have attracted a large and increasing amount of interest due to their outstanding redox and photophysical properties [1–4]. However, most studies have primarily focused on complexes involving rigid heterocyclic ligands such as 2,2′-bipyridine (bpy), 1,10-phenanthroline (phen) and 2,2′:6′,2″-terpyridine (tpy). Over the past decade quite a large amount of data has been accumulated on the changes in the electrochemical and photophysical properties of complexes effected by substitution in the bpy, phen or tpy rings, or replacement of one or both of the pyridine rings with other nitrogen-containing heterocycles [1–9]. On the other hand, the investigations of ruthenium(II) complexes with aliphatic polyamine ligands still remain scarcely touched. In fact, Ru(II) amine complexes display unique photophysical and electrochemical properties, such as lower energy electronic absorption for MLCT transitions, easy oxidation of the metal center and solvatochromic behavior, getting some utilization in probing DNA structure [10,11], sensitizing the local environment [12–14] and metal-containing pharmaceuticals [15].

In order to further understand the solvent-dependent properties of Ru(II) complexes, as well as laying the foundation for the rational design of biological probes and chemical sensors, we report herein the synthesis and characterization of two novel ruthenium amine complexes $[Ru(dppt)(dien)](ClO_4)_2$ and $[Ru(pta)(dien)](ClO_4)_2$ (dppt and pta stand for 3-(1,10-phenanthrolin-2-yl)-5,6-diphenyl-as-triazine and 3-(1,10-phenanthrolin-2-yl)-5,6-diphenyl-as-triazino[5,6-f]-acenaphthylene, respectively), in which an aliphatic polyamine ligand diethylenetriamine (dien) is introduced and this will have a different effect on the properties of ruthenium complexes in comparison with the polyaromatic ligand tpy and its derivatives. The electrochemistry and spectroscopic properties especially solvatochromism of the complexes are also investigated.

* Corresponding authors.
E-mail addresses: ceschh@zsu.edu.cn (H. Chao), cesjln@zsu.edu.cn (L.-N. Ji).

0277-5387/$ - see front matter © 2003 Elsevier Ltd. All rights reserved.
doi:10.1016/j.poly.2003.11.055

2. Experimental

2.1. Materials and preparations

The compounds 3-(1,10-phenanthrolin-2-yl)-5,6-diphenyl-as-triazine (dppt) [16] and 3-(1,10-phenanthrolin-2-yl)-5,6-diphenyl-as-triazino[5,6-f]acenaphthylene (pta) [16] were synthesized according to literature methods. Other materials were commercially available and of reagent grade.

(*Caution*: perchlorate complexes are potential explosives that must be handled in small quantity and with great care.)

2.1.1. Synthesis of Ru(dppt)Cl$_3$

It was synthesized in a similar manner to that described in the literature [17]. A mixture of $RuCl_3 \cdot nH_2O$ (1 mmol, 0.260 g) and dppt (1 mmol, 0.411 g) in 125 ml of absolute ethanol was heated at reflux for 3 h while vigorous magnetic stirring was maintained. After this time the reaction was cooled to room temperature, and the fine brown powder that had appeared was filtered from the reddish yellow solution. The product was washed with 3×30 ml portions of absolute ethanol followed by 3×30 ml portions of Et_2O and air-dried. Yield: 70.3%. (Found: C, 52.17; H, 2.98; N, 11.04%. $C_{27}H_{17}N_5Cl_3Ru$ requires: C, 52.38; H, 2.75; N, 11.32%). ESMS [CH_3OH, m/z]: 583.1 ([M-Cl]$^+$), 273.8 ([M-2Cl]$^{2+}$), 170.8 ([M-3Cl]$^{3+}$).

2.1.2. Synthesis of Ru(pta)Cl$_3$

This complex was synthesized in a similar manner to that described for Ru(dppt)Cl_3, with pta (1 mmol, 0.383 g) in place of dppt. Yield: 65%. (Found: C, 50.76; H, 2.33; N, 11.61%; $C_{25}H_{13}N_5Cl_3Ru$ requires: C, 50.80; H, 2.20; N, 11.85%). ESMS [CH_3OH, m/z]: 555.1 ([M-Cl]$^+$), 259.8 ([M-2Cl]$^{2+}$), 161.38 ([M-3Cl]$^{3+}$).

2.1.3. Synthesis of [Ru(dppt)(dien)](ClO$_4$)$_2 \cdot 2H_2O$

A mixture of Ru(dppt)Cl_3 (0.150 g, 0.243 mmol), dien (0.025 g, 0.243 mmol) and triethylamine (1 cm^3) in ethanol–water (1:1 v/v, 50 cm^3) was refluxed for 8 h, during this time the solution turned reddish purple. After being cooled to room temperature, the ethanol was removed under reduced pressure and a dark purple precipitate was obtained by addition of a saturated aqueous $NaClO_4$ solution. The product was purified by column chromatography on alumina with acetonitrile as eluent. Yield: 63%. (Found: C, 43.85; H, 3.93; N, 13.26. Calc. for $C_{31}H_{30}N_8Cl_2O_8Ru \cdot 2H_2O$: C, 43.76; H, 4.00; N 13.18%). ES-MS [CH_3CN, m/z]: 715.1 ([M-ClO$_4$]$^+$), 308.3 ([M-2ClO$_4$]$^{2+}$). ^{1}H NMR [$(CD_3)_2SO$, aromatic region]: δ 9.52 (d, 1H, H$_c$, $J = 7.5$), 8.87 (dd, 2H, H$_a$, H$_f$, $J_1 = 8$, $J_2 = 8$), 8.57 (d, 1H, H$_g$, $J = 8$), 8.42 (s, 2H, H$_d$, H$_e$), 8.16 (dd, 1H, H$_b$, $J_1 = 5$, $J_2 = 5.5$), 7.77–7.71 (m, 3H, H$_h$, H$_j$), 7.61–7.51 (m, 5H, H$_i$, H$_k$, H$_l$), 7.49 (dd, 2H, H$_m$, $J = 5$).

2.1.4. Synthesis of [Ru(pta)(dien)](ClO$_4$)$_2 \cdot 2H_2O$

This complex (dark purple) was synthesized in an identical manner to that described for [Ru(dppt)(dien)](ClO$_4$)$_2$ with Ru(pta)Cl_3 (0.093 g, 0.243 mmol) in place of Ru(dppt)Cl_3. The product was purified by column chromatography on alumina with acetonitrile–ethanol (v/v, 50:1) as eluent. Yield: 47% (Found: C, 42.41; H, 3.66; N, 13.70. Calc. for $C_{29}H_{26}N_8Cl_2O_8Ru \cdot 2H_2O$: C, 42.34; H, 3.65; N 13.63%). ES-MS [CH_3CN, m/z]: 687.1 ([M-ClO$_4$]$^+$), 294.3 ([M-2ClO$_4$]$^{2+}$). ^{1}H NMR [$(CD_3)_2SO$, aromatic region]: δ 9.72 (d, 1H, H$_c$, $J = 4.5$), 8.89 (dd, 2H, H$_a$, H$_f$, $J_1 = 8$, $J_2 = 7.5$), 8.58–8.50 (m, 3H, H$_g$, H$_h$, H$_j$), 8.41 (s, 2H, H$_d$, H$_e$), 8.18–8.12 (m, 4H, H$_b$, H$_i$, H$_k$, H$_l$), 8.10 (d, 1H, H$_m$, $J = 6$).

2.2. Physical measurements

Microanalyses (C, H and N) were carried out with a Perkin–Elmer 240Q elemental analyser. US/VIS spectra were recorded on a Shimadzu MPS-2000 spectrophotometer. One dimensional ^{1}H NMR spectra and 2D ^{1}H–^{1}H COSY were measured on a Varian-500 NMR spectrometer with $(CD_3)_2SO$ as solvent at room temperature and the residual signal of the solvent was used as an internal standard. Electrospray mass spectra (ES-MS) were recorded on a LCQ system (Finnigan MAT, USA) using methanol as the mobile phase. The spray voltage, tube lens offset, capillary voltage and capillary temperature were set at 4.50 kV, 30.00, 23.00 V and 200 °C, respectively, and the quoted m/z values are for the major peaks in the isotope distribution.

A BioAnalytical Systems 100-W electrochemical analyzer was used to record the cyclic voltammograms. The supporting electrolyte was 0.1 M tetrabutylammonium perchlorate in acetonitrile freshly distilled from phosphorus pentaoxide and deaerated by purging with nitrogen. The electrochemical measurements were made in a standard three-electrode system using a platinum disk working electrode, platinum-wire auxiliary electrode and a Ag/AgCl reference electrode [0.29 V versus NHE, calibrated using the $Fe(C_5H_5)_2/Fe(C_5H_5)_2^+$ couple (0.665 V versus NHE)]. All cyclic voltammograms were recorded at a scan rate of 200 mV/s.

2.3. Molecular orbital calculations

The molecular structures of the free dppt and pta ligands were optimized by the INDO method [18] with the default parameters packaged in the computer program HyperChem Release 6 (HyperCube, Inc.) [19]. Calculations of the electronic structures were carried out using the extended Hückel approximation [20] with the same program using the default parameters.

3. Results and discussion

3.1. Synthesis and characterization

An outline of the syntheses of the ruthenium(II) complexes is illustrated in Scheme 1. Initially, hydrated $RuCl_3$ was reacted with one equivalent dppt or pta in absolute ethanol to obtain the red–brown insoluble $[Ru(dppt)Cl_3]$ or $[Ru(pta)Cl_3]$, respectively. The two precursors were then reacted at reflux with dien in the presence of triethylamine. The resulting ruthenium(II) complexes were isolated as the perchlorates and purified by column chromatography. It is also worth noting that complexes **1** and **2** have relatively strong affinities to the column support Al_2O_3 because of the polar functional group NH or NH_2 in comparison with $[Ru(dppt)_2](ClO_4)_2$ and $[Ru(pta)_2](ClO_4)_2$, bringing difficulty to their elution off the column, so adding a proper quantity of ethanol to the eluent is sometimes necessary.

Electrospray mass spectrometry (ESMS) has recently been shown to be a powerful tool for measuring the molecular mass of non-volatile and thermally unstable compounds [21]. In the ESMS spectra, the two complexes all exhibit the expected peaks due to $[M–ClO_4^-]^+$ and $[M–2ClO_4^-]^{2+}$ cations. The measured molecular weights were consistent with expected values.

All of the new ruthenium(II) complexes give well-defined ^1H NMR spectra. The proton chemical shifts were assigned with the aid of ^1H–^1H COSY experiments and comparison with those of similar compounds [22–25]. A representative ^1H–^1H COSY spectrum of $[Ru(dppt)(dien)]^{2+}$ is shown in Fig. 1. The chemical shifts of all the protons are presented in Section 2. Signals of the protons attached to the phenanthroline moieties, except H_a, appear at lower magnetic fields than those of the free ligands, the downfield shifts of H_c, H_d and H_e, which are at the para position to the coordinated nitrogen, are especially pronounced. At the same time, the protons close to the metal ion all experience much larger shifts, which is most clearly in H_m (0.18 ppm downfield shift for $[Ru(dppt)(dien)]^{2+}$ and 0.65 ppm for $[Ru(pta)(dien)]^{2+}$ in comparison with the corresponding protons of free ligands). This may be mainly attributed to the electron-withdrawing effects of the metal center and indirectly to the σ-donating effect of the trisamine ligand. Furthermore, the difference in chemical shift is strongly pronounced in the pta complex with a planar arrangement of the aromatic rings. In the dppt complex a free rotation of the phenyl rings takes place and therefore the delocalisation of the π-system is less pronounced.

3.2. Molecular orbital calculations

Extended Hückel calculations were carried out in order to obtain compositions and energies of the dppt

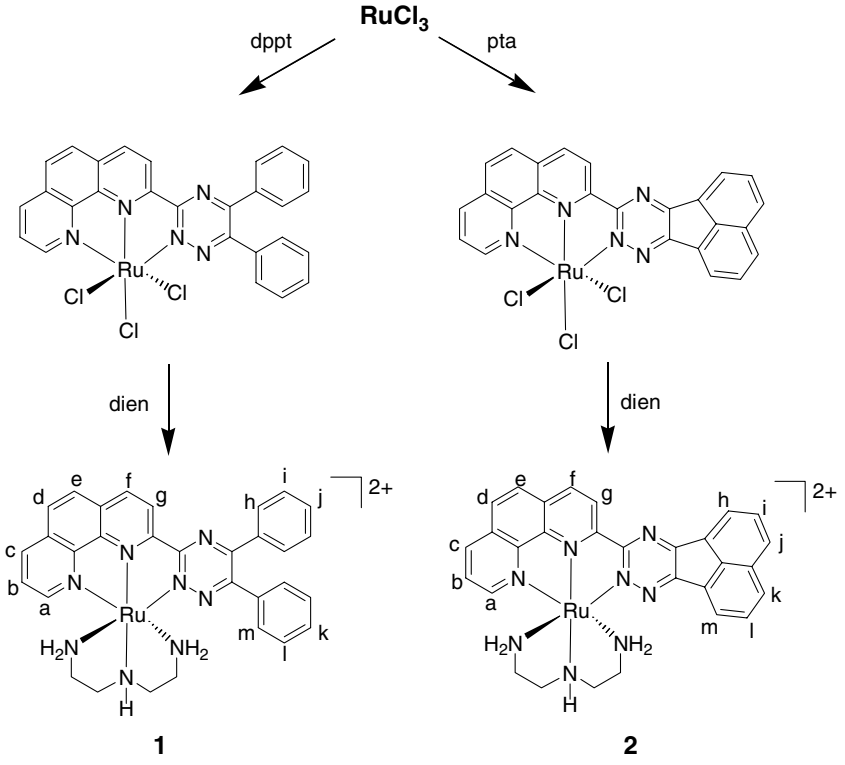

Scheme 1. Synthetic routes for the preparation of the ruthenium(II) complexes.

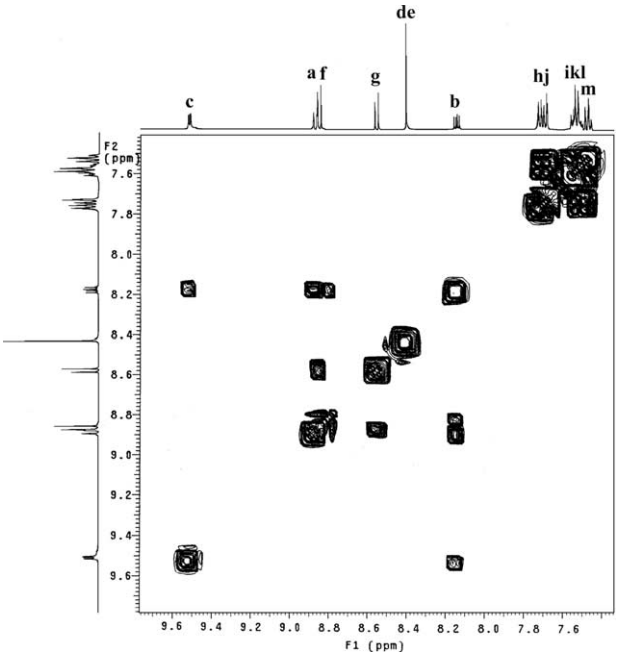

Fig. 1. ^{1}H–^{1}H COSY spectrum of $[Ru(dppt)(dien)]^{2+}$ in $(CD_3)SO$ (500 MHz).

and pta ligand orbitals and to rationalize the electrochemical and spectroscopic results. Fig. 2 shows the graphical illustrations for the three lowest lying unoccupied orbitals of dppt and pta. For the two asymmetric tridentate ligands, we made the following observations: (i) the lowest vacant molecular orbital is centered on the triazine part with the electronic distribution. The LUMO is found at −10.24 eV for complex **1** and −10.29 eV for complex **2**. (ii) The next vacant MO LUMO + 1 lying at higher energy (−9.93 eV for complex **1** and −10.15 eV for complex **2**) is extended on the phenanthroline-type part with a strong weight on the related coordinating nitrogens. (iii) In contrast, the MO LUMO + 2 (−9.64 eV for complex **1** and −9.67 eV for complex **2**) is developed on the phenanthroline-type part, with very little electronic density on the triazine part. This simple electronic approach reflects the non-equivalence of coordinating sites on the asymmetric ligands. This electronic distribution and the orbital energy levels account also for the more pronounced π-acceptor character and the greater energetic stabilization of pta with respect to those of the dppt ligand.

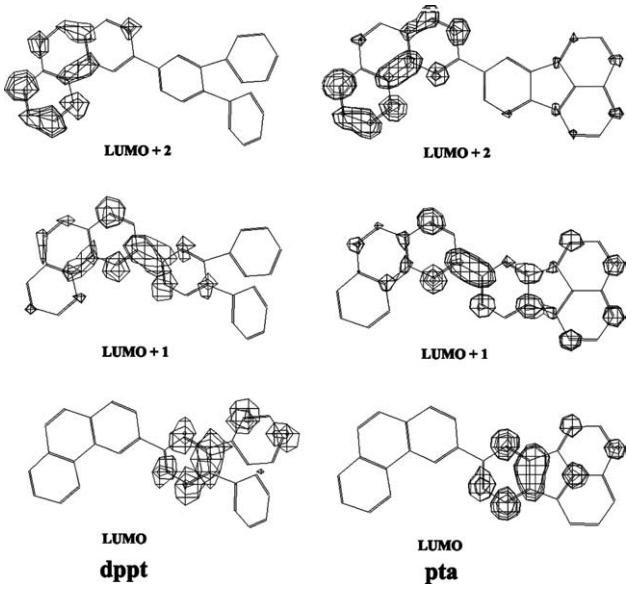

Fig. 2. Graphical illustrations for the three lowest lying unoccupied orbitals of the ligands.

3.3. Electrochemistry

The cyclic voltammograms of complexes **1** and **2** in acetonitrile are shown in Fig. 3. Both complexes exhibit well-defined waves corresponding to the metal-based oxidation and successive ligand-based reductions in the sweep range from −2.0 to 2.0 V, the half-wave potentials of the complexes are collected in Table 1. The anodic

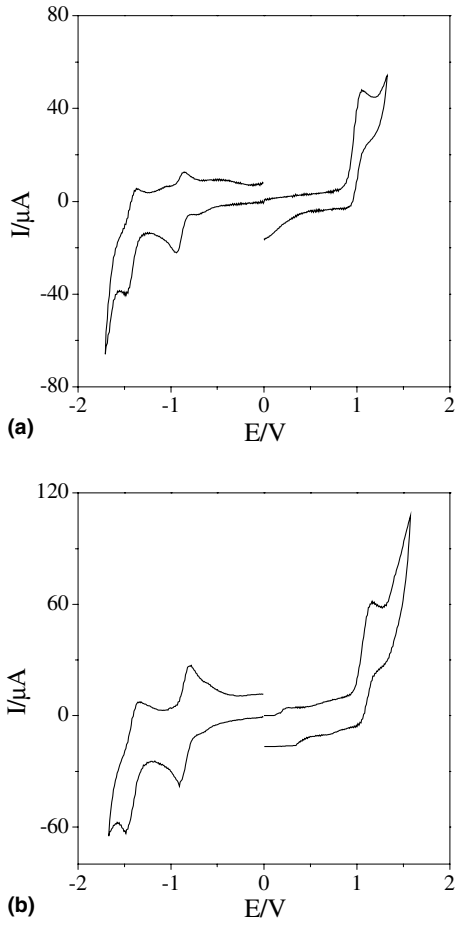

Fig. 3. Cyclic voltammograms of s$[Ru(dppt)(dien)]^{2+}$ (a) and $[Ru(pta)(dien)]^{2+}$ (b) in CH_3CN.

Table 1
Redox potentials for the ruthenium(II) complexes[a]

Complex	Ru^{III}/Ru^{II}	Ligand reduction	
$[Ru(dppt)(dien)]^{2+}$	0.99	−0.92	−1.46
$[Ru(pta)(dien)]^{2+}$	1.11	−0.87	−1.44
$[Ru(dppt)_2]^{2+}$[b]	1.35	−0.83	−1.03
$[Ru(pta)_2]^{2+}$[b]	1.40	−0.75	−0.95

[a] All complexes were measured in 0.1 M NBu_4ClO_4–CH_3CN, error in potentials was ±0.02 V; $T = 23 \pm 1$ °C; scan rate = 100 mV.
[b] Values were taken from [16].

and cathodic peak separations vary from 60 to 73 mV and are nearly scan rate independent, indicating that the processes are reversible one-electron transfers.

Redox processes corresponding to the Ru(III)/Ru(II) couple were observed at 0.99 and 1.10 V for complexes **1** and **2**, respectively. As anticipated, the oxidation of complex **2** shifts to more positive values with the extension of the π framework, which is consistent with the molecular orbital calculation results. At the same time, the oxidation potentials of the complexes are significantly less positive than those of corresponding homoleptic compounds $[Ru(dppt)_2]^{2+}$ and $[Ru(pta)_2]^{2+}$ (Table 1), as a result of the electron-donor capacity of dien that increases the electron density on the Ru(II) center and makes easier for the oxidation of Ru(II) to Ru(III). By comparison with the reductions of similar complexes [13,14,16], the reduction potentials of the two complexes can be rationally attributed to the ligand-based reductions $L^{0/-1}$ and $L^{-1/2}$ (L = dppt, pta).

3.4. Electronic absorption spectra

The absorption spectra of $[Ru(dppt)(dien)]^{2+}$ and $[Ru(pta)(dien)]^{2+}$ were recorded in acetonitrile in the range of wavelengths 250–700 nm (Fig. 4). In order to study the solvatochromic behavior of them, the spectra were obtained in other solvents of increasing polarity (acetone, DMF and DMSO) in the same range of wavelengths (Fig. 5). The absorption spectra for the two complexes are characterized by intense π–π* ligand transitions in the UV and metal-to-ligand charge transfer (MLCT) transitions in the visible region. In $[Ru(dppt)(dien)]^{2+}$ and $[Ru(pta)(dien)]^{2+}$, the absorption maxima of the MLCT bands significantly shift to lower energies compared to those of their homoleptic complexes [16], 488 versus 512 nm for $[Ru(dppt)_2]^{2+}$ versus $[Ru(dppt)(dien)]^{2+}$ and 506 versus 535 nm for $[Ru(pta)_2]^{2+}$ versus $[Ru(pta)(dien)]^{2+}$, respectively. This is consistent with the weak-field ligand character of the amines compared to the aromatic ligand. It is well documented in the literature that the energy of the metal-ligand charge transfer transitions of Ru(II) complexes are influenced by the π-back bonding of ligands [14]. Upon replacing one aromatic ligand with an amine chelate, the back bonding will decrease and the ligand field splitting will be smaller, thus the MLCT transitions will shift to longer wavelengths.

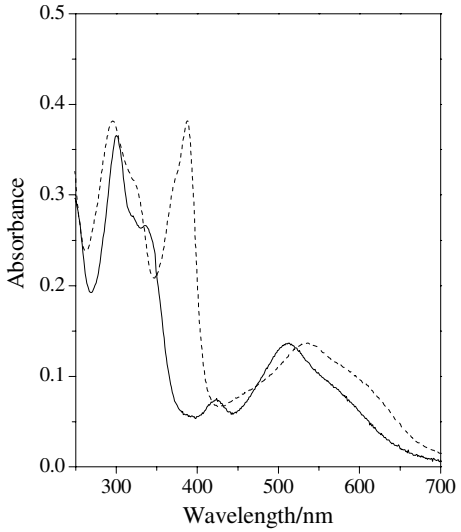

Fig. 4. Absorption spectra of $[Ru(dppt)(dien)]^{2+}$ (solid line) and $[Ru(pta)(dien)]^{2+}$ (dash line) in CH_3CN at room temperature.

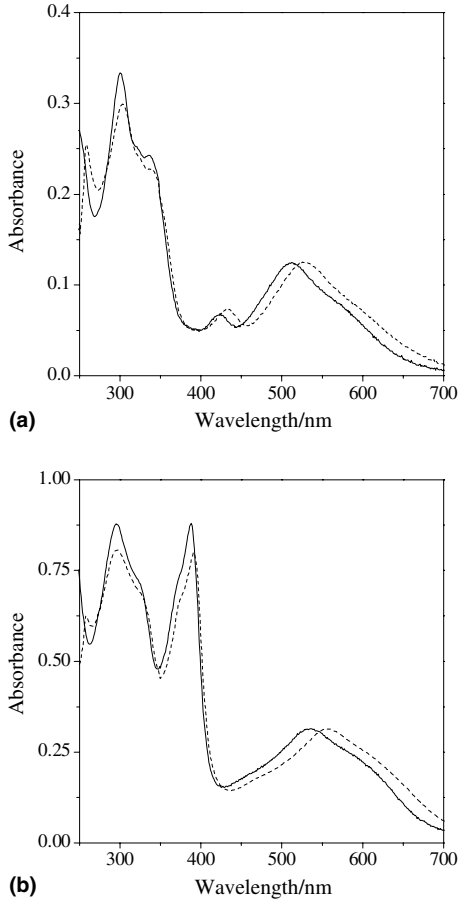

Fig. 5. Absorption spectra of $[Ru(dppt)(dien)]^{2+}$ (a) and $[Ru(pta)(dien)]^{2+}$ (b) in CH_3CN (solid line) and DMSO (dash line) at room temperature.

Table 2
Absorption maxima of the ruthenium(II) complexes in various solvents

Solvent	DN[a]	λ_{max} (nm)	
	(kcal/mol)	$[Ru(dppt)(dien)]^{2+}$	$[Ru(pta)(dien)]^{2+}$
Acetonitrile	14.1	512	535
Acetone	17.1	513	539
Dimethyl-formamide	26.6	524	554
Dimethyl sulfoxide	29.8	525	556

[a] The donor number, DN, is a measure of the electron-pair donating ability of the solvent. DN values were taken from [12].

The MLCT transitions maxima of $[Ru(dppt)(dien)]^{2+}$ and $[Ru(pta)(dien)]^{2+}$ are solvatochromic (Table 2). A pronounced red shift in the position of the MLCT absorption band occurs when the electron-pair donating ability of the solvent is increased (Fig. 5). This behavior had been reported for some ruthenium(II) amine complexes [11–13] and is attributed to the interaction between coordinated amine ligands and solvent molecules, which increases the electron density on the ruthenium and raises the energy of the d-orbitals relative to the ligand π^*-orbitals, thus causing the Ru-L MLCT to shift to longer wavelength in these solvents.

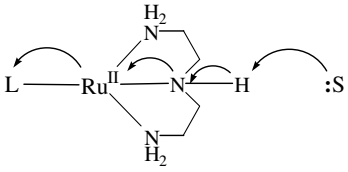

Recent quantum-mechanical calculations also support this idea. Zerner and coworkers [26,27] used a mixed quantum-mechanical/molecular-mechanics method to calculate the electronic spectrum of $[Ru(NH_3)_5(pyridine)]^{2+}$ and they found significant charge transfer from the solvent to the complex. Cacelli and Ferretti [28] performed ab initio calculations on the complex $[Ru(NH_3)_5(pyrazine)]^{2+/3+}$ using a polarizable continuum model for the solvent. They observed electron density to be increasingly shifted toward $Ru^{II/III}$ in stronger electron-donating solvents. In all of these studies, solvation was shown to lead to considerable red-shifts of d–π^* transitions.

In $[Ru(dppt)(dien)]^{2+}$ and $[Ru(pta)(dien)]^{2+}$, the solvatochromism of the MLCT transitions is found to be less remarkable than those of $[Ru(bpy)(NH_3)_4]^{2+}$ and $[Ru(phen)(NH_3)_4]^{2+}$ [12,13]. This may be attributed to the stronger π-acceptor character of dppt and pta, resulting in decreasing electron density on the metal and to some extent rendering the complex less susceptible to solvent. Inspection of Table 2 reveals that $[Ru(pta)(dien)]^{2+}$ is more sensitive to solvent effect than $[Ru(dppt)(dien)]^{2+}$ in spite of stronger electron-withdrawing of pta relative to dppt. Changing the solvent from acetone to DMSO, the absorption maximum of the MLCT band of $[Ru(pta)(dien)]^{2+}$ shifts to longer wavelength by about 21 nm at the most; however in $[Ru(dppt)(dien)]^{2+}$ the largest shifting value is only 13 nm. The detailed mechanism is still unclear but similar observations were made for $[Ru(NH_3)_5(py)]^{2+}$ and $[Ru(NH_3)_5(N\text{-Me-}4,4\text{-bpy})]^{2+}$ wherein the MLCT transitions of the latter are more sensitive to solvent [12].

4. Conclusions

In summary, two novel Ru(II) complexes $[Ru(dppt)(dien)](ClO_4)_2$ (**1**) and $[Ru(pta)(dien)](ClO_4)_2$ (**2**) were synthesized and characterized. Molecular orbital calculations reflect the difference between two asymmetric ligands dppt and pta, this is further testified in the electrochemical studies and absorption spectra. Due to the introduction of dien, the oxidation potentials of complexes **1** and **2** are significantly less positive and the MLCT bands of them shift to lower energies in comparison with those of the homoleptic complexes $[Ru(dppt)_2](ClO_4)_2$ and $[Ru(pta)_2](ClO_4)_2$. At the same time, the two ruthenium(II) amine complexes also exhibit interesting solvatochromic properties.

Acknowledgements

We are grateful to the National Natural Science Foundation of China, the National Science Foundation of Guangdong Province and Research Fund of the Royal Society of Chemistry, UK for their financial support.

References

[1] A. Juris, V. Balzani, F. Barigelletti, S. Campagna, P. Belser, A. Von Zelewsky, Coord. Chem. Rev. 84 (1988) 85.
[2] K. Kalyanasundaram, Photochemistry of Polypyridine and Porphyrin Complexes, Academic Press, London, 1992.
[3] V. Balzani, A. Juris, M. Venturi, S. Campagna, S. Serroni, Chem. Rev. 96 (1996) 756.
[4] A.P. de Silva, H.Q.N. Gunaratne, T. Gunnlangasson, A.J.M. Huxley, C.P. McCoy, J.T. Rademacher, T.E. Rice, Chem. Rev. 97 (1997) 1515.
[5] J.P. Sauvage, J.P. Collin, J.C. Chambron, S. Guillerez, C. Coudret, Chem. Rev. 94 (1994) 993.
[6] A.M.W.C. Thompson, Coord. Chem. Rev. 160 (1997) 1.
[7] L. De Cola, P. Belser, Coord. Chem. Rev. 177 (1998) 301.
[8] Y. Xiong, L.N. Ji, Coord. Chem. Rev. 185–186 (1999) 711.
[9] C. Kaes, A. Katz, M.W. Hosseini, Chem. Rev. 100 (2000) 3553.
[10] D.L. Carlson, D.H. Huchital, E.J. Mantilla, R.D. Sheardy, W.R. Murphy Jr., J. Am. Chem. Soc. 115 (1993) 6424.
[11] R.B. Nair, E.S. Teng, S.L. Kirkland, C.J. Murphy, Inorg. Chem. 37 (1998) 139.
[12] J.C. Curtis, B.P. Sullivan, T.J. Meyer, Inorg. Chem. 22 (1983) 224.
[13] G.A. Mines, J.A. Roberts, J.T. Hupp, Inorg. Chem. 31 (1992) 125.

[14] N. Aydin, C. Schlaepfer, Polyhedron 20 (2001) 37.
[15] M.J. Clarke, Coord. Chem. Rev. 232 (2002) 69.
[16] H. Chao, G. Yang, G.Q. Xue, H. Li, H. Zhang, I.D. Williams, L.N. Ji, X.M. Chen, X.Y. Li, J. Chem. Soc., Dalton Trans. (2001) 1326.
[17] B.P. Sullivan, J.M. Calvert, T.J. Meyer, Inorg. Chem. 19 (1980) 1404.
[18] J.N. Murrell, A.J. Harget, Semi-empirical Self-consistent-field Molecular Orbital Theory of Molecules, Wiley Interscience, New York, 1971.
[19] Hyperchem Release 6.01 for Windows, Hypercube Inc., Gainesville, FL, 2000.
[20] R. Hoffmann, J. Chem. Phys. 39 (1963) 1397.
[21] R. Arakawa, S. Tachiyashiki, T. Matsuo, Anal. Chem. 67 (1995) 4133.
[22] R.R. Ruminski, S. Underwood, K. Vallely, S.J. Smith, Inorg. Chem. 37 (1998) 6528.
[23] Y. Jahng, R.P. Thummel, S.G. Bott, Inorg. Chem. 36 (1997) 3133.
[24] E.C. Constable, M. Maestri, A.M.W. Cargill Thompson, Polyhedron 11 (1992) 2707.
[25] E.C. Constable, J.E. Davies, D. Phillips, P.R. Raithby, Polyhedron 17 (1998) 3989.
[26] K.K. Stavrev, M.C. Zerner, T.J. Meyer, J. Am. Chem. Soc. 117 (1995) 8684.
[27] G.M. Pearl, M.C. Zerner, J. Am. Chem. Soc. 121 (1999) 399.
[28] I. Cacelli, A. Ferretti, J. Chem. Phys. 109 (1998) 8583.

Available online at www.sciencedirect.com
SCIENCE DIRECT®
Polyhedron 23 (2004) 823–829
POLYHEDRON
www.elsevier.com/locate/poly

Synthesis, characterization and in vitro antitumor activity of some arylantimony ferrocenylcarboxylate derivatives and the crystal structures of $[C_5H_5FeC_5H_4C(CH_3)=CHCOO]_2Sb(C_6H_4F\text{-}4)_3$ and $[4\text{-}(C_5H_5FeC_5H_4)C_6H_4COO]_2Sb(C_6H_4F\text{-}4)_3$

Lin Yu [a], Yong-Qiang Ma [a], Run-Chang Liu [a], Guo-Cang Wang [a], Jin-Shan Li [a,*], Guan-Hua Du [b], Juan-Juan Hu [b]

[a] *State Key Laboratory of Elemento-Organic Chemistry, Nankai University, Tianjin 300071, PR China*
[b] *National Engineering Research Center for the Development of New Drugs, Institute of Materia Medica, Chinese Academy of Medical Sciences and Peking Union Medical College, Beijing 100050, PR China*

Received 13 August 2003; accepted 21 November 2003

Abstract

A series of novel arylantimony ferrocenylcarboxylate derivatives with the formulae $[C_5H_5FeC_5H_4C(CH_3)=CHCOO]_2SbAr_3$ and $[4\text{-}(C_5H_5FeC_5H_4)C_6H_4COO]_2SbAr_3$ ($Ar = C_6H_5$, 4-$CH_3C_6H_4$, 4-ClC_6H_4, 4-FC_6H_4) were synthesized and characterized by elemental analysis, IR and ^1H NMR. The crystal structures of $[C_5H_5FeC_5H_4C(CH_3)=CHCOO]_2Sb(C_6H_4F\text{-}4)_3$ and $[4\text{-}(C_5H_5FeC_5H_4)C_6H_4COO]_2Sb(C_6H_4F\text{-}4)_3$ were determined by X-ray diffraction. The two sets of crystal X-ray data show that the antimony atom of the former has a special six-coordinate geometry while that of the latter has a general five-coordinate geometry. Three human neoplastic cell lines (HCT-8, Bel-7402 and KB) were used to screen these compounds. The results indicate that $[C_5H_5FeC_5H_4C(CH_3)=CHCO_2]_2Sb(C_6H_4Cl\text{-}4)_3$ and $[C_5H_5FeC_5H_4C(CH_3)=CHCO_2]_2Sb(C_6H_4F\text{-}4)_3$ at 5 μM show relatively good in vitro antitumor activities.
© 2003 Elsevier Ltd. All rights reserved.

Keywords: Antimony; Ferrocenylcarboxylate; Crystal structures; Antitumor activity

1. Introduction

Numerous main-group metal derivatives have been screened for potential anticancer activity. Among them organotin carboxylates have been most extensively investigated and they exhibit in vitro antitumor activtity against human tumor cell lines, often higher than cisplatin [1,2]. In contrast, organoantimony compounds have received much less attention as potential antitumor drugs. Recently, some organoantimony derivatives have been reported to exhibit marginal antitumor activities [3–7]. Therefore, it was thought worthwhile to explore whether other organoantimony compounds also exhibit antitumor properties. Moreover, it is known that ferrocene derivatives have a wide range of biological activities [8–12]. In this paper, we have prepared a series of arylantimony derivatives of 3-ferrocenyl-2-crotonic acid and 4-ferrocenylbenzoic acid, which contain three active centers, namely the arylantimony(V) moiety and two ferrocenylcarboxylate groups, in order to investigate the influence of the organic ligands at Sb on their antitumor activity.

In addition, the carboxylate ion, RCO_2^-, can coordinate to metals in many ways including as a unidentate ligand, as a chelating ligand, as a bridging bidentate ligand and so on [13]. Therefore, we are also interested in studying the structures of these pentavalent antimony salts of the general formula $Ar_3Sb(O_2CR)_2$ and the influences of electronic and steric effects on the coordination of the antimony atom.

* Corresponding author. Tel.: +862223504230; fax: +862223503438.
E-mail address: yulin77@eyou.com (L. Yu).

0277-5387/$ - see front matter © 2003 Elsevier Ltd. All rights reserved.
doi:10.1016/j.poly.2003.12.002

2. Experimental

2.1. General

All operations were performed in an atmosphere of dry argon using Schlenk techniques. All solvents were dried by standard methods and distilled prior to use. Elemental analyses were determined on a Yanaco CHN Corder MT-3 elemental analyzer. IR spectra were recorded on a Bruker Equinox 55 spectrometer in KBr discs. ^{1}H NMR spectra were measured on a Bruker AC-200 spectrometer in CD_3COCD_3-d_6 solution (**1**–**4**) or $CDCl_3$ solution (**5**–**8**) with TMS as internal standard. 3-Ferrocenyl-2-crotonic acid and 4-ferrocenylbenzoic acid were prepared according to [14,15]. Ar_3SbBr_2 was prepared by the method reported by Lile and Menzies [16].

2.2. Synthesis of the title compounds

The title compounds were synthesized by a more convenient method. Typically, to acid (1 mmol) and triethylamine (0.8 ml) in toluene (40 ml) was added 0.5 mmol of Ar_3SbBr_2. The reaction mixture was stirred at room temperature for 24 h and filtered. The filtrate was evaporated in vacuo. The obtained red solid was recrystallized from CH_2Cl_2/petroleum ether.

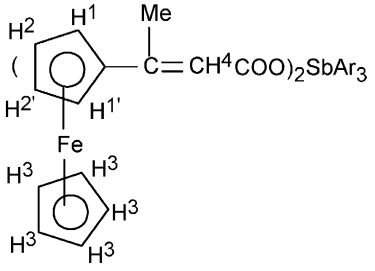

Ar = Ph (**1**); 4-$CH_3C_6H_4$ (**2**); 4-ClC_6H_4(**3**); 4-FC_6H_4 (**4**).

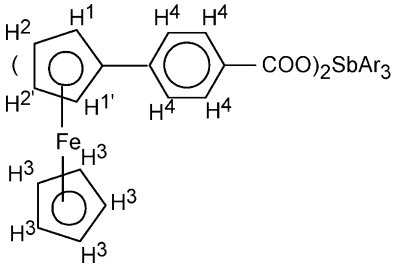

Ar = Ph (**5**); 4-$CH_3C_6H_4$ (**6**); 4-ClC_6H_4(**7**); 4-FC_6H_4 (**8**).

For **1**: yield 77.8%. m.p. 191–193 °C. *Anal*. Calc. for $C_{46}H_{41}Fe_2O_4Sb \cdot CH_2Cl_2$: C, 57.83; H, 4.44. Found: C, 57.67; H, 4.46%. Important infrared data (KBr, cm^{-1}): ν_{asy} (CO_2) 1624, ν_{sym} (CO_2) 1358, $\Delta\nu$ (CO_2) 266, ν (Sb–C) 461. ^{1}H NMR (CD_3COCD_3-d_6, ppm) δ: 4.59 (t, 4H, H^1 $H^{1'}$), 4.37 (t, 4H, H^2 $H^{2'}$), 4.13 (s, 10H, H^3), 6.00 (s, 2H, H^4), 2.43 (s, 6H, Me), 7.16–8.15 (m's, 15H, C_6H_5).

For **2**: yield 89.7%. m.p. 199–200 °C. *Anal*. Calc. for $C_{49}H_{47}Fe_2O_4Sb \cdot CH_2Cl_2$: C, 58.98; H, 4.85. Found: C, 58.51; H, 4.76%. Important infrared data (KBr, cm^{-1}): ν_{asy} (CO_2) 1621, ν_{sym} (CO_2) 1361, $\Delta\nu$ (CO_2) 260, ν (Sb–C) 482. ^{1}H NMR (CD_3COCD_3-d_6, ppm) δ: 4.56 (t, 4H, H^1 $H^{1'}$), 4.36 (t, 4H, H^2 $H^{2'}$), 4.12 (s, 10H, H^3), 6.00 (s, 2H, H^4), 2.38 (s, 6H, Me), 7.29–8.02 (m's, 12H, C_6H_4), 2.34 (s, 9H, CH_3).

For **3**: yield 70.4%. m.p. 207–209 °C. *Anal*. Calc. for $C_{46}H_{38}Cl_3Fe_2O_4Sb \cdot CH_2Cl_2$: C, 52.29; H, 3.73. Found: C, 51.64; H, 3.84%. Important infrared data (KBr, cm^{-1}): ν_{asy} (CO_2) 1613, ν_{sym} (CO_2) 1374, $\Delta\nu$ (CO_2) 239, ν (Sb–C) 486. ^{1}H NMR (CD_3COCD_3-d_6, ppm) δ: 4.58 (t, 4H, H^1 $H^{1'}$), 4.35 (t, 4H, H^2 $H^{2'}$), 4.13 (s, 10H, H^3), 6.01 (s, 2H, H^4), 2.36 (s, 6H, Me), 7.15–8.18 (m's, 12H, C_6H_4).

For **4**: yield 84.6%. m.p. 188–189 °C. *Anal*. Calc. for $C_{46}H_{38}F_3Fe_2O_4Sb \cdot CH_2Cl_2$): C, 54.80; H, 3.91. Found: C, 54.67; H, 4.10%. Important infrared data (KBr, cm^{-1}): ν_{asy} (CO_2) 1615, ν_{sym} (CO_2) 1373, $\Delta\nu$ (CO_2) 242, ν (Sb–C) 477. ^{1}H NMR (CD_3COCD_3-d_6, ppm) δ: 4.58 (t, 4H, H^1 $H^{1'}$), 4.37 (t, 4H, H^2 $H^{2'}$), 4.12 (s, 10H, H^3), 6.00 (s, 2H, H^4), 2.37 (s, 6H, Me), 6.98–8.24 (m's, 12H, C_6H_4).

For **5**: yield 90.3%. m.p. 223 °C (dec). *Anal*. Calc. for $C_{52}H_{41}Fe_2O_4Sb \cdot CH_2Cl_2$: C, 60.73; H, 4.13. Found: C, 60.72; H, 4.19%. Important infrared data (KBr, cm^{-1}): ν_{asy} (CO_2) 1632, ν_{sym} (CO_2) 1322, $\Delta\nu$ (CO_2) 310, ν (Sb–C) 461. ^{1}H NMR ($CDCl_3$, ppm) δ: 4.66 (t, 4H, H^1 $H^{1'}$), 4.34 (t, 4H, H^2 $H^{2'}$), 4.02 (s, 10H, H^3), 7.39–8.14 (m's, 23H, Ar and H^4).

For **6**: yield 70.3%. m.p. 246 °C (dec). *Anal*. Calc. for $C_{55}H_{47}Fe_2O_4Sb \cdot CH_2Cl_2$: C, 61.69; H, 4.53. Found: C, 61.66; H, 4.60%. Important infrared data (KBr, cm^{-1}): ν_{asy} (CO_2) 1639, ν_{sym} (CO_2) 1320, $\Delta\nu$ (CO_2) 319, ν (Sb–C) 481. ^{1}H NMR ($CDCl_3$, ppm) δ: 4.70 (t, 4H, H^1 $H^{1'}$), 4.37 (t, 4H, H^2 $H^{2'}$), 4.06 (s, 10H, H^3), 7.33–8.09 (m's, 20H, Ar and H^4), 2.41 (s, 9H, CH_3).

For **7**: yield 87.5%. m.p. 173–175 °C. *Anal*. Calc. for $C_{52}H_{38}Cl_3Fe_2O_4Sb$: C, 58.55; H, 3.59. Found: C, 58.39; H, 3.61%. Important infrared data (KBr, cm^{-1}): ν_{asy} (CO_2) 1607, ν_{sym} (CO_2) 1326, $\Delta\nu$ (CO_2) 281, ν (Sb–C) 483. ^{1}H NMR ($CDCl_3$, ppm) δ: 4.59 (t, 4H, H^1 $H^{1'}$), 4.26 (t, 4H, H^2 $H^{2'}$), 3.94 (s, 10H, H^3), 7.37–8.05 (m's, 20H, Ar and H^4).

For **8**: yield 69.6%. m.p. 132–134 °C. *Anal*. Calc. for $C_{52}H_{38}F_3Fe_2O_4Sb \cdot 2CH_2Cl_2$: C, 54.63; H, 3.57. Found: C, 54.37; H, 3.92%. Important infrared data (KBr, cm^{-1}): ν_{asy} (CO_2) 1655, ν_{sym} (CO_2) 1316, $\Delta\nu$ (CO_2) 339, ν (Sb–C) 477. ^{1}H NMR ($CDCl_3$, ppm) δ: 4.75 (t, 4H, H^1 $H^{1'}$), 4.44 (t, 4H, H^2 $H^{2'}$), 4.06 (s, 10H, H^3), 7.42–8.14 (m's, 20H, Ar and H^4).

2.3. X-ray crystallography

Diffraction data for compounds **4** and **8** were obtained on a Bruker Smart 1000 CCD diffractometer (graphite monochromatized Mo Kα radiation, $\lambda = 0.71073$ Å). Unit cell dimensions were obtained with least squares refinements and the structure was solved by direct methods using the SHELXS-97 program [17]. Non-hydrogen atoms were refined with anisotropic thermal parameters. All data were corrected using the SADABS method with $T_{max} = 0.8853$ and $T_{min} = 0.7057$. The final refinement was performed by full-matrix least-squares methods with anisotropic thermal parameters for non-hydrogen atoms on F^2. The hydrogen atoms of the compound were added theoretically, riding on the concerned atoms and refined with fixed thermal factors. Crystal data and structure refinement are given in Table 1.

2.4. In vitro antitumor activity assay

The KB cell lines were obtained from the Institute of Cancer of Tianjin. Other cell lines were derived in the Institute of Materia Medica, Chinese Academy of Medical Sciences and Peking Union Medical College. All cell lines were grown in RPMI 1640 medium with 10% fetal bovine serum, in 5% CO_2 atmosphere.

The cytotoxic activity of these compounds was assayed by the 3-(4,5-dimethylthiazol-2-yl)-2,5-diphenyl-2*H*-tetrazolium bromide (MTT, Thiazolyl blue) method [18]. The cell lines, human nasopharyngeal carcinoma (KB), human hepatocellular carcinoma (Bel-7402) and human colo carcinoma (HCT-8) were used for screening. All cell lines were transferred into the 96-wells culture plate. Aliquots of log-phase cells were incubated for 72 h at 37 °C with four dose levels of each organoantimony complex in triplicate. 50 μl of 0.1% MTT (Sigma) was added to each well. After 4 h incubation, the culture medium was removed, and the blue formazan in the cells was dissolved with 150 μl of 2-propanol by vigorous shaking. The optical density of each well was measured at 570 nm wavelength. The cytotoxicity was determined by expressing the mean optical densities for drug-treated cells at each concentration as a percentage of that of untreated cells.

3. Results and discussion

3.1. Preparations

The title compounds were synthesized under mild conditions. These compounds are red solids and are

Table 1
Crystal data and structure refinement for compounds **4** and **8**

Compound	**4**	**8**
Formula	$C_{46}H_{38}F_3Fe_2O_4Sb \cdot CH_2Cl_2$	$C_{52}H_{38}F_3Fe_2O_4Sb \cdot 2CH_2Cl_2$
Formula weight	1030.14	1195.99
T (K)	293(2)	293(2)
λ (Å)	0.71073	0.71073
Crystal system	monoclinic	tetragonal
Space group	$P2_1/c$	$P4_12_12$
Unit cell dimensions		
a (Å)	17.310(4)	9.5699(14)
b (Å)	10.103(3)	9.5699(14)
c (Å)	26.091(5)	54.763(16)
α (°)	90	90
β (°)	108.003(6)	90
γ (°)	90	90
V (Å^3)	4339.5(17)	5015.3(18)
Z	4	4
Density (Mg m^{-3})	1.577	1.584
Absorption coefficient (mm^{-1})	1.457	1.389
$F(000)$	2072	2401
Crystal size (mm)	$0.32 \times 0.22 \times 0.20$	$0.25 \times 0.20 \times 0.10$
θ Range for data collection (°)	1.24–26.40	2.16–25.00
Limiting indices	$-9 \leqslant h \leqslant 21$, $-11 \leqslant k \leqslant 11$, $-32 \leqslant l \leqslant 31$	$-6 \leqslant h \leqslant 11$, $-10 \leqslant k \leqslant 11$, $-64 \leqslant l \leqslant 50$
Reflections collected	19 768	20 287
Independent reflections (R_{int})	8661 (0.0513)	4259 (0.0581)
Completeness to $\theta = 26.40°$	97.2%	95.9%
Absorption correction	none	semi-empirical from equivalents
Refinement method	full-matrix least-squares on F^2	full-matrix least-squares on F^2
Goodness-of-fit on F^2	1.024	0.977
Final R indices [$I > 2\sigma(I)$]	$R_1 = 0.0510$, $wR_2 = 0.1103$	$R_1 = 0.0754$, $wR_2 = 0.1629$
R indices (all data)	$R_1 = 0.1040$, $wR_2 = 0.1389$	$R_1 = 0.0813$, $wR_2 = 0.1665$
Largest diffraction peak and hole (e Å^{-3})	0.819 and −0.576	0.632 and −1.636

stable in air. The compounds are easily soluble in benzene, toluene, CH_2Cl_2, $CHCl_3$ and DMSO, and insoluble in petroleum ether and methanol.

3.2. IR spectra

The infrared spectra of these compounds have been recorded in the range of 4000–400 cm^{-1}. The absorption bands can be assigned on the basis of earlier publications [6,19]. The infrared spectroscopic data provide further support for the molecular constitution of the title compounds. The infrared spectra of all of the organoantimony compounds do not show a strong band in the 3500–3300 cm^{-1} region, due to v (OH), indicating that deprotonation and coordination of the carboxylate group with antimony metal have occurred as expected.

In the majority of organoantimony(V) compounds, antimony has generally a coordination number of five. As the vacant 5d orbital of antimony atom can accept a lone electron pair of ligands, in some cases the antimony may have a coordination number of six [20] or seven [6,19]. The IR stretching vibration frequencies of carbonyl groups in organoantimony carboxylates are very important for determining their structure: When there are interactions between the antimony atom and the carbonyl oxygen atoms of the carboxylate groups, the asymmetric absorption vibration frequencies [v_{asy} (CO_2)] of carboxylate groups decrease, while the symmetric absorption vibration frequencies [v_{sym} (CO_2)] increase. Therefore, their differences [Δv (CO_2)] decrease [2,5]. In the IR spectra of the title compounds, the carboxylate bands are observed in the characteristic regions: v_{asy} (CO_2) between 1655 and 1607 cm^{-1} and v_{sym} (CO_2) between 1374 and 1316 cm^{-1}. On the basis of the difference Δv (CO_2), these compounds can be divided into two categories: Compounds **5**, **6** and **8** show high Δv (CO_2) values (310, 319 and 339 cm^{-1}, respectively) while the other compounds show low Δv (CO_2) values (between 239 and 281 cm^{-1}). To the former, we can assume that there has been weak interaction or no interaction between the antimony atom and the carbonyl oxygen atoms of the carboxylate groups (see the crystal structure of compound **8**). To the latter, we can assume that there has been strong interaction between the carbonyl oxygen atoms of the carboxylate groups and the antimony atom (see the crystal structure of compound **4**). In addition, the frequencies of Sb–C deformations appear between 460 and 510 cm^{-1}, which are consistent with the literature [21,22].

3.3. Crystal structure

3.3.1. Structure of $[C_5H_5FeC_5H_4C(CH_3)=CHCOO]_2Sb(C_6H_4F\text{-}4)_3$

The red crystal of $[C_5H_5FeC_5H_4C(CH_3)=CHCOO]_2Sb(C_6H_4F\text{-}4)_3$ was obtained from a CH_2Cl_2-petroleum ether solution. Fig. 1 shows the molecular structure of compound **4** and gives the atom numbering scheme. Selected bond distances and angles are given in Table 2.

The two ferrocenyl groups and two carboxyl groups in the molecule of compound **4** are all *trans*-configurations. The atoms O(2), C(19), C(20), C(21) and C(22) are coplanar within 0.0228 Å. The distance between O(2) and C(22) is 3.034 Å. The atoms O(4), C(33), C(34), C(35) and C(36) are also coplanar within −0.0332 Å, but the distance between O(4) and C(36) is 4.361 Å, much longer than the corresponding distance between O(2) and C(22). The C=C bond lengths [1.327(8) and 1.331(8) Å] and the Fe–C distances are all consistent with the literature [14,23,24].

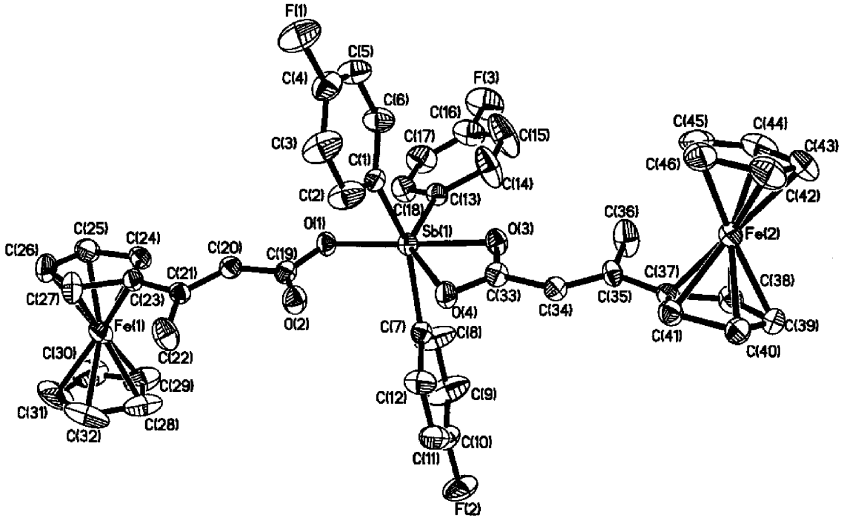

Fig. 1. The molecular structure of $[C_5H_5FeC_5H_4C(CH_3)=CHCOO]_2Sb(C_6H_4F\text{-}4)_3$, showing the atom numbering scheme.

Table 2
Selected bond distances and bond angles of compound **4**

Bond	Distance (Å)	Bond	Angle (°)
Sb(1)–O(3)	2.123(4)	C(1)–Sb(1)–C(13)	105.4(2)
Sb(1)–O(4)	2.647(6)	C(1)–Sb(1)–C(7)	149.5(2)
Sb(1)–C(1)	2.116(5)	O(1)–Sb(1)–O(3)	175.56(15)
Sb(1)–C(7)	2.120(6)	C(13)–Sb(1)–O(3)	88.11(19)
Sb(1)–C(13)	2.119(6)	O(1)–Sb(1)–C(13)	87.6(2)
O(1)–C(19)	1.305(7)	O(1)–Sb(1)–C(7)	90.74(18)
O(2)–C(19)	1.227(7)	C(13)–Sb(1)–C(7)	105.1(2)
O(3)–C(33)	1.317(7)	C(1)–Sb(1)–O(3)	92.99(18)
O(4)–C(33)	1.238(7)	C(7)–Sb(1)–O(3)	89.49(18)
C(20)–C(21)	1.327(8)	O(2)–C(19)–O(1)	121.8(6)
C(34)–C(35)	1.331(8)	O(4)–C(33)–O(3)	118.4(5)
Fe(1)–C(23)	2.043(6)	C(21)–C(23)–Fe(1)	128.0(4)
Fe(1)–C(24)	2.019(6)	C(35)–C(37)–Fe(2)	125.6(4)
Fe(1)–C(25)	2.033(7)	C(23)–Fe(1)–C(28)	110.5(3)
Fe(1)–C(28)	2.011(8)	C(23)–Fe(1)–C(24)	41.2(2)

Carboxylates are versatile ligands which can be either unidentate or bidentate. Antimony–oxygen bond lengths in organoantimony compounds are extremely variable [25], ranging from 1.935 Å in $(Ph_3SbO)_2$ [26] to 2.506 Å in Ph_4SbOSO_2Ph [27], and the Sb–O distances in **4** [Sb(1)–O(1), 2.099(4) Å and Sb(1)–O(3), 2.123(4) Å] lie within this range. However, the Sb(1)–O(2) distance [2.936(6) Å] is rather longer than the Sb(1)–O(4) distance [2.647(6) Å] and both distances are also significantly different from the corresponding distances in $Ph_3Sb(OCOCF_3)_2$ [3.209, 3.231 Å] [28] and $Ph_3Sb(O_2C\overline{CHCMe_2CMe_2})_2$ [2.800(2) Å] [29]. This indicates that there is a relatively strong coordination interaction between Sb(1) and O(4), while almost no interaction between Sb(1) and O(2). The former is a carboxylate as a bidentate ligand, and the latter a unidentate ligand. The C(1)–Sb(1)–C(7) angle, which is affected by the adjacent O(4), is increased to 149.5(2)°, while the C(1)–Sb(1)–C(13) and C(7)–Sb(1)–C(13) angles are decreased to 105.4(2)° and 105.1(2)°, respectively. The corresponding angles in $Ph_3Sb(OCOCF_3)_2$ are 117.52(21)°, 117.99(21)° and 124.47(13)°, and in $Ph_3Sb(O_2C\overline{CHCMe_2CMe_2})_2$ they are 150.0(3)°, 105.1(2)° and 105.1(2)°. Therefore, the molecule of compound **4** consists of a monomer with a six-coordinated antimony atom surrounded by three oxygens and three aryl groups. The atoms O(1), O(3), O(4), C(13) and Sb(1) are coplanar, and the coplanar data is listed in Table 3. The coordination geometry of antimony can be described as a distorted octahedron with two atoms C(1) and C(7) occupying the axial positions.

The unique configuration can be attributed to the −I effect of F of the aryl groups and the steric effect of the two asymmetrical 3-ferrocenyl-2-crotonate groups in the molecule. On one hand, the −I effect of F enhances the Lewis acidity of Sb and leads to the stronger Sb:O═C coordination interaction [6]. On the other hand, the carbonyl oxygens of the two asymmetrical 3-ferrocenyl-2-crotonate groups have theoretically the equal chances to coordinate with the antimony atom. However, when one carbonyl oxygen of the two 2-crotonate groups has coordinated with the antimony atom, the steric effect of the two asymmetrical 2-crotonate groups is such that it is impossible for the other carbonyl oxygen to coordinate with the antimony atom.

Table 3
The coplanar data of compound **4** (Å)

O(1)	O(3)	O(4)	Sb(1)	C(13)
0.0117	0.0278	−0.0210	0.0035	−0.0220

Inspection of the molecular packing of the compound shows that one molecule contains one dichloromethane molecule. This conforms to the result of elemental analysis.

3.3.2. Structure of $[4\text{-}(C_5H_5FeC_5H_4)C_6H_4COO]_2Sb(C_6H_4F\text{-}4)_3$

The red crystal of $[4\text{-}(C_5H_5FeC_5H_4)C_6H_4COO]_2Sb(C_6H_4F\text{-}4)_3$ was also obtained from CH_2Cl_2-petroleum ether solution. One of the approximate dimensions $0.25 \times 0.20 \times 0.10$ mm was mounted in a glass capillary and used for data collection. Fig. 2 shows the molecular structure of compound **8** and gives the atom numbering scheme. The selected bond distances and angles are listed in Table 4.

The crystal structure of compound **8** consists of isolated molecules which have C_2 molecular symmetry, the Sb(1)–C(24)–C(27) atoms forming the C_2 axis. The coordination geometry around the antimony centre is best described as a distorted trigonal bipyramid (TBP), in which two carboxylate groups occupy the apical sites. The O(1A)–Sb(1)–O(1) angle is 174.1(4)°. In the equatorial plane of the molecule of compound **8**, the C(18A)–Sb(1)–C(18), C(18A)–Sb(1)–C(24) and C(18)–Sb(1)–

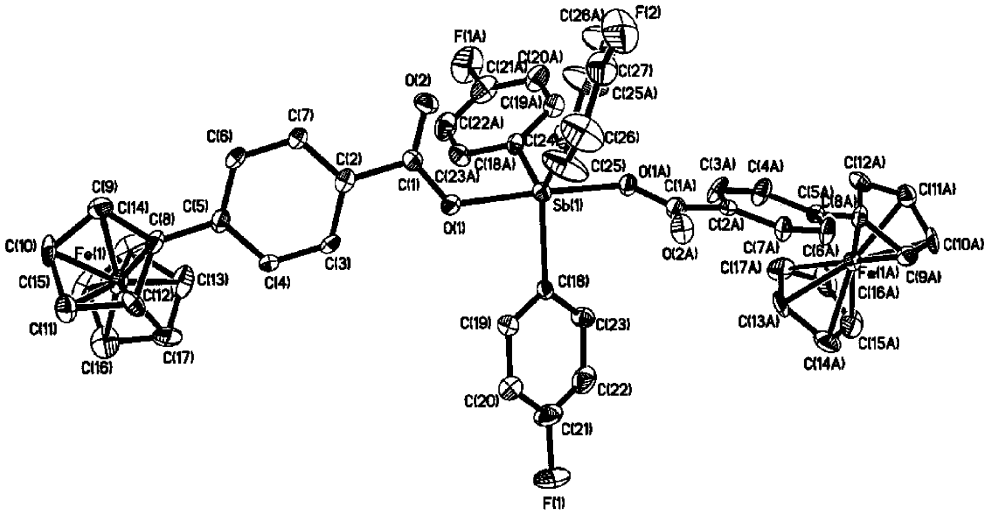

Fig. 2. The molecular structure of $[4\text{-}(C_5H_5FeC_5H_4)C_6H_4COO]_2Sb(C_6H_4F\text{-}4)_3$, showing the atom numbering scheme.

Table 4
Selected bond distances and bond angles of compound **8**

Bond	Distance(Å)	Bond	Angle (°)
Sb(1)–O(1)	2.087(6)	O(1A)–Sb(1)–O(1)	174.1(4)
Sb(1)–O(1A)	2.087(6)	O(1)–Sb(1)–C(18)	84.2(3)
Sb(1)–C(18)	2.123(9)	O(1)–Sb(1)–C(18A)	84.2(3)
Sb(1)–C(18A)	2.123(9)	O(1)–Sb(1)–C(18)	92.9(3)
Sb(1)–C(24)	2.219(15)	O(1)–Sb(1)–C(18A)	92.9(3)
O(1)–C(1)	1.264(12)	C(18A)1–Sb(1)–C(18)	121.8(5)
O(2)–C(1)	1.243(12)	C(18)–Sb(1)–C(24)	119.1(3)
Fe(1)–C(8)	2.057(10)	C(18A)–Sb(1)–C(24)	119.1(3)
Fe(1)–C(15)	1.990(16)	O(1)–Sb(1)–C(24)	92.9(2)
		O(1A)–Sb(1)–C(24)	92.9(2)
		C(9)–Fe(1)–C(8)	41.4(4)
		C(15)–Fe(1)–C(10)	108.8(6)
		O(2)–C(1)–O(1)	124.8(10)

C(24) angles are 121.8(5)°, 119.1(3)° and 119.1(3)°, respectively, which are close to the normal 120°. The Sb–C bond distances [2.123(9) and 2.219(15) Å] are significantly different from the corresponding distances in $Ph_3Sb(OCOCF_3)_2$ [2.078(3), 2.076(3) and 2.092(3) Å] [28]. The Sb–O distances in **8** [both 2.087(6) Å] also lie within the range from 1.935 to 2.506 Å. The non-bonding Sb–O bond, 3.238 Å, is 55% longer than the covalent Sb–O bond and also longer than the corresponding distances in $Ph_3Sb(OCOCF_3)_2$ [3.209 and 3.231 Å]. This indicates that there is no interaction between the metal atom and carbonyl oxygen atoms. For the ferrocenylcarboxylate part, the Fe–C distances are also consistent with the literature [24].

Though the −I effect of F of the aryl groups enhances the Lewis acidity of Sb and leads to the stronger Sb:O═C coordination [6], the large steric effect of the two phenyl groups associated with carboxyl groups outweighs this and results in that the carbonyl oxygen atoms cannot coordinate with the antimony atom.

Inspection of the molecular packing of the compound shows that one molecule contains two dichloromethane molecules. This conforms with the result of elemental analysis, too.

3.4. Antitumor activity

The antitumor activity is assayed by the MTT method [18]. The antitumor activity of the title compounds is listed in Table 5. The results of bioassay indicate that these compounds exhibit certain activities against the three cancer cells in vitro. The compounds **1**–**8** including the ferrocene moiety have relatively higher

Table 5
Antitumor activity of the compounds in vitro

Compound	Inhibition ratio[a] (%) (5 μg/ml)		
	KB	Bel-7402	HCT-8
1	−20.34	−1.30	4.94
2	−2.61	17.53	16.59
3	37.88	72.61	91.19
4	70.76	58.18	73.31
5	−8.42	4.03	12.51
6	4.04	−8.56	1.75
7	58.77	33.96	36.56
8	13.96	8.40	12.51
A[b]	−4.53	−12.31	3.98
B[c]	−3.25	−11.45	−0.11
C[d]	12.66	−32.12	12.24
Cisplatin	92.64	76.25	80.07

[a] Inhibition ratio (%) $= (A_1 - A_2)/A_1 \times 100\%$. Drug is active when the inhibition ratio at 5 μg/ml concentration is $\geqslant 50\%$. A_1, the mean optical densities of untreated cells. A_2, the mean optical densities of drug-treated cells. Negative values indicate that the mean optical densities of drug-treated cells (A_2) is greater than that of untreated cells (A_1), i.e. the drug promoted growth of some tumor cells.

[b] **A**: $C_5H_5FeC_5H_4C(CH_3)$═CHCOOH.

[c] **B**: Ph_3SbBr_2.

[d] **C**: $(PhNHCH_2COO)_2Sb(C_6H_4F\text{-}4)_3$.

antitumor activity than triphenylantimony dibromide. At the same time, the antitumor activity of most of the compounds **1**–**8** is also higher than that of the compound $(PhNHCH_2COO)_2Sb(C_6H_4F\text{-}4)_3$ which is a similar arylantimony carboxylate but not including a ferrocene moiety. The antitumor data indicate that the antitumor activities are affected by the nature of the aryl and the ferrocenylcarboxylate groups. When the ferrocenylcarboxylate group is $C_5H_5FeC_5H_4C(CH_3)=CHCOO$, the compounds whose Ar is $4\text{-}ClC_6H_4$ or $4\text{-}FC_6H_4$ have relatively higher antitumor activities. Specially, the activity of compound **3** against HCT-8 cell is higher than that of cisplatin.

4. Supplementary material

Crystallographic data for the structures reported in this paper have been deposited with the Cambridge Crystallographic Data Centre, CCDC No. 213818 for compound **4** and CCDC No. 212338 for compound **8**. Copies of this information may be obtained free of charge from The Director, CCDC, 12 Union Road, Cambridge, CB2 1EZ, UK (fax: +44-1223-336033; e-mail: deposit@ccdc.cam.ac.uk or http://www.ccdc.cam.ac.uk).

Acknowledgements

We thank Professor Honggeng Wang and Associate Professor Haibin Song for their strong support for our Crystallographic study.

References

[1] C.J. Evans, S. Karpel, Organotin Compounds in Modern Technology, J. Organomet. Chem., Elsevier, Amsterdam, 1985; Library, vol. 16.
[2] J.S. Li, Y.Q. Ma, R.C. Liu, J. Li, Appl. Organomet. Chem. 15 (2001) 227.
[3] C. Silvestru, C. Socaciu, A. Bara, I. Haiduc, Anticancer Res. 10 (1990) 803.
[4] A. Bara, C. Socaciu, C. Silvestru, I. Haiduc, Anticancer Res. 11 (1991) 1651.
[5] J.S. Li, Y.Q. Ma, J.R. Cui, R.Q. Wang, Appl. Organomet. Chem. 15 (2001) 639.
[6] Y.Q. Ma, J.S. Li, Z.A. Xuan, R.C. Liu, J. Organomet. Chem. 620 (2001) 235.
[7] J.S. Li, Y.Q. Ma, L. Yu, J.R. Cui, R.Q. Wang, Synth. React. Inorg. Met.-Org. Chem. 32 (3) (2002) 583.
[8] K.L. Rinehart, R.J. Curby, D.H. Ustafson, J. Am. Chem. Soc. 84 (1962) 3263.
[9] E.I. Edwards, R. Epton, G. Marr, J. Organomet. Chem. 122 (1976) C49.
[10] C.R. Simionescu, T. Lixandru, L. Tataru, I. Mazilu, M. Vata, S.T. Luca, J. Organomet. Chem. 252 (1983) C43.
[11] E.W. Neuse, M.G. Meirim, N.F. Blom, Organometallics 7 (1988) 2562.
[12] W.G. Lu, J.X. Tao, X.Y. Li, Y.Z. Wang, Yingyong Huaxue 17 (2000) 126 (in Chinese).
[13] G.B. Deacon, R.J. Phillips, Coord. Chem. Rev. 33 (1980) 227.
[14] R.J. Yi, C.R. Zhang, Huaxue. Shiji. 13 (2) (1991) 76 (in Chinese).
[15] P. Hu, K.-Q. Zhao, L.-F. Zhang, J. Sichuan. Normal. Univ. 21 (4) (1998) 433 (in Chinese).
[16] W.J. Lile, R.C. Menzies, J. Chem. Soc. (1950) 617.
[17] G.M. Sheldrick, SHELXS-97: Program for Structure Solution, Acta Crystallogr., Sect. A 46 (1990) 467.
[18] F. Denizot, R. Lang, J. Immunol. Methods 89 (1986) 271.
[19] Y.Q. Ma, L. Yu, J.S. Li, Heteroatom. Chem. 13 (4) (2002) 229.
[20] P.L. Millington, D.B. Sowerby, J. Chem. Soc., Dalton Trans. (1992) 1199.
[21] D.H. Whiffen, J. Am. Chem. Soc. (1956) 1350.
[22] R.H. Clark, C.D. Flint, A.J. Hempleman, Spectrochim. Acta 43A (1987) 805.
[23] R.C. Weast, M.J. Astle, Handbook of Chemistry and Physics, 63rd ed., CRC Press, Boca Raton, FL, 1982–1983.
[24] P. Seiler, J.D. Dunitz, Acta Crystallogr., Sect. B B38 (1982) 1741.
[25] G. Ferguson, C. Glidewell, D. Lloyd, S. Metcalfe, J. Chem. Soc., Perkin Trans. 2 (1988) 731.
[26] G. Ferguson, C. Glidewell, B. Kaitner, D. Lloyd, S. Metcalfe, Acta Crystallogr., Sect. C 43 (1987) 824.
[27] R. Ruether, F. Huber, H. Preut, J. Organomet. Chem. 295 (1985) 21.
[28] G. Ferguson, B. Kaitner, C. Glidewell, S. Smith, J. Organomet. Chem. 419 (1991) 283.
[29] J.S. Li, G.Q. Huang, Y.T. Wei, C.H. Xiong, D.Q. Zhu, Q.L. Xie, Appl. Organomet. Chem. 12 (1998) 31.

Available online at www.sciencedirect.com
SCIENCE DIRECT®
Polyhedron 23 (2004) 831–840
POLYHEDRON
www.elsevier.com/locate/poly

Synthesis, structure, spectral and electron-transfer properties of octahedral-$[Co^{III}(L)_2]^+$/$[Zn^{II}(L)_2]$ and square planar-$[Cu^{II}(L)\{OC(=O)CH_3\}]$ complexes incorporating anionic form of tridentate bis(8-quinolinyl)amine $[N^1C_9H_6–N^2–C_9H_6N^3, L^-]$ ligand

Debabrata Maiti [a], Himadri Paul [a], Nripen Chanda [a], Soma Chakraborty [a], Biplab Mondal [a], Vedavati G. Puranik [b], Goutam Kumar Lahiri [a,*]

[a] *Department of Chemistry, Indian Institute of Technology, Powai, Mumbai 400 076, India*
[b] *Physical Chemistry Division, National Chemistry Laboratory, Pune, Maharashtra 411 008, India*

Received 25 August 2003; accepted 21 November 2003

Abstract

The reaction of bis(8-quinolinyl)amine $[N^1C_9H_6–N^2H–C_9H_6N^3$, LH] with $Co^{II}(ClO_4)_2 \cdot 6H_2O$ in methanol under aerobic conditions results in a new class of $[Co^{III}N_6]^+$ ($\mathbf{1}^+$) chromophore incorporating an sp^2-amido nitrogen center (N^2) in the ligand frame. During the course of the reaction, the cobalt ion has been oxidized from its starting +2 oxidation state to +3 state in **1**. The reaction of LH with the Cu-acetate yields monomeric square planar complex, $[Cu^{II}(L)\{OC(=O)CH_3\}]$ (**2**). The same copper complex **2** is also obtained from $Cu(ClO_4) \cdot 6H_2O$ in presence of CH_3COONa as base. On the other hand, the reaction of $Zn(ClO_4) \cdot 6H_2O$ with LH results in octahedral complex $Zn^{II}(L)_2$ (**3**). The Cu(II) complex **2** displays a four-line EPR spectrum at room temperature. Crystal structure of the free ligand (LH) shows that the amine proton [N(2)H] is hydrogen-bonded with the terminal quinoline nitrogen centers [N(1) and N(3)]. The crystal structure of **1** confirms the meridional geometry of the complex cation. The square planar geometry of copper complex **2** is confirmed by its crystal structure where the acetate function behaves as a monodentate ligand. The free ligand, LH, is found to be highly acidic in acetonitrile–water (1:1) medium and correspondingly the amine proton (NH) readily dissociates leading to its L^- form even in absence of any external base. The pK_b value of L^- is determined to be 2.6. Both cobalt and copper complexes do not show any expected spin-allowed d–d transitions, possibly have masked by the intense charge-transfer transitions. However, in case of cobalt complex **1**, one very weak unusual spin-forbidden $^1A_{1g} \rightarrow {}^3T_{1g}$ transition has been observed at 935 nm. The quasi-reversible cobalt (III) $\leftrightharpoons$ cobalt(II) reduction of **1** is observed at E^0, −1.0 V versus SCE.
© 2003 Elsevier Ltd. All rights reserved.

Keywords: Cobalt; Copper; Zinc; Bis(8-quinolinyl)amine; Structures

1. Introduction

Although the ligand bis(8-quinolinyl)amine, LH, was synthesized long back [1,2], the complexation property of LH has been studied only recently to a little extent. The first metal complex of L^- was reported to be a tetrahedral copper-complex, $[Cu^{II}(L)Cl]$ [2]. The crystal structure of the complex reveals the presence of a pairwise interaction between the monomeric units in the solid state, where each ionized amine group occupies an apical co-ordination site of the second Cu(II) center producing a square pyramidal geometry around each copper unit. The crystal structure of the lithium complex of L^- shows a dimeric structure $[Li_2(L)_2]$ in which the two lithium ions and two bridging amido nitrogen centers join together to form a parallelepiped that bisects

* Corresponding author. Tel.: +91-22-2576-7159; fax: +91-22-2572-3480.
E-mail address: lahiri@chem.iitb.ac.in (G. Kumar Lahiri).

0277-5387/$ - see front matter © 2003 Elsevier Ltd. All rights reserved.
doi:10.1016/j.poly.2003.11.053

the dimeric complex, whereas the corresponding Tl^{I} complex Tl(L) exists in the monomeric form [3]. The ligand L^- behaves like a pincer ligand with the divalent Ni^{2+}, Pd^{2+} and Pt^{2+} and the Pt^{2+}complex is reported to perform C–H bond activation process of benzene ring in the presence of a base [4]. The metal complexes of L^- have been essentially restricted to tetra-coordinated species so far, therefore, the present work primarily deals with the hexa-coordinated Co^{III}, Zn^{II} and tetra-coordinated Cu^{II} complexes incorporating L^-.

Herein, we report the synthesis and characterizations of octahedral $[Co^{III}(L)_2]^+$ (**1**), $[Zn^{II}(L)_2]$ (**3**) and square planar $[Cu^{II}(L)\{OC(=O)CH_3\}]$ (**2**) complexes, crystal structures of the free ligand (LH), cobalt and copper complexes and their spectral/electrochemical properties.

2. Experimental

2.1. Materials

Cobalt carbonate and copper nitrate were converted into cobalt perchlorate hexahydrate and copper perchlorate hexahydrate, respectively, by using perchloric acid. 8-Amino quinoline and 8-hydroxy quinoline were purchased from Aldrich, USA. Other chemicals and solvents were reagent grade and used as received. For electrochemical studies, HPLC grade acetonitrile was used. Commercial tetraethyl ammonium bromide was converted to pure tetraethylammonium perchlorate (TEAP) by following an available procedure [5].

2.2. Physical measurements

Solution electrical conductivity was checked using a Systronic conductivity bridge-305. Electronic spectra were recorded using Shimadzu UV-160 (1100–200 nm) and UV-2100 (900–200 nm) spectrophotometer. IR spectra were recorded on a Nicolet spectrophotometer with samples prepared as KBr pellets. ^{1}H NMR spectra were obtained with a 300-MH_z Varian spectrometer. Cyclic voltammetric and coulometric measurements were carried out using a PAR model 273A electrochemistry system. A platinum wire working electrode, a platinum wire auxiliary electrode and a saturated calomel reference electrode (SCE) were used in a standard three-electrode configuration. TEAP was the supporting electrolyte and the solution concentration was ca. 10^{-3} M; the scan rate used was 50 mV s^{-1}. A platinum gauze working electrode was used for coulometric experiments. All electrochemical experiments were carried out under dinitrogen atmosphere, and all redox potentials are uncorrected for junction potentials. The elemental analyses were carried out with a Perkin–Elmer 240C elemental analyzer.

2.3. Preparation of ligand and complexes

2.3.1. Preparation of LH $[N^1C_9H_6–N^2H–C_9H_6N^3]$

The ligand, LH, was synthesized by a modified Bucherer reaction [1,2].

2.3.2. Preparation of $[Co(N^1C_9H_6–N^2–C_9H_6N^3)_2](ClO_4)$ (**1**)

To a solution of $Co(ClO_4)_2\cdot 6H_2O$ (100 mg, 0.273 mmol) in methanol, the ligand, LH (185 mg, 0.682 mmol), was added. The reaction mixture was stirred magnetically for a period of 4 h. The brown colored solid thus obtained was filtered off and washed thoroughly with cold methanol followed by cold water. The product was dried over P_4O_{10} under vacuo. The complex **1** was then recrystallized from benzene–acetonitrile (1:1) mixture. Yield: 124 mg (65%). *Anal.* Calc. for **1**: C, 61.86; H, 3.46; N, 12.02. Found: C, 61.46; H, 3.58; N, 11.40%. Λ_M (Ω^{-1} cm^2 mol^{-1}) in CH_3CN; 117. [^{1}H NMR data in $CDCl_3$: δ, ppm (J, H_z): H(2), 8.45(7.8); H(4), 8.08(8.4); H(5), 8.0(5.1); H(3), 7.85(7.8, 8.4); H(7), 7.26(9.6); H(6), 7.16(5.4, 5.4)].

2.3.3. $[Cu(N^1C_9H_6–N^2–C_9H_6N^3)\{OC(=O)CH_3\}]$ (**2**)

The ligand, LH (156 mg, 0.575 mmol), was added to a methanolic solution of anhydrous copper acetate (50 mg, 0.275 mmol) under stirring condition. The reaction mixture was stirred magnetically for a period of 6 h. The reddish brown colored solid thus formed was filtered off and washed thoroughly with cold methanol followed by cold water. The product was then dried over P_4O_{10} under vacuo. The complex **2** was purified by recrystallization from dichloromethane–hexane (1:1) mixture. Yield: 66 mg (61%). *Anal.* Calc. for **2**: C, 61.14; H, 3.85; N, 10.69. Found: C, 60.43; H, 4.03; N, 11.12%.

2.3.4. $[Zn(N^1C_9H_6–N^2–C_9H_6N^3)_2]$ (**3**)

To a solution of $Zn(ClO_4)_2\cdot 6H_2O$ (100 mg, 0.268 mmol) in methanol was added LH (160 mg, 0.589 mmol). The reaction mixture was stirred magnetically for a period of 4 h. The red colored solid thus obtained was filtered off and washed thoroughly with cold methanol followed by cold water. The product was dried over P_4O_{10} under vacuo. The complex **3** was then recrystallized from dichloromethane–hexane (1:1) mixture. Yield: 94 mg (58%). *Anal.* Calc. for **3**: C, 71.35; H, 3.99; N, 13.87. Found: C, 70.66; H, 3.55; N, 14.15%. ^{1}H NMR data in $CDCl_3$: δ, ppm (J, H_z): H(2), 8.19(8.1); H(4), 8.00(5.9); H(5), 7.92(8.3); H(3), 7.59(8.1, 8.1); H(7), complex multiplet centered at δ, 6.95 ppm; H(6), complex multiplet centered at δ, 6.95 ppm.

2.4. X-ray structure determination

The single crystals of LH were grown by slow evaporation of dichloromethane solution of LH. The single

Table 1
Crystallographic data for $[NC_9H_6–NH–C_9H_6N$ (LH)], $[Co^{III}(L)_2]ClO_4 \cdot 0.5C_6H_6$ (**1**) and $[Cu^{II}(L)\{OC(=O)CH_3\}]$ (**2**)

Formula	$C_{18}H_{13}N_3$	$C_{39}H_{27}N_6ClO_4Co$	$C_{20}H_{15}N_3O_2Cu$
M	271.31	738.07	392.89
Crystal symmetry	monoclinic	triclinic	triclinic
Space group	$C2/c$	$P\bar{1}$	$P\bar{1}$
a (Å)	31.858(3)	9.0439(8)	7.9970(6)
b (Å)	6.2360(4)	12.5407(9)	9.8040(7)
c (Å)	14.5940(10)	14.8085(11)	11.2770(14)
α (°)		101.484(6)	75.217(7)
β (°)	111.524(7)	91.498(7)	85.585(8)
γ (°)		90.455(7)	73.918(6)
V (Å^3)	2697.1(4)	1645.2(2)	821.41(13)
T (K)	293(2)	293(2)	293(2)
μ (mm^{-1})	0.081	0.657	1.350
Z	8	2	2
R_1	0.0455	0.0577	0.0309
wR_2	0.0906	0.1363	0.0769

crystals of complex **1** were grown by slow diffusion of an acetonitrile solution of it in benzene followed by slow evaporation at 298 K. Single crystals of copper complex **2** were grown by slow diffusion of dichloromethane solution of **2** into hexane followed by slow evaporation at 298 K. The X-ray data were collected on a PC-controlled Enraf–Nonius CAD-4 (MACH-3) single crystal X-ray diffractometer using Mo Kα radiation. Significant crystal data and data collection parameters are shown in Table 1. The structures were solved by direct method using SHELXS 86 and refined by full-matrix least-squares on F^2 using SHELXL 97 [6]. The X-ray analysis of the complex **1** shows one ClO_4^- anion and half molecule of benzene as solvent of crystallization in the asymmetric unit. The solvent molecule of benzene is found to be highly disordered and hydrogen atoms for this solvent have not been fixed.

3. Results and discussion

3.1. Synthesis and characterization

The ligand bis(8-quinolinyl)amine $[N^1C_9H_6–N^2H–C_9H_6N^3$, LH] comprising one dissociable amine proton (N^2H) has been synthesized from 8-aminoquinoline and 8-hydroxyquinoline following the reported procedure [1,2]. The direct bonding of N^2 center with the two-electron-withdrawing quinoline moieties makes the amine proton (N^2H) in LH substantially acidic. Thus, the NH proton of LH dissociates in acetonitrile–water (1:1) mixture to give the corresponding conjugate base (L^-). In view of that, the UV–Vis spectrum of the free ligand in 1:1 acetonitrile–water fails to show any noticeable changes in spectral behavior on increasing pH. Therefore the pK_b of L^- of 2.6 has been determined by *pH*-titration (Fig. 1). The strong acidic nature of LH facilitates the dissociation of the NH function under

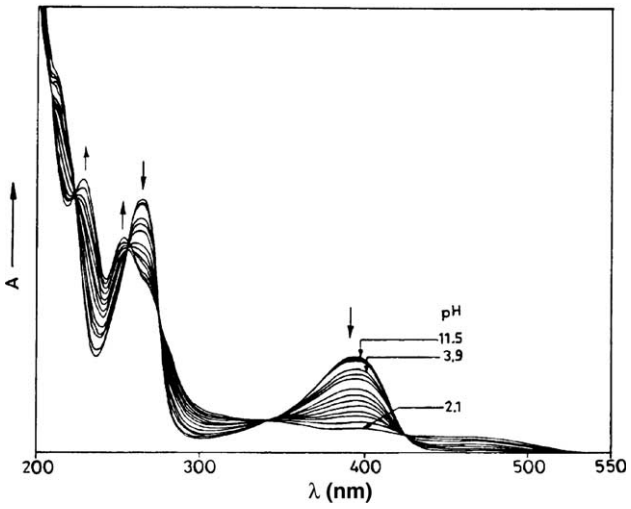

Fig. 1. Electronic spectra of LH at different pH in 1:1 acetonitrile–water. The arrows indicate increase or decrease in band intensities as the reaction proceeds.

normal reaction conditions (Scheme 1). However, in case of peptide bound amide proton [C(=O)–NH] the presence of a base ($NaOCH_3$ or NaOH) is necessary to deprotonate the –NH proton during metallation process [7]. The complex $[Co^{III}(L)_2]ClO_4$ (**1**) has been synthesized from $Co^{II}(ClO_4)_2 \cdot 6H_2O$ and LH in methanol solvent under aerobic condition (Scheme 1). The synthesis of **1** from cobalt (II) starting salt is attained with the metal oxidation. In view of the low Co(III)–Co(II) reduction potential of **1** (see later) it may be logically considered that aerial oxygen is the most probable oxidant [8]. Under a strict dinitrogen atmosphere corresponding cobalt(II) species $\mathbf{1}^-$ can be generated, however, $\mathbf{1}^-$ is found to be oxidized spontaneously in contact with slight amount of air.

The reaction of LH with copper acetate or copper perchlorate in presence of sodium acetate base results in mononuclear tetra-coordinated copper (II) complex of the composition $Cu^{II}(L)\{^-O–C(=O)CH_3\}$ (**2**) (Scheme 1). On the other hand, the reaction of zinc perchlorate hexahydrate with the ligand, LH, yields bis-octahedral neutral complex $Zn^{II}(L)_2$ (**3**) as like the cobalt complex (Scheme 1).

The cobalt and zinc complexes are diamagnetic and behave as 1:1 conductor and neutral, respectively, in acetonitrile. The electrically neutral copper complex **2** exhibits one-electron paramagnetism ($\mu = 1.87$ BM). All the complexes exhibit satisfactory elemental analysis (Section 2).

3.2. Crystal structures of the free ligand $NC_9H_6–NH–C_9H_6N$ (LH), $[Co^{III}(L)_2]ClO_4$ (1) and $[Cu^{II}(L)\{OC(=O)CH_3\}]$ (2)

The formation of LH was confirmed by its crystal structure determination. Crystal structure is shown in

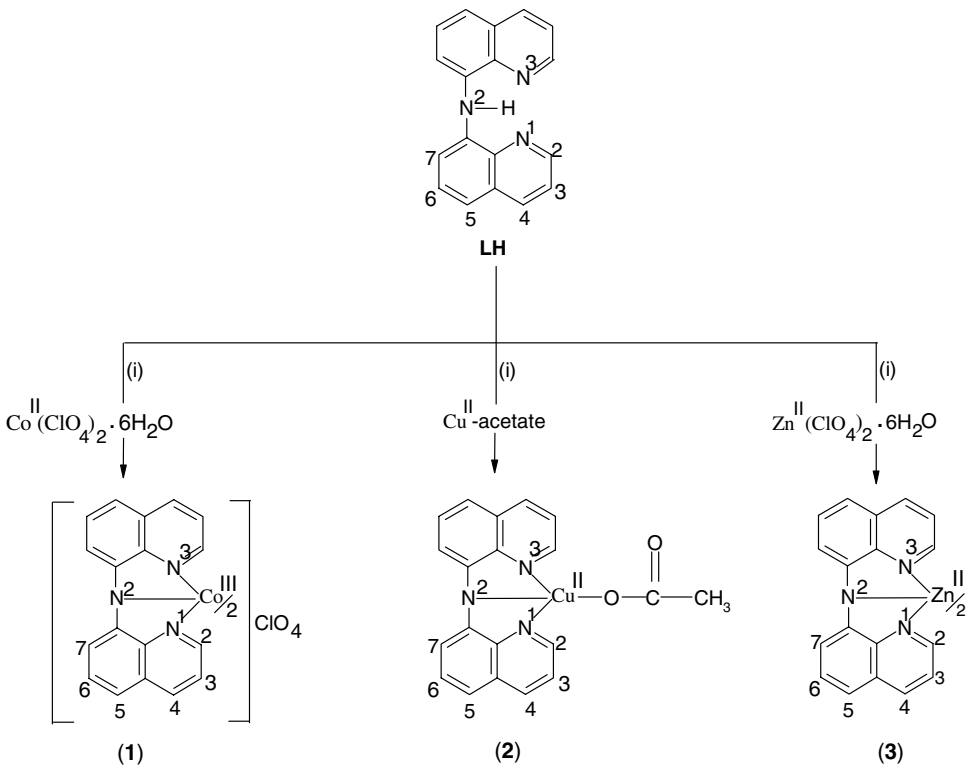

Scheme 1. (i) MeOH, stir.

Fig. 2 and selective bond distances and angles are shown in Table 2. The bond distances and angles are unremarkable. The amido proton N(1)–H(101) has formed intramolecular hydrogen bonding with the nearby two quinolinic nitrogen centers [N(2) and N(3)] (Table 3).

The crystal structure of $[Co^{III}(L)_2]ClO_4 \cdot 0.5C_6H_6$ (**1**) is shown in Fig. 3. Selected bond distances and angles are listed in Table 2. The lattice consists of one type of molecule. The crystal consists of an array of $[Co(L)_2]^+$ cations, $[ClO_4]^-$ anions and benzene of crystallization in a ratio of 1:1:0.5 stoichiometry. The coordination geometry around the cobalt ion is distorted octahedral. The tridentate anionic ligand (L^-) is bonded to the cobalt ion with the terminal quinoline nitrogen atoms being *trans* to each other. The central amido nitrogen centers [N(1) and N(5)] of two L^- around the metal ion are also in *trans* configuration. The two meridional planes are nearly orthogonal. The sp^2 hybridization about each ionized amine group is reflected by the angles Co–N(1)–C(1), Co–N(1)–C(17), C(1)–N(1)–C(17), Co–N(5)–C(26), Co–N(5)–C(28), C(26)–N(5)–C(28), corresponding to 114.9(3)°, 114.1(4)°, 131.0(5)°, 114.6(4)°, 115.7(4)° and 129.6(5)°, respectively. The *trans* angles N(2)–Co–N(3), N(4)–Co–N(6) and N(1)–Co–N(5) are 168.7(2)°, 168.9(2)° and 178.71(19)°, respectively. The observed Co^{III}–N(quinoline) bond distances [1.913(4)–1.929(4) Å] are shorter than the average Co^{III}–N(pyridine) bond distances [1.94–2.00 Å] [9]. The Co-ionized amine bond distances [Co–N(1), 1.889(4) Å and Co–N(5), 1.879(5) Å] are reasonably shorter than the Co–quinoline N bond distances [Co–N(2), 1.913(4) Å; Co–N(3), 1.929(4) Å; Co–N(4), 1.921(4) Å and Co–N(6), 1.916 Å]. The Co^{III}–N(ionized amine) distances in **1** are appreciably shorter than the observed Co^{III}–NH distances [1.929(7)–1.951(7) Å] [10] and Co^{III}–N(amido) distances [1.929(6)–1.942(3)] [11] which are due to the fact of enhanced π-donor property of the ionized amino function. The perchlorate anion is tetrahedral with an average Cl–O distance of 1.410(6) Å and an average O–Cl–O angle of 109.46(4)°.

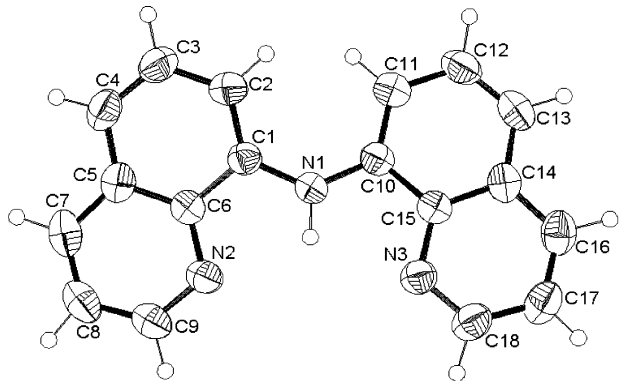

Fig. 2. Crystal structure of $[NC_9H_6–NH–C_9H_6N$, (LH)].

The packing diagram of the complex molecule **1** shows several intramolecular C–H···N and intermolecular C–H···O hydrogen bonding patterns (Table 3). The

Table 2
Selected bond distances and angles and their standard deviation for $[NC_9H_6–NH–C_9H_6N$, (LH)], $[Co(L)_2]ClO_4 \cdot 0.5C_6H_6$ (**1**) and $[Cu(L)\{OC(=O)CH_3\}]$ (**2**)

$NC_9H_6–NH–C_9H_6N$ (LH)		$[Co^{III}(L)_2]ClO_4 \cdot 0.5C_6H_6$		$[Cu^{II}(L)\{OC(=O)CH_3\}]$ (**2**)	
Bond distances (Å)					
N(1)–C(10)	1.382(3)	Co–N(1)	1.889(4)	Cu(1)–N(2)	1.932(2)
N(1)–C(1)	1.385(3)	Co–N(2)	1.913(4)	Cu(1)–O(1)	1.9495(18)
N(2)–C(9)	1.331(3)	Co–N(3)	1.929(4)	Cu(1)–N(3)	1.982(2)
N(2)–C(6)	1.365(3)	Co–N(4)	1.921(4)	Cu(1)–N(1)	1.983(2)
N(3)–C(18)	1.322(3)	Co–N(5)	1.879(5)	O(1)–C(19)	1.272(3)
N(3)–C(15)	1.369(3)	Co–N(6)	1.916(4)	O(2)–C(19)	1.226(3)
Bond angles (°)					
C(10)–N(1)–C(1)	132.4(2)	N(5)–Co–N(1)	178.71(19)	N(2)–Cu(1)–O(1)	175.34(9)
N(1)–C(1)–C(6)	115.4(2)	N(5)–Co–N(2)	96.01(19)	N(2)–Cu(1)–N(3)	82.77(9)
N(2)–C(6)–C(1)	117.3(2)	N(1)–Co–N(2)	84.37(19)	N(2)–Cu(1)–N(1)	82.72(9)
C(9)–N(2)–C(6)	117.1(2)	N(5)–Co–N(6)	84.1(2)	N(3)–Cu(1)–N(1)	164.50(9)
C(2)–C(1)–N(1)	126.7(2)	N(1)–Co–N(6)	94.7(2)	O(1)–Cu(1)–N(3)	98.03(9)
C(2)–C(1)–C(6)	117.9(2)	N(2)–Co–N(6)	89.82(18)	O(1)–Cu(1)–N(1)	96.87(9)
N(1)–C(10)–C(15)	115.5(2)	N(5)–Co–N(4)	84.97(19)	C(19)–O(1)–Cu(1)	107.81(17)
C(10)–C(15)–N(3)	117.3(2)	N(1)–Co–N(4)	96.27(19)	O(2)–C(19)–O(1)	123.7(3)
C(18)–N(3)–C(15)	117.2(2)	N(2)–Co–N(4)	89.63(17)	C(8)–N(2)–C(17)	128.9(2)
C(11)–C(10)–N(1)	126.7(2)	N(1)–Co–N(3)	84.5(2)	O(1)–C(19)–C(20)	116.6(3)
C(11)–C(10)–C(15)	117.8(2)	N(2)–Co–N(3)	168.7(2)		
		N(6)–Co–N(3)	92.45(18)		
		N(4)–Co–N(3)	90.24(17)		
		N(6)–Co–N(4)	168.9(2)		
		N(5)–Co–N(3)	95.2(2)		
		C(1)–N(1)–C(17)	131.0(5)		
		C(28)–N(5)–C(26)	129.6(5)		

Table 3
Hydrogen bonds for $NC_9H_6–NH–C_9H_6N$ (LH) and $[Co^{III}(L)_2]ClO_4 \cdot 0.5C_6H_6$ [Å and (°)]

	D–H···A (°)	*d*(D–H) Å	*d*(H···A) Å	*d*(D···A) Å	D–H···A (°)
$NC_9H_6–NH–C_9H_6N$ (LH)					
Intra- molecular	N(1)–H(101)···N(2)	0.9383	2.1691	2.6592	111.41
	N(1)–H(101)···N(3)	0.9383	2.1984	2.6626	109.48
*$[Co^{III}(L)_2]ClO_4 \cdot 0.5C_6H_6$ (**1**)*					
Intra-molecular	C(8)–H(8)···N(5)	0.97	2.618	3.054	107.45
	C(10)–H(10)···N(5)	0.85	2.606	3.026	111.56
	C(19)–H(19)···N(1)	0.97	2.533	3.080	115.56
	C(35)–H(35)···N(1)	0.98	2.515	3.002	110.37
Inter-molecular	C(16)–H(16)···O(4)^{i}	0.99	2.430	3.305	146.74
	C(30)–H(30)···O(3)^{ii}	0.99	2.533	3.406	146.10

^{i}, $1-x$, $-y$, $1-z$ and ^{ii}, x, y, $-1+z$.

O(3) and O(4) atoms of the perchlorate moiety are involved in intermolecular C–H···O hydrogen bonds, sandwiching the solvent benzene molecule sitting on the symmetry position.

The formation of copper complex **2** has been confirmed by its single crystal X-ray structure. The crystal structure is shown in Fig. 4 and selected bond distances and angles are given in Table 2. The lattice consists of one type of molecule. The square planar geometry around the copper ion in $Cu^{II}N_3O$ coordination environment is evidenced from the angles subtended around the copper center (Table 2). The planarity of coordinated L^- is essentially leading to the square planar geometry. The tridentate anionic ligand is bonded to the copper ion with the terminal quinoline nitrogen centers [N(1) and N(3)] and the central amido nitrogen [N(2)]. The sp^2 hybridization of the ionized amine group is confirmed by the angles Cu(1)–N(2)–C(17), 115.5(17)°; Cu(1)–N(2)–C(8), 115.5(17)° and C(8)–N(2)–C(17), 128.9(2)°. The substantial deviation of the C(8)–N(2)–C(17) angle [128.9(2)°] of the coordinated tridentate ligand (L^-) with respect to the expected sp^2 angle of 120° possibly can account for the observed significant decrease in N–Cu–N *cis* angles [N(1)–Cu(1)–N(2), 82.72(9)° and N(2)–Cu(1)–N(3), 82.77(9)°]. The *trans* angles N(2)–Cu(1)–O(1) and N(1)–Cu(1)–N(3) are

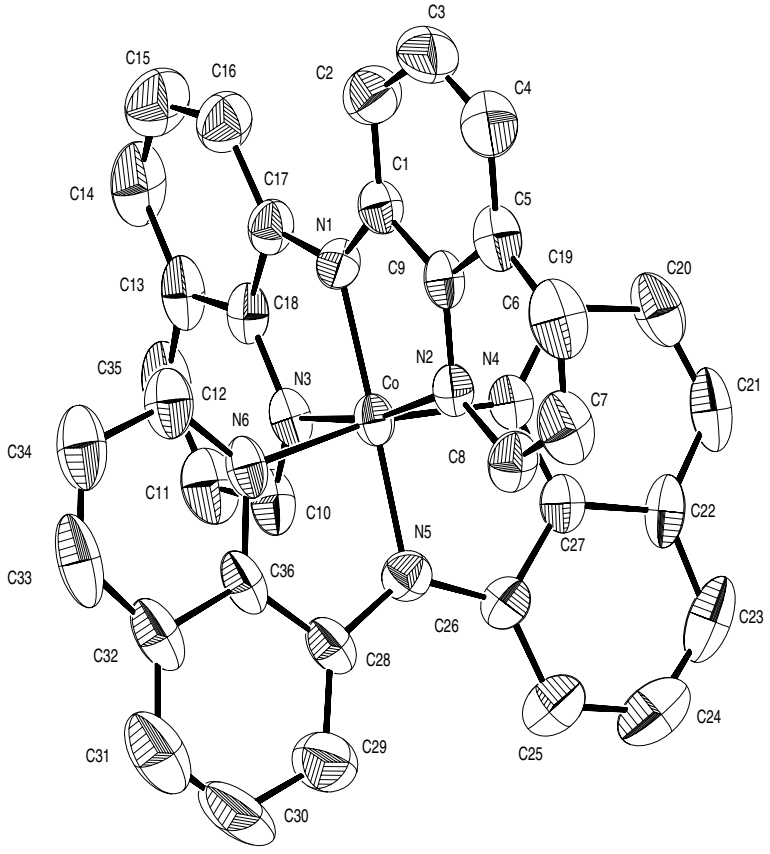

Fig. 3. Crystal structure of $[Co^{III}(L)_2]ClO_4 \cdot 0.5C_6H_6$ (**1**).

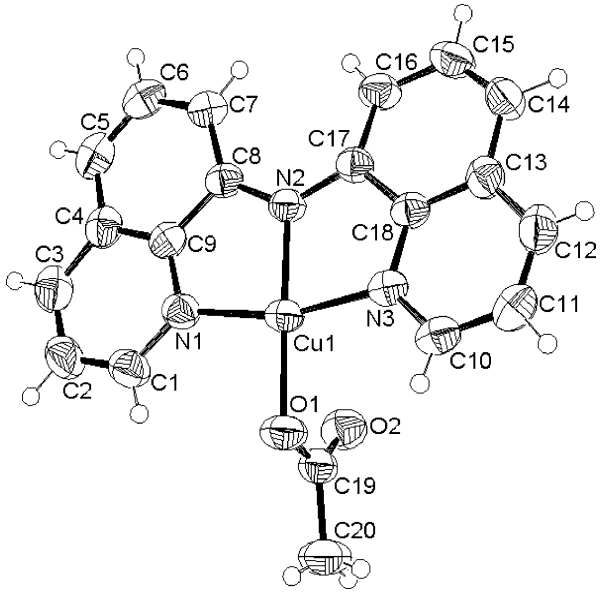

Fig. 4. Crystal structure of $[Cu^{II}(L)\{OC(=O)CH_3\}]$ (**2**).

175.3(9)° and 164.5(9)°, respectively. The Cu^{II}–N (quinoline) distances [Cu(1)–N(1), 1.983(2) Å and Cu(1)–N(3), 1.982(2) Å] are reasonably longer than the corresponding Cu(1)–N(2) (ionized amido nitrogen), 1.932(2) Å which reflects the π-donor ability of the ionized amino function. The Cu(II)–N (quinoline) distances are comparable with those of reported Cu(II)–N (quinoline) distances, 1.972–2.033Å [12]. Cu(1)–O(1) (acetate) distance 1.9495(18) Å is matched well with the reported data of other Cu(II)-monodentate acetate complexes [13]. It is to be noted that the crystal structure of similar reported tetracoordinated $Cu^{II}(L)Cl$ complex shows dimeric interaction through the ionized sp^2 hybridized amido nitrogen [2]. It was proposed that the filled p_z orbital of the sp^2 hybridized amido nitrogen is sufficiently basic to bind to a second copper ion resulting in dimerization. However, any sort of dimerization process has not been observed in the present case which implies that in comparison to the chloro complex the basicity of the amido nitrogen in **2** is significantly less, although the Cu–N(amido nitrogen) distance is almost same in both the complexes [1.932 (2)Å in **2** and 1.935 (2)Å in the corresponding chloro complex $[Cu^{II}(L)Cl]$] [2].

3.3. Spectral properties

The perchlorate vibrations of **1** appeared at 1093 and 629 cm^{-1} in the IR spectrum.

The ^{1}H NMR spectra of **1** and **3** in $CDCl_3$ solvent reveal that half of the individual ligand (L^-) represents the whole molecule due to the presence of internal symmetry (Fig. 5). The absence of NH proton of LH in the NMR spectra supports the bonding of anionic form of the ligand (L^-) to the metal ion in the solution state as well.

The acetonitrile solution of **1** exhibits multiple intense transitions in the UV–Vis region (Fig. 6(a)). [λ_{max}/nm (ε/$M^{-1}\,cm^{-1}$): 505(25 000), 431(9700), 374(5050), 292(57 000) and 217(107 000)]. Based on the high intensities of the visible bands the transitions are assigned to be charge-transfer in nature [14]. Since Co(III) is in the low-spin t_{2g}^6 configuration, the visible energy intense bands at 505 and 431 nm are, therefore, assigned as $L^- \rightarrow e_g(Co^{III})$ ligand-to-metal charge-transfer transitions [8,15]. The UV region moderately strong band at 372 nm and strong bands at 292 and 217 nm are presumably due to intra ligand $n \rightarrow \pi^*$ and $\pi \rightarrow \pi^*$ transitions, respectively [16]. The free ligand (LH) also exhibits strong transitions in the UV-region [λ_{max}/nm (ε/

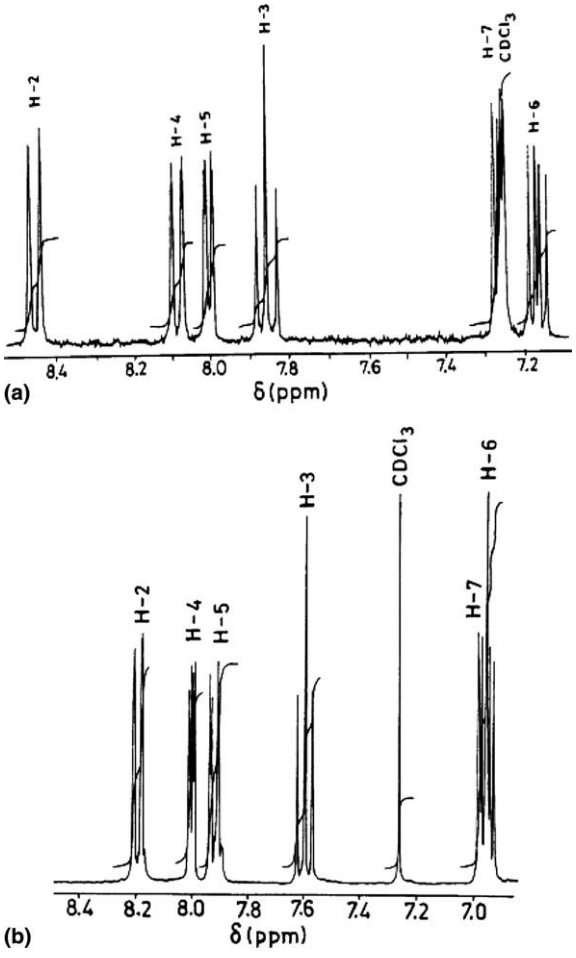

Fig. 5. ^{1}H NMR spectra of: (a) $[Co^{III}(L)_2]ClO_4$ (**1**) and (b) $Zn^{II}(L)_2$ (**3**) in $CDCl_3$.

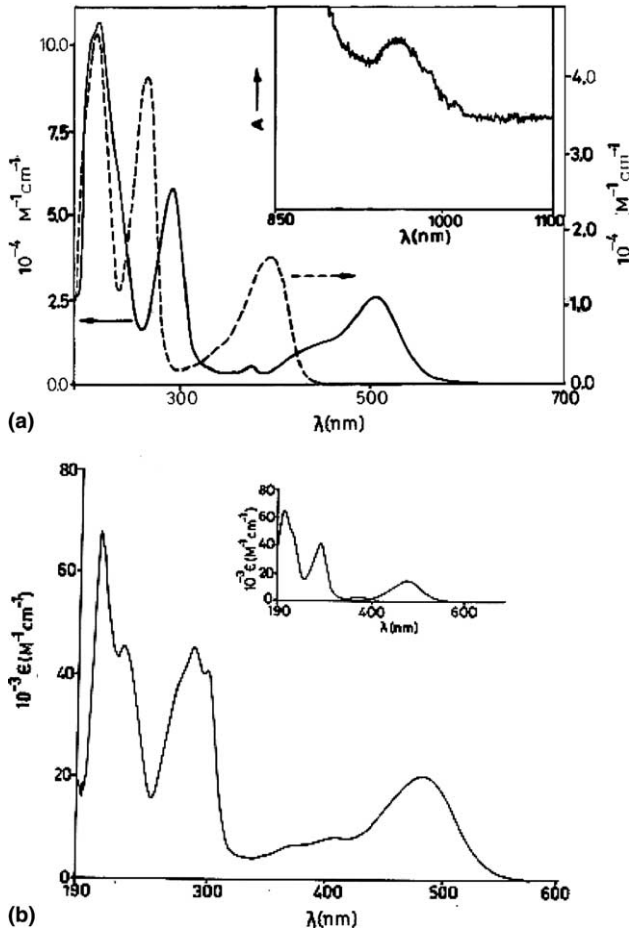

Fig. 6. Electronic spectra of: (a) $[Co^{III}(L)_2]ClO_4$ (**1**) (——) and LH (-----), inset shows the electronic spectrum of **1** in the range of 1100–850 nm; (b) $Zn^{II}(L)_2$ (**3**), inset shows the spectrum of $[Cu^{II}(L)\{OC(=O)CH_3]$ (**2**) in acetonitrile.

$M^{-1}\,cm^{-1}$): 397(16 100); 264(38 900); 214(44 700) in CH_3CN (Fig. 6(a))].

For low-spin octahedral Co(III) complexes having CoN_6 coordination environment the expected two d–d transitions, $^1A_{1g} \rightarrow {}^1T_{1g}$ and $^1A_{1g} \rightarrow {}^1T_{2g}$ usually appear near 500 nm and at a higher energy part, respectively ($\varepsilon \sim 10$–300 $M^{-1}\,cm^{-1}$) [17]. Accordingly, the $[Co(trpy)_2]^{3+}$ and Co(III)-peptide complexes exhibit lowest energy $^1A_{1g} \rightarrow {}^1T_{1g}$ transition near 500 nm [7a,18]. However, in **1** no such d–d transitions are detected in the UV–Vis region. The appearance of low energy intense charge-transfer transitions possibly have masked the expected weak d–d bands [8,19]. On the other hand **1** exhibits a very weak band at 955 nm (ε/$M^{-1}\,cm^{-1}$, 11]) (Fig. 6(a), inset). The existence of spin-allowed d–d band at an energy which is much lower than the observed lowest energy LMCT transition ($\lambda = 505$ nm) particularly in an environment consisting of potent electron-rich ligand function (L^-) and the metal ion in relatively higher oxidation state (Co^{3+}) is hard to conceive. It may, therefore, be logical to look for the possible correspondence of the 955-nm band with the

$^1A_{1g} \rightarrow {}^3T_{1g}$ spin-forbidden singlet–triplet transition as an alternative approach. The characteristics of very weak and relatively low energy of the 955 nm band can possibly justify its origin as $^1A_{1g} \rightarrow {}^3T_{1g}$ spin-forbidden transition. It may be noted that the spin-forbidden singlet–triplet transitions have been detected earlier in few other $Co^{III}N_6$ systems such as $Co(NH_3)_6^{3+}$ and $Co(en)_3^{3+}$ complexes [17,20].

The complex **2** exhibits four intense transition in the UV–Vis region (Fig. 6(b), inset): [λ_{max}/nm (ε/M^{-1} cm^{-1}): 476(14 622), 362(2781), 284(42 625) and 206(65 872)]. The intense transitions are believed to be charge transfer in nature. The lowest energy transition at 476 nm possibly originated from $L^- \rightarrow (Cu^{II})$ LMCT transition. The UV region transitions are possibly originated via intraligand $\pi \rightarrow \pi^*$ and $n \rightarrow \pi^*$ transitions. The expected weak d–d transition in the visible region for **2** has not been detected even with its concentrated solution. It may be lost in the low-energy tail of the intense charge-transfer transition at 476 nm.

The complex **3** shows multiple transitions in the UV–Vis region (Fig. 6(b)): λ_{max}/nm (ε/M^{-1} cm^{-1}): 482(20 227), 229(40 568), 287(45 454), 228(45 340) and 207(67 272). In view of their high intensities the transitions are believed to be charge transfer in nature.

The EPR spectrum (Fig. 7) of **2** is recorded in 1:1 chloroform–toluene mixture at 298 K and it displays an equally spaced four-line spectrum (g_{av}, 2.106 and A_{av}, 80 G) due to hyperfine splitting by the copper nucleus ($I = 3/2$) [21].

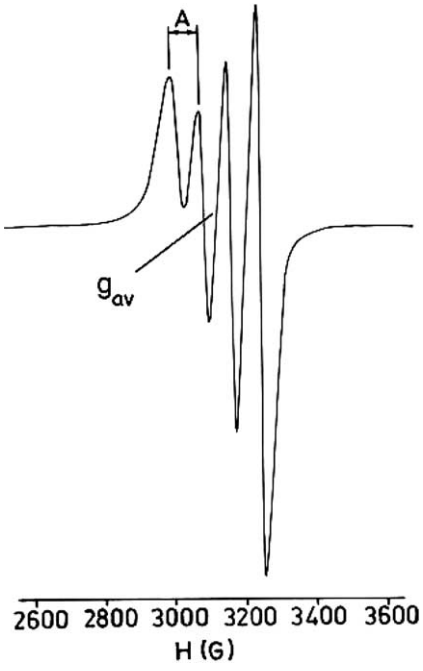

Fig. 7. EPR spectrum of $[Cu^{II}(L)\{OC(=O)CH_3\}]$ (**2**) in 1:1 chloroform–toluene mixture at 298 K.

3.4. Electron-transfer properties

Redox properties of $[Co^{III}(L)_2]^+$ (**1**) and $[Cu^{II}(L)\{OC(=O)CH_3\}]$ (**2**) have been examined in acetonitrile solvent using platinum wire working electrode (Figs. 8 and 9). Cobalt complex **1** displays one quasi-reversible one-electron reductive process E^0, $V(\Delta E_p, mV)$ at −1.0(100) versus SCE (couple-III) (Fig. 8(a)) which is assigned to be $Co(III) \leftrightharpoons Co(II)$ couple. The high negative potential (<−1.0 V) of cobalt(III)–cobalt(II) reduction process can account for the preferential stabilization of cobalt ion in +3 oxidation state in **1** under atmospheric conditions. The cobalt(III)–Cobalt(II) reduction potential of the similar bis octahedral peptido complex {$[Co(L)_2]^+$, $L^- = N$-(2-(4-imidazolyl)ethyl)-pyridine-2-carboxamide} appears at −0.62 V in MeOH, −0.72 V in $(CH_3)_2SO$ and −0.69 V in DMF (acetonitrile data is not available) [22]. The substantial negative shift of Co(III)–Co(II) reduction potential (∼0.3 V) while moving from the deprotonated amido complex to the deprotonated amino complex **1** implies the reasonable difference in basicity between the two sp^2 nitrogen centers. Thus, in case of peptide bound amide proton [C(=O)–NH] the oxidation of cobalt(II) to cobalt(III) takes place only via bubbling of air through the reaction mixture and in the presence of a base ($NaOCH_3$ or NaOH) [22]. The electrochemically generated Co(II) congener $[Co(L)_2]$ ($\mathbf{1}^-$) has been found to be quite unstable, it spontaneously oxidizes to the parent $[Co^{III}(L)_2]^+$ state which has essentially

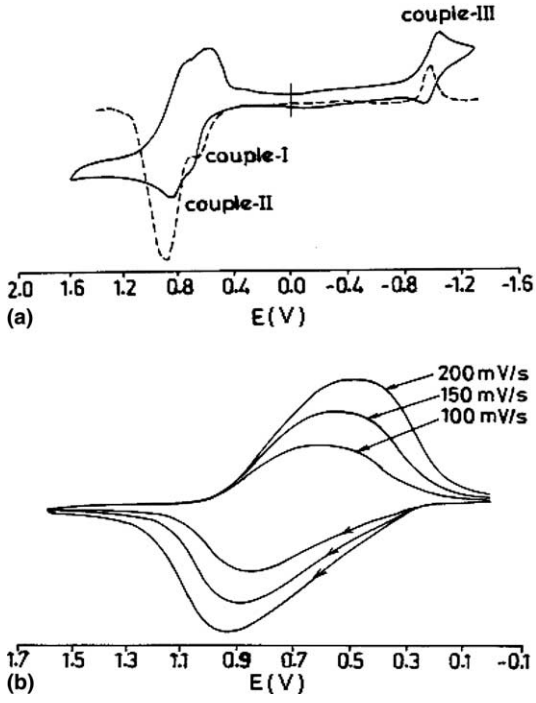

Fig. 8. Cyclic voltammograms of $\sim 10^{-3}$ M solution of $[Co^{III}(L)_2]ClO_4$ (**1**) in acetonitrile: (a) at a scan rate 50 mV s^{-1} and (b) at different scan rates (only for the oxidation processes).

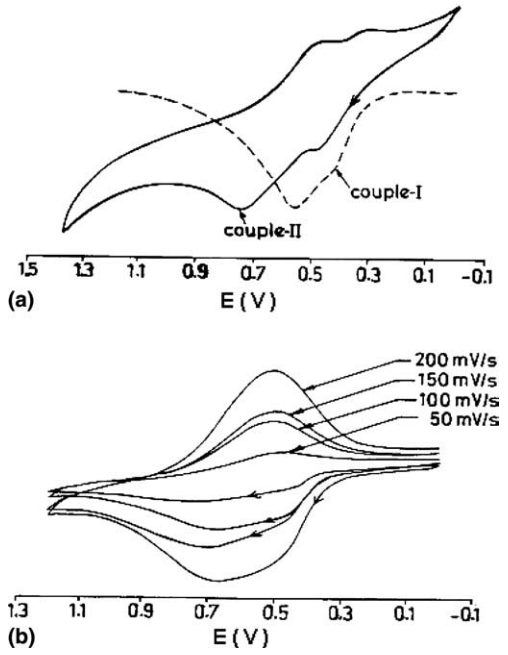

Fig. 9. Cyclic voltammograms of $\sim 10^{-3}$ M solution of $[Cu^{II}(L)\{OC(=O)CH_3\}]$ (**2**) in acetonitrile: (a) at a scan rate 20 mV s^{-1} and (b) at different scan rates (only for the oxidation processes).

precluded the isolation of the corresponding cobalt(II) analogue.

The complex **1** also displays two successive quasi-reversible oxidative responses, E^0, $V(\Delta E_p, \text{mV})$ at 0.64(80) (couple-I) and 0.83(120) (couple-II) (Fig. 8(a)). The one-electron nature of couple-I is confirmed by comparing its differential pulse voltammetric (dpv) current height with that of the Co(III)–Co(II) couple (couple-III). However, relative to couple-I or couple-III, the dpv current height of couple-II appears to be approximately three times greater.

On scan increment (>50 mV s^{-1}), the peaks of the two waves (couples I and II) broaden and merge to a single broad and blunt wave (Fig. 8(b)). The broadness of the profile of voltammograms particularly at a higher scan rate (>50 mV s^{-1}) reveals that the surface based adsorption processes are involved after the usual diffusion controlled based process [23]. In view of this serious electro deposition factor, repeated cleaning of electrode prior to each fresh run is found to be necessary.

The copper(II)-complex **2** shows two successive irreversible oxidation processes E_{pa} at 0.49 and 0.76 V versus SCE at a slower scan rate (20 mV s^{-1}) (Fig. 9(a)). However, on scan increment the shape of the voltammogram changes and at a higher scan rate (>100 mV s^{-1}) it appears to be an overlapping broad wave as like cobalt complex (Fig. 9(b)). Therefore, similar surface confinement processes are also involved during the oxidation steps particularly at a higher scan rate (>20 mV s^{-1}).

The electrogenerated oxidized species decomposes rapidly at room temperature, therefore, further characterization of the oxidized product and subsequent precise assignments of the oxidation processes have not been possible to make.

Since the free ligand (LH) exhibits one irreversible oxidation process at 0.56 V versus SCE in CH_3CN and +4 oxidation state of cobalt ion and +3 state of the copper ion are known to be difficult to stabilize, therefore, it may be logical to assign the oxidative responses as ligand-center based processes.

4. Conclusion

The use of sp^2-amido nitrogen containing tridentate ligand (L^-) leads to the formation of bis chelated octahedral complexes $[Co^{III}(L)_2]^+$ (**1**) and $[Zn^{II}(L)_2]$ (**3**). However, copper ion selectively stabilizes in square planar geometry having $Cu^{II}N_3O$ (**2**) chromophore. The basicity of the anionic sp^2-nitrogen center of L^- is such that it stabilizes the cobalt ion preferentially in trivalent Co^{III} state in **1** under atmospheric conditions. The strongly basic nature of L^- in **1** is also reflected in observed highly negative and reversible $Co^{III} \leftrightharpoons Co^{II}$ couple (−10 V versus SCE). The complexes exhibit strong charge-transfer transitions in UV–Vis region. Although no spin-allowed d–d transition has been observed for both cobalt and copper complexes, the cobalt complex **1** displays one very weak spin-forbidden $^1A_{1g} \rightarrow {}^3T_{1g}$ transition ($\varepsilon/M^{-1}\,cm^{-1}$, 11]) at 955 nm which has so far been rarely observed in few other octahedral Co(III) systems.

5. Supplementary material

Crystallographic data for the structural analysis have been deposited with the CCDC Nos. 216980, 216979 and 216978 for compounds LH, **1** and **2**, respectively. Supplementary data are available from the CCDC, 12 Union Road, Cambridge CB2 1EZ, UK (fax: +44-1223-336033; E-mail: deposit@ccdc.cam.ac.uk or www: http://www.ccdc.cam.ac.uk) on request, quoting the deposition numbers.

Acknowledgements

Financial support received from Council of Scientific and Industrial Research, New Delhi, India, is gratefully acknowledged. The X-ray structural studies were carried out at the National Single Crystal Diffractometer Facility, Indian Institute of Technology, Bombay. Special acknowledgement is made to Sophisticated Analytical Instrument Facility, Indian Institute of

Technology, Bombay for providing the NMR and EPR facilities.

References

[1] K.A. Jensen, P.H. Nielsen, Acta Chem. Scand. 18 (1964) 1.
[2] J.P. Puzas, R. Nakon, J.L. Petersen, Inorg. Chem. 25 (1986) 3837.
[3] J.C. Peters, S.B. Harkins, D.S. Brown, M.W. Day, Inorg. Chem. 40 (2001) 5083.
[4] S.B. Harkins, J.C. Peters, Organometallics 21 (2002) 1753.
[5] D.T. Sawyer, A. Sobkowiak, J.L. Roberts Jr., Electrochemistry for Chemists, Wiley, New York, 1995.
[6] G.M. Sheldrick, SHELXS 97, Program for Crystal Structure Solution and Refinement, University of Göttingen, Germany, 1997.
[7] (a) M. Tsukayama, C.R. Randall, F.S. Santillo, J.C. Dabrowiak, J. Am. Chem. Soc. 103 (1981) 458;
(b) S.J. Brown, M.M. Olmstead, P.K. Mascharak, Inorg. Chem. 28 (1989) 3720;
(c) J.D. Tan, E.T. Farinas, S.S. David, P.K. Mascharak, Inorg. Chem. 33 (1994) 4295;
(d) S.J. Brown, M.M. Olmstead, P.K. Mascharak, Inorg. Chem. 29 (1990) 3229;
(e) R.J. Guajardo, P.K. Mascharak, Inorg. Chem. 34 (1995) 802;
(f) R.J. Guajardo, J.D. Tan, P.K. Mascharak, Inorg. Chem. 33 (1994) 2838;
(g) S.J. Brown, S.E. Hudson, D.W. Stephan, P.K. Mascharak, Inorg. Chem. 28 (1989) 468;
(h) J.C. Dabrowiak, M.J. Tsukayama, J. Am. Chem. Soc. 103 (1981) 7543;
(i) Y. Sugiura, J. Am. Chem. Soc. 102 (1980) 5216;
(j) S.M. Hecht (Ed.), Bleomycin: Chemical, Biochemical and Biological Aspects, Springer-Verlag, New York, 1979.
[8] (a) B.K. Santra, G.K. Lahiri, J. Chem. Soc., Dalton Trans. (1997) 1883;
(b) A. Bharath, B.K. Santra, P. Munshi, G.K. Lahiri, J. Chem. Soc., Dalton Trans. (1998) 2643.
[9] (a) F.A. Chavez, J.M. Rowland, M.M. Olmstead, P.K. Mascharak, J. Am. Chem. Soc. 120 (1998) 9015;
(b) L.A. Tyler, J.C. Noveron, M.M. Olmstead, P.K. Mascharak, Inorg. Chem. 39 (2000) 357.
[10] C. Bombieri, E. Forsellini, A. Delpra, M.L. Tobe, C. Chatterjee, C.J. Cooksey, Inorg. Chim. Acta 75 (1983) 93.
[11] (a) F.A. Chavez, M.M. Olmstesd, P.K. Mascharak, Inorg. Chem. 36 (1997) 6323;
(b) T.J. Collins, R.D. Powell, C. Slebodnick, E.S. Uffelman, J. Am. Chem. Soc. 113 (1991) 8149;
(c) M. Ray, D. Ghosh, Z. Shirin, R.N. Mukherjee, Inorg. Chem. 36 (1997) 3568.
[12] (a) G.J. Palenik, Acta Crystallogr. 17 (1964) 687;
(b) R.G. Little, J.A. Moreland, D.B.W. Yawney, R.J. Doedens, J. Am. Chem. Soc. 96 (1974) 3834;
(c) R.G. Little, D.B.W. Yawney, R.J. Doedens, J. Chem. Soc., Chem. Commun. 4 (1972) 228;
(d) J.A. Bevan, D.P. Graddon, J.F. McConnell, Nature 199 (1963) 373.
[13] (a) T. Nakamura, H. Higuchi, K. Izutsu, Bull. Chem. Soc. Jpn. 62 (1989) 3089;
(b) R.L. Paul, S.M. Couchman, J.C. Jeffery, J.A. McCleverty, Z.R. Reeves, M.D. Ward, J. Chem. Soc., Dalton Trans. 6 (2000) 845.
[14] (a) B.K. Santra, G.K. Lahiri, J. Chem. Soc., Dalton Trans. (1997) 129;
(b) N. Bag, A. Pramanik, G.K. Lahiri, A. Chakravorty, Inorg. Chem. 31 (1992) 40.
[15] (a) I.K. Adzamili, K. Libson, J.D. Lydon, R.C. Elder, E. Deutsch, Inorg. Chem. 18 (1979) 303;
(b) B.A. Lange, K. Libson, E. Deutsch, R.C. Elder, Inorg. Chem. 15 (1976) 2985.
[16] (a) S. Chakraborty, M.G. Walawalkar, G.K. Lahiri, J. Chem. Soc., Dalton Trans. (2000) 2875;
(b) B. Mondal, H. Paul, V.G. Puranik, G.K. Lahiri, J. Chem. Soc., Dalton Trans. (2001) 481.
[17] A.B.P. Lever, Inorganic Electronic Spectroscopy, 2nd ed., Elsevier, Amsterdam, 1984, p. 463.
[18] (a) J.C. Jeffery, E. Schatz, M.D. Ward, J. Chem. Soc., Dalton Trans. (1992) 1921;
(b) N. Maki, Bull. Chem. Soc. Jpn. 42 (1969) 2275.
[19] K.C. Kalia, A. Chakravorty, Inorg. Chem. 7 (1968) 2016.
[20] (a) D.A. Johnson, A.G. Sharpe, J. Chem. Soc. A (1966) 798;
(b) C.K. Jorgensen, Adv. Chem. Phys. 5 (1963) 33.
[21] C. Jubert, A. Mohamadou, J. Marrot, J.P. Barbier, J. Chem. Soc., Dalton Trans. (2001) 1230.
[22] K. Delany, S.K. Arora, P.K. Mascharak, Inorg. Chem. 27 (1988) 705.
[23] R.S. Nicholson, I. Sharin, Anal. Chem. 36 (1964) 706.

Available online at www.sciencedirect.com
SCIENCE DIRECT®
Polyhedron 23 (2004) 841–848
POLYHEDRON
www.elsevier.com/locate/poly

Cobalt(II) complexes of 2-methanol-, 2,6-dimethanol- and 2-ethanolpyridines: syntheses, spectroscopic, thermal and structural characterizations of $[Co_2(\mu\text{-}Cl)_2(mpy)_4]Cl_2 \cdot 2H_2O$, $[Co(dmpy)_2]Cl_2$ and $[Co(Cl)_4](Hpyet)_2$ (mpy = 2-methanolpyridine; dmpy = 2,6-dimethanolpyridine and Hpyet = 2-ethanolpyridinium)

Veysel T. Yilmaz [a,*], Sevim Hamamci [a], Carsten Thöne [b]

[a] Department of Chemistry, Faculty of Arts and Sciences, Ondokuz Mayis University, 55139 Kurupelit, Samsun, Turkey
[b] Institut für Anorganische und Analytische Chemie, Technische Universitat Braunschweig, Postfach 3329, 38023 Braunschweig, Germany

Received 15 October 2003; accepted 24 November 2003

Abstract

Cobalt(II) complexes of 2-methanol-, 2,6-dimethanol- and 2-ethanolpyridines have been prepared by the reaction of the corresponding protonated substituted pyridines with $[Co(sac)_2(H_2O)_4] \cdot 2H_2O$, where sac is saccharinate, and characterised by elemental analyses, IR, UV–Vis, magnetic measurements and single crystal X-ray diffraction. The corresponding 2-methanolpyridine (mpy) complex $[Co_2(\mu\text{-}Cl)_2(mpy)_4]Cl_2 \cdot 2H_2O$ is dimeric with chloro bridges and each cobalt(II) ion has an octahedral coordination with two chloro and two bidentate (N, O) ligands. In the 2,6-dimethanolpyridine (dmpy) complex $[Co(dmpy)_2]Cl_2$, dmpy exhibits a tripodal chelating coordination mode through the N and two hydroxyl O atoms forming a CoN_2O_4 chromophore. The protonated 2-ethanolpyridinium cation Hpyet serves as a non-coordinating, but hydrogen bonded counter ion in $[Co(Cl)_4](Hpyet)_2$. Based on the molecular structures, the electronic, IR spectra and thermal behavior of the complexes are discussed.
© 2003 Elsevier Ltd. All rights reserved.

Keywords: 2-Methanolpyridine; 2,6-Dimethanolpyridine; 2-Ethanolpyridinium; Cobalt(II) complexes; Crystal structures

1. Introduction

Several mixed ligand metal complexes of 2-methanolpyridine (mpy) [1–6], 2,6-dimethanolpyridine (dmpy) [6–10] and 2-ethanolpyridine (pyet) [11–16] have appeared in the literature. Among them, dmpy has received much attention. Mpy and pyet contain two donor sites, namely the py N and hydroxyl O atoms, and behave as chelating bidentate ligands, whereas dmpy acts as a tripodal ligand. These ligands usually form mononuclear complexes. In the case of zinc(II), two polynuclear complexes of mpy were reported [2]. In the protonated form, Hpyet acts as a monodentate ligand through the hydroxyl O atom [17] and it seems that protonation makes the N atom less basic.

In this paper, we report the synthesis, spectroscopic characterization, thermal reactivity and crystal structures of a binuclear cobalt(II) complex of mpy, $[Co_2(\mu\text{-}Cl)_2(mpy)_4]Cl_2 \cdot 2H_2O$ and mononuclear cobalt(II) complexes of dmpy, $[Co(dmpy)_2]Cl_2$, and pyet, $[Co(Cl)_4](Hpyet)_2$.

2. Experimental

2.1. Materials

All reagents were purchased from commercial sources and were used without further purification.

* Corresponding author. Tel.: +90-362-457-6020; fax: +90-362-457-6081.
E-mail address: vtyilmaz@omu.edu.tr (V.T. Yilmaz).

0277-5387/$ - see front matter © 2003 Elsevier Ltd. All rights reserved.
doi:10.1016/j.poly.2003.12.007

2.2. Preparation of metal complexes

About 1.0 mmol (0.53 g) $[Co(sac)_2(H_2O)_4]\cdot 2H_2O$ was dissolved in 30 cm^3 MeOH and mixed with 2.0 mmol of mpy.HCl (0.29 g), dmpy.HCl (0.35 g) and pyet.HCl (0.32 g) dissolved in 1 cm^3 water and stirred for 30 min at 60 °C. Crystals suitable for X-ray diffraction were grown by slow diffusion of ether into the reaction solution at room temperature (r.t.).

$[Co_2(\mu\text{-}Cl)_2(mpy)_4]Cl_2\cdot 2H_2O$: violet. Yield 85%. d.p. 75 °C ($C_{24}H_{32}O_6N_4Cl_4Co_2$ Calc.: C, 39.4; H, 4.4; N, 7.6. Found: C, 39.6; H, 4.2; N, 7.5%). $[Co(dmpy)_2]Cl_2$: pink. Yield 78%. d.p. 88 °C (Found: C, 41.0; H, 4.3; N, 7.0; $C_{14}H_{18}N_2O_4Cl_2Co$ Calc.: C, 41.2; H, 4.4; N, 6.9%) and $[Co(Cl)_4](Hpyet)_2$: blue. Yield 63%. m.p. 79 °C ($C_{14}H_{20}N_2O_2Cl_4Co$ Calc.: C, 37.4; H, 4.5; N, 6.2. Found: C, 37.5; H, 4.3; N, 6.3%).

2.3. Physical measurements

IR spectra were recorded on a Shimadzu FTIR-8900 spectrophotometer as KBr pellets in the frequency range 4000–300 cm^{-1}. Electronic spectra were measured on a Unicam UV2 in the 200–900 nm range. The elemental analyses (C, H and N contents) were performed on a Vario EL Elemental Analyser. Room temperature magnetic susceptibility measurements were carried out using a Sherwood Scientific MXI model Evans magnetic balance. Thermal analysis curves (TG, DTA and DTG) were obtained using a Rigaku TG8110 thermal analyzer in a static air atmosphere. A sample size of 5–10 mg was used.

2.4. X-ray structure determination

The intensity data of the cobalt(II) complexes were collected using a BRUKER SMART 1000 CCD area detector diffractometer (Mo–Kα radiation, $\lambda = 0.71073$ Å) at 133 K. The structures were solved by direct methods using SHELXS-97 [18] and refined by a full-matrix least-squares procedure (SHELXL-97) [19]. The mathematical removal of effects of severely disordered solvent in $[Co(dmpy)_2]Cl_2$ was performed by using the program SQUEEZE incorporated in PLATON [20,21]. All non-hydrogen atoms were refined with anisotropic parameters. Hydrogen atoms bonded to carbon were included using a riding model, while the hydroxyl hydrogen atoms have been refined freely. The details of data collection, refinement and crystallographic data are summarized in Table 1.

Table 1
Crystallographic data for $[Co_2(\mu\text{-}Cl)_2(mpy)_4]Cl_2\cdot 2H_2O$, $[Co(dmpy)_2]Cl_2$ and $[Co(Cl)_4](Hpyet)_2$

Compounds	$[Co_2(\mu\text{-}Cl)_2(mpy)_4]Cl_2\cdot 2H_2O$	$[Co(dmpy)_2]Cl_2$	$[Co(Cl)_4](Hpyet)_2$
Empirical formula	$C_{24}H_{32}O_6N_4Cl_4Co_2$	$C_{14}H_{18}N_2O_4Cl_2Co$	$C_{14}H_{20}N_2O_2Cl_4Co$
M_r	732.20	408.13	449.05
T (K)	133(2)	133(2)	133(2)
Radiation, λ (Å)	0.71073	0.71073	0.71073
Crystal system	triclinic	orthorhombic	triclinic
Space group	$P\bar{1}$	$Cmc2_1$	$P\bar{1}$
a (Å)	7.9154(6)	29.680(3)	8.3989(6)
b (Å)	9.5718(6)	12.9855(12)	8.8289(6)
c (Å)	11.1614(8)	9.3539(8)	14.4913(10)
α (°)	72.121(3)	90	94.739(3)
β (°)	70.460(3)	90	97.817(3)
γ (°)	76.231(3)	90	112.973(3)
V (Å^3)	749.77(9)	3605.1(6)	969.25(12)
Z	1	8	2
D_c (g/cm^3)	1.622	1.504	1.539
μ (mm^{-1})	1.507	1.267	1.444
$F(000)$	374	1672	458
Crystal size (mm)	$0.47\times0.32\times0.29$	$0.50\times0.34\times0.32$	$0.55\times0.41\times0.21$
θ range (°)	2.00–30.03	1.37–30.03	1.43–30.03
Index range (h, k, l)	−11/11, −13/13, −15/15	−41/41, −18/18, −13/13	−11/11, −12/12, −20/20
Reflections collected	14352	34464	18623
Independent reflections (R_{int})	4361 (0.0157)	5330 (0.0333)	5634 (0.0128)
Absorption correction	semi-empirical from equivalents	semi-empirical from equivalents	semi-empirical from equivalents
Maximum and minimum transmission	0.8622 and 0.6763	0.8622 and 0.6439	0.9281 and 0.7760
Data/restraints/parameters	4361/0/197	5330/7/228	5634/0/224
Goodness-of-fit on F^2	1.049	1.030	1.035
Final R indices [$I > 2\sigma(I)$]	0.0204	0.0251	0.0235
R indices (all data)	0.0214	0.0265	0.0254
Largest difference peak and hole (e Å^{-3})	0.445 and −0.303	0.590 and −0.292	0.393 and −0.229

3. Results and discussion

3.1. Synthesis

The aim of the work is to prepare cobalt(II) complexes of saccharinate (sac) with protonated mpy, dmpy and pyet. In order to achieve this goal, the protonated py's were reacted with $[Co(sac)_2(H_2O)_4]\cdot 2H_2O$ in solution. During the reaction, the protonated mpy and dmpy behaved as an acid and protonated the sac anions, forming neutral sacH, mpy and dmpy species. It is well known that sacH in the protonated form is very stable and cannot coordinate to metal ions. Therefore, the coordination sphere around cobalt(II) were filled by mpy and dmpy, resulting in $[Co_2(\mu\text{-}Cl)_2(mpy)_4]Cl_2\cdot 2H_2O$ and $[Co(dmpy)_2]Cl_2$ complexes. In the case of the protonated pyet (Hpyet), the sac ligands were replaced by the chloride ions and Hpyet acted as a counter ion, giving $[Co(Cl)_4](Hpyet)_2$.

$[Co_2(\mu\text{-}Cl)_2(mpy)_4]Cl_2\cdot 2H_2O$ is soluble in water at r.t. and also in hot MeOH and EtOH. $[Co(dmpy)_2]Cl_2$ and $[Co(Cl)_4](Hpyet)_2$ are soluble in water, MeOH and EtOH at r.t. All three complexes are non-hygroscopic and stable in air.

3.2. Spectral and magnetic properties

The most important IR bands of the complexes are listed in Table 2. The broad and intense bands between 3100 and 3380 cm^{-1} are due to the ν(OH) vibrations of the hydrogen bonded hydroxyl group and water molecules. The absorption band centered at 3175 cm^{-1} are characteristic of the ν(NH) vibration of the protonated pyet. The relatively weak absorption bands between 3000 and 2800 cm^{-1} are assigned to the ν(CH) vibrations. The ν(C=N) and ν(CC) vibrations appear in the frequency range 1630–1570 cm^{-1}as strong bands. The N-coordination of mpy and dmpy is also confirmed by the presence of medium bands at around 700 and 435 cm^{-1} due to in- and out-of-plane ring deformation of py [22].

The electronic spectra of the cobalt(II) complexes with mpy and dmpy exhibit a broad ligand field absorption band centered at 500 nm, whereas $[Co(Cl)_4](Hpyet)_2$ displays three distinct bands at 363, 520 and 666 nm due to d–d transitions.

The magnetic moments of the cobalt(II) complexes measured at r.t. clearly indicate that all three complexes are of high-spin type. $[Co_2(\mu\text{-}Cl)_2(mpy)_4]Cl_2\cdot 2H_2O$ has a magnetic moment value of μ_{eff} of 4.3 BM which is noticeably lower than that of the expected value (7.74 BM), indicating an antiferromagnetic interaction in the Co–Co pair. The $[Co(dmpy)_2]Cl_2$ and $[Co(Cl)_4](Hpyet)_2$ complexes have the magnetic moment values of 4.0 and 3.9 BM, respectively, which are similar to the spin-only values.

3.3. Thermal analysis

Thermal decomposition behavior of the complexes were followed up to 700 °C in a static atmosphere of air. Thermoanalytical data including temperature ranges, DTA_{max} and mass loss calculations are presented in Table 3. The suggested decomposition products are based on mass loss calculations. $[Co_2(\mu\text{-}Cl)_2(mpy)_4]Cl_2\cdot 2H_2O$ dehydrates between 35 and 145 °C with a two-step mass loss process and the first dehydration step in the temperature range 35–75 °C corresponds to the endothermic elimination of 0.5 mol of water molecules, while the rest of the lattice water molecules are removed at temperatures up to 145 °C. The experimental mass loss of 4.9% is the same as the calculated value. The degradation of the mpy ligands is a complicated process and takes place in the temperature range 145–515 °C with four endothermic DTA peaks (mass loss: found 58.2%, calc. 59.6%), leaving the $CoCl_2$ residue, which decomposes to Co_3O_4 at 675 °C. The total mass loss of all decomposition process is 82.1% (calc. 83.9%).

$[Co(dmpy)_2]Cl_2$ begins to decompose at 88 °C. The decomposition stage between 88 and 422 °C with two endothermic effects at 136 and 210 °C is related to removal of the two dmy ligands with a mass loss of 50.8% (calc. 51.1%). The resulting $CoCl_2$ intermediate decomposes to Co_3O_4 at 610 °C.

$[Co(Cl)_4](Hpyet)_2$ melts at 79 °C and begins to decompose at 180 °C. The thermal decomposition process of the complex is not easy to understand because of unclear decomposition steps. However, the first two endothermic DTA peaks at 214 and 362 °C peaks may be attributed to the removal of the pyet ligands, while

Table 2
Selected IR spectral data[a] for $[Co_2(\mu\text{-}Cl)_2(mpy)_4]Cl_2\cdot 2H_2O$, $[Co(dmpy)_2]Cl_2$ and $[Co(Cl)_4](Hpyet)_2$

Assignment	$[Co_2(\mu\text{-}Cl)_2(mpy)_4]Cl_2\cdot 2H_2O$	$[Co(dmpy)_2]Cl_2$	$[Co(Cl)_4](Hpyet)_2$
ν(OH)	3285sb	3300–3100sb	3380vs
ν(NH)			3175s
ν(CH)	2918w, 2804w	2877w, 2819vw	2998w, 2847w
ν(CN)	1610vs	1628vs	1609vs
ν(CC)	1569s	1589s	1582vs

[a] Frequencies in cm^{-1}. b, broad; w, very weak; vs, very strong; s, strong.

Table 3
Thermoanalytical data for the cobalt(II) complexes

Complex	Temperature range (°C)	DTA_{max} (°C)[a]	Mass loss (%)		Total mass loss (%)		Solid residue
			Found	Calculated	Found	Calculated	
$[Co_2(\mu\text{-}Cl)_2(mpy)_4]Cl_2 \cdot 2H_2O$	35–145	45(+), 117(+)	4.9	4.9			$[Co_2(\mu\text{-}Cl)_2(mpy)_4]Cl_2$
	145–515	212(+), 319(+), 407(+), 477(+)	58.2	59.6			$2CoCl_2$
	517–675	590(−)	19.0	19.4	82.1	83.9	Co_3O_4 (at 675 °C)
$[Co(dmpy)_2]Cl_2$	88–422	136(+), 210(+)	50.8	51.1			$CoCl_2$
	425–610	470(+), 566(−)	35.1	34.4	85.9	85.6	Co_3O_4 (at 610 °C)
$[Co(Cl)_4](Hpyet)_2$	1180–490	214(+), 362(+), 480(−)	54.9	54.8			$CoCl_2$
	490–610	556(−)	32.1	32.1	87.0	86.9	Co_3O_4 (at 610 °C)

[a] (+): Endothermic, (−): exothermic.

the exothermic DTA peak appearing as a shoulder at 480 °C may be due to formation and/or elimination of 2 mol of HCl. In the last stage, oxidization of $CoCl_2$ to Co_3O_4 takes place at 610 °C. The total experimental mass loss value of 87.0% agrees well with the calculated value 86.9%.

3.4. Description of crystal structures

3.4.1. $[Co_2(\mu\text{-}Cl)_2(mpy)_4]Cl_2 \cdot 2H_2O$

The molecular structure of the title complex with the atom labelling is shown in Fig. 1. The selected bond lengths and angles together with the hydrogen bonding geometry are collected in Table 4. The structure consists of two water molecules, two chloride anions and a $[Co_2(\mu\text{-}Cl)_2(mpy)_4]^{2+}$ unit. In the cation, each cobalt (II) ion is coordinated by two mpy ligands and two chloride anions in a highly distorted octahedral configuration of the $CoN_2O_2Cl_2$ type. Each neutral mpy ligand behaves

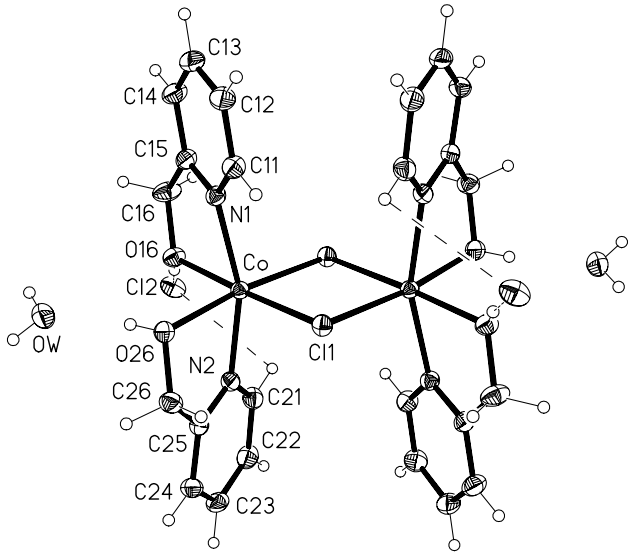

Fig. 1. Dimeric structure of $[Co_2(\mu\text{-}Cl)_2(mpy)_4]Cl_2 \cdot 2H_2O$ with the atom labelling scheme and 50% thermal ellipsoids.

Table 4
Selected bond and hydrogen bonding geometry for $[Co_2(\mu\text{-}Cl)_2(mpy)_4]Cl_2 \cdot 2H_2O$[a]

Bond lengths (Å) and angles (°)			
Co–N1	2.0988(8)	N1–Co–O26	90.38(3)
Co–N2	2.1004(8)	N2–Co–O26	77.56(3)
Co–O16	2.1209(7)	O16–Co–O26	92.33(3)
Co–O26	2.1224(8)	N1–Co–Cl1	101.00(2)
Co–Cl1	2.4620(3)	N(2)–Co–Cl(1)	93.43(2)
Co–$Cl1^{i}$	2.4212(3)	O26–Co–Cl1	87.91(2)
N1–Co–N2	160.87(3)	N1–Co–$Cl1^{i}$	95.30(2)
O16–Co–Cl1	176.92(2)	N2–Co–$Cl1^{i}$	97.80(3)
O26–Co–$Cl1^{i}$	173.36(2)	O16–Co–$Cl1^{i}$	92.40(2)
N1–Co–O16	75.92(3)	Cl1–Co–$Cl1^{i}$	87.617(9)
N2–Co–O16	89.62(3)	Co–Cl1–Co^{i}	92.383(9)

Hydrogen bonds D–H···A	*d*(D–H)	*d*(H···A)	*d*(D···A)	∠(DHA)
OW–HW1···$Cl2^{ii}$	0.80(2)	2.34(2)	3.1418(10)	176(1)
C24–H24···$Cl2^{iii}$	0.95	2.71	3.5372(11)	146
OW–HW2···$Cl2^{iv}$	0.80(2)	2.38(2)	3.1601(11)	169(1)
C22–H22···Cl^{v}	0.95	2.84	3.7588(12)	163
C12–H12···Cl^{vi}	0.95	2.89	3.8300(11)	169
C16–H16···Cl2	0.802(17)	2.204(17)	2.9969(8)	170(1)

[a] Symmetry operations: (i) $-x+1,-y,-z+1$; (ii) $x-1,y,z$; (iii) $-x+1,-y,-z$; (iv) $-x+1,-y+1,-z$; (v) $-x+2,-y,-z$; (vi) $x-1,y,z+1$.

as a bidentate ligand through the N and hydroxyl O atoms forming a five-membered chelate ring, while two of the chloride anions act as a bridge between two cobalt(II) ions and the others remain as counter ions.

The mean Co–N and Co–O bond distances are 2.10 and 2.12 Å, respectively, and are similar to those reported for the bis(mpy)cobalt(II) unit [4]. The Co–Cl bond distances are 2.4212(3) and 2.4620(3) Å. The *trans* bond angles range from 160.87(3)° to 176.92(2)° and the highest deviations in the *cis* bond angles occur at the bite angle of the mpy ligand, N1–Co–O16 [75.92(3)°], and at N1–Co–Cl1 [101.00(2)°] which reflects the highly distorted coordination geometry around the cobalt atom.

The py rings are planar and the OH group significantly deviates from the plane of the py ring. The dihedral angles between two py rings in the same coordination polyhedron is 63(5)°. The Co–Cl–Co^{i}–Cl^{i} bridge is also exactly planar. The Co···Co separation is 3.524 Å and indicates an intermetallic interaction. The crystal structure is stabilized by intermolecular hydrogen bonds involving water molecules, uncoordinated chloride anions and CH_2 and py H atoms as listed in Table 4. The H atoms of the water molecules form relatively strong hydrogen bonds with uncoordinated chloride anions and the $[Co_2(\mu\text{-}Cl)_2(mpy)_4]^{2+}$ units are connected through the hydrogen bonds between the uncoordinated Cl atoms and some H atoms of the py rings and CH_2 group creating a three-dimensional network as shown in Fig. 2.

3.4.2. *[Co(dmpy)$_2$]Cl$_2$*

The molecular structure of $[Co(dmpy)_2]Cl_2$ with the atom labelling is shown in Fig. 3. The selected bond lengths and angles are given in Table 5. In fact, the structure has a highly disordered and unidentifiable solvent, which was eliminated by using the program SQUEEZE incorporated in PLATON [20,21]. Although the structure has two chloride anions, Fig. 3 shows three chloride anions. This is because two chloride anions are occupying special positions (mirror planes) with an occupying factor of 0.5. The structure consists of two chloride anions and a $[Co(dmpy)_2]^{2+}$ cation, in which the cobalt(II) ion sits on the center of symmetry and is octahedrally coordinated by a pair of neutral dmpy molecules, constituting a CoN_2O_4 chromophore. Each dmpy ligand acts as a tripodal and tridentate ligand through the N and two hydroxyl O atoms, forming two five-membered symmetric chelate rings.

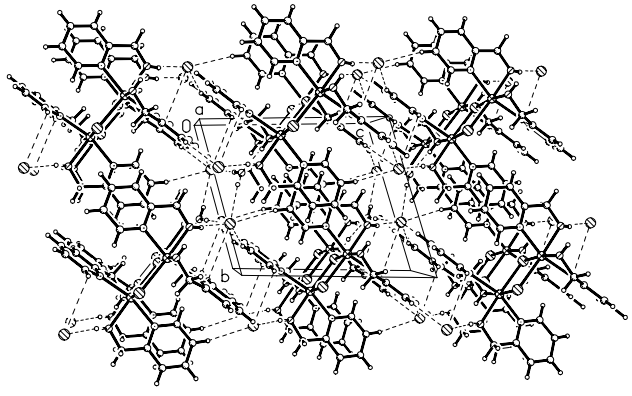

Fig. 2. Packing diagram of $[Co_2(\mu\text{-}Cl)_2(mpy)_4]Cl_2 \cdot 2H_2O$.

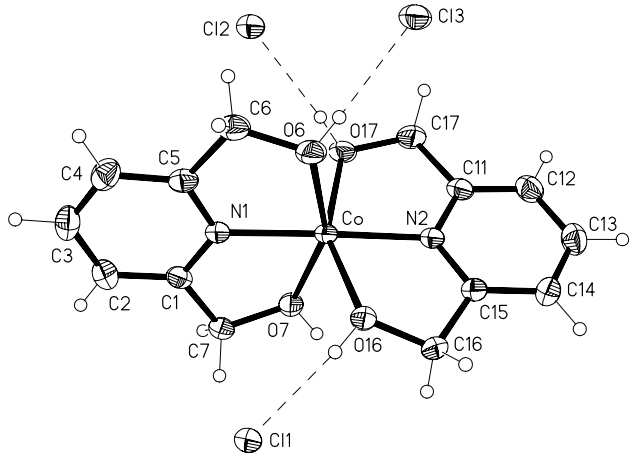

Fig. 3. Molecular structure of $[Co(dmpy)_2]Cl_2$ with the atom labelling scheme and 50% thermal ellipsoids.

The two Co–N bond distances are almost equivalent [2.0220(13) and 2.0241(13) Å], while the Co–O bond distances are in the range 2.1042(11)–2.1406(13) Å. Both Co–N and Co–O bond distances are comparable with those reported for the cobalt(II) complex of dmpy [5]. The Co–N bonds are somewhat shorter than the Co–O bonds and this results in the formation of a compressed distorted octahedral geometry along the Co–N bonds, since the N atoms occupy the axial positions and the O atoms constitute the equatorial plane of the CoN_2O_4 octahedron. Significant distortions in the coordination polyhedra are also deduced from the bond angles. The *trans* and *cis* angles are in the range of 153.20(5)°–177.42(5)° and 76.78(5)°–105.73(5)°. These distortions are presumably a consequence of the steric constraints imposed by the tripodal dmpy ligand.

A packing diagram of $[Co(dmpy)_2]Cl_2$ is shown in Fig. 4 and relevant hydrogen bonds are listed in Table 5. All the hydroxyl hydrogen atoms of the dmpy ligands are involved in hydrogen bonding with the chloride anions, which act as a bridge between the $[Co(dmpy)_2]^{2+}$ units as illustrated in Fig. 4. Additionally, the phenyl H atoms of py also form weak C–H···O and C–H···Cl interactions. The crystal packing of the title complex is determined by these hydrogen bonds forming a three-dimensional network.

3.4.3. *[Co(Cl)$_4$](Hpyet)$_2$*

The structure of the title complex comprises of a tetrachlorocobaltate(II) anion, $[Co(Cl)_4]^{2-}$ and two 2-

Table 5
Selected bond and hydrogen bonding geometry for $[Co(dmpy)_2]Cl_2$[a]

Bond lengths (Å) and angles (°)			
Co–N1	2.0220(13)	N2–Co–O6	105.73(5)
Co–N2	2.0241(13)	N2–Co–O7	100.66(5)
Co–O6	2.1406(13)	N2–Co–O16	76.71(5)
Co–O7	2.1042(11)	N2–Co–O17	77.08(5)
Co–O16	2.1206(11)	O6–Co–O7	153.60(5)
Co–O17	2.1260(14)	O6–Co–O16	92.85(5)
N1–Co–N2	177.42(5)	O6–Co–O17	88.92(5)
N1–Co–O6	76.83(5)	O7–Co–O16	93.99(4)
N1–Co–O7	76.78(5)	O7–Co–O17	96.21(5)
N1–Co–O16	103.60(5)	O161–Co–O17	153.20(5)
N1–Co–O17	102.84(5)		

Hydrogen bonds				
D–H···A	*d*(D–H)	*d*(H···A)	*d*(D···A)	∠(DHA)
O6–H6···Cl3	0.794(17)	2.219(17)	3.0117(14)	177(3)
O16–H16···Cl1	0.798(18)	2.179(18)	2.9753(12)	175(3)
O17–H17···Cl2	0.804(16)	2.208(17)	3.0103(13)	175(2)
C12–H12···Cl3[i]	0.95	2.74	3.6779(17)	168
C4–H4···Cl2[ii]	0.95	2.89	3.8011(17)	162
C4–H4···O17[ii]	0.95	2.60	3.314(2)	132
C4–H4···Cl2[iii]	0.95	2.89	3.8011(17)	162
C14–H14···Cl1[iv]	0.95	2.74	3.6287(17)	156
C2–H2···Cl1[v]	0.95	2.75	3.6376(17)	157
O7–H7···Cl1[vi]	0.815(17)	2.169(17)	2.9824(12)	177(3)

[a] Symmetry operations: (i) $-x,-y,z+1/2$; (ii) $x,-y+1,z-1/2$; (iii) $-x,-y+1,z-1/2$; (iv) $-x+1/2,y-1/2,z$; (v) $x,-y+1,z+1/2$; (vi) $-x+1/2,-y+1/2,z+1/2$.

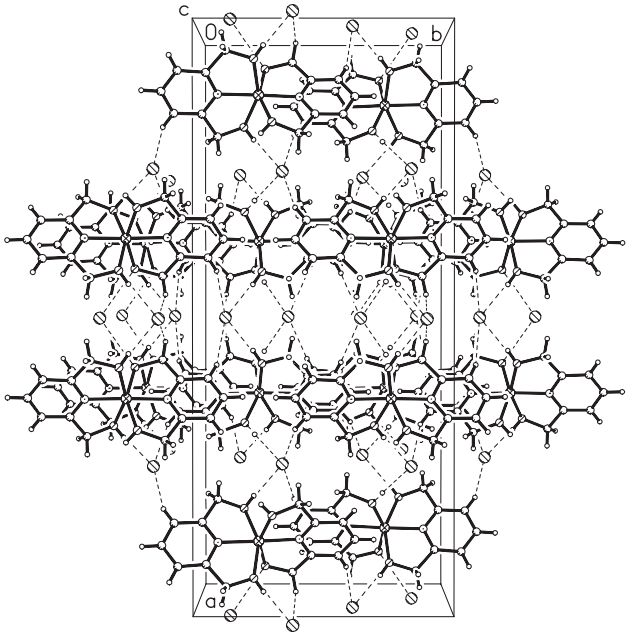

Fig. 4. Packing diagram of $[Co(dmpy)_2]Cl_2$.

ethanolpyridinium (Hpyet) cations as shown in Fig. 5. The geometry about the cobalt atom is essentially tetrahedral. The Co–Cl distances range from 2.2458(4) to 2.3150(3) Å (Table 6), while Cl–Co–Cl bond angles are between 101.921(13)° and 112.243(14)°. The largest differences in Co–Cl bond lengths and Cl–Co–Cl angles are 0.029 Å and 7.76°, respectively, and indicates a significant distortion in the coordination tetrahedron around the cobalt(II) ion. Bond distances and angles are similar to those of other tetrachlorocobaltate anions with protonated amines residing outside the coordination sphere [23].

The two crystallographically distinct, protonated 2-ethanolpyridinium cations serve as non-coordinating, but hydrogen bonded counter ions. As expected, protonation of 2-pyet takes place at the ring nitrogen. The bond lengths of the two independent pyridine rings do not differ significantly and are comparable with those reported for the coordinated Hpyet [17]. The py ring is planar and the ethanol group deviates from the respective pyridine ring plane.

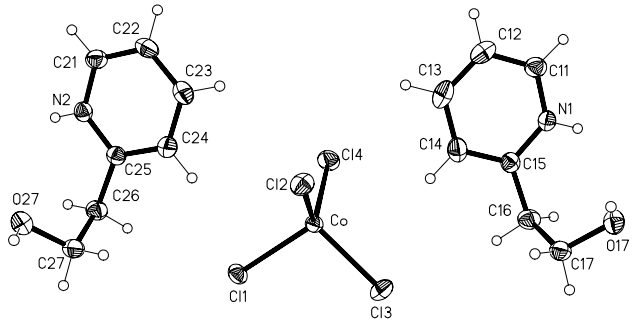

Fig. 5. Molecular structure of $[Co(Cl)_4](Hpyet)_2$ with the atom labelling scheme and 50% thermal ellipsoids.

Table 6
Selected bond and hydrogen bonding geometry for $[Co(Cl)_4](Hpyet)_2$[a]

Bond lengths (Å) and angles (°)				
Co–Cl1	2.3150(3)	Cl1–Co–Cl3	101.921(13)	
Co–Cl2	2.2668(3)	Cl1–Co–Cl4	110.609(13)	
Co–Cl3	2.2796(3)	Cl2–Co–Cl3	111.918(13)	
Co–Cl4	2.2458(4)	Cl2–Co–Cl4	110.337(14)	
Cl1–Co–Cl2	109.518(13)	Cl3–Co–Cl4	112.243(14)	
Hydrogen bonds				
D–H···A	*d*(D–H)	*d*(H···A)	*d*(D···A)	∠(DHA)
C17–H17B···Cl4^{i}	0.99	2.91	3.7782(13)	147
C11–H11···Cl4^{ii}	0.95	2.73	3.6287(14)	158
C16–H16A···Cl3^{iii}	0.99	2.88	3.6847(14)	140
C16–H16A···Cl4^{iii}	0.99	2.98	3.6861(14)	129
C26–H26B···Cl2^{iv}	0.99	2.99	3.5866(13)	120
C21–H21···Cl2^{v}	0.95	2.70	3.5811(13)	154
O27–H27C···Cl1^{vi}	0.86(2)	2.42(2)	3.2366(11)	157(1)
C22–H22···Cl1^{vii}	0.95	2.74	3.5674(13)	146
C12–H12···Cl3^{vii}	0.95	2.75	3.5664(14)	144
O17–H17C···Cl1^{viii}	0.78(2)	2.45(2)	3.1954(10)	160(2)
C11–H11···Cl4^{viii}	0.95	2.92	3.3568(13)	109
N2–H2···O27^{ix}	0.84(2)	1.97(2)	2.8043(14)	173(1)
N1–H1···O17^{x}	0.840(19)	1.916(19)	2.7461(14)	170(1)

[a] Symmetry operations: (i) $x+1, y+1, z$; (ii) $-x, -y+1, -z$; (iii) $-x+1, -y+1, -z$; (iv) $x, y-1, z$; (v) $x-1, y-1, z$; (vi)$-x+1, -y, -z+1$; (vii)$x-1, y, z$; (viii) $x, y+1, z$; (ix)$-x, -y-1, -z+1$; (x) $-x+1, -y+2, -z$.

The hydrogen bond geometry is given in Table 6 and the packing diagram of the complex is shown in Fig. 6. An extensive hydrogen-bonding network connects these ions. These Hpyet species interact by way of strong N–H···O hydrogen bonds with each other and form the O–H···Cl type of hydrogen bonds with the $[Co(Cl)_4]^{2-}$ units. Nine weak C–H···Cl interactions are also observed.

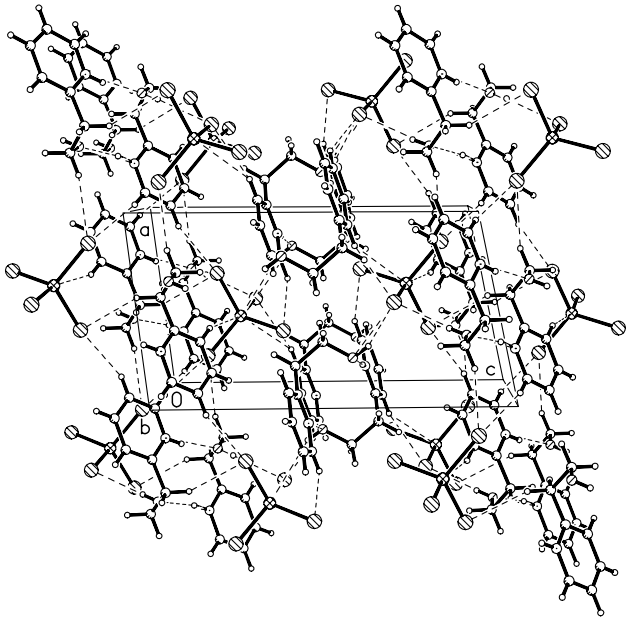

Fig. 6. Packing diagram of $[Co(Cl)_4](Hpyet)_2$.

4. Supplementary material

Crystallographic data for the structures reported in the paper have been deposited at the CCDC as supplementary data, CCDC Nos. 220827, 220828 and 220829 for $[Co(Cl)_4](Hpyet)_2$, $[Co(dmpy)_2]Cl_2$ and $[Co_2(\mu\text{-}Cl)_2(mpy)_4]Cl_2 \cdot 2H_2O$, respectively. Copies of the data can be obtained on application to CCDC, 12 Union Road, Cambridge CB2 1EZ, UK (fax: +44-1223-336033; E-mail: deposit@ccdc.cam.ac.uk or www: http://www.ccdc.cam.ac.uk).

Acknowledgements

This work was supported financially by Ondokuz Mays University. One of us (V.T.Y.) wishes to thank DAAD for the financial support given for his research visit to the Institut für Anorganische und Analytische Chemie of Technische Universität Braunschweig, Germany.

References

[1] N.N. Hoang, F. Valach, M. Dunaj-Jurco, M. Melnik, Acta Crystallogr., Sect. C 48 (1992) 443.
[2] M. Tesmer, B. Müller, H. Vahrenkamp, Chem. Commun. (1997) 721.
[3] V.T. Yilmaz, S. Guney, O. Andac, W.T.A. Harrison, Acta Crystallogr., Sect. C 58 (2002) m427.
[4] V.T. Yilmaz, S. Guney, O. Andac, W.T.A. Harrison, Polyhedron 21 (2002) 2393.

[5] O. Andac, S. Guney, Y. Topcu, V.T. Yılmaz, W.T.A. Harrison, Acta Crystallogr., Sect. C 58 (2002) m17.
[6] V.T. Yilmaz, S. Guney, C. Thöne, Z. Anorg. Allg. Chem. 628 (2002) 1406.
[7] M. Koman, M. Melnik, Polyhedron 16 (1997) 2721.
[8] N. Farfan, H. Hopfl, Heteroatom Chem. 9 (1998) 377.
[9] M. Koman, M. Melnik, J. Moncol, Inorg. Chem. Commun. 3 (2000) 262.
[10] V.T. Yilmaz, S. Guney, O. Andac, W.T.A. Harrison, J. Coord. Chem. 56 (2003) 21.
[11] S. Hamamci, V.T. Yilmaz, C. Thöne, Acta Crystallogr., Sect. E 58 (2002) m369.
[12] V.T. Yilmaz, S. Hamamci, C. Thöne, Cryst. Res. Technol. 37 (2002) 1143.
[13] S. Hamamci, V.T. Yilmaz, C. Thöne, Acta Crystallogr., Sect. E 58 (2002) m700.
[14] V.T. Yilmaz, S. Hamamci, C. Thöne, Acta Crystallogr., Sect. E 58 (2002) m702.
[15] V.T. Yilmaz, S. Hamamci, C. Thöne, Z. Anorg. Allg. Chem. 629 (2003) 711.
[16] V.T. Yilmaz, S. Hamamci, C. Thöne, J. Coord. Chem. 56 (2003) 787.
[17] V.T. Yilmaz, C. Kazak, S. Hamamci, Z. Anorg. Allg. Chem. 629 (2003) 2013.
[18] G.M. Sheldrick, Acta Crystallogr., Sect. A 46 (1990) 467.
[19] G.M. Sheldrick, SHELXL-97, Program for the Refinement of Crystal Structures, University of Göttingen, Göttingen, Germany, 1997.
[20] A.L. Spek, Acta Crystallogr., Sect. A 46 (1990) C34.
[21] P. van der Sluis, A.L. Spek, Acta Crystallogr., Sect. A 46 (1990) 194.
[22] K. Nakamoto, Infrared and Raman Spectra of Inorganic and Coordination Compounds. Part B, 5th ed., Wiley, New York, 1997, p. 23.
[23] J.M. Land, R.G. Baughman, C.A. Hester, Acta Crystallogr., Sect. C 53 (1997) IUC9700016.

Available online at www.sciencedirect.com
SCIENCE DIRECT®
Polyhedron 23 (2004) 849–855
POLYHEDRON
www.elsevier.com/locate/poly

Synthesis and characterization of copper(II) Schiff base complexes derived from salicylaldehyde and glycylglycylglycine ☆

Wen-Long Liu [a], Yang Zou [a], Chun-Lin Ni [a], Zhao-Ping Ni [a], Yi-Zhi Li [a], Yuan-Gen Yao [b], Qing-Jin Meng [a,*]

[a] *Coordination Chemistry Institute, State Key Laboratory of Coordination Chemistry, Department of Chemistry, Nanjing University, 22 Hankou Road, Nanjing 210093, PR China*

[b] *State Key Laboratory of Structural Chemistry, Fujian Institute of Research on the Structure of Matter, Fuzhou 350002, PR China*

Received 7 August 2003; accepted 24 November 2003

Abstract

Two copper(II) tripeptide Schiff base complexes: $[Mg(H_2O)_6][CuL]_2 \cdot 3.5H_2O$ (**1**) and $[Cd(H_2O)_4(CuL)_2] \cdot 3.5H_2O$ (**2**) (H_3L = *N*-salicylideneglycylglycylglycine) have been synthesized and structurally characterized. Single crystal X-ray diffraction analyses showed that the copper atom exhibits square-planar geometry, with the chelating ONNO atoms of the deprotonated Schiff base ligand(L) in the basal plane. In **1**, the anions $[CuL]^-$ and cations $[Mg(H_2O)_6]^{2+}$ are stacked in well-separated columns along the *a*-axis. In **2**, two symmetric $[CuL]^-$ groups coordinate to Cd(II) at an inversion center, each via one carboxylate oxygen atom, to form a heterotrinuclear complex. Variable-temperature magnetic susceptibility measurements revealed the occurrence of an antiferromagnetic interaction in **1** and **2**.
© 2003 Elsevier Ltd. All rights reserved.

Keywords: Copper complexes; Schiff base complexes; Tripeptide complexes

1. Introduction

Transition metal *N*-salicylideneamino acid Schiff base complexes may serve as non-enzymatic models for pyridoxal-amino acid systems, which are of considerable importance as key intermediates in many metabolic reactions of amino acids catalysed by enzymes which require pyridoxal as a cofactor [1–4]. Besides, the complexes of amino-acid Schiff base ligands are considered to constitute a new kind of potential antibacterial and anticancer agent [5–7]. Considerable effort has been devoted to the preparation and structural characterization of Schiff base Cu(II) complexes derived from salicylaldehyde and amino acids [8–21] and reduced salicylidene amino acids [22–24]. However, little attention has been paid to systems in which the Schiff bases are derived from simple peptides [25,26], especially tripeptides, and few such compounds have been synthesized and structurally characterized.

Here, we report the synthesis of two new Schiff base copper(II) complexes with *N*-salicylidene tripeptides. Moreover, the first X-ray structures of mononuclear and carboxylate-bridged trinuclear Schiff base complexes derived from salicylaldehyde and glycylglycylglycine are described.

2. Experimental

2.1. Reagents and physical measurements

The tripeptide, glycylglycylglycine was purchased from Sigma and used without further purification. All other reagents and solvents were purchased from commercial sources and were analytical grade.

☆ Supplementary data associated with this article can be found, in the online version, at doi:10.1016/j.poly.2003.11.049.

* Corresponding author. Tel.: +86-25-3685429/3597266; fax: +86-25-3314502.
E-mail address: mengqj@netra.nju.edu.cn (Q.-J. Meng).

0277-5387/$ - see front matter © 2003 Elsevier Ltd. All rights reserved.
doi:10.1016/j.poly.2003.11.049

The IR spectra were recorded on KBr discs on a Bruker Vector 22 spectrophotometer in the 400–4000 cm^{-1} region. The UV–Vis spectra were recorded with a Shimadzu UV-3100 spectrophotometer. Elemental analyses (C, H, N) were obtained using a Perkin–Elmer 240C elemental analysis instrument. Metallic elements (K, Cu, Cd, Mg) were analyzed using a Perkin–Elmer M2100 atomic absorption spectrophotometer. Electrospray mass spectra were recorded on a LCQ system (Finnigan MAT, USA) using methanol/water as the mobile phase. All ESR spectra were recorded on a Bruker JES-FEIXG spectrometer with the X-band. Variable-temperature magnetic susceptibilities were performed on a CAHN-2000 Faraday balance from 75 to 300 K. Diamagnetic correction for the constituent atoms was made using Pascal's constants.

2.2. Synthesis

2.2.1. Synthesis of the triglycine Schiff base potassium salt ($KH_2L \cdot 1.5H_2O$) (H_3L = N-salicylideneglycylglycylglycine)

Glycylglycylglycine (0.95 g, 5 mmol) was dissolved in 40 cm^3 of aqueous methanol (1:2 by volume mixture) containing KOH (0.28 g, 5 mmol). A solution of salicylaldehyde (0.61 g, 5 mmol) in 10 cm^3 absolute methanol was added dropwise with stirring on a water bath at 35–40 °C for 2 h. The volume of the yellow solution was reduced in vacuo using a rotary evaporator to ca. 5 cm^3. Anhydrous ether was added to deposit a yellowish precipitate, which was then recrystallized from EtOH. Yield: 1.61 g (92%). *Anal.* Calc. for $K(C_{13}H_{14}N_3O_5) \cdot 1.5H_2O$: C, 44.6; H, 4.9; N, 12.0; K, 11.2. Found: C, 44.1; H, 5.2; N, 11.8; K, 11.0%.

2.2.2. Synthesis of Cu(II) Schiff base complex ($K[CuL] \cdot 2H_2O$)

Copper(II) acetate monohydrate (0.40 g, 2 mmol) was dissolved in 10 cm^3 of water. The solution was filtered and added dropwise into 25 cm^3 methanol solution of the triglycine Schiff base potassium salt (0.70 g, 2 mmol). The resulting mixture was adjusted to pH 8–9 with concentrated KOH solution and stirred at 35–40 °C for 2 h, then filtered. The filtrate was concentrated in vacuo using a rotary evaporator to ca. 5 cm^3. The purple product was deposited by adding a large quantity of ethanol with vigorous stirring, recrystallized from water/ethanol, and dried in vacuo at 35 °C over P_2O_5. Yield: 1.88 g (88%). *Anal.* Calc. for $K[Cu(C_{13}H_{12}N_3O_5)] \cdot 2H_2O$: C, 36.40; H, 3.76; N, 9.80; K, 9.12; Cu, 14.82. Found: C, 36.42; H, 3.78; N, 9.75; K, 9.10; Cu, 14.78%. IR (KBr, cm^{-1}): 3381s, 1642s, 1599s, 1551m, 1385m, 1298m. ESI-MS: m/z 353.1 $[CuL]^-$.

2.2.3. Synthesis of Cu(II)–M(II) (M = Mg, Cd) Schiff bases complexes

*2.2.3.1. $[Mg(H_2O)_6][CuL]_2 \cdot 3.5H_2O$ (**1**).* $K[CuL] \cdot 2H_2O$ (1 mmol) was dissolved in 20 cm^3 of H_2O and then filtered. $MgSO_4$ (0.5 mmol) was added to the filtrate with stirring at 25 °C for half an hour. A violet precipitate was obtained, which was recrystallized from hot water (90 °C). The filtrate was allowed to evaporate slowly at room temperature. After several days violet red crystals, which were suitable for X-ray diffraction, were obtained. *Anal.* Calc. for $C_{26}H_{43}N_6O_{19.50}MgCu_2$: C, 34.58; H, 4.80; N, 9.31; Cu, 14.07; Mg, 2.69. Found: C, 34.39; H, 4.88; N, 9.25; Cu, 14.00; Mg, 2.56%. IR (KBr, cm^{-1}): 3417s, 1649s, 1620s, 1544m, 1397m, 1291m.

*2.2.3.2. $[Cd(H_2O)_4(CuL)_2] \cdot 3.5H_2O$ (**2**).* Complex **2** was obtained in similar manner by replacing $MgSO_4$ with $Cd(NO_3)_2 \cdot 6H_2O$. *Anal.* Calc. for $C_{26}H_{39}N_6O_{17.50}CdCu_2$: C, 32.70; H, 4.12; N, 8.80; Cu, 13.31; Cd, 11.77. Found: C, 32.56; H, 4.20; N, 8.66; Cu, 13.11; Cd, 11.52%. IR (KBr, cm^{-1}): 3424s, 1647s, 1600s, 1543m, 1391m, 1303m.

2.3. X-ray crystallography

The diffraction experiments were carried out on a Bruker AXS SMART APEX CCD diffractometer. The structure was solved by direct methods using SHELXTL [27]. All non-hydrogen atoms were refined with anisotropic thermal displacement parameters. Hydrogen atoms were included in the refinement in calculated positions riding on their carrier atoms. A summary of the data collection and structure refinement is listed in Table 1.

3. Results and discussion

3.1. Crystal structure of **1**

An ORTEP plot with non-hydrogen atomic labelling is shown in Fig. 1(a). Selected bond distances and angles are listed in Table 2. The asymmetric unit consists of one $[Mg(H_2O)_6]^{2+}$, two $[CuL]^-$ groups and 3.5 water molecules. The coordination environment of each Cu(II) center is approximately square-planar. The Schiff base ligand is deprotonated, thus acting as a triple negatively charged quadridentate ONNO chelate. The ligand is coordinated to the Cu(II) atom via one phenolic oxygen (Cu(1)–O(1) = 1.851(3) Å, Cu(2)–O(6) = 1.864(3) Å), one imino nitrogen atom (Cu(1)–N(1) = 1.924(3) Å, Cu(2)–N(4) = 1.922(3) Å), one deprotonated amide nitrogen atom (Cu(1)–N(2) = 1.887(3) Å, Cu(2)–N(5) = 1.881(3) Å) and one carbonyl oxygen atom (Cu(1)–

Table 1
Crystal data and structure refinement

	$[Mg(H_2O)_6][CuL]_2 \cdot 3.5H_2O$ (**1**)	$[Cd(H_2O)_4\ (CuL)_2] \cdot 3.5H_2O$ (**2**)
Empirical formula	$C_{26}H_{43}N_6O_{19.50}MgCu_2$	$C_{26}H_{39}N_6O_{17.50}CdCu_2$
Formula weight	903.07	955.11
Crystal system	triclinic	triclinic
Space group	$P\bar{1}$	$P\bar{1}$
Unit cell dimensions		
a (Å)	7.222(1)	7.637(2)
b (Å)	16.175(2)	10.495(2)
c (Å)	17.205(3)	12.462(3)
α (°)	98.83(1)	93.96(1)
β (°)	96.05(1)	96.65(1)
γ (°)	95.06(1)	100.40(1)
V (Å^3)	1963.8(5)	971.7(4)
Z	2	1
D_{calc} (Mg m^{-3})	1.527	1.632
μ(Mo Kα) (cm^{-1})	1.182	1.703
λ(Mo Kα) (Å)	0.71073	0.71073
T (K)	293(2)	293(2)
$F(000)$	934.0	483.0
Crystal size (mm)	$0.3 \times 0.20 \times 0.20$	$0.20 \times 0.15 \times 0.15$
θ range for data collection (°)	1.9 to 25.0	2.7 to 25.0
Index ranges	$-8 \leqslant h \leqslant 8,\ -19 \leqslant k \leqslant 19,\ 0 \leqslant l \leqslant 20$	$-8 \leqslant h \leqslant 9,\ -10 \leqslant k \leqslant 12,\ -14 \leqslant l \leqslant 13,$
Reflections collected	9859	4626
Independent reflections	6804	3341
Refinement method	full-matrix least-squares on F^2	
Data/restraints/parameters	6804/0/499	3341/0/253
R_{int}	0.0374	0.0648
R_1 [$I > 2(I)$]	0.0478	0.0556
wR_2	0.1426	0.1659
Goodness-of-fit on F^2	1.039	1.020
Largest difference: peak and hole (e Å^{-3})	0.99 and −0.44	1.02 and −0.51

O(3) = 1.989(3) Å, Cu(2)–O(8) = 2.002(3) Å. The carbonyl oxygen atoms O(3) and O(8) are here preferred to the peptide nitrogen atoms N(3) and N(6) as metal-binding sites at pHs where the amide proton of the peptide is not dissociated, as have been reported in the tripeptide complexes of Cu(gly-gly-gly)$^+$ [28], Cu(gly-leu-tyr)$^+$ [29], $[Ru(glyglyglyH_{-1})(PPh_3)]_2$ [30] and $[ReO(MECG_2H_2)]_2$ ($MECG_2H_5$ = mercaptoethyl-carbamoyl-methyl-glycylglycine) [31]. The distance from Cu(II) to the deprotonated amide nitrogen atom is shorter than the distance to the imino nitrogen atom. The distance from Cu(II) to the phenolic oxygen is shorter than the distance to the carbonyl oxygen. A slight distortion in the square-planar geometry of Cu(II) is present (observed bond angles vary from 83.1(1)° and 96.9(1)°). The values 1.495(5) Å for the C(8)–N(1) bond and 1.464(6) Å for the N(4)–C(21) bond, shorter than the usual C–N single bond, and 1.249(5) and 1.270(5) Å for the double bonds C(7)–N(1) and N(4)–C(20) are in good agreement with the values of Schiff base type I [32]. The phenyl ring [C(1)–C(6)] and the chelate ring C(1), C(6), C(7), N(1), O(1), Cu(1) make a small dihedral angle of 3.4°, and the phenyl ring [C(14)–C(19)] and the chelate ring C(14), C(19), C(20), N(4), O(6), Cu(2) make a small dihedral angle of 2.4°, suggesting a large π-electron delocalization. The two $[CuL]^-$ groups have alternate spatial arrangements and their Cu chelate planes are almost parallel with a small dihedral angle of 1.2°, where the distance between two neighboring copper(II) ions is 4.67 Å. The Mg(II) center is almost octahedrally coordinated by six aqua ligands. The six Mg–O bonds in the structure are in the range 2.05–2.10 Å.

One of the structural features of **1** is that the anions and cations are stacked in well-separated columns along the a-axis (Fig. 1(b)). Within each anionic columns, the $[CuL]^-$ anions form a chain with alternate spacings. The Cu···Cu distance is 4.67 and 6.16 Å within the $[CuL]^-$ anion chain. The closest Cu···Cu separation between anion chains is 9.89 Å, which is significantly longer than the Cu separation within a chain.

The presence of intermolecular and intramolecular hydrogen bonds plays an important role in the stabilization of the whole structure. These are formed between the N–H of the amide nitrogen in one $[CuL]^-$ group and the carboxylate oxygen of another $[CuL]^-$ group, between the O–H of $[Mg(H_2O)_6]^{2+}$ and water molecules, between the O–H of a water molecule and a phenolic oxygen atom of $[CuL]^-$, between the O–H of a water molecule and a carbonyl oxygen atom of $[CuL]^-$, and between adjacent water molecules. The presence of

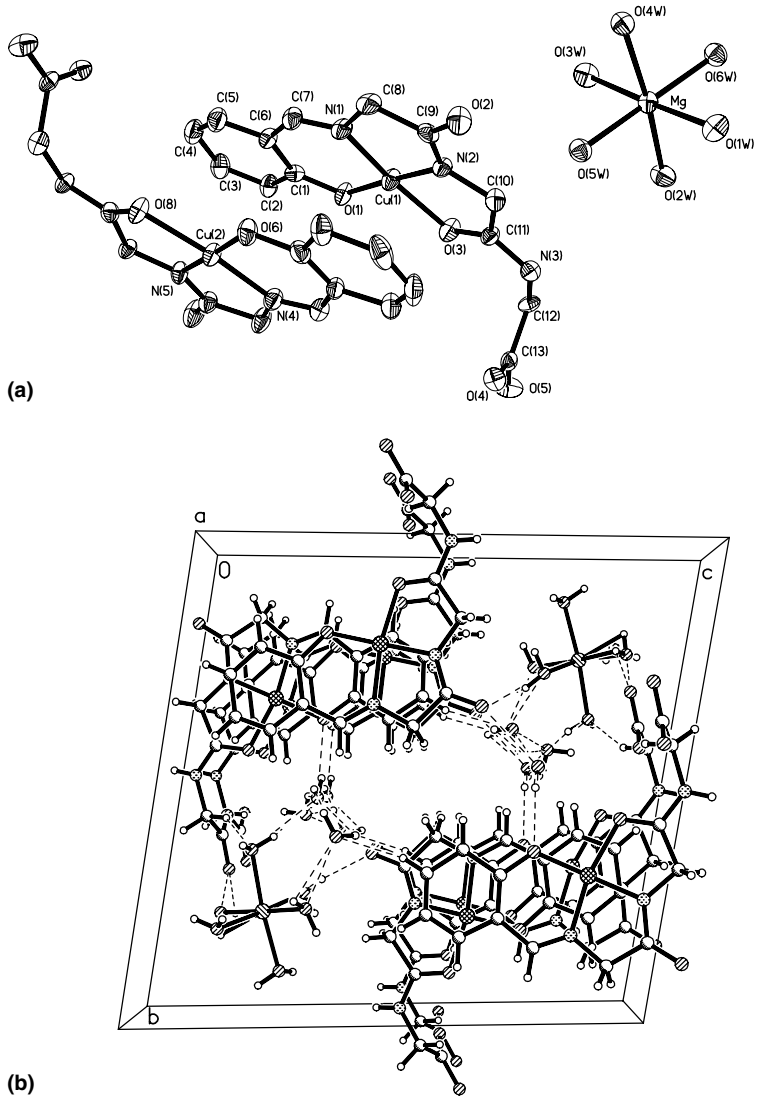

Fig. 1. (a) ORTEP view of **1** with hydrogen atoms and lattice water molecules omitted for clarity. Thermal ellipsoids are drawn at the 35% probability level. (b) The packing diagram of a unit cell of **1** along the *a*-axis.

water molecules and their bridging role with respect to the $[CuL]^-$ and $[Mg(H_2O)_6]^{2+}$ columns allow for the generation of a 3-D hydrogen-bonded network.

The $[CuL]^-$ ligand does not coordinate to the metal ion Mg^{2+} in **1** wherein the Mg^{2+} ion preferentially binds to water molecules, in the form of $[Mg(OH_2)_6]^{2+}$.

3.2. Crystal structure of *2*

Compound **2** consists of a neutral centrosymmetric trinuclear moiety and 3.5 lattice water molecules (Fig. 2(a)). The coordination environment at each Cu(II) center is similar to that in **1**. Selected bond distances and bond angles are given in Table 3.

Comparing with the Mg(II) ion in **1**, the charge–radius ratio of the Cd(II) ion in **2** is higher and Cd(II) is softer than Mg(II). Thus, the Mg(II) ion preferentially binds to harder water molecules in the form of $[Mg(OH_2)_6]^{2+}$ and Cd(II) is propitious to the formation of a bridged polynuclear compound [33,34]. In **2**, each $[CuL]^-$ group coordinates to the Cd(II) center via one carboxylate oxygen atom (O(4)) in a *syn–anti* bridging mode. The Cd(II) center is approximately octahedrally coordinated by two carboxylate oxygens (O(4) and O(4a)) and four aqua ligands.

The most pronounced feature of the crystal structure is the column stacking along the *a*-axis with the $[CuL]^-$ moieties organized in interlaced arrays. The interaction between copper(II) ions and the imino nitrogen atom of an adjacent $[CuL]^-$ group [Cu(II)–N(1A) = 3.301 Å] plays a very important role in the packing scheme. The distance between two copper(II) ions is 3.422 Å. The N(3A)–H proton and one H atom of the ligand water O(7D) hydrogen bond to the carbonyl oxygen atom O(2C) of adjacent $[CuL]^-$ groups to form a 2-D hydrogen-bonded network in the *ab*-plane (Fig. 2(b)).

Table 2
Selected bond distances (Å) and angles (°) for **1**

Bond lengths			
Cu1–O1	1.851(3)	Cu2–O6	1.864(3)
Cu1–O3	1.989(3)	Cu2–O8	2.002(3)
Cu1–N1	1.924(3)	Cu2–N4	1.922(3)
Cu1–N2	1.887(3)	Cu2–N5	1.881(3)
Mg–O1W	2.066(3)	Mg–O4W	2.098(3)
Mg–O2W	2.073(3)	Mg–O5W	2.052(3)
Mg–O3W	2.085(3)	Mg–O6W	2.059(3)
Bond angles			
O1–Cu1–O3	96.2(1)	O6–Cu2–O8	96.9(1)
O1–Cu1–N1	96.4(1)	O6–Cu2–N4	96.2(1)
O3–Cu1–N2	83.1(1)	O8–Cu2–N5	82.6(1)
N1–Cu1–N2	84.2(1)	N4–Cu2–N5	84.2(1)
O2W–Mg–O5W	90.7(1)	O3W–Mg–O5W	92.1(1)
O2W–Mg–O6W	91.3(1)	O3W–Mg–O6W	90.6(1)
O2W–Mg–O3W	88.2(1)	O4W–Mg–O5W	86.2(1)
O4W–Mg–O6W	92.0(1)	O1W–Mg–O5W	89.2(1)
O1W–Mg–O4W	90.6(1)	O1W–Mg–O6W	88.1(1)
O3W–Mg–O4W	87.7(1)	O1W–Mg–O2W	93.6(1)

Table 3
Selected bond distances (Å) and angles (°) for **2**

Bond lengths			
Cu–O1	1.877(5)	Cu–N1	1.932(5)
Cu–O3	2.005(4)	Cu–N2	1.890(5)
Cd–O6	2.315(6)	Cd–O4	2.291(5)
Cd–O7	2.262(5)		
Bond angles			
O1–Cu–O3	97.50(2)	O3–Cu–N2	82.8(2)
O1–Cu–N1	96.2(2)	N1–Cu–N2	83.4(2)
O6–Cd–O7	88.5(2)	O7–Cd–O4	90.5(2)
O6–Cd –O4	91.3(2)		

Symmetry transformations used to generate equivalent atoms: $(-x+1, -y+1, -z+2)$.

In **2**, the N(3)–H proton and the H atoms of two ligand water (O(6), O(7)) and one lattice water (O(8w)) molecules participate in hydrogen bonding. The two H atoms from the ligand water O(6) are all hydrogen bonded to the lattice water oxygen O(8w). Two H atoms from O(8w) are hydrogen bonded to the carbonyl oxygen atom O(2) and the carboxylate oxygen O(4) from another $[CuL]^-$ group, respectively. The hydrogen atom from C(3) in phenyl ring bonds to the carboxylate oxygen O(5) from an adjacent $[CuL]^-$ group forming

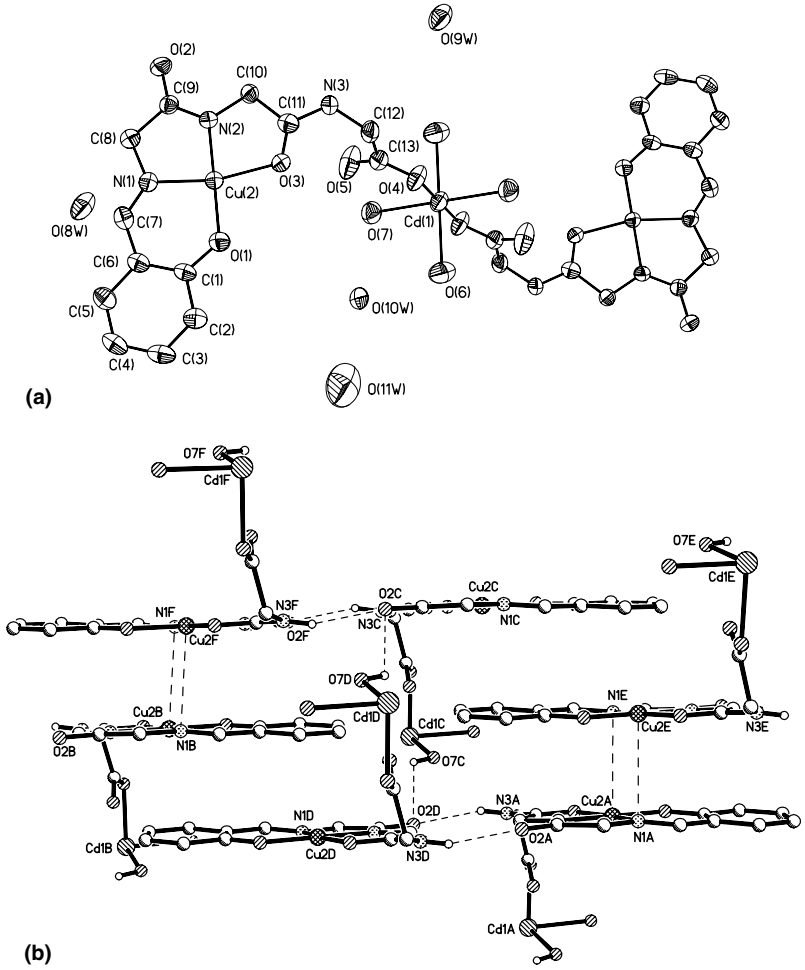

Fig. 2. (a) ORTEP view of **2**, with hydrogen atoms omitted for clarity. Thermal ellipsoids are drawn at the 35% probability level, (b) A view of the packing of **2** along the *c*-axis.

a weak hydrogen bond with the distances C(3)···O(5) = 3.422(9) Å and H···O(5) = 2.58 Å, which is similar to reported values [35,36]. The presence of these intramolecular and intermolecular hydrogen-bondings is an important factor in the stabilization of the whole structure, which allows the compound to form a 3-D network structure.

3.3. Infrared spectra

The infrared spectra of the two compounds show strong typical absorptions at 1649 (**1**) and 1647 cm^{-1} (**2**) related to the ν(C=N) Schiff base imino group. The ν_{as}(COO) is assigned to the strong bands at 1620 (**1**) and 1600 cm^{-1} (**2**) whereas the ν_s(COO) is attributed to the 1397 (**1**) and 1391 cm^{-1} (**2**) peaks. Medium bands present at 1544 (**1**) and 1543 cm^{-1} (**2**) may originate from the vibration of the (Ph–)C–C(=N) bond [37]. Medium bands at 1291 (**1**) and 1303 cm^{-1} (**2**) probably correspond to ν(O–Ph). Both compounds exhibit a broad band in the 3000–3500 cm^{-1} region, which may be ascribed to hydrogen-bonded ν(O–H) and/or ν(N–H), and may also include ν(C–H).

3.4. Electronic spectra

The UV absorption bands observed at 352 (**1**) and 364 nm (**2**) in the two compounds are assigned to the imino n–π^* transitions. The d–d transition spectra of the complexes show broad bands centered at 587 (**1**) and 590 nm (**2**), being suggestive of approximate square-planar geometry at Cu.

3.5. Magnetic properties and ESR spectra

The molar magnetic susceptibility χ_m versus T for each compound shows an antiferromagnetic interaction (Fig. 3). The data for the two compounds have been

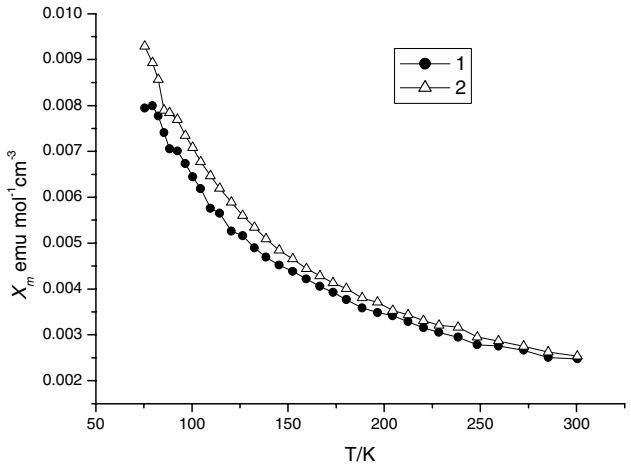

Fig. 3. Temperature dependence of χ_m for **1** (•), **2** (△).

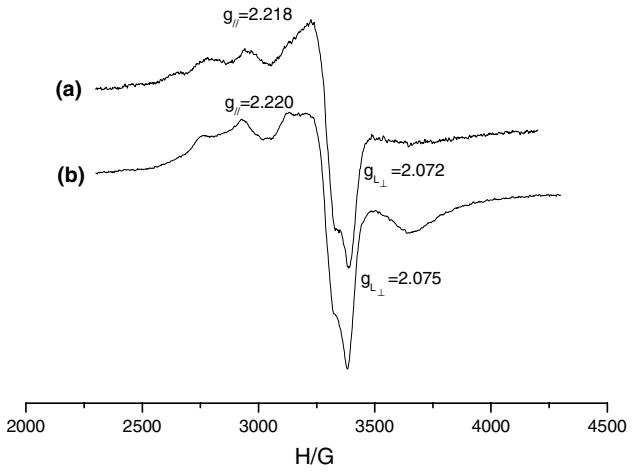

Fig. 4. Experimental ESR spectra of **1** (a) and **2** (b) taken in DMSO at 110 K.

successfully fitted to the Curie–Weiss law ($1/\chi_m = (T-\theta)/C$) (**1**, $C = 0.735$ emu K mol^{-1}, $\theta = -14.430$ K; **2**, $C = 0.734$ emu K mol^{-1}, $\theta = -3.402$ K). The effective magnetic moments are in accordance with diluted monomeric units at 300 K (**1**, $\mu_{eff} = 2.44$ BM; **2**, $\mu_{eff} = 2.47$ BM).

The ESR spectra of **1** and **2** at 110 K in DMSO are shown in Fig. 4. The trends $g_{||}(2.218) > g_\perp(2.072) > g_e(2.0023)$ observed for **1**, $g_{||}(2.220) > g_\perp(2.075) > g_e(2.0023)$ observed for **2** indicate a d(x^2–y^2) ground state. Kivelson and Neiman have shown that $g_{||}$ is a moderately sensitive function for indicating covalence. Relatively speaking, $g_{||} > 2.3$ is characteristic of an ionic environment and $g_{||} < 2.3$ of a covalent environment in M–L bonding [38]. In the present compounds $g_{||}$ indicates a fair degree of covalent character in the Cu–L bonding.

4. Supplementary material

Crystallographic data for the structural analysis have been deposited with the Cambridge Crystallographic Data Centre, CCDC Nos. 213115 for compound **1**, 213114 for compound **2**. Copies of this information may be obtained free of charge from The Director, CCDC, 12 Union Road, Cambridge, CB2 1EZ, UK (fax: +/44-1223-336033; email: deposit@ccdc.cam.ac.uk or www: http://www.ccdc.cam.ac.uk).

Acknowledgements

This work was supported financially by the National Natural Science Foundation of China (No. 20171022, No. 29831010), The Science & Technology Department

of Jiangsu Province, and The Center of Materials Analysis of Nanjing University.

References

[1] R.F. Zabinski, M.D. Toney, J. Am. Chem. Soc. 123 (2001) 193.
[2] S.D. Wetmore, D.M. Smith, L. Radom, J. Am. Chem. Soc. 123 (2001) 8678.
[3] Y. Bkouche-Waksman, J.M. Barbe, A. Kvick, Acta Crystallogr., Sect. B 44 (1988) 595.
[4] J. Kratamar-Smogrovic, M. Blahova, V. Kettmann, Chirality 3 (1991) 503.
[5] T.M. Aminabhavi, N.S. Biradar, S.B. Patil, V.L. Roddabasanagoudar, Inorg. Chim. Acta 107 (1985) 231.
[6] G. Plesch, C. Friebel, O. Svajlenova, J. Kratsmar-Smogrovic, D. Mlynarcik, Inorg. Chim. Acta 151 (1988) 139.
[7] D. Sattari, E. Alipour, S. Shriani, J. Amighian, J. Inorg. Biochem. 45 (1992) 115.
[8] C. Gruning, H. Schmidt, D. Rehder, Inorg. Chem. Commun. 2 (1999) 57.
[9] I. Cavaco, J. Costa Pessoa, M.T.L. Duarte, R.T. Henriques, P.M. Matias, R.D. Gillard, J. Chem. Soc., Dalton Trans. (1996) 1989.
[10] I. Cavaco, J. Costa Pessoa, M.T.L. Duarte, R.D. Gillard, P.M. Matias, Chem. Commun. (1996) 1365.
[11] J. Costa Pessoa, I. Cavaco, I. Correia, M.T. Duarte, R.D. Gillard, R.T. Henriques, F.J. Higes, C. Madeira, I. Tomaz, Inorg. Chim. Acta 293 (1999) 1.
[12] R. Fulwood, H. Schmidt, D. Rehder, J. Chem. Soc., Chem. Commun. (1995) 1443.
[13] A. Garcia-Raso, J.J. Fiol, A. Lopez-Zafra, A. Cabrero, Polyhedron 18 (1999) 871.
[14] V. Vergopoulos, W. Priebsch, M. Fritzsche, D. Rehder, Inorg. Chem. 32 (1993) 1844.
[15] J. Costa Pessoa, I. Cavaco, I. Correia, I. Tomaz, T. Duarte, P.M. Matias, Inorg. Biochem. 80 (2000) 35.
[16] J. Costa Pessoa, M.J. Calhorda, V. Felix, S. Gama, I. Correia, M.T. Duarte, S. Marcao, M.F.M. Piedade, I. Tomaz, J. Inorg. Biochem. 86 (2001) 188.
[17] J. Costa Pessoa, M.T. Duarte, R.D. Gillard, C. Madeira, P.M. Matias, I. Tomaz, J. Chem. Soc., Dalton Trans 23 (1998) 4015.
[18] B. Baruah, S. Das, A. Chakravorty, Inorg. Chem. 41 (2002) 4502.
[19] A. Garcia-Raso, J.J. Fiol, F. Badenas, M. Quiros, Polyhedron 15 (1996) 4407.
[20] A. Garcia-Raso, J.J. Fiol, A. Lopez-Zafra, I. Mata, E. Espinosa, E. Molins, Polyhedron 19 (2000) 673.
[21] A. Garcia-Raso, J.J. Fiol, F. Badenas, E. Lago, E. Molins, Polyhedron 20 (2001) 2877.
[22] L.L. Koh, J.O. Ranford, W. Robinson, J.O. Svensson, A.L.C. Tan, D. Wu, Inorg. Chem. 35 (1996) 6466.
[23] C.T. Yang, B. Moubaraki, K.S. Murray, J.D. Ranford, J.J. Vittal, Inorg. Chem. 40 (2001) 5934.
[24] C.T. Yang, B. Moubaraki, K.S. Murray, J.J. Vittal, J. Chem. Soc., Dalton Trans. 5 (2003) 880.
[25] J. Costa Pessoa, I. Cavaco, I. Correia, D. Costa, R.T. Henriques, R.D. Gillard, Inorg. Chim. Acta 305 (2000) 7.
[26] C.J. Hu, X.M. Ren, C.S. Lu, Y. Zou, W.W. Zhang, C.Y. Duan, Q.J. Meng, Transit. Metal Chem. 28 (2003) 350.
[27] SHELXTL Reference manuals, Version 6.10, Bruker AXS Inc., Madision, WI, 2000.
[28] H.C. Freeman, G. Robinson, J.C. Schoone, Acta Crystallogr. 17 (1964) 719.
[29] W.A. Franks, D. van der Helm, Acta Crystallogr. Sect. B. 27 (1971) 1299.
[30] W.S. Sheldrick, R. Exner, Inorg. Chim. Acta 184 (1991) 119.
[31] M. Lipowska, L. Hansen, X.L. Xu, Inorg. Chem. 41 (2002) 3032.
[32] T. Ueki, T. Ashida, V. Sasada, K. Kakudo, Acta Crystallogr. B25 (1969) 328.
[33] V.W.W. Yam, Y.L. Pui, K.M.C. Wong, K.K. Cheung, Chem. Commun. (2000) 1751.
[34] Y. Yamada, M. Tsumita, A. Hirano, Y. Miyashita, K. Fujisawa, K.I. Okamato, Inorg. Chim. Acta 332 (2002) 108.
[35] V.R. Thalladi, S. Brasselet, D. Bläser, R. Boes, J. Zyss, A. Nangia, G.R. Desiraju, Chem. Commun. (1997) 1841.
[36] S.G. Bodige, R.D. Rogers, S.C. Blackstock, Chem. Commun. (1997) 1669.
[37] J.W. Leadbetter Jr., J. Phys. Chem. 81 (1977) 54.
[38] D. Kivelson, R.R. Neiman, J. Chem. Soc. A (1968) 16.

Available online at www.sciencedirect.com
SCIENCE DIRECT®
Polyhedron 23 (2004) 857–863
POLYHEDRON
www.elsevier.com/locate/poly

Porous coordination networks generated from lanthanum trifluoromethanesulfonate and single/mixed N-oxide spacer linkers

Lin-Ping Zhang [a], Miao Du [a,b], Wen-Jie Lu [a,c], Thomas C.W. Mak [a,*]

[a] *Department of Chemistry, The Chinese University of Hong Kong, Shatin, New Territories, Hong Kong SAR, PR China*
[b] *College of Chemistry and Life Science, Tianjin Normal University, Tianjin 300074, PR China*
[c] *Department of Chemical and Environmental Engineering, Wuyi University, Jiangmen, Guangdong Province, PR China*

Received 4 September 2003; accepted 24 November 2003

Abstract

Three new lanthanum coordination polymers $\{[La(\mu\text{-}L)_2L(H_2O)_2](CF_3SO_3)_3\}_n$ (**1**), $\{[La(\mu\text{-}L')(CF_3SO_3)(H_2O)_2(\mu\text{-}L)_{0.5}L](H_2O)_3(CF_3SO_3)\}_n$ (**2**) and $\{[La(\mu\text{-}L')_2(\mu\text{-}L)](H_2O)_{1.5}(CF_3SO_3)\}_n$ (**3**) have been prepared by the reaction of $La(CF_3SO_3)_3$ with 1,2-bis(4-pyridyl)ethane-*N*,*N*′-dioxide (L), or with mixed N-oxide ligands L and L′ (HL′ = isonicotinic acid N-oxide) in different molar ratios. Single-crystal X-ray analysis showed that **1** possesses a three-dimensional coordination framework connected by L ligands, whereas bridging by both L and L′ spacers in different molar ratios results in coordination polymers **2** and **3** that exhibit two- and three-dimensional networks, respectively. Compounds **2** and **3** represent the first metal complexes containing two different N-oxide bridging ligands. Thermogravimetric analysis studies revealed that ligands L and L′ are bound differently in compounds **1**–**3** due to their distinctive coordination modes.
© 2003 Elsevier Ltd. All rights reserved.

Keywords: Lanthanum trifluoromethanesulfonate; Isonicotinic acid; N-oxide; Mixed ligands; Coordination polymer

1. Introduction

Crystal engineering of metal-organic compounds has developed rapidly in view of their potential applications and unusual topologies [1,2]. It is well established that the assembly processes of coordination networks can be controlled by the choice of metal ions, counter anions, co-existing neutral ligands, temperature, pH and solvents used for crystallization [3–10]. In some instances, two or more complexes of different compositions can be obtained merely by manipulating the ligand/metal molar ratio [11]. The lanthanides have been less studied in this context owing to their weak stereochemical preferences which prevent reliable preconceived molecular assembly in solution [12]. Nevertheless, prior knowledge of persistent structural motifs offers a viable approach to the design of lanthanide coordination networks [13]. A widely applicable strategy using poly(N-oxide) ligands as spacer linkers for assembling coordination networks based on f-block metals has been developed [14]. Recently 4,4′-bipyridine-*N*,*N*′-dioxide [15], 1,2-bis(4-pyridyl)ethane-*N*,*N*′-dioxide and *trans*-1,2-bis(4-pyridyl)ethene-*N*,*N*′-dioxide have been synthesized and used to generate a series of novel lanthanide(III) coordination polymers [16]. Herein, we report the synthesis and structural characterization of $\{[La(\mu\text{-}L)_2L(H_2O)_2](CF_3SO_3)_3\}_n$ (**1**), $\{[La(\mu\text{-}L')(CF_3SO_3)(H_2O)_2(\mu\text{-}L)_{0.5}L](H_2O)_3(CF_3SO_3)\}_n$(**2**) and $\{[La(\mu\text{-}L')_2(\mu\text{-}L)](H_2O)_{1.5}(CF_3SO_3)\}_n$ (**3**), which were self-assembled by La$(CF_3SO_3)_3$ with 1,2-bis(4-pyridly)ethane-*N*,*N*′-dioxide (L) alone, and with both L and L′ (HL′ = isonicotinic acid N-oxide; see Scheme 1) in different molar ratios.

2. Experimental

2.1. General method

IR spectra were recorded with a Nicolet Impact 420 FT-IR spectrometer using KBr pellets. Elemental analyses of C, H and N were performed by MEDAC LTD

* Corresponding author. Tel.: +852-2609-6279; fax: +852-2603-5057.
E-mail address: tcwmak@cuhk.edu.hk (T.C.W. Mak).

0277-5387/$ - see front matter © 2003 Elsevier Ltd. All rights reserved.
doi:10.1016/j.poly.2003.12.004

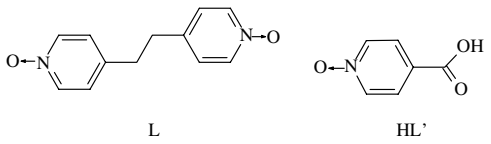

L HL'

Scheme 1.

Brunel Science Centre, UK. Thermal stability of polycrystalline samples **1**–**3** was measured on a Hi-Res TGA 2950 Thermogravimetric Analyzer from 50 to 900 °C under a nitrogen atmosphere at a heating rate of 10 °C/min. 1,2-Bis(4-pyridyl)ethane-*N*,*N*′-dioxide (L) was synthesized as described previously [16]. Lanthanum trifluoromethanesulfonate hydrate and isonicotinic acid N-oxide (HL′) were obtained commercially (Aldrich) and used without further purification.

2.2. Synthesis of $\{[La(\mu\text{-}L)_2L(H_2O)_2](CF_3SO_3)_3\}_n$ (*1*)

To an aqueous solution (3 mL) of $La(CF_3SO_3)_3 \cdot 9H_2O$ (60 mg, 0.08 mmol), an aqueous solution (8 mL) of anhydrous L (100 mg, 0.43 mmol) was added with stirring. The mixture was heated at 70 °C for about 10 min and then filtered. Upon slow evaporation of the filtrate at room temperature, colorless crystals of **1** suitable for X-ray analysis were obtained after several days. Yield ca. 80% (based on $La(CF_3SO_3)_3$). *Anal.* Calc. for $C_{39}H_{40}LaS_3F_9N_6O_{17}$: C, 36.86; H, 3.17; N, 6.61. Found: C, 37.01; H, 3.03; N, 6.32%. IR(KBr, cm^{-1}): 3406sbr, 3117w, 1636w, 1495s, 1453w, 1284s, 1249s, 1171s,1028s, 853m, 771m, 635s, 576w, 510m, 482m.

2.3. Synthesis of $\{[La(\mu\text{-}L')(CF_3SO_3)(H_2O)_2(\mu\text{-}L)_{0.5}L](H_2O)_3(CF_3SO_3)\}_n$ (*2*)

Aqueous solutions of $La(CF_3SO_3)_3 \cdot 9H_2O$ (3 mL; 60 mg, 0.08 mmol) and HL′ (4 mL; 15 mg, 0.1 mmol) were mixed together. Then, an aqueous solution of L (4 mL; 100 mg, 0.2 mmol) was added to the mixture with stirring. After heating at 70 °C for 10 min with stirring, the resultant solution was filtered. Upon slow evaporation of the filtrate at room temperature, colorless crystals of **2** were obtained after several days. Yield ca. 57% (based on $La(CF_3SO_3)_3$). *Anal*. Calc. for $C_{26}H_{32}LaS_2F_6N_4O_{17}$: C, 31.56; H, 3.26; N, 5.66. Found: C, 31.23; H, 3.24; N, 5.44%. IR(KBr, cm^{-1}): 3440sbr, 3120w, 1632w, 1602w, 1548w, 1494m, 1454w, 1407w, 1286s, 1241s, 1175s, 1030s, 856m, 772m, 640s, 576w, 516m, 482m.

2.4. Synthesis of $\{[La(\mu\text{-}L')_2(\mu\text{-}L)](H_2O)_{1.5}(CF_3SO_3)\}_n$ (*3*)

Colorless needle-like crystals of **3** were obtained by a similar procedure to **2** but with a different starting molar ratio of $La(CF_3SO_3)_3$:L:HL′ (1:1:2). Yield ca. 50% (based on $La(CF_3SO_3)_3$). *Anal.* Calc. for $C_{25}H_{23}LaSF_3N_4O_{12.5}$: C, 37.19; H, 2.87; N, 6.94. Found: C, 36.96; H, 2.49; N, 6.72%. IR(KBr, cm^{-1}): 3382sbr, 3115w, 1612w, 1594m, 1546w, 1492s, 1453w, 1406s, 1292s, 1237s, 1174s, 1025s, 859m, 774m, 641s, 485w.

2.5. X-ray crystallography

Selected single crystals of **1**–**3** were used for data collection on a Bruker SMART 1000 CCD diffractometer with graphite monochromated Mo Kα radiation ($\lambda = 0.71073$ Å at 293 K. An empirical absorption correction was applied using the SADABS program [17]. The structures were solved by direct methods and refined by full-matrix least-squares based on F^2 using the SHELXTL program package [18]. The crystallographic data for complexes **1**–**3** are summarized in Table 1.

3. Results and discussion

3.1. Description of the crystal structures

$[La(\mu\text{-}L)_2L(H_2O)_2](CF_3SO_3)_3$ (**1**). The crystal structure of **1** consists of a three-dimensional (3-D) cationic coordination framework $[La(\mu\text{-}L)_2L(H_2O)_2]^{3+}$ and uncoordinated $CF_3SO_3^-$ counter anions. As shown in Fig. 1, each La^{3+} center coordinates to eight oxygen donors from six adjacent L ligands and two water molecules in a square antiprismatic coordination environment. It is notable that all three independent L ligands display different coordination modes in this structure (see Chart 1): (I) monodendate, (II) bidendate (μ-*O*,*O*′) and (III) unusual tridendate (μ-*O*,*O*,*O*′) bridging mode. The dihedral angles between the pyridyl rings within each kind of independent ligand molecule are 138.5°, 53.0° and 57.3°, respectively. The centrosymmetric dimeric La_2O_2 motifs linked by the μ_3 L ligand (with La···La separation of 4.524 Å) can be considered as 4-connected nodes, which are extended into a 3-D architecture by the L ligands exhibiting bridging fashions (II) and (III), as shown in Fig. 2. The channels of the resultant framework are occupied by the monodendate L ligands and the uncoordinated $CF_3SO_3^-$anions, forming O–H···O hydrogen bonding interactions with the aqua ligands O1W–H···O2a, O2W–H···O7b, O2W–H···O1c (a: $-x+2$, $-y+1$, $-z+1$; b: x, $y+1$, $z+1$, c: $-x+3$, $-y+2$, $-z+1$) that further stabilize the overall crystal structure. It is of interest to compare this structure with that of $[La(NO_3)_3(L)(CH_3OH)] \cdot CH_3OH \cdot CH_2Cl_2$ (**1a**) [16]. In the crystal structure of **1a**, the nitrate anions coordinate to the La(III) center in the chelating mode and the L ligands connect the La(III) ions in bidendate (μ-

Table 1
Crystallographic data of complexes **1**–**3**

Complex	**1**	**2**	**3**
Empirical formula	$C_{39}H_{40}F_9LaN_6O_{17}S_3$	$C_{26}H_{32}F_6LaN_4O_{17}S_2$	$C_{25}H_{23}F_3LaN_4O_{12.5}S$
Formula weight	1270.86	989.59	807.44
Crystal size (mm)	$0.28 \times 0.24 \times 0.14$	$0.47 \times 0.27 \times 0.19$	$0.4 \times 0.2 \times 0.13$
Crystal system	monoclinic	triclinic	orthorhombic
Space group	$P2_1/n$ (No. 14)	$P\bar{1}$ (No. 2)	*Fddd* (No. 70)
a (Å)	10.830(1)	10.5878(9)	15.4237(9)
b (Å)	16.713(1)	12.659(1)	25.429(1)
c (Å)	28.085(2)	14.569(1)	30.787(2)
α (°)	90	98.778(2)	90
β (°)	94.967(2)	96.343(2)	90
γ (°)	90	103.102(2)	90
V (Å^3)	5064.6(7)	1858.0(3)	12074(1)
Z	4	2	16
D_{calc} (g/cm^3)	1.688	1.769	1.777
μ(Mo Kα) (mm^{-1})	1.095	1.369	1.573
$F(000)$	2584	990	6416
Reflections collected	34 116	12 830	19 543
Independent reflections (R_{int})	12 242 (0.0908)	8848 (0.0438)	3673 (0.1070)
Observed reflections [$I > 2\sigma(I)$]	6667	6535	2723
Parameters	713	505	244
Goodness-of-fit	0.961	0.988	1.087
$R_1[I > 2\sigma(I)]$ [a]	0.0578	0.0588	0.0489
wR_2 (all data)[b]	0.1574	0.1480	0.1219

[a] $R_1 = \sum ||F_o| - |F_c|| / \sum |F_o|$.
[b] $wR_2 = [\sum[w(F_o^2 - F_c^2)^2] / \sum[w(F_o^2)^2]]^{1/2}$.

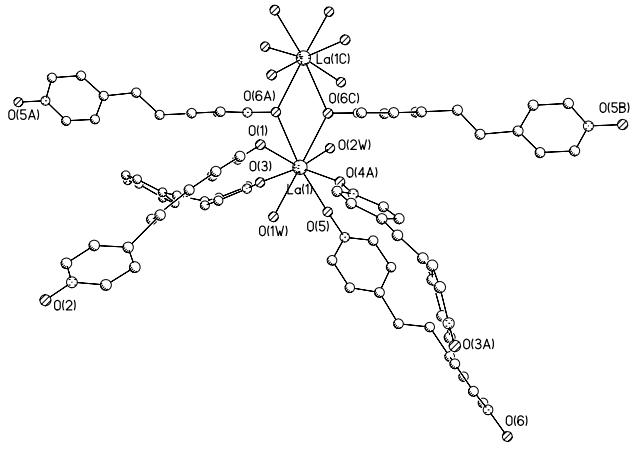

Fig. 1. Coordination geometry of the La(III) center in **1**. Selected bond lengths (Å) and angles (°): La(1)–O(3): 2.339(2), La(1)–O(5): 2.468(2), La(1)–O(4a): 2.360(2), La(1)–O(1): 2.510(2), La(1)–O(1W): 2.545(2); La(1)–O(2W); 2.558(2), La(1)–O(6b): 2.583(2), La(1)–O(6c): 2.66(1); O(3)–La(1)–O(1): 94.43(6), O(3)–La(1)–O(5): 81.21(6), O(5)–La(1)–O(1): 152.08(6). Symmetry codes: a $x-1/2$, $-y+3/2$, $z+1/2$; b $-x+7/2$, $y+1/2$, $-z+3/2$; c $x-1/2$, $-y+3/2$, $z-1/2$.

O,*O*′) and tetradentate (μ-*O*,*O*,*O*′,*O*′) coordination fashions, leading to a two-dimensional square-grid (4,4) coordination network with centrosymmetric dinuclear La_2O_2 nodes. Although the change in the coordination modes of the ligand L gives rise to different coordination frameworks in **1** and **1a**, the nature of the counter anions also play a dominant role in the as-

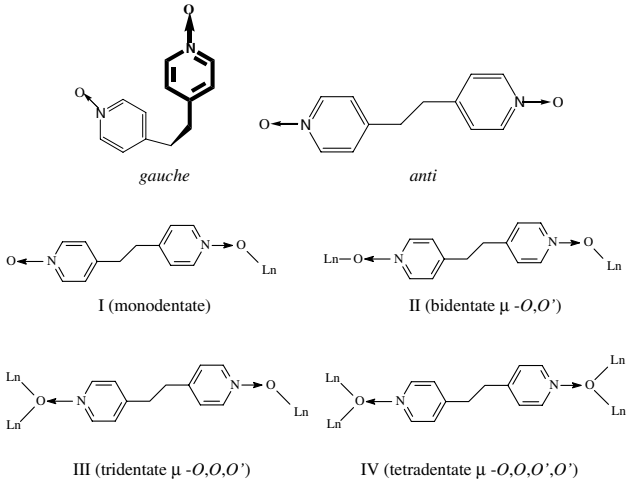

Chart 1.

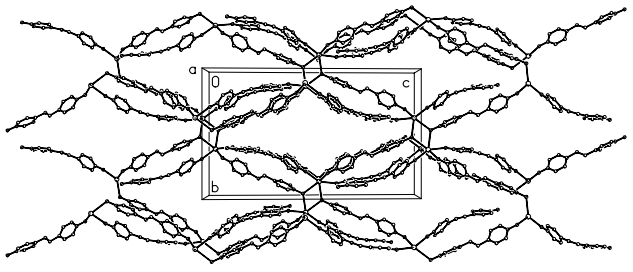

Fig. 2. Three-dimensional coordination network of **1** (the monodendate L ligand and anions are omitted for clarity).

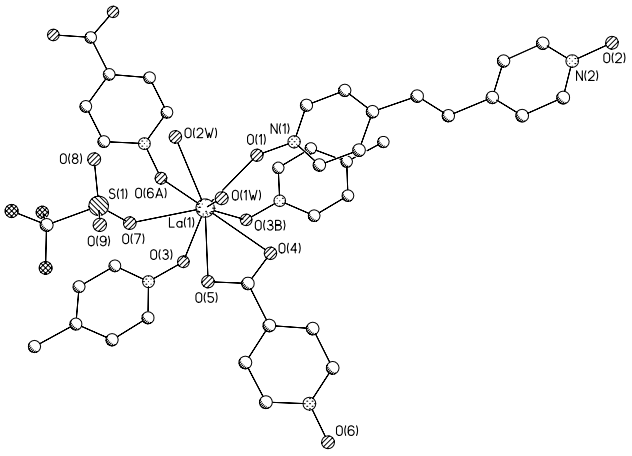

Fig. 3. Coordination geometry of the La(III) center in **2**. Selected bond lengths (Å) and angles (°): La(1)–O(1): 2.413(4), La(1)–O(2W): 2.590(4), La(1)–O(6a): 2.370(4), La(1)–O(3b): 2.609(4), La(1)–O(1W): 2.531(4), La(1)–O(4): 2.624(4), La(1)–O(5): 2.572(4), La(1)–O(7): 2.628(4), La(1)–O(3): 2.583(4); O(1)–La(1)–O(3): 131.6(1), O(1)–La(1)–O(5): 130.1(1), O(5)–La(1)–O(3): 69.7(1), O(1)–La(1)–O(4): 81.5(1), O(5)–La(1)–O(4): 50.7(1), O(3)–La(1)–O(4): 90.0(1), O(1)–La(1)–O(7): 140.9(2), O(5)–La(1)–O(7): 72.5(1), O(3)–La(1)–O(7): 83.2(1), O(4)–La(1)–O(7): 121.1(1). Symmetry codes: a $x-1$, y, z; b $-x+1$, $-y+1$, $-z$.

sembly of these polymeric nets [19]. As observed in **1**, the uncoordinated $CF_3SO_3^-$ anion accounts for subtle templating effects that cause the L ligands to adopt versatile coordination modes.

$[La(\mu\text{-}L')(CF_3SO_3)(H_2O)_2(\mu\text{-}L)_{0.5}L](H_2O)_3(CF_3SO_3)$ (**2**). The anionic ligand L' can coordinate to metals via its N-oxide and/or carboxylate group [20]. By incorporating it as a co-ligand in the formation of **1**, a different coordination architecture **2** was obtained. Here, the central La(III) atom is surrounded by nine oxygen donors from one $CF_3SO_3^-$ anion, two aqua ligands, two L′ and three adjacent L ligands, adopting a tricapped trigonal prismatic geometry as depicted in Fig. 3. In this structure, coordination modes (I) and (III) of L are observed. The dihedral angles between the pair of pyridyl groups within the two independent L molecules are 6.4° and zero (for the one locate at an inversion center). The L′ ligand exhibits the μ_3, end-to-end bridging mode with unusual symmetric bidentate chelatation of the carboxylic group to connect the La(III) centers into a linear chain. The adjacent La···La nonbonding distance within this coordination chain is 10.588 Å. Furthermore, each La center in this chain is cross-linked to another La atom in a neighboring chain by a pair of oxygen donors from two distinct L molecules in coordination mode III, forming a double-chain ladder architecture as shown in Fig. 4. In the centrosymmetric dimeric La_2O_2 motif, the La···La separation is 4.500 Å. Adjacent parallel pyridine rings in the double chain have a center-to-center distance of 3.538 Å, indicating a significant face-to-face π–π stacking interaction [21].

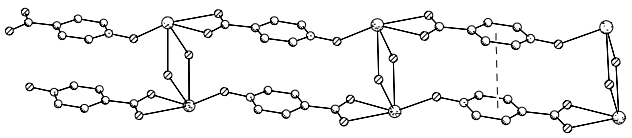

Fig. 4. Double-chain structure of **2** showing π–π stacking interaction.

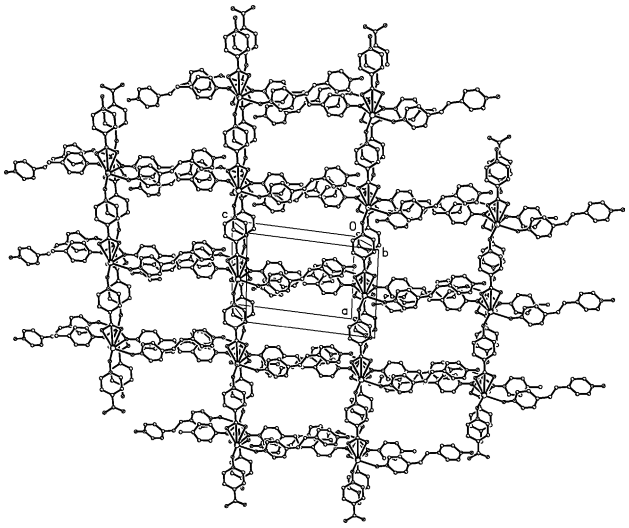

Fig. 5. Square-grid coordination network of **2**.

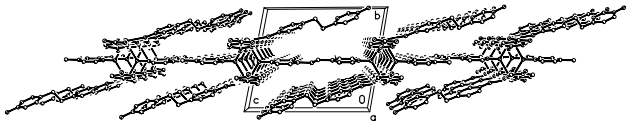

Fig. 6. Side view of the 2-D sheet of **2** showing the outstretched monodendate terminal L ligands.

In addition, these ladder architectures are further connected by the ligand L acting in mode III, resulting in a square grid (see Fig. 5) with the monodendate L ligands protruding at an angle from both sides (see Fig. 6). These 2-D arrays stack along the [0 1 0] direction to generate large channels (representing ca. 24% of the total crystal volume), which are filled by lattice water molecules and anions [22]. The distance between a pair of pyridine rings of the monodendate ligands L from two adjacent layers is only 3.512 Å, indicating significant π–π stacking which further stabilizes the overall 3-D supramolecular system.

$[La(\mu\text{-}L')_2(\mu\text{-}L)](H_2O)(CF_3SO_3)$ (**3**). By altering the starting molar ratio La:L′:L from 1:1:1.5 for **2** to 1:2:1 for **3**, a completely different 3-D coordination polymer was obtained. Here ligand L, occupying a special position of symmetry 2, exhibits bridging mode II in the

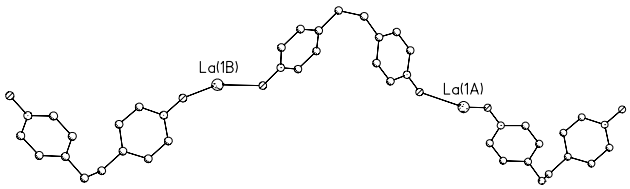

Fig. 7. Infinite zigzag chain bridged by the *gauche* L spacers in **3**.

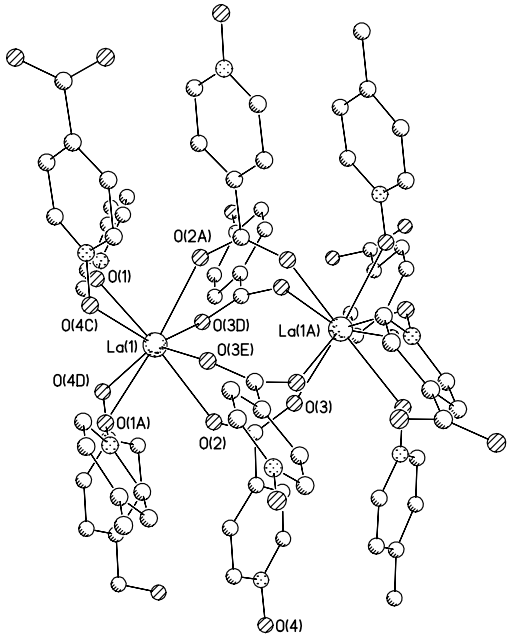

Fig. 8. Coordination geometry of La(III) in the $La_2(L')_4$ paddle wheel of symmetry 222 in **3**. Selected bond lengths (Å) and angles (°): La(1)–O(1): 2.495(2), La(1)–O(2): 2.482(2), La(1)–O(1a): 2.495(2), La(1)–O(3e): 2.527(1), La(1)–O(2a): 2.482(2), La(1)–O(4b): 2.497(1), La(1)–O(4c): 2.497(1), La(1)–O(3d): 2.527(1); O(2)–La(1)–O(1): 141.83(5). Symmetry codes: a $x, -y+5/4, -z+5/4$; b $-x+1, -y+1, -z+1$; c $-x+1, y+1/4, z+1/4$; d $-x+5/4, y, -z+5/4$; e $-x+5/4, -y+5/4, z$.

gauche configuration (the dihedral angle between pyridine rings is 37.3°) to yield an infinite zigzag chain along the [1 1 0] direction, with a nearest La···La separation of 13.081 Å (Fig. 7). The μ_3 spacer L′ takes the end-to-end bridging mode with *syn–syn* coordination of the carboxylic group to La. Each La ion lying on a 2-axis has a LaO_8 square antiprimatic coordination environment, being surrounded by four oxygen donors from the carboxylic groups of four L′, two N-oxide groups of another two L′ and two oxygen atoms from two L molecules. Unlike the dimeric La_2O_2 unit in **1** and **2**, two La(III) centers are connected by four L′ ligands acting in the *syn–syn* carboxylato mode to form a $La_2(L')_4$ paddle wheel of symmetry 222 (Fig. 8) [23]. The La···La distance within this dinuclear unit is 4.637 Å. As shown in Fig. 9, the end-to-end spacers L′ bridge the paddle wheels into a 3-D network with large cavities. As stated above, the ligands L further connect the dimeric units to strengthen the final 3-D framework (Fig. 10). Along the [1 0 0] direction, large channels are occupied by the lattice water molecules and $CF_3SO_3^-$ anions. An analysis of the voids shows 1.49% of empty space even allowing for the guest water molecules and anions in the host framework, and after the removal of them the voids add up to 28.2%.

3.2. TGA studies

It is known that the N-oxide ligand has a higher melting point comparing with the corresponding dipyridine precursor [24], which makes it possible to generate useful porous coordination frameworks with high thermal stability. Thus, thermogravimetric analysis (TGA) of complexes **1**–**3** has been conducted. For

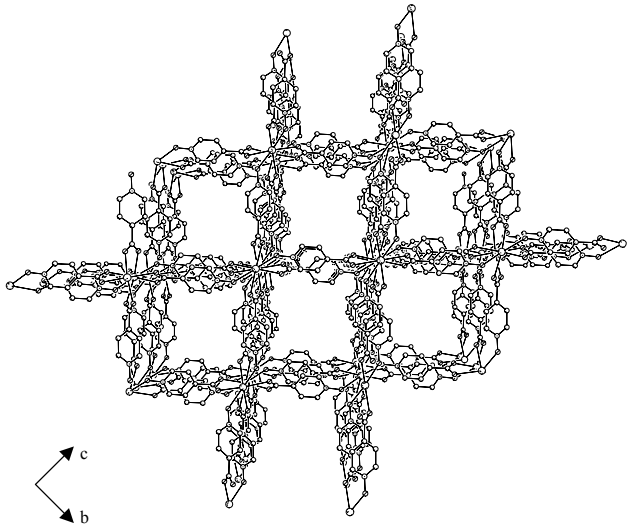

Fig. 9. Three-dimensional framework bridged by L′ ligands viewed along the [1 0 0] direction in **3**.

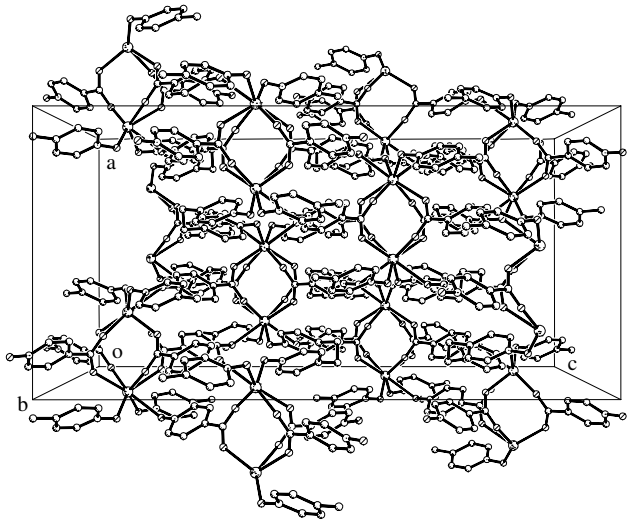

Fig. 10. Three-dimensional framework of **3** viewed along the [0 1 0] direction.

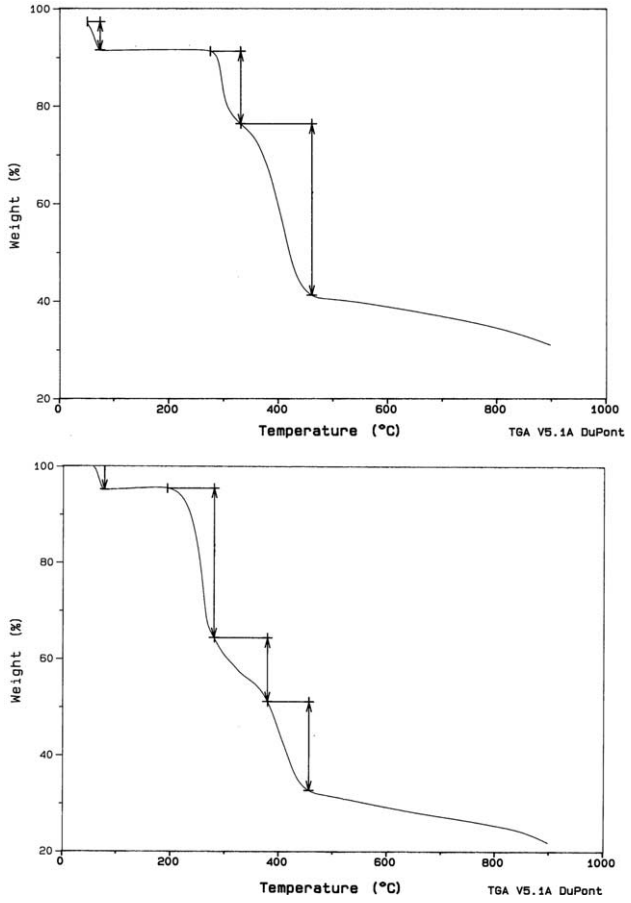

Fig. 11. TGA curves of **2** (top) and **3** (bottom).

complex **1** containing only the L ligand, the first weight loss of 3.18% from 90 to 200 °C corresponds to the loss of two aqua ligands (calculated: 2.83%). The remaining substance does not lose weight upon further heating until two consecutive weight losses occur in the 270–490 °C region (the critical temperature is ca. 340 °C), corresponding to stepwise removal of the first and second L molecules, respectively (observed: 17.17% and 34.55%; calculated: 17.00% and 34.00%). Further heating to 900 °C of the sample indicates a continuous and slow weight loss. For the two-dimensional host framework **2** incorporating both L and L′ spacers (Fig. 11, top), the first weight loss of 6.06% from 50 to 75 °C corresponds to the release of three guest water molecules (calculated: 5.46%). The remaining framework remains intact until two consecutive weight losses occur in the 275–480 °C region (the critical temperature is ca. 330 °C) corresponding to stepwise removal of one L′ molecule plus an aqua ligand (observed: 15.71%; calculated: 15.88%), and 1.5 L plus the second aqua ligand (observed: 34.26%; calculated: 34.56%), respectively. Further heating to 900 °C of the sample only indicates a continuous and slow weight loss. For the 3-D coordination framework **3** (Fig. 11, bottom), the first weight loss of 3.60% from 60 to 85 °C corresponds to the expulsion of 1.5 guest water molecules (calculated: 3.35%). Then, three consecutive weight losses occur in the 200–450 °C region (the critical temperatures are ca. 280 and 380 °C) correspond to stepwise removal of one L molecule (observed: 27.19%; calculated: 26.82%) and two L′ molecules (observed: 35.08%; calculated: 34.52%). Just like **1** and **2**, further heating of **3** to 900 °C indicates a continuous and slow weight loss.

The above observation clearly shows that the thermal behaviors of the frameworks **1**–**3** are quite different, especially in regard to compounds **2** and **3** which have similar compositions but a reversed sequence of weight losses for L and L′. In conformity with the X-ray analysis, this may be attributed to the different coordination/bridging modes of the N-oxide ligands and the co-existing water molecules and $CF_3SO_3^-$ ions, which affect the assembly of the frameworks in the crystal structures.

4. Conclusion

Three novel lanthanum coordination polymers with single or mixed N-oxide ligands have been prepared and structurally characterized. In compound **1**, the flexible ligand 1,2-bis(4-pyridyl)ethane-*N*,*N*′-dioxide (L) exhibits a tridentate (μ-*O*,*O*,*O*′) coordination mode, which together with monodendate and bidendate (μ-*O*,*O*′) bridging modes link the La(III) ions to generate a three-dimensional framework. When the anionic ligand L′ (HL′ = isonicotinic acid N-oxide) was introduced as an added component in the molar ratio of L/L′ (2:1 and 1:2), the network assembly process is greatly affected, leading to two different coordination frameworks **2** and **3**, respectively. TGA studies revealed that due to their different ligation modes, L and L′ show different thermal stabilities in **1**–**3**.

5. Supplementary materials

Crystallographic data for the crystal structures reported in this paper have been deposited with the Cambridge Crystallographic Data Center (CCDC Nos. 217846–217848). This material can be obtained free of charge from the Director, CCDC, 12 Union Road, Cambridge, CB2 1EZ, UK (fax: +44 1223 336033; e-mail: deposit@ccdc.cam.ac.uk or http://www.ccdc.cam.ac.uk).

Acknowledgements

This work is supported by Hong Kong Research Grants Council Earmarked Grant CUHK 4268/00P.

References

[1] (a) S.R Batten, R. Robson, Angew. Chem., Int. Ed. 37 (1998) 1460;
(b) O.M. Yaghi, H. Li, C. Davis, D. Richardson, T.L. Groy, Acc. Chem. Res. 31 (1998) 474;
(c) M. Munakata, L.P. Wu, T. Kuroda-Sowa, Adv. Inorg. Chem. 46 (1999) 173;
(d) A.J. Blake, N.R. Champness, P. Hubberstey, W.-S. Li, M.A. Withersby, M. Schröder, Coord. Chem. Rev. 183 (1999) 117;
(e) D.L. Caulder, K.N. Raymond, Acc. Chem. Res. 32 (1999) 975;
(f) M. Fujita, Acc. Chem. Res. 32 (1999) 53;
(g) S. Leininger, B. Olenyuk, P.J. Stang, Chem. Rev. 100 (2000) 853;
(h) G.F. Swiegers, T. Malefetse, Chem. Rev. 100 (2000) 3483;
(i) B. Multon, M.J. Zaworotko, Chem. Rev. 101 (2001) 1629;
(j) B.J. Holliday, C.A. Mirkin, Angew. Chem., Int. Ed. 40 (2001) 2023;
(k) M. Eddaoudi, D.B. Moler, H. Li, B. Chen, T.M. Reineke, M. O'Keeffe, O.M. Yaghi, Acc. Chem. Res. 34 (2001) 319;
(l) S.L. James, Chem. Soc. Rev. 32 (2003) 276.

[2] (a) M. Fujita, Y.J. Kwon, S. Washizu, K. Ogura, J. Am. Chem. Soc. 116 (1994) 1151;
(b) D. Venkataraman, J.S. Moore, S. Lee, Nature 374 (1995) 792;
(c) R.-G. Xiong, X.-Z. You, B.F. Abrahams, Z. Xue, C.-M. Che, Angew. Chem., Int. Ed. 40 (2001) 4422;
(d) O.R. Evans, W. Lin, Acc. Chem. Res. 35 (2002) 511;
(e) N.L. Rosi, J. Eckert, M. Eddaoudi, D.T. Vodak, J. Kim, M. O'Keeffe, O.M. Yaghi, Science 300 (2003) 1127.

[3] S. Hiraoka, T. Yi, M. Shiro, M. Shionoya, J. Am. Chem. Soc. 124 (2002) 14510.

[4] R. Grommen, P. Manikandan, Y. Gao, T. Shane, J.J. Shane, R.A. Schoonheydt, B.M. Weckhuysen, D. Goldfarb, J. Am. Chem. Soc. 122 (2000) 11488.

[5] S. Aoki, M. Shiro, T. Koike, E. Kimura, J. Am. Chem. Soc. 122 (2000) 576.

[6] O.M. Yaghi, H. Li, C. Davis, D. Richardson, T.L. Groy, Acc. Chem. Res. 31 (1998) 474.

[7] D. Braga, F. Grepioni, G.R. Desiraju, Chem. Rev. 98 (1998) 1375.

[8] A. Kamiyama, T. Noguchi, T. Kajiwara, T. Ito, Cryst. Eng. Commun. 5 (2003) 231.

[9] J.F. Ma, J.F. Liu, X. Yan, H.Q. Jia, Y.H. Lin, J. Chem. Soc., Dalton Trans. (2000) 2403.

[10] L. Pan, X.Y. Huang, J. Li, Y.G. Wu, N.W. Zheng, Angew. Chem., Int. Ed. 39 (2000) 527.

[11] (a) M. Du, S.T. Chen, X.H. Bu, Crystal. Growth Des. 2 (2002) 625;
(b) A.J. Blake, N.R. Brooks, N.R. Champness, P.A. Cooke, A.M. Deveson, D. Fenske, P. Hubberstey, W.-S. Li, M. Schröder, J. Chem. Soc., Dalton Trans. (1999) 2103;
(c) R.W. Saalfrank, I. Bernt, M.M. Chowdhry, F. Hampel, G.B.M. Vaughan, Chem. Eur. J. 7 (2001) 2765.

[12] (a) B. Bocquet, G. Bernardinelli, N. Ouali, S. Floquet, F. Renaud, G. Hopfgartner, C. Piguet, Chem. Commun. (2002) 930;
(b) D.L. Long, A.J. Blake, N.R. Champness, C. Wilson, M. Schröder, Chem. Eur. J. 8 (2002) 2026.

[13] D.-L. Long, A.J. Blake, N.R. Champness, C. Wilson, M. Schröder, J. Am. Chem. Soc. 123 (2001) 3401.

[14] (a) D.-L. Long, A.J. Blake, N.R. Champness, C. Wilson, M. Schröder, Angew. Chem., Int. Ed. 40 (2001) 2444;
(b) S. Tanase, M. Andruh, A. Müller, M. Schmidtmann, C. Mathonière, G. Rombaut, Chem. Commun. (2001) 1084.

[15] (a) D.-L. Long, A.J. Blake, N.R. Champness, M. Schröder, Chem. Commun. (2000) 1369;
(b) A. Nedelcu, Z. Žak, A.M. Madalan, J. Pinkas, M. Andruh, Polyhedron 22 (2003) 789;
(c) S.L. Ma, W.X. Zhu, G.H. Huang, D.Q. Yuan, X. Yan, J. Mol. Struct. 646 (2003) 89.

[16] W.-J. Lu, L.-P. Zhang, H.-B. Song, Q.-M. Wang, T.C.W. Mak, New J. Chem. 26 (2002) 775.

[17] G.M. Sheldrick, SADABS: Program for Empirical Absorption Correction of Area Detector Data, University of Göttingen, Germany, 1996.

[18] G.M. Sheldrick, SHELXTL: Structure Determination Software Progarams, Bruker Analytical X-ray System Inc., Madison, WI, 1997.

[19] M. Du, X.H. Bu, Z. Huang, S.T. Chen, Y.M. Guo, C. Diaz, J. Ribas, Inorg. Chem. 42 (2003) 552.

[20] (a) C.G. Zheng, Y.L. Xie, R.G. Xiong, X.Z. You, Inorg. Chem. Commun. 4 (2001) 405;
(b) J.-G. Mao, H.-J. Zhang, J.-Z. Ni, S.-B. Wang, T.C.W. Mak, Polyhedron 17 (1998) 3999.

[21] C. Janiak, J. Chem. Soc., Dalton Trans. (2000) 3885.

[22] A.L. Spek, J. Appl. Cryst. 36 (2003) 7.

[23] (a) W.J. Evans, D.G. Giarikos, J.W. Ziller, Organometallics 20 (2001) 5715;
(b) A.D. Morales, H.N. de Armas, Acta Cryst. E 58 (2002) m157.

[24] B.Q. Ma, H.L. Sun, S. Gao, G.X. Xu, Inorg. Chem. 40 (2001) 6247.

Available online at www.sciencedirect.com
SCIENCE DIRECT®
Polyhedron 23 (2004) 865–868
POLYHEDRON
www.elsevier.com/locate/poly

The preparation and coordination of 1,3-C_6H_4-{C(O)N(PPh_2)CH_2Ph}$_2$ – a new multidentate ligand

M. Rodriguez i Zubiri, Heather L. Milton, Alexandra M.Z. Slawin, J. Derek Woollins *

School of Chemistry, University of St. Andrews, St. Andrews, Fife KY16 9ST, UK

Received 7 October 2003; accepted 8 December 2003

Abstract

Reaction of isophthaloyl dichloride with two equivalents of benzylamine in the presence of Et_3N gives *N*,*N*′-dibenzyl-1,3-isophthaldiamide which reacts with two equivalents of Ph_2PCl, in the presence of *n*-BuLi at −78 °C to give 1,3-C_6H_4-{C(O)N(PPh_2)CH_2Ph}$_2$ (**1**). Reaction of **1** with [$PtCl_2$(cod)] in dichloromethane gives the *P*, *P*′, *C* tridentate bis-chelate [Pt(Cl){1,3-C_6H_4-{C(O)N(PPh_2)CH_2Ph}$_2$}] (**2**), whilst reaction of **1** with two equivalents of [(C_3H_5)PdCl]$_2$ in thf results in [{PdCl(C_3H_5)}$_2$ {1,3-C_6H_4-{C(O)N(PPh_2)CH_2Ph}$_2$}] (**3**) in which the ligand bridges two palladium centres. The X-ray structures of **2** and **3** are reported.
© 2003 Elsevier Ltd. All rights reserved.

1. Introduction

Imidodiphosphinate anions [$R_2P(E)NP(E')R'_2$]$^-$ (R, R′ = alkyl, aryl or alkoxy; E, E′ = O, S or Se) have received substantial attention in recent years, finding use in applications such as metal extraction agents, NMR shift reagents and in catalytic functions [1–8]. We are currently investigating the chemistry of structurally similar phosphorus(V) derivatised guanidines and amidines $R_2P(E)N{=}C(X)(NH_2)$ (R = alkyl or aryl; E = oxygen or sulfur; X = NH_2 or alkyl). These molecules, readily available from [$R_2P(E)(NCN)$]$^-$ [9–16], possess an ionisable nitrogen-bound proton and have the capacity for delocalisation of the resulting uninegative charge through the π-system of the [$R_2P(E)N{=}C(X)(NH)$]$^-$ anion; hence they could function as *E*,*N*-bidentate ligands in a manner analogous to imidodiphosphinates. We have previously prepared *cis*-[Pt(L^n-*S*,*N*)(PR_3)$_2$]- Cl(PR_3 = PMe_2Ph or 1/2 dppe) from *cis*-[$PtCl_2$(PR_3)$_2$] and the potassium salts of $Me_2P(S)N{=}C(NH_2)_2$, $Ph_2P(S)N{=}C(Me)(NH_2)$ or $Ph_2P(S)N{=}C(NH_2)_2$ in which (L^n)$^-$ form six-membered *S*,*N* chelate rings at platinum(II) [17] and are comparable to [($EPPh_2$)$_2$N]$^-$ (E = S or Se), which generates *cis*-[Pt{($EPPh_2$)$_2$N-*E*,*E*′}(PR_3)$_2$]Cl [18,19]. As part of our continuing studies on phosphine ligands containing P–N bonds [19–23], here we report a new ligand derived from isophthaloyl dichloride which was designed to give six-membered chelate ring systems but surprisingly forms a tridentate and bidentate bridged complexes.

2. Results and discussion

N,*N*′-Dibenzyl-1,3-isophthaldiamide was prepared by reaction of isophthaloyl dichloride with two equivalents of benzylamine in the presence of Et_3N in dichloromethane in the following equation:

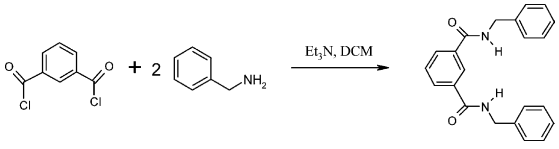

(1)

Reaction of *N*,*N*′-dibenzyl-1,3-isophthaldiamide with two equivalents of Ph_2PCl, in the presence of *n*-BuLi at −78 °C, proceeds in thf to give **1** as a pale yellow solid in 76% yield in the following equation:

* Corresponding author. Tel.: +44-1334-463861; fax: +44-1334-463384.
E-mail address: jdw3@st-andrews.ac.uk (J. Derek Woollins).

0277-5387/$ - see front matter © 2003 Elsevier Ltd. All rights reserved.
doi:10.1016/j.poly.2003.12.005

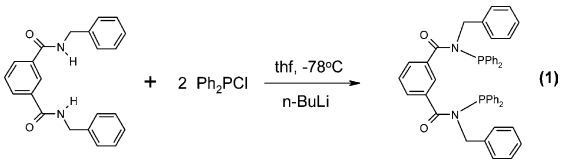

(2)

The $^{31}P–\{^{1}H\}$ NMR spectrum of **1** consists of a singlet at δ (P) 58.5 ppm, the large downfield shift when compared to (1,3-bis(diphenylphosphinoacetyl)benzene, δ (P) 27.2 ppm) [24] reflecting the substitution of the methylene carbon centres in 1,3-bis(diphenylphosphinoacetyl)benzene by nitrogen atoms in **1**.

FAB$^+$ mass spectrometry of **1** shows the expected parent-ion peaks whilst its IR spectrum contains bands that can be assigned to ν(P–N) and ν(C=O) (916 and 1651 cm^{-1}, respectively). Although air- and moisture-stable for short periods in the solid state, **1** is soluble in both thf and dichloromethane and in these solutions it oxidises readily in air.

Reaction of **1** with equimolar quantities of $[PtCl_2(cod)]$ in dichloromethane gives Eq. (3) the P,P',C chelate $[Pt(Cl)\{1,3\text{-}C_6H_4\text{-}\{C(O)N(PPh_2)CH_2Ph\}_2\}]$ (**2**) as a colourless solid in good yield (85%); apart from the expected P,P coordination the central aryl group is metalated by the platinum atom.

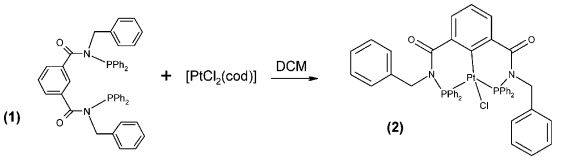

(3)

FAB$^+$ mass spectrometry shows the expected parent-ion peak for **2** (m/z 942 [M]). The IR spectrum of **2** shows bands due to ν(P–N) (915 cm^{-1}) and ν(CO) (1651 cm^{-1}), and a single band characteristic of ν(Pt–Cl) (306 cm^{-1}). The $^{31}P–\{^{1}H\}$ NMR spectrum of **2** consists of a singlet (δ (P) 67.9 ppm) with satellites from coupling to ^{195}Pt and a $[^{1}J\{^{195}Pt–^{31}P\}$ 3080 Hz] which is in agreement with the literature data on similar complexes were the metal center is bound to two phosphorus atoms and to a carbon atom from the ligand backbone ring [25].

The X-ray structure of **2** (Fig. 1) confirms that the ligand is bound in a tridentate mode to the platinum. The ligand contains two fused six-membered Pt–P–N–C–C–C-C rings and the metal centre adopts square planar geometry. The square planar geometry of the platinum centre is distorted, the P–Pt–C angles are narrower than the ideal 90° and P–Pt–Cl angles are larger than 90°. The ligand is not planar and the Ph groups on the phosphorus are on opposite faces of the coordination plane. The P–N and Pt–Cl distances are typical of a single bond.

The reaction of **1** with two equivalents of $[(C_3H_5)PdCl]_2$ in thf gives $[\{PdCl(C_3H_5)\}_2\{1,3\text{-}C_6H_4\text{-}\{C(O)N(PPh_2)CH_2Ph\}_2\}]$ (**3**) in which the ligand bridges two Pd centres in the following equation:

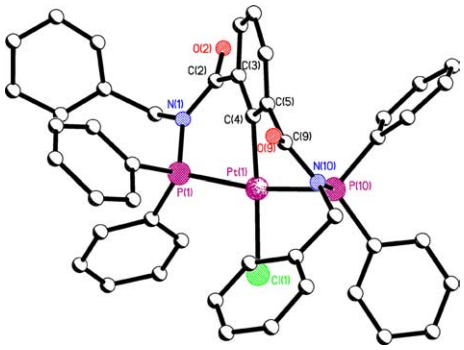

Fig. 1. Solid state structure of $P,P',C[Pt(Cl)\{1,3\text{-}C_6H_4\text{-}\{C(O)N(PPh_2)CH_2Ph\}_2\}]$ (**2**). Selected bond lengths (Å) and angles (°). Numbers in square brackets are the equivalent parameter for the second independent molecule. Pt(1)–C(4) 2.02(1) [2.01(1)], Pt(1)–P(1) 2.259(4) [2.261(4)], Pt(1)–P(10) 2.280(4) [2.273(4)], Pt(1)–Cl(1) 2.357(4) [2.360(4)], P(1)–N(1) 1.73(1) [1.71(1)], N(1)–C(2) 1.37(2) [1.444(18)], N(10)–C(9) 1.397(16) [1.364(17)]; P(1)–Pt(1)–P(10) 168.52(14) [168.68(14)], P(1)–Pt(1)–C(4) 84.5(4) [85.8(4)], P(10)–Pt(1)–C(4) 84.3(4) [83.0(4)], P(1)–Pt(1)–Cl(1) 94.80(13) [94.68(14)], P(10)–Pt(1)–Cl(1) 96.24(14) [96.27(14)].

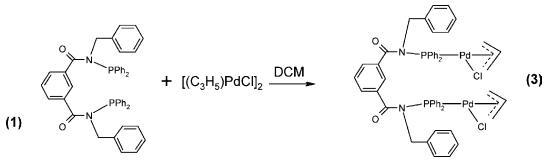

(4)

The $^{31}P–\{^{1}H\}$ NMR spectrum of **3** shows a singlet at δ (P) 72.5 ppm, a downfield shift of approximately 14 ppm from the free ligand. FAB$^+$ mass spectrometry does not show the expected parent-ion peaks and shows instead the fragmentation patterns consistent with the loss of one chloride ion (m/z 1043 [M–Cl$^-$]). Elemental analysis data are in agreement with calculated values and, once again, the IR spectrum of **3** shows bands which can be assigned to ν(P–N) (915 cm^{-1}), ν(C=O) (1648 cm^{-1}) and ν(Pd–Cl) (279 cm^{-1}).

The X-ray structure of **3** (Table 1, Fig. 2) shows that the ligand bridges the palladium atoms, with the molecule having a somewhat helical nature. The P–N and Pd–Cl distances are typical of this type of compound. It is somewhat surprising that the palladium system forms a binuclear product rather than metallating since generally palladium is more prone to metallation than platinum.

In a batch test of the rhodium complex (formed in situ) of **1** as a hydroformylation catalyst for the conversion of 1-hexene at 20 atm CO/H_2 and 100 °C we obtained poor selectivity to aldehyde (29%) with a linear to branched ratio of 1.6:1 suggesting that **1** is only an average ligand for this catalytic process.

3. Experimental

Unless otherwise stated, manipulations were performed under an oxygen-free nitrogen atmosphere using

Table 1
Crystal data and structure refinement details

	2	3
Empirical formula	$C_{46}H_{37}ClN_2O_2P_2Pt$	$C_{53}H_{50}Cl_4N_2O_2P_2Pd_2$
Formula weight	942.26	1163.49
Crystal system	triclinic	triclinic
Space group	$P\bar{1}$	$P\bar{1}$
a (Å)	14.854(2)	11.816(2)
b (Å)	15.754(2)	12.769(2)
c (Å)	18.469(2)	17.579(3)
α (°)	111.581(2)	70.114(3)
β (°)	102.825(2)	83.496(3)
γ (°)	94.704(2)	82.846(3)
V (Å^3)	3854.3(8)	2467.4(7)
Z	4	2
ρ_{calc} (Mg/m^3)	1.624	1.561
M (mm^{-1})	3.835	1.053
Reflections collected	19 093	12 272
Individual reflection (R_{int})	10 749 (0.0301)	6885 (0.0496)
Final R indices [$I > 2\sigma(I)$]	$R_1 = 0.0351$, $wR_2 = 0.0881$	$R_1 = 0.0485$, $wR_2 = 0.1014$

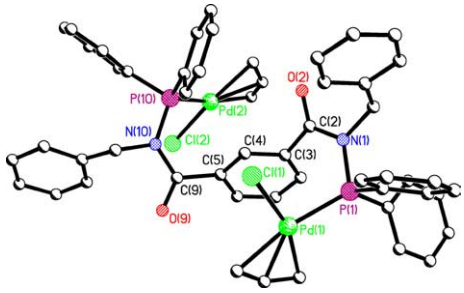

Fig. 2. Solid state structure of [{PdCl(C_3H_5)}$_2${1,3-C_6H_4-{C(O)N(PPh_2)CH_2Ph}$_2$}] (**3**). Selected bond lengths (Å) and angles (°): Pd(1)–P(1) 2.302(2), Pd(1)–Cl(1) 2.386(2), P(1)–N(1) 1.735(5), P(10)–N(10) 1.728(5), N(1)–C(2) 1.380(8), C(2)–C(3) 1.485(9), C(3)–C(4) 1.380(9), C(4)–C(5) 1.385(9), C(5)–C(9) 1.520(9), C(9)–N(10) 1.390(8), Pd(2)–Cl(2) 2.370(2), Pd(2)–P(10) 2.291(2); Pd(1)–P(1)–N(1) 113.23(19), P(1)–N(1)–C(2) 122.7(4), N(1)–C(2)–C(3) 120.5(6), C(3)–C(4)–C(5) 121.5(6), C(4)–C(5)–C(9) 120.5(6), C(9)–N(10)–P(10) 124.4(4), N(10)–P(10)–Pd(2) 111.38(19), Cl(1)–Pd(1)–P(1) 97.32(6), Cl(2)–Pd(2)–P(10) 93.79(7).

predried solvents and standard Schlenk techniques. $^{31}P\{^1H\}$ and ^1H NMR spectra (109.4 and 270.0 MHz, $CDCl_3$) were recorded on a JEOL Delta GSX 270 spectrometer, IR spectra (pressed KBr disks) on a Perkin–Elmer System 2000 FTIR/Raman instrument, elemental analyses were performed by the University of St. Andrews Microanalytical Service. Mass spectroscopy were performed by the National Service in Swansea.

3.1. N,N′-Dibenzyl-1,3-isophthalamide

To a dry and degassed dichloromethane (100 ml) solution of isophthaloyl dichloride (5.890 g, 29.00 mmol) and triethylamine (8.5 ml, 6.160 g, 60.90 mmol) was added a dry and degassed dichloromethane (10 ml) solution of benzylamine (6.3 ml, 6.20 g, 58.00 mmol) dropwise over a period of 30 min. The reaction mixture was stirring for 2 h 30 min, during which time triethylammonium hydrochloride separated from the solution. This precipitate was removed by suction filtration and the filtrate was evaporated to dryness in vacuo to give a white solid product. Recrystallisation from ethanol–water–acetone gave white crystals. Yield: 8.789 g, 88%; Microanalysis: Found (Calc.): C, 76.9 (76.7); H, 5.8 (5.9); N, 8.2 (8.1)%; ^1H NMR: δ 8.19 ppm (t, 1 H, aromatic, $J = 2.74$ Hz), 7.91 ppm (dd, 2H, aromatic, $J = 2.74$ and 8.22 Hz), 7.47 ppm (t, 1H, aromatic, $J = 8.22$ Hz), 7.34-7.22 ppm (m, 10 H, aromatic), 6.60 ppm (t, 2 H, NH, $J = 5.48$ Hz); Selected IR data (KBr): ν(NH) 3290 cm^{-1}, ν(CO) 1635 cm^{-1}; FAB$^+$ MS: m/z 344 [M].

3.2. 1,3-C_6H_4-{C(O)N(PPh_2)CH_2Ph}$_2$ (**1**)

A dry and degassed thf (30 ml) solution of 1,3-C_6H_4-{$CONHCH_2Ph$}$_2$ (0.482 g, 1.4 mmol) was cooled to −78 °C in an acetone-dry ice bath. To the cooled solution was added dropwise a hexane solution of *n*-BuLi (1.2 ml, 2.5 mol dm^{-3}, 2.94 mmol) over 30 min. After the addition the mixture was stirred at −78 °C for 1 h and another 30 additional min at room temperature. The reaction solution was cooled to −78 °C again and to it was added dropwise a solution of diphenylchlorophosphine (0.53 ml, 0.649 g, 2.94 mmol) in thf (10 ml) over 30 min. Stirring was continued for another 1 h at −78 °C. Then the cooling bath was removed and the mixture was stirred overnight at room temperature. The solution was evaporated to dryness in vacuo and dichloromethane (30 ml) was added. Lithium chloride, which precipitated, was removed by filtration under nitrogen and then the volatiles were evaporated in vacuo to leave a white solid.

Yield: 0.758 g, 76%; Microanalysis: Found (Calc.): C, 77.5 (77.4); H, 5.2 (5.4); N, 4.5 (3.9)%; $^{31}P–\{^1H\}$ NMR ($CDCl_3$): 58.5 (s) ppm; Selected IR data KBr (CH_2Cl_2): ν(PN) 916 cm^{-1}, ν(C=O) 1651 cm^{-1}; FAB$^+$ MS: m/z 712 [M], 735 [M + Na]$^+$.

3.3. P,P′,C-[Pt(Cl){1,3-C_6H_4-{C(O)N(PPh_2)CH_2Ph}$_2$}] (**2**)

To a dichloromethane (5 ml) solution of [$PtCl_2$(cod)] (0.035 g, 0.094 mmol) was added a solution of 1,3-C_6H_4-{$CON(PPh_2)HCH_2Ph$}$_2$ (0.071 g, 0.10 mmol) in dichloromethane (5 ml) and the colourless solution stirred for ca. 3 days. The solution was concentrated under reduced pressure to ca. 2 ml and diethyl ether (20 ml) added. The white product was collected by suction filtration and washed with diethyl ether (2 × 10 ml). Yield: 75 mg, 85%; Microanalysis: Found (Calc.): C, 58.6 (58.6); H, 3.3 (4.0); N, 2.8 (3.0)%; $^{31}P–\{^1H\}$ NMR ($CDCl_3$): 67.9 (s) ppm, $^1J(^{195}Pt–^{31}P)$ 3080 Hz; Selected

IR data (KBr): ν(CO) 1651 cm^{-1}, ν(PN) 915 cm^{-1}, ν(PtCl) 306; FAB^+ MS: m/z 942 [M].

3.4. [{Pd(C_3H_5)Cl}$_2${1,3-C_6H_4-{(CO)N(PPh_2)CH_2-Ph}$_2$}] (3)

To a dichloromethane (5 ml) solution of $[(C_3H_5)PdCl]_2$ (0.035 g, 0.09 mmol) was added a solution of 1,3-C_6H_4-{$CON(PPh_2)HCH_2Ph$}$_2$ (0.072 g, 0.10 mmol) in dichloromethane (5 ml) and the colourless solution stirred for ca. 3 days. The solution was concentrated under reduced pressure to ca. 2 ml and diethyl ether (20 ml) added. The white product was collected by suction filtration and washed with diethyl ether (2×10 ml). Yield: 86 mg, 80%; Microanalysis: Found (Calc.): C, 54.4 (54.7); H, 4.2 (4.3); N, 2.3 (2.3)%; ^{31}P–{^1H} NMR ($CDCl_3$): 72.5 (s) ppm; Selected IR data (KBr): ν(CO) 1648 cm^{-1}, ν(PN) 915 cm^{-1}, ν(PdCl) 279 cm^{-1}; FAB^+ MS: m/z 1043 [M–Cl^-].

3.5. Hydroformylation studies

Hydroformylation studies were conducted as described previously [26]. The ligand (0.03 mmol, 0.005 mol dm^{-3}), [$Rh(CO)_2$(acac)] (5.16×10^{-3} g, 0.02 mmol, 0.004 mol dm^{-3}) and toluene (4 ml) were charged into a Schlenk tube and stirred until complexation of the rhodium complex with the phosphine species (total dissolution). The phosphine/rhodium ratio used was 3/2. This solution was placed in a glass lined steel autoclave, CO/H_2 added until 20 bar pressure, the autoclave was heated to 100 °C for the appropiate reaction time and stirred magnetically.

3.6. Crystallography

Crystallography (Table 1) was performed using a Bruker SMART at 125 K; in both cases a minimum of a full hemisphere of data with 0.3 'slices' was collected. Mo Kα radiation was used and multiscan absorption corrections were applied. In **2** because of difficulties with crystal quality the carbon and nitrogen atoms were refined isotropically, all of the other non-H atoms were refined anisotropically with the C–H hydrogen atoms being refined in idealised geometries. All calculations employed the SHELXTL program system [27].

4. Supplementary material

Crystallographic Data for the structural analyses has been deposited with the Cambridge Crystallographic data centre, CCDC Nos. 220834 and 220835. Copies of this information may be obtained free of charge from The Director CCDC, 12 Union Road, Cambridge, CB2 1EZ UK (fax +44-1223-336-033 or e-mail: deposit@ccdc.cam.ac.uk or www: http://www.ccdc.cam.ac.uk).

Acknowledgements

We are grateful to the EPSRC for support, to Johnson Matthey for loans of precious metals and to the JREI for an equipment grant.

References

[1] L. Barkoui, M. Charrouf, M.N. Rager, B. Denise, N. Platzer, H. Rudler, Bull. Chim. Soc. Fr. 134 (1997) 167.
[2] H. Rudler, B. Denise, J.R. Gregario, J. Vaissermann, Chem. Commun. (1997) 2299.
[3] E. Herrmann, O. Navratil, P. Sladek, Phosphorus, Sulfur, Silicon, Relat. Elem. 109–110 (1996) 201.
[4] G. Grossmann, E. Herrmann, O. Navratil, Collect. Czech. Chem. Commun. 55 (1990) 364.
[5] A.M.Z. Slawin, M.B. Smith, J.D. Woollins, J. Chem. Soc., Dalton Trans. (1998) 1537.
[6] D.J. Birdsall, A.M.Z. Slawin, J.D. Woollins, Inorg. Chem. 38 (1999) 4152.
[7] J. Novosad, M. Necas, J. Marek, P. Veltsistas, C. Papadimitriou, I. Haiduc, M. Watanabe, J.D. Woollins, Inorg. Chim. Acta 290 (1999) 256.
[8] T.Q. Ly, J.D. Woollins, Coord. Chem. Rev. 176 (1998) 451.
[9] N. Inguimbert, L. Jäger, M. Taillefer, H.J. Cristau, J. Organomet. Chem. 529 (1997) 257.
[10] J. Münchenberg, O. Böge, A.K. Fischer, P.G. Jones, R. Schmutzler, Phosphorus, Sulfur, Silicon, Relat. Elem. 86 (1994) 103.
[11] A. Schmidpeter, J. Ebeling, Angew. Chem. 70 (1967) 534.
[12] M.A.R. Khayat, F.S. Al-Isa, J. Prakt. Chem. 331 (1988) 149.
[13] R. Appel, Chem. Ber. 105 (1972) 2476.
[14] G. Capozzi, P. Haake, J. Am. Chem. Soc. 94 (1972) 3249.
[15] L. Jäger, N. Inguimbert, M. Taillefer, H.J. Cristau, Synth. Commun. 25 (1995) 2857.
[16] N. Inguimbert, M. Biedermann, H. Stoeckli-Evans, H. Hartung, A. Kolbe, L. Jäger, M. Taillefer, H.J. Cristau, J. Mol. Struct. 519 (2000) 211.
[17] P. Bhattacharyya, A.M.Z. Slawin, J.D. Woollins, Polyhedron 19 (2000) 809.
[18] J.R. Phillips, A.M.Z. Slawin, D.J. Williams, J.D. Woollins, Polyhedron 15 (1996) 3175.
[19] P. Bhattacharyya, A.M.Z. Slawin, D.J. Williams, J.D. Woollins, J. Chem. Soc., Dalton Trans. (1995) 2489.
[20] P. Bhattacharyya, A.M.Z. Slawin, J.D. Woollins, J. Chem. Soc. Dalton (2000) 1545.
[21] T. Appleby, M.L. Clarke, S.M. Aucott, A.M.Z. Slawin, J.D. Woollins, Polyhedron 21 (2002) 2639.
[22] P. Cheshire, A.M.Z. Slawin, J.D. Woollins, Inorg. Chem. Commun. 5 (2002) 803.
[23] S.M. Aucott, A.M.Z. Slawin, J.D. Woollins, Polyhedron 22 (2003) 361.
[24] D. Matt, Polyhedron 10 (1991) 1521.
[25] P. Bhattacharyya, A.M.Z. Slawin, J.D. Woollins, Polyhedron 20 (2001) 1831.
[26] M.R. i Zubiri, M.L. Clarke, D.F. Foster, D.J. Cole-Hamilton, A.M.Z. Slawin, J.D. Woollins, J. Chem. Soc, Dalton (2001) 969.
[27] SHELXTL, Bruker AXS, Madison, 1999.

Available online at www.sciencedirect.com
SCIENCE DIRECT®
Polyhedron 23 (2004) 869–877
POLYHEDRON
www.elsevier.com/locate/poly

Stereocontrol in complexes of cyclam-like macrocycles – influences of chirality

Paul V. Bernhardt [a], Tri Erny Dyahningtyas [b], Sang Cheol Han [b], Jack M. Harrowfield [c,*,1], Il Chool Kim [d], Yang Kim [b,*], George A. Koutsantonis [c], Elisabeth Rukmini [b], Pierre Thuéry [e]

[a] Department of Chemistry, University of Queensland, Brisbane, Qld 4072, Australia
[b] Department of Advanced Materials, Kosin University, 149-1, Dongsam-dong, Yeongdo-gu, Busan 606-701, South Korea
[c] Chemistry, School of Biomedical and Chemical Sciences, University of Western Australia, 35 Stirling Highway, Crawley, WA 6009, Australia
[d] Department of Advanced Materials Engineering, Joongbu University, Chung-Nam, South Korea
[e] CEA/Saclay, DSM/DRECAM/SCM, Bâtiment 125, 91191 Gif-sur-Yvette, France

Received 17 October 2003; accepted 9 December 2003

Abstract

Enforcement of chirality upon a macrocyclic tetramine ligand structure by the introduction of an asymmetric pendent arm which does not significantly modify the macrocycle conformation has no significant effect upon the geometry of the coordination sphere of a bound metal. Where substitution engendering chirality does cause a change in the ligand conformation, in particular for a ligand of restricted stereochemistry, these effects can be much greater. Thus, conversion of 3,7-diazacycloheptane to a macrocycle via attachment of chiral sidearms and ring closure through a template reaction leads to cyclam derivatives with unusual coordination properties.
© 2004 Elsevier Ltd. All rights reserved.

Keywords: Chirality; Tetra-azamacrocycles; Template reaction; Pendent arm; Conformational isomers

1. Introduction

Tetra-azamacrocycles of the cyclam (1,4,8,11-tetra-azacyclotetradecane) type have been prepared with an extraordinary variety of substituents, a common objective of such syntheses being the formation of metal complexes with various pendent arms which facilitate their applications as sensors and catalysts [1]. In the majority of such complexes [2], the macrocycle adopts the "*trans*-III" or *R,S,S,R*-*gauche*-chair-*gauche* conformation which necessarily defines a limited number of pendent arm substituent orientations with respect to the coordinated macrocycle. This conformation is also inherently achiral [3] and appropriate functionalisation of the macrocycle so as to introduce chiral centres is therefore expected, in general, to induce a preference for other conformations. Perhaps the simplest method of generating a chiral cyclam, that of using a chiral amine to provide the central N of a CNC bridge introduced via a template reaction of a tetramine precursor [4–6], might, however, be expected to have a minimal influence [7] and we provide an illustration here of this circumstance. A more elaborate cyclam derivative in which chirality is induced by functionalisation of the ethylene bridges, in contrast, provides an example of more dramatic effects. This cyclam is one of the relatively uncommon group of bridged, bicyclic tetramines which, in many respects, exhibit unusual properties in their metal ion complexes [8,9], so that some differences from unbridged but functionalised cyclams [10] might have been anticipated. Some related, open-chain tetra-aza ligands,

* Corresponding authors. Tel.: +33-03-88-49-32-55; fax: +33-03-90-24-17-19.
E-mail addresses: harrowfield@chimie.u-strasbg.fr (J.M. Harrowfield), ykim@kosin.ac.kr (Y. Kim).
[1] Present address: Universite Louis Pasteur Chimie Inorganique Moleculaire, 1 rue Blaise Pascal, 67008 Strasbourg, France.

0277-5387/$ - see front matter © 2004 Elsevier Ltd. All rights reserved.
doi:10.1016/j.poly.2003.12.014

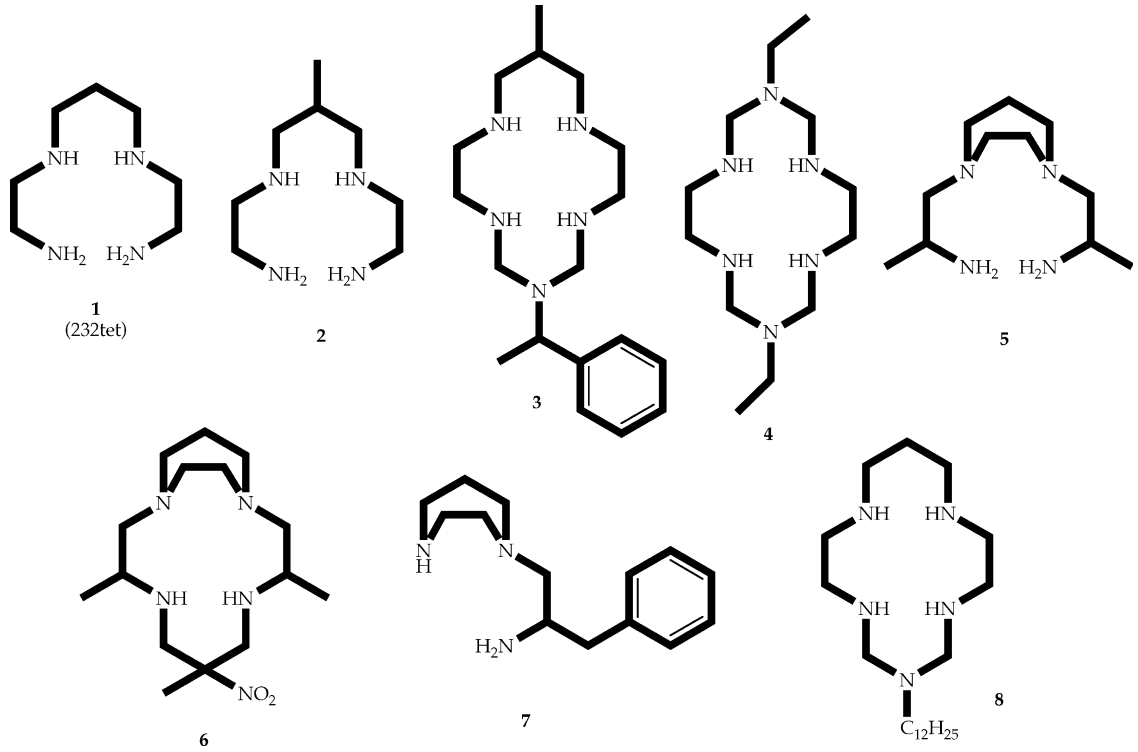

Fig. 1. Polyamine ligands studied in the present work.

derived also from homopiperazine (1,4-diazacycloheptane), are known to be useful as catalysts [11], whereas others are of interest due to their biological activity [12]. All the ligands giving complexes studied in the present work are shown in Fig. 1.

2. Experimental

2.1. Reagents and procedures

(*R*)-1-Phenylethylamine, 3,7-diazaundecane-1,9-diamine ("232tet") (**1**), 1,2-ethanediamine, 1,4-diazacycloheptane, formaldehyde and triethylamine were purchased from the Aldrich Chemical Company and used as received. All organic solvents were distilled prior to use. *N*,*N*′-bis(2-aminoethyl)-2-methylpropane-1,3-diamine (**2**) and its copper(II) complex ([Cu(**2**)]Cl_2) were prepared as described previously [13]. [Cu(**4**)]$(ClO_4)_2$ was prepared by the literature procedure [14] except that the macrocyclic complex was firstly obtained as the chloride and then converted to the perchlorate by precipitation from aqueous solution using $NaClO_4$. *S*,*S*-bis(2-aminopropyl)diazabicyclo[3.2]heptane (**5**) was prepared (from (*S*)-alanine) as a yellowish oil following a literature procedure [15]. Phthaloyl-(*S*)-phenylalanyl chloride was prepared by standard methods [16], as outlined for the alanine analogue in [15].

Ion exchange chromatography was performed under gravity flow using Na^+ form SP-Sephadex C-25 and H^+ form Dowex 50Wx2 (200–400 mesh) cation exchange resins. All eluates were evaporated under reduced pressure (~20 mm Hg) using a Büchi rotary evaporator and a water aspirator.

3. Synthesis

3.1. (3,7-Diazaundecane-1,9-diamine)copper(II) thiocyanate, [Cu(1)NCS]NCS

(This complex was isolated during analysis of the products of a reaction similar to those of present interest but its direct synthesis and structure determination are included here because the structure provides a useful reference point.) 232tet (1.0 g) was added to a solution of $CuCl_2 \cdot 2H_2O$ (1.1 g) in water (50 ml) and the reactants thoroughly mixed. NaNCS (3.0 g) was dissolved in the blue-violet solution produced, a crystalline precipitate then slowly forming as the mixture was cooled on ice. (Yield: 1.3 g.)

3.2. (1,4,6,8,11-Penta-aza-13-methyl-6(1-phenylethyl-cyclotetradecane)copper(II) dithionate (and thiocyanate), [Cu(3)]S_2O_6 (and [Cu(3)]$(NCS)_2$)

(*R*)-1-Phenylethylamine (10 mmol, 0.85 g), triethylamine (22 mmol, 2.5 g) and aqueous formaldehyde (0.1 mol, 8 ml of 37% solution) were added to a methanolic solution (50 ml) of [Cu(**2**)]Cl_2 (10 mmol, 4.1 g) and the

mixture was heated and stirred at 50 °C for 5 h. After evaporation to dryness, the residue was dissolved in water (200 ml) and chromatographed (SP-Sephadex) under elution with 0.3 mol L^{-1} NaCl solution to give a purple leading band of unchanged reactant and a trailing reddish-purple band of the desired macrocyclic product. The second band eluate was taken to dryness and the complex isolated as the chloride, [Cu(**3**]Cl_2(3.2 g), by extraction into ethanol and evaporation of the extract. This was converted to the dithionate by adding $Li_2S_2O_6$ to its concentrated aqueous solution and cooling to ~4 °C. The thiocyanate was obtained similarly, using NaNCS in place of $Li_2S_2O_6$ and the racemic ligand in place of the *R* form. Both compounds formed crystals suitable for diffraction measurements and both structures were solved (see below).

3.3. (9-Methyl-9-nitro-1,4,7,11-tetra-aza-bicyclo[2.3.9] hexadecane)copper(II) perchlorate, [Cu(**6**)]$(ClO_4)_2$ diastereomers

The Cu(II) complex of **5** was prepared by adding $CuCl_2 \cdot 2H_2O$ (1.7 g) to a solution of the crude ligand (2.0 g) in water (100 ml) and was freed of two trace components by chromatography (SP-Sephadex/0.3 mol L^{-1} NaCl). The bulk component eluate was taken to dryness under reduced pressure and the complex extracted from the residue with methanol. Evaporation of the extract gave a blue residue of [Cu(**5**)]Cl_2 which was used directly in the succeeding step. Thus, [Cu(**5**)]Cl_2 (2.0 g) was dissolved in methanol (100 ml) and nitroethane (1.3 g), triethylamine (4 g) and paraformaldehyde (2.2 g) added, before heating the mixture at reflux for three days. The final solution was evaporated to dryness under reduced pressure, dissolved in water (500 ml) and chromatographed on Dowex 50Wx2 with 2 mol L^{-1} HCl to give three bands. Each eluate was evaporated to dryness, giving residues F1 (80 mg), F2 (520 mg) and F3 (880 mg). To obtain crystals suitable for structure determinations, the complexes were converted to their perchlorates by adding $NaClO_4$ to their solutions in ethanol and then adding diethyl ether by vapour diffusion. As in other instances, this resulted in some co-crystallisation with NaCl and $NaClO_4$ but was nonetheless the simplest method for obtaining crystals of sufficient size for the structural work.

3.4. 7 and [Cu(7)Cl]ClO_4

Under a nitrogen atmosphere, a solution of phthaloyl-(*S*)-phenylalanyl chloride (15 g) in DMF (100 ml) was added slowly over 1 h to a cold (0 °C) solution of triethylamine (6 g) and 1,4-diazacycloheptane (2.5 g) in DMF (50 ml). The mixture was stirred overnight and then evaporated to dryness after filtering out a small amount of white solid, presumed to be triethylammonium chloride. A solution of hydrazine hydrate (6 g) in ethanol (500 ml) was added to the residue and the mixture heated at reflux for 3 h. Precipitated phthalhydrazide was filtered out and the filtrate taken to dryness before dissolving the residue in THF (100 ml) and reducing the amide by the gradual addition of $LiAlH_4$ (6 g) under a nitrogen atmosphere, allowing 24 h for reaction. After destroying any excess hydride reagent by the careful addition of water, the reaction mixture was evaporated down to a pasty mass which was transferred to a Soxhlet thimble and the ligand **7** extracted using THF solvent. The extract was evaporated down to a yellow oil. (Yield: 2 g.) Crude ligand (1.0 g) in methanol (100 ml) was mixed with a solution of $CuCl_2 \cdot 2H_2O$ (0.75 g) in methanol (50 ml) and the homogeneous blue solution produced then evaporated to dryness. The residue was dissolved in water (500 ml), absorbed on Na^+ form SP Sephadex C-25 and the column eluted with 0.3 mol L^{-1} NaCl. The bulk of the product eluted rapidly, followed by a very minor, diffuse component which was not further characterised. The blue major-band eluate was evaporated to dryness and the complex extracted into ethanol to separate it from NaCl. Evaporation of the ethanol extract gave 0.7 g of blue powder. Crystals suitable for a structure determination were obtained by vapour diffusion of diethyl ether into an ethanolic solution of the complex containing $NaClO_4$ (see above).

4. Crystallography

The data for [Cu(**6**)($OClO_3$)](ClO_4), [Cu(**6**)(H_2O)]$(ClO_4)_2$ and [Cu(**7**)Cl]ClO_4 were collected in Saclay on a Nonius Kappa-CCD area detector diffractometer [17] using graphite-monochromated Mo Kα radiation (λ 0.71073 Å). The crystals were introduced in glass capillaries with a protecting "Paratone-N" oil (Hampton Research) coating. The unit cell parameters were determined from 10 frames, then refined on all data. A 180° φ-range was scanned with 2° steps during data collection, with a crystal-to-detector distance fixed to 28 mm. The data were processed with DENZO-SMN [18]. The structures were solved by direct methods with SHELXS-97 [19] and subsequent Fourier-difference synthesis and refined by full-matrix least-squares on F^2 with SHELXL-97 [19]. Absorption effects were corrected empirically with the program DELABS from PLATON [20]. The NO_2 and CH_3 groups bound to C10 in [Cu(**6**)(H_2O)]$(ClO_4)_2$ are disordered and have been modelled with two NO_2 groups with occupancy parameters for oxygen atoms constrained to sum to unity, the difference between nitrogen and carbon atoms thus being neglected. All non-hydrogen atoms were refined with anisotropic displacement parameters. The hydrogen atoms bound to nitrogen and oxygen atoms were

found on Fourier-difference maps and all the other ones were introduced at calculated positions. All hydrogen atoms were treated as riding atoms with a displacement parameter equal to 1.2 (NH, OH, CH, CH_2) or 1.5 (CH_3) times that of the parent atom. The Flack parameters [21] were refined to values of −0.01(3) and 0.01(3) for the two structures, respectively. Crystal data and structure refinement parameters are given in Table 1 and selected bond lengths and angles in Fig. 2(c). The molecular plots were drawn using the POVRay option within Xtal 3.7 [22]. All calculations were performed on a Silicon Graphics R5000 workstation.

Intensity data at 296 K for the complexes [Cu(**1**)NCS]NCS, [Cu(**3**)NCS]NCS, [Cu(**3**)OS_2O_5], [Cu(**4**)$(OClO_3)_2$], [Cu(**6**)$(OClO_3)$](ClO_4), and [Cu(**8**)Cl]Cl were collected in Brisbane on an Enraf-Nonius CAD4 four-circle diffractometer using graphite monochromated Mo Kα radiation (λ 0.71073 Å) in the ω-2θ scan mode. Lattice dimensions were determined by a least squares fit of the setting parameters of 25 independent reflections. Data reduction and empirical absorption corrections (ψ-scans) were performed with the WINGX package [23]. Structures were solved by heavy-atom methods with SHELXS and refined by full-matrix least-squares analysis with SHELXL97 [19]. All non-H atoms were refined with anisotropic thermal parameters and H-atoms were constrained at estimated positions. The atomic nomenclature is defined in the figures, Fig. 4(b) being drawn with ORTEP3 [24].

Abnormal features: In the structure of racemic [Cu(**3**)NCS]NCS, disorder in the position of the –C*H$(CH_3)C_6H_5$ group (not shown in the figure ahead) was identified as comprising an approximately equal contribution from the *R* and *S* configurations. Refinement was achieved with the aid of restraints on the geometry of the phenyl ring and isotropic displacement parameters were employed to enable resolution of the different contributors. The relatively weak data for [Cu(**8**)Cl]Cl (16% observed reflections) could not support full anisotropic refinement and only the Cu, Cl and N atoms were refined anisotropically. Nevertheless, the geometry of the complex cation is well defined, albeit at lower precision than the other structures reported here.

5. Results and discussion

The structures of [Cu(**1**)NCS]NCS (Fig. 2(a)), [Cu(**2**)$(OClO_3)_2$] [13], [Cu(**2**)$(O\cdot ClO_2\cdot O)]_{\infty-\infty}ClO_4$ [13] and [Cu(**4**)$(OClO_3)_2$] (Fig. 2(b)), all achiral species, can be regarded as defining constituents of the structure of the chiral complexes of ligand **3**. Note that differences in the nature of the axial ligands in previously known [4,6,7,13,25] such complexes do not seem to give rise to very significant differences in the conformations and

Table 1
Crystal data and structure refinement details

	[Cu(**1**)NCS]NCS	[Cu(**3**)OS_2O_5]	[Cu(**3**)NCS]NCS	[Cu(**4**)$OClO_3$]ClO_4	[Cu(**6**)$OClO_3$]ClO_4	[Cu(**6**)$OClO_3$]ClO_4	[Cu(**6**)(OH_2)]$(ClO_4)_2$	[Cu(**7**)Cl]ClO_4	[Cu(**8**)Cl]Cl·2.5H_2O
Chemical formula	$C_9H_{30}CuN_6S_2$	$C_{18}H_{33}CuN_5O_6S_2$	$C_{20}H_{33}CuN_7S_2$	$C_{12}H_{15}Cl_2CuN_6O_8$	$C_{15}H_{31}Cl_2CuN_5O_{10}$	$C_{15}H_{31}Cl_2CuN_5O_{10}$	$C_{15}H_{33}Cl_2CuN_5O_{11}$	$C_{14}H_{23}Cl_2CuN_5O_4$	$C_{21}H_{52}Cl_2CuN_5O_{2.5}$
M (g mol^{-1})	340.0	543.2	499.2	505.7	575.9	575.9	593.9	431.8	550.1
Space group	$P2_1/n$ (No. 144)[a]	$P3_1$ (No. 144)	*C*2/*c* (No. 15)	$P2_1/n$ (No. 14)[a]	$P2_1$ (No. 4)	$P2_1$ (No. 4)	$P2_12_12_1$ (No. 19)	$P2_12_12_1$ (No. 19)	*C*2/*c* (No. 15)
a (Å)	8.975(1)	8.130(1)	27.511(6)	12.397(2)	8.603(1)	8.538(1)	9.004(2)	6.4582(5)	16.476(1)
b (Å)	14.029(2)	8.130(1)	12.432(1)	10.319(3)	11.2923(8)	11.239(2)	15.271(3)	14.005(1)	6.9765(7)
c (Å)	11.687(2)	31.61(1)	14.827(2)	8.413(3)	12.119(2)	12.007(2)	17.038(3)	19.623(2)	51.847(4)
β (°)	95.35(2)	90	109.17(1)	98.70(1)	101.690(1)	102.084(1)	90	90	96.750(8)
V (Å^3)	1487.7(4)	1809.4(7)	4790(1)	1063.8(4)	1152.9(2)	1126.6(3)	2342.7(8)	1774.9(2)	5888.6(8)
Z	4	3	8	4	2	2	4	4	8
D_{calc} (g cm^{-3})	1.518	1.495	1.384	1.579	1.659	1.698	1.684	1.616	1.241
μ (Mo) (mm^{-1})	1.742	1.327	1.108	1.327	1.240	1.269	1.227	1.555	0.950
λ (Å)	0.71073	0.71073	0.71073	0.71073	0.71073	0.71073	0.71073	0.71073	0.71073
T (K)	296(2)	296(2)	296(2)	298(2)	296(2)	110(2)	100(2)	110(2)	293(2)
R_1[b]	0.0567	0.0599	0.0596	0.0344	0.0436	0.0666	0.0586	0.0469	0.1278
wR_2[c]	0.1456	0.1421	0.1228	0.0775	0.0878	0.1379	0.1314	0.1077	0.2817

[a] Variant of $P2_1/c$.
[b] $R_1 = \sum ||F_o| - |F_c||/|F_o|$ ('observed'' reflections).
[c] $wR_2 = [\sum w(|F_o^2| - |F_c^2|)^2 / \sum w|F_o^2|^2]^{1/2}$ ('observed' reflections).

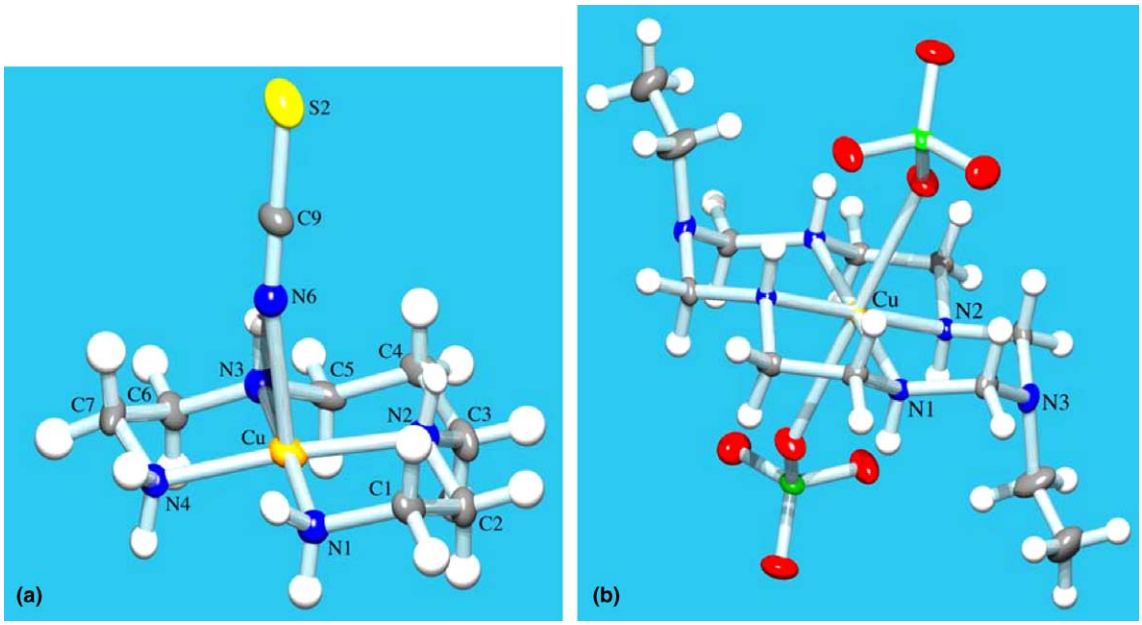

Fig. 2. (a) The complex cation present in the crystal of [Cu(**1**)NCS]NCS. Note that this is actually part of a polymer chain resulting from thiocyanate bridging, with Cu–S 3.240(6) Å. (b) The [Cu(**4**)$(OClO_3)_2$] molecule formally present in crystalline [Cu(**4**)]$(ClO_4)_2$, with Cu–O(ClO_3) 2.586(2) Å. (c) Dimensions (bond angles (upper), bond lengths (lower)) of the essentially planar CuL_4 units found in the present complexes and some reference species.

dimensions of the Cu(II)/tetramine entities. Another example of this is provided in comparing the structure of [Cu(**1**)NCS]NCS with that of [Cu(**1**)$(OClO_3)_2$] [25]. Any differences arising from equatorial vs axial orientations of the methyl substituent in **2** also seem to be slight [13]. The CuN_4 coordination units present in the complexes of ligands **1**, **2** and **4** are identical within NCuN bond angle limits of ±2° and Cu–N bond length limits of ±0.02 Å (Fig. 2(c)) and all, like the complexes of **3**, contain the ligand in a conformation which can be described as *trans*-III. Thus, it is perhaps unsurprising that the chirality of **3** has no dramatic influence on the geometry of the metal ion's primary coordination sphere and that differences associated with the different pendent group and its orientations in the dithionate and thiocyanate complexes of **3** (Figs. 2(c) and 3) are merely comparable to those observed between the other complexes mentioned above. Clearly, if the asymmetry of the pendent arm was to influence reactions at the central metal ion it is unlikely that this could be interpreted in terms of geometric distortions of the coordination geometry. Such differences as are apparent between the dithionate and thiocyanate solids containing $[Cu(\mathbf{3})]^{2+}$ may, of course, reflect that cations of one absolute configuration only are present in the resolved dithionate, whereas enantiomeric species are present in the one lattice for the racemic thiocyanate. That interactions as remote as this must be of negligible influence is, however, suggested by the fact that the geometry of the CuN_4 unit in the complex of a ligand (**8**) analogous to **3** but with a C_{12} chain in place of the phenethyl group [26] and without the methyl substituent lies within the range of those given in Fig. 2(c). Interestingly, when racemic 1-phenylethylamine was used in the synthesis of [Cu(**3**)NCS]NCS, giving crystals belonging to a centric space group, disorder was resolved revealing that the complexes bearing the *R* and *S* forms of the pendent arm occupy the same positions within the lattice with only the C-atoms of the phenylethyl group being disordered. The complex [Cu(**3**)OS_2O_5] obtained from pure (*R*)-1-phenylethylamine of course crystallised in a chiral space group ($P3_1$).

The structure of [Cu(**7**)Cl]ClO_4 (Fig. 4) can be seen as defining part of those of the complexes of **6** and it indicates that both the introduction of a chiral C-centre into a chelate arm and the presence of the mesocyclic homopiperazine moiety have important consequences. The benzyl substituent at the chiral centre is equatorially disposed on the five-membered chelate ring formed in the complex, meaning that the chelate ring must adopt a δ conformation and thus that a 232tet ligand in which both 2-carbon arms are substituted similarly could not coordinate in the usual *gauche*-chair-*gauche* conformation where the two *gauche* units are of opposite chirality (δ and λ). This is well established for many substituted tetramine systems [3,10,27]. Chelation of the homopiperazine unit has perhaps less familiar consequences in that the bond angle subtended at Cu does not lie between those commonly observed for simple 3-carbon and 2-carbon bridges of ~95° and ~85°, respectively, but is considerably smaller than that of a 2-carbon bridge, in [Cu(**7**)Cl]$^+$ being 78.3(2)°. This may to some

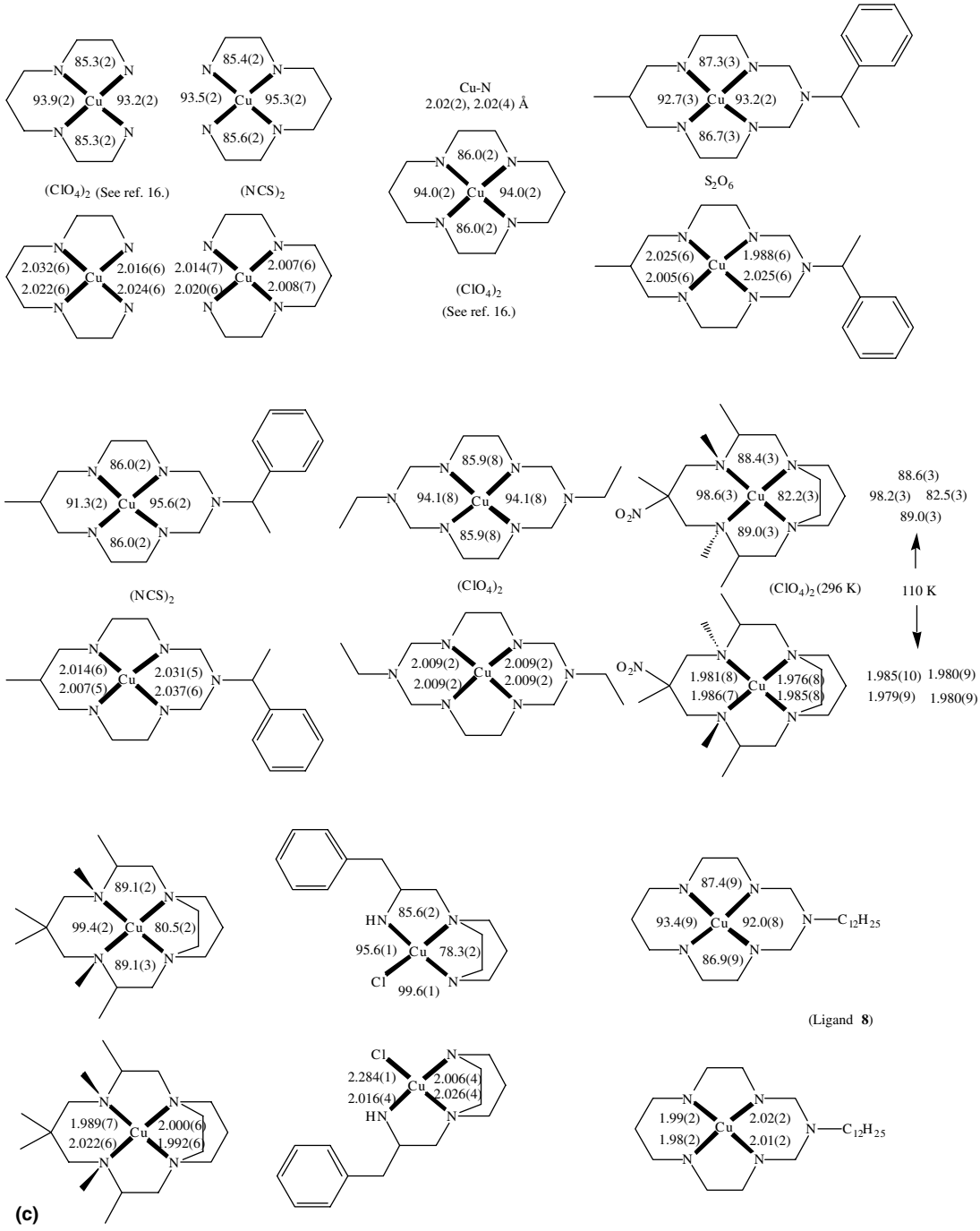

Fig. 2. (*continued*)

extent reflect the fact that there is but a single pendent arm on the mesocycle, since the angle is slightly larger (80.0(2)°) in the Cu(II) complex of a (dipyridyl) tetramine derived from homopiperazine by symmetrical dialkylation of the nitrogen atoms [11], and interestingly this complex has chelate rings formed by the pendent arms which are of the same, rather than opposite, conformation. Thus, it could be said that the small bond angles subtended at Cu(II) by the mesocycle N-donors and the chiral ligand conformations found in complexes of **6** are consistent with their energetics being similar to those of simpler species but the fact that several species are observed indicates that here some factors must be close to being in balance.

Although a clean chromatographic separation of two of the products (F1 and F2) from the reaction leading to the formation of Cu(II) complexes of **6** was achieved, crystal structure determinations on the materials ob-

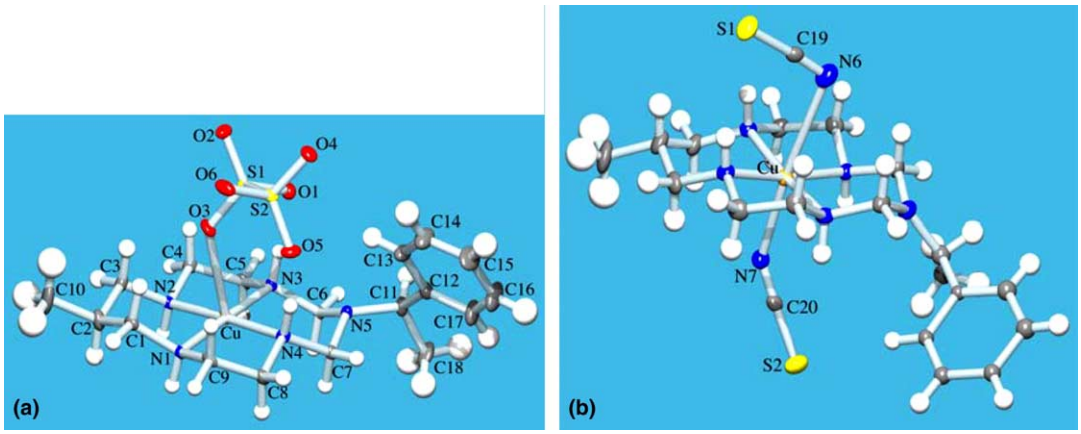

Fig. 3. The coordinated macrocycle units found in (a) the dithionate of optically active $[Cu(\mathbf{3})]^{2+}$ and (b) the thiocyanate of racemic $[Cu(\mathbf{3})]^{2+}$. Disorder not shown in the latter is discussed in the text.

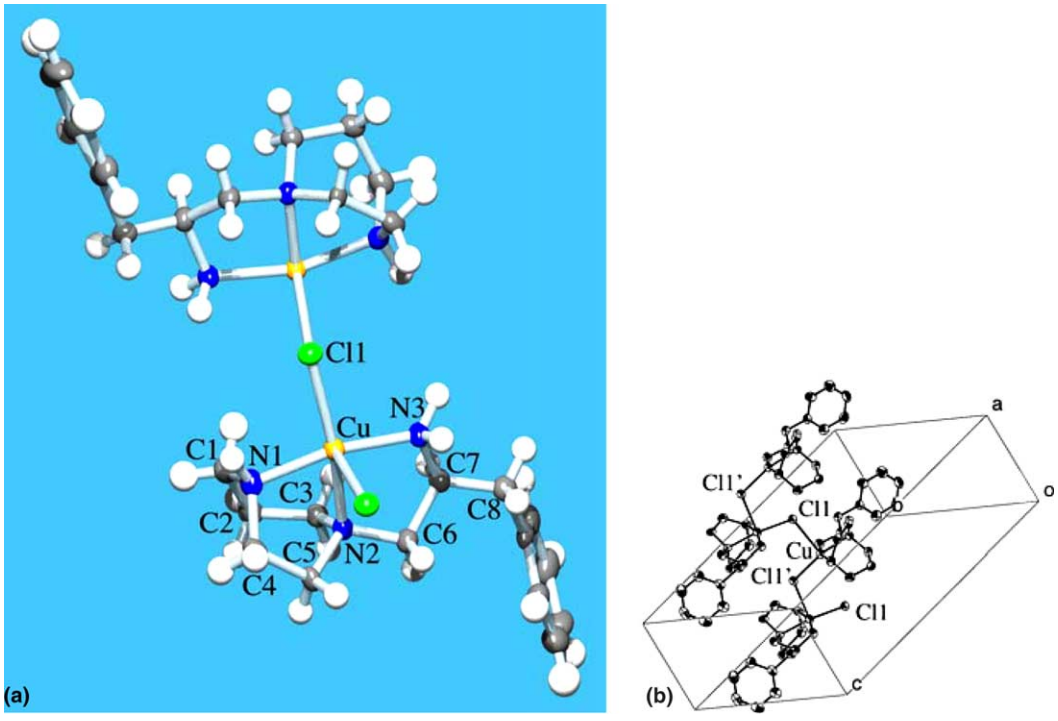

Fig. 4. (a) A view of two $[Cu(\mathbf{7})Cl]^{+}$ entities linked by the chloride bridging which gives rise to their polymerisation. (b) Orientation of the zig-zag $(CuCl)_n$ chains in the unit cell.

tained from the separate eluates proved to be identical. This might be explained by the presence of diastereomers differing with respect to their N-donor configurations which underwent interconversion during the period required for isolation and crystallisation. The result obtained for the structure determination of the product present in F3 of the chromatographic separation, however, requires that the nature of the diastereomer be defined a little more precisely than this.

The two completely independent (Brisbane and Saclay) structure determinations (Fig. 5) on the complex isolated from F1 and F2 are in excellent agreement, especially given a temperature difference of 176 K, the most marked difference being that the bond lengths to perchlorate oxygen atoms (in a tetragonal CuN_4O_2 entity) differ by 0.665 Å at 296 K and by 0.609 Å at 110 K. If indeed it is justified to consider the more remote interaction in both cases as a bond, it is no doubt a very weak one and might therefore be expected to be sensitive to minor structural changes. The structures confirm most obviously the formation of the expected macrocycle, though the 6-membered ring formed by the

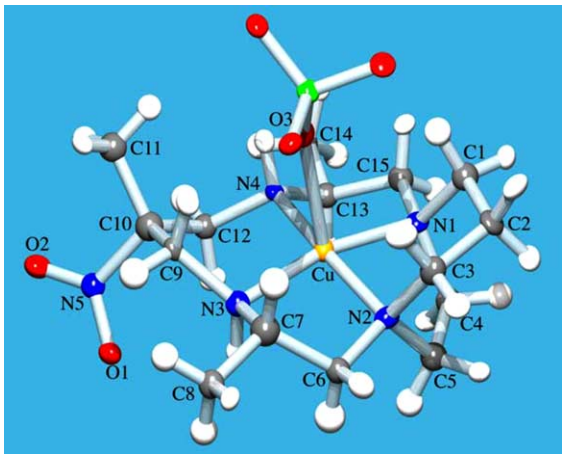

Fig. 5. The complex ion entity formally present in the $[Cu(\mathbf{6})](ClO_4)_2$ species crystallised from the first two chromatographically isolated fractions from the synthesis of the coordinated macrocycle **6**. (Species from the 296 K determination only shown.)

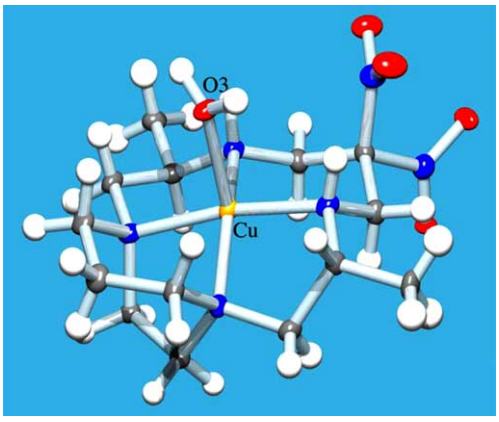

Fig. 6. The complex ion entity formally present in the $[Cu(\mathbf{6})(OH_2)](ClO_4)_2$ species crystallised from the third chromatographically isolated fraction from the synthesis of the coordinated macrocycle **6**. Disorder associated with equal occupancy of both sites on C10 by NO_2 and CH_3 is indicated by showing a nitro group in both positions.

cyclisation reaction is in the uncommon twist-boat conformation, with the two, new chiral-N centres being *R*, *R*. The chiral centres in the 5-membered rings are of the expected *S* configuration (given their derivation from *S*(=L)-alanine), with the methyl substituents equatorial on the rings of δ conformation. There is a stereospecific alignment of the nitro substituent on the side of the near-planar CuN_4 entity bridged by the C_2, rather than the C_3 unit, with one of the nitro-group oxygen atoms being within a hydrogen-bonding distance of one NH. If, by inversion at one N centre, the 6-membered ring were to be converted to its chair form with the nitro substituent in the usual [4,6,13] axial position, the cyclam unit produced would have both 6-membered rings on the same side of the CuN_4 plane, unlike the situation (of being opposite) in the apparently favoured *trans*-III conformation. Though this is hardly a full consideration of the system, it suggests a plausible rationalisation of the observation of two interconverting products, the more stable of which could have the observed structure, as being that there is an unstable diastereomer initially present which does indeed have two chair 6-membered rings, one with an axial nitro substituent, present.

Support for the validity of this argument is provided in the structure obtained for the third reaction product (Fig. 6). Again, the "expected" macrocycle is present but the two chiral N-centres are of opposed configurations (one *R*, one *S*), with the new 6-membered ring being in an essentially chair conformation but defining a cyclam unit where it is on the opposite side of the CuN_4 plane to

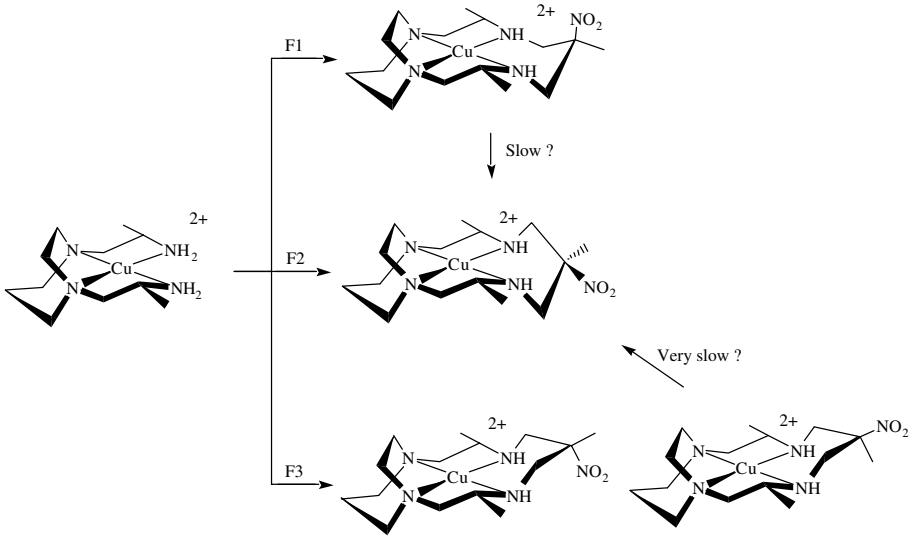

Fig. 7. Proposed products of the reaction of $[Cu(\mathbf{5})]^{2+}$ with HCHO and nitroethane.

the other (derived from the homopiperazine entity). The nitro and methyl substituents on the ring formed by the cyclisation process are disordered equally over axial and equatorial positions, meaning that the isolated material is in fact a mixture of diastereomers. Inversion at the chiral N of *S* configuration would enable the conversion of one of these diastereomers, that where the nitro group is in the "unfavoured" equatorial position, to the same species as that obtained from F1 and F2. This diastereomer is just the other "double chair" species to that postulated to be an unstable form above. Obviously, differences in rates of coordinated-NH deprotonation, coordinated-N inversion or just in stability could explain why one isomer appears to be retained in the system and the other does not. Fig. 7 summarises the proposals presently made for the identity of the various complexes of **6**.

Ignoring features associated with coordination of the macrocycle **6**, the outcome of the cyclisation is such that the reaction may be considered weakly stereoselective, giving the isomer in which the nitro group can be termed "*cis*" with respect to the C_2 bridge of the homopiperazine entity in approximately twice the yield of the "*trans*" isomer. (Although this distribution differs markedly from those for similar isomers observed for 6,13 disubstituted cyclam systems [28], no simple attribution of its cause is obvious.) Presuming the structure determinations to have characterised the predominant species in solution, it appears that it is possible to obtain essentially one Cu(II) complex from each ligand form. The asymmetry of the ligands imposes chirality in different ways upon the metal ion centre, though quantitative measures of these differences remain to be performed. The axial sites of tetragonal Cu(II), occupied here by oxygen atoms from water or perchlorate, are inequivalent but it is not yet clear whether the discrimination is greater or less than that in analogous achiral complexes such as $[Cu(232tet)]^{2+}$. Nonetheless, reduction of the nitro substituent of **6** to an amino group should provide a site for the introduction of various pendent arms upon the macrocycle and thereby allow generation of a group of cyclam-like ligands with properties clearly distinct from those of presently known derivatives.

6. Supplementary materials

CCDC 222031–222039 contain the supplementary crystallographic data for this paper. These data can be obtained free of charge at www.ccdc.cam.uk/conts/retrieving.html [or from the Cambridge Crystallographic Data Centre, 12, Union Road, Cambridge CB2 1EZ, UK; Fax: (internat) +44-1223/336-033; e-mail: deposit@ccdc.cam.ac.uk or www: http://www.ccdc.cam.ac.uk].

Acknowledgements

This work was supported by the Brain Busan 21 Project in 2002.

References

[1] (a) L. Fabbrizzi, F. Foti, M. Licchelli, P.M. Maccarini, D. Sacchi, M. Zema, Chem. Eur. J. 8 (2002) 4965;
(b) K.P. Wainwright, Adv. Inorg. Chem. 52 (2001) 293, and references therein.
[2] M.A. Donnelly, M. Zimmer, Inorg. Chem. 38 (1999) 1650.
[3] J.M. Harrowfield, S.B. Wild, in: G. Wilkinson, J.A. McCleverty, R.D. Gillard (Eds.), Comprehensive Coordination Chemistry, vol. 1, Pergamon Press, Oxford, 1987, p. 179 (Ch. 5).
[4] P.V. Bernhardt, G.A. Lawrance, Coord. Chem. Rev. 104 (1990) 297.
[5] M.P. Suh, Adv. Inorg. Chem. 44 (1997) 93.
[6] (a) P.V. Bernhardt, E.J. Hayes, Inorg. Chem. 42 (2003) 1371;
(b) Inorg. Chem. 41 (2002) 2892;
(c) P.V. Bernhardt, E.G. Moore, M.J. Riley, Inorg. Chem. 41 (2002) 3025;
(d) P. Comba, Y.D. Lampeka, A.Y. Nazarenko, A.I. Prikhod'ko, H. Pritzkow, Eur. J. Inorg. Chem. (2002) 1464.
[7] A. Anastasi, N.F. Curtis, O.P. Gladkikh, T.J.C. Goode, D.C. Weatherburn, Aust. J. Chem. 51 (1998) 673.
[8] R.D. Hancock, M.P. Ngwenya, P.W. Wade, J.C.A. Boeyens, S.M. Dobson, Inorg. Chim. Acta 164 (1989) 73.
[9] C. Hu, T.D. Nguyen, P.S. Wagenknecht, Inorg. Chem. 42 (2003) 742.
[10] M. Rossignoli, P.V. Bernhardt, G.A. Lawrance, M. Maeder, Aust. J. Chem. 50 (1997) 529, and references therein.
[11] J.A. Halfen, J.M. Uhan, D.C. Fox, M.P. Mehn, L. Que Jr., Inorg. Chem. 39 (2000) 4913.
[12] I. Lázár, A. Egri, R. Király, Z. Baranyai, T. Iványi, E. Brücher, Eur. J. Org. Chem. (2002) 351.
[13] M.-H. Choi, J.M. Harrowfield, B.J. Kim, I.-L. Kim, S.-H. Kim, Y. Kim, M.-K. Lee, M. Mocerino, E. Rukmini, B.W. Skelton, A.H. White, J. Chem. Soc., Dalton Trans. (2001) 707.
[14] M.P. Suh, S.-G. Kang, Inorg. Chem. 27 (1988) 2544.
[15] M. Saburi, C. Hattori, S. Yoshikawa, Inorg. Chim. Acta 6 (1972) 427.
[16] J.P. Greenstein, M. Winitz, The Chemistry of the Amino Acids, Wiley, New York, 1961.
[17] Kappa-CCD Software, Nonius BV, Delft, The Netherlands, 1998.
[18] Z. Otwinowski, W. Minor, Methods Enzymol. 276 (1996) 307.
[19] G.M. Sheldrick, SHELXS-97 and SHELXL-97, University of Göttingen, Germany, 1997.
[20] A.L. Spek, PLATON, University of Utrecht, The Netherlands, 2000.
[21] H.D. Flack, Acta Crystallogr., Sect. A 39 (1983) 876.
[22] S.R. Hall, D.J. du Boulay, R. Olthof-Hazekamp (Eds.), Xtal 3.7 System, University of Western Australia, 2000.
[23] L.J. Farrugia, J. Appl. Cryst. 32 (1999) 837.
[24] L.J. Farrugia, J. Appl. Cryst. 30 (1997) 565.
[25] T.G. Fawcett, S.M. Rudich, B.H. Toby, R.A. Lancalette, J.A. Potenza, H.J. Schugar, Inorg. Chem. 19 (1980) 940.
[26] P.V. Bernhardt, Y. Kim, unpublished.
[27] D.A. House, in: G. Wilkinson, J.A. McCleverty, R.D. Gillard (Eds.), Comprehensive Coordination Chemistry, vol. 2, Pergamon Press, Oxford, 1987, p. 23 (Ch. 13).
[28] J.M. Harrowfield, Y. Kim, Y.H. Lee, G.A. Koutsantonis, P. Thuéry, Inorg. Chem. (accepted).

Available online at www.sciencedirect.com
SCIENCE DIRECT®
Polyhedron 23 (2004) 885–894
POLYHEDRON
www.elsevier.com/locate/poly

Synthesis, molecular, crystal and electronic structures of $[(C_6H_6)RuCl(HPz)_2]Cl$ and $[(C_6H_6)RuCl_2(Me_2HPz)]$

J.G. Małecki [a,*], J.O. Dzięgielewski [a], M. Jaworska [b], R. Kruszynski [c,1], T.J. Bartczak [c]

[a] Department of Inorganic and Radiation Chemistry, Institute of Chemistry, University of Silesia, 9th Szkolna St., Katowice 40-006, Poland
[b] Department of Theoretical Chemistry, Institute of Chemistry, University of Silesia, 9th Szkolna St., Katowice 40-006, Poland
[c] X-Ray Crystallography and Crystal Chemistry Group, Institute of General and Ecological Chemistry, Technical University of Łódź, 116 Żeromski St., Łódź 90-924, Poland

Received 24 September 2003; accepted 12 December 2003

Abstract

The reactions of the $(C_6H_6)RuCl_2]_2$ complex with pyrazole and dimethylpyrazole have been examined. The ruthenium complexes, $[(C_6H_6)RuCl(C_3N_2H_4)_2]Cl$ and $[(C_6H_6)RuCl(C_5N_2H_8)_2]$, have been obtained and characterized by IR, UV–Vis and ^1H NMR measurements. Crystal, molecular and electronic structures of the complexes have been determined. The geometries of the complexes were optimized with the DFT method and their UV–VIS spectra were calculated with the TDDFT method.
© 2003 Elsevier Ltd. All rights reserved.

Keywords: Ruthenium arene complexes; Pyrazole; Dimethylpyrazole; X-ray structure; Bond valence

1. Introduction

η^6-Arene ruthenium complexes play a vital role in organometallic chemistry [1a–1e]. Arene ruthenium(II) complexes of the type $[Ru(\eta^6\text{-arene})]^{2+}$ were first made in 1957 by Fisher from anhydrous $RuCl_3$ [2]. These complexes were not convenient precursors to the half-sandwich arene complexes. Winkhaus et al. [3] reported that 1,3-cyclohexadiene undergoes dehydrogenation on reaction with an ethanolic solution of $RuCl_3$ to give the insoluble benzene complex $[(C_6H_6)RuCl_2]_2$. The arene ruthenium halide compounds are key starting materials for the formation of a wide range of natural and cationic ligand derivatives [1d,4a–4d]. The half-sandwich arene ruthenium complexes may serve as excellent catalyst precursors for hydrogenation [4c,5a–5e] and for ring-opening metathesis polymerization [6].

In 1986 McCleverty et al. [7] obtained the complexes $[(C_6H_6)RuCl(HPz)_2]^+$ and $[(C_6H_6)RuCl_2(Me_2HPz)]$. The authors characterized the complexes on the basis of spectroscopic studies (^1H NMR, IR) and noticed that the reaction between $[(C_6H_6)RuCl_2]_2$ and pyrazole gave a mixture, which could not be purified. In this paper we report the syntheses of benzene ruthenium(II) complexes with the pyrazole and dimethylpyrazole ligands and the study of their spectroscopic properties and crystal structures.

2. Experimental

The starting material $[(C_6H_6)RuCl_2]_2$ was synthesized according to the literature procedure [8]. All other reagents were commercially available and were used without further purification.

2.1. Synthesis of $[(C_6H_6)RuCl(HPz)_2]Cl$

A mixture of $[(C_6H_6)RuCl_2]_2$ (0.25 g; 5×10^{-4} mol) and pyrazole (0.21 g; 3×10^{-3} mol) in acetone (100 cm^{-3}) was refluxed for 3 h, cooled and filtered. The yellow crystals suitable for X-ray crystal analysis grew after the reaction mixture was left overnight. Yield 78%. IR(KBr): 3237 ν_{NH}; 3040 $\nu_{CH\text{–pyrazole}}$; 2921, $\nu_{CH\text{–phenyl}}$; 1955, 1872 phenyl; 1569 ν_{CN}, $\nu_{C=C}$; 1480

* Corresponding author. Tel.: +48-32-255911; fax: +48-32-255911.
E-mail addresses: gmalecki@us.edu.pl (J.G. Małecki), kruszyna@ck-sg.p.lodz.pl (T.J. Bartczak).
[1] A holder of the Foundation for Polish Science (FNP) scholarship.

0277-5387/$ - see front matter © 2003 Elsevier Ltd. All rights reserved.
doi:10.1016/j.poly.2003.12.009

$\delta_{(C–CH\ in\ the\ plane)}$; 1432 $\nu_{Ph(P–Ph)}$; 1266 $\delta_{(NH;CH)}$; 1089, 1022 $\delta_{(C–CH\ in\ the\ plane)}$; 813 $\delta_{(C–C\ out\ of\ the\ plane)}$; 746 $\delta_{(C–C\ out\ of\ the\ plane)}$; 695 $\delta_{(C–C\ in\ the\ plane)}$; 590 $\nu_{P–Ph}$. ^{1}H NMR (δ, $CDCl_3$): 11.51 (NH; 2H); 6.10 (s, 6H, C_6H_6); 6.40 (t, 2H, CH pyrazole); 7.72 (d, 2H, CH pyrazole); 8.01 (d, 2H, CH pyrazole); 2.15 *Anal*. Calc. for $C_{12}H_{14}C_{l2}N_4Ru$: C, 37.32; H, 3.65; N, 14.51. Found: C, 36.52; H, 3.15; N, 14.59%.

2.2. Synthesis of $[(C_6H_6)RuCl_2\ (Me_2HPz)]$

A mixture of $[(C_6H_6)RuCl_2]_2$ (0.25 g; 5×10^{-4} mol) and dimethylpyrazole (0.5 g; 3×10^{-3} mol) in acetone (100 cm^{-3}) was refluxed for 4 h, cooled and filtered. The red crystals suitable for X-ray crystal analysis grew after the reaction mixture was left overnight. Yield 64%. IR(KBr): 3240 ν_{NH}; 3040 $\nu_{CH\text{-}pyrazole}$; 2920, $\nu_{CH\text{-}phenyl}$; 1950, 1878 phenyl; 1572 ν_{CN}, $\nu_{C=C}$; 1485 $\delta_{(C–CH\ in\ the\ plane)}$; 1430 $\nu_{Ph(P–Ph)}$; 1262 $\delta_{(NH;CH)}$; 1093, 1025 $\delta_{(C–CH\ in\ the\ plane)}$; 810 $\delta_{(C–C\ out\ of\ the\ plane)}$; 749 $\delta_{(C–C\ out\ of\ the\ plane)}$; 698 $\delta_{(C–C\ in\ the\ plane)}$; 592 $\nu_{P–Ph}$. ^{1}H NMR (δ, $CDCl_3$): 11.01 (NH; H); 5.99 (s, 1H, CH pyrazole); 5.85 (s, 1H, CH pyrazole); 5.76 (s, 6H, C_6H_6); 2.52 (s, 3H, CH_3); 2.21 (s, 3H, CH_3); 1.80 (s, 3H, CH_3) *Anal*. Calc. for $C_{11}H_{14}C_{l2}N_2Ru$: C, 38.16; H, 4.08; N, 8.09. Found: C, 38.10; H, 3.99; N, 8.12%.

2.3. Physical measurements

Infrared spectra were recorded on a Nicolet Magna 560 spectrophotometer in the spectral range 4000–400 cm^{-1} with the sample in the form of a KBr pellet. Electronic spectra were measured on a spectrophotometer Lab Alliance UV-Vis 8500 in the range 800–220 nm in deoxygenated dichloromethane solution. Elemental analyses (C, H, N) were performed on a Perkin–Elmer CHN-2400 analyzer. The ^{1}H NMR spectra were recorded on a Bruker DRX-400 spectrometer in $CDCl_3$ solutions.

2.4. DFT calculations

The GAUSSIAN 03 program [9] was used in the calculations. The geometry optimization was carried out with the DFT method with the use of B3LYP functional [10,11]. The electronic spectrum was calculated with the TDDFT method [12]. LANL2DZ basis set [13] was used on the ruthenium atom, 6-31G(d) on the chlorine, nitrogen and carbon atoms and 6-31G basis on the hydrogen atoms in the calculations.

2.5. Crystal structures determination and refinement

A yellow thin plate crystal of $[(C_6H_6)RuCl(HPz)_2]Cl$ and an orange needle crystal of $[(C_6H_6)RuCl(C_3N_2H_4)_2]$ were mounted on a KM-4-CCD automatic diffractometer equipped with CCD detector and used for data collection. X-ray intensity data were collected with graphite monochromated Mo Kα radiation at a temperature of 293.0(2) K, with the ω scan mode. Forty two and 22 s exposure time, respectively, were used and a quarter and a half of the Ewald sphere was collected up

Table 1
Crystal data and structure refinement for $[(C_6H_6)RuCl(HPz)_2]Cl$ and $[(C_6H_6)RuCl_2(Me_2HPz)]$

Empirical formula	$C_{12}H_{14}C_{l2}N_4Ru$	$C_{11}H_{13}C_{l2}N_2Ru$
Formula weight	386.24	345.20
Crystal system, space group	monoclinic, $P2_1/n$ (No. 14)	triclinic, $P\bar{1}$ (No. 2)
Unit cell dimensions		
a (Å)	12.7755(8)	7.9513(6)
b (Å)	8.8749(4)	9.9764(11)
c (Å)	13.3238(6)	16.8218(9)
α (°)	90	81.944(7)
β (°)	105.164(5)	81.030(5)
γ (°)	90	77.693(8)
Volume (Å^3)	1458.07(13)	1279.86(18)
Z, d_{calc} (Mg m^3)	4, 1.760	4, 1.792
Absorption coefficient (mm^{-1})	1.432	1.616
$F(000)$	768	684
Crystal size (mm)	$0.19 \times 0.13 \times 0.03$	$0.51 \times 0.22 \times 0.15$
Theta range for data collection (°)	3.45–25.11	3.49–25.10
Index ranges	$-15 \leqslant h \leqslant 14$, $0 \leqslant k \leqslant 10$, $0 \leqslant l \leqslant 15$	$-9 \leqslant h \leqslant 9$, $-11 \leqslant k \leqslant 11$, $0 \leqslant l \leqslant 20$
Reflections collected/unique	2600/2600 [$R_{int} = 0.0000$]	4560/4560 [$R_{int} = 0.0000$]
Completeness to $2\theta = 25.11$ (%)	93.3	99.7
Maximum and minimum transmission	0.9624 and 0.7686	0.7901 and 0.4906
Refinement method	full-matrix least-squares on F^2	full-matrix least-squares on F^2
Data/restraints/parameters	2600/0/172	4560/0/293
Goodness-of-fit on F^2	1.095	1.046
Final R indices [$I > 2\sigma(I)$]	$R_1 = 0.0498$, $wR_2 = 0.1145$	$R_1 = 0.0697$, $wR_2 = 0.2372$
R indices (all data)	$R_1 = 0.0710$, $wR_2 = 0.1287$	$R_1 = 0.0727$, $wR_2 = 0.2402$
Largest difference peak and hole (e Å^{-3})	1.223 and −0.622	4.535 and −1.177

to $2\theta = 50.21°$. The unit cell parameters were determined from least-squares refinement of the setting angles of 3513 and 4793 of the strongest reflections respectively. Details concerning crystal data and refinement are given in Table 1. Lorentz, polarization and numerical absorption [14] corrections were applied. The structures were solved by direct methods. All the non-hydrogen atoms were refined anisotropically using the full-matrix, least-squares technique on F^2. All the hydrogen atoms were found from difference Fourier synthesis after four cycles of anisotropic refinement and refined as "riding" on the adjacent atom with an individual isotropic temperature factor equal to 1.2 times the value of the equivalent temperature factor of the parent atom. SHELXS 97 [15], SHELXL 97 [16] and SHELXTL [17] programs were used for all the calculations. Atomic scattering factors were those incorporated in the computer programs.

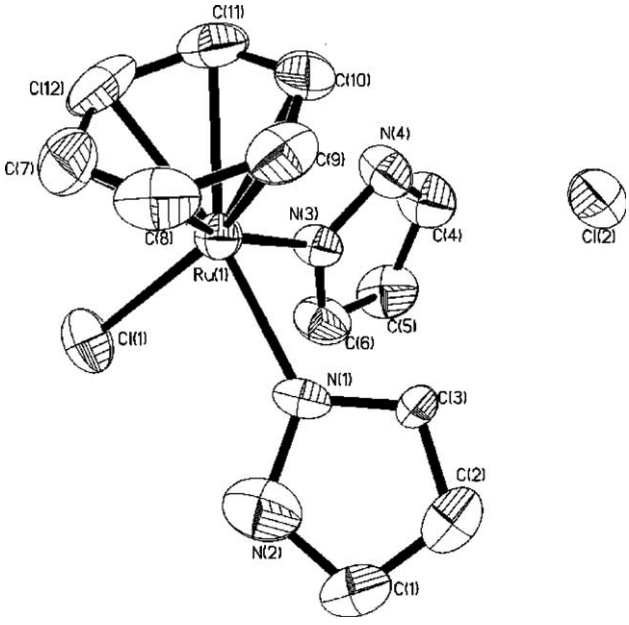

Fig. 1. ORTEP drawing of $[(C_6H_6)RuCl(HPz)_2]Cl$ with 50% probability thermal ellipsoids. Hydrogen atoms have been omitted for clarity.

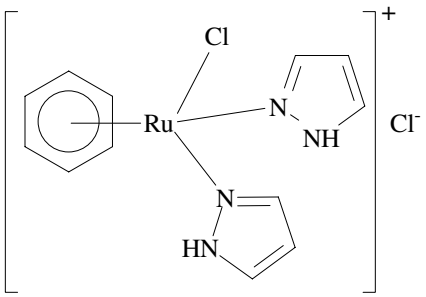

Fig. 2. Structural drawing of $[(C_6H_6)RuCl(HPz)_2]Cl$.

3. Results and discussion

Refluxing of the ruthenium(II) benzene complex $[(C_6H_6)RuCl_2]_2$ with an excess of pyrazole or dimethylpyrazole in acetone leads to the half-sandwich $[(C_6H_6)RuCl(HPz)_2]Cl$ and $[(C_6H_6)RuCl_2(Me_2HPz)]$ complexes in high yield. The elemental analyses of the complexes are in good agreement with their formulation. The characteristic bands of the pyrazole ligand ν(NH) at 3268 cm^{-1} and ν(CN), ν(C=C) at 1516 cm^{-1} are present in the IR spectra of the obtained complexes. The ^1H NMR spectra of the complexes showed the sharp singlets at 6.10 and 5.76 ppm, respectively, characteristic of the coordinated η^6-C_6H_6 ligand. The pyrazole ligand showed a signal at 11.71 ppm (NH) and the sets of signals at 6.40 (t, 2H); 7.72 (d, 2H); 8.01 (d, 2H) from H atoms on different C atoms of the pyrazole ring for the cationic complex and 11.01 (NH); 5.99 (s, 1H); 5.85 (s, 1H); 2.52 (s, 3H); 2.21 (s, 3H); 1.80 (s, 3H) for the complex with the dimethylpyrazole ligand.

3.1. Crystal structures

The $[(C_6H_6)RuCl(HPz)_2]Cl$ complex crystallizes in the monoclinic space group $P2_1/n$. The molecular structure of the compound is shown in Fig. 1 (structural drawing of the complex is presented in Fig. 2). The selected bond lengths and angles are listed in Table 2. The ruthenium atom is in a formally six-coordinate environment, and the structure of the cation complex $[(C_6H_6)RuCl(HPz)_2]^+$ adopts a distorted piano-stool type of geometry with angles around the ruthenium of 82.08(19)° (N(3)–Ru–N(1)), 85.79(14)° (N(3)–Ru–Cl(1)), 87.26(14)° (N(1)–Ru–Cl(1)). The benzene ring is planar and the Ru–C distances are almost equal with an average bond length of 2.182(8) Å (range 2.167(7)–2.194(6) Å). The Ru(1) to benzene centroid distance is 1.676 Å and this is consistent with those values reported for other Ru(II) η^6-arene complexes [4d,18,19]. The Ru–Cl(1) bond length of 2.4026(17) Å is of the same order as in related cationic arene ruthenium(II) compounds [19,20]. The pyrazole Ru–N(1) and Ru–N(2) distances are essentially identical and are in the range of Ru–N distances [21].

Three intermolecular hydrogen bonds [22–24] linking the chlorine anion and pyrazole ring N(4)–H(4)···Cl(2# $-x+1, -y+1, -z$) (D···A distance 3.067(6) Å, D–H···A angle 148.1°), C(1)–H(1)···Cl(2# $-x+1/2, y-1/2, -z-1/2$) (D···A distance 3.559(7) Å, D–H···A angle 147.3°), C(3)–H(3)···Cl(2) (D···A distance 3.068(6) Å, D–H···A angle 175.1°) atoms are observed. Two other intramolecular weak hydrogen bonds are present in the structure of the complex: between arene C(11)–H(11) and Cl(1# $-x+1/2, y+1/2, -z+1/2$) (D···A distance 3.565(8) Å, D–H···A angle 149.7°) and

Table 2
Selected bond lengths (Å) and angles (°) for $[(C_6H_6)RuCl(HPz)_2]Cl$

Bond lengths	
Ru(1)–N(3)	2.106(5)
Ru(1)–N(1)	2.111(5)
Ru(1)–C(12)	2.167(7)
Ru(1)–C(9)	2.177(6)
Ru(1)–C(7)	2.181(7)
Ru(1)–C(11)	2.181(7)
Ru(1)–C(8)	2.192(7)
Ru(1)–C(10)	2.194(6)
Ru(1)–Cl(1)	2.4026(17)
Bond angles	
N(3)–Ru(1)–N(1)	82.08(19)
N(3)–Ru(1)–Cl(1)	85.79(14)
N(3)–Ru(1)–C(11)	93.8(2)
N(3)–Ru(1)–C(9)	122.5(2)
N(3)–Ru(1)–C(7)	154.3(3)
N(1)–Ru(1)–Cl(1)	87.26(14)
N(1)–Ru(1)–C(7)	122.9(3)
N(1)–Ru(1)–C(11)	151.8(3)
N(1)–Ru(1)–C(9)	91.6(2)
N(1)–Ru(1)–C(7)	122.9(3)
C(7)–Ru(1)–Cl(1)	89.1(2)
C(11)–Ru(1)–Cl(1)	120.5(2)
C(9)–Ru(1)–Cl(1)	151.2(2)
C(11)–Ru(1)–C(9)	67.0(3)
C(7)–Ru(1)–C(11)	67.2(3)

between pyrazole N(2)–H(2) and Cl(1# $-x$, $-y$, $-z$) (D···A distance 3.833(7) Å, D–H···A angle 119.7°). In this way an infinite three-dimensional hydrogen-bonded net has been created. The possibility of benzene ring stacking interaction was rejected due to the large distance between parallel rings. There are no unusual intermolecular short contacts, except for the described hydrogen bonds.

The bond valences were computed as $v_{ij} = \exp[(R_{ij} - d_{ij})/B]$ [25–27], where R_{ij} is the bond-valence parameter (in the formal sense R_{ij} is the single-bond length between i and j atoms) [28]. The bond valence parameters [25] have been determined only for: Ru(+4) ($R_{Ru–Cl}$), without specification of the oxidation state of Ru ($R_{Ru–N}$), and $R_{Ru–\pi}$ was never determined. Thus, all these parameters were calculated for Ru(+2). The $R_{Ru–N}$ was determined by fit to the bond lengths method [28] for 282 Ru(+2) six-coordinated complexes found in the literature, [2] where donors were coordinating by nitrogen organic ligands. The computed $R_{Ru–N}$ valence parameter was equal to 1.656 Å, and checking statistics of total Ru valence was: mean error = 0.0071; median = 2.014; mode, 2.052; SD, 0.128; sampling variance = 0.0165; kurtosis = 0.494 and skewness = −0.273. Because both types of structures with chelating and monodendate ligands were used for statistics, there might be a systematic error in analysis resulting from steric restrains of chelating ligands. Thus, all calculations were performed for a group of complexes with monodendate ligands, [2] and $R_{Ru–N} = 1.68$ Å and statistics were: 0.0314, 1.975, cannot be calculated, 0.180, 0.0325, 1.249 and 1.453 in the order as above. According to calculated statistics, the difference of 0.02 Å between $R_{Ru–N}$ comes only from the amount of data, thus the value 1.656 Å was used as a proper $R^{II}_{Ru–N}$ value. Because there exists only eight structures with Ru coordinated only by six Cl atoms [2], the $R_{Ru–Cl}$, parameter was based on the cross and fit to the bond lengths method, using structures with a coordination sphere of the general formula $Ru(N_nCl_{6-n})$, where $n \in \langle 0–5 \rangle$. For 145 structures founded in the literature [2], the obtained $R_{Ru–Cl}$ value is 1.932 Å and statistics are: 0.0144, 1.986, 1.944, 0.184, 0.0337, 1.079 and 0.547 in the order as above. The $R_{Ru–\pi}$ parameter was determined in two different ways: by fit to the bond lengths in 41 π–Ru–π complexes for 54 data [2] and by cross and fit to the bond lengths method in 116 π-$Ru(N_nCl_{3-n})$, where $n \in \langle 0–3 \rangle$ [2]. In first case obtained, valence parameter value was 1.731 Å and statistics, ordered as above, were: 0.0097, 2.005, cannot be calculated, 0.071, 0.0051, −0.041 and 0.123. In second case the obtained valence parameter has a value of 1.725 Å and statistics were: 0.0058, 1.999, 1.974, 0.075, 0.0056, 4.391 and 0.751, in the order as above, thus $R_{Ru–\pi} = 1.731$ Å was chosen as a correct value. The value of B was taken as 0.37 according to the literature [26]. The computed bond valences of the ruthenium are $v_{Ru–Cl} = 0.280$, $v_{Ru–N} = 0.292$, 0.296 and $v_{Ru–\pi} = 1.158$ v.u. (Ru-centroid of aromatic ring distance is 1.6766(6) Å), which shows that the Ru–N and Ru–Cl bonds have the same strength and Ru–π is about four times stronger. The total valence of Ru(1) is 2.027 v.u. which agrees with the formal oxidation state of Ru. This also confirms that the calculated valence parameters have proper values because only violation of the valence-sum rule can indicate mistakes in the interpretation of the structure or structural parameters [28,29].

The complex $[(C_6H_6)RuCl_2\ (Me_2HPz)]$ crystallizes in the triclinic space group $P\bar{1}$ and the crystal structure is built up of two independent molecules in the asymmetric unit. The relative orientation of molecules is depicted in Fig. 3 (the structural drawing is presented in Fig. 4) which also shows the thermal vibration ellipsoids of the non-hydrogen atoms. The coordination about ruthenium is formally six and the structure adopts a distorted piano-stool type of geometry. The selected bond lengths and angles are given in Table 3. The distances and the angles between appropriate atoms in the two molecules are similar. Weighted root mean square deviation of superpositioned molecules is 0.054(7). The most different distance is Ru(1)–C(10) 2.149(11) Å and Ru(51)–C(60) 2.188(11) Å, and the most different angles are

[2] The references were collected from the Cambridge Structural Database v 5.24, November 2002. The list of papers is available as supplementary material on request from R. Kruszyński kruszyna@ck-sg.p.lodz.pl.

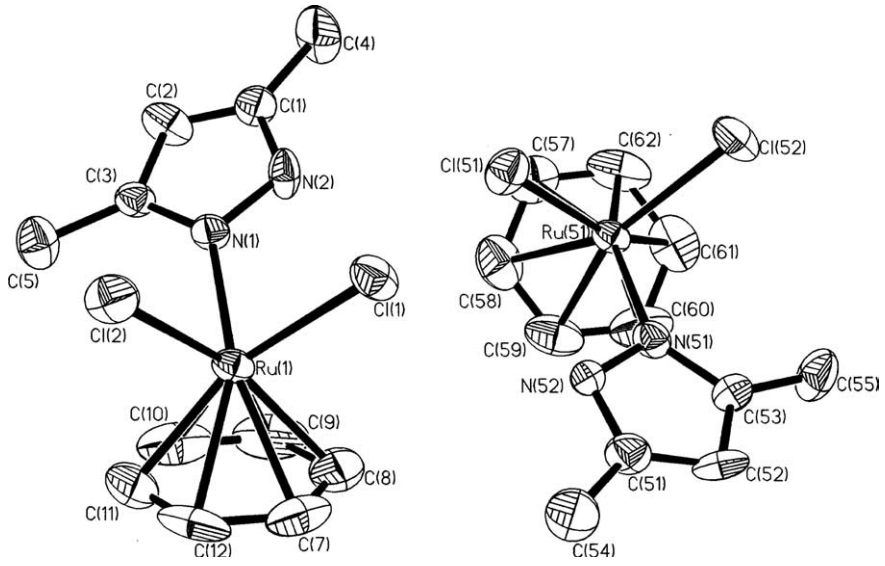

Fig. 3. Relative orientation of the two molecules of $[(C_6H_6)RuCl_2(Me_2HPz)]$ in the asymmetric unit. Thermal vibration ellipsoids scaled to include 50% probability. Hydrogen atoms have been omitted.

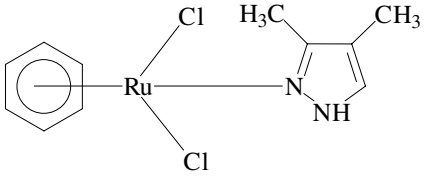

Fig. 4. Structural drawing of $[(C_6H_6)RuCl_2(Me_2HPz)]$.

Cl(1)–Ru(1)–C(7) 92.7(3)° and Cl(51)–Ru(51)–C(57) 91.5(3)°; C(11)–Ru(1)–C(7) 67.0(5)° and N(61)–Ru(51)–C(57) 68.0(5)°. The Ru–Cl bonds length are of the same order as in related compounds (2.423(2) Å for Ru(1)–Cl(1), 2.410(2) Å for Ru(1)–Cl(2), 2.417(2) Å for Ru(51)–Cl(51) and 2.412(2) Å for Ru(51)–Cl(52)). The Me_2HPz ligand displays a Ru–N distance of 2.122(7) Å

Table 3
Selected bond lengths (Å) and angles (°) for $[(C_6H_6)RuCl_2(Me_2HPz)]$

Bond lengths			
Ru(1)–Cl(1)	2.423(2)	Ru(51)–Cl(51)	2.417(2)
Ru(1)–Cl(2)	2.410(2)	Ru(51)–Cl(52)	2.412(2)
Ru(1)–N(1)	2.122(7)	Ru(51)–N(51)	2.125(7)
Ru(1)–C(7)	2.180(10)	Ru(51)–C(57)	2.167(10)
Ru(1)–C(8)	2.155(11)	Ru(51)–C(58)	2.158(11)
Ru(1)–C(9)	2.165(11)	Ru(51)–C(59)	2.170(11)
Ru(1)–C(10)	2.149(11)	Ru(51)–C(60)	2.188(11)
Ru(1)–C(11)	2.151(11)	Ru(51)–C(61)	2.160(11)
Ru(1)–C(12)	2.175(10)	Ru(51)–C(62)	2.177(10)
Bond angles			
Cl(1)–Ru(1)–Cl(2)	88.21(9)	Cl(51)–Ru(51)–Cl(52)	87.59(9)
Cl(1)–Ru(1)–N(1)	85.9(2)	Cl(51)–Ru(51)–N(51)	86.0(2)
Cl(1)–Ru(1)–C(7)	92.7(3)	Cl(51)–Ru(51)–C(57)	91.5(3)
Cl(1)–Ru(1)–C(9)	116.0(5)	Cl(51)–Ru(51)–C(59)	116.1(4)
Cl(1)–Ru(1)–C(11)	157.2(4)	Cl(51)–Ru(51)–C(61)	156.8(4)
Cl(2)–Ru(1)–N(1)	86.3(2)	Cl(52)–Ru(51)–N(51)	86.6(2)
Cl(2)–Ru(1)–C(7)	115.9(3)	Cl(52)–Ru(51)–C(57)	116.4(3)
Cl(2)–Ru(1)–C(9)	155.6(5)	Cl(52)–Ru(51)–C(59)	156.2(4)
Cl(2)–Ru(1)–C(11)	91.4(4)	Cl(52)–Ru(51)–C(61)	91.9(4)
N(1)–Ru(1)–C(7)	157.7(4)	N(51)–Ru(51)–C(57)	156.8(4)
N(1)–Ru(1)–C(9)	92.4(4)	N(51)–Ru(51)–C(59)	92.1(4)
N(1)–Ru(1)–C(11)	116.9(4)	N(51)–Ru(51)–C(61)	117.1(4)
C(11)–Ru(1)–C(7)	67.0(5)	C(61)–Ru(51)–C(57)	68.0(5)
C(11)–Ru(1)–C(9)	67.5(6)	C(61)–Ru(51)–C(59)	67.5(5)
C(9)–Ru(1)–C(7)	68.2(5)	C(57)–Ru(51)–C(59)	68.3(4)

for Ru(1)–N(1) and 2.125(7) Å for Ru(51)–N(51), which are similar and in the range of Ru–N distances. The ruthenium to benzene centroid distance varies from 1.655(9)Å (Ru(1)) to 1.658(2) Å (Ru(51)). The benzene ring is planar and the Ru–C distances are almost equal with an average bond length of 2.166(11) Å (2.163(10) Å for Ru(1)–C to 2.17(11) Å for Ru(51)–C). The computed bond valences of the Ru(1) atom are $v_{Ru-Cl} = 0.265$, 0.275 $v_{Ru-N} = 0.284$ and $v_{Ru-\pi} = 1.225$ v.u. and for the Ru(2) atom are $v_{Ru-Cl} = 0.273$, 0.270 $v_{Ru-N} = 0.282$ and $v_{Ru-\pi} = 1.217$ v.u. (Ru-centroid of aromatic ring distances are 1.656(6) and 1.658(7) Å for molecules indicated by Ru(1) and Ru(2) atoms, respectively), which shows, like in the above described compound, that the Ru–N and Ru–Cl bonds have the same strength and Ru–π is about four times stronger. The total valence of the Ru(1) atom is 2.049 v.u. and that of the Ru(2) atom is 2.049 v.u., which agrees with the formal oxidation state of Ru. This also confirms that the calculated valence parameters have proper values because only violation of the valence-sum rule can indicate mistakes in the interpretation of the structure or structural parameters [28,29].

The molecules of $[(C_6H_6)RuCl_2(Me_2HPz)]$ (Fig. 4) are linked via multiple intermolecular weak C–H···Cl hydrogen bonds [22–24] to generate the infinite three dimensional network (Table 4).

3.2. Geometry optimization and electronic structure

The geometry of the singlet and triplet state was optimized for the $[(C_6H_6)Ru(Hpz)_2Cl]^+$ cation and $[(C_6H_6)RuCl_2(Me_2HPz)]$ molecule. The triplet–singlet energy difference and the optimized geometry parameters for the singlet state are given in Table 5. In Table 6 the energies of several HOMO and LUMO orbitals of $[(C_6H_6)Ru(Hpz)_2Cl]^+$ and $[(C_6H_6)RuCl_2(Me_2HPz)]$ are gathered. In both cases the singlet state is lower in energy, but the triplet–singlet energy difference is smaller for $[(C_6H_6)RuCl_2(Me_2HPz)]$ (6.1 kcal/mol) than for $[(C_6H_6)Ru(Hpz)_2Cl]^+$ (20.9 kcal/mol). This agrees with the smaller HOMO–LUMO gap in $[(C_6H_6)RuCl_2(Me_2HPz)]$ (3.90 eV) than in $[(C_6H_6)Ru(Hpz)_2Cl]^+$ (4.23 eV). The optimized bond distances agree well with the experimental ones, the largest differences are for the metal–benzene carbon bonds. The shortening of the metal–benzene carbon distances in $[(C_6H_6)RuCl_2(Me_2HPz)]$ relatively to $[(C_6H_6)Ru(Hpz)_2Cl]^+$ is reproduced in the optimized structures.

In Fig. 5 several HOMO and LUMO orbitals of $[(C_6H_6)Ru(Hpz)_2Cl]^+$ are depicted. In the free benzene molecule, the π-electron configuration is $\pi_1(a_{2u})^2$ $\pi_2(e_{1g})^2$ $\pi_3(e_{1g})^2$ $\pi_4^*(e_{2u})^0$ $\pi_5^*(e_{2u})^0$ $\pi_6^*(b_{2g})^0$. The bonding between benzene and ruthenium is formed by the two π orbitals of e_{1g} symmetry (π_2 and π_3) and the empty d_{xz} and d_{yz} orbitals of the metal atom (donation from benzene to ruthenium). The resulting bonding orbitals are HOMO − 10, HOMO − 11 and HOMO − 12, HOMO − 11 in $[(C_6H_6)Ru(Hpz)_2Cl]^+$ and $[(C_6H_6)$

Table 5
Triplet–singlet energy difference and optimized geometry parameters for $[(C_6H_6)RuCl(HPz)_2]^+$ and $[(C_6H_6)RuCl_2(Me_2HPz)]$

	$[(C_6H_6)RuCl(HPz)_2]^+$	$[(C_6H_6)RuCl_2(Me_2HPz)]$
ΔE(T–S) (kcal/mol)	20.9	6.1
Ru–C(benz)[a]	2.280 (2.182)	2.250 (2.162)
Ru–N1(Hpz)	2.119 (2.105)	
Ru–N2(Hpz)	2.133 (2.112)	
Ru–N1(Me_2HPz)		2.140 (2.122)
Ru–Cl1	2.452 (2.402)	2.442 (2.410)
Ru–Cl2		2.489 (2.423)

Bond distances in Å (the experimental values are in parentheses).
[a] Average value.

Table 6
Orbital energies for $[(C_6H_6)RuCl(HPz)_2]^+$ and $[(C_6H_6)RuCl_2(Me_2HPz)]$

$[(C_6H_6)RuCl(HPz)_2]^+$		$[(C_6H_6)RuCl_2(Me_2HPz)]$	
H − 11(π_{benz})	−12.95	H − 12(π_{benz})	−9.72
H − 10(π_{benz})	−12.64	H − 11(π_{benz})	−9.41
H − 9(σ_{Cl})	−11.98	H − 10(σ_{Cl})	−8.45
H − 8(π_{Cl})	−11.79	H − 9(σ_{Cl})	−8.23
H − 7(π_{Cl})	−11.36	H − 8(π_{Cl})	−8.11
H − 6(π_{pz})	−11.25	H − 7(π_{Cl})	−7.87
H − 5(π_{pz})	−10.83	H − 6(π_{Cl})	−7.51
H − 4(π_{pz})	−10.74	H − 5(π_{pz})	−7.12
H − 3(π_{pz})	−10.42	H − 4(π_{pz})	−6.68
H − 2(d)	−9.96	H − 3(π_{Cl})	−6.50
H − 1(d)	−9.82	H − 2(d)	−6.32
H(d)	−9.66	H − 1(d)	−6.02
L(d)	−5.43	H(d)	−5.85
L + 1(d)	−5.16	L(d)	−1.95
L + 2(π^*_{benz})	−4.30	L + 1(d)	−1.71
L + 3(π^*_{benz})	−4.17	L + 2(π^*_{benz})	−0.91
L + 4(π^*_{Hpz})	−3.56	L + 3(π^*_{benz})	−0.81
L + 5(π^*_{Hpz})	−3.48	L + 4(π^*_{Hpz})	−0.04

H denotes HOMO, L – LUMO. Energies in eV.

Table 4
Hydrogen-bonds for $[(C_6H_6)RuCl_2(Me_2HPz)]$ (Å and °)

D–H···A	d(D–H)	d(H···A)	d(D···A)	∠(D–H···A)
C(7)–H(7)···Cl(2)#1	0.93	2.72	3.623(11)	163.4
C(9)–H(9)···Cl(52)#2	0.93	2.78	3.696(12)	167.8
C(10)–H(10)···Cl(51)#2	0.93	2.76	3.610(12)	152.9
C(57)–H(57)···Cl(52)#3	0.93	2.79	3.661(12)	156.4

Symmetry transformations used to generate equivalent atoms:#1 $-x+1$, $-y+2$, $-z$; #2 $x+1$, y, z; #3 $-x$, $-y+1$, $-z+1$.

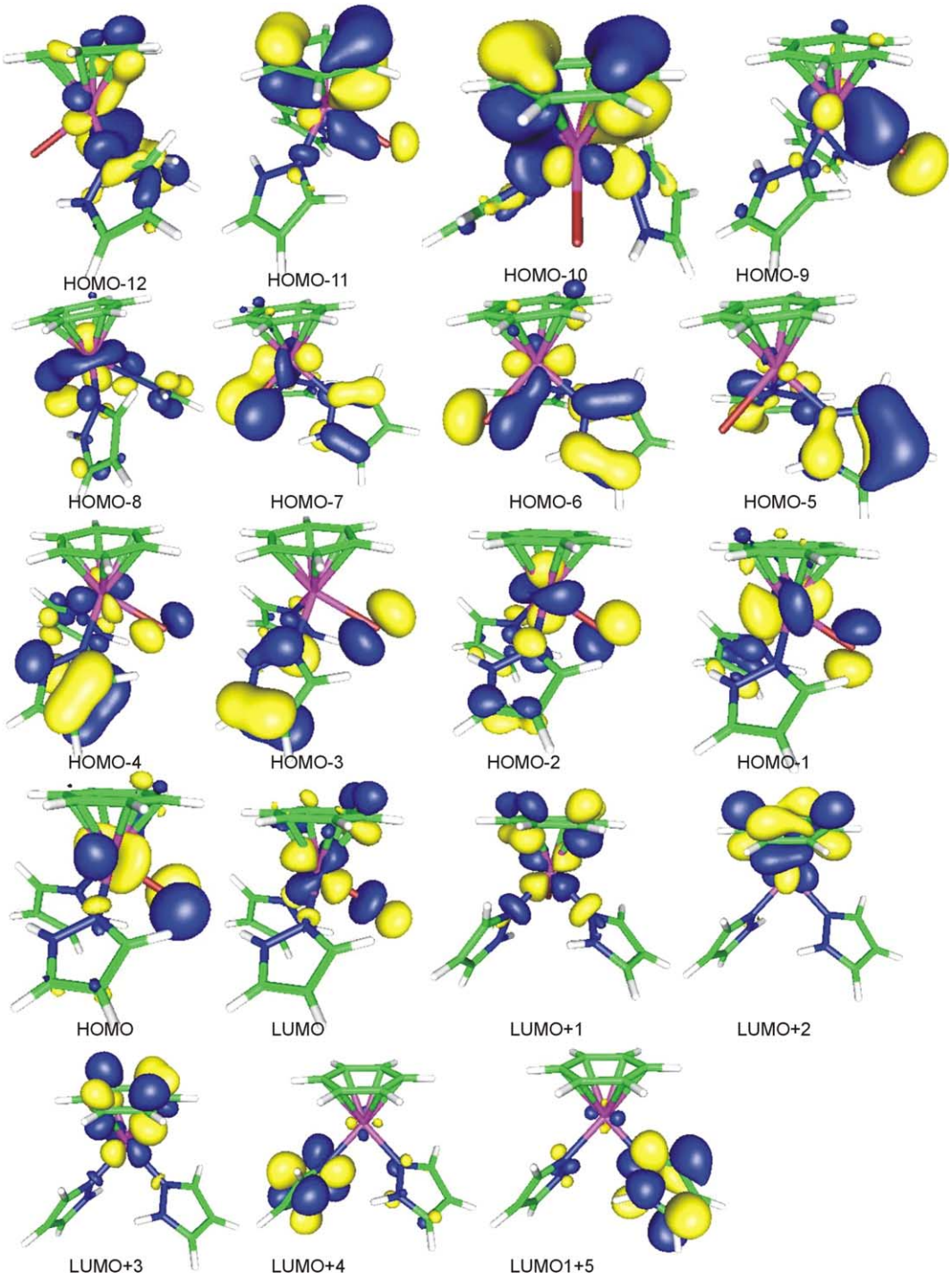

Fig. 5. HOMO and LUMO orbitals of $[(C_6H_6)Ru(Hpz)_2Cl]^+$.

$RuCl_2(Me_2HPz)$], respectively, the antibonding are LUMO and LUMO + 1 (Table 6 and Fig. 5). Since the bonding orbitals are of predominantly benzene character and the antibonding ones are predominantly of metal character, in the electronic transitions the former are described as π_{benz} and the latter as d orbitals. In the back-donation (metal to ligand) the occupied $d_{x_2-y_2}$ and d_{xy} metal orbitals and empty π_4^*, π_5^* benzene orbitals participate (HOMO − 1, HOMO and LUMO + 2, LUMO + 3). However, this interaction is weaker, due to a smaller orbital overlap.

3.3. Electronic spectrum

The spin-allowed, singlet transitions were calculated with the TDDFT method. The calculated electronic

Table 7
Calculated electronic transitions for $[(C_6H_6)RuCl(HPz)_2]^+$ and $[(C_6H_6)RuCl_2(Me_2HPz)]$ with the TDDFT method

The most important orbital excitations		λ (nm)	E (eV)	f	Experimental λ (nm) (E [eV]) ε
$[(C_6H_6)RuCl(HPz)_2]^+$					
H(d) → L(d)		**478.8**	**2.58**	**0.0013**	567.8 (2.18) 28
H − 2(d) → L(d)	**H − 1(d) → L(d)**	**461.9**	**2.68**	**0.0024**	
H − 1(d) → L(d)	**H(d) → L + 1(d)**	**434.9**	**2.85**	**0.0010**	557.8 (2.22) 30
H − 2(d) → L + 1(d)		**422.3**	**2.93**	**0.0011**	
H − 1(d) → L + 1(d)	**H(d) → L + 1(d)**	**379.9**	**3.26**	**0.0046**	405.6 (3.07) 1309
H − 2(d) → L + 1(d)	**H − 1(d) → L + 1(d)**	**371.2**	**3.33**	**0.0025**	
H − 4(π_{Hpz}) → L(d)	**H − 3(π_{Hpz}) → L(d)**	**308.2**	**4.02**	**0.0044**	325.4 (3.81) 1739
H(d) → L + 2(π^*_{benz})		**296.7**	**4.17**	**0.0013**	
H − 3(π_{Hpz}) → L + 1(d)	H − 1(d) → L + 3(π^*_{benz})	285.5	4.34	0.0039	
H − 6(π_{Hpz}) → L + 1(d)	H − 1(d) → L + 2(π^*_{benz})	251.2	4.93	0.0295	
H − 7(π_{Cl}) → L + 1(d)	H − 6(π_{Hpz}) → L + 1(d)	246.0	5.03	0.0301	
H(d) → L + 5(π^*_{Hpz})		231.0	5.36	0.0184	
H − 2(d) → L + 4(π^*_{Hpz})	**H − 1(d) → L + 4(π^*_{Hpz})**	**220.4**	**5.62**	**0.0499**	231.6 (5.35) 15 995
H − 4(π_{Hpz}) → L + 2(π^*_{benz})	**H − 2(d) → L + 5(π^*_{Hpz})**	**216.8**	**5.71**	**0.0355**	
H − 4(π_{Hpz}) → L + 2(π^*_{benz})	**H − 2(d) → L + 5(π^*_{Hpz})**	**216.4**	**5.72**	**0.0156**	
H − 9(σ_{Cl}) → L(d)	**H − 6(π_{Hpz}) → L + 2(π^*_{benz})**	**207.2**	**5.98**	**0.0940**	
$[(C_6H_6)RuCl_2(Me_2HPz)]$					
H(d) → L(d)		542.3	2.28	0.0034	
H − 1(d) → L(d)	H − 1(d) → L + 1(d)	485.0	2.55	0.0016	
H − 2(d) → L(d)	H(d) → L + 1(d)	467.5	2.65	0.0016	
H − 2(d) → L + 1(d)	H − 1(d) → L + 1(d)	450.4	2.75	0.0017	
H − 1(d) → L(d)	**H(d) → L + 1(d)**	**424.9**	**2.91**	**0.0031**	425.0 (2.91) 807
H − 2(d) → L(d)	**H − 2(d) → L + 1(d)**	**385.1**	**3.21**	**0.0069**	370.0 (3.35) 713
H − 3(π_{Cl}) → L(d)		356.9	3.47	0.0021	
H − 4(π_{Hpz}) → L(d)		**331.4**	**3.74**	**0.0033**	337.8 (3.67) 744
H − 3(π_{Cl}) → L + 1(d)	**H(d) → L + 2(π^*_{benz})**	**329.4**	**3.76**	**0.0028**	
H − 4(π_{Hpz}) → L + 1(d)	H − 1(d) → L + 3(π^*_{benz})	311.8	3.97	0.0032	
H − 2(d) → L + 2(π^*_{benz})	**H(d) → L + 3(π^*_{benz})**	**263.1**	**4.71**	**0.0376**	232.0 (5.34) 13 509
H − 4(π_{Hpz}) → L + 2(π^*_{benz})		**246.4**	**5.03**	**0.0127**	
H − 9(σ_{Cl}) → L(d)	H − 9(σ_{Cl}) → L + 1(d)	237.4	5.22	0.0110	
H − 2(d) → L + 4(π^*_{Hpz})		227.4	5.45	0.0107	
H − 10(σ_{Cl}) → L + 1(d)	**H − 3(π_{Cl}) → L + 4 (π^*_{Hpz})**	**216.7**	**5.72**	**0.0433**	216.0 (5.74) 5205
H − 3(π_{Cl}) → L + 4(π^*_{Hpz})		**216.0**	**5.73**	**0.0356**	

The transitions ascribed to the experimental bands are denoted in bold.

transitions are gathered in Table 7. Except for the low energy part of the spectrum, only transitions with oscillator strengths larger than 0.01 are listed.

3.3.1. $[(C_6H_6)Ru(Hpz)_2Cl]^+$

In the calculated electronic spectrum of $[(C_6H_6)Ru(Hpz)_2Cl]^+$, the lowest energy transitions are of d → d origin and they are characterized with small oscillator strengths. The first two (at 478.8 and 461.9 nm) may be attributed to the experimental band at 567.8 nm. The calculated transitions at 434.9 and 422.3 nm, also with d → d character, can be attributed to the experimental band at 557.8 nm. These two experimental bands are of very low intensity ($\varepsilon = 28$ and 30). The next experimental transition occurs at 405.6 nm and has higher intensity ($\varepsilon = 1309$). We attribute this transition to the calculated transition at 379.9 and 371.2 nm also with a d → d character.

The experimental band at 325.4 nm ($\varepsilon = 1739$) can be attributed to the calculated transitions at 308.2. The electronic transitions involved here are of LMCT character (d → π^*_{Hpz}).

The most intense experimental band of $[(C_6H_6)Ru(Hpz)_2Cl]^+$ is found at 231.6 nm ($\varepsilon = 15995$). This band can be attributed to the calculated transitions between 220.4 and 207.2 nm with large oscillator strengths. They are of MLCT (d → π^*_{Hpz}), LLCT ($\pi_{Hpz} \rightarrow \pi^*_{benz}$) and LMCT ($\sigma_{Cl} \rightarrow$ d) character.

3.3.2. $[(C_6H_6)RuCl_2(Me_2HPz)]$

The calculated spectrum for $[(C_6H_6)RuCl_2(Me_2HPz)]$ shows several transitions with small oscillator strengths between 550 and 400 nm. They are LF (d → d) transitions. The first experimental transition at 430.6 nm can be assigned to the calculated transitions at 450.4 and 424.9 nm of LF character. The second experimental band at 370.0 nm may be attributed to the calculated transition at 385.1 nm also of LF type.

The experimental band at 339.2 nm is ascribed to the calculated transitions at 331.4 and 329.4 nm. These

transitions are of LMCT ($\pi_{Hpz} \rightarrow d$, $\pi_{Cl} \rightarrow d$) and MLCT ($d \rightarrow \pi^*_{benz}$) character.

The experimental band at 232.2 nm with $\varepsilon = 13\,509$ can be assigned to the calculated transitions at 263.1 and 246.4 nm with large oscillator strengths. These transitions are of MLCT ($d \rightarrow \pi^*_{benz}$) and LLCT ($\pi_{Hpz} \rightarrow \pi^*_{benz}$) character.

The experimental band at 216.0 nm with $\varepsilon = 5205$ can be attributed to the calculated transitions at 216.7 and 216.0 nm with large oscillator strengths. These transitions are of LMCT ($\sigma_{Cl} \rightarrow d$) and LLCT ($\pi_{Cl} \rightarrow \pi^*_{Hpz}$) type.

The spectra of $[(C_6H_6)Ru(Hpz)_2Cl]^+$ and $[(C_6H_6)RuCl_2(Me_2HPz)]$ according to the TDDFT calculated transitions are similar in the range up to 300 nm. The longest wave transitions are of LF type (567.8, 557.8, 405.6 nm for $[(C_6H_6)Ru(Hpz)_2Cl]^+$ and 430.6, 370.0 for $[(C_6H_6)RuCl_2(Me_2HPz)]$). The bands at 325.4 in $[(C_6H_6)Ru(Hpz)_2Cl]^+$ and 339.2 nm in $[(C_6H_6)RuCl_2(Me_2HPz)]$ arise from $\pi_{Hpz} \rightarrow d$ and $d \rightarrow \pi^*_{benz}$ excitations (plus $\pi_{Cl} \rightarrow d$ in $[(C_6H_6)\ RuCl_2(Me_2HPz)]$). However, in the short wave bands (231.6 for $[(C_6H_6)Ru(Hpz)_2Cl]^+$ and 232.0, 216.0 nm for $[(C_6H_6)RuCl_2(Me_2HPz)]$), a large participation of the pyrazole orbitals is pronounced for the first compound, while the chlorine and benzene orbitals dominate in the transitions of the second one.

4. Supplementary material

Crystallographic data for the structure of the complexes have been deposited at the Cambridge Crystallographic Data Center (CCDC 205958, CCDC 222759). Copies of this information maybe obtained free of charge from The Director, CCDC, 12 Union Road, Cambridge, CB2, IEZ, UK (fax: +44-1223-336-033; e-mail: deposit@ccdc.cam.ca.uk or http://www.ccdc.cam.ac.uk). The list of references concerning to bond valence parameters is available on request from R. Kruszyński kruszyna@p.lodz.pl.

Acknowledgements

The crystallographic part was financed by funds allocated by the State Committee for Scientific Research to the Institute of General and Ecological Chemistry, Technical University of Łódź. The GAUSSIAN 03 calculations were carried out in the Wrocław Centre for Networking and Supercomputing, WCSS, Wrocław, Poland under calculational Grant No. 51/96.

References

[1] (a) H. Le Bozec, D. Touchard, P.H. Dixneuf, Adv. Organomet. Chem. 29 (1989) 163;
(b) R.M. Moriarty, U.S. Gill, Y.-Y. Ku, J. Organomet. Chem. 350 (1988) 157;
(c) R. Noyori, S. Hashiguchi, Acc. Chem. Res. 30 (1997) 97;
(d) M.A. Bennett, in: E.W. Abel, F.G.A. Stone, G. Wilkinson (Eds.), Comprehensive Organometallic Chemistry II, vol. 7, Pergamon Press, Oxford, 1995;
(e) M.A. Bennett, Coord. Chem. Rev. 166 (1997) 225.
[2] E.O. Fischer, R. Böttcher, Z. Anorg. Allgem. Chem. 291 (1957) 305.
[3] G. Winkhaus, H. Singer, J. Organomet. Chem. 7 (1967) 487.
[4] (a) I. de los Rios, M.J. Tenerio, M.A.J. Tenorio, M.C. Puerta, P. Valerga, J. Organomet.Chem. 525 (1996) 57;
(b) A. Schlüter, K. Bieber, W.S. Sheldrick, Inorg. Chim. Acta 340 (2002) 35;
(c) Y. Chen, M. Valentini, P.S. Pregosin, A. Albinati, Inorg. Chim. Acta 327 (2002) 4;
(d) A. Singh, N. Singh, D.S. Pandey, J. Organomet. Chem. 642 (2002) 48.
[5] (a) B. de Clercq, F. Verpoort, J. Mol. Catal. A 180 (2002) 67;
(b) A. Kathó, D. Carmona, F. Viguri, C.D. Remacha, J. Kovács, F. Joó, L.A. Oro, J.Organomet. Chem. 593–594 (2000) 299;
(c) K. Mashima, K. Kusano, N. Sato, Y. Matsumura, K. Nozaki, H. Kumobayashi, N. Sayo, Y. Hori, T. Ishizaki, S. Akutagawa, H. Takaya, J. Org. Chem. 59 (1994) 3064;
(d) S. Hashiguchi, A. Fujii, J. Takehara, T. Ikariya, R. Noyori, J. Am. Chem. Soc. 117 (1995) 7562;
(e) A. Fujii, S. Hashiguchi, N. Uematsu, T. Ikariya, R. Noyori, J. Am. Chem. Soc. 118 (1996) 2521.
[6] A.W. Stumpf, E. Saive, A. Demonceau, A.F. Noels, J. Chem. Soc., Chem. Commun. (1995) 1127.
[7] C.J. Jones, J.A. McCleverty, A.S. Rothin, J. Chem. Soc., Dalton Trans. (1986) 109.
[8] M.A. Bennett, T.-N. Huang, T.W. Matheson, A.K. Smith, Inorg. Synth. 21 (1982) 74.
[9] X-RED, version 1.18. STOE & Cie GmbH, Darmstadt, Germany, 1999.
[10] G.M. Sheldrick, Acta Crystallogr., Sect. A 46 (1990) 467.
[11] G.M. Sheldrick, SHELXL 97. Program for the Solution and Refinement of Crystal Structures, University of Göttingen, Germany, 1997.
[12] G.M. Sheldrick, SHELXTL, release 4.1 for Siemens Crystallographic Research Systems, 1990.
[13] M.J. Frisch, G.W. Trucks, H.B. Schlegel, G.E. Scuseria, M.A. Robb, J.R. Cheeseman, J.A. Montgomery Jr., T. Vreven, K.N. Kudin, J.C. Burant, J.M. Millam, S.S. Iyengar, J. Tomasi, V. Barone, B. Mennucci, M. Cossi, G. Scalmani, N. Rega, G.A. Petersson, H. Nakatsuji, M. Hada, M. Ehara, K. Toyota, R. Fukuda, J. Hasegawa, M. Ishida, T. Nakajima, Y. Honda, O. Kitao, H. Nakai, M. Klene, X. Li, J.E. Knox, H.P. Hratchian, J.B. Cross, C. Adamo, J. Jaramillo, R. Gomperts, R.E. Stratmann, O. Yazyev, A.J. Austin, R. Cammi, C. Pomelli, J.W. Ochterski, P.Y. Ayala, K. Morokuma, G.A. Voth, P. Salvador, J.J. Dannenberg, V.G. Zakrzewski, S. Dapprich, A.D. Daniels, M.C. Strain, O. Farkas, D.K. Malick, A.D. Rabuck, K. Raghavachari, J.B. Foresman, J.V. Ortiz, Q. Cui, A.G. Baboul, S. Clifford, J. Cioslowski, B.B. Stefanov, G. Liu, A. Liashenko, P. Piskorz, I. Komaromi, R.L. Martin, D.J. Fox, T. Keith, M.A. Al-Laham, C.Y. Peng, A. Nanayakkara, M. Challacombe, P.M.W. Gill, B. Johnson, W. Chen, M.W. Wong, C. Gonzalez, J.A. Pople, GAUSSIAN 03, Revision B.03, Gaussian Inc., Pittsburgh, PA, 2003.
[14] A.D. Becke, J. Chem. Phys. 98 (1993) 5648.
[15] C. Lee, W. Yang, R.G. Parr, Phys. Rev. B 37 (1988) 785.
[16] M.E. Casida, in: J.M. Seminario (Ed.), Recent Developments and Applications in Modern Density Functional Theory, Theoretical and Computational Chemistry, vol. 4, Elsevier, Amsterdam, 1996.
[17] P.J. Hay, W.R. Wadt, J. Chem. Phys. 82 (1985) 299.
[18] U. Beck, W. Hummel, H.B. Burgi, A. Ludi, Organometallics 6 (1993) 20.

[19] F.B. McCormick, D.D. Cox, W.B. Gleason, Organometallics 12 (1993) 610.
[20] I. Moldes, E. de la Encarnacion, J. Ros, A. Alvarez.Larena, J.F. Piniella, J. Organomet. Chem. 566 (1998) 165.
[21] (a) R. Tribo, J. Pons, R. Yanez, J.F. Piniella, A. Alvarez-Larena, J. Ros, Inorg. Chem. Commun. 3 (2000) 545;
(b) M. Jahncke, A. Neels, H. Stoeckli-Evans, G. Süss-Fink, J. Organomet. Chem. 561 (1998) 227;
(c) H. Kurosawa, H. Asano, Y. Miyaki, Inorg. Chim. Acta 270 (1998) 87.
[22] G.R. Desiraju, T. Steiner, The Weak Hydrogen Bond in Structural Chemistry and Biology, Oxford University Press, Oxford, 1999.
[23] G.A. Jeffrey, W. Saenger, Hydrogen Bonding in Biological Structures, Springer-Verlag, Berlin, 1994.
[24] R. Taylor, O. Kennard, J. Am. Chem. Soc. 104 (1982) 5063.
[25] M. O'Keeffe, N.E. Brese, Acta Crystallogr., Sect. B 47 (1997) 192.
[26] M. O'Keeffe, N.E. Brese, J. Am. Chem. Soc. 113 (1991) 3226.
[27] I.D. Brown, Bond-length–bond-valence relationship in inorganic solids, in: H.B. Burgi, J.D. Dunitz, J.D. Weinhaim (Eds.), Structure Correlation, Part III, VCH publishers, New York, 1994, pp. 405–429.
[28] L. Sieron, M. Bukowska-Strzyzewska, Acta Crystallogr., Sect. C 55 (1999) 1230.
[29] T.R. Wagner, M.J. O'Keeffe, Solid State Chem. 73 (1998) 211.

Available online at www.sciencedirect.com
SCIENCE DIRECT®
Polyhedron 23 (2004) 895–901
POLYHEDRON
www.elsevier.com/locate/poly

Kinetics of oxidation of glyoxylic acid by [ethylenebis(biguanide)]silver(III) in aqueous media

Amit Das, Subrata Mukhopadhyay *

Department of Chemistry, Jadavpur University, Calcutta 700 032, India

Received 28 October 2003; accepted 16 December 2003

Abstract

The complex cation, [ethylenebis(biguanide)]silver(III), $[Ag(H_2L)]^{3+}$, and its conjugate bases, $[Ag(HL)]^{2+}$ and $[AgL]^{+}$ oxidise glyoxylic acid, $CHOCO_2H$ quantitatively to formic acid and carbon dioxide, themselves being reduced to Ag^{+}. Free ethylenebis(biguanide) was recovered in near-quantitative yield. In the investigated pH range (1.00–7.00), the reaction is first order in both [complex] and total glyoxylate, $[HGX]_T$. The reaction proceeds through four parallel paths: $[Ag(H_2L)]^{3+}$ – HGX (k_1), $[Ag(H_2L)]^{3+}$ – GX^{-} (k_2), $[Ag(HL)]^{2+}$ – GX^{-} (k_3), and $[AgL]^{+}$ – GX^{-} (k_4). The respective rate constants (in 10^4 M^{-1} s^{-1}) are, respectively, 7.34, 112, 40.7 and 19.2 at 25.0 °C and $I = 1.0$ M ($NaNO_3$). Formation of adducts by the reducing species with the metal complex via hydrogen-bonding or electrostriction may be proposed for the low-energy pathway for electron-transfer. A substantial rate retardation in presence of the radical scavenger acrylonitrile suggests successive one-electron changes, $Ag^{III} \rightarrow Ag^{II} \rightarrow Ag^{I}$.
© 2003 Elsevier Ltd. All rights reserved.

Keywords: Kinetics; Mechanism; Redox; Silver; Glyoxylic acid

1. Introduction

The trivalent silver species [ethylenebis(biguanide)]silver(III) (Fig. 1) is an authentic cationic complex of silver [1–3] stable in aqueous solution over a wide pH range against dechelation and intramolecular redox decomposition [4]. Stabilisation of the silver(III) center by the square-planar acyclic tetraaza ligand is so extensive ($\log K = 52$) [5] that the title complex behaves as a milder oxidant [6], more so than Ag^{+} [7]. The complex is freely soluble in aqueous media below pH ca. 4.5 but ~0.2 mM complex can be made soluble up to pH at least 7.0 if alkali is added carefully with stirring to avoid local excesses. Moreover, the silver(III) retains its identity in strongly acidic and in strongly alkaline media, a property unknown in other higher valent silver complexes. In aqueous solutions the complex behaves as a mild dibasic acid ($pK_{a1} = 3.8$, $pK_{a2} = 6.3$) originating from ligand-based protic equilibria [8] and thus the reactivity studies of different silver(III) species connected through protic equilibria is possible because, in spite of the remarkable thermodynamic stability, the silver(III) complex oxidises [9–20] various organic and inorganic species with a variety of electron transfer pathways – inner sphere for weakly reducing ligands [10,11,13,14,19,20], outer sphere for weakly basic but strongly reducing ligands [15,17] and even by Ag^{+} catalysis [9,10,13].

We report herein the kinetics of oxidation of glyoxylic acid and its conjugate base by the title silver(III) complex. Detailed kinetic studies of the oxidation of glyoxylic acid, one of the smallest carboxylic acids, is of importance as in metabolic processes such as glycine catabolism [21] and in plant physiology [22], higher valent metal ions like manganese(III) complexes play an essential role. Glycine oxidation to CO_2 may occur via glyoxylic acid arising from oxidative deamination of glycine by the enzyme glycine oxidase [23]. The silver(III) species, $[Ag(OH)_4]^{-}$ oxidises glycine [24] in strongly alkaline media to NH_3, HCHO and CO_2. $[AuCl_4]^{-}$ also oxidises glycine [25] to NH_3, HCO_2H and CO_2 in weakly acidic media via the intermediate formation of glyoxylic acid. We observed that the title

* Corresponding author. Tel.: +91-33-2867-1181; fax: +91-33-2414-6266.
E-mail address: subrataju@vsnl.net (S. Mukhopadhyay).

0277-5387/$ - see front matter © 2003 Elsevier Ltd. All rights reserved.
doi:10.1016/j.poly.2003.12.006

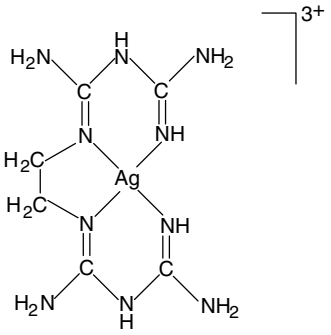

Fig. 1. Structure of [ethylenebis(biguanide)]silver(III) complex.

silver(III) complex reacts very slowly with glycine although it reacts with glyoxylic acid at a moderately fast rate. Under these perspectives it is important to understand the chemistry of Ag(III) – biomolecule interactions. Moreover, the ligand H_2L in $[Ag(H_2L)]^{3+}$ is substitution inert so that Ag^{III} never is released in solution to open extra, complicating pathways in its reduction.

2. Experimental

2.1. Materials

The silver(III) complex, abbreviated as $[Ag(H_2L)]^{3+}$ hereafter, was prepared according to the known procedure [2,3] with a slight modification in the crystallisation process [9]. Aqueous solution of glyoxylic acid were prepared by dissolving solid glyoxylic acid monohydrate (98%, Lancaster) in water and standardised either by standard alkali using Weslow's indicator or spectrophotometrically [26] at 520 nm ($\varepsilon = 17990\ M^{-1}\ cm^{-1}$ as estimated by us, in agreement with the literature [26] value 17 870 $M^{-1}\ cm^{-1}$) after converting glyoxylic acid to 1,5-diphenylformazancarboxylic acid. Both the results agreed well (within 4%). We found that an aqueous solution of ~0.5 M glyoxylic acid is stable for at least one week when kept at low temperature (~5–10 °C) and in the dark. Aqueous solutions of $NaNO_3$ or $NaClO_4$ (both of G.R., E. Merk) were standardised by passing through a Dowex 50W X-8 strong cation exchange resin in the H^+ from and titrating the liberated acid with standard NaOH to a phenolphthalein end point. All measurements were made at 25.0 °C and $I = 1.0$ M ($NaNO_3$ or $NaClO_4$). All solutions were prepared in water, which was deionised and then doubly distilled.

2.2. Physical measurements and kinetics

The acid dissociation constant, K_a of the glyoxylic acid was determined by titrating several aliquots of different strengths with carbonate free deaerated NaOH solution at 1.0 M $NaNO_3$ using a Titrino Autotitrator (Metrohm, 736 GP) at (25 ± 0.1) °C. Production of CO_2 as the gaseous reaction product was qualitatively confirmed by GC analysis. The gaseous product formed during the reaction was collected over a saturated sodium chloride solution and analysed by gas chromatography as described earlier [27] using a Chemito (India) GCHT 8610 equipped with TCD, a Porapack Q and molecular sieve 13X column. Splitless mode injection of 500 μL of sample was used. The oven temperature, injector and detector temperature were kept at 40, 55, and 100 °C, respectively. The carrier hydrogen gas flow was adjusted to 30 ml min^{-1}. All absorbance versus time data were recorded with a Shimadzu (1601 PC) spectrophotometer using 1.00 cm quartz cells. The kinetics was monitored in situ in the 'kinetic mode' of the instrument at 420 nm in the electrically controlled thermostated (25.0 ± 0.1 °C) cell housing (CPS-240A). In this mode the change in absorbance is automatically and continuously recorded. For faster reactions glyoxylic acid solution (adjusted to desired pH) was directly injected into the spectrophotometer cell containing other components of the reaction mixture kept at the same pH. The desired concentration of the complex and reducing agent was achieved after mixing. The solution pH values were adjusted with $HClO_4$ or NaOH. Although the measured pH is usually defined in terms of the activity of hydrogen ions, we used the hydrogen ion concentration by calibrating the pH electrode with analytically prepared solutions as described earlier [28].

2.3. Stoichiometric measurements

The stoichiometry was measured both under kinetic and reverse condition by estimating glyoxylic acid spectrophotometrically and estimating unreacted Ag^{III} in condition when initial $[Ag^{III}]$ is in excess over total glyoxylic acid, $[HGX]_T$ (defined as $[HGX] + [GX^-]$). Excess glyoxylic acid was mixed with the Ag^{III} complex in the pH range 3.0–5.0. After the reaction mixture turned colourless indicating complete reduction of Ag(III) to Ag(I), excess NaCl was added to remove AgCl. Freshly prepared phenylhydrazine hydrochloride (1%) was added (3.0 ml) into each mixture. The resulting solutions were incubated at ~110 °C for 10 min and then cooled to room temperature (~25 °C) followed by successive addition of 2.5 ml each of concentrated HCl and 1% $K_3Fe(CN)_6$. The mixtures were allowed to stand for ~5 min for the quantitative formation of pink coloured formazan derivative of glyoxylic acid [26] that was measured at 520 nm.

Reaction mixtures containing excess Ag^{III} over glyoxylic acid were used to measure the unreacted $[Ag^{III}]$. After completion of reactions (as indicated by no further change in absorbance), measured volumes of dilute HNO_3 were added to reach a final pH within 1.0–2.0

Table 1
Stochiometric results for the oxidation of glyoxylic acid (HGX) by the silver(III) complex at $I = 1.0$ M ($NaNO_3$) and $T = 25$ °C

$[Ag(III)]_T$ (mM)	$[HGX]_T$ (mM)	pH	$[HGX]_{left}$ (mM)	$[Ag(III)]_{left}$ (mM)	$\Delta[HGX]_T/\Delta[Ag(III)]_T$
0.15	0.30	3.1	0.16		0.94
	0.40	4.2	0.24		1.07
	0.60	4.9	0.47		0.87
0.20	0.80	5.3	0.61		0.95
	1.00	4.6	0.79		1.05
0.30	1.00	4.4	0.71		0.97
	1.20	3.9	0.88		1.07
0.45	0.30	3.5		0.13	0.94
1.00	0.50	3.7		0.46	0.93
					Average = 0.98 ± 0.10

and the remaining $[Ag^{III}]$ was estimated at 380 nm ($\varepsilon = 1175\ M^{-1}\,cm^{-1}$) [8]. Both experiments, whether in kinetic or in reverse condition resulted a 1:1 stoichiometry between the redox partners (Table 1).

2.4. Product analysis

Generation of formic acid as one of the oxidation products of the title reaction was tested by the addition of chromotropic acid [29] in the product mixture after removing Ag^+ as AgCl. Formation of CO_2 as the gaseous product was qualitatively confirmed by GC analysis. We also observed that at the end of the reaction, more than 90% of the free ligand (H_2L) can be recovered. For this purpose concentrated (1.0–2.0 mM) solutions of the Ag^{III} complex were reacted with stoichiometric excess glyoxylic acid. Immediately after completion of reaction (absorbance <0.01 at 420 nm), all Ag^+ was precipitated as AgCl and removed by filtration. From the filtrate, the free ligand, ethylenebis(biguanide) was quantitatively isolated [30] as the sparingly soluble [ethylenebis(biguanide)]copper(II) sulfate, and the amount of Cu(II) thus held was estimated iodometrically after decomposing the Cu(II) complex.

3. Results and discussion

3.1. Equilibrium studies and preliminary observations

The pK_a of the glyoxylic acid was found to be 3.20 ± 0.10 at 25.0 °C and at $I = 1.0$ M ($NaNO_3$). Though this value to some extent differs from the reported [31] value (2.91) under similar condition of temperature and ionic strength, we used the value 3.20 for pK_a for the calculation of rate constants. Most of the kinetic runs were performed at 420 nm where all other reaction components except Ag^{III} are transparent. Within the time span of the reactions, autodecomposion of the silver(III) complex was insignificant at the experimental temperature. No external buffer was used in kinetic measurements since buffering (by acetate, for example) affects the spectra of the complex; specific interaction of buffer with the complex was thus indicated. Even in the absence of an external buffer, the media pH before and after the reactions did not change by more than 0.10 units.

3.2. Stoichiometry and the redox reaction

Stoichiometric determination and product analyses clearly indicate the occurrence of reaction (1) in the entire redox process:

$$Ag^{III} + CHOCO_2H + H_2O \rightarrow Ag^{I} + HCO_2H + CO_2 + 2H^+ \quad (1)$$

3.3. Kinetics

No immediate spectrophotometric change was observed on mixing glyoxylic acid with the silver(III) complex over the entire range of experimental pH and total glyoxylate ($[HGX]_T$). However, the absorbance at $\lambda \geqslant 420$ nm gradually decreases to less than 0.01. We measured some k_0 values in the presence of added (1.0 mM) ethylenebis(biguanide) and found to be identical with experiments in its absence within reasonable uncertainties, and we observed no effect of diffused light in our system. The $\log_{10}$ (absorbance) versus time plots were found to be linear for more than 90% completion of reactions and the pseudo-first-order rate constants, k_0, defined by Eq. (2) were obtained from the least-squares slopes of these plots

$$-d[Ag(III)]/dt = k_0[Ag(III)]. \quad (2)$$

Any initial drop in absorbance for faster reactions can be computed from the time of mixing of reactants (~4 s) and the observed-first-order rate constants. Averages of k_0 values from at least three runs were taken and individual runs were reproducible within 3%.

Detailed data of the kinetics of the process were obtained as a function of pH and $[HGX]_T$ and some representative data are summarised in Table 2. Over the entire pH range studied the reaction shows a clear first-order dependence on $[HGX]_T$ and there is no $[HGX]_T$ independent term. The following changes in the reaction conditions had, within the limits of experimental uncertainties, no influence on the values of k_0: a fivefold variation in [Ag(III)] from 0.1 to 0.5 mM, occasional shaking of spectrophotometer cell, presence or absence of dissolved oxygen and a variation in the monitoring wavelength in the range 420–500 nm.

The observed rate constants remarkably depend on the media ionic strength maintained by $NaNO_3$ or $NaClO_4$ (Table 2). A considerable increase in reaction rate at pH > 3.0 with decrease in the ionic strength indicates reaction between oppositely charged ions. [1] However at pH $\leqslant$ 2.0 the reaction rate was found to be practically independent on the media ionic strength probably due to involvement of neutral species glyoxylic acid as the sole reducing component.

Reactions studied in the presence of 6% (v/v) acrylonitrile showed slow polymerisation after ca. 60% consumption of initial Ag^{III}. The $\log_{10}$ (absorbance) versus time plots in this condition showed a definite upward curvature after ca. 50% completion of reactions probably due to heterogeneity in the reaction media. However, the first-order rate constants computed from the initial linear portions of these curves clearly demonstrate much slower reactions in presence of radical scavengers like acrylonitrile.

A plot of k_0 versus pH has a bell shape (Fig. 2) at a particular $[HGX]_T$. Such a pH dependence indicates the involvement of two or more acid–base equilibria [32]. Considering the values for the acid dissociation constants of the complex in aqueous solution [8] (K_{a1} and K_{a2}, which are 1.58×10^{-4} and 5.01×10^{-7} M, respectively) and K_a ($= 6.31 \times 10^{-4}$ M), the measured acid dissociation constant of glyoxylic acid under experimental conditions, Scheme 1 in Eqs. (3)–(9) provides a reasonable explanation for the kinetic observations.

Table 2
Some representative first-order rate constants for oxidation of glyoxylic acid by the silver(III) complex[a]

pH	$[HGX]_T$ (M)	$10^4 k_0$ (s^{-1})
1.00	0.10	0.80 ± 0.02
1.40		0.96 ± 0.03
2.00		1.40 ± 0.03
2.26		1.77 ± 0.06
2.50		2.20 ± 0.05
2.85		3.71 ± 0.06
3.00		4.40 ± 0.09
3.50		$6.09^b \pm 0.08$
4.00		6.00 ± 0.08
4.35		5.30 ± 0.09
4.50		4.90 ± 0.10
5.01		4.20 ± 0.11
5.62		3.72 ± 0.10
6.00		3.34 ± 0.06
6.30		3.00 ± 0.06
6.51		2.80 ± 0.07
6.77		2.46 ± 0.07
7.00		2.30 ± 0.07
2.02	0.20	2.67 ± 0.08
2.01	0.40	5.70 ± 0.12
2.03	0.80	11.0 ± 0.22
3.55	0.20	13.0 ± 0.27
3.52	0.40	25.2 ± 0.35
6.00	0.20	6.55 ± 0.12
5.98	0.40	13.4 ± 0.20

[a] $T = 25.0$ °C, $I = 1.0$ M ($NaNO_3$), [complex] = 0.15 mM.
[b] 10^4 k_0 (s^{-1}) values are 9.25, 14.0 and 19.0 at $I = 0.5$, 0.2 and 0.1 M ($NaNO_3$), respectively.

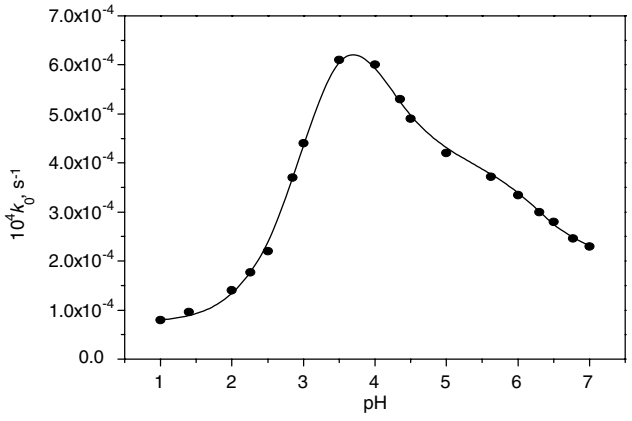

Fig. 2. Dependence of k_0 on pH at $T = 25.0$ °C, $[Ag(III)]_T = 0.15$ mM, $[HGX]_T = 0.10$ M, $I = 1.0$ M ($NaNO_3$). The solid line represents the fit of Eq. (10).

[1] One of the referees suggested that the rate constants might have been changed if $LiClO_4$ is used instead of Na^+ salts for maintaining the ionic strength of the reaction medium. We performed several experiments in presence of varying amount of $LiClO_4$ keeping $I = 1.0$ M. The first-order rate constants thus obtained were found to be substantially higher (15–25%, depending on pH of reaction) than those measured using $NaNO_3$ or $NaClO_4$. The redox partners of the title reaction are oppositely charged and thus conventional metal ion catalysis (M. Gupta, S.K. Saha, P. Banerjee, J. Chem. Soc., Perkin Trans. II (1988) 1781) can be ruled out. A possible reason for the rate enhancement in presence of Li^+ ion may be explained by very high approximate hydration number as estimated by transference data (F.A. Cotton, G. Wilkinson, C.A. Murillo and M. Bochmann, Advanced Inorganic Chemistry (Ch. 3), 6th ed., Wiley, New York, 1999, p. 102) of Li^+ (25.3) than Na^+ (16.6) that results in a major lowering of the effective concentration of solvent water which in turn increases the activity of the redox partners. A similar situation has also been verified with the oxidation of azide by the title silver(III) complex. We also note that the effect of $LiClO_4$ for the rate enhancement is marginal when the reactive form of the reducing agent is uncharged. We will explore in future the finer details of these effects.

$$[Ag(H_2L)]^{3+} \overset{K_{a1}}{\rightleftharpoons} [Ag(HL)]^{2+} + H^+ \quad (3)$$

$$[Ag([HL)]^{2+} \overset{K_{a2}}{\rightleftharpoons} [AgL]^{+} + H^+ \quad (4)$$

$$HGX \overset{K_a}{\rightleftharpoons} H^+ + GX^- \quad (5)$$

$$[Ag(H_2L)]^{3+} + HGX \overset{k_1}{\rightarrow} \text{Products} \quad (6)$$

$$[Ag(H_2L)]^{3+} + GX^- \overset{k_2}{\rightarrow} \text{Products} \quad (7)$$

$$[Ag(HL)]^{2+} + GX^- \overset{k_3}{\rightarrow} \text{Products} \quad (8)$$

$$[AgL]^{+} + GX^- \overset{k_4}{\rightarrow} \text{Products} \quad (9)$$

Scheme 1.

Scheme 1 leads to the rate law

$$k_0[H^+]^3/([HGX]_T\alpha_1\alpha_2) = k_1[H^+]^3 + k_2K_a[H^+]^2 + k_3K_{a1}K_a[H^+] + k_4K_{a1}K_{a2}K_a, \quad (10)$$

where $\alpha_1 = [H^+]^2/([H^+]^2 + K_{a1}[H^+] + K_{a1}K_{a2})$ is the fraction of the silver(III) complex present as $[Ag(H_2L)]^{3+}$ and $\alpha_2 = [H^+]/(K_a + [H^+])$ is the fraction of glyoxylic acid present as HGX.

In the lower pH range (up to pH 2.5), the second dissociation of the dibasic complex may be neglected and reactions (8) and (9) are unnecessary to reproduce the observed k_0 values. On the other hand at pH $\geqslant$ 6.0 we can assume only $[Ag(HL)]^{2+}$ and $[AgL]^+$ as the contributing silver species reacting with GX^-. The rate-laws in these extremes are, respectively,

$$k_0(K_a + [H^+])/[HGX]_T = k_1[H^+] + k_2K_a, \quad (11)$$

$$k_0(K_{a2} + [H^+])/[HGX]_T = k_3[H^+] + k_4K_{a2}. \quad (12)$$

The second-order rate constants (in 10^4 $M^{-1}\,s^{-1}$) evaluated from these linear plots (left-hand sides of Eqs. (11) and (12) versus $[H^+]$) are, respectively, $k_1 = 7.34$, $k_2 = 112$, $k_3 = 40.7$ and $k_4 = 19.2$. They reproduce the observed first-order rate constants satisfactorily (within 10%) using Eq. (10). We also tried to construct a global fit of the left-hand side of Eq. (10) with $[H^+]$; a third-order polynomial fit of the left-hand side of Eq. (10) with $[H^+]$ resulted a very close (within 2%) value of k_1 as found by Eq. (11) and less close agreement for the k_2 value. However, the constant term $k_4K_{a1}K_{a2}K_a$ yielded a negative value that could not be made positive even varying k_1 and k_2 values by more than 50%. We thus used a constant value of the term $k_4K_{a1}K_{a2}K_a$ (using the k_4 values as obtained from Eq. (12) and known K_{a1}, K_{a2} and K_a values) and k_1, and then started iteration to obtain the best values of the coefficients of the $[H^+]^2$ and $[H^+]$ terms, viz. k_2K_a and $k_3K_{a1}K_a$ respectively, until χ^2 for the fitting becomes acceptably small (of the order of 10^{-16}). The rate constants k_2 and k_3 evaluated in this way agree quite well (within 5%) with the values obtained from Eqs. (11) and (12). This is another support for the proposed scheme of reactions.

3.4. Mechanism

The observed sequence of rate constants $k_1 < k_2 > k_3 > k_4$ clearly demonstrates superior kinetic reactivity of protonated oxidants and deprotonated reductant over their counterparts – a trend normally followed in majority of redox reactions [16–19,33–37]. Among the rate constants evaluated (k_1–k_4), we find k_1 is the smallest indicating negligible reactivity of HGX towards the title Ag^{III} complex. We therefore did not include in the scheme the reaction between $[Ag(HL)]^{2+}$ and HGX. Moreover, the acid dissociation constants of $[Ag(H_2L)]^{3+}$ and HGX are quite distant and simultaneous equilibrium generation of both $[Ag(HL)]^{2+}$ and HGX is not appreciable.

The title silver(III) complex is a weak oxidant ($E_{1/2}$ $Ag^{III}/Ag^{II} = 0.05$ V) versus saturated calomel electrode (SCE) [6,38] but the thermodynamics of two electron oxidation of glyoxylic acid is much favourable, estimated to be around 0.3 V versus NHE. [2] Rate retardation in presence of acrylonitrile indicates generation of Ag^{II} and polymerisation initiating radicals, viz. HGX^+ and GX^-. A competitive decay of glyoxylate radicals occurs via fast consumption by Ag^{II} leading to products and initiation of acrylonitrile polymerisation – it explains lowering in reaction rate in presence of acrylonitrile. Generation of glyoxylate radicals by one-electron oxidation of glyoxylic acid is well-established by EPR spectroscopy [39]. However, we observed that the whole reaction course was EPR silent. We infer that the radicals produced from one-electron oxidation of glyoxylic acid react in a fast manner with Ag^{II} before they can escape into bulk solvent, thus evading detection. Unfortunately one electron potential data for HGX/HGX^+ couple as well as its self-exchange rate is unavailable. Thus we are unable to conclude the nature of electron transfer, inner or outer sphere.

Up to pH 2.5, where only $[Ag(H_2L)]^{3+}$ is the kinetically reactive oxidant, preequilibrium formation of any adducts between $[Ag(H_2L)]^{3+}$ and HGX or GX^- is at best poor, estimated to be within a maximum of the order of 10^{-1} M^{-1}. Such a low value does not confirm a

[2] Private communication with Dr. Philip N. Ross, Senior Scientist, Lawrence Berkeley National Laboratory. Glyoxylic acid can thermodynamically be considered as half formic acid and half oxalic acid. The redox potential should therefore be exactly half way between that of formic acid (0.14 V) and oxalic acid (0.49 V).

strong inner sphere attachment of glyoxylic acid with the metal center. Formation of a strong inner sphere adduct by glyoxylate with $[Mn(pd)_2(H_2O)_2]^+$ (Hpd = pentane 2,4 dione) has been proposed [40] and the formation constants of glyoxylate complexes of tripositive rare-earth-metal cations are also high [41]. The in-plane coordinatively saturated Ag^{III} in the title complex makes the situation a different one in aqueous solution where the replaceable water molecules attach only weakly with the axial positions of the Ag^{III} center. Replacement of water molecule by glyoxylate is thus expected to be weak at best. The estimated low value for the formation of adducts in the present study may be assigned to electrostriction [42–45] or any kind of it aided by hydrogen bonding [46,47] in the adducts.

A kinetically indistinguishable scheme where the adducts formed by electrostriction or aided by hydrogen bonding on the basal plane may be proposed. However, this proposition enforces a large separation between the oxidant and the reductant species that inhibits electron transfer within the adduct due to incorrect approach, as it were. Occurrence of electron transfer rather is justified when the reductant approaches the metal center along the axial site of the latter. A comparatively strong adduct formation between the complex and the oxalic acid or bioxalate ion [18] in comparison to glyoxylate indicate a much stronger binding with the more potentially complexing oxalate species inherited by their bidentacy.

Acknowledgements

The award of a Junior Research Fellowship to Amit Das by University Grants Commission, New Delhi and financial assistance from Jadavpur University Research Grant are gratefully acknowledged.

Appendix A. Derivation of Eq. (10)

The acid dissociation constants for the title silver(III) complex are

$$K_{a1} = [Ag(HL)^{2+}][H^+]/[Ag(H_2L)^{3+}], \quad (A.1)$$

$$K_{a2} = [AgL^+][H^+]/[Ag(HL)^{2+}]. \quad (A.2)$$

The analytical concentration of the silver(III) complex, T_c, may be written as

$$T_c = [Ag(H_2L)^{3+}] + [Ag(HL)^{2+}] + [AgL^+],$$

Substituting $[Ag(HL)^{2+}]$ and $[AgL^+]$ in terms of $[Ag(H_2L)^{3+}]$ and rearranging, it results

$$T_c = [Ag(H_2L)^{3+}](1 + K_{a1}/[H^+] + K_{a1}K_{a2}/[H^+]^2),$$

whence we may write,

$$[Ag(H_2L)^{3+}]/T_c$$
= fraction of the silver(III)complex present as $[Ag(H_2L)^{3+}]$
$$= [H^+]^2/([H^+]^2 + K_{a1}[H^+] + K_{a1}K_{a2})$$
$$= \alpha_1 \quad \text{(say)}.$$

Thus, using (A.1) and (A.2) it yields

$$[Ag(H_2L)^{3+}] = \alpha_1 T_c; [Ag(HL)^{2+}] = K_{a1}\alpha_1 T_c$$

and

$$[AgL^+] = K_{a1}K_{a2}\alpha_1 T_c/[H^+]^2.$$

From the glyoxylic acid dissociation equilibrium

$$K_a = [GX^-][H^+]/[HGX],$$

it appears

$$[HGX]/([HGX] + [GX^-])$$
= fraction of glyoxylic acid present as

$$[HGX] = [H^+]/(K_a + [H^+]) = \alpha_2 \quad \text{(say)}.$$

Thus,

$$[HGX] = \alpha_2[HGX]_T$$

and

$$[GX^-] = K_a\alpha_2[HGX]_T/[H^+].$$

Now, for the proposed scheme (see text), rate of the reaction becomes

$$\text{Rate} = k_1\alpha_1\alpha_2 T_c[HGX]_T + k_2K_a\alpha_1\alpha_2 T_c[HGX]_T/[H^+] + k_2K_aK_{a1}\alpha_1\alpha_2 T_c[HGX]_T/[H^+]^2 + k_4K_aK_{a1}K_{a2}\alpha_1\alpha_2[HGX]_T/[H^+]^3,$$

whence, it becomes,

$$k_0[H^+]^3/([HGX]_T\alpha_1\alpha_2) = k_1[H^+]^3 + k_2K_a[H^+]^2 + k_3K_{a1}K_a[H^+] + k_4K_{a1}K_{a2}K_a.$$

References

[1] P. Ray, Nature (London) 151 (1943) 643.
[2] P. Ray, K. Chakravarty, J. Indian Chem. Soc. 21 (1944) 47.
[3] P. Ray, Inorg. Synth. 6 (1960) 74.
[4] R. Banerjee, D. Banerjea, Indian J. Chem. 17A (1979) 246.
[5] D. Sen, N.N. Ghosh, P. Ray, J. Indian Chem. Soc. 27 (1950) 619.
[6] K. Das, R. Banerjee, A. Das, S. Dasgupta, Bull. Electrochem. 5 (1989) 477.
[7] W.M. Latimer, The Oxidation States of the Elements and their Potentials in Aqueous Solutions, second ed., Prentice-Hall, Englewood Cliffs, NJ, 1952, p. 176.
[8] S. Mukhopadhyay, R. Banerjee, Polyhedron 13 (1994) 53.
[9] R. Banerjee, K. Das, A. Das, S. Dasgupta, Inorg. Chem. 28 (1989) 585.
[10] R. Banerjee, A. Das, S. Dasgupta, J. Chem. Soc., Dalton Trans. (1989) 1645.
[11] R. Banerjee, A. Das, S. Dasgupta, J. Chem. Soc., Dalton Trans. (1990) 1207.

[12] R. Banerjee, A. Das, S. Dasgupta, J. Chem. Soc., Dalton Trans. (1990) 2271.
[13] R. Banerjee, R. Das, S. Mukhopadhyay, J. Chem. Soc., Dalton Trans. (1992) 1317.
[14] S. Dasgupta, E. Herlinger, W. Linert, J. Chem. Soc., Dalton Trans. (1993) 567.
[15] R. Banerjee, Proc. Indian Acad. Sci. (Chem. Sci.) 106 (1994) 655.
[16] S.P. Ghosh, M.C. Ghosh, E.S. Gould, Inorg. Chim. Acta 225 (1994) 83.
[17] S. Mukhopadhyay, R. Banerjee, J. Chem. Soc., Dalton Trans. (1994) 1349.
[18] S. Mukhopadhyay, S. Kundu, R. Banerjee, Proc. Indian Acad. Sci. (Chem. Sci.) 107 (1995) 403.
[19] P. Bandopadhyay, S. Mukhopadhyay, Polyhedron 21 (2002) 1893.
[20] P. Bandopadhyay, B.B. Dhar, J. Bhattacharyya, S. Mukhopadhyay, Eur. J. Inorg. Chem. (2003) 4308.
[21] A. White, Principles of Biochemistry, 2nd ed., McGraw-Hill, New York, 1954, p. 548.
[22] E.H. Rodd, in: Chemistry of Carbon Compounds, Part B, vol. 1, Elsevier, Amsterdam, 1952, p. 850.
[23] D.M. Greenberg, Chemical Pathways of Metabolism, vol. 2, 2nd ed., Academic Press, New York, 1961, p. 85.
[24] Y. Sun, L.J. Kirschenbaum, I. Kouadio, J. Chem. Soc., Dalton Trans. (1991) 2311.
[25] J. Zou, Z. Guo, J.A. Parkinson, Y. Chen, P.J. Sadler, J. Chem. Soc., Chem. Commun. (1999) 1359.
[26] D.N. Kramer, N. Klein, R.A. Baselice, Anal. Chem. 30 (1959) 250.
[27] K. Dutta, S. Bhattacharjee, B. Choudhuri, S. Mukhopadhyay, J. Environ. Monit. 4 (2002) 754.
[28] S. Banerjee, U. Roy Choudhury, B.C. Ray, R. Banerjee, S. Mukhopadhyay, Anal. Lett. 34 (2001) 2797.
[29] F. Feigl, Spot Tests in Organic Analysis, 5th ed., Elsevier, London, 1956, pp. 331, 342.
[30] P. Ray, Chem. Rev. 61 (1961) 313.
[31] A.E. Martell, R.M. Smith, in: Critical Stability Constants, vol. 3, Plenum Press, New York, 1997, p. 65.
[32] R.G. Wilkins, The Study of Kinetics and Mechanism of Reactions of Transition Metal Complexes, Allyn & Bacon, Boston, MA, 1974 (Ch. 1), p. 460.
[33] S.K. Ghosh, R.N. Bose, E.S. Gould, Inorg. Chem. 26 (1987) 2688.
[34] K.D. Asmus, M. Bonifacic, P. Toffel, P. O'Neill, D.S. Frohlinde, S. Steenken, J. Chem. Soc., Faraday Trans. 1 (1978) 1820.
[35] K. Lemma, A.M. Sargeson, L.I. Elding, J. Chem. Soc., Dalton Trans. (2000) 1167.
[36] T. Shi, J. Berglund, L.I. Elding, Inorg. Chem. 35 (1996) 3498.
[37] J. Berglund, L.I. Elding, Inorg. Chem. 34 (1995) 513.
[38] B. Chakravarty, J. Inorg. Nucl. Chem. 41 (1979) 757.
[39] B. Neumann, O. Steinbock, S.C. Muller, N.S. Dalal, J. Phys. Chem. 100 (1996) 12342.
[40] R. Banerjee, R. Das, A.K. Chakraburtty, J. Chem. Soc., Dalton Trans. (1990) 3277.
[41] J.E. Powell, Y. Suzuki, Inorg. Chem. 3 (1964) 690.
[42] M.G. Evans, G.H. Nancollas, Trans. Faraday Soc. 49 (1953) 363.
[43] C. Postmus, E.L. King, J. Phys. Chem. 59 (1955) 1208.
[44] F. Basolo, R.G. Pearson, Mechanism of Inorganic Reactions, 2nd ed., Wiley, New York, 1967, p. 34.
[45] M. Grant, R.B. Jordan, Inorg. Chem. 20 (1981) 55.
[46] C.D. Hubbard, A. Gerhard, R. van Eldik, J. Chem. Soc., Dalton Trans. (2001) 1069.
[47] M.C. Ghosh, J.W. Reed, R.N. Bose, E.S. Gould, Inorg. Chem. 33 (1994) 73.

Available online at www.sciencedirect.com
SCIENCE DIRECT®
Polyhedron 23 (2004) 903–911
POLYHEDRON
www.elsevier.com/locate/poly

Synthesis and characterization of *syn–anti* carboxylate-bridged one-dimensional copper(II) complexes with bis(2-pyridylmethyl)amino acids

Ki-Young Choi [a,*], Yong-Man Jeon [a], Haiil Ryu [a], Je-Jik Oh [a], Hae-Hwan Lim [b], Moon-Won Kim [b]

[a] *Department of Chemistry Education, Kongju National University, Kongju 314-701, Republic of Korea*
[b] *Department of Physics, Kongju National University, Kongju 314-701, Republic of Korea*

Received 4 August 2003; accepted 24 September 2003

Abstract

Tetradentate Schiff-base carboxylate-containing ligands, bis(2-pyridylmethyl)amino-2-ethanoic acid (pmea), bis(2-pyridylmethyl)amino-3-propionic acid (pmpa) and bis(2-pyridylmethyl)amino-4-butyric acid (pmba), react with copper(II) perchlorate to give rise to the one-dimensional polymeric chain complexes $\{[Cu(\mu\text{-pmea})](ClO_4)\cdot H_2O\}_n$ (**1**), $\{[Cu(\mu\text{-pmpa})](ClO_4)\cdot 2H_2O\}_n$ (**2**) and $\{[Cu(\mu\text{-pmba})(H_2O)](ClO_4)\cdot 3H_2O\}_n$ (**3**). These complexes have been characterized by X-ray crystallography, UV–Vis spectra and variable-temperature magnetic susceptibility measurements. In complexes **1**–**3**, distorted square-pyramidal copper(II) ions are sequentially bridged by *syn–anti* carboxylate groups. Each of the copper(II) ions exhibit CuN_3O_2 coordination environments with the three nitrogen atoms of the ligand and one oxygen atom belonging to the carboxylate group of an adjacent molecule occupying the basal positions and an oxygen atom (from a carboxylate group in the case of compounds **1**–**2** and from a water molecule in **3**) coordinated in the axial position. The electronic spectra of the complexes are significantly affected by the coordination geometry. Magnetic susceptibility measurements indicate that complexes **1**–**3** exhibit very weak ferromagnetic interactions. The magnetic behavior can be explained on the basis of the structural data.
© 2004 Elsevier Ltd. All rights reserved.

Keywords: Self-assembly; Crystal structures; Bis(2-pyridylmethyl)amino acids; Ferromagnetism; One-dimensional chains; Copper(II) complexes

1. Introduction

Self-assembly of metal ions and multidentate organic ligands has achieved great success in forming coordination polymers and multi-dimensional supramolecular networks [1–24] that can be used as catalysts [5], or exhibit novel properties such as electric conductivities [6], optical properties [7–9] and magnetism [10–24]. The architecture of the metal-organic polymers is based on well-defined coordination chemistry which takes into account the coordination nature of the metal ion, the structure of the organic ligands, and the possible counterion and solvents effects. It is well known that a carboxylate group can bridge two metal ions to give rise to a wide variety of polynuclear complexes ranging from discrete entities to multi-dimensional systems. The inclusion of a carboxylate group into the polydentate ligand allows the formation of trinuclear and tetranuclear complexes with *syn–anti* carboxylate bridging groups and a weak ferromagnetic exchange interaction between the copper(II) ions [18,19]. For example, the *syn–anti* carboxylate bridged linear trinuclear copper(II) complex $[Cu(H_2O)_4\{Cu(HL)\text{-}(H_2O)(ClO_4)\}_2][ClO_4]_2\cdot 2H_2O$ (HL = 6-methylamino-1,3-dimethyl-5-[(2′-carboxyphenyl)azo]uracil) revealed an octahedral and distorted square-pyramidal geometry about the central and terminal copper atoms, which exhibit a weak ferromagnetic interaction between nearest-neighbor copper(II) ions [19]. However, the *syn–anti* conformation corresponds to chain or layer compounds, which are characterized by a weak ferromagnetic

* Corresponding author. Tel.: +82-41-850-8284/8541; fax: +82-41-850-8347/8541.
E-mail address: kychoi@kongju.ac.kr (K.-Y. Choi).

0277-5387/$ - see front matter © 2004 Elsevier Ltd. All rights reserved.
doi:10.1016/j.poly.2003.11.058

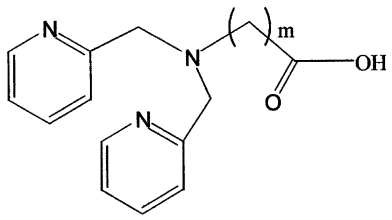

m	Ligand
1	pmea
2	pmpa
3	pmba

Chart 1.

or antiferromagnetic exchange interaction between the copper(II) ions [20–22]. In a zig-zag chain complex [{Cu(L)(Hpz)(H_2O)} · $2H_2O$] (H_2L = 5-[(2-carboxyphenyl)-azo]-1,3-dimethylbarbituric acid; Hpz = pyrazole) [22], the coordination geometry about the copper(II) ions is distorted square-pyramid, which has the *syn–anti* carboxylate bridging groups and reveals a weak intermolecular antiferromagnetic exchange interaction between the copper(II) ions. To further investigate the differences in the magnetic behavior, we have prepared and characterized the one-dimensional carboxylate-bridged copper(II) complexes {[Cu(μ-pmea)](ClO_4) · H_2O}$_n$ (**1**), {[Cu(μ-pmpa)](ClO_4) · $2H_2O$}$_n$ (**2**) and {[Cu(μ-pmba)-(H_2O)]-(ClO_4) · $3H_2O$}$_n$ (**3**) (where pmea = bis(2-pyridylmethyl) amino-2-ethanoic acid, pmpa = bis(2-pyridylmethyl)amino-3-propionic acid and pmba = bis(2-pyridylmethyl)-amino-4-butyric acid) (see Chart 1). The reactions of the tetradentate Schiff-base carboxylate-containing ligands with copper(II) perchlorate lead to *syn–anti* carboxylate-bridged complexes. Because the ligands do not saturate the coordination positions on the copper(II) ions, self-assembly reactions may occur through the deprotonated carboxylate groups, leading to carboxylate-bridged polymeric one-dimensional chains.

2. Experimental

2.1. Materials and physical methods

All the chemicals used in syntheses were of reagent grade and were used without further purification. Infrared spectra were recorded as KBr pellets on a Perkin–Elmer Paragon 1000 FT-IR spectrometer. Solution electronic spectra were obtained on a Jasco Uvidec-610 spectrophotometer. Solid state electronic spectra were measured by the diffuse reflectance method on a Shimadzu UV2401 PC/DRS spectrophotometer. Magnetic susceptibility data were collected in the temperature range 5.0–300 K in an applied field of 0.5 T with the use of a Quantum Design MPMS7 SQUID magnetometer. The diamagnetic corrections were calculated from Pascal's constants. Elemental analyses were carried out on a Perkin-Elmer 240C analyzer. FAB mass spectra were performed by using a Jeol JMS-HA 110A/110A spectrometer.

2.2. Syntheses of bis(2-pyridylmethyl)amino-2-ethanoic acid (pmea)

To a water solution (25 ml) of 2-picolyl chloride hydrochloride (3.61 g, 22 mmol) was added a water solution (25 ml) of glycine (0.75 g, 10 mmol) and sodium hydroxide (1.6 g, 40 mmol). After the mixture was heated to reflux for one day, the solution was extracted with chloroform. The removal of the solvent yielded the crude white product, which was purified by recrystallization from a 1:1 water–ethanol mixture. Yield: 1.72 g (67%). *Anal.* Calc. for $C_{14}H_{15}N_3O_2$: C, 65.35; H, 5.88; N, 16.33. Found: C, 65.46; H, 5.73; N, 16.42%. FAB mass (*m*/*z*): 257 $(M)^+$.

2.3. Syntheses of bis(2-pyridylmethyl)amino-3-propionic acid (pmpa)

The compound pmpa was prepared as colorless crystals in a manner similar to that of pmea by using β-alanine (0.90 g, 10 mmol) instead of glycine. Yield: 2.03 g (75%). *Anal.* Calc. for $C_{15}H_{17}N_3O_2$: C, 66.40; H, 6.32; N, 15.49. Found: C, 66.28; H, 6.40; N, 15.57%. FAB mass (*m*/*z*): 271 $(M)^+$.

2.4. Syntheses of bis(2-pyridylmethyl)amino-4-butyric acid (pmba)

The compound pmba was prepared as colorless crystals in a manner similar to that of pmea by using 4-aminobutyric acid (1.03 g, 10 mmol) instead of glycine. Yield: 2.04 g (72%). *Anal.* Calc. for $C_{16}H_{19}N_3O_2$: C, 67.35; H, 6.71; N, 14.73. Found: C, 67.43; H, 6.62; N, 14.65%. FAB mass (*m*/*z*): 285 $(M)^+$.

2.5. Syntheses of {[Cu(μ-pmea)](ClO_4) · H_2O}$_n$ (1)

A water solution (20 ml) of $Cu(ClO_4)_2 \cdot 6H_2O$ (185 mg, 0.5 mmol) and pmea (129 mg, 0.5 mmol) was heated to reflux for 1 h and then cooled to room temperature. The solution was filtered and left at room temperature until the blue crystals formed. The product was filtered and recrystallized from a hot water/acetonitrile (1:1 v/v, 10 ml) mixture. Yield: 155 mg (71%). *Anal.* Calc. for $C_{14}H_{16}ClCuN_3O_7$: C, 38.45; H, 3.69; N, 9.61. Found: C, 38.54; H, 3.75; N, 9.49%. IR (KBr, cm^{-1}): *ν*(CO) 1610, 1442; pyridine skeleton 1588, 1487, 1426; *ν*(Cl–O) 1092. FAB mass (*m*/*z*): 437 $(M)^+$.

2.6. Syntheses of $\{[Cu(\mu\text{-pmpa})](ClO_4)\cdot 2H_2O\}_n$ (2)

This compound was synthesized as blue crystals in a reaction similar to that of **1**, except for the use of pmpa (136 mg, 0.5 mmol) instead of pmea. Yield: 153 mg (65%). *Anal*. Calc. for $C_{15}H_{20}ClCuN_3O_8$: C, 38.39; H, 4.30; N, 8.95. Found: C, 38.47; H, 4.36; N, 8.87%. IR (KBr, cm^{-1}): ν(CO) 1610, 1439; pyridine skeleton 1558, 1482, 1421; ν(Cl–O) 1091, 1116. FAB mass (m/z): 469 $(M)^+$.

2.7. Syntheses of $\{[Cu(\mu\text{-pmba})(H_2O)](ClO_4)\cdot 3H_2O\}_n$ (3)

This compound was synthesized as blue crystals in a reaction similar to that of **1**, except for the use of pmba (143 mg, 0.5 mmol) instead of pmea. Yield: 174 mg (67%). *Anal*. Calc. for $C_{16}H_{26}ClCuN_3O_{10}$: C, 37.00; H, 5.05; N, 8.09. Found: C, 36.92; H, 5.14; N, 8.17%. IR (KBr, cm^{-1}): ν(CO) 1609, 1443; pyridine skeleton 1589, 1481, 1449; ν(Cl–O) 1092, 1117. FAB mass (m/z): 519 $(M)^+$.

Caution! Perchlorate salts of metal complexes with organic ligands are potentially explosive and should be handled in small quantities with care.

2.8. X-ray crystal structure analysis

Intensity data for the compounds were measured on an Enraf-Nonius CAD4 diffractometer using graphite-monochromated Mo Kα radiation in the ω–2θ scan mode. Accurate cell parameters and an orientation matrix were determined by least-squares fit of 25 reflections. The intensity data were corrected for Lorentz and polarization effects. All data were corrected for empirical absorption. The structure was solved direct methods [25] and the least-squares refinement of the structure was performed by the program SHELXL-97 [26]. For **1**, all non-hydrogen atoms were refined anisotropically. The hydrogen atoms were placed in calculated positions, allowing them to ride on their attached atoms with $U_{iso}(H) = 1.2U_{eq}(C)$. The two hydrogen atoms of the water molecule were not found. The rather higher R_1 and wR_2 values may be attributed mainly to the bad quality of the sample compound. For **2**, all hydrogen atoms except for the water hydrogen atoms Ow(2) were placed in calculated positions with U_{iso} to be 1.2 times the equivalent isotropic displacement of the parent atom. The two hydrogen atoms of Ow(1) were found from the difference Fourier map and their

Table 1
Crystallographic data

	1	**2**	**3**
Empirical formula	$C_{14}H_{16}ClCuN_3O_7$	$C_{15}H_{20}ClCuN_3O_8$	$C_{16}H_{26}ClCuN_3O_{10}$
Formula weight	437.29	469.33	519.39
Temperature (K)	293(2)	293(2)	293(2)
Crystal color/habit	prism/blue	prism/blue	block/deep blue
Crystal system	orthorhombic	monoclinic	orthorhombic
Space group	$P2_12_12_1$	$P2_1/n$	$Pna2_1$
Unit cell dimensions			
a (Å)	10.133(5)	14.236(1)	17.165(3)
b (Å)	11.911(5)	9.523(1)	10.244(1)
c (Å)	14.074(5)	14.554(2)	12.629(1)
β (°)		109.87(1)	
V (Å^3)	1698.6(13)	1855.6(3)	2220.7(5)
Z	4	4	4
D_{calc} (Mg m^{-3})	1.710	1.680	1.553
Absorption coefficient (mm^{-1})	1.487	1.371	1.160
F (0 0 0)	892	964	1076
Crystal size (mm)	$0.35\times0.20\times0.10$	$0.30\times0.20\times0.02$	$0.60\times0.21\times0.15$
θ range (°)	2.24–24.97	1.73–24.97	2.32–25.00
Limiting indices	$-12\leqslant h\leqslant 12$, $0\leqslant k\leqslant 14$, $0\leqslant l\leqslant 15$	$-16\leqslant h\leqslant 15$, $0\leqslant k\leqslant 11$, $0\leqslant l\leqslant 17$	$0\leqslant h\leqslant 20$, $0\leqslant k\leqslant 12$, $-15\leqslant l\leqslant 20$
Reflection collected/unique	3213/2951 ($R_{int} = 0.0459$)	3387/3252 ($R_{int} = 0.0362$)	3899/3899 ($R_{int} = 0.0000$)
Absorption correction	φ-scan	φ-scan	φ-scan
Maximum/minimum transmission	0.8391 and 0.0246	0.9731 and 0.6838	0.9959 and 0.4631
Data/restraints/parameters	2951/0/223	3252/0/248	3899/1/280
Goodness of fit on F^2	1.339	1.042	1.028
Final R indices ($I > 2(I)$)	R_1[a] = 0.0955, wR_2[b] = 0.2744	$R_1 = 0.0541$, $wR_2 = 0.1418$	$R_1 = 0.0525$, $wR_2 = 0.1132$
R indices (all data)	$R_1 = 0.1115$, $wR_2 = 0.2933$	$R_1 = 0.1081$, $wR_2 = 0.1652$	$R_1 = 0.0873$, $wR_2 = 0.1278$
Largest difference peak and hole (e Å^{-3})	1.357 and −0.930	0.946 and −0.642	0.397 and −0.334

[a] $R_1 = \sum||F_o| - |F_c||/\sum|F_o|$.

[b] $wR_2 = [\sum[w(F_o^2 - F_c^2)^2]/\sum[w(F_o^2)^2]]^{1/2}$.

positions were fixed with U_{iso} to be 1.2 times the equivalent isotropic displacement of the parent atom, but the hydrogen atoms of Ow(2) were not located. For **3**, all non-hydrogen atoms were refined anisotropically. All hydrogen atoms except for the water hydrogen atoms were placed in calculated positions with U_{iso} to be 1.2 times the equivalent isotropic displacement of the parent atom. The four hydrogen atoms of Ow(3) and Ow(4) were found from the difference Fourier map and their positions were fixed with U_{iso} to be 1.2 times the equivalent isotropic displacement of the parent atom. The rest of the water molecules were not found. Crystal parameters and details of the data collections and refinement are summarized in Table 1.

3. Results and discussion

3.1. Crystal structures

An ORTEP drawing of $\{[Cu(\mu\text{-pmea})](ClO_4)\cdot H_2O\}_n$ (**1**) with the atomic labelling scheme is shown in Fig. 1 and the selected bond lengths and angles are listed in Table 2. The monodeprotonated pmea ligand acts as a tetradentate ligand toward a copper(II) ion and as a monodentate ligand toward a neighboring copper(II) center. The copper atoms are bridged by a *syn–anti* carboxylate group to form a polymeric one-dimensional chain with an intramolecular Cu···Cu distance of 5.350(1) Å. Each copper(II) ion exhibits a CuN_3O_2 coordination environment with the three nitrogen atoms of the ligand and one oxygen atom belonging to the carboxylate group of an adjacent molecule occupying the basal plane [Cu–N(1) 1.978(9) Å, Cu–N(2) 2.060(8) Å, Cu–N(3) 2.002(8) Å, Cu–O(1) 1.947(7) Å] and an oxygen atom from a carboxylate group coordinated the axial position [Cu–O(2)″ 2.246(7) Å]. The geometry is somewhat distorted from square-pyramidal, as is apparent from the observed τ value of 0.25 (values of 0 and 1 are indicative of idealized square pyramidal and trigonal bipyramidal geometries, respectively) [27]. The copper atom lies 0.082(3) Å above the basal plane toward the carboxylate oxygen atom O(2)″. The N(1)–Cu–N(2) and N(2)–Cu–N(3) bite angles of the five-membered chelate rings are 82.7(4)° and 83.9(3)°, respectively. The dihedral angle (α) between the plane of the carboxylate group and CuN_3O plane is 65.8(7)°. The axial Cu–O(2)″ bond is not perfectly perpendicular to the CuN_3O plane with N–Cu–O(2)″ and O(1)–Cu–O(2)″ angles ranging from 81.8(3)° to 99.9(3)°. The secondary Cu–N(1) and Cu–N(3) bond distances are much shorter than the Cu–N(2) (tertiary amine) distance, indicating comparatively strong coordination.

An ORTEP drawing of $\{[Cu(\mu\text{-pmpa})](ClO_4)\cdot 2H_2O\}_n$ (**2**) with the atomic labelling scheme is shown in Fig. 2 and the selected bond lengths and angles are listed in Table 3. Each copper atom is coordinated by *syn–anti* carboxylate bridges to form a one-dimensional polymeric chain with an intramolecular Cu···Cu distance of 5.800(2) Å. The coordination environment of each copper(II) ion reveals a distorted square-pyramid with three nitrogen atoms and one oxygen atom belonging to the carboxylate group of an adjacent molecule [Cu–N(1) 1.982(5) Å, Cu–N(2) 2.023(4) Å, Cu–N(3) 1.980(4) Å, Cu–O(1) 1.943(4) Å] comprising the basal plane, whereas the apical position is filled by the carboxylate oxygen atom of the pmpa ligand [Cu–O(2)″ 2.393(4) Å]. The distortion τ value is 0.19. The copper atom is displaced 0.027(2) Å from the least-squares plane defined by the N_3O basal plane toward the carboxylate oxygen atom O(2)″. The value of the dihedral angle (α) is 77.7(3)°. The Cu–O(2)″ linkage is bent slightly off the

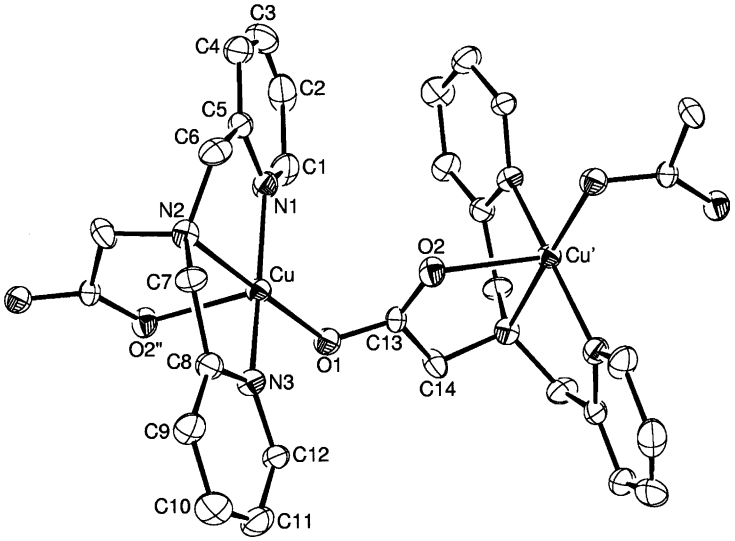

Fig. 1. An ORTEP diagram of $\{[Cu(\mu\text{-pmea})](ClO_4)\cdot H_2O\}_n$ (**1**) with the atom-numbering scheme (30% probability ellipsoids shown). The perchlorate, lattice water molecules and hydrogen atoms are omitted for clarity.

Table 2
Selected bond lengths (Å) and angles (°) for $\{[Cu(\mu\text{-pmea})](ClO_4)\cdot H_2O\}_n$ (**1**)[a]

Bond lengths			
Cu–N(1)	1.978(9)	Cu–N(2)	2.060(8)
Cu–N(3)	2.002(8)	Cu–O(1)	1.947(7)
Cu–O(2)[b]	2.246(7)	C(13)–O(1)	1.277(12)
C(13)–O(2)	1.230(12)	Cu···Cu[b]	5.350(1)
Bond angles			
N(1)–Cu–N(2)	82.7(4)	N(1)–Cu–N(3)	163.3(4)
N(2)–Cu–N(3)	83.9(3)	N(1)–Cu–O(1)	97.5(3)
N(2)–Cu–O(1)	178.2(3)	N(3)–Cu–O(1)	95.6(3)
N(1)–Cu–O(2)[b]	96.7(4)	N(2)–Cu–O(2)[b]	81.8(3)
N(3)–Cu–O(2)[b]	91.1(4)	Cu–O(1)–C(13)	121.8(6)
Cu[c]–O(2)–C(13)	110.6(6)	O(1)–Cu–O(2)[b]	99.9(3)
O(1)–C(13)–O(2)	126.4(8)	O(1)–C(13)–C(14)	112.7(8)
O(2)–C(13)–C(14)	120.6(8)		

[a] Symmetry transformations used to generate equivalent atoms.
[b] $x-1/2,-y+1/2,-z$.
[c] $x+1/2,-y+1/2,-z$.

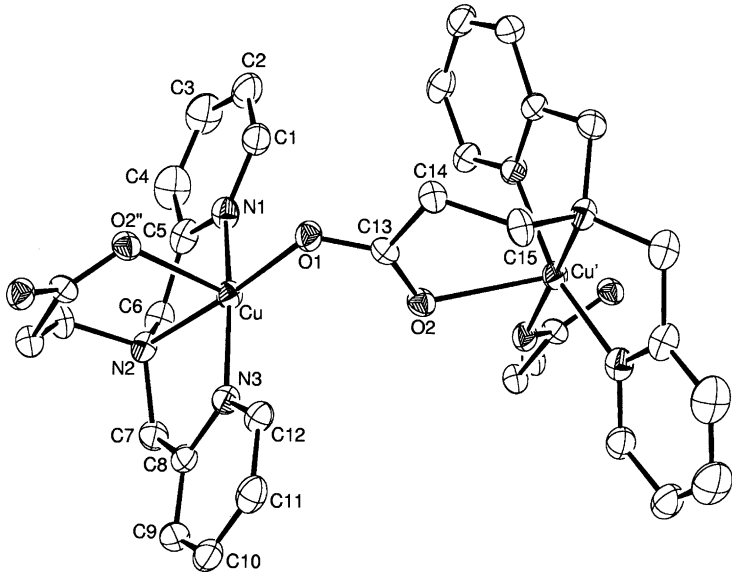

Fig. 2. An ORTEP diagram of $\{[Cu(\mu\text{-pmpa})](ClO_4)\cdot 2H_2O\}_n$ (**2**) with the atom-numbering scheme (30% probability ellipsoids shown). The perchlorate, lattice water molecules and hydrogen atoms are omitted for clarity.

Table 3
Selected bond lengths (Å) and angles (°) for $\{[Cu(\mu\text{-pmpa})](ClO_4)\cdot 2H_2O\}_n$ (**2**)[a]

Bond lengths			
Cu–N(1)	1.982(5)	Cu–N(2)	2.023(4)
Cu–N(3)	1.980(4)	Cu–O(1)	1.943(4)
Cu–O(2)[b]	2.393(4)	C(13)–O(1)	1.261(6)
C(13)–O(2)	1.236(6)	Cu···Cu[b]	5.800(2)
Bond angles			
N(1)–Cu–N(2)	82.8(2)	N(1)–Cu–N(3)	164.2(2)
N(2)–Cu–N(3)	83.7(2)	N(1)–Cu–O(1)	95.3(2)
N(2)–Cu–O(1)	175.7(2)	N(3)–Cu–O(1)	98.7(2)
N(1)–Cu–O(2)	102.1(2)	N(2)–Cu–O(2)[c]	90.3(2)
N(3)–Cu–O(2)[c]	86.2(2)	Cu–O(1)–C(13)	126.2(3)
Cu[c]–O(2)–C(13)	119.6(3)	O(1)–Cu–O(2)[c]	86.3(1)
O(1)–C(13)–O(2)	126.2(5)	O(1)–C(13)–C(14)	113.6(4)
O(2)–C(13)–C(14)	120.2(5)		

[a] Symmetry transformations used to generate equivalent atoms.
[b] $-x+3/2,y-1/2,-z+3/2$.
[c] $-x+3/2,y+1/2,-z+3/2$.

perpendicular to the CuN_3O plane by 0.3–12.1°. The average Cu–N_{py} (secondary) bond distance of 1.981 Å is similar to that found in **1** and shorter than the tertiary Cu–N(2) distance of 2.023(4) Å, giving comparatively strong coordination.

An ORTEP drawing of $\{[Cu(\mu\text{-pmba})(H_2O)](ClO_4)\cdot 3H_2O\}_n$ (**3**) with the atomic labelling scheme is shown in Fig. 3 and the selected bond lengths and angles are listed in Table 4. The copper atoms are bridged by a *syn–anti* carboxylate group of the pmba ligand to form a polymeric one-dimensional chain with an intramolecular Cu···Cu separation of 9.363(2) Å. Each copper(II) ion has a distorted square-pyramidal coordination, in which the basal plane is made up by the three nitrogen atoms of the ligand and one oxygen atom belonging to the carboxylate group of an adjacent molecule [Cu–N(1) 1.978(6) Å, Cu–N(2) 2.022(5) Å, Cu–N(3) 1.979(7) Å, Cu–O(1) 1.927(5) Å], while a water molecule is coordinated at the axial position [(Cu–Ow(1) 2.382(4) Å]. The observed τ value is 0.15. Each copper atom is slightly deviated from the N_3O basal plane by 0.057(2) Å, shifted toward the axially coordinated water molecule Ow(1). The value of the dihedral angle (α) is 86.5(3)°. The Cu–Ow linkage is bent slightly off the perpendicular to the CuN_3O plane by 0.0–5.6°. The average Cu–N (secondary amine) distance of 1.979 Å is shorter than that of Cu–N(2) (tertiary amine) [2.022(5) Å], which is similar to that observed for complex **2**.

3.2. Spectroscopic properties

The infrared spectra of the complexes show ν_{as}(COO) stretching frequencies at 1609–1610 and ν_{sym}(COO) at 1439–1443 cm^{-1}. The difference between ν_{as}(COO) and ν_{sym}(COO) is about 170 cm^{-1}, suggesting a bridging coordination mode for the carboxylate groups. The spectroscopic data of the complexes are listed in Table 5. The UV spectra of the complexes in water and solid state show absorption bands at 254 and 254–255 nm, which are assigned to the intraligand transitions in the complexes. The visible spectra of the complexes in water and solid state also contain broad bands at 675 and 678 nm for **1**, 673 and 675 nm for **2**, and 664 and 667 nm for **3**, characteristic of a copper(II) $d_{zx},d_{yz} \rightarrow d_{x^2-y^2}$

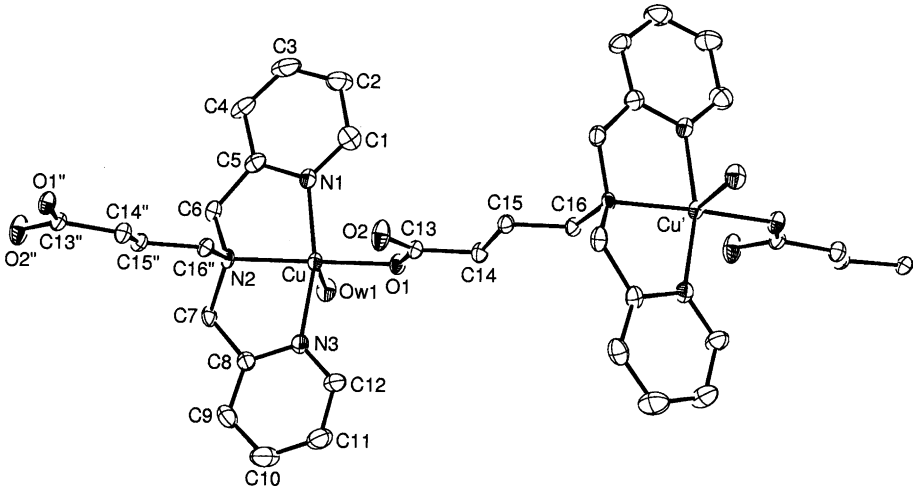

Fig. 3. An ORTEP diagram of $\{[Cu(\mu\text{-pmba})(H_2O)](ClO_4)\cdot 4H_2O\}_n$ (**3**) with the atom-numbering scheme (30% probability ellipsoids shown). The perchlorate, lattice water molecules and hydrogen atoms are omitted for clarity.

Table 4
Selected bond lengths (Å) and angles (°) for $\{[Cu(\mu\text{-pmba})(H_2O)](ClO_4)\cdot 3H_2O\}_n$ (**3**)

Bond lengths			
Cu–N(1)	1.978(6)	Cu–N(2)	2.022(5)
Cu–N(3)	1.979(7)	Cu–O(1)	1.927(5)
Cu–Ow(1)	2.382(4)	C(13)–O(1)	1.278(8)
C(13)–O(2)	1.223(8)	Cu(1)···Cu(2)	9.363(2)
Bond angles			
N(1)–Cu–N(2)	83.0(3)	N(1)–Cu–N(3)	165.2(2)
N(2)–Cu–N(3)	82.4(2)	N(1)–Cu–O(1)	98.0(2)
N(2)–Cu–O(1)	174.3(2)	N(3)–Cu–O(1)	96.4(2)
N(1)–Cu–Ow(1)	94.3(2)	N(2)–Cu–Ow(1)	95.6(2)
N(3)–Cu–Ow(1)	89.1(2)	O(1)–Cu–Ow(1)	90.0(2)
Cu–O(1)–C(13)	113.4(4)	O(1)–C(13)–O(2)	122.3(6)
O(1)–C(13)–C(14)	114.4(6)	O(2)–C(13)–C(14)	123.2(6)

Table 5
Electronic spectral data[a]

Complex	State	λ_{max}, nm (ε = M^{-1} cm^{-1})
$\{[Cu(\mu\text{-pmea})](ClO_4)\cdot H_2O\}_n$ (**1**)	H_2O	254 (1.12×10^3), 675 (109)
	solid	254, 678
$\{[Cu(\mu\text{-pmpa})](ClO_4)\cdot 2H_2O\}_n$ (**2**)	H_2O	254 (1.15×10^3), 673 (108)
	solid	254, 675
$\{[Cu(\mu\text{-pmba})(H_2O)](ClO_4)\cdot 3H_2O\}_n$ (**3**)	H_2O	254 (1.26×10^3), 664 (116)
	solid	255, 667

[a] Solution = water at 20 ± 0.1 °C; solid = diffuse reflectance.

($^2B_1 \rightarrow {}^2E$) [28] transition in a tetragonal ligand field, in which the copper(II) has a distorted square-pyramidal coordination environment. The information obtained from the electronic spectra about the coordination configurations of the copper(II) ions in the complexes is in agreement with those found from the structural data.

3.3. Magnetic properties

The magnetic susceptibilities of the powder samples were investigated in the temperature range 5.0–300 K. The magnetic behaviors of the complexes **1**–**3** are shown in Figs. 4–6 in the form of the magnetic susceptibility (χ_m) and the effective magnetic moment (μ_{eff}) versus T plots. For **1**, as shown in Fig. 4, the μ_{eff} value at room temperature, 1.71 μ_B, is similar to the spin-only value for a copper(II) ion (1.73 μ_B). As the temperature is lowered, the μ_{eff} value gradually increases and exhibits a maximum at 19 K (1.86 μ_B) and rapidly decreases to 1.79 μ_B at 5 K. This behavior is indicative of the predominance of a ferromagnetic interaction. The data were fitted following the Baker et al. equation ($S = 1/2$) [29]

$$\chi_m = \frac{Ng^2\beta^2}{4KT}\left[\frac{1+Ax+Bx^2+Cx^3+Dx^4+Ex^5}{1+Fx+Gx^2+Hx^3+Ix^4}\right]^{2/3}, \quad (1)$$

where $x = |2J|/kT$ and $A = 5.7979916$, $B = 16.902653$, $C = 29.376885$, $D = 29.832959$, $E = 14.036918$, $F = 2.7979916$, $G = 7.0086780$, $H = 8.653644$, $I = 4.5743114$. The best fitting of the variable-temperature data to Eq. (1) gives $J = +0.21$ cm^{-1} with $g = 2.01$. The μ_{eff} value for compound **2** is 1.62 μ_B at room temperature, which is slightly lower than 1.73, increases gradually to 1.76 μ_B at 40 K, and then rapidly decreases to 1.54 μ_B at 5 K (Fig. 5), implying the presence of ferromagnetic interactions between Cu(II) atoms. The best fitting to Eq. (1) gives $J = +0.14$ cm^{-1} with $g = 2.02$. As

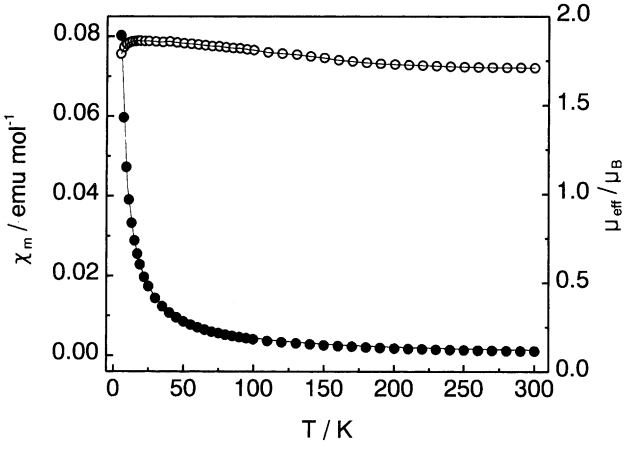

Fig. 4. Plots of χ_m vs. T (•) and μ_{eff} vs. T (○) for **1**. The solid line represents the best fit of the experimental data.

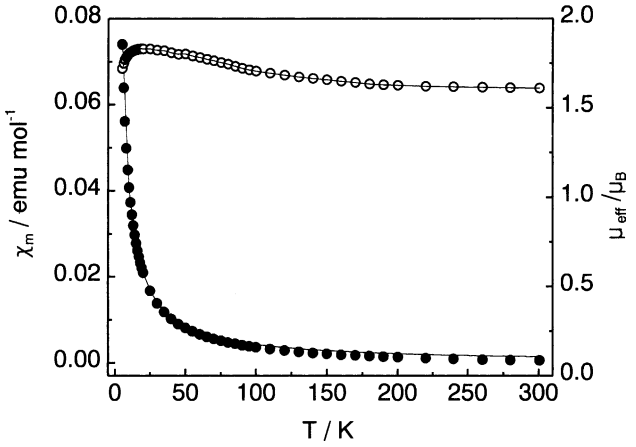

Fig. 5. Plots of χ_m vs. T (•) and μ_{eff} vs. T (○) for **2**. The solid line represents the best fit of the experimental data.

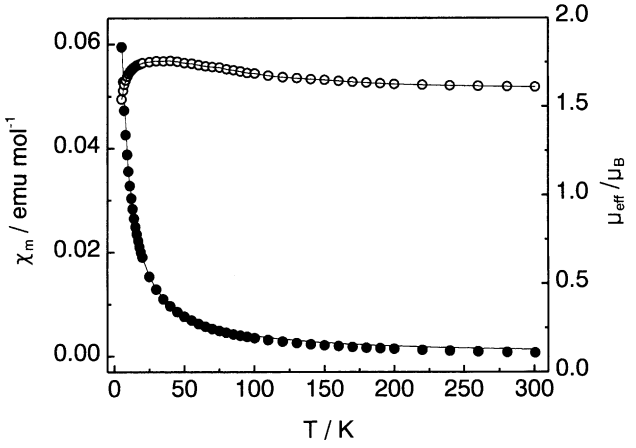

Fig. 6. Plots of χ_m vs. T (•) and μ_{eff} vs. T (○) for **3**. The solid line represents the best fit of the experimental data.

Table 6
Structural and magnetic data of the copper(II) complexes

Complex	Cu–O_{eq} (Å)	Cu–O_{eq} (Å)	α (°)	Cu···Cu (Å)	τ	J (cm^{-1})	g
$\{[Cu(\mu\text{-pmea})](ClO_4)\cdot H_2O\}_n$ (**1**)	1.947	2.246	65.8	5.350	0.25	0.21	2.01
$\{[Cu(\mu\text{-pmpa})](ClO_4)\cdot 2H_2O\}_n$ (**2**)	1.943	2.393	77.7	5.800	0.19	0.14	2.02
$\{[Cu(\mu\text{-pmba})(H_2O)](ClO_4)\cdot 3H_2O\}_n$ (**3**)	1.927	2.382[c]	86.5	9.363	0.15	0.09	2.01
$\{[Cu(\mu\text{-pmae})(H_2O)](ClO_4)\cdot 2H_2O\}_n$[a]	1.972 1.979	2.310[c]		4.844	0.16	4.3	2.01
$\{[Cu(\mu\text{-tana})](ClO_4)\}_n$[b]	1.95	1.98		4.95		2.8	

pmae = 2-pyridylmethyl-2-aminoethanoic acid; tana = 1,4,7-triazacyclononane-N-acetic acid.
[a] Ref. [23].
[b] Ref. [24].
[c] Water molecule.

shown in Fig. 4, the μ_{eff} value for **3** is 1.61 at 300 K, which is slightly lower than 1.73, increases gradually to 1.83 μ_B at 19 K, and then sharply decreases to 1.72 μ_B at 5 K ($J = +0.09$ cm^{-1} with $g = 2.01$), suggesting the existence of very weak ferromagnetic interactions between Cu(II) atoms.

For a comparison purpose, the structural and magnetic data for complexes **1**–**3** are given in Table 6 along with the other *syn–anti* carboxylate-bridged copper(II) complexes. All of the complexes show very weak intramolecular ferromagnetic interactions between the copper(II) centers along the chain via the bridging carboxylate group. The magnetic coupling constant can be expected as a sum of both ferromagnetic and antiferromagnetic contributions [30]. When the copper(II) ions are bridged by polyatomic extended ligands, the ferromagnetic contribution is weak [31]. However, the magnitude of antiferromagnetic interactions is primarily governed by an overlap of two magnetic orbitals centered on the nearest-neighbor copper(II) ions. As pointed out by other authors [18,23,31], for the *syn–anti* conformation of the Cu–O–C–O′–Cu′ bridging network, the contributions between the 2p orbitals of the O and O′ atoms belonging to the magnetic orbitals centered on Cu and Cu′ are unfavorably oriented to give a significant overlap [18,31]. This would lead to a negligible antiferromagnetic contribution so that the weak ferromagnetic one becomes predominant. Furthermore, the non-planarity of the Cu–O–C–O′–Cu′ bridging network is expected to decrease the overlap of the magnetic orbitals in the bridging region, which is favoring ferromagnetic exchange couplings. Similar results are also reported through the carboxylate-bridged copper(II) complexes $\{[Cu(\mu\text{-pmae})(H_2O)](ClO_4)\cdot 2H_2O\}_n$ (pmae = 2-pyridylmethyl-2-aminoethanoic acid, $J = +4.3$ cm^{-1}) [23] and $\{[Cu(\mu\text{-tana})](ClO_4)\}_n$(tana = 1,4,7-triazacyclononane-N-acetic acid, $J = +2.8$ cm^{-1}) [24]. On the other hand, structural factors such as Cu···Cu separation, α dihedral angles and τ parameters seem to be significantly affecting the magnetic magnitude. The values of the ferromagnetic coupling constant decrease in the order **1** > **2** > **3**. This fact may be attributed to the increase of the Cu···Cu separation and α dihedral angles. We can see the distortion parameter (τ) of compounds **1**–**3** and $\{[Cu(\mu\text{-pmae})(H_2O)](ClO_4)\cdot 2H_2O\}_n$, which all exhibit the *syn–anti*-conformation, leading to a ferromagnetic coupling. However, compound **1** shows a smaller J value than $\{[Cu(\mu\text{-pmae})(H_2O)](ClO_4)\cdot 2H_2O\}_n$, in which the τ values are 0.25 and 0.16, respectively. It is indicated that the tetragonal pyramidal geometry with a *syn–anti* bridged copper(II) ion may cause the exchange coupling through the carboxylate group to be less operative in comparison with the geometry close to the square-planar pyramid.

4. Supplementary material

Crystallographic data for the structural analysis have been deposited with the Cambridge Crystallographic Data Center, CCDC No. 215289 for compound **1**, 215290 for compound **2** and 215291 for compound **3**. Copies of this information may be obtained free of charge from the Director, CCDC, 12 Union Road, Cambridge CB2 1EZ, UK (fax: +44-1223-336033; e-mail: deposit@ccdc.cam.ac.uk or http://www.ccdc.cam.ac.uk).

Acknowledgements

This work was supported by a grant (No. R05-2003-000-10536-0) from the Basic Research Program of the Korea Science & Engineering Foundation.

References

[1] Z. Shi, S. Feng, S. Gao, L. Zhang, G. Yang, J. Hua, Angew. Chem., Int. Ed. Engl. 39 (2000) 2325.
[2] O.M. Yaghi, H. Li, C. Davis, D. Richarson, T.L. Groy, Acc. Chem. Res. 31 (1998) 474.
[3] P.J. Hagrman, D. Hagrman, J. Zubieta, Angew. Chem., Int. Ed. Engl. 39 (1999) 2638.
[4] Y.B. Dong, R.C. Layland, M.D. Smith, N.G. Pschirer, U.H.F. Bunz, H.C. Zur Loye, Inorg. Chem. 38 (1999) 3056.

[5] J.S. Seo, D. Whang, H. Lee, S.I. Jun, J. Oh, Y. Jin, K. Kim, Nature 404 (2000) 982.
[6] K. Sinzger, S. Hünig, M. Jopp, D. Bauer, W. Bietsch, J.U. Von Schütz, H.C. Wolf, R.K. Kremer, T. Metzenthin, R. Bau, S.I. Khan, A. Lindbaum, C.L. Lengauer, E. Tillmanns, J. Am. Chem. Soc. 115 (1993) 7696.
[7] O.S. Jung, C.G. Pierpont, J. Am. Chem. Soc. 116 (1994) 2229.
[8] M. Munakata, L.P. Wu, T. Kuroda Sowa, M. Maekawa, Y. Suenaga, K. Furuichi, J. Am. Chem. Soc. 118 (1996) 3305.
[9] O.R. Evans, R. Xiong, Z. Wang, G.K. Wong, W. Lin, Angew. Chem., Int. Ed. Engl. 38 (1999) 536.
[10] O. Kahn, C.J. Martinez, Science 279 (1998) 44.
[11] F. Lloret, G.D. Munno, M. Julve, J. Cano, R. Ruiz, A. Caneschi, Angew. Chem., Int. Ed. Engl. 37 (1998) 135.
[12] S. Han, J.L. Manson, J. Kim, J.S. Miller, Inorg. Chem. 39 (2000) 4182.
[13] W. Lin, M.E. Chapman, Z. Wang, G.T. Yee, Inorg. Chem. 39 (2000) 4169.
[14] K.-Y. Choi, K.M. Chun, I.-H. Suh, Polyhedron 20 (2001) 57.
[15] K.-Y. Choi, S.N. Choi, C.P. Hong, J. Incl. Phenom. Macrocyc. Chem. 40 (2001) 67.
[16] K.-Y. Choi, J. Incl. Phenom. Macrocyc. Chem. 43 (2002) 195.
[17] K.-Y. Choi, H. Ryu, Y.-M. Lim, N.-D. Sung, U.-S. Shin, M. Suh, Inorg. Chem. Commun. 6 (2003) 412.
[18] E. Colacio, J.P. Costes, R. Kivekäs, J.P. Laurent, J. Ruiz, Inorg. Chem. 29 (1990) 4240.
[19] E. Colacio, J.M. Dominguez-Vera, R. Kivekäs, J.M. Moreno, A. Romerosa, J. Ruiz, Inorg. Chim. Acta 212 (1993) 115.
[20] P.K. Coughlin, S.J. Lippard, J. Am. Chem. Soc. 106 (1984) 2328.
[21] E. Colacio, J.M. Dominguez-Vera, J.P. Costes, R. Kivekäs, J.P. Laurent, J. Ruiz, M. Sundberg, Inorg. Chem. 31 (1992) 774.
[22] E. Colacio, J.M. Dominguez-Vera, R. Kivekäs, J. Ruiz, Inorg. Chim. Acta 218 (1994) 109.
[23] E. Colacio, M. Ghazi, R. Kivekäs, J.M. Moreno, Inorg. Chem. 39 (2000) 2882.
[24] D. Schulz, T. Weyhermüller, K. Wieghartdt, C. Butzlaff, A.X. Trautwein, Inorg. Chim. Acta 247 (1996) 387.
[25] G.M. Sheldrick, Acta Crystallogr. Sect. A 46 (1990) 467.
[26] G.M. Sheldrick, SHELXL 97 Program for the Refinement of Crystal Structures, University of Göttingen, Germany, 1997.
[27] A.W. Addison, T.N. Rao, J. Reedijk, J. van Rijn, G.C. Verschoor, J. Chem. Soc., Dalton Trans. (1984) 1349.
[28] B.J. Hathaway, Structure and Bonding (Berlin) 57 (1991) 2801.
[29] G.A. Baker, G.S. Rushbrooke, H.E. Gilbert, Phys. Rev. A 135 (1964) 1272.
[30] J.J. Girard, M.F. Charlot, O. Kahn, Mol. Phys. 34 (1977) 1063.
[31] R.L. Carlin, K. Kopinga, O. Kahn, M. Verdaguer, Inorg. Chem. 25 (1986) 1786.

Available online at www.sciencedirect.com
SCIENCE DIRECT®
Polyhedron 23 (2004) 913–919
POLYHEDRON
www.elsevier.com/locate/poly

Spectroscopic and redox properties of $Rh^{III}Ru^{II}$ and $Ru^{II}Ru^{II}$ complexes derived from 2,2′-bipyridine, pyrazole-3,5-bis(benzimidazole) and 1,2,4-triazole-3,5-dicarboxylic acid as bridging ligands

Sujoy Baitalik, Bula Dutta, Kamalaksha Nag *

Department of Inorganic Chemistry, Indian Association for the Cultivation of Science, Jadavpur, Kolkata 700 032, India

Received 18 August 2003; accepted 30 September 2003

Abstract

The heterovalent heterodinuclear complex $[(bpy)_2Ru^{II}(H_2pzbzim)Rh^{III}(bpy)_2](ClO_4)_4 \cdot 3H_2O$ (**1**) and the isovalent homodinuclear complex $[(bpy)_2Ru^{II}(trzdc)Ru^{II}(bpy)_2](ClO_4) \cdot 5H_2O$ (**2**), where H_3pzbzim = pyrazole-3,5-bis(benzimidazole), H_3trzdc = 1,2,4-triazole-3,5-dicarboxylic acid and bpy = 2,2′-bipyridine, have been synthesized and spectroscopically characterized. Complex **1** undergoes one electron oxidation at 1.20 V (versus Ag/AgCl) in acetonitrile, while for complex **2**, two stepwise oxidations occur at 0.63 and 0.81 V with the comproportionation constant K_c, for the equilibrium $Ru^{II}Ru^{II} + Ru^{III}Ru^{III} \rightleftharpoons 2Ru^{II}Ru^{III}$, equal to 1.11×10^3 at 298 K. The acid dissociation constants of the benzimidazole moieties of complex **1** have been determined in acetonitrile–water (3:2) by spectrophotometric titrations. Both complexes **1** and **2** exhibit luminescence spectra and the quantum yields obtained for methanol–ethanol (1:4) glass (at 77 K) are $\varphi = 3.1 \times 10^{-2}$ for **1** and 3.5×10^{-2} for **2**.
© 2003 Elsevier Ltd. All rights reserved.

Keywords: Diruthenium(II); Rhodium(III) Ruthenium(II); Heterodinuclear complexes; Polypyridine complexes; Electrochemistry

1. Introduction

Intramolecular electron and energy transfer processes in di- and oligonuclear ruthenium(II) and osmium(II) polypyridine complexes whose mononuclear entities are linked by conjugated bridging ligands have received considerable attention [1–6]. The directional flow of electron/or energy gets facilitated when there is asymmetry in the multicomponent system. Such asymmetry can be introduced either by using ligands which differ in donor–acceptor property or using heterometallic sites. The features associated with bridging ligands such as length, rigidity, topology, conjugation, charge and the number of dissociable hydrogen atoms play important roles in this context. Two types of bridging ligands are generally used for this. The first type, which have found maximum use, are electron-poor oligomeric pyridine/pyrazine/pyrimidine derivatives and they mediate metal–metal interaction through low-lying π^* orbitals (LUMO) [1,7–9]. The electron-rich second type of ligands which are triazole, pyrazole or benzimidazole derivatives, on the other hand, participate in intermetallic interactions via hole transfer mechanism [10–12]. The second type of ligand can be made anionic by deprotonating the constituent NH protons.

In earlier publications [12–15], we have reported the synthesis, structure, spectroscopic properties and proton-coupled redox activities of mononuclear and diastereoisomerically pure dinuclear ruthenium(II) and osmium(II) polypyridine complexes with pyrazole-3,5-bis(benzimidazole)[H_3pzbzim] and pyrazole-3,5-bis(benzothiazole)[Hpzbzth] as the bridging ligands. More recently [16], we have reported the comparative physico-chemical properties of the homochiral *rac* ($\Lambda\Lambda/\Delta\Delta$) and heterochiral *meso* ($\Lambda\Delta/\Delta\Lambda$) diastereoisomers of $Ru^{II}Ru^{II}$, $Ru^{II}Os^{II}$ and $Os^{II}Os^{II}$ complexes

* Corresponding author. Tel.: +91-33-2473-4971; fax: +91-33-2473-2805.
E-mail address: ickn@mahendra.iacs.res.in (K. Nag).

0277-5387/$ - see front matter © 2003 Elsevier Ltd. All rights reserved.
doi:10.1016/j.poly.2003.09.035

derived from pyrazole-3,5-dicarboxylic acid (H_3pzdc) and 2,2′-bipyridine (bpy).

The present study is concerned with the chemistry of the heterobimetallic complex $[(bpy)_2Rh^{III}(H_2pzbzim)Ru^{II}(bpy)_2]^{4+}$ on the one hand and 1,2,4-triazole-3,5-dicarboxylic acid [H_3trzdc]-bridged homodinuclear complex $[(bpy)_2Ru^{II}(trzdc)Ru^{II}(bpy)_2]^{+}$ on the other hand.

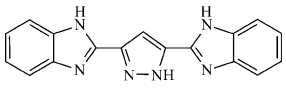

H_3pzbzim

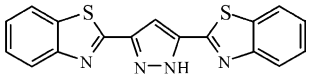

Hpzbzth

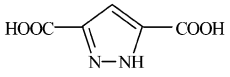

H_3pzdc

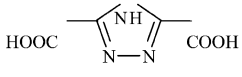

H_3trzdc

2. Experimental

2.1. Materials

All chemicals were obtained from commercial sources and were used as received. Pyrazole-3,5-bis(benzimidazole) [13], *cis*-$[Ru(bpy)_2Cl_2]\cdot 2H_2O$ [17] and *cis*-$[Rh(bpy)_2(H_2O)_2](ClO_4)_3\cdot H_2O$ [18] were prepared according to the reported methods. 1,2,4-triazole-3,5-dicarboxylic acid was prepared by $KMnO_4$ oxidation of 4-amino-3,5-dimethyl-1,2,4-triazole [19] which, in turn, was obtained by a modified method [20]. To a stirred aqueous solution (1 dm^3) of 4-amino-3,5-dimethyl-1,2,4-triazole (25.0 g, 0.22 mol) was added finely ground $KMnO_4$ (158 g, 1 mol) over a period of 2 h, keeping the temperature of the mixture to 90–95 °C. After additional heating and stirring for 8 h, the precipitated MnO_2 was removed by filtration. The filtrate was diluted to ca. 1.5 dm^3, cooled and carefully neutralized with 6 M HCl and then 100 cm^3 of conc. HCl was added. The 1,2,4-triazole-3,5-dicarboxylic acid precipitated was collected by filtration and washed with water, till the washing was free from chloride; yield 28 g (80%).

2.2. Preparation of the complexes

2.2.1. $[(bpy)_2Ru^{II}(H_2pzbzim)Rh^{III}(bpy)_2](ClO_4)_4\cdot 3H_2O$ (**1**)

A mixture of $[(bpy)_2Ru(H_3pzbzim)](ClO_4)_2\cdot 2H_2O$ (0.48 g, 0.5 mmol) [13], triethylamine (0.05 g, 0.5 mmol) and *cis*-$[Rh(bpy)_2(H_2O)_2](ClO_4)_3\cdot H_2O$ (0.38 g, 0.5 mmol) [18] in 50 cm^3 of 1:1 ethanol–water mixture was heated under reflux in a nitrogen atmosphere for 60 h. The solution was rotary evaporated to ca. 20 cm^3 and then filtered. To the filtrate 1 g of $NaClO_4$ dissolved in 5 cm^3 water was added and the mixture was kept at 10 °C for 2 h. A brick red microcrystalline product that separated was collected by filtration. The ^1H NMR spectrum of this product indicated it to be a 3:1 mixture of two diastereoisomers. The major diastereoisomer was isolated in pure form after three successive recrystallization from 2:1 ethanol-acetronitrile mixture. Yield: 0.32 g, 40%. *Anal*. Found: C, 43.16; H, 3.34; N, 12.46. $C_{57}H_{49}Cl_4N_{14}O_{19}RuRh$ requires: C, 43.31; H, 3.10; N, 12.41%. IR (KBr): 3400br, 1625s, 1600s, 1495m, 1480m, 1460s, 1440s, 1420s, 1385m, 1360m, 1310m, 1270s, 1245w, 1100s, br, 770s, 750s, 730m, 630s cm^{-1}.

2.2.2. $[(bpy)_2Ru(trzdc)Ru(bpy)_2](ClO_4)\cdot 5H_2O$ (**2**)

To a stirred suspension of *cis*-$[Ru(bpy)_2Cl_2]\cdot 2H_2O$ (1.04 g, 2 mmol) in ethanol (100 cm^3) was added solid $AgClO_4$ (0.84 g, 4 mmol). The precipitated AgCl was filtered off after 0.5 h and the filtrate was then treated with H_3trzdc (0.16 g, 1 mmol) and triethylamine (0.3 g, 3 mmol). The solution was refluxed for 8 h under nitrogen, after which it was filtered and the filtrate was rotary evaporated to ca. 30 cm^3. The solution was kept in an ice chest, during which time a red orange microcrystalline product deposited. This was collected by filtration and recrystallized twice from methanol. Yield: 0.88 g, 75%. *Anal*. Found: C, 44.75; H, 3.72; N, 13.21. $C_{44}H_{42}ClN_{11}O_{13}Ru_2$ requires: C, 45.14; H, 3.59; N, 13.17%. IR (KBr): 3400br, 1610s, 1590m, 1485m, 1460s, 1425s, 1340m, 1315m, 1100s, br, 845m, 772m, 730m, 665w, 630s, 610w cm^{-1}.

Caution! The perchlorate salts reported in this study are potentially explosive and therefore should be handled with care.

2.3. Physical measurements

The C, H and N analyses were performed on a Perkin–Elmer 2400 elemental analyzer. Infrared spectra were recorded on a Perkin–Elmer 783 spectrophotometer using KBr discs. ^1H NMR spectra were recorded on a Bruker Avance DPX 300 spectrometer using $(CD_3)_2SO$ solutions.

The electrochemical measurements were carried out with a BAS 100 B electrochemistry system using a three-electrode assembly comprising a Pt or glassy carbon working electrode, Pt auxiliary electrode and an aqueous Ag/AgCl reference electrode. The electrochemical measurements (CV, DPV and SWV) were carried out at 25 °C under a nitrogen atmosphere in an acetonitrile solution of the complex (ca. 1 mmol dm^{-3}) with tetraethylammonium perchlorate (0.1 mol dm^{-3}) as the supporting electrolyte. The reference electrode was separated from the bulk electrolyte by a salt bridge containing the supporting electrolyte in 1:1 acetonitrile–water. The potentials measured were automatically compensated for the *iR* drop and under this condition

the ferrocene/ferrocenium couple occurred at 0.36 V with a peak-to-peak separation of 62 mV.

Electronic absorption spectra were recorded on a Shimadzu UV-2100 spectrophotometer. For determining the acid dissociation constants of the bridging ligand in complex **1**, spectrophotometric titrations were carried out with a series of acetonitrile–water (3:2) solutions containing the same amount of the complex and buffer solutions were added to adjust the pH in the range 2–12 keeping the ratio of acetonitrile to water (3:2) fixed.

Emission spectra were recorded on a Perkin–Elmer LS 55 fluorescence spectrophotometer in methanol–ethanol (1:4) solution at 298 and 77 K. Quantum yields of the complexes at both the temperatures were determined by a relative method using $[Ru(bpy)_3]^{2+}$ in the same solvent mixture as the standard. The quantum yields were calculated [21] using the following equation:

$$\varphi = \varphi_{std}(A_{std}/A)(I/I_{std})\left(\eta^2/\eta^2_{std}\right), \quad (1)$$

where φ and φ_{std} are the quantum yields of unknown and standard samples, A and A_{std} are the absorbances at the excitation wavelength and η and η_{std} are the refractive indices of the solutions.

3. Results and discussion

3.1. $[(bpy)_2Ru^{II}(H_2pzbzim)Rh^{III}(bpy)_2](ClO_4)_4 \cdot 3H_2O$ (*1*)

The heterodinuclear complex **1** was obtained by reacting one equivalent each of $[(bpy)_2Ru(H_3pzbzim)](ClO_4)_2 \cdot 2H_2O$ [13], *cis*-$[(bpy)_2Rh(H_2O)_2](ClO_4)_3 \cdot H_2O$ [18] and triethylamine over a long period in ethanol–water (1:1) solution. As shown in Scheme 1, due to the inherent chirality for each of the metal centres the heterobimetallic complex **1** should have two pairs of homochiral ($\Lambda\Lambda/\Delta\Delta$) and heterochiral ($\Lambda\Delta/\Delta\Lambda$) diastereoisomers.

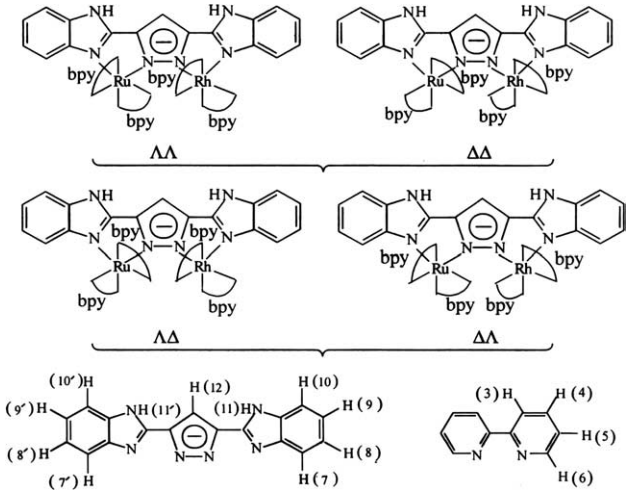

Scheme 1.

3.1.1. ^1H NMR spectra

In a previous publication [13], we have reported that in the homodinuclear ruthenium(II) complexes $[(ppy)_2Ru(H_2pzbzim)Ru(ppy)_2]^{3+}$ (ppy = polypyridine), the aromatic H(7) proton of the bridging ligand (see Scheme 1 for numbering) is most shielded due to the anisotropic ring current effect of the polypyridine ligands. In contrast, the benzimidazole H(11) proton appears at the lowest field. The small but significant differences in chemical shifts observed for the H(7) doublet or the H(11) singlet of the homochiral ($\Lambda\Lambda/\Delta\Delta$) and heterochiral ($\Lambda\Delta/\Delta\Lambda$) diastereoisomers have been used as the markers to identify and quantify the relative amounts of the diastereoisomers in a mixture. In the case of $[(bpy)_2Ru(H_2pzbzim)Ru(bpy)_2]^{3+}$, the H(7) and H(11) resonances of the *meso* ($\Lambda\Delta$) form are observed at 5.04 and 14.38 ppm, respectively, as against those observed at 5.06 and 14.46 ppm for the rac ($\Lambda\Lambda/\Delta\Delta$) form.

As compared to the homodinuclear complexes, the ^1H NMR spectrum of the heterodinuclear complex $[(bpy)_2Ru(H_2pzbzim)Rh(bpy)_2]^{4+}$ (**1**) will be more complex because in this case the two-halves of the bridging ligand $(H_2pzbzim)^-$ are no longer equivalent. Indeed, the ^1H NMR spectrum of complex **1**, as isolated, showed a large number of overlapping signals, including two pairs of doublets at 4.80 and 5.12 ppm (major pair) and 5.07 and 5.21 ppm (minor pair) and two pairs of singlets at 14.44 and 14.36 ppm (major pair) and 14.50 and 14.62 ppm (minor pair). The ratio between the areas of major and minor signals was found to be about a 3:1, indicating that complex **1**, as isolated, contained two diastereoisomers in a 3:1 ratio. The major diastereoisomer was separated in the pure form by recrystallizing the mixture three times from ethanol–acetonitrile (2:1) and its ^1H NMR spectrum is shown in Fig. 1. It should be noted that of the two doublets at 4.80 and 5.12 ppm, the more shielded one can be attributed to H(7 or 7′) in the vicinity of the electron rich

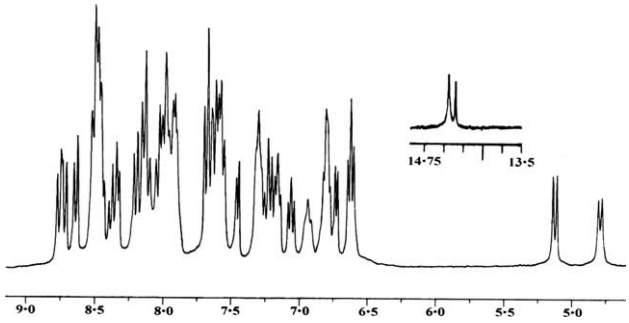

Fig. 1. ^1H NMR spectrum of the major diastereoisomer of $[(bpy)_2Ru(H_2pzbzim)Rh(bpy)_2]^{4+}$ (**1**) in $(CD_3)_2SO$.

ruthenium(II) site. The same consideration applies to the NH(11/11′) proton.

3.1.2. Redox behavior

The redox activities of complex **1** have been studied in acetonitrile solution over the potential range from +1.5 to −2.2 V (versus Ag/AgCl) using CV, DPV and SWV techniques. Fig. 2 shows the cyclic voltammogram of the compound in the positive potential regime. A reversible redox couple due to Ru^{II}/Ru^{III} with $E_{1/2} = 1.20$ V and a peak-to-peak separation of 65 mV is observed. The values of $E^{ox}_{1/2}$ obtained from DPV and SWV have agreed within 5 mV. In the negative potential range from −1 to −2.2 V, the compound undergoes three quasi-reversible reduction processes with $E^{red}_{1/2} = -2.06$, −1.90 and −1.62 V. The current height of the first couple, both in the CV and DPV, is twice that of the second or third, indicating that the first electron transfer process is dielectronic. It should be noted that these electron transfers occur to the π-LUMO of bpy, each of which can accept two electrons.

It is of interest to compare the Ru^{II}/Ru^{III} oxidation potential $E^{ox}_{1/2}$ of $[(bpy)_2Ru^{II}(H_2pzbzim)Rh^{III}(bpy)_2]^{4+}$ ($E^{ox}_{1/2} = 1.20$ V) with those of $[(bpy)_2Ru(H_3pzbzim)]^{2+}$ ($E^{ox}_{1/2} = 0.89$ V) [15] and $[(bpy)_2Ru^{II}(H_2pzbzim)Ru^{II}(bpy)_2]^{3+}$ ($E^{ox}_{1/2} = 1.01$ and 1.23 V). As compared to the dicationic mononuclear complex ($E_{1/2} = 0.89$ V), the first metal centre in the tricationic homodinuclear complex is oxidized at a more positive potential (1.01 V). On the other hand, the removal of an electron from the tetrapositively charged $[Ru^{II}Rh^{III}]^{4+}$ cation (1.20 V) is almost as difficult as that of the similarly charged $[Ru^{II}Ru^{III}]^{4+}$ cation (1.23 V). Clearly, the redox behavior of these complex species are strongly dependent on the overall charge of the complex species. Further, when complex **1** is treated with two equivalents of a strong base the two benzimidazole protons of the bridging ligand get deprotonated to produce $[(bpy)_2Ru^{II}(pzbzim)Rh^{III}(bpy)_2](ClO_4)_2$. The $E_{1/2}$ of this dicationic species is shifted to a considerably low positive potential, 0.86 V. This value, in turn, is close to that of the mononuclear dipositively charged $[(bpy)_2Ru^{II}(H_3pzbzim)]^{2+}$ cation (0.89 V).

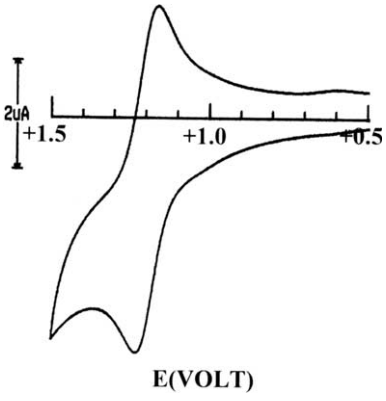

Fig. 2. Cyclic voltammogram of $[(bpy)_2Ru^{II}(H_2pzbzim)Rh^{III}(bpy)_2]^{4+}$ (**1**) in acetonitrile.

3.1.3. Absorption spectra and protonic equilibria

The absorption spectrum of complex **1** in acetonitrile exhibits four bands at 295 (67 400), 315sh (49 200), 490 (5490) and 480 nm (6050) with their molar absorptivities (ε/dm^3 mol^{-1} cm^{-1}) given in parentheses. The two bands observed at 295 and 315 nm, which also appeared in a similar region in the mononuclear and homodinuclear ruthenium(II) complexes, are considered to be due to intraligand π–π^* transition. The other two bands at 440 and 480 nm with comparable intensities are due to metal-to-ligand $Ru(d\pi) \rightarrow bpy(\pi^*)$ charge transfer transitions.

Inasmuch as the imidazole NH group of the bridging ligand can be subjected to deprotonation, we have been interested to determine the pK_a values for $[(bpy)_2Ru^{II}(H_2pzbzim)Rh^{III}(bpy)_2]^{4+}$ and compare them with those obtained for $[(bpy)_2Ru^{II}(H_3Pzbzim)]^{2+}$ [15] and $[(bpy)_2Ru^{II}(H_2pzbzim)Ru^{II}(bpy)_2]^{3+}$ [13]. The influence of pH on the absorption spectral behavior of complex **1** in acetonitrile–water (3:2) is shown in Fig. 3. With the increase of pH, the intensity of the peak at 430 nm decreases with a concomitant increase of the peak intensity at 490 nm. The consecutive absorption curves pass through two isosbestic points at 395 and 440 nm and indicate the occurrence of the following acid–base equilibria:

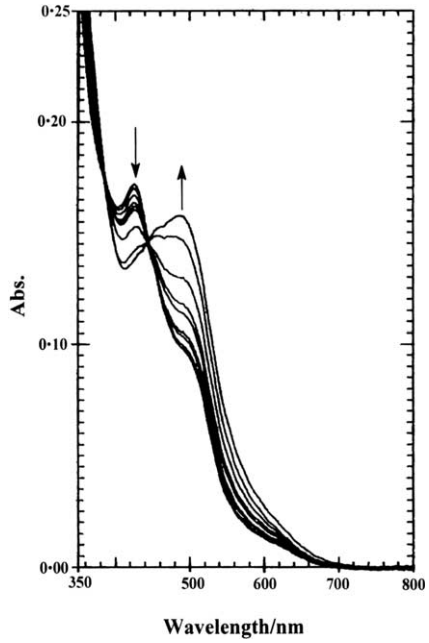

Fig. 3. Changes in the absorption spectrum of $[(bpy)_2Ru(H_2pzbzim)Rh(bpy)_2]^{4+}$ (**1**) with the variation of pH in acetonitrile–water (3:2).

$$\begin{array}{c}[(bpy)_2Ru^{II}(H_2pzbzim)Rh^{III}(bpy)_2]^{4+}\\ K_1 \Uparrow\Downarrow\\ [(bpy)_2Ru^{II}(Hpzbzim)Rh^{III}(bpy)_2]^{3+} + H^+\\ K_2 \Uparrow\Downarrow\\ [(bpy)_2Ru^{II}(pzbzim)Rh^{III}(bpy)_2]^{2+} + H^+\end{array} \quad (2)$$

The pK values have been evaluated from the absorption data pertaining to the pH ranges 4–8 for pK_1 and 8–12 for pK_2 using the following equation:

$$pH = pK - \log\frac{A - A_0}{A_f - A}, \quad (3)$$

where A_0, A_f and A refer to the absorbances at the initial, final and intermediate pH values of a given wavelength. The pK values thus obtained are p$K_1 = 5.45(5)$ and p$K_2 = 9.85(5)$. Clearly, pK_1 refers to the dissociation constant of the benzimidazole unit attached to the relatively more electron withdrawing Rh^{III}, while pK_2 is related to the corresponding unit bound to Ru^{II}. It is interesting to note that for $[(bpy)_2Ru^{II}(H_2pzbzim)Ru^{II}(bpy)_2]^{3+}$ p$K_1 = 7.95$ and p$K_2 = 9.75$ [13]. Thus, relative to the Ru^{II} site, coordination of (H_2pzbzim) to Rh^{III} leads to considerable diminution of its first acid dissociation constant, albeit the second dissociation constant remains almost unchanged.

3.1.4. Emission spectrum

The emission spectral behavior of complex **1** has been studied at 298 and 77 K in methanol–ethanol (1:4) solutions and glass, respectively. As shown in the inset of Fig. 4, at room temperature a very weak and broad emission occurs at about 655 nm. On the other hand, at 77 K, excitation of either of the MLCT bands at 435 and 480 nm gives rise to a well defined luminescence spectrum with its peak at 632 nm. The quantum yield of this emission process is 3.1×10^{-2}. It may be mentioned that in the case of $[(bpy)_2Ru(H_2pzbzim)Ru(bpy)_2]^{3+}$, the emission spectrum at 77 K shows its peak at 640 nm with a quantum yield of 7.5×10^{-2} [13].

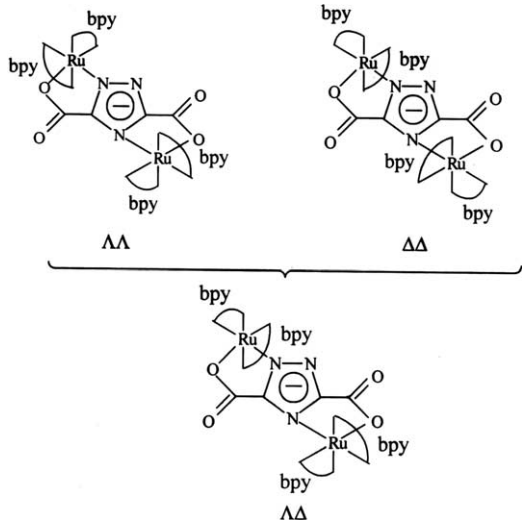

Scheme 2.

3.2. $[(bpy)_2Ru(trdc)Ru(bpy)_2](ClO_4)\cdot 5H_2O$ (2)

The homodinuclear ruthenium(II) complex **2** was obtained by reacting two equivalents of in situ generated $[(bpy)_2Ru(EtOH)_2]^{2+}$ with one equivalent of 1,2,4-triazole-3,5-dicarboxylic acid (H_3trzdc) and three equivalents of triethylamine in ethanol. As shown in Scheme 2, complex **2** will be formed as a mixture of homochiral (ΛΛ/ΔΔ) *rac* and heterochiral (ΛΔ) *meso* diastereoisomers.

3.2.1. ^1H NMR spectrum

The ^{1}H NMR spectrum of complex **2** is shown in Fig. 5. Since each of the bipyridine signals, if fully resolved, should represent a pair of protons, the observed spectrum on that basis accounts for the presence of 64

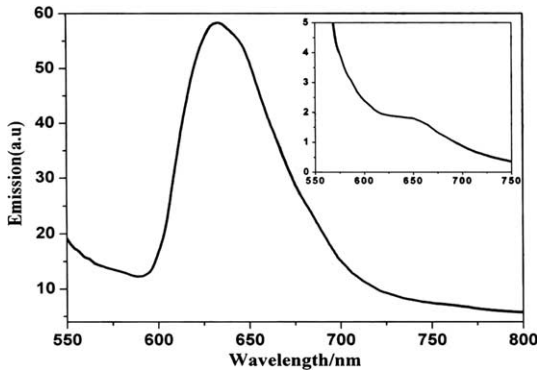

Fig. 4. Luminescence spectrum observed for $[(bpy)_2Ru(H_2pzbzim)Rh(bpy)_2]^{4+}$ (**1**) in frozen methanol–ethanol (1:4) glass at 77 K. Inset shows the spectrum observed at 298 K.

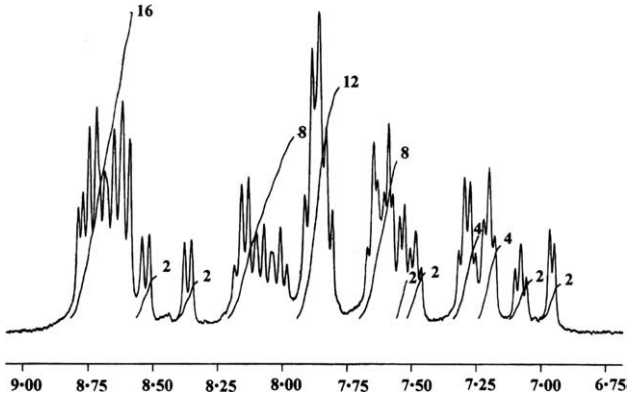

Fig. 5. ^{1}H NMR spectrum of $[(bpy)_2Ru(trzdc)Ru(bpy)_2]^+$ (**2**) in $(CD_3)_2SO$. The integral traces indicate the number of protons involved.

protons, which, however, is double the number of protons that $[(bpy)_2Ru(trzdc)Ru(bpy)_2]^+$ (**2**) contains. Clearly, this indicates that complex **2** is a 1:1 mixture of the homochiral and heterochiral diastereoisomers. This is further borne out by the fact that the proton integral traces in Fig. 5 consistently show 1:1 correspondence of the two diastereoisomers. The separation of the diastereoisomers based on fractional recrystallization turned out to be an unsatisfactory experience. So far, we have not been able to isolate the pure diastereoisomers and consequently subsequent studies have been made with the mixture.

3.2.2. Redox behavior

The electrochemical characteristics of complex **2** have been examined by cyclic voltammetry (CV), square wave voltammetry (SWV) and differential pulse voltammetry (DPV). Fig. 6 shows the occurrence of two fully reversible $Ru^{II}Ru^{II}/Ru^{II}Ru^{III}$ and $Ru^{II}Ru^{III}/Ru^{III}Ru^{III}$ redox couples each with peak-to-peak separation (ΔE_p) of 60 mV. The two $E^{ox}_{1/2}$ values are 0.63 and 0.81 V and the separation between these two redox couples is 0.18 V. It may be mentioned that in the case of the two diastereoisomers of the pyrazolate-3,5-dicarboxylate-bridged diruthenium complex $[(bpy)_2Ru(pzdc)\text{-}Ru(bpy)_2]^+$ the following values were obtained [16]:

$$rac: E^{ox}_{1/2} = 0.75, 0.92\ \text{V}; \quad \Delta E_{1/2} = 0.17\ \text{V},$$

$$meso: E^{ox}_{1/2} = 0.71, 0.91\ \text{V}; \quad \Delta E_{1/2} = 0.20\ \text{V}.$$

Thus, relative to either of the above mentioned diastereoisomers, complex **2** undergoes stepwise oxidations more easily. However, the $\Delta E_{1/2}$ value of **2** is almost same as that of the 1:1 mixture of *rac* and *meso* diastereoisomers of $[(bpy)_2Ru(pzdc)Ru(bpy)_2]^+$. Accordingly, the equilibrium constant K_c for the comproportionation reaction, $Ru^{II}Ru^{II} + Ru^{III}Ru^{III} \rightleftharpoons 2Ru^{II}Ru^{III}$ ($K_c = \exp[nF\Delta E_{1/2}/RT]$), is similar for the two cases ($K_c = 1.11 \times 10^3$ for **2** at 298 K).

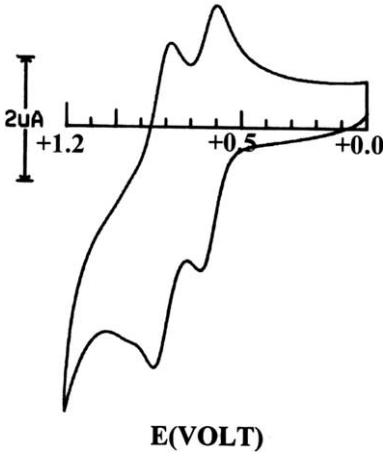

Fig. 6. Cyclic voltammogram of $[(bpy)_2Ru(trzdc)Ru(bpy)_2]^+$ (**2**) in acetonitrile.

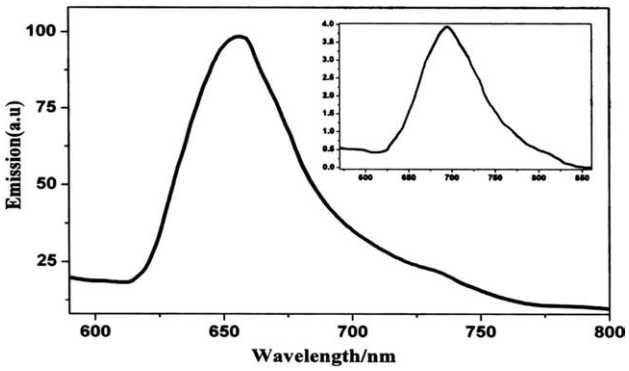

Fig. 7. Luminescence spectrum of $[(bpy)_2Ru(trzdc)Ru(bpy)_2]^+$ (**2**) in frozen methanol–ethanol (1:4) glass at 77 K. Inset shows the spectrum observed at 298 K.

The electrochemical response of complex **2** in the reductive mode is indicative of the occurrence of two bipyridine-based two-electron reductions at −1.65 and −2.10 V. The simultaneous transfer of one electron to two complimentary bipyridine moieties could not be resolved by square wave or differential pulse voltammetric techniques.

3.2.3. Absorption and emission spectra

The absorption spectrum of complex **2** in methanol–ethanol (1:4) solution exhibits two strong bands in the visible region at 420 nm ($\varepsilon = 10\,520$ dm^3 mol^{-1} cm^{-1}) and 500 nm ($\varepsilon = 13\,840$ dm^3 mol^{-1} cm^{-1}), which are considered to be due to metal-to-ligand $Ru(d\pi) \rightarrow bpy(\pi^*)$ charge transfer transitions. The emission spectra of complex **2** have been recorded at 298 and 77 K in methanol–ethanol (1:4) solution and glass, respectively, and the spectra observed are shown in Fig. 7. As shown in the inset of Fig. 7, excitation of the MLCT band at 500 nm at room temperature gives rise to a luminescent band with its peak at 695 nm. This band appears to be due to the emission from a ^{3}MLCT excited state, corresponding to a spin-forbidden $Ru \rightarrow bpy^*$ transition [22]. As compared to the fluid solution spectrum, the luminescence peak of complex **2** in frozen glass at 77 K gets blue-shifted to 655 nm (Fig. 7) with considerable increase in intensity. The quantum yield of complex **2** at 77 K ($\varphi = 3.5 \times 10^{-2}$) is about twenty five times greater than that at 298 K ($\varphi = 1.4 \times 10^{-3}$).

4. Conclusion

Using the bridging ligands pyrazole-3,5-bis(benzimidazole)[H_3pzbzim] and 1,2,4-triazole-3,5-dicarboxylic acid [H_3trzdc] the heterodinuclear complex $[(bpy)_2Ru^{II}(H_2pzbzim)Rh^{III}(bpy)_2](ClO_4)_4 \cdot 3H_2O$ (**1**) and the homodinuclear complex $[(bpy)_2Ru^{II}(trzdc)\text{-}Ru^{II}\text{-}(bpy)_2](ClO_4) \cdot 5H_2O$ (**2**) have been synthesized. The

physico-chemical properties of the major diastereoisomeric form of complex **1** and the 1:1 mixture of the *rac* and *meso* forms of complex **2** have been investigated. The redox potentials for the $Ru^{II}Rh^{III}/Ru^{III}Rh^{III}$ couple in complex **1** ($E_{1/2} = 1.20$ V) has been found to be almost equal to that of the $Ru^{II}Ru^{III}/Ru^{III}Ru^{III}$ couple in the $[(bpy)_2Ru^{II}(H_2pzbzim)Ru^{III}(bpy)_2]^{4+}$ species ($E_{1/2} = 1.23$ V). On the other hand, the deprotonated $[(bpy)_2Ru^{II}(pzbzim)Rh^{III}(bpy)_2]^{2+}$ cation undergoes oxidation at a much less positive potential ($E_{1/2} = 0.86$ V). When the acid dissociation constants determined for the benzimidazole units of complex **1** ($pK_1 = 5.45$ and $pK_2 = 9.85$) are compared with those of $[(bpy)_2Ru^{II}(H_2pzbzim)Ru^{II}(bpy)_2]^{3+}$ ($pK_1 = 7.95$ and $pK_2 = 9.75$) the pK values indicate considerable augmentation of acidity of the benzimidazole unit bound to Rh^{III}. The homodinuclear complex **2** undergoes stepwise oxidations at 0.63 and 0.81 V and the comproporationation constant K_c for the equilibrium $Ru^{II}Ru^{II} + Ru^{III}Ru^{III} \rightleftharpoons 2Ru^{II}Ru^{III}$ is 1.11×10^3 at 298 K. Both complexes **1** and **2** in frozen methanol–ethanol (1:4) glass at 77 K on excitation of their MLCT bands give rise to fairly strong luminescence spectra with their peaks at 632 and 655 nm, respectively, and the corresponding quantum yields are 3.1×10^{-2} for **1** and 3.5×10^{-2} for **2**.

Acknowledgements

K.N. is thankful to the Council of Scientific and Industrial Research, India for funding this study.

References

[1] V. Balzani, A. Zuris, M. Venturi, S. Campagna, S. Serroni, Chem. Rev. 96 (1996) 759.
[2] J.-P. Collin, P. Gavina, H. Heitz, J.-P. Sauvage, Eur. J. Inorg. Chem. (1998) 1.
[3] M.D. Ward, Chem. Soc. Rev. (1995) 121.
[4] G. Giuffrida, S. Campagna, Coord. Chem. Rev. 135/136 (1994) 517.
[5] R. Ziessel, M. Hissler, A. El-ghayoury, A. Harriman, Coord. Chem. Rev. 178–180 (1998) 1251.
[6] (a) L. De Cola, P. Belser, Coord. Chem. Rev. 177 (1998) 301; (b) A. Belser, P. Belser, Coord. Chem. Rev. 230 (2002) 29.
[7] J.-P. Sauvage, J.-P. Collin, J.-C. Chambron, S. Gullierez, C. Coudret, V. Balzani, F. Barigelletti, L. De Cola, L. Flamingini, Chem. Rev. 94 (1994) 993.
[8] E.C. Constable, Prog. Inorg. Chem. 42 (1994) 67.
[9] F.R. Keene, Chem. Soc. Rev. 27 (1998) 185.
[10] (a) R. Hage, J.G. Haasnoot, H.A. Nieuwenhuis, J. Reedijk, D.J.A. de Ridder, J.G. Vos, J. Am. Chem. Soc. 112 (1990) 9245; (b) L. De Cola, F. Barigelletti, V. Balzani, R. Hage, J.G. Haasnoot, J. Reedijk, J.G. Vos, Chem. Phys. Lett. 178 (1991) 491; (c) J.H. Van Dieman, R. Hage, J.G. Haasnoot, H.E.B. Lempers, J. Reedijk, J. Vos, L. De Cola, F. Barigelletti, V. Balzani, Inorg. Chem. 31 (1992) 3518; (d) H.E.B. Lempers, J.G. Haasnoot, J. Reedijk, R. Hage, F.M. Weldon, J.G. Vos, Inorg. Chim. Acta 225 (1994) 67.
[11] S. Serroni, S. Campagna, G. Denti, T.E. Keyes, J.G. Ves, Inorg. Chem. 35 (1996) 4513.
[12] (a) M. Haga, T. Ano, K. Kano, S. Yannabe, Inorg. Chem. 30 (1991) 3843; (b) T. Ohono, K. Nozaki, M. Haga, Inorg. Chem. 31 (1992) 4256; (c) M. Haga, M. Ali, S. Koeski, A. Yoshimura, K. Nozaki, T. Ohono, Inorg. Chim. Acta 226 (1994) 17; (d) M. Haga, T. Ano, T. Ishizaki, K. Kano, K. Nakazaki, T. Ohono, J. Chem. Soc., Dalton Trans. (1994) 263; (e) M. Haga, M. Ali, H. Maegawa, K. Nozaki, A. Yoshimura, T. Ohono, Coord. Chem. Rev. 132 (1994) 99.
[13] S. Baitalik, U. Flörke, K. Nag, Inorg. Chem. 38 (1999) 3296.
[14] S. Baitalik, U. Flörke, K. Nag, J. Chem. Soc., Dalton Trans. (1999) 719.
[15] S. Baitalik, P. Bag, K. Nag, Polyhedron 21 (2002) 2481.
[16] (a) S. Baitalik, U. Flörke, K. Nag, Inorg. Chim. Acta 337 (2002) 439; (b) S. Baitalik, P. Bag, U. Flörke, K. Nag, Inorg. Chim. Acta 357 (2003) 699.
[17] B.P. Sullivan, T.J. Meyer, Inorg. Chem. 17 (1978) 3334.
[18] P.M. Gidney, R.D. Gillard, B.T. Heaton, J. Chem. Soc., Dalton Trans. (1972) 2621.
[19] T.N. Vereshchagina, K.L. Krupin, V.A. Lopyrov, Tr. Sev-Zap. Zaoch. Politekh. Inst. (USSR) 6 (1969) 49, Chem. Abs. 76 (1978) 334.
[20] G.A. Van Albada, R.A.G. de Graff, J.G. Haasnoot, J. Reedijk, Inorg. Chem. 23 (1984) 1404.
[21] J. Van Houten, R.J. Watts, J. Am. Chem. Soc. 98 (1976) 4853.
[22] K. Kalyansundaram, Photochemistry of Polypyridine and Porphyrin Complexes, Academic Press, London, 1992.

Available online at www.sciencedirect.com
SCIENCE DIRECT®
Polyhedron 23 (2004) 921–928
POLYHEDRON
www.elsevier.com/locate/poly

Preparation, structure and catalytic activity of palladium(II) complexes with a carboxyferrocenylphosphine and an ortho-metallated C,N-ligand

Petr Štěpnička *, Martin Lamač, Ivana Císařová

Department of Inorganic Chemistry, Faculty of Science, Charles University, Hlavova 2030, 128 40 Prague 2, Czech Republic

Received 28 July 2003; accepted 12 November 2003

Abstract

The ortho-palladated dimer *trans*-[{Pd(μ-Cl)($C_6H_4CHNMe_2$-κ^2C^1,P)}$_2$] (**1**) reacts with methyl 1′-(diphenylphosphino)ferrocenecarboxylate (**2**) under bridge cleavage to afford [SP-4-4]-[PdCl($C_6H_4CH_2NMe_2$-κ^2C^1,P){Fe(η^5-$C_5H_4PPh_2$-κP)(η^5-$C_5H_4CO_2Me$)}] **(3)** while a reaction between the cationic complexes [Pd($C_6H_4CHNMe_2$-κ^2C^1,P)(MeCN)$_2$]X (**4**, X = ClO_4 (**a**) and BF_4 (**b**)) with **2** gives the products of replacement of one acetonitrile ligand *trans* to nitrogen, [SP-4-3]-[Pd($C_6H_4CHNMe_2$-κ^2C^1,P){Fe(η^5-$C_5H_4PPh_2$-κP(η^5-$C_5H_4CO_2Me$)}(MeCN)]X (**5a**, **5b**). The crystal structures of **4a** and **5a** have been determined by X-ray crystallography. Compounds **3**, **5b** and other in situ generated complexes with the related ferrocene phosphines were tested as catalysts in Suzuki–Miyaura coupling of 4-bromotoluene and phenylboronic acid.
© 2004 Elsevier Ltd. All rights reserved.

Keywords: Palladium; Ferrocene; Phosphine; Suzuki–Miyaura coupling; Ortho-metallated complexes; X-ray crystallography

1. Introduction

Chemistry of hybrid carboxyphosphine ligands, including the very basic one, $Ph_2PCH_2CO_2H$, has received considerable attention in the recent past since the acid and closely related compounds, particularly esters, have found applications in synthesis and catalysis [1]. As it has been demonstrated even for the case of one transition metal with a specific coordination environment such as palladium(II) ligated by ortho-metallated *N*,*N*-benzylamine, these functionalized phosphines can coordinate as carboxyphosphines or, after deprotonation, as the respective phosphinocarboxylates(1–) and functionalized alkyls (or enolates) [Ph_2PCHCO_2Et]$^-$. Besides, they may act as normal phosphine ligands with non-coordinated carboxy functions and also as bidentate bridging or chelating ligands [2].

We have recently described the coordination chemistry in an analogous system involving palladium(II) chelated with the 2-(dimethylaminomethyl)phenyl ligand and ligands derived from *rac*-[2-(diphenylphosphino)ferrocenyl]acetic acid: the acid itself, the corresponding acetate (1 –) and methyl ester [3]. This report deals with differences in reactivity observed in an analogous series but with another ferrocene carboxyphosphine, 1′-(diphenylphosphino) ferrocene carboxylic acid (Hdpf), and its methyl ester [4]. We describe the crystal structures of [Pd($C_6H_4CHNMe_2$-κ^2C^1,P) ((MeCN)$_2$]ClO_4 (**4a**) and [SP-4-3]-[Pd($C_6H_4CHNMe_2$-κ^2C^1,P){Fe(η^5-$C_5H_4PPh_2$-κP)(η^5-$C_5H_4CO_2Me$)}(Me- CN)]X, where X = ClO_4 (**5a**) and BF_4 (**5b**), and also the catalytic activity of the obtained products in Suzuki–Miyaura cross-coupling in a comparison with other systems based on related ferrocene phosphines.

2. Results and discussion

The metathesis of ortho-palladated dimer **1** with methyl 1′-(diphenylphosphino)ferrocenecarboxylate (**2**)

* Corresponding author. Tel.: +420-221-952-356/951-260; fax: +420-221-952-378/951-253.
E-mail addresses: stepnic@mail.natur.cuni.cz, stepnic@natur.cuni.cz (P. Štěpnička).

0277-5387/$ - see front matter © 2004 Elsevier Ltd. All rights reserved.
doi:10.1016/j.poly.2003.11.057

gives the expected product of the bridge-cleavage reaction, complex **3**. On the other hand, the reaction between cationic bis(acetonitrile) complexes **5**, prepared by reacting stoichiometric amounts of **1** and the appropriate silver(I) salt in acetonitrile with one equivalent of **2**, proceeds under a replacement of only one acetonitrile ligand, affording acetonitrile-phosphine complexes [SP-4-3]-[Pd($C_6H_4CHNMe_2$-κ^2C^1, P){Fe(η^5-$C_5H_4PPh_2$-κP)(η^5-$C_5H_4CO_2Me$)} (MeCN)]X, X = ClO_4 (**5a**) and BF_4 (**5b**) (Scheme 1). Perchlorate **5a** can be also synthesized from **3** by removal of a chloride ligand with a stoichiometric amount of $AgClO_4$. The formation of phosphine complexes **5** instead of the anticipated P,O-chelates analogous to [SP-4-3]-[Pd($C_6H_4CHNMe_2$-κ^2C^1, P){Fe(η^5-1-(CH_2CO_2Me-κO^2)-2-(PPh_2-κP)C_5H_3)(η^5-C_5H_5)}]-ClO_4 [3] undoubtedly reflects different steric properties of the involved phosphinoester ligands, pointing to an unfavourable geometry of a Pd(**2**-κ^2P, O) motif [5].

Reactivity of **5a** in substitution reactions towards selected donors was studied on a small scale by ^{1}H and ^{31}P NMR spectroscopy. The experiments revealed that **5a** (0.20 M in $CDCl_3$) does not react within 24 h at room temperature with 2,3-dimethylbut-2-ene (≈50 equiv.) or diphenylacetylene (1 equiv.) but decomposes to complex mixtures upon addition of 1 equiv. of trimethylphosphine, triphenylphosphine and trimethylphosphite under otherwise identical reaction conditions.

Compounds **3** and **5** are air stable and can be stored under ambient conditions for months. Complexes **4** deposit metallic palladium upon prolonged standing but can be easily purified by dissolving in acetonitrile, filtration and crystallization (or precipitation) with diethyl ether. All compounds were characterized by spectral methods and elemental analysis. The ^{1}H and ^{13}C NMR spectra of **3** and **5**, particularly the $^4J_{PH}$ and $^3J_{PC}$ (cf. [2,3]) coupling constants, indicate the complexes to have *trans*-P–N geometry, in accordance with the solid-state structures of **5a** and **5b** determined by X-ray diffraction (see below). The exclusive *P*-coordination of **2** is nicely reflected by ^{31}P NMR spectra, showing a single, downfield shifted resonance [^{31}P coordination shifts, $\Delta_P = \delta_{complex} - \delta_{ligand}$: 50.0 (**3**), 48.6 (**5a**) and 48.7 (**5b**)]. IR spectra of **3** and **5** display virtually unaffected $\nu_{C=O}$ bands (cf. $\nu_{C=O}$ 1710 cm^{-1} for **2**, [4]) and thus rule out any significant involvement of the ester group in coordination. In addition, the spectra show characteristic $\nu_{C\equiv N}$ stretching bands and bands due to the anions (e.g., strong ν_3 bands of ClO_4 and BF_4).

2.1. Solid-state structures

The molecular structure of **4a** (Fig. 1, Table 1) corroborates the expected planar coordination environment around palladium, which is asymmetric only negligibly in the Pd-donor bond lengths but significantly more in the

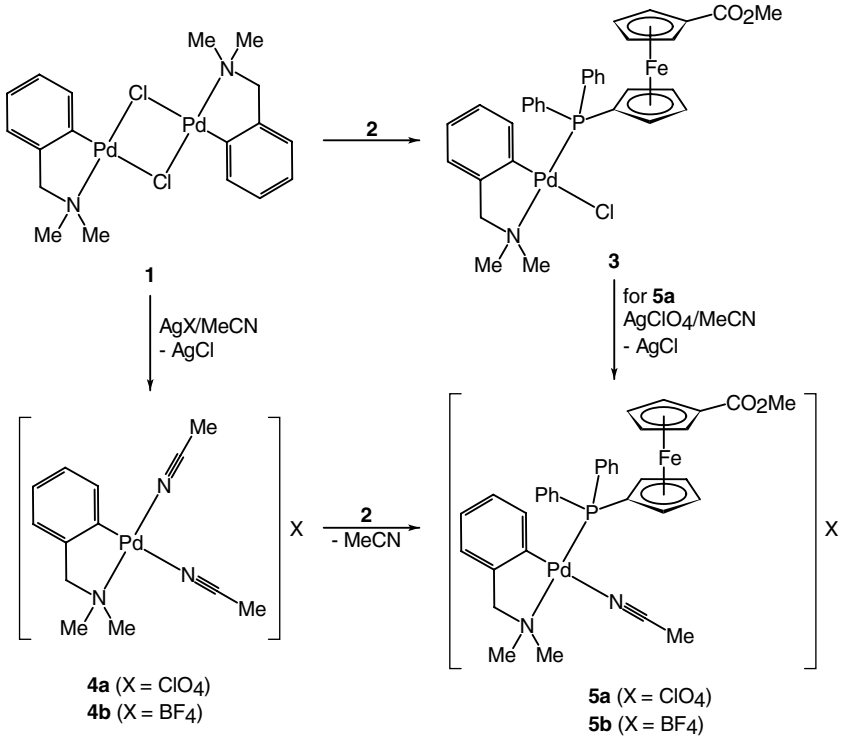

Scheme 1.

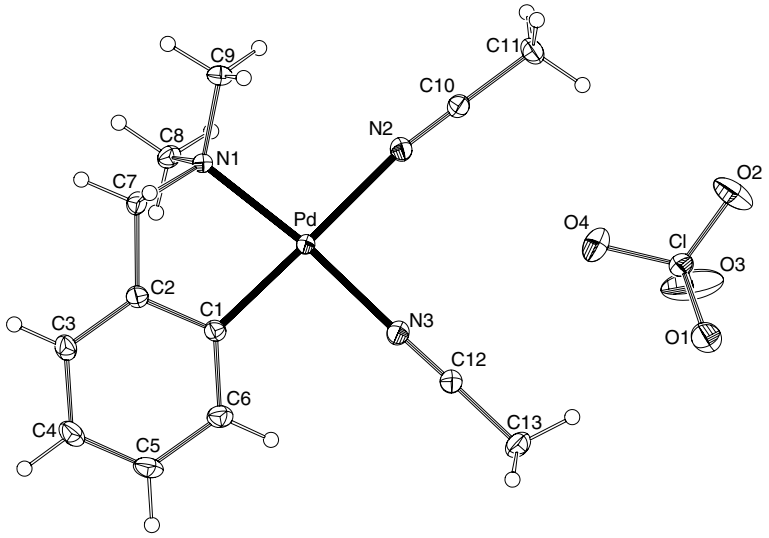

Fig. 1. A view of the molecular structure of **4a**, showing the atom labelling scheme. The thermal motion ellipsoids are drawn at the 30% probability level.

Table 1
Selected geometric parameters for **4b**[a]

Pd–N(1)	2.069(2)	N(1)–Pd–N(2)	96.85(7)
Pd–N(2)	2.126(2)	N(2)–Pd–N(3)	88.78(8)
Pd–N(3)	2.017(2)	N(1)–Pd–C(1)	81.89(8)
Pd–C(1)	1.978(2)	N(3)–Pd–C(1)	92.48(8)
N(1)–C(7)	1.498(3)	N(1)–C(7)–C(2)	107.4(2)
C(2)–C(7)	1.501(3)	C(7)–C(2)–C(1)	115.8(2)
N(2)–C(10)	1.133(3)	N(2)–C(10)–C(11)	179.5(2)
N(3)–C(12)	1.134(3)	N(3)–C(12)–C(13)	179.0(3)

[a] Further data: Pd–N(1)–C angles: 106.0(1)–115.1(1)°. Parameters of the counter ion: Cl–O(1) 1.434(2), Cl–O(2) 1.422(2), Cl–O(3) 1.427(3), Cl–O(4) 1.402(2) Å ; O–Cl–O angles: 108.2(2)–110.7(2)°.

interligand angles, though without any tetrahedral deformation as evidenced by the sum of the interligand angles of exactly 360°. In accordance with a larger *trans*-influence of the aryl ligand, the Pd–N(2) distance is elongated by ≈5% as compared to Pd–N(3). This, as well as the individual bond lengths, correspond well to parameters reported for, e.g., (*R*)-bis(acetonitrile)-{9-[1-(dimethylamino)ethyl-κN] phenanthren-10-yl-κC^{10}}palladium(II) perchlorate [6] and bis(acetonitrile)-{2-[1-(dimethylamino)methyl-κN]-3-methylnaphth-1-yl-κC^1} palladium (II) trifluoromethanesulfonate [7].

The metallated phenyl ring in **4a** is rotated from the coordination plane along the C(1)–C(4) axis at a dihedral angle of 19.12(9)° and the adjacent five-membered palladacycle adopts an envelope conformation (ring puckering parameters [8]: $Q_2 = 0.443(2)$ Å, $\phi_2 = 213.5(3)°$). The solid-state packing of **4a** is molecular, the most prominent intermolecular contact being an interaction between the palladium and a neighbouring aromatic π-electron system (Pd···C(5)^i 3.498(2) Å, *i*. $(1 + x, y, z)$), which interconnects the cations into infinite chains running along the *shortest* lattice parameter *a*. Since solid-state packing is further aided only by weak C–H···O(ClO_4) (C···O 3.4–3.5 Å) and C–H···π-ring (phenyl) interactions, it likely affects macroscopic properties of the crystals, which are obtained as thin needles, readily bent, loosing internal integrity upon only a slight pressure (see Section 3).

As revealed by the solid-state structure of **5a** (Fig. 2, Table 2), the replacement of the acetonitrile ligand with **2** brings about a more pronounced deformation of the coordination sphere. The plane defined by the palladium centre and the four directly bonded atoms (PdL_4) is twisted, the maximum deviation from the least-squares plane being 0.165(2) Å for N(1), which is about 10 times higher than the maximum deviation observed for **4a** [0.012(2) Å for C(1)]. The Pd-donor bond lengths are similar to the respective distances in (S)-acetonitrile-{[1-(dimethylamino)ethyl-κN]phenyl-κC^1}-(3,4-dimethyl-1-phenylphosphole-κP)palladium(II) perchlorate [9] and [(cyanomethylene)triphenylphosphorane-κN]-{[(dimethylamino)methyl-κN]phenyl-κC^1}-(trimethylphosphite)-palladium(II) perchlorate [10]. The palladacycle in **5a** adopts an envelope conformation very much similar to that of **4a** ($Q_2 = 0.429(2)$ Å, $\phi_2 = 212.6(3)°$). Likewise, the phenyl plane is rotated in a similar manner (around the C(25)–C(28) axis) but more than in **4a** (the respective dihedral angle is 27.9(1)°).

The geometry of the carboxyphosphine ligand, apart from a changed conformation of the 1,1′-disubstituted ferrocene core which is *anti*-eclipsed with the torsion angle C(1)–Cg(1)–Cg(2)–C(6) of −145.2(2)°, differs only marginally from an uncoordinated form (e.g., by a slight opening of the C–P–C angles) [4]. The ferrocene unit is rotated with respect to the coordination plane at a dihedral angle between the phosphinylated cyclopentadienyl-ring and PdL_4 plane of 54.9(1)°.

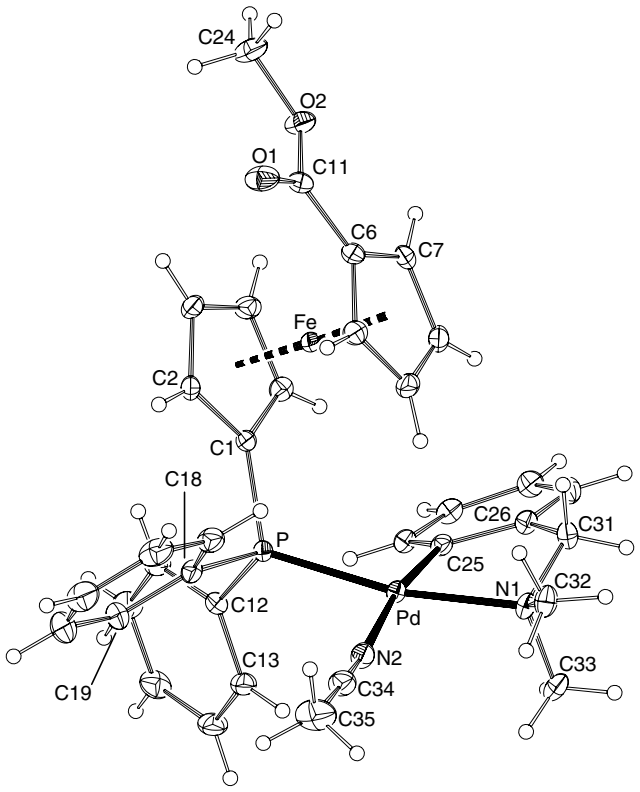

Fig. 2. A view of the cation in the structure of **5a**. The thermal ellipsoids enclose 30% probability level.

Table 2
Selected geometric parameters for **5b**[a]

Pd–P	2.2677(6)	P–Pd–N(2)	93.17(6)
Pd–N(1)	2.134(2)	P–Pd–C(25)	94.22(7)
Pd–N(2)	2.087(2)	N(1)–Pd–N(2)	91.54(8)
Pd–C(25)	2.004(2)	N(1)–Pd–C(25)	82.05(8)
N(2)–C(34)	1.134(4)	N(2)–C(34)–C(35)	177.3(3)
Fe–Cg(1)	1.653(1)	Cg(1)–Fe–Cg(2)	176.45(6)
Fe–Cg(2)	1.655(1)	O(1)–C(11)–O(2)	124.1(2)
C(11)–O(1)	1.203(3)	C(11)–O(2)–C(24)	116.1(2)
C(11)–O(2)	1.339(3)		
O(2)–C(24)	1.440(4)		

[a] Cg(1) and Cg(2) are the centroids of the C(1–5) and C(6–10) cyclopentadienyl rings, respectively. Further data: P–C(1) 1.810(2), P–C(12) 1.816(2), P–C(18) 1.826(2) Å; C–P–C angles 101.7(1)–105.2(1)°; N(2)–C(34) 1.134(4), C(34)–C(35) 1.450(4); Cl–O distances: O(11) 1.427(2) O(12) 1.406(3), O(13) 1.410(4), O(14) 1.397(3) Å; O–Cl–O angles: 107.2(2)–112.5(2)°.

2.2. Suzuki–Miyaura cross-coupling reactions

The Suzuki–Miyaura cross-coupling is a widely used method for the preparation of aromatic compounds [11]. As a benchmark test for complexes **3** and **5b**, and some related compounds, we used the reaction between 4-bromotoluene and phenylboronic acid in the presence of 1 mol.% of palladium catalyst and potassium carbonate as the base (2 equiv.) in hot toluene. The results obtained with **3**, **5b** (entries 1, 2), defined model compounds (entries 3, 4 and 10) and catalysts generated in situ from Pd-precursors and ferrocenephosphines (entries 5–9) are summarized in Table 3. Generally, the coupling reaction proceeded very well with the expected formation of 4-methylbiphenyl without any apparent formation of homocoupling products and deboronation. The only exception was the reaction with the catalyst formed in situ from $[Pd(cod)Cl_2]$ (cod = η^2:η^2-cycloocta-1,5-diene) and Hdpf (entry 5), where the product was obtained in a rather low yield and contaminated with the educts. Notably, when 4-bromotoluene was replaced with the significantly less reactive 4-chlorotoluene [12], the coupling reactions catalyzed with $[Pd(OAc)_2]$/2 Hpdf or $[PdCl_2(PPh_3)_2]$ did not proceed satisfactorily under otherwise identical conditions: as revealed by GC-MS and NMR analysis, the crude product contained mainly 4-chlorotoluene and biphenyl, the product of homocoupling of the boronic acid, but only traces of 4-methylbiphenyl.

Table 3
Suzuki–Miyaura coupling of 4-bromotoluene and $PhB(OH)_2$[a]

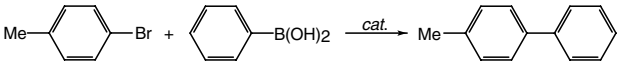

Entry	Catalyst	Isolated yield of 4-methylbiphenyl (%)
1	**3**	80
2	**5b**	85
3	$[PdCl^2(Hdpf\text{-}\kappa P)_2$	80
4	$[PdCl^2(Hdpf\text{-}\kappa P)_2$/2 Hdpf	89
5	$[Pd(cod)Cl_2]$/2 Hdpf[b]	44[c]
6	$[Pd(OAc)_2]$/2 Hdpf[b]	96
7	$[Pd(OAc)_2]$/5 Hdpf[b]	86
8	$[Pd(OAc)_2]$/2 **2**[b]	96
9	$[Pd(OAc)_2]$/2 $FcPPh_2$[b]	94
10	$[PdCl_2(PPh_3)_2]$	80

[a] The yields are based on 4-bromotoluene. For conditions see Section 3.
[b] Catalyst generated in situ by mixing these precursors.
[c] Contaminated with unreacted educts.

The results clearly indicate that the presence of the carboxyl group in the structure of ferrocene phosphine has virtually no influence on the performance of catalysts generated thereof and, hence, can be used for a further catalyst modification (e.g., immobilization). Further work in this area is currently in progress.

3. Experimental

3.1. General comments

All syntheses were carried out under argon with an exclusion of direct daylight. Toluene was dried by standing with potassium metal and freshly distilled under argon. Dichloromethane was dried over anhydrous potassium carbonate. Solvents for crystallizations and chromatography were used without purification. *Trans*-di-μ-chlorobis{(2-(dimethylaminomethyl-κN)phenyl-

κC[1]}dipalladium(II) (**1**) [13], Hdpf, **2** [4], $FcPPh_2$ [14], **4a** [3], $[Pd(cod)Cl_2]$ [15], $[Pd(OAc)_2]$ [16] and $[PdCl_2(Hdpf\text{-}\kappa P)_2]$ [17] were prepared by the literature procedures. All other chemicals were used as obtained from commercial sources.

NMR spectra were recorded on a Varian UNITY Inova 400 spectrometer (^1H, 399.95; ^{13}C, 100.58; ^{31}P, 161.9 MHz) at 298 K. Chemical shifts (δ (ppm)) are given relative to internal tetramethylsilane. The assignment of the NMR signals is based on ^1H,^1H-COSY, ^{13}C APT, ^{13}C gHSQC and ^{13}C gHMBC experiments. IR spectra were recorded on an FT IR Nicolet Magna 650 instrument in the range of 400–4000 cm^{-1}. Melting points were determined on a Kofler apparatus and are uncorrected.

3.2. Synthesis of [SP-4-4]-[PdCl($C_6H_4CH_2NMe_2\kappa^2C^1,P$){Fe($\eta^5$-$C_5H_4PPh_2$-κP)($\eta^5$-$C_5H_4CO_2Me$)}] (3)

Dimer **1** (55.2 mg, 0.10 mmol) and **2** (86.0 mg, 0.20 mmol) were dissolved in dichloromethane (2 ml), and the mixture was stirred for 30 min at room temperature. Then, the product was precipitated by addition of hexane, filtered off, washed with hexane and dried under vacuum (60 °C/0.5 Torr for 1 h) to afford **3** as an orange solid (123.1 mg, 88%).

^1H NMR ($CDCl_3$): δ 2.86 (d, $^4J_{PC} = 2.8$ Hz, 6H, N*Me*$_2$), 3.75 (s, 3H, O*Me*), 4.14 (d, $^4J_{PC} = 2.4$ Hz, 6H, NC*H*$_2$), 4.37 (ddd, $J \approx 1.0$, 1.9, 2.9 Hz, 2H), 4.49 (apparent q, $J \approx 1.9$ Hz, 2H), 4.92–4.95 (m, 4H) (fc, 4 × C*H*); 6.22–7.59 (m, 14H, aromatics). $^{31}P\{^1H\}$ NMR ($CDCl_3$): δ 32.6 (s). $^{13}C\{^1H\}$ NMR ($CDCl_3$): δ 50.15 (d, $^3J_{PC} = 3$ Hz, N*Me*$_2$), 51.71 (O*Me*), 71.48 (fc, *C*H), 72.18 (fc, C_{ipso}), 73.60 (d, $J_{PC} = 7$ Hz, fc, *C*H), 73.65 (d, $^3J_{PC} \approx 2$ Hz, NCH_2), 74.92 (fc, *C*H), 75.24 (d, $^1J_{PC} \approx 60$ Hz, fc, C_{ipso}), 76.68 (fc, *C*H), 122.49, 123.76, 124.89 (d, $^3J_{PC} = 5$ Hz) (C_6H_4, *C*H); 128.00 (d, $J_{PC} = 11$ Hz, PPh_2, *C*H), 130.63 (d, $J_{PC} = 3$ Hz, PPh_2, *C*H), 131.28 (d, $^1J_{PC} = 50$ Hz, PPh_2, C_{ipso}), 134.37 (d, $J_{PC} = 12$ Hz, PPh_2, *C*H), 138.35 (d, $J_{PC} = 10$ Hz, C_6H_4, *C*H); 148.16 (d, $J_{PC} = 2$ Hz), 152.23 (C_6H_4, C_{ipso}); 171.52 (*C*O_2Me). IR (Nujol): $\tilde{\nu}/cm^{-1}$ $\nu_{C=O}$ 1716 s, 1706 s; 1281 s, 1194 w, 1166 w, 1138 m, 1099 m, 1032 m, 994 w, 972 m, 834 m, 745 m, 696 m, 521 m, 508 m. *Anal.* Calc. for $C_{33}H_{33}ClFeNO_2P$: C, 56.28; H, 4.72; N, 1.99%. Found: C, 56.22; H, 4.69; N, 1.94%.

3.3. Synthesis of [Pd($C_6H_4CH_2NMe_2$-κ^2C^1,P)(MeCN-κN)$_2$]BF_4 (4b)

A solution of $AgBF_4$ (0.390 g, 2.00 mmol) in acetonitrile (5 ml) was added into a solution of **1** (0.552 g, 1.00 mmol) in dichloromethane (10 ml). The mixture turned immediately from yellow to only slightly yellowish and an off-white volumious precipitate (AgCl) separated. The mixture was stirred for 15 min in the dark, the precipitate was removed by filtration and the filtrate evaporated under reduced pressure. The oily residue was dissolved in acetonitrile (5 ml) and the product precipitated by addition of diethyl ether. The product was filtered off and dried under vacuum (at 2 Torr for 3 h). Yield: 0.710 g (87%), white solid.

^1H NMR ($CDCl_3$): δ 2.37, 2.50 (2 × s, 3H, *Me*CN); 2.84 (s, 6H, N*Me*$_2$), 3.93 (s, 2H, NCH_2), 6.88–7.08 (m, 4H, aromatics). $^{13}C\{^1H\}$ NMR ($CDCl_3$): δ 2.57, 3.22 (*Me*CN); 52.82 (N*Me*$_2$), 73.23 (NCH_2), 120.23, 121.01 (Me*C*N); 122.32, 125.81, 126.00, 133.33 (C_6H_4, *C*H); 142.15, 147.21 (C_6H_4, C_{ipso}). IR (Nujol): $\tilde{\nu}$ (cm^{-1}) $\nu_{C\equiv N}$ 2333, 2320, 2306, 2293 m; 1580 m, 1564 w, 1289 m; $\nu_3(BF_4)$ 1098 s, 1057 vs br composite; 871 m, 746 vs; 622 m, 521 m, 432 m. *Anal.* Calc. for $C_{13}H_{18}BF_4N_3Pd$: C, 38.13; H, 4.43; N, 10.26%. Found: C, 38.43; H, 4.14; N, 10.02%.

3.4. Synthesis of [SP-4-3]-[Pd($C_6H_4CH_2NMe_2$-κ^2C^1,P){Fe(η^5-$C_5H_4PPh_2$-κP)(η^5-$C_5H_4CO_2Me$)}(MeCN-κN)]X, X = ClO_4 (5a) and BF_4 (5b)

Solid **4a** (105.6 mg, 0.25 mmol) was added into a solution of **2** (112.4 mg, 0.26 mmol) in dichloromethane (3 ml). The solid dissolved quickly to give a clear orange solution, which was crystallized by a careful addition of hexane (as a top layer) and diffusion at room temperature for several days. The crystalline solid formed during several days was filtered off, washed with diethyl ether and dried under vacuum (0.5 Torr for 1 h). Yield of **5a**: 192.1 mg (95%), a rusty orange crystalline solid.

^1H NMR ($CDCl_3$): δ 1.94 (s, 3H, *Me*CN), 2.87 (d, $^4J_{PH} = 2.9$ Hz, N*Me*$_2$), 3.75 (s, 3H, O*Me*), 4.12 (d, $^4J_{PH} = 2.3$ Hz, NCH_2), 4.15 (apparent q, 2H), 4.45 (br s, 2H), 4.48 (apparent q, 2H), 4.85 (apparent t, 2H) (fc, 4 × C*H*); 6.35–7.76 (m, 14H, aromatics). $^{31}P\{^1H\}$ NMR ($CDCl_3$): δ 31.2 (s). $^{13}C\{^1H\}$ NMR ($CDCl_3$): δ 2.54 (*Me*CN), 50.76 (br s, N*Me*$_2$), 52.02 (O*Me*), 71.83 (fc, *C*H), 72.12 (d, $^3J_{PC} = 4$ Hz, NCH_2), 72.59, 73.68 (d, $^1J_{PC} = 56$ Hz) (2 × fc, C_{ipso}); 73.78 (d, $J_{PC} = 7$ Hz), 73.87, 75.45 (d, $J_{PC} = 11$ Hz) (3 × fc, *C*H); ≈120.9 (br, Me*C*N), 123.58, 125.42 (d, $J_{PC} = 5$ Hz), 125.56 (C_6H_4, *C*H); 128.82 (d, $J_{PC} = 11$ Hz, PPh_2, *C*H), 129.74 (d, $^1J_{PC} = 51$ Hz, PPh_2, C_{ipso}), 131.69 (d, $J_{PC} = 2$ Hz), 134.10 (d, $J_{PC} = 12$ Hz (PPh_2, *C*H); 137.47 (d, $J_{PC} = 12$ Hz, C_6H_4, *C*H), 144.39 (br), 148.87 (C_6H_4, C_{ipso}), 171.24 (*C*O_2Me). IR (Nujol): $\tilde{\nu}$ (cm^{-1}) $\nu_{C\equiv N}$ 2323, 2299 m; $\nu_{C=O}$ 1717 vs; 1285 s; 1203 m, 1151 m; $\nu_3(ClO_4)$ 1102 s composite; 977 m, 844 m, 836 m, 777 m, 749 s, 697 s, $\nu_4(ClO_4)$ 623 s; 542 m, 522 s, 507 s, 480 s. *Anal.* Calc. for $C_{35}H_{36}ClFeN_2O_6PPd$: C, 51.94; H, 4.48; N, 3.46%. Found: C, 51.63; H, 4.39; N, 3.24%.

Compound **5a** was also obtained by reacting a solution of **3** (35.6 mg, 0.051 mmol) in dichloromethane with $AgClO_4$ (10.8 mg, 0.052 mmol) dissolved in acetonitrile

(1 ml). A white precipitate which formed immediately (AgCl) was, after stirring for 15 min, filtered off and washed with a little dichloromethane. The clear orange filtrate was evaporated to dryness, redissolved in a mixture of dichloromethane (2 ml) and acetonitrile (five drops), and crystallized by liquid-phase diffusion of diethyl ether over several days. Yield: 36.2 mg (88%), rusty brown needles (identified by IR and NMR spectra).

Complex **5b** was obtained from **4b** (409.6 mg, 1.00 mmol) and **2** (434.0 mg, 1.01 mol) as given above for **5a**. Yield: 771.6 mg (97%), a rusty brown solid. Single crystals were grown by recrystallization from dichloromethane–hexane.

^{1}H NMR ($CDCl_3$): δ 1.90 (s, 3H, *Me*CN), 2.86 (d, $^4J_{PH} = 2.9$ Hz, N*Me*$_2$), 3.75 (s, 3H, O*Me*), 4.12 (d, $^4J_{PH} = 2.1$ Hz, NC*H*$_2$), 4.15 (apparent q, 2H), 4.42 (br apparent t, 2H), 4.50 (apparent q, 2H), 4.86 (br s, 2H) (fc, 4 × C*H*); 6.35–7.77 (m, 14H, aromatics). ^{31}P{^{1}H} NMR ($CDCl_3$): δ 31.3 (s). ^{19}F NMR ($CDCl_3$): δ −153.02 (s, 80%, $^{11}BF_4$), −152.97 (s, 20%, $^{10}BF_4$). ^{13}C{^{1}H} NMR ($CDCl_3$): δ 2.29 (*Me*CN), 50.75 (d, $^3J_{PC} \approx 2$ Hz, N*Me*$_2$), 52.11 (O*Me*), 71.95 (fc, *C*H), 72.11 (d, $^3J_{PC} = 4$ Hz, N*C*H$_2$), 72.48 (br), ≈73.56 (d, $^1J_{PC} \approx 60$ Hz) (2 × fc, C_{ipso}); 73.79 (d, $J_{PC} = 8$ Hz), 73.86, 75.44 (d, $J_{PC} = 11$ Hz) (3 × fc, *C*H); ≈121.5 (br, Me*C*N), 123.56, 125.40 (d, $J_{PC} = 5$ Hz), 125.61 (C_6H_4, *C*H); 128.88 (d, $J_{PC} = 11$ Hz, PPh_2, *C*H), 129.81 (d, $^1J_{PC} = 52$ Hz, PPh_2, C_{ipso}), 131.74 (d, $J_{PC} = 2$ Hz), 134.03 (d, $J_{PC} = 12$ Hz (PPh_2, *C*H); 137.47 (d, $J_{PC} = 12$ Hz, C_6H_4, *C*H), 144.57, 148.99 (C_6H_4, C_{ipso}), ≈171.2 (br, *C*O$_2$Me). IR (Nujol): $\tilde{\nu}$ (cm^{-1}) $\nu_{C\equiv N}$ 2329, 2300 m; $\nu_{C=O}$ 1716 vs, 1704 sh; 1286 s; 1203 m, 1162 s; ν_3 (BF_4) 975–1096 s br composite; 844 m, 836 m, 777 m, 758 m, 750 s, 699 s, 542 m, 522 s, 507 s, 480 s. $C_{35}H_{36}BF_4FeN_2O_2PPd$: C, 52.76; H, 4.55; N, 3.52%. Found: C, 52.48; H, 4.41; N, 3.24%.

3.5. Typical procedure for Suzuki–Miyaura cross-coupling

4-Bromotoluene (1.00 mmol), $PhB(OH)_2$ (1.05 mmol), K_2CO_3 (2.0 mmol) and catalyst (1 mol.% Pd; added as a defined complex or a mixture of a Pd-source and a ligand, see Table 3) were placed into a Schlenk tube equipped with a stirring bar. The tube was sealed with a septum and repeatedly evacuated by an oil pump and filled with argon. Toluene (2 ml, distilled under argon) was added, and the tube was once again evacuated and filled with argon (when the reaction was performed with 4-chlorotoluene, this was added as the last, mixed with the solvent). Then, the mixture was heated in an oil bath kept at 110 °C with stirring overnight (20 h). After cooling to room temperature, the mixture was washed with water (5 × 3 ml), the organic layer was filtered and transferred to a flask with a syringe. The solvent was evaporated under reduced pressure to give crude crystalline product, which was further purified by flash chromatography (silica gel, CH_2Cl_2). Removal of the solvent under vacuum afforded pure 4-methylbiphenyl as a colourless crystalline solid (for yields see Table 3). NMR ($CDCl_3$): δ_H 2.39 (s, 3H, *Me*), 7.21–7.61 (m, 9H, aromatics); δ_C 21.08 (*Me*), 126.96, 126.97, 126.99, 128.70, 129.47 (aromatic *C*H); 137.00, 138.36, 141.16 (aromatic C_{ipso}). M.p. 47–8 °C (hexane; [18], 47–8 °C).

3.6. X-ray crystallography

Compound **4a** was crystallized by liquid-phase diffusion of diethyl ether into an acetonitrile solution and obtained as elongated colourless needles. The crystals were somewhat waxy and could not be cut without an elastic deformation. Hence, a needle with a cross-section ≈0.13 × 0.20 mm^2, exceeding the primary beam area by its length, had to be selected for the measurement. Due to the crystal shape, no explicit absorption correction was applied except for an averaging of the equivalent diffractions (which however gives reliable data, see parameters in Table 4). Single crystals of **5a** were grown from hexane/dichloromethane (rusty orange prism,

Table 4
Crystallographic data, data collection and structure refinement (see also Section 3)

Compound	**4a**	**5a**
Formula	$C_{13}H_{18}ClN_3O_4Pd$	C_{34} $H_{36}ClFeN_2O_2PPd$
M (g mol^{-1})	422.15	809.33
Crystal system	triclinic	monoclinic
Space group	$P\bar{1}$ (no. 2)	$P2_1/n$ (no. 14)
a (Å)	6.0832(2)	10.1958(1)
b (Å)	11.0496(4)	17.5035(3)
c (Å)	12.3660(4)	19.3172(3)
α (°)	86.180(2)	90
β (°)	85.961(2)	100.8424(8)
γ (°)	88.783(2)	90
V (Å^3)	827.18(5)	3385.85(9)
Z	2	4
D_c (g cm^{-3})	1.695	1.588
μ (Mo Kα) (mm^{-1})	1.303	1.134[e]
Total number of diffraction	6233	54,217
Unique/observed[a] diffractions	3716/3531	7748/6678
R_{int} (%)[b]	1.75[d]	2.81
Number of parameters	203	428
R observed diffractions (%)[c]	2.57	3.13
R, wR all data (%)[c]	2.72, 6.69	4.00, 7.84
$\Delta\rho$ (e Å^{-3})	0.90, 0.73	1.94,[f] −0.74

[a] Diffractions with $I_o > 2\sum(I_o)$.
[b] $R_{int} = \sum |F_o^2 - \langle F_o^2 \rangle| / \sum F_o^2$.
[c] $R(F) = \sum ||F_o| - |F_c|| / \sum |F_o|$, $wR(F^2) = \{\sum[w(F_o^2 - F_c^2)^2] / \sum[w(F_o^2)^2]\}^{1/2}$.
[d] For an averaged data set (see Section 3).
[e] Corrected for absorption, the range of transmission coefficients: 0.791–0.870.
[f] See Section 3.6 for discussion of a high residual electron density.

$0.13 \times 0.18 \times 0.38$ mm). In both cases, the full-set of diffraction data ($\pm h \pm k \pm l$) with $2\theta \leqslant 55°$ were collected on a Nonius KappaCCD diffractometer equipped with Cryostream Cooler (Oxford Cryoystems) at 150 K using graphite monochromatized Mo Kα radiation ($\lambda = 0.71073$ Å and analyzed with the HKL program package by Nonius BV (Table 4).

The structures were solved by direct methods (SIR92 [19]) and refined by weighted full-matrix least-squares procedure on F^2 (SHELXL97 [20]). Final geometric calculations were carried out with a recent version of the Platon program [21]. All non-hydrogen atoms were refined with anisotropic thermal motion parameters whilst all hydrogen atoms were included in the calculated positions [CH bond lengths: 0.93 (aromatic), 0.97 (methylene) and 0.96 (methyl) Å and assigned $U_{iso}(H) = 1.2U_{eq}(C)$ (aromatic and methylene) or 1.5 $U_{eq}(C)$ (methyl).

In the case of **5a**, the final difference electron density maps showed an unusually high residual electron density (1.94 e Å^{-3} in 1.9 Å distance from Pd). A closer inspection revealed that the first two maxima on the map (1.94 and 0.56 e Å^{-3}; intensity of the next most intense positive peak: 0.50 e Å^{-3}) are as distant as Pd and P atoms in the molecule of **5a**, and can be independently refined as Pd and P with equal occupancies of 3%, thus decreasing the *R*-value by 0.3% (another possibly observable maximum due to the iron atom could not be identified because of overlaps). Since these maxima were observed reproducibly in the crystals resulting from different experiments, at different temperatures, and also in the structure of isostructural complex **5b**, [1] these features seem to reflect *the* real structure of crystals, where some parts are rotated with respect to the dominant repeating unit (the bulky ferrocene ligand can act as the pivot in the case of **5a** and **5b**).

4. Supplementary data

Crystallographic data (CIF files) have been deposited with the Cambridge Crystallographic Data Centre under the deposition numbers CCDC-213739 (**4a**) and -213740 (**5a**). Copies of the data may be obtained free of charge upon request to CCDC, 12 Union Road, Cambridge CB2 1EZ, UK (fax: +44-1223-336033, e-mail: deposit@ccdc.cam.ac.uk, www: http://www.ccdc.cam.ac.uk).

[1] Individual geometric parameters for **5b** do not differ significantly from those of the isostructural perchlorate **5a** [**5b**: $C_{35}H_{36}BF_4FeN_2O_2PPd$, $P2_1/n$ (no. 14), $a = 10.1319(1)$, $b = 17.4440(2)$, $c = 19.2608(2)$ Å; $\beta = 101.2538(7)°$, $Z = 4$ at 120 K]. Crystallographic data have been deposited at the Cambridge Crystallographic Data Centre (deposition number CCDC-213741) and will not be discussed here.

Acknowledgements

This work was supported by Grant Agency of the Czech Republic (grant Nos. 203/01/P002, 104/02/0571, and 203/99/M037) and is a part of a long-term Research plan of the Faculty of Sciences, Charles University.

References

[1] (a) For instance in alkene oligomerization, polymerization and copolymerization: S. Mecking, Angew. Chem., Int. Ed. 40 (2001) 534;
(b) G.J.P. Britovsek, V.C. Gibson, D.F. Wass, Angew. Chem., Int. Ed. 38 (1999) 429;
(c) K. Nomura, Recent Res. Devel. Pure Appl. Chem. 12 (1998) 473;
(d) M. Peuckert, W. Keim, Organometallics 2 (1983) 594;
(e) Catalytic hydrogenation: M. Onishi, K. Hiraki, M. Yamaguchi, J. Morishita, Inorg. Chim. Acta 195 (1992) 151;
(f) (Amides) F. Joo, E. Trocsanyi, J. Organomet. Chem. 231 (1982) 63;
(g) Pd-catalyzed allylic substitution (amides): H. Lam, X. Cheng, J.W. Steed, D.J. Aldous, K.K.M. Hii, Tetrahedron Lett. 43 (2002) 5875;
(h) Synthesis of functionalized dendrimers: P. Lange, A. Schier, H. Schmidbaur, Inorg. Chim. Acta 235 (1995) 263;
(i) Extractive recovery of rare metals: A. Jegorov, J. Podlaha, Catal. Lett. 8 (1991) 9.
[2] (a) P. Braunstein, D. Matt, Y. Dusausoy, L. Ricard, J. Fischer, A. Mitschler, New J. Chem. 4 (1980) 493;
(b) P. Braunstein, D. Matt, Y. Dusausoy, J. Fischer, A. Mitschler, L. Ricard, J. Am. Chem. Soc. 103 (1981) 5115;
(c) P. Braunstein, D. Matt, Y. Dusausoy, J. Fischer, Organometallics 2 (1983) 1410;
(d) P. Braunstein, J. Fischer, D. Matt, M. Pfeffer, J. Am. Chem. Soc. 106 (1984) 410;
(e) P. Braunstein, D. Matt, D. Nobel, D.-E. Bouaoud, D. Grandjean, J. Organomet. Chem. 301 (1986) 401.
[3] P. Štěpnička, Organometallics 22 (2003) 1728.
[4] J. Podlaha, P. Štěpnička, I. Císařová, J. Ludvík, Organometallics 15 (1996) 543.
[5] Coordination of the dpf$^-$ anion as a P, O-chelate was reported in a series of square-planar Rh(I) complexes [RhL(CO)(dpf-κ^2P, O)] P. Štěpnička, I. Císařová, J. Chem. Soc., Dalton Trans. (1998) 2807.
[6] P.-H. Leung, K.-H. Ng, Y. Li, A.J.P. White, D.J. Williams, Chem. Commun. (1999) 2435.
[7] J.-M. Valk, R. van Belzen, J. Boersma, A.L. Spek, G. van Koten, J. Chem. Soc., Dalton Trans. (1994) 2293.
[8] D. Cremer, J.A. Pople, J. Am. Chem. Soc. 97 (1975) 1354.
[9] N. Gül, J.H. Nelson, Organometallics 19 (2000) 91.
[10] L.R. Falvello, S. Fernández, R. Navarro, E.P. Urriolabetia, Inorg. Chem. 36 (1997) 1136.
[11] (a) N. Miyaura, A. Suzuki, Chem. Rev. 95 (1995) 2457;
(b) A. Suzuki, in: F. Diedrich, P.J. Stang (Eds.), Metal-catalyzed cross-coupling reactions, Wiley, Weinheim, 1998, pp. 49–97, Ch. 2;
(c) A. Suzuki, in: E. Negishi (Ed.), Handbook of Organopalladium Chemistry for Organic Synthesis, vol. 1, Wiley, New York, 2002, pp. 249–261 (Ch. III.2.2);
(d) See also: N. Miyaura, A. Suzuki, Synth. Commun. 11 (1981) 513.
[12] A.F. Littke, G.C. Fu, Angew. Chem. Int. Ed. 41 (2002) 4176.
[13] A.C. Cope, E.C. Friedrich, J. Am. Chem. Soc. 90 (1968) 909.

[14] (a) G.P. Sollott, H.E. Mertwoy, S. Portnoy, J.L. Snead, J. Org. Chem. 28 (1963) 1090;
(b) J.C. Kotz, C.L. Nivert, J. Organomet. Chem. 52 (1973) 387.
[15] D. Drew, J.R. Doyle, A.G. Shaver, in: F.A. Cotton (Ed.), Inorganic Synthesis, vol. 13, McGraw-Hill, New York, 1972, p. 47.
[16] T.A. Stephenson, S.M. Morehouse, A.R. Powell, J.P. Heffer, G. Wilkinson, J. Chem. Soc. (1965) 363.
[17] P. Štěpnička, J. Podlaha, R. Gyepes, M. Polášek, J. Organomet. Chem. 552 (1998) 293.
[18] L. Gattermann, Justus Liebigs Ann. Chem. 347 (1906) 347.
[19] A. Altomare, M.C. Burla, M. Camalli, G. Cascarano, C. Giacovazzo, A. Guagliardi, G. Polidori, J. Appl. Cryst. 27 (1994) 435.
[20] G.M. Sheldrick, SHELXL97. Program for Crystal Structure Refinement from Diffraction Data, University of Göttingen, Göttingen, 1997.
[21] A.L. Spek, Platon, a multipurpose crystallographic tool (2001). Available from interrefhttp://www.cryst.chem.uu.nl/platon/urlhttp://www.cryst.chem.uu.nl/platon/.

Available online at www.sciencedirect.com
SCIENCE DIRECT®
Polyhedron 23 (2004) 929–936
POLYHEDRON
www.elsevier.com/locate/poly

Layered $[BaMn_{1-x}M_x(C_3H_2O_4)_2(H_2O)_4]$ (M = Fe, Co or Cu) solid solutions: thermal, spectroscopic and magnetic properties ☆

Izaskun Gil de Muro, Luis Lezama, Maite Insausti, Teófilo Rojo *

Dpto. Química Inorgánica, Facultad de Ciencias, UPV/EHU, Apdo. 644, 48080 Bilbao, Spain

Received 6 October 2003; accepted 25 November 2003

Abstract

Metallo-organic complexes with the formula $[BaMn_{1-x}M_x(C_3H_2O_4)_2(H_2O)_4]$, where M = Fe, Co or Cu ($0 \leqslant x \leqslant 1$), were synthesised and characterised. All of them are isostructural and crystallise in the space group *Pccn*. The crystal structure has been described as a two-dimensional (2D) arrangement of M–malonate layers extended along the (0 1 0) crystallographic plane. Octahedral polyhedra of transition metallic ions are coordinated by bridging malonate ligands, through the O–C–O atoms. The evolution of the cell volume follows Vegard's law. Spectroscopic data are consistent with the transition metallic ions in a high-spin octahedral symmetry, confirming the substitution of the metallic cations. All the iron and cobalt compounds exhibit 2D antiferromagnetic interactions with the presence of weak ferromagnetism. The copper solid solution also shows 2D antiferromagnetic interactions, unlike the $[BaCu(C_3H_2O_4)_2(H_2O)_4]$ complex, which exhibited ferromagnetic ones.
© 2004 Elsevier Ltd. All rights reserved.

Keywords: Malonate complexes; 2D antiferromagnets; Weak ferromagnetism

1. Introduction

The chemistry of heteronuclear complexes involving bridging carboxylato ligands has created a high interest aimed at designing polynuclear extended systems with specific dimensionality, the results concerning the magnetic properties being of special interest.

The malonate, with two neighbouring carboxylato groups, is a very versatile ligand. It can simultaneously adopt monodentate, various bischelating coordination modes and different carboxylato bridging modes (*syn–syn*, *syn–anti*, and *anti–anti*) giving rise to a variety of structures and being a useful tool for connecting different metals and transmitting different magnetic interactions. The exchange coupling through the carboxylato ligand is dependent, apart from the nature of the metallic ion, on the conformation of the bridge between the interacting metal centers [1–4]. In this way, ferromagnetically [5] or antiferromagnetically [6] coupled dimers, alternating chains [3,4,7], polymeric trinuclear antiferromagnetic complexes [8], two-dimensional ferromagnetic and antiferromagnetic compounds [9,10], and more extended structures [1] have been obtained with the malonate ligand.

In this sense, we have recently reported the study of different malonate complexes with the formula $[AM(C_3H_2O_4)_2(H_2O)_4]$, where AM is SrMn, SrCu, BaMn, BaFe, BaCo and BaCu [9,11]. All of them were found to be isostructural and showed interesting spectroscopic and magnetic properties. The structure was visualised as a lamellar network with MO_6 polyhedra coordinated by bridging malonate ligands. Two-dimensional (2D) magnetic interactions were also found in all compounds, with the presence of antiferromagnetic interactions for manganese(II), iron(II) and cobalt(II) compounds and ferromagnetic for the copper(II) complexes. Furthermore, these complexes can be used as precursors in the synthesis of mixed oxides, being an alternative to the ceramic method. The thermal decomposition of heterometallic complexes permits the preparation of highly homogeneous phases at lower

☆ Supplementary data associated with this article can be found, in the online version, at doi:10.1016/j.poly.2003.12.015.

* Corresponding author. Tel.: 34-94-6012458; fax: 34-94-4648500.
E-mail address: qiproapt@lg.ehu.es (T. Rojo).

0277-5387/$ - see front matter © 2004 Elsevier Ltd. All rights reserved.
doi:10.1016/j.poly.2003.12.015

temperatures and with smaller grain sizes than those obtained from the ceramic method. So, taking into account that all of them are isostructural. $[BaMn_{1-x}M_x(C_3H_2O_4)_2(H_2O)_4]$ solid solutions with M = Fe, Co or Cu and $0 \leqslant x \leqslant 1$ have been synthesised, characterised and their spectroscopic, magnetic and thermal properties studied. The complexes will be abbreviated as BaMnFe, BaMnCo and BaMnCu.

2. Experimental

Manganese(II) chloride, cobalt(II) chloride, copper(II) chloride and malonic acid were purchased from Fluka, iron(II) and barium chloride was purchased from Aldrich Co. and sodium carbonate from Merck. All of them were used without further purification.

To a solution of 2.5 mmol of disodium malonate, previously formed from 2.5 mmol (0.2601 g) of malonic acid neutralised with 2.5 mmol (0.7419 g) of sodium carbonate, the stoichiometric amounts of the corresponding transition metallic chlorides were added. The mixture was stirred for 30 min, after which 1 mmol of barium chloride was added. Polycrystalline powders of all the phases were obtained in a few seconds and stirred for 1–2 h for a complete precipitation. For the iron compounds, a closed system with a nitrogen atmosphere was needed to prevent oxidation. The products obtained were filtered and washed in ethanol/water followed by diethyl ether. The complexes were obtained as polycrystalline powders of several colours, white in the case of BaMnFe, light pink for BaMnCo compounds and light blue for BaMnCu ones. The analyses of the C, H and metals agree with the $BaMn_{1-x}M_xC_6H_{12}O_{12}$ stoichiometries and are given as Supplementary Material.

3. Physical measurements

Microanalyses were performed with a LECO CHNS-932 elemental analyzer. Analytical measurements were carried out in an ARL 3410+ICP with Minitorch equipment. The powder X-ray diffraction (XRD) pattern was taken using a Philips X'pert diffractometer equipped with graphite-monochromated Cu Kα1 radiation. Data were collected by scanning in the 2θ range 5–80° with increments of 0.02°. Thermogravimetric measurements were performed in a TA instruments-STD 2960 (simultaneous DSC-TGA) instrument. Crucibles containing 20 mg of sample were heated at 5° min^{-1} under dry air atmosphere. Diffuse reflectance spectra were carried out in a CARY 2415 spectrometer in the range 5000–45 000 cm^{-1}. EPR spectra were recorded on a Bruker ESP300 spectrometer, equipped with a standard Oxford low-temperature device operating at X band. The magnetic field was measured with a Bruker BNM 200 gaussmeter, and the frequency was determined by using a Hewlett-Packard 5352B microwave frequency counter. Magnetic susceptibilities of powdered samples were carried out in the temperature range 1.8–300 K using a Quantum Design MPMS-7 Squid magnetometer. The magnetic measurements were performed at magnetic fields between 0 and 7 T.

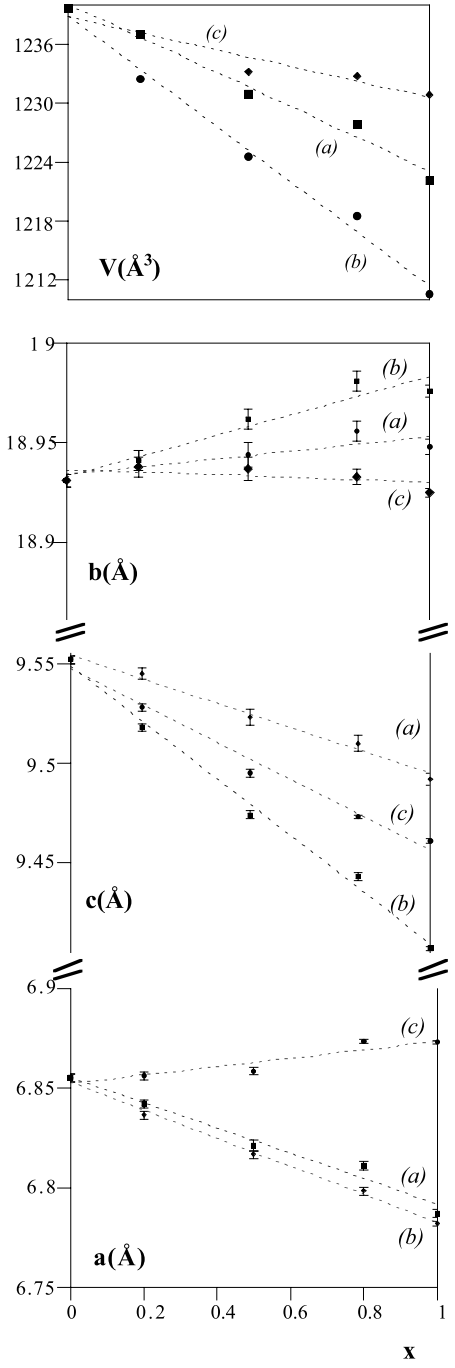

Fig. 1. Variation of the crystallographic parameters with the composition for the $[BaMn_{1-x}M_x(C_3H_2O_4)_2(H_2O)_4]$ (M = Fe, Co, Cu). (a) BaMnFe (●), (b) BaMnCo (■) and (c) BaMnCu (◆) solid solutions.

4. Results and discussion

4.1. Crystallographic study

Powder X-ray diffraction patterns of the products were performed in the 2θ range 5–80°. Indexation of the diffraction profile and refinement of the cell parameters were made by FULLPROF (pattern-matching analysis) [12] on the basis of the space group *Pccn* and the cell parameters found for a single crystal of [SrCu-$(C_3H_2O_4)_2(H_2O)_4$], previously published [9]. The variation of the calculated crystallographic parameters versus the composition is represented in Fig. 1 (for more information see Supplementary Material). Notable is the gradual decrease of the *a* and *c* crystallographic parameters when the iron and cobalt contents increase, in agreement with the smaller size of these cations in comparison with the manganese one. However, in the case of the copper solid solution, the *a* parameter increases. This fact is due to the Jahn–Teller effect in the copper(II) compounds, which causes the elongation of the metal coordination polyhedra in this direction. The *b* parameter remains practically invariable or slightly increases for the BaMnCo phases. In any case, the cell volume linearly diminishes with the amount of the inserted cations following Vegard's law, according to their smaller size.

Taking these results into account, we consider all the phases as isostructural to the previously characterised SrCu phase. The structure consists of layered networks of octahedral polyhedra of transition metallic ions coordinated by malonate ligands. These carboxylato bridging arrangements form infinite sheets, extended along the (0 1 0) crystallographic plane where the shortest M ··· M exchange distance is found through the O–C–O atoms (see Fig. 2). The alkaline earth cations are located between the M–malonate layers.

4.2. Thermal study

The thermal decomposition steps of the compounds were obtained from their TG curves shown in Fig. 3. Decomposition occurs following three consecutive processes: dehydration, ligand pyrolysis and inorganic residue formation.

The first process takes place in the 75–100 °C temperature range and corresponds to the loss of the four water molecules. This process seems to occur in only one

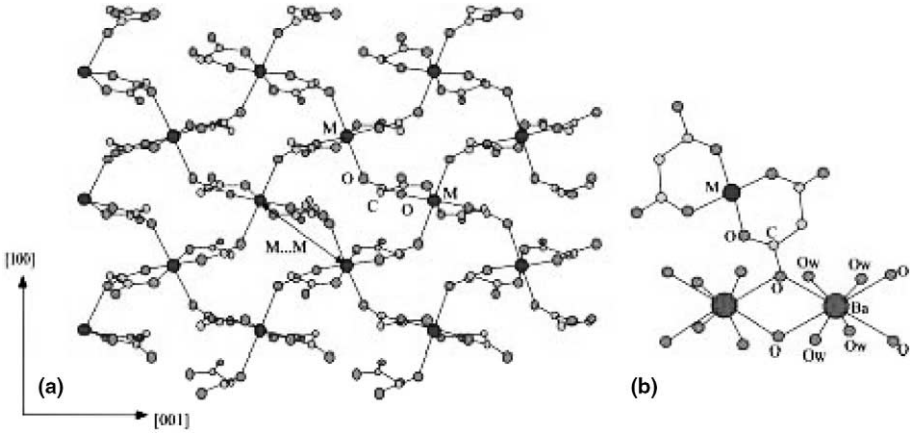

Fig. 2. (a) Two-dimensional network of transition metal polyhedra and (b) alkaline earth centre and linkage to transition metal polyhedra in $[AM(C_3H_2O_4)_2(H_2O)_4]$.

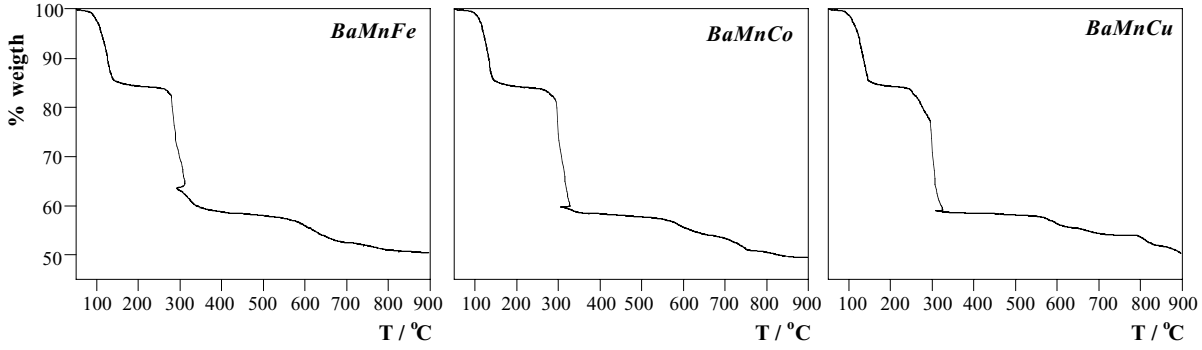

Fig. 3. TG curves in air, for the $BaMn_{0.5}Fe_{0.5}$, $BaMn_{0.5}Co_{0.5}$ and $BaMn_{0.5}Cu_{0.5}$ compounds.

step, suggesting that all the water molecules are similar, as was deduced from the crystallographic data of the SrCu compound. After that, the decarboxylation of the ligand comes and a sharp mass loss in the 250–450 °C temperature range is observed. The weight loss agrees with the formation of $BaCO_3$ and the corresponding transition metal oxides. Above 500 °C, the TG curves show a gradual mass loss, when the carbonate decomposes to yield the mixed oxides. In the case of the BaMnFe and BaMnCo precursors, the evolution of the inorganic residue seems to take place in two steps, concluding in a very slight mass loss. The X-ray diffractograms of the obtained residues indicated the presence of a $BaMn_{1-x}M'_xO_{3-\delta}$ oxide, together with slight amounts of some impurities. The last weight-constant plateau corresponds to the formation of a stable oxide so the attainment of the $BaMn_{1-x}Fe_xO_{3-\delta}$ and $BaMn_{1-x}Co_xO_{3-\delta}$ oxides may occur near 750 °C in both cases. In the case of the BaMnCu precursor, the evolution of the inorganic residue finishes at 850 °C in a slight mass loss step. The residue has been identified as a mixture of $BaMn_{1-x}Cu_xO_{3-\delta}$ and CuO oxides. Consequently, the optimum reaction temperature in order to obtain the $BaMn_{1-x}Cu_xO_{3-\delta}$ oxide could be near 850 °C.

4.3. Diffuse reflectance spectroscopy

The reflectance spectra were recorded at room temperature in the 5000–45 000 cm^{-1} range. Several bands corresponding to high spin iron(II), cobalt(II) and copper(II) ions in octahedral geometry can be seen in the spectra of Fig. 4. The bands due to the manganese(II) ions cannot be observed because they come from forbidden transitions. The assignment of these bands are summarized in Table 1. The intensities change depending on the inserted metal content. For the BaMnFe phases, a single band is observed at around 11 400 cm^{-1}, which is characteristic of a high-spin d^6 configuration in octahedral coordination. The spectra of the BaMnCo compounds show three bands, at around 8200, 18 000 and 21 500 cm^{-1}, which are characteristic of a cobalt(II) compound in octahedral geometry. Finally, the spectra for the copper doped compounds show a main band at 13 800 cm^{-1} (725 nm) and another one at around 6800 cm^{-1} (1470 nm). These bands are typical of copper(II) (d^9) compounds where the copper ion is in tetragonally elongated octahedral coordination [13].

4.4. EPR spectroscopy

The room temperature X-band EPR spectra of some BaMnCu powdered samples are shown in Fig. 5(a). All of them, except the BaCu compound, show isotropic signals centred at around $g = 2$. The presence of only one signal, different from the signal of the parent compounds, indicates that the two different transition metallic ions in the compounds are magnetically coupled,

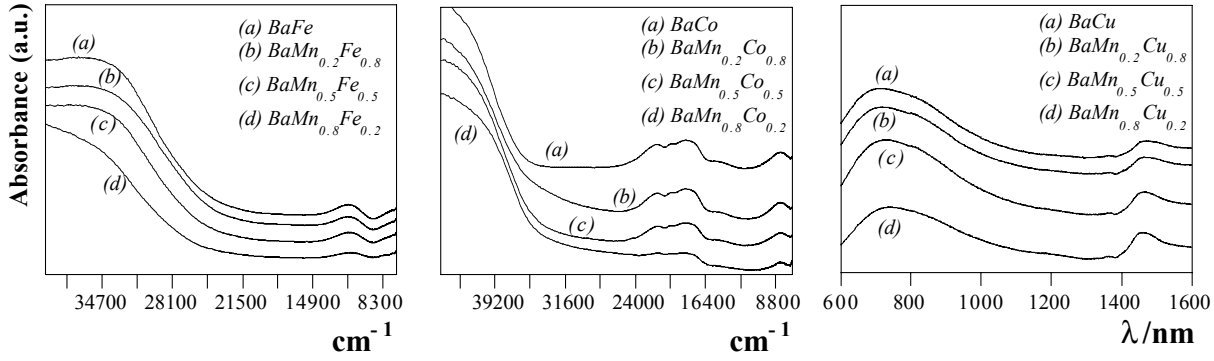

Fig. 4. Diffuse reflectance spectra for the BaMnFe, BaMnco and BaMnCu systems.

Table 1
Assignment of the diffuse reflectance bands for the BaMnFe, BaMnCo and BaMnCu solid solutions

	Position (cm^{-1})	Transition	Metallic cation
BaMnFe	1400	$^5E_g \leftarrow {}^5T_{2g}$	Octahedral Fe^{II} d^6
BaMnCo	8200	$^4T_{2g} \leftarrow {}^4T_{1g}(F)$	Octahedral Co^{II} d^7
	18 000	$^4A_{2g} \leftarrow {}^4T_{1g}(F)$	
	21 500	$^4T_{1g}(P) \leftarrow {}^4T_{1g}(F)$	
BaMnCu		$^2E_g(d_{yz}\,d_{xz}) \leftarrow {}^2B_{1g}(d_{x^2-y^2})$	
	13 600 (730 nm)	$^2B_{2g}(d_{xy}) \leftarrow {}^2B_{1g}(d_{x^2-y^2})$	Tetragonally elongated octahedral Cu^{II} d^9
	6850 (1460 nm)	$^2A_{1g}(d_{z^2}) \leftarrow {}^2B_{1g}(d_{x^2-y^2})$	

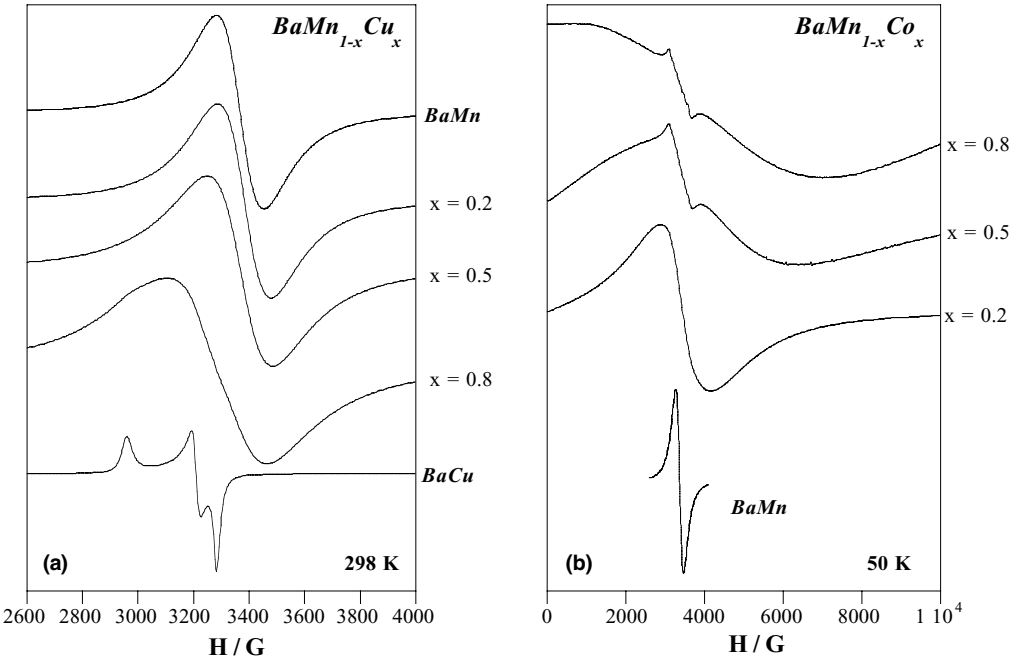

Fig. 5. (a) X-band EPR spectra at room temperature of the BaMnCu family and (b) X-band EPR spectra at 50 K of the BaMnCo family.

confirming the presence of both cations in the structure. It is also worth mentioning the absence of satellite signals from impurities present, and so co-precipitation of the parent compounds can be rejected.

The X-band spectra of the BaMnFe and BaMnCo solid solutions were also measured at room temperature, but the linewidth increased with the iron or cobalt contents and the resolution was really poor. The spectra for the BaMnCo system at 50 K are shown in Fig. 5(b). The linewidth of the signals of the BaMnCo complexes are wider than those of the BaMn compound, and get wider with increasing cobalt content. This fact agrees with the existence of Mn^{II}–Co^{II} interactions, confirming the presence of both metallic cations in the structure. However, at high cobalt contents, the appearance of the hyperfine signal corresponding to the manganese(II) ions indicates the presence of a small paramagnetic impurity in the sample. At lower temperatures (4 K), the main signal becomes wider again, suggesting the presence of significant magnetic interactions.

4.5. Magnetic properties

Variable-temperature magnetic susceptibility measurements were performed on $[BaMn_{1-x}M_x(C_3H_2O_4)_2(H_2O)_4]$ (M = Fe, Co and Cu) powdered samples in the 1.8–300 K temperature range, under a magnetic field of 1 kG. The plots $\chi_m T$ versus T for the $BaMn_{0.5}Fe_{0.5}$ and $BaMn_{0.5}Co_{0.5}$ complexes are shown in Fig. 6 as representative examples. The obtained magnetic parameters

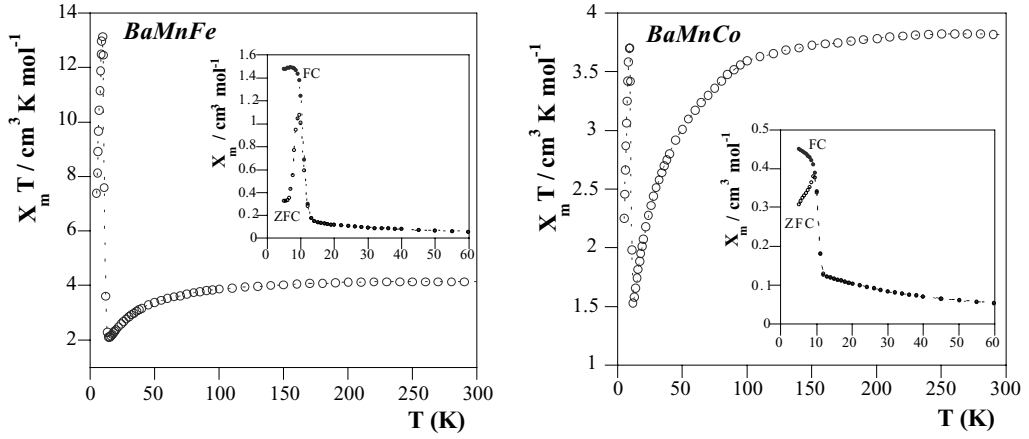

Fig. 6. $\chi_m T$ vs. T curves for $BaMn_{0.5}Fe_{0.5}$ and $BaMn_{0.5}Co_{0.5}$ compounds. χ_m vs. T, FC and ZFC curves in the insets.

Table 2
Magnetic parameters of the $[BaMn_{1-x}M_x(C_3H_2O_4)_2(H_2O)_4]$ (M = Fe, Co, Cu) compounds

		T_N (K)	C_m ($cm^3\,K\,mol^{-1}$)	θ (K)	μ_{eff} (μ_B)
BaMn [9]	AF + weak FM	7	4.34	−13.8	5.76
BaFe [11]	AF + weak FM	13.2	3.64	−19.3	5.23
BaCo [11]	AF + weak FM	13	3.59	−48.9	4.96
$BaMn_{0.5}Fe_{0.5}$	AF + weak FM	12	4.37	−12.7	5.75
$BaMn_{0.5}Co_{0.5}$	AF + weak FM	11.5	4.02	−13.5	5.52
$BaMn_{0.8}Cu_{0.2}$	AF		3.49	−10.6	5.17
$BaMn_{0.5}Cu_{0.5}$	AF		2.60	−10.0	4.48
$BaMn_{0.2}Cu_{0.8}$	AF		1.09	−6.4	2.91
BaCu [9]	FM		0.41	1.8	1.89

The parameters of the parent compounds are given for comparison.

are collected in Table 2. The μ_{eff} values measured at room temperature are 5.75 and 5.52 μ_B for the iron and cobalt compounds, respectively, in accordance with a paramagnetic behaviour of both systems, being in high-spin states. The magnetic moments ($\mu_{eff} = \sqrt{8}\chi_m T$) slowly diminish with decreasing temperature, reaching a minimum value at around 12 K, then sharply increase and near 10 K a maximum appears. From χ_m^{-1} versus T curves Curie–Weiss behaviours have been deduced above 30 K. The values of the Weiss and Curie constants are $\theta = -12.7$ and −13.5 K and $C_m = 4.37$ and 4.02 $cm^3\,K\,mol^{-1}$, for $BaMn_{0.5}Fe_{0.5}$ and $BaMn_{0.5}Co_{0.5}$, respectively. The progressive decrease of both $\chi_m T$ curves up to 15 K, together with the negative values of θ, indicate the presence of antiferromagnetic interactions. Nevertheless, below 15 K the sudden increase of the magnetic moment suggests that total antiparallel alignment of the spins is not reached, with the appearance of a small ferromagnetic component.

Magnetization measurements at low temperatures for $BaMn_{0.5}Fe_{0.5}$ and $BaMn_{0.5}Co_{0.5}$ have been carried out and the curves are represented in Fig. 7. At 5 K, both compounds show small M versus H hysteresis loops with coercive fields near 3000 G and remnant magnetization values of 0.20 and 0.06 (in $N\beta$ units) for the iron and cobalt complexes, respectively. The thermoremnant magnetization curves show Néel temperatures of 12 and 11.5 K for BaMnFe and BaMnCo, respectively. Below T_N, the saturation is rapidly reached with M_r values of 0.20 and 0.06 (in $N\beta$ units), similar to the average value of the parent compounds. Both curves confirm the presence of a small ferromagnetic component at low temperatures.

In the case of the copper compounds, different magnetic behaviours were observed. The magnetic susceptibility data of the $BaMn_{0.8}Cu_{0.2}$, $BaMn_{0.5}Cu_{0.5}$ and $BaMn_{0.2}Cu_{0.8}$ powdered samples are represented in Fig. 8. The μ_{eff} values measured at room temperature are 5.17, 4.48 and 2.91 μ_B (see Table 2), which correspond to the values of paramagnetic behaviour for both spin systems (6.04 and 1.89 μ_B for BaMn and BaCu, respectively). These values decrease with decreasing temperature, suggesting the existence of antiferromagnetic interactions with Néel temperatures below 5 K. The χ_m^{-1} curves were fitted to a Curie–Weiss behaviour with values of θ, −10.6, −10.0, −6.4 K for $BaMn_{0.8}Cu_{0.2}$, $BaMn_{0.5}Cu_{0.5}$ and $BaMn_{0.2}Cu_{0.8}$, in agreement with the presence of antiferromagnetic interactions. Finally, in the case of the $BaMn_{0.8}Cu_{0.2}$ compound, the small minimum observed in the $\chi_m T$ curve at 6 K seems to indicate the presence of a weak ferromagnetic component below 5 K.

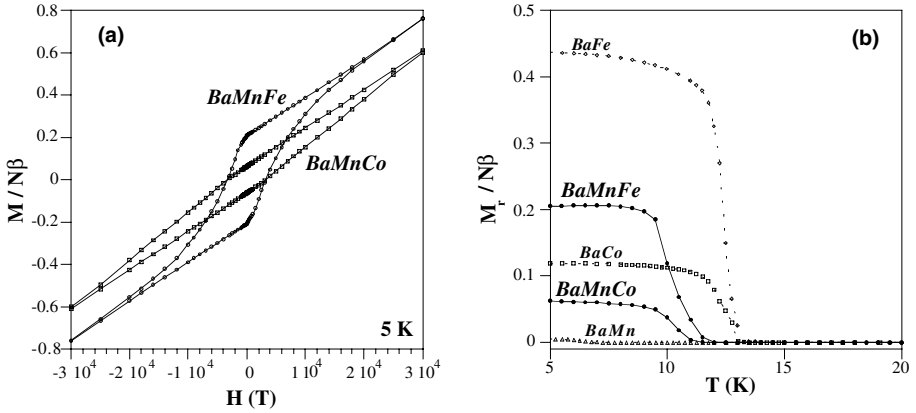

Fig. 7. (a) Hysteresis curves measured at 5 K for $BaMn_{0.5}Fe_{0.5}$ and $BaMn_{0.5}Co_{0.5}$ compounds and (b) zero field magnetization vs. T curves after cooling the samples under a magnetic field of 100 G. BaMn, BaFe and BaCo thermoremnant curves are given for comparison.

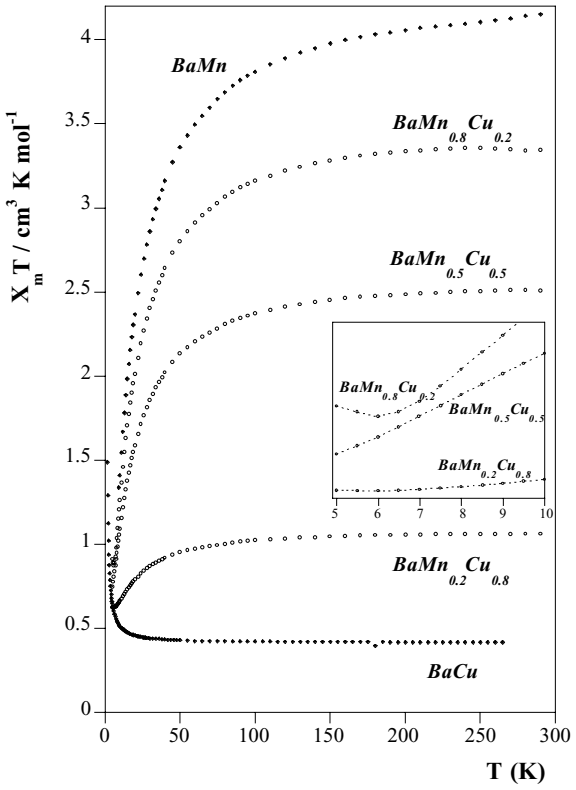

Fig. 8. $\chi_m T$ vs. T curves for $BaMn_{0.8}Cu_{0.2}$, $BaMn_{0.5}Cu_{0.5}$ and $BaMn_{0.2}Cu_{0.8}$ compounds. Low temperature data are magnified in the inset. The curves for BaMn and BaCu are included for comparison.

The magnetic behaviour described for the solid solutions is very similar to that observed for the parent compounds. The BaMn, BaFe and BaCo susceptibility data were fitted to a 2D Heisenberg antiferromagnetic model above T_N [9,11], whereas the BaCu data were fitted to a 2D Heisenberg ferromagnetic model [9]. Therefore, it can be concluded that the BaMnFe and BaMnCo solid solutions exhibit 2D Heisenberg antiferromagnetic behaviour above 15 K, due to a weak intralayer antiferromagnetic interaction between $M^{II}\cdots M^{II}$ cations, through O–C–O bridges. Below this temperature, the misalignment of the spins (or canting) in the layer causes a subsequent long-range ferromagnetic arrangement between layers. Moreover, the magnetization values do not agree with a $Mn^{II}\cdots M^{II}$ ferrimagnetic ordering, so a Mn–M ordered sequence can be rejected. The higher ferromagnetic component, found for the iron compounds, can be mainly attributed to the anisotropy of the metallic cations, but other parameters such as exchange magnetic interactions (bond and angles) should be also considered. Finally, the low Néel temperatures found in the solid solutions can be related to the presence of structural disorder in these phases.

The BaMnCu solid solution also exhibits 2D antiferromagnetic interactions. In this way, the ferromagnetic interactions found for the BaCu compound disappear even with a small content of manganese. This transition can be due to the high spin of the manganese(II) ion (d^5, $S = 5/2$), compared to the spin of the copper(II) ion (d^9, $S = 1/2$). The higher spin of the manganese implies that more magnetic orbitals are present in the different exchange pathways, and therefore more interactions could be competing between them. As a result, the antiferromagnetic interactions can become the more significant ones and the ferromagnetic interactions found in BaCu vanish.

5. Conclusions

The $[BaMn_{1-x}M_x(C_3H_2O_4)_2(H_2O)_4]$ (M = Fe, Co, Cu) solid solutions were synthesised and studied. All the phases are isostructural and exhibit 2D arrangements of M–malonate networks.

Two-dimensional (2D) antiferromagnetic interactions have been proposed for almost all the compounds. In the case of the BaMnFe and BaMnCo systems, weak ferromagnetism below Néel temperatures (12 K) was also detected, as a consequence of a long-range magnetic ordering of the canted spins between layers. The magnitude of this ferromagnetic component can be mainly attributed to the anisotropy of the metallic cations.

Unlike the BaCu phase, which shows ferromagnetic interactions, the BaMnCu solid solution exhibits antiferromagnetic interactions. This fact can be explained as being due to the higher spin of the manganese(II) ions ($S = 5/2$), which implies more exchange pathways, the antiferromagnetic interactions becoming the main ones in this system.

Acknowledgements

This work has been carried out with the financial support of the MCYT (MAT 2001-0064) and the Universidad del País Vasco/Euskal Herriko Unibertsitatea (Project 169.310-13494/2001).

References

[1] T.K. Maji, S. Sain, G. Mostafa, T.-H. Lu, J. Ribas, M. Monfort, N.R. Chaudhuri, Inorg. Chem. 42 (2003) 709.
[2] C. Ruiz-Pérez, J. Sanchiz, M. Hernández-Molina, F. Loret, M. Julve, Inorg. Chem. 39 (2000) 1363.
[3] C. Ruiz-Pérez, J. Sanchiz, M. Hernández-Molina, F. Loret, M. Julve, Inorg. Chim. Acta 298 (2000) 202.
[4] C. Ruiz-Pérez, M. Hernández-Molina, P. Lorenzo-Luis, F. Lloret, J. Cano, M. Julve, Inorg. Chem. 39 (2000) 3845.

[5] R.P. Scaringe, W.E. Hatfield, D.J. Hodgson, Inorg. Chem. 16 (1977) 1600.
[6] D. Chattopadhyay, S.K. Chattopadhyay, P.R. Lowe, C.H. Schwalke, S.K. Mazumber, A. Rana, S. Ghosh, J. Chem. Soc., Dalton Trans. (1993) 913.
[7] S.H. Saadeh, K.L. Trojan, J.W. Kampf, W.E. Hatfield, V.L. Peroraro, Inorg. Chem. 32 (1993) 3034.
[8] Y.-G. Wei, S.-W. Zhang, M.-C. Shao, Q. Liu, Y.-Q. Tang, Polyhedron 15 (1996) 4303.
[9] I. Gil de Muro, F.A. Mautner, M. Insausti, L. Lezama, M.I. Arriortua, T. Rojo, Inorg. Chem. 37 (1998) 3243.
[10] Y. Rodriguez-Martín, C. Ruiz-Pérez, J. Sanchiz, F. Loret, M. Julve, Inorg. Chim. Acta 318 (2001) 159.
[11] I. Gil de Muro, M. Insausti, L. Lezama, T. Rojo, Eur. J. Inorg. Chem. (2003) 2948.
[12] J. Rodríguez-Carvajal, Physica B 192 (1993) 55.
[13] A.B.P. Lever, Inorganic Electronic Spectroscopy, 2nd ed., Elsevier, New York, 1986.

Available online at www.sciencedirect.com
SCIENCE DIRECT®
Polyhedron 23 (2004) 937–942
POLYHEDRON
www.elsevier.com/locate/poly

Syntheses, crystal structures and thermoanalyses of thiostannates $[Ni(en)_3]_2Sn_2S_6$ and $[Ni(dien)_2]_2Sn_2S_6$

Ding-Xian Jia [a], Jie Dai [a,b,*], Qin-Yu Zhu [a], Yong Zhang [a], Xiao-Mei Gu [a]

[a] *Department of Chemistry and Chemical Engineering, Suzhou University, Suzhou 215006, PR China*
[b] *State Key Laboratory of Coordination Chemistry, Nanjing University, Nanjing 210093 PR China*

Received 19 August 2003; accepted 26 November 2003

Abstract

Two thiostannates $[Ni(en)_3]_2Sn_2S_6$ (**1**) (en = ethylenediamine) and $[Ni(dien)_2]_2Sn_2S_6$ (**2**) (dien = diethylenetriamine) were prepared by the reaction of $SnCl_4 \cdot 5H_2O$, $NiCl_2 \cdot 6H_2O$ and S_8 in a molar ratio of Sn/Ni/S = 1:1:4 (or $SnCl_4$:$NiCl_2$:S_8 = 1:1:0.5) under solvothermal conditions. Both compounds are composed of the discrete $[Sn_2S_6]^{4-}$ anion. The coordinated cations $[Ni(en)_3]^{2+}$ and $[Ni(dien)_2]^{2+}$ act as structure directing agents which lead to different packing of the $[Sn_2S_6]^{4-}$ anions. Compounds **1** and **2** decompose at 291 and 310 °C, respectively, and both of them lose all of their organic ligands in one step under a nitrogen stream. The hydrogen bonds are considered to be one of the important reasons for their difference in decomposition temperature.
© 2003 Elsevier Ltd. All rights reserved.

Keywords: Solvothermal synthesis; Thiostannates; Nickel; Crystal structures; Thermoanalysis

1. Introduction

Open framework materials based on main group chalcogenometalates are of increasing interest because of their unique properties and potential applications, such as semiconductors [1–3], photoconductivity [4], non-linear optics [5], catalysis [6] and ion exchange capability [7]. Recently, two types of polythiostannates $[Sn_3S_7]^{2-}$ [7–11] and $[Sn_4S_9]^{2-}$ [11–14], which are denoted SnS-1 and SnS-3, respectively, have been synthesized and described. SnS-1 and SnS-3 are synthesized by a hydrothermal reaction using Sn or SnS_2 and S_8 as reactants and amine or tetra-alkylammonium hydroxide as the mineralizer. The dimeric anion $[Sn_2S_6]^{4-}$ is a precursor of SnS-1 which can be obtained from an aqueous solution of $[Sn_2S_6]^{4-}$ simply by precise control of pH through bubbling CO_2 into the mother-liquor [9,11]. The dimeric anion is the predominant tin-containing species in the synthetic systems of Sn/S/amine and a basic building block for the SnS-*n* framework [11].

In most of the thiostannates compounds, the cations, which compensate the anions charge in the structure, are either protonated amine or tetra-alkylammonium [7–13] ions or metal cations [14,15]. Thiostannates which combine with transition metal complex cations as counterions are still a less explored area [16]. The transition metal complex cations may serve as structure-directing agents in growing chalcogenometalates crystals [17]. Bensch et al. [18] very recently reported four compounds of this kind with $[Sn_2S_6]^{4-}$ anions, using elemental nickel, tin and sulphur as starting reactants. In this work, we have successfully prepared thiostannates $[Ni(en)_3]_2Sn_2S_6$ and $[Ni(dien)_2]_2Sn_2S_6$ from the Ni(II)/Sn(IV)/S/en (or dien) (en = ethylenediamine, dien = diethylenetriamine) system under mild solvothermal conditions. This combination of transition metal ions may endue thiostannates with new properties that the transition metals have. The structures of compounds $[Ni(en)_3]_2Sn_2S_6$ and $[Ni(dien)_2]_2Sn_2S_6$ are described and their thermal behaviors have been investigated.

* Corresponding author. Tel./fax: +86-512-65224783.
E-mail address: daijie@suda.edu.cn (J. Dai).

0277-5387/$ - see front matter © 2003 Elsevier Ltd. All rights reserved.
doi:10.1016/j.poly.2003.12.008

2. Experimental

2.1. Synthesis of $[Ni(en)_3]_2Sn_2S_6$ (1)

The source materials of $NiCl_2 \cdot 6H_2O$ (0.7131 g, 3 mmol), $SnCl_4 \cdot 5H_2O$ (1.052 g, 3 mmol) and S_8 (0.3848 g, 1.5 mmol) dissolved in 10 ml en and were carefully mixed, and then loaded into a Teflon-lined stainless steel autoclave whose volume was about 15 ml. Then the sealed autoclave was heated to 180 °C over 4 h and maintained at this temperature for four days. After cooling to room temperature, purple cubic crystals were isolated and washed with ethanol and ether (yield 65%, based on Sn). IR (cm^{-1}): 3221vs, 3121vs, 2920m, 2870m, 1671w, 1578m, 1451m, 1385m, 1323m, 1281m, 1273m, 1092m, 1011vs, 864m, 675s, 525m, 486m. Elemental analysis Found: C, 15.64; H, 5.38; N, 18.42%. $C_{12}H_{48}Ni_2N_{12}Sn_2S_6$ requires: C, 15.88; H, 5.33; N, 18.52%.

2.2. Synthesis of $[Ni(dien)_2]_2Sn_2S_6$ (2)

The pink prism-like crystals of $[Ni(dien)_2]_2Sn_2S_6$ were prepared by a similar method used in the synthesis of the crystals of **1** except that ethylenediamine was replaced by diethylenetriamine (yield 65%, based on Sn). IR (cm^{-1}): 3237m, 3133m, 2967w, 2863w, 1621m, 1574m, 1470s, 1385m, 1323m, 1281m, 1238m, 1181m, 1080vs, 1042m, 995m, 961vs, 860m, 783m, 675m, 633m, 598s, 532s. Elemental analysis Found: C, 20.08; H, 5.62; N, 17.46%. $C_{16}H_{52}Ni_2N_{12}Sn_2S_6$ requires: C, 20.02; H, 5.46; N, 17.51%.

2.3. Physical measurements

FT-IR spectra were recorded with a Nicolet Magna-IR 550 spectrometer in dry KBr pellets. Elemental analysis was carried out on an EA-1110 elemental analyzer. Thermogravimetric (TG) analysis was conducted on a SDT 2960 TGA-DCS microanalyzer. All the samples were heated under a nitrogen stream of 100 ml/min with a heating rate of 5 °C/min.

2.4. Single crystal structure determination

The measurement was carried out on a Rigaku Mercury CCD diffractometer using the ω-scan method with graphite monochromated Mo Kα radiation ($\lambda = 0.07107$ nm) at -80 ± 1 °C. The X-ray diffraction data of single crystals were collected to a maximum 2θ value of 55.0° for both **1** and **2**. An empirical absorption correction was applied for all compounds and the data were corrected for Lorentz and polarization effects. The structure of **1** was solved by direct methods using the program of SHELX 97 and the structure of **2** was solved by heavy-atom Patterson methods using PATTM (the DIRDIF program system). Both of the structures were expanded using Fourier techniques DIRDIF 99. The non-hydrogen atoms were refined anisotropically. Hydrogen atoms were refined using the riding model for compound **2**, while the hydrogen atoms of **1** were not dealt with due to the disorder of en. The final cycle of full-matrix least-squares refinement on F^2 was based on definite observed reflections and variable parameters, and converged with unweighted and weighted agreement factors of R_1 and wR_2. A summary of the experimental details and selected results for compounds **1** and **2** is given in Table 1.

Table 1
Crystallographic data for $[Ni(en)_3]_2Sn_2S_6$ (**1**) and $[Ni(dien)_2]_2Sn_2S_6$ (**2**)

Compound	1	2
Empirical formula	$C_{12}H_{48}Ni_2N_{12}Sn_2S_6$	$C_{16}H_{52}Ni_2N_{12}Sn_2S_6$
F_w	907.73	959.81
Crystal size (mm)	$0.50\times0.45\times0.40$	$0.30\times0.15\times0.12$
Colour, habit	purple, cubic	pink, prism
Crystal system	orthorhombic	monoclinic
Space group	*Pbca* (No. 61)	$P2_1/n$ (No. 14)
a (Å)	11.5212(8)	9.9168(10)
b (Å)	18.631(2)	14.392(1)
c (Å)	15.2368(11)	12.0589(11)
β (°)	90.00	91.906(5)
V (Å^3)	3270.5(4)	1720.1(3)
Z	4	2
T (K)	193	193
$D_{calc.}$ (g cm^{-3})	1.843	1.853
μ (cm^{-1})	30.52	29.07
2θ(max) (°)	55.0	55.0
Reflections collected	31,956	17,214
Unique reflections	3499	3922
R_{int}	0.044	0.029
Observations	3134 ($I > 3\sigma(I)$)	3588 ($I > 2\sigma(I)$)
Variables	208	202
R_1	0.036 ($I > 3\sigma(I)$)	0.022 ($I > 2\sigma(I)$)
wR_2 (for all reflections)	0.129	0.047
Goodness of fit indicator	1.058	0.99

3. Results and discussion

3.1. Synthesis of the compounds

Single crystals of $[Ni(en)_3]_2Sn_2S_6$ (**1**) and $[Ni(dien)_2]_2Sn_2S_6$ (**2**) are obtained by using the reaction of $SnCl_4 \cdot 5H_2O$, $NiCl_2 \cdot 6H_2O$ and S_8 in the same molar ratio of Sn/Ni/S = 1:1:4 ($SnCl_4$:$NiCl_2$:S_8 = 1:1:0.5) under mild solvothermal conditions in en and dien solvent, respectively. Stannic chloride was used as the source material instead of Sn powder which is usually used in synthesis of thiostannates under hydrothermal or solvothermal conditions [9,10,18]. The Ozin group had studied the Sn/S/amine (water solution) system in detail and isolated dimeric $[Sn_2S_6]^{4-}$ and $[S_2O_3]^2$ reaction in-

termediates from the solution [11]. The redox disproportionation reaction of S_8 is believed to be one of the sources of the S^{2-} ion (as Eq. (1) [19]) which is used to form the $[Sn_2S_6]^{4-}$ anion.

$$1/2S_8 + 9H_2O \rightarrow 2S^{2-} + S_2O_3^{2-} + 6H_3O^+ \quad (1)$$

In the case of the Sn^{4+}/S/en (dien) system in this work, the S^{2-} ions which are necessary to form $[Sn_2S_6]^{4-}$ might also come from disproportionation of S_8 as Eq. (1), since the metal salts used are hydrated and the solvents are also not absolutely anhydrous. On the other hand, the ethylenediamine in this system might not only act as a solvent, but also offer a source of S^{2-} (or S_m^{2-}) by reacting with elemental sulphur:

$$S + en \rightarrow S^2(\text{or } S_m^{2-}) + (Hen)^+ + \text{oxidized product of amine} \quad (2)$$

Reaction (2) is complicated and has not been studied in detail. When the sulphur reacts with en, a dark brown color is developed immediately and the species of S^{2-}, S_m^{2-} and $(Hen)^+$ have been confirmed by the products, such as $(enH)_4[Sn_2S_6]$, $(enH)_4[Sn_2Se_6]\cdot en$, $(enH)_4[Sn_2Te_6]\cdot en$ [20] and $[Mn(en)_3]Te_4$ [21]. However, the mechanism of the synthetic reaction needs to be further confirmed.

It is noteworthy that transition metal cations $[Ni(en)_3]^{2+}$ and $[Ni(dien)_2]^{2+}$ are likely better mineralizers than the protonated amines such as enH^+ and $dienH^+$, because the products from the Ni^{2+}/Sn^{4+}/S/en (dien) system are $[Ni(en)_3]_2Sn_2S_6$ and $[Ni(dien)_2]_2Sn_2S_6$ rather than $(enH)_4Sn_2S_6$ and $(dienH)_4Sn_2S_6$. If the nickel salts were not introduced into these systems under the same experimental conditions, crystallization of $(enH)_4[Sn_2S_6]$ is very difficult and the crystals were only obtained after the reaction solution had been left for about one month at room temperature.

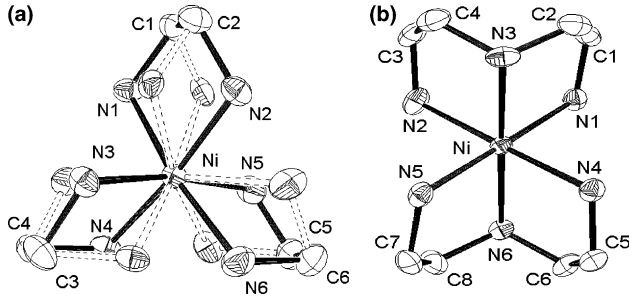

Fig. 1. The structures of the transition metal complex cations in **1** (a) and **2** (b) with the labelling scheme and ellipsoids at 50% probability. Hydrogen atoms have been omitted for clarity.

3.2. Description of the structures

The crystal structures of compounds **1** and **2** were determined by the single-crystal X-ray diffraction method. The results show that compound **1** crystallizes in the orthorhombic space group of *Pbca* (No. 61) and compound **2** in the monoclinic space group of $P2_1/n$ (No. 14). Both compounds consist of discrete $[Sn_2S_6]^{4-}$ anions with $[Ni(en)_3]^{2+}$ or $[Ni(dien)_2]^{2+}$ cations as counterions.

The structure of compound **1** is essentially the same as that of $[Ni(en)_3]_2Sn_2S_6$ which was very recently synthesized by the Bensch group, but they use elemental nickel, tin and sulphur as starting reactants [18]. The Ni^{2+} ion is coordinated by six N atoms of three bidentate ethylenediamine ligands with Ni–N distances ranging from 2.097(4) to 2.146(5) Å. The conformation of $[Ni(en)_3]^{2+}$ cation is difficult to fix due to the disorder of the ethylenediamine ligands. The configurations of the ligands are disordered with Λ ($\delta\delta\delta$):Δ ($\lambda\lambda\lambda$) [or Δ ($\lambda\lambda\lambda$) :Λ ($\delta\delta\delta$) in inversion position] occupation ratios of 0.76:0.24 (Fig. 1(a)). In compound **2**, the Ni^{2+} ion is coordinated by six N atoms of two trichelating dieth-

Table 2
Selected bond distances (Å) and angles (°) for $[Ni(en)_3]_2Sn_2S_6$ (**1**) and $[Ni(dien)_2]_2Sn_2S_6$ (**2**)

	1	**2**		**1**	**2**
Bond distances					
Ni–N1	2.108(4)	2.118(2)	Ni–N4	2.097(4)	2.133(2)
Ni–N2	2.133(4)	2.143(2)	Ni–N5	2.116(4)	2.113(2)
Ni–N3	2.137(4)	2.090(2)	Ni–N6	2.146(5)	2.102(2)
Sn–S1	2.338(1)	2.354(1)	Sn–S3	2.453(1)	2.461(1)
Sn–S2	2.347(1)	2.334(1)	Sn–S3′	2.457(1)	2.453(1)
Bond angles					
(1) N–Ni–N$^{trans.}$	172.3(2)	179.47(7)	(2) N–Ni–N$^{trans.}$	172.3(2)	177.52(8)
(3) N–Ni–N$^{trans.}$	169.7(2)	177.56(7)			
S1–Sn–S2	111.52(4)	114.48(2)	S2–Sn–S3′	113.18(3)	112.07(2)
S1–Sn–S3	114.58(4)	113.24(2)	S3–Sn–S3′	91.61(4)	93.013(19)
S2–Sn–S3	112.40(3)	111.53(2)	Sn–S3–Sn′	88.39(4)	86.987(19)
S1–Sn–S3′	112.20(3)	110.59(2)			

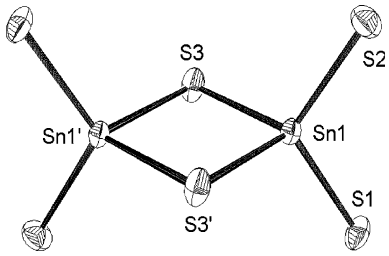

Fig. 2. The structure of the $[Sn_2S_6]^{4-}$ anion with the labelling scheme and ellipsoids at 50% probability.

ylenetriamine ligands. The conformation of octahedral $[Ni(dien)_2]^{2+}$ is s-facial (Fig. 1(b)).

In compounds **1** and **2**, The Ni–N bond lengths are within the range for compounds containing $[Ni(en)_3]^{2+}$ and $[Ni(dien)_2]^{2+}$ cations [22,23]. The $[Ni(en)_3]^{2+}$ and $[Ni(dien)_2]^{2+}$ octahedral coordination spheres are distorted, which can be seen from the N–Ni–N_{trans} angles varying from 169.7(2)° to 172.3(2)° and 177.52(8)° to 179.47(7)°, respectively. The three octahedral axial N–Ni–N_{trans} angles of the coordination octahedra are listed in Table 2.

The $[Sn_2S_6]^{4-}$ anion, which is formed by the connection of two SnS_4 tetrahedra sharing a common edge, can be described as a planar Sn_2S_2 four-membered ring with each Sn atom having two terminal Sn–S bonds (Fig. 2). The terminal Sn–S_t bond lengths, being between 2.334(1) and 2.354(1) Å, are shorter than those of the bridging Sn–S_b bonds which vary from 2.461(1) to 2.453(1) Å. Both kinds of bond lengths are in good agreement with corresponding bond lengths in other compounds containing $[Sn_2S_6]^{4-}$ anions [20,24]. The two SnS_4 tetrahedra in the $[Sn_2S_6]^{4-}$dimer are slightly distorted, which is demonstrated by the S_t–Sn–S_t and S_t–Sn–S_b angles deviating from the ideal value of 109.5° (Table 2).

The packing of $[Sn_2S_6]^{4-}$ anions in compounds **1** and **2** is different (shown in Fig. 3). There are eight $[Sn_2S_6]^{4-}$ anions at corners and six at crystal faces per unit cell of **1**, while there are four $[Sn_2S_6]^{4-}$ anions at crystal edges and two at crystal faces of [0 0 1] per unit cell of **2**. One $[Sn_2S_6]^{4-}$ anion is surrounded by four $[Ni(en)_3]^{2+}$ cations in **1**, and by six $[Ni(dien)_2]^{2+}$ cations in **2**.

Between the anion and cation in compound **2**, a lot of short intermolecular N–H···S interactions, which indicate weak hydrogen bonding, are found and one Sn_2S_6 unit is hydrogen bonded to six different cations (Fig. 4(b)). The terminal S(1) and S(2) atoms form hydrogen bonds to H–N groups of $[Ni(dien)_2]^{2+}$ cations with H···S distances ranging from 2.508(3) to 2.888(2) Å and N–H···S angles ranging from 145.0(2)° to

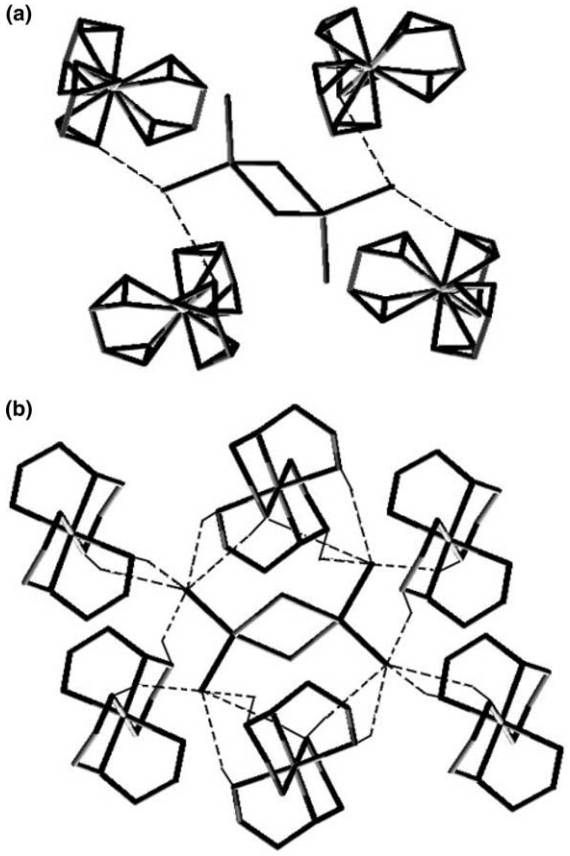

Fig. 4. The views of the $[Sn_2S_6]^{4-}$ anion hydrogen bonding interaction with cations in **1** (a) and **2** (b). Hydrogen atoms have been omitted for clarity.

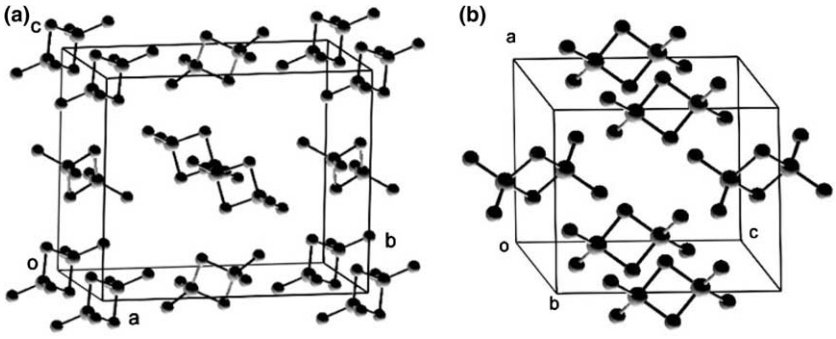

Fig. 3. The packing of the $[Sn_2S_6]^{4-}$ anions in **1** (a) and **2** (b), the cations have been omitted for clarity.

Table 3
Selected H···S distances (Å) and N–H···S angles (°) in $[Ni(dien)_2]_2Sn_2S_6$

N–H	S	N–H	H···S	N···S	N–H···S
N(1)–H(1)	S(1)	0.761(3)	2.812(2)	3.484(2)	148.5(2)
N(2)–H(4)	S(1)	0.875(4)	2.888(2)	3.639	145.0(2)
N(4)–H(15)	S(1)	0.897(3)	2.571(2)	3.453(2)	168.2(2)
N(5)–H(17)	S(1)	0.885(3)	2.583(2)	3.461(2)	171.7(2)
N(6)–H(18)	S(1)	0.900(3)	2.527(2)	3.394(2)	161.6(2)
N(1)–H(2)	S(2)	0.915(3)	2.582(2)	3.419(2)	152.2(2)
N(3)–H(5)	S(2)	0.924(3)	2.705(2)	3.561(2)	154.5(2)
N(4)–H(14)	S(2)	0.942(3)	2.508(2)	3.407(2)	159.7(2)
N(5)–H(16)	S(2)	0.906(3)	2.846(2)	3.676	153.0(2)

171.7(2)° (Table 3). In compound **1**, the number of interion interactions is less than that in **2** (Fig. 4(a)) and this difference might be the reason of disorder of the ethylenediamine in **1**. The results show that $[Ni(en)_3]^{2+}$ and $[Ni(dien)_2]^{2+}$ cations have different structure-directing effects, although both of them are actually synthesized under the same conditions except for the amine.

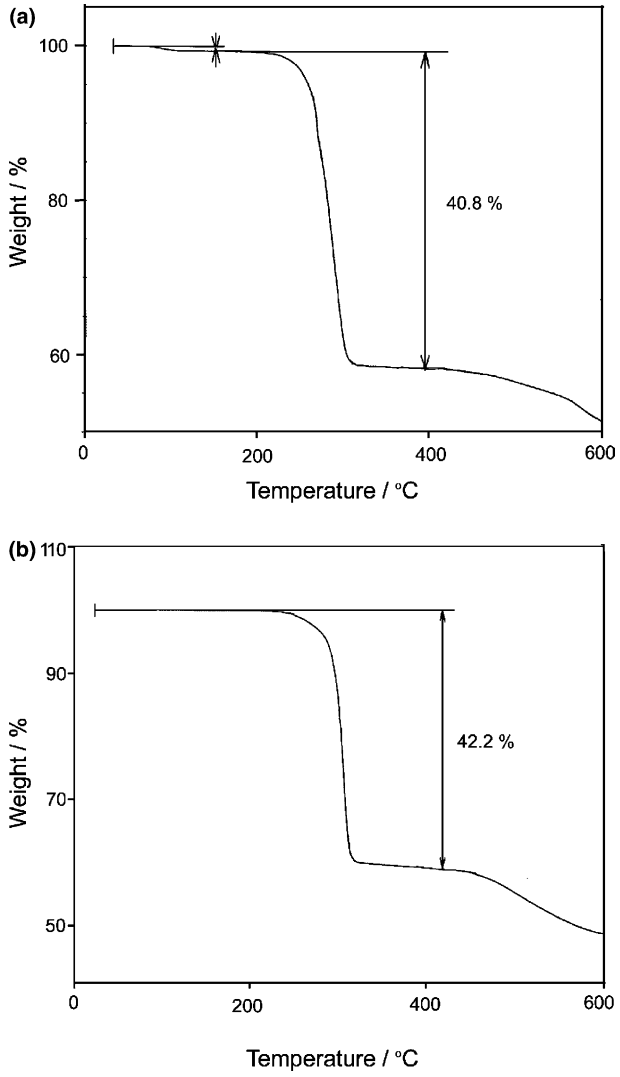

Fig. 5. Thermogravimetric analyses curves of compounds **1** (a) and **2** (b).

3.3. Thermal analysis

The thermal behavior of the title compounds were measured between temperatures of 20 and 600 °C with the DSC-TGA method under nitrogen. The results are shown in Fig. 5. The first step mass loss of **1** (about 0.56% below 100 °C) is attributed to desorption of water (Fig. 5(a)). Compound **1** is decomposed at 291 °C accompanied by one endothermic peak in the DSC curve (peak temperature, T_p). The corresponding loss of 40.8% is in accordance with the complete mass loss of six en ligands (Calc. 39.7% for 6 en).

The decomposition of **2** is at 310 °C (T_p of DSC) and the corresponding loss of 42.2% is in good agreement with the complete mass loss of the four dien ligands (Calc. 43.0% for 4 dien). From the behaviors of thermal decomposition, it is obvious that compounds **1** and **2** remove all of their organic amine ligands in one step under nitrogen. The decomposition temperature of **2** is higher than that of **1** by about 20 °C. This result can be explained reasonably by the structure analysis that shows compound **2** has more N–H···S hydrogen bonds than compound **1**, which makes the organic ligands in **2** more difficult to remove.

4. Conclusions

Single crystals of $[Ni(en)_3]_2Sn_2S_6$ and $[Ni(dien)_2]_2$-Sn_2S_6 can be obtained by reaction of $SnCl_4 \cdot 5H_2O$, $NiCl_2 \cdot 6H_2O$ and S_8 under mild solvothermal conditions. The results presented in this paper demonstrate that the transition metal complex cations can act as a mineralizer in the synthesis of $[Sn_2S_6]^{4-}$ thiostannates from the Ni(II)/Sn(IV)/S/en (dien) system using solvothermal techniques. The $[Ni(en)_3]^{2+}$ and $[Ni(dien)_2]^{2+}$ cations are likely a better mineralizer than protonated amines, such as enH^+ and $dienH^+$.

The different structure directing effect of $[Ni(en)_3]^{2+}$ and $[Ni(dien)_2]^{2+}$ cations is one of the reasons that $[Sn_2S_6]^{4-}$ anions arrange in a different way in the crystal structures of compounds **1** and **2**. Both title compounds lose all of their amine ligands in one step under nitrogen. The decomposition temperature of **2** is higher than that of **1** by about 20 °C, accounting for the N–H···S hydrogen bonding.

5. Supplementary data

Crystallographic data for the structural analyses have been deposited with the Cambridge Crystallographic Data Centre, CCDC nos. 217522 and 217523 for com-

pounds **1** and **2**, respectively. These data can be obtained free of charge via www.ccdc.cam.ac.uk/conts/retrieving.html or from the Cambridge Crystallographic Data Centre, 12 Union Road, Cambridge CB2 1EZ, UK; fax: (+44) 1223-336-033, or e-mail: deposit@ccdc.cam.ac.uk.

Acknowledgements

This work was supported by the National Natural Science Foundation (20071024, 20371033), P.R. China. The authors are also grateful to the Key Laboratory of Organic Synthesis of Jiangsu Province, Suzhou University, for financial support.

References

[1] C.L. Bowes, G.A. Ozin, Adv. Mater. 8 (1996) 13.
[2] J. Llanos, C. Mujica, V. Sánchez, O. Peña, J. Solid State Chem. 173 (2003) 78.
[3] C.R. Evenson IV, P.K. Dorhout, Z. Anorg. Allg. Chem. 627 (2001) 2178.
[4] U. Simon, F. Schüth, S. Schunk, X. Wang, F. Liebau, Angew. Chem. Int. Ed. Engl. 36 (1977) 1121.
[5] R.L. Glitzendanner, F.L. Di Salvo, Inorg. Chem. 35 (1996) 2623.
[6] R.R. Chianelli, T.A. Pecoraro, T.R. Halber, W.-H. Pan, E.I. Stiefel, J. Catal. 86 (1984) 226.
[7] J.B. Parise, Y. Ko, J. Rijssenbeek, D.M. Nellis, K. Tan, S. Koch, J. Chem. Soc. Chem. Commun. (1994) 527.
[8] J. Li, H. Kessler, Micropor. Mesopor. Mater. 27 (1999) 57.
[9] T. Jiang, A. Lough, G.A. Ozin, Adv. Mater. 10 (1998) 42.
[10] H. Ahari, Ö. Dag, S. Petrov, G.A. Ozin, J. Phys. Chem. B 102 (1998) 2356.
[11] T. Jiang, A. Lough, G.A. Ozin, R.L. Bedard, J. Mater. Chem. 8 (1998) 733.
[12] T. Jiang, A. Lough, G.A. Ozin, R.L. Bedard, R. Broach, J. Mater. Chem. 8 (1998) 721.
[13] Y. Ko, K. Tan, D.M. Nellis, S. Koch, J.B. Parise, J. Solid State Chem. 114 (1995) 506.
[14] G.A. Marking, M. Evain, V. Petricek, M.G. Kanatzidis, J. Solid State Chem. 141 (1998) 17.
[15] J. Liao, C. Varotsis, M.G. Kanatzidis, Inorg. Chem. 32 (1993) 2453.
[16] J. Li, Z. Chen, R.J. Wang, D.M. Proserpio, Coord. Chem. Rev. 190–192 (1999) 707.
[17] R. Stähler, W. Bensch, Eur. J. Inorg. Chem. 12 (2001) 3073.
[18] M. Behrens, S. Scherb, C. Näther, W. Bensch, Z. Anorg. Allg. Chem. 629 (2003) 1367.
[19] W.F. Gigenbach, Inorg. Chem. 13 (1974) 1724.
[20] S. Dehnen, C. Zimmermann, Z. Anorg. Allg. Chem. 628 (2002) 2463.
[21] Z. Chen, R.-J. Wang, X.-Y. Huang, J. Li, Acta Crystallogr. Section C 56 (2000) 1100.
[22] M. Ohba, N. Maruono, H. kawa, T. Enoki, J.-M. Latour, J. Am. Chem. Soc. 116 (1994) 11566.
[23] W. Bensch, C. Näther, R. Stähler, Chem. Commun. (2001) 477.
[24] J. Li, B. Marler, H. Kessler, M. Soulard, S. Kallus, Inorg. Chem. 36 (1997) 4697.

Available online at www.sciencedirect.com
SCIENCE DIRECT®
Polyhedron 23 (2004) 943–948
POLYHEDRON
www.elsevier.com/locate/poly

Two novel heterometallacrowns: syntheses and crystal structures of two copper(II) complexes with malonate and *o*-pthalate

Hong-Lei Liu, Hong-Yan Mao, Hong-Yun Zhang *, Chen Xu, Qing-An Wu, Gang Li, Yu Zhu, Hong-Wei Hou

Department of Chemistry, Zhengzhou University, Henan 450052, PR China

Received 9 August 2003; accepted 27 November 2003

Abstract

Two copper(II) sodium(I) coordination compounds of formula $[C_{16}H_{12}CuNa_2O_{10}]$ (**1**) and $[C_6H_8CuNa_2O_{10}]$ (**2**) were prepared and their structures were characterized by single-crystal X-ray diffraction, IR spectra and thermal analyses. In complex **1**, the sodium atom is six coordinated with four carboxylate oxygens from two *o*-pthalate ligands, another one oxygen atom from one *o*-pthalate and one water molecule building a distorted octahedron. All the four oxygen atoms in one *o*-pthalate participate in coordination, two of which bridge one sodium and one copper atoms, with another one bridging two sodium atoms and the fourth coordinating one sodium atom. As for complex **2**, the sodium atom is also six-coordinated with tetrakis-monodentate malonate oxygen atoms and two water molecules building a distorted octahedron. For every malonate, three oxygens coordinate out of the total four. Every carboxylate offers an oxygen atom bridging one sodium and one copper atom with the remaining one bridging two sodium atoms. In both cases, each copper atom is in a square planar environment formed by four carboxylate-oxygens from four *o*-pthalates and two malonates respectively. The IR spectra also testify the structure detection. Thermal analyses of the two complexes were also carried out.
© 2004 Elsevier Ltd. All rights reserved.

Keywords: Herometallacrown; Malonate; *o*-Pthalate; Cu(II) complexes

1. Introduction

Malonate as a bridging ligand has versatile modes in Cu(II) complexes [1–7]. The variety of the coordination modes of the malonate ligand (bidentate through two carboxylate-oxygens and different carboxylate-bridging modes) accounts for the structural complexity of the malonate complexes [8]. The *o*-pthalate ligand can also act as a bidentate or bis-(bidentate) ligand. The coordination ability and versatility of malonate and *o*-pthalate as ligands induced us to investigate the coordination of the mixed-ligand species with the copper(II) ion. Two copper(II) sodium(I) complexes $[C_{16}H_{12}CuNa_2O_{10}]$ (**1**) and $[C_6H_8CuNa_2O_{10}]$ (**2**) have been prepared by the reaction of *o*-pthalic acid anhydride, sodium hydroxide and sodium malonate with $CuCl_2$. Complex **1** belongs to the monoclinic system, $P2_1/c$ space group. Its crystallographic data are: $a = 11.086(2)$ Å, $b = 6.6480(13)$ Å, $c = 12.195(2)$ Å, $\alpha = 90°$, $\beta = 101.88(3)°$, $\gamma = 90°$. The crystal structure data indicates that the Cu(II) ion is coordinated through four oxygen atoms from four *o*-pthalate ligands. The Cu(II) ion has four coordination in the center of a square plane. The Na(I) ion is coordinated with five carboxylate oxygen atoms and one water molecule in a more complicated mode. The crystal is stabilized by π–π stacking interactions between neighboring planes. As for complex **2**, it belongs to the orthorhombic system, *Pbca* space group. The crystallographic data are: $a = 6.8403(14)$ Å, $b = 9.5226(19)$ Å, $c = 16.402(3)$ Å, $\alpha = 90°$, $\beta = 90°$, $\gamma = 90°$. The crystal structure data shows that the Cu(II) ion is coordinated through four oxygen atoms from two bidentate malonates. Cu(II) ion is four coordinate in the center of a square plane. The

* Corresponding author. Tel.: +86-371-776-3675; fax: +86-371-776-1744.
E-mail address: wzhy917@zzu.edu.cn (H.-Y. Zhang).

0277-5387/$ - see front matter © 2004 Elsevier Ltd. All rights reserved.
doi:10.1016/j.poly.2003.11.059

Na(I) ion is six coordinated with four malonate oxygen atoms and two water molecules in a more complicated mode. These two complexes both qualify as metallacrowns, metal complexes with a structure analogy to crown ethers [9].

2. Experimental

2.1. Materials and physical measurements

The chemicals for the syntheses of the compounds were all of analytical pure grade, purchased from Zhengzhou Chemical Reagent Company and used without further purification. IR spectra were recorded on a Nicolt IR-470 spectrophometer as KBr pellets in the range 4000–400 cm^{-1}. A single crystal was measured on a Rigaku-Raxis-IV X-ray diffractometer and thermal analyses were done with a MKV thermal analyzer in air atmosphere from room temperature to 400 °C.

2.2. Syntheses of complexes *1* and *2*

An aqueous solution containing *o*-pthalic acid anhydride (0.06 g, 0.4 mmol) and sodium malonate (0.06 g, 0.4 mmol) was neutralized to pH 7 with 0.5 M NaOH solution. 2 ml 0.5 M aqueous solution of $CuCl_2$ was added to the above-mentioned solution. Then the resulting mixture was run into a small vial and allowed to evaporate naturally at room temperature. Filtered, washed with anhydrous ethanol and dried naturally, two different color crystals suitable for single-crystal X-ray diffraction analysis were obtained after about three months. One is complex **1**, deep blue; the other is complex **2**, pale blue.

2.3. X-ray crystallography

Intensity data of complexes **1** and **2** were measured with a Rigaku-Raxis-IV X-ray diffractometer using monochromated Mo Kα ($\lambda = 0.71073$ Å) radiation at 291 K. 2859 reflections were measured over the ranges $1.88 \leqslant$

Table 1
Crystallographic data and structure refinement for complexes **1** and **2**

	Complex **1**	Complex **2**
Formula	$C_{16}H_{12}CuNa_2O_{10}$	$C_6H_8CuNa_2O_{10}$
M	473.78	349.64
Crystal system	monoclinic	orthorhombic
Space group	$P2_1/c$	*Pbca*
a (Å)	11.086(2)	6.8403(14)
b (Å)	6.6480(13)	9.5226(19)
c (Å)	12.195(2)	16.402(3)
α (°)	90	90
β (°)	101.88(3)	90
γ (°)	90	90
V (Å^3)	879.5(3)	1068.4(4)
D_c (Mg m^{-3})	1.789	2.161
Z	2	4
μ (mm^{-1})	1.348	2.175
Reflections collected/unique	2859/1687 [$R_{int} = 0.0209$]	3484/1129 [$R_{int} = 0.0588$]
Data/restraints/parameters	1687/0/142	1129/0/97
R[a]	0.0321	0.0412
R_w[b]	0.0771	0.1147
Goodness-of-fit on F^2	1.118	1.132
$\Delta\rho_{min}$ and $\Delta\rho_{max}$ (e Å^{-3})	−0.496 and 0.355	−1.014 and 0.721

[a] $R = \sum ||F_o| - |F_c|| / \sum |F_o|$.
[b] $R_w = \left[\sum (||F_o| - |F_c||)^2 / \sum w|F_o|^2\right]^{1/2}$.

Table 2
Selected bond distances (Å) and angles (°) for complex **1**

Bond distances			
Cu(1)–O(1)	1.9445(18)	Na(1)–O(5)#1	2.296(2)
Cu(1)–O(1)#1	1.9445(17)	Na(1)–O(1)	2.3660(19)
Cu(1)–O4)#2	1.9725(16)	Na(1)–O(2)#4	2.425(2)
Cu(1)–O(4)#3	1.9725(16)	Na(1)–O(3)#4	2.448(2)
Cu(1)–Na(1)	3.3828(11)	Na(1)–O(2)#3	2.523(2)
Cu(1)–Na(1)#1	3.3828(11)	Na(1)–O(4)#3	2.770(2)
Bond angles			
Na(1)–Cu(1)–Na(1)#1	180.0	O(5)–Na(1)–O(2)#2	151.79(9)
O(5)–Na(1)–O(1)	80.31(8)	O(1)–Na(1)–O(2)#2	86.80(7)
O(5)–Na(1)–O(2)#4	82.05(8)	O(2)#4–Na(1)–O(2)#2	106.38(6)
O(1)–Na(1)–O (2)#4	161.38(7)	O(3)#4–Na(1)–O(2)#2	80.85(7)
O(5)–Na(1)–O(3)#4	127.33(9)	O(5)–Na(1)–O(4)#2	84.37(8)
O(1)–Na(1)–O(3)#4	114.08(7)	O(1)–Na(1)–O(4)#2	65.28(6)
O(2)#4–Na(1)–O(3)#4	81.59(6)	O(2)#4–Na(1)–O(4)#2	107.10(6)
O(3)#4–Na(1)–O(4)#2	148.28(7)	C(1)–O(1)–Cu(1)	119.61(14)
O(2)#2–Na(1)–O(4)#2	67.44(6)	O(1)–C(1)–C(1)	115.4(2)
O(5)–Na(1)–Cu(1)	67.87(7)	Cu(1)–O(1)–Na(1)	102.97(7)

Symmetry transformations used to generate equivalent atoms: #1 $-x, -y-2, -z$; #2 $x, -y-5/2, z+1/2$; #3 $-x, y+1/2, -z-1/2$; #4 $x, y+1, z$; #5 $-x, y-1/2, -z-1/2$; #6 $x, y-1, z$.

$2\theta \leqslant 27.53$, $0 \leqslant h \leqslant 14$, $-8 \leqslant k \leqslant 8$, $-15 \leqslant l \leqslant 15$ yielding 1687 unique reflections for complex **1**. For the case of the second complex, 3484 reflections were measured over the ranges $2.48 \leqslant 2\theta \leqslant 27.49$, $-8 \leqslant h \leqslant 8$, $0 \leqslant k \leqslant 12$, $-19 \leqslant l \leqslant 19$, and yielded 1129 unique reflections. Raw data were corrected and the structures were solved using the SHELX-97 program. Non-hydrogen atoms were located by direct phase determination and subjected to anisotropic refinement. The full-matrix least-squares calculation on F^2 were applied on the final refinement. The refinement converged at $R_1 = 0.0321$ and $wR_2 = 0.0771$ values for reflections with $I > 2\sigma$ for complex **1**, and $R_1 = 0.0412$ and $wR_2 = 0.1147$ values for reflections with $I > 2\sigma$ for complex **2**. Details of the crystal structure determinations are summarized in Tables 1 and 2 of this paper. Full atomic data are available as a file in CIF format.

3. Results and discussion

3.1. IR spectra

In the IR spectrum of either complex **1** or **2**, a strong and broad band in the 3500–3300 cm^{-1} region (O–H stretching vibration) indicates the presence of coordinated water molecules. In the IR spectrum of complex **1**, the presence of malonate accounts for the weak intensity peaks at 2936 cm^{-1} for νC–H, strong peaks at 1606 and 1577 cm^{-1} for ν_{as}COO and medium intensity peaks at

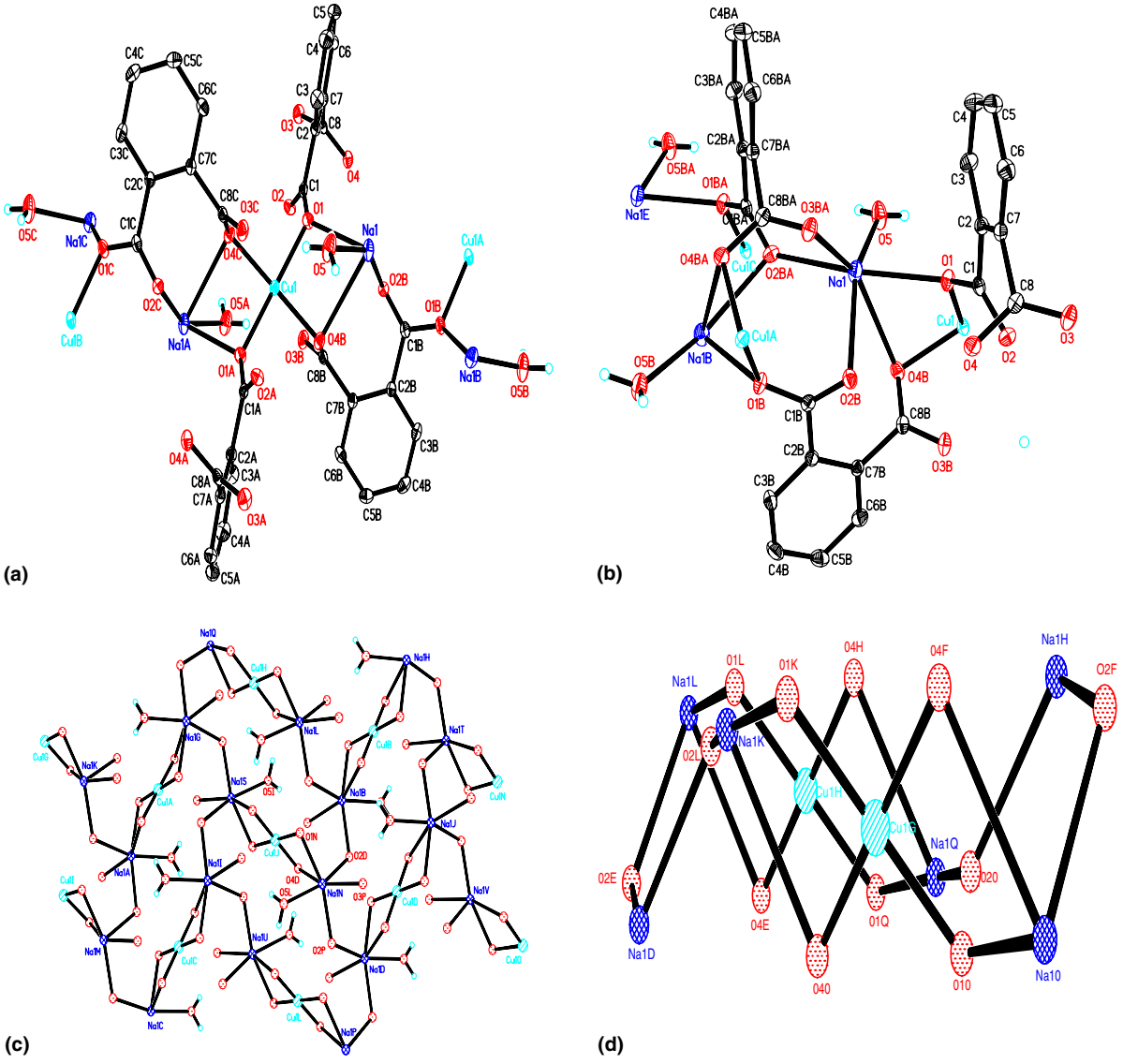

Fig. 1. Perspective drawings of (a) the copper (II) and (b) sodium (I) environments in complex **1** along with the atom numbering. Thermal ellipsoids are drawn at the 50% probability level, (c) two dimensional network of **1**, (d) core of complex **1** as a metallacrown.

1407 and 1366 cm^{-1} for v_sCOO. In the IR spectrum of complex **2**, the medium intensity peaks at 1638, 1572 and 1487 cm^{-1} are consistent with the existence of a benzene cycle. The other strong peaks at 1611 and 1592 cm^{-1}, 1407 and 1366 cm^{-1} can be attributed to v_{as}COO, v_sCOO, respectively.

3.2. Crystal structure of complex *1*

Crystal data and structure determination summaries for complexes **1** and **2** are shown in Table 1. Four oxygen atoms from four *o*-pthalate groups coordinate to the central copper atom and build a near square around it, which is shown in the angle data: O1–Cu1–O1A = 180.0°, O1–Cu1–O4B = 89.12(7)° and O4B–Cu1–O4C = 180°. The values of the copper–oxygen bond lengths are somewhat different [1.9445 Å for Cu1–O1 and Cu1–O1A, 1.9725 Å for Cu1–O4B and Cu1–O4C] (Fig. 1(a)).

Four oxygen atoms from two bidentate *o*-pthalates, another one oxygen atom from a monodentate *o*-pathalate and one water molecule participate in coordinating to the central sodium atom and make a distorted octahedron. O5, O3BA, O2B and O4B build the equatorial plane with O1and O2BA occupying the axial positions (Fig. 1(b)). The selected bond lengths and angles are shown in Table 3.

For each carboxylate there is one oxygen atom bridging a sodium and a copper atom. One of the remaining oxygen atoms in a certain *o*-pthalate group bridges two sodium atoms and the other one coordinate a sodium atom.

The sodium atoms build zigzag chains owing to the coordination of *o*-pthalate groups. These chains are linked through 4-coordinated copper atoms and form macrocycles, which constitute further parallel planes. The distance between neighboring planes is about 10.9 Å. The ring normal and the vector between the ring centroids form an angle of about 47°, with a centroid – centroid distance of 4.639 Å, which indicates that this dimensional structure is stabilized by interplanar π–π stacking between the benzene rings in neighboring planes [10]. The intraplanar structure can be seen in Fig. 1(c).

3.3. Crystal structure description of complex *2*

The copper atoms are 4-coordinated CuO_4. Four oxygen atoms from two bidentate malonate ligands describe a parallelogram environment around the copper atom, as is shown in these angles: O3C–Cu1–O3 = 180.0°, O3C–Cu1–O1C = 93.45(9)°, O1C–Cu1–O1 = 180.00(10)°. And the copper–oxygen bond lengths are 1.9494 Å for Cu1–O3C and Cu1–O3, 1.960(2) Å for Cu1–O1C and Cu1–O1 (Fig. 2(a)).

The sodium atoms are 6-coordinated NaO_6. Four oxygen atoms from four different malonate ligands and two water molecules form a distorted octahedron. Three oxygen atoms from malonate ligands and one water molecule occupy the equatorial sites. The 4th malonate oxygen atom and the other water molecule hold the axial positions. The sodium-water oxygen bond lengths [Na1A–O5A = 2.366(3) Å and Na1A–O5E = 2.387(3) Å] are longer than those of sodium-malonate oxygen bonds [Na1A–O1 = 2.456(2) Å, Na1A–O4A = 2.462(3) Å, Na1A–O4FC = 2.580(3) Å and Na1A–O3C = 2.584(3) Å]. Three oxygen atoms O1, O3C, O4C from malonate and one water molecule oxygen O5E occupy the equatorial sites with large deviations from the ideal value of 90° being observed

Table 3
Selected bond distances (Å) and angles (°) for complex **2**

Bond distances			
Cu(1)–O(1)	1.960(2)	Na(1)#1–O(1)	2.456(2)
Cu(1)–O(1)#3	1.960(2)	Na(1)#1–O(3)#3	2.584(3)
Cu(1)–O(3)	1.9494(19)	Na(1)#1–O(4)#1	2.462(3)
Cu(1)–O(3)#3	1.9494(19)	Na(1)#1–O(4)#6	2.580(3)
Cu(1)–Na(1)#1	3.5364(15)	Na(1)#1–O(5)#1	2.366(3)
Cu(1)–Na(1)#2	3.5364(15)	Na(1)#1–O(5)#5	2.387(3)
Bond angles			
O(3)#3–Cu(1)–O(3)	180.0	O(5)#5–Na(1)#1–O(1)	141.84(11)
O(3)#3–Cu(1)–O(1)#3	93.45(9)	O(5)#1–Na(1)#1–O(4)#1	177.48(11)
O(3)–Cu(1)–O(1)	93.45(9)	O(5)#5–Na(1)#1–O(4)#1	79.32(9)
O(1)#3–Cu(1)–O(1)	180.00(10)	O(1)–Na(1)#1–O(4)#1	89.90(9)
Na(1)#1–Cu(1)–Na(1)#2	180.00(4)	O(5)#1–Na(1)#1–O(4)#6	77.35(9)
O(5)#1–Na(1)#1–O(5)#5	101.95(10)	O(5)#5–Na(1)#1–O(4)#6	98.60(9)
O(5)#1–Na(1)#1–O(1)	90.38(10)	O(1)–Na(1)#1–O(4)#6	119.41(9)
O(4)#1–Na(1)#1–O(4)#6	100.34(9)	O(1)–Na(1)#1–O(3)#3	64.18(8)
O(5)#1–Na(1)#1–O(3)#3	84.18(9)	O(4)#1–Na(1)#1–O(3)#3	98.20(9)
O(5)#5–Na(1)#1–O(3)#3	81.13(9)	O(4)#6–Na(1)#1–O(3)#3	161.08(9)

Symmetry transformations used to generate equivalent atoms: #1 $-x+2,-y-1,-z$; #2 $x-1/2,-y-1/2,-z$; #3 $-x+5/2,y-1/2,z$; #4 $x-1/2,y,-z+1/2$; #5 $x+1/2,-y-1/2,-z$; #6 $x+1/2,y,-z+1/2$; #7 $-x+5,y+1/2,z$.

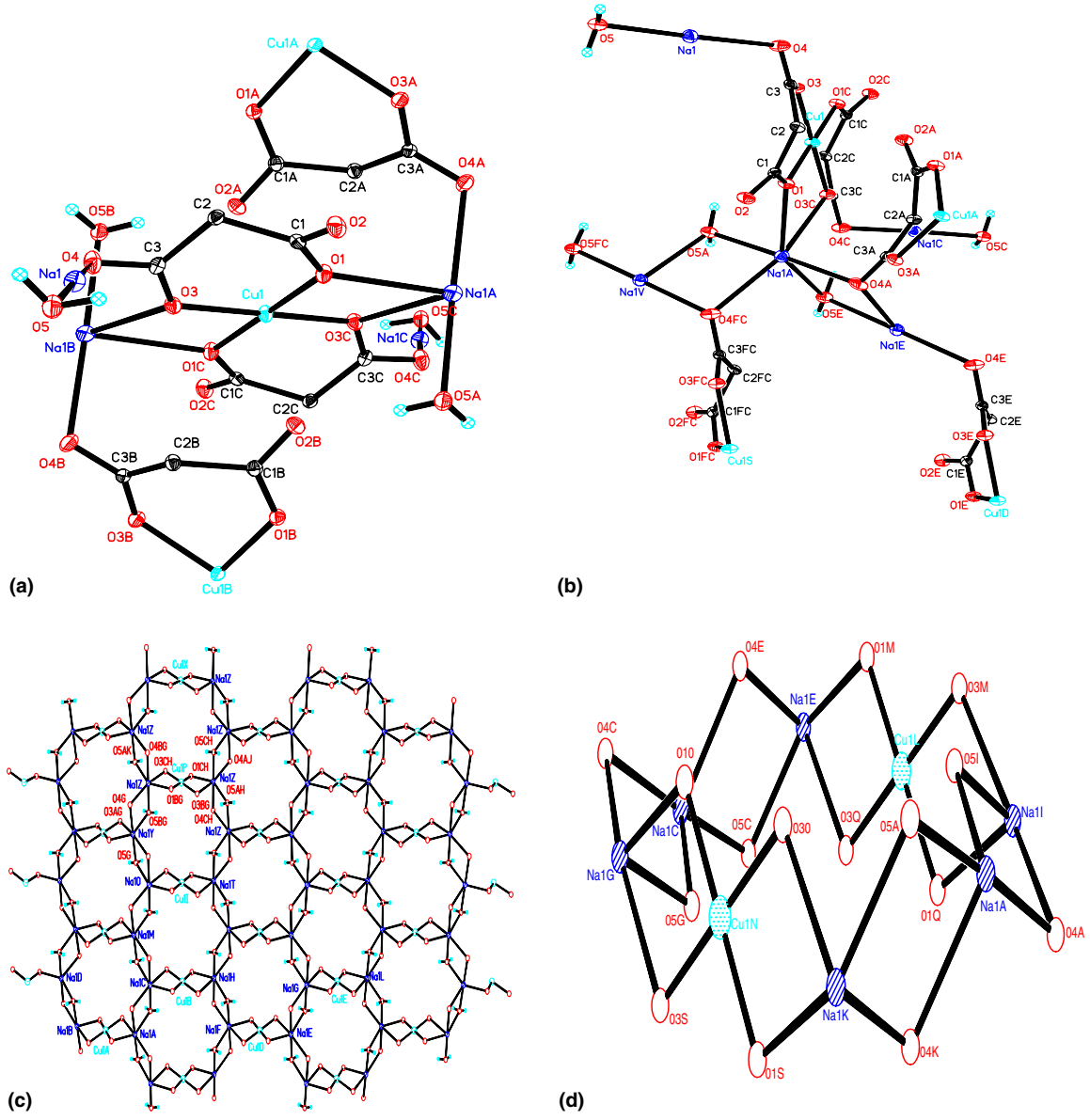

Fig. 2. Perspective drawings of (a) the copper (II) and (b) sodium (I) environments in complex **2** along with the atom numbering. Thermal ellipsoids are drawn at the 50% probability level, (c) diagram of one planar structure in complex **2**, (d) core of complex **2** as a metallacrown.

for some bond angles around the sodium atom [100.34(9)°, 64.18(8)° and 98.20(9)° for O4A–Na1A–O4FC, O1–Na1A–O3C and O4A–Na1A–O3C, respectively]. Some selected bond angles are shown as follows: Cu1–O1–Na1B = 105.87(10)°, Cu1–O3–Na1C = 101.63(9)°, Na1A–O4A–Na1E = 97.46(9)°, Na1A–O5A–Na1V = 105.79(11)° (Fig. 2(b)).

For every malonate ligand there are three oxygen atoms participating in coordinating out of the total four with the other one being free. One oxygen atom from each carboxylate bridges one sodium and one copper atom and the remaining coordinating oxygen atom bridges two sodium atoms.

For each sodium atom there are two coordinating water molecules each of which bridge two different sodium atoms. The oxygen atom from one water molecule exists not only in the equatorial site for one sodium coordination environment, but also at the axial position for another sodium atom's unit.

The sodium atoms form zigzag chains through the coordination of water molecules and malonate-oxygen atoms. These chains are linked by 4-coordinated copper atoms and build 2-D planes (Fig. 2(c)), which constitute further a complicated 3-D structure owing to the coordination effect of the remaining water molecules and malonate-oxygen atoms.

It can be found that the malonate's coordination mode in complex **2** is different not only from those in past copper(II) complexes [1–7], but also from those in other metal complexes [11–14].

The other important characteristic of this crystal structure is that 6 sodium atoms and 2 copper atoms build an 8-center metallocycle through coordination with malonate ligands and water molecules just as in complex **1** (Figs. 1(d) and 2(d)). Both complexes **1** and **2** seem to be so-called heterometallacrown.

3.4. Thermal analysis

Thermogravimetic analysis of compound **1** reveals that it loses two coordinating water molecules at $T < 176$ °C. The decomposition of *o*-pthalate occurs in two steps at about $T = 280$ and $T = 372$ °C. Similarly, the thermogravimetic analysis of compound **2** indicates that it loses a total of two coordinating water molecules at $T < 220$ °C. The decomposition of *o*-pthalate occurs in two steps at $T > 350$ °C.

3.5. Conclusion

The core of complex **1** illustrates that it is a 16-metallacrown-8. Complex **2** has an overall ring structure similar to that of complex **1**. From Figs. 1(d) and 2(d) it can be seen that these two complexes qualify as authentic examples of 16-metallacrown-8 structure types. The difference between them is the different linking system between the copper and sodium atoms replacing the carbon atoms of the 16-crown-8 ether.

4. Supplementary material

Crystallographic data for the structural analysis have been deposited with the Cambridge Crystallographic Data Centre, CCDC Nos. 217021 and 217022 for compounds **1** and **2**, respectively. Copies of this information may be obtained free of charge from The Director, CCDC, 12 Union Road, Cambridge, CB2 1EZ, UK (fax: +44-1223-336033; e-mail: deposit@ccdc.cam.ac.uk or www:http://www.ccdc.cam.ac.uk).

Acknowledgements

This work was supported by the Natural Science Foundation of Henan Education Department (200011500027) and the Natural Foundation of Henan Province (0211020300).

References

[1] D. Chattopadhyay, S.K. Chattopadhyay, P.R. Lowe, C.H. Schwalke, S.K. Mazumber, A. Rana, S. Ghosh, J. Chem. Soc., Dalton Trans. (1993) 913.
[2] I. Gil de Muro, F.A. Mautner, M. Insausti, L. Lezama, M.I. Arriortua, T. Rojo, Inorg. Chem. 37 (1998) 3243.
[3] C. Ruiz-Pérez, J. Sanchiz, M. Hernández-Molina, F. Lloret, M. Julve, Inorg. Chim. Acta 298 (2000) 202.
[4] E. Suresh, M.H. Bhadbhade, Acta Crystallogr., Sect. C 53 (1997) 193.
[5] C. Ruiz-Pérez, M. Hernández-Molina, P. Lorenzo-Luis, F. Lloret, J. Cano, M. Julve, Inorg. Chem. 39 (2000) 3845.
[6] C. Ruiz-Pérez, J. Sanchiz, M. Hernández-Molina, F. Lloret, M. Julve, Inorg. Chem. 39 (2000) 1363.
[7] I.G. de Muro, M. Insausti, L. Lezama, M.K. Urtiaga, M.I. Arriortua, T. Rojo, J. Chem. Soc., Dalton Trans. (2000) 3360.
[8] Y. Rodrÿguez-Martÿna, J. Sanchiz, C. Ruiz-Pérez, F. Lloret, M. Julve, Inorg. Chim. Acta 326 (2001) 20.
[9] B.R. Gibney, A.J. Stemmler, S. Pilotek, J.W. Kampf, U.L. Pecoraro, Inorg. Chem. 32 (1993) 6008.
[10] C. Janiak, J. Chem. Soc., Dalton Trans. (2000) 3885.
[11] I. Gil de Muro, F.A. Mautner, Inorg. Chem. 37 (1998) 3243.
[12] C. Ruiz-Pérez, M. Hernández-Molina, Inorg. Chim. Acta 298 (2000) 245.
[13] Y.-G. Wei, S.-W. Zhang, Polyhedron 15 (23) (1996) 4303.
[14] S.M. Saadeh, K.L. Trojan, Inorg. Chem. 32 (1993) 3034.

Available online at www.sciencedirect.com
SCIENCE DIRECT®
Polyhedron 23 (2004) 949–954
POLYHEDRON
www.elsevier.com/locate/poly

A novel manganese(III) quadridentate Schiff-base dimeric complex: synthesis, crystal structure and magnetic properties ☆

Ruma Karmakar [a], Chirantan Roy Choudhury [a], Georges Bravic [b], Jean-Pascal Sutter [b,*], Samiran Mitra [a,*]

[a] *Department of Chemistry, Jadavpur University, Kolkata 700 032, India*
[b] *Institut de Chimie de la Matière Condensée de Bordeaux UPR 9048 CNRS, Ave Dr. Schweitzer, F-33608 PESSAC, France*

Received 9 September 2003; accepted 1 December 2003

Abstract

One new dimeric manganese(III) complex $[MnL(H_2O)]_2(ClO_4)_2 \cdot H_2O$ **(1)** where [L = *N*,*N*′-bis(2-hydroxyacetophenylidene)-1,2-diaminopropane] has been synthesised and characterised by spectroscopic and electrochemical study, and the single crystal structure of the complex was determined. The crystal structure features the presence of two independent molecules in the asymmetric unit. The dimeric unit is formed by a double Mn–O bridge of one molecule with its centrosymmetric homologue. Low temperature magnetic susceptibility measurements show a ferromagnetic intra-dimer interaction.
© 2004 Elsevier Ltd. All rights reserved.

Keywords: Dimeric complex; Manganese(III); Crystal structure; Ferromagnetic behaviour

1. Introduction

Exchange interaction between paramagnetic centres of a large number of multi-nuclear complexes has already been investigated. The nature and the tuning of magnetic interactions between metal centres are crucial points in the conception of molecule-based magnetic materials [1]. Binuclear manganese(III) Schiff base compounds are of increasing interest because such dinuclear systems are known to act as a paramagnetic building block for multidimensional expanded structures [2] as well as for their important roles in biological systems, e.g., in many metalloenzymes, redox and non-redox proteins [3,4] and also as a catalyst in olefin epoxidation [5]. Moreover in nature, the oxygen evolving complexes of photosystem II are believed to be catalysed by a cluster of manganese ions. Manganese(III) salen-type complexes are very well studied because this type of Schiff base ligands present suitable biometric properties that can mimic the structural feature of the active site [5,6].

The manganese(III) salen-type compounds are generally in equilibrium between the monomeric and the dimeric species, their solid state form depends on the steric characteristics of the salen-type Schiff bases [1a]. Dimeric manganeses(III) complexes generally exhibit an antiferromagnetic intra-dimer interaction which is very well explored [7–13], but a few examples of ferromagnetic interactions have been reported as well [14–17]. These type of ferromagnetic dimers afford an unusual $S = 4$ ground spin state making themselves appealing candidates for a building block to design new magnetic materials.

Here, for the synthesis of a manganese(III) complex with tetradentate N_2O_2 donor set Schiff base ligands, we employed the poorly coordinating perchlorate ion so that water would be able to complete the coordination sphere of the metal ions and expected an intramolecular interaction between these species, resulting in a dimer.

In this report, we present the synthesis, characterisation, single crystal X-ray structure and low temperature

☆ Supplementary data associated with this article can be found, in the online version, at doi:10.1016/j.poly.2003.12.012.

* Corresponding authors. Tel.: +91-33-2668-4193/2017; fax: +91-33-2414-6266.
E-mail addresses: jpsutter@icmcb.u-bordeaux.fr (J.-P. Sutter), smitra_2002@yahoo.com (S. Mitra).

0277-5387/$ - see front matter © 2004 Elsevier Ltd. All rights reserved.
doi:10.1016/j.poly.2003.12.012

magnetic behaviour study of one novel out-of-plane manganese(III) Schiff base dimer where two independent molecules are in the asymmetric unit. This phenomenon is very rare in the literature [10]. The dimeric unit is formed by the double Mn–O bridge of one molecule with its centrosymmetric homologue. Interestingly, this complex displays ferromagnetic behaviour at low temperature.

2. Experimental

2.1. Physical measurements

The infrared spectrum was recorded on a Perkin–Elmer FT-IR spectrophotometer as a KBr pellet and the electronic spectrum on a Perkin–Elmer Lambda-40 spectrophotometer using acetonitrile as solvent. Elemental analyses were carried out on a Perkin–Elmer 2400-II instrument. Electrochemical studies were performed on a CH 600A cyclic voltameter instrument using acetonitrile as solvent and tetrabutyl ammonium perchlorate as the supporting electrolyte. Variable-temperature magnetic susceptibility measurements were carried out with a Quantum Design MPMS-5S SQUID magnetometer under an applied magnetic field of 1000 Oe. Diamagnetic corrections were estimated from Pascal tables and magnetic data were corrected for diamagnetic contributions of the sample holder [18].

2.2. Materials

Reagent grade 2-hydroxy acetophenone, 1,2-diaminopropane (Fluka) and manganese(II) perchlorate hexahydrate (Fluka) were obtained commercially. All the solvents used were of reagent grade.

2.3. Preparation

2.3.1. Synthesis of the ligand and complexes

2.3.1.1. Synthesis of the Schiff base ligand. The Schiff base ligand $[HOC_6H_4C(CH_3)NCH_2CH(CH_3)NC(CH_3)C_6H_4OH]$ (H_2L) was obtained by refluxing a methanolic solution (25 ml) of 2-hydroxy acetophenone (2 mmol) and 1,2-diaminopropane (1 mmol) for 30 min. The resulting orange-yellow solution containing the ligand was used without further purification.

Caution! Perchlorate salts are potentially explosive and should be used in small quantities with much care.

2.3.2. Synthesis of the title compound $[MnL(H_2O)]_2(ClO_4)_2 \cdot H_2O$ (**1**)

To a methanolic solution of manganese perchlorate (0.362 g, 1 mmol), a methanolic solution of the Schiff base (1 mmol) was added with constant stirring. The resulting solution was stirred for 5 min at room temperature. After three days crystals suitable for X-ray diffraction were collected and the rest were filtered and air-dried. Yield: 60%. *Anal.* calc. for $C_{19}H_{23}ClMnN_2O_{7.5}$, C, 44.89; H, 4.92; N, 5.51; Mn, 10.82. Found: C, 44.81; H, 4.86; N, 5.48; Mn, 10.79%.

2.4. Crystallographic structure determination of compound **1**

A crystal was mounted on an ENRAF-NONIUS K-CCD diffractometer and analysed using monochromated Mo-Kα X-ray radiation ($\lambda = 0.71073$ Å). The structure was solved by direct methods with the SIR97 program. Least-squares structure refinements based on F^2 were carried out by a user defined block-diagonal matrix. Locations of hydrogen atoms, except some water ones, were generated geometrically (C–H = 1.0 Å) and included in the refinement with isotropic thermal parameters. All non-hydrogen atoms were refined with anisotropic thermal parameters. Atom scattering factors were taken from the International Tables for

Table 1
Crystal data for compound **1**

Crystal data	
Formula	$C_{38}H_{46}N_4O_{15}Cl_2Mn_2$
M (g mol^{-1})	979.6
Crystal system	monoclinic
Space group	$P2_1/n$
a (Å)	12.8459(2)
b (Å)	23.7900(3)
c (Å)	15.0533(2)
β (°)	113.512(1)
V(Å^3)	4218.4(2)
Z	4
D_{calc} (Mg m^{-3})	1.549
Mo Kα radiation, λ (Å)	0.71073
μ (mm^{-1})	0.832
Data collection	
Enraf-Nonius K-CCD diffractometer	ω scans of 1°
θ range (°)	$6 \rightarrow 27.5$
hkl ranges	$h - 16 \rightarrow 16$; $k - 30 \rightarrow 30$; $l - 19 \rightarrow 19$
Absorption correction	scalepack
Measured reflections	17 994
Independent reflections	9510
Observed reflections [$I > 3\sigma$]	6185
R_{int}	0.023
Refinement	
Based on F^2, reflections used	9428
N_r of parameters	727
R[a]	0.049
wR[a]	0.157
S(Goodness-of-fit)	0.999
Δ/σ_{max}	0.200
Residual density (e Å^{-3})	1.45

[a] $R = \sum ||F_o| - |F_c|| / \sum |F_o|$ for observed reflections, $wR = [\sum w(F_o^2 - F_c^2)^2 / \sum (wF_o)^2]^{1/2}$, $w = 1/(\sigma^2(F_o^2) + 0.04F^2)$, $F = (2F_o + F_c)/3$.

Crystallography. Unit-cell parameters were obtained by least-square refinement from 9428 reflections in the range $6.1° \leqslant \theta \leqslant 27.4°$. 268 frames were collected during 15 h by ω scans of 2° giving 17 994 measured reflections. Crystal data and details of data collection are given in Table 1. Final reliability factors converged to $R(F) = 0.049$ and $wR(F^2) = 0.157$. A final difference Fourier map showed residual density of 1.45 e Å.

3. Results and discussion

3.1. Infrared spectrum

The infrared spectrum of compound **1** is very much consistent with the structural data presented in this paper. The bands in the range 3524 and 1620 cm^{-1} are attributable to O–H stretching and bending of coordinated water ligands or water of crystallisation. This also indicates the presence of hydrogen bonding in the complex [19]. The ν(C=N) band appears at 1598 cm^{-1}. The phenolic C–O stretching is present at 1274 and 1286 cm^{-1} [19,20]. Bands in agreement with non-coordinated anions could also be observed for perchlorate compounds, 1172, 1161–1086, 969 cm^{-1} [20,21]. Ligand coordination to the manganese centre is substantiated by two bands appearing at 476 and 456 cm^{-1}, attributable to ν(Mn–N) and ν(Mn–O), respectively.

3.2. Electronic spectrum

Although the electronic spectra of the manganese complexes with multidentate Schiff base ligands is not in general a good indicator of geometry, it can act as a supporter of it [22].

The complex displays two strong absorption bands in the region 225 and 276 nm, which can be assigned to the charge transfer from the ligands to the Mn(III) transition. As usual, the spectrum shows very weak low-intensity absorption bands associated with d–d transitions in the range 490–500 nm for compound **1**.

3.3. Electrochemical study

The electrochemical study of the compound was performed using acetonitrile as the solvent and tetrabutylammonium perchlorate as the supporting eletrolyte at a scan rate of 50 mV s^{-1}. Cyclic voltammetry on compound **1** shows (Fig. 1) two reductive responses on the negative side of SCE (at −0.30, −0.47 V) due to the Mn(II)/Mn(III) redox couple, both of which are irreversible in nature. The observed potential gap (170 mV) between the two reductions indicates the effective communication between the Mn(III) centres through the two phenoxo-bridges. Two irreversible oxidation responses

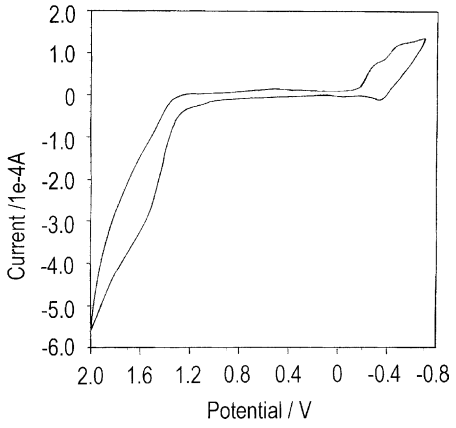

Fig. 1. Cyclic voltammogram of compound **1** in acetonitrile.

are also expected for such a system, but only one such oxidation is observed on the positive side of SCE at 1.57 V [due to oxidation of Mn(III) to Mn(IV)], as the solvent itself oxidises at 2.0 V.

3.4. Crystal structure of compound *1*

The crystal structure determination revealed that compound **1** associates as a dimer in the solid state and two slightly different dimers were found. These are the result of the presence of two independent molecules of **1** in the asymmetric unit. The ORTEP diagram of the independent molecules in the asymmetric unit are depicted in Fig. 2 and a view of the dimer is shown in Fig. 3.

The two independent molecules present in the asymmetric unit are structurally identical except for a slight variation in bond lengths and angles. The presence of a chiral carbon atom on the ligand could have been anticipated to introduce a segregation among the complex units even for a racemic mixture. This is not the case because the compound crystallizes in a centro-symmetric space group. In both independent cationic units **A** and **B**, the Mn(III) ion adopts a distorted octahedral geometry in which the equatorial plane is formed by the coordination of the Schiff base ligand, i.e., two imino-nitrogen and two phenolic-oxygen atoms, and the axial sites are occupied by oxygen atoms of the coordinated water molecule and the bridging O atom. For both molecules **A** and **B**, the equatorial bond distances are slightly shorter than the axial bond distances and the Mn atoms are 0.1040(5) and 0.0897(5) Å out of the equatorial planes. Consequently the environment around each manganese atom can be described as a distorted $N_2O_2O'_2$ octahedron as a result of Jahn–Teller distortion.

Each cationic moiety associates with an identical unit in dimers, **AA** and **BB**, in which the Mn-centers are doubly bridged by two μ-phenoxo oxygen atoms from the Schiff base ligands. Each molecule of a pair is related

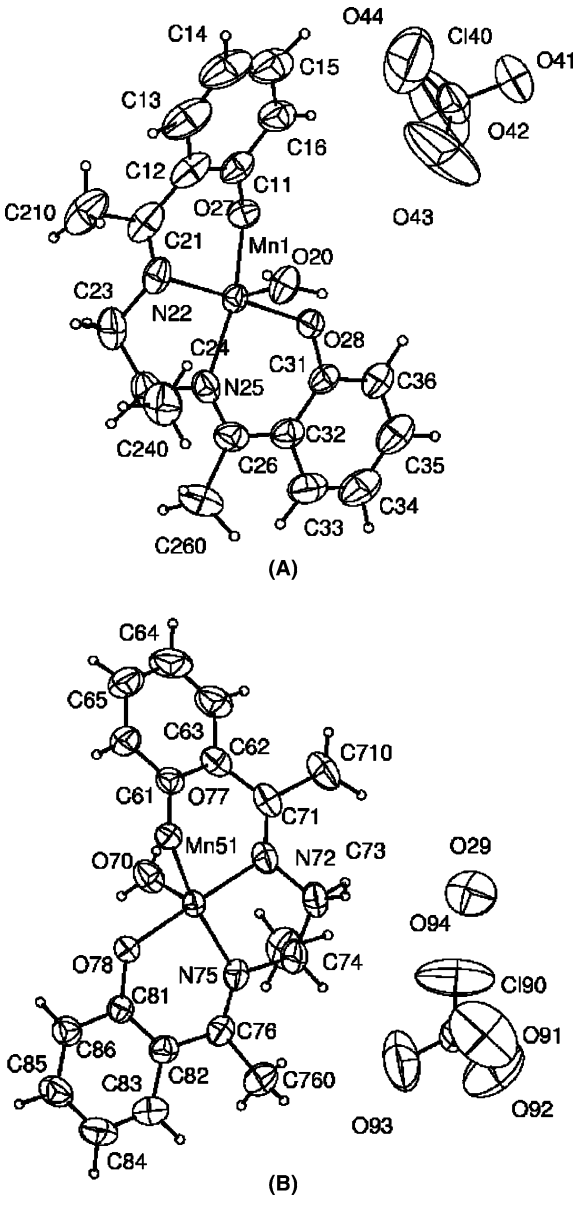

Fig. 2. ORTEP plot of the two independent molecules showing half of a dimer (**A** and **B**) present in the asymmetric units. The thermal ellipsoids are represented at 50% probability level. Selected bond lengths (Å) and angles (°): Unit **A**: Mn1–N22, 1.964(4); Mn1–N25, 1.997(4); Mn1–O27, 1.894(3); Mn1–O28, 1.853(3); Mn1–O20, 2.189(4); Mn1–O27* $(1-x,-y,1-z)$, 2.411(3). Mn1–O27–Mn1*, 100.4. Unit **B**: Mn51–N72, 1.972(4); Mn51–N75, 1.991(4); Mn51–O77, 1.892(3); Mn51–O78, 1.856(3); Mn51–O70, 2.220(4) and Mn51–O77* $(1-x,-y,-z)$, 2.401(3). Mn51–O77–Mn51*, 100.9.

to the other by centro-symmetry therefore whereas the asymmetric carbon atom of one has *R* configuration, the second has *S*. The bridging Mn–O bond distances are 2.411(3) Å for **AA** and 2.401(3) Å for **BB** and intra-dimer Mn–Mn separations are 3.325(1) and 3.326(1) Å, respectively.

The two Mn linked water molecules enable H-bonds between the different dimers (O(20)···O(78), 2.795(5) Å and O(70)···O(28), 2.787(5) Å) as well as with a per-

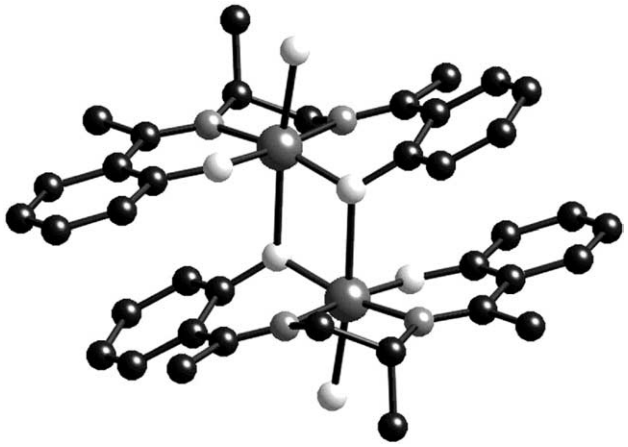

Fig. 3. View of the molecular arrangement for a cationic dimer unit of compound **1** (H atoms are omitted for clarity).

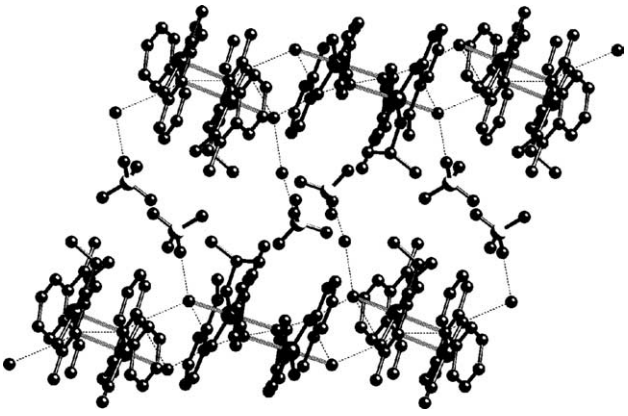

Fig. 4. Packing diagram of compound **1**.

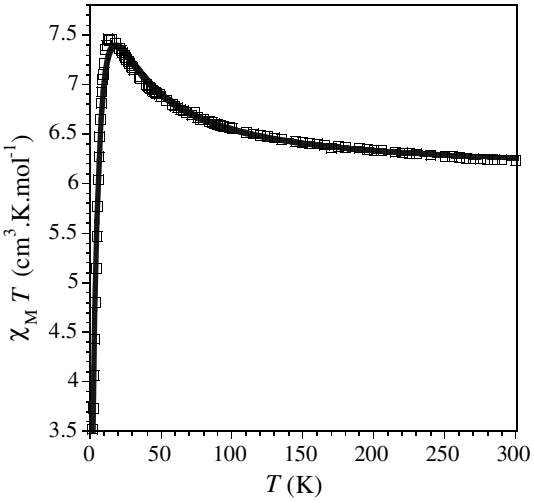

Fig. 5. Temperature dependence of the experimental (□) and calculated (—) $\chi_M T$ for dimer **1**. Best fit yielded $J = 3.7 \pm 0.1$ cm^{-1}, $zJ' = 0.41$ cm^{-1} and $g = 2.015$ (see text).

chlorate ion (O(70)···O(47), 2.78 (1) Å). The free H_2O is linked by H-bonds with the coordinated H_2O of molecule **A** (O(29)···O(20), 2.741(7) Å) and with the perchlorate oxygen O(94) (2.85(1) Å). The packing diagram of compound **1** is shown in Fig. 4.

3.5. Magnetic properties

The temperature dependence of the molar magnetic susceptibility, χ_M, for compound **1** was measured on a polycrystalline sample in the temperature range 2–300 K. Results are depicted in a graph of $\chi_M T$ versus T in Fig. 5. At 300 K, the value for $\chi_M T$ is 6.25 cm^3 K mol^{-1} in good agreement with the expected contribution of two non-interacting Mn(III) ions with $S = 2$ spin. For lower temperature, the value of $\chi_M T$ steadily increases to reach 7.45 cm^3 K mol^{-1} at 15 K before suddenly dropping to 3.50 cm^3 K mol^{-1} for 2 K, the lowest temperature investigated. The behavior in the 300–15 K temperature domain is indicative of a ferromagnetic interaction between the Mn(III) ions within the dimer, whereas the drop of $\chi_M T$ for lower temperatures can be ascribed to two possible contributions. One is due to the zero field splitting (ZFS) of the states of the Mn(III) ions, the second arises from intermolecular exchange interactions and they might be concomitant. The X-ray features for compound **1** show that the dimers are linked through hydrogen bonds established between the H_2O ligands and the phenolate oxygen atoms of neighboring molecules. Such links are known to mediate an exchange interaction between magnetic centers [23,24]. Moreover, the maximum value reached for $\chi_M T$, 7.45 cm^3 K mol^{-1}, is lower than the 10 cm^3 K mol^{-1} expected for a $S = 4$ ground state (assuming $g = 2$) confirming indeed that the decrease of $\chi_M T$ can be ascribed to inter-dimer exchange interactions.

Therefore, the magnetic properties were analyzed by a theoretical model considering the interaction between two $S = 2$ spin centers and, to account for the low temperature behavior, a contribution arising from inter-dimer interactions. The total spin Hamiltonian taking into account the Zeeman perturbation for the dimer is given in Eq. (1) [1c], where J represents the Mn–Mn exchange parameter and S_{Mn} and g_{Mn}, respectively, the spin and the local g-tensor associated to Mn(III). The intermolecular interactions were considered in the mean-field approximation and appear as zJ' in the expression of $\chi_M T$ used to analyze the experimental data (Eq. (2)). The best fit to the experimental data (Fig. 3) was obtained for $J = 3.7 \pm 0.1$ cm^{-1}, $zJ' = 0.41$ cm^{-1} and $g = 2.015$

$$\mathrm{H} = -J_{\hat{S}_{Mn1}\cdot\hat{S}_{Mn2}} + g_{Mn}\beta(\hat{S}_{Mn1} + \hat{S}_{Mn2})\cdot H, \quad (1)$$

$$\chi_M T = \frac{Ng^2\beta^2 F(J,T)T}{kT - zJ'F(J,T)}, \quad (2)$$

with

$$F(J,T) = \frac{60 + 2\exp(-9J/kT) + 10\exp(-7J/kT) + 28\exp(-4J/kT)}{9 + 3\exp(-9J/kT) + 5\exp(-7J/kT) + 7\exp(-4J/kT) + \exp(-10J/kT)}.$$

4. Concluding remarks

Compared to related {Mn(III)salen} dimers, the ferromagnetic interaction for compound **1** is amongst the strongest reported so far. The strength of this exchange coupling is in line with the rather short Mn–O bonds linking the mononuclear units. This bond for compound **1** is very similar to that observed for the salen derivative [5] and shorter than that for salen derivatives with functionalized diaminoethane units [1]. Obviously, the intramolecular separation for such compounds is affected by the steric constraint introduced by the substituents. For compound **1** this does not apply because the methyl group on the diaminoethane moiety of the ligand points outwards; this permits the fragments of the dimer to come close and results in a stronger exchange interaction.

5. Supplementary material

Crystallographic data for structural analysis has been deposited with the Cambridge Crystallographic Data Centre, CCDC No. 214703 for **1**. Copies of this information may be obtained free of charge from The Director, CCDC, 12 Union Road, Cambridge, CB2 1EZ, UK (fax: +44-1223-336033; deposit@ccdc.cam.ac.uk or www.ccdc.cam.ac.uk).

Acknowledgements

This work was supported by the grants from DST, CSIR, UGC, New Delhi, India. Our thank is also extended to Dr. S. Bhattacharya, Department of Chemistry, Jadavpur University, for his valuable discussion in the cyclic voltametric studies.

References

[1] (a) H. Miyasaka, R. Clérac, T. Ishii, H.-C. Chang, S. Kitagawa, M. Yamashita, J. Chem. Soc., Dalton Trans. (2002) 1528;
(b) Reviews: O. Kahn, Molecular Magnetism, VCH, Weinheim, Germany, 1993;
(c) O. Kahn, Struct. Bond. (Berlin) 68 (1987) 89;
(d) J.S. Miller, A.J. Epstein, Angew. Chem. Int. ed. Engl. 33 (1994) 385;

(e) D. Gatteschi, Adv. Mater. 6 (1994) 635;
(f) M. Verdaguer, A. Bleuzen, V. Marvaud, J. Vaissermann, M. Seuleiman, C. Desplanches, A. Scuiller, C. Train, R. Garde, G. Gelly, C. Lomenech, I. Rosenman, P. Veillet, C. Cartier, F. Villain, Coord. Chem. Rev. 190–192 (1999) 1023;
(g) C. Mathonière, J.-P. Sutter, J.V. Yakhmi, in: J.S. Miller, M. Drillon (Eds.), Magnetism: Molecules to Materials, vol. 4, VCH, Weinheim, 2002, pp. 1–40.

[2] S. Sailaja, K. Rajender Reddy, M.V. Rajasekharan, C. Hureau, E. Rivière, J. Cano, J.-J. Girerd, Inorg. Chem. 42 (2003) 180.

[3] J.J.R. Fraústo da Silva, R.J.P. Williams, The Biological Chemistry of the Elements, Clarendon Press, Oxford, 1991, p. 370 (Chapter 14).

[4] V.L. Pecoraro (Ed.), Manganese Redox Enzymes, VCH, New York, 1992.

[5] H.-L. Shyu, H.-H. Wei, Y. Wang, Inorg. Chim. Acta 290 (1999) 8, and references therein.

[6] Y. Cringh, S.W. Gordon-Wylie, R.E. Norman, G.R. Clark, S.T. Weintraub, C.P. Horwitz, Inorg. Chem. 36 (1997) 4968.

[7] C.E. Hulme, M. Watkinson, M. Haynes, R.G. Pritchard, C.A. McAuliffe, N. Jaiboon, B. Beagley, A. Sousa, M.R. Bermejo, M. Fondo, J. Chem. Soc., Dalton Trans. (1997) 1805.

[8] N. Matsumoto, Z.J. Zhong, H. Ōkawa, S. Kida, Inorg. Chim. Acta 160 (1989) 153.

[9] N. Matsumoto, N. Takemoto, A. Ohyosi, H. Ōkawa, Bull. Chem. Soc. Jpn. 61 (1988) 2984.

[10] M.R. Bermejo, A. Castiñeiras, J.C. Garcia-Monteagudo, M. Rey, A. Sousa, M. Watkinson, C.A. McAuliffe, R.G. Pritchard, R.L. Beddoes, J. Chem. Soc., Dalton Trans. (1996) 2935.

[11] A. Garcia-Deibe, A. Sousa, M.R. Bermejo, P.P. MacRory, C.A. McAuliffe, R.G. Pritchard, M. Helliwell, J. Chem. Soc., Chem Commun. (1991) 728.

[12] (a) M. Mikuriya, Y. Yamato, T. Tokii, Bull. Chem. Soc. Jpn. 65 (1992) 1466;
(b) H. Li, Z.J. Zhong, C. Duan, X. You, T.C.W. Mac, B. Wu, J. Coord. Chem. 41 (1997) 183.

[13] B.J. Kennedy, K. Murray, Inorg. Chem. 24 (1985) 1552.

[14] H. Miyasaka, N. Matsumoto, H. Ōkawa, N. Re, E. Gallo, C. Floriani, J. Am. Chem. Soc. 118 (1996) 98.

[15] Y. Sato, H. Miyasaka, N. Matsumoto, H. Ōkawa, Inorg. Chim. Acta 247 (1996) 57.

[16] N. Matsumoto, H. Okawa, S. Kida, T. Ogawa, A. Ohyoshi, Bull. Chem. Soc. Jpn. 62 (1989) 3812.

[17] H.-L. Shyu, H.-H. Wie, Y. Wang, Inorg. Chim. Acta 290 (1999) 8.

[18] P. Pascal, Ann. Chim. Phys. 19 (1910) 5.

[19] (a) C.T. Yang, B. Moubaraki, K.S. Murray, J.D. Ranford, J.J. Vittal, Inorg.Chem. 40 (2001) 5934;
(b) N.N. Murthy, M.M. Tahir, K.D. Karlin, J. Am. Chem. Soc. 115 (1993) 10404.

[20] (a) Y. Agnus, R. Louis, B. Metz, C. Boudon, J.P. Gisselbrecht, M. Gross, Inorg. Chem. 30 (1991) 3155;
(b) K. Nakamoto, Infrared and Raman Spectra of Inorganic and Coordination Compounds, 4th ed., Wiley Interscience, New York, 1986.

[21] S. Ferrer, J.G. Haasnoot, J. Reedijk, E. Müller, M.B. Cingi, M. Lanfranchi, A.M.M. Lanfredi, J. Ribas, Inorg. Chem. 39 (2000) 1859.

[22] M. Suzuki, A. Uehara, Bull. Chem. Soc. Jpn. 57 (1984) 3134.

[23] C. Rancurel, N. Daro, O. Benedi Borobia, E. Herdtweck, J.-P. Sutter, Eur. J. Inorg. Chem. (2003) 167.

[24] C. Desplanches, E. Ruiz, A. Rodriguez-Fortea, A. Alvarez, J. Am. Chem. Soc. 124 (2002) 5197.

Available online at www.sciencedirect.com
SCIENCE DIRECT®
Polyhedron 23 (2004) 955–961
POLYHEDRON
www.elsevier.com/locate/poly

^{11}B NMR study on the interaction of boric acid with Azomethine H

Hidenobu Matsuo [a], Yoshinobu Miyazaki [b], Hiroyuki Takemura [a], Shiro Matsuoka [a], Hirofumi Sakashita [c], Kazuhisa Yoshimura [a,*]

[a] *Department of Chemistry, Faculty of Sciences, Kyushu University, Ropponmatsu, Chuo-ku, Fukuoka 810-8560, Japan*
[b] *Department of Chemistry, Fukuoka University of Education, Akamabunkyo-machi, Munakata, Fukuoka 811-4192, Japan*
[c] *The Center of Advanced Instrumental Analysis, Kyushu University, Kasuga, Fukuoka 816-8580, Japan*

Received 8 October 2003; accepted 2 December 2003

Abstract

^{11}B NMR spectroscopy provided direct evidence that boric acid reacts with Azomethine H to form a 1:1 bischelate complex. A new peak with a −17.9 ppm chemical shift is due to the chelate complex containing tetrahedral boron. It has been quantitatively confirmed that the reaction includes two chemical equilibria; one is related to the ligand formation and the other to the complex formation. The formation constant for the ligand is small, less than 10, whereas that for the complex is relatively large, greater than 10^5. Azomethine H is hydrolyzed in aqueous solution because of its low stability, and the ligand formation is responsible for the nature of its complexation with boric acid.
© 2004 Elsevier Ltd. All rights reserved.

Keywords: Borate complex; Azomethine H; Boric acid; Complexation; ^{11}B NMR

1. Introduction

A large number of spectrophotometric studies have focused on the development of methods which enable one to determine the concentration of boric acid in an aqueous solution under moderate conditions. The Azomethine H method, proposed by Capelle in 1964 [1], has been employed for the boron analyses of natural and waste waters, soils and plants [2–10]. Azomethine H (8-hydroxy-1-(salicylideneamino)-3,6-naphthalenedisulfonic acid, Fig. 1) is a Schiff base of salicylaldehyde and H-acid (1-amino-8-naphthol-3,6-disulfonic acid), and its solution exhibits an absorption maximum at 412 nm in the presence of boric acid.

A number of studies have been performed for optimization of conditions for boron determination using Azomethine H as a coloring agent. For this purpose, it is very important to understand well the interaction between boric acid and Azomethine H. It has been pointed out in some papers that Azomethine H reacts with boric acid to form chelate complexes in solution, and then the complexes exhibit an absorption maximum in the visible region [4–6]. Some possible complexes are shown in Fig. 2, i.e., a 1:1 monochelate complex of trigonal boric acid (I), a 1:1 bischelate complex with tetrahedral boron (II), a 1:1 monochelate complex with tetrahedral boron (III), and its corresponding 1:2 complex (IV) [4–11]. On the contrary, Harp has suggested that the absorption maximum is due only to the Azomethine H species [7]. However, direct evidence regarding the coloring processes and the structure of the borate complex has not been provided until now.

^{11}B NMR spectroscopy is an excellent tool for studying the reaction of boric acid/borate with chelating ligands. In our previous studies, the nature of the interaction between boric acid/borate and boron-selective adsorbents such as crosslinked dextran gels, chelating resins with functional groups of *N*-methylglucamine and chromotropic acid-presorbed resin had been elucidated [12–17]. In this study, characteristics of the complexation of boric acid with Azomethine H will be discussed using the ^{11}B NMR method.

* Corresponding author. Tel.: +81-92-726-4743; fax: +81-92-726-4842.
E-mail address: kazz@chem.rc.kyushu-u.ac.jp (K. Yoshimura).

0277-5387/$ - see front matter © 2004 Elsevier Ltd. All rights reserved.
doi:10.1016/j.poly.2003.12.016

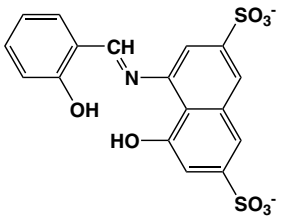

Fig. 1. Chemical structure of Azomethine H.

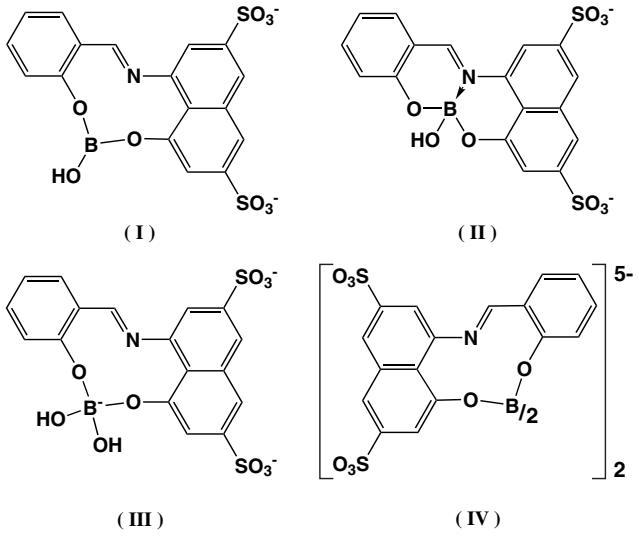

Fig. 2. Possible complexes of boric acid with Azomethine H.

2. Experimental

2.1. Reagents

All chemicals except Azomethine H and H-acid were of analytical reagent grade. All solutions of chelating agents were freshly prepared. Azomethine H (reagent grade), purchased from Dojindo (Japan) as the disodium salt, was used without further purification. A 20.0 mmol dm^{-3} Azomethine H solution was prepared by dissolving 0.467 g of the reagent in 50 cm^3 of a 10 mmol dm^{-3} ascorbic acid solution. A 20.0 mmol dm^{-3} salicylaldehyde solution was prepared by dissolving 0.122 g of salicylaldehyde in 50 cm^3 water with the addition of a small amount of KOH solution. The H-acid, 1-amino-8-naphthol-3,6-disulfonic acid, was received as a reagent grade monosodium salt (86.1%, Tokyo Kasei, Japan) and was used without further purification. A 10.0 mmol dm^{-3} H-acid solution was prepared by dissolving 0.449 g of H-acid in 100 cm^3 water with the addition of a small amount of KOH solution. Deionized water prepared with a Milli-Q SP system (Millipore, USA) was used throughout. The pH of the solution was adjusted with a 0.1 mol dm^{-3} acetate buffer, phosphate buffer, HEPES buffer, or KOH solution and was measured with a Horiba pH meter, Model F-22. The ionic strength was kept at 0.10 mol dm^{-3} with potassium chloride.

2.2. NMR measurements

^{11}B NMR spectra were recorded on a JEOL JNM-GSX 500 spectrometer (the Center of Advanced Instrumental Analysis, Kyushu University) at a resonance frequency of 160.0 MHz with a 10 mm multinuclear probe at 25 ± 1 °C. The sample solution ($I = 0.10$ mol dm^{-3}, KCl) containing known amounts of boric acid/borate and ligand was prepared, and the pH was adjusted with a small amount of buffer solution. After being allowed to stand for about 1 day, the solution was used for the NMR measurement. The standard NMR parameters were as follows: the flip angle was ca. 90° (36 μs), the pulse repetition time was 1 s, and the spectral width was 31 kHz. The chemical shifts were determined with reference to a 0.1 mol dm^{-3} boric acid solution as an external standard. On this scale the signal of BF_3–OEt_2, the generally accepted reference, came at −19.4 ppm.

3. Results and discussion

3.1. ^{11}B NMR spectra of the boric acid–Azomethine H system

The values of the ^{11}B NMR chemical shifts allow us to estimate the structures of the boron species [18–22]. If free boric acid of a trigonal planer structure is used as an external reference, the signal due to free borate anion having the tetrahedral structure appears around −17.7 ppm. When boric acid reacts with chelating ligands to form a complex with a six-membered ring structure, the 1:1 monochelate complexation shows a signal around −18.3 ppm, and further 1:2 bischelate complexation adds a new peak around −18.9 ppm.

The ^{11}B NMR spectra of boric acid in the presence of Azomethine H in weakly acidic regions varied with a change in the total concentration ratio of Azomethine H to boron. Fig. 3 shows that a new peak due to the complex appears in addition to that of free boric acid and that the chemical shift value for the complex is −17.9 ppm. Moreover, it was apparent that there was only one complex in this system, because no more peaks were observed even at higher Azomethine H concentrations.

The relative peak areas of the ^{11}B NMR spectra are directly proportional to the relative concentration of the respective boron species [19–21]. Fig. 3 shows that the concentration of the complex depends on the relative concentration ratio of ligand to boric acid. On the assumption that the complexation is a simple reaction expressed by Eq. (1), we calculated the concentration quotients, Q, using Eq. (2) and the concentrations estimated by ^{11}B NMR measurements

$$\text{Azomethine H} + \text{B(OH)}_3 \rightleftharpoons \text{complex} \quad (1)$$

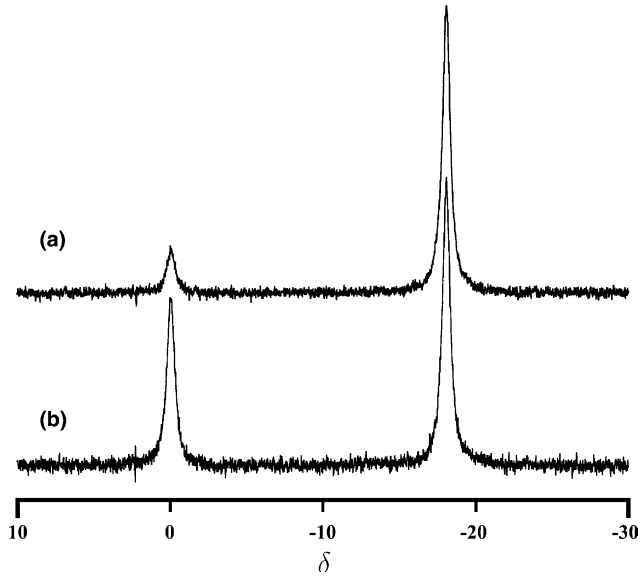

Fig. 3. ^{11}B NMR spectra for the solution containing 10.0 mmol dm^{-3} Azomethine H (pH 6.5). ((a): 5.00 mmol dm^{-3}, (b): 10.0 mmol dm^{-3} boric acid/borate).

$$Q = \frac{[\text{complex}]}{[\text{Azomethine H}][\text{B(OH)}]_3}. \quad (2)$$

The calculated Q had significantly different values when the concentration ratios of boric acid to the total Azomethine H were different, suggesting that such a simple equation could not explain the complexation reaction (Table 1), and therefore some other reactions may be involved in this system.

3.2. ^{11}B NMR spectra of the starting material systems

Azomethine H is a Schiff base and hydrolyzes to yield salicylaldehyde and an H-acid. The ^{11}B NMR spectra for boric acid solutions with the starting materials of Azomethine H are shown in Fig. 4. Both spectra showed not only the peak of free boric acid/borate but also those of complex species with a chemical shift around −17.7 ppm. In the salicylaldehyde system, the peak of the complex species was not observed in weakly acidic solutions. The relative peak areas of chelating boron species were much smaller than that of boric acid–Azomethine H, even if the molar ratios of these ligands to boric acid were higher than that for the Azomethine H system. Thus, the interaction of boric acid only with

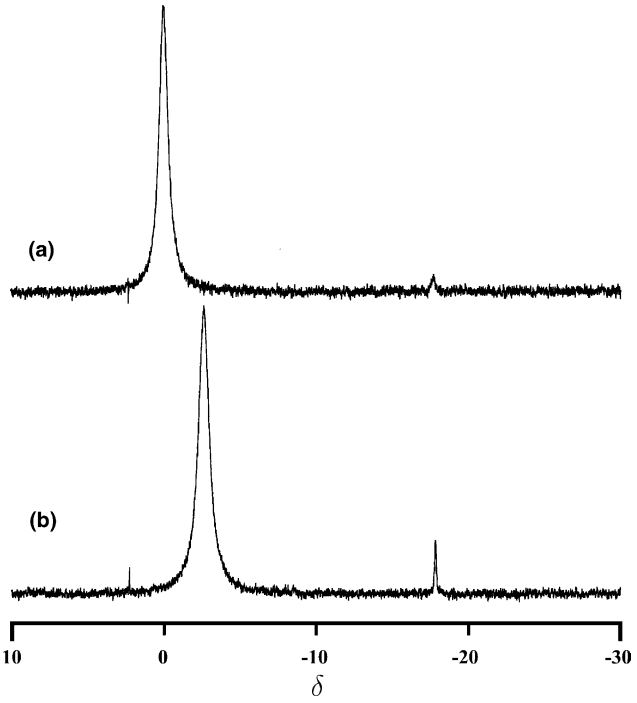

Fig. 4. ^{11}B NMR spectrum for the 10.0 mmol dm^{-3} boric acid/borate solutions containing H-acid or salicylaldehyde. ((a): 10.0 mmol dm^{-3} H-acid, pH 6.5; (b): 50.0 mmol dm^{-3} salicylaldehyde, pH 8.5).

salicylaldehyde or H-acid is negligible in the weakly acidic region. ^{11}B NMR spectra for weakly basic solutions containing ascorbic acid, Azomethine H and boric acid/borate also gave new peaks due to the interaction between borate and ascorbic acid [23], but these peaks were not recorded under weakly acidic conditions.

3.3. The structure of the boric acid–Azomethine H complex

As mentioned above, the interaction of boric acid with Azomethine H gave only one complex with a new peak in the ^{11}B NMR spectrum. The chemical shift value for the complex was −17.9 ppm, indicating that the structure of the chelate complex consisted of tetrahedral boron, not of trigonal boron such as (I) in Fig. 2. The results under the condition of $C_B/C_L = 1.0$ in Table 1 indicate that the boric acid–Azomethine H complex should not be a 1:2 chelate such as in Fig. 2 (IV) but a 1:1 chelate complex, because the equilibrium concentrations of the complex exceeded more than half of the

Table 1
Concentration quotients for the boric acid and Azomethine H system

C_B :C_L[a]	pH	[Free B]/mmol dm^{-3}	[complex]/mmol dm^{-3}	log(Q/mol^{-1} dm^3)
1.0:1.0	4.72	3.8	6.2	2.5
	6.50	3.7	6.3	2.5
0.5:1.0	4.72	0.60	4.4	3.0
	6.43	0.65	4.3	3.0

[a] C_L, total concentration of Azomethine H, 10.0 mmol dm^{-3}; C_B, total concentration of boric acid

total concentrations of the ligand. Moreover, the equilibrium concentrations of the complex were independent of the pH of the solutions in weakly acidic regions if other conditions were the same. The complexation of boric acid under acidic conditions progresses with a nucleophilic attack of the ligand on the empty orbital of boric acid [16]. The 1:1 monochelate complex presented in Fig. 2 (III) is excluded as the boric acid–Azomethine H complex, because the complexation equilibrium must be affected by pH, as expressed by Eq. (3).

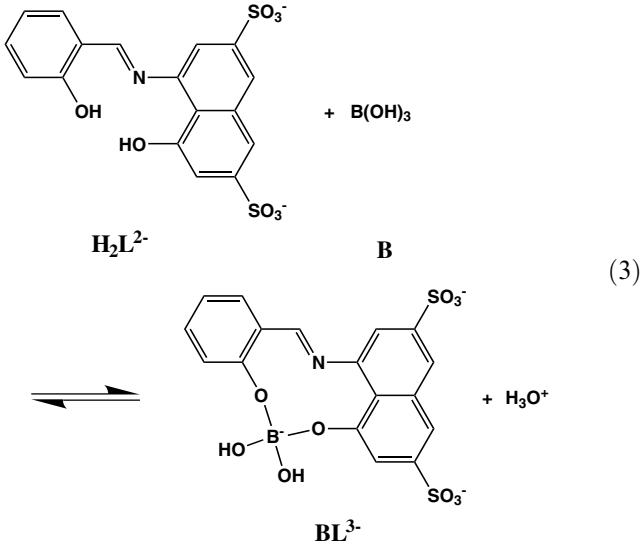

(3)

Intramolecular hydrogen bonding may suppress the protonation of the nitrogen atom of Azomethine H. In addition, it has been reported that the chemical shift value of the complex with coordination via the nitrogen atom is similar to those generally observed for the complex having a B–O bond [18]. Therefore, the possible structure of the Azomethine H–boric acid complex should be a 1:1 chelate complex having a coordination bond with the nitrogen atom of Azomethine H such as (II) in Fig. 2. As expressed by Eq. (4), such a complexation equilibrium does not involve proton dissociation.

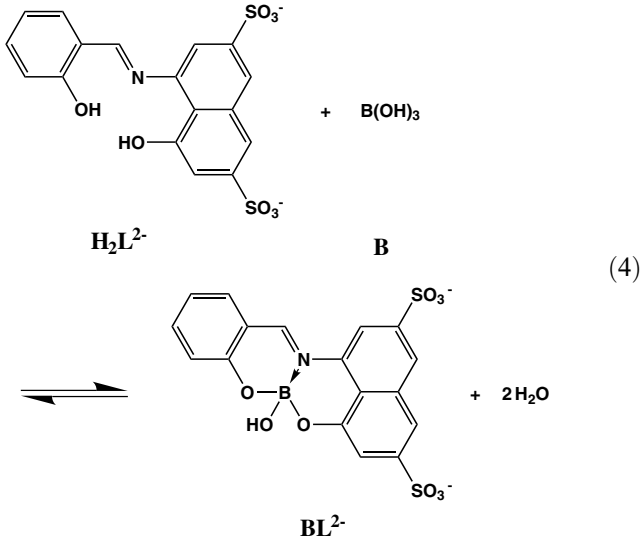

(4)

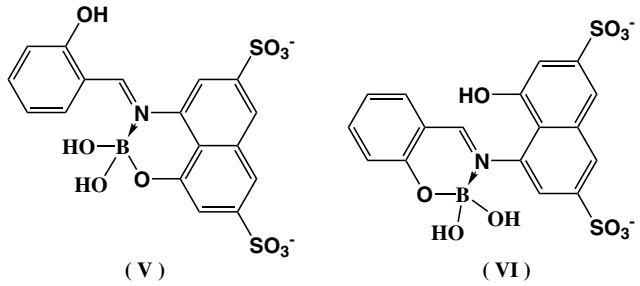

Fig. 5. Possible Azomethine H–boric acid complexes having a coordination bond with a nitrogen atom.

Fig. 5 also shows possible structures of the Azomethine H–boric acid monochelate complex having a coordination bond via the nitrogen atom. According to the ^{11}B NMR spectrum of the H-acid system in Fig. 4, the possibility of the monochelate complex shown in Fig. 5 (V) will be small. Regardless of the presence of 100 mmol dm^{-3} amine derivatives such as 4-aminobenzenesulfonic acid and 6-amino-1,3-naphthalenedisulfonic acid, the solutions containing 10 mmol dm^{-3} boric acid/borate and 50 mmol dm^{-3} salicylaldehyde gave the same spectra as those shown in Fig. 4, indicating that the monochelate complex such as (VI) in Fig. 5 will be unstable. These results suggest that the possible structure is the 1:1 bischelate complex represented by (II) in Fig. 2. If there is a chelate complex with the boron atom having multiple chelate rings, more than one peak is usually observed in the ^{11}B NMR spectrum. In this system, both of the two 1:1 monochelate complexes illustrated in Fig. 5 may not be very stable and may immediately form the bischelate complex. These are the reasons why the interaction between boric acid and Azomethine H provides only one complex.

3.4. Complexation equilibria of the boric acid–Azomethine H system

Similar NMR measurements were performed for solutions containing boric acid, salicylaldehyde and H-acid. The ^{11}B NMR spectra of 5.00 mmol dm^{-3} boric acid and salicylaldehyde solutions to which H-acid had been added at various concentrations at pH 4.94 showed the same peak as that assigned to the complex (Fig. 6). The relative peak area was dependent on the total concentration of H-acid.

Because the reaction of boric acid only with salicylaldehyde or H-acid can be negligible as mentioned above, it was confirmed that the reaction between boric acid and Azomethine H involves two chemical equilibria: one is related to the ligand formation (Eq. (5)) and the other to the complex formation (Eq. (4)).

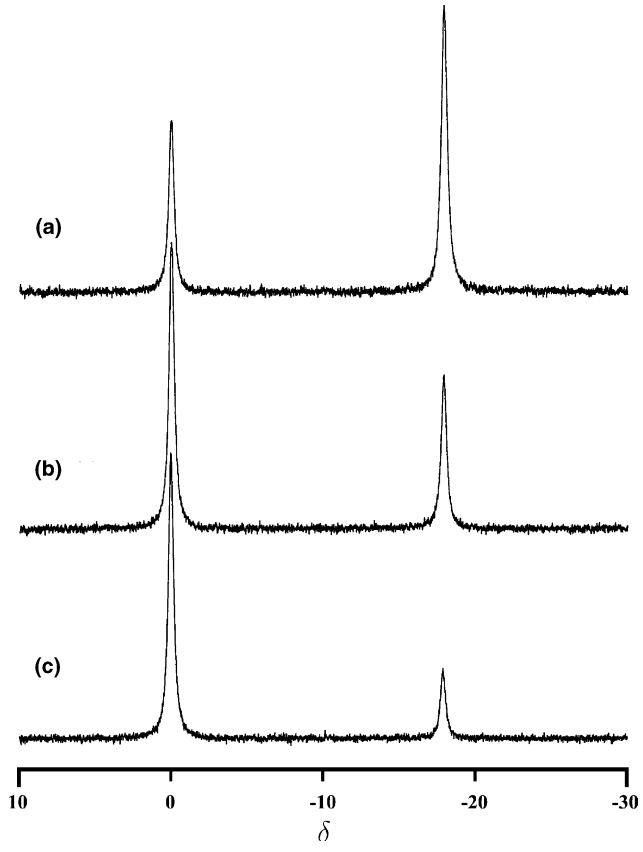

Fig. 6. ^{11}B NMR spectra for the solution containing 5.00 mmol dm^{-3} boric acid, 5.00 mmol dm^{-3} salicylaldehyde and various concentration of H-acid (pH 4.94). ((a) 5.00 mmol dm^{-3}; (b) 2.00 mmol dm^{-3}; (c) 1.00 mmol dm^{-3} H-acid).

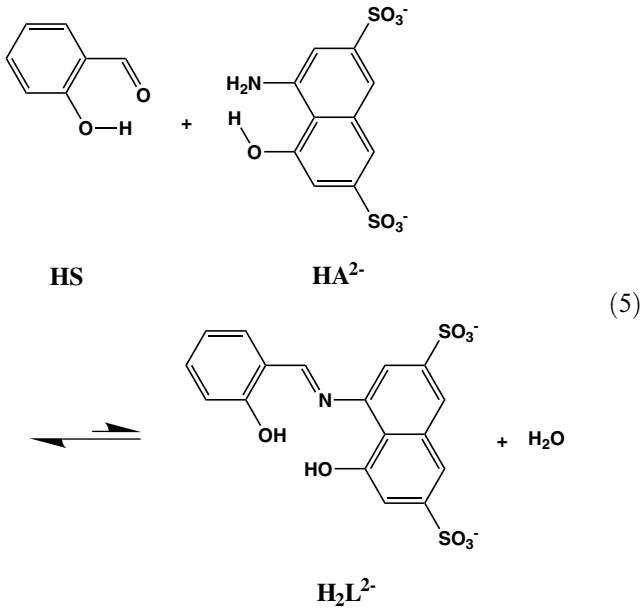

(5)

When dissolved in aqueous solution, almost all of the Azomethine H is hydrolyzed to yield its starting materials. It is well-known that H-acid is unstable in aqueous solution and that the color of Azomethine H solution

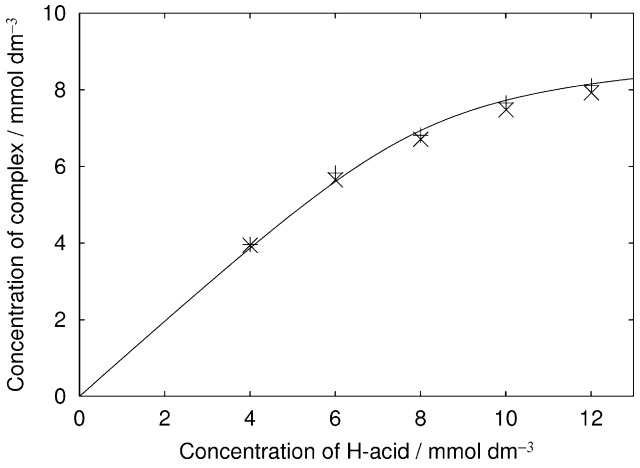

Fig. 7. Effect of increasing concentration of H-acid on the equilibrium concentration of the complex (9.60 mmol dm^{-3} salicylaldehyde, 10.0 mmol dm^{-3} boric acid/borate solution at pH 6.67. Standing time: 1 day (+), 1 week (×)). Solid line: calculated concentration of the complex using the $K_{f(LC)}$ value.

turns brown if the solution is allowed to stand for a long period [2,4,6–8]. The sample solutions containing boric acid, salicylaldehyde and H-acid became apparently browner with the increase in the concentration of uncomplexed H-acid. Fig. 7 shows variations in the equilibrium concentrations of the complex with time at different concentrations of H-acid. Although the changes in sample color resulted in a higher reagent blank for the boron determination, a decrease in the equilibrium concentrations of the complex was not observed. These results indicate that the decomposition of the starting materials of Azomethine H is involved in the reaction.

Fig. 8 shows that the complexation equilibrium is independent on the pH of the solution at least under weakly acidic conditions. Both starting materials of

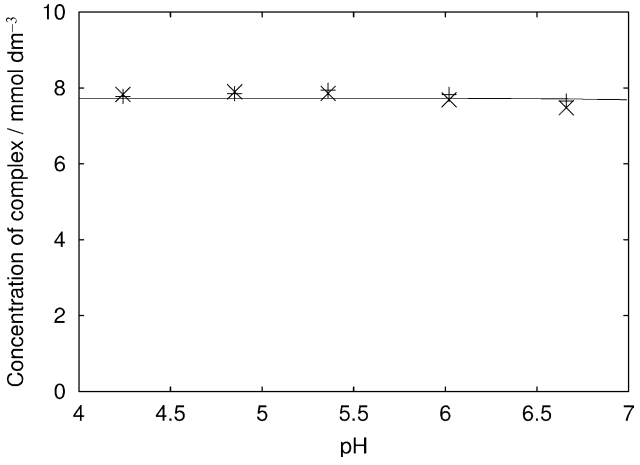

Fig. 8. pH dependence of the equilibrium concentration of the complex (10.0 mmol dm^{-3} salicylaldehyde, boric acid/borate, and H-acid solution. Standing time: 1 day (+), 1 week (×)). Solid line: calculated concentration of the complex using the $K_{f(LC)}$ value.

Azomethine H contain functional groups relating to acid dissociation reactions expressed as follows:

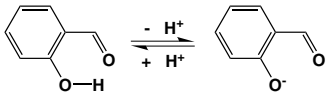

(6)

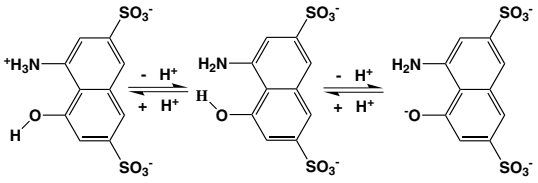

H_2A^- HA^{2-} A^{3-} (7)

Because the Schiff base formation from primary amine and aldehyde proceeds by nucleophilic attack of free amine on the aldehyde [3,24,25], salicylaldehyde condenses with HA^{2-} or A^{3-} of the H-acid species to form Azomethine H. The acid dissociation constant of salicylaldehyde was determined spectrophotometrically to be $10^{-8.14}$ ($I = 0.1$ mol dm^{-3}, KCl, 25 °C), and therefore HS in Eq. (6) is predominant in acidic solution. In the case of H-acid, acid dissociation constants for Eq. (7) were not available from the literature, but the predominant species is supposed to be HA^{2-} in the weakly acidic region because it can form intramolecular hydrogen bonding.

It was concluded that the reaction includes two chemical equilibria with respect to Eqs. (4) and (5). The equilibrium constants ($K_{f(L)}$ and $K_{f(C)}$) are defined by Eqs. (8) and (9), respectively.

$$K_{f(L)} = \frac{[H_2L^{2-}]}{[HS][HA^{2-}]}, \tag{8}$$

$$K_{f(C)} = \frac{[BL^{2-}]}{[H_2L^{2-}][B]}. \tag{9}$$

However, the $K_{f(L)}$ value was too small and could not be experimentally obtained, because the mixed solution of the starting materials did not give any measurable absorption bands due to Azomethine H in the UV and visible regions. Therefore, the overall equilibrium constant, $K_{f(LC)}$, defined by Eq. (10) and the product of $K_{f(L)}$ and $K_{f(C)}$, was estimated

$$K_{f(LC)} = K_{f(L)}K_{f(C)} = \frac{[BL^{2-}]}{[HS][HA^{2-}][B]}. \tag{10}$$

Eq. (11) may account for the overall reaction in this system

$$HS + HA^{2-} + B \rightleftharpoons BL^{2-} + 3H_2O \tag{11}$$

The mass balance equations for the total concentrations of salicylaldehyde (C_S), H-acid (C_A) and boric acid (C_B) are then expressed as follows:

$$C_S = [HS] + [BL^{2-}], \tag{12}$$

$$C_A = [HA^{2-}] + [BL^{2-}], \tag{13}$$

$$C_B = [B] + [BL^{2-}]. \tag{14}$$

The $K_{f(LC)}$ value could be determined based on the relative intensities of the ^{11}B NMR signals. Table 2 shows that the $K_{f(LC)}$ value is constant at $10^{5.91\pm0.07}$ under different conditions.

The equilibrium concentrations of the complex calculated using the constant are compared with those observed experimentally as a function of the total H-acid concentration or pH (Figs. 7 and 8). While almost all of the H-acid reacts to form the bischelate complex in

Table 2
Formation constant for complexation of boric acid with salicylaldehyde and H-acid

pH	C_B[a] /mmol dm^{-3}	C_S[b]/mmol dm^{-3}	C_A[c]/mmol dm^{-3}	[Free B]/mmol dm^{-3}	[complex]/mmol dm^{-3}	log($K_{f(LC)}$/mol^{-2} dm^6)
4.24	10.0	9.57	10.0	2.21	7.79	5.94
4.85			10.0	2.15	7.85	5.99
4.94	5.00	4.96	1.00	4.06	0.94	5.95
			2.00	3.22	1.78	5.89
			3.00	2.53	2.47	5.86
			4.00	2.04	2.96	5.84
			5.01	1.71	3.29	5.82
5.36	10.0	9.57	10.0	2.05	7.95	6.06
6.02			10.0	2.16	7.84	5.98
6.67			8.01	3.17	6.83	5.83
			10.0	2.33	7.67	5.87
			12.0	1.88	8.12	5.89
						5.91 ± 0.07

[a] C_B, total concentration of boric acid.
[b] C_S, total concentration of salicylaldehyde.
[c] C_A, total concentration of H-acid.

the presence of excessive amounts of boric acid and salicylaldehyde, increased proportions of the H-acid did not produce any new peaks due to other unexpected complexation reactions. The experimental results were on the calculated solid lines. These figures show that the lines reproduce well the experimental results and that the $K_{f(LC)}$ value can be applicable to any experiments under different conditions. Our results, thus obtained, offer some useful information for optimization of the conditions for boron determination. The Azomethine H method can be performed using a mixed solution of the salicylaldehyde and H-acid instead of their condensation product, as suggested by Harp [10] and Staden [7]. By keeping the H-acid concentration low enough to form the chelate complex, the reagent blank for the boron determination due to the decomposition of H-acid can be reduced as much as possible.

As mentioned above, the $K_{f(L)}$ value was too small and could not be experimentally obtained. On the assumption that the molar absorptivities of Azomethine H are similar to those of its boric acid complex (e.g., 10^3 mol^{-1} dm^3 cm^{-1} at 412 nm), the $K_{f(L)}$ value was roughly calculated. The absorbance of the mixture solution of the starting materials at 10^{-3} mol dm^{-3} was almost the same as the sum of the absorbances of their individual solutions and the difference was less than 0.01. The equilibrium Azomethine H concentration in the mixture solution was estimated to be lower than 10^{-5} mol dm^{-3} and the $K_{f(L)}$ value to be less than 10. Therefore, the $K_{f(C)}$ value should be greater than 10^5. This complexation constant is comparable to those of the most stable 1:2 bischelate complexes (approximately 10^6) [16]. On the contrary, the 1:1 bischelate complex formation constant is much greater than that of the corresponding complex with triethanolamine [18]. Such a large stability is due to the structures of the complex and the ligand. The bischelate complex may be stabilized by the delocalized sp^2 character of the ligand. Intramolecular hydrogen bonding allows the conformation of the free ligand to be that shown in Fig. 1, and the structure is suitable for interaction with boric acid to form the complex.

4. Conclusion

The Azomethine H method is a practical spectrophotometric method for boron analysis applicable under mild conditions. However, the interaction of boric acid with Azomethine H has been unclear for a long time. There are some possible complexes shown in Fig. 2, or a possibility that light absorption in the visible region can only be due to the free ligand. In this work, the complexation of boric acid with Azomethine H could be quantitatively clarified by a ^{11}B NMR study: the starting materials of Azomethine H (H-acid and salicylaldehyde) yield the 1:1 bischelate complex including B–N bonding only in the presence of boric acid.

Acknowledgements

This work was partially supported by the Steel Industry Foundation for the Advancement of Environmental Protection Technology.

References

[1] R. Capelle, Anal. Chim. Acta 24 (1964) 555.
[2] W.D. Basson, R.G. Böhmer, D.A. Stanton, Analyst 94 (1969) 1135.
[3] W.D. Basson, P.P. Pille, A.L. Du Preez, Analyst 99 (1974) 168.
[4] D.A. Oxspring, S. Mclean, E. O'Kane, W.F. Smyth, Anal. Chim. Acta 317 (1995) 295.
[5] R.A. Edwards, Analyst 105 (1980) 139.
[6] M.K. John, H.H. Chuab, J.H. Neufeld, Anal. Lett. 8 (1975) 559.
[7] D.L. Harp, Anal. Chim. Acta 346 (1997) 373.
[8] K. Nose, M. Zenki, Y. Shimoishi, Bunseki Kagaku 42 (1993) 351.
[9] F.J. Krug, J. Mortatti, L.C.R. Pessenda, E.A.G. Zagatto, H. Bergamin F, Anal. Chim. Acta 125 (1981) 29.
[10] J. Koos, F. van Staden, T.A. van der Merwe, Analyst 125 (2000) 2094.
[11] K. Ishihara, Y. Mouri, S. Funahashi, M. Tanaka, Inorg. Chem. 30 (1991) 2356.
[12] K. Yoshimura, Y. Miyazaki, S. Sawada, H. Waki, J. Chem. Soc., Faraday Trans. 92 (1996) 651.
[13] T.M. Suzuki, D.A.P. Tanaka, T. Yokoyama, Y. Miyazaki, K. Yoshimura, J. Chem. Soc., Dalton Trans. 10 (1999) 1639.
[14] K. Yoshimura, Y. Miyazaki, F. Ota, S. Matsuoka, H. Sakashita, J. Chem. Soc., Faraday Trans. 94 (1998) 683.
[15] C. Shao, Y. Miyazaki, S. Matsuoka, K. Yoshimura, H. Sakashita, Macromolecules 33 (1) (2000) 19.
[16] C. Shao, S. Matsuoka, Y. Miyazaki, K. Yoshimura, T.M. Suzuki, D.A.P. Tanaka, J. Chem. Soc., Dalton Trans. (2000) 3136.
[17] Y. Miyazaki, K. Yoshimura, Y. Miura, H. Sakashita, K. Ishimaru, Polyhedron 22 (2003) 909.
[18] A. Sonoda, N. Takagi, K. Ooi, T. Hirotsu, Bull. Chem. Soc. Jpn. 71 (1998) 161.
[19] M. van Duin, J.A. Peters, A.P.G. Kieboom, H. van Bekkum, Tetrahedron 40 (1984) 2901.
[20] M. van Duin, J.A. Peters, A.P.G. Kieboom, H. van Bekkum, Tetrahedron 41 (1985) 3411.
[21] J.G. Dawber, S.I.E. Green, J.C. Dawber, S. Gabrail, J. Chem. Soc. Faraday Trans. 1 84 (1988) 41.
[22] S. Chapelle, J.-F. Verchere, Tetrahedron 44 (1988) 4469.
[23] N. Obi, M. Katayama, J. Sano, Y. Kojima, Y. Shigemitsu, B. Takada, New J. Chem. 22 (1998) 933.
[24] C.V. McDonnell Jr., M.S. Michailidis, R.B. Martin, J. Phys. Chem. 74 (1970) 26.
[25] E.H. Cordes, W.P. Jencks, J. Am. Chem. Soc. 85 (1963) 2843.

Available online at www.sciencedirect.com
SCIENCE DIRECT®
Polyhedron 23 (2004) 963–967
POLYHEDRON
www.elsevier.com/locate/poly

Synthesis and crystal structure of a mononuclear iron(III) (η^2-acetato) complex of a β-*cis* folded salen type ligand ☆

Jesús Sanmartín *, Ana M. García-Deibe, Matilde Fondo, Débora Navarro, Manuel R. Bermejo

Departemento de Química Inorgánica, Facultade de Química, Universidade de Santiago de Compostela, Campus Sur, Santiago de Compostela 15782, Spain

Received 25 November 2003; accepted 3 December 2003

Abstract

$Fe(H_2SB)(\eta^2\text{-}O_2CMe)\cdot MeCN$ [H_4SB: *N*,*N*′-bis(5-hydroxysalicylidene)-1,4-diaminobutane] was synthesised via an electrochemical procedure and its crystal structure was determined. The metal ion assumes a distorted octahedral coordination geometry that involves the two O-atoms of a chelating acetate and the N_2O_2 compartment of the bisdeprotonated diimine, which is asymmetrically folded in a β-*cis* arrangement. Moderate hydrogen bonds between adjacent complex molecules, which also interact with lattice acetonitrile molecules, lead to a linear interaction, predominant in the crystal packing.
© 2004 Elsevier Ltd. All rights reserved.

Keywords: Iron complexes; Acetate ligands; η^2-Coordination modes; Schiff bases; β-Cis arrangements

1. Introduction

Iron(III) complexes of salen type ligands have received considerable attention as potential models for biologically important enzymes [1] and oxidation catalysts [2]. As a result, some crystal structures of Fe(salen)X complexes, where X is a potentially chelating or bridging ligand such as catecol, hydroquinone, phenanthrenesemiquinone or acetylacetone, have been described [3].

Carboxylato complexes in general and acetato ones, in particular, have also been subject to much interest [4], since they are present in some important enzymes. Among the coordinating modes of the acetate ligand, η^1 and μ modes are very common, whereas the chelating behaviour is not very frequent both for iron proteins and complexes [5].

In the course of our efforts to prepare building-blocks [6] capable of linking two remote moieties yielding trinuclear complexes [7], we have obtained $Fe(H_2SB)(\eta^2\text{-}O_2CMe)\cdot MeCN$, where H_4SB is *N*,*N*′-bis(5-hydroxysalicylidene)-1,4-diaminobutane (Fig. 1).

2. Experimental

2.1. Materials and methods

Chemicals of the highest commercial grade available (Aldrich) were used as received. An iron metal plate (Aldrich) was washed with a dilute hydrochloric acid solution prior to electrolysis.

Elemental analyses were performed on a Carlo Erba EA 1108 analyser. Mass spectra (ES) were recorded on a LC/MSD Hewlett–Packard 1100 spectrometer with methanol and formic acid (3%) as solvent. The samples had been previously dissolved in dimethylsulfoxide. NMR spectra were recorded on a Bruker 300 AC spectrometer, using DMSO as solvent. Infrared spectra were recorded as KBr pellets on a Bio-Rad FTS 135 spectrophotometer in the range of 4000–600 cm^{-1}. Magnetic susceptibility measurements were performed

☆ Supplementary data associated with this article can be found, in the online version, at doi:10.1016/j.poly.2003.12.011.

* Corresponding author. Tel.: +34-981-591076; fax: +34-981-597525.
E-mail address: qisuso@usc.es (J. Sanmartín).

0277-5387/$ - see front matter © 2004 Elsevier Ltd. All rights reserved.
doi:10.1016/j.poly.2003.12.011

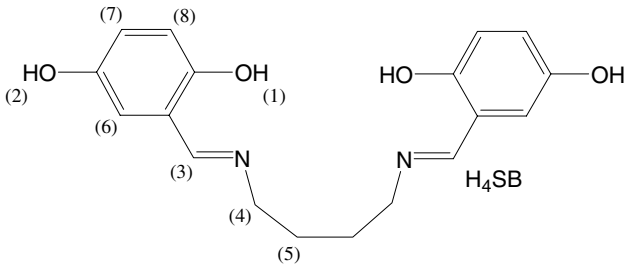

Fig. 1. Schematic representation of H_4SB.

at room temperature on pulverised samples using a Sherwood Scientific magnetic susceptibility balance.

2.2. Ligand synthesis

N,*N*′-Bis(2,5-dihydroxybencylidene-1,4-diaminobutane), H_4SB, has been prepared by condensation in chloroform (80 ml) of 2,5-dihydroxybenzaldehyde (1.0 g, 7.2 mmol) with 1,4-diaminobutane (0.32 g, 3.6 mmol). The solution was heated at reflux over a 3 h period and subsequently concentrated in vacuum. The orangey precipitate formed was collected by filtration, washed with diethyl ether (15 ml), and dried in vacuum. Yield: 1.11 g (93%). m.p.: 195 °C. *Anal.* Calc. for $C_{18}H_{20}N_2O_4$: C, 65.85; H, 6.10; N, 8.54. Found: C, 65.56; H, 5.89; N, 8.38%. ES-MS (0 V): 329.0 m/z (82%, M^+). FT-IR (KBr): ν(O–H)$_{OH}$ 3434 (b) and 3258 (b), ν(C=N) 1643 (s), ν(C–H) 1461 (vs), ν(C–O) 1258 (m). ^{1}H NMR (DMSO-d_6, 300 MHz) 12.71 (2H, s, H_1), 8.99 (2H, s, H_2), 8.46 (2H, s, H_3), 6.72–6.40 (6H, m, H_{6-8}), 3.60 (4H, t, H_4), 1.67 (4H, t, H_5).

2.3. Complex synthesis

An acetonitrile solution (80 cm^3) of H_4SB (0.100 g, 0.305 mmol), dipyridyl ketone (0.112 g, 0.609 mmol) and acetic acid (0.036 g, 0.609 mmol), containing about 40 mg of tetramethylammonium perchlorate, was electrolysed [8] for 1 h 40 min using a 10 mA current intensity with an initial voltage of 11.1 V. **Caution:** *Although no problem has been encountered in this work, all perchlorate compounds are potentially explosive, and should be handled in small quantities with great care*! After filtration of the resulting solution, its slow evaporation allowed the obtaining of blackish plate-shaped crystals of Fe(H_2SB)(η^2-O_2CMe)·MeCN, suitable for X-ray diffraction studies. Yield: 0.037 g (25%). *Anal.* Calc. for $C_{22}H_{24}FeN_3O_6$: C, 54.79; H, 5.02; N, 8.71. Found: C, 53.97; H, 4.99; N, 8.53%. ES-MS: 383.1 m/z (100%, M^+–O_2CMe–MeCN). FT-IR (KBr): ν(O–H)$_{OH}$ 3323 (s), ν(C=N) 1613 (vs), $\nu_{asym}(CO_2)$ 1558 (s), ν(C–H) 1472 (vs), $\nu_{sym}(CO_2)$ 1455 (sh,s) ν(C–O) 1296 (vs) cm^{-1}. μ (295 K): 6.2 BM.

Table 1
Crystal and structure refinement data for Fe(H_2SB)(η^2-O_2CMe)·MeCN

Empirical formula	$C_{22}H_{24}FeN_3O_6$
Molecular weight	482.29
Crystal system	monoclinic
Space group	$P2_1/n$ (No. 14)
a (Å)	10.417(2)
b (Å)	19.244(3)
c (Å)	12.179(2)
β (°)	113.481(3)
V (Å^3)	2239.1(6)
T (K)	293(2)
Z	4
μ (Mo Kα) (mm^{-1})	0.717
Number of reflections collected	9331
Number of independent reflections	3783
R_{int}	0.0589
Data/restraints/parameters	3783/0/298
R_1, $wR_2[I > 2\sigma(I)]$	0.0495, 0.0963
R_1, wR_2 (all data)	0.1147, 0.1242
Residuals (e Å^{-3})	0.605, −0.507

2.4. Single-crystal X-ray diffraction studies

X-ray data were collected at room temperature on a Bruker Smart-CCD-1000 diffractometer, using graphite-monochromated Mo Kα radiation ($\lambda = 0.71073$ Å). Data collection and processing were carried out using the Bruker SMART programs [9] and empirical absorption correction was applied using SADABS [10]. The structure was solved by direct methods, and refined by full-matrix least-squares based on F^2 using SHELX-97 software [11]. All non-hydrogen atoms were anisotropically refined. Hydrogen atoms were included at geometrically calculated positions with thermal parameters derived from the parent atoms. Table 1 provides a summary of crystal data, data collection and refinement parameters.

3. Results and discussion

The obtaining of H_4SB had been previously reported [7], however, its detailed synthesis and characterisation had not been previously described. With respect to Fe(H_2SB)(η^2-O_2CMe)·MeCN, this was obtained by an electrochemical method [8] in an attempt to prepare an iron complex of di-2-pyridylmethanediol and *N*,*N*′-bis(5-hydroxysalicylidene)-1,4-diaminobutane ligands.

The analytical, ES-MS and IR data led us to postulate the obtaining of Fe(H_2SB)(η^2-O_2CMe)·MeCN, its magnetic moment at room temperature being in agreement with a high-spin d^5 octahedral configuration [12]. The substantial decrease of the ν(C=N) band (30 cm^{-1}) joint to the increase of the ν(C–O) frequency (38 cm^{-1}), compared to the free ligand spectrum, are in agreement with the participation of the phenol and imine donor

atoms in the coordination to the metal centre [8]. The observation of only one of the O–H vibration bands, at about 3323 cm^{-1}, reveals the bideprotonation of H_2SB^{2-}, where the 5-hydroxy positions on each benzylidene ring remain protonated. The two strong bands arising from the C–O stretching vibrations show a frequency difference of 103 cm^{-1}, which according to the literature [5e] corresponds to a chelating coordination mode of the acetate group.

3.1. Single-crystal X-ray diffraction studies of $Fe(H_2SB)(\eta^2\text{-}O_2CMe)\cdot MeCN$

The molecular structure of the complex is represented in Fig. 2, with the atom labelling scheme used in Table 2, which lists the most relevant bond distances and angles. The asymmetric unit consists of a discrete molecule of $Fe(H_2SB)(\eta^2\text{-}O_2CMe)$ interacting with a lattice acetonitrile molecule.

In $Fe(H_2SB)(\eta^2\text{-}O_2CMe)\cdot MeCN$, the iron(III) centre is coordinated in a distorted octahedral fashion by H_2SB^{2-} acting as a typical N_2O_2-donor and a chelating acetate ligand. The latter occupies two of the equatorial coordination sites [O(5) and O(6)], whilst the Schiff base fills a meridian [O(4)N(2)N(1)] of the octahedron and the remaining equatorial position [O(1)]. This asymmetric folding of the diimine conforms to the β-*cis* arrangement shown in Fig. 3. Despite it being easier to achieve with a flexible spacer such as $(CH_2)_4$, it is a not very frequent arrangement in mononuclear octahedral complexes of salen-type ligands. The majority of these are *trans* arranged (Fig. 3), but the β-*cis* conformation is adopted by Fe(salen)X complexes when X behaves as *cis* chelating [3a]. Electrochemical studies on $M(R_2\text{-salen})(N'Bu)_2$ (where M = Mo or W) allowed the conclusion that the adoption of the β-*cis* conformation is apparently dictated by electronic rather than steric factors [13].

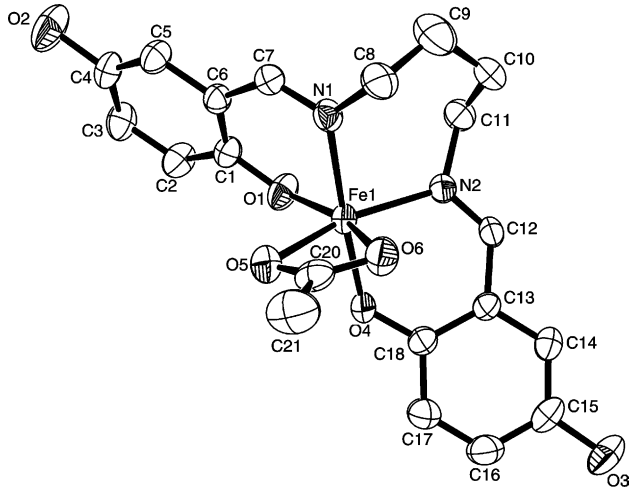

Fig. 2. ORTEP view of $Fe(H_2SB)(\eta^2\text{-}O_2CMe)$. Ellipsoids are drawn at 50% probability. The acetonitrile molecule and parentheses are omitted for clarity.

Table 2
Selected bond distances (Å) and bond angles (°) for $Fe(H_2SB)(\eta^2\text{-}O_2CMe)\cdot MeCN$

Bond lengths				
Fe(1)–O(1)	1.863(3)			
Fe(1)–O(4)	1.903(3)			
Fe(1)–N(1)	2.136(4)			
Fe(1)–N(2)	2.081(4)			
Fe(1)–O(5)	2.131(3)			
Fe(1)–O(6)	2.186(3)			
Fe(1)–C(20)	2.505(5)			
Bond angles				
O(1)–Fe(1)–O(4)	96.24(14)			
O(1)–Fe(1)–N(1)	87.82(14)			
O(1)–Fe(1)–N(2)	107.49(15)			
O(1)–Fe(1)–O(5)	97.82(15)			
O(1)–Fe(1)–O(6)	157.62(14)			
O(4)–Fe(1)–N(1)	175.86(14)			
O(4)–Fe(1)–N(2)	87.85(14)			
O(4)–Fe(1)–O(5)	91.53(14)			
O(4)–Fe(1)–O(6)	90.73(13)			
N(1)–Fe(1)–O(6)	85.79(14)			
N(2)–Fe(1)–O(5)	154.60(14)			
N(2)–Fe(1)–O(6)	93.97(14)			
N(2)–Fe(1)–N(1)	90.16(15)			
O(5)–Fe(1)–N(1)	88.71(14)			
O(5)–Fe(1)–O(6)	60.64(13)			
Torsion angles				
N(1)–C(8)–C(9)–C(10)	−69.9(7)			
C(8)–C(9)–C(10)–C(11)	63.1(8)			
C(9)–C(10)–C(11)–N(2)	−88.9(6)			
H bonds				
D–H···A	*d*(D–H)	*d*(H···A)	*d*(D···A)	∠(DHA)
O(2)–H(2A)···O(6)[a]	0.68(5)	2.09(6)	2.741(6)	162(7)
O(3)–H(3A)···N(1S)	0.67(5)	2.15(6)	2.782(9)	158(8)

[a] Symmetry transformations used to generate equivalent atoms: $x-1, y, z$.

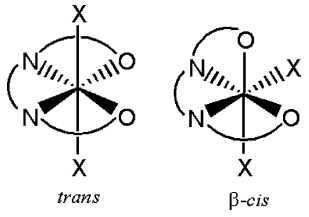

Fig. 3. Schematic representation and nomenclature of two possible geometries for complexes of the type $M(N_2O_2)X_2$.

Although the ribonucleotide reductase iron protein (RR B2) [5c] and other model polynuclear iron complexes, such as $[Fe_2(Py)_2(O_2CMe)_5(OH_2)]Et_4N$ or $[Fe_3(O)(O_2CMe)_7(OH_2)]Et_4N$ [5d], contain terminal η^2-acetato groups, this coordination mode is rather infrequent both for Fe(III) and Fe(II) ions [5]. Thus, to the best of our knowledge $Fe(H_2SB)(\eta^2\text{-}O_2CMe)\cdot MeCN$ is the first example of a mononuclear iron (η^2-acetato)

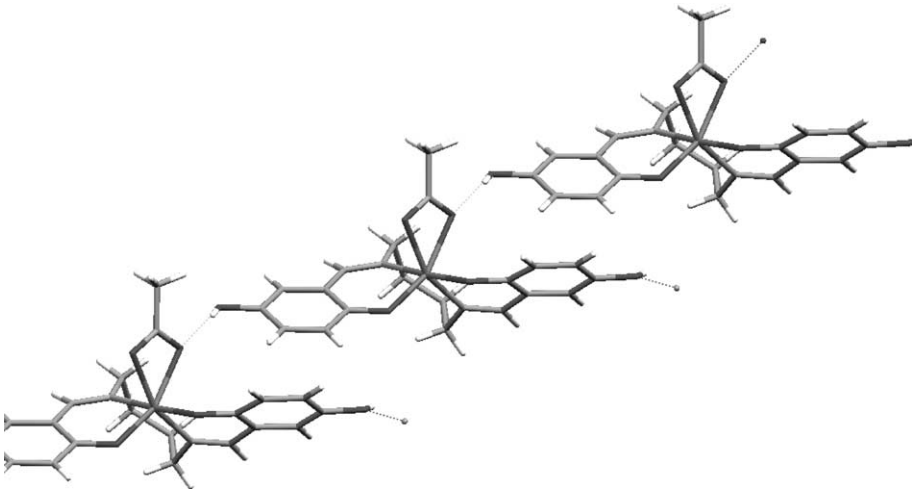

Fig. 4. Stick representation of three molecules of $Fe(H_2SB)(\eta^2\text{-}O_2CMe)$ connected by H bonds between the acetate and one of the outer phenol groups. Each complex molecule is also interacting with an acetonitrile molecule through the remaining protonated phenol group but they have been omitted for clarity.

complex, at least of salen type ligands. This *cis* chelating behaviour of the acetate ligand could be allowed by the flexibility of the Schiff base ligand. Thus, $[Fe^{III}(salen)(\mu\text{-}O_2CMe)]_n$ shows linear polymerisation through bridging bidentate acetate groups [14] with a typical *trans* arrangement of the more rigid ligand (Fig. 3). By contrast, $salbn^{2-}$, which contains the same spacer as $H_2SB_2^-$, assumes the β-*cis* folding even with monodentate ligands such as MeO^- in $[Fe(salbn)(\mu\text{-}OMe)]_2$ [12]. The flexibility, as well as the strain, of the *gauche* conformed $(CH_2)_4$ chain of $H_2SB_2^-$ is revealed by the torsion angles, that also show that one of the bonds is almost eclipsed (Table 2).

In general, although the Fe–N and Fe–O distances related to the Schiff base ligand could be considered within the usual ranges reported for Fe(III) complexes of N,O-donor ligands [14–16], the equatorial bonds (in *trans* positions with respect to the acetate group) are shorter than the apical ones, Fe(1)–(O1) being especially short. With regard to the acetate group, both angles and distances are within the common ranges found for Fe(III) complexes [5d,15] and even for Fe(II) ones [5b,5d], since they are not very different in that respect.

The presence of the outer phenol groups is significant, since they give rise to an H bonding scheme, apart from some C–H$\cdots\pi$ interactions, that is essential for the crystal packing. One of the external phenolic O atoms, O(3), interacts with an acetonitrile molecule, whereas the other one is connected to an acetate group of a neighbouring complex molecule. This interaction leads to an almost linear ''polymerisation'' based on moderate H bonds [17] along the *a* direction (Fig. 4). Since the external phenolic groups, O(2) and O(3), remain protonated and uncoordinated, they allow the additional, and previously confirmed, possibility to behave as a building-block [7].

4. Conclusions

We have synthesised by an electrochemical procedure $Fe(H_2SB)(\eta^2\text{-}O_2CMe)\cdot MeCN$. The Fe(III) ion assumes a distorted octahedral coordination geometry, afforded by the N_2O_2-donor set of the dianionic diimine and two oxygen atoms of an acetate group. Despite its simplicity, two features of $Fe(H_2SB)(\eta^2\text{-}O_2CMe)\cdot MeCN$ can provide some interest from the point of view of the coordination chemistry: (i) the acetate is coordinated in a hitherto unfamiliar η^2 mode for mononuclear iron complexes; (ii) the Schiff base ligand is β-*cis* folded. These seem to be related, since the atypical chelating coordination of the acetate group could be favoured by the diimine flexibility, and the *cis* chelating behaviour of the acetate involves the β-*cis* folding of the Schiff base.

5. Supplementary material

Crystallographic data for the structural analysis are deposited with the Cambridge Crystallographic Data Centre, CCDC with deposition number CCDC 220996. Copies of this information can be obtained from Cambridge Crystallographic Data Centre, 12 Union Road, Cambridge CB2 1EZ, UK (fax: +44-1223-336033; e-mail: deposit@ccdc.cam.ac.uk or www: http://www.ccdc.cam.ac.uk).

Acknowledgements

The authors are grateful to Xunta de Galicia (PGIDIT03PXIB20901PR) for financial support.

References

[1] (a) L. Que Jr., A.E. True, Prog. Inorg. Chem. 38 (1990) 97;
(b) L. Que Jr., Coord. Chem. Rev. 50 (1983) 73.

[2] A. Boettcher, M.W. Grinstaff, J.A. Labinger, H.B. Gray, J. Mol. Catal. A 113 (1996) 191.

[3] (a) R.B. Lauffer, R.H. II Heistand, L. Que Jr., Inorg. Chem. 22 (1983) 50;
(b) R.H. II Heistand, A.L. Roe, L. Que Jr., Inorg. Chem. 21 (1982) 676.

[4] (a) W.H. Armstrong, A. Spool, G.C. Papaevthymiou, R.B. Frankel, S.J. Lippard, J. Am. Chem. Soc. 106 (1984) 3653;
(b) I.M. Arafa, H.M. Goff, S.S. David, B.P. Murch, L. Que Jr., Inorg. Chem. 26 (1987) 2779.

[5] (a) S. Ogo, R. Yamahara, M. Roach, T. Suenobu, M. Aki, T. Ogura, T. Kitagawa, H. Masuda, S. Fukuzumi, Y. Watanabe, Inorg. Chem. 41 (2002) 5513;
(b) D. Coucouvanis, R.A. III Reynolds, W.R. Dunham, J. Am. Chem. Soc. 117 (1995) 7570;
(c) P. Nordlund, H. Eklund, J. Mol. Biol. 232 (1993) 123;
(d) R.A. Reynolds III, W.R. Dunham, D. Coucouvanis, Inorg. Chem. 37 (1998) 1232;
(e) P. Poganiuch, S. Liu, G.C. Papaefthymiou, S.J. Lippard, J. Am. Chem. Soc. 113 (1991) 4645.

[6] J. Sanmartín, A.M. García-Deibe, M. Fondo, D. Navarro, M.R. Bermejo, Inorg. Chem. Commun. 7 (2004) 311.

[7] (a) S.M. Kagwanja, D.J. Jones, J.P. Maher, J.A. McCleverty, Polyhedron 13 (1994) 2615;
(b) S.M. Kagwanja, D.J. Jones, J.A. McCleverty, Polyhedron 16 (1997) 1439.

[8] J. Sanmartín, M.R. Bermejo, A.M. García-Deibe, M. Maneiro, C. Lage, A.J. Costa-Filho, Polyhedron 19 (2000) 185.

[9] SMART: Bruker Molecular Analysis Research Tool V 5.5054, Bruker AXS Inc., Madison, WI, USA, 1998.

[10] SADABS: Area-Detector Absorption Correction, Siemens Industrial Automation Inc., Madison, WI, USA, 1996.

[11] G.M. Sheldrick, SHELX-97 (SHELXS-97 and SHELXL-97): Programs for Crystal Structure Analyses, University of Göttingen, Göttingen, Germany, 1998.

[12] S. Negoro, H. Asada, M. Fujiwara, T. Matsushita, Inorg. Chem. Commun. 6 (2003) 357.

[13] M. Motevalli, A.D. Oduwole, B.C. Parkin, R. Ramnauth, A.C. Sullivan, N. Kaltsoyannis, J. Chem. Soc., Dalton Trans. (2003) 3591.

[14] G. Liu, A.M. Arif, F.W. Bruenger, S.C. Miller, Inorg. Chim. Acta 287 (1999) 109.

[15] M. Mikuriya, Y. Hashimoto, S. Nakashima, Chem. Commun. (1996) 295.

[16] (a) L. He, Q.-F. Shi, S.-H. Gou, M. Qian, C.-Y. Duan, Acta Crystallogr., Sect. C 46 (1999) 46;
(b) T. Nakamura, E. Kuranuki, K. Niwa, M. Fujiwara, T. Matsushita, Chem. Lett. (2000) 248;
(c) J. Reglinski, M. Patykiewicz, Acta Crystallogr., Sect. E 58 (2002) m543;
(d) Y. Miyasato, Y. Nogami, M. Ohba, H. Sakiyama, H. Okawa, Bull. Chem. Soc. Jpn. 76 (2003) 1009.

[17] T. Steiner, Angew. Chem. Int. Ed. 41 (2002) 48.

Available online at www.sciencedirect.com
SCIENCE DIRECT®
Polyhedron 23 (2004) 969–978
POLYHEDRON
www.elsevier.com/locate/poly

Synthesis, EPR and Mössbauer spectral studies of new iron(III) complexes with 2-benzoylpyridine-N(4), N(4)-(butane-1,4-diyl) thiosemicarbazone (HBpypTsc): X-ray structure of $[Fe(BpypTsc)_2]FeCl_4 \cdot 2H_2O$ and the free ligand

Anandaram Sreekanth [1], M.R. Prathapachandra Kurup *

Department of Applied Chemistry, Cochin University of Science and Technology, Kochi 682 022, Kerala, India

Received 11 August 2003; accepted 9 December 2003

Abstract

Three novel iron(III) complexes of 2-benzoylpyridine N(4), N(4)-(butyl-1,4-diyl) thiosemicarbazone (HBpypTsc), $[Fe(BpypTsc)_2]ClO_4$ (**1**), $[Fe(BpypTsc)_2]NO_3$ (**2**) and $[Fe(BpypTsc)_2]FeCl_4$ (**3**) were synthesized and physico-chemically characterized by means of partial elemental analyses, magnetic measurements (polycrystalline state), UV–Vis and IR spectroscopies. The spin Hamiltonian parameters, isomer shifts and quadrupolar splitting values of the complexes were assigned by variable temperature EPR and Mössbauer spectra. The presence of a spin-paired iron(III) cation with $d_{xz}^2 d_{yz}^2 d_{xy}^1$ ground state is revealed by the simulated EPR spectral data. The structures of the free ligand HBpypTsc and one of the complexes $[Fe(BpypTsc)_2]FeCl_4$ (**3**) were solved by single crystal X-ray diffraction which authenticated a FeN_4S_2 octahedral coordination in the complex, as envisaged from the spectral data. All complexes except $[Fe(BpypTsc)_2]FeCl_4$ (**3**) were found to be low-spin $S = 1/2$ ($^2T_{2g}$), whereas **3** was found to have both low-spin ($^2T_{2g}$) and high-spin ($^6A_1$) centres.
© 2004 Elsevier Ltd. All rights reserved.

Keywords: Iron(III) complexes; Thiosemicarbazone; Single crystal X-ray diffraction; Mössbauer spectra; EPR spectra; IR spectra

1. Introduction

The discovery of a low-spin ($S = 1/2$) non-heme $[Fe^{III}N_2S_3]$ centre in the enzyme nitrile hydratase has raised interest in mononuclear model iron(III) complexes with N, S coordination [1,2]. Several groups have structurally characterized iron(III) complexes with N_xS_y coordination and compared their spectroscopic properties with the biological iron site [3,4]. The well-documented biological activities of several heterocyclic thiosemicarbazones have often attributed to a chelation phenomenon with transition metal ions [5]. The success in therapeutic applications of N-heterocyclic thiosemicarbazones for removing excess iron from iron-loaded mice through chelation therapy is quite remarkable [6]. We have previously examined the chelation behavior of some O–N–S and N–N–S donor thiosemicarbazones with several transition metal ions with the aim of gaining more information about their nature of coordination and related structural, spectral and biological properties [7–11]. There are some interesting reports on the iron(III) complexes of biologically active 2-acetylpyridine thiosemicarbazones [12,13]. This paper discusses the syntheses and spectral studies of three iron(III) complexes with the title ligand 2-benzoylpyridine N(4), N(4)-(butane-1,4-diyl)thiosemicarbazone (HBpypTsc) (Scheme 1). A previously reported complex of a 2-acetylpyridine thiosemicarbazone prepared from $FeCl_3$, gave a stoichiometry $FeLCl_2$ which suggested it to be a five-coordinate iron(III) complex having an

* Corresponding author. Tel.: +91-484-2575804; fax: +91-484-2577595.
E-mail addresses: sran@esr.phys.chem.ethz.ch (A. Sreekanth), mrp@cusat.ac.in (M.R.P. Kurup).
[1] Present address: Laboratorium für Physikalische Chemie, Eidgenössische Technische Hochschule, Honggerberg, CH-8093, Zurich, Switzerland. Tel.: +41-1-6325702; fax: +41-1-6321538.

0277-5387/$ - see front matter © 2004 Elsevier Ltd. All rights reserved.
doi:10.1016/j.poly.2004.01.006

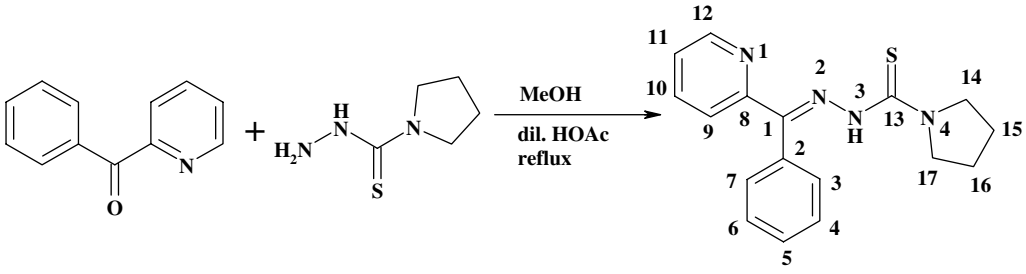

Scheme 1.

intermediate spin state [14]. However the structural information as well as the spectral information obtained for a similar compound, **3** in our case, confirmed that the previous report could be incorrectly formulated.

2. Experimental

2.1. General

2-Benzoylpyridine (Lancaster), ferric chloride (Merck) and ferric nitrate (Merck) was used as received. Ferric perchlorate was prepared from ferric carbonate by digesting it with perchloric acid followed by evaporating the solution on a sand bath followed by subsequent cooling. *Caution! Perchlorate salts are potentially explosive and should be handled with care.* Pyrrolidine-1-thiocarboxylic acid hydrazide was synthesized by adopting and modifying a reported procedure [15]. All solvents were distilled before use.

2.2. Synthesis of HBpypTsc

To a solution of pyrrolidine-1-thiocarboxylic acid hydrazide (0.1 mol) and 2-benzoylpyridine (0.1 mol) in 20 mL methanol, 2 drops of conc. acetic acid was added and the reaction mixture was heated under reflux for 5 h. The reaction mixture was kept for 3 days where the deep yellow colored crystals of HBpypTsc began to separate in a decent yield with satisfactory analytical data. X-ray quality single crystals of the compound were grown from a solution of the compound HBpypTsc in chloroform layered with methanol in 3 days. Melting point 185–186 °C. ^{1}H NMR δ (ppm): NH, 14.3, singlet 1H; 8.73, doublet, aromatic, 1H, $J = 7.5$ Hz; 8.5, aromatic, doublet, 1H; 7.1–7.8, aromatic, multiplet, 7H, 3.8, aliphatic, multiplet, 4H, 1.9, aliphatic, multiplet, 4H.

2.3. Synthesis of $[Fe(BpypTsc)_2]ClO_4$ (**1**)

To a methanolic solution of ferric perchlorate (1 mmol) was added a solution of HBpypTsc (2 mmol) in chloroform and the mixture was refluxed for 30 min. The resulting deep green colored solution was evaporated to half its volume. On cooling dark brown shining crystals of compound **1** separated out and were washed with ether and dried over P_4O_{10} in vacuo.

2.4. Synthesis of $[Fe(BpypTsc)_2]NO_3$ (**2**)

To a methanolic solution of ferric nitrate (1 mmol) was added a solution of HBpypTsc (2 mmol) in chloroform and the mixture was refluxed for 30 min. The resulting deep green colored solution was evaporated to half of its volume. On cooling dark brown shining crystals of compound **2** separated out and were washed with ether and dried over P_4O_{10} in vacuo.

2.5. Synthesis of $[Fe(BpypTsc)_2]FeCl_4$ (**3**)

To a methanolic solution of ferric chloride (1 mmol) was added a solution of HBpypTsc (1 mmol) in chloroform and the mixture was refluxed for 30 min. The resulting deep green colored solution was evaporated to half its volume. On cooling dark brown shining crystals of compound **3** separated out and were washed with ether and dried over P_4O_{10} in vacuo. X-ray quality single crystals of the compound were grown by the slow evaporation of a methanolic solution of the complex in 7 days.

2.6. Physical methods

Microanalyses were carried out using a Heraeus Elemental Analyzer at CDRI, Lucknow, India. Infrared spectra were recorded on a Shimadzu DR 8001 series FT-IR instrument as KBr pellets in the range 400–4000 cm^{-1} and far-IR spectra were recorded in the range 50–500 cm^{-1} on a NICOLET MAGNA 550 FT-IR spectrometer using polyethylene pellets at RSIC, IIT, Bombay, India. Electronic spectra were recorded in the 900–250 nm range in a diffused reflectance mode in MgO matrix in Ocean Optics SD 200 fiber optic Spectrophotometer. Magnetic measurements were made in the polycrystalline state on a home built simple Gouy balance using $Hg[Co(SCN)_4]$ as calibrant. EPR spectra were recorded in a Bruker ESP300, X-band CW spectrometer operating at 9.52 GHz equipped with a liquid

Table 1
Crystal data and structure refinement parameters

	HBpypTsc	$[Fe(BpypTsc)_2]FeCl_4 \cdot 2H_2O$ (**3**)
Empirical formula	$C_{17}H_{18}N_4S$	$C_{34}H_{38}Cl_4Fe_2N_8O_2\ S_2$
Formula weight, M	310.41	908.34
Temperature, T (K)	298(2)	293(2)
Wavelength, Mo Kα (Å)	0.70930	0.70930
Crystal system	orthorhombic	triclinic
Space group	$P2_1P2_1P2_1$	$P\bar{1}$
Unit cell dimensions		
a (Å)	9.95	9.64
b (Å)	10.77	15.15
c (Å)	14.89	16.24
α (°)	90.00	114.57
β (°)	90.00	93.79
γ (°)	90.00	101.76
Volume, V (Å^3)	1596.3	2082.1
Z, Calculated density, ρ (Mg m^{-3})	4, 1.292	2, 1.449
Absorption coefficient, μ (mm^{-1})	0.205	1.094
$F(000)$	656	932
Crystal size (mm)	$0.35 \times 0.35 \times 0.30$	$0.275 \times 0.175 \times 0.150$
θ Range for data collection	2.33–24.90	1.40–24.92
Limiting indices	$0 \leqslant h \leqslant 11$, $0 \leqslant k \leqslant 12$, $0 \leqslant l \leqslant 17$	$0 \leqslant h \leqslant 11$, $-17 \leqslant k \leqslant 17$, $-19 \leqslant l \leqslant 19$
Reflections collected/Unique	1526/1526 [$R_{int} = 0.000$]	5912/5912 [$R_{int} = 0.000$]
Completeness to 2θ (°, %)	24.90, 94.1	24.92, 80.8
Maximum and minimum transmission	1.000 and 0.989	1.000 and 0.969
Goodness-of-fit on F^2	1.075	1.134
Final R indices [$I > 2\sigma(I)$]	$R_1 = 0.0332$, $wR_2 = 0.0777$	$R_1 = 0.0605$, $wR_2 = 0.1535$
R indices (all data)	$R_1 = 0.0387$, $wR_2 = 0.0825$	$R_1 = 0.0895$, $wR_2 = 0.1726$
Largest difference peak and hole (e Å^{-3})	0.174 and −0.224	1.287 and −0.405

nitrogen cryostat. The spectra were measured with a modulation amplitude of 0.05(0.1) mT and 100 kHz modulation frequency, and the field was calibrated by using 2,2-diphenyl-1-picrylhydrazyl (DPPH) with a g value of 2.0036. NMR spectra were recorded on a Bruker DRX 500 instrument using $CDCl_3$ as the solvent and TMS as the internal reference at the Sophisticated Instruments Facility, Indian Institute of Science, Bangalore, India. The tentative structure of the compound HBpypTsc was assigned on the basis of different NMR experiments, based on the couplings and connectivities of the signals observed. The ^{1}H resonances were assigned on the basis of chemical shifts, multiplicities and coupling constants from ^{1}H NMR experiments. The assignments of the NH and OH hydrogens were made by comparison with the spectra recorded on deuterium exchange. The carbon types were determined by ^{13}C-Spin Echo Fourier Transform (SEFT) experiments. Mössbauer spectra were recorded on a constant-acceleration spectrometer with multi channel analyzer using a ^{57}Co source in a Rhodium matrix at Inter University Consortium, Indore, India.

2.7. X-ray crystallography

A dark brown triclinic crystal of the $[Fe(BpypTsc)_2]$-$FeCl_4$ (**3**) and a deep yellow orthorhombic crystal of HBpypTsc having appropriate dimensions were sealed in a glass capillary, and intensity data were measured at room temperature (293 K) on an Nonius MACH3 diffractometer equipped with graphite-monochromated Mo Kα ($\lambda = 0.71073$ Å) radiation. The trial structure was obtained by direct methods using SHELXL-97 and refined by full-matrix least squares on F^2 (SHELXS-97) [16,17]. The non-hydrogen atoms were refined with anisotropic thermal parameters. All hydrogen atoms were geometrically fixed and allowed to refine using a riding model. Absorption corrections were employed using ψ-scan. The crystallographic data along with details of structure solution refinements are given in Table 1.

3. Results and discussions

3.1. Syntheses

The ligand HBpypTsc was synthesized by a direct condensation of the ketone with the thiosemicarbazide. In the ^{1}H NMR spectrum the signal for N(2)H is observed at a low field of $\delta = 14.35$ ppm and this signal disappears on deuterium exchange, which is consistent with the Z configuration of the thiosemicarbazone moiety. The low frequency multiplets at $\delta = 3.8$ (4H)

and 1.9 (4H) ppm were attributed to pyrrolidine ring protons C14 and C15, respectively, which are chemically and magnetically equivalent with C17 and C16 (the numbering scheme of HBpypTsc is given in Scheme 1). Aromatic protons of the pyridine and phenyl ring appear at $\delta = 8.73$, doublet, aromatic, 1H, $J = 7.5$ Hz; 8.5, aromatic, doublet, 1H and 7.1–7.8, aromatic, multiplet, 7H, respectively. The carbon atoms were assigned on the basis of proton decoupled ^{13}C and ^{13}C- Spin Echo Fourier Transform NMR spectra. Eighteen signals were observed in the ^{13}C NMR spectrum, which are assigned as follows. Signals at $\delta = 177.0$ and 177.6 ppm were attributed to C(1)=N(2) and C(13)=S(1) of the thiosemicarbazone moiety. Aromatic carbons of the pyridine and phenyl ring of the 2–benzoylpyridine moiety appear at $\delta = 121.5$ (C5), 123.8 (C4), 126.1 (C6), 128.4 (C10), 129.2 (C11), 129.6 (C3), 129.9 (C9), 137.3 (C7), 143.9 (C2), 148.0 (C9), 149.2 (C12), 152.8 (C8), whereas the peaks at $\delta = 53.4$, 50.4, 26.6 and 24.3 were assigned to aliphatic carbons C14, C17, C15 and C16, respectively, of the pyrrolidine ring.

All complexes were dark brown and are readily soluble in polar organic solvents. Their stoichiometries and partial elemental analysis data are shown in Table 2. Analytical data shows a 1:2:1 ratio of iron, ligand and anions for FeL_2X [$X = ClO_4$, $FeCl_4^-$, NO_3]. From the analytical data obtained for compound **3** two formulations are possible: $[Fe(BpypTsc)_2]FeCl_4$ or $[FeBpypTscCl_2]$, but from the crystallographic as well as the spectroscopic data it is clear the compound isolated is the former one consisting of an ion pair. The compounds were 1:1 electrolytes [18] in DMF with Λ_m values near to 95 $\Omega^{-1}\,cm^2\,mol^{-1}$. The cation centre of all the complexes are expected to contain two deprotonated ligands attached to an iron(III) centre. Magnetic moments have been determined for all the complexes at room temperature in the polycrystalline state. Iron(III) is known to exist in three states with $S = 5/2$ ($^6A_1$, $\mu = 5.92$ BM), 3/2 ($^4A_2$, $\mu = 3.87$ BM) and 1/2 ($^2T_2$, $\mu = 1.73$ BM)[19]. The magnetic moments of the compounds **1** and **2** are 1.89 and 2.33 BM, respectively, indicating these compounds are typical low spin compounds. The high values of susceptibility for compound **3** indicate the presence of a high spin centre in the molecule [20,21]. The complete assignment of the spin states of the complexes were done on the basis of EPR and Mössbauer measurements.

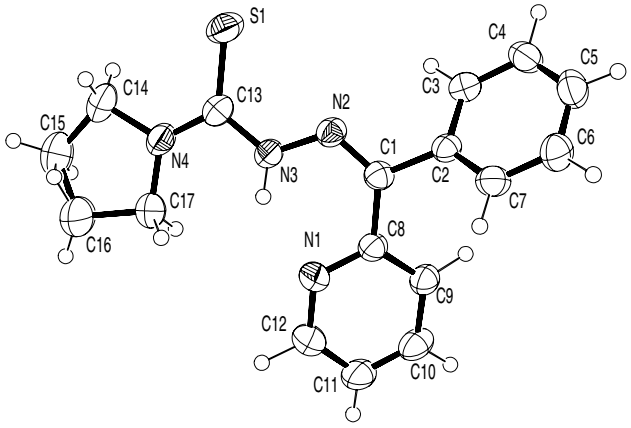

Fig. 1. ORTEP diagram of the compound HBpypTsc, with 54% ellipsoidal probability. Hydrogen atoms are shown as smaller spheres of arbitrary radii.

3.2. Molecular and crystal structure of compound HBpypTsc

Fig. 1 shows the molecular structure of the compound along with the atom numbering scheme. The molecule exists in the E conformation around the N2–N3 bond. The structure reveals quasicoplanarity in the plain of the thiosemicarbazone but both the aromatic rings are bifurcated. The molecular structure reveals that the compound exists in the thione form. Table 3 illustrates selected bond lengths and angles.

The compound has two double bonds in the thiosemicarbazone moiety viz. C1–N2 1.295 Å and C13–S1 1.681 Å which are consistent with the previously reported cases. The planarity in the thiosemicarbazone is revealed by a smaller dihedral angle of the N2–N3–C13–S1 (0.9°) skeleton. A considerable amount of ring bifurcation from the plane of the thiosemicarbazone is indicated by the dihedral angles C1–N2–N3–C13 (−176.9°) and C8–C1–C2–C7 (−44.7°). The S and pyridyl N1 atoms are in E configuration with respect to the C1–N2 bond. The five-membered pentamethyleneimine (pyrrolidine) ring is not planar and tends towards an envelope conformation [22]. The smaller dihedral angles between the pyridyl ring and the phenyl ring of the 2-benzoylpyridine moiety and thiosemicarbazone moiety C2–C1–C8–C9 (−28.2°) and N3–N2–C1–C8 (2.2°), is due to a resonance effect between the π systems. Pyridyl nitrogen N1 is intramolecularly hydrogen bonded to

Table 2
Stoichiometries and partial elemental analysis of the complexes

Compounds	Stoichiometries	*Anal.* Calc. (Found) (%)			μ (BM)
		C	H	N	
$[Fe(BpypTsc)_2]ClO_4$ (**1**)	$C_{34}H_{34}ClFeN_8O_4S_2$	52.74 (52.75)	4.40 (4.43)	14.45 (14.48)	1.89
$[Fe(BpypTsc)_2]NO_3$ (**2**)	$C_{34}H_{34}FeN_9O_3S_2$	55.40 (55.43)	4.65 (4.65)	17.09 (17.11)	2.33
$[Fe(BpypTsc)_2]FeCl_4$ (**3**)	$C_{34}H_{34}Cl_4Fe_2N_8S_2$	46.80 (46.81)	3.93 (3.93)	12.85 (12.85)	4.38

Table 3
Selected bond lengths (Å) and angles (°) of HBpypTsc

Bond lengths		Bond angles	
S(1)–C(13)	1.681(3)	C(1)–N(2)–N(3)	118.4(2)
N(1)–C(12)	1.341(4)	C(13)–N(3)–N(2)	121.1(2)
N(1)–C(8)	1.342(4)	N(1)–C(8)–C(9)	121.7(3)
N(2)–C(1)	1.295(4)	N(1)–C(8)–C(1)	117.5(2)
N(2)–N(3)	1.366(3)	N(1)–C(12)–C(11)	123.9(4)
N(3)–C(13)	1.360(4)	N(3)–C(13)–S(1)	124.0(2)
X–H···Cg	H···Cg (Å)	X···Cg (Å)	∠X– H···Cg (°)
C12–H12···Cg(3)[a]	2.8518	3.6071	126.85
C16–H16···Cg(2)[b]	3.2937	4.1282	145.44
D–H···A	H···A (Å)	D···A (Å)	∠D–H···A (°)
N3–H103···N1[c]	1.94	2.659	136
C11–H11···N2[c]	2.59	3.409	153

Cg(2) = N1, C8, C9, C10, C11, C12; Cg(3) = C2, C3, C4, C5, C6, C7.
Cg, centroid; D, donor and A, acceptor.
[a] Equivalent position code: $1/2 - x, 1 - y, 1/2 + z$.
[b] Equivalent position code: $1 - x, -1/2 + y, 1/2 - z$.
[c] Equivalent position code: x, y, z.

N3–H10 at 2.65 Å distance forming a six-membered ring.

3.3. Molecular and crystal structure of compound 3

The compound $Fe(BpypTsc)_2FeCl_4 \cdot 2H_2O$ (**3**) crystallizes with two molecules of water of crystallization. Table 4 presents the selected bond lengths and angles. Fig. 2 shows the molecular structure of the compound along with the atom numbering scheme. The low-spin iron(III) ion has a distorted octahedral geometry in the complex. The pattern of coordination is similar to that observed in similar types of complexes [23]. The two molecules of monodeprotonated ligand, coordinate to iron via pyridyl nitrogens, azomethine nitrogens and thiolato sulfur atoms to form four five membered che-

Table 4
Selected bond lengths and angles of compound **3**

Bond lengths (Å)		Bond angles (°)	
Fe(1)–N(2)	1.916(4)	N(2)–Fe(1)–N(6)	175.4(2)
Fe(1)–N(6)	1.928(5)	N(2)–Fe(1)–N(5)	102.2(2)
Fe(1)–N(5)	1.980(5)	N(6)–Fe(1)–N(5)	81.6(2)
Fe(1)–N(1)	1.984(5)	N(2)–Fe(1)–N(1)	81.1(2)
Fe(1)–S(2)	2.201(19)	N(6)–Fe(1)–N(1)	101.9(2)
Fe(1)–S(1)	2.225(19)	N(5)–Fe(1)–N(1)	86.8(2)
S(1)–C(13)	1.749(6)	N(2)–Fe(1)–S(2)	91.06(15)
N(2)–C(1)	1.309(7)	N(6)–Fe(1)–S(2)	85.55(16)
N(2)–N(3)	1.358(6)	N(5)–Fe(1)–S(2)	165.38(15)
Fe(2)–Cl(4)	2.156(2)	N(1)–Fe(1)–S(2)	89.13(16)
Fe(2)–Cl(3)	2.168(2)	N(2)–Fe(1)–S(1)	85.30(15)
Fe(2)–Cl(2)	2.171(2)	N(6)–Fe(1)–S(1)	92.03(15)
Fe(2)–Cl(1)	2.196(2)	N(5)–Fe(1)–S(1)	90.19(16)
C–H···π	H···Cg (Å)	X···Cg (Å)	X–H···Cg (°)
C12–H12···Cg(4)[a]	2.7053	3.1962	113.95
C29–H29···Cg(3)[a]	2.7790	3.1651	104.77
H-bonding interactions	H···A (Å)	D···A (Å)	D–H···A (°)
O1–H102···O2[b]	0.94	2.0425	131
O2–H103···O1[c]	1.70	2.3247	128
O1–H104···O2[d]	1.65	2.3247	122
C14–H14A···S2	2.78	3.6489	145

Cg(3) = Fe1, N1, C8, C1, N2, Cg(4) = Fe1, N5, C25, C18, N6.
[a] x, y, z.
[b] $2 - x, 1 - y, -z$.
[c] $1 + x, 1 + y, z$.
[d] $1 - x, 1 - y, -z$.

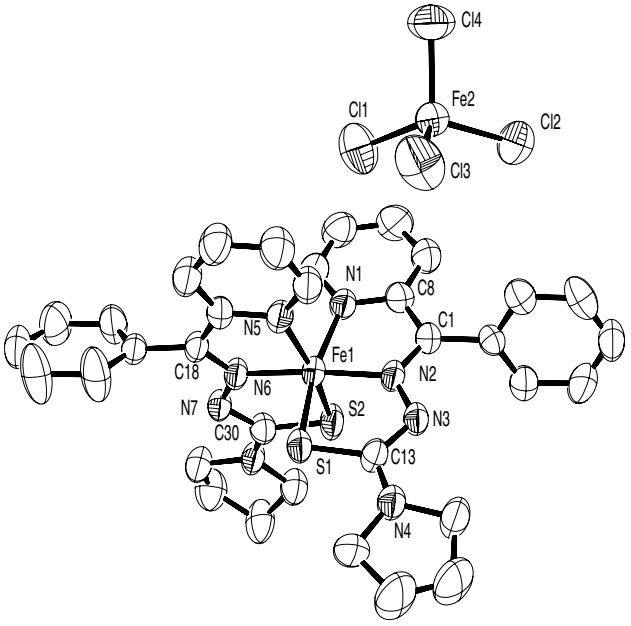

Fig. 2. ORTEP diagram of the compound[Fe(BpypTsc)$_2$]FeCl$_4$ · 2H$_2$O (**3**) with 50% ellipsoidal probability. Hydrogen atoms and lattice water molecules are omitted for clarity.

late rings. The crystallographic asymmetric unit contains a [Fe(BpypTsc)$_2$] cation and a tetrachloroferrate ($FeCl_4^-$) anion along with two molecules of lattice water.

Coordination lengthens the ligands C13–S1 and C1–N2 bonds to 1.749 and 1.309 Å, respectively, and this is an explicit indication of the deprotonation followed by the coordination of the ligand moiety. There is a slight shortening of the Fe–N(azomethine) bond distance compared to Fe–N(py) distances; this may be attributed to the fact that the azomethine nitrogen is a stronger base compared with the pyridyl nitrogen. The two azomethine nitrogen atoms are *trans* to each other, while the pyridyl nitrogen atoms and thiolato sulfur atoms are in *cis* positions. The ligands are orthogonal to the metal ion, with the NNS coordination in a meridonal fashion [24]. The chelate rings are almost planar. There exist strong C–H$\cdots\pi$ interactions between these metal containing chelate rings Cg(3) and Cg(4) with pyridyl ring protons. The tetrachloroferrate anion present in the molecule is slightly distorted tetrahedral with equal bond lengths (~2.187 Å) and angles (~109.46°).

3.4. IR spectra

In Table 5 we have compiled the assignments of IR bands most useful for the establishment of the mode of coordination of thiosemicarbazone ligands in their iron(III) coordination. Coordination of the azomethine nitrogen is indicated by the lowering of the band at 1630 cm^{-1} by 30–50 cm^{-1}. The band is not a pure vibrational band of C=N stretching, but it is a combination band of C=C vibrations of the pyridyl ring also [25]. Two bands ≈1340 and 840 cm^{-1} were assigned to the C–S stretching and bending mode of vibrations. These bands also shift to lower energies in all complexes compared to the ligand, indicating the coordination of the thiolato sulfur. Another band which is considered to be sensitive to coordination is ν(N–N) which is raised in energy due to coordination because of the increased double bond character. The newly formed C=N bond due to the deprotonation of the ligand is also observed ≈1630 cm^{-1}. The spectra of the complexes showed an increase in pyridyl ring in-plane and out-of-plane bending mode of vibrations at ≈440 and 650 cm^{-1}.

Table 6 shows the polyatomic anionic vibrations along with the M–L stretching vibrations observed in the far-IR and IR regions. Fig. 3 shows the far-IR spectra of the complexes. The spectra of compound **1**

Table 5
Ligand vibrational data of the complexes

Compound	ν(C=N)	ν(N=C)	ν(N=N)	ν/δ(C=S)
HBpypTsc	1630 s		1118 s	1342 s, 842 w
[Fe(BpypTsc)$_2$]ClO$_4$ (**1**)	1594 s	1627 s	1163 s	1240 m, 843 w
[Fe(BpypTsc)$_2$]NO$_3$ (**2**)	1594 s	1628 s	1108 s	1202 s, 839 w
[Fe(BpypTsc)$_2$]FeCl$_4$ (**3**)	1595 m	1645 m	1111 s	1204 s, 844 w

All values are in cm^{-1}.

Table 6
Far-IR and anionic vibrational data of the complexes

Compound	ν(Fe–N$_{azo}$)	ν(Fe–N$_{py}$)	ν(Fe–S)	ν(X^a)
[Fe(BpypTsc)$_2$]ClO$_4$ (**1**)	515 w	354 w	452 w	470 w, 1105 s, 619 w
[Fe(BpypTsc)$_2$]NO$_3$ (**2**)	585 w	364 w	450 w	698 w, 839 w, 1379 s, 1289 s
[Fe(BpypTsc)$_2$]FeCl$_4$ (**3**)	528 w	352 s	419 s	374 s, 320 s, 134 w, 110 s

All values are in cm^{-1}.
[a] ClO$_4$, FeCl$_4$, NO$_3$.

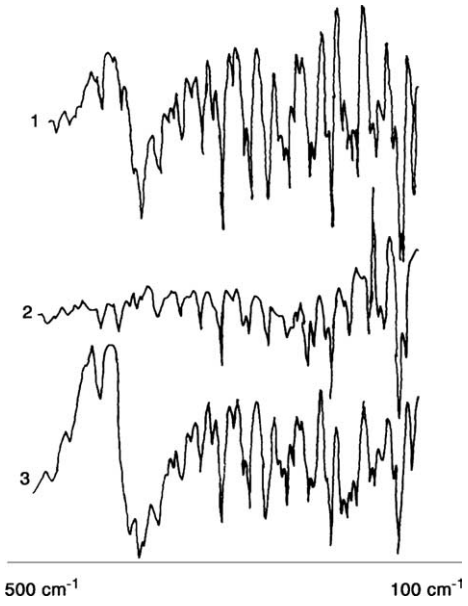

Fig. 3. Far-IR spectra of the iron(III) complexes.

had broad split bands assignable to $\nu_3(ClO_4) \approx 1105$ cm^{-1}, it is unlikely that the perchlorate ion is bound directly to the iron(III) centre since there is no indication of splitting of $\nu_4(ClO_4) \approx 619$ cm^{-1}. This is also confirmed by the absence of $\nu_1(ClO_4) \approx 920$ cm^{-1}. Besides these $\nu_2(ClO_4)$ is also observed ≈ 470 cm^{-1}. All these bands are split due to the strong H-bonding interactions in the molecule [26]. A similar splitting occurs in the $\nu_3(FeCl_4) \approx 374$ cm^{-1} band in the spectrum of compound **3**. This splitting may be due to the steric factors which reduce the symmetry from tetrahedral [27]. Similarly the band corresponding to $\nu_4 \approx 134$ cm^{-1} is also found to be split due to site effects. The other two stretching modes ν_1 and ν_2 are found at approximately 330 and 114 cm^{-1}, respectively, in the spectrum of compound **3**. The spectrum of compound **2** has two strong bands at 1389 and 1289 cm^{-1} corresponding to ν_1 and ν_4 of the nitrato group. The absence of a combination band ≈ 1740 cm^{-1} assignable to $\nu_1 + \nu_4$ indicates the ionic nature of the group [28]. Bands at ≈ 515 and 355 cm^{-1} are assigned to the Fe–N vibrations of the azomethine and pyridyl nitrogen coordination, respectively. Fe–S bond stretching vibrations are found approximately at 420 cm^{-1} in the spectra of the complexes.

3.5. Electronic spectra

Table 7 shows the electronic spectral values in solid-state DRS mode. Fig. 4 shows the electronic spectrum of compound **3**. The UV region is dominated by two intense intra ligand bands at ~36 000 and 29 000 cm^{-1} assigned to $\pi \rightarrow \pi^*$ and $n \rightarrow \pi^*$ transitions.

Usually $n \rightarrow \pi^*$ transitions involving N and S atoms occur at a lower energy than $\pi \rightarrow \pi^*$. Bands which are between 36 000 and 30 000 cm^{-1} in the spectrum of the complexes having pyridyl ligands have been assigned to $\pi \rightarrow \pi^*$ and $n \rightarrow \pi^*$ transitions and the bands between 15 000 and 27 000 cm^{-1} are assigned to $d \rightarrow \pi^*$ transitions, $S \rightarrow Fe$ and other ligand-to-metal charge transfer transitions. The bands below 15 000 cm^{-1} are due to $d \rightarrow d$ bands which correspond to a $^2T_{2g} \rightarrow {}^2T_{1g}$ transition of the d^5 spin-paired systems [29]. A comparison of the spectra of **1**, **2** and **3** shows no significant differences indicating that electronic spectra of the cations dominate the spectral properties [30]. Therefore the spin forbidden transitions between 13 700 and 16 600 cm^{-1} of $[FeCl_4]^-$ are too weak to be observed. Unfortunately the electronic spectra of low-spin iron(III) compounds have not been adequately characterized.

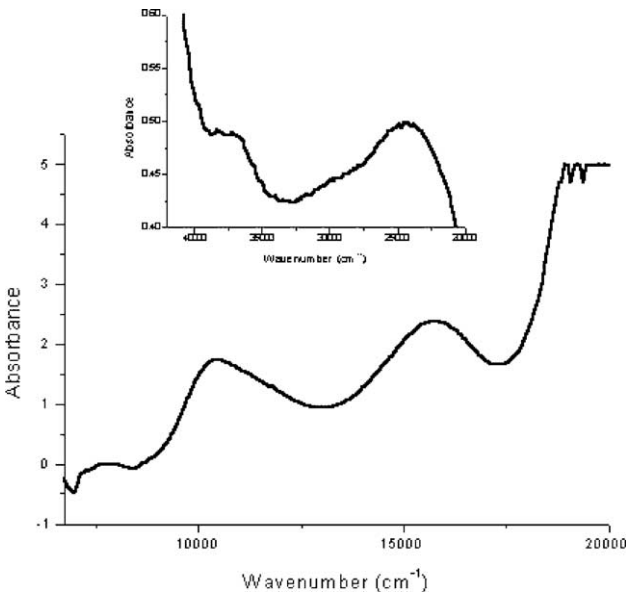

Fig. 4. UV–Vis-NIR spectrum of compound 3 (insight: UV region).

Table 7
Electronic spectral data of the complexes

Compound	$\pi \rightarrow \pi^*$	$n \rightarrow \pi^*$	LMCT	$d \rightarrow d$
HBpypTsc	43 300	29 240, 29 760	–	–
$[Fe(BpypTsc)_2]ClO_4$ (**1**)	36 5136	30 487	26 737, 15 503	10 362
$[Fe(BpypTsc)_2]NO_3$ (**2**)	36 630	29 585	24 509, 15 822	10 373
$[Fe(BpypTsc)_2]FeCl_4$ (**3**)	37 037	30 211	24 390, 211 416, 15 974	10 438

All values are in cm^{-1}.

3.6. Electron paramagnetic resonance spectra

The EPR spin Hamiltonian parameters of the iron(III) complexes obtained after the spectral simulations performed by EasySpin package [31] are presented in Table 8. Figs. 5–7 show the EPR spectra of the complexes recorded under different conditions. The EPR of the d^5 iron(III) is expressed by the spin Hamiltonian [32,33],

$$H = \beta[g_x H_x \cdot S_x + g_y H_y \cdot S_y + g_z H_z \cdot S_z]$$

with $S = 1/2$ and $g = 2.00$.

The polycrystalline EPR spectra of compound **3** consist of a single broad line with a Δpk (peak-to-peak) value ~27 mT and a comparatively higher g value ~2.25. This feature does not change even when the temperature is lowered to 100 K. This is indicative of the presence of a mixture of spin species in the system. The observed g value ≈2.0 and a nearly isotropic spectra indicate spin–spin relaxation via dipole–dipole interactions. However the solid-state spectra of the other two compounds **1** and **2** are rhombic in nature with three g values. This type of feature is common for low spin octahedral complexes [34]. The observed anisotropic character is due to rhombic distortion common for spin paired iron(III) complexes.

The isotropic spectrum of complex **3** in the polycrystalline state changes to a rhombic spectrum in frozen solution in DMF. Since the g_{av} values obtained at both temperatures are similar, it is likely that lattice effects in the solid state may account for this change from isotropic to rhombic and it is common for spin paired iron(III) complexes. The small deviation of the anisotropic g values from 2.0 suggests that the unpaired electron is in the d_{xy} orbital with a $d_{xz}^2 d_{yz}^2 d_{xy}^1$ ground state configuration. It was interesting to note a sharp but small signal corresponding to $g = 4.2603$ indicating the presence of a high spin species which was identified as the $[FeCl_4]^-$ anion. The spectra of the compounds **1** and **2** recorded in dichloromethane at 100 K also show anisotropic spectra with three g values corresponding to a low spin octahedral iron(III) system. However the spectral features were not resolved probably due to poor glass formation.

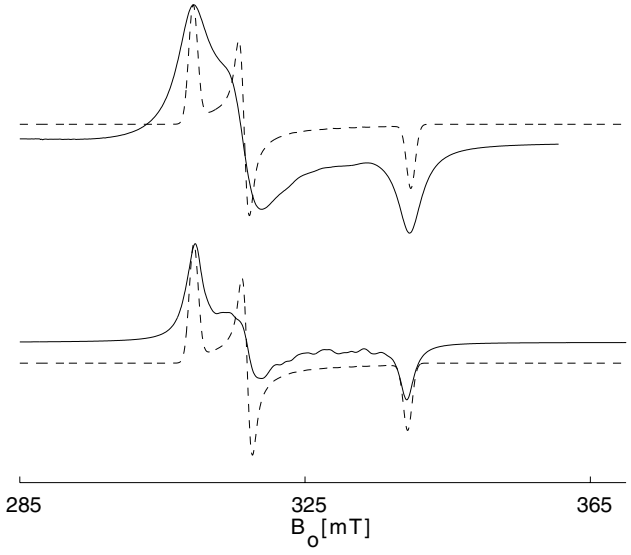

Fig. 5. EPR spectrum of compound **1** in the polycrystalline state: upper trace at 298 K, lower trace at 100 K. Dotted lines shows the simulated best fit spectra of the compound.

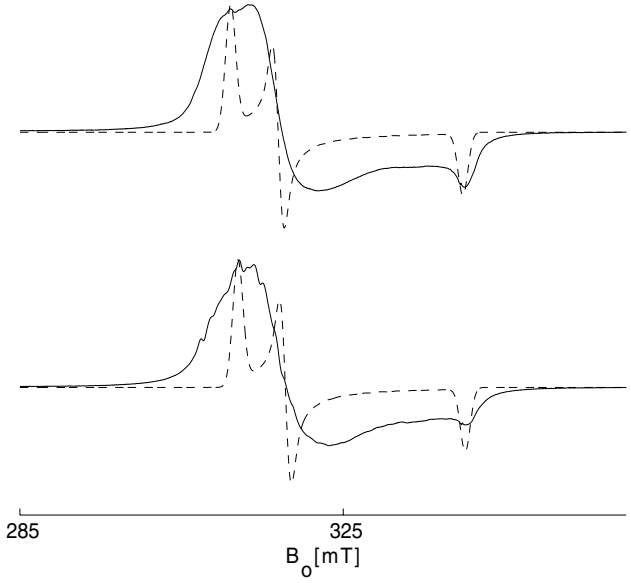

Fig. 6. EPR spectrum of compounds **1** and **2** in a solution of dichloromethane at 100 K: upper trace compound **1**, lower trace compound **2**. Dotted lines show the simulated best fit spectra of the compounds.

Table 8
EPR spectral data of the complexes

Compound	State	Temperature (K)	g_1	g_2	g_3
$[Fe(BpypTsc)_2]ClO_4$ (**1**)	powder	298	2.1990	2.1495	2.0026
	powder	100	2.1984	2.1466	2.0052
	CH_2Cl_2	100	2.1803	2.1400	2.0010
$[Fe(BpypTsc)_2]NO_3$ (**2**)	powder	298	2.1899	2.1465	2.0036
	powder	100	2.1897	2.1462	2.0032
	CH_2Cl_2	100	2.1866	2.1460	2.0027
$[Fe(BpypTsc)_2]FeCl_4$(**3**)	powder	298			2.2594, $\Delta pk = 30$ mT
	powder	100			2.1490, $\Delta pk = 27$ mT
	DMF	100	2.1935	2.1432	1.9981, 4.2603

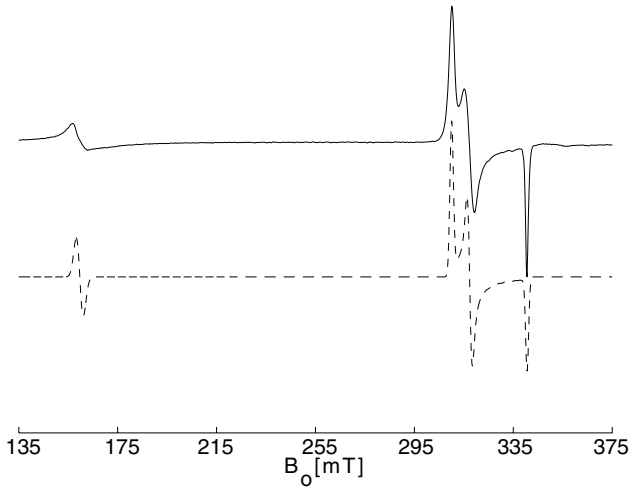

Fig. 7. EPR spectrum of compound **3** in a solution of DMF at 100 K: upper trace experimental spectrum, lower trace simulated best fit spectrum.

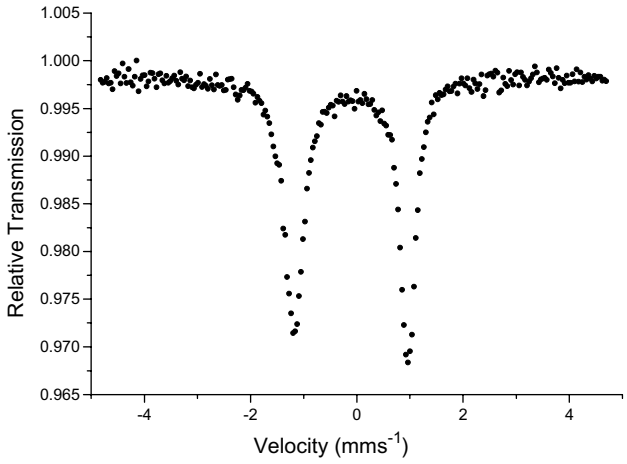

Fig. 8. Mössbauer spectrum of compound **1** (298 K).

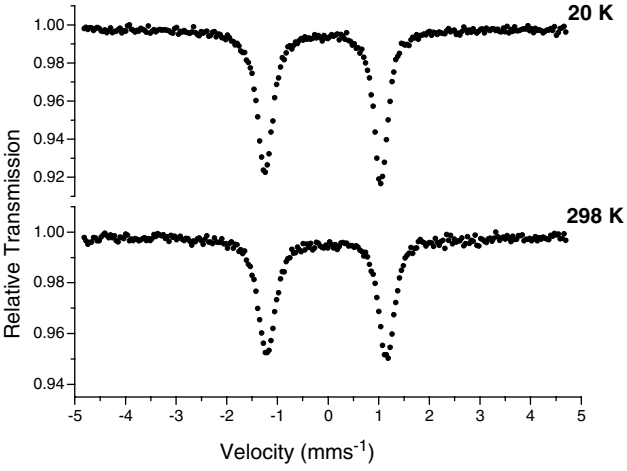

Fig. 9. Mössbauer spectra of compound **2** at different temperatures.

3.7. Mössbauer spectra

Mössbauer spectra of the complexes were recorded at 298 and 20 K in order to understand and confirm the spin behavior of the systems. The Mössbauer parameters calculated from the spectra are presented in Table 9, and Figs. 8–10 show the spectra of the complexes. All values were compared with α-iron as a standard.

The high intensity doublet in the spectra of all the complexes with an isomer shift approximately at −0.12 mm s^{-1}, characterized by a quadrupolar splitting $\Delta E_q \approx 2.1$ mm s^{-1}, is ascribed to the low spin $^2T_{2g}$ ground state of low spin iron(III) [35]. These values change a little when the temperature is lowered. The signals in the low temperature spectra were more intense. The 1:1 ratio between the quadrupole split spectra is not strictly observed due to the anisotropic absorption known as the Goldansky–Karyagin effect. The spectra of compound **3** is unusually interesting with the presence of another broad signal corresponding to $\delta^{is} \approx 0.12$ mm s^{-1} $\Delta E_q \approx 0.67$ mm s^{-1}, ascribed to a tetrahedral high spin iron(III) species [36]. The observation of the broad line with unresolved quadrupolar splitting is assumed to be due to much slower spin relaxation due to the orbital electrons of iron. The high spin signal is temperature dependent and in the 20 K spectrum of compound **3** the signal is found to be shifted compared to the 298 K spectrum, and it was found to be more intensified. There are no changes between the 298 and 20

Table 9
Mössbauer spectral data of the complexes

Compound	Temperature (K)	Spin	δ^{is} (mm s^{-1})	ΔE_q (mm s^{-1})
[Fe(BpypTsc)$_2$]ClO$_4$ (**1**)	298	1/2	−0.17 ($^2T_{2g}$)	2.231 ($^2T_{2g}$)
[Fe(BpypTsc)$_2$]NO$_3$ (**2**)	298	1/2	−0.11 ($^2T_{2g}$)	2.351 ($^2T_{2g}$)
	20	1/2	−0.12 ($^2T_{2g}$)	2.352 ($^2T_{2g}$)
[Fe(BpypTsc)$_2$]FeCl$_4$ (**3**)	298	1/2	−0.10 ($^2T_{2g}$)	2.110 ($^2T_{2g}$)
	20	1/2	−0.11 ($^2T_{2g}$)	2.241 ($^2T_{2g}$)
	298	5/2	0.17 ($^6A_1$)	0.925 ($^6A_1$)
	20	5/2	0.12 ($^2T_{2g}$)	0.625 ($^2T_{2g}$)

All values are relative to α-iron.

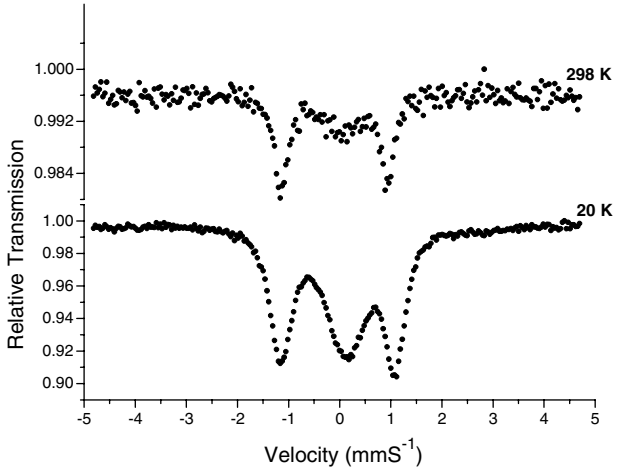

Fig. 10. Mössbauer spectra of compound **3** at different temperatures.

K spectra of the signal due to the spin-paired iron moiety showing the presence of a stable spin system without any magnetic interactions in the molecules [37].

3.8. Supplementary information

Crystallographic data for the structural analysis has been deposited with the Cambridge Crystallographic Data centre, CCDC 217178 for compound HBpypTsc and CCDC 217177 for compound $[Fe(BpypTsc)_2]$-$FeCl_4 \cdot 2H_2O$ (**3**). Copies of this information may be obtained free of charge from The Director, CCDC, 12 Union Road, Cambridge, CB2 IEZ, UK (fax: +44-1223-336-033; E-mail: deposit@ccdc.cam.ac.uk or http://www.ccdc.cam.ac.uk).

Acknowledgements

One of the authors (A.S.) thanks the Cochin University of Science and Technology for a Research Fellowship. The authors are thankful to the National Single Crystal X-ray Diffraction Facility, IIT, Bombay for the X-ray diffraction studies and Dr. Ajay Gupta, Inter-university Consortium, Indore, India for Mössbauer spectral experiments. M.R.P. Kurup is thankful to the Science, Technology and Environment Department (STED), Govt. of Kerala for financial assistance.

References

[1] M.J. Nelson, H. Jin, I.M. Turner Jr., G. Grove, R.C. Scarrow, B.A. Brennan, L. Que Jr., J. Am. Chem. Soc. 113 (1991) 7072.
[2] R.C. Scarrow, B.A. Brennan, J.G. Cummings, H. Jin, D.J. Duong, J.T. Kindit, M.J. Nelson, Biochemistry 35 (1996) 100078.
[3] T. Bessel, K.S. Burger, G. Vogit, K. Wieghardt, C. Butzlaff, A.X. Trautwein, Inorg. Chem. 32 (1993) 124.
[4] J.C. Noveron, R. Herradora, M.M. Olmstead, P.K. Mascharak, Inorg. Chim. Acta 282 (1999) 269.
[5] A.E. Liberta, D.X. West, Biometals 5 (1992) 121.
[6] R. Raina, T.S. Srivastava, Inorg. Chim. Acta 67 (1982) 83.
[7] R.P. John, A. Sreekanth, M.R.P. Kurup, S.M. Mobin, Polyhedron 21 (2002) 2515.
[8] R.P. John, A. Sreekanth, M.R.P. Kurup, A. Usman, I.A. Razak, H.K. Fun, Spectrochim. Acta A 59 (2003) 1349.
[9] A. Sreekanth, S. Sivakumar, M.R.P. Kurup, J. Mol. Struct. 655 (2003) 47.
[10] A. Sreekanth, M.R.P. Kurup, Polyhedron 22 (2003) 3321.
[11] P. Bindu, M.R.P. Kurup, T.R. Satyakeerthy, Polyhedron 18 (1999) 321.
[12] B.S. Garg, M.R.P. Kurup, S.K. Jain, Y.K. Bhoon, Transition Met. Chem. 13 (1988) 247.
[13] B.S. Garg, M.R.P. Kurup, S.K. Jain, Y.K. Bhoon, Synth. React. Inorg. Met.- Org. Chem. 28 (1998) 1415.
[14] Y.K. Bhoon, J.P. Scovill, D.L. Klayman, Transition Met. Chem. 7 (1982) 264.
[15] J.P. Scovill, Phosphorous Sulfur Silicon Relat. Elem. 60 (1991) 15.
[16] G.M. Sheldrick, Program for the Solution of Crystal Structures, University of Göttingen, Göttingen, Germany, 1997.
[17] G.M. Sheldrick, Program for the Solution of Crystal Structures, University of Göttingen, Göttingen, Germany, 1997.
[18] W.J. Geary, Coord. Chem. Rev. 7 (1971) 81.
[19] S.A. Cotton, Coord. Chem. Rev. 8 (1978) 185.
[20] N.C. Saha, A. Saha, R.J. Butcher, S. Chaudhuri, N. Saha, Inorg. Chim. Acta 339 (2002) 348.
[21] S. Vasudevan, H.N. Vasan, C.N.R. Rao, Chem. Phys. Lett. 65 (1979) 444.
[22] A. Usman, I.A. Razak, S. Chantrapromma, H.K. Fun, V. Philip, A. Sreekanth, M.R.P. Kurup, Acta Crystallogr., Sect. C. Cryst. Struc. Commun. C 58 (2002) o652.
[23] N.C. Saha, R.J. Butcher, S. Chaudhari, N. Saha, Polyhedron 22 (2003) 375.
[24] A. Usman, I.A. Razak, S. Chantrapromma, H.K. Fun, A. Sreekanth, S. Sivakumar, M.R.P. Kurup, Acta Crystallogr., Sect. C. Cryst. Struct. Commun. C 58 (2002) m461.
[25] D.X. West, P.M. Ahrweiler, G. Ertem, J.P. Scovill, D.L. Klayman, J.L.F. Anderson, R. Gilardi, C. George, L.K. Pannel, Transition Met. Chem. 10 (1985) 264.
[26] K. Nakamoto, Infrared and Raman Spectra of Inorganic and Coordination Compounds, 5th ed., Wiley, New York, 1997.
[27] J.S. Avery, C.D. Burbridge, D.M.L. Goodgame, Spectrochim. Acta, Part A 24 (1968) 1721.
[28] I. Nakagwa, J.L. Walter, J. Chem. Phys. 51 (1969) 1389.
[29] A.H. Ewald, R.L. Martin, E. Sinn, A.H. White, Inorg. Chem. 8 (1968) 1837.
[30] E. Konig, K. Madeja, Spectrochim. Acta Part A 23 (1967) 45.
[31] St. Stoll, Spectral simulations in solid-state EPR, PhD Thesis, ETH, Zurich, 2003.
[32] B. Bleaney, M.C.M. O'Brien, Proc. Phys. Soc. London Sect. B 69 (1956) 1216.
[33] J.S. Griffith, The Theory of Transition Metal Ions, Cambridge University Press, London, 1961.
[34] Y. Nishida, A. Sumita, K. Hayashida, H. Olishima, S. Kida, Y. Maedo, J. Coord. Chem. 9 (1979) 261.
[35] S. Floquet, M.L. Boillot, E. Riviere, F. Varret, K. Boukheddaden, D. Morineau, P. Negrier, New. J. Chem. 27 (2003) 341.
[36] N.A. Bell, J.S. Brooks, J.K. Robinson, S.C. Thrope, J. Chem. Soc., Faraday Trans. 94 (1998) 3155.
[37] A.G. Maddock, Mössbauer Spectroscopy, Principles and Applications of the Techniques, Ellis Horwood, Chichester, 1997.

Available online at www.sciencedirect.com
SCIENCE DIRECT®
Polyhedron 23 (2004) 979–985
POLYHEDRON
www.elsevier.com/locate/poly

Synthesis and structures of unsymmetrical bis- and tris-cyclotriphosphazenes

N. Satish Kumar, K.C. Kumara Swamy *

School of Chemistry, University of Hyderabad, Hyderabad 500046, AP, India

Received 10 September 2003; accepted 10 December 2003

Abstract

Synthesis and characterization of several unsymmetrical bis- and tris-spirocyclic cyclotriphosphazenes that include the ones with chiral 1,1′-bi-2-naphthol are reported. Specifically, the compounds $N_3P_3(OCH_2CMe_2CH_2O)(HNCH_2CMe_2CH_2NH)Cl_2$ (**1**), $N_3P_3(OCH_2CMe_2CH_2O)(HNCH_2CMe_2CH_2NH)[(2,2'\text{-}OC_6H_4)_2]$ (**2**), $N_3P_3(OCH_2CMe_2CH_2O)[(2\text{-}OC_{10}H_6)_2CH_2]Cl_2$ (**3**), $N_3P_3(OCH_2CMe_2CH_2O)[1,1'\text{-}O_2(C_{10}H_6)_2]Cl_2$ (**4**), $N_3P_3(OCH_2CMe_2CH_2O)(HNCH_2CMe_2CH_2NH)$ $(1,1'\text{-}O_2(C_{10}H_6)_2)$ (**5**) and $N_3P_3(OCH_2CMe_2CH_2O)[1,1'\text{-}O_2(C_{10}H_6)_2]_2$ (**6**) are prepared by starting with the mono-spiro compound $N_3P_3(OCH_2CMe_2CH_2O)Cl_4$. No ansa type of compound was isolated from these reactions. X-ray structures of **1** and **2** have been determined. Synthesis of the tris-spiro compound $N_3P_3[1,1'\text{-}O_2(C_{10}H_6)_2]_3$ (**7**), possessing the 1,1′-bi-2-naphthoxy residue is also reported.
© 2003 Elsevier Ltd. All rights reserved.

Keywords: Cyclophosphazenes; Chiral; Spirocyclic; X-ray structure

1. Introduction

The chemistry of phosphazenes $[NPX_2]_n$ [X = Cl, F] is attractive in view of the diversity of the products that can be obtained by simple substitution of the halogens on phosphorus [1–4]. Cyclophosphazenes are also valuable precursors for speciality polymers [5–8]. While the reaction of monofunctional reagents with halogenocyclophosphazenes leads to, primarily, geminal or nongeminal substitution products, polyfunctional reagents can lead to a greater variety of products that include 'spiro', 'ansa' or 'intermolecular' condensation products in which the phosphazene ring is retained [9–15]. We have been interested in the chemistry of spirocyclic cyclophosphazenes [10,16] and in particular, the unsymmetrically substituted ones of type **I**, because they could be potential molecularly chiral compounds that may be amenable for resolution and use in asymmetric synthesis. In this connection it is noted that although several tris-spirocyclic cyclotriphosphazenes are known [11,17–19], none with three different difunctional reagents has yet been characterized. Such a compound is useful in comparing the variation in bond parameters at phosphorus. Although we have not been able to get a compound of type **I** so far to check the chirality aspects, we have succeeded in obtaining the tris(spiro) derivative **2** with three different difunctional residues, by starting with the bis(spiro) compound **1**. This paper deals with the synthesis and X-ray structural studies on these two compounds. In addition to these, we also report the synthesis of other bis and tris derivatives **3**–**7**. Of these, **4**–**7** possess a 1,1′-bi-2-naphthoxy residue. The latter compounds were synthesized for possible use as bases in asymmetric synthesis at a later stage.

* Corresponding author. Tel.: +91-40-23010682; fax: +91-40-23012460.
E-mail address: kckssc@uohyd.ernet.in (K.C. Kumara Swamy).

0277-5387/$ - see front matter © 2003 Elsevier Ltd. All rights reserved.
doi:10.1016/j.poly.2003.12.024

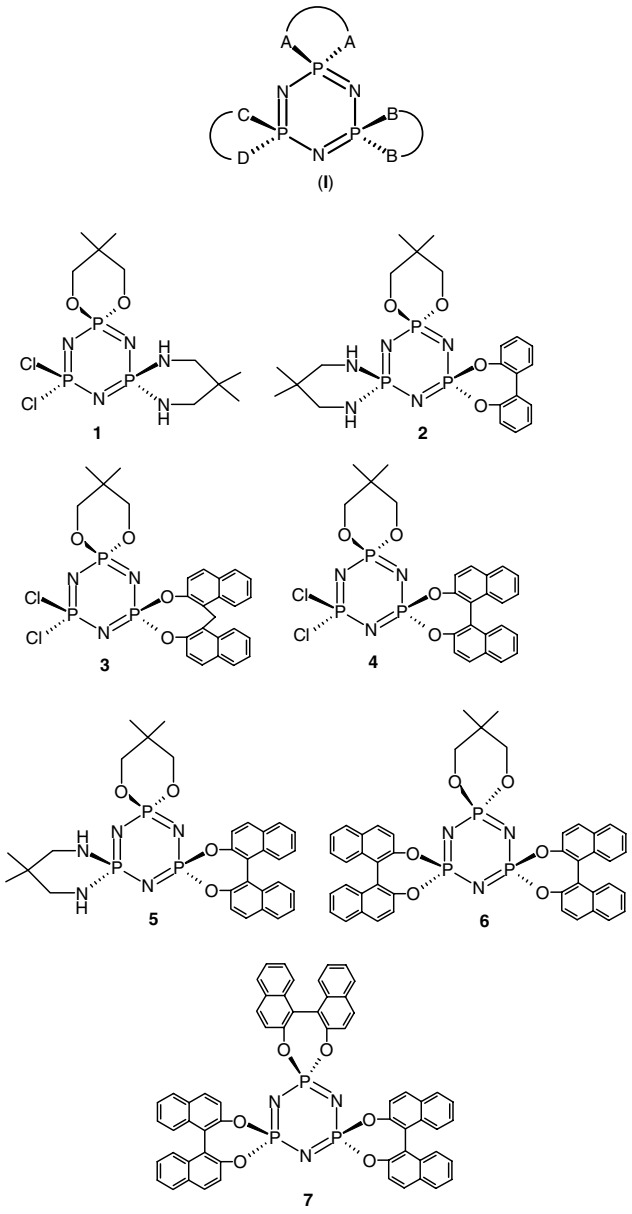

2. Experimental

Chemicals were procured from Aldrich/Fluka or from local manufacturers; they were purified when required. Solvents were purified according to standard procedures [20]. All reactions, unless stated otherwise, were performed under dry nitrogen atmosphere. ^{1}H and $^{31}P\{H\}$ NMR spectra were recorded on a Bruker 200 MHz spectrometer in $CDCl_3$, with shifts referenced to $SiMe_4$ ($\delta = 0$) or 85% H_3PO_4 ($\delta = 0$). Elemental analyses were carried out on a Perkin–Elmer 240C CHN analyzer.

2.1. Synthesis of *1*

A solution of 2,2-dimethyl-1,3-propane diamine (1.02 g, 1.19 mL, 10 mmol) and triethylamine (2.02 g, 20 mmol) in toluene (10 mL) was added dropwise over a period of 10 min with continuous stirring to a solution of $N_3P_3(OCH_2CMe_2CH_2O)Cl_4$ [21], (3.79 g, 10 mmol) in toluene (10 mL) and the reaction mixture was then heated to reflux for 30 h. The triethylamine hydrochloride formed was filtered off. Removal of solvent toluene from the filtrate led to compound **1**. Crystallization (colourless crystals) was done using toluene–hexane (2:1). Yield: 3.1 g (76%). M.p. 166–170 °C. IR (KBr, cm^{-1}): 3426, 3250, 1471, 1379, 1213, 1059, 1013. ^{1}H NMR ($CDCl_3$): δ 0.95, 0.98, 1.10, 1.25 (4 s, 12 H, CH_3), 2.68 (br s, 2 H, N*H*), 2.80–3.10 (m, 4 H, NHCH_2), 3.80–4.28 (m, 4 H, OCH_2). ^{13}C NMR: δ 20.8, 22.1, 24.4, 24.9 (4 s, *C*H_3), 31.7 (*C*(CH_2NH–)$_2$), 31.8 (d, ^{3}J(P–C) = 4.6 Hz, *C*(CH_2O)$_2$), 52.6 (s, NH*C*H_2), 76.4 (s, O*C*H_2). ^{31}P NMR: δ 6.9 (dd to t, ^{2}J(P–P)$\sim$67.0 Hz, O_2P(spiro)), 12.0 (dd to t, ^{2}J(P–P)$\sim$67.0 Hz, N_2P(spiro)), 23.4 (dd to t, ^{2}J(P–P)$\sim$67.0 Hz, *P*Cl_2). *Anal.* Calc. for $C_{10}H_{22}N_5O_2Cl_2$: C, 29.42; H, 5.43; N, 17.15. Found: C, 29.45; H, 5.48; N, 17.22%.

2.2. Synthesis of *2*

To a stirred suspension of NaH (0.05 g, $\sim$2.0 mmol) in THF (20 mL) at 0 °C was added 2,2′-biphenol (0.18 g, 1.0 mmol). After ca. 0.5 h, **1** (0.41 g, 1.0 mmol) was added and the reaction mixture was refluxed for 36 h. After cooling to room temperature, the reaction mixture was carefully quenched with ice, washed with water, extracted with dichloromethane (2×15 mL) and dried (Na_2SO_4). The solvent was removed to obtain a solid, which was purified by column chromatography (ethyl acetate–hexane 6:1). Crystallization (colourless crystals) was done using a dichloromethane–hexane mixture (1:2). Yield: 0.29 g (55%). M.p. >270°C. IR (KBr, cm^{-1}): 3389, 3329, 1475, 1440, 1383, 1246, 1186, 1060, 1016. ^{1}H NMR: δ 0.87, 0.95, 1.00, 1.22 (4 s, 12 H, CH_3), 2.64 (br m, 2 H, N*H*), 2.94, 3.00 (2 d or dd, $J = 6.0$, 11.2 Hz, 4 H, NHCH_2), 3.83–4.30 (m, 4 H, OCH_2), 7.23–7.55 (m, 8 H, Ar–H). ^{13}C NMR: δ 21.0, 22.3, 24.6 (3 s, *C*H_3), 31.5, 32.0 (2 d, ^{3}J(P–C) = 4.8 Hz each, *C*(CH_2O)$_2$ and *C*(CH_2NH)$_2$), 52.8 (s, NH*C*H_2), 75.9 (d, ^{2}J(P–C) = 6.1 Hz, O*C*H_2), 122.1, 125.6, 129.2, 129.4, 148.6, 148.8 (all Ar–*C*). ^{31}P NMR: δ 12.8 (dd to t, ^{2}J(P–P)$\sim$70.0 Hz, O_2P(spiro, 6-membered)), 17.3 (dd to t, ^{2}J(P–P)$\sim$70.0 Hz, N_2P(spiro)), 24.9 (dd to t, ^{2}J(P–P)$\sim$70.0 Hz, O_2P(spiro, 7-membered)). The X-ray structure was taken for the crystals from dichloromethane–hexane, that showed the CH_2Cl_2 peak at δ 5.2 ppm in the ^{1}H NMR.

2.3. Synthesis of *3*

A solution of bis(2-hydroxy-1-naphthyl)methane [22] (0.30 g, 1.0 mmol) and triethylamine (0.20 g, 0.28 mL, 2.0 mmol) in toluene (5 mL) was added dropwise over a

period of 10 min with continuous stirring to a solution of $N_3P_3(OCH_2CMe_2CH_2O)Cl_4$ (0.38 g, 1.0 mmol) in toluene (10 mL) and the reaction mixture was then heated to reflux for 30 h. The triethylamine hydrochloride formed was filtered off and the removal of solvent toluene from the filtrate led to compound **3**. Yield: 0.42 g (70%). M.p. 265 °C. IR (KBr, cm^{-1}): 1595, 1512, 1464, 1386, 1192, 1053, 1003. ^1H NMR: δ 1.03, 1.08 (2 s, 6 H, CH_3), 3.96 (dd, 2 H, ^2J(H–H) = 10.7 Hz, ^3J(P–H) = 13.0 Hz, OCH_2(A)), 3.96 (dd to t, 2 H, ^2J(H–H) = ^3J(P–H) = 10.7 Hz, 2 H, OCH_2(B)), 5.00 (s, 2 H, $ArCH_2$), 7.31–8.34 (m, 12 H, Ar*H*). ^{13}C NMR: δ 21.2, 21.6 (2 s, CH_3), 23.9 (s, $ArCH_2$), 32.2 (s, $C(CH_3)_2$), 76.5 (d, ^2J(P–C) = 10.5 Hz, OCH_2), 121.4, 123.5, 124.2, 125.2, 127.1, 128.9, 129.0, 132.0, 132.8, 148.8 (all Ar- = *C*). ^{31}P NMR: δ 4.9 (A portion of ABX, ^2J(P–P)∼70.6 Hz each, O_2P (spiro, 8-membered)), 6.7 (B portion of ABX, ^2J(P–P)∼70.6 Hz each, O_2P (spiro, 6-membered)), 26.0 (∼ t, ^2J(P–P) = 70.6 Hz each, PCl_2). *Anal.* Calc. for $C_{26}H_{24}N_3O_3P_3Cl_2$: C, 51.50; H, 3.98; N, 6.93. Found: C, 52.4; H, 4.43; N, 6.86%.

2.4. Synthesis of *4*

The procedure was the same as for **2** using 1,1′-bi-2-naphthol (0.29 g, 1 mmol) and $N_3P_3(OCH_2CMe_2CH_2O)Cl_4$ (0.38 g, 1 mmol). Yield: 0.38 g (65%). M.p. 158–162 °C. IR (cm^{-1}): 1591, 1508, 1464, 1373, 1265, 1182, 1059, 974. ^1H NMR: δ 1.05, 1.08 (2 s, 6 H, CH_3), 3.95–4.28 (m, 4 H, OCH_2), 7.35–8.15 (m, 12 H, Ar*H*). ^{13}C NMR: δ 21.3, 21.5 (2 s, CH_3), 32.1 (d, ^3J(P–C)∼6 Hz, $C(CH_3)_2$), 76.7 (d, ^2J(P–C) = 6 Hz, OCH_2), 110.9, 117.8, 121.0, 121.6, 124.0, 124.2, 125.6 126.6, 127.1, 127.2, 127.4, 128.4, 129.5, 130.9, 131.1, 131.4, 131.9, 132.5, 146.8, 152.8 (all Ar–*C*). ^{31}P NMR: δ 7.4 (dd to t, ^2J(P–P)∼70.3 Hz, O_2P (spiro, 6-membered)), 19.8 (dd to t, ^2J(P–P) ∼ 70.3 Hz, O_2P (spiro, 7-membered)), 27.1 (dd to t, ^2J(P–P)∼70.3 Hz, PCl_2). *Anal.* Calc. for $C_{25}H_{22}N_3O_4P_3Cl_2$: C, 50.69; H, 3.74; N, 7.09. Found: C, 50.72; H, 3.76; N, 7.15%.

2.5. Synthesis of *5*

The procedure was the same as that for **2** using 1,1′-bi-2-naphthol (0.29 g, 1.0 mmol) and **1** (0.41 g, 1.0 mmol). Yield: 0.39 g (62%). M.p. 249–252 °C. IR (KBr, cm^{-1}): 3350, 1591, 1508, 1467, 1371, 1240, 1182, 1057, 1010, 972. $[\alpha]_D = -195.1$ (*c* 1.0, $CDCl_3$). ^1H NMR: δ 0.85, 0.93, 1.00, 1.23 (4 s, 12 H, CH_3), 2.65 (br s, 2 H, N*H*), 2.85–3.10 (m, 4 H, $NHCH_2$), 3.70–4.28 (m, 4 H, OCH_2), 7.25–7.95 (m, 12 H, Ar–H). ^{13}C NMR: δ 20.9, 22.3, 24.6, 24.7 (4 s, CH_3), 31.5, 32.0 (2 d, ^3J(P–C) = 8.0, 5.4 Hz, $C(CH_2O)_2$and$C(CH_2NH)_2$, respectively), 52.8 (s, $NHCH_2$), 75.9 (d, ^2J (P–C) = 6.1 Hz, OCH_2), 121.7, 125.2, 126.2, 127.2, 127.3, 128.3, 130.4, 130.5, 131.6, 132.6, 147.7, 147.9 (all Ar–*C*). ^{31}P NMR: δ 12.9 (dd to t, ^2J(P–P)∼71.0 Hz, O_2P (spiro, 6-membered)), 17.0 (dd to t, ^2J(P–P)∼71.0 Hz, N_2P(spiro)), 25.7 (dd to t, ^2J (P–P)∼71.0 Hz, O_2P (spiro, 7-membered)). *Anal.* Calc. for $C_{30}H_{34}N_5O_4P_3$: C, 57.92; H, 5.58; N, 11.25. Found C, 57.98; H, 6.02; N, 11.32%.

2.6. Synthesis of *6*

The procedure was the same as that for **2** using 1,1′-bi-2-naphthol (0.57 g, 2.0 mmol). and $N_3P_3(OCH_2CMe_2CH_2O)Cl_4$ (0.38 g, 1.0 mmol). Yield: 0.59 g (73%). M.p. >280 °C. IR (KBr, cm^{-1}): 1589, 1506, 1466, 1369, 1263, 1207, 1184, 1068, 974. $[\alpha]_D = -197.8$ (*c* 1.1, $CHCl_3$). ^1H NMR: δ 1.03 (s, 6 H, CH_3), 4.08 (d, ^3J(P–H) = 13.0 Hz, 4 H, OCH_2), 7.26–8.06 (m, 24 H, Ar–*H*). ^{13}C NMR: δ 21.5 (s, CH_3), 32.1 (br s, $C(CH_3)_2$), 76.4 (OCH_2), 121.7, 125.2, 125.4, 126.2, 126.3, 127.2, 127.3, 128.3, 128.4, 130.8, 131.6, 131.8, 132.3, 132.6, 147.5 (all Ar–*C*). ^{31}P NMR: δ 13.1 (t, ^2J (P–P)∼91.0 Hz, O_2P (spiro, 6-membered)), 26.4 (d, ^2J(P–P) ∼91.0 Hz, O_2P (spiro, 7-membered)). *Anal.* Calc. for $C_{45}H_{34}N_3O_6P_3$: C, 67.08; H, 4.25; N, 5.21. Found C, 67.22; H, 4.28; N, 5.26%.

2.7. Synthesis of *7*

The procedure was the same as that for **2** using 1,1′-bi-2-naphthol (0.86 g, 3.0 mmol) and $N_3P_3Cl_6$ (0.35 g, 1.0 mmol). Yield: 0.67 g (68%). M.p. >280 °C. IR (KBr, cm^{-1}): 1591, 1606, 1466, 1277, 1207, 1184, 1068, 979. $[\alpha]_D = -42.5$ (*c* 0.8, $CDCl_3$). ^1H NMR: δ 7.18–7.85 (m, Ar*H*). ^{13}C NMR: δ 121.6, 121.9, 125.2, 126.2, 127.3, 127.5, 128.4, 130.8, 131.6, 132.3 (all Ar–*C*). ^{31}P NMR: δ

Table 1
Crystal data for **1** and **2**

Compound	**1**	**2**
Formula	$C_{20}H_{44}Cl_4N_{10}O_4P_6$	$C_{23}H_{32}Cl_2N_5O_4P_3$
Formula weight	816.27	606.35
Crystal system	triclinic	orthorhombic
Size (mm)	0.4 × 0.3 × 0.2	0.3 × 0.3 × 0.2
Space group	$P\bar{1}$	*Pccn*
a (Å)	10.888(3)	10.865(3)
b (Å)	11.166(3)	25.263(6)
c (Å)	15.934(4)	20.648(4)
α (°)	84.57(2)	90.0
β (°)	80.47(2)	90.0
γ (°)	78.35(2)	90.0
V (Å^3)	1867.3(10)	5667(2)
Z	2	8
D_{calc} (g cm^{-3})	1.452	1.421
μ (mm^{-1})	0.616	0.437
F(0 0 0)	848	2528
Data/restraints/ parameters	6572/0/421	4988/0/338
S	1.028	1.049
$R_1[I > 2\sigma(I)]$	0.0483	0.0625
wR_2 [all data]	0.1525	0.1809
Maximum/minimum residual electron density (e Å^{-3})	0.608/−0.389	0.763/−0.750

26.6 (s, O_2P(spiro)). *Anal.* Calc. for $C_{60}H_{36}N_3O_6P_3$: C, 72.95; H, 3.67; N, 4.25. Found C, 73.00; H, 3.69; N, 4.29%.

X-ray data were collected on an Enraf-Nonius-MACH3 X-ray diffractometer at 293 K using Mo K_α ($\lambda = 0.71073$ Å) radiation with the crystals mounted on a glass fibre. The structures were solved by direct methods [23]; all non-hydrogen atoms were refined anisotropically. For the hydrogen atoms except the NH hydrogen atoms in **1**, the riding model was used. The crystal data are summarized in Table 1.

3. Results and discussion

3.1. Synthesis and spectra

Synthesis of all the compounds reported herein is straightforward and utilizes the reaction of the phosphazene precursor with the diamine in the presence of a base or with a diol (as a sodium salt or in the presence of triethylamine).

Among the compounds **1**–**6** with the 1,3,2-dioxaphosphorinane ring, in **1**–**5** the OCH_2 protons show up as a multiplet and the two methyls of the $C(CH_3)_2$ group show two peaks suggesting that this ring is fairly rigid in these compounds. This feature is analogous to that observed for a many other tetra-coordinate compounds bearing this ring [24–28]. When racemic 1,1′-bi-2-naphthol was used in the preparation of **5**, we expected to see separated signals for the possible diastereomers [due to the chirality of the 1,1′-bi-2-naphthoxy residue and possible molecular chirality at the phosphazene due to rigid ring systems], but did not. Compound **5** obtained by starting with either racemic or chiral 1,1′-bi-2-naphthol showed the same ^{31}P NMR spectra.

For compounds **3** and **4** an ABX and AMX pattern, respectively, are observed in the ^{31}P NMR spectra [Fig. 1]. These are consistent with the spirocyclic structures as assigned, but not with the *ansa* products (**II**) or (**III**) wherein an AB_2 (or AX_2) pattern would be expected.

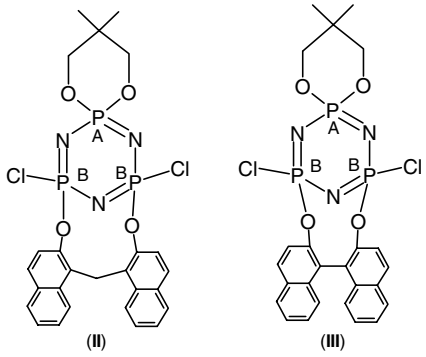

It can be noted the δ(P) values for the P(spiro) atoms with phosphorus being a part of the seven-membered ring system [cf. **2**, **4**–**7**] are always downfield to those with P(spiro) atoms as part of six- or eight-membered rings [cf. **1**–**6**]. For example, in **2**, δ(P) values for O_2P (spiro, 7-membered) and O_2P (spiro, 6-membered) are, respectively, 24.9 and 12.8. Previously such an observation on hypervalent phosphorus compounds has been made by others and by us [29–32]. This feature was rationalized earlier by invoking the rigidity of the seven-membered rings used in these studies [29]. However, it should be noted that the δ(P) values for the tri-coordinate compounds $PhOP(OCH_2CH{=}CHCH_2O)$ [130.4] and $PhOP(OCH_2CH_2CH_2CH_2O)$ [127.3] possessing more flexible seven-membered rings are also quite downfield to $PhOP(OCH_2CMe_2CH_2O)$ [114.6] which possesses a six-membered ring [33]. These observations suggest that phosphorus is shielded when it is a part of an even-membered [six or eight] ring and gets deshielded when it is a part of an odd-membered [five or seven] ring. Earlier workers have, however, have noticed that presence of five-membered rings also deshields phosphorus relative to six-membered rings [29–32,34].

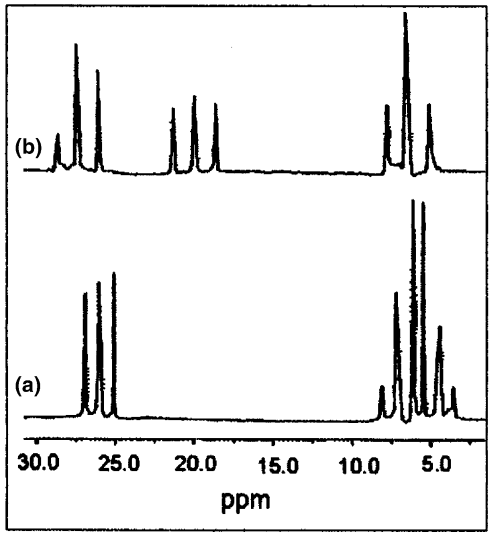

Fig. 1. The ^{31}P NMR spectra of (a) **3** and (b) **4**.

3.2. X-ray structures of *1* and *2*

The structure of **1**, with both the molecules in the asymmetric unit and with hydrogen bonding, is shown in Fig. 2; bond parameters are given in Table 2. The phosphazene P–N bond distances in **1** [1.550–1.618 Å] are in the normal range expected for such compounds [1,35].The variation in the mean P–N distances, considering both the molecules in the asymmetric unit, is in the order: Cl_2P–N<O_2P(spiro)–N<N_2P(spiro)–N. However, the exocyclic P–N single bond distances are fairly close to the phosphazenic P–N bond distances. This suggests substantial additional π-character at the exocyclic P–N bonds. This feature is also reflected in the

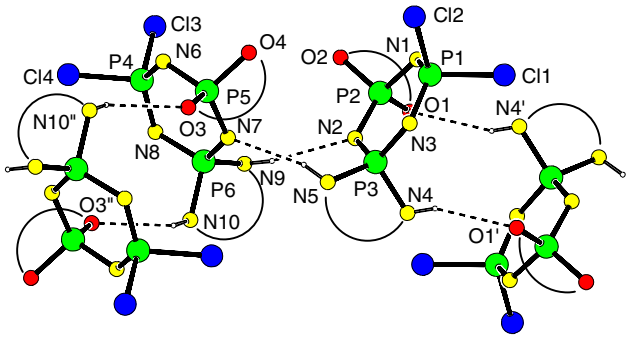

Fig. 2. Molecular structure of **1** showing all non-hydrogen atoms. Curved lines represent the $-CH_2CMe_2CH_2-$ residue. Selected hydrogen bond parameters (Å, °): N(4)–HN(4)···O(1′) 0.75 (4), 2.29 (4), 2.994 (4), 157(4); N(5)–HN(5)···N(7) 0.81 (4), 2.19 (5), 2.975 (4), 163(4); N(9)–HN(9)···N(2) 0.81 (4), 2.36 (5), 3.151 (5), 165(4); N(10)–HN(10)···O(3′) 0.76 (5), 2.34 (5), 2.993 (4), 144(4).

sum of the bond angles at the exocyclic nitrogen atoms N(4), N(5), N(9) and N(10) which are, respectively, 358°, 360°, 347° and 350°; the larger deviation at N(9) and N(10) may be due to higher uncertainties associated with the hydrogen positions. As regards phosphazenic bond angles, there is a marked deviation from the expected 120° at P(3) and P(6) (each connected to four nitrogen atoms); such a feature was observed previously in the spirocyclic compound $N_3P_3(HNCH_2CH_2CH_2NH)Cl_4$ [1,36].

The phosphazene ring in the two molecules of the asymmetric unit of **1** can be considered to be slightly distorted planar with the maximum deviation of 0.125 Å at N(2) and 0.095 Å at N(8) from the respective mean planes. This deviation is to be expected since the susbtituents at the three phosphorus atoms are all different.

Interestingly, the conformations of the 1,3,2-diazaphosporinane rings for the two molecules present in the asymmetric unit of **1** are different. Whereas this saturated ring at P(6) shows the normal chair conformation with P(6) and C(17) on the opposite sides of the mean plane comprising the atoms N(9), N(10), C(16) and C(18), the ring at P(3) has a 'tub' conformation with N(5) and C(6) at the two unique positions [Fig. 3]. It should be noted that the *tub* conformation for a saturated phosphorinane ring is *not common* for tetracoordinate P(V) compounds [21,37–39] and is found mostly for pentacoordinate phosphorus species [31,40]. We believe that this change in conformation in **1** is a result of the hydrogen bonding present in this compound (see below).

As shown in Fig. 2, both the NH protons of the 1,3,2-diazphosphorinane ring are engaged in hydrogen bonding [41,42]. While the ones at N(5) and N(9) are

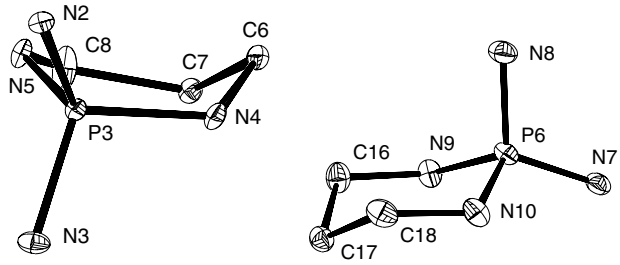

Fig. 3. A drawing showing the different conformations of the 1,3,2-diazaphosphorinane ring in **1**.

Table 2
Selected bond lengths (Å) and bond angles (°) for **1** and **2** with esd's

Compound **1**			Compound **2**		
Bond lengths					
P(1)–N(1)	1.573(3)	P(4)–N(6)	1.550(4)	P(1)–N(1)	1.581(5)
P(1)–N(3)	1.551(3)	P(4)–N(8)	1.553(3)	P(1)–N(3)	1.595(4)
P(1)–Cl(1)	2.002(2)	P(4)–Cl(3)	2.015(2)	P(1)–N(4)	1.628(4)
P(1)–Cl(2)	2.012(2)	P(4)–Cl(4)	1.989(2)	P(1)–N(5)	1.611(4)
P(2)–N(1)	1.577(3)	P(5)–N(6)	1.579(4)	P(2)–N(1)	1.554(4)
P(2)–N(2)	1.575(3)	P(5)–N(7)	1.580(3)	P(2)–N(2)	1.584(4)
P(2)–O(1)	1.582(3)	P(5)–O(3)	1.570(3)	P(2)–O(1)	1.587(4)
P(2)–O(2)	1.572(3)	P(5)–O(4)	1.566(3)	P(2)–O(2)	1.595(3)
P(3)–N(2)	1.605(3)	P(6)–N(7)	1.583(3)	P(3)–N(2)	1.576(4)
P(3)–N(3)	1.615(3)	P(6)–N(8)	1.618(3)	P(3)–N(3)	1.578(4)
P(3)–N(4)	1.627(3)	P(6)–N(9)	1.626(3)	P(3)–O(3)	1.588(4)
P(3)–N(5)	1.607(3)	P(6)–N(10)	1.636(3)	P(3)–O(4)	1.595(3)
Bond angles					
N(1)–P(1)–N(3)	120.8(2)	N(6)–P(4)–N(8)	121.3(2)	N(1)–P(1)–N(3)	116.3(2)
N(1)–P(2)–N(2)	118.1(2)	N(6)–P(5)–N(7)	117.1(2)	N(1)–P(2)–N(2)	117.7(2)
N(2)–P(3)–N(3)	111.6(2)	N(7)–P(6)–N(8)	113.7(2)	N(2)–P(3)–N(3)	118.8(2)
P(1)–N(1)–P(2)	118.9(2)	P(4)–N(6)–P(5)	119.6(2)	P(1)–N(1)–P(2)	123.8(3)
P(2)–N(2)–P(3)	123.8(2)	P(5)–N(7)–P(6)	125.1(2)	P(2)–N(2)–P(3)	120.9(2)
P(1)–N(3)–P(3)	123.3(2)	P(4)–N(8)–P(6)	120.8(2)	P(1)–N(3)–P(3)	120.2(3)

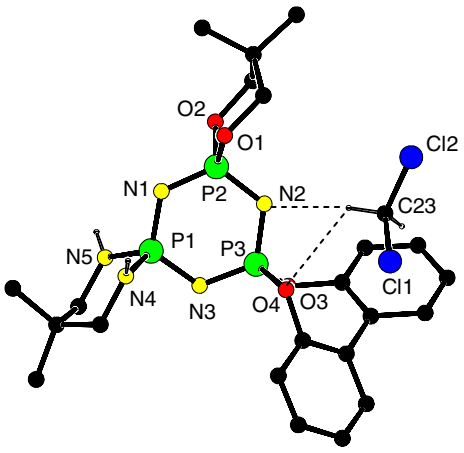

Fig. 4. Molecular structure of **2** showing all the non-hydrogen atoms. The hydrogen bonding interactions involving the solvent CH_2Cl_2 are also shown. Selected (possible) hydrogen bond parameters (Å, °): N(5)–HN(5)···O(2′) 0.86, 2.94, 3.252 (5), 103.8; C(23)–H(23B)···O(4) 0.97, 2.70, 3.289 (8), 119.9; C(23)–H(23B)···N(2) 0.97, 2.64, 3.557 (7), 157.1.

hydrogen bonded to the phosphazene ring nitrogen atoms N(7) and N(2) leading to a dimeric formulation, the hydrogens at N(4) and N(10) are hydrogen bonded to O(1) and O(3) of the 1,3,2-dioxaphosphorinane rings, respectively. It is important to note that the hydrogen bond acceptor sites N(2) and N(7) are elelctron-rich because of the proximity to the phosphorus bearing the 1,3,2-diazaphosphorinane residue which could push some electron density to the phosphazene ring system.

Compound **2** [Fig. 4, Table 2], to our knowledge, is the first unsymmetrical tris-spirocyclic cyclotriphosphazene to be structurally characterized. The phosphazene ring in **2** is planar with a maximum deviation of 0.103 Å at N(3) from the mean plane. The mean phosphazenic P–N bond distances in **2** are shorter at the P(spiro) bearing the oxygen atoms compared to those at the P(spiro) with the 1,3,2-diazaphosphorinane ring, as expected. The P–N single bonds in the 1,3,2-diazaphosphorinane ring are only slightly longer [within 0.02 Å] compared to the phosphazenic P–N bonds, thus showing substantial π-character; these nitrogen atoms [N(4), N(5)] are essentially planar [sum of the angles ~360°]. Both the N–P–N and the P–N–P angles are fairly close to 120° despite the fact the three phosphorus atoms carry *different* non-phosphazenic rings. The saturated six-membered rings have a *chair* conformation [cf. compound **1** above].

In contrast to what is observed for **1**, only very weak intermolecular hydrogen bonding between one of the NH hydrogens and an oxygen atom [O(2)] of the saturated 1,3,2-dioxaphosphorinane ring is present in **2** [not shown in Fig. 4]. The second NH proton does not appear to be participating in hydrogen bonding. Interestingly, a dichloromethane molecule sits very close to the phosphazene ring with a bifurcated C–H···O hydrogen bond involving one of the methylene protons, N(2) of the phosphazene ring and O(4) of the 1,3,2-dioxaphosphocin ring.

4. Summary and outlook

Synthesis and structures of an unsymmetrical bis-spirocyclic cyclotriphosphazene and the first example of an unsymmetrical tris-spirocyclic cyclotriphosphazene has been accomplished. Several new chiral and racemic spirocyclic cyclotriphosphazenes have also been synthesized. The utility of these compounds in the possible chiral induction [e.g. synthesis of hydroxyphosphonates via the Pudovik reaction] has to be investigated further. However, characterization of a cyclotriphosphazene with chirality solely at phosphorus is an interesting target that still has to be accomplished.

5. Supplementary data

Supplementary data are available from the CCDC, 12 Union Road, Cambridge CB2 1EZ, UK (fax: +44-1223-336033; E-mail: deposit@ccdc.cam.ac.uk or www:http://www.ccdc.cam.ac.uk) on request, quoting the Deposition Nos. CCDC 219286 and 219287.

Acknowledgements

This work was supported by the Department of Science and Technology (DST), New Delhi. N.S.K. thanks the Council of Scientific and Industrial Research (CSIR), New Delhi for a fellowship. The National Single Crystal Diffractometer Facility at the University of Hyderabad funded by DST (New Delhi) is gratefully acknowledged.

References

[1] V. Chandrasekhar, K.R.J. Thomas, Struct. Bond. 81 (1993) 41.
[2] C.W. Allen, Chem. Rev. 91 (1991) 133.
[3] V. Chandrasekhar, V. Krishnan, Adv. Inorg. Chem. 53 (2002) 159.
[4] A.J. Elias, J.M. Shreeve, Adv. Inorg. Chem. 52 (2001) 335 (fluorophosphazene review).
[5] J.E. Mark, H.R. Allcock, R. West, Inorganic Polymers, Prentice-Hall, New Jersey, 1992.
[6] Y. Chang, E.S. Powell, H.R. Allcock, S.M. Park, C. Kim, Macromolecules 36 (2003) 2568.
[7] T.J. Hartle, N.J. Sunderland, M.B. McIntosh, H.R. Allcock, Macromolecules 33 (2000) 4307.
[8] Y. Chang, R. Prange, H.R. Allcock, S.C. Lee, C. Kim, Macromolecules 35 (2002) 8556.
[9] R.A. Shaw, Phosphorus Sulfur Silicon 45 (1989) 103.
[10] S. Kumaraswamy, M. Vijjulatha, C. Muthiah, K.C. Kumara Swamy, U. Engelhardt, J. Chem. Soc., Dalton Trans. (1999) 891.

[11] O.-S. Jung, Y.T. Kim, Y.-A. Lee, Y.J. Kim, H.K. Chae, Inorg. Chem. 38 (1999) 5457.
[12] K. Brandt, I.P. Czomperlik, M. Siwy, T. Kupka, R.A. Shaw, S. Ture, A. Clayton, D.B. Davies, M.B. Hursthouse, G.D. Sykara, J. Org. Chem. 64 (1999) 7299.
[13] D.B. Davies, T.A. Clayton, R.E. Eaton, R.A. Shaw, A. Egan, M.B. Hursthouse, G.D. Sykara, I.P. Czomperlik, M. Siwi, K. Brandt, J. Am. Chem. Soc. 122 (2000) 12447.
[14] K. Brandt, M. Siwy, I.P. Czomperlik, J. Silberring, J. Org. Chem. 66 (2001) 5701.
[15] K. Muralidharan, P. Venugopalan, A.J. Elias, Inorg. Chem. 42 (2003) 3176.
[16] P. Kommana, S. Kumaraswamy, K.C. Kumara Swamy, Inorg. Chem. Commun. 6 (2003) 394.
[17] H.R. Allcock, A.D. Primrose, E.N. Silverberg, K.B. Visscher, A.L. Rheingold, I.A. Guzei, M. Parvez, Chem. Mater. 12 (2000) 2530.
[18] H.R. Allcock, L.A. Siegel, J. Am. Chem. Soc. 86 (1964) 5140.
[19] H.R. Allcock, M.T. Stein, J. Am. Chem. Soc. 96 (1974) 49.
[20] D.D. Perrin, W.L.F. Armarego, D.R. Perrin, Purification of Laboratory Chemicals, Pergamon, Oxford, 1986.
[21] N. Satish Kumar, K.C. Kumara Swamy, Acta Crystallogr., Sect. C. 57 (2001) 1421.
[22] Y. Ogata, A. Kawasaki, T. Goto, Tetrahedron 25 (1969) 2589.
[23] G.M. Sheldrick, SHELX-97, University of Göttingen, Germany, 1997.
[24] J.G. Verkade, D.W. White, R.D. Bertrand, G.K. McEwen, J. Am. Chem. Soc. 92 (1970) 7125.
[25] L.D. Hall, R.B. Malcolm, Can. J. Chem. 50 (1972) 2092.
[26] S. Kumaraswamy, R.S. Selvi, K.C. Kumara Swamy, Synthesis (1997) 207.
[27] C. Muthiah, K. Praveen Kumar, C. Aruna Mani, K.C. Kumara Swamy, J. Org. Chem. 65 (2000) 3733.
[28] N. Satish Kumar, S. Kumaraswamy, M.A. Said, K.C. Kumara Swamy, Org. Proc. Res. Develop. 7 (2003) 925.
[29] R.R. Holmes, T.K. Prakasha, S.D. Pastor, in: L.D. Quin, J.G. Verkade (Eds.), Phosphorus-31 NMR Spectral Properties in Compound Characterization and Structural Analysis, VCH, New York, 1994, p. 27.
[30] M.A Said, M. Pülm, R. H-Irmer, K.C. Kumara Swamy, J. Am. Chem. Soc. 118 (1996) 9481.
[31] M.A. Said, M. Pülm, R. Herbst-Irmer, K.C. Kumara Swamy, Inorg. Chem. 36 (1997) 3044.
[32] C. Muthiah, M.A. Said, M. Pülm, R. Herbst-Irmer, K.C. Kumara Swamy, Polyhedron 19 (2000) 63.
[33] A.C. Guimaraes, J.B. Robert, Tetrahedron Lett. (1976) 473.
[34] See for example, D.G. Gorenstein, in: Progr. Nucl. Magn. Reson. Spectrosc. 16 (1983) 1.
[35] D.E.C. Corbridge, Phosphorus – An Outline of its Chemistry, Biochemistry and Technology, 4th ed., Elsevier, Amsterdam, 1990, p. 47.
[36] A.H. Alkubaisi, W.F. Deutch, M.B. Hursthouse, H.G. Parkes, L.S. Shaw (neé Gözen), R.A. Shaw, Phosphorus Sulfur Silicon 28 (1986) 229.
[37] B.E. Maryanoff, R.O. Hutchins, C.A. Maryanoff, Top. Stereochem. 11 (1979) 187.
[38] M.J. Gallager, in: J.G. Verkade, L.D. Quin (Eds.), Phosphorus-31 NMR Spectroscopy in Stereochemical Analysis, VCH, Deerfield Beach, FL, 1987 (Chapter 9).
[39] W.G. Bentrude, W.N. Setzer, in: J.G. Verkade, L.D. Quin (Eds.), Phosphorus-31 NMR Spectroscopy in Stereochemical Analysis, VCH, Deerfield Beach, FL, 1987 (Chapter 11).
[40] K.C. Kumara Swamy, S.D. Burton, J.M. Holmes, R.O. Day, R.R. Holmes, Phosphorus Sulfur Silicon 53 (1990) 437.
[41] For a discussion on NH···N hydrogen bonding in the fully substituted aminophosphazenes, $(RNH)_6P_3N_3$, see: J.F. Bickley, R. Bonar-Law, G.T. Lawson, P.I. Richards, F. Rivals, A. Steiner, S. Zacchini, J. Chem. Soc., Dalton Trans. (2003) 1235.
[42] (Amino)cyclophosphazenes, $N_3P_3(NH_2)_2(OR)_4$, show a complex three dimensional hydrogen-bonded network. See: J.K. Fincham, H.G. Parkes, L.S. Shaw (nèe Gözen), R.A. Shaw, M.B. Hursthouse, J. Chem. Soc., Dalton Trans. (1988) 1169.

Available online at www.sciencedirect.com
SCIENCE DIRECT®
Polyhedron 23 (2004) 987–991
POLYHEDRON
www.elsevier.com/locate/poly

Transformation of maleato manganese(II): temperature effect and coordination modes ☆

Hong-Bin Chen, Hui Zhang, Jin-Mei Yang, Zhao-Hui Zhou *

Department of Chemistry and State Key Laboratory for Physical Chemistry of Solid State Surface, Xiamen University, Xiamen 361005, China

Received 20 July 2003; accepted 11 December 2003

Abstract

Two maleato bipyridine manganese(II) coordination polymers $[Mn(male)(bpy)(H_2O)]_n \cdot 2nH_2O$ (**1**) and $[Mn(male)(bpy)]_n$ (**2**) (H_2male = maleic acid, bpy = 2,2′-bipyridine) were prepared in an ice-bath and at room temperature respectively, and were spectroscopically and structurally characterized. Complex **1** obtained at low temperature, possesses a one-dimensional helical chain in the solid state with hepta-coordination number at the manganese center. At room temperature, the hydrated complex **1** was irreversibly converted into the thermodynamically stable dehydrated product **2** with octahedral coordination. A similar dehydration effect was observed for the maleato manganese(II) complex with a more conjugated phenanthroline (phen) ligand. The maleato manganese(II) coordination polymer $[Mn(male)(phen)]_n \cdot nH_2O$ (**3**) can be converted into the dehydrated product $[Mn(male)(phen)]_n$ (**4**) upon heating, while the resultant product retains a similar pattern of coordination mode.
© 2004 Elsevier Ltd. All rights reserved.

Keywords: Manganese maleate; Coordination polymer; Temperature effect; Helical architecture; Hydrogen bonds; π–π interactions

1. Introduction

Metal-directed self-assembly of coordination polymers with well-defined architectures has presently been one topic of intense interest in the field of supra-molecular chemistry owing to their original topologies, desired properties and potential applications in multidisciplinary areas, e.g., catalysis, nonlinear optics, magnetism, luminescence, gas storage and chemical absorption [1]. Considerable efforts have been made to construct such extended solid materials with manipulated and tunable functionalities. The most common used strategy is to employ appropriate organic building blocks with several metal centers through direct bond formation. However, it still remains a challenge for synthetic chemists to predict and control the way of molecular components assembled in the crystalline phase. This is because the self-assembly processes are heavily influenced by subtle factors, such as templates [2], choice of solvents and counterions [3], and pH values [4]. When the reaction conditions are deliberately controlled, infinite networks with novel topologies can be gained. Though it was clear long ago that temperature can dramatically affect the extended structure of the networks, the influence of temperature in the formation of coordination polymers is less well understood and systematic studies are rare [5]. It is known that in the self-assembly of both synthetic and biological systems the thermodynamic product is usually favored, the kinetic product may also be obtained if the shape of the energy hypersurface is such that the system becomes trapped in local minima [6]. To develop the better understanding of temperature effects on the formation of coordination polymers, in the present contribution, two new maleato manganese(II) polymers formulated as $[Mn(male)(bpy)(H_2O)]_n \cdot 2nH_2O$ (**1**) and $[Mn(male)\ (bpy)]_n$ (**2**) were temperature-dependently prepared and structurally characterized. Irreversible conversion from kinetic maleato manganese **1** to the dehydrate product **2** was investigated.

☆ Supplementary data associated with this article can be found, in the online version, at doi:10.1016/j.poly.2004.01.005.

* Corresponding author. Tel.: +86-592-2184531; fax: +86-592-2183047.
E-mail address: zhzhou@xmu.edu.cn (Z.-H. Zhou).

0277-5387/$ - see front matter © 2004 Elsevier Ltd. All rights reserved.
doi:10.1016/j.poly.2004.01.005

2. Experimental

All chemicals were commercially available and used without further purification. Elemental microanalyses (C, H and N) were performed on an EA 1100 elemental analyzer. Infrared spectra were recorded from KBr pellets on a Nicolet FT-IR 360 spectrophotometer in the range of 4000–400 cm^{-1}.

2.1. Preparation of $[Mn(male)(bpy)(H_2O)]_n \cdot 2nH_2O$ (1)

Manganese maleate was prepared in situ at 0 °C by mixing $MnCl_2 \cdot 4H_2O$ (0.99 g, 5 mmol) and an equimolar amount of sodium maleate, dissolving in 20 ml double distilled water. After stirring the mixture for 15 min, an equimolar amount of 2,2′-bipyridine (0.780 g, 5 mmol), dissolved in 10 ml methanol, was slowly added and stirring was continued for another 10 min. The solution was kept in the refrigerator. Block-like crystals suitable for single crystal diffraction analysis were obtained a few days later. Yield: 85%. *Anal.* Calcd. for $C_{14}H_{16}N_2O_7Mn$: C, 44.3; H, 4.2; N, 7.4. Found: C, 43.0; H, 4.1; N, 7.3%. IR (KBr, cm^{-1}): ν(O–H) 3377_{vs}, ν_{as}(C=O) 1578_{vs}, ν_s(C=O) 1439_s, ν(Mn–O) 773_s.

2.2. Preparation of $[Mn(male)(bpy)]_n$ (2)

The preparation of **2** was similar to the hydrate product **1** except the reaction was proceeded at ambient temperature. Plate single crystals suitable for X-ray diffraction were obtained after a few weeks. Yield: 90%. *Anal.* Calcd. for $C_{14}H_{10}N_2O_4Mn$: C, 51.7; H, 3.1; N, 8.6. Found: C, 52.2; H, 3.2; N, 8.9%. IR (KBr, cm^{-1}): ν_{as}(C=O) 1593_s, 1547_{vs}, ν_s(C=O) 1429_m, 1398_m, ν(Mn–O) 774_m.

2.3. Conversion of $[Mn(male)(bpy)(H_2O)]_n \cdot 2nH_2O$ (1) to $[Mn(male)(bpy)]_n$ (2)

The crystals of **1** were picked out and put in a beaker with some mother liquid at ambient temperature. A few days later, the block-like yellow crystals segmented into 'chaos' and IR spectra justified it was converted into thermodynamic product **2**.

2.4. Conversion of $[Mn(male)(phen)]_n \cdot nH_2O$ (3) to $[Mn(male)(phen)]_n$ (4)

The maleato phenanthroline manganese complexes **3** and **4** were prepared as reported very recently [7]. Crystals of **3** (0.37g, 1 mmol) in 5 ml water were warmed in a 50 °C warm bath for 8 h. The resultant product was showed to be the dehydrated maleato manganese complex **4** by IR spectra.

2.5. X-ray data collection, structure solution and refinement

Intensity data were collected on a Bruker SMART APEX CCD using Mo Kα radiation ($\lambda = 0.71073$ Å). Both structures were solved by direct methods and refined by full-matrix least squares based on F^2 using

Table 1
Crystallographic data for $[Mn(male)(bpy)(H_2O)]_n \cdot 2nH_2O$ (**1**) and $[Mn(male)(bpy)]_n$ (**2**)

Compounds	1	2
Empirical formula	$C_{14}H_{16}N_2O_7Mn$	$C_{14}H_{10}N_2O_4Mn$
Formula weight	379.23	325.18
Crystal system	monoclinic	monoclinic
Space group	$P2_1/c$	$P2_1/c$
a (Å)	8.0194(2)	11.4546(3)
b (Å)	8.6486(1)	13.3064(4)
c (Å)	23.3306(4)	8.8076(3)
β (°)	92.059(1)	111.455(1)
V (Å^3)	1617.09(5)	1249.42(7)
Z	4	4
$D_{calcd.}$ (g cm^{-3})	1.558	1.729
Crystal size (mm)	$0.061 \times 0.051 \times 0.035$	$0.066 \times 0.200 \times 0.216$
F_{000}	780	660
θ range (°)	$1.75 \leqslant \theta \leqslant 28.82$	$1.91 \leqslant \theta \leqslant 28.94$
T (K)	296	296
μ (mm^{-1})	0.855	1.075
$R[I > 2\sigma(I)]$	$R = 0.0554$, $R_w = 0.1499$	$R = 0.0383$, $R_w = 0.0816$
R (all data)	$R = 0.0595$, $R_w = 0.1553$	$R = 0.0524$, $R_w = 0.0865$
	$w^{-1} = \sigma^2(F_o^2) + 0.1245P^2$ $P = (F_o^2 + 2F_c^2)/3$	$w^{-1} = \sigma^2(F_o^2) + 0.0373P^2 + 0.1049P$, $P = (F_o^2 + 2F_c^2)/3$
Goodness-of-fit	0.912	1.027
Minimum and maximum residual density (e Å^{-3})	−1.130 and 0.727	−0.345 and 0.335

Table 2
Selected bond lengths (Å) and angles (°) for 1[a] and 2[b]

*[Mn(male)(bpy)(H$_2$O)]$_n$·2nH$_2$O (**1**)*					
Bond lengths					
Mn1–O1	2.3666(2)	Mn1–O2	2.2344(2)	Mn1–O3^{i}	2.362(2)
Mn1–O4^{i}	2.3600(2)	Mn1–Ow1	2.1375(2)	Mn1–N1	2.2528(2)
Mn1–N2	2.2540(2)				
Bond angles					
O1–Mn1–O2	56.67(5)	O1–Mn1–O3^{i}	137.79(6)	O1–Mn1–O4^{i}	158.97(7)
O1–Mn1–O1w	82.99(6)	O1–Mn1–N1	88.21(6)	O1–Mn1–N2	97.58(6)
O2–Mn1–O3^{i}	84.96(6)	O2–Mn1–O4^{i}	139.62(6)	O2–Mn1–O1w	95.68(7)
O2–Mn1–N1	139.66(6)	O2–Mn1–N2	91.65(6)	O3–Mn1–O4	54.67(7)
O3–Mn1–O1w^{i}	84.23(7)	O3–Mn1–N1^{i}	133.59(7)	O3^{i}–Mn1–N1^{i}	100.36(6)
O4–Mn1–Ow1^{i}	81.97(7)	O4–Mn1–N1^{i}	79.80(6)	O4–Mn1–N2^{i}	94.97(7)
Ow1–Mn1–N1	99.23(7)	Ow1–Mn1–N2	171.69(7)	N1–Mn1–N2	72.57(6)
Hydrogen bonding					
Bond lengths					
O1w···O2^{i}	2.727(3)	O1w···O3w	2.730(2)	O2w···O1^{ii}	2.810(3)
O2w···O4^{iii}	2.756(3)	O2w···O2w^{ii}	2.863(3)	O3w···O4^{iv}	2.805(4)
*[Mn(male)(bpy)]$_n$ (**2**)*					
Bond lengths					
Mn1–O1	2.1812(2)	Mn1–O2^{i}	2.1499(2)	Mn1–O3	2.1157(2)
Mn1–O4^{ii}	2.1733(2)	Mn1–N1	2.2688(2)	Mn1–N2	2.3286(2)
Bond angles					
O1–Mn1–O2^{i}	94.16(7)	O1–Mn1–O3	82.89(6)	O1–Mn1–O4^{ii}	176.65(6)
O1–Mn1–N1	86.74(6)	O1–Mn1–N2	93.61(6)	O2–Mn1–O3^{i}	99.63(6)
O2^{i}–Mn1–O4^{ii}	84.15(6)	O2–Mn1–N1^{i}	89.82(6)	O2–Mn1–N2^{i}	159.24(7)
O3–Mn1–O4^{ii}	94.53(6)	O3–Mn1–N1	166.42(6)	O3–Mn1–N2	100.42(6)
O4^{ii}–Mn1–N1	96.14(6)	O4^{ii}–Mn1–N2	88.95(6)	N1–Mn1–N2	71.44(7)

[a] Symmetry transformation: (i) $1-x, 1/2+y, 1/2-z$; (ii) $1-x, -y, -z$; (iii) $-1+x, -1/2-y, -1/2+z$; (iv) $x, 1+y, z$.
[b] Symmetry transformation: (i) $x, 1/2-y, 1/2+z$; (ii) $1-x, -y, 1-z$.

SHELX-97 software [8]. All non-hydrogen atoms were anisotropically refined. Hydrogen atoms were included at geometrically calculated positions with thermal parameters derived from the parent atoms, except those bonded to the water molecules. The water hydrogen atoms were located in the difference map and included at these sites, with a fixed isotropic displacement factor of $U(\mathrm{H}) = 1.2U_{\mathrm{eq}}(\mathrm{O})$. Crystal data, data collection and refinement parameters are summarized in Table 1. Selected bond lengths and bond angles are listed in Table 2.

3. Results and discussion

Based on IR spectra, we can deliberately diagnose the coordination nature of the maleato group in complexes **1** and **2**. Specifically, asymmetric stretching vibrations ν_{as}(COO) appear near 1578 cm^{-1} for **1** and between 1593 and 1547 cm^{-1} for **2**, and the symmetric stretching vibrations ν_s(COO) are observed near 1439 cm^{-1} for **1** and between 1429 and 1398 cm^{-1} for **2**. The separations [ν_{as}(COO)–ν_s(COO)] of complexes **1** and **2** (139 and 118 cm^{-1}) are much smaller than the value of 200 cm^{-1} for the free maleato group, indicating that the coordinated carboxyl group is in a bidentate bridging or chelating mode [9,10].

X-ray diffraction analysis reveals the maleato manganese dihydrate **1** possesses 1D helical chains with the basic building unit Mn(male)(bpy)(H$_2$O). Each manganese atom is primarily coordinated by four oxygen atoms from two bidentated maleates, two nitrogen atoms from bpy and one water molecule, in an irregular pentagonal-bipyramidal configuration (Fig. 1). The carboxyl oxygen atoms O1, O2 chelate to central manganese with an O1–Mn1–O2 bond angle of 56.7°, while O3, O4 of the other carboxyl group bind another manganese center. Thus each maleato unit serves as a bis(bidentate) ligand to link two manganese atoms and yields a half turn of the helical structure. All the carbon atoms of the maleato unit form a common plane, from which both terminal carboxyl groups O1–C1–O3 and O3–C4–O4 are twisted from the carbon backbone by 20.0° and 72.1°, respectively. The four Mn–O bond distances are different from each other to some extent (Table 2), with that to O2 being particularly short [2.2344(2) Å]. Unexpectedly, the shortest bond distance is that to the coordinated water molecule [Mn1–O1w 2.1375(2) Å]. So far, a great majority of structurally characterized Mn(II) complexes take invariably a

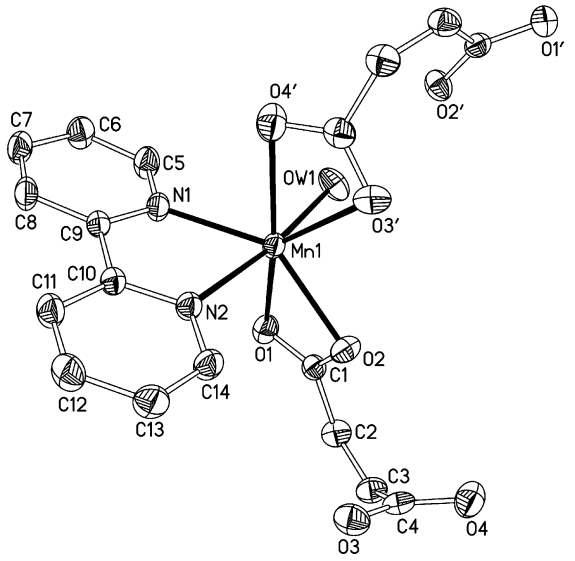

Fig. 1. One of the asymmetric units of $[Mn(male)(bpy)(H_2O)]_n \cdot 2nH_2O$ (**1**) in the Λ-configuration; hydrogen atoms and water molecules were omitted for clarity; thermal ellipsoids are drawn at 30% probability.

six-coordinate octahedral geometry around the metal atom. Complexes with coordination numbers exceeding six are limited to a few examples [11]. To the best of our knowledge, a helical coordination polymer based on a hepta-coordinated manganese center has not yet been documented hitherto. Extension of the basic building unit along the crystallographic 2_1 axis in the *b* direction gives an infinite 1D helical architecture with a long pitch of 8.649 Å. The helical chain is decorated by 2,2′-bpy ligands alternatively at the two sides and the 2,2′-bpy planes on the same side are absolutely parallel one another, while they have a dihedral angle of 42.8° with those on the other side (Fig. 2). The helical chains are further extended through hydrogen bonds between water molecules and carboxyl oxygen atoms into a two-dimensional network.

The asymmetric unit of **2** consists of one manganese center, one maleato group and one bpy ligand. Each manganese center primarily coordinates to two nitrogen atoms from 2,2′-bpy and four carboxylate oxygen atoms from three maleato groups, in a geometry which is best described as a distorted octahedron (Fig. 3). The Mn1–N1 bond distance [2.2688(2) Å] is slightly shorter than the Mn1–N2 bond [2.3286(2) Å] in the same ligand, suggesting some twist in the 2,2′-bpy ligand (dihedral angle 11.5° between the two pyridyl rings). *Cis*-fashioned oxygen atoms O1 and O3 at the two termini of the maleato unit bind the manganese center into a seven-member chelate ring with an O1–Mn1–O3 bond angle of 82.89°, while O2 and O4 bind to the other two manganese atoms. In this way, each maleato group acts as a tetradentate ligand to coordinate three manganese atoms. The dihedral angle (45.0°) between O1–C1–O3 and O3–C4–O4 is much smaller than that in **1** (67.9°). Both terminal carboxyl groups O1–C1–O2 and O3–C4–O4 twist from the carbon backbone C1–C2–C3–C4 by 45.9°and 1°, respectively. The conformations of the maleato units in the two complexes are so different that the explanation why two different topological products were obtained becomes obvious. The coordination mode of the maleato group is to some extent similar to those previously reported for $[Mn_4(male)_2(bpy)_8](ClO_4)_4 \cdot (MeOH)_2(H_2O)_2$ [12], $[Mn(male)(\mu\text{-}4,4'\text{-}bpy)]_n \cdot 0.5nH_2O$ [13] and [Mn(male)(phen)]$_n$ [7,14]. However, the extension of the basic unit and the packing style are different from those related compounds, thus giving rise to topologically different products. In addition, dimeric $[Mn_2(male)_2(bpy)_2]$ may

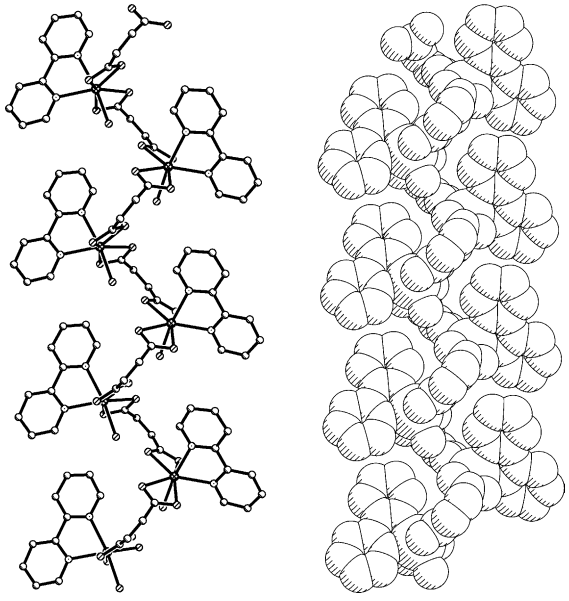

Fig. 2. One of the perspective views of a single helical chain of $[Mn(male)(bpy)(H_2O)]_n \cdot 2nH_2O$ (**1**) in the M-configuration.

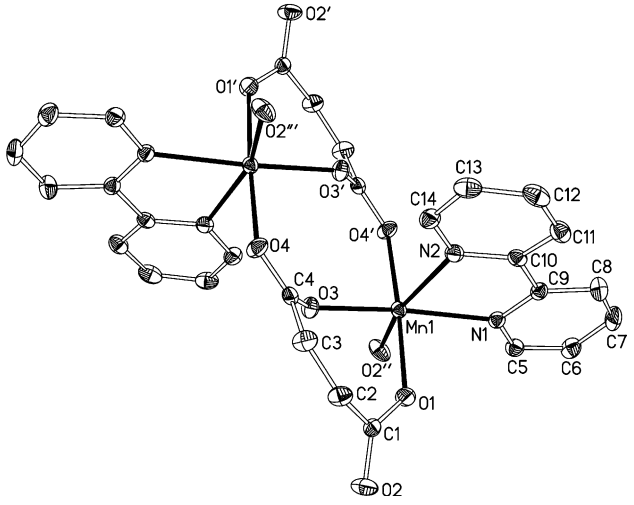

Fig. 3. Asymmetric unit of $[Mn(male)(bpy)]_n$ (**2**) with atom numbering scheme; hydrogen atoms were omitted for clarity; thermal ellipsoids are drawn at 30% probability.

be better as a secondary building unit (SBU) than monomeric [Mn(male)(bpy)] for clearly describing the crystal structure. In the dimeric model, the extension directions of O2 and O2′, O2″ and O2‴ are opposite to each other, respectively, linking and being linked by another four SBUs into a two-dimensional zigzag structure. π–π stacking interactions between bipyridyl planes further extend the two-dimensional structure into a three-dimensional network.

The formation of both maleato manganeses complexes is temperature-dependent. When the reaction proceeded at 0 °C, only the one-dimensional coordination polymer **1** was separated. Whereas at ambient temperature, only the thermodynamic product **2** was isolated. Furthermore, the irreversible conversion from **1** to **2** was observed when **1** was exposed to an ambient temperature for a few days and this reaction could be qualitatively traced by IR spectra. As to the details of how the conversion proceeds requires further theoretical deduction and kinetic measurements. Here the possible mechanism of transformation is depicted as follows. In the first step, the manganese maleate species $[Mn(male)(H_2O)_2]_n \cdot nH_2O$ was formed according to previous reports [15]. Addition of 2,2′-bipyridine ligand replaces the water molecules to complete the formation of the kinetic product $[Mn(male)(bpy)(H_2O)]_n \cdot 2nH_2O$ (**1**) with hepta-coordination. On warming to room temperature, the maleato manganese complex **1** was further compelled into the thermodynamically stable product $[Mn(male)(bpy)]_n$ **2** with dehydration. Very recently, the stable maleato bipyridine manganese species **2** has been separated as the only product in the Mn^{2+}/maleate/bipyridine system in ethanol solution [7]. However, a similar condition with phenanthroline results in the formation of the hydrated product $[Mn(male)(phen)]_n \cdot nH_2O$ (**3**), which can be converted into the dehydrated maleato phenanthroline manganese(II) $[Mn(male)(phen)]_n$ (**4**) [7,14] upon heating in our experiment. This is much related, but having the more conjugated phenanthroline ring in the complexes. The detailed transformations of the maleato manganese complexes is shown in Scheme 1.

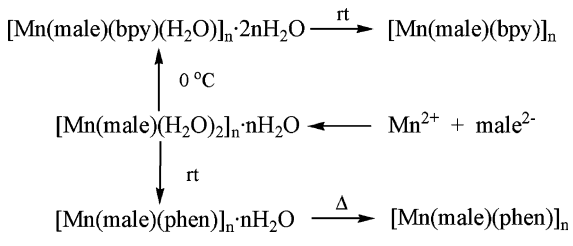

Scheme 1. Transformations of maleato manganese complexes with 2,2-bipyridine and phenanthroline groups.

4. Supplementary materials

Crystallographic data for the structural analyses have been deposited with the Cambridge Crystallographic Data Centre, CCDC No. 215790 for compound **1** and 215791 for compound **2**. Copies of this information may be obtained free of charge from The Director, CCDC, 12 Union Road, Cambridge, CB2 1EZ, UK (fax: +44-1223-336033; e-mail: deposit@ccdc.cam.ac.uk or www: http://www.ccdc.cam.ac.uk).

Acknowledgements

Financial supports from the Ministry of Science and Technology (001CB108906) and the National Science Foundation of China (No. 20171037, 20021002) are gratefully acknowledged.

References

[1] B. Moulton, M.J. Zaworotko, Chem. Rev. 101 (2001) 1629.
[2] H. Gudbjartson, K. Biradha, K.M. Poirier, M.J. Zaworotko, J. Am. Chem. Soc. 121 (1999) 2599.
[3] (a) H.P. Wu, C. Janiak, G. Rheinwald, H. Lang, J. Chem. Soc., Dalton Trans. (1999) 183;
(b) M.A. Withersby, A.J. Blake, N.R. Champness, P.A. Cooke, P. Hubberstey, W.S. Li, M. Schröder, Inorg. Chem. 38 (1999) 2259.
[4] N. Niklas, F. Hampel, R. Alsfasser, Chem. Commun. (2003) 1586.
[5] Z.H. Zhou, J.J. Ye, Y.F. Deng, G. Wang, J.X. Gao, H.L. Wan, Polyhedron 21 (2002) 787.
[6] B. Hasenknopf, J.M. Lehn, N. Boumediene, E. Leize, A. Van Dorssellaer, Angew. Chem., Int. Ed. 37 (1998) 3265.
[7] C.B. Ma, C.N. Chen, Q.T. Liu, F. Chen, D.Z. Liao, L.C. Li, L.C. Sun, Eur. J. Inorg. Chem. (2003) 2872.
[8] G..M. Sheldrick, SHELX-97 (SHELXS-97 and SHELXL-97), Programs for Crystal Structure Analyses, University of Göttingen, Germany, 1998.
[9] G..B. Deacon, R.J. Phillips, Coord. Chem. Rev. 33 (1980) 227.
[10] D.N. Sathyanarayana, V.V. Savant, Z. Anorg. Allg. Chem. 385 (1971) 329.
[11] (a) T. Tanase, S. Tamakoshi, M. Doi, M. Mikuriya, H. Sakurai, S. Yano, Inorg. Chem. 39 (2000) 692, and references therein;
(b) M. Devereux, M. McCann, V. Leon, M. Geraghty, V. McKee, J. Wikaira, Polyhedron 19 (2000) 1205.
[12] M.X. Li, G.Y. Xie, S.L. Jin, Y.D. Gu, M.Q. Chen, J. Liu, Z. Xu, X.Z. You, Polyhedron 15 (1996) 535.
[13] Z. Shi, L.R. Zhang, S. Gao, G.Y. Yang, J. Hua, L. Gu, S.H. Feng, Inorg. Chem. 39 (2000) 1990.
[14] Y.Q. Zheng, Z.P. Kong, J. Coord. Chem. 55 (2002) 1241.
[15] (a) T. Lis, Acta. Crystallogr. C 39 (1983) 39;
(b) M.P. Gupta, B. Mahanta, Cryst. Struct. Commun. 7 (1978) 179.

Available online at www.sciencedirect.com
SCIENCE DIRECT®
Polyhedron 23 (2004) 993–998
POLYHEDRON
www.elsevier.com/locate/poly

Synthesis, spectroscopy, crystal structure and magnetism of tetrakis(2-aminopyrimidine)bis(μ-methoxo)bis(perchlorato) dicopper(II): a rare case of distortion isomerism

Gerard A. van Albada [a], Ilpo Mutikainen [b], Urho Turpeinen [b], Jan Reedijk [a,*]

[a] Leiden Institute of Chemistry, Gorlaeus Laboratories, Leiden University, P.O. Box 9502, 2300 RA Leiden, The Netherlands
[b] Laboratory of Inorganic Chemistry, Department of Chemistry, University of Helsinki, P.O. Box 55 (A.I.Virtasen aukio 1), 00014, Finland

Received 19 November 2003; accepted 11 December 2003

Abstract

The dinuclear compound $[Cu(ampym)_2(\mu\text{-}CH_3O)(ClO_4)]_2$ (ampym = 2-aminopyrimidine) has been synthesized and characterized by X-ray crystallography and infrared spectroscopy. In addition, EPR and magnetic measurements have been performed and related to the dinuclear structural details.

The compound crystallizes in the monoclinic space group $P2_1/c$, with $a = 8.0190(13)$, $b = 18.2500(11)$, $c = 10.955(2)$ Å, $\beta = 116.390(13)°$, $V = 1436.2(4)$ Å^3 and $Z = 2$. The coordination geometry around the Cu(II) ion is distorted square pyrimidal with the basal plane formed by two nitrogen atoms of two ampym molecules (Cu–N distances 2.002(3) and 2.031(3) Å) and two oxygen atoms of the bridging methoxo molecules (Cu–O distances of 1.936(2) and 1.937(3) Å). The apical position is occupied by a semi-coordinated oxygen of a perchlorate anion (Cu–O distance 2.442(2) Å). The H-bonds, formed by the amino group and the un-coordinated pyrimidine nitrogen atom of a neighbouring ampym molecule, give rise to an interesting Watson–Crick type pairwise aggregation of ampym ligands.

In the far-IR, the Cu–N vibrations are observed at 443 and 265 cm^{-1}, and the Cu–O are observed at 353 and 240 cm^{-1}. At room temperature the compound gives an EPR silent behaviour and magnetic susceptibility measurements, down to 4 K, agree with a strong antiferromagnetic interaction having a very large singlet–triplet splitting ($J = -621$ cm^{-1}). The title compound appears to be a distortion isomer of a recently reported X-ray structure of identical stoichiometry.
© 2004 Elsevier Ltd. All rights reserved.

Keywords: Copper; Structure; Magnetism; Dinuclear; EPR

1. Introduction

The ligand used in this study, 2-aminopyrimidine (abbreviated as ampym), with two H-bond donor atoms and two H-bond acceptor atoms, is particularly attractive as a very simple self-complementary prototype for chain formation with other organic molecules [1–9]. Metal compounds with ampym as the only organic ligand, or present as a complementary organic ligand, have been increasingly used [10–25]. Quite a few Cu(II) X-ray structures with ampym acting as a complementary organic ligand, together with a variety of other organic ligands, have recently become available in the literature; in these cases ampym is found to act as a monodentate co-ligand [10–14], or as a bridging didentate ligand [15–20].

Different Cu(II) compounds with ampym were investigated by X-ray crystallography depending on the nature of the anion and the synthetic method. With halides as anions, mononuclear and polymeric compounds have been obtained in which ampym acts as a monodentate or a didentate ligand [22–25]. With other anions like sulfate [26,27], triflate [28], nitrate [29] and dicyanamide [30], mononuclear or polynuclear Cu(II) compounds are obtained, all with ampym acting as a monodenate ligand. X-ray structures of a dinuclear Cu(II) methoxo-bridged [31] and a hydroxo-bridged Cu(II) compound [32] were

* Corresponding author. Tel.: +715274450; fax: +715274671.
E-mail address: reedijk@chem.leidenuniv.nl (J. Reedijk).

0277-5387/$ - see front matter © 2004 Elsevier Ltd. All rights reserved.
doi:10.1016/j.poly.2003.12.019

also recently obtained, again with ampym acting as a monodentate ligand. With tetrafluoroborate as an anion surprisingly a very complicated trinuclear-based polymeric structure was obtained [33].

It should also be mentioned that the ligand ampym is known to be useful as a starting material for template synthesis with Cu(II) triflate, forming completely new organic compounds [34,35], in which additions have taken place.

In this study we present the synthesis, characterization and X-ray structure of the dinuclear methoxo-bridged Cu(II) compound $[Cu(ampym)_2(\mu\text{-}CH_3O)(ClO_4)]_2$, together with spectroscopic and magnetic measurements.

In a recent publication [31], the crystal structure and magnetic measurements have been published of the differently synthesized compound with exactly the same geometry, $[Cu(ampym)_2(\mu\text{-}CH_3O)]_2(ClO_4)_2$, almost similar to the compound used in this study, however, with quite diffferent structural and magnetic properties. The two compounds appear to be distortion isomers, which cannot converted into one another.

2. Experimental

2.1. General

C,H,N determinations were performed on a Perkin–Elmer 2400 Series II analyser. UV–vis spectra were obtained on a Perkin–Elmer Lambda 900 spectrophotometer using the diffuse reflectance technique, with MgO as a reference. X-band powder EPR spectra were obtained on a Jeol RE2x electron spin resonance spectrometer using DPPH ($g = 2.0036$) as a standard. FTIR spectra were obtained on a Perkin–Elmer Paragon 1000 FTIR spectrophotometer equipped with a Golden Gate ATR device, using the reflectance technique (4000–300 cm^{-1}, res. 4 cm^{-1}). Far-FTIR spectra were obtained on a Bruker 113v infrared spectrophotometer as polyethylene mulls (500–100 cm^{-1}, res. 2 cm^{-1}).

Magnetic susceptibility measurement (5–300 K) were carried out (at 0.1 T) using a Quantum Design MPMS-5 5T SQUID magnetometer. Data were corrected for the magnetization of the sample holder and for diamagnetic contributions, which were estimated from Pascal constants.

2.2. Synthesis

The ampym ligand was obtained commercially and used without purification. The title compound was obtained by adding 0.2 M ampym dissolved in methanol to a solution of 0.1 M copper(II) perchlorate in methanol. Upon standing at RT, dark green crystals were formed within a few days.Yield 78%, elemental analysis for $C_{18}H_{26}Cl_2Cu_2N_{12}O_{10}$ [found (calc.)]: C, 27.9 (28.1); H, 3.5 (3.4)%; N, 21.8 (21.9)%.

Table 1
Crystallographic data for $[Cu(ampym)_2(\mu\text{-}CH_3O)(ClO_4)]_2$

Formula	$C_{18}H_{26}Cl_2Cu_2N_{12}O_{10}$
Molecular weight	768.49
Crystal system	monoclinic
Space group	$P2_1/c$ (No. 14)
a (Å)	8.0190(13)
b (Å)	18.2500(11)
c (Å)	10.955(2)
β (°)	116.390(13)
V (Å^3)	1436.2(4)
Z	2
D_{calc} (g cm^{-3})	1.777
$F(000)$	780
μ (mm^{-1})	1.741
Crystal size (mm)	$0.18 \times 0.08 \times 0.03$
Temperature (K)	173(2)
θ_{min}, θ_{max} (°)	5.11, 27.54
Wavelength (Mo Kα)	0.71073 (graphite monochromator)
Total reflections	10 742
Total unique reflections	3283 ($R_{int} = 0.101$)
Observed reflections ($I > 2(I)$)	2134
No. of refined parameters	199
R^a, $wR_2{}^b$, S	0.0473, 0.0971, 0.983
Minimum and maximum residual densities (e/Å^3)	−0.474 and 0.105

[a] $R_1 = \sum ||F_o| - |F_c|| / \sum |F_o|$.
[b] $wR_2 = [\sum[w(F_o^2 - F_c^2)^2] / \sum[w(F_o^2)^2]]^{1/2}$.

2.3. X-ray crystallography

A crystal was selected and mounted to the glass fiber using the oil-drop method; data were collected on a Nonius KappaCCD diffractometer (graphite-monochromated Mo Kα radiation, $\omega - 2\theta$ scans). The intensity data were corrected for Lorentz and polarization effects, for absorption (psiscan absorption correction) and extinction. The structures were solved by direct methods. The programs COLLECT [36], SHELXS 97 [37] and SHELXL 97 [38] were used for data reduction, structure solution and structure refinement, respectively. Refinement of F^2 was done against all reflections. The weighted R factor, wR, and goodness-of-fit S are based on F^2, the conventional R factor is based on F, with F set to zero for negative F^2. All non-hydrogen atoms were refined anisotropically. The H atoms were introduced in calculated positions and refined with fixed geometry with respect to their carrier atoms. Crystallographic data are collected in Table 1.

3. Results and discussion

3.1. Crystal structure of $[Cu(ampym)_2(\mu\text{-}CH_3O)(ClO_4)]_2$

The structure of the compound is depicted in Fig. 1, with relevant bond length and bond angle information

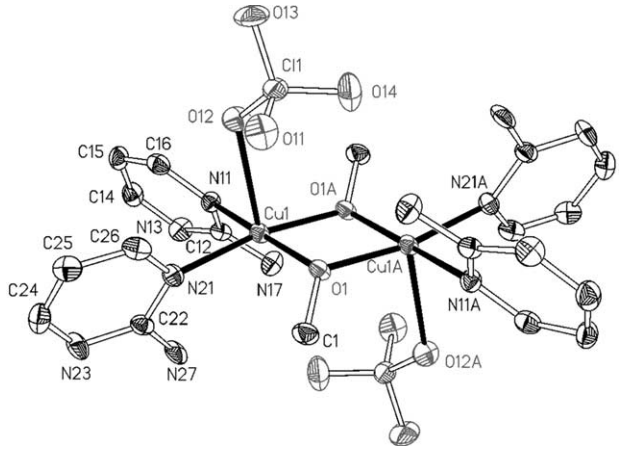

Fig. 1. Atomic displacement plot (50% probability level) of the molecular structure of $[Cu(ampym)_2(\mu\text{-}CH_3O)(ClO_4)]_2$. Hydrogen atoms are omitted for clarity.

given in Table 2. The dinuclear unit has a centre of symmetry located on the Cu–Cu centre.

The Cu atom has a square–pyramidal geometry with the basal plane consisting of two nitrogens from two ampym ligands (N11, N21) with Cu–N distances of 2.002(3) and 2.031(3) Å and two oxygen atoms of the briding methoxo groups (O1, O1A) with Cu–O distances of 1.936(2) and 1.937(3) Å. The apical position is occupied by an oxygen atom of the coordinating perchlorate anion (Cu–O12 = 2.443(3) Å). In fact this distance is one of the shortest $Cu–O_{(ClO4)}$ distances found so far in Cu(II) methoxo-bridged dinuclear compounds, as related distances found in literature vary from 2.675 to >3.6 Å [31,39–43]. In the isomeric compound $[Cu(ampym)_2(\mu\text{-}CH_3O)]_2(ClO_4)_2$ [31] all $Cu–O_{(ClO4)}$ distances are >3.3 Å. The angles of the nearly square basal plane are deviating between 8° and 11° from planarity, while the Cu–O–Cu angle is 102.21(12)° and the Cu–Cu distance 3.0143(8) Å. In the isomeric compound without coordinating perchlorate anions [31], these angles and distances are 100.0(1)° and 2.951(1) Å, respectively. The distances and angles for the title compound are consistent with other Cu(II) dinuclear methoxo-bridged compounds in the literature [31,39–43].

The crystal lattice is stabilized by a H-bonding system (Watson–Crick type) between the amino nitrogen N17 and the uncoordinated pyrimidine nitrogen atom N13 of a neighbouring ampym ligand (N13···N17 3.061(4) Å). A similar H-bonding pattern was reported earlier for compounds containing ampym as a ligand [31,44,45]. Furthermore some intramolecular H-bonds occur, and more details are given in Table 2.

Another distinct difference between the title compound and the isomeric compound published recently by Zhu et al. [31] is the fact that the two ampym ligands are in *cis* position for the title compound, but in a *trans* position for the compound made by Zhu et al. [31] (Fig. 2). This ligand conformational difference might be responsible for the fact that the perchlorate anion is semi-coordinating in the title compound and non-coordinating in the isomeric compound of Zhu et al. [31], thereby explaining also why both isomers cannot be converted into one another without decomposition.

3.2. Spectroscopy

The ligand-field transition band measured as a solid with the diffuse reflectance technique is found at 17.1×10^3 cm^{-1}, which is a normal ligand field transition for a CuN_2O_2 or a $CuN_2O_2(O)_x$ chromophore

Table 2
Selected bond lengths (Å) and angles (°) for $[Cu(ampym)_2(\mu\text{-}CH_3O)(ClO_4)]_2$

Bond lengths				
Cu1–O1	1.938(3)	Cu1–O12	2.443(3)	
Cu1–N11	2.030(3)	Cu1–N21	2.002(3)	
Cu1–Cu1A	3.0143(8)	Cu1–O1A	1.938(2)	
Bond angles				
O1–Cu1–O12	98.40(9)	O1–Cu1–N11	172.37(11)	
O1–Cu1–N21	95.57(12)	O1–Cu1–O1A	77.89(10)	
O12–Cu1–N11	86.91(11)	O12–Cu1–N21	94.39(11)	
Cu1–O1–Cu1A	102.21(12)			
Hydrogen-bonding parameters				
D–H···A	D–H (Å)	H···A (Å)	D···A (Å)	D–H···A (°)
N(17)–H(171)···N(13) [$2-x,\ -y,\ 1-z$]	0.880	2.243	3.047(4)	151.7
N(17)–H(172)···O(1) [$2-x,\ -y,\ -z$]	0.880	2.286	3.032(4)	142.6
N(17)–H(172)···O(11) [$2-x,\ -y,\ -z$]	0.880	2.406	2.995(4)	124.7[a]
N(17)–H(172)···O(14) [$2-x,\ -y,\ -z$]	0.880	2.575	3.109(5)	120.0[a]
N(27)–H(271)···O(13) [$1+x,\ y,\ 1+z$]	0.880	2.070	2.946(4)	173.3
N(27)–H(272)···O(14) [$2-x,\ -y,\ -z$]	0.880	2.219	2.968(4)	142.8

A: $2-x,\ -y,\ -z$.

[a] Bifurcated hydrogen bond; the sum of the angles involving H(172) is 357.2°.

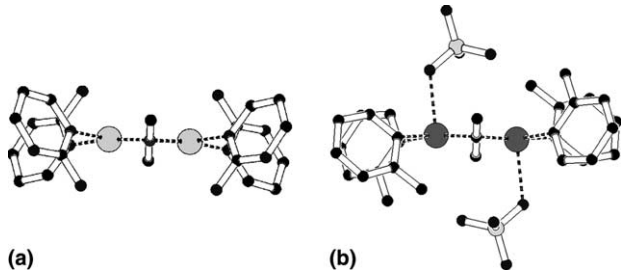

Fig. 2. Figure showing *cis*/*trans* positions of the ligands of (a) $[Cu(ampym)_2(\mu\text{-}CH_3O)]_2(ClO_4)_2$ [31] and (b) $[Cu(ampym)_2(\mu\text{-}CH_3O)(ClO_4)]_2$.

[41,42,46]. In addition, a second strong and sharp band is found at 26.0×10^3 cm^{-1}, which is known to be characteristic for dinuclear copper(II) compounds, with a square planar $Cu_2O_2N_4$ chromophore and has been assigned to an $(O) \rightarrow (Cu)$ charge-transfer band [41,42,47,48].

In the IR spectra of the title compound, one strong and one somewhat weaker bands are present at 3347 and 3449 cm^{-1}, which can be attributed to OH and NH stretching vibrations. The vibrations of the perchlorate anion were observed as two strong broad bands around 1117 and 1043 cm^{-1}, in agreement with semi-coordination.

In the far-IR region (500–100 cm^{-1}) in general the Cu–N and Cu–O vibrations are observed [49,50]. In an earlier study of methoxo-bridged Cu(II) compounds with the ligand bis(2-benzimidazolyl)propane [41], the Cu–N vibrations were observed at 439–441, 351–357 and 290–285 cm^{-1}. The Cu–O vibrations were found at 390 and 229–231 cm^{-1} [41]. The title compound has promiment bands at 443, 353, 265 and 240 cm^{-1}. Also a sharp, less prominent band is observed at 429 cm^{-1}, but as the free ampym ligand also has an absorption at 405 cm^{-1}, that band may originate from the ligand. So we can assign the Cu–N vibrations for the title compound at 443 and 265 cm^{-1} and the Cu–O at 353 and 240 cm^{-1}. Almost the same observation has been made for the compound $[Cu(ampym)_2(\mu\text{-}CH_3O)(CF_3SO_3)]_2$ for which the same bands are observed at 446, 271 cm^{-1} and 356, 223 cm^{-1} [51]. More evidence comes from the mononuclear compound $Cu(ampym)(NO_3)_2$ in which the Cu–N vibrations are found at 439, 284 cm^{-1}, while the Cu–O vibrations are shifted to 334, 217 cm^{-1} [29].

3.3. Magnetic properties

The EPR of the title compound, measured as a polycrystalline powder at RT, is EPR silent, while at 77 K a weak signal is observed with a $g_\perp = 2.06$, $g_\parallel = 2.32$ and $A_\parallel = 16.1$ mT. The absence of an EPR signal indicates already a very strong AF interaction (vide infra), while the weak signal at 77 K most probably originate from a small mononuclear impurity, which is usually present in dinuclear compounds. Absence of EPR signals is also known for other Cu(II) dinuclear methoxo-bridged compounds [40–42].

The magnetic susceptibility of a powdered sample was measured from 5 to 300 K. The magnetic properties of the complex are depicted in Fig. 3 in the form of μ_{eff} versus T for two Cu(II) ions. At 300 K, the μ_{eff} starts at a value of about 1.16 BM (much below the spin only value for two Cu ions of 2.83 BM) and the μ_{eff} decreases at 300 K to about 0.10 BM. This behaviour indicates a very strong antiferromagnetic interaction.

The theoretical expression for the magnetic susceptibility for two interacting $S = 1/2$ centres, which is based on the general Hamiltonian [52] is: $H_{ex} = -JS_1S_2$, in which the exchange parameter J is negative for antiferromagnetic and positive for ferromagnetic interaction.

The magnetic data were fitted to the equation given in the literature for dinuclear copper compounds [52]:

$$X_m = (2Ng^2\beta^2)[kT - 2zJ'/(3 + \exp(-J/kT))]^{-1} \times [3 + \exp(-J/kT)]^{-1}(1 - p) + X_p p,$$

in which N, g, β, k and T have their usual meanings. The parameter p denotes the fraction of paramagnetic impurity in the sample and zJ' the interaction between neighbouring dinuclear identities. The fit was accomplished by minimization of

$$R = \sum (X_m \cdot T_{calc} - X_m \cdot T_{obs})^2/(X_m \cdot T_{obs})^2$$

by a least-squares procedure. The best fit was obtained for $J = -621$ cm^{-1}, $g = 1.95$, $zJ' = -0.02$ cm^{-1}, $p = 0.005$, with a final R of 7×10^{-2} (see Fig. 3).

With the isomeric methoxo-bridged compound $[Cu(ampym)_2(\mu\text{-}CH_3O)]_2(ClO_4)_2$ [31], a similar magnetic behaviour was observed, but with a much less strong AF interaction of $J = -275$ cm^{-1}, which can be understood from the different Cu–Cu distances and Cu–O–Cu angles

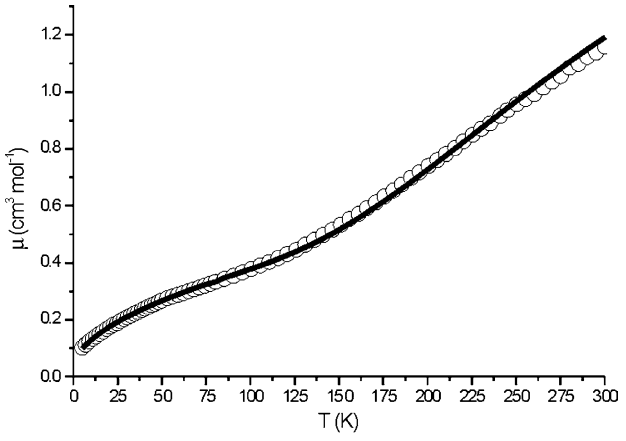

Fig. 3. A plot of the temperature dependence of μ_{eff} vs. T for $[Cu(ampym)_2(\mu\text{-}CH_3O)(ClO_4)]_2$. The solid line represents the calculated curve for the parameters $J = -621$ cm^{-1}, $g = 1.95$, $zJ' = -0.02$ cm^{-1} (see text).

of both compounds (3.0143(8) Å, 102.21(12)° and 2.951(1) Å, 100.0(1)°, for the title compound and the isomeric compound [31], respectively).

4. Concluding remarks

A methoxo-bridged Cu(II) compound with the ligand 2-aminopyrimidine is reported in this study and is compared with a differently prepared isomeric compound, recently published [31]. The difference in the properties originates from the fact that in the first compound, $[Cu(ampym)_2(\mu\text{-}CH_3O)(ClO_4)]_2$ (**1**), which is synthesized by a straightforward procedure, the perchlorate anions are coordinated to the Cu atom. In the isomeric compound, $[Cu(2\text{-aminopyridine})_2(\mu\text{-}CH_3O)]_2(ClO_4)_2$ (**2**), synthesized with adding terephthalaldehyde [31] to the system, the perchlorate anions are not coordinated to the Cu atom. As shown in this study this difference has a significant influence in the geometry of the compound (*cis*/*trans* orientations of the ligands), as well in the strength of the antiferromagnetic interaction between the Cu atoms, which is $J = -621$ and -275 cm^{-1}, for **1** and **2**, respectively. It appeared impossible to convert our compound into the isomeric species by heating, cooling, or recrystallization. Apparently the presence of terephthalaldehyde in [31] must have some kind of template effect. So we clearly deal with a case of distortion isomerism for two compounds of identical composition and quite similar structures. Only a few related cases are known in the literature [53–55] and usually also involve Cu(II).

5. Supplementary material

Crystallographic data (excluding structure factors) for the structure reported in this paper have been deposited with the Cambridge Crystallographic Data Centre as supplementary publication no. CCDC220300. Copies of available material can be obtained, free of charge, on application to the Director, CCDC, 12 Union Road, Cambridge CB2 1EZ, UK (fax: +44(0)1223336033; email: deposit@ccdc.cam.ac.uk or www: http://www.ccdc.cam.ac.uk).

Acknowledgements

The work described in this paper was supported by the Leiden University Study group WFMO (Werkgroep Fundamenteel Materialen Onderzoek) and the Council for Chemical Sciences of the Netherlands Organization for Scientific Research (CW-NWO). Part of the was supported financially by the Graduate Research School Combination NRSC "Catalysis".

References

[1] D.E. Lynch, T. Latif, G. Smith, K.A. Byriel, C.H.L. Kennard, J. Chem. Crystallogr. 27 (1997) 567.
[2] D.E. Lynch, T. Latif, G. Smith, K.A. Byriel, C.H.L. Kennard, S. Parsons, Aust. J. Chem. 51 (1998) 403.
[3] V. Bertolasi, P. Gilli, V. Ferretti, G. Gilli, Acta Crystallogr., Sect. B 57 (2001) 591.
[4] S. Goswami, R. Mukherjee, K. Ghosh, I.A. Razak, S.S.S. Raj, H.-K. Fun, Acta Crystallogr., Sect. C 56 (2001) 477.
[5] G. Smith, C.H.L. Kennard, K.A. Byriel, Polyhedron 10 (1991) 873.
[6] G. Smith, E.J. O'Reilly, H.L. Carrell, C.J. Carrell, C.H.L. Kennard, Polyhedron 15 (1996) 1995.
[7] K. Kobayashi, T. Shirasaka, K. Yamaguchi, S. Sakamoto, E. Horn, N. Furukawa, Chem. Commun. (2000) 41.
[8] A. García-Raso, J.J. Fiol, F. Bádenas, E. Lago, E. Molins, Polyhedron 20 (2001) 2877.
[9] A.J. Blake, P. Hubberstey, C.L. Sampson, Acta Crystallogr., Sect. E 58 (2002) m99.
[10] E.J. O'Reilly, G. Smith, C.H.L. Kennard, A.H. White, Aust. J. Chem. 36 (1983) 183.
[11] E.J. O'Reilly, G. Smith, C.H.L. Kennard, Inorg. Chim. Acta 90 (1984) 63.
[12] C.H.L. Kennard, S.W. Stewart, E.J. O'Reilly, G. Smith, A.H. White, Polyhedron 4 (1985) 697.
[13] T.C.W. Mak, C.H.L. Kennard, G. Smith, E.J. O'Reilly, D.S. Sagatys, J.C. Fulwood, Polyhedron 6 (1987) 855.
[14] D.E. Lynch, Acta Crystallogr., Sect. C 57 (2001) 158.
[15] G. Smith, E.J. O'Reilly, C.H.L. Kennard, A.H. White Soc., J. Chem., Dalton Trans. (1985) 243.
[16] G. Smith, C.H.L. Kennard, K.A. Byriel, Polyhedron 10 (1991) 873.
[17] G. Smith, E.J. O'Reilly, H.L. Carrell, C.J. Carrell, C.H.L. Kennard, Polyhedron 15 (1996) 1995.
[18] D.E. Lynch, Acta Crystallogr., Sect. C 56 (2000) e425.
[19] A. García-Raso, J.J. Fiol, F. Bádenas, E. Lago, E. Molins, Polyhedron 20 (2001) 2877.
[20] A.J. Blake, P. Hubberstey, C.L. Sampson, Acta Crystallogr., Sect. E 58 (2002) m99.
[21] Q.-H. Jin, X.-M. Lu, H.-J. Zhu, X.-P. Ji, Chin. J. Chem. 18 (2000) 928.
[22] C. Zanchini, R.D. Willett, Inorg. Chem. 29 (1990) 3027.
[23] T. Manfredini, G.C. Pellacani, A. Bonamartini-Corradi, L.P. Battaglia, G.G.T. Guarini, J.G. Giusti, G. Pon, R.D. Willett, D.X. West, Inorg. Chem. 29 (1990) 2221.
[24] R. Corzo-Suárez, S. García-Granda, I. Díaz, V. Fernández-Herrero, J. Luis Martínez, Acta. Crystallogr., Sect. C 53 (1997) 1786.
[25] G. Pon, R.D. Willett, B.A. Prince, W.T. Robinson, M.M. Turnbull, Inorg. Chim. Acta 255 (1997) 325.
[26] P.O. Lumme, P. Kekarainen, H. Knuuttila, T. Kurkirinne, M. Latvala, L. Rönkönharju, S. Salonen, Finn. Chem. Lett. (1981) 25.
[27] P.O. Lumme, H. Knuuttila, E. Lindell, Acta Crystallogr., Sect. C 52 (1996) 51.
[28] G.A. van Albada, W.J.J. Smeets, A.L. Spek, J. Reedijk, J. Chem. Crystallogr. 30 (2000) 11.
[29] G.A. van Albada, I. Mutikainen, U. Turpeinen, J. Reedijk, Acta Crystallogr., Sect. E 58 (2002) m55.
[30] G.A. van Albada, M.E. Quiroz-Castro, I. Mutikainen, U. Turpeinen, J. Reedijk, Inorg. Chim. Acta 298 (2000) 221.
[31] H.-L. Zhu, C.-X. Ren, X.-M. Chen, J. Coord. Chem. 55 (2002) 667.
[32] G.A. van Albada, I. Mutikainen, W.J.J. Smeets, A.L. Spek, U. Turpeinen, J. Reedijk, Inorg. Chim. Acta 327 (2002) 134.

[33] G.A. van Albada, O. Roubeau, I. Mutikainen, U. Turpeinen, J. Reedijk, New J. Chem. 27 (2003) 1693.
[34] G.A. van Albada, I. Mutikainen, U. Turpeinen, J. Reedijk, Eur. J. Inorg. Chem. (1998) 547.
[35] G.A. van Albada, P.J. van Koningsbruggen, I. Mutikainen, U. Turpeinen, J. Reedijk, Eur. J. Inorg. Chem. (1999) 2269.
[36] Nonius, COLLECT, Nonius BV, Delft, The Netherlands, 2002.
[37] G.M. Sheldrick, SHELXS 97, Program for Crystal Structure Determination, University of Göttingen, Germany, 1997.
[38] G.M. Sheldrick, SHELXL 97, Program for the Refinement of Crystal Structures, University of Göttingen, Germany, 1997.
[39] G.A. van Albada, I. Mutikainen, I. Riggio, U. Turpeinen, J. Reedijk, Polyhedron 21 (2002) 141.
[40] S. Amani Komaei, G.A. van Albada, I. Mutikainen, U. Turpeinen, J. Reedijk, Polyhedron 18 (1999) 1991.
[41] G.A. van Albada, M.T. Lakin, N. Veldman, A.L. Spek, J. Reedijk, Inorg. Chem. 34 (1995) 4910.
[42] G.A. van Albada, W.J.J. Smeets, A.L. Spek, J. Reedijk, Inorg. Chim. Acta 260 (1997) 151.
[43] R.-H. Wang, W.-P. Su, R. Cao, Y.-J. Zhao, M.-C. Hong, Chin. J. Struct. Chem. 20 (2001) 37.
[44] G.A. van Albada, M.E. Quiroz-Castro, I. Mutikainen, U. Turpeinen, J. Reedijk, Inorg. Chim. Acta 298 (2000) 221.
[45] G.A. van Albada, W.J.J. Smeets, A.L. Spek, J. Reedijk, J. Chem. Crystallogr. 30 (2000) 11.
[46] B.J. Hathaway, in: G. Wilkinson, R.D. Gillard, J.A. McCleverty (Eds.), Comprehensive Coordination Chemistry, vol. 5, Pergamon Press, Oxford, 1987.
[47] M. Yamashita, H. Ito, T. Ito, Inorg. Chem. 22 (1983) 2102.
[48] S. Kida, Y. Nishida, M. Sakamoto, Bull. Chem. Soc. Jpn. 46 (1973) 2428.
[49] J.R. Ferraro, Low Frequency Vibrations of Inorganic and Coordination Compounds, Plenum Press, New York, 1971.
[50] E. Ghomashchi, Spectrosc. Lett. 27 (1994) 829.
[51] G.A. van Albada (2003), unpublished work.
[52] O. Kahn, Molecular Magnetism, VCH Publishers, New York, 1993.
[53] S. Youngme, N. Chaichit, N. Koonsang, Inorg. Chim. Acta 335 (2002) 36.
[54] R. Uggla, M. Melník, J. Valo, A. Pajunen, M.R. Sundberg, Acta Chem. Scand. 49 (1995) 585.
[55] M. Brophy, G. Murphy, C. O'Sullivan, B. Hathaway, B. Murphy, Polyhedron 18 (1999) 611.

Available online at www.sciencedirect.com
SCIENCE DIRECT®
Polyhedron 23 (2004) 999–1002
POLYHEDRON
www.elsevier.com/locate/poly

Synthesis and characterization of coordination polymers of Zn(II) with 1,3-bis(4-pyridyl)propane and 4,4′-pyridine ligands

Ting-Wai Lee, Jasmine Po-Kwan Lau, Wing-Tak Wong *

Department of Chemistry, The University of Hong Kong, Pokfulam Road, Hong Kong, PR China

Received 4 September 2003; accepted 15 December 2003

Abstract

Two new metal-coordination polymers, $[Zn_2(bpy)(OAc)_4]_n$ (**1**) and $[Zn(bpp)(NO_3)_2]_n$ (**2**) were prepared by the layering method using Zn(II) ions, bpy and bpp ligands, and structurally characterized by single-crystal X-ray diffraction analyses. Complexes **1** and **2** were both found to be one-dimensional coordination polymers. The periodic length of the chain between two alternate Zn(II) ions in compound **1** is 26.92 Å which is more than twice the length of compound **2** ($26.92 > 11.92 \times 2$).
© 2004 Elsevier Ltd. All rights reserved.

Keywords: Zinc; 1,3-Bis(4-pyridyl)propane; 4,4′-Pyridine; Polymeric network; X-ray crystallography

1. Introduction

The metal–organic coordination polymers [1–4] of bpy [4,4′-pyridine] [5–7] and bpp [1,3-bis(4-pyridyl)propane] ligands [8–10] have attracted continuous attention in recent years. A subtle change in the use of conformationally flexible ligands as spacers in the design and construction of coordination polymers may lead to new polymeric networks. The bpy and bpp ligands have been shown to be versatile, and may coordinate to metal ions as spacers through the N atoms. The coordination versatility, together with the coordination requirements of specific metal ions, allows the construction of novel new structures. The chemistry of the new coordination polymers is of considerable interest for potential application in optoelectronic [11], magnetic [12] and microporous materials [13]. In earlier efforts, we have used the bpp [1,3-bis(4-pyridyl)propane] ligand with nickel and manganese ions to form three new metal–organic coordination polymers, $\{[Ni(bpp)_2](ClO_4)_2 \cdot 2H_2O \cdot 2CHCl_3\}_n$, $[Mn(bpp)_2Cl_2 \cdot 2CHCl_3]_n$ and $\{[Mn(bpp)_2(H_2O)_2](ClO_4)_2 \cdot bpp \cdot H_2O\}_n$ [14]. As a continuation of our work, we herein report the synthesis and solid structure of two new compounds, namely $[Zn_2(bpy)(OAc)_4]_n$ (**1**), and $[Zn(bpp)(NO_3)_2]_n$ (**2**) using zinc(II) ions, bpy and bpp ligands.

2. Experimental

2.1. General procedures

All materials were used as received from commercial sources (Sigma–Aldrich, Lancaster, ARCOS or STREM). Elemental analysis for C, H and N of compounds **1** and **2** were carried out on their crystal samples by the Department of Biology and Chemistry at the City University of Hong Kong. Their IR spectra were recorded in the wave number range 4000–400 cm^{-1} on a BIO-RAD FTS-135 Spectrometer that was calibrated with a thin film of polystyrene.

2.2. Preparation of $[Zn_2(bpy)(OAc)_4]_n$ (1)

Crystals of compound **1**, of considerable size (ca. 0.2 mm), formed in 5 days at room temperature upon the slow evaporation of a solution of $Zn(OAc)_2$ (1.010 g, 5.505 mmol; FW: 183.48) and bpy (0.106 g, 0.679 mmol; MW: 156.19) in methanol (5 ml). *Anal.* Calc. for $Zn_2C_{18}H_{20}N_2O_8$: C, 41.33; H, 3.85; N, 5.35. Found: C,

* Corresponding author. Tel.: +28592157; fax: +(852)25472933/+(852)28571586/+25472933.
E-mail address: wtwong@hkucc.hku.hk (W.-T. Wong).

0277-5387/$ - see front matter © 2004 Elsevier Ltd. All rights reserved.
doi:10.1016/j.poly.2003.12.020

41.75; H, 4.19; N, 5.39%. IR (KBr) ν/cm^{-1}: 3073m, 3046m, 2923m, 2857m, 1613vs, 1491m, 1419s, 1396s, 1338m, 1218w, 1073m, 1047w, 1016m, 813m, 727w, 679w, 643m, 619w, 490w.

2.3. Preparation of $[Zn(bpp)(NO_3)_2]_n$ (2)

A solution of $Zn(NO_3)_2 \cdot 6H_2O$ (1.005 g, 3.378 mmol; FW: 297.49) in acetone (3 mL) was layered on a solution of bpp (0.100 g, 0.504 mmol; MW: 198.27) in chloroform (3 mL). Crystals of compound **2**, of considerable size (ca. 0.5 mm), formed at the interface in 5 weeks at room temperature. *Anal.* Calc. for $ZnC_{13}H_{14}N_4O_6$: C, 40.28; N, 14.45, O, 24.76. Found: C, 40.25; N, 14.20; O, 24.55%. IR (KBr) ν/cm^{-1}: 3062m, 3048m, 2952m, 2938m, 2859m, 1654m, 1624s, 1561m, 1491s, 1434s, 1388s, 1292s, 1229m, 1069m, 1033s, 1014s, 856m, 823m, 760w, 620m, 581w, 529m, 518m.

2.4. X-ray crystallography

All pertinent crystallographic data and other experimental details are summarized in Table 1. Crystals suitable for X-ray analyses were glued on glass fibres with epoxy resin or sealed in 0.3 mm glass capillaries. Intensity data were collected at ambient temperature on a Bruker AXS SMART CCD diffractometer that was equipped with graphite-monochromated Mo Kα radiation ($\lambda = 0.71073$ Å). All structures were solved by direct methods (SIR 92) [15] and expanded by Fourier-difference technique (DIRDIF 94) [16]. Non-hydrogen atoms were refined anisotropically for all compounds. Hydrogen atoms were generated in their ideal positions and included in the structure factor calculations, but not refined. Calculations were performed on a Silicon Graphics computer using the teXsan [17] crystallographic software package. Tables 2 and 3 list the selected bond lengths and angles.

Table 1
Crystallographic data and data collection parameters for complexes (**1**) and (**2**)

Compound	**1**	**2**
Empirical formula	$C_{18}H_{20}N_2O_8Zn_2$	$C_{13}H_{14}N_4O_6Zn$
Formula weight	523.12	387.66
Crystal dimension (mm)	$0.15 \times 0.10 \times 0.05$	$0.50 \times 0.50 \times 0.50$
Crystal system	orthorhombic	monoclinic
Space group	$Pna2_1$ (#33)	$P2_1/n$ (#14)
a (Å)	26.918(1)	11.698(1)
b (Å)	7.9710(5)	11.351(1)
c (Å)	10.4560(7)	11.923(1)
α (°)		
β (°)		96.21(1)
γ (°)		
V (Å^3)	2243.5(2)	1573.9(2)
Z value	4	4
D_c (g cm^{-3})	1.549	1.636
$F(000)$	1064.00	792.00
μ(Mo Kα) (cm^{-1})	21.83	15.99
Temperature (K)	298	298
Reflection collected	13 771	9672
Unique reflection	2926	3707
Observed reflection $[I > 1.50\sigma(I)]$	2308	2669
R	0.036	0.051
R_w	0.042	0.059

Table 2
Selected bond distances (Å) and angles (°) for **1**

Bond distances			
Zn(1)–O(1)	1.981(3)	Zn(1)–O(4)	2.056(4)
Zn(1)–N(1)	2.019(3)	Zn(1)–N*(2)	2.008(3)
Bond angles			
O(1)–Zn(1)O(4)	97.0(1)	O(1)–Zn(1)–N(1)	115.9(1)
O(1)–Zn(1)–N(2)	117.5(1)	O(4)–Zn(1)–N(1)	92.6(1)
O(4)–Zn(1)–N*(2)	124.9(2)	N(1)–Zn(1)–N*(2)	107.0(1)

Table 3
Selected bond distances (Å) and angles (°) for **2**

Bond distances			
Zn(1)–O(1)	2.160(6)	Zn(1)–O(2)	2.182(5)
Zn(1)–O(3)	2.060(6)	Zn(1)–O(5)	2.011(5)
Zn(1)–O(7)	2.150(4)	Zn(1)–N(1)	2.150(3)
Zn(2)–O(4)	1.964(7)	Zn(2)–O(6)	1.937(8)
Zn(2)–O(7)	2.170(5)	Zn(2)–O(8)	2.178(6)
Zn(2)–N(2)	2.038(3)		
Bond angles			
O(1)–Zn(1)–O(2)	59.8(1)	O(1)–Zn(1)–O(3)	156.1(2)
O(1)–Zn(1)–O(5)	97.3(2)	O(1)Zn(1)–O(7)	90.3(3)
O(1)–Zn(1)–N(1)	91.3(2)	O(2)Zn(1)–O(3)	96.3(2)
O(2)–Zn(1)–O(5)	157.0(2)	O(2)Zn(1)–O(7)	95.5(3)
O(2)–Zn(1)–N(1)	90.0(2)	O(3)Zn(1)–O(5)	106.5(1)
O(3)–Zn(1)–O(7)	92.7(4)	O(3)–Zn(1)–N(1)	88.0(3)
O(5)–Zn(1)–O(7)	86.1(3)	O(5)–Zn(1)–N(1)	88.4(2)
O(7)–Zn(1)–N(1)	174.4(3)	O(4)–Zn(2)–O(6)	111.0(2)
O(4)–Zn(2)–O(7)	105.6(4)	O(4)Zn(2)–O(8)	103.9(3)
O(4)–Zn(2)–N(2)	97.4(3)	O(6)–Zn(2)–O(7)	97.9(4)
O(6)–Zn(2)–O(8)	140.5(3)	O(6)–Zn(2)–N(2)	102.4(3)
O(7)–Zn(2)–O(8)	54.2(2)	O(7)–Zn(2)–N(2)	141.4(1)
O(8)–Zn(2)–N(2)	90.6(2)		

3. Results and discussion

3.1. Crystal structure of $[Zn_2(bpy)(OAc)_4]_n$ (1)

The molecular structure and selected bond parameters of complex **1** are shown in Fig. 1 and Table 2, respectively. Complex **1** is an infinite one-dimensional coordination polymer in which bpy (spacers) are connected to each other by $Zn(OAc)_2$ dimeric units (nodes), thus forming a zig-zag chain. In each $Zn(OAc)_2$ dimeric unit, two Zn(II) ions are bridged by the carboxylate groups of the two OAc^- ions that are centered at C(7) and C(7*), and O(4) atom of the OAc^- ion centered at C(11). The O(5) atom of the OAc^- ion that is centered

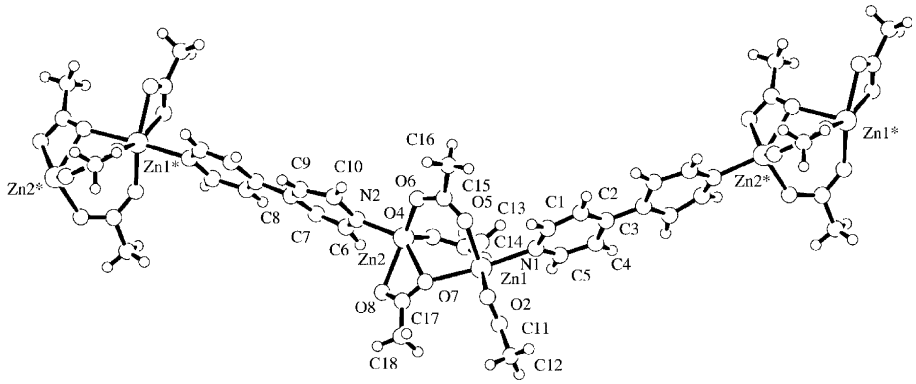

Fig. 1. The molecular structure of $[Zn_2(bpy)(OAc)_4]_n$ (**1**) with the atom numbering scheme.

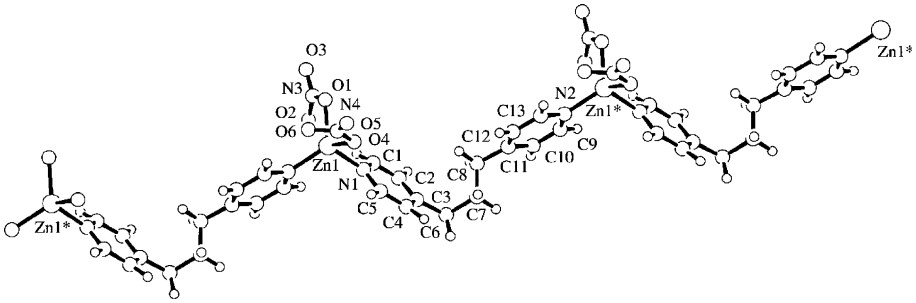

Fig. 2. The molecular structure of $[Zn(bpp)(NO_3)_2]_n$ (**2**) with the atom numbering scheme.

at C(11) coordinates with the Zn(II)(2) ion and exhibits static disorder (not shown for clarity). Consequently, including coordination by bpy, the Zn(II)(1) ion is octahedrally coordinated and the Zn(II)(2) ion is trigonal-pyrimidally coordinated. The periodic length of the chain between two alternate Zn(II)(1) ions is 26.92 Å. The distance between two Zn(II) ions in the $Zn(OAc)_2$ dimeric unit is 3.33 Å. Adjacent polymer chains $[Zn_2(bpy)(OAc)_4]_n$ in the unit cell propagate in two stacks along the *a*-axis and pack along the *b*-axis. Despite the stacking structure, 3% of the crystal volume is available for occupying guest molecules. This network is closely related to another Zn(II)-containing zig-zag chain, $[Zn(pyrazine)Br_2]_n$ [18]. The periodic length of compound **1** is longer than that of $[Zn(pyrazine)Br_2]_n$, due to the use of longer spacers (bpy), and the extension of the zig-zag chain by $Zn(OAc)_2$ dimeric units in **1**.

3.2. Crystal structure of $[Zn(bpp)(NO_3)_2]_n$ (2)

The coordination geometry in compound **2** is shown in Fig. 2. The molecular structure is a one-dimensional coordination polymer in which the ligand 1,3-bis(4-pyridyl)propane, bpp, (spacers) are connected to each other by $Zn(NO_3)_2$ units (nodes). The Zn(II) ion is tetrahedrally coordinated by two $NO_3^{2-}$and two bpp ligands. Each bpp is required by the coordination geometry of the Zn(II) ion to head downward but twist in its trimethylene group. This mode of coordination gives a sinusoidal chain (period 11.92 Å), with the ligand in a TT conformation. The periodic length of compound **1** is more than twice the length of compound **2** ($26.92 > 11.92 \times 2$), even though bpy is shorter than bpp by the length of a trimethylene group. The twisting of the bpp ligand in compound **2** shortens the distance between the two pyridyl N atoms, and the $Zn(OAc)_2$ dimeric units extend the chain in compound **1**. Despite having a conformationally flexible bpp ligand as its spacer, compound **2** is not a helical chain. The type of conformation is also observed in reported systems such as $\{[Ag(bpp)](NO_3)\}_n$ [19], which is a one-dimensional coordination polymer with a Ag(I) ion as the node and bpp as the spacer. This is also not a helical chain, but a sinusoidal chain. Compound **2** propagates in three chains long the *c*-axis and packs long the *a*-axis. Adjacent chains to the *b*-axis have a translational relationship of $c/2$ along the *c*-axis. No significant void volume was found for this compound.

4. Supplementary data

The crystallographic data (excluding structure factors) for the structures reported in this paper have been deposited with the Cambridge Crystallographic Data Centre (CCDC) as supplementary publication no. CCDC 211891–CCDC 211892. Copies of the data can be obtained free of charge on application to CCDC, 12 Union Road, Cambridge CB2 1EZ, UK (fax: (+44) 1223

336-033; deposit@ccdc.cam.ac.uk or www: http://www.ccdc.cam.ac.uk).

Acknowledgements

We gratefully acknowledge financial support from the Hong Kong Research Grants Council and The University of Hong Kong. J.P.K. Lau acknowledges the receipt of a postgraduate studentship (2002–2003) and a Hung Hing Ying Scholarship (2003–2004).

References

[1] O.R. Evans, W. Lin, Acc. Chem. 35 (2002) 511.
[2] B.J. Holliday, C.A. Mirkin, Angew. Chem., Int. Ed. 40 (2001) 2022.
[3] M.J. Zaworotko, Angew. Chem., Int. Ed. 39 (2000) 3052.
[4] A.K. Cheetham, G. Ferey, T. Loiseau, Angew. Chem., Int. Ed. 38 (1999) 3268.
[5] W. Dong, Q.-L. Wang, S.-F. Si, D.-Z. Liao, Z.-H. Jiang, S.-P. Yan, P. Cheng, Inorg. Chem. Commun. 6 (2003) 873.
[6] X.-M. Zhang, X.-M. Chen, Eur. J. Inorg. Chem. 3 (2003) 413.
[7] S.-I. Noro, R. Kitaura, M. Kondo, S. Kitagawa, T. Ishii, H. Matsuzaka, M. Yamashita, J. Am. Chem. Soc. 124 (2002) 2568.
[8] M.J. Plater, M.R.St.J. Foreman, T. Gelbrich, S.J. Coles, M.B. Hursthouse, J. Chem. Soc., Dalton Trans. (2000) 3065.
[9] M.-L. Tong, Y.-M. Wu, J. Ru, X.-M. Chen, H.-C. Chang, S. Kitagawa, Inorg. Chem. 41 (2002) 4846.
[10] E.-Q. Gao, S.-Q. Bai, Z.-M. Wang, C.-H. Yan, J. Chem. Soc., Dalton Trans. (2003) 1759.
[11] W. Lin, Z. Wang, L. Ma, J. Am. Chem. Soc. 121 (1999) 11249.
[12] O. Kahn, Acc. Chem. Res. 33 (2000) 647.
[13] P. Long, E.B. Woodlock, X. Wang, Inorg. Chem. 39 (2000) 4174.
[14] T.-W. Lee, J.P.-K. Lau, W.-T. Wong, in preparation.
[15] A. Altomare, M.C. Burla, M. Camalli, M. Cascarano, C. Giacovazzo, A. Guagliardi, G. Polidori, J. Appl. Crystallogr. 27 (1994) 435.
[16] DIRDIF94: B.T. Beurskens, G. Admiroal, G. Beurskens, W.P. Bosman, R. de Gelder, R. Isrel, J.M.M. Smits, Technical Report of the Crystallography Laboratory, University of Nijmegen, 1994.
[17] teXsan, Crystal Structure Analysis Package, Molecular Structure Corporation, Houston, TX, 1985, 1992.
[18] S.A. Bourne, M. Kilkenny, L.R. Nassimbeni, J. Chem. Soc., Dalton Trans. (2001) 1176.
[19] S.R. Batten, J.C. Jeffery, M.D. Ward, Inorg. Chim. Acta 292 (1999) 231.

Available online at www.sciencedirect.com
SCIENCE DIRECT®
Polyhedron 23 (2004) 1003–1009
POLYHEDRON
www.elsevier.com/locate/poly

Syntheses and structures of 1D, 2D, 3D cadmium(II) coordination polymers with oxalate and aromatic co-ligands ☆

Sheng-Qing Xia, Sheng-Min Hu, Jing-Cao Dai, Xin-Tao Wu *, Zhi-Yong Fu, Jian-Jun Zhang, Wen-Xin Du

State Key Laboratory of Structural Chemistry, Fujian Institute of Research on the Structure of Matter, Chinese Academy of Sciences, Fuzhou, Fujian 350002, China

Received 27 October 2003; accepted 15 December 2003

Abstract

Four mixed-ligand complexes, $\{Na_2[Cd_2(Htma)_2(ox)(H_2O)_2]\}_n$(**1**) (tma = trimesate, ox = oxalate), $\{[Cd_2(2,2'\text{-bipyridine})_2(ox)_2]\cdot 2H_2O\}_n$ (**2**), $\{Cd_3(4,4'\text{-trimethylenedipyridine})_3(ox)_3\}_n$ (**3**), and $\{Na_2[Cd_4(isonicotinate)_4(ox)_3]\}_n$ (**4**) were synthesized by hydrothermal reactions. The structures of **1**, **2**, **3** and **4** consist of 1D ladder-like chains, 1D zigzag chains, a 2D square network and a 3D framework, respectively, featuring dinuclear (for **1** and **2**), trinuclear (for **3**) and tetranuclear (for **4**) units. The TGA experiments showed that these four complexes were quite thermally stable.
© 2004 Elsevier Ltd. All rights reserved.

Keywords: Cadmium; Coordinate; Polymers; Ligands; Supramolecular

1. Introduction

In recent years, much interest has been focused on the design and synthesis of supramolecular compounds, for their interesting structure motifs and potential applications in ion exchange, porous materials and molecular adsorbents [1–3]. In the process of fabricating these kinds of complexes, some organic N-donors such as bipyridine and related species [4,5] are often chosen as rigid 'tectons' to bind the metal centers. Other approaches to obtain analogous coordination polymers include the reaction of metal ions with multifunctional ligands containing O-donors or mixed N/O-donors such as oxalate, trimesate, isonicotinate ligands and poly-aromatic acids [6–8].

The oxalate ion has been known to function as a bis-bidentate ligand, and its coordination to transition metal ions has been widely researched due to its remarkable ability to mediate strong magnetic interactions between the metal centers [9–12]. By employing different templating cations, a good many infinite 2D and 3D magnetic polymers with the formula $[M^{II}M^{III}(ox)_3]_n^{n-}$ (M^{II} = V, Cr, Mn, Fe, Co, Ni, Cu, Zn; M^{III} = V, Cr, Fe) were synthesized in the last decade [13–15].

Polynuclear cadmium compounds [16,17] have been studied for their novel open-framework structure motifs with channels [18,19]. In this paper, we report four infinite 1D, 2D and 3D mixed-ligand cadmium polymers (**1**–**4**) with oxalate and aromatic co-ligands prepared by hydrothermal synthesis, which exhibit high thermal stabilities.

2. Experimental

All syntheses were performed in poly(tetrafluoroethylene)-lined stainless steel autoclaves under autogenous pressure. Chemicals were commercially purchased and used as received. Elemental analyses were carried out by the Elemental Analysis Laboratory of our Institute, and TGA (thermal gravimetric analysis) was performed under nitrogen at a heating rate of 10 °C min^{-1} using a

☆ Supplementary data associated with this article can be found, in the online version, at doi:10.1016/j.poly.2003.12.021.

* Corresponding author. Tel.: +86-591-3792837; fax: +86-591-3714946.
E-mail address: wxt@ms.fjirsm.cn (X.-T. Wu).

0277-5387/$ - see front matter © 2004 Elsevier Ltd. All rights reserved.
doi:10.1016/j.poly.2003.12.021

TA5200/MDSC2910 system by the Thermal Analysis Laboratory of Huaqiao University. Infrared spectra (KBr pellets) were recorded in the range from 4000 to 400 cm^{-1} on a Nicolet Magna 750 FTIR spectrometer.

2.1. Syntheses, elemental analyses and IR spectra

2.1.1. $\{Na_2[Cd_2(Htma)_2(ox)(H_2O)_2]\}_n$ (1)

Complex **1** was synthesized hydrothermally from the reaction of $Cd(NO_3)_2 \cdot 4H_2O$ (1.0 mmol), H_3 (tma) (1.0 mmol), $Na_2C_2O_4$ (1.0 mmol) and H_2O (10 ml) at 120 °C for two days, and then the reactant was cooled at a rate of 0.3 °C min^{-1} to give a 31% yield of **1** based on Cd as colorless crystals, which were collected by mechanical isolation and washed with water and absolute alcohol. *Anal.* Calc. (Found): C, 29.62 (29.76); O, 35.51 (35.22); H, 1.49 (1.35)%. IR (KBr, cm^{-1}): 3338 (w), 3089 (w), 2066 (w), 1700 (s), 1618 (s), 1579 (s), 1532 (s), 1435 (s), 1385(s), 1322 (m), 1233(m), 1186 (s), 1112 (m), 801 (m), 735 (s), 680 (s), 536 (m).

2.1.2. $\{[Cd_2(2,2'\text{-bipyridine})_2(ox)_2]\cdot 2H_2O\}_n$ (2)

Compound **2** was synthesized and purified by the method like **1**, except that the reactants were $Cd(NO_3)_2 \cdot 4H_2O$ (1.0 mmol), 2,2′-bipyridine (1.0 mmol), $Na_2C_2O_4$ (1.0 mmol) and H_2O (10 ml). The experiment gave colorless crystals with about 37% yield based on Cd. *Anal.* Calc. (Found): C, 38.47 (38.72); O, 21.35 (21.68); H, 2.69 (2.55); N, 7.47 (7.21)%. IR (KBr, cm^{-1}): 3377 (w), 3097 (w), 3066 (w), 1649 (m), 1600 (s), 1579 (s), 1474 (m), 1435 (s), 1311 (s), 1240 (m), 1166 (m), 1011 (m), 770 (s), 735 (m), 649 (m), 621 (m), 528 (m).

2.1.3. $\{Cd_3(4,4'\text{-trimethylenedipyridine})_3(ox)_3\}_n$ (3)

The synthesis and purification of compound **3** were similar to compound **1**, and the reaction of $Cd(NO_3)_2 \cdot 4H_2O$ (1.0 mmol), 4,4′-trimethylenedipyridine (1.0 mmol), $Na_2C_2O_4$ (1.0 mmol) and H_2O (10 ml) gave a 23% yield of **3** based on Cd as yellow crystals. *Anal.* Calc. (Found): C, 45.19 (45.34); O, 16.05 (16.41); H, 3.51 (3.47); N 7.02 (6.85)%. IR (KBr, cm^{-1}): 3455 (w), 3050 (w), 2926 (w), 2860 (w), 1634 (s), 1603 (s), 1556 (m), 1501 (w), 1427 (s), 1303 (s), 1221 (m), 1073 (m), 1014 (m), 793 (s), 582 (w), 501 (m).

2.1.4. $\{Na_2[Cd_4(isonicotinate)_4(ox)_3]\}_n$ (4)

Compound **4** was synthesized by the hydrothermal reaction of $Cd(NO_3)_2 \cdot 4H_2O$ (1.0 mmol), isonicotinic acid (1.0 mmol), $Na_2C_2O_4$ (1.0 mmol) and H_2O (10 ml) to give a 45% yield of **4** based on Cd as colorless crystals. *Anal.* Calc. (Found): C, 28.87 (29.03); O, 25.64 (25.71); H, 1.29 (1.02); N 4.49 (4.33)%. IR (KBr, cm^{-1}): 3451 (w), 3058 (w), 1645 (s), 1614 (s), 1595 (s), 1552 (m), 1420 (s), 1385 (s), 1322 (s), 1217 (m), 1073 (m), 1014 (m), 870 (m), 790 (s), 700 (s), 516 (m).

2.2. The TGA data

Thermogravimetric analysis (TGA) was performed on polycrystalline samples under N_2. The aqua ligands in **1** and co-crystallized water in **2** began to dissociate when the temperature reached ca. 150 and 80 °C, respectively. There was no obvious weight loss until the temperature was increased to 410, 320, 305 and 420 °C for **1**, **2**, **3** and **4**, correspondingly, which showed fairly high thermal stabilities, especially for **1** and **4**.

2.3. Crystal structure determination

Intensity data for the four complexes were collected at 293(2) K on a Siemens Smart CCD diffractometer with Mo Kα radiation ($\lambda = 0.71073$ Å). The structures

Table 1
Crystal data collection and structure refinement parameters for **1**–**4**

	1	**2**	**3**	**4**
Empirical formula	$C_{20}H_{12}Cd_2Na_2O_{18}$	$C_{24}H_{20}Cd_2N_4O_{10}$	$C_{45}H_{42}Cd_3N_6O_{12}$	$C_{30}H_{16}Cd_4N_4Na_2O_{20}$
Formula weight	811.08	749.24	1196.05	1248.05
Crystal system	triclinic	monoclinic	triclinic	monoclinic
Space group	$P\bar{1}$	C_2/c	$P\bar{1}$	$P2_1/c$
a (Å)	6.6981(4)	14.7964(3)	8.986(1)	9.444(1)
b (Å)	8.6266(6)	13.0218(7)	11.230(1)	18.666(2)
c (Å)	10.3659(7)	15.6888(6)	12.140(1)	10.388(1)
α (°)	96.286(3)	90	83.058(2)	90
β (°)	107.42(0)	115.508(2)	87.426(2)	92.744(2)
γ (°)	91.431(2)	90	66.880(2)	90
Volume (Å^3)	566.99(6)	2728.2(0)	1118.4(2)	1829.1(3)
Z	1	4	1	2
$d_{calc.}$ (g cm^{-3})	2.375	1.824	1.776	2.266
T (K)	293(2)	293(2)	293(2)	293(2)
λ(Mo Kα) (Å)	0.71073	0.71073	0.71073	0.71073
μ(Mo Kα) (mm^{-1})	2.013	1.620	1.483	2.409
R	0.0704	0.0683	0.0646	0.0797
wR	0.1539	0.1065	0.1337	0.1445

$R = \sum(||F_o| - |F_c||)/\sum|F_o|$, $R_w = \{\sum w[(F_o^2 - F_c^2)^2]/\sum w[(F_o^2)^2]\}^{0.5}$, $w = [\sigma^2(F_o^2) + (aP)^2 + b2P]^{-1}$, where $P = (F_o^2 + 2F_c^2)/3$.

Table 2
Selected bond lengths (Å) and bond angles (°); symmetry codes: (A) $x, y, z-1$, (B) $-x+2, -y, -z+1$, for **1**, (A) $-x+1/2, -y+3/2, -z$, (B) $-x, -y+2, -z$, for **2**, (A) $-x+1, -y+1, -z+1$, (B) $-x+2, -y, -z+2$, for **3**, (A) $-x, 1-y, -z$; (B) $-x, 1-y, 1-z$; (C) $-1+x, y, z$; (D) $1+x, y, z$; (E) $x, 1/2-y, 1/2+z$ for **4**

*Compound **1***			
Bond lengths			
Cd1–O1	2.189(7)	Cd1–O4A	2.241(8)
Cd1–O7B	2.286(8)	Cd1–O8	2.317(8)
Cd1–O9	2.424(8)	Cd1–O3A	2.621(9)
Bond angles			
O1–Cd1–O9	89.0(3)	O7B–Cd1–O8	71.9(3)
O4A–Cd1–O3A	52.7(3)	O7B–Cd1–O3A	85.7(3)
O4A–Cd1–O9	90.2(3)	O1–Cd1–O8	127.5(3)
*Compound **2***			
Bond lengths			
Cd1–O2A	2.266(6)	Cd1–O1	2.280(7)
Cd1–O4B	2.283(7)	Cd1–O3	2.289(7)
Cd1–N2	2.298(8)	Cd1–N1	2.302(7)
Bond angles			
N2–Cd1–N1	72.0(3)	O2A–Cd1–O1	73.4(2)
O4B–Cd1–O3	72.7(2)	O4B–Cd1–N2	106.8(3)
O1–Cd1–N1	101.2(2)	O2A–Cd1–N2	94.5(3)
*Compound **3***			
Bond lengths			
Cd1–O6	2.271(6)	Cd1–O4	2.283(6)
Cd1–O3	2.288(7)	Cd1–O5A	2.290(6)
Cd1–N3	2.319(8)	Cd1–N2	2.335(8)
Cd2–O1	2.285(7)	Cd2–O2	2.280(6)
Cd2–N1	2.328(8)		
Bond angles			
O6–Cd1–O5A	72.8(2)	O4–Cd1–O3	72.7(2)
N3–Cd1–N2	90.6(3)	O3–Cd1–N3	87.7(3)
O6–Cd1–N3	99.2(3)	O6–Cd1–N2	92.2(2)
O3–Cd1–N2	97.9(3)	O2–Cd2–O1	74.4(2)
O2–Cd2–N1	88.3(3)	O1–Cd2–N1	86.5(3)
O2–Cd2–N1B	91.7(3)	O1–Cd2–N1B	93.5(3)
*Compound **4***			
Bond lengths			
Cd1–O4C	2.19(1)	Cd1–N2	2.30(1)
Cd1–O10B	2.370(9)	Cd1–O8	2.383(9)
Cd1–O5A	2.48(1)	Cd1–O6	2.50(1)
Cd1–O10	2.591(9)	Cd2–O8E	2.273(9)
Cd2–O6E	2.301(9)	Cd2–O7	2.33(1)
Cd2–O9	2.355(9)	Cd2–N1	2.37(1)
Cd2–O2D	2.39(1)	Cd2–O1D	2.54(1)
Bond angles			
O4C–Cd1–O10B	94.9(4)	O4C–Cd1–O8	86.2(4)
O8–Cd1–O10	64.1(3)	O8–Cd1–O6	65.2(3)
O5A–Cd1–O6	65.3(3)	N2–Cd1–O6	91.7(4)
O6E–Cd2–N1	84.6(4)	O10B–Cd1–O5A	96.2(3)
O8E–Cd2–O6E	70.4(3)	O2D–Cd2–O1D	53.3(4)

were solved by direct methods using SHELXS-97 [20] and refined by full-matrix least-squares methods using SHELXL-97 [21]. Anisotropic displacement parameters were used for all non-hydrogen atoms. No attempt was made to locate the hydrogen atoms of water, and the other hydrogen atoms were added in the riding model but not refined. The crystallographic data are summarized in Table 1, and the selected bond lengths and bond angles of the four compounds are listed in Table 2.

3. Results and discussion

3.1. Syntheses

In this paper, four cadmium oxalate polymers with aromatic ligands have been synthesized by hydrothermal reactions. We have made a probe on the reaction of cadmium (II) with mere oxalate ligand under the same conditions. When the molar proportion of ligand versus metal was about 1:1, we got a colorless crystal $\{Cd_2(ox)_2(H_2O)_4\}_n \cdot 2nH_2O$ (**5**) with a 2D layered structure, which has been reported by Orioli et al. [22]. The coordination geometry about each cadmium atom in this complex was approximately that of a pentagonal bipyramid with two coordinated water molecules in the apical and equatorial positions. So it was natural to see whether the two coordinated sites of water could be replaced by other co-ligands such as aromatic ligands and what changes on the structure would take place if these co-ligands were introduced. We tried lots of aromatic ligands and found the following four aromatic ligands H_3 tam, 2,2′-bipyridine, 4,4′-trimethylenedipyridine and isonicotinic acid would coordinate to cadmium with oxalate and form mixed-ligand polymers. Due to the different coordination conformations and abilities of these aromatic ligands with cadmium, the structures showed abundant variation, not only on motifs of the frameworks, but also on coordination modes of cadmium ions with oxalate ligands. Only in **4** did the structure of cadmium with oxalate ligands still exhibit a layer motif. While for **2** and **3** with pyridine co-ligands introduced, they changed to chain structures. In complex **1**, the oxalate only acted as a bridging ligand to bind two metal centers, and the linkages among these binuclear units were accomplished by the Htma ligands.

According to the literatures to date, there are five coordination modes of the oxalate ligand when coordinated to cadmium(II) ions, as shown in Scheme 1. Through one or two combined modes, various architectures have been observed [16,17]. For the polymers reported in this paper, the main coordination modes include (a), (c) and (d), and mode (d) is a new one as far as we know.

These four complexes are very stable in air, insoluble in the usual polar or non-polar solvents such as acetone, chloroform, benzene, H_2O, methanol, CH_3CN, DMF, etc.

3.2. Infrared spectra

All complexes showed the characteristic bands of aromatic and carboxylate ligands. The stretching vibration

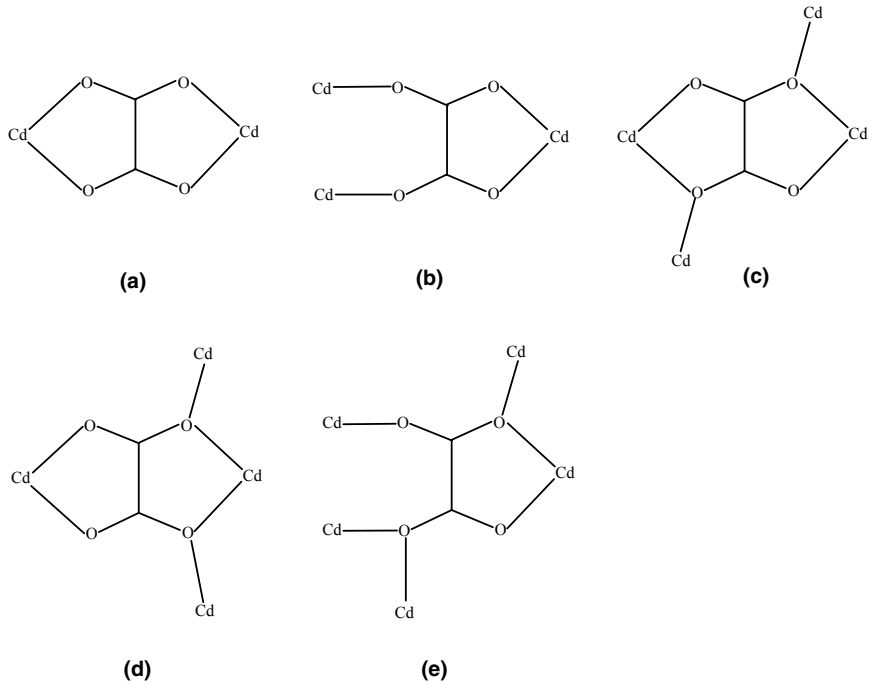

Scheme 1. Coordination modes of oxalate to cadmium ions: (a) chelate bis-bidentate; (b) chelate bis-bidentate and bidentate; (c) chelate/bridging bis-bidentate; (d) chelate/bridging bis-bidentate and chelate bis-bidentate; (e) chelate/bridging bis-bidentate and chelate/bridging bidentate.

bands of Ar–H were at 3089 cm^{-1} for **1**, 3097 cm^{-1} for **2**, 3050 cm^{-1} for **3** and 3058 cm^{-1} for **4**. The C–H stretching vibration bands for methylene in **3** were at 2926 and 2860 cm^{-1}. The δ_{Ar-H} (out-of-plane bending vibration) bands appeared at 680, 735 and 801 cm^{-1} for **1**, 735 and 770 cm^{-1} for **2**, 793 cm^{-1} for **3**, 700 and 790 cm^{-1} for **4**. The C=C or C=N stretching vibrations for these four complexes all gave absorption bands from 1474 to 1600 cm^{-1} in the corresponding spectra. The asymmetric and symmetric C=O stretching vibration bands of oxalate groups emerged at 1649, 1435 cm^{-1} for **2** and 1634, 1427 cm^{-1} for **3**, suggesting the chelate bis-bidentate coordination mode of the oxalate ligands. While in **1** and **4**, due to C=O vibrations of the aromatic carboxylate groups, the absorption peaks around these bands split and made the spectra become more complicated. The peak appearing at 1700 cm^{-1} in complex **1** might be assigned to the C=O stretching vibration for the uncoordinated carboxylate group of Htma.

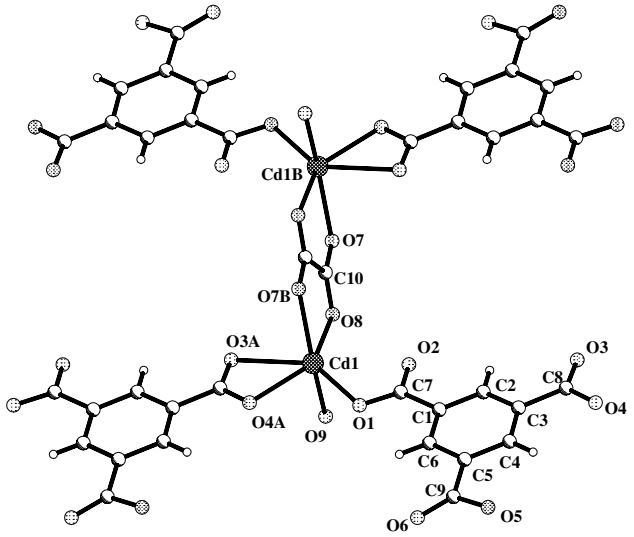

Fig. 1. Perspective view of the coordination environments of Cd1 with atomic labels in **1**.

3.3. Crystal structures

3.3.1. Crystal structure of $\{Na_2[Cd_2(Htma)_2(ox)(H_2O)_2]\}_n$ (1)

Compound **1** exhibits a 1D infinite chain structure motif, in which each cadmium atom has an O_6 distorted octahedral configuration formed by an aqua ligand (Cd1–O9 = 2.424(8) Å), two oxygen atoms from oxalate ions and three oxygen atoms provided by Htma ligands, as shown in Fig. 1. For the oxalate ligand, there is only one kind of coordination fashion (Scheme 1(a)), through which two cadmium atoms are bridged to each other with Cd1–O7B = 2.286(8) Å and Cd1–O8 = 2.317(8) Å. Of the three carboxylate groups in the Htma ligand, there are only two bonding modes; one is unidentate (Cd1–O1 = 2.189(7) Å) and the other is chelating bis-bidentate (Cd1–O3A = 2.621(9) Å and Cd1–O4A = 2.241(8) Å). In this coordination fashion, a centrosymmetric bi-nuclear $[Cd_2(Htma)_2(ox)(H_2O)_2]$ unit is

formed and the connectivity of these units through Htma ligands results in an interesting 1D "ladder-like" linear chain (Fig. 2), which has not been reported previously among related oxalate coordination polymers.

3.3.2. Crystal structure of $\{[Cd_2(2,2'\text{-bipyridine})_2(ox)_2]\cdot 2H_2O\}_n$ (2)

The structure motif of compound **2** is also a 1D infinite chain, yet each octahedron around the cadmium atom is composed of four oxygen atoms from oxalate ions and two nitrogen atoms from 2,2′-bipyridine, as shown in Fig. 3. The two nitrogen atoms are bonded to a cadmium atom to form a five-membered chelating ring ($\angle$N1–Cd1–N2 = 72.0(3)°), which restrains the spacial extension of the cadmium oxalate unit in compound **2**. Thus centrosymmetric di-nuclear $[Cd_2(C_{10}H_8N_2)_2(ox)_2]$ units are constructed, which are interlinked to each other through oxalate ligands, as shown in Fig. 4, to form a 1D zigzag chain. A similar chain has been reported in the structure of $\{Cu(C_{10}H_8N_2)(C_2O_4)\cdot 2H_2O\}_n$ [23].

3.3.3. Crystal structure of $\{Cd_3(4,4'\text{-trimethylenedipyridine})_3(ox)_3\}_n$ (3)

Fig. 5 shows the coordination environment of Cd1 and Cd2 in compound **3**. Each cadmium atom lies inside a distorted octahedron composed of four oxygen atoms from oxalate ions and two nitrogen atoms provided by different 4,4′-trimethylenedipyridine ligands. In the octahedron cage containing Cd1, two nitrogen atoms are adjacent to each other ($\angle$N3–Cd1–N2 = 90.6(3)°), while in the one containing Cd2, the two nitrogen atoms occupy two polar sites. The bonding distances of N2–Cd1, N3–Cd1 and N1–Cd2 are almost equal to each other (2.335(8), 2.319(8) and 2.328(8) Å). The trimethylene units ($-CH_2-CH_2-CH_2-$) in the 4,4′-trimethylenedipyridine ligands are disordered, as shown in Fig. 5 (C18 and C19, C38 and C38C).

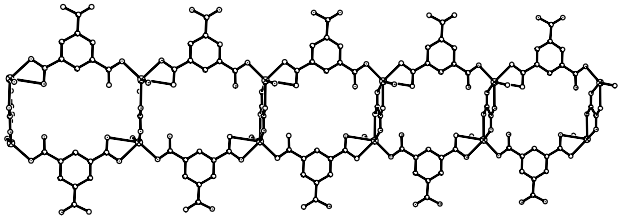

Fig. 2. The "ladder-like" 1D chain structure of **1** featuring dinuclear units.

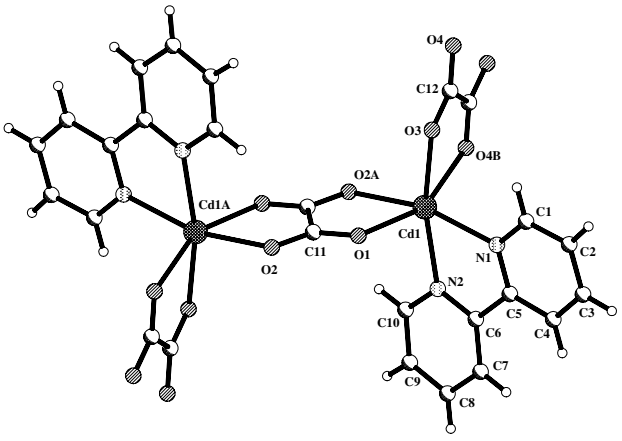

Fig. 3. Perspective view of the coordination environments of Cd1 with atomic labels in **2**.

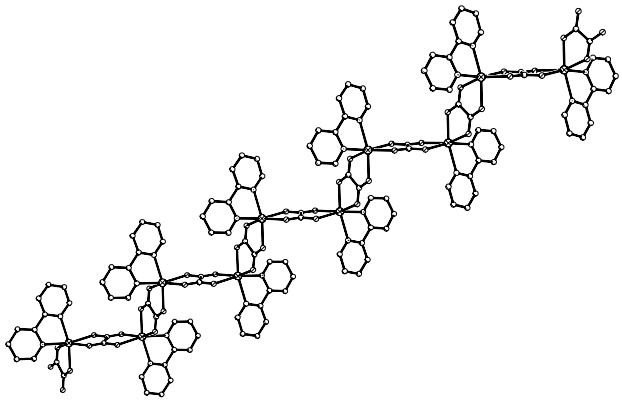

Fig. 4. The 1D zigzag chain structure of **2** viewed along the *c*-axis, featuring dinuclear units.

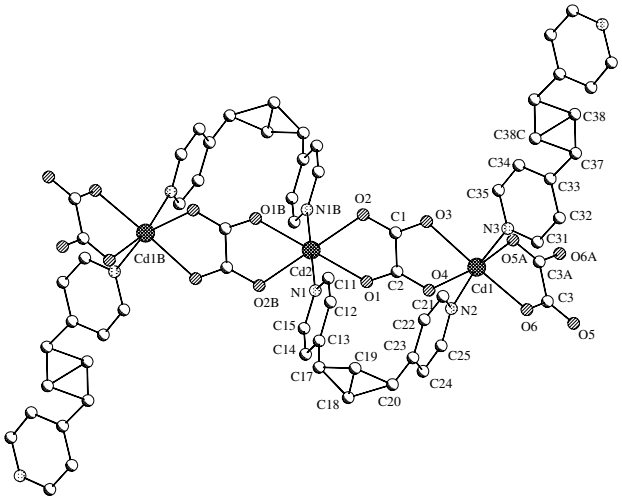

Fig. 5. Perspective view of the coordination environment of Cd atoms with atomic labels in **3**. Noting the trimethylene units ($-CH_2-CH_2-CH_2-$) in 4,4′-trimethylenedipyridine are disordered (C18 and C19, C38 and C38C (symmetry: $-x, -y, 1-z$)).

It has been reported that 1,2-bis(4-pyridyl)ethane can act as a "spacer" in cobalt nitrate polymers by adopting the *gauche* (angular) or *anti* (linear) conformation [24]. It is interesting that the 4,4′-trimethylenedipyridine ligands exhibit a similar coordination mode in this complex. In each tri-nuclear $[Cd_3(C_{13}H_{14}N_2)_3(ox)_3]$ unit, there are also two centrosymmetric *gauche* spacers, exhibiting a "sine-function-like" shape. There is one chelating bis-bidentate oxalate and the remaining *anti* spacers then connect these trinuclear units to fabricate a

novel 2D eight-metal "brick-wall-like" square network with a hole size of about 8×13 Å (Fig. 6).

3.3.4. Crystal structure of $\{Na_2[Cd_4(isonicotinate)_4(ox)_3]\}_n$ (4)

Compound **4** exhibits a 3D structure motif, whose coordination environment of Cd1 and Cd2 are shown in Fig. 7. Unlike the previous three structures, the coordination number of the cadmium atom is seven in this polymer. Around each cadmium atom, the coordination environment includes six oxygen atoms and one nitrogen atom. However, the arrangement of the ligand atoms around Cd1 leads to the formation of a distorted pentagonal bipyramid, while for Cd2 it changes to a distorted mono-capped octahedron. These results are of note since the Cd atom is generally octahedrally coordinated where the coordination number is six, just as described in **1**, **2** and **3**. Furthermore, for the oxalate ligand, there are two types of coordination modes, one is chelate/bridging bis-bidentate (Scheme 1(c)), and the other is chelate/bridging bis-bidentate and chelate bis-bidentate (Scheme 1(d)). A centrosymmetric tetra-nuclear unit, $[Cd_4(ox)_3]$, can be observed from the constructed 2D cadmium oxalate layers viewed along the bc plane, which is shown in Fig. 8(a). As a rigid binding tecton, the isonicotinate ligands then play a role in sustaining these layers to form a novel 3D architecture, as shown in Fig. 8(b).

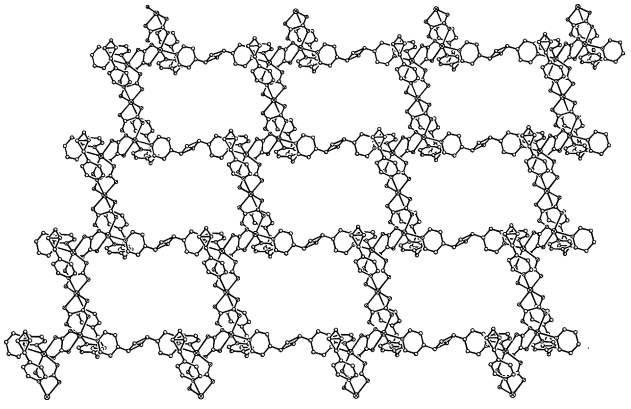

Fig. 6. The "brick-wall-like" square eight-metal network observed in **3** viewed along the *c*-axis, featuring trinuclear units.

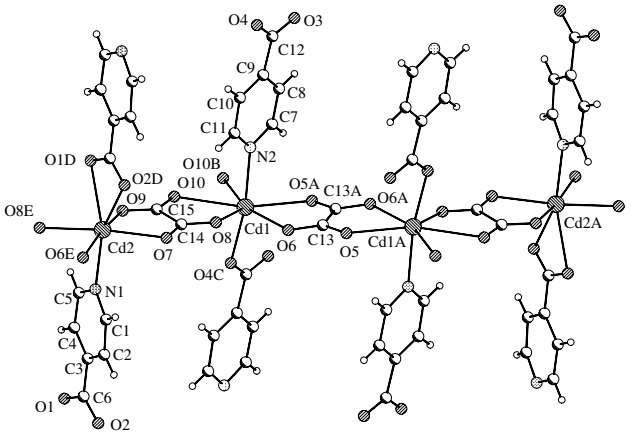

Fig. 7. Perspective view of the coordination environments of Cd atoms with atomic labels in **4**.

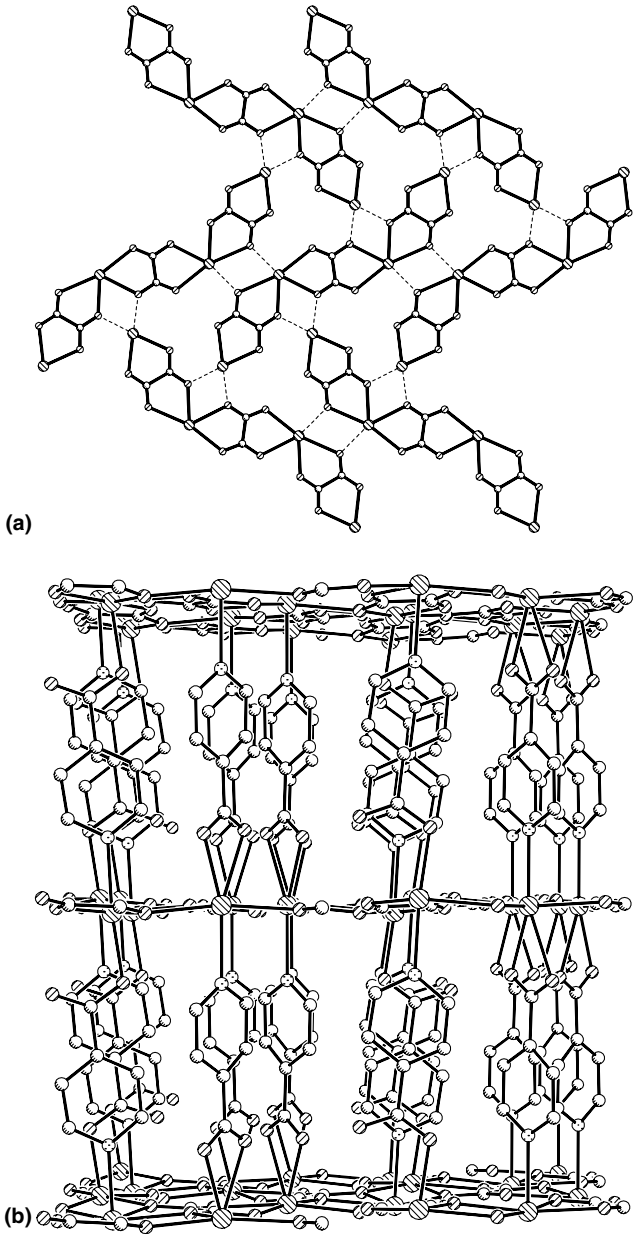

Fig. 8. (a) The layer structure of cadmium oxalate in **4** viewed along *bc* plane, featuring the tetranuclear units (the bonds among the units are shown as dash lines for clarity). (b) The 3D architecture in **4** viewed along the *c*-axis, showing the layers are sustained by the isonicotinate tectons along the *a*-axis.

4. Conclusions

The use of oxalate and different co-ligands in hydrothermal synthesis generates interesting structure

motifs in new cadmium polymers, with dimensions ranging from 1D to 3D, which feature dinuclear, trinuclear and tetranuclear units correspondingly and show relatively high thermal stabilities.

5. Supplementary material

Crystallographic data for the structural analysis have been deposited with the Cambridge Crystallographic Data Centre, CCDC Nos. CCDC 214532–214535 (for compound **1** to **4**, respectively) contain the supplementary crystallographic data for this paper. These data can be obtained free of charge via www.ccdc.cam.ac.uk/conts/retrieving.html (or from the Cambridge Crystallographic Data Centre, 12 Union Road, Cambridge CB2 1EZ, UK; fax: (+44) 1223-336-033; or e-mail: deposit@ccdc.cam.ac.uk).

Acknowledgements

This research was supported by grants from the State Key laboratory of Structural Chemistry, Fujian Institute of Research on the Structure of Matter, the Chinese Academy of Sciences (CAS), the Ministry of Science and Technology of China (001CB1089), the National Science Foundation (20273073, 90206040) of China and Fujian Province (2001J026, 2002F014, 2002J007, 2003J042) for research funding support.

References

[1] M.J. Plater, M.R.St.J. Foreman, T. Gelbrich, M.B. Hursthouse, J. Chem. Soc., Dalton Trans. (2000) 1995.
[2] S. Noro, S. Kitagawa, M. Kondo, K. Seki, Angew. Chem. Int. Ed. Engl. 39 (2000) 2082.
[3] J.-C. Dai, X.-T. Wu, Z.-Y. Fu, C.-P. Cui, S.-M. Hu, W.-X. Du, L.-M. Wu, H.-H. Zhang, R.-Q. Sun, Inorg. Chem. 41 (2002) 1391.
[4] P.J. Hagman, D. Hagrman, J. Zubieta, Angew. Chem. Int. Ed. Engl. 38 (1999) 2638.
[5] Z.-Y. Fu, P. Lin, W.-X. Du, L. Chen, C.-P. Cui, W.-J. Zhang, X.-T. Wu, Polyhedron 20 (2001) 1925.
[6] P.A. Prasad, S. Neeraj, S. Natarajan, C.N.R. Rao, Chem. Commun. (2000) 1251.
[7] T.J. Prior, M.J. Rosseinsky, Chem. Commun. (2001) 495.
[8] C.J. Kepert, M.J. Rosseinsky, Chem. Commun. (1998) 31.
[9] M. Julve, M. Verdaguer, A. Gleizes, M. Philoche-Levisalles, O. Kahn, Inorg. Chem. 23 (1984) 3808.
[10] S. Alvarez, M. Julve, M. Verdaguer, Inorg. Chem. 29 (1990) 4500.
[11] M. Ohba, H. Tamaki, N. Matsumoto, H. Okawa, Inorg. Chem. 32 (1993) 5385.
[12] J. Glerup, P.A. Goodson, D.J. Hodgson, K. Michelsen, Inorg. Chem. 34 (1995) 6255.
[13] H. Tamaki, Z.J. Zhong, N. Matsumoto, S. Kida, M. Koikawa, N. Achiwa, Y. Hashimoto, H. Okawa, J. Am. Chem. Soc. 114 (1992) 6974.
[14] C. Mathonière, C.J. Nuttal, S.G. Carling, P. Day, Inorg. Chem. 35 (1996) 1201.
[15] S. Decurtins, H.W. Schmalle, R. Pellaux, P. Schneuwly, A. Hauser, Inorg. Chem. 35 (1996) 451.
[16] R. Vaidhyanathan, S. Natarajan, C.N.R. Rao, J. Solid State Chem. 162 (2001) 150.
[17] R. Vaidhyanathan, S. Neeraj, P.A. Prasad, S. Natarajan, C.N.R. Rao, Angew. Chem. Int. Ed. Engl. 39 (2000) 3470.
[18] Z.-Y. Fu, X.-T. Wu, J.-C. Dai, L.-M. Wu, C.-P. Cui, S.-M. Hu, Chem. Commun. (2001) 1856.
[19] L.-Y. Zhang, G.-F. Liu, S.-L. Zheng, B.-H. Ye, X.-M. Zhang, X.-M. Chen, Eur. J. Inorg. Chem. (2003) 2965.
[20] G.M. Sheldrick, SHELXS-97, Program for X-ray Crystal Structure Solution, University of Göttingen, Göttingen, 1997.
[21] G.M. Sheldrick, SHELXS-97, Program for X-ray Crystal Structure Refinement, University of Göttingen, Göttingen, 1997.
[22] P. Orioli, B. Bruni, M. Di Varia, L. Messori, F. Piccioli, Inorg. Chem. 41 (2002) 4312.
[23] H. Oshio, U. Nagashima, Inorg. Chem. 31 (1992) 3295.
[24] T.L. Hennigar, D.C. MacQuarrie, P. Losier, R.D. Rogers, M.J. Zaworotko, Angew. Chem. Int. Ed. Engl. 36 (1997) 972.

Available online at www.sciencedirect.com
SCIENCE DIRECT®
Polyhedron 23 (2004) 1011–1017
POLYHEDRON
www.elsevier.com/locate/poly

Helical zinc complexes of pyrazine–pyridine hybrids

S.I.G. Dias [a], Fenton Heirtzler [a,*], T. Bark [b], Gael Labat [c], Antonia Neels [c]

[a] School of Physical Sciences, Chemical Laboratory, University of Kent, Canterbury, Kent CT2 7NH, UK
[b] Department of Chemistry, University of Fribourg, Pérolles, 1700 Fribourg, Switzerland
[c] Institute of Chemistry, University of Neuchâtel, Avenue de Bellevaux 51, 2000 Neuchâtel, Switzerland

Received 1 October 2003; accepted 19 December 2003

Abstract

The zinc(II) complexes **1a**$ZnCl_2$ and **1b**$ZnCl_2$ (**1a**: 2-(6′,2″-bipyrid-2′-yl)-3-(2-pyridyl)pyrazine; **1b**: 2-(6′,2′-bipyrid-2′-yl)-5,6-dinitrilo-3-(2-pyridyl)pyrazine) were prepared by treatment of the ligands with $ZnCl_2$. The structures of both were investigated by X-ray crystallography and ^{1}H NMR spectroscopy. Both complexes display proton deshielding phenomena that are attributed to a twisted solution-state molecular conformation. In the solid state, **1a**$ZnCl_2$ exhibits a high degree of torsion about the axis through the uncomplexed pyridine ring and the pendant chlorine atoms. The solid-state structure and solution-state self-associative behavior of **1b**$ZnCl_2$ are indicative of a partial self-assembly motif.
© 2004 Elsevier Ltd. All rights reserved.

Keywords: Pyrazine; Pyridine; X-ray; NMR; Stacking; Twist

1. Introduction

Recently, we described several examples of so-called pyrazine–pyridine hybrids, which self-assemble with particular metal salts to π-stacked, dimeric complexes [1–4]. In unsymmetrical ligands such as **1a**, the 2,3-disubstitution pattern of oligopyridyl chains on the pyrazine ring [5–8] is decisive in a preference for tetrahedral metals [2–4]. The angular arrangement of divergent binding sites leads to a bis-bidentate, instead of bidentate/terdentate complexation mode (Fig. 1). Such complexes also organize through homopyrazine π-stacking, affording a chiral, $\Delta\Delta/\Lambda\Lambda$-configuration, and via the solid-state π-stacking of metallo-cyclophane cations, to provide a high degree of parallel lattice ordering [4,7]. In the native ligands, twisting interactions induce a single-helical molecular conformation [7].

Metallo-organic supramolecular complexes of zinc(II) and oligopyridine-type ligands are attracting attention on account of their excellent excited-state dipolar properties, which render them relevant to applications based on non-linear optical effects [9–12]. These bulk properties can be enhanced through incorporation into highly ordered and polar lattices [12–16]. Symmetrical 2,5-dipyridylpyrazine-type ligands and their 2,6′-bipyridyl homologues self-assemble with zinc(II) salts to linear or bridged polymeric as well as macrocyclic-polymetallic structures and through which stereochemical and chiral features may be efficiently expressed [17,18]. Whereas single-enantiomer chirality is an additional means of organizing transition dipole moments, i.e., via non-centrosymmetric crystal-lattice ordering [16,19], so far equilibrating mixtures of *meso*/chiral metallo-cyclophanes containing octahedral di-zinc(II) have been reported [20,21]. Thus, we were attracted to the use of zinc(II) metallo-cyclophanes and related complexes as novel metallo-organic photonic materials. Preliminary work dictated examining the currently available 2,3-disubstituted ligands' interaction with practical zinc(II) salts, with an emphasis on coordination [22] and ligand geometry, intra/intermolecular stacking effects and long-range interactions. Since the synthesis of analogous 2,3-dicyanopyrazine ligands is possible through our previously-introduced methodology [8], and nitrile substitution increases dipolar alignment [23–26], these materials were also of interest.

* Corresponding author. Tel.: +44-1227-827-041; fax: +44-1227-827-724.
E-mail address: heirtzler@web.de (F. Heirtzler).

0277-5387/$ - see front matter © 2004 Elsevier Ltd. All rights reserved.
doi:10.1016/j.poly.2003.12.013

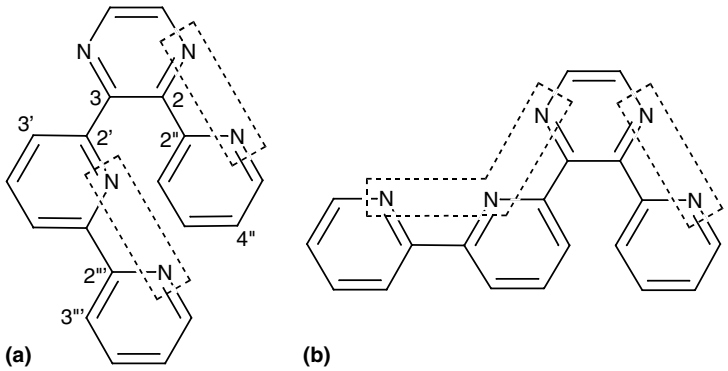

Fig. 1. Potential binding domains in ligand **1a**.

2. Results and discussion

Ligand **1a** was available from earlier studies [7]. Heating of the unsymmetrical α-diketone **2** [8] with one equivalent of diaminomaleonitrile in glacial acetic acid afforded dinitrile-substituted ligand **1b** in 67% yield after purification (Scheme 1). Treatment of **1a** and **1b** with zinc dichloride in acetonitrile or acetonitrile-chloroform under reflux conditions resulted in the precipitation of sparingly-soluble solids that could be recrystallized from hot nitromethane. The results of combustion analyses on these complexes were in agreement with a 1:1:2 stoichiometry of **1a/1b**:Zn:Cl. While the electrospray- and FAB-mass spectra of both complexes displayed m/z signals of monomeric materials, the base signal of the complex from **1b** corresponded to $[\mathbf{1b}_2\mathrm{Zn}]^+$. There was thus just cause to investigate their solid-state structures through X-ray crystal structure analysis, as well as to clarify their organizational priorities (see Section 4 for full details).

The complexation domain of $\mathbf{1a}ZnCl_2$ contains η^3-coordination of **1a** to the metal and has a monomeric constitution (Fig. 2(a)). The metal-nitrogen bond lengths (Table 1) and deviations of the constituent aza-aromatics from co-planarity are indicative of a lopsided terdentate coordination. In particular, the Zn–N lengths to pyridine are shorter than to pyrazine, and the torsional angle between C_5H_3N pyridine and pyrazine is significantly greater than that between the adjacent pyridine rings. The pendant chlorine atoms occupy pseudo-axial positions. While the zinc–chlorine bonding distances are unremarkable, the halogens' orientation with respect to the overall molecular geometry warrants comment. One of these, Cl1, is within 0.05 Å of the mean plane of the C_5H_3N ring, while the other (Cl2) lies 3.04 Å on the other side of the same plane. The zinc–chlorine bond angles to nitrogen of C_5H_3N are correspondingly deformed. The uncomplexed pyridine ring is twisted with respect to and deflected out of the plane of the pyrazine ring. Both of the pyridyl–pyrazine torsions occur at the cost of atomic deviations from the mean plane of pyrazine (0.01–0.09 Å). The location of the uncomplexed C_5H_4N ring on the opposite side to Cl2 gives the entire molecule a shallow helical pitch.

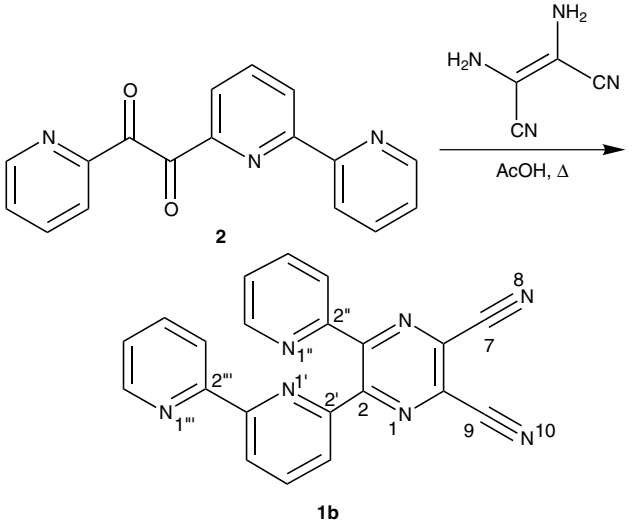

Scheme 1. Synthesis of nitrile disubstituted **1b**.

Two different intermolecular parallel stacking interactions are apparent in the lattice of $\mathbf{1a}ZnCl_2$. The complexed bipyridyl domains stack in offset, anti-parallel pairs related by an inversion center (Fig. 2(b)). Thus, while the individually stacking C_5H_4N and C_5H_3N rings are canted 9.83° overall, the bipyridyl rings are co-planar, with atomic distances from the respective mean ring planes in the 3.14–3.81 Å range. Also, columns of homochiral helices are interdigitated by their racemates (Fig. 2(c)). This interpenetration occurs via anti-parallel pyridylpyrazine stacking interactions, which besides minimizing contact between the $ZnCl_2$ centers, generates an inversion center between them. Short H···Cl contacts [27] to the uncomplexed pyridine ring (Cl1···H5‴ and Cl2···H4‴) between the interdigitating columns are apparent.

The complex $\mathbf{1b}ZnCl_2$ is surprisingly monomeric, and occurs as a solvate with a 2:1 – ratio of nitromethane to complex. Strikingly, layers of nitromethane are sepa-

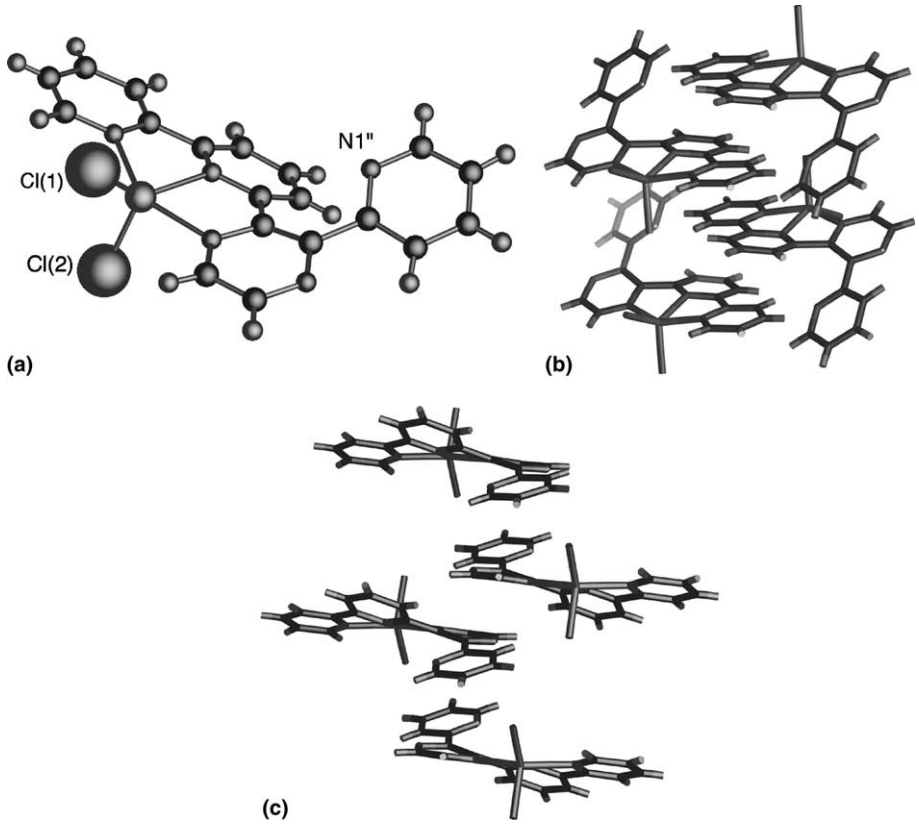

Fig. 2. Crystal structure of complex **1a**$ZnCl_2$: (a) single molecule, emphasizing twist with respect to N(1″) pyridine ring; (b) parallel stacking of complexed 2,6′-bipyridyl domains; (c) mirror-image columns of stacked 3-(2′-pyridyl)pyrazine subunits.

Table 1
Bonding- and non-bonding parameters associated with **1a**$ZnCl_2$ and **1b**$ZnCl_2$

Substance	**1a**$ZnCl_2$	**1b**$ZnCl_2$	Substance	**1a**$ZnCl_2$	**1b**$ZnCl_2$
Bond lengths					
N(1)–Zn	2.2175 Å	2.523 Å	*Distances from mean plane:*		
N(1′)–Zn	2.1120 Å	2.074 Å	Cl(1)–C_5H_3N	0.048 Å	1.761 Å
N(1‴)–Zn	2.1668 Å	2.097 Å	Cl(2)–C_5H_3N	−3.042 Å	−1.983 Å
Cl(1)–Zn	2.2411 Å	2.2116 Å			
Cl(2)–Zn	2.2784 Å	2.2215 Å	*Extra-annular torsional angles:*		
			Pyrazine-C_5H_3N	28.61°	22.618°
Bond angles			C_5H_3N–C_5H_4N	9.83°	1.294°
N(1)–Zn–N(1′)	73.570°	70.06°	Pyrazine-C_5H_4N	22.35°	30.767
N(1′)–Zn–N(‴)	75.026°	78.05°			
N(1)–Zn–Cl(1)	98.179°	93.01°			
N(1′)–Zn–Cl(1)	136.994°	112.02°			
N(1‴)–Zn–Cl(1)	99.386°	108.43°			
N(1)–Zn–Cl(2)	98.043°	91.93°			
N(1′)–Zn–Cl(2)	108.721°	126.62°			
N(1‴)–Zn–Cl(2)	99.189°	99.25°			

rated by sheet-like **1b**$ZnCl_2$ complexation domains (Fig. 3(a)). The repeating distance between these two layers is ≈11.8 Å. While the complexation domain observed for **1b**$ZnCl_2$ superficially resembles that of **1a**$ZnCl_2$, significant differences in molecular geometry are apparent (Fig. 3(b)). An increased dissymmetry of the 2,2′:6′,2″-terpyridyl-like binding domain occurs, e.g. the Zn–N(1) (pyrazine) bond length increases by 14% relative to **1a**$ZnCl_2$ (Table 1). The origins of this effect either plausibly involve electronic factors or steric interaction with chlorine atoms (closest contacts of Cl1 and Cl2 to nitrile carbons: 4.29 and 3.41 Å, respectively). The constituent atoms of the dicyanopyrazine ring deviate by 0.01–0.07 Å from their mean plane. This situation appears to reduce the overall ligand strain around the terdentate site, as reflected in extra-annular torsional angles. Deformation of the metal-halogen bonds with respect to the η^3-binding domain is relieved,

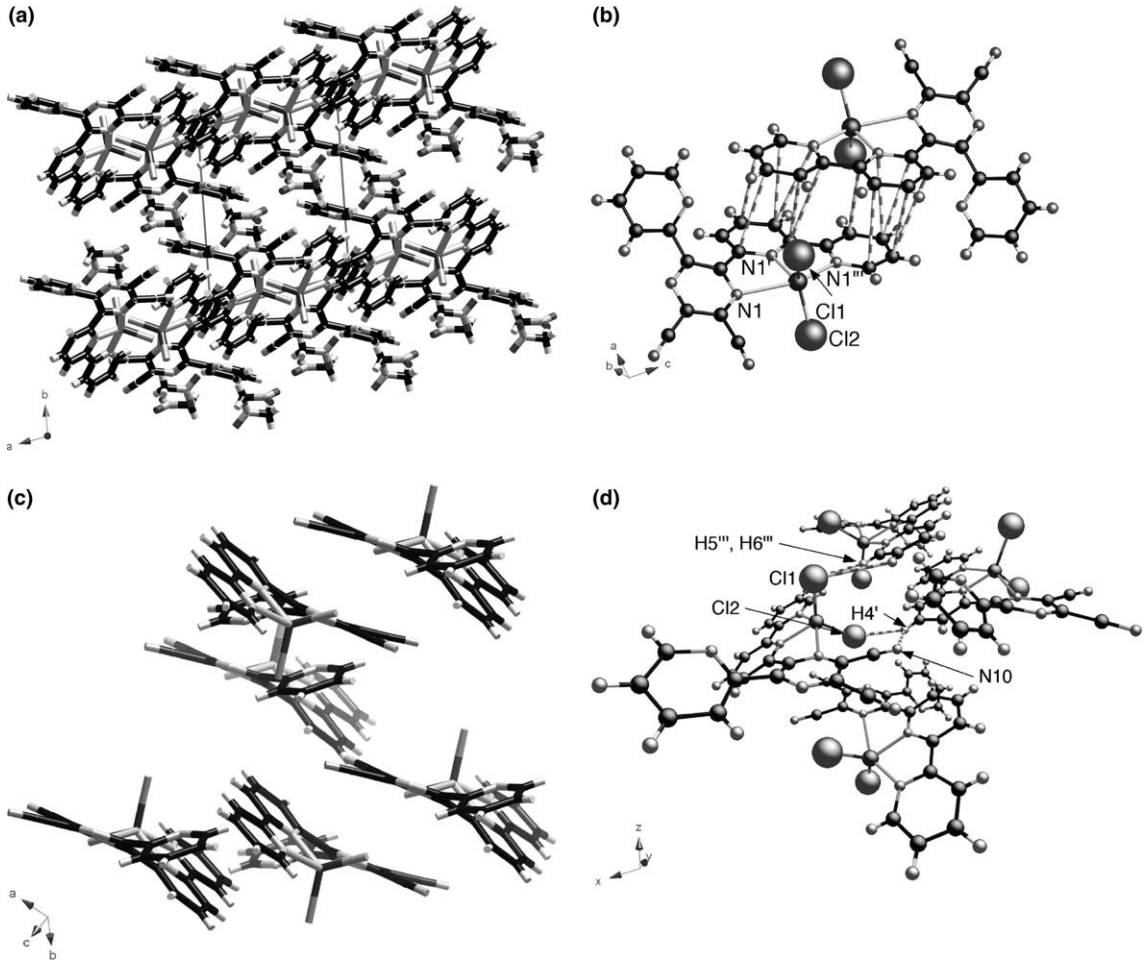

Fig. 3. Complex **1b**$ZnCl_2$ in the solid state: (a) alternating strata of complex and nitromethane; (b) stacked dimeric pairs; (c) stacked 3-(2′-pyridyl)pyrazine subunits [vertical orientation]; (d) likely close contacts.

as shown by the distances of the halogens from the mean plane of C_5H_3N pyridine. The bond angles and atom-to-plane distances involving N of C_5H_3N and the halogen atoms indicate that the Zn–Cl bond vectors are pointed marginally toward, and not away from the un-complexed C_5N_4N ring.

The most prominent intermolecular interaction of **1b**$ZnCl_2$ involves the stacking of inversion center-related pairs of bipyridyl sub-units in **1b** (Fig. 3(b)). These are coplanar to within 0.38° and are characterized by atom-to-mean plane distances in the 3.02–3.30 Å range and closest intermolecular atomic distances of 3.49–3.75 Å. Within this situation, the uncomplexed pyridine rings adapt, as in the case of **1a**$ZnCl_2$, an approximately *anti*-conformation with respect to the pyrazine ring, but are intriguingly twisted inward towards their inversion-related stacking partners to afford estimated short intermolecular $N1'' \cdots H4'''$ contacts of ~2.73 Å; no $Cl \cdots H$ distances within 3 Å are observed. Overall, the geometry and stacking interactions of this situation resemble those in the dicopper(I) metallo-cyclophane of **1a** (atom-to-plane stacking distances: 3.08–3.47 Å).

Another stacking interaction involves the synthon represented by the uncomplexed pyridylpyrazine fragment. This associates with itself to afford atom-to-plane separations and closest-neighbor distances (3.42–3.47 and 3.49–3.75 Å, respectively), bespeaking of an intermediate offset parallel stacking arrangement [28]. Each stacked pyridyl-pyrazinyl pair is coplanar to within 0.61°, although the individual stacking rings are tilted by 3.9° to each other.

Parallel alignment also occurs through the dicyanopyrazine groups, that are oriented in an anti-parallel, dimeric manner (Fig. 3(c)). But also, the nitrile groups interconnect the closely stacked **1b**$ZnCl_2$ pairs from the opposite side of the dicyanopyrazine plane (Fig. 3(d)). For a given equivalent of **1b**$ZnCl_2$, these involve short distances from both nitrile N10 and Cl2 to H4′, as well as $Cl2 \cdots H5'$, on a single molecular neighbor (2.78, 2.67 and 3.72 Å, respectively). Contacts from Cl1 to H5‴ and H6‴ on yet another adjoining molecule (3.56 and 3.11 Å) complete this aspect.

To compare the solid- and solution-state structures of the zinc complexes, their proton NMR spectra were

analysed and assigned. Since the ligand **1b** is previously unreported, its ^{1}H NMR spectrum deserves brief comment. The outstanding feature in this substance is the upfield resonance of H3‴, which is indicative of an edge-on-face stacking interaction between the spatially proximate C_5H_4N pyridine rings containing N1‴ and N1″ [7]. Thus, the presence of the nitrile groups does not interfere with the expected conformational preferences of this heterocyclic system. For the complexes, spectra were assigned with the assistance of pulse field gradient COSY spectra (Fig. 4). The downfield shift of H3‴ and its coupling constants are consistent with those of other terdentate pyridine–pyrazine complexes [29] and are indicative of complexation involving C_5H_4N pyridine of the 2,6′-bipyridyl substituent.

Also in both of the zinc(II) complexes, H3″ of C_5H_4N pyridine undergoes an unusual upfield shift (**1a**$ZnCl_2$ and **1b**$ZnCl_2$: $\Delta\delta$ relative to ligands in $CDCl_3$: 0.51 δ 7.31 and 1.03, respectively). Initially, the assignment of the upfield doublet to H3″ (as opposed to H3′ of the C_5H_3N ring) was not straightforward. However, similar experiments on **1b**$ZnCl_2$ at 270 MHz clearly indicated the connectivity of this shift to the remaining three protons of the uncomplexed C_5H_4N ring. A similar shifting of this position occurs in dimeric metallo-cyclophanes, but in that case arises from an edge-on-face interaction of the orthogonally directed bipyridyl complexation domains [2,3]. Insight into the origins of this new effect is provided through molecular model studies. Orthogonal stacking of the uncomplexed C_5H_4N pyridine ring against the C_5H_3N ring should induce a shielding effect in spatially adjacent positions in the later, but not the former ring. However, other η^3-metalloorganic complexes of 2,3-disubstituted pyrazine–pyridine hybrids exist in highly twisted solution-state geometries [29,30], suggesting that long-range effects, to cause shielding of H3″ by the chlorine atoms, may occur for the current zinc(II) complexes. Since, however no dynamic signal broadening width was observed at 25 °C, any such fluxional processes involving the uncomplexed pyridine ring are rapid on the ^{1}H NMR spectroscopic time scale.

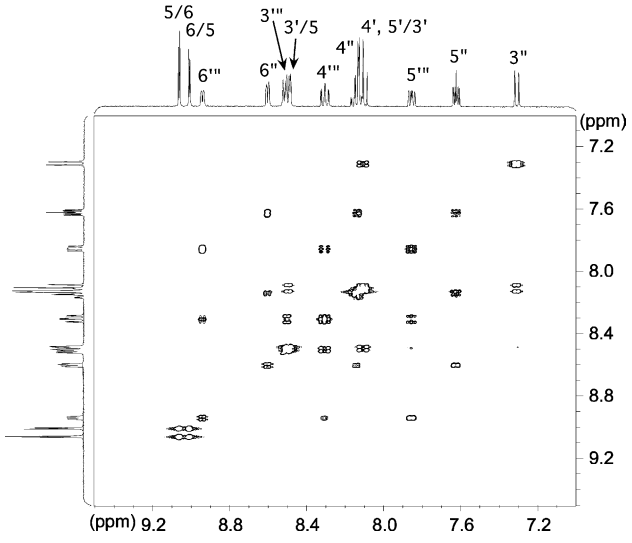

Fig. 4. Pulsed field gradient ^{1}H–^{1}H correlation spectrum for **1a**$ZnCl_2$ (CD_3NO_2, 400 MHz).

3. Concluding remarks

Complexation of the sterically hindered bipyridyl-pyridylpyrazine hybrids **1a** and **1b** with zinc(II) induces a change from bis-bidentate to terdentate complexation geometry, while maintaining related long-range stacking and organizational features as for dimeric metallo-cyclophanes. Tantalizingly, the appearance of mass spectral signals from $[\mathbf{1b}_2Zn]^+$, the weakened Zn–N (pyrazine) bond and the dimeric, multi-interaction solid-state stacking motif of **1b**$ZnCl_2$ suggest that this complex is on the brink of an oligomeric self-assembly program. For both new complexes, solid-state atropisomeric chirality in the form of helicity is observed, and is also probable in solution, a feature that compliments the point chirality of the metallo-cyclophanes. Thus, the precise molecular and crystal lattice topology can be controlled through appropriate substitution of the ligand scaffolding. Indeed, highly polar nitrile substitution, which is desirable from the point of excited-state dipole moment tuning, is tolerated by the observed complexation mode. These studies have revealed to us the complexity of the organizational and topological phenomena possible for such pyrazine–pyridine hybrids, and will aid in the design of monomeric and dimeric zinc(II) complexes appropriate for evaluation excited-state dipolar properties.

4. Experimental

4.1. General procedures and starting materials

Electrospray mass spectra (ES-MS) were recorded on a ThermoFinnigan LCQ Classic by direct injection into a flow of acetonitrile at 5 μl/min, needle voltage 3.5 kV, capillary voltage 30 V and capillary temperature 60 °C. Data was collected manually in Tune Plus and visualised in the Qual Browser of the Excalibur software. FAB-MS spectra were recorded on a VG Instruments 7070E instrument with a FAB inlet system. Infrared spectra were recorded in a Mattson FT-IR spectrometer as KBr disks. UV spectra were recorded on a Unicam apparatus. Elementary analyses were obtained in a Carlo Erba Elemental Analyser. ^{1}H NMR spectra were recorded at 25 °C on Jeol 270 GSX and Bruker Avance 400 spectrometers. ^{13}C NMR spectra were recorded at 67.5 MHz

on the Jeol 270 GSX instrument. All NMR spectra were referred to Me_4Si at δ 0.0 ppm. Except for diketone **2**, all starting materials and solvents were commercially available and used without further purification.

4.2. Syntheses

4.2.1. Ligand *1b*

To a solution of diketone **2** [8] (0.30 g, 1.0 mmol) in AcOH (15 ml) was added diaminomaleonitrile (0.10 g, 1.0 mmol). The reaction was refluxed for 1 h. Afterwards, the mixture was cooled to room temperature, the product extracted (CH_2Cl_2, 3×10 ml), the combined organic extracts were washed (H_2O, 3×10 ml), dried ($MgSO_4$) and the solvent removed by rotary evaporation at atmospheric pressure to give a brown solid. The product was purified by column chromatography (CH_2Cl_2:EtOAc 1:1, alumina, activity stage III) and recrystallized ($CHCl_3$/hexane) to afford colourless crystals in 67% yield. M.p. 185–186 °C; Calc. for $C_{21}H_{11}N_7$: C, 69.80; H, 3.07; N, 27.13. Found: C, 69.79; H, 3.02; N, 26.85; EI-MS (70 eV) m/z (relative intensity): 360 ([**1b**-H] $^+$, 100%); 283 ([**1b**-C_5H_4N] $^+$, 14%); 128 ($[C_8H_6N_2]^+$, 12%); 78 ($[C_5H_4N]^+$, 32%); ν(cm^{-1}) (KBr): 2362 (C≡N); 1562 (C=C); 669 (Ar–H); ^{1}H NMR ($CDCl_3$, 270 MHz) δ (ppm): 8.60 (1H, br d, $J = 4.9$ Hz, H6‴); 8.47 (1H, d, $J = 7.9$ Hz, H3′/H5′); 8.33 (1H, br d, $J = 4.7$ Hz, H6″); 8.23 (1H, d, $J = 7.7$ Hz, H5′/H3′); 8.07 (1H, d, $J = 7.9$ Hz, H3″); 8.05 (1H, t, $J = 7.8$ Hz, H4′); 7.94 (1H, d, t, $J = 1.6$ 7.7 Hz, H4″); 7.51 (1H, d, t, $J = 1.6$ 7.9 Hz, H4‴); 7.30–7.07 (2H, m, H5″, H5‴); 7.08 (1H, d, $J = 7.9$ Hz, H3‴); ^{13}C NMR ($CDCl_3$, 67.5 MHz) δ (ppm): 155.00 (1C, C); 154.78 (2C, C); 152.42 (1C, C); 152.28 (2C, C); 149.12 (1C, C); 149.05 (1C, C); 138.33 (1C, CH); 136.86 (1C, CH); 136.48 (1C, CH); 130.05 (1C, CH); 124.63 (1C, CH); 124.40 (2C, CH); 124.35 (1C, CH); 124.05 (1C, CH); 122.28 (1C, CH); 120.33 (1C, CH); 112.95 (2C, CN); λ_{max}(CH_3CN) (nm): 240 ($\log \varepsilon = 4.30$); 283 (4.35); 327 (4.11).

4.2.2. *1aZnCl$_2$*

From a stock solution of anhydrous $ZnCl_2$ (53.9 mg, 0.395 mmol) in MeCN (20.0 ml) was added 1.00 ml (0.0198 mmol $ZnCl_2$) to a solution of **1a** (6.15 mg, 0.0198 mmol) in $CHCl_3$ (1 ml). A white solid separated from solution. Further MeCN (2 ml) was added and the mixture heated to reflux for 1 h. The solvent was removed in vacuo and the residue recrystallized from hot nitromethane to give 7.1 mg (0.026 mmol, 80%) of clear, brick-shaped crystals after filtration and drying in vacuo. This material was also suitable for X-ray diffraction studies. M.p. 284 °C (decomp.); IR ν(cm^{-1}) (KBr): 1594 (m, C=C); 1456 (s, C=C); 783 (vs, Ar–H); Calc. for $C_{19}H_{13}Cl_2N_5Zn$: C, 50.98; H, 2.93; N, 15.65. Found: C, 50.88; H, 2.84; N, 15.31; FAB-MS (NBA) m/z 409.8 (**1a**$ZnCl^+$, 42%), 375.8 (**1a**Zn^+, 2%), 154 (NBA, 100%); ^{1}H NMR (400 MHz, CD_3NO_2) δ (ppm): 9.07 (d, $J = 2.5$ Hz, 1H, H-5/6), 9.01 (d, $J = 2.3$ Hz, 1H, H6/5), 8.94 (br d, $J = 5.0$ Hz, 1H, H6‴), 8.60 (br d, $J = 4.8$ Hz, 1H, H6″), 8.50 (d, t, $J = 0.8$, 8.1 Hz, 1H, H3′/5′), 8.50 (t,

Table 2
Crystal data, data collection parameters and details of structure refinement for **1a**$ZnCl_2$ and **1b**$ZnCl_2$

Substance	**1a**$ZnCl_2$	**1b**$ZnCl_2$
Crystal shape	pale yellow block	yellow block
Empirical formula	$C_{19}H_{13}Cl_2N_5Zn$	$C_{23}H_{17}Cl_2N_9O_4Zn$
M	447.61	619.73
Crystal size (mm)	$0.50 \times 0.30 \times 0.30$	$0.50 \times 0.50 \times 0.50$
System	monoclinic	triclinic
Space group	$P2_1/n$	$P\bar{1}$
a (Å)	7.6358(6)	9.7292(10)
b (Å)	12.4493(8)	11.8291(12)
c (Å)	18.9321(15)	12.1358(13)
α (°)	90	91.244(8)
β (°)	100.519(9)	106.679(9)
γ (°)	90	100.429(8)
U (Å^3)	1769.4(2)	1311.8(2)
Z	4	2
D_c (g cm^{-3})	1.680	1.569
T (K)	153(2)	293(2)
Θ range (°)	1.97–25.86	1.76–25.00
Measured, independent and observed reflections ($I > 2\sigma I$)	13070, 3415 and 2937	6477, 4224 and 3689
R_{int}	0.0515	0.0751
Data, restraints, parameters	3415, 0, 296	4224, 0, 354
Absorption correction	semi-empirical from equivalents	empirical
Final $R_1(I > 2\sigma I)$	0.0251 (wR_2 0.0628)	0.0631 (wR_2 0.1586)
H-locating and refining method	localized	calculated
Largest peak and hole (e Å^3)	+0.392 and −0.379	+0.921 and −1.087
Maximum and minimum transmission	0.566 and 0.411	0.755 and 0.325

$J = 7.8$ Hz, 1H, H3‴), 8.31 (d, t, $J = 1.6$, 8.0 Hz, 1H, H4″), 8.15 (d, t, $J = 1.5$, 7.8 Hz, 1H, H4″), 8.09–8.14 (m, 2H, H − 5′/3′, H4′), 7.86 (ddd, $J = 1.0$, 5.0, 8.6 Hz, 1H, H5‴), 7.62 (ddd, $J = 2.0$, 4.8, 6.8 Hz, 1H, H5″), 7.31 (dd, $J = 0.5$, 8.1 Hz, 1H, H3″).

4.2.3. *1bZnCl₂*

To a solution of **1b** (0.0124 g, 0.034 mmol) in degassed acetonitrile (2 ml) was added $ZnCl_2$ (0.004 g, 0.03 mmol) under N_2. After a few minutes, a white precipitate was formed. This mixture was refluxed for an hour then cooled to room temperature and the solvent evaporated to give a green solid. Recrystallization from hot nitromethane, followed by slow cooling over 24 h afforded colourless crystals suitable for X-ray diffraction studies. M.p. 290 °C (decomp.); $\nu(cm^{-1})$ (KBr): 1596 (C=C); 1574 (C=C); 785 (Ar–H); no absorptions from the nitrile groups were visibile; Calc. for $C_{21}H_{11}Cl_2N_7Zn(CH_3NO_2)$: C, 48.89%; H, 2.39%; N, 19.89%. Found: C, 48.71; H, 2.26; N, 19.63; ES-MS (CH_3COOH/MeCN) m/z (relative intensity): 462 ([**1b**ZnCl]$^+$, 25%), 785 ([**1b**$_2$Zn]$^+$, 100%); $\lambda_{max}(CH_3CN)$ (nm): 244 ($\log \varepsilon = 4.02$); 283 (3.99); 320 (3.93); ^{1}H NMR ($(CD_3)_2SO$, 270 MHz) δ (ppm) 8,61 (br d, $J = 4.7$ Hz, 1H, H6″), 8.41 (dd, $J = 1.9$, 7.2 Hz, 1H, H3′/5′), 8.34 (br d, $J = 5.1$ Hz, 1H, H6‴), 8.14–8.23 (m, 2H, H4′, H5′/3′), 8.04–8.12 (m, 2H, H3‴, H4‴), 7.67 (d, t, $J = 1.7$, 7.6 Hz, 1H, H4″), 7.35–7.44 (m, 2H, H5″, H5‴), 7.04 (d, $J = 8.0$ Hz, 1H, H3″).

4.3. Crystal structure determination and data collection

Data collection occurred on a Stoe Image Plate Diffraction system, using graphite-monochromated Mo Kα radiation ($\lambda = 0.71073$ Å). Image plate distance: 70 mm, ϕ oscillation scans 0–190°, step $\Delta\phi = 1°$. The structures were solved by direct methods (SHELXS-97) and refined anisotropically on F^2 (SHELXL-97). The crystal data and particulars associated with data collection and refinement for each structure are collected in Table 2.

5. Supplementary material

CCDC-219660 (**1a**$ZnCl_2$) and CCDC-219661 (**1a**$ZnCl_2$) contain the supplementary crystallographic data for this paper. These data can be obtained free of charge at http://www.ccdc.cam.ac.uk/conts/retrieving.html or from the Cambridge Crystallographic Data Centre, 12 Union Road, Cambridge CB2 1EZ, UK (fax: +44-1223-336033; e-mail: deposit@ccdc.cam.ac.uk).

Acknowledgements

We are grateful to the Engineering and Physical Sciences Research Council (EPSRC) for financial support (Grant R/R09138) and the Treubel-Fond (Universität Basel) for partial support of this work. We thank Prof. A. von Zelewsky (University of Fribourg) for his interest and support, as well as Drs. K. Howland and D. Smith (both University of Kent) and Mr. F. Nydegger (University of Fribourg) for assistance in the acquisition of spectra. Our thanks also go out to Prof. H. Stoeckli-Evans (Universite de Neuchâtel) for supporting the X-ray data acquisitions and the EPSRC Mass Spectrometry Centre for analytical support.

References

[1] F. Heirtzler, T. Weyhermüller, J. Chem. Soc., Dalton Trans. (1997) 3653.
[2] T. Bark, T. Weyhermüller, F. Heirtzler, Chem. Commun. (1998) 1475.
[3] P.J. Cragg, F.R. Heirtzler, M.J. Howard, I. Prokes, T. Weyhermüller, in press.
[4] F. Heirtzler, S.I.G. Dias, M. Neuburger, in press.
[5] F.R. Heirtzler, M. Neuburger, M. Zehnder, E.C. Constable, Liebigs Ann.-Recl. (1997) 297.
[6] F.R. Heirtzler, Chimia 53 (1999) 204.
[7] F. Heirtzler, M. Neuberger, K. Kulike, J. Chem. Soc., Perkin Trans. 1 (2002) 809.
[8] F.R. Heirtzler, Synlett (1999) 1203.
[9] D. Roberto, F. Tessore, R. Ugo, S. Bruni, A. Manfredi, S. Quici, Chem. Commun. (2002) 846.
[10] A. Hilton, T. Renouard, O. Maury, H. Le Bozec, I. Ledoux, J. Zyss, Chem. Commun. (1999) 2521.
[11] W.B. Lin, L. Ma, O.R. Evans, Chem. Commun. (2000) 2263.
[12] T. Salditt, Q.R. An, A. Plech, J. Peisl, C. Eschbaumer, C.H. Weidl, U.S. Schubert, Thin Solid Films 354 (1999) 208.
[13] S. Aitipamula, P.K. Thallapally, R. Thaimattam, M. Jaskolski, G.R. Desiraju, Org. Lett. 4 (2002) 921.
[14] G.R. Desiraju, J. Mol. Struct. 374 (1998) 191.
[15] S.P. Anthony, T.P. Radhakrishnan, Chem. Commun. (2001) 931.
[16] A. Jouaiti, M.W. Hosseini, N. Kyritsakas, Chem. Commun. (2002) 1898.
[17] A. Neels, H. Stoeckli-Evans, Inorg. Chem. 38 (1999) 6164.
[18] T. Bark, M. Duggeli, H. Stoeckli-Evans, A. von Zelewsky, Angew. Chem., Int. Ed. 40 (2001) 2848.
[19] J.D. Wright, Molecular Crystals, Cambridge University Press, Cambridge, 1995.
[20] A. Bilyk, M.M. Harding, P. Turner, T.W. Hambley, J. Chem. Soc., Dalton Trans. (1994) 2783.
[21] A. Bilyk, M.M. Harding, P. Turner, T.W. Hambley, J. Chem. Soc., Dalton Trans. (1995) 2549.
[22] C.E. Housecroft, A.G. Sharpe, Inorganic Chemistry, Prentice Hall, Harlow, 2000.
[23] D.S. Reddy, Y.E. Ovchinnikov, O.V. Shishkin, Y.T. Struchkov, G.R. Desiraju, J. Am. Chem. Soc. 118 (1996) 4085.
[24] B.L.V. Prasad, H. Sato, T. Enoki, S. Cohen, T.P. Radhakrishnan, J. Chem. Soc., Dalton Trans. (1999) 25.
[25] J.H. Kim, S.R. Shin, M. Matsuoka, K. Fukunishi, Dyes Pigm. 41 (1999) 183.
[26] J.Y. Jaung, M. Matsuoka, K. Fukunishi, Synthesis (1998) 1347.
[27] R. Taylor, O. Kennard, J. Am. Chem. Soc. 104 (1982) 5063.
[28] C.A. Hunter, J.K.M. Sanders, J. Am. Chem. Soc. 112 (1990) 5525.
[29] F.R. Heirtzler, M. Neuburger, M. Zehnder, S.J. Bird, K.G. Orrell, V. Sik, J. Chem. Soc., Dalton Trans. (1999) 565.
[30] F. Heirtzler, P. Jones, M. Neuburger, M. Zehnder, Polyhedron 18 (1999) 601.

Available online at www.sciencedirect.com
SCIENCE DIRECT®
Polyhedron 23 (2004) 1019–1025
POLYHEDRON
www.elsevier.com/locate/poly

Copper(II) and zinc(II) complexes of amide pendant-armed cross-bridged tetraamine ligands

Weijun Niu [a], Edward H. Wong [a,*], Gary R. Weisman [a,*], Lev N. Zakharov [b], Chris D. Incarvito [c], Arnold L. Rheingold [b]

[a] Department of Chemistry, Parsons Hall, University of New Hampshire, Durham, NH 03824-3598, USA
[b] Department of Chemistry and Biochemistry, University of California, San Diego, La Jolla, CA 92093-0358, USA
[c] Department of Chemistry and Biochemistry, University of Delaware, Newark, DE 19716, USA

Received 11 August 2003; accepted 23 December 2003

Abstract

Copper(II) and zinc(II) complexes of cross-bridged cyclam and cyclen with primary amide pendant arms (ligands **1** and **2**) have been prepared and structurally characterized. The copper complex of cyclam-derived **1** has a Jahn–Teller distorted Cu(II) octahedral coordination geometry with both amide arms coordinated through the carbonyl oxygens. The Cu(II) complex of the cyclen analogue **2** has been found to exist in three slightly different forms. Both zinc complexes also adopt full N_4O_2 coordination from these potentially hexadentate cross-bridged ligands. These structural data confirm the exclusive *cis*-folded ligand configuration in all four complexes as well as the significantly better fit of ligand **1** towards both Cu(II) and Zn(II) cations when compared to **2**. The complexes of **1** provide the first examples of a [2233]/[2233] cross-bridged cyclam conformation, as opposed to the previously observed [2323]/[2323] conformation.
© 2004 Elsevier Ltd. All rights reserved.

1. Introduction

Polyazamacrocylic complexes of copper(II) and zinc(II) are of relevance in coordination, catalytic, biological, as well as radiopharmaceutical chemistry [1–4]. We have designed, prepared and studied ethylene cross-bridged cyclam and cyclen ligands (Fig. 1) and their derivatives [5], which have proven to be excellent chelators for a variety of metal ions including Cu(II) and Zn(II) [6–8]. Others have also taken up the study of the coordination chemistry of these interesting ligands [9]. An excellent review of the area by Springborg has recently appeared [10]. The enhanced resistance of the metal complexes of these ligands towards common decomplexation pathways when compared to unbridged tetraamine macrocycles have been amply confirmed [9,11]. This kinetic inertness can be of major significance in their potential applications [12]. A further augmentation of this desirable property can be achieved through attachment of coordinating pendant arms at the two secondary amine sites. Both cyclam and cyclen ligands with amide pendant arms have already received much attention in MRI and biomimetic research areas [2,13–16]. We have previously reported a synthesis of the first copper complex of a diamide-armed cross-bridged cyclam, **1** (4,11-bis(carbamoylmethyl)-1,4,8,11-tetraazabicyclo[6.6.2]hexadecane) [7]. Herein we present the synthesis, spectral, and structural characterization of the Cu(II) and Zn(II) complexes of **1** and its cyclen analogue **2** (4,10-bis(carbamoylmethyl)-1,4,7,10-tetraaazabicyclo[5.5.2]tetradecane) (Fig. 1).

2. Experimental

Ligand **1** was prepared as described previously [7]. Ligand **2**, which has been described in the patent literature [17], was prepared by a variation of our general approach [6,7]. All other reagents and solvents were obtained commercially and used without further

* Corresponding authors. Tel.: +1-603-862-1788/2304; fax: +1-603-862-4278.
E-mail addresses: ehw@cisunix.unh.edu (E.H. Wong), gary.weisman@unh.edu (G.R. Weisman).

0277-5387/$ - see front matter © 2004 Elsevier Ltd. All rights reserved.
doi:10.1016/j.poly.2003.12.017

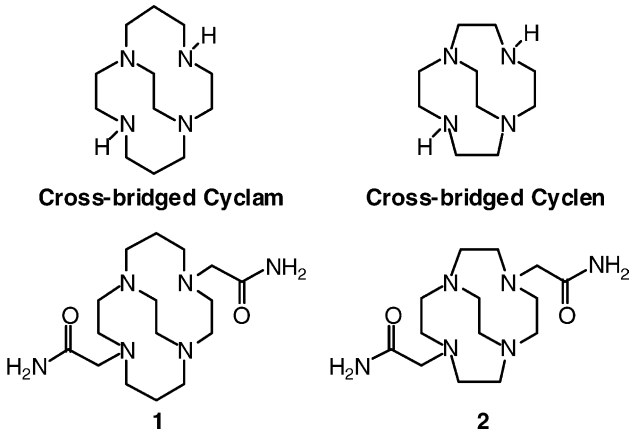

Fig. 1. Cross-bridged cyclam, cross-bridged cyclen, and ligands **1** and **2**.

purification. Reactions were performed under a nitrogen atmosphere. Recrystallizations, however, were carried out in closed containers without special precautions to exclude either air or moisture. Electronic spectra were run on a Cary 5E spectrophotometer while ^{1}H and ^{13}C NMR data were collected on either a Bruker AM-360 or Varian Inova-400 spectrometer. FT-IR (KBr) of the complexes were recorded on a Nicolet MX-1 FT spectrophotometer. Elemental analysis were performed by Atlantic Microlab, Norcross, GA.

2.1. $[Cu \cdot \mathbf{1}](NO_3)_2$

A mixture of $\mathbf{1} \cdot (H_2O)_{0.5}$ (136.9 mg, 0.392 mmol) and $Cu(NO_3)_2 \cdot 3H_2O$ (95.8 mg, 0.397 mmol) in MeOH (16 mL) was refluxed for 17 h to form a dark-blue MeOH solution and some bluish brown precipitate. The MeOH solution was isolated by centrifugation. Et_2O vapor diffusion into this solution yielded 138.7 mg of a blue crystalline solid, which was dissolved in H_2O/MeOH (1:1) and diffused by acetone vapor to form blue crystals. Electronic spectrum (H_2O): $\lambda_{max}(\varepsilon) = 286$ nm (1.348 M^{-1} cm^{-1}), 625 (34 M^{-1} cm^{-1}). IR (KBr): 3285, 3139 cm^{-1} (ν_{OH} and ν_{NH}), 1678(s) $\nu_{C=O}$, 1604 (medium) cm^{-1}. *Anal.* Calc. for $CuC_{16}H_{32}N_6O_2(NO_3)_2H_2O$: C, 35.19; H, 6.28; N, 20.52. Found: C, 34.93; H, 6.24; N, 20.32%.

2.2. $[Cu \cdot \mathbf{2}](ClO_4)_2$

A mixture of ligand $\mathbf{2} \cdot H_2O$ (16.8 mg, 0.0508 mmol) and $Cu(ClO_4)_2 \cdot 6H_2O$ (22.1 mg, 0.0596 mmol) in MeOH (11 mL) was refluxed for 1 day. After cooling to room temperature, this solution was diffused with Et_2O vapor to yield 21.0 mg (72%) of blue crystals. Electronic spectrum (H_2O): $\lambda_{max}(\varepsilon) = 283$ nm (3.351 M^{-1} cm^{-1}), 633 nm (76 M^{-1} cm^{-1}). IR (KBr): 3439, 3359, 3309, 3256 cm^{-1} (ν_{OH} and ν_{NH}), 1682(s), 1661(s) cm^{-1} $\nu_{C=O}$, 1612 (medium), 1593 (medium) cm^{-1} ($\nu_{C=O}$ or NH_2bending). *Anal.* Calc. for $CuCl_2C_{14}H_{28}N_6O_{10}$: C, 29.25; H, 4.91; N, 14.62. Found: C, 29.09; H, 5.19; N, 14.59%.

2.3. $[Zn \cdot \mathbf{1}](ClO_4)_2$

To a MeOH solution (5 mL) of $\mathbf{1} \cdot (H_2O)_{0.5}$ (46.3 mg, 0.132 mmol) which was about 95% pure, a MeOH solution (6 mL) of $Zn(ClO_4)_2 \cdot 6H_2O$ (50.3 mg, 0.135 mmol) was added. This resulting solution was refluxed for 27 h to form a cloudy solution. This solution was then centrifuged to remove the white precipitate. Et_2O vapor diffusion into this supernatant yielded 52.9 mg of a white solid, which was recrystallized from acetone and washed by $CHCl_3$. Then it was redissolved in MeCN and ether diffused into this solution to form pure $[Zn \cdot \mathbf{1}](ClO_4)_2$ as needle-shaped crystals (15.6 mg, 20%). IR (KBr): 3442, 3337, 3293 and 3232 cm^{-1} (ν_{OH} and ν_{NH}), 1673, 1659 cm^{-1} ($\nu_{C=O}$), 1590 cm^{-1} (w, NH_2 bending). ^{1}H NMR in CD_3CN: δ 7.31(2H, s, NH_2), 6.94 (2H, s, NH_2), 3.66 (2H, br A of AB in CH_2CONH_2 arms), 3.47 (2H, B of AB in CH_2CONH_2 arms), 3.35–3.44 (2H, m) 3.15–3.29 (4H, m), 3.08 (4H, broad td, $J = 12.9$, 2.4 Hz), 2.59–2.87 (10H, m), 2.17–2.31 (2H, m, β-CH_{ax}), 1.68 (2H, dp, $J = 17.6$, 2.5 Hz, β $CH_{eq}H$); $^{13}C\{^{1}H\}$ data in CD_3CN: δ 176.88, 62.13, 60.68, 59.71, 58.53, 52.35, 51.52, 23.80. *Anal.* Calc. for $ZnC_{16}H_{32}N_6O_2(ClO_4)_2$: C, 31.78; H, 5.33; N, 13.90. Found: C, 31.99; H, 5.39; N, 13.78%.

2.4. $[Zn \cdot \mathbf{2}](ClO_4)_2$

A mixture of ligand $\mathbf{2} \cdot H_2O$ (74.1 mg, 0.224 mmol) in MeOH (5 mL) and $Zn(ClO_4)_2 \cdot 6H_2O$ (84.0 mg, 0.226 mmol) in MeOH (2 mL) was refluxed for one day. After cooling to room temperature, needle-shaped crystals (53.0 mg) grew out and were centrifuged from this solution. Ether was diffused into the supernatant to produce another 27.2 mg of colorless crystals. The combined yield was 62%. IR (KBr): 3413, 3370, 3296, 3241 cm^{-1} (ν_{NH} or ν_{OH}), 1682(s), 1663(s) cm^{-1} ($\nu_{C=O}$ stretches) 1597 (medium) cm^{-1} (OH or NH_2 bending). ^{1}H NMR of N-deuterated complex in CD_3OD: δ 3.94 (4H, s, CH_2COND_2), 3.32–3.49 (8H, m), 3.11 (4H, s, cross-bridging CH_2CH_2), 3.05 (4H, dd, $J = 12.1$, 4.8 Hz), 2.94 (4H, td, $J = 12.3$, 7.1 Hz); in D_2O (400 MHz): δ 3.98 (4H, s, CH_2COND_2), 3.38 (8H, br dd, $J = 9.4$, 3.0 Hz), 3.07 (4H, s, cross-bridging CH_2CH_2), 2.89–3.06 (8H, m); $^{13}C\{^{1}H\}$ NMR in CD_3OD (N–D complex): δ 177.90, 63.08, 61.73, 57.81, 50.58; in D_2O (N–D complex):δ 77.09, 62.27, 60.98, 56.73, 49.98. *Anal.* Calc. for $ZnCl_2C_{14}H_{28}N_6O_{10}$: C, 29.16; H, 4.89; N, 14.57. Found: C, 29.23; H, 4.98; N, 14.31%.

2.5. X-ray crystal structure determination

Diffraction intensity data were collected with a Siemens P4/CCD ($[Zn \cdot \mathbf{1}](ClO_4)_2$ and $[Zn \cdot \mathbf{2}](ClO_4)_2$) and a Bruker Smart Apex CCD ($[Cu \cdot \mathbf{1}](NO_3)_2$ and $[Cu \cdot \mathbf{2}](ClO_4)_2$) diffractometers. Crystal data, data col-

Table 1
Crystal data, data collection, and refinement parameters

	$[Cu \cdot \mathbf{1}](NO_3)_2 \cdot (CH_3OH) \cdot (H_2O)$	$[Cu \cdot \mathbf{2}](ClO_4)_2 \cdot 0.3(CH_3OH)$	$[Zn \cdot \mathbf{1}](ClO_4)_2$	$[Zn \cdot \mathbf{2}](ClO_4)_2$
Chemical formula	$C_{17}H_{38}CuN_8O_{10}$	$C_{14.33}H_{29.33}CuCl_2N_6O_{10.33}$	$C_{16}H_{32}Cl_2N_6O_{10}Zn$	$C_{14}H_{28}Cl_2N_6O_{10}Zn$
Color and habit	blue block	blue block	colorless needle	colorless block
Size (mm)	$0.20 \times 0.25 \times 0.35$	$0.10 \times 0.30 \times 0.40$	$0.10 \times 0.10 \times 0.25$	$0.20 \times 0.30 \times 0.50$
Crystal system	monoclinic	monoclinic	monoclinic	monoclinic
Space group	$C2/c$	$P2_1/c$	$C2/c$	$P2_1/c$
a (Å)	17.2993(8)	23.287(2)	21.491(14)	8.9473(5)
b (Å)	14.9664(7)	15.4289(14)	9.282(7)	18.6467(10)
c (Å)	18.9985(9)	18.1376(17)	15.388(11)	13.3839(7)
α (°)	90.00	90.00	90.00	90.00
β (°)	106.3400(10)	106.845(2)	131.588(10)	93.8770(10)
γ (°)	90.00	90.00	90.00	90.00
Z, Z'	8, 1	12, 3	4, 0.5	4, 1
λ (Å)	0.71073 (Mo Kα)	0.71073 (Mo Kα)	0.71073 (Mo Kα)	0.71073 (Mo Kα)
T (K)	150(2)	153(2)	223(2)	173(2)
Reflections independent	5507 [$R_{int} = 0.0229$]	14495 [$R_{int} = 0.0206$]	1660 [$R_{int} = 0.0312$]	5130 [$R_{int} = 0.0269$]
Reflections with $I > 2\sigma(I)$	4580	12680	1428	4259
Parameters	426	861	223	298
R (observed data)[a]	0.0456	0.0394	0.0276	0.0513
$R(\omega F^2)$ (observed data)[b]	0.1235	0.1274	0.0738	0.1260

[a] $R = \sum \|F_o| - |F_c\| / \sum |F_o|$.
[b] $R(\omega F^2) = \{\sum[\omega(F_o^2 - F_c^2)^2] / \sum[\omega(F_o^2)^2]\}^{1/2}$; $\omega = 1/[\sigma^2(F_o^2) + (aP)^2 + bP]$, $P = [2F_c^2 + \max(F_o, 0)]/3$.

lection, and refinement parameters are given in Table 1. The structure was solved using direct methods, completed by subsequent difference Fourier syntheses, and refined by full matrix least-squares procedures on F^2. SADABS absorption correction was applied for all data. All non-hydrogen atoms were refined with anisotropic displacement coefficients. In $[Cu \cdot \mathbf{2}](ClO_4)_2$ and $[Zn \cdot \mathbf{2}](ClO_4)_2$ the positions of the H atoms were calculated and in $[Cu \cdot \mathbf{1}](NO_3)_2$ and $[Zn \cdot \mathbf{1}](ClO_4)_2$ the H atoms were found on the difference F-map and refined with isotropic thermal parameters. In $[Cu \cdot \mathbf{1}](NO_3)_2$ disordered solvent molecules (CH_3OH and H_2O) non-involved in coordination of the main molecule were treated by SQUEEZE (Van der Sluis, P., Spek, A.L., Acta Crystallogr., Sect. A 46 (1990) 194–201). Correction of the X-ray data by SQUEEZE (107 electron/cell) was close to the required values (107 electron/cell). All software and sources of scattering factors are contained in the SHELXTL (5.10) program package (G. Sheldrick, Bruker XRD, Madison, WI).

3. Results and discussion

3.1. Synthesis and spectral characterization

Both zinc(II) and copper(II) complexes of ligands **1** and **2** were readily prepared from respective metal salts and ligand in methanol. Diethyl ether diffusion into methanol or acetonitrile solutions of the crude products yielded X-ray quality crystals.

Infra-red spectra of all four complexes feature amide carbonyl stretching bands between 1659 and 1682 cm^{-1}. These data are consistent with O-coordination of the amide pendant arms in the solid-state [18–21] as confirmed by their X-ray structures presented below. Electronic spectra of the copper complexes reveal a charge-transfer as well as a broad d–d band for both $[Cu \cdot \mathbf{1}](NO_3)_2$ (λ_{max} (H_2O) 286 and 625 nm) and $[Cu \cdot \mathbf{2}](ClO_4)_2$ (λ_{max} (H_2O) 283 and 633 nm).

Solution NMR spectra of the zinc complexes confirmed the existence of a single isomer in each case. The $^{13}C\{^1H\}$ NMR spectrum of $[Zn \cdot \mathbf{1}](ClO_4)_2$ contains only eight resonances, consistent with a C_2-symmetric solution species. $[Zn \cdot \mathbf{2}](ClO_4)_2$ exhibits only five distinct

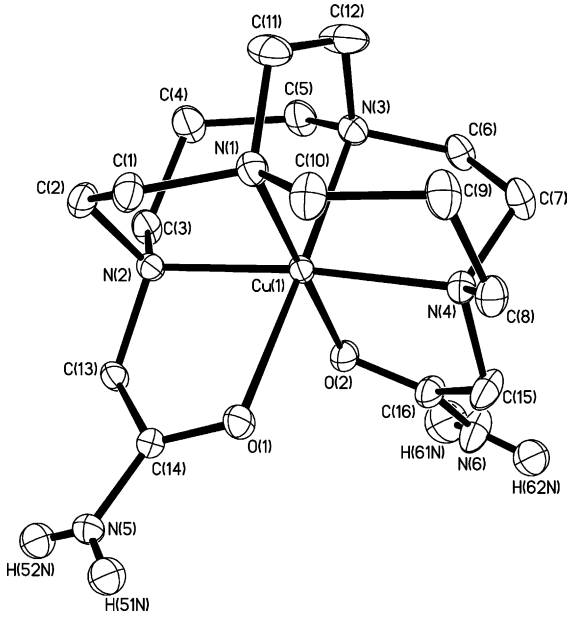

Fig. 2. Molecular structure of $[Cu \cdot \mathbf{1}](NO_3)_2$. Nitrate anions and hydrogens omitted except on the amide nitrogens.

Table 2
Selected bond distances (Å) and bond angles (°) for $[Cu \cdot \mathbf{1}](NO_3)_2$

Cu(1)–O(1)	2.2643(18)	O(1)–Cu(1)–O(2)	89.93(7)
Cu(1)–O(2)	2.0423(19)	N(1)–Cu(1)–O(2)	179.09(8)
Cu(1)–N(1)	2.043(2)	N(2)–Cu(1)–N(4)	174.38(8)
Cu(1)–N(2)	2.044(2)	N(3)–Cu(1)–O(1)	177.64(8)
Cu(1)–N(3)	2.178(2)	N(1)–Cu(1)–N(2)	86.98(8)
Cu(1)–N(4)	2.061(2)	N(1)–Cu(1)–N(4)	97.44(8)
		N(1)–Cu(1)–N(3)	86.93(9)
		N(2)–Cu(1)–N(3)	98.50(8)
		N(3)–Cu(1)–N(4)	85.24(8)

SD in parentheses.

^{13}C resonances and has singlet ^{1}H resonances for both its cross-bridging ethylene and pendant-arm methylene protons in accord with C_{2v} symmetry in solution. Since retention of the solid-state structure (vide infra) of $[Zn \cdot \mathbf{2}](ClO_4)_2$ in solution would result in only C_2 spectral symmetry, the observed NMR data require onset of dynamic enantiomerization, a process which might or might not involve dissociation of one or more amide pendant arms from the zinc. Proton spectra obtained down to −80 °C revealed extensive signal broadening but unfortunately no slow-exchange data were accessible to allow further delineation of this process.

3.2. X-ray structures

The X-ray structure of $[Cu \cdot \mathbf{1}](NO_3)_2$ reveals a fully enveloped metal center with both amide pendant arms coordinated through their oxygens (Fig. 2). Important bond angles and distances are listed in Table 2. The familiar Jahn–Teller elongation of six-coordinated Cu(II) is manifested along the O(1)–Cu(1)–N(3) axis. Thus the Cu(1)–O(1) bond at 2.264(2) Å is significantly longer than the Cu(1)–O(2) distance of 2.042(2) Å. Similarly, the Cu(1)–N(3) bond-length of 2.178(2) Å can be contrasted with the shorter Cu(1)–N(1) bond at 2.043(2) Å. In the reported structure of the carboxylate-armed analogue of this complex, a similar elongation is observed along one O–Cu–N axis [7]. The good fit of

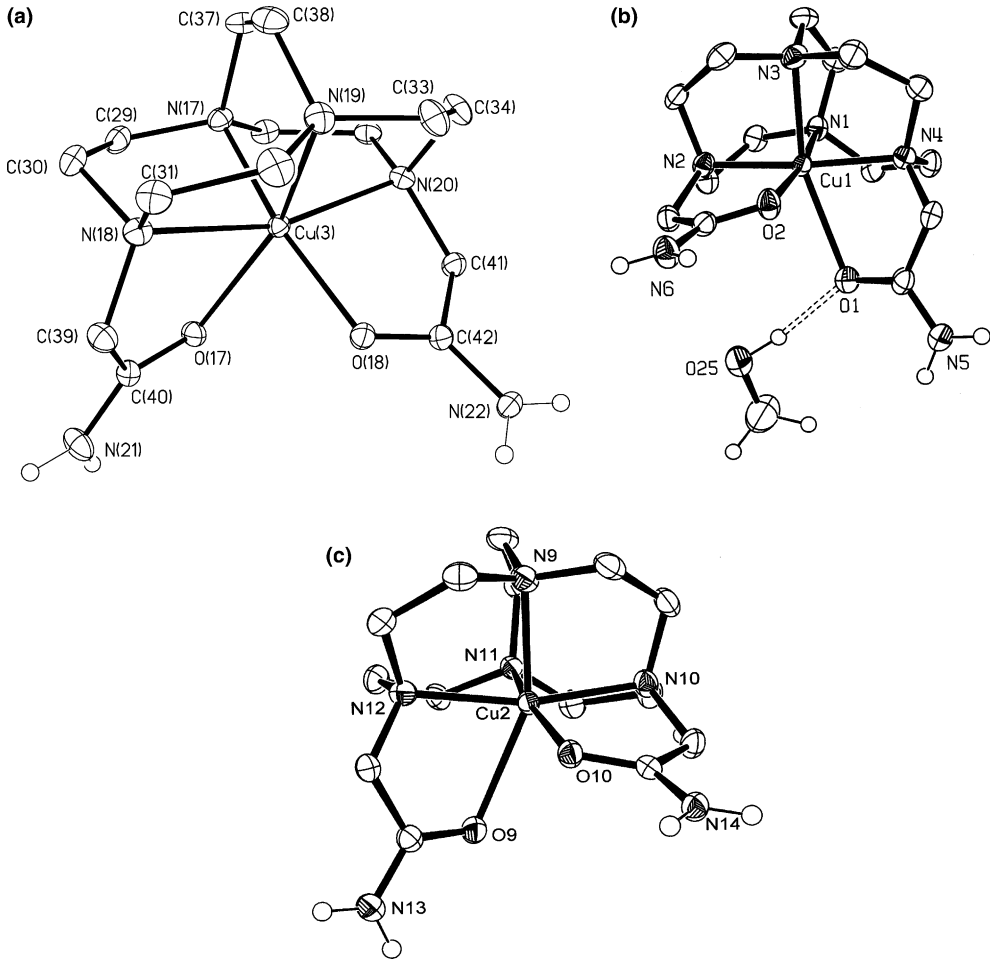

Fig. 3. (a)The first structure of $[Cu \cdot \mathbf{2}](ClO_4)_2$. Perchlorate anions and hydrogens omitted except on the amide nitrogens. (b) The second structure of $[Cu \cdot \mathbf{2}](ClO_4)_2$. Perchlorate anions and hydrogens omitted except on the methanol and amide nitrogens. (c) The third structure of $[Cu \cdot \mathbf{2}](ClO_4)_2$. Perchlorate anions and hydrogens omitted except on the amide nitrogens.

Cu(II) inside the cleft of ligand **1** is confirmed by the near-linear bond angles for N(2)–Cu(1)–N(4) of 185.62(8)°, N(3)–Cu(1)–O(1) of 177.64(8)°, and N(1)–Cu(1)–O(2) of 179.09(8)°. Most literature reports of copper(II) complexes of carbamoylmethyl-armed cyclam and cyclam derivatives have the common *trans-III* configuration and feature axially coordinated amide oxygens [21–23].

Three distinct forms of the $[Cu \cdot \mathbf{2}](ClO_4)_2$ complex are found in its X-ray structure. The first is a direct analogue of the $[Cu \cdot \mathbf{1}](NO_3)_2$ structure featuring full envelopment of the Cu(3) center within the ligand's N_4O_2 donor set (Fig. 3(a)). The Jahn–Teller elongation is along the O(17)–Cu(3)–N(19) axis with long Cu–O (2.231(2) Å) and Cu–N (2.156(2) Å) bonds. The significantly poorer fit of six-coordinate Cu(II) inside the cyclen-derived **2** is revealed in the non-linear bond angles for N(18)–Cu(3)–N(20) of 162.20(7)°, N(19)–Cu(3)–O(17) of 156.87(7)°, and N(17)–Cu(3)–O(18) of 167.62(7)°. The other two structural forms of $[Cu \cdot \mathbf{2}](ClO_4)_2$ both feature more substantial Jahn–Teller elongations with significantly longer axial Cu–O bonds of 2.465(2) and 2.445(2) Å as well as Cu–N bonds of 2.194(2) and 2.176(2) Å, respectively (Figs. 3(b) and (c)). A noteworthy difference between these two structures is the presence of H-bonding between the more loosely coordinated amide oxygen and a methanol solvent molecule in one of them (Fig. 3(b)). Other relevant structural data of all three Cu(II) coordination spheres are listed in Table 3. Surprisingly, no previous structural reports of carbamoylmethyl-functionalized cyclen Cu(II) complexes for comparison purposes are found in a search of the *Cambridge Structural Database*. A single 2-carbamoylethyl-armed cyclen Cu(II) complex has the ligand in the familiar *trans-I* configuration with only a single coordinated amide arm [20].

Overall the X-ray structure of $[Zn \cdot \mathbf{1}](ClO_4)_2$ is similar to that of $[Cu \cdot \mathbf{1}](NO_3)_2$ with the cation fully coordinated by the hexadentate ligand (Fig. 4). Important bond distances and angles are presented in Table 4. Here the complex has exact C_2 symmetry. The Zn(II) cation subtends an obtuse N(2)–Zn(1)–N(2A) angle of 183.9(1)° indicative of its being inside the ligand cleft. Other near-linear angles are O(1)–Zn(1)–N(1A) and O(1A)–Zn(1)–N(1) both at 176.9(7)°. The single structural report of a bis(carbamoylmethyl)-armed dibenzocyclam features a *trans-III* ligand configuration with axially coordinated amide oxygens [18].

The significantly poorer fit of six-coordinate Zn(II) inside ligand **2** in the structure of $[Zn \cdot \mathbf{2}](ClO_4)_2$ is

Table 3
Selected bond distances (Å) and bond angles (°) for the three forms of $[Cu \cdot \mathbf{2}](ClO_4)_2$

Cu(1)–N(2)	1.9696(17)	N(2)–Cu(1)–N(4)	173.02(8)
Cu(1)–N(4)	1.9885(18)	N(4)–Cu(1)–O(2)	103.27(7)
Cu(1)–O(2)	2.0223(16)	N(2)–Cu(1)–N(1)	87.92(7)
Cu(1)–N(1)	2.0439(18)	N(4)–Cu(1)–N(1)	85.62(8)
Cu(1)–N(3)	2.1935(19)	O(2)–Cu(1)–N(1)	171.06(7)
Cu(1)–O(1)	2.4650(16)	N(2)–Cu(1)–N(3)	88.34(7)
		N(4)–Cu(1)–N(3)	88.00(7)
Cu(2)–O(10)	1.9576(14)	O(10)–Cu(2)–N(11)	166.53(7)
Cu(2)–N(11)	1.9686(18)	N(11)–Cu(2)–N(10)	84.58(7)
Cu(2)–N(10)	2.0593(17)	O(10)–Cu(2)–N(12)	104.43(6)
Cu(2)–N(12)	2.1021(19)	N(11)–Cu(2)–N(12)	87.60(7)
Cu(2)–N(9)	2.1763(19)	N(10)–Cu(2)–N(12)	165.80(7)
Cu(2)–O(9)	2.4450(14)	N(11)–Cu(2)–N(9)	87.01(7)
		N(10)–Cu(2)–N(9)	85.91(7)
		N(12)–Cu(2)–N(9)	81.86(7)
Cu(3)–O(18)	1.9524(15)	O(18)–Cu(3)–N(17)	167.62(7)
Cu(3)–N(17)	1.9625(18)	N(17)–Cu(3)–N(20)	84.03(7)
Cu(3)–N(20)	2.0926(18)	N(17)–Cu(3)–N(19)	87.47(7)
Cu(3)–N(19)	2.1556(19)	N(20)–Cu(3)–N(19)	84.56(7)
Cu(3)–N(18)	2.172(2)	N(17)–Cu(3)–N(18)	85.80(7)
Cu(3)–O(17)	2.2306(16)	N(20)–Cu(3)–N(18)	162.20(7)
		N(19)–Cu(3)–N(18)	80.42(7)
		N(19)–Cu(3)–O(17)	156.87(7)

SD in parentheses.

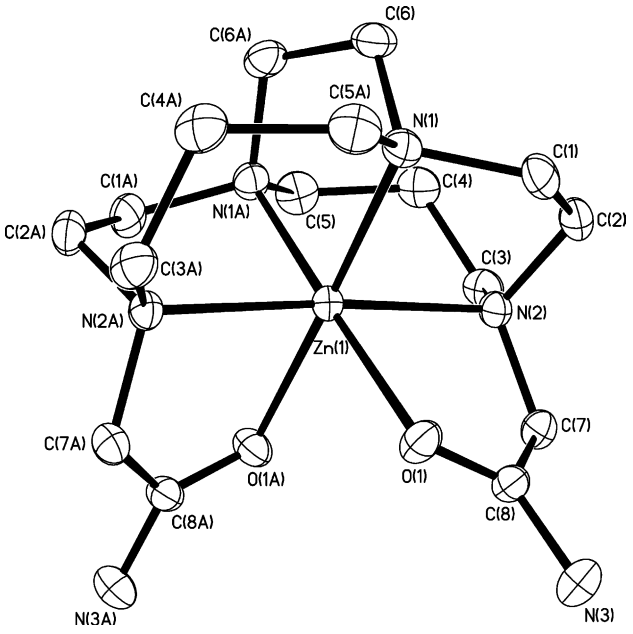

Fig. 4. Molecular structure of $[Zn \cdot \mathbf{1}](ClO_4)_2$ with counterions and hydrogens omitted.

Table 4
Selected bond distances (Å) and bond angles (°) for $[Zn \cdot \mathbf{1}](ClO_4)_2$

Zn(1)–N(1)	2.087(2)	N(1)–Zn(1)–N(1A)	86.36(14)
Zn(1)–N(1A)	2.087(2)	N(1)–Zn(1)– O(1A)	176.91(7)
Zn(1)–O(1)	2.099(2)	N(1A)– Zn(1)–O(1)	176.91(7)
Zn(1)–O(1A)	2.099(2)	O(1)– Zn(1)–O(1A)	85.10(13)
Zn(1)–N(2A)	2.147(3)	N(1)– Zn(1)–N(2)	97.36(10)
Zn(1)–N(2A)	2.147(3)	N(1)– Zn(1)–N(2)	85.48(9)
		N(1)–Zn(1)–N(2)	97.36(10)
		N(2)–Zn(1)–N(2A)	176.13(11)

SD in parentheses.

clearly shown in Fig. 5. Here its protrusion from the ligand cleft is best gauged by its nonlinear N(2)–Zn(1)–N(4) angle of 159.1(1)°. Angles similarly severely distorted from ideal values are O(1)–Zn(1)–N(1) at 157.1(1)° and O(2)–Zn(1)–N(3) at 158.0(1)°. Other relevant structural data are presented in Table 5. Three structures have been reported for Zn(II) complexes of carbamoylmethyl-functionalized cyclen. Interestingly, each of these features a distinct coordination number ranging from five to six to seven [2,24,25]. The five-coordinate structure, however, contains a deprotonated amide nitrogen which is coordinating instead of the oxygen [24].

The conformation of the bicyclo[6.6.2] ligand backbone in the structures of $[Cu \cdot \mathbf{1}](NO_3)_2$ and $[Zn \cdot \mathbf{1}](ClO_4)_2$ was a surprise. Instead of the [2323]/[2323] distorted diamond-lattice conformation that has been observed in all previously published structures of complexes of cross-bridged cyclams, these structures exhibit a new [2233]/[2233] bicyclic conformation. In this conformation, the ethylene cross-bridge torsion angle is of opposite sign and each of the 10-rings is in the quadrangular [2233] conformation [26,27]. As a result, the axial (non-bridgehead) nitrogen lone pairs tend to cant in toward the cleft, making this a slightly more convergent conformation in our estimation. Indeed, both structures exhibit slightly concave N(axial)–M–N(axial) angles. We had been aware of this possibility for some time on the basis of Monte Carlo searches of conformational space of cross-bridged cyclam ligands, but such studies using a variety of force fields also showed the [2233]/[2233] conformation to be higher in steric energy than the [2323]/[2323] conformation by several kcal/mol. Preliminary molecular mechanics (*PCModel* v.8, Serena Software, Bloomington, IN, 2003) suggest that this is also true for the pendant-arm ligand **1** in the complexing conformation of $[Zn \cdot \mathbf{1}](ClO_4)_2$. Why then the adoption of this conformation in both Cu and Zn complexes? We hypothesize that this conformation allows the carbonyls of the relatively short carbamoylmethyl arms to better reach the metals for efficient ligation.

We believe that these structural data confirming the coordination of both pendant amide arms of ligands **1** and **2** with both Cu(II) and Zn(II) anticipate enhanced inertness towards decomplexation. Further, it is expected that the better fit of ligand **1** than **2** should be reflected in relative kinetic stabilities. Relevant studies of pendant-armed cross-bridged ligand complexes of main group and transition metals are in progress.

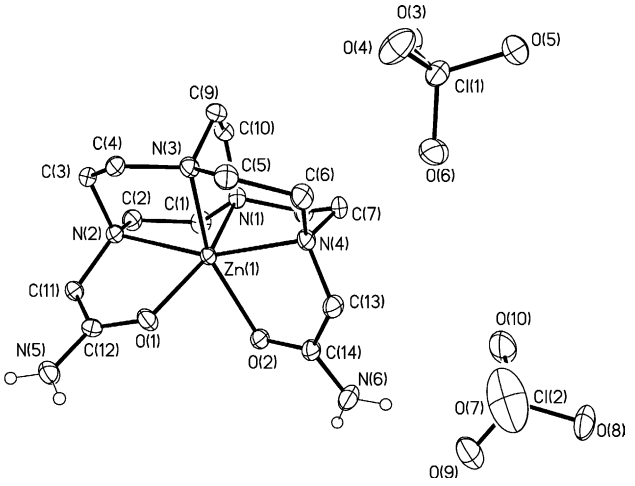

Fig. 5. Molecular structure of $[Zn \cdot \mathbf{2}](ClO_4)_2$ with hydrogens omitted except on the amide nitrogens.

Table 5
Selected bond distances (Å) and bond angles (°) for $[Zn \cdot \mathbf{2}](ClO_4)_2$

Zn(1)–O(1)	2.016(2)	O(1)–Zn(1)–N(1)	157.07(10)
Zn(1)–N(1)	2.076(3)	O(1)–Zn(1)–N(3)	100.39(11)
Zn(1)–N(3)	2.107(3)	N(1)–Zn(1)–N(3)	85.48(11)
Zn(1)–O(2)	2.167(2)	N(3)–Zn(1)–O(2)	158.02(10)
Zn(1)–N(4)	2.172(3)	O(1)–Zn(1)–N(4)	117.38(10)
Zn(1)–N(2)	2.244(3)	N(1)–Zn(1)–N(4)	85.35(10)
		N(3)–Zn(1)–N(4)	80.79(10)
		O(2)–Zn(1)–N(4)	77.53(9)
		O(1)–Zn(1)–N(2)	78.75(9)
		N(1)–Zn(1)–N(2)	79.97(10)
		N(3)–Zn(1)–N(2)	83.34(10)
		O(2)–Zn(1)–N(2)	118.58(9)
		N(4)–Zn(1)–N(2)	159.14(10)

SD in parentheses.

4. Supplementary data

Additional details of the crystal structural determinations and data tables have been deposited at the Cambridge Crystallographic Data Centre (CCDC Nos. 215754–215757). Copies of this information may be obtained free of charge from the Director, CCDC, 12 Union Road, Cambridge, CB2 1EZ, UK (Fax: +44-1223-336-033; e-mail: deposit@ccdc.ac.uk or www: http://www.ccdc.cam.ac.uk).

Acknowledgements

Financial support of this research was from NIH Grants CA93375 and GM55916-01 at UNH and an NSF instrumentation grant at the University of Delaware.

References

[1] C.J. Anderson, F. Dehdashti, P.D. Cutler, S.W. Schwarz, R. Laforest, L.A. Bass, J.S. Lewis, D.W. McCarthy, J. Nucl. Med. 42 (2001) 213.
[2] S. Aoki, H. Kawatani, T. Goto, E. Kimura, M. Shiro, J. Am. Chem. Soc. 123 (2001) 1123.
[3] L.A. Bass, M. Wang, M.J. Welch, C.J. Anderson, Bioconjugate Chem. 11 (2000) 527.

[4] W.B. Edwards, C.J. Anderson, G.B. Fields, M.J. Welch, Bioconjugate Chem. 12 (2001) 1057.
[5] G.R. Weisman, M.E. Rogers, E.H. Wong, J.P. Jasinski, E.S. Paight, J. Am. Chem. Soc. 112 (1990) 8604.
[6] G.R. Weisman, E.H. Wong, D.C. Hill, M.E. Rogers, D.P. Reed, J.C. Calabrese, J. Chem. Soc., Chem. Commun. (1996) 947.
[7] E.H. Wong, G.R. Weisman, D.C. Hill, D.P. Reed, M.E. Rogers, J.P. Condon, M.A. Fagan, J.C. Calabrese, K.-C. Lam, I.A. Guzei, A.L. Rheingold, J. Am. Chem. Soc. 122 (2000) 10561.
[8] W. Niu, E.H. Wong, G.R. Weisman, K.-C. Lam, A.L. Rheingold, Inorg. Chem. Commun. (1999) 361.
[9] T.J. Hubin, Coord. Chem. Rev. 241 (1–2) (2003) 27.
[10] J. Springborg, Dalton Trans. (2003) 1653.
[11] W. Niu, Ph.D. Thesis, University of New Hampshire, Durham, NH, 2003.
[12] C.J. Anderson, M.J. Welch, Chem. Rev. 99 (1999) 2219.
[13] A. Bianchi, L. Calabi, C. Giorgi, P. Losi, P. Mariani, P. Paoli, P. Rossi, B. Valtancoli, M. Virtuani, Dalton Trans. (2000) 697.
[14] S. Aime, A. Barge, J.I. Bruce, M. Botta, J.A.K. Howard, J.M. Moloney, D. Parker, A.S. de Sousa, M. Woods, J. Am. Chem. Soc. 121 (1999) 5762.
[15] P. Cocolios, R. Guilard, C. Gros, PCT Int. Appl., 1996, 9611189.
[16] R.S. Dickins, S. Aime, A.S. Batsanov, A. Beeby, M. Botta, J.I. Bruce, J.A.K. Howard, C.S. Love, D. Parker, R.D. Peacock, H. Puschmann, J. Am. Chem. Soc. 124 (2002) 12697.
[17] D.A. Moore, PCT Int. Appl., 1994, 9404485.
[18] R. Mattes, U. Voet, Z. Naturforsch. B 54 (1999) 321.
[19] C. Bucher, E. Duval, J.-M. Barbe, J.-N. Verpeaux, C. Amatore, R. Guilard, C.R. Acad. Sci., Ser. IIc 3 (2000) 211.
[20] D.-Y. Kong, Y.-Y. Xie, Polyhedron 19 (2000) 1527.
[21] K.-Y. Choi, H.-H. Lee, B.B. Park, J.H. Kim, J. Kim, M.-W. Kim, J.-W. Ryu, M. Suh, I.-H. Suh, Polyhedron 20 (2001) 2003.
[22] E. Espinosa, M. Meyer, D. Berard, R. Guilard, Acta Crystrallogr., Sect. C 58 (2002) m119.
[23] H. Kurosaki, C. Bucher, E. Espinosa, J.-M. Barbe, R. Guilard, Inorg. Chim. Acta 322 (1 and 2) (2001) 145.
[24] E. Kimura, T. Gotoh, S. Aoki, M. Shiro, Inorg. Chem. 41 (2002) 3239.
[25] H. Maumela, R.D. Hancock, L. Carlton, J.H. Reibenspies, K.P. Wainwright, J. Am. Chem. Soc. 117 (1995) 669.
[26] J. Dale, Acta Chem. Scand. 27 (1973) 1115.
[27] J. Dale, Top. Stereochem. 9 (1976) 199.

Available online at www.sciencedirect.com
SCIENCE DIRECT®
Polyhedron 23 (2004) 1027–1035
POLYHEDRON
www.elsevier.com/locate/poly

Monobranched and hyperbranched dendrimers based on cyclophosphazene containing nitrile and phosphine donors and their Fe and Ru organometallic derivatives

Carlos Díaz *, Miguel Barbosa, Zaida Godoy

Departamento de Química, Facultad de Ciencias, Universidad de Chile, Las Palmeras 3425, Casilla 653, Santiago, Chile

Received 25 July 2003; accepted 28 December 2003

Abstract

The series of complexes $[N_3P_3(OC_6H_5)_5X.ML_n]PF_6$, $X = OC_6H_4CH_2CN$, $N(CH_3)(CH_2)_2CN$ or $OC_6H_4PPh_2$, and $[N_3P_3(X)_6 \cdot (ML_n)_6](PF_6)_6$, X = $OC_6H_4CH_2CN$ or $N(CH_3)(CH_2)_2CN$ with ML_n = CpFe(dppe) and $CpRu(PPh_3)_2$ have been synthesized by reaction of the corresponding cyclophosphazene ligands: $N_3P_3(OC_6H_5)_5OC_6H_4CH_2CNL_1$, $N_3P_3(OC_6H_5)_5N(CH_3)(CH_2)_2CNL_2$, $N_3P_3(OC_6H_5)_5OC_6H_4PPh_2L_3$, $N_3P_3(OC_6H_4\ CH_2CN)_6L_4$ and $N_3P_3(N(CH_3)(CH_2)_2CN)_6L_5$ with the respective organometallic CpFe(dppe)I and $CpRu(PPh_3)_2Cl$ in CH_3OH as solvent and in presence or of NH_4PF_6. The new compounds were characterized by elemental analysis and IR, UV–Visible and multinuclear NMR spectroscopy. Cyclic voltammetry studies indicate that the cyclophosphazene dendrimers act as insulators between the organometallic centers.
© 2004 Elsevier Ltd. All rights reserved.

Keywords: Dendrimers; Cyclophosphazene; Metal–nitrile complexes; Iron complexes

1. Introduction

Dendrimers chemistry is a rapid developing field of research [1]. Dendrimers offer the prospect of novel material with advantageous properties allowing them to serve, as soluble catalysts [2], dendritic boxes [3], and other supramolecular dendritic arrangements. Since the initial report on this class of molecules by Vögtle in 1978 [4] many different structural classes of dendritic macromolecules have been reported. Two main classes of dendrimers can be distinguished: the classical organic dendrimers [1] and the emergent inorganic dendrimers [5].

The incorporation of transition-metal complexes in both organic and inorganic dendrimers lead to new and interesting materials with specific properties such as the capability to absorb visible light, to give luminescence and to undergo reversible multielectron redox processes [6]. Such species, in fact could find applications as components in molecular electronic and as a photochemical molecular devices for solar energy conversion, information storage and in catalysis [6]. In general metal-containing dendrimers can be classified in two ways: according to the nature of the dendrimer and acording to the nature of the metal. With regarding to the nature of the dendrimer three categories can be distinguished: (see Scheme 1):

(a) Dendrimers with coordination centers at the core.
(b) Dendrimers with coordination centers through all layers and
(c) Dendrimers with coordination centers on the periphery.

On the other hand, with regard to the nature of the metal, dendrimers can be clasified in (i) those that the metal fragments are coordination units and (ii) those that the metal fragments are organometallic units.

Although dendrimers with coordination centers on the periphery have been reported [1,2,6], for those with the dendrimer – core being organic, few examples of inorganic dendrimers with metal coordination or organometallic derivatives on the surface have been reported

* Corresponding author. Tel.: +56-2-6787396; fax: +56-2-2713888.
E-mail address: cdiaz@uchile.cl (C. Díaz).

0277-5387/$ - see front matter © 2004 Elsevier Ltd. All rights reserved.
doi:10.1016/j.poly.2003.12.018

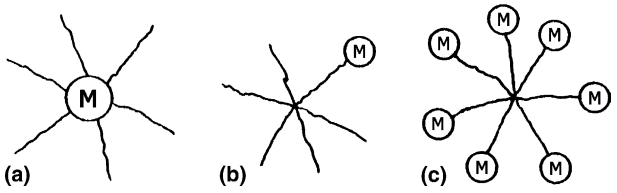

Scheme 1. Schematic representation of three class of metallodendrimers.

[5–8]. In spite of that dendrimers based on cyclophosphazenes have been reported [5], relatively few metal [9] and organometallic [5,8,10] derivatives have been reported. We have recently reported some organometallic derivatives of partially branched cyclophosphazene derivatives [10] and some single transition metal chlorides derivatives [9].

In continuation of our studies, we aimed to investigate the electronic communication between the metallic centers in dendrimers containing six organometallics groups in the peripheral (ligands **L4** and **L5**, see Scheme 2) as well as the influence of the X spacer and the nature of the metal, on the electronic transfer between the phosphorus (ring) atom and the metallic center (ligands **L1**–**L3**).

This communication reports the synthesis and characterization of new inorganic dendrimers based on cyclophosphazene having nitrile and phosphine donor groups and containing their Fe and Ru organometallic derivatives on the surface.

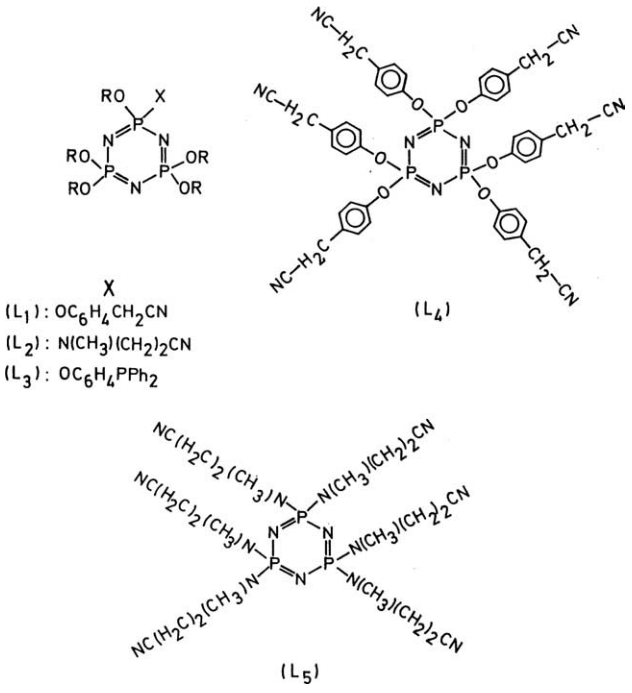

Scheme 2. Formulas for the ligands.

2. Results and discussion

2.1. Synthesis of the ligands

The synthesized ligands are shown in Scheme 2. As expected the synthesis of the dendrimers **L1**, **L3** and **L4** was made by the divergent strategy [1], by reaction of $N_3P_3Cl_6$ or $N_3P_3(OC_6H_5)_5Cl$ with $HO{-}_6H_4CH_2CN$ in acetone and in presence of the K_2CO_3 [9,10]. The ligands **L2** and **L5** were prepared by a similar strategy by reaction of the amine $HN(CH_3)CH_2CH_2CN$ with $N_3P_3Cl_6$ or $N_3P_3(OC_6H_5)_5Cl$ using triethylamine as HCl abstractor. As commonly observed for $N_3P_3(OC_6H_5)_{6-n}(C_6H_5)_n$ or $N_3P_3(OC_6H_5)_{6-}(NHR)_n$ derivatives, the products **L1**, **L3**, **L4** and **L5** were obtained as yellow or white oil, while **L2** was obtained as a white solid. All the new compounds were fully characterized by elemental analisis (or mass spectra for **L1** and **L4**) as well as IR, UV–Visible and ^1H ^{31}P and ^{13}C NMR spectroscopy. The compounds exhibits the typical IR bands of the $N_3P_3(OC_6H_5)_{6-n}(C_6H_5)_n$ ring [11]: ν(C-OP) arounds 1200 cm^{-1}, ν(PN) around 1100 cm^{-1} and ν(P-OC) around 1000 cm^{-1}. Additionally the expected, ν(CN) bands for **L1** , **L2**, **L4** and **L5** were observed in the range 2245–2228 cm^{-1}, see Table 1.

The ^{31}P NMR spectra of the ligands **L1**, **L4** and **L5** exhibit the typical singlet signal expected for these systems while that the ^{31}P NMR spectra for **L2** and **L3** show one triplet and one doublet corresponding to a AB_2 systems. These values are shown in Table 2.

For the ligands **L1**, **L3** and **L4**, their ^{13}C spectra exhibit all the expected signals for the groups (OC_6H_5), (OC_6H_4X) and $P(C_6H_5)_2$ (accordingly correspond see Section 3). Thus the signal of the CN and CH_2 groups were observed around 117 and 24 ppm, respectively. Full data are shown in Section 3.

2.2. Synthesis of the organometallic derivatives

2.2.1. Iron and ruthenium derivatives of ligands L_1, L_4

Using a previously reported methodology [10], the iron and ruthenim organometallic derivatives of the nitrile ligand **L1** and **L4** were prepared by reaction of the respective dendrimer ligands with the organometallic CpFe(dppe)I and $CpRu(PPh_3)_2Cl$ respectively, in methanol as solvent and using NH_4PF_6 as halide abstractor:

(**1**) $[CpFe(dppe)(L_1)][PF_6]$
(**2**) $[CpRu(PPh_3)_2(L_1)][PF_6]$
(**3**) $[[CpFe(dppe)]_6\ (L_4)][PF_6]_6$
(**4**) $[[CpRu(PPh_3)_2]_6(L_4)][PF_6]_6$

Compounds were characterized by elemental analyses, IR, ^1H ^{31}P, and ^{13}C NMR as well as UV–Visible and cyclic voltammetric methods. The IR spectra of the complexes exhibit the expected bands due to ν(N=P) and ν(CN) modes of the free ligand as well as the $\nu(PF_6)$

Table 1
Selected Ir bands for of the ligands L_1–L_5 and of their Fe and Ru complexes **1**–**11**

	ν(PO–C_6H_5)	ν(PN)	ν(P–OC_6H_5)	ν(CN)	C_5H_5	C_6H_5
Ligands						
L_1	1259	1177	1117	2245		
L_2		1177		2247		
L_3	1271	1212,1170	1154			
L_4	1265	1171	1100	2247		
L_5	1273	1192	1125	2252		
Complexes						
(**1**)	1268	1177,1161	1096	2280		711
(**2**)	1258	1177		2129	1091	696
(**3**)	1273	1192,1145	1145	2252	1099	690
(**4**)	1187	1187	1176	2270	1089	696
(**5**)	1266	1195,1177	1161		1090	705
(**6**)	1267	1197,1176	1163		1093	680
(**7**)	1285				1120	696
(**8**)	1253	1177	1161	2280	1096	696
(**9**)	1268	1178	1160	2280	1089	692
(**10**)	1273	1192	1145	2252		696
(**11**)	1241	1164	1094	2270	1097	698

Table 2
Formulas and ^{31}P NMR data for the ligands L_1–L_5 and of their Fe and Ru complexes **1**–**11**

	^{31}P(JP-P,Hz)	(dppe)	PPh_3	PPh_2
Ligands				
L_1 $N_3P_3(OC_6H_5)_5OC_6H_4CH_2CN$	11.66s			
L_2 $N_3P_3(OC_6H_5)_5$ $N(CH_3)CH_2)_2CN$	18.11t; 2.79d (82.9)			
L_3 $N_3P_3(OC_6H_5)_5OC_6H_4PPh_2$	18.1t; 2.78d(81.4)			−10.47 (s)
L_4 $N_3P_3(OC_6H_4CH_2CN)_6$	11.89 (s)			
L_5 $N_3P_3(N(CH_3)(CH_2)_2CN)_6$	18.5 (s)			
Complexes				
(**1**) $[CpFe(dppe)(L_1)][PF_6]$	11.42	100.25		
(**2**) $[CpRu(PPh_3)_2(L_1)][PF_6]$	10.89		44.0	
(**3**) $[CpFe(dppe)]_6(L_4)][PF_6])_6$	11.30	100.20		
(**4**) $[CpRu(PPh_3)_2]_6(L_4)][PF_6]$	11.50		42.26	
(**5**) $[CpFe(dppe)(L_3)][PF_6]$	17.6t; 2.76d(79.3)	92.4		24.0
(**6**) $[CpRu(PPh_3)_2(L_3)][PF_6]$	18.1t; 2.48d(78.6)		34.6	24.8
(**7**) $[CpFe(dppe)PPh_2C_6H_4OH][PF_6]$		93		4.6
(**8**) $[CpFe(dppe)(L_2][PF_6]$	18.1t; 2.78d (82.98)	86		
(**9**) $[CpRu(PPh_3)_2(L_2)][PF_6]$	18.09t; 2.77d (82.5)		37.8	
(**10**) $[CpFe(dppe)]_6(L_5)][PF_6]_6$	18.54	93.6		
(**11**) $[CpRu(PPh_3)_2]_6(L_5)][PF_6]_6$	18.0		34.93	

An heptuplet signal at −148 ppm corresponding to PF_6 anion was also observed.

band. Values are displayed in Table 1. Characteristic splitting of the ν(N=P) bands due to coordination of metal halide to CN groups for dendrimer L_1 and L_4 have been observed recently [9a]. A similar but lesser effect was observed for complexes (**1**)–(**4**). Thus, this splitting pattern appears to be typical of metal coordination [9,10]. The complexes (**1**)–(**4**) exhibit the expected ^{31}P signal for the N_3P_3 ring namely a singlet sligtly shifted to lower values by coordination effects. This small decrese in the ^{31}P chemical shift is typical of coordination of organometallic fragments [10]. On the other hand the ^{31}P signal of the dppe ligand ligated to CpFe fragment for the complexes (**1**) and (**3**) was observed as normal at 100 ppm while the signal of PPh_3 coordinated to the fragment CpRu was normally observed at 44 and 42 ppm. The PF_6 anion was normally observed as a septuplet around −148 ppm. From the ^{13}C NMR spectrum of complexes, it can be clearly corroborated the presence of the groups (OC_6H_5), (OC_6H_4X) $X = CH_2CN$, PPh_2, of the ligands as well as the typical signals of the fragments $P(C_6H_5)_3$ and C_5H_5 (see Section 3).

Thus, these data compare well with those of the nitrile mononuclear model complexes {CpFe(dppe)-NCR][PF_6]} [12], as well as other cyclophosphazene organometallic derivatives [10].

2.2.2. The iron and ruthenium derivatives of the ligand L_3

Following a previously reported procedure [13], the complexes:

(5) [CpFe(dppe)(L_3)][PF_6]

(6) [CpRu(PPh_3)$_2$(L_3)][PF_6]

were synthesized from the reaction of the respective organometallic with L_3 in methanol as solvent and using NH_4PF_6 as halide abstractor. As model, we have also prepared the new complex:

(7) [CpFe(dppe)$PPh_2C_6H_4OH$][PF_6]

by reaction of the known $PPh_2C_6H_4OH$ [8d] with the iron organometallic.

The new complexes (**5**)–(**6**) were characterized by elemental analyses, IR, ^{1}H and ^{31}P NMR, UV–Visible and cyclic voltammetric methods. IR and NMR data for the complexes are not unusual and they are displayed in Tables 1–3 and in Section 3. It is interesting to mention the ν(OH) of (**7**) at 3420 cm^{-1} and the ^{31}P signal of the PPh_2 group at 4.6 ppm significantly shifted from the free value −10 ppm. Similar shifting for the complexes (**5**) and (**6**) were observed. As observed for another cyclophosphazenes and polyphosphazenes containing phosphines [8d] a small fraction of phosphine phosphorus as $O=PPh_2$ was detected by the signals at 28.63 and 26.61 ppm for **5** and **6**, respectively.

2.2.3. Iron and ruthenium derivatives of the ligands L_2 *and* L_5

These compounds were synthesized using the usual methodology for preparing iron–nitrile and ruthenium–nitrile complexes [10,12]:

(8) [CpFe(dppe)($\mathbf{L}_2$)][PF_6]

(9) [CpRu(PPh_3)$_2$($\mathbf{L}_2$)][PF_6]

(10) [[CpFe(dppe)]$_6$ ($\mathbf{L}_5$)][PF_6]$_6$

(11) [[CpRu(PPh_3)$_2$]$_6$($\mathbf{L}_5$)][PF_6]$_6$

Table 3
Electrochemical data for complexes **1**–**11**

	$E1/2$ (V)	ΔE (V)
1	0.81	0.11
2	0.53	0.06
3	0.81	0.14
4	0.50	0.06
5	0.88	0.10
6	0.570	0.088
7	0.884	0.092
8	0.775	0.080
9	0.613	0.073
10	0.767	0.263
11	0.590	0.091

Potential referenced against Ag/AgCl, at 100 mV s^{-1} scan rate, in a 0.1 mol dm^{-3} n-Bu_4N[PF_6].

The compounds were characterized by elemental analyses, IR, ^{1}H, ^{31}P, as well as UV–Visible and cyclic voltammetric methods. The IR spectra of complexes exhibit the expected bands due to ν(N=P) and ν(CN) modes of the free ligand as well as the ν(PF_6) band. Values are displayed in Table 1, The characteristic spliting of ν(N=P) upon coordination was also observed. A decrease of the ν(CN) band upon coordination suggest the link of the ligand through the CN group instead of the N(CH_3) group of the ligand. The complexes (**8**)–(**11**) exhibit the expected ^{31}P signal for the N_3P_3 ring, namely, a singlet (for (**10**) and (**11**)) or a triplet and doublet signals (for (**8**) and (**9**)) at sligthly shifted lower values by coordination effects. As previously mentioned this small decrease of the ^{31}P chemical shift is typical of organometallic fragments coordination [10]. On the other hand, the ^{31}P signal of the dppe ligand ligated to CpFe fragment for the complexes (**8**) and (**10**) was normally observed at 92.4 and 93.6 ppm, respectively. The signal of PPh_3 coordinated to the fragment CpRu was observed at 34.6 and 34.9 ppm for (**9**) and (**11**), respectively. The PF_6 anion was normally observed as a septuplet around −142 ppm. Relatively fast decomposition of the samples in solution precludes the measurements of good ^{13}C NMR spectrum for the complexes.

As previously reported [10c] the ^{31}P chemical shift parameter $\Delta = |\delta\ ^{31}\text{P(free ligand)} - \delta\ ^{31}\text{P(complex)}|$ in the systems similar to the organometallic derivatives (**1**), (**2**), (**5**), (**6**), (**8**) and (**9**) is a measure of the electron transfer between the phosphorus atom and the metal atom. From ^{31}P NMR data shown in Table 2 it can be viewed that the Δ parameter is greater for the ruthenium derivatives than for the iron complexes. Thus this parameter does not correlates with the distance of the X spacer as found in another similar systems [10c].

2.2.4. UV–Visible spectra of the complexes

The UV–Visible spectrum of the complexes is dominated by both, the organometallic chromophore and by the nature of the CN or PPh_2 groups linked to the metal. Iron complexes having the CpFe(dppe) moiety exhibits well defined absorption maxima arounds 450 nm depending of the N or P donor interaction [10,12,13]. Less intense shoulders arounds 526 and 600 nm have been assigned to the metal–ligand charge transfer transitions (MLCT) [12]. Fig. 1 exhibits the UV–Visible spectrum of (**8**). Data are shown in Section 3. On the contrary the ruthenium containing dendrimers (**9**) and (**11**) exhibits a tail beginning around 500 nm, of a more intense absorption band centered at 350 nm. Thus these absorption patterns are typical of [CpFe(dppe)NCR][PF_6], [10,12] of [CpFe(dppe)PPh_2-R][PF_6] [13], [CpRu(PPh_3)$_2$ NCR][PF_6] [10,12] and [CpRu(PPh_3)$_2$$PPh_2$-R][$PF_6$] [13] complexes.

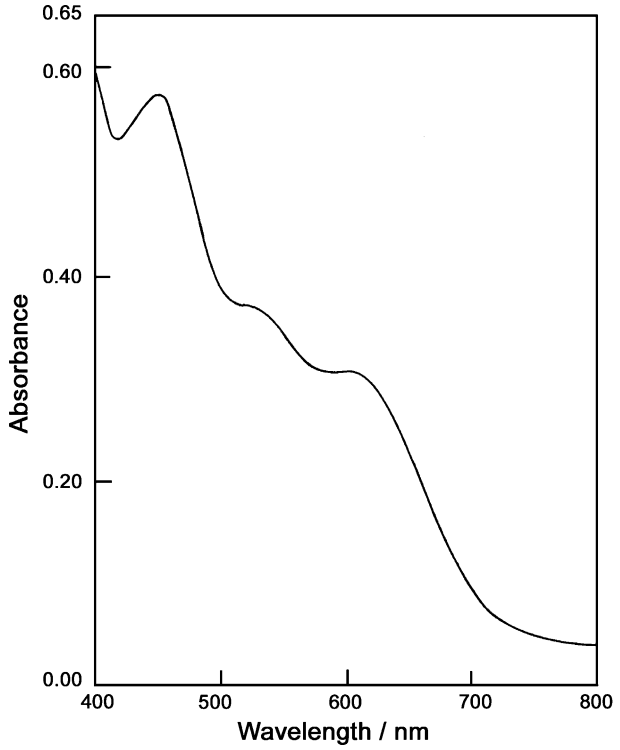

Fig. 1. UV–Visible spectrum for (**8**) in CH_2Cl_2 solution at room temperature.

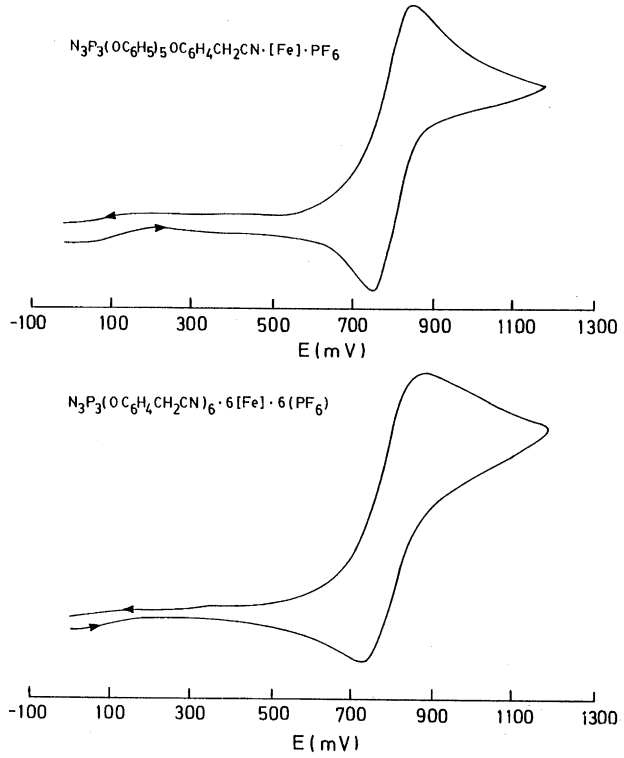

Fig. 2. Cyclic voltammogram of complexes (**1**) and (**3**) on a graphite electrode ($v = 100$ mV s^{-1}) of a CH_2Cl_2(n-$Bu_4N^+PF_6^-$ solution) containing: complex (**1**), (2.11×10^{-3}M) curve upper, and complex (**3**), (3.4×10^{-4}M) curve lower.

2.2.5. Cyclic voltammetry studies

There are few reports of electrochemical studies on cyclophosphazene metal complexes [8–10], Cyclic voltammetry for these type of systems provides some insight into the communication degree between the metal centers along the cyclophosphazene [4]. For all the studied complexes one single oxidation wave was observed. In Fig. 2, the cyclic voltammogram of complex (**1**) having one fragment CpFe(dppe) (symbolized [Fe] in the figure) is compared with that containing six iron group the complex (**3**). As shown in Fig. 2, similar CV (similar intensities and shapes) are obtained, being the concentration of the dendrimer (**1**) six times more larger than the complex (**3**), which indicated that their oxidation wave involves the transfer of six electrons at the same potential. Then, the six CpFe(dppe) groups behave as six electroactive non-interacting redox centers around the periphery of the cyclosphosphazene ring.

As is usually observed for this type of organometallic compounds [8–10], only quasi-reversible waves were observed in all the cases. From Table 3 it can be observed that the potential values clearly depend on the π-acceptor capacity of the group linked to the organometallic fragment. For the fragment CpFe(dppe) the most π-acceptor phosphorus induce the highest electron witdrawing effect provoking the most highest potential value, ≈0.88 V. Consistent with this, the weakest π-acceptor ligand nitrile, decrease their potential values in an amount which depend on the nature of the spacer (X in the Scheme 2). In the $CpRu(PPh_3)_2$ series the opposite tendency was observed. In this case, inductive effects of the group spacer increasing in the order $-C_6H_4O >$ $N(CH_2)_2$ could explain the observed order of the potential.

3. Experimental

3.1. General considerations

Infrared spectra were recorded on a FT-Bruker-66V spectrophotometer in Nujol. NMR spectra were recorded on a Bruker AMX 300 spectrometer in chloroform-d_1 with TMS (H) $\delta = 0.0$ ppm as internal standard or 85% H_3PO_4 and downfield positive to the reference as external standard for the ^{31}P measurements.

UV–Visible absorption spectra were recorded using a Varian DMS-90 spectrophotometer with 1 cm optical path cuvettes in CH_2Cl_2 solutions. Elemental analyses were performed on Fisons-Carlo Erba EA 1108, apparatus by CEPEDEQ, Universidad de Chile.

Mass spectra were recorded with a ICP-MS Fisons VG Plasma Quad mass spectrometers.

Electrochemical measurements were made on a Parc model 370 electrochemistry system, using a three electrode device, employing a carbon glassy working electrode, platinum wire counter electrode and saturated calomel reference electrode. Solutions were 10^{-3} M in the complex and 0.1 M in $[NBu_4]PF_6$ as supporting electrolyte. Under the same experimental conditions, $E1/2$ for the ferrocene–ferrocenium complex was 0.64 V with peak separations of about 0.060 V (internal standard). Reactions were carried out under nitrogen using standard Schlenk-tube techniques. Diethylether and *n*-hexane were dried over sodium and distilled.

$N_3P_3Cl_6$, HO–C_6H_4–CH_2CN, $HNCH_3CH_2CH_2CN$, NH_4PF_6 and $CpRu(PPh_3)_2Cl$ were purchased from Aldrich. CpFe(dppe)I was prepared by a previously reported method [9,10]. $N_3P_3(O–C_6H_5)_5Cl$ was prepared using a previously reported method [10b].

3.2. Preparation of ligand and complexes

3.2.1. Ligands

3.2.1.1. Synthesis of $N_3P_3(O–C_6H_5)_5(O–C_6H_4–CH_2–CN)$ (L_1). A mixture of $N_3P_3(O–C_6H_5)_5Cl$ 2.3 g, (3.62 mmol); HO–C_6H_4–CH_2–CN 0.5 g; (3.75 mmol), K_2CO_3 0.97 g; (7.02 mmol) and $[Bu_4N]Br$ 1.7 g; (5.27 mmol) was refluxed in acetone (40 ml) for 20.17 h. The solution was filtered through celite and the solvent evaporated in vacuo. The red oil residue was extracted with toluene to give a red solution. *n*-Hexane was added to obtain a ligth red oil, which was washed with *n*-hexane and dried under reduce pressure. Mass spectrum (m/e) 732 M^+. Calc. (732); 691 (M^+-CH_3CN)-^{1}H NMR ($CDCl_3$): 7.1–6.9 (m, OC_6H_5), 6.83–6.73 (m OC_6H_4), 3.71, 3.53 (s, CH_2). ^{13}C NMR ($CDCl_3$, ppm): 150.91, 129.9, 125.46, 121.24, 117.87 (OC_6H_4X), 150.91, 129.21, 121.24, 117.87 ($P(OC_6H_5)$), 116.95 (CN), 24.19 (CH_2). UV/Vis(CH_2Cl_2): $\lambda = 232$ nm.

3.2.1.2. Synthesis of $N_3P_3(O–C_6H_4–CH_2–CN)_6$ (L_4). A mixture of $N_3P_3Cl_6$ 0.26 g, (0.75 mmol); HO–C_6H_4–CH_2–CN 0.8 g; (6 mmol), K_2CO_3 1.54 g; (11.14 mmol) and $[Bu_4N]Br$ 1.5 g; (4.65 mmol) was refluxed in acetone (30 ml) for 51 h. The red solution was filtered through celite and the solvent evaporated in vacuo. The red oil residue was dried in vacuum and extracted with dichloromethane and filtered through celite and dried to obtain a ligth red oil, which was dried under reduce pressure. Mass spectrum (m/e) 927 M^+ Calc. (927), 886 (M^+-CH_3CN). ^{1}H NMR (CD_2Cl_2): 7.21–6.93 (m, OC_6H_4) 1.63, 1.43(s, CH_2). ^{13}C NMR ($CDCl_3$): 129.73, 125.63, 121.79, 118.54 (OC_6H_4X): 117.36 (CN), 24.43 (CH_2). UV/Vis(CH_2Cl_2): $\lambda = 234$ nm.

3.2.1.3. Synthesis of $N_3P_3(OC_6H_5)_5N(CH_3)(CH_2)_2CN$ (L_2). A mixture of $N_3P_3(O–C_6H_5)_5Cl$ 1.05 g, (1.65 mmol); $HN(CH_3)(CH_2)_2CN$ 0.154 ml; (1.65 mmol), NEt_3 0.229 ml; (1.65 mmol) were refluxed in benzene (35 ml) for 72 h. The solution was evaporated in vacuo and the yellow pale oil residue was poured into water and was extracted with dichloromethane. The extract was dried over sodium sulphate and filtered trough celite and the same solvent evaporated under vacuum to give a white solid. *Anal.* Calc. for $C_{34}H_{27}O_5N_5P_3$: C, 59.76; H, 4.68; N, 10.25; P, 13.01. Found: C, 57.67; H, 4.25; N, 6.96; P, 13.61%. ^{1}H NMR (CD_2Cl_2): 7.3–7.0 (m, C_6H_5), 2.56 (d, CH_3 $J_{PNH} = 11$ Hz), 2.99 (m, CH_2), 2.03 (t, CH_2). ^{13}C NMR ($CDCl_3$, ppm): 150.59, 129.82, 125.49, 121.35 (P-OC_6H_5), 118.54(CN), 45.56(CH_2), 34.158CH_2), 17.14(CH_3).). UV/Vis(CH_2Cl_2): $\lambda = 261$ nm.

3.2.1.4. Synthesis of $N_3P_3(N(CH_3)(CH_2)_2CN)_6$ (L_5). A mixture of $N_3P_3Cl_6$ 5 g, (14.38 mmol); $HN(CH_3)(CH_2)_2CN$ 8.068 ml (86.31 mmol), in NEt_3 11.96 ml; (86.31 mmol) were refluxed in bencene (50 ml) for 10 h. The pale yellow solution was filtered and the solvent evaporated in vacuo. The oil residue was redissolved in a *n*-hexane/dichloromethane mixture. Purification of the product mixture was made by chromatography using neutral alumna. Elution with a *n*-hexane/dichloromethane mixture and collection of the transparent fraction followed by evaporation under vacuum afford a ligth yellow oil, which was dried under reduce pressure. *Anal.* Calc. for $C_{24}H_{42}N_{15}P_3$; C, 45.51; H, 6.63; N, 33.18; P, 14.30. Found: C, 43.24; H, 6.71; N, 28.03; P, 14.69%. ^{1}H NMR ($CDCl_3$): 2.78 (m C**H**$_2$CN), 2.69(s, CH_3), 2.6(m C**H**$_2$N). ^{13}C NMR ($CDCl_3$): 118.47 (CN), 45.71 (CH_2), 33.58 (CH_2), 17.60(CH_3).

3.2.1.5. Synthesis of $N_3P_3(O–C_6H_5)_5(O–C_6H_4–PPh_2)$ (L_3). A mixture of $N_3P_3(O–C_6H_5)_5Cl$ 0.3052 g, (0.48 mmol); HO–C_6H_4–PPh_2 0.1214 g; (0.849 mmol), Cs_2CO_3 0.294 g; (0.9 mmol) were refluxed in acetone (30 ml) for 2 h. The solution was filtered through celite and the solvent evaporated in vacuo. The yellow pale oil residue was extracted with toluene to give a red solution. *n*-Hexane was added to obtain a ligth red oil, which was washed with *n*-hexane and dried under reduce pressure. *Anal.* Calc. for $C_{48}H_{39}O_6N_3P_4$: C, 65.67; H, 4.78; N, 4.78; P, 13.9. Found: C, 64.28; H, 4.26; N, 4.26; P, 14.14%. ^{1}H NMR (CD_3Cl): 7.1–7.3 (m OC_6H_5), 7.0–6.9 (m, C_6H_4), 3.75 (s, CH_2). ^{13}C NMR ($CDCl_3$, ppm): 151.06, 134.96, 133.47, 125.2, 121.22, 115.87 (OC_6H_4X) 135.74, 133.47, 129.46, 128.76 (–PPh_2), 150.17, 128.41, 124.88, 120.97 (P–OC_6H_5). UV/Vis(CH_2Cl_2): $\lambda = 230$ nm.

3.2.2. Complexes

*3.2.2.1. Synthesis of $[N_3P_3(O–C_6H_5)_5(O–C_6H_4–CH_2–CN)\cdot Fe(Cp)dppe]PF_6$ (**1**).* A mixture of $N_3P_3(O–C_6H_5)_5(O–C_6H_4–CH_2–CN)$ 0.23 g (0.31 mmol), and

CpFe(dppe)I 0.2 g (0.31 mmol) in methanol (20 ml), in presence of NH_4PF_6 0.2 g (1.23 mmol) was stirred for 21 h at room temperature. The solvent was removed under reduced pressure and the residue extracted with CH_2Cl_2 and filtered through celite and concentrated to ≈10 ml. A *n*-hexane/diethylether 4:1 mixture was added and the red powdered precipitate was twice washed with the same solvent mixture and dried under reduced pressure.

Yield: 0.25 g, 49%. *Anal*. Calc. for $C_{69}H_{60}F_6O_6N_4P_6Fe$: C, 61.99; H, 5.00; N, 4.01; P, 13.32. Found: C, 62.9; H, 4.7; N, 3.9; P, 12.32%. ^{1}H NMR (CD_3Cl): 7.73(m), 7.75(m), 7.35(m), 7.26(m), 7.18(m OC_6H_5), 6.98(m), 6.77(m OC_6H_4), 4.3 (s, C_5H_5), 3.7 (CH_2P), 1.27 (CH_2C). ^{13}C NMR ($CDCl_3$): 156.7, 129.95, 125.3, 121.3, 116.45 (OC_6H_4X), 156.7; 129,6, 120.18, 116.45 $P(OC_6H_5)$, 137, 133.19, 133.13, 132.56, 131.68, 131.55 131.55, 127.97 ($P(C_5H_5)$), 79.3 (C_5H_5), 29.26 (CH_2CN), 20.13.3 (CH_2P). UV/Vis(CH_2Cl_2): $\lambda = 366$ and 466 nm.

*3.2.2.2. Synthesis of [N_3P_3(O-C_6H_5)$_5$(O-C_6H_4-CH_2-CN) · Ru(Cp)(PPh_3)$_2$]PF_6 (**2**).* A solution of CpRu(PPh_3)$_2$Cl 0.14 g (0.19 mmol) in CH_3OH (20 ml) was stirred with [N_3P_3(O–C_6H_5)$_5$(O–C_6H_4–CH_2–CN) 0.22 g (0.3 mmol) in the presence of NH_4PF_6 0.2 g (1.22 mmol) at room temperature for 23 h. The solvent was removed under reduced pressure and the residue extracted with CH_2Cl_2 (15 ml) and filtered through celite. Then reduced in volume and *n*-hexane/dithylether 4:1 mixture was added. The yellow solid precipitate was twice washed with the same mixture and dried.

Yield: 0.41 g, 97%. *Anal*. Calc. for $C_{79}H_{66}F_6O_6N_4P_6Ru$: C, 60.46; H, 4.20; N, 3.0. Found: C, 60.5; H, 6.3; N, 3.57%. ^{1}H NMR (CD_3Cl): 7.3, 7.42 ($P(C_5H_5)$), 6.94–6.83, 6.72, 6.64, (OC_6H_4X), 4.43 (s, C_5H_5), 1.13(CH_2). ^{13}C NMR ($CDCl_3$): 156, 133.58, 129.14, 123.38, 121.44 (OC_6H_4X), 156, 128.7, 119.44, 116.44 ($P(OC_6H_5)$), 134.11, 133.58, 130.56, 130.38, 129.73, 127.33 ($P(C_5H_5)$). 115.22 CN; 81.47 (C_5H_5); 24,12 (CH_2CN); 19.99,13.66 CH_2P.

*3.2.2.3. Synthesis of [N_3P_3(O–C_6H_4–CH_2–CN)$_6$ · (Fe(Cp)dppe)$_6$]$[PF_6]_6$ (**3**).* A mixture of N_3P_3(O–C_6H_4–CH_2–CN)$_6$ 0.21 g (0.23 mmol), and CpFe(dppe)I 0.17 g (0.26 mmol) in methanol (30 ml), in presence of NH_4PF_6 0.2 g (1.23 mmol) was stirred for 24 h at room temperature. The solvent was removed under reduced pressure and the residue extracted with CH_2Cl_2 and filtered through celite and concentrated to ≈10 ml. *n*-Hexane was added and the red powdered precipitate was twice washed with the same solvent and dried under reduced pressure.

Yield: 0.25, g. 49%. *Anal*. Calc. for $C_{234}H_{210}F_{36}O_6N_9P_{21}Fe_6$: C, 54.37; H, 4.03; N, 2.05. Found: C, 54.76; H, 5.7; N, 2.64%. ^{1}H NMR (CD_3Cl): 7.3(m), 7.25(m), 7.13(m), 6.97(m), (OC_6H_4X /PC_6H_5), 5.33(sC_5H_5), 1.01(CH_2). ^{13}C NMR($CDCl_3$): 156, 129.96, 125.49; 121.73 129.54, 121.73 (OC_6H_4X): 133.13, 133.07, 131.63, 130.91 ($P(OC_6H_5)$), 79.54 (C_5H_5); 24.22 (**C**H_2CN), 20.45, 23.66 (**C**H_2P). UV/Vis(CH_2Cl_2): $\lambda = 340$ and 440 nm.

*3.2.2.4. Synthesis of [N_3P_3(O–C_6H_4–CH_2–CN)$_6$ · (Ru(Cp)(PPh_3)$_{26}$]$[PF_6]_6$ (**4**).* A solution of CpRu(PPh_3)$_2$Cl 0.2 g (0.27 mmol) in CH_3OH (30 ml) was stirred with [N_3P_3(O–C_6H_4–CH_2–CN)$_6$ 0.085 g. (0.09 mmol) in the presence of NH_4PF_6 0.25 g (1.5 mmol) at room temperature for 74 h. The solvent was removed under reduced pressure and the yellow–orange residue extracted with CH_2Cl_2 (15 ml) and filtered through celite. Then reduced in volume and *n*-hexane/dithylether 4:1 mixture was added. The yellow solid precipitate was twice washed with the same mixture and dried.

Yield: 0.41 g, 97%. *Anal*. Calc. for $C_{102}H_{86}F_{36}O_6N_9P_{21}Ru_6$; C, 59.34; H, 4.34; N, 2.0. Found: C, 58.79; H, 4.48; N, 2.12%. ^{1}H NMR (CD_3Cl): 6.6–7.68(m C_6H_4), 4.36 (s,C_5H_5). ^{13}C NMR ($CDCl_3$):156, 129.13, 127,85 (OC_6H_4X): 134.14, 133.57, 132.38, 132.25, 128.96, 128.80, 127.85 ($P(OC_6H_5)$), 81.04 (C_5H_5), 24.0 (CH_2).

*3.2.2.5. Synthesis of [N_3P_3(O–C_6H_5)$_5$(O–C_6H_4–PPh_2) · Fe(Cp)dppe)]PF_6 (**5**).* A mixture of N_3P_3(O–C_6H_5)$_5$(O–C_6H_4–PPh_2) 0.2478 g (0.28 mmol), and CpFe(dppe)I 0.182 g (0.254 mmol) in methanol (20 ml), in presence of NH_4PF_6 0.0937 (0.575 mmol) was stirred for 19 h at room temperature. The solvent was removed under reduced pressure and the residue extracted with CH_2Cl_2 and filtered through celite and concentrated to ≈10 ml. A *n*-hexane/diethylether 4:1 mixture was added and the red powdered precipitate was twice washed with the same solvent mixture and dried under reduced pressure.

Yield: 0.25 g, 49%. *Anal*. Calc. for $C_{79}H_{68}F_6O_6N_3P_6Fe$**.**$CH_2Cl_2$; C, 58.68; H, 4.28; N, 2.3; P, 13.9. Found: C, 58.81; H, 4.53; N, 1.9, P, 14.14%. ^{1}H NMR (CD_3Cl): 8.6–8.3 (m PC_6H_5), 7.4,7.8 (m OC_6H_5), 7.25–7.18 ($P(C_6H_5)_3$), 6.93, 6.91 (mOC_6H_4P)4. 9(sC_5H_5), 3.5(m.b.CH_2). UV/Vis(CH_2Cl_2): 239, 268, 448 and 526 nm(sh), 602 nm(sh).

*3.2.2.6. Synthesis of [N_3P_3(O–C_6H_5)$_5$(O–C_6H_4–PPh_2) · (Ru(Cp)(PPh_3)$_2$)]PF_6 (**6**).* A mixture of N_3P_3(O–C_6H_5)$_5$(O–C_6H_4–PPh_2 0.2478 g (0.28 mmol) and (Ru(Cp)(PPh_3)$_2$Cl 0.182 g (0.254 mmol) in methanol (20 ml), in presence of NH_4PF_6 0.0937 (0.575 mmol) was stirred for 19 h at room temperature. The solvent was removed under reduced pressure and the residue extracted with CH_2Cl_2 and filtered through celite and

concentrated to ≈10 ml. A *n*-hexane/diethylether 4:1 mixture was added and the red powdered precipitate was twice washed with the same solvent mixture and dried under reduced pressure.

Yield: 0.25 g, 49%. *Anal*. Calc. for $C_{89}H_{74}F_6O_6N_3P_6Ru$; C, 62.38; H, 4.73; N, 4.32; P, 10.50. Found: C, 63.05; H, 4.73; N, 2.16; P, 10.86%. ^{1}H NMR (CD_3Cl): 7.8–7.7 (OC_6H_5), 7.2–7.0 ($P(C_6H_5)_3$), 6.94–6.88 (OC_6H_4P), 4,9(s, C_5H_5).). UV/Vis(CH_2Cl_2): $\lambda = 239$ nm, 268 nm (sh), 302 nm(sh), 353 nm.

*3.2.2.7. Synthesis of [HO–C_6H_4–PPh_2·Fe(Cp)dppe]-PF_6 (**7**)*. A mixture of HO–C_6H_4–PPh_2 0.2478 g (0.28 mmol), and CpFe(dppe)I 0.182 g (0.254 mmol) in methanol (20 ml), in presence of NH_4PF_6 0.0937 (0.575 mmol) was stirred for 19 h at room temperature. The solvent was removed under reduced pressure and the residue extracted with CH_2Cl_2 and filtered through celite and concentrated to ≈10 ml. A *n*-hexane/diethylether 4:1 mixture was added and the red powdered precipitate was twice washed with the same solvent mixture and dried under reduced pressure.

Yield: 0.25 g, 49%. *Anal*. Calc. for $C_{49}H_{44}F_6OP_2Fe{\bullet}CH_2Cl_2$: C, 58.68; H, 4.28; N, 2.3. Found: C, 58.81; H, 4.53; N, 1.9%. ^{1}H NMR (CD_3Cl): 6.6–6.7 (m C_6H_4) 4.27(s, C_5H_5). 3.04 (CH_2). ^{13}C NMR ($CDCl_3$): 156.7, 129.6 129.95 (OC_6H_4X) 133.13, 131.62, 130.95, 127.97, 125.3, 121.3 ($P(C_6H_5)_2$), 120.18 (CN), 79.3 (C_5H_5), 24.2 (CH_2). UV/Vis(CH_2Cl_2): $\lambda = 255$, 476 and 617 nm.

*3.2.2.8. Synthesis of [$N_3P_3(OC_6H_5)_5N(CH_3)(CH_2)_2$-CNFe(Cp)dppe]$PF_6$ (**8**)*. A mixture of $N_3P_3(OC_6H_5)_5N(CH_3)(CH_2)CN$ 0.20 g (0.29 mmol) and CpFe(dppe)I 0.195 g (0.295 mmol) in methanol (20 ml), in presence of NH_4PF_6 0.097 (0.67 mmol) was stirred for 19 h at room temperature. The solvent was removed under reduced pressure and the residue extracted with CH_2Cl_2 and filtered through celite and concentrated to ≈10 ml. A *n*-hexane/diethylether 4:1 mixture was added and the red powdered precipitate was twice washed with the same solvent mixture and dried under reduced pressure.

Yield: 0.25 g, 49%. *Anal*. Calc. for $C_{65}H_{56}F_6O_5N_5P_6Fe$: C, 61.99; H, 5.00; N, 5.19; P, 13.8. Found: C, 62.9; H, 4.7; N, 5.0; P, 13.0%. ^{1}H NMR (CD_3Cl): 7.3–6.9 (m) 6.4 (PC_6H_5) 4.32 (s, C_5H_5), 1.54(m CH_3), 1.25 (CH_2). ^{13}C NMR ($CDCl_3$): 156.7, 129.95, 125.3 121.3 ($P(OC_6H_5)$), 133.13, 131.62, 130.95, 129.6, 127.97 ($P(C_5H_5)$), 120.18 (CN) 79.3 (C_5H_5), 24.2 (CH_2). UV/Vis(CH_2Cl_2): $\lambda = 233$, 467 and 623 nm.

*3.2.2.9. Synthesis of [$N_3P_3(O–C_6H_5)_5(N(CH_3)(CH_2)_2CN)$·Ru(Cp)$(PPh_3)_2$]$PF_6$ (**9**)*. A solution of $CpRu(PPh_3)_2Cl$ 0.2155 g (0.297 mmol) in CH_3OH (20 ml) was stirred with $[N_3P_3(O–C_6H_5)_5(O–C_6H_4–CH_2–CN)$ 0.2 g (0.29 mmol) in the presence of NH_4PF_6 0.098 g (0.67 mmol) at room temperature for 23 h. The solvent was removed under reduced pressure and the residue extracted with CH_2Cl_2 (15 ml) and filtered through celite. Then reduced in volume and *n*-hexane/dithylether 4:1 mixture was added. The yellow solid precipitate was twice washed with the same mixture and dried.

Yield: 0.41 g, 97%. *Anal*. Calc. for $C_{75}H_{62}F_6O_5N_5P_6Ru$: C, 60.46; H, 4.20; N, 4.6; P, 12.12. Found: C, 60.5; H, 6.3; N, 3.5; P, 11.08%. ^{1}H NMR (CD_3Cl): 7.8–7.0 (OC_6H_5), 4.1 (s, C_5H_5) 1.55 CH_3. ^{13}C NMR ($CDCl_3$): 129.14, 128.70, 121.44 $P(OC_6H_5)$, 133.58; 130.56; 129.14 128.70 ($P(C_5H_5)$), 121.44 (CN), 84.5 (C_5H_5), 24.12 (CH_2). UV/Vis (CH_2Cl_2): $\lambda = 233$ and 350 nm.

*3.2.2.10. Synthesis of [$N_3P_3(N(CH_3)(CH_2)_2CN)_6$·(Fe(Cp)dppe)$_6$][$PF_6$]$_6$ (**10**)*. A mixture of $[N_3P_3(O–C_6H_4–CH_2–CN)_6$ 0.0235 g (0.037 mmol) and CpFe(dppe)I 0.1207 g (0.18 mmol) in methanol (20 ml), in presence of NH_4PF_6 0.1123 g (0.77 mmol) was stirred for 12 h at room temperature. The solvent was removed under reduced pressure and the residue extracted with CH_2Cl_2 and filtered through celite and concentrated to ≈10 ml. *n*-Hexane was added and the red powdered precipitate was twice washed with the same solvent and dried under reduced pressure.

Yield: 0.25 g, 49%. *Anal*. Calc. for $C_{210}H_{216}F_{36}O_5N_9P_{18}Fe_6$: C, 54.37; H, 4.03; N, 5.19; P, 13.79. Found: C, 54.76; H, 5.7; N, 4.07; P, 13.90%. ^{1}H NMR (CD_3Cl): 7.81(m), 7.74(m), 7.58(m), 7.42(m)(PC_6H_5), 4.36 (s,C_5H_5), 2.16 (CH_3), 0.1 (CH_2). UV/Vis(CH_2Cl_2): $\lambda = 230$ and 451 nm.

*3.2.2.11. Synthesis of [$N_3P_3(N(CH_3)(CH_2)_2CN)_6$·(Ru(Cp)$(PPh_3)_2$)$_6$][$PF_6$]$_6$ (**11**)*. A solution of $CpRu(PPh_3)_2Cl$ 0.1569 g (0.27 mmol) in CH_3OH (30 ml) was stirred with $[N_3P_3(O–C_6H_4–CH_2–CN)_6$ 0.02182 g (0.034 mmol) in the presence of NH_4PF_6 0.6741 g (0.41 mmol) at room temperature for 1 h. The solvent was removed under reduced pressure and the yellow–orange residue extracted with CH_2Cl_2 (15 ml) and filtered through celite. Then reduced in volume and *n*-hexane/dithylether 4:1 mixture was added. The yellow solid precipitate was twice washed with the same mixture and dried.

Yield: 0.41g, 97%. *Anal*. Calc. for $C_{270}H_{252}F_{36}N_{15}P_{18}Ru_6$: C, 59.34; H, 4.34; N, 4.46; P, 11.53. Found: C, 58.79; H, 4.48; N, 2.31; P, 11.9%. ^{1}H NMR (CD_3Cl): 7.8–7.0 (m PC_6H_5), 4.5 (s, C_5H_5), 1.6 (CH_3) 1.3, 0.8 (CH_2). ^{13}C NMR ($CDCl_3$): 134.14, 133.57, 132.38, 132.25, 129.13, 128.96, 128.80($P(C_5H_5)$), 127.85 (CN),

81.8 (C_5H_5), 24.2 (CH_2). UV/Vis(CH_2Cl_2): $\lambda = 235$ and 349 nm.

Acknowledgements

Financial support from FONDECYT, project 1030515, and beca DID,PG-85/2002 (M.B.) U. de Chile, is gratefully acknowledged.

References

[1] (a) G.R. Newkome, E. He, C.H. Moorefield, Chem. Rev. 99 (1999) 1689;
(b) F. Zeng, S.C. Zimmerman, Chem. Rev. 97 (1999) 1681.
[2] M.T. Reetz, G. Lohmer, R. Schwickardi, Angew.Chem. Int. Ed. Engl. 36 (1997) 1526.
[3] F.G.A. Jansen, E.M.M. de Brabander-van den Berg, E.W. Meiser, Recl. Trav. Chim., Pays Bas 114 (1995) 225.
[4] E. Buhleier, W. Wehnen, F. Vögtle, Synthesis 155 (1978).
[5] I.P. Majoral, A.M. Caminade, Chem. Rev. 99 (1999) 845.
[6] V. Balzani, S. Campagna, G. Denti, A. Juris, S. Serroni, M. Venturi, Acc. Chem. Res. 31 (1998) 26.
[7] G.J. Mccubbin, F.J. Stoddart, T. Welton, A.J.P. White, D.J. Williams, Inorg. Chem. 37 (1998) 3753.
[8] (a) R. Schneider, C. Köllner, I. Welbey, A. Togni, J. Chem. Soc. Chem. Commu. 2415 (1999);
(b) M. Gleria, R. Bertani, G. Facchim, F. Noe, R.A. Michelin, M. Mazzon, A.J.L. Pombeiro, M.F.C.G. Da Silva, I.L.F. Machado, J. of, Inorg. Organomet. Polym. 6 (1999) 145;
(c) K.R.J. Thomas, V. Parthasarathy Pal, S.R. Scott, R. Haldford, A.W. Cordes, Inorg. Chem. 32 (1993) 606;
(d) G.A. Carriedo, F.J. Garcia Alonso, P.A. Gonzalez, P. Gomez-Elipe, Polyhedron 18 (1999) 2853.
[9] (a) C. Díaz, M.L. Valenzuela, Polyhedron 21 (2002) 909;
(b) C. Díaz, M.L. Valenzuela, Bol. Soc. Quim 45 (2002) 527.
[10] (a) C. Díaz, I. Izquierdo, F. Mendizabal, N. Yutronic, Inorg. Chim. Acta 294 (1999) 207;
(b) C. Díaz, I. Izquierdo, Polyhedron 18 (1999) 1479;
(c) C. Diaz, F. Mendizabal, Bol. Soc. Chil. Quim. 46 (2001) 293.
[11] (a) For IR data and discussion of IR spectra of $N_3P_3X_6$ and $N_3P_3(OR)_6$ compounds see: S.S. Krishnamurthy, C. Sau, Adv. Inorg. Chem. Radiochem. 21 (1978) 41;
(b) H.R. Allcock, L.J. Wagner, M.L. Levin, J. Am. Chem. Soc. 105 (1983) 1321;
(c) A. Carriedo, F.J.G. Alonso, P.A. Gonzalez, J.R. Menendez, J. Raman Spectrosc. 29 (1998) 27.
[12] C. Diaz, Bol. Soc. Chil. Quim. 44 (1997) 1775.
[13] (a) N.G. Connelly, O.M. Hicks, G.R. Lewis, A. Guy Orpen, A.J. Wood, J. Chem. Soc., Chem. Commun. 517 (1998);
(b) D. Astruc, Electron Transfer and Radical Processes in Transition Metal Chemistry, Wiley, New York, 1995, p. 116, (Chapter 2).

Available online at www.sciencedirect.com
SCIENCE DIRECT®
Polyhedron 23 (2004) 1037–1043
POLYHEDRON
www.elsevier.com/locate/poly

Coupled electron-transfer and spin-exchange reactions of metal–bis[tris(pyrazolyl)methane] complexes

Josie R. Sheets, Franklin A. Schultz *

Department of Chemistry, Indiana University-Purdue University Indianapolis, 402 North Blackford Street, Indianapolis, IN 46202-3274, USA

Received 15 September 2003; accepted 2 January 2004

Abstract

Coupled electron-transfer and spin-exchange reactions of metal(II)–bis[tris(pyrazolyl)methane] complexes, $[M(tpm)_2]^{2+}$, with M = Mn, Fe, Co, or Ni and tpm = $HC(pz)_3$ or $HC(3,5\text{-}Me_2pz)_3$ are reported. Apparent heterogeneous electron-transfer rate constants, $(k_{s,h})_{app}$, for $[M(tpm)_2]^{2+}$ to $[M(tpm)_2]^{3+}$ oxidations are determined from the scan rate dependence of cyclic voltammetric peak potential separations, ΔE_p. Consistent with the expectation that electron-transfer reactions that are accompanied by a change in spin-state are slower than those that are not, $(k_{s,h})_{app}$ for oxidation of high-spin (HS) $\{Fe[HC(3,5\text{-}Me_2pz)_3]_2\}^{2+}$ to low-spin (LS) $\{Fe[HC(3,5\text{-}Me_2pz)_3]_2\}^{3+}$ is 10 times smaller than the value for oxidation of predominantly LS $\{Fe[HC(pz)_3]_2\}^{2+}$ to LS $\{Fe[HC(pz)_3]_2\}^{3+}$. In addition, very small values of $(k_{s,h})_{app}$ are observed for the one-electron oxidations of HS $\{Co[HC(pz)_3]_2\}^{2+}$ and HS $\{Mn[HC(3,5\text{-}Me_2pz)_3]_2\}^{2+}$. The electrochemical, magnetic, and spectroscopic properties of $[M(tpm)_2]^{2+}$ complexes are similar to those of the corresponding tris(pyrazolyl)borate (pzb^-) complexes with the exception that, because of net charge considerations, the M(III/II) potential is ~1 V more positive for $[M(tpm)_2]^{3+/2+}$ than for $[M(pzb)_2]^{+/0}$ couples. The stability of $[M(tpm)_2]^{2+}$ complexes in CH_3CN and DMF solution is investigated by positive ion electrospray ionization mass spectrometry. It is demonstrated that $\{Fe[HC(pz)_3]_2\}^{2+}$ undergoes ligand dissociation in DMF.
© 2004 Elsevier Ltd. All rights reserved.

Keywords: Electron-transfer reactions; Spin-exchange reactions; Bis[tris(pyrazolyl)methane] complexes; Low-spin configurations; High-spin configurations

1. Introduction

Poly(pyrazolyl)borate (pzb^-) ligands are well known for their ability to modulate the magnetic, spectroscopic, and catalytic properties of transition metal compounds [1–3]. Complexes containing the isoelectronic tris(pyrazolyl)methane ligand (tpm, Chart 1) [4] also possess this quality, and interest in these compounds is increasing [5]. Both pzb^- [6–8] and tpm [9,10] support spin-state isomerization in their homoleptic iron(II)-bis(ligand) complexes. Two interesting observations have been reported in this regard. (1) In the solid state, $\{Fe[HC(3,5\text{-}Me_2pz)_3]_2\}(BF_4)_2$ undergoes a thermally induced spin-state transition in which the $Fe^{II}N_6$ center converts from all high-spin (HS, $S = 2$) above 206 K to a 50:50 mixture of HS and low-spin (LS, $S = 0$) forms below 200 K; the composition of the mixture does not change upon further decrease in temperature to 5 K [11–13]. (2) In *N*,*N*-dimethylformamide (DMF) solution, $\{Fe[HC(pz)_3]_2\}^{2+}$ is reported to exist as a slowly equilibrating mixture of LS and HS forms detectable by ^1H NMR spectroscopy [14]. Observation of such behavior is unusual [15], because spin-state conversions are rapid processes in solution [16].

Our laboratory is interested in the mechanism and energetics of coupled electron-transfer and spin-exchange reactions [17–21]. These transformations occur as closely coupled events in many chemical and biological systems, and underlie important catalytic processes [22]. Recently, in surveying the electrochemical, magnetic, and spectroscopic properties of metal–bis(pzb) complexes, we detected examples of coupled electron-transfer and spin-exchange and reported on the influence of metal and ligand structure on such behavior

* Corresponding author. Tel.: +1-317-278-2027; fax: +1-317-274-4701.
E-mail address: schultz@chem.iupui.edu (F.A. Schultz).

0277-5387/$ - see front matter © 2004 Elsevier Ltd. All rights reserved.
doi:10.1016/j.poly.2004.01.004

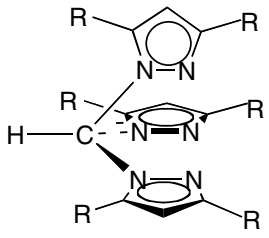

$HC(pz)_3$ R = H

$HC(3,5\text{-}Me_2pz)_3$ R = CH_3

Chart 1. Structures of tris(pyrazolyl)methane (tpm) ligands.

[21]. The present article extends this study to the analogous $[M(tpm)_2]^{2+}$ complexes with M = Mn, Fe, Co, or Ni and tpm = $HC(pz)_3$ or $HC(3,5\text{-}Me_2pz)_3$. Its objectives are to identify additional examples of coupled electron-transfer and spin-exchange and to compare behavior with that of the corresponding pzb^- complexes. In addition, some observations regarding the behavior of $\{Fe[HC(pz)_3]_2\}^{2+}$ in DMF solution are reported.

2. Experimental

2.1. Materials

The $HC(pz)_3$ and $HC(3,5\text{-}Me_2pz)_3$ ligands were prepared from chloroform and the appropriate pyrazole following procedures closely adapted from those of Reger et al. [23]. Details are given in [24]. $\{M[HC(pz)_3]_2\}(BF_4)_2$ and $\{M[HC(3,5\text{-}Me_2pz)_3]_2\}(BF_4)_2$ with M = Fe, Co, and Ni were prepared by drop wise addition of an acetone or tetrahydrofuran (THF) solution of the ligand (2.0 mmol in 10 ml) to a stirred aqueous solution of the hydrated metal(II) tetrafluoroborate (Aldrich, 1.0 mmol in 10 ml). The $HC(pz)_3$ complexes formed as insoluble salts almost immediately. The $HC(3,5\text{-}Me_2pz)_3$ complexes began to form within 5–15 min. These reaction mixtures were stirred overnight to insure complete product formation. $\{Fe[HC(3,5\text{-}Me_2pz)_3]_2\}(BF_4)_2$ formed more slowly than the other complexes. In this case, a 2.5:1 ligand-to-metal mole ratio in THF solvent was employed. Product formation was observed to begin after ca. 30 min, and the reaction mixture was stirred overnight. $\{Mn[HC(3,5\text{-}Me_2pz)_3]_2\}(NO_3)_2$ was prepared in a manner analogous to the other $HC(3,5\text{-}Me_2pz)_3$ complexes by use of hydrated manganese(II) nitrate. A manganese(II) complex with $HC(pz)_3$ could not be prepared. Products were isolated by filtration, washed with water and acetone, and air-dried. Yields were 52–82%. Elemental analyses were performed by Huffman Laboratories (Golden, CO).

Acetonitrile and DMF used for electrochemical and spectroscopic studies were obtained as high purity Burdick and Jackson reagents from VWR and used as received. Tetra-*n*-butylammonium hexafluorophosphate ($TBAPF_6$) supporting electrolyte was used as received from Aldrich.

2.2. Methods

Cyclic voltammetry (CV) experiments were performed by use of a Bioanalytical Systems (BAS) CV-50W potentiostat and employed a three-electrode cell consisting of a BAS glassy carbon working electrode (0.071 cm^2 area), a BAS Ag/AgCl reference electrode (0.236 V versus NHE [25]), and a Pt wire auxiliary electrode. The glassy carbon electrode was polished with diamond paste or an aqueous slurry of alumina prior to each trial. CV experiments were conducted in CH_3CN or DMF solutions containing 1 mM complex and 0.1 M $TBAPF_6$. Solutions were deoxygenated with argon gas and maintained under a blanket of Ar during measurements. Formal potentials were evaluated as $E^{0\prime} = (E_{pa} + E_{pc})/2$, where E_{pa} and E_{pc} are the anodic and cathodic peak potentials. Peak potential separations were evaluated as $\Delta E_p = |E_{pa} - E_{pc}|$. The ferrocene/ferricenium couple ($Fc^{+/0}$) exhibits an $E^{0\prime}$ value of 0.43 V versus Ag/AgCl in 0.1 M $TBAPF_6/CH_3CN$.

Apparent values of the standard heterogeneous electron-transfer rate constant, $(k_{s,h})_{app}$, were determined from cyclic voltammetric peak potential separations as a function of scan rate [26]. Measured values of ΔE_p were corrected for uncompensated solution resistance as described in [27] using a value of $\rho = 1.3 \times 10^2$ Ω cm [28] for the specific resistance of 0.1 M $TBAPF_6/CH_3CN$. The relationship between ΔE_p and $(k_{s,h})_{app}$ was established by digital simulation (DigiSim 3.03, Bioanalytical Systems [29]) using values of $\alpha = 0.50$, $D = 8.0 \times 10^{-6}$ $cm^2\ s^{-1}$, and $T = 295$ K.

The magnetic susceptibilities of solid samples of the complexes were determined by use of a Johnson Matthey MSB-1 balance at ambient temperature (295 K). The molar susceptibility, χ_M, determined as $\chi_M = \chi_V \times MW/\rho$ from the volume susceptibility (χ_V), density (ρ), and molecular weight (MW) of the sample, was corrected for the diamagnetic contributions of the ligands, metal core electrons, and counter ions [30] to yield $\chi_{M'}$. The effective magnetic moment was calculated as $\mu_{eff} = 2.83(\chi_{M'} \times T)^{1/2}$.

Electrospray ionization mass spectrometry was performed by use of a PE Sciex API III mass analyzer. Dinitrogen, obtained as the boil-off of liquid N_2, was employed as the curtain gas (0.8–1.0 l min^{-1}). The normal operating pressure and temperature were ca. 3×10^{-5} atm and 17 K, respectively. A syringe pump set

at a flow rate of 2–10 μl min^{-1} was used to introduce 1×10^{-3} M solutions of the complexes in CH_3CN or DMF.

Electronic spectra were obtained by use of an Agilent 8453A or a PE Lambda 19 spectrometer. Variable temperature measurements were conducted on the PE instrument equipped with a Neslab RTE-111 temperature control unit.

3. Results

3.1. Synthesis

The complexes were formed by addition of an acetone or THF solution of the ligand to an aqueous solution of the hydrated metal salt. Either acetone or THF is a suitable solvent for these preparations, but a more lustrous microcystalline product is obtained by use of acetone. All results reported are for acetone derived materials with the exception of $\{Fe[HC(3,5\text{-}Me_2pz)_3]_2\}(BF_4)_2$, in which case it is necessary to use THF as solvent. Elemental analyses are presented in Table 1 and are consistent with the formulation of the products as metal(II)–bis[tris(pyrazolyl)methane] complexes.

3.2. Magnetism and spectroscopy

Magnetic moments of the divalent bis(tpm) salts are collected in Table 1. Results are consistent with a high-spin metal(II) center in all cases except $\{Fe[HC(pz)_3]_2\}(BF_4)_2$, where the value $\mu_{eff} = 0.98\ \mu_B$ is indicative of predominantly low-spin Fe(II). The red-violet color of $\{Fe[HC(pz)_3]_2\}(BF_4)_2$ in comparison with the colorless appearance of $\{Fe[HC(3,5\text{-}Me_2pz)_3]_2\}(BF_4)_2$ is consistent with this observation. The spin-equilibrium behavior of $\{Fe[HC(pz)_3]_2\}^{2+}$ in CH_3CN solution was investigated by visible spectroscopy. The complex exhibits a ligand field absorption band at 523 nm, which obeys Beer's law at 295 K. The intensity of the band increases upon cooling. Analysis of the temperature-dependent absorbance, $A(T)$, from 283 to 338 K by use of following equation [31]:

$$A(T) = A(0)/[\exp(\Delta S^0_{SE}/R)\exp(-\Delta H^0_{SE}/RT) + 1], \quad (1)$$

where $A(0)$ is the absorbance at 0 K (obtained by extrapolation), yields values of $\Delta H^0_{SE} = 25$ kJ mol^{-1}, $\Delta S^0_{SE} = 63$ J mol^{-1} K^{-1}, $\varepsilon_{LS} = 81$ M^{-1} cm^{-1}, and $K^{298}_{SE} = 0.08$ for the $LS \leftrightarrows HS$ equilibrium of $\{Fe[HC(pz)_3]_2\}^{2+}$. These findings are in agreement with the results of McGarvey et al. [9] and indicate the

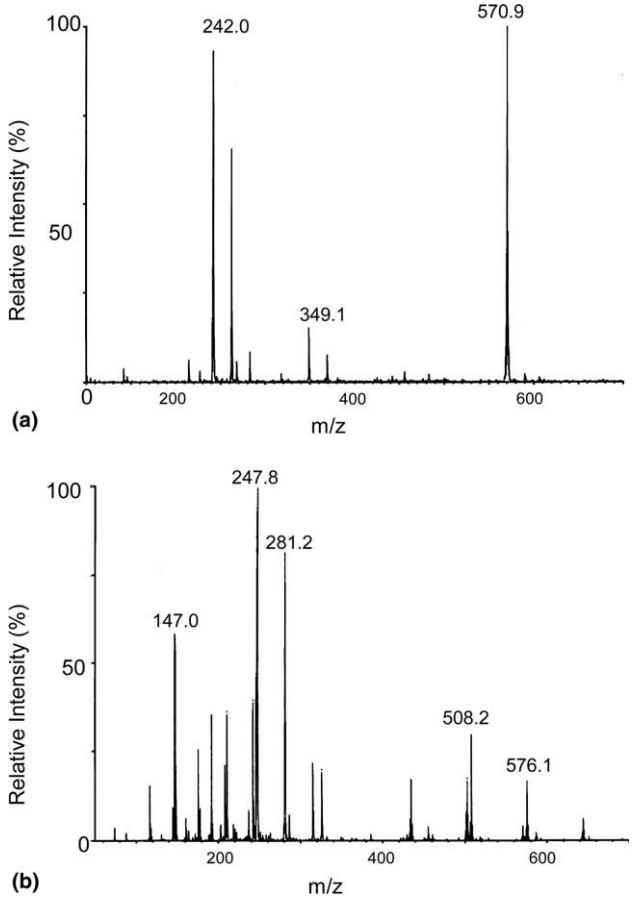

Fig. 1. Positive ion electrospray mass spectrum of $\{Fe[HC(pz)_3]_2\}(BF_4)_2$ in (a) CH_3CN and (b) DMF.

Table 1
Analytical, magnetic, and mass spectrometric data for $[M(tpm)_2]^{2+}$ complexes

Complex	Anal. Calc. (found) (%)			μ_{eff} (μ_B)[a]	m/z Calc. (found)	
	C	H	N		$[M(tpm)_2]^{2+}$	$\{[M(tpm)_2](BF_4)\}^+$
$\{Fe[HC(pz)_3]_2\}(BF_4)_2$	36.51 (36.06)	3.06 (3.22)	25.55 (24.74)	0.98	242.1 (242.0)	571.1 (570.9)
$\{Co[HC(pz)_3]_2\}(BF_4)_2$	36.34 (36.68)	3.05 (3.15)	25.43 (25.15)	4.79	243.6 (243.3)	574.1 (573.0)
$\{Ni[HC(pz)_3]_2\}(BF_4)_2$	36.35 (36.25)	3.05 (3.16)	25.44 (25.00)	2.94	243.1 (242.0)	573.1 (572.0)
$\{Mn[HC(3,5\text{-}Me_2pz)_3]_2\}(NO_3)_2$	49.55 (49.30)	5.71 (5.83)	25.27 (24.93)	6.18		
$\{Fe[HC(3,5\text{-}Me_2pz)_3]_2\}(BF_4)_2$	46.52 (45.55)	5.37 (5.35)	20.34 (19.55)	5.28	326.2 (324.9)	739.3 (738.9)
$\{Co[HC(3,5\text{-}Me_2pz)_3]_2\}(BF_4)_2$	46.34 (46.46)	5.35 (5.50)	20.27 (19.84)	4.60	327.7 (326.9)	742.3 (741.7)
$\{Ni[HC(3,5\text{-}Me_2pz)_3]_2\}(BF_4)_2$	46.36 (46.27)	5.35 (5.43)	20.27 (19.92)	2.95	327.2 (326.3)	741.3 (742.0)

[a] At 295 K.

presence of ~7% high-spin $\{Fe[HC(pz)_3]_2\}^{2+}$ in CH_3CN solution at 295 K. In contrast, the red-violet color of $\{Fe[HC(pz)_3]_2\}^{2+}$ and its 523-nm absorption band disappear when $\{Fe[HC(pz)_3]_2\}(BF_4)_2$ is dissolved in DMF. These features are partially restored by addition of excess $HC(pz)_3$.

The principal peaks observed by positive ion electrospray mass spectrometry of acetonitrile solutions of the complexes are collected in Table 1. The major signals observed are those corresponding to the doubly charged molecular ion, $[M(tpm)_2]^{2+}$, and to its 1:1 ion pair, $\{[M(tpm)_2](BF_4)\}^{+}$. The mass spectrum of $\{Fe[HC(pz)_3]_2\}(BF_4)_2$ in CH_3CN (Fig. 1(a)), which exhibits peaks at $m/z = 242.0$ ($\{Fe[HC(pz)_3]_2\}^{2+}$) and $m/z = 570.9$ ($\{Fe[HC(pz)_3]_2(BF_4)\}^{+}$), illustrates this behavior. Surprisingly, this compound exhibits a very different mass

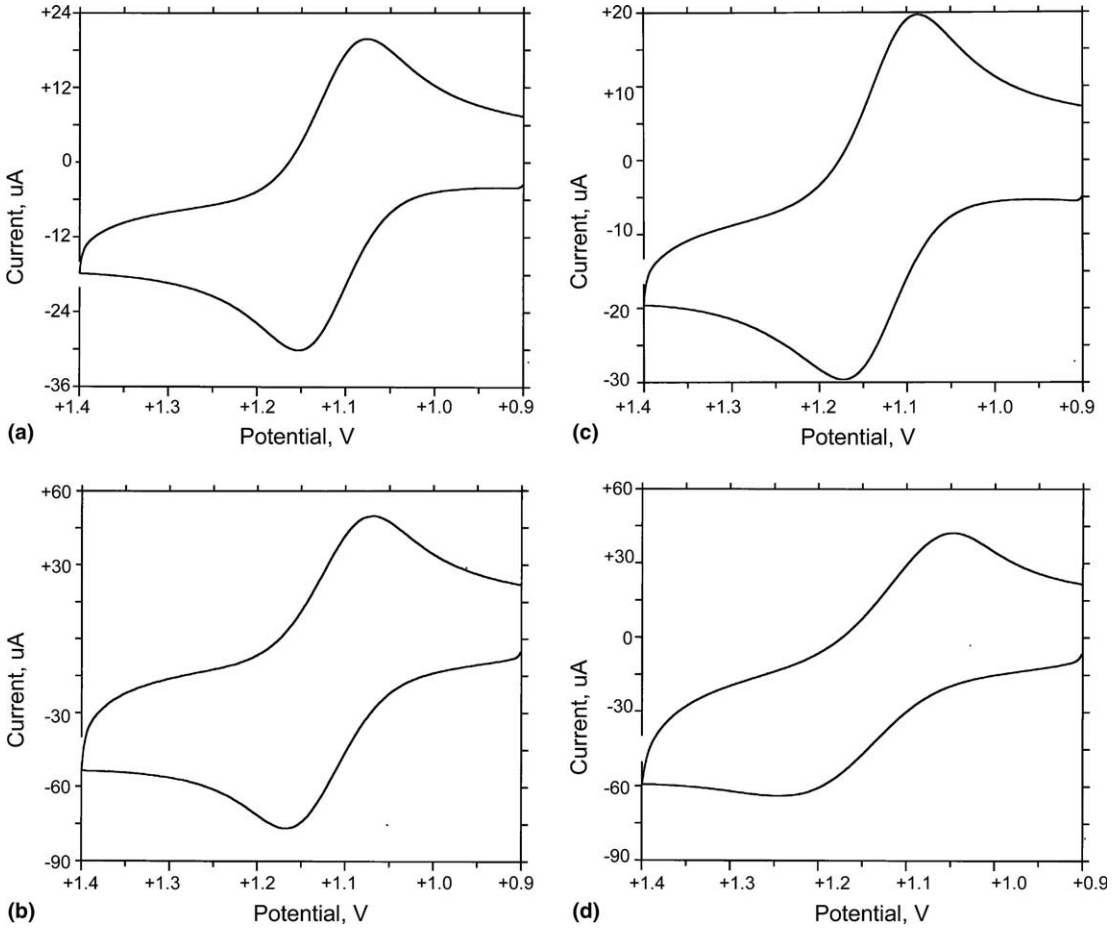

Fig. 2. Cyclic voltammetry in 0.1 M $TBAPF_6/CH_3CN$ of 1×10^{-3} M $\{Fe[HC(pz)_3]_2\}(BF_4)_2$ at (a) $v = 0.2$ V s^{-1}, (b) $v = 1.0$ V s^{-1} and of 1×10^{-3} M $\{Fe[HC(3,5\text{-}Me_2pz)_3]_2\}(BF_4)_2$ at (c) $v = 0.2$ V s^{-1}, (d) $v = 1.0$ V s^{-1}.

Table 2
Cyclic voltammetric data for oxidation of iron(II)-bis[tris(pyrazolyl)methane] complexes[a]

$\{Fe[HC(pz)_3]_2\}(BF_4)_2$					$\{Fe[HC(3,5\text{-}Me_2pz)_3]_2\}(BF_4)_2$			
v (V s^{-1})	$E^{0\prime}$ (V)[b]	ΔE_p (mV)	i_{pr}/i_{pf}	$i_p/v^{1/2}$ AC (μA $s^{1/2}$ $V^{-1/2}$ cm^{-2} mM^{-1})	$E^{0\prime}$ (V)[b]	ΔE_p (mV)	i_{pr}/i_{pf}	$i_p/v^{1/2}$ AC (μA $s^{1/2}$ $V^{-1/2}$ cm^{-2} mM^{-1})
0.05	1.12	69	1.1	800	1.13	75	1.1	750
0.10	1.12	68	1.1	800	1.13	79	1.1	750
0.20	1.12	74	1.1	810	1.13	81	1.1	770
0.40	1.12	80	1.0	770	1.13	110	1.0	640
0.60	1.12	83	1.1	750	1.14	110	1.0	620
0.80	1.11	88	1.1	770	1.14	130	1.0	580
1.00	1.11	91	1.1	770	1.13	170	1.1	520

[a] Recorded in 0.1 M $TBAPF_6/CH_3CN$.
[b] V vs. Ag/AgCl.

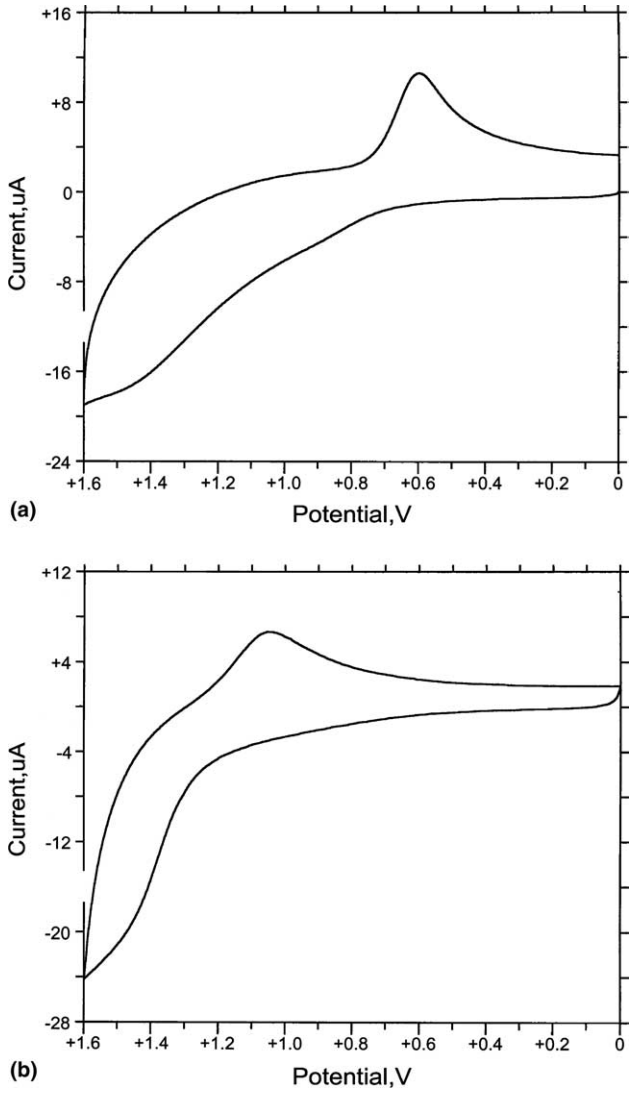

Fig. 3. Cyclic voltammetry in 0.1 M $TBAPF_6/CH_3CN$ of (a) 1×10^{-3} M $\{Co[HC(pz)_3]_2\}(BF_4)_2$ at $v = 0.2$ V s^{-1} and (b) 1×10^{-3} M $\{Mn[HC(3,5\text{-}Me_2pz)_3]_2\}(NO_3)_2$ at $v = 0.05$ V s^{-1}.

spectral response in DMF. As shown in Fig. 1(b), peaks corresponding to the molecular ions are absent and are replaced by peaks assignable to species such as $[Fe(DMF)_6]^{2+}$ ($m/z = 247.8$), $\{Fe[HC(pz)_3]\text{-}(DMF)_4\}^{2+}$ ($m/z = 281.2$), $[Fe(DMF)_5(BF_4)]^{+}$ ($m/z = 508.2$), and $\{Fe[HC(pz)_3](DMF)_3(BF_4)\}^{+}$ ($m/z = 576.1$). In contrast, the mass spectrum of $\{Fe[HC(3,5\text{-}Me_2pz)_3]_2\}(BF_4)_2$ in DMF is unchanged from that in CH_3CN.

3.3. Electrochemistry

The electrochemical behavior of the $[Fe(tpm)_2]^{2+}$ complexes in CH_3CN is illustrated in Fig. 2. Cyclic voltammetric data as a function of scan rate (v) are collected in Table 2. Each complex exhibits a chemically reversible oxidation at ca. 1.1 V corresponding to the electrode reaction in Eq. (2) with M = Fe

$$[M(tpm)_2]^{2+} \leftrightarrows [M(tpm)_2]^{3+} + e^- \quad E^{0\prime}, (k_{s,h})_{app} \qquad (2)$$

For $\{Fe[HC(pz)_3]_2\}^{2+}$, i_p varies linearly with $v^{1/2}$, $i_p/v^{1/2}$ AC exhibits a constant value of 780 ± 20 μA $s^{1/2}$ $V^{-1/2}$ cm^{-2} mM^{-1} that is consistent with a one-electron transfer in CH_3CN [32], and ΔE_p increases to a small extent above the anticipated value of 58 mV [26] as v increases from 0.05 to 1.0 V s^{-1}. These increments in ΔE_p are only 5–10 mV larger than the amounts calculated to arise from the uncompensated solution resistance of 0.1 M $TBAPF_6/CH_3CN$ [27] and are consistent with a value of $(k_{s,h})_{app} \geqslant 0.2$ cm s^{-1} for the $\{Fe[HC(pz)_3]_2\}^{3+/2+}$ couple. For $\{Fe[HC(3,5\text{-}Me_2pz)_3]_2\}^{2+}$, the anodic wave broadens, the variation of i_p with $v^{1/2}$ is not rigorously linear, and ΔE_p increases to a much greater extent as v is increased over the same scan rate interval. These results are consistent with charge-transfer limitation of the electrode reaction [26]. Comparison of the experimental scan rate dependence of ΔE_p with that obtained by digital simulation leads to a value of $(k_{s,h})_{app} = 1.7 \pm 0.7 \times 10^{-2}$ cm s^{-1} for $\{Fe[HC(3,5\text{-}Me_2pz)_3]_2\}^{3+/2+}$.

The electrochemical behavior of $\{Fe[HC(3,5\text{-}Me_2pz)_3]_2\}^{2+}$ in DMF is similar to that observed in CH_3CN. However, the anodic and cathodic responses that are characteristic of Eq. (2) with M = Fe vanish

Table 3
Electrochemical data for $[M(tpm)_2]^{3+/2+}$ and $[M(pzb)_2]^{+/0}$ redox couples

Metal	Pyrazole	$[M(tpm)_2]^{3+/2+}$ [a]		$[M(pzb)_2]^{+/0}$ [b]	
		$E^{0\prime}$ (V) vs. $Fe^{+/0}$	$(k_{s,h})_{app}$ (cm s^{-1})	$E^{0\prime}$ (V) vs. $Fe^{+/0}$	$(k_{s,h})_{app}$ (cm s^{-1})
Fe	Pz	0.69	$\geqslant 2\times10^{-1}$	−0.27	2×10^{0} [c]
	3,5-Me_2pz	0.70	1.7×10^{-2}	−0.44	9×10^{-2} [c]
Co	Pz	0.61	1.3×10^{-6}	−0.53	1.9×10^{-4}
	3,5-Me_2pz	[d]	[d]	−0.58	2.2×10^{-5}
Mn	Pz	[d]	[d]	0.06	5.3×10^{-5}
	3,5-Me_2pz	0.85	7.6×10^{-5}	−0.13	5.9×10^{-4}

[a] In 0.1 M $TBAPF_6/CH_3CN$.
[b] In 0.1 M $TBAPF_6$/1,2-dichloroethane from [21].
[c] In 1:1 acetone/tetrahydrofuran containing 0.1 M $TBAPF_6$ from [20].
[d] Not observed.

when $\{Fe[HC(pz)_3]_2\}(BF_4)_2$ is dissolved in DMF. They are replaced by a kinetically sluggish electrode reaction whose characteristics ($E^{0\prime} = 0.6$ V, $i_{pr}/i_{pf} \sim 1$, $\Delta E_p =$ mV at $v = 0.3$ V s^{-1}) are similar to those that appear when $[Fe(H_2O)_6](BF_4)_2$ is added to 0.1 M $TBAPF_6$/DMF. Addition of excess $HC(pz)_3$ to either $\{Fe[HC(pz)_3]_2\}(BF_4)_2$ or $[Fe(H_2O)_6](BF_4)_2$ dissolved in DMF partially restores the voltammetric response at 1.1 V.

The complexes $\{Co[HC(pz)_3]_2\}^{2+}$ and $\{Mn[HC(3,5\text{-}Me_2pz)_3]_2\}^{2+}$ also are electrochemically active in CH_3CN. $\{Co[HC(pz)_3]_2\}^{2+}$exhibits a broad anodic wave extending from 0.8 to 1.6 V that is followed by a more well-defined cathodic peak at 0.6 V on scan reversal (Fig. 3(a)). $\{Mn[HC(3,5\text{-}Me_2pz)_3]_2\}^{2+}$ undergoes oxidation at 1.2–1.6 V followed by a cathodic peak at 1.0 V (Fig. 3(b)). A poorly defined voltammetric oxidation wave (not shown) is observed for $\{Co[HC(3,5\text{-}Me_2pz)_3]_2\}^{2+}$ in CH_3CN. The Ni(II) complexes could not be oxidized within the potential window of the solvent.

The electrochemical responses illustrated in Fig. 3 are assigned to the one-electron electrode reactions described by Eq. (2) with M = Co or Mn. The reactions are electrochemically irreversible, and it is evident based on peak potential separations that the heterogeneous electron-transfer kinetics of these couples are much slower than those of the $[Fe(tpm)_2]^{3+/2+}$ couples. Values of $(k_{s,h})_{app} = 1.3 \times 10^{-6}$ and 7.6×10^{-5} cm s^{-1} are estimated for $\{Co[HC(pz)_3]_2\}^{3+/2+}$ and $\{Mn[HC(3,5\text{-}Me_2pz)_3]_2\}^{3+/2+}$, respectively. Electrochemical data for all $[M(tpm)_2]^{3+/2+}$ couples are summarized in Table 3, where they are compared with results for the corresponding $[M(pzb)_2]^{+/0}$ complexes in 1,2-dichloroethane. Because of the difference in solvents, electrode potentials are referred to the $E^{0\prime}$ of $Fc^{+/0}$.

4. Discussion

4.1. Electrochemical, magnetic, and spectroscopic properties

The homoleptic $[M(tpm)_2]^{2+}$ complexes with M = Mn, Co, and Ni exhibit magnetic and spectroscopic properties that are consistent with assignment of these compounds as HS metal(II) species (Table 1). The magnetic properties of the $[Fe(tpm)_2]^{2+}$ complexes are influenced by the identity of the pyrazole ring substituents. $\{Fe[HC(3,5\text{-}Me_2pz)_3]_2\}^{2+}$ is entirely HS, whereas $\{Fe[HC(pz)_3]_2\}^{2+}$participates in a LS ⇆ HS equilibrium that produces ~7% HS Fe(II) in solution at 295 K. The corresponding $Fe[HB(3,5\text{-}Me_2pz)_3]_2$ and $Fe[HB(pz)_3]_2$ complexes exhibit similar behavior [6–8,20].

Although the magnetic and spectroscopic properties of metal–bis(tpm) and metal–bis(pzb) complexes are quite similar, their electrochemical properties are distinct. As documented in Table 3, values of $E^{0\prime}$ are about 1 V more positive for $[M(tpm)_2]^{3+/2+}$ than for $[M(pzb)_2]^{+/0}$ couples. The difference reflects the importance of net charge on the metal-centered oxidation potentials. However, it is noteworthy that the $\{M[HC(pz)_3]_2\}^{3+/2+}$ potentials also are 0.9–1.7 V more positive than the $E^{0\prime}$ values of the corresponding $[M(tacn)_2]^{3+/2+}$ (tacn = 1,4,7-triazacyclononane) complexes and approximately equal to (or in the case of $\{Co[HC(pz)_3]_2\}^{3+/2+}$ more positive than) the $E^{0\prime}$ values of $[M(bpy)_2]^{3+/2+}$ (bpy = 2,2′-bipyridine) [21]. These observations indicate that tris(pyrazolyl)methane is highly effective in stabilizing M(II) versus M(III) oxidation states.

The tris(pyrazolyl)methane complexes described in this work also undergo coupled electron-transfer and spin-exchange reactions. As shown in Table 3, the apparent kinetics of reaction (2) are a function of the metal ion and the ligand. These factors also influence spin-state distributions. On the basis of ligand field considerations [33], the M(III) species are assigned a low-spin configuration. This is based on the observation that in the corresponding $[M(pzb)_2]^+$ and $[M(tacn)_2]^{3+}$ complexes, where pzb^- and tacn exhibit a ligand field strength comparable to that of tpm [21], the metals also are low-spin. Thus, the largest value of $(k_{s,h})_{app}$ for $[M(tpm)_2]^{3+/2+}$ couples is observed for the reaction in which predominantly LS $\{Fe[HC(pz)_3]_2\}^{2+}$ is oxidized to LS $\{Fe[HC(pz)_3]_2\}^{3+}$. Oxidation of HS $\{Fe[HC(3,5\text{-}Me_2pz)_3]_2\}^{2+}$ to LS $\{Fe[HC(3,5\text{-}Me_2pz)_3]_2\}^{3+}$, which is accompanied by spin conversion, exhibits a value of $(k_{s,h})_{app}$ that is 10 times smaller. The relative values of $(k_{s,h})_{app}$ for $Fe[HB(pz)_3]_2^{+/0}$ and $Fe[HB(3,5\text{-}Me_2pz)_3]_2^{+/0}$ are quite similar (Table 3). These results are consistent with the expectation [34–36] that electron-transfer reactions that are accompanied by a change in spin state are slower than those that are not. Such behavior can be interpreted [19,20] in terms of the mechanistic pathway shown in Fig. 4 (an electrochemical scheme of squares [37]), wherein spin-exchange is viewed as a rapidly established chemical equilibrium that decreases $(k_{s,h})_{app}$ by depleting the population of forms involved in electron-transfer. Relationships between $(k_{s,h})_{app}$ and the thermodynamic spin-equilibrium parameters that describe these distributions are derived in [19,20].

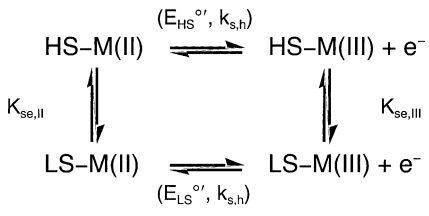

Fig. 4. Mechanism of coupled electron-transfer and spin-exchange.

Slow charge transfer also is observed for $\{Co[HC(pz)_3]_2\}^{3+/2+}$ and $\{Mn[HC(3,5\text{-}Me_2pz)_3]_2\}^{3+/2+}$. In these cases, $(k_{s,h})_{app}$ is much smaller than it is for $\{Fe[HC(pz)_3]_2\}^{3+/2+}$ or $\{Fe[HC(3,5\text{-}Me_2pz)_3]_2\}^{3+/2+}$. Moreover, $(k_{s,h})_{app}$ is uniformly 10–100 times smaller for all $[M(tpm)_2]^{3+/2+}$ couples in comparison to $[M(pzb)_2]^{+/0}$. These observations illustrate that metal ion and ligand can alter the apparent kinetics of reactions that involve coupled electron-transfer and spin-exchange. A possible explanation of this behavior is that reactions of this type must proceed through minor HS-M(III) or LS-M(II) intermediates, the populations of which can be very dependent on metal ion or ligand. Investigation of the basis for the observed range of kinetic behavior is continuing in our laboratory.

4.2. Solution behavior of $[Fe(tpm)_2]^{2+}$ complexes

The integrity of $[Fe(tpm)_2]^{2+}$ complexes is maintained in CH_3CN solution. However, $\{Fe[HC(pz)_3]_2\}(BF_4)_2$ undergoes ligand dissociation when dissolved in DMF. Mass spectrometry provides the strongest evidence of this behavior. Ligand dissociation also is evident by visible spectroscopy and electrochemistry. Although discrete complexes such as $\{Fe[HC(3,5\text{-}Me_2pz)_3](H_2O)_3\}^{2+}$ [38] and $[Fe(1,4,7\text{-trimethyl-}1,4,7\text{-triazacyclononane})(CH_3CN)_3]^{2+}$ [39] have been produced under particular conditions, the mass spectrum in Fig. 1(b) suggests that a range of solvated products including completely dissociated forms is produced. Our results support the interpretation of Toftlund [15] that ligand dissociation rather than slow exchange of LS and HS forms of $\{Fe[HC(pz)_3]_2\}^{2+}$ [14] occurs in DMF.

$\{Fe[HC(3,5\text{-}Me_2pz)_3]_2\}(BF_4)_2$ exhibits no evidence of ligand dissociation when dissolved in DMF. The difference in behavior between $\{Fe[HC(pz)_3]_2\}^{2+}$ and $\{Fe[HC(3,5\text{-}Me_2pz)_3]_2\}^{2+}$ is surprising, because it is anticipated that the HS character of the latter complex would promote ligand dissociation. However, it was noted during synthesis that a longer reaction time and excess ligand were required to form $\{Fe[HC(3,5\text{-}Me_2pz)_3]_2\}(BF_4)_2$, whereas $\{Fe[HC(pz)_3]_2\}(BF_4)_2$ was produced quickly. Thus, the kinetics of ligand binding and dissociation may be slower in the case of $\{Fe[HC(3,5\text{-}Me_2pz)_3]_2\}^{2+}$.

Acknowledgements

Support of this research by the National Science Foundation (CHE-9988694) is gratefully acknowledged. The authors thank James Ashworth for helpful preliminary experiments and Dr. Bruce Young for help with mass spectrometry.

References

[1] S. Trofimenko, Chem. Rev. 93 (1993) 943.
[2] N. Katijima, W.B. Tolman, Prog. Inorg. Chem. 43 (1995) 419.
[3] S. Trofimenko, Scorpionates–The Coordination Chemistry of Polypyrazolylborate Ligands, Imperial College Press, London, 1999.
[4] S. Trofimenko, J. Am. Chem. Soc. 92 (1970) 5118.
[5] D.L. Reger, Comments Inorg. Chem. 21 (1999) 1.
[6] J.P. Jesson, S. Trofimenko, D.R. Eaton, J. Am. Chem. Soc. 89 (1967) 3158.
[7] J.K. Beattie, R.A. Binstead, R.J. West, J. Am. Chem. Soc. 100 (1968) 3044.
[8] Th. Buchen, P. Gütlich, Inorg. Chim. Acta 231 (1995) 221.
[9] J.J. McGarvey, H. Toftlund, A.H.R. Al-Obaidi, K.P. Taylor, S.E.J. Bell, Inorg. Chem. 32 (1993) 2469.
[10] P.A. Anderson, T. Astley, M.A. Hitchman, F.R. Keene, B. Moubaraki, K.S. Murray, B.W. Skelton, E.R.T. Tiekink, H. Toftlund, A.H. White, J. Chem. Soc., Dalton Trans. (2000) 3505.
[11] D.L. Reger, C.A. Little, A.L. Rheingold, M. Lam, T. Concolino, A. Mohan, G.J. Long, Inorg. Chem. 39 (2000) 4674.
[12] D.L. Reger, C.A. Little, V.G. Young Jr., M. Pink, Inorg. Chem. 40 (2001) 2870.
[13] D.L. Reger, C.A. Little, M.D. Smith, G.J. Long, Inorg. Chem. 41 (2002) 4453.
[14] D.L. Reger, C.A. Little, A.L. Rheingold, M. Lam, L.M. Liable-Sands, B. Rhagitan, T. Concolino, A. Mohan, G.J. Long, V. Briois, F. Grandjean, Inorg. Chem. 40 (2001) 1508.
[15] H. Toftlund, Monatsh. Chem. 132 (2001) 1269.
[16] J.K. Beattie, Adv. Inorg. Chem. 32 (1988) 1.
[17] J.W. Turner, F.A. Schultz, Inorg. Chem. 38 (1999) 358.
[18] J.W. Turner, F.A. Schultz, Inorg. Chem. 40 (2001) 5296.
[19] J.W. Turner, F.A. Schultz, Coord. Chem. Rev. 219–221 (2001) 81.
[20] J.W. Turner, F.A. Schultz, J. Phys. Chem. B 106 (2002) 2009.
[21] D.C.L. DeAlwis, F.A. Schultz, Inorg. Chem. 42 (2003) 3616.
[22] D. Schröder, S. Shaik, H. Schwarz, Acc. Chem. Res. 33 (2000) 139.
[23] D.L. Reger, T.C. Grattan, K.J. Brown, C.A. Little, J.J.S. Lamba, A.L. Rheingold, R.D. Sommer, J. Organomet. Chem. 607 (2000) 126.
[24] J. Sheets, M.S. Thesis, Indiana University-Purdue University Indianapolis, IN, 2003.
[25] Q. Yu, C.A. Salhi, E.A. Ambundo, M.J. Heeg, L.A. Ochrymowycz, D.B. Rorabacher, J. Am. Chem. Soc. 123 (2001) 5720.
[26] A.J. Bard, L.R. Faulkner, Electrochemical Methods: Fundamentals and Applications, 2nd ed., Wiley, New York, 2001.
[27] W.J. Bowyer, E.E. Engelman, D.H. Evans, J. Electroanal. Chem. 262 (1989) 67.
[28] K.M. Kadish, J.Q. Ding, T. Malinski, Anal. Chem. 56 (1984) 1741.
[29] M. Rudolph, D.R. Reddy, S. Feldberg, Anal. Chem. 66 (1994) 589A.
[30] R.S. Drago, Physical Methods for Chemists, 2nd ed., Surfside Scientific Publishers, Gainesville, FL, 1992.
[31] L.L. Martin, R.L. Martin, A.M. Sargeson, Polyhedron 13 (1994) 1969.
[32] J.R. Bradbury, F.A. Schultz, Inorg. Chem. 25 (1986) 4408.
[33] B.N. Figgis, M.A. Hitchman, Ligand Field Theory and Its Applications, Wiley–VCH, New York, 2000.
[34] H. Yasuda, K. Suga, S. Aoyagui, J. Electroanal. Chem. 86 (1978) 259.
[35] K.M. Kadish, C.H. Su, L.J. Wilson, Inorg. Chem. 21 (1982) 2312.
[36] P. Hendry, A. Ludi, Adv. Inorg. Chem. 35 (1990) 117.
[37] S.A. Lerke, D.H. Evans, S. Feldberg, J. Electroanal. Chem. 296 (1990) 299.
[38] D.L. Reger, C.A. Little, A.L. Rheingold, R. Sommer, G.J. Long, Inorg. Chim. Acta 316 (2001) 65.
[39] D.W. Blakesley, S.C. Payne, K.S. Hagen, Inorg. Chem. 39 (2000) 1979.

Available online at www.sciencedirect.com
SCIENCE DIRECT®
Polyhedron 23 (2004) 1045–1053
POLYHEDRON
www.elsevier.com/locate/poly

Synthesis and reactivity of $[Re(ClCH_2Cl)(CO)_3L][A]$ and $[Re(OSO_2CF_3)(CO)_3L]$ ($L = Ph_2PO(CH_2)_2OPPh_2$; $A = BF_4$, $[B\{3,5\text{-}(CF_3)_2C_6H_3\}_4]$): the crystal structure of $[Re(OSO_2CF_3)(CO)_3L]$ and $[Re(NCCH_3)(CO)_3L][BF_4]$

María C. Rodríguez [a], Jorge Bravo [a], Eduardo Freijanes [a], Enrique Oñate [b], Soledad García-Fontán [a,*], Pilar Rodríguez-Seoane [a]

[a] Departamento de Química Inorgánica, Universidade de Vigo, E-36200 Vigo, Spain
[b] Departamento de Química Inorgánica, Universidad de Zaragoza, Spain

Received 28 October 2003; accepted 5 January 2004

Abstract

The previously reported complex $[ReBr(CO)_3L]$ (L = 1,2-bis[diphenylphosphinite]ethane) was reacted with $AgBF_4$ in dichloromethane to yield *fac*-$[Re(ClCH_2Cl)(CO)_3L][BF_4]$ (**1**). By contrast, reaction of the same starting material with AgOTf (OTf = OSO_2CF_3) afforded the neutral complex *fac*-$[Re(OTf)(CO)_3L]$ (**2**). When **2** was treated with $NaBAr_F$ ($BAr_F = [B\{3,5\text{-}(CF_3)_2C_6H_3\}_4]$) in the same solvent, the complex *fac*-$[Re(ClCH_2Cl)(CO)_3L][BAr_F]$ (**3**) was formed. Substitution of the loosely held ligand CH_2Cl_2 in **1** and **3** resulted in the formation of compounds of the type $[Re(X)(CO)_3L][A]$ ($X = H_2O$, CH_3CN; $A = BF_4^-$, BAr_F^-), whereas the removal of OTf in **2** only was possible to form $[Re(NCCH_3)(CO)_3L][OTf]$. All the new complexes were characterized by ^1H, $^{13}C\{^1H\}$, $^{31}P\{^1H\}$ and $^{19}F\{^1H\}$ NMR as well as by IR spectroscopies. In the case of compounds **2** and $[Re(NCCH_3)(CO)_3L][BF_4]$, X-ray suitable crystals were isolated. In both cases, the Re atom adopts six-coordination by bonding to the three CO ligands, the two P atoms of L and either the oxygen atom of the OTf anion or the N atom of CH_3CN.
© 2004 Elsevier Ltd. All rights reserved.

Keywords: Rhenium(I); Phosphinite ligands; Dichloromethane complexes; Crystal structures

1. Introduction

The synthesis of solvent-coordinated cationic complexes possessing a non-coordinating anion is a matter of considerable interest, since they are useful as a source of other species resulting from the substitution of the coordinated solvent for a more basic ligand [1–8]. Furthermore, the lability of the solvent ligand gives easily rise to a highly reactive 16e electrophilic fragment able to activate small molecules such as H_2, alkanes, silanes, etc., and, so that, to provide an important step in many chemical processes. However, the success in isolating this kind of compounds stems, on the one hand, from the good fortune in the choice of the appropriate solvent (polar enough to provide adequate solubility of the ionic complex but not basic enough to bind irreversibly with the metal centre); on the other, from the presence of a non-interacting counterion. In this respect, the isolation of stable dichloromethane complexes where CH_2Cl_2 behaves as either monodentate or bidentate ligand towards a cationic metal centre has been the object of a number of reports, despite this compound has been traditionally considered as a non-coordinating solvent [9,10].

We describe in this paper the synthesis and characterization of some new cationic complexes containing CH_2Cl_2 as a monodentate ligand and BF_4 or BAr_F as counterions, as well as the substitution of dichloromethane, either for tetrafluoroborate (normally thought to be a low-interacting anion), or for more active ligands

* Corresponding author. Tel.: +34-986-812-549; fax: +34-986-813-798.
E-mail address: erivas@uvigo.es (S. García-Fontán).

0277-5387/$ - see front matter © 2004 Elsevier Ltd. All rights reserved.
doi:10.1016/j.poly.2004.01.003

such as H_2O and acetonitrile. The crystal structures of two of the prepared complexes are also reported.

2. Experimental

2.1. Materials and instrumentation

All synthetic operations were performed under dry argon. A standard vacuum system and Schlenk type glassware were used in handling metal complexes. Solvents were pre-dried over sodium wire or calcium chloride before reflux and subsequent distillation, under argon, from a suitable drying agent. Deuterated solvents for NMR measurements (Aldrich) were dried over molecular sieves. All the commercially available reagents were used as supplied.

Elemental analyses were performed with a Fisons EA-1108 apparatus. Melting points were determined using a GallenKamp MFB-595 apparatus and were uncorrected. Conductivity measurements were carried out on a Crison GLP-32 conductivity meter. IR spectra of samples in KBr pellets were recorded on a Bruker Vector IFS28 FT spectrophotometer, and NMR spectra (at room temperature) on a Bruker AMX 400 spectrometer. ^1H and $^{13}C\{^1H\}$ signals are referred to internal TMS, $^{31}P\{^1H\}$ chemical shifts to 85% H_3PO_4, and $^{19}F\{^1H\}$ signals to $CFCl_3$ with downfield shifts considered positive. Mass spectra were recorded in the LSIMS, Cs^+ mode on a Micromass Autospec M instrument.

2.2. X-ray diffraction

Crystallographic data were collected on a Bruker Smart 1000 CCD diffractometer at 293 K (complex **2**) or at 120 K (complex **1a**) using Mo Kα radiation ($\lambda = 0.71073$ Å) and were corrected for Lorentz and polarization effects. The frames were integrated with the Bruker *SAINT* [11] software package and the data were corrected for absorption using the program SADABS [12]. The structures were solved by direct methods using the program SHELXS 97 [13]. All non-hydrogen atoms were refined with anisotropic thermal parameters by full-matrix least-squares calculations on F^2 using the program SHELXL 97 [14]. Hydrogen atoms were inserted at calculated positions and constrained with isotropic thermal parameters. Neutral atom scattering factors and anomalous dispersion corrections were taken from *International Tables for X-ray Crystallography* [15]. Drawings were produced with *PLATON* [16].

Crystallographic data and structure refinement parameters are listed in Table 1. The poor quality of the single crystal led to worse structure refinement parameters in the case of the second compound.

Table 1
Crystal data and structure refinement parameters for the complexes

	[Re(OSO$_2$CF$_3$)(CO)$_3$L]	[Re (NCCH$_3$)(CO)$_3$L][BF$_4$]
Empirical formula	$C_{30}H_{24}F_3O_8P_2ReS$	$C_{31}H_{27}NO_5P_2ReBF_4$
Formula weight	849.69	828.49
Temperature (K)	293(2)	120(2)
Wavelength (Å)	0.71073	0.71073
Crystal system	monoclinic	triclinic
Space group	$P2_1/c$	$P\bar{1}$
Unit cell dimensions:		
a (Å)	9.9850(5)	9.6790(7)
b (Å)	19.0949(11)	13.3972(10)
c (Å)	16.9130(9)	13.5348(10)
α (°)	90	95.6040(10)
β (°)	91.6990(10)	109.3350(10)
γ (°)	90	110.2120(10)
V (Å^3)	3223.3(3)	1508.89(19)
Z	4	2
Absorption coefficient (mm^{-1})	3.999	4.200
$F(000)$	1664	812
Crystal size (mm)	$0.35 \times 0.22 \times 0.04$	$0.28 \times 0.10 \times 0.04$
θ range for data collection (°)	1.61–28.00	1.64–28.52
Index ranges	$-13 \leqslant h \leqslant 11, -24 \leqslant k \leqslant 25, -22 \leqslant l \leqslant 21$	$-12 \leqslant h \leqslant 12, -17 \leqslant k \leqslant 17, -18 \leqslant l \leqslant 18$
Reflections collected	19,381	18,126
Independent reflections	7460 [$R_{int} = 0.0562$]	6973 [$R_{int} = 0.0534$]
Data/restraints/parameters	7460/0/406	6973/0/407
Goodness-of-fit on F^2	0.856	0.947
Final R indices [$I > 2\sigma(I)$]	$R_1 = 0.0344$	$R_1 = 0.0384$
R indices (all data)	$wR_2 = 0.0620$	$wR_2 = 0.0663$
Largest different peak and hole (e Å^{-3})	1.110 and −0.727	1.737 and −2.265

2.3. Synthesis of complexes

2.3.1. *fac*-[Re(ClCH$_2$Cl)(CO)$_3$L][BF$_4$] (**1**)

To a mixture of [ReBr(CO)$_3$L] (100 mg, 0.1 mmol) and AgBF$_4$ (38 mg, 0.2 mmol) 20 ml of dichloromethane were added. The solution was refluxed for 1 h, and the brown precipitate (AgBr) was filtered off through cellite. After sucking dry, the resulting oil was triturated with hexane (4 ml) and a brown solid was formed. Yield: 58 mg (52%). M.p. 183 °C. Λ_M (nitromethane): 66.3 Ω^{-1} cm^2 mol^{-1}. *Anal.* Calc. for $C_{30}H_{26}Cl_2O_5P_2BF_4Re$ (872.40): C, 41.30; H, 3.00%. Found: C, 41.48; H, 3.03. IR (KBr pellets, cm^{-1}): 2048s, 1974s, 1921s, ν(CO); 1097s, ν(BF$_4$). ^{1}H NMR (CHCl$_3$-d, 400 MHz): δ (ppm) = 4.00–4.30 (m, 4H, –CH$_2$CH$_2$–); 7.26–7.65 (m, 20H, –Ph). ^{31}P{^{1}H} NMR (CHCl$_3$-d, 161 MHz): δ(ppm) = 120.2 (s). ^{19}F{^{1}H} (CH$_2$Cl$_2$-d_2, 376 MHz): δ(ppm) = −151.3 (s). MS: m/z (referred to the most abundant isotopes): 701 [M-(BF$_4$, CH$_2$Cl$_2$)]; 673 [M-(BF$_4$, CH$_2$Cl$_2$, CO)]; 645 [M-(BF$_4$, CH$_2$Cl$_2$, 2CO)].

2.3.2. *fac*-[Re(OSO$_2$CF$_3$)(CO)$_3$L] (**2**)

Hundred milligram of [ReBr(CO)$_3$L] (0.1 mmol) were mixed with 49 mg of AgOTf (0.2 mmol) and 20 ml of dichloromethane were added. After refluxing for 3 h protected from light, the solid (AgBr) was filtered off, the solution was dried in vacuo and the resulting oil was taken into ether (4 ml), furnishing a white solid. This solid was separated, washed with ether and vacuum dried. Yield: 73 mg (67%). M.p. 244 °C. Λ_M (nitromethane): 4.9 Ω^{-1} cm^2 mol^{-1}. *Anal.* Calc. for $C_{30}H_{24}SO_8P_2F_3Re$ (849.73): C, 42.41; H, 2.85. Found: C, 41.83; H, 2.86%. IR (KBr pellets, cm^{-1}): 2046s, 1967s, 1926s, ν(CO); 1321s, $\nu(\eta^1$-OSO$_2$CF$_3$). ^{1}H NMR (CHCl$_3$-d, 400 MHz): δ(ppm) = 4.08–4.18 (m, 4H, –CH$_2$CH$_2$–); 7.16–7.70 (m, 20H, –Ph). ^{13}C{^{1}H} NMR (CHCl$_3$-d, 100 MHz): δ(ppm) = 189.6 (m, C_AO, C_BO); 189.6 (t, C_EO); $^2J_{C-P}$ = 7.3 Hz. 66.4 (s, –CH$_2$–CH$_2$–); 118 (q, CF$_3$); $^2J_{C-F}$ = 319 Hz. ^{31}P{^{1}H} NMR (CHCl$_3$-d, 161 MHz): δ(ppm) = 117.4 (s). ^{19}F{^{1}H} (CHCl$_3$-d, 376 MHz): δ(ppm) = −76.9 (s). MS: m/z (referred to the most abundant isotopes): 850 [M]; 701 [M–O$_3$SCF$_3$]; 673 [M–(O$_3$SCF$_3$, CO)]; 645 [M–(O$_3$SCF$_3$, 2CO)]. Single crystals were obtained by slow evaporation of an EtOH/CHCl$_3$ (10:2, v/v) solution.

2.3.3. *fac*-[Re(ClCH$_2$Cl)(CO)$_3$L][BAr$_F$] (**3**)

A mixture of complex **2** (100 mg, 0.1 mmol) and NaBAr$_F$ (166 mg, 0.2 mmol) was solved in dichloromethane (20 ml). After 1 h stirring at room temperature a precipitate of NaOTf was formed and filtered off. The remaining solution was dried in vacuo and the resulting oil was taken into hexane (4 ml) after which a yellow precipitate was formed. Yield: 190 mg (98%). M.p. 132 °C. Λ_M (nitromethane): 71.4 Ω^{-1} cm^2 mol^{-1}. *Anal.* Calc. for $ReC_{62}H_{38}Cl_2O_5P_2BF_{24}$ (1648.81): C, 45.16; H, 2.32. Found: C, 45.34; H, 2.45%. IR (KBr pellets, cm^{-1}): 2053s, 1984s, 1938s, ν(CO). ^{1}H NMR (CHCl$_3$-d, 400 MHz): δ(ppm) = 4.24 (m, 4H, –CH$_2$CH$_2$–); 7.40–7.69 (m, 20H, –Ph). ^{13}C{^{1}H} NMR (CH$_2$Cl$_2$-d$_2$, 100 MHz): δ(ppm) = 190.4 (m, C_AO, C_BO); 192.6 (t, C_EO); $^2J_{C-P}$ = 8.0 Hz. 66.2 (s, –CH$_2$–CH$_2$–); 124.9 (q, CF$_3$); $^2J_{C-F}$ = 271 Hz. ^{31}P{^{1}H} NMR (CHCl$_3$-d, 161 MHz): δ(ppm) = 124.2 (s). ^{19}F{^{1}H} (CHCl$_3$-d, 376 MHz): δ(ppm) = −62.5 (s). MS: m/z (referred to the most abundant isotopes): 757 [M–(BAr$_F$, CO)]; 701 [M–(BAr$_F$, CH$_2$Cl$_2$)]; 673 [M–(BAr$_F$, CH$_2$Cl$_2$, CO)]; 645 [M–(BAr$_F$, CH$_2$Cl$_2$, 2CO)].

Attempts to synthesize this complex by reacting [ReBr(CO)$_3$L] with AgBAr$_F$ were unsuccessful.

2.3.4. *fac*-[Re(NCCH$_3$)(CO)$_3$L][BF$_4$] (**1a**)

To a mixture of [ReBr(CO)$_3$L] (100 mg, 0.1 mmol) and AgBF$_4$ (38 mg, 0.2 mmol) 20 ml of dichloromethane were added. After filtration of the formed solid (AgBr), the solution was treated with CH$_3$CN (7 ml), refluxed for 4 h and vacuum dried, resulting in an oil which was triturated with EtOH (4 ml). The formed white solid was dried in vacuo. Yield: 49 mg (45%). M.p. 229 °C. Λ_M (nitromethane): 93.1 Ω^{-1} cm^2 mol^{-1}. *Anal.* Calc. for $ReC_{31}H_{27}O_5P_2NBF_4$ (828.52): C, 44.94; H, 3.28. Found: C, 44.34; H, 3.53%. IR (KBr pellets, cm^{-1}): 2053s, 1990s, 1934s, ν(CO); 2325w, 2295w, ν(CN); 1100s, ν(BF$_4$). ^{1}H NMR (CHCl$_3$-d, 400 MHz): δ(ppm) = 1.91 (s, 3H, CH$_3$CN) 4.16–4.32 (m, 4H, –CH$_2$CH$_2$–); 7.26–7.60 (m, 20H, –Ph). ^{13}C{^{1}H} NMR (CHCl$_3$-d, 100 MHz): δ(ppm) = 186.9 (dd, C_AO); $^2J_{CP(trans)}$ = 47, $^2J_{CP(cis)}$ = 25 Hz; 186.6 (dd, C_BO); $^2J_{CP(trans)}$ = 47 Hz, $^2J_{CP(cis)}$ = 25 Hz; 190.2 (t, C_EO); $^2J_{CP(cis)}$ = 8.4 Hz. 66.1 (s,–CH$_2$–CH$_2$–); 125.8 (s, CN–); 2.6 (s, CH$_3$–). ^{31}P{^{1}H} NMR (CHCl$_3$-d, 161 MHz): δ(ppm) = 115.3 (s). ^{19}F{^{1}H} (CHCl$_3$-d, 376 MHz): δ(ppm) = −153.2 (s). MS: m/z (referred to the most abundant isotopes): 742 [M–BF$_4$]; 701 [M–(BF$_4$, CH$_3$CN)]; 673 [M–(BF$_4$, CH$_3$CN, CO)]; 645 [M–(BF$_4$, CH$_3$CN, 2CO)]. By slow evaporation of an EtOH/CH$_2$Cl$_2$ (10:2, v/v) solution, crystals suitable for X-ray diffractometry were isolated.

2.3.5. *fac*-[Re(OH$_2$)(CO)$_3$L][BF$_4$] (**1b**)

To a mixture of [ReBr(CO)$_3$L] and AgBF$_4$ (100 mg, 0.1 mmol and 38 mg, 0.2 mmol, respectively) 20 ml of CH$_2$Cl$_2$ were added. After 1 h reflux, the precipitate (AgBr) was filtered off and 15 μl of water were added to the solution. After being maintained for 2 h at room temperature the solvent was eliminated in vacuo furnishing a solid which was treated with 5 ml of hexane to yield a grey solid. Yield: 37 mg (39%). M.p. 173 °C. Λ_M (nitromethane): 66.4 Ω^{-1} cm^2 mol^{-1}. *Anal.* Calc. for $ReC_{29}H_{26}O_6P_2BF_4$ (805.48): C, 43.24; H, 3.25. Found: C, 43.59; H, 3.54%. IR (KBr pellets, cm^{-1}): 2046s, 1969s, 1923s, ν(CO); 2000s, ν(BF$_4$); 3443m, ν(OH$_2$). ^{1}H NMR (CHCl$_3$-d, 400 MHz): δ(ppm) = 1.72 (s, 2H,

OH_2); 4.04–4.17 (m, 4H, $-CH_2CH_2-$); 7.26–7.68 (m, 20H, –Ph). $^{13}C\{^1H\}$ NMR ($CHCl_3$-d, 100 MHz): δ(ppm) = 189.0 (m, *trans*-C_AO, C_BO); 190.4 (t, *cis*-C_EO); $^2J_{CP(cis)} = 7$ Hz. 66.8 (s, $-CH_2-CH_2-$). $^{31}P\{^1H\}$ NMR ($CHCl_3$-d, 161 MHz): δ(ppm) = 119.8 (s). $^{19}F\{^1H\}$ ($CHCl_3$-d, 376 MHz): δ(ppm) = −151.5 (s). MS: *m*/*z* (referred to the most abundant isotopes): 701 [M–(BF_4, H_2O)]; 673 [M–(BF_4, H_2O, CO)]; 645 [M–(BF_4, H_2O, 2CO)], 617 [M-(BF_4, H_2O, 3CO)].

2.3.6. *fac*-[Re(NCCH$_3$)(CO)$_3$L][OTf] (**2a**)

Five milliliter of CH_3CN was added to a solution of complex **2** (100 mg, 0.1 mmol) in toluene (20 ml). The mixture was refluxed for 1 h and vacuum dried. The resulting oil was taken into hexane (5 ml) and the formed colourless solid was filtered out and washed with hexane. Yield: 40 mg (38%). M.p. 232 °C. Λ_M (nitromethane): 47.0 $\Omega^{-1}\,cm^2\,mol^{-1}$. *Anal*. Calc. for $ReC_{32}H_{27}O_8P_2NSF_3$ (890.78): C, 43.15; H, 3.06; N, 1.57. Found: C, 42.52; H, 3.19; N, 1.75%. IR (KBr pellets, cm^{-1}): 2053s, 1992s, 1935s, ν(CO); 2321w, 2292w, ν(CN); 1265s, $\nu(O_3SCF_3)$. ^1H NMR ($CHCl_3$-d, 400 MHz): δ(ppm) = 1.80 (s, 3H, CH_3CN) 4.08–4.21 (m, 4H, $-CH_2CH_2-$); 7.16–7.61 (m, 20H, –Ph). $^{13}C\{^1H\}$ NMR ($CHCl_3$-d, 100 MHz): δ(ppm) = 186.9 (dd, C_AO); $^2J_{CP(trans)} = 47$, $^2J_{CP(cis)} = 24$ Hz; 186.6 (dd, C_BO); $^2J_{CP(trans)} = 47$ Hz, $^2J_{CP(cis)} = 24$ Hz; 190.3 (t, C_EO), $^2J_{cis} = 8.4$ Hz; 66.0 (s, $-CH_2-CH_2-$); 120.8 (q, CF_3), $^2J_{CF} = 321$ Hz; 125.5 (s, CN–); 2.8 (s, CH_3–). $^{31}P\{^1H\}$ NMR ($CHCl_3$-d, 161 MHz): δ(ppm) = 115.6 (s). $^{19}F\{^1H\}$ ($CHCl_3$-d, 376 MHz): δ(ppm) = −78.3 (s). MS: *m*/*z* (referred to the most abundant isotopes): 742 [M–O_3SCF_3]; 701 [M–(O_3SCF_3, CH_3CN)]; 673 [M–(O_3SCF_3, CH_3CN, CO)]; 645 [M–(O_3SCF_3,CH_3CN, 2CO)].

2.3.7. *fac*-[Re(NCCH$_3$)(CO)$_3$L][BAr$_F$] (**3a**)

A solution of complex 3 (100 mg, 0.1 mmol) in dichloromethane (20 ml), after adding 5 ml of acetonitrile, was stirred for 4 h at room temperature and dried in vacuo. An oil was formed, which was triturated with hexane (5 ml), resulting in a yellow solid that was filtered off and hexane washed. Yield: 35 mg (36%). M.p. 256 °C. Λ_M (nitromethane): 57.7 $\Omega^{-1}\,cm^2\,mol^{-1}$. *Anal*. Calc. for $ReC_{63}H_{39}O_5P_2NBF_{24}$ (1604.93): C, 47.15; H, 2.45; N, 0.87. Found: C, 46.44; H, 2.56; N, 0.78%. IR (KBr pellets, cm^{-1}): 2060s, 2005m, 1956s, ν(CO); 2367vw, 2342vw, ν(CN). ^1H NMR ($CHCl_3$-d, 400 MHz): δ(ppm) = 1.60 (s, 3H, CH_3CN) 4.20 (m, 4H, $-CH_2CH_2-$); 7.26–7.70 (m, 20H, –Ph). $^{13}C\{^1H\}$ NMR ($CHCl_3$-d, 100 MHz): δ(ppm) = 186.6 (dd, C_AO); $^2J_{CP(trans)} = 45$, $^2J_{CP(cis)} = 22$ Hz; 186.4 (dd, C_BO); $^2J_{CP(trans)} = 45$ Hz, $^2J_{CP(cis)} = 22$ Hz; 190.3 (t, C_EO), $^2J_{CP(cis)} = 8.8$ Hz; 65.25 (s, $-CH_2-CH_2-$); 124.5 (q, CF_3), $^2J_{CF} = 272$ Hz; 122.7 (s, CN–); 1.4 (s, CH_3–). $^{31}P\{^1H\}$ NMR ($CHCl_3$-d, 161 MHz): δ (ppm) = 117.3 (s). $^{19}F\{^1H\}$ ($CHCl_3$-d, 376 MHz): δ(ppm) = −62.5 (s). MS: *m*/*z* (referred to the most abundant isotopes): 742 [M–BAr_F]; 701 [M–(BAr_F, CH_3CN)]; 673 [M–(BAr_F, CH_3CN, CO)]; 645 [M–(BAr_F, CH_3CN, 2CO)].

2.3.8. *fac*-[Re(OH$_2$)(CO)$_3$L][BAr$_F$] (**3b**)

To a solution of complex **3** (100 mg, 0.1 mmol) in dichloromethane (20 ml) 7 μl of H_2O were added. After refluxing for 2 h, the mixture was vacuum dried and the formed oil was taken into hexane (5 ml) affording a yellow solid. Yield: 30 mg (32%). M.p. 138 °C. Λ_M (nitromethane): 74.6 $\Omega^{-1}\,cm^2\,mol^{-1}$. *Anal*. Calc. for $ReC_{61}H_{38}O_6P_2BF_{24}$ (1581.90): C, 46.32; H, 2.42. Found: C, 46.14; H, 2.18%. IR (KBr pellets, cm^{-1}): 2052s, 1989m, 1970m, 1941s, ν(CO); 3426m, $\nu(OH_2)$. ^1H NMR ($CHCl_3$-d, 400 MHz): δ(ppm) = 1.61 (s, 2H, OH_2) 4.26 (m, 4H, $-CH_2CH_2-$); 7.26–7.68 (m, 20H, –Ph). $^{13}C\{^1H\}$ NMR (CH_2Cl_2-d_2, 100 MHz): δ(ppm) = 193.0 (t, C_EO), $^2J_{CP(cis)} = 7$ Hz; 190.5 (m, C_AO, C_BO); 66.31 (s, $-CH_2-CH_2-$); 162.2 (q, CF_3), $^2J_{CF} = 49$ Hz. $^{31}P\{^1H\}$ NMR ($CHCl_3$-d, 161 MHz): δ(ppm) = 123.9 (s). $^{19}F\{^1H\}$ ($CHCl_3$-d, 376 MHz): δ(ppm) = −62.5 (s). MS: *m*/*z* (referred to the most abundant isotopes): 701 [M–(BAr_F, H_2O)]; 673 [M–(BAr_F, H_2O, CO)]; 645 [M–(BAr_F, H_2O, 2CO)].

3. Results and discussion

3.1. Crystal structures

3.1.1. [Re(OTf)(CO)$_3$L] (**2**)

Fig. 1 shows the displacement ellipsoid plot for complex **2** with the atom numbering scheme, and Table 2 lists the chief bond distances and bond angles. The structure consists of discrete [ReOTf$(CO)_3$L] pseudo-octahedral units with the Re atom coordinated to the two phosphorus donors from the bidentate L ligand, one oxygen atom of the OSO_2CF_3 (OTf) anion and the three CO ligands in a *facial* disposition. The Re–P bond lengths have values in the range described for other Re(I) complexes with similar ligands [17], and they are unremarkable. The CO ligand *trans* to the O atom of the triflate anion lies closer to the metal atom [1.889(5) Å] than the other two, *trans* to the P atoms [1.942(5) and 1.970(5) Å, respectively], as expected from both the π-donor character of the oxygen and the *trans* influence of the phosphorus. Moreover, the shortest C–O bond length [1.140(5) Å] corresponds logically with the longest Re–C distance [1.970(5) Å]. The values of the internal distances in the OTf anion denote an S–O donor bond [1.477(3) Å] weaker than the other two S–O bonds [1.425(3), 1.422(3) Å respectively], even though it is quite shorter than an S–O single bond (about 1.70 Å) [18]. All

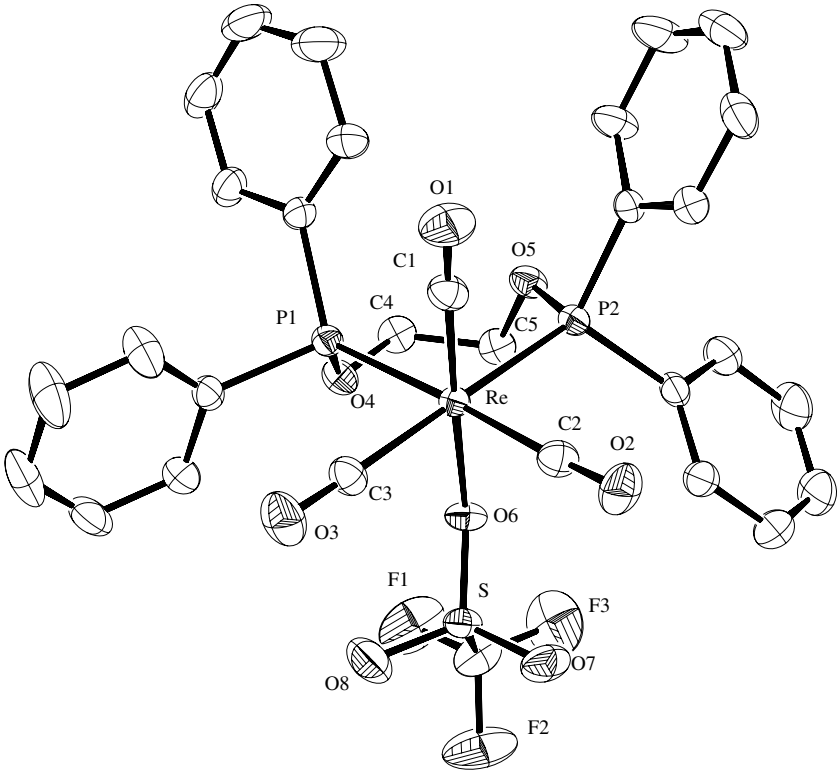

Fig. 1. Displacement ellipsoid plot for complex **2** with the atom numbering scheme. Ellipsoids at 30% probability.

Table 2
Selected bond lengths [Å] and angles [°] for the new species

	$[Re(OSO_2CF_3)(CO)_3L]$	$[Re(NCCH_3)(CO)_3L]^+$
Bond lengths		
Re–C(1)	1.889(5)	1.904(5)
Re–C(2)	1.942(5)	1.949(5)
Re–C(3)	1.970(5)	1.948(5)
Re–P(1)	2.4811(11)	2.4522(13)
Re–P(2)	2.4478(11)	2.4529(13)
C(1)–O(1)	1.157(5)	1.168(6)
C(2)–O(2)	1.145(5)	1.156(5)
C(3)–O(3)	1.140(5)	1.152(5)
Re–O(6)	2.206(3)	
S–O(6)	1.477(3)	
S–O(7)	1.425(3)	
S–O(8)	1.422(3)	
Re–N		2.133(4)
N–C(6)		1.121(6)
Bond angles		
P(1)–Re–P(2)	88.16(4)	89.20(4)
C(1)–Re–C(2)	84.79(19)	92.1(2)
C(2)–Re–C(3)	89.00(19)	89.0(2)
C(1)–Re–P(1)	96.92(14)	96.24(14)
C(1)–Re–P(2)	93.89(14)	90.54(14)
C(1)–Re–C(3)	89.8(2)	90.4(2)
C(2)–Re–P(2)	93.67(13)	92.77(14)
C(3)–Re–P(1)	89.07(13)	88.88(15)

the bond angles around the Re atom have values very close to 90°, even the P–Re–P angle [88.16(4)°] despite the bite of the bidentate ligand.

3.1.2. $[Re(CH_3CN)(CO)_3L]^+$

The formation of crystals suitable for X-ray crystallography in the case of the compound **1a** allowed the structural study of the cation present in this complex as well as in **2a** and **3a**. The displacement ellipsoid plot for this cation is shown in Fig. 2. As in the structure commented above, the coordination polyhedron around the Re atom is again a pseudo-octahedron formed by the two P atoms of the bidentate L ligand, the N atom of the acetonitrile and three CO ligands in a *facial* arrangement. The two carbonyl ligands *trans* to the P donors are located at practically the same distance from Re [1.949(5) and 1.948(5) Å, respectively] (see Table 2), whereas the third CO (*trans* to the acetonitrile) is nearer [1.904(5) Å]. Furthermore, the C–O bond length in the latter is slightly longer [1.168(6) Å] than in the other two [1.152(5), 1.156(5) Å], and the internal C–N bond length in the acetonitrile ligand [1.121(6) Å] is slightly shorter than in the free ligand (1.158 Å) [18].

3.2. Characterization and reactivity of the complexes

The molar conductivities showed all the new species to be 1:1 electrolytes in nitromethane, with the only exception of complex **2** which is non-ionogenic in this solvent [19].

In the case of complex **1**, its $^{31}P\{^1H\}$ NMR spectrum shows two singlets at 120.2 ppm, which we state as due

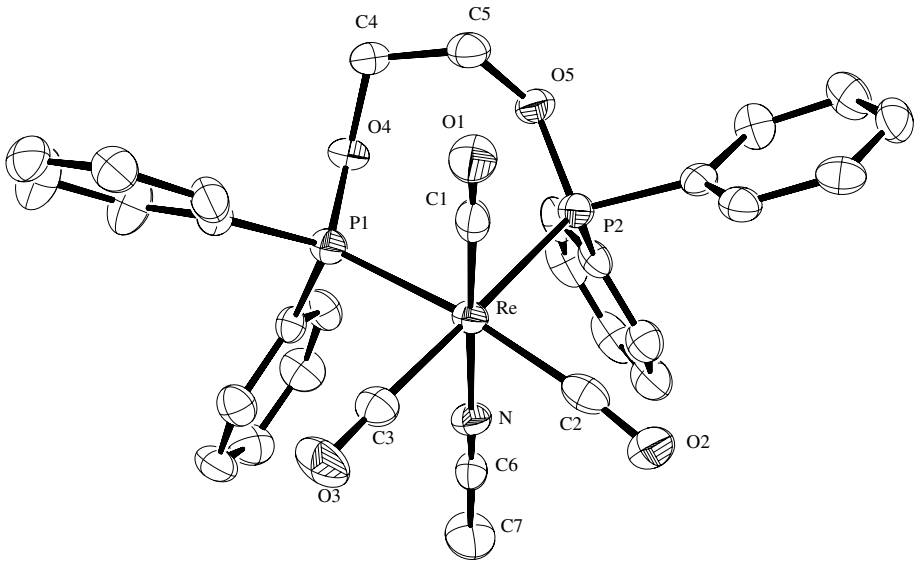

Fig. 2. Displacement ellipsoid plot of the cation $[Re(CH_3CN)(CO)_3L]^+$ with the atom numbering scheme. Ellipsoids at 30% probability.

to the complex containing CH_2Cl_2 as a ligand, and at 120.9 ppm (less intense) which denotes the existence of another species in solution, presumably arisen from the equilibrium:

$$[Re(ClCH_2Cl)(CO)_3L][BF_4] \rightleftharpoons [Re(FBF_3)(CO)_3L] + CH_2Cl_2$$

The existence of this equilibrium seems to be confirmed by the $^{19}F\{^1H\}$ NMR spectrum in dichloromethane at room temperature, which shows, apart from the singlet due to the free BF_4 anion (at −151.3 ppm), another broad signal downfield (at −149.3 ppm, Fig. 3) attributable to the BF_4 ion attached to the Re atom.

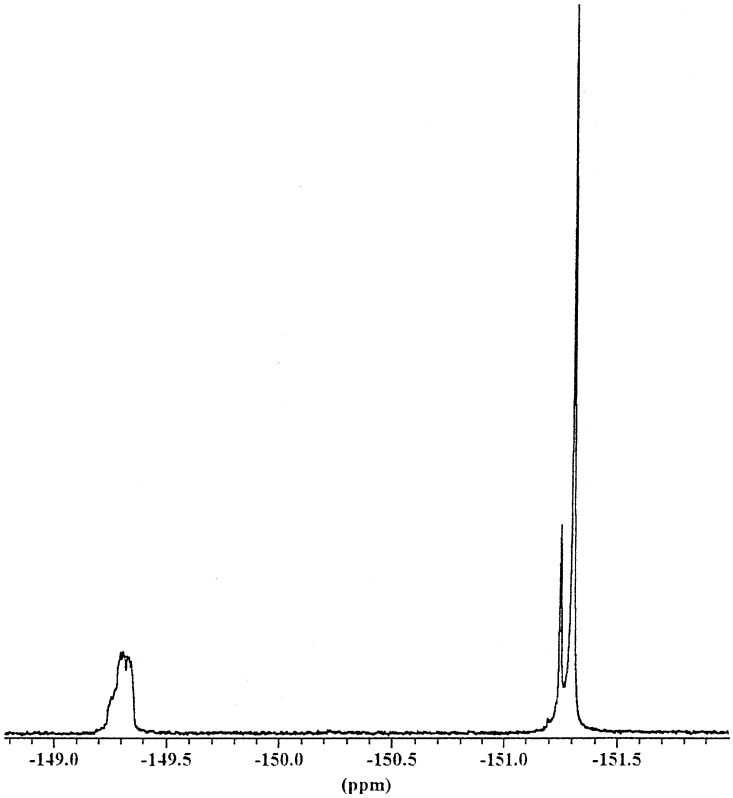

Fig. 3. $^{19}F\{^1H\}$ NMR spectrum of complex **1**.

This signal is located at a position close to that found in similar systems [20].

In order to seek to confirm this supposition, and provided that the ubiquitous *aqua* ligand is very difficult to avoid, the $^{31}P\{^1H\}$ and $^{19}F\{^1H\}$ NMR spectra of this complex in $CDCl_3$ were recorded after adding H_2O to the solution. As a consequence of the presence of water, the signal at 120.2 ppm (presumably due to the $ClCH_2Cl$ complex) disappears in the $^{31}P\{^1H\}$ NMR spectrum, whereas a new signal is observed at 119.8 ppm (attributable to the *aqua* complex), and the singlet located at 120.9 ppm remains, even though it becomes less intense. This seems to indicate that *some* of the BF_4 anions remain attached to Re despite the presence of H_2O. Regarding the $^{19}F\{^1H\}$ spectrum, the two signals commented above survive after adding the water, denoting the existence of both types of BF_4 anion (free and coordinated to Re). These results showed that H_2O takes immediately the place of dichloromethane in the attachment to the metal atom, whereas the displacement of the BF_4 anion takes a longer term. When water is added in excess, the $^{19}F\{^1H\}$ and $^{31}P\{^1H\}$ NMR spectra denote the non-survival of BF_4 as a ligand and no compound but the *aqua* complex is present. By contrast, the spectroscopic studies of complex **3** did not provide any evidence of the existence of such a type of equilibrium, as expected from the non-coordinating character of the BAr_F anion.

The ^1H NMR spectra of complexes **1**, **2** and **3** show the Ph and (CH_2–CH_2) ligand signals at the expected positions, while the singlet due to the $ClCH_2Cl$ ligand is located at about 4.8 ppm in **1** and is not observable in **3,** presumably obscured by the ligand signals.

On the other hand, the $^{13}C\{^1H\}$ NMR spectrum of complex **3** in dichloromethane showed a splitting of the CH_2Cl_2-d_2 signal (Fig. 4). In fact, the quintuplet at 53.8 ppm is accompanied by another less intense signal downfield, at 54.0 ppm, which we attribute to the dichloromethane attached to the metal, despite the fast interchange with the free solvent that usually makes it impossible to observe in the NMR spectra at room temperature [21].

With the aim of testing the liability of both ligands CH_2Cl_2 and OTf against some bases, the three complexes were treated with MeCN and H_2O (see Scheme 1). The substitution of dichloromethane in complexes **1** and **3** by either acetonitrile or water was quite easy in smooth conditions. However, the triflate anion is more difficult to remove, so that its substitution by MeCN to give **2a** needed more drastic requirements (toluene reflux for 1 h), whereas any attempt to displace OTf by H_2O was unsuccessful.

The characterization of the new species **1a**, **2a** and **3a,** arised from the reaction of the complexes **1–3** with MeCN, was carried out by IR and NMR spectroscopies,

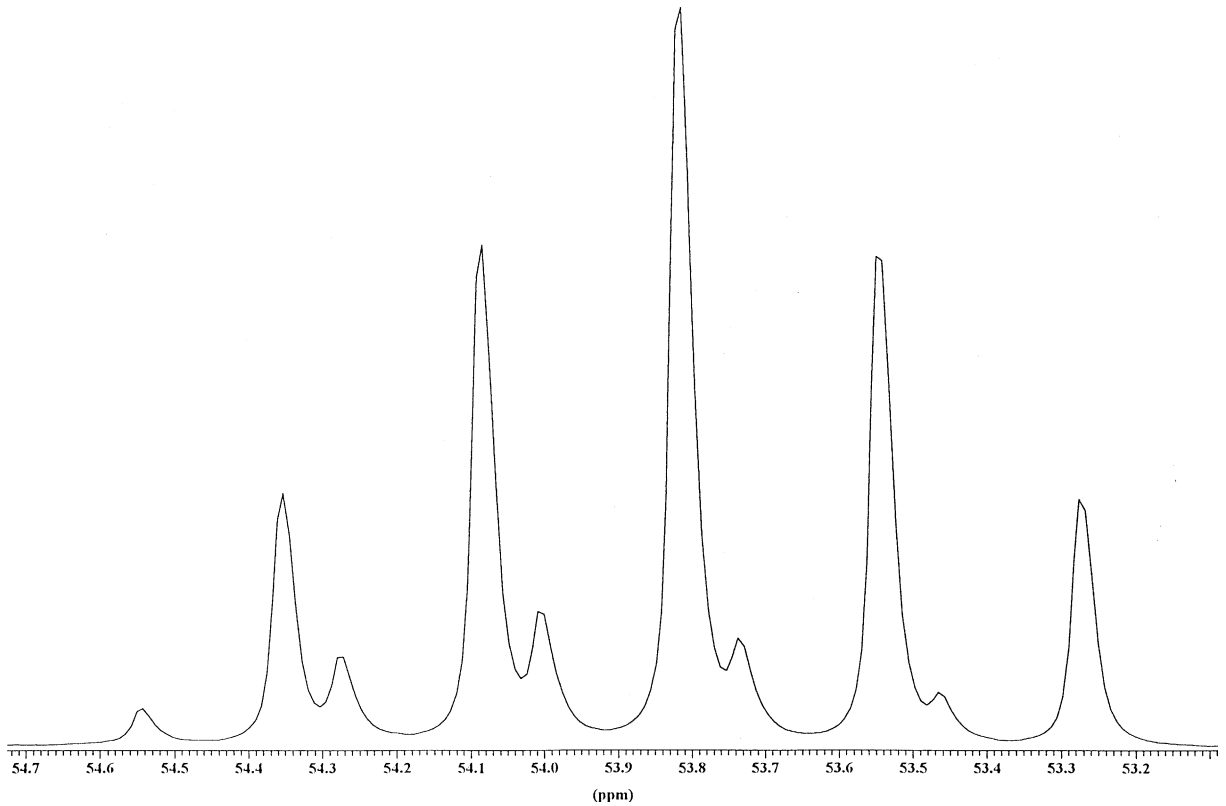

Fig. 4. $^{13}C\{^1H\}$ NMR spectrum of complex **3**.

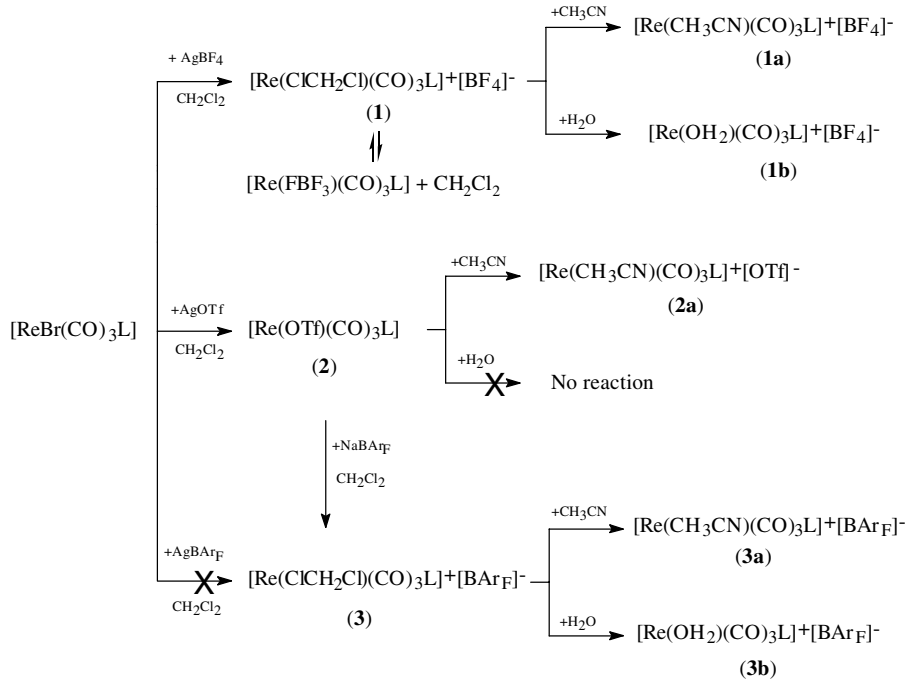

Scheme 1.

and, in the case of complex **1a**, by X-ray diffraction studies, which allowed the structural elucidation of the cation $[Re(CH_3CN)(CO)_3L]^+$ present in all the three compounds.

The IR bands attributable to C–O stretching modes of the carbonyl ligands are in the range reported for similar systems [22,23]. The substitution of CH_2Cl_2 by MeCN causes in these bands only a very slight shift to higher wavenumber, despite the strengthening in the C–O bond to be expected from the π-acceptor character of MeCN in contrast with the π-donor behaviour of the Cl atom of dichloromethane. The acetonitrile complexes exhibit CN stretches in the IR spectra as two weak or very weak bands at higher wavenumber than in the free ligand (2252 cm^{-1}). These bands are in the range 2367–2292 cm^{-1} described previously [24], and are consistent with the strengthening of the C–N bond in MeCN under coordination to the metal as commented in the crystal structure discussion (see above). The singlet in the ^1H NMR spectra of the complexes in $CDCl_3$ (at 1.9, 1.8 and 1.6 ppm for **1a**, **2a** and **3a**, respectively), is consistent with the existence of CH_3CN bound to the metal, whereas the ^{13}C NMR spectra in the same solvent show two singlets, one at 2.6, 2.8 and 1.4 ppm (for **1a**, **2a** and **3a**, respectively), attributable to the methyl group of MeCN, and the other at 125.8, 125.5 and 122.7 ppm, corresponding to the CN group of the same ligand [22,24]. A triplet at around 190 ppm [$J(^{13}C–^{31}P) = 9$ Hz] and two double doublets at 186 ppm [$J_{cis}(^{13}C–^{31}P) \approx 22$ Hz, $J_{trans}(^{13}C–^{31}P) \approx 50$ Hz) are due to the carbonyl ligands. The $^{31}P\{^1H\}$ spectra show a singlet at 115.3, 116.6 and 117.3 ppm for **1a**, **2a** and **3a**, respectively, indicating the magnetic equivalence of the two P nuclei.

Whereas the substitution of the OTf ligand by H_2O was not possible in complex **2,** (even in drastic conditions), the displacement of CH_2Cl_2 in complexes **1** and **3** afforded the new *aqua* complexes **1b** and **3b**, respectively. Both complexes behave as 1:1 electrolytes in nitromethane, as denoted by the values of their molar conductivities in this solvent (see Section 2). The broad singlet in the ^1H NMR spectra at 1.72 and 1.61 ppm for **1b** and **3b**, respectively, indicates the presence of the *acuo* ligand, whereas the singlets at −151.5 (**1b**) and −62.5 ppm (**3b**) in the $^{19}F\{^1H\}$ NMR spectra confirm the existence of the BF_4 and BAr_F anions in the former and the latter, respectively. Finally, the $^{31}P\{^1H\}$ NMR spectra show one singlet for both compounds, denoting the magnetic equivalence of the P atoms of the bidentate ligand.

4. Supplementary material

Crystallographic data for the structural analysis have been deposited with the Cambridge Crystallographic Data Centre, CCDC nos. 213341 and 213342. Copies of this information may be obtained free of charge from The Director, CCDC, 12 Union Road, Cambridge, CB2

1EZ, UK (fax: +44-1223-336033; e-mail: deposit@ccdc.cam.ac.uk or http://www.ccdc.cam.ac.uk).

References

[1] J.A. Davies, F.R. Hartley, Chem. Rev. 81 (1981) 79.
[2] F.R. Hartley, J.A. Davies, Rev. Inorg. Chem. 4 (1982) 27.
[3] J.A. Davies, Adv. Inorg. Chem. Radiochem. 24 (1981) 115.
[4] W. Beck, K. Sünkel, Chem. Rev. 88 (1988) 1405.
[5] S.H. Strauss, Chem. Rev. 93 (1993) 927.
[6] G.A. Lawrence, Adv. Inorg. Chem. 34 (1989) 145.
[7] D.M. Tellers, R.G. Bergman, Organometallics 20 (2001) 4819.
[8] R.V. Honeychuck, W.H. Hersh, Inorg. Chem. 28 (1989) 2869.
[9] W. Beck, K. Schloter, Z. Naturforsch B 33 (1978) 1214.
[10] K. Snkel, G. Urban, W. Beck, J. Organomet. Chem. 252 (1983) 187.
[11] SMART (control) and SAINT (integration) Software. Bruker Analytical X-ray Systems, Madison, WI, 1994.
[12] G.M. Sheldrick, SADABS. An Empirical Absorption Correction Program for Area Detector Data, University of Göttingen, Germany, 1996.
[13] G.M. Sheldrick, SHELXS97. Program for the Solution of Crystal Structures from X-ray Data, University of Göttingen, Germany, 1997.
[14] G.M. Sheldrick, SHELXL97. Program for the Refinement of Crystal Structures from X-ray Data, University of Göttingen, Germany, 1997.
[15] A.J.C. Wilson, in: International Tables for Crystallography, vol. C, Kluwer Academic Publishers, Dordrecht, 1992.
[16] A.L. Spek, PLATON. A Multi-purpose Crystallographic Tool, University of Utrecht, 2000.
[17] V.I. Zdanovich, A.S. Batsanov, I.E. Zanin, Y.T. Struchkov, M.G. Ezernitskaya, B.V. Lokshin, Metallorg. Khim. (Organomet. Chem. in the USSR) 4 (1991) 551.
[18] J.E. Huheey, E.A. Keiter, R.L. Keiter, Inorganic Chemistry. Principles of Structure and Reactivity, 4th ed., Harper, New York, 1993.
[19] W.J. Geary, Coord. Chem. Rev. 7 (1971) 81.
[20] R. Carballo, A. Castiñeiras, S. García-Fontán, P. Losada-González, U. Abram, E.M. Vázquez-López, Polyhedron 20 (2001) 2371.
[21] D. Tellers, R.G. Bergman, Organometallics 20 (2001) 4819.
[22] J.Y.K. Cheng, Kung-Kai Cheung, M.C.W. Chan, Kwok-Yin Wong, Chi-Ming Che, Inorg. Chim. Acta 272 (1998) 176.
[23] P. Bergamini, F.F. DeBiani, L. Marvelli, N. Mascellani, M. Peruzzini, R. Rossi, P. Zanello, New J. Chem. (1999) 207.
[24] R.H. Reimann, E. Singleton, J. Organomet. Chem. 59 (1973) C24.

Available online at www.sciencedirect.com
SCIENCE DIRECT®
Polyhedron 23 (2004) 1055–1061
POLYHEDRON
www.elsevier.com/locate/poly

Copper(II) complexes of bis- and tetrakis-(2-pyridylsulfanylmethyl)benzenes

David A. McMorran *, Christopher M. Hartshorn, Peter J. Steel

Department of Chemistry, University of Canterbury, Christchurch, Dunedin, New Zealand

Received 12 December 2003; accepted 5 January 2004

Abstract

Reactions of copper(II) salts with the ligand 1,2-bis(2-pyridylsulfanylmethyl)benzene ($\mathbf{L}_1$) and the isomeric ligands 1,2,3,4-tetrakis(2-pyridylsulfanylmethyl)benzene ($\mathbf{L}_2$) and 1,2,4,5-tetrakis(2-pyridylsulfanylmethyl)benzene ($\mathbf{L}_3$) give copper(II) complexes, some of which have been characterised by X-ray crystallography. $[Cu(\mathbf{L}_1)Cl_2]$ is found to be a one-dimensional coordination polymer, containing two subtly different copper atom environments. By contrast, $[Cu_2(\mathbf{L}_2)Cl_4]$ and $[Cu_2(\mathbf{L}_3)(NO_3)_4]$ are discrete species with, in each case, the copper atoms chelated by adjacent ligand arms.
© 2003 Elsevier Ltd. All rights reserved.

Keywords: Copper; *N*-ligands; Thioethers; Multi-armed ligands; X-ray structures; Coordination polymer

1. Introduction

The construction of metallosupramolecular assemblies, in which organic ligand components are "glued" together by transition metal ions, continues to be an area of great interest [1–6]. A wide variety of assemblies, such as squares [7–9], cubes [10], tetrahedra [11,12] and helicates [13,14], as well as a range of one-, two- and three-dimensional coordination polymers [15–20], are now known. In each case, the metallosupramolecular architecture is the result of the particular structural characteristics of its constituent components. It is clear that components with new geometrical and structural properties might give rise to new and interesting supramolecular assemblies. In particular, so-called multi-armed molecules [21], incorporating donor groups at the ends of each arm, might serve as potential bridging ligands with a number of different coordination modes. Variation in the number, length and relative arrangement of the arms in such ligands might be expected to generate assemblies of varying dimensionalities, with novel structural and functional properties.

As a part of our continuing studies into the consequences for metal-ion binding of incorporating flexible spacers into poly-*N*-heterocyclic ligands [22–28], we have recently reported the synthesis of a series of new multi-armed ligands, in which a benzene, or biphenylene, core unit was appended by up to eight pyridylsulfanylmethyl arms [29]. Silver(I) adducts of some of these have been reported [30] and X-ray crystallographic analyses showed these adducts to be either 2 + 2 metallocyclic or one-dimensional polymeric species. In each case, weak Ag···S interactions played a role in determining the overall structures. We now report the synthesis and structural characterization of copper(II) adducts of three of these ligands, $\mathbf{L}_1$–$\mathbf{L}_3$ (Scheme 1). Each ligand was reacted with copper(II) chloride and copper(II) nitrate to give, in most cases, insoluble green or blue compounds. Three of the products were able to be characterised by X-ray crystallography. Reaction of copper(II) chloride with 1,2-bis(2-pyridylsulfanylmethyl)benzene ($\mathbf{L}_1$) results in the formation of a one-dimensional polymeric structure, with each ligand bridging two dissimilar copper atoms. Reaction of the four-armed ligands 1,2,3,4-tetrakis(2-pyridylsulfanylmethyl)benzene ($\mathbf{L}_2$) and 1,2,4,5-tetrakis(2-pyridylsulfa-

* Corresponding author. Present address: Department of Chemistry, University of Otago, P.O. Box 56, Dunedin, New Zealand. Tel.: +64-3-479-7934; fax: +64-3-479-7906.
E-mail address: davidm@alkali.otago.ac.nz (D.A. McMorran).

0277-5387/$ - see front matter © 2003 Elsevier Ltd. All rights reserved.
doi:10.1016/j.poly.2004.01.001

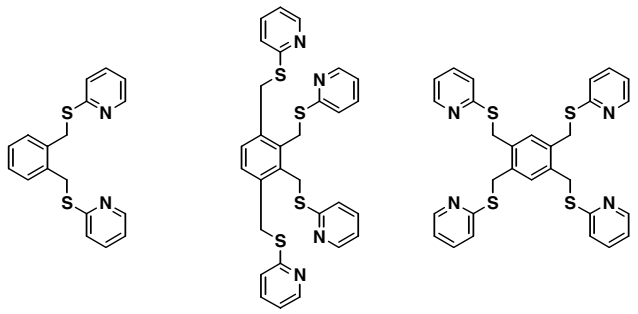

Scheme 1.

nylmethyl)benzene ($\mathbf{L}_3$) with copper(II) chloride and copper(II) nitrate, respectively, gave discrete bimetallic complexes. As was found for the silver adducts, weak sulfur-to-metal bonding interactions are observed in the present complexes in the solid state and, in one case, such bonding appears to be present in solution.

2. Experimental

2.1. General procedure

Ligands $\mathbf{L}_1$ [30], $\mathbf{L}_2$ and $\mathbf{L}_3$ [29] were prepared as described previously. UV–Vis spectra were recorded on a GBC UV/VIS 920 spectrometer. Elemental analyses were performed by the Campbell Microanalytical Laboratory at the University of Otago.

2.2. Preparation of $[Cu(\mathbf{L}_1)(NO_3)_2]$

$Cu(NO_3)_2 \cdot 3H_2O$ (19 mg, 0.080 mmol) in hot methanol (1 mL) was added to $\mathbf{L}_1$ (25 mg, 0.080 mmol) in hot methanol (2 mL) to give a pale green solution. The solvent was removed and the deep green residue redissolved in acetone (2 mL). Addition of diethyl ether gave a blue flocculent precipitate which was filtered off, washed with diethyl ether and dried. Yield: 31 mg (79%). *Anal.* Calc. for $C_{18}H_{16}N_4S_2O_6Cu$: C, 42.22; H, 3.15; N, 10.94. Found: C, 42.10; H, 3.11; N, 10.63%.

2.3. Preparation of $[Cu(\mathbf{L}_1)Cl_2] \cdot CH_3OH$

$CuCl_2 \cdot 2H_2O$ (38 mg, 0.22 mmol) and $\mathbf{L}_1$ (73 mg, 0.22 mmol) were stirred in hot methanol (10 mL). On cooling, green crystals formed which were suitable for X-ray analysis. Yield: 90 mg (83%). *Anal.* Calc. for $C_{18}H_{16}N_2S_2CuCl_2 \cdot CH_3OH$: C, 46.48; H, 4.11; N, 5.71. Found: C, 46.54; H, 3.83; N, 5.75%.

2.4. Preparation of $[Cu_2(\mathbf{L}_2)(NO_3)_4]$

A solution of $Cu(NO_3)_2 \cdot 3H_2O$ (34 mg, 0.14 mmol) in hot acetonitrile (3 mL) was added to a solution of $\mathbf{L}_2$ (40 mg, 0.070 mmol) in hot acetonitrile (3 mL) to give a clear, deep green solution, which rapidly deposited a blue precipitate. The hot suspension was stirred for 10 min, then cooled and the solid filtered off, washed with diethyl ether and dried, giving a pale blue solid. Yield: 60 mg (91%). *Anal.* Calc. for $C_{30}H_{26}N_8S_4O_{12}Cu_2$: C, 38.10; H, 2.77; N, 11.84. Found: C, 38.35; H, 2.97; N, 10.95%.

2.5. Preparation of $[Cu_2(\mathbf{L}_2)Cl_4] \cdot CH_3CN \cdot H_2O$

A solution of $CuCl_2 \cdot 2H_2O$ (19 mg, 0.11 mmol) in hot acetonitrile (2 mL) was added to a solution of $\mathbf{L}_2$ (31 mg, 0.054 mmol) in hot acetonitrile (3 mL) to give a heavy green precipitate. The hot suspension was stirred for 10 min, then cooled and the solid filtered off, washed with diethyl ether and dried, giving a yellow-brown microcrystalline solid. Yield: 39 mg (86%). *Anal.* Calc. for $C_{30}H_{26}N_4S_4Cu_2Cl_4 \cdot CH_3CN \cdot H_2O$: C, 42.76; H, 3.47; N, 7.78. Found: C, 42.22; H, 3.22; N, 7.75%. Crystals suitable for X-ray analysis were obtained by slowly diffusing a solution of $CuCl_2$ (12 mg, 0.014 mmol) in acetonitrile (3 mL) into a solution of $\mathbf{L}_2$ (40 mg, 0.070 mmol) in acetonitrile (3 mL), giving clumps of golden yellow plates. Yield: 20 mg (68%). *Anal.* Calc. for $C_{30}H_{26}N_4S_4Cu_2Cl_4 \cdot 3H_2O \cdot 1/2CH_3CN$: C, 40.72; H, 3.69; N, 6.89. Found: C, 41.18; H, 3.62; 6.98%.

2.6. Preparation of $[Cu_2(\mathbf{L}_3)(NO_3)_4]$

A solution of $Cu(NO_3)_2 \cdot 3H_2O$ (34 mg, 0.14 mmol) in hot acetonitrile (3 mL) was added to a solution of $\mathbf{L}_3$ (40 mg, 0.070 mmol) in hot acetonitrile (3 mL) to give, initially, a dark green solution, which became orange-brown and finally deep green as the $Cu(NO_3)_2$ solution was added. On complete addition, the clear, hot solution was stirred for 10 min, then cooled to give a dark green solid. This was filtered off, washed with diethyl ether and dried to give a green solid. Yield: 47 mg (71%). *Anal.* Calc. for $C_{30}H_{26}N_8S_4O_{12}Cu_2$: C, 38.10; H, 2.77; N, 11.84. Found: C, 38.01; H, 2.78; N, 10.48%. Crystals suitable for X-ray analysis were obtained by carefully layering a solution of $Cu(NO_3)_2 \cdot 6H_2O$ (8.5 mg, 0.035 mmol) in acetonitrile (1 mL) onto a solution of $\mathbf{L}_3$ (10 mg, 0.0017 mmol) in dichloromethane (1 mL), with 2 mL of acetonitrile as a buffer region. On standing, clumps of deep green plates formed. Yield: 12 mg (72%). *Anal.* Calc. for $C_{30}H_{26}N_8S_4O_{12}Cu_2$: C, 38.10; H, 2.77; N, 11.84. Found: C, 38.07; H, 2.56; N, 10.77%.

2.7. Preparation of $[Cu_2(\mathbf{L}_3)Cl_4]$

A solution of $CuCl_2 \cdot 2H_2O$ (15 mg, 0.088 mmol) in hot acetonitrile (1 mL) was added to a solution of $\mathbf{L}_3$ (25 mg, 0.044 mmol) in hot acetonitrile (3 mL) to give a deep red solution which rapidly deposited a green-brown precipitate. The hot suspension was stirred for 10 min, then

cooled and the solid filtered off, washed with diethyl ether and dried, to give an olive green solid. Yield: 32 mg (87%). *Anal*. Calc. for $C_{30}H_{26}N_4S_4Cu_2Cl_4$: C, 42.91; H, 3.12; N, 6.67. Found: C, 42.62; H, 3.16; N, 6.69%.

2.8. X-ray crystallography

The crystal data, data collection and refinement parameters are listed in Table 1. All measurements were made with a Siemens CCD area detector using graphite monochromatised Mo Kα ($\lambda = 0.71073$ Å) radiation. Intensities were corrected for Lorentz and polarisation effects and for absorption. The structures were solved by direct methods using SHELXS [31], and refined on F^2 using all data by full-matrix least-squares procedures with SHELXL-97 [32]. All non-hydrogen atoms were refined with anisotropic displacement parameters. Hydrogen atoms were included in calculated positions with isotropic displacement parameters 1.3 times the isotropic equivalent of their carrier carbons. The function minimised was $\sum w(F_o^2 - F_c^2)$, with $w = [\sigma^2(F_o^2) + aP^2 + bP]^{-1}$, where $P = [\max(F_o)^2 + 2F_c^2]/3$. In the case of $[Cu_2(\mathbf{L}_3)(NO_3)_4]$, one of the nitrate nitrogens was refined isotropically.

3. Results and discussion

The new copper(II) complexes were prepared by reaction of either copper(II) chloride or copper(II) nitrate with the ligand in acetonitrile or methanol solutions. In each case, the coloured products precipitated from the cooled solutions in good to high yield. These products were, however, poorly soluble and only solutions in dimethyl formamide (dmf) could be obtained. Microanalysis suggested that the product of the reaction of $CuCl_2$ and the bidentate ligand $\mathbf{L}_1$ had a 1:1 Cu:ligand ratio, whereas a 2:1 Cu:ligand ratio was found for the copper complexes of the tetradentate ligands $\mathbf{L}_2$ and $\mathbf{L}_3$. The reactions of the ligands $\mathbf{L}_2$ and $\mathbf{L}_3$ with copper(II) nitrate were also carried out in dmf, giving coloured solutions. However, attempts to isolate a solid product, by slow evaporation or by addition of solvents such as diethyl ether to induce precipitation, gave only ligand.

In the course of the addition of an acetonitrile solution of $Cu(NO_3)_2$ to one of $\mathbf{L}_3$, the reaction mixture underwent an intriguing series of colour changes. On adding the first drops of the copper(II) solution, a dark green solution was obtained. This then changed to a yellow-brown solution and then finally to a green solution, from which a green solid then rapidly precipitated. When the reaction was repeated in dmf solution, only the yellow and final green solutions, and not the initial dark green solution, were observed. On complete addition, the green dmf solution was stable. The colour changes were followed by UV–Vis spectroscopy and it was found that, in the intermediate yellow solution, intense bands in the region up to ca. 500 nm were present, which were not present in the spectra of the free ligand or of the final green species. By contrast, similar be-

Table 1
Crystal data, data collection and refinement parameters

	$[Cu(\mathbf{L}_1)Cl_2]\cdot CH_3OH$	$[Cu_2(\mathbf{L}_2)Cl_4]\cdot 3H_2O\cdot 1/2CH_3CN$	$[Cu_2(\mathbf{L}_3)(NO_3)_4]$
Formula	$C_{19}H_{20}N_2S_2OCuCl_2$	$C_{31}H_{33.5}N_{4.5}S_4O_3Cu_2Cl_4$	$C_{30}H_{26}N_8S_4O_{12}Cu_2$
Molecular weight	490.93	914.24	945.41
Crystal system	triclinic	triclinic	triclinic
a (Å)	8.785(4)	12.060(4)	8.523(6)
b (Å)	11.075(5)	13.171(4)	8.994(5)
c (Å)	12.090(5)	14.735(5)	13.052(8)
α (Å)	97.10(3)	112.157(4)	106.75(2)
β (Å)	102.87(3)	112.631(4)	91.72(2)
γ (Å)	112.28(3)	95.384(4)	107.01(2)
V (Å)^3	1032.5(8)	1920.9(10)	909.0(10)
Space group	$P\bar{1}$	$P\bar{1}$	$P\bar{1}$
Z	2	2	1
$F(000)$	502	930	480
μ (mm^{-1})	1.531	1.641	1.474
ρ_{calcd} (g cm^{-1})	1.579	1.581	1.728
Dimensions (mm)	$0.41 \times 0.26 \times 0.10$	$0.55 \times 0.50 \times 0.03$	$0.75 \times 0.32 \times 0.12$
Temperature (K)	158(2)	168(2)	168(2)
$2\theta_{max}$	50	50	50
Number of reflections measured	4681	22 500	10 767
Number of unique reflections	2949	6691	3188
Number of reflections with $I > 2\sigma(I)$	1397	4599	2541
Weighting, a/b	0.0096/0.0000	0.0396/0.7565	0.0763/0.8169
Parameters	249	486	248
wR (all data)	0.1027	0.0967	0.1297
R_1 ($I > 2\sigma I$)	0.0560	0.0403	0.0460

haviour was not observed on mixing $Cu(NO_3)_2$ solutions with either $\mathbf{L}_1$ or $\mathbf{L}_2$. Further, analysis of spectral changes on reaction of $Cu(NO_3)_2$ with 2-pyridylsulfanylmethylbenzene, the "one-armed" ligand, also showed no evidence of an intermediate yellow solution.

It has been reported that copper(II) complexes with thioether donors exhibit strong $S\sigma \rightarrow Cu(II)$ LMCT bands, at around 450 nm [33–35]. It is therefore possible that this intermediate species might involve a complex of the type shown in Scheme 2, with a weak Cu···S bond(s). Though rare, complexes involving four-membered chelate rings of this type have been reported [30,36–38]. However, why such a complex should form under these concentration conditions, and for only $\mathbf{L}_3$, is unclear. [1]

Analytically pure crystalline samples were eventually prepared, in good yield, by mixing copper(II) solutions and ligand solutions very slowly, either by layering or by diffusion. In each case, a discrete complex, with adjacent arms of the ligand chelating the copper atom(s), or a polymeric structure, in which the ligand bridges copper atoms, are possible. X-ray crystal structures of the three complexes were therefore undertaken.

Mixing methanol solutions of copper(II) chloride and $\mathbf{L}_1$ yielded green crystals suitable for X-ray analysis. Fig. 1 shows a perspective view of the structure, which crystallises in the triclinic space group $P\bar{1}$ and is found to be a one-dimensional coordination polymer. The asymmetric unit contains two copper atoms, each of which lies on a crystallographic centre of inversion, one $\mathbf{L}_1$ ligand and a methanol solvate molecule. Each copper atom has a square planar geometry, with the pyridine donors lying *trans* to each other. In addition to this, however, each of the sulfur atoms forms weak interactions with the copper, with distances of 3.116(3) Å (Cu1···S10) and 3.019(3) Å (Cu2···S20), giving the copper atoms a tetragonally distorted octahedral geometry. The mean-planes of the pyridine rings are inclined at angles of 87.2(8)° and 53.7(8)° to the central benzene ring and lie at an angle of 56.1(8)° to each other. The two arms of the ligand lie on opposite sides of the central benzene ring. The ligand separates the two copper atoms by 8.693(3) Å.

The methanol solvate molecule is hydrogen bonded to one of the coordinated chlorides, with a Cl···H distance of 2.538 Å and a Cl···H–O angle of 151.0°. Its presence leads to the distinct differences in the environments of the two copper atoms, as depicted in Fig. 2.

Fig. 3 shows an extended view of the one-dimensional polymeric nature of the structure. The chains form a sinusoidal arrangement and propagate perpendicular to

[1] Preliminary investigations of the reaction of $Cu(NO_3)_2$ solutions with hexakis(2-pyridylsulfanylmethyl)benzene also shows these colour changes and gives an intermediate spectrum containing a band at ca. 500 nm, similar to that observed with $\mathbf{L}_3$.

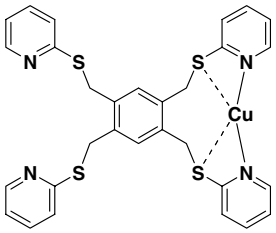

Scheme 2.

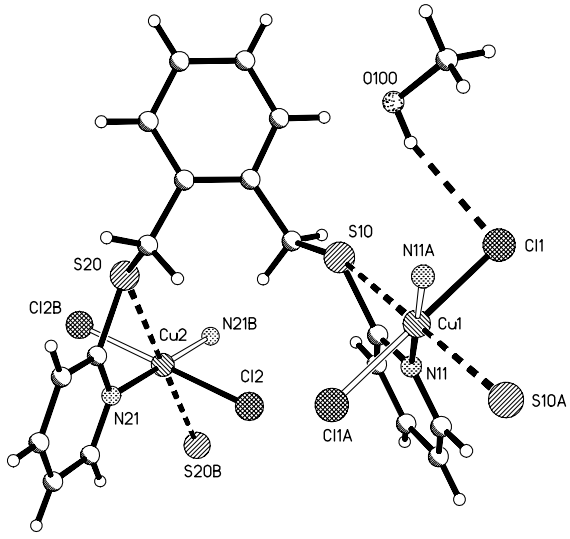

Fig. 1. Perspective view of $[Cu(\mathbf{L}_1)Cl_2]\cdot CH_3OH$, showing atomic labelling. Atom X is related to atoms XA and XB by the symmetry transformations $[-x+1,-y,z+1]$ and $[-x-1,-y-1,-z]$, respectively. Selected bond lengths (Å) and angles (°). Cu1–N11 1.995(7); Cu1–Cl1 2.220(2); Cu2–N21 1.986(6); Cu2–Cl2 2.243(2); Cu1–S10 3.116(3); Cu2–S20 3.019(2); N11–Cu1–Cl1 90.96(18); N11–Cu1–S10 124.09(19) N21–Cu2–Cl2 90.53(19); N21–Cu2–S20 58.3(2).

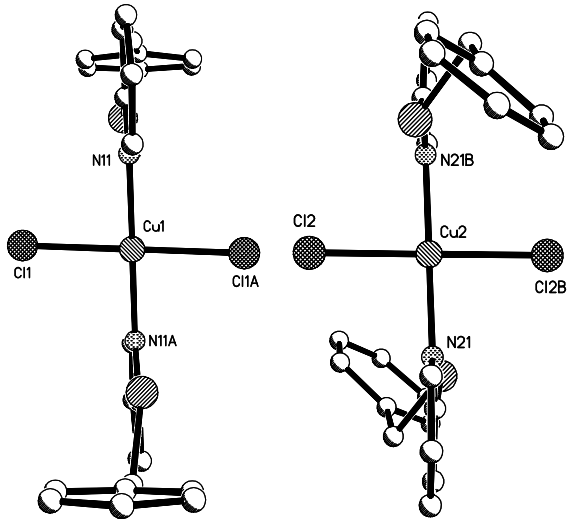

Fig. 2. Different ligand conformations about the two different copper atoms in $[Cu(\mathbf{L}_1)Cl_2]\cdot CH_3OH$.

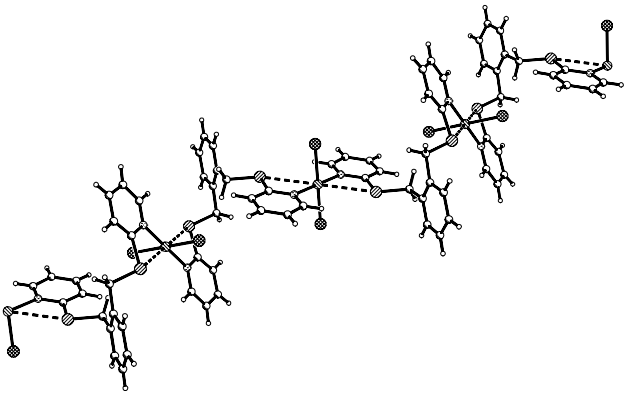

Fig. 3. View of the extended one-dimensional structure of $[Cu(\mathbf{L}_1)Cl_2]\cdot CH_3OH$.

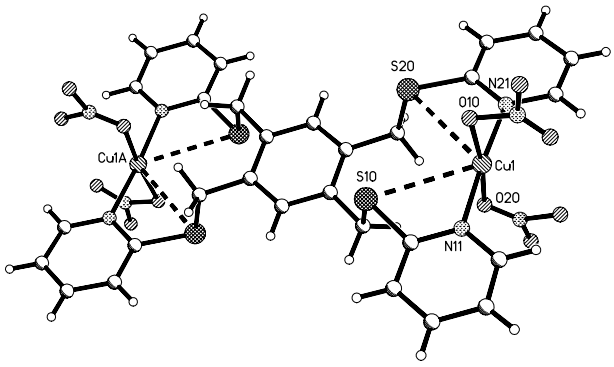

Fig. 5. Perspective view of the structure of $[Cu_2(\mathbf{L}_3)(NO_3)_4]$. Atom XA is related to atom X by the symmetry transformation $[-x,-y,-z]$. Selected bond lengths (Å) and angles (°). Cu1–N11 2.012(3); Cu1–N21 2.014(3); Cu1–O10 1.963(3); Cu1–O20 2.013(4); Cu1–S10 3.155(4); Cu1–S20 3.149(4); N11–Cu1–N21 176.1(2); O10–Cu1–O20 172.4(2); N11–Cu1–O10 91.1(2); N11–Cu1–O20 89.9(2); N11–Cu1–S10 57.1(2); O10–Cu1–S10 85.4(2); S10–Cu1–S20 69.2(2).

the *c* axis. Adjacent chains interact via hydrogen bonding interactions between coordinated chlorides and pyridine hydrogens (Cl···C 3.54 Å, Cl···H–C 152.1°) and also via S···H–C interactions (S···H 2.934 Å, S···H–C 127.4°).

Diffusion of an acetonitrile solution of copper(II) chloride into an acetonitrile solution of $\mathbf{L}_2$ led to the formation of golden yellow crystals suitable for X-ray analysis. Fig. 4 shows a perspective view of the structure of the complex, which crystallises in the triclinic space group $P\bar{1}$. The asymmetric unit contains one $\mathbf{L}_2$ ligand, two copper atoms, four chlorides, three water solvate molecules and half an acetonitrile solvate molecule. The acetonitrile and one of the half water molecules share the occupancy of a site with the second of the half water molecules. Each copper atom is coordinated by two, mutually *trans*, pyridine nitrogens from adjacent arms of the ligand, and two chlorides, which coordinate with Cl–Cu–Cl angles of 137.61(5)° and 127.36(5)°. The copper atoms further form relatively strong bonding interactions to sulfur atoms, with distances between 2.890(4) Å (Cu2···S30) and 3.077(4) Å (Cu1···S10). It appears to be these interactions, which lie approximately *trans* to the coordinated chlorides, which push the chlorides away from being co-planar with the nitrogen donors, giving the copper atoms a highly distorted octahedral geometry. The ligand arms

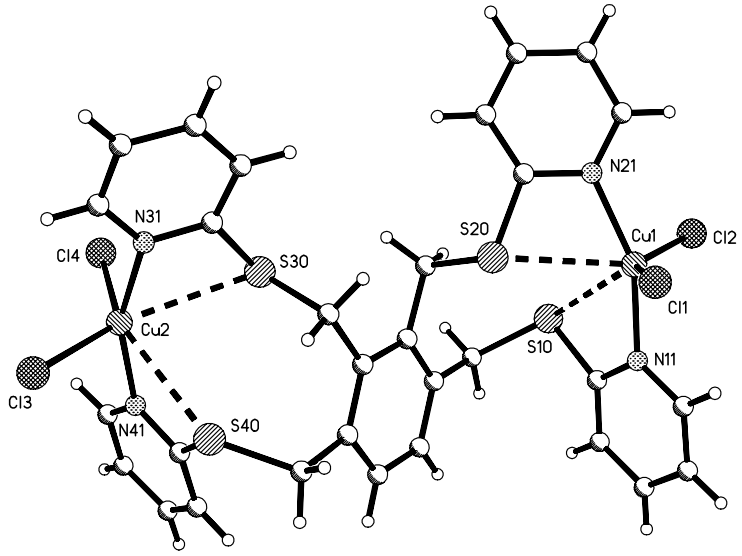

Fig. 4. Perspective view of the structure of $[Cu_2(\mathbf{L}_2)Cl_4]\cdot 3H_2O\cdot 1/2CH_3CN$. Solvate molecules are omitted for clarity. Selected bond lengths (Å) and angles (°). Cu1–N11 1.991(4); Cu1–N21 1.997(3); Cu1–Cl1 2.2879(13); Cu1–Cl2 2.2651(13); Cu1–S10 3.077(4); Cu1–S20 2.896(4); Cu2–N31 1.978(4); Cu2–N41 1.979(3); Cu2–Cl3 2.2983(14); Cu2–Cl4 2.3217(14); Cu2–S30 2.890(4); Cu2–S40 2.998(4); N11–Cu1–N21 156.73(14); Cl1–Cu1–Cl2 137.61(5); S10–Cu1–S20 73.5(10); N11–Cu1–Cl1 95.56(10); N11–Cu1–Cl2 93.16(10); N11–Cu1–S10 58.8(10); N11–Cu1–S20 99.3(10); N31–Cu2–N41 156.51(13); Cl3–Cu2–Cl4 127.36(5); S30–Cu2–S40 74.0(10); N31–Cu2–Cl3 95.39(10); N31–Cu2–Cl4 93.17(11); N31–Cu2–S30 62.2(10); N31–Cu2–S40 101.3(10).

adopt an up–up–down–down arrangement with respect to the central benzene ring. The two outer pyridine rings lie almost orthogonal to the central benzene ring, with angles between the mean-planes of 101.0(1)° (N11–C16) and 98.4(1)° (N41–C46), while the other two, inner, pyridine rings lie at angles of 45.9(1)° (N21–C26) and 40.7(1)° (N31–C36). The angle between the mean-planes of the pyridine rings are 60.4(1)°, for the rings coordinated to Cu1, and 62.1(1)°, for the rings coordinated to Cu2. The ligand separates the two copper atoms by 10.142(4) Å.

Consideration of the molecular packing shows that adjacent molecules are held together by numerous CH···O, OH···N and OH···Cl hydrogen bonding interactions between each other and to the acetonitrile and water solvate molecules.

Careful layering of a solution of copper(II) nitrate in acetonitrile onto a solution of $\mathbf{L}_3$ in dichloromethane resulted in the formation of deep green crystals suitable for X-ray analysis. Fig. 5 shows a perspective view of the complex, which crystallises in the triclinic space group $P\bar{1}$. The asymmetric unit contains one copper atom, half of a $\mathbf{L}_3$ ligand and two nitrates. The centroid of the central benzene ring of the ligand lies on a crystallographic centre of inversion. As a result, the ligand arms adopt an up–up–down–down arrangement with respect to the central benzene ring. The copper atom enjoys a square planar geometry, being coordinated by the pyridine nitrogens of two adjacent ligand arms and the oxygens of two monodentate nitrate anions. Because of the up–up arrangement of the ligand arms, the nitrogen donors coordinate *trans* to each other and are both coplanar with the two sulfur atoms. An interaction between the copper and the sulfurs, of the type observed for $[Cu_2(\mathbf{L}_2)Cl_4]^{2+}$, would then lead, in this case, to the nitrogen donors being pushed out of the coordination plane. This cannot occur, and so the Cu···S distances are longer than in the case of $[Cu_2(\mathbf{L}_2)Cl_4]^{2+}$, at 3.155(4) Å (Cu1···S10) and 3.149(4) Å (Cu1···S20). The plane containing the two pyridine rings and the copper atom is almost parallel with that of the central benzene ring (angle between the mean planes is 5.2°), giving the molecule a 'stepped' appearance. The ligand separates the two copper atoms by 11.574(4) Å.

The molecules arrange themselves in sheets parallel to the *a* axis, with the uncoordinated oxygens of each of the nitrates forming intramolecular CH···O hydrogen bonding interactions, with O···C distances of 3.24 Å and 3.39 Å and O···H–C angles of 165.4° and 160.4°, respectively: each molecule enjoys such interactions with four neighbouring molecules. Adjacent molecules also form offset π-stacking interactions, parallel to the *c* axis, between the central benzene ring of one molecule and a pyridine ring of the other, with a closest C–C distance of 3.46 Å.

4. Conclusions

We have prepared a series of copper(II) complexes with the ligands $\mathbf{L}_1$, $\mathbf{L}_2$ and $\mathbf{L}_3$. Three of these have been characterised by X-ray crystallography and these show that the solid state structures of the complexes are, at least in part, determined by weak Cu···S bonding interactions. Indeed, in the case of $[Cu_2(\mathbf{L}_3)(NO_3)_4]$, this pseudo-chelating nature of the ligand is perhaps the reason why a discrete dimetallic species, rather than the expected polymeric species, is obtained. Further, we have shown that there is some evidence for such interactions playing a role in the solution chemistry of one of the ligands, $\mathbf{L}_3$. These results provide further evidence that the structures adopted by metallosupramolecular assemblies are the result of a variety of sometimes very subtle interactions. Exploration of the coordination chemistry of these and related ligands continues.

5. Supplementary material

CCDC 220138, 220139 and 220140 contains the supplementary crystallographic data for this paper. These data can be obtained free of charge via www.ccdc.cam.ac.uk/conts/retrieving.html (or from the CCDC, 12 Union Road, Cambridge CB2 1EZ, UK; fax: +44 1223 336033; e-mail: deposit@ccdc.cam.ac.uk).

Acknowledgements

We thank the Royal Society of New Zealand Marsden Fund for financial support.

References

[1] W.-Y. Sun, M. Yoshizawa, T. Kusukawa, M. Fujita, Curr. Opin. Chem. Biol. 6 (2002) 757.
[2] R.S. Seidel, P.J. Stang, Acc. Chem. Res. 35 (2002) 972.
[3] G.F. Swiegers, T.J. Malefetse, Coord. Chem. Rev. 225 (2002) 91.
[4] B.J. Holliday, C.A. Mirkin, Angew. Chem., Int. Ed. 40 (2001) 2022.
[5] G.F. Swiegers, T.J. Malefetse, Chem. Rev. 100 (2000) 3483.
[6] S. Leininger, B. Olenyuk, P.J. Stang, Chem. Rev. 100 (2000) 853.
[7] M. Schweiger, S.R. Seidel, A.M. Arif, P.J. Stang, Inorg. Chem. 41 (2002) 2556.
[8] E. Iengo, R. Minatel, B. Milani, L.G. Marzilli, E. Alessio, Eur. J. Inorg. Chem. (2001) 609.
[9] F.A. Cotton, L.M. Daniels, C. Lin, C.A. Murillo, S.-Y. Yu, J. Chem. Soc., Dalton Trans. (2001) 502.
[10] S. Roche, C. Haslam, S.L. Heath, J.A. Thomas, Chem. Commun. (1998) 1681.
[11] D.L. Caulder, C. Brueckner, R.E. Powers, S. Koenig, T.N. Parac, J.A. Leary, K.N. Raymond, J. Am. Chem. Soc. 123 (2001) 8923.
[12] D.L. Caulder, K.N. Raymond, J. Chem. Soc., Dalton Trans. (1999) 1185.
[13] M. Albrecht, Chem. Rev. 101 (2001) 3457.

[14] C. Piguet, G. Bernardinelli, G. Hopfgartner, Chem. Rev. 97 (1997) 2005.
[15] C. Janiak, Dalton Trans. (2003) 2781.
[16] S.L. James, Chem. Soc. Rev. 32 (2003) 276.
[17] O.R. Evans, W. Lin, Acc. Chem. Res. 35 (2003) 511.
[18] M.J. Zaworotko, Chem. Commun. (2001) 1.
[19] A.N. Khlobystov, A.J. Blake, N.R. Champness, D.A. Lemenovskii, A.G. Majouga, N.V. Zyk, M. Schröder, Coord. Chem. Rev. 222 (2001) 155.
[20] R. Robson, J. Chem. Soc., Dalton Trans. (2000) 3735.
[21] D.D. MacNicol, G.A. Downing, in: Comprehensive Supramolecular Chemistry, vol. 6, Elsevier, Oxford, 1996, pp 421–464, and references therein..
[22] D.A. McMorran, P.J. Steel, Inorg. Chem. Commun. 6 (2003) 43.
[23] D.A. McMorran, P.J. Steel, Chem. Commun. (2002) 2120.
[24] D.A. McMorran, S. Pfadenhauer, P.J. Steel, Aust. J. Chem. 55 (2002) 519.
[25] D.A. McMorran, P.J. Steel, J. Chem. Soc., Dalton Trans. (2002) 3321.
[26] D.A. McMorran, P.J. Steel, Supramol. Chem. 14 (2002) 79.
[27] D.A. McMorran, S. Pfadenhauer, P.J. Steel, Inorg. Chem. Commun. 5 (2002) 449.
[28] P.J. Steel, C.J. Sumby, Chem. Commun. (2002) 322.
[29] D.A. McMorran, P.J. Steel, Tetrahedron 59 (2003) 3701.
[30] C.M. Hartshorn, P.J. Steel, J. Chem. Soc., Dalton Trans. (1998) 3935.
[31] G.M. Sheldrick, Acta Crystallogr., Sect A 46 (1990) 467.
[32] G.M. Sheldrick, SHELXL-97, University of Göttingen, Germany, 1997.
[33] S.G. Murray, F.R. Hartley, Chem. Rev. 81 (1981) 365.
[34] V.M. Miskowski, J.A. Thich, R. Solomon, H.J. Schugar, J. Am. Chem. Soc. 98 (1976) 8344.
[35] A.R. Amundsen, J. Whelan, B. Bosnich, J. Amer. Chem. Soc. 99 (1977) 6730.
[36] K. Umakoshi, I. Kinoshita, K. Matsumoto, S. Ooi, Nippon Kagaku Kaishi (1986) 1517.
[37] M.C. Durrant, C. Hauser, D.L. Hughes, M.J. Maguire, R.L. Richards, J. Organomet. Chem. 476 (1994) 219.
[38] R. Scopelliti, G. Bruno, C. Donato, G. Tresoldi, Inorg. Chim. Acta 313 (2001) 43.

Available online at www.sciencedirect.com
SCIENCE DIRECT®
Polyhedron 23 (2004) 1063–1067
POLYHEDRON
www.elsevier.com/locate/poly

Structural and reactivity changes in ruthenium ammines induced by the NO ligand

Welter C. Silva [a,1], Eduardo E. Castellano [b], Douglas W. Franco [a,*]

[a] Departamento de Química e Física Molecular, Instituto de Química de São Carlos, Universidade de São Paulo, Av. do Trabalhador Sao Carlense, Cx. Postal 780, CEP, São Carlos, SP 13560270, Brazil
[b] Instituto de Física de São Carlos, Universidade de São Paulo, CEP, São Carlos, SP 13560-970, Brazil

Received 9 October 2003; accepted 6 January 2004

This paper is dedicated in memoriam to our colleague and friend Rex E. Shepherd, University of Pittsburgh, Pittsburgh, PA, USA

Abstract

The crystal structure of $[Ru(NH_3)_5(OH_2)]_2(S_2O_6)_3 \cdot 2H_2O$ has been solved by X-ray diffraction techniques. The relevant average interatomic distances are Ru–$(NH_3)_{eq} = 2.09$ Å, Ru–$(NH_3)_{ax} = 2.08$ Å and Ru–$(OH_2)_{ax} = 2.11$ Å. The aquation rate (k_{H_2O}) and the activation parameters for the reaction

$$trans\text{-}[RuNO(NH_3)_4Cl]^{2+} + H_2O \overset{k_{H_2O}}{\rightarrow} trans\text{-}[RuNO(NH_3)_4(H_2O)]^{3+} + Cl^-$$

have been calculated as 8.4×10^{-6} s^{-1} (0.10 mol L^{-1} CF_3COOH, $\mu = 0.10$ mol L^{-1}, 40 °C), $\Delta H^{\neq}_{-1} = 2.3$ kcal mol^{-1}, $\Delta S^{\neq}_{-1} = 24.0$ cal deg^{-1} mol and $\Delta G^{\neq}_{-1} = 8.6$ kcal mol^{-1}. A comparison between the structural data, kinetic and thermodynamic reactivities of $[Ru(NH_3)_5(OH_2)]^{3+}$ and *trans*-$[RuNO(NH_3)_4(OH_2)]^{3+}$ ions strongly suggests that the substitution of the *trans* NH_3 ligand in the coordination sphere of $[Ru(NH_3)_5(OH_2)]^{2+}$ by NO confers a character of Ru(III) to the formally Ru(II) center.
© 2004 Elsevier Ltd. All rights reserved.

Keywords: Crystal structure; Back-bonding; Ruthenium complex; NO; Reactivity; Molecular

1. Introduction

There is a growing interest in the research involving nitric oxide (NO) chemistry as this molecule is directly involved in various biological processes such as vasodilatation and neurotransmission, as well as in a number of pathologies including inflammatory and immune diseases [1,2].

Metal complexes are extremely useful to activate the nitric oxide molecule. There is a great deal of effort in many laboratories aiming to develop coordination compounds able to act as NO carriers in biological media [3–7]. One of the key issues for modeling NO delivers or scavengers is to understand the mutual influences of both NO and the ligands *trans* positioned to NO on the coordination sphere, in their respective reactivities [8–10].

The purpose of this paper is to use ruthenium ammines as a model to understand the reactivity and structural effects induced by the presence of NO in the *trans*-$[RuNO(NH_3)_4(OH_2)]^{3+}$ complex as a whole by the comparison between the chemical properties (internuclear distances, pK_a and kinetic and thermodynamic data) of the $[Ru(NH_3)_5(OH_2)]^{3+}$ and *trans*-$[RuNO(NH_3)_4(OH_2)]^{3+}$ ions, and their respective chlorides derivatives.

2. Experimental

2.1. Reagents and materials

All chemicals were reagent grade quality (Aldrich and Merck) and used without further purification. The

* Corresponding author. Tel.: +55-16-273-9970; fax: +55-16-273-9976.
E-mail address: douglas@iqsc.usp.br (D.W. Franco).
[1] This manuscript is a part of the PhD thesis by Welter C. Silva.

0277-5387/$ - see front matter © 2004 Elsevier Ltd. All rights reserved.
doi:10.1016/j.poly.2004.01.007

solvents were purified as described in the literature [11]. Doubly distilled water was used throughout the experiments. Ruthenium trichloride ($RuCl_3 \cdot xH_2O$) was the starting material for the synthesis of the ruthenium complexes. All reactions and measurements were performed under an argon atmosphere, using standard techniques for the manipulations of air-sensitive compounds [12].

2.2. Synthesis of the ruthenium compounds

trans-$[RuNO(NH_3)_4Cl]Cl_2$ [13], $[Ru(NH_3)_5Cl]Cl_2$ [14] and $[Ru(NH_3)_5(H_2O)](CF_3SO_3)_3$ [15] were prepared according to the methods found in the literature, and their characteristics were checked by UV–visible, IR spectroscopy and electrochemical techniques.

2.3. Instrumentation

The elemental analysis were performed on a Perkin–Elmer elemental analyzer 2400 CHN. Ultraviolet and visible spectra were obtained on a Hitachi spectrophotometer model 3501-U. For EPR experiments, a Bruker ESP300e spectrometer operating with an X-band microwave bridge was used at the liquid N_2 temperature.

The electrochemical measurements were taken using a PARC system model 173 potentiostat/galvanostat, a model 175 universal programmer and a model 264A polarographic analyzer. Glassy carbon, saturated calomel (SCE) and platinum wire electrodes were used as working, reference and auxiliary electrodes, respectively.

The aquation for *trans*-$[RuNO(NH_3)_4Cl]Cl_2$ complex [13] was followed using the Hitachi spectrophotometer model 3501-U. The temperatures of the experiments were 40, 45, 49 and 60 ± 0.5 °C and controlled by a thermostated Tecnal TE 184 temperature bath. The solutions were prepared by dissolving the solid in degassed 0.10 mol L^{-1} CF_3COOH, $\mu = 0.10$ mol L^{-1} and quickly transferred, using teflon tubing, to a 1–5 cm quartz glass-sealed cell. The rate constants were graphically obtained from plots of $\log(A_t - A_\infty)$ versus time. The plots were linear from at least three half-lives. The activation parameters were calculated from specific rate constant data at different temperatures, using the Eyring plot ($\ln k/T$ against $1/T$) [16].

2.4. X-ray crystallographic study

The $[Ru(NH_3)_5(OH_2)]_2(S_2O_6)_3 \cdot 2H_2O$ crystals were obtained from the mother-liquor solution resulting from the syntheses of the $[Ru(NH_3)_5(OH_2)](CF_3SO_3)_3$ complex kept in a refrigerator for 2 days. The composition of these crystals was confirmed by elemental analysis and their cyclic voltammetry, electronic and EPR spectroscopy data were compared with the ones described in the literature for the $[Ru(NH_3)_5(OH_2)]^{3+}$ ion. $E_{1/2} = -210$ mV versus SCE [15,17]. UV–visible bands [15,17]: 268 ($\varepsilon = 675$ mol^{-1} L cm^{-1}) and 321 nm ($\varepsilon = 215$ mol^{-1} L cm^{-1}). The EPR spectra powder at different temperatures for $[Ru(NH_3)_5(OH_2)](CF_3SO_3)_3$ exhibit $g_\perp$ equal to 2.60. The $g_\parallel$ peak cannot be detected [18]. The simulation of $[Ru(NH_3)_5(OH_2)](CF_3SO_3)_3$ solid at 77 K gives $g_\perp = 2.62$ and $g_\parallel = 0.6 \geqslant g \geqslant 0$ [18].

Diffraction measurements were performed on an Enraf–Nonius Kappa-CCD diffractometer with graphite monochromated Mo Kα ($\lambda = 0.71073$ Å) radiation. The structure was first solved in P_m by the Heavy Atom Patterson method. The structure was refined to an R_1 value of 0.0274. Routine search for further symmetry using the method of Le Page [19] indicated that a center of inversion could have been overlooked. As it turned out, most atom coordinates could be transformed to comply with the $P_{2/m}$ super group symmetry except for the water molecule, which in this group is symmetric related to the NH_3 moiety *trans* to it, by a crystallographic inversion center. Since the Ru–N and Ru–O interatomic distances are equal within experimental error, we decided to describe the structure more economically as a somewhat disordered one but in the higher symmetry space group $P_{2/m}$. A nitrogen atom and

Table 1
Crystal data and structure refinement for $[Ru(NH_3)_5(H_2O)]_2(S_2O_6)_3 \cdot 2H_2O$

Empirical formula	$H_{38}N_{10}O_{22}Ru_2S_6$
Formula weight	924.90
Temperature (K)	120(2)
Wavelength (Å)	0.71073
Crystal system	monoclinic
Space group	$P2/m$, #10
Unit cell dimensions	
a (Å)	6.6365(2)
b (Å)	7.5620(2)
c (Å)	14.5879(4)
β (°)	98.834(1)
Volume (Å^3)	723.41(4)
Z, D_{calc} (Mg m^{-3})	1, 2.123
Absorption coefficient (mm^{-1})	1.577
$F(000)$	468
Crystal size (mm)	$0.28 \times 0.18 \times 0.12$
θ range for data collection (°)	3.04–25.99
Index ranges	$-8 \leqslant h \leqslant 6$, $-9 \leqslant k \leqslant 9$, $-17 \leqslant l \leqslant 17$
Reflections collected/unique	7248/1509 [$R_{int} = 0.0294$]
Completeness to $2\sigma = 25.99$ (%)	97.9
Absorption correction method	multi-scan
Maximum and minimum transmission	0.8333 and 0.6665
Refinement method	full-matrix least-squares on F^2
Data/restraints/parameters	1509/4/122
Goodness-of-fit on F^2	1.037
Final R indices [$I > 2\sigma(I)$]	$R_1 = 0.0297$, $wR_2 = 0.0716$
R indices (all data)	$R_1 = 0.0311$, $wR_2 = 0.0726$
Largest difference peak and hole (e Å^{-3})	1.108 and −0.924

an oxygen one, both with one half occupation factors, were assigned to the site of the water oxygen bonded to ruthenium and were constrained to have the same coordinates and thermal parameters. This model of a partially disordered structure refined to a final R_1 value of 0.0297, somewhat higher than the previous one, as expected, since the number or refined parameters was almost halved. Table 1 shows the data collection and refinement conditions.

3. Results and discussion

3.1. Molecular and crystal structure

There are two independent $[Ru(NH_3)_5OH_2]^{3+}$ moieties in the asymmetric unit, both displaying crystallographic mirror symmetry. The O-atom of the water molecule, the NH_3 *trans* to it and the heavy atom are sited on the crystallographic mirror plane, and the four equatorial NH_3 molecules are related in pairs by this same plane. The three counter-ions are also sited in special positions, each having two sulfur and two oxygen atoms on the crystallographic mirror plane and two other oxygen atoms in general positions. The resulting stoichiometry of three anions $S_2O_6^{2-}$ to two cations $[Ru(NH_3)_5OH_2]^{3+}$ is consistent with the one expected for the Ru(III) oxidation state.

It is interesting to note that in an earlier study [18] on the EPR and NMR of $[(M)(NH_3)_5(OH_2)]^{3+}$ species ($M = Os^{III}$, Ru^{III}), the presence of two forms of $[Os(NH_3)_5(OH_2)]^{3+}$ in the crystalline form was noted due to the presence of two EPR signals. The two forms in the related ruthenium compound could not be detected because the $g_{\|}$ region of the spectrum was outside the range of the spectrometer.

Attempts to obtain good crystals from $[Ru(NH_3)_5(OH_2)](CF_3SO_3)_3$ solutions were unsuccessful in the past [15,17], thus we believe that the $[Ru(NH_3)_5(OH_2)]^{3+}$ fragments prefer to use the $S_2O_6^{2-}$ as counter-ions rather than $CF_3SO_3^-$. In the present reported complex, two ions of the aqua-complex, three $S_2O_6^{2-}$ as counter-ions and two water molecules compose the unit cell $[Ru(NH_3)_5(OH_2)]_2(S_2O_6)_3 \cdot 2H_2O$.

Table 1 shows the X-ray data for $[Ru(NH_3)_5(OH_2)]_2(S_2O_6)_3 \cdot 2H_2O$ and Table 2 shows the relevant observed interatomic distances for this complex as well as for other related ones.

The average interatomic distance Ru–NH_3 in the equatorial plane is 2.09 Å, which is similar to the one found in other ruthenium complexes, such as $[RuCl(NH_3)_5]Cl_2$ (2.10 Å) [14], $[Ru(NH_3)_6]Cl_3$ (2.11 Å) [17] and *trans*-$[RuNO(NH_3)_4(OH_2)]Cl_3 \cdot 3H_2O$ (2.10 Å) [20]. The average interatomic distance Ru–OH_2 (2.11 Å) in the axial plane of the $[Ru(NH_3)_5(OH_2)]^{3+}$ ion, i.e., a Ru(III) species, is larger than the one observed for *trans*-$[RuNO(NH_3)_4(OH_2)]Cl_3 \cdot 3H_2O$ (2.04 Å) [20], where the metal center is formally in the oxidation state II. This Ru(II)–OH_2 distance shortening by replacing the *trans* NH_3 ligand by NO in the Ru(II) species is attributed to the strong $4d_\pi \rightarrow \pi^*NO$ back-bonding (Table 2), which would induce the OH_2 ligand to donate electrons to the Ru(II) center through the np ligand $\rightarrow Ru(II)d_\pi$.

A similar behavior is observed when comparing the Ru–Cl distance [17,20] in the $[Ru^{III}(NH_3)_5Cl)]^{2+}$ and *trans*-$[Ru^{II}NO(NH_3)_4(Cl)]^{2+}$ species, where the Ru–Cl distances for pentaammine and the nitrosyl-tetraammine species are 2.36 and 2.34 Å [19], respectively.

In *trans*-$[Ru^{II}NO(NH_3)_4(Cl)]^{2+}$ and *trans*-$[Ru^{II}NO(NH_3)_4(OH_2)]^{3+}$ species, the Ru–N–O angle is 180.0° and 178.1°, and NO stretching frequency values (ν_{NO}) equal at 1850 and 1912 cm^{-1}. Furthermore, both

Table 2
Interatomic distances (Å) selected for ruthenium species

Compound	Equatorial plane[a] (Ru–NH_3), Å	Axial plane (Ru–NH_3), Å	Axial plane (Ru–OH_2), Å	Angle (Ru–N–O), °
$[Ru(NH_3)_6]Cl_3$[b]	2.11			
$[Ru(NH_3)_5Cl]Cl_2$[b]	2.10			
$[Ru(NH_3)_5NO]Cl_3$[c]	2.10	2.02		172.8
$[Ru(NH_3)_5pz](CF_3SO_3)_3 \cdot H_2O$[d]	2.11			
$[Ru(NH_3)_5Mepz]I_3$[e]	2.12	2.17		
$[Ru(NH_3)_5Mepz](tos)_4 \cdot 5H_2O$[e]	2.11	2.10		
trans-$[RuNO(NH_3)_4OH]Cl_2$[c]	2.10			173.8
trans-$[RuNO(NH_3)_4(OH_2)]Cl_3 \cdot 3H_2O$[f]	2.11		2.04	178.1
$[Ru(NH_3)_5(OH_2)]_2[S_2O_6]_3 \cdot 2H_2O$[g]	2.09	2.06	2.11[a]	

[a] The values show the average interatomic distances.
[b] Ref. [17].
[c] Ref. [14].
[d] Ref. [23], pz = pyrazine.
[e] Ref. [21a], Mepz (1-methylpyrazinium, tos = tosylate(*p*-toluenosulfonate).
[f] Ref. [20].
[g] This work.

complexes are EPR silent, therefore it is quite reasonable assume the [$Ru^{II}NO^+$] formulation for both species, in which the NO^+ ligand withdrawing the electronic density of the metallic center (II) [20b]. Thus, the Ru–X distance are similar (or even shorter) to the one expected for the Ru(III) center through a cooperative effect along the NO–Ru–X axis (X = Cl^- and OH_2).

The π acidity of NO^+, measured as the Ru–X distance (X = the ligand *trans* to NO), is even higher than the one exhibited by the well-known strong π-acceptor Mepz (1-methylpyrazinium), so-called "organic NO" [21b], as observed from the Ru–NH_3 (*trans*) distance in $[Ru(NH_3)_5(Mepz)]I_3$ (2.17 Å) [21a] and $[Ru(NH_3)_5(NO)]Cl_3$ (2.02 Å) [22] species.

3.2. Kinetic reactivities

Besides the structural effects, the NO influences on the complex ion behavior are easily noticed in solution. A good example is the pK_a value for the coordinated water molecule in such complexes:

$$[Ru(NH_3)_5(H_2O)]^{2+} + H_2O \rightleftharpoons [Ru(NH_3)_5(OH)]^{+} + H_3O^+ \quad (1)$$

$$[Ru(NH_3)_5(H_2O)]^{3+} + H_2O \rightleftharpoons [Ru(NH_3)_5(OH)]^{2+} + H_3O^+ \quad (2)$$

The pK_a values for reactions (1) and (2) are 13.1 [24] and 4.1 [24], respectively, which are consistent with the 2+ and 3+ charges of the aqua species. Enormous change in the acidity of the Ru(II) center, and then in the acidity of the OH_2 ligand, is observed when the NO ligand is present in the coordination sphere, as expressed by the pK_a value of 3.1 [20] for the following reaction:

$$trans\text{-}[RuNO(NH_3)_4(H_2O)]^{3+} + H_2O \rightleftharpoons trans\text{-}[RuNO(NH_3)_4(OH)]^{2+} + H_3O^+ \quad (3)$$

Again, the higher acidity exhibited by the formally Ru(II) center in the *trans*-$[RuNO(NH_3)_4(OH_2)]^{3+}$ species (ν_{NO} = 1912 cm^{-1}, EPR silent, Ru–N–O angle = 178.1°) [20], as compared to the one of the Ru(III) center in the $[Ru(NH_3)_5(OH_2)]^{3+}$ species, is consistent with the smaller Ru–OH_2 distance in the nitrosyl complex (Table 2).

The kinetic reactivity of the metal center is also strongly influenced by the NO presence. The aquation rate constant (k_{H_2O}) values for the chloro-pentaammine species (4), $[Ru(NH_3)_5Cl]^{2+}$ and $[Ru(NH_3)_5Cl]^{+}$, are 5.4×10^{-6} s^{-1} (40 °C) [25] and 2.0×10 s^{-1} (43 °C) [26], respectively. Under comparable experimental conditions (0.10 mol L^{-1} CF_3COOH, μ = 0.10 mol L^{-1}, 40 °C), the k_{H_2O} for *trans*-$[RuNO(NH_3)_4Cl]^{2+}$ species (5) is 8.4×10^{-6} s^{-1}

Table 3
Experimental rate constants for $[Ru(NH_3)_5L]^{n+}$ and *trans*-$[RuNO(NH_3)_4L]^{2+}$ species, where L = Cl^-, the measurement corresponds to k_{H_2O}

Species	k_{H_2O} (s^{-1})	T (°C)
$[Ru(NH_3)_5Cl]^{+}$	20.2[a]	43
$[Ru(NH_3)_5Cl]^{2+}$	5.4×10^{-6}[b]	40
	8.5×10^{-6}[b]	45
	2.3×10^{-5}[b]	53
	6.5×10^{-5}[b]	64
trans-$[RuNO(NH_3)_4Cl]^{2+}$	8.4×10^{-6}[c]	40
	9.4×10^{-6}[c]	45
	2.0×10^{-5}[c]	49
	6.2×10^{-5}[c]	60

[a] Values measured by cyclic voltammetric method [26].
[b] Interpolated from Eyring plot using the experimental data of [25] ($\Delta H^{\neq}_{-1}$ = 2.4 kcal mol^{-1}, $\Delta S^{\neq}_{-1}$ = 30.0 cal deg^{-1} mol and $\Delta G^{\neq}_{-1}$ = 6.5 kcal mol^{-1}).
[c] This paper ($\Delta H^{\neq}_{-1}$ = 2.3 kcal mol^{-1}, $\Delta S^{\neq}_{-1}$ = 24.0 cal deg^{-1} mol^{-1} and $\Delta G^{\neq}_{-1}$ = 8.6 kcal mol^{-1}).

$$[Ru(NH_3)_5Cl]^{2+} + H_2O \xrightarrow{k_{H2O}} [Ru(NH_3)_5(H_2O)]^{3+} + Cl^- \quad (4)$$

$$trans\text{-}[RuNO(NH_3)_4Cl]^{2+} + H_2O \xrightarrow{k_{H2O}} trans\text{-}[RuNO(NH_3)_4(H_2O)]^{3+} + Cl^- \quad (5)$$

The above data clearly stress that the rate of Cl^- dissociation from the Ru(II) center is much slower when the *trans* NH_3 ligand is replaced by NO. Thus, the *trans*-$[RuNO(NH_3)_4Cl]^{2+}$ species exhibits an inertness to Cl^- aquation comparable to the Ru(III) pentaammine complex ions (Table 3).

It is well accepted that the substitution reactions in octahedral complexes follow a dissociate pathway [16]. According to this model, the rate determining step is controlled by a bond breaking process [16]. Therefore, in a series of related compounds the $\Delta H^{\neq}_{-1}$ values, for the dissociation of the same ligand X, will provide an idea of the relative metal–X bond strength.

The activation parameter data ($\Delta H^{\neq}_{-1}$, $\Delta S^{\neq}_{-1}$ and $\Delta G^{\neq}_{-1}$) for *trans*-$[RuNO(NH_3)_4Cl]^{2+}$ complex are 2.3 kcal mol^{-1}, 24.0 cal deg^{-1} mol^{-1} and 8.6 kcal mol^{-1}, respectively. The activation parameter data for *trans*-$[RuNO(NH_3)_4Cl]^{2+}$ complex (Table 3) are similar to the ones reported for $[Ru(NH_3)_5Cl]^{2+}$ complex ($\Delta H^{\neq}_{-1}$ = 2.4 kcal mol^{-1}, $\Delta S^{\neq}_{-1}$ = 30.0 cal deg^{-1} mol and $\Delta G^{\neq}_{-1}$ = 6.5 kcal mol^{-1}), and consistent with the charge of both complex ions and their respective Ru–Cl bond strength.

Thus, all the present experimental data indicate that the ruthenium(II) center bonded to the NO ligand exhibits kinetic and thermodynamic properties similar to the ones of a ruthenium(III) center.

4. Conclusions

According to experimental data (IR, X-ray diffraction and EPR spectroscopies), the *trans*-$[RuNO(NH_3)$-

$_4(H_2O)]^{3+}$ are better represented as $[Ru^{II}NO^+]$, than as $[Ru^{III}NO^0]$. The presence of the nitric oxide ligand in the coordination sphere of $[Ru(NH_3)_4(H_2O)]^{2+}$ moiety shortens to 2.04 Å the Ru^{II}–OH_2 interatomic distance, which is smaller than the value of 2.11 Å observed for the Ru^{III}–OH_2 in $[Ru(NH_3)_5(H_2O)]^{3+}$, thus making the ruthenium(II) center a stronger Lewis acid than the ruthenium(III) center. This behavior is also supported by pK_a values of 3.1 and 4.1 for aqua-nitrosyl-tetraammine(II) and aqua-pentaammine(III) species and by the lower rate of Cl^- replacement in *trans*-$[RuNO(NH_3)_4Cl]^{2+}$ regarding $[Ru(NH_3)_5Cl)]^{2+}$.

5. Supplementary material

Crystallographic data for the structure in this paper have been deposited with the Fachinformationszentrum Karlsruhe (FIZ) as supplementary publication on CSD No. 391231.

Acknowledgements

The authors acknowledge Angela Cristina Pregnolato Giampedro and Bruce R. McGarvey for reading the manuscript and the Brazilian agencies FAPESP (Proc. 99/0719-9), CAPES and CNPq for the financial support.

References

[1] D. Ricard-Jané, M. Llobera, M.D. López-Tejero, Nitric Oxide: Biol. Chem. 6 (2002) 178.
[2] F. Herencia, M.P. López-García, A. Ubeda, L.M. Ferrándiz, Nitric Oxide: Biol. Chem. 6 (2002) 242.
[3] J.C. Toledo Jr., L.G.F. Lopes, A.A. Alves, L.P. Silva, D.W. Franco, J. Inorg. Biochem. 89 (2002) 267.
[4] Y. Chen, R.E. Shepherd, J. Inorg. Biochem. 68 (1997) 183.
[5] M. De Leo, P.C. Ford, J. Am. Chem. Soc. 121 (1999) 1980.
[6] L.V. Andreasen, I.M. Lorkovic, G.B. Richter-Addo, P.C. Ford, Nitric Oxide: Biol. Chem. 6 (2002) 228.
[7] A.D Torsoni, B.F. Barros, J.C. Toledo Jr., M. Haun, M.H. Krieger, E. Tfouni, D.W. Franco, Nitric Oxide: Biol. Chem. 6 (2002) 247.
[8] S.S.S Borges, C.U. Davanzo, E.E. Castellano, J. Z-Schpector, S.C. Silva, D.W. Franco, Inorg. Chem. 37 (1998) 2670.
[9] M.G. Gomes, C.U. Davanzo, S.C. Silva, L.G.F. Lopes, P.S. Santos, D.W. Franco, J. Chem. Soc., Dalton Trans. (1998) 601.
[10] D.R Lang, J.A. Davis, L.G.F. Lopes, A.A. Ferro, L.C.G. Vasconcellos, D.W. Franco, E. Tfouni, A. Wieraszko, M.J. Clarke, Inorg. Chem. 39 (2000) 2294.
[11] D.D. Perrin, W.L.F. Armarego, D.R. Perrin, Purification of Laboratory Chemicals, Pergamon Press, New York, 1983.
[12] D.F. Shriver, The Manipulation of Air-sensitive Compounds, McGraw-Hill, New York, 1969.
[13] A.F. Schreiner, S.W. Lin, P.J. Hauser, E.A. Hopcus, D.J. Hamm, J.D. Gunter, Inorg. Chem. 3 (1972) 880.
[14] A.D. Allen, F. Bottomley, R.D. Harris, V.P. Reinsalu, C.V. Senoff, Inorg. Synth. 12 (1970) 2.
[15] H. Krenztien, Mixed valence ruthenium ammine dinitrile and related complexes, Ph.D. Thesis, Stanford University, 1976.
[16] E.S. Lewis, Techniques of Chemistry, Investigation of Rates and Mechanisms of Reactions VI, Wiley, New York, 1974, and literature cited.
[17] E.A. Seddon, K.R. Seddon, The Chemistry of Ruthenium, Elsevier, New York, 1984, p. 230.
[18] B.R. McGarvey, N.C. Batista, C.W.B. Bezerra, M.S. Schultz, D.W. Franco, Inorg. Chem. 37 (1998) 2865.
[19] (a) MISSYM Algorithm: Y. LePage, J. Appl. Crystallogr. 20 (1987) 264;
(b) A.L. Spek, J. Appl. Crystallogr. 21 (1988) 578.
[20] (a) C.W.B. Bezerra, S.C. Silva, M.T.P. Gambardella, R.H.A. Santos, L.M.A. Plicas, E. Tfouni, D.W. Franco, Inorg. Chem. 38 (1999) 5660;
(b) E. Tfouni, M. Krieger, B.R. McGarvey, D.W. Franco, Coor. Chem. Rev. 236 (2003) 57.
[21] (a) J.F. Wishart, A. Bino, H. Taube, Inorg. Chem. 25 (1986) 3318;
(b) E. Waldhor, W. Kaim, J.A. Olabe, L.D. Slep, J. Fiedler, Inorg. Chem. 36 (1997) 2969.
[22] F. Bottomley, J. Chem. Soc., Dalton Trans. (1974) 1600.
[23] M.E. Gress, C. Creutz, C.O. Quicksall, Inorg. Chem. 20 (1981) 1522.
[24] (a) P.C. Ford, R.D.F. Gaunder, P. Rudd, H. Taube, J. Am. Chem. Soc. 90 (1968) 1187;
(b) E. Tfouni, P.C. Ford, Inorg. Chem. 19 (1980) 72;
(c) H. Taube, Pure Appl. Chem. 51 (1979) 901.
[25] J.A. Broomhead, F. Basolo, R.G. Pearson, Inorg. Chem. 3 (1964) 826.
[26] G.N. Coleman, J.W. Gesler, F.A. Shirley, J.R. Kuempel, Inorg. Chem. 12 (1973) 1036.

Available online at www.sciencedirect.com
SCIENCE DIRECT®
Polyhedron 23 (2004) 1069–1073
POLYHEDRON
www.elsevier.com/locate/poly

Reactivity studies of cyclopentadienyl bis(triphenylphosphine)ruthenium(II) complex towards some polypyridyl ligands

R. Lalrempuia [a], P. Govindaswamy [a], Yurij A. Mozharivskyj [b], Mohan Rao Kollipara [a,*]

[a] Department of Chemistry, North Eastern Hill University, Shillong 793 022, India
[b] Ames Laboratory, Iowa State University of Science and Technology, Ames, Iowa, IA 50011, USA

Received 5 December 2003; accepted 7 January 2004

Abstract

The reaction of $[CpRu(PPh_3)_2Cl]$ (**1**) ($Cp = \eta^5$-C_5H_5) with excess of some potentially bridging ligands viz. 2,3-bis(α-pyridyl)pyrazine (bpp), 2,3-bis(α-pyridyl)quinoxaline (bpq), 1,3,5-tris(pyridyl)-2,4,6-triazine (tptz) and 2,3,5,6-tetrakis(pyridyl)pyrazine (tppz) yielded cationic mononuclear complexes of the type $[CpRu(PPh_3)(bpp)]^+$ (**2**), $[CpRu(PPh_3)(bpq)]^+$ (**3**), $[CpRu(PPh_3)(tptz)]^+$ (**4**) and $[CpRu(PPh_3)(tppz)]^+$ (**5**), respectively. These complexes have been isolated as hexafluorophosphate salts. They were characterized by FT-IR, ^1H NMR and ^{31}P $\{^1H\}$ NMR spectroscopy. The molecular structures of representative complexes **3** and **5** have been solved by single crystal X-ray crystallography.
© 2004 Elsevier Ltd. All rights reserved.

Keywords: Ruthenium; Cyclopentadienyl; 2,3-Bis(α-pyridyl)pyrazine; 1,3,5-Tris(pyridyl)-2,4,6-triazine; 2,3,5,6-Tetrakis(pyridyl)pyrazine

1. Introduction

As part of our investigation of the complexes of areneruthenium(II) [1], cyclopentadienylruthenium(II) [2], osmium(II) [3] and indenylruthenium(II) [4] with a variety of nitrogen-based ligands, we here report on complexes of cyclopentadienylruthenium(II) system with some potentially bridging polypyridyl ligands. The current interest in complexes of polypyridyl ligands, 2,2′-bipyridine, 1,10-phenanthroline, 2,2′:6′,2″-terpyridine, etc., is associated with the extremely interesting electrochemical, photophysical and photoelectrochemical properties that they exhibit [5–8]. Complexes with these ligands are also DNA intercalators, showing an ability to inhibit nucleic acid synthesis in vivo [9]. The recent report on the reactivity studies of arene ruthenium(II) with the ligands (Scheme 1) showed that the ligands L = bpp and bpq cleanly cleaved the halide bridge complex $[(\eta^6$-*p*-cymene$)RuCl_2]_2$ to give two products of the formula $[(\eta^6$-*p*-cymene$)RuCl(L)]^+$ and $[\{(\eta^6$-*p*-cymene$)RuCl\}_2(L)]^{2+}$ [1] and the ligands L = tppz, tptz and py-terpy displaced arene moiety as well as chloride ligands to form dicationic complexes of the formula $[LRuL']^{2+}$. However, py-terpy can also acts as a monodentate ligand binding the metal with nitrogen of the pendant 4-pyridyl group to form $[(\eta^6$-*p*-cymene$)RuCl_2$(py-terpy)] when the reaction medium is diethylether [10]. In the present case, we do not observe the formation of dimeric complexes that could be due to the presence of sterically demanding bulky triphenylphosphine.

2. Experimental

The solvents were purified and dried by standard methods and all reactions were carried out under dry nitrogen atmosphere. Infrared spectra were recorded as KBr pellets using on a Perkin–Elmer Model 983 spectrophotometer. ^1H and ^{13}C $\{^1H\}$ NMR spectra were recorded on a Bruker ACF 300, spectrometer and

* Corresponding author. Tel.: +91-364-272-2620; fax: +91-364-255-0076.
E-mail addresses: kmrao@nehu.ac.in, mrkollipara@yahoo.com (M.R. Kollipara).

0277-5387/$ - see front matter © 2004 Elsevier Ltd. All rights reserved.
doi:10.1016/j.poly.2004.01.002

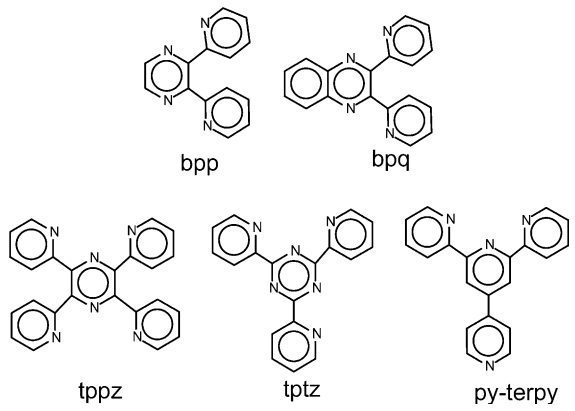

Scheme 1. Ligands used in this work.

referenced to external tetramethylsilane. ^{31}P $\{^1H\}$ NMR chemical shifts are reported relative to H_3PO_4 (85%). Elemental analyses were performed by RSIC, Shillong.

The ligands 2,3-bis(α-pyridyl)pyrazine (bpp), 2,3-bis(α-pyridyl)quinoxaline (bpq), 2,3,5,6-tetrakis(pyridyl)pyrazine (tppz) [11] and py-terpy [12] and $[CpRu(PPh_3)_2Cl]$ [13] were synthesized according to the literature methods. 1,3,5-tris(pyridyl)-2,4,6-triazine (tptz) was purchased from Loba Chemie Private Limited and used as such.

2.1. Preparation of the complexes 2–5

The following general procedure was used for the preparation of these mononuclear complexes.

The mixture of the complex $[CpRu(PPh_3)_2Cl]$ (0.1 g, 0.110 mmol), the ligand (0.220 mmol) and NH_4PF_6 (0.220 mmol) were refluxed in methanol (40 ml) whereby the orange color suspension gradually changes to intense dark red color. It was refluxed for 5 h, then the solvent was rotary evaporated. The residue was extracted with $CHCl_3$ and filtered through short silica gel column to remove insoluble material, the filtrate was again concentrated to about 2 ml and addition of excess diethylether precipitated the product as red-brown solid.

2.1.1. $[CpRu(PPh_3)(bpp)]PF_6$ (**2**PF_6)

^1H NMR (δ, $CDCl_3$): 9.53 (s, 1H), 9.32 (d, 1H, $J = 4.8$ Hz), 8.63 (d, 1H, $J = 4.7$), 8.32 (s, 1H), 8.02 (t, 1H, $J = 6.8$ Hz), 7.65 (d, 1H, $J = 7.6$ Hz), 7.54 (t, 1H, $J = 7.6$ Hz), 7.33–6.98 (m, 17H), 6.56 (d, 1H, $J = 8.2$ Hz), 4.84 (s, 5H).

^{31}P $\{^1H\}$ NMR (δ, $CDCl_3$): 48.81 (s), −143 (sept).

Anal. Calc. for $C_{37}H_{20}N_4RuP_2F_6$: C, 55.02; H, 3.74; N, 6.96. Found: C, 55.20; H, 3.78; N, 7.00%.

UV–Vis (CH_2Cl_2, 10^{-3} M): $\lambda_{max} = 489$ nm.

2.1.2. $[CpRu(PPh_3)(bpq)]PF_6$ (**3**PF_6)

^1H NMR (δ, CD_3CN): 9.23 (d, 1H, $J = 5.4$ Hz), 8.74 (d, 1H, $J = 8.9$ Hz), 8.58 (d, 1H, $J = 4.3$ Hz), 8.10 (t, 1H, $J = 8.1$ Hz), 8.01–7.86 (m, 3H), 7.79 (t, 1H, $J = 6.8$ Hz), 7.60 (t, 1H, $J = 6.9$ Hz), 6.39–7.71 (m, 9H), 7.09 (t, 1H, $J = 9.9$ Hz), 6.90 (m, 7H), 6.76 (d, 1H, 8.4), 5.04 (s, 5H).

^{31}P $\{^1H\}$ NMR (δ, $CDCl_3$): 52.66 (s), −143(sept).

Anal. Calc. for $C_{41}H_{32}N_4RuP_2F_6$: C, 57.41; H, 3.73; N, 6.52. Found: C, 57.56; H, 3.82; N, 6.44%.

UV–Vis (CH_2Cl_2, 10^{-3} M): $\lambda_{max} = 486$ nm.

2.1.3. $[CpRu(PPh_3)(tptz)]PF_6$ (**4**PF_6)

^1H NMR (δ, CD_3CN): 9.30 (d, 1H, $J = 5.2$ Hz), 8.91 (d, 1H, $J = 4.2$ Hz), 8.68 (d, 1H, $J = 7.9$ Hz), 8.64 (d, 1H, $J = 8$ Hz), 8.39 (d, 1H, $J = 4.8$ Hz), 8.03–7.84 (m, 3H), 7.56–7.46 (m, 4H), 8.36–6.96 (m, 17H), 4.53 (s, 5H, Cp).

^{31}P $\{^1H\}$ NMR (δ, $CDCl_3$): 48.98 (s), −143 (sept).

Anal. Calc. for $C_{41}H_{32}N_6RuP_2F_6$: C, 55.60; H, 3.64; N, 9.49. Found: C, 55.83; H, 3.72; N, 9.63%.

UV–Vis (CH_2Cl_2, 10^{-3} M): $\lambda_{max} = 477$ nm.

2.1.4. $[CpRu(PPh_3)(tppz)]PF_6$ (**5**PF_6)

^1H NMR (δ, $CDCl_3$): 8.95 (m, 1H), 8.63 (d, 1H, $J = 6$ Hz), 8.19 (m, 1H), 8.03 (t, 1H, $J = 6.6$), 7.92 (m, 1H), 7.62–6.75 (m, 26H), 4.95 (s, 5H, Cp).

^{31}P $\{^1H\}$ NMR (δ, $CDCl_3$): 46.21 (m), −143 (sept).

Anal. Calc. for $C_{47}H_{36}N_6RuP_2F_6$: C, 58.69; H, 3.74; N, 8.73. Found: C, 58.75; H, 3.67; N, 8.81%.

UV–Vis (CH_2Cl_2, 10^{-3} M): $\lambda_{max} = 461$ nm.

3. Crystal structure determination of 3PF_6 and 5PF_6

Suitable single crystals of **3**PF_6 were grown by slow diffusion of hexane into acetone solution and of **5**PF_6 were grown from hexane into chloroform solution. A suitable size crystal of complex **3**PF_6 was mounted on the end of the glass fiber and mounted on a Nonius MACH3 diffractometer where as complex **5**PF_6 was mounted on Bruker Smart Apex CCD system equipped with graphite monochromatized Mo Kα ($\lambda = 0.70930$ Å) radiation at a temperature of 293 K for the cell determination and intensity data collection. Crystal data collection parameters are summarized in Table 1. The structure was solved by direct methods [14] (SHELXS-1997). Refinement was by full-matrix least-squares based on F^2 using SHELXL-93 [15]. Lorentz and polarization corrections were applied. Non-hydrogen atoms were refined anisotropically only in the case of complex **3**PF_6 and hydrogen atoms were refined using a "riding" model. Figs. 1 and 2 are the ORTEP [16] representation of the molecules with 50% probability thermal ellipsoids displayed. Selected bond distances and angles are given in Tables 2 and 3 for complexes **3**PF_6 and **5**PF_6, respectively.

Table 1
Crystal data and structure refinement for complex $\mathbf{5}PF_6 \cdot 3CHCl_3$ and complex $\mathbf{3}PF_6 \cdot C_3H_2O$

Empirical formula	$C_{50}H_{39}Cl_9F_6N_6P_2Ru$	$C_{44}H_{34}F_6N_4P_2ORu$
Formula weight	1319.93	911.79
T (K)	293 (2)	293 (2)
Wavelength (Å)	0.71073	1.5418
Crystal system	orthorhombic	monoclinic
Space group	*Pbca*	$P21/n$
Unit cell dimensions		
a (Å)	15.2504(12)	14.2780(10)
b (Å)	19.1960(15)	9.9760(10)
c (Å)	37.199(3)	28.9110(10)
β (Å)		103.48
V (Å^3)	10889.8(15)	4004.6(5)
Z	8	4
D_{calc} (Mg m^{-3})	1.610	1.512
Crystal size (mm)	$0.6 \times 0.5 \times 0.3$	$0.6 \times 0.6 \times 0.2$
θ range for data collection (°)	1.73–15.07	0–70
Index ranges	$-11 \leqslant h \leqslant 11$,	$0 \leqslant h \leqslant 17$,
	$-14 \leqslant k \leqslant 13$,	$0 \leqslant k \leqslant 12$,
	$-27 \leqslant l \leqslant 27$	$-35 \leqslant l \leqslant 34$
Reflections collected	22 053	7411
Independent reflections	2214 ($R_{int} = 0.0583$)	5586
Absorption coefficient (mm^{-1})	0.851	4.517
$F(000)$	5296	1848
Absorption correction	empirical (SADABS)	empirical
Refinement method	full-matrix least-squares on F^2	
Data/restraints/parameters	2214/9/352	5586/0/524
Goodness-of-fit on F^2	1.002	1.162
Final R indices [$I > 2\sigma(I)$]	$R_1 = 0.0665$, $wR_2 = 0.1598$	$R_1 = 0.0819$, $wR_2 = 0.2046$
R indices (all data)	$R_1 = 0.0789$, $wR_2 = 0.1717$	$R_1 = 0.1134$, $wR_2 = 0.2418$
Largest different peak and hole (e Å^{-3})	0.546 and −0.471	

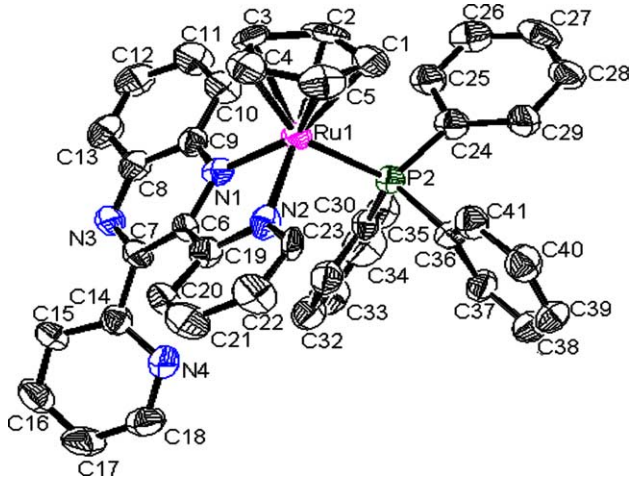

Fig. 1. Molecular structure of $[CpRu(PPh_3)(bpq)]PF_6$ (**3**). The entire hydrogen atoms, PF_6 and part of acetone molecules are removed for clarity.

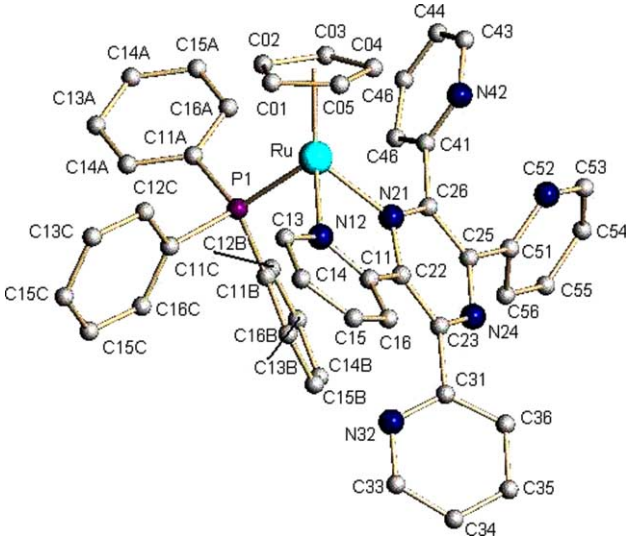

Fig. 2. Molecular structure of $[CpRu(PPh_3)(tppz)]PF_6$ (**3**). The entire hydrogen atoms, PF_6 and chloroform molecules are removed for clarity.

4. Results and discussion

The reaction of the complex $[CpRu(PPh_3)_2Cl]$ (**1**) where $Cp = \eta^5$-$C_5H_5$with excess of the ligands (Scheme 1) in methanol under refluxing condition resulted in the dissociation of one of the triphenylphosphines and chloride ligand to yield the monomeric chelate complexes **2**–**5** (Scheme 2). We are unable to isolate the anticipated dimeric complexes by changing the molar ratio of the starting complex to the corresponding ligand. These complexes are soluble in most of the polar solvents.

All these complexes showed a sharp singlet in the region of 4.53–5.04 ppm in ^{1}H NMR spectra, which can

Table 2
Selected bond lengths (Å) and bond angles (°) for $[CpRu(PPh_3)(bpq)]PF_6$ (**3**PF_6)

Bond lengths	
Ru(1)–N(1)	2.090 (7)
Ru(1)–C(5)	2.172 (9)
Ru(1)–C(3)	2.217 (8)
Ru(1)–N(2)	2.070 (7)
Ru(1)–C(1)	2.188 (9)
Ru(1)–C(4)	2.203 (9)
Ru(1)–P(2)	2.322 (2)
Ru(1)–C(2)	2.230 (8)
Bond angles	
N(2)–Ru(1)–N(1)	76.11 (2)
N(1)–Ru(1)–P(2)	94.00 (17)
N(2)–Ru–P(2)	95.01 (19)

Table 3
Selected bond lengths (Å) and bond angles (°) for $[CpRu(PPh_3)(tppz)]PF_6 \cdot 3CHCl_3$ (**5**PF_6)

Bond lengths	
Ru(1)–N(12)	2.093(12)
Ru(1)–C(01)	2.207(11)
Ru(1)–C(04)	2.214(11)
P(1)–C(11B)	1.837(9)
Ru(1)–N(21)	2.113(12)
Ru(1)–C(02)	2.193(11)
Ru(1)–C(05)	2.220(11)
P(1)–C(11A)	1.849(10)
Ru(1)–P(1)	2.336(5)
Ru(1)–C(03)	2.197(10)
P(1)–C(11C)	1.834(9)
Bond angles	
N(12)–Ru–N(21)	75.9(5)
N(21)–Ru–P(1)	92.4(3)
N(12)–Ru–P(1)	93.7(3)

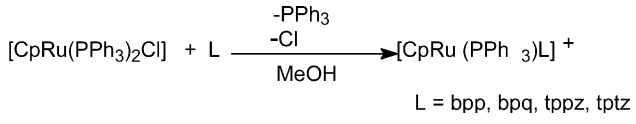

Scheme 2.

be assigned unambiguously to the resonance of cyclopentadienyl ligand. The analytical data, integration of the spectrum and a rather complicated peaks originating from the potentially bridging ligands in the ^1H NMR spectrum suggest the unsymmetrical coordinating nature of this ligand to the metal center, i.e. two nitrogens chelate the ruthenium centre leaving other pyridyl groups uncoordinated which inturn reflects the monomeric nature of the complexes. The peaks corresponding to the protons of the triphenylphosphine and the chelate ligands appear in the aromatic region in the range of 7–9 ppm. The ^{31}P $\{^1H\}$ NMR spectrum of these complexes showed single peak at around 48 ppm and septet at −143 ppm for triphenylphosphine and PF_6^- ion, respectively. In the case of complex **5** a multiplet was observed at 46 ppm for triphenylphosphine, which may be due to the interaction between the phosphorus and the protons of the highly strained tppz ligand.

In contrast to the above reactions, the product isolated from the reaction between complex **1** and py-terpy contains a mixture of products. The ^1H NMR spectrum shows three equally intense cyclopentadienyl peaks at 4.4, 4.38 and 4.36 ppm suggesting the presence of three different environments for the cyclopentadienyl ligand. ^{31}P $\{^1H\}$ NMR spectrum is also complicated and shows peaks at 49.7 ppm (singlet), 45.9 ppm (singlet) and 42.8 ppm (multiplets). The UV–Vis spectrum also shows two very broad bands at 450 and 520 nm. An attempt to separate the mixture by crystallization and column chromatography was unsuccessful.

5. Crystal structures

The complex $[CpRu(PPh_3)(bpq)]PF_6$ (**3**PF_6) crystallizes with one acetone per molecule but only two protons of the acetone were located. The geometry about the metal atom can be regarded as distorted octahedral with the bpq ligand chelating the ruthenium atom with two nitrogen atoms and the other coordination sites occupied by triphenylphosphine and a pentahapto bound cyclopentadienyl ligand. The average Ru–C (Cp) bond length is 2.202 Å where the individual bond length falls within the range of 2.172–2.230 Å. The two nitrogens chelate the ruthenium (N1–Ru–N2) with an angle of 76.11° and the bond lengths are almost the same with 2.090 and 2.070 Å for Ru–N1 and Ru–N2, respectively. The angle subtended by N1–Ru–P2 and N2–Ru–P2 is 94° and 95.01°, respectively. The distance between the ruthenium atom and phosphorus atom of the triphenylphosphine ligand is 2.322 Å. Even with the low accuracy of the results from the X-ray determination, all the metrical parameters are in a close agreement with those of complex **5** and other related works [1,2].

The complex $[CpRu(PPh_3)(tppz)]PF_6$ (**5**PF_6) crystallized with three molecules of chloroform per molecule. The crystal diffracts weakly and the maximum angle at which $I > 2\sigma(I)$ is 15°. Due to the small ratio of data to parameter, only the PF_6 and chloroform units were refined anisotropicaly and the rest was refined isotropicaly. The average Ru–C (Cp) bond length is 2.211 Å. The nitrogen atoms N12 and N21 chelate the ruthenium atom with an angle of 75.9°. The bond distance between the ruthenium and N12, N21 and P of PPh_3 is 2.093, 2.113 and 2.336 Å, respectively. The angle subtended by N12–Ru–P1 and N21–Ru–P1 is 93.7° and 92.4°, respectively. The bond angles and bond lengths are comparable in both these structures as well as with those of related complexes.

6. Conclusion

The reaction of $[CpRu(PPh_3)_2Cl]$ with equimolar or excess amount of some potential bridging polypyridyl ligands L, where L = bpp, bpq, tppz and tptz in methanol in refluxing condition yielded mononuclear complexes of the formulations $[CpRu(PPh_3)(L)]^+$ which apparently results from the dissociation of one triphenylphosphine and the chloride ligands.

7. Supplementary material

Crystallographic data for the structural analysis have been deposited at the Cambridge Crystallographic Data Centre (CCDC), CCDC Nos. 222042 for complex **3** and 222043 for complex **5**, respectively. Copies of this information may be obtained free of charge from The Director, CCDC, 12 Union Road, Cambridge, CB2 1EZ, UK (fax: +44-1223-336033; email: deposit@ccdc.cam.ac.uk or www: http://www.ccdc.cam.ac.uk).

Acknowledgements

K.M.R. thanks the DST (DST SERC: SP/S1/F-22/98), New Delhi for financial support. We also thanks the S. Dey and T.P. Singh, AIIMS, New Delhi for providing help in solving single crystal structure.

References

[1] (a) R. Lalrempuia, M.R. Kollipara, P.J. Carroll, Polyhedron 22 (2003) 605;
(b) R. Lalrempuia, M.R. Kollipara, Polyhedron 22 (2003) 3155.
[2] K.M. Rao, C.R.K. Rao, P.S. Zacharias, Polyhedron 16 (1997) 2369.
[3] R. Lalrempuia, P.J. Carroll, M.R. Kollipara, Polyhedron 22 (2003) 1391.
[4] M.R. Kollipara, E.K. Rymmai, Polyhedron 22 (2003) 307.
[5] (a) A.M.W. Thompson, Coord. Chem. Rev. 160 (1997) 1;
(b) J.P. Sauvage, J.P. Collin, J.C. Chambron, S. Guillerez, C. Coudret, V. Balzani, F. Barigelletti, L. De Cola, L. Flamigni, Chem. Rev. 94 (1994) 993.
[6] (a) E.C. Constable, Adv. Inorg. Chem. 34 (1989) 1;
(b) E.C. Constable, Adv. Inorg. Chem. Radiochem. 30 (1986) 69;
(c) E.C. Constable, Prog. Inorg. Chem. 42 (1994) 67.
[7] F. Fagalde, N.E. Katz, J. Chem. Soc., Dalton Trans. (1993) 571.
[8] (a) J.A. Bailey, V.M. Miskowski, H.B. Gray, Inorg. Chem. 32 (1993) 369;
(b) H.K. Yip, L.K. Cheng, K.K. Cheng, C.M. Che, J. Chem. Soc., Dalton Trans. (1993) 2933.
[9] W.I. Sundquist, S.J. Lippard, Coord. Chem. Rev. 100 (1990) 293.
[10] R. Lalrempuia, unpublished work.
[11] H.A. Goodwin, F. Lions, J. Am. Chem. Soc. 81 (1959) 6415.
[12] E.C. Constable, A.M.W. Cargill Thompson, J. Chem. Soc., Dalton Trans. (1992) 2947.
[13] M.I. Bruce, N.J. Windsor, Aust. J. Chem. 30 (1977) 1601.
[14] SIR-92: A. Altomare, M.C. Burla, M. Camalli, M. Cascarano, C. Giacovazzo, A. Guagliardi, G. Polidoro, J. Appl. Crystallogr. 27 (1994) 435.
[15] G.M. Sheldrick, SHELXL-93: Program for the Refinement of Crystal Structures, University of Göttingen, Göttingen, Germany, 1993.
[16] C.K. Johnson, ORTEP-II: A Fortran Thermal Ellipsoid Plot Program for Crystal Structure Illustrations, ORNL-5138, 1976.

Available online at www.sciencedirect.com
SCIENCE DIRECT®
Polyhedron 23 (2004) 1075–1080
POLYHEDRON
www.elsevier.com/locate/poly

Syntheses and crystal structures of bis(tetrahydrofurfurylindenyl) lanthanocene chlorides $(C_4H_7OCH_2C_9H_6)_2LnCl$ (Ln = La, Lu)

Jianhua Cheng [a], Dongmei Cui [a,b], Wenqi Chen [a], Tao Tang [a,*], Baotong Huang [a]

[a] *State Key Laboratory of Polymer Physics and Chemistry, Changchun Institute of Applied Chemistry, Chinese Academy of Sciences, Changchun 130022, China*
[b] *Department of Chemical Engineering, Changchun University of Technology, Changchun 130012, China*

Received 15 August 2003; accepted 9 January 2004

Abstract

Reaction of two equivalents of tetrahydrofurfuryl indenyl lithium with anhydrous lanthanide trichlorides in THF afforded bis(tetrahydrofurfurylindenyl) lanthanide chlorides $(C_4H_7OCH_2C_9H_6)_2LnCl$, Ln = La(**1**), Pr(**2**), Lu(**3**). Complexes **1** and **3** are characterized by single-crystal analysis. The results of crystal structural determination reveal that they are 9-coordinate monomeric intramolecular complexes with a *trans* arrangement of both the sidearms and indenyl rings in the solid state. The effects of rare earth ionic radii on the structures of $(C_4H_7OCH_2C_9H_6)_2LnCl$ are discussed.
© 2004 Elsevier Ltd. All rights reserved.

Keywords: Tetrahydrofurfurylindenyl; Lanthanide chlorides; Crystal structure; Ionic radius

1. Introduction

Due to their large radii and relatively low oxidation, rare earth elements generally form complexes which have high coordination numbers and weak metal–ligand bonds. Under the same reaction conditions, reaction of the same reactants with different rare earth elements may afford a series of complexes with uniform molecular formula but different structure, such as $(C_5H_5)_3Ln \cdot THF$ [1], $(C_9H_7)_3Ln \cdot THF$ [2] and $(CH_3OCH_2CH_2C_5H_4)_2$-LnCl [3,4].

So far, most of the organolanthanides bear two substituted or unsubstituted cyclopentadienyl or indenyl ligands. The attempts to synthesize bis-ligand type lanthanides are often frustrated because of the lanthanide contraction and coordination unsaturation (especially, the light rare earth complexes) [5]. Recently, considerable efforts have been devoted to exploring the organometallic chemistry of metallocenes with donor-functionalized side chains [6], because the donor-functionalized side chains can increase the stability of highly reactive organolanthanide complexes by forming an intramolecular chelating coordination with the central metal, and for the light lanthanide complexes, the enhanced stability facilitates the synthesis of the desired complexes. Most of the ligands used are those with ether- or amino-substituted cyclopentadienyl groups. To complete the series of the complexes $(C_4H_7OCH_2$-$C_9H_6)_2LnCl$ [7,8], complexes La(**1**), Pr(**2**) and Lu(**3**) were synthesized, and **1** and **3** were X-ray characterized. Detailed relations between the rare earth ionic radii and the structures of these complexes are described.

2. Results and discussion

2.1. Synthesis

Two equivalents of $C_4H_7OCH_2C_9H_6Li$ and $LnCl_3$-(Ln = La, Pr and Lu) were reacted in THF, followed by centrifugation, removal of the solvent and extraction with mixed solvents (toluene/THF). Crystals of the corresponding complexes were obtained in moderate yields (Scheme 1) after being kept at −10 °C for several days. These complexes are soluble in polar solvents like

* Corresponding author. Tel: +86-431-5262004; fax: 86-431-5685653.
E-mail address: ttang@ciac.jl.cn (T. Tang).

0277-5387/$ - see front matter © 2004 Elsevier Ltd. All rights reserved.
doi:10.1016/j.poly.2004.01.020

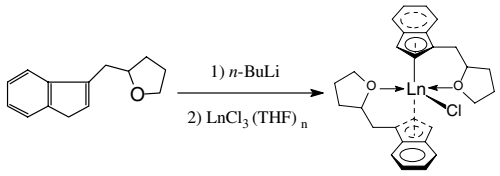

Ln = La(**1**), Pr(**2**), Lu(**3**)

Scheme 1.

THF, only dissolved in aromatic solvents such as toluene on heating. All complexes in solution are air- and moisture-sensitive, but their crystals can be kept for long time in air.

The complexes were characterized by elemental analysis, IR and mass spectrometry. The IR spectra of these complexes showed similar patterns and displayed the characteristic absorption peaks of the aromatic group at about 3030, 1600, 750 cm^{-1}, η^5-indenyl moieties at about 3060, 1430, 1290, 1030, 780 cm^{-1}, and the C–O–C band at 1060, 870, 840 cm^{-1}. The EI-MS data of these complexes displayed characteristic fragments, such as $[M]^+$, $[M–Cl]^+$, $[M–L]^+$, $[C_4H_7O]^+$, etc.

Under similar conditions, with the molar ratio of $C_4H_7OCH_2C_9H_6Li$ to $LnCl_3 = 0.8$ or 3, (Ln = La, Pr and Lu), the attempt to synthesize mono- or tri-tetrahydrofurfurylindenyl lanthanides was defeated, only bis(tetrahydrofurfurylindenyl) lanthanocene chlorides were found.

2.2. Crystal structure of *1* and *3*

Due to their similar crystal data with the same crystal system (orthorhombic) and space group ($P2_12_12_1$), complexes **1** and **3** are isostructural. The molecular structure of **1** is shown in Fig. 1. Although the compounds crystallize from mixed solutions (including THF), they remain unsolvated 9-coordinate monomeric complexes in the solid state. The coordination geometry

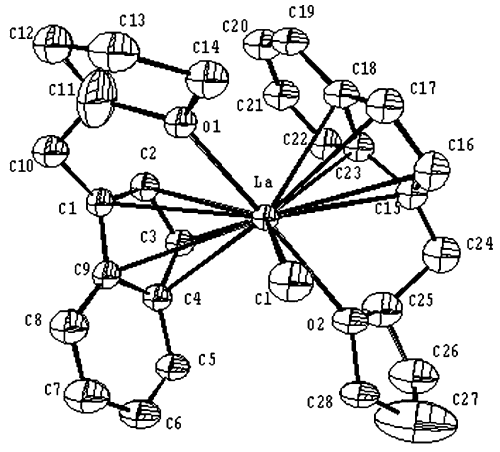

Fig. 1. ORTEP drawing of $(C_4H_7OCH_2C_9H_6)_2LaCl$(**1**) with 40% thermal ellipsoids. Hydrogen atoms are omitted for clarity.

around the central metal atom can be described as a distorted trigonal bipyramid. Two oxygen atoms lie at both apices, and the chlorine atom, the central metal atom and the two centroids of cyclopentadienyl rings of indene form the equatorial plane.

The angles of Cent(1)–La(Lu)–Cl (119.7°, 115.5°), Cent(2)–La(Lu)–Cl (112.2°, 114.7°), Cent(1)–La(Lu)–Cent(2) (128.1°, 129.8°) are close to the ideal angle (120°) of trigonal bipyramid geometry, while the angles of O(1)–La(Lu)–O(2) (161.85°, 159.9°) show large deviation from the ideal angle (180°).

2.3. Effects of ionic radii on the structures of $(C_4H_7OCH_2C_9H_6)_2LnCl$

Including our previous work, effects of the rare earth ionic radii on the structures of $(C_4H_7OCH_2C_9H_6)_2LnCl$ are discussed.

Unlike other series of lanthanides complexes, such as $(C_5H_5)_3Ln \cdot THF$ [1], $(C_9H_7)_3Ln \cdot THF$ [2] and $(CH_3OCH_2CH_2C_5H_4)_2LnCl$ [3,4], all the complexes $(C_4H_7OCH_2C_9H_6)_2LnCl$ (Ln = La, Nd, Sm, Gd, Dy, Y, Ho, Er, Yb, Lu) show the same structure. So, the changes of rare earth ionic radius only influence the bond lengths and bond angles of this series of complexes.

The distances between the metal ion and the carbon atoms of these complexes are listed in Table 3. Compared with the bond lengths within this series of complexes, the bond distances of Ln–C(ring) almost follow a trend (going from La to Lu): the smaller the ionic radii, the shorter the average bond length, and the wider the bond length range. The bond lengths of complex **1** range from 2.797 to 2.883 Å (0.086 Å), and average 2.844 Å; while the bond lengths of complex **3** range from 2.565 to 2.809 Å (0.244 Å), and average 2.687 Å.

The size of the tetrahydrofurfurylindenyl ligand can be calculated as the difference between the mean bond length of Ln–C(ring) and ionic radius [9] (ionic radius vary in different coordination space). The changes of the rare earth ionic radii show little influence on the size of ligand (from 1.626 to 1.654 Å).

The distances between the metal ion and the centroid of the indenyl groups of these complexes show the same trend as the bond lengths of Ln–C(ring) (Fig. 2). This trend is also consistent with the lanthanide contraction. The difference between the bond lengths of Ln–Cent(1) and Ln–Cent(2) is small, ranging from 0.025 Å (Sm) to 0.002 Å (Lu).

The slip parameter ΔM–C [10], which quantifies the η^5–η^3 slippage within indenyl metal complexes, ranging from 0.0663 (0.0343) Å for complex **1** to 0.1763 (0.078) Å for complex **3**, is shown in Fig. 3. Although it is not a rectilinear trend, the slip distortion gradually increases with the decrease of the radii size of the central metals. Thereto, the pitch of ΔM–C(1) is higher than ΔM–C(2). It can also be described as follows: with the decrease of

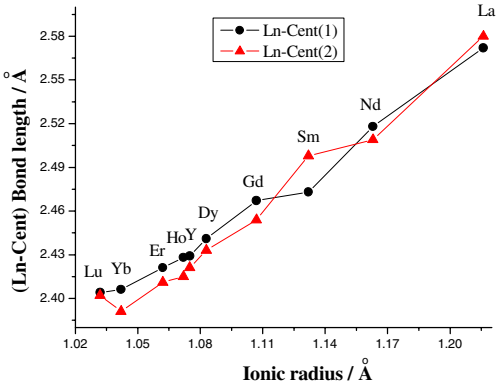

Fig. 2. Bond lengths of Ln–Cent.

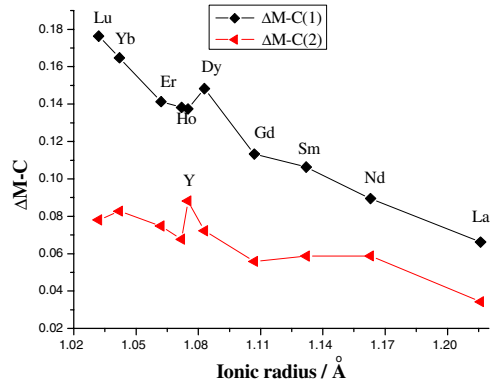

Fig. 3.

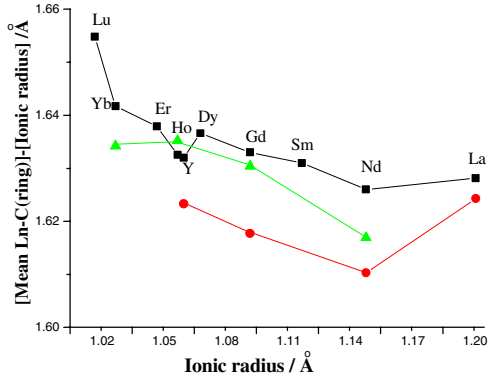

Fig. 4. Comparison between three ligands ■: $(C_4H_7OCH_2\ C_9H_6)_2$ LnCl; ●: $(CH_3OCH_2CH_2C_9H_6)_2LnCl$; ▲: $O(CH_2CH_2C_9H_6)_2LnCl$-THF.

the ionic radii, one indenyl plane almost keeps no slippage, and the other inclines gradually. In the Lu complex, it is noted that one indenyl ligand shows η^5-coordination to the Lu atom, while the another is almost bonded in η^3-mode.

The dihedral angle of indene planes ranging from 51.5° (Y, Ho) to 52.9° (La) and the RA angle [11] ranging from 152.11° (Yb) to 157.73° (Nd) show no obvious relation with ionic radii.

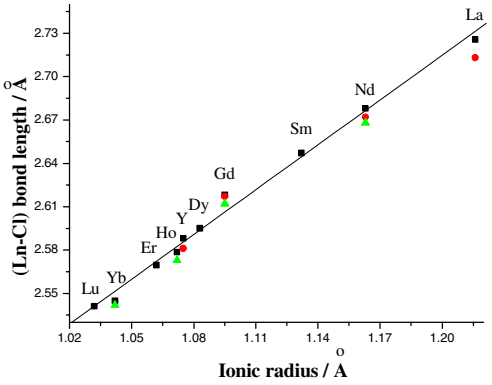

Fig. 5. Bond lengths of Ln–Cl ■: $(C_4H_7OCH_2C_9H_6)_2LnCl$; ●: $(CH_3OCH_2CH_2C_9H_6)_2LnCl$; ▲: $O(CH_2CH_2C_9H_6)_2LnCl \cdot THF$.

Compared with some other 9-coordinate lanthanocene chlorides of indenyl ligands bearing pendant O-donors, $(CH_3OCH_2CH_2C_9H_6)_2LnCl$ (Ln = La, Nd, Gd, Y [12] and $[O(CH_2CH_2C_9H_6)_2]$ LnCl · THF (Ln = Nd, Gd, Ho) [13] (Fig. 4), it is concluded that the space coordination environment of tetrahydrofurfurylindenyl is similar to the above two ligands. The distances between Ln–Cl of these three kinds of complexes are shown in Fig. 5 and their bond lengths are very close, and well accorded with the lanthanide contraction, which also support the above conclusion.

3. Conclusion

Ten stable lanthanocene chloride complexes (from La to Lu) with the tetrahydrofurfurylindenyl ligand have been synthesized and X-ray characterized. The investigation results indicate that they are isostructural, the side chain oxygen atoms displace THF to coordinate with the metal atom to form stable intramolecular bis-indenyl-type complexes. The changes of the bond length of Ln–C(ring), Ln–Cent, Ln–Cl, and ΔM–C are consistent with lanthanide contraction, while no obvious connections are found between the dihedral angles of indene planes and the RA angles with the rare earth radius.

4. Experiments

4.1. General procedures

All operations involving organometallic compounds were carried out under an inert atmosphere of argon using standard Schlenk techniques. Tetrahydrofuran, toluene and hexane were distilled under argon from sodium/potassium alloy with benzophenone ketyl prior to use. Anhydrous lanthanide chlorides [14], tetrahydrofurfurylindenyl lithium [7] were prepared according to

Table 1
Details of the crystal data and structure refinements for Complexes **1** and **3**

Complex	**1**	**3**
Formula	$C_{28}H_{30}O_2ClLa$	$C_{28}H_{30}O_2ClLu$
Formula weight	572.88	608.94
Crystal size (mm)	$0.25 \times 0.24 \times 0.19$	$0.46 \times 0.25 \times 0.21$
Color	colorless	green
Crystal system	orthorhombic	orthorhobmic
Space group	$P2_12_12_1$ (No. 19)	$P2_12_12_1$ (No. 19)
a (Å)	10.3630(4)	10.5054(6)
b (Å)	14.7448(3)	14.7599(5)
c (Å)	15.6170(4)	14.9938(6)
Volume (Å^3)	2386.28(12)	2324.92(18)
Z	4	4
$D_{calc.}$ (g cm^{-1})	1.595	1.740
μ (mm^{-1})	1.925	4.384
$F(000)$	1152	1208
θ_{max}(°)	27.48	27.48
Reflections collected	4114	3016
Independent reflections	3087	3016
Goodness-of-fit	0.996	0.985
Final R indices [$I > 2\sigma(I)$]	$R_1 = 0.0248, wR_2 = 0.0617$	$R_1 = 0.0294, wR_2 = 0.0642$
R indices (all data)	$R_1 = 0.02796, wR_2 = 0.0760$	$R_1 = 0.0347, wR_2 = 0.0815$
$\Delta p_{max/min}$ (e Å^{-3})	0.862/−1.065	0.980/−1.281

published procedures; the analysis of rare earth metals and chlorine were accomplished using direct complexometric titration with disodium EDTA and the Volhard method, respectively. Carbon and hydrogen analysis were carried out by the combustion method. IR spectra were recorded on a Bio-Rad FTS135 spectrometer in the form of KBr pellets. Mass spectra were recorded on a LGQ spectrometer.

4.2. Synthesis of bis(tetrahydrofurfurylindenyl) lanthanum chloride(*1*)

Tetrahydrofurfurylindenyl lithium (0.006 mol) in 15 mL of THF was added slowly to a suspension of $LaCl_3$ (0.7376 g, 0.003 mol in 20 mL THF) at low temperature (≈−60 °C). The reaction mixture was allowed to naturally warm to r.t and stirred for 24 h. After centrifugation the solvent was evaporated in vacuo. The residues were extracted with 30 mL toluene/THF (4:1) and kept at −10 °C. Colorless crystals were obtained in 35% yield. *Anal*. Calc. (%) for $C_{28}H_{30}O_2ClLa$: La, 24.33; Cl, 6.20; C, 58.65; H, 5.24. Found (%): La, 24.81; Cl, 6.82; C, 60.02; H, 5.61. EI-MS m/z (fragment, relative intensity %): 572 ([M]$^+$, 25), 536 ([M–Cl]$^+$, 10), 373 ([M–L]$^+$, 55), 139 ([La]$^+$, 8), 71 ([C_4H_7O]$^+$, 100). IR (cm^{-1}): 3065(m), 3035(m), 1600(m), 1425(w), 1338(s), 1295(m), 1070(m), 1027(s), 956(m), 945(s), 868(m), 840(w), 789(s), 745(s), 441(s).

4.3. Synthesis of bis(tetrahydrofurfurylindenyl) praseodymium chloride(*2*)

The procedure followed was similar to that for **1**. Yellow crystals were obtained in 57% yield. *Anal*. Calc.

Table 2
Selected bond lengths (Å) and bond angles (°) for complexes **1** and **3**

Complex	La(**1**)	Lu(**3**)
Bond length (Å)		
Ln–Cl	2.7257(14)	2.541(2)
Ln–O(1)	2.543(4)	2.414(6)
Ln–O(2)	2.560(4)	2.403(6)
Ln–C(1)	2.817(5)	2.622(7)
Ln–C(2)	2.797(5)	2.565(7)
Ln–C(3)	2.826(5)	2.669(8)
Ln–C(4)	2.883(5)	2.809(7)
Ln–C(9)	2.876(5)	2.781(8)
ΔM–C(ring1)[a]	0.0663	0.1763
Ln–Cent(1)[b]	2.572	2.404
Ln–C(15)	2.836(6)	2.675(8)
Ln–C(16)	2.824(6)	2.614(9)
Ln–C(17)	2.844(6)	2.671(9)
Ln–C(18)	2.874(6)	2.737(9)
Ln–C(23)	2.864(5)	2.725(8)
ΔM–C(ring2)	0.0343	0.078
Ln–Cent(2)	2.580	2.402
Bond angle (°)		
O(1)–Ln–Cl	82.01(10)	79.75(17)
O(2)–Ln–Cl	79.84(10)	80.18(15)
O(1)–Ln–O(2)	161.85(13)	159.9(2)
Cl–Ln–Cent(1)	119.7	115.5
Cl–Ln–Cent(2)	112.2	114.7
O(1)–Ln–Cent(1)	88.2	97.8
O(1)–Ln–Cent(2)	100.8	92.4
O(2)–Ln–Cent(1)	100.0	89.8
O(2)–Ln–Cent(2)	86.9	96.8
Cent(1)–Ln–Cent(2)	128.1	129.8
RA	153.95	152.25
Dihedral angle of indene planes	52.9	51.9

[a] Ring **1** and ring **2** indicate C(1)–C(4) and C(9), C(15)–(18) and C(23), respectively.
[b] Cent(1) and Cent(2) are the centroids of ring **1** and ring **2**.

Table 3
Metrical data for $(C_4H_7OCH_2C_9H_6)_2LnCl$ (/Å)

$(C_4H_7OCH_2C_9H_6)_2LnCl$	Ionic radii[a]	Ln–C(ring)			[Mean Ln–C(ring)] – [Ionic radius]
		High	Low	Mean	
La	1.216	2.883	2.797	2.844	1.628
Nd	1.163	2.857	2.730	2.789	1.626
Sm	1.132	2.822	2.688	2.763	1.631
Gd	1.107	2.828	2.672	2.740	1.633
Dy	1.083	2.837	2.642	2.719	1.637
Y	1.075	2.820	2.627	2.707	1.632
Ho	1.072	2.821	2.635	2.705	1.633
Er	1.062	2.800	2.610	2.700	1.638
Yb	1.042	2.812	2.582	2.680	1.642
Lu	1.032	2.809	2.565	2.687	1.654

[a] These ionic radii are only effective for 9-coordinate lanthanides.

(%) for $C_{28}H_{30}O_2ClPr$: Pr, 24.53; Cl, 6.18; C, 58.49; H, 5.22. Found (%): Pr, 24.71; Cl, 6.52; C, 60.12; H, 5.56. EI-MS m/z (fragment, relative intensity %): 574 ($[M]^+$, 29), 538 ($[M–Cl]^+$, 17), 375 ($[M–L]^+$, 65), 141 ($[Pr]^+$, 16), 71 ($[C_4H_7O]^+$, 100). IR (cm^{-1}): 3065(m), 3035(m), 1602(m), 1425(m), 1338(s), 1295(m), 1070(s), 027(s), 955(m), 945(s), 865(w), 837(w), 788(s), 749(s), 441(s).

4.4. Synthesis of bis(tetrahydrofurfurylindenyl) lutetium chloride(*3*)

The procedure followed was similar to that for **1**. Green crystals were obtained in 65% yield. *Anal*. Calc. (%) for $C_{28}H_{30}O_2ClLu$: Lu, 28.76; Cl, 5.83; C, 55.22; H, 4.93. Found (%): Lu, 28.85; Cl, 6.11; C, 56.23; H, 5.55. EI-MS m/z (fragment, relative intensity %): 610 ($[M]^+$, 6), 574($[M–Cl]^+$, 18), 412 ($[M–L]^+$, 25), 175 ($[Lu]^+$, 10), 71 ($[C_4H_7O]^+$, 100). IR (cm^{-1}): 3061(w), 3035(m), 1615(w), 1430(w), 1338(m), 1297(w), 1068(s), 1027(m), 959(m), 945(m), 877(w), 836(w), 772(s), 745(m), 442(s).

4.5. Crystal structure determination

A suitable crystal was sealed in thin-walled glass capillary under argon. Data were collected on a Rigaku Rapid Diffractometer with graphite-monochromated Mo-Kα ($\lambda = 0.071073$ Å) radiation using the $\omega - 2\theta$ technique at 293 K. Crystal data and experimental details are listed in Table 1, while selected bond lengths and bond angles are given in Table 2. The crystal structures were solved by direct methods and refined on F^2 by full-matrix least-squares methods, expanded using Fourier techniques [15]. All hydrogen atoms were added according to theoretical models with isotropic thermal parameters related to those of the supporting carbon atoms, but were not included in refinement. All calculations were performed using the SHELXS-97 crystallographic software package [16].

5. Supplementary material

Crystallographic data for the structural analyses have been deposited with the Cambridge Crystallographic Data Centre, CCDC No. 198715 and 198716 for compounds **1** and **3**. Copies of this information may be obtained free of charge from The Director, CCDC, 12 Union Road, Cambridge CB2 1EZ, UK (Fax: +44-1223-336033; E-mail: deposit@ccdc.cam.ac.uk or www: http://www.ccdc.cam.ac.uk).

Acknowledgements

Financial support from the special funds for Major State Basic Research Projects (Project No. G1999064801) is gratefully acknowledged.

References

[1] W. Chen, G. Lin, J. Xia, G. Wei, Y. Zhang, Z. Jin, J. Organomet. Chem. 467 (1994) 75.
[2] J. Guan, S. Qi, R.D. Fischer, J. Organomet. Chem. 549 (1997) 203.
[3] C. Qian, B. Wang, D. Deng, J. Hu, J. Chen, G. Wu, P. Zheng, Inorg. Chem. 33 (1994) 3382.
[4] B. Wang, D. Deng, C. Qian, New J. Chem. 19 (1995) 515.
[5] D.M. Cui, T. Tang, J.H. Cheng, W.Q. Chen, B.T. Huang, Chem. J. Chin. Univ. 23 (2002) 188.
[6] Review articles:
(a) C. Müller, D. Vos, P. Jutzi, J. Organomet. Chem. 600 (2000) 127;
(b) U. Siemeling, Chem. Rev. 100 (2000) 1495;
(c) H. Butenschön, Chem. Rev. 100 (2000) 1527;
(d) Y.H. Qian, J.L. Huang, Chin. J. Chem. 19 (2001) 1009.
[7] J.H. Cheng, D.M. Cui, W.Q. Chen, T. Tang, B.T. Huang, J. Organomet. Chem. 658 (2002) 153.
[8] J.H. Cheng, D.M. Cui, W.Q. Chen, T. Tang, B.T. Huang, Chem. J. Chin. Univ. 24 (2003) 973.
[9] R.D. Shannon, Acta. Crystallogr. Sect. A. 32 (1976) 752.
[10] (a) S.A. Westcott, A.K. Kakkar, G. Stringer, N.J. Taylor, T.B. Marder, J. Organomet. Chem. 394 (1990) 777;
(b) R.T. Bakerm, T.H. Tulip, Organometallics 5 (1986) 839.

[11] M.J. Calhorda, V. Félix, L.F. Veiros, Coord. Chem. Rev. 230 (2002) 49.
[12] C.T. Qian, G. Zou, J. Sun, J. Organomet. Chem. 566 (1998) 21.
[13] C.T. Qian, G. Zou, J. Sun, J. Chem. Soc., Dalton Trans. (1998) 1607.
[14] M.D. Toylor, C.P. Carter, J. Inorg. Nucl. Chem. 24 (1962) 387.
[15] SHLXTL PLUS, Siemens Analytical X-ray Institute Inc., XS: Program for Crystal Structure Solution, XL: Program for Crystal Structure Determination, XP: Interactive Molecular Graphics, (1990).
[16] G.M. Sheldrick, SHELXL-97, Program for the refinement of the crystal structure, University of Göttingen, Germany, 1997.

Available online at www.sciencedirect.com
SCIENCE DIRECT®
Polyhedron 23 (2004) 1081–1088
POLYHEDRON
www.elsevier.com/locate/poly

Synthesis, X-ray crystal structures, physicochemical and magnetic studies on copper(II) *N*-(2-carboxyphenyl) iminodiacetate polymers ☆

Susmita Bandyopadhyay [a], Ansuman Das [a], G.N. Mukherjee [a,*], Andrea Cantoni [b], Gabriele Bocelli [b], Siddhartha Chaudhuri [c], Joan Ribas [d]

[a] *Department of Chemistry, University College of Science, University of Calcutta, 92, Acharya Prafulla Chandra Road, Kolkata 700 009, India*
[b] *CSSD-CNR, Palazzo Chimico Parco Area delle Scienze, Parma, Italy*
[c] *R.S.I.C., Bose Institute, 93, Acharya Prafulla Chandra Road, Kolkata 700 009, India*
[d] *Department de Química Inorgànica, Universitat de Barcelona, Diagonal, 647, 08028 Barcelona, Spain*

Received 9 December 2003; accepted 19 January 2004

Abstract

Two polymeric Cu(II) complexes with *N*-(2-carboxyphenyl)iminodiaceticacid (H_3cpida) have been synthesized and characterized by elemental analysis, conductance, spectral, thermogravimetric, magnetic measurements and single-crystal X-ray diffraction. Green crystals of $\{[Cu(Hcpida)]\cdot H_2O\}_n$ (**1**) are obtained by digesting $Cu(OH)_2$ with hot aqueous solution of H_3cpida in 1:1 molar proportion. Blue crystals of $\{[Cu(Hcpida)(H_2O)]\cdot H_2O\}_n$ (**2**) are obtained by slow cooling of hot aqueous solution of **1**. Coordination environment of Cu(II) ion in the green compound **1** (λ_{max} 749, 365 nm) is five-coordinated distorted square pyramidal, which on hydration, is transformed to six-coordinated distorted octahedral blue compound **2** (λ_{max} 768, 315 nm). Single-crystal X-ray diffraction experiments indicate that the structures of both **1** and **2**, are made up of 1D polymeric Cu(II) units linked by carboxylato bridges in *syn–anti* bonding mode, stabilized via inter-chain hydrogen bonds and π–π stacking interactions of the phenyl rings. Crystal lattice of **2** contains channels that host the lattice water molecules. Variable temperature (2–300 K) magnetic measurements indicate that the Cu(II) ions in both **1** and **2** exist as magnetically quasi-isolated spin doublets ($g > 2$) involving weak ferromagnetic coupling among the Cu(II) ions through the carboxylato bridges resulting in J values of 3.60 cm^{-1} for **1** and 5.69 cm^{-1} for **2**.
© 2004 Elsevier Ltd. All rights reserved.

Keywords: Copper(II); Aminopolycarboxylate; Ferromagnetic coupling; π–π stacking; Cylindrical channels

1. Introduction

Extended frameworks of coordination polymers, based on complexes of transition metals and multifunctional bridging ligands, are of great research interest due to their potential applications in the fields of catalysis, electrical conductivity, molecular magnetic materials and host–guest chemistry [1]. Construction of coordination polymers with multi-dimensional frameworks has focused on the use of directional interactions such as H-bonding and π–π stacking that control the aggregation of molecular species [2]. The carboxylato group is one of the most widely used bridging ligands for designing polynuclear complexes having novel structural features and interesting magnetic properties. Versatility of this group as a ligand is illustrated by the variety of its coordination modes when acting as a bridge [3], the most common being the *syn–syn* and *syn–anti* conformations that mediate large antiferromagnetic [4] and weak antiferromagnetic or ferromagnetic interactions [5]. Complexes containing the much less known *anti–anti* conformation show both antiferromagnetic and ferromagnetic couplings [5l]. Transition metal complexes with aminopolycarboxylates, functioning as chelating as well as bridging

☆ Supplementary data associated with this article can be found, in the online version, at doi:10.1016/j.poly.2004.01.009.

* Corresponding author. Tel.: +91-33-23508386; fax: +91-33-23519755.
E-mail address: gmchem@rediffmail.com (G.N. Mukherjee).

0277-5387/$ - see front matter © 2004 Elsevier Ltd. All rights reserved.
doi:10.1016/j.poly.2004.01.009

ligands are well known. Extensive structural studies have been carried out on the metal chelates with simple aminopolycarboxylates, viz. iminodiacetate (ida) and N-substituted ida [6]. In contrast there are only a few reports of such studies on the complexes with tripodal quadridentate aminopolycarboxylate ligands like *N*-(2-carboxyphenyl)iminodiaceticacid (H_3cpida) [7]. In this paper, we report the synthesis, characterization, physicochemical studies, single-crystal X-ray diffraction and variable temperature magnetic measurements and magneto structural correlation of the two 1D coordination polymers $\{[Cu(Hcpida)]\cdot H_2O\}_n$ (**1**) and $\{[Cu(Hcpida)(H_2O)]\cdot H_2O\}_n$ (**2**), obtained as a hydration product of **1**. Compound **2** was found to be identical with the one reported by Shkolnikova et. al. [8], who synthesized the compound by a different procedure. Both the complexes **1** and **2** are made up of zigzag polymeric chains with carboxylato groups bridging the adjacent Cu(II) units in the *syn–anti* bonding mode. The interpenetrating chains are stabilized via inter-chain hydrogen bonds and π–π stacking interactions among the phenyl rings [2e]. Crystal lattice of **2** contains cylindrical channels that appear to host the lattice water molecules.

2. Experimental

2.1. Materials and measurements

All reagents were of A.R. grade obtained commercially and used without further purification. Elemental analyses (C, H and N) were done with a Perkin–Elmer 2400 CHNS/O analyzer and the copper (%) in the complexes were determined titrimetrically [9]. Molar conductance values of the complexes in aqueous solution were measured with a Systronics 304 digital conductivitymeter. The electronic spectra of the complexes in solid state and in aqueous solution were recorded on a Hitachi U-3501 spectrophotometer. IR spectra in KBr pellets were recorded using a Perkin–Elmer RXI FT-IR spectrophotometer. Thermal analyses were carried out on a Metler Toledo TGA/SDTA 851 thermal analyzer in a dynamic atmosphere of dinitrogen (flow rate: 30 ml min^{-1}). Magnetic measurements were carried out on polycrystalline samples (0.03 g) with a Quantum Design MPMS XL-5 SQUID susceptometer operating at a magnetic field of 0.1 T between 2 and 300 K. The diamagnetic corrections were evaluated from Pascal's constants. Magnetization measurements were made in the same SQUID at 2 K.

2.2. Synthesis

2.2.1. N-(2-carboxyphenyl)iminodiacetic acid (H_3cpida)

The ligand H_3cpida was prepared by condensing anthranilic acid with monochloroacetic acid in presence of Na_2CO_3 following the reported procedure [10], m.p. 210 °C. *Anal*. Calc. for $C_{11}H_{11}NO_6$: C, 52.17; H, 4.34; N, 5.53. Found: C, 52.25; H, 4.29; N, 5.71%. IR (KBr disk, ν/cm^{-1}): ν(OH) 3671s; ν(CO) 1728vs; ν_{as}(COO) 1599s; ν(CN) 1553s; ν_s(COO) 1381s.

2.2.2. $\{[Cu(Hcpida)]\cdot H_2O\}_n$ (**1**)

To a suspension of freshly precipitated alkali free copper(II) hydroxide obtained from $CuSO_4\cdot 5H_2O$ (2.75 g, 11 mmol) in 40 ml water, H_3cpida (2.53 g, 10 mmol) was added with stirring and the mixture was digested at 60–70 °C for 1 h. Unreacted $Cu(OH)_2$ was filtered off and the resulting green solution was evaporated carefully at 60 °C to ~25 ml. Green prismatic crystals of **1**, suitable for X-ray diffraction were obtained on standing (yield: ca. 75%). *Anal*. Calc. for $C_{11}H_{11}CuNO_7$: C, 39.70; H, 3.31; N, 4.21; Cu, 19.09. Found: C, 39.55; H, 3.40; N, 4.16; Cu, 18.82%. λ_{max}/nm (solid state) 749, 365; λ_{max}/nm (H_2O) 759 (ε/mol^{-1} 1 cm^{-1}, 76). Molar conductivity (H_2O, S cm^2 mol^{-1}): 332.4. IR (KBr disk, ν/cm^{-1}):, ν(OH) 3618s, 3507s; ν(CO) 1713vs; ν_{as}(COO)1599s; ν(CN)1403s; ν_s(COO) 1360s. TG: found loss of 5.52% in the temperature range 95–160 °C, calc. for $1H_2O$, 5.41%, corresponding to the dehydration processes, $[Cu(Hcpida)]\cdot H_2O \rightarrow [Cu(Hcpida)]$.

2.2.3. $\{[Cu(Hcpida)(H_2O)]\cdot H_2O\}_n$ (**2**)

The green compound **1** (0.66 g, 2 mmol) was dissolved in boiling water (25 ml) and the solution was filtered hot. Shining blue prismatic crystals of **2**, suitable for X-ray diffraction, were obtained on cooling the filtrate at room temperature (yield: ca. 67%). *Anal*. Calc. (%) for $C_{11}H_{13}$ $CuNO_8$: C, 37.66; H, 3.71; N, 3.99; Cu, 18.11. Found: C, 37.5; H, 3.86; N, 4.15; Cu, 18.25%. λ_{max}/nm (solid state) 768, 315; λ_{max}/nm (H_2O) 766 (ε/mol^{-1} 1 cm^{-1}, 85). Molar conductivity (H_2O, S cm^2 mol^{-1}): 305. IR (KBr disk, ν/cm^{-1}): ν(OH) 3602s, 3511s, 3363s; ν(CO) 1722s; ν_{as}(COO) 1647vs; ν(C–N) 1412s; ν_s(COO) 1366s. TG: found loss of 10.45% in the temperature range 90–165 °C, calc. for $2H_2O$: 10.27%, corresponding to the dehydration processes, $[Cu(Hcpida)(H_2O)]\cdot H_2O \rightarrow [Cu(Hcpida)]$.

2.3. Crystal structure determination

Table 1 summarizes the pertinent crystallographic data together with refinement details, for $\{[Cu(Hcpida)]\cdot H_2O\}_n$ (**1**) and $\{[Cu(Hcpida)(H_2O)]\cdot H_2O\}_n$ (**2**) and Table 2 lists some of the selected bond lengths and bond angles. The X-ray single-crystal diffraction data were collected at 293 K for complex **1** on a Bruker AXS Smart single-crystal diffractometer and for complex **2** an Enraf Nonius CAD4 single-crystal diffractometer was used. The data were corrected for Lorentz, polarization and absorption effects. The crystal structures of the complexes were solved by direct methods using SIR-97

Table 1
Crystal data and structure determination summery for complexes **1** and **2**

	1	2
Formula	$C_{11}H_{11}NO_7Cu$	$C_{11}H_{13}NO_8Cu$
Molecular weight	332.75	350.77
Crystal system	monoclinic	orthorhombic
Space group	$P2_1/c$	*Pbca*
a (Å)	9.494(2)	15.158(2)
b (Å)	7.175(3)	22.677(4)
c (Å)	17.299(2)	7.508(2)
α (°)	90	90
β (°)	94.66(2)	90
γ (°)	90	90
V (Å^3)	1174.5(6)	2580.8(9)
T (K)	293	293
Z	4	8
μ (mm^{-1})	1.893 (Mo Kα)	2.812 (Cu Kα)
Reflections measured	11 891	2417
Unique reflections collected	2669	2417
Observed reflections $[I > 2\sigma(I)]$	2450	1613
Refined parameters	214	239
$wR(F^2)$[a]	0.1214	0.1638
$R_1[I > 2\sigma(I)]$[b]	0.0428	0.0571
R_{int}	0.032	0.000
S	1.103	1.055

[a] $wR_2 = \left[\sum w\left(F_o^2 - F_c^2\right)^2 \Big/ \sum w(F_o^2)^2\right]^{1/2}$.
[b] $R_1 = \sum ||F_o| - |F_c|| / \sum |F_o|$.

Table 2
Bond distances (Å) and angles (°) around the Cu(II) ions in complexes **1** and **2**

	1	2
Bond distances		
Cu(1)–O(9)	1.962(3)	1.905(4)
Cu(1)–O(18)	1.927(3)	1.919(4)
Cu(1)–N(15)	2.036(3)	2.078(4)
Cu(1)–O(10)[a]	1.927(2)	1.974(3)
Cu(1)–O(11)	2.306(3)	2.296(3)
Cu(1)–O(2W)		2.651(5)
Bond angles		
O(9)–Cu(1)–N(15)	89.03(11)	89.89(16)
O(9)–Cu(1)–O(10)[a]	93.26(10)	86.30(16)
O(9)–Cu(1)–O(18)	159.69(11)	175.80(18)
O(18)–Cu(1)–N(15)	85.70(10)	87.54(16)
O(18)–Cu(1)–O(10)[a]	94.56(10)	96.82(16)
O(10)[a]–Cu(1)–N(15)	172.30(10)	169.01(14)
O(9)–Cu(1)–O(11)	90.05(11)	94.22(18)
O(18)–Cu(1)–O(11)	107.73(11)	88.65(17)
N(15)–Cu(1)–O(11)	76.80(10)	80.90(16)
O(10)[a]–Cu(1)–O(11)	95.83(9)	89.10(16)
O(9)–Cu(1)–O(2W)		93.16(19)
O(18)–Cu(1)–O(2W)		83.49(19)
O(11)–Cu(1)–O(2W)		167.65(14)
N(15)–Cu(1)–O(2W)		89.23(16)
O(10)[a]–Cu(1)–O(2W)		101.26(19)

[a] Designates the symmetry related atoms at $-x, y - 1/2, -z + 3/2$ for complex **1** and those at $-x + 1/2, -y, z + 1/2$ for complex **2**.

[11] and SHELXS-97 [12] and refined by using SHELXL-97 [12]. The non-hydrogen atoms were refined anisotropically. The hydrogen atoms in complexes **1** and **2** were refined using isotropic thermal parameters, except the carboxylic acid hydrogens (H13) in both the complexes, which were made to 'ride' on the atoms to which they were bonded (O13). Because of high thermal vibration, the hydrogen atoms of the water molecule in **1** could not be located. Neutral atom scattering factors were taken from Cromer and Weber [13] and anomalous dispersion effects were included in F_c [14]. The crystallographic illustrations were prepared using ORTEP-3 [15].

3. Results and discussion

Compound **1** obtained from the reaction of equimolar amounts of freshly precipitated alkali free $Cu(OH)_2$ with H_3cpida. In hot aqueous solution it is slowly transformed to compound **2**. Such transformation of **1** to **2** occurs with remarkable structural and spectral changes, as coordinately unsaturated square pyramidal Cu(II) ion in **1** becomes coordinately saturated distorted octahedral in complex **2** through hydration reaction (Scheme 1).

3.1. Physicochemical studies

Diffuse reflectance spectra of the green complex **1** (λ_{max} 749, 365 nm) and the blue complex **2** (λ_{max} 768, 315 nm) show significant differences. The d–d band ($^2B_{1g} \rightarrow {}^2B_{2g}$) shows a red shift of ~20 nm in going from **1** to **2** as a consequence of higher CFSE of Cu(II) (d^9) ion in a square pyramidal geometry in **1** than that in a distorted octahedral geometry in **2**. On the other hand, the LMCT band shows a blue shift of ~50 nm in going from **1** to **2** obviously due to stronger metal–ligand orbital overlap permitted in a distorted octahedral geometry than that in a square pyramidal geometry [16]. The IR bands in the range (3430–3618 cm^{-1}) confirm the presence of lattice water in both the compounds **1** and **2** [17]. This is further supported by the weight loss percent observed in the temperature range 90–165 °C. The asymmetric ν_{as}(COO) and the symmetric ν_s(COO) stretching bands of the Cu(II)-complexes fall in the region 1599–1647 and 1332–1366 cm^{-1}, respectively. The difference between ν_{as}(COO) and ν_s(COO) stretching frequencies suggests both terminal as well as bridging modes of coordination of the carboxylate groups [18,3a]. High molar conductance values of **1** and **2** in

$$\{[Cu(Hcpida)].H_2O\}_n \xrightarrow{nH_2O} \{[Cu(Hcpida)(H_2O)] \cdot H_2O\}_n$$

1, green **2**,blue

Scheme 1.

H_2O (332.5 and 305 S cm^2 mol^{-1}, respectively) indicate their electrolytic nature, obviously due to the presence of COOH groups coordinated to Cu(II) ions through their carbonyl oxygen atoms, as a result of which these coordinated COOH groups ionize almost completely in aqueous solution (pH∼3). Thus the complexes **1** and **2** in aqueous solution, possibly exist as complex acids, $\{H^+[Cu(cpida)]^-\}_n$ and $\{H^+[Cu(cpida)(H_2O)]^-\}_n$, respectively, similar to the Co(III)–dimethylglyoxime (H_2dmg) complex, $[Co(H_2dmg)(Hdmg)Cl_2]$ which exists as $H^+[Co(Hdmg)_2Cl_2]^-$ giving a molar conductance of 374 S cm^2 mol^{-1} in freshly prepared aqueous solution at room temperature [19]. In spite of different types of bonding of the two water molecules (one coordinated water and one lattice water) in compound **2**, both the water molecules are lost in an overlapping step in the temperature range 90–165 °C, possibly due to longer bond distance (Table 2) between Cu(II) and the coordinated water molecule [Cu–O2W = 2.651(5) Å] rendering the latter loosely bound.

3.2. Description of crystal structures

The crystal structure of **1** (Fig. 1) consists of asymmetric units containing Cu(II) ion in distorted square pyramidal environment (4 + 1 type) with O(9) and O(18) from two carboxylate groups, the amino-nitrogen N(15) and a carboxylate-oxygen O(10)^{i} of the carboxylate group attached to the phenyl ring (symmetry code $i = -x, y - 1/2, -z + 3/2$) occupying the four basal positions. The coordination at the apical position is completed by the carbonyl-oxygen O(11) of a carboxylate group of the ligand. The four closest donors [O(9), N(15), O(18), O(10)^{i}] define a mean equatorial plane (deviations from −0.253(3) to −0.260(3) Å for O(18) and O(9) to +0.147(2) and +0.249(3) Å for O(10)^{i} and N(15), respectively). The Cu(II) ion lies at +0.065(1) Å from this plane towards O(11). The percentage of distortion of this square pyramidal stereochemistry towards a hypothetical trigonal one is obtained from the value of $\tau = 21.01$ [5n]. The two glycinate like fragments of the ligand form five-membered puckered chelate rings at the Cu(II) ion. A mean plane drawn through one of the rings is almost coplanar with the basal plane (dihedral angle 13.28(9)°), while that through the other ring is nearly perpendicular to it (dihedral angle 104.30(7)°). The 'equatorial' ring, defined by the atoms Cu(1)–N(15)–C(16)–C(17)–O(18) (deviations from −0.202(3) to 0.282(3) Å from the mean plane) is less distorted than the 'perpendicular' one, consisting of the atoms Cu(1)–N(15)–C(14)–C(12)–O(11) (deviations from −0.264(3) to 0.322(4) Å). Both the rings have conformations intermediate between envelope and half-chair (q, ϕ values for 'equatorial' and 'perpendicular' rings are 0.337(3) Å, 313.8(5)° and 0.462(2) Å, 351.4(4)°, respectively) [20]. The phenyl ring is directed downward from the pyramid (i.e., on the opposite side of O(11)) and its mean plane makes a dihedral angle of 60.96(9)° with the basal plane.

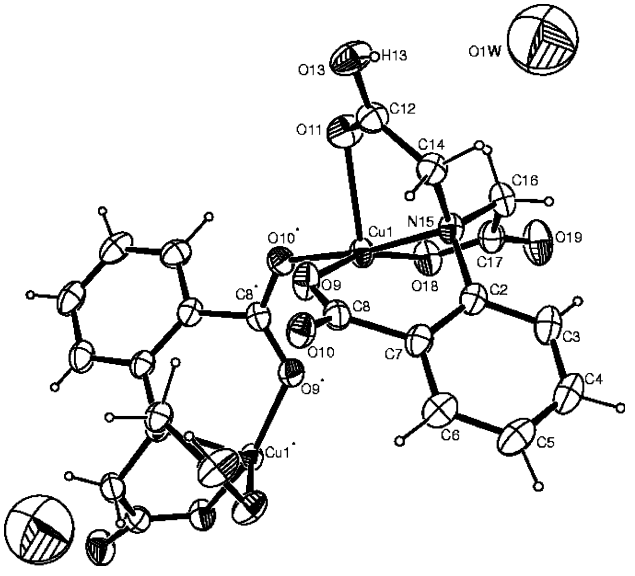

Fig. 1. ORTEP view of $\{[Cu(Hcpida)]\cdot H_2O\}_n$ (**1**) with atom labeling scheme. Thermal ellipsoids are shown at 50% probability.

Complex **1**, like other Cu(II)–(ida/substituted ida) complexes [6], crystallizes in the polymeric form with carboxylate moieties bridging the symmetry related Cu(II) ions in *syn–anti* bonding mode having Cu–Cu separation of 5.02 Å through this bridge. But the novelty of this complex is that the carboxylate group attached to the phenyl ring, rather than the carboxylate group of the glycinate like fragments, is responsible for the formation of polymeric chains along the *b*-axis. The torsion angle between the basal planes of the consecutive Cu(II) units is found to be 58.5(1)°. The carboxylic acid hydrogen atom (H13) reinforces the cohesion of the chains through H-bond formation with the O(18)^{ii} atom (symmetry code $ii = x, y + 1, z$) of the alternate Cu(Hcpida) units of the same chain (Table 3). Although the H atoms of the water molecule could not be located, there are some potential acceptors for water hydrogen atoms, which are possibly involved in H-bonding to link the two adjacent chains and thus contribute to crystal packing. The crystal packing is further reinforced by π–π stacking interactions [2e] between parallel phenyl rings ($\alpha = 0.03°$) of adjacent chains (related by symmetry code $iii = -x, -y, -z - 2$) with a shortest distance of 3.638(2) Å ($\beta = \gamma = 23.79°$) (Fig. 2).

Complex **2**, obtained as a hydration product of complex **1**, retains the similar polymeric nature as its parent. In this complex the atoms O(9), O(11) and O(18) from the three carboxylate groups, the amino nitrogen N(15), the carboxylate oxygen O(10)^{iv} of the carboxylate group attached to the phenyl ring (symmetry code $iv = -x + 1/2, -y, z + 1/2$) from an adjacent asymmetric unit and a water O(2W) atom define the asymmetrically

Table 3
Hydrogen bond distances (Å) and angles (°) for complexes **1** and **2**

D–H	*d*(D–H)	*d*(H···A)	∠DHA	*d*(D···A)	A	Symmetry
Complex **1**						
O13–H13	0.82	1.79	166.3	2.599(4)	O18	$[x, y+1, z]$
Complex **2**						
O13–H13	0.82	1.81	166.4	2.618(6)	O2W	$[-x-1/2, y-1/2, z]$
O1W–HA1W	0.75	2.46	124.0	2.948(8)	O11	$[-x-3/2, y-1/2, z]$
O1W–HB1W	0.61	2.22	168.0	2.821(8)	O18	$[x+1/2, -y+1/2, -z-1]$
O2W–HA2W	0.73	2.56	166.0	3.271(8)	O10	$[x, y, z+1]$
O2W–HA2W	0.73	2.35	128.0	2.854(6)	O9	$[x+1/2, -y+1/2, -z]$
O2W–HB2W	0.79	1.89	163.0	2.660(9)	O1W	

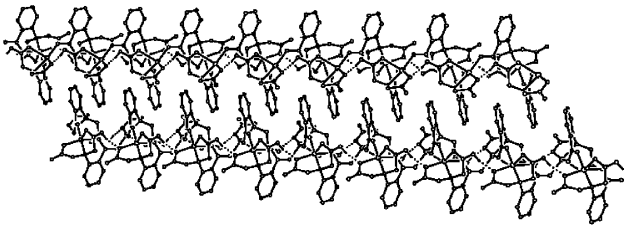

Fig. 2. 1D polymeric framework of $\{[Cu(Hcpida)]\cdot H_2O\}_n$ (**1**) showing π–π stacking between phenyl rings of two adjacent chains. H-bonds are shown by dotted lines.

elongated octahedral coordination of the Cu(II) ion (type 4 + 1 + 1) with unequally disposed *trans*-axial long Cu(1)–O(11) and Cu(1)–O(2W) bonds (Fig. 3). Both the Cu-glycinate like chelate rings are less distorted (deviations of 'equatorial' ring from −0.186(8) to 0.089(5) Å, and deviations of 'perpendicular' ring from −0.109(5) to 0.205(7) Å) compared to complex **1**. The conformation of the 'equatorial' ring has changed to envelope (*q*, ϕ values for 'equatorial' and 'perpendicular' rings are 0.186(5) Å, 147.3(16)° and 0.219(4) Å, 335.6(14)°, respectively) [20]. Dihedral angles between the basal plane and these two rings have changed to 4.51(13)° and 89.44(13)°. The plane of the phenyl ring has also rotated to make a dihedral angle of 35.73(13)° with the basal plane. Torsion angle between the basal planes of the consecutive Cu(II) units has been increased to 65.4(1)°.

The carboxylic acid hydrogen (H13) in complex **2** is involved in H-bonding with oxygen, $O(2W)^{v}$, of a $[Cu(Hcpida)(H_2O)]$ unit of the adjacent chain (related by symmetry code $v = -x-1/2, y-1/2, z$) and this closes a cylindrical channel along *b*-axis that hosts the lattice water molecule (Fig. 4). All the hydrogen atoms of both coordinated and uncoordinated water molecules take part in intra- and inter-chain H-bonding to reinforce the cohesion and contribute to crystal packing (Table 3). The conformational changes associated with the hydration reaction (Scheme 1) bring the copper atoms of the chains closer to each other with Cu–Cu separation of 4.87 Å through the bridge.

Although **2** is structurally similar to the compound described by Shkolnikova et al. [8], the bond lengths are slightly different, particularly the Cu–N(15) and the C12–O13 bonds, which are 2.078(4) and 1.304(6) Å, respectively, in **2** as compared to 2.058(5) and 1.325(7) Å in the other. Moreover, the novel feature of **2** is its

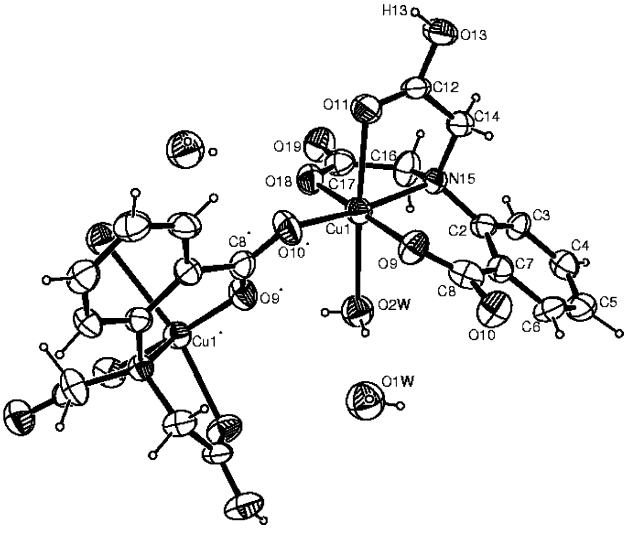

Fig. 3. ORTEP view of $\{[Cu(Hcpida)(H_2O)]\cdot H_2O\}_n$ (**2**) with atom labeling scheme. Thermal ellipsoids are shown at 50% probability.

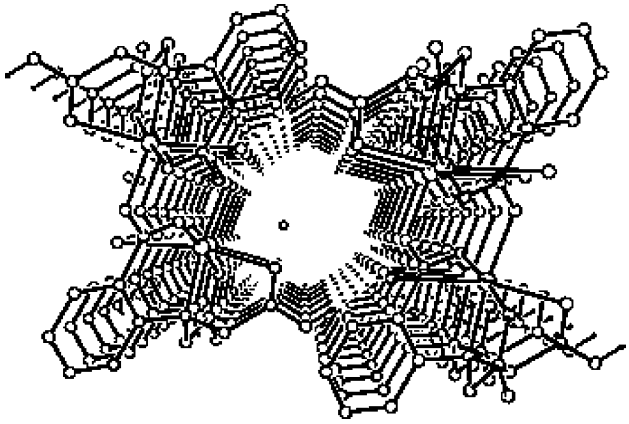

Fig. 4. Perspective view showing the cylindrical channel and the location of the guest water molecules in the lattice of $\{[Cu(Hcpida)(H_2O)]\cdot H_2O\}_n$ (**2**). H-bonds are shown by dotted lines.

ability to form cylindrical channels for hosting the H_2O molecules (Fig. 4).

3.3. Magnetic properties

The magnetic properties of complexes **1** and **2** are very similar, which seem logical taking into consideration the coincidence in the chemical pathway in their structures (carboxylato bridge in *syn–anti* equatorial–equatorial coordination mode). $\chi_M T$ versus T plot of **1** is shown in Fig. 5, that of **2** is quite similar. The values of $\chi_M T$ at 300 K are 0.45 $cm^3\ mol^{-1}$ K for **1** and 0.47 $cm^3\ mol^{-1}$ K for **2**, which are as expected for one magnetically quasi-isolated spin doublet ($g > 2.00$). Starting from the room temperature, $\chi_M T$ values smoothly increase up to 0.80 $cm^3\ mol^{-1}$ K for **1** and 0.96 $cm^3\ mol^{-1}$ K for **2** at 2 K. The shapes of these curves clearly indicate weak ferromagnetic coupling among the Cu(II) ions. The mathematical formula derived by Baker et al. [21] for ferromagnetic 1D systems with $S = 1/2$ is valid only for relatively high temperatures. Thus, when the ferromagnetic coupling is weak, this formula is not very accurate. For this reason the fit of the experimental data for complexes **1** and **2** was performed in numerical form from a full-matrix diagonalization of the Hamiltonian corresponding to a ring of 12 local $S = 1/2$ centers with the adequate J coupling parameters (through the carboxylato in *syn–anti* coordination mode) using the CLUMAG program [22]. With this program, the use of 12 cycled centers gives a good approximation for the system, which is actually infinite. The best J and g values are 3.6 and 2.18 cm^{-1} for **1** and 5.69 and 2.24 cm^{-1} for **2**. In the two cases R is 2.5×10^{-5} and 1.3×10^{-5}, respectively, where R is the agreement factor defined as $\sum_i[(\chi_M T)_{obs} - (\chi_M T)_{calc}]^2 / \sum_i[(\chi_M T)_{obs}]^2$. The reduced molar magnetization ($M/N\beta$) per Cu entity tends to $1N\beta$ (electron) (Fig. 5, inset) for both complexes **1** and **2**, but the shapes of the experimental curves are clearly above the theoretical ones for the Brillouin law. These features agree to the global ferromagnetic coupling within the copper(II) ions in **1** and **2**.

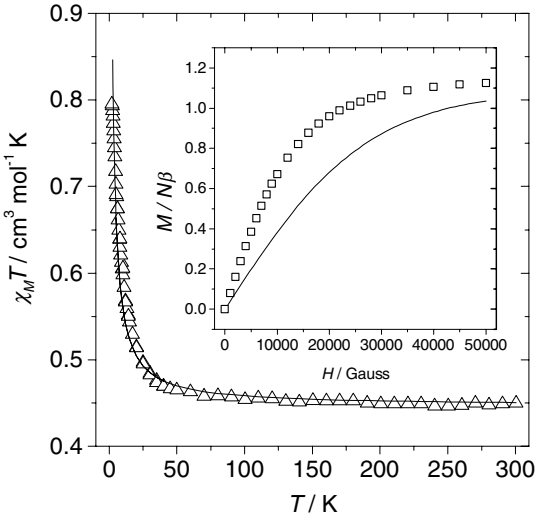

Fig. 5. Plot of the $\chi_M T$ vs. T of $\{[Cu(Hcpida)]\cdot H_2O\}_n$ (**1**). Solid line represents the best fit data. Inset: $M/N\beta$ vs. H. Solid line indicates the Brillouin curve with the calculated g value.

3.4. Magneto-structural correlations

From crystallographic analysis, it is evident that the Cu(II) ions in both the complexes **1** and **2**, are linked by carboxylato groups in *syn–anti* conformation with equatorial–equatorial coordination mode. For complex **1**, the Cu(II) center has almost perfectly square-pyramidal geometry while it is distorted octahedral for **2**. Small overlap between the magnetic orbitals ($d_{x^2-y^2}$) of the copper atoms for a planar Cu–O–C–O–Cu skeleton through the *syn–anti* carboxylato bridge account for the weak magnetic coupling observed. This overlap is significantly reduced for cases in which the Cu–O–C–O–Cu skeleton deviates from planarity (out-of-phase exchange pathway), which reduces the antiferromagnetic contribution, and as a result the ferromagnetic term becomes dominant (Scheme 2) [5d–5l]. This is true for both the complexes **1** and **2**. The higher J value for **2** can be explained by the greater dihedral angle between the two adjacent copper(II) planes of this complex compared to **1** (dihedral angles are 58.5(1)° and 65.4(1)° for complexes **1** and **2**, respectively). Theoretical DFT calculations corroborate these general features [5m]. Magneto structural data of some selected ferromagnetically coupled carboxylato bridged Cu(II) complexes along with those of **1** and **2** are presented in Table 4. From this table, it is easy to realize that the dihedral (or torsion) angle between the equatorial Cu(II) planes is important but not the exclusive factor that can influence J values. Dihedral angles for the complexes $\{[Cu(H_2O)_3][Cu(mal)_2(H_2O)]\}_n$ and **1** are very different, such as 85.95° (very close to the limit of 90°) and 58.5°, respectively (Table 4), but these two compounds have very similar J values (+3.0 and +3.6 cm^{-1}, respectively). Again, the

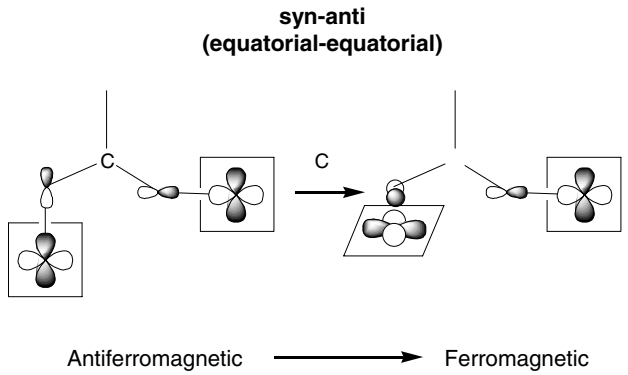

Scheme 2.

Table 4
Relevent magneto structural data of some selected[a] complexes with *syn–anti* carboxylato bridges in *equatorial–equatorial* (*basal–basal*) coordination mode: (HL^1 = 6-methylamino-1,3-dimethyl-5-[(2-carboxyphenyl)azo]uracil; L^2 = 1,3-dimethyl-5-((2-carboxyphenyl)azo)barbiturate; L^3 = condensation product of pyridine-2-carboxaldehyde with anthranilic acid; mal = malonate)

Compound	*d*(Cu–O) (Å)	Dihedral angle (°)[b]	*J* (cm^{-1})	Reference
$[Cu(H_2O)_4\{(CuHL^1)(H_2O)(ClO_4)\}_2(ClO_4)_2 \cdot 2H_2O]$	1.949 1.880	94.9	+2.7	[5d]
$[Cu(H_2O)L^2]_n$	1.995 1.902	46.4	+3.3	[5j]
$[Cu_2(mal)_2(H_2O)(4,4'\text{-bpy})]$	1.922 1.957	72.72	+12.4	[5g]
$[\{Cu_4(L^3)_4(H_2O)_4\} \cdot 3.5NO_3 \cdot 0.5N_3]$	1.957 1.936	86.8 (average)	+6.88	[5h]
$\{[Cu(H_2O)_3][Cu(mal)_2(H_2O)]\}_n$	1.989 1.947	85.95	+3.0	[5e]
Complex **1**	1.962 1.927	58.5	+3.6	this work
Complex **2**	1.974 1.905	65.4	+5.7	this work

[a] Only those complexes for which the authors indicate the dihedral angle.
[b] Between adjacent copper(II) planes.

greatest *J* value (+12.4 cm^{-1}) does not correspond to the greatest dihedral angle (only 72.7°) (Table 4). Thus, other parameters, such as distances, other distortions, etc may be important and should be studied theoretically.

4. Conclusion

In this work, we report two 1D polymeric Cu(II) complexes, $\{[Cu(Hcpida)] \cdot H_2O\}_n$ (**1**) and $\{[Cu(Hcpida)(H_2O)] \cdot H_2O\}_n$ (**2**), derived from *N*-(2-carboxyphenyl)iminodiacetic acid (H_3cpida). Transformation of **1** to **2** through hydration is accompanied by remarkable structural (Cu(II)-square pyramidal to Cu(II)-distorted octahedral) and spectral changes. The carboxylato group attached to the phenyl ring of the coordinated $Hcpida^{2-}$ ion is responsible for the formation of the polymeric chain like structure in both **1** and **2**. Extensive H-bonding involving the H-atoms of water molecules and unionized carboxylic acid H-atom of the ligand reinforces the crystal packing, which is further reinforced by π–π stacking of the phenyl rings of the adjacent chains held parallel in the polymeric network. Such packing in **2** forms cylindrical channels that host the lattice water molecules. Both the complexes show ferromagnetic coupling between the Cu(II) ions through carboxylato bridge in *syn–anti* (equatorial–equatorial) coordination modes with Cu–Cu distances of 5.02 and 4.78 Å, respectively.

5. Supplementary data

Crystallographic data for the structural analysis have been deposited with the Cambridge Crystallographic Data Centre, CCDC Nos. 206860, 206861 for complexes **1** and **2**, respectively. Copies of this information may be obtained free of charge from The Director, 12 Union Road, Cambridge CB2 1EZ, UK (fax: +44-1223-336033; e-mail: deposit@ccdc.cam.ac.uk or www: http://www.ccdc.cam.ac.uk).

Acknowledgements

Authors grateful thanks are due to the Council of Scientific and Industrial Research (New Delhi) and University Grants Commission (New Delhi) for the award of research fellowships to A.D. and S.B., respectively. Financial support to J.R. given by the Spanish Government (Grant: BQU2000-0791) is gratefully acknowledged.

References

[1] (a) M. Fujita, Y.J. Kwon, S. Washizu, K. Ogura, J. Am. Chem. Soc. 116 (1994) 1151;
(b) S. Decurtins, H. Schmalle, R. Pellaux, New J. Chem. 22 (1998) 117;
(c) A. Aumuller, P. Erk, G. Klebe, S. Hunig, J.U. von Schutz, H.P. Warner, Angew. Chem., Int. Ed. Engl. 25 (1986) 740;
(d) A.J. Blake, N.R. Champness, P. Hubberstey, W.-S. Li, M.A. Withersby, M. Schröder, Coord. Chem. Rev. 183 (1999) 117;
(e) S.-K. Yoo, J.Y. Ryu, J.Y. Lee, C. Kim, S.-J. Kim, Y. Kim, J. Chem. Soc., Dalton Trans. (2003) 1454;
(f) Y. Qi, Y. Wang, C. Hu, M. Cao, L. Mao, E. Wang, Inorg. Chem. 42 (2003) 8519;
(g) A. Grirrane, A. Pastor, A. Galindo, A. Ienco, C. Mealli, P. Rosa, Chem. Commun. 4 (2003) 512;
(h) R. Vaidhyanathan, S. Natarajan, C.N.R. Rao, J. Chem. Soc., Dalton Trans. (2003) 1459;
(i) D. Cheng, M.A. Khan, R.P. Houser, J. Chem. Soc., Dalton Trans. (2002) 4555;

(j) E. Colacio, M. Ghazi, R. Kivekas, J.M. Moreno, Inorg. Chem. 39 (2000) 2882.
[2] (a) G.R. Desiraju, Acc. Chem. Res. 29 (1996) 441;
(b) O. Félix, M.W. Hosseini, A. De Cian, J. Fischer, Chem. Commun. (2000) 281;
(c) D. Braga, F. Grepioni, Acc. Chem. Res. 33 (2000) 601;
(d) P.V. Bernhardt, Inorg. Chem. 38 (1999) 3481;
(e) C. Janiak, J. Chem. Soc., Dalton Trans. (2000) 3885;
(f) Y. Li, H. Zhang, E. Wang, N. Hao, C. Hu, Y. Yan, D. Hall, New J. Chem. 11 (2002) 1619;
(g) E. Tynan, P. Jensen, P.E. Kruger, A.C. Lees, M. Nieuwenhuyzen, J. Chem. Soc., Dalton Trans. (2003) 1223;
(h) C.-T. Yang, B. Moubaraki, K.S. Murray, J.J. Vittal, J. Chem. Soc., Dalton Trans. (2003) 880.
[3] (a) G.B. Deacon, R.J. Phillips, Coord. Chem. Rev. 33 (1980) 227;
(b) M. Melnik, Coord. Chem. Rev. 36 (1981) 1;
(c) M. Kato, Y. Muto, Coord. Chem. Rev. 92 (1988) 45;
(d) C. Oldham, in: G. Wilkinson, R.D. Gillard, J.A. McCleverty (Eds.), Comprehensive Coordination Chemistry, vol. 2, Pergamon Press, Oxford, 1987.
[4] (a) R.J. Doedens, Prog. Inorg. Chem. 38 (1990) 97;
(b) B. Bleaney, K.D. Bowers, Proc. R. Soc. London, Ser., A 214 (1952) 451;
(c) B.N. Figgis, R.L. Martin, J. Chem. Soc. (1956) 3837.
[5] (a) K.K. Nanda, A.W. Addison, E. Sinn, L.K. Thompson, Inorg. Chem. 35 (1996) 5966;
(b) E. Bakalbassi, C. Tsipis, A. Bozopoulos, W. Dreissing, H. Harti, J. Mrozinski, Inorg. Chim. Acta 186 (1991) 113;
(c) R. Carling, K. Kopinga, O. Kahn, M. Verdaguer, Inorg. Chem. 25 (1986) 1786;
(d) E. Colacio, J.M. Domínguez-Vera, R. Kivekas, J.M. Moreno, A. Romerosa, J. Ruiz, Inorg. Chim. Acta 212 (1993) 115;
(e) C. Ruiz-Pérez, J. Sanchiz, M.H. Molina, F. Lloret, M. Julve, Inorg. Chem. 39 (2000) 1363, and references therein;
(f) C. Ruiz-Pérez, M. Hernández-Molina, P. Lorenzo-Luis, F. Lloret, J. Cano, M. Julve, Inorg. Chem. 39 (2000) 3845, and references therein;
(g) Y. Rodríguez-Martín, C. Ruiz-Pérez, J. Sanchiz, F. Lloret, M. Julve, Inorg. Chim. Acta 318 (2001) 159;
(h) S.K. Dey, B. Bag, K.M.A. Mali, M.S. El Fallah, J. Ribas, S. Mitra, Inorg. Chem. 42 (2003) 4029;
(i) E. Colacio, J.P. Costes, R. Kivekas, J.P. Laurent, J. Ruiz, Inorg. Chem. 29 (1990) 4240;
(j) E. Colacio, J.M. Domínguez-Vera, J.P. Costes, R. Kivekas, J.P. Laurent, J. Ruiz, M. Sundberg, Inorg. Chem. 31 (1992) 774;
(k) M. Murugesu, R. Clérac, B. Pilawa, A. Mandel, C.E. Anson, A.K. Powell, Inorg. Chim. Acta 337 (2002) 328;
(l) E. Colacio, J.M. Domínguez-Vera, M. Ghazi, R. Kivekas, M. Klinga, J.M. Moreno, Eur. J. Inorg. Chem. (1999) 441, and references therein;
(m) A. Rodríguez-Fortea, P. Alemany, S. Alvarez, E. Ruiz, Chem. Eur. J. 7 (2001) 627;
(n) A.W. Addison, T.N. Rao, J. Reedjik, J. van Rijn, C.J. Verschoor, J. Chem. Soc., Dalton Trans. (1984) 1349.
[6] (a) M.J. Román-Alpiste, J.D. Martín-Ramos, A. Castiñeiras-Campos, E. Bugella-Altamirano, A.G. Sicilia-Zafra, J.M. González-Pérez, J. Niclós-Gutiérrez, Polyhedron 18 (1999) 3341;
(b) A. Castiñeiras Campos, A.G. Sicilia Zafra, J.M. González Pérez, J. Niclós Gutiérrez, E. Chinea, A. Mederos, Inorg. Chim. Acta 241 (1996) 39;
(c) E. Bugella-Altamirano, J.M. González-Pérez, D. Choquesillo-Lazarte, R. Carballo, A. Castiñeiras, J. Niclós-Gutiérrez, Inorg. Chem. Commun. 6 (2003) 71;
(d) D. Choquesillo-Lazarte, B. Covelo, J.M. González-Pérez, A. Castiñeiras, J. Niclós-Gutiérrez, Polyhedron 21 (2002) 1485;
(e) Marc Anton Walters, Vadim Vapnyar, Adam Bolour, Chris Incarvito, Arnold L. Rheingold, Polyhedron 22 (2003) 941.
[7] (a) K. Swaminathan, U.C. Sinha, C. Chatterjee, V.S. Yadava, V.M. Padmanabhan, Acta Crystallogr., Sect. C 45 (1989) 21;
(b) K. Swaminathan, U.C. Sinha, C. Chatterjee, Acta Crystallogr., Sect. C 44 (1988) 447.
[8] L.M. Shkolnikova, V.S. Fundamenski, A.L. Poznyak, Zh. Neorg. Khim. 37 (1992) 583.
[9] A.I. Vogel, Textbook of Quantitative Inorganic Analysis, fifth ed., Longman Scientific and Technical, New York, 1989.
[10] A. Young, T.R. Sweet, J. Am. Chem. Soc. 80 (1958) 800.
[11] A. Altomare, G. Cascarano, C. Giacovazzo, A. Guagliardi, A.G.G. Moliterni, M.C. Burla, G. Polidori, M. Camalli, R. Spagna, Private communication, 1997.
[12] G.M. Sheldrick, SHELX-97: Program for the Refinement of Crystal Structure, University of Göttingen, Göttingen, Germany, 1997.
[13] D.T. Cromer, J.T. Weber, in: International Tables for X-ray Crystallography (Table 2.2A), vol. IV, Kynoch Press, Birmingham, 1994.
[14] J.A. Ibers, W.C. Hamilton, Acta Crystallogr. 17 (1964) 781.
[15] L.J. Farrugia, ORTEP-3 for Windows, University of Glasgow, Glasgow, UK, 1999.
[16] A.B.P. Lever, Inorganic Electronic Spectroscopy, Elsevier, Amsterdam, 1984.
[17] J.R. Ferraro, Low-frequency Vibrations of Inorganic and Coordination Compounds, Plenum Press, New York, 1971.
[18] (a) C. Djordjevic, M. Lee, E. Sinn, Inorg. Chem. 28 (1989) 719;
(b) M. Tsaramyrsi, M. Kaliva, A. Salifoglou, C.P. Raptopoulou, A. Terzis, V. Tangorlis, J. Giapintzakis, Inorg. Chem. 40 (2001) 5772.
[19] J. Roy, D. Banerjea, J. Indian Chem. Soc. 53 (1976) 221.
[20] (a) D. Cremer, J.A. Pople, J. Am. Chem. Soc. 97 (1975) 1354;
(b) J.C.A. Boyens, J. Cryst. Mol. Struct. 8 (1978) 31.
[21] G.A. Baker, G.S. Rushbrooke, H.E. Gilbert, Phys. Rev. A 135 (1964) 1272.
[22] D. Gatteschi, L. Pardi, Gazz. Chim. Ital. 123 (1993) 231.

Available online at www.sciencedirect.com
SCIENCE DIRECT®
Polyhedron 23 (2004) 1089–1096
POLYHEDRON
www.elsevier.com/locate/poly

Di-protonated 1,4,8,11-tetramethyl-1,4,8,11-tetraazacyclotetradecane tetra-*N*-oxide, a bulky di-cation that induces the assembly of unusual lanthanide(III) complexes ☆

Wen-Jie Lu [a,b], Lin-Ping Zhang [b], Hoi-Shan Chan [b], Tze-Lock Chan [b], Thomas C.W. Mak [b,*]

[a] *Department of Chemical and Environmental Engineering, Wuyi University, Jiangmen, Guangdong Province, PR China*
[b] *Department of Chemistry, The Chinese University of Hong Kong, New Territories, Hong Kong SAR, PR China*

Received 27 November 2003; accepted 20 January 2004

Abstract

Di-protonated 1,4,8,11-tetramethyl-1,4,8,11-tetraazacyclotetradecane tetra-*N*-oxide takes the *RSSR* configuration and is stabilized by a pair of charge-assisted intramolecular $[O–H\cdots O]^+$ hydrogen bonds; the di-cation induces the formation of lanthanide(III) complexes $[Ln(NO_3)_6]^{3-}$ (Ln = Ce, La, Nd), $[Er(NO_3)_3(H_2O)_3]$ and *catena*-$[Ce(NO_3)_4(\mu\text{-}NO_3)]_n^{2n-}$, the latter being a novel linear coordination polymer constructed by a bridging nitrate ligand functioning in the $\mu\text{-}O, O, O', O''$ mode.
© 2004 Elsevier Ltd. All rights reserved.

Keywords: Proton sponge; Macrocyclic tetramine; Lanthanide complex; 1,4,8,11-tetramethyl-1,4,8,11-tetraazacyclotetradecane

1. Introduction

Proton sponges [1] continue to attract much current interest due to their unusually high basicity, low nucleophilicity, slow deprotonation, and applications in modeling of low energetic enzymatic catalysis [2]. With mineral or organic acids, proton sponges of the diamine type form very stable ionic complexes consolidated by low-barrier intramolecular $[N–H\cdots N]^+$ hydrogen bonding, a primary example being 1,8-bis(dimethylamino) naphthalene [3]. Subsequent effort to explore other classes of *N*-donor proton sponges focused on cyclam-like macrocyclic tetramines [4] and, more recently, bowl and cage adamanzanes [5]. In this context, 1,4,8,11-tetramethyl-1,4,8,11-tetraazacyclotetradecane (Me_4cyclam), which has been widely employed as a polydentate ligand to bind labile metal moieties [6], is readily protonated in acid solution [7]. Our recent studies on metal complexes with polydentate ligands [8] prompted us to synthesize 1,4,8,11-tetramethyl-1,4,8,11-tetraazacyclotetradecane tetra-*N*-oxide ($Me_4cyclamO_4$) (**1**) as a potentially new type of proton sponge that features charge-assisted intramolecular $[N\rightarrow O–H\cdots O\leftarrow N]^+$ hydrogen bonding. Our attempt in using this tetra-*N*-oxide as a multidirectional linker for $[Ln(NO_3)_x]^{(x-3)-}$ nodes in coordination network construction was unsuccessful thus far, but rath- er yielded its diprotonated cation that led to the isolation of the crystalline complexes $[Me_4cyclam(OHO)_2]_2$ $[Ln(NO_3)_6](NO_3)\cdot H_2O$ (Ln = Ce **2**, La **3** and Nd **4**), $2[Me_4cyclam(OHO)_2](NO_3)_2\cdot[Er(NO_3)_3(H_2O)_3]\cdot 2H_2O\cdot CH_3OH$ **5** and $\{[Me_4cyclam(OHO)_2][Ce(NO_3)_4(\mu\text{-}NO_3)]\}_n$ **6**, the structures of which have been determined by X-ray crystallography.

☆ Supplementary data associated with this article can be found, in the online version, at doi:10.1016/j.poly.2004.01.008.

* Corresponding author. Tel.: +852-2609-6279; fax: +852-2603-5057.
E-mail address: tcwmak@cuhk.edu.hk (T.C.W. Mak).

0277-5387/$ - see front matter © 2004 Elsevier Ltd. All rights reserved.
doi:10.1016/j.poly.2004.01.008

2. Experimental

2.1. General procedures

IR spectra were recorded with a Nicolet Impact 420 FT-IR spectrometer using KBr pellets. Elemental analyses of C, H and N were performed by MEDAC LTD, Vrunel Science Centre, United Kingdom. 1,4,8,11-Tetramethyl-1,4,8,11-tetraazacyclotetradecane (Me_4cyclam) and the lanthanide salts were purchased from Aldrich and used in this work without further purification.

2.2. Synthesis of 1,4,8,11-tetramethyl-1,4,8,11-tetraazacyclotetradecane-N-tetroxide ($Me_4cyclamO_4$) (**1**)

A mixture of 1,4,8,11-tetramethyl-1,4,8,11-tetraazacyclotetradecane (Me_4cyclam, 2.0 g, 7.81 mmol), acetic acid (20 cm^3) and 35% hydrogen peroxide (10 cm^3) was heated at 80–85 °C for 1 h. Then hydrogen peroxide (7 cm^3) was added and the mixture kept at 80–85 °C for 1 h with stirring. An additional portion of hydrogen peroxide (7 cm^3) was introduced, and heating was continued for a further 9 h. The excess acetic acid and water were removed under vacuum, water (20 cm^3) was added twice, and each time the mixture was concentrated to dryness under vacuum. Acetone (100 cm^3) was then added to the remaining oil to yield a colorless precipitate, which was filtered off and washed with hot acetone to remove un-reacted Me_4cyclam. The solid mixtures were separated by LC on aluminum oxide 90 with MeOH-EtOAC (1:1 v/v) and then with MeOH to give $Me_4cyclamO_4$ as a powdery product. Colorless crystals of the hexahydrate $Me_4cyclamO_4 \cdot 6H_2O$ **1** (2.0 g, yield 60%) were grown by vapor diffusion of diethyl ether into a solution of the powder in MeOH-H_2O (4:1, v/v) at room temperature. *Anal.* Calc. for $C_{14}H_{32}N_4O_4 \cdot 6H_2O$: C, 39.25; H, 10.28; N, 13.08. Found: C, 38.94; H, 10.21; N, 13.30%. ^{1}H NMR (300 MHz, D_2O): δ 2.29 (4H, m, β-CH_2), 3.19 (12H, s, N–CH_3), 3.75 (16H, t, α-CH_2), 4.77 (w, H_2O); all shifted down field with reference to the parent Me_4cyclam [9]. IR (KBr, cm^{-1}): 3460*s*, 1649*s*, 1474*m*, 950*m*, 729*m*.

2.3. Synthesis of {[$Me_4cyclam(OHO)_2$]$_2$[$Ce(NO_3)_6$]-(NO_3)·(H_2O)} (**2**)

A solution of $Me_4cyclamO_4 \cdot 6H_2O$ **1** (85.6 mg, 0.20 mmol) in H_2O (1.5 cm^3, pH 4–5) and MeOH (6.5 cm^3) was carefully layered over a solution of Ce(NO_3)$_3 \cdot 6H_2O$ (43.4 mg, 0.10 mmol) in MeOH (3.0 cm^3) and CH_2Cl_2 (5.0 cm^3) in a test tube. Over a period of several days, colorless crystals were grown on the wall of the test tube and collected to give 55.0 mg of **2**. Yield: 44.5%. *Anal.* Calc. for $C_{28}H_{70}CeN_{15}O_{30}$: C, 27.18; H, 5.66; N, 16.99. Found: C, 26.98; H, 5.64; N, 16.77%. ^{1}H NMR (DMSO-d_6): δ 9.00 (O–H–O, w). Analogous ^{1}H spectra were also observed for complexes **3**–**6** at δ 9.00–10.00 ppm.

2.4. Synthesis of {[$Me_4cyclam(OHO)_2$]$_2$[$La(NO_3)_6$]-(NO_3)·(H_2O)} (**3**)

Colorless crystals of compound **3** were prepared in the same manner as **2**. Yield: 45.0%. *Anal.* Calc. for $C_{28}H_{70}LaN_{15}O_{30}$: C, 27.21; H, 5.67; N, 17.00. Found: C, 26.97; H, 5.70; N, 16.76%.

2.5. Synthesis of {[$Me_4cyclam(OHO)_2$]$_2$[$Nd(NO_3)_6$]-(NO_3)·(H_2O)} (**4**)

Pale pink crystals of compound **3** were prepared in the same manner as **2**. Yield: 44.0%. *Anal.* Calc. for $C_{28}H_{70}NdN_{15}O_{30}$: C, 27.09; H, 5.64; N, 16.93. Found: C, 26.91; H, 5.63; N, 16.67%.

2.6. Synthesis of 2[$Me_4cyclam(OHO)_2$](NO_3)$_2$·[Er(NO_3)$_3$(H_2O)$_3$]·2H_2O·CH_3OH (**5**)

Pale pink crystals of **5** were prepared in the same manner as **2**. Yield: 45.0%. *Anal.* Calc. for $C_{29}H_{82}ErN_{15}O_{35}$: C, 25.45; H, 5.99; N, 15.36. Found: C, 25.32; H, 5.95; N, 15.58%.

2.7. Synthesis of {[$Me_4cyclam(OHO)_2$][$Ce(NO_3)_4(\mu$-$NO_3)$]}$_n$ (**6**)

A solution of $Me_4cyclamO_4 \cdot 6H_2O$ **1** (85.6 mg, 0.20 mmol) in H_2O (1.5 cm^3, pH 6–7) and MeOH (6.5 cm^3) was carefully layered over a solution of Ce(NO_3)$_3 \cdot 6H_2O$ (43.4 mg, 0.10 mmol) in MeOH (3.0 cm^3) and CH_2Cl_2 (5.0 cm^3). Colorless crystals of **6** were obtained after several days. Yield: 46.0%. *Anal.* Calc. for $C_{14}H_{34}CeN_9O_{19}$: C, 21.76; H, 4.40; N, 16.32. Found: C, 21.93; H, 4.42; N, 16.60%.

2.8. X-ray crystallography

Selected single crystals of **1**–**5** sealed inside Lindemann glass capillaries were used for data collection on a Bruker SMART 1000 CCD diffractometer with graphite monochromatized Mo Kα radiation ($\lambda = 0.71073$ Å) at 293 K. Intensity data was obtained in the range $1.5° < \theta < 28°$. An empirical absorption correction was applied using the SADABS program [10]. The data collection of compounds **6** was performed on a Rigaku AFC7R four-circle diffractometer in the variable ω-scan mode [11] using Mo Kα radiation ($\lambda = 0.71073$ Å) at 293 K. Intensity data was recorded in the range $2.3° < \theta < 25°$, and an empirical absorption correction was applied using ψ-scan data for selected strong reflections. The structures were solved by direct methods

and refined by full-matrix least squares based on F^2 using the SHELXTL program package [12].

3. Results and discussion

3.1. Synthesis of 1,4,8,11-tetramethyl-1,4,8,11-tetraazacyclotetradecane tetra-N-oxide and its lanthanide(III) complexes

The tetra-*N*-oxide was obtained by exhaustive oxidation of 1,4,8,11-tetramethyl-1,4,8,11-tetraazacyclotetradecane (Me_4cyclam) with acetic acid and hydrogen peroxide. The workup procedure employing alumina and organic solvents ensured that the purified product was neutral $Me_4cyclamO_4$, rather than the acetate salt of its di-protonated form. Structural characterization of $Me_4cyclamO_4$ was performed by X-ray analysis of its crystalline hexahydrate $Me_4cyclamO_4 \cdot 6H_2O$ **1**.

Compound **2**–**6** were obtained by the reaction of $Ln(NO_3)_3$ (Ln = Ce **2**, **6**; La **3**; Nd **4**; Er **5**) with $Me_4cyclamO_4 \cdot 6H_2O$ **1** using a "diffusion solvent mixture" composed of the MeOH–H_2O and MeOH–H_2O–CH_2Cl_2 systems. The main function of dichloromethane is to slow down the rate of the reaction and facilitate crystal growth. The reaction of $Ce(NO_3)_3$ and $Me_4cyclamO_4$ in aqueous acidic solution (pH 4–5) yielded compound **2** containing the $[Ce(NO_3)_6]^{3-}$anion. In contrast, under weakly acidic or neutral condition (pH 6–7), compound **6** was obtained which features a novel *catena*-$[Ce(NO_3)_4(\mu\text{-}NO_3)]_n^{2n-}$ chain bridged by μ-O,O,O',O'' nitrate ligands. This shows that formation of the lanthanide complexes can be controlled by changing the pH.

3.2. Crystal structures

The tetra-*N*-oxide molecule is located at a site of symmetry $\bar{1}$ and exhibits the *RSSR* configuration [13] (Fig. 1). The four nitrogen atoms are necessarily co-planar, with O1 and O2A pointing to one side, and O2 and O1A to the other, and the O···O distance is 4.676 Å. The plane of C6, N1 and O1 makes a dihedral angle of 94.9° with the plane of the four nitrogen atoms, and the plane of C7, N2 and O2 make a corresponding dihedral angle of 68.0°. The $Me_4cyclamO_4$ molecule forms acceptor O–H···O hydrogen bonds with water molecules O1W and O2W, generating a layer structure (Fig. 2). Such layers are further inter-connected through hydrogen bonds involving O3W, thus leading to a three-dimensional network (Fig. 3).

In $[Me_4cyclam(OHO)_2]_2[Ce(NO_3)_6](NO_3) \cdot H_2O$ **2**, the Ce(III) ion located at an inversion center is coordinated by six chelating nitrate ions (Ce–O, 2.617–2.669 Å), exhibiting an icosahedral coordination geometry similar to that found in $[(C_4H_9)_3NH]_3[La(NO_3)_6]$ [14] (Fig. 4(a)). The vertices of the coordination polyhedron constitute three co-planar sets: O11, O12, O11A, O12A and Ce1 (**I**); O21, O22, O21A, O22A and Ce1 (**II**), and O31, O32, O31A, O32A and Ce1 (**III**). These planes are almost orthogonal to one another, the dihedral angles being 92.8° between **I** and **II,** 90.5° between **II** and **III**, and 85.3° between **I** and **III** (Fig. 4(b)). Though the *N*-oxide group is known to be a good donor to coordinate the lanthanide(III) ion [15], each pair of contiguous *N*-oxide groups in $Me_4cyclamO_4$ sequestrates a proton from the solvent, forming a charge-assisted intramolecular

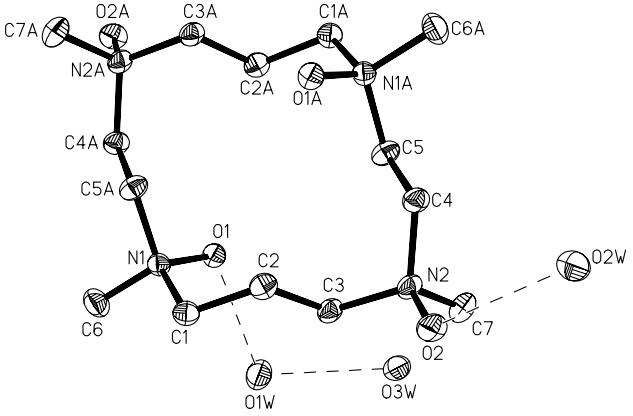

Fig. 1. The centrosymmetric 1,4,8,11-tetramethyl-1,4,8,11-tetraazacyclotetradecane tetra-*N*-oxide molecule taking the *RSSR* configuration, and independent lattice water molecules involved in hydrogen bonding, in Me4cyclamO4 · $6H_2O$ **1**. Hydrogen atoms are omitted for clarity.

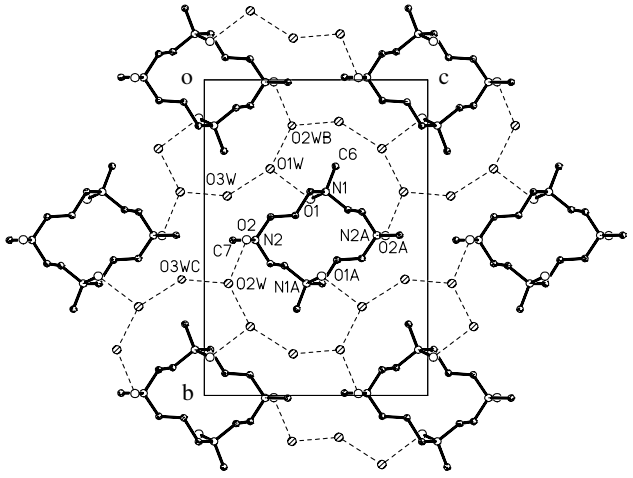

Fig. 2. Hydrogen-bonded layer structure of $Me_4cyclamO_4 \cdot 6H_2O$ **1** projected normal to the *a* axis. Hydrogen bonding: O1W–H···O1 177(3)°, O1W···O1 2.723(2) Å; O2W–H···O2 170(3)°, O2W···O2 2.708(2) Å; O3W–H···O1W 174(3)°, O3W···O1W 2.792(3) Å; O1W–H···O2WB 170(3)°, O1W···O2WB 2.712(2) Å; and O2W–H···O3WC 177(3)°, O2W···O3WC 2.758(2) Å (A: $-x+1,-y+1,-z+1$; B: $-x+1,y-1/2,-z+1/2$; C: $-x+1,-y+1,-z$).

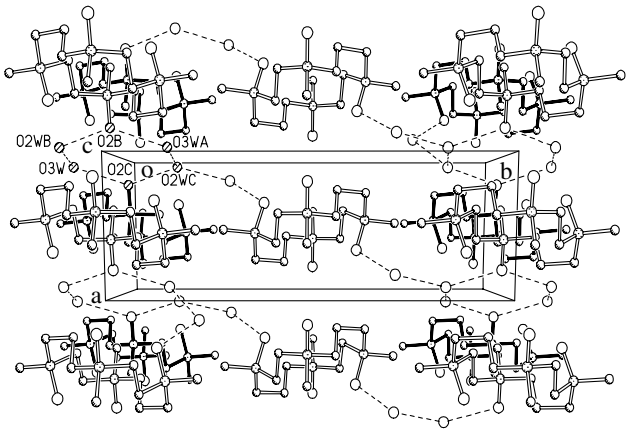

Fig. 3. Hydrogen-bonded three-dimensional framework of **1** viewed along the *c* axis.

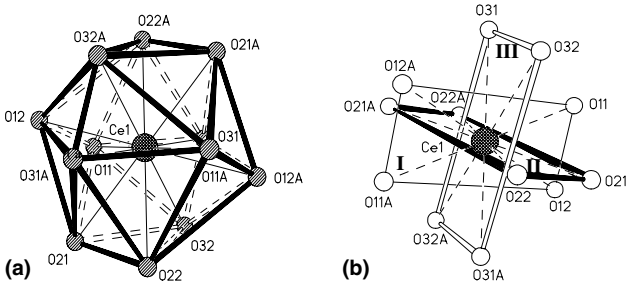

Fig. 4. (a) Icosahedral coordination polyhedron of the Ce(III) ion in **2**. (b) Ligand atoms arranged in three mutually perpendicular planes.

$[O–H\cdots O]^+$ hydrogen bond. The O···O distance between O1 and O1A is 2.538 Å, much shorter than that of 4.676 Å in **1**. The crystal structure of **2** consists of a packing of the $[Ce(NO_3)_6]^{3-}$ anion and two independent $[Me_4cyclam(OHO)_2]^{2+}$ ions (one of which is disordered), all three being located in sites of symmetry $\bar{1}$, together with a disordered discrete nitrate ion and a lattice water molecule.

Compounds **3** and **4** are isomorphous to **2** with Ce(III) replaced by La(III) in **3** and Nd(III) in **4**, respectively.

$2[Me_4cyclam(OHO)_2](NO_3)_2\cdot[Er(NO_3)_3(H_2O)_3]\cdot 2H_2O\cdot CH_3OH$ (**5**) can be considered as a double salt with co-crystallized water and methanol solvate molecules. The $[Er(NO_3)_3(H_2O)_3]$ molecule is located at a site of symmetry *m*, being coordinated by three chelating nitrate groups and three aqua ligands in a distorted tricapped trigonal prismatic environment (Fig. 5). The non-ligating nitrate ion, the lattice water molecule, and the disordered methanol molecule are connected to the uncharged $[Er(NO_3)_3(H_2O)_3]$ complex through hydrogen bonds to generate an infinite $\{[Er(NO_3)_3(H_2O)_3](NO_3)_3\cdot H_2O\cdot CH_3OH\}_n^{n-}$ chain, which is surrounded by $[Me_4cyclam(OHO)_2]^{2+}$ cations and discrete nitrate ions in the resulting crystal packing (Fig. 6).

In compound **6** SADABS $\{[Me_4cyclam(OHO)_2][Ce(NO_3)_4(\mu\text{-}NO_3)]\}_n$, the asymmetric unit contains three independent $[Me_4cyclam(OHO)_2]^{2+}$ cations (Fig. 7), two of which are located at inversion centers; all three have the same *RSSR* configuration consolidated by a pair of charge-supported asymmetric $[O–H\cdots O]^+$ hydrogen

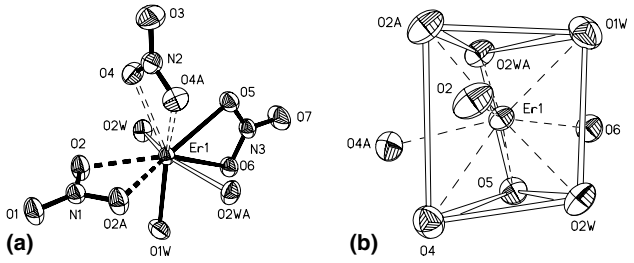

Fig. 5. (a) Molecular structure of $[Er(NO_3)_3(H_2O)_3]$ in **5**. The O1, N1, O3, N2, O5, O6, O7, N3, O1W and Er1 atoms are located on a mirror plane. (b) Tricapped trigonal prismatic coordination geometry of Er(III) in **5**.

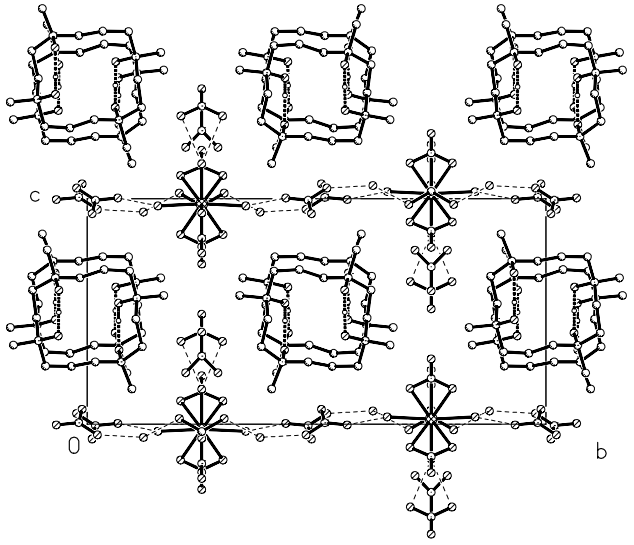

Fig. 6. Crystal structure of compound **5**.

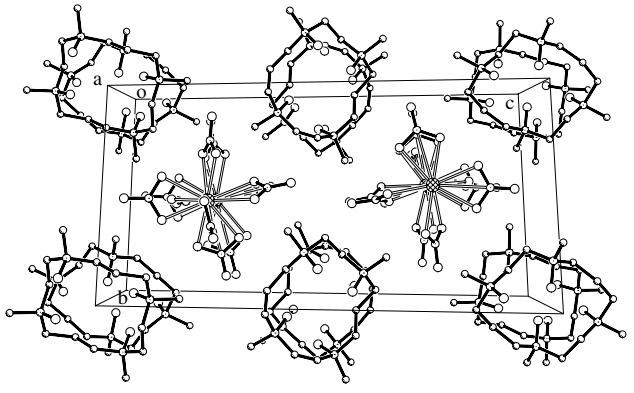

Fig. 7. Packing diagram of compound **6**, viewed along the *a* axis.

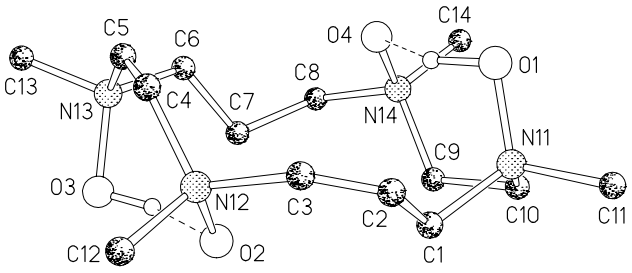

Fig. 8. $[Me_4cyclam(OHO)_2]^{2+}$ cation exhibiting the RSSR configuration and asymmetric $[O–H\cdots O]^+$ hydrogen bonds.

bonds (Fig. 8). Each of the two independent Ce(III) ions in the unit is surrounded by twelve oxygen atoms from six chelating nitrate ions, leading to an icosahedral coordination geometry analogous to that in **2**. Two of these nitrate groups act as consecutive μ-O, O, O', O'' linkers to bridge the Ce(III) ions (Fig. 9(a)), thus generating an unprecedented *catena*-$[Ce(NO_3)_4(\mu\text{-}NO_3)]_n^{2n-}$ linear chain running parallel to the *a* axis (Fig. 9(b)). The literature contains several metal complexes in which the nitrate group functions in the μ-O, O, O', O'' mode to form binuclear [16], linear polymeric [17], and zeolite-like network [18] structures. However, in the reported nitrato-bridged binuclear and polymeric complexes, for example $[(dien)Pb(NO_3)_2]_n$ [17a], the coordination sphere about the metal center also comprises other types of ligands. To our knowledge, the $[Ce(NO_3)_4(\mu\text{-}NO_3)]_n^{2n-}$ chain of compound **6** and the host framework of $C_{60}\{Ag(NO_3\}_5$ are the only polymeric structures that are constructed entirely with nitrate ligands.

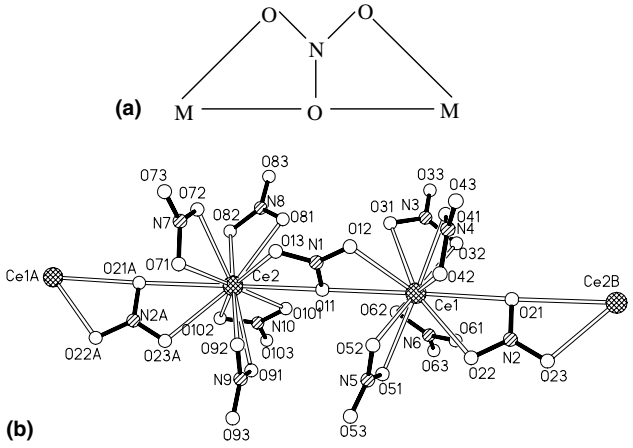

Fig. 9. (a) The nitrate ion acting in the μ-O, O, O', O'' mode to bridge two metal ions. (b) Polymeric chain *catena*-$[Ce(NO_3)_4(\mu\text{-}NO_3)]_n^{2n-}$ running parallel to the *a* axis in **6**, successive pairs of lanthanide centers being bridged by a μ-O, O, O', O'' nitrate group.

Table 1
Crystallographic data of complexes **1**–**6**

	Complex **1**	Complex **2**	Complex **3**	Complex **4**	Complex **5**	Complex **6**
Empirical formula	$C_{14}H_{44}N_4O_{10}$	$C_{28}H_{70}CeN_{15}O_{30}$	$C_{28}H_{70}LaN_{15}O_{30}$	$C_{28}H_{70}NdN_{15}O_{30}$	$C_{29}H_{78}ErN_{15}O_{35}$	$C_{14}H_{70}NdN_{15}O_{30}$
Formula weight	428.53	1237.11	1235.90	1241.23	1368.36	772.64
Crystal size (mm)	$0.35 \times 0.30 \times 0.27$	$0.36 \times 0.30 \times 0.25$	$0.28 \times 0.22 \times 0.18$	$0.88 \times 0.48 \times 0.45$	$0.52 \times 0.39 \times 0.37$	$0.57 \times 0.30 \times 0.28$
Crystal system	monoclinic	triclinic	triclinic	triclinic	monoclinic	triclinic
Space group	$P2_1/c$ (No. 14)	$P\bar{1}$ (No. 2)	$P\bar{1}$ (No. 2)	$P\bar{1}$ (No. 2)	$P2_1$/m (No. 11)	$P\bar{1}$ (No. 2)
a (Å)	5.648(1)	9.5474(5)	9.5496(7)	9.5545(5)	10.6722(4)	11.384(2)
b (Å)	17.035(3)	10.9671(6)	10.9826(8)	10.9610(6)	23.144(1)	11.823(2)
c (Å)	11.955(2)	12.7522(7)	12.7631(9)	12.7376(7)	12.0525(5)	22.598(5)
α (°)	90	93.356(1)	93.383(2)	93.354(1)	90	85.90(3)
β (°)	102.109(4)	92.507(1)	92.499(2)	92.328(1)	109.310(1)	77.92(3)
γ (°)	90	93.365(1)	93.418(2)	93.351(1)	90	69.82(3)
V (Å^3)	1124.5(3)	1329.2(1)	1332.4(2)	1328.1(1)	2809.5(2)	2792(1)
Z	2	1	1	1	2	4
D_{calc} (g/cm^3)	1.266	1.546	1.540	1.552	1.618	1.838
μ (Mo Kα) (mm^{-1})	0.105	0.958	0.903	1.079	1.603	1.730
F (0 0 0)	472	641	640	643	1418	1564
Reflections collected	7621	9140	9219	8957	19198	10348
Independent reflections	2707(0.0402)	6315(0.0397)	6353(0.0642)	6270(0.0343)	6926(0.0656)	9828(0.0285)
Observed reflections [$I > 2\sigma(I)$]	1810	5640	3193	6209	5735	6679
Parameters	146	406	406	406	403	787
Goodness-of-fit	1.024	1.106	0.983	1.140	1.000	1.045
R_1 [$I > 2\sigma(I)$][a]	0.0536	0.0745	0.0900	0.0665	0.0538	0.0428
wR_2 (all data)[b]	0.1542	0.2086	0.2496	0.1849	0.1503	0.1189

[a] $R_1 = \sum \|F_o| - |F_c\| / \sum |F_o|$.

[b] $wR_2 = \left[\sum[w(F_o^2 - F_c^2)^2] / \sum[w(F_o^2)^2]\right]^{1/2}$.

Table 2
Selected bond lengths (Å) and angles (°) for compounds **2**–**6**

*Complex **2***			
Bond lengths			
Ce(1)–O(11)	2.632(5)	Ce(1)–O(12)	2.669(5)
Ce(1)–O(21)	2.642(5)	Ce(1)–O(22)	2.648(5)
Ce(1)–O(31)	2.617(4)	Ce(1)–O(32)	2.648(5)
Bond angles			
O(11)–Ce(1)–O(21)	67.2(2)	O(11)–Ce(1)–O(32)	70.3(2)
O(21)–Ce(1)–O(12)	64.4(2)	O(11)–Ce(1)–O(22)	110.4(2)
O(21)–Ce(1)–O(22)	47.9(2)	O(11)–Ce(1)–O(12)	47.6(1)
O(31)–Ce(1)–O(12)	109.5(2)	O(22)–Ce(1)–O(12)	108.5(2)
O(31)–Ce(1)–O(21)	109.9(2)	O(31)–Ce(1)–O(32)	48.5(2)
O(32)–Ce(1)–O(22)	65.6(2)	O(31)–Ce(1)–O(11)	65.10(1)
O(32)–Ce(1)–O(12)	112.0(2)	O(31)–Ce(1)–O(22)	112.0(2)
O(32)–Ce(1)–O(21)	68.8(1)		
*Complex **3***			
Bond lengths			
La(1)–O(11)	2.650(6)	La(1)–O(12)	2.679(6)
La(1)–O(21)	2.667(7)	La(1)–O(22)	2.673(7)
La(1)–O(31)	2.638(6)	La(1)–O(32)	2.655(6)
Bond angles			
O(11)–La(1)–O(22)	110.7(2)	O(11)–La(1)–O(32)	70.3(2)
O(11)–La(1)–O(12)	47.5(2)	O(11)–La(1)–O(21)	67.8(2)
O(31)–La(1)–O(11)	65.0(2)	O(21)–La(1)–O(12)	64.6(2)
O(31)–La(1)–O(32)	47.9(2)	O(21)–La(1)–O(22)	47.5(2)
O(31)–La(1)–O(21)	109.7(2)	O(22)–La(1)–O(12)	108.2(2)
O(31)–La(1)–O(12)	109.7(2)	O(31)–La(1)–O(22)	112.0(2)
O(32)–La(1)–O(21)	68.9(2)	O(32)–La(1)–O(12)	111.8(2)
O(32)–La(1)–O(22)	66.2(2)		
*Complex **4***			
Bond lengths			
Nd(1)–O(11)	2.600(4)	Nd(1)–O(12)	2.633(4)
Nd(1)–O(21)	2.616(4)	Nd(1)–O(22)	2.623(4)
Nd(1)–O(31)	2.593(4)	Nd(1)–O(32)	2.619(4)
Bond angles			
O(11)–Nd(1)–O(22)	110.6(1)	O(11)–Nd(1)–O(12)	48.2(3)
O(11)–Nd(1)–O(32)	69.9(1)	O(11)–Nd(1)–O(21)	67.1(2)
O(21)–Nd(1)–O(32)	68.5(1)	O(21)–Nd(1)–O(22)	48.4(1)
O(21)–Nd(1)–O(12)	64.9(1)	O(22)–Nd(1)–O(12)	109.2(1)
O(31)–Nd(1)–O(11)	65.3(1)	O(32)–Nd(1)–O(12)	112.3(1)
O(31)–Nd(1)–O(22)	112.2(1)	O(32)–Nd(1)–O(22)	65.8(1)
O(31)–Nd(1)–O(21)	110.2(1)	O(31)–Nd(1)–O(32)	48.9(1)
O(31)–Nd(1)–O(12)	110.0(1)		
*Complex **5***			
Bond lengths			
Er(1)–O(1W)	2.330(5)	Er(1)–O(2)	2.405(4)
Er(1)–O(2W)	2.308(3)	Er(1)–O(6)	2.407(5)
Er(1)–O(4)	2.472(4)	Er(1)–O(5)	2.409(5)
Bond angles			
O(1W)–Er(1)–O(2)	78.8(2)	O(1W)–Er(1)–O(5)	124.6(2)
O(1W)–Er(1)–O(6)	72.2(2)	O(1W)–Er(1)–O(4)	149.6(1)
O(2W)–Er(1)–O(6)	74.5(1)	O(2W)–Er(1)–O(5)	80.9(1)
O(2W)–Er(1)–O(1W)	85.0(1)	O(2W)–Er(1)–O(2)	77.1(1)
O(2W)–Er(1)–O(4)	74.1(1)	O(2)–Er(1)–O(6)	140.7(1)
O(2)–Er(1)–O(5)	146.1(1)	O(2)–Er(1)–O(4)	75.2(1)
O(5)–Er(1)–O(4)	74.2(2)	O(6)–Er(1)–O(5)	52.4(2)
O(6)–Er(1)–O(4)	121.0(2)		

Table 2 (*continued*)

Complex **6**			
Bond lengths			
Ce(1)–O(11)	2.796(4)	Ce(1)–O(12)	2.647(4)
Ce(1)–O(21)	2.807(4)	Ce(1)–O(22)	2.622(4)
Ce(1)–O(31)	2.625(4)	Ce(1)–O(32)	2.580(4)
Ce(1)–O(41)	2.660(5)	Ce(1)–O(42)	2.584(4)
Ce(1)–O(51)	2.602(5)	Ce(1)–O(52)	2.580(4)
Ce(1)–O(61)	2.627(4)	Ce(1)–O(62)	2.661(4)
Ce(2)–O(71)	2.602(4)	Ce(2)–O(72)	2.602(4)
Ce(2)–O(81)	2.619(4)	Ce(2)–O(82)	2.610(4)
Ce(2)–O(91)	2.624(4)	Ce(2)–O(92)	2.576(4)
Ce(2)–O(101)	2.609(4)	Ce(2)–O(102)	2.587(4)
Ce(2)–O(11)	2.809(4)	Ce(2)–O(13)	2.628(4)
Ce(2)–O(21a)	2.982(4)	Ce(2)–O(23a)	2.635(5)
Bond angles			
O(12)–Ce(1)–O(11)	46.8(1)	O(22)–Ce(1)–O(21)	46.7(1)
O(32)–Ce(1)–O(31)	48.6(1)	O(42)–Ce(1)–O(41)	48.6(1)
O(52)–Ce(1)–O(51)	49.1(1)	O(61)–Ce(1)–O(62)	47.7(1)
O(71)–Ce(2)–O(72)	48.7(1)	O(82)–Ce(2)–O(81)	48.7(1)
O(92)–Ce(2)–O(91)	48.8(2)	O(102)–Ce(2)–O(101)	49.1(1)
O(81)–Ce(2)–O(13)	66.6(1)	O(101)–Ce(2)–O(13)	112.2(1)
O(71)–Ce(2)–O(23a)	68.8(2)	O(102)–Ce(2)–O(23a)	71.4(2)
O(91)–Ce(2)–O(13)	105.6(2)	O(101)–Ce(2)–O(11)	67.5(1)
O(13)–Ce(2)–O(11)	46.7(1)	O(71)–Ce(2)–O(21a)	67.0(1)
O(23a)–Ce(2)–O(21a)	44.5(1)		

Symmetry codes: a $-x+1,-y+1,-z+1$ for **2**–**4**; a $x-1,y,z$ for **6**.

4. Conclusions

Only a few compounds bearing multiple *N*-oxide groups have been reported in the literature, and they are generally derived from nitrogen heterocyclic systems. Known examples include the tri-*N*-oxides of pyrido[3,2-*f*]-quinoxaline [19] and benzo-*asym*-triazine [20], the tetra-*N*-oxide of hexamethylbipyrazine [21], and 1,2,3,4-tetrazino[5,6-*f*]benzo-1,2,3,4-tetrazine 1,3,7,9-tetra-*N*-oxides [22]. Another synthetic approach to tetra-*N*-oxides is based on the incorporation of a pair of 2,2′-bipyridine units into either an acyclic skeleton [23] or a macrocycle [24]. $Me_4cyclamO_4$ differs from all these in that it possesses two pairs of contiguous *N*-oxide groups.

Hydrophobic bulky organic cations such as PPh_4^+ [25], and $[Ph_3PNPPh_3]^+$ [26], $(Ph_3PCH{=}CHPPh_3)^{2+}$ [27], and $[Ph_3P(CH_2)_3PPh_3]^{2+}$[27] have been used to advantage to induce co-crystallization with a wide variety of inorganic and organometallic anionic species, most often in non-aqueous media. We envisage that the di-positive cation $[Me_4cyclam(OHO)_2]^{2+}$ may well play an analogous and complementary role in the stabilization of unusual mono- and poly-nuclear complexes in aqueous solution that leads to their isolation in the crystalline state, such as the *catena*-$[Ce(NO_3)_4(\mu\text{-}NO_3)]_n^{2n-}$ linear chain in complex **6** (see Tables 1 and 2).

5. Supplementary data

Crystallographic data for the structural analysis have been deposited with the Cambridge Crystallographic Data Center, CCDC No. 216202-216207 for compounds **1**–**6**. Copies of this information may be obtained free of charge from the Director, CCDC, 12 Union Road, Cambridge, CB2 1EZ, UK (fax: +44-1233-336033; deposit@ccdc.cam.ac.uk or www.ccdc.cam.ac.uk).

Acknowledgements

This work is supported by Hong Kong Research Grants Council Earmarked Grant CUHK 4268/00P and CUHK 402003, and a Croucher Visiting Scholarship to W.-J. Lu.

References

[1] (a) R.W. Alder, Acc. Chem. Res. 16 (1983) 321;
(b) R.W. Alder, Chem. Rev. 89 (1989) 1215;
(c) H.A. Staab, T. Saupe, Angew. Chem., Int. Ed. Engl. 27 (1988) 865;
(d) K. Woniak, H. He, J. Klinowski, E. Grech, J. Phys. Chem. 99 (1995) 1403;
(e) P.R. Mallinson, G.T. Smith, C.C. Wilson, E. Grech, K. Woniak, J. Am. Chem. Soc. 125 (2003) 4259;
(f) A.J. Bieko, Z. Latajka, W. Sawka-Dobrowolska, L. Sobczyk, V.A. Ozeryanskii, A.F. Pozharskii, E. Grech, J. Nowicka-Scheibe, J. Chem. Phys. 119 (2003) 4313;
(g) J. Nelson, V. McKee, G. Morgan, Prog. Inorg. Chem. 47 (1998) 167.
[2] (a) W.W. Cleland, M.M. Kreevoy, Science 264 (1994) 1887;
(b) W.W. Cleland, M.M. Kreevoy, Science 269 (1995) 104;
(c) P.A. Frey, Science 269 (1995) 194;
(d) J.A. Gerlt, M.M. Kreevoy, W.W. Cleland, P.A. Frey, Chem. Biol. 4 (1997) 259;

(e) W.W. Cleland, P.A. Frey, J.A. Gerlt, J. Biol. Chem. 273 (1998) 25529;
(f) E. Kimura, Y. Zasshi, J. Pharm. Soc. Jpn. 122 (2002) 219.
[3] R.W. Alder, P.S. Bowman, W.R.S. Steele, D.R. Winterman, J. Chem. Soc., Chem. Commun. (1968) 723.
[4] (a) Y. Miyahara, K. Goto, T. Inazu, Tetrahedron Lett. 42 (2001) 3097;
(b) L. Broge, I. Sotofte, C.E. Olsen, J. Springborg, Inorg. Chem. 40 (2001) 3124;
(c) E.H. Wong, G.R. Weisman, D.C. Hill, D.P. Reed, M.E. Rogers, J.S. Condon, M.A. Fagan, J.C. Calabrese, K.C. Lam, I.A. Guzei, A.L. Rheingold, J. Am. Chem. Soc. 122 (2000) 10561.
[5] (a) Y. Miyahara, Y. Tanaka, K. Aminmoto, T. Akazawa, T. Sakuragi, H. Kobayashi, K. Kubota, M. Suenaga, H. Koyama, T. Inazu, Angew. Chem., Int. Ed. Engl. 38 (1999) 956;
(b) J. Springborg, Dalton Trans. (2003) 1653.
[6] (a) Q.M. Wang, H.K. Lee, T.C.W. Mak, New J. Chem. 26 (2002) 513;
(b) C.-M. Che, V.W.-W. Yam, K.-C. Cho, H.B. Gray, J. Chem. Soc., Chem. Commum. (1987) 948;
(c) C.-M. Che, S.-S. Kwong, C.-K. Poon, T.-F. Lai, T.C.W. Mak, Inorg. Chem. 24 (1985) 1359.
[7] K.R. Adam, I.M. Atkinson, S. Farquhar, A.J. Leong, L.F. Lindoy, M.S. Mahinay, P.A. Tasker, D. Thorp, Pure Appl. Chem. 70 (1998) 2345.
[8] (a) Q.-M. Wang, T.C.W. Mak, Chem. Commun. (2001) 807;
(b) W.-J. Lu, L.-P. Zhang, H.-B. Song, Q.-M. Wang, T.C.W. Mak, New J. Chem. 26 (2002) 775;
(c) C.-Y. Su, B.-S. Kang, H.-Q. Liu, Q.-G. Wang, T.C.W. Mak, Chem. Commun. (1998) 1551;
(d) C.-Y. Su, B.-S. Kang, H.-Q. Liu, Q.-G. Wang, Z.-N. Chen, Z.-L. Lu, Y.-X. Tong, T.C.W. Mak, Inorg. Chem. 38 (1999) 1374;
(e) C.-Y. Su, B.-S. Kang, Q.-C. Yang, T.C.W. Mak, J. Chem. Soc., Dalton Trans. (2000) 1857.
[9] E.K. Barefield, F. Wanger, Inorg. Chem. 12 (1973) 2435.
[10] G.M. Sheldrick, SADABS: Program for Empirical Absorption Correction of Area Detector Data, University of Göttingen, Germany, 1996.
[11] R.A. Sparks, in: F.R. Ahmed (Ed.), Crystallography, Computing Techniques, Munksgaard, Copenhagen, 1976, p. 452.
[12] G.M. Sheldrick, SHELXTL: Structure Determination Software Programs, Bruker Analytical X-ray Systems Inc, Madison, WI, 1997.
[13] T.W. Hambley, J. Chem. Soc., Dalton Trans. (1986) 565.
[14] (a) C.-H. Yan, Y.-W. Zhang, S. Gao, B.-G. Li, C.-H. Huang, G.-X. Xu, Alloys Compounds 225 (1995) 385;
(b) R.B. King, J. Am. Chem. Soc. 22 (1970) 6460.
[15] (a) D.L. Long, A.J. Blake, N.R. Champness, C. Wilson, M. Schröder, J. Am. Chem. Soc. 123 (2001) 3401;
(b) B.-Q. Ma, S. Gao, H.-L. Sun, G.-X. Xu, J. Chem. Soc., Dalton Trans. (2001) 130;
(c) A. Nedelcu, Z. Žak, A.M. Madalan, J. Pinkas, M. Andruh, Polyhedron 22 (2003) 789;
(d) S. Tanase, M. Andruh, A. Müller, M. Schmidtmann, C. Mathonière, G. Rombaut, Chem. Commun. (2001) 1084.
[16] (a) C.L. Lengauer, G. Giester, Acta Cryst. C 53 (1997) 870;
(b) M. Hashimoto, M. Takata, A. Yagasaki, Inorg. Chem. 39 (2000) 3712.
[17] (a) J.M. Harrowfield, H. Miyamae, B.W. Skelton, A.A. Soudi, A.H. White, Aust. J. Chem. 49 (1996) 1029;
(b) J.M. Harrowfield, H. Miyamae, B.W. Skelton, A.A. Soudi, A.H. White, Aust. J. Chem. 49 (1996) 1081;
(c) K. Lashgari, M. Kritikos, K. Lashgari, G. Westin, Acta Cryst. C 54 (1998) 1794.
[18] M.M. Olmstead, K. Maitra, A.L. Balch, Angew. Chem., Int. Ed. Engl. 38 (1999) 231.
[19] F. Linsker, R.L. Evans, J. Am. Chem. Soc. 68 (1946) 874.
[20] N.G. Argyropoulos, J.K. Gallos, Z.Y. Zhang, G.J. Palenik, J. Chem. Soc., Chem. Commun. (1989) 986.
[21] B.J. McGee, L.J. Sherwood, M.L. Greer, S.C. Blackstock, Org. Lett. 2 (2000) 1181.
[22] A.E. Frumkin, A.M. Churakov, Y.A. Strelenko, V.V. Kachala, V.A. Tartakovsky, Org. Lett. 1 (1999) 721.
[23] M.D. Best, E.V. Anslyn, Chem. Eur. J. 9 (2003) 51.
[24] M. Pietrazkiewicz, S. Pappalardo, P. Finocchiaro, A. Mamo, J. Karpiuk, J. Chem. Soc., Chem. Commun. (1990) 1907.
[25] M. Scudder, I. Dance, J. Chem. Soc., Dalton Trans. (1998) 3155.
[26] G.R. Lewis, I. Dance, J. Chem. Soc., Dalton Trans. (2000) 299.
[27] S. Costea, M. Bujoli-Doeuffa, G. Louarnb, D. Massiotc, R. Breca, S. Jobic, New J. Chem. (2003) 1228.

Available online at www.sciencedirect.com
SCIENCE DIRECT®
Polyhedron 23 (2004) 1097–1107
POLYHEDRON
www.elsevier.com/locate/poly

Synthesis of new dinuclear and mononuclear peroxovanadium(V) complexes containing biogenic co-ligands: a comparative study of some of their properties

Swapnalee Sarmah, Diganta Kalita, Pankaj Hazarika, Ruli Borah, Nashreen S. Islam *

Department of Chemical Sciences, Tezpur University, Tezpur 784 028, India

Received 12 June 2003; accepted 20 November 2003

Abstract

Dinuclear peroxo complexes of vanadium, $[V_2O_2(O_2)_3(asn)_3]\cdot H_2O$ (**1**) and $[V_2O_2(O_2)_3(gln)_3]\cdot H_2O$ (**2**) have been synthesized from the reaction of V_2O_5 with H_2O_2 and the respective amino acid ligand at pH ca. 2. Similar reactions conducted at pH ca. 5 afforded the monomeric complexes, $Na[VO(O_2)_2(asn)]\cdot H_2O$ (**3**) and $Na[VO(O_2)_2(gln)]\cdot H_2O$ (**4**). The compounds were characterized by elemental analysis and spectral studies. In complexes **1** and **2,** the two V(V) centres are bridged by a peroxo group and an amino acid ligand occurring as a zwitterion. The monomeric complexes **3** and **4** contain peroxo groups bonded in a side-on fashion and an amino acid co-ligand binding the V(V) centre through O (carboxylate) atoms. The complexes **1** and **2** rapidly degraded in solution with release of O_2 and formation of diperoxovanadate and decavanadate as shown by ^{51}V NMR spectra whereas complexes **3** and **4** remained stable in solution for over 24 h. Extent and rate of oxygen released from the two types of complexes under the effect of catalase action further evidenced the differences in their $V{:}O_2^{2-}$ content and mode of peroxide binding in these species. The μ-peroxovanadate complexes **1** and **2** instantaneously oxidized bromide to a bromination competent intermediate in phosphate buffer at physiological pH, and also efficiently mediated bromination of organic substrates in aqueous-organic media. Complexes **3** and **4** were inactive for bromination under analogous conditions. These findings make the dinuclear complexes **1** and **2** possible candidates of mimic in the action of vanadium in bromoperoxidase.
© 2004 Elsevier Ltd. All rights reserved.

Keywords: Dinuclear peroxovanadate; Peroxo-bridged divanadate; Peroxidative bromination; Heteroligand peroxovanadate; Amino acid containing peroxovanadates

1. Introduction

Vanadium and its compounds are increasingly being recognized to have biological functions [1–4]. Potential usage of vanadium compounds as therapeutic anti-diabetic agents has been the subject of a number of recent reviews [5,6]. There has been a continuous upsurge in interest in the chemistry of vanadium peroxides mainly owing to their insulin-mimetic properties [5–7], their ability to oxidize organic and inorganic substrates [8] as well as their potential as models for understanding vanadium dependent biogenic systems [6]. Studies on synthetic peroxovanadate complexes as functional and structural models of bromoperoxidase [8–12], the enzyme involved in the biosynthesis of a variety of naturally occurring brominated products, have been immensely useful in helping to elucidate the details of the mechanism of the action of the enzyme and have provided diverse approaches to this area [8–14].

The majority of known synthetic hetero-ligand peroxovanadate(V) complexes represent anionic mono, di or tetraperoxo complexes containing the peroxo group bonded to vanadium in a side-on fashion [8]. Reports related to dinuclear peroxovanadium(V) compounds with a bridging peroxo group are limited [15–20] and it is an area needing exploration. Such peroxovanadate species have been implicated as intermediates in some biochemical processes [21,22]. The existence of a dimeric

* Corresponding author. Tel.: +91-3712-267173 (Off.)/237549 (Res.); fax: +91-3712-267006.
E-mail address: nsi@tezu.ernet.in (N.S. Islam).

0277-5387/$ - see front matter © 2004 Elsevier Ltd. All rights reserved.
doi:10.1016/j.poly.2003.11.060

species of the type, $(VO)_2(O_2)_3$ in an acidic solution and its being the possible critical oxidant of bromide has been reported [11] however, its exact identity in solution has yet to be ascertained. Thus the paucity of information on peroxo bridged divanadates and the current intensive search for bio-relevant vanadium complexes [5,6,9] prompted us to direct our efforts in establishing viable synthetic routes to new dimeric peroxovanadates in a biogenic ligand environment. We have recently achieved the synthesis of new members of peroxo bridged compounds of the type $[V_2O_2(O_2)_3(\text{dipeptide})_3]\cdot H_2O$ [18] and $[V_2O_2(O_2)_3(\text{tripeptide})_2]\cdot H_2O$ [19]. These triperoxo divanadate complexes distinguished themselves in terms of their spectral as well as solution properties from the known peroxovanadium complexes possessing exclusively terminally bound peroxo groups. The complexes exhibited unique redox properties and could act as a bromide oxidant with good activity at physiological pH [18,19], an essential requirement of a biomimetic model. Based on detailed investigations in solution, we have proposed that a μ-peroxo intermediate VOOV, is likely to be the active intermediate in such bromination reactions.

With an objective to provide further evidence to this proposal and in continuation of our work on peroxovanadates we have now synthesized additional members of dinuclear μ-peroxovanadate and monomeric peroxovanadate complexes stabilized by coordinatively versatile amino acids with polar side chains viz., glutamine and asparagine as heteroligands. It was considered imperative to investigate the possible similarities or differences in spectral, redox or solution properties which may exist between the μ-peroxovanadate and monomeric peroxovanadate complexes in analogous coligand environment.

In this paper, the synthesis and physicochemical characterization of complexes of the type $[V_2O_2(O_2)_3L_3]\cdot H_2O$ and $Na[VO(O_2)_2L]\cdot H_2O$, (L = asparagine and glutamine) are presented. The two types of complexes synthesized provided a means of undertaking a comparative study of their various properties.

2. Materials and methods

The chemicals used were all reagent grade products. Catalase was obtained from Sigma–Aldrich Chemical Company. The water used for solution preparation was deionised and distilled.

2.1. Synthesis of dimeric peroxovanadate complexes, $[V_2O_2(O_2)_3(asn)_3]\cdot H_2O$ (1) and $[V_2O_2(O_2)_3(gln)_3]\cdot H_2O$ (2)

In a typical reaction solid V_2O_5 (0.25 g, 1.37 mM) was mixed with amino acid in a 250 ml beaker maintaining the molar ratio of V:amino acid as 1:2, to which 15 ml of 30% H_2O_2 (132.3 mM) was added gradually with constant stirring. The reaction mixture was then stirred for ca.15 min in an ice bath keeping the temperature below 4 °C. During this period the solid dissolved yielding a clear reddish yellow solution. The pH of the solution was recorded to be 2.0. No attempt was made to adjust the pH of the reaction solution. On adding pre-cooled ethanol (ca. 50 ml) to the above solution under continuous stirring, an orange–yellow coloured pasty mass separated out. After allowing to stand for about 10 min in the ice bath, the supernatant liquid was decanted and the residue was treated repeatedly with an acetone:ethanol (3:1 v/v) mixture under scratching until it became a microcrystalline solid. The product was separated by centrifugation, washed with cold ethanol and dried in vacuo over concentrated sulfuric acid. In the solid state these complexes were found to be stable for several weeks stored dry at <20 °C but tended to be hygroscopic at ambient conditions and decomposed in a few days.

Anal. Calc. for $[V_2O_2(O_2)_3(asn)_3]\cdot H_2O$: V, 15.82; O_2^{2-}, 14.91; C, 22.36; N, 13.00; H, 3.83. Found: V, 15.82; O_2^{2-}, 14.90; C, 22.59; N, 13.10; H, 4.01. Yield: approximately 50%.

Anal. Calc. for $[V_2O_2(O_2)_3(gln)_3]\cdot H_2O$: V, 14.87; O_2^{2-}, 13.99; C, 26.24; N, 12.24; H, 4.37. Found: V, 14.80; O_2^{2-}, 14.10; C, 26.10; N, 12.30; H, 4.50. Yield: approximately 47%.

2.2. Synthesis of monomeric peroxovanadate complexes, $Na[VO(O_2)_2(asn)]\cdot H_2O$ (3) and $Na[VO(O_2)_2(gln)]\cdot H_2O$ (4)

The procedure adopted for the synthesis is common to both complexes. This consisted of gradual addition of 12 ml H_2O_2 (30% solution, 105.84 mM) to a mixture of V_2O_5 (0.25 g, 1.37 mM) and amino acid at a molar ratio of V:amino acid of 1:1 with continuous stirring. Keeping the temperature below 4 °C in an ice bath, the mixture was stirred for ca. 15 min until all solids dissolved. At this stage the pH of the solution was recorded to be ca. 2. Concentrated sodium hydroxide solution (conc. ca. 8 M) was added dropwise with constant stirring to raise the pH of the reaction medium to ca. 5. On adding precooled ethanol (about 50 ml) to this mixture under vigorous stirring a yellow coloured pasty mass separated out. After standing for about 15 min in the ice bath, the supernatant liquid was decanted, and the residue was treated repeatedly with acetone:ethanol (3:1 v/v) mixture under scratching until it became a microcrystalline solid. The product was separated by centrifugation, washed with cold ethanol and dried in vacuo over concentrated sulfuric acid. In the solid state these complexes were found to be stable for several months stored dry at <25 °C.

Anal. Calc. for $Na[VO(O_2)_2(asn)]\cdot H_2O$: Na, 7.56; V, 16.77; O_2^{2-}, 21.05; C, 15.79; N, 9.21; H, 2.30. Found: Na, 7.69; V, 16.89; O_2^{2-}, 20.90; C, 15.44; N, 9.15; H, 2.23. Yield: approximately 43%.

Anal. Calc. for $Na[VO(O_2)_2(gln)]\cdot H_2O$: Na, 7.23; V, 16.03; O_2^{2-}, 20.12; C,15.78; N, 9.21; H, 2.63. Found: Na, 7.32; V, 16.34, O_2^{2-}, 20.04; C, 15.62; N, 9.29; H, 2.49. Yield: approximately 40%.

2.3. Elemental analysis

The compounds were analyzed for C, H, N and Na at Regional Sophisticated Instruments Centre, North-Eastern Hill University, Shillong, India and at the Department of Organic Chemistry, Indian Institute of Science, Bangalore, India. Vanadium and peroxide were estimated by methods mentioned in earlier papers [23].

2.4. Spectroscopic measurements

Spectra in the visible and ultraviolet region were recorded in a Hitachi model 2001 recording spectrophotometer in 1 cm quartz cuvettes. The absorbance values are denoted as, e.g., A_{592}, A_{340}, at the wavelengths indicated. The infrared (IR) spectra were recorded with samples as KBr pellets in a Nicolet model Impact 410 FTIR spectrophotometer and also in a Perkin–Elmer Model 983 spectrophotometer. The spectra were recorded at ambient temperatures by making pressed pellets of the compounds. The ^{1}H NMR spectra were recorded in deuterated chloroform in a Varian EM–390 90 MHz spectrophotometer using TMS as the internal standard. The ^{51}V NMR spectra were recorded in a Brucker AMX 400 FT spectrometer at vanadium frequency 105.190 MHz with the samples in a 10 mm spinning tube with a sealed co-axial tube containing D_2O, which provided the lock signal. The chemical shift data are shown as negative values of ppm with reference to $VOCl_3$ at 293 K. HPLC analyses were performed using a Waters Tm 2487 dual λ detector and assayed at fixed wavelengths using a C_{18} column (Nova-Pak C_{18}, 3.9×150 mm, Waters).

2.5. Measurement of bromination activity in solution

The method of de Boer et al. [24] of introducing four bromine atoms into the molecule of phenol red (ε^{433}mM = 19.7) to form bromophenol blue (ε^{592}mM = 67.4) was used to measure bromination activity. Phenol red acts as an efficient trap of active bromine species without influencing the rate of reaction until it is exhausted. The reaction mixture contained phosphate buffer (50 mM, pH 5.5), KBr (2 M) and phenol red (20 μM). The redox activity was tested by adding a weighed amount of the solid compounds, and by monitoring the possible change in absorbance at 592 nm at 30 °C. The volume of the reaction mixture was kept at 25 ml to enable accurate weighing of small amounts of the solid samples of peroxovanadates added. Aliquots were transferred to the spectrophotometer immediately after mixing to record the jump in A_{592}. The added bridging-peroxo complexes acted directly as a bromide oxidant producing instant change in A_{592} and therefore represented as 'instant activity'. The steady rate of increase that followed due to residual peroxovanadate is referred to as 'secondary rate'.

2.6. Bromination of organic substrates and products analysis

In a representative procedure, organic substrate (0.5 mM) was added to a solution of acetonotrile:water (1:1) (3 ml) containing KBr (1.5 mM). A weighed amount of solid peroxovanadate complex **2** (0.25 mM) was then added to the reaction mixture at room temperature under continuous stirring. The stirring was continued for ca.1 h. Reaction products as well as unreacted organic substrates were then extracted with diethyl ether and dried over anhydrous Na_2SO_4. Products were then separated by TLC and HPLC. ^{1}H NMR spectroscopy and melting point determinations were made to interpret the products.

2.7. Stability of complexes in solution – measurement of oxygen release from the peroxovanadium complexes

A Gilson 5/6 H oxygraph fitted with a Clark oxygen electrode was used for measuring changes in the concentration of dissolved oxygen (0.224 mM at 30 °C) in the medium. The changes were recorded in units of μM of dissolved oxygen. The rate and total amount of oxygen released from a 0.2 mM solution of the compound in phosphate buffer (50 mM, pH 7.0) on adding catalase (0.08 mg protein/ml) were measured. In the middle of the chart paper the recorder pen was set for measuring the release of oxygen into the medium. The machine was standardized by the increases in dissolved oxygen obtained on adding catalase to buffered solutions containing known amounts of H_2O_2. Oxygen release from H_2O_2 was complete within 10 s under these conditions, but a maximum of only about 200 μM of O_2 can be measured before it comes out in the form of bubbles. This limits the concentration of the substrate to 0.2 mM in this method.

3. Results

3.1. Synthesis and characterization

The methodology for the successful synthesis of the orange coloured dinuclear peroxovanadate complexes **1**

and **2** was based on the reaction of $V_2O_5$with H_2O_2 and the respective amino acid in aqueous acidic solution. Since our primary aim was to isolate complexes with a $(VO)_2(O_2)_3$ moiety which has been reported to exist in acidic solution, the pH value of ca. 2 attained spontaneously during the reactions was not raised. In a solution of vanadate and excess H_2O_2 at a $pH > 5$, formation of diperoxoxvanadate (DPV) species is favoured [25,26]. Thus a comparatively higher pH of ca. 5 of the reaction medium is likely to be responsible for the formation of the yellow alkali oxodiperoxovanadate complexes **3** and **4**.

The compounds **1**–**4** were diamagnetic in nature as was evident from the magnetic susceptibility measurements, in conformity with the presence of vanadium(V) in each case.

From the elemental analysis data, the ratio of V:O_2^{2-} and V:amino acid was ascertained to be 2:3 for complexes **1** and **2** in agreement with their formulation as $[V_2O_2(O_2)_3L_3]\cdot H_2O$ and suggesting a dimeric nature for the complexes. The elemental analysis results for complexes **3** and **4** indicated the presence of two peroxide groups and one amino acid per vanadium centre which could be fitted with the formula $Na[VO(O_2)_2L]\cdot H_2O$.

Each of the amino acid containing triperoxodivanadates(V) and mononuclear diperoxovanadate complexes displayed characteristic spectral patterns in the infrared region involving absorptions due to ν(V=O), coordinated peroxide, amino acid ligands and lattice water. The strong absorption at ca. 960 cm^{-1} in the spectra of the complexes was consistent with the presence of a terminally bonded V=O group [26,27] in each case.

A triangularly bonded peroxo group exhibits a diagnostic IR pattern with ν(O–O) appearing at ca. 870 cm^{-1} and ν_2 and ν_3 which involve metal–oxygen stretches appearing in the region 500–600 cm^{-1} [27]. In the spectra of complexes **1** and **2** in addition to the strong ν(O–O) absorption appearing at ca. 870 cm^{-1}, an additional weak intensity but well resolved band has been observed at ca. 810 cm^{-1} which has been assigned to the ν(O–O) band of the bridging peroxo group [28,29]. The peroxo bands observed in the spectra of complexes **3** and **4** (Table 1) were in the range characteristic of triangularly bonded peroxide. Significantly, no band appeared in the 810 cm^{-1} region in the spectra of the monomeric complexes **3** and **4**. These results suggest the presence of two different types of peroxo groups, the terminal chelated and the bridging type in complexes **1** and **2**, and the presence of terminal bidentate peroxide in complexes **3** and **4** and thus support the original formulations. Similar observations were made earlier for compounds wherein the side-on bound and the bridging type of peroxo groups were encountered simultaneously [17–20,28,29]. Synthesis and structural characterization of a complex, $[F(O_2)\{VO(O_2)F\}_2]^{3-}$, was reported earlier by Schwendt et al. [15,16] having a bridging peroxo moiety bonded in a $\mu-\eta^2{:}\eta^2$ fashion. IR spectra of these complexes displayed the ν(O–O) stretch at a relatively higher frequency of ca. 900 and 870 cm^{-1} indicating that the mode of peroxide coordination is probably different in these complexes from that in dinuclear peroxovanadates reported here and in our earlier papers [18,19].

Existence of coordinated amino acids in the complexes **1**–**4** was evident from their IR spectra which showed characteristic differences between the spectral pattern originating from amino acids of the complexes and the spectra of the free amino acids [30,31]. The N–H stretching bands were observed in the 3300–3000 cm^{-1} region as expected from the $-N^+H_3$ group and the amino group of the amino acid side chains. The rocking modes of N^+H_3 occurred at ca. 1050 and 1160 cm^{-1}. A band appearing at 1660–1670 cm^{-1} has been assigned to the ν(C=O) mode of the amide group of the amino acid side chain. The band was observed to be slightly shifted from its free ligand value of ca. 1680 cm^{-1} probably owing to its participation in hydrogen bonding. The absorption attributable to ν_{as}(COO) of the coordinated carboxylate group appeared in the 1650–1640 cm^{-1} region in the spectra of the complexes [30]. The symmetric stretching vibration of the carboxylate group of uncoordinated asparagine and glutamine occur at 1411 and at 1430 cm^{-1}, respectively. The spectra of complexes **1** and **2** displayed a medium intensity band at ca. 1360 cm^{-1} which may be assigned to ν_s(COO). The shifting of this band to lower frequency with the difference

Table 1
Infrared and ultraviolet spectral data of the peroxovanadate complexes

Compound	IR peak (cm^{-1})				UV peak	
	ν_s(V–O_2)	ν_{as}(V–O_2)	ν(O–O)	ν(V=O)	nm	A (1 mM)
$[V_2O_2(O_2)_3(asn)_3]\cdot H_2O$	562m	631m	859s 803m	954s	320	0.70
$[V_2O_2(O_2)_3(gln)_3]\cdot H_2O$	562m	640m	870m 809m	955s	328	0.40
$Na[VO(O_2)_2(asn)]\cdot H_2O$	557m	640m	869s	949s	324	0.63
$Na[VO(O_2)_2(gln)]\cdot H_2O$	540m	660m	873s	953s	321	0.72
DPV	522m	602s	877s	935s	325	0.60

$v_{as} - v_s \approx 250$ cm^{-1} is characteristic of monodentate coordination of the carboxylate group via the O(carboxylate) atom [30]. The spectra of complexes **1** and **2** exhibited another distinct band at 1405 cm^{-1} in the case of complex **1** and at 1412 cm^{-1} in the case of complex **2**, attributable to a bridging carboxylate group ($v_{as} - v_s \approx 200$ cm^{-1}). The symmetric stretching frequencies of the coordinated carboxylate group of the amino acid ligands in complexes **3** and **4**, on the other hand, were found to be shifted to higher values of 1420 and 1435 cm^{-1}, respectively, compared to their free ligand values. The spectra of these complexes displayed the v_{as}(COO) in the 1635–1640 cm^{-1} region. The shift of the v_s(COO) band to a higher frequency and the decrease in Δ value [$\Delta \approx v_{as}$(COO) – v_s(COO)] is typical of an amino acid bonded in a bidentate fashion through the carboxylate group [30]. The presence of glutamine and asparagine as a zwitterion in these complexes with protonated N^+H_3 was ascertained from the spectrum as mentioned in the foregoing discussions. Presence of lattice water in each of the complexes, **1**–**4** was indicated by the strong ν(OH) absorptions displayed at 3500–3400 cm^{-1}. However, the bending mode of water could not be assigned with certainty as it occurred in the carbonyl frequency region. The IR spectral data thus suggest that in each of the complexes, **1**–**4** amino acid occurring as zwitterion binds the V(V) centers through O(carboxylate) atoms. Based on these observations a structure of the type shown in Fig. 1 has been proposed for complexes **1** and **2**, which is shown for the asparagine complex as a representative example. For complexes **3** and **4** a structure of the type shown in Fig. 2 has been envisaged.

3.2. Nature and stability of the complexes in solution

The stability of the monomeric diperoxovanadate complexes **3** and **4** in solution was observed to be much

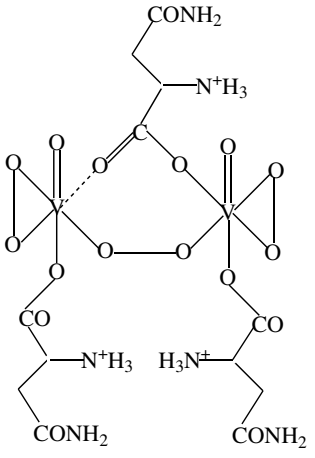

Fig. 1. Proposed structure of the dimeric peroxovanadate compounds shown with $[V_2O_2(O_2)_3(asn)_3]\cdot H_2O$ as representative.

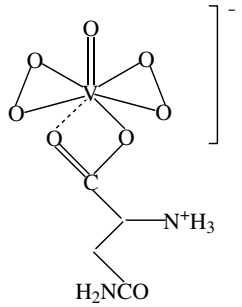

Fig. 2. Proposed structure of the monomeric peroxovanadate compounds shown with $Na[VO(O_2)_2(asn)]\cdot H_2O$ as representative.

higher as compared to that of dinuclear complexes **1** and **2**. Instability of the complexes **1** and **2** in water and degradative loss of the peroxide groups were evident from the oxygen evolution taking place from the complexes on adding the compounds to water. As a means of determining the stability of the complexes in solution, the rate of oxygen released from the complexes in solution was measured with an Oxygraph. Immediately on adding the compounds (ca. 2 mg/ml) to water the rate of oxygen release was exceedingly high, with a value of about 10 μM /min for a brief period of ca. 15 min.

In order to further investigate the nature of the species remaining in solution after oxygen evolution ceased to appear, we were interested to study their activity with the enzyme catalase. On addition of catalase to the solutions of **1** and **2** after the oxygen evolution ceased, further slow release of oxygen was recorded (Table 2) which revealed that the products in such solutions were indeed peroxovanadates. A maximum of 1.5 O_2 per mole of the compound would be released if all the three peroxides were retained. Lower values of 0.7 and 0.4 O_2 per mole of the compound were recorded since part of the peroxide was initially lost during the making of the solution in water. The subsequent secondary rates of oxygen release, calculated from the data, paralleled the residual peroxide concentrations.

The extent and rate of oxygen released under the effect of catalase action from complexes **3** and **4** (Table 2) were found to be comparable to that of the aquo oxodiperoxvanadate complex (DPV) [32] indicating their similarity with respect to number of peroxides and probably the pattern of their coordination to the V(V) centre. On incubation with catalase DPV was found to be degraded releasing half the molecular equivalent of oxygen at a rate of 36 μM/min from a solution of 0.2 mM [32]. The stability of the complexes **1**–**4** were also studied by estimating the peroxide content at different time intervals which revealed the variation in stability of the complexes. Whereas compounds **1** and **2** lost their peroxide rapidly, compounds **3** and **4** remained stable for a period of 24 h or more.

The electronic spectra of compounds **1**–**4** in aqueous solution exhibited a weak intensity broad LMCT band at

Table 2
Catalase dependent oxygen release from peroxovanadium compounds

Compound	Conc. (mM)	Oxygen release		ΔO_2/compound (mol. ratio)
		μM/min	Total (μM)	
$[V_2O_2(O_2)_3(asn)_3]\cdot H_2O$	0.2	17.6	145	0.72
$[V_2O_2(O_2)_3(gln)_3]\cdot H_2O$	0.2	11.2	87	0.44
$Na[VO(O_2)_2(asn)]\cdot H_2O$	0.2	32.2	185	0.92
DPV	0.2	36.0	192	0.96

310–320 nm (Table 1) originating from coordinated peroxide. Variations in absorbance values indicate partial loss of peroxide on making solutions of these compounds. In case of complexes **1** and **2** the intensity of this band was found to decrease with time, consistent with the loss of peroxide from these complexes and their unstable nature.

Further information regarding the nature of the complexes in solution was derived from ^{51}V NMR studies. Interaction of vanadium with amino acids and peptides is of considerable biological importance and has been studied extensively in solution [33–37]. The assignment of the peaks in the present study was on the basis of available data [33,38–40]. The solutions of **1** and **2** being acidic, it may be expected that free vanadate formed on depletion of its peroxide will oligomerize to the decameric form (V_{10}). The spectra of the complexes **1** and **2** displayed three peaks at −427, −509 and −527 ppm with an intensity ratio of 1:2:2 which have been assigned to V_{10}. The major signal at −694 ppm indicated the presence of diperoxovanadate as the predominant species. The small variations from the reported chemical shift values may be due to the presence of the coordinated ligands in some of the products and to variation of pH. The less intense peak observed at −545 ppm has been identified as monoperoxovanadate species. The two weak resonances appearing near −714 ppm were probably due to the presence of diperoxovanadate species containing an amino acid ligand coordinated through the carboxylate group [33,34]. Thus from the NMR spectral studies it was further evident that peroxo bridged dimeric complexes **1** and **2** undergo rapid degradation in water and hence provide no direct information regarding the nature of the original solid compound. The spectrum of complexes **3** and **4** displayed a predominant peak at −695 ppm characteristic of a diperoxovanadate species. Indication of the presence of traces of vanadates appeared in the spectra of the mononuclear complexes recorded 30 min after the preparation of the solutions.

3.3. Redox activity of the complexes in bromination reactions

3.3.1. Reaction with solid peroxovanadium compounds

The bromination of phenol red to bromophenol blue was employed to investigate the bromination activity of the complexes **1**–**4** in solution. Addition of a weighed amount of solid compound **1** or **2** to the standard reaction of bromide in phosphate buffer with phenol red as a trap for oxidized bromine resulted in instantaneous colour change of the solution from yellow to blue. The spectrum recorded showed a peak at A_{592} characteristic of the product bromophenol blue and a decrease in absorbance of the peak at A_{433} due to loss of phenol red (Fig. 3). After the initial very fast bromination activity referred as "instant" activity, a slow increase in A_{592} indicated a secondary rate of bromination (Fig. 4). The data in Table 3 show the instant and secondary bromination activities of dinuclear complexes **1** and **2**.

A similar reaction when carried out in the absence of phenol red displayed a peak at 262 nm with a shoulder at 237 nm on addition of compound **1** or **2**. Addition of phenol red to this solution resulted in the decrease in A_{262} nm and a peak at 592 nm appeared indicating the formation of bromophenol blue. The 262 nm peak, therefore, represents a bromination competent oxidized species of bromide, probably an equilibrium mixture of BrOH, Br_2 and Br_3^- as proposed earlier [1].

The results of the aforementioned experiments suggest the occurrence of two distinct types of bromination reaction. The fast bromination reaction which give a large increase in A_{592} indicates the presence of an active

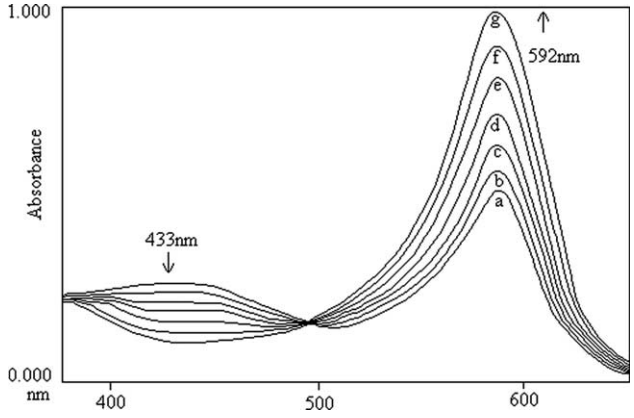

Fig. 3. Bromination activity with dinuclear peroxovanadate complex **2**. (a) The spectrum recorded immediately after adding the solid compound to the reaction mixture showing the "instant activity"; (b–g) spectral changes at 5 min intervals. The reaction mixture contained phosphate buffer (0.05 M, pH 5.5), KBr (2 M) and phenol red (0.02 mM).

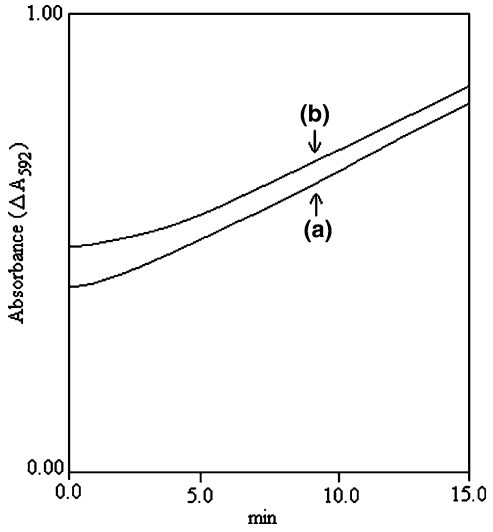

Fig. 4. The increase of A_{592} indicating the secondary rate of bromination: (a) with complex **1**; (b) with complex **2**. The reaction mixture contained phosphate buffer (0.05 M, pH 5.5), KBr (2 M) and phenol red (0.02 mM).

group in the peroxo bridged complexes that readily oxidizes bromide. It is evident that the degradation products of the compounds formed in solution are responsible for the slow secondary bromination reaction. The instant activity of 37–43% recorded, although small, substantiated the oxidant capacity of the original compounds in spite of their being highly unstable in solution.

Significantly, the monomeric diperoxovanadate compounds **3** and **4** were totally inactive in bromination under identical conditions. Under these conditions DPV (1 mM) was inactive on its own, however, in presence of vanadate showed the secondary rate but not the instant activity (Table 3).

3.3.2. Reaction with solutions of peroxovanadate compounds

Reactions conducted by addition of an aliquot of **1** or **2** from a freshly prepared solution, instead of the solid compound, to the standard reaction mixture gave a good rate of increase in A_{592}. The rate progressively decreased when equal aliquots were tested from this stock solution at 2–4 min intervals, followed by total loss of activity after about 2 h of making the solution. These experiments further confirmed that the vanadate products derived from the peroxo bridged complexes, responsible for the secondary slow bromination reaction, also undergo further inactivation.

These rapid inactivation processes constrained our studies on the kinetics of the reaction. Data collected by using a freshly prepared solution for each experiment indicated that increases in rates are nonlinear with increase in concentrations of complexes **1** or **2**. The rate showed a linear relationship when plotted against the square of the concentration of bromide indicating a second order dependence with respect to KBr (data not shown).

3.3.3. Effect of buffer

Omission of phosphate buffer from the reaction medium had no significant effect on the instant bromination activity of the complexes, although a small decrease of about 10% was observed in the secondary rate of bromination. This indicated that the presence of phosphate was not essential for such activity of dinuclear peroxovanadate complexes. This is in contrast to the requirement of phosphate with the vanadate–H_2O_2 system as bromide oxidant [41]. Vanadate is known to react with most of the compounds used in buffers including phosphate [42]. With respect to vanadates, Hepes is fairly inert and is the recommended buffer [42,43]. However, in the present study fast bromination activity was found to be suppressed when Hepes (pH 6.5) was used as the buffer indicating possible interaction between Hepes and the bimetallic peroxovanadate compounds. In investigations dealing with peroxovanadates, a near neutral phosphate buffer was found to be reasonably inert and its use proved to be satisfactory in several studies [18,19,43–45]. Instant bromination activity was realized with the compounds **1** and **2** in phosphate buffer at pH 7.0. The data in Table 3 were obtained at pH 5.5 in order to record the secondary activity.

3.3.4. Inhibition of bromination reaction

Inhibitor studies are valuable in giving clues on the involvement of reactive species. The effect of H_2O_2 and EDTA on the bromination reaction under standard assay conditions was tested. The initial fast bromination reaction was inhibited only to the extent of 5–10% with

Table 3
Bromination of phenol red with peroxovanadate complexes **1** and **2**

Compound	Conc.		Instant activity			Secondary rate (extrapolated to 1 mM compound) μM Br/min
	mg/ml	mM	ΔA_{592}	Bromine transfer		
				Total (μM)	μM/mM compound	
$[V_2O_2(O_2)_3(asn)_3]\cdot H_2O$	0.10	0.15	0.406	24.09	160.6	7.05
$[V_2O_2(O_2)_3(gln)_3]\cdot H_2O$	0.12	0.17	0.535	31.74	86.7	7.29

H_2O_2 (10 mM) and ca. 20% with EDTA (10 mM). After the initial jump in A_{592} the peak intensity remained unchanged with time in contrast to its slow increase in the absence of inhibitors, indicating complete inhibition of the secondary reaction. It is thus inferred that the peroxo bridged dimeric vanadate is probably the most proximate intermediate in bromide oxidation as it is only partly inhibited by H_2O_2 and EDTA which terminate the secondary bromination reaction carried out by degradation products of the dinuclear complex.

3.3.5. Substrate bromination in aqueous-organic media

The high bromination activity exhibited by the complexes in aqueous solution prompted us to explore the efficacy of complexes **1** and **2** in mediating bromination of organic substrates in the presence of inorganic bromide in aqueous-organic media. Reactions were carried out in the absence of buffer. Bromination of several activated aromatics into their corresponding bromo-organics were achieved in moderate yields in the presence of the dinuclear complex **1** or **2** (Table 4). Preferential bromination at either ortho or para positions of the aromatic ring leading to mono substitution indicate an electrophilic bromination mechanism. That the brominating species was 'Br^+' and not a Br· radical in these reactions was further evident from the ring substituted products obtained from the substrate, 2-methoxy toluene (Table 4). Bromination through radical reaction would have produced benzyl bromide instead of bromo-methoxy toluene [11]. Attempted bromination using complex **3** did not yield brominated products as anticipated.

4. Discussion

The reaction of vanadium with H_2O_2 is highly sensitive to pH and it is known that the number of peroxo groups per vanadium center increases with increasing pH of the reaction medium [25]. In the present study, it has been possible to isolate two types of peroxovanadates viz., molecular dimeric complexes $[V_2O_2(O_2)_3L_3]\cdot H_2O$ and anionic monomeric complexes $Na[VO(O_2)_2L]\cdot H_2O$, (L = asparagine or glutamine), by varying the pH of the reaction medium. The low pH apparently favoured the coordination of the amino acids in their zwitterionic form thereby stabilizing the $V_2O_2(O_2)_3$ moiety and leading to the synthesis of the desired molecular complexes **1** and **2**.

Bonding of more than one amino acid to the same metal center in different coordination modes as observed in the case of complexes **1** and **2** may appear unusual, however, it is not unprecedented [46]. Depending on the pH of the reaction solution and the nature of the metal, a tridentate amino acid of the glutamine and asparagine type provides several alternative coordination sites to the metal, viz., terminal amino and carboxylate groups as well as the amide groups of the side chain. Thus the chosen ligands can act as mono, bi or tridentate ligands with different combinations of donor atoms and can occur in complexes in either neutral zwitterionic form or the anionic form. In addition, they are known to form bridges between metal atoms leading to the formation of dinuclear or polynuclear structures [46]. Peroxovanadium compounds having a bridging peroxo moiety, bonded in a $\mu-\eta^1{:}\eta^1$ fashion, could so far be synthesized only in the presence of amino acids and peptides [17–20]. These ligands are likely to impart additional stability to the highly reactive 'VOOV' species by forming hydrogen bonds between their side chains.

The stabilization provided by the amino acid co-ligands to the μ-peroxovanadate moiety formed in solution, affording their isolation into solid state, would presumably be lost in aqueous solution resulting in the break up of the VOOV group with subsequent release of oxygen. The peroxo groups which are retained in the degradation products and are responsible for the further release of oxygen under the effect of catalase action, are the ones bonded in a side-on fashion as indicated by their ^{51}V NMR and electronic spectra. Since the diperoxovanadium complexes **3** and **4** contain side-on bound peroxo groups they appear to be relatively much more stable in solution and degrade steadily under the action of catalase releasing the amount of oxygen corresponding to two peroxo groups per molecule, consistent with their formulae.

The work of several groups on redox chemistry of vanadyl, vanadate and peroxovanadates are pertinent in explaining the reactions involved in the present study [21,47–50]. It has been known that oxidation of bromide by H_2O_2 to hypobromous acid, capable of transferring a bromine atom to an acceptor molecule, occurs at a pH < 3.0 but is ineffective in near neutral pH > 5.0. The reaction is catalyzed by vanadium compounds such as $VOSO_4$ [47] or V_2O_5 [12]. The most probable oxidants of bromide, monoperoxovanadate (MPV) and diperoxovanadate (DPV), are readily formed on adding excess H_2O_2 to vanadate solution [25,47,50], with DPV predominating at pH > 5.0. However, synthetic DPV or MPV, or compounds containing such moieties were catalytically incompetent in bromide oxidation at neutral pH [49]. A dimeric triperoxovanadate(V) intermediate presumed to be formed from a combination of MPV and DPV was then proposed to be the active oxidant [11]. However, this dimeric species was found only in highly acidic medium (pH < 5).

The observation that inactive DPV requires the presence of vanadyl or vanadate to gain oxidant activity at pH > 5, led to the proposal that the μ-peroxo bridged divanadate intermediate, $[OVOOV(O_2)]^{3+}$, formed by complexation between these two species is the proximate oxidant of bromide [41]. Support for such an interme-

Table 4
Bromination of aromatic substrates mediated by $[V_2O_2(O_2)_3(gln)_3]\cdot H_2O$

Substrates	Products		%Yield	
Aniline	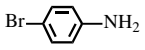 a	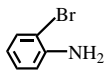 b	a: 35	b: 23
o-Nitroaniline	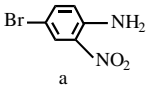 a	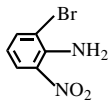 b	a: 50	b: 20
m-Nitroaniline	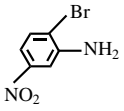 a	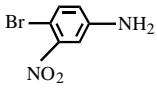 b	a: 40	b: 22
p-Nitroaniline	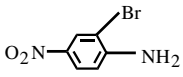		71	
o-Aminophenol	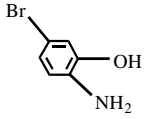		42	
m-Aminophenol	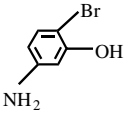 a	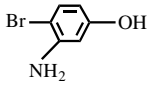 b	a: 39	b: 11
p-Aminophenol	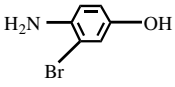		43	
Quinol	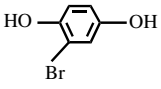		30	
o-Methoxytoluene	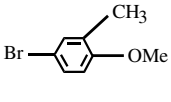 a	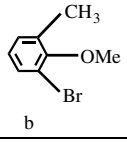 b	a: 40	b: 20

diate came from our investigations on a series of synthetic compounds with a VOOV bridge which were found to be active in oxidative bromination at physiological pH [18,19]. Results of the present study lend further support to this contention.

A scheme of reactions, shown in Fig. 5, is proposed which is based on our results and work of some other laboratories [21,41,47–50]. The μ-peroxo group of the 'VOOV' moiety appears to be amenable for reductive cleavage by bromide which produces a bromination competent intermediate, –BrOVO(O_2), that can transfer the bromine atom to the substrate AH (reaction a and b in Fig. 5). On its dissolution the compound dissociates into MPV and DPV species (Fig. 5 reaction c) as identified by ^{51}V NMR with subsequent loss of instant bromination activity. These observations and the marginal effects of H_2O_2 and EDTA, which considerably inhibit vanadate dependent bromination activity, lend support to our earlier proposal that 'VOOV'' is the active group and is the likely primary oxidant of bromide at near neutral pH. The secondary bromination activity results from the formation of DPV and vanadate formed as

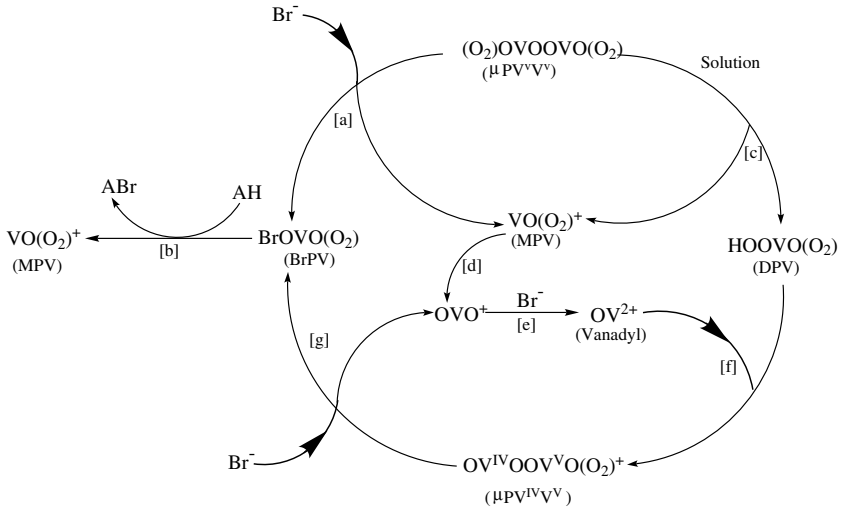

Fig. 5. Schematic representation of reactions occurring with peroxo bridged divanadate compounds: (a) formation of active bromine compound BrPV and MPV when solid is added to a bromide solution; (b) transfer of bromine to acceptor AH (phenol red); (c) dissociation of the dinuclear complex on dissolution in water into MPV and DPV (in absence of bromide) with concomitant loss of bromination activity; (d) reduction of MPV to vanadate; (e) reduction of vanadate to vanadyl by acid and bromide; (f) formation of μ-peroxo compound from DPV + vanadyl; (g) breakdown of μ-peroxo group and oxidation of bromide yielding BrPV. Amino acid ligands in the compounds are not shown. Valency state of reduced vanadium is shown as V^{IV} and all others are V^{V}. No attempt is made to show the exact stoichiometry of the reaction.

dissociation products of the dinuclear complex in solution (Fig. 5 reaction d). Dismutation of MPV generates vanadate which is then reduced to vanadyl by bromide (reaction d and e) as demonstrated experimentally in earlier work [41]. Vanadyl then complexes with DPV to form a μ-peroxovanadate dimer (reaction f) [48]. This complex can then oxidize bromide and produce a bromination competent intermediate that can be recycled till phenol red is completely consumed (reaction g). The striking feature of the essentiality of vanadyl V(IV) for converting DPV into an effective bromide oxidant was thus accommodated as V^{IV}–O–O–V^{V} in the reaction pathway in Fig. 5. Bromide is needed in two steps, in recycling vanadyl by reduction of vanadate and in interacting with the peroxo bridged intermediate, which explains the slow reaction being second order with respect to KBr concentration. Inhibition of the secondary reaction in the presence of excess H_2O_2 is evidently owing to the conversion of vanadate into DPV which is inactive in bromination. EDTA inhibits reaction g by complexing with V(V) and V(IV) centers of the μ-peroxovanadate intermediate as was demonstrated experimentally in earlier studies [51].

To summarize this investigation concerning the synthesis and some aspects of the chemistry of dinuclear and mononuclear peroxovanadate complexes, we would like to emphasize that the dimeric complexes with a μ-peroxovanadate moiety are distinctly different in nature, stability and reactivity from the monomeric anionic complexes possessing exclusively chelated bidentate peroxo groups. The heteroligand plays an important role in imparting stability to the VOOV group permitting its isolation in the solid state. Present experiments confirm the reactivity of the synthetic μ-peroxovanadate dimer in producing a bromination competent intermediate. The proposed reaction pathway confers the status of a selective bromide oxidant, at physiological pH, on the VOOV group. However, it is not completely clear as to why a peroxo bridged divanadate moiety is much more reactive in oxidative bromination than a peroxo group bonded to V(V) in a side-on fashion. Theoretical computations are expected to provide valuable insights into this aspect and such studies are being initiated. We are constrained in concluding that any of the above reactions are involved in the action of the enzymes in view of lack of direct evidence. However, since crystal structures of haloperoxidase proteins showed dimeric subunits with a vanadium per subunit [52], the possibility of the active site in the protein having a vanadium dimer cannot be ruled out.

Acknowledgements

Financial assistance from the Council of Scientific and Industrial Research, New Delhi, is gratefully acknowledged. We express our sincere gratitude to Prof. T. Ramasarma, Department of Biochemistry, Indian Institute of Science, Bangalore, for valuable discussion and for allowing us to use the oxygraph. We thank Aparna V.S. Rao (IISC) for performing the oxygen release measurements and Prof. K. Ramanathan of the Sophisticated Instrumental Facility (IISC) for the NMR spectra. We would like to thank Mr. Kalyan K. Haza-

rika of the Department of Molecular Biology and Biotechnology, Tezpur University for carrying out HPLC analyses.

References

[1] E. de Boer, Y. Van Kooyk, M.G.M. Tromp, R. Wever, Biochem. Biophys. Acta 869 (1986) 48.
[2] H. Vilter, D. Rehder, Inorg. Chim. Acta 136 (1987) L7.
[3] D. Rehder, Coord. Chem. Rev. 182 (1999) 297.
[4] L.C. Cantley, L. Josephson, R. Warner, M. Yanagisawa, C. Lechana, G. Guidotti, J. Biol. Chem. 252 (1977) 7421.
[5] K.H Thompson, J.H. McNeill, C. Orvig, Chem. Rev. 99 (1999) 2561.
[6] Y. Shechter, G. Eldberg, A. Shisheva, D. Gefel, N. Sekar, S. Qian, R. Bruck, E. Gershonov, D.C. Crans, Y. Goldwasser, M. Fridkin, J. Li, in: A.S. Tracey, D.C. Crans (Eds.), Vanadium Compounds. Chemistry, Biochemistry and Therapeutic Applications, Oxford University Press, New York, 1998, pp. 308–315.
[7] K.H Thompson, C. Orvig, J. Chem. Soc., Dalton Trans. (2000) 2885.
[8] A. Butler, M.J. Clague, G.E. Meister, Chem. Rev. 94 (1994) 625.
[9] D. Rehder, M. Bashirpoor, S. Jantzen, H. Schmidt, M. Farahbakhsh, H. Nekola, in: A.S. Tracey, D.C. Crans (Eds.), Vanadium Compounds. Chemistry, Biochemistry and Therapeutic Applications, Oxford University Press, New York, 1998, pp. 60–70.
[10] A. Butler, Coord. Chem. Rev. 187 (1999) 17.
[11] M.J. Clague, A. Butler, J. Am. Chem. Soc. 117 (1995) 3475.
[12] M. Bhattacharjee, Polyhedron (1992) 2817.
[13] G.J. Colpas, B.J. Hamstra, J.W. Kampf, V.L. Pecoraro, J. Am. Chem. Soc. 118 (1996) 3469.
[14] V. Conte, O. Bortolini, M. Carraro, S. Moro, J. Inorg. Biochem. 80 (2000) 41.
[15] P. Schwendt, D. Joniakova, Thermochim. Acta 68 (1983) 297.
[16] P. Schwendt, D. Gyepesova, Acta Cryst. C 46 (1990) 1753.
[17] M. Bhattacharjee, M.K. Chaudhuri, N.S. Islam, P.C. Paul, Inorg. Chim. Acta 169 (1990) 97.
[18] S. Sarmah, N.S. Islam, J. Chem. Res. (S) (2001) 172.
[19] S. Sarmah, P. Hazarika, N.S. Islam, A.V.S. Rao, T. Ramasarma, Mol. Cell. Biochem. 236 (2002) 95.
[20] M.K. Chaudhuri, P.C. Paul, Ind. J. Chem. A 31 (1992) 466.
[21] H.N. Ravishankar, M.K. Chaudhuri, T. Ramasarma, Inorg. Chem. 33 (1994) 3788.
[22] H.N. Ravishankar, T. Ramasarma, Arch. Biochem. Biophys. 316 (1995) 319.
[23] M.K. Chaudhuri, S.K. Ghosh, N.S. Islam, Inorg. Chem. 24 (1985) 2706.
[24] E. de Boer, H. Plat, M.G.M. Tromp, R. Wever, M.C.R. Franssen, H.C. van der Plas, H.C. Meijer, H.E. Schoemaker, Biotech. Bioeng. 30 (1987) 607.
[25] J.A. Connor, E.A.V. Ebsworth, Adv. Inorg. Chem. Radiochem. 6 (1964) 292.
[26] A.B.P. Lever, H.B. Gray, Acc. Chem. Res. 11 (1978) 348.
[27] N.J. Campbell, A.C. Dengel, W.P. Griffith, Polyhedron 8 (1989) 1379.
[28] G.V. Jere, G.D. Gupta, J. Inorg. Nucl. Chem. 32 (1970) 537.
[29] K. Nakamoto, Infrared and Raman Spectra of Inorganic and Coordination Compounds, 4th ed., J. Wiley and Sons, New York, 1986, p. 298.
[30] K. Nakamoto, Infrared and Raman Spectra of Inorganic and Coordination Compounds. Part B, 5th ed., J. Wiley and Sons, New York, 1997, p. 71.
[31] R.A. Meyers (Ed.), Encyclopedia of Analytical Chemistry, vol. 2, Wiley, New York, 2000, pp. 546–559.
[32] H.N. Ravishankar, A.V.S. Rao, T. Ramasarma, Arch. Biochem. Biophys. 321 (1995) 477.
[33] A.S. Tracey, J.S. Jaswal, J. Am. Chem. Soc. 114 (1992) 3835.
[34] J.S. Jaswal, A.S. Tracey, J. Am. Chem. Soc. 115 (1993) 5600.
[35] J. Costa Pessoa, S.M. Luz, R.D. Gillard, J. Chem. Soc., Dalton Trans. (1997) 569.
[36] D.C. Crans, P.M. Ehde, P.K. Shin, L. Pettersson, J. Am. Chem. Soc. 113 (1991) 3728.
[37] F.W.B. Einstein, R.J. Batchelar, S.J. Angus-Dunne, A.S. Tracey, Inorg. Chem. 35 (1996) 1680.
[38] D. Rehder, H. Holst, W. Priebsch, H. Vilter, J. Inorg. Biochem. 41 (1991) 171.
[39] O.W Howarth, J.R. Hunt, J. Chem. Soc., Dalton Trans. (1979) 1388.
[40] V. Conte, F. Di Furia, S. Moro, J. Mol. Catal. A 120 (1997) 93.
[41] A.V.S. Rao, H.N. Ravishankar, T. Ramasarma, Arch. Biochem. Biophys. 334 (1996) 121.
[42] D.C. Crans, Comments Inorg. Chem. 16 (1994) 1.
[43] A. Shaver, J.B. Ng, D.A. Hall, B.I. Posner, Mol. Cell. Biochem. 153 (1995) 5.
[44] R.M. Totaro, P.A.M. Williams, M.C. Apella, M.A. Blesa, E.J. Baran, J. Chem. Soc., Dalton Trans. (2000) 4403.
[45] A.V.S. Rao, N.S. Islam, T. Ramasarma, Arch. Biochem. Biophys. 342 (1997) 289.
[46] S.T. Chow, C.A. McAuliffe, in: S. Lippared (Ed.), Progress in Inorganic Chemistry, vol. 19, Wiley Interscience, New York, 1975, pp. 15–104.
[47] H. Sakurai, K. Tsuchiya, FEBS Lett. 260 (1990) 109.
[48] H. Brooks, F. Sicilio, Inorg. Chem. 10 (1971) 2530.
[49] M. Bhattacharjee, S. Ganguly, J. Mukherjee, J. Chem. Res. (S) (1995) 80.
[50] J.S. Jaswal, A.S. Tracey, Inorg. Chem. 30 (1991) 3718.
[51] S. Sarmah, P. Hazarika, N.S. Islam, Polyhedron 21 (2002) 389.
[52] M.N. Isupov, A.R. Dalby, A.A. Brindley, Y. Izumi, T. Tanabe, G.N. Murshudov, J.A. Littlechild, J. Mol. Biol. 299 (2000) 1035.

Available online at www.sciencedirect.com
SCIENCE DIRECT®
Polyhedron 23 (2004) 1109–1113
POLYHEDRON
www.elsevier.com/locate/poly

Structural characterization and luminescence properties of an isonicotinic acid N-oxide Mn(II) complex

N. Can [a,*], S.E. Sözerli Can [b], A. Ataç [a], F. Bardak [a]

[a] Department of Physics, Faculty of Arts and Sciences, Celal Bayar University 45030 Manisa, Turkey
[b] Department of Chemistry, Faculty of Arts and Sciences, Celal Bayar University 45030 Manisa, Turkey

Received 20 November 2003; accepted 11 December 2003

Abstract

An isonicotinic acid N-oxide Mn(II) compound was synthesized and characterized on the basis of elemental analysis and X-ray crystallography. In the complex, Mn(II) ions are coordinated by six water molecules, and the coordination number of the Mn(II) ion is six. FTIR spectra of the compound free isonicotinic acid N-oxide (INO) have been recorded in the range 4000–400 cm^{-1}. Cathodoluminescence (CL) spectra from the Mn(II) complex have been recorded. The luminescence data were interpreted in terms of the emission band at 480 nm. The green luminescence (~480 nm) arises from the Mn^{2+} transition $^4T_1$ (^4G) → $^6A_1$ (^6S). It shows weak vibronic structure, short lifetimes less than 250 μs, and indicates that Mn^{2+} is octahedrally coordinated, occupying sites with similar distortions. The lifetime and intensity of the signal is temperature dependent, and the parameters are reported for the 480 nm emission line.
© 2004 Elsevier Ltd. All rights reserved.

Keywords: Mn(II) complex; Isonicotinic acid; N-oxide; Crystal structure; Luminescence

1. Introduction

Lanthanide complexes of three isomers of pyridine carboxylic acid, namely nicotinic acid, isonicotinic acid and picolinic acid, have been extensively investigated [1–3]. Pyridine carboxylic acid N-oxides have an oxygen atom in place of the nitrogen donor site, but studies on ligand behavior toward lanthanides are limited, as so far only one dimeric lanthanium complex of 6-methylpicolinic acid N-oxide (6-mepicno) has been structurally examined [4,5]. N-oxide functionalization of nicotinic acid and isonicotinic acid should increase the flexibility of the resulting ligands in addition to enhancement of their capacities for coordination and or hydrogen bonding. Therefore their lanthanide complexes are expected to exhibit different characteristics as compared with the corresponding lanthanide nicotinates and isonicotinates. So far, only the molecular structure of monomeric $Mn[(SPPh_2)_2N]_2$ [6,7] and $Mn[(OPPh_2)_2N]_3$ [8], which exhibit tetrahedral MnS_4 and octahedral MnO_6, respectively, have been reported. By contrast, the Mn(II) acetylacetonate derivative is a trimer, with all manganese atoms exhibiting octahedral MnO_6 cores as a result of the bimetallic triconnective coordination of the ligands [9]. Recently the synthesis of $Mn[(XPR_2)(YPR'_2)N]_2$ (X, Y = 0, S; R, R′ = Me, Ph) complexes and the X-ray structure of monomeric $Mn[(OPPh_2)(SPPh_2)N]_2$ have been reported [10]. We wish to report here the molecular structure of a manganese (II) complex of INO and its luminescence properties. It has been known for many decades that some organic and inorganic materials emit light when bombarded by electrons (cathodoluminescence, CL), and that the nature of that emission in the complex could contain significant information. CL is a very sensitive technique to probe the surface state and changes in the crystal field resulting, for example, from pressure changes. The excitation density in this case is very high compared to X-ray irradiation, which enhances the light output. CL is an attractive option since, by varying the electron energy, it is possible to probe to successively deeper depths below the surface. The spectral

* Corresponding author. Tel.: +90-236-241-21-56; fax: +90-236-241-21-58.
E-mail address: nurdogan.can@bayar.edu.tr (N. Can).

0277-5387/$ - see front matter © 2004 Elsevier Ltd. All rights reserved.
doi:10.1016/j.poly.2003.12.022

information aids identification of different types of defect but it is not an accurate quantitative route since the luminescence efficiency is strongly modified by the presence of defects, dislocations and surface states. Normally the emitted light level increases with higher incident energy, in part because there is luminescence quenching from the damage surface (i.e. dislocations) on the signal. CL is not a passive surface probe and it must be borne in mind that repeated measurements with energetic electron beams may contribute to surface modifications which range from the familiar degradation of halides, to relaxations giving improved crystallinity of $LiNbO_3$.

In order to understand the limitations and/or problems of the surface it is necessary to find surface sensitive techniques to assess the quality of some inorganic materials. These should be non-destructive, so methods such as transmission electron microscopy (TEM) are of minimal value in routine assessment. Whilst scanning electron microscopy (SEM) or atomic force microscopy (AFM) offer views of the outer surface and can include compositional data, they are of limited use for characterization of this kind of material. More appropriate measurements are optical absorption and luminescence. Note absorption and luminescence offer wavelength discrimination between different defect types. Numerous examples have been summarized for simple inorganic materials in a recent review [11] with particularly clear examples being seen for ammonium bromide, strontium titanate and potassium niobate. The approach has been effective not only for the simple inorganic materials but also for fullerenes and even superconductors. However, it has not been attempted previously with inorganic materials comprising of large molecular units. As far as we are concerned, there is no previous literature about luminescence of Mn(II) complexes. Therefore we believe that this is the first such work using luminescence.

2. Experimental

2.1. Synthesis

All chemicals were reagent grade (Aldrich) and were used without further purification. One millimole (0.35 g) $MnBr_2 \cdot 4H_2O$ was dissolved in absolute hot ethanol (10 ml). Two millimole (0.28 g) isonicotinic acid N-oxide was dissolved in hot ethanol and added to the solution. Workup as described above, single crystals were formed at the interface and also at the bottom of the solution at 2 °C.

2.2. Elemental analysis

The prepared complex was analyzed for C, H, N using a CHN (LECO, CHN-600) with the following results (found (%)/calculated (%));$[Mn(H_2O)_6]$ $[O–C_6H_4NO_2]_2$ C = 32.76/32.80, H = 4.53/4.58, N = 6.40/6.37.

2.3. Crystal structure determination

Data were collected at 173(2) K on an Enraf-Nonius CAD4 diffractometer at Sussex University using monochromated Mo Kα radiation (0.17073 Å) and corrected for Lorenz and polarization effects. The structures were determined by direct methods, with SHELXL 97 programs used for structure solution and refinement on F^2 using all reflections. In the ORTEP-3 plots the thermal ellipsoids are shown at the 50% probability level. All hydrogen atoms were located on a difference map and were refined.

2.4. Physical measurements

The IR spectra (KBr discs) of the free ligand and the compound $[Mn(H_2O)_6][O–C_6H_4NO_2]_2$ were recorded on a Mattson 1000 FTIR spectrometer in the range 4000–400 cm^{-1}, which was calibrated using polystyrene bands. The vibrational wavenumbers and proposed assignments of INO and Mn(INO) complex are discussed in Section 3.

CL time resolved spectroscopy was performed on an apparatus designed and built at the University of Sussex [12]. The acceleration potential was 10 kV and the current was 20 nA, corresponding to an incident power density of 0.8 mW cm^{-2}. The primary electron beam was pulsed using a Thandor TG501 5 MHz function generator as a sine function with a frequency of 90 Hz, except for the lifetime measurement. The CL response was gated using an EgandG Ortholoc-SC 9505 two-phase lock-in amplifier. Spectra were measured in the temperature range 40–300 K using an $f/4$ scanning monochromator and a cooled red-sensitive photomultiplier tube.

3. Results and discussion

The molecular geometry of INO and the Mn(II) compound was shown by an X-ray diffraction study to have the structure depicted in Fig. 1 (with the geometrical data shown in Table 2). If we assume the amido group (–COOH) has a single mass point all the molecules under consideration would belong the C_{2v} point group. This simplified model leads to 30 normal vibrations of which 21 are planar and nine are non-planar. In addition to these 30-ring vibrations there would be six vibrations due to the substituent carboxyl group. These vibrations cannot be classified as to their symmetry, with respect to the molecular plane as the carboxyl group makes the molecule non-planar.

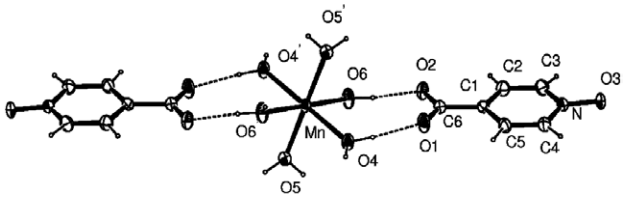

Fig. 1. Molecular structure of $[Mn(H_2O)_6][O–C_6H_4NO_2]_2$.

Information concerning crystallographic data and structure refinement of the Mn(II) complex is summarized in Table 1. Selected bond lengths and angles are presented Table 2.

The luminescence data were quite limited, but there have been room temperature structural characterizations of related rare earth complexes with nicotinic and isonicotinic acid N-oxides [13] that included data for erbium and europium site distortions from the changes of the photoluminescence and absorption of the rare-earth line spectra. Immediate initial effects of the isonicotinic acid N-oxide Mn(II) compound are seen in Fig. 2 for CL measurements. At a modulation frequency of just 9 Hz (i.e. effectively continuous ~ dc excitation) the main signal peaks near 480 nm in both cases, but there are poorly resolved additional features in the tails of the central region. The green luminescence of about 480–520 nm is generally attributed to the transition $^4T_1(^4G) \rightarrow {}^6A_1\ (^6S)$ between the lowest energy levels of Mn^{2+} in an octahedral coordination. Such a luminescence peak appears even at concentrations as low as 10 ppm [14]. It cannot be excluded, however, that some Mn^{2+} ions occupy very large (dodecahedral) sites which can also produce a small ligand field splitting Dq and green luminescence [15,16]. The remarkable similarity of the position and the shape of the Mn^{2+} green emission band (Fig. 2) strongly suggests that Mn^{2+} is octahedrally coordinated and occupies sites with similar ion–ligand interactions. At 40 K the position of the green luminescence peak in the sample remains practically the same. The independence of the band position on temperature might indicate that Mn^{2+} occupies sites with rigid Mn–O bonds which practically do not change with temperature.

The computer system used in the CL analysis records only the magnitude of the emission and not the sign and, therefore, the data are always a positive number. For cosine dependence, the data are always a positive number. For cosine dependence, data extend from positive to negative values, and hence we have converted sections of the data to negative values where they pass through zero. ϕ_c is related to the decay lifetime (τ) of the emission and frequency of the pulsed primary beam (f) for isolated luminescence bands by the expression $\tan\phi_c = 2\pi f\tau$. Unfortunately in the present CL system the maximum chopping frequency is only 100 kHz and this is slow compared with the luminescence lifetimes being considered. Nevertheless, attempts to estimate the

Table 1
Crystal data and structure refinement for $[Mn(H_2O)_6][O–C_6H_4NO_2]_2$

Empirical formula	$C_{12}H_{20}MnN_2O_{12}$
Formula weight	439.24
Temperature (K)	173(2)
Wavelength (Å)	0.71073
Crystal system	triclinic
Space group	$P\bar{1}$ (No.2)
Unit cell dimensions	
a (Å)	7.5380(3)
b (Å)	7.6939(3)
c (Å)	7.9118(4)
α (°)	100.276(2)
β (°)	102.091(2)
γ (°)	92.371(2)
Volume (Å^3)	440.00(3)
Z	1
Density, calculated (Mg/m^3)	1.66
Absorption coefficient (mm^{-1})	0.82
$F(0\,0\,0)$	227
Crystal size (mm)	$0.10 \times 0.05 \times 0.02$
θ range for data collection (°)	4.03–24.77
Index ranges	$-8 \leqslant h \leqslant 8$, $-8 \leqslant k \leqslant 9$, $-9 \leqslant l \leqslant 8$
Reflections collected	4655
Independent reflections	1491 [$R_{int} = 0.031$]
Reflections with $I > 2\sigma(I)$	1401
Completeness to $\theta = 24.77°$	99.0%
Refinement method	full-matrix least-squares on F^2
Data/restraints/parameters	1491/0/164
Goodness-of-fit on F^2	0.756
Final R indices [$I > 2\sigma(I)$]	$R_1 = 0.028$, $wR_2 = 0.078$
R indices (all data)	$R_1 = 0.031$, $wR_2 = 0.081$
Largest difference peak and hole (e Å^{-3})	0.25 and −0.24

Table 2
Selected bond lengths [Å] and angles [°]

Bond lengths	
Mn–O(6)	2.1309(16)
Mn–O(4)	2.1805(16)
Mn–O(5)	2.1844(16)
O(1)–C(6)	1.250(3)
O(2)–C(6)	1.259(3)
C(1)–C(6)	1.512(3)
Bond angles	
O(6)′–Mn–O(6)	180
O(6)′–Mn–O(4)	93.56(7)
O(6)–Mn–O(4)	86.44(7)
O(4)–Mn–O(4)′	180
O(6)′–Mn–O(5)	91.04(7)
O(6)–Mn–O(5)	88.96(7)
O(4)–Mn–O(5)	90.94(6)
O(4)′–Mn–O(5)	89.06(6)
O(5)′–Mn–O(5)	180
C(5)–C(1)–C(6)	120.86(19)
C(2)–C(1)–C(6)	121.42(19)
O(1)–C(6)–O(2)	125.2(2)
O(1)–C(6)–C(1)	117.79(19)
O(2)–C(6)–C(1)	116.96(19)

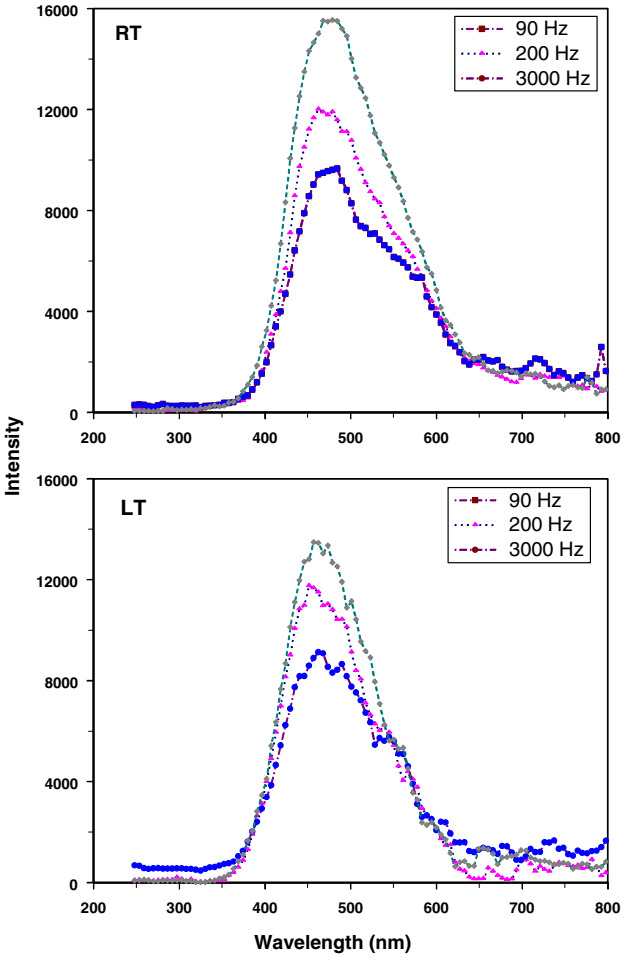

Fig. 2. Room and low temperature CL spectra of the Mn(II) complex obtained using a lock-in amplifier. The spectra are corrected for the efficiency variations of the optical system. The electron energy used was 10 kV.

lifetime of the 480 nm emission gives a value near 215 μs at room temperature (RT), and near 235 μs at 40 K.

In this study time resolved luminescence spectra of the Mn complex have been measured. The following features can be deducted from the cathodoluminescence emission spectra. One type of emission spectra is observed and the decay of the green luminescence is non-exponential. Analysis of the luminescence spectra shows that Mn^{2+} occupies a similar and well defined octahedral site. The Mn^{2+}–water interactions are weak and affect the lifetime of the green band.

Isonicotinic acid N-oxides give two donor sites (a) carboxyl group and (b) pyridine N-oxides (N=O). In this kind of ligand the bonding may take place through the carboxyl oxygen or N=O.

The vibrational assignments for isonicotinamide and nicotinamide were made and structural characterization and spectroscopic features of their metal halogen compounds were investigated in previous works [17–20]. Also the vibrational assignments of isonicotinic acid for a few bands were made experimentally [21] and theoretically [22]. In this paper the vibrational wavenumbers and proposed assignments of INO for a few bands were made by comparing the results.

Significant absorption bands in the infrared spectrum of INO are observed at 3550(m), 1656(m) and 1606(m) cm^{-1}. They are assigned to ν(OH), ν(CO) and ν(RN=O). The absorption band in the infrared spectrum of $[Mn(H_2O)_6] \cdot [O - C_6H_4NO_2]_2$ at 1656 cm^{-1}, due to the carboxyl group (ν(CO)), is observed at 1639 cm^{-1}. Significant negative shift of the carboxyl group takes place because of the coordination through the carboxyl oxygen. This situation indicates that coordination of INO take place via the carboxyl oxygen to the metal ion (Mn).

4. Supplementary material

Crystallographic data for the structural analyses have been deposited with the Cambridge Crystallographic Data Centre, CCDC no 222424. Copies of this information may be obtained free of charge from The Director, CCDC, 12 Union Road, Cambridge CB2 1EZ, UK (Fax. +44-1223-336033; e-mail: deposit@ccdc.cam.ac.uk or www.http://ccdc.cam.ac.uk).

Acknowledgements

We would like to thank Prof. P.D. Townsend for giving kind permission to use his equipment in Sussex. Crystal structure determination was carried out at the Department of Chemistry, University of Sussex. The assistance of Peter B. Hitchcock is gratefully acknowledged.

References

[1] P. Starynowicz, Acta Crystallogr. C 47 (1991) 294.
[2] J.-F. Ma, Z.-S. Jin, J.-Z. Ni, Polyhedron 14 (1995) 563.
[3] J.-F. Ma, Z.-S. Jin, J.-Z. Ni, Polyhedron 15 (1996) 1797.
[4] G.F. De Sa, F.R.G. eSilva, O.L. Malta, J. Alloys Compd. 207 (1994) 457.
[5] L. Yan, J.-M. Liu, X. Wang, R.-D. Yang, F.-L. Song, Polyhedron 14 (1995) 3545.
[6] O. Siman, M. Wrighton, H.B. Gray, J. Coord. Chem. 2 (1972) 159.
[7] O. Siman, H.B. Gray, Inorg. Chem. 13 (1974) 1185.
[8] N. Zuniga-Villareal, M. Reyes Lezama, S. Hernandez-Ortega, C. Silvestru, Polyhedron 17 (1998) 2679.
[9] S. Shibata, S. Onuma, H. Inoue, Inorg. Chem. 24 (1985) 1723.
[10] I. Szekely, C. Silvestru, J.E. Drake, G. Balazs, S.I. Farcas, I. Haiduc, Inorg. Chim. Acta 299 (2000) 247.
[11] P.D. Townsend, M. Maghrabi, B. Yang, Nucl. Instrum. Meth. B 191 (2002) 767.
[12] P.D. Townsend, A. Rowlands, Cathodoluminescence in Geosciences, Springer, Berlin, 2000, pp. 41–57.

[13] J-G. Mao, H-J. Zhang, J-Z. Ni, S-B. Wang, T.C.W. Mak, Polyhedron 17 (1998) 3999.
[14] B. Andrianasolo, B. Champagnon, E. Duvad, Phys. Chem. Glasses 30 (1989) 215.
[15] D.S. McClure, J. Chem. Phys. 36 (1962) 2757.
[16] M.A. Noginov, G.B. Loutts, M. Warren, J. Opt. Soc. Am. (B) 16 (1999) 475.
[17] E. Şahin, S. İde, A. Ataç, Ş Yurdakul, J. Mol. Struct. 616 (2002) 253.
[18] S. Yurdakul, A. Ataç, E. Şahin, S. İde, Vibrat. Spectrosc. 31 (2003) 41.
[19] S. Bayarı, A. Ataç, S. Yurdakul, J. Mol. Struct. 655 (2003) 163.
[20] S. İde, A. Ataç, Ş Yurdakul, J. Mol. Struct. 605 (2002) 103.
[21] M.S. Afifi, A. Shabana, Analysis 10 (1982) 239.
[22] P. Koczon, J.Cz. Dobrowolski, W. Lewandowski, A.P. Mazurek, J. Mol. Struct. 655 (2003) 89.

Available online at www.sciencedirect.com
SCIENCE DIRECT®
Polyhedron 23 (2004) 1115–1123
POLYHEDRON
www.elsevier.com/locate/poly

Synthesis and characterization of $[Cu_2(L)_2(OCOCH_3)(OCH_3)]ClO_4$ {L = 2-[(4-methyl-pyridin-2-ylimino)-methyl]-phenol}: EPR and X-ray studies

R. Srinivasan [a], I. Sougandi [a], K. Velavan [a], R. Venkatesan [a], Babu Verghese [b], P. Sambasiva Rao [a,*]

[a] *Department of Chemistry, Pondicherry University, R.V. Nagar, Kalapet, Pondicherry 605 014, India*
[b] *RSIC, Indian Institute of Technology, Chennai 600 036, India*

Received 22 July 2003; accepted 6 January 2004

Abstract

A dicopper complex of a Schiff's base, 2-[(4-methyl-pyridin-2-ylimino)-methyl]-phenol, with a bridging acetato ligand has been synthesized and characterized by single crystal XRD, EPR, magnetic susceptibility, IR, UV–Vis, CV and elemental analysis. The X-ray analysis indicates that the system belongs to the triclinic space group $P\bar{1}$. One of the copper atoms in the binuclear complex adopts a square-pyramidal geometry consisting of the tridentate *N*-salicylidimine dianions, the neutral monodentate pyridine ligand in the basal plane and the solvent molecule in the apical position, while the other copper assumes a square-planar geometry. A seven line pattern observed at half-field in the frozen solution EPR spectrum confirms the interaction between the two copper ions. The cyclic voltametric studies point to a two-step electron transfer indicating the reduction of the two copper ions to copper(I), i.e., Cu(II)Cu(II) ↔ Cu(II)Cu(I) ↔ Cu(I)Cu(I). The molar conductance for the complex measured in methanol solvent indicates that the complex is a 1:1 electrolyte.
© 2004 Elsevier Ltd. All rights reserved.

Keywords: Binuclear copper complex; EPR; Half-field; Superhyperfine; X-ray; Electrochemical

1. Introduction

Polynuclear complexes with redox-active transition metal centers play an important role in biological processes because of facilitated electron transfer in redox reactions. Copper(II) complexes of tridentate Schiff base type, especially with dimeric units, are therefore suitable as bioinorganic model compounds. Numerous EPR spectroscopic studies, along with a few structural results of copper(II) complexes with tridentate Schiff base anions of the *N*-salicylideneamino acetate type have shown a variety of coordination geometries and cooperative ordering effects [1–4], which depend on Lewis basicity and the stereochemical properties of additional bidentate donor ligands. These ligands are essential for saturating the copper(II) coordination sphere of the tridentate Schiff base copper fragments. Also, the local distortion of the coordination polyhedra around the copper ion may vary from elongated square-pyramid to square-planar. However, in every case, it has been modified by an orthorhombic component, observable by spectroscopic means, such as EPR. The arrangement of the ligand molecules (monomer or dimer) in the crystal structure can be classified into three groups: the molecules appear as monomers [5]; can form phenoxy O-bridged dimeric units [6]; or may be connected to polymeric chains via an apically bound carboxylate oxygen atom of the respective neighbouring molecule [2,7]. In order to understand the nature of copper atoms in the complexes to see their viability as model compounds, a series of complexes have been prepared in our laboratory having dicopper with various bridging moieties [8–15]. The results are interesting, but the

* Corresponding author. Tel.: +914132255485; fax: +914132665991.
E-mail address: psr52in@yahoo.co.in (P. Sambasiva Rao).

0277-5387/$ - see front matter © 2004 Elsevier Ltd. All rights reserved.
doi:10.1016/j.poly.2004.01.016

interaction has not been confirmed by X-ray studies due to the failure of obtaining good single crystals. Hence, the present study has been undertaken, where we were able to obtain a good single crystal suitable for X-ray study. The results obtained with other techniques are also reported in this communication.

2. Experimental

2.1. Preparation of the ligand

The selected Schiff's base ligand [16] was synthesized by direct mixing of a 1:1 molar ratio of 4-methyl-2-aminopyridine (2.12 g) with salicylaldehyde (4 ml) under reflux for about 6 h in double distilled dry ethanol. Slow evaporation resulted in the formation of yellow diamond crystals. The ligand has been characterized by elemental analysis, IR, UV–Vis, NMR and mass techniques. The ligand, 2-[(4-methyl-pyridin-2-ylimino)-methyl]-phenol, is abbreviated as Hsalamp.

2.2. Preparation of the complex

To a methanolic solution of the ligand Hsalamp (2.12 g, 0.01 mol), a methanolic solution of copper acetate (0.998 g, 0.005 mol) was added, and the color of the solution changed from yellow to green. Further addition of a methanolic solution of lithium perchlorate (0.80 g 0.005 mol) turned the solution to dark green. The whole solution was then kept under reflux for 8 h at around 330 K. Slow evaporation of this solution resulted in the formation of a green colored powder, which when dissolved in methanol for crystallization by slow evaporation resulted in the formation of small crystals of shiny green color suitable for X-ray study. Fig. 1 gives the systematic procedure for the preparation of the copper complex, the structure of which has been confirmed by X-ray and EPR studies (vide infra). The analytical data for the complex is: molecular formula $Cu_2C_{29}H_{29}N_4O_9Cl$ Calculated (Found): %C = 47.0(44.6), %H = 3.9(3.6), %N = 7.5(6.8), %Cu = 17.2(17.0). The molar conductance for the complex measured in methanol solvent is $126\Lambda_m$ ($S\,cm^2\,mol^{-1}$), indicating that the complex is ionic and univalent in type.

2.3. Instrumentation

Infrared spectra were recorded on a Perkin–Elmer IR 598 spectrophotometer on KBr disks in the range of 4000–250 cm^{-1}. ^1H NMR (400 MHz) spectra were recorded using a model JEOL FX-400 FT NMR spectrometer in $CDCl_3$ solution using TMS as the internal

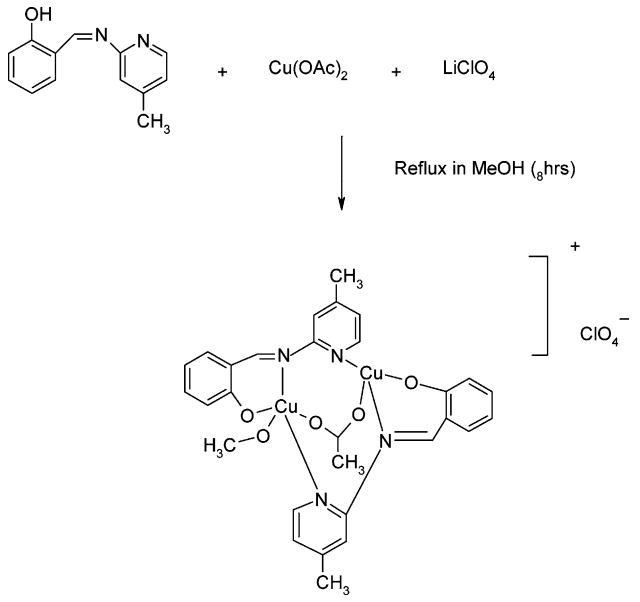

Fig. 1. Schematic representation of the preparation of the dimeric copper complex, $[Cu_2(Hsalamp)_2(OCOCH_3)(OCH_3)]ClO_4$.

standard. Elemental (C, H, N) analysis was performed with a Heraus rapid analyzer. Cu was estimated by AAS using a model 2380 Perkin–Elmer spectrophotometer. Electron impact (EI) mass spectra were recorded on a JEOL D-300 mass spectrometer. Fast atom bombardment (FAB) mass spectra were recorded on a JEOL SX 102/DA-6000 mass spectrometer using Ar/Xe (6 kV, 10 mA) as the FAB gas and m-nitrobenzyl alcohol as the matrix (NBA). Electronic spectral studies were conducted on an Ocean Optics SD1000 miniature fiber optics spectrometer using a 1 cm quartz cuvette in the wavelength range of 200–800 nm. Molar conductance (Λ_m) values were measured using a control dynamics conductivity meter in DMF solvent. The electro chemical measurements were performed at room temperature in DMF under O_2 free conditions using an Autolab PGSTAT 12 controlled by general purpose electrochemical system software (GPES). A three-electrode assembly comprising a Pt disc-working electrode, a Pt rod auxiliary electrode and a saturated calomel reference electrode (SCE) was used. The supporting electrolyte was tetra-*n*-butylammonium perchlorate (TBAP) 0.1 M, and all solutions were about 10^{-3} M in concentration. Magnetic susceptibility data of the powdered samples were measured in the 80–300 K range using a Princeton Applied Research Model 155 VSM instrument operating at 5000 G magnetic field. The instrument had been calibrated using metallic Ni. Diamagnetic corrections were evaluated by using Pascal's constants. ESR spectra were recorded with a JEOL TES 100 ESR spectrometer. Low temperature measurements were made at a liquid nitrogen temperature (77 K) using an insertion type Dewar.

3. Results and discussion

3.1. X-ray crystal structure of the complex

Crystals of suitable dimensions were selected for X-ray analysis. The intensity data were collected at room temperature using a Siemens SMART CCD area detector three-circle diffractometer [17] equipped with graphite monochromated Mo Kα ($\lambda = 0.71073$ Å) radiation. The data collection nominally covered over a full hemisphere of reciprocal space by a combination of three sets of exposures; each set had a different ϕ angle in the crystal and each exposure covered 0.3° in ω. The crystal-to-detector distance was 5.89 cm. Coverage of the unique set was over 86% complete to at least 25.6° in θ. The substantial redundancy in data allowed empirical absorption corrections [18] to be applied using multiple measurements of equivalent reflections. Depending on the intensity of the data, data frames were collected for 10–30 s/frames, giving an overall time for data collection of 7–18 h. The data frames were integrated using SAINT [19] and were merged to give a unique data set.

The structure was solved by automated Patterson methods and subsequent difference Fourier techniques using DIRDIF-98 [20] and was refined on F^2 using full-matrix least squares techniques using SHELXL-97 [21]. All hydrogen atoms were included at calculated positions using a riding model. The U_{iso} of H atoms of CH and CH_2 groups and the methyl group were taken as $1.2U_{eq}$ and $1.5U_{eq}$ of their carrier atoms, except for the water hydrogen atoms, which could not be identified. All non-hydrogen atoms were refined with anisotropic thermal parameters. The final R value was 0.064 for 4679 observed reflections with $I > 2\sigma(I)$ and 0.113 for all data (7401). The residual electron density of 0.84 e/Å^3 and the deepest hole of −0.66 e/Å^3 was close to the O8 and O6 atoms of the perchlorate solvent molecule. Anomalous dispersion effects for all atoms were included in the final calculation. The atomic scattering factor values were taken from the International Tables for X-ray Crystallography (1974). The crystal data, intensity data collection details and refinement parameters are summarized in Table 1. Fig. 2 shows the ZORTEP plot [22] of the molecule with the numbering scheme (thermal ellipsoids are drawn at the 50% probability level). Bond geometry calculations were performed using the software CIFTAB [25] and PARST [23]. Selected bond angles and bond distances are given in Table 2.

The copper ions in the complex take up two different coordination environments. Cu1 adopts a (4 + 1) square-pyramidal geometry defined by the bidentate *N*-salicylidimine dianions and the neutral monodentate pyridine ligand in the basal plane. The apical position is occupied by a solvent methanol molecule at a distance of 2.337(4) Å. In the polymeric structure of (3,5-dimethylpyridine)(*N*-salicylidimine copper(II)) [24], the apical distance is 2.386(2) Å. Both the copper ions are connected by an acetate bridge. The Cu–$O_{(acetate)}$ distances 1.965(4) and 1.957(4) Å are in agreement with those found in the related Cu(II) complex [25]. The Cu1 atom lies above the plane O1N2N4O3 by 0.133(1) Å and is displaced towards atom O5. The Cu–O [Cu1–O1 1.906(3) and Cu1–O3 1.965(4) Å] and Cu–N distances [Cu–N2 2.042(4) and Cu1–N4 2.012(4) Å] lie in the range reported in closely related structures [26,27]. Cu2 adopts a square-planar geometry and deviates from the base plane O1N2O3N4 by 0.019(1) Å. The Cu2–O2 distance is 1.877(4) Å, which is slightly shorter than Cu1–O1, due to solvent coordination, which may be involved in this slight weakening. The intramolecular distance between the two metal centers Cu1···Cu2 is 2.832(1) Å. The equatorial position is occupied by oxygen atoms from an adjacent chelate at an apical distance of [O3···O4] 2.236(5) Å. The pyridine ring (N2-C8) is inclined with respect to the basal plane (through O1N2N4O3) at an

Table 1
Summary of crystal data, data collection and refinement

Crystal data	
Chemical formula	$C_{29}H_{29}N_4O_5Cu_2(ClO_4)$
Formula weight (M_r)	740.0
Crystal system	triclinic
Space group	$P\bar{1}$
Unit cell dimensions	
a (Å)	8.9532(1)
b (Å)	12.7423(3)
c (Å)	14.9012(1)
α (°)	73.767(1)
β (°)	75.322(1)
γ (°)	77.496(1)
Volume (Å^3)	1559.4(5)
Z	2
D_c (calculated) (Mg/m^3)	1.576
Wavelength (γ, Å) Mo Kα	0.71073
Absorption coefficient (μ, mm^{-1})	1.508
Temperature (T, K)	293
Crystal size (mm)	0.44×0.40×0.28
$F(000)$	756
Data collection	
Diffractometer	Siemens SMART CCD area detector
Index ranges	$-11 \leqslant h \leqslant 11$ $-16 \leqslant k \leqslant 16$ $-19 \leqslant l \leqslant 14$
θ_{max}(°)	28
Reflections measured	10 764
Independent reflections	7401
Reflections with $I > 2\sigma(I)$	
Refinement	
Refinement method	on F^2
Reflections used	7401
Refinement parameters	406
Goodness-of-fit (S)	1.017
Final R indices [$I > 2\sigma(I)$]	$R_1 = 0.064$, $wR_2 = 0.159$
Largest difference peak and hole (e/Å^3)	0.837, −0.662

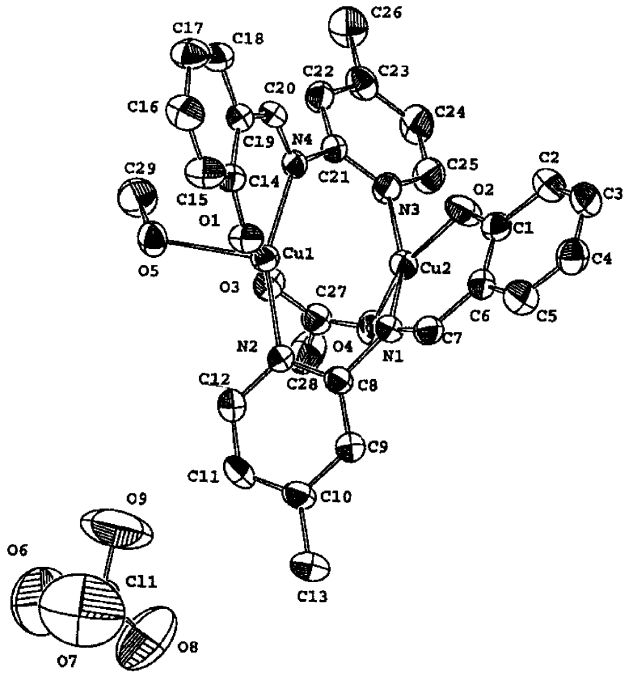

Fig. 2. ZORTEP diagram of the dimeric copper complex with numbering scheme. Thermal ellipsoids are drawn at 50% probability level.

angle of 79.6(2)°. The second pyridine ring (N3–C21) is twisted from the mean plane O2N1O4N3 through an angle of 86.3(1)°. These two pyridine rings are inclined to each other at an interplanar angle of 59.0(2)°. Both the six-membered rings (O1C14C19C20N4Cu1 and O2ClC6C7N1Cu2) involving metal ions adopt half-boat conformations. The ring puckering parameters are [28]: $q_2 = 0.282(4)$, $q_3 = 0.146(4)$, $Q_T = 0.317(4)$ Å, $\phi_2 = -62(1)°$ and $\theta_2 = 63(1)°$ for the ring involving Cu1, and $q_2 = 0.180(4)$, $q_3 = 0.100(4)$, $Q_T = 0.206(3)$ Å, $\phi_2 = -51(1)°$ and $\theta_2 = 61(1)°$ for the ring involving the Cu2 ion. Two eight-membered rings (including the metal ions) are formed by the donor atoms of the Schiff bases and the acetate bridges and both are in a twist-boat conformation. The ring puckering parameters are: $Q_T = 1.104(4)$, $q_2 = 1.085(4)$, $q_3 = 0.019(5)$, $q_4 = -0.201(4)$ Å, $\phi_2 = 176.8(2)°$, $\phi_3 = -75(11)°$, $\theta_2 = 89.0(3)°$ and $\theta_3 = 175(1)°$ for ring (N1Cu1N3C21N4-Cu1N2C8), and $Q_T = 2.015(3)$, $q_2 = 1.933(4)$, $q_3 = 0.164(4)$, $q_4 = 0.544(4)$ Å, $\phi_2 = 112.7(1)°$, $\phi_3 = 175(1)°$, $\theta_2 = 85.2(1)°$ and $\theta_3 = 16.8(4)°$ for ring (N1Cu2O4-C27O3Cu1N2C8). The packing of the molecular structure viewed down the a-axis is shown in Fig. 3.

The primary interactions between the molecules are Van der Waal's in nature. The perchlorate oxygen atoms O8 and O9 are the potential acceptors involved in two intermolecular hydrogen bonds with symmetry related molecules [C28–H28A···O8 and C29–H–29C···O9]. The layers lie parallel to the *xy* plane. In addition to the above, a few more C–H···O and O–H···O type of weak interactions are present to stabilize the molecular packing arrangement.

3.2. IR and UV–Vis studies

The IR spectra of the copper complex, recorded in KBr pellets and in polyethylene, show peaks in the region 1435–1465 cm^{-1}, assigned to the stretching vibrations of the aromatic skeleton of the salicylaldehyde portion. The one at 1094 cm^{-1} is due to the uncoordinated perchlorate ion [29]. The C=N stretching frequency is observed at 1612 cm^{-1}, showing a shift of about 15 cm^{-1}in relation to the free ligand. The phenolic C–O observed at 1299 cm^{-1}, further confirms the participation of the phenolic oxygen in the coordination with the metal ion [30]. It has been reported that if an

Table 2
Some standard bond distances (Å) and angles (°) in the structure of the dimeric copper complex, $[Cu_2(Hsalamp)_2(OCOCH_3)(OCH_3)]ClO_4$

Bond distances			
Cu1–O1	1.906(3)	Cu1–O3	1.965(4)
Cul–N4	2.012(4)	Cu1–N2	2.042(4)
Cul–O5	2.337(4)	Cul–Cu2	2.8324(8)
Cu2–O2	1.877(4)	Cu2–O4	1.957(4)
Cu2–N1	1.978(4)	Cu2–N3	2.021(4)
Bond angles			
O1–Cu1–O3	170.24(16)	O1–Cu1–N4	93.04(15)
O3–Cu1–N4	92.37(15)	O1–Cu1–N2	89.19(15)
N4–Cu1–N2	153.68(16)	O1–Cu1–O5	87.08(15)
O3–Cu1–O5	84.31(15)	N4–Cu1–O5	95.74(15)
N2–Cu1–O5	110.57(15)	O1–Cu1–Cu2	110.32(12)
O3–Cu1–Cu2	79.02(11)	N4–Cu1–Cu2	73.61(11)
N2–Cu1–Cu2	81.03(11)	O5–Cu1–Cu2	159.68(10)
O2–Cu2–O4	158.64(17)	O2–Cu2–N1	94.19(16)
O4–Cu2–N1	95.34(16)	O2–Cu2–N3	89.42(17)
O4–Cu2–N3	88.36(16)	N1–Cu2–N3	159.37(17)
O2–Cu2–Cu1	122.32(14)	O4–Cu2–Cu1	78.54(11)
N1–Cu2–Cu1	76.87(12)	N3–Cu2–Cu1	84.04(12)

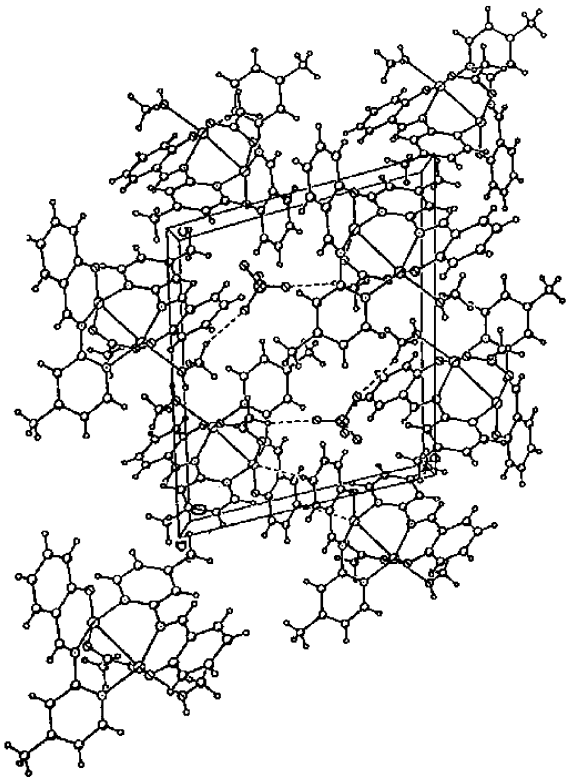

Fig. 3. Packing of molecular structure of the dimeric copper complex, as viewed from the *a*-axis.

acetate bridge joins two copper centers, then the difference in the frequencies of ν_{asyCOO} and ν_{symCOO} should be less than 154 cm^{-1}. For a copper complex, if the difference is around 107 cm^{-1}, then the two copper ions in the complex are joined by a monoatomic acetate bridge [29,31]. In our case, the difference between the two frequencies is around 122 cm^{-1} as the asymmetric and symmetric values are 1557 and 1435 cm^{-1}. On similar lines mentioned in the literature, this value confirms the presence of mono acetate bridging in the copper complex. The deprotonation of the phenolic OH and subsequent coordination of oxygen with the copper metal ion has been confirmed by the reduction in the intensity of the peak in the region 2915–2935 cm^{-1}, compared to the corresponding band in the ligand. The bands at 360 and 301 cm^{-1} are assigned to the Cu–N and Cu–O modes, respectively [32].

The electronic spectrum of the complex, recorded in methanol solvent, shows three bands in the region 396, 288 and 235 nm. The calculated molar absorbtivity values are 5850, 16 160 and 22 280 (ε/l mol^{-1} cm^{-1}). When compared with the pure ligand spectrum, a shift in the bands is noticed, due to the formation of the complex. A peak or shoulder in the region 430–380 nm can be assigned to the nitrogen (pyridile/imino) to copper transitions [33]. The peak at 396 nm in the present system corresponds to the pyridile nitrogen to copper charge transition. The band at 288 nm corresponds to n-π^* and the one at 235 nm to π–π^* transitions. A broad band around 680 nm is assigned to a d–d transition in the metal complex. The redshift in the λ_{max} value is indicative of distortion in its coordination geometry.

3.3. EPR studies

As we were unable to get good single crystals suitable for EPR studies, only the solution and powder results are reported below. The sample was nicely powdered and the EPR spectrum was recorded both at RT and 77 K. The EPR spectra obtained at RT and 77 K are almost identical, except for a change in intensity of the resonance lines. The EPR spectrum obtained at RT is given in Fig. 4. It consists of a strong line at the center, a broad line at low field and two broad lines on either side of the strong line. This is a triplet spectrum, having appreciable zero-field splitting (D) [34–36]. When $S = 1$, it gives rise to two states $|\pm 1\rangle$ and $|0\rangle$, separated by D. The degenerate $|\pm 1\rangle$ state splits into $|+1\rangle$ and $|-1\rangle$ once an external magnetic field is applied. Now, two EPR lines are expected due to the allowed transitions of $|-1\rangle$ to $|0\rangle$ and $|0\rangle$ to $|+1\rangle$. The separation between these two lines is approximately equal to $2D$, to first-order. The deviation from axial symmetry in D values is estimated by a parameter known as E. In a few cases, the forbidden transition from $|-1\rangle$ to $|+1\rangle$ is also seen [34,35]. This is also known as half-field transition, since it occurs at approximately half the field at which the main allowed transitions are expected. As mentioned earlier, the intensity ratio of high field transition to low field transition is slightly decreased as the temperature is lowered from RT to 77 K. This suggests that the ground state is $|-1\rangle$. Further, as expected hyperfine resonance lines from copper nuclei are not seen, due to dipolar broadening. The solid state structure from X-ray analysis indicates that the two Cu(II) ions are out of plane (see X-ray data) thus showing a weaker ferromagnetic interaction. This spectrum can be divided into three parts: the first one, the resonance line at low field; the second one consisting of the strong central line and the third one corresponding to the two weak shoulders, like features on either side of the central strong line. The strong resonance at the center with a g value close to 2.1

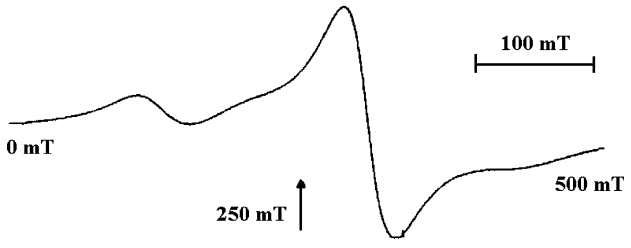

Fig. 4. EPR powder spectrum of the dimeric copper complex at 298 K. The presence of broad lines on either side of the strong line, indicate the zero-field splitting from $S = 1$. $\nu = 9.40041$ GHz.

is due to monomer impurity, as confirmed by the absence of hyperfine lines from the copper nucleus. On the other hand, the low field line is due to the half-field transition, arising from the coupling of the two copper ions and corresponds to the forbidden transition from $|-1\rangle$ to $|+1\rangle$. Here, one should expect seven hyperfine lines from the two interacting copper nuclei. This was not noticed here; however, it is clearly seen in the solution spectrum of the sample recorded at 77 K (see below). From the third part, two g and D values are calculated. Here, we want to mention that the broad nature of the central line is not only due to the unresolved hyperfine structure from the copper nucleus, but also from the small D value. This assumption has been made considering the 77 K solution spectrum (see below). The calculated spin Hamiltonian parameters obtained from RT and LNT EPR spectra are (the second D value is within the line width and hence is not calculated)

$$\text{RT}: \quad g_1 = 2.13, \quad g_2 = 2.23, \quad D_1 = 113(3)\ \text{mT},$$

$$\text{LNT}: \quad g_1 = 2.15, \quad g_2 = 2.25, \quad D_1 = 115(2)\ \text{mT}.$$

In order to understand and further confirm this dimeric phenomenon, a solution spectrum of the sample has been measured both at RT and 77 K. The copper sample is dissolved in dry ethanol and the EPR spectrum of the solution sample, recorded at RT, is shown in Fig. 5. This clearly indicates a four-line pattern due to the interaction of the single unpaired electron with a copper nucleus ($I = 3/2$). The broad nature of the first hyperfine line and the presence of two lines on the higher field of the strong line, indicates the presence of two Cu(II) ions, with different g and A values. In the solution EPR spectrum, due to isotropic exchange interaction, one expects an averaged spectrum, having isotropic spin Hamiltonian parameters. However, since the D tensor is traceless, it averages out to zero in solution samples and will not be shown in the EPR spectrum. The calculated isotropic g and A values for the two copper(II) centers are

$$\text{Center 1}: \quad g_{\text{iso}} = 2.166(4), \quad A_{\text{iso}} = 4.67\ \text{mT},$$

$$\text{Center 2}: \quad g_{\text{iso}} = 2.118(1), \quad A_{\text{iso}} = 6.25\ \text{mT}.$$

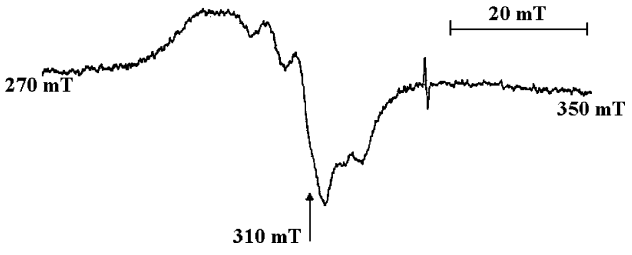

Fig. 5. EPR solution spectrum of the dimeric copper complex in ethanol solvent at 298 K. The sharp line in here and in other figures corresponds to DPPH. $\nu = 9.11610$ GHz.

The copper hyperfine structure, which is not seen in the powder spectrum due to dipolar–dipolar broadening, appeared in solution due to the very low concentration of the solution. At higher concentrations of the sample, the four copper hyperfine lines collapsed to a single broad line. The sample was then cooled to 77 K and the EPR spectrum recorded at 77 K in the magnetic field region of 210–410 mT is shown in Fig. 6. This clearly differs from the RT powder EPR spectrum. As mentioned earlier in the RT powder spectrum discussion, this also represents a clear triplet spectrum with an orthorhombic g tensor. As the line widths of the EPR spectrum are larger at RT compared to 77 K, the zero-field lines are not well resolved in the RT EPR spectrum. As the sample is cooled to 77 K, the two perpendicular components have split, resulting in orthorhombic symmetry for the copper complex. The calculated spin Hamiltonian parameters are

$$g_1 = 2.07, \quad g_2 = 2.13, \quad g_3 = 2.05,$$

$$D_1 = 77.5\ \text{mT}, \quad D_2 = 44.6\ \text{mT}, \quad D_3 = 1.6\ \text{mT}.$$

The g value obtained by taking the average of the three g values obtained in the solution spectrum at 77 K is 2.09. Alternatively, one can think of two g values only, with the central line at $g = 2.05$ arising from monomer impurity, whose concentration might have increased after dissolving the complex in the solvent. With this type of assumption, the calculated spin Hamiltonian parameters are

$$g_1 = 2.07, \quad g_2 = 2.13,$$

$$D_1 = 77.5\ \text{mT}, \quad D_2 = 44.6\ \text{mT}.$$

The average of these two g values obtained in the solution spectrum at 77 K is 2.11. The isotropic g value obtained from the solution spectrum at RT is 2.166. The latter assumption of two g values looks more appropriate. However, single crystal work at X-band and/or measurement at 77 K with Q-band will further help to confirm our hypothesis. As of now, these two could not be done. This difference in the g values could be due to a

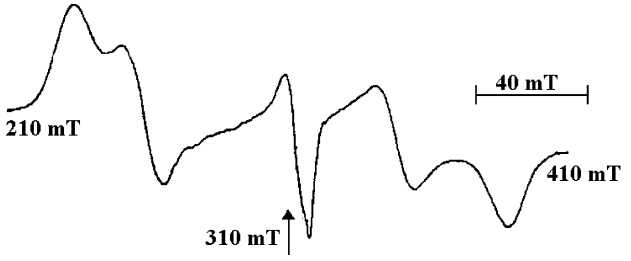

Fig. 6. EPR solution spectrum of the dimeric copper complex in ethanol solvent at 77 K in the range 210–410 mT. One can notice orthorhombic g and zero-field splitting from the two copper nuclei. $\nu = 9.04918$ GHz.

small structural change that might have occurred during dissolution in the solvent ethanol. However, when the EPR spectra are recorded in various solvents, the average g value is in the range 2.10–2.25. Hence, the indication of a small structural change has not been completely ruled out. The same type of observation was also noticed in some of our previous studies [8–15]. Although the X-ray data have suggested two types of copper ions, one in square-planar geometry and the other in square-pyramidal geometry, we did not notice two types of resonances from the two different copper ions. However, even if the resonances are present, they might not have appeared in powder samples due to the broadness of the resonance lines (line width around 10 mT). In addition, in the solution sample at RT, again due to rapid motion of ions, the resonances are averaged out. Even at 77 K, the resonance lines are still broad ruling out the possibility of observing two separate signals for the two copper ions.

An interesting observation of the present study is the presence of resonance lines at half-field transitions. This kind of result has been rarely reported in the EPR literature [34–37]. Here, we want to mention that even in the room temperature powder spectrum, the half-field line is noticed; however without any hyperfine splitting from the two copper nuclei. The EPR spectrum of the solution sample recorded at 77 K in the region 100–180 mT is shown in Fig. 7. One can clearly notice a seven line pattern with a rough intensity ratio of 1:2:3:4:3:2:1. The average hyperfine coupling constant is 6.1 mT. As discussed in the X-ray structural analysis, the distance between the two copper ions is 2.832 Å. It has been known that if the separation distance between the two metal centers is more than 3.5 Å, an interaction is not expected. In addition, the dihedral angle between the two copper atoms and the connecting ligand atoms also plays an important role in deciding the extent of the interaction. The half-field resonances are due to the transition between the $|-1\rangle$ and $|+1\rangle$ level in the triplet EPR spectrum [38]. However, it is forbidden, as the selection rule for this transition has been ± 2. The normal allowed transition is ± 1. Hence, it is not generally observed in most the EPR spectra, even though a small interaction is present between the two metal ions.

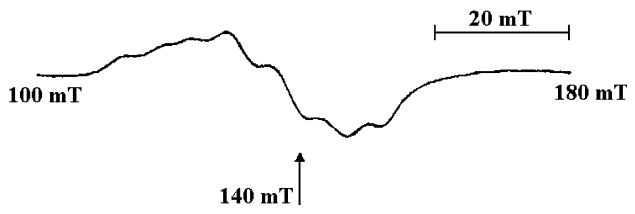

Fig. 7. EPR solution spectrum of the dimeric copper complex in ethanol solvent at 77 K in the region 100–180 mT, indicating hyperfine lines from two copper nuclei at half-field position. $\nu = 9.04918$ GHz.

The intensity pattern arises due to the two copper ions, having a total nuclear spin of 3. Hence, a seven-line pattern is expected and observed. Using the point dipole approximation and the measured D, the Cu–Cu separation (r) is calculated using the empirical formula [39]

$$r(\text{Å}) = [0.65 \times g_{\|}^2/D(\text{cm}^{-1})]^{1/3}.$$

By assuming a $g_{\|}$ value of 2.23 and D around 0.126 cm^{-1}, the calculated distance between the copper ions is 2.94 Å, and this value is close to that observed in the X-ray structural analysis (2.832 Å). However, the important observation is that the distance is sufficiently small to have an interaction between the two ions.

3.4. Magnetic study

The magnetic susceptibility of a powdered sample of the complex was measured in the temperature range 77–300 K using a vibrating sample magnetometer. Analysis has been carried out using the modified Bleaney–Bowers equation [40]

$$\chi_{\text{m}} = \{Ng^2\beta^2/KT\}[3 + \exp(-2J/KT)]^{-1}(1-p) + (Ng_{\text{i}}^2\beta^2/KT)p + N_{\alpha},$$

where χ_{m} is the paramagnetic susceptibility per molecule after the correction for diamagnetism, p is the paramagnetic impurities; g_{i} is the average g factor of the paramagnetic impurity. $-2J$ is the singlet–triplet energy separation, N_{α} is the TIP which is assumed to be 60×10^{-6} $\text{cm}^3\,\text{mol}^{-1}$ for Cu(II) dimers [41]. A best fit to the experimental value for the complex is summarized in Table 3. The observed J value is about 17.8 cm^{-1}. This suggests a weak ferromagnetic interaction between the two Cu(II) centers and also confirms the observation of EPR spectrum. The hydroxo bridged complexes exhibit a weak antiferromagnetic interaction when compared to nitrito and acetato bridged complexes, due to a π type overlap between the out of plane copper orbital and the non-bonding pair on oxygen (p_x). This will be more significant than the σ type overlap and hence gives rise to enhanced antiferromagnetism in the case of trigonal-planar oxygen and reduced antiferromagnetism in pyramidal oxygen [43,44]. Since the observed J value is made up of antiferromagnetic and ferromagnetic contributions, which in turn are influenced by a variety of structural and electronic factors, the detailed reasons for these variations in J can be quite complex. The ferromagnetic behaviour is generally due to the non-coplanarity of the two Cu chromophores. This "folding" feature is akin to the "roof shaped" geometry noted by Kahn [42] in various symmetrically bridged dihydroxo dimers. The consequent accidental orthogonality of the Cu $d_{x^2-y^2}$ magnetic orbitals postulated by Kahn to be responsible for reducing the $J_{\text{antiferro}}$ contribution relative

Table 3
Magnetic susceptibility data for the Complex $[Cu_2(Hsalamp)_2(OCOCH_3)(OCH_3)]ClO_4$

Temperature (K)	$10^3\ \chi_M$ (cm^3/M)		μ_{eff} (BM)	
	Observed	Calculated	Observed	Calculated
79	4.10	4.11	1.611	1.612
90	3.55	3.57	1.600	1.604
100	3.18	3.19	1.596	1.598
110	2.87	2.88	1.590	1.593
130	2.41	2.42	1.584	1.586
150	2.07	2.08	1.577	1.581
190	1.62	1.63	1.570	1.575
230	1.33	1.35	1.565	1.573
270	1.13	1.15	1.563	1.574
296	1.04	1.05	1.570	1.575

to J_{ferro} seems to broadly hold true in the case of asymmetrical species. The same compound also contains very tight Cu–O–Cu angles and short Cu–Cu distances within two coplanar *cis*-disposed square-pyramidal chromophores. However, in the present case, a ferromagnetic interaction is observed between the two copper ions, in relation to the previous studies. It has been reported that if the geometry around the copper ion is square-pyramidal, the magnetic orbital is $d_{x^2-y^2}$ and the lobes are pointed towards the ligands [45]. However, if the geometry is trigonal bipyramidal, the magnetic orbital is d_z^2 with lobes pointing towards the bonding ligands.

3.5. Cyclic voltammetric study

The cyclic voltammetric studies for the dimeric copper complex were performed in dried acetonitrile solvent. The most cathodic response is observed at an E_{pc} value of −0.88 V [44]. This has been assigned to a one-step two-electron reduction process, i.e., Cu(II)–Cu(II) → Cu(I)–Cu(I) redox process. The anodic scan following an initial cathodic scan is associated with a sharp feature at −0.08 V, which is characteristic of desorption of the electrogenarated copper(0) species. We observed a decrease in the intensities of the E_{pc} values in the multiple scan voltammogram performed at 50 mV/s, compared to the values obtained for 200, 100 and 50 mV/s. The $E_{1/2}$ value is found to be approximately at −1.00 V. It has been concluded from the differential pulse voltammogram that the initial process is the reduction of the two copper ions from +2 to +1 state and then +1 state to 0 state, as reported earlier [42]. This is achieved at the same $E_{1/2}$ value of about approximately −1.00 V, due to the broad feature observed in the differential pulse voltammogram. Further conformation of this reduction is obtained in a previous study, in which the two reductions were obtained at −0.54 and −0.86 V [46]. However, in the present case, due to the broad feature, we have observed both the reductions at −1.0 V.

4. Conclusions

The copper–copper dimer complex with the ligand Hsalamp has given very interesting results. Single crystal X-ray studies on this system have indicated that the two metal centers are in different geometries and the distance between them is appropriate for metal–metal interaction. The notable feature of the structure is that the Schiff base acts as a bidentate ligand (phenolic O– and imine –N=) with one of the copper ions and the hetero nitrogen atom coordinating with the other copper ion. The intramolecular distance between the two metal centers is 2.832(1) Å. The six-membered rings in the structure adopt a half-boat conformation, whereas the eight-membered rings assume a twist-boat conformation. The molecules are stabilized by C–H···O and O–H···O type weak hydrogen bond like interactions. The EPR results on this complex confirm the interaction between the two copper atoms and a well-resolved seven-line pattern is observed for the half-field transition, with a hyperfine value of 6.1 mT, nearly half of the value observed for a single electron on a copper nucleus. The assumption of axially symmetric or orthorhombic g needs confirmation from single crystal EPR studies at X-band or low temperature solution studies at Q-band. CV studies indicate a one-step two-electron reduction process, i.e., Cu(II)–Cu(II) → Cu(I)–Cu(I) redox process. Magnetic studies suggest a weak ferromagnetic interaction between the two Cu(II) centers and also confirms the observation of EPR spectrum.

5. Supplementary data

Supplementary data are available from the CCDC, 12 Union Road, Cambridge CB2 1EZ, UK (fax: +44-1223-336033; E-mail: deposit@ccdc.cam.ac.uk or www: http://www.ccdc.cam.ac.uk) on request, quoting the Deposit No. 208446.

Acknowledgements

Recognition and support in the form of DST-FIST by DST to the Department of Chemistry, Pondicherry University, Pondicherry is highly appreciated. The authors thank the Council of Scientific & Industrial Research (CSIR) 01(1771)/02/EMR-II, the Department of Science & Technology (DST), the University Grant Commission (UGC), New Delhi for financial assistance.

References

[1] G. Plesch, C. Friebel, O. Švajlenová, J. Krătsmăr-Šmogrovič, Inorg. Chim. Acta 81 (1987) 129.
[2] J. Sivý, V. Kettmannn, J. Krătsmăr-Šmogrovič, O. Švajlenová, C. Friebel, G. Plesch, Z. Anorg. Allg. Chem. 55 (1990) 583.
[3] G. Plesch, C. Friebel, O. Švajlenová, J. Krătsmăr-Šmogrovič, Polyhedron 10 (1991) 893.
[4] G. Plesch, C. Friebel, O. Švajlenová, J. Krătsmăr-Šmogrovič, Polyhedron 14 (1995) 1185.
[5] T. Ueki, T. Ashida, Y. Sasada, M. Kakudo, Acta Crystallogr., Sect. B 25 (1969) 328.
[6] F. Pavelčik, J. Krătsmăr-Šmogrovič, O. Švajlenová, J. Majer, Collect. Czech. Chem. Commun. 46 (1981) 3186.
[7] T. Ueki, T. Ashida, Y. Sasada, M. Kakudo, Acta Crystallogr. 22 (1967) 870.
[8] T.M. Rajendiran, R. Venkatesan, P. Sambasiva Rao, M. Kandaswamy, Polyhedron 17 (1998) 3427.
[9] I. Rekha Naganthan, R. Venkatesan, P. Sambasiva Rao, T.M. Rajendiran, Proc. Indian Acad. Sci. (Chem.l Sci.) 110 (1998) 397.
[10] T.M. Rajendiran, R. Kannappan, R. Venkatesan, P. Sambasiva Rao, M. Kandaswamy, Polyhedron 18 (1999) 3085.
[11] R. Srinivasan, R. Venkatesan, T.M. Rajendiran, P. Sambasiva Rao, Proc. Indian Acad. Sci. (Chem. Sci.) 112 (2000) 359.
[12] S. Sujatha, T.M. Rajendiran, R. Kannappan, R. Venkatesan, P. Sambasiva Rao, Proc. Indian Acad. Sci. (Chem. Sci.) 112 (2000) 559.
[13] S. Karthikeyan, T.M. Rajendiran, R. Kannappan, R. Mahalakshmy, R. Venkatesan, P. Sambasiva Rao, Proc. Indian Acad. Sci. (Chem. Sci.) 113 (2001) 245.
[14] I. Sougandi, R. Mahalakshmi, R. Kannappan, T.M. Rajendiran, R. Venkatesan, P. Sambasiva Rao, Trans. Metal Chem. 27 (2002) 512.
[15] R. Kannappan, R. Mahalakshmy, T.M. Rajendiran, R. Venkatesan, P. Sambasiva Rao, Proc. Indian Acad. Sci. (Chem. Sci.) 115 (2003) 1.
[16] R. Srinivasan, R. Venkatesan, P. Sambasiva Rao, Proc. Indian Acad. Sci. (Chem. Sci.) 115 (2003) 91.
[17] Siemens, SAINT, Software Reference Manual Version 4.0. Siemens Analytical X-ray instruments Inc., Madison, WI, 1996.
[18] G.M. Sheldrick, SADABS. Program for empirical absorption correction, University of Gottingen, Germany, 1996.
[19] Siemens, SMART Software References Manual, Siemens Analytical X-ray Instruments Inc., Madison, WI, 1996.
[20] P.T. Beurskens, G. Beurskens, R. De Galder, S. Garcia-Granda, R.O. Gould, R. Israel, J.M.M. Smits, The DIRDIF-98 program system, Crystallography Laboratory, University of Nijimegen, The Netherlands, 1998.
[21] G.M. Sheldrick, SHELXL-97. Program for crystal structure refinement, University of Göttingen, Göttingen, Germany, 1997.
[22] L. Zsolnai, ZORTEP, Interactive graphics program for crystal structure illustrations, University of Heidelberg, Germany, 1997.
[23] M. Nardelli, J. Appl. Cryst. 28 (1995) 659.
[24] S.A. Warda, Acta Cryst. C 53 (1997) 1010.
[25] D.J. Elliot, L.L. Martin, M.R. Taylor, Acta. Cryst. C 54 (1998) 1259.
[26] S.A. Warda, Acta Cryst. C 54 (1998) 187.
[27] S.A. Warda, Acta Cryst. C 54 (1998) 768.
[28] Cremer, J.A. Pople, J. Chem. Soc. 97 (1975) 1354.
[29] G.B. Deacon, R.J. Phillips, Coord. Chem. Rev. 33 (1980) 227.
[30] H.A. Tijmir, Polyhedron 2 (1983) 723.
[31] K. Nakamoto, Infrared and Raman Spectra of Inorganic and Coordination Compounds, 4th ed., Wiley, New York, 1986, pp. 147–150, 227–233, 251–253.
[32] K. Nakamoto, C.W. Schaipfer, Inorg. Chim. Acta 6 (1972) 70.
[33] A.B.P. Lever, Inorganic Electronic Spectroscopy, 2nd ed., Elsevier, Amsterdam, 1984, pp. 356, 553–572, 636–638.
[34] S.S. Eaton, K.M. More, B.M. Sawant, G.R. Eaton, J. Am. Chem. Soc. 105 (1983) 6560.
[35] J.V. Folgado, R. Ibanez, E. Coronado, D. Beltran, J.M. Savariault, J. Galy, Inorg. Chem. 27 (1988) 19.
[36] P. Chaudhuri, K. Oder, J. Chem. Soc., Dalton Trans. 1597 (1990).
[37] O. Kahn, Angew. Chem., Int. Ed. 834 (1985) 24.
[38] A. Abragam, B. Bleaney, Electron Paramagnetic Resonance of Transition Metal Ions, Clarendon Press, Oxford, 1970.
[39] R.L. Dutta, A. Syamal, Elements of Magneto Chemistry, S. Chand and Company, 1990, p. 82.
[40] B. Bleaney, K.D. Bowers, Proc. R. Soc., London, Ser. A 214 (1952) 415.
[41] L.K. Thompson, N.D. Donald, E. William, J.F. Banks, R.M. Buchanan, H. Rougchay, R.J. Webb, D.N. Hendrickson, Inorg. Chem. 29 (1990) 1058.
[42] O. Kahn, R. Claude, H. Coundanne, Nouv. J. Chim. 4 (1980) 167.
[43] W.J. Geary, Coord. Chem. Rev. 7 (1971) 81.
[44] I.E. Dickson, R. Robson, Inorg. Chem. 13 (1974) 1301.
[45] G. Christou, S.P. Perlepes, E. Libby, K. Folting, J.C. Huffman, R.J. Webb, D.N. Hendrickson, Inorg. Chem. 29 (1990) 3657.
[46] R. Gupta, S. Mukherrjee, R. Mukherjee, J. Chem. Soc., Dalton Trans. (1999) 4025.

Available online at www.sciencedirect.com
SCIENCE DIRECT®
Polyhedron 23 (2004) 1125–1129
POLYHEDRON
www.elsevier.com/locate/poly

A novel potassium-centered highly symmetrically polynuclear zirconium complex: $K[\{(Cp^*Zr)_3(\mu_3\text{-}N)(\mu_3\text{-}NH)(\mu\text{-}NH_2)_3\}_4(NH_2)_5(NH_3)_7]$

Guangcai Bai, Denis Vidovic, Herbert W. Roesky *, Jörg Magull

Institut für Anorganische Chemie der Universität, Tammannstrasse 4, D-37077 Göttingen, Germany

Received 26 November 2003; accepted 15 January 2004

Abstract

Treatment of $[Cp^*ZrCl_3]$ (**1**; $Cp^* = C_5Me_5$) with KH in liquid ammonia and toluene at −78 °C resulted in the complete removal of chloride and formation of the nitrogen-containing zirconium potassium complex $K[\{(Cp^*Zr)_3(\mu_3\text{-}N)(\mu_3\text{-}NH)(\mu\text{-}NH_2)_3\}_4(NH_2)_5(NH_3)_7]\cdot 6C_7H_8$ (**2**). X-ray structure analysis revealed this complex contains four $[(Cp^*Zr)_3(\mu_3\text{-}N)(\mu_3\text{-}NH)(\mu\text{-}NH_2)_3(NH_2)(NH_3)_2]$ building blocks where one of the protons is replaced by an interstitial potassium cation. Each of the four building blocks contains three Zr atoms forming a perfect equilateral triangular core, which is capped inside by a nitrido (N) and outside by an imido (NH) group, and furthermore symmetrically bridged by amido (NH_2) groups.
© 2004 Elsevier Ltd. All rights reserved.

Keywords: Ammonolysis; Liquid ammonia/toluene two-phase system; Potassium; Zirconium

1. Introduction

Thin films of early transition metal nitrides have many applications as technologically important materials due to their unique properties [1–9]. In general, the nitrides have been prepared using chemical vapor deposition (CVD) techniques [10–15]. The development of synthesis in solution to yield solid-state materials via molecular precursors represents an intriguing challenge in the field of materials [16–19]. The interest in using transition metal nitrides has promoted studies on the intermediates with amido (NH_2), imido (NH) and nitrido (N) groups formed during the ammonolysis of transition metal compounds. Although some nitrogen-containing early transition metal compounds have been isolated and structurally characterized [20–28], polynuclear zirconium amide, imide and nitride species are very rare.

Wolczanski and co-worker [29] isolated the $[\{(t\text{Bu}_3\text{CO})\text{Zr}\}_5(\mu_5\text{-N})(\mu_3\text{-NH})_4(\mu\text{-NH}_2)_4]$ cluster from the ammonolysis of $[(t\text{Bu}_3\text{CO})\text{Zr}(\text{CH}_2\text{Ph})_3]$. Meanwhile, the pseudo-octahedral $[\{(t\text{Bu}_3\text{CO})\text{Zr}\}_6(\mu_6\text{-N})(\mu_3\text{-NH})_6(\mu\text{-NH}_2)_3]$ and the dodecaamido square pyramidal $[\{(t\text{Bu}_3\text{CO})\text{Zr}\}_5(\mu_5\text{-N})(\mu\text{-NH}_2)_{12}]$ compounds were obtained and characterized using ^{1}H, ^{13}C$\{^1$H$\}$, and ^{15}N NMR investigations. Our recent demonstration that the liquid ammonia/toluene two-phase system is highly effective for the ammonolysis and hydrolysis of transition metal compounds has led to the preparation of the amido, imido or nitrido group 4 complexes $[(\text{LTi})_6(\mu_3\text{-N})_2(\mu_3\text{-NH})_6\cdot 6(C_7H_8)]$ [30], $[\{(\text{MeC}_5\text{H}_4)\text{Zr}\}_5(\mu_5\text{-N})(\mu_3\text{-NH})_4(\mu\text{-NH}_2)_4]$ [31], and $[(\eta^3\text{-L})\text{Zr}(\mu\text{-NH})]_2$ ($\text{L} = (\text{PN}t\text{Bu})_2(t\text{BuN})_2$) [32], and related systems [33–40]. Herein we report the ammonolysis of a group 4 organometallic halide in a two-phase system, yielding a polynuclear zirconium anion.

2. Experimental

2.1. General data

All experimental manipulations were carried out under an atmosphere of purified nitrogen using standard Schlenk techniques. Samples prepared for spectral

* Corresponding author. Tel.: +49-551-39-3000/3001; fax: +49-551-39-3373.
E-mail address: hroesky@gwdg.de (H.W. Roesky).

0277-5387/$ - see front matter © 2004 Elsevier Ltd. All rights reserved.
doi:10.1016/j.poly.2004.01.017

measurements as well as for reactions were manipulated in a glove-box. Solvents were dried using conventional procedures, distilled under nitrogen and degassed prior to use. Deuterated NMR solvents were treated with K/Na alloy, distilled, and stored under nitrogen.

The NMR spectra were recorded on Bruker AM 250 spectrometer with $SiMe_4$ as external standard. Mass spectra were recorded on a Finnigan MAT 8230 mass spectrometer using the EI-MS method. The most intensive peak of an isotope distribution is tabulated. IR spectra are recorded on Bio-Rad FTS-7 spectrometer as nujol mulls between KBr plates. Elemental analyses were performed at the Analytical Laboratory of the Institute of Inorganic Chemistry, University of Göttingen.

2.2. Preparation of 2

Ammonia (50 ml) was condensed onto a suspension of **1** (1.37 g, 4.12 mmol) and KH (0.51 g, 12.76 mmol) in toluene (80 ml) at −78 °C under stirring. The stirring of the mixture was continued for 1 h at this temperature. Then the excess of ammonia was allowed to evaporate from the reaction mixture over a period of 4 h. During this time, the mixture was warmed slowly to room temperature. After filtration and subsequent concentration (to 15 ml) in vacuo, the resulting colorless solution was kept at −20 °C for two months to isolate colorless crystals of **2** (0.12 g). After isolating the crystals, and subsequent removal of the solvent, the colorless mother liquor was maintained at −20 °C for one week, from which additional crystals of **2** (0.15 g) were obtained. Total yield 0.27 g (21%); m.p. > 410 °C; IR (Nujol): $\tilde{\nu} = 3384, 1261, 1095, 1018, 801, 724, 666\ cm^{-1}$; ^1H NMR (300 MHz, C_6D_6): $\delta = 2.24$–1.62 (m, C_5Me_5), 2.05, 1.35, 1.18, 0.91, −0.12 (br, μ_3-N*H*, μ_2-NH_2, NH_2 and NH_3); EI-MS: *m/z* (%): 1498 (4) [M^+–2{(Cp*Zr)$_3$(μ_3-N)(μ_3-NH)(μ-NH$_2$)$_3$(NH$_2$)(NH$_3$)$_2$}–6C$_7$H$_8$–8NH$_3$–NH$_2$], 1364 (21) [M^+–2{(Cp*Zr)$_3$(μ_3-N)(μ_3-NH)(μ-NH$_2$)$_3$(NH$_2$)(NH$_3$)$_2$}–6C$_7$H$_8$–7NH$_3$–2NH$_2$–Cp*], 121 (100) [Cp*–CH$_2$]. Elemental *Anal.* Calc. for $C_{162}H_{287}KN_{32}Zr_{12}$ (3817.0): C, 51.0; H, 7.6; N, 11.7. Found: C, 51.0; H, 7.6; N, 10.7%.

2.3. Crystallographic measurement

Single crystals of **2** suitable for X-ray structural analysis were obtained from toluene by maintaining the reaction mixture at −20 °C for two months. Data for the structure were collected on a STOE IPDS II diffractometer. Intensity measurement was performed on a rapidly cooled crystal in an oil drop in the range $4.84° \leqslant 2\theta \leqslant 49.62°$. The structure was solved by direct methods (SHELXS-97) [41] and refined with all data by full-matrix least-squares on F^2 (SHELXL-97) (145 parameters) [42]. The hydrogen atoms of C–H bonds were added in idealized positions. $R_1 = 0.0471$ for $I > \sigma(I)$, $wR_2 = 0.1112$ for all data. The final difference Fourier synthesis gave a min/max residual electron density −0.521/+0.930 e Å^{-3}. Other details of the data collection, structure solution, and refinement are listed in Table 1.

Table 1
Crystallographic data for K[{(Cp*Zr)$_3$(μ_3-N)(μ_3-NH)(μ-NH$_2$)$_3$}$_4$(NH$_2$)$_5$(NH$_3$)$_7$]·6C$_7$H$_8$ (**2**)

Empirical formula[a]	$C_{162}H_{228}KN_{32}Zr_{12}$
Formula weight	3757.50
Crystal class	cubic
Space group	*I*23
Unit cell parameters	
a (Å)	20.640(2)
b (Å)	20.640(2)
c (Å)	20.640(2)
V (Å^3)	8792.6(18)
Z	2
ρ_{calc} (g cm^{-3})	1.419
μ (mm^{-1})	0.758
T (K)	133(2)
F(000)	3846
2θ range (°)	4.82–29.62
Total number of reflections	5100
Independent reflections R_{int}	2402 (0.0458)
R^b, $wR^c(I > 2\sigma(I))$	0.0471, 0.1056
R, wR_2 (all data), *w*;	0.0609, 0.1112
Goodness-of-fit, S^d	0.874
Data/restraints/parameters	2402/0/144
Largest difference peak and hole (e Å^{-3})	0.930 and −0.521

[a] Including six toluene molecules; the 59 hydrogen atoms of N–H bonds cannot be determined by X-ray diffraction.

[b] $R = \sum ||F_o| - |F_c|| / \sum |F_o|$.

[c] $wR_2 = \left[\sum w(F_o^2 - F_c^2)^2 \Big/ \sum w(F_o^2)^2\right]^{1/2}$.

[d] $S = \left[\sum w(F_o^2 - F_c^2)^2 \Big/ \sum (n-p)\right]^{1/2}$.

3. Results and discussion

Treatment of [Cp*ZrCl$_3$] (**1**) with KH (1:3 molar ratio) in liquid ammonia and toluene at −78 °C yields K[{(Cp*Zr)$_3$(μ_3-N)(μ_3-NH)(μ-NH$_2$)$_3$}$_4$(NH$_2$)$_5$(NH$_3$)$_7$]·6C$_7$H$_8$ (**2**; Scheme 1). Obviously, the hydride converts the ammonia to amide NH_2^- [43], and furthermore converts the resulting metal amide ($ZrNH_2$) to the corresponding imide (ZrNH) and nitride (ZrN) via inter-or intramolecular ammonia or hydrogen elimination.

Compound **2** is a colorless crystalline solid with unusual thermal stability. The melting point of **2** exceeds 410 °C (*no obvious decomposition was observed*). The IR spectrum of **2** shows a weak and broad absorption at 3384 cm^{-1}, assignable to the N–H stretching frequencies. Compound **2** exhibits the fragments [M^+-2{(Cp*Zr)$_3$(μ_3-N)(μ_3-NH)(μ-NH$_2$)$_3$(NH$_2$)(NH$_3$)$_2$}-6C$_7$H$_8$-8NH$_3$-NH$_2$] and [M^+–2{(Cp*Zr)$_3$(μ_3-N)(μ_3-NH)-(μ-NH$_2$)$_3$(NH$_2$)(NH$_3$)$_2$}–6C$_7$H$_8$–7NH$_3$–2NH$_2$–Cp*] at 1498 (4%) and 1364 (21%) in the EI mass spectrum of **2**, which indicates that two of the neutral building blocks

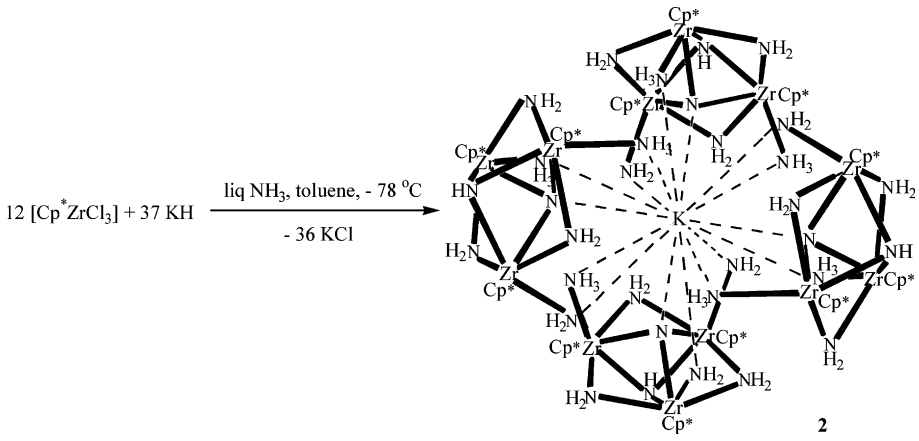

Scheme 1. Synthesis of **2**. Cp* = C_5Me_5.

of **2** are easily eliminated under EI-MS condition. The ^{1}H NMR spectral data of **2** show a series of resonances (from 2.24 to 1.62 ppm) for the protons of the Cp* groups and very broad resonances (2.05, 1.35, 1.18, 0.91 and −0.12 ppm) for the protons of the N–H moieties, indicative of the dissociation of **2** by dissolution.

Single crystals of **2** suitable for X-ray structural analysis were obtained from toluene by maintaining the reaction mixture at −20 °C for two months. Compound **2** crystallizes in the cubic space group *I*23. The molecular structure of **2** is shown in Fig. 1. In the crystal, **2** is a highly symmetrical complex, which consists of four $[(Cp^*Zr)_3(\mu_3\text{-}N)(\mu_3\text{-}NH)(\mu\text{-}NH_2)_3(NH_2)(NH_3)_2]$ building blocks where one of the protons is replaced by an interstitial potassium cation. Each of the four building blocks contains three Zr atoms forming a perfect equilateral triangular core, which is capped inside by a nitrido (N) and outside by an imido (NH) group, and

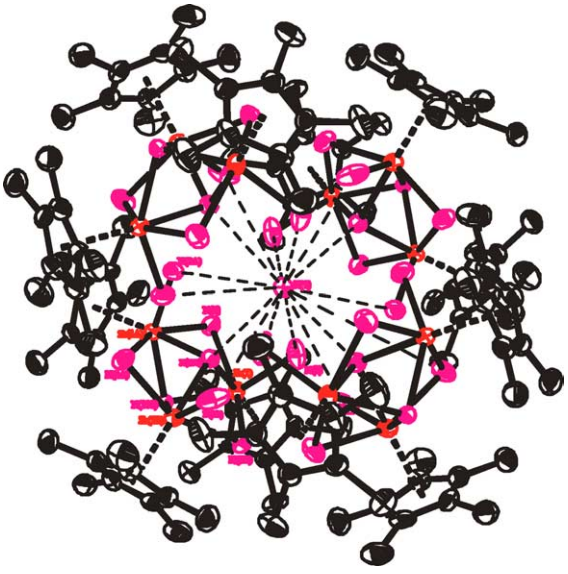

Fig. 1. The molecular structure of **2**. The hydrogen atoms and the toluene molecules are omitted for clarity.

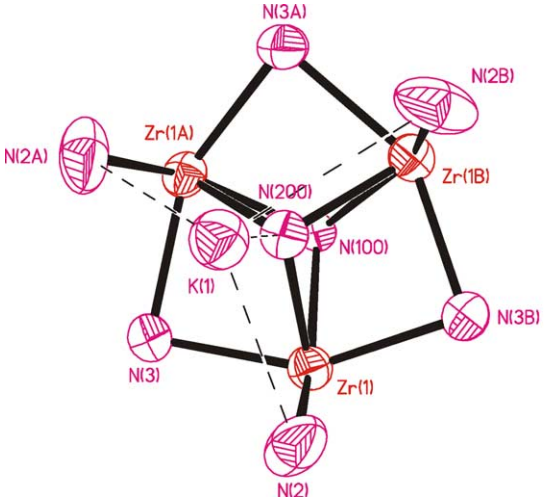

Fig. 2. The core structure of the building block $[(Cp^*Zr)_3(\mu_3\text{-}N)(\mu_3\text{-}NH)(\mu\text{-}NH_2)_3(NH_2)_2(NH_3)]$ with potassium.

furthermore symmetrically bridged by amido (NH_2) groups (Fig. 2 shows the core structure of one of the building blocks with potassium). The distorted octahedral coordination sphere of each zirconium is completed by a terminally bonded NH_3 or an amido NH_2 group oriented toward the inside of the cluster and a Cp* ligand tilted outside, leading to a geometry similar to that of trinuclear polyoxozirconium chloride $[\{(Cp^*ZrCl)(\mu\text{-}OH)\}_3(\mu_3\text{-}OH)(\mu_3\text{-}O)\cdot 2THF]$ [44].

The Zr(1)–N(100) (Zr–(μ_3-NH) 2.231(5) Å), Zr(1)–N(200) (Zr–(μ_3-N) 2.192(5) Å), Zr(1)–N(3) and Zr(1)–N(3B) (Zr–(μ-NH_2) 2.285(6) and 2.329(7) Å) bond lengths and the Zr···Zr (3.220(1) Å) distances are comparable to those found in $[\{(MeC_5H_4)Zr\}_5(\mu_5\text{-}N)(\mu_3\text{-}NH)_4(\mu\text{-}NH_2)_4]$ [1] and in $[\{(tBu_3CO)Zr\}_5(\mu_5\text{-}$

[1] Zr_a–(μ_3-NH) 2.253 Å, Zr_b–(μ_3-NH) 2.186 Å, Zr_a–(μ_5-N) 2.210 Å, Zr_b–(μ_5-N) 2.232 Å, Zr_b–(μ-NH_2) 2.296 Å, $Zr_a\cdots Zr_b$ 3.143 Å, $Zr_b\cdots Zr_b$ 3.1566 Å; Zr_a and Zr_b represent the one apical and the four basal zirconium atoms of the square pyramidal cluster, respectively [28].

Table 2
Selected bond lengths (Å) and bond angles (°) for $K[\{(Cp^*Zr)_3(\mu_3\text{-}N)(\mu_3\text{-}NH)(\mu\text{-}NH_2)_3\}_4(NH_2)_5(NH_3)_7]\cdot 6C_7H_8$ (**2**)

Bond lengths			
Zr(1)–N(100)	2.231(5)	Zr(1)–N(200)	2.192(5)
Zr(1)–N(2)	2.256(8)	Zr(1)–N(3)	2.285(6)
Zr(1)–N(3B)	2.329(7)	Zr(1)···Zr(1A)	3.220(1)
N(2)==N(3B)	3.114	N(3)==N(100)	2.966
N(2)==N(200)	2.839	N(3)==N(200)	2.712
K(1)–N(2)	3.818	K(1)–N(200)	3.670
Bond angles			
N(100)–Zr(1)–N(200)	65.5(3)	N(100)–Zr(1)–N(2)	144.3(3)
N(100)–Zr(1)–N(3)	82.08(19)	N(200)–Zr(1)–N(2)	79.0(3)
N(200)–Zr(1)–N(3)	74.63(18)	N(2)–Zr(1)–N(3)	92.9(3)
Zr(1)–N(100)–Zr(1B)	92.4(3)	Zr(1)–N(200)–Zr(1A)	94.5(3)
Zr(1)–N(3)–Zr(1A)	88.5(2)	Zr(1A)–Zr(1)–Zr(1B)	60.0

$N)(\mu_3\text{-}NH)_4(\mu\text{-}NH_2)_4]$. [2] The bond lengths of Zr–(μ-NH_2) are longer than those of the Zr–(μ-NH) bonds in $[(\eta^3\text{-}L)Zr(\mu\text{-}NH)]_2$ (2.039(8) and 2.057(8) Å) [32]. The Zr···Zr distances are also similar with those exhibited by $[(\eta^3\text{-}L)Zr(\mu\text{-}NH)]_2$ (3.168(2) Å) and the polyoxozirconium cluster $[\{(EtMe_4C_5)Zr\}_6(\mu_6\text{-}O)(\mu_3\text{-}O)_8]\cdot(C_7H_8)$ (from 3.1542(9) to 3.1709(11) Å, av. 3.1635 Å) [33,34]. The Zr–NH_2 and Zr–NH_3 bond lengths (Zr(1)–N(2) 2.256(8) Å) are slightly shorter than those of Zr–(μ-NH_2) bonds, but a little bit longer than those of the Zr–(μ_3-NH) bonds (see Table 2).

The N···N distances N(3)···N(200) ((μ-NH_2)···μ_3-N) 2.715 Å), N(3)···N(2), N(3)···N(2A) ((μ-NH_2)···NH_2/NH_3 3.290 and 3.107 Å), and N(200)···N(2) ((μ_3-N)···NH_2/NH_3 2.830 Å), indicate the possibility of formation of hydrogen bonds (free NH_3 molecules may be involved) when the building blocks were formed. The K(1)–N(200) (K–(μ_3-N) 3.664 Å) and the K(1)–N(3) (K–NH_2/NH_3 3.815 Å) distances are significantly longer than those of the K–N bonds found in $[(\eta^1\text{-}LH)Zr(N\mathit{t}Bu)\{(N\mathit{t}Bu)_2PPN\mathit{t}Bu\}^-\{K(\eta^6\text{-}C_7H_8)\}^+\cdot 0.5C_7H_8]$ (2.859(3), 2.892(4), and 3.086(3) Å) [45] and in $[(tmp)_{12}K_6Mg_6(C_6H_5)_6]$ (tmp = 2,2,6,6-tetramethylpiperidide; (3.191(4) and 3.090(4) Å)) [46,47]. Obviously, potassium links the four blocks together to yield a highly symmetrical complex via sixteen weak K–N bonds. The argument that there are only weakly coordinating interactions between different blocks and potassium, suggests that **2** should easily dissociate in solution or under EI-MS condition, which is indeed supported by the ^1H NMR and EI-MS spectral data of **2**.

For the formation of **2** it seems likely that first the four trinuclear zirconium units are formed, of which one $[(Cp^*Zr)_3(\mu_3\text{-}N)(\mu_3\text{-}NH)(\mu\text{-}NH_2)_3(NH_2)(NH_3)_2]$ is deprotonated. In this case, three of the Cp* ligands should be in the *cis*-arrangement at the $(ZrNH_2)_3$ ring in the trinuclear zirconium precursor, because all of the Cp* ligands are oriented outside the ball resembled core of **2**. However, it has been demonstrated that two of the Cp* and one of the terminal chlorine atoms lie on the same side of the $(ZrOH)_3$ ring, while the remaining Cp* ligands and chlorine atoms are arranged in the opposite position in the trinuclear zirconium compound $[\{(Cp^*ZrCl)(\mu\text{-}OH)\}_3(\mu_3\text{-}OH)(\mu_3\text{-}O)\cdot 2THF]$ [44]. Furthermore, it should be difficult to convert the trimer from the *trans*- to the *cis*-position during the aggregation process. We assume liquid ammonia and potassium are important as well for generating the *cis*-building block as for the formation of **2**.

4. Conclusions

We have shown that the novel potassium-centered highly symmetrical polynuclear zirconium complex **2** has been prepared by the ammonolysis of the alkyl substituted cyclopentadienyl zirconium trichloride in the presence of KH in a two-phase system (NH_3/toluene). A potassium cation is surrounded by four trinuclear zirconium species in **2**. To the best of our knowledge, **2** represents the biggest nitrogen-containing zirconium cluster. So far, we were not able to obtain crystalline products using sodium cation. Further work is concentrated on other cations.

5. Supplementary materials

CCDC-202641 (**2**) contains the supplementary crystallographic data for this paper. These data can be obtained free of charge via www.ccdc.cam.ak/conts/retrieving.htm (or from the Cambridge Crystallographic Data Centre, 12 Union Road, Cambridge CB21EZ, UK; (fax: +44-1223-336-033; or deposit@ccdc.cam.ac.uk).

[2] Zr_a–(μ_3-NH) 2.27 Å, Zr_b–(μ_3-NH) 2.19 Å Zr_a–(μ_5-N) 2.35 Å, Zr_b–(μ_5-N) 2.23 Å, Zr_b–(μ-NH_2) 2.31 Å, $Zr_a\cdots Zr_b = Zr_b\cdots Zr_b$ 3.146 Å, respectively [26].

Acknowledgements

This work was supported by the Deutsche Forschungsgemeinschaft, the Göttinger Akademie der Wissenschaften and the Fonds der Chemischen Industrie.

References

[1] R. Fix, R.G. Gordon, D.M. Hoffman, Chem. Mater. 3 (1991) 1138.
[2] R. Fix, R.G. Gordon, D.M. Hoffman, Chem. Mater. 5 (1993) 614.
[3] W.D. Munz, D. Hofmann, K. Hartig, Thin Solid Films 96 (1982) 79.
[4] R. Buhl, H.K. Pulker, E. Moll, Thin Solid Films 80 (1981) 265.
[5] M.-A. Nicolet, Thin Solid Films 52 (1978) 415.
[6] S. Kanamori, Thin Solid Films 136 (1986) 195.
[7] M. Wittmer, B. Studer, H. Melchior, J. Appl. Phys. 52 (1981) 5722.
[8] M. Veszelei, E. Veszelei, Thin Solid Films 236 (1993) 46.
[9] M.K. Wahlstrom, E. Johansson, E. Veszelei, P. Bennich, M. Olsson, S. Hogmark, Thin Solid Films 220 (1992) 315.
[10] D.M. Hoffman, Polyhedron 13 (1994) 1169.
[11] S.R. Kurtz, R.G. Gordon, Thin Solid Films 140 (1986) 277.
[12] W. Rockensüß, H.W. Roesky, Adv. Mater. 5 (1993) 443.
[13] R.M. Fix, R.G. Gordon, D.M. Hoffman, J. Am. Chem. Soc. 112 (1990) 7833.
[14] L.H. Dubois, Polyhedron 13 (1994) 1329.
[15] N. Yokoyama, K. Hinode, Y. Homma, J. Electrochem. Soc. 138 (1991) 190.
[16] A.L. Robinson, Science 233 (1986) 25.
[17] G.W. Parshall, Organometallics 6 (1987) 687.
[18] H.-P. Baldus, M. Jansen, Angew. Chem. 109 (1997) 338.
[19] H.-P. Baldus, M. Jansen, Angew. Chem. Int. Ed. 36 (1997) 328.
[20] M.M.B. Holl, P.T. Wolczanski, G.D. Van Duyne, J. Am. Chem. Soc. 112 (1990) 7989.
[21] M.M.B. Holl, M. Kersting, B.D. Pendley, P.T. Wolczanski, Inorg. Chem. 29 (1990) 1518.
[22] A. Abarca, P. Gómez-Sal, A. Martín, M. Mena, J.M. Poblet, C. Yélamos, Inorg. Chem. 39 (2000) 642.
[23] P. Gómez-Sal, A. Martín, M. Mena, C. Yélamos, J. Chem. Soc., Chem. Commun. (1995) 2185.
[24] A. Martín, M. Mena, A. Pérez-Redondo, C. Yélamos, Organometallics 21 (2002) 3308.
[25] A. Abarca, A. Martín, M. Mena, C. Yélamos, Angew. Chem. 112 (2000) 3602.
[26] A. Abarca, A. Martín, M. Mena, C. Yélamos, Angew. Chem. Int. Ed. 39 (2000) 3460.
[27] H.W. Roesky, Y. Bai, M. Noltemeyer, Angew. Chem. 101 (1989) 788.
[28] H.W. Roesky, Y. Bai, M. Noltemeyer, Angew. Chem. Int. Ed. 28 (1989) 754.
[29] M.M.B. Holl, P.T. Wolczanski, J. Am. Chem. Soc. 114 (1992) 3854.
[30] G. Bai, H.W. Roesky, M. Noltemeyer, H. Hao, H.-G. Schmidt, Organometallics 19 (2000) 2823.
[31] G. Bai, P. Müller, H.W. Roesky, I. Usón, Organometallics 19 (2000) 4675.
[32] G. Bai, H.W. Roesky, H.-G. Schmidt, M. Noltemeyer, Organometallics 20 (2001) 2962.
[33] G. Bai, H.W. Roesky, P. Lobinger, M. Noltemeyer, H.-G. Schmidt, Angew. Chem. 113 (2001) 2214.
[34] G. Bai, H.W. Roesky, P. Lobinger, M. Noltemeyer, H.-G. Schmidt, Angew. Chem. Int. Ed. 40 (2001) 2156.
[35] G. Bai, H.W. Roesky, J. Li, T. Labahn, F. Cimpoesu, J. Magull, Organometallics 22 (2003) 3034.
[36] G. Bai, H.W. Roesky, P. Müller, Bull. Pol. Acad. Sci. Chem. 50 (1) (2002) 1.
[37] G. Bai, Y. Peng, H.W. Roesky, J. Li, H.-G. Schmidt, M. Noltemeyer, Angew. Chem. 115 (2003) 1164.
[38] G. Bai, Y. Peng, H.W. Roesky, J. Li, H.-G. Schmidt, M. Noltemeyer, Angew. Chem. Int. Ed. 42 (2003) 1132.
[39] G. Bai, H.W. Roesky, J. Li, H.-G. Schmidt, M. Noltemeyer, Angew. Chem. 115 (2003) 5660.
[40] G. Bai, H.W. Roesky, J. Li, H.-G. Schmidt, M. Noltemeyer, Angew. Chem. Int. Ed. 42 (2003) 5502.
[41] G.M. Sheldrick, Acta Crystallogr., Sect. A 46 (1990) 467.
[42] G.M. Sheldrick, SHELXL-93: Program for Crystal Structure Refinement, Universität Göttingen, Göttingen, 1993.
[43] D. Nicholls, Inorganic Chemistry in Liquid Ammonia, Monograph 17, New York, 1979, p. 7.
[44] L.M. Babcock, V.W. Day, W.G. Klemperer, J. Chem. Soc., Chem. Commun. (1988) 519.
[45] G. Bai, H.W. Roesky, M. Noltemeyer, H.-G. Schmidt, J. Chem. Soc., Dalton Trans. (2002) 2437.
[46] P.C Andrews, A.R. Kennedy, R.E. Mulvey, C.L. Raston, B.A. Roberts, R.B. Rowlings, Angew. Chem. 112 (2000) 2036.
[47] P.C Andrews, A.R. Kennedy, R.E. Mulvey, C.L. Raston, B.A. Roberts, R.B. Rowlings, Angew. Chem. Int. Ed. 39 (2000) 1960.

Available online at www.sciencedirect.com
SCIENCE DIRECT®
Polyhedron 23 (2004) 1131–1137
POLYHEDRON
www.elsevier.com/locate/poly

Chiral copper(II) complexes of optically active Schiff bases: syntheses, crystal structure and asymmetric oxidation of methyl phenyl sulfide with hydrogen peroxide

Hai-Bin Zhu [a], Zhen-Ya Dai [b], Wei Huang [a], Kai Cui [a], Shao-Hua Gou [a,b,*], Cheng-Jian Zhu [b,*]

[a] *State Key Laboratory of Coordination Chemistry, Nanjing University, Nanjing 210093, China*
[b] *Department of Chemistry, Nanjing University, Nanjing 210093, China*

Received 13 November 2003; accepted 16 January 2004

Abstract

Several chiral copper(II) complexes of optically active Schiff bases (*R*,*R*)-**4a-c**, which have central seven-membered chelate rings, have been synthesized and characterized. X-ray single crystal analysis of a typical compound indicated that the complex is monomeric and the geometry around the metal atom is very distorted tetrahedral. All the complexes have been tested as catalysts for asymmetric oxidation of methyl phenyl sulfide. The mechanism of the catalytic reaction in the presence of these complexes has been tentatively elucidated.
© 2004 Elsevier Ltd. All rights reserved.

Keywords: Asymmetric oxidation; Chiral copper(II) complexes; Schiff base; Sulfide; Seven-membered

1. Introduction

Metal complexes with Schiff base ligands, despite a vast literature, continue to be of current interest for their application in asymmetric catalysis [1–5]. So far, a large number of these kinds of complexes have resulted from the coordination reaction between transition metals and chiral salen-type Schiff base ligands derived from the condensation of salicylaldehyde derivatives and optically active diamines such as 1,2-diphenyl-ethylenediamine or 1,2-diaminocyclohexane. Generally, five-membered or six-membered metal chelate rings have been generated in the formation of the complexes with the above-mentioned ligands, and they play an important structural role when these complexes act as catalysts for asymmetric synthesis. Although Schiff base metal complexes with 1,4-diamines derivatives have been reported, much attention has been focused on their stereochemical aspects [6–11]. Chiral metal complexes of this type with seven-membered chelate rings, however, have been rarely involved in the area of asymmetric catalysis [12]. To explore the catalytic function of the category of complexes with this notable structural feature, we herein report the synthesis and crystal structure of a few of chiral copper(II) complexes together with an examination of their potential as asymmetric oxidation catalysts for the conversion of sulfides to sulfoxides.

2. Experimental

2.1. General remarks

All solvents were of analytical grade and dried with standard methods and distilled before use. 3,5-di-*tert*-butyl-2-hydroxybenzaldehyde was prepared according to a literature method [13]. Elemental analyses were measured with a Perkin–Elmer 1400C analyzer. Infrared spectra (4000–400 cm^{-1}) were recorded on a Bruker Vector 22 FT-IR spectrophotometer. ^1H NMR spectra were obtained in a Bruker DRX 500 MHz spectrometer.

* Corresponding authors. Tel./fax: +862-53-59-5068.
E-mail address: sgou@netra.nju.edu.cn (S.-H. Gou).

0277-5387/$ - see front matter © 2004 Elsevier Ltd. All rights reserved.
doi:10.1016/j.poly.2004.02.005

Electrospray ionization (ES) mass spectra were recorded employing a Finnigan MAT SSQ 710 mass spectrometer in a scan range 100–1200 amu. Preparative thin layer chromatography was performed on 0.5 mm × 20 cm × 20 cm E. Merck silica gel plate (60F-254).

2.2. Synthesis of chiral 1,4-diaminobutane (*R,R*)-*1a–c*

Chiral 1,4-diaminobutane (*R,R*)-**1a–c** were prepared by literature methods [14].

(*R,R*)-**1a**: IR (KBr, cm^{-1}): 3369 br, s; 3300 br, s; 1588 s; 1194 m; 1095 s. ^1H NMR (500 MHz, $CDCl_3$, 25 °C, TMS): $\delta = 4.72$ (dd, 1H, CH), 3.70 (m, 2H, CH), 2.75 (m, 4H, CH_2), 1.74 (m, 1H, CH), 1.38 (s, 4H, NH_2), 0.88 (dd, 6H, CH_3). ESI-MS *m/z* (%): 175.1 (100) $[\mathbf{1a}+H]^+$. *Anal*. Calc. for $C_8H_{18}N_2O_2$: C, 55.15; H, 10.41; N, 16.08. Found: C, 55.17; H, 10.33; N, 16.17%.

(*R,R*)-**1b**: IR (KBr, cm^{-1}): 3400 br, s; 3375 br, s; 1637 m; 1592 m; 1221 m; 1174 m; 1159 m; 1094 m; 1066 m; 1026 m. ^1H NMR (500 MHz, $CDCl_3$, 25 °C, TMS): $\delta = 7.38 - 7.26$ (m, 5H, phenyl), 5.76 (s, 1H, CH), 3.78 (m, 2H, CH), 2.83–2.69 (m, 4H, CH_2), 1.37 (s, 4H, NH_2). ESI-MS *m/z* (%): 209.1 (100) $[\mathbf{1b}+H]^+$. *Anal*. Calc. for $C_{11}H_{16}N_2O_2$: C, 63.44; H, 7.74; N, 13.45. Found: C, 63.49; H, 7.65; N, 13.29%.

(*R,R*)-**1c**: IR (KBr, cm^{-1}): 3367 br, s; 3300 br, s; 1590 m; 1247 m; 1217 m; 1160 m; 1057 m. ^1H NMR (500 MHZ, $CDCl_3$, 25 °C, TMS): $\delta = 3.61$ (m, 2H, CH), 2.65 (m, 4H, CH_2), 1.52 (s, 4H, NH_2), 1.22 (s, 6H, CH_3). ESI-MS *m/z* (%): 161.1 (100) $[\mathbf{1c}+H]^+$. *Anal*. Calc. for $C_7H_{16}N_2O_2$: C, 52.48; H, 10.07; N, 17.49. Found: C, 52.50; H, 10.13; N, 17.52%.

2.3. Synthesis of Schiff bases (*R,R*)-*3a–c*

Schiff bases (*R,R*)-**3a–c** were prepared by a modification of the method reported by Jacobsen and coworkers [13].

(*R,R*)-**3a**: Yield, 80%; m.p. 142–143 °C. $[\alpha]_D^{15} = +30.6$ ($c = 1$, $CHCl_3$). IR (KBr, cm^{-1}): 3403 br, w; 1632 s; 1470 m. ^1H NMR (500 MHz, $CDCl_3$, 25 °C, TMS): $\delta = 13.48$ (br, 2H, OH), 8.44 (s, 2H, HC=N), 7.42 (s, 2H, phenyl), 7.12 (s, 2H, phenyl), 4.89 (d, 1H, CH), 4.24 (t, 1H, CH), 4.19 (t, 1H, CH), 3.93-3.84 (m, 4H, CH_2), 1.87 (m, 1H, CH), 1.47 (s, 18H, CH_3), 1.33 (s, 18H, CH_3), 0.96 (d, 6H, CH_3). ESI-MS *m/z* (%): 607.4 (100) $[\mathbf{3a}+H]^+$. *Anal*. Calc for $C_{38}H_{58}N_2O_4$: C, 75.21; H, 9.63; N, 4.62. Found: C, 75.17; H, 9.53; N, 4.81%.

(*R,R*)-**3b**: Yield, 73%; m.p. 82–84 °C. $[\alpha]_D^{15} = +3.2$ ($c = 1$, $CHCl_3$). IR (KBr, cm^{-1}): 3424 br, w; 1634 s; 1473 m. ^1H NMR (500 MHz, $CDCl_3$, 25 °C, TMS): $\delta = 13.50$ (br, 2H, OH), 8.50 (s, 1H, HC=N), 8.44 (s, 1H, HC=N), 7.50 (m, 2H, phenyl), 7.43 (s, 2H, phenyl), 7.36 (m, 3H, phenyl), 7.14 (s, 1H, phenyl), 7.09 (s, 1H, phenyl), 6.01 (s, 1H, CH), 4.48 (m, 2H, CH), 4.01–3.94 (m, 4H, CH_2), 1.49 (s, 18H, CH_3), 1.34 (s, 18H, CH_3). ESI-MS *m/z* (%): 641.3 (100) $[\mathbf{3b}+H]^+$. *Anal*. Calc. for $C_{41}H_{56}N_2O_4$: C, 76.84; H, 8.81; N, 4.37. Found: C, 76.88; H, 8.86; N, 4.44%.

(*R,R*)-**3c**: Yield, 70%; m.p. 122–124 °C. $[\alpha]_D^{15} = +49.5$ ($c = 1$, $CHCl_3$). IR (KBr, cm^{-1}): 3449 br, w; 1632 s; 1470 m. ^1H NMR (500 MHz, $CDCl_3$, 25 °C, TMS): $\delta = 13.48$ (br, 2H, OH), 8.42 (s, 2H, HC=N), 7.39 (s, 2H, phenyl), 7.09 (s, 2H, phenyl), 4.21 (m, 2H, CH), 3.91 (m, 2H, CH_2), 3.84 (m, 2H, CH_2), 1.58 (s, 6H, CH_3), 1.44 (s, 18H, CH_3), 1.30 (s, 18H, CH_3). ESI-MS *m/z* (%): 593.4 (100) $[\mathbf{3c}+H]^+$. *Anal*. Calc. for $C_{37}H_{56}N_2O_4$: C, 74.96; H, 9.52; N, 4.73. Found: C, 74.92; H, 9.61; N, 4.82%.

2.4. Preparation of chiral copper(II) complexes (*R,R*)-*4a–c*

A general procedure is described here. To the solution of a salen ligand (0.1 mmol) in methanol was added $Cu(OAc)_2 \cdot H_2O$ (0.02 g, 0.1 mmol) and the reaction mixture was stirred under reflux for 2 h. The precipitated solids were filtered, washed with methanol and dried in vacuum.

(*R,R*)-**4a**: Yield, 73%. IR (KBr, cm^{-1}): 1609 s; 1530 m; 1462 m. ESI-MS *m/z* (%): 668.4 (100) $[\mathbf{4a}+H]^+$. *Anal*. Calc. for $C_{38}H_{56}CuN_2O_4$: C, 68.28; H, 8.44, N, 4.19. Found: C, 68.04; H, 8.55, N, 4.25%.

(*R,R*)-**4b**: Yield, 72%. IR (KBr, cm^{-1}): 1613 s; 1530 m; 1461 m. ESI-MS *m/z* (%) 702.3 (100) $[\mathbf{4b}+H]^+$. *Anal*. Calc. for $C_{41}H_{54}CuN_2O_4$: C, 70.11; H, 7.75; N, 3.99. Found: C, 70.42; H, 7.56, N, 4.18%.

(*R,R*)-**4c**: Yield, 57%. IR (KBr, cm^{-1}): 1605 s; 1531 m; 1461 m. ESI-MS *m/z* (%) 654.4 (100) $[\mathbf{4c}+H]^+$. *Anal*. Calc. for $C_{37}H_{54}CuN_2O_4$: C, 67.91; H, 8.32; N, 4.28. Found: C, 67.85; H, 8.39; N, 4.29%.

2.5. Asymmetric oxidation

General procedure for asymmetric oxidation: Thioanisole (1.00 mmol) and the catalyst (0.01 mmol) were dissolved in acetonitrile at room temperature. To the solution was added hydrogen peroxide (1.10 mmol) at the same temperature and the mixture was stirred for 24 h, and filtrated through a pad of Celite. No sulfone was detected by TLC analysis of the filtrate. The filtrate was concentrated and purified by thin layer chromatography on silica gel (petroleum:ethylacetate = 3:1) to yield methyl phenyl sulfoxide. The enantiomeric excess of the sulfoxide was determined by HPLC analysis Daicel Chiralcel OD (hexane:*i*-PrOH = 9:1).

2.6. Crystallographic data for (*R,R*)-*4c*

A single crystal of (*R,R*)-**4c** was measured on a Bruker CCD-4K diffractometer using graphite-monochromated MoKα ($\lambda = 0.71073$ Å) radiation at 293(2) K. The data were collected using SMART and reduced

Table 1
Summary of crystal data for complex (*R*,*R*)-**4c**

Empirical formula	$C_{37}H_{54}CuN_2O_4$
Formula weight	654.36
Crystal size (mm)	$0.36 \times 0.40 \times 0.44$
Crystal system	monoclinic
Wavelength (Mo Kα) (Å)	0.71073
Space group	$P2_1$
Unit cell dimensions	
a (Å)	11.341(1)
b (Å)	24.277(3)
c (Å)	14.828(2)
β (°)	103.35(1)
V (Å^3)	3972.4(8)
Z	4
D_{calc} (Mg m^{-3})	1.094
F(000)	1404
μ (mm^{-1})	0.585
Temperature (K)	293(2)
Index ranges	$-13 \leqslant h \leqslant 13$; $-28 \leqslant k \leqslant 19$; $-17 \leqslant l \leqslant 15$
Reflections collected/unique (R_{int})	11138/5710 (0.0838)
Refinement method	full-matrix least-squares on F^2
Absorption correction	empirical
Data/parameters	11138/793
Goodness-of-fit on F^2	1.056
Final *R* indices [$I > 2\sigma(I)$]	$R_1 = 0.0914$ $wR_2 = 0.1222$
R indices (all data)	$R_1 = 0.1708$ $wR_2 = 0.1415$
Flack value	0.02(2)
Maximum/minimum, Δρ (e Å^{-3})	0.418 and −0.391

by using the program SAINT [15]. Empirical absorption correction was done by using the SADABS program [16]. The structure was solved by direct methods and refined by least squares method on F^2_{obs} by using the SHELXTL-PC software package [17]. The anisotropic thermal parameters of all non-hydrogen atoms were refined by the full-matrix least-squares procedure and the hydrogen atom positions were geometrically fixed and allowed to ride on the attached atoms. The experimental details and refinement results for (*R*,*R*)-**4c** are listed in Table 1.

3. Results and discussion

3.1. Synthesis and molecular structure of the copper(II) complexes

Following a modified literature procedure [13], condensation of optical 1,4-diamines (*R*,*R*)-**1a**–**c** with 3,5-di-*tert*-butyl-2-hydroxybenzaldehyde **2** in ethanol at 80 °C yielded the corresponding Schiff base derivatives (*R*,*R*)-**3a**–**c**. Complexation of copper(II) acetate monohydrate by (*R*,*R*)-**3a**–**c** readily afforded complexes (*R*,*R*)-**4a**–**c** (Scheme 1).

Electrospray ionization mass spectra of these compounds revealed that all the copper(II) complexes were mononuclear. Slow evaporation of the acetonitrile solution of (*R*,*R*)-**4c** gave dark brown crystals suitable for X-ray analysis. The other two complexes (*R*,*R*)-**4a** and (*R*,*R*)-**4b** were consistently obtained as feathery needles unsuitable for crystallographic analysis. The molecular structure of (*R*,*R*)-**4c** is given in Fig. 1.

As shown, the presence of bulky substituents on the phenyl ring has made the two aromatic rings not co-planar. The copper(II) atom of (*R*,*R*)-**4c**, which is four-coordinate, has a geometry of very distorted tetrahedral. The dihedral angle between the Cu(1), N(2), C(22), C(16), C(17), O(2) plane and its counter-part is 48.7°, which is slightly larger than that [42.6(3)°] of the analogous (salen) Cu(II) complex reported by Nathan et al. [18]. This difference in dihedral angle can be explained by the steric repulsion of *tert*-butyl groups as well as the more flexible chain (four carbon atoms) of our salen-type ligand. The Cu–N distances and Cu–O distances are in the range 1.95–1.99 and 1.89–1.90 Å, respectively, comparable to the corresponding bond lengths found in the complex [Cu(sal-4)] reported earlier [18]. It is anticipated that the two imine-N atoms and its carbon chain form a seven-membered chelate ring with the metal atom in the complex. The chelate bite angle in the seven-membered ring is 101.3(3)°, and the C(32), C(33), O(4), C(35), O(3) atoms constitute a five-membered ring close to an ideal half-chair conformation in its neighbor.

3.2. Asymmetric oxidation of methyl phenyl sulfide

The oxidation of prochiral sulfides to sulfoxides has been catalyzed by a range of chiral vanadyl complexes [19], manganese complexes [20] and titanium complexes [21] of Schiff base ligands. Recently Cross and coworkers [22] have described the asymmetric oxidation of sulfide with copper(II) complexes. Using 10 mol % of the copper(II) complex as the catalyst and hydrogen peroxide as the oxygen source, they obtained enantioselectivity of only up to 14% e.e. However, to date there have been no reports of this reaction catalyzed by chiral Schiff base metal complexes with 1,4-diamines derivatives. To explore the effect of such a kind of metal complex as enantioselective catalysts, complexes (*R*,*R*)-**4a**–**c** were tested as catalysts for H_2O_2 oxidation of PhMeS (Scheme 2).

It is found that in acetonitrile catalysts (*R*,*R*)-**4a**–**c** were effective with good chemical yields (>80%), but only (*R*,*R*)-**4c** produced a reasonable enantiomeric excess (17%). To our knowledge, reaction at lower temperature may improve the enantioselectivity. In our further examination of the temperature effect on enantioselectivity, however, the reaction at 0 °C turned out to proceed very slowly. We also examined the oxidation of methyl phenyl sulfide in the presence of various solvents. Compared with acetonitrile, *n*-hexane

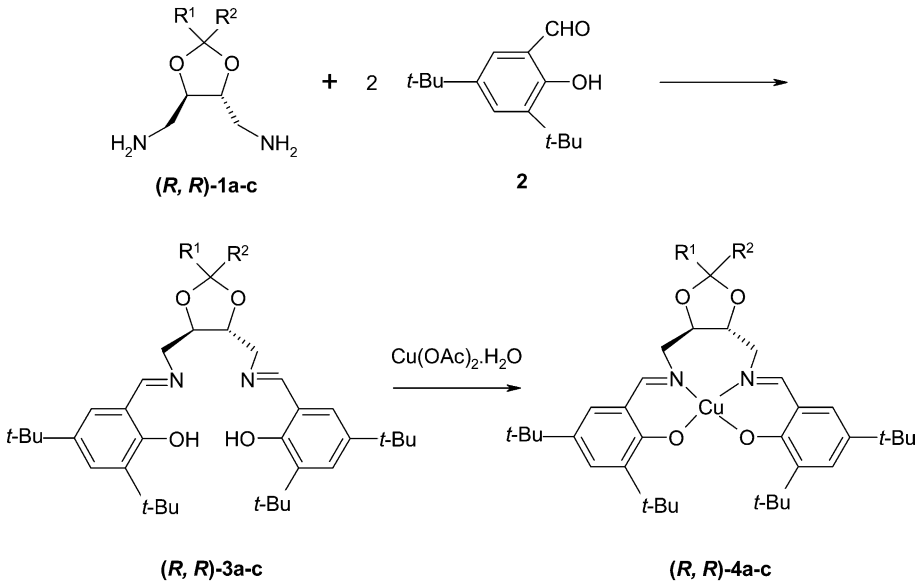

1,3,4	a	b	c
R^1	H	H	Me
R^2	*i*-Pr	Ph	Me

Scheme 1. Preparation of Schiff base ligands (*R*,*R*)-**3a**–**c** and their copper(II) complexes (*R*,*R*)-**4a**–**c**.

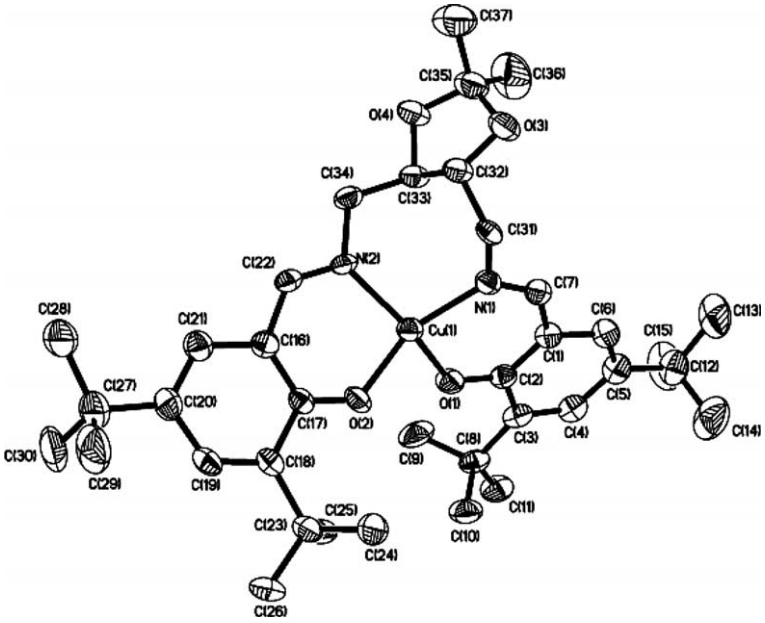

Fig. 1. ORTEP drawing of the complex (*R*,*R*)-**4c** (30% thermal probability) with the atom numbering scheme. Hydrogen atoms are omitted for clarity. Selected bond lengths (Å) and angles (°) (standard deviations in parentheses): Cu(1)–O(1): 1.892(6); Cu(1)–O(2): 1.891(7); Cu(1)–N(1): 1.953(8); Cu(1)–N(2): 1.990(8). O(1)–Cu(1)–O(2): 89.2(3); N(1)–Cu(1)–N(2): 101.3(3); O(1)–Cu(1)–N(1): 92.5(3); O(2)–Cu(1)–N(2): 94.0(3); O(1)–Cu(1)–N(2): 149.6(3); N(1)–Cu(1)–O(2): 146.0(3).

slightly improved chemical yield but with negligible (<2%) e.e., while $CHCl_3$ and CH_2Cl_2 lower the chemical yield without generating significant enantiomeric excess. It is noted that the use of DMF as a solvent caused the decomposition of the catalysts. When Bu^{t}OOH was used as an oxidant instead of aqueous H_2O_2, the reac-

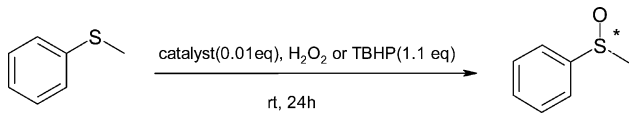

Scheme 2. Asymmetric oxidation of methyl phenyl sulfide catalyzed by (*R*,*R*)-**4a**–**c**.

tion proceeded smoothly but with lower e.e. (< 6%). In all cases of our reaction, no sulfone was observed.

The mechanism of the asymmetric oxidation of sulfide catalyzed by a chiral copper(II) complex with Schiff base ligands is still unclear at present. Recently Decinti and coworkers [23] have proposed that the mechanism of styrene epoxidation with iodosylbenzene in the presence of copper(II) Schiff base complexes involved the formation of copper–iodosylbenzene adducts as intermediates. We also performed the reaction of complex (*R*,*R*)-**4c** with hydrogen peroxide in the absence of substrate under the same conditions as a catalytic process in attempt to identify the reactive species. Spectrometric measurements in the UV-Vis region of metal complexes–hydrogen peroxide mixtures showed that the characteristic spectral bands of complex (*R*,*R*)-**4c** undergo a decrease in absorbance with increasing reaction time, which reflects a decrease in the concentration of the metal complex. Moreover it is observed that the rates of the spectral changes in different solvents are not the same (Fig. 2). We postulated that an analogous intermediate, copper–hydrogen peroxide adducts, may also be involved in our performed reaction. Differences in the observed rates of the spectral changes in different solvents may suggest that the stability of the copper–hydrogen peroxide adducts vary in the sequence $CH_3CN > n\text{-}C_6H_{14} > CHCl_3$. The instability of this adduct is also supported in the experiment by the observation of slow decomposition of the catalyst. It is known that the enantioselectivity of the reaction originates from the stereochemical communication between the substrate and catalytic species. The stability of the catalytic species is crucial for full stereochemical communication in the transition state. So the observation of relatively higher enatioselectivity in CH_3CN compared with other solvents may be interpreted on the basis of the above considerations. At 0 °C under the same conditions the absorbance of spectral bands of the copper(II) complex showed a slight change, perhaps indicative of no obvious interaction between (*R*,*R*)-**4c** and H_2O_2. It maybe suggested that at 0 °C no e.e. could be obtained in our catalytic system. Investigations are currently underway to improve the efficiency of the catalysts and to determine which copper species is responsible for the observed enantioselectivity.

The observation of lower enantioselectivity in the sulfide oxidation may also be interpreted on the basis of the molecular structure of the copper(II) complex (*R*,*R*)-**4c**. For the sake of comparison, we also performed

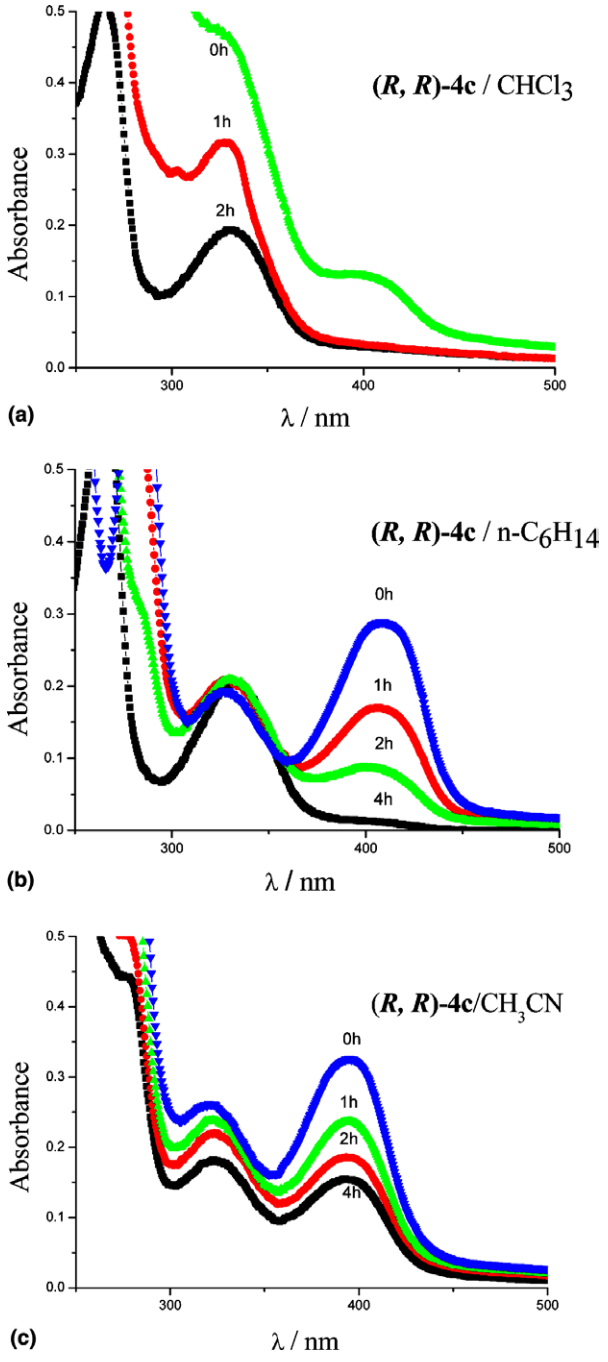

Fig. 2. Absorption spectra in the d–d band region of complex (*R*,*R*)-**4c** at room temperature in different solvents: in the absence of H_2O_2 ($t = 0$); in the presence of excess H_2O_2 at different time intervals ($t = 1$ h, $t = 2$ h, $t = 4$ h).

molecular mechanics (UFF) optimization calculations on copper(II) complexes (*R*,*R*)-**4a**–**b** with the GAUSSIAN 98 package [24]. The results revealed that the diol-protected groups in the complexes (*R*,*R*)-**4a**–**c** are far away from apical coordinating site of the central metal and exhibited no interaction with the oncoming sulfide approaching the metal along the orientations of two Cu–N bonds with similar ease (Fig. 3). Accordingly,

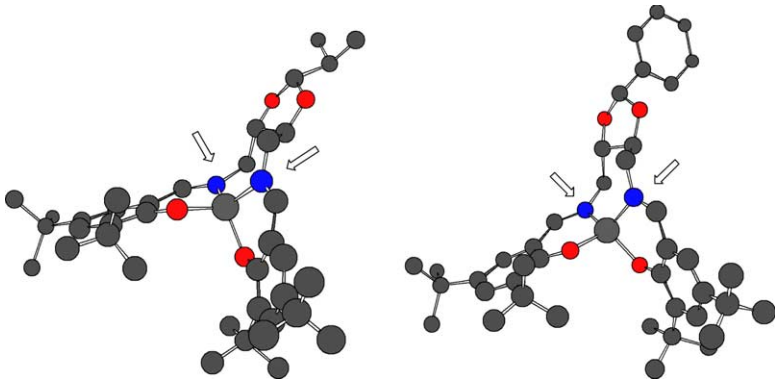

Fig. 3. Molecular structures of (*R*,*R*)-**4a** and (*R*,*R*)-**4b** optimized by molecular mechanics (UFF).

high asymmetric induction was not realized in the oxidation of sulfide with (*R*,*R*)-**4a**–**c**. On the other hand, it is not excluded that the accelerating non-catalytic oxidation reaction at room temperature may also contribute to low e.e.

4. Conclusion

Overall we have prepared three new chiral copper(II) complexes of an optically active schiff base (*R*,*R*)-**4a**–**c** with a central seven-membered ring. Although useful enantioselectivity has not yet been attained in sulfide oxidation with the system thus far, it is likely that significant improvements will result from further modification of the steric and electronic properties of these and related catalysts.

5. Supplementary materials

CCDC-221370 contains the supplementary crystallographic data for this paper. These data can be obtained free of charge at www.ccdc.cam.ac.uk/conts/retrieving.html or from the Cambridge Crystallographic Data Centre, 12, Union Road, Cambridge CB2 1EZ, UK; fax: (internat.) +44-1223/336-033; e-mail: deposit@ccdc.cam.ac.uk.

Acknowledgements

The authors are grateful to the referees' helpful suggestions. Thanks are due to the financial support by the National Natural Science Foundation of China (projects 20271026 and 20391001). S.G. is also indebted to the State Department of Education for Boshidian funding.

References

[1] (a) W. Zhang, J.L. Loebatch, E.N. Jacobsen, J. Am. Chem. Soc. 112 (1990) 2801;
(b) W. Zhang, E.N. Jacobsen, J. Org. Chem. 56 (1991) 2296;
(c) N. Hosoya, A. Hatayama, R. Irie, H. Sasaki, T. Kastuki, Tetrahedron 50 (1994) 4311;
(d) P. Mosset, A. Scheurer, Tetrahedron 55 (1999) 1063.
[2] (a) M. Tokunaga, J.F. Larrow, F. Kakiuchi, E.N. Jacobsen, Science 277 (1997) 936;
(b) S.E. Schaus, B.D. Brandes, J.F. Larrow, M. Tokunaga, K.B. Hansen, A.E. Gould, M.E. Furrow, E.N. Jacobsen, J. Am. Chem. Soc. 124 (2002) 1307;
(c) B.D. Brandes, E.N. Jacobsen, Tetrahedron: Asymmetry 8 (1997) 3927.
[3] (a) L.E. Martínez, J.L. Leighton, D.H. Carsten, E.N. Jacobsen, J. Am. Chem. Soc. 117 (1995) 5897;
(b) E.N. Jacobsen, F. Kakjuchi, R.G. Konsler, J.F. Larrow, M. Tokunaga, Tetrahedron Lett. 38 (1997) 773;
(c) H. Lebel, E.N. Jacobsen, Tetrahedron Lett. 40 (1999) 7303.
[4] (a) T. Fukuda, T. Katsuki, Tetrahedron 53 (1997) 7201;
(b) T. Niimi, T. Uchida, R. Irie, T. Katsuki, Tetrahedron Lett. 41 (2000) 3647;
(c) T. Uchida, B. Saha, T. Katsuki, Tetrahedron Lett. 42 (2001) 2521;
(d) B. Saha, T. Uchida, T. Katsuki, Tetrahedron: Asymmetry 14 (2003) 823.
[5] (a) K. Aikawa, R. Irie, T. Katsuki, Tetrahedron 57 (2001) 845;
(b) Y.N. Belokon, M. North, V. Kublitski, N.S. Ikonnikov, P.E. Krasik, V.I. Maleev, Tetrahedron Lett. 40 (1999) 6105;
(c) Y.N. Belokon, G.R. Davies, M. North, Tetrahedron Lett. 41 (2000) 7245.
[6] S. Yamada, Coord. Chem. Rev. 190–192 (1999) 537.
[7] (a) M. Mathew, A.J. Carty, G.J. Palenik, J. Am. Chem. Soc. 92 (1970) 3197;
(b) G.A. Kolawole, K.S. Patel Soc., J. Chem. Dalton Trans. (1981) 1241;
(c) P.E. Riley, V.L. Pecoraro, C.J. Carrano, J.A. Bonadies, K.N. Raymond, Inorg. Chem. 25 (1986) 154.
[8] (a) M. Calvin, C.H. Barkelew, J. Am. Chem. Soc. 68 (1946) 2267;
(b) H. Weigold, B.O. West, J. Chem. Soc. (A) (1967) 1310;
(c) A.E. Martell, M. Calvin, Chemistry of the Metal Chelate Compounds, Prentice-Hall, New York, 1952, p. 266;
(d) M. Hariharan, F.L. Urbach, Inorg. Chem. 8 (1969) 556.
[9] R.H. Holm, J. Am. Chem. Soc. 82 (1960) 5632.
[10] G.E. Batley, D.P. Graddon, Aust. J. Chem. 20 (1967) 885.
[11] (a) S.K. Shaikhutdinov, A.N. Shupik, E.M. Trukhan, J. Chem. Soc., Faraday Trans. 89 (1993) 3959;
(b) G.E. Batley, D.P. Graddon, Aust. J. Chem. 21 (1968) 267;
(c) G.E. Batley, D.P. Graddon, Aust. J. Chem. 21 (1968) 1473.
[12] W. Zhang, Ph.D. Thesis, University of Illinois, September 1991.
[13] J.F. Larrow, E.N. Jacobsen, J. Org. Chem. 59 (1994) 1939.
[14] D.K. Kim, G. Kim, J. Gam, Y.B. Cho, H.T. Kim, J.H. Tai, K.H. Kim, W.S. Hong, J.G. Park, J. Med. Chem. 37 (1994) 1471, and references therein.

[15] Siemens, SAINT v4 Software Reference Manual, Siemens Analytical X-ray Systems, Inc., Madison, WI, 1996.
[16] G.M. Sheldrick, sc sadabs, Program for Empirical Absorption Correction of Area Dectector Data, University of Gottingen, Germany, 1996.
[17] Siemens, SHELXTL, Version 5 Reference Manual, Siemens Analytical X-ray Systems, Inc., Madison, WI, 1996.
[18] L.C. Nathan, J.E. Koehne, J.M. Gilmore, K.A. Hannibal, W.E. Dewhirst, T.D. Mai, Polyhedron 22 (2003) 887.
[19] (a) K. Nakajima, M. Kojima, J. Fujita, Chem. Lett. (1986) 1483;
(b) C. Bolm, F. Bienewald, Angew. Chem. Int. Ed. Engl. 34 (1995) 2640;
(c) K. Nakajima, K. Kojima, M. Kojima, J. Fujita, Bull. Chem. Soc. Jpn. (1990) 620;
(d) J. Skarżewski, E. Ostrycharz, R. Siedlecka, Tetrahedron: Asymmetry 10 (1999) 3457;
(e) A.H. Vetter, A. Berkessel, Tetrahedron Lett. 39 (1998) 1741;
(f) B. Pelotier, M.S. Anson, I.B. Campbell, S.J.F. Macdonald, G. Priem, Synlett. (2002) 1055.
[20] (a) M. Palücki, P. Hanson, E.N. Jacobsen, Tetrahedron Lett. 33 (1992) 7111;
(b) K. Noda, N. Hosoya, R. Irie, Y. Yamashita, T. Katsuki, Tetrahedron 50 (1994) 9609.
[21] (a) S. Colonna, A. Manfredi, M. Spadoni, L. Casella, M. Gulloti, J. Chem. Soc., Perkin Trans. I (1981) 71;
(b) C. Sasaki, K. Nakajima, M. Kojima, J. Fujita, Bull. Chem. Soc. Jpn. 64 (1991) 1318.
[22] S. Bunce, R.J. Cross, L.J. Farrugia, S. Kunchandy, L.L. Meason, K.W. Muir, M. O'Donnell, R.D. Peacock, D. Stirling, S.J. Teat, Polyhedron 17 (1998) 4179.
[23] S. Zolezzi, E. Spodine, A. Decinti, Polyhedron 22 (2003) 1653.
[24] M.J. Frisch, G.W. Trucks, H.B. Schlegel, G.E. Scuseria, M.A. Robb, J.R. Cheeseman, V.G. Zakrzewski, J.A. Montgomery Jr., R.E. Stratmann, J.C. Burant, S. Dapprich, J.M. Millam, A.D. Daniels, K.N. Kudin., M.C. Strain, O. Farkas, J. Tomasi, V. Barone, M. Cossi, R. Cammi, B. Mennucci, C. Pomelli, C. Adamo, S. Clifford, J. Ochterski, G.A. Petersson, P.Y. Ayala, Q. Cui, K. Morokuma, N. Rega, P. Salvador, J.J. Dannenberg, D.K. Malick, A.D. Rabuck, K. Raghavachari, J.B. Foresman, J. Cioslowski, J.V. Ortiz, A.G. Baboul, B.B. Stefanov, G. Liu, A. Liashenko, P. Piskorz, I. Komaromi, R. Gomperts, R.L. Martin, D.J. Fox, T. Keith, M.A. Al-Laham, C.Y. Peng, A. Nanayakkara, M. Challacombe, P.M.W. Gill, B. Johnson, W. Chen, M.W. Wong, J.L. Andres, C. Gonzalez, M. Head-Gordon, E.S. Replogle, J.A. Pople, GAUSSIAN 98, Revision A.11.3, Gaussian, Inc., Pittsburgh, PA, 2002.

Available online at www.sciencedirect.com
SCIENCE DIRECT®
Polyhedron 23 (2004) 1139–1144
POLYHEDRON
www.elsevier.com/locate/poly

Preparation and crystal structure of (2,2′-bibenzimidazole)dihalobis(triphenylphospine)rhenium(III) halides

François Baril-Robert, André L. Beauchamp *

Département de chimie, Université de Montréal, C.P. 6128, Succursale Centre-ville, Montréal, QC, Canada H3C 3J7

Received 3 September 2003; accepted 18 January 2004

Abstract

The reaction of $ReOX_3(PPh_3)_2$ (where X = Cl, Br) with 2,2′-bibenzimidazole ($bibzimH_2$) in the presence of excess PPh_3 yields the rhenium(III) cationic complexes $[ReX_2(PPh_3)_2(bibzimH_2)]X$, in which the phosphines are *trans* to one another, whereas the plane perpendicular to this direction includes the chelating bidentate $bibzimH_2$ and two *cis* halogen ligands. The third halogen is a halide counter-ion, attached to the complex cation via a pair of $N–H\cdots X^-$ hydrogen bonds involving the two N–H groups of $bibzimH_2$. Crystallographic work on the chloro compound indicates that the departure from octahedral geometry is controlled by the bite of the $bibzimH_2$ ligand and that the presence of the phenylene groups does not introduce substantial steric hindrance. Despite the fact that the species is paramagnetic, the ^1H NMR spectra were fully assigned.
© 2004 Elsevier Ltd. All rights reserved.

Keywords: Rhenium; Benzimidazole; Bibenzimidazole; Crystal structure; Paramagnetic NMR

1. Introduction

In the recent years, our laboratory has become interested in the complexation of 2,2′-biimidazole ($biimH_2$, Scheme 1) to various metal centers. In the formally neutral form, two nitrogen donors in coplanar rings can adopt a *syn* orientation leading to chelates similar to those of bipyridine. However, $biimH_2$ differs from bipyridine by the presence of five-membered rings, which change the bite angle for chelate formation and allow for more conformational freedom about the connecting C2–C2′ bond, thereby leading to oligomeric or polymeric structures [1–3]. In both cases, the residual N–H bonds generate in the crystal particular hydrogen-bond patterns from which supramolecular assemblies can be constructed. Extra structural features appear when biimidazole coordinates in the monoanionic form, since one of the uncoordinated nitrogens is protonated and the other is not. Hydrogen bonding then takes place with donors, acceptors, or more interestingly, with units containing one of each, including monodeprotonated biimidazolate itself, which gives access to an enlarged variety of patterns for crystal engineering. This versatility is well illustrated by the series of compounds reported by Takodoro et al. [4–7]. Finally, fully deprotonated dianionic biimidazolate can behave as a bis-bidentate/chelating unit like the oxalate dianion and link two metal centers into larger building blocks [8–10] that could be considered in the development of molecular devices [11,12].

In our previous contributions [13,14], we reported that the Re(V) precursors $ReOX_3(PPh_3)_2$ and $ReO(OEt)X_2(PPh_3)_2$ are reduced cleanly by PPh_3 in the presence of $biimH_2$, giving good yields of the rhenium(III) cationic complexes *cis*,*trans*-$[ReX_2(PPh_3)_2(biimH_2)]X$ with X = Cl, Br and I. The residual N–H protons of coordinated $biimH_2$ were found to be moderately acidic and to participate in strong hydrogen-bonding interactions, leading to tight ion pairs with halide or carboxylate counter-ions. By using the smaller phosphine PMe_3, neutral complexes containing monodeprotonated

* Corresponding author. Tel.: +514-343-6446; fax: +514-343-7586.
E-mail address: andre.beauchamp@umontreal.ca (A.L. Beauchamp).

0277-5387/$ - see front matter © 2004 Elsevier Ltd. All rights reserved.
doi:10.1016/j.poly.2004.01.012

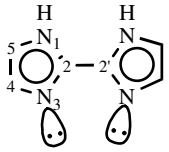

Scheme 1.

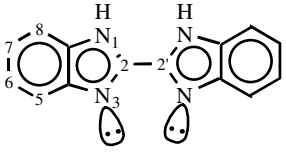

Scheme 2.

biimidazole could be isolated as dimers assembled by a pair of complementary N–H···N hydrogen bonds. This study is being extended here to 2,2-bibenzimidazole ($bibzimH_2$, Scheme 2), in which the presence of phenylene units opens a number of possibilities for ligand tuning via substitution on the ring. We wish to report the preparation and structural characterization of the compounds $[ReX_2(PPh_3)_2(bibzimH_2)]X$, which show that the extra phenylene rings do not introduce appreciable steric or other undesirable effects and that the chemistry of the Re(III)-$biimH_2$ systems is applicable to the bulkier $bibzimH_2$ system.

2. Experimental

2.1. Reactants and methods

$KReO_4$ and all other reactants were obtained from Aldrich and used without further purification. $ReOCl_3(PPh_3)_2$ [15] and $ReOBr_3(PPh_3)_2$ [16] were prepared by literature methods. Deuterated solvents were purchased from Aldrich or CDN Isotopes.

The NMR spectra were measured with Bruker ARX-400 or AMX-300 spectrometers. For the ^1H spectra, the residual solvent signals (DMSO-d_6, 2.50 ppm; $CDCl_3$, 7.26 ppm) were used as internal references and the chemical shifts are expressed in ppm versus $SiMe_4$. Electronic spectra were recorded as $CHCl_3$ solutions in quartz cells with a UV–Vis–NIR Cary 5E spectrometer. FAB^+ mass spectra in NBA were measured at the Centre de Spectrométrie de Masse de l'Université de Montréal. Elemental analyses were run at the Laboratoire d'Analyse Élémentaire de l'Université de Montréal.

2.2. Preparation of the ligand

2,2′-Bibenzimidazole was prepared as described by Fieselmann et al. [17]. In our hands, the purification by recrystallization from ethylene glycol was not totally efficient and an extra purification step was introduced. The yellow solid was dissolved in boiling NaOH, 0.25 M, and refluxed for 2 days. Some insoluble material was filtered off and the dark-brown solution was neutralized with concentrated HCl. The light-violet solid was filtered, transferred into water and refluxed for 1 h to remove any ionic form of the molecule. Finally, the solid was filtered, washed with water, ethanol and diethyl ether, and dried in air. Yield: 24%.

2.3. Preparation of $[ReX_2(PPh_3)_2(bibzimH_2)]X$

A suspension of PPh_3 (0.238 g; 0.91 mmol) and $bibzimiH_2$ (0.123 g; 0.52 mmol) in 40 mL $CHCl_3$ is heated to the boiling point, and $ReOCl_3(PPh_3)_2$ (0.354 g; 0.42 mmol) is added. The lime-green solution darkens quickly and the mixture is refluxed for 2.5 h. It is filtered hot and evaporation of the resulting dark-red solution yields a sticky dark-red material. Upon dropwise addition of diethyl ether, a red powder is obtained, which is filtered and washed with diethyl ether. Crystals of the solvent-free material are obtained by slow diffusion of diethyl ether into a CH_2Cl_2 solution.

2.3.1. $[ReCl_2(PPh_3)_2(bibzimH_2)]Cl$

Yield: 77%. ^1H NMR ($CDCl_3$): see text. MS FAB^+ (*m*/*z*): 1014 $[M]^+$, 752 $[M-PPh_3]^+$, 717 $[M-PPh_3-Cl]^+$. UV–Vis (λ (nm) (ε (M^{-1} cm^{-1}))): 558 (670), 522 (675), 469 (1350), 434 (1400), 404 (1200), 360 (8700), 341 (8750), 330 (6500). Composition was determined by X-ray diffraction on a crystal picked up in the morphologically homogeneous sample.

2.3.2. $[ReBr_2(PPh_3)_2(bibzimH_2)]Br$

Same as above, from $ReOBr_3(PPh_3)_2$. Yield: 72%. *Anal.* Calc. for $C_{50}H_{40}Br_3N_4P_2Re$: C, 50.69; H, 3.40; N, 4.73. Found: C, 50.94; H, 3.42; N, 4.72%. ^1H NMR ($CDCl_3$): see text. MS FAB^+ (*m*/*z*): 1102 $[M]^+$, 843 $[M-PPh_3]^+$, 762 $[M-PPh_3\text{-}Br]^+$.

2.4. X-ray diffraction study

To grow the crystals used for X-ray work, the powder was placed in a vial and covered with acetone, the vial was closed tightly and left at room temperature for a few days. The powder dissolved slowly and reprecipitated as less soluble red blocks of the solvate *cis*-$[ReCl_2(PPh_3)_2(bibzimH_2)]Cl\cdot 3(CH_3)_2CO$. The X-ray data were collected with a Bruker Smart 2K CCD diffractometer using the graphite-monochromatized Cu Kα radiation, as described elsewhere [18]. The data were interpreted with the SHELXTL software [19]. The XPREP procedure [20] was used to apply an absorption correction based on crystal morphology. The non-hydrogen atoms were generally refined anisotropically. The hydrogens were first placed at idealized positions and allowed to ride

Table 1
Crystal data for $[ReCl_2(PPh_3)_2(bibzimH_2)]Cl \cdot 3(CH_3)_2CO$

Formula	$C_{59}H_{58}Cl_3N_4O_3P_2Re$
Formula weight	1225.58
T (K)	220(2)
Diffractometer	Bruker Smart CCD 2K
Crystal system	monoclinic
Space group	$P2_1/n$ (no. 14)
a (Å)	14.4209(2)
b (Å)	23.6633(4)
c (Å)	16.7633(2)
β (deg)	94.860(1)
Volume (Å^3)	5699.8(1)
Z	4
d_{calc} (g/cm^3)	1.428
Reflection cell parameters	50 312
Crystal dimensions (mm)	$0.16 \times 0.26 \times 0.38$
Radiation (λ, Å)	Cu Kα (1.54178)
μ (cm^{-1})	63.60
Transmission range	0.185–0.361
Reflections measured	68 215
Reflections independent	11 165 ($R_{int} = 0.07$)
Reflections observed ($I > 2\sigma$)	9843
R^* ($I > 2\sigma$)	0.0555
$wR_2{}^*$ ($I > 2\sigma$)	0.1582
S^* ($I > 2\sigma$)	1.076

$^* R = \sum \|F_o| - |F_c\| / \sum |F_o|$, $wR_2 = \{\sum[w(F_o^2 - F_c^2)^2] / \sum w(F_o^2)^2\}^{1/2}$, $S = \{\sum[w(F_o^2 - F_c^2)^2] / (N_{obs} - N_{param})\}^{1/2}$.

on the supporting atom. No disorder was detected in the $[ReCl_2(PPh_3)_2(bibzimH_2)]^+$ unit, but the chloride counter-ion and the three acetone molecules of the asymmetric unit were disordered. Each of these acetone sites was modeled with three different sets of positions. The FLAT option was used to keep the molecule planar, whereas constraints were applied on interatomic distances, based on the average data for solvate acetone in the Cambridge Crystallographic Database [21] [C=O, 1.21 Å; C–CH_3, 1.47 Å; O···CH_3, 2.33 Å; CH_3···CH_3, 2.51 Å]. A very small tolerance on the distances had to be applied to stabilize the refinement. The occupancies were first refined with a constraint applied to normalize their sum to unity, then they were rounded off to the nearest 0.05 and fixed (0.60/0.20/0.20) for the rest of the refinement. The chloride ion was described by means of two positions located on each side of the plane through $bibzimH_2$. These positions were initially refined separately, then simultaneously. The occupancies were refined as above and fixed (0.60/0.40) in the last least-squares cycles. The final R factor of 0.055 is considered to be satisfactory, considering the severe disorder present in the structure. The crystal data are collected in Table 1.

A data set was also collected on red plates of the solvent-free complex salt, grown by slow diffusion of diethyl ether into a saturated CH_2Cl_2 solution of the raw material. These crystals belong to space group *Pbca*, with $a = 11.199$, $b = 23.455$, $c = 34.567$ Å and $Z = 8$ molecules per cell. The complex showed the same structure as the Tris–acetone solvate, except for a two-fold orientation disorder around the Re–P bond for one of the PPh_3 ligands. Because of disorder and poor crystal quality, the R factor could not be reduced below of 0.12. No further efforts were devoted to this material, since better crystals of the solvate had become available in the meantime.

3. Results and discussion

Good yields of the bromo and chloro complexes $[ReX_2(PPh_3)_2(bibzimH_2)]X$ are obtained by heating $ReOX_3(PPh_3)_2$ and bibenzimidazole in $CHCl_3$ in the presence of excess PPh_3 (Scheme 3). Infrared spectra confirm the presence of PPh_3 and $bibzimH_2$ in the compounds. A definite proof for the structure is provided by the X-ray diffraction results discussed below. The presence of the $[ReX_2(PPh_3)_2(bibzimH_2)]^+$ ion in the solid is consistent with the FAB^+ spectra showing the parent-ion pattern with the expected isotopic distribution, together with fragments resulting from the loss of PPh_3 and X. The good solubility in solvents like CH_2Cl_2 and $CHCl_3$ agrees with the presence of tight ion pairs, as noted for the biimidazole complexes [13]. The compounds were fully characterized by ^1H NMR.

In the free ligand, the two benzimidazole units connected via the C2–C2′ bond are symmetry equivalent (Scheme 2). In addition, the N–H protons are involved in a fast tautomeric exchange between the ring N atoms, which renders the H_5/H_8 pair (and H_6/H_7 pair) chemically, but not magnetically, equivalent. Accordingly, only two signals are observed (AA′BB′ system, Fig. 1), but they are not first order. The chemical shifts and coupling constants (Table 2) were determined from the method described by Sohar [22].

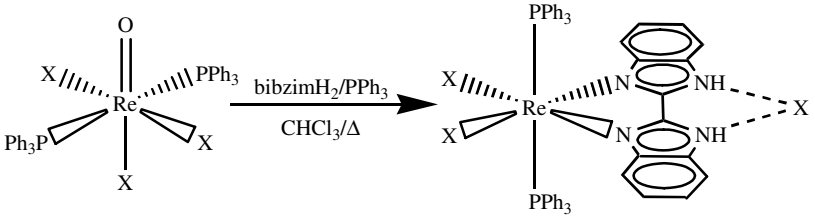

Scheme 3.

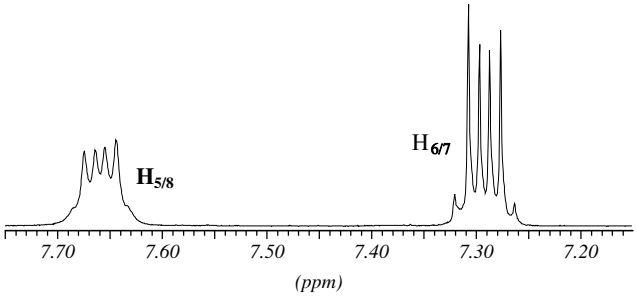

Fig. 1. ^{1}H NMR signals (DMSO-d_6) of the aromatic protons of free bibenzimidazole.

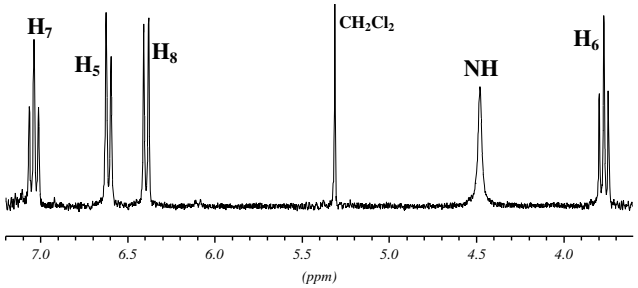

Fig. 2. Signals of the coordinated bibenzimidazole protons in the ^{1}H NMR spectrum ($CDCl_3$) of $[ReCl_2(PPh_3)_2(bibzimH_2)]Cl$. The CH_2Cl_2 signal results from residual traces of the recrystallization solvent.

Table 2
^{1}H NMR chemical shifts (ppm) and coupling constants (Hz) of bibzimH_2 (DMSO-d_6)

δ, $H_{5/8}$	7.66 ppm (m)
δ, $H_{6/7}$	7.29 ppm (m)
$^3J_{56} = {}^3J_{78}$	7.9 Hz
$^3J_{67}$	6.5 Hz
$^4J_{57} = {}^4J_{68}$	1.3 Hz
$^5J_{58}$	0.0 Hz

The low-spin d^4 center in rhenium(III) monomers is paramagnetic. Despite this fact, the ^{1}H NMR spectra are relatively clean, integrations are reliable and couplings are often observed. The data for the bibzimH_2 complexes are collected in Table 3. The PPh_3 signals appear at the same positions as for the related complexes of biimidazole [13] and they are readily identified from multiplicities and integrations. The *ortho* protons, close to the metal center, undergo a considerable shift (13.3 ppm) downfield from their normal position (7–8 ppm). Since the Re–N bonds are non-labile, bibzimH_2 gives four C–H signals between ~7 and ~3.7 ppm (Fig. 2). In contrast with those of PPh_3, they are shifted upfield by paramagnetism. The second-order effects noted for the free ligand have now disappeared, since the signals have been shifted considerably. H_5 and H_8 appear as doublets and can be distinguished from H_6 and H_7, which give pseudo-triplets because of couplings with two adjacent protons. One of the latter protons appears at much higher field (~4 ppm) than the other. Semi-empirical PM3 calculations [23] suggest that the orbitals containing the unpaired electrons are more concentrated on H_6 than on any other proton, whereas its neighbor H_7 is predicted to be the least affected by the unpaired electrons. Accordingly, the higher-field triplet (3.76 (Cl); 4.25 (Br) ppm) is assigned to H_6, whereas the other triplet (7.03 (Cl); 6.71 (Br) ppm) must correspond to H_7. A COSY 2D experiment for $[ReBr_2(PPh_3)_2(bibzimH_2)]Br$ indicates proximity for the protons appearing at 6.22 and 4.25 ppm, respectively. This allows us to assign the doublet at 6.22 ppm to H_5 and the other doublet at 6.01 ppm to H_8. The acidic N–H protons give a broad peak at 4.44 (Cl) or 4.89 (Br) ppm.

3.1. Crystal structures

The $[ReCl_2(PPh_3)_2(bibzimH_2)]Cl$ unit is shown in Fig. 3. The octahedral environment of rhenium(III) includes one non-deprotonated bidentate bibzimH_2 ligand, two phosphines *trans* to one another and two chlorines. The third chlorine is actually the counter ion forming two N–H···Cl^- hydrogen bonds with bibzimH_2. Selected interatomic distances and bond angles are compared with those of the biimidazole analog [13] in Table 4.

Most of the departure from octahedral coordination originates from the small bite angle (76.7(2)°) of bibzimH_2, which allows the opposite Re–Cl bonds to move away from each other (Cl(1)–Re–Cl(2) = 96.97(5)°). The Re–P bonds, perpendicular to the $ReCl_2N_2$ plane, are not exactly collinear (P(1)–Re–P(2) = 175.21(4)°), but

Table 3
^{1}H NMR data for the $[ReX_2(PPh_3)_2(bibzimH_2)]X$ complexes (in $CDCl_3$)

	$[ReCl_2(PPh_3)_2(bibzimH_2)]Cl$	$[ReBr_2(PPh_3)_2(bibzimH_2)]Br$
PPh_3, H_o	13.31 (d, 12H), $^3J = 7.0$ Hz	13.32 (d, 12H), $^3J = 7.1$ Hz
PPh_3, H_p	8.42 (t, 6H), $^3J = 7.1$ Hz	8.38 (t, 6H), $^3J = 7.4$ Hz
PPh_3, H_m	8.18 (t, 12H), $^3J = 7.5$ Hz	8.11 (t, 12H), $^3J = 7.6$ Hz
bibzimH_2, H_7	7.03 (t, 2H), $^3J = 8.0$ Hz	6.71 (t, 2H), $^3J = 8.1$ Hz
bibzimH_2, H_5	6.60 (d, 2H), $^3J = 8.2$ Hz	6.22 (d, 2H), $^3J = 8.4$ Hz
bibzimH_2, H_8	6.38 (d,2H), $^3J = 8.6$ Hz	6.01 (d, 2H), $^3J = 8.3$ Hz
bibzimH_2, (N)H	4.44 (s broad, 2H)	4.89 (s broad, 2H)
bibzimH_2, H_6	3.76 (t, 2H), $^3J = 7.7$ Hz	4.25 (t, 2H), $^3J = 7.7$ Hz

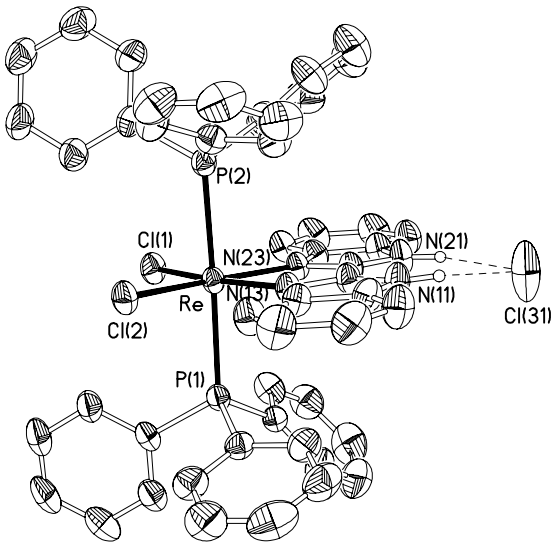

Fig. 3. ORTEP drawing of the $[ReCl_2(PPh_3)_2(bibzimH_2)]Cl$ ion pair. For simplicity, the carbon-bonded hydrogens are omitted.

Table 4
Selected distances (Å) and angles (deg) in the $[ReCl_2(PPh_3)_2(LH_2)]Cl$ compounds

LH_2	$bibzimH_2$	$biimH_2$ [13]
Bond lengths		
Re–N(13)	2.127(4)	2.114(3)
Re–N(23)	2.145(4)	2.129(3)
Re–P(1)	2.496(1)	2.476(1)
Re–P(2)	2.494(1)	2.466(1)
Re–Cl(1)	2.360(1)	2.381(1)
Re–Cl(2)	2.369(1)	2.354(1)
Bond angles		
N(13)–Re–N(23)	76.7(2)	76.0(1)
P(1)–Re–P(2)	175.21(4)	177.24(3)
Cl(1)–Re–Cl(2)	96.97(5)	99.38(4)
P(1)–Re–N(13)	89.4(1)	90.8(1)
P(1)–Re–N(23)	92.3(1)	90.0(1)
P(1)–Re–Cl(1)	91.51(5)	89.98(4)
P(1)–Re–Cl(2)	88.15(5)	90.22(4)
P(2)–Re–N(13)	88.9(1)	91.0(1)
P(2)–Re–N(23)	91.7(1)	88.5(1)
P(2)–Re–Cl(1)	90.96(5)	87.93(4)
P(2)–Re–Cl(2)	87.48(5)	91.91(4)
Cl(1)–Re–N(13)	169.0(1)	173.2(1)
Cl(1)–Re–N(23)	92.3(1)	97.3(1)
Cl(2)–Re–N(13)	94.0(1)	87.3(1)
Cl(2)–Re–N(23)	170.7(1)	163.3(1)
N(11)–C(12)–C(22)	130.7(5)	133.9(4)
N(13)–C(12)–C(22)	117.0(4)	115.4(4)
N(21)–C(22)–C(12)	128.8(5)	132.5(4)
N(23)–C(22)–C(12)	117.5(4)	117.0(4)
C(12)–N(13)–Re	114.4(3)	116.5(3)
C(14)–N(13)–Re	140.1(4)	137.3(3)
C(22)–N(23)–Re	114.3(3)	115.1(3)
C(24)–N(23)–Re	140.8(3)	138.8(3)

the deviation is small. The Re–N and Re–Cl bond lengths compare well with those of the $biimH_2$ complex, but the Re–P bonds are ~0.02 longer here, probably because the extra phenylene rings leave less space for the phosphine phenyl rings.

The two benzimidazole halves of the coordinated ligand are coplanar (dihedral angle = 1.7(3)°). As depicted in Fig. 4, ring closure induces in-plane distortions to improve the overlap between the metal orbitals and the ligand σ lone pairs, leading to a large difference between the $N_3–C_2–C_2'$ and $N_1–C_2–C_2'$ angles. In the present $bibzimH_2$ complex, this difference is somewhat smaller (~117° versus ~130°) than for the $biimH_2$ complexes (~116° versus ~133°). Thus, the phenylene rings act as bulky α substituents counteracting ligand distortion, which explains that the Cl–Re–Cl angle is smaller here (~97°) than in the $biimH_2$ analog (~99°).

The N–H groups form hydrogen bonds with the chloride counter-ion (Fig. 3 and Table 5). The N···Cl distances of ~3.06 Å and the N–H···Cl angles (~154°) close to linearity correspond to moderately strong interactions [24]. The reduction of ligand distortion is a favorable factor, since it allows the N···Cl distance and the N–H···Cl angle to be greater than for the $biimH_2$ complexes (~3.16 Å and ~147°, respectively) [13].

The phosphines are related by an approximate mirror plane. Two phenyl groups of each phosphine are positioned above (or below) the $bibzimH_2$ ligand, whereas the third phenyl ring is roughly parallel to the Re–P bond and the ortho hydrogen is nested between the two chloro ligands. A similar conformation has been observed for $[ReCl_2(PPh_3)_2(biimH_2)]Cl$ [13]. However, in contrast with the latter case, there are no appreciable π interactions between the phosphine phenyl rings and those of the $bibzimH_2$, since these rings are not parallel (dihedral angle of 20.5° and 25.0°) and the inter-ring distances are relatively large (3.49 and 3.65 Å).

The ion pairs form columns along the unit cell *b* direction and the acetone solvent molecules occupy channels between these columns.

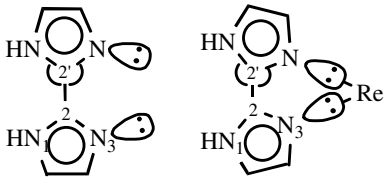

Fig. 4. Undistorted biimidazole molecule (left) and distorted coordinated ligand (right).

Table 5
Geometry of the hydrogen bonds in $[ReCl_2(PPh_3)_2(bibzimH_2)]Cl$

D–H···A	D–A (Å)	H–A (Å)	D–H–A (°)
N(11)–H(11)···Cl(31)[a]	3.000(9)	2.18	155.8
N(21)–H(21)···Cl(31)[a]	3.078(8)	2.27	154.3
N(11)–H(11)···Cl(32)[a]	3.128(9)	2.33	152.2
N(21)–H(21)···Cl(32)[a]	3.018(8)	2.21	155.0

[a] Occupancies: Cl(31), 0.60; Cl(32), 0.40.

4. Conclusion

This work shows that the extra aromatic rings in bibzimH_2 do not preclude the formation of the [ReX_2(PPh_3)$_2$(LH_2)]X complexes observed with biimidazole and that they introduce only small structural differences due to steric effect. Therefore, this system, with the extra advantage of tunability by substitution on the phenylene unit, could provide a valuable starting point to prepare bimetallic compounds by coordination of an extra metallic center to the external N donors.

5. Supplementary material available

Crystallographic information as a CIF file has been deposited with the Cambridge Crystallographic Data Centre (CCDC No. 215000). Copies of the data can be obtained free of charge via www.ccdc.cam.ac.uk/conts/retrieving.html or from the Cambridge Crystallographic Data Centre, 12, Union Road, Cambridge CB2 1EZ, UK; fax: +44 1233 336033; or e-mail: deposit@ccdc.cam.ca.uk.

Acknowledgements

We thank the Natural Sciences and Engineering Research Council of Canada for financial support, and Dr. M. Simard and F. Bélanger-Gariépy for assistance in the interpretation of the X-ray diffraction data.

References

[1] S. Fortin, A.L. Beauchamp, Inorg. Chem. 39 (2000) 4886.
[2] C.A. Hester, H.L. Collier, R.G. Baughman, Polyhedron 15 (1996) 4255.
[3] C.A. Hester, R.G. Baughman, H.L. Collier, Polyhedron 16 (1997) 2893.
[4] M. Tadokoro, H. Kanno, T. Kitajima, H. Shimada-Umemoto, N. Nakanishi, K. Isobe, K. Nakasuji, Proc. Natl. Acad. Sci. USA 99 (2002) 4950.
[5] M. Takodoro, K. Nakasuji, Coord. Chem. Rev. 198 (2000) 205.
[6] M. Takodoro, K. Isobe, H. Uekusa, Y. Ohasi, J. Toyoda, K. Tashiro, K. Nakasuji, Angew. Chem., Int. Ed. Engl. 38 (1999) 95.
[7] M. Takodoro, J. Toyoda, K. Isobe, T. Itoh, A. Miyasaki, T. Enoki, K. Nakasuji, Chem. Lett. (1995) 613.
[8] S. Rau, T. Büttner, C. Temme, M. Ruben, H. Görls, D. Walther, M. Duati, S. Fanni, J.G. Vos, Inorg. Chem. 39 (2000) 1621.
[9] M. Haga, T. Matsumura-Inoue, S. Yamabe, Inorg. Chem. 26 (1987) 4148.
[10] P. Majumbar, S.-M. Peng, S. Goswami, J. Chem. Soc., Dalton Trans. (1998) 1569.
[11] A.P. de Silva, H.Q.N. Gunaratne, T. Gunnlaugsson, A.J.M. Huxley, C.P. McCoy, J.T. Rademacher, T.E. Rice, Chem. Rev. 97 (1997) 1515.
[12] M.D. Ward, Chem. Soc. Rev. (1995) 121.
[13] S. Fortin, A.L. Beauchamp, Inorg. Chem. 40 (2001) 105.
[14] S. Fortin, A.L. Beauchamp, J. Chem. Soc., Dalton Trans. (2001) 3520.
[15] J. Chatt, G.A. Rowe, J. Chem. Soc. (1962) 4019.
[16] N.P. Johnson, C.J.L. Lock, G. Wilkinson, J. Chem. Soc. (1964) 1054.
[17] B.F. Fieselmann, D.N. Hendrickson, G.D. Stucky, Inorg. Chem. 17 (1978) 2078.
[18] C. Tessier, A.L. Beauchamp, F.D. Rochon, Inorg. Chem. 41 (2002) 6527.
[19] G.M. Sheldrick, SHELXTL, The Complete Software Package for Single Crystal Structure Determination, Release 5.10., Bruker AXS Inc., Madison, WI, 1997.
[20] XPREP, X-ray Data Preparation and Reciprocal Space Exploration Program, Release 5.10, Bruker AXS Inc., Madison, WI, 1997.
[21] Cambridge Structural Database, Version 5.4, November 2002 release with February 2003 updates, Cambridge Crystallographic Data Centre, Cambridge, UK.
[22] P. Sohar, Nuclear Magnetic Resonance Spectroscopy, Chemical Rubber Company Press, Boca Raton, FL, 1983.
[23] PCSpartan Pro 1.0.6, Wavefunction Inc., Irvine, CA, 2001.
[24] G.H. Stout, L.H. Jensen, X-Ray Structure Determination, A Practical Guide, Macmillan, New York, 1968, p. 467.

Available online at www.sciencedirect.com
SCIENCE DIRECT®
Polyhedron 23 (2004) 1145–1152
POLYHEDRON
www.elsevier.com/locate/poly

A new octamolybdate: observation of the θ-isomer in $[Fe(tpyprz)_2]_2[Mo_8O_{26}] \cdot 3.7H_2O$ (tpyprz = tetra-2-pyridylpyrazine)

Damian G. Allis *, Eric Burkholder, Jon Zubieta *

Department of Chemistry, Syracuse University, Syracuse, NY 13244, USA

Received 18 December 2003; accepted 18 January 2004

Abstract

The hydrothermal reaction of $Fe(CH_3CO_2)_2$, tetra-2-pyridylpyrazine (tpyprz) and $(NH_4)_6Mo_7O_{24} \cdot 4H_2O$ yields purple crystals of $[Fe(tpyprz)_2]_2[Mo_8O_{26}] \cdot 3.7H_2O$. The discrete octamolybdate anions represent a new isomeric form, θ-$[Mo_8O_{26}]^{4-}$. The cluster anion consists of four octahedra, two square pyramids, and two tetrahedra in an edge- and corner-sharing arrangement. A computational study of the isomer using both a single-point energy calculation of the crystallographic coordinates and a geometry optimization of the isomer at the Restricted Hartree–Fock level of theory illustrates the similarities of the θ-isomer and the low energy δ-isomer reported previously.
© 2004 Elsevier Ltd. All rights reserved.

Keywords: Octamolybdate; Hydrothermal synthesis; Three-dimensional oxide; Organic–inorganic hybrid; Building block approach; Hartree–Fock calculations

1. Introduction

The contemporary interest in inorganic oxides reflects their extensive compositional range, considerable structural diversity, and physical properties related to applications ranging from heavy construction to microelectronics [1–4]. In addition to a wealth of solid state materials [5], the polyoxometalates represent a subclass of molecular oxide species [6,7].

In the specific case of molybdenum polyoxoanions, these clusters have been extensively explored as analogues to oxide surfaces and as potential catalysts [8], as well as molecular building blocks in the synthesis of oxide solid phase materials [9]. A common example is the octamolybdate anion $[Mo_8O_{26}]^{4-}$, for which seven isomeric forms, α through η, have been reported. The α- and β-forms are selectively crystallized from aqueous solutions of molybdate acidified to pH 3–4, followed by addition of appropriate cations [10–14]. The γ-form has been prepared from aqueous solution by appropriate choice of cations [15]. The δ-isomer has been isolated by both conventional and hydrothermal methods [16]. All isomeric forms have been observed under hydrothermal conditions in the presence of secondary metal–ligand coordination cations. Thus, the α-isomer has been observed for $[\{Cu(bpe)\}_4Mo_8O_{26}]$ [17]; the β-form for $[\{Cu(Me\text{-}pyz)\}_4Mo_8O_{26}]$ [18], $[\{Cu(Me_2pyrm)\}_4Mo_8O_{26}]$ [18], $[\{Cu(pyr_2\text{-}S)\}_4Mo_8O_{26}]$ [19], $[\{Cu(dpa)\}_2Mo_8O_{26}]$ [20], $[\{Cu(pyr)\}_4Mo_8O_{26}]$ [21], and $[\{Cu(4,4'\text{-}bpy)(nic)(H_2O)\}_2Mo_8O_{26}$ [22]; the γ-isomer in $[\{Cu(en)_2Mo_8O_{26}]$ [23] and $[\{Cu(pyrd)\}_4\ H_4Mo_8O_{26}]$ [24]; and the δ-isomer for $[\{Cu(4,4'\text{-}bpy)\}_4Mo_8O_{26}]$ [25]. An ε-isomer has been reported for the Ni(II) species $[\{Ni(4,4'\text{-}bpy)_2(H_2O)_2\}_2Mo_8O_{26}]$ [25]. More recently, the η-isomer has been described for the structure of $[\{Cu(t\text{-}Bu_2bpy)\}_2Mo_8O_{26}]$ [26] and the ζ-form has been described in $[\{Cu_2(tpyprz)\}_2Mo_8O_{26}]$ [27].

As part of our continuing studies of the hydrothermal chemistry of polyoxomolybdates, we have prepared yet another isomeric form, the θ-type, in the structure of $[Fe(tpyprz)_2]_2[Mo_8O_{26}] \cdot 3.7H_2O$ (**1** $\cdot 3.7H_2O$).

* Corresponding authors. Fax: +1-315-443-4070.
E-mail addresses: dgallis@syr.edu (D.G. Allis), jazubiet@syr.edu (J. Zubieta).

0277-5387/$ - see front matter © 2004 Elsevier Ltd. All rights reserved.
doi:10.1016/j.poly.2004.01.011

2. Experimental methods

2.1. Synthesis and spectroscopy

Chemicals were used as obtained without further purification. Iron(II) acetate anhydrous, ammonium paramolybdate, and 1,2-ethylene diphosphonic acid were purchased from Alfa Aesar; tetra-2-pyridinylpyrazine (tpyprz) was purchased from Aldrich. The synthesis was carried out in 23 ml poly(tetrafluoroethylene) lined stainless steel containers under autogenous pressure. The reactants were stirred briefly and the initial pH measured before heating. Water was distilled in-house above 3 MΩ using a Barnstead Model 525 Biopure Distilled Water Center. The initial and final pH of the reaction was measured using Hydrion pH sticks. Syntheses were carried out in Parr acid digestion bombs with 23 ml poly(tetrafluoroethylene) liners. Infrared spectra were obtained on a Perkin–Elmer 1600 series FTIR spectrometer.

2.2. Synthesis of $[Fe(tpyryz)_2]_2[Mo_8O_{26}]\cdot 3.7H_2O$ ($\mathbf{1}\cdot 3.7H_2O$)

A mixture of $(NH_4)_6Mo_7O_{24}\cdot 4H_2O$ (0.197 g, 0.159 mmol), $Fe(II)(CH_3CO_2)_2$ (0.078 g, 0.45 mmol), tpyprz (0.086 g, 0.22 mmol), $H_2O_3P(CH_2)_2PO_3H_2$ (0.083 g, 0.44 mmol), and H_2O (10.053 g, 558 mmol) in the mole ratio 0.9:2.0:1.0:2.0:2500 was placed in a Parr acid digestion bomb. After heating at 150 °C for 96 h, purple crystals were isolated in 60% yield based on iron. Initial pH, 4.5; final pH, 4.0. Attempts to synthesize $\mathbf{1}\cdot 3.7H_2O$ in the absence of 1,2-ethylene-diphosphonic acid have proved unsuccessful. IR (KBr pellet, cm^{-1}): 3400 (m, br), 1380 (s), 910 (s, br), 850 (m), 810 (s).

2.3. X-ray crystallography

Crystallographic data for **1** were collected with a Bruker P4 diffractometer equipped with a SMART CCD system [28] and using Mo Kα radiation ($\lambda = 0.71073$ Å). The data were collected at 90 K and corrected for Lorentz and polarization effects [29]. Absorption corrections were made using SADABS [30]. The structure solution and refinement were carried out using the SHELXTL [31] crystallographic software package. The structures were solved using direct methods and all of the non-hydrogen atoms were located from the initial solution. After locating all of the non-hydrogen atoms in each structure, the model was refined against F^2, initially using isotropic then anisotropic thermal displacement parameters, until the final value of Δ/σ_{max} was less than 0.001. Crystal data for **1** are summarized in Table 1. Selected bond lengths and angles for compound **1** are collected in Table 2. CCDC reference number 225745.

Table 1
Crystal data and structure refinement for $[Fe(tpyprz)_2]_2[Mo_8O_{26}]\cdot 3.7H_2O$ ($\mathbf{1}\cdot 3.7H_2O$)

Empirical formula	$C_{48}N_{12}H_{35.75}FeMo_4O_{14.75}$
Formula weight	1456.25
Crystal system	monoclinic
Space group	$P2_1/n$
a (Å)	15.0644(8)
b (Å)	15.8456(8)
c (Å)	21.1678(11)
β (°)	94.108(1)
Volume (Å^3)	5039.9(5)
Z	4
Density (calculated) (Mg/m^3)	1.919
Absorption coefficient (mm^{-1})	1.332
Temperature (K)	90(2)
Wavelength (Å)	0.71073
Independent reflections	16749 [$R_{int} = 0.0504$]
Goodness-of-fit on F^2	1.080
Final R indices [$I > 2\sigma(I)$]	$R_1 = 0.0663, wR_2 = 0.1492$

2.4. Computational methods

The computational study of the θ-isomer consisted of both a single-point energy calculation of the crystallographic coordinates and a geometry optimization of the isomer at the Restricted Hartree–Fock (RHF) level of theory using the 6-31G* basis set for oxygen and the SBKJC effective core potential for molybdenum [32]. Calculations were performed using the PC-GAMESS version [33] of the GAMESS-US Quantum Chemistry package [34]. The single-point energy calculation was performed on the crystallographic coordinates in the absence of symmetry restrictions. As the isomer is of nearly C_i symmetry, the geometry optimization was performed on a position-averaged C_i symmetry structure with the same basis sets and convergence criteria employed previously for the complete octamolybdate isomer series [27]. A consequence of imposing symmetry in GAMESS, where the retention of the point group symmetry is enforced by the use of symmetry-unique input coordinates, is that the structure is never able to optimize to a lower symmetry minimum energy structure.

3. Results and discussion

3.1. Synthesis and structure

The bimetallic oxide of this study was prepared by conventional hydrothermal methods, which avoid thermal decomposition of the organic component while providing conditions which overcome the differential solubilities of the organic and inorganic components and which are optimal for crystal growth [35–37]. In this fashion, the reaction of $Fe(CH_3CO_2)_2$, $(NH_4)_6Mo_7O_{24}\cdot 4H_2O$, ethylenediphosphonic acid, and tetra-2-pyridylpyrazine yielded $[\{Fe_2(tpyprz)\}_2Mo_8O_{26}]\cdot$

Table 2
Selected bond lengths (Å) and angles (°) for $[Fe(tpyprz)_2]_2[Mo_8O_{26}]\cdot 3.7H_2O$

Bond lengths	
Mo(1)–O(2)	1.699(4)
Mo(1)–O(3)	1.699(4)
Mo(1)–O(4)	1.902(4)
Mo(1)–O(1)	1.982(4)
Mo(1)–O(11)#1	2.280(4)
Mo(1)–O(5)	2.365(3)
Mo(2)–O(7)	1.693(4)
Mo(2)–O(6)	1.700(4)
Mo(2)–O(4)	1.904(4)
Mo(2)–O(8)	1.939(3)
Mo(2)–O(12)#1	2.328(4)
Mo(2)–O(5)	2.355(3)
Mo(3)–O(9)	1.702(4)
Mo(3)–O(10)	1.708(4)
Mo(3)–O(8)	1.856(4)
Mo(3)–O(1)#1	1.858(4)
Mo(3)–O(11)	2.522(4)
Mo(4)–O(13)	1.698(4)
Mo(4)–O(12)	1.752(3)
Mo(4)–O(11)	1.791(4)
Mo(4)–O(5)	1.810(3)
Fe(1)–N(2)	1.864(4)
Fe(1)–N(5)	1.875(4)
Fe(1)–N(3)	1.950(4)
Fe(1)–N(6)	1.955(4)
Fe(1)–N(4)	1.963(4)
Fe(1)–N(1)	1.970(4)
Bond angles	
O(2)–Mo(1)–O(3)	104.0(2)
O(2)–Mo(1)–O(4)	99.4(2)
O(3)–Mo(1)–O(4)	101.8(2)
O(2)–Mo(1)–O(1)	100.0(2)
O(3)–Mo(1)–O(1)	95.1(2)
O(4)–Mo(1)–O(1)	150.29(16)
O(2)–Mo(1)–O(11)#1	93.4(2)
O(3)–Mo(1)–O(11)#1	160.77(19)
O(4)–Mo(1)–O(11)#1	83.20(15)
O(1)–Mo(1)–O(11)#1	73.38(16)
O(2)–Mo(1)–O(5)	165.2(2)
O(3)–Mo(1)–O(5)	89.87(19)
O(4)–Mo(1)–O(5)	72.15(13)
O(1)–Mo(1)–O(5)	83.78(14)
O(11)#1–Mo(1)–O(5)	73.86(15)
O(7)–Mo(2)–O(6)	104.7(2)
O(7)–Mo(2)–O(4)	101.87(19)
O(6)–Mo(2)–O(4)	99.17(18)
O(7)–Mo(2)–O(8)	100.81(19)
O(6)–Mo(2)–O(8)	96.68(18)
O(4)–Mo(2)–O(8)	147.92(15)
O(7)–Mo(2)–O(12)#1	86.91(18)
O(6)–Mo(2)–O(12)#1	168.2(2)
O(4)–Mo(2)–O(12)#1	80.25(15)
O(8)–Mo(2)–O(12)#1	78.63(16)
O(7)–Mo(2)–O(5)	161.40(19)
O(6)–Mo(2)–O(5)	93.8(2)
O(4)–Mo(2)–O(5)	72.35(13)
O(8)–Mo(2)–O(5)	78.95(13)
O(12)#1–Mo(2)–O(5)	74.76(15)
O(9)–Mo(3)–O(10)	105.4(2)
O(9)–Mo(3)–O(8)	102.18(19)
O(10)–Mo(3)–O(8)	107.34(18)
O(9)–Mo(3)–O(1)#1	100.5(2)
O(10)–Mo(3)–O(1)#1	111.37(19)
O(8)–Mo(3)–O(1)#1	127.31(16)
O(9)–Mo(3)–O(11)	165.71(19)
O(10)–Mo(3)–O(11)	88.16(17)
O(8)–Mo(3)–O(11)	77.51(14)
O(1)#1–Mo(3)–O(11)	69.58(15)
O(13)–Mo(4)–O(12)	107.28(19)
O(13)–Mo(4)–O(11)	108.95(19)
O(12)–Mo(4)–O(11)	110.47(18)
O(13)–Mo(4)–O(5)	109.3(2)
O(12)–Mo(4)–O(5)	108.25(19)
O(11)–Mo(4)–O(5)	112.41(18)

Symmetry transformation used to generate equivalent positions: $\#1\ -x, -y+2, -z+2$.

$3.7H_2O$ ($\mathbf{1}\cdot 3.7H_2O$) in 60% yield as purple crystals. Curiously, a crystalline phase could be obtained only in the presence of the diphosphonate, suggesting the preformation of a molybdenum reservoir in the form of a molybdophosphonate cluster. The infrared spectrum of **1** exhibited strong bands in the 800–960 cm^{-1} range, attributed to υ (Mo=O) and υ (Mo–O–Mo). A group of peaks in the 1000–1500 cm^{-1} region is characteristic of the tpypyz ligand.

The structure of **1** consists of discrete $\{Fe(tpyprz)_2\}^{2+}$ cations and $\{\theta\text{-}Mo_8O_{26}\}^{4-}$ anions. The cations consist of distorted $\{FeN_6\}$ octahedra. The Fe(II) site coordinates to three nitrogen donors from each of two tpypyz ligands, with average distances of 1.870(4) and 1.960(4) Å to the pyrazine and pyridyl nitrogen donors, respectively. The nitrogen donors of each of the tpypyz ligands adopt a *meridional* arrangement about the metal center.

The structure of the $\{\theta\text{-}Mo_8O_{26}\}^{4-}$ anion is shown in Fig. 1. The cluster may be described as a ring of four $\{MoO_6\}$ octahedra and two $\{MoO_5\}$ square pyramids in an edge- and corner-sharing arrangement, capped on either face by tetrahedral $\{MoO_4\}$ subunits in a corner-

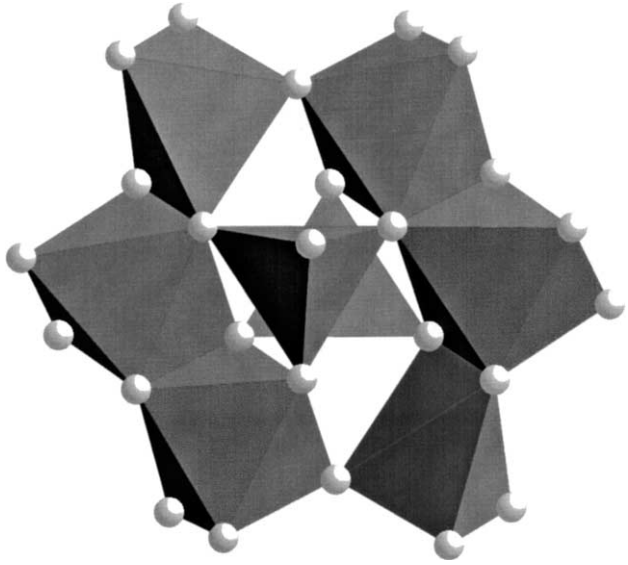

Fig. 1. A polyhedral representation of the structure of $\theta\text{-}[Mo_8O_{26}]^{4-}$.

Table 3
Polyhedral components and oxo-group types of the octamolybdate isomers

Isomer	Polyhedra	Oxo-group types
α-$Mo_8O_{26}^{4-}$	6 octahedra, 2 tetrahedra	14t, $6\mu^2$, $6\mu^3$
β-$Mo_8O_{26}^{4-}$	8 octahedra	14t, $6\mu^2$,$4\mu^3$, $2\mu^5$
γ-$Mo_8O_{26}^{4-}$	6 octahedra, 2 square pyramids (Type A)	14t, 10^2, $2\mu^3$
δ-$Mo_8O_{26}^{4-}$	4 octahedra, 4 tetrahedra	14t,$10\mu^2$, $2\mu^3$
ε-$Mo_8O_{26}^{4-}$	6 square pyramids, 2 octahedra	16t, $4\mu^2$, $6\mu^3$
ζ-$Mo_8O_{26}^{4-}$	4 octahedra, 4 square pyramids	14t, $6\mu^2$, $6\mu^3$
η-$Mo_8O_{26}^{4-}$	6 octahedra, 2 square pyramids (Type B)	14t, $4\mu^2$, $8\mu^3$
θ-$Mo_8O_{26}^{4-}$	4 octahedra, 2 square pyramids, 2 tetrahedra	14t, $8\mu^2$, $4\mu^3$

sharing mode. The ring is constructed of pairs of edge-sharing octahedra linked through the square pyramidal sites. Each square pyramid edge-shares with one binuclear unit of octahedra and corner-shares with the second. The tetrahedral sites share three oxo-groups with the equatorial ring and project a terminal oxo-group in a direction approximately normal to the ring plane. Each $\{MoO_4\}$ site contributes one oxo-group as a μ^3-bridge between the tetrahedral site and one octahedral and one square pyramidal center of the ring, a second μ^3-bridge between the tetrahedral site and a pair of octahedra and a μ^2-bridge to an octahedral site. Consequently, the structure exhibits 14 terminal, 8 doubly bridging and 4 triply bridging oxo-groups.

Seven isomeric forms of octamolybdate have been described previously, as noted in Table 3. The θ-form of this study is a unique example of an octamolybdate constructed from three polyhedral subunits. The structure of the θ-isomer is clearly related to that of the α- and δ-isomers by the breaking of two bonds and the making of two bonds, respectively, as shown in Fig. 2. Since the relative single-point energies of the seven previously reported isomers have been calculated, a computational study of the θ-isomer was undertaken.

3.2. Computational studies

Two views of the θ-isomer are shown in Fig. 3, including top-down and side view pairs from the crystallographic coordinates and the C_i symmetry structure obtained from the RHF geometry optimization. Within the ability of the RHF calculations to reproduce the actual form of the isolated octamolybdate, this comparison is meant to demonstrate the changes to the structure of the θ-isomer that occur in the absence of crystallographic forces. The major structural changes that occur in the RHF energy minimization are (1) a general expansion of the isomer (a change consistent with all previous RHF calculations of the octamolybdates, [27]), (2) a separation of the equatorial square pyramids (Mo3) away from the center of the isomer, resulting in an elongated Mo3–O11 bond, and (3) a small shift of the two apical tetrahedra away from a central plane composed of the two apical Mo4 centers and the two O4 atoms. The θ-isomer expands 0.021 Å along the axis composed of the two O4 atoms, 0.238 Å along the axis composed of the two Mo4 apical tetrahedral centers, and 0.928 Å along the axis composed of the two Mo3 square pyramids.

The symmetry-unique bond lengths of the crystallographic and calculated isomer are summarized in Table 4. While some of the overall changes in the larger structure are found to be significant during the optimization procedure, many of the Mo–O bonds are found to agree quite well between the crystallographic and calculated structures. The average difference between crystal and calculation is 0.074 Å, with sixteen of the symmetry-unique bonds within 0.05 Å of the crystallo-

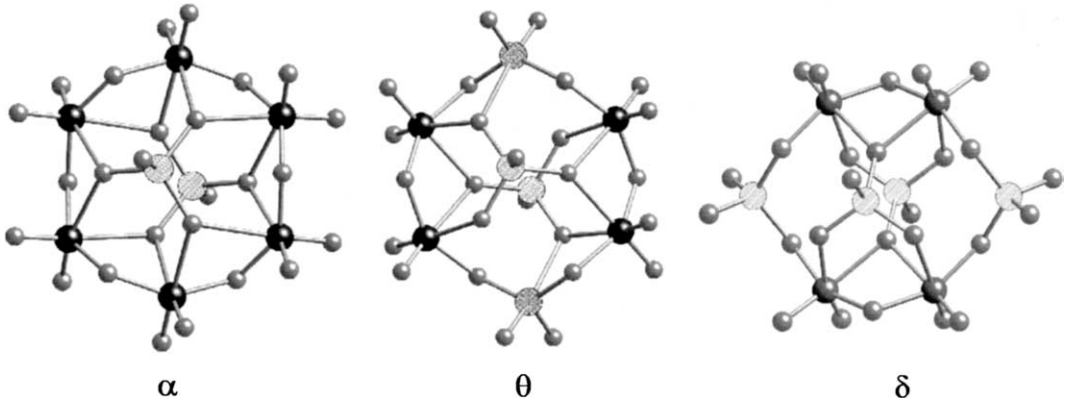

Fig. 2. The structures of the α-, δ- and θ-isomers of $[Mo_8O_{26}]^{4-}$.

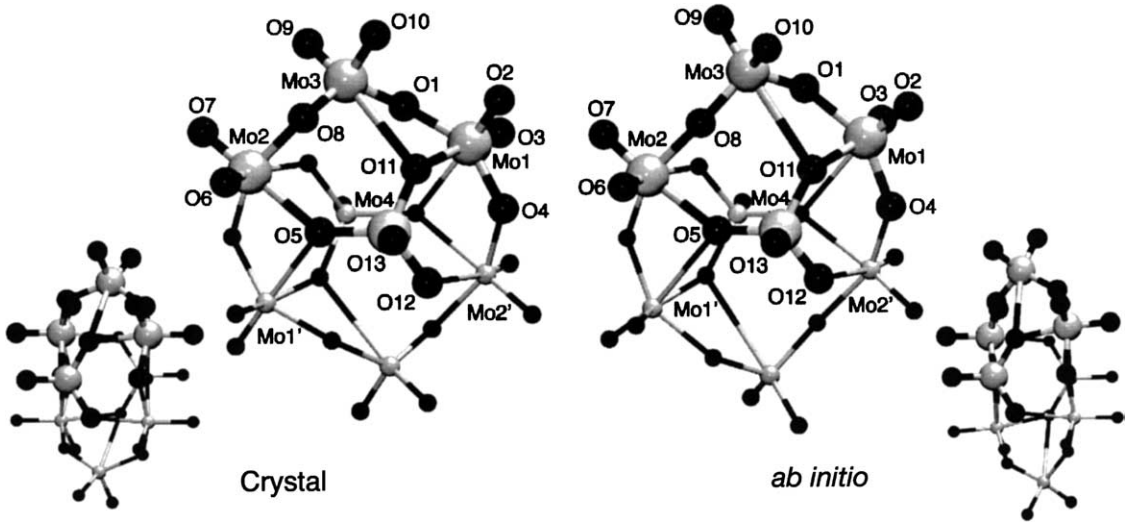

Fig. 3. Crystallographic (left) and calculated (right) structural comparison and labeling scheme for the new θ-isomer. Top-down and side view pairs are to scale with one another. Figures were generated with VMD [40].

Table 4
Mo–O bond lengths for the symmetry-unique atoms of the crystal and calculated θ-isomer

	Mo–O bond	Crystal (Å)	RHF (Å)		Mo–O bond (Å)	Crystal (Å)	RHF (Å)
Mo1 octahedral	Mo1–O1	1.982	2.021	Mo2 octahedral	Mo2–O5	2.355	2.320
	Mo1–O2	1.699	1.677		Mo2–O6	1.700	1.674
	Mo1–O3	1.699	1.679		Mo2–O7	1.693	1.677
	Mo1–O4	1.902	1.901		Mo2–O8	1.939	2.016
	Mo1–O11	2.280	2.167		Mo2′–O4	1.904	1.935
	Mo1′–O5	2.365	2.867		Mo2′–O12	2.328	2.331
Mo3 square pyramidal	Mo3–O1	1.858	1.832	Mo4 tetrahedral	Mo4–O5	1.810	1.793
	Mo3–O8	1.856	1.823		Mo4–O11	1.791	1.793
	Mo3–O9	1.702	1.695		Mo4–O12	1.752	1.747
	Mo3–O10	1.708	1.695		Mo4–O13	1.698	1.694
	Mo3–O11	2.522	3.076				

See Fig. 3 for the atom labels. Crystallographic values represent the average Mo–O bond length where differences exist.

graphic bond lengths. Three metal–oxygen bonds are found to change by more than 0.1 Å and, together, are the changes responsible for the major differences between theory and experiment. The bond Mo1–O11 decreases in the calculated structure by 0.113 Å while the bond Mo3–O11 increases by 0.554 Å. In this pair, the μ^3-O11 atom increases bonding character in one shorter (Mo1–O11, 2.280 Å) crystallographic bond at the expense of lost bonding character in one longer (Mo3–O11, 2.522 Å) metal–oxygen bond. This weakening of the Mo3–O11 bond and enhancement of the Mo1–O11 bond permits both the elongation that occurs between the Mo3 and Mo3′ atoms and the pull of each apical tetrahedron (Mo4) towards one of the octahedral Mo1 centers. This pull between one pair of Mo1 and Mo4 atoms through O11 also leads to an elongation of the Mo1–O5 bond formed in the crystal between, as shown in Fig. 3, Mo1′ and O5 (the symmetry-related Mo1 center in the C_i symmetry structure). The Mo–O bonds in the apical tetrahedra change little from the crystallographic values upon energy minimization and these tetrahedra are found to shift as complete units in the direction of Mo1. The most pronounced bond length changes occur in the longest Mo–O bonds in the structure. These longer Mo–O interactions are, by their length, weaker than the majority of the bonds in the θ-isomer and are expected to be the most susceptible to shifting during a structural rearrangement.

The single point and geometry-optimized energies of the θ-isomer are compared with the seven previously examined isomers in Table 5. Both the crystal coordinates and minimum energy θ-structures are found to agree best in their respective calculations with the δ-isomer. Apparent from the comparison of the δ- and θ-isomers in Fig. 4 are the similarities of the two forms and a straightforward rearrangement pathway between two mirror image forms of the θ-isomer by way of a δ-isomer intermediate. The mirror plane in the "transition structure" through which the mirror image forms are related is, in fact, the mirror plane of the D_{2h}

Table 5
Relative energies (in kJ/mol) of the eight octamolybdate isomers as calculated from their crystallographic coordinates (left) and RHF energy minimizations (right)

	Crystal structures			RHF calculations	
	6-31G* $\Delta E_{relative}$	6-31G* $\Delta E_{neighbor}$		6-31G* $\Delta E_{relative}$	6-31G* $\Delta E_{neighbor}$
θ	0.00	0.00	θ	0.00	0.00
δ	3.78	3.78	δ	0.97	0.97
α	26.78	23.00	α, η[a], ε[a], ζ[a]	25.30	24.33
ε	69.78	43.01	γ(ζ)[b]	36.19	10.88
ζ	86.82	17.04	β	150.19	113.97
γ	101.74	14.92			
η	162.44	60.70			
β	196.98	34.54			

Both the energy differences relative to the lowest-energy form (relative) and the energy difference between neighboring isomers (neighbor) are provided. Isomer energies for α–η are taken from [27].

[a] The η-, ε-, ζ-isomers were found to optimize to the D_{3d}-symmetry α-isomer. See [27].

[b] The ζ-isomer optimizes to the γ-isomer or the α-isomer depending on the starting coordinates. See [27].

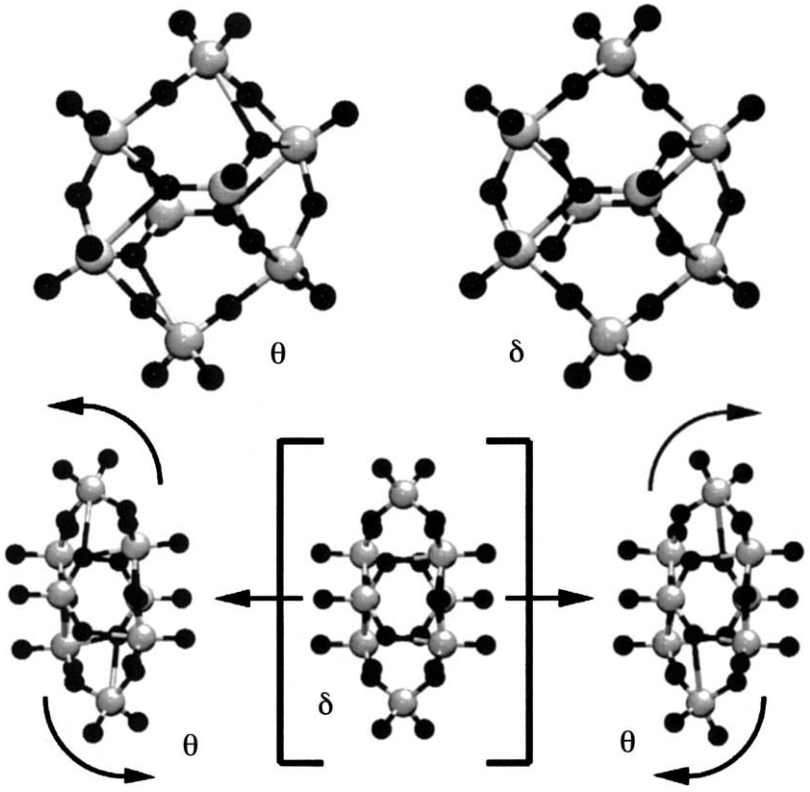

Fig. 4. RHF structure comparison (to scale) of the θ-isomer (left) and δ-isomer (right), and the rearrangement pathway between mirror image forms of the θ-isomer through a higher-symmetry δ-isomer intermediate (bottom). Figures were generated with VMD [40].

δ-isomer. The single-point energy analysis places the θ-isomer 3.78 kJ/mol more stable in energy than the δ-isomer, making it the new lowest energy form at the RHF/6-31G* level of theory and with the selected basis set and effective core potential combination. Geometry optimization changes this relative energy difference to 0.97 kJ/mol, a remarkably small value given the large perceived difference in structure. The δ-isomer was recalculated with imposed C_i symmetry in an effort to determine if the D_{2h} symmetry constraints prevented it from falling to a lower energy θ-isomer structure. With no geometry change calculated at this lower symmetry, it is predicted that the δ-isomer is a stable local minimum. While higher-level calculations are required to more accurately determine the energy difference between these two structures, the RHF re-

sults show with reasonable accuracy that these two structures are far closer to one another in energy that either is to the remaining isomers of the octamolybdate series.

It is important to acknowledge at the end of the crystal/calculated analysis of this isomer, and the known octamolybdate series in general, that each of these data sets provides information about the isolated isomers in limited ways. Both RHF and DFT calculations [38] have been used in the analysis of these isomers, and agree in the general ordering of isomer energies, indicating that this ordering is reasonably accurate for the isolated forms. The calculations are obviously limited by their lack of treatment of the crystal environment into which these various isomers have been isolated. The calculated energies are, within the limited sampling size of available crystal forms, in contradiction with the relative abundances of the isomers in their crystals. The β-isomer is seen by all computational methods as a very high-energy octamolybdate form, yet it is most prevalent from among the available crystal structures. Its existence in solution, however, is found most prominently only under very acidic conditions [39] that presumably mimic the charge features of their crystal environments through either direct contact or surrounding effects. The importance of environment, then, cannot be understated in performing comparisons of energy and structure between the isomers.

4. Conclusions

Hydrothermal synthesis has been exploited in the isolation of yet another isomeric form of octamolybdate. The θ-isomer is unique in containing three polyhedral building blocks, four octahedra, two square pyramids and two tetrahedra.

Single point and geometry-optimized energies of the θ-isomer reveal its similarities to the δ-isomer and suggest a rearrangement pathway between the two minor images of the θ-isomer through a δ-intermediate. While the calculations suggest that the θ-isomer is the new lowest energy structure, the previously lowest energy δ-isomer appears to be a stable local minimum.

5. Supplementary material

The supplementary materials, including atomic positional parameters, hydrogen atom positions, anisotropic thermal parameters and full tables of bond lengths and angles have been deposited with the Cambridge Crystallographic Data Centre, 12 Union Road, Cambridge CB2 IEZ, UK (fax: +44-1223-336033; E-mail: deposit@ccdc.cam.ac.uk or www: http://www.ccdc.cam.ac.uk), as supplementary material CCDC 225745 and can be obtained by contacting the CCDC, quoting the article details and the corresponding SUP number.

Acknowledgements

This work was supported by a grant from the National Science Foundation, CHE-0242153.

References

[1] N.N. Greenwood, A. Earnshaw, Chemistry of the Elements, Pergamon Press, New York, 1984.
[2] (a) W. Büchner, R. Schiebs, G. Winter, K.H. Büchel, Industrial Inorganic Chemistry, VCH, New York, 1989;
(b) B. Cockayne, D.W. Jones, in: D.W. Jones (Ed.), Modern Oxide Materials, Academic Press, New York, 1972.
[3] W.H. McCarroll, in: R.B. King (Ed.), Encyclopedia of Inorganic Chemistry, vol. 6, Wiley, New York, 1994, pp. 2903–2946.
[4] A.K. Cheetham, Science 264 (1994) 794.
[5] A.K. Cheetham, P. Day, Solid State Chemistry, Clarendon Press, Oxford, 1992.
[6] M.T. Pope, Heteropoly and Isopoly Oxometalates, Springer, New York, 1983.
[7] M.T. Pope, A. Müller (Eds.), Polyoxometalate Chemistry, Kluwer Academic, Dordrecht, 2001.
[8] C.L. Hill, R. Renneke, J. Am. Chem. Soc. 108 (1986) 3528.
[9] P.J. Hagrman, D. Hagrman, J. Zubieta, Angew. Chem., Int. Ed. Engl. 38 (1999) 2639.
[10] K.H. Tytko, Z. Naturforsch. B 31 (1976) 757.
[11] A.F. Masters, S.F. Ghellu, R.T. Brownlee, M.J. O'Connor, A.G. Wedd, Inorg. Chem. 19 (1980) 3866.
[12] M.T. Pope, Prog. Inorg. Chem. 39 (1991) 255.
[13] (a) For other examples of the α-molybdate form see: V.W. Day, M.F. Fredrich, W.G. Klemperer, W. Shum, J. Am. Chem. Soc. 99 (1977) 952;
(b) W. Yang, C. Lu, H. Zhuang, J. Chem. Soc., Dalton Trans. (2002) 2879.
[14] (a) For other examples of the β-molybdate isomer see: X.-M. Lu, W.-J. Li, X.-A. Mao, Jiegou Huaxe 19 (2000) 163;
(b) R.Z. Wang, J.Q. Xu, G.Y. Yang, W.M. Bu, Y.H. Xing, D.M. Li, S.Q. Liu, L. Ye, Y.G. Fan, Polish J. Chem. 73 (1999) 1909;
(c) X.-M. Lu, S.-C. Liu, Y. Liu, X.-H. Bu, S.-L. Hong, Huaxue Xuebao 55 (1997) 1009;
(d) A. Kitamura, T. Ozeki, A. Yagasaki, Inorg. Chem. 36 (1997) 4275;
(e) C.J. Gomez-Garcia, E. Coronado, S. Triki, L. Ouahab, P. Delhar, Adv. Mater. 5 (1993) 283;
(f) D. Attanasio, M. Bonamico, V. Fores, L. Suber, J. Chem. Soc., Dalton Trans. (1992) 2523;
(g) X. Wang, X. Xu, Q. Wang, Y. Zhai, Polyhedron 11 (1992) 1423;
(h) J. Fuchs, I. Bruedgam, Z. Naturforsch. B 32B (1977) 853;
(i) W.G. Klemperer, W. Shum, J. Am. Chem. Soc. 98 (1976) 8291;
(j) J. Fuchs, H. Hartl, Angew. Chem. 88 (1976) 385.
[15] (a) γ-molybdate: M.C. Niven, J.J. Cruywagen, J.B.B. Heyns, J. Chem. Soc., Dalton Trans. (1991) 2007;
(b) M. Inoue, T. Yamase, Bull. Chem. Soc. Japan 68 (1995) 3055.
[16] δ-molybdate: R. Xi, B. Wang, K. Isobe, T. Nishioka, K. Toriumi, Y. Ozawa, Inorg. Chem. 33 (1994) 833.
[17] D. Hagrman, C. Sangregorio, C.J. O'Connor, J. Zubieta, J. Chem. Soc., Dalton Trans. (1998) 3707.
[18] R.N. Devi, J. Zubieta, Inorg. Chim. Acta 332 (2002) 72.
[19] D. Hagrman, J. Zubieta, C.R. Acad. Sci., Ser. Iic 3 (2000) 231.

[20] R.S. Rarig, J. Zubieta, J. Solid State Chem. 167 (2002) 370.
[21] D. Hagrman, P. Hagrman, J. Zubieta, Inorg. Chim. Acta 300–302 (2000) 212.
[22] C.-Z. Lui, C.-D. Wu, H.-H. Zhuang, J.-S. Huang, Chem. Mater. 14 (2002) 2649.
[23] J.R.D. DeBord, R.C. Haushalter, L.M. Meyer, D.J. Rose, P.J. Zapf, J. Zubieta, Inorg. Chim. Acta 256 (1997) 165.
[24] D. Hagrman, C. Sangregorio, C.J. O'Connor, J. Zubieta, J. Chem. Soc., Dalton Trans. (1998) 3707.
[25] D. Hagrman, C. Zubieta, R.C. Haushalter, J. Zubieta, Angew. Chem., Int. Ed. Engl. 36 (1997) 873.
[26] R.S. Rarig, L. Bewley, E. Burkholder, J. Zubieta, Ind. J. Chem. 42A (2003) 2235.
[27] D.G. Allis, R.S. Rarig, E. Burkholder, J. Zubieta, J. Mol. Struct. 688 (2004) 11.
[28] SMART, Data Collection Software, version 4.050, Siemens Analytical Instruments Inc., Madison, WI, 1996.
[29] SAINT, Data Reduction Software, version 4.050, Siemens Analytical Instruments Inc., Madison, WI, 1996.
[30] G.M. Sheldrick, SADABS, University of Göttingen, Germany, 1996.
[31] SHELXTL PC, Siemens Analytical X-ray Instruments Inc., Madison, WI, 1993.
[32] W.J. Stevens, M. Krauss, H. Basch, P.G. Jasien, Can. J. Chem. 70 (1992) 612.
[33] A.A. Granovsky, Available from: http://classic.chem.msu.su/gran/gamess/index.html.
[34] M.W. Schmidt, K.K. Baldridge, J.A. Boatz, S.T. Elbert, M.S. Gordon, J.J. Jensen, S. Koseki, N. Matsunaga, K.A. Nguyen, S. Su, T.L. Windus, M. Dupuis, A.J. Montgomery, J. Comp. Chem. 14 (1993) 1347.
[35] R.C. Finn, R.C. Haushalter, J. Zubieta, Prog. Inorg. Chem. 51 (2003) 451.
[36] J. Gopalakrishnan, Chem. Mater. 7 (1995) 1265.
[37] A. Stein, S.W. Keller, T.G. Mallouk, Science 259 (1993) 1558.
[38] A.J. Bridgeman, J. Phys. Chem. A 106 (2002) 12151.
[39] W.G. Klemperer, W. Shum, J. Am. Chem. Soc. 98 (1976) 8291.
[40] W. Humphrey, A. Dalke, K. Schulten, J. Mol. Graphics 14 (1996) 33.

Available online at www.sciencedirect.com
SCIENCE DIRECT®
Polyhedron 23 (2004) 1153–1158
POLYHEDRON
www.elsevier.com/locate/poly

Preparation, crystal structure and spectroscopic characterization of novel *N*-*R*-sulfonyldithiocarbimate platinum(II) complexes

Marcelo R.L. Oliveira [a,*], Mayura M.M. Rubinger [a], Silvana Guilardi [b], Eduardo de Faria Franca [b], Javier Ellena [c], Vito M. De Bellis [d]

[a] *Departamento de Química, Universidade Federal de Viçosa, Viçosa MG, CEP 36571-000, Brazil*
[b] *Instituto de Química, Universidade Federal de Uberlândia, Uberlândia MG, CEP 38408-100, Brazil*
[c] *Instituto de Física de São Carlos, Universidade de São Paulo, São Carlos SP, CEP 13560-970, Brazil*
[d] *Departamento de Química, ICEx, Universidade Federal de Minas Gerais, Belo Horizonte MG, CEP 31270-901, Brazil*

Received 8 October 2003; accepted 20 January 2004

Abstract

Potassium *N*-*R*-sulfonyldithiocarbimates, $K_2(RSO_2N{=}CS_2)$, react with $K_2[PtCl_4]$ in water/methanol to yield complex anions bis(*N*-*R*-sulfonyldithiocarbimato)platinate(II), $[Pt(RSO_2N{=}CS_2)_2]^{2-}$, (R = C_6H_5 (**1**) and 4-BrC_6H_4 (**2**)) which were isolated as their *n*-Bu_4N^+ salts.The single crystal X-ray analysis showed that $(Bu_4N)_2[Pt(C_6H_5SO_2N{=}CS_2)_2]$ crystallizes in the triclinic space group $P\bar{1}$, and $(Bu_4N)_2[Pt(4\text{-}BrC_6H_4SO_2N{=}CS_2)_2]$ crystallizes in the monoclinic space group $P2_1/c$ with disorder in the two chains of the two univalent Bu_4N^+ cation and 4-BrC_6H_4 groups of the anion. All complexes present a similarly distorted square-planar configuration due to the asymmetric bidentate chelation by two sulfur atoms. In both compounds the Pt atoms are in the crystallographic center of symmetry. Elemental analyses, IR spectra and electronic spectra were also consistent with the formation of platinum–sulfur diamagnetic square planar complexes. The ^{1}H NMR, ^{13}C NMR and ^{195}Pt NMR spectra showed the expected signals for the *n*-Bu_4N^+ cation and the anionic complexes.
© 2004 Elsevier Ltd. All rights reserved.

Keywords: Dithiocarbimates; Platinum complexes; Crystal structures

1. Introduction

Dithiocarbamate salts and dithiocarbamate complexes are well known compounds, their wide range of applications being described in the literature. For example, dithiocarbamate and their derivatives are very active accelerators in vulcanization [1]. Many dithiocarbamates, anions and complexes, show biological activity and are used as fungicides [2,3]. The interest in platinum(II) complexes containing S donors has increased in recent years, with the aim of synthesizing anti-tumor drugs having reduced toxicity with respect to *cis*platin [4].

We became interested in the synthesis and characterization of dithiocarbimate metal complexes because they are similar to dithiocarbamates and have been less studied. The platinum(II) bisdithiocarbimate complexes are necessarily anionic species. Thus, the use of active counter ions could improve their biological activity and different cations should also allow a variation in the solubility of these platinum–sulfur compounds.

Here, we describe the synthesis of two bis(*N*-*R*-sulfonyldithiocarbimato)platinate(II) tetra-*n*-butylammonium salts. The anionic complexes are the first examples of platinum complexes with dithiocarbimates derived from sulfonamides. These compounds were characterized by IR, electronic spectra, ^{1}H, ^{13}C and ^{195}Pt NMR spectra, elemental analyses for C, H, N, Pt and by single X-ray diffraction techniques.

2. Experimental

2.1. Materials and methods

Solvents (acetonitrile, dichloromethane, dimethylformamide, ethanol and methanol) were purchased from

* Corresponding author. Tel.: +31-3899-3059; fax: +31-3899-3065.
E-mail address: marcelor@ufv.br (M.R.L. Oliveira).

0277-5387/$ - see front matter © 2004 Elsevier Ltd. All rights reserved.
doi:10.1016/j.poly.2004.01.021

Merck and were used as supplied. Benzenesulfonamide, 4-bromobenzenesulfonyl chloride, potassium tetrachloroplatinate(II) and tetra-*n*-butylammonium bromide were purchased from Aldrich. The 4-bromobenzenesulfonamide was prepared from the 4-bromobenzenesulfonyl chloride as described elsewhere [5]. Potassium *N*-phenylsulfonyldithiocarbimate and potassium *N*-4-bromophenylsulfonyldithiocarbimate were prepared from sulfonamides using procedures described in the literature for analogous compounds [6,7]. These salts, which are soluble in H_2O and insoluble in most organic solvents, were recrystallized from hot ethanol/water mixtures. KOH and CS_2 were purchased from Vetec. IR spectra were recorded with a Perkin–Elmer 1000 FT-IR spectrophotometer using CsI pellets. The electronic spectra were recorded with a Beckman DU 640 spectrometer. The NMR spectra were recorded with a Bruker DRX-400 spectrophotometer in $CDCl_3$ with TMS or $K_2[PtCl_4]$ (for the ^{195}Pt NMR) as internal standards. Microanalyses for C, H and N were obtained from a Perkin–Elmer 2400 CHN elemental analyzer. Platinum was analyzed by atomic absorption on a Hitachi Z-8200 atomic absorption spectrophotometer. Uncorrected melting points were measured with a Mettles FP5 melting point apparatus.

2.2. Syntheses

The syntheses of the platinum complexes were performed according to Scheme 1. Potassium tetrachloroplatinate(II) (0.415 g; 1.0 mmol) and tetra-*n*-butylammonium bromide (0.647 g; 2.0 mmol) were added to a solution of potassium *N*-*R*-sulfonyldithiocarbimate dihydrate (2.0 mmol) in methanol/water 1:1 (10 mL). The reaction mixture was stirred for 3 h at room temperature. The yellow solid obtained was filtered, washed with distilled water and dried under reduced pressure for one day, yielding $(Bu_4N)_2[Pt(RSO_2N{=}CS_2)_2]$ (ca. 70% based on the $K_2[PtCl_2]$). Suitable crystals for X-ray structure analyses were obtained after slow evaporation of solutions of the compounds in methanol/water 4:1.

2.2.1. Tetrabutylammonium bis(N-phenylsulfonyldithiocarbimato)platinate(II) (1)

Elemental *Anal.* Calc.: C, 48.35; H, 7.23; N, 4.90; Pt, 17.07. Found: C, 48.10; H, 7.16; N, 4.80; Pt, 17.45%; m.p. (°C): 150.0–152.0. IR (most important bands) (cm^{-1}): 1395 ν(CN), 1274 $\nu(SO_{2ass})$, 1137 $\nu(SO_{2sym})$, 934 $\nu(CS_{2ass})$, 300 ν(PtS). UV/Vis [λ (nm), ε (l mol^{-1} cm^{-1})]: 259 (43343) ($\pi \rightarrow \pi^*$ (SCS)), 375 (21890) ($n \rightarrow \pi^*$ (S)), 430 (1836) (CT). ^{1}H NMR (complex anion signals) (δ): 8.00–7.96 (m, 4H, H2 and H6), 7.48–7.32 (m, 6H, H3, H4 and H5). ^{13}C NMR (complex anion signals) (δ): 212.74 ($N{=}CS_2$), 143.63 (C1), 131.05 (C4), 127.87 (C3, C5), 127.67 (C2, C6). ^{195}Pt NMR (δ): −3857.

2.2.2. Tetrabutylammonium bis(N-4-bromophenylsulfonyldithiocarbimato)platinate(II) (2)

Elemental *Anal.* Calc.: C, 42.49; H, 6.20; N, 4.31; Pt, 15.00. Found: C, 41.40; H, 6.00; N, 4.15; Pt, 14.50%; m.p. (°C): 170.0–171.9. IR (most important bands) (cm^{-1}): 1380 ν(CN), 1300, 1290, $\nu(SO_{2ass})$, 1135 $\nu(SO_{2sym})$, 930 $\nu(CS_{2ass})$, 320 ν(PtS). UV/Vis [λ (nm), ε (l mol^{-1} cm^{-1})]: 235 (30590) ($\pi \rightarrow \pi^*$ (NCS)), 263 (41670) ($\pi \rightarrow \pi^*$ (SCS)), 376 (17380) ($n \rightarrow \pi^*$ (S)), 437 (2105) (CT). ^{1}H NMR (complex anion signals) (δ): 7.88–7.85 (m, 4H, H2 and H6), 7.51–7.48 (m, 4H, H3 and H5). ^{13}C NMR (complex anion signals) (δ): 213.29 ($N{=}CS_2$), 142.58 (C1), 130.87 (C3 and C5), 129.56 (C2 and C6), 125.46 (C4). ^{195}Pt NMR (δ): −3872.

2.3. X-ray diffraction experiments

Intensity data of the compounds **1** and **2** were collected on an Enraf-Nonius Kappa-CCD diffractometer with graphite monochromated Mo Kα ($\lambda = 0.71073$ Å), provided with a cryogenic device operating at 120 K. Data collection were made using the COLLECT program [8] up to 55° in 2θ with a redundancy of 4 in both cases. The final lattice parameters were based on all reflections. Integration and scaling of the reflections, correction for Lorentz and polarization effects were performed with the HKL Denzo-Scalepack system of programs [9]. The face-indexed numerical absorption was calculated by the method Gaussian using the PLATON program [10].

The structures were solved by direct methods with SHELXS 97 [11] and refined on F^2 by full-matrix least-squares using SHELXL 97 [12]. All non-hydrogen atoms were modelled anisotropically, while hydrogen atoms were stereochemically positioned and refined with the riding model [12]. Hydrogen atoms of the aromatic rings and CH_2 were set isotropic with isotropic thermal parameters of $1.2U_{eq}$ of the carbon atoms joined directly to

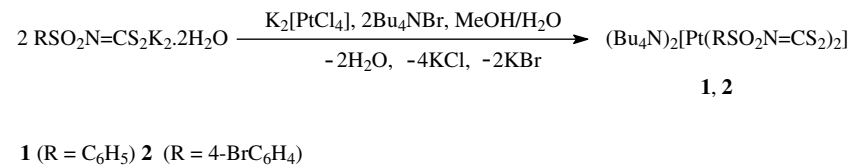

Scheme 1.

Table 1
Crystal data

Compound	1	2
Empirical formula	$C_{46}H_{82}N_4O_4S_6Pt$	$C_{46}H_{80}Br_2N_4O_4S_6Pt$
Formula weight	1142.61	1300.41
Crystal system	triclinic	monoclinic
Space group	$P\bar{1}$	$P2_1/c$
a (Å)	9.8946(1)	8.9729(2)
b (Å)	10.7316(2)	12.4964(1)
c (Å)	13.5726(2)	24.0690(3)
α (°)	80.744(1)	90
β (°)	81.993(1)	93.671(1)
γ (°)	66.594(1)	90
Volume (Å^3)	1300.86(3)	2693.29(7)
Z	1	2
Crystal size (mm)	$0.137 \times 0.035 \times 0.016$	$0.076 \times 0.010 \times 0.010$
ρ_{calc} (g cm^{-3})	1.459	1.604
μ(Mo Kα) (mm^{-1})	2.981	4.365
Minimum/maximum transmission	0.5486/0.8713	0.6779/0.9173
θ Range (°)	3.40–27.48	3.68–27.48
Index ranges	$-12, 12$; $-13, 13$; $-17, 17$	$-11, 11$; $-16, 16$; $-31, 31$
Reflection collected	40 023	51 871
Number of unique reflections	5975	6153
Number of observed reflection, $I > 2\sigma(I)$	5915	4543
Number of parameters refined	282	357
R^a, Rw^b [$I > 2\sigma(I)$]	0.0214, 0.0493	0.0369, 0.0710
R^a, Rw^b (all data)	0.0218, 0.0496	0.0647, 0.0802
S^c	1.029	1.030
RMS (e Å^{-3})	1.362	0.899

[a] $R = \sum ||F_o| - |F_c|| / \sum |F_o|$.
[b] $Rw = [\sum w(F_o^2 - F_c^2)^2 / \sum w(F_o^2)^2]^{1/2}$, $w = 1/\sigma^2(F_o^2)$.
[c] $S = [\sum w(F_o^2 - F_o^2)^2 / (N_{obs} - N_{param})]^{1/2}$.

Table 2
Selected bond lengths (Å) and angles (°)

	1	2
Bond lengths		
Pt–S(1)	2.3208(5)	2.352(4)
Pt–S(2)	2.3227(5)	2.289(4)
C(1)–S(1)	1.733(2)	1.732(4)
C(1)–S(2)	1.750(2)	1.737(4)
C(1)–N(1)	1.293(3)	1.313(4)
N(1)–S(3)	1.623(2)	1.619(3)
O(1)–S(3)	1.443(2)	1.441(3)
O(2)–S(3)	1.446(2)	1.438(3)
C(2)–S(3)	1.781(2)	1.79(4)
Bond angles		
S(1)–Pt–S(2)	74.65(2)	74.69(13)
S(1^i)–Pt–S(2)	105.35(2)	107.49(16)
C(1)–S(1)–Pt	88.94(7)	87.01(15)
C(1)–S(2)–Pt	88.48(7)	88.92(13)
S(1)–C(1)–S(2)	107.87(11)	108.5(2)
S(1)–C(1)–N(1)	131.25(16)	130.0(3)
S(2)–C(1)–N(1)	120.88(16)	121.5(3)
O(1)–S(3)–O(2)	116.35(10)	116.93(16)
O(1)–S(3)–N(1)	112.81(9)	111.99(16)
O(2)–S(3)–N(1)	105.63(10)	105.79(16)
O(1)–S(3)–C(2)	107.96(10)	107.15(17)
O(2)–S(3)–C(2)	106.19(9)	105.4(14)
N(1)–S(3)–C(2)	107.39(9)	107.2(11)
S(3)–N(1)–C(1)	122.06(15)	121.5(3)

(i) $-x, -y+1, -z+1$ for **1** and $-x+1, -y+1, -z$ for **2**.

the hydrogen atoms and CH_3 group with isotropic parameters of $1.5U_{eq}$ of the methyl carbon atom.

Data collection and experimental details for compounds **1** and **2** are summarized in Table 1. Selected bond lengths and angles are listed in Table 2.

3. Results and discussion

The compounds **1** and **2** are yellow crystalline solids stable at the ambient conditions. They are soluble in most of organic solvents and insoluble in water.

Their electronic spectra in ethanol showed three bands for **1** and four bands for **2**. The band around 400 nm was assigned to the charge transfer transition. This band is also observed in the spectra of other diamagnetic planar platinum(II)–bisdithiocarbimato complexes [13]. The other bands were assigned to the internal transitions of the ligands. The $\pi \rightarrow \pi^*$ (NCS) band in the spectrum of **1** was obscured by the very intense band assigned to $\pi \rightarrow \pi^*$ (SCS).

There are no strong or medium bands in the 1450–1550 cm^{-1} region in the IR spectra of the potassium dithiocarbimates related to the complexes here prepared, the ν(CN) band being observed at 1267 and 1258 cm^{-1}

for $C_6H_5SO_2N{=}CS_2K_2\cdot 2H_2O$ and 4-$BrC_6H_4SO_2N{=}CS_2K_2\cdot 2H_2O$, respectively. A strong band observed around 1390 cm^{-1} in the spectra of the compounds **1** and **2** was assigned to the ν(CN). These bands are in higher wavenumbers when compared with the spectra of $(Bu_4N)_2[Ni(C_6H_5SO_2N{=}CS_2)_2]$ and $(Bu_4N)_2[Ni(4\text{-}BrC_6H_4SO_2N{=}CS_2)_2]$ [14]. In the case of the dithiocarbimates here studied, the CN bond is formally a double bond. However, because of the SO_2 neighbor group, the canonical forms (a) and (b) (Scheme 2) contribute appreciably to the resonance hybrid. This fact explains the low values for de ν(CN) band wavenumbers. The spectra of the complexes $[Pt(C_6H_5N{=}CS_2)_2]^{2-}$ [13] and $[Pt(N\text{-}4\text{-}NH_2C_6H_2N{=}CS_2)_2]^{2-}$ [15] that does not have the SO_2 group, show the ν(CN) band at 1520 cm^{-1} and 1501 cm^{-1}, respectively. The $\nu(CS_{2ass})$ were observed at higher frequencies in the spectra of the potassium salts of dithiocarbimates (971 and 973 cm^{-1} for $C_6H_5SO_2N{=}CS_2K_2\cdot 2H_2O$ and 4-$BrC_6H_4SO_2N{=}CS_2K_2\cdot 2H_2O$, respectively) than in the spectra of the compounds **1** and **2** ($\sim$930 cm^{-1}). The shifts observed in the $\nu(CS_{2ass})$ and ν(CN) bands of the complexes when compared to the spectra of the free ligands, are consistent with the increased importance of the canonical form (c) after complexation (Scheme 2). The spectra of the compounds **1** and **2** also show the expected medium/strong band in the 300–400 cm^{-1} range assigned to the ν(PtS).

The NMR spectra were typical for diamagnetic species and were consistent with the proposed structures. The integration curves on the ^{1}H NMR spectra were consistent with a 2:1 proportion between the tetra-*n*-butylammonium cation and the complex anion. In the ^{13}C NMR spectra of the compounds **1** and **2** the signal of the quaternary carbon of the dithiocarbimate moiety is shifted upfield when compared to the correspondent signal in the potassium dithiocarbimate spectra. Although the spectra were obtained in different solvents (the potassium *N*-*R*-dithiocarbimate were only soluble in water), this fact is also consistent with the increase in the contribution of canonical form (c) after the complexation (Scheme 2). The ^{195}Pt NMR spectra show a singlet at $\delta = -3857$ and $\delta = -3872$ for **1** and **2**, respectively. These values are close to those observed for compounds containing the PtS_4 chromophore, such as $[Pt(Et_2CNS_2)_2]$ (−3835), $[Pt(^iPr_2CNS_2)_2]$ (−3779) and $[Pt(^nBu_2CNS_2)_2]$ (−3843) [16].

The crystal structure of the anions of the compounds **1** and **2** are illustrated in Figs. 1 and 2, respectively. The

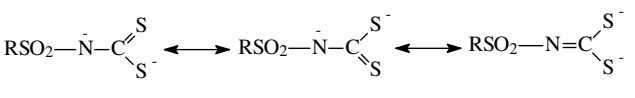

Scheme 2.

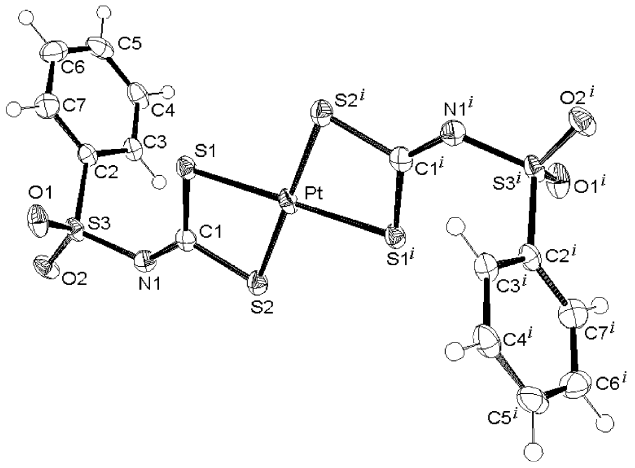

Fig. 1. ORTEP 3 [18] view of the anion of compound **1**, showing displacement ellipsoids at 50% probability level. Symmetry code (i) $-x, -y+1, -z+1$.

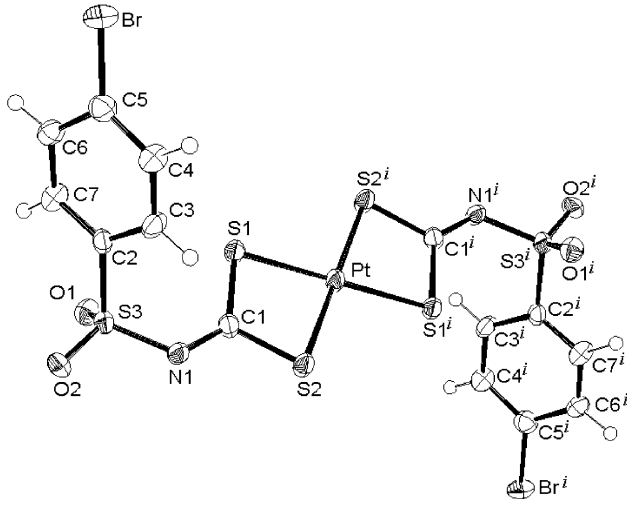

Fig. 2. ORTEP 3 [18] view of the anion of compound **2**, showing displacement ellipsoids at 50% probability level. Symmetry code (i) $-x+1, -y+1, -z$.

$[Pt(RSO_2N{=}CS_2)_2]^{2-}$ anions and two univalent *n*-Bu_4N^+ cations are related by an inversion centre at Pt. In the compound **2**, two of the chains of the *n*-Bu_4N^+ cation and 4-BrC_6H_4 groups were found to be disordered.

In both complex anions, the platinum(II) is coordinated by the four sulfur atoms of the two *N*-*R*-sulfonyldithiocarbimate ligands into a distorted square planar configuration. The S(1)–Pt–S(2) angle is smaller than 90° due to the asymmetric bidentate chelation.

The $N{=}CS_2$ fragments of the complexes show interesting features. In the compounds **1** and **2**, the CS bond lengths are nearly equal and are slightly shorter than typical C–S single bond lengths (ca. 1.81 Å) due to the partial π-delocalization in the S–C–S group (Scheme 2). However, in the $C_6H_5SO_2N{=}CS_2K_2\cdot 2H_2O$ they are quite different [7] (Table 3). Their differences can be

Table 3
Comparison between the CS_2 bonds (lengths and angles) in the dithiocarbimate potassium salts and complexes of nickel(II) and platinum(II) with dithiocarbimate anions

Substances	C(1)–S(1) (Å)	C(1)–S(2) (Å)	S(1)–C(1)–S(2) (°)
$K_2(C_6H_5SO_2N{=}CS_2)\cdot 2H_2O$[a]	1.701(7)	1.745(7)	119.4(4)
$[Ni(C_6H_5SO_2N{=}CS_2)_2]^{2-}$[b]	1.70(1)	1.72(1)	109.2(7)
$[Pt(C_6H_5SO_2N{=}CS_2)_2]^{2-}$	1.733(2)	1.750(2)	107.87(11)
$[Ni(4\text{-}BrC_6H_4SO_2N{=}CS_2)_2]^{2-}$[c]	1.722(10)	1.722(11)	108.4(6)
$[Pt(N\text{-}4\text{-}BrC_6H_4SO_2N{=}CS_2)_2]^{2-}$	1.732(4)	1.737(4)	108.5(2)

[a] Ref. [7].
[b] Ref. [17].
[c] Ref. [14].

Table 4
Comparison between crystallographic and spectroscopic data for the CN bond in the dithiocarbimate anions

Substances	ν(CN) (cm^{-1})	^{13}C NMR (NCS_2) (ppm)	CN length (Å)
$C_6H_5SO_2N{=}CS_2K_2\cdot 2H_2O$[a]	1267	223.19	1.342(9)
$[Ni(C_6H_5SO_2N{=}CS_2)_2]^{2-}$[b]	1380	210.63	1.32(2)
$[Pt(C_6H_5SO_2N{=}CS_2)_2]^{2-}$	1395	212.74	1.293(3)
$4\text{-}BrC_6H_4SO_2N{=}CS_2K_2\cdot 2H_2O$	1258	225.74	
$[Ni(N\text{-}4\text{-}BrC_6H_5SO_2N{=}CS_2)_2]^{2-}$[c]	1370	210.97	1.321(12)
$[Pt(N\text{-}4\text{-}BrC_6H_4SO_2N{=}CS_2)_2]^{2-}$	1380	213.29	1.313(4)

[a] Crystallographic data from [7].
[b] Crystallographic data from [17], spectroscopic data from [14].
[c] Ref. [14].

explained by the greater repulsive interaction between S(2) and the lone-pair located on the nitrogen [7] than the repulsion between S(1) and the RSO_2 group. When the complexation occurs two factors must be considered. First, the S(1)–C(1)–S(2) angle decreases. This fact weakens the interaction between S(2) and the nitrogen lone-pair shortening the difference between the C(1)–S(1) and the C(1)–S(2) bond lengths (Table 3). Another interesting point to consider is the greater C–S bond lengths in the Pt complexes when compared to the Ni analogous. This fact is probably due to the fact that the platinum(II) is a softer acid than nickel(II) which favors the M–S linkage and the canonical form (c) (Scheme 2). The increase on the importance of the canonical form (c) reflects on the CN bond length. This bond in **1** and **2** have approximately the same lengths and are shorter than the CN bonds in $C_6H_5SO_2N{=}CS_2K_2\cdot 2H_2O$ (Table 4). Besides, the CN bonds in the anionic complexes **1** and **2** are shorter than those on the analogous nickel(II) complexes [14,17].

4. Conclusion

Two novel platinum(II) dithiocarbimates complexes were described. Their tetra-*n*-butylammonium salts were obtained in crystalline form and were characterized by X-ray diffraction techniques. There is an interesting relationship between the spectroscopic data and the X-ray experiments results (Table 4) that pointed to an increase of the contribution of the canonical form (c) to the resonance hybrid from the ligands to the complexes, and from nickel(II) complexes to platinum(II) complexes, with a consequent increase of the CN double bond character. Thus, in the IR spectra the wavenumbers of the ν(CN) are smaller for the ligands than for the complexes, the ^{13}C NMR spectra show that the carbon atoms of the dithiocarbimate moiety are more shielded in the complexes than in $C_6H_5SO_2N{=}CS_2K_2\cdot 2H_2O$, and the crystallographic data show that the CN bond are shorter in the complexes than in $C_6H_5SO_2N{=}CS_2K_2\cdot 2H_2O$.

5. Supplementary material

Crystallographic data for the structural analysis have been deposited with the Cambridge Crystallographic Data Centre, CCDC Nos. 219805 and 219806 for **1** and **2**, respectively. Copies of this information may be obtained free of charge from The Director, CCDC, 12 Union Road, Cambridge, CB2 1EZ, UK (fax: +44-1223-336-033; e-mail: deposit@ccdc.cam.ac.uk or http://www.ccdc.cam.ac.uk).

Acknowledgements

This work has been supported by FAPEMIG (Grant CEX 1123/90), FINEP, CNPq and CAPES (Brazil).

References

[1] A. Manohar, K. Ramalingam, G. Bocelli, L. Righi, Inorg. Chim. Acta 314 (2001) 177.
[2] P. Leroux, Pestic. Sci. 47 (1996) 191.
[3] D. Coucouvanis, Prog. Inorg. Chem. 11 (1969) 233.
[4] G. Faraglia, D. Fregona, S. Sitran, L. Giovagnini, C. Marzano, F. Baccichetti, U. Casellato, R. Graziani, J. Inorg. Biochem. 83 (2001) 31.
[5] A.I. Vogel, A Textbook of Practical Organic Chemistry Including Qualitative Organic Analysis, Logmans Green and CO. LTDA, London, 1996.
[6] K. Hartke, Achiv der Pharmazie 299 (1966) 164.
[7] H.U. Hummel, U.Z. Korn, Naturforsch 44B (1989) 24.
[8] E. Nonius, COLLECT 1997–2000, Nonius BV, Delft, The Netherlands, 2000.
[9] Z. Otwinowski, W. Minor, H.K.L. Denzo, H.K.L. Scalepack, in: C.W. Carter Jr., R.M. Sweet (Eds.), Methods in Enzymology, vol. 276, Academic Press, New York, 1997, pp. 307–326.
[10] A.L. Spek, Acta Crystallogr. A46 (1990) 194.
[11] G.M. Sheldrick, SHELXS 97. Program for Crystal Structure Resolution, University of Göttingen, Göttingen, Germany, 1997.
[12] G.M. Sheldrick, SHELXL 97. Program for Crystal Structure Analysis, University of Göttingen, Göttingen, Germany, 1997.
[13] C.C. Hadjikostas, G.A. Katsoulos, S.K. Shakhatreh, Inorg. Chim. Acta 133 (1987) 129.
[14] M.R.L. Oliveira, R. Diniz, V.M. De Bellis, N.G. Fernandes, Polyhedron 22 (2003) 1561.
[15] Y.P. Tian, C.Y. Duan, Z.L. Lu, X.Z. You, H.K. Fun, B.C. Yip, Polyhedron 15 (9) (1996) 1495.
[16] R. Colton, T.A. Stephenson, Polyhedron 3 (2) (1984) 231.
[17] H.U. Hummel, U.Z. Korn, Naturforsch 44B (1989) 29.
[18] L.J. Farrugia, J. Appl. Crystallogr. 30 (1997) 565.

Available online at www.sciencedirect.com
SCIENCE DIRECT®
Polyhedron 23 (2004) 1159–1168
POLYHEDRON
www.elsevier.com/locate/poly

Platinum(II) and palladium(II) complexes containing a mixed donor 'P_2N' multidentate ligand

Eric W. Ainscough *, Andrew M. Brodie *, Anthony K. Burrell [1], Andreas Derwahl, Geoffrey B. Jameson, Steven K. Taylor

Chemistry, Institute of Fundamental Sciences, Massey University, Private Bag 11 222, Palmerston North, New Zealand

Received 10 December 2003; accepted 22 January 2004

Abstract

The 'P_2N' mixed donor ligand 2-(diphenylphosphino)-*N*-[2-(diphenylphosphino)benzylidene]benzeneamine (PNCHP) reacts with [MCl_2(1,5-cyclooctadiene)] and [$M(CH_3)Cl$(1,5-cyclooctadiene)] to give the complexes [M(PNCHP-κ^3P,N,P)Cl]Cl (M = Pt or Pd) and [Pd(PNCHP-κ^3P,N,P)(CH_3)]Cl, respectively. The ionic chloride can be exchanged with BF_4^- by reaction with $AgBF_4$. Abstraction of the covalent chloride with $AgBF_4$ in the presence of acetonitrile yields [Pt(PNCHP-κ^3P,N,P)(CH_3CN)]$^{2+}$. The acetonitrile ligand of this dication can be substituted with a variety of ligands to afford complexes of the type, [Pt(PNCHP-κ^3P,N,P)L]$^{2+}$ (L = the monodentate ligands: triphenylphosphine, 2-picoline, 3-picoline or the chelate ligands: 1,10-phenanthroline, 2,2′-bipyridine, bis(diphenylphosphino)ethane, 2,2′:6′,2″-terpyridine). The latter ligands all bind in a bidentate fashion to give five-coordinate complexes. The compounds have been characterised by spectroscopic and analytical means. The single crystal structures of the four-coordinate complexes, [Pt(PNCHP-κ^3P,N,P)Cl]Cl and [Pt(PNCHP-κ^3P,N,P)(PPh_3)]$(BF_4)_2$, and the five-coordinate complexes, [Pt(PNCHP-κ^3P,N,P)L]$(BF_4)_2$ (L = 1,10-phenanthroline and 2,2′:6′,2″-terpyridine), have been determined.
© 2004 Elsevier Ltd. All rights reserved.

Keywords: Crystal structure; Platinum; Palladium; Phosphorus–nitrogen donor

1. Introduction

Interest in the chemistry of the platinum group metals with mixed-donor, multidentate ligands [1] tends to be driven by interest in these systems as potential catalysts [1a,2]. To date, studies which involve ligands containing mixed phosphorus and nitrogen donor atoms have generally focussed on bidentate ligands [1,2c,3]. In contrast, mixed donor terdentate ligands, such as the 'P_2N' ligand, 2-(diphenylphosphino)-*N*-[2-(diphenylphosphino)benzylidene]benzeneamine (PNCHP), have received considerably less attention. PNCHP contains two inequivalent 'soft' phosphorus donor atoms and a 'borderline' nitrogen donor atom [4] (see Scheme 1). Therefore, with respect to the Hard and Soft Acid and Base (HSAB) principle, the ligand should be well suited to binding to platinum(II) and palladium(II). The favourable 'soft'–'soft' interactions of the phosphorus donor atoms of the PNCHP ligand with the low valent metal atom of concern are expected to anchor the ligand to the platinum(II) or palladium(II) metal centre. On one hand, the 'borderline'-'soft' nitrogen–metal atom interaction will have the potential for facile dissociation, and consequently the metal–PNCHP complex could exhibit interesting reactivity patterns [5]. For example, ring-opening, which is considered to be an important step in the mechanism of successful CO insertions 'into' metal–methyl bonds involving other terdentate ligands, allows an incoming CO ligand to bind to a coordination site in the square plane *cis* to the methyl group [6]. On the other hand, PNCHP has shown preference for terdentate coordination, occupying three sites of a square plane and has shown no previous signs of ring-opening [7]. Therefore, in this study we have concen-

* Corresponding authors. Tel.: +64-6-350-5102; fax: +64-6-350-5682.
E-mail address: a.brodie@massey.ac.nz (A.M. Brodie).
[1] Present address: Actinide, Catalysis and Separations Chemistry, C-SIC, Mail Stop J514, Los Alamos National Laboratory, Los Alamos, NM 87545, USA.

0277-5387/$ - see front matter © 2004 Elsevier Ltd. All rights reserved.
doi:10.1016/j.poly.2004.01.015

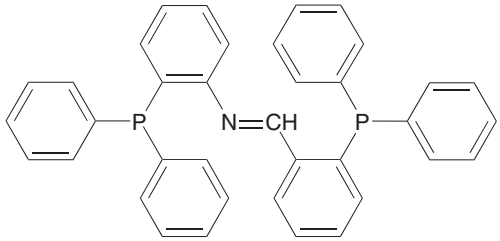

PNCHP

Scheme 1.

trated on the replacement of the chloride group with 'strong' bidentate ligands, such as 1,10-phenanthroline (phen), 2,2′-bipyridine (bipy) and bis(diphenylphosphino)ethane (diphos) as well as the terdentate, 2,2′:6′,2″-terpyridine (terpy) and report that these additional ligands are forced to bind to the fifth coordination site of the metal to give five-coordinate d^8 metal complexes.

2. Results and discussion

2.1. Synthesis of [Pt(PNCHP-κ³P,N,P)(MeCN)](BF₄)₂ (3) and related compounds

The syntheses of [M(PNCHP-κ^3P,N,P)Cl]Cl (M = Pd **1a** or Pt **1b**) and [Pd(PNCHP-κ^3P,N,P)-(CH_3)]Cl (**7**) are depicted in Scheme 2. PNCHP coordinates to platinum(II) and palladium(II) in a terdentate fashion by displacing 1,5-cyclooctadiene (COD) and one chloride from [M(COD)Cl_2] to yield complexes of the type [M(PNCHP-κ^3P,N,P)Cl]Cl (M = Pd **1a** and M = Pt **1b**). Attempts to isolate [M(PNCHP-κ^2P,P)Cl_2] were unsuccessful. However, several intermediates, which were suggestive of mono- and bidentate PNCHP species, were observed when monitoring the synthesis of [M(PNCHP-κ^3P,N,P)Cl]Cl by ^{31}P NMR. PNCHP

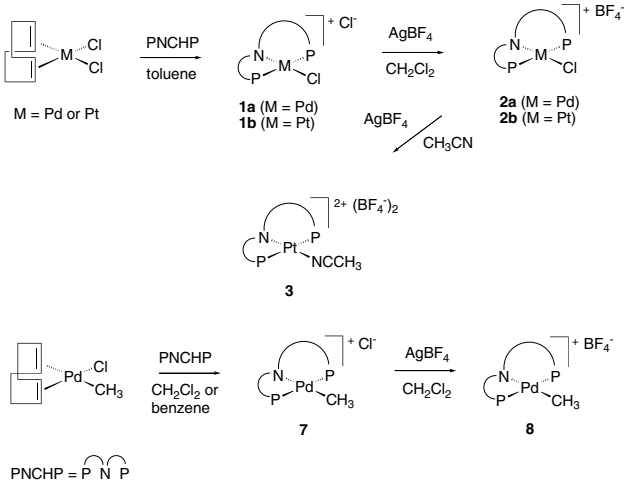

Scheme 2.

displaces COD and the chloro group from [Pd(COD)(-CH_3)Cl] yielding the compound [Pd(PNCHP-κ^3P,N,P)(CH_3)]Cl (**7**).

The ionic chloride of both **1a** and **1b** can be exchanged for a BF_4^- ion to give [M(PNCHP-κ^3P,N,P)Cl]BF_4 (M = Pd **2a** and M = Pt **2b**). In the presence of acetonitrile (MeCN) a second chloride of **1b** can be abstracted with $AgBF_4$ to give [Pt(PNCHP-κ^3P,N,P)(MeCN)]-(BF_4)$_2$ **3**. The chloride of **7** is easily exchanged for BF_4^- by a metathetical reaction of **7** with $AgBF_4$, affording the compound [Pd(PNCHP-κ^3P,N,P)(CH_3)]BF_4 **8**. When compound **8** was subjected to CO (7 atm) at room temperature there was no evidence for the formation of a CO adduct or for an insertion reaction. This is in contrast to palladium complexes with terdentate nitrogen ligands [6a], where insertion likely occurs via a mechanism involving dissociation of one of the distal nitrogen atoms to from a four-coordinate intermediate. In **8** the PNCHP ligand cannot dissociate a distal phosphorus atom [6a].

The reaction of **3** with monodentate ligands, L (L = 2-picoline, 3-picoline or triphenylphosphine) results in the substitution of the coordinated acetonitrile to give four-coordinate, dicationic complexes of the type [Pt(PNCHP-κ^3P,N,P)(L-κ^1)]$^{2+}$ (**4**) (Scheme 3). Analogous substitution reactions with the bidentate ligands (L–L), 2,2′-bipyridine (bipy), 1,10-phenanthroline (phen) or bis(diphenylphosphino)ethane (diphos)] gave complexes of the type [Pt(PNCHP-κ^3P,N,P)(L–L-κ^2)]$^{2+}$ (**5**), where the metal is now considered to be five-coordinate. Reaction of **3** with the potentially terdentate ligand 2,2′:6′,2″-terpyridine (terpy) also gives rise to a five-coordinate complex, [Pt(PNCHP-κ^3P,N,P)(terpy-κ^2N,N)]$^{2+}$ (**6**).

2.2. Single crystal X-ray diffraction studies

The X-ray determined crystal structures of **1b, 4a, 5a**, and **6** are shown as ORTEP plots of the cations in Figs. 1–4, respectively, and selected bond lengths and angles are given in Table 2.

2.2.1. Crystal structure of [Pt(PNCHP-κ³P,N,P)Cl]-Cl·2CH₂Cl₂ (1b)

The structure of the cation [Pt(PNCHP-κ^3P,N,P)Cl]$^+$ of **1b** (Fig. 1) contains a four-coordinate platinum atom with the two phosphorus atoms [P(1) and P(2)] and the imine nitrogen atom (N′ or N″) of PNCHP and one chloride [Cl(1)] atom making up the four donor atoms. A second chloride (ionic) and two molecules of dichloromethane are also present but omitted from Fig. 1 for clarity. The coordination geometry around the platinum atom is slightly distorted square planar which can be attributed to the steric requirements of the coordinated PNCHP ligand. The mean C(1)=N imine bond length at 1.272 Å is similar to the value found for the free ligand (1.266 Å) [4] as well

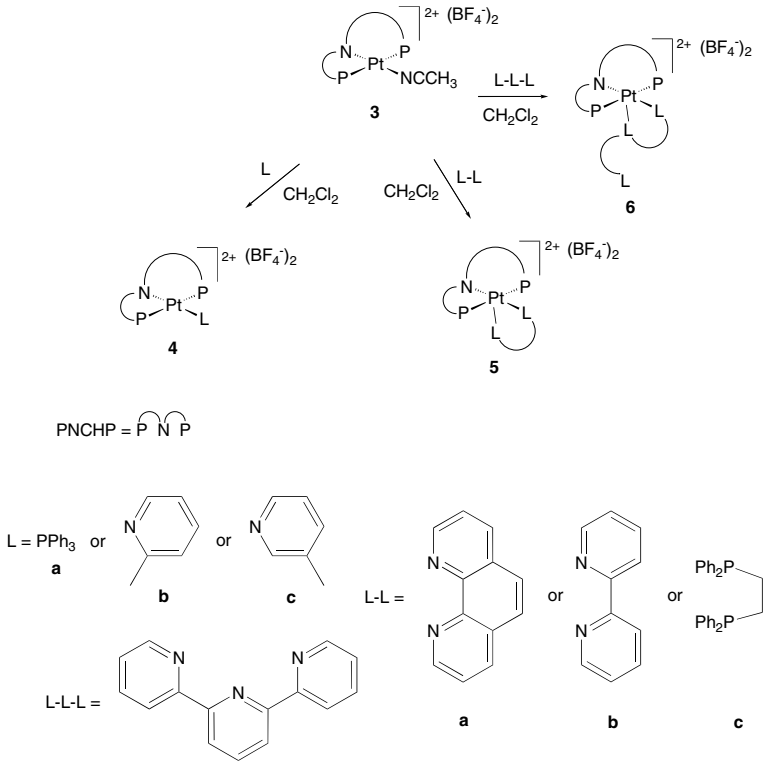

Scheme 3.

as for the related compounds, **4a**, **5a** and **6** [1.290(6)–1.297(15) Å] reported in this study.

*2.2.2. Crystal structure of [Pt(PNCHP-κ³P,N,P)-(PPh₃)](BF₄)₂ (**4a**)*

The structure of the dication, [Pt(PNCHP-κ^3P,N,P)(PPh_3)]$^{2+}$ **4a** (Fig. 2), shows the two phosphorus atoms [P(1) and P(2)] and nitrogen atom (N) of PNCHP and the phosphorus atom of a triphenylphosphine [P(3)] coordinated to a central platinum atom (Pt). As for **1b**, the coordination geometry of the platinum is slightly distorted square planar. Calculation of a plane involving the platinum atom and the four donor atoms, N, P(1), P(2) and P(3), shows a significant deviation from coplanarity of 0.146 Å, much greater than in the structure discussed above (0.095 for molecule A and 0.024 Å for molecule B). The Pt–P bond lengths to PNCHP [Pt–P(1), 2.3151(12) Å and Pt–P(2), 2.3247(12) Å] are similar

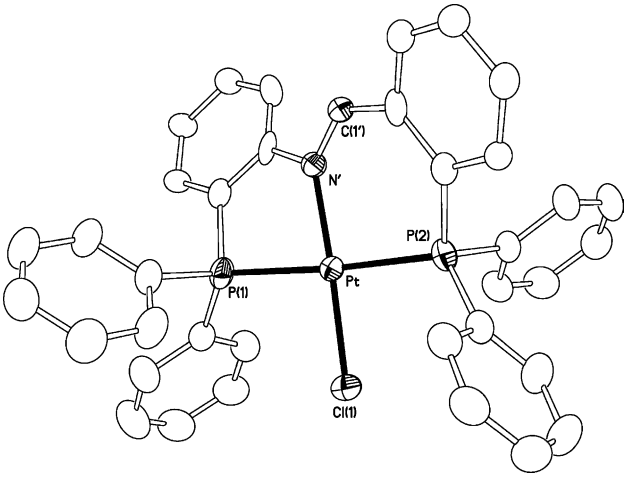

Fig. 1. ORTEP diagram of the cation of complex **1b** (major disorder part) showing the numbering system used. Thermal ellipsoids are at the 50% probability level. Hydrogen atoms have been omitted for clarity.

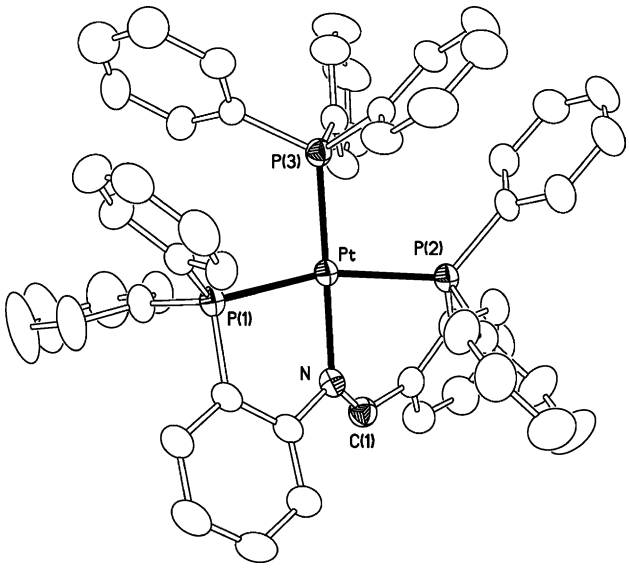

Fig. 2. ORTEP diagram of the cation of complex **4a** showing the numbering system used. Thermal ellipsoids are at the 50% probability level. Hydrogen atoms have been omitted for clarity.

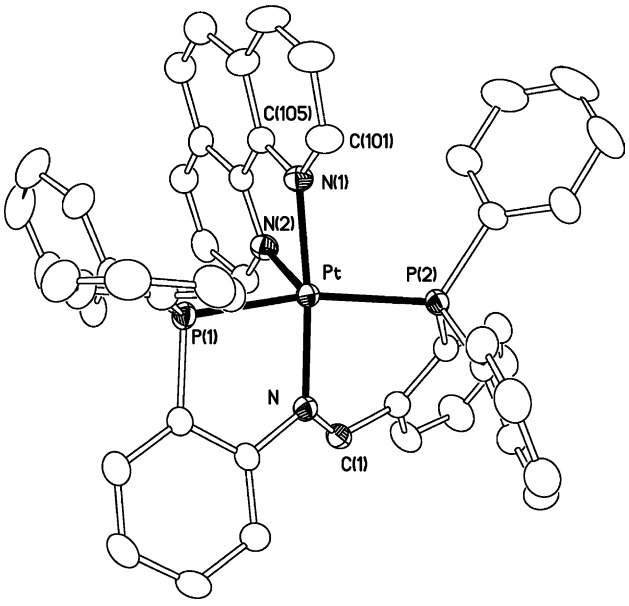

Fig. 3. ORTEP diagram of the cation of complex **5a** showing the numbering system used. Thermal ellipsoids are at the 50% probability level. Hydrogen atoms have been omitted for clarity.

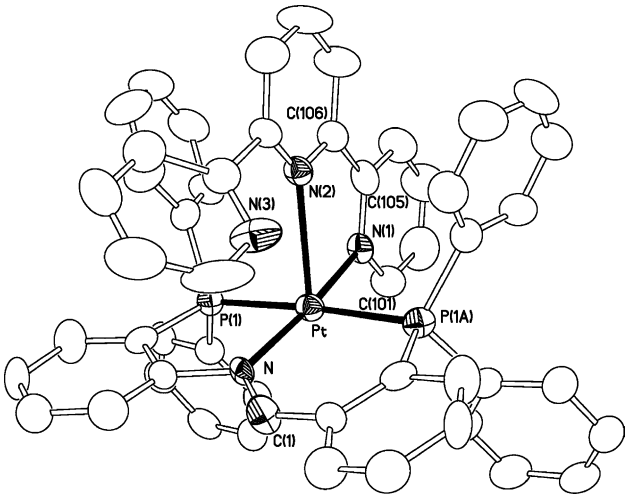

Fig. 4. ORTEP diagram of the cation of complex **6** showing the numbering system used. Thermal ellipsoids are at the 50% probability level. Hydrogen atoms have been omitted for clarity.

[2.332(2)–2.347(2) Å] to other square planar d^8 complexes of platinum for compounds with two phosphines *trans* to each other [8] Pt–P and Pt–N bond lengths are similar to those found in the complexes *cis*-$[Pt(PNH_2)]^{2+}$ and *trans*-$[Pt(PNH_2)]^{2+}$ ($PNH_2 = o$-aminophenyldiphenylphosphine) [9]. However, the bond lengths Pt–P(1) and Pt–P(2) are significantly longer (by 0.0215 and 0.0390 Å, respectively) than those found for [Pt(PNCHP-κ^3P,N,P)Cl]$^+$ (**1b**), which is consistent with the greater steric requirement of the mutually *cis* coordinated triphenylphosphine ligand – effectively there are three bulky triphenylphosphino moieties in close proximity.

2.2.3. Crystal structure of [Pt(PNCHP-κ^3P,N,P)-(phen–κ^2N,N)](BF$_4$)$_2\cdot$CH$_2$Cl$_2$ (**5a**)

For the dication, [Pt(PNCHP-κ^3P,N,P)(phen–κ^2N,N)]$^{2+}$ of **5a** (Fig. 3), the platinum atom is five-coordinate with a slightly distorted square-pyramidal geometry. The PNCHP ligand occupies three sites of the basal plane, coordinating through the two phosphorus atoms [P(1) and P(2)] and the nitrogen atom (N). The remaining coordination site of the basal plane is filled by one of the nitrogen atoms [N(1)] of the 1,10-phenanthroline (phen) ligand. The second nitrogen atom [N(2)] of the 1,10-phenanthroline is located at the apex of the square pyramid. There is no significant difference between the Pt–N(imine) [2.038(2) Å] and Pt–N(1)(phen) [2.043(2) Å] bond lengths, which are *trans* to one another in the basal plane. The axial phen–N(2)–Pt distance of 2.526(2) Å is considerably greater than the equatorial N(1)–Pt distance of 2.043(2) Å, the latter being typical for platinum(II)-1,10-phenanthroline species [10]. Due to the rigid structure of 1,10-phenanthroline, the second nitrogen atom is forced to be in the vicinity of the metal, making it difficult to decide whether or not the axial nitrogen atom-to-metal distance N(2)–Pt corresponds to a weak bond. However, in **5a** the phen is considered to be bidentate for the following reasons: (i) The platinum atom is displaced from the basal plane by 0.1052(8) Å towards the N(2) atom. (ii) The ratio of the axial/equatorial phen–N–Pt bond lengths at 1.24 is close to values for accepted five coordinate species [11]. For example, ratios of 1.17 are found for the five coordinate species $[Ni(CN)_5]^{2-}$ and 1.14 for the five coordinate $[PtI_2(CO)(dmphen)]$ (dmphen = 2,9-dimethyl-1,10-phenanthroline), where the phenanthroline ligand is bound in an axial-to-equatorial bidentate mode. By contrast, in $[PtCl(phen)(PEt_3)_2]^+$, where the phen ligand is considered monodentate, the ratio is 1.33 [12]. (iii) The N(1)–Pt–N(2) angle of 74.54(8)° lies close to the average phen N–M–N angle of 79.5° when the ligand is clearly bidentate [11]. For comparison, the equivalent angles in $[Pt(CN)(phen)_2]^+$ and $[PtCl(phen)(PEt_3)_2]^+$, where the phen ligand is monodentate, are 69.7(2)° and 68.2°, respectively [13,14]. (iv) The difference between the Pt–N(1)–C(105) and Pt–N(1)–C(101) angles of only −2.7°, is indicative of a phenanthroline ligand bound to both the basal plane and the apical site of the metal atom [15]. (v) Lastly, the axial phen–N–Pt distance [2.526(2) Å] in **5a** is considerably shorter than the analogous distances in $[Pt(CN)(phen)_2]^+$ and $[PtCl(phen)(PEt_3)_2]^+$ [2.761(5) and 2.843(20) Å, respectively], which are considered to be too long for a bonding interaction.

2.2.4. Crystal structure of [Pt(PNCHP-κ^3P,N,P)(terpy-κ^2N,N)](BF$_4$)$_2$ (**6**)

The geometry around the metal in [Pt(PNCHP-κ^3P,N,P)(terpy-κ^2N,N)]$^{2+}$ **6** (Fig. 4) is similar to that

Table 1
Crystal data and structure refinement for the complexes **1b**, **4a**, **5a**, and **6**

Compound	**1b**	**4a**	**5a**	**6**
Empirical formula	$C_{39}H_{33}Cl_6NP_2Pt$	$C_{57}H_{48}B_2Cl_4F_8NP_3Pt$	$C_{50}H_{39}B_2Cl_2F_8N_3P_2Pt$	$C_{52}H_{40}B_2F_8N_4P_2Pt$
M	985.39	1350.38	1183.39	1151.53
T (K)	203(2)	203(2)	203(2)	200(2)
Crystal system	triclinic	monoclinic	triclinic	monoclinic
Space group	$P\bar{1}$	$P2(1)/c$	$P\bar{1}$	$P2(1)/m$
a (Å)	10.7207(1)	13.1722(1)	10.3338(1)	11.289(2)
b (Å)	13.8244(2)	21.81280(10)	12.9595(2)	16.021(3)
c (Å)	14.5320(2)	19.7670(2)	18.5480(2)	13.684(3)
α (°)	114.840(2)	90	87.012(1)	90
β (°)	91.402(1)	91.942(1)	88.389(1)	107.97(3)
γ (°)	96.559(1)	90	76.211(1)	90
U (Å^3)	1935.45(4)	5676.24(8)	2408.78(5)	2354.3(8)
Z	2	4	2	2
Absorption coefficient (mm^{-1})	4.152	2.810	3.160	3.122
Reflections measured	18848	31955	20996	19782
Independent reflections	8348 ($R_{int} = 0.0244$)	12425 ($R_{int} = 0.0285$)	9682 ($R_{int} = 0.0130$)	4368 ($R_{int} = 0.0992$)
Final R indices [$I > 2\sigma(I)$]	$R_1 = 0.0268$, $wR_2 = 0.0654$	$R_1 = 0.0449$, $wR_2 2 = 0.0996$	$R_1 = 0.0207$, $wR_2 = 0.0547$	$R_1 = 0.0458$, $wR_2 = 0.1047$
R indices (all data)	$R_1 = 0.0301$, $wR_2 = 0.0673$	$R_1 = 0.0603$, $wR_2 = 0.1095$	$R_1 = 0.0220$, $wR_2 = 0.0559$	$R_1 = 0.0627$, $wR_2 = 0.1119$

Table 2
Selected bond lengths (Å) and angles (°) for the complexes **1b**, **4a**, **5a**, and **6** with estimated standard deviations in parentheses

	1b	**4a**	**5a**	**6**
Bond lengths				
Pt–P(1)	2.2936(8)	2.3151(12)	2.2997(6)	2.3058(16)
Pt–P(2)	2.2857(8)	2.3247(12)	2.2947(6)	2.3058(16)
Pt–N	2.038(4)–N′, 2.106(7)-N″	2.107(4)	2.038(2)	2.044(10)
Pt–Cl(1)	2.2875(9)			
Pt–N(1)			2.043(2)	2.061(7)
Pt–N(2)			2.526(2)	2.625(7)
Pt–P(3)		2.2688(13)		
N–C(1)	1.301(6)-A, 1.242(8)-B	1.290(6)	1.295(3)	1.297(15)
Bond angles				
P(1)–Pt–P(2)	174.84(3)	160.96(5)	161.34(2)	175.30(8)
N–Pt–Cl(1)	169.83(10)-A, 168.20(14)-B			
N–Pt–P(3)		175.68(12)		
N–Pt–N(1)			172.52(8)	170.3(2)
P(1)–Pt–N	80.85(10)-A, 98.08(16)-B	82.23(11)	84.66(6)	80.3(2)
P(2)–Pt–N	95.13(10)-A, 77.34(16)-B	83.37(11)	86.84(6)	99.4(2)
P(1)–Pt–Cl(1)	93.14(3)			
P(2)–Pt–Cl(1)	91.29(3)			
P(1)–Pt–P(3)		98.80(5)		
P(2)–Pt–P(3)		96.49(5)		
P(1)–Pt–N(1)			91.98(6)	90.07(4)
P(2)–Pt–N(1)			98.25(6)	90.07(4)
P(1)–Pt–N(2)			94.69(5)	92.26(4)
P(2)–Pt–N(2)			103.04(5)	92.26(4)
N(1)–Pt–N(2)			74.54(8)	72.6(3)
N–Pt–N(2)			99.03(8)	109.1(3)

found in [Pt(PNCHP-κ^3P,N,P)(phen)]$^{2+}$. Again, the platinum atom is square pyramidal with the two phosphorus atoms [P(1) and P(2)] and one nitrogen atom (N) of PNCHP occupying three equatorial sites, with the fourth site occupied by one of the terminal nitrogen atoms [N(1)] of the 2,2′,6′2″-terpyridine ligand. The central nitrogen atom [N(2)] of the terpy occupies the axial site with the axial Pt–N(2) distance at 2.625(7) Å being longer than the equatorial Pt–N(1) distance of 2.061(7) Å. The Pt–N(2) distance is considered to cor-

respond to a bonding interaction since the same arguments put forth to describe the nature of the axial Pt–N(2) bond in [Pt(PNCHP)(phen–$\kappa^2 N,N$)]$^{2+}$ (**5a**) also hold for **6**, although the interaction is weaker: the platinum atom is displaced from the basal donor atom plane by only 0.0349(8) Å towards the N(2) atom, the axial/equatorial ratio is slightly larger at 1.27 and difference between the M–N(1)–C(105) and M–N(1)–C(101) angles is also slightly larger at +5.0°. In addition, unlike the phen ligand in **5a**, the pyridyl ring containing the axial bound nitrogen atom is free to rotate around the C(105)–C(106) axis and therefore is not required to orientate itself for bonding with the metal, as it does. The two rings containing the N(1) and N(2) atoms lie in one plane. In contrast, the mean plane of the pyridyl ring containing the non-bonding nitrogen atom N(3) is tilted 47.7° relative to the mean plane of the middle pyridyl ring.

2.3. NMR spectroscopy

The ^{31}P NMR data for selected compounds are collected in Table 3. All the platinum(II) compounds displayed similar spectra, showing two doublets with platinum-195 satellites which are assigned to the two phosphorus atoms of the PNCHP ligand with ^2J(P,P) coupling between the two inequivalent phosphorus nuclei and ^1J(Pt,P) coupling due to the spin 1/2 nucleus ^{195}Pt, found in 33% abundance. In general, for all the platinum(II) compounds discussed here, one of the phosphorus atoms gives rise to a high frequency resonance (δ 45.9–28.7) and the other to a low frequency resonance (δ 19.5–12.3). The former resonances can reasonably assigned to the phosphorus atoms involved in the five-membered ring, due to the ring contribution (ΔR) effect [16,17]. The ^2J(P,P) coupling constants ranged from 306 to 422 Hz which is indicative of a *trans* arrangement of inequivalent phosphorus atoms [18]. Coupling constants of larger magnitude were exhibited by the monocationic complexes, whilst those of smaller magnitude were displayed by the dicationic complexes. ^1J(P,Pt) coupling constants ranged from 2353 to 2789 Hz and were typical of *trans*-platinum(II) complexes [18]. The ^1J(P,Pt) coupling constants associated with the higher frequency resonances, i.e. those from δ 45.9–28.7, were on average 30 Hz higher than their lower frequency counterparts at δ 19.5–12.3, further supporting the assignment of the signals at high frequency to the phosphorus atoms involved in the five-membered ring, again due to the ring contribution (ΔR) effect [18].

The spectra of the two complexes, [Pt(PNCHP-$\kappa^3 P,N,P$)(PPh$_3$)](BF$_4$)$_2$ (**4a**) and [Pt(PNCHP-$\kappa^3 P,N,P$)-(diphos)](BF$_4$)$_2$ (**5c**) contain additional phosphorus signals due to their phosphine co-ligands. For **4a**, where the ancillary ligand is triphenylphosphine, an additional resonance at δ 5.1, with ^2J(P,P) coupling constants of 18 and 21 Hz and a ^1J(P,Pt) of 3397 Hz, was observed. The relatively large ^1J(P,Pt) coupling constant for the triphenylphosphine ligand, relative to those observed for PNCHP, is due to the poorer *trans* influence of the ni-

Table 3
NMR data for selected compounds

Compound	^{31}P {^{1}H}NMR[a]			^{1}H NMR[b]	
	δ	^2J(PP)/Hz	^1J(PPt)/Hz	δ (C*H*=N)[c]	^3J(HPt)/Hz
[Pd(PNCHP)Cl]Cl (**1a**)	37.3, 22.6	478		10.61	
[Pt(PNCHP)Cl]Cl (**1b**)	32.0, 18.8	421	2542, 2495	10.87	106.5
[Pt(PNCHP)(PPh$_3$)](BF$_4$)$_2$ (**4a**)	38.5, 19.5, 5.1[e]	337, 21, 18	2496, 2367, 3397	8.62(dd)[d]	63.9 [^4J(HP) 11.6, 1.1]
[Pt(PNCHP)(2-pico)](BF$_4$)$_2$ (**4b**)	33.4, 18.5 [g]	363	2493, 2490	9.48[f]	92.2
[Pt(PNCHP)(3-pico)](BF$_4$)$_2$ (**4c**)	34.4, 19.3[g]	366	2499, 2505	9.46[f]	90.3
[Pt(PNCHP)(phen)](BF$_4$)$_2$ (**5a**)	29.9, 14.4	354	2789, 2757	9.42[h]	91.6
[Pt(PNCHP)(bipy)](BF$_4$)$_2$ (**5b**)	29.7, 15.2	363	2731, 2722	8.95	90.9
[Pt(PNCHP)(diphos)](BF$_4$)$_2$ (**5c**)	45.9, 12.3	396	2435, 2353	[i]	
	42.6[j] , 38.3[j]	[k]	[k] 3088		
[Pt(PNCHP)(terpy)](BF$_4$)$_2$ (**6**)	28.7, 13.6	306	2698, 2669	9.04[h]	95.7
[Pd(PNCHP)Me]Cl (**7**)	33.6, 27.5	392		10.29	

[a] Recorded at 109 MHz, chemical shifts are in ppm relative to 85% H_3PO_4, solvent $CDCl_3$ unless stated otherwise.
[b] Recorded at 270 MHz, chemical shifts are in ppm relative to $Si(CH_3)_4$, solvent $CDCl_3$ unless stated otherwise.
[c] In addition, compounds **4b**, **4c** and **7** show C*H*$_3$-resonances at δ 2.24, 1.97 and 0.56, respectively. **5c** shows $Ph_2PCH_2CH_2PPh_2$resonances at δ 3.02.
[d] In CD_3CN.
[e] Ph_3P resonance.
[f] In $(CD_3)_2CO$
[g] In CH_3CN.
[h] In CD_2Cl_2.
[i] Obscured by aromatic C*H* resonances in the range δ 7.95 – 5.94.
[j] $Ph_2PCH_2CH_2PPh_2$resonance.
[k] Not resolved.

trogen when compared to the phosphorus atom. The chemical shift is similar to other triphenylphosphine platinum(II) compounds [19] with the ^2J(P,P) coupling constant being typical of phosphorus atoms in a *cis* arrangement [18]. Free diphos contains equivalent phosphorus atoms but on coordination in **5c**, these become inequivalent, exhibiting one resonance at 42.6 and the other at δ 38.3, values which support both diphos phosphorus atoms being coordinated to the platinum atom. The ^1J(P,Pt) coupling constant of 3088 Hz is typical of diphos coordinated in square planar platinum(II) complexes [20,21] and consistent with P *trans* to N. The expected second ^1J(P,Pt) coupling constant could not be resolved.

The phosphorus-31 NMR spectra of the palladium complexes are similar to those of the platinum compounds, but with the expected absence of phosphorus-to-metal coupling. All spectra displayed two doublet signals, which are assigned to the inequivalent phosphorus atoms of PNCHP. As for the platinum compounds, chemical shifts are indicative of phosphorus-transition metal coordination. The ^2J(P,P) coupling constants were typical of the PNCHP ligand bound to palladium(II) with its two phosphorus atoms *trans* to one another. As previously reported [18], chemical shifts and coupling constants for the palladium complexes were significantly larger than those for their platinum analogues.

All the compounds listed in Table 3 displayed a signal in the range δ 10.9–8.6 which can be assigned to the imine proton of coordinated PNCHP with coupling to ^{195}Pt (60 – 110 Hz) being observed for the platinum complexes. As the ancillary ligand is changed from a halogen to a nitrogen to a phosphorus donor ligand, the chemical shift of the imine proton moves to lower frequency and the ^3J(H,Pt) coupling constant decreases. The shift to lower frequency can be explained using the relative *trans* influence of the donor atom of the ancillary ligand. For example, when the ancillary donor atom is phosphorus (high in the *trans* influence series), as it is in [Pt(PNCHP-κ^3P,N,P)(PPh_3)]$(BF_4)_2$ (**4a**) and [Pt(PNCHP-κ^3P,N,P)(diphos)]$(BF_4)_2$ (**5c**), the imine proton exhibits its lowest frequency shifts.

3. Conclusions

For the d^8 metals, platinum(II) and palladium(II), the PNCHP ligand coordinates to three sites of the square-plane, using the two phosphorus atoms and the imino-nitrogen atom. In the compound [Pt(PNCHP-κ^3P,N,P)(MeCN)]$(BF_4)_2$ (**3**), the acetonitrile ancillary ligand, which occupies the fourth site of the square-plane, can be substituted with monodentate ligands, such as 2- and 3-picoline and triphenylphosphine. Reaction of **3** with the bidentate ligands 2,2′-bipyridine, 1,10-phenanthroline and bis(diphenylphosphino)ethane, does not result in any observable competition with the PNCHP ligand for coordination sites. Instead, these ligands act in a bidentate fashion, with one of their donor atoms occupying the fourth site of the square-plane, and the second donor atom the apical site of a square pyramid to give five-coordinate dicationic complexes. The potentially tridentate ligand, 2,2′,6′,2″-terpyridine, also behaves as a bidentate, forming the five-coordinate complex [Pt(PNCHP-κ^3P,N,P)(terpy-κ^2N,N)]$^{2+}$ (**6**).

4. Experimental

4.1. Materials and instrumentation

Spectral measurements were performed as previously described [7]. Microanalyses were performed by the Campbell Microanalytical Laboratory, University of Otago. Many of the compounds contained solvated CH_2Cl_2 which was readily lost and the analytical data reflect this. The PNCHP ligand [4], [Pt(COD)Cl_2], [Pd(COD)Cl_2] and [Pd(COD)(Me)Cl] [22] were prepared according to literature preparations. All reactions were carried out under an inert atmosphere. Solvents were dried by standard procedures [23].

4.2. Preparation of the complexes

4.2.1. [Pd(PNCHP-κ^3P,N,P)Cl]Cl (**1a**)

A mixture of [Pd(COD)Cl_2] (0.100 g, 0.350 mmol) and PNCHP (0.193 g, 0.351 mmol) in benzene (12 mL) was heated to reflux for 1 h. The resulting yellow precipitate was isolated by filtration, washed with *N*-pentane and air dried to yield **1a** (0.235 g, 86.9%) as a yellow powder. *Anal.* Calc. for $C_{37}H_{29}Cl_2NP_2Pd \cdot 0.5\ CH_2Cl_2$: C, 58.54; H, 3.93; N, 1.82. Found: C, 58.41; H, 3.99; N, 1.78%.

4.2.2. [Pt(PNCHP-κ^3P,N,P)Cl]Cl (**1b**)

A mixture of [Pt(COD)Cl_2] (0.100 g, 0.267 mmol) and PNCHP (0.147g, 0.267 mmol) in benzene (12 mL) was stirred at room temperature for 40 min, giving a yellow precipitate. The mixture was heated to reflux for 30 min and allowed to cool. The resulting yellow precipitate was isolated by filtration, washed with diethylether and air dried to yield **1b** (0.146 g, 60.7%) as a yellow powder. The compound can be crystallised from dichloromethane/*N*-hexane. M.p: 294-296 °C (dec). *Anal.* Calc. for $C_{37}H_{29}Cl_2NP_2Pt \cdot 1.5CH_2Cl_2$: C, 49.04; H, 3.42; N, 1.49. Found: C, 48.78; H, 2.75; N, 1.52%.

4.2.3. [Pd(PNCHP-κ^3P,N,P)Cl]BF_4 (**2a**)

A mixture of **1a** (0.202 g, 0.263 mmol) and $AgBF_4$ (0.054 g, 0.277 mmol) in dichloromethane (12 mL) was

exposed to ultrasound for 1 h resulting in yellow and white precipitates. This mixture was filtered through kieselguhr and the trapped yellow precipitate dissolved and washed through into the filtrate with acetonitrile, leaving the insoluble white precipitate behind. The filtrate was taken to dryness in vacuo and the resulting yellow residue crystallised from dichloromethane/*n*-hexane. Compound **2a** (0.169 g, 82.6%) was isolated as large yellow crystals, washed with a dichloromethane/*N*-pentane mixture and air-dried. *Anal.* Calc. for $C_{37}H_{29}BClF_4NP_2Pd$: C, 57.10; H, 3.76; N, 1.80. Found: C, 56.68; H, 3.70; N, 1.90%.

4.2.4. [Pt(PNCHP-κ^3P,N,P)Cl]BF_4 (**2b**)

A mixture of **1b** (0.300 g, 0.333 mmol) and $AgBF_4$ (0.071 g, 365 mmol) in dichloromethane (12 mL) was exposed to ultrasound for 1 h, resulting in yellow and white precipitates. The mixture was filtered through kieselguhr and the trapped yellow precipitate dissolved and washed through into the filtrate using acetonitrile, leaving the insoluble white precipitate behind. The filtrate was taken to dryness in vacuo and the resulting yellow residue crystallised from dichloromethane/*N*-hexane overnight. Compound **2b** (0.248 g, 79.9%) was isolated as orange crystals, washed with a dichloromethane/*N*-pentane mixture and air-dried. M.p. 198–200 °C. *Anal.* Calc. for $C_{37}H_{29}BClF_4NP_2Pt \cdot 0.75CH_2Cl_2$: C, 48.72; H, 3.30; N, 1.51. Found: C, 48.55; H, 3.29; N, 1.56%.

4.2.5. [Pt(PNCHP-κ^3P,N,P)(MeCN)]$(BF_4)_2$ (**3**)

A mixture of **2b** (0.401 g, 0.431 mmol) and $AgBF_4$ (0.0899 g, 401 mmol) in acetonitrile (c.a. 15 mL) was heated to reflux for 27 h, giving a dark-orange solution. The solvent was removed in vacuo and the resulting orange residue crystallised from dichloromethane/*N*-hexane to yield **3** (0.369 g, 96.0%). *Anal.* Calc. for $C_{39}H_{32}B_2F_8N_2P_2Pt \cdot 0.5CH_2Cl_2$: C, 47.36; H, 3.32; N, 2.80. Found: C, 47.89; H, 3.45; N, 2.81%.

4.2.6. [Pt(PNCHP-κ^3P,N,P)(PPh_3)]$(BF_4)_2$ (**4a**)

A mixture **2b** (0.101 g, 0.108 mmol) and $AgBF_4$ (0.0226 g, 0.116 mmol) in acetonitrile (12 mL) was heated to reflux for ca. 25 min, giving a white precipitate. PPh_3 (0.0306 g, 0.117 mmol) was added to the reaction mixture and refluxing continued for a further 30 min. This mixture was filtered through kieselguhr and the trapped yellow precipitate dissolved and washed through into the filtrate with dichloromethane, leaving the original white precipitate behind. The filtrate solvent was evaporated in vacuo and the resulting yellow residue precipitated from dichloromethane/*N*-hexane overnight. Compound **4a** (0.103 g, 80.8%) was isolated as a very pale yellow powder, washed with *N*-pentane and air-dried. The powder can be recrystallised from a CH_2Cl_2/*N*-hexane vapour diffusion to yield colourless crystals. *Anal.* Calc. for $C_{55}H_{44}B_2F_8NP_3Pt \cdot CH_2Cl_2$: C, 53.15; H, 3.66; N, 1.11. Found: C, 53.36; H, 3.80; N, 1.18%.

4.2.7. [Pt(PNCHP-κ^3P,N,P)(2-pico)]$(BF_4)_2$ (**4b**)

A mixture of **2b** (0.162 g, 0.174 mmol) and $AgBF_4$ (0.0360 g, 0.185 mmol) in acetonitrile (12 mL) was heated to reflux for 30 min, giving a white precipitate. 2-Picoline (2-pico) (0.0183 mL, 0.185 mmol) was added to the reaction mixture and refluxing continued for a further 30 min. The white precipitate was removed by filtration through kieselguhr and the filtrate taken to dryness in vacuo. The resulting yellow residue converted to a white and brown mixture over two days. The white product was separated from the insoluble brown product by dissolving in dichloromethane, followed by filtration. Crystallisation was initiated by addition of *N*-hexane to the filtrate. Compound **4b** (0.1354 g, 72.4%) was isolated as white microcrystals, washed with diethylether and dried in vacuo. *Anal.* Calc. for $C_{43}H_{36}B_2F_8N_2P_2Pt$: C, 51.06; H, 3.59; N, 2.78. Found: C, 51.04; H, 3.48; N, 2.79%.

4.2.8. [Pt(PNCHP-κ^3P,N,P)(3-pico)]$(BF_4)_2$ (**4c**)

A mixture of **2b** (0.154 g, 0.165 mmol) and $AgBF_4$ (0.0343 g, 0.176 mmol) in acetonitrile (12 mL) was heated to reflux for ca. 25 min, giving a white precipitate. 3-Picoline (3-pico) (0.016 mL, 0.18 mmol) was added to the reaction mixture and refluxing continued for a further 30 min. The white precipitate was removed by filtration through kieselguhr and the filtrate taken to dryness in vacuo. The resulting yellow residue was taken into solution with acetonitrile, followed by addition of diethylether to precipitate out the desired product. Compound **4c** (0.101 g, 56.5%) was isolated as a very pale yellow powder, washed with diethylether and air-dried. *Anal.* Calc. for $C_{43}H_{36}B_2F_8N_2P_2Pt \cdot CH_2Cl_2$: C, 48.20; H, 3.49; N, 2.56. Found: C, 47.88; H, 3.31; N, 3.05%.

4.2.9. [Pt(PNCHP-κ^3P,N,P)(phen)]$(BF_4)_2$ (**5a**)

A mixture of **3** (0.114 g, 0.119 mmol) and 1,10-phenanthroline (phen) (0.024 g, 0.133 mmol) in benzene (15 mL) was heated to reflux for 1 h, giving an orange toffee-like solid. The solvent was removed in vacuo and the resulting orange residue taken up into dichloromethane and heated to reflux overnight. The orange solution was subject to vapour diffusion using *N*-hexane giving **5a** (0.126 g, 96.4%) as chunky orange crystals. *Anal.* Calc. for $C_{49}H_{37}B_2F_8N_3P_2Pt \cdot CH_2Cl_2$: C, 50.75; H, 3.32; N, 3.55. Found: C, 51.05; H, 2.95; N, 3.52%.

4.2.10. [Pt(PNCHP-κ^3P,N,P)(bipy)]$(BF_4)_2$ (**5b**)

A yellow solution of **2b** (0.194 g, 0.209 mmol) and $AgBF_4$ (0.0436 g, 0.224 mmol) in acetonitrile (12 mL) was heated to reflux for 20 h. The resulting orange solution was filtered through kieselguhr. 2,2′-Bipyridine

(bipy) (0.033 g, 0.21 mmol), dissolved in acetonitrile, was added to the filtrate and refluxing continued for a further 1 h, giving an intense orange solution. The solution was allowed to cool, followed by solvent removal in vacuo. Additional white precipitate was removed by filtration through kieselguhr and washed with acetonitrile, and the filtrate plus washings were taken to dryness in vacuo. The resulting yellow residue was recrystallised from dichloromethane/*N*-hexane. Compound **5b** (0.141 g, 62.7%) was isolated as orange crystals, washed with *N*-pentane and air-dried. M.p: 259-260 °C. *Anal.* Calc. for $C_{47}H_{37}B_2F_8N_3P_2Pt \cdot 0.5CH_2Cl_2$: C, 51.08; H, 3.43; N, 3.76. Found: C, 51.22; H, 3.26; N, 3.85%.

4.2.11. [Pt(PNCHP-κ^3P,N,P)(diphos)]$(BF_4)_2$ (**5c**)

Compound **3** (0.100 g, 0.104 mmol) and bis(diphenylphosphino)ethane (diphos) (0.0420 g, 0.105 mmol) were dissolved together in dichloromethane (12 mL) and heated to reflux for 3 h. A small amount of the by-product $[Pt(diphos)_2](BF_4)_2$ (0.015 g, 24.5%), as a yellow precipitate, was removed by filtration and the filtrate set up for vapour diffusion with *N*-hexane. Compound **5c** was isolated as a yellow powder which on exposure to air, slowly turns green. *Anal.* Calc. for $C_{63}H_{53}B_2F_8NP_4Pt \cdot 2CH_2Cl_2$: C, 52.52; H, 3.86; N, 0.94. Found: C, 52.60; H, 3.79; N, 0.58%.

4.2.12. [Pt(PNCHP-κ^3P,N,P)(terpy)]$(BF_4)_2$ (**6**)

Compound **3** (0.100 g, 0.105 mmol) and 2,2′,6′,2″-terpyridine (terpy) (0.0244 g, 0.105 mmol) were dissolved together in dichloromethane (c.a. 12 mL) and heated to reflux for ca. 3 h. The reaction mixture was filtered and set up for vapour diffusion in *N*-hexane. Compound **6** (0.0919 g, 76.9%) was isolated as orange crystals, washed with *N*-pentane and air dried. *Anal.* Calc. for $C_{52}H_{40}B_2F_8N_3P_2Pt$: C, 54.24; H, 3.50; N, 4.87. Found: C, 53.97; H, 3.50; N, 4.85%

4.2.13. [Pd(PNCHP-κ^3P,N,P)(CH_3)]Cl (**7**)

A mixture of [Pd(COD)(CH_3)Cl] (0.101 g, 0.381 mmol) and PNCHP (0.208 g, 0.378 mmol) in dichloromethane (12 mL) was stirred at room temperature for 1 h, giving a yellow solution. *N*-Hexane was added until a slight cloudiness was observed. Very pale yellow microcrystals resulted after standing overnight. These were isolated by filtration, washed with *N*-pentane and air dried to yield **7** (0.239 g, 89.4%). *Anal.* Calc. for $C_{38}H_{32}ClNP_2Pd$: C, 64.60; H, 4.57; N, 1.98. Found: C, 64.30; H, 4.64; N, 2.01%.

4.2.14. [Pd(PNCHP-κ^3P,N,P)(CH_3)]BF_4 (**8**)

Compound **7** (164 g, 0.232 mmol) and $AgBF_4$ (0.0447 g, 0.230 mmol) were combined in dichloromethane (ca. 12 mL) and heated to reflux for 1 h. The reaction mixture was filtered through kieselguhr. *N*-Pentane was vapour diffused into the filtrate over a weekend. Compound **8** (0.114 g, 61.9%) was isolated as pale yellow microcrystals, washed with *N*-pentane and dried in vacuo. *Anal.* Calc. for $C_{38}H_{32}BF_4NP_2Pd \cdot 0.5CH_2Cl_2$: C, 57.78; H, 4.16; N, 1.75. Found: C, 58.15; H, 4.18; N, 1.83%.

4.3. Crystallography

Single crystals of the compounds, **1b**, **4a**, **5a** and **6**, were grown as described under their respective syntheses and attached to the ends of glass fibres with cyanoacrylate glue. Data collection and refinement were performed as previously described [24]. Table 1 lists the crystal data for the compounds. For **1b**, the imine bond of the PNCHP ligand and contiguous phenyl rings are disordered over two sites, A and B, and were refined with a free variable giving the occupancy of these as 0.67 and 0.33, respectively. In the case of **6**, the platinum atom and the two pyridyl rings of the terpy ligand lie on a mirror plane and were refined with special position constraints. The PNCHP ligand is disordered about this mirror plane and the two single phenyl rings and the phosphorus are assigned with occupancies of 1. When the imine link between the two phosphorus atoms was refined with an occupancy of 0.5 (as this was indicated by the large temperature factors in this part of the molecule in the initial refinement) with the N constrained to lie on the mirror plane, unreasonable C=N bond distances resulted. Removing the special position constraint allowed the imine nitrogen, N, and carbon, C(1), to take their respective disordered positions slightly above and below the mirror plane, hence giving bond distances in the usual range.

5. Supplementary material

CCDC 213469 (**1b**), 213470 (**5a**), 213471 (**4a**) and 213472 (**6**) contain the supplementary crystallographic data for this paper. These data can be obtained free of charge via www.ccdc.cam.ac.uk/conts/retrieving.html (or from the Cambridge Crystallographic Data Centre, 12, Union Road, Cambridge CB2 1EZ, UK; fax: +44-1223-336033; or data_request@ccdc.cam.ac.uk).

Acknowledgements

We thank Associate Professor C.F. Rickard, University of Auckland, for X-ray data collection, Dr. P.J.B. Edwards for assistance with NMR spectra and the Massey University Research Fund for financial support.

References

[1] (a) G. Sánchez, J. Vives, J.L. Serrano, J. Pe'rez, G. Lo'pez, Inorg. Chim. Acta 328 (2002) 74, and references therein;
(b) A.D. Getty, K.I. Goldberg, Organometallics 20 (2001) 2545;
(c) K.R. Reddy, K. Surekha, G.-H. Lee, S.-M. Peng, J.-T. Chen, S.-T. Liu, Organometallics 20 (2001) 1292;
(d) M.A. Jalil, S. Fujinami, H. Nishikawa, J. Chem. Soc., Dalton Trans. (2001) 1091;
(e) M. Konrad, S. Wuthe, F. Meyer, E. Kaifer, Eur. J. Inorg. Chem. (2001) 2233;
(f) S.M. Aucott, A.M.Z. Slawin, J.D. Woollins, J. Chem. Soc., Dalton Trans. (2000) 2559;
(g) A. Habtemariam, B. Watchman, B.S. Potter, R. Palmer, S. Parsons, A. Parkin, P.J. Sadler, J. Chem. Soc., Dalton Trans. (2001) 1306.

[2] (a) P.-Y. Shi, Y.-H. Liu, S.-M. Peng, S.-T. Liu, Organometallics 21 (2002) 3203;
(b) Y.-C. Chen, C.-L. Chen, J.-T. Chen, S.-T. Liu, Organometallics 20 (2001) 1285;
(c) H. Yoshida, Y. Honda, E. Shirakawa, T. Hiyama, Chem. Commun. (2001) 1880.

[3] (a) F. Stöhr, D. Sturmayr, G. Kickelbick, U. Schubert, Eur. J. Inorg. Chem. (2002) 2305;
(b) C. Müller, C.N. Iverson, R.J. Lachicotte, W.D. Jones, J. Am. Chem. Soc. 123 (2001) 9718.

[4] E.W. Ainscough, A.M. Brodie, A.K. Burrell, X. Fan, M.J.R. Halstead, S.M.F. Kennedy, J.M. Waters, Polyhedron 19 (2000) 2585.

[5] (a) E.W. Ainscough, A.M. Brodie, A.K. Burrell, S.M.F. Kennedy, J. Am. Chem. Soc. 123 (2001) 10391;
(b) E.W. Ainscough, A.M. Brodie, A.K. Burrell, S.M.F. Kennedy, J. Organomet. Chem. 609 (2000) 2;
(c) E.W. Ainscough, A.M. Brodie, A.K. Burrell, A. Derwahl, S.K. Taylor, Inorg. Chim. Acta (2004) in press.

[6] (a) J.H. Groen, A. de Zwart, M.J.M. Vlaar, J.M. Ernsting, P.W.N.M. van Leeuwen, K. Vrieze, H. Kooijman, W.J.J. Smaates, A.L. Spek, P.H.M. Budzelaar, Q. Xiang, R.P. Thummel, Eur. J. Inorg. Chem. (1998) 1129;
(b) P. Wehman, R.E. Rülke, V.E. Kaasjager, P.C.J. Kamer, H. Kooijman, A.L. Spek, C.J. Elsevier, K. Vrieze, P.W.N.M. van Leeuwen, J. Chem. Soc., Chem. Commun. (1995) 331.

[7] E.W. Ainscough, A.M. Brodie, P.D. Buckley, A.K. Burrell, S.M.F. Kennedy, J.M. Waters, J. Chem. Soc., Dalton Trans. (2000) 2663.

[8] L.M. Engelhardt, J.M. Patrick, C.L. Raston, P. Twiss, A.H. White, Aust. J. Chem. 37 (1984) 2193.

[9] M.K. Cooper, J.M. Downes, H.J. Goodwin, M. McPartlin, Inorg. Chim. Acta 76 (1983) L157.

[10] A. Hazell, A. Mukhopadhyay, Acta Crystrallogr. B 36 (1980) 1647.

[11] G.W. Bushnell, K.R. Dixon, M.A. Khan, Can. J. Chem. 52 (1974) 1367, and references therein.

[12] K.N. Raymond, T.G. Spiro, A. Terzis, Inorg. Chem. 9 (1970) 2415.

[13] O. Wernberg, A. Hazell, J. Chem. Soc., Dalton Trans. (1980) 973.

[14] G.W. Bushnell, K.R. Dixon, M.A. Khan, Can. J. Chem. 56 (1978) 450.

[15] L. Cavallo, R. Cini, J. Kobe, L.G. Marzilli, G. Natile, J. Chem. Soc., Dalton Trans. (1991) 1867.

[16] S. Berger, S. Braun, H.-O. Kalinowski, NMR Spectroscopy of the Non-metallic Elements, Wiley, Chichester, 1997, p. 837.

[17] G. Dyer, J. Roscoe, Inorg. Chem. 35 (1996) 4098, and references therein.

[18] J. Mason (Ed.), Multinuclear NMR, Plenum Press, New York, 1987.

[19] D.V. Khasnis, M. Lattman, U. Siriwardane, Inorg. Chem. 28 (1989) 681.

[20] H.E. Bryndza, J.C. Calabrese, M. Marsi, D.C. Roe, W. Tam, J.E. Bercaw, J. Am. Chem. Soc. 108 (1986) 4805.

[21] G. Banditelli, A.L. Bandini, B. Bovio, Inorg. Chim. Acta 96 (1985) 213.

[22] A. Buijs, G.P.C.M. Dekker, C.J. Elsevier, W.J.J. Smeets, A.L. Spek, C.H. Stam, P.W.N.M. van Leeuwen, K. Vrieze, Y.F. Wang, Organometallics 11 (1992) 1937, and references therein.

[23] D.D. Perrin, W.L.F. Armarego, Purification of Laboratory Chemicals, 3rd ed., Pergamon, Oxford, 1988.

[24] S.E. Page, K.C. Gordon, A.K. Burrell, Inorg. Chem. 37 (1998) 4452.

Available online at www.sciencedirect.com
SCIENCE DIRECT®
Polyhedron 23 (2004) 1169–1173
POLYHEDRON
www.elsevier.com/locate/poly

A novel tetranuclear copper(II) complex with 3,5-pyridinedicarboxylate bridges

Jingcai Yao [a,b], Wei Huang [a], Haibin Zhu [a], Jianglin Fang [a], Shaohua Gou [a,*]

[a] State Key Laboratory of Coordination Chemistry, Nanjing University, Nanjing 210093, China
[b] Department of Chemistry, Luoyang Normal College, Luoyang 471022, China

Received 5 November 2003; accepted 24 January 2004

Abstract

An unprecedented tetranuclear complex bridged by 3,5-pyridinedicarboxylate (abbreviated as 3,5-PDC) with an empirical formula $[Cu_2(2,2'\text{-bpy})_3(3,5\text{-PDC})]_2(ClO_4)_4 \cdot 2(H_2O)$, has been synthesized and spectrally characterized. X-ray structural analysis reveals that there are two types of copper(II) centers, one is penta-coordinate with a distorted pyramidal geometry, while the other is tetra-coordinate with a distorted square planar geometry. 3,5-PDC serves as a tridentate ligand linking three adjacent metals with its one nitrogen and two monodentate carboxylic donors.
© 2004 Published by Elsevier Ltd.

Keywords: Tetranuclear copper(II) complex; Structural elucidation; Hydrogen bonds

1. Introduction

In recent years, supramolecular frameworks, including transitional metal polynuclear complexes, have been extensively studied for generating new materials with expected structures, prescribed functions and interesting magnetic properties [1]. Among those complexes certain tetranuclear examples that have been well characterized structurally and magnetically have attracted much attention for designing metal clusters with heterocubane cores [2]. Tetranuclear copper(II) species are of interest in bioinorganic modeling, multi-electron transfer processes, catalysis and magneto-structure research. Of the many known Cu_4 species, the most common strategy to obtain these compounds is metal self-association induced by bridging ligands like hydroxo [3], imidazolate [4], oximate [5], diazine [6] and carboxylate [7]. On the other hand, coordination polymers of multi-carboxylate ligands such as 1,3-benzenedicarboxylate and 1,3,5-benzene-tricarboxylate anions possessing high symmetry have been widely investigated [8,9].

The high symmetry 3,5-$PDCH_2$ molecule is a potential rigid multidentate ligand containing a pyridine ring and two carboxylic groups, which can be used as a terminal ligand or a bridging ligand with different coordination numbers when coordinated with various metal ions. In addition to its versatile coordinating modes, 3,5-PDC may take part in hydrogen bonding interactions and π–π interactions with its N, O donors and pyridine ring. So far, only three papers involving mononuclear Ni(II), Co(II) and Pd(II) complexes with 3,5-PDC have been postulated [10], but there are a few examples to elucidate the feature of 3,5-PDC as a bridging ligand connecting two or more metals. In this report, we describe a novel tetranuclear copper(II) complex, by self-assembly utilizing 3,5-PDC as the multifunctional bridge and 2,2′-bipyridine as a metal protecting block, whose crystal structure has been explored. To our knowledge, this represents the first tetranuclear copper(II) complex involving 2,2-bpy protecting metal

* Corresponding author. Tel.: +86-25-359-5068; fax: +86-25-331-4502.
E-mail address: sgou@netra.nju.edu.cn (S. Gou).

0277-5387/$ - see front matter © 2004 Published by Elsevier Ltd.
doi:10.1016/j.poly.2004.01.010

blocks and four Cu(II) centers that are bridged by two tridentate 3,5-PDC ligands.

2. Experimental

2.1. Materials and measurements

Cu(2,2′-bpy)Cl_2 was prepared by the literature method [11], other reagents were commercially available and used as received. Microanalysis was carried out on a Perkin–Elmer 1400C element analyzer. Metal contents were measured by a Jarrell-Ash 1100 + 2000 type quantometer. Infrared spectra (4000–400 cm^{-1}) were recorded using a Nicolet FT-IR 170X spectrophotometer on KBr disks. Electrospray ionization mass spectra (ESMS) were recorded on a Finnigan MAT SSQ 710 mass spectrometer in a scan range of 200–1500 amu.

2.2. Preparation of the tetranuclear Cu(II) complex

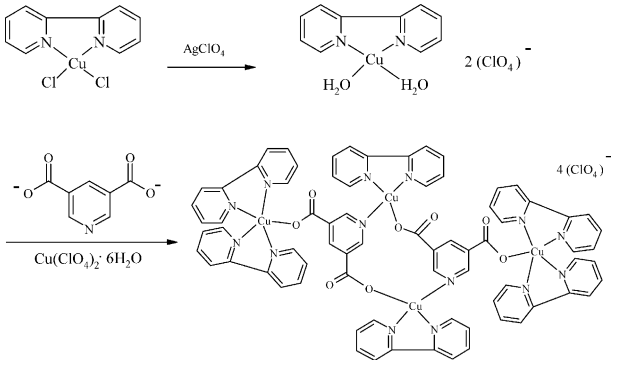

Treatment of Cu(2,2′-bpy)Cl_2 (0.29 g, 1 mmol) dissolved in ethanol (20 cm^{-3}) and water (10 cm^{-3}) with stoichiometric $AgClO_4$ aqueous solution (5 cm^{-3}) formed a solution of Cu(2,2′-bpy)$\cdot(ClO_4)_2$, then 20 cm^{-3} of ethanol containing $Cu(ClO_4)_2 \cdot 6H_2O$ (0.37 g, 1 mmol) was added at 50 °C. After 2 h, the above-mentioned blue solution was added to 3,5-PDCNa_2 (0.21 g, 1 mmol) in a mixed solution of ethanol/water (20 cm^{-3}/10 cm^{-3}). The final blending solution was stirred for another 18 h at 50 °C, the deep blue filtrate was allowed to stand for self-evaporation in the atmosphere at room temperature. After 5 days, blue block-shaped single crystals were obtained that were suitable for X-ray structure analysis. Yield: 64%. *Anal.* Calc. for $Cu_4C_{74}H_{58}Cl_4N_{14}O_{26}$: C, 45.46; H, 2.99; N, 10.03. Found: C, 45.17; H, 2.96; N, 10.01%. Metal contents calc. for $Cu_4C_{74}H_{58}Cl_4N_{14}O_{26}$: Cu, 13.00. Found: 12.6%. IR (KBr disk, cm^{-1}): 3416 (b), 3141 (s), 2945 (m), 2864 (m), 1638 (s), 1619 (s), 1569 (m), 1515 (w), 1458 (m), 1407 (w), 1363 (w), 1287 (w), 1232 (w), 1163 (m), 1086 (m), 833 (w), 758 (m) and 626 (m). ES-MS: m/z 385 [Cu(2,2′-bpy)(3,5-PDCH)]$^+$.

2.3. Crystallographic data for $[Cu_2(2,2'\text{-bpy})_3(3,5\text{-PDC})]_2(ClO_4)_4 \cdot 2(H_2O)$

A blue single crystal with approximate dimensions of $0.20 \times 0.30 \times 0.40$ mm was measured on a Bruker CCD-4K diffractometer using graphite-monochromated Mo Kα ($\lambda = 0.71073$ Å) radiation at 293 K. The data were collected using SMART and reduced by using the program SAINT [12]. Empirical absorption correction was done by using the SADABS program [13]. The structure was solved by direct methods and refined by the least squares method on F^2_{obs} by using the SHELXTL PC software package [14]. The anisotropic thermal parameters of all non-hydrogen atoms were refined by the full-matrix least-squares procedure and the hydrogen atom positions were geometrically fixed and allowed to ride on the attached atoms. The summary of the crystal data, experimental details and refinement results for the title complex is listed in Table 1, while selected bond distances and bond angles are given in Table 2.

Table 1
Summary of crystal data for complex $[Cu_2(2,2'\text{-bpy})_3(3,5\text{-PDC})]_2(ClO_4)_4 \cdot 2(H_2O)$

Formula	$C_{37}H_{29}Cl_2N_7O_{13}Cu_2$
Formula weight	977.65
Crystal system	triclinic
Space group	$P\bar{1}$
Unit cell dimensions	
a (Å)	9.036(2)
b (Å)	14.803(3)
c (Å)	15.345(3)
α (°)	104.59(1)
β (°)	102.71(1)
γ (°)	100.42(1)
Volume (Å^3)	1876.0(7)
Z	2
Density calculated (g cm^{-3})	1.731
Absorption coefficient (mm^{-1})	1.356
Crystal size (mm)	$0.20 \times 0.30 \times 0.40$
Temperature (K)	293(2)
θ range for data collection	1.43–25.04
Index ranges	$-10 \leqslant h \leqslant 10$, $-14 \leqslant k \leqslant 17$, $-16 \leqslant l \leqslant 18$
Number of reflections collected	9735
Number of independent reflections/parameters	6489/552
Observed data [$I > 2\sigma(I)$]	4464
Goodness-of-fit on F^2	0.993
F (000)	992.0
R_{int}	0.0415
Final R indices [$I > 2\sigma(I)$]	$R_1 = 0.0459$ $wR_2 = 0.0829$
R indices (all data)	$R_1 = 0.0713$ $wR_2 = 0.0880$
Largest differential peak and hole (e Å^{-3})	0.534 and −0.406

Table 2
Selected bond lengths (Å) and angles (°)

Bond lengths			
Cu (1)–N(1)	1.980(4)	Cu (1)–N(2)	2.056(3)
Cu (1)–N(5)	2.168(4)	Cu (1)–N(6)	1.973(4)
Cu (1)–O(1)	1.955(3)	Cu(2)–O(3)	1.971(3)
Cu(2)–N(3)	2.005(4)	Cu(2)–N(4)	1.975(3)
Cu(2)–N(7)b	2.001(3)		
O(1)–C(28)	1.276(5)	O(2)–C(28)	1.227(5)
O(3)–C(37)	1.274(5)	O(4)–C(37)	1.221(5)
Cu(1)···O(17)c	2.724(4)	Cu(1)···O(1W)	2.529(4)
Cu(1)···Cu(2)	9.664	Cu(1)···Cu(2A)	6.914
Cu(1)···Cu(1A)	15.099	Cu(2)···Cu(2A)	7.378
Bond angles			
O(1)–Cu(1)–N(6)	93.75(13)	O(1)–Cu(1)–N(1)	92.43(14)
O(1)–Cu(1)–N(2)	151.47(14)	O(1)–Cu(1)–N(5)	102.71(13)
N(1)–Cu(1)–N(2)	80.60(15)	N(1)–Cu(1)–N(5)	97.47(14)
N(6)–Cu(1)–N(1)	173.43(14)	N(6)–Cu(1)–N(2)	94.94 (15)
N(6)–Cu(1)–N(5)	79.00(15)	N(2)–Cu(1)–N(5)	105.61(13)
O(3)–Cu(2)–N(4)	95.69(14)	O(3)–Cu(2)–N(3)	158.39(13)
N(4)–Cu(2)–N(3)	81.29(16)	N(4)–Cu(2)–N(7)b	164.61(13)
N(3)–Cu(2)–N(7)b	95.31(15)	O(3)–Cu(2)–N(7)b	92.84 (13)
C(35)–N(7)–C(36)	117.0(3)	C(35)–N(7)–Cu(2)	116.4 (3)
C(36)–N(7)–Cu(2)	124.5(3)	O(3)–Cu(2)–O(17)c	81.54 (12)
O(17)c–Cu(2)–N(3)	79.64 (12)	O(17)c–Cu(2)–N(4)	110.86(13)
O(17)c–Cu(2)–N(7)b	83.03 (13)	H(1W)a–O(1W)–H(1W)b	106.4

Symmetry transformations used to generate equivalent atoms: (b) $-x, -y, -z$; (c) $-x, -y, 1-z$.

3. Results and discussion

Four copper ions in our tetranuclear complex are confirmed more by the ICP analysis than by the X-ray determination. The asymmetric and symmetric vibrations of the carboxylate moiety in the infrared spectrum of the title compound were observed at ν_{as}(COO): 1638, 1619cm^{-1} and ν_s(COO): 1407, 1363 cm^{-1}, respectively. The Δ values of 212 and 275 cm^{-1} frequencies between the ν_{as}(COO) and the ν_s(COO) are indicative of the existence of monodentate carboxylic groups. Meanwhile, the typical stretching bands of perchlorate ions were observed at 1086 and 626 cm^{-1}, and a broad peak at 3416 cm^{-1} revealed the presence of weakly coordinating water molecules. Though the molecular ion peak of $[Cu_2(2,2'\text{-bpy})_3(3,5\text{- PDC})]_2(ClO_4)_4$ has not been found, the electro-spray ionization mass spectra demonstrates that a mono-charged peak corresponding to $[Cu(2',2\text{-bpy})(3'5\text{-PDCH})]^+$ is present. The structure of the compound has been further confirmed by X-ray diffraction determination.

The crystal structure of $[Cu_2(2,2'\text{-bpy})_3(3,5\text{- PDC})]_2(ClO_4)_4 \cdot 2(H_2O)$ is revealed by an X-ray diffraction study of a suitable blue single crystal. An ORTEP drawing of the compound with the atom numbering scheme is shown in Fig. 1. In the unit cell, there are two kinds of crystallographically independent copper(II) atoms with different coordination geometries that are bridged by two 3,5-PDC ligands. The Cu_4 core is composed of two kinds of Cu(II) atoms [namely, Cu(1) and Cu(2)]. The four copper ions, which lie on a plane, form a parallelogram array which is similar to the $[Cu_4O_4]^{4+}$ macrocyclic complex we reported previously [15]. The inter-atomic distances between the crystallographically independent Cu(II) atoms, Cu(1)···Cu(2) and Cu(1)···Cu(2A), which compose the long and the short sides of the parallelogram, are 9.664 and 6.914 Å, respectively. The two diagonals of the parallelogram, Cu(1)···Cu(1A) and Cu(2)···Cu(2A), are 15.099 and 7.378 Å in length, respectively.

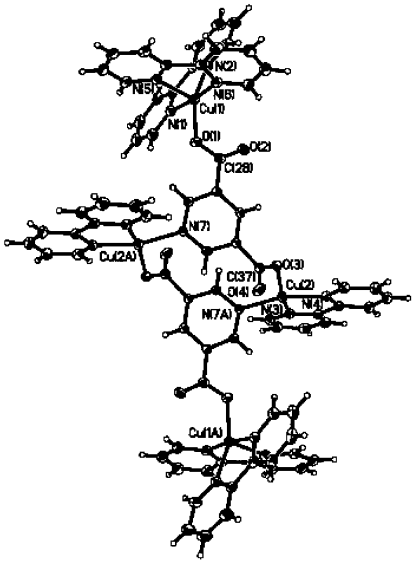

Fig. 1. ORTEP drawing of the complex cation species (30% thermal probability) with the atom-numbering scheme. Lattice water molecules, hydrogen atoms and perchlorate anions are omitted for clarity.

The Cu(1) atom is in a five-coordinate distorted pyramidal environment composed of one oxygen atom from

Table 3
Hydrogen-bonding interactions

Hydrogen bonding	D–H	H...A	D–A	D–H...A	Symmetry transformations
O(1W)–H(1W)A...O(4)	0.850	2.000	2.696(5)	139.00	$1+x,1+y,1+z$
O(1W)–H(1W)B...O(12)	0.900	1.990	2.863(5)	162.00	$-1+x,-1+y,-1+z$
C(1)–H(1)A...O(4)	0.930	2.550	3.481(6)	177.00	$1+x,y,1+z$
C(5)–H(5)A...O(2)	0.930	2.500	3.179(7)	130.00	$1+x,y,z$
C(6)–H(6)A...O(17)	0.930	2.520	3.365(7)	151.00	$-1-x,-y,1-z$
C(18)–H(18)A...O(2)	0.930	2.280	3.139(6)	154.00	$1-x,-y,1-z$
C(19)–H(19)A...O(10)	0.930	2.370	3.222(8)	151.00	$1-x,-y,1-z$
C(22)–H(22)A...O(16)	0.930	2.500	3.427(7)	178.00	$-1+x,-1+y,-1+z$
C(35)–H(35)A...O(1W)	0.930	2.520	2.840(6)	101.00	$1-x,1-y,1-z$
C(36)–H(36)A...O(17)	0.930	2.520	3.143(6)	125.00	$x,y,-1+z$

one carboxylate of one 3,5-PDC ligand and four nitrogen atoms from two terminal 2, 2′-bpy molecules. The equatorial plane consists of N(1), N(2), N(6) and O(1) atoms with bond distances of Cu–N: 1.973(4)–2.056(3) Å and Cu(1)–O(1): 1.955(3) Å and bond angles of 80.60(15)–94.94(15)°. The apical site of the copper square plane is occupied by N(5) from one 2, 2′-bpy molecule with a relatively longer Cu(1)–N(5) bond distance of 2.168(4) Å. The corresponding bond angles between N(5) and those atoms in the basal plane are in the range 79.00(15)–105.61(13)°.

The geometry of the other metal atom may be described as a tetra-coordinate distorted square plane. Cu(2) is coordinated by one 2, 2′-bpy molecule, one nitrogen atom of a 3,5-PDC ligand and one carboxylate nitrogen atom of another neighboring 3,5-PDC ligand. The coordination plane around the Cu(2) atom is composed of N(3), N(4), O(3), N(7A) atoms with the normal Cu–N distances of 1.975(3)–2.005(4) Å and the bond angles of 81.29(16)°–95.30(16)°. The bond distance of Cu(2)–O(3) is 1.971(3) Å and the four bond angles of the square plane are in the range 81.29(16)°–95.69(14)°. It is noted that O(1)–C(28) and O(3)–C(37) are 1.276(5) and 1.274(5) Å long, respectively, which appear to be somewhat longer than the O(2)–C(28) and O(4)–C(37) distances of 1.227(5) and 1.221(5) Å, indicating the presence of some double-bond character in the O(2)–C(28) and O(4)–C(37) bonds. The water molecule and one perchlorate anion, with rather longer Cu(1)···O(1W) and Cu(2)···O(17A) distances of 2.522(4) and 2.724(4) Å, respectively, are positioned above and below the Cu(2) coordination plane, which may arise from the Jahn–Teller effect. In this sense, the coordination environment around Cu(2) may be described as a six-coordinate elongated octahedron.

It is worthy to note that 3,5-PDC functions as a bridging tridentate ligand connecting three adjacent copper(II) ions via its one nitrogen and two monodentate carboxylate donors, and two bridging 3,5-PDC ligands and two symmetry related copper(II) ions form a 12-membered supramolecular chelating ring. In addition, six 5-membered rings consist of 2,2′-bpy and copper(II) centers in the tetranuclear copper(II) complex. The Cu···Cu separations are 6.914 Å [Cu(1)···Cu(2)], 7.378 Å [Cu(2)···Cu(2A)], and 15.099 Å [Cu(1)···Cu(1A)].

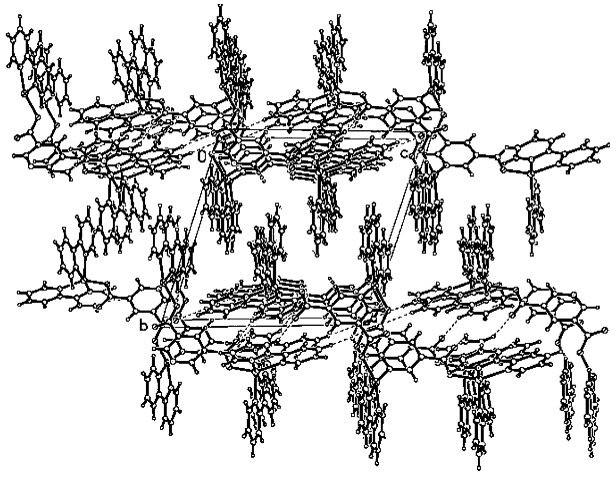

Fig. 2. View of the 3D network depicting the connection via non-classic hydrogen bonds down the *a*-axis. For clarity, crystal water molecules and percholate anions are omitted.

The dihedral angles between the pyridine ring and three 5-membered rings are 100.2°, 70.8° and 6.2°. It is found that there exists a small cavity of ca. 4.24×4.05 Å^2 from the 12-membered ring. Furthermore, the tetranuclear copper(II) centers form an absolutely coplanar structure exhibiting centrosymmetry.

Another interesting structural feature of the compound is the formation of a 3D hydrogen bond network. The corresponding data of H-bonds are listed in Table 3 and illustrated in Fig. 2. Two kinds of O–H···O intramolecular hydrogen bonds are observed between the same water molecule O(1W) and the uncoordinated carboxylic oxygen atom O(4) and perchlorate oxygen atom O(12), respectively. Intermolecular and intramolecular C–H···O hydrogen bonding interactions are common in this compounds with the donor–acceptor bond distances and the donor–H–acceptor bond angles varying from 2.840(6)–3.481(6) Å and 101.00°–178.00°, respectively.

4. Conclusion

One of the research aims of our group is to obtain dinuclear or multinuclear complexes [16] instead of infinite

networks. As we know, coordination polymers are often yielded when pyridine-based carboxylate derivatives are treated directly with metal ions. Using certain capped groups is a good strategy to prevent polymerization and interpenetration. But it does not always works. On the one hand, only certain organic compounds with suitable size and geometry are qualified for this purpose. On the other hand, only certain metal centers with flexible coordinating numbers or weakly coordinated groups (such as an aqua ligand which can be easily replaced) can serve as templating ions to direct the further assembly. In view of these we have used 2,2′-bipyridine protected copper(II) species as a building unit to react with 3,5-PDC bridging ligands in order to cap the ends of a potentially polymeric system. As a result, we have prepared successfully the first tetranuclear copper(II) complex partly capped by 2,2-bpy with four Cu(II) centers that are bridged by two tridentate 3,5-PDC ligands. In our case, the geometries of two metal centers have changed from tetra-coordinate square planar to penta-coordinate pyramidal. The other two metal ions have maintained their original geometries, but their coordinating water molecules have been replaced by ligands possessing higher coordinating abilities, namely the nitrogen atoms of pyridines as well as the oxygen atoms of carboxylic groups.

5. Supplementary materials

Crystallographic data (excluding structural factors) for the structure of **1** have been deposited with the Cambridge Crystallographic Data Center with the CCDC number 200969. Copies of the data can be obtained free of charge on application to CCDC, 12 Union Road, Cambridge CB2 1EZ, UK (fax: +44-1223-336-033; e-mail: deposit@ccdc.cam.ac.uk for www: http://www.ccdc.cam.ac.uk).

Acknowledgements

We thank the National Natural Science Foundation of China (project 20271026 and 20301009) and the Jiangsu Province Department of Science and Technology (project BK2001031) for financial aid. S.G. is also indebted to the State Department of Education for Boshidian funding.

References

[1] (a) M.W. Wemple, D.K. Coggin, J.B. Vincent, J.K. McCusker, W.E. Streib, J.C. Huffman, D.N. Hendrickson, G. Christou, J. Chem. Soc., Dalton Trans. 4 (1998) 719;
(b) C. He, C.Y. Duan, C.J. Fang, Y.J. Liu, Q.J. Meng, J. Chem. Soc., Dalton Trans. 7 (2000) 1207;
(c) R. Konecny, J. Li, C.L. Fisher, V. Dillet, D. Bashford, L. Noodleman, Inorg. Chem. 38 (1999) 940;
(d) R.H. Holm, P. Kennepohl, E.I. Solomon, Chem. Rev. 96 (1996) 2239;
(e) M.J. Plater, M.R.S.J. Foreman, R.A. Howie, J.M.S. Skakle, A.M.Z. Slawin, Inorg. Chim. Acta 315 (2001) 126.

[2] (a) G.B. Karet, Z. Sun, D.D. Heinrich, J.K. McCusker, K. Folting, W.E. Streib, J.C. Huffman, D.N. Hendrickson, G. Christou, Inorg. Chem. 35 (1996) 6450;
(b) A.L. Barra, A. Caneschi, A. Cornia, F. Fabrizi de Biani, D. Gatteschi, C. Sangregorio, R. Sessoli, L. Sorace, J. Am. Chem. Soc. 121 (1999) 5302;
(c) J. Yoo, E.K. Brechin, A. Yamaguchi, M. Nakano, J.C. Huffman, A.L. Maniero, L.-C. Brunel, K. Awaga, H. Ishimoto, G. Christou, D.N. Hendrickson, Inorg. Chem. 39 (2000) 3615.

[3] (a) J. Sletten, A. Sørensen, M. Julve, Y. Journaux, Inorg. Chem. 29 (1990) 5054;
(b) I.I. Mathews, H. Manohar, J. Chem. Soc., Dalton Trans. (1991) 2139.

[4] (a) P. Chaudhuri, I. Karpenstein, M. Winter, M. Lengen, C. Butzlaff, E. Bill, A.X. Trautwein, U. Floerke, H.J. Haupt, Inorg. Chem. 32 (1993) 888;
(b) M. Mimura, T. Matsuo, T. Nakashima, N. Matsumoto, Inorg. Chem. 37 (1998) 3553.

[5] E. Colacio, C. López-Magana, V. Mckee, A. Romerosa, J. Chem. Soc., Dalton Trans. (1999) 2923.

[6] C.J. Mattews, K. Avery, Z.Q. Xu, L.K. Thompson, L. Zhao, D.O. Miller, K. Biradha, K. Poirier, M.J. Zaworotko, C. Wilson, A.E. Goeta, J.A.K. Howard, Inorg. Chem. 38 (1999) 5266.

[7] (a) E. Colacio, M. Ghazi, R. Kivekäs, J.M. Moreno, Inorg. Chem. 39 (2000) 2882;
(b) R. Acevedo-Chávez, M.E. Costas, S. Bernès, G. Medina, L. Gasque, J. Chem. Soc., Dalton Trans. (2002) 2553.

[8] (a) H. Li, C.E. Davis, T.L. Groy, D.G. Kelley, O.M. Yaghi, J. Am. Chem. Soc. 120 (1998) 2186;
(b) T.M. Reineke, M. Eddaoudi, M. O'Keeffe, O.M. Yaghi, Angew. Chem. Int. Ed. 38 (1999) 2590;
(c) L. Pan, N.-W. Zheng, Y. Wu, S. Han, R. Yang, X.-Y. Huang, J. Li, Inorg. Chem. 40 (2001) 828;
(d) S.A. Bourne, J.-J. Lu, A. Mondal, B. Moulton, M.J. Zaworotko, Angew. Chem., Int. Ed. 40 (2001) 2111.

[9] (a) O.M. Yaghi, G.M. Li, H.L. Li, Nature 378 (1995) 703;
(b) O.M. Yaghi, C.E. Davis, G. Li, H.L. Li, J. Am. Chem. Soc. 119 (1997) 2861;
(c) O.M. Yaghi, H.L. Li, T.L. Groy, J. Am. Chem. Soc. 118 (1996) 9096;
(d) J.W. Ko, K.S. Min, M.P. Suh, Inorg. Chem. 41 (2002) 2151.

[10] (a) H. Xu, N. Zheng, H. Xu, Y. Wu, R. Yang, E Ye, X. Jin, J. Mol. Struct. 606 (2002) 117;
(b) D. Min, S.S. Yoon, J.H. Lee, M. Suh, S.W. Lee, Inorg. Chem., Commun. 4 (2001) 297;
(c) Z.Q. Qin, M.C. Jennings, R.J. Puddephatt, K.W. Muir, Inorg. Chem. 41 (2002) 5174.

[11] G. Eugenio, M. Giovanni, S. Daniele, S.-E. Liliana, Inorg. Chim. Acta 299 (2000) 253.

[12] Siemens, SAINT v4 Software Reference Manual, Siemens Analytical X-ray Systems, Inc., Madison, WI, USA, 1996.

[13] G.M. Sheldrick, SADABS, Program for Empirical Absorption Correction of Area Dectector Data, University of Gottingen, Germany, 1996.

[14] Siemens, SHELXTL, Version 5 Reference Manual, Siemens Analytical X-ray Systems, Inc., Madison, WI, USA, 1996.

[15] S. Gou, M. Qian, Z. Yu, C. Duan, X. Sun, W. Huang, J. Chem. Soc., Dalton Trans. (2001) 3232.

[16] (a) W. Huang, D. Hu, S. Gou, H. Qian, H.-K. Fun, S.S.S. Raj, Q. Meng, J. Mol. Struct. 649 (2003) 269;
(b) W. Huang, S. Gou, D. Hu, S.S.S. Raj, H.-K. Fun, Q. Meng, Inorg. Chem. 40 (2001) 1712.

Available online at www.sciencedirect.com
SCIENCE DIRECT®
Polyhedron 23 (2004) 1175–1184
POLYHEDRON
www.elsevier.com/locate/poly

Cobalt and nickel complexes of a tetradentate phthalazine ligand – mononuclear, dinuclear and trinuclear derivatives

Laurence K. Thompson [a,*], Virginie Niel [a], Hilde Grove [a], David O. Miller [a], Michael J. Newlands [a], Peter H. Bird [b], Wasantha A. Wickramasinghe [b], A.B.P. Lever [c]

[a] Department of Chemistry, Memorial University, St. John's, NL, Canada A1B 3X7
[b] Department of Chemistry and Biochemistry, Concordia University, 1455 de Maisonneuve Blvd. W, Montreal, Canada PQ H3G 1M8
[c] Department of Chemistry, York University, 4700, Keele St., Toronto, Canada ON M3J 1P3

Received 3 October 2003; accepted 25 January 2004

Abstract

Examples of mononuclear (Ni(II)), dinuclear (Ni(II), Co(III)) and trinuclear (Ni(II)) complexes of the ligand 1,4-di-2′-pyridyl-aminophthalazine (pap) are reported. In the dinuclear complexes two metal ions are bridged by phthalazine (N–N) groups and two water molecules (Ni(II)), and two hydroxide ions (Co(III)). A novel $Ni_3(\mu_3\text{-}OH)_2$ central core exists in the trinuclear example, with additional phthalazine (N–N) bridges linking the Ni(II) centers. The polynuclear nickel complexes exhibit antiferromagnetic exchange through combinations of diazine (N–N) and water and hydroxide bridges ($J(Ni_2) = -4.9, -5.25\ cm^{-1}$; $J(Ni_3) = -15.7\ cm^{-1}$). The Co(III) complex is diamagnetic.
© 2004 Elsevier Ltd. All rights reserved.

1. Introduction

The ligand 1,4-di-2′-pyridyl-aminophthalazine (pap) has been studied in detail, and has produced numerous dinuclear copper(II) complexes involving combinations of diazine (N–N) and other bridges (X) (e.g. $X = OH^-$, N_3^-, Cl^-, Br^-, IO_3^-) [1–17]. These examples have formed the basis for a detailed understanding of magnetic exchange interactions in this type of complex, and magneto-structural correlations within related series of complexes have provided fundamental insights into the geometrical and electronic properties of the bridge group (X), particularly N_3^- and OH^-, as it pertains to modern theoretical interpretations of exchange mechanisms. Complexes with other metals are less well characterized, and full structural details are not well documented. Some early reports highlighted complexes of Ni(II), Co(II) and Co(III) with pap and its alkyl substituted congeners, with evidence for dinuclear and mononuclear systems, based largely on elemental and spectroscopic evidence [18,19]. However, a lack of structural and magnetic details left the broad picture of these systems largely unexplored, despite some preliminary structural details reported for $[Co_2(pap)_3(OH)_2]Br_4 \cdot 9H_2O$ and $[Ni_2(pap)_3(H_2O)_2]Br_4 \cdot 6H_2O$ [19]. These structures were not reported fully at the time, but revealed dinuclear Co(III) and Ni(II) structures, respectively, with $\{\mu_2\text{-}N\text{–}N(\mu_2\text{-}O)_2\}$ triple bridges between metal centers ($O{=}OH^-$ (Co), H_2O (Ni)). Complex formation with these ligands was found to be pH dependent, and in acidic aqueous solvents protonated ligand complexes were produced as well, with a structurally characterized mononuclear example with Cu(II) ($[Cu(papH)_2(H_2O)_2](BF_4)_4$) [2].

We have revisited these systems in part to document the structural details of the Ni(II) and Co(III) complexes of the ligand pap in more detail, which were largely unavailable before, but also to examine the variable temperature magnetic properties. In this report, we describe the molecular structures of the complexes $[Ni(papH)_2(H_2O)_2](BF_4)_4 \cdot 4H_2O$ (**1**), $[Ni_2(pap)_3(H_2O)_2](NO_4)_4 \cdot 5H_2O$ (**2**), $[Ni_3(pap)_3(OH)_2](BF_4)_3F \cdot xH_2O$ (**5**),

* Corresponding author. Tel.: +1-709-737-8750; fax: +1-709-737-3702.
E-mail address: lthomp@mun.ca (L.K. Thompson).

0277-5387/$ - see front matter © 2004 Elsevier Ltd. All rights reserved.
doi:10.1016/j.poly.2004.01.022

which has a novel, and previously unobserved trinuclear structural motif, and $[Co_2(pap)_3(OH)_2](NO_4)_4 \cdot 9.5H_2O$ (**4**). Variable temperature magnetic properties for **2**, **5**, and the previously reported dinuclear complex $[Ni_2(pap)_3(H_2O)_2]Br_4 \cdot 3.5H_2O$ (**3**) [19] are also reported, all of which exhibit intramolecular antiferromagnetic exchange coupling.

2. Experimental

2.1. Physical measurements

Infrared spectra were recorded as Nujol mulls using a Mattson Polaris FTIR instrument. UV–Vis spectra were obtained as Nujol mulls with a Cary 5E spectrometer. C, H, N analyses on vacuum dried samples were performed by the Canadian Microanalytical Service, Delta, BC, Canada. Variable temperature magnetic data were obtained with a Quantum Design MPMS5S SQUID magnetometer operating at 0.1 T in DC mode (2–300 K), and with an Oxford Instruments Faraday magnetometer operating at 1.0 T with a field gradient of 10 T m^{-1} (5–300 K). Calibrations were carried out using a palladium standard cylinder, and $HgCo(NCS)_4$. Diamagnetic corrections for the sample holders and diamagnetic components of the complexes were applied.

2.2. Synthesis of the complexes

2.2.1. $[Ni(papH)_2(H_2O)_2](BF_4)_4$ (**1**)

Pap [1] (0.75 g, 2.4 mmol) was added to a solution of $Ni(BF_4)_2 \cdot 6H_2O$ (0.85 g, 2.5 mmol) in water (75 ml), and the mixture refluxed for 2 h. A small amount of pale green precipitate was filtered off and discarded, and the green solution concentrated until a green crystalline product formed (Yield: 0.56 g). Recrystallization from a water/methanol mixture gave pale green crystals suitable for structural analysis. These were kept under mother liquor prior to structural analysis because they desolvate on exposure to air. Elemental analysis (dried sample): *Anal*. Calc. for $(C_{18}H_{15}N_6)_2Ni(H_2O)_2(BF_4)_4$: C, 40.30; H, 3.17; N, 15.70. Found: C, 40.32; H, 3.27; N, 15.75%.

2.2.2. $[Ni_2(pap)_3(H_2O)_2](NO_3)_4 \cdot 5H_2O$ (**2**), $[Ni_2(pap)_3(H_2O)_2]Br_4 \cdot 3.5H_2O$ (**3**)

Pap (0.314 g, 1.00 mmol) was added to a solution of $Ni(NO_3)_2 \cdot 6H_2O$ (0.300 g, 1.00 mmol) in water/methanol (15/2 ml), and the mixture warmed. The ligand dissolved to form a purple solution, which produced turquoise green crystals on standing (Yield: 0.30 g). Crystals for structural analysis were kept under mother liquor because of instability on exposure to air. **3** was prepared in a similar manner [19]. Elemental analysis: *Anal*. Calc. for $(C_{18}H_{14}N_6)_3Ni_2(H_2O)_7(NO_3)_4$: C, 45.21; H, 3.90; N, 21.48. Found (**2**): C, 45.67; H, 3.63; N, 21.48%. Elemental analysis: *Anal*. Calc. for $(C_{18}H_{14}N_6)_3Ni_2(H_2O)_{5.5}Br_4$: C, 43.85; H, 3.61; N, 17.05. Found (**3**): C, 43.80; H, 3.42; N, 16.93%.

2.2.3. $[Co_2(pap)_3(OH)_2](NO_3)_4 \cdot 9.5H_2O$ (**4**)

Pap (0.314 g, 1.00 mmol) was added to a solution of $Co(NO_3)_2 \cdot 6H_2O$ (0.290 g, 1.00 mmol) in water (25 ml) and the mixture warmed with stirring in air becoming dark brown in color after 24 h. The solution was filtered and allowed to stand. Dark brown crystals suitable for structural analysis formed after several days (Yield: 0.25 g). Elemental analysis: *Anal*. Calc. for $(C_{18}H_{14}N_6)_3Co_2(OH)_2(H_2O)_{9.5}(NO_3)_4$: C, 42.83; H, 4.16; N, 20.35. Found: C, 42.92; H, 3.98; N, 20.30%.

2.2.4. $[Ni_3(pap)_3(OH)_2](BF_4)_3F \cdot 9H_2O$ (**5**)

$Ni(BF_4)_2 \cdot 6H_2O$ (1.6 g, 4.7 mmol) was dissolved in water (45 ml) and the pH adjusted to 5.5 by addition of NaF. Pap (1.0 g, 2.9 mmol) was added, and the mixture heated forming a deep blue solution. The solution was filtered and reduced in volume with the formation a turquoise green crystalline product (Yield: 1.2 g), which contained some white crystals, presumed to be NaF. The combined product was recrystallized from methanol, to give turquoise green crystals, which were filtered off and air dried. They were observed to desolvate on exposure to air. A final recrystallization of a portion of this product from water gave turquoise crystals that were kept under mother liquor for structural analysis. This sample was used for magnetic analysis. Elemental analysis: *Anal*. Calc. for $(C_{18}H_{14}N_6)_3Ni_3(OH)_2(H_2O)_9F(BF_4)_3$: C, 40.70; H, 3.89; N, 15.82. Found: C, 40.62; H, 3.17; N, 15.91%.

2.2.5. Synthesis of $Ni(BF_4)_2$ complexes

The synthetic procedures for compounds **1** and **5** were based on those outlined in [18]. Structural data have now correctly identified **1**, but **5** has turned out to be a trinuclear complex, rather than the dinuclear complex proposed previously on the basis of elemental and spectroscopic data.

2.3. X-ray crystallography

The diffraction intensities of a green crystal of **1** were collected with graphite-monochromatized Mo-Kα X-radiation (rotating anode generator) using a Bruker P4/CCD diffractometer at 193(1) K to a maximum 2θ value of 52.8°. The data were corrected for Lorentz and polarization effects. The structure was solved by direct methods [20,21]. All atoms except hydrogens were refined anisotropically. Hydrogen atoms were placed in calculated positions with isotropic thermal parameters set to 20% greater than their bonded partners, and were not refined. Neutral atom scattering factors [22] and anomalous-dispersion terms [23,24] were taken from the

Table 1
Summary of crystallographic data for **1**, **2**, **4** and **5**

Compound	**1**	**2**	**4**	**5**
Empirical formula	$C_{36}H_{34}N_{12}O_2B_4F_{16}Ni$	$C_{54}H_{59}N_{22}O_{21.5}Ni_2$	$C_{54}H_{60}N_{22}O_{22}Co_2$	$C_{54}H_{58}N_{18}O_9B_3Ni_3$
Formula weight	1072.66	1477.59	1487.07	1539.68
Space group	*Pbcn* (#60)	$P\bar{1}$ (#2)	$P2_1/n$ (#14)	$C2/c$ (#15)
a (Å)	9.6727(7)	13.942(2)	18.580(5)	15.769(2)
b (Å)	19.643(1)	14.324(2)	14.066(4)	16.816(2)
c (Å)	22.712(2)	16.547(2)	25.86(1)	24.798(3)
α (°)	90	81.118(3)	90	90
β (°)	90	78.366(2)	104.70(3)	95.749(2)
γ (°)	90	79.434(2)	90	90
V (Å^3)	4315.2(5)	3158.0(7)	6536(4)	6542(1)
ρ_{calc} (g cm^{-3})	1.651	1.554	1.511	1.563
Z	4	2	4	4
μ (cm^{-1})	5.71	6.92	6.01	9.57
λ (Å)	0.71073	0.71073	0.71073	0.71073
T (K)	193(1)	193(1)	299(1)	193(1)
R_1	0.070	0.076	0.116	0.088
wR_2	0.191	0.228	0.118	0.294

$R_1 = \sum ||F_o| - |F_c|| / \sum |F_o|$, $wR_2 = [\sum[w(|F_o|^2 - |F_c|^2)^2] \Big/ \sum[w(|F_o|^2)^2]]^{1/2}$.
$R = \sum ||F_o| - |F_c|| / \sum |F_o|$, $R_w = [\sum w(|F_o| - |F_c|)^2 \Big/ \sum wF_o^2]^{1/2}$.

usual sources. All other calculations were performed with the teXsan [1] crystallographic software package using a PC computer. One tetrafluoroborate anion was found to have rotational disorder, and occupancy factors were set to averages of the refined values. The three fluorine atoms (occupancy 0.3) were refined isotropically, and all other non-hydrogen atoms were refined anisotropically. All aromatic hydrogen atoms were found and placed at ideal positions with riding thermal parameters. Hydrogen atoms on nitrogen atoms and those on water molecules were found and refined with riding positional and thermal parameters. Abbreviated crystal data are given in Table 1. **2** and **5** were treated in similar manner and crystal data are given in Table 1. For **2** hydrogen atoms (amino and hydroxyl) were introduced in calculated or difference map positions with isotropic thermal parameters set 20% greater than those of their bonding partners at the time of their inclusion. They were not refined. Of the four nitrates in the model two (N22, N23) are present at half occupancy and disordered. Nitrate N23 is also paired with a half occupancy disordered water molecule, and was fixed for the final round of refinement. For **5** hydrogen atoms were introduced in calculated or difference map positions, with isotropic thermal parameters set 20% greater than those of their bonding partners at time of their inclusion. Amine hydrogen atoms were placed in difference map positions and optimized by positional refinement, but fixed for the final round of refinement. Other hydrogen atoms were not refined. One BF_4^- ion is disordered over two sites, with what has been modeled as a partial occupancy water in close proximity. These atoms were fixed for the final round of refinement. A charge imbalance occurs in the expanded model, effectively associated with a missing fluoride ion. However, the acidic conditions used in the preparation of **5**, the neutral nature of the ligands, and the sensible elemental analysis suggests that an additional fluoride ion is present.

The diffraction intensities of a dark red-brown single crystal of **4** were collected with graphite-monochromated Mo Kα X-radiation using a Rigaku AFC6S diffractometer at 299(1) K and the ω–2θ scan technique to a 2θ value of 55.1°. The data were corrected for Lorentz and polarization effects. The structure was solved by direct methods and expanded using Fourier techniques [20,21]. Some non-hydrogen atoms were refined anisotropically, while the rest were refined isotropically. Hydrogen atoms were included but not refined. The final cycle of full-matrix least-squares refinement on F was based on 5722 observed reflections ($I > 2.00\sigma(I)$) and 797 variable parameters and converged (largest parameter shift was 0.01 times its esd) with unweighted and weighted agreement factors of: $R = 0.116$, and $R_w = 0.118$. The standard deviation of an observation of unit weight was 3.04. The weighting scheme was based on counting statistics and included a factor ($p = 0.007$) to downweight the intense reflections. The maximum and minimum peaks on the final difference Fourier map corresponded to 1.35 and −2.44 e$^-$/Å^3, respectively. Neutral atom scattering factors [22] and anomalous-dispersion terms [23,24] were taken from the usual sources. All calculations were performed with the teXsan [1] crystallographic software package using a PC computer. Hydrogen atoms were introduced in calculated or difference map positions with isotropic thermal parameters set 20% greater than those of their bonded partners at the time of their inclusion. They were not

[1] teXsan for Windows: Crystal Structure Analysis Package, Molecular Structure Corporation (1997).

refined. Hydrogen atoms have not been included on the lattice water molecules and one ligand amino group. Two nitrate anions were found to be loose and were fixed for the final round of refinement. The crystal studied diffracted weakly, with a low percentage of observed data. However, the essential features of the structure are clearly revealed. Abbreviated structural details for **4** are listed in Table 1.

3. Results and discussion

3.1. Structure of $[Ni(papH)_2(H_2O)_2](BF_4)_4$ (**1**)

The structure of the cation in **1** is shown in Fig. 1, and selected bond distances and angles are listed in Table 2. Two bidentate, protonated ligands are bound to an octahedral Ni(II) center, coordinating via adjacent pyridine and phthalazine nitrogen atoms. Two *cis*-water molecules fill the two remaining coordination sites. Ni–N and Ni–O distances (Ni–L 2.064–2.085 Å) are typical for Ni(II) complexes of this sort, and bond angles around the metal ion indicate only slight distortion from regular octahedral geometry. Proton H(61) located on the uncoordinated pyridine nitrogen N(6) appears to form an internal hydrogen bond to phthalazine nitrogen N(4) (H(61)–N(4) 1.833 Å; N(6)–H(61)–N(4) 139.1°), thus preventing metal ion coordination at this ligand site. The uncoordinated pyridine rings (e.g. N(6)) are close to coordinated pyridine rings (e.g. N(1_4), with an N–N separation of 3.855 Å, and equivalent C–C distances in the range 3.77–4.42 Å). They are not parallel, but their proximity, and the possible π interactions between the aromatic rings, may contribute to the stability of the unusual structural arrangement.

Table 2
Selected bond lengths (Å) and angles (°) for **1**

Bond lengths	
Ni1–N3	2.064(3)
Ni1–N1	2.077(4)
Ni1–O1	2.085(3)
Bond angles	
N3–Ni1–N3	91.40(19)
N3–Ni1–N1	83.19(15)
N3–Ni1–N1	92.63(15)
N1–Ni1–N1	174.0(2)
N3–Ni1–O1	178.40(15)
N3–Ni1–O1	90.08(14)
N1–Ni1–O1	96.15(16)
N1–Ni1–O1	88.14(16)
N3–Ni1–O1	90.08(14)
N3–Ni1–O1	178.40(14)
N1–Ni1–O1	88.13(16)
O1–Ni1–O1	88.4(2)

3.2. Structure of $[Ni_2(pap)_3(H_2O)_2](NO_3)_4 \cdot 5H_2O$ (**2**)

The structure of the dinuclear cation in **2** is shown in Fig. 2, and selected bond lengths and angles are listed in Table 3. Three neutral ligands are bound to two pseudo-octahedral *cis*-N_4O_2 nickel(II) ions, with one ligand coordinating in a tetradentate manner through two external pyridine nitrogen atoms, and the phthalazine N–N, which acts as a bridge between the metal centers. This ligand spans the dinuclear center with the pyridine rings arranged in a *trans* conformation relative to the two Ni(II) atoms. The other two ligands are bidentate

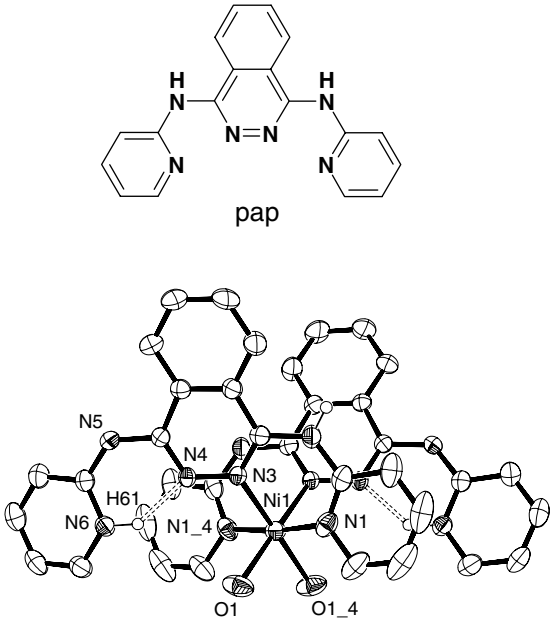

Fig. 1. Structural representation of the cation in **1** (40% thermal ellipsoids).

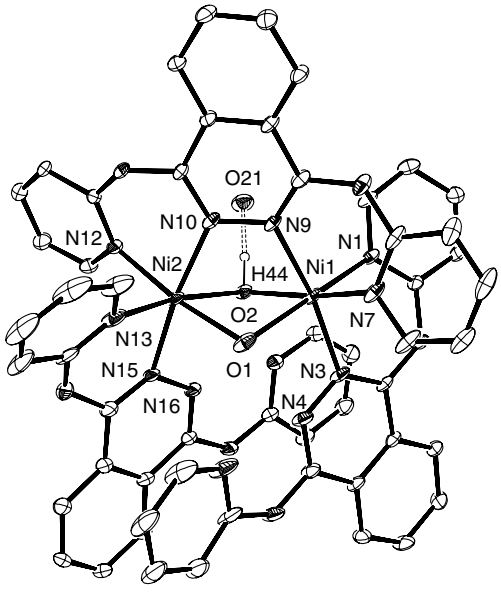

Fig. 2. Structural representation of the cation in **2** (40% thermal ellipsoids).

Table 3
Selected bond lengths (Å) and angles (°) for **2**

Bond lengths	
Ni1–N3	2.043(4)
Ni1–N7	2.060(5)
Ni1–N1	2.063(4)
Ni1–N9	2.070(4)
Ni1–O1	2.108(4)
Ni1–O2	2.138(4)
Ni2–N15	2.051(5)
Ni2–N10	2.059(4)
Ni2–N12	2.065(5)
Ni2–N13	2.081(5)
Ni2–O2	2.116(3)
Ni2–O1	2.138(4)
Bond angles	
N3–Ni1–N7	95.67(18)
N3–Ni1–N1	88.78(17)
N7–Ni1–N1	90.17(18)
N3–Ni1–N9	170.45(18)
N7–Ni1–N9	85.70(17)
N1–Ni1–N9	100.68(16)
N3–Ni1–O1	87.95(16)
N7–Ni1–O1	97.05(17)
N1–Ni1–O1	172.33(16)
N9–Ni1–O1	82.50(15)
N3–Ni1–O2	92.47(16)
N7–Ni1–O2	171.01(14)
N1–Ni1–O2	93.82(15)
N9–Ni1–O2	85.65(15)
O1–Ni1–O2	79.40(14)
N15–Ni2–N10	171.39(16)
N15–Ni2–N12	97.14(19)
N10–Ni2–N12	86.48(17)
N15–Ni2–N13	87.9(2)
N10–Ni2–N13	99.8(2)
N12–Ni2–N13	91.20(19)
N15–Ni2–O2	89.01(15)
N10–Ni2–O2	82.67(15)
N12–Ni2–O2	99.65(15)
N13–Ni2–O2	169.02(17)
N15–Ni2–O1	90.91(18)
N10–Ni2–O1	85.38(16)
N12–Ni2–O1	171.86(16)
N13–Ni2–O1	90.28(18)
O2–Ni2–O1	79.22(14)
Ni1–O1–Ni2	94.78(15)
Ni2–O2–Ni1	94.55(13)

with one pyridine and one phthalazine nitrogen filling *cis* coordination positions at each nickel center. Two water molecules complete the triple bridging arrangement between the nickel atoms. Ni–N distances are in the range 2.043–2.083 Å, typical for systems of this sort. The Ni–O(H_2O) distances are much longer (2.109–2.139 Å), as expected for bond connections to neutral water molecules. The Ni(1)–Ni(2) distance is 3.126 Å, and Ni–O–Ni angles are 94.5° and 94.8° (O(2), O(1)). The presence of four nitrate groups in the lattice, and normal bonding distances within the ligands, confirms the assignment of O(1) and O(2) as water molecules, assuming that the nickel ions are Ni(II) (vide infra). This dinuclear $[(pap)_3Ni_2(H_2O)_2]^{4+}$ structural arrangement has been observed before in the complex $[Ni_2(pap)_3(H_2O)_2]Br_4 \cdot 3.5H_2O$ (**3**), which has been published in a preliminary form [19]. Ni–N and Ni–O distances are very slightly longer, with a Ni–Ni distance of 3.151(3) Å, and Ni–O–Ni angles of 94.3(4)° and 94.5(4)°.

The unusual dinuclear structure raises the question of why two ligands are bidentate, which is untypical of this class of compounds. Clearly, there are too many potential nitrogen donors (12) to be accommodated in a simple dinuclear structure and it begs the question as to whether a third metal can be accommodated (vide infra). However, some interesting structural features appear to have a stabilizing effect on the structure of **2**. Fig. 3 shows an alternate view with the superposition of some aromatic rings not fully involved in coordination. Very close cross ring contacts are observed between the phthalazine ring (N(3)–N(4)) and phthalazine ring N(15)–N(16) (N(4)–N(16) 3.020 Å, C(13)–C(49) 3.385 Å, C(6)–N(18) 3.360 Å, C(7)–C(50) 3.523 Å, C(12)–N(17) 3.555 Å), indicating significant π interactions between the rings, perhaps contributing to the stability of the structure.

3.3. Structure of $[Co_2(pap)_3(OH)_2](NO_3)_4 \cdot xH_2O$ (**4**)

The molecular structure of the cation in **4** is shown in Fig. 4, and selected bond distances and angles are listed in Table 4. The structure of the cation is similar to that of $[Co_2(pap)_3(OH)_2]Br_4 \cdot 9H_2O$ reported in an earlier publication in preliminary form [19]. Two Co(III) centers are bridged by two hydroxide ions, and the N–N fragment of a tetradentate pap ligand. Each Co(III) ion has a CoN_4O_2 coordination environment, with two bidentate ligands completing the coordination sphere. Co–L distances are quite short (1.89–1.96 Å) consistent with the Co(III) oxidation state. The Co(1)–Co(2) distance is consistently short (2.777(3) Å), with Co–O–Co angles of 93.3(5)° and 94.2(5)° (O(1), O(2), respectively). The 2:3 (metal:ligand) stoichiometry is the same as in **2**

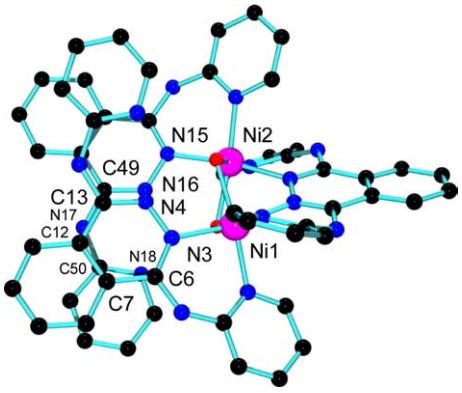

Fig. 3. Structural representation of the cation in **2** showing overlapping aromatic rings.

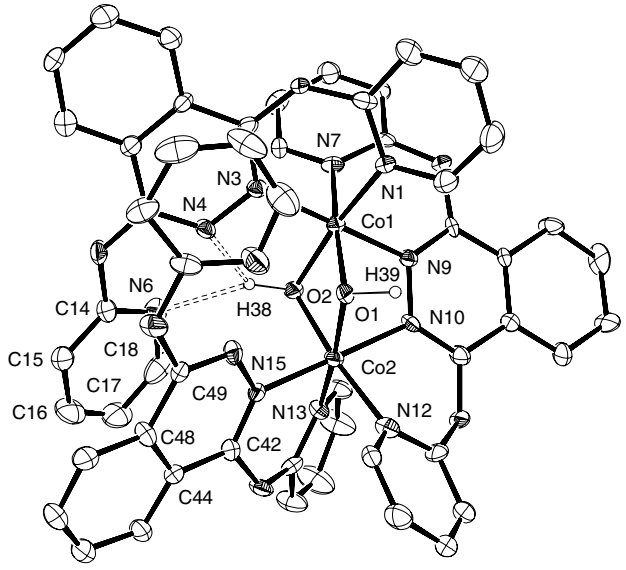

Fig. 4. Structural representation of the cation in **4** (40% thermal ellipsoids).

and **3**, with an almost identical structural arrangement. Structural features that stabilize the arrangement of ligands are similar to those in **2** and **3**. Proton H(38), bound to bridging oxygen O(2), is close to nitrogen atoms N(4) and N(6) on one bidentate ligand (H–N distances 1.832, 2.198 Å, respectively), and may provide a significant hydrogen bonding contact, and be partly responsible for stabilizing the structure. Overlapping aromatic ring components again appear to play an important structural role. Close contacts between phthalazine ring atoms N(15)–N(16) and the adjacent pyridine ring (N(6)) fall in the range 3.37–3.68 Å, clearly indicating significant π contacts across the rings, which contribute to the stability of the structure. A similar situation exists with the corresponding pair of rings in the other half of the molecule.

3.4. Structure of $[Ni_3(pap)_3(OH)_2](BF_4)_3F\cdot xH_2O$ (5)

The structure of the cation in **5** is shown in Fig. 5, and selected bond distances and angles are listed in Table 5. Three tetradentate ligands are bound to a triangular, trinuclear Ni(II) center, with the three nickel ions bridged externally by three phthalazine N–N diazine groups, and internally by two μ_3-OH groups. Three BF_4^- ions show up in the lattice, and given the neutral nature of the ligands (vide infra), and the fact that F^- ion was added in the reaction mixture to synthesize **5**, it is reasonable to assume that one of the residual peaks in the lattice can be assigned to fluoride, and that the bridging oxygen atoms are hydroxides. The cation has twofold symmetry through Ni(1), with Ni(1)–Ni(2) and Ni(2)–Ni(2′) distances of 3.027 and 2.998 Å, respectively. The Ni–N distances fall in the range 2.043–2.129 Å, slightly longer than in **2**, with Ni–O distances in the range 2.093–2.116 Å, shorter than in **2** and consistent with the presence of OH bridges. There are no unusually short Ni–N contacts, which would indicate any coordinated anionic sites due to proton loss from the ligands, and C–N distances to the exocyclic ligand nitrogen atoms are typical for C–N single bonds, thus indicating the neutral nature of the ligands.

The triangular core structure is shown in Fig. 6, highlighting the three N–N, and two μ_3-OH bridges. The three Ni(II) centers form a roughly planar triangle and the Ni–N–N-Ni torsional angles (19.8°, 22.4°) indicate that the $Ni_3(\mu_2\text{-N–N})_3$ ring is only slightly dis-

Table 4
Selected bond lengths (Å) and angles (°) for **4**

Bond lengths	
Co1–Co2	2.777(3)
Co1–O1	1.92(1)
Co1–O2	1.90(1)
Co1–N1	1.93(1)
Co1–N3	1.91(1)
Co1–N7	1.95(1)
Co1–N9	1.89(1)
Co2–O1	1.902(9)
Co2–O2	1.89(1)
Co2–N10	1.91(1)
Co2–N12	1.96(1)
Co2–N13	1.94(1)
Co2–N15	1.93(1)
Bond angles	
O1–Co1–O2	81.2(4)
O1–Co1–N1	91.1(5)
O1–Co1–N3	97.4(5)
O1–Co1–N7	172.6(5)
O1–Co1–N9	86.3(5)
O2–Co1–N1	172.0(5)
O2–Co1–N3	93.1(5)
O2–Co1–N7	95.0(5)
O2–Co1–N9	84.0(5)
N1–Co1–N3	90.1(5)
N1–Co1–N7	92.4(5)
N1–Co1–N9	93.3(5)
N3–Co1–N7	89.1(5)
N3–Co1–N9	174.9(6)
N7–Co1–N9	87.0(5)
O1–Co2–O2	82.0(4)
O1–Co2–N10	83.2(5)
O1–Co2–N12	97.6(5)
O1–Co2–N13	171.3(5)
O1–Co2–N15	92.2(5)
O2–Co2–N10	86.5(5)
O2–Co2–N12	173.1(5)
O2–Co2–N13	89.4(5)
O2–Co2–N15	95.4(5)
N10–Co2–N12	86.6(5)
N10–Co2–N13	94.9(5)
N10–Co2–N15	174.7(5)
N12–Co2–N13	90.7(5)
N12–Co2–N15	91.5(5)
N13–Co2–N15	90.1(5)
Co1–O1–Co2	93.3(5)
Co1–O2–Co2	94.2(5)

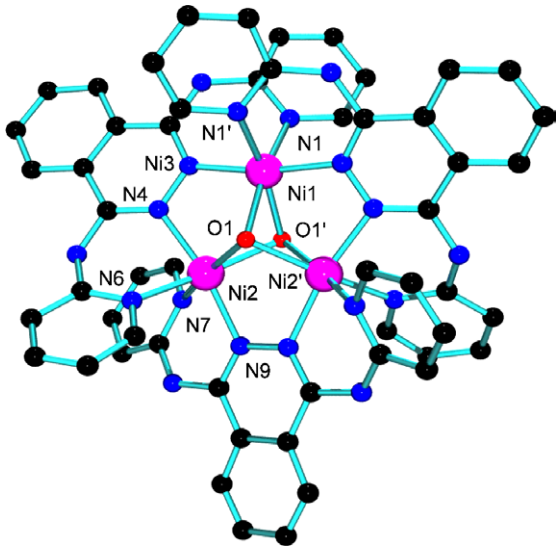

Fig. 5. Structural representation of the cation in **5**.

torted from a plane. The oxygen bridging atoms are displaced from this pseudo-plane, by virtue of the octahedral geometry at each nickel center, and the Ni(1)–O(1)–Ni(2), Ni(1)–O(1)–Ni(2′) and Ni(2)–O(1)–Ni(2′) angles (91.96°, 91.85°, and 91.34°, respectively) indicate significant pyramidal distortion at each oxygen bridge (solid angle 275.15°).

3.5. Magnetic properties

The mononuclear complex **1** has a room temperature moment of 3.13 μ_B, which drops slightly on cooling to 3.00 μ_B at 30 K, followed by a more pronounced drop to 2.37 μ_B at 2 K. This is typical behavior for a mononuclear Ni(II) complex with the low temperature drop associated with zero field splitting. Compound **4** has a magnetic moment of <1 μ_B in this temperature range, indicating the presence of low spin Co(III) centers, as expected based on the structural results. The variable temperature magnetic data for **2** are presented in Fig. 7 as χ_{mol}, and the sharp rise in χ as temperature is lowered to a maximum at 8 K signifies the presence of weak intra-molecular anti-ferromagnetic exchange between the Ni(II) centers. The data were fitted to an isotropic exchange expression based on the exchange Hamiltonian $H = -JS_1 \cdot S_2$ (Eq. (1)) within the software package MAGMUN4.0. [2] The spin state combinations and their

[2] MAGMUN4.0 is available free of charge from http://www.ucs.mun.ca/~lthomp/index.html. It has been developed by Dr. Zhiqiang Xu (Memorial University), in conjunction with Dr. O. Waldmann (waldmann@mps.ohio-state.edu). We do not distribute the source codes. The programs may be used only for scientific purposes, and economic utilization is not allowed. If the routine is used to obtain scientific results, which are published, the origin of the programs should be quoted.

Table 5
Selected bond lengths (Å) and angles (°) for **5**

Bond lengths	
Ni1–N3	2.054(5)
Ni1–N3	2.054(5)
Ni1–N1	2.096(5)
Ni1–N1	2.096(5)
Ni1–O1	2.114(4)
Ni1–O1	2.114(4)
Ni2–N4	2.049(5)
Ni2–N9	2.057(5)
Ni2–O1	2.089(4)
Ni2–N6	2.094(5)
Ni2–O1	2.094(4)
Ni2–N7	2.124(6)
Ni2–Ni2	2.9971(15)
Bond angles	
N3–Ni1–N3	170.5(3)
N3–Ni1–N1	89.55(19)
N3–Ni1–N1	83.9(2)
N3–Ni1–N1	83.9(2)
N3–Ni1–N1	89.55(19)
N1–Ni1–N1	93.4(3)
N3–Ni1–O1	90.45(17)
N3–Ni1–O1	97.50(18)
N1–Ni1–O1	166.84(19)
N1–Ni1–O1	99.64(18)
N3–Ni1–O1	97.51(18)
N3–Ni1–O1	90.45(17)
N1–Ni1–O1	99.64(18)
N1–Ni1–O1	166.85(19)
O1–Ni1–O1	67.3(2)
N4–Ni2–N9	168.3(2)
N4–Ni2–O1	92.88(17)
N9–Ni2–O1	97.5(2)
N4–Ni2–N6	83.6(2)
N9–Ni2–N6	89.7(2)
O1–Ni2–N6	97.82(18)
N4–Ni2–O1	96.03(18)
N9–Ni2–O1	92.74(18)
O1–Ni2–O1	68.1(2)
N6–Ni2–O1	165.93(18)
N4–Ni2–N7	88.2(2)
N9–Ni2–N7	82.7(3)
O1–Ni2–N7	168.08(19)
N6–Ni2–N7	94.1(2)
O1–Ni2–N7	100.0(2)
Ni2–O1–Ni1	91.98(16)

$$H = -JS_1 \cdot S_2, \tag{1}$$

$$\chi_{M'} = \frac{N\beta^2 g^2}{3k(T-\theta)} \frac{\sum S'(S'+1)(2S'+1)\,e^{-E(S')/kT}}{\sum (2S'+1)\,e^{-E(S')/kT}}, \tag{2}$$

$$\chi_M = \chi_{M'}(1-\rho) + \frac{4S(S+1)N\beta^2 g^2 \rho}{3kT} + \mathrm{TIP}, \tag{3}$$

energies were permuted using normal vector summation methods [25] within the software and substituted into the van Vleck equation (2). Corrections were applied for paramagnetic impurity fraction (ρ), Weiss-like temperature factor (θ) and temperature independent paramagnetism (TIP) (Eqs. (2) and (3)). An excellent data fit

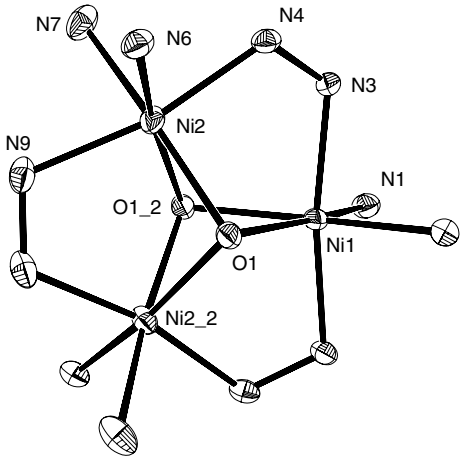

Fig. 6. Structural representation of the trinuclear core in **5** (30% thermal ellipsoids).

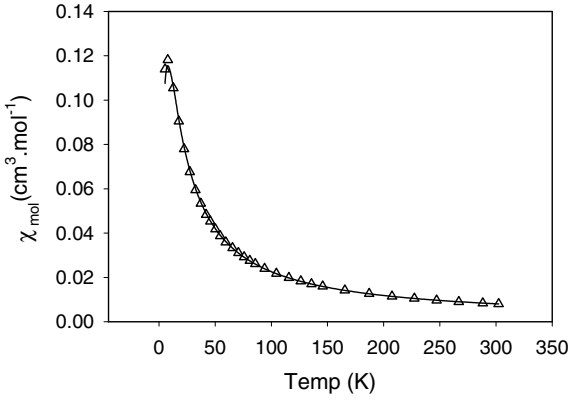

Fig. 7. Magnetic data for **2**. The solid line represents the best to Eq. (3), with $g = 2.169(3)$, $J = -5.25(9)$ cm^{-1}, $\rho = 0.014$, TIP $= 395\times10^{-6}$ cm^3 mol^{-1}, $\theta = -1$ K.

was obtained for $g = 2.169(3)$, $J = -5.25(9)$ cm^{-1}, $\rho = 0.014$, and TIP $= 395\times10^{-6}$ cm^3 mol^{-1} ($10^2R = 0.71$; $R = [\sum(\chi_{obs} - \chi_{calc})^2/\sum\chi^2_{obs}]^{1/2}$). The solid line in Fig. 7 was calculated with these values. The experimental susceptibility data for **3** are shown in Fig. 8, and correspond closely, as expected, with **2**. A similar data treatment for **3** gave $g = 2.206(1)$, $J = -4.88(2)$ cm^{-1}, $\rho = 0.008$, and TIP $= 440\times10^{-6}$ cm^3 mol^{-1} ($10^2R = 0.30$). Comparable J values are obtained, in agreement with the similarities in structure. Inclusion of zero field splitting terms in these analyses gave inferior data fittings, and so the magnetic data appear to be dominated mainly by exchange effects.

Magnetic data for **5**, plotted as μ_{mol}/temperature, are shown in Fig. 9, and the smooth drop in moment as temperature is lowered is indicative of quite strong antiferromagnetic exchange. The data were fitted using MAGMUN4.0 to an isotropic exchange expression based on the exchange Hamiltonian (Eq. (4)) for three $S = 1$ spin centers arranged in an equilateral triangle

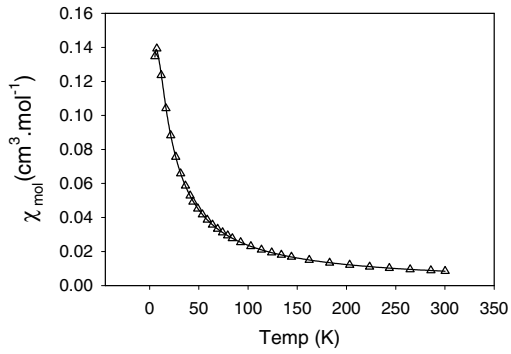

Fig. 8. Magnetic data for **3**. The solid line represents the best to Eq. (3), with $g = 2.206(1)$, $J = -4.88(2)$ cm^{-1}, $\rho = 0.008$, TIP $= 440\times10^{-6}$ cm^3 mol^{-1}, $\theta = 0$ K.

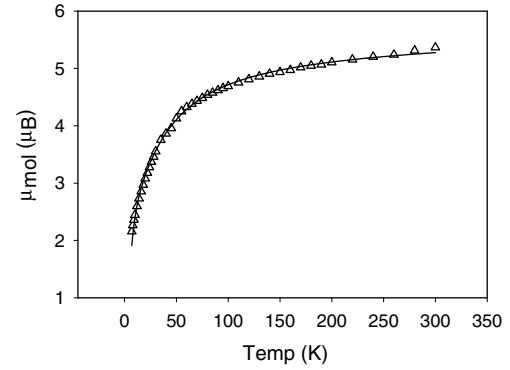

Fig. 9. Magnetic data for **5**. The solid line represents the best to Eq. (4), with $g = 2.214(6)$, $J = -15.7(4)$ cm^{-1}, $\rho = 0.05$, TIP $= 500\times10^{-6}$ cm^3 mol^{-1}, $\theta = -1$ K.

with a single J value. This combines the effects of the two different bridges which connect adjacent pairs of nickel centers. A good fit gave $g = 2.214(6)$, $J = -15.7$ cm^{-1}, $\rho = 0.05$, TIP $= 500\times10^{-1}$ cm^3 mol^{-1}, $\theta = -1$ K, $10^2R = 1.8$. The solid line in Fig. 9 was calculated with these parameters

$$H = -J\{S_{12} + S_{23} + S_{13}\}. \quad (4)$$

The magnetic properties of **2**, **3** and **4** are the result of the combination of the exchange effects of two different bridging groups connecting the Ni(II) centers. Since it is not possible to differentiate the contributions of two groups in the overall exchange process the J values obtained are the resultants of these combined effects. The exchange effects of phthalazine bridges have been studied widely in polynuclear copper(II) complexes, and it is generally accepted that coupling is always antiferromagnetic, with moderate $-2J$ values, e.g. 100–200 cm^{-1} [26]. In nickel chemistry there are few examples of systems with just phthalazine bridges, and a study by Ball and Blake on $[Ni_2(DHPH)_2(H_2O)_4]X_4$ (X = Cl, Br, I; DHPH = 1,4-dihydrazino-phthalazine) involving a double bridged $Ni_2(\mu\text{-N–N})_2$ dinuclear center, led to $-J$

values in the range 20–25 cm^{-1} ($H = -2JS_1 \cdot S_2$) [27]. For an analogous di-copper(II) system $[Cu_2(DHPH)(H_2O)_2(ClO_4)_2](ClO_4)_2$ a much larger exchange integral was observed ($-2J = 489\ cm^{-1}$) [28].

Hydroxide bridges are renowned for their ability to propagate exchange coupling between metal ions, e.g. copper(II), with an exchange dependence on bridge angle between the active metal magnetic orbitals, and magneto-structural correlations on a range of related complexes have shown that for Cu–O–Cu angles >97.5° anti-ferromagnetic coupling is observed, while ferromagnetic exchange occurs at smaller angles [29,30]. Magneto-structural correlations for H_2O bridged systems appear not to have been studied. The small Ni–O–Ni angles in **2** and **3** (94.3°–94.8°) might suggest that the water bridges could be responsible for a ferromagnetic exchange component in comparison with hydroxide. However, the phthalazine bridge is likely to have a dominant anti-ferromagnetic effect, and so the small $-J$ values observed for **2** and **3** (4.88, 5.25 cm^{-1}) could well be the resultant of two antagonistic exchange effects. The Ni–OH–Ni bridge angles in **5** are even smaller (91°–92°), and might again be candidates for a ferromagnetic exchange contribution. However, the larger exchange coupling in **5** indicates that efficient N–N phthalazine bridging must again dominate the exchange situation.

4. Conclusions

The ligand pap shows considerable versatility in its coordination chemistry with Ni(II) and Co(III), with examples of mononuclear, dinuclear and trinuclear complexes. The dinuclear and trinuclear Ni(II) complexes are bridged by combinations of N–N (phthalazine) and water and hydroxide bridges, respectively, with magnetic properties that result from a combination of two bridging interactions. All examples are anti-ferromagnetically coupled.

5. Supplementary material

Crystallographic data for the structural analyses have been deposited with the Cambridge Crystallographic Data Center, CCDC Nos. 232257–232260. Copies of this information may be obtained free of charge from The Director, CCDC, 12, Union Road, Cambridge CB2 1EZ, UK (fax: +44-1223-336033; e-mail: deposit@ccdc.cam.ac.uk; www: http://www.ccdc.cam.ac.uk).

Acknowledgements

This study was supported by the Natural Sciences and Engineering Research Council of Canada (NSERC) and the Research Council of Norway (H.G.). We thank Dr. R. McDonald, University of Alberta, for structural data.

References

[1] L.K. Thompson, V.T. Chacko, J.A. Elvidge, A.B.P. Lever, R.V. Parish, Can. J. Chem. 47 (1969) 4141.
[2] J.C. Dewan, L.K. Thompson, Can. J. Chem. 60 (1982) 121.
[3] D.V. Bautista, J.C. Dewan, L.K. Thompson, Can. J. Chem. 60 (1982) 2583.
[4] G. Bullock, F.W. Hartstock, L.K. Thompson, Can. J. Chem. 61 (1983) 57.
[5] L.K. Thompson, Can. J. Chem. 61 (1983) 579.
[6] L.K. Thompson, A.W. Hanson, B.S. Ramaswamy, Inorg. Chem. 23 (1984) 2459.
[7] S.K. Mandal, L.K. Thompson, A.W. Hanson, J. Chem. Soc., Chem. Commun. (1985) 1708.
[8] L.K. Thompson, F.W. Hartstock, L. Rosenberg, T.C. Woon, Inorg. Chim. Acta 97 (1985) 1.
[9] S.K. Mandal, L.K. Thompson, M.J. Newlands, F.L. Lee, Y. LePage, J.-P. Charland, E.J. Gabe, Inorg. Chim. Acta 122 (1986) 199.
[10] S.K. Mandal, T.C. Woon, L.K. Thompson, M.J. Newlands, E.J. Gabe, Aust. J. Chem. 39 (1986) 1007.
[11] L.K. Thompson, S.K. Mandal, L. Rosenberg, Inorg. Chim. Acta 133 (1987) 81.
[12] L.K. Thompson, F.L. Lee, E.J. Gabe, Inorg. Chem. 27 (1988) 39.
[13] S.S. Tandon, L.K. Thompson, M.E. Manuel, J.N. Bridson, Inorg. Chem. 33 (1994) 5555.
[14] L.K. Thompson, S.S. Tandon, M.E. Manuel, Inorg. Chem. 34 (1995) 2356.
[15] S.S. Tandon, L.K. Thompson, D.O. Miller, J. Chem. Soc., Chem. Commun. (1995) 1907.
[16] L.K. Thompson, S.S. Tandon, Comments Inorg. Chem. 18 (1996) 125.
[17] C.L. Sheppard, S.S. Tandon, L.K. Thompson, J.N. Bridson, D.O. Miller, M. Handa, F. Lloret, Inorg. Chim. Acta 250 (1996) 227.
[18] J.A. Doull, L.K. Thompson, Can. J. Chem. 58 (1980) 221.
[19] G. Bullock, A. Cook, A. Foster, L. Rosenberg, L.K. Thompson, Inorg. Chim. Acta 103 (1985) 207.
[20] (a) G.M. Sheldrick, SHELX-97, 1997;
(b) A. Altomare, M. Cascarano, C. Giacovazzo, A. Guagliardi, SIR-97, J. Appl. Cryst. 26 (1993) 343.
[21] P.T. Beurskens, G. Admiraal, G. Beurskens, W.P. Bosman, R. de Gelder, R. Israel, J.M.M. Smits, DIRDIF-94: The DIRDIF-94 program system, Technical Report of the Crystallography Laboratory, University of Nijmegen, The Netherlands, 1994.
[22] D.T. Cromer, J.T. Waber, in: International Tables for X-ray Crystallography, vol. IV, The Kynoch Press, Birmingham, 1974, Table 2.2 A.
[23] J.A. Ibers, W.C. Hamilton, Acta Crystallogr. 17 (1964) 781.
[24] D.C. Creagh, W.J. McAuley, in: A.J.C. Wilson (Ed.), International Tables for Crystallography, vol. C, Kluwer Academic Publishers, Boston, MA, 1992, pp. 219–222, Table 4.2.6.8.
[25] K. Kambe, J. Phys. Soc. Jpn. 5 (1950) 48.
[26] (a) L.K. Thompson, S.S. Tandon, M.E. Manuel, Inorg. Chem. 34 (1995) 2356;
(b) S.S. Tandon, L.K. Thompson, M.E. Manuel, J.N. Bridson, Inorg. Chem. 33 (1994) 5555, and references therein.

[27] P.W. Ball, A.B. Blake, J. Chem. Soc. A (1969) 1415.
[28] S.S. Tandon, L.K. Thompson, R.C. Hynes, Inorg. Chem. 31 (1992) 2210.
[29] V.H. Crawford, H.W. Richardson, J.R. Wasson, D.J. Hodgson, W.E. Hatfield, Inorg. Chem. 15 (1976) 2107.
[30] L.K. Thompson, F.L. Lee, E.J. Gabe, Inorg. Chem. 27 (1988) 39.

Available online at www.sciencedirect.com
SCIENCE DIRECT®
Polyhedron 23 (2004) 1185–1189
POLYHEDRON
www.elsevier.com/locate/poly

Organosulfur donor with hydroxy groups and its conducting salt: crystal structures and physical properties

Shi-Xia Liu [a,*], Antonia Neels [b], Helen Stoeckli-Evans [b], Melanie Pilkington [c], John D. Wallis [c], Silvio Decurtins [a,*]

[a] *Departement für Chemie und Biochemie, Universität Bern, Freiestrasse 2, Bern CH-3012, Switzerland*
[b] *Institut de Chimie, Université de Neuchâtel, Avenue Bellevaux 51, Neuchâtel CH-2007, Switzerland*
[c] *Department of Chemistry and Physics, The Nottingham Trent University, Clifton Lane, Nottingham NG11 8NS, UK*

Received 16 December 2003; accepted 27 January 2004

Abstract

Crystal structures of organosulfur donor 2-(5′,6′-dihydro[1,3]dithiolo[4,5-b][1,4]-dithiin-2′-ylidene)-6,7-di-hydro-5H-[1,3]dithiolo[4,5-b][1,4]dithiepine-6,6-dimethanol (**D**) and its conducting salt $\mathbf{D}_2\mathrm{I}_3$ are described. Conductivity properties of $\mathbf{D}_2\mathrm{I}_3$ are also discussed.
© 2004 Elsevier Ltd. All rights reserved.

Keywords: Radical salts; Bis(ethylenedithio)tetrathiafulvalene (ET); Crystal structures; Electrical conductivity

1. Introduction

The radical cation salts based on bis(ethylenedithio)tetrathiafulvalence (ET) are the major class of organic quasi-two-dimensional metals and superconductors [1]. Their conductive properties are highly sensitive to chemical modifications of the ET framework, and considerable efforts have been devoted to the search for molecular superconductors presenting higher critical temperatures (T_c) by the synthetic chemistry methods [2–4]. Most of these chemical modifications were aimed to increase the dimensionality of these materials which can suppress the Peierls distortions at low temperature by favoring the intermolecular interaction among electron donors and acceptors (or counter anions). To introduce the possibility of strong hydrogen bonding some ET derivatives with hydroxy groups have been synthesised [5–9].

We report here the crystal structures of the title donor **D** (Fig. 1) and its conducting salt $\mathbf{D}_2\mathrm{I}_3$.

2. Experimental

2.1. Materials and equipment

Unless stated otherwise, all reagents were purchased from commercial sources and used without additional purification. Organosulfur donor (**D**) and the supporting electrolyte n-$\mathrm{Bu_4NI_3}$ were prepared according to literature procedures [6,10]. Conductivity was measured by the four-probe technique on a compressed pellet.

2.2. Synthesis of $\boldsymbol{D_2I_3}$

The conducting salt $\mathbf{D}_2\mathrm{I}_3$ was obtained by electrocrystallization. Single crystals were grown on a platinum wire anode as brown thin plates by anodic oxidation of **D** in the presence of n-$\mathrm{Bu_4NI_3}$ at constant low-current density (1 $\mu\mathrm{A\,cm^{-2}}$) in $\mathrm{CH_3CN}$.

2.3. Crystallography

Intensity measurements were collected on a Stoe Image Plate Diffraction System [11] for donor **D** and a Stoe Mark II-Image Plate Diffraction System [12] for its salt $\mathbf{D}_2\mathrm{I}_3$, equipped with graphite monochromated Mo

* Corresponding authors. Tel.: +41-31-6314245; fax: +41-31-6313993 (S.-X. Liu).
E-mail addresses: liu@iac.unibe.ch (S.-X. Liu), silvio.decurtins@iac.unibe.ch (S. Decurtins).

0277-5387/$ - see front matter © 2004 Elsevier Ltd. All rights reserved.
doi:10.1016/j.poly.2004.01.013

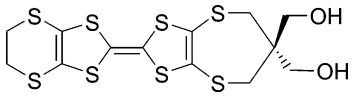

Fig. 1. Organosulfur donor **D**.

Kα radiation ($\lambda = 0.71073$ Å) using the $\omega - 2\theta$ scan technique. The structures were solved by Direct methods using the programme SHELXS 97 [13]. The refinement and all further calculations were carried out using SHELXL 97 [14].

For donor **D**, the H-atoms were either located from Fourier difference maps and refined isotropically or included in calculated positions and treated as riding atoms using SHELXL default parameters. The non-H atoms were refined anisotropically, using weighted full-matrix least-squares on F^2. The crystal diffracted weakly and only 1/3 of the reflections can be considered to be observed [$I > 2\sigma(I)$]. Owing to the extremely long *b*-axis, a certain fraction of the reflections (ca. 12%) was overlapped and eliminated from the *hkl* file. The molecule is structurally disordered, with the terminal $-C_2H_4$ group having two conformations.

For its salt $\mathbf{D}_2I_3$, the hydrogen atoms were included in calculated positions and treated as riding atoms using SHELXL 97 default parameters. The non-H atoms were refined anisotropically, using weighted full-matrix least-squares on F^2. An absorption correction was applied using DIFABS [15] ($T_{min} = 0.325$, $T_{max} = 0.755$).

Table 1
Crystallographic data for donor **D** and its salt $\mathbf{D}_2I_3$

	D	$\mathbf{D}_2I_3$
Molecular formula	$C_{13}H_{14}O_2S_8$	$C_{26}H_{28}I_3O_4S_{16}$
Molecular weight	458.72	1298.14
Crystal dimensions (mm)	$0.40 \times 0.40 \times 0.10$	$0.500 \times 0.275 \times 0.025$
Crystal system	monoclinic	orthorhombic
Space group	$P2_1/c$	$Pbn2_1$
Unit cell dimensions		
a (Å)	6.4287(7)	8.2240(5)
b (Å)	42.420(7)	11.7860(7)
c (Å)	7.1209(8)	42.170(3)
β (°)	114.705(12)	90.000(0)
U (Å^3)	1764.2(4)	4087.5(5)
Z	4	4
D_{calc} (g cm^{-3})	1.727	2.109
Absorption coefficient (mm^{-1})	1.016	3.146
R_{int}	0.1316	0.0701
Measured reflections	8562	14 708
Independent reflections	3004	7099
Reflections with $I > 2\sigma(I)$	1110	5762
R_1 (observed)	0.0714	0.0849
wR_2 (all data)	0.2189	0.2372
Goodness-of-fit	0.821	1.026

The crystallographic data of donor **D** and its salt $\mathbf{D}_2I_3$ are collected in Table 1. Selected bond lengths and angles are given in Table 2.

Table 2
Selected bond lengths (Å) and angles (°) for donor **D** and its salt $\mathbf{D}_2I_3$

D		$\mathbf{D}_2I_3$			
Bond lengths					
C(1)–C(4)	1.342(11)	C(1)–C(4)	1.372(16)	C(14)–C(17)	1.369(17)
C(1)–S(1)	1.741(11)	C(1)–S(1)	1.742(10)	C(14)–S(9)	1.744(11)
C(4)–S(4)	1.750(11)	C(4)–S(4)	1.725(13)	C(17)–S(12)	1.740(12)
C(5)–C(6)	1.325(14)	C(5)–C(6)	1.416(17)	C(18)–C(19)	1.370(16)
C(5)–S(4)	1.756(9)	C(5)–S(4)	1.731(12)	C(18)–S(9)	1.721(11)
C(5)–S(1)	1.777(9)	C(5)–S(1)	1.728(11)	C(18)–S(12)	1.744(12)
C(6)–S(5)	1.749(9)	C(6)–S(5)	1.717(12)	C(19)–S(13)	1.744(11)
C(6)–S(8)	1.759(9)	C(6)–S(8)	1.729(11)	C(19)–S(16)	1.750(10)
C(7)–C(11)	1.354(9)	C(7)–C(11)	1.316(18)	C(20)–C(24)	1.364(16)
C(7)–S(5)	1.745(10)	C(7)–S(5)	1.779(11)	C(20)–S(13)	1.726(12)
C(11)–S(8)	1.733(11)	C(11)–S(8)	1.744(11)	C(24)–S(16)	1.735(10)
O(1)–C(12)	1.441(14)	O(1)–C(12)	1.395(17)	O(3)–C(25)	1.416(15)
O(2)–C(13)	1.436(12)	O(2)–C(13)	1.466(15)	O(4)–C(26)	1.403(14)
Bond angles					
C(4)–C(1)–S(1)	116.6(8)	C(4)–C(1)–S(1)	116.7(8)	C(17)–C(14)–S(9)	117.2(9)
C(1)–C(4)–S(4)	118.3(8)	C(1)–C(4)–S(4)	116.8(9)	C(14)–C(17)–S(12)	116.3(9)
S(4)–C(5)–S(1)	113.4(6)	S(1)–C(5)–S(4)	116.2(7)	S(9)–C(18)–S(12)	116.0(7)
S(5)–C(6)–S(8)	113.9(7)	S(5)–C(6)–S(8)	116.6(7)	S(13)–C(19)–S(16)	114.5(6)
C(11)–C(7)–S(5)	115.4(8)	C(11)–C(7)–S(5)	115.2(9)	C(24)–C(20)–S(13)	116.9(9)
C(7)–C(11)–S(8)	118.9(8)	C(7)–C(11)–S(8)	119.4(9)	C(20)–C(24)–S(16)	117.2(8)
O(1)–C(12)–C(9)	111.0(11)	O(1)–C(12)–C(9)	112.0(11)	O(3)–C(25)–C(22)	112.7(10)
O(2)–C(13)–C(9)	115.0(12)	O(2)–C(13)–C(9)	111.3(10)	O(4)–C(26)–C(22)	111.8(11)
C(13)–C(9)–C(12)	115.1(10)	C(13)–C(9)–C(12)	109.9(10)	C(26)–C(22)–C(25)	110.0(10)

3. Results and discussion

3.1. Structure of *D*

Organosulfur donor **D** was recrystallised from THF/CH_3CN to afford single crystals. The X-ray crystal analysis revealed that in the crystal lattice, the molecules are linked by a 1D polymer arrangement of some conventional O–H···O hydrogen bonds (Table 3), so forming zig-zag chains along the *b*-axis (Fig. 2). The donor molecules are quasi-parallel caused by asymmetric hydrogen-bonds and mutually shifted with interplanar distances of 4.17 Å and stacked along the *c*-axis. There are intermolecular S···S contacts in the range of 3.29–3.60 Å.

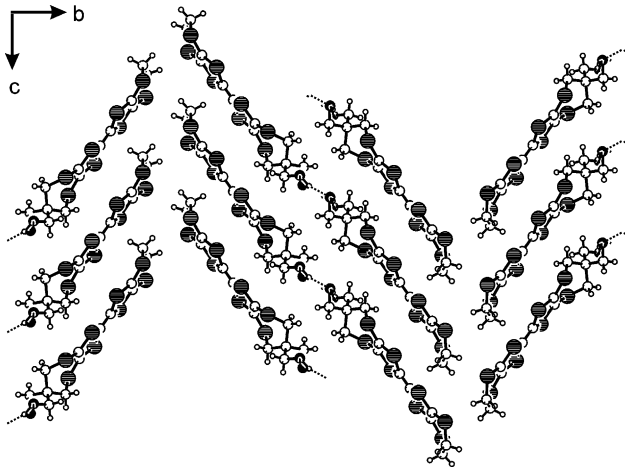

Fig. 2. Crystal packing of the neutral donor **D** showing hydrogen bonding (dashed lines) between stacks.

3.2. Synthesis, conductivity properties and structure of D_2I_3

In order to obtain the conducting salts of **D**, standard electrocrystallizations were examined in the presence of various tetrabutylammonium (TBA) salts as the electrolyte: these included linear (I_3^-), tetrahedral (ClO_4^-), and octahedral (PF_6^-) anions. However, only the electrocrystallization at a constant current (1.0 μA) in CH_3CN with TBA· I_3 gave crystalline salts as brown thin plates. The room-temperature conductivity measured by a four-probe technique on a compressed pellet showed a relatively high conductivity ($\sigma_{rt} = 2.95$ S cm^{-1}). The temperature dependence of the resistivity is shown in Fig. 3. From room temperature to about 240 K, its electrical resistance varies very little. But when the temperature is lowered further, the electrical resistance increases strongly, showing semiconducting behaviour with the activation energy being about 0.35 eV.

Table 3
Hydrogen bonds (Å, °) for donor **D**

D–H···A	*d*(D–H)	*d*(H···A)	*d*(D···A)	D–H···A (°)
O(2)–H(2)···O(1)^{i}	1.05(11)	1.85(11)	2.884(10)	170(11)
O(1)–H(1)···O(2)^{ii}	1.00(13)	1.76(13)	2.719(11)	159(12)

Symmetry transformations used to generate equivalent atoms: (i) $1x-1,\ y,\ z$; (ii) $-x+2,\ -y,\ -z+1$.

The X-ray analyses showed that the charge-transfer complex D_2I_3 crystallises with two positively charged donor molecules A and B and one disordered I_3^- anion per asymmetric unit (Fig. 4). The molecular structures of the two donor units (A and B) are only slightly different. For both units A and B in the salt, the central TTF units are coplanar with deviations from the least-squares plane being less than 0.047 Å. Apparently, in the oxidation state the TTF units show less deviations from planarity

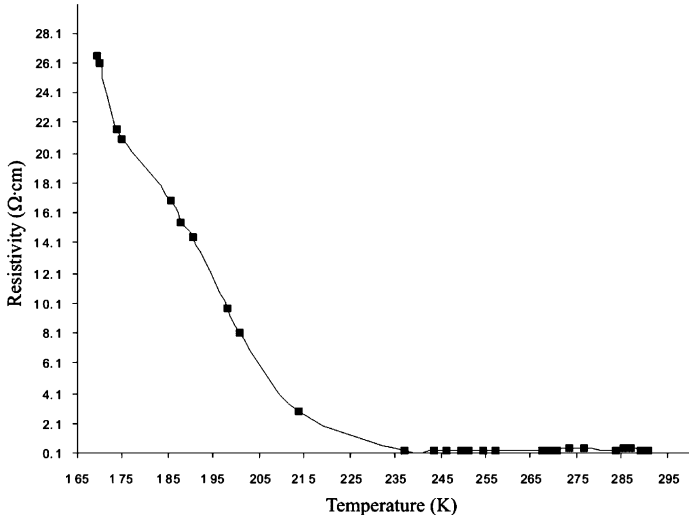

Fig. 3. Temperature dependence of the resistivity for D_2I_3.

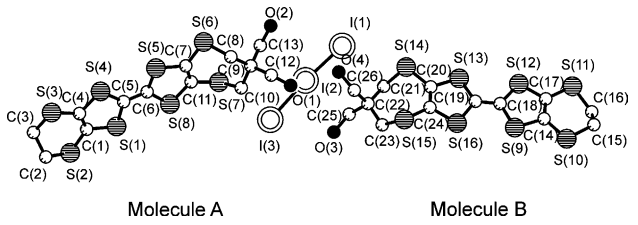

Fig. 4. Crystal structure of the conducting salt $\mathbf{D}_2\mathrm{I}_3$. Hydrogen atoms are omitted for clarity.

than those in the neutral state (largest deviation is 0.064 Å). The bond lengths of the central C=C [C(5)–C(6); C(18)–C(19)] bonds are 1.416 and 1.370 Å, respectively, in the salt (Table 2). As compared to that of the neutral donor **D** (1.325 Å), it can be inferred that the TTF units in salt $\mathbf{D}_2\mathrm{I}_3$ are partially oxidised according to the correlation between the oxidation states of TTF derivatives and bond lengths of the central C=C bonds [16]. As depicted in Fig. 5, the donor molecules are dimerised in 'head-to-head' manner, which might increase the effective overlap area of the molecules and stabilise the electronic state with van der Waals attractive force [17]. Dimers are orthogonally arranged to each other along the *b*-axis. The dihedral angles between the molecules are 84.6° and 72.3° for pairs A–A and B–B, respectively. The donor array of the present salt is classified as the so-called κ-type. There are S···S contacts (3.46–3.62 Å, sum of van der Waals radii 3.70 Å) and weak hydrogen bonds (C–H···S = 3.49–3.76 Å and C–H···O = 2.84–2.91 Å) between neighboring dimers. Whereas between A and B stacks, some conventional O–H···O hydrogen bonds with 1D polymer arrangement (Table 4 and Fig. 5), a short S···I contact (3.63 Å) and weak hydrogen bonds C–H···I (3.74–3.95 Å) are observed.

In both **D** and $\mathbf{D}_2\mathrm{I}_3$, no intramolecular hydrogen bonds are observed which can be explained by strong competition of bimolecular ring motifs [18]. The hydrogen bond pattern in these two compounds is different, as shown by the graph-set analysis following the accepted proposition of Etter et al. [19]. In donor **D**, one kind of hydrogen bond gives rise to chains and two other different kinds of hydrogen bond give rise to rings, which form a higher-order network. Therefore, the graph-set for **D** is $C(6)\ R_4^4(8)\ R_2^2(12)\ R_4^4(16)$. Whereas in its salt, $\mathbf{D}_2\mathrm{I}_3$, one kind of hydrogen bond gives rise to chains and another kind of hydrogen bond gives rise to a ring, two of which make up a higher-order network. Thus, the graph-set for $\mathbf{D}_2\mathrm{I}_3$ is $C(6)\ R_3^3(10)\ R_4^4(16)$.

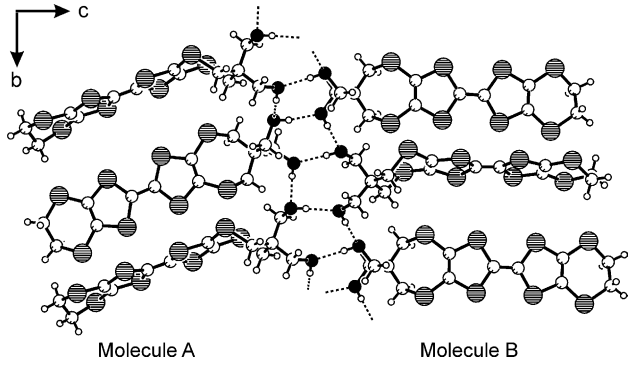

Fig. 5. Crystal packing of the conducting salt $\mathbf{D}_2\mathrm{I}_3$ showing hydrogen bonding (dashed lines). I_3^- anions are omitted for clarity.

Table 4
Hydrogen bonds (Å, °) for $\mathbf{D}_2\mathrm{I}_3$

D–H···A	*d*(D–H)	*d*(H···A)	*d*(D···A)	D–H···A (°)
O(1)–H(1)···O(2)^{i}	0.84	1.85	2.664(12)	162.9
O(2)–H(2)···O(3)	0.84	1.88	2.706(12)	167.3
O(3)–H(3)···O(4)^{i}	0.86	1.87	2.728(11)	179.4
O(4)–H(4)···O(1)^{ii}	0.85	1.90	2.744(12)	179.1

Symmetry transformations used to generate equivalent atoms: (i) $-x-3/2,\ y+1/2,\ z$; (ii) $-x-3/2,\ y-1/2,\ z$.

4. Conclusions

In conclusion, the title donor has yielded a conducting salt $\mathbf{D}_2\mathrm{I}_3$ and shows a unique crystal structure. Thus, compound **D** can be expected to be a suitable donor for exploring organic metals in the future.

5. Supplementary material

Crystallographic data for the structure reported in this paper have been deposited with the Cambridge Crystallographic Data Centre, CCDC No. 218114–218115 for compounds **D** and $\mathbf{D}_2\mathrm{I}_3$. Copies of the data can be obtained free of charge on application to CCDC, 12 Union Road, Cambridge CB2 1EZ, UK (fax: +44-1223-336033; e-mail: deposit@ccdc.cam.ac.uk or www: http://www.ccdc.cam.ac.uk).

Acknowledgements

We thank both Prof. Lahcéne Ouahab and Dr. Stéphane Golhen for their help and useful discussions about conductivity measurements. This work was supported by the SNF programme (Grant No. 200021-100432).

References

[1] J.M. Williams, J.R. Ferraro, R.J. Thorn, K.D. Carlson, U. Geiser, H.H. Wang, A.M. Kini, M.-H. Whangbo, Organic Superconductor (Including Fullerenes), Prentice-Hall, Englewood Cliffs, NJ, 1992.

[2] H. Nishikawa, T. Morimoto, T. Kodama, I. Ikemoto, K. Kikuchi, J. Yamada, H. Yoshino, K. Murata, J. Am. Chem. Soc. 124 (2002) 730.
[3] C. Rovira, S. LeMoustarder, D. Belo, J. Veciana, M. Almeida, V. Gama, M.T. Duarte, Synth. Met. 120 (2001) 717.
[4] S. LeMoustarder, P. Hudhomme, C. Durand, N. Mercier, M.T. Azcondo, P. Delhaes, A. Riou, A. Gorgues, J. Mater. Chem. 10 (2000) 617.
[5] N. Saygili, R.J. Brown, P. Day, R. Hoelzl, P. Kathirgamanathan, E.R. Mageean, T. Ozturk, M. Pilkington, M.M.B. Qayyum, S.S. Turner, L. Vorwerg, J.D. Wallis, Tetrahedron 57 (2001) 5015.
[6] T. Ozturk, N. Saygili, S. Ozkara, M. Pilkington, C.R. Rice, D.A. Tranter, F. Turksoy, J.D. Wallis, J. Chem. Soc., Perkin Trans. 1 (2001) 407.
[7] G.A. Horley, T. Ozturk, F. Turksoy, J.D. Wallis, J. Chem. Soc., Perkin Trans. 1 (1998) 3225.
[8] H.-X. Li, D.-Q. Zhang, W. Xu, L.-Z. Fan, D.-B. Zhu, Synth. Met. 106 (1999) 111.
[9] (a) P. Blanchard, K. Boubekeur, M. Sallé, G. Duguay, M. Jubault, A. Gorgues, J.D. Martin, E. Canadell, P. Auban-Senzier, D. Jérome, P. Batail, Adv. Mater. 4 (1992) 579;
(b) S.A. Baudron, N. Avarvari, P. Batail, C. Coulon, R. Clérac, E. Canadell, P. Auban-Senzier, J. Am. Chem. Soc. 125 (2003) 11583.
[10] J.M. Williams, T.J. Emge, H.H. Wang, M.A. Beno, P.T. Copps, L.N. Hall, K.D. Carlson, G.W. Crabtree, Inorg. Chem. 23 (1984) 2558.
[11] Stoe and Cie, IPDS Software, Stoe and Cie GmbH, Darmstadt, Germany, 2000.
[12] G.M. Sheldrick, Acta Crystallogr., Sect. A 46 (1990) 467.
[13] G. Sheldrick, SHELXL 97, Universität Göttingen, Göttingen, Germany, 1999.
[14] Stoe and Cie, X-Area V1.17 and X-RED32 V1.04 Software, Stoe and Cie GmbH, Darmstadt, Germany, 2002.
[15] A.L. Spek, Acta Crystallogr., Sect. A 46 (1990) C-34.
[16] C. Katayama, M. Honda, H. Kumagai, J. Tanaka, G. Saito, H. Inokuchi, Bull. Chem. Soc. Jpn. 58 (1985) 2272.
[17] H. Fujiwara, Y. Misaki, M. Taniguchi, T. Yamabe, T. Kawamoto, T. Mori, H. Mori, S. Tanaka, J. Mater. Chem. 8 (1998) 1711.
[18] T. Steiner, Angew. Chem., Int. Ed. 41 (2002) 48.
[19] M.C. Etter, J.C. MacDonald, J. Bernstein, Acta Crystallogr., Sect. B 46 (1990) 256.

Available online at www.sciencedirect.com
SCIENCE DIRECT®
Polyhedron 23 (2004) 1191–1197
POLYHEDRON
www.elsevier.com/locate/poly

Structural studies of bis-(2,6-diacetylpyridine-bis-(phenylhydrazone)) and X-ray structure of its Y(III), Pr(III), Sm(III) and Er(III) complex

Farba Bouyagui Tamboura [a], Pepe Marcel Haba [a], Mohamed Gaye [a,*], Abdou Salam Sall [a], Aliou Hamady Barry [b], Tahar Jouini [c]

[a] *Département de Chimie, Faculté des Sciences et Techniques, Université Cheikh Anta Diop, BP 5199, DakarFann, Sénégal*
[b] *Département de Chimie, Faculté des Sciences, Université de Nouakchott, Nouakchott, Mauritania*
[c] *Département de Chimie, Faculté des Sciences, Campus Universitaire, 1060 Tunis, Tunisia*

Received 18 December 2003; accepted 27 January 2004

Abstract

Reaction of 2,6-bis(phenylhydrazone)pyridine with $Ln(NO_3)_3 \cdot 6H_2O$ nitrate (Ln = Y, Pr, Sm and Er) produces mononuclear complexes. The crystal structures of $[Ln(C_{23}H_{19}N_5O_2)(H_2O)(NO_3)]$ (Ln = Y or Er) and $\{[Ln(C_{23}H_{19}N_5O_2)(C_{23}H_{20}N_5O_2)](H_2O)_2((CH_3)_2SO)\}$ (Ln = Pr or Sm) were determined. Coordination of the dianionic and the monoanionic ligands in the complexes is via the pyridyl nitrogen, hydrazino nitrogen and iminol oxygen. The crystal structures were determined.

In the isostructural complexes (Ln = Y, Er) the lanthanide ion have exactly the same coordination, being an irregular polyhedron with coordination number of eight.

In the isostructural complexes (Ln = Pr, Sm) the lanthanide ion assumes a ten co-ordinated geometry for both metal ions. The coordination polyhedron around each lanthanide atom in both complexes is best described as a distorted bicapped square antiprism.
© 2004 Elsevier Ltd. All rights reserved.

Keywords: Hydrazones; Complex; Lanthanide; X-ray; Spectroscopy; Crystal structures

1. Introduction

Owing to the ramifying applications of the lanthanides macrocyclic complexes in applied and fundamental sciences, this field continues to receive much attention. They are used as catalysts [1] in transesterification, as radiopharmaceuticals [2] and as fluoroimmuno assay reagents [3,4]. Certain Eu(III) and Nd(III) complexes have been reported to have laser property [5].

Our research interest in the synthesis and the study of the physicochemical properties of lanthanides(III) complexes derived from macroacyclic ligand molecules with N_5O_2 inners. We have recently reported the synthesis of lanthanides complexes of a N_3O_2 ligand [6].

The lanthanide in their trivalent state, complexes with strongly chelating species containing highly electronegative donors atoms [7,8]. 2,6-diacetylpyridine and benzoylhydrazide possesses potential nitrogen and oxygen donors. They can interact together to form 2,6-diacetylpyridine-bis-(benzoylhydrazone) which can acts with metal ion to form stable complexes [9,10].

In view of these facts, reaction of some lanthanides nitrates and 2,6-diacetylpyridine-bis-(benzoylhydrazone) has been carried out and structures of the resulting complexes were investigated using spectroscopic techniques and X-ray diffraction. The results of this study are reported in this present paper.

* Corresponding author. Tel.: +221-555-58-91; fax: +221-824-63-18.
E-mail address: mlgayeastou@yahoo.fr (M. Gaye).

0277-5387/$ - see front matter © 2004 Elsevier Ltd. All rights reserved.
doi:10.1016/j.poly.2004.01.014

2. Experimental

2.1. Reagents materials

All chemicals and solvents used were of reagent grade. All metal(III) salts were used as nitrates. NMR spectrum was recorded on a Bruker 400 spectrometer, infrared spectra were recorded on a Nicolet 5SXC FT-IR spectrophotometer using KBr pellets or Nujol mulls. Elemental analysis of C, H and N was performed by the analytical laboratory of the Department of Inorganic Chemistry (University of Padua, Italy). Molar conductance measurement was made using a WTW LF-330 conductivity meter with a WTW conductivity cell on about 1 mmol dm^{-3} dimethylformamide solution at room temperature. Room temperature magnetic susceptibility measurements were made on solid complexes using a Johnson Mattey balance with $Hg[Co(SCN)_4]$ as the calibrator. Melting point were recorded on a Büchi apparatus and are uncorrected.

2.2. Preparation of the Schiff base (H_2L)

To a solution of 2,6-diacetylpyridine (1.63 g, 10 mmol) in 60 ml of methanol was added a solution of benzoylhydrazine (2.72 g, 20 mmol) in 10 ml of the same solvent. Two drops of glacial acetic acid were added and the resulting mixture was refluxed under stirring for 2 h. On cooling the white precipitate, which appeared, was filtered off, washed with 2×10 ml of methanol and 2×20 ml of ether before dried under vacuum. The yield is 93%, m.p. 224 °C. *Anal.* Calc. for $C_{23}H_{21}N_5O_2 \cdot 1/2H_2O$. C, 67.63; H, 5.43; N, 17.15. Found: C, 67.49; H, 5.65; N, 17.26%. Mass spectrum (EI): $m/z = 408$ ($[C_{23}H_{21}N_5O_2 \cdot 0.5H_2O]^+$). IR ($cm^{-1}$, Nujol mulls) $\nu_{C=N}$ 1667; ν_{N-N} 1018. ^1H NMR ($(CD_3)_2SO$, 400 MHz): 2.55 (s, 6H), 7.7 (m, 13 H), 10.9 (s, 2H) ppm. ^{13}C NMR ($(CD_3)_2SO$, 75 MHz): 12.54, 120.58, 128.35, 131.65, 134.10, 137.24, 154.30.

2.3. Preparation of [Y(L) (H_2O)(NO_3)] (1)

To a suspension of H_2L (2 mmol) in absolute ethanol (20 ml) was added $Y(NO_3)_3 \cdot 6H_2O$ (2 mmol) in 10 ml of absolute ethanol. The white suspension turns to yellow immediately. After 20 min under stirring a solution of LiOH (4 mmol) in 5 ml of absolute ethanol was added. The yellow precipitate disappears and the solution was refluxed for two hours. On cooling the deep yellow precipitate, which was formed, was filtered off, washed with 2×10 ml of absolute ethanol and dried under vacuum (yield, 78%). Crystals suitable for X-ray analysis were grown by dissolving 0.5 g of this compound in minimum amount of dimethylsulfoxide (4–5 cm^3) to yield a saturated solution. The resulting solution was allowed to evaporate slowly at room temperature for several days to yield fine crystals. *Anal.* Calc. for $YC_{23}H_{21}N_6O_6$ C, 48.78 (48.73), H, 3.74 (3.73), N, 14.84 (14.82)%. IR (cm^{-1}, Nujol mulls) ν(C=N) 1645, ν(N–N) 1018, $\nu(NO_3^-)$ 1453, 1307, 1032, $\Delta\nu$ 146, $\nu(H_2O)$ 3225. Λ_M (S cm^2 mol^{-1}), 23 (dmf solution).

2.4. Preparation of [Er(L)(H_2O)(NO_3)] (2)

Complex **2** was prepared in the form of yellow powder as described for **1**. Crystallization from dimethylsulfoxide solution gave crystal suitable for X-ray analyses. The yield is 79%. *Anal.* Calc. for $ErC_{23}H_{21}N_6O_6$ C, 42.85; H, 3.28; N, 13.03. Found: C, 42.82; H, 3.25; N, 13.01%. IR (cm^{-1}, Nujol mulls) ν(C=N) 1639, ν(N–N) 1018, $\nu(NO_3^-)$ 1450, 1303, 1032, $\Delta\nu$ 147, $\nu(H_2O)$ 3225 ; $\mu_{eff} = 9.72$ μ_B; $\Lambda_M = 72$ S cm^2 mol^{-1}.

2.5. Preparation of {[Pr(HL)(L)](H_2O)$_2$($(CH_3)_2SO$)} (3)

To a solution of H_2L (2 mmol) in absolute ethanol (20 ml) was added $Pr(NO_3)_3 \cdot 6H_2O$ (1 mmol) in 10 ml of absolute ethanol. The white suspension turns to yellow immediately. After 20 min under stirring a solution of LiOH (3 mmol) in 5 ml of absolute ethanol was added. The yellow precipitate disappears and the solution was refluxed for two hours. On cooling no precipitate was observed. A yellow solid was obtained after slow evaporation. Crystallization from dimethylsulfoxide solution gave crystal suitable for X-ray analyses. The yield is 70%. *Anal.* Calc. for $PrC_{48}H_{49}N_{10}O_7S$ C, 54.86; H, 4.70; N, 13.33; S, 3.05. Found: C, 54.83; H, 4.68; N, 13.29; S, 3.08%. IR (cm^{-1}, Nujol mulls) $\nu_{C=N}$ 1645; ν_{N-N} 1018 ; $\mu_{eff} = 3.20$ μ_B; $\Lambda_M = 34.3$ S cm^2 mol^{-1}.

2.6. Preparation of {[Sm(HL)(L)](H_2O)$_2$($(CH_3)_2SO$)} (4)

Complex **4** was prepared in the form of yellow powder as described for **3**. Crystallization from dimethylsulfoxide solution gave crystal suitable for X-ray analyses. The yield is 72%. *Anal.* Calc. for $SmC_{48}H_{49}N_{10}O_7S$ C, 54.37; H, 4.66; N, 13.21; S, 3.02. Found: C, 54.34; H, 4.63; N, 13.17; S, 3.04%. IR (cm^{-1}, Nujol mulls) $\nu_{C=N}$ 1637; ν_{N-N} 1018; $\mu_{eff} = 1.67$ μ_B; $\Lambda_M = 25.4$ S cm^2 mol^{-1} (see Table 1).

2.7. X-ray data collection and reduction

Yellow crystals of [Y(L)(H_2O)(NO_3)], [Er(L)(H_2O)-(NO_3)], {[Pr(HL)(L)](H_2O)$_2$($(CH_3)_2SO$)} and {[Sm(HL)-(L)](H_2O)$_2$($(CH_3)_2SO$)} obtained by slow evaporation of dimethylsulfoxide were mounted on glass fibers and used for data collection. Data were collected on CAD 4 diffractometer using Mo Kα radiation ($\lambda = 0.71073$ Å).

Table 1
Crystal data and structure refinement for complexes (**1**), (**2**), (**3**), (**4**)

Empirical formula	$C_{23}H_{21}N_6O_6Y$	$C_{23}H_{21}N_6O_6Er$	$C_{48}H_{49}N_{10}O_7SPr$	$C_{48}H_{49}N_{10}O_7SSm$
Color; habit	yellow; prism	yellow; prism	yellow; prism	yellow; prism
Formula weight	566.4	644.7	1051.0	1060.4
Temperature (K)	293(2)	293(2)	293(2)	293(2)
Crystal size (mm)	$0.80 \times 0.60 \times 0.35$	$0.3 \times 0.20 \times 0.30$	$0.30 \times 0.30 \times 0.30$	$0.35 \times 0.35 \times 0.35$
Crystal system	monoclinic	monoclinic	orthorhombic	orthorhombic
Space group	$P2_1/n$	$P2_1/n$	$Pn2_1a$	$Pn2_1a$
Unit cell dimensions				
a (Å)	8.174(3)	8.1428(0)	13.149(2)	13.125(4)
b (Å)	10.099(4)	10.0871(0)	15.819(3)	15.930(5)
c (Å)	29.423(6)	29.3186(0)	23.487(6)	23.347(8)
β (°)	90.23(2)°	90.325(0)		
V (Å^3)	2428.73(9)	2408.11(0)	4885.4(2)	4881(3)
Z	4	4	4	4
Density (Mg m^{-3})	1.55	1.78	1.430	1.443
Absorption coefficient (mm^{-1})	2.452	3.536	1.100	1.306
θ range for data collected (°)	1.38–21.98	2.1–25.5	1.55–26.97	1.55–21.97
Index ranges	$-8 \leqslant h \leqslant 8$, $0 \leqslant k \leqslant 10$, $0 \leqslant l \leqslant 30$	$0 \leqslant h \leqslant 9$, $0 \leqslant k \leqslant 12$, $-35 \leqslant l \leqslant 35$	$-1 \leqslant h \leqslant 16$, $0 \leqslant k \leqslant 20$, $0 \leqslant l \leqslant 29$	$-13 \leqslant h \leqslant 0$, $-16 \leqslant k \leqslant 0$, $-1 \leqslant l \leqslant 24$
Absorption correction	Ψ-scan	Ψ-scan	Ψ-scan	Ψ-scan
Reflections collected	3039	4799	5983	3298
Independent reflections (R_{int})	2973(0.0171)	4465(0.165)	5505(0.040)	3110(0.042)
Data/restraints/parameters	2973/0/326	4465/0/146	5505/1/605	3110/1/365
Final R indices ($I > 2\sigma(I)$)	$R_1 = 0.064$, $wR_2 = 0.044$	$R_1 = 0.056$, $wR_2 = 0.132$	$R_1 = 0.0626$, $wR_2 = 0.1405$	$R_1 = 0.0671$, $wR_2 = 0.1613$
R Indices (all data)	$R_1 = 0.127$, $wR_2 = 0.116$	$R_1 = 0.078$, $wR_2 = 0.148$	$R_1 = 0.1269$, $wR_2 = 0.1694$	$R_1 = 0.1104$, $wR_2 = 0.1861$
Goodness-of-fit	1.031	1.054	1.108	1.125
Largest difference peak/hole (e Å^{-3})	0.565/−0.257	2.790/−3.133	1.403/−1.704	1.802/−1.165

The structure were solved by direct methods which revealed the positions of all non-hydrogen atoms, and refined on F^2 by full-matrix least-square procedure using anisotropic displacement parameters. Molecular graphics are from PLATON or ORTEP.

3. Results and discussion

3.1. Formation of the Schiff base

H_2L (2,6-diacetylpyridine-bis-(benzoylhydrazone)) was prepared according to the Scheme 1. N_3O_2 Schiff base was obtained from the condensation of 2,6-diacetylpyridine and two equivalent of benzoylhydrazide. The resulting compound is insoluble in ethanol and methanol. The ^{1}H and ^{13}C NMR data for the Schiff base, the analytical and spectral data are consistent with the proposed structure. Infrared spectra of the compound show the appearance of some bands in the region 1700–1600 cm^{-1} characteristic of the amide (N–C=O) and the imine (C=N) bonds in the Schiff base and a band at 1018 cm^{-1} characteristic of N–N vibrations. The ^{1}H NMR data show the appearance of **H**O–C(=N)–Ph hydrogen resonance at 10.9 ppm which suggested the transformation of the amide groups in iminol groups in solution (Scheme 1). This is confirmed by the infrared data. No band characteristic of HO bending vibrations was observed in the solid state.

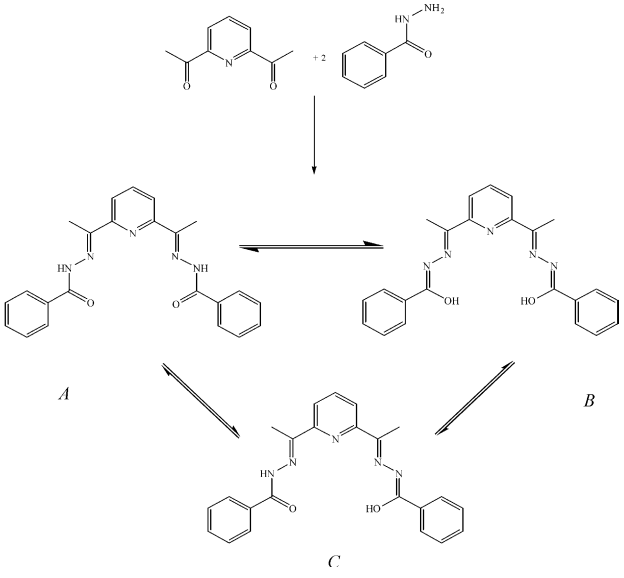

Scheme 1. The three isomeric forms in solution of the ligand H_2L.

3.2. Characterization and spectroscopic studies

The mononuclear Ln(III) complexes were prepared by mixing equimolecular amount of penta or hexahydrated lanthanide nitrate salts and 2,6-diacetylpyridine-bis-(benzoylhydrazone) (H_2L) in absolute ethanol at reflux. H_2L results from the 1/1 Schiff base condensation of 2,6-diacetylpyridine with benzoylhydrazide in ethanol. The immediate color change of the H_2L solution upon addition of the $Ln(NO_3)_3$ and LiOH indicated instant occurrence of the formation of the complex. For Er^{3+} and Y^{3+} most of the compound precipitated out during refluxing and stirring. Unlike the lanthanide complexes of Sm^{3+} and Pr^{3+} had considerable solubility in hot ethanol. The yields are quite high for the lanthanide complexes (70–85%). The elemental analyses of the complexes were consistent with the composition of $[Ln(L)(H_2O)(NO_3)]$ for Y and Er and $\{[Ln(L)(HL)](H_2O)_2((CH_3)_2SO)\}$ for Pr and Sm where HL denotes a monodeprotonated ligand and L a dideprotonated ligand molecules. All the complexes are characterized by elemental analysis, infrared study, molar conductance, magnetic measurements and X-ray crystallography.

All complexes show a strong IR band in the region 1650–1630 cm^{-1} assigned to the ν(C=N) vibration. In the spectra of **1** and **2** the bands at ca. 3225 and 820 cm^{-1} are characteristic of co-ordinated water molecules [11]. In the spectra of **3** and **4** the broad band of medium intensity occurring in the range 3450–3380 cm^{-1} is due to the stretching vibration of the HO of the lattice water molecules. All the spectra show band at 1580 cm^{-1} as expected for the highest-energy pyridine ring vibration. The weak band of moderate intensity at 1018 cm^{-1} is due to the N–N vibrations [12]. Comparison to the literature values of IR data gives information regarding to the possible bonding modes of the nitrate anion. The bands in the range 1420–1460 cm^{-1} (ν5), at ca. 1305 cm^{-1} (ν1) and at ca. 1032 cm^{-1} (ν2) clearly identify the nitrates as co-coordinated species in the complexes **1** and **2** [13]. The molar electrical conductivity was measured in dimethylformamide for freshly prepared solution and after standing for two weeks. The values are quite constant for all the complexes. No replacement of a co-coordinated site by dmf molecules was observed. The Λ_M values of the complexes **3** is higher than the expected value for a 2:1 electrolyte and those of complexes **1**, **2** and **4** are consistent with the expected value for a 1:1 electrolyte [14]. The μ_{eff} of the lanthanide complexes show that these are paramagnetic except for the complex **1** which is diamagnetic in nature. This paramagnetic behaviour is consistent with the presence of unpaired 4f electrons. The observed μ_{eff} values are close proximity of the values for the free metal ions reported by Van Vleck and Frank [15]. These observations suggest that the 4f electrons of the lanthanide(III) do not take part in bond formation in these species.

3.3. Crystal structures of $[Y(L)(H_2O)(NO_3)]$ and $[Er(L)(H_2O)(NO_3)]$

In the reaction of 2,6-diacetylpyridine-bis-(phenylhydrazone) with yttrium(III) or erbium(III) nitrate, the two iminol protons are exchanged. The coordination of the hydrazone to lanthanide(III) results in the formation of five membered (two LnOCNN and two LnNCCN) chelating rings in which the lanthanide ion is eight coordinated. The complexes **1** and **2** crystallized in monoclinic space group $P2_1/n$. Each unit cell contains four molecules. ORTEP drawing with the atoms numbering scheme for $[Y(L)(HL)(H_2O)(NO_3)]$ and $\{[Er(L)(HL)(H_2O)(NO_3)]$ are shown in Figs. 1 and 2. Relevant interatomic distances and angles are given in Table 2. The coordination polyhedron is described by one nitrate group coordinated as bidentate, five donors atoms (two iminolic oxygen and three nitrogen) of the ligand and one coordinated water molecule. The five angles involving adjacent equatorial atoms namely O1–Y–O2, O2–Y–N2, O1–Y–N4, N1–Y–N2 and N1–Y–N4 are not differ notably, being 100.94(14)°, 165.59(15)°,

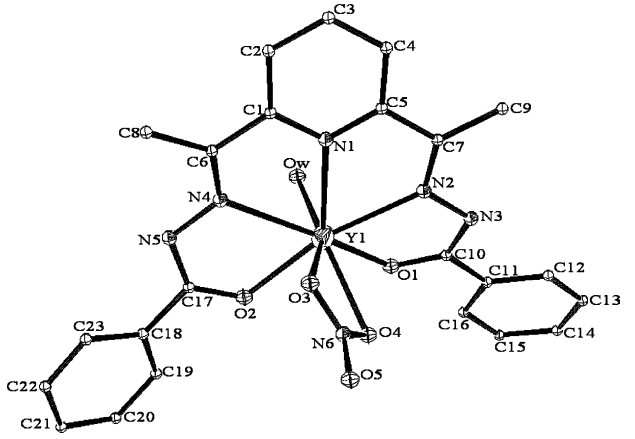

Fig. 1. ORTEP drawing of $[Y(L)(NO_3)(H_2O)]$ with atom numbering scheme.

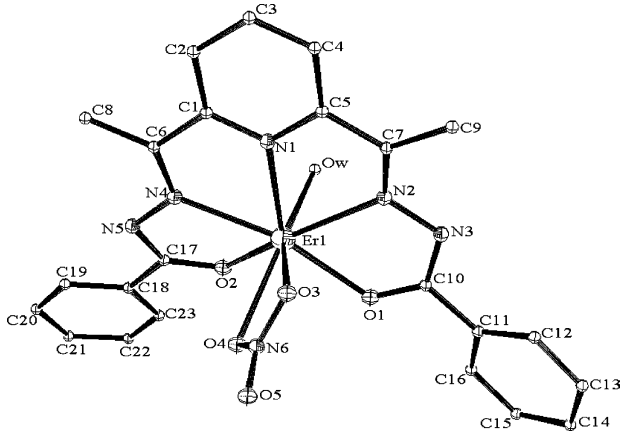

Fig. 2. ORTEP drawing of $[Er(L)(NO_3)(H_2O)]$ with atom numbering scheme.

Table 2
Selected bond distances (Å) and angles (°) for complexes **1** and **2**

Bond	Ln = Y	Ln = Er	Angle	Ln = Y	Ln = Er
O1–C10	1.286(7)	1.282(12)	O2–Ln–N2	165.59(15)	155.6(2)
O2–C17	1.290(7)	1.296(11)	O3–Ln–O4	51.80(14)	52.0(2)
N2–C7	1.297(7)	1.286(12)	O2–Ln–N4	65.58(15)	66.1(2)
N3–C10	1.321(7)	1.332(13)	N2–Ln–N4	128.83(16)	129.5(3)
N4–C6	1.297(8)	1.283(12)	O1–Ln–N1	126.61(15)	130.9(3)
N5–C17	1.335(8)	1.327(12)	O2–Ln–N1	130.11(15)	127.2(3)
O3–N6	1.278(6)	1.270(10)			
O4–N6	1.258(6)	1.258(10)			
O5–N6	1.229(6)	1.228(10)			

156.69(15)°, 64.28(16)° and 64.60(15)°, respectively, (O1–Er–O2, O2–Er–N2, O1–Er–N4, N4–Er–N3 and N2–Er–N3 are 99.5(2)°, 155.6(2)°, 164.5(3)°, 65.0(3)° and 64.5(3)°, respectively). Four types of Ln-ligand interatomic distances have been found: Y–O (hydrazonic) 2.265(4) and 2.268(4) Å, (Er–O (hydrazonic) 2.252(7) and 2.267(7) Å), Y–N (hydrazonic) 2.429(5) and 2.468(5) Å (Er–N (hydrazonic) 2.418(8) and 2.450(8) Å), Y–O (nitrate) 2.449(4) and 2.463(4) Å (Er–O (nitrate) 2.447(7) and 2.449(8) Å) and Y–O (H_2O) 2.330(4) Å (Er–O (H_2O) 2.318(7) Å). As found in the infrared study the nitrate acts as bidentate in both complexes [3].

According to the infrared and NMR data of the 2,6-diacetylpyridine-bis-(benzoylhydrazone) the imine group (O=C–NH) is transformed in iminol group in solution (**HO**–C(=N)). In solution the ligand acts with the lanthanide ion in his iminol form. In both complexes the C10–N3 and C17–N5 distances are consistent with a double bond while the C10–O1 and C17–O2 distances are consistent with a single bond.

3.4. Crystal structures of {[Pr(HL)(L)](H₂O)₂((CH₃)₂SO)} and {[Sm(HL)(L)](H₂O)₂((CH₃)₂SO)}

In both complexes, the lanthanide(III) ion has a coordination number of ten binding the two imines nitrogen, the pyridine nitrogen and the two anionic oxygen of one ligand molecule and the two imines nitrogen, the pyridine nitrogen, the one anionic oxygen and the one neutral oxygen of the other ligand molecule.

The complexes **3** and **4** crystallized in orthorhombic space group $Pn2_1a$. Each unit cell contains four molecules. ORTEP drawing with the atoms numbering scheme for {[Pr(L)(HL)](H_2O)$_2$((CH_3)$_2$SO)} and {[Sm(L)(HL)](H_2O)$_2$((CH_3)$_2$SO)} are shown in Figs. 2 and 3. Relevant interatomic distances and angles are given in Table 3. The lanthanides ions are ten-coordination in the complexes. In addition to the three anionic oxygen, Ln(III) complete their coordination spheres with six neutral nitrogen from the ligand molecules and one neutral oxygen. The dmso and the water molecules was not linked to the metal ion. The coordination of the hydrazone to Ln results in the formation of five membered (two LnOCNN and two LnNCCN) chelating rings. In the two complexes the Ln–N(pyridine) bonds are the largest metal-ligand distances (Pr–N1 is 2.715(10) and Pr–N6 is 2.733(11) Å) while Sm–N1 and Sm–N6 are 2.697(16) and 2.707(16) Å, respectively. The Ln–N bonds involving the hydrazone's nitrogen are essentially equal (2.595(10), 2.661(10), 2.667(10) and 2.673(12) Å for {[Pr(L)(HL)](H_2O)$_2$((CH_3)$_2$SO)}; 2.562(16), 2.629(15), 2.645(19) and 2.650(2) Å for {[Sm(L)(HL)](H_2O)$_2$((CH_3)$_2$SO)}. The Ln–O bonds involving the hydrazonic oxygen are in the range (2.376–2.680 Å) and are comparable in the two complexes.

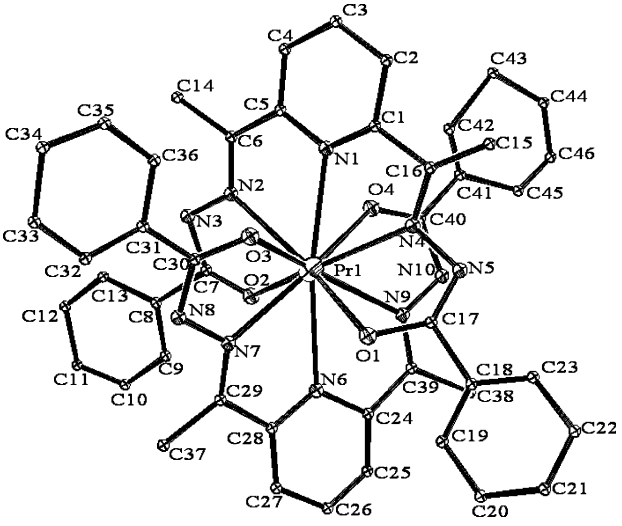

Fig. 3. ORTEP drawing of [Pr(L)(HL)] with atom numbering scheme, H_2O and (CH_3)$_2$SO) are omitted for clarity.

In praseodymium complex one ligand molecule have two ionic oxygen while the other one have one neutral oxygen and one ionic oxygen. The C7–O2, C17–O1 and C30–O3 distances are consistent with a single bond while the C7–N3, C17–N5 and C30–N8 distances are consistent with a double. The remaining bond distances of the hydrazone moiety, as well as C40–N10 and C40–O4 are consistent with a single and a double bond, respectively. In the case of the samarium complex the C17–O1 distance appears to be consistent with a double bond; both ligand molecules present one neutral oxygen and one ionic oxygen.

Table 3
Selected bond distances (Å) and angles (°) for complexes **3** and **4**

Bond	Ln = Pr	Ln = Sm	Angle	Ln = Pr	Ln = Sm
Ln–O1	2.503(9)	2.477(15)	O2–Ln–O1	130.8(3)	129.3(5)
Ln–O2	2.462(10)	2.402(14)	O1–Ln–N2	159.5(3)	159.1(5)
Ln–O3	2.411(11)	2.376(16)	O2–Ln–N4	156.2(4)	155.4(6)
Ln–O4	2.680(12)	2.668(17)	N2–Ln–N4	119.1(3)	121.2(5)
N3–C7	1.319(17)	1.30(3)	O3–Ln–N9	160.5(4)	159.3(6)
N5–C17	1.317(18)	1.32(3)	N7–Ln–N9	118.7(4)	119.9(6)
N8–C30	1.331(18)	1.34(3)	O3–Ln–O4	130.5(3)	130.2(5)
N10–C40	1.39(2)	1.34(3)	N7–Ln–O4	156.8(5)	155.4(7)
O2–C7	1.315(16)	1.29(2)	O2–Ln–N1	117.2(3)	117.7(5)
O1–C17	1.285(16)	1.23(3)	O1–Ln–N1	112.0(3)	113.0(5)
O3–C30	1.293(17)	1.30(3)			
O4–C40	1.234(19)	1.21(3)			

The bond angles (Table 3) of the two ligands, which involve the Ln(III) ions, are similar in both complexes. In particular the angles involving donor atoms (O, N) within the same ligand are very close proximity. The greatest difference occurs in comparing analogous angles between the two ligands; for example in the {[Pr(L)(HL)](H$_2$O)$_2$((CH$_3$)$_2$SO)} complex, O2–Pr–N2 is 60.2(3)°, but O3–Pr–N7 is 61.3(4)°. The difference is even smaller in {[Sm(L)(HL)](H$_2$O)$_2$((CH$_3$)$_2$SO)}, O1–Sm–N4 is 58.8(5)°, but O4–Sm–N9 is 57.7(6)°). As would be expected due to the comparable sizes of praseodymium(III) and samarium(III) the bond angles involving the metals ions in both complexes are not notably different (see Fig. 4).

Two possible coordination polyhedra with ten vertexes are known. The coordination polyhedron around each lanthanide atom in both complexes is better described as a distorted bicapped square antiprism in which N1 and N6 are the caps as shown in Fig. 5. In fact, considering those to be a bicapped dodahedron, severe distortions have to be take in account.

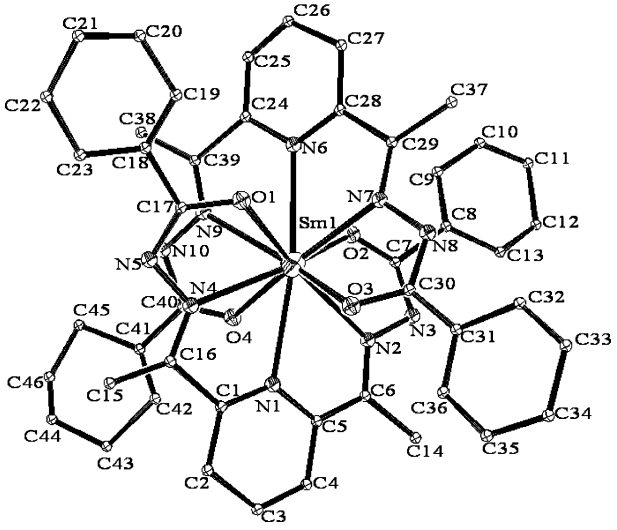

Fig. 4. ORTEP drawing of [Sm(L)(HL)] with atom numbering scheme, H$_2$O and (CH$_3$)$_2$SO) are omitted for clarity.

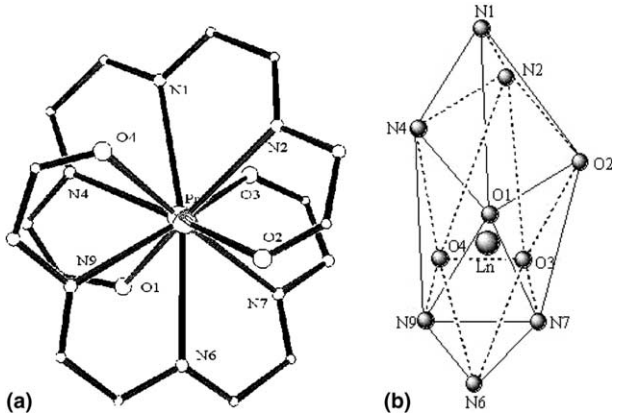

Fig. 5. (a) Coordination polyhedron around the lanthanide ion (e.g., Pr); (b) coordination polyhedron around the lanthanide ion described as a distorted bicapped square antiprism.

4. Supplementary material

Crystallographic data for the structures reported in this paper have been deposited with the Cambridge Crystallographic Data Center as supplementary publication no. CCDC 206711 for [Y(L)(H$_2$O)(NO$_3$)], CCDC-224955 for [Er(L)(H$_2$O)(NO$_3$)], CCDC-208792 for {[Pr(L)(HL)](H$_2$O)$_2$((CH$_3$)$_2$SO)} and CCDC-208834 for [Sm(L)(HL)](H$_2$O)$_2$((CH$_3$)$_2$SO)}. Copies of available material can be obtained, free of charge, on application to the Director, CCDC, 12 Union Road, Cambridge CB2 1ZE, UK (fax: +44-1223-336033 or e-mail: deposit@ccdc.cam.ac.uk or http://www.cam.ac.uk).

Acknowledgements

The authors thank Professor Oumar Sarr and the Third World Academy of Science for financial support (Grant Research Number 97-034 RG/CHE/AF/AC).

References

[1] D.W. Knoeppel, J. Liu, E.A. Meyers, S.G. Shore, Inorg. Chem. 37 (1998) 4828.

[2] V. Alexander, Chem. Rev. 95 (1995) 273.
[3] P. Caraven, J.J. Ellison, T.J. McMurry, R.B. Lauffer, Chem. Rev. 99 (1999) 2293.
[4] D. Parkers, J.A. Williams, J. Chem. Soc., Dalton Trans. (1996) 3613.
[5] L.M. Vallarino, J. Less-Common Met. 149 (1989) 121.
[6] M. Diop, F.B. Tamboura, M. Gaye, A.S. Sall, A.H. Barry, T. Jouini, Inorg. Chem. Commun. 6 (2003) 1004.
[7] T. Moeller, D.E. Martin, L.C. Thompson, R. Ferrus, G.R. Feistel, W.J. Pandal, Chem. Rev. 65 (1965) 1.
[8] T. Moeller, in: J.C. Bailar, H.J. Emeleus., R.S. Nyholm, A.F. Trotman-Dickenson (Eds.), Comprehensive Inorganic Chemistry, vol. 4, Pergamon, Oxford, 1973, p. 1.
[9] O. Diouf, D.G. Sall, M. Gaye, A.S. Sall, U. Casellato, R. Graziani, Z. Kristallogr. 214 (1999) 493.
[10] O. Diouf, M. Gaye, A.S. Sall, F.B. Tamboura, A.H. Barry, T. Jouini, Z. Kristallogr. 216 (2001) 421.
[11] K. Nakamoto, Infrared and Raman Spectra of Inorganic and Coordination Compounds, 3rd ed., Wiley–Interscience, New York, 1978.
[12] P.A. Kumar, Synth. React. Inorg. Met. Org. Chem. 28 (5) (1998) 699.
[13] V.A.J. Aruna, V.J. Alexander, Chem. Soc., Dalton Trans. (1996) 1867.
[14] W.J. Geary, Coord. Chem. Rev. 7 (1971) 81.
[15] J.H. Van Vleck, A. Frank, Phys. Rev. 34 (1929) 1494, 1625.

Available online at www.sciencedirect.com
SCIENCE DIRECT®
Polyhedron 23 (2004) 1199–1206
POLYHEDRON
www.elsevier.com/locate/poly

Laser ablation synthesis of new phosphorus and phosphorus-sulfur clusters and their TOF mass spectrometric identification

Ondrej Šedo [a], Zbyněk Voráč [b], Milan Alberti [b,*], Josef Havel [a]

[a] Department of Analytical Chemistry, Faculty of Science, Masaryk University, Kotlářská 2, 611 37 Brno, Czech Republic
[b] Department of Inorganic Chemistry, Faculty of Science, Masaryk University, Kotlářská 2, 611 37 Brno, Czech Republic

Received 11 December 2003; accepted 29 January 2004

Abstract

Laser ablation of elemental phosphorus, sulfur, their mixtures or some phosphorus sulfides in connection with Time-Of-Flight (TOF) mass spectrometry was studied. Laser ablation of pure red phosphorus leads to formation of singly charged P_n^+ ($n = 1$–189) and P_n^- ($n = 1$–225) clusters. Much higher n values than those known in the literature were proved. Similarly, laser ablation of elemental sulfur produces S_m^+ ($m = 1$–11) and S_m^- ($m = 1$–15) species. Via laser ablation of P_4S_3 and P_4S_{10} compounds, the formation of several clusters with different P:S ratio was observed. Their stoichiometry was estimated from the mass spectra and natural abundance of sulfur isotopes. Similarly to laser ablation of red phosphorus, the amounts of P_nS_m clusters generated from P_4S_3 and P_4S_{10} with an odd number of phosphorus atoms were much higher than those with an even number. Generation of various mixed P–S clusters was also reached via direct laser ablation of a mixture of the elements. Higher yield of the mixed clusters was obtained when the mixture was first homogenized using ultrasound. Partially, some reactions were also initiated by ultrasound itself.

Totally, at least 68 new P_nS_m clusters were formed and detected. The laser ablation synthesis either from phosphorus sulfides or from elemental mixtures represents a new possibility of forming and studying mixed clusters of these elements.
© 2004 Elsevier Ltd. All rights reserved.

Keywords: Phosphorus; Sulfur; Clusters; Phosphorus sulfides; Laser ablation synthesis; TOF mass spectrometry

1. Introduction

Phosphorus and sulfur exist in several allotropic modifications. Atoms of these elements can be connected in many ways, usually to polymeric non-linear chains or rings [1]. Concerning the mixed 15/16 group elements clusters, some of them are known for a long time. Alchemists were attracted by bright golden yellow color of realgar (As_4S_4) and orpiment (As_2S_3) mixtures with cheaper metals such as lead to form "gold" [2]. In modern chemistry wide scale of phosphorus sulfides has been synthesized and characterized. From the literature compounds P_4S_m ($m = 2$–7, 9, 10) [1,3] are known, usually synthesized by heating elements at the temperature higher than the melting point of sulfur, or adding sulfur to P_4S_3 or P_4S_7. These phosphorus sulfides, mostly P_4S_{10} and P_4S_3, have wide range of technological applications in the organic synthesis, respectively, for "strike anywhere" matches manufacturing [1] and therefore studying their properties is a scope of several papers. Infrared and Raman spectra of P_4S_3, P_4S_7, P_4S_{10} were studied in [4,5]. The intramolecular bonding in crystalline tetraphosphorus trisulfide was studied by Raman spectroscopy in [6]. ^{31}P NMR has been successfully applied in studies of P_4S_3 [7,8], P_4S_9 and P_4S_{10} [9]. Tattershall et al. [10–12] by NMR provided the evidence for phosphorus-rich phosphorus sulfide cage compounds derivatived from P_4S_3.

Laser ablation of red phosphorus leads to the formation of several homo-atomic poly-anions and cations with single charge [13,14]. Phosphorus clusters P_n^- (up to $n = 40$) and their cations P_n^+ (up to $n = 91$) were

* Corresponding author. Tel.: +420-441-129-344; fax: +420-541-211-214.
E-mail address: alberti@chemi.muni.cz (M. Alberti).

0277-5387/$ - see front matter © 2004 Elsevier Ltd. All rights reserved.
doi:10.1016/j.poly.2004.01.018

synthesized in the gas phase by laser ablation of crystalline red phosphorus. The neutral P_n clusters are found to be even-numbered with the local abundance maxima at $n = 8$, 10, 14, and 40. On the contrary, the cationic clusters are preferentially odd-numbered with P_{21}^+ being the most abundant ion.

It is suggested that dodecahedral fullerene-like P_{20}, stabilized with an additional phosphorus ion in the laser plasma can be significantly stable [13]. A theoretical study of the isomers of neutral, cationic and anionic phosphorus clusters P_5, P_7, P_9, P_8 and P_9 was performed using the B3LYP, DFT method to predict the most stable isomers of these compounds present in the spectra [15–17].

Time-Of-Flight (TOF) mass spectrometric observations of gaseous phosphorus sulfides and oxysulfides were made in [18]. Bews and Glidewell [19] studied structures and energies of mass spectral fragments for P_4S_3 and its molecular ion $P_4S_3^+$ and for further spectral fragment pairs. Electronic structures of P_4S_n ($n = 5$, 6) were investigated using ab initio methods [20]. Electronic structures of phosphorus sulfide P_4S_{10} and P_4S_7 and phosphorus oxide P_4O_{10} are discussed in [21].

Recently, we have shown a new approach to the synthesis using laser ablation of a mixture of the elements. New tellurium–sulfide clusters were formed by a laser while simultaneous chemical analysis of the products formed by TOF mass spectrometry was done [22]. The aim of this work is to continue development and evaluation of this new perspective synthetic approach of inorganic chemistry and to study systematically possibilities of laser ablation as a method for generation of new phosphorus–sulfide clusters and to characterize the fragments or mixed P_nS_m clusters formed by TOF mass spectrometry.

2. Experimental

2.1. Chemicals and reagents

Elemental red phosphorus was purchased from R. de Haën (Hannover, Germany) and elemental sulfur was from Spolek pro chemickou a hutní výrobu (Ústí n/L, Czech Republic). Benzene was from Lachema a.s. (Brno, Czech Republic). Bradykinin, α-cyano-4-hydroxycinnamic acid, guanosine-5′-monophosphate and harmane were all purchased from Sigma (Steinheim, Germany). P_4S_{10} was purchased from Sigma (Steinheim, Germany) and P_4S_3 from Fluka AG (Buchs, Switzerland). All these chemicals were of analytical grade purity, except bradykinin, the purity of which was 98%.

2.2. Apparatus

Mass spectra measurements were carried out on AXIMA CFR (Kratos Analytical, Manchester, United Kingdom) mass spectrometer equipped with a nitrogen laser wavelength of 337 nm from Laser Science Inc. (Franklin, MA, USA). For the calibration of positive mode, molecular ions $[M+H]^+$ of α-cyano-4-hydroxycinnamic acid and bradykinin were used. In case of negative mode, $[M-H]^-$ ions of harmane and guanosine-5′-monophosphate were applied. Each mass spectrometric analysis was performed using at least 100 shots and the obtained data were accumulated. The ultrasound UC 006 DM1 bath was from Tesla (Rožnov pod Radhoštěm, Czech Republic).

2.3. Procedure of synthesis

Synthetic procedure by means of laser ablation used in this work is similar to that one described earlier [22]. A suspension of either fine powdered sulfur or red phosphorus, eventually a suspension of sulfur-phosphorus powder mixture in benzene in volume of 1 μl (suspension containing 1 mg ml^{-1}) was pipetted on a sample plate and dried at room temperature in an air stream. Synthesis was then initiated by laser pulses and mass spectrometric analyses of the products formed were carried out with pulsed extraction in negative and positive modes, either in linear or reflectron arrangement.

3. Results and discussion

The first part of the paper focuses on the mass spectra obtained using LDI–TOF MS with the aim to follow similarities or differences between modes and laser energies. Even if the formation of sulfur species [14] and phosphorus clusters [13,14] is described in the literature, in the first stage we studied carefully the formation of pure elemental clusters under the laser energy conditions used later on in this work for synthesis of P_nS_m clusters.

3.1. Phosphorus P_n^+ and P_n^- clusters

Phosphorus clusters were synthesized by laser pulses from elemental red phosphorus and the products were analyzed by TOF mass spectrometry, both in positive and negative modes. Applying the laser power of 2.2 mW results in formation of charged phosphorus clusters up to P_{65}^+ and P_{57}^-. In agreement with the literature [13], we also observed that clusters containing an even number of phosphorus atoms are less abundant than odd ones. All these compounds are stable enough, as they can be detected also in the reflectron mode prolonging ion flight time. Exceeding the laser power of 2.6 mW results in the formation of higher cluster ions. Due to lower stability of these higher clusters the signals were not observed in the reflectron modes. An example of mass spectra concerning laser ablation of red phospho-

rus using high laser power is given in Fig. 1. It is evident that negatively charged clusters consisting of up to 225 atoms are produced with maximum abundance for P_{27}^- of the low mass region and P_{103}^- for the high mass region. In the literature [13] only clusters up to P_{91}^+ and P_{40}^- have been described. Almost no clusters with an even number of atoms are observed in the negative mode. In the mass spectra obtained in the positive mode (Fig. 2),

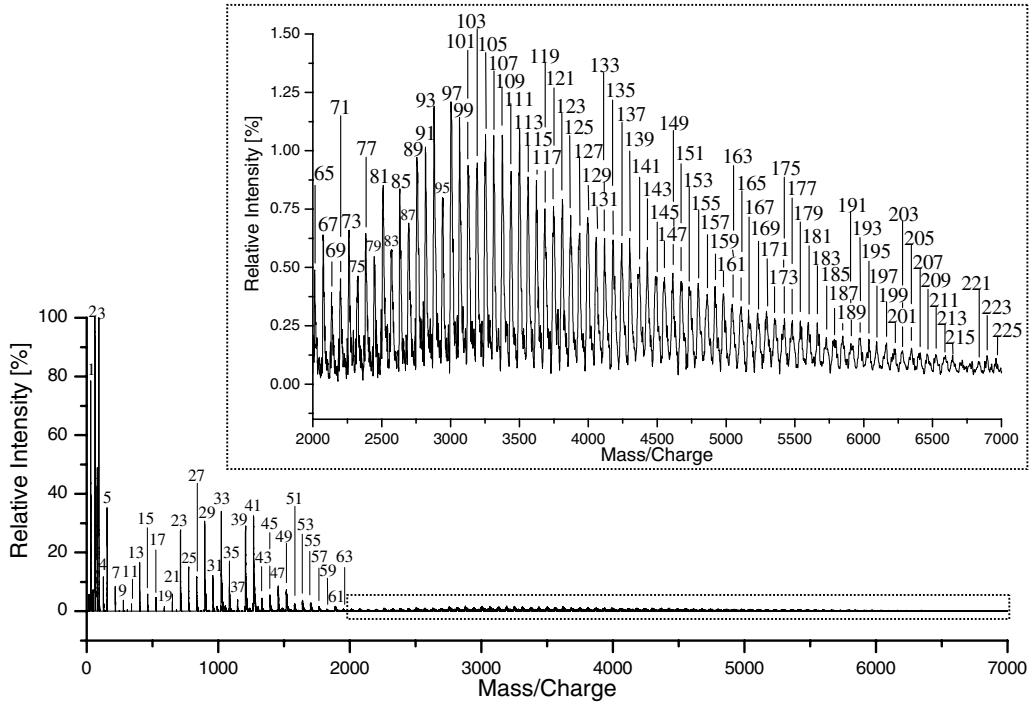

Fig. 1. Mass spectra of negatively charged phosphorus clusters produced during laser ablation of red phosphorus powder. Linear negative mode with pulsed extraction, laser power of 2.67 mW.

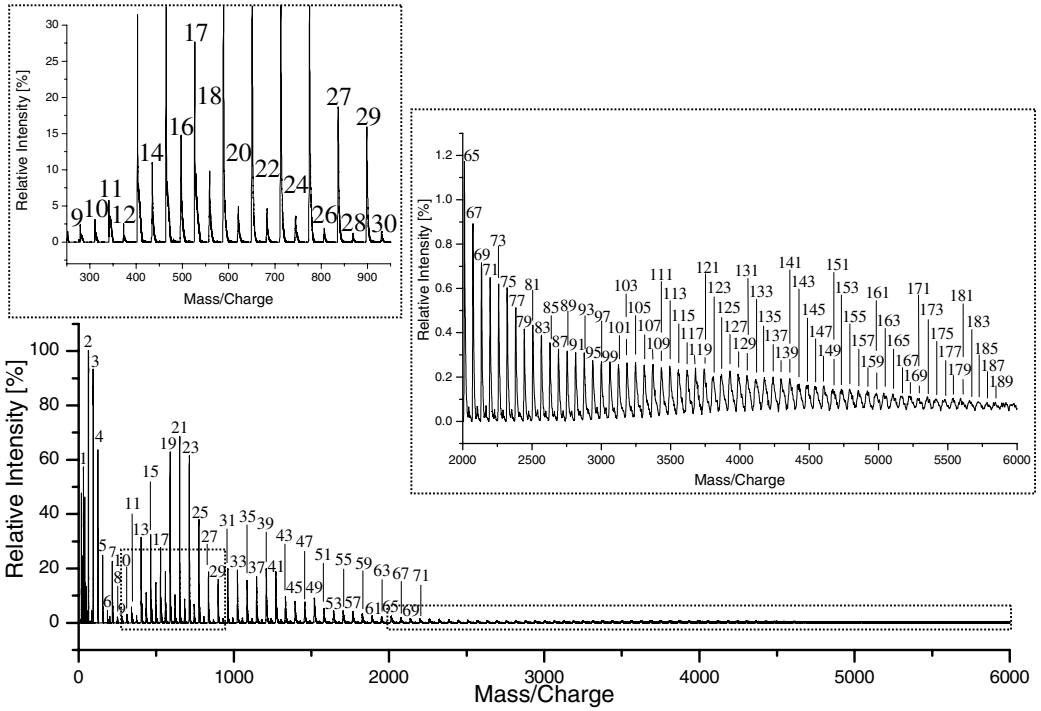

Fig. 2. Mass spectra of positively charged phosphorus clusters produced during laser ablation of red phosphorus powder. Linear positive mode with pulsed extraction, laser power of 2.67 mW.

the highest observed cluster P_n^+ contains 189 phosphorus atoms. Similarly to the negative mode, clusters with an odd number of atoms dominate in the spectra. On the other hand, several signals corresponding to an even number of phosphorus atoms present in the clusters with local intensity maximum around P_{18}^+ are formed.

Concerning the structure of P_n clusters there is some discussion in the literature. For example Chen et al. [16] did a theoretical study for the possible structure of the isomers of neutral, cationic and anionic phosphorus clusters P_5, P_7, P_9. In another study [15] about the structure of P_{20} cluster it is suggested that the smallest fullerene cage (dodecahedron with I_h symmetry) is the most stable. A positively charged P_{20}^+ cluster was observed here but not a negatively charged one. Although P_4 tetrahedron is the basic structural unit for several phosphorus compounds, LDI TOF mass spectra show dominant abundance of P_n clusters with an odd number of atoms. However, only clusters that are charged can be detected by the instrumentation and therefore, there is a probability that various uncharged, even more stable structures formed during the laser ablation process can be formed, but these neutral molecules are not observed in the mass spectra.

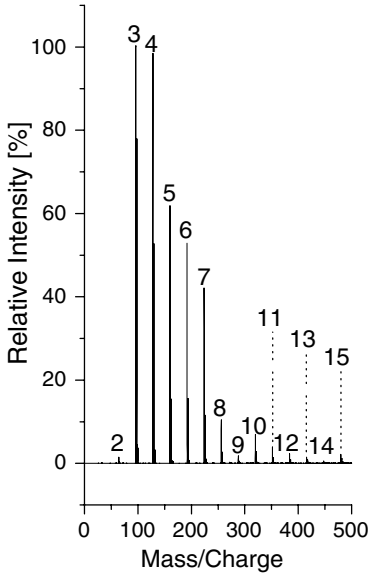

Fig. 3. Mass spectra of negatively charged sulfur species produced during laser ablation of fine sulfur powder. Linear negative mode with pulsed extraction, laser power of 3.17 mW.

3.2. Sulfur S_n^+ and S_n^- species

Sulfur species synthesized via laser ablation were observed both in the positive and the negative modes. An example of mass spectra concerning laser ablation of elemental sulfur is given in Fig. 3, where S_n^- anions up to S_{15}^- can be seen, while in the positive mode S_n^+ ($n = 1$–11) cations are observed. On the contrary to phosphorus, there is not any significant difference between intensities of the signals of even and odd species. The results concerning sulfur LDI–TOF MS are in agreement with the literature [14].

3.3. Synthesis of mixed P_nS_m clusters from a mixture of the elements

Red phosphorus is highly polymeric and insoluble in any solvent. Therefore, its suspension with sulfur in

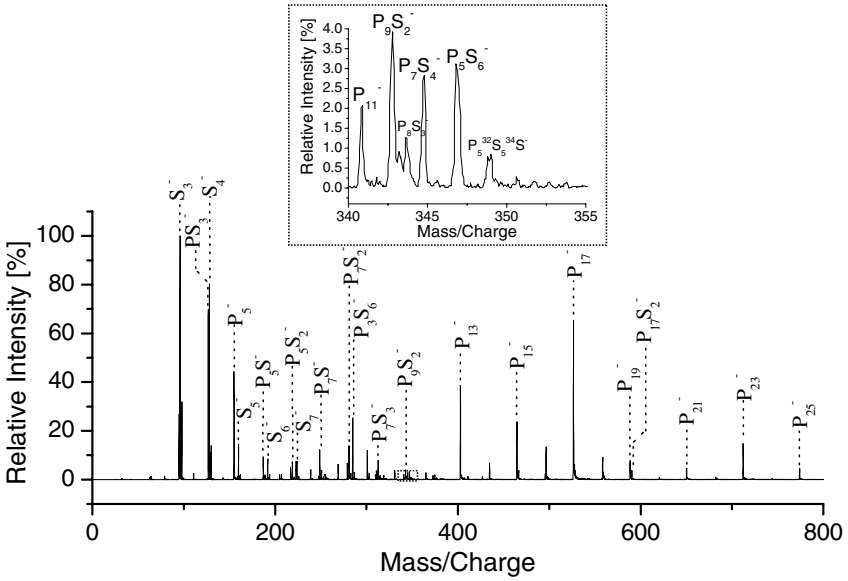

Fig. 4. Mass spectra obtained from laser ablation of a mixture of red phosphorus and sulfur (in molar ratio 1:1). Linear negative mode with pulsed extraction, laser power of 2.67 mW. Detailed view on section 340–355 Da with dominant component formulas added.

benzene was used for the synthesis. An excess of one of the components causes problems as the ablation of pure elements is too intensive and interferes with the observation of mixed clusters. When the suspension of elements (1:1, w/w) was mixed by stirring only with a glass stick, the generation of P_nS_m compounds was observed only from a few "sweet spots" and quite high laser power was needed for the mixed clusters generation. An example of mass spectra obtained from laser ablation of such P:S mixture is given in Fig. 4. A section of the spectrum containing P_{11}^-, $P_9S_2^-$, $P_8S_3^-$, $P_7S_4^-$ and $P_5S_6^-$ clusters is magnified. It follows from this figure that the resolution of the signals allows distinguishing isotopic patterns of the cluster signals, allowing the use of the isotopic pattern modeling for unambiguous identification of the species. The dominant peak in the magnified section corresponds to $P_9{}^{32}S_2^-$. However, $P_9S_2^-$ cluster ion is also induced in isotopic forms of $P_9{}^{32}S^{34}S^-$ and several other less abundant species. According to the natural distribution of sulfur isotopes, the peak of $P_9{}^{32}S^{34}S^-$ which cannot be under given conditions separated from the $P_7S_4^-$ signal, should possess $\approx 8\%$ of $P_9{}^{32}S_2^-$ intensity. Therefore, it is clear that the $P_7S_4^-$ cluster signal is also present in the mass spectra. All peaks from the mass spectra were analyzed in a similar way. The review of the compounds identified from mass spectra is given in Table 1.

For better homogenization of the mixture we used the ultrasound as well. An example of the mass spectrum obtained from the ultrasound homogenized mixture

Table 1
Review of $P_nS_m^-$ clusters stoichiometry identified in the mass spectra of a mixture of red phosphorus and sulfur (displayed in Fig. 4)

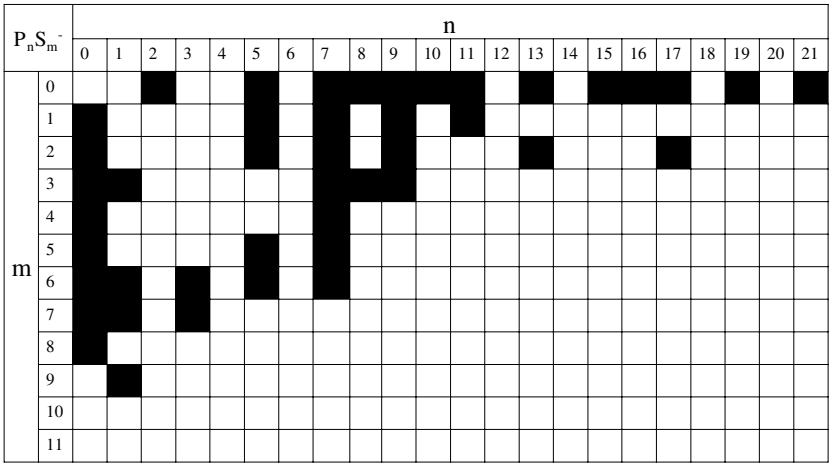

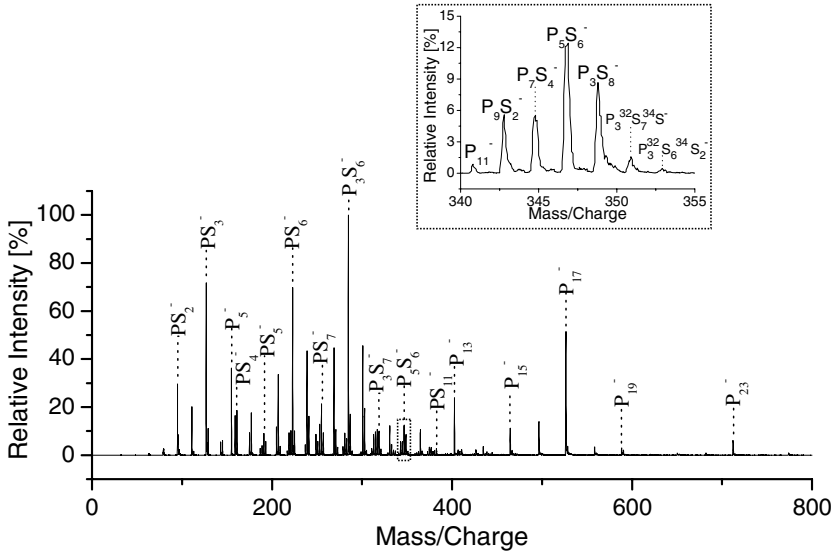

Fig. 5. Mass spectra obtained from laser ablation of the mixture of red phosphorus and sulfur (in the molar ratio 1:1) homogenized by the ultrasound. Linear negative mode with pulsed extraction, laser power of 1.67 mW. Detailed view on section 340–355 Da with dominant component formulas added.

(1:1, w/w) is given in Fig. 5. Complete review of mixed P_nS_m clusters identified from mass spectra is given in Table 2. It is possible to see that the ultrasound application leads to significant increase in the number of the mixed P_nS_m clusters. Mostly, the number of sulfur atoms in the clusters is higher compared to previous results obtained without the ultrasound homogenization. This effect can be related to reactions initiated by the ultrasound itself. After the homogenization we noticed that the suspension produced a sulfane-like odor. However, the increase of the number of species might be related to the improved contact between the two elements during the laser ablation process caused by enhanced homogeneity of the mixture. The ultrasound can initiate several reactions, radicals are formed and thus the reactivity of the components is increased.

3.4. Formation of clusters from P_4S_3 and P_4S_{10}

The compounds P_4S_3 and P_4S_{10} are well characterized as stable compounds built of phosphorus and sulfur atoms which are derived from different structural models. Ablating these sulfides we wanted to study their fragmentation and to compare structure of clusters formed with those generated from phosphorus and sulfur mixture ablation. Eventually, the idea was to use these two compounds as precursors for the synthesis of new P_nS_m clusters.

Table 2
Review of $P_nS_m^-$ clusters stoichiometry identified in the mass of the mixture of red phosphorus and sulfur homogenized with the ultrasound spectra (displayed in Fig. 5)

$P_nS_m^-$	n: 0	1	2	3	4	5	6	7	8	9	10	11	12	13	14	15	16	17	18	19	20	21
m: 0						■				■		■		■		■		■		■		■
1		■				■		■		■		■		■		■		■		■		
2		■		■		■		■		■		■		■		■		■		■		
3	■	■		■		■		■		■		■										
4		■		■		■		■		■												
5		■		■		■		■		■												
6		■		■		■		■														
7		■		■		■																
8		■		■		■																
9				■																		
10				■																		
11		■		■																		

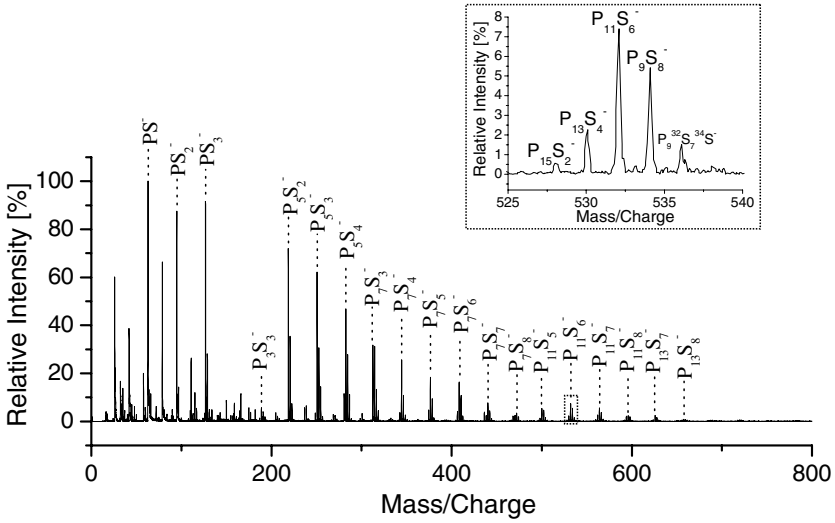

Fig. 6. Mass spectra of the mixed phosphorus–sulfur clusters produced during laser ablation of fine powder of pure P_4S_3. Linear negative mode with pulsed extraction, laser power of 3.33 mW. Detailed view on section 525–540 Da with dominant component formulas added.

Mass spectra obtained from ionization of P_4S_3 measured in the negative mode, which are shown in Fig. 6, are similar to those obtained from phosphorus and sulfur mixtures. There are only few clusters containing an odd number of phosphorus atoms. The number of sulfur atoms in observed clusters is rather high. Stoichiometries of the clusters identified from the mass spectra are summarized in Table 3. In the positive mode of the mass spectra measurement, formation of low molecular weight clusters was observed.

Although P_4S_{10} molecule contains more sulfur atoms, laser ablation from P_4S_{10} produces lower number of mixed clusters. An example of mass spectra concerning P_nS_m clusters obtained via laser ablation of P_4S_{10} is displayed in Fig. 6 and the stoichiometries of the clusters formed are reviewed in Table 4. Both studied phosphorus sulfides are not ionized in a form of a molecular ion. Mass spectra obtained in the positive mode are similar to those measured in the negative one, where only signals of $P_5S_8^+$, $P_5S_9^+$ and $P_5S_{10}^+$ were additionally observed.

From the comparison of the mass spectra between all mixed P_nS_m clusters spectra (Figs. 4–7) several similarities can be observed. Clusters with an odd number of phosphorus atoms are preferably formed in all cases, not depending on the original nature of the P–S system ionized (elemental mixture or phosphorus sulfides). That means that application of laser pulses results in cleavage of bonds in the phosphorus sulfides and the atoms or ions in the plasma plume are then reorganized always in a similar way forming similar mixed clusters.

Table 3
Review of $P_nS_m^-$ clusters stoichiometry identified in the mass spectra of P_4S_3 (displayed in Fig. 6)

$P_nS_m^-$	n																					
	0	1	2	3	4	5	6	7	8	9	10	11	12	13	14	15	16	17	18	19	20	21
m 0																						
1		■														■						
2								■		■				■		■						
3		■				■		■		■		■		■		■						
4						■		■		■				■								
5				■		■		■		■				■								
6				■		■		■		■				■								
7				■		■		■		■				■								
8						■		■		■		■										
9						■				■		■										
10						■				■												
11																						

Table 4
Review of $P_nS_m^-$ clusters stoichiometry identified in the mass spectra of P_4S_{10} (displayed in Fig. 7)

$P_nS_m^-$	n																					
	0	1	2	3	4	5	6	7	8	9	10	11	12	13	14	15	16	17	18	19	20	21
m 0																						
1		■										■										
2		■										■										
3		■										■										
4		■		■								■										
5				■																		
6		■		■																		
7		■		■																		
8		■		■																		
9		■		■																		
10		■		■																		
11				■		■																

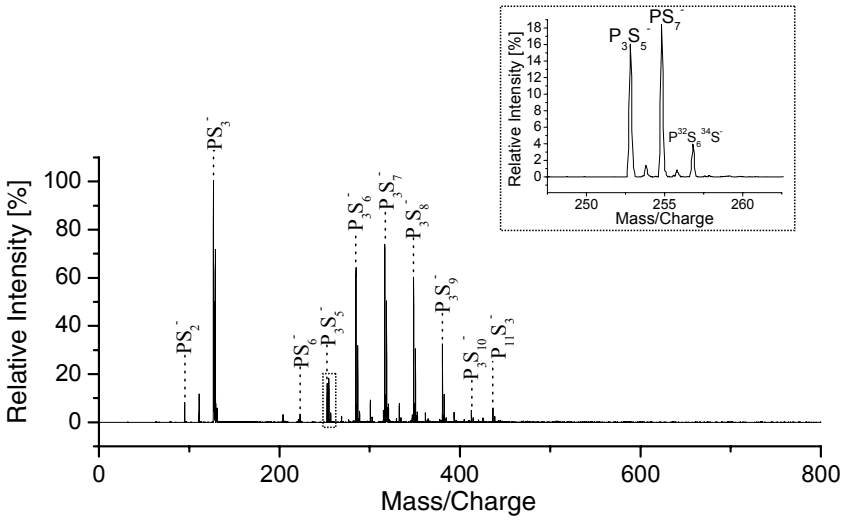

Fig. 7. Mass spectrum of mixed phosphorus–sulfur clusters produced during laser ablation of fine powder of pure P_4S_{10}. Linear negative mode with pulsed extraction, laser power of 2.67 mW. Detailed view on section 245–265 Da with dominant component formulas added.

4. Conclusions

Via laser ablation of red phosphorus, the formation of singly charged P_n^+ ($n = 1$–189) and P_n^- ($n = 1$–225) clusters was observed. Much higher values of cluster molecular weights than those reported earlier in the literature were found. Laser ablation of elemental sulfur produces S_m^+ ($m = 1$–11) and S_m^- ($m = 1$–15) species. Laser ablation of phosphorus and sulfur mixture leads to formation of a wide range of P_nS_m clusters with various P:S ratio. Clusters P_1S_m ($m = 1$–8, 11), P_3S_m ($m = 2$–11), P_5S_m ($m = 1$–8), P_7S_m ($m = 1$–6), P_9S_m ($m = 1$–6), $P_{11}S_m$ ($m = 1$–3), $P_{13}S_m$ ($m = 1$–2), $P_{15}S_m$ ($m = 1$–2), $P_{17}S_m$ ($m = 1$–2) and $P_{19}S_m$ ($m = 1$–2) were detected. The number of mixed P_nS_m clusters formed can be enhanced when the ultrasound is used for homogenization of the elemental mixture. Species similar to those ionized from the phosphorus–sulfur mixture can be generated by laser ablation of P_4S_3 and P_4S_{10} phosphorus sulfides. The stoichiometry of new clusters not described in the literature before was determined.

Acknowledgements

This work was supported by the Ministry of Education, Youth and Sports, Grant No. MSM 143 1000 11.

References

[1] N.N. Greenwood, A. Earnshaw (Eds.), Chemistry of the Elements, 2, Pergamon Press, Oxford, 1997, pp. 506–510.
[2] G.W. Drake, J.W. Kolis, Coord. Chem. Rev. 137 (1994) 131.
[3] H. Nowottnick, R. Blachnik, Z. Anorg, Allg. Chem. 625 (1999) 1966.
[4] J.O. Jensen, D. Zeroka, J. Mol. Struct. 487 (1999) 267.
[5] J.O. Jensen, D. Zeroka, A. Banerjee, J. Mol. Struct. (Theochem) 505 (2000) 31.
[6] G.R. Burns, J.R. Rollo, J. Phys. Chem. Solids 48 (1987) 347.
[7] E.R. Andrew, W.S. Hinshaw, M.G. Hutchins, A. Jasinski, Chem. Phys. Lett. 27 (1974) 96.
[8] E.R. Andrew, W.S. Hinshaw, A. Jasinski, Chem. Phys. Lett. 24 (1974) 399.
[9] E.R. Andrew, W. Vennart, G. Bonnard, R.M. Croiset, M. Demarcq, E. Mathieu, Chem. Phys. Lett. 43 (1976) 317.
[10] B.W. Tattershall, Kendall Nigel L., Polyhedron 13 (1994) 2629.
[11] B.W. Tattershall, Kendall Nigel L., Polyhedron 13 (1994) 1507.
[12] R. Blachnik, K. Hackmann, B.W. Tattershall, Polyhedron 15 (1996) 1415.
[13] A.V. Bulgakov, O.F. Bobrenok, V.I. Kosyakov, Chem. Phys. Lett. 320 (2000) 19.
[14] A.K. Hearley, B.F.G. Johnson, J.S. McIndoe, D.G. Tuck, Inorg. Chim. Acta 334 (2002) 105.
[15] B. Song, P. Cao, Phys. Lett. A 291 (2001) 343.
[16] M.D. Chen, R.B. Huang, L.S. Zheng, Q.E. Zhang, C.T. Au, Chem. Phys. Lett. 325 (2000) 22.
[17] M.D. Chen, R.B. Huang, L.S. Zheng, C.T. Au, J. Mol. Struct. (Theochem) 499 (2000) 195.
[18] D.W. Muenow, J.L. Margrave, J. Inorg. Nucl. Chem. 34 (1972) 89.
[19] J.R. Bews, C. Glidewell, J. Mol. Struct. (Theochem) 86 (1982) 217.
[20] P.G. Perkins, Inorg. Chim. Acta 73 (1983) 45.
[21] Y. Tahri, H. Chermette, G. Hollinger, J. Electron Spectrosc. Rel. Phen. 56 (1991) 51.
[22] M. Alberti, O. Šedo, J. Havel, Polyhedron 22 (2003) 2601.

Available online at www.sciencedirect.com
SCIENCE DIRECT®
Polyhedron 23 (2004) 1207–1216
POLYHEDRON
www.elsevier.com/locate/poly

Synthesis and crystal structures of diorganotin dicyanoethylene-1,2-dithiolate compounds and their derivatives with 4,4′-Bipy or Phen

Chunlin Ma [a,b,*], Yinfeng Han [a], Dacheng Li [a]

[a] Department of Chemistry, Liaocheng University, 34 Wenhua Road, Liaocheng 252059, PR China
[b] Taishan University, Taishan 271021, PR China

Received 23 November 2003; accepted 30 January 2004

Abstract

Six diorganotin(IV) compounds with dicyanoethylene-1,2-dithiolate (mnt) of the type $[R_2Sn(mnt)Cl_nL]\cdot Y$ (when $n = 0$, L = 0: R = CH_3, Y = 0, **1**; R = *n*-Bu, Y = 0, **2**; R = C_6H_6, Y = 0.5C_6H_6, **3**; R = CH_3, Y = 1.5(4,4′-Bipy), **4**; when $n = 1$, L = 0, R = CH_3, Y = 4,4′-Bipy, **5**; when $n = 0$, L = Phen, R = CH_3, Y = 0, **6**; 4,4′-Bipy = 4,4′-bipyridyl; Phen = 1,10-phenanthroline) are synthesized by the reaction of diorganotin dichloride and disodium maleonitriledithiolate (Na_2mnt) in the presence of 4,4′-Bipy or Phen. All the compounds **1**–**6** are characterized by elemental, IR, ^{1}H NMR spectroscopy and X-ray crystallography analyses. The X-ray data showed the geometries of all the tin atoms in compounds **1**–**4** are tetrahedral, and those in **5** and **6** are trigonal bipyramidal and distorted octahedral, respectively. Co-crystallization is found in crystals of compounds **3** and **4**. The co-crystallized solvents are benzene and 4,4′-Bipy, respectively. Compound **5** is a stannate with a five-coordinated tin(IV) atom. Compound **6** is a six-coordinated dimethyltin(IV) derivative from mixed ligands of mnt and Phen.
© 2004 Elsevier Ltd. All rights reserved.

Keywords: Diorganotin; Dicyanoethylene-1,2-dithiolate; 4,4′-Bipyridyl; 1,10-Phenanthroline; X-ray crystal structure; Co-crystallization

1. Introduction

The environmental and biological chemistry of organotin(IV) complexes have been subjects of interest for some time due to their wide use [1,2]. In particular, organotin(IV) 1,2-dithiolate complexes have been studied extensively due to the diversity of their commercial application and the richness of their structural chemistry [3–5]. A uniform view has been formed in previous reports that the tin center in neutral diorganotin(IV) dicyanoethylene-1,2-dithiolate compounds is clearly unsaturated and will coordinate, at least in the solid state, beyond four if steric effects allow. Consequently, it is possible to synthesize some diorganotin(IV) dicyanoethylene-1,2-dithiolate compounds of mixed ligands such as 4,4′-Bipy or Phen (4,4′-Bipy = 4,4′-bipyridyl; Phen = 1,10-phenanthroline).

Out of the above consideration, we designed a series of experiments of diorganotin dichloride and Na_2mnt in the presence of 4,4′-Bipy or Phen. To our surprise, we obtained six compounds of the type $[R_2Sn(mnt)Cl_nL]\cdot Y$ [when $n = 0$, L = 0: R = CH_3, Y = 0 (**1**); R = *n*-Bu, Y = 0 (**2**); R = C_6H_6, Y = 0.5C_6H_6 (**3**); R = CH_3, Y = 1.5(4,4′-Bipy) (**4**); when $n = 1$, L = 0: R = CH_3, Y = 4,4′-Bipy (**5**); when $n = 0$, L = Phen, R = CH_3, Y = 0 (**6**)]. Determinations by elemental, IR, ^{1}H NMR spectroscopy and X-ray crystallography analyses of all the compounds **1**–**6** are given, among which only IR and NMR data of compounds **1** and **2** have been reported previously [6,7]. The X-ray data show the geometries of all the tin atoms in compounds **1**–**4** are tetrahedral, and those in **5** and **6** are trigonal bipyramidal and distorted octahedral, respectively.

* Corresponding author. Tel.: +86-635-8238121; fax: +86-635-8238274.
E-mail address: macl@lctu.edu.cn (C. Ma).

0277-5387/$ - see front matter © 2004 Elsevier Ltd. All rights reserved.
doi:10.1016/j.poly.2004.01.019

2. Experimental

2.1. Materials and measurements

Dimethyltin dichloride, di-*n*-butyltin dichloride, diphenyltin dichloride, 4,4′-bipyridyl and 1,10-phenanthroline are commercially available and they were used without further purification. Na_2mnt was prepared by a standard method as reported in the literature [8]. The melting points were obtained with Kofler micro melting point apparatus and are uncorrected. Infrared-spectra were recorded on a Nicole-460 spectrophotometer using KBr discs and sodium chloride optics. ^1H NMR spectra were recorded on a FX-90Q Spectrometer. The chemical shifts are given in ppm relative to Me_4Si in $CDCl_3$ solvent. Elemental analyses were performed with a PE-2400II apparatus.

2.2. Synthesis of the compounds **1**–**6**

2.2.1. $[(CH_3)_2Sn(mnt)]$ (**1**)

The reaction was carried out under nitrogen atmosphere. Na_2mnt (0.372 g, 2 mmol) and dimethyltin dichloride (0.439 g, 2 mmol) were added to a solution of absolute ethanol (20 ml) in a Schlenk flask. The mixture was stirred for 12 h at 40 °C and then filtered. The filtrate was gradually removed by evaporation under vacuum until a solid product was obtained. The solid was then recrystallized from benzene. Buff crystal compound **1** was formed. Yield: 81%; m.p. >250 °C. *Anal*. Calc. for $C_6H_6N_2S_2Sn$: C, 24.94; H, 2.09; N, 9.70. Found: C, 24.88; H, 2.16; N, 9.58%. IR (KBr, cm^{-1}): ν(Sn–S), 288 and 351; ν_{as}(Sn–C), 555; ν_s(Sn–C), 450; ν(C–S), 1200 and 1234; ν(C≡N), 2208; ν(C=C), 1490. ^1H NMR ($CDCl_3$, ppm): 1.22 [s, $^2J(^{119}Sn–^1H)$, 74.7 Hz, Me].

2.2.2. $[(n\text{-}Bu)_2Sn(mnt)]$ (**2**)

Compound **2** was prepared in the same way as compound **1**, by adding di-*n*-butyltin dichloride (0.607 g, 2 mmol) instead of dimethyltin dichloride. Yield: 80%; m.p. 176–178 °C. *Anal*. Calc. for $C_{12}H_{18}N_2S_2Sn$: C, 38.63; H, 4.86; N, 7.51. Found: C, 38.51; H, 4.78; N, 7.53%. IR (KBr,cm^{-1}): ν(Sn–S), 290 and 355; ν_{as}(Sn–C), 575; ν_s(Sn–C), 457; ν(C–S), 1190 and 1220; ν(C≡N), 2217; ν(C=C), 1474. ^1H NMR ($CDCl_3$, ppm): 1.15 (t, 6H, CH_3), 1.56–1.78 (m, 12H, $CH_2CH_2CH_2$).

2.2.3. $[Ph_2Sn(mnt)]\cdot 0.5C_6H_6$ (**3**)

The compound **3** is prepared in the same way as that of compound **1**, by adding diphenyltin dichloride (0.687 g, 2 mmol) instead of dimethyltin dichloride. Yield: 85%; m.p. 200–202 °C. *Anal*. Calc. for $C_{19}H_{13}N_2S_2Sn$: C, 50.47; H, 2.90; N, 6.19. Found: C, 50.22; H, 3.01; N, 6.10%. IR (KBr,cm^{-1}): ν(Sn–S), 291 and 358; ν_{as}(Sn–C), 585; ν_s(Sn–C), 460; ν(C–S), 1182 and 1150; ν(C≡N), 2190; ν(C=C), 1464. ^1H NMR ($CDCl_3$, ppm): 7.39–7.85 (m, 26H, $2C_6H_5 + C_6H_6$).

2.2.4. $[(CH_3)_2Sn(mnt)]\cdot 1.5(4,4'\text{-}Bipy)$ (**4**)

The reaction was carried out under nitrogen atmosphere. Na_2mnt (0.372 g, 2 mmol) and dimethyltin dichloride (0.439 g, 2 mmol) were added to a solution of absolute ethanol (20 ml) in a Schlenk flask and stirred. After 4,4′-Bipy (0.468 g, 3 mmol) was added to the flask, the mixture was stirred for 12 h at 40 °C and then was filtered. The filtrate was gradually removed by evaporation under vacuum until solid product was obtained. The solid was then recrystallized from benzene. Buff crystal compound **4** was formed. Yield: 78%; m.p. 246–248 °C. *Anal*. Calc. for $C_{21}H_{18}N_5S_2Sn$: C, 48.21; H, 3.47; N, 13.39. Found: C, 48.33; H, 3.59; N, 13.18%. IR (KBr,cm^{-1}): ν(Sn–S), 262 and 276; ν_{as}(Sn–C), 551; ν_s(Sn–C), 455; ν(C–S), 1190 and 1210; ν(C≡N), 2207; ν(C=C), 1480; ν(C=N), 1178. ^1H NMR ($CDCl_3$, ppm): 1.20 [s, $^2J(^{119}Sn–^1H)$, 75.1 Hz, Me], 7.68 (d, 6H, $C_{10}H_8N_2$), 8.51 (d, 6H, $C_{10}H_8N_2$).

2.2.5. $[4,4'\text{-}BipyH]^+[(CH_3)_2SnCl(mnt)]^-$ (**5**)

The reaction was carried out under nitrogen atmosphere. Na_2mnt (0.372 g, 2 mmol) and 4,4′-Bipy (0.468 g, 3 mmol) were added to a solution of absolute ethanol (20 ml) in a Schlenk flask and stirred. After dimethyltin dichloride (0.439 g, 2 mmol) was added to the flask, the mixture was stirred for 12 h at 40 °C and then was filtered. The solid was then recrystallized from benzene. Yield: 83%; m.p. 208–210 °C. *Anal*. Calc. for $C_{16}H_{15}ClN_4S_2Sn$: C, 39.91; H, 3.14; N, 11.63. Found: C, 39.78; H, 3.03; N, 11.88%. IR (KBr,cm^{-1}): ν(Sn–S), 260 and 278; ν_{as}(Sn–C), 557; ν_s(Sn–C), 451; ν(Sn–Cl), 280; ν(C–S),1186 and 1198; ν(C≡N), 2199; ν(C=C), 1490; ν(C=N), 1201, ν(N–H), 3418. ^1H NMR ($CDCl_3$, ppm): 1.16 [s, $^2J(^{119}Sn–^1H)$, 78.2 Hz, Me], 7.75 (d, 4H, $C_{10}H_8N_2$), 8.43 (d, 4H, $C_{10}H_8N_2$).

2.2.6. $[(CH_3)_2Sn(mnt)(Phen)]$ (**6**)

Compound **6** was prepared in the same way as compound **5**, by using Phen (0.360 g, 2 mmol) instead of 4,4′-Bipy. Yield: 76%; m.p. 192–194 °C. *Anal*. Calc. for $C_{18}H_{14}N_4S_2Sn$: C, 46.08; H, 3.01; N, 11.94. Found: C, 46.10; H, 3.24; N, 11.71%. IR (KBr,cm^{-1}): ν(Sn–S), 258 and 275; ν_{as}(Sn–C), 558; ν_s(Sn–C), 453; ν(Sn–N), 420 and 457; ν(C–S), 1180 and 1206; ν(C≡N), 2197; ν(C=C), 1450; ν(C=N), 1180. ^1H NMR ($CDCl_3$, ppm): 1.17 [s, $^2J(^{119}Sn–^1H)$, 65 Hz, Me], 7.26–7.81 (m, 8H, $C_{12}H_8N_2$).

2.3. X-ray crystallography

All X-ray crystallographic data were collected on a Bruker Smart CCD 1000 diffractometer. Criterion of

Table 1
Crystal, data collection and structure refinement parameters for all compounds **1–6**

Compound	**1**	**2**	**3**	**4**	**5**	**6**
Empirical formula	$C_6H_6N_2S_2Sn$	$C_{12}H_{18}N_2S_2Sn$	$C_{38}H_{26}N_4S_4Sn$	$C_{21}H_{18}N_5S_2Sn$	$C_{16}H_{15}ClN_4S_2Sn$	$C_{18}H_{14}N_4S_2Sn$
Formula weight	288.94	373.09	904.25	523.21	481.58	469.14
Wavelength (Å)	0.71073	0.71073	0.71073	0.71073	0.71073	0.71073
Crystal system	orthorhombic	orthorhombic	monoclinic	monoclinic	monoclinic	orthorhombic
Space group	*pnnm*	*pnma*	$P2_1/c$	$P2/n$	$P2_1/c$	*Pca*2
Unit cell dimensions						
a (Å)	12.394(4)	14.812(10)	16.514(6)	18.692(15)	13.109(7)	19.763(8)
b (Å)	7.904(3)	13.947(9)	15.787(5)	12.706(10)	10.367(6)	7.164(3)
c (Å)	9.752(4)	7.975(5)	15.676(5)	18.692(15)	14.494(8)	13.152(5)
β (°)	90	90	109.693(5)	101.721(9)	91.937(9)	90
V (Å^3)	955.3(6)	1647.4(19)	3848(2)	4347(6)	1968.7(18)	1826.0(12)
Z	4	4	4	8	4	4
D_{calc} (Mg m^{-3})	2.009	1.504	1.561	1.599	1.625	1.674
$F(000)$	552	744	1784	2088	952	928
μ (mm^{-1})	3.051	1.788	1.547	1.385	1.651	1.604
Crystal size (mm)	0.40 × 0.12 × 0.08	0.29 × 0.25 × 0.17	0.26 × 0.22 × 0.15	0.50 × 0.45 × 0.40	0.26 × 0.21 × 0.13	0.21 × 0.15 × 0.07
θ range for data collection (°)	2.66–25.03	2.75–25.01	1.31–25.03	1.40–25.03	2.06–25.03	2.06–25.03
Index ranges	$-14 \leqslant h \leqslant 14$; $-9 \leqslant k \leqslant 8$; $-10 \leqslant l \leqslant 11$	$-17 \leqslant h \leqslant 17$; $-16 \leqslant k \leqslant 16$; $-9 \leqslant l \leqslant 54$	$-19 \leqslant h \leqslant 19$; $-17 \leqslant k \leqslant 18$; $-18 \leqslant l \leqslant 18$	$-19 \leqslant h \leqslant 22$; $-15 \leqslant k \leqslant 14$; $-21 \leqslant l \leqslant 22$	$-14 \leqslant h \leqslant 15$; $-12 \leqslant k \leqslant 11$; $-17 \leqslant l \leqslant 10$	$-23 \leqslant h \leqslant 21$; $-8 \leqslant k \leqslant 8$; $-13 \leqslant l \leqslant 15$
Reflections collected	4761	8081	20 151	16 073	10 161	9304
Unique reflections (R_{int})	902 (0.0393)	1517 (0.0346)	6781 (R0.0440)	5854 (0.1732)	3473 (0.0891)	2909 (0.0646)
Absorption corrections	multi-scan	semi-empirical from equivalents	semi-empirical from equivalents	semi-empirical from equivalents	semi-empirical from equivalents	semi-empirical from equivalents
Maximum/minimum transmission	0.7924, 0.3750	0.7509, 0.6252	0.8011, 0.6892	0.6073, 0.5443	0.8140, 0.6735	0.8960, 0.7293
Data, restraints, parameters	902, 0	1517, 0	6781, 0	5854, 60	3473, 0	2909, 1
Goodness of fit on F^2	0.978	1.020	0.883	0.921	0.926	0.895
Final R indices [$I > 2\sigma(I)$]	$R_1 = 0.0223$, $wR_2 = 0.0490$	$R_1 = 0.0274$, $wR_2 = 0.0638$	$R_1 = 0.0323$, $wR_2 = 0.0783$	$R_1 = 0.0693$, $wR_2 = 0.0967$	$R_1 = 0.0487$, $wR_2 = 0.1061$	$R_1 = 0.0367$, $wR_2 = 0.0719$
R indices (all data)	$R_1 = 0.0297$, $wR_2 = 0.0512$	$R_1 = 0.0391$, $wR_2 = 0.0673$	$R_1 = 0.0620$, $wR_2 = 0.0853$	$R_1 = 0.2050$, $wR_2 = 0.1357$	$R_1 = 0.0803$, $wR_2 = 0.1337$	$R_1 = 0.0721$, $wR_2 = 0.1096$
Largest difference peak, hole (e Å^3)	0.425, −0.404	0.204, −0.825	0.684, −0.374	0.972, −0.413	0.829, −0.994	0.405, −0.487

observability was used for the solution and refinement. The structure was solved by direct methods and refined by a full-matrix least-squares procedure based on F^2 using the SHELXL 97 program system. All data were collected at 298(2) K using graphite-monochromated Mo Kα radiation ($\lambda = 0.71073$ Å) and corrected for Lorentz and polarization effects for absorption. The positions of partly hydrogen atoms are retained, and their contributions in structural factor calculations are included. Table 1 lists the crystal data and structure refinement parameters for compounds **1–6**.

3. Results and discussion

3.1. Synthesis of compounds *1–6*

The synthesis procedures are shown in Scheme 1.

3.2. Spectroscopic studies

3.2.1. IR spectroscopic studies of compounds *1–6*

The assignment of IR bands of these compounds has been made by comparison with IR spectra of their related precursors. The spectra of all six compounds **1–6** show some common characters. The frequencies appearing in the region 258–280 cm^{-1} are assigned to the Sn–S stretching mode of vibration, all of which are consistent with those detected in a number of organotin(IV)–sulfur complexes [9–11]. IR bands at about 2000, 1460 and 1200 cm^{-1} have been assigned to ν(C≡N), ν(C=C) and ν(C–S), respectively, among which those related to the C=C and C–S stretching modes show a genuine positive shift [6].

Some obvious differences among the spectra of the six compounds **1–6** are also observed. For compound **5**, new vibrations appear at 280 and 3418 cm^{-1}, which can

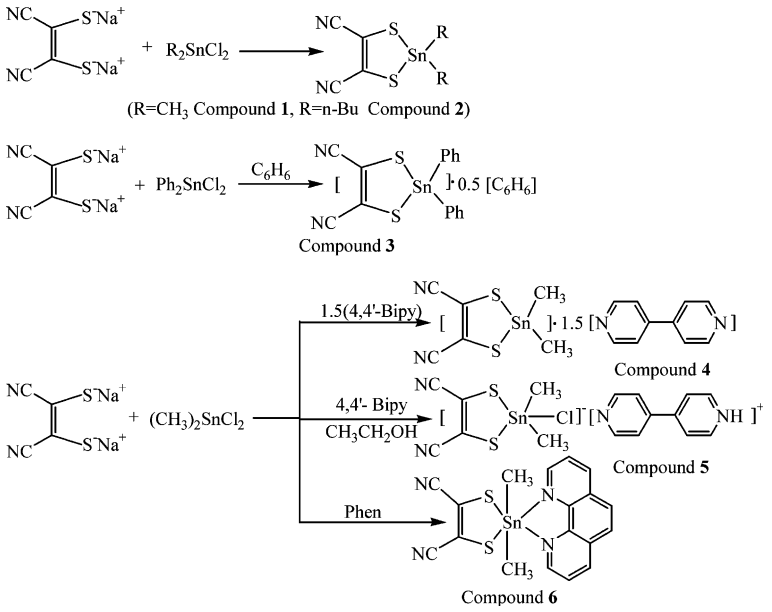

Scheme 1.

be assigned to the vibrations of ν(Sn–Cl) and ν(N–H), respectively, indicating the nature of a one-substituted compound. For compound **6**, new vibrations appearing at about 420 and 457 cm^{-1}, attributed to Sn–N bonds between the tin atom and two nitrogen atoms of Phen, further testify the coordinated format of compound **6**. These formations are consistent with the following X-ray structure analyses.

3.2.2. ^1H NMR spectroscopic studies of compounds 1–6

^1H NMR spectra shows that the chemical shifts of the methyl groups, 1.16–1.27 ppm in compound **1** and compounds **4**–**6**, the butyl group in compound **2**, 1.56–1.78 ppm, and the phenyl group in compound **3**, 7.34–7.67 ppm, are all shifted upfield as compared with their corresponding precursors, similar to those appearing in the literature [12,13]. In addition, the resonances appearing at 7.68–8.51 ppm for compounds **4** and **5** are attributed to the protons of 4,4′-Bipy and the resonance at 7.26–7.81 ppm for compound **6** is assigned to the protons of Phen [14,15].

Moreover, the $^2J(^{119}Sn–^1H)$ of dimethyltin derivatives **1** and **4** have values of 74.7 and 75.1 Hz respectively, typical of tetra-coordinated tin species. While complexes **5** and **6** have values of 78.2 and 65 Hz, respectively, consistent with those of five- or *cis*-six-coordinated tin species, respectively. On the basis of Lockarts's Eq. [16], the Me–Sn–Me angle are estimated to be approximately 124.6° for compound **1**, 125.1° for compound **4**, 128.7° for compound **5** and 115.6° for compound **6**, which are all in agreement with those values found in the crystal structures.

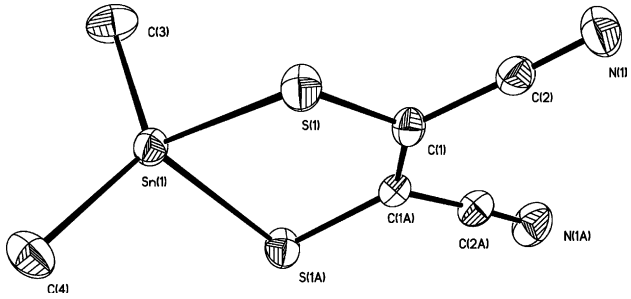

Fig. 1. Molecular structure of compound **1**.

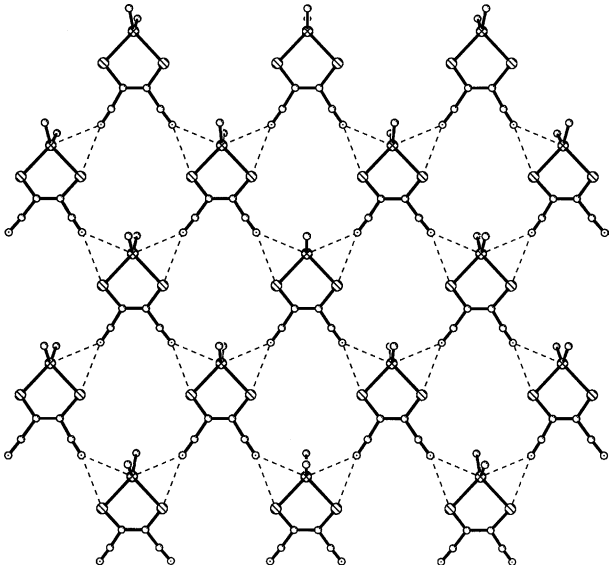

Fig. 2. A network of compound **1**.

3.3. X-ray studies

From X-ray crystal structure analysis, we note that the geometries of all the tin atoms in compounds **1**–**4** are tetrahedral, and those in **5** and **6** are trigonal bipyramidal and distorted octahedral, respectively. Co-crystallization is found in crystals of compounds **3** and **4**. The co-crystallized solvents are benzene and 4,4′-Bipy, respectively. Compound **5** is a stannate with a five-coordinated tin atom. Compound **6** is a six-coordinated dimethyltin(IV) derivative from mixed ligands of mnt and Phen. Detailed analysis on all the compounds **1–6** follows.

3.3.1. Crystal structures of $(CH_3)_2Sn(mnt)$ (1), $(n\text{-}Bu)_2Sn(mnt)$ (2) and $[Ph_2Sn(mnt)]\cdot 0.5C_6H_6$ (3)

The crystal structure and unit cell of compounds **1**, **2** and **3** are shown in Figs. 1–6, respectively, and selected bond lengths and bond angles are listed in Table 2. For compounds **1**, **2** and **3**, the geometry of the tin atoms is distorted tetrahedral and the tin atom forms four primary bonds: two to the methyl (butyl or phenyl) groups and two to sulfur atoms. Two weak intermolecular Sn···N and S···N interactions are recognized. The former exists between the Sn atom and two nitrogen atoms from two adjacent molecules. The latter exists between two sulfur atoms of the same molecule and two nitrogen atoms from two adjacent molecules. The corresponding intermolecular Sn···N and S···N distances are 3.068 and 3.174 Å for compound **1**, 2.828 and 3.060 Å for compound **2**, 2.867 and 3.222 Å for compound **3**, respectively. These Sn···N bond distances are similar to the values recorded in the Cambridge Crystallographic Database [17], and are much shorter than the sum of the van der Waal's radii of Sn and N (3.75 Å) [18,19]. Thus by the two weak intermolecular Sn···N and S···N

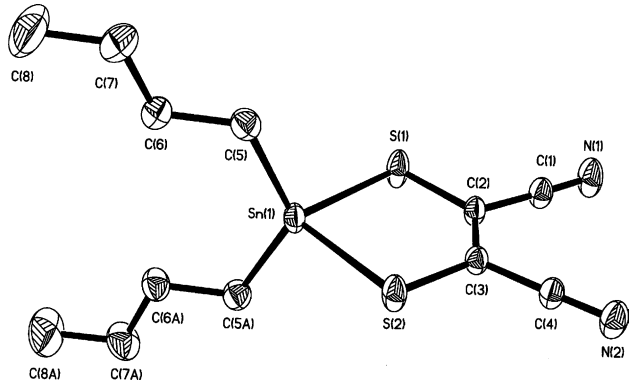

Fig. 3. Molecular structure of compound **2**.

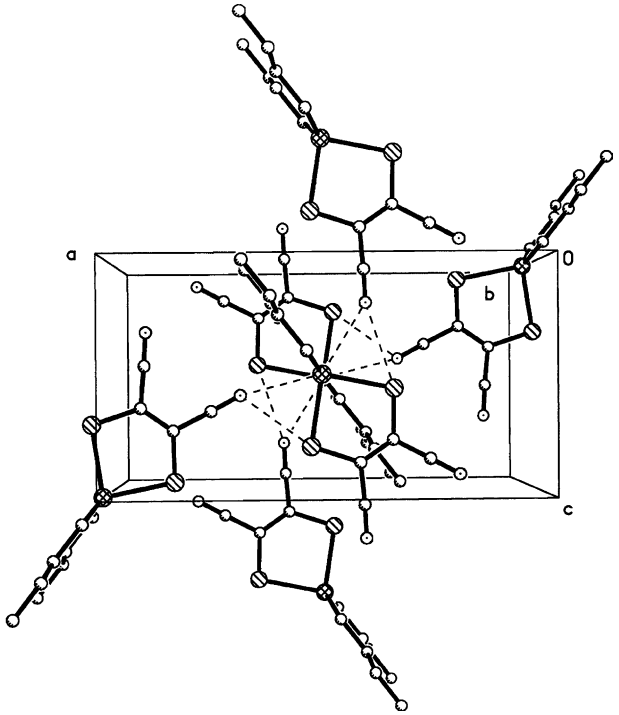

Fig. 4. Unit cell of compound **2**.

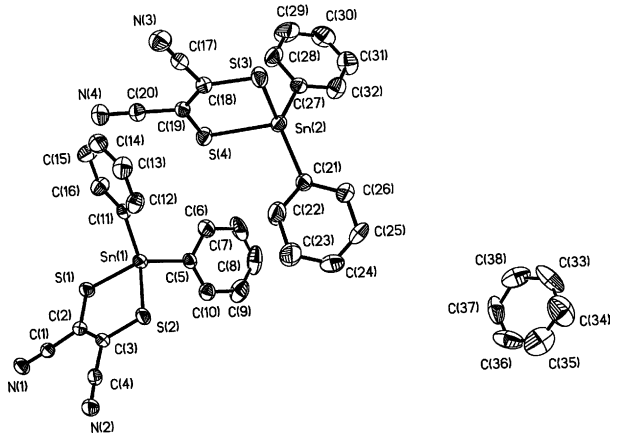

Fig. 5. Molecular structure of compound **3**.

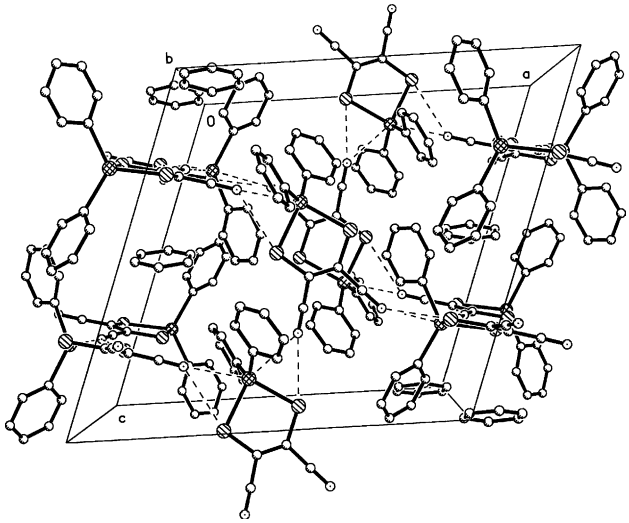

Fig. 6. Unit cell of compound **3**.

Table 2
Selected bond lengths (Å) and bond angles (°) for compounds **1**, **2** and **3**

$[(CH_3)_2Sn(mnt)]$ (***1***)			
Bond lengths			
Sn(1)–C(3)	2.112(5)	Sn(1)–S(1)	2.4604(11)
Sn(1)–C(4)	2.098(4)	Sn(1)–S(1)#1	2.4604(11)
Bond angles			
C(4)–Sn(1)–C(3)	124.2(2)	C(3)–Sn(1)–S(3)	109.80(11)
C(4)–Sn(1)–S(1)	109.84(11)	C(3)–Sn(1)–S(1)#1	109.80(11)
C(4)–Sn(1)–S(1)#1	109.84(11)	S(1)–Sn(1)–S(1)#1	87.09(5)
$(n\text{–}Bu)_2Sn(mnt)$ (***2***)			
Bond lengths			
Sn(1)–C(5)	2.126(3)	Sn(1)–S(1)	2.479(2)
Sn(1)–C(5)#1	2.126(3)	Sn(1)–S(2)	2.488(2)
Bond angles			
C(5)–Sn(1)–C(5)#1	127.39(19)	C(5)–Sn(1)–S (2)	108.44(10)
C(5)–Sn(1)–S(1)	109.03(10)	C(5)#1–Sn(1)–S(2)	108.44(10)
C(5)#1–Sn(1)–S(1)	109.03(10)	S(1)–Sn(1)–S(2)	87.08(4)
$[Ph_2Sn(mnt)]\cdot 0.5C_6H_6$ (***3***)			
Bond lengths			
Sn(1)–C(5)	2.114(5)	Sn(2)–C(27)	2.109(5)
Sn(1)–C(11)	2.126(5)	Sn(2)–C (21)	2.118(5)
Sn(1)–S(1)	2.4460(15)	Sn(2)–S(3)	2.4551(16)
Sn(1)–S(2)	2.4520(16)	Sn(2)–S(4)	2.4687 (15)
Bond angles			
C(5)–Sn(1)–C(11)	118.45(18)	C(27)–Sn(2)–C(21)	127.99(19)
C(5)–Sn(1)–S(1)	116.36(13)	C(27)–Sn(2)–S(3)	107.08(13)
C(11)–Sn(1)–S(1)	110.93(13)	C(21)–Sn(2)–S(3)	113.54(14)
C(5)–Sn(1)–S(2)	106.41(14)	C(27)–Sn(2)–S(4)	107.78(13)
C(11)–Sn(1)–S(2)	111.55(14)	C(21)–Sn(2)–S(4)	104.73(13)
S(1)–Sn (1)–S(2)	89.04(4)	S(3)–Sn(2)–S(4)	88.08(5)

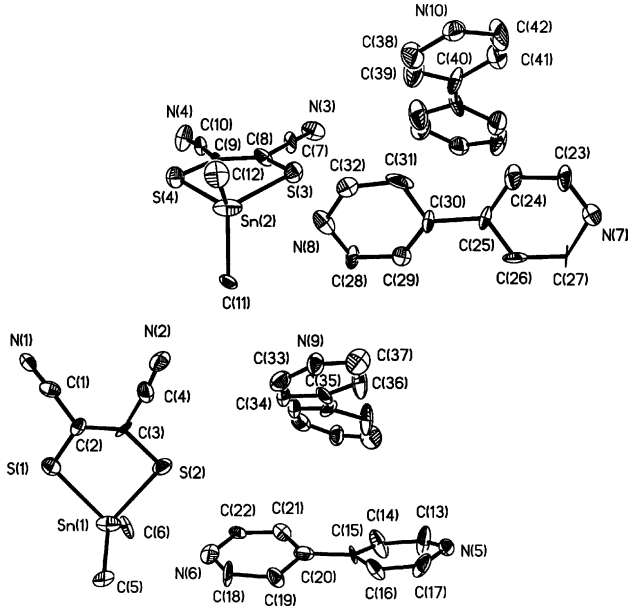

Fig. 7. Molecular structure of compound **4**.

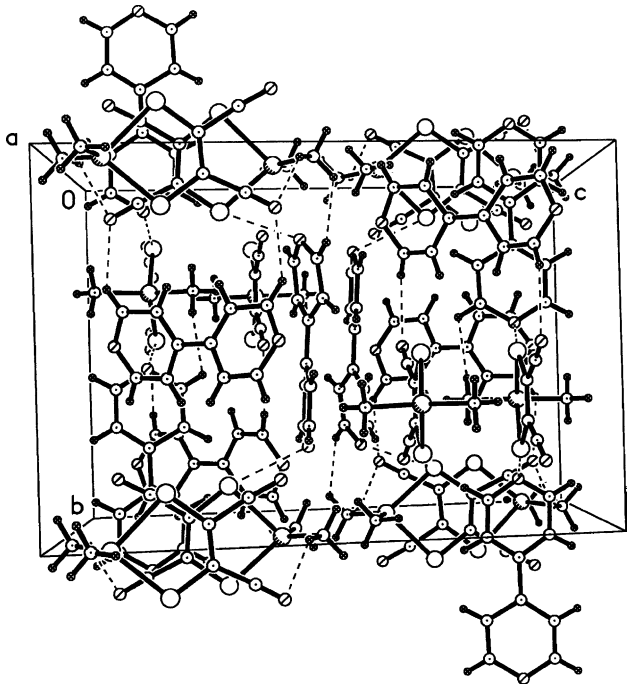

Fig. 8. Unit cell of compound **4**.

interactions, a similar network structure is constructed in all the crystals of **1**–**3**.

For compound **3**, co-crystallization is found in the crystals and the co-crystallized solvent is benzene, with a molar ratio of $Ph_2Sn(mnt)$: C_6H_6 of 2:1. For the main component, $Ph_2Sn(mnt)$, there exist two monomers in the asymmetric unit which are almost the same with regard to the conformation, but are different from a crystallographic point of view, with small differences in bond lengths and bond angles.

3.3.2. Structure of $[(CH_3)_2Sn(mnt)]\cdot 1.5(4,4'\text{-Bipy})$ (**4**)

The crystal structure and unit cell of compound **4** are shown in Figs. 7 and 8, respectively, and selected bond lengths and bond angles are listed in Table 3. For compound **4**, similar to compound **3**, co-crystallization is found but the co-crystallized solvent is 4,4′-Bipy with a molar ratio of $(CH_3)_2Sn(mnt)$: 4,4′-Bipy of 2:3. Two monomers of the main component, $(CH_3)_2Sn(mnt)$, exist in the asymmetric unit which are almost the same with regard to the conformation, but with small differences in bond lengths and bond angles. The geometry of the tin atoms involved is a distorted tetrahedron. Distortion from strict tetrahedral coordination is partly because of the variation of the sulfur bonding, and the sulfur atoms occupying *cis* positions [S(1)–Sn(1)–S(2)] 84.69(10)° and [S(4)–Sn(2)–S(3)] 85.09(11)°,. There also exist two intermolecular Sn···N and S···N interactions but the function atoms involved differ. The weak Sn···N interactions exist between the Sn atom and two nitrogen atoms from two adjacent 4,4′-Bipy molecules while the S···N interactions exist between two sulfur atoms of the same molecule and two nitrogen atoms from two adja-

Table 3
Selected bond lengths (Å) and bond angles (°) for compounds **4**, **5** and **6**

$[(CH_3)_2Sn(mnt)]\cdot 1.5(4,4'\text{-Bipy})$ (**4**)			
Bond lengths			
Sn(1)–C(5)	2.081(7)	Sn(2)–C(12)	1.981(9)
Sn(1)–C(6)	2.116(8)	Sn(2)–C(11)	2.052(8)
Sn(1)–S(1)	2.455(3)	Sn(2)–S(4)	2.496(3)
Sn(1)–S(2)	2.555(3)	Sn(2)–S(3)	2.498(3)
Bond angles			
C(5)–Sn(1)–C(6)	125.6(4)	C(12)–Sn(2)–C(11)	118.3(5)
C(5)–Sn(1)–S(1)	113.6(3)	C(12)–Sn(2)–S(4)	113.9(3)
C(6)–Sn(1)–S(1)	112.0(3)	C(11)–Sn(2)–S(4)	109.2(3)
C(5)–Sn(1)–S(2)	106.4(3)	C(12)–Sn(2)–S(3)	113.6(3)
C(6)–Sn(1)–S(2)	105.8(2)	C(11)–Sn(2)–S(3)	112.0(3)
S(1)–Sn(1)–S(2)	84.69(10)	S(4)–Sn(2)–S(3)	85.09(11)
$[4,4'\text{-BipyH}]^+[(CH_3)_2SnCl(mnt)]^-$ (**5**)			
Bond lengths			
Sn(1)–C(5)	2.114(7)	Sn(1)–S(2)	2.644(2)
Sn(1)–C(6)	2.104(7)	Sn(1)–Cl(1)	2.554(2)
Sn(1)–S(1)	2.449(2)		
Bond angles			
C(6)–Sn(1)–C(5)	127.8(4)	S(1)–Sn(1)–Cl(1)	83.49(6)
C(6)–Sn(1)–S(1)	115.1(3)	C(6)–Sn(1)–S(2)	92.2(3)
C(5)–Sn(1)–S(1)	117.1(2)	S(1)–Sn(1)–S(2)	83.23(6)
C(6)–Sn(1)–Cl(1)	93.5(3)	C(5)–Sn(1)–S(2)	92.9(2)
C(5)–Sn(1)–Cl(1)	93.0(2)	Cl(1)–Sn(1)–S(2)	166.72(7)
$[(CH_3)_2Sn(mnt)(Phen)]$ (**6**)			
Bond lengths			
Sn(1)–C(18)	2.151(10)	Sn(1)–N(3)	2.431(7)
Sn(1)–C(17)	2.175(12)	Sn(1)–S(1)	2.550(3)
Sn(1)–N(4)	2.346(11)	Sn(1)–S(2)	2.637(3)
Bond angles			
C(18)–Sn(1)–C(17)	109.7(5)	N(4)–Sn(1)–S(1)	160.1(3)
C(18)–Sn(1)–N(4)	93.8(4)	N(3)–Sn(1)–S(1)	96.7(2)
C(17)–Sn(1)–N(4)	94.6(4)	C(18)–Sn(1)–S(2)	92.8(3)
C(18)–Sn(1)–N(3)	158.9(5)	C(17)–Sn(1)–S(2)	157.5(4)
C(17)–Sn(1)–N(3)	83.8(5)	N(4)–Sn(1)–S(2)	82.0(3)
N(4)–Sn(1)–N(3)	68.3(4)	N(3)–Sn(1)–S(2)	74.3(3)
C(18)–Sn(1)–S(1)	97.7(3)	S(1)–Sn(1)–S(2)	81.29(10)
C(17)–Sn(1)–S(1)	96.7(4)		

cent 4,4′-Bipy molecules. The corresponding intermolecular Sn···N and S···N distances are 2.708 and 2.935 Å, respectively. Compared with that in complex **1**, the Sn···N bond distances are much shorter. Meanwhile, hydrogen bonding is formed between 4,4′-Bipy and nitrogen atoms from an adjacent $(CH_3)_2Sn(mnt)$ (H(37)···N(1) 2.409, H(33)···N(2) 2.726 and H(28)···N(9) 2.712 Å). Thus by all three weak interactions, a network is constructed.

3.3.3. Structure of $[4,4'\text{-BipyH}]^+[(CH_3)_2SnCl(mnt)]^-$ (**5**)

The crystal structure and unit cell of compound **5** are shown in Figs. 9 and 10, respectively, and selected bond lengths and bond angles in Table 3. X-ray crystal structure analysis revealed compound **5** is a ionic stannate and contains a penta-coordinated tin atom. The geometry of the tin atom of the anion $[(CH_3)_2SnCl(mnt)]^-$ is distorted trigonal bipyramidal with Cl(1) and S(2) occupying the axial sites and the S(2)–Sn–Cl(1) is 166.72(7)°. The Sn–Cl bond lengths are in the region usually found in those bipyramidal complexes [20] while those Sn–S bond lengths (2.449(2) and 2.644(2) Å) are appreciably less than those for the trigonal bipyramidal neutral compound $[Me_2ClSnS_2\text{-}CNMe_2]$ (Sn–S(*ax*) 2.79(1) and Sn–S(*eq*) 2.48(2) Å), indicating the strong coordination at these sites [21].

The weak hydrogen bonds of N···H between cations help the construction of one dimension infinite chain. The N(3)H(3)···N(4) is 2.678 Å. Furthermore, weak CH···Cl (H(16)···Cl(1), 4.005 Å) and CH···N (H(7)···N(2), H(11)···N(2) 3.762 Å) hydrogen bonds between anion and cation are recognized, which link two component into a layer.

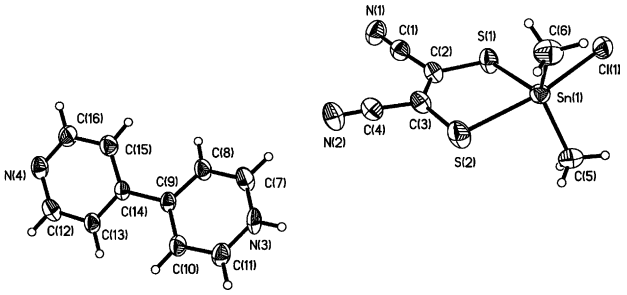

Fig. 9. Molecular structure of compound **5**.

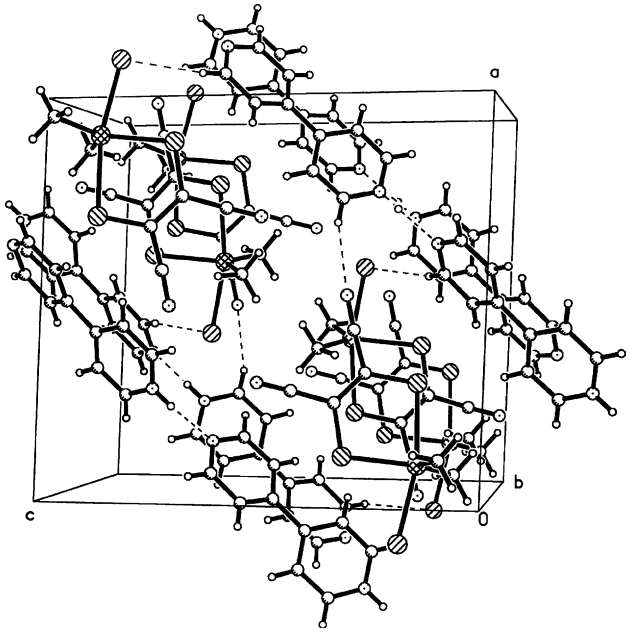

Fig. 10. Unit cell of compound **5**.

3.3.4. Structure of $[(CH_3)_2Sn(mnt)(Phen)]$ (**6**)

The crystal structure and unit cell of compound **6** are shown in Figs. 11 and 12, respectively, selected bond lengths and bond angles are listed in Table 3. Compound **6** contains a hexa-coordinated tin atom and has a distorted octahedral environment. Two carbons of methyl and two sulfur atoms of mnt are covalently linked to the tin atom. The valence extension is performed via two nitrogen atoms of Phen. The carbons are situated in

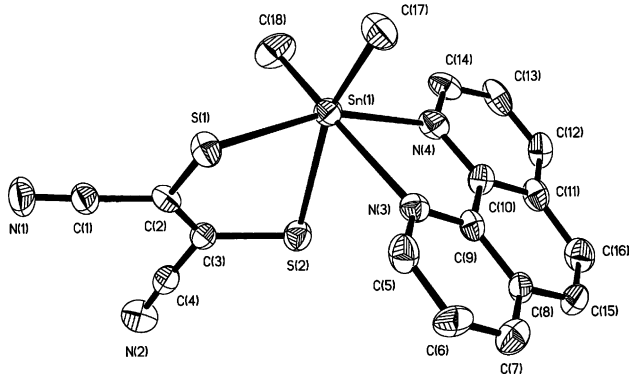

Fig. 11. Molecular structure of compound **6**.

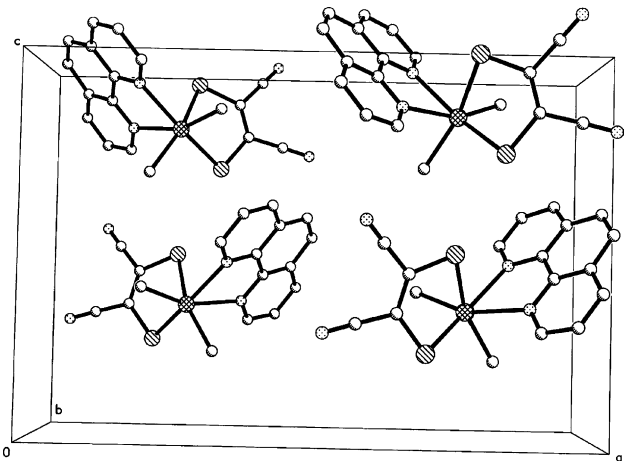

Fig. 12. Unit cell of compound **6**.

Table 4
Sn–S bond lengths (Å) and S–Sn–S bond angles (°) for all compounds **1**–**6**

Compound	Sn–S	Bond lengths	S–Sn–S	Angles (°)
1	Sn(1)–S(1)	2.4604(11)	S(1)–Sn(1)–S(1)#1	87.09(5)
	Sn(1)–S(1)#1	2.4604(11)		
4	Sn(1)–S(1)	2.455(3)	S(1)–Sn (1)–S(2)	84.69(10)
	Sn(1)–S(2)	2.555(3)	S(3)–Sn(2)– S(4)	85.09(11)
	Sn(2)–S(3)	2.496(3)		
	Sn(2)–S(4)	2.498(3)		
5	Sn(1)–S(1)	2.449(2)	S(1)–Sn(1)–S(2)	83.23(6)
	Sn(1)–S(2)	2.644(2)		
6	Sn(1)–S(1)	2.550(3)	S(1)–Sn(1)–S(2)	81.29(10)
	Sn(1)–S(2)	2.637(3)		

a *cis* position to each other (C(17)–Sn(1)–C(18) = 109.7(5)). One Sn(1)–C(17) is trans to the sulfur atom S(2) of mnt and the other Sn(1)–C(18) is trans to a nitrogen N(3) of Phen. Sn(1), N(3), N(4), C(18) and S(1) are almost coplanar with the tin atom deviating from the best plane by 0.2892 Å. Distortion from strict octahedral coordination is partly because of the variation of the sulfur bonding, and the sulfur atoms occupying *cis* positions (S(1)–Sn(1)–S(2), 81.29(10)°).

Sn–S bond lengths and S–Sn–S bond angles are shown in Table 4. Comparing Sn–S bond lengths of compounds **1**, **4**, **5** and **6**, which belong to dimethyltin(IV) derivatives from mnt, we find that when these dimethyltin(IV) derivatives are four-coordinated (**1** and **4**), two Sn–S bond are symmetric and lie in the range 2.45–2.56 Å. However, when the tin atom coordination number is greater than four, as in the case of compounds **5** and **6**, the Sn–S bond lengths are asymmetric with the longer at about 2.64(3) Å and the shorter at about 2.55 Å. Meanwhile, we find that S–Sn–S bond angles lessen when the coordination number of the tin atom increases. The above differences in Sn–S bond lengths and S–Sn–S angles among compounds **1**, **4**, **5** and **6** are attributed to the distinction of the coordination numbers of the central tin atoms.

It is noted that despite using a 1:1:1 molar ratio of Na_2mnt:(n-Bu)$_2SnCl_2$ (or Ph_2SnCl_2): Phen(or 4,4′-Bipy), we did not obtain the product with mixed ligands. The result suggested that the spatial resistances from two butyl (two phenyl) groups are strong enough to prevent another ligand chelating to the central tin atom.

4. Supplementary material

Crystallographic data (excluding structure factors) for the structure analysis of compounds **1**–**6** have been deposited with the Cambridge Crystallographic Data Center, CCDC no. 220164 **1**, 220169 **2**, 220178 **3**, 221137 **4**, 221133 **5** and 220170 **6**. Copies of this information may be obtained free of charge from The Director, CCDC, 12 Union Road, Cambridge, CB2 1EZ, UK (fax: +44-1223-336033; e-mail: deposit@ccdc.cam.ac.uk or http://www.ccdc.cam.ac.uk).

Acknowledgements

We thank the National Nature Science Foundation of China (20271025) and the National Nature Science Foundation of Shandong Province for financial support.

References

[1] M. Gielen, Appl. Organomet. Chem. 16 (2002) 481.
[2] A.H. Penninks, P.M. Punt, M. Bol-Schoenmakers, H.J.M. Van Rooijen, W. Seinen, Silicon Germanium Tin Lead Comp. 9 (1986) 367.
[3] (a) A.C. Sau, R.O. Day, R.R. Holmes, J. Am. Chem. Soc. 103 (1981) 1264;
(b) Z.H. Chohan, R.A. Howie, J.L. Wardell, J. Organomet. Chem. 577 (1999) 140;
(c) R.R. Holmes, S. Shafieezad, V. Chandrasekhar, A.C. Sau, J.M. Holmes, R.O. Day, J. Am. Chem. Soc. 110 (1988) 1168;
(d) S.S.V. Doidge-Harrison, R.A. Howie, J.T.S. Irvine, G. Spencer, J.L. Wardell, J. Organomet. Chem. 414 (1991) C5;
(e) A.P.G. de Sousa, R.M. Silva, A. Cesar, J.L. Wardell, J.C. Huffman, A. Abras, J. Organomet. Chem. 605 (2000) 82.
[4] A.C. Sau, R.O. Day, R.R. Holmes, Inorg. Chem. 20 (1981) 3076.
[5] R.O. Day, J.M. Holmes, S. Shafieezad, V. Chandrasekhar, R.R. Holmes, J. Am. Chem. Soc. 110 (1988) 5377.
[6] N. Singh, S. Gupta, G. Nath, Appl. Organomet. Chem. 14 (2000) 484.
[7] E.S. Bretschneider, C.W. Allen, Inorg. Chem. 12 (1973) 623.
[8] G. Bahr, G. Schleitzer, Chem. Ber. 90 (1957) 438.
[9] C.V. Rodarte de Moura, A.P.G. de Sousa, R.M. Silva, A. Abras, M. Hörner, A.J. Bortoluzzi, C.A.L. Filgueiras, J.L. Wardell, Polyhedron 18 (1999) 2961.
[10] C.L. Ma, Q. Jing, R.F. Zhang, Appl. Organomet. Chem. 17 (2003) 623.
[11] J.S. Casas, E.G. Martinez, J. Sordo, M.L. Jorge, U. Russo, Appl. Organomet. Chem. 15 (2001) 204.
[12] C.L. Ma, Q. Jing, J.H. Zhang, R.F. Zhang, Polyhedron 22 (2003) 2767.

[13] Y. Ye, Q. Zeng, L.Z. Liu, Synth. Commun. 31 (2001) 2373.
[14] H.A. Cruse, N.E. Leadbeater, Inorg. Chem. 38 (1999) 4149.
[15] I. Lange, E. Wieland, P.G. Jones, A. Blaschette, J. Organomet. Chem. 458 (1993) 57.
[16] T.P. Lockhart, W.F. Manders, Inorg. Chem. 25 (1986) 892.
[17] F.H. Allen, S.A. Bellard, M.D. Brice, B.A. Cartwright, A. Doubleday, H. Higgs, T. Hummelink, B.G. Hummelink-Peters, O. Kennard, W.D.S. Motherwell, J.R. Rogers, D.G. Watson, Acta Crystallogr. B 35 (1979) 2331.
[18] J.S. Casas, A. Castineiros, E.G. Martinez, A.S. Gonzales, A. Sanchez, J. Sordo, Polyhedron 16 (1997) 795.
[19] R. Barbieri, F. Huber, L. Pellerito, G. Ruisi, A. Silvestri, 119mSn Mossbauer studies on tin compounds, in: P.J. Smith (Ed.), Chemistry of Tin, 2nd ed., Blackie, London, 1998.
[20] A.C. Sau, R.O. Day, R.R. Holmes, J. Am. Chem. Soc. 103 (1981) 1264.
[21] K. Furue, T. Kimura, N. Yasuoka, N. Kasai, M. Kakudo, Bull. Chem. Soc. Jpn. 43 (1970) 1661.

Available online at www.sciencedirect.com
SCIENCE DIRECT®
Polyhedron 23 (2004) 1217–1224
POLYHEDRON
www.elsevier.com/locate/poly

Synthesis and characterization of three 5-(4-pyridyl)tetrazolato complexes obtained by reaction of 4-cyanopyridine with metal azides from aqueous solutions

Franz A. Mautner [a,*], Christian Gspan [a], Karl Gatterer [a], Mohamed A.S. Goher [b], Morsy A.M. Abu-Youssef [b], Edith Bucher [c], Werner Sitte [c]

[a] *Institut für Physikalische und Theoretische Chemie, Technische Universität Graz, Rechbauerstr. 12, A-8010 Graz, Austria*
[b] *Faculty of Science, Department of Chemistry, Alexandria University, P.O. Box 426 Ibrahimia, 21321 Alexandria, Egypt*
[c] *Institut für Physikalische Chemie, Montanuniversität Leoben, A-8700 Leoben, Austria*

Received 15 December 2003; accepted 2 February 2004

Abstract

Three metal complexes with the 5-(4-pyridyl)tetrazolate anion, $(4\text{-PTZ})^-$, as ligand were obtained by the reaction of 4-cyanopyridine with corresponding metal azides in aqueous solution. Isomorphic complexes of composition $[M(4\text{-PTZ})_2(H_2O)_4]\cdot 2H_2O$ with M = Mn(II) (**1**) and Cd(II) (**2**) were obtained, whereas $[Ca_{1.5}((4\text{-PTZ})_2H)(N_3)_2(H_2O)_5](H_2O)_{0.3}$ (**3**) was separated from calcium azide solutions. The IR spectra and the thermal behaviour of the complexes are measured and discussed. The single crystal X-ray diffraction revealed that the isomorphous structures of **1** and **2** consist of octahedrally coordinated metal centers, where two 4-PTZ anions act as monodentate ligands via their pyridine-N atoms in *trans*-positions. The structures also contain six water molecules, four act as monodentate ligands and the remaining two as lattice water molecules. Hydrogen bonds of the types O–H...O and O–H...N connect the mononuclear units to a three-dimensional network structure. The chain structure of complex **3** features octahedrally coordinated Ca(1); dinuclear subunits of pentagonal-bipyramidal Ca(2) centers; azide groups acting in end-on and end-to-end bridging mode; a $(4\text{-PTZ})_2H$ ligand in its zwitter ionic form coordinated via N(1) atom of the tetrazole ring to Ca(2), as well as lattice and ligand water molecules. Again, a complicated hydrogen bond system connects the chains of polyhedra to form a 3-D network structure.
© 2004 Elsevier Ltd. All rights reserved.

Keywords: Cadmium(II); Calcium(II); Manganese(II); Synthesis; Crystal structures; Tetrazolate complexes

1. Introduction

Tetrazole as functional group plays an increasingly important role in coordination chemistry as ligand [1], in medical chemistry as a metabolically stable surrogate for a carboxylic acid group [2] and in various materials science applications, including special explosives [3]. Also of great potential are the many useful transformations that make tetrazoles versatile intermediates for substituted tetrazoles, in particular of other 5-ring heterocycles via the Huisgen rearrangement [4]. Sharpless and Demko [5] have recently reported an environmentally friendly, relatively simple synthetic approach for generating 5-substituted 1H-tetrazoles. In the general [2+3] cycloaddition reaction, the tetrazoles are prepared by the addition of azide to nitriles in water with the aid of Zn^{2+} as Lewis acid; and for the reaction of PhCN with $ZnBr_2$ and NaN_3 $Zn(PhCN_4)_2$ has been postulated as solid intermediate. Subsequent density functional theory calculations result a reduction of the energy barrier of the zinc catalyzed reaction by 5–6 kcal/mol [6]. Very recently, Xue et al. [7] reported two novel Cd(II) coordination polymers employing the 5-(4-pyridyl)tetrazolate anion $(4\text{-PTZ})^-$ as a bridging ligand. The reaction of $CdCl_2$ with 4-cyanopyridine in the presence of NaN_3 and water under hydrothermal conditions yielded

* Corresponding author. Tel.: +00-43-316-873-8234; fax: +00-43-316-873-8225.
E-mail address: mautner@ptc.tu-graz.ac.at (F.A. Mautner).

0277-5387/$ - see front matter © 2004 Elsevier Ltd. All rights reserved.
doi:10.1016/j.poly.2004.02.001

$Cd_3(OH)_2Cl_2(4\text{-PTZ})_2$ while $Cd(4\text{-PTZ})_2(H_2O)_2$ was obtained by the treatment of 4-H-PTZ with $CdCl_2$ and H_2O under similar experimental conditions. The structure of the latter complex consists of sheets of *trans*-coordinated Cd(II) octahedra, with the 4-PTZ anions acting as bidentate bridging N-donor ligands (via pyridine and tetrazole N atoms). The 2D system of the first complex is more complicated with the 4-PTZ anions acting as tridentate ligands, thus demonstrating the bridging abilities of the 4-PZT anions. Bidentate bridging 4-PTZ anions were also found in the 2D layered network (4-PTZ)Zn(OH)(H_2O), also reported by this group [8].

In the course of our systematic investigations of molecular magnets based on metal azido complexes containing pyridine derivative ligands [9–13] we observed that the intermediate reaction of 4-cyanopyridine with azide ion

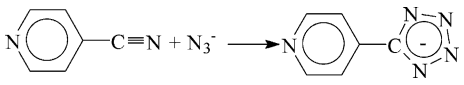

takes place at even milder experimental conditions and we separated three metal complexes with 4-PZT anions as ligand.

2. Experimental

2.1. Materials and instrumentation

Infrared spectra were recorded by a Bruker IFS-125 model FT-IR spectrophotometer as KBr pellets [14]. 4-Cyanopyridine has been purchased from Aldrich Company and other chemicals were of analytical grade quality and used without further purification. C,H,N analyses were carried out using a Perkin–Elmer analyzer [15], metal analyses by complexometric titration [16].

Caution: Metal azide complexes are potential explosives. Only a small amount of material should be prepared and handled with caution.

2.2. Synthesis

2.2.1. $[Mn(4\text{-PTZ})_2(H_2O)_4](H_2O)_2$ (**1**)

The complex was prepared by combining 8 ml of an aqueous solution of NaN_3 (0.32 g, 5.0 mmol) saturated with hydrazoic acid [16], with an aqueous solution (20 ml) of $Mn(NO_3)_2 \cdot 4H_2O$ (1.00 g, 0.4 mmol) and 4-cyanopyridine (0.1 g, 0.96 mmol), followed by subsequent heating of the reaction solution to 80 °C for 6–8 h to complete the tetrazol reaction. The final clear solution was cooled to room temperature and prism shaped, colorless crystals of the complex were separated within several days. Yield: 75%. *Anal*. Calc.: C, 31.7; H, 4.4; N, 30.8; Mn, 12.1. Found: C, 31.5; H, 4.2; N, 30.6; Mn, 12.3%. IR, KBr (cm^{-1}) (v very, s strong, m medium, w weak, br broad): 3205 vs, br, 1623 s, 1445 m, 1431 s, 1378 m, 1219 ms, 1156 wm, 1071 mw, 1043 w, 1014 ms, 877 w, 836 m, 750 m, 728 m, 712 s, 528 m, 446 mw.

2.2.2. $[Cd(4\text{-PTZ})_2(H_2O)_4](H_2O)_2$ (**2**)

A similar procedure as for **1** was used for synthesis. The complex was prepared by combining 31 ml of an aqueous solution of NaN_3 (0.32 g, 5.0 mmol) saturated with hydrazoic acid [16], with an aqueous solution (20 ml) of $3CdSO_4 \cdot 8H_2O$ (0.50 g, 1.95 mmol Cd) and 4-cyanopyridine (0.20 g, 1.9 mmol), followed by subsequent heating of the reaction mixture to 75 °C for 10 h to obtain the tetrazol. The clear solution was slowly cooled to room temperature and the first undefined precipitate filtered. From the mother liquor needle shaped, colorless crystals of the complex were separated within several days. Yield: 80%. *Anal*. Calc.: C, 28.1; H, 3.9; N, 27.3; Cd, 21.9. Found: C, 27.9; H, 3.7; N, 27.5; Cd, 21.8%. IR, KBr(cm^{-1}): 3200 vs, br, 1622 s, 1446 m, 1432 s, 1375 m, 1219 ms, 1156 wm, 1073 mw, 1045 w, 1019 s, 874 w, 834 m, 750 m, 728 m, 713 s, 527 m, 454 mw.

2.2.3. $[Ca_{1.5}((4\text{-PTZ})_2H)(N_3)_2(H_2O)_5](H_2O)_{0.3}$ (**3**)

Compound **3** was synthesized by adding 4-cyanopyridine (0.11 g, 1.0 mmol) to 10 ml of an aqueous solution of $Ca(N_3)_2$ (4.97 g, 40 mmol Ca), saturated with HN_3 (pH 5.5–6.0) [16] and subsequent heating of the mixture to 80 °C for 6 h. After slow cooling of the final clear solution to room temperature irregular shaped, colorless and transparent crystals of **3** were separated within a few days. Yield: 70%. *Anal*. Calc: C, 27.0; H, 3.7; N, 42.1; Ca, 11.3. Found: C, 27.2; H, 3.9; N, 42.0; Ca, 11.2%. IR KBr (cm^{-1}): 3260 vs, br, 2056 s, 2037 s, 1664 ms, 1622 s, 1523 w, 1445 ms, 1431 s, 1409 m, 1151 m, 1039 w, 1008 m, 874 m, 843 ms, 754 ms, 710 s, 641 m, 527 m, 456 m.

2.3. X-ray crystallography

Single crystal X-ray data were measured at 90(2) K on a modified STOE four circle diffractometer using graphite crystal-monochromatized Mo Kα radiation ($\lambda = 0.71069$ Å). The intensities were corrected for Lorentz-polarisation effects and for absorption [range of normalized transmission factors: 1.000–0.638; 1.000–0.491 and 1.000–0.526, for **1**–**3**, respectively]. Crystallographic data and processing parameters are given in Table 1. The structures were solved by direct methods and subsequent Fourier analyses. The program DIFABS [17] and SHELXTL/PC program package [18] were used for computations. Analytical expressions of neutral-atom scattering factors were employed, and anomalous dispersion corrections were incorporated. Anisotropic displacement parameters were applied to non-hydrogen

Table 1
Crystallographic data and processing parameters

Compound	**1**	**2**	**3**
Empirical formula	$C_{12}H_{20}MnN_{10}O_6$	$C_{12}H_{20}CdN_{10}O_6$	$C_{12}H_{19.6}Ca_{1.5}N_{16}O_{5.3}$
Formula mass	455.32	512.78	532.96
System	triclinic	triclinic	triclinic
Space group	$P\bar{1}$	$P\bar{1}$	$P\bar{1}$
a (Å)	7.385(3)	7.421(3)	9.096(3)
b (Å)	7.852(3)	7.891(3)	10.703(4)
c (Å)	8.563(3)	8.671(3)	12.039(5)
α (°)	91.07(3)	90.53(3)	82.59(3)
β (°)	93.03(3)	92.13(3)	75.14(3)
γ (°)	100.74(3)	100.36(3)	85.69(3)
V (Å^3)	487.0(3)	499.1(3)	1122.3(7)
Z	1	1	2
μ(Mo Kα) (mm^{-1})	0.731	1.146	0.458
D_{calc} (Mg/m^3)	1.553	1.706	1.577
Approximate crystal size (mm)	$0.30 \times 0.20 \times 0.07$	$0.40 \times 0.20 \times 0.20$	$0.30 \times 0.30 \times 0.24$
θ range (°)	2.81–24.98	2.79–25.00	2.75–29.85
Reflections collected	2084	2129	5907
Independent reflections/R_{int}	1711/0.0220	1719/0.0224	5175/0.0211
Parameters	154	154	369
Goodness-of-fit on F^2	1.068	1.138	1.059
$R1/wR2$	0.0339/0.0866	0.0294/0.0783	0.0380/0.0986
Largest peak/hole (e/Å^3)	0.307/−0.327	0.683/−0.663	0.553/−0.464

atoms in full-matrix least-squares refinements based on F^2. All hydrogen atoms were located from difference Fourier maps assigned with isotropic displacement factors and included in the final refinement cycles as follows: (a) pyridine hydrogen atoms bonded to carbon by geometrical restraints using the HFIX utility of SHELXTL/PC package; (b) disordered H(7) and H(8) of **3** with HFIX utility and split occupancy of 0.50; (c) water hydrogens by use of O–H distance restraints. The occupancy of disordered lattice water molecule O(6) of **3** was refined to 0.296(6) and finally fixed to 0.30. Selected bond distances and bond angles are given in Tables 2–4, for complexes **1**–**3**, respectively.

2.4. Thermogravimetry, differential thermal analysis, and mass spectroscopy

All experiments were performed in simultaneous TG/DTA/MS mode. TG/DTA data were obtained using a symmetric thermobalance (Setaram, model TAG 2416) compensating the buoyancy effect. The samples were heated in Al_2O_3 crucibles from 20 to 260 °C with a ramp rate of 5 °C/min. Ar (5.0) was used as carrier gas with flow rates of 1 l/h. The thermobalance was coupled to a quadrupole mass spectrometer (Pfeiffer Vacuum, model ThermoStar GSD 301 T1, max. 100 amu). MS data were recorded in multiple ion detection mode.

Table 2
Selected bond lengths (Å) and angles (°) for **1**

Bond lengths			
Mn(1)–O(3)	2.163(2)	Mn(1)–O(3A)	2.163(2)
Mn(1)–O(2)	2.164(2)	Mn(1)–O(2A)	2.164(2)
Mn(1)–N(1A)	2.301(2)	Mn(1)–N(1)	2.301(2)
C(3)–C(6)	1.463(3)	C(6)–N(2)	1.337(3)
C(6)–N(5)	1.342(3)	N(2)–N(3)	1.339(3)
N(3)–N(4)	1.320(3)	N(4)–N(5)	1.345(3)
Bond angles			
O(3)–Mn(1)–O(2)	91.03(7)	O(3)–Mn(1)–N(1A)	91.12(7)
O(2)–Mn(1)–N(1)	92.67(7)	N(2)–C(6)–N(5)	111.3(2)
N(2)–C(6)–C(3)	124.5(2)	N(5)–C(6)–C(3)	124.2(2)
C(6)–N(2)–N(3)	105.0(2)	N(4)–N(3)–N(2)	109.7(2)
N(3)–N(4)–N(5)	109.2(2)	C(6)–N(5)–N(4)	104.9(2)
Hydrogen bonds			
O(3)...O(1)	2.741(2)	O(3)...N(5B)	2.792(2)
O(2)...N(4C)	2.864(3)	O(2)...O(1D)	2.731(2)
O(1)...N(3C)	2.764(3)	O(1)...N(2E)	2.805(3)

Symmetry codes: (A) $-x, -y, -z$; (B) $x, y, z+1$; (C) $x, y-1, z+1$; (D) $-x+1, -y, -z$; (E) $-x+1, -y+1, -z$.

Table 3
Selected bond lengths (Å) and angles (°) for **2**

Bond lengths			
Cd(1)–O(2A)	2.282(3)	Cd(1)–O(2)	2.282(3)
Cd(1)–O(3)	2.290(3)	Cd(1)–O(3A)	2.290(3)
Cd(1)–N(1A)	2.329(3)	Cd(1)–N(1)	2.329(3)
C(3)–C(6)	1.466(5)	C(6)–N(5)	1.332(5)
C(6)–N(2)	1.342(5)	N(2)–N(3)	1.336(4)
N(3)–N(4)	1.319(4)	N(4)–N(5)	1.346(4)
Bond angles			
O(2)–Cd(1)–O(3)	92.22(10)	O(2)–Cd(1)–N(1)	93.23(10)
O(3A)–Cd(1)–N(1)	90.76(10)	N(5)–C(6)–N(2)	111.6(3)
N(5)–C(6)–C(3)	124.4(3)	N(2)–C(6)–C(3)	124.0(3)
N(3)–N(2)–C(6)	104.5(3)	N(4)–N(3)–N(2)	110.0(3)
N(3)–N(4)–N(5)	108.9(3)	C(6)–N(5)–N(4)	105.0(3)
Hydrogen bonds			
O(3)...O(1)	2.726(4)	O(3)...N(5B)	2.798(4)
O(2)...N(4C)	2.848(4)	O(2)...O(1D)	2.729(4)
O(1)...N(3C)	2.770(4)	O(1)...N(2E)	2.799(4)

Symmetry codes: (A) $-x, -y, -z$; (B) $x, y, z+1$; (C) $x, y-1, z+1$; (D) $-x+1, -y, -z$; (E) $-x+1, -y+1, -z$.

Table 4
Selected bond lengths (Å) and angles (°) for **3**

Bond lengths			
Ca(1)–O(1A)	2.320(2)	Ca(1)–O(2A)	2.377(2)
Ca(1)–N(11)	2.460(2)	Ca(1)...Ca(2)	6.811(3)
Ca(2)...Ca(2B)	4.318(2)	Ca(2)–N(21)	2.599(2)
Ca(2)–O(3)	2.301(2)	Ca(2)–O(5)	2.381(2)
Ca(2)–N(13)	2.454(2)	Ca(2)–O(4)	2.517(2)
Ca(2)–N(1)	2.581(2)	Ca(2)–N(21B)	2.597(2)
N(11)–N(12)	1.182(2)	N(12)–N(13)	1.166(2)
N(21)–N(22)	1.191(2)	N(22)–N(23)	1.173(2)
N(1)–N(2)	1.343(2)	N(2)–N(3)	1.322(2)
N(1)–C(1)	1.343(2)	N(4)–C(1)	1.341(2)
N(3)–N(4)	1.340(2)	N(10)–C(7)	1.340(2)
N(7)–C(7)	1.340(2)	N(7)–N(8)	1.345(2)
N(8)–N(9)	1.323(2)	N(9)–N(10)	1.337(2)
Bond angles			
O(1)–Ca(1)–O(2)	93.41(6)	O(2A)–Ca(1)–N(11)	93.38(7)
O(1)–Ca(1)–N(11A)	90.45(6)	O(3)–Ca(2)–O(5)	108.33(6)
O(3)–Ca(2)–N(13)	97.62(7)	O(5)–Ca(2)–N(13)	130.68(6)
O(3)–Ca(2)–O(4)	75.53(6)	O(5)–Ca(2)–O(4)	70.17(6)
N(13)–Ca(2)–O(4)	77.11(6)	O(3)–Ca(2)–N(1)	168.64(5)
O(5)–Ca(2)–N(1)	80.00(6)	N(13)–Ca(2)–N(1)	81.82(6)
O(4)–Ca(2)–N(1)	115.17(5)	O(3)–Ca(2)–N(21B)	80.17(6)
O(5)–Ca(2)–N(21B)	145.63(5)	N(13)–Ca(2)–N(21B)	78.56(6)
O(4)–Ca(2)–N(21B)	142.69(5)	N(1)–Ca(2)–N(21B)	88.62(6)
O(3)–Ca(2)–N(21)	77.86(6)	O(5)–Ca(2)–N(21)	81.45(6)
N(13)–Ca(2)–N(21)	146.13(6)	O(4)–Ca(2)–N(21)	131.92(6)
N(1)–Ca(2)–N(21)	96.23(6)	N(21B)–Ca(2)–N(21)	67.58(6)
N(12)–N(11)–Ca(1)	134.78(14)	N(13)–N(12)–N(11)	178.4(2)
N(12)–N(13)–Ca(2)	177.2(2)	N(22)–N(21)–Ca(2B)	119.68(12)
N(22)–N(21)–Ca(2)	127.48(13)	Ca(2B)–N(21)–Ca(2)	112.42(6)
N(23)–N(22)–N(21)	179.8(2)	N(2)–N(1)–Ca(2)	107.32(11)
C(1)–N(1)–Ca(2)	146.43(12)	N(2)–N(1)–C(1)	104.84(14)
N(3)–N(2)–N(1)	109.23(14)	N(2)–N(3)–N(4)	109.77(14)
N(3)–N(4)–C(1)	104.69(14)	N(4)–C(1)–N(1)	111.5(2)
N(4)–C(1)–C(2)	122.5(2)	N(1)–C(1)–C(2)	126.0(2)
C(7)–N(7)–N(8)	104.6(2)	N(9)–N(8)–N(7)	109.5(2)
N(8)–N(9)–N(10)	109.31(14)	N(9)–N(10)–C(7)	105.1(2)
N(7)–C(7)–N(10)	111.5(2)	N(7)–C(7)–C(8)	124.9(2)
N(10)–C(7)–C(8)	123.6(2)		
Hydrogen bonds			
O(1)...N(9E)	2.831(3)	O(1)...N(8C)	2.764(2)
O(2)...N(23F)	2.864(3)	O(2)...N(7C)	2.816(3)
O(3)...N(3D)	2.776(3)	O(3)...N(2B)	2.787(2)
O(4)...N(4D)	2.898(2)	O(4)...N(11G)	3.068(3)
O(5)...N(10H)	2.777(3)	O(5)...O(2G)	3.371(3)
O(6)...N(23I)	2.851(6)	O(6)...N(23)	2.902(6)
N(5)...N(6)	2.631(3)		

Symmetry codes: (A) $-x, 2-y, -z$; (B) $-x, 1-y, 1-z$; (C) $1-x, 1-y, -1-z$; (D) $-1+x, y, z$; (E) $x, 1+y, 1+z$; (F) $x, 1+y, -1+z$; (G) $-x, 1-y, -z$; (H) $x, y, 1+z$; (I) $-x, -y, 1-z$.

3. Results and discussion

The reaction of 4-cyanopyridine with aqueous solutions of their divalent metal azides at temperatures of 60–80 °C formed $[M(4\text{-PTZ})_2(H_2O)_4]\cdot 2H_2O$, [M = Mn, Cd; (4-PTZ = 5-(4-pyridyl)tetrazolate)] and $[Ca_{1.5}((4\text{-PTZ})_2H)(N_3)_2(H_2O)_5](H_2O)_{0.3}$. In the calcium compound the tetrazolate ligands are observed in their protonated zwitter ionic form. The [2+3] cycloaddition reaction was not observed with 3-cyanopyridine and similar experimental conditions; instead the 2D system $[Cd(3\text{-CNpy})(N_3)_2]_n$ [19] was obtained. The $[Mn(4\text{-CNpy})_2(N_3)_2]_n$ 2-D system was formed at lower reaction temperatures [20]. However, under hydrothermal conditions (105 °C), the monomeric $[Zn(2\text{-PTZ})_2(H_2O)_2]$ and the 3D diamondoid-like network $[Zn(3\text{-PTZ})_2]_n$ were obtained by the [2+3] cycloaddition reaction with 2- and 3-cyanopyridine, respectively [8].

3.1. Structures

The single crystal X-ray diffraction revealed that the isomorphous structures of **1** and **2** consist of octahedrally coordinated metal centers, where two 4-PTZ anions act as monodentate ligands via their pyridine-N atoms in *trans*-positions [Mn(1)–N(1) 2.301(2); Cd(1)–N(1) 2.329(2) Å]. The structures also contain six water molecules, four act as monodentate ligands [Mn–O 2.163(2), 2.164(2) Å; Cd–O 2.282(3), 2.290(3) Å] and the remaining two as lattice water molecules. Selected bond parameters are listed in Tables 2 and 3, respectively; the principle structural features of complex **1** are shown in Fig. 1. Hydrogen bonds of type O–H...O and O–H...N connect the mononuclear units to a three-dimensional network structure (Fig. 2). The four N-donor atoms of the tetrazolato group are not coordinated to metal centers, but act as acceptor of the O–H...N hydrogen bonds. The six-membered pyridine ring and the five-membered tetrazolate ring of the 4-PTZ ligands are both planar and their mean planes have acute angles of 12.67(10)° and 12.47(15)°, for **1** and **2**, respectively. Adjacent mononuclear units show alternate stacking of their 4-PTZ ligands along the *a*-axis of the triclinic unit cell. The shortest separation of tetrazole ring centers from pyridine ring centers is 3.571(2) and 3.602(3) Å, for **1** and **2**, respectively.

A perspective view of compound **3** is given in Fig. 3, selected bond parameters are summarized in Table 4. The chain structure (Fig. 4) of compound **3** features octahedrally coordinated Ca(1); dinuclear subunits of pentagonal-bipyramidal Ca(2) centers; azide groups acting in end-on and end-to-end bridging mode; a $(4\text{-PTZ})_2H$ ligand in its zwitter ionic form coordinated via N(1) atom of the tetrazole ring to Ca(2); lattice and ligand water molecules. Again, a complicated hydrogen bond system connects the chains of polyhedra to form a 3-D network structure. Ca(1) centers are located at inversion centers. Their *trans*-coordinated octahedra are formed by oxygen atoms of four water molecules and the nitrogen atoms of two end-to-end azido bridges [Ca(1)–O(1) 2.320(2), Ca(1)–O(2) 2.377(2), Ca(1)–N(11) 2.460(2) Å]. The basal positions of the pentagonal bipyramids of Ca(2) centers are occupied by nitrogen atoms N(13), N(21) and N(21B) of azido groups [Ca(2)–N(13) 2.454(2), Ca(2)–N(21) 2.599(2), Ca(2)–N(21B) 2.597(2) Å] and oxygen atoms O(4) and O(5) of two water molecules [Ca(2)–O(4) 2.517(2), Ca(2)–O(5) 2.381(2) Å], which deviate −0.76 and +0.69 Å, respectively, from the mean basal plane. The apical positions are occupied by O(3) of water molecule and N(1) of monodentate tetrazolate ligand [Ca(2)–O(3) 2.301(2), Ca(2)–N(1) 2.581(2) Å, O(3)–Ca(2)–N(1) 168.64(5)°]. Two centrosymmetrically related polyhedra of Ca(2) have common basal edges via N(21) and N(21B) of end-on bridging azido groups. The Ca(2)...Ca(2B) separation is 4.318(2) Å, the Ca(2)–N(21)–Ca(2B) bridge angle is 112.42(6)°. Pentagonal bipyramidal Ca polyhedra also connected by two common end-on azido bridges to dinuclear subunits have been observed in the crystal structures of $CsCa(N_3)_3 \cdot H_2O$ [21], $Cs_5Ca_2(N_3)_9 \cdot 2H_2O$ [22], and $Cs_7Ca_4(N_3)_{15}$ [23]. The octahedra of Ca(1) are linked by end-to-end bridging azido groups with the dinuclear subunits of Ca(2) centers to form a 1D chain

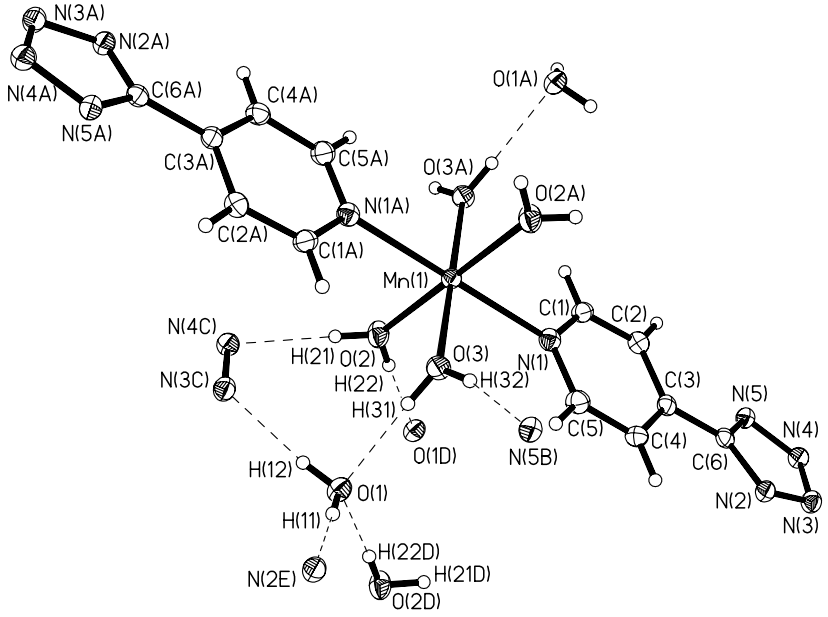

Fig. 1. Perspective view and atom labeling scheme of $[Mn(4\text{-PTZ})_2(H_2O)_4] \cdot 2H_2O$ (**1**). Broken lines indicate hydrogen bonds . Symmetry codes according to Table 2.

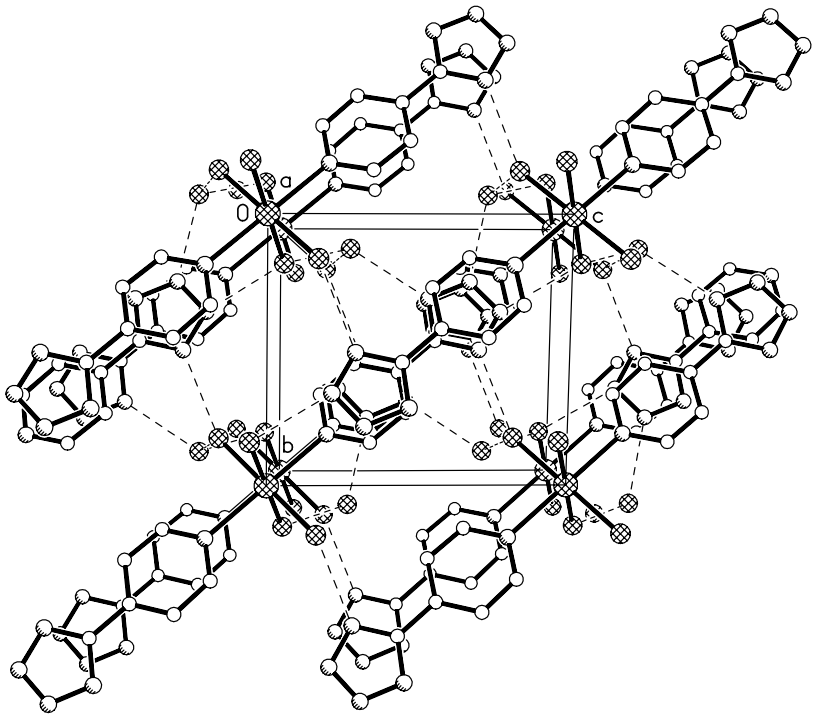

Fig. 2. Packing plot of $[Mn(4\text{-}PTZ)_2(H_2O)_4]\cdot 2H_2O$ (**1**) along *a*-axis of unit cell. Hydrogen bonds are indicated by broken lines.

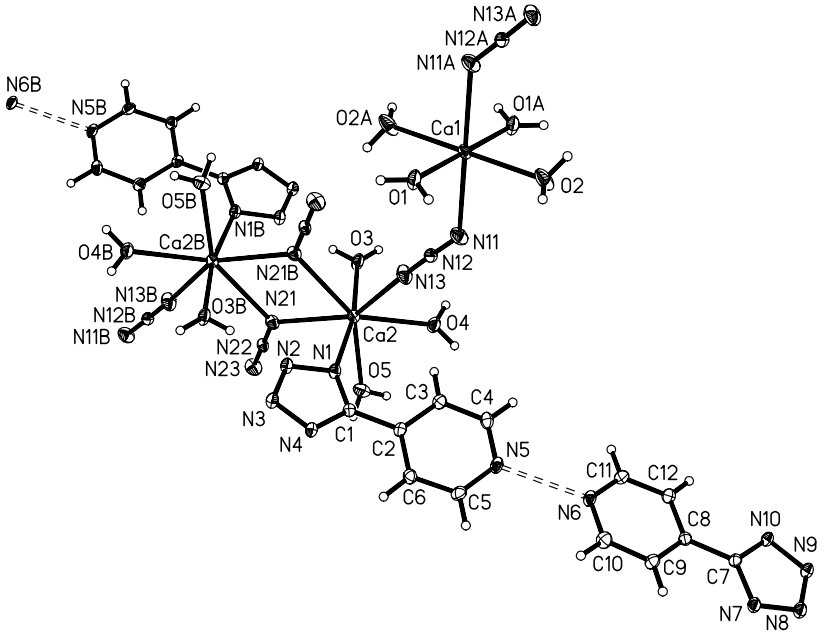

Fig. 3. Perspective view of $[Ca_{1.5}((4\text{-}PTZ)_2H)(N_3)_2(H_2O)_5](H_2O)_{0.3}$ (**3**) with atom labeling scheme. Disordered atoms are omitted for clarity. Symmetry codes according to Table 4.

systems along [0 1 −1] direction (Fig. 4). The Ca(1)...Ca(2) centers are separated by 6.811(2) Å. The Ca(2)–N(13)–N(12) bond angle is almost linear [177.2(2)°], whereas Ca(1)–N(11)–N(12) is 134.78(14)°. The Ca(1)–N(11)...N(13)–Ca(2) torsion angle is 176.6(4)°.

In contrast to complexes **1** and **2** the monodentate 4-PTZ ligand is not coordinated via its pyridine nitrogen

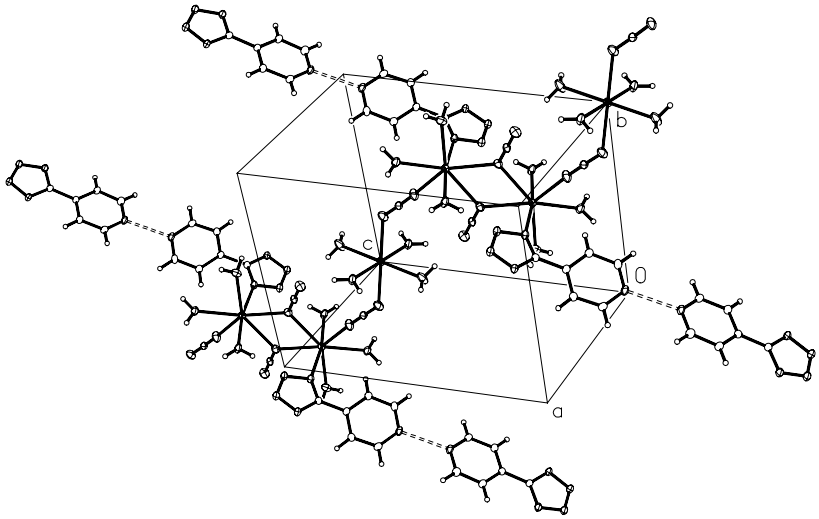

Fig. 4. Propagation of the chain structure of $[Ca_{1.5}((4\text{-}PTZ)_2H)(N_3)_2(H_2O)_5](H_2O)_{0.3}$ (**3**) along the [0 1 −1] direction of the unit cell.

atom to the metal center. Instead, a zwitter ion pair is formed with a second, non-coordinated 4-PTZ anion, with a N(5)...N(6) separation of 2.631(3) Å. The four aromatic rings of the zwitter ion are not coplanar. The tetrazole rings form acute angles of 14.92(9)° and 5.22(11)° with their pyridine rings, respectively, whereas the acute angle between central pyridine rings is 17.00(8)°. Except N(1), which is coordinated to Ca(2), all tetrazolate N-donor atoms are involved in hydrogen bonds of type N...H–O. The 1D chains of Ca-polyhedra form layers extended parallel to the *bc*-planes of the triclinic unit cell. Along the *a*-axis these layers are separated by sheets of alternate stacked $(4\text{-}PTZ)_2H^+$ zwitter ions. The shortest separations between adjacent ring centers are 3.577(2) and 3.688(2) Å.

Bond lengths and bond angles of the tetrazolate groups of the $(4\text{-}PTZ)_2H^+$ zwitter ion of **3** and of the 4-PTZ ligands of **1** and **2** agree well with values reported in a series of bis-tetrazolate-dianions [24]. The N2–N3 bond opposite to C in position 5 is significantly shorter [1.319(4)–1.323(2) Å] than other interatomic distances within the heterocycle despite of the aromatic nature of the five-membered ring. In case of 5-phenyl tetrazolate anion (5-PhTZ) the deprotonation had also led to a noticeable elongation of the N2–N3 bond from 1.247 to 1.307(3) Å, in excellent agreement with ab initio calculations [25].

3.2. IR spectra

The dominating feature in the IR spectra of compounds **1**–**3** is the strong and very broad band in the region 3550–3000 cm^{-1} originating from the extensive hydrogen bonded water molecules. The IR spectra of isomorphic complexes **1** and **2** are practically identical in shape and positions of their vibrational bands. The absence of any bands in 2200–1700 cm^{-1} region confirms ring formation to the tetrazolate ligand by [2+3] cycloaddition. Neither vibrations associated with ν(CN) of 4-CNpy (expected weak to medium bands centered around 2240 cm^{-1}) nor strong bands associated with $\nu_{as}(N_3)$ in the 2150–2000 cm^{-1} region are present [26]. In agreement with the crystal structure, the IR spectrum of **3** shows two additional very strong bands at 2056 and 2037 cm^{-1}, due to $\nu_{as}(N_3)$. The former band at 2056 cm^{-1} may be assigned to the μ-1,1 azide bridge, and the latter one to the μ-1,3 azide bridge [27,28].

3.3. Thermoanalytic investigations

The thermal decomposition of the three compounds was studied by thermogravimetry with simultaneous differential thermal analysis and mass spectrometry. Onset of dehydration of the Cd compound (**2**) is observed at 61 °C. Mass spectrometry confirms that the mass loss is due to emission of H_2O ($m/z = 18$). The TG signal indicates that the departure of water can be described as a two-step process. Correspondingly, DTG, DTA, and MS signals show two partly overlapping peaks. From the TG signal a loss of 5.8 mol H_2O can be calculated which is somewhat smaller than the theoretically expected loss of 6 mol H_2O. The third step of weight loss, with onset temperature at about 200 °C, can be assigned to the decomposition of tetrazole rings by release of N_2 ($m/z = 28$). The calculated amount of 2.5 mol N_2 is larger than the theoretically expected loss of 2 mol N_2. However, as the MS signal indicates an overlap in the emission of H_2O and N_2 separation of these two effects is difficult.

The Mn compound (**1**) shows a thermal behavior which is analogous to (**2**). Dehydration starts at 66 °C and is characterized by two superimposed peaks which

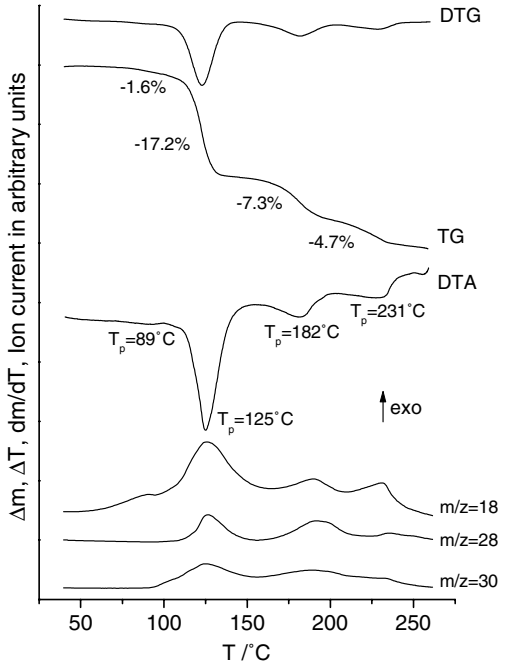

Fig. 5. TG, DTG, DTA, and MS curves for compound (**3**) (simultaneous measurement); powder weight: 10.66 mg; heating rate: 5 °C/min; dynamic argon atmosphere; flow rate: 1 l/h; $m/z = 18$ (H_2O); $m/z = 28$ (N_2); $m/z = 30$ (NO).

correspond to the removal of all water molecules (calculated amount: 5.9 mol H_2O; theoretically expected amount: 6 mol H_2O). Further decomposition of the sample, with onset temperature at 225 °C, is due to departure of N_2 (calculated amount: 2.3 mol N_2; theoretically expected amount: 2 mol N_2).

Compared with (**1**) and (**2**) the behavior of the Ca compound (**3**) is more complex (Fig. 5). Onset of mass loss upon heating occurs at approximately 55 °C. Four overlapping peaks in DTA and DTG signals as well as mass spectrometer signal ($m/z = 18$) indicate that dehydration takes place in four steps. Additionally, the simultaneous departure of N_2 ($m/z = 28$) and NO ($m/z = 30$) with H_2O is detected by mass spectrometry which makes a quantitative separation of the effects difficult. However, the experimentally observed total mass loss of 30.7% is in agreement with a theoretically expected mass loss of 28.4% associated with release of 5.30 mol H_2O and 2 mol N_2 (from tetrazole).

4. Supplementary material

Supplementary data are available from the CCDC, 12 Union Road, Cambridge CB2 1EZ, UK (fax: +44-1223-336033; E-mail: deposit@ccdc.cam.ac.uk or www: http://www.ccdc.cam.ac.uk) on request, quoting the deposition numbers: CCDC-225740 to CCDC-225742 for **1**–**3**, respectively.

Acknowledgements

F.A.M. thanks Prof. Kratky and Prof. Belaj (Univ. Graz) for the use of the STOE 4-circle diffractometer.

References

[1] R.N. Butler, in: A.R. Katrizky, C.W. Rees, E.F.V. Scriven (Eds.), Comprehensive Heterocyclic Chemistry, vol. 4, Pergamon, Oxford, UK, 1996.
[2] H. Singh, A.S. Chawla, V.K. Kapoor, D. Paul, R. Malhotra, Prog. Med. Chem. 17 (1980) 151.
[3] (a) V.A. Ostrovskii, M.S. Pevzner, T.P. Kofmna, M.B. Shcherbinin, I.V. Tselinskii, Targets Heterocycl. Syst. 3 (1999) 467;
(b) M. Hiskey, D.E. Chavez, D.L. Naud, S.F. Son, H.L. Berghout, C.A. Bome, Proc. Pyrotech. Semin. 27 (2000) 3.
[4] D.J. Moderhack, J. Prakt. Chem. 340 (1988) 687.
[5] Z.P. Demko, K.B. Sharpless, J. Org. Chem. 66 (2001) 7945.
[6] F. Himo, Z.P. Demko, L. Noodleman, K.B. Sharpless, J.Am. Chem. Soc. 125 (2003) 9983.
[7] X. Xue, X.-S. Wang, L.-Z. Wang, R.-G. Xiong, B.F. Abrahams, X.-Z. You, Z.-L. Xue, C.-M. Che, Inorg. Chem. 41 (2002) 6544.
[8] L.-Z. Wang, Z.-R. Qu, H. Zhao, X.-S. Wang, R.-G. Xiong, Z.-L. Xue, Inorg. Chem. 42 (2003) 3969.
[9] R. Cortes, L. Lezama, F.A. Mautner, T. Rojo, in: M.M. Turnbull, T. Sugimoto, L.K. Thompson (Eds.), Molecule-Based Magnetic Materials, Theory, Techniques and Applications; ACS Symposium Series, no. 644, ACS, Washington, DC, 1996.
[10] J. Ribas, A. Escuer, M. Monfort, R. Vicente, R. Cortes, L. Lezama, T. Rojo, Coord. Chem. Rev. 193–195 (1999) 1027.
[11] M.A.M. Abu-Youssef, A. Escuer, M.A.S. Goher, F.A. Mautner, G. Reiss, R. Vicente, Angew. Chem., Int. Ed. Engl. 39 (2000) 1624.
[12] A. Escuer, J. Cano, M.A.S. Goher, Y. Journaux, F. Lloret, F.A. Mautner, R. Vicente, Inorg. Chem. 39 (2000) 4688.
[13] A. Escuer, R. Vicente, F.A. Mautner, M.A.S. Goher, M.A.M. Abu-Youssef, Chem. Commun. (2002) 64.
[14] M.A.S. Goher, F.A. Mautner, M.A.M. Abu-Youssef, A.K. Hafez, A.M.A. Badr, J. Chem. Soc., Dalton Trans. (2002) 3309.
[15] M.A.S. Goher, F.A. Mautner, A.K. Hafez, M.A.M. Abu-Youssef, C. Gspan, A.M.A. Badr, Polyhedron 22 (2003) 975.
[16] F.A. Mautner, Doctoral Thesis, Technische Universität Graz, 1988.
[17] H. Walker, D. Stuart, Acta Crystallogr. A39 (1983) 158.
[18] SHELXTL/PC 5.03, Siemens Analytical Automation Inc., Madison, WI, 1995.
[19] M.A.S. Goher, F.A. Mautner, M.A.M. Abu-Youssef, A.K. Hafez, A.M.A. Badr, C. Gspan, Polyhedron 22 (2003) 3137.
[20] A. Escuer, R. Vicente, M.A.S. Goher, F.A. Mautner, Inorg. Chem. 36 (1997) 3440.
[21] H. Krischner, F.A. Mautner, C. Kratky, Acta Crystallogr. C39 (1983) 941.
[22] A.I. Saracoglu, H. Krischner, C. Kratky, Z. Kristallogr. 165 (1983) 79.
[23] H. Krischner, F.A. Mautner, C. Kratky, Z. Kristallogr. 167 (1984) 83.
[24] A. Hammerl, G. Holl, T.M. Klapötke, P. Mayer, H. Nöth, H. Piotrowski, M. Warchhold, Eur. J. Inorg. Chem. (2002) 834.
[25] I.A. Guzei, G.A. Bikzhanova, Acta Crystallogr. E58 (2002) o937.
[26] K. Nakamoto, Infrared Spectra of Inorganic and Coordination Compounds, 2nd ed., Wiley, New York, 1978.
[27] I. Agrell, Acta Chem. Scand. 25 (1971) 2965.
[28] M.A.S. Goher, Acta Chim. Hung. 127 (1990) 213.

Available online at www.sciencedirect.com
SCIENCE DIRECT®
Polyhedron 23 (2004) 1225–1233
POLYHEDRON
www.elsevier.com/locate/poly

Structural and spectral studies of nickel(II) complexes of di-2-pyridyl ketone N^4,N^4-(butane-1,4-diyl) thiosemicarbazone

Varughese Philip [a], V. Suni [a], Maliyeckal R. Prathapachandra Kurup [a,*], Munirathinam Nethaji [b]

[a] *Department of Applied Chemistry, Cochin University of Science and Technology, Kochi 682 022, Kerala, India*
[b] *Department of Inorganic and Physical Chemistry, Indian Institute of Science, Bangalore 560 012, India*

Received 25 September 2003; accepted 3 February 2004

Abstract

An interesting series of three Ni(II) complexes with the general formula $[NiLX]\cdot\frac{1}{2}H_2O$ (X = Cl, N_3 and NCS) were synthesized using di-2-pyridyl ketone N^4,N^4-(butane-1,4-diyl) thiosemicarbazone (HL). The structures of the compounds NiLCl (**1**) and $NiL(N_3)$ (**2**) have been solved by single crystal X-ray crystallography with $P\bar{1}$ and *Pbca* space groups, respectively. Electronic spectral data suggests a square planar geometry around nickel(II) in all the complexes. X-ray diffraction studies reveal that the thiosemicarbazone is bonded to the nickel(II) centre as an NNS donor ligand coordinating through one of the pyridine nitrogens, azomethine nitrogen and thiolate sulfur. Magnetic susceptibility measurements at room temperature indicate the diamagnetic nature of all the complexes. ^{1}H NMR, UV/Vis and IR spectroscopic data are consistent with the structures of compounds **1** and **2** derived from the crystallographic results and the spectral data for compound NiL(NCS) (**3**) suggest a structure similar to the chloro and azido derivatives.
© 2004 Elsevier Ltd. All rights reserved.

Keywords: Di-2-pyridyl ketone; Thiosemicarbazone; Ni(II) thiosemicarbazone complex; Electronic spectra; IR spectra; X-ray crystal structure

1. Introduction

Metal complexes of thiosemicarbazones possess significant biological activity and are nowadays widely used as potential drugs [1]. It has been shown that metal complexes derived from substituted thiosemicarbazones from 2-acetylpyridine exhibit antimalarial activity. There are also some reports on the anticancer activity of some of the transition metal complexes of thiosemicarbazones [2]. The biological activity of thiosemicarbazones is related to its chelating ability with transition metal ions, bonding through nitrogen, nitrogen and sulfur [3] or oxygen, nitrogen and sulfur [4]. In the case of α-N heterocyclic carbaldehyde thiosemicarbazones, the biological activity depends on the parent aldehyde or ketone [5,6]. Compared to the extensive studies on 2-acetylpyridine thiosemicarbazones [7–9], there are only few reports on the metal complexes of thiosemicarbazones derived from di-2-pyridyl ketone [10]. We have recently reported the synthesis, spectral characterization and structural studies of the present thiosemicarbazone with the aim to correlate the structural features and chelating ability [11]. Di-2-pyridyl ketone N^4,N^4-(butane-1,4,diyl) thiosemicarbazone resonates into thione and thiol forms and as a result a small negative charge resides on the nitrogen atom of the pyridine ring, which enhances its biological activity [12,13]. This paper deals with the synthesis, spectral and structural studies of Ni(II) complexes of the potential tetradentate ligand, di-2-pyridyl ketone N^4,N^4-(butane-1,4-diyl) thiosemicarbazone (Fig. 1). An interesting aspect of the present study is that the quadridentate HL behaves as a tridentate ligand in all the complexes under study, since only one of the pyridyl nitrogens is coordinated to the metal. The Ni(II) complexes are square planar in

* Corresponding author. Tel.: +91-484-2575804; fax: +91-484-2577595.
E-mail address: mrp@cusat.ac.in (M.R. Prathapachandra Kurup).

0277-5387/$ - see front matter © 2004 Elsevier Ltd. All rights reserved.
doi:10.1016/j.poly.2004.02.004

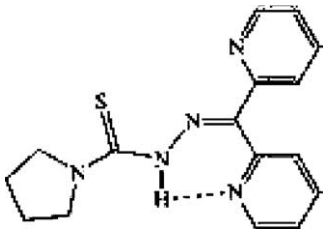

Fig. 1. Structure of di-2-pyridyl ketone N^4, N^4-(butane-1,4-diyl)thiosemicarbazone.

geometry with the fourth coordination site occupied by Cl, N_3 or NCS in compounds **1**, **2** and **3**, respectively.

2. Experimental

2.1. Synthesis of ligand

Di-2-pyridyl ketone N^4,N^4-(butane-1,4-diyl) thiosemicarbazone was prepared by the earlier reported method [11].

2.2. Synthesis of complexes

2.2.1. Synthesis of $[NiLCl]\cdot\frac{1}{2}H_2O$

A solution of the ligand HL (0.311 g, 1 mmol) in 20 ml of hot ethanol was treated with an ethanolic solution of $NiCl_2\cdot 6H_2O$ (0.237 g, 1 mmol). The solution was heated under reflux for 2 h. The resulting solution was allowed to stand at room temperature and after slow evaporation, dark brown crystals of compound **1** separated out, which were collected, washed with water, followed by ether and dried over P_4O_{10} in vacuo.

2.2.2. Synthesis of $[NiL(N_3)]\cdot\frac{1}{2}H_2O$

A solution of the ligand HL (0.311 g, 1 mmol) in 20 ml of hot ethanol was treated with an ethanolic solution of $Ni(OAc)_2\cdot 4H_2O$ (0.248 g, 1 mmol). The solution was heated under reflux and sodium azide (0.065 g, 1 mmol) was added in portions to the solution and further refluxed for 2 h. The resulting solution was allowed to stand at room temperature for few days and upon slow evaporation gave dark brown crystals of compound **2**. The crystals separated out were collected, washed with water, followed by ether and dried over P_4O_{10} in vacuo.

2.2.3. Synthesis of $[NiL(NCS)]\cdot\frac{1}{2}H_2O$

A solution of the ligand HL (0.311 g, 1 mmol) in 20 ml of hot ethanol was treated with an ethanolic solution of $Ni(OAc)_2\cdot 4H_2O$ (0.248 g, 1 mmol). The solution was heated under reflux and an ethanolic solution of potassium thiocyanate (0.097 g, 1 mmol) was added to the solution and further refluxed for 2 h. The resulting solution was allowed to stand at room temperature and after slow evaporation, dark brown crystals of compound **3** separated out, which were collected, washed with water, followed by ether and dried over P_4O_{10} in vacuo.

2.3. Physical measurements

Elemental analyses were carried out using a Heraeus Elemental Analyzer at the Regional Sophisticated Instrumentation Center, Central Drug Research Institute, Lucknow, India. Molar conductance measurements of the complexes were carried out in DMF solvent at 28 ± 2 °C on a Centuary CC-601 digital conductivity meter with dip type cell and platinum electrode. Approximately 10^{-3} M solutions were used. The magnetic susceptibility measurements were made using a simple Gouy balance at room temperature using mercury tetrathiocyanatocobaltate(II), $Hg[Co(NCS)_4]$ as calibrant. Infrared spectra were recorded on a Shimadzu DR 8001 series FTIR instrument as KBr pellets for spectra run from 4000 to 400 cm^{-1}, and using polyethylene for the range 500–100 cm^{-1} in a Nicolet Magna 550 FTIR instrument. Solid state reflectance spectra in the 200–900 nm range were recorded on an Ocean Optics SD 2000 Fibre Optic Spectrometer. ^1H NMR spectra were recorded in an AMX 400 MHz FT-NMR Spectrometer using $CDCl_3$ as a solvent and TMS as an internal standard at the Sophisticated Instruments Facility, Indian Institute of Science, Bangalore, India.

2.4. X-ray crystallography

Single crystals of compound **1** for X-ray analysis were grown by slow evaporation of the complex in methanol. A dark brown crystal of [NiLCl] (**1**) was mounted on a glass fiber using epoxy cement. The X-ray diffraction data were measured in frames with increasing ω (width of 0.3°/frame) at room temperature (293 K) using a Bruker SMART APEX CCD diffractometer, equipped with a fine focus sealed tube X-ray source. Selected crystal data and data collection parameters are given in Table 2. SMART software was used for data acquisition and SAINT software for data extraction [14]. Empirical absorption corrections were made on the intensity data [15]. The structure was solved by the heavy atom method and refined by full-matrix least squares using the SHELX system of programs [16] and the graphics tool was PLATON for windows [17]. All non-hydrogen atoms of the complex cations were refined anisotropically. Some hydrogen atoms were located from the difference Fourier map, and the rest were generated, assigned isotropic thermal parameters, and refined using a riding model. The hydrogen atoms were used for structure factor calculation only. A dark brown crystal of the compound $[NiLN_3]$ (**2**) was analyzed in a similar way and the crystallographic data along with the structural refinements are also given in Table 2.

3. Results and discussion

3.1. Synthesis of complexes

Colours, elemental analyses and stoichiometries of the ligand (HL) and its nickel(II) complexes are presented in Table 1. Elemental data for all the complexes are consistent with the 1:1:1 ratio of the metal:thiosemicarbazone:gegenion. All the complexes are found to be brown in colour, which is common to complexes involving thiosemicarbazone coordination, resulting from the sulfur to metal charge transfer bands [18,19]. Conductivity measurements in 10^{-3} DMF solution indicate that all complexes are non-electrolytes in this solution [20]. The non-electrolytic nature of complexes indicates that the ligand, which behaves as a uninegative ion, coordinates to Ni(II) along with the chloride, azide or thiocyanate ions giving the formula [NiLX] $\cdot\frac{1}{2}H_2O$ (where X = Cl, N_3 and NCS). The square planar geometry around Ni(II) in the complexes is also evident from their magnetic moment measurements.

3.2. Crystal structures of [NiLCl] and [NiL(N_3)]

The molecular structures of [NiLCl] (**1**) and [NiL(N_3)] (**2**) along with the atomic labelling are shown in Figs. 2 and 3, and selected bond lengths and bond angles are summarized in Table 3. The ligand behaves as

Table 1
Elemental analyses, colours and molar conductivities of Ni(II) complexes

Compound	Colour	λ_M	Found (Calc.) %		
			C	H	N
HL	yellow		62.10 (61.71)	5.56 (5.50)	22.43 (22.49)
[NiLCl] $\cdot\frac{1}{2}H_2O$	brown	12	46.64 (46.47)	3.98 (4.14)	16.81 (16.93)
[NiL(N_3)] $\cdot\frac{1}{2}H_2O$	brown	15	45.81 (45.74)	3.98 (4.08)	26.29 (26.67)
[NiL(SCN)] $\cdot\frac{1}{2}H_2O$	brown	10	46.75 (46.81)	3.72 (3.93)	19.00 (19.27)

Table 2
Crystal data, data collection and structure refinement parameters for [NiLCl] and [NiL(N_3)]

Parameters	[NiLCl]	[NiL(N_3)]
Empirical formula	$C_{16}H_{16}ClN_5NiS$	$C_{16}H_{16}N_8NiS$
Formula weight, M	404.56	411.14
Temperature, T (K)	293(2)	293(2)
Wavelength, Mo Kα (Å)	0.71073	0.71073
Crystal system	triclinic	orthorhombic
Space group	$P\bar{1}$	*Pbca*
Lattice constants		
a (Å)	5.3295(12)	14.483(3)
b (Å)	11.390(3)	11.962(2)
c (Å)	13.930(3)	20.344(4)
α (°)	99.721(4)	90
β (°)	91.871(4)	90
γ (°)	98.720(4)	90
Volume V (Å^3)	822.3(3)	3524.5(12)
Z	2	8
Calculated density (Mg m^{-3})	1.634	1.550
Absorption coefficient, μ (mm^{-1})	1.477	1.238
F (0 0 0)	416	1696
Crystal size (mm)	0.30 × 0.25 × 0.20	0.30 × 0.25 × 0.20
θ range for data collection	1.49–27.88	2.00–26.04
Limiting indices	$-6 \leqslant h \leqslant 6$, $-14 \leqslant k \leqslant 14$, $-18 \leqslant l \leqslant 17$	$-17 \leqslant h \leqslant 17$, $-14 \leqslant k \leqslant 14$, $-25 \leqslant l \leqslant 25$
Reflections collected	9069	25,988
Unique reflections	3551 [$R_{int} = 0.0266$]	3470 [$R_{int} = 0.0227$]
Completeness to θ	27.88 (91.1%)	26.04 (99.9%)
Absorption correction	none	none
Maximum and minimum transmission	0.7566 and 0.6657	0.7899 and 0.7078
Refinement method	full-matrix least-squares on F^2	full-matrix least-squares on F^2
Data/restraints/parameters	3551/0/281	3470/0/299
Goodness-of-fit on F^2	1.114	1.079
Final R indices [$I > 2\sigma(I)$]	$R_1 = 0.0413$, $wR_2 = 0.0949$	$R_1 = 0.0258$, $wR_2 = 0.0657$
R indices (all data)	$R_1 = 0.0488$, $wR_2 = 0.0983$	$R_1 = 0.0310$, $wR_2 = 0.0688$
Largest difference peak and hole (e Å^{-3})	0.455 and −0.189	0.276 and −0.166

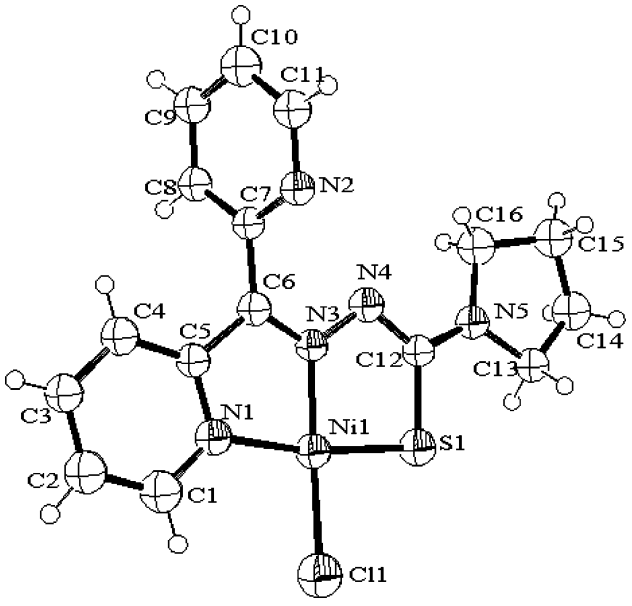

Fig. 2. ORTEP diagram for compound [NiLCl], displacement ellipsoids are drawn at 50% probability level and hydrogen atoms are shown as small spheres of arbitrary radii.

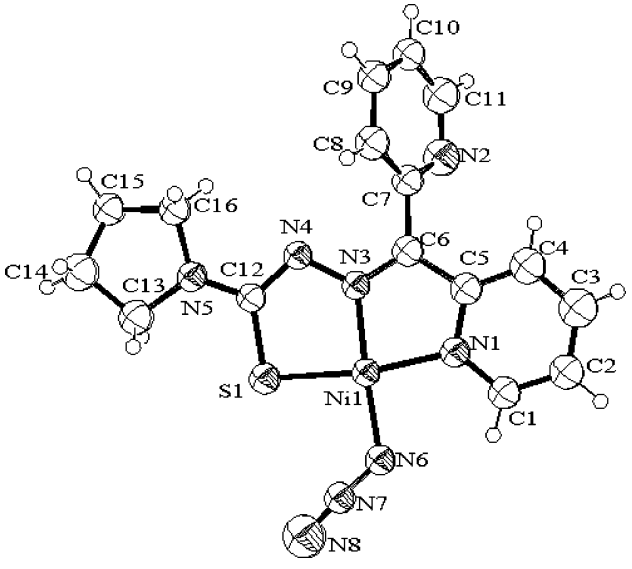

Fig. 3. ORTEP diagram for compound [$NiLN_3$], displacement ellipsoids are drawn at 50% probability level and hydrogen atoms are shown as small spheres of arbitrary radii.

NNS tridentate, coordinating via its pyridine nitrogen, azomethine nitrogen and the thiolate sulfur atom giving a distorted square planar geometry around the nickel atom. The configuration of the thiosemicarbazone chain about the C(6)–N(3) bond changes *Z* to facilitate the coordination of the thiolate sulfur to Ni(1) in both complexes. The Ni(II) coordination is almost square planar in compound **1**, with a maximum value for the mean deviation of the pyridine N(1), imino N(3), thiosemicarbazone S(1) and chloride Cl(1) atoms from their own plane of 0.0447 Å. Compared to this, greater distortion from square planar configuration is observed in **2** as evident from the maximum mean deviation value of 0.2042 Å for the plane constituted by N(1), N(3), S(1) and N(6). The bond angles, S(1)–Ni(1)–N(3) (87.07°) and Cl(1)–Ni(1)–N(1) (96.99°) of [NiLCl] (**1**) and N(3)–Ni(1)–N(1) (83.54°) and S(1)–Ni(1)–N(6) (95.40°) of [$NiL(N_3)$] (**2**) also reveal the distortion of the square planes comprising of Ni(1), Cl(1), N(1), N(3) and S(1) atoms in compound **1** and Ni(1), N(1), N(3), N(6) and S(1) in compound **2**, respectively. The bond angles Ni(1)–N(3)–C(6) (116.68°) and Ni(1)–N(1)–C(5) (112.16°) in compound **1** and Ni(1)–N(3)–C(6) (117.11°) and Ni(1)–N(1)–C(5) (112.9°) in compound **2** are almost identical. Similarly, the bond angles N(1)–Ni(1)–Cl(1) (96.99°); N(3)–Ni(1)–S(1) (87.07°) in compound **1** and N(2)–Ni(1)–N(6) (93.84°); N(3)–Ni(1)–S(1) (87.32°) in compound **2** are also analogous, as expected on the basis of the similar square planar nature for both complexes. The dihedral angles formed by the least square planes Cg(1) and Cg(2) are 2.29° and 42.14° respectively for **1** and **2**. This strongly supports the distorted square planar conformation of both the molecules where greater distortion is observed for compound **2**. The C(6)–N(3)

Table 3
Comparison of selected bond lengths (Å) and bond angles (°) of HL, [NiLCl] and [$NiLN_3$]

	HL	[NiLCl]	[$NiLN_3$]
Bond lengths			
Ni(1)–N(3)		1.853(2)	1.8557(13)
Ni(1)–N(1)		1.922(2)	1.9145(14)
Ni(1)–S(1)		2.1374(8)	2.1419(5)
S(1)–C(12)	1.671(4)	1.741(3)	1.7422(16)
N(3)–C(6)	1.308(4)	1.293(3)	1.308(2)
N(3)–N(4)	1.371(4)	1.373(3)	1.3669(19)
N(4)–C(12)	1.386(4)	1.331(3)	1.329(2)
Ni(1)–Cl(1)		2.1592(8)	
Ni(1)–N(6)			1.8723(15)
N(6)–N(7)			1.196(2)
N(7)–N(8)			1.146(2)
Bond angles			
N(3)–Ni(1)–S(1)		87.07(7)	87.32(5)
N(3)–Ni(1)–N(1)		84.00(9)	83.54(6)
N(1)–Ni(1)–S(1)		170.96(6)	169.90(5)
C(12)–S(1)–Ni(1)		95.43(9)	94.93(6)
C(1)–N(1)–Ni(1)		129.50(19)	127.71(13)
C(5)–N(1)–Ni(1)		112.16(16)	112.97(11)
C(6)–N(3)–Ni(1)		116.68(17)	117.11(12)
N(4)–N(3)–Ni(1)		124.42(15)	123.62(10)
C(6)–N(3)–N(4)	118.6(3)	118.8(2)	119.25(14)
N(1)–Ni(1)–Cl(1)		96.99(6)	
N(1)–Ni(1)–N(6)			93.84(7)
N(3)–Ni(1)–Cl(1)		176.82(7)	
N(3)–Ni(1)–N(6)			176.95(6)
S(1)–Ni(1)–Cl(1)		92.01(3)	
N(6)–Ni(1)–S(1)			95.41(5)
N(7)–N(6)–Ni(1)			124.25(14)
N(8)–N(7)–N(6)			175.9(2)

bond distances in the complexes are observed to be 1.293(3) and 1.308(2) Å in compounds **1** and **2** respectively and compared to the corresponding C(6)–N(3) bond distance in the ligand, this bond length is much shorter in **1**. This indicates stronger coordination of the azomethine nitrogen in compound **1** compared to compound **2**. Also, this implies a partial double bond character for the C(6)–N(3) bond in compound **1** [21]. The delocalisation of electron density from the coordinating nitrogen onto the central metal atom gives rise to an elongated N(3)–N(4) bond compared to the uncomplexed thiosemicarbazone in both complexes. The loss of the proton bound to N(4) in HL produces a negative charge, which is delocalised on the N(3)–N(4)–C(12) system. This is indicated by the lengthening of the bond S(1)–C(12), 1.741 Å in **1** and 1.7422 Å in **2**, compared to the value of 1.671 Å in the ligand. The decrease in the bond length of C(12)–N(4), 1.331 Å in compound **1** and 1.329 Å in compound **2**, from the value of 1.384 Å of the thiosemicarbazone also supports thiolate formation. Ring puckering analyses and least-square plane calculations show that the Cg(3) ring comprising of N5, C13, C14, C15 and C16 adopts an envelope conformation on C(15) in both complexes **1** and **2**. These observations are consistent with the work on nickel(II) complexes of di-2-pyridyl ketone N(4) substituted thiosemicarbazones by West et al. [22,23].

The molecules of [NiLCl] are packed in a 'face to face' manner within the unit cell (Fig. 4). However, the molecules of [NiL(N_3)] adopt a 'zig-zag' arrangement as is evident from Fig. 5. The unit cell is viewed down the *a* axis and 2 and 8 molecules of compound **1** and **2** respectively are arranged in their unit volume cell. The assemblage of molecules in the respective manner in the unit cell is resulted by the diverse π–π stacking, CH–π and ring–metal interactions depicted in Tables 4 and 5. The metal chelate rings Cg(1) and Cg(2) are involved in π–π interactions with the pyridyl ring of the neighbouring unit at average distances of 3.7897 and 3.7733 Å in compounds **1** and **2**, respectively. In addition to the π–π stacking, the CH–π interactions of the pyridyl hydrogens with the metal chelate rings of the neighbouring molecules contribute to the stability of the unit cell packing. Short ring–metal interaction of the chelate ring Cg(4) is observed at a distance of 3.586 Å from the Ni centre in compound **1**, while they are perceived at 3.788 Å for Cg(5) from the metal in the packed molecules of compound **2**. The crystal structure of **1** is further stabilized by the two CH–π interactions, viz. C(3)–H(3)–Cg(5) and C(13)–H(132)–Cg(1) while stability is enhanced by the C(2)–H(2)–Cg(1) and C(16)–H(162)–Cg(2) interactions in compound **2**. These π–π, CH–π and ring–metal interactions point out the possibility for metalloaromaticity – a classic concept recently reviewed by Masui [24].

3.3. Infrared spectra

Selected IR bands are listed in Table 6. The assignments of IR bands are observed to be in good agreement with the X-ray structural data. The spectrum of the ligand exhibits a medium band at 3049 cm^{-1}, which is assigned to *ν*(NH) vibration. The absence of *ν*(NH) in the spectra of the complexes provides strong evidence for the ligand coordination around the Ni(II) ion in its deprotonated form. The spectra of the complexes exhibit a systematic shift in the position of the bands in the region 1600–1350 cm^{-1} due to *ν*(C=C) and *ν*(C=N) vibrational modes, and their mixing patterns are different from those present in the ligand spectrum. As a result of coordination, the band corresponding to azomethine nitrogen, *ν*(C=N) shifts to higher wavenumbers by ca. 10 cm^{-1} in the complexes [25–28]. The band at 810 cm^{-1}, which is assigned to *ν*(C=S) in the free ligand, is shifted to lower wavenumbers in the complexes suggesting the change of bond order and strong electron-delocalisation upon

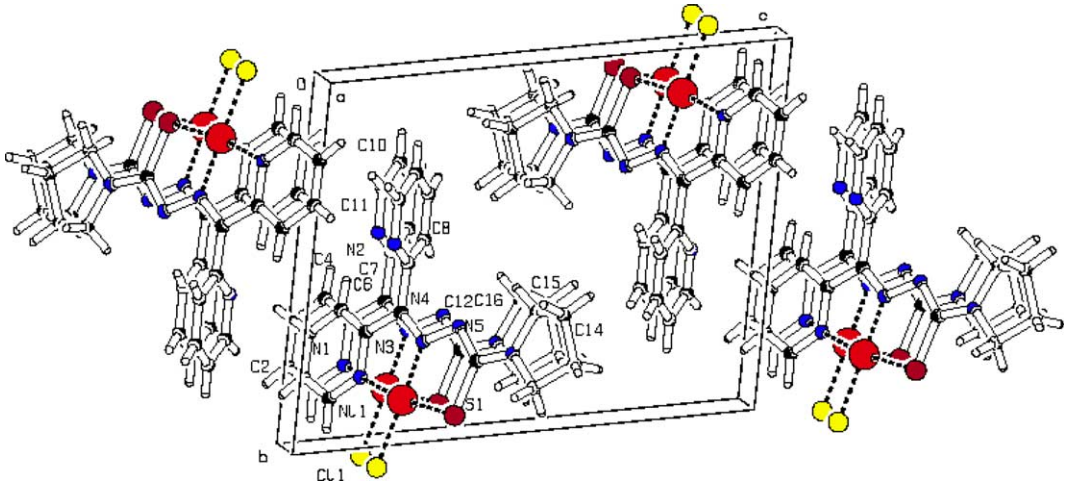

Fig. 4. Unit cell packing diagram of complex NiLCl, viewed down the *a*-axis.

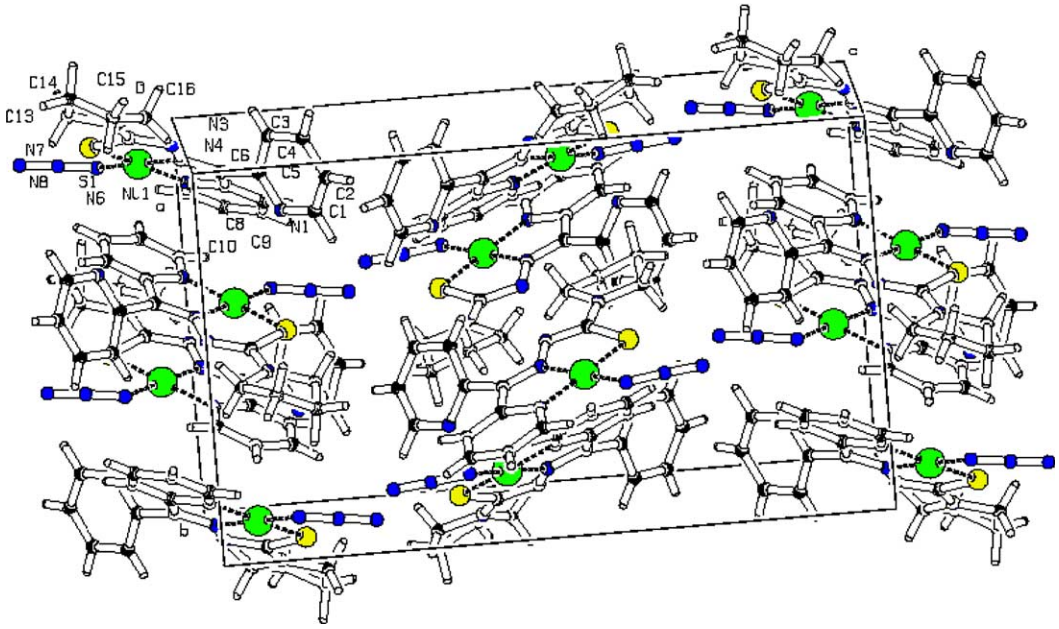

Fig. 5. Unit cell packing diagram of complex $NiLN_3$ viewed down the *a*-axis.

Table 4
Interaction parameters of the compound [NiLCl]

π–π interactions			
Cg(I)–Res(1)–Cg(J)	Cg–Cg (Å)	$\alpha°$	$\beta°$
Cg(1) [1] -> Cg(4)[a]	3.6176	2.29	24.97
Cg(2) [1] -> Cg(4)[a]	3.9617	4.11	28.56
Cg(4) [1] -> Cg(2)[b]	3.9617	4.11	32.55

Equivalent position codes: $a = 1 + x, y, z$; $b = -1 + x, y, z$
Cg(1) = N(1), S(1), C(12), N(4), N(3); Cg(2) = Ni(1), N(1), C(5), C(6), N(3); Cg(4) = N(1), C(1), C(2), C(3), C(4), C(5);
Cg(5) = N(2), C(7), C(8), C(9), C(10), C(11)

CH–π interactions			
XH(I)–Cg(J)	H···Cg (Å)	X–H···Cg (°)	X···Cg (Å)
C(3)–H(3)[1] -> Cg(5)[e]	2.9502	134.61	3.6194
C(13)–H(132) [1] -> Cg(1)[f]	2.8596	151.14	3.7287

Equivalent position code: $e = -1 - x, 1 - y, -z$; $f = 1 + x, y, z$

D: Donor, A: Acceptor, Cg: Centroid, α: dihedral angles between planes I and J, β: angle Cg(1)–Cg(J).

Table 5
Interaction parameters of the compound [$NiLN_3$]

π–π interaction			
Cg(I)–Res(I)–Cg(J)	Cg–Cg (Å)	α (°)	β (°)
Cg(1)-[1]–Cg(5)[a]	3.6650	7.99	18.30
Cg(2)-[1]–Cg(2)[a]	3.8815	0.02	31.20
Cg(5)-[1]–Cg(1)[a]	3.6650	7.99	26.21

Equivalent position codes: $a = -x, -y, -z$
Cg(1) = Ni(1), S(1), C(12), N(4), N(3); Cg(2) = Ni(1), N(1), C(5), C(6), N(3); Cg(5) = N(1), C(1), C(2), C(3), C(4), C(5)

CH–π interactions			
X–H(I)–Cg(J)	H···Cg(Å)	X–H···Cg (°)	X···Cg (Å)
C(2)–H(2)–Cg(1)[e]	2.8692	153.22	3.7304
C(16)–H(162)–Cg(2)[f]	3.0502	152.71	3.9291

Equivalent position code: $e = -1/2 + x, 1/2 - y, -z$; $f = 1/2 - x, -1/2 + y, z$

D: Donor, A: Acceptor, Cg: Centroid, α: dihedral angles between planes I and J, β: angle Cg(1)–Cg(J).

Table 6
Infrared spectral assignments (cm^{-1}) for HL and its Ni(II) complexes

Compound[a]	ν(NH)	ν(CN)	ν(CS)	ν(NiNazomethine)	ν(NiS)	ν(NiCl)	ρ(NiNpy)
HL	3049 s	1582 s	810 m				
[NiLCl]		1592 m	777 m	473 w	351m	304 m	281m
[NiL(N_3)]		1586 s	783 m	473 m	358 m		281m
[NiL(SCN)]		1591m	787 m	465 sh	354 m		

[a] Hydrate waters are omitted for convenience.

chelation [29]. The appearance of a new peak at ca. 1540 cm^{-1} in the complex is due to the asymmetric stretching vibration of the newly formed C(12)=N(4) bond. A medium band around 470 cm^{-1} further supports azomethine nitrogen coordination. The spectrum of the chloro complex exhibits bands at 351 and 304 cm^{-1} corresponding to ν(Ni–S) and ν(Ni–Cl), respectively.

The azido complex (compound **2**) exhibits a strong band at 2037 cm^{-1} corresponding to the ν_a(NNN) stretching vibration [30] of the coordinating azido group. The broad bands at 575 and 440 cm^{-1}, assigned to δ(NNN) and ν(Ni–N), respectively [31], are not prominent, suggesting that Ni–N–N–N is not linear. Compound **3** shows a sharp band at 2101 cm^{-1}, which is assigned to ν(C–N) of the thiocyanato group, indicating coordination through the thiocyanate sulfur [32]. A weak band at 700 cm^{-1} and several weak bands near 420 cm^{-1} corresponding to ν(C–S) and δ(NCS) of the thiocyanato group further supports sulfur coordination of the thiocyanate anion with the nickel centre [33–36].

3.4. Electronic spectra

Solid state electronic spectra of compounds **1**, **2** and **3** were determined in the region 200–900 nm. The data are given in Table 7. The ligand (HL) has absorption maxima at 36,240 and 35,100 cm^{-1} due to the $\pi \rightarrow \pi^*$ transition of the pyridyl ring and the imine function of thiosemicarbazone moiety, respectively. There are two bands at 30,880 and 29,150 cm^{-1} corresponding to the $n \rightarrow \pi^*$ transition of the pyridyl nitrogen and thioamide function, respectively. These bands suffer marginal shifts on complexation. The broad band at 31,150 cm^{-1} in [NiLCl] is assigned for both $n \rightarrow \pi^*$ transitions and Cl $\rightarrow$ Ni(II) charge transfer transitions [37]. The shift of the $\pi \rightarrow \pi^*$ bands to the longer wavelength region is the result of the C=S bond being weakened and conjugation system being enhanced after the formation of the complex [38]. The absence of bands below 10,000 cm^{-1} confirms the planar nature of the complexes. The $d \rightarrow d$ spectral transitions can be assigned to $^1A_{1g} \rightarrow {}^1E_g$, $^1A_{1g} \rightarrow {}^1A_{2g}$ and $^1A_{1g} \rightarrow {}^1B_{1g}$ in the order of decreasing energy [39]. The d–d bands appearing as weak shoulders centered around the 20,000 cm^{-1} region are typical of square planar monoligated Ni(II) complexes [40]. The presence of intense $\pi \rightarrow \pi^*$ and $n \rightarrow \pi^*$ transitions cause the lower energy d–d bands and LMCT bands to appear as weak shoulders, bringing about difficulty in the assignment of bands.

3.5. ^1H NMR spectra

^1H NMR spectral measurements are assigned as previously reported on di-2-pyridyl ketone N(4)-methyl and N(4)-dimethyl thiosemicarbazone and its metal complexes [23]. Table 8 shows that the N4H resonance is obtained at 15.0 ppm in HL. The large downfield shift of this proton indicates its involvement in hydrogen

Table 7
Electronic spectral assignments, cm^{-1} for HL and its nickel(II) complexes

Compound[a]	$\pi \rightarrow \pi^a$	$n \rightarrow \pi^a$	LMCT	d–d
HL	36240 35100	29150 30880 sh		
[NiLCl]	32780 sh	31150	23640 22880 sh	19340 sh 18150 sh 17210 sh
[NiL(N_3)]	32360 sh	30490	23750 22370 sh	19190 sh 17510 sh 16920 sh
[NiL(SCN)]	32680	30670	23750	19450 sh 17700 sh 17030 sh

[a] Hydrate waters are omitted for convenience.

Table 8
^{1}H NMR assignments of ligands HL and its nickel(II) complexes (δ in ppm)

Compound[a]	Solvent	N4H	C1H	C2H	C3H	C4H	C8H	C9H	C10 H	C11H
HL	$CDCl_3$	15.00	8.71,2H,d	7.34,2H,t	6.80,2H,t	7.00,2H,d				
[NiLCl]	$CDCl_3$		8.70,1H,d	7.75,1H,d	7.32,1H,d	7.87,1H,d	7.47,1H,d	7.74,1H,t	7.70,1H,t	8.63,1H,d
[NiL(N_3)]	$CDCl_3$		8.68,1H,d	7.73,2H,d	7.30,1H,t	7.87,1H,d	7.19.,1H,t	7.50,1Ht	7.73,2H,d	8.13,1H,d
[NiL(SCN)]	$CDCl_3$		8.69,1H,d	7.76,2H,t	7.30,2H,t	7.85,1H,d	7.54,1H,d	7.30,2H,t	7.76,2H,t	8.16,1H,d

[a] Hydrate waters are omitted for convenience.

bonding with the pyridyl nitrogen atom. This disappears in the spectra of complexes, which supports the enolisation and coordination of sulfur to Ni(II) in the thiolate form after deprotonation. The signals corresponding to aromatic protons are shifted downfield by 0.2–0.4 ppm on complexation. This is due to the electron withdrawal from the aromatic ring during the coordination of pyridyl nitrogen with the metal. The protons corresponding to the two pyridyl rings of di-2-pyridyl ketone appear as separate signals in the complexes, indicating its loss of equivalence due to imposition of a rigid geometry around the metal ion after complexation. This observation is consistent with the resonance of HL protons with C(1)H and C(11)H at $\delta = 8.71$ ppm (2H, doublet), C(2)H and C(10)H at $\delta = 7.34$ ppm (2H, triplet), C(4)H and C(8)H at $\delta = 7.00$ ppm (2H, doublet), C(3)H and C(9)H at $\delta = 6.8$ ppm (2H, triplet), which on complexation resonate at different fields. Due to the hydrogen bonding and CH–π interactions, the resonance absorptions of protons of the pyridyl ring are shifted downfield, which is further supported by X-ray crystallography.

4. Supplementary data

Crystallographic data for the structural analysis has been deposited with the Cambridge Crystallographic Data Center, CCDC 216757 for compound NiLCl (**1**) and CCDC 216756 for compound NiL(N_3) (**2**). Copies of this information may be obtained free of charge from The Director, CCDC, 12 Union Road, Cambridge, CB2 IEZ, UK (fax: +44-1223-336-033; e-mail: deposit@ccdc.cam.ac.uk or http://www.ccdc.cam.ac.uk).

Acknowledgements

The authors are thankful to the Regional Sophisticated Instrumentation Centre, CDRI, Lucknow, India, for the elemental analysis and the Sophisticated Instruments Facility, IISc Bangalore for NMR measurements. M. R.P. Kurup is thankful to the State Committee on Science, Technology and Environment, Thiruvanathapuram, India and V. Suni acknowledges the Cochin University of Science and Technology, for financial support.

References

[1] D.L. Klayman, J.P. Scovill, J.F. Bartosevich, J. Bruce, J. Med. Chem. 26 (1983) 35, and references therein.
[2] A.G. Quiroga, J.M. Pérez, E.I. Montero, D.X. West, C. Alonso, C. Navarro-Ranninger, J. Inorg. Biochem. 75 (1999) 293.
[3] A.C. Sartorelli, K.C. Agrawal, A.S. Tisftsoglou, E.C. Moore, Adv. Enzyme Reg. 15 (1977) 117.
[4] P. Bindu, M.R.P. Kurup, T.R. Satyakeerthy, Polyhedron 18 (1999) 321.
[5] S. Padhye, G.B. Kauffman, Coord. Chem. Rev. 63 (1985) 127.
[6] R. Restivo, G.J. Palenik, Acta Crystallogr. Sect. B 27 (1970) 1397.
[7] B.S. Garg, M.R.P. Kurup, S.K. Jain, Y.K. Bhoon, Transition Met. Chem. 13 (1988) 92.
[8] D.X. West, C.S. Carlson, A.C. Whyte, Transition Met. Chem. 15 (1990) 43.
[9] B.S Garg, M.R.P. Kurup, S.K. Jain, Y.K. Bhoon, Transition Met. Chem. 13 (1988) 247.
[10] C.-Y. Duan, B.-M. Wu, T.C.W. Mak, J. Chem. Soc., Dalton Trans. (1996) 3485.
[11] A. Usman, I.A. Razak, S. Chantrapromma, H.K. Fun, Varughese Philip, A. Sreekanth, M.R.P. Kurup, Acta Crystallogr., Sect. C 58 (2002) o652.
[12] G.J. Palenik, D.F. Rendle, W.S. Carter, Acta Crystallogr., Sect. B 30 (1974) 2390.
[13] R. Restivo, G.J. Palenik, Acta Crystallogr., Sect. B 30 (1970) 26.
[14] Siemens, SMART and SAINT, Area Detector Control and Integration Software, Siemens Analytical X-ray Instruments Inc., Madison, WI, 1996.
[15] R.H. Blessing, Acta Crystallogr. Sect. A 51 (1995) 33.
[16] G.M. Sheldrick, SHELXS-97 Program for the Solution of Crystal Structures, University of Göttingen, Göttingen, Germany, 1997.
[17] A.L. Speck, PLATON, A Multipurpose Crystallographic Tool, Utrecht University, Utrecht, The Netherlands, 1999.
[18] H. Beraldo, L.P. Boyd, D.X. West, Transition Met. Chem. 23 (1998) 67.
[19] H. Beraldo, S.B. Kaisner, J.D. Turner, I.S. Billeh, J.S. Ives, D.X. West, Transition Met. Chem. 22 (1997) 459.
[20] W.J. Geary, Coord. Chem. Rev. 7 (1971) 81.
[21] N. Gokhale, S. Padhye, D. Rathbone, D. Billington, P. Lowe, C. Schwalbe, C. Newton, Inorg. Chem. Commun. 4 (2001) 26.
[22] J.K. Swearingen, W. Kaminsky, D.X. West, Transition Met. Chem. 27 (2002) 7.
[23] J.K. Swearingen, D.X. West, Transition Met. Chem. 26 (2001) 252.
[24] H. Masui, Coord. Chem. Rev. 219–221 (2001) 957.
[25] A. Sreekanth, M.R.P. Kurup, Polyhedron 22 (2003) 3321.
[26] M.J.M. Campbell, Coord. Chem. Rev. 15 (1975) 279.
[27] B.S. Garg, M.R.P. Kurup, S.K. Jain, Y.K. Bhoon, Transition Met. Chem. 13 (1988) 309.
[28] B.S. Garg, M.R.P. Kurup, S.K. Jain, Y.K. Bhoon, Transition Met. Chem. 16 (1991) 111.
[29] R. Mayer, in: M. Jansen (Ed.), Organosulfur Chemistry, Interscience, New York, 1967, p. 219.

[30] K. Nakamoto, Infrared and Raman Spectra of Inorganic and Coordination Compounds, 5th ed., Wiley, New York, 1997.
[31] R.P. John, A. Sreekanth, M.R.P. Kurup, S.M. Mobin, Polyhedron 21 (2002) 2515.
[32] R.A. Bailey, S.L. Kozak, T.W. Michelsen, W.N. Mills, Coord. Chem. Rev 6 (1971) 407.
[33] C.H. Mitchel, R.J.P. Williams, J. Chem. Soc. (1960) 1912.
[34] A. Turco, C. Pecile, Nature 191 (1961) 66.
[35] J. Lewis, R.S. Nyholm, P.W. Smith, J. Chem. Soc. (1960) 1912.
[36] A. Sabatini, I. Bertini, Inorg. Chem. 4 (1965) 959.
[37] M. Suzuki, H. Kanatomi, H. Koyama, I. Murase, Bull. Chem. Soc. Japan 53 (1980) 1961.
[38] Q. Li, H. Tang, Y. Li, M. Wang, L. Wang, C. Xia, J. Inorg. Biochem. 78 (2000) 167.
[39] L.D. Dave, P. Frances, Indian J. Chem. 22A (1983) 422.
[40] M. Akbar Ali, S.M.G. Hossain, S.M.M.H. Majumder, M. Nazimuddin, M.T.H. Tazafder, Polyhedron 6 (1987) 1653.

Available online at www.sciencedirect.com
SCIENCE DIRECT®
Polyhedron 23 (2004) 1235–1242
POLYHEDRON
www.elsevier.com/locate/poly

Near-IR absorption due to supramolecular electronic interaction in an extended 3D hydrogen-bonding network material: synthesis, crystal structure and properties of [4,4′-H_2bpy][Cu(mnt)$_2$] ☆

V. Madhu, Samar K. Das *

School of Chemistry, University of Hyderabad, Hyderabad 500046, India

Received 21 November 2003; accepted 3 February 2004

Abstract

The synthesis and single-crystal X-ray structure of an ion-pair complex, [4,4′-H_2bpy][Cu(mnt)$_2$] (**1**), is described. In the crystal structure, the interactions between anions and cations via bifurcated (bpyN)–H···(NC–mnt)$_2$ hydrogen bonds give rise to a three-dimensional supramolecular network having well-defined channels. Complex **1** exhibits two redox waves at +0.44 and −0.36 V (versus SCE) in dimethylformamide corresponding to the Cu(mnt)$_2]^{1-}$/Cu(mnt)$_2]^{2-}$ and [4,4′-H_2bpy]$^{2+}$/[4,4′-H_2bpy]$^{1+}$ couples, respectively. The near-IR absorption at 1225 nm in the solid state has been attributed to the charge transfer from the copper dithiolate anion, [Cu(mnt)$_2]^{2-}$, to the bipyridinium cation, [4,4′-H_2bpy]$^{2+}$.
© 2004 Elsevier Ltd. All rights reserved.

Keywords: Ion pair complex; Hydrogen bonding network; Non-covalent interaction; Charge transfer; Near-IR absorption

1. Introduction

The supramolecular construction of specific architectures from well-defined molecular building blocks has been an active area of chemical research over the past few years because such molecular assemblies may have new exciting properties and thereby can be used as functional materials [1,2]. The basis of supramolecular assembly is the reliable and meaningful connections between molecular structures based on non-covalent intermolecular interactions such as H-bonding. The use of metal–(bis)dithiolene complexes as building units in the construction of such molecule based framework materials has received considerable attention due to their potential applications in the areas of near-infrared (near-IR) dyes [3], conducting [4], magnetic [5] and non-linear optical materials [6]. The near-IR absorption is of special interest among these properties. There is a practical need for obtaining materials that give rise to a strong absorption in the near-IR region for the application in Q-switching infrared lasers [3]. The origin of such low energy absorption from metal (bis)dithiolene complexes may be discussed under two headings: (i) The HOMO and LUMO are delocalized over both dithiolene ligands, and the electronic transition between these orbitals gives rise to a strong absorption in the near-IR region. Donor substituents in the parent dithiolene raise the energy of the HOMO more than that of LUMO resulting in a shift of the low energy band to lower frequencies. (ii) Ion-pair charge transfer (IPCT) complexes $\{A^{2+}[ML_2]^{2-}\}$, M = Ni, Pd, Pt and Cu, between bipyridinium acceptors and (dithiolene)metalate donors exhibit IPCT bands in the near-IR region [7]. IPCT complexes of the type [M(Me$_2$-pipdt)$_2$][M(mnt)$_2$] (M = Pd, Pt) have recently been reported with near-IR absorption properties [8]. The present work deals with an IPCT complex. Although this ion-pair charge-transfer has been described as a supramolecular electronic interaction between the components, any supramolecular network based on such an ion pair is not yet known.

☆ Supplementary data associated with this article can be found, in the online version, at doi:10.1016/j.poly.2004.02.002.

* Corresponding author. Tel.: +91-40-23011007; fax: +91-40-2301-2460.
E-mail address: skdsc@uohyd.ernet.in (S.K. Das).

0277-5387/$ - see front matter © 2004 Elsevier Ltd. All rights reserved.
doi:10.1016/j.poly.2004.02.002

This is because bipyridinium derivatives have always been used, the parent dication $[4,4'\text{-}H_2bpy]^{2+}$ (simply protonated) has not been previously utilized as a redox active acceptor. Taking advantage of the ability of protons on bipyridine-nitrogen donors to form bifurcated H-bonding with cyano-nitrogens of the mnt ligand, we wish to report here that the $[Cu(mnt)_2]^{2-}$ anion undergoes N–H$\cdots$ N linking with the $[4,4'\text{-}H_2bpy]^{2+}$ cation to form a new type of 3D supramolecular network in $[4,4'\text{-}H_2bpy]_n[Cu(mnt)_2]_n$ (**1**).

2. Experimental

2.1. General methods

Elemental analyses were performed using a Perkin–Elmer 240C analytical instrument. Infrared (IR) spectra were recorded on KBr pellets with a JASCO FT/IR-5300 spectrometer in the region of 400–4000 cm^{-1}. Electronic spectra were obtained on a UV-3101PC/UV–VIS–NIR spectrophotometer (Shimadzu), equipped with a diffuse reflectance accessory (reflectance spectra were recorded on KBr pellets). The diffuse reflectance spectra obtained were then Kubelka-Munk corrected. The ESR spectra were recorded on a (JEOL) JES-FA200 ESR Spectrometer. A Cypress model CS-1090/CS-1087 electroanalytical system was used for cyclic voltammetric experiments. The electrochemical experiments were measured in DMF containing $[Bu_4N][ClO_4]$ as a supporting electrolyte, using a conventional cell consisting of two platinum wires as working and counter electrodes, and a saturated calomel electrode (SCE) as reference. The potentials reported here are uncorrected for junction contributions. Electrical resistivities of compacted pellets were checked by the conventional two-probe technique. Powder X-ray diffraction data were collected on a Phillips PW 3710 diffractometer.

2.2. Materials

Disodium maleonitriledithiolate (Na_2mnt) was prepared using a synthetic procedure described in the literature [9]. $[Bu_4N]_2[Cu(mnt)_2]$ was prepared following a method as reported by Davison and Holm [10]. 4,4′-Bipyridine was purchased from Merck and used as received. Solvents were purified by standard methods. The preparations and measurements were carried out in diffuse light since dithiolene complexes are known to be light sensitive.

2.3. Synthesis of $[4,4'\text{-}H_2bpy][Cu(mnt)_2]$ (**1**)

2.3.1. Method 1

To a solution of 4,4′-bipyridine (0.31 g, 2.0 mmol) in CH_3CN (25 ml) kept in an oil bath, was added a solution of $CuCl_2\cdot 2H_2O$ (0.17 g, 1 mmol) in water (10 ml). A solution of $[Bu_4N]_2[Cu(mnt)_2]$ (0.83 g, 1 mmol) in CH_3CN (10 ml) was subsequently added to the resulting dark red reaction mixture, which was then refluxed with stirring for 2 h. The insoluble material, formed during this time, was removed by filtration and the filtrate was allowed to stand for three days at room temperature. This resulted in the formation of deep-red, prismatic crystals, which were filtered off and washed with *i*PrOH/Et_2O and then air-dried at room temperature. Yield: 0.090 g (9%, based on 4,4′-bipyridine). Elemental *Anal.* Calc. for $C_{18}H_{10}CuN_6S_4$: C, 43.06; H, 2.01; N, 16.74. Found: C, 43.12; H, 1.98; N, 16.68%. IR (cm^{-1}): 3200m (ν_{N-H}), 3132m (ν_{N-H}), 3090w (ν_{N-H}), 3070w (ν_{N-H}), 2205vs (ν_{CN}), 1471m ($\nu_{C=C}$), 862w (ν_{C-S}). The compound was additionally characterized by UV–Vis and ESR spectroscopy, cyclic voltammetry and single-crystal X-ray structural analysis.

2.3.2. Method 2

To a solution of 4,4′-bpy (0.10 g, 0.64 mmol) in methanol (5 ml), HCl (0.2 ml, 36%) was added slowly, resulting in the precipitation of $[4,4'\text{-}H_2bpy]Cl_2$ as colorless crystalline compound. It was filtered, washed with methanol-diethylether and dried in vacuum. Yield: 0.127 g (86% based on 4,4′-bipyridine used). Elemental *Anal.* Calc. for $C_{10}H_{10}N_2Cl_2$: C, 52.42; H, 4.40; N, 12.23. Found: C, 53.01; H, 4.31; N, 12.02%. IR (cm^{-1}): 3054m (ν_{N-H}), 2733br, 1630m, 1593s, 1481s, 1232m, 1194m, 787s.

An aqueous solution (5 ml) of $[4,4'\text{-}H_2bpy]Cl_2$(0.12 g, 0.52 mmol) was slowly added to an acetone solution (15 ml) of $[Bu_4N]_2[Cu(mnt)_2]$ (0.48 g, 0.58 mmol) and the reaction mixture was stirred for 10 min at room temperature. Subsequently, it was heated on a water bath for 5 min resulting in the formation of a dark red microcrystalline solid. The solid was filtered off, washed with acetone and dried under vaccum. This compound was recrystallized by slow diffusion of diethylether into its DMF solution at 10 °C for 48 h. The dark red plate-shaped crystals, appearing during this time, were filtered, washed with diethylether and dried in vacuum. Yield: 0.192 g (65%, based on $[Bu_4N]_2[Cu(mnt)_2]$). This compound was identified as **1**. Elemental *Anal.* Calc. for $C_{18}H_{10}CuN_6S_4$: C, 43.06; H, 2.01; N, 16.74. Found: C, 42.98; H, 1.95; N, 16.65%. The compound exhibited identical IR spectrum, X-ray powder diffraction pattern, cyclic voltammograms, electronic and ESR spectra as shown by compound **1**, obtained in method 1. Crystals, suitable for single-crystal X-ray diffraction study, were grown in a λ-shaped diffusion glass-tube set-up by dissolving $[Bu_4N]_2[Cu(mnt)_2]$ (0.22 g, 27 mmol) in acetone in one arm and $[4,4'\text{-}H_2bpy]Cl_2$ in water in the other arm of the λ-shaped set-up. The remaining gap, inside the tubes, was carefully filled up with acetone and the set-up was kept at room temperature for 20 days. Deep-red

prismatic crystals, precipitated inside the tubes, were identified as **1** using the above-mentioned routine techniques and gave identical unit cell parameters ($a = 12.742(1)$ Å, $b = 7.462(9)$ Å, $c = 21.041(5)$ Å, orthorhombic, $V = 2000(3)$ Å^3) as shown by the crystals obtained in method 1.

2.4. X-ray crystallography

A deep-red prismatic crystal of size $0.68 \times 0.68 \times 0.52$ mm^3 was mounted on an Enraf-Nonius CAD4 diffractometer and the data were collected at 20 °C temperature using graphite-monochromated Mo Kα ($\lambda = 0.71073$ Å) radiation. An empirical absorption correction based on a series of ψ scans was applied. The structure was solved by the direct method (SHELXS-97) [11a] and refined by the full-matrix least-squares on F^2 method (SHELXL-97) [11b]. All non-hydrogen atoms were refined anisotropically. Hydrogen atoms were introduced at calculated positions and included in the refinement riding on their respective parent atoms. The crystallographic data and the parameters of structure refinement are summarized in Table 1.

2.5. X-ray powder diffraction studies

The X-ray powder diffraction pattern of the crystals, synthesized by method 2, and the computer simulated [12] pattern obtained from the single-crystal X-ray data of the crystal, isolated in method 1, were practically identical (see Supplementary information).

Table 1
Crystal data and structure refinement for **1**

Empirical formula	$C_{18}H_{10}CuN_6S_4$
Formula weight	502.10
T (K)	293(2)
λ (Å)	0.71073
Crystal system	orthorhombic
Space group	$Pca2_1$
a (Å)	12.757(4)
b (Å)	7.487(8)
c (Å)	21.074(9)
V (Å^3)	2013(2)
Z	4
D_{calc} (Mg m^{-3})	1.657
Absorption coefficient (mm^{-1})	1.518
$F(000)$	1012
Crystal size (mm)	$0.68 \times 0.68 \times 0.52$
θ range for data collection (°)	1.93–27.48
Reflections collected/unique	2377/2377
Refinement method	full-matrix least-squares on F^2
Data/restraints/parameters	2377/1/258
Goodness-of-fit on F^2	1.050
Final R indices [$I > 2\sigma(I)$]	$R_1 = 0.0318$, $wR_2 = 0.0795$
R indices (all data)	$R_1 = 0.0379$, $wR_2 = 0.0829$
Largest difference peak and hole (e Å^{-3})	0.285 and −1.025

3. Results and discussion

3.1. Synthesis

Compound **1** has been synthesized (in method 1) by heating a ~3:1 acetonitrile/water solution of $[Bu_4N]_2[Cu(mnt)_2]$, $CuCl_2 \cdot 2H_2O$ and 4,4′-bipyridine. The dissolution of $CuCl_2$ lowers the pH of the reaction mixture by generating HCl acid, whereby 4,4′-bipyridine gets protonated with the formation of the $[4,4'\text{-}H_2bpy]^+$ cation. However, the yield in method 1 is very poor. **1** can easily be obtained in a high yield synthesis (method 2) simply by using $[4,4'\text{-}H_2bpy]Cl_2$ and $[Bu_4N]_2[Cu(mnt)_2]$ as shown in the following reaction:

$$[4,4'\text{-}H_2bpy]Cl_2 + [Bu_4N]_2[Cu(mnt)_2] \rightarrow [4,4'\text{-}H_2bpy][Cu(mnt)_2] + 2Bu_4NCl \quad (1)$$

3.2. Description of the structure

1 crystallizes in the orthorhombic space group $Pca2_1$. A thermal ellipsoidal plot of **1** with non-hydrogen atom labelling is presented in Fig. 1. This shows the abundance of $[4,4'\text{-}H_2bpy]^{2+}$ and $[Cu(mnt)_2]^{2-}$ as an ion-pair. The crystallographic details are summarized in Table 1 and relevant bond lengths and angles for the complex are described in Table 2. In the anion, the geometry around the copper atom, which is coordinated by four sulfur atoms from two mnt ligands, is considerably distorted, with a dihedral angle of 30.28° between the mnt planes. The two pyridine rings of the $[4,4'\text{-}H_2bpy]^{2+}$ cation also exhibit non-coplanar geometry with a dihedral angle of 37.84° between the least-square planes of the two rings (Table 3). The non-planarity around the metal ion, which is not very common in bis-dithiolene complexes, is generally caused by dimerization via metal sulfur interactions as observed in complexes, $Co_2[S_2C_2(CF_3)_2]_4$ [13], $[Bu_4N]_2[Co_2(S_2C_6Cl_4)_4]$ [14], $[Bu_4N_2[Fe_2(mnt)_4]$ [15], $[Bu_4N]_2[Fe_2(edt)_4]$ [16] and $[Et_4N]_2[Mn_2(edt)_4]$ [17,18]. Deviations from planarity were also found in copper bis-dithiolene complexes $[epy]_2[Cu(dmit)_2]$ [19], $[NMe_4]_2[Cu(mnt)_2]$ [20] and $[methyleneblue]_2[Cu(mnt)_2] \cdot Me_2CO$ [21] with dihedral angles of 57.3°, 41° and 47.4°, respectively. These deviations are ascribed to a close H···S distance of 2.9 Å, the presence of several short contacts between the atoms of the anion and cations, and the introduction of stacked, large methylene blue molecules, respectively. Non-planarity between two mnt ligands in the present ion pair complex **1** seems to be caused by the supramolecular interactions between the cation and anion through all possible hydrogen bonding sites of both components as described in the following section.

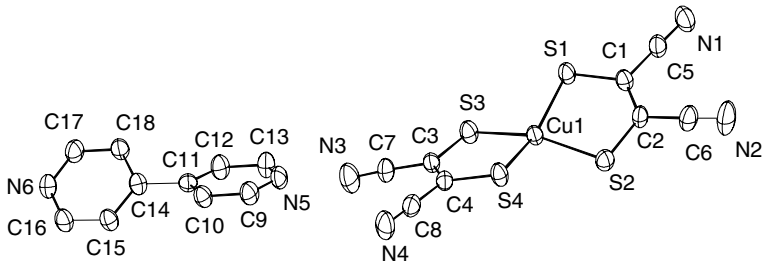

Fig. 1. Thermal ellipsoid plot of **1** (50% probability).

There are two H-bonding donors for the [4,4′-H_2bpy]$^{2+}$ dication and four H-bonding acceptors for the Cu(mnt)$_2$]$^{2-}$ dianion. Supramolecular interactions are thus expected between the cations and anions via bifurcated H-bonds. This is indeed the case as depicted in Fig. 2. The bifurcated hydrogen bonding, which is observed in other bipyridinium containing compounds, involves the interactions between the N–H groups of bipyridinium cations and the CN groups of mnt ligands. In the crystal structure, each bipyridinium dication interacts with four complex anions and each complex anion communicates with four bipyridinium dications (Fig. 2). The hydrogen bonding interactions between non-planar components (cation and anion) of the ion pair complex **1** gives rise to a three-dimensional supramolecular network having well-defined channels as shown in Fig. 3. Whereas one type of channel is found in the views along the crystallographic *a*- and *c*-axes (see Supplementary information), two types of channels (20 and 30 membered rings) are clearly shown in Fig. 3, viewed along cystallographic *b*-axis. There are four types of N–H···N hydrogen bonds through out this supramolecular network of **1**. The relevant distances and angles of hydrogen bonding contacts are summarized in Table 4.

Table 2
Selected bond lengths (Å) and angles (°) for **1**

Bond lengths			
Cu(1)–S(1)	2.2757(12)	Cu(1)–S(2)	2.2628(14)
Cu(1)–S(3)	2.2599(14)	Cu(1)–S(4)	2.2617(13)
S(1)–C(1)	1.729(4)	S(2)–C(2)	1.725(4)
S(3)–C(3)	1.731(4)	S(4)–C(4)	1.727(4)
C(1)–C(2)	1.367(6)	C(1)–C(5)	1.441(6)
C(2)–C(6)	1.440(6)	C(3)–C(4)	1.375(6)
C(3)–C(7)	1.420(5)	C(4)–C(8)	1.434(6)
C(5)–N(1)	1.141(6)	C(6)–N(2)	1.136(7)
C(7)–N(3)	1.143(6)	C(8)–N(4)	1.144(6)
N(5)–C(9)	1.324(6)	N(5)–C(13)	1.339(6)
N(6)–C(17)	1.333(6)	N(6)–C(16)	1.339(6)
C(9)–C(10)	1.378(6)	C(10)–C(11)	1.392(6)
C(11)–C(12)	1.377(6)	C(14)–C(18)	1.389(6)
Bond angles			
S(3)–Cu(1)–S(4)	92.16(5)	S(3)–Cu(1)–S(2)	158.92(6)
S(4)–Cu(1)–S(2)	90.70(5)	S(3)–Cu(1)–S(1)	93.43(5)
S(4)–Cu(1)–S(1)	157.52(6)	S(2)–Cu(1)–S(1)	91.85(5)
C(1)–S(1)–Cu(1)	100.78(14)	C(2)–S(2)–Cu(1)	100.74(14)
C(3)–S(3)–Cu(1)	100.89(14)	C(4)–S(4)–Cu(1)	100.95(15)
C(2)–C(1)–C(5)	117.8(4)	C(2)–C(1)–S(1)	122.7(3)
C(5)–C(1)–S(1)	119.5(3)	C(1)–C(2)–C(6)	118.3(4)
C(1)–C(2)–S(2)	123.8(3)	C(6)–C(2)–S(2)	117.9(3)
C(4)–C(3)–C(7)	119.0(4)	C(4)–C(3)–S(3)	123.0(3)
C(7)–C(3)–S(3)	118.0(3)	C(3)–C(4)–C(8)	119.9(4)
C(3)–C(4)–S(4)	123.0(3)	C(8)–C(4)–S(4)	117.1(3)
N(3)–C(7)–C(3)	177.8(6)	N(4)–C(8)–C(4)	179.3(6)
C(9)–N(5)–C(13)	122.7(4)	C(17)–N(6)–C(16)	122.3(4)

3.3. IR spectroscopy

Compound [Bu_4N]$_2$[Cu(mnt)$_2$] exhibits a ν(CN) band at 2190 cm^{-1} in the IR spectrum. Upon (bpyN)–H···(NC–mnt)$_2$ hydrogen-bond formation (Fig. 2) in **1**, the ν(CN) shifts to a higher frequency (2205 cm^{-1}). The cyanide group acts as a donor by donating electrons to the proton of the [4,4′-H_2bpy]$^{2+}$ cation from an orbital which is weakly antibonding in nature [22]. Thus the ν(CN) of the hydrogen bonded-complex **1** is higher than the value obtained in [Bu_4N]$_2$[Cu(mnt)$_2$]. The ν(NH) vibrations appear at 3054 cm^{-1} in the IR spectrum of [4,4′-H_2bpy]Cl_2. Four weak features are observed at 3200, 3132, 3090 and 3070 cm^{-1} for ν(NH) vibrations in the IR spectrum of **1**. This shifting of ν(NH) bands to higher frequencies in **1** is not unexpected because strong N–H···Cl hydrogen bonding is anticipated in [4,4′-H_2bpy]Cl_2.

3.4. Electrochemistry

The cyclic voltammogram of **1** in DMF exhibits two quasi-reversible redox waves at $E_{1/2} = -0.36$ V versus SCE ($\Delta E_p = 98$ mV) and 0.44 V versus SCE ($\Delta E_p = 79$ mV). Both electrochemical responses, displayed by the complex, are quasi-reversible processes. The first response at 0.44 V is assigned to the Cu(mnt)$_2$]$^{1-}$/Cu(mnt)$_2$]$^{2-}$ couple. This data agrees well with that reported for the [Bu_4N]$_2$[Cu(mnt)$_2$] complex [23]. The second reductive response at −0.36 V can be described as the [4,4′-H_2bpy]$^{2+}$ + e ⇌ [4,4′-H_2bpy]$^{1+}$ process.

3.5. Electronic spectra

The UV–Vis solution spectra of **1**, [Bu_4N]$_2$[Cu(mnt)$_2$] and [4,4′-H_2bpy]Cl_2 are displayed in Fig. 4. The ab-

Table 3
Least-square planes for the cation and the anion in [4,4′-H_2bpy][Cu(mnt)$_2$]

	Plane 1	Plane 2	Plane 3	Plane 4
P	−3.5878	4.4532	2.7315	3.7732
Q	6.8480	6.9391	7.0308	−7.0570
R	6.1190	2.9162	5.6668	−3.2708
S	0.3605	7.0154	4.6551	1.0487

Deviations from planes (Å)

Plane 1		Plane 2		Plane 3		Plane 4	
C14	0.0061	C11	−0.0069	Cu1	0.0161	Cu1	0.0267
C15	−0.0039	C12	0.0005	S4	−0.0179	S1	−0.0264
C16	−0.0017	C13	0.0061	C4	0.0113	C1	0.0111
N6	0.0051	N5	−0.0061	C3	0.0061	C2	0.0181
C17	−0.0026	C9	−0.0007	S3	−0.0157	S2	−0.0294
C18	−0.0030	C10	0.0072	C7	0.0612	C5	0.0641
				C8	0.0201	C6	0.1074
				N3	0.1483	N1	0.1504
				N4	0.0147	N2	0.2202

Plane 1: C14, C15, C16, N6, C17, C18; Plane 2: C11, C12, C13, N5, C9, C10; Plane 3: Cu1, S4, C4, C3, S3, C7, C8, N3, N4; Plane 4: Cu1, S1, C1, C2, S2, C5, C6, N1, N2; Plane equation: $Px + Qy + Rz = S$.

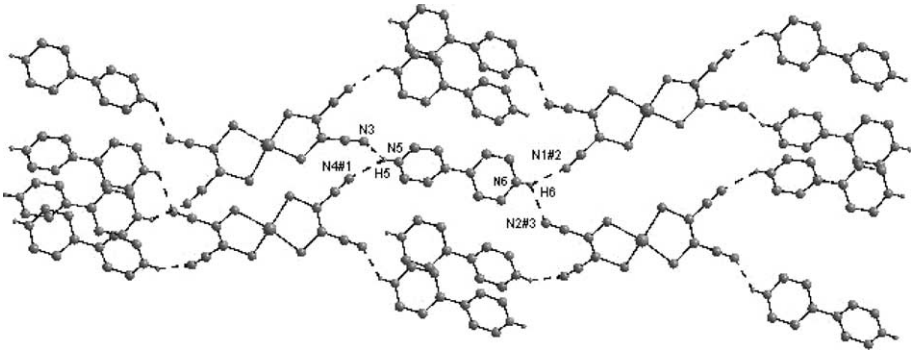

Fig. 2. Bifurcated H-bonding interactions between the N–H groups of the bipyridinium cation and the CN groups of the mnt^{2-} ligands of the complex anion. Each bipyridinium cation is hydrogen bonded to four complex anions and each complex anion is hydrogen bonded to four bipyridinium cations.

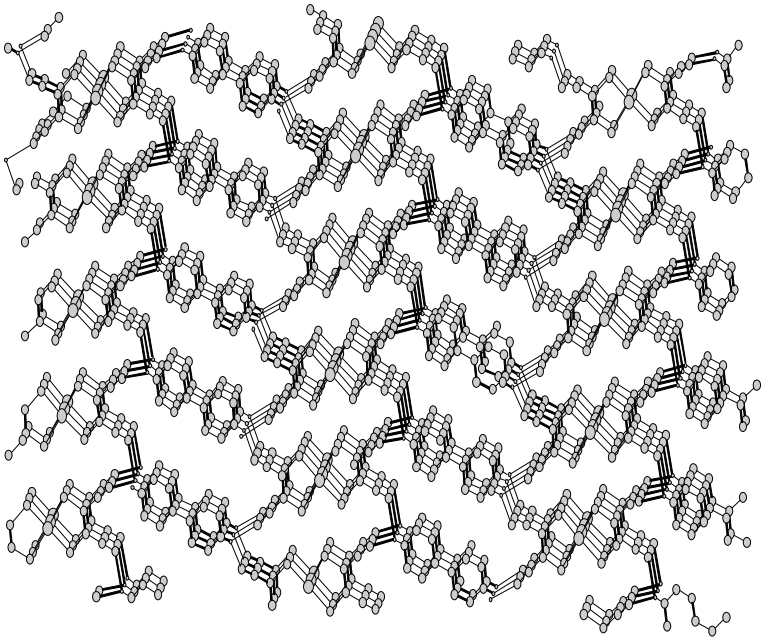

Fig. 3. Three-dimensional supramolecular network viewed down the crystallographic *b*-axis.

Table 4
Hydrogen bonds for **1** (Å and °) (see Fig. 2)

D–H···A	*d*(D···H)	*d*(H···A)	*d*(D···A)	∠DHA
N(5)–H(5)···N(3)	0.86	2.18	2.875(6)	137.8
N(5)–H(5)···N(4)#1	0.86	2.37	3.017(6)	132.1
N(6)–H(6)···N(1)#2	0.86	2.29	3.041(5)	145.9
N(6)–H(6)...N(2)#3	0.86	2.40	2.976(6)	124.8

Symmetry transformations used to generate equivalent atoms: #1: $x-0.5,-y+1,z$; #2: $x,y+1,z-1$; #3: $x-0.5,-y+1,z-1$.

sorption bands at 325 and 375 nm are due to L(π)–L(π*) transitions and bands in the 490 nm region are assigned to MLCT absorptions for the metal dithiolene parts [7e]. In solution, the bipyridinium cation does not absorb above 300 nm. As compared to the tetrabutylammonium salt, the band positions remain unchanged in 4,4′-bipyridinium salt **1**. The broad and weak absorption bands appear at ~1200 nm (Fig. 4(b)). The intensity of this near-IR band of **1** ($\varepsilon = 110$ M^{-1} cm^{-1}) is higher than that of $[Bu_4N]_2[Cu(mnt)_2]$ ($\varepsilon = 70$ M^{-1} cm^{-1}).

In the solid state, compound **1** exhibits a band at 1225 nm (in the near-IR region) of much higher intensity and a sharp band at 760 nm in its diffuse reflectance spectrum; the complex $[Bu_4N]_2[Cu(mnt)_2]$ does not show any intense band in the near-IR region, but shows a moderate absorption at 810 nm in the solid state as shown in Fig. 5. Whereas the peak at ~1200 nm is predominant in the diffuse reflectance spectrum of **1**, this peak is weaker but recognisable in the solid state electronic spectrum of $[Bu_4N]_2[Cu(mnt)_2]$ (Fig. 5). The molar extinction coefficient of this peak (~1200 nm) in the solution absorption spectrum of $[Bu_4N]_2[Cu(mnt)_2]$ is 70 M^{-1} cm^{-1}. We, therefore, tentatively assign this 1225 nm band in the solid state electronic spectrum of **1** to a d–d absorption overlapped by an IPCT-band. The absorptions at 760 and 810 nm of compounds **1** and $[Bu_4N]_2[Cu(mnt)_2]$, respectively, in their solid states (Fig. 5) are not visible in the corresponding solution absorption spectra (Fig. 4). These solid state bands are tentatively assigned to an anion–cation type intermolecular interaction in their corresponding solid states. The diffuse reflectance spectrum of $[4,4'\text{-}H_2bpy]Cl_2$ shows a broad band in the region of 450–700 nm (Fig. 5). A similar broad feature (with little shift) is observed in the solid state electronic spectrum of $[4,4'\text{-}H_2bpy](BF_4)_2$. However, in the absence of further studies, mainly theoretical calculations, the assignment of these bands is difficult.

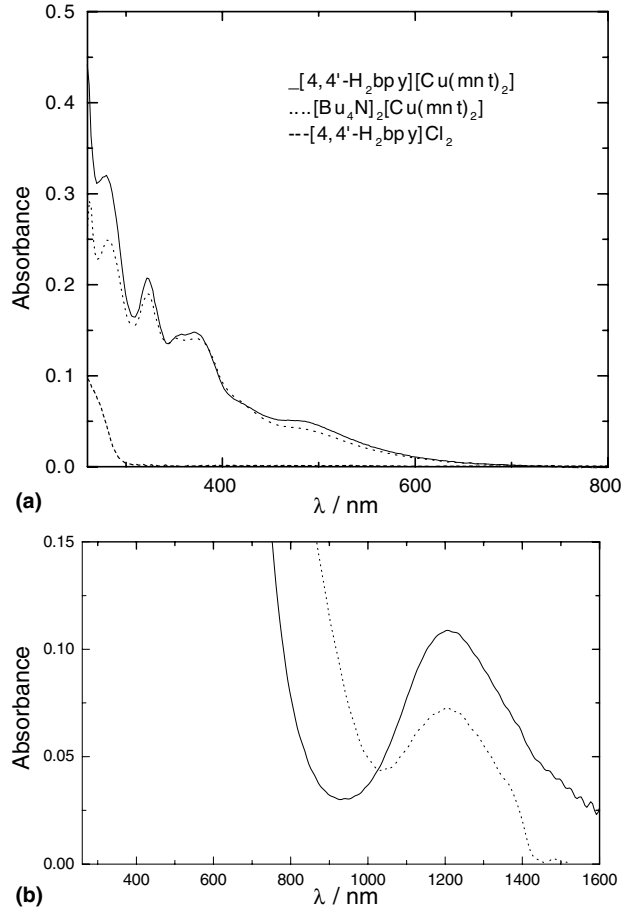

Fig. 4. (a) UV–Vis spectra in DMF (1×10^{-5} M). (b) 1×10^{-3} M in DMF, —, $[4,4'\text{-}H_2bpy][Cu(mnt)_2]$; ···, $[Bu_4N]_2[Cu(mnt)_2]$.

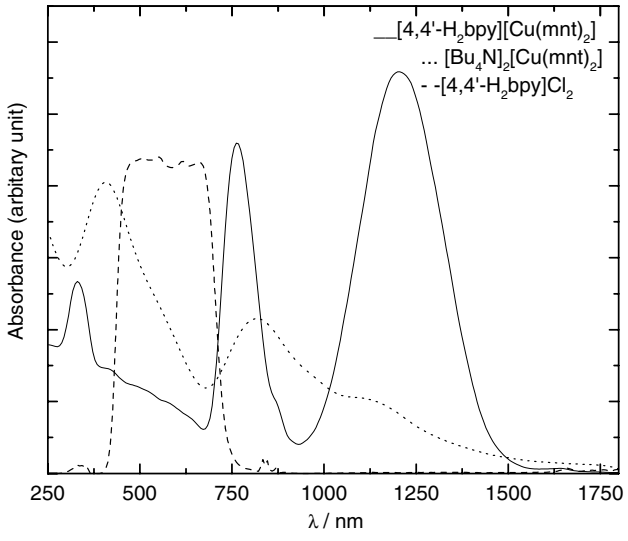

Fig. 5. The diffuse refletance spectra of $[4,4'\text{-}H_2bpy][Cu(mnt)_2]$ (**1**), $[NBu_4]_2[Cu(mnt)_2]$ and $[4,4'\text{-}H_2bpy]Cl_2$.

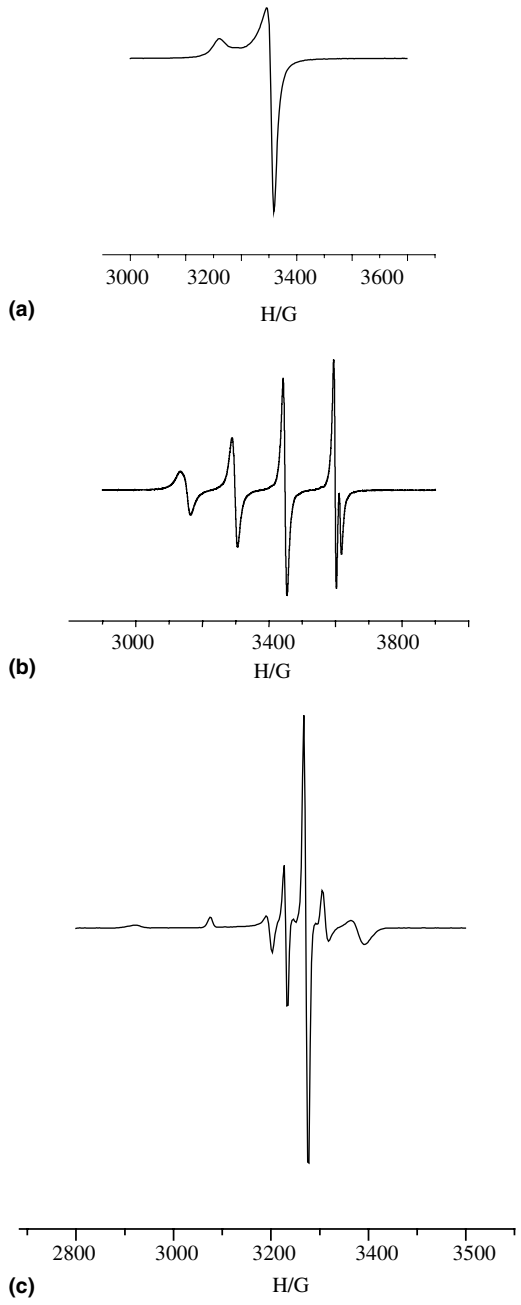

Fig. 6. The ESR spectra of [4,4′-H_2bpy][Cu(mnt)$_2$] (**1**) at room temperature: (a) in the solid state, (b) in DMF. (c) The ESR spectrum of [4,4′-H_2bpy][Cu(mnt)$_2$] (**1**) in the solid state at liquid nitrogen temperature.

3.6. ESR spectroscopy

Fig. 6 illustrates the ESR spectra of **1** in the solid-state and in solution at room temperature. The g values ($g_{\|} = 2.08$, $g_{\perp} = 2.03$) observed in the room temperature solid-state ESR spectrum (Fig. 6(a)) are very close to those ($g_{\|} = 2.090$, $g_{\perp} = 2.024$ and $g_{\|} = 2.092$, $g_{\perp} = 2.026$) of the non-planar Cu(II)–dithiolene complexes, [mb]$_2$[Cu(mnt)$_2$]·Me_2CO (mb = methylene blue) [20] and [epy]$_2$[Cu(dmit)$_2$] (epy = N-ethylpyridinium, H_2dmit = 4,5-dimercapto-1,3-dithiole-2-thione) [19], respectively. These g values are also close to those ($g_1 = 2.023$, $g_2 = 2.026$, $g_3 (= g_{\|}) = 2.086$) of the planar Cu-mnt complex, [Bu_4N]$_2$[Cu(mnt)$_2$] [24]. The isotropic ^{63,65}Cu hyperfine structure is observed ($g_0 = 2.052$, $|A_0| = 7.648$ mT) in the solution spectrum of **1** (Fig. 6(b)). The solid-state ESR spectrum of **1** at liquid nitrogen temperature exhibits hyperfine structure due to ^{63,65}Cu nuclei as shown in Fig. 6(c). Interestingly, both $g_{\|}$ and $g_{\perp}$ features get resolved due to ^{63,65}Cu hyperfine coupling, which is very rarely observed in metal–dithiolene complexes. The average value of the hyperfine coupling parameters (determined from $|A_{\|}| = 15.28$ mT and $|A_{\perp}| = 4.39$ mT) is 8.02 mT, which is close to that (7.648 mT) of the solution ESR spectrum at room temperature.

4. Conclusions

A series of ion-pair charge-transfer (IPCT) complexes {$A^{2+}[ML_2]^{2-}$}, M = Ni, Pd, Pt, and Cu, between bipyridinium acceptors and (dithiolene)metalate donors, that exhibit IPCT bands in the near-IR region, has been reported in literature. In these complexes, the acceptors are always bipyridinium derivatives, not the parent bipyridinium (protonated) cation. The results, presented herein, show that the protonated bipyridnium dication, not only forms an ion pair charge transfer complex with a metal dithiolate dianion showing a sharp absorption in the near-IR region, but also it undergoes hydrogen bonding interactions with cyano ligands of the mnt complex constructing a three-dimensional supramolecular network in the crystal of **1**.

5. Supplementary material

Crystallographic data for the structural analysis have been deposited with the Cambridge Crystallographic Data Centre, CCDC No. 204645 for compound **1**. Copies of this information may be obtained free of charge from The Director, CCDC, 12 Union Road, Cambridge CB2 1EZ, UK (fax: +44-1223-336033; e-mail: deposit@ccdc.cam.ac.uk or www: http://www.ccdc.cam.ac.uk).

Acknowledgements

We are grateful for the financial support of the Council of Scientific and Industrial Research (CSIR), Government of India (Project No. 01(1737)/02/EMR-II). The national X-ray diffractometer facility at the University of Hyderabad, by the Department of Science and Technology, Government of India, is gratefully

acknowledged. The authors thank Dr. S. Pal and Mr. S. Pal for providing electrochemical data for this work. We thank UGC, Government of India for the infrastructure facility at the University of Hyderabad under UPE (University with potential for excellence) grant.

References

[1] (a) J.-M. Lehn, Supramolecular Chemistry: Concepts and Perpectives, VCH, Weinheim, 1995;
(b) J.-M. Lehn, in: J.-P. Behr (Ed.), Perspectives in Supramolecular Chemistry, vol. 1, Wiley, Chichester, 1994;
(c) J.-M. Lehn, in: A.D. Hamilton (Ed.), Perspectives in Supramolecular Chemistry, vol. 3, Wiley, Chichester, 1996;
(d) F. Vögtle, Supramolecular Chemistry, Wiley, Chichester, 1991;
(e) B. Dietrich, P. Viout, J.-M. Lehn, Macrocyclic Chemistry: Aspects of Organic and Inorganic Supramolecular Chemistry, VCH, Weinheim, 1992.

[2] (a) V.G. Albano, M.C. Aragoni, M. Arca, C. Castellari, F. Demartin, F.A. Devillanova, F. Isaia, V. Lippolis, L. Loddo, G. Verani, Chem. Commun. (2002) 1170;
(b) T. Suzuki, H. Fujii, T. Miyashi, J. Org. Chem. 57 (1992) 6744;
(c) B.N. Figgis, E.S. Kucharski, M. Vrtis, J. Am. Chem. Soc. 115 (1993) 176.

[3] (a) F. Bigoli, P. Deplano, F.A. Devillanova, V. Lippolis, P.J. Lukes, M.L. Mercuri, M.A. Pellinghelli, E.F. Trogu, J. Chem. Soc., Chem. Commun. (1995) 371;
(b) U.T. Mueller-Westerhoff, B. Vance, D.I. Yoon, Tetrahedron 47 (1991) 909.

[4] (a) H. Tanaka, H. Kobayashi, A. Kobayashi, J. Am. Chem. Soc. 124 (2002) 10002;
(b) H. Tanaka, Y. Okano, H. Kobayashi, W. Suzuki, A. Kobayashi, Science 291 (2001) 285.

[5] (a) A.T. Coomber, D. Beljonne, R.H. Friend, J.K. Bredas, A. Charlton, N. Robertson, A.E. Underhill, M. Kurmoo, P. Day, Nature 380 (1996) 144;
(b) N. Robertson, L. Cronin, Coord. Chem. Rev. 227 (2002) 93.

[6] (a) F. Bigoli, C.-T. Chen, W.-C. Wu, P. Deplano, M.L. Mercuri, M.A. Pellinghelli, L. Pilia, G. Pintus, A. Serpe, E.F. Trogu, Chem. Commun. (2001) 2246;
(b) C.S. Winter, C.A.S. Hill, A.E. Underhill, Appl. Phys. Lett. 58 (1991) 107.

[7] (a) C. Handrosch, R. Dinnebier, G. Bondarenko, E. Bothe, F. Heinemann, H. Kisch, Eur. J. Inorg. Chem. (1999) 1259;
(b) G. Schmauch, F. Knoch, H. Kisch, Chem. Ber. 127 (1994) 287;
(c) I. Nunn, B. Eisen, R. Benedix, H. Kisch, Inorg. Chem. 33 (1994) 5079;
(d) H. Kisch, Coord. Chem. Rev. 125 (1993) 155;
(e) W. Dmler, H. Kisch, New J. Chem. 15 (1991) 649.

[8] F. Bigoli, P. Deplano, M.L. Mercuri, M.A. Pellinghelli, L. Pilia, G. Pintus, A. Serpe, E.F. Trogu, Inorg. Chem. 41 (2002) 5241.

[9] E.I. Stiefel, L.E. Bennett, Z. Dori, T.H. Crawford, C. Simo, H.B. Gray, Inorg. Chem. 9 (1970) 281.

[10] A. Davison, R.H. Holm, Inorg. Synth. 10 (1967) 8.

[11] (a) G.M. Sheldrick, SHELXS-97: A Program for Structure Solution, University of Göttingen, Germany, 1997;
(b) G.M. Sheldrick, SHELXL-97: A Program for Structure Refinement, University of Göttingen, Germany, 1997.

[12] W. Kraus, G. Nolze, Powder Cell for Windows, Version 2.3, Berlin, 1999.

[13] J.H. Enemark, W.N. Lipscomb, Inorg. Chem. 4 (1965) 1729.

[14] M.J. Baker-Hawkes, Z. Dori, R. Eisenberg, H.B. Gray, J. Am. Chem. Soc. 90 (1968) 4253.

[15] W.C. Hamilton, I. Bernal, Inorg. Chem. 6 (1967) 2003.

[16] M.R. Snow, J.A. Ibers, Inorg. Chem. 12 (1973) 249.

[17] T. Costa, J.R. Dorfman, K.S. Hagen, R.H. Holm, Inorg. Chem. 22 (1983) 4091.

[18] G. Christou, J.C. Huffman, J. Chem. Soc., Chem. Commun. (1983) 558.

[19] G. Matsubayashi, K. Takahashi, T. Tanaka, J. Chem. Soc., Dalton Trans. (1988) 967.

[20] C. Mahadevan, M. Seshasayee, J. Crystallogr. Spectrosc. Res. 14 (1984) 215.

[21] D. Snaathorst, H.M. Doesburg, J.A.A.J. Perenboom, C.P. Keijzers, Inorg. Chem. 20 (1981) 2526.

[22] K. Nakamoto, Infrared and Raman Spectra of Inorganic and Coordination Compounds, Wiley, New York, 1986.

[23] A. Davison, N. Edelstein, R.H. Holm, A.H. Maki, Inorg. Chem. 2 (1963) 1227.

[24] A.H. Maki, N. Edelstein, A. Davison, R.H. Holm, J. Am. Chem. Soc. 86 (1964) 4580.

Available online at www.sciencedirect.com
SCIENCE DIRECT®
Polyhedron 23 (2004) 1243–1248
POLYHEDRON
www.elsevier.com/locate/poly

Synthesis and characterization of copper(II) azide complexes containing polyamines as co-ligands

Jun Luo [a], Xi-Geng Zhou [a,*], Song Gao [b], Lin-Hong Weng [a], Ze-Huai Shao [a], Chun-Mei Zhang [a], Yan-Rong Li [a], Jie Zhang [a], Rui-Fang Cai [a]

[a] *Department of Chemistry, Fudan University, Handan Road 220, Shanghai 200433, PR China*
[b] *State Key Laboratory of Rare Earth Materials Chemistry and Applications, College of Chemistry, Peking University, Beijing 100871, PR China*

Received 4 December 2003; accepted 3 February 2004

Abstract

Two new copper(II) azide complexes $Cu_2(pn)_2(N_3)_4$ (**1**) and $Cu_3(dien)_2(N_3)_6$ (**2**) (pn = 1,3-diaminopropane and dien = diethylenetriamine) have been synthesized and characterized by single crystal X-ray diffraction. In complex **1** each copper(II) atom is coordinated to six nitrogen atoms from four azide anions and one 1,3-diaminopropane molecule in a distorted octahedral geometry. Successive pairs of copper(II) atoms are linked by two end-on azide bridges to form a polymeric chain. In centrosymmetric complex **2** the central copper(II) is coordinated by two monodentate azide anions and linked to two terminal copper atoms by double end-on azide bridges to give a linear trinuclear unit. The coordination geometry around each of the terminal copper atoms is square pyramidal, being surrounded by two nitrogen atoms of the bridging azide anions and three nitrogen atoms of the diethylenetriamine ligand. Magnetic susceptibility measurement of complex **2** in the range 2–300 K showed weak antiferromagnetic exchange between the copper(II) ions ($J = -2.09(8)$ cm^{-1}) through the double end-on azide bridges.
© 2004 Elsevier Ltd. All rights reserved.

Keywords: Azides; Polyamines; Copper(II) complexes; Crystal structures; Magnetic properties; Coordination polymers

1. Introduction

Great efforts have been devoted to the study of transition metal azide complexes because of their diverse structural types and fascinating magnetic properties [1–4]. To clarify the magneto-structural correlation of azide-bridged complexes, diverse co-ligands were introduced and the structures as well as magnetic properties of the adjusted complexes have been systematically investigated. Numerous complexes including dinuclear [5,6], trinuclear [7,8] and tetranuclear [9–11] species, together with one- [12,13], two- [14–16] and three-dimensional [17] coordination polymers have been well documented. On the other hand, the investigation results indicate that the introduction of polyamine co-ligands to the copper(II) azide complex system may bring about some interesting structures and magnetic properties due to the coordination functionality of various nitrogen donor atoms of the co-ligands [18–26]. To better understand the influence of the polyamine co-ligands on the structures and properties of the copper(II) azide complexes, we herein report the synthesis and characterization of two new copper(II) azide complexes $Cu_2(pn)_2(N_3)_4$ (**1**) and $Cu_3(dien)_2(N_3)_6$ (**2**).

2. Experimental

2.1. Materials and physical measurements

All reagents were commercial grade and were used as received. Elemental analyses for C, H, N were carried

* Corresponding author. Tel.: 86-21-65643769; fax: 86-21-65641740.
E-mail address: xgzhou@fudan.edu.cn (X.-G. Zhou).

0277-5387/$ - see front matter © 2004 Elsevier Ltd. All rights reserved.
doi:10.1016/j.poly.2004.02.003

out on an Elementar Vario EL-III analyzer, metal was determined by the ICP method. Magnetic measurement was performed on an Oxford Maglab2000 system in the temperature range of 2–300 K under a 30 kOe field. Diamagnetic corrections were made with Pascal's constants for all constituent atoms and magnetic moments were calculated by the equation $\mu_{\text{eff}} = 2.828(\chi_M T)^{1/2}$.

2.2. Preparation of the complexes

2.2.1. $Cu_2(pn)_2(N_3)_4$ (1)

A 2 ml ethanol solution of 1,3-diaminopropane (44 mg, 0.60 mmol) was added dropwise to a 3 ml ethanol solution of $CuCl_2 \cdot 2H_2O$ (51 mg, 0.30 mmol) under stirring. A 2 ml aqueous solution of NaN_3 (78 mg, 1.20 mmol) was added to a 3 ml ethanol solution of $MnCl_2 \cdot 4H_2O$ (59 mg, 0.30 mmol) and the mixture was stirred for another 5 min. Then the above two solutions were mixed, and a deep blue solution was formed and filtered, the filtrate evaporated slowly in air. After two weeks, deep blue block crystals of $Cu_2(pn)_2(N_3)_4$ (**1**) were obtained in 22% yield. *Anal.* Found: C, 15.71; H, 5.14; N, 50.27; Cu, 27.13. Calc. for $C_6H_{20}Cu_2N_{16}$: C, 16.25; H, 4.55; N, 50.54; Cu, 28.66%.

2.2.2. $Cu_3(det)_2(N_3)_6$ (2)

A 4 ml ethanol solution of diethylenetriamine (31 mg, 0.30 mmol) and a 4 ml ethanol solution of copper acetate (60 mg, 0.30 mmol) were mixed and stirred for 5 min. To the resulting deep-blue mixture was added dropwise a 2 ml aqueous solution of sodium azide (20 mg, 0.30 mmol). After stirring for another 5 min, the solution was filtered and the filtrate evaporated slowly in air. After one month, deep blue block crystals of $Cu_3(dien)_2(N_3)_6$ (**2**) were separated in 17% yield. *Anal.* Found: C, 14.53; H, 4.45; N, 52.33. Calc. for $C_8H_{26}Cu_3N_{24}$: C, 14.80; H, 4.04; N, 51.79%.

2.3. X-ray crystallography

Data collection for **1** and **2** was carried out on a Bruker Smart APEX CCD diffractometer equipped with graphite monochromated Mo Kα radiation ($\lambda =$ 0.71073 Å) at 298 K. Intensities were corrected for empirical absorption based on SADABS scan technique [27]. Both structures were solved by direct methods and refined by full-matrix least-squares on F^2 [28]. All non-H atoms were refined anisotropically, the H atoms attached to C atoms were added at calculated positions and the H atoms linked to N atoms were located from the difference Fourier map and refined freely with N–H distances 0.71(3)–0.87(5) Å. Table 1 gives crystallographic data of the two complexes. Tables 2 and 3 list the selected bond parameters and hydrogen bond parameters of complex **1**. Tables 4 and 5 show the selected bond parameters and hydrogen bond parameters of complex **2**.

Table 1
Crystallographic data for the two title complexes

	1	**2**
Empirical formula	$C_6H_{20}Cu_2N_{16}$	$C_8H_{26}Cu_3N_{24}$
Formula weight	443.46	649.15
Temperature (K)	298(2)	298(2)
Wavelength (Å)	0.71073	0.71073
Crystal system	monoclinic	monoclinic
Space group	$P2_1/n$	$P2_1/n$
Unit cell dimensions		
a (Å)	6.835(2)	6.826(2)
b (Å)	6.751(2)	12.800(3)
c (Å)	18.367(4)	13.606(3)
β (°)	99.543(3)	98.248(4)
V (Å^3)	835.8(3)	1176.4(5)
Z	2	2
D_{calc} (Mg m^{-3})	1.762	1.833
Absorption coefficient (mm^{-1})	2.547	2.740
$F(0\,0\,0)$	452	658
Crystal size (mm)	$0.50 \times 0.40 \times 0.35$	$0.20 \times 0.10 \times 0.10$
θ Range for data collection (°)	3.05–26.00	2.20–25.01
Index ranges	$-6 \leqslant h \leqslant 8$, $-7 \leqslant k \leqslant 8$, $-19 \leqslant l \leqslant 22$	$-8 \leqslant h \leqslant 8$, $-15 \leqslant k \leqslant 10$, $-15 \leqslant l \leqslant 16$
Reflections collected	3698	4851
Refinement method	full-matrix least-squares on F^2	full-matrix least-squares on F^2
Data $[I > 2\sigma(I)]$/parameters	1648/125	2073/180
Goodness-of-fit on F^2	1.041	0.830
R_1 indices ($I > 2\sigma(I)$)	0.0388	0.0337
wR_2 indices (all data)	0.1088	0.0549
Largest difference peak and hole (e Å^{-3})	0.506 and −0.448	0.525 and −0.361

Table 2
Selected bond distances (Å) and bond angles (°) for $Cu_2(pn)_2(N_3)_4$ (**1**)

Bond distances			
Cu(1)–N(7)	1.994(3)	Cu(1)–Cu(1C)	6.835(2)
Cu(1)–N(4)	2.006(3)	N(1)–N(2)	1.173(4)
Cu(1)–N(8)	2.006(3)	N(2)–N(3)	1.137(5)
Cu(1)–N(1)	2.461(3)	N(4)–N(5)	1.180(4)
Cu(1)–N(3B)	2.856(5)	N(5)–N(6)	1.149(4)
Cu(1)–Cu(1A)	3.3088(9)		
Bond angles			
N(7)–Cu(1)–N(4)	88.3(1)	N(8)–Cu(1)–N(1)	90.8(1)
N(4)–Cu(1)–N(1A)	91.8(1)	N(7)–Cu(1)–N(3B)	82.6(1)
N(7)–Cu(1)–N(8)	95.4(1)	N(4)–Cu(1)–N(3B)	96.8(2)
N(1A)–Cu(1)–N(8)	84.6(1)	N(1A)–Cu(1)–N(3B)	97.8(1)
N(7)–Cu(1)–N(1)	94.7(1)	N(8)–Cu(1)–N(3B)	79.8(2)
N(4)–Cu(1)–N(1)	92.8(1)	Cu(1)–N(1)–Cu(1A)	95.0(1)
N(1A)–Cu(1)–N(1)	85.0(1)		

Symmetry transformations used to generate equivalent atoms:(A) $-x+1, -y+1, -z$;(B) $x-1, y, z$;(C) $x+1, y, z$.

Table 3
Hydrogen bonds for $Cu_2(pn)_2(N_3)_4$ (**1**) (Å and °)

D–H···A	d(D–H)	d(H···A)	d(D···A)	<(DHA)
N(7)–H(7A)···N(4)#4	0.81(4)	2.33(5)	3.107(4)	159(4)
N(7)–H(7B)···N(6)#5	0.80(5)	2.29(5)	3.068(5)	163(5)
N(8)–H(8A)···N(4)#1	0.87(5)	2.48(5)	3.331(5)	169(4)
N(8)–H(8B)···N(6)#6	0.81(5)	2.40(5)	3.194(5)	164(4)

Symmetry transformations used to generate equivalent atoms: #1 $-x+1,-y+1,-z$; #2 $x-1,y,z$; #3 $x+1,y,z$; #4 $-x+1,-y+2,-z$; #5 $-x,-y+2,-z$; #6 $-x,-y+1,-z$.

Table 4
Selected bond distances (Å) and bond angles (°) for $Cu_3(dien)_2(N_3)_6$ (**2**)

Bond distances			
Cu(1)–N(4)	2.011(3)	Cu(1)–Cu(2)	3.3509(8)
Cu(1)–N(10)	2.012(3)	N(4)–N(5)	1.188(3)
Cu(1)–N(7)	2.531(3)	N(5)–N(6)	1.154(4)
Cu(2)–N(7)	1.971(3)	N(7)–N(8)	1.190(4)
Cu(2)–N(2)	1.994(4)	N(8)–N(9)	1.148(4)
Cu(2)–N(3)	1.996(4)	N(10)–N(11)	1.184(4)
Cu(2)–N(1)	1.996(4)	N(11)–N(12)	1.149(4)
Cu(2)–N(4)	2.448(3)		
Bond angles			
N(4)–Cu(1)–N(10)	89.8(1)	N(7)–Cu(2)–N(4)	84.6(1)
N(4)–Cu(1)–N(7)	81.6(1)	N(2)–Cu(2)–N(4)	101.7(1)
N(10)–Cu(1)–N(7)	90.2(1)	N(3)–Cu(2)–N(4)	90.3(2)
N(7)–Cu(2)–N(3)	94.9(2)	N(1)–Cu(2)–N(4)	99.9(2)
N(2)–Cu(2)–N(3)	84.3(2)	Cu(1)–N(4)–Cu(2)	96.9(1)
N(7)–Cu(2)–N(1)	95.4(2)	Cu(2)–N(7)–Cu(1)	95.4(1)
N(2)–Cu(2)–N(1)	84.4(2)		

Table 5
Hydrogen bonds for $Cu_3(dien)_2(N_3)_6$ (**2**) (Å and °)

D–H···A	d(D–H)	d(H···A)	d(D···A)	<(DHA)
N(2)–H(2C)···N(9)#2	0.71(3)	2.38(3)	3.057(5)	160(4)
N(3)–H(3C)···N(7)#3	0.81(3)	2.58(4)	3.157(5)	130(3)
N(1)–H(1D)···N(6)#4	0.75(3)	2.37(3)	3.092(5)	161(4)
N(1)–H(1C)···N(12)#1	0.78(3)	2.51(3)	3.283(6)	170(4)
N(3)–H(3D)···N(10)	0.76(3)	2.33(4)	3.037(6)	156(4)

Symmetry transformations used to generate equivalent atoms: #1 $-x,-y+2,-z+1$; #2 $x-1/2,-y+3/2,z-1/2$; #3 $-x+1,-y+2,-z+1$; #4 $x+1/2,-y+3/2,z+1/2$.

3. Results and discussion

3.1. Description of the structures

The copper(II) coordination environment of complex **1** is depicted in Fig. 1. Each Cu(1) atom is surrounded by one terminal azide N atom (N(4)), one bridging azide N atom (N(1A)) and two N atoms (N(7), N(8)) of one 1,3-diaminopropane molecule in the basal plane, along with two bridging azide N atoms (N(1), N(3B)) in the apical sites to form a distorted octahedral geometry. Two copper(II) atoms are connected by two end-on azide bridges to define a centrosymmetric dimeric unit, and each dimeric units is linked together to form a chain

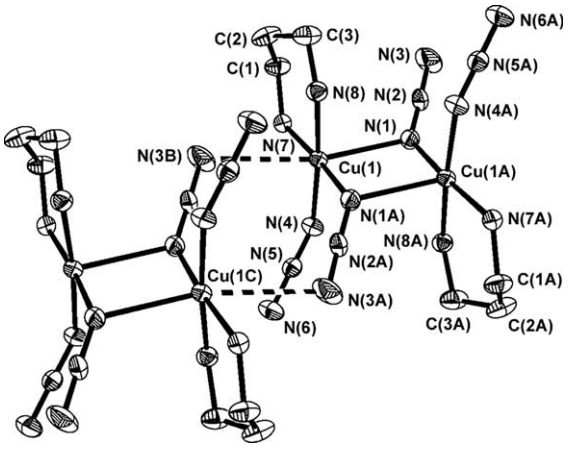

Fig. 1. The copper(II) coordination environment of complex **1**. Thermal ellipsoids are at 50% probability level.

structure via weak interactions ($Cu\cdots N = 2.856(5)$ Å). Finally, these chains are crosslinked via hydrogen bonds involving the terminal azide N atoms and the amino H atoms of the pn group ($N\cdots N = 3.068(5)$–$3.194(5)$ Å, $H\cdots N = 2.29(5)$–$2.40(5)$ Å and $N–H\cdots N = 159(4)°$–$164(4)°$), thus forming a two dimensional network structure (Fig. 2). In complex **1** the bridging azide anions exhibit two types of coordination modes: end-on fashion within the dimeric unit and end-to-end fashion between neighboring dimeric units. The $Cu\cdots Cu$ distance within the dimer is 3.3088(9) Å, and that between two dimers is 6.835(2) Å.

The molecular structure of the trinuclear complex **2** is depicted in Fig. 3. The central copper(II) atom adopts a *cis*-octahedral geometry, being linked to four basal nitrogen atoms (N(4), N(4A), N(10) and N(10A)) and two apical nitrogen atoms (N(7), N(7A)) from end-on bridging azide groups. Each of the two terminal copper(II) atoms adopts a square pyramidal geometry, with the azide nitrogen atom N(7) and three nitrogen atoms (N(1), N(2) and N(3)) from one diethylenetriamine ligand in the basal plane, along with azide nitrogen atom N(4) in the apical site. The distances between two adjacent copper(II) atoms is 3.3509(8) Å. Complex **2** is the first trinuclear copper(II) azide complex with polyamine co-ligands [18–26]. Intermolecular hydrogen-bonding interactions between the N atoms of the azide groups and the amino H atoms of the dien group ($N\cdots N$ 3.057(5)–3.157(5) Å, $H\cdots N$ 2.37(3)–2.58(4) Å and $N–H\cdots N$ 130(3)°–161(4)°) lead to the construction of a three-dimensional network structure (Fig. 4).

In complex **1** and **2** the $Cu–N_{basal}$ distances show no significant difference. The $Cu–N_{pn}$ distances in complex **1** (1.994(3)–2.006(3) Å) are almost equal to the $Cu–N_{dien}$ distances in complex **2** (1.994(4)–1.996(4) Å), and are consistent with the corresponding distances in aliphatic amine-copper complexes [29,30]. In complex **1** the axial $Cu–N_{azide}$ distances (2.461(3)–2.856(5) Å) are markedly

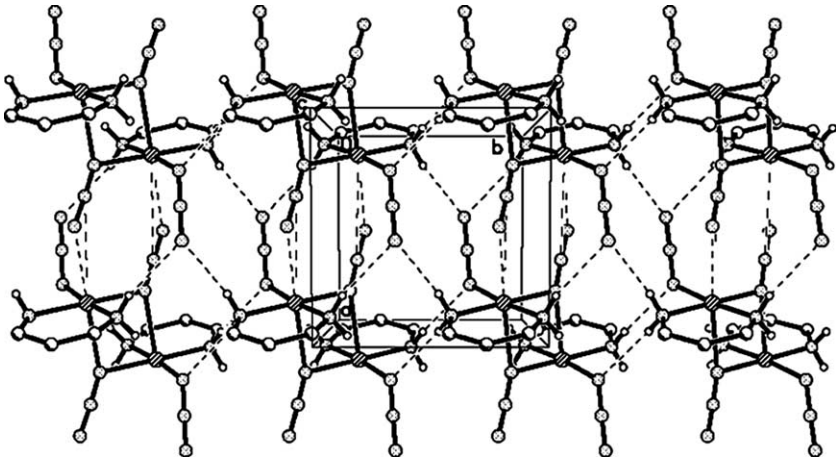

Fig. 2. The two-dimensional network structure of complex **1** form by hydrogen-bonding interactions (dashed lines).

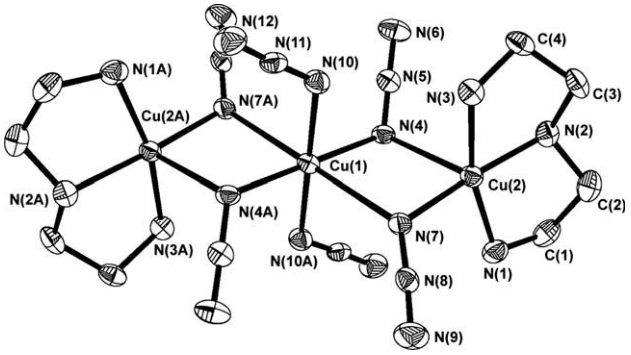

Fig. 3. The molecular structure of complex **2**. Thermal ellipsoids are at 50% probability level.

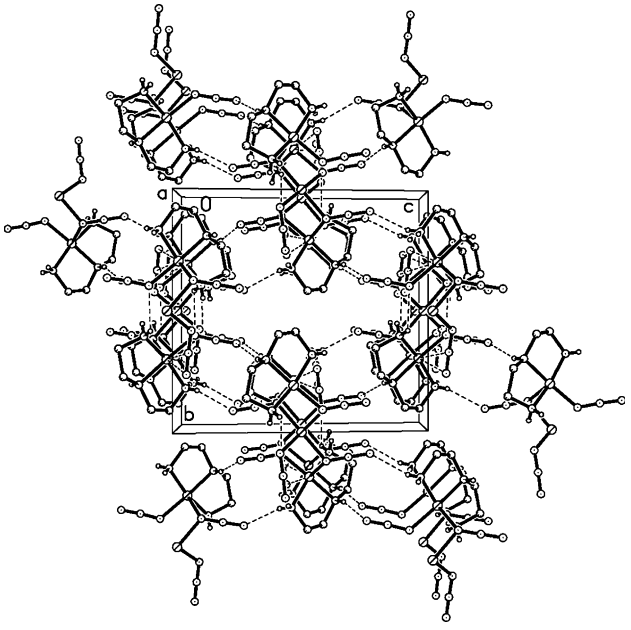

Fig. 4. The three-dimensional network structure of complex **2** formed by hydrogen-bonding interactions (dashed lines).

longer than the basal Cu–N_{azide} distance (2.006(3) Å); a similar situation is also observed in complex **2** and this axial elongation could be attributed to the Jahn–Teller distortion of copper(II) ions. The Cu–N_{azide} distances of the two complexes are respectively comparable to the corresponding distances in other copper(II) azide complexes [8,25,31]. In **2** the N_{basal}–Cu–N_{basal} (two neighboring basal N atoms) and N_{apical}–Cu–N_{basal} angles for the central copper(II) atom are in the ranges 89.8(1)°–90.2(1)° and 81.6(1)°–98.4(1)°, respectively, while the corresponding values for the terminal copper(II) atoms are 84.3(2)°–95.4(2)° and 84.6(1)°–101.7(1)°, indicating that the geometry of the terminal copper(II) atoms are more distorted than that for the central one. Further comparison also reveals that the geometry of complex **1** is more distorted than that of complex **2**.

It is interesting to note that the replacement of pn by dien results in the change of the coordination mode of the copper(II) atom with polyamine ligands from octahedral for **1** to square pyramidal for **2**. Obviously, this may be attributed to the larger steric effect of dien, which prohibits other azide groups from further coordination to the terminal copper, therefore favoring formation of trinuclear complex **2**. The steric effect of two aliphatic amines is also reflected by the relatively larger N(4)–Cu(2)–N(2) angle (101.7(1)°) in complex **2** as compared to the N(7)–Cu(1)–N(1) angle (94.7(1)°) in complex **1**.

3.2. Magnetic properties

The magnetic susceptibilities of complex **2** have been measured in the temperature range of 2–300 K at 30 kOe, and the plots of $\chi_M T$ and ${\chi_M}^{-1}$ vs T are shown in Fig. 5. The magnetic susceptibility above 20 K obeys the Curie–Weiss law with the Weiss constant $\theta = -0.5$ K, and a Curie constant $C = 1.14$ cm^3 mol^{-1} K. The C value is very close to the value (1.13 cm^3 mol^{-1} K) of three non-interacting Cu^{II} ions with $g = 2.0$. With the

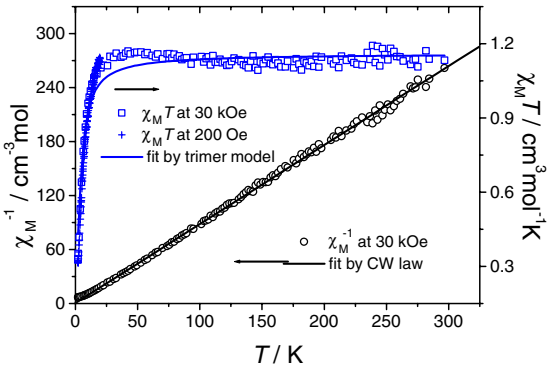

Fig. 5. Plot of $\chi_M T$ at 30 kOe (open square), $\chi_M T$ at 200 Oe (cross) and χ_M^{-1} (open circle) vs. T for complex **2**; the solid line shows the best fit theoretical curves for complex **2**.

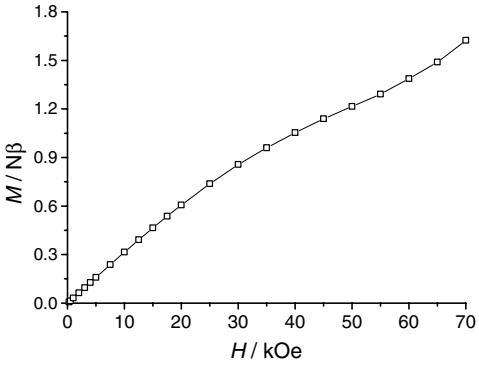

Fig. 6. Magnetization (open square) for complex **2** at 1.86 K as a function of the applied magnetic field (0–70 kOe).

decrease of the temperature, $\chi_M T$ remains almost constant to ca. 20 K, and then decreases rapidly, reaching a minimum of 0.33 cm^3 mol^{-1} K at 2.2 K. The $\chi_M T$ measured at low field (200 Oe) below 20 K also shows a decrease, suggesting the occurrence of antiferromagnetic interactions between adjacent Cu(II) ions. These may be attributed to magnetic coupling in end-on azide-bridging copper(II) complexes in which large Cu–N (EO azide nitrogen) distances above 2.05 Å often promote antiferromagnetic coupling between adjacent copper(II) atoms [32]. In complex **2** the Cu(1)–N(7) and Cu(2)–N(4) distances are 2.531(3) and 2.448(3) Å, respectively, leading to antiferromagnetic coupling within the trinuclear unit.

The magnetic data of the complex **2** were fitted using a trinuclear Cu^{II} model [33].

$$\chi_M = \frac{Ng^2\beta^2}{4kT}\,\frac{1+\exp\left(\frac{-2J}{kT}\right)+10\exp\left(\frac{J}{kT}\right)}{1+\exp\left(\frac{-2J}{kT}\right)+2\exp\left(\frac{J}{kT}\right)}. \qquad (1)$$

In Eq. (1), N, β, and g have their usual meaning and J is the exchange coupling constant describing the magnetic interaction between two adjacent copper(II) ions within the trinuclear unit. The fitted values are in good agreement with the experimental data and the parameters $J = -2.09(8)$ cm^{-1}, $g = 2.031(3)$ and $R = 1 \times 10^{-3}$ ($R = \Sigma[(\chi_M)\text{obs} - (\chi_M)\text{calc}]^2/\Sigma[(\chi_M)\text{obs}^2$ further confirm antiferromagnetic exchange coupling within the trimers. It is interesting to compare the magnetic properties of complex **2** with [Cu(4-Etpy)(N$_3$)$_2$]$_2$ [6]. Both complexes are homo-azide end-on bridged copper(II) complexes; the former shows weak antiferromagnetic coupling while the latter displays ferromagnetic coupling between adjacent copper(II) ions. The ferromagnetic properties for the latter complex originate from the fact that the Cu–N (EO azide nitrogen) distances of [Cu(4-Etpy)(N$_3$)$_2$]$_2$ are in the normal range (1.970(10)–1.979(9) Å) and the Cu–N–Cu bond angles within each dimeric unit is 103.0(5)°, which is slightly less than 104°. These bond parameters are known to lead to ferromagnetic interaction between the two nearest-neighbouring spin doublets in homo-azide end-on bridged copper(II) complexes [32].

The field dependence of the magnetization (0–70 kOe) measured at 1.86 K is shown in Fig. 6, where M, N, β and H are magnetization, Avogadro's number, electron Bohr magneton and applied magnetic field, respectively. The magnetization increases with the increase of magnetic field, reaching ca. 1.2 $N\beta$ per Cu$_3$ unit around 50 kOe, being consistent with the expected value of $1N\beta$ for an anti-parallel linear alignment of three Cu^{II} magnetic moments with $S_T = 1/2$. Above 50 kOe, the magnetization increases further, indicating that the spins deviate from antiferromagnetic coupling and align with the applied field.

In conclusion, the interaction between double end-on azide bridges of complex **2** is weak antiferromagnetic.

4. Supplementary data

Crystallographic data for the structural analysis have been deposited with the Cambridge Crystallographic Data Centre, CCDC Nos. 222993 and 222994 for complexes **1** and **2**. Copies of this information may be obtained free of charge from The Director, CCDC, 12 Union Road, Cambridge CB2 1EZ, UK (+44-1223-336033; e-mail: deposit@ccdc.cam.ac.uk or www:http://www.ccdc.cam.ac.uk).

Acknowledgements

The project was supported by National Natural Science Foundation of PR China and the New Century Distinguished Scientist of the Ministry of Education of China.

References

[1] J. Ribas, M. Monfort, B.K. Ghosh, X. Solans, Angew. Chem. Int. Ed. Engl. 33 (1994) 2087.

[2] G. De Munno, M. Julve, G. Viau, F. Lloret, J. Faus, D. Viterbo, Angew. Chem. Int. Ed. Engl. 35 (1996) 1807.
[3] C.S. Hong, Y. Do, Angew. Chem. Int. Ed. 38 (1999) 193.
[4] Z. Shen, J.-L. Zuo, S. Gao, Y. Song, C.-M. Che, H.-K. Fun, X.-Z. You, Angew. Chem. Int. Ed. 39 (2000) 3633.
[5] U. Ray, B. Chand, G. Mostafa, J. Cheng, T.-H. Lu, C. Sinha, Polyhedron 22 (2003) 2587.
[6] M.A.S. Goher, A. Escuer, F.A. Mautner, N.A. Al-Salem, Polyhedron 20 (2001) 2971.
[7] H.-J. Chen, Z.-W. Mao, S. Gao, X.-M. Chen, Chem. Commun. (2001) 2320.
[8] J.-C. Liu, D.-G. Fu, J.-Z. Zhuang, C.-Y. Duan, X.-Z. You, J. Chem. Soc., Dalton Trans. (1999) 2337.
[9] G.S. Papaefstathiou, A. Escuer, M. Font-Bardía, S.P. Perlepes, X. Solans, R. Vicente, Polyhedron 21 (2002) 2027.
[10] J. Ribas, M. Monfort, R. Costa, X. Solans, Inorg. Chem. 32 (1993) 695.
[11] B. Kersting, G. Steinfeld, D. Siebert, Chem. Eur. J. 7 (2001) 4253.
[12] C.S. Hong, J.-E. Koo, S.-K. Son, Y.S. Lee, Y.-S. Kim, Y. Do, Chem. Eur. J. 7 (2001) 4243.
[13] M.A.S. Goher, A. Escuer, F.A. Mautner, N.A. Al-Salem, Polyhedron 21 (2002) 1871.
[14] J.L. Manson, A.M. Arif, J.S. Miller, Chem. Commun. (1999) 1479.
[15] A. Escuer, R. Vicente, M.A.S. Goher, F.A. Mautner, Inorg. Chem. 35 (1996) 6386.
[16] R. Cortés, M.K. Urtiaga, L. Lezama, J.L. Pizarro, M.I. Arriortua, T. Rojo, Inorg. Chem. 36 (1997) 5016.
[17] A.-H. Fu, X.-Y. Huang, J. Li, T. Yuen, C.L. Lin, Chem. Eur. J. 8 (2002) 2239.
[18] X.-H. Bu, M. Du, Z.-L. Shang, L. Zhang, Q.-H. Zhao, R.-H. Zhang, M. Shionoya, Eur. J. Inorg. Chem. (2001) 1551.
[19] N.K. Karan, S. Mitra, T. Matsushita, V. Gramlich, G. Rosair, Inorg. Chim. Acta. 332 (2002) 87.
[20] P. Manikandan, R. Muthukumaran, K.R. Justin Thomas, B. Varghese, G.V.R. Chandramouli, P.T. Manoharan, Inorg. Chem. 40 (2001) 2378.
[21] B. Graham, M.T.W. Hearn, P.C. Junk, C.M. Kepert, F.E. Mabbs, B. Moubaraki, K.S. Murray, L. Spiccia, Inorg. Chem. 40 (2001) 1536.
[22] T.-H. Lu, S.-C. Lin, H. Aneetha, K. Panneerselvam, C.S. Chung, J. Chem. Soc., Dalton Trans. (1999) 3385.
[23] H.-L. Zhu, P. Huang, C.-Y. Duan, L.-M. Zheng, Y.-J. Liu, M.-F. Wu, W.-X. Tang, Trans. Met. Chem. 24 (1999) 380.
[24] A. Escuer, M. Font-Bardía, E. Peñalba, X. Solans, R. Vicente, Polyhedron 18 (1998) 211.
[25] O.L. Casagrande, S.I. Klein, A.E. Mauro, K. Tomita, Trans. Met. Chem. 14 (1989) 45.
[26] O. Kahn, S. Sikorav, J. Gouteron, S. Jeannin, Y. Jeannin, Inorg. Chem. 22 (1983) 2877.
[27] G.M. Sheldrick, SADABS A Program for Empirical Absorption Correction, University of Göttingen, Germany, 1996.
[28] G.M. Sheldrick, SHELXS-97 and SHELXL-97, University of Göttingen, Germany, 1997.
[29] P.J. Baesjou, W.L. Driessen, J. Reedijk, A.L. Spek, Inorg. Chim. Acta. 306 (2000) 237.
[30] L.A. Kovbasyuk, I.O. Fritsky, V.N. Kokozay, T.S. Iskenderov, Polyhedron 16 (1997) 1723.
[31] M.A.S. Goher, A. Escuer, F.A. Mautner, N.A. Al-Salem, Polyhedron 20 (2001) 2971.
[32] E. Ruiz, J. Cano, S. Alvarez, P. Alemany, J. Am. Chem. Soc. 120 (1998) 11122.
[33] E. Sinn, in: A. Townshend (Ed.), Encyclopaedia of Analytical Chemistry, Academic Press, London, 1995, pp. 2765–2780.

Available online at www.sciencedirect.com
SCIENCE DIRECT®
Polyhedron 23 (2004) 1249–1255
POLYHEDRON
www.elsevier.com/locate/poly

Synthesis, structure and anti-fungal activity of dimeric Ag(I) complexes containing bis-imidazole ligands

Suaad Abuskhuna [a], John Briody [a], Malachy McCann [a,*], Michael Devereux [b], Kevin Kavanagh [c], Julia Barreira Fontecha [d], Vickie McKee [d]

[a] Department of Chemistry, St. Patrick's College, National University of Ireland Maynooth, Maynooth, Co. Kildare, Ireland
[b] Dublin Institute of Technology, Cathal Brugha Street, Dublin, Ireland
[c] Department of Biology, National University of Ireland Maynooth, Maynooth, Co. Kildare, Ireland
[d] Department of Chemistry, Loughborough University, Loughborough, Leics LE11 3TU, UK

Received 10 November 2003; accepted 4 February 2004

Abstract

Five Ag(I) complexes containing the ligands bis(imidazol-2-yl)methane (2-BIM) and its derivatives were prepared and $[Ag_2(2\text{-}BIM)_2](ClO_4)_2$ and $[Ag_2(2\text{-}BIM(Bz)OH)_2](ClO_4)_2 \cdot EtOH$ were characterised using X-ray crystallography. In each dimer the two Ag(I) ions are two-coordinate and there are small but definite argentophilic Ag–Ag (d^{10}–d^{10}) interactions. All of the complexes display anti-fungal activity when tested in vitro against the fungal pathogen *Candida albicans*.
© 2004 Elsevier Ltd. All rights reserved.

Keywords: Bis-imidazole; Bis(imidazol-2-yl)methane; X-ray structures; Silver(I); Argentophilicity; Anti-fungal; Candida albicans

1. Introduction

In our efforts to develop new metal complexes that would greatly inhibit the growth of the human fungal pathogen *Candida albicans* [1–4] we have found that, to date, the most active drug tested in aqueous media is the Ag(I) complex $[Ag(phendio)_2]ClO_4$ (phendio = 1,10-phenanthroline-5,6-dione) [5]. As part of these ongoing studies into the synthesis and in vitro testing of new metal-based anti-fungal drugs we report here the preparation of five Ag(I) complexes containing bis(imidazole) ligands. Bis(imidazol-2-yl)methane (2-BIM) and its derivatives (Fig. 1), in which the two imidazole rings are linked via a single tetrahedral carbon atom, can be viewed as primitive models for multi-histidine coordination in biological systems. Such bis(imidazole) ligands have been shown to form stable six-membered chelate rings with a variety of transition metals [6–12], and the Pt(II) complex $[Pt(2\text{-}BIM(Me)OH)Cl_2]$ (2-BIM(Me)OH = bis(*N*-methylimidazol-2-yl)carbinol) [10] has been reported to exhibit notable antitumor activity.

2. Results and discussion

In the current study, $AgClO_4$ was reacted at room temperature with methanolic solutions of the five bis(imidazole) ligands shown in Fig. 1 to give the respective Ag(I) complex in moderate to good yield. The complexes were soluble in hot acetonitrile and DMSO and insoluble in water. The X-ray crystal structure of $[Ag_2(2\text{-}BIM)_2](ClO_4)_2$ (Fig. 2 and Table 1) showed the complex to be centrosymmetric, containing two $Ag(2\text{-}BIM)^+$ units. The two metal ions are two-coordinate and have identical atoms in the plane of the chelating ligand. Using its two imine N atoms each 2-BIM ligand bridges the pair of Ag(I) ions. All four N atoms (N1, N4A, N4, N1A) are coplanar and the two imidazole groups in each 2-BIM ligand have an interplanar angle of 75.52(8)°. The two Ag(I) ions are only weakly interacting, the distance separating them being 3.2612(4) Å. The binding of the two 2-BIM ligands is similar to that

* Corresponding author. Tel.: +353-1-708-3767; fax: +353-1-708-3815.
E-mail address: mmcann@may.ie (M. McCann).

0277-5387/$ - see front matter © 2004 Elsevier Ltd. All rights reserved.
doi:10.1016/j.poly.2004.02.006

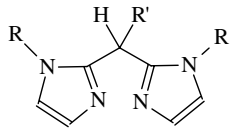

	R	R'
2-BIM	H	H
2-BIM(Bz)OH	$PhCH_2$	OH
2-BIM(Me)	Me	H
2-BIM(CN)	$NC(CH_2)_2$	H
2-BIM(ClBz)	Cl_2PhCH_2	H

Fig. 1. Ligand symbols and structures.

observed for the $Biim^{2-}$ ligand ($Biim^{2-}$ = 2,2′-biimidazolate) in the heteropolynuclear complex, $[\{Ru(pap)_2(Biim)\}_2Ag_2](ClO_4)_2 \cdot H_2O$ (pap = 2-(phenylazo)pyridine) [13]. The shorter Ag–Ag separation in the latter species is (2.8899 Å) is mainly a consequence of the smaller size of the $Biim^{2-}$ ligand compared to 2-BIM (no methylene bridge between the two imidazole rings in $Biim^{2-}$). The formula unit of $[Ag_2(2\text{-}BIM)_2](ClO_4)_2$ is completed by two lattice perchlorate, which are involved in hydrogen bonding to the hydrogen atoms of the imidazole nitrogen atoms (N2 and N3, and N2A and N3A, respectively). The lattice perchlorate anions show unsymmetric bridging interactions with Ag(I) ions of neighbouring cations ($AgOClO_3$ 2.965(2) and 3.264(2) Å). There are hydrogen bonding interactions along the *a* and *b* directions which link the units together in the lattice, forming sheets. However, there are no hydrogen bonds in the *c* direction, that is to say, between the sheets. There are some intermolecular π–π interactions involving the imidazole rings on adjacent dimer molecules and there is also evidence of some interdimer C–H···π interactions between neighbouring imidazole functions. A perspective view of the cell packing is shown in Fig. 3.

The X-ray crystal structure of $[Ag_2(2\text{-}BIM(Bz)OH)_2](ClO_4)_2 \cdot EtOH$ (Fig. 4 and Table 2) shows the asymmetric unit containing one $[Ag_2(2\text{-}BIM(Bz)OH)_2]^{2+}$ unit, two perchlorate anions and a solvate ethanol. The two Ag(I) ions are again bridged by the two ligands and each metal is approximately linearly coordinated to a pair of imine nitrogens. There are additional longer interactions with the perchlorate anions. The metal-metal distance of 3.018(4) Å is considerably shorter than in $[Ag_2(2\text{-}BIM)_2](ClO_4)_2$. Within the $[Ag_2(2\text{-}BIM(Bz)OH)_2](ClO_4)_2 \cdot EtOH$ complex molecule there appears to be some degree of intramolecular π–π interaction between the imidazole and phenyl rings of the opposing two 2-BIM(Bz)OH ligands in the dimer. Interestingly, the angles N(1A)–Ag(1)–Ag(2) and N(4B)–Ag(1)–Ag(2) are very different to one another (168.30(12)° and 68.35(8)°, respectively). One of the perchlorate anions in the complex is disordered and was modeled with two alternative sets of oxygen atom positions (50% occupancy each). The ethanol solvate is also disordered and was modeled as 50% occupancy of two alternative positions. Hydrogen atoms attached to carbon were inserted at calculated positions, whilst those attached to the 2-BIM(Bz)OH alcohol groups were located from difference maps and not further refined, those bonded to the disordered oxygen atom of the ethanol solvate were not located or included in the model. One view of the packing in the crystal is illustrated in Fig. 5.

Repeated attempts to grow crystals of $[Ag_2\{2\text{-}BIM(Me)\}_2](ClO_4)_2$, $[Ag_2\{2\text{-}BIM(CN)\}_2](ClO_4)_2$ and $[Ag_2\{2\text{-}BIM(BzCl)\}_2](ClO_4)_2$ suitable for X-ray structural anal-

Table 1
Selected bond lengths (Å) and angles (°) for $[Ag_2(2\text{-}BIM)_2](ClO_4)_2$

Bond lengths (Å)	
Ag(1)–N(4)#1	2.0953(17)
Ag(1)–N(1)	2.0957(17)
Ag(1)–Ag(1)#1	3.2612(4)
Ag(1)–O(11)#2	2.965(2)
Ag(1)–O(11)#3	3.264(2)
Bond angles (°)	
N(4)#1–Ag(1)–N(1)	167.80(7)
N(4)#1–Ag(1)–Ag(1)#1	91.08(5)
N(1)–Ag(1)–Ag(1)#1	99.94(5)

Symmetry transformations used to generate equivalent atoms: #1 $-x+1, -y+1, -z+1$; #2 $1+x, 1+y, z$; #3 $1-x, -y, 1-z$.

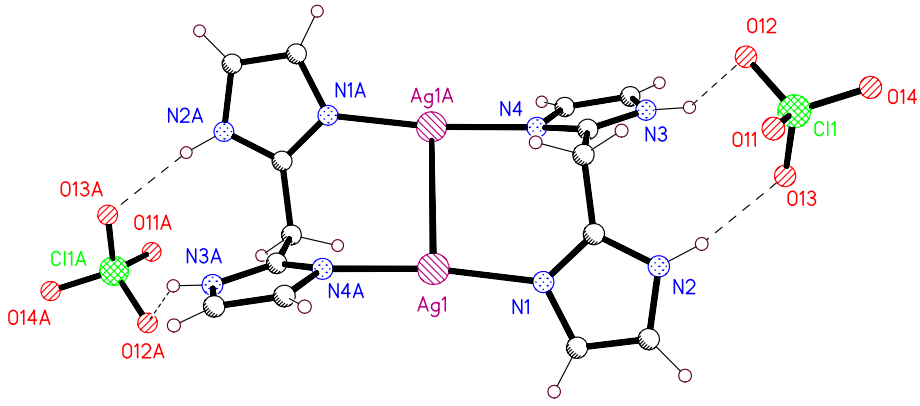

Fig. 2. X-ray crystal structure of $[Ag_2(2\text{-}BIM)_2](ClO_4)_2$.

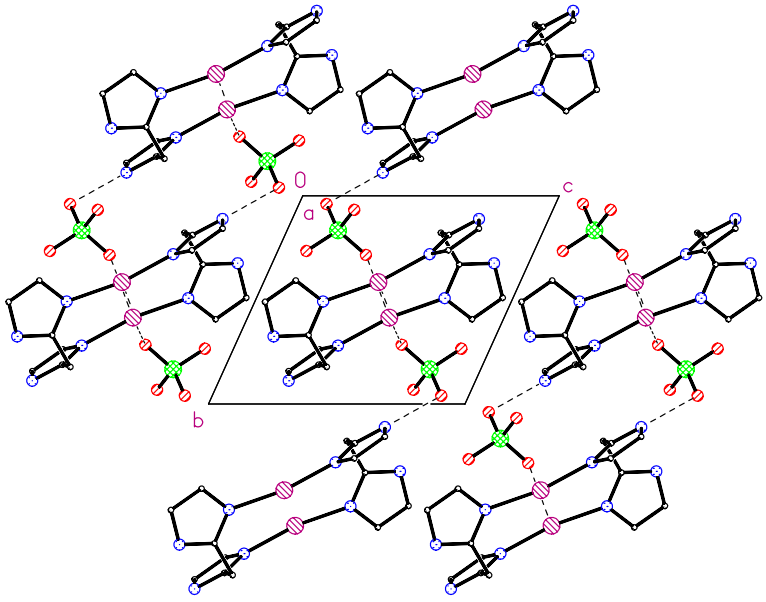

Fig. 3. Packing diagram for $[Ag_2(2\text{-}BIM)_2](ClO_4)_2$.

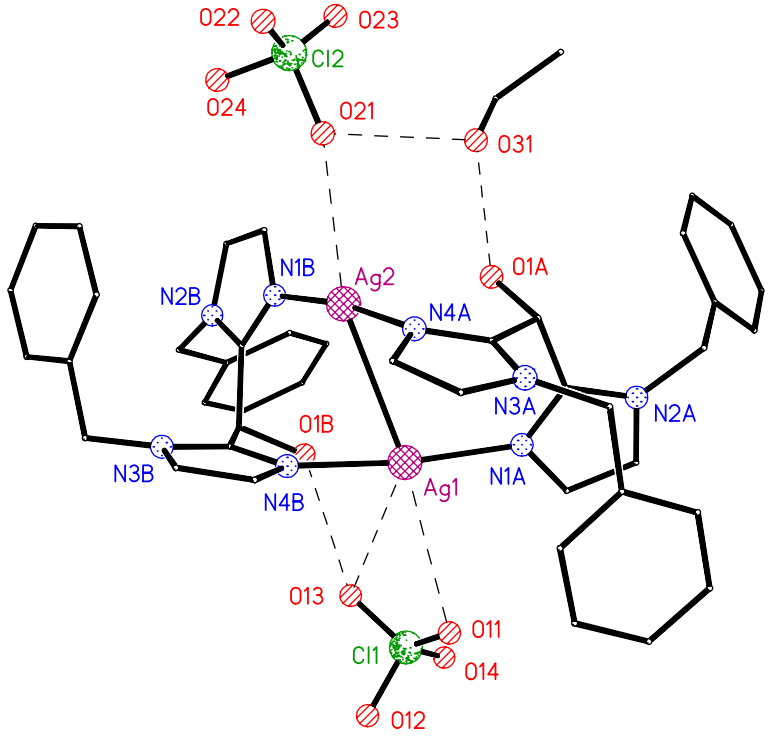

Fig. 4. X-ray crystal structure of $[Ag_2(2\text{-}BIM(Bz)OH)_2](ClO_4)_2 \cdot EtOH$.

ysis were unsuccessful. However, given the close similarities in the core structures of all five bis(imidazole) ligands the latter three silver complexes are thought to be essentially isostructural with $[Ag_2(2\text{-}BIM)_2]$ $(ClO_4)_2$ and $[Ag_2(2\text{-}BIM(Bz)OH)_2](ClO_4)_2 \cdot EtOH$ and are thus also formulated as dimers. For $[Ag_2\{2\text{-}BIM(CN)\}_2](ClO_4)_2$ there is also the possibility of the pendant cyano groups participating in the bonding to the metal since Ag(I) has a high affinity for organonitrile donors.

2.1. In vitro anti-Candida studies

All of the metal-free bis(imidazole) ligands and the Ag(I) complexes were screened for their ability to inhibit the growth of *C. albicans*. The minimum inhibitory concentration (MIC) is the concentration of drug (expressed as μg of complex per 1 cm^3 of aqueous growth medium solution) required to totally inhibit the growth of the fungal cells at 37 °C. As the complexes and the

Table 2
Selected bond lengths (Å) and angles (°) for $[Ag_2(2\text{-BIM(Bz)OH})_2](ClO_4)_2 \cdot EtOH$

Bond lengths (Å)	
Ag(1)–N(1A)	2.111(3)
Ag(1)–N(4B)	2.134(3)
Ag(1)–Ag(2)	3.0184(4)
Ag(1)–O(11)	3.211(6)
Ag(1)–O(13)	3.312(7)
Ag(2)–N(1B)	2.119(3)
Ag(2)–N(4A)	2.141(3)
Ag(2)–O(21)	3.012(7)
Ag(2)–O(21′)	3.234(14)
Bond angles (°)	
N(1A)–Ag(1)–N(4B)	168.30(12)
N(1A)–Ag(1)–Ag(2)	103.65(8)
N(4B)–Ag(1)–Ag(2)	68.35(8)
N(1A)–Ag(1)–O(11)	82.69(13)
N(4B)–Ag(1)–O(11)	105.55(13)
Ag(2)–Ag(1)–O(11)	173.58(10)
N(1A)–Ag(1)–O(13)	109.69(14)
N(4B)–Ag(1)–O(13)	81.74(14)
Ag(2)–Ag(1)–O(13)	133.53(10)
O(11)–Ag(1)–O(13)	41.35(13)
N(1B)–Ag(2)–N(4A)	172.79(12)
N(1B)–Ag(2)–O(21)	92.53(19)
N(4A)–Ag(2)–O(21)	93.9(2)
N(1B)–Ag(2)–Ag(1)	99.97(8)
N(4A)–Ag(2)–Ag(1)	74.23(8)
O(21)–Ag(2)–Ag(1)	164.88(17)
N(1B)–Ag(2)–O(21′)	76.8(2)
N(4A)–Ag(2)–O(21′)	109.3(2)
Ag(1)–Ag(2)–O(21′)	174.4(2)

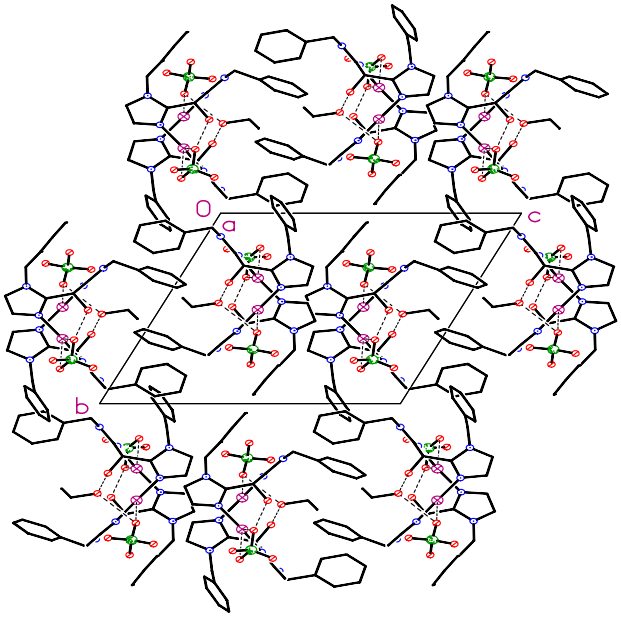

Fig. 5. Packing diagram for $[Ag_2(2\text{-BIM(Bz)OH})_2](ClO_4)_2 \cdot EtOH$.

ligands were essentially water insoluble the tests were carried out as suspensions of the complexes in the aqueous growth medium. In addition, because the complexes were soluble in DMSO a series of anti-fungal tests were also conducted using DMSO/water solutions of the complexes (see Section 3). In all cases, the activity of the complexes were compared to that of a control system in which the cells were grown in the absence of any added complex or free ligand (under these conditions the fungal cell replication was rapid). In addition, under the present biological test conditions an aqueous suspension of the anti-*Candida* prescription drug ketoconazole had an MIC value of ca. 2.5 $\mu g\,cm^{-3}$.

All of the metal-free ligands were found to be inactive against the fungal cells. As aqueous suspensions, the silver complexes were moderately active with MIC value ranges indicated in brackets: $[Ag_2(2\text{-BIM})_2](ClO_4)_2$ (10–20 $\mu g\,cm^{-3}$); $[Ag_2(2\text{-BIM(Bz)OH})_2](ClO_4)_2 \cdot EtOH$ (50–100 $\mu g\,cm^{-3}$); $[Ag_2\{2\text{-BIM(Me)}\}_2](ClO_4)_2$ (20–50 $\mu g\,cm^{-3}$); $[Ag_2\{2\text{-BIM(CN)}\}_2](ClO_4)_2$ (20–50 $\mu g\,cm^{-3}$). A considerable improvement in anti-fungal activity was observed upon administering the complexes as DMSO/water solutions as opposed to aqueous suspensions: $[Ag_2(2\text{-BIM})_2](ClO_4)_2$ (5–10 $\mu g\,cm^{-3}$); $[Ag_2(2\text{-BIM(Bz)-OH})_2](ClO_4)_2 \cdot EtOH$ (2.5–5 $\mu g\,cm^{-3}$); $[Ag_2\{2\text{-BIM(Me)}\}_2](ClO_4)_2$ (2.5–5 $\mu g\,cm^{-3}$); $[Ag_2\{2\text{-BIM(CN)}\}_2](ClO_4)_2$ (5–10 $\mu g\,cm^{-3}$); $[Ag_2\{2\text{-BIM(BzCl)}\}_2](ClO_4)_2$ (5–10 $\mu g\,cm^{-3}$). Besides greatly increasing the solubility of the complexes the DMSO is also thought to make the cells more permeable to the complexes so that they can enter the cells and exert their effects on the organism. In comparison, as an aqueous suspension $[Ag(phen\text{-}dio)_2]ClO_4$ has an MIC value of 0.3 $\mu g\,cm^{-3}$ [5].

3. Experimental

Chemicals were purchased from commercial sources and, unless specified, were used without further purification. Literature methods were used to prepare 2-BIM [14,15], 2-BIM(Me) [7,16] and 2-BIM(OH)Bz [17]. The preparation of the silver complexes was conducted in the absence of light and the samples were stored in the dark. Infrared spectra of solids (in a KBr matrix) were recorded in the region 4000–400 cm^{-1} on a Nicolet FT-IR Impact 400D infrared spectrometer and ^1H NMR spectra were run on a Bruker Avance 300 MHz instrument. Microanalytical data were provided by the Microanalytical Laboratory, National University of Ireland, Cork, Ireland.

3.1. 2-BIM(CN)

Acrylonitrile (3.6 g, 67 mmol) was added to a mixture of 2-BIM (5.0 g, 34 mmol), and triethylamine (6.8 g, 67 mmol) in acetonitrile (150 cm^3). The reaction mixture was refluxed with stirring for 5 h. The solvent was removed under reduced pressure giving a white solid, which was recrystallised from acetone. Yield: 4.7 g (55%). Mp 170 °C. *Anal.* Calc. C, 61.40; H, 5.50; N,

33.07. Found: C, 61.26; H, 5.47; N, 32.76%. ^{1}H NMR(DMSO-d_6): 7.17 (2H, d, $J = 1.3$ Hz), 6.8 (2H, d, $J = 1.3$ Hz), 4.3 (4H, t, $J = 6.7$ Hz), 4.2 (2H, s), 3.0 (4H, t, $J = 6.7$ Hz) ppm. ^{13}C NMR(DMSO-d_6): 143.6, 127.3, 120.8, 118.8, 25.4, 19.2 ppm. IR: 3125, 2932, 2264, 1485, 1447, 1383, 1287, 1166, 1134, 1089, 926, 722, 743, 705 cm^{-1}. Mass spec.: m/z: 254 (M^+, 4%), 200 (4), 173 (8), 161 (6), 148 (10), 134 (11), 120 (14), 107 (14), 94 (28), 82 (84), 66 (20), 54 (100).

3.2. 2-BIM(BzCl)

2,6-Dichlorobenzyl chloride (0.53 g, 2.7 mmol) was added to a stirred mixture of 2-BIM (0.2 g, 1.3 mmol) and sodium hydride (0.06 g, 2.5 mmol) in dry DMF (15 cm^3). The mixture was stirred overnight at room temperature and the solvent removed under reduced pressure. Water (20 cm^3) was added and the product extracted with dichloromethane, and the dichloromethane solution was then dried over magnesium sulphate. After filtration the solvent was removed under reduced pressure. The resulting brown oily residue was digested in cyclohexane and the white product precipitated upon cooling. Yield: 0.34 g (54%). Mp 93 °C. *Anal*. Calc. C, 54.10; H, 3.43; N, 12.02. Found: C, 54.09; H, 3.58; N, 11.73%. ^{1}H NMR ($CDCl_3$): 7.4 (2H, d, $J = 2$ Hz), 7.1 (2H, dd, $J = 8.3$ Hz), 6.9 (2H, d, $J = 1.3$ Hz), 6.7 (2H, d, $J = 1.3$ Hz), 6.5 (2H, d, $J = 8.3$ Hz), 5.2 (4H, s), 4.2 (2H, s). ^{13}C NMR ($CDCl_3$): 143, 134.5, 133.6, 132.7, 129.5, 129.1, 128.1, 127.5, 120.5, 47, 27 ppm. IR: 2945, 1593, 1485, 1447, 1389, 1274, 1121, 1057, 849, 733, 682 cm^{-1}. Mass spec.: m/z: 466 (M^+, 16%), 429 (4), 305 (26), 269 (8), 205 (8), 159 (100), 147 (8), 123 (16), 99 (6), 89 (16), 81 (38), 63 (10).

3.3. $[Ag_2(2\text{-}BIM)_2](ClO_4)_2$

Silver perchlorate (0.70 g, 3.37 mmol) was added to a stirred solution of 2-BIM (0.5 g, 3.37 mmol) in methanol (15 cm^3) and the mixture stirred for 1 h at room temperature. The precipitated white was filtered off, washed with methanol and air-dried. Yield: 1.00 g (83%). *Anal*. Calc. C, 23.64; H, 2.25; N, 15.76. Found: C, 23.58; H, 2.13; N, 15.78%. IR: 3344, 3151, 1293, 1095, 759, 624 cm^{-1}. ^{1}H NMR (ppm DMSO): 6.8 (8H, s), 4 (4H, s). The complex was soluble in hot acetonitrile and DMSO, and crystals suitable for X-ray analysis were obtained by recrystallising from acetonitrile.

3.4. $[Ag_2(2\text{-}BIM(Bz)OH)_2](ClO_4)_2 \cdot EtOH$

This white complex was prepared and recrystallised in a similar way to $[Ag_2(2\text{-BIM})_2](ClO_4)_2$ using silver perchlorate (0.06 g, 0.17 mmol) and 2-BIM(Bz)OH (0.1 g, 0.29 mmol). Yield: 0.11 g (68%). *Anal*. Calc. C, 43.87; H, 3.48; N, 9.70. Found: C, 44.21; H, 3.45; N, 9.69%. IR: 2485, 3138, 2971, 1497, 1459, 1287, 1102, 827, 717, 624 cm^{-1}. ^{1}H NMR (ppm DMSO): 5.2 (8H, dd), 6.4 (2H, d), 7.1 (8H, s), 7.35 (20H, m). The complex was soluble in hot acetonitrile, hot acetone and DMSO.

3.5. $[Ag_2\{2\text{-}BIM(Me)\}_2](ClO_4)_2$

To a solution of silver perchlorate (0.10 g, 0.48 mmol) in methanol (3 cm^3) was added a solution of 2-BIM(Me) (0.10 g, 0.56 mmol) in methanol (3 cm^3). A white precipitate formed immediately and the reaction mixture was stirred for 20 min at room temperature. The white product was filtered off, washed with methanol and then dried in air. Yield: 0.13 g (62%). *Anal*. Calc. C, 28.10; H, 3.13; N, 14.60. Found: C, 27.5; H, 3.00; N, 14.13%. IR: 3485, 3138, 2971, 1497, 1414, 1293, 1102, 772, 627 cm^{-1}. ^{1}H NMR (ppm DMSO): 3.5 (12H, s), 4.36 (4H, s), 6.8 (4H, s), 7.2 (4H, s). The complex was soluble in hot acetonitrile, hot acetone and DMSO.

3.6. $[Ag_2\{2\text{-}BIM(CN)\}_2](ClO_4)_2$

This white complex was prepared in a similar way to $[Ag_2\{2\text{-BIM(Me)}\}_2](ClO_4)_2$ using silver perchlorate (0.10 g, 0.48 mmol) and 2-BIM(CN) (0.20 g, 0.78 mmol). Yield: 0.32 g (89%). *Anal*. Calc. C, 33.81; H, 3.03; N, 18.20. Found: C, 33.46; H, 2.92; N, 18.20%. IR: 3511, 3138, 2984, 2264, 1497, 1427, 1287, 1102, 756, 627 cm^{-1}. ^{1}H NMR (ppm DMSO): 7.3 (4H, s), 6.8 (4H, s), 4.4 (4H, s), 4.2 (8H, t), 2.9 (8H, t). The complex was soluble in hot acetonitrile, hot acetone and DMSO.

3.7. $[Ag_2\{2\text{-}BIM(BzCl)\}_2](ClO_4)_2$

This white complex was prepared in a similar way to $[Ag_2\{2\text{-BIM(Me)}\}_2](ClO_4)_2$ using silver perchlorate (0.08 g, 0.38 mmol) in 3 ml methanol was added to 2-BIM(BzCl) (0.20 g, 0.43 mmol). Yield: 0.16 g (57%). *Anal*. Calc. C, 37.43; H, 2.37; N, 8.31. Found: C, 37.03; H, 2.41; N, 8.04%. IR: 3511, 3138, 1593, 1491, 1395, 1274, 1102, 836, 749, 628 cm^{-1}. ^{1}H NMR (ppm DMSO): 7.9 (4H, d), 7.56 (4H, dd), 7.5 (4H, d),7.25 (4H, d) 6.8 (4H, d), 5.5 (8H, s), 4.8 (4H, s). The complex was soluble in hot acetonitrile, hot acetone and DMSO.

3.8. Anti-Candida testing

Candida albicans ATCC 10231 was obtained from the American Type Culture Collection (Manasas, VA, USA). Cultures were grown on Sabouraud dextrose agar (SDA) plates at 37 °C and maintained at 4 °C for short-term storage. Minimum inhibitory concentrations (MICs) were determined as follows. RPMI-1640 broth medium was used for the anti-*Candida* susceptibility testing. RPMI (5.15 g) was dissolved in cold distilled water (425 cm^3) in a 1-l Duran bottle and the pH

adjusted to 4.0 using a few drops of HCl (ca. 2 M). The resulting solution was autoclaved and then allowed to cool to approximately 50 °C. Morpholinepropanesulfonic acid (MOPS) (17.3 g) and L-glutamate (0.15 g) were dissolved together with stirring in distilled water (50 cm^3) and the resulting solution filter sterilized. The MOPS and L-glutamate solution was added to the warm RPMI and the pH of the mixture adjusted to 7.0 using sterile NaOH (6 M). Prior to MIC testing, cells were grown on SDA at 37 °C for 24 h. Cell suspensions were prepared in sterile phosphate buffered saline (PBS, pH 7.2) and cells were counted microscopically following dilution with PBS. A microtitre plate was inoculated with cells at a density of 5×10^5 cells cm^{-3}. Test suspensions (in water) and solutions (in aqueous DMSO) of the silver complexes were each prepared as follows. *Suspensions in water*: the complex (0.02 g) was suspended in distilled water (10 cm^3) to yield a stock suspension of concentration 2000 $\mu g\,cm^{-3}$. Doubling dilutions of the stock suspension were made to yield a series of test suspensions ranging in complex concentration from 20 to 1.25 $\mu g\,cm^{-3}$. *Solutions in DMSO*: the complex (0.02 g) was dissolved in DMSO (10 cm^3) to yield a stock solution of concentration 2000 $\mu g\,cm^{-3}$. Doubling dilutions of the stock solution were made using distilled water to yield a series of test solutions ranging in complex concentration from 20 to 1.25 $\mu g\,cm^{-3}$. The DMSO concentration (% v/v) in the test solutions ranged from 1.0% to 0.06% (note that a 2% DMSO aqueous solution, without added complex, does not inhibit the growth of the microorganism whereas a 3% DMSO aqueous solution will arrest cell growth totally). For the aqueous test suspensions and the aqueous-DMSO test solutions the complex/cell mixtures were incubated at 37 °C for 24 h with continuous shaking and the assays were performed in triplicate. Plates were read using a Labsystems iEMS Reader MF (absorbance at $\lambda = 540$ nm) and data were statistically analysed.

3.9. X-ray crystallography

All of the data were collected at 150 K on a Bruker SMART 1000 diffractometer using Mo Kα radiation ($\lambda = 0.71073$ Å). The structures were solved by direct methods and refined by full-matrix least-squares on F^2 using all the reflections. One of the prechlorate anions in $[Ag_2(2\text{-BIM(Bz)OH})_2](ClO_4)_2 \cdot EtOH$ is disordered and was modeled with two alternative sets of oxygen atom positions (50% occupancy each). The ethanol solvate is also disordered and was modeled as 50% occupancy of two alternative positions. All non-hydrogen atoms were refined with anisotropic atomic displacement parameters and hydrogen atoms bonded to carbon were inserted at calculated positions. Hydrogen atoms bonded to nitrogen ($[Ag_2(2\text{-BIM})_2](ClO_4)_2$) or the ligand alcohol group ($[Ag_2(2\text{-BIM(Bz)OH})_2](ClO_4)_2 \cdot EtOH$) were located from difference maps and not further refined; those bonded to the disordered oxygen of the ethanol solvate in $[Ag_2(2\text{-BIM(Bz)OH})_2](ClO_4)_2 \cdot EtOH$ were not included in the model. All programmes used in the structure solution and refinement are included in the SHELXTL package [18] and data collection and refinement details are summarised in Table 3.

Table 3
X-ray crystallographic data. Crystal data and structure refinement for $[Ag_2(2\text{-BIM})_2](ClO_4)_2$ and $[Ag_2(2\text{-BIM(Bz)OH})_2](ClO_4)_2 \cdot EtOH$

Identification code	$[Ag_2(2\text{-BIM})_2](ClO_4)_2$	$[Ag_2(2\text{-BIM(Bz)OH})_2](ClO_4)_2 \cdot EtOH$
Empirical formula	$C_{14}H_{16}Ag_2Cl_2N_8O_8$	$C_{44}H_{46}Ag_2Cl_2N_8O_{11}$
Formula weight	710.99	1149.53
Crystal system	triclinic	triclinic
Space group	$P\bar{1}$	$P\bar{1}$
a (Å)	7.8149(10)	10.9636(7)
b (Å)	8.9902(11)	14.7743(9)
c (Å)	9.2559(11)	16.0180(10)
α (°)	108.046(2)	114.3870(10)
β (°)	98.283(2)	98.2900(10)
γ (°)	114.763(2)	95.8410(10)
Volume ($Å^3$)	532.47(11)	2300.6(2)
Z	1	2
F (0 0 0)	348	1164
Crystal size (mm)	$0.16 \times 0.25 \times 0.31$	$0.37 \times 0.25 \times 0.14$
θ range for data collection (°)	2.44–28.65	1.54–25.00
Reflections collected	4544	16522
Independent reflections [$R_{(int)}$]	2396 [0.0186]	8050 [0.0159]
Absorption correction	multiscan	multiscan
Maximum and minimum transmission	1.0000 and 0.8116	1.000000 and 0.912980
Data/restraints/parameters	2396/0/154	8050/98/667
R_1, wR_2 [$I > 2\sigma(I)$]	0.0198, 0.0526	0.0356, 0.0877
R_1, wR_2 (all data)	0.0204, 0.0530	0.0455, 0.0942

4. Supplementary data

X-ray supplementary data for $[Ag_2(2\text{-}BIM)_2](ClO_4)_2$ and $[Ag_2(2\text{-}BIM(Bz)OH)_2](ClO_4)_2 \cdot EtOH$ are available from the Cambridge Crystallographic Data Centre, 12 Union Road, Cambridge CB2 1EZ, England (fax: +44-1223-336033; E-mail: deposit@ccdc.cam.ac.uk or www: http://www.ccdc.cam.ac.uk), on request quoting the deposition numbers CCDC 219908 and CCDC 219909, respectively.

Acknowledgements

S. Abuskhuna acknowledges financial support from the Libyan Higher Education Department.

References

[1] B. Coyle, K. Kavanagh, M. McCann, M. Devereux, M. Geraghty, BioMetals 16 (2003) 321.
[2] B. Coyle, P. Kinsella, M. McCann, M. Devereux, R. O'Connor, M. Clynes, K. Kavanagh, Toxicology in Vitro 18 (2004) 63.
[3] M. Geraghty, J.F. Cronin, M. Devereux, M. McCann, BioMetals 13 (2000) 1.
[4] M. McCann, B. Coyle, J. Briody, F. Bass, N. O'Gorman, M. Devereux, K. Kavanagh, V. McKee, Polyhedron 22 (2003) 1595.
[5] M. McCann, B. Coyle, S. McKay, P. McCormack, K. Kavanagh, M. Devereux, V. McKee, P. Kinsella, R. O'Connor, M. Clynes, Biometals (2004), in press.
[6] C. Place, J.-L. Zimmermann, E. Mulliez, G. Guillot, C. Bois, J.-C. Chottard, Inorg. Chem. 37 (1998) 4030.
[7] S. Elgafi, B.A. Messerle, T.W. Hambley, P. Turner, J. Chem. Soc. Dalton Trans. (1997) 2341.
[8] R. Bhalla, M. Helliwell, C.D. Garner, J. Chem. Soc., Chem. Commun. (1996) 921.
[9] X.-M. Chen, Z.-T. Xu, T.C.W. Mak, Polyhedron 14 (1995) 319.
[10] M.J. Bloemink, H. Engelking, S. Karentzopoulos, B. Krebs, J. Reedijk, Inorg. Chem. 35 (1996) 619.
[11] M. Grehl, B. Krebs, Inorg. Chem. 33 (1994) 3877.
[12] S. Abuskhuna, J. Briody, M. McCann, M. Devereux, K. Kavanagh, V. McKee, Polyhedron, to be published.
[13] P. Majumdar, K.K. Kamar, A. Castiñeiras, S. Goswami, J. Chem. Soc., Chem. Commun. (2001) 1292.
[14] M. Joseph, T. Leigh, M.L. Swain, Synthesis 7 (1977) 459.
[15] R.S. Brown, R.G. Clewely, J. Org. Chem. 52 (1987) 1216.
[16] B.P. Cantwell, Ph.D. Thesis, NUI Maynooth, 1992.
[17] A.M. Roe, J. Chem. Soc. (1963) 2195.
[18] G.M. Sheldrick, SHELXTL version 6.12, Bruker AXS, Madison, WI, 2001.

Available online at www.sciencedirect.com
SCIENCE DIRECT®
Polyhedron 23 (2004) 1257–1262
POLYHEDRON
www.elsevier.com/locate/poly

Hydrothermal syntheses, structures and magnetic properties of two transition metal coordination polymers with a square grid framework

Xiang-Jun Zheng [a], Li-Cun Li [b], Song Gao [c], Lin-Pei Jin [a,*]

[a] Department of Chemistry, Beijing Normal University, Beijing 100875, PR China
[b] Department of Chemistry, Nankai University, Tianjin 300071, PR China
[c] State Key Laboratory of Rare Earth Materials Chemistry and Applications, College of Chemistry and Molecular Engineering, Peking University, Beijing 100871, PR China

Received 1 December 2003; accepted 6 February 2004

Abstract

Two coordination polymers, $[M(NDA)(4,4'\text{-bpy})(H_2O)_2]\cdot nH_2O$ (M = Co, $n = 1$ (**1**); M = Ni, $n = 0.5$ (**2**), NDA = 1,4-naphthalenedicarboxylate, 4,4′-bpy = 4,4′-bipyridine) have been synthesized by the hydrothermal reaction of $MCl_2\cdot 6H_2O$, NDA and 4,4′-bpy. Single-crystal X-ray diffraction analysis shows that they are isostructural and represent the first examples of a square grid metal-organic framework constructed by a transition metal, dicarboxylate and 4,4′-bpy with each edge formed by one ligand. The layers are assembled together through hydrogen bonding, resulting in a 3-D supramolecular architecture. Magnetic susceptibility studies reveal that there is a weak antiferromagnetic exchange interaction between the Co(II) ions in the 2-D square grid network of **1**, and a weak ferromagnetic exchange interaction between the Ni(II) ions in **2**.
© 2004 Elsevier Ltd. All rights reserved.

Keywords: Hydrothermal synthesis; Coordination polymer; Magnetic property; Transition metal; Square grid structure; 1,4-Naphthalenedicarboxylic acid

1. Introduction

In recent years, great attention has been paid to the design and synthesis of functional metal-organic frameworks (MOFs) for their potential application as porous materials [1–7], as well as magnetic materials [8,9]. In constructing MOFs, polycarboxylates, especially dicarboxylates, are usually selected because they may act as both counteranions and bridging ligands to extend the architecture to 1-D chain [10], 2-D layer [11] and 3-D network [12]. The coordination of the metal with NDA is less investigated [1,13,14]. In this paper, NDA is utilized to build coordination networks for two reasons. On one hand, they can furnish the directional conformation of structures via coordination interactions with versatile bonding modes as well as via non-covalent bonding interactions such as hydrogen bonding and π–π stacking interactions. On the other hand, it can construct MOFs with channels because of its linear structure. 4,4′-Bpy is also a neutral linear bifunctional ligand that is widely used as an excellent spacer in the construction of supramolecular architectures [5,15–20]. Both ligands are of length ca. 7.0 Å, which is favorable for the formation of a square grid or cubic framework. The reported structures of MOFs constructed by carboxylates and 4,4′-bpy are 1-D chains [20–23], 2-D grids (square grids [19,25] or others [24]) and 2-D sheet pillared by 4,4′-bpy to form a 3-D network [16–18]. Each edge of the square grid is mostly built by the linkage of two ligands. Here, we report the first square grid metal-organic framework constructed by a transition metal, dicarboxylate and 4,4′-bpy, with each ligand constituting one edge.

* Corresponding author. Tel.: +86-10-6220-5522; fax: +86-10-6220-0567/86-10-6220-2075.
E-mail address: lpjin@bnu.edu.cn (L.-P. Jin).

0277-5387/$ - see front matter © 2004 Elsevier Ltd. All rights reserved.
doi:10.1016/j.poly.2004.02.007

2. Experimental

All chemicals and reagents were used as received.

2.1. Measurements

Elemental analyses were performed with an Elementar Vario EL analyzer. The IR spectrum was recorded with a Nicolet Avatar 360 FT-IR spectrometer using the KBr pellet technique. Thermogravimetric analysis was performed with a ZRY-2P Thermal Analyzer. The magnetic susceptibility measurements were performed in the range of 2–300 K on crystal sample using an oxford MagLab System 2000 magnetometer. The experimental susceptibilities were corrected for the sample holder and the diamagnetism contributions estimated from Pascal's constants. Effective magnetic moments were calculated using the equation $\mu_{\text{eff}} = 2.828(\chi_{\text{M}}T)^{1/2}$, where χ_{M} is the molar magnetic susceptibility.

2.2. Preparation of the title complexes

2.2.1. [Ni(NDA)(4,4′-bpy)(H$_2$O)$_2$]·0.5H$_2$O

A mixture of $NiCl_2 \cdot 6H_2O$ (0.024 g, 0.1 mmol), 1,4-naphthalenedicarboxylic acid (0.033 g, 0.15 mmol), 4,4′-bpy·2H$_2$O (0.02 g, 0.1 mmol), NaAc·3H$_2$O (0.04 g, 0.3 mmol), H$_2$O (12 ml) and aqueous NaOH (0.4 ml, 0.26 mmol) was sealed in a 25-ml stainless steel reactor with a Teflon liner and slowly heated to 150 °C for 96 h, then cooled to room temperature. Green crystals were obtained and washed with ethanol (yield: 0.025 g, 52.7%). *Anal.* Calc. for $C_{22}H_{19}N_2NiO_{6.5}$: C, 55.74; H, 4.04; N, 5.91. Found: C, 55.75; H, 3.49; N, 5.86. FT-IR data (cm^{-1}): 3562s, 3425s, 3255s, 1607s, 1557s, 1510m, 1464m, 1414s, 1361s, 814m, 632m.

2.2.2. [Co(NDA)(4,4′-bpy)(H$_2$O)$_2$]·H$_2$O

A mixture of $CoCl_2 \cdot 6H_2O$ (0.024 g, 0.1 mmol), 1,4-naphthalenedicarboxylic acid (0.022 g, 0.10 mmol), 4,4′-bpy·2H$_2$O (0.02 g, 0.1 mmol), NaAc·3H$_2$O (0.04 g, 0.3 mmol), H$_2$O (12 ml) and a drop of aqueous NaOH solution (0.65 mol L^{-1}) was sealed in a 25-ml stainless steel reactor with a Teflon liner and slowly heated to 120 °C for 96 h, then cooled to room temperature. Pink crystals were obtained and washed with ethanol (yield: 0.002 g, 4.2%). *Anal.* Calc. for $C_{22}H_{20}CoN_2O_7$: C, 54.67; H, 4.17; N, 5.80. Found: C, 55.18; H, 3.72; N, 5.76%. FT-IR data (cm^{-1}): 3565s, 3430s, 1606s, 1557s, 1415s, 1363s, 1219m, 1084m, 812m, 630m.

2.3. X-ray crystallographic analyses

The single-crystal X-ray data collection for the title complexes was performed with a Bruker Smart 1000 CCD diffractometer, using graphite-monochromated Mo Kα radiation ($\lambda = 0.71073$ Å). Semi-empirical absorption corrections were applied using the SADABS program. The structure was solved by direct methods and refined by full-matrix least-squares on F^2 using the SHELXTL 97 program [26]. All non-hydrogen atoms were refined with anisotropic displacement parameters. The hydrogen atoms on water molecules were located by difference Fourier synthesis and refined isotropically, while the other hydrogen atoms were generated geometrically and treated by a mixture of independent and constrained refinement. The crystal data for **1** and **2** are summarized in Table 1. Selected bond distances and bond angles for **1** and **2** are listed in Table 2.

Table 1
Crystal data of complexes **1** and **2**

Compound	**1**	**2**
Empirical formula	$C_{22}H_{20}CoN_2O_7$	$C_{22}H_{19}N_2NiO_{6.50}$
Formula weight	483.33	474.10
Temperature (K)	293(2)	293(2)
Crystal system	monoclinic	monoclinic
Space group	$P2/c$	$P2/c$
a (Å)	9.849(3)	9.766(3)
b (Å)	11.484(3)	11.382(4)
c (Å)	9.799(3)	9.738(3)
α (°)	90	90
β (°)	109.870(4)	109.555(5)
γ (°)	90	90
V (Å^3)	1042.4(5)	1020.0(6)
Z	2	2
D_c (g cm^{-3})	1.54	1.544
μ (mm^{-1})	0.871	0.997
Reflections collected, unique, R_{int}	5600, 2132, 0.0530	4732, 2000, 0.0339
R indices [$I > 2\sigma(I)$]	$R_1 = 0.0392$, $wR_2 = 0.0751$	$R_1 = 0.0370$, $wR_2 = 0.0708$
R indices (all data)	$R_1 = 0.0655$, $wR_2 = 0.0823$	$R_1 = 0.0540$, $wR_2 = 0.0754$

Table 2
Selected bond distances (Å) and bond angles (°) for **1** and **2**

1		**2**	
Co(1)–O(1)	2.084(2)	Ni(1)–O(1)	2.066(2)
Co(1)–O(3)	2.092(2)	Ni(1)–O(3)	2.069(2)
Co(1)–N(1)	2.163(3)	Ni(1)–N(1)	2.166(3)
Co(1)–N(2)[b]	2.226(3)	Ni(1)–N(2)[b]	2.115(3)
O(1)[a]–Co(1)–O(3)	90.77(7)	O(1)[c] –Ni(1)–O(3)	88.87(7)
O(1)–Co(1)–O(3)	89.25(7)	O(1)–Ni(1)–O(3)	91.14(7)
O(1)–Co(1)–O(3)[a]	90.77(7)	O(1)–Ni(1)–O(3)[c]	88.87(7)
O(1)–Co(1)–N(1)	89.42(6)	O(1)–Ni(1)–N(1)	90.48(5)
O(3)–Co(1)–N(1)	91.18(5)	O(3)–Ni(1)–N(1)	88.99(5)
O(1)–Co(1)–N(2)[b]	90.58(5)	O(1)–Ni(1)–N(2)[b]	89.52(5)
O(3)–Co(1)–N(2)[b]	88.82(6)	O(3)–Ni(1)–N(2)[b]	91.01(5)

[a] $-x+2,\ y,\ -z+3/2$.
[b] $x,\ y+1,\ z$.
[c] $-x+1,\ y,\ -z+1/2$.

3. Results and discussion

3.1. Crystal structures

Complex **1** is isostructural to complex **2**. Therefore, only the structure of complex **2** will be discussed in detail. The coordination environment around the Ni^{2+} ion is shown in Fig. 1. The Ni^{2+} ion is located in a slightly distorted octahedral surrounding with two oxygen atoms from two water molecules and two oxygen atoms from two carboxylate groups of two NDA anions [Ni(1)–O(1) = Ni(1)–O(1A) 2.066(2); Ni(1)–O(3) = Ni(1)–O(3A) 2.069(2) Å] building the equatorial plane, and two nitrogen atoms from two 4,4′-bpy molecules [Ni(1)–N(1) 2.166(3); Ni(1)–N(2A) 2.115(3) Å] in the axial positions. The two aromatic rings of 4,4′-bpy make a dihedral angle of 46.8°. Each 4,4′-bpy molecule acts as an *N*,*N*′-bis(monodentate) ligand, bridging the Ni^{2+} ions in the [0 1 0] direction, whereas each carboxylate group of each NDA anion adopts the monodentate coordination mode, making the ligand NDA bridge the Ni^{2+} ions in the [1 0 1] direction. The dihedral angle of the two carboxylate groups of a NDA ligand is 60.8° and they are not in the plane of the naphthalene ring. Based on the bridging of 4,4′-bpy and NDA, a square grid coordination polymer is constructed (Fig. 2) with dimensions of 11.25×11.38Å and the adjacent edges are represented by 4,4′-bpy and NDA, respectively.

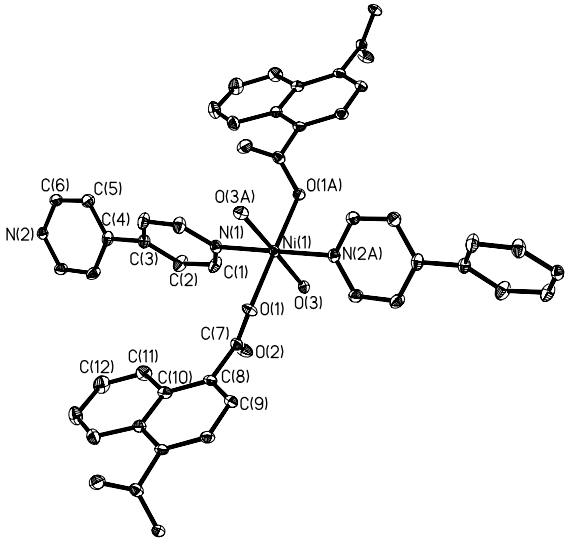

Fig. 1. Coordination environment of complex **2**. The asymmetric unit and the related coordinated atoms are labelled. The lattice water molecule (O4) and all hydrogen atoms are omitted for clarity. Thermal ellipsoids are shown at 30% probability.

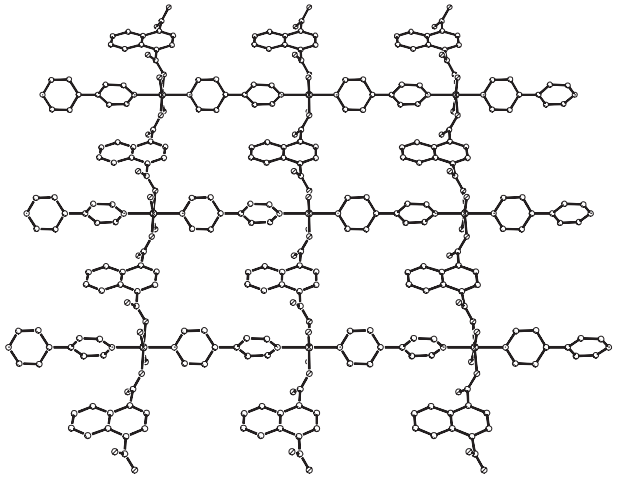

Fig. 2. Perspective view of the 2-D square grid structure of complex **2** viewed along the *c*-axis.

There are abundant hydrogen bonds in the crystal of complex **2** (Table 3). The coordinated water molecules are involved in both an intramolecular hydrogen bond with the uncoordinated carboxylate oxygen atom of NDA from the same asymmetrical unit and an intermolecular hydrogen bond with the coordinated carboxylate oxygen atom of NDA from the adjacent layer. The lattice water molecule is located in the layer of the square grid. As a bridging center, it is simultaneously hydrogen bonded to two uncoordinated carboxylate oxygen atoms of two NDA ligands from its neighboring two layers. Thus, every two adjacent layers are organized by hydrogen bonds between coordinated water molecules and coordinated carboxylate oxygen atoms of NDA, whereas every two separate layers are assembled together through the hydrogen bond between the lattice water and uncoordinated oxygen atoms of NDA (Fig. 3). Interestingly, the adjacent two square grids are stacked parallel but in a staggered manner on each other along the [1 0 $\bar{1}$] direction, with an interlayer separation of 3.98 Å and an interlayer Ni···Ni separation of 5.22 Å, which are much shorter than the intralayer Ni···Ni separations (11.38 and 11.25 Å). The arrangement of layers in such a staggered manner leads to cavities with small dimensions as shown in Fig. 4. Every square grid

Table 3
Hydrogen bonds geometry (Å and °) in complex **2**

D–H	*d*(D–H)	*d*(H···A)	∠DHA	*d*(D···A)	A
O3–H3A	0.804	1.954	153.86	2.699	O2
O3–H3B	0.781	1.994	168.65	2.765	O1 $[x, -y+2, z-1/2]$
O4–H4A	0.851	1.915	171.24	2.759	O2 $[x-1, y, z]$
O4–H4B	0.852	1.894	177.25	2.745	O2 $[-x+1, y, -z+1/2]$

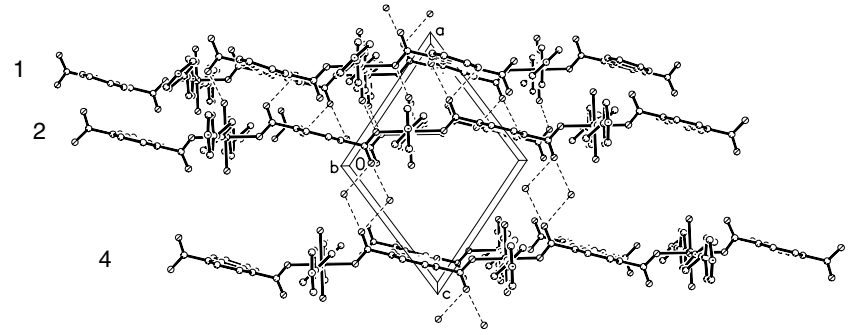

Fig. 3. The hydrogen-bonding interactions between the neighboring layers and two separate layers of complex **2**. For the interest of clarity, the third layer and all the hydrogen atoms are omitted.

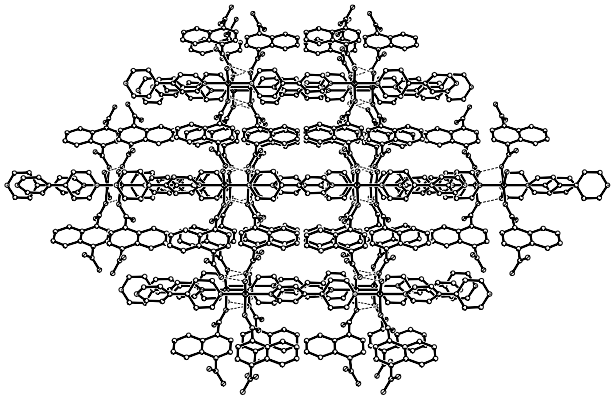

Fig. 4. Packing diagram of complex **2**, showing the cavities viewed along the *c*-axis. For the interest of clarity, all hydrogen atoms and lattice water molecules are omitted.

is divided into two parts by two naphthalene rings, and the dimension of every cavity is 9.5×3.0 Å. The 4,4′-bpy rings in the neighboring layers are not parallel to each other, whereas the NDA rings in the neighboring layers are parallel to each other, but not overlapped. Therefore, no π–π stacking interactions were observed in the crystal.

3.2. Magnetic properties

The variable temperature magnetic susceptibility data of the title complexes were measured in the range of 2–300 K under a magnetic field of 1 T. The plots of χ_M and effective magnetic moment μ_{eff} versus T for **1** and **2** are shown in Figs. 5(a) and (b), respectively. It can be seen from Fig. 5(a) that the μ_{eff} value decreases gradually upon cooling and the μ_{eff} value at 300 K is 4.69 μ_B, which is much larger than that expected for the spin-only case of Co ($\mu_{eff}^{so} = 3.87\mu_B$), indicating that an important orbital contribution is involved.

Complex **1** can be regarded as 1-D chains built by NDA and Co(II) ions, and the magnetic interactions transferred by 4,4′-bpy and hydrogen bonds should be very weak. The antiferromagnetic chain model ($S = 3/2$) was applied to **1** and the expression of the magnetic susceptibility is given below: $\chi_M = (Ng^2\beta^2/kT)[A + Bx^2][1 + Cx + Dx^3]^{-1}$, with $x = |J|/kT$ and $A = 1.2500$, $B = 17.041$, $C = 6.7360$ and $D = 238.47$ [27]. Considering the weak magnetic coupling transferred by 4,4′-bpy and hydrogen bonds, the mean field approximation, zJ' was introduced [28]. The total magnetic susceptibility is $\chi_{total} = \chi_M/[1 - \chi_M(2zJ'/Ng^2\beta^2)]$. The best fit (line in Fig. 5(a)) for the magnetic data (2–300 K) leads to $g = 2.49$, $J = -0.12$ cm^{-1}, $zJ' = -0.03$ cm^{-1},

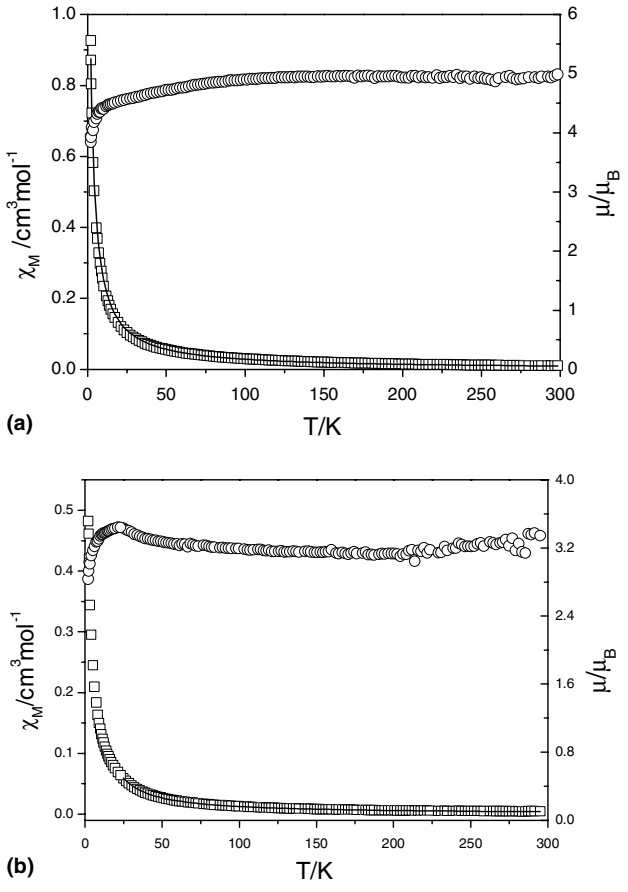

Fig. 5. Plot of the temperature dependence of χ_M (□) and μ_{eff} (○) for complex **1** (a) and **2** (b).

$R = 1.76 \times 10^{-3}$ (the value R is defined as $\sum[(\chi_M)_{obs} - (\chi_M)_{calc}]^2 / \sum[(\chi_M)_{obs}]^2$). The fitting results show that the exchange coupling between the Co(II) ions through the NDA bridge is weakly antiferromagnetic. The antiferromagnetic interactions transferred by 4,4′-bpy and hydrogen bonds are much weaker.

For complex **2**, upon cooling, the μ_{eff} value increases up to a maximum value of $3.43\mu_B$ around 25 K. Below 25 K, the μ_{eff} value abruptly decreases to $2.83\mu_B$ at 2 K. The magnetic behavior of **2** indicates a weak ferromagnetic exchange interaction between the Ni(II) ions in the 2-D square grid network. The structure of **2** was treated with the same method as **1** and the magnetic data of **2** have been fitted at 25 K by means of a 1-D ($S = 1$) ferromagnetic chain model [29]. [1] The expression of the magnetic susceptibility is $\chi_M = (2/3)(Ng^2\beta^2/kT)(AX^3 + BX^2 + CX + 1)/(DX^2 + EX + 1)$, with $X = J/kT$ and for $\alpha = 1$, $A = 0.14709$, $B = -0.788967$, $C = 0.866426$, $D = 0.096573$ and $E = -0.624929$. The best fit (line in Fig. 5(b)) for the magnetic data leads to $g = 2.17$, $J = 2.92\ cm^{-1}$, $R = 1.85 \times 10^{-4}$, indicating a weak ferromagnetic interaction between Ni(II) ions transferred through NDA. The abrupt decrease in the μ_{eff} versus T plot below 25 K may result from a possible zero-field splitting effect of Ni(II) ions in axially elongated octahedral surroundings [30], and antiferromagnetic interactions transferred by 4,4′-bpy and hydrogen bonds. However, the zero-field splitting of Ni(II) will be effective since the antiferromagnetic interactions transferred by 4,4′-bpy and hydrogen bonds are very weak as shown in complex **1**.

In the title complexes, weak ferro- or antiferromagnetic interactions between metal ions via NDA ligand were observed. Thus, the NDA ligand will be useful for the design of a range of magnetically interesting molecule materials.

3.3. Thermogravimetric analysis

Thermogravimetric analysis of complex **2** was carried out to examine its thermal stability. The TGA curve shows that the first weight loss of 9.6%, which occurs between 103.5 and 186 °C, corresponds to the loss of two coordinated water molecules and half an uncoordinated water molecule (calculated: 9.5%). Further decomposition begins at 308 °C and ends at 695.7 °C with residue NiO being obtained in 17.4% yield (calculated: 15.8%).

[1] The model is 1-D chain ($S = 1$) with alternating ferro-ferromagnetic coupling and when α is equal to 1, the model can be applied for ferromagnetic 1-D chain ($S = 1$).

4. Supplementary material

Crystallographic data for the structures reported in this paper have been deposited at the Cambridge Crystallographic Data Center as supplementary publication: CCDC Nos. 223356 and 205533 for **1** and **2**, respectively. Copies of the data can be obtained free of charge on application to CCDC, 12 Union Road, Cambridge CB2 1EZ, UK (fax: +44-1223-336-033; e-mail: deposit@ccdc.cam.ac.uk or www: http://www.ccdc.cam.ac.uk).

Acknowledgements

This work is supported by the National Natural Science Foundation of China (20331010) and the State Key Project of Fundamental Research (G1998061308).

References

[1] M. Eddaoudi, J. Kim, N. Rosi, D. Vodak, J. Wachter, M. O'Keeffe, O.M. Yaghi, Science 295 (2002) 469.
[2] M.J. Zaworotko, Chem. Commun. (2001) 1.
[3] M. Eddaoudi, H. Li, O.M. Yaghi, J. Am. Chem. Soc. 122 (2000) 1391.
[4] S.-I. Noro, S. Kitagawa, M. Kondo, K. Seki, Angew. Chem., Int. Ed. 39 (2000) 2082.
[5] E.J. Cussen, J.B. Claridge, M.J. Rosseinsky, C.J. Kepert, J. Am. Chem. Soc. 124 (2002) 9574.
[6] B.F. Abrahams, B.F. Hoskins, D.M. Michail, R. Robson, Nature 369 (1994) 727.
[7] M. Fujita, Y.J. Kwon, S. Washizu, K. Ogura, J. Am. Chem. Soc. 116 (1994) 1151.
[8] O. Kahn, C.J. Martinez, Science 279 (1998) 44.
[9] H.Z. Kou, S. Gao, J. Zhang, G.H. Wen, G. Su, R.K. Zheng, X.X. Zhang, J. Am. Chem. Soc. 123 (2001) 11809.
[10] X.M. Zhang, M.L. Tong, M.L. Gong, X.M. Chen, Eur. J. Inorg. Chem. (2003) 138.
[11] H.X. Zhang, B.S. Kang, A.W. Xu, Z.N. Chen, Z.Y. Zhou, A.S.C. Chan, K.B. Yu, C. Ren, J. Chem. Soc., Dalton Trans. (2001) 2559.
[12] P. Ayyappan, O.R. Evans, W.B. Lin, Inorg. Chem. 40 (2001) 4627.
[13] D.T. Vodak, M.E. Braun, J. Kim, M. Eddaoudi, O.M. Yaghi, Chem. Commun. (2001) 2534.
[14] J.Y. Lu, V. Schauss, Inorg. Chem. Commun. (2002) 1028.
[15] B.W. Sun, S. Gao, B.Q. Ma, Z.M. Wang, New J. Chem. 24 (2000) 953.
[16] J. Tao, M.L. Tong, X.M. Chen, J. Chem. Soc., Dalton Trans. (2000) 3669.
[17] S. Dalai, P.S. Mukherjee, E. Zangrando, F. Lloret, N.R. Chaudhuri, J. Chem. Soc., Dalton Trans. (2002) 822.
[18] S.M.-F. Lo, S.S.-Y. Chui, L.Y. Shek, Z.Y. Lin, X.X. Zhang, G.H. Wen, I.D. Williams, J. Am. Chem. Soc. 122 (2000) 6293.
[19] Y. Rodriguez-Martin, C. Ruiz-Pérez, J. Sanchiz, F. Lloret, M. Julve, Inorg. Chim. Acta 318 (2001) 159.
[20] B. Conerney, P. Jensen, P.E. Kruger, B. Moubaraki, K.S. Murray, Cryst. Eng. Commun. 5 (2003) 454.
[21] H.Y. Shen, D.Z. Liao, Z.H. Jiang, S.P. Yan, B.W. Sun, G.L. Wang, X.K. Yao, H.G. Wang, Polyhedron 17 (1998) 1953.
[22] R. Carballo, A. Castineiras, B. Covelo, E.M. Vazquez-Lopez, Polyhedron 20 (2001) 899.

[23] F.P. Liang, Z.L. Chen, R.X. Hu, H. Liang, K.B. Yu, Z.H. Zhou, Acta Chim. Sinica 59 (2001) 405.
[24] J. Tao, Y. Zhang, M.L. Tong, X.M. Chen, T. Yuen, C.L. Lin, X.Y. Huang, J. Li, Chem. Commun. (2002) 1342.
[25] J.M. Li, Y.G. Zhang, J.H. Chen, L. Rui, Q.M. Wang, X.T. Wu, Polyhedron 19 (2000) 1117.
[26] G.M. Sheldrick, SHELXTL 97, Program for the Refinement of Crystal Structures, University of Göttingen, Germany, 1997.
[27] W. Hiller, J. Strähle, A. Datz, M. Hanack, W.E. Hatfield, L.W. Ter Haar, P. Gütlich, J. Am. Chem. Soc. 106 (1984) 329.
[28] A.P. Ginsberg, M.E. Lines, Inorg. Chem. 11 (1972) 2289.
[29] M. Monfort, I. Resino, M.S.E. Fallah, J. Ribas, X. Solans, M. Font-Bardia, H. Stoeckli-Evans, Chem. Eur. J. 7 (2001) 280.
[30] R. Vicente, A. Escuer, X. Solans, M. Font-Bardía, Inorg. Chim. Acta 248 (1996) 59.

Available online at www.sciencedirect.com
SCIENCE DIRECT®
Polyhedron 23 (2004) 1263–1270
POLYHEDRON
www.elsevier.com/locate/poly

Synthesis and structure of diphenylphosphine derivatives of molybdenocene

Sofia S.M.C. Godinho [a], Beatriz Royo [a], Maria T. Lobato [b], Eberhardt Herdtweck [c], Carlos C. Romão [a,*]

[a] *Instituto de Tecnologia Química e Biológica da Universidade Nova de Lisboa, Quinta do Marquês, EAN, Apt 127, 2781-901 Oeiras, Portugal*
[b] *Escola Secundária Fernando Lopes Graça, Av. Comandante Gilberto Duarte, no. 470, 2775-200 Parede, Portugal*
[c] *Anorganisch-chemisches Institut der Technischen Universität München, Lichtenbergstraße 4, D-85747 Garching bei München, Germany*

Received 21 November 2003; accepted 9 February 2004

Abstract

The phosphino molybdenocene complex $[Cp_2Mo(PPh_2H)_2][BF_4]_2$ **(1)** (Cp = η^5-C_5H_5) was prepared by reaction of Cp_2MoI_2 with PPh_2H and excess of $TlBF_4$ in NCMe. The monocation $[Cp_2MoI(PPh_2H)]^+$ (**2**) as the BF_4^- or I^- salt was synthesised by treatment of $Cp_2MoI(SPh)$ with HBF_4 followed by addition of PPh_2H, or by reaction of Cp_2MoI_2 with PPh_2H, respectively. The indenyl phosphine complex $[IndMo(CO)_2(PPh_2H)_2]BF_4$ (**3**) (Ind = η^5-C_9H_7) was prepared by reaction of $IndMo(CO)_2(\eta^3$-$C_3H_5)$ with HBF_4 followed by addition of PPh_2H. Deprotonation of **1** with *dabco* led to the formation of the phosphinophosphido molybdenocene $[Cp_2Mo(PPh_2)(PPh_2H)][BF_4]$ (**4**). Treatment of **1** with two equivalents of LiBu in thf at −30 °C formed a thermally unstable complex (**5**) which could not be isolated. ^{31}P NMR and protonation to reform **1** support its formulation as $CpMo(PPh_2)_2$. The molecular structures of $[Cp_2Mo(PPh_2H)_2][BF_4]_2$ and $[Cp_2MoI(PPh_2H)]^+$ have been determined by single-crystal X-ray diffraction.
© 2004 Elsevier Ltd. All rights reserved.

Keywords: Cyclopentadienyl; Indenyl; Phosphino; Phosphido; Molybdenum; Metallocenes

1. Introduction

Following the pioneering studies of Green and co-workers on the synthesis of polynuclear complexes derived from organometallic ligands, namely of type $Cp_2M(\mu$-$SR)_2M'L_n$ (M = Mo, W, Nb; $M'L_n$ several transition metal fragments) [1], the related bis-phosphido derivatives $Cp_2M(\mu$-$PR_2)_2M'L_n$ (M = Zr, Hf) were first reported simultaneously by three groups in 1985 [2–4].

Extension of this work to the metallocenes of group 5 led to the synthesis of $Cp_2ML(PPh_2)$ (M = Nb, Ta; L = CO, PMe_2Ph, $P(OMe)_3$) and its PPh_2 bridged adduct with $Cr(CO)_5$ [5]. The corresponding Mo and W complexes of formula $Cp_2MH(PPh_2)$ and their adducts with $CpMn(CO)_2$ were reported in 1990 [6]. Both these groups **5** and **6** complexes are obtained by deprotonation of $Cp_2ML(PPh_2H)]^+$ (M = Nb, Ta) or $[Cp_2MH(PPh_2H)]^+$ (M = Mo, W). In turn, the PPh_2H cations were obtained by reaction of PPh_2Cl with Cp_2MLH (M = Nb, Ta) [7] and Cp_2MH_2 (M = Mo, W) [6] respectively. The search for bis-phosphido derivatives of the Cp_2Nb fragment was carried out by reaction of $Cp'_2NbH(PPh_2H)$ with PR_2Cl (R = Me, [8] Ph [9]) that leads to the cations $[Cp'_2Nb(PPh_2H)_2]^+$ (Cp′ = MeCp) [9] and $[Cp_2Nb(PPh_2H)PMe_2H)]^+$ [8]. Deprotonation of these cations forms $Cp_2Nb(PPh_2)(PMe_2H)$ [8], $Cp'_2Nb(PPh_2H)(PPh_2)$ and $[Cp'_2Nb(PPh_2)_2]M'$ (M′ = Li, Na) [9]. The latter product is more stable as the Na salt the Li salt decomposing readily at room temperature.

The co-ordination chemistry of $Cp_2Nb(PPh_2)(PMe_2H)$ was briefly examined [10].

The recent report on the synthesis and the crystal structure of $Cp_2Nb(PPh_2H)(PPh_2)$ includes a large literature coverage of this topic [11].

* Corresponding author. Tel.: +351-214418407; fax: +351-214411277.
E-mail address: ccr@itqb.unl.pt (C.C. Romão).

0277-5387/$ - see front matter © 2004 Elsevier Ltd. All rights reserved.
doi:10.1016/j.poly.2004.02.010

In the present work we report our findings on the synthesis and chemistry of molybdenocene derivatives of PPh_2H and our attempts to prepare the corresponding phosphido indenyl analogues.

2. Results and discussion

2.1. Synthesis of cationic complexes containing the phosphine ligand PPh_2H

Refluxing a solution of Cp_2MoI_2 with PPh_2H in NCMe in the presence of excess $TlBF_4$, followed by filtration of TlI and recrystallisation of the remaining residue from NCMe/Et_2O, gave orange–yellow crystals of $[Cp_2Mo(PPh_2H)_2][BF_4]_2$ (**1**) in ≈72% yield (see Scheme 3). The ^{31}P NMR spectrum of **1** shows only one doublet at δ 20.45 ppm (J_{P-H} = 396.0 Hz, P–H). Its ^1H NMR spectrum shows a doublet at δ 7.60 ppm (J_{P-H} = 396.0 Hz, P–H) assigned to the P–H proton of the phosphine ligands. The resonance of the Cp protons appears in the region usually observed for other dications of type $[Cp_2Mo(PR_3)_2]^{2+}$ [12], a triplet at δ 5.99 ppm. The coupling of the Cp protons with the two equivalent P atoms is very small, 2 Hz.

In the absence of $TlBF_4$ the above reaction mixture produced a modest yield (24%) of the red complex $[Cp_2MoI(PPh_2H)]I$ (**2, I**) (see Scheme 1). This compound was best prepared as the BF_4 salt by reaction of PPh_2H with the reaction mixture obtained by treatment of $Cp_2MoI(SPh)$ [13] with 1 equivalent of HBF_4 in Et_2O (see Scheme 2). Under these conditions a good yield of $[Cp_2MoI(PPh_2H)]BF_4$ (**2, BF_4**) was obtained. The ^{31}P NMR spectra of both salts of **2** in dichloromethane show one doublet slightly shielded compared to that of **1**, with slightly different chemical shifts for each anion. As expected, the resonance of the Cp protons in the ^1H NMR spectrum reveals a higher shielding (≈0.5 ppm) as compared to that of **1**. The crystal structure of the BF_4^- salt of **2** was also solved by X-ray diffraction (see below).

Starting from $IndCpMoX_2$ (X = Cl, I), we were unable to prepare any of the indenyl containing analogues of both **1** and **2**. Highly coloured dichroic products containing both PPh_2H and indenyl were observed by ^1H and ^{31}P NMR but the syntheses were totally irreproducible. This is a surprising and unexplained result

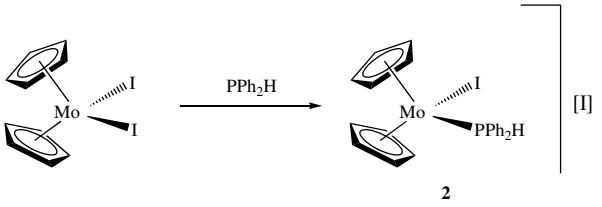

2

Scheme 1. Synthesis of $[Cp_2MoI(PPh_2H)][I]$.

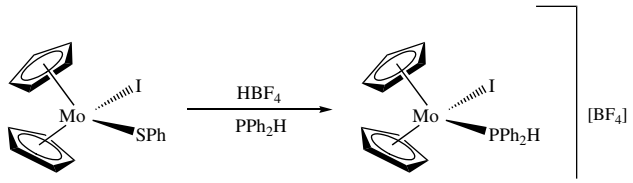

2

Scheme 2. Synthesis of $[Cp_2MoI(PPh_2H)][BF_4]$.

having in mind the similar chemistry of both Cp_2Mo and IndCpMo fragments [16]. On the other hand, reaction of PPh_2H with the species formed in situ by addition of one equivalent of HBF_4 on $IndMo(CO)_2(\eta^3\text{-}C_3H_5)$, gave a moderate yield of a yellow compound formulated as $[IndMo(CO)_2(PPh_2H)_2]BF_4$ (**3**) by means of IR and NMR spectroscopy. The ^1H NMR spectrum of **3** is consistent with the presence of a pentahapto indenyl ring as observed in similar examples with other phosphines. The P–H protons appear at δ 7.27 ppm (J_{P-H} = 392.7 Hz) in the ^1H NMR spectrum. Accordingly, the ^{31}P NMR spectrum shows only one doublet at δ 34.55 ppm (J_{P-H} = 393.6 Hz). The IR spectrum shows the two strong vibrations of the *cis*-CO ligands in the region expected for a Mo(II) complex with this charge and structure. In spite of the lack of X-ray diffraction data, the spectroscopic data are consistent with the given formulation that corresponds to a very wide variety of indenyl containing piano stool complexes.

2.2. Crystallography studies

The molecular structures of **1** and **2** have been determined by X-ray diffraction. Their cationic moieties are shown in Figs. 1 and 2, respectively. Bond lengths and bond angles are listed in Table 1. A search in the Cambridge Structural Database revealed five Mo^{IV} compounds in addition with the same Mo-core geome-

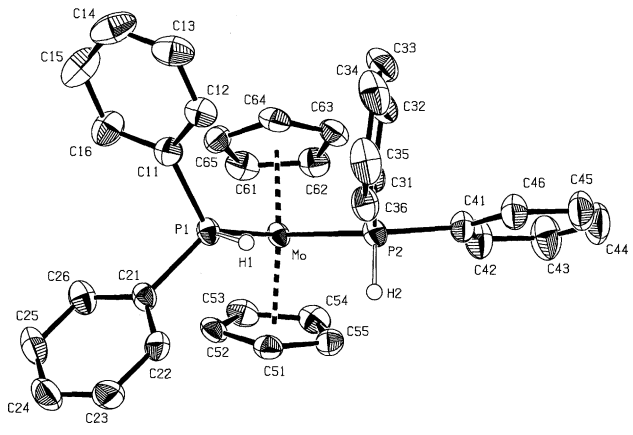

Fig. 1. ORTEP style plot of the di-cationic part of **1** in the solid state. Thermal ellipsoids are drawn at the 50% probability level. Hydrogen atoms are omitted for clarity.

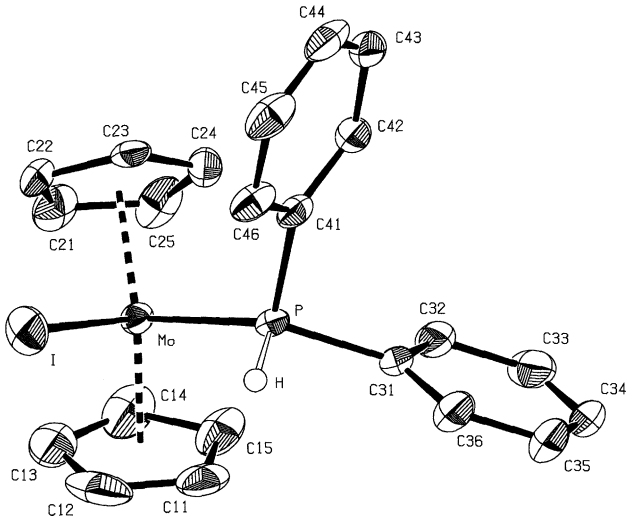

Fig. 2. ORTEP style plot of the mono-cationic part of **2** in the solid state. Thermal ellipsoids are drawn at the 50% probability level. Hydrogen atoms are omitted for clarity.

try $Mo(\eta^5\text{-}C_5H_4R)_2E_2$ with R = H, ^{t}but and one E = PR'_3 [14]. The results are given in Table 1, too. As expected from the NMR and IR data all three Mo-cations are monomeric. The cyclopentadienyl ligands are bound to molybdenum in a typical η^5 manner. No ring slippage is observed in the planar rings. The values of the Cp–Mo–Cp bent angles of 135.41°, 136.20°, and 134.79° in comparison to the other five compounds (Table 1) indicates that they are relatively insensitive to the nature of the E ligand and its steric demands. More pronounced, and caused by the steric repulsion, are the observed differences in the E–Mo–E angle (≈74–92°). All other intramolecular distances and angles lie in the typical ranges and need no further discussion.

2.3. Reactivity studies on the PPh_2H complexes 1–3

The cationic nature of the complexes **1**–**3** suggests facile deprotonation of the PPh_2H ligands with formation of phosphido complexes, much in the same way as has been reported for the Nb complexes mentioned above. Indeed, treatment of a suspension of **1** in CH_2Cl_2 with excess NEt_3 gives a bright orange solution. Concentration and addition of Et_2O gives an orange crystalline product formulated as $[Cp_2Mo(PPh_2)(PPh_2H)]BF_4$ (**4**). The same product is, however, best prepared using *dabco* (1,4-diazabicyclo[2.2.2]octane) instead of NEt_3 since the protonated form of *dabco* precipitates out and allows an easier purification of the product (see Scheme 3). Treatment of a CH_2Cl_2 solution of **4** with HBF_4 in Et_2O immediately precipitates the yellow dication **1,** as ascertained by ^{31}P and ^1H NMR. The ^1H NMR of **4** in CD_2Cl_2 at room temperature shows a set of signals between δ 7.60 and 7.10 ppm and one signal at δ 4.96 ppm assigned to the Cp protons. The ^{31}P NMR in the same solvent shows two resonances: a doublet at δ 41.1 ppm (J_{P-H} = 364 Hz) and a singlet at δ −11.9 ppm. The former signal is assigned to the Ph_2PH ligand and the latter to the PPh_2 ligand. A similar upfield resonance of the P atom was found in $Cp_2MoH(PPh_2)$ at δ −10.3 ppm [2]. In the isoelectronic Nb complex, $Cp_2Nb(PPh_2)(HPPh_2)$ two P resonances are found at δ 66.2 and 5.9 ppm [11]. The proton resonance of the Ph_2P–H ligand is certainly hidden under the other aromatic signals, like in $Cp_2Nb(PPh_2)(HPPh_2)$. A value of δ 7.60 ppm is given for the complex $[Cp_2Nb(PPh_2H)(PMe_2H)]Cl$ [8]. The ^1H NMR spectrum remains essentially unchanged on lowering the temperature down to 185 K.

Although air sensitive in solution, **4** is clearly much more thermally stable than its isoelectronic Nb congener

Table 1
Characteristic bond lengths [Å], angles [°], for **1**, **2**, **BF_4** and related compounds $Mo(\eta^5\text{-}C_5H_4R)_2E_2$

	1 R: H E: $P(Ph)_2H$	**2,BF_4**[b] R: H E1: I E2: $P(Ph)_2H$	[18][b] R: H E: PMe_3	[19][b] R: ^{t}but E1: Me E2: PMe_3	[20][b] R: H E1: Me E2: PPh_3	[20][b] R: H E1: H E2: PPh_3	[21][b] R: H E1: OCH_2CF_3 E2: $P(^n but)_3$
Bond lengths							
Mo–E1	2.5181(9)	2.7989(3)	2.516(2)	2.287(8)	2.269(5)	1.74(7)	2.020(9)
Mo–E2	2.4928(10)	2.4697(8)	2.516(2)	2.491(3)	2.526(2)	2.501(2)	2.539(4)
Mo–Cg1[a]	1.989	1.971	1.978	1.996	1.988	1.970	1.974
Mo–Cg2[a]	1.979	1.980	1.982	1.992	1.984	1.980	1.967
Bond angles							
E1–Mo–E2	82.77(2)	79.60(2)	91.55(8)	77.4(2)	84.1(2)	77(3)	74.4(3)
E1–Mo–Cg1	105.58	108.10	106.67	106.5	103.3	99	107.2
E1–Mo–Cg2	108.92	106.13	104.83	105.4	105.3	107	109.6
E2–Mo–Cg1	105.15	103.86	106.66	107.1	108.1	108.3	111.1
E2–Mo–Cg2	106.42	110.67	104.81	105.6	108.2	107.8	105.0
Cg1–Mo–Cg2	135.41	134.79	134.21	138.3	135.5	139.2	133.7

[a] Cg1 (Cg2) denotes the centre of gravity of the cyclopentadienyl moiety C51–C55 (C61–C65).
[b] The atom labels are adapted to the numbering scheme used in **1**.

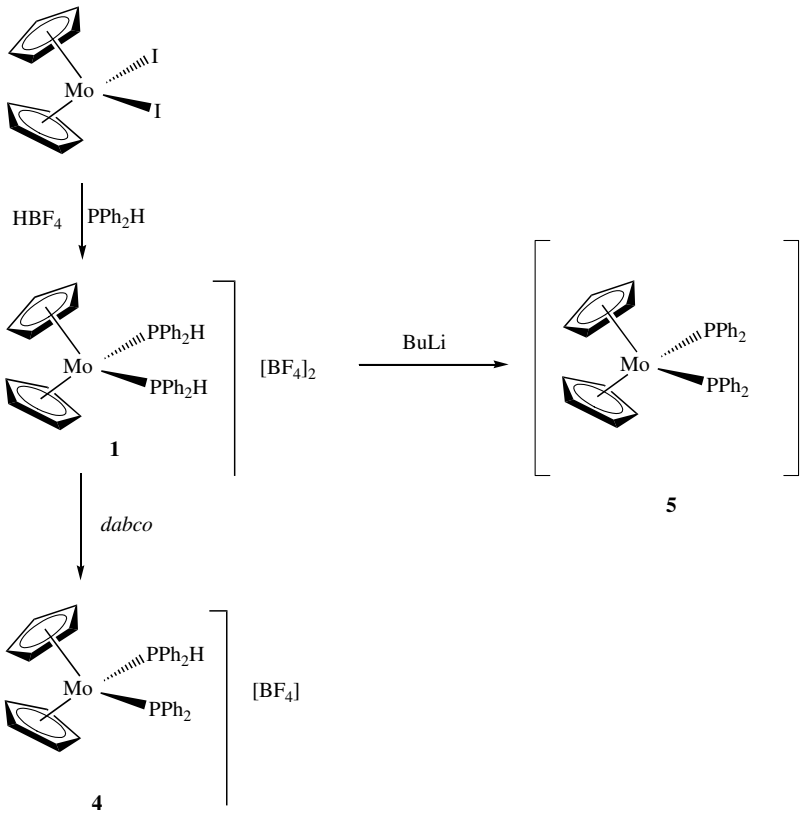

Scheme 3. Synthesis of the molybdenum derivatives **1**, **4** and **5**.

$Cp_2Nb(PPh_2H)(PPh_2)$ which decomposes readily to the ortho-metallated species [$Cp_2Nb(PHPh–C_6H_4–)$] [11].

Further deprotonation was attempted in order to obtain the neutral bis-phosphido complex $Cp_2Mo(PPh_2)_2$, isoelectronic with the well known thiolato ligands $Cp_2Mo(SR)_2$ and $[Cp'_2Nb(PPh_2)_2]^-$. Reaction of **1**, suspended in thf, with LiOMe, $LiNEt_2$, HNa, LiBu, always at a temperature below −30 °C affords a red solution (see Scheme 3). This fact suggests that deprotonation has occurred since the cations **1** and **4** are insoluble in thf and $Cp_2Mo(PPh_2)_2$ (**5**) is expected to be freely soluble in this solvent. However, the solution is very unstable and decomposes above −30 °C giving a brown intractable residue. Similar behavior is observed in a MeOH/LiOMe system. In order to attempt the characterization of **5** in situ the reaction of **1** with BuLi was carried out in a NMR tube at −50 °C. The ^{31}P NMR spectrum of the red solution in thf-d_8 at −40 °C shows *only one* singlet resonance at δ −24.7 ppm revealing the presence of only one product, the equivalence of the two P atoms, and the absence of a PPh_2H ligand that should give a doublet resonance. The integrity of the Cp_2Mo fragment was ascertained by the fact that treatment of the red solution of **5** with $HBF_4 \cdot Et_2O$ led to the precipitation of **1** in essentially quantitative yield. These observations strongly support the formulation of **5** as the bis-phosphido complex $Cp_2Mo(PPh_2)_2$ (**5**).

The instability of $Cp_2Mo(PPh_2)_2$ is not unexpected. The crystal structure of $Cp_2Zr(PPh_2)_2$ clearly showed that the Zr–P bonds are unequal, one of them exhibiting a clear shortening due to P to Zr backdonation which results in a partial double bond character [15]. Of course, in the Cp_2Mo (IV) fragment the corresponding metallocene a1 frontier orbital is filled, thereby preventing this stabilisation and actually creating a destabilising interaction between both P lone pairs and the filled a1 orbital. One might envisage a possibility of avoiding this repulsion either by a ring-slippage mechanism capable of lowering the electronic density at the Mo atom or by a rotation of the lone pairs of the P atoms away from the a1 orbital. The latter possibility should also exist in the isoelectronic Nb(III) complexes [$Cp'_2Nb(PPh_2)_2$]- and $Cp_2Nb(PPh_2)(PMe_2H)$. However, both of them are rather unstable in contrast to the formally 16 electron $Cp_2Zr(PPh_2)_2$, suggesting that this rotation is not enough to stabilise the complexes. The fact that indenyl slippage would be more favourable for the indenyl than for the Cp ring, justified our attempts to synthesize the analogous compounds for the IndCpMo fragment. Unfortunately, we were unable to obtain any of the necessary precursors, namely [$IndCpMo(PPh_2H)_2]^{2+}$.

The cation $[IndMo(CO)_2(PPh_2H)_2]BF_4$ (**3**) also undergoes deprotonation by addition of NEt_3 or NaH, but

the solutions obtained are unstable and no products could be clearly identified.

One alternative possibility of stabilizing the structure of **5** would be its coordination to electrophilic species capable of coordinating the P donor atoms. This was attempted by reacting the solution of **5** at −30 °C with electrophilic, unsaturated metal fragments or precursors like $CoBr_2(thf)_2$, $NiBr_2(thf)_2$, $(NBD)Mo(CO)_4$, $Mo(\eta^3\text{-}C_3H_5)(CO)_2(NCMe)_2Cl$. In no case was there possible to isolate some compound corresponding to the adducts of general type $Cp_2Mo(\mu\text{-}PPh_2)_2M'Ln$. Instead, successive color changes and or mixtures of products were obtained. The reaction of **1** with Cp_2ZrMe_2 expected to liberate CH_4 and form $[Cp_2Mo(\mu\text{-}PPh_2)_2ZrCp_2]^{2+}$ was also unsuccessful. Clearly, the reactivity of $Cp_2Mo(PPh_2)_2$ (**5**) seems to be rather complex and simple adduct formation with other metal centers is not the main reaction pathway.

3. Conclusions

Several diphenylphospine derivatives of molybdenocene were prepared, two of them characterised by X-ray diffraction. The dication $[Cp_2Mo(PPh_2H)_2]^{2+}$ (**1**) can be deprotonated to the mono-phosphido complex $[Cp_2Mo(PPh_2)(PPh_2H)][BF_4]$ (**4**) by Et_3N or dabco. In thf, deprotonation with LiBu at −40 °C forms the bis-phosphido complex $Cp_2Mo(PPh_2)_2$ (**5**). Due to its thermal instability **5** was only characterised by its ^{31}P NMR spectrum, showing a singlet at δ −24.7 ppm, and by its reaction with HBF_4 to give **1**. Disappointingly, the high reactivity of $Cp_2Mo(PPh_2)_2$ seems to limit its use as an organometallic ligand in contrast to the isostructural $Cp_2Zr(PPh_2)_2$ and the isoelectronic $Cp_2Mo(SR)_2$ both of which have a rich chemistry in this regard.

4. Experimental

All operations were carried out under an atmosphere of dinitrogen with standar Schlenk line and glove-box techniques. Solvents were purified by conventional methods and distilled under nitrogen prior to use. ^1H and ^{31}P NMR spectra were measured on a Bruker CXP 300 spectrometer (H, 300 MHz, ^{31}P, 121.49 MHz), referenced internally to $SiMe_4$ and externally to 85% H_3PO_4, respectively. IR spectra were measured on an Unicam Mattson model 7000 FTIR spectrometer. Elemental analyses were performed by Maria Conceição Almeida in the Elemental Analysis Service of ITQB.

All common chemicals and solvents were purchased from commercial suppliers. The synthesis of $[CpMo(\eta^5\text{-}C_5H_6)(CO)_2][BF_4]$ [16], $[IndMo(\eta^5\text{-}C_5H_6)(CO)_2][BF_4]$ [16], Cp_2MoI_2 [16], Cp_2MoCl_2 [12], was done according to literature procedures.

4.1. Preparation of $[Cp_2Mo(PPh_2H)_2][BF_4]_2$ (**1**)

A suspension of Cp_2MoI_2 (0.3 g, 0.62 mmol) in NCMe (20 ml) was treated with PPh_2H (0.36 ml, 1.49 mmol) and the reaction mixture was stirred overnight under reflux in the absence of light. To the resulting greyish solution was added an excess of $TlBF_4$ and the mixture was left under reflux for another 2 h, in the absence of light. The solution was filtered through celite to separate the TlI, the filtrate was taken to dryness and the residue washed with Et_2O and dried under vacuum to yield the title compound **1** as a yellow powder. Recrystallisation from NCMe/Et_2O affords orange–yellow crystals. When Cp_2MoCl_2 or the corresponding dibromide was used as a starting material, under the same conditions, similar results were obtained. Yield: 0.34 g (72.5%). Selected IR (KBr, cm^{-1}): 2211, broad, ν(PH), 1085, vs, ν(BF). *Anal.* Calc. for $C_{34}H_{32}B_2F_8MoP_2$: C, 52.89; H, 4.18. Found: C, 52.78; H, 4.07%. ^1H NMR (Me_2CO-d^6, δ ppm): 7.60–7.53 (m, 20H, Ph), 7.60 (d, 2H, J_{P-H} = 405 Hz, P–H), 5.99 (t, 10H, J_{P-H} = 2 Hz, Cp). ^{31}P NMR (CD_2Cl_2/NCMe-d^3, δ ppm): 20.45 (d, J_{P-H} = 396.0 Hz, P–H).

4.2. Preparation of $[Cp_2MoI(PPh_2H)]^+$

4.2.1. Preparation of $[Cp_2MoI(PPh_2H)][BF_4]$ (**2**, BF_4)

A solution of $Cp_2MoI(SPh)$ (0.88 g, 1.91 mmol) in CH_2Cl_2 (50 ml) was treated with a slight excess of $HBF_4 \cdot Et_2O$ giving a dark green solution, which was stirred for 15 min. Then, in the absence of light, a slight excess of PPh_2H (0.4 ml) was added and the solution was stirred for another 30 min giving a brownish solution. The volume was reduced to a fifth and the solution was filtered. The resulting precipitate was washed twice with Et_2O, further washed with CH_2Cl_2 and hexane and dried under vacuum. Recrystallisation from a mixture of Me_2CO, EtOH and Et_2O at 4 °C gave red single crystals of $[Cp_2MoI(PPh_2H)][BF_4]$ suitable for X-ray analysis. Yield: 0.63 g (53%). Selected IR (KBr, cm^{-1}): 2295, w, ν(PH), 1084, vs, ν(BF). *Anal.* Calc. for $C_{22}H_{21}BF_4IMoP$: C, 42.21; H, 3.38. Found: C, 42.35; H, 3.41%. ^1H NMR (NCMe-d^3, δ ppm): 7.67–7.51 (m, 10H, Ph); 7.82 (d, 1H, J_{P-H} = 404.0 Hz, P–H); 5.47 (s, 10H, Cp). ^{31}P NMR (CD_2Cl_2/NCMe-d^3, δ ppm): 27.53 (d, J_{P-H} = 405.8 Hz, P–H).

4.2.2. Preparation of $[Cp_2MoI(PPh_2H)]I$ (**2**,**I**)

A suspension of Cp_2MoI_2 (0.3 g, 0.63 mmol) in NCMe (20 ml) was treated with 2 equivalents of PPh_2H. The reaction mixture was stirred overnight under reflux, in the absence of light. The resulting purple solution was filtered and the filtrate was concentrated to yield $[Cp_2MoI(PPh_2H)]I$ as a bordeaux solid. Yield: 0.19 g (24%). Selected IR (KBr, cm^{-1}): 2309, w, ν(PH), 1099, vs, ν(BF). *Anal.* Calc. for $C_{22}H_{21}I_2MoP$: C, 39.67; H,

3.18. Found: C, 39.88; H, 3.31%. ^{1}H NMR (CD_2Cl_2/NCMe-d^3, δ ppm): 7.78–7.19 (m, 10H, Ph); 7.11 (d, 1H, J_{P-H} = 402.0 Hz, P–H); 5.54 (s, 10H, Cp). ^{31}P NMR (CD_2Cl_2/NCMe-d^3, δ ppm): 24.58 (d, J_{P-H} = 403.4 Hz, P–H).

4.3. Preparation of $[IndMo(CO)_2(PPh_2H)_2][BF_4]$ (3)

A solution of $IndMo(\eta^3\text{-}C_3H_5)(CO)_2$ (0.34 g, 1.10 mmol) in CH_2Cl_2 (15 ml) was treated with 1 equiv of $HBF_4 \cdot Et_2O$. After 5 min stirring at room temperature, the deep red solution was cooled in an ice bath and was treated with 2 equiv of PPh_2H in the absence of light. The solution was allowed to warm up to room temperature and after stirring for 1 h, the volume was reduced to half and Et_2O (30 ml) was added to precipitate a red powder. The solid was further washed with Et_2O and the product was recrystallised from a mixture of Me_2CO, EtOH and Et_2O at room temperature to afford yellow crystals of the title compound **3**. Yield: 0.33 g (42%). *Anal*. Calc. for $C_{35}H_{29}BF_4MoP_2$: C, 60.55; H, 4.21. Found: C, 60.68; H, 4.22%. Selected IR (KBr, cm^{-1}): 2068, w, ν(PH), 1977, vs, ν(CO), 1898, vs, ν(CO), 1081, vs, ν(BF). ^{1}H NMR (Me_2CO-d^6, δ ppm): 7.69–7.53 (m, 20H, Ph); 7.39–7.35 (m, 2H, H$^{5-8}$); 7.28–7.15 (m, 2H, H$^{5-8}$); 7.27 (d, 2H, J_{P-H} = 392.7 Hz, P–H); 6.08 (d, 2H, H$^{1/3}$); 6.02 (t, 1H, H^2). ^{31}P NMR (Me_2CO-d^6, δ ppm): 34.55 (d, J_{P-H} = 393.6 Hz, P–H).

4.4. Preparation of $[Cp_2Mo(PPh_2)(PPh_2H)][BF_4]$ (4)

A slight excess of *dabco* (0.12 g, 1.07 mmol) was added to a solution of $[Cp_2Mo(PPh_2H)_2][BF_2]_2$ (0.4 g, 0.56 mmol) in dichloromethane (30 ml). The solution immediately changed from the initial yellow colour to an orange solution with a white precipitate. The mixture was stirred for 1 h and the solution was filtered. The filtrate was concentrated to dryness and the residue was washed with ether to yield the title compound **4** as an orange solid. Yield: 0.35 g (92%). Selected IR (KBr, cm^{-1}): 1084, vs, ν(BF). *Anal*. Calc. for $C_{34}H_{31}BF_4MoP_2$: C, 59.68; H, 4.57. Found: C, 59. 86; H, 4.62%. ^{1}H NMR (Me_2CO-d^6, δ ppm): 7.80–7.20 (m, 20H, Ph); 5.34 (t, 10H, Cp). ^{31}P NMR (Me_2CO-d^6, δ ppm): 41.1 (d, J_{P-H} = 393.6 Hz, $\underline{P}Ph_2H$); −11.9 (s, $\underline{P}Ph_2$).

4.5. Reaction of $[Cp_2Mo(PPh_2H)_2][BF_4]_2$(1) with BuLi

A suspension of **1** in thf-d^8 was prepared in a NMR tube and cooled to −50 °C. Solution of BuLi in hexanes (1.6 M) was added dropwise. The yellow suspension instantaneously changed to a deep red solution. The ^{31}P NMR spectra was recorded at −40 °C showing a singlet resonance at −24.7 ppm. ^{31}P NMR (thf-d^8, δ ppm): −24.7 (s, $\underline{P}Ph_2$).

4.6. Single crystal X-ray structure determination experiments

4.6.1. Structure determination of compound 1

Details of the X-ray experiment, data reduction, and final structure refinement calculation are summarized in Table 2. Crystals of complex **1** suitable for an X-ray structure determination were grown from a saturated solution of **1** in a NCMe/Et_2O. A clear orange–yellow fragment ($0.20 \times 0.40 \times 0.50$ mm) was stored under perfluorinated ether, transferred in a Lindemann capillary, fixed and sealed. Preliminary examination and data collection were carried out on a four-circle diffractometer (NONIUS CAD4) at the window of a sealed tube (NONIUS FR590; 50 kV; 30 mA; 1.5 kW) and graphite monochromated Mo Kα radiation ($\lambda = 0.71073$ Å). The unit cell parameters were obtained by full-matrix least-squares refinement of 24 high angle reflections. Data collection was performed at 193 K within a Θ-range of $1.52° < \Theta < 24.97°$ and an exposing time of maximum 90 s per scan (omega scans; scan width $(1.00 + 0.25 \tan \Theta)° \pm 25\%$ at each side of the reflection to determine the background). A total of 6295 intensities were collected [17a]. Raw data were corrected for Lorentz and polarization effects. Corrections for absorption effects (based

Table 2
Crystal data and summary of intensity data collection and structure refinement of **1** and **2,BF$_4$**

	1	**2,BF$_4$**
Formula	$C_{34}H_{32}B_2F_8MoP_2$	$C_{22}H_{21}BF_4IMoP$
Formula weight	772.10	626.01
Color/shape	orange–yellow/fragment	bordeaux/fragment
Crystal system	monoclinic	monoclinic
Space group	$P2_1/c$ (No. 14)	$P2_1/n$ (No. 14)
a (Å)	13.736(4)	10.3922(3)
b (Å)	14.240(2)	18.1898(4)
c (Å)	17.322(5)	11.7510(4)
β (°)	102.45(1)	90.202(1)
V (Å^3)	3308.5(14)	2221.30(11)
Z	4	4
ρ_{calcd} (g cm^{-3})	1.550	1.872
μ (mm^{-1})	0.563	2.092
Diffractometer	NONIUS CAD4	NONIUS KAPPACCD
λ (Å)	Mo Kα 0.71073	Mo Kα 0.71073
T (K)	193	123
Reflections collected	6295	10037
hkl range	h: −16,15; k: 0,16; l: 0,20	h: ±12; k: −14,22; l: ±14
Independent reflections (R_{int})	5820/0.0125	4448/0.025
Observed reflections ($I > \sigma(I)$)	4739	4143
Parameters refined	580	374
R_1 (oberved/all data)	0.0254/0.0446	0.0296/0.0322
wR_2 (observed/all data)	0.0562/0.0610	0.0834/0.0852
GOF (observed/all data)	1.043/1.043	1.053/1.053

on psi-scans) were applied [17b]. No decay was observed during the measurement. After merging ($R_{int} = 0.0125$) and rejecting of the systematically absent intensities a sum of 5820 (all data), 4739 ($I > \sigma(I)$), respectively, remained and all were used in the further calculations. The structure was solved by Patterson methods [17c] and difference Fourier syntheses [17d]. All non-hydrogen atoms of the asymmetric unit were refined with anisotropic thermal displacement parameters. All hydrogen atoms were found and refined with individual isotropic displacement parameters. Full-matrix least-squares refinements with 580 parameters were carried out by minimizing $\sum w(F_o^2 - F_c^2)^2$ with SHELXL-97 weighting scheme and stopped at shift/err <0.001. In compound **1** a disorder 0.556(6):0.444(6) of three fluorine atoms of one BF_4 anion could be resolved clearly. Neutral atom scattering factors for all atoms and anomalous dispersion corrections for the non-hydrogen atoms were taken from INTERNATIONAL TABLES FOR CRYSTALLOGRAPHY [17e]. All calculations were performed on a DEC 3000 AXP workstation and an Intel Pentium II PC, with the STRUX-V system [17f], including the programs PLATON [17g], MOLEN [17b], and SHELXL-97 [17d].

4.6.2. Structure determination of compound ***2****,* ***BF_4***

Crystal data and details of the structure determination are presented in Table 2. Suitable single crystals for the X-ray diffraction study were grown from a mixture of Me_2CO, EtOH and Et_2O at 4 °C. A red colored fragment ($0.18 \times 0.23 \times 0.38$ mm) was stored under perfluorinated ether, transferred in a Lindemann capillary, fixed and sealed. Preliminary examination and data collection were carried out on an area detecting system (NONIUS KAPPACCD) at the window of a rotating anode (NONIUS FR951) and graphite monochromated Mo Kα radiation ($\lambda = 0.71073$ Å). The unit cell parameters were obtained by full-matrix least-squares refinement of 11,993 reflections. Data collection were performed at 123 K within a Θ-range of $2.06° < \Theta < 26.40°$; two sets with 206 films were measured in rotation modus with $\Delta\varphi/\Delta\Omega = 1.0°$. A total of 10,037 intensities were integrated [17h]. Raw data were corrected for Lorentz, polarization, decay and absorption effects [17i]. After merging ($R_{int} = 0.025$) a sum of 4448 (all data), 4143 ($I > \sigma(I)$), respectively, remained and were used for all calculations. The structure was solved by a combination of direct methods [17j] and difference Fourier syntheses [17d]. All non-hydrogen atoms were refined anisotropically. All hydrogen atoms could be located and were allowed to refine with individual isotropic displacement parameters freely. Full-matrix least-squares refinements with 374 parameters were carried out by minimizing $\sum w(F_o^2 - F_c^2)^2$ with SHELXL-97 weighting scheme and stopped at shift/err <0.001. A disorder 0.52(4):0.48(4) of two fluorine atoms of the BF_4 anion could be resolved clearly. Neutral atom scattering factors for all atoms and anomalous dispersion corrections for the non-hydrogen atoms were taken from INTERNATIONAL TABLES FOR CRYSTALLOGRAPHY [17e]. All calculations were performed on a DEC 3000 AXP workstation and an Intel Pentium II PC, with the STRUX-V system [17f], including the programs PLATON [17g], SIR92 [17j], and SHELXL-97 [17d].

5. Supporting information available

Crystallographic data (excluding structure factors) for the structures reported in this paper have been deposited with the Cambridge Crystallographic Data Centre as supplementary publication nos. CCDC-211212 (**1**) and CCDC-211213 (**2**). Copies of the data can be obtained free of charge on application to CCDC, 12 Union Road, Cambridge CB2 1EZ, UK (fax: +44-1223-336-033; e-mail: deposit@ccdc.cam.ac.uk or www: http://www.ccdc.cam.ac.uk).

Acknowledgements

This work was supported by FCT through project POCTI/36127/QUI/2000. S. S.M.C. Godinho thanks Praxis XXI for a Ph.D. grant BD3805/96 and B. Royo thanks Praxis XXI for a postdoctoral grant. We wish to acknowledge Maria da Conceição Almeida for providing data from the Elemental Analyses Service at the Instituto de Tecnologia Química e Biológica, Universidade Nova de Lisboa, Oeiras, Portugal.

References

[1] W.E. Douglas, M.L.H. Green, J. Chem. Soc. Dalton Trans. (1972) 1796.
[2] R.T. Baker, T.H. Tulip, S.S. Wreford, Inorg. Chem. 24 (1985) 1379.
[3] T.S. Targos, R.P. Rosen, R.R. Whittle, G.L. Geoffroy, Inorg. Chem. 24 (1985) 1375.
[4] L. Gelmini, L.C. Matassa, D.W. Stephan, Inorg. Chem. 24 (1985) 2585.
[5] G. Boni, P. Sauvageot, C. Moïse, J. Organomet. Chem. 489 (1995) C32.
[6] C. Barre, M.M. Kubicki, J.-C. Leblanc, C. Moïse, Inorg. Chem. 29 (1990) 5244.
[7] G. Bonnet, O. Lavastre, J.-C. Leblanc, C. Moïse, New J. Chem. 12 (1988) 551.
[8] G. Bonnet, O. Lavastre, G. Boni, J.-C. Leblanc, C. Moïse, C.R. Acad. Sci. Paris (1994) 1293.
[9] G.I. Nikonov, D.A. Lemenovskii, Organometallics 13 (1994) 3127.
[10] P. Oudet, C. Moïse, M.M. Kubicki, Inorg. Chim. Acta 247 (1996) 263.
[11] G.I. Nikonov, D.A. Lemenovskii, K.Y. Dorogov, A.V. Churakov, Polyhedron 18 (1999) 1159.

[12] (a) M.L.H. Green, J.A. McCleverty, L. Pratt, G. Wilkinson, J. Chem. Soc. (1961) 4854;
(b) R. Davis, L.A.P. Kane-Meguire, in: G. Wilkinson, F.G.A. Stone, E.W. Abel (Eds.), Comprehensive Organometallic Chemistry, vol. 3, Pergamon Press, New York, 1982, pp. 1321–1384, and references therein.
[13] Prepared by a similar procedure to the one, used for the synthesis of $Cp_2WI(SPh)$, described in Carlos C. Romão Thesis, Instituto Superior Técnico de Lisboa, 1979.
[14] (a) The Cambridge Structural Database: a quarter of a million crystal structures and rising, F.H. Allen, Acta Crystallogr. B 58 (2002) 380;
(b) New Software for searching the Cambridge Structural Database and visualizing crystal structures, I.J. Bruno, J.C. Cole, P.R. Edgington, M. Kessler, C.F. Macrae, P. McCabe, J. Pearson, R. Taylor, Acta Crystallogr. B 58 (2002) 389.
[15] R.T. Baker, T.H. Tulip, Organometallics 5 (1986) 839.
[16] (a) J.R. Ascenso, C.G. de Azevedo, I.S. Gonçalves, E. Herdtweck, D.S. Moreno, C.C. Romão, J. Zühlke, Organometallics 13 (1994) 429;
(b) I.S. Gonçalves, C.C. Romão, J. Organomet. Chem. 486 (1995) 155;
(c) J.R. Ascenso, C.G. de Azevedo, I.S. Gonçalves, E. Herdtweck, D.S. Moreno, M. Pessanha, C.C. Romão, Organometallics 14 (1995) 3901.
[17] (a) L. Straver, CAD4 Operating System, Version 5.0, B.V. ENRAF-NONIUS, Delft, The Netherlands, 1989;
(b) C.K. Fair, MOLEN: An Interactive Intelligent System for Crystal Structure Analysis, ENRAF-NONIUS, Delft, The Netherlands, 1990
(c) G.M. Sheldrick, SHELXS-86, University of Göttingen, Göttingen, Germany, 1986;
(d) G.M. Sheldrick, SHELXL-97, University of Göttingen, Göttingen, Germany, 1998;
(e) A.J.C. Wilson (Ed.), International Tables for Crystallography, vol. C, Tables 6.1.1.4 (pp. 500–502), 4.2.6.8 (pp. 219–222), and 4.2.4.2 (pp. 193–199), Kluwer Academic Publishers, Dordrecht, The Netherlands, 1992;
(f) G. Artus, W. Scherer, T. Priermeier, E. Herdtweck, STRUX-V: A Program System to Handle X-Ray Data, TU München, Garching, Germany, 1997;
(g) A.L. Spek, PLATON: A Multipurpose Crystallographic Tool, Utrecht University, Utrecht, The Netherlands, 1999;
(h) Data Collection Software for NONIUS KAPPACCD devices, Delft, The Netherlands, 1997;
(i) Z. Otwinowski, W. Minor, Meth. Enzymol. 276 (1997) 307ff;
(j) A. Altomare, G. Cascarano, C. Giacovazzo, A. Guagliardi, M.C. Burla, G. Polidori, M. Camalli, SIR92, J. Appl. Crystallogr. 27 (1994) 435.
[18] CCDC code GEBFAU. B.S. McGilligan, T.C. Wright, G. Wilkinson, M. Motevalli, M.B. Hursthouse, J. Chem. Soc. Dalton Trans. (1988) 1737.
[19] CCDC code QOMJIL. J.H. Shin, W. Savage, V.J. Murphy, J.B. Bonanno, D.G. Churchill, G. Parkin, J. Chem.Soc. Dalton Trans. (2001) 1732.
[20] CCDC codes SIFCUF, SIFCOZ. C.G. Azevedo, M.J. Calhorda, M.A.A.F. de, C.T. Carrondo, A.R. Dias, V. Felix, C.C. Romao, J. Organomet. Chem. 391 (1990) 345.
[21] CCDC code ZUJPAV. J.-G. Ren, H. Tomita, M. Minato, T. Ito, K. Osakada, M. Yamasaki, Organometallics 15 (1996) 852.

Available online at www.sciencedirect.com
SCIENCE DIRECT®
Polyhedron 23 (2004) 1271–1277
POLYHEDRON
www.elsevier.com/locate/poly

2,2′-Bipyrimidine (bpym) in iron(III) carboxylate chemistry: preparation and characterization of $[Fe_2O(O_2CMe)_2(bpym)_2(H_2O)_2](ClO_4)_2$, and the influence of weak interactions in the formation of metal clusters

Athanassios K. Boudalis [a], Catherine P. Raptopoulou [b], Aris Terzis [b], Spyros P. Perlepes [b,*]

[a] *Department of Chemistry, University of Patras, 26504 Patras, Greece*
[b] *Institute of Materials Science, NCSR "Demokritos", 153 10 Aghia Paraskevi Attikis, Greece*

Received 14 November 2003; accepted 17 February 2004

Abstract

The full investigation of the synthetic possibilities in the $Fe(ClO_4)_3 \cdot 6H_2O/NaO_2CMe/bpym$ reaction system, where bpym is 2,2′-bipyrimidine, in MeCN has provided access to only one product. This is the dinuclear complex $[Fe_2O(O_2CMe)_2(bpym)_2(H_2O)_2](ClO_4)_2 \cdot H_2O \cdot 2MeCN$ (**3** $\cdot H_2O \cdot 2MeCN$). Its cation contains the (μ-oxo)bis(μ-carboxylato)diiron(III) core, while a chelating bpym molecule and one aquo ligand complete a distorted octahedral coordination at each metal ion. The complex cations participate in intercationic hydrogen bonds creating chains along the *b* axis, which form pairs due to π–π interactions between bpym rings of adjacent chains. The complex has been characterized by IR spectroscopy; characteristic bands are discussed in terms of the known structure and the coordination modes of the ligands. The room-temperature effective magnetic moment of **3** is 1.81 BM, a value indicating the presence of relatively strong antiferromagnetic interaction. The $Fe^{III}/ClO_4^-/MeCO_2^-$/bpym chemistry is compared to the already well-developed $Fe^{III}/ClO_4^-/MeCO_2^-$/bpy (bpy = 2,2′-bipyridine) chemistry.
© 2004 Elsevier Ltd. All rights reserved.

Keywords: 2,2′-Bipyrimidine complexes; Iron(III) carboxylate complexes; Oxo-bridged iron(III) complexes; π–π stacking interactions; X-ray crystal structure

1. Introduction

Dinuclear and polynuclear iron(III) carboxylate complexes have been much investigated in recent years owing to their relevance as models for the active sites of various non-heme iron proteins [1,2], and the interesting magnetic properties that some of them possess [3,4]. The continuing development of these areas requires the discovery of new examples on a regular basis, and several groups have thus been investigating new synthetic procedures capable of allowing access to new structural types. One approach has been the use of appropriately chosen chelating ligands to encourage aggregation while ensuring discrete products that are soluble and can be purified, crystallized and studied in solution. Restricting further discussion to 2,2′-bipyridine (bpy) or its derivatives, the up to now structurally characterized members of this family are $[Fe_2O(O_2CMe)_2Cl_2(bpy)_2]$ [5], $[Fe_2O(O_2CCH_2Cl)_2(bpy)_2(H_2O)_2](NO_3)_2$ [6], $[Fe_4O_2(O_2CMe)_7(bpy)_2]X$ (X = ClO_4 (**1**) [7], Cl [8]), $[Fe_4O_2(O_2CEt)_7(bpy)_2]X$ (X = ClO_4 [9], PF_6 [10]), $[Fe_4O_2Cl_2(O_2CMe)_6(bpy)_2]$ [11], $[Fe_4(OHO)(OH)_2(O_2CMe)_4(bpy)_4](ClO_4)_3$ (**2**) [12], $[Fe_6O_3(OEt)_2(O_2CMe)_9(bpy)_2](ClO_4)$ [13] and $[Fe_2O(O_2CCF_3)_2(Me_2bpy)_4](ClO_4)_2$ [14], where Me_2bpy is 4,4′-dimethyl-2,2′-bipyridine. In

* Corresponding author. Tel.: +30-2610-997146; fax: +30-2610-997118.
E-mail address: perlepes@patreas.upatras.gr (S.P. Perlepes).

0277-5387/$ - see front matter © 2004 Elsevier Ltd. All rights reserved.
doi:10.1016/j.poly.2004.02.008

all cases, the metal ions are held together by O-based monatomic bridges such as O^{2-}, OH^- and OR^-.

More recently we have decided to extend the above studies by using bis(chelating) aromatic N-donors to investigate to what extent such ligands might affect the identity of products obtained compared to normal bpy and to what extent this might thus prove a route to new cluster types. Our hope was that such ligands could provide access to new types of clusters involving repeating cluster units (available as discrete species with bpy) rather than repeating mononuclear centres, although isolation of coordination polymers could not a priori be ruled out. Christou's group has introduced and successfully developed this approach by using the bis(bipyridine) ligand 1,2-bis(2,2′-bipyridyl-6-yl)ethane (L) and isolating complexes with novel 3d-metal cluster types such as the face-sharing triple cubane core of $[Co_8O_4(OH)_4(O_2CMe)_6L_2]^{2+}$ [15], the "dimer-of-dimers" topology of $[Mn_4O_2(O_2CMe)_4L_2]^{2+}$ [16], the "four-rung ladder" cores of $[Fe_6O_4Cl_4(O_2CPh)_4L_2]^{2+}$ [17] and $[Mn_4O_2(OMe)_3(O_2CPh)_2L_2(MeOH)]^{2+}$ [16], and the "six-rung ladder" motif of $[Fe_6O_6(O_2CPh)_3\ L_3(H_2O)_2]^{3+}$ [18]. In addition, and irrespective of the identities of possible products, we wanted to thoroughly examine the elementary underlying chemistry of this general reaction system, by fully exploring its "parameter space" through subtle changes in reaction parameters, such as the nature of the aromatic N-donors.

Our first choice was 2,2′-bipyrimidine (bpym). Although strictly speaking this molecule is not a bis(2,2′-bipyridine) ligand, it can adopt the bis(chelating) bridging coordination mode [19] (Fig. 1) seen in normal bis(bpy) ligands. Of particular interest is the ability of bridging bpym to transmit antiferromagnetic coupling between paramagnetic 3d-metal ions separated by more than 5 Å [20]. In contrast to the great number of studies devoted to Mn(II), Fe(II), Co(II), Ni(II) and Cu(II) complexes of bpym [19–26], practically nothing is known for the coordination chemistry of bpym with iron(III). Only two iron(III)-bpym complexes have been structurally characterized [27]. These are the mononuclear complex $[FeCl_3(bpym)(H_2O)]$ in which bpym acts as a bidentate terminal(chelating) ligand (Fig. 1) and the dinuclear complex $[Fe_2(bpym)Cl_6(H_2O)_2]$ in which bpym behaves as a bis(chelating) bridging ligand (Fig. 1).

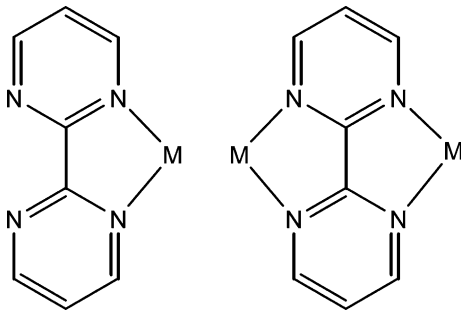

Fig. 1. The chelating (left) and bis(chelating) bridging (right) coordination modes of 2,2′-bipyrimidine (bpym).

The synthetic investigation of the reaction system $Fe(ClO_4)_3\cdot 6H_2O/NaO_2CMe/bpym$ in MeCN is herein reported. The *analogous* reaction system with bpy gave complexes **1** [7] and **2** [12], see Eqs. (1) and (2), respectively, depending on the Fe^{III}:bpy reaction ratio. Complex **1** has a bent ("butterfly") disposition of four Fe^{III} atoms with the pyramidal μ_3-O^{2-} groups on the same side of the fused Fe_3 planes, whereas **2** contains the novel rectangular $[Fe_4(\mu_4\text{-}OHO)\ (\mu\text{-}OH)_2]^{7+}$ core:

$$4Fe(ClO_4)_3\cdot 6H_2O + 7NaO_2CMe\cdot 3H_2O + 2bpy \xrightarrow{MeCN} [Fe_4O_2(O_2CMe)_7(bpy)_2](ClO_4) + 7NaClO_4 + 4HClO_4 + 43H_2O \quad (1)$$

$$4Fe(ClO_4)_3\cdot 6H_2O + 4NaO_2CMe\cdot 3H_2O + 4bpy \xrightarrow{MeCN} [Fe_4(OHO)(OH)_2(O_2CMe)_4(bpy)_4](ClO_4)_3 + 4NaClO_4 + 5HClO_4 + 32H_2O \quad (2)$$

We wondered whether bpym would have the ability to assemble new cluster types with Fe^{III} not available with bpy. Not surprisingly for 3d-metal cluster chemistry, our efforts resulted in the isolation of a dinuclear compound, whose X-ray structure and characterization are herein described. This work can be regarded as a step in a broad programme [28–36] concerned with developing synthetic routes and strategies to polynuclear complexes of middle- and late-3d metals at intermediate oxidation states.

2. Experimental

2.1. Materials

All reagents and solvents were of analytical grade and used as received. The synthesis was carried out under aerobic conditions. *Warning*: Although no such tendency was observed during the present work, perchlorate salts are potentially explosive and should be handled with caution "and" in small quantities.

2.2. Synthesis of $[Fe_2O(O_2CMe)_2(bpym)_2(H_2O)_2](ClO_4)_2$ (3)

To a solution of $Fe(ClO_4)_3\cdot 6H_2O$ (0.234 g, 0.51 mmol) and $NaO_2CMe\cdot 3H_2O$ (0.124 g, 0.89 mmol) in MeCN (6 ml) was added a solution of bpym (0.080 g, 0.51 mmol) in the same solvent (7 ml). The color of the solution changed from deep red to dark green. The solution was left undisturbed in a closed flask and after ca 1 week dark green prismatic crystals of $\mathbf{3}\cdot H_2O\cdot 2MeCN$ formed, along with a few colorless prisms, which were

identified as $NaClO_4$ by their IR spectra. The dark green crystals were manually separated, washed with MeCN and dried in vacuo. Typical yields are in the range 50–55%. The dried sample analysed as solvent-free. *Anal.* Calc. for $C_{20}H_{22}Cl_2Fe_2N_8O_{15}$: C, 30.13; H, 2.79; N, 14.06. Found: C, 30.05; H, 2.59; N, 13.54%. IR data (KBr, cm^{-1}): 3374m, 3096m, 1578s, 1562s, 1534s, 1442s, 1406s, 1358w, 1334w, 1302w, 1270w, 1246w, 1216w, 1146s, 1118sb, 1032s, 1020s, 988w, 916m, 820w, 758s, 692m, 660s, 620m, 556m.

2.3. Measurements

Microanalyses (C, H, N) were performed by the Microanalytical Laboratory of the Laboratoire de Chimie de Coordination at Toulouse (France). Infrared spectra (4000–500 cm^{-1}) were recorded as KBr disks on a Perkin–Elmer 16PC spectrometer with samples prepared as KBr pellets. Magnetic susceptibility measurements at ambient temperature were carried out on a Faraday balance equipped with a SARTORIUS micro-electrobalance and a DRUSH electromagnet; diamagnetic corrections were estimated from Pascal's constants.

2.4. X-ray crystallography

A crystal of $\mathbf{3}\cdot H_2O\cdot 2MeCN$, with approximate dimensions of $0.05\times0.25\times0.50$ mm, was mounted in a capillary. Diffraction measurements were made on a Crystal Logic Dual Goniometer diffractometer using graphite-monochromated Mo radiation. Crystal data and parameters for data collection and processing are reported in Table 1. Unit cell dimensions were determined and refined by using the angular settings of 25 automatically centred reflections in the range $11° < 2\theta < 23°$. Intensity data were recorded using a θ–2θ scan to $2\theta_{max} = 50°$ with scan speed $3.0°\,min^{-1}$ and scan range 2.0° plus $\alpha_1\alpha_2$ separation. Three standard reflections monitored every 97 reflections showed less than 3% variation and no decay. Lorentz, polarization and Ψ-scan absorption corrections were applied using Crystal Logic software.

The structure was solved by direct methods using SHELXS-86 [37] and refined by full-matrix least squares techniques on F^2 with SHELXL-97 [38]. All hydrogen atoms were introduced at calculated positions as riding on bonded atoms, except those on the water molecules which were located by difference maps and were refined isotropically. All non-hydrogen atoms were refined using anisotropic thermal parameters.

Table 1
Crystallographic data for complex $\mathbf{3}\cdot H_2O\cdot 2MeCN$

Formula	$C_{24}H_{30}Cl_2Fe_2N_{10}O_{16}$
Formula weight	897.18
Crystal system	triclinic
Space group	$P\bar{1}$
T (K)	298
Unit cell dimensions	
a (Å)	12.575(9)
b (Å)	11.398(8)
c (Å)	15.48(1)
α (°)	92.75(3)
β (°)	108.49(3)
γ (°)	116.14(2)
V (Å^3)	1842(2)
Z	2
ρ_{calc} ($g\,cm^{-3}$)	1.617
Radiation, λ (Å)	Mo Kα, 0.71073
μ (mm^{-1})	1.015
Reflections collected/unique	6743/6481 [$R_{int} = 0.0259$]
Data with $I > 2\sigma(I)$	4668
Parameters refined	513
$(\Delta\rho)_{max}(\Delta\rho)_{min}$ (e Å^{-3})	0.622, −0.593
w[a]	$a = 0.0327,\ b = 1.8889$
Goodness-of-fit on F^2	1.025
R_1,[b] wR_2[c] (all data)	0.0709, 0.1132
R_1,[b] wR_2[c] ($I > 2\sigma(I)$)	0.0414, 0.0994

[a] $w = 1/[\sigma^2(F_o^2) + (aP)^2 + bP]$ and $P = (\max(F_o^2, 0) + 2F_c^2)/3$.
[b] $R_1 = \sum(|F_o| - |F_c|)/\sum(|F_o|)$.
[c] $wR_2 = \{\sum[w(F_o^2 - F_c^2)^2]/\sum[w(F_o^2)^2]\}^{1/2}$.

3. Results and discussion

3.1. Synthetic comments

The reaction that leads to **3** – which contains terminal bpym ligands (vide infra) – can be summarized in balanced Eq. (3), based on the reasonable assumption that H_2O from the starting materials and/or the solvent is the source of the O^{2-} ion:

$$2Fe(ClO_4)_3\cdot 6H_2O + 2NaO_2CMe\cdot 3H_2O + 2bpym \xrightarrow[20°C]{MeCN} [Fe_2O(O_2CMe)_2(bpm)_2(H_2O)_2](ClO_4)_2 + 2NaClO_4 + 2HClO_4 + 15H_2O \quad (3)$$

The Fe^{III}:$MeCO_2^-$:bpym ratio initially employed in the reaction mixture was the same that led to the isolation of complex **2**, i.e., 1:1.75:1 (see Section 2.2). This ratio was chosen in order to allow for a direct comparison of the chemistry of bpym and bpy in the present system. With the identity of **3** established by X-ray crystallography, our next goal was either to try to "force" a percentage of bpym to act as a bis(chelating) bridging ligand (thus favoring aggregates based on the tetranuclear cluster unit $[Fe_4(OHO)(OH_2)(O_2CMe)_4(bpym)_4]^{3+}$, i.e. the bpym analogue of discrete **2**), or to prepare the bpym analogue of **1**, i.e., $[Fe_4O_2(O_2CMe)_7(bpym)_2](ClO_4)$. It seemed logical to us that one (or both) of the above goals would be realized by increasing the Fe^{III}:bpym molar ratio. Unfortunately, we could not confirm this synthetic expectation. Use of the same reaction system in MeCN but employing the 2:*x*:1 Fe^{III}:$MeCO_2^-$:bpym ratios ($x = 1.0, 1.2, 1.4, 1.6, 1.8, 2.0$) and a variety of crystallization conditions, led repeatedly

to the isolation of pure **3** in various yields. The facts that in all cases the bpym-based yields are lower than 60% and the final filtrates are intensely coloured probably indicate additional bpym-containing iron(III) species in solution. Also, directed attempts to obtain the above-mentioned desired polynuclear complexes, or even a tetranuclear cluster that would be the bpym analogue of **2**, from reactions of the pre-isolated **1** or **2** with bpym resulted always in the isolation of **3**.

It is clear that the potential of the bis(chelating) bridging coordination mode for bpym is not realized in the $Fe(ClO_4)_3 \cdot 6H_2O/NaO_2CMe$/bpym reaction system in MeCN. It should be reminded at this point that bpym does have the ability to bridge Fe^{III} atoms [27]. A preliminary examination of the above-described experimental adventures is not informative about the reasons that lead to the isolation of the dinuclear complex **3** instead of higher nuclearity species. However, a careful examination of the molecular and crystal structure of **3** helps us to understand its exclusive isolation (vide infra).

3.2. Description of structure

The cation of complex $\mathbf{3} \cdot H_2O \cdot 2MeCN$ is shown in Fig. 2. Selected interatomic distances and bond angles are presented in Table 2.

Complex **3** crystallizes in the triclinic space group $P\bar{1}$. Its structure consists of the dinuclear $[Fe_2O(O_2CMe)_2(bpym)_2(H_2O)_2]^{2+}$ cation, two ClO_4^- anions, and solvate H_2O and MeCN molecules; the latter three will not be further discussed. The complex cation contains two Fe^{III} atoms bridged by one μ-O^{2-} group and two $\eta^1{:}\eta^1{:}\mu_2$-$MeCO_2^-$ ligands, forming a $\{Fe_2(\mu\text{-}O)(\mu\text{-}O_2CMe)_2\}^{2+}$ core. The distorted octahedral geometry at each Fe^{III} is completed with one chelating bpym molecule and one aquo ligand. The Fe(1)–N(4) bond *trans* to the oxo bridge is longer (2.234(3) Å) than its counterpart in the *cis* position (Fe(1)–N(1) = 2.181(3) Å) as a result of the powerful *trans* influence of the short Fe(μ-O^{2-}) bond [6,39]. A similar trend is seen in the Fe(2)–O(W2) bond which is *trans* to the oxo bridge; this bond is longer (2.127(3) Å) than the Fe(1)–O(W1) bond (2.063(4) Å) which is *cis* to the oxo bridge.

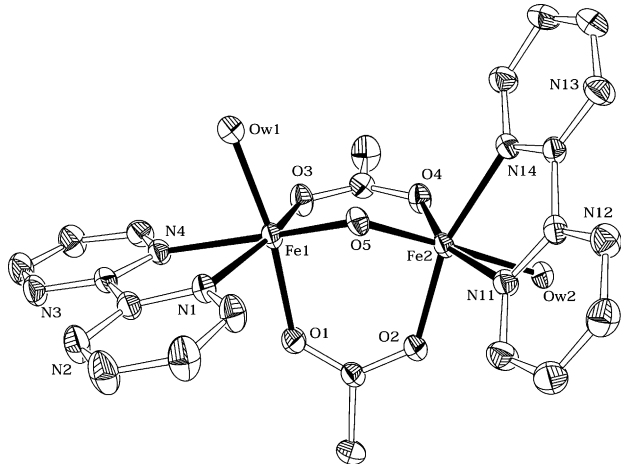

Fig. 2. Partially labelled ORTEP plot of the cation of complex $\mathbf{3} \cdot H_2O \cdot 2MeCN$ at the 30% probability level. Hydrogen atoms have been omitted for clarity.

Table 2
Selected interatomic distances (Å) and bond angles (°) for complex $\mathbf{3} \cdot H_2O \cdot 2MeCN$

Interatomic distances			
Fe(1)–O(1)	2.045(3)	Fe(2)–O(2)	1.995(3)
Fe(1)–O(3)	2.022(3)	Fe(2)–O(4)	2.021(3)
Fe(1)–O(5)	1.783(2)	Fe(2)–O(5)	1.787(3)
Fe(1)–O(W1)	2.063(4)	Fe(2)–O(W2)	2.127(3)
Fe(1)–N(1)	2.181(3)	Fe(2)–N(11)	2.187(3)
Fe(1)–N(4)	2.234(3)	Fe(2)–N(14)	2.166(3)
Bond angles			
O(1)–Fe(1)–O(W1)	169.7(1)	O(2)–Fe(2)–N(14)	163.0(1)
O(3)–Fe(1)–N(1)	162.0(1)	O(4)–Fe(2)–N(11)	162.9(1)
O(5)–Fe(1)–N(4)	169.8(1)	O(5)–Fe(2)–O(W2)	178.1(1)
N(1)–Fe(1)–N(4)	73.4(1)	N(11)–Fe(2)–N(14)	75.1(1)
Fe(1)···Fe(2)	3.098(1)	Fe(1)–O(5)–Fe(2)	120.4(1)

Complex **3** joins a family of structurally characterized dinuclear complexes containing the (μ-oxo)bis(μ-carboxylato)diiron(III) core [39]. Close precedents to **3** are complexes $[Fe_2O(O_2CMe)_2Cl_2(bpy)_2]$ [5] and $[Fe_2O(O_2CCH_2Cl)_2(bpy)_2(H_2O)_2](NO_3)_2$ [6]. In Table 3 are compared selected structural parameters for the three complexes. A comparison of these structural parameters for **1** and the other two complexes reveals a general similarity. The slightly smaller Fe–O–Fe angle in **3** is associated with a slightly shorter Fe···Fe separation. However, there are also some slight structural differences. In the bpy complexes, both donor atoms *trans* to the oxo group are nitrogen atoms. Thus, the two monodentate terminal ligands are positioned *cis* to the bridging oxo group and are in an *anti* arrangement with respect to the Fe–O–Fe plane. In the bpym-containing complex **3**, only one nitrogen atom [N(4)] is *trans* to the bridging oxo group, the other *trans* donor atom being a water oxygen [O(W2)]. Thus, only one monodentate terminal ligand [O(W1)] is positioned *cis* to the oxo group. The two terminal aqua ligands are neither in an *anti* nor in a *syn* arrangement with respect to the Fe–O–Fe plane; O(W1) is 1.520(4) Å above this plane, while O(W2) is practically on the plane (it lies only 0.064(4) Å below the Fe–O–Fe plane).

The crystal structure is stabilized by a network of strong intermolecular hydrogen bonds. Details of the hydrogen bonds are provided in Table 4. A partial crystal packing diagram of $\mathbf{3} \cdot H_2O \cdot 2MeCN$ is shown in Fig. 3. Of particular interest is an intercationic hydrogen bond of medium strength with the coordinated H_2O oxygen O(W2) as donor and the "free" (uncoordinated)

Table 3
Comparison of selected structural parameters (Å, °) for complexes $[Fe_2O(O_2CMe)_2Cl_2(bpy)_2]$, $[Fe_2O(O_2CCH_2Cl)_2(bpy)_2(H_2O)_2](NO_3)_2$ and $[Fe_2O(O_2CMe)_2(bpym)_2(H_2O)_2](ClO_4)_2$ (**3**)

Complex	Fe···Fe	Fe-(μ-O^{2-})[a]	Fe–N_{cis} [a,b]	Fe–N_{trans} [a,b]	Fe–O–Fe
$[Fe_2O(O_2CMe)_2Cl_2(bpy)_2]$	3.151(1)	1.785(4)	2.151(5)	2.208(5)	123.9(2)
$[Fe_2O(O_2CCH_2Cl)_2(bpy)_2(H_2O)_2](NO_3)_2$	3.111(1)	1.784(2)	2.121(2)	2.183(2)	121.5(1)
3	3.098(1)	1.785(3)	2.174(3)	2.234(3)	120.4(1)

[a] Average values except the Fe–N_{trans} bond length for **3** which represents a single value.
[b] Fe–$N_{cis/trans}$ describes iron-nitrogen bonds *cis* or *trans* to the bridging oxo ligand.

Table 4
Hydrogen bonding details[a] for complex $\mathbf{3}\cdot H_2O\cdot 2MeCN$

D–H···A	D···A (Å)	H···A (Å)	D–H···A (°)	Symmetry equivalence of A
O(W1)–HA(OW1)···O(7)	2.847	2.143	173.3	x, y, z
O(W1)–HB(OW1)···O(W3)	2.599	1.869	175.7	x, y, z
O(W2)–HA(OW2)···N(31)	2.819	2.012	172.2	$1+x, y, z$
O(W2)–HB(OW2)···N(3)	2.851	2.142	167.5	$x, -1+y, z$
O(W3)–HA(OW3)···O(6)	2.861	1.997	154.5	$-x, -y, -z$
O(W3)–HB(OW3)···O(11)	2.806	1.793	151.6	$x, 1+y, z$

A, acceptor; D, donor.
[a] Atoms O(6), O(7) and O(11) belong to ClO_4^- counteranions.

bpym nitrogen N(3) of an adjacent cation as acceptor. This ligand–ligand hydrogen bond connects the dinuclear cations and creates one-dimensional (1D) assemblies (chains) parallel to the crystallographic *b* axis. There are also π–π interactions [40] between bpym rings that belong to different chains connecting them into pairs. These π–π interactions are shown as a single line in Fig. 3, joining the centre of the C(14)–C(15) bond between the two symmetrically related bpym ligands.

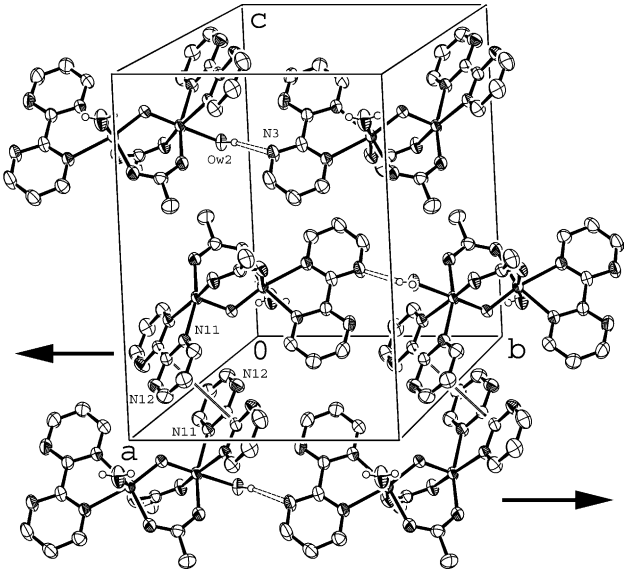

Fig. 3. Crystal packing diagram of complex **3**. Hydrogen bonds (dotted lines) connect the dinuclear cations forming 1D chains along the *b* axis, while π–π interactions (single lines) between the bpym aromatic rings form pairs of such chains. Counteranions, solvate molecules and hydrogen atoms (except those of the aqua ligands) have been omitted for clarity. The arrows indicate the directions of the H-bonds' donor–acceptor vectors (O–H···N) of each chain.

The average distance between the best mean planes of the two symmetrically related bpym ligands (the symmetry code is $1-x, -y, -z$) is 3.48 Å. The complex cations that share π–π interactions are symmetry related to each other by an inversion centre between them and, thus, the π–π interacting chains run the crystal lattice in antiparallel to each other, as can be seen by the opposite orientations of the H-bond donor–acceptor vectors (N···H–O and O–H···N).

The existence of the above described interactions stabilizes the obtained product and therefore it accelerates its precipitation, in contrast with complexes **1** and **2**, where such interactions do not operate in an analogous manner. It is obvious from the labile nature of these systems, confirmed by ^1H NMR experiments in previous studies [34], that many species coexist in solution and that a combination of stability and solubility factors determines which species will precipitate. This example illustrates how secondary interactions (hydrogen bonds, π–π stackings) can have an effect on the identity of the product isolated from a complicated reaction mixture.

3.3. IR spectroscopy

In the $\nu(OH)_{water}$ region, the spectrum of dried **3** shows one medium band at 3374 cm^{-1}, assignable to coordinated water [41]. The spectrum of **3** presents two strong bands at 1534 and 1406 cm^{-1}, attributed to the antisymmetric and symmetric stretching vibrations of the carboxylate group, respectively [42,43]. The difference $\Delta = \nu_{as}(COO) - \nu_s(COO)$ is equal to 128 cm^{-1}, lower than that of NaO_2CMe (164 cm^{-1}), as expected for the crystallographically established bidentate bridging mode of the acetate ligation [43].

The ν(C⎓C) and ν(C⎓N) stretching vibrations of free 2,2′-bipyrimidine at 1565, 1556, 1432 and 1404 cm^{-1} shift to slightly higher frequencies upon complexation and appear at 1577, 1561 and 1405 cm^{-1} in **3**, with the band at 1432 cm^{-1} being masked by the carboxylate symmetric stretch. This appearance of two bands (in the form of a quasi –symmetric doublet) at 1580–1560 cm^{-1} is in accordance with the terminal coordination of bpym [26,44,45]; the lower frequency band does not appear when bpym is bridging(bis-chelating) [23]. The γ(CH) vibration of free bpym (830 and 820 cm^{-1}) appears as a single medium intensity band at 820 cm^{-1} [44]. The Fe–O–Fe antisymmetric stretch, ν_{as}(Fe–O–Fe), is located at 758 cm^{-1} [39,46]. Finally the strong and broad band around 1100 cm^{-1} and the medium band at 620 cm^{-1} are attributed to the $\nu_3(F_2)$ and $\nu_4(F_2)$ modes of the uncoordinated T_d perchlorate anions [42]. The broad character and signs of splitting of the band at ~1100 cm^{-1} both indicate the involvement of the ClO_4^- ions in hydrogen bonding [47].

3.4. Magnetic susceptibility at room temperature

For complex **3** the effective magnetic moment (μ_{eff}) value per Fe_2 is 1.81 BM at 300 K. This value is considerably less than the 8.37 BM value expected for a dinuclear species containing non-interacting Fe^{III} ($S = 5/2$) ions, suggesting the presence of a relatively strong antiferromagnetic interaction in the complex [18]. However, since the magnetic properties of similar dinuclear complexes containing the $\{Fe_2(\mu\text{-}O)(\mu\text{-}O_2CR)_2\}^{2+}$ core have been exhaustively studied [5,6,18,48], no variable-temperature studies were further pursued.

4. Conclusions

In this study, the chemistry of the $Fe^{III}/MeCO_2^-$/L–L systems previously explored with L–L = bpy, was expanded to include 2,2′-bipyrimidine (bpym), in an attempt to obtain different and – if possible – larger clusters, but also in order to examine the basic chemistry of this general system. The use of the bpym ligand in Fe^{III} acetate chemistry has provided access to one dinuclear complex containing the (μ-oxo)bis(μ-carboxylato)diiron(III) core and exhibiting an interesting supramolecular structure. Although one of the goals of this study, i.e., the preparation of larger molecular aggregates, was not attained, we managed to further elucidate some of the factors governing the formation of metal clusters in the above general system. Consideration of synthetic parameters, in combination with careful analysis of the crystal structure of the complex, allowed us to reach some conclusions regarding the reasons that led to the complex obtained. A rational extension of the work reported here is to study the $Fe^{III}/PhCO_2^-$/bpym system in order to investigate the different electronic and steric nature, and the π–π capability of the benzoate ligand. Our results will be reported in due course.

5. Supplementary material

Crystallographic data for the structural analysis have been deposited with the Cambridge Crystallographic Data Centre, CCDC No. 220156. Copies of this information may be obtained free of charge from The Director, CCDC, 12 Union Road, Cambridge, CB2 1EZ, UK (fax: +44-1233-336033; e-mail: deposit@ccdc.cam.ac.uk or www: http://www.ccdc.cam.ac.uk).

Acknowledgements

The authors thank the Greek General Secretariat of Research and Technology (Grant 99ED139) for support of this work and Prof. Jean-Pierre Tuchagues for microanalytical and magnetic measurements at the Laboratoire de Chimie de Coordination du CNRS at Toulouse.

References

[1] D.M. Kurtz Jr., J. Biol. Inorg. Chem. 2 (1997) 159.
[2] M.A. Pavlosky, E.I. Solomon, J. Am. Chem. Soc. 116 (1994) 11610.
[3] C. Canada-Vilalta, E. Rumberger, E.K. Brechin, W. Wernsdorfer, K. Folting, E.R. Davidson, D.N. Hendrickson, G. Christou, J. Chem. Soc., Dalton Trans. (2002) 4005.
[4] A. Caneschi, D. Gatteschi, C. Sangregorio, R. Sessoli, L. Sorace, A. Cornia, M.A. Novak, C. Paulsen, W. Wernsdorfer, J. Magn. Magn. Mater. 200 (1999) 182.
[5] J.B. Vincent, J.C. Huffman, G. Christou, Q. Li, M.A. Nanny, D.N. Hendrickson, R.H. Fong, R.H. Fish, J. Am. Chem. Coc. 110 (1988) 6898.
[6] K.L. Taft, A. Maschelein, S. Liu, S.J. Lippard, D. Garfinkel-Shweky, A. Bino, Inorg. Chim. Acta 198–200 (1992) 627.
[7] J.K. McCusker, J.B. Vincent, E.A. Schmitt, M.L. Mino, K. Shin, D.K. Coggin, P.M. Hagen, J.C. Huffman, G. Christou, D.N. Hendrickson, J. Am. Chem. Soc. 113 (1991) 3012.
[8] W.-Y. Pan, X.-F. Yu, Chin. J. Chem. 12 (1994) 534.
[9] X.-F. Yu, Y.-Q. Jiang, Huaxue Xuebao 51 (1993) 579.
[10] B. Yan, Z.-D. Chen, Inorg. Chem.Commun. 4 (2001) 138.
[11] W.W. Wemple, D.K. Coggin, J.B. Vincent, J.K. McCusker, W.E. Streib, J.C. Huffman, D.N. Hendrickson, G. Christou, J. Chem. Soc., Dalton Trans. (1998) 719.
[12] A.K. Boudalis, N. Lalioti, G.A. Spyroulias, C.P. Raptopoulou, A. Terzis, V. Tangoulis, S.P. Perlepes, J. Chem. Soc., Dalton Trans. (2001) 955.
[13] E.J. Seddon, J.C. Huffman, G. Christou, J. Chem. Soc., Dalton Trans. (2000) 4446.
[14] S. Ménage, J.-M. Vincent, C. Lambeaux, G. Chottard, A. Grand, M. Fontecave, Inorg. Chem. 32 (1993) 4766.

[15] V.A. Grillo, Z. Sun, K. Folting, D.N. Hendrickson, G. Christou, Chem. Commun. (1996) 2233.
[16] E.C. Sañudo, V.A. Grillo, M.J. Knapp, J.C. Bollinger, J.C. Huffman, D.N. Hendrickson, G. Christou, Inorg. Chem. 41 (2002) 2441.
[17] C.M. Grant, M.J. Knapp, W.E. Streib, J.C. Huffman, D.N. Hendrickson, G. Christou, Inorg. Chem. 37 (1998) 6065.
[18] E.J. Seddon, J. Yoo, K. Folting, J.C. Huffman, D.N. Hendrickson, G. Christou, J. Chem. Soc., Dalton Trans. (2000) 3640.
[19] G. De Munno, G. Viau, M. Julve, F. Lloret, J. Faus, Inorg. Chim. Acta 257 (1997) 121, and references therein.
[20] G. De Munno, R. Ruiz, F. Lloret, J. Faus, R. Sessoli, M. Julve, Inorg. Chem. 34 (1995) 408.
[21] D. Armentano, G. De Munno, F. Lloret, M. Julve, Inorg. Chem. 38 (1999) 3744, and references therein.
[22] G. De Munno, T. Poerio, M. Julve, F. Lloret, J. Faus, A. Caneschi, J. Chem. Soc., Dalton Trans. (1998) 679, and references therein.
[23] R. Cortés, M.K. Urtiaga, L. Lezama, J.L. Pizarro, M.I. Arriortua, T. Rojo, Inorg. Chem. 36 (1997) 5016.
[24] G. De Munno, M. Julve, F. Lloret, J. Faus, A. Caneschi, J. Chem. Soc., Dalton Trans. (1994) 1175, and references therein.
[25] G. De Munno, M. Julve, F. Lloret, A. Derory, J. Chem. Soc., Dalton Trans. (1993) 1179.
[26] J.-A. Real, H. Bolvin, A. Bousseksou, A. Dworkin, O. Kahn, F. Varret, J. Zarembowitch, J. Am. Chem. Soc. 114 (1992) 4650.
[27] G. De Munno, W. Ventura, G. Viau, F. Lloret, J. Faus, M. Julve, Inorg. Chem. 37 (1998) 1458.
[28] For very recent representative literature, see Refs. [29–36]. For a review, see: G.S. Papaefstathiou, S.P. Perlepes, Comments Inorg. Chem. 23 (2002) 249.
[29] C.J. Milios, E. Kefalloniti, C.P. Raptopoulou, A. Terzis, A. Escuer, R. Vicente, S.P. Perlepes, Polyhedron 23 (2004) 83.
[30] C.J. Milios, C.P. Raptopoulou, A. Terzis, F. Lloret, R. Vicente, S.P. Perlepes, A. Escuer, Angew. Chem. 43 (2004) 210.
[31] C.J. Milios, C.P. Raptopoulou, A. Terzis, R. Vicente, A. Escuer, S.P. Perlepes, Inorg. Chem. Commun. 6 (2003) 1056.
[32] C.J. Milios, E. Kefalloniti, C.P. Raptopoulou, A. Terzis, R. Vicente, N. Lalioti, A. Escuer, S.P. Perlepes, Chem. Commun. (2003) 819.
[33] A.K. Boudalis, F. Dahan, A. Bousseksou, J.-P. Tuchagues, S.P. Perlepes, Dalton Trans. (2003) 3411.
[34] A.K. Boudalis, N. Lalioti, G.A. Spyroulias, C.P. Raptopoulou, A. Terzis, A. Bousseksou, V. Tangoulis, J.-P. Tuchagues, S.P. Perlepes, Inorg. Chem. 41 (2002) 6474.
[35] G.S. Papaefstathiou, A. Escuer, M. Font-Bardia, S.P. Perlepes, X. Solans, R. Vicente, Polyhedron 21 (2002) 2027.
[36] E. Diamantopoulou, C.P. Raptopoulou, A. Terzis, V. Tangoulis, S.P. Perlepes, Polyhedron 21 (2002) 2117.
[37] G.M. Sheldrick, Acta Crystallogr., Sect. A 46 (1990) 467.
[38] G.M. Sheldrick, SHELXL-97, Crystal Structure Refinement Program, University of Göttingen, Göttingen, Germany, 1997.
[39] D.M. Kurtz Jr., Chem. Rev. 90 (1990) 585.
[40] C.A. Hunter, Chem. Soc. Rev. (1994) 101.
[41] L.S. Gelfand, F.J. Iaconiani, L.L. Pytlewski, A.N. Speca, C.M. Mikulski, N.M. Karayannis, J. Inorg. Nucl. Chem. 42 (1980) 377.
[42] K. Nakamoto, Infrared and Raman Spectra of Inorganic and Coordination Compounds, 4th ed., Wiley, New York, 1986.
[43] G.B. Deacon, R.J. Phillips, Coord. Chem. Rev. 33 (1980) 227.
[44] I. Castro, M. Julve, G. De Munno, G. Bruno, J.A. Real, F. Lloret, J. Faus, J. Chem. Soc., Dalton Trans. (1992) 1739.
[45] M. Julve, M. Verdaguer, G. De Munno, J.A. Real, G. Bruno, Inorg. Chem. 32 (1993) 795.
[46] J.C. Plakatouras, Th. Bakas, C.J. Huffman, J.C. Huffman, V. Papaefthymiou, S.P. Perlepes, J. Chem. Soc., Dalton Trans. (1994) 2737.
[47] V. Tangoulis, C.P. Raptopoulou, A. Terzis, S. Paschalidou, S.P. Perlepes, E. Bakalbassis, Inorg. Chem. 36 (1997) 3996.
[48] S.M. Gorun, S.J. Lippard, Inorg. Chem. 30 (1991) 1625.

Available online at www.sciencedirect.com
SCIENCE DIRECT®
Polyhedron 23 (2004) 1279–1285
POLYHEDRON
www.elsevier.com/locate/poly

Electrochemical, spectroelectrochemical, and pyridine binding properties of tetrathia macrocycle-bridged dimeric cobalt phthalocyanine

Ismail Yilmaz *, Makbule Burkut Koçak

Department of Chemistry, Technical University of Istanbul, Maslak, Istanbul 34469, Turkey

Received 31 December 2003; accepted 17 February 2004

Abstract

Tetrathia macrocycle-bridged dimeric cobalt phthalocyanine, $[(RS)_6CoPc]_2CR$ where $R = C_6H_{13}$, CR = [1,4,7,10-tetrathia-(12-crown-4)], was investigated electrochemically and spectroelectrochemically. Pyridine binding properties of the complex were also investigated by spectrophotometric technique in the solution of dichloromethane. The neutral complex undergoes two quasi-reversible two-electron-oxidations and two quasi-reversible two-electron-reductions in CH_2Cl_2 containing 0.1 M tetra-*n*-butylammonium perchlorate (TBAP). The half-wave potentials for oxidation of the hexylthio substituted complex are located at $E_{1/2} = 0.65$ and 1.28 V, while the two reductions are located at $E_{1/2} = -0.38$ and −1.37 V vs. SCE. These potentials of the complex show little or no difference compared to those of unsubstituted CoPc and other SR substituted phthalocyanines under the same experimental condition, thus suggesting the weak electron-donating properties of the peripheral hexylthio substituents on the phthalocyanine rings. Evaluation of the well-defined UV–Vis spectra of the neutral complex and its electrochemically oxidized and reduced, $\{[(RS)_6Co(2+)Pc(-)]_2CR\}^{2+}$, $\{[(RS)_6Co(+)Pc(2-)]_2CR\}^{2-}$, and $\{[(RS)_8Co(+)Pc(3-)]_2CR\}^{4-}$, species obtained with applied potentials in thin layer cell showed that neutral and mono-oxidized species remained its highly aggregation properties while mono- and doubly reduced complexes behave as monomeric form in the solution as a result of a weak coupling effect. The complex was also investigated as to pyridine-binding ability in dichloromethane/pyridine mixtures. Spectroscopic changes were monitored by UV–Vis spectrophotometry where the Q band of the neutral complex resulted in an increase in intensity, which was associated with the formation of pyridine mono-adduct for binuclear cobalt phthalocyanine complex, $[(RS)_6CoPc]_2CR$.
© 2004 Elsevier Ltd. All rights reserved.

Keywords: Phthalocyanine; Electrochemistry; Spectroelectrochemistry; Pyridine binding

1. Introduction

Metallophthalocyanines (MPc) are well studied as molecular electronics [1,2], non-linear optics [3], liquid crystals [4,5], gas sensors [6], photosensitizers [7], catalysts [8–13], semiconductive materials [14], photovoltaic cells [15], and electrochromic displays [16,17] over the last few years. Especially, the cobalt phthalocyanine (CoPc) and its derivatives are shown to catalyze reactions like the reduction of oxygen, CO_2, formic acid, formaldehyde, trichloro acetic acid, and cysteine-containing proteins. The catalytic behavior of CoPc complexes is associated with the redox activity of the central metal which undergoes oxidation and reduction related with Co(3+)/Co(2+) and Co(2+)/Co(I) in electrochemical reaction [8–13]. The values of the oxidation or reduction potentials of the central metal in CoPc thus strongly influence the catalytic behavior of the complexes which are essential for the design of more efficient catalysts. The spectroelectrochemical studies of the phthalocyanines facilitate the understanding of the nature of the redox processes which may occur at either the central metal atom or the phthalocyanine ring, but this cannot usually be distinguished by using electrochemistry alone. The spectroelectrochemical studies of the phthalocyanines are also important with regard to their

* Corresponding author. Tel.: +90-212-285-6831; fax: 90-212-285-6386.
E-mail address: iyilmaz@itu.edu.tr (I. Yilmaz).

0277-5387/$ - see front matter © 2004 Elsevier Ltd. All rights reserved.
doi:10.1016/j.poly.2004.02.009

possible use as electrochromic materials where display several colors depend on applied potential on the electrode surface [18–20].

In these respects, the synthesis [21–23], the electrochemical [24–26], spectroelectrochemical [24,26–28] and electrocatalytic behavior [8–13] of cobalt phthalocyanines derivatives have been extensively investigated under different experimental conditions. In particular, multinuclear cobalt phthalocyanines having various kinds of linkage have been the subject of interest in electrocatalysis for the reduction of oxygen at fuel cell cathode because the electrocatalyst can participate in a concerted fashion with the multielectron reduction which makes effective oxygen reduction catalysts to hydrogen peroxide [26].

The present paper reports the electrochemical and spectroelectrochemical characterization and pyridine binding properties of tetrathia macrocycle-bridged dimeric cobalt phthalocyanine, $[(RS)_6CoPc]_2CR$ where R = C_6H_{13}, CR = [1,4,7,10-tetrathia-(12-crown-4)] (Chart 1) in CH_2Cl_2.

No detailed study on the spectroelectrochemistry of macrocycle-bridged dimeric cobalt phthalocyanines has been carried out with the exception of a few reports [24,26]. The synthesis of $[(RS)_6CoPc]_2CR$ was afforded with the reaction of $[(RS)_6H_2Pc]_2CR$ (metal-free phthalocyanines) and cobalt chloride in quinoline. Long-alkyl chains substituted on the peripheral position of phthalocyanine units in the molecule provide high solubility in non-coordinating solvents (e.g., dichloromethane, chloroform, diethylether, *n*-hexane) such as has been observed for long-alkyl chains or bulky-groups substituted mono, unsymmetrical, double-decker phthalocyanines and quinoxaline or some oxime complexes [29–32].

The purpose of this work was to understand the redox behavior of neutral and electrogenerated tetrathia macrocycle-bridged dimeric cobalt phthalocyanine $[(RS)_6CoPc]_2CR$ using electrochemical and spectroelectrochemical techniques, as well as to determine aggregation behaviour and the number of pyridine adduct for the axially ligation of the complex in CH_2Cl_2. The pyridine binding experiment also provides the first example on axially ligation for the binuclear cobalt phthalocyanines in CH_2Cl_2 although there have been some experiments on ligation with pyridine for monophthalocyanines in DMSO [33].

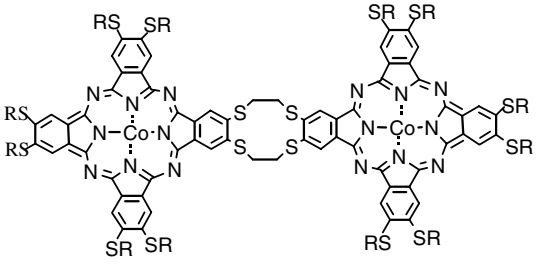

$[(RS)_6CoPc]_2CR$

Chart 1.

2. Experimental

2.1. Chemicals and reagents

Dichloromethane (CH_2Cl_2) was three times treated with H_2SO_4 and distilled over P_2O_5 and CaH_2 prior to use. Dimethylsulfoxide (DMSO) was freshly distilled after drying over alumina. Tetra-*n*-butylammonium perchlorate (TBAP, Fluka Chemical Co.) was recrystallized from ethyl alcohol and dried in a vacuum oven at 40 °C for at least 1 week prior to use. Ferrocene was recrystallized from ethyl alcohol, before use. The target molecule in this work is tetrathia macrocycle-bridged dimeric cobalt phthalocyanine bearing hexylthio substituents on the periphery, which was accomplished by the reaction of $[(RS)_6H_2Pc]_2CR$ (metal-free phthalocyanine) [34] and cobalt chloride in quinoline. The synthesis of $[(RS)_6CoPc]_2CR$ was adopted from a procedure similar to that used for the synthesis of the zinc phthalocyanine complex $[(RS)_6ZnPc]_2CR$ [34]. Purification was achieved by column chromatography over silica gel using CH_2Cl_2 as eluent. The compound was highly soluble in dichloromethane, chloroform, carbon tetrachloride, diethlyether, and *n*-hexane due to the introduction of long-hexylthio chains on the peripheral position of two phthalocyanine cores.

2.2. Instrumention

Cyclic voltammograms (CV) was carried out using CV measurements with a Princeton Applied Research Model 273 potentiostat controlled by an external PC. Current–voltage curves were recorded using an X–Y recorder (RE 0091). A three electrode system was used for CV measurements in CH_2Cl_2 and consisted of a glassy carbon working electrode, a platinum wire counter electrode and a saturated calomel reference electrode (SCE). The reference electrode was separated from the bulk solution by a fritted-glass bridge filled with the solvent/supporting electrolyte mixture. The ferrocene/ferrocenium couple (Fc/Fc^+) was used as an internal standard but all potentials in the paper are referenced to the SCE. Solutions containing $[(RS)_6CoPc]_2CR$ were deoxygenated by a stream of high purity nitrogen for at least 5 min. prior to running the experiment and the solution was protected from air by a blanket of nitrogen during the experiment. Controlled potential electrolysis (CPE) was performed with the Princeton Applied Research Model 273 potentiostat/Galvanostat. An "H" type cell with a fritted glass to separate the cathodic and

anodic portions of the cell was used for bulk electrolysis. The working and counter electrodes were platinum and the reference electrode was an SCE. The sample and solvent were transferred into the electrolysis cell under nitrogen. UV–Vis spectroelectrochemical experiments were performed with a home-built thin-layer cell that utilized a light transparent platinum gauze working electrode. Potentials were applied and monitored with an Princeton Applied Research Model 273 potentiostat. Time-resolved UV–Vis spectra and spectrophotometric titration experiments were recorded with a Unicam UV2 Model spectrophotometer.

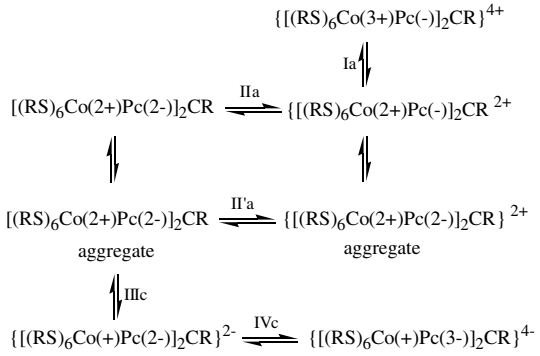

Scheme 1.

3. Results and discussion

3.1. Electrochemistry

The electrochemistry of CoPc is classified into two sections, that referring to donor solvents and non-donor solvents. Whether the metal or the ring is oxidized first depending on the nature of solvent is the principal difference for the redox couples of CoPc. Doner solvents such as dimethylsulfoxide, dimethylformamide, and acetonitrile or coordinating counter anions in non-donor solvents such as dichlorobenzene and dichloromethane are known to strongly favour Co(3+)Pc species. But, the ring oxidized is seen first in non-donor solvents in the absence of coordinating counter anions [25,26].

Fig. 1 shows a typical cyclic voltammogram of the investigated compound, in that $[(RS)_6CoPc]_2CR$ undergoes a two quasi-reversible two-electron-oxidations and two quasi-reversible two-electron-reductions in CH_2Cl_2 containing 0.1 M TBAP. These reactions are schematically illustrated in Scheme 1 where the oxidations are labeled as reactions I and II and the reductions as reactions III and IV.

The half-wave potentials for the reduction of $[(RS)_6CoPc]_2CR$ in CH_2Cl_2, 0.1 M TBAP are located at

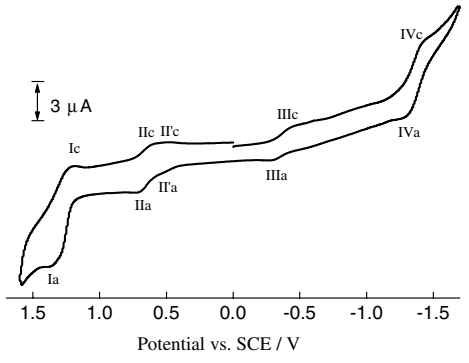

Fig. 1. Cyclic voltammograms of $[(RS)_6CoPc]_2CR$ in CH_2Cl_2 solution containing 0.1 M TBAP. Scan rate = 0.02 V/s.

$E_{1/2} = -0.38$ and -1.37 V, while the two oxidations are located at $E_{1/2} = 0.65$ and 1.28 V vs. SCE. The half-wave potentials of $[(RS)_6CoPc]_2CR$ and some selected mono and dimeric cobalt phthalocyanines are given in Table 1.

Introduction of electron–donating substituents to the phthalocyanine cores should lead to an increase in the electron density of the central metal atom ion thereby making the MPc complex more easily oxidized and less easily reduced [35,36]. However, the investigated compound here and available reports on alkylthio substituted cobalt phthalocyanines show little or no difference in their reduction potentials compared to the unsubstituted CoPc [37]. For example, the first reduction potential ($E_{1/2}$) for the CoPc in dimethylformamide is −0.37 V vs. SCE, while it is −0.38 and −0.34 V vs. SCE for the $[(RS)_6CoPc]_2CR$ and $CoPc(SC_2H_4OH)_8$ [38] in CH_2Cl_2 and DMSO, respectively. These data indicate the weak electron-donating influence of the alkylthio substituents on the average electron density of the metal phthalocyanines. It is also seen that there is little difference between the reduction potentials of $[(RS)_6CoPc]_2CR$, monomeric CoTNPc [25], and dimeric Et-MeO(5)[CoTrNPc] [34] (TN = tetraneopentoxy substituent, electron-donation influence of which is almost similar to that of the alkylthio substituents). We also observed the same weak electron-donating influence of the alkylthio-substituents for previously investigated $[(C_6H_{13}S)_8Pc]_2Lu$, $[(C_{12}H_{25}S)_4Pc]_2Lu$ complexes under the same experimental conditions [18–20].

The redox processes of $[(RS)_6CoPc]_2CR$ were examined as a function of potential scan rate in order to ascertain the mode of mass transport. The cathodic and anodic currents for the oxidation and reduction couples in CH_2Cl_2 each increased in direct proportion to the square root of scan rate between 0.02 and 0.25 V/s, thus suggesting the redox reactions in solution are controlled by diffusion [39].

The investigated compound, $[(RS)_6CoPc]_2CR$, is a relatively planar binuclear molecule which can be regarded as having low flexibility in the plane connecting

Table 1
Half-wave potentials of $[(RS)_6CoPc]_2CR$ and selected mono and dimeric cobalt phthalocyanines

Solvent/condition	Compound	Ox_2(**I**)	Ox_1 (**II**)	Red_1 (**III**)	Red_2(**IV**)	Reference
CH_2Cl_2	$[(RS)_6CoPc]_2CR$	1.28 (0.10)	0.65 (0.08)	−0.38 (0.09)	−1.37 (0.01)	tw
DMF	CoPc		0.54	−0.37	−1.40	[37]
DMSO	$CoPc(SC_2H_4OH)_8$			−0.34	−1.22	[38]
DCB	CoTNPc	1.10	0.54	−0.40	−1.56	[24,37]
DCB	EtMeO(5)[CoTrNPc]$_2$		0.56	−0.42	−1.56	[24,37]

Values of $\Delta E_p (= E_{pa} - E_{pc})$ for $[(RS)_6CoPc]_2CR$ are given in parenthesis. tw: this work.

two phthalocyanines units. That is to say, two phthalocyanines units do not rotate from the standpoint of constrains of tetrathia macrocycle-bridges between two phthalocyanines units. Thus, no splitting of the redox peaks could be expected for binuclear cobalt complex, $[(RS)_6CoPc]_2CR$, such as has been observed for the Co(2+)/Co(+) couple of a clamshell cobalt porphyrin and the Co(2+)/Co(+) and Co(2+)/Co(+) couples of face-to-face cobalt porphyrins [40,41] due to interactions between the two cobalt atoms, which are held in close proximity by the ligand geometry. But intermolecular interaction between phthalocyanine molecules should result in aggregation which is expected to show an additional wave (II'a) corresponding to the reduction of aggregated species as observed in Fig. 1, if there is an equilibrium between the aggregated and non-aggregated species where the equilibrium is slow relative to the electrochemical timescale [42]. Therefore, II'a and IIa in Fig. 1 should be assigned to the oxidation of aggregated and non-aggregated $[(RS)_6CoPc]_2CR$ species as shown in Scheme 1. Aggregation appears to be influenced by the net charge on the phthalocyanine units, being more important with positively charged than with negatively charged species. The results were also confirmed with spectroscopic date obtained from spectroelectrochemical measurement of the $[(RS)_6CoPc]_2CR$ in a thin layer cell. In the case of the binuclear cobalt phthalocyanine $[(RS)_6CoPc]_2CR$ studied here, the two phthalocyanine units of each molecule oxidize and reduce simultaneously although some mixed-valence species were seen for the binuclear phthalocyanines in the literature [24]. The controlled potential coulometric (CPC) study indicated that the number of electrons transferred for electrochemical reactions of the complex is two for each oxidation and reduction processes. The redox potentials of $[(RS)_6CoPc]_2CR$ measured in this work are consistent with those of binuclear cobalt phthalocyanines reported in the literature [25].

3.2. UV–Vis spectra of electrooxidized and electroreduced complexes

Typical absorption spectra for neutral $[(RS)_6CoPc]_2CR$ and its electrochemically generated species, $\{[(RS)_6Co(2+)Pc(-)]_2CR\}^{2+}$, $\{[(RS)_6Co(+)Pc(2-)]_2CR\}^{2-}$, and $\{[(RS)_8Co(+)Pc(3-)]_2CR\}^{4-}$, are shown in Figs. 2 and 3(a)–(c). Spectroscopic data for neutral and electrochemically generated species are also given in Table 2.

The typical UV–Visible spectra of neutral $[(RS)_6CoPc]_2CR$ exhibited characteristic Q and B bands, one in the visible region at 700 nm (Q-band) attributed to the $\pi \rightarrow \pi^*$ transition from the highest occupied molecular orbital (HOMO) to the lowest unoccupied molecular orbital (LUMO) of the Pc(-2) ring, and the other in the UV region at 321 nm (B-band) arising from the deeper π-levels $\rightarrow$ LUMO transition. Neutral $[(RS)_6CoPc]_2CR$ shows an additional band centered at ca. 50 nm to the blue of the normal Q band as a result of aggregation through exciton coupling of phthalocyanine units [26].

The intensity of Q band relative to B is also low (Fig. 2, as shown solid line). These results are similar to those previously observed for binuclear cobalt phthalocyanines [25]. Both B and Q bands of $[(RS)_6CoPc]_2CR$ are slightly shifted to longer wavelengths compared to unsubstituted CoPc. Such a red shift is an indication that the energy gap between the highest occupied molecular orbital (HOMO) and lowest unoccupied molecular orbital (LUMO) of the complex are narrower than those of the CoPc, thereby increasing the electroconductivity of the molecule [19].

$[(RS)_6CoPc]_2CR$ was stepwise oxidized or reduced in a thin-layer cell and the resulting UV–Vis spectra were

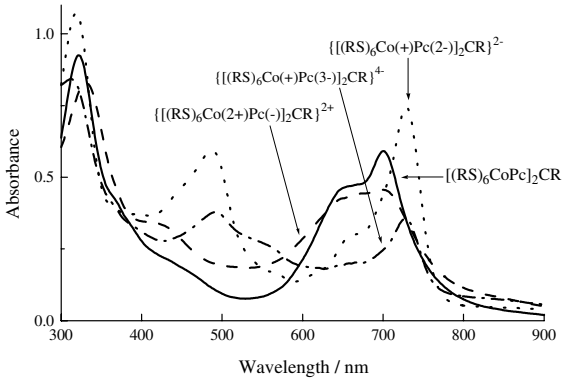

Fig. 2. UV–Vis spectra of $[(RS)_6CoPc]_2CR$ (solid line), $\{[(RS)_6Co(+)Pc(2-)]_2CR\}^{2-}$ (dot line), $\{[(RS)_8Co(+)Pc(3-)]_2CR\}^{4-}$ (dash dot line), and $\{[(RS)_6Co(2+)Pc(-)]_2CR\}^{2+}$ (dash line) in CH_2Cl_2 containing 0.2 M TBAP.

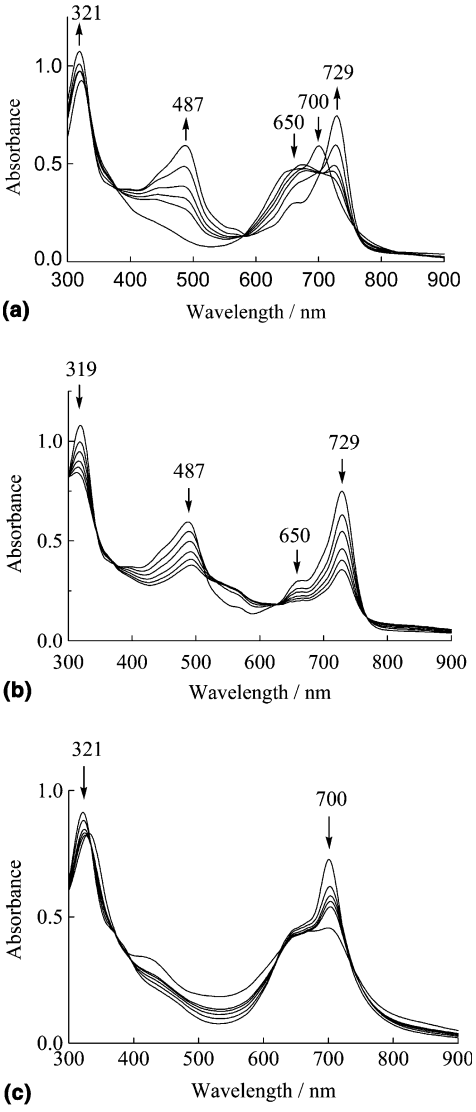

Fig. 3. Time-resolved UV–Vis spectral changes of $[(RS)_6CoPc]_2CR$ (a) during the first reduction at $E_{app} = -0.7$ V, (b) during the second reduction at $E_{app} = -1.5$ V (c) during the first oxidation at $E_{app} = 0.9$ V in CH_2Cl_2 solution containing 0.2 M TBAP.

measured as a function of time. Examples of the time-resolved spectra are shown in Fig. 3(a)–(c) and summary of the spectroscopic data is given in Table 2.

The evolution of the UV–Vis spectral changes upon the first reduction of $[(RS)_6CoPc]_2CR$ results in the spectroscopic changes are shown in Fig. 3(a) and Fig. 2 (dot line) for the final spectrum of $\{[(RS)_6Co(+)Pc(2-)]_2CR\}^{2-}$ and accompanies with a change of color from green to yellow. Isobesting points are observed at 334, 377, 581, 766 nm. The spectrum is typical of a Co(+)Pc(−2) species, characterized by the appearance of strong band at 487 nm, assigned as a metal-to-ligand charge transfer from Co(+)Pc(2−) $[d(xz, yz)] \rightarrow \pi$ (1b1u) Pc(2−), a red shift, and an increase in intensity of the Q band centered at 729 nm [25,26,43]. The Co(I) species is expected to be much less intermolecularly coupled than the Co(2+) species as a result of the negative charge on the cobalt atoms giving rise to weak coupling effect. Thus, the intensity of the band at 650 nm decreases as seen in Figs. 2 and 3(a). An equilibrium between aggregated and non-aggregated products could not be expected following the first reduction process of $[(RS)_6CoPc]_2CR$ based on the metal centered, which is consistent with CV of $[(RS)_6CoPc]_2CR$. This shows that the reduced species of the complex $\{[(RS)_6Co(+)Pc(2-)]_2CR\}^{2-}$ behaves as a monomeric form in the solution, which could be expected for common MPc molecules in their solution state of electrochemistry. The electron transfer reaction was reversible on the spectroelectrochemical timescale and the original spectrum (and color) of the compounds was obtained upon re-oxidation. Thus, the reduced phthalocyanine remained fully stable throughout the experiment. The well-defined UV–Vis spectral changes during the second reduction of $[(RS)_6CoPc]_2CR$ are shown in Fig. 3(b) and Fig. 2 (dash dot line) for the final spectrum of $\{[(RS)_8Co(+)Pc(3-)]_2CR\}^{4-}$. The reduction product results in a color change from yellow to pink. Isobesting points are observed at 342, 372, 627, 766 nm. The observed small red shift of the MLCT band and decrease in intensity of the Q and B bands relative to that of the first reduction product are similar to those mentioned for monomeric [44] and dimeric [25] cobalt phthalocyanines in literature. Re-oxidation of ring-reduced species at a positive potential generates the starting material with the same Q band intensity.

UV–Vis spectral changes upon the first oxidation of $[(RS)_6CoPc]_2CR$ in CH_2Cl_2 are shown in Fig. 3(c) and Fig. 2 (dash line) for the final spectrum of $\{[(RS)_6Co(2+)Pc(-)]_2CR\}^{2+}$. Isobesting points are observed at 333, 394, 622, 734 nm. The decreases in the intensity of the Q and B bands with small red shift are observed but no drastic color change was seen as previously

Table 2
UV–Vis spectral data of $\{[(RS)_8CoPc]_2CR\}^n$ in CH_2Cl_2 containing 0.2 M TBAP

Charge, n	Species	λ (nm) (log ε)			
0	$[(RS)_6CoPc]_2CR$	321 (5.62)		650 (5.32)	700 (5.43)
−2	$[(RS)_6CoPc]_2CR$	319 (5.70)	487 (5.43)	650 (5.08)	729 (5.54)
−4	$[(RS)_6CoPc]_2CR$	313 (5.58)	493 (5.23)	650 (4.9)	729 (5.21)
+2	$[(RS)_6CoPc]_2CR$	331 (5.57)		650 (5.29)	700 (5.31)

mentioned [25]. The broad, low-intensity spectrum is very similar in appearance to those reported for the ring oxidations of phthalocyanines [25,45] and metalloporphyrins [46] to form the phthalocyanine and porphyrin cation radical species.

Re-reduction at a negative potential of ring-oxidized species generates the starting material with the same Q band intensity which means the oxidized product remains stable during the spectroelectrochemical process. The aggregation band corresponding to the first oxidizided species is centered at 650 nm which is similar to that of neutral molecule with the exception of the almost same height of bands as shown Fig. 3(c). This aggregation effect could be also observed in CV of $[(RS)_6CoPc]_2CR$ corresponding to the equilibrium between aggregation and non-aggregation species (Fig. 1 and Scheme 1).

3.3. Formation of mono-pyridine adduct and equilibrium measurement

The binding of pyridine to $[(RS)_6CoPc]_2Cr$ was carried out at 296 K in dichloromethane and the reaction was monitored by UV–Vis spectroscopy. The absorbance data can be fitted to the Hill equation (1) [47]

$$\log[(A_i - A_o)/(A_f - A_i)] = \log K + p\log[py], \quad (1)$$

where A_i is the absorbance at a specific concentration of pyridine; A_o the initial absorbance, where $[py] = 0$, and A_f the final absorbance, where the fully ligated $[(RS)_6CoPc]_2CR$ is the only species present. The value for log K was obtained from the intercept of the regression line $\log[(A_i - A_o)/(A_f - A_i)]$ vs. log [py]. The slope, p, should be equal to the number of axially coordinated ligands. The concentration of the $[(RS)_6CoPc]_2CR$ for the measurement was $\sim 10^{-5}$ M and that of pyridine was in the range of 10^{-5} to 0.5 M. The binuclear cobalt complex, $[(RS)_6CoPc]_2CR$ was investigated as to pyridine binding ability in dichloromethane/pyridine mixtures. The addition of pyridine to dichloromethane solution of $[(RS)_6CoPc]_2CR$ leads to an increase in intensity for the Q band of the neutral complex. The new spectra are formed with isobesting points at 661, 715 nm for the measurement of dichloromethane solution. Further addition of pyridine had no effect on the position of maxima.

The first axial ligand in MPc complexes generally occurs at a fast rate causing very minor spectroscopic changes that are difficult to observe [33,48]. The spectral changes are associated with pyridine adduct for $[(RS)_6CoPc]_2CR$ as shown in Eq. (2) for the $[(RS)_6CoPc]_2CR$, whose spectrum in dichloromethane and neat pyridine is illustrated in Fig. 4(a) and (b).

$$[(RS)_6Co(2+)Pc(2-)]_2CR + 2py \rightleftharpoons [(RS)_6Co(3+)Pc(2-)(py)_2]_2CR \quad (2)$$

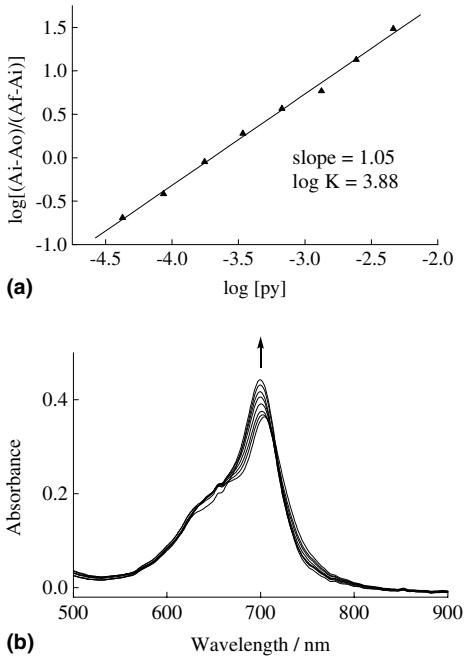

Fig. 4. (a) Plots of $\log[(A_i - A_o)/(A_f - A_i)]$ vs. log [py] for the formation of $[(RS)_6Co(3+)Pc(2-)(py)_2]_2CR$ in CH_2Cl_2 and (b) Absorbtion spectral changes of $[(RS)_6CoPc]_2CR$ on addition of pyridine in CH_2Cl_2.

The spectral changes associated with the conversion of $[(RS)_6CoPc]_2CR$ to its pyridine adducts are shown in Fig. 4(b) and, when analyzed by the Hill plot of $\log[(A_i - A_o)/(A_f - A_i)]$ vs. log [py] shown as Fig. 4(a), give a slope of 1.05, consistent with the binding of one pyridine molecule per cobalt atom in the two phthalocyanine units to form $[(RS)_6Co(III)Pc(-2)(py)_2]_2CR$. The value of log K for the axially ligation of pyridine in $CH_2Cl_2$is 3.88 as shown in Fig. 4(a), which is higher than that of CoPc in DMSO where axial ligand exchange reaction with pyridine in $CoPc(DMSO)_2$ was reported [33].

Acknowledgements

The support of Research Fund of Technical University of Istanbul is gratefully acknowledged.

References

[1] J. Simon, P. Bassoul (Eds.), Design of Molecular Materials: Supramolecular Engineering, Wiley, Chichester, 2000, pp. 197–291.
[2] W. Gopel, Synth. Met. 41 (1991) 1087.
[3] M.A. Diaz Garcia, I. Ledoux, J.A. Duro, T. Torres, F. Agullo-Lopez, J. Zyss, J. Phys. Chem. 98 (1994) 8761.
[4] H. Eichhorn, D. Wöhrle, D. Pressner, Liq. Cryst. 22 (1997) 643.
[5] D. Lelievre, M.A. Petit, J. Simon, Liq. Cryst. 4 (1989) 707.

[6] J.D. Wright, P. Roisin, G.P. Rigby, R.J.M. Nolte, M.J. Cook, S.C. Thorpe, Sensor Actuators B 13 (1993) 276.
[7] I. Rosenthal, in: C.C. Leznoff, A.B.P Lever (Eds.), The Phthalocyanines Properties and Applications, vol. 4, VCH, New York, 1996, pp. 485–514.
[8] J.H. Zagal, Coord. Chem. Rev. 119 (1992) 89.
[9] P. Janda, N. Kobayashi, P.R. Auburn, H. Lam, C.C. Leznoff, A.B.P. Lever, Can. J. Chem. 67 (1989) 1109.
[10] N. Kobayashi, W.A. Nevin, Appl. Organomet. Chem. 10 (1996) 579.
[11] W.J. Todd, F. Bailly, J. Pavez, P.W. Faguy, R.P. Baldwin, R.M. Buchanan, J. Am. Chem. Soc. 120 (1998) 4887.
[12] M.K. Halbert, R.P. Baldwin, Anal. Chem. 57 (1985) 591.
[13] E. Karmann, D. Schlettwein, N.I. Jaeger, J. Electroanal. Chem. 405 (1996) 149.
[14] R. Zhou, F. Josse, W. Gopel, Z.Z. Özturk, O. Bekarolu, Appl. Organomet. Chem. 10 (1996) 557.
[15] D. Wöhrle, L. Kreienhoop, G. Schnurpfeil, J. Elbe, B. Tennigkeit, S. Hiller, D. Schlettwein, J. Mater. Chem. 5 (1995) 1819.
[16] N. Toshima, T. Tominaga, S. Kawamura, B. Chem. Soc. Jpn. 69 (1996) 245.
[17] B. Lukas, J. Silver, Dr. Lovett, M.J. Cook, Chem. Phys. Lett. 241 (1995) 351.
[18] K.M. Kadish, T. Nakanishi, A. Gürek, V. Ahsen, I. Yilmaz, J. Phys. Chem. B 105 (2001) 9817.
[19] I. Yilmaz, T. Nakanishi, A. Gürek, K.M. Kadish, J. Porhyrins Phthalocyanines 7 (2003) 227.
[20] T. Nakanishi, I. Yilmaz, N. Nakashima, K.M. Kadish, J. Phys. Chem. B 107 (2003) 12789.
[21] M. Kandaz, I. Yilmaz, O. Bekarolu, Polyhedron 19 (2000) 19115.
[22] I. Yilmaz, O. Bekarolu, Chem. Ber. 129 (1996) 967.
[23] M. Koçak, A.G. Gürek, A. Gül, O. Bekarolu, Chem. Ber. 127 (1994) 355.
[24] N. Kobayashi, H. Lam, W.A. Nevin, P. Janda, C.C. Leznoff, T. Koyama, A. Monden, H.J. Shirai, Am. Chem. Soc. 116 (1994) 879.
[25] W.A. Nevin, M.R. Hempstead, W. Liu, C.C. Leznoff, A.B.P. Lever, Inorg. Chem. 26 (1987) 570.
[26] W.A. Nevin, W. Liu, M.R. Hempstead, S.M. Marcuccio, M. Melnik, C.C. Leznoff, A.B.P. Lever, Inorg. Chem. 26 (1987) 891.
[27] K.J. Balkus, A.G. Gabrielov, S.l. Bell, F. Bedioui, L. Roue, Devynck, J. Inorg. Chem. 33 (1994) 67.
[28] A.B.P. Lever, Inorg. Chim. Acta. 203 (1993) 171.
[29] A.G. Gurek, O. Bekarolu, J. Chem. Soc., Dalton Trans. (1994) 1419.
[30] S. Dabak, A. Gül, O. Bekaroğlu, Chem. Ber. 127 (1994) 2001.
[31] M. Kandaz, S.Z. Coruhlu, I. Yilmaz, A.R. Ozkaya, Transit. Met. Chem. 27 (2002) 877.
[32] I. Yilmaz, O. Bekarolu, J. Chem. Res. (1998) 374.
[33] T. Nyokong, Polyhedron 14 (1995) 2325.
[34] A.G. Gürek, O. Bekarolu, J. Porhyrins Phthalocyanines 1 (1997) 67.
[35] D. Wöhrle, V.J. Schmidt, J. Chem. Soc., Dalton Trans. (1998) 549.
[36] A. Louati, M. Elmeray, J.J. Andre, J. Simon, K.M. Kadish, M. Gross, A. Giraudeau, Inorg.Chem. 24 (1985) 1175.
[37] A.B.P. Lever, E.L. Milaeva, E. Speier, in: C.C. Leznoff, A.B.P. Lever (Eds.), The Phthalocyanines Properties and Applications, vol. 3, VCH, New York, 1993, pp. 42–69.
[38] A.R. Özkaya, E. Hamuryudan, Z.A. Bayr, O. Bekaroglu, J. Porhyrins Phthalocyanines 4 (2000) 689.
[39] A.J. Bard, L.R. Faulkner (Eds.), Electrochemical Methods: Fundamentals and Applications, 2nd ed., Wiley, New York, 2001, pp. 228–234.
[40] Y. Lemest, M. L'Her, J. Courtotcoupez, J.P. Collman, E.R. Evitt, C.S. Bencosme, J. Electroanal. Chem. 184 (1985) 331.
[41] J.P. Collman, M. Marrocco, C.M. Elliott, M. L'Her, J. Electroanal. Chem. 124 (1981) 113.
[42] A. Giraudeau, A. Louati, M. Gross, J.J. Andre, J. Simon, C.H. Su, K.M. Kadish, J. Am. Chem. Soc. 105 (1983) 2917.
[43] P.C. Minor, M. Gouterman, A.B.P. Lever, Inorg. Chem. 24 (1985) 1894.
[44] D.W. Clack, J.R. Yandle, Inorg. Chem. 11 (1972) 1738.
[45] T. Nyokong, Z. Gasyna, M.J. Stillman, Inorg. Chim. Acta. 112 (1986) 11.
[46] J. Fajer, D.C. Borg, A. Forman, D. Dolphin, R.H. Felton, J. Am. Chem. Soc. 92 (1970) 3451.
[47] P.E. Ellis, J.E. Linard, T. Szymanski, R.D. Jones, J.R. Budge, F. Basolo, J. Am. Chem. Soc. 102 (1980) 1889.
[48] T. Nyokong, Polyhedron 14 (1995) 643.

Available online at www.sciencedirect.com
SCIENCE DIRECT®
Polyhedron 23 (2004) 1287
POLYHEDRON
www.elsevier.com/locate/poly

Erratum

Erratum to: "Synthesis, characterization and crystal structures of (*Z*)-1-(triarylstannyl)-3-phenyl-1-buten-3-ols and their arylhalostannyl derivatives" [Polyhedron 22 (2003) 3523] ☆,☆☆

Dong-Sheng Zhu [a,b], Ze-Min Mei [a], Chun-Sheng Lü [a], Wei Gao [a], Yue-Tao Zhang [a], Ying Mu [a,c,*], Zong-Mu Wang [a]

[a] *School of Chemistry, Jilin University, Changchun 130023, PR China*
[b] *School of Chemistry, Northeast Normal University, Changchun 130024, PR China*
[c] *Key Laboratory for Supramolecular Structure and Materials of the Ministry of Education, Jilin University, Changchun 130023, PR China*

Received 15 July 2003; accepted 26 August 2003

While processing the article for publication an incorrect acceptance date was inadvertently used in the original article. The correct date should be 26 August 2003.

☆ PII of original article: S0277-5387(03)00566-7.
☆☆ DOI of original article: 10.1016/j.poly.2003.09.012.
* Corresponding author. Tel.: +864318499136; fax: +864318949334.
E-mail address: ymu@mail.jlu.edu.cn (Y. Mu).

0277-5387/$ - see front matter © 2004 Elsevier Ltd. All rights reserved.
doi:10.1016/j.poly.2003.08.020

Available online at www.sciencedirect.com
SCIENCE DIRECT®
Polyhedron 23 (2004) 1289
POLYHEDRON
www.elsevier.com/locate/poly

Erratum

Erratum to: "Effect of free and chelating phosphine coordination environments on the NiS_2P_2 chromophore: synthesis, NMR and other spectral studies. Crystal and molecular structures of (*N*,*N*-dipropyldithiocarbamato)di(triphenylphosphine)nickel(II) perchlorate and (*N*,*N*-dipropyldithiocarbamato)1,2-bis((diphenylphosphino)ethane)nickel(II) tetraphenylborate" [Polyhedron 23 (2004) 77] ☆,☆☆

B. Arul Prakasam [a], Kuppukkannu Ramalingam [a,*], M. Saravanan [a], Gabriele Bocelli [b], Andrea Cantoni [b]

[a] *Department of Chemistry, Annamalai University, Annamalainagar, Annamalainagar 608 002, India*
[b] *IMEM, CNR, Parma, Italy*

Received 26 July 2003; accepted 29 August 2003

While processing the article for publication an incorrect acceptance date was inadvertently used in the original article. The correct acceptance date should be 29 August 2003.

☆ PII of original article: S0277-5387(03)00565-5.
☆☆ DOI of original article: 10.1016/j.poly.2003.09.013.
* Corresponding author. Tel.: +914132202834; fax: +914132202834.
E-mail address: krchem@rediffmail.com (K. Ramalingam).

0277-5387/$ - see front matter © 2004 Elsevier Ltd. All rights reserved.
doi:10.1016/j.poly.2003.08.021

Available online at www.sciencedirect.com
SCIENCE DIRECT®
Polyhedron 23 (2004) 1291
POLYHEDRON
www.elsevier.com/locate/poly

Erratum

Erratum to: "Synthesis and X-ray crystal structures of hydridotris(3,5-dimethylpyrazolyl)borate (Tp′) molybdenum(VI) bis(imido) complexes" [Polyhedron 23 (2004) 189] ☆,☆☆

Vernon C. Gibson [a], Carl Redshaw [b,*], William Clegg [c], Mark R.J. Elsegood [d], Ulrich Siemeling [e], Thomas Türk [e]

[a] *Department of Chemistry, Imperial College, South Kensington, London SW7 2AY, UK*
[b] *Wolfson Materials and Catalysis Centre, School of Chemical Sciences and Pharmacy, The University of East Anglia, Norwich NR4 7TJ, UK*
[c] *School of Natural Sciences (Chemistry), University of Newcastle, Newcastle upon, Tyne NE1 7RU, UK*
[d] *Department of Chemistry, Loughborough University, Loughborough, Leicestershire LE11 3TU, UK*
[e] *Department of Science, University of Kassel, Heinrich-Plett-Str. 40, D-34132 Kassel, Germany*

Received 5 August 2003; accepted 16 September 2003

While processing the article for publication an incorrect acceptance date was inadvertently used in the original article. The correct acceptance date should be 16 September 2003.

☆ PII of original article: S0277-5387(03)00589-8.
☆☆ DOI of original article: 10.1016/J.poly.2003.10.005.
* Corresponding author. Tel.: +44-1604-593137; fax: +44-1603-592003.
E-mail address: carl.redshaw@uea.ac.uk (C. Redshaw).

0277-5387/$ - see front matter © 2003 Elsevier Ltd. All rights reserved.
doi:10.1016/j.poly.2003.09.038

Available online at www.sciencedirect.com
SCIENCE DIRECT®
Polyhedron 23 (2004) 1293–1302
POLYHEDRON
www.elsevier.com/locate/poly

Complexes of zinc(II) halides with *N*-benzyl- and *N*-*p*-tolyl-2-oxo-1-naphthylideneamine – preparation and characterization

Zora Popović [a,*], Vibor Roje [a], Gordana Pavlović [b], Dubravka Matković-Čalogović [a], Maša Rajić [c], Ivan Leban [d]

[a] *Faculty of Science, Laboratory of General and Inorganic Chemistry, Department of Chemistry, University of Zagreb, Ul. kralja Zvonimira 8, HR-10000 Zagreb, Croatia*
[b] *Faculty of Textile Technology, University of Zagreb, Pierottijeva 6, HR-10000 Zagreb, Croatia*
[c] *Laboratory for Thermal Analysis, Brodarski Institute – Marine Research and Special Technology, Av. V. Holjevca 20, HR-10000 Zagreb, Croatia*
[d] *Laboratory of Inorganic Chemistry, Faculty of Chemistry and Chemical Technology, University of Ljubljana, P.O. Box 537, 1001 Ljubljana, Slovenia*

Received 22 July 2003; accepted 8 December 2003
Available online 9 April 2004

Dedicated to Professor Milan Sikirica on the occasion of his 70th birthday

Abstract

A series of novel complexes, dihalo-bis(*N*-benzyl-2-oxo-1-naphthylideneamine-*O*)zinc(II), $ZnX_2(bznapH)_2$ (**1**–**3**), dihalo-bis(*N*-*p*-tolyl-2-oxo-1-naphthylideneamine-*O*)zinc(II), $ZnX_2(tolnapH)_2$ (**4**–**6**), of the general formula $[ZnX_2(LH)_2]$ X = Cl, Br, I, have been prepared. The crystal structures of four compounds (**1**–**4**) reveal four coordinated zinc centres by two halogen and two oxygen atoms from the Schiff-base in the form of distorted tetrahedra. Complex **4** crystallizes as the one-to-one solvate with ethanol.

The tetrahedral distortion is most pronounced in the structure of $ZnI_2(bznapH)_2$ complex. X-ray structural data showed that the Schiff-base ligand in the naphthylideneamine tautomeric form is weakly bound to Zn atom in **1**–**4** (being in the range from 1.952(3) Å in **2** to 2.002(3) Å in **4**). The molecular structures of **1**–**4** are governed by the type of halide and the corresponding Schiff-base. Although the structure comparison of $ZnX_2(bznapH)_2$ vs. $ZnX_2(tolnapH)_2$ leads to the conclusion that ligand spatial accomodation (non-planar bznapH with aliphatic interruption vs. aromatic tolnapH) is the dominating factor in the crystal structures. The crystal structures of **2**–**4** are dominated by van der Waals forces. There is a weak intermolecular hydrogen bond of the C–H···Cl type in **1** (3.710(5) Å joining molecules into endless chains. The UV–Vis and ^{1}H NMR spectra, obtained in ethanolic and acetone solution indicate that the complexes do not exist in the solutions.
© 2004 Elsevier Ltd. All rights reserved.

Keywords: Zinc complexes; Schiff-bases; Crystal structures; IR; UV and NMR spectroscopy; Thermal analysis

1. Introduction

In the context of our investigation of mercury(II) compounds with Schiff-bases [1], we undertook the investigation of the analogous zinc(II) compounds in order to make more complete the coordination chemistry of the group 12 metals. It is well known that zinc and Schiff-bases play important roles in biological systems; zinc mainly as a part of metalloenzymes [2] and Schiff-bases as the intermediates in aminoacid metabolism [3,4].

This paper reports the synthesis, IR, NMR and UV characterization as well as thermal studies of a series of 1:2 complexes of zinc(II) halides with *N*-benzyl-, *N*-*p*-tolyl-2-oxo-1-naphthylideneamine. The crystal structures of the complexes **1**–**4** have been determined by crystal X-ray diffractometry.

* Corresponding author. Tel.: +385-1-4606652; fax: +385-1-4611191.
E-mail address: zpopovic@chem.pmf.hr (Z. Popović).

0277-5387/$ - see front matter © 2004 Elsevier Ltd. All rights reserved.
doi:10.1016/j.poly.2003.12.023

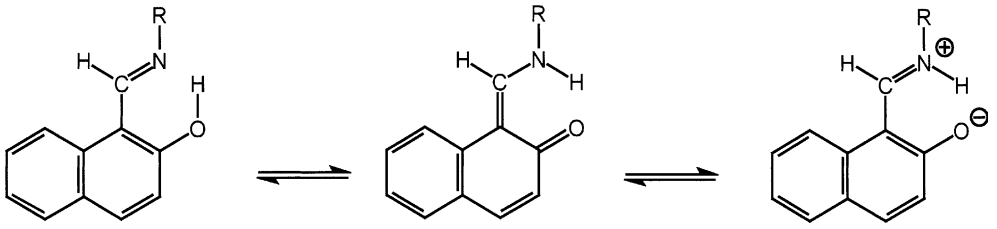

Scheme 1.

Schiff-bases derived from *O*-hydroxy aromatic aldehydes such as salicylaldehyde and 2-hydroxy-1-naphthaldehyde with the *N*,*O*-donor set react with the zinc ion to yield two different types of compounds, i.e. metal chelates and adducts of general formulas ZnL_2 and $ZnX_2 \cdot 2LH$, respectively, both containing a four-coordinated zinc metal centre [5]. The chelate zinc complexes of the ZnL_2 type where L = salicylaldiminato ligand are well known, but according to the Cambridge Structural Database [6a,6b] there are only two zinc(II) complexes with the Schiff-bases derived from 2-hydroxy-1-naphthaldehyde that are structurally characterized. One of them (refcode: POGJAW) [7] contains a five-coordinated zinc atom (three nitrogen atoms, one oxygen atom and one bromine atom) and the other has a tetrahedrally coordinated zinc atom (refcode: SUQWOK) [8]. According to our best knowledge, there is only one more zinc(II) complex with a Schiff-base derived from 2-hydroxy-1-naphthaldehyde and that has only been characterized spectroscopically [9]. There is no structural characterization of zinc adducts with the naphthaldimine type of Schiff-bases.

The crystal structures of these non-coordinated ligands have not been determined up until now. The tautomeric equilibrium of the Schiff-bases derived from 2-hydroxy-1-naphthaldehyde and amines (1:1 molar ratio), in the solid state [10–12] as well as in solution [3], is usually shifted toward the keto-amine tautomeric form (Scheme 1). There are also examples of the structures of this Schiff-base type that in the solid state exist in the enol-imine tautomeric form [13].

2. Experimental

All reagents used were purchased from Aldrich, solvents from Kemika-Zagreb and were used without further purification. C, H and N analysis was provided by the Analytical Services Laboratory of the Ruđer Bošković Institute. The IR spectra of all mentioned compounds were recorded in a Perkin–Elmer Fourier Transform 1600 spectrometer in the range of 4000–450 cm^{-1} as KBr discs. The UV–Vis spectra were recorded using a Varian Cary 300 operating in the range 190–900 nm. The ^1H NMR spectra were recorded in a Varian Gemini 300 spectrometer, at 20 °C. All chemical shifts, in parts per million (ppm), are referred to TMS. Digital resolution was 0.32 Hz per point. The thermal measurements were performed using a simultaneous TGA–DTA analyser (TA Instruments, SDT Model 2960 coupled with MS). The samples were placed in small alumina sample pans. The TGA and DTA curves were obtained by placing the samples of about 2 mg in mass, in open sample pans, with a heating rate of 10 °C min^{-1} and argon (purity above 99.996%) flowing at the rate of 50 ml min^{-1}. The SDT was calibrated with indium.

2.1. Preparation of the ligands and basic analytical data

The Schiff-bases *N*-benzyl-2-oxo-1-naphthylideneamine (bznapH) [14] and *N*-*p*-tolyl-2-oxo-1-naphthylideneamine (tolnapH) were prepared by the conventional condensation method.

[bznapH]. Chemical analysis: found (required for $C_{18}H_{15}NO$) C, 82.73 (82.89); H, 6.18 (5.79); N, 5.66 (5.36). Melting point: 98.5 °C. Selected IR-max (KBr disc, cm^{-1}): 1629vs (C=O), 1542s and 1209m-s (C–N). Selected UV–Vis absorptions (EtOH): λ_{max}/nm (ε/dm^3 mol^{-1} cm^{-1}) 231 (45370), 307 (10920) and 420 (11010). ^1H NMR peaks (d_6-acetone): 14.98 (s, 1H, –O*H*), 9.36 (s, 1H, *H*C=N), 8.14-6.92 (m, 11H, Ar–*H*), 4.91 (s, 2H, –CH_2–).

[tolnapH]. Chemical analysis: found (required for $C_{18}H_{15}NO$) C, 82.05 (82.89); H, 5.77 (5.79); N, 5.46 (5.36). Melting point: 131 °C. Selected IR-max (KBr disc, cm^{-1}): 1619vs (C=O), 1543s and 1211m-s (C–N). Selected UV–Vis absorptions (EtOH): λ_{max}/nm (ε/dm^3 mol^{-1} cm^{-1}) 233 (47420), 318 (13810) and 440 (16370). ^1H NMR peaks (d_6-acetone): 15.73 (s, 1H, –O*H*), 9.68 (s, 1H, *H*C=N), 8.44-7.06 (m, 10H, Ar–*H*), 2.36 (s, 3H, –CH_3).

2.2. Preparation of the complexes and basic analytical data

2.2.1. General procedure

Ethanolic solutions of the corresponding zinc(II) salts and the appropriate Schiff-base in a 1:2 molar ratio were refluxed for several hours. The reaction mixture was then left to stand for two days. The compounds were filtered off, washed with ethanol and dried in vacuo. After standing for a few days, the filtrates **1**–**4**

Table 1
General and crystal data and summary of intensity data collection and structure refinement for **1**, **2**, **3** and **4**

Compound	**1**	**2**[a]	**3**[b]	**4**
Formula	$C_{36}H_{30}Cl_2N_2O_2Zn$	$C_{36}H_{30}Br_2N_2O_2Zn$	$C_{18}H_{15}INOZn_{0.5}$	$C_{36}H_{30}Cl_2N_2O_2Zn \cdot EtOH$
M_r	658.91	747.81	420.90	698.93
Colour and habit	colourless, prism	yellow, plate	yellow, needle	yellow, plate
Crystal system	monoclinic	monoclinic	monoclinic	triclinic
Space group	*Cc* (No. 9)	$P2_1/n$ (No. 14)	$P2/c$ (No. 13)	$P\bar{1}$ (No. 2)
Crystal dimensions (mm)	0.596×0.498×0.284	0.29×0.28×0.09	0.10×0.05×0.01	0.40×0.20×0.01
Temperature (K)	293	200	200	293
Unit cell parameters				
a (Å)	13.4309(15)	12.6821(1)	12.1548(3)	10.089(5)
b (Å)	19.7654(19)	38.3182(4)	8.6508(2)	11.571(3)
c (Å)	12.049(4)	13.1555(2)	17.7188(4)	16.318(5)
α (°)				108.758(19)
β (°)	93.33(2)	94.179(1)	92.452(2)	102.52(3)
γ (°)				92.76(2)
V (Å^3)	3193.2(12)	6375.99(13)	1861.40(8)	1746.5(12)
Z	4	8	4	2
D_{calc} (g cm^{-3})	1.371	1.558	1.502	1.329
μ (mm^{-1})	0.971	3.3	2.348	0.9
$F(000)$	1360	3008	824	
θ range for data collection (°)	3–30	3–55	4–54	2–27
h, k, l range	−18 to 18; 18 to 27; −11 to 16	−16 to16; −46 to 48; −17 to 17	−15 to 15; −11 to 10; −22 to 22	−12 to 12; −14 to 13; 0 to 20
Diffractometer	PW 1100 upgraded by Stoe	Nonius Kappa CCD area-detector diffractometer	Nonius Kappa CCD area-detector diffractometer	PW 1100 upgraded by Stoe
Scan type	ω	ω	ω	ω
Number of measured reflections	6321	16243	6713	7519
Number of independent reflections (R_{int})	6137 (0.031)	9606 (0.026)	3895 (0.024)	7519 (0.00)
Number of refined parameters	388 (two restraints)	792	199	421
Number of observed reflections $I \geqslant 2\sigma(I)$	3532	6507	2571	1812
Range of transmission factors minimum, maximum[c]	0.6117; 0.7776			
Crystal face indices, distances from centroid (mm)	(1 0 0; −1 0 0) 0.298 (1 0 −1; −1 0 1) 0.249 (0 1 0; 0 −1 0) 0.142			
R[d] wR[e] $I \geqslant \sigma(I)$]	0.043; 0.124	0.046; 0.089	0.047; 0.151	0.048; 0.1396
R, wR (all data)	0.094; 0.106	0.088; 0.078	0.078; 0.128	0.099; 0.257
g_1, g_2 in w[f]	0.0844; 0	0.0227; 6.8592	0.0805; 1.2948	0.0624; 0
Goodness-of-fit on F^2, S[g]	0.91	1.08	1.002	0.705
Maximum and minimum electron density (e Å^{-3})	0.44 and −0.28	−0.40 and 0.44	0.652 and −0.69	0.34 and −0.60
Flack parameter	0.006(14)			
Maximum Δ/σ	0.001	0.001	0.001	0.001
Extinction coefficent		0.00025(8)		

[a] The asymmetric unit contains two crystallographically independent molecules.
[b] The iodine atom lies on the twofold axis.
[c] Absorption correction type: numerical Gaussian for **1**; only scaling for **2** and **3**; not applied for **4**.
[d] $R = \sum ||F_o| - |F_c|| / \sum |F_o|$.
[e] $wR = \left[\sum (F_o^2 - F_c^2)^2 \Big/ \sum w(F_o^2)^2\right]^{1/2}$.
[f] $w = 1/[\sigma^2(F_o^2) + [(g_1P)^2 + g_2P]$ where $P = (F_o^2 + 2F_c^2)/3$.
[g] $S = \sum [w(F_o^2 - F_c^2)^2/(N_{obs} - N_{param})]^{1/2}$.

yielded crystals of good quality for X-ray diffraction experiment.

*[ZnCl$_2$(bznapH)$_2$] (**1**)*. Reaction time: 4 h. Colour: yellow-brownish Yield: 60%. *Anal.* Found (required for $C_{36}H_{30}Cl_2N_2O_2Zn$): C, 64.78 (65.62); H, 4.85 (4.59); N, 4.20 (4.25); Zn, 10.17 (9.92%). Selected IR-max (KBr disc, cm^{-1}): 1634vs (C=O), 1548s (C=C) and 1212m-s (C–N).

*[ZnBr$_2$(bznapH)$_2$] (**2**)*. Reaction time: 4 h. Colour: yellow. Yield: 76%. *Anal.* Found (required for $C_{36}H_{30}Br_2N_2O_2Zn$): C, 57.85 (57.82); H, 4.00 (4.04); N, 3.75 (3.75); Zn, 8.43 (8.74%). Selected IR-max (KBr discs, cm^{-1}): 1633vs (C=O), 1548s (C=C) and 1211m-s (C–N).

*[ZnI$_2$(bznapH)$_2$] (**3**)*. Reaction time: 6 h. Colour: yellow. Yield: 76%. *Anal.* Found (required for $C_{36}H_{30}I_2N_2O_2Zn$): C, 51.27 (51.36); H, 3.78 (3.59); N, 3.39 (3.33); Zn, 7.97 (7.77%). Selected IR-max (KBr discs, cm^{-1}): 1633vs (C=O), 1548s (C=C) and 1211m-s (C–N).

*[ZnCl$_2$(tolnapH)$_2$] (**4**)*. Reaction time: 4 h. Colour: yellow. Yield: 90%. *Anal.* Found (required for $C_{36}H_{30}Cl_2N_2O_2Zn$): C, 65.31 (65.62); H, 4.75 (4.59); N, 4.17 (4.25); Zn, 9.60 (9.92%). Selected IR-max (KBr discs, cm^{-1}): 1626vs (C=O), 1548s (C=C) and 1216m-s (C–N).

*[ZnBr$_2$(tolnapH)$_2$] (**5**)*. Reaction time: 1 h. Colour: yellow. Yield: 89%. *Anal.* Found (required for $C_{36}H_{30}Br_2N_2O_2Zn$): C, 57.76 (57.82); H, 4.26 (4.04); N, 3.87 (3.75); Zn, 8.53 (8.74%). Selected IR-max (KBr discs, cm^{-1}): 1626vs (C=O), 1548s (C=C) and 1217m-s (C–N).

*[ZnI$_2$(tolnapH)$_2$] (**6**)*. Reaction time: 4 h. Colour: yellow. Yield: 86%. *Anal.* Found (required for $C_{36}H_{30}I_2N_2O_2Zn$): C, 51.74 (51.36); H, 4.27 (3.59); N, 3.21 (3.33); Zn, 7.87 (7.77%). Selected IR-max (KBr discs, cm^{-1}): 1622vs (C=O), 1547s (C=C) and 1216m-s (C–N).

2.3. X-ray single crystal analyses of the compounds *1, 2, 3 and 4*

Relevant data on the summary of intensity data collection for the structures **1**–**4** are given in Table 1. Data collection for **1** and **4** were controlled by the STADI4 program [15]. Lattice constants were obtained by the least-squares refinement from the settings of 46 reflections ($10° \leqslant \theta \leqslant 16°$) for **1** and 21 reflections ($8° \leqslant \theta \leqslant 15°$) for **4**. 7383 reflections with $1° \leqslant \theta \leqslant 28°$ and 3409 reflections with $1° \leqslant \theta \leqslant 28°$ were used for unit cell refinement for structures **2** and **3**, respectively. Two sets of 311 frames and one of 167 frames were collected at the crystal-detector distance of 70 mm, 0.6° scans, 12 s per frame for structure **2** and two sets of 187 and 62 frames at the crystal-detector distance of 45 mm, 1.0° scans, 30 s per frame for structure **3**.

Reference reflections were monitored periodically showing no significant intensity decay for all four structures. The data were corrected for Lorentz-polarization by the X-RED [16] program for **1** and **4** and by DENZO-SMN [17] for **2** and **3**. The Gaussian absorption correction based on the crystal dimensions by the X-RED [16] program was performed for **1**, but for **2** and **3** only scaling based on all symmetrically dependent reflections were applied.

The structures were solved by direct methods implemented in the SHELXS [18] program. The applied refinement procedure based on the F^2 values against all reflections included the anisotropic model for all non-H atoms using the SHELXL [19] program. The hydrogen atoms were generated at ideal geometrical positions [Csp^2–H 0.93, Csp^3–H 0.97 Å, Csp^3–H 0.96 Å for phenyl, methylene and methyl carbon atoms with $U_{iso}(H) = 1.2$ or 1.5 $U_{eq}(C)$] and refined applying the riding model. In the structure of compound **1** the hydrogen atoms belonging to the nitrogen atoms of the C=N group were found, but finally refined at idealized stereochemical positions (N–H 0.86 Å) by the riding model procedure. Structurally identical hydrogen atoms in **2** and **3** were found in the electron density difference Fourier maps and refined freely [N1–H1N 0.74(4) Å and N2–H2N 0.83(4) Å in **2** and N1–H1N 0.64(4) Å in **3**].

In the structure of compound **4**, due to the poorer quality X-ray diffraction data (data-to-parameter ratio is less than 4.5), the positional disorder of the atoms C1, C2 and O3 of the ethanol molecule could not be refined, thus hydrogen atoms belonging to C1, C2 and O3 were not modelled. The hydrogen atom which belongs to the N2 atom is found in the electron density difference Fourier map and is refined freely, but the hydrogen atom which belongs to N1 atom could not be found and it was generated at an ideal position and refined by the riding model procedure (N–H 0.86 Å). The standard deviations of the molecular geometry of **4** are significantly larger than in **1**, **2** and **3** making the comparison of its geometry to the other ones impossible. Only the main stereochemical features of the solid state structure of **4** could be obtained, but not the fine structural details. Graphical work has been performed by the program PLATON-98 [20].

3. Results and discussion

3.1. General aspects

The reactions of zinc(II) halides with *N*-benzyl-2-oxo-1-naphthylideneamine and *N*-*p*-tolyl-2-oxo-1-naphthylideneamine in ethanolic solution, give complexes of the general formula [ZnX$_2$(HL)$_2$] (X = Cl, Br, I) (Scheme 2). The isolated compounds are stable in air at room temperature, but do not exist in DMSO, DMF, pyridine, chloroform, acetone or ethanol solutions, i.e. they undergo decomposition, which is revealed by ^{1}H NMR and UV spectra. Compound **4** crystallizes as an ethanolic solvate, but its crystals, losing the ethanol, slowly decompose into the unsolvated compound at room temperature.

$$ZnX_2 + 2LH \underset{\text{reflux}}{\overset{\text{EtOH}}{\rightleftharpoons}} ZnX_2(LH)_2$$

LH = *N*-benzyl-2-oxo-1-naphthylideneamine (bznapH)
N-*p*-tolyl-2-oxo-1-naphthylideneamine (tolnapH)

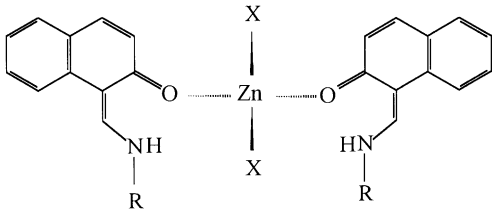

$ZnX_2(bznapH)_2$ [X = Cl (**1**), Br (**2**), I (**3**)]
$ZnX_2(tolnapH)_2$ [X = Cl (**4**), Br (**5**), I (**6**)]

Scheme 2.

3.2. Spectroscopic studies

The IR spectra of the free Schiff-bases and compounds **1**–**6** are quite similar in the "finger print" region. The common feature of all these spectra is a very weak and broad stretching band in the 3000–1800 cm^{-1} region that can be assigned as the ν(NH) stretching band. The very strong absorption band in the region of 1630–1610 cm^{-1}, is due to the C=O stretching vibrations and indicates the presence of the keto-amine tautomeric form of the Schiff-base, both in the free ligand and in the complexes. Furthermore, the strong absorption bands in the region of 1550–1540 cm^{-1} that can be assigned to the C=C stretching accompanied with that in the region of 1220–1210 cm^{-1} that suggests C=N stretching, confirm the existence of the keto-amine tautomeric form of the Schiff-base [21–23], suggesting metal-to-ligand coordination via the carbonyl oxygen atom.

The UV–Vis absorption spectra measured for the absolute ethanolic solution of the zinc complexes (**1**–**6**) suggest that they decompose when dissolved. Such a conclusion can be drawn because of the similarity of the spectra of the free ligands with those measured for the solution of the complexes. Moreover, that is quite consistent with the our previous results obtained for the mercury(II) halide adducts with the same ligand [1]. The spectra reveal a predominance of the keto-amine tautomeric form of both ligands [24,25].

We also measured the ^{1}H NMR spectra in acetone. The NMR measurements show that complexes **1**–**6** are not stable in acetone either. This conclusion was drawn from the fact that there are no significant changes in the ^{1}H NMR chemical shifts of the dissolved compounds in comparison with those of the free ligands. In the ^{1}H NMR spectrum of bznapH the signals of azomethine and hydroxyl protons appear at 9.36 and 14.98 ppm, while in tolnapH they appear at 9.68 and 15.73 ppm, respectively. The signals corresponding to Ar–*H* appear in the region 6.9–8.2 ppm and 7.0–8.5 ppm for bznapH and tolnapH, respectively. At 4.91 ppm the signal corresponding to the two methylene protons for bznapH have been observed and that at 2.36 ppm corresponds to the three methyl protons for tolnapH [8,26,27].

3.3. X-ray structural studies

The structural study of the four zinc complexes **1**–**4** was undertaken in order to establish the general mode of ligating of this type of Schiff-base, dependence of the zinc coordination sphere geometry on the type of zinc halide (chloride, bromide and iodide) and to compare results with the 1:1 mercury halide adducts of the same Schiff-base which have been previously structurally characterized by us [1].

In the $ZnX_2 \cdot 2LH$ adducts or in the $[ZnX_2(LH)_2]$ complexes zinc retains X^- ions in the coordination sphere and thus neutral LH Schiff-base completes the coordination sphere bonding monodentately by either oxygen or nitrogen ligating centre, but not with both donor atoms. Contrary to the ZnL_2 complexes where the Schiff-base is bound in an anionic form, the intramolecular hydrogen bond of the O–H···N or N–H···O type is preserved in the adducts or in the $[ZnX_2(LH)_2]$ type of complexes. Usually, the type of intramolecular hydrogen bond found in the adduct or in the $[ZnX_2(LH)_2]$ complexes and non-coordinated Schiff-base is different, thus leading to the change of the tautomeric form of the Schiff-base ligand upon complexation [5]. Adducts of the type $ZnX_2 \cdot 2LH$ are only known for salicylaldimine Schiff-bases and according to the Cambridge Structural Database [6a,6b] there are three such adducts: *N*-isopropylsalicylaldimine with ZnI_2 (refcode: VATROX) [28], dichloro-bis(2-(*o*-tolyliminomethyl)phenolato-O)-zinc(II) (refcode: XAXVIB) [29] and bis(1-anilinomethylidene-2-oxo-1H,2H-naphthalene-chloro)-zinc (refcode: VIRVUN) [30]. The common feature of these three adducts is stronger Zn–X bonds (2.564(1)–2.587(1) Å range for the Zn–I bond in VATROX, 2.2401(7) Å for the Zn–Cl bond in XAXVIB and 2.203(7), 2.226(7), 2.201(7) and 2.217(8) Å for the Zn–Cl bonds in VIRVUN) and weaker Zn–O bonds being in the range from 1.955 Å (mean value) in VATROX to 2.00(1) Å in VIRVUN. These Zn–O bond distances are longer than in the chelate ZnL_2 complexes (the average Zn–O bond distance value in the ZnL_2 complexes with salicylaldimine Schiff bases is 1.926 Å). This elongation is the consequence of the Schiff-base ligation in the neutral form in the adducts and the participation of N,O-donor atoms in the intramolecular hydrogen bond formation. The length of the N–H···O intramolecular hydrogen bond varies from 2.499 Å in VIRVUN to 2.636 Å in VATROX.

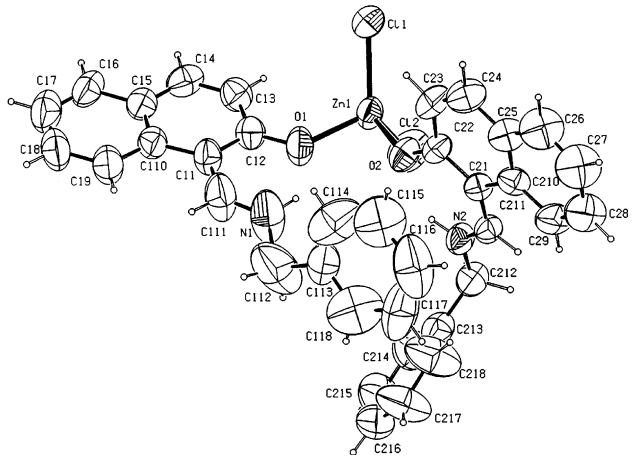

Fig. 1. ORTEP drawing of $ZnCl_2(bznapH)_2$ (**1**) with the atom numbering scheme. The thermal ellipsoids are at the 50% probability level.

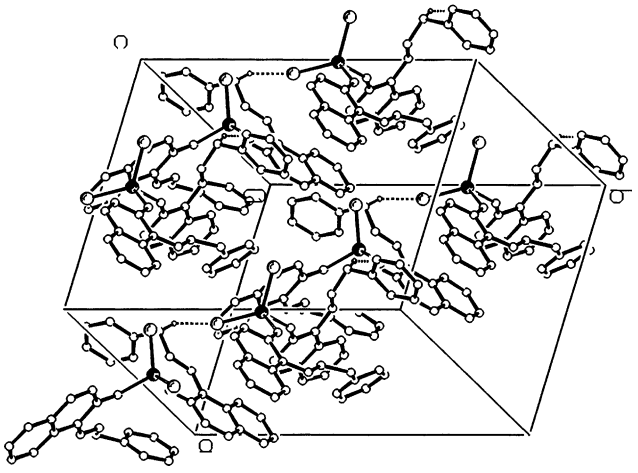

Fig. 2. The crystal packing of $ZnCl_2(bznapH)_2$ (**1**) showing the intermolecular C212–H21A···Cl1 hydrogen bonds by dashed lines that link molecules into endless chains parallel to the *y*-axis. The other hydrogen atoms are omitted for clarity.

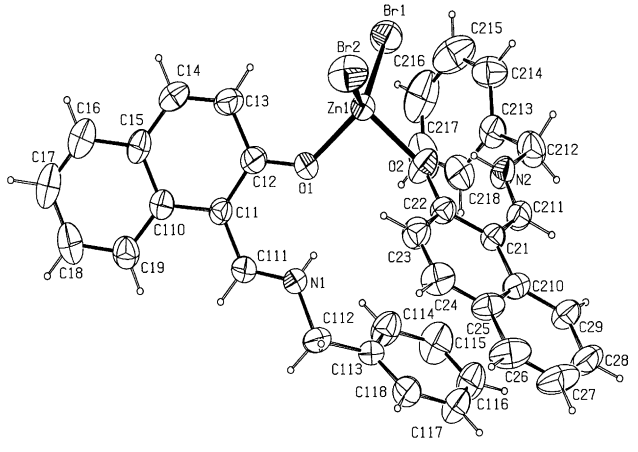

Fig. 3. ORTEP drawing of $ZnBr_2(bznapH)_2$ (**2**) with atom the numbering scheme. The thermal ellipsoids are at the 50% probability level. There are two crystallographically independent molecules within the asymmetric unit. Only one is shown for clarity.

The crystal structures of the two isostructural adducts, $HgX_2(bznapH)$ (X = Cl, Br) revealed dimers formed by bridging halogen atoms and generated a 2 + 2 effective coordination sphere of the mercury atoms [1]. The dimers are joined only by the van der Waals contacts.

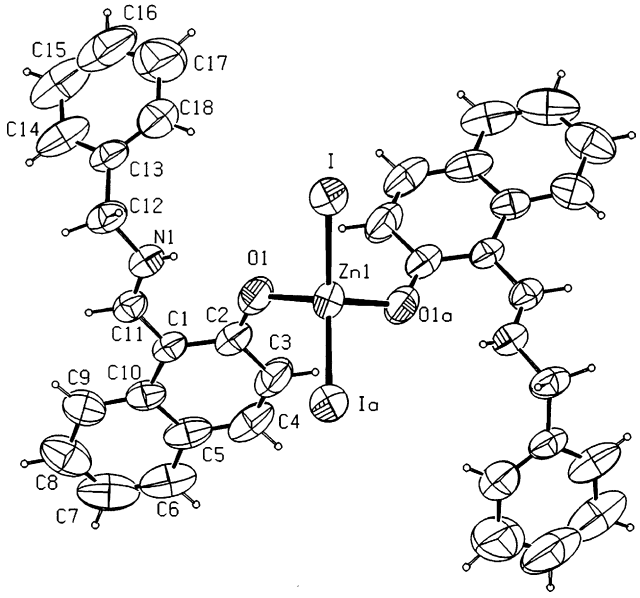

Fig. 4. ORTEP drawing of $ZnI_2(bznapH)_2$ (**3**) with the atom numbering scheme. The thermal ellipsoids are at the 50% probability level. Symmetry code: (a): $1-x, y, 3/2-z$.

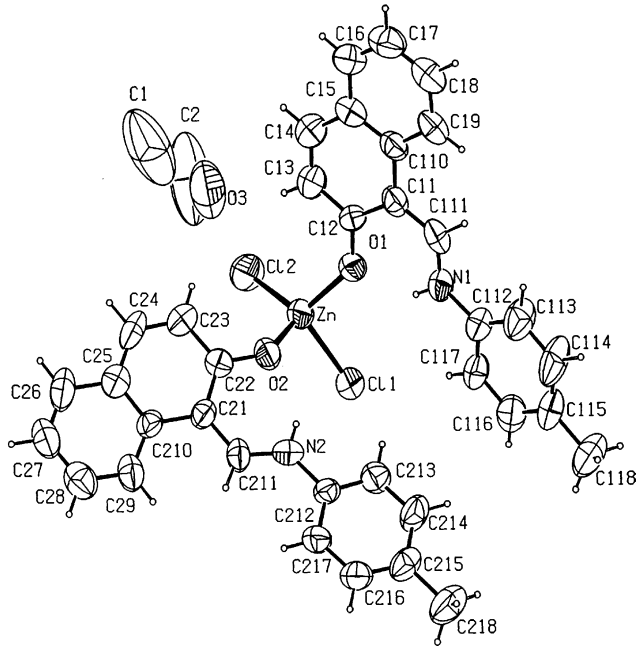

Fig. 5. ORTEP drawing of $ZnCl_2(tolnapH)_2 \cdot EtOH$ (**4**) with the atom numbering scheme. The thermal ellipsoids are at the 50% probability level.

In the zinc complexes **1**–**4** the common feature is the distorted tetrahedral coordination sphere of the zinc atom formed by two halogen atoms [Zn1–Cl1 2.215(2) and Zn1–Cl2 2.229(2) Å in **1**; Zn1–Br1 2.344(1), Zn1–Br2 2.356(1), Zn2–Br3 2.371(1) and Zn2–Br4 2.355(1) Å in **2** and Zn1–I1 2.564(1) Å in **3**, Zn–Cl1 2.255 (2) and Zn–Cl2 2.204 (2) in **4**] and two oxygen atoms from two neutral monodentate Schiff bases [Zn1–O1 1.968(4) and Zn1–O2 1.982(3) Å in **1**, Zn1–O1 1.960(3), Zn1–O2 1.975(3), Zn2-O3 1.957(3) and Zn2–O4 1.952(3) Å in **2**, Zn1–O1 1.968(4) Å in **3**, Zn–O1 1.976(3) and Zn–O2 2.002(3) Å in **4**] (Figs. 1, 3, 4 5). The Zn–O bond distance values are comparable with those found in zinc complexes with salicylaldimines (VATROX, XAXVIB, VIRVUN) and are longer than in the chelate complexes.

In the structures of complexes **1**–**4** the X1–Zn–X2 bond angles are the most deformed from ideal tetrahedral geometry. The degree of deformation is most pronounced in the iodo derivative [X1–Zn–X2 bond angles values are 118.81(7)° in **1**, 119.49(3)° in **2**, 123.49(4)° in **3** and 120.94(7)° in **4**].

The dihedral angles between planes of the naphthalene rings and phenyl rings of the *N*-substituents (Table 3) indicate non-planarity of the ligands in the **1**–**3** complexes, while in **4** the corresponding dihedral angles are remarkably smaller, but still the molecules are not planar [20.3(2)° and 22.2(3)° in **4** vs. the range from 56.2(5)° to 81.7(2)° for **1**, **2** and **3**]. The tendency of a stacking arrangement of planar tolnapH molecules is observed in the structure of $HgCl_2$(tolnapH) [1] causing the needle-shaped crystal morphology.

In **2**, the rings 1 and 2 are oriented to each other by approx. 70°, while other rings (3–8) do not deviate significantly from planarity (Table 3).

The molecules are mutually connected only by van der Waals interactions, except in **1** where weak intermolecular hydrogen bonds of the C–H···Cl type link molecules into endless chains parallel to the *y*-axis.

Table 2
Relevant interatomic distances (Å) and angles (°) for the compounds **1**, **2**, **3** and **4**

	1	**2**	**3**	**4**
Interatomic distances				
Zn1–X1[a]	2.2149(15)	2.3435(7)	2.5639(6)	2.255(2)
Zn1–X2[a]	2.2292(18)	2.3558(8)		2.204(2)
Zn2–X3[a]		2.3708(8)		
Zn2–X4[a]		2.3551(8)		
Zn1–O1	1.968(4)	1.960(3)	1.968(4)	1.976(4)
Zn1–O2	1.982(3)	1.975(3)		2.002(3)
Zn2–O3		1.957(3)		
Zn2–O4		1.952(3)		
O1–C12[b]	1.283(6)	1.305(5)	1.298(6)	1.310(6)
O2–C22	1.285(5)	1.298(5)		1.319(7)
O3–C32		1.301(5)		
O4–C42		1.294(5)		
N1–C111[c]	1.294(10)	1.298(6)	1.280(6)	1.307(8)
N2–C211	1.299(5)	1.291(5)		1.327(7)
N3–C311		1.300(6)		
N4–C411		1.302(6)		
Bond angles				
X1–Zn1–X2[a,d]	118.81(7)	119.49(3)	123.49(4)	120.94(7)
X1–Zn1–O1	112.37(12)	116.03(9)	103.06(11)	99.22(13)
X1–Zn1–O2[e]	117.59(10)	100.65(8)	108.25(11)	98.34(10)
X2–Zn1–O1[f]	112.42(13)	109.31(9)	110.59(15)	116.32(11)
X2–Zn1–O2	101.01(9)	114.53(10)		114.06(12)
O1–Zn1–O2	90.93(14)	93.61(12)		105.18(15)
Br3–Zn2–Br4		116.92(3)		
Br3–Zn2–O3		119.66(9)		
Br3–Zn2–O4		96.54(11)		
Br4–Zn2–O3		107.00(9)		
Br4–Zn2–O4		120.70(10)		
O3–Zn2–O4		94.37(14)		

[a] X1 = Cl1 in **1**, Br1 in **2** and I in **3**;X2 = Cl2 in **1** and Br2 in **2**; X3 = Br3 in **2**; X4 = Br4 in **2**.
[b] O1–C2 in **3**.
[c] N1–C11 in **3**.
[d] I–Zn–I^{i} in **3** (i = $1-x, y, 3/2-z$).
[e] I–Zn–O1^{i} in **3** (i = $1-x, y, 3/2-z$).
[f] O1–Zn–O1^{i} in **3** (i = $1-x, y, 3/2-z$).

Table 3
Dihedral angles between planes defined by the naphtahlene and phenyl rings atoms in **1**, **2**, **3** and **4**

Number of plane	Plane defined by atoms	Dihedral angle (°)
*Compound **1***		
1	C11–C110	1,2 56.2(5)
2	C113–C118	
3	C21–C210	3,4 62.0(5)
4	C213–C218	
*Compound **2***		
1	C11–C110	1,2 70.1(2)
2	C113–C118	
3	C21–C210	3,4 81.7(2)
4	C213–C218	
5	C31–C310	5,6 80.5(2)
6	C313–C318	
7	C41–C410	7,8 80.3(2)
8	C413–C418	
*Compound **3***		
1	C1–C10	1,2 70.5(4)
2	C13–C18	
*Compound **4***		
1	C11–C110	1,2 20.3(2)
2	C112–C116	
3	C21–C210	3,4 22.2(3)
4	C212–C216	

(Table 4, Fig. 2.) [31,32]. This hydrogen bond does not influence the Zn–Cl1 bond distance since it is comparable with the Zn–Cl2 bond distance (atom Cl2 does not participate in hydrogen bond formation) [Zn1–Cl1 2.215(2) and Zn1–Cl2 2.229(2) Å in **1**].

The significant difference of the Zn–Cl1 and Zn–Cl2 bond distances in **4** (Table 2) can indicate the participation of the Cl1 atom in the O–H···Cl intermolecular hydrogen bond formation with the O3 atom of an ethanol molecule (Cl1···O3 distance is 3.266(7) Å).

So, the conclusion is that the geometry of the zinc coordination sphere in the three complexes **1**–**3** is not affected by the crystal packing forces (i.e. intermolecular hydrogen bonds). Therefore, the bond distances and angles values within the coordination sphere are mutually comparable.

3.4. Description of the ligands

The bznapH and tolnapH Schiff-bases exist in the keto-amine tautomeric form in all four complexes (**1**–**4**) revealing the N–H···O resonance assisted intramolecular hydrogen bond (RAHB) [range for the N···O distance is 2.565(5)–2.599(5) Å] (Table 4). The same tautomeric form is found in the crystal structures of the analogous 1:1 adducts with mercury(II) halides [1].

The C=N bond distance values are in the range from 1.280(6) Å in **3** to 1.299(5) Å in **1**. The C–O bond distance values (1.283(6)–1.301(5) Å) are shortened in relation to the Csp^2–OH bond distance value in phenols (1.36 Å) [33]. These two bonds, C=N and Csp–O, are the most sensitive indicators of the proton location, on the oxygen or nitrogen site, i.e. on the type of the tautomer. In the mercury analogues the intramolecular hydrogen bond N–H···O is 2.58(1) Å in the chloro derivative and 2.59(1) Å in the bromo derivative.

The geometry of the ligands in the complexes **1**–**4** are comparable with the similar non-coordinated naphthaldimines in the keto-amine form, indicating the labile bounding of the ligands with the zinc centre.

3.5. Thermal analysis

The samples of the free ligands, bznapH and tolnapH, as well as the zinc complexes **1**–**6** were heated from room temperature up to 700 °C.

Table 4
Hydrogen bond geometry (Å, °) in **1**, **2** and **3**

D–H···A	*d*(D–H)	*d*(H···A)	∠DHA	*d*(D···A)
1				
N1–H1···O1	0.86	1.984	127	2.591(8)
N2–H2···O2	0.86	1.938	133	2.599(5)
C212–H21A ···Cl1^{i}	0.97	2.800	157	3.710(5)
2				
N1–H1N···O1	0.74(4)	1.99(5)	137(5)	2.576(5)
N2–H2N···O2	0.83(4)	1.91(4)	135(4)	2.565(5)
N3–H3N···O3	0.90(5)	1.89(4)	132(4)	2.589(5)
N4–H4N···O4	0.69(4)	2.05(5)	133(5)	2.574(6)
3				
N1–H1N··· O1	0.64(4)	2.13(4)	128(5)	2.571(6)
4				
N1–H1···O1	0.86	1.856	2.552(6)	137
N2–H2···O2	0.79(3)	1.95(3)	2.602(6)	141(4)

Symmetry code (i): $-1/2+x, -1/2-y, -1/2+z$.

Table 5
Thermoanalytical data for bznapH and tolnapH and its Zn(II) complexes

Compound	Process	Temperature (°C)	Accumulated weight loss (%)	
			Found	Calculated
BznapH	Melting (endo)	98.50		
	Degradation (endo)	150–400	88	100
	Residue	400	12	
TolnapH	Melting (endo)	139.22		
	Degradation (endo)	100–300	100	100
$ZnCl_2(bznapH)_2$ (**1**)	Degradation of ligand (endo)	200–380	70.4	79.3
	Elimination of Cl (exo)	340–550	9.83	10.77
	Residue	550	19.77	9.93
$ZnBr_2(bznapH)_2$ (**2**)	Degradation of ligand (endo)	200–375	61.6	69.86
	Elimination of Br (exo)	330–600	20.37	21.64
	Residue	600	18.03	8.05
$ZnI_2(bznapH)_2$ (**3**)	Degradation of ligand (endo)	200–365	54.56	62.05
	Elimination of Br (exo)	325–650	29.43	30.17
	Residue	650	16.01	7.78
$ZnCl_2(tolnapH)_2$ (**4**)	Melting (endo)	211.82		
	Degradation of ligand (endo)	200–310	31.54	39.65
	Degradation of ligand (endo)	310–365	31.35	39.65
	Elimination of Cl (exo)	365–500	9.21	10.77
	Residue	500	27.9	9.93
$ZnBr_2(tolnapH)_2$ (**5**)	Degradation of ligand (endo)	200–300	26.32	34.93
	Degradation of ligand (endo)	300–370	27.76	34.93
	Elimination of Br (exo)	370–600	20.54	21.64
	Residue	600	25.38	8.75
$ZnI_2(tolnapH)_2$ (**6**)	Degradation of ligand (endo)	200–305	23.21	31.03
	Degradation of ligand (endo)	305–385	24.27	31.03
	Elimination of I (exo)	385–640	28.96	30.17
	Residue	640	23.56	7.78

The DTA curves of the complexes **1**–**3** were dominated by the typical endothermic minima, which correspond to the melting points (Table 5). Degradation of bznapH (ca. 88%) was observed in the range of 200–400 °C and was characterized by the endothermic peak in the DTA-curve. On heating the samples **1**–**3** up to 600 °C elimination of halogen occurred which was determined by an exothermic peak but still ca. 20% of the initial mass of the samples was left as a mixture of carbonated residue and zinc.

Thermal analysis of the complexes **4**–**6** showed that only the zinc chloride complex **4** melts, while **5** and **6** initially underwent degradation over two consecutive endothermic processes. Elimination of halogen was represented by the exothermic peak. As for **1**–**3**, there was also ca. 25% of the initial mass left in the sample pan.

4. Supplementary material

Atomic coordinates and equivalent isotropic displacement parameters, calculated hydrogen atom parameters, anisotropic thermal parameters and bond lengths and angles have been deposited and allocated deposition numbers at the Cambridge Crystallographic Data Centre (CCDC Nos. 198366–198369 for structures **1**, **2**, **3** and **4**, respectively). Copies of this information may be obtained free of charge from The Director, CCDC, 12 Union Road, Cambridge CB2 1EZ, UK (fax: +44-1223-336033; email: deposit@ccdc.caom.ac.uk or www.ccdc.com.ac.uk). All structural factor tables are available from the authors upon request.

Acknowledgements

This research was supported by the Ministry of Science and Technology of the Republic of Croatia (Grant Nos. 0119633, 0119632 and 01920202). The crystallographic data for structures **2** and **3** were collected on the KappaCCD Nonius diffractometer in the Laboratory of Inorganic Chemistry, Faculty of Chemistry and Chemical Technology, University of Ljubljana, Slovenia. We acknowledge with thanks the financial contribution of the Ministry of Education, Science and Sport, Republic of Slovenia through grants X-2000 and PO-511-103,

which thus made the purchase of the apparatus possible. We thank the INA d.d. Zagreb, Division of Strategic Development, Research and Investment for allowing us to record the UV–Vis spectra on their instrument.

References

[1] Z. Popović, V. Roje, G. Pavlović, D. Matković-Čalogović, M. Rajić, G. Giester, Inorg. Chim. Acta 332 (2001) 65.
[2] R.H. Prince, Zinc and Cadmium, in: G. Wilkinson (Ed.), Comprehensive Coordination Chemistry, vol. 5, Pergamon Press, Oxford, 1987, p. 1001.
[3] J. Costamagna, J. Vargas, R. Lattore, A. Alvarado, G. Mena, Coord. Chem. Rev. 119 (1992) 67.
[4] W. Kaim, B. Schwederski, Bioinorganic Chemistry: Inorganic Elements in the Chemistry of Life, Wiley, Chichester, 1994.
[5] A.D. Garniovskii, A.L. Nivorozhkin, V.I. Minkin, Coord. Chem. Rev. 126 (1993) 1.
[6] (a) Cambridge Structural Database, V5.24, Cambridge Crystallographic Data Centre, 12 Union Road, Cambridge, England, November, 2002
(b) F.H. Allen, Acta Crystallogr., Sect. B 58 (2002) 380.
[7] J. Ondráček, B. Kratochvíl, V. Haber, Collect. Czech. Chem. Commun. 59 (1994) 1809.
[8] T. Hökelek, Z. Kl, M. Iklan, M. Toy, J. Mol. Struct. 523 (2000) 61.
[9] B.B. Mahapatra, M.K. Raval, A.K. Behera, A.K. Das, J. Indian, Chem. Soc. 72 (1995) 161.
[10] M. Gavranić, B. Kaitner, E. Meštrović, J. Chem. Crystallogr. 26 (1996) 23.
[11] B. Kaitner, G. Pavlović, Acta Crystallogr., Sect. C 52 (1996) 2573.
[12] G.O. Dudek, J. Am. Chem. Soc. 85 (1963) 694.
[13] B. Kaitner, E. Meštrović, G. Pavlović, J. Chem. Crystallogr. 28 (1998) 77.
[14] G. Pavlović, Ph.D. Thesis, University of Zagreb, 1998 (abstract in English).
[15] Stoe & Cie, STADI4, Diffractometer Control Program for Windows, Darmstadt, Germany, 1995.
[16] Stoe & Cie, X-RED, Data Reduction Program for Windows, Darmstadt, Germany, 1995.
[17] Z. Otwinowski, W. Minor, in: C.W. Carter Jr., R.M. Sweet (Eds.), Methods in Enzymology, Macromolecular Crystallography – Part A, vol. 276, Academic Press, London, 1997, p. 307.
[18] G.M. Sheldrick, SHELXS-97: Program for the Solutions of Crystal Structures, University of Göttingen, Germany, 1997.
[19] G.M. Sheldrick, SHELXL-97: Program for the Refinement of Crystal Structures, University of Göttingen, Germany, 1997.
[20] A.L. Spek, Acta Crystallogr., Sect. A 46 (1990) 34.
[21] S.R. Salman, N.A.I. Saleh, Spectrosc. Lett. 30 (1997) 1289.
[22] J.W. Ledbetter Jr., J. Phys. Chem. 81 (1977) 54.
[23] T. Yuzawa, H. Takahashi, H. Hamaguchi, Chem. Phys. Lett. 202 (1993) 221.
[24] L. Antonov, W.M.F. Fabian, D. Nedeltcheva, F.S. Kamounah, J. Chem. Soc., Perkin Trans. 2 (2000) 1173.
[25] P. Nagy, R. Herzfeld, Spectrosc. Lett. 31 (1998) 221.
[26] J.-C. Zhuo, Magn. Res. Chem. 37 (1999) 259.
[27] H. Ünver, Spectrosc. Lett. 34 (2001) 783.
[28] F.A. Bottino, P. Finocchiaro, E. Libertini, G. Mattern, Z. Kristallogr. 187 (1989) 71.
[29] D. Ülkü, C. Arc, M.N. Tahir, O. Atakol, Acta Crystallogr., Sect. C 56 (2000) 1298.
[30] V.S. Sergienko, A.E. Mistryukov, V.V. Litvinov, M.I. Knyazhanskii, A.D. Garnovskii, M.A. Porai-Koshits, Koord. Khim. 16 (1990) 168.
[31] R. Taylor, O. Kennard, J. Am. Chem. Soc. 104 (1982) 5063.
[32] G.R. Desiraju, T. Steiner, The Weak Hydrogen Bond, IUCr, Oxford Science Publications, Oxford, 2001.
[33] F.H. Allen, O. Kennard, D.G. Watson, L. Brammer, A.G. Orpen, R. Taylor, J. Chem. Soc. Perkin Trans. II (1987) S1.

Available online at www.sciencedirect.com
SCIENCE DIRECT®
Polyhedron 23 (2004) 1303–1308
POLYHEDRON
www.elsevier.com/locate/poly

Crystal structure, magnetic and spectral properties of tetrakis(2-nitrobenzoato)di(aqua)dicopper(II) dihydrate

Petra Stachová [a,*], Dušan Valigura [a], Marián Koman [a], Milan Melník [a], Maria Korabik [b], Jerzy Mroziński [b], Tadeusz Glowiak [b]

[a] Department of Inorganic Chemistry, Slovak Technical University, Radlinskeho 9, 812 37 Bratislava, Slovakia
[b] Faculty of Chemistry, University of Wroclaw, 50-383 Wroclaw, Poland

Received 2 October 2003; accepted 11 December 2003
Available online 22 April 2004

Abstract

The synthesis, characterization and structure of $[Cu_2(2\text{-}NO_2bz)_4(H_2O)_2]\cdot 2H_2O$ are reported. The structure is centrosymmetric and the copper(II) atom has a square–pyramidal coordination by four oxygen atoms of carboxylate groups with a mean Cu–O distance of 1.964(1) Å which creates a plane, and the apical position is occupied by a water molecule at a Cu–OH_2 bond distance of 2.111(1) Å.

The electronic and infrared spectra exhibit typical features consistent with the observed structure. The EPR spectrum of a microcrystalline sample is consistent with a dimeric structure with the Hamiltonian parameters $g_\perp = 2.018$, $g_\parallel = 2.315$, $D = 0.343$ and $E = 0.003$ cm^{-1}. The magnetic susceptibility measurements of a polycrystalline sample proved the dimeric structure and gives at 300 K an effective magnetic moment of 1.33 BM and at 70 K $\mu_{eff} \cong 0.04$ BM. The magnetic susceptibility data best fitting to a Bleaney–Bowers equation gives $2J = -332$ cm^{-1}.
© 2004 Elsevier Ltd. All rights reserved.

Keywords: Copper; Crystal structure; Dimer; Spectral properties; Magnetic properties

1. Introduction

Copper(II) carboxylates including copper(II) benzoates have been extensively studied from different points of view because the carboxylato anions exhibit different bonding modes that are related to their properties, e.g. basicity of the anion, position of substituent on the aromatic ring [1–3]. A bulky benzene ring substituent in an *ortho* position to the carboxylato group is believed to prefer the dimeric copper(II) benzoate structure [4] and that was the reason of their wider structural study [5–21]. In general, copper(II) carboxylates exhibit a dimeric paddle-wheel cage structure. Some 250 X-ray crystal structures containing the $Cu_2(OOCR)_4$ core can be found in the Cambridge Structural Database, of which about 200 are of the type $[Cu_2(OOCR)_4L_2]$, where L is an apical ligand with an oxygen or a nitrogen donor atom [3].

In this paper we present our results on the structural, spectroscopic and magnetic properties of the dimeric $[Cu_2(2\text{-}NO_2bz)_4(H_2O)_2]\cdot 2H_2O$ (2-NO_2bz = 2-nitrobenzoate anion). These studies are important to establish the structure of the active components of pharmaceutical preparations.

2. Experimental

2.1. Preparation of the complex

Green crystals of $[Cu_2(2\text{-}NO_2bz)_4(H_2O)_2]\cdot 2H_2O$ were prepared by the reaction of an aqueous solution of copper(II) acetate (1 mmol) with 2-nitrobenzoic acid (2 mmol). The blue–green solution obtained after the

* Corresponding author. Tel.: +421-2-5932-5611; fax: +421-2-5249-3198.
E-mail address: stachovap@chtf.stuba.sk (P. Stachová).

0277-5387/$ - see front matter © 2004 Elsevier Ltd. All rights reserved.
doi:10.1016/j.poly.2003.12.025

reaction was left for crystallization at room temperature (about 20 days) and green crystals were filtered off. *Anal.* Calc. for $C_{14}H_{10}N_2O_9Cu$: Cu, 14.71; C, 38.94; H, 2.80; N, 6.49. Found: Cu, 14.38; C, 39.57; H, 2.76; N, 6.40%.

2.2. Spectral analysis

The electronic spectrum (190–1100 nm) of the complex was measured in Nujol suspension with a SPECORD 200 (Carl Zeiss Jena) spectrophotometer, and the infrared spectrum in the region of 4000–100 cm^{-1} was measured with a Nicolet MAGNA 750 IR spectrometer using both KBr pellet and Nujol suspension techniques for the 4000–400 cm^{-1} region and a polyethylene pellet for 400–100 cm^{-1}.

An EPR spectrum of a powdered sample was obtained using an EPR Bruker ER 200E-SRC at room temperature.

2.3. Magnetic susceptibility measurements

Magnetic susceptibility measurements in the temperature range of 1.9–300 K were carried out on powdered samples of the complex, at the magnetic field 5 kG, using a Quantum Design SQUID Magnetometer (type MPMS-XL5). Corrections for diamagnetism of the constituting atoms were calculated using Pascal constants [1,2] and the value of 60×10^{-6} $cm^3\,mol^{-1}$ was used as the temperature-independent paramagnetism of the copper(II) ion. The effective magnetic moments were calculated from the expression

$$\mu_{\text{eff}} = 2.83\sqrt{\chi_{\text{M}}^{\text{corr}} \cdot T}\ (\text{BM}).$$

2.4. Analytical methods

The copper content was determined by electrolysis of a water solution obtained by the sample mineralization with a mixture of sulfuric acid and potassium peroxodisulfate. Carbon, hydrogen and nitrogen analysis were performed on a Carlo Erba instrument.

2.5. X-ray measurement

Data collection and cell refinement of presented complex were carried out using a Kuma KM4 CCD diffractometer [22]. Intensity data were corrected for Lorenz and polarization factors. The structure was solved by the heavy atom method with SHELX 86 [23], and subsequent Fourier synthesis using SHELXL 93 [24]. Geometrical analysis was performed using SHELXL 97 [25] and the structure was drawn using the ORTEP-3 for Windows program [26]. Final crystal data and structure refinement parameters are given in Table 1.

Table 1
Crystal data and structure refinement for $[Cu_2(2\text{-}NO_2bz)_4(H_2O)_2]\cdot 2H_2O$

Identification code	tg24a
Empirical formula	$C_{14}H_{12}N_2O_{10}Cu$
Formula weight	431.80
Temperature (K)	293(2)
Wavelength (Å)	0.71073
Crystal system	monoclinic
Space group	$C2/c$
Unit cell dimensions	
a (Å)	14.998(3)
b (Å)	10.800(2)
c (Å)	19.723(4)
β (°)	98.33(3)
V (Å^3)	3161.0(11)
Z	8
$D_{\text{calc.}}$ (Mg/m^3)	1.782
Absorption coefficient (mm^{-1})	1.446
$F(0\,0\,0)$	1752
θ Range for data collection (°)	3.68–28.72
Index ranges	$-19 < h < 19$, $-13 < k < 14$, $-25 < l < 25$
Reflection collected	9919
Independent reflections	3716
Refinement method	full matrix least squares on F^2
Data/restrains/parameters	3716/0/244
Goodness-of-fit on F^2	0.979
Final R indices [$I > 2\sigma I$)]	$R_1 = 0.0279$, $wR_2 = 0.0628$
R indices (all data)	$R_1 = 0.0316$, $wR_2 = 0.0647$
Largest difference peak and hole (e Å^{-3})	0.41, −0.42

3. Results and discussion

3.1. Spectroscopic properties

All the typical features of the IR spectrum of the compound are clearly compatible with the structural characteristics of $[Cu_2(2\text{-}NO_2bz)_4(H_2O)_2]\cdot 2H_2O$. The IR spectrum of the title compound shows a strong and broad absorption band in the area 3620–3300 cm^{-1}, and the deformation band at 1637 cm^{-1} belongs to water in the crystal structure. Carboxylate stretching frequencies were found, with $\nu_{as}(COO^-)$ at 1626 cm^{-1} and $\nu_s(COO^-)$ at 1413 cm^{-1}. The difference between the symmetric and asymmetric stretching vibrations of 213 cm^{-1} is about 24 cm^{-1} larger than that in 2-nitrobenzoic acid (189 cm^{-1}) and 20 cm^{-1} larger than in sodium 2-nitrobenzoate (193 cm^{-1}) which indicates [27] that the 2-nitrobenzoate anion is coordinated as a ligand with a bidentate bridging carboxylic group (see Section 3.2).

The solid state electronic spectrum of the complex shows a broad band (band I) at 14,164 cm^{-1} which could assigned to a $d_{xz}, d_{yz} \rightarrow d_{x^2-y^2}$ transition [28]. Moreover, the spectrum displays a shoulder at 33,000 cm^{-1} (band II). Band II has been assigned to a charge-transfer LMCT absorption [29] and is believed to be indicative of a dimer complex [30]. Finally, the complex displays bands I and II in the usual range for copper(II)

complexes with a square–pyramidal CuO_4O' environment [31].

The EPR spectrum of the powdered sample of the complex was made at room temperature (Fig. 1). The spectrum exhibits features typical of those for dimeric carboxylatocopper(II) complexes [1,2], absorptions at low and high field ($H_{z1} \approx 300$ and $H_{z2} \approx 6000$ G, respectively) and line $H_{\perp 2} \approx 4700$ G. The EPR spectrum was interpreted by using the effective spin Hamiltonian [32] for a randomly oriented triplet state $S = 1$

$$\hat{H} = g\beta H\hat{S} + D\hat{S}_{z^2} + E(\hat{S}_{z^2} - \hat{S}_{z^2}) - 2/3D,$$

where D and E are the axial and rhombic zero-field splitting parameters, and x, y, z are the principal axes of the coordinate system fixed with respect to the Cu–Cu axes. The calculated spin Hamiltonian parameters are $g_\perp = 2.018$, $g_\parallel = 2.315$, $D = 0.343$ and $E = 0.003$ cm^{-1}. These parameters are "classical" for dimeric copper(II) carboxylate complexes [1,2].

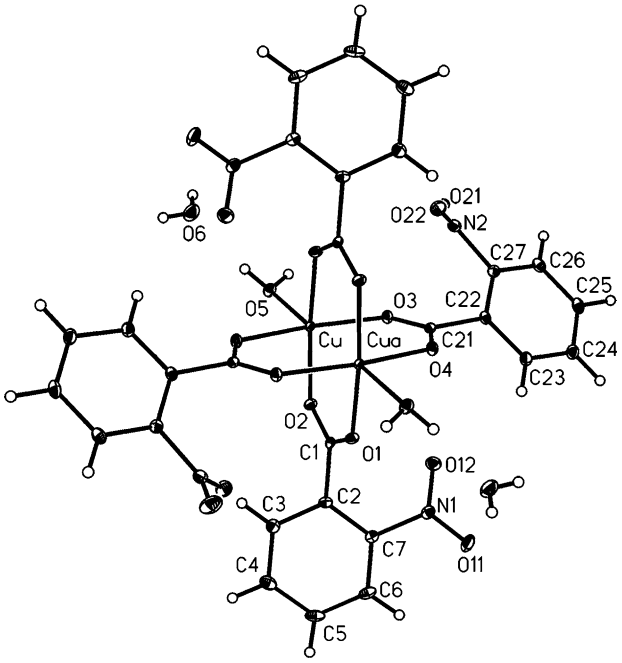

Fig. 1. The molecular structure and atom numbering of $[Cu_2(2\text{-}NO_2bz)_4(H_2O)_2] \cdot 2H_2O$.

3.2. Crystal structure

The molecular structure and atomic numbering scheme are shown in Fig. 2. The structure consists of the centrosymmetric dimer molecule $[Cu_2(2\text{-}NO_2bz)_4(H_2O)_2]$ in which two copper(II) atoms are bridged via four carboxylato anions thus forming a square base of four oxygen atoms (Table 2) around each copper (average Cu–O distance 1.964(1) Å). The apical position of the square pyramidal coordination polyhedron is occupied by the oxygen atom O5 of a water molecule (Cu–O5 distance 2.111(1) Å). The copper atoms are displaced from the respective basal planes towards the apical oxygen atoms by 0.184(1) Å, and the Cu–Cu separation within the dimer was found to be 2.5954(6) Å. The

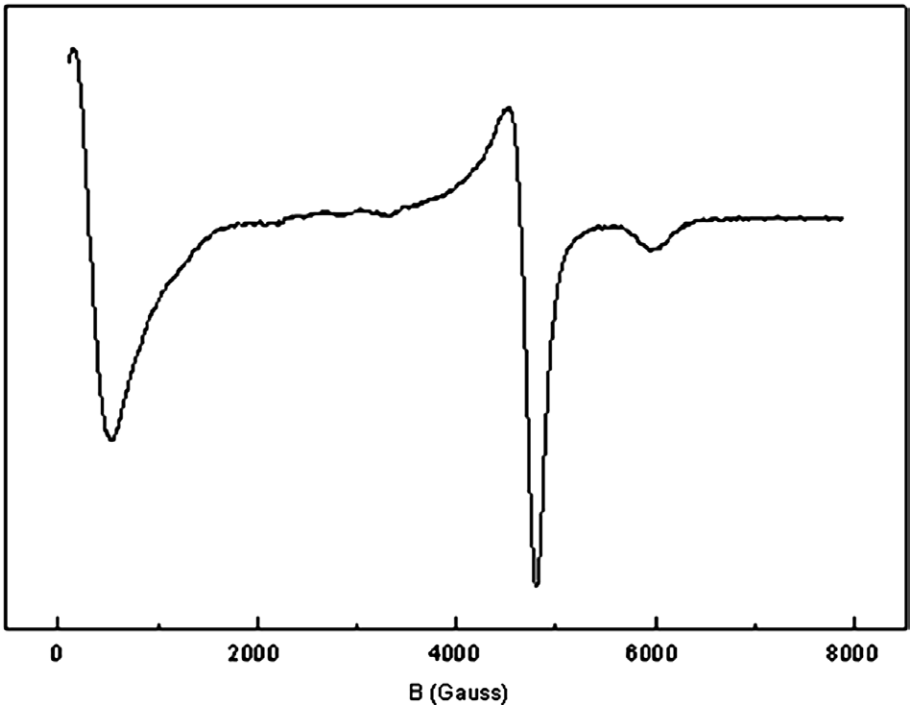

Fig. 2. The EPR spectrum of $[Cu_2(2\text{-}NO_2bz)_4(H_2O)_2] \cdot 2H_2O$.

Table 2
Selected bond lengths (Å) and angles (°) for $[Cu_2(2\text{-}NO_2bz)_4(H_2O)_2]\cdot 2H_2O$

Bond lengths			
Cu–O3	1.9552(12)	Cu–Cu	2.5954(6)
Cu–O4	1.9563(12)	O1–C1	1.250(2)
Cu–O1	1.9704(12)	O2–C1	1.247(2)
Cu–O2	1.9756(12)	O3–C21	1.252(2)
Cu–O5	2.1108(12)	O4–C21	1.240(2)
Bond angles			
O3–Cu–O4	169.19(5)	O2–Cu–O5	99.08(5)
O3–Cu–O1	88.40(5)	O3–Cu–Cu	83.03(4)
O4–Cu–O1	89.91(5)	O4–Cu–Cu	86.16(4)
O3–Cu–O2	90.60(6)	O1–Cu–Cu	81.97(4)
O4–Cu–O2	89.07(6)	O2–Cu–Cu	87.28(4)
O1–Cu–O2	169.25(5)	O5–Cu–Cu	172.96(3)
O3–Cu–O5	99.83(5)	O2–C1–O1	126.19(15)
O4–Cu–O5	90.89(5)	O4–C21–O3	126.66(15)
O1–Cu–O5	91.64(5)		

crystal structure of $[Cu_2(2\text{-}NO_2bz)_4(H_2O)_2]\cdot 2H_2O$ is completed by a crystalline water molecule that is hydrogen bonded (Table 3) to the water molecule that is coordinated to the copper atom (O5–H51–O6 with a O6–H51 distance of 1.914 Å) and to the nitro-group oxygen atom of neighbouring dimeric units (O6–H61–O1 with a O1–H61 distance of 2.154 Å and O6–H62–O22 with a O22–H62 distance of 2.639 Å).

X-ray analysis of the similar $[Cu_2(2\text{-}NO_2bz)_4(DMSO)_2]$ shows [19] significantly longer Cu–O distances both in the equatorial positions (average Cu–O distance 1.984 Å) and in the apical position 2.138 Å. The analysis of dimeric structures of composition $[Cu_2(2\text{-}Xbz)_4(H_2O)_2]$ (where X = benzoyl [6], methoxy [15], Cl [20] and NO [3]) shows that in the 2-NO_2bz complex the Cu–O(apical) distance is the shortest, together with the smallest displacement of the copper atom from the basal plane towards the apical ligand. Further analysis of the Cu–O(apical) and Cu–(basal plane) distances within the group of known structures [5–21] showed that only within the group of $[Cu_2(2\text{-}Xbz)_4(H_2O)_2]$ (where X = benzoyl [6], methoxy [15], Cl [20] and NO [3]) could the linear correlation between the Cu–O(apical) and Cu–(basal plane) distances be found (Fig. 3). In addition to that the smallest displacement of the copper atom from the basal plane in our 2-NO_2bz complex results in the shortest Cu–Cu distance 2.5954(6) Å in comparison to those for the benzoyl [6] (2.638 Å), methoxy [15] (2.613 Å) and Cl [20] (2.599 Å) derivatives. These structural features were the base for further study of the magnetic properties of the title compound.

3.3. Magnetic properties

The magnetic susceptibility of the complex has been measured in the temperature range 70–300 K. Fig. 4 shows the plots of χ_M and/or $\chi_M \times T$ versus T. The value of $\chi_M \times T$ continuously decreases with the lowering of the temperature. At 300 K the observed value of $\chi_M \times T$ is 0.22 ($cm^3\,K\,mol^{-1}$) and the effective magnetic moment is equal to 1.33 BM. At the temperature 70 K $\chi_M \times T \cong 0$ and $\mu_{eff} \cong 0.04$ BM. At temperatures lower than 70 K diamagnetic properties of the dimer are observed. This trends indicates an antiferromagnetic exchange interaction between the two copper(II) magnetic centers of the dimeric unit and depopulation of the excited triplet ($S = 1$) state [33]. The magnetic data of the complex were fitted to a susceptibility equation derived from a spin Hamiltonian

$$H = -2JS_1S_2,$$

with a Bleaney–Bowers equation [34]

$$\chi_M = \frac{N\beta^2 g^2}{3kT}\left[1 + \frac{1}{3}\exp\left(\frac{-2J}{kT}\right)\right]^{-1} + N\alpha,$$

where N is the Avogadro's number, g is the spectroscopic splitting factor, β is the Bohr magneton, k is the Boltzmann's constant and J is the exchange parameter.

The best fitting parameters are $J = -166$ cm^{-1} and $g = 2.17_2$ obtained with a good agreement factor $R = 3.382 \times 10^{-8}$, where

$$R = \frac{\sum_{i=1}^{n}\left(T_i\chi_i^{exp} - T_i\chi_i^{calc}\right)^2}{\sum_{i=1}^{n}\left(T_i\chi_i^{exp}\right)^2}.$$

In spite of the shortest Cu–Cu distance found in the structure of $[Cu_2(2\text{-}NO_2bz)_4(H_2O)_2]\cdot 2H_2O$, the energy separation between the triplet state and singlet ground state, the $-2J$ value, exhibits a "normal" value in the range 300–350 cm^{-1}. The "normal" $-2J$ value for the complex under study could be taken as a proof of mutual relation between the $-2J$ value and the structure of the Cu–O–C–O′–Cu′ bridges which can be described by the ϕ_{bend} angle that is defined [35] as the angle between

Table 3
Selected hydrogen bond for $[Cu_2(2\text{-}NO_2bz)_4(H_2O)_2]\cdot 2H_2O$

D–H	d(D–H)	d(H···A)	⟨DHA	d(D···A)	A (symmetry)
O5–H51	0.829	1.914	172.94	2.739	O6 $[x, y-1, z]$
O5–H52	0.786	2.195	156.89	2.935	O11 $[-x, -y, -z+1]$
O6–H61	0.735	2.154	170.98	2.882	O1 $[-x, -y+1, -z+1]$
O6–H62	0.704	2.639	124.72	3.094	O22 $[-x, -y+1, -z+1]$
O6–H62	0.704	2.654	147.47	3.269	O21 $[-x, -y+1, -z+1]$

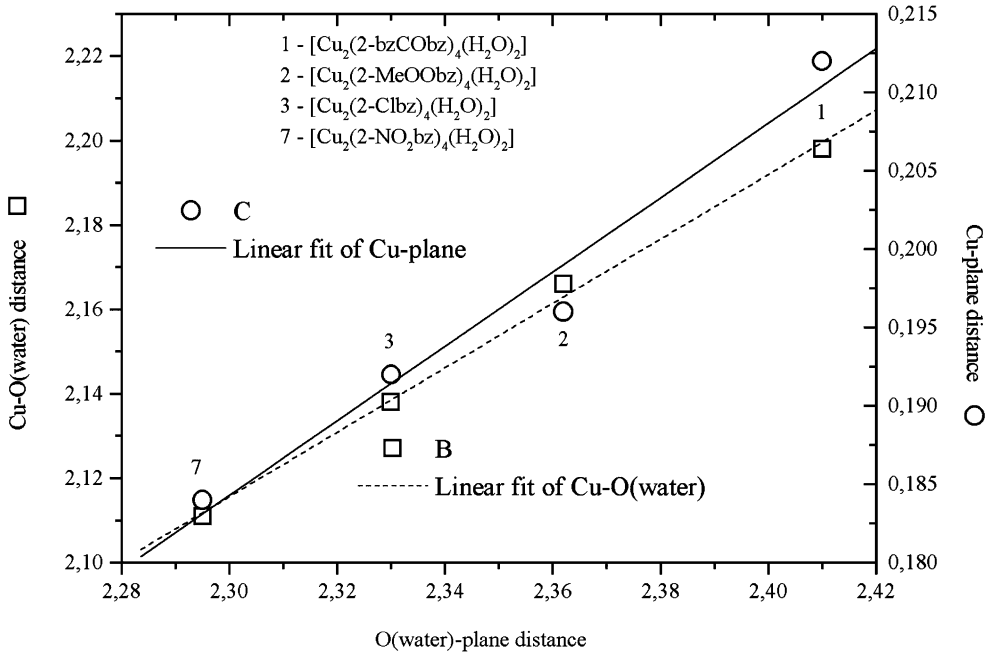

Fig. 3. Plot of the Cu–O(apical) distance and/or Cu–basal plane displacement versus the O(apical) to basal plane distance together with the linear fit of the data used.

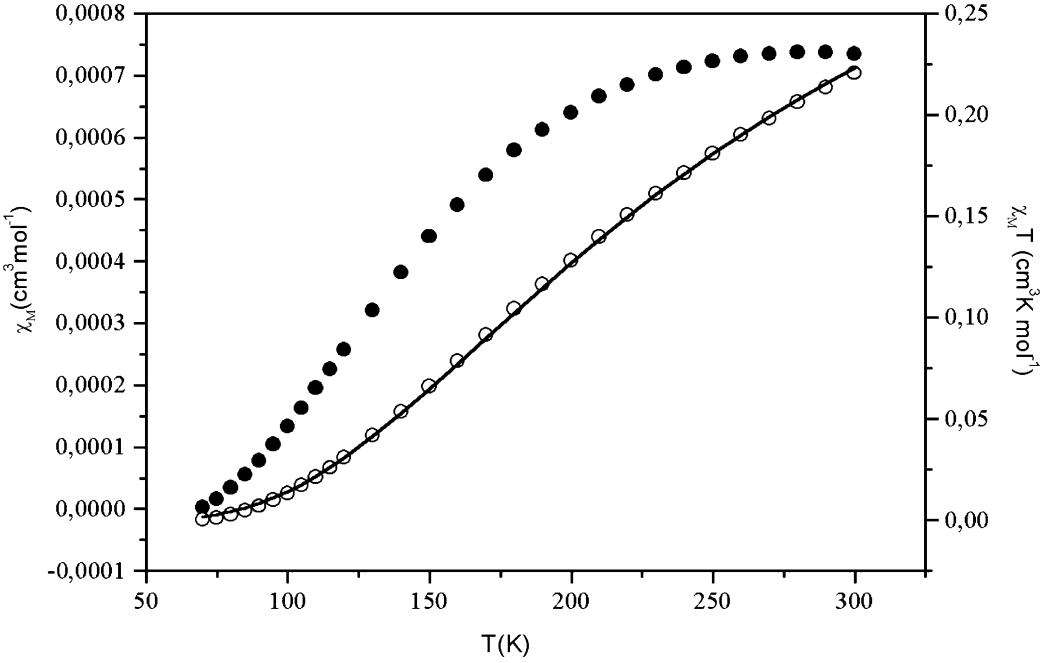

Fig. 4. Plots of the magnetic data versus temperature; $\chi_M^{exptl.}$ (•), $\chi_M^{exptl.} \times T$ (○) and $\chi_M^{calcd.} \times T$ (full line) vs. T using calculated results from the Bleaney–Bowers equation.

CuOO′Cu′ and OCO′ planes. Both structurally independent bridges are nearly planar and exhibit small values of the ϕ_{bend} angle, 1.28(14)° and 1.94(17)°. The orientation of the benzene rings with respect to the carboxylato bridge probably has no influence on the magnetic interaction between the copper centres.

4. Supplementary material

Supplementary material including all atomic coordinates ($\times 10^4$), anisotropic displacement parameters for non-hydrogen atoms and all interatomic distances and bond angles have been deposited with the Cambridge

Crystallographic Centre, CCDC No. 220840 for the compound $[Cu_2(2\text{-}NO_2bz)_4(H_2O)_2]\cdot 2H_2O$. Copies of this information may be obtained free of charge from The Director, CCDC, 12 Union Road, Cambridge, CB2 1EZ, UK (fax: +44-1233-336-033; e-mail: deposit@ccdc.cam.ac.uk or www: http://www.ccdc.cam.ac.uk).

Acknowledgements

The authors thank the Ministry of Education of the Slovak Republic (APVT foundation 2001902 and VEGA 1/9251/02) and Polish Ministry of the Science and Computerization (Grant No. 4T09A 11523) for the financial support of this work.

References

[1] M. Melnik, Coord. Chem. Rev. 36 (1981) 287.
[2] M. Melnik, Coord. Chem. Rev. 42 (1982) 259.
[3] M. Melník, M. Kabešová, M. Koman, L'. Macášková, J. Garaj, C.E. Holloway, A. Valent, J. Coord. Chem. 45 (1998) 147.
[4] W. Harrison, S. Rettig, J. Trotter, J. Chem. Soc., Dalton Trans. (1972) 1852.
[5] S. Batsanov, Yu.T. Struchkov, A.S. Grigo'eva, E.E. Kriss, N.F. Konakhovich, Yu.A. Fialkov, Koord. Khim. 7 (1981) 784.
[6] T. Usubaliev, F.N. Musaev, A.N. Shnulin, Kh.S. Mamedov, Koord. Khim. 8 (1982) 1400.
[7] M.G. Mys'kiv, V.V. Olijnik, A.S. Grigo'eva, E.E. Kriss, N.F. Konakhovich, A.S. Grigo'eva, Koord. Khim. 8 (1982) 1415.
[8] G. Facchin, M.H. Torre, E. Kremer, O.E. Piro, E.J. Baran, Z. Anorg. Allg. Chem. 624 (1998) 2025.
[9] V.Kh. Sabirov, A.S. Batsanov, Yu.T. Struchkov, A.S. Grigo'eva, E.E. Kriss, N.F. Konakhovich, Yu.A. Fialkov, Koord. Khim. 10 (1984) 1474.
[10] L.S. Erre, G. Micera, P. Piu, F. Cariati, G. Ciani, Inorg. Chem. 24 (1985) 2297.
[11] F. Valach, M. Tokarèík, T. Maris, D.J. Watkin, C.K. Prout, Z. Kristallogr. 215 (2000) 56.
[12] T.C.W. Mak, Wai-Hing Zip, C.H.L. Kennard, G. Smith, Polyhedron 9 (1990) 1667.
[13] B. Yatsimirskii, M.G. Mys'kiv, A.S. Grigori'eva, E.E. Kriss, E.I. Gladyshevskii, Dokl. Akad. Nauk. SSSR 247 (1979) 1204.
[14] M.G. Mys'kiv, V.V. Olijnik, E.E. Kriss, N.F. Konakhovich, A.S. Grigori'eva, Koord. Khim. 8 (1982) 1415.
[15] V. Adelskold, L. Eriksson, P.-E. Werner, M. Westdahl, B. Lučanská, J. Krätsmar- šmogrovič, A. Valent, Acta Chem. Scand. 43 (1989) 855.
[16] G. Facchin, M.H. Torre, E. Kremer, O.E. Piro, E.J. Baran, Z. Naturforsch. Teil B 53 (1998) 871.
[17] W. Brzyska, W. Wolodkiewicz, Z. Rzaczynska, T. Glowiak, Monatsch. Chem. 126 (1995) 285.
[18] Ueyama, Y. Yamada, J. Takeda, T. Okamura, W. Mori, A. Nakamura, Chem. Commun. (1996) 1377.
[19] M. Klinga, M.R. Sundberg, M. Melník, J. Mrozinski, Inorg. Chim. Acta 162 (1989) 39.
[20] T. Kawata, S. Ohba, T. Tokii, Y. Muto, M. Kato, Acta Crystallogr. C 48 (1992) 1590.
[21] K. Yoneda, K. Uchiyama, B. Boettcher, Y. Inouye, Bull. Chem. Soc. Jpn. 66 (1993) 3815.
[22] Kuma Diffraction, KM4CCD System Software, Version 1.149, Kuma Diffraction Instruments and Université de Lausanne, Switzerland, 1998.
[23] G.M. Sheldrick, SHELXS-86, in: G.M. Sheldrick, C. Kruger, R. Goddard (Eds.), Crystallographic Computing, 3, Oxford University Press, Oxford, 1985, pp. 175–189.
[24] G.M. Sheldrick, SHELXL93. Program for Crystal Structure Refinement, University of Göttingen, 1993.
[25] G.M. Sheldrick, SHELXL97. Program for Crystal Structure Refinement, University of Göttingen, 1997.
[26] L.J. Farrugia, J. Appl. Cryst. 30 (1997) 565.
[27] K. Nakamoto, Infrared and Raman Spectra of Inorganic and Coordination Compounds, Wiley–Interscience, New York, 1997.
[28] M. Kato, Y. Muto, Coord. Chem. Rev. 92 (1988) 45.
[29] J. Catterick, P. Thorton, Adv. Inorg. Chem. Radiochem. 20 (1977) 291.
[30] M. Melník, I. Potočňák, L'. Macášková, D. Mikloš, Polyhedron 15 (1996) 2159.
[31] A.B.P. Lever, Inorganic Electronic Spectroscopy, Elsevier, Amsterdam, 1984.
[32] A. Abragam, B. Bleaney, Electron Paramagnetic Resonance of Transition Ions, Clarendon Press, Oxford, 1971.
[33] O. Kahn, Molecular Magnetism, VCH Publisher, Weinheim, 1993.
[34] B. Bleaney, K.D. Bowers, Proc. R. Soc. Lond. A 214 (1952) 451.
[35] T. Kawata, H. Uekusa, S. Ohba, T. Furukawa, T. Tokii, Y. Muto, M. Kato, Acta Crystallogr. B 48 (1992) 253.

Available online at www.sciencedirect.com
SCIENCE DIRECT®
Polyhedron 23 (2004) 1309–1316
POLYHEDRON
www.elsevier.com/locate/poly

Synthesis of new pyrazole-containing binuclear and mononuclear Cu(II) complexes: crystal structure, EPR, magnetic and spectroscopic properties

Barbara Barszcz [a,*], Tadeusz Głowiak [b], Julia Jezierska [b], Alina Tomkiewicz [b]

[a] *Institute of Chemistry, Pedagogical University, Chęcińska 5, 25-020 Kielce, Poland*
[b] *Faculty of Chemistry, University of Wrocław, F.Joliot-Curie 14, 50-383 Wrocław, Poland*

Received 26 November 2003; accepted 8 January 2004
Available online 9 April 2004

Abstract

Reaction of 1-hydroxymethyl-3,5-dimethylpyrazole (LOH) with copper(II) salts yields new dinuclear $[CuLLONO_3]_2$ (**1**) or mononuclear $CuL_3(NO_3)_2$ (**2**) co-ordination compounds, where L – (3,5-dimethylpyrazole), LO – (1-methoxy-3,5-dimethylpyrazole). The type of the obtained complex strongly depends on the solvent used during the preparation (propan-2-ol,T = 298K for **1** and a mixture of solvents: methanol, propan-2-ol, trimethyl orthoformate, $T = 333K$ for **2**). The crystal and molecular structure for both of the compounds were determined by single-crystal X-ray diffraction. The structure **1** consists of a dicopper complex with two bridging methoxide groups with a Cu–Cu separation of 2.958 (1) Å. Each copper atom is in a N_2O_3 donor set. The coordination geometry of the copper centres is described as distorted square-pyramidal with one of the oxygen atoms of the NO_3^- anion at the apex. The structure of **1** is compared with those observed previously for two similar $[CuL(LO)X]_2$ complexes where $X = BF_4^-$ (**3**) or ClO_4^- (**4**) instead of NO_3^- (**1**). Variable-temperature EPR spectra (77–295 K) and magnetic susceptibility measurements (1.9–300 K) indicate the antiferromagnetic exchange interaction is dependent on the compensating ligand; it is apparently smaller for the complex with $X = NO_3^-$ than for those with $X = BF_4^-$ and ClO_4^-, in agreement with the same order of increase of the Cu(II)–Cu(II) distances and bond angles of the bridging atoms. The structure of **2** is very close to regular square-pyramidal a with CuN_3O_2 chromophore formed by three L and one NO_3^- ligand, giving a trigonal distortion parameter (τ) of 0.094. The results of spectroscopic studies, IR, UV–Vis and EPR, of the compounds **1** and **2** appear to be in a good accord with the molecular structure determined by single-crystal X-ray analysis.
© 2004 Elsevier Ltd. All rights reserved.

Keywords: Dinuclear copper(II) complex; Magnetic properties; Bidentate ligand; Crystal structure; UV–Vis, EPR and IR spectra

1. Introduction

The occurrence of a pair of Cu–Cu or Cu–Zn ions at the active site of metalloenzymes, which are all involved in the redox chemistry in cellular life, has stimulated much interest in modelling the active-site structure to the research of the physicochemical properties of such metalloenzymes. The use of chelating ligands incorporating pyrazole derivatives has drawn strong interest in modelling such biological systems [1–3]. Driessen et al. [4,5] discussed coordination properties of 1-(2-hydroxyethyl)-3,5-dimethylpyrazole (N-hed) towards several first-row transition metal ions. They concluded that N-hed in the complexes with Cu(II) was in the neutral form $[Cu(HL)_2X_2]$ (X = Cl, NCS or NO_3), or in the dehydrogenated form $[Cu_2L_2X_2]$ (X = Cl, Br and NO_3) or in both the neutral and the dehydrogenated forms $[Cu_2(HL)_2L_2(ClO_4)_2$. Additionally, the pyrazole has been extensively employed in pyrazolylborates to stabilize a variety of organometallic and coordination compounds [6]. Our studies on the coordination chemistry of Cu(II) complexes with diazoles containing the hydrox-

* Corresponding author. Tel.: +48-41-361-6011; fax: +48-41-361-4942.
E-mail address: basiab@pu.kielce.pl (B. Barszcz).

0277-5387/$ - see front matter © 2004 Elsevier Ltd. All rights reserved.
doi:10.1016/j.poly.2004.01.024

ymethyl substituent situated in position 2 of the imidazole ring led us to the conclusion that in aqueous solution [7–9] and in the solid state [10,11], the oxygen atom of the substituent interacts with the Cu(II) ion, participating in a five-membered chelate ring together with the imidazole nitrogen.

In light of our previous results we extended the investigations to 1-hydroxymethyl-3,5-dimethylpyrazole (LOH), providing the same hydroxymethyl substituent in the α position of the pyridine-like nitrogen atom of the pyrazole ring. The protonation constants ($pK_a = 3.48$) of LOH and the equilibrium stability constants of the complexes with the copper(II) ion, determined by the pH potentiometric technique at 298 K [$I = 0.5$ mol/dm^3 (KNO_3)] ($\log\beta_1 = -6.10$, $\log\beta_2 = 2.68 \pm 0.02$), clearly indicate that the donor properties of the ligand depend on electron density located on the pyridine-like nitrogen atom of the pyrazole ring. The 1-hydroxymethyl-3,5-dimethylpyrazole forms very weak complexes in water solution because the H_2O molecules efficiently compete as ligands with the pyrazole derivatives in Cu(II) coordination [12]. Now continuing the studies on the synthesis and characterization of copper(II) complexes as simply models of the active-site of metalloenzymes, we attempted to obtain dinuclear Cu(II) complexes in the solid state using 1-hydroxymethyl-3,5-dimethylpyrazole as a starting ligand in the reaction with the Cu(II) ion. Special attention was paid by us not only to the conditions of the complex preparation but also to the structural effect of the compensative anions: NO_3^-, BF_4^- and ClO_4^-, acting as the apical monodentate ligands, on the magnetic exchange between the coupled copper centers in terms of the change of metal–metal separation, bond angles at the bridging atoms, dihedral angles between the planes containing the copper(II) ions and other details of the metal ion stereochemistry of the particular dimers. Thus, determination of the crystal structure (**1** and **2**), measurements of magnetic susceptibility as a function of temperature (**1**, **3** and **4**) and spectroscopic (EPR IR, UV–Vis) studies of all these complexes have been undertaken by us.

2. Experimental

2.1. Materials and methods

Copper(II) nitrate trihydrate, copper(II) perchlorate hexahydrate, copper(II) tetrafluoroborate hydrate and 1-hydroxymethyl-3,5-dimethylpyrazole (Aldrich Chemical Company) were reagent grade and were used without further purification.

Magnetic measurements in the temperature range 1.72–300 K were determined using a Quantum Design SQUID-based MPMSXL-5-type magnetometer. The SQUID magnetometer was calibrated with a palladium rod sample (Materials Research Corporation, measured purity 99.9985%) for which the gram magnetic susceptibility was taken as 5.30×10^{-6} cm^3 g^{-1} at 293 K (National Bureau of Standards, USA) [13]. All susceptibility measurements were made at a field of 5 kG. The corrections for diamagnetism of the constituent atoms were calculated from the Pascal constants [14]. Electron paramagnetic resonance (EPR) spectra were performed at 77 K on a Bruker ESP 300E spectrometer at the X-band frequency (about 9.45 GHz) and equipped with a Bruker NMR gaussmeter ER 035M and a Hewlett-Packard microwave frequency counter HP 5350B. The spectra were analysed by a computer simulation program based on resonance fields calculated according to the method of Sakaguchi et al. [15,16]. Elemental analyses were run on a Model 240 Perkin–Elmer CHN Analyser. FAB mass spectra were obtained on an AMD 604 mass spectrometer.

The infrared spectra (4000–400 cm^{-1}) in KBr and FIR spectra (400–30 cm^{-1}) in Nujol with specimens applied as a suspension of the complexes in Nujol onto a polyethylene window, were recorded on a Perkin–Elmer 180 spectrophotometer.

The absorption spectra were recorded using a Specord M-40 (Carl Zeiss Jena). The reflectance spectra were measured on a Cary 5 UV–Vis–near IR spectrometer.

2.2. Synthesis of the coordination compounds

2.2.1. $[CuLLONO_3]_2$ (**1**)

The sea green dinuclear Cu(II) complex (L = 3,5DMePz, LO = 1-CH_2O-3,5-DMePz) was prepared in the open air using propan-2-ol as the solvent and the molar ratio Cu:L was 1:4. A solution of 1-CH_2OH-3,5-DMePz (0.5046 g, 4 mmol) in 20 cm^3 of propan-2-ol was added dropwise to a solution of $Cu(NO_3)_2 \cdot 3H_2O$ (0.2416 g, 1 mmol) dissolved in 20 cm^3 of propan-2-ol. The reaction was carried out at room temperature for 25 min, all the time stirring. The solution was filtered and the filtrate was left to stand at room temperature for about three weeks and the resulting sea green crystals were filtered and washed with cold Et_2O. After that, the crystals were dried for three days in a vacuum box.

Yield: 0.1476 g, 42.6%. (Found: C, 38.2; H, 4.9; N, 20.1%. $C_{22}H_{34}N_{10}O_8Cu_2$ requires: C, 38.1; H, 5.0; N, 20.2).

Positive ion FAB mass spectrum; $m/z = 504$ [$Cu_2Pz(PzCH_2O)_2(NO_3)_2$]$^+$; 440 [$Cu_2(PzCH_2O)_2(NO_3)_2$]$^+$; 379 [$Cu_2(PzCH_2O)_2NO_3$]$^+$; 317 [$Cu(PzCH_2O)_2NO_3$]$^+$; 255 [$Cu(PzCH_2O)_2$]$^+$; 223 [$CuPz(PzCH_2O)$]$^+$; 159 [$CuPzCH_2O$]$^+$; 107 [$CuNCH_2O$]$^+$, where (Pz = pyrazole).

The other $[CuL(LO)X]_2$ complexes containing $X = BF_4^-$ (**3**) [17] and ClO_4^- (**4**) anions were prepared by a method similar to that used for complex **1**. Sat-

isfactory elemental analysis results were obtained in all cases.

Caution! Perchlorate salts are potentially explosive. Although no detonation tendencies have been observed with $[CuL(LO)ClO_4]_2$, caution is advised and handling of only small quantities is recommended.

2.2.2. $CuL_3(NO_3)_2$ (2)

The ligand 1-hydroxymethyl-3,5-dimethyl pyrazole (1-CH_2OH-3,5-DMePz), 0.2523 g, 2 mmol was dissolved in 20 cm^3 of the mixture (1:1) methanol and propan-2-ol and added dropwise to the solution which contained the salt of $Cu(NO_3)_2 \cdot 3H_2O$ (0.1208 g, 0.5 mmol) dissolved in 20 cm^3 of the mixture of trimethyl orthoformate and methanol, while stirring. The synthesis was carried out at 333 K or at room temperature. The solution was filtered and the filtrate was left to stand at room temperature for 2–3 weeks and the resulting blue crystals were filtered and washed with cold Et_2O. Crystals which were more suitable for X-ray diffraction study were obtained by recrystallizing the product from after boiling the mixture of methanol and propan-2-ol. After that, the obtained complex was formulated as $[CuL_3(NO_3)_2]$, where L = 3,5DMePz (yield 36%). (Found: C, 37.9; H, 5.0; N, 23.3%. $C_{15}H_{24}N_8O_6Cu$ requires: C, 37.9; H, 5.1; N, 23.5).

Positive-ion FAB mass spectrum; $m/z = 413$ $[CuL_3NO_3]^+$; 317 $[CuL_2NO_3]^+$; 255 $[CuL_2]^+$; 159 $[CuL]^+$; 106 $[Cu–N–C–CH_3]^+$.

2.3. Single crystal structure determinations

For (**1**) and (**2**) respectively, sea green and blue prisms with dimensions of $0.15 \times 0.18 \times 0.20$ and $0.12 \times 0.10 \times 0.07$ mm were measured on a KUMA KM4 (**1**) and KM-4CCD (**2**) diffractometer with graphite monochromator and Cu Kα (**1**), Mo Kα (**2**) radiation. The crystallographic data and the refinement procedure details are given in Table 1. The structures were solved by direct methods using the SHELXS97 [18] program system and refined by the full-matrix least-squares method on all F^2 data using the SHELXL97 [19] program. Non-hydrogen atoms were refined with anisotropic thermal parameters. The hydrogen atoms for (**1**) were included from the difference maps and were refined with isotropic thermal parameters; for (**2**) were included in calculated positions from the geometry of molecules. The absorption corrections were applied for (**1**) empirically [20] and for (**2**) from indexed faces [21].

3. Results and discussion

The type of coordination compounds which have been obtained in the reaction of 1-hydroxymethyl-3,5-dimethylpyrazole with the copper(II) ion strongly depends on the kind of solvent which has been used during the preparation. It is one of the factors affecting the redox potential of the Cu(II) ion. Preparing the mixture of the solvent (trimethyl orthoformate, methanol and propan-2-ol), for the molar ratio Cu:L of 1:2 or 1:4 only one type of mononuclear Cu(II) complex, $[CuL_3(NO_3)_2]$, has been obtained. For all stoichiometries used the ligand decomposed to HCOH and 3,5-dimethylpyrazole (L) according to Scheme 1.

Table 1
Crystal data and structure refinement for complexes **1** and **2**

	1	**2**
Empirical formula	$C_{22}H_{34}N_{10}O_8Cu_2$	$C_{15}H_{24}N_8O_6Cu$
Formula weight	693.67	475.97
T (K)	293(2)	100
Wavelength	1.54180(Cu Kα)	0.71073(Mo Kα)
Crystal system	triclinic	monoclinic
Space group	$P\bar{1}$	$P2_1/c$
a (Å)	8.648(2)	14.6759(16)
b (Å)	9.532(2)	12.4401(11)
c (Å)	9.964(2)	11.5544(12)
α (°)	85.43 (3)	
β (°)	64.81(3)	93.852(9)
γ (°)	88,87(3)	
V (Å^3)	740.8(3)	2104.7(4)
Z	1	4
D_c (g/cm^{-3})	1.555	1.502
Goodness-of-fit (F^2)	1.085	1.198
R_1, wR_2 [$I > 2s(I)$]	0.0417, 0.1170	0.0786, 0.1385
R_1, wR_2 (all data)	0.0444, 0.1195	0.1255, 0.1553

Carrying out the coordination reaction using only propan-2-ol as the solvent and with the Cu:L molar ratio of 1:4, in the open air, a new type of dinuclear complex with mixed ligands, $[CuL(LO)X]_2$ (X = NO_3, BF_4, ClO_4) has been obtained. During the coordination process half of the stoichiometrically used ligand decomposes to HCOH and 3,5-dimethylpyrazole (L) (Scheme 1) and another part undergoes dehydronation giving 1-methoxy-3,5-dimethylpyrazole (LO) according to Scheme 2.

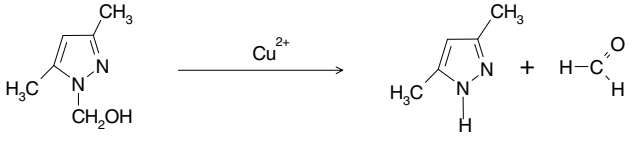

Scheme 1. The ligand reaction during the formation of the monodentate Cu(II) complex.

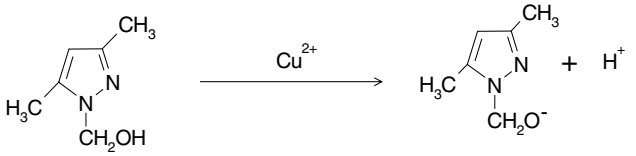

Scheme 2. The process of dehydronation during the formation of $[CuL(LO)X]_2$ complexes.

A similar dinuclear complex with the ClO_4^- anion was obtained by Oki et al. [22] but in a different way using as a starting ligand not only 1-hydroxymethyl-3,5-dimethylpyrazole but also 3,5- dimethylpyrazole.

3.1. Description of the structures

3.1.1. Crystal structure of $[CuLLONO_3]_2$ (1)

A perspective view of complex **1** is depicted in Fig. 1 along with the atomic numbering scheme. Selected interatomic distances and angles are given in Table 2. The crystal structure reveals that the dimeric Cu(II) complex contains three kinds of ligands: 3,5-dimethylpyrazole (L), 1-methoxy-3,5-dimethylpyrazole (LO), which are received during the coordination process, and the NO_3^- anion. The molecular structure consists of a dicopper complex with two bridging methoxide groups with a Cu–Cu separation of 2.958 (1) Å and Cu–O(11)–Cu_a bond angle of 99.21(9)°. Each copper atom is in a N_2O_3 donor set. A description of the geometry of the five-coordinated centres can be obtained by determining the structural index τ defined by Addison et al. [23]. The application of this method yields values τ of 0.39. The coordination geometry of the copper centres is therefore best described as a distorted square pyramidal with one of the oxygen atom of the NO_3^- anion at the apex. The Cu–O(1) bond distance is 2.256(2) Å. The four basal positions are comprised of one nitrogen atom (N21) of the pyrazole ring from the L the nitrogen (N11) and two bridging methoxide oxygen atoms (O11 and $O11_a$) from LO. The latter ligand acts as a bidentate ligand, forming a five-membered chelate ring with the central ion. The chelation is rather symmetric because Cu–N(11) (1.983(3)) Å and Cu–O(11) (1.936(2)) Å have a similar length. The overall stability of this complex in the solid state depends on the contribution of the extensive intramolecular hydrogen bonding between the pyrazole NH and the oxygen atoms of the nitrate ions, with a N(22)–H(22)$\cdots$O(1)$(-x, -y+1, -z)$ distance of 2.34 Å. By comparison of the structural data of compound **1**

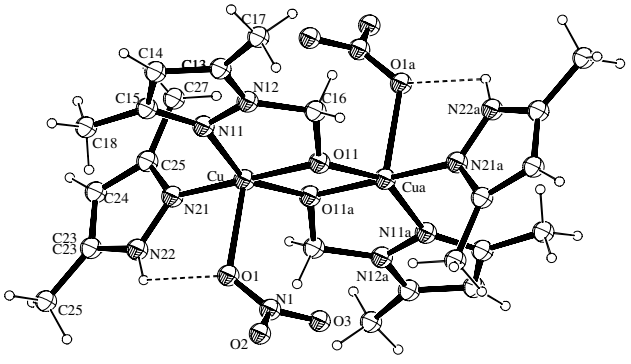

Fig. 1. Molecular structure of dinuclear $[CuLLONO_3]_2$ (**1**) showing the atom numbering scheme. Fifty percent probability amplitude displacement ellipsoids are shown.

Table 2
Selected bond lengths (Å) and bond angles (°) for **1** and **2**

1		**2**	
Bond lengths			
Cu–O (11)	1.936(2)	Cu–N (11)	1.966(4)
Cu–O (11_a)	1.949(2)	Cu–N (21)	2.010(4)
Cu–N (21)	1.973(2)	Cu–N (31)	2.010(4)
Cu–N (11)	1.983(3)	Cu–O (1)	2.015(3)
Cu–O (1)	2.256(2)	Cu–O (4)	2.324(3)
Cu–Cu_a	2.958(1)		
Bond angles			
O(11)–Cu–O(11_a)	80.79(9)	N(11)–Cu–N(21)	90.41(16)
O(11)–Cu–N(21)	175.30(9)	N(11)–Cu–N(31)	91.85(16)
O(11_a)–Cu–N(21)	94.76(10)	N(31)–Cu–N(21)	176.15(17)
O(11)–Cu–N(11)	82.09(10)	N(11)–Cu–O(1)	170.49(14)
O(11_a)–Cu–N(11)	151.82(10)	N(21)–Cu–O(1)	91.42(15)
N(21)–Cu–N(11)	101.42(10)	N(31)–Cu–O(4)	88.73(14)
O(11)–Cu–O(1)	94.91(9)	N(11)–Cu–O(4)	102.56(14)
O(11_a)–Cu–O(1)	101.77(10)	N(21)–Cu–O(4)	93.82(14)
N(21)–Cu–O(1)	87.46(10)	N(31)–Cu–O(4)	88.73(14)
N(11)–Cu–O(1)	101.85(11)	O(1)–Cu–O(4)	86.63(12)
O(11)–Cu–Cu_a	40.56(6)	N(1)–O(1)–Cu	103.7(3)
O(11_a)–Cu–Cu_a	40.23(6)	N(2)–O(4)–Cu	137.2(3)
N(21)–Cu–Cu_a	134.97(8)	C(15)–N(11)–Cu	133.2(3)
N(11)–Cu–Cu_a	119.38(7)	N(12)–N(11)–Cu	120.7(3)
O(1)–Cu–Cu_a	100.98(7)		
C(16)–O(11)–Cu	115.37(18)		
C(16)–O(11)–Cu_a	126.41(19)		
Cu–O(11)–Cu_a	99.21(9)		
N(1)–O(1)–Cu	125.6(2)		
C(15)–N(11)–Cu	143.2(2)		
N(12) – N(11)–Cu	110.99(18)		
C(25)–N(21)–Cu	130.0(2)		
N(22)–N(21)–Cu	124.05(18)		

Symmetry transformations used to generate equivalent atoms: (a) $-x, -y+1, -z$.

with those determined previously for similar $[CuL(LO)X]_2$ complexes in which instead of $X = NO_3$ (**1**), the apical site is occupied by $X = BF_4^-$ (**3**) [17] or ClO_4^- (**4**) [22] anions, some differences in the bond lengths and bond angles are observed. The Cu–Cu separation being 3.0031(8) Å and 3.022(1) Å for **3** and **4**, respectively, is considerably longer than that of **1**. This fact changes drastically the Cu–O–Cu bond angles of 102.91(9)° and 103.(1)° for **3** and **4**, respectively. The similar ligand, 1-(2-hydroxyethyl-3,5-dimethylpyrazole (N-hed), which is different from LOH only in the length of the substituent in position 1, behaves quite differently during the coordination process with the Cu(II) ion. Driessen et al. [4] reported that the geometry of three dinuclear compounds $[Cu(N\text{-}oed)X]_2$ ($X = Cl$, Br, NO_3, N-oed – the dehydronated form of the N-hed) corresponds to square planar coordination with e.g. the Cu–Cu distance of 3.042(4) Å for $[Cu(N\text{-}oed)Br]_2$ being longer than those observed by us for $[CuL(LO)X]_2$ complexes. The greatest metal–metal distance of 3.07(6) Å was determined for the compound $[Cu(HL)L]_2(ClO_4)_2$ [5], containing the ligand (N-hed) both in the neutral form (HL) and in the dehydronated form (L)

with two Cu(II) ions bridged by the oxygen atoms of two L ligands.

3.1.2. Crystal structure of $CuL_3(NO_3)_2$ (2)

Complex **2** was characterized by single-crystal X-ray crystallography. Selected bond lengths and angles are given in Table 2. A perspective view of the molecule is shown in Fig. 2. Complex **2** has a binary structure consisting of 3,5-dimethylpyrazole, which has been obtained in the reaction of 1-hydroxymethyl-3,5-dimethylpyrazole with the Cu(II) ion and NO_3^- anions. While the basal plane is occupied by three nitrogen atoms of the pyrazole rings and the oxygen atom (O1) of the NO_3^- anion, the oxygen atom (O4) of the second nitrate anion is involved in axial bonding in the 4+1 coordination geometry of the CuN_3O_2 chromophore. The axial Cu–O(4) bond length of 2.324(3) Å is longer than that of **1**. The structure of **2** is very close to regular square pyramidal, giving a trigonal distortion parameter (τ) value of 0.094 [23]. The crystal structure of **2** is stabilized by a network of hydrogen bonds (Table 3). Additionally, the hydrogen atoms of the pyrazole N–H(22) and N–H(32) are engaged in hydrogen bonding with the next molecule of **2** (Fig. 3).

3.2. Spectroscopic properties

In the infrared spectra of the free LOH ligand, which is used as a starting ligand for the synthesis, the OH-stretching band lies at 3152 cm^{-1} and is very broad due to the strong inter- and intramolecular hydrogen bond $\nu(O\cdots H\cdots N)$ vibrations. This band disappears in the infrared spectra of Cu(II) complexes, $[CuL(LO)NO_3]_2$ (**1**), $CuL_3(NO_3)_2$ (**2**) or $[CuL(LO)BF_4]_2$ (**3**). This fact

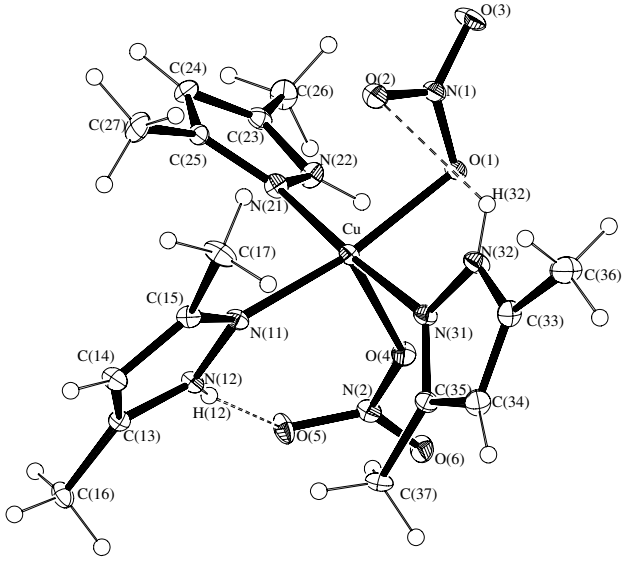

Fig. 2. Molecular structure of mononuclear $CuL_3(NO_3)_2$ (**2**). Details as for Fig. 1.

Table 3
Probable hydrogen bond lengths (Å) and bond angles(°) for **2**

D–H···A	d(H···A)	d(D···A)	∠(DHA)
N(32)–H(32)···O(6)^{ii}	2.17	2.954(3)	150
N(32)–H(32)···O(2)	2.53	3.084(7)	123
N(12)–H(12)···O(5)	1.92	2.754(1)	162
N(22)–H(22)···O(2)^{i}	2.07	2.898(2)	159
N(32)–H(32)···O(4)^{ii}	2.55	3.234(2)	136

Symmetry transformations used to generate equivalent atoms: (i) $[x, 3/2-y, -1/2+z]$, (ii) $[x, 3/2-y, 1/2+z]$.

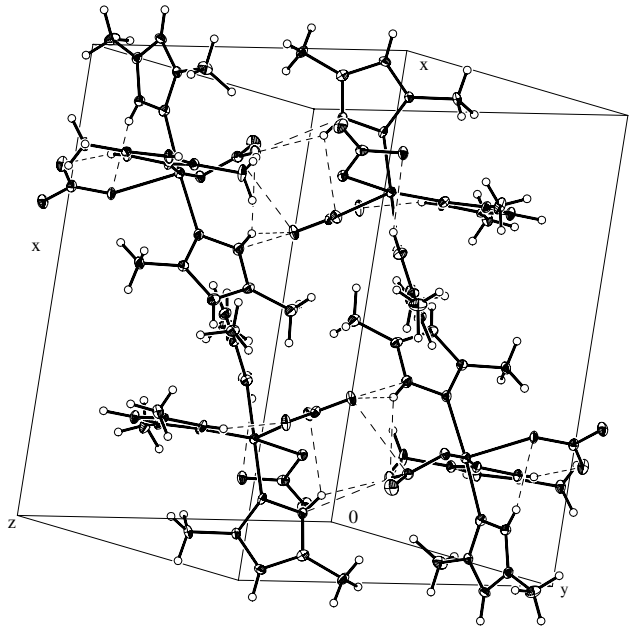

Fig. 3. Intermolecular hydrogen bond system of **2**.

and new absorption bands at 3288, 3304 and 3352 cm^{-1} for **1**, **2** and **3**, respectively, which can be assigned to ν(N–H), confirmed that the complexes contain new ligands, L and LO, received during the coordination reaction with the Cu(II) ion. The broadness and rather low position of the N–H band of (**1**) are indicative of a strong intramolecular hydrogen bonding between the NH of L and the oxygen atoms of the nitrate ions in accord with the crystal structure (Fig. 1). Dinuclear (**1**, **3**) and mononuclear (**2**) Cu(II) complexes show new bands, compared to the ligand spectra, at 352, 353 and 257 cm^{-1}, respectively, which arise from ν(Cu–N) stretches as well as at 408, 414 and 350 cm^{-1}, respectively, due to the Cu–oxygen bonds vibrations.

The reflectance spectra of **1** and **3** (solid state) show the bands at 14 200 and 15 600 cm^{-1}, respectively, characteristic of a d → d transition for compounds with a square pyramidal geometry of the individual copper(II) ions with a $d_{x^2-y^2}$ ground state [24]. At the highest energy the spectra exhibit a very broad intense absorption with poorly marked maxima between ca. 21 000 and 50 000 cm^{-1}. It contains most likely several

transitions associated with the ligand to copper charge transfer transitions which correspond to the peak position established by means of the Gaussian distribution at 26 700, 26 500 [$O \rightarrow Cu(II)$], 34 200, 33 200 [$\pi_{2(pirazol)} \rightarrow \sigma^*(Cu(II)$] and 49 200, 48 000 $cm^{-1}(\pi \rightarrow \pi^*$, $\sigma_{(N)} \rightarrow \sigma^*$, respectively. The transition in the 25 000–33 000 cm^{-1} region is usually used as a good evidence of the formation of alkoxo bridged complexes [25–28].

The reflectance spectrum of mononuclear complex **2** displays bands at 11 000 and 16 900 cm^{-1} which correlates with a square pyramidal environment of copper(II) ions. Additionally, using the Gaussian distribution of the absorption in the highest-energy the following peak positions are established: 27 500 [$\pi_{1(pirazol)} \rightarrow \sigma^*(Cu(II)$], 34 100 [$\pi_{2(pirazol)} \rightarrow \sigma^*(Cu(II)$] 47 900 cm^{-1} ($\pi \rightarrow \pi^*$). The proposed assignments are in agreement with the data reported for the Cu(II) complexes with 3.5-dimethylpyrazole [29].

3.3. EPR spectroscopy

The EPR spectra of the polycrystalline dimers are presented in Fig. 4. Only in the case of the dimer with $X = NO_3^-$ does the spectrum exhibit two signals – a stronger one at 550 mT and a weak, broad one at about 200 mT, which are associated with the transitions within $S = 1$ levels. The spectrum was simulated using the following Spin Hamiltonian parameters: $D = 0.59\ cm^{-1}$, $E = 0.01\ cm^{-1}$, $g_{\|} = 2.20$, $g_{\perp} = 2.06$. The smallest gap between $S = 1$ and $S = 0$ levels for the complex with $X = NO_3^-$ is most likely the reason of its exceptional EPR properties as compared to those when $X = ClO_4^-$ and BF_4^- and for other alkoxo bridged dimers derived from 1-(hydroxyethyl)-3,5-dimethylpyrazole[4,5] which exhibit stronger antiferromagnetic interactions and are EPR-silent.

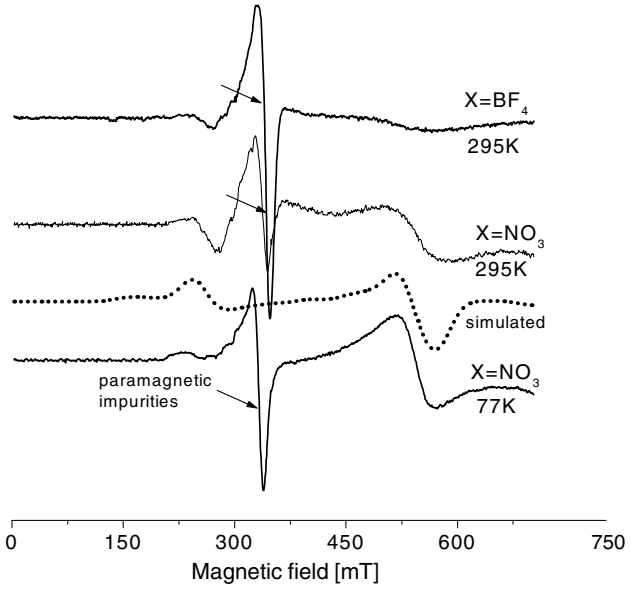

Fig. 4. EPR spectra of polycrystalline [CuLLOHX] at 295 K, the arrows indicate the signal due to paramagnetic impurities.

The EPR spectra of polycrystalline complex **2** at 295 and 77 K are resolved in the parallel region due to hyperfine interaction with the copper nuclei. The spectral parameters, $g_{\|} = 2.270$, $g_{\perp} = 2.055$ and $A_{\|} = 180 \times 10^{-4}$ cm^{-1}, are characteristic of axial symmetry of the Cu(II) coordination sphere. The parameters values are in a good correspondence with the N_3O donor set in the Cu(II) *xy* plane evidenced by the crystal structure analysis.

3.4. Magnetic properties

The magnetic properties of complexes **1**, **3** and **4** under the form of $\chi_M T$ versus T and χ_M versus T (χ_M being the molar magnetic susceptibility) are shown in Figs. 5–7, respectively.

$\chi_M T$ at room temperature for **1** is close to 0.66 $cm^3\,mol^{-1}\,K$ and is smaller than the spin-only value of 0.75 $cm^3\,mol^{-1}\,K$ expected for an uncoupled dicopper(II) system. It decreases slightly up to 120 K, then rapidly and finally reaches a plateau below approxi-

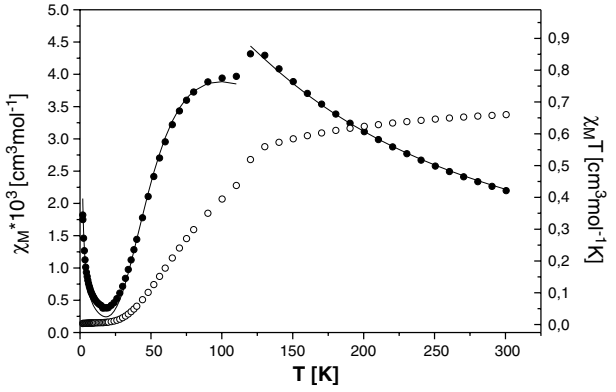

Fig. 5. Temperature dependence of χ_M (•) and $\chi_M T$ (○) for [CuLLONO$_3$]. The solid lines are the calculated curves.

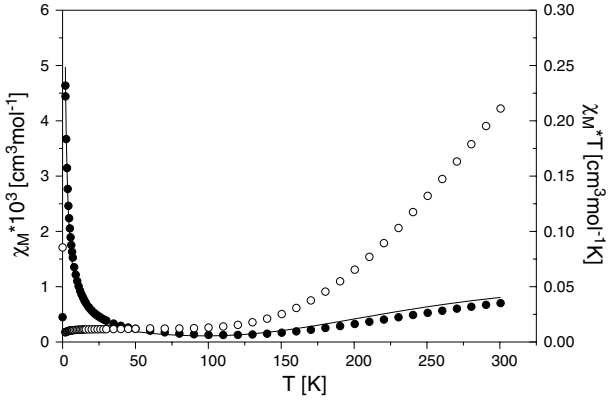

Fig. 6. Temperature dependence of χ_M (•)and $\chi_M T$ (○) for [CuLLOBF$_4$]. The solid lines are the calculated curves.

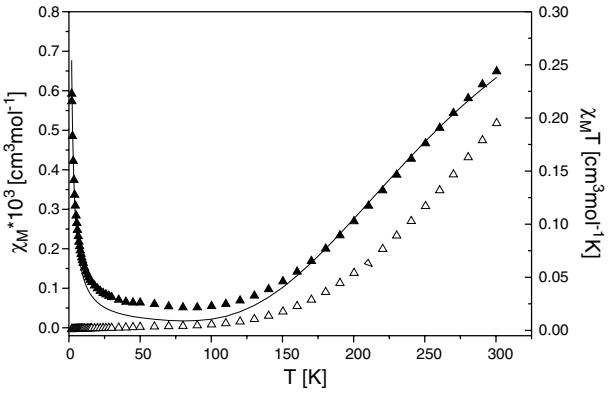

Fig. 7. Temperature dependence of χ_M (▲) and $\chi_M T$ (△) for [CuLLOClO$_4$]. The solid lines are the calculated curves.

mately 25 K with a value of 0.35×10^{-2} cm^3 mol^{-1} K. This behavior indicates an antiferromagnetic interaction between the two Cu(II) centers [30]. Upon cooling from room temperature the χ_M increases and achieves a maximum value of 4.09×10^{-3} cm^3 mol^{-1} at ca. 120 K. At this temperature a structural phase transition of the first order is observed. The systematic studies of the order–disorder and thermodynamic characteristics of this phase transition by X-ray diffraction and calorimeter methods are in progress and will be published elsewhere. When the temperature is lowered below 120 K, one can observe that the χ_M decreases, reaches a minimum at 19 K and increases rapidly between 19 and 1.90 K. This increase indicates the presence of a paramagnetic impurity. The impurity accounts for the plateau value of χ_MT in the low temperature region. In the case of complexes **3** and **4** the values of χ_MT are at room temperature close to 0.211 cm^3 mol^{-1} K and 0.19 cm^3 mol^{-1}, respectively, which are significantly below the spin-only value suggesting the presence of stronger antiferromagnetic intramolecular interactions than for **1**. Both χ_M and $\chi_M T$ decrease as the temperature is lowered from room temperature to 110 K. At lower temperatures a rapid increase in the magnetic susceptibility, preceded by a plateau for **4**, is next observed as a result of a small amount of monomeric Cu(II) ion.

The temperature dependence of the magnetic susceptibility measured between 1.9 and 300 K was analysed on the basis of the isotropic Heisenberg model, $\hat{H} = -2J(\hat{S}_1 \cdot \hat{S}_2)$, using the modified Bleaney–Bowers equation [31]:

$$\chi_M = \frac{Ng_{dim}^2\beta^2}{3kT}\left[1 + \frac{1}{3}\exp\left(\frac{-2J}{kT}\right)\right]^{-1}(1-x) + \left(\frac{Ng_{mon}\beta^2}{4kT}\right)x, \quad (1)$$

where x is the proportion of the paramagnetic impurity (presumably non-coupled monomeric copper(II) complex), $2J$ is the interaction parameter between two spin carriers and the other symbols have their usual meaning.

The best least-squares fitting of the experimental data through this expression leads to $2J = -58$ cm^{-1} $g_{dim} = 2.11$, $g_{mon} = 2.13$, $x = 0.5\%$ (in the temperature range 1.9–110 K) and $2J = -45$ cm^{-1}, $g_{dim} = 2.11$, $g_{mon} = 2.13$, $x = 0.5\%$ (in the temperature range 120–300 K) for complex **1**, $2J = -269$ cm^{-1}, $g_{dim} = 2.25$, $g_{mon} = 2.06$, $x = 1.20\%$ for complex **3**, $2J = -288$ cm^{-1}, $g_{dim} = 2.18$, $g_{mon} = 2.20$, $x = 0.14\%$ for complex **4**. The agreement factor R, defined as $[R = \sum(\chi_{exp}T - \chi_{calc}T)^2/\sum(\chi_{exp}T)^2]$, is 4.93×10^{-4} for **1** (1.9–110 K), 3.34×10^{-4} for **1** (120–300 K), 6.97×10^{-4} for **3**, 1.28×10^{-3} for **4**. The large negative $2J$ values in the cases confirm a very strong antiferromagnetic interaction between the two Cu(II) centers. This interaction can be understood in term of the non-zero overlap between the copper(II) magnetic $d_{x^2-y^2}$ orbitals, depending on the coordination geometry around the metal ions [32–35].

In such dimeric copper(II) complexes these magnetic interactions occur via the double oxygen bridge. For the studied complexes the antiferromagnetic exchange interaction tends to increase according to the series of compensative ligands: $NO_3^- \ll BF_4^- < ClO_4^-$. Replacement of NO_3^- by BF_4^- or ClO_4^- anions results in the increase of the Cu(II)–Cu(II) distance and consequently substantially increases the bond angles of the bridging atoms. With increasing bond angles the magnetic orbitals of both Cu(II) ions are favorably oriented and delocalized towards the bridging network, which leads to a very large overlap and hence to a very strong antiferromagnetic interaction [35]. It is well know [36] that for the hydroxide-bridged dimers the way of exchange interaction characteristically depends on the bridge angle implying a crossover from antiferromagnetic to ferromagnetic coupling at about 97.6°. The studies of a chlorine-bridged dimeric system [37] (Cu–Cl–Cu) have shown that the crossover-bridging angle is at 95.1°. A similar relation between Cu–O–Cu bridge angles (99.21(9)° for 1, 102.91(9)° for **3** and 103(1)° for **4**) and the exchange coupling, antiferromagnetic in nature, is observed by us for the new dinuclear complexes. The ferromagnetic coupling for **4** was postulated erroneously in the previous work [22] as a too rash interpretation of the solution paramagnetic susceptibility measured by ^{1}H shift in the NMR spectra only at room temperature.

3.5. Conclusion

By carrying out the synthesis in a special way and using only 1-hydroxymethyl-3,5-dimethylpyrazole as the starting ligand in the presence of copper(II) salts, new dinuclear Cu(II) complexes of [CuL(LO)X]$_2$ or mononuclear [CuL$_3$(NO$_3$)](NO$_3$) where L – (3,5-dimethylpyrazole), LO – (1-methoxy-3,5-dimethylpyrazole), X = NO_3^-, BF_4^-, ClO_4^-) have been obtained. In particular, the kind of solvent used plays an important role in the synthesis of the complexes. Moreover, in the three

examples of Cu(II) dimers characterized in this paper, the coordinating anions significantly contribute to the magnetic behaviour. With the increase of the volume of the anions, parallel to the change in Cu(II)–Cu(II) bond length and bond angle, the spin super-exchange interaction measured by the energy gap between the singlet and triplet states increases. So it is interesting to point out that the antiferromagnetic exchange interaction tends to increase according to the series of compensative ligands: $NO_3^- \ll BF_4^- < ClO_4^-$.

4. Supplementary material

Crystallographic data for the structural analysis have been deposited with the Cambridge Crystallographic Data Centre, CCDC Nos. 218201 (**1**) and 218200 (**2**). Copies of this information may be obtained free of charge from The Director, CCDC, 12 Union Road, Cambridge, CB2 1EZ, UK (fax: +44-1223-336033; e-mail: deposit@ccdc.cam.ac.uk or www.ccdc.cam.ac.uk).

References

[1] J.C. Bayon, P. Esteban, G. Net, P.G. Rasmussen, K.N. Baker, C.W. Hahn, M.M. Gumz, Inorg. Chem. 30 (1991) 2572.
[2] N. Kitajma, K. Fujisawa, Y. Moro-Oka, Inorg. Chem. 29 (1990) 3657.
[3] T.N. Donovan, D.E. Williams, J. Banks, R.M. Buchanan, H.R. Chang, R.J. Webb, D.N. Hendrikson, Inorg. Chem. 29 (1990) 1058.
[4] W.L. Driessen, S. Gorter, W.G. Haanstra, L.J.J. Laarhoven, J. Reedijk, K. Goubitz, F.R. Seljee, Recl. Trav. Chim. Pay-Bas 112 (1993) 309.
[5] W.L. Driessen, B. Maase, J. Reedijk, H. Kooijman, M.T. Lakin, A.L. Spek, Inorg. Chim. Acta 300–302 (2000) 1099.
[6] S. Trofimenko, Prog. Inorg. Chem. 34 (1986) 115.
[7] J. Kulig, B. Barszcz, B. Lenarcik, Polish J. Chem. 66 (1992) 79.
[8] B. Barszcz, J. Kulig, J. Chem. Soc., Dalton Trans. (1993) 1559.
[9] B. Barszcz, J. Kulig, J. Jezierska, J. Lisowski, Polish J. Chem. 73 (1999) 447.
[10] B. Barszcz, T. Głowiak, J. Jezierska, Polyhedron 18 (1999) 3713.
[11] K. Kurdziel, T. Głowiak, J. Jezierska, Polyhedron 21 (2002) 1857.
[12] J. Kulig, unpublished data.
[13] H.V.A. Briscoe, P.L. Robinson, A.J. Rudge, J. Chem. Soc. (1931) 3219.
[14] E. König, Magnetic Properties of Coordination and Organometallic Transition Metal Compounds, Springer, Berlin, 1966.
[15] U. Sakaguchi, Y. Arata, S. Fujiwara, J. Magn. Res. 9 (1973) 118.
[16] A. Ozarowski, unpublished program.
[17] B. Barszcz, T. Głowiak, J. Jezierska, K. Kurdziel, Inorg. Chem. Commun. 5 (2002) 1056.
[18] G.M. Sheldrick, SHELXS97, Program for Solution of Crystal Structure, University of Göttingen, Göttingen, Germany, 1997.
[19] G.M. Sheldrick, SHELXL97, Program for Refinement of Crystal Structure, University of Göttingen, Götingen, Germany, 1997.
[20] N. Walker, D. Stuart, Acta Cryst. A 39 (1989) 158.
[21] CrysAlis RED-CCD 166, Kuma Diffraction Software, Wrocław, Poland, 1999.
[22] A.R. Oki, J. Sanchez, R.J. Morgan, J. Coord. Chem. 36 (1995) 167.
[23] A.W. Addison, T.N. Rao, J. Reedijk, J. van Rijn, G.C. Verschoor, J. Chem. Soc., Dalton Trans. (1984) 1349.
[24] A.B.P. Lever, Inorganic Electronic Spectroscopy, Elsevier, Amsterdam, 1984.
[25] Y. Ismura, Y. Nonaka, S. Kida, Bull. Chem. Soc. Jpn. 46 (1973) 3728.
[26] S.J. Loeb, J.W.L. Martin, Ch. J. Willis, Inorg. Chem. 18 (1979) 3160.
[27] E.J. Salomon, K.W. Penfield, D.E. Wilcox, Struct. Bonding (Berlin) 53 (1983) 1.
[28] M. Jeżowska-Bojczuk, H. Kozłowski, S. Lamotte, P. Decock, A. Temeriusz, I. Zajączkowski, J. Stępiński, J. Chem. Soc., Dalton Trans. (1995) 2657.
[29] E. Bernaducci, W.F. Schwindinger, I.V.J.L. Hughey, K. Krogh-Jespersen, H.J. Schugar, J. Am. Chem. Soc. 103 (1981) 1686.
[30] Y. Journaux, J. Sletten, O. Kahn, Inorg. Chem. 24 (1985) 4063.
[31] B. Bleaney, K.D. Bowers, Proc. Roy. Soc. A 214 (1952) 451.
[32] O. Kahn, Angew. Chem., Int. Ed. Engl. 24 (1985) 834.
[33] A. Garcia, R. Costa, J. Ribas, T. Mallah, Y. Journaux, J. Sletten, X. Solans, V. Rodriguez, Inorg. Chem. 32 (1993) 3733.
[34] R. Costa, A. Garcia, R. Sanchez, J. Ribas, X. Solans, V. Rodriguez, Polyhedron 21 (1993) 2697.
[35] E.-Q. Gao, H.-Y. Sun, D.-Z. Liao, Z.-H. Jiang, S.-P. Yan, Polyhedron 21 (2002) 359.
[36] D.J. Hodgson, Prog. Inorg. Chem. 19 (1975) 173.
[37] S.G.N. Roundhill, D.M. Roundhill, D.R. Bloomquist, C. Landee, R.D. Willett, D.M. Dooleg, H.B. Gray, Inorg. Chem. 18 (1979) 831.

Available online at www.sciencedirect.com
SCIENCE DIRECT®
Polyhedron 23 (2004) 1317–1323
POLYHEDRON
www.elsevier.com/locate/poly

Crystal structure and electrochemistry of copper(II) macrocycles containing terpyridine

V.E. Marquez [a], Juan R. Anacona [b,*], Daniel Loroño [c]

[a] Departamento de Química Aplicada, Instituto Universitario de Tecnología, Apartado Postal 255, Cumaná, Venezuela
[b] Departamento de Química, Universidad de Oriente, Apartado Postal 208, Cumaná, Venezuela
[c] School of Chemistry, University of Edinburgh, West Mains Road, Edinburgh EH9 3JJ, UK

Received 28 July 2003; accepted 25 January 2004
Available online 22 April 2004

Abstract

The macrocycle L, prepared by template condensation of bis-6,6″-(α-methylhidrazino)-4′-phenyl-2,2′:6″,2′-terpyridine with glyoxal, forms a stable crystalline complex of copper(II) $[Cu(L)(H_2O)_2][PF_6]_2$ which has been used as a starting material to prepare, for electrochemical studies, a series of seven coordinate copper(II) complexes $[Cu(L)X_2][PF_6]_2$ (X = pyridine, 4-cyanopyridine, 4-aminopyridine, 4-dimethylaminopyridine, pyrazine, imidazole, 1-methylimidazole, 2-methylimidazole, and trimethylphosphite). Cyclic voltammetry of the aquo complex in DMSO show one reversible reduction wave at −0.36 V versus $Ag/AgBF_4$ reference electrode and controlled potential electrolysis in the presence of trimethylphosphite affords a diamagnetic species which has been assigned as a mononuclear d^{10} Cu(I) species. The crystal and molecular structure of $[Cu(L)(imidazole)_2][PF_6]_2$ shows the metal to be in a pentagonal bipyramidal N_7 environment.
© 2004 Elsevier Ltd. All rights reserved.

Keywords: Macrocyclic complexes; Cyclic voltammetry; X-ray crystallography; Imidazole

1. Introduction

Earlier studies [1,2] reported the electrochemical investigation of the redox behaviour in acetonitrile solution of the copper(II) complexes with 14-membered saturated tetraaza macrocycles. It was found that controlled potential electrolysis performed both in oxidation and reduction did not produce the corresponding copper(III) and copper(I) complexes, in contrast to the nickel analogues. However, cyclic voltammetry performed at high potential scan rate showed both in oxidation and in reduction a reversible one electron redox process, ascribed to the formation of copper(III) and copper(I) complex cations, respectively.

The reduction of transition metal complexes of potential π-acceptor macrocyclic ligands such as **L** is of interest because of the possibility of forming either metal reduced species or metal-stabilized ligand radical species in which the electron resides mainly on the macrocyclic ligand.

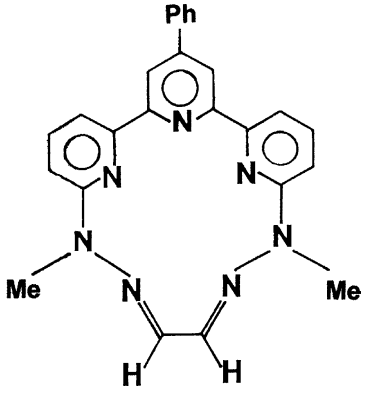

As previously shown [3–15], these redox properties may be highly dependent on the axial ligation. Continuing with early studies [16–24] we have studied the redox chemistry of copper(II) complexes of **L** in the presence of a series of axial ligands in order to determine whether variations in redox properties are observed.

* Corresponding author. Fax: +58-93317485.
E-mail address: juananacona@hotmail.com (J.R. Anacona).

0277-5387/$ - see front matter © 2004 Elsevier Ltd. All rights reserved.
doi:10.1016/j.poly.2004.01.023

2. Experimental

2.1. Physical measurements

IR spectra were recorded on a Perkin–Elmer Model 983 spectrophotometer using KBr pellets. The spectra were calibrated against the 1603 cm^{-1} band of polystyrene. Conductance measurements were made using a Wayne Kerr Universal Bridge. The conductivity cell was calibrated with aqueous KCl. Microanalyses were performed on a Leco 932 CHNS elemental analyzer. Electrochemical measurements were recorded on a Model 170 Electrochemistry System (Princeton Applied Research). All readings were taken using a three electrode potentiostatic system in MeCN with 0.1 mol dm^{-3} (n-Bu)$_4$NBF$_4$ as supporting electrolyte. The potentials are referenced against a saturated calomel electrode (SCE). CV studies were carried out using Pt wires as auxilliary and working electrodes and a Ag–AgBF$_4$ reference electrode with sample concentrations of 10^{-3}–10^{-4} mol dm^{-3}. EPR spectra were measured at 77 K on a Varian E109 spectrophotometer (X band) and calibrated with diphenylpicrylhydrazyl (dpph; $g = 2.0037$). Magnetic susceptibilities were measured on a Johnson Matthey susceptibility balance at room temperature using HgCo(NCS)$_4$ as calibrant.

2.2. Materials

Published methods were used to prepare H$_2$L[PF$_6$]$_2$ by the template condensation of bis-6,6″-(α-methylhidrazino)-4′-phenyl-2,2′:6″,2′-terpyridine with glyoxal about Cr^{3+} or $SnMe_2Cl_2$ [16–19]. Solvents were distilled over appropriate drying agents prior to use. All other chemicals were commercial materials of analytical grade. Unless otherwise stated the reactions were carried out under dry N_2.

2.3. Preparation of [Cu(L)(H$_2$O)$_2$][PF$_6$]$_2$

The free macrocycle H$_2$L[PF$_6$]$_2$ (0.029 g, 0.04 mmol) and Cu(O$_2$CMe)$_2\cdot$4H$_2$O (0.025 g, 0.1 mmol) in of dry MeOH (50 cm^3) were boiled under reflux, until a clear solution was obtained. A solution of [NH$_4$][PF$_6$] (0.033 g, 0.2 mmol) in MeOH was added to the hot solution, which was allowed to cool slowly. Copper(II) complex was obtained as a brown precipitate.

2.4. Preparation of [Cu(L)(X)$_2$][PF$_6$]$_2$ (X = pyridine (Py), 4-cyanopyridine (4-NCPy), 4-aminopyridine (4-H$_2$NPy), 4-dimethylaminopyridine (4-Me$_2$NPy), pyrazine, imidazole (Im), 1-methylimidazole (1-MeIm), 2-methylimidazole (2-MeIm) and trimethylphosphite (P(OMe)$_3$))

The complex [Cu(L)(H$_2$O)$_2$][PF$_6$]$_2$ (0.090 g. 0.11 mmol) was dissolved in boiling methanol (50 cm^3), excess of X ligand was added, and the reaction mixture was refluxed for 25 min. Addition of a concentrated methanolic solution of ammonium hexafluorophosphate to the hot solution gave a precipitate of the pure product, which was collected, washed copiously with diethyl ether and dried in vacuo. The yield was quantitative. Completion of reaction could be determined by the absence of the two water ν(O–H) resonances in the infrared spectrum near 3500 cm^{-1}.

2.5. X-ray crystallography: structure of [Cu(L)(Im)$_2$][PF$_6$]$_2$

Green prismatic crystals were obtained by recrystallization of the complex from acetone and diethyl ether. For X-ray structural determination a single crystal with approximate dimensions $0.35\times0.28\times0.20$ mm was selected. Data were collected on a Brucker SMART APEX diffractometer equipped with an Oxford Cryosystem low temperature device at 150 K. The initial unit cell was indexed using a least-squares analysis of a random set of reflections collected from three series of 0.3° wide ω-scans, 10 s per frame and 25 frames per series that were well distributed in reciprocal space. Data frames were collected [Mo Kα ($\lambda = 0.71073$ Å)] with 0.3° wide ω-scans, 10 s per frame and 600 frames per series. Four complete series were collected at varying ϕ angles ($\phi = 0°$, 90°, 180° and 240°). The crystal to detector distance was 6.0 cm, this providing a set of $3.48° \leqslant 2\theta \leqslant 52.80°$. A total of 15 601 reflections were collected and performed using SAINT [25], while absorption correction was applied using SADABS [26] with 7928 unique [$R_{int} = 0.0297$]. System symmetry, systematic absences and intensity statistics indicated the unique triclinic space group $P\bar{1}$. The structure was determined by direct methods with the location of the nearly all non-hydrogen atoms using the program SHELXS [27] and refined by full-matrix least-squares on F^2 using SHELXL [28]. All non-hydrogen atoms were refined anisotropically, while hydrogen atoms were placed in calculated positions, constrained to ride on their carbon atoms with group U_{iso} values assigned ($U_{iso}(H) = 1.20U_{iso}$ for aromatic carbons and $1.50U_{iso}$ for methyl atoms).

3. Results and discussion

Although complexes of 6,6″-bis(α-methylhydrazino)-4′-phenyl-2,2′:6″,2′-terpyridine have been prepared with a wide range of transition metal and main group metal ions, the condensation with glyoxal only proceeded in a satisfactory way with nickel(II) or manganese(II) as the template. However, the metal-free macrocycle L may be obtained as its dication from condensations in which the transient template ions Cr^{3+} or $[SnMe_2]^{2+}$ are used [18].

The elemental analyses and some physical properties of $H_2(L)[PF_6]_2$ and the substituted complexes $[Cu(L)(X)_2][PF_6]_2$ are given in Table 1. The molar conductivities of 10^{-3} mol dm^{-3} solutions in $MeNO_2$, MeCN or DMSO fall in the range expected for 1:2 electrolytes [29]. This is supported by the IR spectrum where two bands at 842 and 558 cm^{-1} characteristic of the non-coordinated hexafluorophosphate anion are present.

The spectrum of L itself is devoid of any evidence for the presence of either a ketonic carbonyl (1700 cm^{-1}) or primary amine groups (3300, 3200 cm^{-1}). This and the presence of a strong C=N stretching band in the range 1580–1620 cm^{-1} provide assurance that the required Schiff base linkages have formed. The spectra of the complexes show similarities to one another and include absorptions characteristic for L. The bands assigned to the pyridine ring vibrations are shifted to lower frequencies, which is a good indication of the coordination of the heterocyclic nitrogen atoms. The shifting of the ν(C=N) band to lower wavenumbers relative to the free ligand results from a decrease in the C=N double bond character upon coordination. In all the compounds the band assigned to the monosubstituted benzene falls in the range 740–730 cm^{-1}. The spectrum of the aquo complex showed in addition to the O–H stretching vibration at 3500–3400 cm^{-1} a broad band of moderate intensity at 605 cm^{-1}, which is usually assigned to wagging or rocking modes of coordinated water [30].

The UV–Vis spectrum of $[Cu(L)(H_2O)_2]^{2+}$ macrocyclic complex presents a broad band of low intensity at very low energy (6993 cm^{-1} in DMSO and 8547 cm^{-1} in acetonitrile) which parallel the spectral band at 7400 cm^{-1} observed in pentagonal bipyramidal complexes of copper(II) and assigned to the transition $^2A_1' \rightarrow {}^2E_2'$ in D_{5h} symmetry [31]. Pentagonal bipyramidal complexes of copper(II) present another band at 11 900 cm^{-1} assigned to the transition $^2A_1' \rightarrow {}^2E_1''$ which could not be detected in the present work. The high energy band observed at 20 800 cm^{-1} in nitromethane solvent appears to be too far red-shifted to tentatively assign to the aforementioned transition.

The room temperature magnetic moment of the compound $[Cu(L)(H_2O)_2][PF_6]_2$ is 1.75 μ_B, which is characteristic of high spin d^9 systems with one unpaired electron. The X-band EPR spectrum of the complex in acetonitrile glass at 77 K shows a typical pattern of magnetically dilute $S = 1/2$ centres with spectral characteristics ($g_\parallel = 2.26$, $g_\perp = 2.06$ and $A_\parallel = 170$ G) resembling those of copper(II) in other six and seven coordinate geometries. The EPR hyperfine structure (four lines) is due to interaction of the unpaired electron with the ^{63}Cu and ^{65}Cu nuclei which have the same nuclear spin $I = 3/2$.

3.1. Electrochemical studies

Cyclic voltammetry measurements on the axially substituted copper(II) complexes were made in DMSO solution where an equilibrium between the solvated species $[Cu(L)(DMSO)_n]^{2+}$ and the species incorporating the axial X substituent $[Cu(L)(X)_2]^{2+}$ should be expected. Therefore, in order to force the equilibrium in favour of the axially substituted adducts, an excess of the neutral substituent was added into the electrochemical cell. Electrolyte concentrations of 0.1 M were used in all electrochemical experiments and all solutions were degassed with argon prior to use. A well resolved reduction wave was observed for the copper(II) aquo complex at −0.36 V (less than free macrocycle $E_{1/2} = -0.94$ V) which is assigned to the Cu(II)/Cu(I) reduction.

Further electrochemical studies of axially substituted derivatives were carried out and Table 2 shows the $E_{1/2}$ values of the different reversible waves detected in our experiments. In general, the shift in $E_{1/2}$ compared with the value for the aquo species reflects a relative stabilization of the divalent metal ion. The most contrasting

Table 1
The elemental analyses and molar conductances of H_2L^{2+} and its complexes

Compound	Found (calcd) (%)			Λ_M (Ω^{-1} C m^2 mol^{-1})		
	C	H	N	$MeNO_2$	MeCN	DMSO
$H_2L[PF_6]_2$	42.53 (42.19)	3.56 (3.23)	13.42 (13.78)	134	243	52
$[Cu(L)(H_2O)_2][PF_6]_2$	34.08 (37.11)	3.65 (3.10)	11.50 (12.12)	138	278	68
$[Cu(L)(Py)_2][PF_6]_2$	45.52 (45.14)	3.65 (3.33)	13.48 (13.54)	158	279	53
$[Cu(L)(4\text{-}NCPy)_2][PF_6]_2$	45.44 (45.28)	3.25 (2.96)	15.57 (15.71)	168	253	57
$[Cu(L)(4\text{-}H_2NPy)_2][PF_6]_2$	44.73 (43.73)	3.72 (3.44)	16.38 (16.03)	145	273	54
$[Cu(L)(4\text{-}Me_2NPy)_2][PF_6]_2$	46.37 (46.04)	4.34 (4.03)	15.52 (15.15)	155	286	47
$[Cu(L)(pyrazine)_2][PF_6]_2$	42.84 (42.47)	3.16 (3.11)	16.46 (16.51)	132	247	58
$[Cu(L)(Im)_2][PF_6]_2$	40.99 (40.95)	2.99 (3.19)	17.27 (16.95)	165	224	65
$[Cu(L)(1\text{-}MeIm)_2][PF_6]_2$	42.84 (42.29)	3.75 (3.52)	16.21 (16.44)	163	283	54
$[Cu(L)(2\text{-}MeIm)_2][PF_6]_2$	42.28 (42.29)	3.37 (3.52)	16.63 (16.44)	153	238	58
$[Cu(L)(P(OMe)_3)_2][PF_6]_2$	36.59 (36.45)	3.56 (3.82)	9.43 (9.60)	144	273	62
$[Cu(L)(H_2O)_2][BF_4]$	43.87 (43.60)	3.46 (3.34)	14.16 (14.24)	80	145	35

Table 2
CV data for the axially substituted copper(II) complexes[a]

Complex	$E_{1/2}$ (V)	$E_{pa} - E_{pc}$ (mV)
$[Cu(L)(H_2O)_2]^{2+}$	−0.36	80
$[Cu(L)(Py)_2]^{2+}$	−0.36	70
$[Cu(L)(4\text{-}NCPy)_2]^{2+}$	−0.34	70
$[Cu(L)(4\text{-}H_2NPy)_2]^{2+}$	−0.41	90
$[Cu(L)(4\text{-}Me_2NPy)_2]^{2+}$	−0.40	90
$[Cu(L)(pyrazine)_2]^{2+}$	−0.36	110
$[Cu(L)(Im)_2]^{2+}$	−0.50	70
$[Cu(L)(1\text{-}MeIm)_2]^{2+}$	−0.54	80
$[Cu(L)(2\text{-}MeIm)_2]^{2+}$	−0.37	80
$[Cu(L)(P(OMe)_3)_2]^{2+}$	−0.10	120

[a] All potentials are relative to a Ag/Ag^+ reference electrode at room temperature in DMSO solution. Scan rate: 100 mV s^{-1}.

behaviour can be appreciated when imidazole or 1-methylimidazole (π donor properties) and the triphenylphosphine (π acceptor properties) are separately added to the electrochemical cell.

The bis-(1-MeIm) adduct of the copper(II) macrocycle displays a shift in the half wave potential from −0.36 V (aquo ligand) to −0.54 V which is consistent with the strong σ/π donor effects of 1-MeImidazole. The more difficult reduction of the axial 1-MeImidazole species in comparison with the aquo complex reflects the relative stabilization of the Cu(II) oxidation state towards reduction. On the other hand, the more easy reduction of the axial trimethylphosphite species (−0.10 V) in relation with the aquo complex reflects the stabilization of the copper(I) oxidation state.

Controlled potential electrolysis of $[Cu(II)(L)(P(OMe)_3)_2][PF_6]_2$ in DMSO in the presence of excess of trimethylphosphite at −0.06 V under a constant stream of argon gas led to the reduction of the copper(II) species with change of colour from dark orange to green. On completion of reduction the reaction mixture was transferred by syringe to a Schlenk tube and the copper(I) species was isolated as a green precipitate of $[Cu(L)(H_2O)_2][BF_4]$ by the addition of dry, oxygen-free diethyl ether. To confirm that the green colour is due to the formation of a copper(I) complex the compound $[Cu(L)(H_2O)_2][BF_4]_2$ was also prepared and shows the same orange colour than the starting material $[Cu(L)(H_2O)_2][PF_6]_2$. The infrared spectrum for the copper(I) complex shows similarities with the spectrum of the copper(II) complex but the PF_6 group was changed for BF_4 group from the supporting electrolyte. The B–F stretching frequency is quite broad, centred around 1084 cm^{-1} and is typical of complexes having tetrafluoroborate counter ions. The electrical conductance value in acetonitrile, nitromethane and DMSO solutions fall in the range expected for 1:1 electrolytes and the elemental analysis (Table 1) agrees well with the proposed formulae. A 400-MHz ^1H NMR spectrum of a $(CD_3)_2SO$ solution was consistent with the formulation and the mass spectrum of the salt showed a peak at m/z 417 which corresponds to the parent ion of the free macrocycle. The reduction was also followed by EPR spectroscopy, which showed the gradual loss of signal assigned to high spin d^9 copper(II), and on completion of the reduction no EPR signal could be observed at 77 K as DMSO glass. The EPR spectrum of the isolated green material exhibited no signals at all. This was consistent with the formation of a low spin d^{10} copper(I) species and confirming the process as a metal centred reduction following Nelson's criteria [32].

The electrochemical results described above are analogous to the redox properties observed for $[Co(L)(H_2O)_2]^{2+}$ $E_{1/2} = -1.35$ V [21] in which reduction occurs also at the metal centre. This is in contrast to the redox properties of Ni(II) [24], Mn(II) [23] and Fe(II) [22] complexes of L which on addition of $P(OMe)_3$ to their solutions in the electrochemical cell showed essentially no shifts in the value of $E_{1/2}$ for the above reduction process. No metal(I) species could be detected in the quantitative reductions of such solutions. These are ligand centred processes.

The CV of $[Cu(L)(H_2O)_2]^{2+}$, $[Cu(L)(1\text{-}MeIm)_2]^{2+}$ and $[Cu(L)(P(OMe)_3)_2]^{2+}$ in DMSO is shown in Fig. 1. Finally, the cyclic voltammetry in most cases showed peak separation ($E_{pa} - E_{pc}$) near 80 mV suggesting that the electrode reactions approached Nernstian behaviour. All the attempts to crystallize reduced species were not successful.

3.2. Structure of $[Cu(L)(Im)_2][PF_6]_2$

X-ray crystallographic study revealed that the structure comprises a cationic macrocyclic coppert(II) complex (see Fig. 2), two PF_6^- counter anions and a

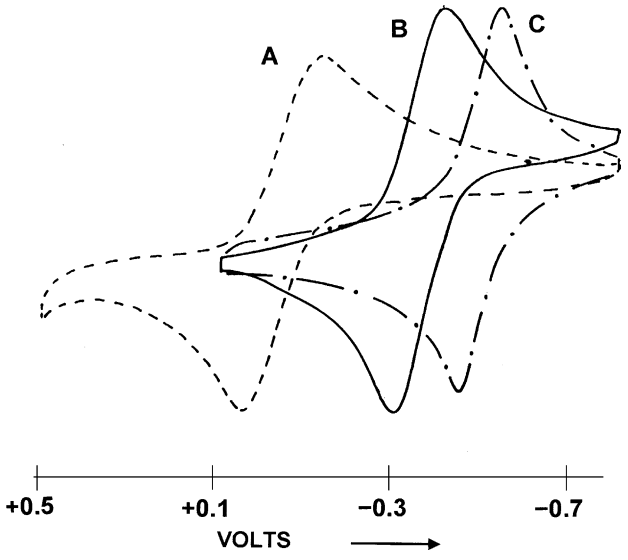

Fig. 1. Voltammogram of copper(II) systems: (A) $[Cu(L)(H_2O)_2]^{2+}$ (B) $[Cu(L)(I\text{-}MeIm)_2]^{2+}$ and (C) $[Cu(L)(P(OMe)_3)_2]^{2+}$.

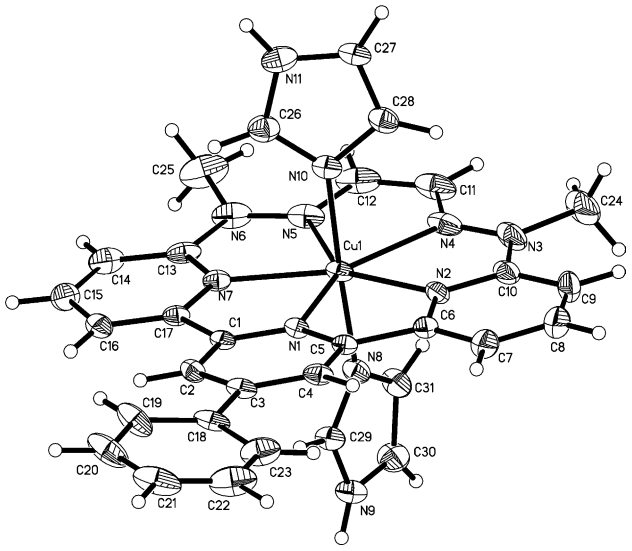

Fig. 2. Perspective view of the macrocyclic cationic complex showing the atomic numbering scheme.

molecule of imidazole of solvation, these both species are involved in strong hydrogen bonds in order to give extra stabilization to the complex. The central copper(II) ion is seven coordinated with five sites within the macrocycle, three pyridyl and two diamine nitrogen atoms [Cu(1)–N(1) 2.170(2), Cu(1)–N(2) 2.189(2), Cu(1)–N(7) 2.195(2), Cu(1)–N(4) 2.255(2) and Cu(1)–N(5) 2.223(2) Å], and to two nitrogens of two imidazole molecules [Cu(1)–N(8) 2.035(2) and Cu(1)–N(10)

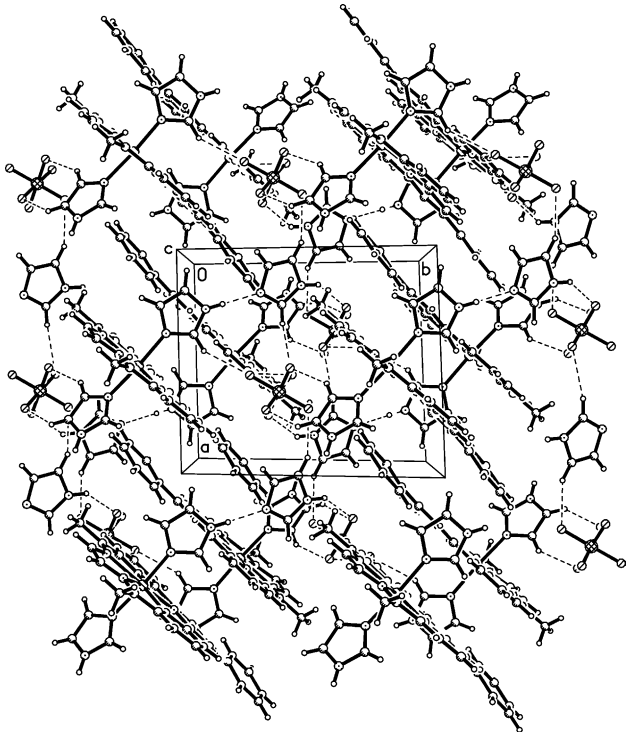

Fig. 3. A view of packing of the macrocyclic cation along the *c*-axis.

Table 3
Crystal data summary of intensity data collection and structure refinement for $[Cu(L)(Im)_2][PF_6]_2 \cdot C_3H_4N_2$[a]

Empirical formula	$C_{34}H_{33}CuF_{12}N_{13}P_2$
Crystal system	triclinic
Space group	$P\bar{1}$
Unit cell dimensions	
a (Å)	10.322(3)
b (Å)	12.292(4)
c (Å)	16.053(5)
α (°)	72.722(5)
β (°)	83.021(5)
γ (°)	86.329(5)
V (Å^3)	1929.6(10)
Z	2
Formula weight	977.22
D_{calc} (g cm^{-3})	1.682
Absorption coefficient (mm^{-1})	0.755
$F(000)$	990
Reflections collected	15 601
Independent reflections (R_{int})	7928 (2.97)
Data/restraints/parameters	7928/0/571
Final R indices ($I > 2\sigma(I)$) (%)	$R_1 = 4.33$, $wR_2 = 10.66$
Final R indices (all data)	$R_1 = 5.83$, $wR_2 = 11.45$
Goodness-of-fit on F^2	1.025
Largest difference peak and hole (e Å^{-3})	0.428 and −0.310

[a] Temperature 150 (2) K. θ range for data collection 1.74–26.40°. Scan type: ϕ and ω scans. Index ranges: $-12 \leqslant h \leqslant 12$, $-15 \leqslant k \leqslant 15$, $-20 \leqslant l \leqslant 20$. Solution: direct method. Quantity minimized: $wR_2 = \{[\sum w(F_o^2 - F_c^2)^2]/\sum wF_o^4\}^{0.5}$. Weighting scheme $w = [\sigma^2(F_o^2) + (xP)^2 + yP]^{-1}$, where $P = (F_o^2 + 2F_c^2/3)$.

Table 4
Selected bond lengths (Å) and angles (°)

Bond lengths	
Cu(1)–N(1)	2.170(2)
Cu(1)–N(2)	2.189(2)
Cu(1)–N(7)	2.195(2)
Cu(1)–N(10)	2.041(2)
Cu(1)–N(8)	2.035(2)
Cu(1)–N(5)	2.223(2)
Cu(1)–N(4)	2.255(2)
Bond angles	
N(1)–Cu(1)–N(2)	73.61(8)
N(1)–Cu(1)–N(7)	72.67(8)
N(2)–Cu(1)–N(7)	146.26(8)
N(1)–Cu(1)–N(10)	91.93(8)
N(2)–Cu(1)–N(10)	89.74(8)
N(7)–Cu(1)–N(10)	90.14(9)
N(1)–Cu(1)–N(8)	91.99(8)
N(2)–Cu(1)–N(8)	90.78(8)
N(7)–Cu(1)–N(8)	91.61(8)
N(10)–Cu(1)–N(8)	176.03(8)
N(1)–Cu(1)–N(5)	143.72(9)
N(2)–Cu(1)–N(5)	142.54(9)
N(7)–Cu(1)–N(5)	71.08(9)
N(10)–Cu(1)–N(5)	86.55(8)
N(8)–Cu(1)–N(5)	90.64(8)
N(1)–Cu(1)–N(4)	143.82(9)
N(2)–Cu(1)–N(4)	70.24(9)
N(7)–Cu(1)–N(4)	143.39(9)
N(10)–Cu(1)–N(4)	86.48(9)
N(8)–Cu(1)–N(4)	89.99(8)
N(5)–Cu(1)–N(4)	72.33(10)

Table 5
Hydrogen bond distances (Å) and angles (°)

D–H···A	D–H	H···A	D···A	⟨D–H···A
N(9)–H(9N)···N(12)^{i}	0.84(3)	1.96(4)	2.794(3)	169(3)
N(11)–H(11N)···F(3)^{ii}	0.87(4)	2.64(4)	3.312(4)	135(3)
N(11)–H(11N)···F(6)^{ii}	0.87(4)	2.47(4)	2.960(3)	116(3)
N(13)–H(13N)···F(8)^{iii}	0.89(2)	2.32(4)	3.099(4)	146(5)
C(8)–H(8)···F(9)^{iv}	0.95	2.54	3.482(4)	170.2
C(8)–H(8)···F(10)^{iv}	0.95	2.52	3.244(4)	133.1
C(15)–H(15)···F(2)^{v}	0.95	2.47	3.260(4)	140.5
C(25)–H(25B)···F(1)^{vi}	0.98	2.49	3.269(4)	136.5
C(26)–H(26)···N(7)	0.95	2.58	3.077(4)	112.6
C(26)–H(26)···F(1)^{vi}	0.95	2.48	3.074(4)	120.2
C(27)–H(27)···F(6)^{ii}	0.95	2.55	3.010(3)	110.3
C(27)–H(27)···F(12)	0.95	2.48	3.246(4)	138.0
C(28)–H(28)···F(7)	0.95	2.35	3.175(3)	144.7
C(29)–H(29)···F(9)^{vii}	0.95	2.49	3.289(3)	142.1
C(32)–H(32)···F(10)^{viii}	0.95	2.53	3.402(4)	152.0
C(33)–H(33)···F(11)^{iv}	0.95	2.31	3.191(4)	153.5

Symmetry transformations used to generate equivalent atoms: (i) $-x+2,-y,-z+1$; (ii) $-x+1,-y+1,-z$; (iii) $x+1,y,z$; (iv) $-x+1,-y+1,-z+1$; (v) $-x+1,-y,-z$; (vi) $x-1,y,z$; (vii) $x,y-1,z$; (viii) $-x+2,-y+1,-z+1$.

2.041(2) Å]. The coordination geometry of the Cu(II) is a pentagonal bipyramid [N–Cu–N angles within the five coordination planes are: 73.61(8)°, 70.24(9)°, 72.33(10)°, 71.08(9)°, 72.67(8)° and the angle between axial nitrogens N(8)–Cu(1)–N(10) is 176.03(8)°].

The coordinated imidazole molecules are situated quite perpendicular to the main coordination macrocyclic plane (on average value of 90.02°). Coordinated imidazoles are rotated between each other by 65.0° and the phenyl substituent of one of the macrocyclic pyridyl groups is rotated to the main coordination plane by 13.30°. A view of packing of the structure along the *c*-axis is given in Fig. 3 which shows the accommodation of the main coordination plane of the complex cation in a diagonal distribution, and its hydrogen bonding interactions. The relevant crystal data and structure parameters are summarized in Table 3, selected bond lengths and angles are given in Table 4 and hydrogen bonds distances are given in Table 5.

4. Supplementary data

Crystallographic data for the structural analysis have been deposited with the Cambridge Crystallographic Data Centre, 12 Union Road, Cambridge CB2 1EZ, UK (fax: +44-1223-336033; E-mail: deposit@ccdc.cam.ac.uk or www: http://www.ccdc.cam.ac.uk) CCDC No. 205590.

Acknowledgements

V.E.M. is very much indebted to Professor Lord J. Lewis, Professor E.C. Constable and Dr. S. McQueen for their support and continuous encouragement. D.L. thanks to the Universidad de Oriente for support.

References

[1] P. Zanello, R. Seeber, A. Cinquantini, G. Mazzocchin, L. Fabbrizzi, J. Chem. Soc., Dalton Trans. (1982) 893.
[2] L. Fabbrizzi, A. Poggi, P. Zanello, J. Chem. Soc., Dalton Trans. (1983) 2191.
[3] F.F. Lovecchio, E.S. Gore, D.H. Busch, J. Am. Chem. Soc. 96 (1974) 3109.
[4] D.C. Olson, J. Vasilevskis, Inorg. Chem. 8 (1969) 1611.
[5] D.C. Olson, J. Vasilevskis, Inorg. Chem. 10 (1971) 463.
[6] C.W.G. Ansell, J. Lewis, P.R. Raithby, J.N. Ramsden, M. Schröder, J. Chem. Soc., Chem. Commun. (1982) 546.
[7] C.W.G. Ansell, J. Lewis, M.C. Liptrot, P.R. Raithby, M. Schröder, J. Chem. Soc., Dalton Trans. (1982) 1593.
[8] M.M. Bishop, J. Lewis, T.D. O' Donoghue, P.R. Raithby, J. Chem. Soc., Chem. Commun. (1978) 476.
[9] J. Lewis, T.D. O' Donoghue, P.R. Raithby, J. Chem. Soc., Dalton Trans. (1980) 1383.
[10] J. Lewis, M. Schröder, J. Chem. Soc., Dalton Trans. (1982) 1085.
[11] R.R. Gagné, J.L. Allison, R.S. Gall, C.A. Koval, J. Am. Chem Soc. 99 (1977) 7170.
[12] A.W. Addison, M. Carpenter, L.K.-M. Lau, W. Wicholas, Inorg. Chem. 17 (1978) 1545.
[13] R.R. Gagné, J.L. Allison, D.M. Ingle, Inorg. Chem. 18 (1979) 2767.
[14] R.R. Gagné, D.M. Ingle, J. Am. Chem. Soc. 102 (1980) 1444.
[15] V.L. Goedken, S.-M. Peng, J. Chem. Soc., Chem. Commun. (1974) 914.
[16] E.C. Constable, J. Lewis, Polyhedron 1 (1982) 303.
[17] E.C. Constable, J. Lewis, M. Liptrot, P.R. Raithby, M. Schröder, Polyhedron 2 (1983) 301.
[18] E.C. Constable, J. Lewis, M. Liptrot, P.R. Raithby, J. Chem. Soc., Dalton Trans. (1984) 2177.
[19] E.C. Constable, F.K. Khan, J. Lewis, M.C. Liptrot, P.R. Raithby, J. Chem. Soc., Dalton Trans. (1985) 333.
[20] V.E. Marquez, J.R. Anacona, Polyhedron 16 (1997) 2375.
[21] V.E. Marquez, J.R. Anacona, Polyhedron 20 (2001) 1885.

[22] V.E. Marquez, J.R. Anacona, Transition Met. Chem. 25 (2000) 188.
[23] V.E. Marquez, J.R. Anacona, Transition Met. Chem. (2004) in press.
[24] V.E. Marquez, J.R. Anacona, J. Coord. Chem. 49 (2000) 281.
[25] SAINT Bruker 2002, Bruker-AXS, Madison, WI, USA.
[26] G.M. Sheldrick, SADABS: Version 2.06, University of Göttingen, Germany, 2001.
[27] G.M. Sheldrick, SHELXS-97, University of Göttingen, Germany, 1997.
[28] G.M. Sheldrick, SHELXL-97, University of Göttingen, Germany, 1997.
[29] W.J. Geary, Coord. Chem. Rev. 7 (1971) 81.
[30] M.G.B. Drew, J. Grimshaw, P.D.A. McIlroy, S.M. Nelson, J. Chem. Soc., Dalton Trans. (1976) 1388.
[31] S.M. Nelson, C.V. Knox, J. Chem. Soc., Dalton Trans. (1983) 2525.
[32] S.M. Nelson, M. McCann, C. Stevenson, M.G.B. Drew, J. Chem. Soc., Dalton Trans. (1979) 1477.

Available online at www.sciencedirect.com
SCIENCE DIRECT®
Polyhedron 23 (2004) 1325–1331
POLYHEDRON
www.elsevier.com/locate/poly

Template condensation reactions of formaldehyde with amines and 2,3-butanedihydrazone: preparation and properties of nickel(II) complexes of 18-membered decaaza macrocycles

Masoud Salavati-Niasari *, Mostafa Rezai-Adaryani

Department of Chemistry, University of Kashan, Kashan 4354365567, Iran

Received 4 October 2003; accepted 30 January 2004
Available online 10 April 2004

Abstract

Six new square-planar nickel(II) complexes of 18-membered decaaza macrocyclic ligands 5,6,14,15-tetramethyl-1,3,4,7,8,10,12,13,16,17-decaazacyclooctadecane $[Ni(Me_4[18]aneN_{10})](ClO_4)_2$ (**1**); 1,10-dimethyl-$[Ni(Me_2Me_4[18]aneN_{10})](ClO_4)_2$ (**2**); 1,10-diethyl-$[Ni(Et_2Me_4[18]aneN_{10})](ClO_4)_2$ (**3**); 1,10-dipropyl-$[Ni(Pr_2Me_4[18]aneN_{10})](ClO_4)_2$ (**4**); 1,10-dibutyl^{iso}-$[Ni(Bu_2Me_4[18]aneN_{10})](ClO_4)_2$ (**5**); 1,10-dibenzyl-5,6,14,15-tetramethyl-1,3,4,7,8,10,12,13,16,17-decaazacyclooctadecane $[Ni((Benzyl)_2Me_4[18]aneN_{10})](ClO_4)_2$ (**6**); $[Ni(Me_4[18]aneN_{10})](PF_6)_2$ (**7**); $[Ni(Me_2Me_4[18]aneN_{10})](PF_6)_2$ (**8**); $[Ni(Me_4Me_4[18]aneN_{10})](PF_6)_2$ (**9**); $[Ni(Pr_2Me_4[18]aneN_{10})](PF)_2$ (**10**); $[Ni(Bu_2Me_4[18]aneN_{10})](PF_6)_2$ (**11**); $[Ni((Benzyl)_2Me_4[18]aneN_{10})](PF_6)_2$ (**12**); $[Ni(Me_4[18]aneN_{10})(NCS)_2]$ (**13**); $[Ni(Me_2Me_4[18]aneN_{10})(NCS)_2]$ (**14**); $[Ni(Et_2Me_4[18]aneN_{10})(NCS)_2]$ (**15**); $[Ni(Pr_2Me_4[18]aneN_{10})(NCS)_2]$ (**16**); $[Ni(Bu_2Me_4[18]aneN_{10})(NCS)_2]$ (**17**) and $[Ni((Benzyl)_2Me_4[18]aneN_{10})(NCS)_2]$ (**18**) have been prepared from the one-pot template condensation reaction of formaldehyde, 2,3-butanedihydrazone with alkyl and benzyl amine in the presence of the nickel(II) ion. Elemental analyses, IR, UV–Vis spectroscopy, conductometric and magnetic measurements have been used to characterize the nickel(II) complexes of these decaaza macrocycles. The spectra of $[Ni(R_2Me_4[18]aneN_{10})](ClO_4)_2$ shows that the four nitrogen (α-diimine) atoms are coordinated to the nickel(II) ion. The hydrazones of the (α-diimine) function have the *anti–anti* configuration yielding a macrocyclic species with D_{2h} symmetry. The nickel(II) complexes are diamagnetic and four coordinate, exhibiting only weak interactions with different solvents. The physical and chemical properties of the complexes are compared with other closely related complexes.
© 2004 Elsevier Ltd. All rights reserved.

Keywords: Template synthesis; Decaazacyclooctadecane; Nickel(II) complexes; Macrocycle

1. Introduction

Metal template syntheses often provide selective routes toward products that are not obtainable in the absence of metal ions. Especially, template reactions involving formaldehyde and amines facilitate the preparation of saturated polyaza multidenatate, macrocyclic and macropolycyclic complexes [1–6]. The reactions are simple "one-pot reactions", cheap and high yielding. Metal template condensation reactions involving amines and formaldehyde have been employed in the preparation of various saturated polyazamacrocyclic complexes [7–13].

A wide variety of amines, both "free" and coordinated, are known to react with aldehydes to form a more complicated amine ligand. The products of these reactions can be of many different types, although the innumerable Schiff-base ligands represent the largest class of these ligands. Related types of reactions include the well-known reaction of ammonia with formaldehyde to yield hexamethylenetetramine (I) [14]. More recent examples of polydentate and macrocyclic ligand syntheses from the reaction of amines with formaldehyde (II, III) are illustrated [13,15,16].

The octaazamacrocyclic complexes,(VII), obtained by the metal template condensation of 2,3-butanedihydrazone with aldehydes have uncoordinated secondary nitrogen atoms which are capable of under-

* Corresponding author. Tel.: +98-361-555-333; fax: +98-361-552-930.
E-mail address: salavati@kashanu.ac.ir (M. Salavati-Niasari).

0277-5387/$ - see front matter © 2004 Elsevier Ltd. All rights reserved.
doi:10.1016/j.poly.2004.02.016

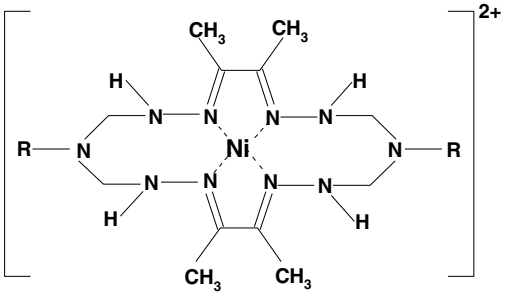

R	complex	complex number
H	$[Ni(Me_4[18]aneN_{10})](ClO_4)_2$	1
Methyl	$[Ni(Me_2Me_4[18]aneN_{10})](ClO_4)_2$	2
Ethyl	$[Ni(Et_2Me_4[18]aneN_{10})](CLO_4)_2$	3
Propyl	$[Ni(Pr_2Me_4[18]aneN_{10})](ClO_4)_2$	4
Iso-buthyl	$[Ni(Bu_2Me_4[18]aneN_{10})](ClO_4)_2$	5
Benzyl	$[Ni((Benzyl)_2Me_4[18]aneN_{10}](ClO_4)_2$	6
H	$[Ni(Me_2Me_4[18]aneN_{10})](PF_6)_2$	7
Methyl	$[Ni(Me_2Me_4[18]aneN_{10})](PF_6)_2$	8
Ethyl	$[Ni(Et_2Me_4[18]aneN_{10})](PF_6)_2$	9
Propyl	$[Ni(Pr_2Me_4[18]aneN_{10})](PF_6)_2$	10
Iso-buthyl	$[Ni(Bu_2Me_4[18]aneN_{10})](PF_6)_2$	11
Benzyl	$[Ni((Benzyl)_2Me_4[18]aneN_{10}](PF_6)_2$	12
H	$[Ni(Me_4[18]aneN_{10})(NCS)_2]$	13
Methyl	$[Ni(Me_2Me_4[18]aneN_{10})(NCS)_2]$	14
Ethyl	$[Ni(Et_2Me_4[18]aneN_{10})(NCS)_2]$	15
Propyl	$[Ni(Pr_2Me_4[18]aneN_{10})(NCS)_2]$	16
Iso-buthyl	$[Ni(Bu_2Me_4[18]aneN_{10})(NCS)_2]$	17
Benzyl	$[Ni((Benzyl)_2Me_4[18]aneN_{10}(NCS)_2]$	18

Scheme 1.

going further reactions with aldehydes [17]. It was therefore expected that (VII) might undergo a further condensation reaction with formaldehyde and ammonia to yield a tricyclic macro ring ligand (VIII) in which two triazacyclohexan rings were fused to the original 14-membered macrocyclic ring. The products obtained in all cases were of type (IX) that formally results from the condensation of four molecules of formaldehyde with the macrocyclic complexes of type (VII) [18].

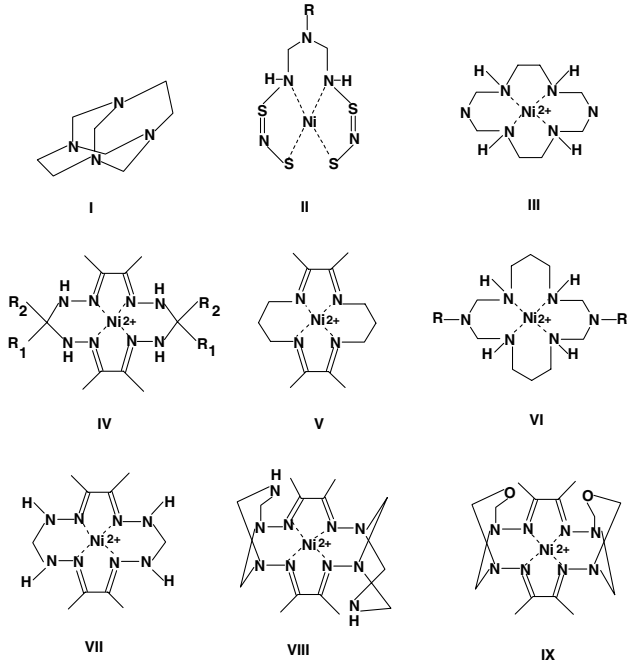

In this paper, we report the synthesis, characterization and properties of the new square planar nickel(II) complexes of 5,6,14,15-tetramethyl-1,3,4,7,8,10,12,13,16,17-decaazacyclooctadecane $[Ni(Me_4[18]aneN_{10})](ClO_4)_2$ (**1**), 1,10-dimethyl-$[Ni(Me_2Me_4[18]aneN_{10})](ClO_4)_2$ (**2**), 1,10-diethyl-$[Ni(Et_2Me_4[18]aneN_{10})](ClO_4)_2$ (**3**), 1,10-dipropyl-$[Ni(Pr_2Me_4[18]aneN_{10})](ClO_4)_2$ (**4**), 1,10-dibutyl^{iso}-$[Ni(Bu_2Me_4[18]aneN_{10})](ClO_4)_2$ (**5**), 1,10-dibenzyl-5,6,14,15-tetramethyl-1,3,4,7,8,10,12,13,16,17-decaazacylooctadecane $[Ni((Benzyl)_2Me_4[18]aneN_{10})](ClO_4)_2$ (**6**), $[Ni(Me_4[18]aneN_{10})](PF_6)_2$ (**7**), $[Ni(Me_2Me_4$ [18]aneN$_{10}$)$](PF_6)_2$ (**8**), $[Ni(Me_4Me_4[18]aneN_{10})](PF_6)_2$ (**9**), $[Ni(Pr_2Me_4[18]aneN_{10})](PF)_2$ (**10**), $[Ni(Bu_2Me_4[18]$ aneN$_{10}$)$](PF_6)_2$ (**11**), $[Ni((Benzyl)_2Me_4[18]aneN_{10})](PF_6)_2$ (**12**), $[Ni(Me_4[18]aneN_{10})(NCS)_2]$ (**13**), $[Ni(Me_2Me_4[18]$ aneN$_{10}$)$(NCS)_2]$ (**14**), $[Ni(Et_2Me_4[18]aneN_{10})(NCS)_2]$ (**15**), $[Ni(Pr_2Me_4[18]aneN_{10})(NCS)_2]$ (**16**), $[Ni(Bu_2Me_4$ [18]aneN$_{10}$)$(NCS)_2]$ (**17**) and $[Ni((Benzyl)_2Me_4[18]aneN_{10})(NCS)_2]$ (**18**), which are given in Scheme 1.

2. Experimental

2.1. Materials and measurements

Safety note. Perchlorate salts of transition metal complexes with organic ligands are often explosive and should be handled with caution. All chemicals and solvents used in the syntheses were of reagent grade and were used without further purification. For the spectroscopic measurements, water was distilled and organic solvents were purified according to the literature method [19]. Electronic absorption spectra were obtained with a Shimadzu UV–Vis scanning spectrophotometer (Model 2101 PC), FTIR spectra with a Shimadzu Varian 4300 spectrophotometer, ^{1}H NMR spectra with a Bruker AC 80 (in CH_3NO_2-d_3 as solvent), and conductance measurements with a Metrohm Herisau conductometer E 518. The elemental analyses (carbon, hydrogen and ni-

trogen) of the complexes were obtained from a Carlo ERBA Model EA 1108 analyser. Magnetic moments were calculated from magnetic susceptibility data obtained using a Johnson Matthey MK-1 magnetic susceptibility balance. Atomic Absorption Spectra (AAS) were recorded on a Perkin–Elmer 4100-1319 spectrophotometer.

2.2. Preparation of 2,3-butanedihydrazone

2,3-butanedihydrazone was prepared by the method of Bush and Bailar [20].

2.3. Preparation of [Ni(Me_2Me_4[18]$aneN_{10}$)]$(ClO_4)_2$ (**2**)

To a stirred methanol solution (500 ml) of $NiCl_2 \cdot 6H_2O$ (10.00 g, 42.07 mmol) were slowly added 2,3-butanedihydrazone (9.61 g, 84.20 mmol), 36% formaldehyde (13 ml) and 36% methylamine (10.47 ml, 84.20 mmol). One drop of concentrated perchloric acid was added to catalyse the condensation reaction. The mixture was heated at reflux for 24 h until a dark red solution resulted. The solution was cooled to room temperature and filtered to remove nickel hydroxide. Excess percholoric acid or lithium perchlorate dissolved in methanol was added to the filtrate, and the mixture was kept in the refrigerator until a red-brown solid formed. The red-brown solid was filtered, washed with diethyl ether, and air-dried. The product was crystallized from hot water. Yield: ~48%. *Anal*. Calc. for (**2**); Ni, 9.85; C, 28.21; H, 5.07; N, 23.50. Found Ni, 9.76; C, 28.11; H, 5.01; N, 23.61%.

2.4. Preparation of [Ni(Me_4[18]$aneN_{10}$)]$(ClO_4)_2$ (**1**)

The procedure followed was similar to that for [Ni(Me_2Me_4[18]$aneN_{10}$)]$(ClO_4)_2$, except that 25% ammonia (6.3 ml, 84.20 mmol) was used instead of methylamine. Yield: ~41%. *Anal*. Calc. for (**1**): Ni, 10.33; C, 25.37; H, 4.61; N, 24.66%. Found: Ni, 10.24; C, 25.27; H, 4.50; N, 24.72%.

2.5. Preparation of [Ni(Et_2Me_4[18]$aneN_{10}$)]$(ClO_4)_2$ (**3**)

This complex was prepared by a method similar to that for [Ni(Me_2Me_4[18]$aneN_{10}$)]$(ClO_4)_2$, except 50% ethylamine (8.72 ml, 84.20 mmol) was used instead of methylamine. Yield: ~38%. *Anal*. Calc. for (**3**): Ni, 9.40; C, 30.79; H, 5.49; N, 22.22. Found: Ni, 9.28; C, 30.68; H, 5.41; N, 22.51%.

2.6. Preparation of [Ni(Pr_2Me_4[18]$aneN_{10}$)]$(ClO_4)_2$ (**4**)

The procedure followed was similar to that for [Ni(Me_2Me_4[18]$aneN_{10}$)]$(ClO_4)_2$, except that propylamine (6.91 ml, 84.2 mmol) was used instead of methylamine. Yield: ~39%. *Anal*. Calc. for (**4**): Ni, 8.99; C, 33.15; H, 5.87; N, 21.48. Found: Ni, 8.81; C, 33.04; H, 5.78; N, 21.56%.

2.7. Preparation of [Ni($Bu^{iso}_2Me_4$[18]$aneN_{10}$)]$(ClO_4)_2$ (**5**)

This complex was prepared by a method similar to that for [Ni(Me_2Me_4[18]$aneN_{10}$)]$(ClO_4)_2$, except *iso*-butylamine (8.36 ml, 84.20 mmol) was used instead of methylamine. Yield: ~42%. *Anal*. Calc. for (**5**): Ni, 8.63; C, 35.31; H, 6.22; N, 20.59. Found: Ni, 8.54; C, 35.22; H, 6.09; N, 20.64%.

2.8. Preparation of [Ni($(Benzyl)_2Me_4$[18]$aneN_{10}$)]$(ClO_4)_2$ (**6**)

This complex was prepared by a method similar to that for [Ni(Me_2Me_4[18]$aneN_{10}$)]$(ClO_4)_2$, except benzyl amine (9.2 ml, 84.20 mmol) was used instead of methylamine. Yield: ~52%. *Anal*. Calc. for (**6**): Ni, 7.84; C, 41.74; H, 5.12; N, 18.72. Found: Ni, 7.76; C, 41.69; H, 5.01; N, 18.93%.

2.9. Preparation of [Ni(R_2Me_4[18]$aneN_{10}$)](PF_6) (**7**)–(**12**)

A solution of 3.1 mmol NH_4PF_6 in 5 ml of H_2O was added to a solution of 1.2 mmol [Ni(R_2Me_4[18]$aneN_{10}$)]$(ClO_4)_2$ (**1**)–(**6**) in 10 ml of H_2O. The brown-orange product that precipitated was filtered, washed with H_2O and dried in air. *Anal*. Calc. for (**7**) (Yield: ~70%): Ni, 8.90; C, 21.86; H, 3.98; N, 21.25. Found: Ni, 8.74; C, 21.74; H, 3.89; N, 21.32%. *Anal*. Calc. for (**8**) (Yield: ~71%): Ni, 8.54; C, 24.47; H, 4.40; N, 20.38. Found: Ni, 8.42; C, 24.31; H, 4.36; N, 20.42%. *Anal*. Calc. for (**9**) (Yield: ~73%): Ni, 8.21; C, 26.87; H, 4.79; N, 19.58. Found: Ni, 8.13; C, 26.80; H, 4.68; N, 19.71%. *Anal*. Calc. for (**10**) (Yield: ~75%): Ni, 7.95; C, 29.29; H, 4.61; N, 18.95. Found: Ni, 7.86; C, 29.21; H, 4.51; N, 19.05%. *Anal*. Calc. for (**11**) (Yield: ~76%): Ni, 7.66; C, 31.33; H, 4.96; N, 18.26. Found: Ni, 7.58; C, 31.23; H, 4.83; N, 18.32%. *Anal*. Calc. for (**12**) (Yield: ~78%): Ni, 7.03; C, 37.41; H, 4.07; N, 16.77. Found: Ni, 6.91; C, 37.33; H, 3.92; N, 16.85%.

2.10. Preparation of [Ni(R_2Me_4[18]$aneN_{10}$)][$(NCS)_2$] (**13**)–(**18**)

A saturated solution of NaNCS in 10 ml of CH_3CN was added to a solution containing 0.2 g of [Ni(R_2Me_4[18]$aneN_{10}$)]$(ClO_4)_2$ (**1**)–(**6**) in 20 ml of CH_3CN. The solution was allowed to stand at room temperature and then the pink precipitate that formed was filtered, washed with acetonitrile, and dried in vacuum. *Anal*. Calc. for (**13**) (Yield: ~52%): Ni, 12.09;

C, 34.65; H, 5.40; N, 34.64. Found: Ni, 11.86; C, 34.49; H, 5.31; N, 34.78%. *Anal.* Calc. for (**14**) (Yield: ~53%): Ni, 11.43; C, 37.44; H, 5.89; N, 32.75. Found: Ni, 11.30; C, 37.29; H, 5.76; N, 32.89%. *Anal.* Calc. for (**15**) (Yield: ~55%): Ni, 10.84; C, 39.94; H, 6.33; N, 31.05. Found: Ni, 10.71; C, 9.78; H,. 22; N, 31.21%. *Anal.* Calc. for (**16**) (Yield: ~56%): Ni, 10.31; C, 42.19; H, 6.73; N, 29.52. Found: Ni, 10.20; C, 42.01; H, 6.59; N, 29.66%. *Anal.* Calc. for (**17**): (Yield: ~57%): Ni, 9.82; C, 44.22; H, 7.09; N, 28.13%. Found: Ni, 9.71; C, 44.11; H, 6.89; N, 28.28%. *Anal.* Calc. for (**18**): (Yield: ~59%): Ni, 8.82; C, 50.53; H, 5.76; N, 25.26. Found: Ni, 8.69; C, 50.41; H, 5.61; N, 25.34%.

2.11. Preparation of [Ni($C_{14}H_{28}N_{10}$)] (*XII*)

Triethylamine (0.5ml) was added to a deaerated solution of 200 mg of (**2**) in 15 ml of CH_3CN. The red-brown solution changed to an intense dark red colour upon mixing the reagents. The air-sensitive product, which began precipitating within minutes, was filtered after 0.5 h under a nitrogen atmosphere, washed with anhydrous ethanol, and dried in vacuum. IR (KBr, cm^{-1}): 1598 ($\nu_{C=N}$). *Anal.* Calc. for [Ni($C_{14}H_{28}N_{10}$)]: Ni, 14.84; C, 42.58; H, 7.09; N, 35.45. Found: Ni, 14.77; C, 14.77; H, 6.91; N, 35.53%.

3. Results and discussion

Decaaza bis (α-diimine) macrocyclic nickel(II) complexes were prepared by reacting 2 equivalents of 2,3-butanedihydrazone, 4 equivalents of formaldehyde with 2 equivalents of the appropriate amine in the presence of the nickel(II) ion (Schemes 1, 2). It was observed that the 18-membered decaaza macrocyclic product obtained from the reaction was largely affected by the molar ratio of the reactants. The cyclization process is acid catalysed, but large excesses of acid destroy the complexes. The crude product often contained a small amount of the octaazabis (α-diimine) macrocyclic (VII) complex as a by-product. However, the mononuclear complex can be readily isolated by fractional recrystallization of the product from ca. 0.05 M $HClO_4$ aqueous solutions.

The free amino groups of coordinated 2,3-butanedihydrazone are ideally oriented for ring closure by reaction with carbonyl functions to give six-membered chelated rings and ultimately octaaza-14-membered ring macrocyclic complexes, with the 2,3,9,10-tetramethyl-1,4,5,7,8,11,12,14-octaazacyclotetradeca-1,3,8,10-tetraene ligand (IV). This type of reaction closely parallels that reported by Kerwin and Melson [21] in which tetradentate ligands were formed by the condensation of benzil monohydrazone in the presence of Ni(II). In the

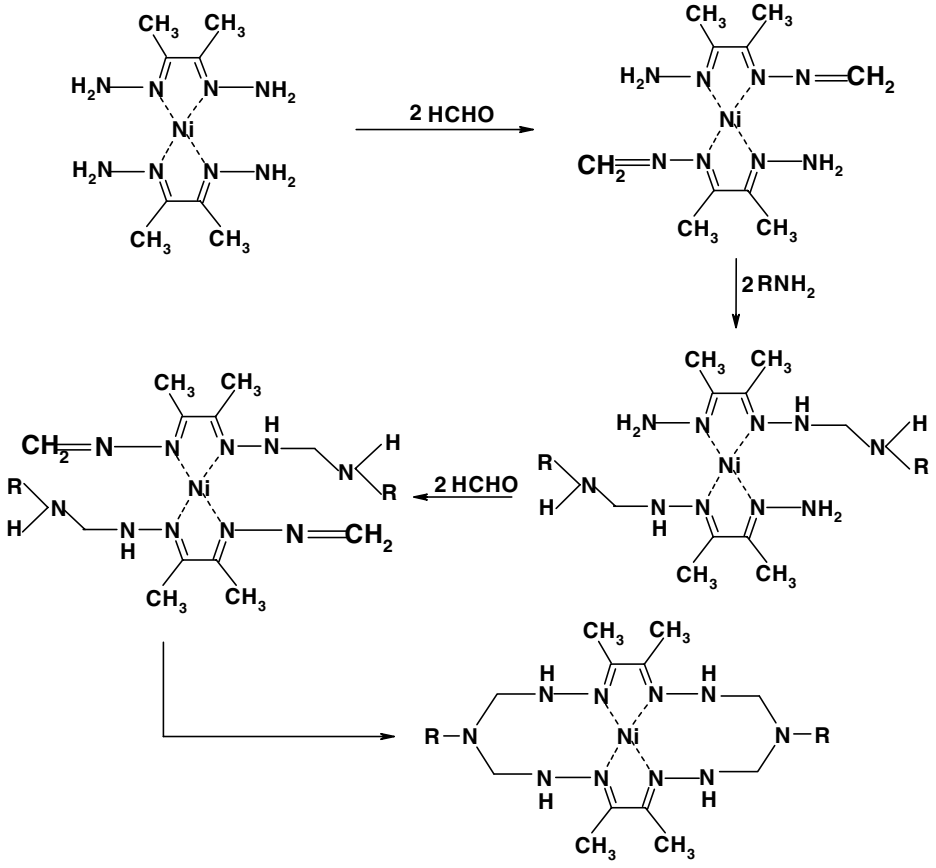

Scheme 2.

absence of added carbonyls, the 2,3-butanedihydrazone complexes described by Stouffer and Busch [22] are formed.

The complexes in this paper (Scheme 1) were expected to have physical properties very similar to those of the metal complexes of 2,3,9,10-tetramethyl-1,4,8,11-tetraazacyclotetradeca-1,3,8, 10-tetraene(V) [23,24], but to be much more chemically reactive for a number of reasons. The 18-membered decaazamacrocycle contains hydrazone linkages, which are more reactive than the 1,3-diaminopropane ring (V) complexes. In addition, C–N linkages are easier to oxidize than C–C single bonds. Other possible reactions include (a) reduction of the C=N double bonds (the resulting completely saturated complexes should have no particularly unusual physical properties, however, reoxidation of the ligand should occur at the N–N linkages in the 18-membered decaaza macrocycle yielding a new type of chelate ring), (b) nucleophilic attack on C=N double bonds, (c) deprotonation of hydrazine protons, (d) further condensation reaction which can occur at the secondary N–H centers. The decaazabis(α-diimine) macrocyclic ligands are strong-field ligands and promote spin pairing whenever possible. The magnetic moments (−0.10 to $-0.51\mu_B$) of the nickel(II) complexes measured in the solid state correspond to the square-planar coordination geometry of the complexes.

The possibility of *syn–anti* and *anti–anti* isomerization among the free dihydrazone ligands and their decaaza complexes were considered. Both isomers of 2,3-butanedihydrazone are capable of forming metal chelates with the *syn–anti* configuration forming six-membered chelate rings, while the *anti–anti* configuration yield five-membered α-diimine chelate rings.

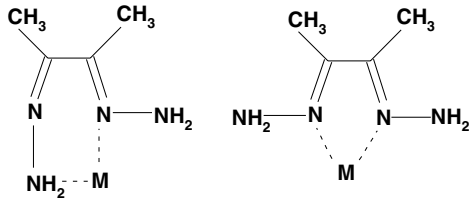

X XI

The *syn–anti* configuration of a number of cyclic 1,2-dihydrazones was observed by Baldwin et al. [25]. However, the NMR spectrum of 2,3-butanedihydrazone indicates the *anti–anti* configuration. The π-acceptor property of the α-diimine moieties enhances their chelating tendency with metals of significant π-donor tendency. Therefore the cyclization products of XI obtained from condensation of 2,3-butanedihydrazone with formaldehyde and amine are expected to yield products having the symmetrical *anti–anti* structure of 18-membered decaaza macrocycle nickel(II) complexes.

$[Ni(R_2Me_4[18]aneN_{10})]^{2+}$ react with excess NaNCS in aqueous solution to form tetragonal complexes $[Ni(R_2Me_4[18]aneN_{10})(NCS)_2]$, whose IR spectra (Table 1) show that the nitrogen atoms of the NCS^- ligands are coordinated to the Ni(II) ion [26]. Pink complexes of thiocyanate are not soluble in most solvents such as CH_3CN, EtOH, DMF and in H_2O.

The infrared spectra of the complexes, $[Ni(R_2Me_4[18]aneN_{10})](ClO_4)_2$, are all very similar to one another

Table 1
IR, UV–Vis, magnetic and conductance data of 18-membered decaaza macrocyclic nickel(II) complexes at 25 °C

Complex	IR (cm^{-1})			UV–Vis	μ_B	Λ_M[a] (Ω^{-1} cm^{-2} M^{-1})
	ν_{N-H}	$\nu_{C=N}$	ν_{CS}, ν_{CN}	Λ_{max} (nm (ε, M^{-1} cm^{-1}))		
1	3294	1608		428(sh, 2300), 349(sh, 6100), 297(21 800)	−0.11	251
2	3287	1606		429(sh, 2320), 348(sh, 6150), 298(21 800)	−0.12	262
3	3260	1603		427(sh, 2290), 346(sh, 6160), 297(21 800)	−0.23	254
4	3250	1601		428(sh, 2310), 347(sh, 6100), 298(21 800)	−0.24	254
5	3241	1596		429(sh, 2320), 348(sh, 6170), 297(21 800)	−0.32	257
6	3307	1612		426(sh, 2330), 349(sh, 6100), 298(21 800)	−0.36	264
7	3291	1607		423(sh, 2450), 351(sh, 6200), 298(23 000)	−0.18	238
8	3286	1605		431(sh, 2460), 351(sh, 6300), 299(23 000)	−0.19	243
9	3260	1602		433(sh, 2420), 352(sh, 6200), 298(23 000)	−0.23	253
10	3255	1601		434(sh, 2430), 351(sh, 6200), 297(23 000)	−0.37	253
11	3250	1600		431(sh, 2420), 351(sh, 6210), 298(23 000)	−0.41	255
12	3305	1610		434(sh, 2490), 350(sh, 6300), 298(23 000)	−0.51	239
13	3298	1609	2056, 783	423(sh, 2400), 341(sh, 6200), 298(22 800)	−0.14	
14	3291	1615	2048, 784	424(sh, 2300), 349(sh, 6100), 297(22 800)	−0.15	
15	3267	1612	2039, 784	423(sh, 2300), 349(sh, 6100), 297(22 800)	−0.17	
16	3261	1610	2034, 783	425(sh, 2310), 350(sh, 6110), 297(22 800)	−0.18	
17	3258	1609	2036, 784	426(sh, 2310), 349(sh, 6100), 296(22 800)	−0.22	
18	3314	1630	2031, 783	421(sh, 2400), 349(sh, 6100), 297(22 800)	−0.34	

[a] In nitromethane solution unless other wise specified.

and support the ligand structure proposed in Scheme 1. The most diagnostic absorption bands are the N–H and C=N stretching modes, as well as those attributable to free perchlorate anions. Some of the representative N–H and C=N stretching frequencies are tabulated in Table 1. There were no other absorption bands present which could be assigned to uncondensed functional groups, e.g., such as $-NH_2$ or C=O, of the starting materials.

A comparison of the spectra of the 18-membered decaaza macrocycles $[Ni(R_2Me_4[18]aneN_{10})](ClO_4)_2$ with those of the closely related divalent metal complexes of $Me_4[14]1,3,8,10$-tetraeneN_4 (V) and $Me_4[14]$-1,3,8,10-tetraeneN_8 (VII) reveals some differences in the C=N stretching frequency region of the spectra [23,24]. The intensity and position of the C=N stretching frequency of our 18-membered decaaza macrocycle complexes are strong and sharp and are one indication of the difference in dipole strength of the hydrazone's C=N as compared to the α-diimine C=N bond.

The electronic spectra (Table 1) of the Ni(II) complexes are comparable to those of square-planar Ni(II) complexes with tetraaza macrocycles, V, VII, IV, indicating that the decaaza ligands of this study do not differ significantly from the tetraaza ligands with respect to the ligand field strength [23,24]. The UV–Vis spectra of these intensely coloured complexes are dominated by intense charge-transfer absorptions in the visible and UV portions of the spectra. The spectra are tabulated for identification purpose only; no detailed assignment will be made due to the overlap of ligand field and charge-transfer absorptions. Generally, the lowest energy bands of the spectra for Ni(II) complexes are $d \rightarrow \pi^*$ charge-transfer bands which have been extensively studied and characterized in other α-diimine complexes [27].

The 18-membered decaaza macrocyclic nickel(II) complexes undergo intense colour changes due to deprotonation of the macrocyclic ligand in the presence of amine bases such as pyridine and triethylamine. Similar N–H deprotonation reactions have been observed with other metal complexes containing hydrazones linkages [28,29]. For the Ni(II) complex, triethylamine is sufficiently basic for the formation of the molecular complex. The C=N stretching frequency of this compound [Ni ($C_{14}H_{28}N_{10}$)], 1598 cm^{-1}, is reduced significantly from its dicationic precursor, $[Ni(C_{14}H_{30}N_{10})](ClO_4)_2$, 1606 cm^{-1}. The C=N stretching frequencies, together with the change in the electronic bands (lowering of the energy of charge-transfer bands and increased intensity) indicate that the loss of these protons is accompanied by increased delocalization which includes the deporotonated hydrazine linkage.

The deprotonated macrocyclic complexes are very susceptible to ligand dehydrogenation reactions with dioxygen, double bonds being introduced into the six-membered chelate rings [28–35].

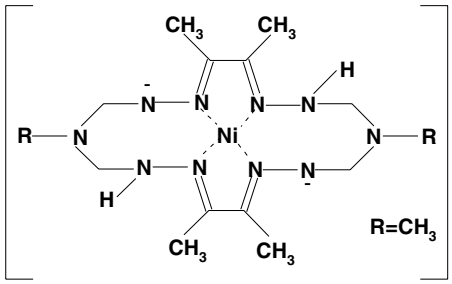

XII

The ^1H NMR spectrum of $[Ni(Me_2Me_4[18]aneN_{10})](PF_6)_2$ in nitromethane showed the methyl resonance of the 2,3-butanedihydrazone linkage occurring in the vicinity of 2.0–3.0 ppm (δ) and appearing as a singlet, confirming the symmetrical D_{2h} structure of Scheme 1. There was no observable coupling between the protons of these methyl groups and the N–H protons of the six-membered rings. The $-CH_2$ groups of $[Ni(Me_2Me_4[18]aneN_{10})](ClO_4)_2$ exhibit a triplet in the vicinity of 4.85 ppm due to the coupling with the hydrogen atoms of the adjacent nitrogen atoms. The N–H resonance appears as a broad band near 6.7 ppm, the broad nature of absorption being attributable to the combined effects of the quadrupole moment of nitrogen, rapid exchange of N–H protons, and motion of these protons (resulting from configuration inversion about the nitrogen atom) in the anisotropic magnetic field created by the square-planar coordination environment of the metal ions. The methylene resonances of the amine linkage in $[Ni(Me_2Me_4[18]aneN_{10})](ClO_4)_2$ are also broader than usual and attributable to rapid equilibrium between the conformers depicted below and to the anisotropic nature of the magnetic field of a low spin d^8 system.

4. Conclusions

New square planar decaaza bis (α-diimine) macrocyclic nickel(II) complexes, $[Ni(R_2Me_2[18]aneN_{10})]^{2+}$, can be prepared by the simple metal template condensation of 2 moles of 2,3-butanedihydrazone, 4 moles of CH_2O with 2 moles of amine. The spectra of the complexes show that the four nitrogen (α-diimine) atoms are coordinated to the nickel(II) ion.

References

[1] J.B. Harrowfield, A.J. Herbit, P.A. Lay, A.M. Sargeson, A.M. Bond, J. Am. Chem. Soc. 105 (1983) 5503.
[2] M.P. Suh, W. Shin, D. Kim, S. Kim, Inorg. Chem. 23 (1984) 618.
[3] M.P. Suh, D. Kim, S. Kim, Inorg. Chem. 24 (1985) 3712.
[4] M.P. Suh, W. Shin, H. Kim, C.H. Koo, Inorg. Chem. 26 (1987) 1846.
[5] M.P. Suh, S.-G. Kang, Inorg. Chem. 27 (1988) 2544.

[6] M.P. Suh, W. Shin, S.-G. Kang, M.S. Lah, T.-M. Chung, Inorg. Chem. 28 (1989) 1602.
[7] (a) N.F. Curtis, Coord. Chem. Rev. 3 (1968) 3;
(b) N.F. Curtis, J. Chem. Soc., Chem. Commun. 524 (1966);
(c) P. Comba, N.F. Curtis, G.A. Lawrence, A.M. Sargeson, B.W. Skelton, A.H. White, Inorg. Chem. 25 (1987) 4260.
[8] (a) M.P. Suh, S.-G. Kang, V.L. Goedken, S.-H. Park, Inorg. Chem. 30 (1991) 365;
(b) M.P. Suh, D. Kim, Inorg. Chem. 24 (1985) 3712;
(c) M.P. Suh, W. Shin, H. Kim, C.H. Koo, Inorg. Chem. 26 (1987) 1846.
[9] A.D. Blas, G.D. Santis, L. Fabbrizzi, M. Licchelli, A.M.M. Lanfredi, P. Morosi, P. Pallavici, F. Ugozzoli, J. Chem. Soc., Dalton Trans. (1993) 1411.
[10] (a) S.-G. Kang, J.-S. Choi, Bull. Korean Chem. Soc. 15 (1994) 374;
(b) S.-G. Kang, J.-S. Choi, S.-J. Choi, S.-J. Kim, Bull. Korean Chem. Soc. 16 (1997) 518.
[11] R.W. Hay, A. Dan by, P. Lightfoot, Y.D. Lampeka, Polyhedron 16 (1997) 2777.
[12] (a) S.-G. Kang, K. Ryu, M.P. Suh, J.H. Jeong, Inorg. Chem. 36 (1997) 2478, and references therein;
(b) M.P. Suh, W. Shin, S.-G. Kang, M.S. Lah, T.M. Chung, Inorg. Chem. 28 (1989) 1602.
[13] M. Salavati-Niasari, H. Najafian, Polyhedron 22 (2003) 2633.
[14] F.G. Riddell, P. Murray-Rust, J. Chem. Soc., Chem. Commun. (1970) 1075.
[15] U. Thewalt, J. Weiss, Z. Anorg. Chem. 348 (1966) 238.
[16] U. Thewalt, C.E. Bugg, Chem. Ber. 105 (1972) 1614.
[17] S.-M. Peng, V.L. Goedken, J. Chem. Soc., Chem. Commun. (1973) 62.
[18] S.-M. Peng, V.L. Goedken, Inorg. Chem. 17 (1978) 820.
[19] D.D. Perrin, W.L.F. Armarego, D.R. Perrin, Purification of Laboratory Chemicals, 2nd ed., Pergamon Press, Oxford, 1980.
[20] D.H. Bush, J.C. Bailar, J. Am. Chem. Soc. 78 (1956) 1137.
[21] C.M. Kerwin, G.A. Melson, Inorg. Chem. 11 (1972) 726.
[22] R.C. Stouffer, D.H. Busch, J. Am. Chem. Soc. 78 (1956) 6016.
[23] S.C. Jackels, K. Farmery, E.K. Barefield, N.J. Rose, D.H. Busch, Inorg. Chem. 11 (1972) 2893.
[24] D.A. Baldwin, R.M. Pfeiffer, D.W. Reichgott, N.J. Rose, J. Am. Chem. Soc. 95 (1973) 5152.
[25] J.E. Baldwin, R.H. Holm, R.W. Harper, J. Huff, S. Koch, T.J. Truex, Inorg. Nucl. Chem. Lett. 8 (1972) 393.
[26] K. Nakamato, Infrared and Raman Spectra of Inorganic and Coordination Compounds, 3rd ed., Wiley, New York, 1978, p. 270.
[27] P. Krumholz, Struct. Bonding (Berlin) 9 (1971) 129.
[28] V.L. Goedken, S.-M. Peng, J. Am. Chem. Soc. 95 (1973) 5774.
[29] V.L. Goedken, S.-M. Peng, J. Chem. Soc., Chem. Commun., (1975) 258s.
[30] G.J. Palenik, Acta Crystallogr. 17 (1964) 696.
[31] F. Bigoli, A. Breibanti, M.A. Pellinghelli, A. Tiripicchio, Acta Crystallogr., Sect. B 29 (1973) 2344.
[32] C.W. Reimann, S. Block, A. Perloff, Inorg. Chem. 5 (1966) 1185.
[33] H.S. Preston, C.H.L. Kennard, J. Chem. Soc. A (1969) 1956.
[34] N.C. Baenziger, R.J. Schultz, Inorg. Chem. 10 (1971) 661.
[35] G. Zakrzewski, E.C. Lingefelter, Inorg. Chim. Acta 4 (1970) 251.

Available online at www.sciencedirect.com
SCIENCE DIRECT®
Polyhedron 23 (2004) 1333–1339
POLYHEDRON
www.elsevier.com/locate/poly

Synthesis of a cyano-bridged Fe_2Mn linear unit and a Fe_2Mn_2 square unit by using the [*fac*-Fe{HB(pz)$_3$}(CN)$_3$]$^-$ building block

Jinkwon Kim [a,*], Sujin Han [a], In-Ku Cho [a], Ki Young Choi [b], Min Heu [c], Seokwon Yoon [c], Byoung Jin Suh [c]

[a] *Department of Chemistry, Kongju National University, 182 Shinkwan, Kongju, Chungnam 314-701, Republic of Korea*
[b] *Department of Chemical Education, Kongju National University, 182 Shinkwan, Kongju, Chungnam 314-701, Republic of Korea*
[c] *Department of Physics, The Catholic University of Korea, Puchon 420-743, Republic of Korea*

Received 17 November 2003; accepted 2 February 2004
Available online 15 April 2004

Abstract

Mononuclear $(LH_2)[Fe\{HB(pz)_3\}(CN)_3]_2 \cdot 2H_2O \cdot 2MeOH$ (**2**) (L = C-*meso*-3,14-dimethyl-2,6,13, 17-tetraazatricyclo[16.4.0.0^{7,12}] docosane) and two cyano-bridged bimetallic complexes $[\{Fe\{HB(pz)_3\}(CN)_3\}_2Mn(MeOH)_4] \cdot 2MeOH$ (**3**) and $[Mn_2Fe_2\{HB(pz)_3\}_2(CN)_6(4,4'\text{-bipyridine})_2](ClO_4)_2 \cdot 4MeCN$ (**4**) have been prepared and their structures and magnetic properties studied. A crystal structure analysis of complex **2** revealed a hydrogen bonded dimeric structure of two $[Fe\{HB(pz)_3\}(CN)_3]^-$ anions and two water molecules. The structure of **3** consists of a neutral Fe^{III}–Mn^{II}–Fe^{III} molecule and two crystal methanol molecules. The manganese ion is coordinated by two $[Fe\{HB(pz)_3\}(CN)_3]^-$ moieties through cyanide bridging ligands with *trans* geometry, resulting in a linear trinuclear structure. Reaction of the 2,2′-bipyridine ligand with complex **3** resulted in the formation of complex **4**. The crystal structure of **4** consists of a discrete tetranuclear square Fe_2Mn_2 complex, two perchlorate anions and four acetonitrile solvent molecules. The manganese ions are surrounded by two 2.2′-bipyridine ligands and bridged by two $[Fe(tbp)(CN)_3]^-$ moieties through cyanide bridging ligands to form a cyclic tetranuclear structure. The magnetic properties of **3** and **4** are found to be dominated by a weak antiferromagnetic interaction of low-spin Fe^{III} ($S = 1/2$) and high-spin Mn^{II} ($S = 5/2$). The Fe^{III}–Mn^{II} coupling constant J was determined to be −5.90(9) or −7.6(2) cm^{-1} for **3** and −2.29(3) cm^{-1} for **4**.
© 2004 Elsevier Ltd. All rights reserved.

Keywords: Cyanide bridged clusters; Iron(III) complex; Tris(pyrazolyl)borate; Magnetic properties

1. Introduction

Hexacyanide complexes of the first transition metal elements have been used as useful building blocks to synthesize molecular based magnets possessing the Prussian blue structure type [1–5]. Several cyano-bridged three dimensional molecular magnets display their Curie temperature (T_c) above room temperature and may find application in many areas, including memory storage and magneto-optic devices [6–10]. To understand the correlation between crystal structure and molecular magnetism of cyano-bridged molecular magnets, various heterobimetallic systems with different dimensionalities have been extensively investigated by using $[M(CN)_6]^{3-}$ (M = Cr, Mn, Fe), $[Mo(CN)_7]^{4-}$ and $[Mo(CN)_8]^{3-}$ molecular building blocks [11–14]. Furthermore, many research efforts of cyano-bridged clusters has focused on exploring new single-molecule magnets, which possess an energy barrier for magnetic moment reversal due to high spin (S) and negative magnetic anisotropy (D), and exhibit new physical phenomena of magnetic quantum tunneling. Various cyano-bridged polynuclear complexes were prepared by using molecular building blocks such as $[M(CN)_6]^{3-}$ (M = Cr, Fe), $[Mo(CN)]^{3-}$ and *fac*-$[M(L_3)(CN)_3]$ [15–22]. The cyanide-bridged cluster having the highest ground-state spin value ($S = 51/2$) is known to be a $Mn_9^{II}Mo_6^{V}$ cluster which does not exhibit molecular

* Corresponding author. Tel.: +82-41-850-8496; fax: +82-41-850-8479.
E-mail address: jkim@kongju.ac.kr (J. Kim).

0277-5387/$ - see front matter © 2004 Elsevier Ltd. All rights reserved.
doi:10.1016/j.poly.2004.02.026

hysteresis and slow relaxation of the magnetization [18], whereas the $Mn_9^{II}W_6^{V}$ cluster ($S = 39/2$) shows some indication of slow relaxation [19]. The well-characterized cyano-bridged single-molecule magnet is the trigonal prismatic cluster $[(Me_3tacn)_2MnCr_6(CN)_{18}]^{2+}$ (Me_3tacn = 1,4,7-trimethyltriazacyclononane), showing temperature dependence in out-of-phase ac susceptibility [23]. In order to expand such a molecular chemistry for magnetic materials, we utilized a new molecular building block, [*fac*-Fe{HB(pz)$_3$}(CN)$_3$]$^-$ {HB(pz)$_3$ = hydrotris(1-pyrazolyl)borate}, and successfully synthesized the trinuclear cyano-bridged complex, $[MnFe_2\{HB(pz)_3\}_2(CN)_6(CH_3OH)_4]$ and the tetranuclear square complex, $[Mn_2Fe_2\{HB(pz)_3\}_2(CN)_6(4,4'\text{-bipyridine})_2](ClO_4)_2$. All the complexes were characterized by X-ray crystallographic analyses and magnetic measurements.

2. Experimental

2.1. Materials and measurements

$(LH_2)Cl_2$ was prepared as described previously [24]. The chemicals were purchased from Aldrich and used without further purification.

Infrared spectra (400–4000 cm^{-1}) were recorded from KBr pellets on a Perkin–Elmer FT-IR spectrometer. Elemental analyses were performed at the Korea Basic Science Institute, Seoul, Korea. Variable temperature (2.0–300 K) magnetic susceptibility measurements were carried out with a Quantum Design MPMS-XL SQUID magnetometer under an applied magnetic field of 1000 Oe. Magnetic data were corrected for diamagnetic contribution of diamagnetic moieties according to Pascal tables.

2.2. Synthesis of K[Fe{HB(pz)$_3$}(CN)$_3$] (1)

The synthetic method used for complex 1 is a modification of a known method [25]. K{HB(pz)$_3$} (126 mg, 0.5 mmol) and KCN (160 mg, 2.5 mmol) in 20 cm^3 of H_2O was added into a solution of $FeCl_3 \cdot 4H_2O$ (100 mg, 0.5 mmol) in 20 cm^3 of methanol. The solution color changed immediately to dark red and a red brown powder was precipitated. After heating at 70 °C for 2 h, the solution was filtered to remove insoluble KCl. An orange powder was collected by filtration from the concentrated solution and recrystallization from methanol–diethyl ether solution gave orange crystals of **1**. Yield: 53%. IR (KBr, cm^{-1}): ν_{CN}, 2129.

2.3. Synthesis of (LH_2)[Fe{HB(pz)$_3$}(CN)$_3$]$_2 \cdot 2H_2O \cdot$ 2MeOH (2)

To a solution of $(LH_2)Cl_2$ (L = C-*meso*-3,14-dimethyl-2,6,13,17-tetraazatricyclo[16.4.0.0^{7,12}]docosane) (50 mg, 0.1 mmol) in 10 cm^3 of water, was added K[Fe{HB(pz)$_3$}(CN)$_3$] (85 mg, 0.2 mmol) in 20 cm^3 of water–methanol mixed solvents. An orange solid was formed immediately. The reaction mixture was stirred for 1 h at ambient temperature. The orange solid was collected by filtration and recrystallized from MeOH–Et_2O solution. Analytically pure crystals were obtained by slow diffusion of diethyl ether into a methanol solution. Yield: 60%. *Anal.* Calc. for $C_{46}H_{72}B_2Fe_2N_{22}O_4$: C, 48.9; H, 6.4; N, 27.3. Found: C, 48.4; H, 6.6; N, 27.6%. IR (KBr, cm^{-1}): ν_{CN}, 2122.

2.4. Synthesis of {Fe{HB(pz)$_3$}(CN)$_3$}$_2$Mn(MeOH)$_4$] · 2MeOH (3)

To a slurry of $MnBr_2 \cdot 4H_2O$ (130 mg, 0.45 mmol) and $KClO_4$ (104 mg, 0.75 mmol) in 10 cm^3 of water, was added K[Fe{HB(pz)$_3$}(CN)$_3$] (60 mg, 0.15 mmol). The reaction mixture was stirred for 30 min at ambient temperature. A dark red crystalline powder was collected by filtration and dissolved in a small amount of methanol solvent. Analytically pure red crystals were obtained by slow diffusion of diethyl ether into methanol solution. Yield: 78%. *Anal.* Calc. for $C_{30}H_{44}B_2Fe_2MnN_{18}O_6$: C, 38.3; H, 4.7; N, 26.8. Found: C, 38.1; H, 4.7; N, 26.4%. IR (KBr, cm^{-1}): ν_{CN}, 2128, 2151.

2.5. Synthesis of [Mn$_2$Fe$_2${HB(pz)$_3$}$_2$(CN)$_6$ (4,4′-bipyridine)$_2$](ClO$_4$)$_2$ · 4MeCN (4)

To a solution of [{Fe{HB(pz)$_3$}(CN)$_3$}$_2$Mn(HOMe)$_4$] (**3**) (220 mg, 0.2 mmol) in 100 cm^3 of MeOH, was added $[Mn(2,2'\text{-bipy})_2(H_2O)_2](ClO_4)_2$ (240 mg, 0.4 mmol) in 20 cm^3 of MeOH. The resulting deep red solution was stirred for 1 h and treated with Et_2O to result in precipitation. Analytically pure dark red crystals were obtained after recrystallization from MeCN–Et_2O solution. Yield: 34%. *Anal.* Calc. for $C_{64}H_{52}B_2Cl_2Fe_2Mn_2N_{26}O_8$: C, 47.2; H, 3.2; N, 22.4. Found: C, 47.4; H, 3.3; N, 22.7%. IR (KBr, cm^{-1}): ν_{CN}, 2148.

2.6. Crystallography

The data collections were performed on an Enraf-Nonius CAD4 diffractometer (complexes **2** and **3**) and a Bruker SMART CCD diffractometer (complex **4**) with graphite-monochromated Mo Kα radiation (λ = 0.71073 Å). The structures of the compounds were solved by direct methods and refined by the full-matrix least-squares method on all F^2 data using SHELX-97 [26]. The anisotropic thermal parameters for all non-hydrogen atoms were included in the refinements. All hydrogen atoms bonded to carbon atoms were included in calculated positions. The C–H bond distances were fixed and the U values were assigned based approxi-

Table 1
Details of the crystallographic data collection for **2**, **3** and **4**

	2	**3**	**4**
Chemical formula	$C_{46}H_{72}B_2Fe_2N_{22}O_4$	$C_{30}H_{44}B_2Fe_2MnN_{18}O_6$	$C_{72}H_{64}B_2Cl_2Fe_2Mn_2N_{30}O_8$
Chemical formula weight	1130.58	941.09	1791.63
Space group	$P\bar{1}$	$P2_1c$	$P\bar{1}$
a (Å)	11.380(2)	9.3572(6)	12.457(3)
b (Å)	11.447(1)	16.581(3)	13.440(3)
c (Å)	13.553(1)	14.442(1)	13.863(3)
α (°)	79.55(1)	90.0	84.25(2)
β (°)	67.69(1)	94.752(5)	78.15(2)
γ (°)	60.90(1)	90.0	62.94(2)
V (Å^3)	1427.2(3)	2233.0(5)	2022.9(8)
Z	1	2	1
ρ_{calc} (g cm^{-3})	1.315	1.400	1.471
μ (mm^{-1})	0.570	0.979	0.796
Number of unique reflections	5013	3903	9123
Number of observed reflections ($I_o > 2\sigma I_o$)	4254	3254	6064
$2\theta_{max}$ (°)	50	50	56
Number of parameters refined	345	269	534
$R(F)$, $wR(F^2)$	0.0410, 0.1085	0.0381, 0.0995	0.0467, 0.1195
Goodness-of-fit	1.051	1.037	0.946

mately on the U value of the attached atom. The crystal and refinement data are summarized in Table 1.

3. Results and discussion

The cyanide stretching frequency of **2** is slightly shifted to lower energy compared to that of **1** because of hydrogen bonding interactions between the cyanides and water molecules. For **3** and **4**, a CN stretching band is shifted to a higher wavenumber, suggesting formation of CN^- bridges, as observed in other cyanide bridged transition metal complexes.

3.1. Description of the structures

The crystal structure of **2** consists of one LH_2^{2+} cation, two $[Fe\{HB(pz)_3\}(CN)_3]^-$ anions, two water molecules and two methanol molecules. Two $[Fe\{HB(pz)_3\}(CN)_3]^-$ anions are linked by hydrogen bonds between cyanide ligands and water molecules, as displayed in Fig. 1. The geometry of the $[Fe\{HB(pz)_3\}(CN)_3]^-$ anion is not quite the same as the structure analyzed for the PPh_4^+ salt of the $[Fe\{HB(pz)_3\}(CN)_3]^-$ anion [25]. The Fe^{III} ion of the $[Fe\{HB(pz)_3\}(CN)_3]^-$ anion is coordinated by one $HB(pz)_3^-$ anion and three cyanide anions with octahedral geometry. The values of the three Fe–C distances are in the very narrow range of 1.923(3)–1.930(3) Å, and these values are somewhat longer than those found in $(PPh_4)[Fe\{HB(pz)_3\}(CN)_3]$ [1.910(6)–1.929(6) Å] [25] and $(PPh_4)[Fe(bipy)(CN)_4]$ [1.87(2)–1.91(2) Å] [27] which have a low spin Fe^{III} ($S = 1/2$) ion. The Fe-N distances are also in a very narrow range of 1.977(2)–1.981(2) Å. The Fe···Fe distance of the hydrogen bonded dimeric unit is 9.172 Å, while the shortest Fe···Fe distance is 7.841 Å. The hydrogen bonded N···O distances are 2.885(4) and 2.905(4) Å and N···H–O angles are 162.1° and 169.1° (see Table 2).

The structure of complex **3** consists of the neutral $[\{Fe\{HB(pz)_3\}(CN)_3\}_2Mn(MeOH)_4]$ molecule and two methanol molecules. The manganese ion is placed in a crystallographic inversion center and coordinated by two $[Fe(tbp)(CN)_3]^-$ moieties through cyanide bridging

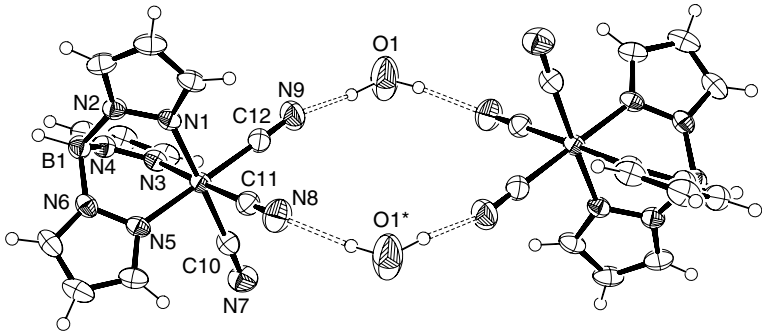

Fig. 1. ORTEP diagram with atom labelling scheme of **2**.

Table 2
Selected bond lengths (Å) and bond angles (°) for complex **2**

Bond lengths			
Fe1–C10	1.925(3)	Fe1–C11	1.930(3)
Fe1–C12	1.923(3)	Fe1–N1	1.977(2)
Fe1–N3	1.981(2)	Fe1–N5	1.980(2)
Bond angles			
C10–Fe1–C11	88.2(1)	C10–Fe1–C12	88.6(1)
C11–Fe1–C12	88.0(1)	C10–Fe1–N1	178.3(1)
C11–Fe1–N1	92.0(1)	C12–Fe1–N1	93.1(1)
C10–Fe1–N3	92.1(1)	C11–Fe1–N3	178.4(1)
C12–Fe1–N3	90.4(1)	C10–Fe1–N5	91.1(1)
C11–Fe1–N5	92.9 (1)	C12–Fe1–N5	179.0(1)
N1–Fe1–N3	87.8 (1)	N1–Fe1–N5	87.2(1)
N3–Fe1–N5	88.7(1)	Fe1–C10–N7	178.2(2)
Fe1–C11–N8	179.6(3)	Fe1–C12–N9	177.7(3)

Table 3
Selected bond lengths (Å) and bond angles (°) for complex **3**

Bond lengths			
Fe1–C10	1.918(3)	Fe1–C11	1.934(3)
Fe1–C12	1.925(3)	Fe1–N1	1.981(2)
Fe1–N3	1.968(2)	Fe1–N5	1.985(2)
Mn1–N7	2.179(2)	Mn1–N7*	2.179(2)
Mn1–O1	2.189(2)	Mn1–O2	2.192(2)
C10–N7	1.136(4)	C11–N8	1.138(4)
C12–N9	1.146(4)		
Bond angles			
C10–Fe1–C11	87.5(1)	C10–Fe1–C12	86.9(1)
C11–Fe1–C12	89.5(1)	C11–Fe1–N1	93.5(1)
C10–Fe1–N1	176.5(1)	C12–Fe1–N1	89.7(1)
C10–Fe1–N3	90.3(1)	C11–Fe1–N3	177.1(1)
C12–Fe1–N3	92.3(1)	C10–Fe1–N5	95.3(1)
C11–Fe1–N5	89.9(1)	C12–Fe1–N5	177.7(1)
N1–Fe1–N3	88.9(1)	N1–Fe1–N5	88.1(1)
N3–Fe1–N5	88.4(1)	N7–Mn1–O1	89.3(1)
N7–Mn1–O1*	90.7(1)	N7–Mn1–O2	90.3(1)
N7–Mn1–O2*	89.8(1)	O1–Mn1–O2	87.1(1)
O1–Mn1–O2*	92.9(1)	C10–N7–Mn1	167.3(2)
C13–O1–Mn1	131.1(2)	C14–O2–Mn1	126.0(2)

Symmetry transformations used to generate equivalent atoms (*): $-x, -y+2, -z+1$.

ligands with *trans* geometry. The four residual coordination sites of Mn^{II} are occupied by methanol molecules. The arrangement of the trinuclear unit is shown in Fig. 2. The Fe^{III}–C and Fe^{III}–N bond distances are 1.918(3)–1.934(3) and 1.968(2)–1.985(2) Å, respectively, while Mn^{II}–N and Mn^{II}–O bond distances are 2.179(2) and 2.191(2) Å, respectively. The Mn–N–C–Fe structural unit is almost linear with Fe–C–N and Mn–N–C angles of 176.9(3)° and 167.3(2)°, respectively. The Fe···Mn distance is 5.1931(5) Å, which is comparable to the values found in other Fe^{III}–CN–Mn^{II} connectivities [28] (see Table 3).

The crystal structure of **4** consists of a discrete tetranuclear mixed metal complex, two perchlorate anions and four acetonitrile solvent molecules. An ORTEP diagram of complex of **4** is displayed in Fig. 3. The overall structure of the cationic complex can be best described as a tetranuclear square composed of low-spin Fe^{III} ions and high-spin Mn^{II} ions. The $[Fe\{HB(pz)_3\}(CN)_3]^-$ ion coordinates to two adjacent Mn ions with its two linear cyano bridges [C10–N7–Mn1, 161.1(2)°; C11–N8–Mn1 172.0(2)°]. The Mn^{II} ion has a slightly distorted octahedral geometry. The Fe^{III}–C and Fe^{III}–N bond distances are 1.912(3)–1.927(3) and 1.965(2)–1.981(2) Å, respectively, while Mn^{II}–N bond distances are 2.180(3) and 2.291(3) Å. The intramolecular Fe···Mn distances are 5.174(1) and 5.220(1) Å. The intramolecular Fe···Fe and Mn···Mn distances are 7.310(1) and 7.389(1) Å, respectively (see Table 4).

3.2. Magnetic properties

Magnetic susceptibilities for **3** and **4** were measured down to 2.0 K. The resulting plot of $\chi_m T$ versus T for **3** is given in Fig. 4. As shown in the figure, the $\chi_m T$ value is 6.29 cm^3 K mol^{-1} at room temperature and it decreases gradually with lowering temperature to reach 1.3 cm^3 K mol^{-1} at $T = 2$ K. The $\chi_m T = 6.29$ cm^3 K mol^{-1} at 300 K is close to but somewhat larger than the spin-only value of $\chi_m T = 5.13$ cm^3 K mol^{-1} for the uncorrelated three-spin system consisting of two low-spin Fe^{III} ($S = 1/2$) and one high-spin Mn^{II} ($S = 5/2$) with

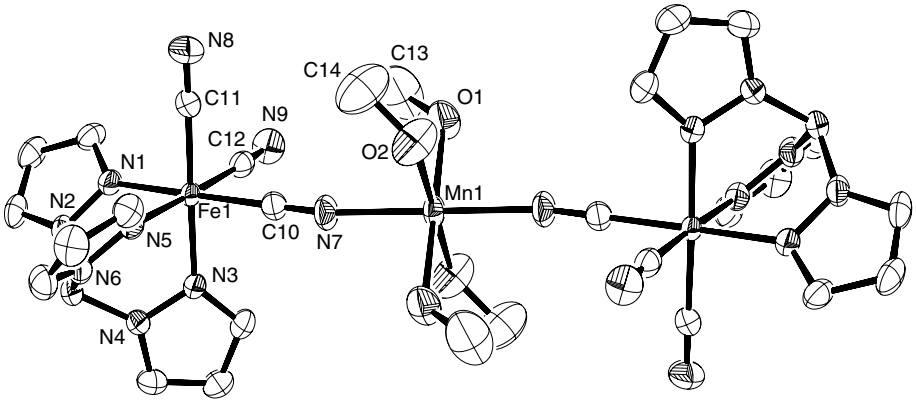

Fig. 2. ORTEP diagram with atom labelling scheme of **3**.

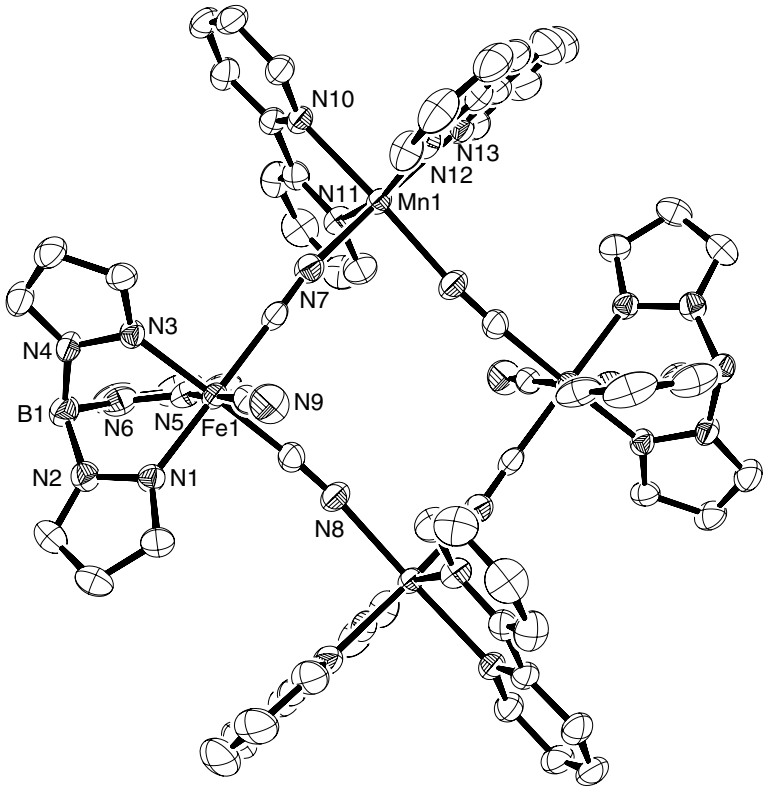

Fig. 3. ORTEP diagram with atom labelling scheme of **4**.

Table 4
Selected bond lengths (Å) and bond angles (°) for complex **4**

Bond lengths			
Fe1–N1	1.967(2)	Fe1–N3	1.981(2)
Fe1–N5	1.965(3)	Fe1–C10	1.927(3)
Fe1–C11	1.912(3)	Fe1–C12	1.924(3)
Mn1–N7	2.180(3)	Mn1–N8*	2.182(3)
Mn1–N10	2.253(2)	Mn1–N11	2.253(3)
Mn1–N12	2.230(3)	Mn1–N13	2.291(3)
N7–C10	1.146(4)	N8–C11	1.150(4)
N9–C12	1.144(4)		
Bond angles			
C10–Fe1–C11	89.8(1)	C10–Fe1–C12	89.0(1)
C11–Fe1–C12	86.1(1)	C10–Fe1–N1	179.1(1)
C11–Fe1–N1	90.6(1)	C12–Fe1–N1	91.9(1)
C10–Fe1–N3	91.9(1)	C11–Fe1–N3	177.9(1)
C12–Fe1–N3	92.8(1)	C10–Fe1–N5	90.5(1)
C11–Fe1–N5	91.6(1)	C12–Fe1–N5	177.6(1)
N1–Fe1–N3	87.8(1)	N1–Fe1–N5	88.7(1)
N3–Fe1–N5	89.6(1)	N7–Mn1–N8*	89.9(1)
N7–Mn1–N10	95.4(1)	N7–Mn1–N11	99.6(1)
N7–Mn1–N12	97.6(1)	N7–Mn1–N13	169.8(1)
N8–Mn1–N10	165.8(1)	N8–Mn1–N11	93.4(1)
N8–Mn1–N12	98.3(1)	N8–Mn1–N13	88.9(1)
N10–Mn1–N11	72.8(1)	N10–Mn1–N12	94.1(1)
N10–Mn1–N13	88.2(1)	N11–Mn1–N12	159.2(1)
N11–Mn1–N13	90.6(1)	N12–Mn1–N13	72.5(1)
C10–N7–Mn1	161.1(2)	C11–N8–Mn1*	172.0(2)

Symmetry transformations used to generate equivalent atoms (*): $-x+1, -y+1, -z$.

$g = 2.00$. Since the temperature dependence of $\chi_m T$ indicates that Fe^{III} and Mn^{II} ions are coupled antiferromagnetically through cyanide bridges, we expect, within the linear three-spin model [29], the $S_{total} = 3/2$ ground-state spin of the molecule and $\chi_m T \cong 1.9$ cm^3 K mol^{-1} for $g = 2.0$ at $T = 2$ K, which is in good agreement with the experimental result $\chi_m T \cong 1.3$ cm^3 K mol^{-1} at $T = 2$ K. Thus, we include the exchange interactions in the spin Hamiltonian as $H = -2J(S_{Fe1} \cdot S_{Mn} + S_{Fe2} \cdot S_{Mn})$ and fit the magnetization data of **3**. The solid and dashed curves in Fig. 4 are the fitting results using the model Hamiltonian and the following two parameter sets: $J = -5.90(9)$ cm^{-1}, $g_{Fe} = 2.83(3)$, $g_{Mn} = 2.12(1)$ (solid line in Fig. 4) or $J = -7.6(2)$ cm^{-1} and $g_{Fe} = g_{Mn} = 2.22(1)$ (dashed line in Fig. 4). Both curves agree with the experimental results reasonably well.

Shown in Fig. 5 is the plot of $\chi_m T$ versus T for **4**. Overall, the temperature dependence of $\chi_m T$ is similar to that of **3**, whereby $\chi_m T$ gradually decreases with lowering temperature and reaches 3.23 cm^3 K mol^{-1} at $T = 2$ K. This similar behavior is rather surprising, in particular due to the small value of $\chi_m T$ at low temperatures. Suppose, as we did for **3**, that Fe^{III} is in the low-spin state ($S = 1/2$) and Mn^{II} is in the high-spin state ($S = 5/2$) for **4**. Then the $\chi_m T = 10.61$ cm^3 K mol^{-1} at 300 K is reasonably close to the spin-only

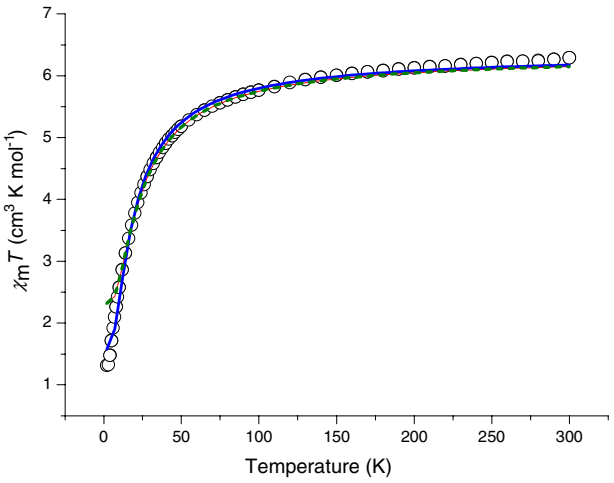

Fig. 4. The plot of $\chi_m T$ vs. T for **3**. The solid line and dashed line represent the best fit of the data. The dashed line is not visible clearly since it almost overlaps with the solid line.

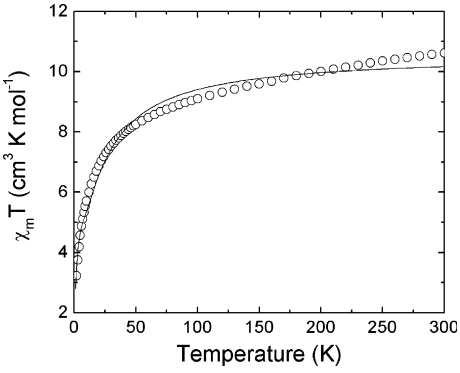

Fig. 5. The plot of $\chi_m T$ vs. T for **4**. The solid line represents the best fit of the data.

value $\chi_m T = 9.50$ cm^3 K mol^{-1} for uncorrelated two low-spin Fe^{III} ($S = 1/2$) and two high-spin Mn^{II} ($S = 5/2$) with $g = 2.00$. However, if only the antiferromagnetic interactions between Fe^{III} and Mn^{II} ions are considered, the ground-state spin is $S_{total} = 4$ and $\chi_m T \cong 10$ cm^3 K mol^{-1} for $g = 2.0$ at $T = 2$ K, which is much larger than the experimental value $\chi_m T \cong 3.23$ cm^3 K mol^{-1} at $T = 2$ K. Thus, in order to find a reasonable model to fit the magnetization data of **4**, we include the exchange interactions between the same kind of ions as well as between different kinds of ions in the spin Hamiltonian, as $H = -2J_1(S_{Fe1} \cdot S_{Mn1} + S_{Fe1} \cdot S_{Mn2} + S_{Fe2} \cdot S_{Mn1} + S_{Fe2} \cdot S_{Mn2}) - 2J_2 S_{Mn1} \cdot S_{Mn2} - 2J_3 S_{Fe1} \cdot S_{Fe2}$. The solid curve in Fig. 5 is the fitting result using the model Hamiltonian and the parameters: $J_1 = -2.29(3)$ cm^{-1}, $J_2 = -0.76(1)$ cm^{-1}, $|J_3| < 10^{-4}$ cm^{-1}, $g_{Fe} = g_{Mn} = 2.10(1)$. Although the model Hamiltonian fits the experimental results reasonably, no strong argument on the antiferromagnetic interaction between Mn^{II} and Mn^{II} ions can be attached at the moment. However, it should be noted that the low-spin state of Fe^{III} and the high-spin state of Mn^{II} are still valid for **4** since, as it has been mentioned previously, the $\chi_m T$ value at room temperature is reasonably close to the spin-only value for uncorrelated two low-spin Fe^{III} ($S = 1/2$) and two high-spin Mn^{II} ($S = 5/2$) with $g = 2.00$.

4. Supplementary material

X-ray crystallographic files, in CIF format, for the structure determination of **2**, **3** and **4** are available from the CCDC, 12 Union Road, Cambridge CB2 1EZ, UK (fax: +44-1223-336033; E-mail: deposit@ccdc.cam.ac.uk or www: http://www.ccdc.cam.ac.uk) on request, quoting the deposition numbers 210062, 210061 and 210060, respectively.

Acknowledgements

We gratefully acknowledge the financial support from the NRL program of the ministry of Science and Technology, Korea. We also thank Center for Molecular Design and Synthesis, Korea Advanced Institute of Science and Technology for providing a Bruker SMART CCD diffractometer. S.Y. and B.J.S. acknowledge support by KOSEF via eSSC at POSTECH.

References

[1] M. Verdauer, A. Bleuzen, V. Marvaud, J. Vaissermann, M. Seuleiman, C. Desplanches, A. Scuiller, C. Train, R. Garde, G. Gelly, C. Lomenech, I. Rosenman, P. Veillet, C. Cartier, F. Villain, Coord. Chem. Rev. 190–192 (1999) 1023.
[2] T. Mallah, S. Thiébaut, M. Verdaguer, P. Veillet, Science 262 (1993) 1544.
[3] R.W. Entley, G.S. Girolami, Science 268 (1995) 397.
[4] W.E. Buschmann, S.C. Paulson, C.M. Wynn, M. Girtu, A.J. Epstein, H. White, J.S. Miller, Adv. Mater. 9 (1997) 645.
[5] O. Sato, T. Iyoda, A. Fujishima, K. Hashimoto, Science 271 (1996) 49.
[6] S. Ferlay, T. Mallah, R. Ouahès, P. Vsillet, M. Verdaguer, Nature 378 (1995) 701.
[7] Ø. Halevik, W.E. Buschmann, J. Zhang, J. Manson, J.S. Miller, Adv. Mater. 11 (1999) 914.
[8] J.S. Miller, Adv. Mater. 6 (1994) 322.
[9] O. Sato, T. Iyoda, A. Fujishima, K. Hashimoto, Science 272 (1996) 704.
[10] M. Mizuno, S.-I. Ohkoshi, K. Hashimoto, Adv. Mater. 12 (2000) 1955.
[11] M. Ohba, H. Ōkawa, Coord. Chem. Rev. 198 (2000) 313.
[12] W.E. Buschmann, J. Ensling, P. Gütlich, J.S. Miller, Chem. Eur. J. 5 (1999) 3019.
[13] O. Kahn, J. Larionova, L. Ouahab, Chem. Commun. (1999) 945.
[14] A.K. Sra, M. Andruh, O. Kahn, S. Golhen, L. Ouahab, J.V. Yakhmi, Angew. Chem. Int. Ed. 38 (1999) 2606.
[15] A. Scillier, T. Mallah, M. Verdaguer, A. Nivorozkhin, J.L. Tholence, P. Veillet, New J. Chem. 20 (1996) 1.
[16] K.E. Vostrikova, D. Luneau, W. Wersdorfer, P. Rey, M. Verdaguer, J. Am. Chem. Soc. 122 (2000) 718.

[17] G. Rogez, A. Marvilliers, E. Rivière, J.-P. Audière, F. Lloret, F. Varret, A. Goujon, N. Mendenez, J.-J. Girerd, T. Mallah, Angew. Chem. Int. Ed. 39 (2000) 2885.
[18] J. Larionova, M. Gross, M. Pilkingto, H. Andres, H. Stoeckli-Evans, H.U. Güdel, S. Decurtins, Angew. Chem. Int. Ed. 39 (2000) 1605.
[19] Z.J. Zhong, H. Seino, Y. Mizobe, M. Hidai, A. Fujishima, S.-I. Ohkoshi, K. Hashimoto, J. Am. Chem. Soc. 122 (2000) 2952.
[20] J.L. Henrich, P.A. Berseth, J.R. Long, Chem. Commun. (1998) 1231.
[21] J.J. Sokol, M.P. Shores, J.R. Long, Inorg. Chem. 41 (2002) 3052.
[22] J.Y. Yang, M.P. Shores, J.J. Sokol, J.R. Long, Inorg. Chem. 42 (2003) 1403.
[23] J.J. Sokol, A.G. Hee, J.R. Long, J. Am. Chem. Soc. 124 (2002) 7656.
[24] S.-G. Kang, J.K. Kweon, S.-K. Jung, Bull. Korean Chem. Soc. 12 (1991) 483.
[25] R. Lescouezec, J. Vaissermann, F. Lloret, M. Julve, M. Verdaguer, Inorg. Chem. 41 (2002) 5943.
[26] G.M. Sheldrick, SHELX-97, Universität of Göttingen, Göttingen, Germany, 1997.
[27] R. Lescouezec, F. Lloret, M. Julve, J. Vaissermann, M. Verdaguer, Inorg. Chem. 41 (2002) 818.
[28] R. Lescouezec, F. Lloret, M. Julve, J. Vaissermann, M. Verdaguer, R. Llusar, S. Uriel, Inorg. Chem. 40 (2001) 2065.
[29] O. Kahn, in: Molecular Magnetism, VCH, New York, 1993.

Available online at www.sciencedirect.com
SCIENCE DIRECT®
Polyhedron 23 (2004) 1341–1350
POLYHEDRON
www.elsevier.com/locate/poly

The origin of optical activity in complexes of the type [Co(diimine)$_2$carbohydrate]$^{2+}$

José Parada *, Guillermo Larrazábal

Departamento de Química Inorgánica y Analítica, Facultad de Ciencias Químicas y Farmacéutica, Universidad de Chile, Casilla 233, Santiago, Chile

Received 24 September 2003; accepted 8 February 2004
Available online 9 April 2004

Abstract

Complexes of the type Δ- and Λ-[Co(diimine)$_2$carbohydrate]$^{2+}$ were synthesized with the diimines: 1,10-phenanthroline and 2,2′-bipyridine and with the carbohydrates: aminosugars, hexoses, pentoses and sucrose, with the aim of finding out which are the determining factors of the resultant chirality in these compounds. The optical characteristics of the complexes obtained were determined through measurement of their absorption and circular dichroism spectra. All the complexes synthesized exhibited an excitonic effect in the UV spectral region. Assignment of the circular dichroism bands in the visible could be performed by applying ligand field theory treatment and assuming a D_2 local symmetry to the optically active bands in the region of the d–d* absorption bands corresponding to the $^1A_1 \rightarrow {}^1B_2$ and $^1A_1 \rightarrow {}^1B_3$ transitions. Rotatory strength of these bands can be ascribed to coupling of the magnetic moments of the d–d* bands with the electric moments of the $\pi \rightarrow \pi^*$ transitions, polarized along the short axis of the diimine molecules, which turned out to be almost parallel in the Δ- and Λ-[Co(diimine)$_2$carbohydrate]$^{2+}$ complexes.
© 2004 Elsevier Ltd. All rights reserved.

Keywords: Carbohydrate; Cobalt complex; Absorption spectra; Circular dichroism; Optical activity

1. Introduction

Carbohydrates, such as aminosugars: D-glucosamine, D-galactosamine, D-mannosamine; hexoses: D-glucose, D-galactose, D-mannose; pentoses: D- and L-arabinose, D- and L-xylose, D-ribose and sucrose (Scheme 1), react stereoselectively with the species Δ-, Λ-[Co(phen)$_2$Cl$_2$]$^+$ with the exception of D-glucose (Table 1) [1–6]. The products thus obtained are of the type Δ- and Λ-[Co(phen)$_2$carbohydrate]$^{2+}$, where the carbohydrate behaves as a bidentate ligand and is monodeprotonated. The chiral preference in the formation of these compounds may be caused by different structural factors, such as: interatomic distances, bonding angles, etc., leading to differences in the steric interactions of the diastereomers as a result of bigger or smaller distances of the carbohydrate to the phenanthroline molecules in the coordination sphere (Fig. 1) [1–6]. The degree of stereoselectivity, though, does not change on replacing the phenanthroline ligands bipyridine (Scheme 2), in order to obtain compounds of the type Δ- and Λ-[Co(bipy)$_2$carbohydrate]$^{2+}$. Results appearing in Table 2 [1] show that the higher degree of flexibility of the bipyridine molecule, compared to that of the phenanthroline, has no influence on the chiral preference in the process of formation of these complexes.

The monosaccharides, which adopt mainly the anomeric forms α or β, coordinate to the metallic ion through the ligand groups O^--1 and NH_2 or OH-2, adopting an axial, equatorial disposition or viceversa (Fig. 1) [1–5]. The coordinated anomer has one of the chair conformations: $^4C_1$ or $^1C_4$, slightly distorted, [7–9] compared to that of the free monosaccharide in water solution. On the other hand, coordination of the anomer (α or β) is independent of the nature of the aromatic diimine, thus coinciding with the independence of stereoselectivity with the nature of these ligands. Sucrose coordinates as a bidentate ligand,

Abbreviations: D-Glucosamine: 2-amino-2-deoxy-glucose; D-Galactosamine: 2-amino-2-deoxy-galactose; D-Mannosamine: 2-amino-2-deoxy-mannose; phen: 1,10′-phenanthroline; bipy: 2,2′-bipyridine.

* Corresponding author.
E-mail address: jparada@ciq.uchile.cl (J. Parada).

0277-5387/$ - see front matter © 2004 Elsevier Ltd. All rights reserved.
doi:10.1016/j.poly.2004.02.020

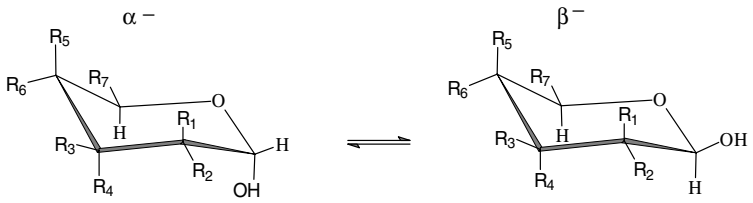

	R_1	R_2	R_3	R_4	R_5	R_6	R_7
D-glucopyranose	H	OH	OH	H	H	OH	CH_2OH
D-glucosamine	H	NH_2	OH	H	H	OH	CH_2OH
D-galactopyranose	H	OH	OH	H	OH	H	CH_2OH
D-galactosamine	H	NH_2	OH	H	OH	H	CH_2OH
D-mannopyranose	OH	H	OH	H	H	OH	CH_2OH
D-mannosamine	NH_2	H	OH	H	H	OH	CH_2OH
D-xylopiranose	H	OH	OH	H	H	OH	H
D-ribopyranose	H	OH	H	OH	H	OH	H

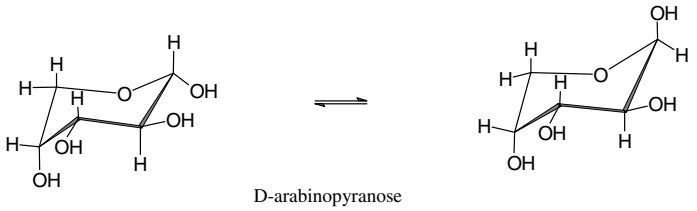

D-arabinopyranose

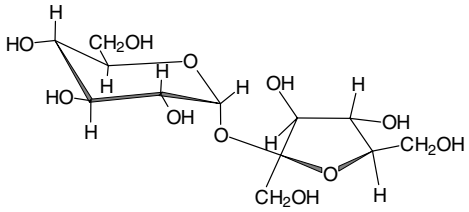

Sucrose (α-D-glucopyranosyl-β-D-fructofuranosyde)

Scheme 1.

Table 1
Preferred absolute configuration in complexes of the type $[Co(phen)_2carbohydrate]^{2+}$ and percentage of the Δ diastereomer

Complex	Preferred absolute configuration	Percentage of the Δ form[a]
$[Co(phen)_2$D-glucosamine$]^{2+}$	Δ	94
$[Co(phen)_2$D-galactosamine$]^{2+}$	Δ	95
$[Co(phen)_2$D-mannosamine$]^{2+}$	Δ	∼100
$[Co(phen)_2$D-galactose$]^{2+}$	Δ	∼100
$[Co(phen)_2$D-mannose$]^{2+}$	Δ	98
$[Co(phen)_2$D-glucose$]^{2+}$	Δ ≈ Λ	∼50
$[Co(phen)_2$D-arabinose$]^{2+}$	Δ	67
$[Co(phen)_2$D-ribose$]^{2+}$	Λ	37
$[Co(phen)_2$D-xylose$]^{2+}$	Λ	33
$[Co(phen)_2$D-sucrose$]^{2+}$	Δ	100

[a] The percentage values were obtained from the relation: $([\Delta]/([\Delta]+[\Delta]))\times 100$.

through the O^--2 fragment of glucopyranose and through OH-1 of fructofuranose [6]. Conformation of coordinated sucrose does not change significantly compared to that of this ligand in its crystalline form [6].

The higher coordinating power of the amino group in the aminosugars [10] does not exert influence on the chiral preference nor on the degree of stereoselectivity of the resulting complexes [1]. In relation with this point, the complexes with aminosugars, as well as those with hexoses reach a higher degree of product with absolute configuration Δ during the synthetic process (Table 1). Besides, when the CH_2OH group in the position 5 of the hexopyranoses and of the aminohexopyranoses (Scheme 1) is replaced by an hydrogen atom, thus turning into a pentopyranose (Scheme 1), this last confers higher flexibility and higher entropy to the coordinated carbohydrate on both diastereomers [7–9], and the degree of chiral preference lowers (Table 1).

In complexes of the same type with the aminoalcohol "ephedrine", which shows a higher degree of flexibility than the carbohydrates, the products obtained do not show chiral preference [11]. Considering the evidence previously mentioned it is possible to correlate the "rigidity" [7–9] of the ligand with the degree of chiral preference in the systems here studied. Additionally, a direct relationship is observed between the size of the carbohydrate (Scheme 1) and the chiral preference. In this way,

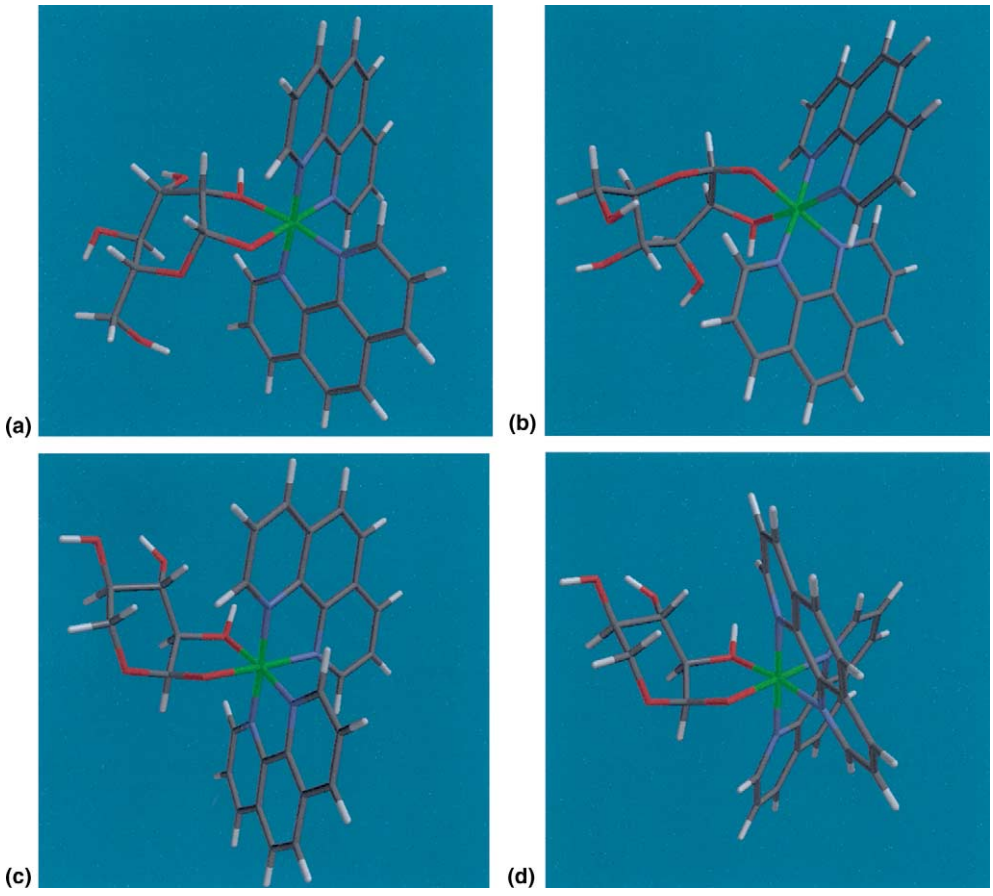

Fig. 1. The most likely structures of the complex ions: (a) Δ-[Co(phen)$_2$β-D-mannopyranose]$^{2+}$, (b) Λ-[Co(phen)$_2$β-D-mannopyranose]$^{2+}$, (c) Δ-[Co(phen)$_2$α-D-xylopyranose]$^{2+}$, (d) Λ-[Co(phen)$_2$α-D-xylopyranose]$^{2+}$, obtained with the semiempirecal PM3 (tm) method, SPARTAN program [26].

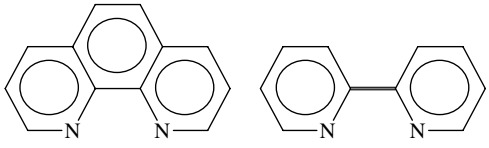

1,10-phenanthroline(phen) 2,2′-bipyridine (bipy)

Scheme 2.

Table 2
Preferred absolute configuration in complexes of the type [Co(bipy)$_2$carbohydrate]$^{2+}$

Complex	Preferred absolute configuration
[Co(bipy)$_2$D-glucosamine]$^{2+}$	Δ
[Co(bipy)$_2$D-galactosamine]$^{2+}$	Δ
[Co(bipy)$_2$D-mannosamine]$^{2+}$	Δ
[Co(bipy)$_2$D-galactose]$^{2+}$	Δ
[Co(bipy)$_2$D-mannose]$^{2+}$	Δ
[Co(bipy)$_2$D-glucose]$^{2+}$	Δ ≈ Λ
[Co(bipy)$_2$D-arabinose]$^{2+}$	Δ
[Co(bipy)$_2$D-ribose]$^{2+}$	Λ
[Co(bipy)$_2$D-xylose]$^{2+}$	Λ

sucrose, which has a bigger size than the remaining carbohydrates here studied, can enter into the coordination sphere of the complexes Δ- and Λ-[Co(phen)$_2$Cl$_2$]$^+$ with a minimum steric hindrance for the diastereomer of Δ configuration, which is formed exclusively [7]. From the previously mentioned evidence, it is possible to correlate the degree of stereoselectivity in the process of formation of the complexes Δ- and Λ-[Co(phen)$_2$carbohydrate]$^{2+}$ with both the rigidity of the ligand molecule and their relative size, according to the sequence [1]

sucrose > aminosugars ≈ hexopyranoses

> pentopyranoses.

This work covers also the study of the absorption and circular dichroism spectra of the complexes in terms of the "ligand-field" [12,13] and "perturbation" theories [14] in order to discover the origin of the optical activity in the visible spectral region.

2. Experimental

2.1. Synthesis of the bis-(diimine)(carbohydrate) Co(III) complexes

All the reagents and solvents used were p.a. and were used without further purification.

The complexes here synthesized, of the type bis-(diimine)(carbohydrate) cobalt(III), were prepared from complex salts of the general formula *cis*-[Co(diimine)$_2$Cl$_2$]Cl which, in turn, were obtained by the technique described by Ablov [15], to obtain *cis*-[Co(phen)$_2$Cl$_2$]Cl. This last compound, in our case, is the "precursor" complex. The same method was applied to obtain the precursor complex with 2,2′-bipyridine.

The compounds formed by Co(III), a carbohydrate molecule, and the previously mentioned diimines were obtained according to the following general procedure: 1 mmol of [Co(diimine)$_2$Cl$_2$]Cl and 2 mmol of a carbohydrate were mixed in 40 ml of water and the pH of the solution was adjusted to 8, with 0.1 M NaOH. The total volume was completed to 50 ml in a volumetric flask that was then sealed and introduced into a thermoregulated Haake K-F3 Model bath, where it was kept for one week at 25 °C. During that period the pH of the solution and its optical activity were controlled at intervals of 2 h in a Jobin Yvon CD-6 spectropolarimeter.

Once the maximum value of the optical activity was reached, the solution was transferred to an SP-Sephadex C25 chromatographic column (1 m long and 2 cm diameter) maintaining a speed of elution of 3 ml/min. The eluant used was NaCl in water in a gradient of 0.05–0.1 M concentrations. The fractions were gathered in an automatic collector (Advance SF-2120) and their circular dichroism and absorption spectra were recorded both in the visible as in the ultraviolet regions. The fractions showing the same sequence of optical activity signals were mixed in order to know the amount of complex through the concentration of cobalt. The fractions corresponding to the complexes of general formula Δ- and Λ-[Co(diimine)$_2$carbohydrate]$^{2+}$ showed a brownish colour in the case of the aminosugars and a red colour in the complexes formed by the hexoses, pentoses and sucrose. In all these cases, yellow coloured products remained at the top of the column. They could be eluted with an NaCl 0.5 M solution. They corresponded to a racemic product, the complex [Co(diimine)$_3$]$^{3+}$ [16].

The complexes of Δ and Λ configuration, once isolated chromatographically, were precipitated with 0.1 M KI_3 as complex salts of this anion.

The solid products obtained were suspended in water and sonnicated, so as to remove the NaCl salt, that coprecipitated with the complex in the presence of the triiodide anion. The composition of the salts obtained was known through elemental analysis (Table 3). The compounds which do not appear in the table were only studied in solution.

2.2. Spectral measurements

Optical rotation measurements were performed in a Perkin–Elmer 141 spectropolarimeter, at 475 and 550 nm wavelength, at 25 °C in cells of 1 and 5 cm width.

The circular dichroism spectra were obtained in a Jobin Yvon CD-6 spectropolarimeter with 10^{-3}–10^{-4} M solutions of the complexes in the visible and 10^{-5}–10^{-6} M solutions in the ultraviolet spectral region, in quartz cells 0.1, 0.5 and 1 cm widths, in such a way as to have a maximum absorbance not greater than 0.8 absorbance units. Measurements of the absorption spectra were carried out in the same way as was described for the measurement of the circular dichroism, in the Jobin Yvon CD-6 and Unicam UV3 spectrophotometers, both in the visible and in the ultraviolet regions.

The cobalt content of the complexes in the solutions as in the solid compounds was found out by atomic absorption spectroscopy, with a Perkin–Elmer 1100B spectrophotometer.

Table 3
Elemental analysis of the complexes [Co(diimine)$_2$aminosugar](I$_3$)$_3$ and [Co(phen)$_2$carbohydrate](I$_3$)$_2$

Complex	% C	% H	% N	% Co
Δ-[Co(phen)$_2$D-glucosamine](I$_3$)$_3$	20.75(20.68)	1.65(1.67)	4.09(4.02)	3.50(3.39)
Δ-[Co(bipy)$_2$D-glucosamine](I$_3$)$_3$	18.80(18.43)	1.67(1.65)	4.25(4.13)	3.60(3.48)
Δ-[Co(phen)$_2$D-mannosamine](I$_3$)$_3$	19.65(20.68)	1.55(1.67)	4.14(4.02)	3.54(3.39)
Δ-[Co(bipy)$_2$D-mannosamine](I$_3$)$_3$	18.95(18.43)	1.63(1.65)	4.30(4.13)	3.72(3.48)
Δ-[Co(phen)$_2$D-galactosamine](I$_3$)$_3$	20.98(20.68)	1.78(1.67)	4.12(4.02)	3.56(3.39)
Δ-[Co(phen)$_2$galactose](I$_3$)$_2$	25.82(26.47)	2.04(1.99)	4.11(4.12)	4.20(4.23)
Δ-[Co(phen)$_2$mannose](I$_3$)$_2$	25.45(26.47)	1.82(1.99)	4.35(4.12)	4.00(4.23)
Δ-[Co(phen)$_2$glucose](I$_3$)$_2$	26.13(26.47)	2.07(1.99)	4.45(4.12)	4.32(4.23)
Δ-[Co(phen)$_2$sucrose](I$_3$)$_2$	28.43(28.38)	2.54(2.43)	3.81(3.68)	3.94(3.88)
Δ-[Co(phen)$_2$D-xylose](I$_3$)$_2$	26.00(26.17)	1.75(1.88)	3.94(4.21)	4.21(4.44)
Δ-[Co(phen)$_2$L-xylose](I$_3$)$_2$	26.39(26.17)	1.83(1.88)	4.48(4.21)	4.31(4.44)
Δ-[Co(phen)$_2$L-arabinose](I$_3$)$_2$	26.07(26.17)	1.60(1.88)	4.61(4.21)	4.00(4.44)
Λ-[Co(phen)$_2$L-arabinose](I$_3$)$_2$	26.47(26.17)	1.87(1.88)	4.36(4.21)	4.32(4.44)
Δ-[Co(phen)$_2$D-ribose](I$_3$)$_2$	26.65(26.17)	1.84(1.88)	4.46(4.21)	4.14(4.44)
Λ-[Co(phen)$_2$D-ribose](I$_3$)$_2$	25.98(26.17)	1.75(1.88)	4.37(4.21)	4.09(4.44)

Calculated values are inside parenthesis.

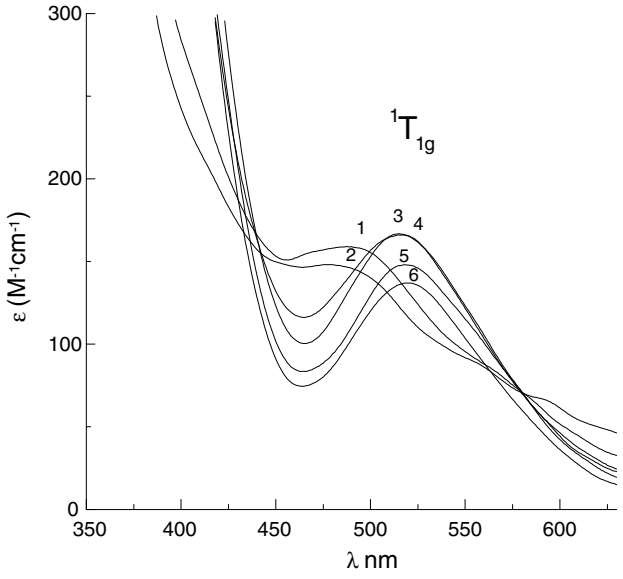

Fig. 2. Absorption spectra in the visible region of complexes Δ- and Λ-[Co(diimine)$_2$carbohydrate]$^{2+}$: (1) Δ-[Co(phen)$_2$D-galactosamine]$^{2+}$, (2) Δ-[Co(bipy)$_2$D-galactosamine]$^{2+}$, (3) Δ-[Co(phen)$_2$D-arabinose]$^{2+}$, (4) Δ-[Co(phen)$_2$D-galactose] $^{2+}$, (5) Λ-[Co(phen)$_2$D-glucose]$^{2+}$, (6) Δ-[Co(phen)$_2$sucrose]$^{2+}$.

Elemental analysis of C, H and N on the compounds synthesized were performed on a Fisons-Carlo Erba EA 1108 micro-analyzer.

3. Results and discussion

All of the Co(III) compounds formed by two molecules of an aromatic diimine and a carbohydrate, be it an aminosugar, an aldose (hexoses, pentoses) or sucrose, exhibit only one absorption band in the visible region (Fig. 2 and Tables 4–6) [1–6]. It is located in the region of 480–519 nm, corresponding to the $^1T_{1g}$ state in octahedral symmetry. This spectral range of absorption coincides with the expected one, according to the average field rule of the ligands [12,13,17,18], indicating, thus, that coordination of the aminosugar occurs through the NH_2 and OH groups. The remaining carbohydrates coordinate through two OH groups. On comparing the location of the $^1T_{1g}$ state of the complexes with aminosugars with that of complexes formed by the corresponding carbohydrates, it can be observed that the positions of the absorption band maxima are shifted ~30 nm towards shorter wavelength (Fig. 2).

The energy level scheme included is a qualitative one and shows the sequence for octahedral (O_h) complexes of Co(III) and the resulting levels produced by rhombic distortion, assuming that they turn out to be orthoaxial, with holohedrized symmetry D_2 [16,24] (see Scheme 3). In regular octahedral complexes the Cartesian orbitals are split by symmetry in the e_g "class" that gives origin to σ bonds and the t_{2g} "class"

Table 4
Average values of absorption and circular dichroism for complexes Δ- and Λ-[Co(diimine)$_2$aminosugar]$^{2+}$[a]

	Absorption		CD	
	λ (nm)	log ε	λ (nm)	Δε (M^{-1} cm^{-1})
Δ-[Co(phen)$_2$D-aminosugar]$^{2+}$[b]	225sh	4.81	236	+9.5
	272	4.65	267	+13.3
			281	−19.4
	319sh	3.83	318	+4.0
	371.5sh	2.90	357	−1.2
	485	2.33	418	+1.2
			502	−2.8
			598sh	−0.13
Δ-[Co(bipy)$_2$D-aminosugar]$^{2+}$			260	+5.0
	305	4.23	299	+2.3
			319	−3.8
			337	+0.4
			353	−0.4
	482	2.10	424	+0.8
			501	−2.1
			599sh	−0.11
Λ-[Co(bipy)$_2$D-aminosugar]$^{2+}$			256	−3.45
	304	4.21	298.5	−2.15
			320.5	+2.25
			340.5	−0.55
			364	+0.14
	485	2.08	420.5	−0.4
			503.5	+1.2
			577sh	+0.35

[a] Diimines: 1,10-phenthroline and 2,2′-bipyridine and the D-aminosugars are: D-glucosamine, D-galactosamine and D-mannosamine.
[b] Values for D-glucosamine were published in [27]; those for D-galactosamine and D-mannosamine appear in [4].

Table 5
Average values of absorption and circular dichroism for complexes Δ- and Λ-[Co(diimine)$_2$carbohydrate]$^{2+}$ [a]

	Absorption		CD	
	λ (nm)	log ε	λ (nm)	$\Delta\varepsilon$ (M^{-1} cm^{-1})
Δ-[Co(phen)$_2$carbohydrate]$^{2+}$	226.7sh	4.9	228.5	−10.4
	270	4.65	267	+9.8
			280	−12.1
	324sh	3.75	322.5	+2.71
	357sh	3.22	364	−1.28
	517	2.21	414	+2.52
			512	−4.18
			608sh	−0.42
Λ-[Co(phen)$_2$carbohydrate]$^{2+}$	227sh	4.84	228	+9.2
	270	4.63	267	−8.8
			280	+10.6
	321sh	3.76	321	−2.9
	352.5sh	3.53	364	+1.1
	515	2.18	414	−2.37
			513	+3.85
			609sh	−0.25

[a] Carbohydrates are: D-galactose [5], D-mannose, D-glucose, D-, L-arabinose [5], D-, L-xylose, D-ribose and sucrose [6].

Table 6
Average values of absorption and circular dichroism for complexes Δ- and Λ-[Co(bipy)$_2$carbohydrate]$^{2+}$ [a]

	Absorption		CD	
	λ (nm)	log ε	λ (nm)	$\Delta\varepsilon$ (M^{-1} cm^{-1})
Δ-[Co(bipy)$_2$carbohydrate]$^{2+}$	305	4.28	270	+5.1
			315	−3.5
			329	+1.75
			363	−0.73
	510	2.16	407.5	+2.19
			504	−3.51
			600sh	−0.11
Λ-[Co(bipy)$_2$carbohydrate]$^{2+}$	303	4.26	270	−5.61
			316	+3.1
			326	−1.6
			358	+1.44
	508	2.15	411	−2.32
			505	+3.78
			605sh	−0.15

[a] The carbohydrates are: D-galactose, D-mannose, D-, L-arabinose, L-xylose and D-ribose.

that forms π bonds. This classification can be applied to a Cartesian system of coordinates whose origin is placed at the nucleus of the central ion, in such a way that the axis addresses through the nuclei of the ligands. The chromophores that belong to this class are named orthoaxial. Holohedrized symmetry has been applied to such a structure where any interaction that takes place along the x, y and z axes is divided in halfs: one half addresses through $-x, -y, -z$, while the other half does it through x, y and z [16a,24]. On lowering the symmetry, three energy levels: $^1B_1$, $^1B_2$ and $^1B_3$ are expected for each singlet state of Co(III). Table 7 shows the three energy levels originating from the $^1T_{1g}$ and $^1T_{2g}$ octahedral levels on applying crystal field calculations [12,13]. The energy differences between these levels are small and the observed spectral absorption band covers the three separate bands. The circular dichroism spectra, though, show two bands in this region.

Calculations of the rotatory strength based on the perturbation theory and considering D_2 symmetry show that only two out of the three transitions are optically active and of opposite signs. These last correspond to transitions between the fundamental, $^1A_1$ state to the $^1B_2$ and $^1B_3$ excited states.

These results coincide with the experimental evidence showing two circular dichroism signs in the region of the $^1T_{1g}$ state for each one of the complexes studied (Fig. 3).

Optical activity of the d–d transitions in the complexes Δ- and Λ-[Co(diimine)$_2$carbohydrate]$^{2+}$ may rise

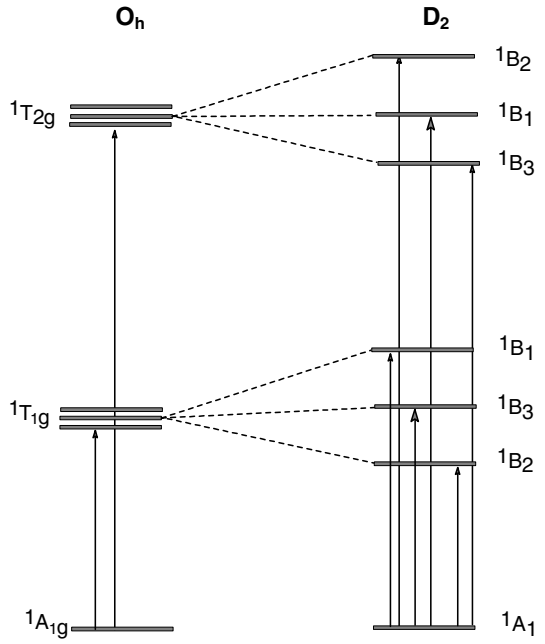

Scheme 3.

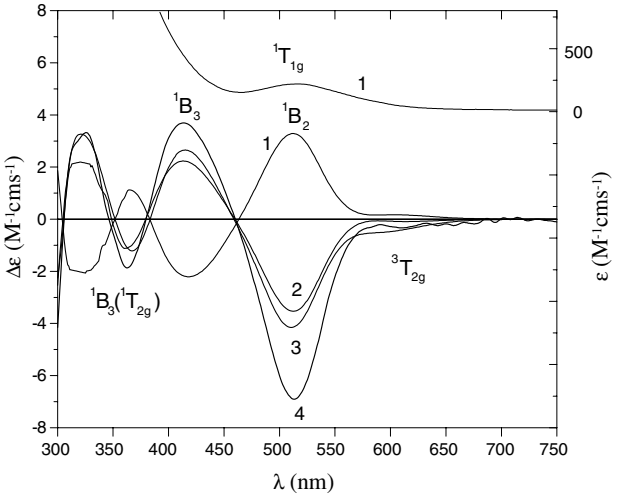

Fig. 3. Absorption and circular dichroism spectra in the visible region of complexes Δ- and Λ-[Co(phen)$_2$carbohydrate]$^{2+}$: (1) Λ-[Co(phen)$_2$D-arabinose]$^{2+}$, (2) Δ-[Co(phen)$_2$D-galactose]$^{2+}$, (3) Δ-[Co(phen)$_2$D-arabinose]$^{2+}$, (4) Δ-[Co(phen)$_2$sucrose]$^{2+}$.

as the result of coupling of the magnetic moments in these transitions (m^*_{dd}) with the electric moments of the π–π* transitions of the diimines (α band), that are polarized along the short axis of the diimine molecule ($\mu^*_{\pi\pi}$), both of which turn out to be parallel in all of the obtained compounds [14,19,20] and their rotatory strengths are of opposite signs.

Calculations of the energy levels of the complexes [Co(diimine)$_2$carbohydrate]$^{2+}$ having origin in the $^1T_{1g}$ state once split by rhombic distortion (D_2) (Table 7) give an average value of $Dq^{O^-} = 2033$ cm^{-1}, corresponding to the splitting of the energy levels produced by the alcoxide group.

The calculated value for Dq^{O^-} is similar to that of other Co(III) complexes, where the donor group is also O^-, as is the case for the oxalate or carbonate ions [17,21–24].

Regarding the absorption and circular dichroism bands in the zone of the d–d* transitions, the calculated energy level values for the Dq^{OH} parameter show an average of 2118 cm^{-1} for the complexes [Co(diimine)$_2$carbohydrate]$^{2+}$, (carbohydrate: hexoses, pentoses and sucrose). This value is also similar to those obtained for other Co(III) complexes with ligands coordinated through O^- and OH, as is the case with H_2O [17,21–24]. Results indicate that the carbohydrates as ligands coordinate through the O^- bonded to the carbon atoms 1 or 3 and through the NH_2 group bonded to the carbon atom 2 in the complexes with aminosugars. In complexes with sugars coordination is established through two OH groups, one of which is deprotonated.

Values obtained for B (Racah parameter) of d–d* transitions related to interelectronic repulsions (Table 8) are placed in the range of ~500 cm^{-1}. This value is in the order of magnitude of those calculated for other [CoN_5O_1] and [CoN_4O_2] systems [12,13]. It is generally

Table 7
Energies of transitions from the fundamental state $^1A_1$ to the excited state $^1B_1$, $^1B_2$ and $^1B_3$ (rhombic symmetry, D_2) for both $^1T_{1g}$ and $^1T_{2g}$ states

Complex[a,b]	$^1A_{1g} \rightarrow {}^1T_{1g}$ (cm^{-1})		
	$^1A_1 \rightarrow {}^1B_1$	$^1A_1 \rightarrow {}^1B_2$	$^1A_1 \rightarrow {}^1B_3$
[Co(diimine)$_2$aminosugar]$^{2+}$	20449(489)	20640(485)	20199(495)
[Co(diimine)$_2$carbohydrate]$^{2+}$	19336(517)	19432(515)	19931(502)
	$^1A_{1g} \rightarrow {}^1T_{2g}$		
	$^1A_1 \rightarrow {}^1B_1$	$^1A_1 \rightarrow {}^1B_2$	$^1A_1 \rightarrow {}^1B_3$
[Co(diimine)$_2$aminosugar]$^{2+}$	28156(355)	28059(356)	27809(360)
[Co(diimine)$_2$carbohydrate]$^{2+}$	28218(354)	28121(357)	28717(348)

[a] Diimines correspond to: 1,10-phenanthroline and 2,2′-bipyridine.
[b] Calculations did not consider the values of Ds, which are the same for all of these complexes, corresponding to 5/84 of the respective Dq values. Values inside parenthesis correspond to the wave lengths in nm.

Table 8
Spectral parameters in cm^{-1} obtained by measurements of the absorrtion and circular dichroism spectra of complexes [Co(diimine)$_2$carbohydrate]$^{2+a,b}$

Complex	$^1A_{1g} \rightarrow {}^3T_{2g}$ (cm^{-1})	$^1A_{1g} \rightarrow {}^1T_{1g}$ (cm^{-1})	$^1A_{1g} \rightarrow {}^1T_{2g}$ (cm^{-1})	B (cm^{-1})	C (cm^{-1})
[Co(diimine)$_2$aminosugar]$^{2+c}$	16682	20640	28396	485	3919
[Co(diimine)$_2$carbohydrate]$^{2+d}$	16584	19432	27950	532	3552

[a] The energy values, cm^{-1}, correspond to the average of the experimental values, both for complexes with aminosugars as for those with sugars, standard deviation: 110 cm^{-1}.
[b] Diimines corresponds to 1,10-phenanthroline and 2,2′-bipyridine.
[c] Aminosugars are: D-glucosamine, D-galactosamine and D-mannosamine.
[d] Carbohydrates are: D-glucose, D-galactose, D-mannose, D-, L-arabinose, D-, L-xylose, D-ribose and sucrose.

considered that the Racah parameter C (Table 8) reflects the radial expansion of the d orbitals in complexes [12,13]. Values of 3866 cm^{-1} were obtained for complexes with aminosugars and of: 3673, 3689 and 3682 cm^{-1} for complexes with hexoses, pentoses and sucrose, respectively.

Comparison of the values 3873 cm^{-1} for $[Co(NH_3)_4C_2O_4]^+$ and 3720 cm^{-1} for $[Co(NH_3)_4CO_3]^+$ [12,13,25] shows that expansion by delocalization towards the ligands via π system is relatively unimportant in these cases.

In the present work the absolute configurations Δ and Λ of complexes [Co(diimine)$_2$carbohydrate]$^{2+}$ were identified by their circular dichroism spectra, according to the sign sequence of the "excitonic" effect [18] of the $\pi \rightarrow \pi^*$ transition at ~270 nm for compounds with phenanthroline and of ~300 nm for complexes with 2,2′-bipyridine (p band) [16], in the complexes having two diimine molecules as ligands (Fig. 4, Tables 4–6). The "excitonic" effect [18] consists of the presence of two

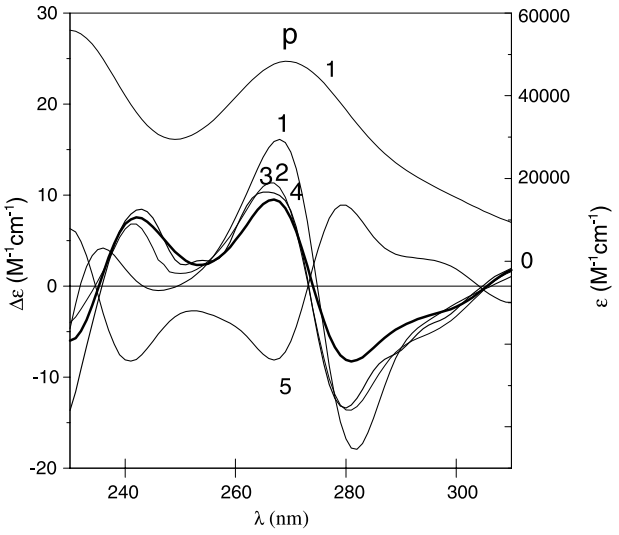

Fig. 4. Absorption and circular dichroism spectra in the UV region of complexes Δ-[Co(phen)$_2$carbohydrate]$^{2+}$: (1) D-mannosamine, (2) sucrose [6], (3) D-galactose [5], (4) D-arabinose [5] and (5) Λ-[Co(phen)$_2$D-arabinose]$^{2+}$ [5].

circular dichroism bands of opposite signs under the p absorption band, as a result of electrostatic coupling of the dipolar moments of the electric transitions in the individual diimine ligand molecules in these type of complexes. Besides the previously mentioned signals, a circular dichroism band is observed in the UV region, localized in the range of 241–243 nm (β band), that should correspond to a transition polarized along the major axis of the diimine molecule and calculated by self consistent field [13] to be at 260 nm. The corresponding absorption band is generally masked. The band of phenanthroline appears as a shoulder at ~320 nm in the absorption spectrum and gives a neat circular dichroism band at this wavelength (Fig. 3).

This last band is overlapped by the "p" band in the absorption spectra of the complexes [Co(bipy)$_2$carbohydrate]$^{2+}$. In the circular dichroism spectra, though, it can be observed at ~340 nm (Tables 4–6).

Correlation among the circular dichroism spectra in the visible region and configuration around Co(III) in the *tris*-chelate complexes is based on the location of the $^1A_2$ and ^1E states in D_3 symmetry (or $^1B_1$, $^1B_2$ and $^1B_3$ in the systems of D_2 symmetry), corresponding to the first excited state [14,19]. It has been found that the transition of ^1E symmetry shows a positive circular dichroism signal, whereas, in that of $^1A_2$ symmetry, the signal is negative when the complex has a Λ configuration (the signs will be the apposite ones for a complex of Δ configuration). It has to be born in mind also that the signal corresponding to the ^1E transition is always more intense than that of the $^1A_2$ transition, making it possible to identify them in the corresponding spectrum [17,21–24]. In the complexes of the type [Co(diimine)$_2$AB], where AB is a bidentate ligand, one of the components of the first excited state, the one deriving from the ^1E state in D_3 symmetry ($^1B_2$ under D_2 symmetry), dominates the circular dichroism spectrum. This is the one responsible for the positive or negative Cotton effect in the circular dichroism curve in the visible region, and is correlated with the absolute configuration of the *tris*-chelate Co(III) complex [1,18,21–24].

In all of the circular dichroism spectra examined, whose configuration has been known through the exci-

tonic effect, it can be seen that the first signal in the visible spectra is located at 502–513 nm. This is the band showing higher rotatory strength (higher $\Delta\varepsilon$) and has a negative sign in the complexes of Δ configuration and a positive sign for those of Λ configuration (Fig. 3 and Tables 4–6). This band corresponds to the $^1A_1 \rightarrow {}^1B_2$ transition under D_2 symmetry, according to the calculated rotatory strength for the complexes [14,19,20]. The band located at 410–415 nm has a lower $\Delta\varepsilon$ value, is of opposite sign to that of the previously mentioned one and it should correspond to the $^1B_3$ state under D_2 symmetry. It was assigned, as it was previously described [14,19,20]. In all of these complexes the states $^1B_3$ and $^1B_2$ in D_2 symmetry (region of the $^1T_{1g}$ state in O_h symmetry) are those that coincide with the sign sequence of the excitonic effect and, consequently, with the absolute configuration of the complexes [13,21]. Under the first absorption band in the visible region, corresponding to the $^1T_{1g}$ state there are two circular dichroism signals of opposite signs (Fig. 3 and Tables 4–6) under the first absorption band in the visible region, corresponding to the $^1T_{1g}$ state. The two circular dichroism signals arise from the partition of the $^1T_{1g}$ state of Co(III) under rhombic distortion, as a result of coordination of two molecules of an aromatic diimine plus one molecule of a carbohydrate around the metallic ion (Table 7) [12,13].

The p and α bands of the aromatic diimine overlap part of the absorption spectrum of Co(III) in all the Δ- and Λ-[Co(diimine)$_2$carbohydrate]$^{2+}$ complexes. Nevertheless, the corresponding circular dichroism spectra reveal a clear signal at ~364 nm. (Fig. 3 and Tables 4–6), that can be assigned to the $^1T_{2g}$ state in octahedral symmetry and, under D_2 symmetry, it would correspond to the transition from the fundamental $^1A_1$ state to the $^1B_3$ excited state [14,19,20]. The transition from the $^1A_1$ to the $^1B_2$ state in this region is expected to show optical activity of opposite sign to that of the $^1B_3$ state. This point could not be checked experimentally, since in the complexes Δ-, Λ-[Co(phen)$_2$carbohydrate]$^{2+}$ (Fig. 3, Tables 6–8) the circular dichroism spectra of these bands are overlapped by the α band, whereas in the complexes Δ- and Λ-[Co(bipyridine)$_2$carbohydrate]$^{2+}$ they are overlapped by the p and α bands (Table 6).

It could be observed also that the $^1A_1 \rightarrow {}^1B_1$ transition is not optically active in these complexes [14,19,20]. This result is in agreement with the number of signals of these compounds in the region of the $^1T_{2g}$ state [1–6].

In the circular dichroism spectra of the Δ and Λ isomers examined, a weak signal appears at the lower energy side of the $^1T_{1g}$ state band, that can be isolated by gaussian analysis: its location and $\Delta\varepsilon$ value lead to associate it to the $^3T_{2g}$ state of Co(III) in the complexes (Fig. 3 and Tables 4–6). Location of this spectral signal coincides with that of spin-forbbiden bands in Co(III) complexes with a similar coordination sphere [17,21].

Summarizing, it is worthwhile to remark the following features for the type of complexes here studied.

The circular dichroism spectra of the complexes show remarkable regularity in the number of spectral bands, sign sequence and intensity of the signals, independently of the nature of the carbohydrate ligands, number of asymmetric centers present in the chiral ligands; distribution of the asymmetric centers (*R* or *S*) of the C atoms bonded to N or O atoms that establish coordination, nor the conformation of the ring around the metallic ion. The same can be said about the different aromatic diimines 1,10-phenanthroline and 2,2′-bipyridine.

The spectra of the complexes here studied make it possible to spot the circular dichroism bands corresponding to singlet–triplet electronic transitions, which are rarely observed.

It is also worthwhile remarking that the carbohydrates as ligands, when bonded to Co(III) and form *tris*-quelate complexes with a particular configuration, make it possible to observe, as few other ligands do, the majority of the electronic transitions of this ion.

References

[1] J. Parada, Doctoral Thesis in Chemistry, University of Chile, 2003.

[2] A. Blasko, C.A. Bunton, S. Bunel, E. Moraga, C. Ibarra, J. Parada, Bol. Soc. Chil. Quím. 40 (1995) 449.

[3] S. Bunel, C. Ibarra, E. Moraga, J. Parada, A. Blasko, C.A. Bunton, Bol. Soc. Chil. Quím. 42 (1997) 109.

[4] S. Bunel, C. Ibarra, E. Moraga, J. Parada, A. Blasko, C. Whiddon, C.A. Bunton, Carbohydr. Res. 312 (1998) 191.

[5] J. Parada, S. Bunel, C. Ibarra, E. Mogara, N.D. Gillitt, C.A. Bunton, Polyhedron 20 (2001) 2223.

[6] (a) J. Parada, S. Bunel, C. Ibarra, G. Larrazábal, E. Moraga, Carbohydr. Res. 329 (2000) 195;
(b) J. Parada, S. Bunel, C. Ibarra, G. Larrazábal, E. Moraga, N.D. Gillitt, C.A. Bunton, Carbohydr. Res. 333 (2001) 185;
(c) J. Parada, S. Bunel, C. Ibarra, G. Larrazábal, E. Moraga, N. Gillitty, C.A. Bunton, Polyhedron 21 (2002) 2215.

[7] (a) P.L. Durette, D. Horton, Adv. Carbohydr. Chem. Biochem. 26 (1971) 49;
(b) M.K. Kaloustian, J. Chem. Educ. 51 (1974) 777.

[8] (a) E.L. Eliel, N.L. Allinger, S.J. Angyal, G.A. Morrison, Conformational Analysis, Interscience Publishers, New York, 1965;
(b) E.L. Eliel, S.H. Wilen, L.M. Mander, Stereochemistry of Organic Compounds, Wiley, New York, 1994.

[9] J.F. Stoddart, Stereochemistry of Carbohydrates, Wiley–Interscience, New York, 1971.

[10] W.J. Jolly, Modern Inorganic Chemistry, 2nd ed., McGraw-Hill, New York, 1991.

[11] C. Ortega, Licenciate Thesis in Chemistry, University of Chile, 1997.

[12] J. Ferguson, C.J. Hawkins, N.A.P. KaneMaguire, H. Lip, Inorg. Chem. 8 (1969) 771.

[13] N. Sanders, P. Day, J. Chem. Soc. A (1970) 1190.

[14] I. Tinoco, Adv. Chem. Phys. 4 (1962) 113.

[15] K. Bock, R.U. Lemieux, Carbohydr. Res. 100 (1982) 63.

[16] (a) C.J. Hawkins, Absolute Configurations of Metal Complexes, Wiley–Interscience, New York, 1971;

(b) K. Nakanishi, N. Berova, R.W. Woody, Circular Dichroism, Principles and Applications, VCH Publishers, New York, 1994.
[17] A.P.B. Lever, Inorganic Electronic Spectroscopy, Elsevier, Amsterdam, 1984.
[18] B. Bosnich, Acc. Chem. Res. 2 (1969) 266.
[19] (a) F.S. Richardson, J. Chem. Phys. 54 (1971) 2453;
(b) J.S. Griffith, The Theory of Transition Metal Ions, University Press, Cambridge, 1964.
[20] R.D. Gillard, Prog. Inorg. Chem. 7 (1966) 215.
[21] T. Yasui, B.E. Douglas, Inorg. Chem. 10 (1971) 97.
[22] (a) B.E. Douglas, S. Yamada, Inorg. Chem. 4 (1965) 1561;
(b) J.H. Dunlop, R.D. Gillard, J. Chem. Soc. (1965) 6351;
(c) K. Kawasaki, J. Yoshii, M. Shibata, Bull. Chem. Soc. Jpn. 43 (1970) 3819.
[23] V.S. Sastri, C.H. Langford, Can. J. Chem. 47 (1969) 4237.
[24] (a) C.E. Schäffer, C.H.R.K. Jorgensen, Mat. Fys. Medd. Dan. Vid. Selsk 34 (1965) 1;
(b) J. Josephsen, C.E. Schäffer, Acta Chem. Scand. A 31 (1977) 813.
[25] M. Ban, J. Csaszar, Acta Chim. Acad. Sciet. Hung. 57 (1968) 153.
[26] (a) J.J.R. Stewart, J. Comp. Chem. 10 (1989) 209;
(b) J.J.R. Stewart, J. Comp. Chem. 11 (1990) 543;
(c) J.J.R. Stewart, J. Comp. Chem. 12 (1991) 320.
[27] S. Bunel, C. Ibarra, E. Moraga, V. Calvo, A. Blaskóy, C.A. Bunton, Carbohydr. Res. 239 (1993) 185.

Available online at www.sciencedirect.com
SCIENCE DIRECT®
Polyhedron 23 (2004) 1351–1359
POLYHEDRON
www.elsevier.com/locate/poly

5,6-Dicyano-2,3-dithiopyrazine (dcdmp) chemistry: synthesis and crystal structure of Au(III)(dcdmp)$_2$ complexes and 2,3,7,8-tetracyano-1,4,6,9-tetraazothianthrene

D. Belo, I.C. Santos, M. Almeida *

Departamento de Química, Instituto Tecnológico e Nuclear, P 2686-953 Sacavém, Portugal

Received 5 November 2003; accepted 11 February 2004
Available online 9 April 2004

Abstract

As an effort to explore new complexes of the 2,3-dicyano-5,6-dimercaptopyrazyne (dcdmp) ligand with different transition metals, different salts containing both the Au(dcdmp)$_2^-$ complex and the new species 2,3,7,8-tetracyano-1,4,6,9-tetraazothianthrene (tctata), were obtained and characterized. *n*-Bu$_4$N Au(dcdmp)$_2$ crystallises in monoclinic space group $C2/c$, $Z = 8$ with unit cell parameters $a = 35.147(4)$, $b = 9.527(1)$, $c = 21.792(2)$ Å and $\beta = 109.626(8)°$. Its crystal structure consist of almost regular columns of [Au(dcdmp)$_2$]$^-$, stacked along b, surrounded by *n*-Bu$_4$N$^+$ cations. *n*-Bu$_4$N AuBr$_2$ (tctata) crystallises in triclinic space group $P\bar{1}$, $Z = 2$, with unit cell parameters $a = 10.986(1)$, $b = 13.230(2)$, $c = 13.791(1)$ Å, $\alpha = 79.150(9)°$, $\beta = 69.663(6)°$, $\gamma = 70.254(9)°$. The crystal packing is made by zig-zag chains of tctata separated by layers of cations, with AuBr$_2$ anions located in alternated cavities between the tctata chains and the cation layers. At last, *n*-Bu$_4$N[Au(dcdmp)$_2$] (tctata) crystallises in monoclinic space group $P2_1/n$, $Z = 4$, with unit cell parameters $a = 10.693(2)$, $b = 40.308(7)$, $c = 10.870(1)$ Å, $\beta = 92.16(1)°$. Its crystal structure can be seen has a mix of those of the two preceding compounds. It consists of bidimensional layers composed of out of registry parallel zig-zag chains of alternating tctata and [Au(dcdmp)$_2$]$^-$ units. The adjacent layers are separated by layers of [*n*Bu$_4$N]$^+$. In the last two compounds the tctata appears as a planar molecule.
© 2004 Elsevier Ltd. All rights reserved.

Keywords: S ligands; Coordination chemistry; Aurates; Thianthrenes

1. Introduction

Transition metal bisdithiolene complexes have, since their earlier studies during the sixties, attracted a great interest due to a rich variety of coordination geometry, and vivid redox behaviour [1]. These characteristics made them as choice building blocks for molecular materials displaying unconventional electrical and magnetic properties [2]. One of the key aspects in the versatility of these complexes, making them so attractive in the design of magnetic properties of molecular materials, is that both by change in the transition metal and in the oxidation state they can display different magnetic moments.

Square planar coordination geometry with these ligands is frequently observed in the anionic form with metals of Ni and Cu groups and such complexes have been used as counterions in charge transfer solids with a variety of donors. This planar geometry often favours solid state structures presenting more or less regular staking of the planar units providing chains of extended interactions in the solid, which can give rise to interesting properties such as ferromagnetism [3], metallic conductivity [4] or even superconductivity [5,6].

In these type of complexes both the accessibility to different oxidation states and the magnitude of the solid state interactions is expected to be favoured by ligands with more extended π-systems. While sulfur rich ligands have been extensively explored significantly less effort has been devoted to the study of other extended dithiolene π-ligands containing different heteroatoms like

* Corresponding author. Tel.: +351-219946171; fax: +351-219941455.
E-mail address: malmeida@itn.pt (M. Almeida).

0277-5387/$ - see front matter © 2004 Elsevier Ltd. All rights reserved.
doi:10.1016/j.poly.2004.02.019

N and O. These heteroatoms are expected to act also as an extra coordinating site which may provide an additional degree of freedom in crystal engineering of these solids, as recently demonstrated for pyrazinediselenate [7] and pyrazinedithiolate [8] Cu complexes. With the 2,3-dicyano-5,6-dimercaptopyrazyne (dcdmp) ligand the only reported complexes previously to our work are with nickel in the monoanionic form, $Ni(dcdmp)_2^-$ [9] and with it a few charge transfer salts with TTF and other related donors have been also described.

Preliminary data on charge transfer salts of $Au(dcdmp)_2^-$ with TTF type donors were previously reported by us [10]. In this paper we report the synthesis and characterization of the $Au(dcdmp)_2^-$ complex, and we describe two salts containing the new species 2,3,7,8-tetracyano-1,4,6,9-tetraazothianthrene (tctata) obtained as the product of a side reaction between the ligand with its precursor.

2. Experimental

2.1. Synthesis

To a suspension of sodium sulfate monohydrated in acetone (241 mg, 1×10^{-3} mol) was added, under stirring, an acetone solution of 2,3-dichloro-5,6-dicianopyrazine (100 mg, 5.02×10^{-4} mol). The formed red solution was filtered and added to a solution (2 ml) of potassium tetrachloroaurate (95 mg, 2.51×10^{-4} mol) in acetone, turning to a brown mixture. The inorganic precipitate was removed and the liquor added to 1 ml of a solution of tetrabutylammonium bromide (81 mg, 2.51×10^{-4} mol) in acetone, giving rise to an orange-gold solution. The stirring was maintained, in all steps, until no visible modification was observed. This solution was then filtered and allowed to a slow evaporation of the solvent in inert atmosphere. The orange solid obtained was filtered and recrystallised in acetone-diethyl ether, to afford needle shape crystals with three different colours. There are red (**3**) and yellow (**4**) crystals dominating the sample, but some green (**5**) crystals can be found also. In all cases, the crystals were suitable for X-ray diffraction measurements, revealing three different compositions. Visual separation of the crystals afforded the following characterisation data.

3: Tetrabutylammonium salt of gold(III)-bis-5,6-dicyano-2,3-dithiopyrazine, *n*-Bu_4N $Au(dcdmp)_2$, m.p. 258.3–260.5 °C (followed by decomposition). IR (KBr): $\widetilde{V} = 434$ (w, Au–S), 735 (m, CH_2–S–CH_2), 1172 (S, C–N), 1266 (m), 1301 (S), 1455 (m), 1481 (w, C=N–C), 2233 (m, C≡N), 2879–2966 (m, C–H alifat) cm^{-1}. UV–Vis (CH_3CN): $\lambda_{max} = 1413$, 1721, 1911, 2275, 2496 nm. *Anal.* Calc. for CHNS ($C_{28}H_{36}N_9S_4Au$): C, 40.82; H, 4.40; N, 15.30; S, 15.56. Found: C, 42.38; H, 3.70; N, 15.64; S, 15.71%. MS: *m*/*z* (%) 580.9 [M^-] (100) [$C_{12}N_8S_2Au$], 242.3 [M^+] (100) [$C_{16}H_{36}N$].

4: Tetrabutylammonium salt of gold dibromide with 2,3,7,8-tetracyano-1,4,6,9-tetraazothianthrene, *n*-Bu_4N $AuBr_2$ (tctata), m.p. 189.2–191.3 °C (followed by decomposition). IR (KBr): $\widetilde{V} = 428$ (S, Au–Br), 742 (m, CH_2–S–CH_2), 884 (m), 1170 (S, C–N), 1235 (m), 1325 (S), 1381 (m), 1485 (m, C=N–C), 1507 (m), 2240 (w, C≡N), 28877–2966 (m, C–H alifat) cm^{-1}. UV–Vis (CH_3CN): $\lambda_{max} = 1413$, 1721, 1911, 2275, 2496 nm. *Anal.* Calc. for CHNS ($C_{28}H_{36}N_9S_2AuBr_2$): C, 36.57; H, 3.94; N, 13.71; S, 6.97. Found: C, 38.54; H, 3.61; N, 14.04; S, 6.68%. MS: *m*/*z* (%) 288.0 (100) [$C_{12}N_8S^-$], 250.0 (39) [$C_{12}N_7S^-$], 356.8 (28) [$AuBr_2^-$], 197.0 (100) [Au^+], 242.3 (78) [$C_{16}H_{36}N^+$].

5: Tetrabutylammonium salt of gold(III)-bis-5,6-dicyano-2,3-dithiopirazine with 2,3,7,8-tetracyano-1,4,6,9-tetraazothianthrene, *n*-$Bu_4N[Au(dcdmp)_2]$ (tctata): the isolated amount of this compound was not enough to any characterization further than its structure determined by X-ray diffraction.

2.2. X-ray structure determination

The data collection was performed on two different Enraf-Nonius CAD4 diffractometer, one equipped with a graphite monochromatised Mo Kα radiation ($\lambda = 0.71069$ Å) and the other equipped with a graphite monochromatised Cu Kα radiation ($\lambda = 1.54150$ Å), in the $\omega - 2\theta$ scan mode. The structures were solved by direct methods using SIR97 [11] and refined by full-matrix least-squares methods using the program SHELXL97 [12] and the WINGX software package[13]. All non-hydrogen atoms were refined anisotropically. Hydrogen atoms were placed in idealised positions and allowed to refine riding on the parent C atom. Molecular graphics were prepared using ORTEP3 [14] and SCHAKAL-97 [15]. Crystal data and structure refinement of are summarized in Table 1.

3. Results and discussion

3.1. Synthesis

The synthesis of the gold complex **3** was performed following a standard procedure for the preparation of dithiolates from dichlorides, (Scheme 1) also used to prepare the Ni analogue [9]. The dithiolate ligand (**2**) in solution was obtained from the corresponding chloride salt (**1**) by treatment with Na_2S, in acetone. This ligand, without intermediate isolation was successively reacted with potassium tetrachloroaurate and *n*-Bu_4NBr, also in acetone solutions, followed by slow evaporation of the solvent in inert atmosphere, to give the gold(III) complex that was obtained as a red needle

Table 1
Crystallographic data for compounds **3**, **4** and **5**

Compound	**3**	**4**	**5**
Crystal size (mm)	$0.70 \times 0.32 \times 0.14$	$0.7 \times 0.3 \times 0.2$	$0.50 \times 0.25 \times 0.14$
Crystal system	monoclinic	triclinic	monoclinic
Crystal color/shape	red/needle	yellow/needle	green/needle
Space group	$C2/c$	$P\bar{1}$	$P2_1/n$
Lattice constants (Å, °)	$a = 35.147(4)$	$a = 10.986(1)$	$a = 10.693(2)$
	$b = 9.527(1)$	$b = 13.230(2)$	$b = 40.308(7)$
	$c = 21.792(2)$	$c = 13.791(1)$	$c = 10.870(1)$
		$\alpha = 79.150(9)$	
	$\beta = 109.626(8)$	$\beta = 69.663(7)$	$\beta = 92.16(1)$
		$\gamma = 70.254(9)$	
Volume (Å^3)	6873.3(1)	1763.3(3)	4682(1)
Formula sum	$C_{28}H_{36}AuN_9S_4$	$C_{28}H_{36}AuBr_2N_9S_2$	$C_{40}H_{36}AuN_{17}S_6$
Formula weight	823.86	919.56	1144.18
Z	8	2	4
ρ_{calc} (Mg/m^3)	1.592	1.732	1.623
Absorption coefficient (mm^{-1})	4.557	6.588	8.824
$F(000)$	3280	896	2280
Wavelength	Mo Kα (0.71069 Å)	Mo Kα (0.71069 Å)	Cu Kα (1.54150 Å)
T (K)	273(2)	293(2)	293(2)
θ range (°)	2.22–26.00	2.07–26.03	4.28–72.87
Index range (h, k, l)	−43/40, 0/11, 0/26	−12/13, −16/16, 0/16	−12/0, 0/48, −12/12
Scan type	$\omega - 2\theta$	$\omega - 2\theta$	$\omega - 2\theta$
Number of collected reflections	6906	7136	8842
Number of unique reflections/R_{int}	6718/0.0756	6840/0.0211	8425/0.1277
T_{max} and T_{min}	0.9975/0.4966	0.9864/0.7158	
Goodness-of-fit on F^2	0.901	1.045	1.017
Number of refined parameters	379	379	578
R (observed reflections)	0.0666	0.0669	0.0684
wR_2 (observed reflections)	0.1047	0.1480	0.1582

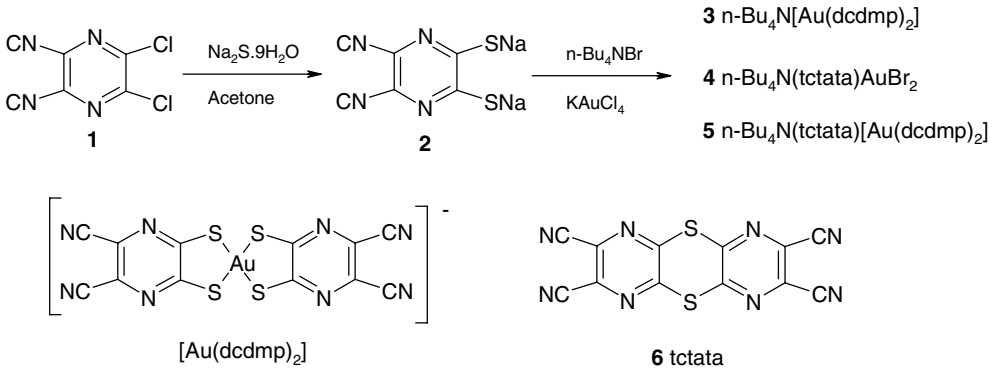

Scheme 1.

shaped crystals. The elemental analysis is consistent with a 1:1 stoichiometry, as confirmed by the X-ray crystal structure determination. Unexpectedly two other different kind of complexes were obtained, *n*-$Bu_4N[Au(dcdmp)_2]$ (tcdpdt) (**4**), as yellow needles and *n*-Bu_4NAuBr_2(tcdpdt) (**5**) as green needle shaped crystals, both containing the new species (tctata) (**6**). The structures of **3**, **4** and **5** were solved by single crystal X-ray diffraction (Scheme 1).

The unprecedented formation of the tetracyanotetraazathianthrene **6** incorporated in the structure of **4** and **5**, can be explained by a side reaction, taking place between the starting dichloride **1** and the dithiolate ligand **2**. The dithiolate acts as a nucleophilic agent, and substitutes the chlorine atoms in the pyrazine ring through an aromatic nucleophilic substitution mechanism which is activated by the cyano groups and further helped by the presence of the nitrogen atoms in the aromatic ring. Both the cyano groups and the nitrogen atoms are electroattractors, enhancing an electronic deficiency on the carbon atoms linked to chlorine (Scheme 2).

This explanation is supported by the fact that the above proposed reaction is similar to that previously

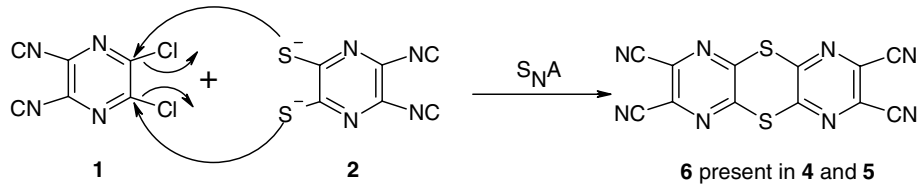

Scheme 2.

used to prepare other thiantrenes [16,18], but wewere not successful in isolating **6** as a pure compound.

Cyclic voltammetry of *n*-$Bu_4NAu(dcdmp)_2$ (**3**) in acetonitrile (Fig. 1, full line) shows a pair of symmetric reversible redox waves at $E_{1/2} = -0.629$ V vs Ag/AgCl ascribed to the couple $Au(dcdmp)_2^{2-}/Au(dcdmp)_2^{-}$. The cyclic voltammetry of **4** in the same conditions (Fig. 1, dashed line) shows three irreversible waves at −0.604, −0.349 and +0.732 V. The last wave is close to the values reported for the reaction $AuBr_2^- \leftrightarrow Au+2Br^-$ [17] but the two first waves are ascribed to tctata.

3.2. Structural characterisation

The crystal quality made possible to solve the crystal structure of compounds **3**, **4** and **5**. The geometry of the $Au(dcdmp)_2^-$ complex in **3** and **5** is identical, with average Au–S bond lengths of 2.307(3) and 2.320(3) Å, respectively (see Table 2). These values are in the upper side of the range of values reported for other gold(III) dithiolates that extend from 2.29 to 2.34 Å, with an average value of 2.305 Å. In both cases the complex is almost planar, with significant non planar deviations

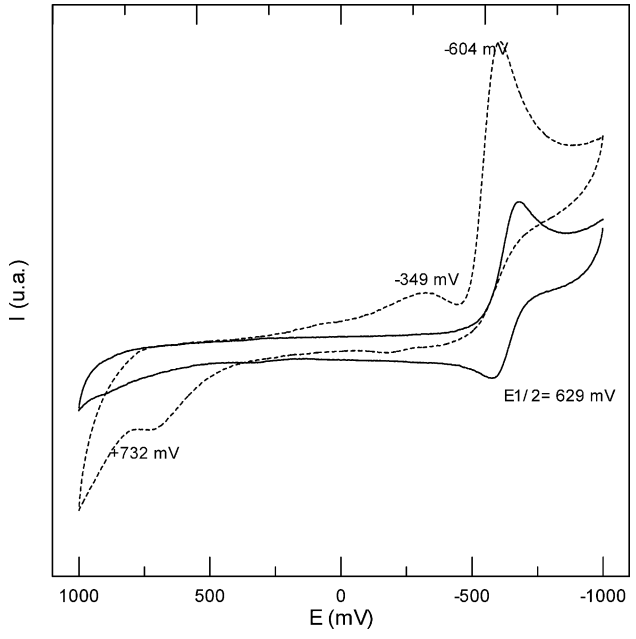

Fig. 1. Cyclic voltammetry of *n*-$Bu_4N[Au(dcdmp)_2]$ (solid line) and *n*-$Bu_4N(tctata)AuBr_2$ (dashed line), in acetonitrile.

Table 2
Selected bond lengths (Å) of $[Au(dcdmp)_2]^-$ complexes in **3** and **5**

	3	**5**
Au1–S1	2.303(3)	2.314(3)
Au1–S2	2.309(3)	2.322(3)
Au1–S3	2.303(3)	2.325(3)
Au1–S4	2.313(3)	2.317(3)
S1–C1	1.72(1)	1.73(1)
S2–C2	1.73(1)	1.73(3)
S3–C7	1.73(1)	1.72(1)
S4–C8	1.74(1)	1.72(1)
C1–C2	1.47(1)	1.44(1)
C7–C8	1.43(1)	1.45(1)
C1–N1	1.32(1)	1.35(1)
C2–N2	1.32(1)	1.34(1)
C7–N5	1.30(1)	1.34(1)
C8–N6	1.32(1)	1.32(2)
N1–C3	1.32(1)	1.34(1)
N2–C4	1.33(1)	1.34(1)
N5–C9	1.35(1)	1.31(2)
N6–C10	1.34(1)	1.34(1)
C3–C4	1.42(1)	1.37(1)
C9–C10	1.40(1)	1.39(2)
C3–C5	1.42(2)	1.41(2)
C4–C6	1.44(2)	1.45(2)
C9–C11	1.50(2)	1.43(2)
C10–C12	1.47(2)	1.45(2)
C5–N3	1.16(2)	1.14(2)
C6–N4	1.12(2)	1.16(2)
C11–N7	1.11(2)	1.14(2)
C12–N8	1.17(2)	1.14(2)

observed only in the terminal cyano groups, which are displaced towards opposite directions giving rise to a very small chair type distortion (Figs. 2 and 3). In both complexes the dcdmp ligands are identical within experimental uncertainty and with a geometry close to that found in the corresponding Ni analogue [9].

The new tetracyanothianthrene tctata species, present in complexes **4** and **5**, has bond lengths and angles identical to the corresponding ones in the dcdmp ligand in the dithiolates and an almost planar geometry in good agreement with that found in the unsubstituted analogue tetraazothiaantrene [18] (Figs. 3 and 4, Table 3). The two tctata molecules in **4**, are identical with an almost planar geometry, with a small twist of the terminal cyano groups, in opposite directions. The angles of the central ring range from 126.1° to 127.9°, in the case of the C=C–S angles, and show the values of 105.6° and 105.9° for the C–S–C angle. In the crystal structure of **5**, the tctata molecule shows a slight deviation from pla-

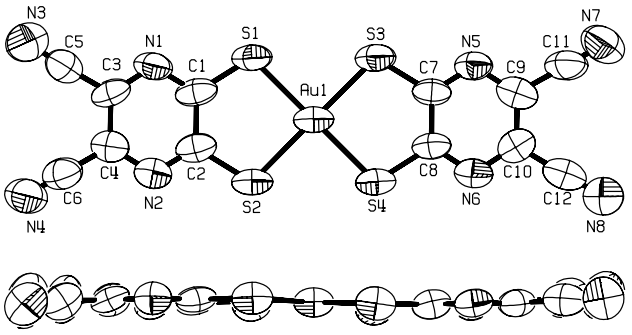

Fig. 2. ORTEP views and atomic numbering scheme of $Au(dcdmp)^{2-}$, in **3**, with thermal ellipsoids at 40% probability.

narity. There is a significant deviation of the sulphur atom, relatively to the average plane of the molecule and therefore the dihedral angle between the two half of the molecule is 174°. The non planarity is also denoted by the central ring bond angles that in the case of C=C–S bonds range from 125.5° to 126.6° while those of the C–S–C bonds are 107.7° and 106.3°. The deviation of the S atoms from the average molecular plane is certainly due to short contacts between these atoms and gold and carbon atoms in neighbouring ditiolate species (see Table 6).

To the best of our knowledge tctata, together with bis(quinoxaline)-2,2′,3,3′-disulfide [19] and 1,4,6,9-tetraazathianthrene [18], are the only azathiaantrenes displaying an essentially planar geometry, while all others present significant molecular dihedral angles ranging from 132° to 143°.

The tetrabutylammonium salt **3**, crystallises in the monoclinic system, space group $C2/c$, $Z = 8$. The unit cell contains one independent $[Au(dcdmp)_2]^-$complex and one independent tetrabutylammonium cation in general positions. The crystal structure consists of columns of $[Au(dcdmp)_2]^-$pairs, stacked along b (Fig. 5). The normal to complex plane makes an angle of 51.6° with this axis. There are two different overlap modes between complexes characterised by a different displacement along their long axis. The distance between the average plane of $[Au(dcdmp)_2]^-$ complexes are almost identical, being 3.49 and 3.47 Å, between and within the pairs of dithiolates, respectively. The stacks of the complexes are completely surrounded by $[n\text{-}Bu_4N]^+$ cations which prevent any contact between neighbouring stacks (Fig. 6).

The adopted overlap mode between stacked complexes at such a short distance corresponds to the existence of several short interatomic contacts (see Table 4),

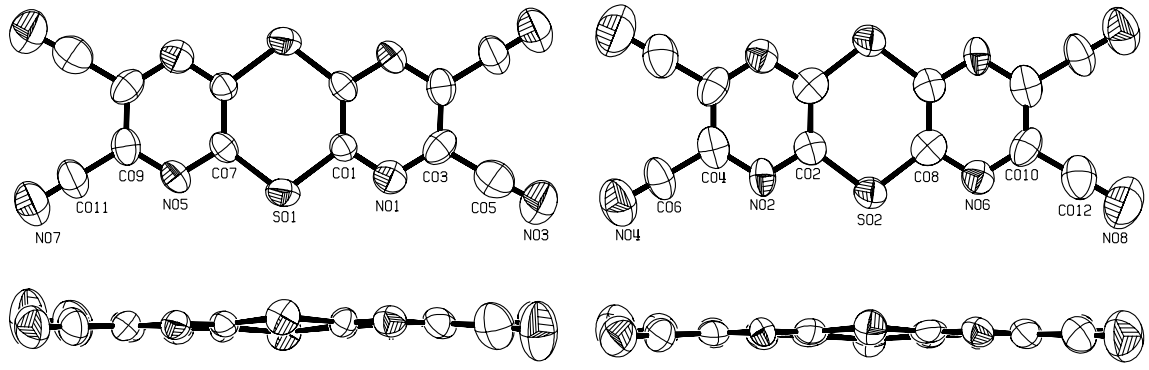

Fig. 3. ORTEP views and atomic numbering scheme of tctata units in **4**, with thermal ellipsoids at 40% probability.

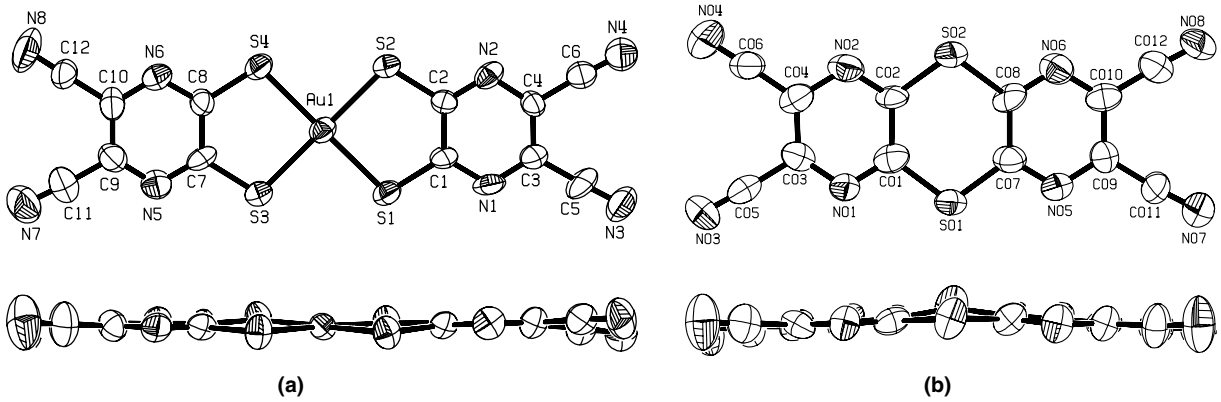

Fig. 4. ORTEP views and atomic numbering scheme of $Au(dcdmp)^{2-}$ (a) and tctata (b), in **5**, with thermal ellipsoids at 40% probability.

Table 3
Selected bond lengths (Å) of **6** in **4** and **5**

	5	**4** mol1	**4** mol2
S01–C01	1.75(2)	1.758(8)	
S01–C07	1.74(1)	1.732(9)	
S02–C02	1.75(1)		1.74(1)
S02–C08	1.74(1)		1.72(1)
C01–N01	1.31(2)	1.29(1)	
C07–N05	1.31(1)	1.31(1)	
C02–N02	1.30(1)		1.30(1)
C08–N06	1.31(1)		1.33(1)
C01–C02	1.45(1)		
C07–C08	1.45(1)		
C03–N01	1.32(2)	1.35(1)	
C09–N05	1.33(1)	1.35(1)	
C04–N02	1.38(2)		1.33(1)
C010–N06	1.32(1)		1.32(1)
C04–C03	1.37(2)		
C010–C09	1.40(2)		
C03–C05	1.50(2)	1.47(2)	
C09–C011	1.42(2)	1.44(1)	
C04–C06	1.41(2)		1.44(1)
C010–C012	1.44(2)		1.42(2)
C05–N03	1.13(2)	1.17(2)	
C011–N07	1.14(2)	1.11(1)	
C06–N04	1.16(2)		1.12(1)
C012–N08	1.14(2)		1.19(2)

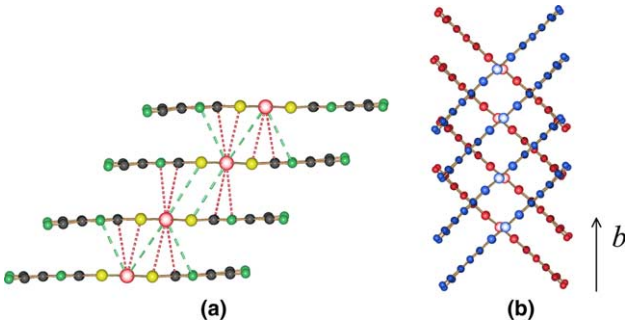

Fig. 5. Partial views of the crystal structure of **3** (a) view showing the short contacts between molecules along the dithiolate columns: the shortest contacts (dotted line) and contacts exceeding no more than 4% the sum of the van der Waals radii (dashed line); (b) view along *c*, showing the relative positions of dithiolates in two columns.

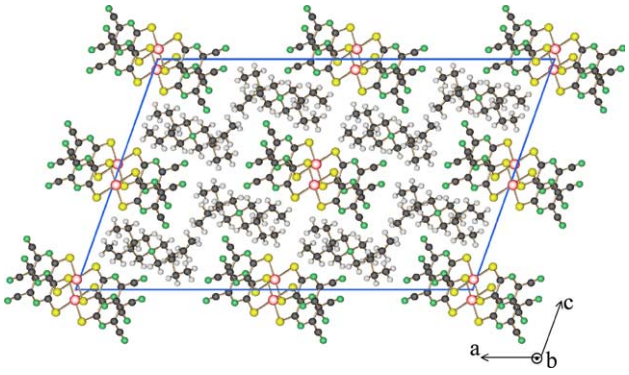

Fig. 6. View of the crystal structure of **3** along *b*.

Table 4
Hydrogen bonds and short contacts in the crystal structure of **3**

	d (Å)	Angle (°)	*d* (Å)/Σr_{vdw}
Au···S4	3.688		0.89
Au···N2	3.576		0.94
Au···C2	3.824		0.98
Au···C8	3.768		0.97
S1···H23a–C23	2.961	161.56	0.97
S4···H24a–C24	3.026	132.78	0.99
N3···H44a–C44	2.589	173.05	0.96
Au···Au	4.630		1.01
Au···S2	4.202		1.03
Au···N6	3.960		1.04
Au···C4	3.965		1.02

Σr_{vdw} = van der Waals radii sum

some clearly below the sum of van der Waals radii (dotted lines in Fig. 5), the shortest one being Au···S1 (3.71 Å). Other interactions are noticed slightly above the sum of van der Waals radii, as Au···Au exceeding by 1% that sum (dashed line in Fig. 5).

The interactions between the dithiolate complexes and the tetrabuthylamonium cations are established though several hydrogen bonds (Fig. 7, Table 4), only one through a pyrazinic nitrogen atom. Clearly the crystal structure of **3** is determined by the short complex interactions through both Au–S and Au–Au contacts and π–π interactions between ligands.

Compound **4** crystallises in the triclinic system, space group $P\bar{1}$, $Z = 2$. The unit cell has two independent units of tctata located at inversion centres, one independent tetrabutylamonium cation and one independent $AuBr_2$ anion. The crystal packing is made by zig-zag chains of tctata, separated by layers of the tetrabutylammonium cations parallel to the *b*, *a*–*c* plane (Fig. 8). The tctata units along the chains are connected by short S···S

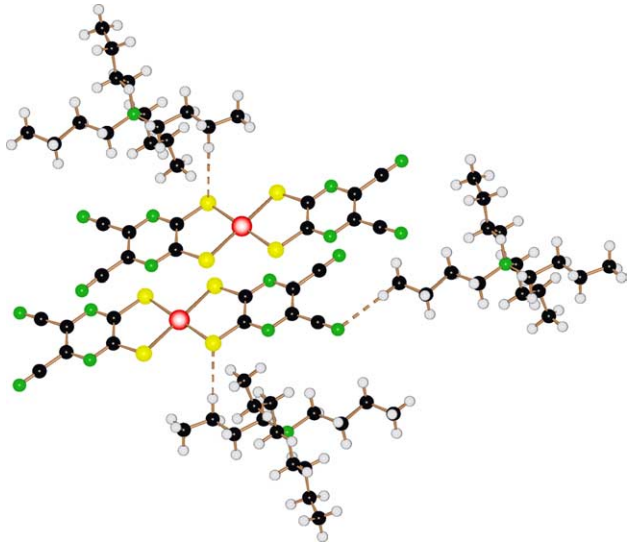

Fig. 7. Hydrogen bonds between the dithiolate anions and neighbouring cations, in the crystal structure of **3**.

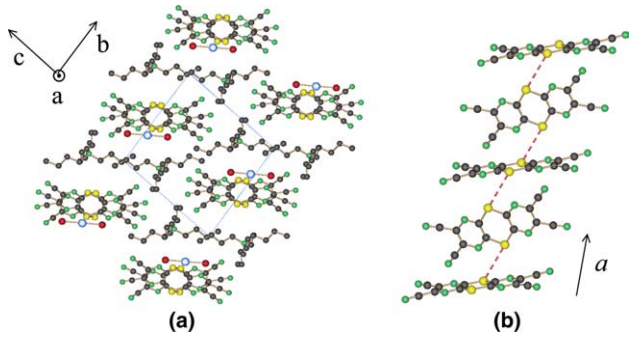

Fig. 8. (a) View of the crystal structure of **4** along *b*. (b) Partial view of the tctata zig-zag chains emphasising the S···S short contact, along the chain.

contacts at 3.586 Å and the angle between the average planes of these species is 76.1°. The $AuBr_2$units, with a linear geometry typical of monoanionic state, are located in alternated cavities between the tctata chains and cationic planes (Fig. 9). There are several short contacts (≈4 Å) between the gold atom and the sulphur atoms of the tctata unit and hydrogen bonds between the Au atom and the surrounding tetrabuthylamonium cations (see Table 5). The interactions between the tctata units and the tetrabuthylamonium cation are made through several hydrogen bonds (Table 5, Fig. 9), none of them involving the pyrazinic nitrogen atoms.

The last salt, **5**, crystallises in the monoclinic system, space group $P2_1/n$, $Z = 4$. The unit cell contains one independent molecule of tctata, one independent tetrabutylamonium cation and one independent $[Au(dcdmp)_2]^-$ complex all located in general in general positions. Its crystal structure can be seen as a combination of those of the two preceding compounds. It consists of bidimensional layers, in the *a*, *c* plane, composed of out of registry parallel zig-zag chains of alternating tctata and $[Au(dcdmp)_2]^-$ units (Fig. 11). The adjacent layers are separated by cation layers $[nBu_4N]^+$, along *b*, (Fig. 10). Several short contacts, within layer, can be noticed. With exception of the S3···S3 interaction between the anions in neighbouring

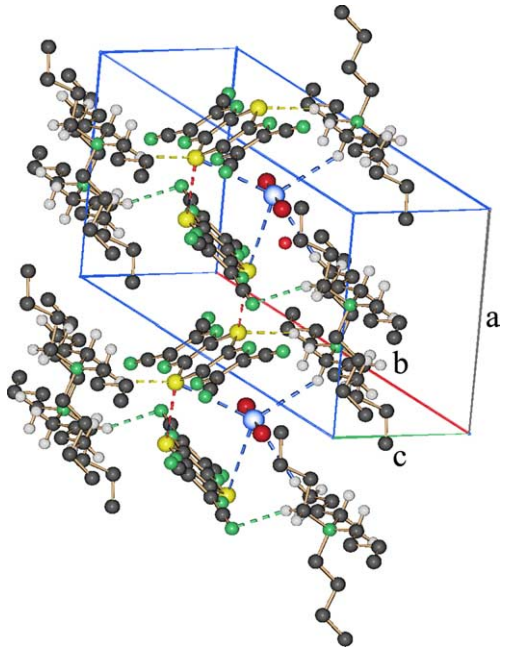

Fig. 9. Partial view of the crystal structure of **4**, showing the short contacts between the different species.

Table 5
Hydrogen bonds and short contacts in the crystal structure of **4**

	d (Å)	Angle (°)
C51–H51a···N04	2.551	152
C31–H31b···S02	2.943	149
C21–H21a···Au	3.291	145
C24–H24b···Au	3.247	163
Au···S02	4.026	
Au···S01	3.924	
S01···S02	3.586	

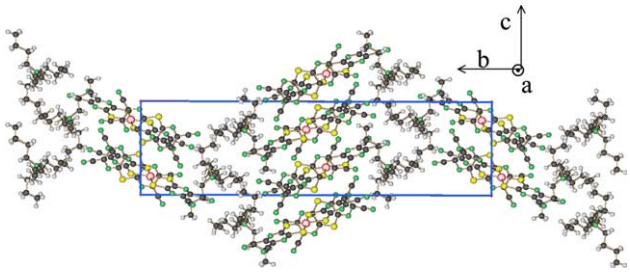

Fig. 10. View of the crystal structure of **5** along *a*.

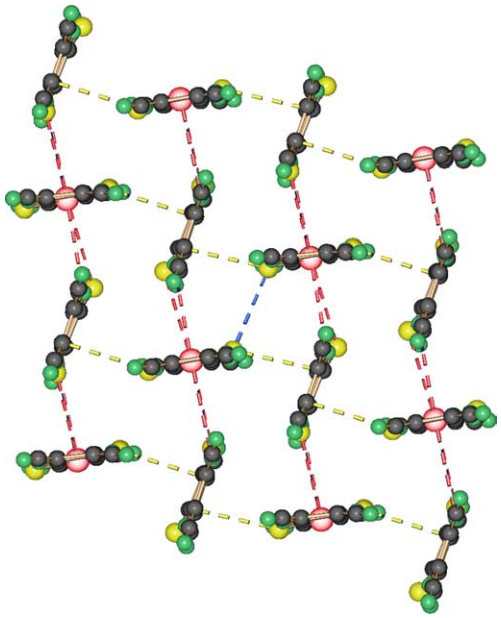

Fig. 11. View of the tctata and $[Au(dcdmp)_2]^-$ layer, in the *a*, *c* plane, in the crystal structure of **5,** emphasising the short contact responsible for the bidimensional network.

Table 6
Hydrogen bonds and short contacts in the crystal structure of **5**

	d (Å)	Angle (°)
C–H13a···N6	2.641	159.83
C–H14e···N7	2.633	174.50
C–H13b···N07	2.503	154.04
Au···S01	4.004	
Au···S02	3.730	
Au···N01	4.041	
Au···N06	3.648	
S3···S3	3.664	
S01···C9	3.380	
S02···C9	3.431	

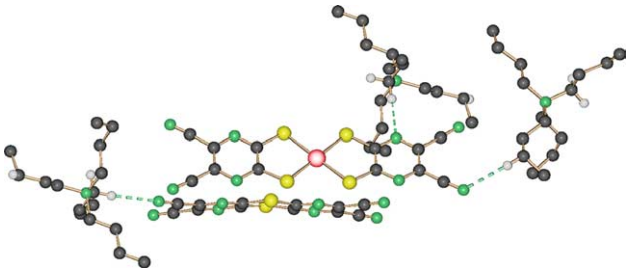

Fig. 12. Hydrogen bonds between the tctata and $[Au(dcdmp)_2]^-$ molecules and neighbouring cations, in the crystal structure of **5**.

chains, all short contacts are between different species and involve the sulphur atom of the neutral complex and the carbon atom of the pyrazine ring in the anion. The short contacts along the chain are of the Au···S type and the angle between the units is 62.7° (Fig. 11, Table 6). The neutral tctata and the $Au(dcdmp)_2^-$ anions in the layer are connected with the tetrabutylammonium through C–H···N hydrogen bonds. The nitrogen atoms involved in this interaction, are available both from the anion and the neutral specie (Fig. 12, Table 6), only one trough the pyrazinic N6 atom. The crystal structure of this compound is dominated by strong interactions between tctata and $Au(dcdmp)_2^-$ involving S–S and S–Au contacts as in **3** which determine the formation of layers.

4. Conclusion

In conclusion the $Au(dcdmp)_2$ complex was prepared and the structure of two salts described in detail. Although tetracyanotetraazothianthrene could no be isolated as a pure compound, two salts containing this new thianthrene derivative were obtained. In both cases this thianthrene derivative presents an almost planar geometry.

At variance with other pyrazinediselenate [7] or pyrazinedithiolate [8] salts where the N heteroatom acted as a new coordination centre in these compounds with the dicyanopyrazine ligand no such role is observed. However the pyrazinic ring contributes to electron delocalisation and allows π–π interactions between ligands of different complexes.

5. Supplementary material

Crystallographic data (excluding structure factors) for the structures reported in this paper have been deposited in the Cambridge Crystallographic Data Centre. The deposition numbers are CCDC 222525, CCDC 222526 and CCDC 222527 for compounds **3**, **4** and **5** respectively. Copies of the data can be obtained free of charge upon application to the director of CCDC, 12 Union Road, GB, Cambridge CB12 1EZ. [Fax: +441223/336/033, E-mail deposit@ccdc.cam.ac.uk, or on the web: http://www.ccdc.cam.ac.uk].

Acknowledgements

This work was partially supported by FCT-Portugal (Contract POCTI/35342/QUI/2000) and also benefited from COST action D14.

References

[1] (a) J.A. McLeverty, Prog. Inorg. Chem 10 (1968) 29;
(b) D. Coucouvanis, Prog. Inorg. Chem. 11 (1970) 233;
(c) R. Eisenberg, Prog. Inorg. Chem 12 (1970) 295;
(d) L. Alcácer, H. Novais, in: J.S. Miller (Ed.), Extended Linear Chain Compounds, vol. 3, Plenum Press, New York, 1983, p. 319 (Chapter 6);
(e) S. Alvarez, V. Ramon, R. Hoffman, J. Am. Chem. Soc. 107 (1985) 6253.
[2] N. Robertson, L. Cronin, Coord. Chem. Rev. 227 (2002) 93.
[3] A.T. Coomber, D. Beljonne, R.H. Friend, J.L. Bredas, A. Charlton, N. Robertson, A.E. Underhill, M. Kurmoo, P. Day, Nature 380 (1996) 144.
[4] (a) M. Ahamad, A.E. Underhill, J. Chem. Soc., Chem. Commun. (1981) 67;
(b) M.M. Ahamad, D.J. Turner, A.E. Underhill, C.S. Jacobsen, K. Mortensen, K. Carneiro, Phys. Rev. B 29 (1984) 4796.
[5] P. Cassoux, L. Valade, in: D.W. Bruce, D. O'Hare (Eds.), Inorganic Materials, 2nd ed., Wiley, Chichester, 1996, p. 1.
[6] P. Cassoux, J.S. Miller, in: L.V. Interrante, M.J. Hampden-Smith (Eds.), Chemistry of Advanced Materials, Wiley–VCH, New York, 1998, p. 19.
[7] X. Ribas, J. Dias, J. Morgado, K. Wurst, M. Almeida, J. Veciana, C. Rovira, Cryst. Eng. Commun. 93 (2002) 4.
[8] X. Ribas, J.C. Dias, J. Morgado, K. Wurst, E. Molins, E. Ruiz, M. Almeida, J. Veciana, C. Rovira, Chem. – Eur. J. (2004) 1318.
[9] M. Tomura, S. Tanaka, Y. Yamashita, Synth. Met. 24 (1994) 197.
[10] D. Belo, J. Morgado, E.B. Lopes, I.C. Santos, V. Gama, R.T. Henriques, M. Almeida, Synth. Met. 102 (1999) 1751.
[11] A. Altomare, M.C. Burla, M. Camalli, G. Cascarano, G. Giacovazzo, A. Guagliardi, A.G.G. Moliterni, G. Polidori, R. Spagna, J. Appl. Cryst. 32 (1999) 115.

[12] G.M. Sheldrick, SHELXL97, A Program for Crystal Structure Refinement, University of Göttingen, Germany, 1997.
[13] L.J. Ferrugia, J. Appl. Cryst. 32 (1999) 837.
[14] L.J. Ferrugia, J. Appl. Cryst. 30 (1997) 565.
[15] E. Keller, SCHAKAL-97, A Computer Program for the Representation of Molecular and Crystallographic Models, Kristallographisches Institut der Universität Freiburg i. Br., Germany, 1997.
[16] H.E. Simmons, R.D. Vest, D.C. Blomstrom, J.D.R. Roland, T.L. Cairns, J. Am. Chem Soc. 84 (1962) 4746.
[17] C.D. Hodgmam (Ed.), Handbook of Chemistry and Physics, The Chemical Rubber Publishing Co., Cleveland, OH, 1960, p. 1743.
[18] V.M. Lynch, S.H. Simonsen, B.E. Davis, G.E. Martin, M.J. Musmar, W.W. Lam, K. Smith, Acta Cryst. C 50 (1994) 1470.
[19] A.G. Pignedoly, G. Peyronel, L. Antolini, J. Cryst. Mol. Struct. 7 (1977) 173.

Available online at www.sciencedirect.com
SCIENCE DIRECT®
Polyhedron 23 (2004) 1361–1369
POLYHEDRON
www.elsevier.com/locate/poly

Heteroleptic platinum(II) complexes with crown thioethers and diimine ligands: the crystal structures of [Pt(9S3)(2,2′-bipy)]$(PF_6)_2$ and [Pt(9S3)(4,4-dimethyl-2,2′-bipy)]$(PF_6)_2 \cdot 2.5CH_3NO_2$ ☆

Gregory J. Grant [a,*], Ketankumar N. Patel [a], Monte L. Helm [a], Larry F. Mehne [b], David W. Klinger [b], Donald G. VanDerveer [c,1]

[a] Department of Chemistry, The University of Tennessee at Chattanooga, TN, USA
[b] Department of Chemistry, Covenant College, GA, USA
[c] School of Chemistry and Biochemistry, Georgia Institute of Technology, Atlanta, GA, USA

Received 13 November 2003; accepted 13 February 2004
Available online 9 April 2004

Abstract

We wish to report the synthesis, crystal structures, spectroscopic and electrochemical properties of new Pt(II) heteroleptic complexes with two diimines (2,2′-bipyridine, 4,4′-dimethyl-2,2′-bipyridine), and the crown trithioether 9S3 (1,4,7-trithiacyclononane). In addition, we report the synthesis and spectroscopic properties of three related 9S3/diimine (4,4′-di-*t*-butyl-2,2′-bipyridine, 4,4′-dinonyl-2,2′-bipyridine, 3,4,7,8-tetramethyl-1,10-phenanthroline) complexes as well as an examination of the spectroscopic and electrochemical properties of the reported [Pt(9S3)(1,10-phenanthroline)]$(PF_6)_2$. All complexes have the general formula [Pt(9S3)(N_2)](PF_6) (N_2 = diimine) and form similar structures in which the Pt(II) center is surrounded by a *cis* arrangement of the two N donors from the diimine chelate and two sulfur atoms from the 9S3 ligand. The ^{195}Pt NMR chemical shifts for all six complexes show a value near −3290 ppm, consistent with a *cis*-PtS_2N_2 coordination sphere. The third sulfur in each structure forms a longer interaction with the platinum resulting in an elongated square pyramidal structure. These distances, however, are approximately 0.2 Å longer than with the analogous diphosphine complexes, demonstrating that better π acids, in fact, do not result in shorter Pt–S axial distances as has previously been proposed.
© 2004 Elsevier Ltd. All rights reserved.

Keywords: Thioether complexes; Platinum complexes; Trithiacyclononane; Platinum nuclear magnetic resonance; Diimine complexes; Crown thioethers

1. Introduction

Over the past 10 years several research groups have examined the coordination chemistry of crown thioether ligands, such as 1,4,7-trithiacyclononane (9S3), in a number of areas including transition metal complexes, main group compounds, and organometallic complexes [1–6]. A key metal ion in thiacrown coordination chemistry is platinum(II) due to the high stability of Pt–S bonds, the relevance of this type of bond in catalysis, and the physicochemical properties exhibited by complexes with platinum group metals [7–11]. An interesting and unusual structural feature in 9S3/Pt(II) complexes is the presence of longer distance Pt–S interactions between the metal and axial sulfur atoms in the coordinated thioether macrocycle. Two equatorial Pt–S bonds in the coordinated 9S3 are observed close to the expected range of 2.2–2.4 Å, but there are longer axial

☆ Contribution from the Department of Chemistry, The University of Tennessee at Chattanooga, Chattanooga, TN 37403; Department of Chemistry, Covenant College, Lookout Mountain, Georgia 30750 and School of Chemistry and Biochemistry, Georgia Institute of Technology, Atlanta, GA 30332.

* Corresponding author.
E-mail address: greg-grant@utc.edu (G.J. Grant).
[1] Present address: Department of Chemistry, Clemson University, Clemson, SC 29366, USA.

0277-5387/$ - see front matter © 2004 Elsevier Ltd. All rights reserved.
doi:10.1016/j.poly.2004.02.023

interactions present which show a great variation in distance, ranging anywhere between 2.6 and 3.3 Å. The long distance interactions result in Pt(II) structures best described as elongated square pyramids [$S_4 + S_1$ coordination] [7] or elongated octahedra [$S_4 + S_2$ coordination] [9,11]. The Pt–S axial interactions alter the electrochemical and spectroscopic properties of the platinum(II) ion and are of theoretical interest as they possibly contain a weak attractive component [12]. Indeed, all of the observed Pt–S axial distances fall between the covalent bond distance and the sum of the Van der Waals radii for a platinum(II)–sulfur interaction [13]. [2] The anomalous behavior of crown thioether complexes of Pt(II) and related metal ions results from their unusual long distance interactions [14].

There is current interest in platinum(II) complexes involving long distance interactions such as these because they can serve as models for transition states of associative substitution reactions involving d^8 metal ions [15]. Recent reports by our group and others have extended work to include heteroleptic 9S3 platinum(II) complexes ($[Pt(9S3)(L)]^{2+}$), and it is observed that the Pt–S axial interaction is highly dependent upon the nature of the ancillary ligand (L) [16–24]. When the initial observations of the phenomena were made, it was proposed that the platinum–axial sulfur distance was controlled by the π-acceptor ability of the ancillary ligand [15,16]. The hypothesis was that the Pt d_{xz} and d_{yz} orbitals would function as donor orbitals, and electron density would be transferred via back bonding into the π^* orbitals on the ancillary ligand. Accordingly, the increasing positive charge on the metal would then draw the axial sulfur closer to it through electrostatic interactions. In order to examine this hypothesis more fully, we undertook the current study of a series of complexes with diimine ligands such as 2,2-bipyridine (bipy), a class of ligands well known to be excellent π acceptors. We have reported a recent series of papers involving 9S3/Pt(II) complexes with a variety of diphosphine ligands as the ancillary ligand [21–24]. There have also been previous reports describing heteroleptic complexes with Pt(II) and 9S3 containing halides [20] and both σ and π carbon donors [17,25] as the second ligand, but previous work with diimine ligands was limited to one compound, 1,10-phenanthroline (phen) [15]. Another key factor in diimine/Pt(II) chemistry is the importance of these complexes in the development of molecular photochemical devices, and a review of the photochemistry of Pt(II) complexes with diimines has recently appeared [26]. A listing for the different diimine structures used in our study is given in Scheme 1, and we wish to report the syntheses and spectroscopic properties for

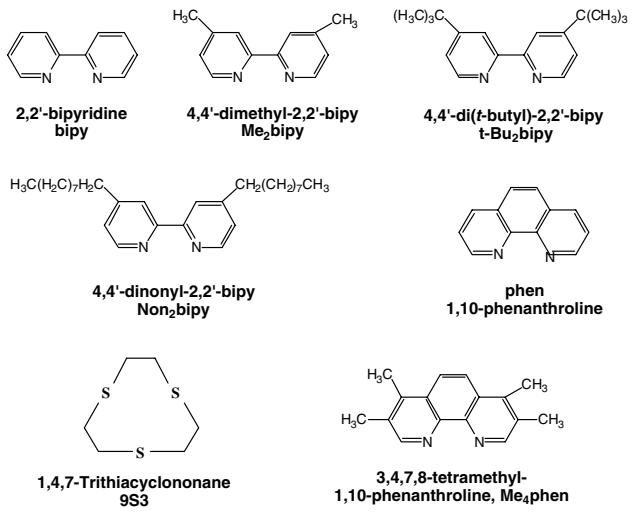

Scheme 1. Ligands discussed in this report.

five new Pt(II) heteroleptic complexes containing a series of diimine ligands. The complexes all have the general formula $[Pt(9S3)(N_2)](PF_6)_2$ where N_2 is a diimine ligand [N_2 = 2,2-bipyridine (bipy), 4,4′-dimethyl-2,2-bipyridine (Me_2bipy), 4,4′-di-*t*-butyl-2,2-bipyridine (t-Bu_2bipy), 4,4′-di-nonyl-2,2-bipyridine (Non_2bipy), and 3,4,7,8-tetramethyl-1,10-phenanthroline (Me_4phen)]. Additionally, full spectroscopic and electrochemical data for the analogous and previously reported with 1,10-phenanthroline (phen) [15] is given. Platinum-195 NMR serves as an excellent tool to probe these complexes, and we also include the study of the six thioether–diimine complexes employing this technique [27].

2. Experimental

2.1. Materials and measurements

All solvents and reagents were purchased from Aldrich Chemical Company and used as received. The starting complex $[Pt(9S3)Cl_2]$ was prepared by the published method [20]. Elemental analyses were performed by Atlantic Microlab, Inc., of Atlanta, GA. Fourier transform infrared spectra were obtained using a Galaxy FT-IR 5000 spectrophotometer and ultraviolet-visible spectra were obtained on a Varian DMS 200 UV–Vis spectrophotometer. Carbon-13 and proton NMR spectra were recorded on a Varian Gemini 300 NMR spectrometer using CD_3NO_2 for both the deuterium lock and reference. Carbon connectivity was confirmed via distortionless enhancement by polarization transfer (DEPT) experiments. Platinum-195 NMR spectra were recorded at 20 °C and 64.270 MHz using aqueous solutions of $[PtCl_6]^{2-}$ (0 ppm) as an external reference and delay time of 0.01 s. Referencing was verified versus authentic samples of $[PtCl_4]^{2-}$ which was

[2] The sum of the van der Waals radii for platinum and sulfur is 3.50 Å.

found to have a chemical shift at −1626 ppm, in agreement with the reported value of −1624 ppm. [27]. A Biological Analytical Systems CV50W Analyzer was used for all electrochemical measurements. The supporting electrolyte was 0.1 M $(Bu)_4NBF_4$ in CH_3CN, and sample concentrations were approximately 3 mM. All voltammograms were recorded at a scan rate of 100 mV/s. The standard three-electrode configuration was as follows: Pt-disk working electrode, Pt-wire auxiliary electrode, and Ag/0.01 M Ag(I) pseudo-reference electrode. All reported potentials were referenced against Fc/Fc^+ couple.

2.2. Preparation of the 9S3/bipy complexes

2.2.1. Preparation of [Pt(9S3)(bipy)](PF6)2

A mixture of [Pt(9S3)Cl_2] (100 mg, 0.224 mmol) and 2,2′-bipyridine (34.9 mg, 0.224 mmol) was refluxed in 50 mL of nitromethane for 3 h. A mass of NH_4PF_6 (73.0 mg, 0.448 mmol) was added, and the mixture refluxed an additional 30 min. The solution was filtered whilst hot, and then concentrated to 2/3 its original volume. Ether was then diffused overnight into the nitromethane solution. A yellow-orange precipitate formed which is filtered, washed with ethanol (3 × 15 mL), ether (3 × 15 mL), and then recrystallized by ether diffusion into a nitromethane to yield dark brown crystals (113 mg, 61.5%) of [Pt(9S3)(bipy)]$(PF_6)_2$ suitable for X-ray diffraction studies. The electronic absorption spectrum measured in acetonitrile showed three λ_{max}'s at 396 nm ($\varepsilon = 1750$), 329 nm ($\varepsilon = 1960$), and 308 nm ($\varepsilon = 8500$). FT-IR (KBr, cm^{-1}): 3141, 2952, 2825, 1642, 1588, 1425, 1410, 1248, 1149, 1079, 849 (s, PF_6^-), 763, 649 (C–S), 563. *Anal*. Calc. for $C_{16}F_{12}H_{20}N_2P_2PtS_3$: C, 23.39; H, 2.45; N, 3.41; S, 11.71. Found: C, 23.54; H, 2.55; N, 3.45; S, 11.76%. ^{1}H NMR (CD_3NO_2): δ (ppm), 9.04 (m, $^3J_{Pt-H} = 36$ Hz, $^3J_{H-H} = 5.7$ Hz, *bipy*, 2H), 8.60 (m, *bipy*, 2H), 8.52 (m, *bipy*, 2H), 7.90 (m, *bipy*, 2H), 3.36 (m, broad, *9S3*, 12H) ppm. $^{13}C\{^1H\}$ NMR (CD_3NO_2): δ (ppm), 157.5 (s, *bipy*, 2C), 151.5 (s, *bipy*, 2C), 144.0 (s, *bipy*, 2C), 130.6 (s, *bipy*, 2C), 126.5 (s, *bipy*, 2C), 34.5 (s, *9S3*, 6C). $^{195}Pt\{^1H\}$ NMR(CD_3NO_2), δ ($v_{1/2}$): singlet at −3261 ppm (726 Hz). The complex showed an irreversible oxidation at +0.94 V and an irreversible reduction at −1.22 V.

2.2.2. Preparation of [Pt(9S3)(Me2bipy)](PF6)2·2.5 CH3NO2

A mixture of [Pt(9S3)Cl_2] (100 mg, 0.224 mmol) and 4,4-dimethyl-2,2′-bipyridine (Me_2bipy) (41.3 mg, 0.224 mmol) was refluxed in 50 mL of CH_3NO_2 for 3 h. A mass of NH_4PF_6 (73.0 mg, 0.448 mmol) was added, and the mixture refluxed an additional 30 min. The solution was filtered whilst hot, and then concentrated to 2/3 its original volume. Ether was then diffused overnight into the nitromethane concentrate. Yellow-orange crystals had formed which were filtered, washed with ethanol (3 × 15 mL), ether (3 × 15 mL). The yield was 124 mg (64.7%) of [Pt(9S3)(Me_2bipy)]$(PF_6)_2 \cdot 2.5\ CH_3NO_2$. Recrystallization using ether diffusion into a nitromethane yielded crystals suitable for X-ray diffraction studies. The electronic absorption spectrum measured in acetonitrile showed two λ_{max}'s at 382 nm ($\varepsilon = 2720$) and 277 nm ($\varepsilon = 17\,500$) and shoulders at 319 ($\varepsilon = 11\,800$) and 308 ($\varepsilon = 12\,000$). FT-IR (KBr, cm^{-1}): 3090, 2978, 1698, 1616, 1439, 1400, 1215, 1038, 848 (s, PF_6^-), 662 (C–S), 555, 422. *Anal*. Calc. for $C_{20.50}H_{31.50}F_{12}N_{4.50}O_5P_2PtS_3$: C, 24.57; H, 3.11; S, 9.60; N, 6.29. Found: C, 24.77; H, 3.05; S, 9.61; N, 6.49%. ^{1}H NMR (CD_3NO_2): δ (ppm), 8.83 (m, $^3J_{Pt-H} = 36$ Hz, $^3J_{H-H} = 5.6$ Hz, *bipy*, 2H), 8.41 (s, *bipy*, 2H), 7.68 (m, $^3J_{H-H} = 5.6$ Hz, *bipy*, 2H), 3.36 (m, broad, *9S3*, 12H, 2.67 (s, –C*H*$_3$, 6H). $^{13}C\{^1H\}$ NMR (CD_3NO_2): δ (ppm) 157.7 (s, *bipy*, 2C), 157.0 (s, *bipy*, 2C), 150.5 (s, *bipy*, 2C), 130.9 (s, *bipy*, 2C), 127.0 (s, *bipy*, 2C), 34.4 (s, *9S3*, 6C), 21.9 (s, –*C*H$_3$, 2C) ppm. $^{195}Pt\{^1H\}$ NMR(CD_3NO_2), δ ($v_{1/2}$): singlet at −3279 ppm (678 Hz). The complex showed an irreversible oxidation at +0.97 V and an irreversible reduction at −1.48 V.

2.2.3. Preparation of [Pt(9S3)(t-Bu2bipy)](PF6)2

A mixture of [Pt(9S3)Cl_2] (50.0 mg, 0.112 mmol) and $AgPF_6$ (56.6 mg, 0.224 mmol) was stirred in the dark in 10 mL of CH_3CN for 24 h. The white precipitate of AgCl was then filtered and a mass of 4,4′-di-tertiary-butyl-2,2′-bipyridyl (*t*-Bu_2bipy), (30.1 mg, 0.112 mmol) was added. The solution was then stirred for an additional 48 h. The solution was concentrated to 1/3 its original volume, and ether was then diffused overnight into the acetonitrile concentrate to form yellow crystals. The crystals were filtered, washed with ethanol (3 × 15 mL), ether (3 × 15 mL) to yield 84.2 mg (80.5%) of [Pt(9S3)(t-Bu_2bipy)]$(PF_6)_2$. The electronic absorption spectrum measured in acetonitrile showed two λ_{max}'s at 386 nm ($\varepsilon = 2230$) and 309 nm ($\varepsilon = 13\,200$) and a shoulder at 319 ($\varepsilon = 11\,100$). FT-IR (KBr, cm^{-1}): 3004, 2957, 2901, 2866, 1616, 1543, 1482, 1418, 1254, 1073, 836 (s, PF_6^-), 740, 663 (C–S), 555. *Anal*. Calc. for $C_{24}H_{36}F_{12}N_2P_2PtS_3$: C, 30.87; H, 3.89; N, 3.00; S, 10.30. Found: C, 30.77; H, 3.85; N, 3.24; S, 10.19%. ^{1}H NMR (CD_3NO_2): δ (ppm), 8.88 (m, $^3J_{Pt-H} = 36$ Hz, $^3J_{H-H} = 5.6$ Hz, *bipy*, 2H), 8.55 (d, $^4J_{H-H} = 2.4$ Hz, *bipy*, 2H), 7.87 (d of d, $^3J_{H-H} = 5.6$ Hz, $^4J_{H-H} = 2.4$ Hz, *bipy*, 2H), 3.41 (m, broad, *9S3*, 12H), 1.47 (s, –C(C*H*$_3$)$_3$, 18H). $^{13}C\{^1H\}$ NMR (CD_3NO_2): δ (ppm) 169.4 (s, *bipy*, 2C), 157.2 (s, *bipy*, 2C), 150.9 (s, *bipy*, 2C), 127.7 (s, *bipy*, 2C), 123.5 (s, *bipy*, 2C), 37.4 (s, –*C*(CH$_3$)$_3$, 2C), 34.5 (s, *9S3*, 6C), 30.3 (s, –C(*C*H$_3$)$_3$, 6C). $^{195}Pt\{^1H\}$ NMR(CD_3NO_2), δ ($v_{1/2}$): singlet at −3289 ppm (539 Hz).

2.2.4. Preparation of [Pt(9S3)(Non2bipy)](PF6)2

A mixture of [Pt(9S3)Cl_2] (50.0 mg, 0.112 mmol) and $AgPF_6$ (56.6 mg, 0.224 mmol) was stirred in the dark in

10 mL of CH_3CN for 24 h. The white precipitate of AgCl was then filtered and a mass of 4,4′-di-nonyl-2,2′-bipyridyl (Non_2bipy), (45.7 mg, 0.112 mmol) was added. The solution was then stirred for an additional 48 h. The solution was concentrated to 1/3 its original volume, and ether was then diffused overnight into the acetonitrile concentrate to form yellow crystals. The crystals were filtered, washed with ethanol (3 × 15 mL), ether (3 × 15 mL) to yield 95.1 mg (79.1%) of [Pt(9S3)(Non_2bipy)]$(PF_6)_2$. The electronic absorption spectrum measured in acetonitrile showed two λ_{max}'s at 386 nm ($\varepsilon = 2530$) and 319 nm ($\varepsilon = 11\,400$) and a shoulder at 308 ($\varepsilon = 10\,400$). FT-IR (KBr, cm^{-1}): 3090, 2922, 2849, 1616, 1555, 1491, 1422, 1284, 1137, 1038, 835 (s, PF_6^-), 654 (C–S), 555. *Anal*. Calc. for $C_{34}H_{56}F_{12}N_2P_2PtS_3$: C, 37.95; H, 5.43; N, 2.61; S, 8.94. Found: C, 38.05; H, 5.30; N, 2.75; S, 9.07%. ^1H NMR (CD_3NO_2): δ (ppm), 8.84 (m, $^3J_{Pt-H} = 36$ Hz, $^3J_{H-H} = 5.8$ Hz, *bipy*, 2H), 8.44 (s, *bipy*, 2H), 7.70 (m, $^3J_{H-H} = 5.8$ Hz, *bipy*, 2H), 3.28 (m, *9S3*, 12H), 2.95 (t, $^3J_{H-H} = 7.4$ Hz, $-CH_2(CH_2)_7CH_3$, 4H), 1.79 (q, $^3J_{H-H} = 6.9$ Hz, $-CH_2CH_2CH_2(CH_2)_5CH_3$, 4H), 1.39 (b, m, $-CH_2CH_2(CH_2)_2(CH_2)_4CH_3$, 8H), 1.29 (b, m, $-CH_2CH_2(CH_2)_2(CH_2)_4CH_3$, 16H), 0.87 (t, $^3J_{H-H} = 6.6$ Hz, $-CH_2CH_2(CH_2)_2(CH_2)_4CH_3$, 6H). $^{13}C\{^1H\}$ NMR (CD_3NO_2): δ (ppm), 162.0 (s, *bipy*, 2C), 157.2 (s, *bipy*, 2C), 150.8 (s, *bipy*, 2C), 130.3 (s, *bipy*, 2C), 126.4 (s, *bipy*, 2C), 34.5 (s, *9S3*, 6C), 36.7 (s, $-C_9H_{19}$, 2C), 33.0 (s, $-C_9H_{19}$, 2C), 31.1 (s, $-C_9H_{19}$, 2C), 30.6 (s, $-C_9H_{19}$, 2C), 30.4 (s, $-C_9H_{19}$, 2C), 30.3 (s, $-C_9H_{19}$, 2C), 30.2 (s, $-C_9H_{19}$, 2C), 23.7 (s, $-C_9H_{19}$, 2C), 14.5 (s, $-C_9H_{19}$, 2C) ppm. $^{195}Pt\{^1H\}$ NMR(CD_3NO_2), δ ($\nu_{1/2}$): singlet at −3284 ppm (353 Hz).

2.3. Preparation of the 9S3/phen complexes

2.3.1. Preparation of [Pt(9S3)(phen)](PF6)2

The synthesis of this compound has been previously reported using a different route [15]. We include the new synthesis as well as additional spectroscopic and electrochemical data. A mixture of [Pt(9S3)Cl_2] (100 mg, 0.224 mmol) and 1,10-phenanthroline (phen) (40.4 mg, 0.224 mmol) was refluxed in 50 mL of CH_3NO_2 for 3 h. The resulting solution was cooled slightly before a mass of NH_4PF_6 (73.0 mg, 0.448 mmol) was added, and the mixture refluxed an additional 30 min. The solution is filtered whilst hot and concentrated to 2/3 of its original volume. Ether was then diffused overnight into the nitromethane solution. A yellow-orange precipitate formed which is filtered, washed with ethanol (3 × 15 mL), ether (3 × 15 mL), and then recrystallized by ether diffusion into a nitromethane to yield dark brown crystals (143 mg, 75.4%) of [Pt(9S3)(phen)]$(PF_6)_2$. The electronic absorption spectrum measured in acetonitrile showed two λ_{max}'s at 393 nm ($\varepsilon = 2780$) and 275 nm ($\varepsilon = 31\,700$). ^1H NMR (CD_3NO_2): δ, 9.37 (m, $^3J_{Pt-H} = 37$ Hz, $^3J_{H-H} = 5.8$ Hz, *phen*, 2H), 9.08 (m, $^3J_{H-H} = 7.9$ Hz, *phen*, 2H), 8.36 (s, *phen*, 2H), 8.21 (m, $^3J_{H-H} = 7.2$ Hz, *phen*, 2H), 3.40 (m, broad, *9S3*, 12H) ppm. $^{13}C\{^1H\}$ NMR (CD_3NO_2): δ, 152.1 (s, *phen*, 2C), 148.1 (s, *phen*, 2C), 143.2(s, *phen*, 2C), 133.5 (s, *phen*, 2C), 130.0 (s, *phen*, 2C), 128.5 (s, *phen*, 2C), 34.6 (s, *9S3*, 6C) ppm. $^{195}Pt\{^1H\}$ NMR(CD_3NO_2), δ ($\nu_{1/2}$): singlet at −3292 ppm (754 Hz). The complex showed no oxidative electrochemistry and an irreversible reduction at −1.18 V.

2.3.2. Preparation of [Pt(9S3)(Me4phen)](PF6)2

A mixture of [Pt(9S3)Cl_2] (88.0 mg, 0.197 mmol) and 3,4,7,8-tetramethyl-1,10- phenanthroline (Me_4phen) (21.1 mg, 0.0892 mmol) was refluxed in 50 mL of CH_3NO_2 for 3 h. The resulting solution was cooled slightly before a mass of NH_4PF_6 (64.2 mg, 0.394 mmol) was added, and the mixture refluxed an additional 30 min. The solution is filtered whilst hot and concentrated to 2/3 of its original volume. Ether was then diffused overnight into the nitromethane solution to form brown crystals. These were washed with washed with ethanol (3 × 15 mL), ether (3 × 15 mL), and then recrystallized by ether diffusion into a nitromethane to yield dark brown crystals (96.0 mg, 54.1%) of [Pt(9S3)(Me_4phen)]$(PF_6)_2$. The electronic absorption spectrum measured in acetonitrile showed three λ_{max}'s at 377 nm ($\varepsilon = 3780$), at 336 nm ($\varepsilon = 4290$), and 276 nm ($\varepsilon = 62\,000$). FT-IR (KBr, cm^{-1}): 3055, 2970, 1615 1555, 1439, 1417, 1283, 1098, 840 (s, PF_6^-), 654 (C–S), 555. *Anal*. Calc. for $C_{22}F_{12}H_{28}N_2P_2PtS_3$: C, 29.30; H, 3.13; N, 3.11; S, 10.67. Found: C, 29.20; H, 3.16; N, 3.34; S, 10.67%. ^1H NMR (CD_3NO_2): δ, 8.99 (m, $^3J_{Pt-H} = 36$ Hz, *phen*, 2H), 8.44 (s, *phen*, 2H), 3.48 (m, broad, *9S3*, 12H) 2.93 (s, $-CH_3$, 6H), 2.69 (s, $-CH_3$, 6H) ppm. $^{13}C\{^1H\}$ NMR (CD_3NO_2): δ, 152.4 (s, *phen*, 2C), 151.6 (s, *phen*, 2C), 151.6 (s, *phen*, 2C), 137.9 (s, *phen*, 2C), 131.7(s, *phen*, 2C), 125.9 (s, *phen*, 2C), 34.4 (s, *9S3*, 6C), 18.0 (s, $-CH_3$, 2C), 15.8 (s, $-CH_3$, 2C) ppm. $^{195}Pt\{^1H\}$ NMR(CD_3NO_2), δ ($\nu_{1/2}$): singlet at −3313 ppm (822 Hz).

Data collection and processing. Suitable crystals of all complexes were grown by slow diffusion of ether into a nitromethane solution, and summary of key crystallographic details for the structures is presented in Table 1. For all structures, intensity data were collected on a Siemens SMART 1K CCD diffractometer [28,29], and the structures were solved using direct methods [28]. For the bipy complex, the *h*, *k*, *l* ranges used during its structure solution and refinement were −13/11, −13/13, −13/12. For 10 346 measured reflections 5023 were unique. The merging *R*-values on intensities were 0.0366. The structure was refined by a full-matrix least squares on F^2 using 5023 unique reflections and 340 parameters. The residuals were as follows: for reflections having $I > 2\sigma(I)$ $R = 0.0329$, $R_w = 0.0730$ and GoF = 1.054; for all reflections $R = 0.0396$, $R_w = 0.0754$. The secondary extinction coefficient was 0.0088(18) μm. For the Me_2bipy complex, the *h*, *k*, *l* ranges used during its structure solution and refinement were −32/33, −24/22,

Table 1
Crystallographic data summary for $[Pt(9S3)(2,2'\text{-bipy})](PF_6)_2$ (**1**), $[Pt(9S3)(4,4'\text{-dimethyl-}2,2'\text{-bipy})](PF_6)_2 \cdot 2.5CH_3NO_2$ (**2**)

	[1]	[2]
Empirical formula	$C_{16}H_{20}F_{12}N_2P_2PtS_3$	$C_{20.50}H_{31.50}F_{12}N_{4.50}O_5P_2PtS_3$
fw (amu)	821.55	1002.21
Size (mm)	$0.25 \times 0.24 \times 0.17$	$0.31 \times 0.17 \times 0.14$
Appearance	brown, needles	orange,needles
Crystal system	triclinic	monoclinic
Space group	$P\bar{1}$	Cc
a (Å)	10.3577(5)	26.055(3)
b (Å)	10.8912(5)	18.509(2))
c (Å)	10.9256(5)	16.494(2)
α (°)	83.7920(10)	90
β (°)	84.1930(10)	121.767(2)
γ (Å)	87.5590(10)	90
V (Å^3)	1218.35(10)	6763.1(15)
Z	2	8
ρ_{calcd} (g cm^{-3})	2.239	1.969
μ (mm^{-1})	6.249	4.535
T (K)	303(2)	193(2)
Reflections collected	5023	10 255
Reflections unique	4447	9691
R_{merge}	0.0396	0.0561
R_1[a]	0.0329	0.0527
wR_2[b]	0.0754	0.1281

[a] $R_1 = \Sigma||F_o| - |F_c||/\Sigma|F_o|$ for observed data ($I > 2\sigma(I)$).
[b] $wR_2 = \{\Sigma[wF_o^2 - F_c^2)^2]/\Sigma[wF_o^2)^2]\}^{1/2}$ for all data.

−17/21. For 10 255 measured reflections 9691 were unique. The merging R-values on intensities were 0.0503. The structure was refined by a full-matrix least squares on F^2 using 9691 unique reflections and 897 parameters. The residuals were as follows: for reflections having $I > 2\sigma(I)$ $R = 0.0527$, $R_w = 0.1281$ and GoF = 1.035; for all reflections $R = 0.0561$, $R_w = 0.1314$.

3. Results and discussion

3.1. Synthesis, spectra, and electrochemistry

All of complexes are readily prepared by the reaction of $[Pt(9S3)Cl_2]$ with one equivalent of diimine ligand which replaces the two chloride donors. In four cases, this is accomplished by the refluxing of the reaction mixture in nitromethane followed by metathesis to the hexafluorophosphate salt as shown below. We would like to note that this reaction proceeds more cleanly and in better yield than starting with the $[Pt(diimine)Cl_2]$ complex as previously described [15]. For the cases involving the more sterically hindered *t*-butyl and nonyl disubstituted bipy ligands, the procedure either did not work or gave poor yields. Therefore, we successfully employed an alternative preparation whereby $[Pt(9S3)Cl_2]$ was dechlorinated with silver ion in acetonitrile, followed by the addition of the diimine ligand at room temperature. Lastly, we would note that we have been unable to obtain the analogous diimine complexes when electron-withdrawing groups are present on the diimine ring. Similar reactions with dibromo and dicarboxylic acid substituted bipyridines did not give the desired products, probably due to electron-withdrawing effects on their substituent groups.

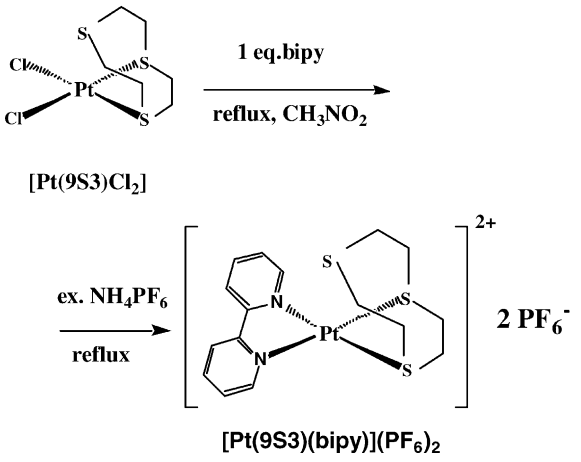

The composition of the new complexes is confirmed using a variety of spectroscopic techniques and elemental analysis. The proton NMR spectra of the six complexes show resonances for all protons in the appropriate ratios and splittings. The 12 protons of the 9S3 appear as a broad, complex ABCD pattern, in contrast to the characteristic $AA'BB'$ pattern commonly observed for 9S3 in phosphine and halide complexes [20–24]. The hydrogen *ortho* to the nitrogen of the pyridine rings for the six ligands exhibits a distinctive $^3J_{(Pt-H)}$ coupling at 36 Hz. In addition, ^{13}C DEPT experiments confirm carbon connectivity in all complexes. As expected, the 9S3 ligand is fluxional in solution resulting in a single ^{13}C NMR resonance for the thioether ligand, showing all six carbon atoms to be equivalent. The fluxionality has been proposed to occur via rapid intramolecular exchanges of sulfur atoms (1,4-metallotropic shift) [15,30] and has been observed in the presence of a variety of ancillary ligands. All six complexes show this feature in their carbon NMR spectra. For the Non_2bipy complex, even at −90 °C, we have not been able to observe a slow exchange of 9S3 in the carbon-13 NMR spectrum, suggesting a very low barrier to rotation. [3]

[3] The Non_2bipy complex has excellent acetone solubility so we had hoped to observe a slow ligand exchange in its ^{13}C NMR spectrum. Although the 9S3 resonance appears as a singlet at 20 °C, cooling down sequentially to −90 °C results first in broadening, then a collapse of this peak into the baseline. The slow exchange of 9S3 is not observed even at this temperature. [15] does report decoalescence of the 9S3 resonances in the proton NMR spectrum of the phen complex at −80 °C.

Table 2
Solid state structures of platinum(II) crown thioether complexes, [Pt(9S3)L], and their ^{195}Pt NMR chemical shifts

Complex	Geometry	^{195}Pt NMR δ (ppm)
$[Pt(9S3)(bipy)]^{2+}$ [a]	$S_2N_2 + S_1$	−3261
$[Pt(9S3)(Me_2\ bipy)]^{2+}$ [a]	$S_2N_2 + S_1$	−3279
$[Pt(9S3)(t\text{-}Bu_2\ bipy)]^{2+}$ [a]	$S_2N_2 + S_1$	−3289
$[Pt(9S3)(Non_2\ bipy)]^{2+}$ [a]	$S_2N_2 + S_1$	−3284
$[Pt(9S3)(phen)]^{2+}$ [a]	$S_2N_2 + S_1$	−3292
$[Pt(9S3)(Me_4\ phen)]^{2+}$ [a]	$S_2N_2 + S_1$	−3313
$[Pt(9S3)Cl_2]$ [b]	$S_2Cl_2 + S_1$	−3605
$[Pt(9S3)Br_2]$ [b]	$S_2Br_2 + S_1$	−3779
$[Pt(9S3)I_2]$ [b]	$S_2I_2 + S_1$	−4147
$[Pt(9S3)_2]^{2+}$ [c]	$S_4 + S_2$	−4117
$[Pt(9S3)(PPh_3)_2]^{2+}$ [d]	$S_2P_2 + S_1$	−4347
$[Pt(9S3)(dppe)]^{2+}$ [d]	$S_2P_2 + S_1$	−4069
$[Pt(9S3)(dppf)]^{2+}$ [d]	$S_2P_2 + S_1$	−4407
$[Pt(9S3)(dppbe)]^{2+}$ [d]	$S_2P_2 + S_1$	−4618
$[Pt(9S3)(dppv)]^{2+}$ [d]	$S_2P_2 + S_1$	−4731
$[Pt(9S3)(Chiraphos)]^{2+}$ [d]	$S_2P_2 + S_1$	−4452

dppe, 1,2-bis(diphenylphosphino)ethane; dppbe,1,2-bis(diphenylphosphino)benzene; dppf, 1,1′-bis(diphenylphosphino)ferrocene; dppv, *cis*-1,2-bis(diphenylphosphino)ethylene; *R*,*R*-Chiraphos, 2,3-bis(diphenylphosphino)butane.

[a] This work.

[b] Ref. [20].

[c] Ref. [7].

[d] Ref. [21–24].

A summary of the ^{195}Pt NMR chemical shifts for all six complexes appears in Table 2. All are shifted downfield compared to other 9S3 Pt(II) complexes and average −3286 ppm. It is interesting to note that this chemical shift lies intermediate between the values for $[Pt(9S3)Cl_2]$/$[Pt(bipy)Cl_2]$ and $[Pt(9S3)Br_2]$/$[Pt(bipy)Br_2]$, illustrating how the platinum chemical shift is sensitive to the average ligand environment [31]. [4] One surprising aspect of our data is how little variation there is in the chemical shifts of the different diimine complexes. For example, as also seen in Table 2, a comparable set of six diphosphine complexes exhibit ^{195}Pt NMR chemical shifts that vary by almost 700 ppm while the six diimines complexes vary by only about 50 ppm.

Both the bipy and Me_2bipy complexes show similar electrochemical behavior with an irreversible oxidation close to +0.95 V and an irreversible reduction between −1.22 and −1.48 V, respectively. In contrast, the phen complex shows no oxidation waves, but does exhibit a reduction at a similar value of −1.18 V. The lack of an oxidation wave of the phen complex may reflect enhanced π backbonding for that complex. Electrochemical measurements on the Pd(II) 9S3 analogs of the bipy and phen complexes show reversible one-electron reductions, but no oxidation waves [16]. It has been proposed that the Pt dπ orbital is involved in the oxidation process while the π* orbital on the diimine is involved in the reduction process, a hypothesis supported by our data on these compounds [32].

[4] The compound $[Pt(bipy)Cl_2]$ shows a ^{195}Pt NMR resonance at −2315 ppm. The resonances for the bromo analog are shifted upfield to −2544 ppm.

3.2. Structures

Crystallographic data for the two complexes are presented in Table 1, selected bond distances and angles appear in Table 3, and thermal ellipsoid plots of the two structures are presented in Fig. 1, 2. Both complexes show an elongated square pyramidal structure which is common for heteroleptic crown trithioether complexes of Pt(II) and Pd(II) [4,21–24]. The square plane is comprised of a *cis* arrangement of the two nitrogen donors of the diimine and two sulfur donors from the 9S3. The third 9S3 sulfur shows a long distance axial interaction to complete the elongated square pyramidal structure. In the bipy complex, the Pt(II) ion is raised slightly (by 0.1008(14) Å) above the mean square equatorial plane and directed towards the axial sulfur donor, and the four atoms in the equatorial plane have an average displacement of 0.0425 Å. The Me_2bipy complex crystallizes with two independent but similar cations in the asymmetric unit. For both structures the Pt(II) is raised slightly less than in the bipy structure, 0.0747(0.0037) and 0.0860(0.0036) Å from the equatorial plane which has an average displacement of 0.0297 and 0.0303 Å, respectively. There are several contrasts between the two complexes resulting from the presence of the two methyl groups in *para* positions of the Me_2bipy ligand. Its Pt(II)/9S3 complex shows a larger N–Pt–N chelate angle, shorter Pt–N distances, and also shorter Pt–S equatorial distances.

Table 3
Selected bond distances (Å) and angles (°) for $[Pt(9S3)(2,2'\text{-bipy})](PF_6)_2$ (**1**) and $[Pt(9S3)(4,4'\text{-dimethyl-}2,2'\text{-bipy})](PF_6)_2 \cdot 2.5\ CH_3NO_2$ (**2a** and **2b**)

	[1]	[2a]	[2b]
Bond distances			
$Pt–S1_{axial}$	2.8599(16)	2.914(3)	2.907(3)
Pt–S4	2.2745(15)	2.264(3)	2.265(3)
Pt–S7	2.2656(13)	2.265(3)	2.259(3)
Pt–N1	2.055(4)	2.083(8)	2.063(9)
Pt–N2	2.050(3)	2.060(9)	2.051(9)
Bond angles			
S4–Pt–S7	88.22(5)	88.51(10)	88.80(10)
N1–Pt–N2	79.70(18)	79.3(4)	80.1(4)
S1–Pt–S4	85.64(5)	84.96(7)	85.91(7)
S1–Pt–S7	85.21(5)	84.95(7)	85.06(7)
S1–Pt–N1	103.64(13)	101.624(6)	99.95(6)
S1–Pt–N2	99.91(14)	98.540(6)	97.74(6)
S4–Pt–N1	170.43(14)	172.5(3)	173.1(3)
S4–Pt–N2	96.59(14)	96.2(3)	95.6(3)
S7–Pt–N1	94.80(13)	95.7(3)	95.3(3)
S7–Pt–N2	173.20(14)	174.4(3)	174.9(3)

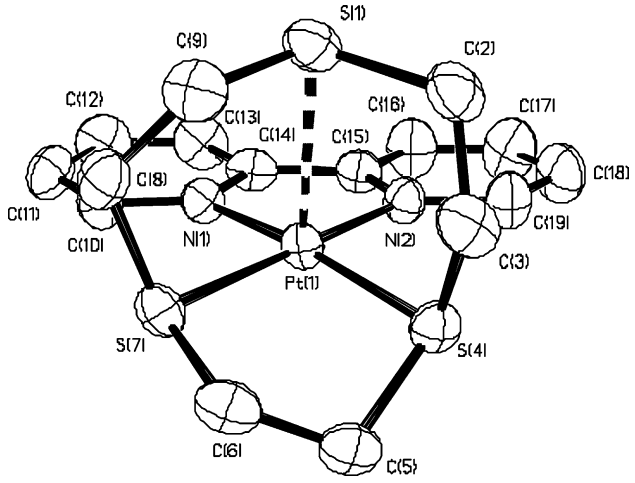

Fig. 1. Thermal ellipsoid perspective (50% probability) of cation in [Pt(9S3)(2,2′-bipy)]$(PF_6)_2$.

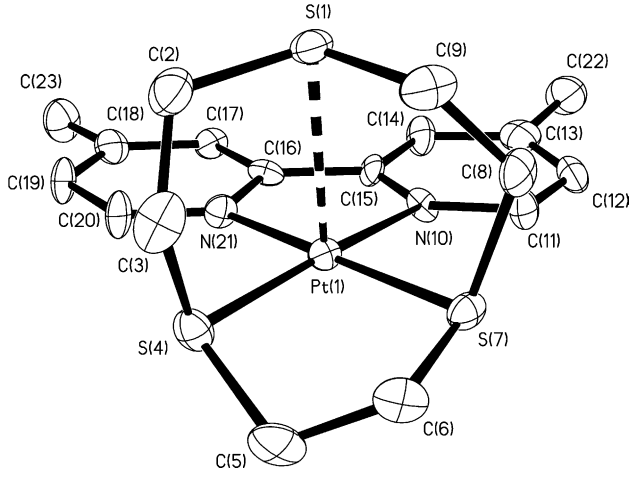

Fig. 2. Thermal ellipsoid perspective (50% probability) of cation in [Pt(9S3)(4,4′-dimethyl-2,2′-bipy)]$(PF_6)_2 \cdot 2.5CH_3NO_2$.

The two pyridine rings in both the bipy and Me_2bipy structures are inclined towards each other (3–4°) and away from the axial sulfur. This bow deformation of the diimine ligand is also seen in the crystal structures of the related Pd(II) complexes, [Pd(9S3)(bipy)]$(PF_6)_2$ and [Pd(9S3)(phen)]$(PF_6)_2$, which show a similar degree of tilting of their rings [16]. In order to accommodate complexation of the platinum by the thiacrown, the diimine ligand distorts from a planar structure via this inward bowing. The bowing of the bipy rings is especially seen in the C–N–N–C dihedral angles which measure, 24.2° (C10–N1–N2–C19) and 26.8° (C20–N21–N10–C11), respectively, for the two Pt(II) complexes. It is interesting to note that this bowing distortion is also observed in the analogous [Pt(9S3)(phen)]$(PF_6)_2$ structure [15]. However, the bowing for the phen ligand is even more pronounced and noticeably larger, by almost a factor of two, compared to what is observed for the two bipy structures. One would have anticipated that the more rigid phen ligand would distort less, not more, and the distortion suggests an enhanced π interaction with the metal center, as supported by our electrochemical data.

One particular structural feature of interest is the distance between the axial sulfur donor and the platinum center since this distance is quite sensitive to the nature of the ancillary ligand. Table 4 summarizes the Pt–S equatorial and axial distances for a series of heteroleptic 9S3 complexes. [5] When the axial distances in the diimine complexes are compared to phosphines, the axial distances are significantly longer. Initial observations of the sulfur axial interactions in heteroleptic Pt(II) and Pd(II) complexes of 9S3 led to the proposal that better π acids, such as bipy and phen, would result in shorter M–S axial distances through π backbonding between the metal d_{yz} and d_{xz} orbitals and the π^* orbitals of the diimine [15,16]. Similarly, better σ donating ligands would result in longer M–S axial distances. However, as our data demonstrates, this is, in fact, not the case. Rather, better π acceptors like bipy and phen and their methyl-substituted derivatives, have longer Pt–S axial distances than do any of the phosphines donors. [6] Phosphines are both stronger σ donor and weaker π acceptor ligands than are diimines. According to the original hypothesis, they should show longer, not shorter, Pt–S axial interactions since their Pt centers would have less positive charge.

We have noticed a general trend in the structural data presented in Table 4. Ligands, which have the shorter equatorial Pt–S distances, generally have longer axial distances and vice versa. Pi donor ligands such as halides have the shortest equatorial and longest axial distances. Phosphine ligands which are better σ donors show the longest equatorial, but the shortest axial distances. Based upon this collection of data, we would like to propose an alternative hypothesis concerning the metal–axial sulfur interaction in the approximately fifty Pt(II) and Pd(II) complexes of trithiacrowns. The role of the ancillary ligand is certainly very important, but it is predominately one for controlling the equatorial M–S distances and not increasing the positive charge on the metal. We would note that the Pt–N distances are longer in the 9S3 complexes with diimines than in the dichloro complexes for bipy (average: 2.008(10) versus 2.053(3) Å) [33]. This suggests that the presence of the 9S3 ligand weakens the Pt–diimine interaction compared to a chloride donor. The balance of the electron density at

[5] The sum of the two equatorial Pt–S bonds and the axial Pt–S distance is surprisingly constant, averaging 7.40 (±0.19) Å for the full set of diimine, thioether, and phosphine complexes.

[6] We have attempted to solve the structure for [Pt(9S3)(Me_4phen)]$(PF_6)_2$ but the *R* value remains fairly high at 10%. However, the axial/equatorial Pt–S distances are very similar to the values given in Table 4 with Pt–S equatorial distances of 2.26 Å and axial distances of 2.88 Å.

Table 4
Pt–S axial and equatorial distances (Å) for [Pt(NS3)L] complexes

([N]S3), (L)	Pt–S_{axial}	Pt–S_{eq} (**1**)	Pt–S_{eq} (**2**)
Diimines			
9S3 × bipy[a]	2.86	2.27	2.27
9S3 × Me_2bipy[a]	2.91	2.27	2.27
9S3, phen[b]	2.82	2.27	2.27
Halides			
9S3, 2 × Cl[c]	3.26	2.22	2.24
9S3, 2 × Br[c]	3.24	2.24	2.25
9S3, 2 × I[c]	3.21	2.25	2.27
Thioethers			
9S3 × 2[d]	2.89	2.25	2.31
9S3 × 2[e]	3.04	2.29	2.29
9S3 × 2[e]	3.07	2.29	2.29
Diphosphines			
9S3, 2 × PPh_3[f]	2.64	2.36	2.49
9S3, dppm[f]	2.67	2.35	2.36
9S3, dppe[f]	2.74	2.37	2.37
9S3, *R*,*R*-Chiraphos[f]	2.70	2.36	2.38
9S3, dppbe[f]	2.72	2.34	2.38

dppm, 1,1′-bis(diphenylphosphino)methane; dppe, 1,2-bis(diphenylphosphino)ethane; dppbe, 1,2-bis(diphenylphosphino)benzene; Chiraphos, *R*,*R*-2,3-bis(diphenylphosphino)butane.

[a] This work.

[b] Ref. [15].

[c] Ref. [20].

[d] Ref. [7].

[e] Ref. [35], we have recently determined the structures for $[Pt(9S3)_2](PF_6)_2$, CCDC 219803 and $[Pt(9S3)_2](BF_4)_2$, CCDC 219804, BF_4^- and PF_6^- salts, respectively.

[f] Refs. [21–24].

the metal center by the σ and π interactions involving the ancillary ligand influences the positioning of the axial sulfur donor. Depending upon the donor/acceptor characteristics of the ancillary ligand, the equatorial sulfur atoms are pushed or pulled towards the metal in the equatorial plane by the lengthening or shortening of the metal–sulfur bonds. Due to the rigidity of the 9S3, however, the third sulfur donor will approach the metal more closely if the equatorial sulfurs are pushed back or it will move away if they are pulled towards the metal. We feel that the original hypothesis proposing that σ donor ligands will exhibit longer axial interactions while π acceptor ligands will show shorter ones no longer fits the structural data that has now been accumulated for this series of compounds [34]. [7]

[7] In their study of 9S3-phen fused ligands, Lippolis and co-workers noted that the metal–axial sulfur distances did not fit the increased positive charge hypothesis. We note that their data fits this hypothesis regarding longer axial distances being seen with shorter equatorial ones.

4. Conclusions

One equivalent of a variety of diimines readily reacts with $[Pt(9S3)Cl_2]$ forming heteroleptic thioether–diimine complexes of the formula $[Pt(9S3)(N_2)](PF_6)$ (N_2 = diimine) with elongated square pyramidal structures $[S_2N_2 + S_1]$ in the solid state. The presence of a *cis*-PtS_2N_2 coordination sphere for the six complexes is supported by ^{195}Pt NMR chemical shifts. The third sulfur in each structure forms a longer interaction with the platinum resulting in an elongated square pyramidal structure. These distances, however, are approximately 0.2 Å longer than with the analogous diphosphine complexes, demonstrating that better π acids, in fact, do not result in a shorter Pt–S axial distance compared to better σ donor ligands as has previously been proposed.

5. Supplementary material

Crystallographic data for the two structures reported in this paper have been deposited with the Cambridge Crystallographic Data Centre as 223510 and 223511. Copies of the data can be obtained free of charge upon application to CCDC, 12 Union Road, Cambridge, CB2 1 EZ UK (fax: +44-1223-336-033); email: deposit@ccdc.cam.ac.uk or on the web: http://www.ccdc.cam.ac.uk.

Acknowledgements

This research was generously supported by grants from the Petroleum Research Fund, administered by the American Chemical Society, the Grote Chemistry Fund, the Camille and Henry Dreyfus Foundation, the National Science Foundation RSEC Program, and the William L. Wheeler Center for Odor Research at the University of Tennessee at Chattanooga.

References

[1] A.J. Blake, M. Schröder, in: A.G. Sykes (Ed.), Advances in Inorganic Chemistry, vol. 35, Academic Press, New York, 1990, p. 2.
[2] S.R. Cooper, Acc. Chem. Res. 21 (1988) 141.
[3] S.R. Cooper, S.C. Rawle, Struct. Bonding (Berlin) 72 (1990) 1.
[4] M. Schröder, Pure Appl. Chem. 60 (1988) 517.
[5] W.N. Setzer, E.L. Cacioppo, Q. Guo, G.J. Grant, D.D. Kim, J.L. Hubbard, D.G. VanDerveer, Inorg. Chem. 29 (1990) 2672.
[6] R.D. Adams, S.B. Falloon, K.T. McBride, J.H. Yamamoto, Organometallics 14 (1995) 1739.
[7] A.J. Blake, R.O. Gould, A.J. Holder, T.I. Hyde, A.J. Lavery, M.O. Odulate, M. Schröder, J. Chem. Soc., Chem. Commun. (1987) 118.
[8] A.J. Blake, A.J. Holder, G. Reid, M. Schröder, J. Chem. Soc., Dalton Trans. (1994) 627.
[9] A.J. Blake, R.O. Gould, A.J. Lavery, M. Schröder, Angew. Chem., Int. Ed. Engl. 25 (1986) 274.

[10] S.J. Loeb, J.R. Mansfield, Can. J. Chem. 74 (1996) 1377.
[11] A.J. Blake, R.D. Crofts, M. Schröder, J. Chem. Soc., Dalton Trans. (1993) 2259.
[12] T.W. Hambley, Inorg. Chem. 37 (1998) 3767.
[13] J.E. Huheey, E.A. Keiter, R.L. Keiter, Inorganic Chemistry, 4th ed., Harper Collins, New York, 1993, p. 292.
[14] G.J. Grant, N.S. Spangler, W.N. Setzer, D.G. VanDerveer, Inorg. Chim. Acta 246 (1996) 41.
[15] H. Nikol, Hans-Beat Bürgi, K.I. Hardcastle, H.B. Gray, Inorg. Chem. 34 (1995) 6319.
[16] A.J. Blake, Y.V. Roberts, M. Schröder, J. Chem. Soc., Dalton Trans. (1996) 1885.
[17] M.A. Bennett, J.K. Felixberger, A.C. Willis, Gazz. Chim. Ital. 123 (1993) 405.
[18] G.J. Grant, I.M. Poullaos, D.F. Galas, D.G. VanDerveer, J.D. Zubkowski, E.J. Valente, Inorg. Chem. 40 (2001) 564.
[19] G.-H. Lee, Acta Crystallogr. C54 (1998) 906.
[20] G.J. Grant, C.G. Brandow, D.F. Galas, J.P. Davis, W.T. Pennington, J.D. Zubkowski, E.J. Valente, Polyhedron 20 (2001) 3333.
[21] G.J. Grant, I.M. Poullaos, D.F. Galas, S.C. Carter, D.G. VanDerveer, J. Chem. Soc., Dalton Trans. (2002) 2973.
[22] G.J. Grant, D.F. Galas, D.G. VanDerveer, Polyhedron 21 (2002) 879.
[23] G.J. Grant, S.M. Carter, I.M. Poullaos, A.L. Russell, D.G. VanDerveer, J. Organomet. Chem. 637–639 (2001) 683.
[24] G.J. Grant, J.D. Pool, D.G. VanDerveer, J. Chem. Soc., Dalton Trans. (2003) 3981.
[25] M.A. Bennett, A.J. Canty, J.K. Felixberger, L.M. Rendina, C. Sunderland, A.C. Willis, Inorg. Chem. 32 (1993) 1951.
[26] M. Hissler, J.E. McGarrah, W.B. Connick, D.K. Geiger, S.D. Cummings, R. Eisenberg, Coord. Chem. Rev. 208 (2000) 115.
[27] P.S. Pregosin, in: P.S. Pregosin (Ed.), Transition Metal Nuclear Magnetic Resonance, Elsevier, New York, 1991, p. 251, and references cited therein.
[28] The programs used for data collection, solution and refinement of this structure were: SMART 5.054, SAINT$^+$ 6.01, SHELXTL 5.1, 1998-1999, Bruker AXS, Madison, WI, USA.
[29] SABABS R.H. Blessing, Acta Crystallogr. A51 (1995) 33.
[30] E.W. Abel, P.D. Beer, I. Moss, K.G. Orrell, V. Sik, P.A. Bates, M.B. Hurthouse, J. Chem. Soc., Chem. Commun. (1987) 978.
[31] E.G. Hope, W. Levason, N.A. Powell, Inorg. Chim. Acta 115 (1986) 187.
[32] V. Anbalagan, R. Srinivasan, K.S. Pallavi, Trans. Met. Chem. 26 (2002) 603.
[33] R.H. Herber, M. Croft, M.J. Coyer, B. Bilash, A. Sahiner, Inorg. Chem. 33 (1994) 2422.
[34] F. Contu, F. Demartin, F.A. Devillanova, A. Garau, F. Isaia, V. Lippolis, A. Salis, G. Verani, J. Chem. Soc., Dalton Trans. (1997) 4410.
[35] G.J. Grant, W. Chen, A.M. Goforth, K.N. Patel, C.L. Baucom, P. Repovic, D.G. VanDerveer, W.T. Pennington, Crystal Growth and Design, submitted.

Available online at www.sciencedirect.com
SCIENCE DIRECT®
Polyhedron 23 (2004) 1371–1374
POLYHEDRON
www.elsevier.com/locate/poly

Oxidatively induced one-electron reductive elimination of pentafluorophenyl from $[Mo(C_6F_5)(CO)_5]^-$

Jungsook Kim, Stephen L. Gipson *

Department of Chemistry, Baylor University, Waco, TX 76798, USA

Received 11 December 2003; accepted 15 February 2004
Available online 12 April 2004

Abstract

The anionic molybdenum(0) complex $[Mo(C_6F_5)(CO)_5]^-$ displays a one-electron oxidation by cyclic voltammetry that is only partially chemically reversible. The partial chemical reversibility is caused by a slow chemical reaction following oxidation. This reaction has been shown to be cleavage of the $Mo–C_6F_5$ bond in a one-electron reductive elimination process. Chemical oxidation by ferrocenium in the presence of nucleophiles yields known $Mo(CO)_5L$ (L = Py, PPh_3) complexes, while oxidation with tropylium traps the C_6F_5 radical as $C_7H_7C_6F_5$. NMR and mass spectrometry were used to identify the oxidation products. Simulated cyclic voltammograms have been used to estimate the rate constant for cleavage of the $Mo–C_6F_5$ bond in the presence of pyridine as approximately 700 $M^{-1}\,s^{-1}$.
© 2004 Elsevier Ltd. All rights reserved.

Keywords: Molybdenum complexes; Carbonyl complexes; Pentafluorophenyl; Oxidation; Bond cleavage; Reductive elimination

1. Introduction

For some years now we have been studying the redox-induced chemistry of pentafluorophenylmolybdenum carbonyl complexes. We have shown that the cycloheptatrienyl derivative $Mo(C_6F_5)(CO)_2(\eta\text{-}C_7H_7)$ undergoes an inefficient oxidatively induced CO insertion [1], while upon reduction it dimerizes by coupling of the cycloheptatrienyl rings to give the ditropyl complex $[\{Mo(C_6F_5)(CO)_2\}_2(\eta^6{:}\eta'^6\text{-}C_{14}H_{14})]^{2-}$ [2]. Displacement of the ditropyl ligand from the dimeric dianion by $P(OMe)_3$ yields *cis-mer*-$[Mo(C_6F_5)(CO)_2\{P(OMe)_3\}_3]^-$ [3], which undergoes other substitution reactions and an oxidatively induced isomerization [4]. In an effort to find a more convenient entry into related Mo(0) chemistry, we developed a synthesis of the $[Mo(C_6F_5)(CO)_5]^-$ anion [5]. We have now concluded an investigation of the oxidative chemistry of this complex, in which it was demonstrated that oxidation is followed by relatively slow one-electron, homolytic reductive elimination via cleavage of the $Mo–C_6F_5$ bond to yield the 16-electron $Mo(CO)_5$ fragment and a pentafluorophenyl radical.

While the possibility of one-electron reductive elimination from transition metal organometallic compounds has long been discussed, the literature contains relatively few reported examples. The chemical oxidation of R_4Pb (R = Me, Et), $Me_2Pt(PPh_3)_2$ and $Et_2Pt(PMe_2Ph)_2$ by $IrCl_6^{2-}$ is believed to be followed by metal–carbon bond cleavage to yield alkyl radicals which subsequently react with additional $IrCl_6^{2-}$ to yield RCl as the organic product of one-electron reductive elimination [6,7]. Similarly, chemical or electrochemical oxidation of tetramethylaurate [8] and dimethylcobalt macrocyclic chelates [9] produces methyl radicals. One-electron oxidation of several group 4 dicyclopentadienyl complexes Cp_2MR_2 (M = Ti, Zr; R = Me, Ph, Bz) produces organic radicals which subsequently dimerize [10–12]. Chemical or electrochemical oxidation of $Cp^*Ir(DMSO)Me_2$ in DMSO as solvent yields CH_4 through $Ir–CH_3$ bond cleavage followed by hydrogen abstraction from adventitious water, while oxidation of the rhodium analog yields instead the two-

* Corresponding author. Tel.: +254-710-3311; fax: +254-710-2403.
E-mail address: stephen_gipson@baylor.edu (S.L. Gipson).

0277-5387/$ - see front matter © 2004 Elsevier Ltd. All rights reserved.
doi:10.1016/j.poly.2004.02.022

electron reductive elimination product ethane [13]. Oxidation of Cp^*RuL_2R ($L = PMe_3$, PMe_2Ph, $R = Me$; $L = PMe_3$, $R = CH_2CMe_3$) and $CpRu(PPh_3)_2Me$ yield RH via Ru–C bond cleavage followed by H-atom abstraction from one of the other ligands [14]. In a similar study of the oxidations of $CpRu(CO)(PR_3)Me$ ($R = Cy$, Ph), it was concluded that coordination of solvent to the $17e^-$ cation precedes Ru–Me bond cleavage [15]. The only reported example of one-electron reductive elimination from group 6 compounds is that of Cp_2MX_2 ($M = Mo$, W; $X =$ halide, thiolate) [16]. We report here the first oxidatively induced metal–carbon bond cleavage (one-electron reductive elimination) in a molybdenum complex, $[Mo(C_6F_5)(CO)_5]^-$, which also has the distinction of not having any hydrogen-containing ligands.

2. Experimental

2.1. Reagents

All reactions were carried out under argon using Schlenk techniques or in a nitrogen-atmosphere glovebox. All solvents were distilled from appropriate drying agents and stored under nitrogen. The compounds $PPN[Mo(C_6F_5)(CO)_5]$ [5] (PPN = bis(triphenylphosphoranylidene)ammonium) and Cp_2FeBF_4 [17] were prepared by published methods. All other reagents were obtained commercially and were used as received.

2.2. Instrumentation

IR spectra were obtained using a Mattson Instruments Genesis II FTIR and a cell with CaF_2 windows separated by a 0.1 mm spacer. ^1H, ^{31}P, and ^{19}F NMR spectra were obtained on a Bruker DPX 300 MHz NMR spectrometer. NMR chemical shifts were referenced to residual protons in the solvent (for ^1H), 85% H_3PO_4 external standard (for ^{31}P), or $CFCl_3$ external standard (for ^{19}F). Mass spectra were obtained on a VG/Fisons Prospec 3000 double focusing spectrometer using EI ionization. Peaks in the mass spectrum were referenced to perfluorokerosene.

Cyclic voltammetry was performed using a Bioanalytical Systems BAS 100B/W electrochemical analyzer. Solutions contained approximately 0.1 M $[Bu_4N]PF_6$ supporting electrolyte. Electrodes consisted of a 0.5 mm Pt disk working electrode, Pt wire auxiliary electrode, and Ag/AgCl reference electrode. Potentials were referenced to the formal potential of the decamethylferrocenium–decamethylferrocene couple ($Cp^*_2Fe^+/Cp^*_2Fe$), which we measure as approximately −0.1 V vs. Ag/AgCl. Simulations of the cyclic voltammetry were run using Bioanalytical Systems DigiSim 3.0 software.

3. Results and discussion

3.1. Cyclic voltammetry of $PPN[Mo(C_6F_5)(CO)_5]$

The cyclic voltammetry of $PPN[Mo(C_6F_5)(CO)_5]$ in CH_2Cl_2 displays a partially chemically reversible one-electron oxidation at +0.66 V vs. $Cp^*_2Fe^+/Cp^*_2Fe$. The ratio of the cathodic to the anodic peak currents for this couple ranges from near zero at scan rates below 20 mV/s to near unity at scan rates above 5 V/s. This change in chemical reversibility suggests that the presumed product of the oxidation, the neutral 17-electron complex $Mo(C_6F_5)(CO)_5$, undergoes a relatively slow chemical reaction. In THF and MeCN solvents the chemical reversibility is even lower, with the peak current ratio for a given scan rate decreasing in the order $CH_2Cl_2 >$ THF > MeCN. Given that this is the same order as the coordinating ability of the solvents, these results suggest that the decomposition of the 17-electron species involves nucleophilic attack by solvent.

The participation of nucleophiles in the chemical reaction following oxidation of $[Mo(C_6F_5)(CO)_5]^-$ is further supported by the observation that the addition of ligands such as pyridine and triphenylphosphine to CH_2Cl_2 solutions of $PPN[Mo(C_6F_5)(CO)_5]$ causes a decrease in chemical reversibility of the oxidation. At a scan rate of 0.2 V/s, the peak current ratio for a 1.0 mM solution of $PPN[Mo(C_6F_5)(CO)_5]$ in CH_2Cl_2 decreases from 0.72 in the absence of pyridine to essentially zero with 5.0 mM added pyridine. All of these observations are consistent with an EC mechanism for the oxidation of $[Mo(C_6F_5)(CO)_5]^-$.

3.2. Chemical oxidation of $PPN[Mo(C_6F_5)(CO)_5]$ by ferrocenium and tropylium

In order to identify the products of the reaction of $Mo(C_6F_5)(CO)_5$ with nucleophiles, $PPN[Mo(C_6F_5)(CO)_5]$ was treated with the mild oxidants Cp_2FeBF_4 and $C_7H_7BF_4$. The oxidations with ferrocenium (1 equiv.) were conducted in the presence of pyridine or triphenylphosphine (2 equiv.) in $CDCl_3$ as solvent. NMR spectroscopy of the resulting solutions identified the products as $Mo(CO)_5L$ (by ^1H and ^{31}P, L = Py or PPh_3), C_6F_5H (by ^1H and ^{19}F), and Cp_2Fe (by ^1H). Thus, the 16-electron $Mo(CO)_5$ fragment produced by the Mo–C_6F_5 bond cleavage was trapped as a stable 18-electron complex by the added ligand, while the C_6F_5 radical most likely abstracted a hydrogen atom from adventitious water to yield the pentafluorobenzene.

The reaction of $PPN[Mo(C_6F_5)(CO)_5]$ with $C_7H_7BF_4$ could not be performed in the presence of nucleophiles since the tropylium reacted more rapidly with the nucleophiles than with the Mo complex. Nevertheless, a slow reaction between $PPN[Mo(C_6F_5)(CO)_5]$ and $C_7H_7BF_4$ did occur in the absence of added nucleophile

in $CDCl_3$ and the NMR spectra of the product solution were consistent with $C_7H_7C_6F_5$ being the pentafluorophenyl-containing product. Isolation of this species by preparative TLC followed by mass spectral analysis gave a parent ion at *m/z* 258.11 ($C_7H_7C_6F_5$) and fragments at 167.03 (C_6F_5) and 91.08 (C_7H_7). Thus the oxidation of $[Mo(C_6F_5)(CO)_5]^-$ by $C_7H_7BF_4$ is believed to involve the following sequence of reactions:

$$[Mo(C_6F_5)(CO)_5]^- + C_7H_7^+ \rightarrow Mo(C_6F_5)(CO)_5 + C_7H_7^{\cdot}$$

$$Mo(C_6F_5)(CO)_5 + S \rightarrow Mo(CO)_5S + C_6F_5^{\cdot}$$

$$C_7H_7^{\cdot} + C_6F_5^{\cdot} \rightarrow C_7H_7C_6F_5$$

where S in the above reactions could be solvent, the BF_4^- anion, or adventitious water.

3.3. Simulation of cyclic voltammetry

In order to understand more about the mechanism of the apparent one-electron reductive elimination of C_6F_5 from $Mo(C_6F_5)(CO)_5$, we have simulated the cyclic voltammetry of PPN[$Mo(C_6F_5)(CO)_5$] in CH_2Cl_2 in the presence of pyridine using the reactions in Scheme 1.

At reasonably fast scan rates in the absence of pyridine, the electron transfer reaction appears chemically and electrochemically reversible and can be simulated using a slightly slow electron transfer with a rate constant of 0.06 cm/s and a transfer coefficient of 0.5. Fig. 1 shows the effect of pyridine concentration on the apparent chemical reversibility of experimental and simulated cyclic voltammograms of 1.0 mM PPN[$Mo(C_6F_5)(CO)_5$] at a scan rate of 0.2 V/s. In the absence of pyridine, simulations gave an optimum fit using a first-order rate constant for reaction (1) of 0.22 s^{-1}. This reaction almost certainly involves some nucleophile, but since this species can be neither conclusively identified nor quantitated, the reaction was modeled as a first-order process.

With all other parameters held constant at values given in Table 1, simulations were then run to obtain the second-order rate constant, k_2, for the reaction of pyridine with $Mo(C_6F_5)(CO)_5$, reaction (2). Optimum fits were obtained with k_2 values ranging from 646 to 1041 $M^{-1}\,s^{-1}$. Fig. 2 illustrates the effect of scan rate on the apparent chemical reversibility of experimental and simulated cyclic voltammograms of 1.0 mM PPN[$Mo(C_6F_5)(CO)_5$] in the presence of 5.0 mM pyridine. Using the same values for other parameters as in

$$[Mo(C_6F_5)(CO)_5]^- \rightleftharpoons Mo(C_6F_5)(CO)_5 + e^- \quad (E)$$

$$Mo(C_6F_5)(CO)_5 \rightarrow Mo(CO)_5S + C_6F_5 \quad (1)$$

$$Mo(C_6F_5)(CO)_5 + Py \rightarrow Mo(CO)_5Py + C_6F_5 \quad (2)$$

Scheme 1.

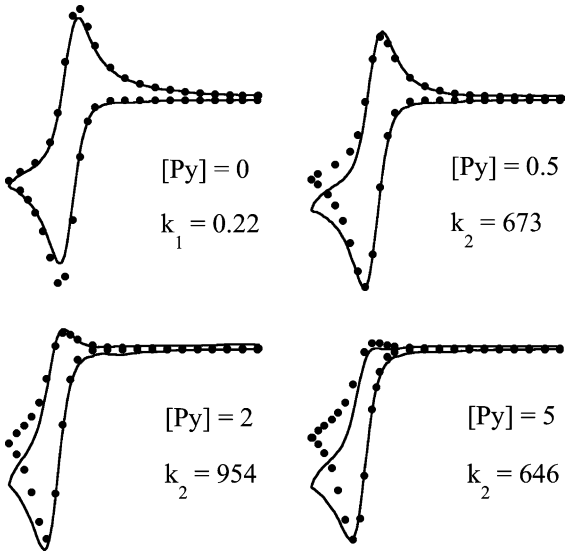

Fig. 1. Experimental (solid lines) and simulated (circles) cyclic voltammograms of 1.0 mM PPN[$Mo(C_6F_5)(CO)_5$] + pyridine in CH_2Cl_2/0.1 M $[Bu_4N]PF_6$ at a 0.5 mm diameter Pt disk electrode at 0.2 V/s. Concentrations of pyridine labeled in mM. Optimized rate constant for k_1 labeled in s^{-1} and for k_2 in $M^{-1}\,s^{-1}$.

Fig. 1, optimization of k_2 gave values ranging from 482 to 823 $M^{-1}\,s^{-1}$. Generally excellent agreement between experimental and simulated results was thus achieved using the parameters shown in Table 1 and an average value for k_2 of approximately 700 $M^{-1}\,s^{-1}$. This corresponds to a relatively slow reaction, much slower than the elimination of methyl radical from dimethylcobalt(IV) macrocycles [9], though significantly faster than the reaction of $CpRu(CO)(PR_3)CH_3$ with CH_3CN [15].

The mechanism of the oxidatively induced one-electron reductive elimination is proposed to involve nucleophilic attack (association) of the incoming ligand at the Mo, followed by extrusion of the C_6F_5 radical. Essentially identical results could be obtained by modeling the reaction with pyridine as either a rate-limiting pre-equilibrium between $Mo(C_6F_5)(CO)_5$ and pyridine followed rapid extrusion of C_6F_5 or a rapid pre-equilibrium followed by a rate-determining homolysis of the Mo–C_6F_5 bond. Therefore, the combination of nucleo-

Table 1
Parameters used in simulation of cyclic voltammetry of PPN[$Mo(C_6F_5)(CO)_5$] in CH_2Cl_2 in the presence of pyridine

α	0.5	Electrode area	0.0023 cm^2
k_E	0.06 cm s^{-1}	Double layer capacitance	0.0013 μF
k_1	0.22 s^{-1}	Uncompensated resistance	2000 Ω
K_{eq1}	2.2×10^6		
K_{eq2}	2.7×10^8		

α, transfer coefficient; k_E, standard heterogeneous rate constant for electron transfer; k_1, first-order rate constant for reaction in absence of nucleophile; K_{eq}, equilibrium constants for reactions (1) and (2) (see Scheme 1).

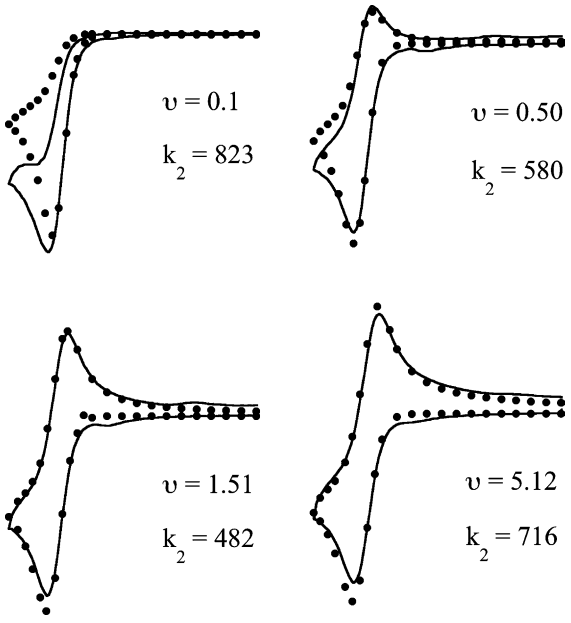

Fig. 2. Experimental (solid lines) and simulated (circles) cyclic voltammograms of 1.0 mM PPN[$Mo(C_6F_5)(CO)_5$] + 5.0 mM pyridine in CH_2Cl_2/0.1 M $[Bu_4N]PF_6$ at a 0.5 mm diameter Pt disk electrode. Scan rates labeled in V/s. Optimized rate constants labeled in $M^{-1}\,s^{-1}$.

philic attack and bond homolysis were modeled as the single second-order reaction shown in Scheme 1. Consistent with qualitative observations of the cyclic voltammetry, the reductive elimination in the presence of added nucleophile is significantly more rapid than in pure solvent. This observation lends support to the proposed associative nature of the overall reaction.

4. Conclusions

On the basis of experimentally observed cyclic voltammetry, simulations of this cyclic voltammetry, and products observed from chemical oxidation, a mechanism for the oxidatively induced one-electron reductive elimination of C_6F_5 from PPN[$Mo(C_6F_5)(CO)_5$] has been proposed. An initial one-electron oxidation produces the 17-electron species $Mo(C_6F_5)(CO)_5$. In agreement with previously published results for other systems [15], further reaction of this species is believed to involve prior association of the incoming ligand. The resulting 19-electron species then undergoes cleavage of the metal–carbon bond, effecting a one-electron reductive elimination reaction. The products of the reaction have all been identified by a combination of IR, NMR, and mass spectrometries.

Acknowledgements

We thank the Robert A. Welch Foundation (Grant No. AA-1083) and Baylor University, in part, for support of this research.

References

[1] S.L. Gipson, K. Kneten, Inorg. Chim. Acta 157 (1989) 143.
[2] M. Su, S.L. Gipson, D.F. Mullica, E.L. Sappenfield, D.H. Leschnitzer, J. Chem. Soc., Dalton Trans. (1993) 3323.
[3] S.L. Gipson, D.F. Mullica, E.L. Sappenfield, M.L. Hander, D.H. Leschnitzer, J. Chem. Soc., Dalton Trans. (1992) 521.
[4] D.F. Mullica, S.L. Gipson, M. Su, E.L. Sappenfield, Polyhedron 14 (1995) 2215.
[5] W.J. Doucette, J. Kim, J.A. Kautz, S.L. Gipson, Inorg. Chim. Acta 304 (2000) 237.
[6] H.C. Gardner, J.K. Kochi, J. Am. Chem. Soc. 97 (1975) 1855.
[7] J.Y. Chen, J.K. Kochi, J. Am. Chem. Soc. 99 (1977) 1450.
[8] D. Zhu, S.V. Lindeman, J.K. Kochi, Organometallics 18 (1999) 2241.
[9] W.H. Tamblyn, R.J. Klingler, W.S. Hwang, J.K. Kochi, J. Am. Chem. Soc. 103 (1981) 3161.
[10] S.L. Borkowsky, N.C. Baenziger, R.F. Jordan, Organometallics 12 (1993) 486.
[11] M.J. Burk, W. Tumas, M.D. Ward, D.R. Wheeler, J. Am. Chem. Soc. 112 (1990) 6133.
[12] R.F. Jordan, R.E. LaPointe, C.S. Bajgur, S.F. Echols, R. Willett, J. Am. Chem. Soc. 109 (1987) 4111.
[13] E. Fooladi, T. Graham, M.L. Turner, B. Dalhus, P.M. Maitlis, M. Tilset, J. Chem. Soc., Dalton Trans. (2002) 975.
[14] P. Diversi, M. Fontani, M. Fuligni, F. Laschi, S. Matteoni, C. Pinzino, P. Zanello, J. Organomet. Chem. 626 (2001) 145.
[15] T. Aase, M. Tilset, V.D. Parker, J. Am. Chem. Soc. 112 (1990) 4974.
[16] J.C. Kotz, W. Vining, W. Coco, R. Rosen, Organometallics 2 (1983) 68.
[17] D.N. Hendrickson, Y.S. Sohn, H.B. Gray, Inorg. Chem. 10 (1971) 1559.

Available online at www.sciencedirect.com
SCIENCE DIRECT®
Polyhedron 23 (2004) 1375–1378
POLYHEDRON
www.elsevier.com/locate/poly

Cis-$[PtCl_2(p\text{-}TPPTP(H)_7)_2]Cl_2 \cdot 4H_2O \cdot (CH_3CH(OH)CH_3)$: a platinum phosphine complex exhibiting both inter- and intra-molecular hydrogen bonding

Terence L. Schull [a,*], Ray Butcher [b], Walter J. Dressick [a], Susan L. Brandow [a], Laura K. Byington [c], D. Andrew Knight [c,*]

[a] *Center for Bio/Molecular Science and Engineering, Code 6900, US Naval Research Laboratory, 4555 Overlook Avenue, S. W., Washington, DC 20375-5348, USA*
[b] *Department of Chemistry, Howard University, Washington, DC 20009, USA*
[c] *Department of Chemistry, Loyola University, 6363 St. Charles Avenue, New Orleans, LA 70118, USA*

Received 15 December 2003; accepted 17 February 2004
Available online 9 April 2004

Abstract

The title compound, *cis*-$[PtCl_2(p\text{-}TPPTP(H)_7)_2]Cl_2 \cdot 4H_2O \cdot (CH_3CH(OH)CH_3)$ (TPPTP = triphenylphosphine triphosphonate), is formed via crystallization from a water-isopropanol solution of *cis*-$[PtCl_2(TPPTP(H_6))_2]$. The coordination geometry around platinum is distorted square planar with two coordinated chloride ligands, and two free chloride ions in the crystal lattice. Two of the phosphonic acid groups are protonated $-PO_3H_3^+$ and the complex contains extensive intra- and inter-molecular hydrogen bonding.
© 2004 Elsevier Ltd. All rights reserved.

Keywords: Phosphine; Phosphonic acid; Platinum

1. Introduction

Phosphonic acid functionalized complexes of transition metals are currently being explored as water-soluble homogeneous catalysts, photo-catalysts and supported catalysts. The $-PO_3H_2$ functional group has a number of desirable attributes which can be exploited: (1) due to the dianionic nature of the $[PO_3]^{2-}$ group, both functionalized organic and inorganic species are expected to be highly water-soluble and highly organophobic, two characteristics which are important for the design of biphasic/aqueous phase homogeneous catalysts [1]; (2) organophosphonic acids are known to form two- and three-dimensional supramolecular arrays stabilized by hydrogen bonding. This property has piqued the interest of crystal engineers who can make use of the wide variety of H-bonding motifs for the design of new functional solids [2]; (3) the phosphonate group forms strong covalent bonds with inorganic oxides such as SiO_2, Al_2O_3 and TiO_2 and thus provides a suitable tether for anchoring the molecular species for the purposes of heterogenizing organometallic and coordination complexes. Bujoli and co-workers [3] have recently prepared a titanium phosphonate supported rhodium/2,2′-bipyridine complex for hydrogenation of ketones and carbon–carbon multiple bonds. We have demonstrated the utility of a phosphine–phosphonic acid complex of palladium, anchored to silica, for catalytic carbon–phosphorus bond formation [4]. Our research has mainly focused on the synthesis of phosphonic acid and phosphonate functionalized phosphine complexes of late transition metals. In 1996, we reported the synthesis and use of *m*-TPPMP (triphenylphosphine monophosphonate disodium salt) in aqueous phase palladium catalyzed carbonylation [5]. More recently, we described the use of a *p*-$TPPTP(H)_6$ (TPPTP = triphenylphosphine triphosphonate) [6,7] derivative of molybde-

* Corresponding authors. Fax: +1-504-865-2269.
E-mail address: daknight@loyno.edu (D.A. Knight).

0277-5387/$ - see front matter © 2004 Elsevier Ltd. All rights reserved.
doi:10.1016/j.poly.2004.02.021

num(0) for monolayer functionalization of aluminum, and a *p*-TPPTP complex of palladium for the aqueous phase phosphonylation of phenyl triflate [4].

2. Experimental

Reagents and solvents were obtained from commercial sources and used as received. *Cis*-[$PtCl_2$(*p*-TPPTP$(H)_6)_2$] was prepared according to the literature procedure [4]. Yellow crystals of **1**·$4H_2O$·($CH_3CH(OH)CH_3$) suitable for X-ray diffraction were isolated from H_2O/2-propanol (slow diffusion at room temperature).

3. Crystal data structure and refinement

Crystal data and details of structure determination for **1** are given in Table 1. Single-crystal X-ray diffraction measurements were carried out using Mo Kα radiation ($\lambda = 0.71073$ Å) at 198 K. The structure was solved by direct methods using Fourier techniques. The non-hydrogen atoms were refined anisotropically. Hydrogen atoms attached to O, O(3A), O(2E), O(3E), and O(2F) were first located in difference Fourier maps and were then idealized with the X–O–H tetrahedral angle. The hydrogen atoms attached to water oxygens were located in difference Fourier maps and then idealized by fixing the O–H distance at 0.85 Å and refining the H···H distance for all water hydrogen atoms as a variable. The final value (1.36517 Å) corresponds to a H–O–H angle of 106.8°. All hydrogen atoms attached to carbons were idealized using SHELXL default values for each type of carbon. Data collection and cell refinement were performed using SMART [12]. SAINT and XPREP [13,14] were used for data reduction, and SHELX-97 programs [13] were used to refine the structure.

4. Results and discussion

The reaction of 1.6 equivalents of *p*-TPPTP$(H)_6$ with K_2PtCl_4 in water, followed by precipitation with ethanol, gives *cis*-[$PtCl_2$(*p*-TPPTP$(H)_6)_2$] as a cream powder. When an aqueous solution of *cis*-[$PtCl_2$(*p*-TPPTP$(H)_6)_2$] is layered with 2-propanol, yellow crystals of *cis*-

Table 1
Crystal data and structure refinement for **1**

Identification code	**1**
Empirical formula	$C_{39}H_{44}Cl_4O_{23}P_8Pt$
Formula weight	1465.39
T (K)	198(2)
λ (Å)	1.54178
Crystal system	triclinic
Space group	$P\bar{1}$
Unit cell dimensions	
a (Å)	14.3000(10)
b (Å)	14.6560(10)
c (Å)	15.6710(10)
α (°)	104.505(4)
β (°)	115.330(3)
γ (°)	100.078(4)
V (Å^3)	2720.5(3)
Z	2
ρ_{calc} (Mg/m^3)	1.789
Absorption coefficient (mm^{-1})	9.552
$F(000)$	1456
Crystal size (mm)	0.36×0.08×0.06
θ range for data collection (°)	3.29–65.18
Index ranges	$-16 \leqslant h \leqslant 16$, $-17 \leqslant k \leqslant 16$, $-18 \leqslant l \leqslant 17$
Reflections collected	13 217
Independent reflections (R_{int})	7921 (0.0602)
Completeness to $\theta = 65.18°$ (%)	85.2
Absorption correction	semi-empirical from equivalents
Maximum and minimum transmission	0.928697 and 0.634023
Refinement method	full-matrix least-squares on F^2
Data/restraints/parameters	7921/12/707
Goodness-of-fit on F^2	0.982
Final R indices [$I > 2\sigma(I)$]	$R_1 = 0.0757$, $wR_2 = 0.1909$
R indices (all data)	$R_1 = 0.0887$, $wR_2 = 0.1982$
Largest difference peak and hole (e Å^{-3})	5.091 and −2.828

$[PtCl_2(p\text{-}TPPTP(H)_7)_2]Cl_2 \cdot 4H_2O \cdot (CH_3CH(OH)CH_3)$ (**1**) form on standing.

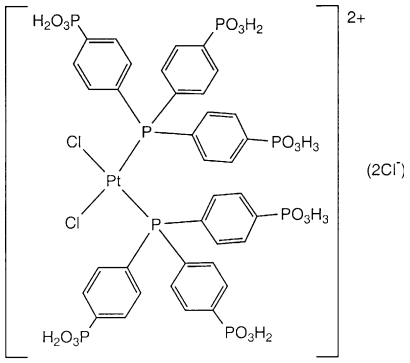

1

Here, we report the crystal structure of **1** which shows extensive inter-molecular hydrogen bonding as well as a novel intra-molecular hydrogen bonded interaction. The ORTEP representation of **1** is shown in Fig. 1 and selected bond lengths and angles are listed in Table 2. Only three crystal structures containing the subunit *cis*-$[PtCl_2L_2]$ (L = triarylphosphine) were found in the Cambridge Crystallographic Database for comparison of geometric parameters and **1** shows some interesting differences with these structures. Compound **1** crystallizes in space group $P\bar{1}$ and with two discreet molecules in the unit cell. The geometry around the central platinum atom is best described as distorted square planar with two phosphorus atoms of the phosphine ligands coordinated in a *cis* fashion, and two chloride ligands similarly disposed. Deviation of atoms from the least squares plane for the central platinum and the four coordinated atoms are: Pt, 0.006 Å; P(1), −0.085 Å; P(2), 0.106 Å; Cl(1), −0.143 Å; Cl(2), 0.115 Å. These deviations from the plane are much greater than those found for the complex *cis*-$[PtCl_2(PPh_3)_2]$ [8] in which the maximum deviation of any atom from the least square planes is only 0.006 Å, possibly reflecting the distortion imposed by hydrogen bonding in **1**. The Pt–Cl bond distances in **1** are 2.355(3) and 2.328(3) Å for Pt–Cl(1) and PtCl(2), respectively. This asymmetry in Pt–Cl bond lengths was noted in a report of the structure of *cis*-$[PtCl_2(PPh_3)_2]$ in which the longest Pt–Cl bond was *trans* to the shortest Pt–P bond and vice versa. This is not the case in complex **1** in which the longest Pt–Cl is in fact *trans* to the longest Pt–P bond (Pt–P(1)). The sum of *trans* Pt–Cl and Pt–P bonds are thus quite different and this suggests that other factors, in addition to electronic properties of the ligands, are affecting the *trans*-influences of Cl and phosphine ligands in **1**. It is not surprising that the P(1)–Pt–P(2) angle (98.30(10)°) is significantly larger than ideal (90°) presumably to overcome steric crowding of the phosphine ligands. This angle is larger than any previously reported for the structures of *cis*-$[PtCl_2L_2]$ (L = triarylphosphine) complexes: $L = PPh_3$, [97.8°] [8]; $L = P(C_6H_4C_6F_{13}\text{-}4)_3$ [97.73(9)°] [9]; $L = P(C_6H_5)_2(C_6H_4COOH\text{-}3)$ [96.18(16)°] [10]. Similarly, the Cl(1)–Pt–Cl(2) angle is compressed in **1** (88.04(10)°).

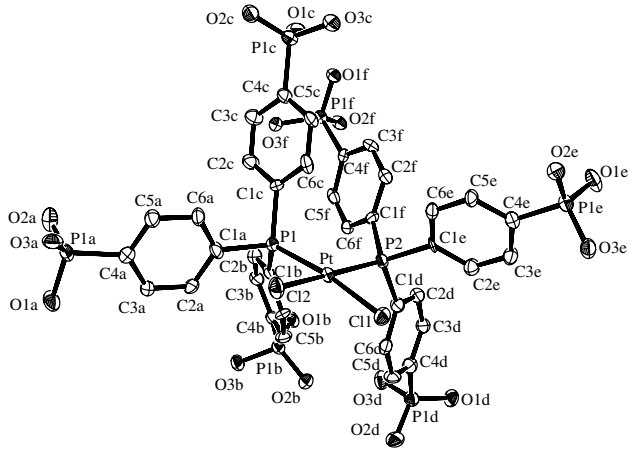

Fig. 1. ORTEP representation of **1** showing the atom numbering scheme. Ellipsoids are shown at the 50% probability level.

Table 2
Selected bond lengths (Å) and bond angles (°) for **1**

Bond lengths	
Pt–P(2)	2.266(3)
Pt–P(1)	2.271(3)
Pt–Cl(2)	2.328(3)
Pt–Cl(1)	2.355(3)
O–H···O(2A)	2.780(13)
O(3A)···O(2D)#1	2.448(11)
O(2E)···O(4W)	2.501(13)
O(3E)···O(3F)#2	2.509(11)
O(2F)···O(3F)#3	2.643(10)
O(1W)···O#4	2.715(14)
O(1W)···O(1D)	2.784(14)
O(3W)···O(3C)	2.504(12)
O(3W)···O(3A)#6	2.751(12)
O(4W)···O(1W)#7	2.683(13)
O(4W)···O(2C)#2	2.684(12)
Bond angles	
P(2)–Pt–P(1)	98.30(10)
P(2)–Pt–Cl(2)	172.05(10)
P(1)–Pt–Cl(2)	88.01(10)
P(2)–Pt–Cl(1)	86.19(10)
P(1)–Pt–Cl(1)	172.60(9)

One of the more interesting features of compound **1** is the presence of both intra- and inter-molecular hydrogen bonding. The phosphonic acid group can act both as hydrogen acceptor (P=O) and hydrogen donor (P–OH) and the presence of water molecules and a 2-propanol molecule results in an extended three-dimensional hydrogen bonded network. The intra-molecular hydrogen bonding occurs between *para*-substituted phenyl phosphonic acid groups on adjacent phenyl rings on one of the triarylphosphine ligands. This is illustrated in Fig. 2.

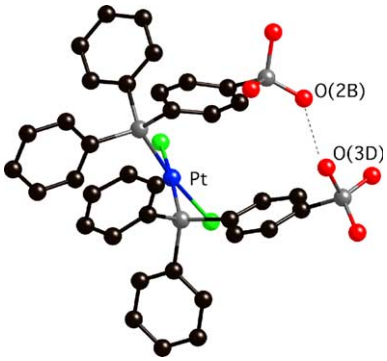

Fig. 2. Portion of **1** showing intra-molecular hydrogen bonding. Hydrogen atoms, solvate molecules and non-intra-molecular H-bonded phosphonic acid groups omitted for clarity.

A hydrogen bond is located between O(2B) and O(3D)–H (D···A = 2.600 Å). Inter-molecular phosphonic acid hydrogen bonding occurs between O(3A)–H and O(2D) (D···A = 2.448(11) Å), O(3E)–H and O(3F) (D···A = 2.509(11) Å) and O(2F)–H and O(3F) (D···A = 2.643(10) Å). Four water molecules are also hydrogen bonded to the phosphonate groups and chloride anions forming an extended 3D array.

A second interesting feature is the presence of two acidic protons located between phosphonate oxygen atoms on each ligand, and two water molecules. The P–O bond lengths are consistent with a structure intermediate between a protonated phosphonic acid group and a hydronium ion [11]. The presence of two extra protons per molecule gives an overall charge of 2+ on the molecule that is balanced by the presence of two free chloride anions in the crystal lattice.

5. Supplementary data

Copies of this information may be obtained free of charge from the Director, CCDC, 12 Union Road, Cambridge CB2 1EZ, UK (fax: +44-1223-336-033; e-mail: deposit@ccdc.cam.ac.uk or www: http://www.ccdc.cam.ac.uk) quoting the deposition No. 221745.

Acknowledgements

We thank the Office of Naval Research under the Naval Research Core Program and the ASEE for Summer Faculty Research Fellowships (to R.B. and D.A.K.).

References

[1] N. Pinault, D.W. Bruce, Coord. Chem. Rev. 241 (2003) 1.
[2] A.H. Mahmoudkhani, L. Langer, J. Mol. Struct. 609 (2002) 97.
[3] C. Maillet, P. Janvier, M.-J. Bertrand, T. Praveen, B. Bujoli, Eur. J. Org. Chem. (2002) 1689.
[4] B.A. Harper, D.A. Knight, C. George, S.L. Brandow, W.J. Dressick, C.S. Dalcey, T.L. Schull, Inorg. Chem. 42 (2003) 516.
[5] T.L. Schull, J.C. Fettinger, D.A. Knight, Inorg. Chem. 35 (1996) 6717.
[6] W.J. Dressick, C. George, S.L. Brandow, T.L. Schull, D.A. Knight, J. Org. Chem. 65 (2000) 5059.
[7] T.L. Schull, S.L. Brandow, W.J. Dressick, Tetrahedron Lett. 42 (2001) 5373.
[8] G.K. Anderson, H.C. Clark, J.A. Davies, G. Ferguson, M. Parvez, J. Cryst. Spectrosc. Res. 12 (1982) 449.
[9] J. Fawcett, E.G. Hope, R.D.W. Kemmitt, D.R. Paige, D.R. Russell, A.M. Stuart, J. Chem. Soc., Dalton Trans. (1998) 3751.
[10] V. Ravindar, H. Schumann, H. Hemling, J. Blum, Inorg. Chim. Acta 240 (1995) 145.
[11] F. Adani, E. Montoneri, P.J. Squattrito, Acta Crystallogr., Sect. C 56 (2000) 463.
[12] Bruker, SMART, Version 5.059, Bruker AXS Inc., Madison, WI, USA, 1999.
[13] Bruker, SAINT, Version 6.02A and SHELX-97, Version 6.10, Bruker AXS Inc., Madison, WI, USA, 2000.
[14] Bruker, XPREP, Version 5.1, Bruker AXS Inc., Madison, WI, USA, 1997.

Available online at www.sciencedirect.com
SCIENCE DIRECT®
Polyhedron 23 (2004) 1379–1384
POLYHEDRON
www.elsevier.com/locate/poly

Synthesis, crystal structures and magnetic studies of terephthalato-bridged binuclear nickel(II) complexes

Chang Seop Hong *, Young Sin You

Department of Chemistry, Korea University, Seoul 136-701, Republic of Korea

Received 27 January 2004; accepted 17 February 2004
Available online 9 April 2004

Abstract

Two binuclear compounds $[Ni_2(pmdtn)_2(tp)(H_2O)_2](ClO_4)_2(H_2O)_4$ (**1**) and $[Ni_2(pmdtn)_2(tp)(N_3)_2](H_2O)_4$ (**2**) have been prepared by using the multibinding terephthalate (= tp) dianion and the tridentate capping ligand *N*,*N*,*N*′,*N*′,*N*″-pentamethyldiethyltriamine (= pmdtn) and have been characterized by X-ray crystallography and magnetic measurements. The crystal structures of both complexes show distorted octahedral geometries around the Ni(II) centers linked by the tp bridges in a bisbidentate fashion. The dihedral angles between the benzene rings and carboxylate groups correspond to 14.2° for **1** and 21.5° for **2**. The intradimer distance of Ni···Ni through the tp ligand for **1** and **2** are 10.731 and 10.800 Å, respectively. The magnetic data reveal weak antiferromagnetic interactions transmitted by the tp bridge with $J = -0.18$ cm^{-1} (**1**) and -0.02 cm^{-1} (**2**), which is explained by the structural parameters.
© 2004 Elsevier Ltd. All rights reserved.

Keywords: Nickel(II) compounds; Crystal structures; Terephthalate ligand; Binuclear complexes; Magnetic properties

1. Introduction

There has been considerable interest in molecule-based magnets due to possible applications to magnetic devices [1,2]. It is essential to gain an intimate understanding of the magnetic exchange phenomena between paramagnetic metal ions, which helps to design magnetic systems with desirable properties. Bridging ligands that can mediate magnetic interactions between spin carriers become one of crucial ingredients to achieve coordination materials exhibiting intriguing magnetic behaviors. The basic question related to the current subject is how far the magnetic exchange couplings can propagate. To test this matter it is appropriate to utilize the tp ligand that connects paramagnetic metal ions within 10–11 Å, along with a variety of binding modes, generating compounds ranging from discrete molecules to 1D, 2D and to 3D networks [3–7]. To probe the underlying magnetic interaction mechanism especially in tp-linked magnetic systems, we have studied nickel compounds with the tp ligand, due to the fact that examples of such Ni(II) compounds are limited to date [8–10]. Herein, we report the syntheses, structures and magnetic behaviors of two new binuclear compounds $[Ni_2(pmdtn)_2(tp)(H_2O)_2](ClO_4)_2(H_2O)_4$ (**1**) and $[Ni_2(pmdtn)_2(tp)(N_3)_2](H_2O)_4$ (**2**) (tp = terephthalate, pmdtn = *N*,*N*,*N*′,*N*′,*N*″-pentamethyldiethyltriamine). The tp unit in both compounds acts as bisbidentate and communicates weak antiferromagnetic interactions depending on structural parameters.

2. Experimental

2.1. Materials

All chemicals and solvents were purchased from commercial sources and used without further purification. Potassium tp was readily prepared by reacting terephthalic acid with a stoichiometric amount of KOH in water.

* Corresponding author. Tel.: +82232903138; fax: +82232903121.
E-mail address: cshong@korea.ac.kr (C.S. Hong).

0277-5387/$ - see front matter © 2004 Elsevier Ltd. All rights reserved.
doi:10.1016/j.poly.2004.02.017

2.2. Preparation of $[Ni_2(pmdtn)_2(tp)(H_2O)_2](ClO_4)_2\cdot(H_2O)_4$ (1)

To a 10 ml aqueous solution of nickel(II) perchlorate hexahydrate (2.0 mmol) was added an aqueous solution (10 ml) of pmdtn (2.0 mmol) and potassium tp (1.0 mmol) with stirring. Green precipitates were immediately formed and redissolved by adding methanol (10 ml). The resulting deep green solution was filtered and left undisturbed, giving green crystals of **1** in a yield of 70% based on Ni. *Anal*. Calc. for $C_{26}H_{62}N_6O_{18}Cl_2Ni_2$: C, 33.4; H, 6.68; N, 8.99. Found: C, 33.1; H, 6.62; N, 9.11%. Selected IR data (cm^{-1}, KBr pellet): 3618 (m), 3536 (m), 3470 (m), 3352 (m), 3019 (m), 2887 (m), 2904 (m), 2904 (m), 2815 (w), 1698, 1647 (m, HOH bendings), 1553 (vs, tp $\nu_a(CO_2^-)$), 1513 (m), 1477 (s), 1450 (s), 1411 (vs, tp $\nu_s(CO_2^-)$), 1306 (m), 1285 (w), 1244 (w), 1127, 1079 (vs, Cl–O stretchings), 1019 (m), 988 (m), 936 (m), 889 (w), 855 (m), 801 (w), 755 (m), 623 (m), 520 (m). UV–Vis (MeOH) [λ_{max}, nm (M^{-1} cm^{-1})]: 238 (5510), 388 (114), 636 (47), 1056 (22).

2.3. Preparation of $[Ni_2(pmdtn)_2(tp)(N_3)_2](H_2O)_4$ (2)

To a 10 ml aqueous solution of nickel(II) nitrate hexahydrate (2.0 mmol) was added an aqueous solution (10 ml) of pmdtn (2.0 mmol) and potassium tp (1.0 mmol) with stirring. Green precipitates immediately formed which were redissolved by adding methanol (10 ml) and then treated with sodium azide (1.0 mmol). The filtrate of the resulting solution was allowed to stand for several days, providing green crystals of **2** in a yield of 60% based on Ni. *Anal*. Calc. for $C_{26}H_{58}N_{12}O_8Ni_2$: C, 39.8; H, 7.45; N, 21.4. Found: C, 39.3; H, 7.31; N, 21.0%. Selected IR data (cm^{-1}, KBr pellet): 3500 (m), 3452 (m), 2980 (w), 2890 (w), 2846 (w), 2041 (vs, $\nu_a(N_3^-)$), 1645, 1620 (w, HOH bendings), 1550 (s, tp $\nu_a(CO_2^-)$), 1516 (w), 1465 (m), 1414 (s, tp $\nu_s(CO_2^-)$), 1292 (w), 1248 (w), 1177 (w), 1154 (w), 1130 (w), 1102 (w), 1044 (w), 1026 (m), 990 (w), 943 (w), 900 (w), 882 (w), 851 (m), 802 (m), 781 (w), 751 (m), 510 (m), 391 (w). UV–Vis (MeOH) [λ_{max}, nm (M^{-1} cm^{-1})]: 234 (2080), 384 (151), 640 (51), 1068 (24). The reaction of **1** with one or two equiv of sodium azide in water-methanol (1:1 v/v) solvent yielded an identical product to **2**.

2.4. Physical measurements

Elemental analyses for C, H and N were performed at the Elemental Analysis Service Center of the Korea Basic Science Institute. Infrared spectra were obtained from KBr pellets with an EQUINOX 55 spectrometer. Electronic spectra were obtained and manipulated by using a Shimadzu UV-3100S spectrophotometer. Magnetic susceptibilities for **1** and **2** were carried out using a Quantum Design MPMS-7 SQUID susceptometer. Diamagnetic corrections were estimated from Pascal's tables.

2.5. Crystallographic data collection and structure determination

Data were collected at 293 K using an Enraf-Nonius CAD4TSB diffractometer with graphite monochromated Mo Kα radiation ($\lambda = 0.71073$ Å) in the $\omega/2\theta$ scan mode. The unit cell parameters were calculated by least-squares refinement of 25 well-centered reflections. All data were corrected for Lorentz polarization effects. A total of 3501 (**1**) and 2731 (**2**) reflections with the maximum 2θ of 49.94° (**1** and **2**) were measured, and 2361 (**1**) and 2024 (**2**) reflections were assumed to be observed applying the condition $F_o > 4\sigma(F_o)$. Crystallographic data and details of data collection are listed in Table 1.

The structures were solved with the SIR-92 program and refined by least-squares analysis using anisotropic thermal parameters for non-hydrogen atoms with the SHELXL-93 program [11,12]. H atoms were calculated at idealized positions ($d_{CH} = 0.970$ Å for methylene, 0.960 Å for methyl and 0.930 Å for phenyl) and refined riding on the corresponding carbon atoms with isotropic thermal parameters [$U = 1.2U(C_{methylene})$, $1.5U(C_{methyl})$ and $1.2U(C_{phenyl})$]. The goodness-of-fit for all observed reflections was 1.178 (**1**) and 1.092 (**2**). Maximum and minimum peaks in the final difference synthesis were

Table 1
Crystallographic data

	1	**2**
Chemical formula	$C_{26}H_{62}N_6O_{18}Cl_2Ni_2$	$C_{26}H_{58}N_{12}O_8Ni_2$
Formula weight	935.14	784.26
Crystal system	monoclinic	monoclinic
Space group	$P2_1/c$	$P2_1/n$
a (Å)	12.438(1)	9.161(2)
b (Å)	11.570(2)	14.784(1)
c (Å)	15.234(3)	13.827(1)
β (°)	106.15(1)	90.33(1)
V (Å^3)	2105.9(5)	1872.7(5)
Z	4	4
$F(000)$	988	836
D_{calc} (g cm^{-3})	1.475	1.391
μ (mm^{-1})	1.096	1.065
T (K)	293(2)	293(2)
Maximum 2θ (°)	49.94	49.94
Index range	$+h, +k, \pm l$	$-h, -k, \pm l$
Total reflections	3501	2731
Observed reflections[a]	2361	2024
Number of parameters	244	217
R_1[b]	0.0550	0.0497
wR_2[c]	0.1223	0.1135
$\Delta\rho_{max}$, $\Delta\rho_{min}$ (e Å^{-3})	0.714, −0.297	0.742, −0.529

[a] $F_o > 4\sigma(F_o)$.
[b] $R_1 = \sum ||F_o| - |F_c|| / \sum |F_o|$.
[c] $wR_2 = \left[\sum w(F_o^2 - F_c^2)^2 / \sum w(F_o^2)^2\right]^{1/2}$.

0.714 and −0.297 e Å^{-3} for **1**, 0.742 and −0.529 e Å^{-3} for **2**, respectively.

3. Results and discussion

3.1. Syntheses and characterization

Compound **1** was prepared by the reaction of the Ni(II) ion with a mixture of pmdtn as a capping ligand and dicarboxylate dianion as a bridging ligand. In the IR spectrum of **1**, the most interesting features are the COO stretching bands occurring at 1563 and 1411 cm^{-1}. The binding modes of carboxylate ligands can be assessed on the basis of the difference (Δ) between asymmetric stretching $\nu_a(CO_2^-)$ and symmetric stretching $\nu_s(CO_2^-)$. Accordingly, the calculated Δ value of 152 cm^{-1}, which is compared with the value ($\Delta = 170$ cm^{-1}) of potassium tp, allows one to assume the bridging mode of the tp ligand as bidentate [13]. It appears that the broad bands in the O–H region show the presence of hydrogen bonds. In the UV–Vis spectrum, the strong absorption at 238 nm ($\varepsilon = 5510$ M^{-1} cm^{-1}) can be assigned to the charge transfer transition. The other three bands are associated with the spin-allowed transitions from the $^3A_{2g}$ ground state to the excited triplet states: $^3A_{2g}$ (F) $\rightarrow$ $^3T_{1g}$ (P) for 388 nm ($\varepsilon = 114$ M^{-1} cm^{-1}), $^3A_{2g}$ (F) $\rightarrow$ $^3T_{1g}$ (F) for 636 nm ($\varepsilon = 47$ M^{-1} cm^{-1}), and $^3A_{2g}$ (F) $\rightarrow$ $^3T_{2g}$ (P) for 1056 nm ($\varepsilon = 22$ M^{-1} cm^{-1}). The magnitude of the absorptions in the d-d transitions is stronger than that of $Ni(H_2O)_6^{2+}$, indicating that the geometry about the nickel center can be described as a distorted octahedron [14]. From the Tanabe-Sugano diagram, values of 10 Dq and B (Racah parameter) are estimated to be 9820 and 727 cm^{-1}, respectively. The β value, defined as $\beta = B_{complex}/B_{gaseous}$, demonstrates that there is a reduction to 70% of the free ion value for interelectronic repulsion, due to some degree of covalency of the metal-ligand bond.

The further reaction of **1** with one or two equiv of sodium azide produced the binuclear compound **2** where the coordinated water molecules are replaced by the azide ligands. It is evident that **2** is very stable since **2** is exclusively formed regardless of the amount of sodium azide used. In situ generated **1** also leads to the formation of **2** in the presence of sodium azide. The IR spectrum of **2** is distinguished from that of **1** due to the existence of the stretching frequency of the azide ligand instead of the perchlorate anion. In addition, the disappearance of the peak occurring at 3618 cm^{-1} that can be assigned to the coordinated water molecules implies the coordination of the azide ligands to the nickel centers. The UV–Vis spectrum of **2** is analogous to that of **1**. The assignment of each band is as follows: the charge transfer transition for 234 ($\varepsilon = 2080$ M^{-1} cm^{-1}), $^3A_{2g}$ (F) $\rightarrow$ $^3T_{1g}$ (P) for 384 nm ($\varepsilon = 151$ M^{-1} cm^{-1}), $^3A_{2g}$ (F) $\rightarrow$ $^3T_{1g}$ (F) for 640 nm ($\varepsilon = 51$ M^{-1} cm^{-1}), and $^3A_{2g}$ (F) $\rightarrow$ $^3T_{2g}$ (P) for 1068 nm ($\varepsilon = 24$ M^{-1} cm^{-1}). The estimated 10 Dq value of 10 600 cm^{-1} designates that the effect of the ligand field on the complex formation in **2** is stronger than that of **1**. The β value of 85% can be derived from a B value of 881 cm^{-1}.

3.2. Description of the structures

A perspective view of **1** with the atom-numbering scheme is shown in Fig. 1. Selected bond distances and angles are reported in Table 2. The Ni1 atom is in a distorted octahedral arrangement comprising three nitrogen atoms of the pmdtn ligand [Ni1–N1 = 2.141(4) Å, Ni1–N2 = 2.132(4) Å, and Ni1–N3 = 2.143(4) Å], two oxygen atoms of the tp bridge [Ni1–O2 = 2.113(3) Å and Ni1–O3 = 2.178(4) Å] and one oxygen atom of a water

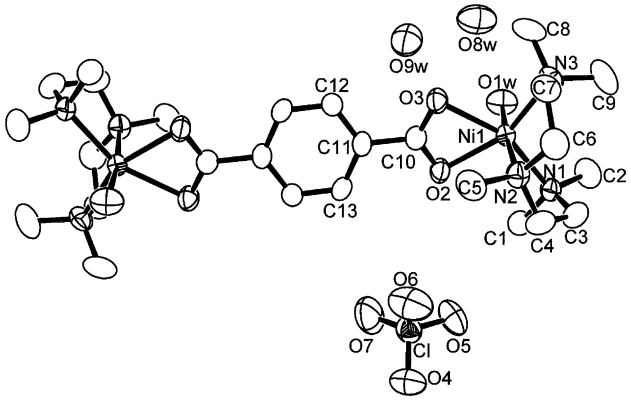

Fig. 1. Molecular structure of **1** with the atom numbering scheme.

Table 2
Selected bond distances (Å) and angles (°) for **1**

Bond lengths			
Ni1–O1W	2.074(4)	Ni1–O2	2.113(3)
Ni1–N2	2.132(4)	Ni1–N1	2.141(4)
Ni1–N3	2.143(4)	Ni1–O3	2.178(4)
Ni1–C10	2.468(5)	O2–C10	1.247(6)
O3–C10	1.271(6)		
Bond angles			
O1W–Ni1–O2	89.8(2)	O1W–Ni1–N2	173.7(2)
O2–Ni1–N2	93.5(2)	O1W–Ni1–N1	89.8(2)
O2–Ni1–N1	95.25(15)	N2–Ni1–N1	84.6(2)
O1W–Ni1–N3	94.3(2)	O2–Ni1–N3	154.5(2)
N2–Ni1–N3	85.0(2)	N1–Ni1–N3	109.9(2)
O1W–Ni1–O3	91.5(2)	O2–Ni1–O3	61.29(13)
N2–Ni1–O3	94.8(2)	N1–Ni1–O3	156.49(15)
N3–Ni1–O3	93.4(2)	O1W–Ni1–C10	91.4(2)
O2–Ni1–C10	30.4(2)	N2–Ni1–C10	94.1(2)
N1–Ni1–C10	125.6(2)	N3–Ni1–C10	124.2(2)
O3–Ni1–C10	30.95(15)	C3–N1–Ni1	105.2(3)
C1–N1–Ni1	109.5(3)	C2–N1–Ni1	117.1(4)
C6–N2–Ni1	106.2(3)	C4–N2–Ni1	104.8(3)
C5–N2–Ni1	115.9(3)	C9–N3–Ni1	118.8(4)
C8–N3–Ni1	110.4(4)	C7–N3–Ni1	101.1(3)
C10–O2–Ni1	90.8(3)	C10–O3–Ni1	87.2(3)
O2–C10–O3	120.7(5)	O2–C10–Ni1	58.9(3)
O3–C10–Ni1	61.8(3)	C11–C10–Ni1	174.3(4)

molecule [Ni1–O1w = 2.074(4) Å]. The O2, O3, N1 and N3 atoms constitute the equatorial plane in which the small bite angle of the carboxylate group [O2–Ni1–O3 = 61.29(13)°] gives the main distortion on the octahedral geometry, while the axial positions are filled by the O1w and N2 atoms. The bite angle in **1** is slightly more acute than that (61.9(1)°) reported for $[Ni_2(tp)(bpy)_4](ClO_4)_2$ (bpy = 2,2′-bipyridine), indicating that the octahedron around the Ni atom in **1** is rather more distorted [10]. The tp ligand behaves as a bidentate ligand as expected from the IR data. The dihedral angle between the carboxylate group and the benzene ring of the tp ligand is 14.2°. The intradimer Ni···Ni distance is 10.713 Å.

Hydrogen bonds make the binuclear entity extend toward a higher dimensional system. In **1**, the coordinated water molecule (O1w) undergoes hydrogen bonding to the perchlorate oxygen atom (O6a; a = $1-x, 0.5+y, 0.5-z$) with a distance of 2.850 Å and then the other oxygen atom (O5b; b = $1-x$, $-0.5+y, 0.5-z$) of the anion forms a hydrogen bond to the lattice water oxygen atom (O9w) [O5b··· O9w = 2.902 Å]. The O9w atom is additionally hydrogen-bonded to the carboxylate oxygen atom (O3) [O9w···O3 = 2.768 Å]. The resulting structural overview can be described as a ladder-like array running along the *b*-axis as illustrated in Fig. 2(a). Linkage between the 1D arrays is formed by taking into account that the O1w atom has another hydrogen bond to the lattice water atom (O8w) [O1w···O8w = 2.692 Å] that is close to the other lattice water oxygen (O9wc; c = $-x, -y, -z$) with a distance of 2.749 Å. Consequently, these hydrogen bonds fabricate a 2D network as shown in Fig. 2(b) in the *ca*-plane. The shortest intermolecular distance of Ni···Ni is 8.155 Å.

The molecular structure of **2** resembles that of **1** except the absence of the perchlorate anions and the coordinated water molecules are replaced by the azido groups (Fig. 3). Selected bond distances and angles are reported in Table 3. Each nickel atom adopts a distorted octahedral coordination sphere. The equatorial plane is composed of two oxygen atoms of the tp ligand [Ni1–O1 = 2.187(4) Å and Ni1–O2 = 2.186(3) Å] with a small bite angle of 60.23(13)° and two nitrogen atoms of the pmdtn ligand [Ni1–N1 = 2.135(4) Å and Ni1–N3 = 2.145(5) Å]. The dihedral angle between the carboxylate group and benzene ring of the tp bridge is 21.5°, larger than that of **1**. The intradimer distance of Ni···Ni is 10.800 Å, slightly longer than that of **1**.

As found in **1**, there are plenty of hydrogen bonds in the lattice of **2**. The oxygen atom (O1a; a = $-0.5+x, 0.5-y, 0.5+z$) of the carboxylate group of the tp bridge is connected via a hydrogen bond to the oxygen atom (O4w) of the lattice water molecule [O1a···O4w = 2.892 Å] that is also linked to the other lattice water oxygen atom (O3w) [O3w···O4wb = 2.830 Å; b = $0.5-x, 0.5+y, 1.5-z$]. This lattice water (O3w) is connected to the carboxylate oxygen atom (O2) of the other binuclear entity [O3w···O2b = 2.868 Å] and the nitrogen atom (N4) of another binuclear unit [O3w···N4c = 2.934 Å; c = $-x, 1-y, 1-z$]. In this way, these hydrogen bonds construct a 3D network system as seen in Fig. 4. The shortest intermolecular distance of Ni···Ni is 7.707 Å, shorter than that of **1**.

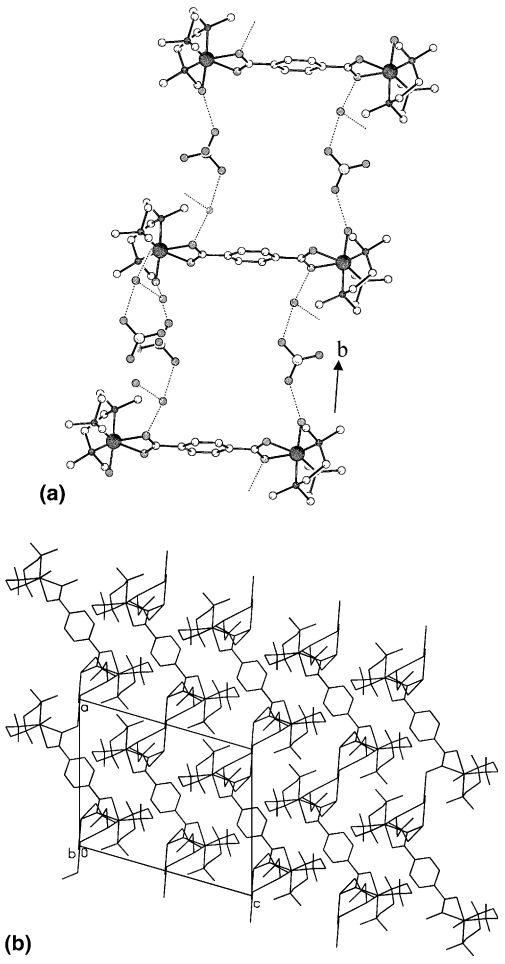

Fig. 2. View of the 2D array (a) along the *b*-axis and (b) in the *ca*-plane.

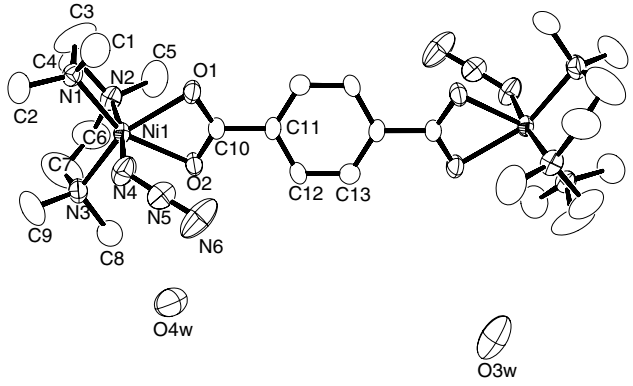

Fig. 3. Molecular structure of **2** with the atom numbering scheme.

Table 3
Selected bond distances (Å) and angles (°) for **2**

Bond lengths			
Ni1–N4	2.063(5)	Ni1–N2	2.129(4)
Ni1–N1	2.135(4)	Ni1–N3	2.145(5)
Ni1–O2	2.186(3)	Ni1–O1	2.187(4)
Ni1–C10	2.515(5)	O1–C10	1.264(6)
O2–C10	1.264(6)		
Bond angles			
N4–Ni1–N2	173.3(2)	N4–Ni1–N1	92.3(2)
N2–Ni1–N1	84.4(2)	N4–Ni1–N3	91.8(2)
N2–Ni1–N3	84.0(2)	N1–Ni1–N3	109.7(2)
N4–Ni1–O2	92.0(2)	N2–Ni1–O2	93.5(2)
N1–Ni1–O2	154.23(15)	N3–Ni1–O2	95.54(15)
N4–Ni1–O1	92.1(2)	N2–Ni1–O1	93.9(2)
N1–Ni1–O1	94.23(15)	N3–Ni1–O1	155.6(2)
O2–Ni1–O1	60.23(13)	N4–Ni1–C10	90.2(2)
N2–Ni1–C10	96.4(2)	N1–Ni1–C10	124.4(2)
N3–Ni1–C10	125.7(2)	O2–Ni1–C10	30.18(14)
O1–Ni1–C10	30.18(14)	C2–N1–Ni1	118.6(4)
C3–N1–Ni1	103.6(3)	C1–N1–Ni1	109.3(4)
C6–N2–Ni1	106.1(4)	C5–N2–Ni1	116.1(4)
C4–N2–Ni1	106.5(3)	C8–N3–Ni1	108.6(4)
C9–N3–Ni1	117.1(4)	C7–N3–Ni1	105.5(4)
N5–N4–Ni1	121.5(4)	C10–O1–Ni1	89.4(3)
C10–O2–Ni1	89.5(3)	O1–C10–O2	120.3(5)
O1–C10–Ni1	60.4(3)	O2–C10–Ni1	60.4(2)
C11–C10–Ni1	174.0(4)		

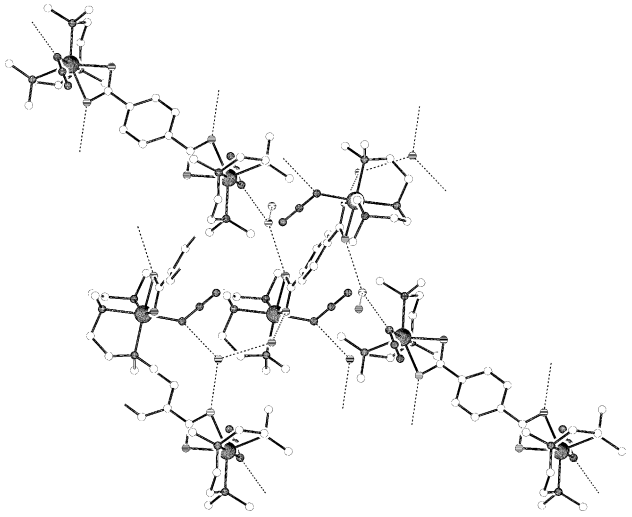

Fig. 4. Perspective view of the 3D network in **2** with hydrogen bonds.

3.3. Magnetic results

The variable temperature magnetic susceptibility data were measured for **1** in the temperature range 5–300 K. Plots of χ_m and the $\chi_m T$ product versus temperature are presented in Fig. 5. At 300 K, the value of $\chi_m T$ is 2.38 cm^3 K mol^{-1}, which falls in the normal range of two non-coupled Ni(II) ions. On cooling, the $\chi_m T$ value decreases continuously, finally reaching a value of 2.06

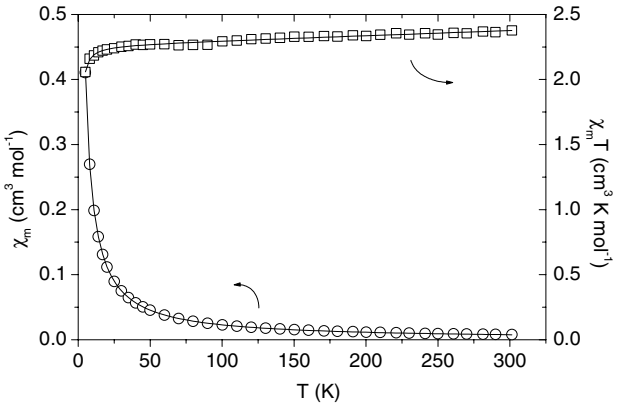

Fig. 5. Plots of χ_m and $\chi_m T$ vs. T for **1**. The solid line shows the best theoretical fit.

m^3 K mol^{-1} at 5 K, suggesting the presence of an antiferromagnetic interaction. A quantitative analysis can be performed on the basis of a spin Hamiltonian $H = -JS_1 \cdot S_2 - D(S_{1z}^2 + S_{2z}^2)$, where D is the zero-field parameter [15]. The experimental data were fitted including the temperature-independent paramagnetism (TIP). Least-squares fitting of the magnetic data gives parameters of $g = 2.12$, $J = -0.18$ cm^{-1}, $D = -2.4$ cm^{-1} and TIP = 0.00039 cm^3 mol^{-1}. The measure of the goodness-of-fit R, defined as $R = [\Phi/(n-k)]^{1/2}$ where n is the number of data points, k is the number of parameters, and $\Phi = \sum[(\chi_m T)_i^{obs} - (\chi_m T)_i^{calc}]^2$, is equal to 7.0×10^{-5}. The J value consistent with the reported value ($J = -0.6$ cm^{-1}) for the nickel dimer bridged by the tp ligand indicates the presence of a weak antiferromagnetic interaction, which is operating via the extended tp ligand [16]. As seen in Fig. 6, the $\chi_m T$ plot of **2** is similar to that of **1**. Magnetic data were fitted using the same equation as **1**, affording magnetic parameters of $g = 2.18$, $J = -0.02$ cm^{-1}, $D = -2.4$ cm^{-1} and TIP = 0.00041 cm^3 mol^{-1} with $R = 2.7 \times 10^{-4}$. The tp ligand in **2** mediates a weaker antiferromagnetic coupling than that in **1**.

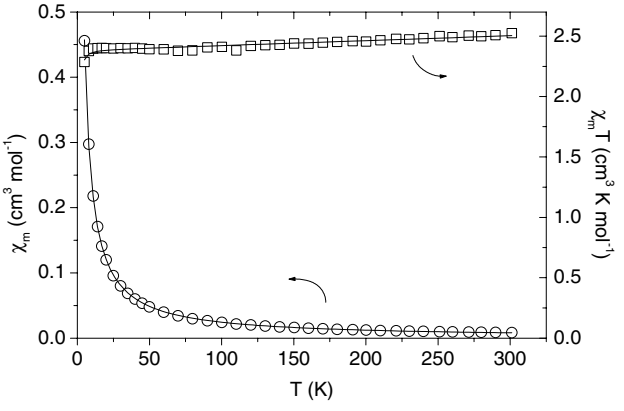

Fig. 6. Plots of χ_m and $\chi_m T$ vs. T for **2**. The solid line presents the best theoretical fit.

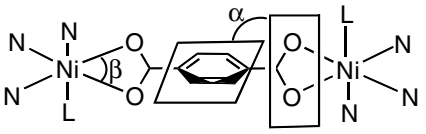

Scheme 1.

Table 4
Magnetic and structural parameters for tp-bridged Ni(II) binuclear complexes

Compound	α (°)	β (°)	d_{Ni-Ni} (Å)	J (cm^{-1})
1	14.2	61.29	10.731	−0.18
2	21.5	60.23	10.800	−0.02
$[Ni_2(bpy)_4(tp)](ClO_4)_2$[a]	5.2	61.9	9.449	−0.6

[a] Refs. [10,16].

It is worth comparing the magnetic properties of **1** and **2**. The magnetic orbitals on the nickel(II) centers that are parallel to the basal plane can be propagated through the tp unit. The magnitude of the magnetic exchange for **1** and **2** likely depends on three factors observed in the structure (Scheme 1): the bite angle (β), the dihedral angle (α), and the intramolecular distance between Ni···Ni (d_{Ni-Ni}). The first factor (β) is related to the orientation of the magnetic orbitals that are delocalized more effectively over the oxygen atoms of the tp ligand when the bite angle is closer to 90°. It is known that the greater the dihedral angle (α) and metal–metal separation (d_{Ni-Ni}) are, the weaker the magnetic interaction between metal centers would be [16]. From the structural parameters, **1** has the larger β, the smaller α, and the shorter d_{Ni-Ni} than **2**. On these criteria, as summarized in Table 4, it is reasonably understood that the magnetic interaction of **1** is stronger than that of **2**.

4. Supplementary material

Crystallographic data for the structural analysis have been deposited with the Cambridge Crystallographic Data Center, CCDC Nos. 229699 and 229700 for complexes **1** and **2**, respectively. Copies of this information may be obtained free of charge from The Director, CCDC, 12 Union Road, Cambridge CB2 1EZ, UK (fax: +44-1223-336-033; email: deposit@ccdc.cam.ac.uk or http://www.ccdc.cam.ac.uk).

Acknowledgements

This work is supported by the Korea Research Foundation (Grant No. KRF-2003-003-C00073).

References

[1] O. Kahn, Acc. Chem. Res. 33 (2000) 647.
[2] E. Coronado, F. Palacio, J. Veciana, Angew. Chem. Int. Ed. 42 (2003) 2570.
[3] C.E. Xanthopoulos, M.P. Sigalas, G.A. Katsoulos, C.A. Tsipis, A. Terzis, M. Mentzafos, A. Hountas, Inorg. Chem. 32 (1993) 5433.
[4] K.-S. Burger, P. Chaudhuri, K. Wieghardt, B. Nuber, Chem. Eur. J. 1 (1995) 583.
[5] L. Yang, F. Bian, S. Yan, D. Liao, P. Cheng, Z. Jiang, Inorg. Chem. Commun. 6 (2003) 1188.
[6] L. Deakin, A.M. Arif, J.S. Miller, Inorg. Chem. 38 (1999) 5072.
[7] C.S. Hong, Y. Do, Inorg. Chem. 36 (1997) 5684.
[8] T.-B. Lu, H. Xiang, R.L. Luck, Z.-W. Mao, X.-M. Chen, L.-N. Ji, Inorg. Chim. Acta 355 (2003) 229.
[9] K.-Y. Choi, K.M. Chun, I.-H. Suh, Polyhedron 20 (2001) 57.
[10] Z.-L. Deng, J. Shi, Z.-H. Jiang, D.-Z. Liao, S.-P. Yan, G.-L. Wang, Polyhedron 11 (1992) 885.
[11] A. Altomare, G. Cascarano, C. Giacovazzo, A. Guagliardi, M.C. Burla, G. Polidor, M.J. Camallio, J. Appl. Cryst. 27 (1994) 435.
[12] G.M. Sheldrick, SHELXL-93: User Guides, University of Göttingen, Göttingen,Germany, 1993.
[13] K. Nagamoto, Infrared and Raman Spectra of Inorganic and Coordination Compounds. Part B: Applications in Coordination, Organometallic and Bioinorganic Chemistry, 5th ed., Wiley, New York, 1997, p. 59.
[14] B.N. Figgis, Introduction to Ligand Fields, Wiley, New York, 1966, p. 220.
[15] G. De Munno, M. Julve, F. Lloret, A. Derory, J. Chem. Soc., Dalton Trans. (1993) 1179.
[16] J. Cano, G. De Munno, J.L. Sanz, R. Ruiz, J. Faus, F. Lloret, M. Julve, A. Caneschi, J. Chem. Soc., Dalton Trans. (1997) 1915.

Available online at www.sciencedirect.com
SCIENCE DIRECT®
Polyhedron 23 (2004) 1385–1392
POLYHEDRON
www.elsevier.com/locate/poly

Synthesis, characterization and bio-activity of metal complexes of bidentate N–S isomeric Schiff bases derived from *S*-methyldithiocarbazate (SMDTC) and the X-ray structure of the bis[*S*-methyl-β-*N*-(2-furyl-methylketone) dithiocarbazato]cadmium(II) complex

Kar-Beng Chew [a], M.T.H. Tarafder [a,1], Karen A. Crouse [a,*], A.M. Ali [b], B.M. Yamin [c], H.-K. Fun [d]

[a] *Department of Chemistry, Universiti Putra Malaysia, 43400 Serdang, Selangor, Malaysia*
[b] *Laboratory of Molecular and Cell Biology, Institute of Bioscience, Universiti Putra Malaysia, 43400 Serdang, Selangor, Malaysia*
[c] *School of Chemical Sciences and Food Technology, Universiti Kebangsaan Malaysia, 43600 Bangi, Selangor, Malaysia*
[d] *X-ray Crystallography Unit, School of Physics, Universiti Sains Malaysia, 11800 Minden, Penang, Malaysia*

Received 4 November 2003; accepted 19 February 2004
Available online 10 April 2004

Abstract

Condensation of SMDTC with 2-furyl-methylketone and 5-methyl-2-furaldehyde gave isomeric Schiff bases, (NS) and (NS′). The metal complexes of these uninegatively charged bidentate Schiff base ligands with cadmium, tin, iron, lead and cobalt have been prepared. The complexes have been characterized by a variety of physico-chemical techniques. X-ray crystallographic analysis shows that the Cd(II) complex, bis[*S*-methyl-β-*N*-(2-furylmethylketone)dithiocarbazato]cadmium(II), consists of two molecules with distorted octahedral structure. The Co(II) complexes are paramagnetic with a square-planar stereochemistry. The diamagnetic Sn(II), Fe(III) and Pb(II) complexes also have square-planar structures while the diamagnetic $[Cd(NS')_2]\cdot 3H_2O$ complex is tetrahedral. The $[Cd(NS')_2]\cdot 3H_2O$, $[Sn(NS)_2]$ and $[Co(NS)_2]$ showed clear inhibition of almost all bacteria and fungi tested However, $[Cd(NS)_2]$, $[Fe(NS)]Cl_2$, $[Pb(NS)_2]$ and $[Pb(NS')_2]$ were inactive against all bacteria assayed while $[Cd(NS)_2]$, $[Fe(NS)]Cl_2$ and $[Pb(NS)_2]$ showed clear inhibition of some fungi. The $[Cd(NS)_2]$, $[Cd(NS')_2]\cdot 3H_2O$ and $[Co(NS)_2]$ were found to be very active against Human cell T-lymphoblastic leukemia (CEM-SS) and cervical cancer cells (HELA) with CD_{50} values between 1.8 and 3.6 $\mu l\,cm^{-3}$.
© 2004 Elsevier Ltd. All rights reserved.

Keywords: *S*-methyldithiocarbazate (SMDTC); NS Schiff base; Crystal structure of Cd(II) complex; Dithiocarbazate derivatives

1. Introduction

Dithiocarbazate, $NH_2NHCS_2^-$, and its substituted derivatives have been synthesized and investigated over the past few decades [1–12]. Dithiocarbazic acid and the Schiff bases derived from its *S*-alkyl and aryl esters form an interesting series of ligands and metal complexes. Researchers in this area have been continuing the syntheses of new nitrogen–sulfur donor ligands through Schiff base condensation with various aldehydes and ketones. The number of ligands synthesized continues to increase because of the intriguing observation that different ligands show different biological properties, although they may differ only slightly in their molecular structures [1,4]. Indeed, carcinostatic activities have already been found for some metal complexes of dithiocarbazic acid and some Schiff bases derived from its *S*-methyl ester [3]. As part of our ongoing study of Schiff bases derived from dithiocarbazate, we report herein the

* Corresponding author. Tel.: +60-3-8946-6788; fax: +60-3-8943-5380.
E-mail address: crouse@pc.jaring.my (K.A. Crouse).
[1] Present address: Department of Chemistry, Rajshahi University, Rajshahi-6205, Bangladesh.

0277-5387/$ - see front matter © 2004 Elsevier Ltd. All rights reserved.
doi:10.1016/j.poly.2004.02.018

coordination chemistry and bioactivity of some transition and non-transition metal complexes containing nitrogen–sulfur donor SMDTC derivatives.

2. Experimental

2.1. Preparation of S-methyldithiocarbazate (SMDTC)

This compound was synthesized as previously reported [10]. Potassium hydroxide (22.8 g, 0.4 mol) was dissolved completely in 90% ethanol (140 ml) and the mixture was cooled in ice. To the mixture, hydrazine hydrate (20 g, 0.4 mol) was added slowly with stirring. Carbon disulfide (30.4 g, 0.4 mol) was then added dropwise with vigorous stirring. The temperature of the reaction mixture was not allowed to rise above 6 °C during the period of addition of carbon disulfide. The resulting yellow oil was separated by means of a separatory funnel and dissolved in 40% ethanol (40 ml) and the solution was cooled in ice. Methyl iodide (58 g, 0.4 mol) was added slowly with vigorous stirring. The white product was separated by filtration, washed with water and dried in air. The crude product was recrystallized from ethanol. Yield, 20 g (40%). The melting point was 81 °C (Lit. 81–82 °C) [10].

2.2. General method for preparation of the Schiff bases

The Schiff bases were synthesized as previously reported [11]. SMDTC (0.2 mol) was dissolved in absolute ethanol (35 ml). To this solution was added an aldehyde or ketone, also in absolute ethanol (30 ml). The mixture was heated while being stirred for 15 min and later allowed to stand for 20 min. The precipitate was filtered and dried over silica gel. Crude products were recrystallized from ethanol.

2.3. General method for preparation of the metal complexes

Schiff base (0.2 mol) in 40 ml of absolute ethanol was added to a solution containing a stoichiometric amount of metal salt in absolute ethanol (40 ml). The mixture was heated while being stirred. The precipitate was filtered, washed with ice-cold alcohol and dried over silica gel. The yield and melting point of each product was determined. The metal salts used were $Cd(CH_3COO)_2 \cdot 2H_2O$, $SnCl_2$, $FeCl_3$, $Pb(CH_3COO)_2 \cdot 3H_2O$ and $CoCl_2 \cdot 6H_2O$.

2.4. Physical measurements

Carbon, hydrogen, nitrogen and sulfur analyses were carried out using a LECO CHNS-932 instrument. The IR spectra were recorded as KBr pellets, in the 4000–400 cm^{-1} region, on a Perkin–Elmer 1750X FTIR spectrometer. Metal determinations were carried out using a Perkin–Elmer Plasma 1000 Emission Spectrometer. The molar conductances of 10^{-3} M solutions of the metal complexes in DMSO were measured at 30 °C using a Jenway 4310 conductivity meter and a dip-type cell with platinized electrode. The UV–Vis spectra were run on a Shimadzu UV-2501 PC spectrophotometer (900–200 nm). Melting points were determined using an Electrothermal digital melting point apparatus. Magnetic susceptibility measurements were carried out using a Sherwood Scientific MSB-AUTO magnetic susceptibility balance at 298 K.

2.5. X-ray structure determination

Beautiful yellow crystals of the Cd(II) complex formed when the dimethylsulfoxide (DMSO) solution was allowed to slowly evaporate for a couple of weeks. The selected crystal of the Cd(II) complex was mounted on a SMART CCD diffractometer at the X-ray Crystallography Unit, School of Physics, University of Science Malaysia (USM). Reflection data were measured at 20 °C using graphite monochromated Mo Kα ($\lambda = 0.71073$ Å) radiation with a detector distance of 4 cm and a swing angle of −35°. The data collected were reduced using a program SAINT [13] and a multi-scan absorption correction was carried out using SADABS [14]. The structure was solved using direct methods and refined using the full-matrix least-squares methods on F^2_{obs} using the SHELXTL [15] software package. The non-H atoms were anisotropically refined. The hydrogen atoms were located by difference syntheses and later were fixed geometrically and allowed to ride on their parent C atoms, with C–H = 0.93–0.96 Å. The molecular graphics were created using SHELXTL. Atomic scattering factors and anomalous dispersion correction were taken from the International Table for X-ray crystallography [16].

2.6. Bioactivity

2.6.1. Qualitative antimicrobial assay

Eight pathogenic microbials were used to test the biological potential of the compounds: (i) Methicillin resistant *staphylococcus* (MRSA), (ii) *Bacillus subtilis* wild type (B29), (iii) *Bacillus subtilis* mutant defective DNA repair (B28), (iv) *Pseudomonas aeruginosa* (60690), (v) *Candida albicans* (CA), (vi) *Aspergillus ochraceous* (398), (vii) *Saccharomyces cerevisiae* (20341) and (viii) *Candida lypolytica* (2075). The sources of microbes and culture maintenance were as previously described [17]. The antimicrobial activity of each compound was determined qualitatively through the modified disc diffusion method [18]. A lawn of microorganisms was prepared by pipetting and evenly spreading 10 μl of inoculum (adjusted turbidometrically to 10^5–10^6 CFU/cm^3; CFU, colony forming units) onto agar set in petri

dishes. Nutrient agar (NA) was used for bacteria while potato dextrose agar (PDA) was used for fungi. Filter paper discs (Whatman No. 1) measuring 6mm in diameter were impregnated with dimethylsulfoxide (DMSO) stock solution of the compounds (100 mg/cm^3) and dried under sterile conditions. The dried discs were then placed on the previously inoculated agar surface. The plates were inverted and incubated for 24 h at 37 °C for the bacteria and 30 °C for the fungi. Antimicrobial activity was indicated by the presence of clear inhibition zones around the discs.

2.6.2. Quantitative antimicrobial assay

Compounds that showed positive antimicrobial activity with the disc diffusion assay were subjected to the broth dilution method for the qualitative measurement of microbiostatic (inhibitory) activity as described by Hufford and Clark [19]. The lowest concentration that completely inhibited visible microbial growth was recorded as the minimum inhibitory concentration (MIC, μg/ml). Streptomycin and nystatin (Sigma, USA) were used as positive controls for bacteria and fungi, respectively.

2.6.3. Cytotoxic assay

Two types of cell line were used, CEM-SS (Human cell T-lymphoblastic leukemia) and HELA (cervical cancer cells). The CEM-SS and HELA cell lines were obtained from the National Cancer Institute, USA. Cytotoxicity was evaluated using MTT (3-[4,5-dimethylthiazo-2-yl]-2,5-diphenyltetrazolium bromide) (Sigma, USA) assay following Mosmann's method [17] as previously reported [12]. Cytotoxicity is shown as the minimum concentration required to reduce the absorbance of treated cells by 50% with reference to the untreated cells (CD_{50}). Doxorubicin and tamoxifen were used as cytotoxic standards.

3. Results and discussion

Condensation of SMDTC with 2-furyl-methylketone (NS) and 5-methyl-2-furaldehyde (NS′) gave the isomeric uninegatively charged bidentate Schiff bases. These coordinated with metal ions through the thiolo sulfur and the azomethine nitrogen as reported previously [11].

Analytical data and yields for the Schiff bases and their metal complexes are given in Table 1. Significant IR bands of the Schiff bases and their metal complexes are given in Table 2. The absence of ν(S–H) absorbance at ca. 2570 cm^{-1} in the spectrum of the Schiff bases indicates that in the solid state, they exist primarily in the thione form. These thione groups are relatively unstable in the monomeric form and tend to convert to the more stable thiolo forms by enethiolization in solution [2]. The ^{1}H NMR spectra of the Schiff bases in DMSO

Table 1
Analytical data for the Schiff bases and their complexes

Compound	Color	m.p. (°C)	Found (Calc.) (%)					Yield (%)
			C	H	N	S	M	
NS[a] (**1**)	Orange	123.7	44.71 (44.86)	4.86 (4.67)	13.55 (13.08)	29.75 (29.91)		80.6
NS′[a] (**2**)	Light yellow	130.4	44.80 (44.86)	4.89 (4.67)	13.60 (13.08)	29.46 (29.91)		85.3
$[Cd(NS)_2]$ (**3**)	Orange	187.0	35.77 (35.65)	3.27 (3.37)	10.31 (10.39)	24.48 (23.79)	20.58 (20.86)	60.5
$[Cd(NS')_2]\cdot 3H_2O$ (**4**)	Yellow	202.9	32.07 (32.40)	3.83 (4.080)	9.68 (9.448)	21.62 (21.63)	18.39 (18.96)	56.8
$[Sn(NS)_2]$ (**5**)	Yellow	171.5	35.49 (35.24)	3.64 (3.332)	9.86 (10.27)	23.09 (23.52)	21.26 (21.77)	62.8
$[Sn(NS')_2]\cdot 3H_2O$ (**6**)	Yellow	232.8	31.40 (32.07)	4.19 (4.037)	9.50 (9.352)	21.40 (21.40)	20.46 (19.81)	57.3
$[Fe(NS)]Cl_2$ (**7**)	Brown	163.8	28.72 (28.26)	2.368 (2.668)	8.59 (8.24)	18.36 (18.86)	16.98 (16.42)	65.9
$[Fe(NS')]Cl_2$ (**8**)	Black	140.3	28.49 (28.26)	2.60 (2.668)	8.69 (8.24)	18.65 (18.86)	16.02 (16.42)	71.2
$[Pb(NS)_2]$ (**9**)	Yellow	210.8	30.07 (30.32)	2.85 (2.863)	8.99 (8.840)	21.00 (20.23)	33.28 (32.69)	62.7
$[Pb(NS')_2]$ (**10**)	Yellow	217.8	30.34 (30.32)	2.88 (2.863)	8.95 (8.840)	20.18 (20.23)	32.03 (32.69)	63.8
$[Co(NS)_2]$ (**11**)	Green	247.8	39.01 (39.58)	3.75 (3.737)	11.56 (11.54)	26.02 (26.42)	12.56 (12.14)	55.8
$[Co(NS')_2]$ (**12**)	Dark purple	217.3	39.71 (39.58)	3.76 (3.737)	11.81 (11.54)	26.22 (26.42)	12.68 (12.14)	59.1

NS = SMDTC + 2-furyl-methylketone.
NS′ = SMDTC + 5-methyl-2-furaldehyde.
[a] Ref. [11].

Table 2
Significant IR bands of the Schiff bases and their complexes

Compound	ν(N–H)	ν(C=N)	ν(C=S)	ν(C–S)	Reference
NS	3210	1572	1064		[11]
NS′	3114	1618	1094		[11]
$[Cd(NS)_2]$		1551		1000	
$[Cd(NS')_2]\cdot 3H_2O$		1558		1031	
$[Sn(NS)_2]$		1530		1028	
$[Sn(NS')_2]\cdot 3H_2O$		1564		1024	
$[Fe(NS)]Cl_2$		1558		1008	
$[Fe(NS')]Cl_2$		1563		1027	
$[Pb(NS)_2]$		1542		1024	
$[Pb(NS')_2]$		1568		1022	
$[Co(NS)_2]$		1516		1025	
$[Co(NS')_2]$		1572		1028	

showed a peak at ca. δ 4.00 ppm attributed to the S–H proton [11], indicating that the thiolo tautomer was present in solution. The ν(C=S) bands at 1064 and 1094 cm^{-1} observed in the free ligands were not observed in the spectra of the metal complexes, thus supporting the suggestion that coordination was through the thione sulfur. The disappearance of ν(N–H) bands in the IR spectra of the metal complexes suggest that the ligand lost one proton on complexation, thus acting as a uninegative ligand. The lowering in frequency of the azomethine (C=N) band is evidence that the Schiff bases are bonded to the metal ions as bidentate NS chelating agents. Consequently the ν(C–S) mode is observed in the spectra of the complexes confirming that complexation occurred. There is no important displacement of the frequency of the ring breathing, ν(C–O–C) vibration at 1250 cm^{-1} [20] and there was also no absorption observed at ca. 450 cm^{-1} that can be assigned to metal–oxygen bond stretching. This confirms that there was no coordination of furyl ring oxygen to central metal atom except for complex (**3**), in which case it has been proven by X-ray crystallography that there is long distance contact between furyl ring oxygen and the central Cd ion. This can be further proved by the IR spectrum of complex (**3**) where complex (**3**) has the significant displacement of the frequency of the ring breathing, ν(C–O–C) vibration at 1230 cm^{-1} and absorption was observed at 449 cm^{-1} which can be attributed to metal–oxygen bond stretching.

The molar conductance data (Table 3) showed that complexes (**4**), (**5**), (**6**), (**9**), (**10**), (**11**) and (**12**) were non-electrolytes, indicating that the ligand is coordinated to the metal ions as a uninegatively charged bidentate species. Complexes (**7**) and (**8**) exhibit the behavior of 1:2 electrolytes in DMSO [21]. Presumably these complexes undergo solvation to release chloride ions as has been proposed for similar complexes under the same conditions [12].

The magnetic susceptibility measurements (Table 3) showed that complexes (**11**) and (**12**) were paramagnetic at room temperature with magnetic moments of 1.98 and 1.92 B.M., respectively, characteristic of a square-planar structure. The diamagnetic complexes (**5**), (**6**), (**7**), (**8**), (**9**) and (**10**) have square-planar structures whereas complex (**4**) is expected to be tetrahedral [22]. The electronic spectra of the Schiff bases display two

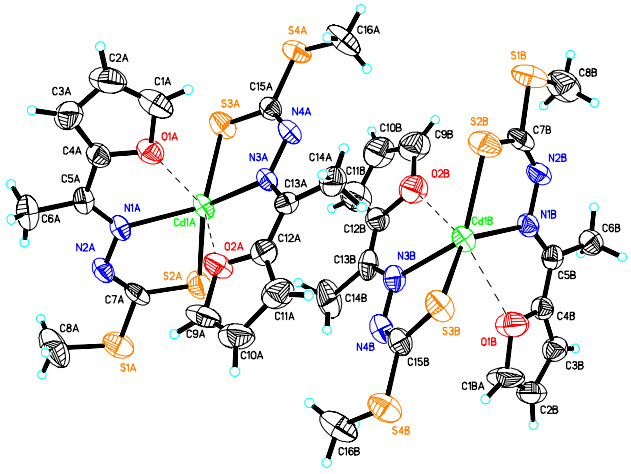

Fig. 1. ORTEP diagram of bis[*S*-methyl-β-*N*(furylmethylketone)dithiocarbazato]cadmium(II) with 50% probability displacement ellipsoids.

Table 3
Physical properties of the metal complexes

Compound	UV–Vis spectra,[a] λ_{max} (nm)	Molar conductance (Ω^{-1} cm^2 mol^{-1})	μ_{eff} (BM)
NS[b]	298 (3.2), 349 (2.3)		
NS′[b]	297 (3.4), 356 (2.2)		
$[Cd(NS)_2]$	295 (3.3), 327 (3.1), 380 (2.1)	2.36	Diamagnetic
$[Cd(NS')_2]\cdot 3H_2O$	330 (3.3), 378 (2.8)	3.49	Diamagnetic
$[Sn(NS)_2]$	297 (4.0), 327 (3.5), 452 (2.4)	29.86	Diamagnetic
$[Sn(NS')_2]\cdot 3H_2O$	289 (4.3), 324 (3.4), 459 (2.2)	3.28	Diamagnetic
$[Fe(NS)]Cl_2$	308 (3.2), 378 (2.3)	62.59	Diamagnetic
$[Fe(NS')]Cl_2$	298 (3.4), 374 (2.1)	59.67	Diamagnetic
$[Pb(NS)_2]$	312 (4.3), 355 (3.4), 412 (2.3)	4.37	Diamagnetic
$[Pb(NS')_2]$	320 (3.4), 357 (2.3)	2.62	Diamagnetic
$[Co(NS)_2]$	338 (3.4), 387 (2.8)	2.73	1.98
$[Co(NS')_2]$	330 (3.1), 392 (2.3)	1.82	1.92

[a] Log ε (cm^{-1} mol^{-1} l) are given in parentheses.
[b] Ref. [11].

bands in the 356–349 and 298–297 nm ranges which can be assigned to the $n \rightarrow \pi^*$ and $\pi \rightarrow \pi^*$ transitions of the azomethine group, respectively. The spectra of metal complexes display two absorptions at 363–324 and 297–289 nm which can be assigned to the intra-ligand transitions of the azomethine group in each case [23]. The bands at 462–452 and 392–387 nm may be assigned as combination of the $^1A_{1g} \rightarrow {}^1E_g$ (d–d) and $S \rightarrow M$ (charge-transfer) transitions. LMCT bands of the type $S \rightarrow M$ are quite common in metal complexes of thiosemicarbazone ligands [24,25] and therefore are not unexpected in the complexes under study here.

3.1. The structure of $Cd(NS)_2$

The molecular structure of the complex with its atom numbering scheme is depicted in Fig. 1. The crystal data and refinement are given in Table 4. The asymmetric unit consists of 2 molecules.

The geometry of the central Cd1A (Table 5) atom is distorted octahedral with atoms O1A and S2A in the axial positions. The O1A–Cd1A–S2A bond angle is 140.10(10)°. The O2A, N1A, S3A and N3A atoms occupy the equatorial positions with bond angles between 64.10(16)° and 118.20(13)° about the central Cd1A ion (Table 5). The Cd1A···O1A and Cd1A···O2A bond lengths of 2.710(4) and 2.654(6) Å, respectively, are slightly longer than normal [26] but bonds of this length have been observed in compounds such as $[Cd\{C_2(COO)_2\}(H_2O)_3]\cdot H_2O$ [27] and $[Cd_2(NO_3)_2(C_6H_{12}N_4)_2](NO_3)_2$ [28].

In the second molecule, the octahedral geometry about Cd1B is severely distorted with long range Cd1B···O2B and Cd1B···O1B bond lengths of 2.850(6) and 2.763(5) Å, respectively. Such a long Cd–O bond length has been previously reported in Λ-$[Cd(C_{20}H_{44}N_4O_4)](C_6H_2N_3O_7)_2\cdot CH_3CN$ for Cd···O(H) (2.845(2) Å) [29]. The lengthening of this Cd1B···O2B bond may be due to interaction in the packing of the molecules. The furyl ring O2B–C9B–C10B–C11B–C12B and Cd1B are planar with maximum deviation for Cd1B of only 0.032(1) Å from the mean plane. However, the central atom, Cd1B is deviated by −0.610(1) Å from the opposite furyl ring, O1B–C1B–C2B–C3B–C4B. The two furyl fragments are almost perpendicular to one another (83.5(5)°). In the first molecule, the central atom, Cd1A, is deviated from both furyl rings O1A–C1A–C2A–C3A–C4A and O2A–C9A–C10A–C11A–C12A by −0.938(1) and −0.641(1) Å, respectively, with dihedral angle between the furyl rings of 66.2(5)°. Both Cd central atoms chelated to the thiolo sulfur, β-azomethine nitrogen and furyl oxygen in a tridentate manner.

In the second molecule, the O1B and S2B atoms occupy the axial position with O1B–Cd1B–S2B bond angle of 138.17(12)°. The O2B, N1B, S3B and N3B atoms occupy the equatorial positions with angles between 61.68(18)° and 138.29(13)°. The bond lengths and angles in the Schiff bases are typical of dithiocarbazate Schiff bases [11]. However the elongation of the S1B–C8B bond to 1.819(9) Å in comparison to the other S–C(Me) bonds (1.767(8)–1.793(8) Å) is possibly the result of vibration.

The chelated fragments Cd1A–N1A–N2A–C7A–S2A (maximum deviation 0.034(6) Å for N1A) and Cd1A–N3A–N4A–C15A–S3A (maximum deviation 0.0014(5) Å for N3A) in the first molecule are planar. The angle between the two fragments is 82.76(19)°. In the second molecule, the chelated fragments Cd1B–N1B–N2B–C7B–S2B and Cd1B–N3B–N4B–C15B–S3B are less planar with maximum deviations of 0.151(6) and 0.182(5) Å for N1B and N3B atoms, respectively, with dihedral angle of 68.2(2)°.

Table 4
Crystal data, data collection and structure refinement parameters for the $[Cd(C_8H_9N_2S_2O_1)_2]$ complex

Compound	$[Cd(C_8H_9N_2O_1S_2)_2]$
Empirical formula	$C_{16}H_{18}N_4O_2S_4Cd$
Formula weight	538.98
Temperature (K)	293 (2)
Wavelength (Å)	0.71073
Crystal system	triclinic
Space group	$P\bar{1}$
Unit cell dimensions	
a (Å)	12.9874 (6)
b (Å)	13.6194 (6)
c (Å)	13.6576 (6)
α (°)	83.728(1)
β (°)	64.744 (1)
γ (°)	87.421 (1)
Volume (Å^3)	2171.76 (17)
Z	4
Calculated density (Mg m^{-3})	1.648
Absorption coefficient (mm^{-1})	1.408
$F(0\,0\,0)$	1080
Crystal size (mm)	$0.40 \times 0.24 \times 0.20$
Theta range (°)	1.50–26.50
Limiting indices	$-15 \leqslant h \leqslant 16$, $-17 \leqslant k \leqslant 13$, $-16 \leqslant l \leqslant 17$
Reflections collected/unique	13 514/8557 ($R_{int} = 0.0885$)
Completeness to theta = 29.61	95%
Absorption correction	empirical
Maximum and minimum transmission	0.7659 and 0.6027
Refinement method	full-matrix least-squares on F^2
Data/restraints/parameters	8557/0/488
Goodness-of-fit on F^2	0.943
Final R indices [$I > 2\sigma(I)$]	$R_1 = 0.0596$, $wR_2 = 0.1572$
R indices (all data)	$R_1 = 0.0853$, $wR_2 = 0.1736$
Extinction coefficient	0.0106 (9)
Largest difference peak and hole	1.24 and −1.71 (e Å^{-3})

3.2. Biological activities

3.2.1. Antimicrobial activity

The complexes (**4**), (**5**) and (**11**) show clear inhibition of all the bacteria and fungi tested, with the exception

Table 5
Selected bond lengths (Å) and bond angles (°) for the $[Cd(C_8H_9N_2S_2O_1)_2]$ complex

Bond lengths			
Cd(1A)–N(3A)	2.288(5)	Cd(1A)–N(1A)	2.308(5)
Cd(1A)–S(3A)	2.4833(16)	Cd(1A)–S(2A)	2.4955(17)
Cd(1A)–O(1A)	2.710(4)	Cd1A–O(2A)	2.654(6)
Cd(1B)–N(1B)	2.298(5)	Cd(1B)–N(3B)	2.313(5)
Cd(1B)–S(3B)	2.4746(16)	Cd(1B)–S(2B)	2.4880(16)
Cd(1B)–O(1B)	2.763(5)	Cd(1B)–O(2B)	2.850(6)
S(1A)–C(7A)	1.758(5)	S(1A)–C(8A)	1.779(10)
S(2A)–C(7A)	1.727(7)	S(3A)–C(15A)	1.740(6)
S(4A)–C(15A)	1.751(6)	S(4A)–C(16A)	1.793(8)
S(1B)–C(7B)	1.747(6)	S(1B)–C(8B)	1.819(9)
S(2B)–C(7B)	1.752(7)	S(3B)–C(15B)	1.740(6)
S(4B)–C(15B)	1.762(6)	S(4B)–C(16B)	1.767(8)
N(1A)–C(5A)	1.301(7)	N(1A)–N(2A)	1.409(6)
N(2A)–C(7A)	1.288(8)	N(3A)–C(13A)	1.295(7)
N(3A)–N(4A)	1.411(6)	N(4A)–C(15A)	1.306(8)
N(1B)–C(5B)	1.287(7)	N(1B)–N(2B)	1.421(6)
N(2B)–C(7B)	1.270(8)	N(3B)–C(13B)	1.290(7)
N(3B)–N(4B)	1.423(7)	N(4B)–C(15B)	1.283(8)
O(1A)–C(4A)	1.360(7)	O(1A)–C(1A)	1.382(7)
O(2A)–C(12A)	1.378(8)	O(2A)–C(9A)	1.382(7)
O(1B)–C(4B)	1.357(7)	O(1B)–C(1B)	1.405(9)
O(2B)–C(12B)	1.367(7)	O(2B)–C(9B)	1.396(9)
Bond angles			
O(1A)–Cd(1A)–S(2A)	140.10(10)	N(3A)–Cd(1A)–N(1A)	134.16(16)
N(3A)–Cd(1A)–S(3A)	79.49(12)	N(1A)–Cd(1A)–S(3A)	118.20(13)
N(3A)–Cd(1A)–S(2A)	127.79(12)	O(2A)–Cd(1A)–N(3A)	64.10(16)
N(1A)–Cd(1A)–O(2A)	84.29(17)	N(1A)–Cd(1A)–S(2A)	78.31(12)
S(3A)–Cd(1A)–S(2A)	125.68(6)	O(1A)–Cd(1A)–O(2A)	78.22(15)
O(2A)–Cd(1A)–S(3A)	142.48(11)	O(1A)–Cd(1A)–N(1A)	63.90(15)
O(1A)–Cd(1A)–N(3A)	77.16(16)	S(2A)–Cd(1A)–O(2A)	89.19(12)
N(1B)–Cd(1B)–N(3B)	113.01(17)	N(1B)–Cd(1B)–S(3B)	138.27(13)
N(3B)–Cd(1B)–S(3B)	78.91(13)	N(1B)–Cd(1B)–S(2B)	79.49(12)
N(3B)–Cd(1B)–S(2B)	132.99(14)	S(2B)–Cd(1B)–O(1B)	138.17(12)
S(3B)–Cd(1B)–S(2B)	122.77(6)	O(1B)–Cd(1B)–O(2B)	108.66(17)
N(3B)–Cd(1B)–O(2B)	61.68(18)	O(1B)–Cd(1B)–N(3B)	81.20(18)
O(1B)–Cd(1B)–N(1B)	62.69(17)	N(1B)–Cd(1B)–O(2B)	78.44(18)
S(2B)–Cd(1B)–O(2B)	78.46(12)	O(2B)–Cd(1B)–S(3B)	136.27(12)

that (**4**) and (**5**) were inactive toward Methicillin resistant *staphylococcus* (MRSA) and *Candida albicans* (CA), respectively. However, complexes (**3**), (**7**) and (**9**) were inactive toward all bacteria. Complex (**3**) was active against *Candida albicans* (CA) and *Saccharomyces cerevisiae* (20341) while complexes (**7**) and (**9**) showed

Table 6
Qualitative antimicrobial assay (100 mg cm^{-3})[a]

Compound	(B28)	(60690)	(MRSA)	(B29)	(20341)	(C.A.)	(2075)	(398)
$[Cd(NS)_2]$	10	13	9	13	16	27	9	3
$[Cd(NS')_2]\cdot 3H_2O$	16	21	13	18	40	38	22	25
$[Sn(NS)_2]$	19	26	17	20	25	6	45	35
$[Sn(NS')_2]\cdot 3H_2O$	6	16	16.5	15	6	6	30	22
$[Fe(NS)]Cl_2$	6	7	7	6.5	6	8	15	14
$[Fe(NS')]Cl_2$	7	6	6.5	7	8	7	7	13
$[Pb(NS)_2]$	6	7	6.5	6.5	6	6	14	15
$[Pb(NS')_2]$	6	6	6.5	6.5	6	6	13	7
$[Co(NS)_2]$	20	15	18	18	20	22	27	22
$[Co(NS')_2]$	6	6	6	6	6	6	6	6
Streptomycin (control)	30	30	31	30				
Nystatin (control)					24	21	27	25

Bacillus subtilis (mutant-defective DNA repair) (B28), *Pseudomonas aeruginosa* (60690, Methicillin resistant *Staphylococcus* (MRSA), *Bacillus subtilis*-wild type (B29), *Saccharomyces cerevisiae* (20341), *Candida albicans* (C.A.), *Candida lypolytica* (2075), *Aspergillus ochraceous* (398).

[a] Inhibition diameter in millimeters. Inhibition diameter 15 mm – strongly active.

Table 7
Quantitative antimicrobial assay (MIC value, $\mu g\,ml^{-3}$)[a]

Compound	(B28)	(60690)	(MRSA)	(B29)	(20341)	(C.A.)	(2075)	(398)
$[Cd(NS)_2]$					50 000	6250		
$[Cd(NS')_2]\cdot 3H_2O$	3125	6250		390	6250	3125	390	390
$[Sn(NS)_2]$	6250	3125	6250	6250	6250		3125	3125
$[Sn(NS')_2]\cdot 3H_2O$		12 500	6250	12 500			6250	12 500
$[Fe(NS)]Cl_2$							12 500	
$[Pb(NS)_2]$								12 500
$[Co(NS)_2]$	781	1562	781	781	6250	6250	781	1562
Streptomycin (control)	48.8	12.2	12.2	48.8				
Nystatin (control)					6250	3125	6250	3125

Bacillus subtilis (mutant-defective DNA repair) (B28), *Pseudomonas aeruginosa* (60690, Methicillin resistant *Staphylococcus* (MRSA), *Bacillus subtilis*-wild type (B29), *Saccharomyces cerevisiae* (20341), *Candida albicans* (C.A.), *Candida lypolytica* (2075), *Aspergillus ochraceous* (398).

[a] MIC ($\mu g\,ml^{-3}$), minimum inhibitory concentration, i.e. the lowest concentration to completely inhibit microbial growth. Complexes (**4**), (**5**), (**6**) and (**11**) indicate that they are less active than the standard drug, streptomycin.

clear inhibition of *Candida lypolytica* (2075) and *Aspergillus ochraceous* (398), respectively. Complex (**6**) showed activity against three bacteria [*Pseudomonas aeruginosa* (60690), Methicillin resistant *Staphylococcus* (MRSA) and *Bacillus subtilis*-wild type (B29)] and two fungi [*Candida lypolytica* (2075) and *Aspergillus ochraceous* (398)]. Complexes (**8**), (**10**) and (**12**) were inactive toward all bacteria and fungi. Qualitative antimicrobial results are shown in Table 6. Compounds that showed clear inhibition zones of 15 mm and above were considered active and attempts were made to determine the minimum inhibitory concentration (MIC) (Table 7). The MIC values against bacteria ($=390$–$12\,500\ \mu g\,cm^{-3}$) for complexes (**4**), (**5**), (**6**) and (**11**) indicate that they are less active than the standard drug, streptomycin. The MIC values for complexes (**4**) and (**11**) against *Candida lypolytica* (2075) and *Aspergillus ochraceous* (398) were higher than the standard drug, nystatin; however, complexes (**3**) and (**7**) were less active than nystatin toward *Saccharomyces cerevisiae* (20341) and *Candida lypolytica* (2075), respectively, while complexes (**6**) and (**9**) were less active against *Aspergillus ochraceous* (398) than nystatin. The activities of the remainder were comparable to nystatin.

Table 8
Cytotoxic activity

Compound	CD_{50} (μg/ml)	
	T-lymphoblastic leukemic cells (CEM-SS)	Cervical cancer cells (HELA)
NS	>25	>25
NS′	>25	>25
$[Cd(NS)_2]$	1.8	1.8
$[Cd(NS')_2]\cdot 3H_2O$	2.0	1.8
$[Sn(NS)_2]$	>25	na
$[Sn(NS')_2]\cdot 3H_2O$	>25	na
$[Fe(NS)]\cdot Cl_2$	>25	na
$Fe(NS')]\cdot Cl_2$	>25	>25
$[Pb(NS)_2]$	>25	na
$[Pb(NS')_2]$	>25	na
$[Co(NS)_2]$	2.1	3.6
$[Co(NS')_2]$	>25	>25
$CdBr_2\cdot 4H_2O$	14.0	na
$SnCl_2\cdot 2H_2O$	>25	na
$FeCl_2$	>25	na
$PbNO_3$	>25	na
$CoCl_2\cdot 6H_2O$	12.0	na
Doxorubicin (standard)	0.10	11.0
Tamoxifen (standard)	36.0	7.0

Note. na, not available; CD_{50}, <5.0 μg/ml – strongly active; CD_{50}, 5.0 to <10.0 μg/ml – moderately active; CD_{50}, 10.0–25.0 μg/ml – weakly active; CD_{50}, >25.0 μg/ml – not active.

3.2.2. Cytotoxic activity

Complexes $[Cd(NS)_2]$ (**3**); $[Cd(NS')_2]\cdot 3H_2O$ (**4**) and $[Co(NS)_2]$ (**11**) (where NS and NS′ are the 2-furylmethylketone and 5-methyl-2-furaldehyde Schiff bases of SMDTC) were found to be very active against T-lymphoblastic leukemic cells (CEM-SS) and cervical cancer cells (HELA) with CD_{50} values between 1.8 and 3.6 $\mu l\,cm^{-3}$. While both Schiff bases utilized in this work had been shown to be inactive [11] in their uncomplexed state, Tarafder et al. [22] reported that the 5-methyl-2-furaldehyde Schiff base of the closely related S-benzyldithiocarbazate (SBDTC) exhibited strong activity against CEM-SS. It is of note that the inactive 2-furylmethylketone Schiff base of SMDTC became active on complexation with Cd(II) (**3**) while for the SBDTC derivative, the opposite was the case, the Cd(II) complex was found [22] to be inactive against CEM-SS. Interestingly, the Cd(II) complexes of 5-methyl-2-furaldehyde Schiff bases of both SBDTC and SMDTC (**4**) showed good activity towards CEM-SS. However, Pb(II) complexation of the 5-methyl-2-furaldehyde Schiff bases of both SBDTC [22] and SMDTC (**10**) did not alter their activity towards CEM-SS. Complexes (**8**) and (**12**) were found to be inactive toward both cell lines. Complexes (**5**), (**6**), (**7**), (**9**) and (**10**) were tested against only CEM-SS and were found to be inactive (Table 8). In all cases the simple inorganic metal salts were no more than weakly active at the maximum concentrations used in the assay of the complexes. It is clear that more

comparative data must be collected for Schiff bases containing different functional groups and complexed to different metal ions before a pattern of activity can be determined.

4. Supplementary material

Crystallographic data for the structural analysis have been deposited with the Cambridge Crystallographic Data Centre, CCDC No. 215299. Copies of this information may be obtained free of charge from The Director, CCDC, 12 Union Road, Cambridge, CB2 1EZ, UK (fax: +44-1223-336033; e-mail: deposit@ccdc.cam.ac.uk or www: http://www.ccdc.cam.ac.uk).

Acknowledgements

The authors thank the referees for constructive comments and M. Ibrahim M. Tahir (UPM) for valuable discussion. We thank the Department of Chemistry and the Institute of Bioscience, at University Putra Malaysia, for the provision of laboratory facilities. We also thank the Ministry of Science, Technology and the Environment, Malaysia, for funding this research under the Intensification of Research in Priority Areas Scheme (IRPA Grant No. 09-02-04-0296).

References

[1] M.A. Ali, M. Nazimuddin, R. Shaha, R.J. Butcher, J.C. Bryan, Polyhedron 17 (1998) 3955, and references therein.
[2] M.A. Ali, M.T.H. Tarafder, J. Inorg. Nucl. Chem. 39 (1977) 1785.
[3] S.M.M.H. Majumder, M.A. Ali, F.E. Smith, M.A.U. Mridha, Polyhedron 7 (1988) 2183.
[4] M.T.H. Tarafder, M.A. Ali, N. Saravanan, W.Y. Weng, K. Saravanan, N. Umar-Tsafe, K.A. Crouse, Transition Met. Chem. 25 (2000) 295, and references therein.
[5] Y.P. Tian, C.Y. Duan, X.Z. You, Transition Met. Chem. 23 (1998) 17, and references therein.
[6] Z. Xu, E.C. Alyea, G. Ferguson, M.C. Jennings, Polyhedron 10 (1991) 1625.
[7] C.Y. Zhao, C.Y. Duan, Y.P. Tian, X.Z. You, T.C.W. Mak, Acta Crystallogr. C 53 (1997) 1151.
[8] Z. Zhou, K. Yu, S. Gou, X. You, Z. Xu, Polyhedron 10 (1991) 37.
[9] X.H. Zhu, S.H. Liu, Y.J. Liu, J. Ma, C.Y. Duan, X.Z. You, Y.P. Tian, F.X. Xie, S.S. Ni, Polyhedron 19 (1998) 181.
[10] M. Das, S.E. Livingstone, Inorg. Chim. Acta 19 (1976) 5.
[11] M.T.H. Tarafder, Kar-Beng Chew, K.A. Crouse, A.M. Ali, B.M. Yamin, H.-K. Fun, Polyhedron 21 (2002) 2683.
[12] M.T.H. Tarafder, M.A. Ali, N. Saravanan, W.Y. Weng, K. Saravanan, N. Umar-Tsafe, K.A. Crouse, Transition Met. Chem. 25 (2000) 295.
[13] G.M. Sheldrick, SAINT V4, Software Reference Manual, Siemens Analytical X-ray System, Madison, WI, USA, 1996.
[14] G.M. Sheldrick, SADABS, Program for Empirical Absorption Correction of Area Detector Data, University of Göttingen, Göttingen, Germany, 1996.
[15] G.M. Sheldrick, SHELTXL V 5.1, Software Reference Manual, Bruker AXS, Inc., Madison, WI, USA, 1997.
[16] A.L. Spek, Acta Crystallogr. A 46 (1996) C-34.
[17] M. Mosmann, J. Immunol. Methods 65 (1983) 55.
[18] A.W. Bauer, M.D.K. Kirby, J.C. Sherris, M.D. Turck, Am. J. Clin. Pathol. 45 (1966) 493.
[19] C.D. Hufford, A.M. Clark, in: Atta-ur-Rahman (Ed.), Studies in Natural Products Chemistry, vol. 2, Elsevier, Amsterdam, 1988, p. 421.
[20] M.A. Ali, R.N. Bose, J. Inorg. Nucl. Chem. 39 (1977) 265.
[21] W.J. Geary, Coord. Chem. Rev. 7 (1971) 81.
[22] M.T.H. Tarafder, Teng-Jin Khoo, K.A. Crouse, A.M. Ali, B.M. Yamin, H.-K. Fun, Polyhedron 21 (2002) 2691.
[23] M.A. Ali, A.H. Mirza, R.J. Butcher, M.T.H. Tarafder, T.B. Keat, A.M. Ali, J. Inorg. Biochem. 92 (2002) 141.
[24] D.X. West, C.S. Carlson, A.E. Liberta, J.N. Albert, C.R. Daniel, Transition Met. Chem. 15 (1990) 383.
[25] D.X. West, M.A. Lockwood, A. Liberta, X. Chen, R.D. Willett, Transition Met. Chem. 18 (1993) 221.
[26] F.H. Allen, Acta Crystallogr. B 58 (2002) 380.
[27] U. Ruschewits, I. Pantenburg, Acta Crystallogr. C 58 (2002) 483.
[28] J. Cai, S.W. Ng, Acta Crystallogr. E 59 (2003) 692.
[29] C.B. Smith, S.F. Lincoln, M.R. Taylor, K.D. Wainwright, Acta Crystallogr. C 59 (2003) 358.

Available online at www.sciencedirect.com
SCIENCE DIRECT®
Polyhedron 23 (2004) 1393–1399
POLYHEDRON
www.elsevier.com/locate/poly

Phosphanylalkylcyclopentadienyl ligands: synthesis, molecular structures and catalytic properties of [{(η^5-C_5H_4)CMe_2PHR}$CrCl_2(PMe_2Ph)$] (R = Ph, ^{t}Bu)

Thomas Höcher [a], Brian A. Salisbury [b], Klaus H. Theopold [b], Evamarie Hey-Hawkins [a,*]

[a] *Institut für Anorganische Chemie der Universität, Johannisallee 29, D-04103 Leipzig, Germany*
[b] *Department of Chemistry and Biochemistry, Center for Catalytic Science and Technology, University of Delaware, Newark, DE 19716, USA*

Received 5 January 2004; accepted 19 February 2004
Available online 12 April 2004

Abstract

Li[(C_5H_4)CMe_2PHPh] reacted with [$CrCl_3(THF)_3$] with formation of a mixture of products, among which only [{(η^5-C_5H_4)CMe_2PPh}$CrCl]_2$ (**1**) could be isolated. However, when [$CrCl_3(PMe_2Ph)_3$] was treated with Li[(C_5H_4)CMe_2PHR], the complexes [{(η^5-C_5H_4)CMe_2PHR}$CrCl_2(PMe_2Ph)$] (R = Ph (**2**), ^{t}Bu (**3**)) were obtained in moderate yield. Complexes **1** and **2** were characterised by X-ray crystallography, **1–3** by IR spectroscopy. In the solid state, a phosphanido-bridged dimer is observed for **1**, while **2** and **3** are monomeric complexes without coordination of the phosphanyl group of the cyclopentadienyl ring. **2** and **3** were also characterised by mass spectrometry and NMR and UV–Vis spectroscopy, and their magnetic moments were determined. **2** and **3** were studied in the catalytic polymerisation of ethylene with methylalumoxane (MAO) as cocatalyst.
© 2004 Elsevier Ltd. All rights reserved.

Keywords: Phosphanylalkylcyclopentadienyl ligands; Chromium complexes; Polymerisation studies

1. Introduction

After the discovery of α-olefin polymerisation [1], numerous metallocene and monocyclopentadienyl derivatives with different steric and electronic properties were synthesised and employed as catalysts in polymerisation reactions. *Ansa*-metallocene dichlorides of Ti, Zr, and Hf (especially chiral ones) are important catalysts for the methylalumoxane-promoted isotactic polymerisation of olefins. Therefore, intensive research is being carried out towards the synthesis of improved catalysts [2–5]. Recently, monocyclopentadienyl derivatives in which the cyclopentadienyl ring has a heteroatom-functionalised side chain were prepared and employed in the polymerisation and copolymerisation of olefins [6]. These studies were also extended to phospholyl ligands [7].

While numerous cyclopentadienyl ligands with *O*- and *N*-functionalised side chains are known, the number of cyclopentadienes with a *P*-functionalised alkyl or silyl side chain is still small [8], and it was only in 1994 that Heidemann and Jutzi [9] reported the first compound in which the P atom bears a reactive P–H bond. We extended this class of compounds to other derivatives in 1999 [10,11]. The lithium salts [Li(TMEDA)]$_2$[(C_5H_4)-CMe_2PPh] [12] and [Li(TMEDA)][(C_5H_4)CMe_2PR_2] (R = Ph, Me) [13], 1-$SiMe_2PHMes^*C_5Me_4H$ and its dimeric dipotassium salt [$K(THF)_2]_2$[(C_5Me_4)$SiMe_2$-PMes*] (Mes* = 2,4,6-$^t Bu_3C_6H_2$) [14] have been structurally characterised. Such compounds should be useful precursors for dianionic bifunctional ligands in transition metal chemistry. In addition, the presence of a P-containing group is advantageous for reactivity studies by ^{31}P NMR spectroscopy.

We previously reported the synthesis of the PH-functionalised ferrocene derivatives *rac*-[Fe{(η^5-C_5H_4)CMe_2PHR}$_2$] [R = Ph, 2,4,6-$Me_3C_6H_2$ (Mes)] [15] the monosubstituted phosphanylalkylcyclopentadienyl

* Corresponding author. Tel.: +493419736151; fax: +493419739319.
E-mail address: hey@rz.uni-leipzig.de (E. Hey-Hawkins).

0277-5387/$ - see front matter © 2004 Elsevier Ltd. All rights reserved.
doi:10.1016/j.poly.2004.02.011

complexes of group 4 metals, [{(η^5-C_5H_4)$SiMe_2PHR$}-$ZrCl_3$] (R = Ph, Cy) and [{(η^5-C_5H_4)CMe_2PH^tBu}-MCl_3] (M = Ti, Zr) [16] and of the metallocene derivatives [{(η^5-C_5H_4)CMe_2PHR}$_2ZrCl_2$] and [{(η^5-C_5H_4)CMe_2PHR}$_2$TiCl] (R = Ph, ^{t}Bu). The last-named slowly decompose on recrystallisation from THF, Et_2O or toluene with formation of [{(η^5-C_5H_4)$_2CMe_2$}MCl_2] (M = Zr, Ti) and $(PR)_n$ (R = Ph, n = 4–6, R = ^{t}Bu, n = 4) and PH_2R [17]. Recently, Erker and coworkers [18] reported the synthesis and catalytic properties in the polymerisation of olefins of the constrained-geometry catalysts [{(C_5H_4)CMe_2PCy}$M(NR_2)_2$] (M = Ti, R = Me, M = Zr, R = Et). Hou and coworkers [14] reported the synthesis of [{(η^5-C_5Me_4)$SiMe_2PMes$*}-$Ln(L)_n$] (Ln = Sm: L = THF, n = 1 or 3; L = $MeOCH_2$-CH_2OMe, n = 2; L = $PO(NMe_2)_3$, n = 2; Ln = Yb, L = THF, n = 3) and the polymerisation of ethene, ε-caprolactone and 1,3-butadiene with the Sm^{II} mono-THF complex.

We now report the synthesis and catalytic properties of the first PH-functionalised phosphanylalkylcyclopentadienyl complexes of chromium(III), [{(η^5-C_5H_4)CMe_2PHR}$CrCl_2$(PMe_2Ph)] (R = Ph (**2**), ^{t}Bu (**3**)), and the first constrained-geometry chromium complex with a phosphanidoalkylcyclopentadienyl ligand, [{(η^5-C_5H_4)CMe_2PPh}CrCl]$_2$ (**1**).

Only a limited number of chromium complexes with chelating tertiary phosphanylalkylcyclopentadienyl ligands is known [19]. [{(η^5-C_5H_4)$CH_2CH_2PR_2$}$CrCl_2$] (R = Me, Et, Pr, ^{i}Pr, ^{i}Bu, ^{t}Bu, neopentyl, hexyl, Cy, Ph, *o*-tolyl, 1-naphthyl) are accessible from the corresponding lithium cyclopentadienide and [$CrCl_3(THF)_3$] [19]; reaction with MeLi and R′MgCl gave the corresponding dimethyl and dialkyl derivatives (R′ = Me, Pr, Cy, ^{t}Bu). The dichloride complex can be used with methyl alumoxane (Al:Cr = 100:1) as a catalyst for the polymerisation of ethene [20].

2. Results and discussion

The lithium reagents Li[(C_5H_4)CMe_2PHR] (R = Ph [10], ^{t}Bu [17]) are readily accessible by reaction of LiPHR with 6,6-dimethylfulvene. The reaction of Li[(C_5H_4)CMe_2PHPh] with [$CrCl_3(THF)_3$] yielded a pale blue powder, from which a small amount of blue crystals of [{(η^5-C_5H_4)CMe_2PPh}CrCl]$_2$ (**1**) was obtained on recrystallisation from toluene/hexane (Eq. (1)). Attempts to synthesise **1** in better yield (a) by heating to reflux after addition of Li[(C_5H_4)CMe_2PHPh] to [$CrCl_3(THF)_3$]; (b) by reaction of [{(η^5-C_5H_4)CMe_2-$PHPh$}$CrCl_2$(PMe_2Ph)] with DBU (DBU = 1,8-diazabicyclo[5.4.0]undec-7-ene); or (c) by reaction of Li[(C_5H_4)CMe_2PHPh] with [$CrCl_3(THF)_3$] in the presence of DBU failed. The molecular structure (vide infra) shows a phosphanido-bridged dimer. However, the presence of a PH band at 2289 cm^{-1} in the IR spectrum of the pale blue powder indicates that a mixture of products was obtained. The other product(s) could, however, not be obtained in pure form by fractional crystallisation, extraction or thin-layer chromatography. The formation of 6,6-dimethylfulvene in the reaction mixture, shown by ^{1}H NMR spectroscopy, indicated decomposition of the phosphanylalkylcyclopentadienyl ligand. Similarly, decomposition of Li[(C_5H_4)C-Me_2PHPh] was observed on protonation with HCl gas in diethyl ether (formation of PH_2Ph, LiCl and 6,6-dimethylfulvene) and in reactions with $AlCl_3$, for which elimination of HCl is proposed as the first reaction step [21]. A similar reaction is proposed here, with attack of $CrCl_3$ on the cyclopentadienyl ring (with elimination of LiCl) and/or at the phosphanyl group (with elimination of HCl).

Activation of the PH proton and elimination of HCl can be avoided if [$CrCl_3(PMe_2Ph)_3$] is employed as starting material, as this prevents attack at the phosphanyl group, as well as subsequent reactions after formation of the cyclopentadienyl complexes, because coordination of the phosphanyl group to chromium is prevented. Dark green [$CrCl_3(PMe_2Ph)_3$] is readily obtained from the reaction of $CrCl_3$ with three equivalents of PMe_2Ph in refluxing THF/toluene (if less PMe_2Ph is employed, unconsumed insoluble $CrCl_3$ remains) [22]. After filtration, the solution of the phosphine complex was treated in situ with a solution of Li[(C_5H_4)C-Me_2PHR] in THF at −50 °C, and the blue chromium(III) complexes [{(η^5-C_5H_4)CMe_2PHR}$CrCl_2$(PMe_2Ph)] (R = Ph (**2**), ^{t}Bu (**3**)) were obtained in high yield (Eq. (1)).

Crystals of **2** and **3** are only slowly oxidised in air, while a blue solution of **3** in THF, toluene or CH_2Cl_2 slowly turns green on prolonged exposure to air. In the IR spectra, complexes **2** and **3** exhibit a sharp PH absorption at 2278 (**2**) and 2276 cm^{-1} (**3**). The $^{31}P\{^1H\}$ NMR spectra (CH_2Cl_2/C_6D_6) show very broad signals ($v_{1/2}$ ca. 900 Hz) at 92 (**2**) and 111 ppm (**3**) (cf. Li[(C_5H_4)CMe_2PHR]: −1.2 ppm (R = Ph) [10]), 26.0 ppm (R = ^{t}Bu) [17]. Typical of half-sandwich Cr^{III} complexes, the ^{1}H NMR spectra of **2** and **3** (C_6D_6) show several broad and isotropically shifted resonances ranging in chemical shift approximately from +11 to −30 ppm. Consistent with the structural similarity of **2** and **3**, both spectra feature a series of very similar peaks, namely, those at 10.5, 5.0, ca 0.0 and ca. −28 ppm. These are likely associated with the PMe_2Ph ligand and the geminal methyl groups of the cyclopentadienyl substituent, although the greater signal intensity at 0.0 ppm in **3** suggests accidental coincidence with the resonance of the *tert*-butyl group. The spectrum of **2** exhibits a few minor additional peaks, which are attributed to the P-bound phenyl ring. In summary, the ^{1}H NMR spectra of paramagnetic organometallics can rarely be unambi-

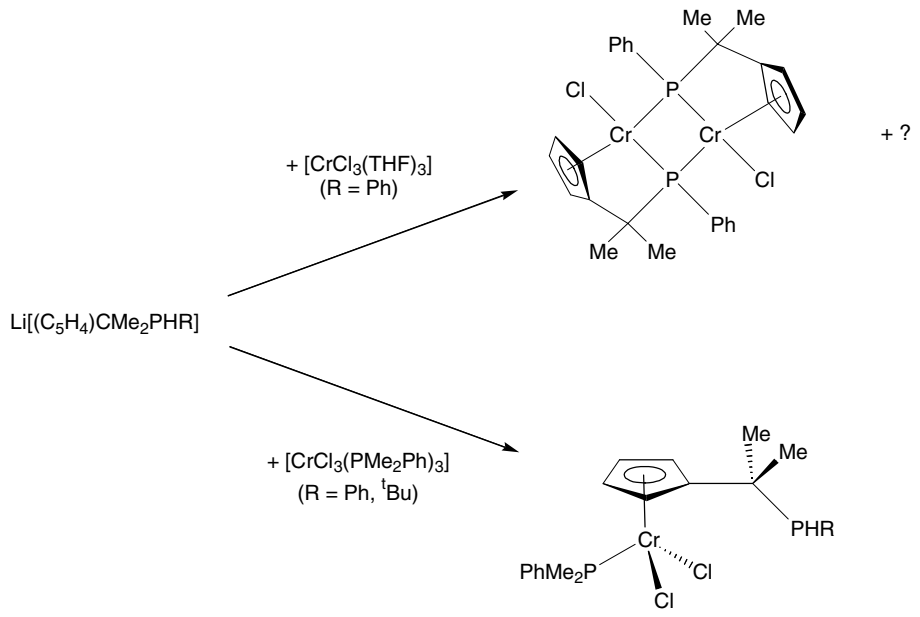

(1)

R = Ph (**2**), ^{t}Bu (**3**)

gously assigned. However, the spectra of **2** and **3** clearly show them to be closely related and are entirely consistent with the crystal structures. The cyclopentadienyl protons are probably too far shifted and broadened to be readily detectable.

In the UV–Vis spectra the blue complexes **2** and **3** show absorptions at $\lambda = 661$ ($\log(\varepsilon/\mathrm{cm}^2\ \mathrm{mol}^{-1}) = 4.69$) and 667 nm ($\log(\varepsilon/\mathrm{cm}^2\ \mathrm{mol}^{-1}) = 4.72$), respectively.

No meaningful mass spectrum was obtained for **2**, while for **3**, a molecular ion peak as well as fragmentation products thereof were observed in the FAB mass spectrum.

2.1. Molecular structures of *1* and *2*

Crystals of **2** suitable for X-ray crystallography were obtained from a concentrated solution in diethyl ether at −30 °C. Compound **3** crystallises in very thin plates regardless of the solvent used for crystallisation. Therefore, only a poor data set was obtained, but it was sufficient to elucidate the structural motif, which is similar to that of **2**.

Compounds **1** and **3** crystallise in the monoclinic space group $P2_1/c$ with 2 and 8 formula units in the unit cell, respectively; **2** crystallises in the triclinic space group $P\bar{1}$ with 4 formula units in the unit cell.

In **1**, the centre of the Cr_2P_2 ring coincides with a crystallographic centre of inversion. The Cr_2P_2 ring forms a parallelogram with a Cr···Cr distance of 2.9383(1) Å and a P–Cr–P bond angle of 102.75(2)° (Table 1). The cyclopentadienyl ring and the Cr_2P_2 ring form an angle of 32.4(1)°; the cyclopentadienyl and phenyl rings form an angle of 35.8°. The chromium atom, C1 of the cyclopentadienyl ring, C12 of the methylene bridge and P1 form a planar four-membered ring; this plane forms an angle of 54.8(1)° with the Cr_2P_2 ring (see Fig. 1).

There are two independent molecules in the asymmetric unit of **2**, which differ mainly in the configuration of the chiral P atoms, P1 and P3. One has *R*, and the other *S* configuration (see Fig. 2).

In **1**, the Cr–P bond is 0.09 Å shorter than the coordinative Cr–P(PMe$_2$Ph) bond in **2** (2.439(1) and 2.447(1) Å). Similar Cr–P bond lengths are observed in the phosphanido-bridged complexes [{(η^5-C_5Me_5)Cr}$_2$(μ-

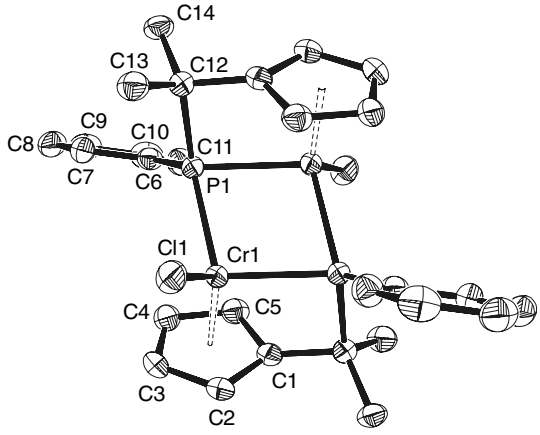

Fig. 1. Molecular structure of [{(η-C_5H_4)CMe_2PPh}CrCl]$_2$ (**1**) showing the atom-numbering scheme employed (ORTEP plot, 50% probability, SHELXTL PLUS; XP [26]). Hydrogen atoms are omitted for clarity.

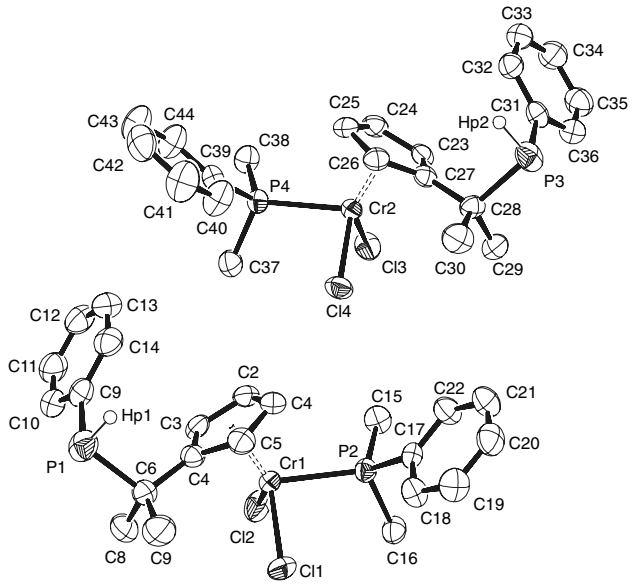

Fig. 2. Molecular structure of $[\{(\eta^5\text{-}C_5H_4)CMe_2PHPh\}CrCl_2(PMe_2Ph)]$ (**2**) showing the atom-numbering scheme employed (ORTEP plot, 50% probability, SHELXTL PLUS; XP [26]). Hydrogen atoms (other than PH) are omitted for clarity. There are two independent molecules in the unit cell.

$PPh_2)_n(\mu\text{-}Cl)_{3-n}]^+$ ($n = 1$, 2; Cr–P 2.385(2)–2.404(4) Å) [23] and the phosphine complexes $[\{(\eta^5\text{-}C_5H_4)CH_2\text{-}CH_2PR_2\}CrCl_2]$ (2.459(1) (R = Cy), 2.447(1) Å (R = Ph)) [19]. The different environment of Cr in **1** and **2** has only minor influence on the Cr–C (cyclopentadienyl ring) and Cr–Cl distances (see Table 1).

2.2. Ethylene polymerisation catalysis

Cyclopentadienyl chromium(III) complexes are known to catalyse the polymerization of ethylene, and in view of the structural novelty of the complexes described above their catalytic activity was evaluated. 10 mg of chromium compound and 100 equivalents of methylalumoxane (MAO) were dissolved in 50 ml toluene ([Cr] $\approx 10^{-6}$ M) and exposed to 1.4 MPa of ethylene for 1 h at room temperature. Under these conditions both **2** and **3** produced moderate amounts of polyethylene (**2**, 0.54 g; **3**, 1.38 g). Characterisation of the resulting polymers by ^{13}C NMR spectroscopy showed them to be highly linear polyethylene with negligible branching (**2**, 0.9 branches per 1000 backbone C atoms; **3**, 1.9 branches per 1000 backbone C atoms). However, molecular weight determination by gel permeation chromatography (GPC) revealed a surprising difference between the two samples. Polyethylene obtained with **3** had a very narrow molecular weight distribution ($M_n = 2220$, $M_w = 4710$, $M_w/M_n = 2.12$), consistent with a homogeneous single-site catalyst. In contrast, the polymer produced by **2** was at least trimodal and accordingly had a much higher

Table 1
Selected distances [Å] and bond angles [°] for **1** and **2**

$[\{(\eta\text{-}C_5H_4)CMe_2PPh\}CrCl]_2$ (**1**)			
Cr(1)–C	2.203(2)–2.255(2)	C(6)–P(1)–C(12)	107.9(1)
Cr(1)–P(1)	2.347(1)	C(1)–Cr(1)–P(1)	126.23(5)
Cr(1)–P(1a)	2.360(1)	Cl(1)–Cr(1)–P(1)	103.47(2)
Cr(1)···Cr(1a)	2.9383(1)	P(1)–Cr(1)–P(1a)	102.75(2)
P(1)–Cr(1a)	2.360(1)	C(6)–P(1)–Cr(1)	121.43(6)
P(1)–C(6)	1.817(2)	C(12)–P(1)–Cr(1)	126.05(6)
P(1)–C(12)	1.894(2)	C(1a)1–C(12)–P(1)	93.2(1)
Cr(1)–Cl(1)	2.278(1)	P(1)···P(1a)	3.678(1)
$[\{(\eta^5\text{-}C_5H_4)CMe_2PHPh\}CrCl_2(PMe_2Ph)]$ (**2**)			
Molecule 1		Molecule 2	
Cr(1)–C	2.191(3)–2.282(3)	Cr(2)–C	2.209(3)–2.290(3)
Cr(1)–Cl	2.278(1)–2.292(1)	Cr(2)–Cl	2.288(1)–2.290(1)
Cr(1)–P(2)	2.439(1)	Cr(2)–P(4)	2.447(1)
P(1)–C(6)	1.910(4)	P(3)–C(28)	1.895(3)
P(1)–H(p1)	1.36(4)	P(3)–H(p2)	1.34(4)
C(9)–P(1)–C(6)	104.1(2)	C(31)–P(3)–C(28)	104.6(1)
C(9)–P(1)–H(p1)	101.1(2)	C(31)–P(3)–H(p2)	101.2(1)
C(6)–P(1)–H(p1)	98.2(2)	C(28)–P(3)–H(p2)	98.8(2)
C(16)–P(2)–C(17)	103.2(2)	C(38)–P(4)–C(37)	104.2(2)
C(15)–P(2)–C(16)	103.9(2)	C(38)–P(4)–C(39)	106.0(2)
C(15)–P(2)–C(17)	105.9(2)	C(37)–P(4)–C(39)	104.6(2)
C(15)–P(2)–Cr(1)	113.7(1)	C(39)–P(4)–Cr(2)	115.59(1)
C(16)–P(2)–Cr(1)	112.1(1)	C(38)–P(4)–Cr(2)	113.6(2)
C(17)–P(2)–Cr(1)	116.7(1)	C(37)–P(4)–Cr(2)	111.9(1)
Cl(1)–Cr(1)–Cl(2)	97.97(4)	Cl(4)–Cr(2)–Cl(3)	97.5(1)
Cl(1)–Cr(1)–P(2)	92.94(4)	Cl(4)–Cr(2)–P(4)	92.7(1)
Cl(2)–Cr(1)–P(2)	89.61(4)	Cl(3)–Cr(2)–P(4)	91.4(1)

polydispersity ($M_n = 4830, M_w = 617000, M_w/M_n = 127.8$). The reasons for this disparity are not clear, given the subtle structural differences between the two catalyst precursors.

3. Experimental

3.1. General

All experiments were carried out under purified dry nitrogen. Solvents were dried and freshly distilled under argon. The NMR spectra were recorded with an AVANCE DRX 400 spectrometer (Bruker): ^{1}H NMR (400.13 MHz): internal standard solvent, external standard TMS; ^{31}P NMR (161.9 MHz): external standard 85% H_3PO_4. The IR spectra were recorded on an FT-IR spectrometer Perkin–Elmer System 2000 (KBr) in the range 350–4000 cm^{-1}. UV–Vis spectra were recorded with a LAMBDA 900 (Perkin–Elmer). The magnetic moments were determined with a magnetic susceptibility balance of Johnson Mathey Alfa Products. EI MS: MAT 212 (Varian); FAB: ZAB-HSQ-VG Analytical Manchester. The melting points were determined in sealed capillaries under nitrogen and are uncorrected (Boetius). Li[$(C_5H_4)CMe_2PHPh$] [10] Li[$(C_5H_4)CMe_2PH^tBu$] [17] and [$CrCl_3(PMe_2Ph)_3$] [24] were prepared according to the literature procedures. $CrCl_3$ is commercially available (Merck).

3.2. Synthesis of [{(η-C_5H_4)CMe_2PPh}$CrCl$]$_2$ (1)

At ca. −50 °C a solution of Li[$(C_5H_4)CMe_2PHPh$] (1.7 g, 7.7 mmol) in THF (10 ml) was slowly added to a suspension of [$CrCl_3(THF)_3$] (2.9 g, 7.7 mmol) in THF (25 ml). During the addition, [$CrCl_3(THF)_3$] slowly dissolved, and the initially colorless solution turned dark green after addition of several drops of the solution of the Li salt. The solution was stirred for 24 h at r.t., after which it had turned blue. Then the solvent was evaporated in vacuum and the slimy blue residue was washed with *n*-hexane to give 2.0 g of a blue powder after drying in vacuo. The blue powder was dissolved in toluene (15 ml) and layered with *n*-hexane. A blue powder was obtained and a small amount of blue crystals of **1** suitable for X-ray structure determination formed at the interface between the two solvents.

3.3. Synthesis of [{(η^5-C_5H_4)CMe_2PHPh}$CrCl_2$-(PMe_2Ph)] (2)

$CrCl_3$ (1.2 g, 7.6 mmol) was suspended in toluene (25 ml), and THF (25 ml) and PMe_2Ph (3.3 ml, 22.8 mmol) were added quickly. The mixture slowly turned green and was refluxed for ca. 2 h, after which the reaction was complete. The solution was filtered and the filtrate cooled to −50 °C. A solution of Li[$(C_5H_4)CMe_2PHPh$] (1.7 g, 7.6 mmol) in THF (25 ml) was slowly added to this solution. During the addition, the initially green solution turned blue. The solution was stirred for 12 h at r.t. Then the solvent was evaporated in vacuo and the blue residue dissolved in CH_2Cl_2 (25 ml). LiCl was separated from the blue solution by filtration and extracted twice with CH_2Cl_2 (10 ml). The CH_2Cl_2 fractions were combined and the solvent was evaporated in vacuum. The blue residue was washed with hexane (2×20 ml) and extracted repeatedly with Et_2O (70 ml) to give 1.8 g (50%) of **2**; m.p. 114–117 °C. Blue crystals were obtained from a concentrated Et_2O solution at −30 °C.

^{1}H NMR (C_6D_6): $\delta = -28.3$ (br s), 0.3 (s), 4.5 (sh), 5.0 (s), 5.8 (s), 10.5 (s). ^{31}P NMR (CH_2Cl_2/C_6D_6): $\delta = 92$ ppm. IR: 3076 (w, CH, C_5H_4), 3054 (w, CH, Ph), 2964, 2910 (m, CH, CH_3 (CMe)), 2866 (w, CH, CH_3 (PMe)), 2278 (m, PH), 1476, 1365 (m-st, CH_3 (CMe)), 1435 (st, CH_3 (PMe)), 1282, 1106 (w-m, PC (PMe_2Ph), 955, 924, 829, 913 (st, CH, CH_3 (PMe)) 745, 694 (st, CH, Ph) 485 (m, PC (PMe_2Ph)) cm^{-1}. UV–Vis: log(ε/cm^2 mol^{-1}) = 4.69 ($\lambda = 661$ nm). $\mu_{eff} = 4.0$ B.M. ($\mu_{calc} = 3.8$). *Anal*. Calc. for $C_{22}H_{27}Cl_2CrP_2$ (476.3): C, 55.5; H, 5.7. Found: C 53.9, H 5.3%.

3.4. Synthesis of [{(η^5-C_5H_4)CMe_2PH^tBu}$CrCl_2$-(PMe_2Ph)] (3)

$CrCl_3$ (1.3 g, 8.2 mmol) was suspended in toluene (25 ml), and THF (25 ml) and PMe_2Ph (3.5 ml, 24.2 mmol) were added quickly. The mixture slowly turned green and was refluxed for ca. 2 h, after which the reaction was complete. The solution was filtered and the filtrate cooled to −50 °C. A solution of Li[$(C_5H_4)CMe_2PH^tBu$] (1.65 g, 8.2 mmol) in THF (10 ml) was slowly added to this solution. During the addition, the initially green solution turned blue. The solution was stirred at r.t. for 2 h and then refluxed for 1 h. Then the solvent was evaporated in vacuum and the blue residue dissolved in CH_2Cl_2 (25 ml). LiCl was separated from the blue solution by filtration and extracted twice with CH_2Cl_2 (10 ml). The CH_2Cl_2 fractions were combined and the solvent was evaporated in vacuum. The blue residue was washed with hexane (2×25 ml) and extracted repeatedly with Et_2O (50 ml) to give 1.9 g (51%) of **3** as blue crystals; m.p. 143 °C.

^{1}H NMR (C_6D_6): $\delta = -28.3$ (br s), 0.0 (s), 5.0 (s), 8.9 (br s), 10.5 (s). ^{31}P NMR (CH_2Cl_2/C_6D_6): $\delta = 111$ ppm. IR: 3080 (w, CH, C_5H_4), 3054 (w, CH, Ph), 2953, 2892 (m-st, CH, CH_3 (CMe)), 2859 (m-st, CH, CH_3 (PMe)), 2295, 2276 (m, PH), 1474, 1365 (m-st, CH_3 (CMe)), 1436 (m-st, CH_3 (PMe)), 1411 (m-st, CH_3 (^{t}Bu)) 1280, 1107 (m, PC (PMe_2Ph)), 955, 924, 829, 913 (st, CH, CH_3 (PMe)) 744, 694 (st, CH, Ph) 485 (m, PC (PMe_2Ph)), 408

Table 2
Crystal data and structure refinement for **1** and **2**

	1	**2**
Empirical formula	$C_{28}H_{30}Cl_2Cr_2P_2$	$C_{22}H_{27}Cl_2CrP_2$
M_r	603.36	476.30
Temperature (K)	220(2)	220(2)
Crystal system	monoclinic	triclinic
Space group	$P2_1/c$ (no. 14)	$P\bar{1}$ (no. 2)
a (Å)	8.7224(4)	13.738(2)
b (Å)	8.9261(4)	13.764(2)
c (Å)	17.0822(8)	13.885(2)
α (°)	90	88.986(3)
β (°)	96.4(1)	72.509(3)
γ (°)	90	72.607(3)
V (Å^3)	1321.7(1)	2382.0(6)
Z	2	4
ρ_{calc} (Mg m^{-3})	1.516	1.328
$F(000)$	620	988
Crystal size (mm)	$0.70 \times 0.20 \times 0.05$	$0.3 \times 0.2 \times 0.2$
Absorption coefficient (mm^{-1})	1.162	0.844
Θ range (°)	2.35–28.74	1.56–29.45
Reflections collected	13076	15394
Independent reflections	3239	11272
R_{int}	0.0391	0.0271
Parameters	211	495
$R[I > 2\sigma I)]$	0.0300	0.0514
$wR2$ (all data)	0.0756	0.0999
Δ/ρ_{min} (e Å^{-3})	0.306	0.312
Δ/ρ_{max} (e Å^{-3})	−0.313	−0.369

(st, CrCl?) cm^{-1}. FAB MS: m/z (%) = 455 (12) [M$^+$], 420 (49) [M$^+$ − Cl], 317 (25) [M$^+$ − PMe$_2$Ph], 282 (62) [M$^+$ − Cl − PMe$_2$Ph], 139 (100) [PMe$_2$Ph + H$^+$], and fragmentation products thereof. EI MS: $m/z = 362$ [M$^+$ − C$_6$H$_5$CH$_3$], 317 [M$^+$ − PMe$_2$Ph], 281 [M$^+$ − HCl − PMe$_2$Ph], 225 [M$^+$ − HCl − PMe$_2$Ph − ^{t}Bu], 193 [M$^+$ − PMe$_2$Ph − PH^{t}Bu − Cl], 138 [PMe$_2$Ph]$^+$, 123 [PMePh], and fragmentation products thereof. UV–Vis: log(ε/cm^2 mol^{-1}) = 4.72 (λ = 667 nm). μ_{eff} = 3.8 B.M. (μ_{calc} = 3.8). *Anal.* Calc. for $C_{20}H_{31}Cl_2CrP_2$ (456.3): C, 52.6; H, 6.8. Found: C, 52.0; H, 7.1%

3.5. Data collection and structural refinement of **1** and **2**

Data (λ(Mo Kα) = 0.71073 Å) were collected with a Siemens CCD (SMART) diffractometer. All observed reflections were used for refinement (SAINT) of the unit-cell parameters. Empirical absorption correction with SADABS [25]. The structures were solved by direct methods (SHELXTL PLUS) [26]. For **1** and **2**, Cr, P, Cl, and C atoms were refined anisotropically; H atoms were located by difference maps and refined isotropically (see Table 2).

4. Supplementary material

CCDC-221773 (**1**) and -221774 (**2**) contain the supplementary crystallographic data for this paper. These data can be obtained free of charge via www.ccdc.cam.ac.uk/conts/retrieving.html (or from the Cambridge Crystallographic Data Centre, 12 Union Road, Cambridge CB2 1EZ, UK; fax: (+44)-1223-336-033; or deposit@ccdc.cam.uk).

Acknowledgements

We gratefully acknowledge financial support from the *Deutscher Akademischer Austauschdienst* (315/PPP/ab) and the *US National Science Foundation* (CHE-9876426 to KHT). We thank ChevronPhillips Chemical Co. for characterisation of the polymers.

References

[1] K. Ziegler, E. Holzkamp, H. Breil, H. Martin, Angew. Chem. 67 (1955) 541.
[2] N. Schneider, M.E. Huttenloch, U. Stehling, R. Kirsten, F. Schaper, H.H. Brintzinger, Organometallics 16 (1997) 3413, and references therein.
[3] W. Kaminsky, O. Rabe, A.-M. Schauwienold, G.U. Schupfner, J. Hanss, J. Kopf, J. Organomet. Chem. 497 (1995) 181.
[4] S.T. Chacon, E.B. Coughlin, L.M. Henling, J.E. Bercaw, J. Organomet. Chem. 497 (1995) 171.
[5] (a) W. Kaminsky, K. Külper, H.H. Brintzinger, F.R.W.P. Wild, Angew. Chem. 97 (1985) 507; Angew. Chem. Int. Ed. Engl. 24 (1985) 507;
(b) H.H. Brintzinger, D. Fischer, R. Mülhaupt, B. Rieger, R.M. Waymouth, Angew. Chem. 107 (1995) 1255; Angew. Chem. Int. Ed. Engl. 34 (1995) 1143;
(c) G. Fink, R. Mülhaupt, H.H. Brintzinger, Ziegler Catalysts – Recent Scientific Innovations and Technological Improvements, Springer-Verlag, Berlin, 1995.
[6] (a) P.J. Shapiro, E. Bunel, W.P. Schaefer, J.E. Bercaw, Organometallics 9 (1990) 867;
(b) P.J. Shapiro, W.D. Cotter, W.P. Schaefer, J.A. Labinger, J.E. Bercaw, J. Am. Chem. Soc. 116 (1994) 4623;
(c) J.C. Flores, J.C.W. Chien, M.D. Rausch, Organometallics 13 (1994) 4140;
(d) H.G. Alt, K. Föttinger, W. Milius, J. Organomet. Chem. 572 (1999) 21;
(e) M. Galan-Fereres, T. Koch, E. Hey-Hawkins, M. Eisen, J. Organomet. Chem. 580 (1999) 145;
(f) A.L. McKnight, R.M. Waymouth, Chem. Rev. 98 (1998) 2587;
(g) J.A.M. Canich, Eur. Patent 420 436, 1991;
(h) G.F. Schmidt, F.J. Timmers, G.W. Knight, S.-Y. Lai, P.N. Nickias, R.K. Rosen, J.C. Stevens, D.R. Wilson, Eur. Patent 416 815, 1991.
[7] (a) S.J. Brown, X. Gao, D.G. Harrison, L. Koch, R.E.V.H. Spence, G.P.A. Yap, Organometallics 17 (1998) 5445;
(b) F. Mathey, Chem. Rev. 88 (1988) 429;
(c) C. Janiak, K.C.H. Lange, U. Versteeg, D. Lentz, P. Budzelaar, Chem. Ber. 129 (1996) 1517;
(d) C. Janiak, U. Versteeg, K.C.H. Lange, R. Weimann, E. Hahn, J. Organomet. Chem. 501 (1995) 219.
[8] H. Butenschön, Chem. Rev. 100 (2000) 1527.
[9] T. Heidemann, P. Jutzi, Synthesis (1994) 777.
[10] T. Koch, E. Hey-Hawkins, Polyhedron 18 (1999) 2113, and references therein.

[11] C.S. Slone, D.A. Weinberger, C.A. Mirkin, Prog. Inorg. Chem. 48 (1999) 233.
[12] U.J. Bildmann, G. Müller, Z. Naturforsch. 55B (2000) 895.
[13] U.J. Bildmann, M. Winkler, G. Müller, Z. Naturforsch. 55B (2000) 1005.
[14] O. Tardif, Z. Hou, M. Nishiura, T. Koizumi, Y. Wakatsuki, Organometallics 20 (2001) 4565.
[15] T. Höcher, S. Blaurock, E. Hey-Hawkins, Eur. J. Inorg. Chem. (2002) 1174.
[16] T. Koch, E. Hey-Hawkins, M. Galan Fereres, M.S. Eisen, Polyhedron 21 (2002) 2445.
[17] T. Koch, S. Blaurock, F.B. Somoza Jr., A. Voigt, R. Kirmse, E. Hey-Hawkins, Organometallics 19 (2000) 2556.
[18] K. Kunz, G. Erker, S. Döring, R. Fröhlich, G. Kehr, J. Am. Chem. Soc. 123 (2001) 6181.
[19] A. Döhring, V.R. Jensen, P.W. Jolly, W. Thiel, J.C. Weber, Organometallics 20 (2001) 2234.
[20] P.W. Jolly, K. Jonas, G.P.J. Verhovnik, A. Döhring, J. Göhre, J.C. Weber, (Studiengesellschaft Kohle mbH). Patent PCT, WO 98/04570, DE 197 10 615.3 (14.03.97), 1998.
[21] S. Kohn, Diplomarbeit, Universität Leipzig, 2001.
[22] For the related complex $[CrCl_3(Me_2PCH_2)_3CMe]$ see: E. Thaler, K. Folting, J.C. Huffman, K.G. Caulton, Inorg. Chem. 26 (1987) 374.
[23] P. Wei, D.W. Stephan, Organometallics 22 (2003) 1712.
[24] T. Höcher, Dissertation, Universität Leipzig, 2004.
[25] G.M. Sheldrick, SADABS – a program for empirical absorption correction, Göttingen, 1998.
[26] SHELXTL PLUS, Siemens Analyt. X-ray Inst. Inc., 1990, XS: program for crystal structure solution, XL: program for crystal structure determination, XP: interactive molecular graphics.

Available online at www.sciencedirect.com
SCIENCE DIRECT®
Polyhedron 23 (2004) 1401–1408
POLYHEDRON
www.elsevier.com/locate/poly

Nickel(II) and copper(II) Schiff base complexes bearing benzo-15-crown-5 functionalities as probes for spectroscopic recognition of lanthanide ions

Carla Sousa, Paula Gameiro, Cristina Freire *, Baltazar de Castro

REQUIMTE, Departamento de Química, Faculdade de Ciências, Universidade do Porto, Rua do Campo Alegre 687, 4169-007 Porto, Portugal

Received 4 December 2003; accepted 20 February 2004
Available online 9 April 2004

Abstract

A combination of host guest and coordination chemistry in the design of a spectroscopic sensor for lanthanide and aluminium ions is described. Nickel(II) and copper(II) complexes with a N_2O Schiff base ligand and bearing two benzo-15-crown-5 moieties as flexible arms have been prepared and characterised by FAB-MS, UV–Vis and FTIR spectroscopies and, depending on the transition metal, by ^1H NMR or EPR. Recognition studies of alkaline, alkaline-earth, aluminium and lanthanide ions have been attempted in dmf by UV–Vis spectroscopy. Charge transfer and intraligand electronic bands of the Ni(II) and Cu(II) complexes show significant changes only in the presence of the M^{3+} ions used, lanthanides (Er^{3+}, Gd^{3+} and Pr^{3+}) and Al^{3+}. Spectral changes induced by increasing M^{3+} concentrations have allowed the calculation of stability constants associated with the coordination of one trivalent ion in each crown ether moiety, corresponding to the formation of 1:2 adducts (metal complex:M^{3+}), with values of $\log \beta_{21}$ in the range 8.2–9.5. No apparent correlation is perceptible between $\log \beta_{21}$ values and the transition metal, but a cavity effect was detected for each metal complex since $\log \beta_{21}$ values increased as lanthanide radii increased.
© 2004 Elsevier Ltd. All rights reserved.

Keywords: Ion recognition; Schiff base complexes; Crown ether; UV–Vis; Lanthanides

1. Introduction

Molecular recognition is the first step in the design of molecular sensors for detection of ions or neutral species in organic or aqueous media. In the presence of the target species, the molecular sensor is designed to exhibit a physical response which must be easily detected.

The traditional approach of host–guest chemistry has focused primarily on systems, such as crown ethers, calixarenes and cryptands, which have shown to act as selective hosts for ions and neutral species [1–3]. Upon specific functionalisation they can act as excellent platforms to append several sensing moieties, allowing the preparation of panoply of molecular sensors which will detect the target species by using specific physicochemical properties of the attached sensing block.

There has been an increasing interest in the preparation of the referred host groups with appended transition metal complexes, and examples of this work include as signalling moieties ferrocene and other organometallic compounds [4–7], Schiff base complexes [7–9], metalloporphyrins and phthalocyanines [7,10–12]. These systems, owing to intrinsic properties of transition metals, constitute versatile spectroscopic and electrochemical responsive receptors for charged and neutral guests.

We have been interested in the preparation of Schiff base complexes functionalised with crown ether and pseudo-crown ether moieties for ion recognition, both in solution and as polymeric films deposited onto Pt and ITO electrodes. We have grafted dibenzo18-crown-6- and benzo-15-crown-5-ether onto N_2O_2 Schiff base ligands [13] and explored their properties to sense representative and lanthanide cations, both in solution [14] and as-deposited polymeric films [15]. Currently, we are pursuing the synthesis of Schiff base ligands

* Corresponding author. Tel.: +351226082890; fax: +351226082959.
E-mail address: acfreire@fc.up.pt (C. Freire).

0277-5387/$ - see front matter © 2004 Elsevier Ltd. All rights reserved.
doi:10.1016/j.poly.2004.02.014

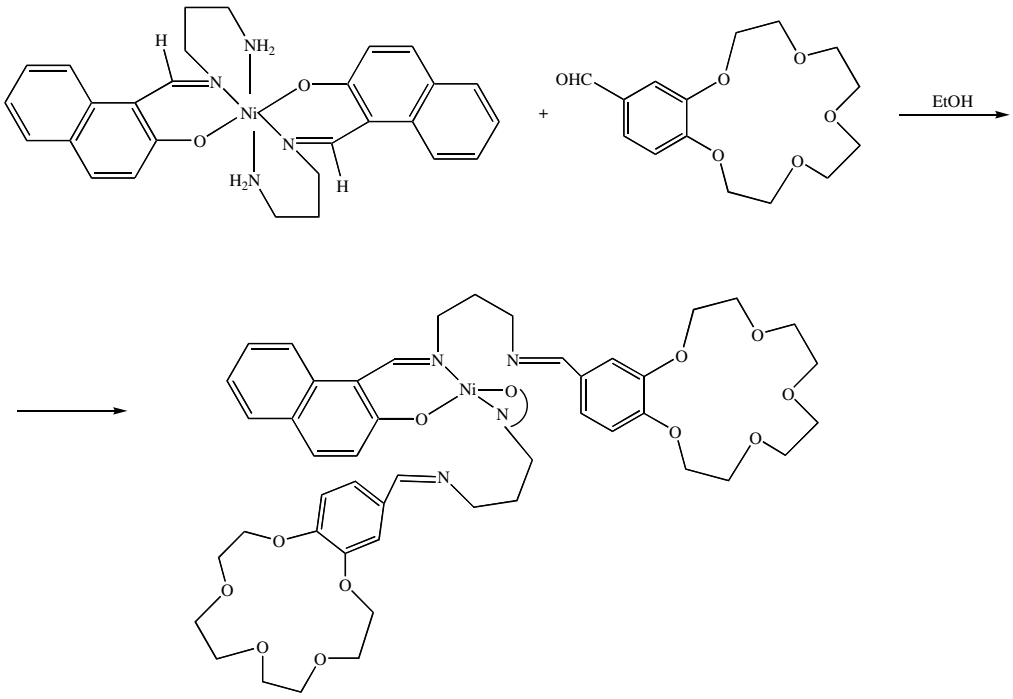

Scheme 1. Reaction steps used in the preparation of $[Ni(nlpb15)_2]$.

functionalised with the same motif, but including the crown ether moiety as flexible appended arms.

In a preceding paper we have reported the synthesis of nickel(II) complexes of general formula NiL_2, where L is an asymmetric N_2O tridentate ligand obtained by Schiff condensation of propane-1,3-diamine with salicylaldehyde or a derivative [16]. The nickel(II) complexes have amine groups that can react with formyl groups of crown-ether derivatives yielding Schiff base nickel(II) and copper(II) complexes with two appended flexible crown ether arms, as depicted in Scheme 1. The introduction of a transition metal complex moiety into the crown ether framework allows the exploitation of its spectroscopic and electrochemical properties to sense s-block, aluminium and lanthanide ions.

2. Experimental

2.1. Reagents and solvents

All reagents and solvents were used as received. Solvents for syntheses were of reagent grade and those for electrochemical and UV–Vis studies of analytical grade. Nickel acetate tetrahydrate, copper acetate monohydrate, dimethylglyoxime, potassium perchlorate, sodium perchlorate hydrate and calcium nitrate tetrahydrate were from Merck; strontium nitrate, barium perchlorate and magnesium perchlorate from Fluka; lithium perchlorate, rubidium chloride, cesium fluoride, erbium perchlorate (40 wt% solution in water) and gadolinium trifluoromethanesulfonate from Aldrich; praseodymium nitrate from Alfa Aesar; and aluminium nitrate nonohydrate from J.T. Baker. Tetraethylammonium perchlorate (TEAP) was from Fluka and was kept in an oven at 60 °C prior to use.

Caution! perchlorates are hazards may explode.

2.2. Synthesis

The compound 4′-formylbenzo-15-crown-5 was prepared by a procedure described in literature [17], by reacting 3,4-dihydroxybenzaldehyde with 1,11-dichloro-3,6,9-trioxaundecane. The parent nickel complex, $[Ni(nlp)_2]$, was synthesised by the procedure described in [16].

2.2.1. Preparation of bis[o-(3-(benzo-15-crown-5-formimidoyil)propylformimidoyil)naphtholate-O,N]nickel [Ni(nlpb15)$_2$]

A solution of 4′-formylbenzo-15-crown-5 (0.85 g; 2.9 mmol) in EtOH was added to an ethanolic solution of $[Ni(nlp)_2]$ (0.62 g; 1.2 mmol) and the mixture was refluxed for 6 h. A light-green solid was collected, washed with EtOH and dried over vacuum. Yield 0.65 g (51%).

MS (FAB), m/z: 1069 $[M+H]^+$ (5%), 1092 $[M+Na+H]^+$ (27); high resolution: 1069. Calc. for $NiC_{58}H_{67}N_4O_{12}$: 1069.410896. Found: 1069.412454. ^{1}HNMR $CDCl_3$: $\delta = 9.08$ (s; 2H; –CHN), 8.52 (s; 2H; –CHN), 7.80–7.77 (d; 2H; –H arom), 7.66–7.64 (d; 2H; –H arom), 7.51–7.48 (d; 2H; –H arom), 7.42–7.35 (t; 4H; –H arom), 7.22–7.17 (t; 2H; –H arom), 7.05–7.03 (d; 2H;

–H arom), 6.84–6.78 (t; 4H; –H arom), 4.15–4.13 (m; 8H; $-CH_2$), 3.94–3.76 (m; 32H; $-CH_2$); 2.36 (s; 4H; $-CH_2$); 1.71 (s; 2H; $-H_2O$). IR(KBr) (ν/cm^{-1}): 3457, 2931, 2853, 1643, 1619, 1602, 1562, 1540, 1516, 1460, 1435, 1401, 1370, 1345, 1326, 1270, 1239, 1208, 1177, 1131, 1087, 1053, 1016, 975, 923, 860, 830, 777, 752, 687, 662, 640, 620, 535, 473, 429. UV–Vis λ_{max} (dmf)/nm ($\varepsilon \times 10^3$/dm^3 mol^{-1} cm^{-1}): 345 (15.5), 403 sh (6.52), 423 (8.0), 445 sh (4.8).

2.2.2. Preparation of bis[o-(3-(benzo-15-crown-5-formimidoyil)propylformimidoyil)naphtholate-O, N]copper [Cu(nlpb15)$_2$]

A solution of [Ni(nlpb15)$_2$] (0.11 g; 0.10 mmol) in $CHCl_3$was added to a solution of dimethylglyoxime (H_2dmg) (0.024 g; 0.21 mmol) in EtOH and the mixture was stirred for 14 h at room temperature. The red nickel complex, [Ni(dmg)$_2$], was filtered off and rejected. An ethanolic solution of copper(II) acetate (0.021 g; 0.10 mmol) was added to the filtrate and the mixture was stirred for 6 h. A light-brown solid was collected, washed with diethyl ether and dried over vacuum. Yield 0.016 g (15%).

MS (FAB), m/z: 1074 $[M+H]^+$ (5%), 1097 $[M+Na+H]^+$ (15); high resolution: 1074. Calc. for $CuC_{58}H_{67}N_4O_{12}$: 1074.405149. Found: 1074.409683. IR(KBr) (ν/cm^{-1}): 2915, 2867, 1641, 1615, 1606, 1560, 1541, 1512, 1461, 1438, 1414, 1400, 1365, 1344, 1323, 1270, 1238, 1208, 1179, 1129, 1103, 1052, 1017, 984, 938, 888, 858, 829, 779, 749, 666, 649, 602, 519, 502, 473, 417. UV–Vis λ_{max} (dmf)/nm ($\varepsilon \times 10^3$/dm^3 mol^{-1} cm^{-1}): 382 (3.4), 396 (33.9), 422 sh (13.8).

No accurate elemental analysis could be obtained for the functionalised complexes due to the high capacity of crown ether cavities for solvation; for this reason purity of the complexes were checked by high resolution mass spectra.

2.3. Physical measurements

Mass spectra were obtained at 'Departamento de Química da Universidade de Aveiro' (Portugal). ^{1}H NMR spectra were recorded with a Bruker AC 200 in $CDCl_3$ and the chemical shifts are reported relative to Me_4Si, used as an internal standard. Infrared spectra (KBr pellets) were recorded in the range 4000–400 cm^{-1} using a BioRad FTS 155 spectrometer. EPR spectra were obtained at 120 K with a Bruker ESP 300 (X-band); the magnetic field was calibrated by using Mn^{2+} in MgO, and diphenylpicrylhydrazyl was used as internal reference (dpph; $g = 2.0037$).

Cyclic voltammetry was performed using an Autolab PGSTAT20 potentiostat/galvanostat. A Pt disk electrode with an area of 0.0314 cm^2 was used as the working electrode, a Pt electrode as the counter electrode and an Ag/AgCl (1 mol dm^{-3} NaCl) as the reference electrode. Prior to use, the Pt working electrode was polished with an aqueous suspension of 0.05 μm alumina (Beuhler) on a Master-Tex (Beuhler) polishing pad, then rinsed with water and dried. All solutions were deareated by a stream of argon.

Room temperature electronic spectra of the complexes in dmf and $CHCl_3$ were recorded with a Unicam UV 2 spectrophotometer in the range 335–1100 nm, using standard 1-cm quartz cells; complex concentrations were 1×10^{-3} mol dm^{-3} (d–d bands) and 1×10^{-5} mol dm^{-3} (CT and intra ligand bands). Spectrophotometric titrations were carried out at 25.0 ± 0.1 °C in dmf and the spectra recorded in the wavelength range 335–550 nm, using a slit width of 2 nm. To a series of solutions of [M(nlpb15)$_2$], M = Ni(II) or Cu(II), with concentrations in the range 1×10^{-5}–2×10^{-4} mol dm^{-3} were added increasing concentrations of ions of representative metals (Al^{3+}, Li^+, Na^+, K^+, Rb^+, Cs^+, Mg^{2+}, Ca^{2+}, Sr^{2+} and Ba^{2+}) or of lanthanides (Er^{3+}, Pr^{3+} and Gd^{3+}), spanning the range 1.0×10^{-6}–1.0×10^{-4} mol dm^{-3} and the respective spectra recorded. The Beer–Lambert law was obeyed for solutions of the complex at the experimental conditions used (5.0×10^{-6}–2.5×10^{-4} mol dm^{-3}); solutions of lanthanide ions ($< 1 \times 10^{-4}$ mol dm^{-3}) did not absorb in the wavelength range used. The stability constants (β_{21}), the equilibrium concentrations of the species in solution and the extinction coefficients at selected wavelengths were determined using the programme SQUAD [18].

Stock solutions of the representative metal ions (Li^+, Na^+, K^+, Rb^+, Cs^+, Mg^{2+}, Ca^{2+}, Sr^{2+}, Ba^{2+} and Al^{3+}) and of the lanthanides ions (Er^{3+}, Pr^{3+} and Gd^{3+}) (0.01 mol dm^{-3}) were prepared in dmf.

3. Results and discussion

3.1. Complex preparation and characterisation

The four-coordinate functionalised complex [Ni(nlpb15)$_2$] was prepared by Schiff condensation of the coordinated amine groups of [Ni(nlp)$_2$] [16] with the formyl group of formylbenzo-15-crown-5 (Scheme 1). The homologous Cu complex, [Cu(nlpb15)$_2$], was prepared by demetalation of [Ni(nlpb15)$_2$] with dimethylglyoxime and addition of copper acetate, as it was not possible to prepare the parent copper compound, [Cu(nlp)$_2$].

The FAB mass spectrum of [Ni(nlpb15)$_2$] shows peaks at $m/z = 1069$ and 1092, which correspond to $[M+H]^+$ and $[M+Na+H]^+$, respectively. That of the copper(II) complex shows not only fragments with $m/z = 1074$ and 1097, values associated with $[M+H]^+$ and $[M+Na+H]^+$, but also a peak at $m/z = 1139$ which corresponds to protonated binuclear species $[Cu_2(nlpb15)_2+H]^+$; formation of protonated binuclear

species have also been observed in the FAB mass spectrum of [Ni(nlp)$_2$] [16].

Solutions of [Ni(nlpb15)$_2$] in $CDCl_3$ exhibit ^{1}H NMR spectra with chemical shifts typical of a diamagnetic Ni(II) compound, what provides a first indication that upon reaction of the transition metal complex amine groups with crown ether formyl functionalities, the nitrogen atoms of the newly formed imine bonds are not bound to the metal centre, with the implication that the novel complex exhibits an almost N_2O_2 square planar geometry. In the ^{1}H NMR spectrum of [Ni(nlpb15)$_2$] the two resolved singlets at $\delta = 9.08$ and 8.52 ppm are assigned to the two C(H)=N protons, that of the ether and the aldehyde moieties, respectively. The observation of these two singlets provides confirmation of Schiff base reaction between amine groups of the complex and formylbenzo-15-crown-5.

The signals of the aromatic protons appear at 7.80 and 6.78 pm, the multiplet at 4.15 ppm is assigned to crown ether methylene groups, and that at 3.76 pm to terminal CH_2 of the imine bridge and the protons of the central CH_2 in this bridge appear at 2.36 pm.

The EPR spectrum of [Cu(nlpb15)$_2$] in frozen dmf solution is similar to those of copper(II) complexes with tetradentate Schiff base ligands [19–21]; it is of apparent axial symmetry and exhibits in all magnetic regions well-resolved hyperfine couplings with copper (^{63}Cu/^{65}Cu, $I = 3/2$), although no superhyperfine splitting with ligand nitrogen atoms could be observed in any of the g regions, probably due to the large bandwidth associated with the spectrum in dmf. The similarity between this spectrum, and those observed for other four-coordinate copper Schiff base complexes, allows for the same orientation scheme for the g tensor: $g_1 = g_z$, $g_2 = g_x$, $g_3 = g_y$, where g_1 and g_3 refer to the lowest and highest magnetic fields g values (obviously, $|A_1| = |A_z|$, $|A_2| = |A_x|$ and $|A_3| = |A_y|$ [19–21]. Simulation of the spectrum using a rhombic spin Hamiltonian yields: $g_z = 2.312$, $g_x = 2.139$, $g_y = 2.131$, $A_z(\mathrm{Cu}) = 180$ G, $A_x(\mathrm{Cu}) = A_y(\mathrm{Cu}) = 25$ G; $a_z(\mathrm{N}) = 20$ and $a_x(\mathrm{N}) = a_y(\mathrm{N}) = 10$ G. The value of the copper hyperfine coupling in the z region is typical of almost square planar complexes (or with incipient axial coordination), which combined with the fact that $g_z > g_x, g_y$ indicates that the complex has a $d_{x^2-y^2}$ ground state and an almost square planar geometry.

The IR spectra of [Ni(nlpb15)$_2$] and [Cu(nlpb15)$_2$] are very similar, a consequence of their expected structural similarity. The most sticking difference between the spectrum of Ni(nlpb15)$_2$] and that of the parent complex [Ni(nlp)$_2$] [16] is the disappearance of two sharp bands at 3345 and 3276 cm^{-1}, assigned to the symmetric and anti-symmetric stretchings of –NH_2 in the six-coordinate complex, thus providing further indication that condensation between NH_2 groups of [Ni(nlp)$_2$] and formylbenzo-15-crown-5 has occurred; no comparison between the spectra of [Cu(nlp)$_2$] and [Cu(nlpb15)$_2$] was possible, as the latter was prepared by demetalation of the corresponding nickel complex. The C=N stretching vibration is observed at 1619 cm^{-1} for [Ni(nlpb15)$_2$] and at 1615 cm^{-1} for [Cu(nlpb15)$_2$] [16,22,23], the shift to lower energies on going from nickel to copper reflects the increase in the system reduced mass. Moreover, the bands due to Ar–O–C (crown ether) and to C–O–C (crown ether) vibrations [24,25] are detected in the ranges: 1270–1131 cm^{-1} for [Ni(nlpb15)$_2$] and 1270–1103 cm^{-1} for [Cu(nlpb15)$_2$].

Electronic spectra of the two complexes are very similar, either in dmf and $CHCl_3$, although the bands of the copper complex are shifted to higher energies. They are typical of square planar complexes, as they show one broad medium intensity band at $\lambda \approx 600$ nm ($\varepsilon = 130$–140 dm^3 mol^{-1} cm^{-1}) due to several d–d transitions of similar energies: $d_{x^2-y^2} \leftarrow (d_{z^2}; d_{xy}; d_{xz}; d_{xy})$; as example, the electronic spectra for nickel complex are depicted in Fig. 1 [26]. These observations further confirm that the complexes have similar structures, and that after crown ether functionalisation the imine nitrogens are not bound to the metal. The profile of the d–d bands contrasts with that of the nickel precursor complex, which shows d–d bands in the NIR–Vis region (λ in the range 500–1100 nm), a consequence of its octahedral geometry [16]. In the region of $\lambda < 460$ nm, both nickel and copper complexes show several high intensity CT and intra-ligand bands.

Both compounds show, in the potential range 0–1.3 V, an irreversible oxidation process, whereas their reductive electrochemical behaviour is more complex. The cyclic voltammogram of [Ni(nlpb15)$_2$] shows in the potential range −0.30 to −1.90 V (0.50 V s^{-1}), one cathodic wave at −1.57 V and three anodic waves at −1.43, −1.06 and −0.58 V. Similarly, [Cu(nlpb15)$_2$] shows in the potential range −0.3 to −1.8 V (0.020 V s^{-1}), two cathodic waves at −0.99 and −1.59 V and two low intensity anodic waves at −0.73 and 0.06 V. As these results suggest that charge transfer in both complexes is associated with chemical reactions involving the metal and the ligand [27], no further characterisation of their electrochemical behaviour was pursed.

3.2. Metal ion recognition studies

Metal ion recognition was performed by monitoring the CT and $\pi \rightarrow \pi^*$ band region (from $\lambda = 335$ to 550 nm) of the nickel and copper complexes upon incremental addition of dmf solutions of the target metal ions.

Addition of alkaline (Li^+, Na^+, K^+, Rb^+ and Cs^+) and alkaline-earth (Mg^{2+}, Ca^{2+}, Sr^{2+} and Ba^{2+}) ions causes no significant changes in the energy of the CT and $\pi \rightarrow \pi^*$ bands of any of the complexes. However, incremental additions of aluminium and of lanthanide

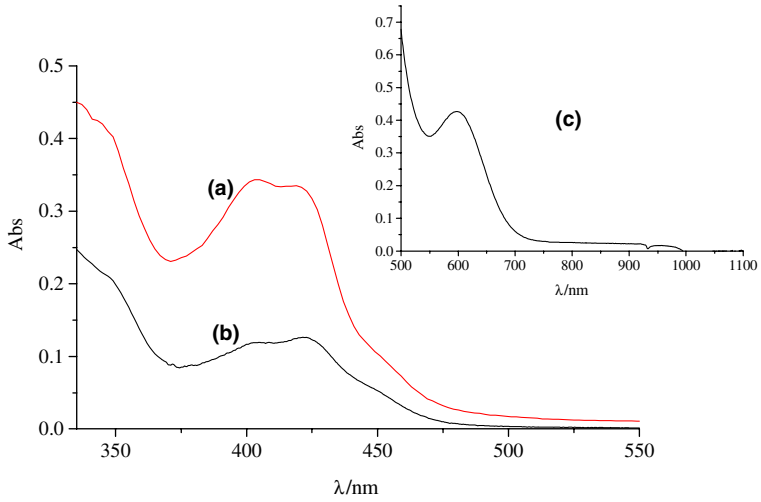

Fig. 1. UV–Vis spectra of $[Ni(nlpb15)_2]$: (a) in dmf $\lambda = 335$–550 nm; (b) in $CHCl_3$ $\lambda = 335$–550 nm; (c) in $CHCl_3$ $\lambda = 550$–1000 nm.

ions (Er^{3+}, Gd^{3+} and Pr^{3+}) induce large changes in the electronic band profile, and that are similar for both complexes (typical responses are depicted in Fig. 2). For solutions of $[Ni(nlpb15)_2]$ and upon aluminium and lanthanide additions the absorbance of the electronic band at 345 nm decreases until practically zero, and the band at 400 increases in intensity and exhibits a small hypsochromic shift; for the corresponding copper(II) complex the band at 381 practically vanishes and the band at 421 not only increases in intensity but is slightly shifted to lower energies. Moreover, for the nickel complex, the shoulder at 455 nm also decreases in intensity.

The changes in absorbance as a function of added ion concentration give rise to sharp isosbestic points at $\lambda = 363$ and 435 nm for the nickel complex, and at $\lambda = 350$, 395 and 441 nm for the copper complex, thus providing a strong indication of the presence of two absorbing species in solution [28–30]: the original transition metal complexes and their Ln^{3+} or Al^{3+} adducts.

The spectral change induced by Ln^{3+} and Al^{3+} ions is a consequence of adduct formation between the metal complexes and the added metal cations. Based on the structure of the nickel precursor complex, $[Ni(nlp)_2]$ [16], we propose that the bidentate ligands in the functionalised complexes are in *trans* conformation. This conformation prevents electrostatic interactions between phenolic oxygen atoms bound to the transition metal centre and the added cations, a behaviour that has been observed for nickel and copper complexes with *cis*-N_2O_2-type tetradentate Schiff base ligands [31–33]. Consequently, for these crown ether functionalised complexes the coordination sites for extrinsic cations are the two crown ethers moieties.

Two types of adduct formation mechanism can be proposed (Scheme 2): (i) complexation of one cation to one of the two crown ethers, 1:1 adduct formation (Eq.

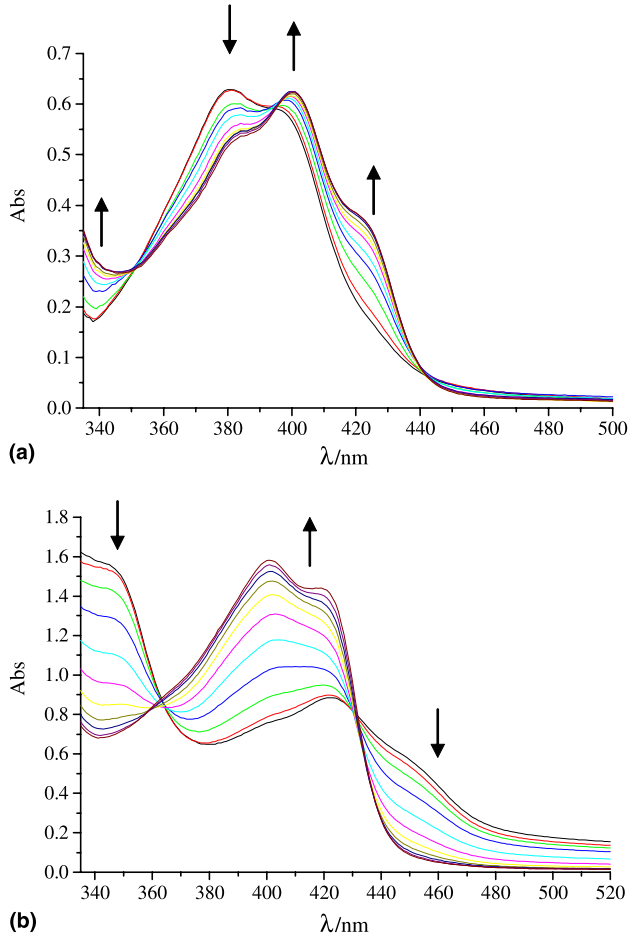

Fig. 2. (a) UV–Vis spectra of $[Cu(nlpb15)_2]$ ($C_{complex} = 5.002 \times 10^{-5}$ mol dm^{-3}, dmf) after addition of increasing quantities of Er^{3+}; $[Cu(nlpb15)_2]$:Er^{3+}molar ratio from 1:0.2 to 1:1.2. (b) UV–Vis spectra of $[Ni(nlpb15)_2]$ ($C_{complex} = 1.669 \times 10^{-4}$ mol dm^{-3}, dmf) after addition of increasing quantities of Al^{3+}; $[Ni(nlpb15)_2]$:Al^{3+}molar ratio from 1:0.2 to 1:1.2.

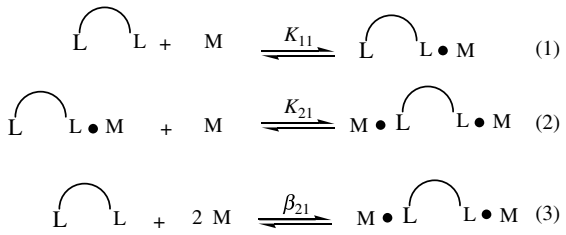

Scheme 2. Solution equilibria for metal complex adduct formation.

(1)), followed by coordination of a second metal ion to the free crown ether moiety, 1:2 adduct (Eq. (2)) or (ii) simultaneously coordination of *two* metal ions to the crown ether cavities, 1:2 adduct (Eq. (3)).

Preliminary information on the adduct formation mechanism can be gathered by considering the system, upon addition of the metal ions, a 1:1 adduct, and apply linear functions, as the double reciprocal and Scatchard plots, to absorbance and metal ion concentration [34]. As the plots obtained with these functions, for all the systems studied, were non-linear it is possible to conclude that the nickel and copper complexes must form adducts with a stoichiometry higher than 1:1. Furthermore, the use of graphical methods [34] to determine the number of species in solution permit to conclude that, upon metal cation addition, there are only two absorbing species in solution. The coupling of these results suggests a model for adduct formation that comprises concomitant coordination of *two* metal ions to each metal complex, one in each crown ether cavity as depicted in (Eq. (3)), Scheme 2.

Taking into account the proposed adduct formation mechanism, we have used the program SQUAD to quantify the interaction between the nickel and copper complexes and the added cations (β_{21} in (Eq. (3)), Scheme 2) using the UV–Vis spectral changes, and the results obtained are summarised in Table 1. Further confirmation for the absence of 1:1 adducts was obtained by the impossibility to determine stability constants associated with coordination of only one cation to the transition metal complexes, although data in the range where these species could exist were used ($C_{\text{complex}} \gg C_{\text{M}}^{n+}$).

Table 1
$\log \beta_{21}$ values for $\{[Ni(nlpb15)_2]\cdot 2M^{3+}\}$ and $\{[Cu(nlpb15)_2]\cdot 2M^{3+}\}^{+}$ adducts in dmf at 25 °C

Complex	M^{3+}	$\log \beta_{21}$
$[Ni(nlpb15)_2]$	Al^{3+}	8.60 ± 0.12
	Er^{3+}	8.28 ± 0.05
	Gd^{3+}	8.70 ± 0.08
	Pr^{3+}	9.01 ± 0.10
$[Cu(nlpb15)_2]$	Al^{3+}	9.08 ± 0.10
	Er^{3+}	7.99 ± 0.05
	Gd^{3+}	8.21 ± 0.10
	Pr^{3+}	9.45 ± 0.15

The agreement between the experimental and calculated spectra (using data from SQUAD) supports the model proposed for adduct formation by simultaneous coordination of *two* metal ions to each transition metal centre, one in each crown ether cavity. In Fig. 3 are depicted the calculated and experimental spectra of $\{[Ni(nlpb15)_2]\cdot 2M^{3+}\}$ and $\{[Cu(nlpb15)_2]\cdot 2M^{3+}\}$ ($M = Ln^{3+}$, Al^{3+}).

As no crystals with diffractometric quality could be obtained for any of the adducts, no definitive information on the coordination number of the lanthanide ions upon complexation into the crown cavities was gathered; nevertheless, we assume that a high coordination number must occur and thus water or solvent molecules must also be bonded to the lanthanide cations.

The absence of any spectral changes upon addition of alkaline and earth-alkaline ions prevented the determination of stability constants using this technique. But this negative result can not exclude the existence of interactions between the representative ions and the crown ether groups.

Our data suggest that ion charge density is determinant in the recognition process using the spectroscopic properties of the metal complexes, as significant changes on the electronic spectra could only be observed after

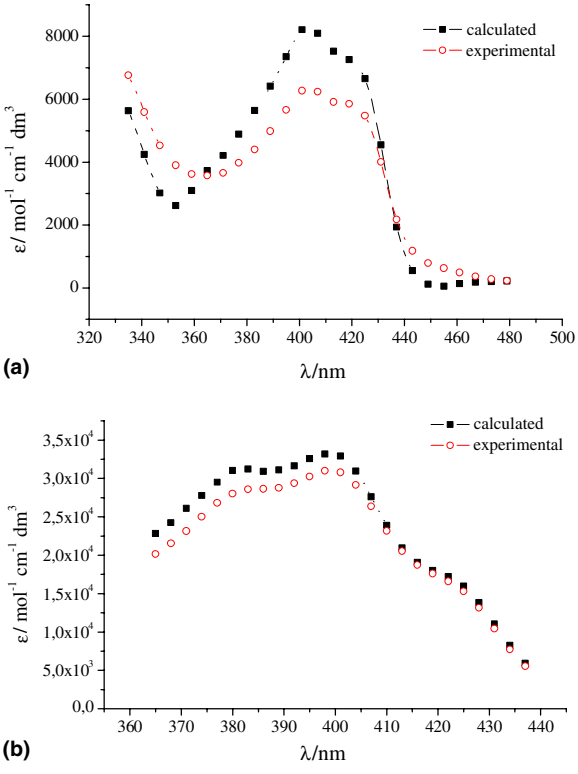

Fig. 3. Calculated and experimental spectra of: (a) $[Ni(nlpb15)_2]\cdot 2Al^{3+}$ and (b) $[Cu(nlpb15)_2]\cdot 2Pr^{3+}$.

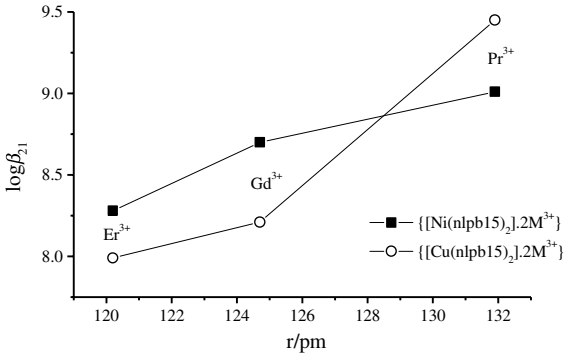

Fig. 4. Plots of $\log \beta_{21}$ vs. M^{3+} radii: [Cu(nlpb15)$_2$] and [Ni(nlpb15)$_2$]. M^{3+} radii (coordination number 9) from [38].

addition of trivalent cations. The spectral bands used in this study are associated with charge transfer and intraligand naphthaldehyde derivative) transitions and thus spectroscopic recognition has occurred mainly through chemical bonds. The energy of the electronic states involved in the transitions was found to be influenced only when cations with charge density higher than 0.025 pm^{-1} (coordination number 6) are bound to the crown ether groups, a consequence of the length of the spacer between naphthaldehyde fragment and the crown ether group.

No correlation was detected between $\log \beta_{21}$ values and the transition metal complex used, although the nickel complex tends to exhibit larger $\log \beta_{21}$ values. However, for each complex there is a rough linear correlation between the $\log \beta_{21}$ values and the lanthanide ionic radii, as depicted in Fig. 4: the larger the lanthanide ionic radii the higher the $\log \beta_{21}$. These results indicate the existence of the cavity effect, as the lanthanide cation with the larger radii, which is closer to that of Na^+, that is known to provide a better fit to the 15-crown-5 cavity [35–37], is the one that exhibits the larger stability constant.

4. Concluding remarks

Nickel and copper complexes functionalised with flexible crown ether moieties were shown to behave as spectroscopic probes for Al^{3+} and lanthanide cations in organic media, by making use of spectral changes in the charge transfer and naphthaldehyde intraligand based bands. It was possible to calculate the stability constants for 1:2 adducts (metal complex:cation), and for each complex there is a linear correlation between the $\log \beta_{21}$ values and the lanthanide ionic radii, what indicates the existence of a cavity effect, an important property for the design of selective chemosensors.

However, no detectable changes were observed in the UV–Vis spectra of the nickel(II) and copper(II) complexes upon addition of alkaline and alkaline earth ions, what was taken as an indication that ion recognition occurs mainly via chemical bonds and that space effects are not relevant, although the ligand has been designed to have flexible arms to allow for such type of molecular sensing mechanism.

Acknowledgements

C. Sousa thanks the Fundação para a Ciência e a Tecnologia (Lisboa) and ESF for a fellowship (BPD/SFRH/5678/2001). We thank Mrs. Felisberta Machado for recording UV–Vis spectra.

References

[1] C.J. Pederson, H.K. Frensdorf, Angew. Chem., Int. Ed. 11 (1972) 16.
[2] G. Gokel, Crown Ethers and Cryptands, RSC, Cambridge, 1991.
[3] J.L. Atwood, J.E.D. Davies, D.D. MacNicol, F. Vogtle, K.S. Suslick (Eds.), Comprehensive Supramolecular Chemistry, vol. 1, Pergamon, New York, 1996.
[4] P.D. Beer, P.A. Gale, G.Z. Chen, Coord. Chem. Rev. 185–186 (1999) 3.
[5] T.Y. Dong, C.K. Chang, C.H. Cheng, K.J. Lin, Organometallics 18 (1999) 1911.
[6] P.D. Beer, Chem. Soc. Rev. 18 (1989) 409.
[7] F.C.J.M. van Veggel, W. Verboom, D.N. Reinhoudt, Chem. Rev. 94 (1994) 279.
[8] S. Karaböcek, N. Karaböcek, Polyhedron 16 (1997) 1774.
[9] S. Turconi, C.P. Horwirtz, Y. Ciringh, S.T. Weintraub, J.T. Warden, J.H.A. Nugent, M.C.W. Evans, J. Chem. Soc., Dalton Trans. (1997) 4075.
[10] X. Li, Y. Chen, H. Xu, J. Mater. Chem. 9 (1999) 1415.
[11] Y. Diskin-Posner, R.K. Kumar, I. Goldberg, New J. Chem. 23 (1999) 885.
[12] M.J. Gunter, T.P. Jeynes, M.R. Johnston, P. Turner, Z. Chen, J. Chem. Soc., Perkin Trans. 1 (1998) 1945.
[13] C. Sousa, J. Enrique, C. Freire, C. Romão, B. Castro, Het. Commun. 6 (2000) 323.
[14] C. Sousa, Ph.D. Thesis, Faculdade de Ciências, Universidade do Porto, 2001.
[15] M. Martins, C. Freire, A.R. Hillman, Chem. Commun. (2003) 434.
[16] C. Sousa, C. Freire, B. Castro, J. Coord. Chem. 54 (2001) 1.
[17] R. Ungaro, B. El Haj, J. Smid, J. Am. Chem. Soc. 98 (1976) 5198.
[18] D.J. Leggett, W.A.E. McBryde, Anal. Chem. 47 (1975) 1065.
[19] A.H. Maki, B.R. McGarvey, J. Chem. Phys. 29 (1958) 31.
[20] A.H. Maki, B.R. McGarvey, J. Chem. Phys. 29 (1958) 35.
[21] Y. Nishida, S. Kida, Coord. Chem. Rev. 27 (1978) 273.
[22] K. Nakamoto, Infrared and Raman Spectra of Inorganic and Coordination Compounds, Wiley, New York, 1997.
[23] H. Almadfa, A.A. Said, E.M. Nour, Bull. Soc. Chim. Fr. 128 (1991) 137.
[24] A. Gül, A.I. Okur, A. Cihan, N. Tan, Ö. Bekâroglu, Synth. React. Inorg. Met., Org. Chem. 16 (1986) 871.
[25] A. Gül, Ö. Bekâroglu, J. Chem. Soc., Dalton Trans. (1983) 2537.
[26] A.B.P. Lever, Inorganic Electronic Spectroscopy, Elsevier, New York, 1984.
[27] A.J. Bard, L.R. Faulkner, Electrochemical Methods – Fundamentals and Applications, Wiley, New York, 1998.

[28] R. Ostaszewski, A. Bozek, M. Palys, Z. Stojek, J. Chem. Soc., Perkin Trans. 2 (1999) 1193.
[29] S. Pellet-Rostaing, F. Chitry, L. Nicod, M. Lemaire, J. Chem. Soc., Perkin Trans. 2 (2001) 1426.
[30] G.D. Brindley, O.D. Fox, P.D. Beer, J. Chem. Soc., Dalton Trans. (2000) 4354.
[31] L. Carbonaro, M. Isola, P. La Pegna, L. Senatore, F. Marchetti, Inorg. Chem. 38 (1999) 5519.
[32] D. Cunningham, P. McArdle, M. Mitchell, N.N. Chonchubhair, M. O'Gara, F. Franceschi, C. Floriani, Inorg. Chem. 39 (2000) 1639.
[33] C.-C. Cheng, M.-C. Liu, Tetrahedron Lett. 41 (2000) 10047.
[34] K.A. Connors, Binding Constants – The Measurement of Molecular Complex Stability, Wiley, New York, 1987.
[35] Y. Liu, T.-B. Lu, M.-Y. Tan, T. Hakushi, Y. Inoue, J. Phys. Chem. 97 (1993) 4548.
[36] J.-C.G. Bünzli, F. Pilloud, Inorg. Chem. 28 (1989) 2638.
[37] J. Massaux, J.F. Desreux, J. Am. Chem. Soc. 104 (1982) 2967.
[38] J.E. Huheey, E.A. Keiter, R.L. Keiter, Principles of Structure and Reactivity – Inorganic Chemistry, Harper Collins College Publishers, New York, 1993.

Available online at www.sciencedirect.com
SCIENCE DIRECT®
Polyhedron 23 (2004) 1409–1417
POLYHEDRON
www.elsevier.com/locate/poly

New examples of the unusual X-phenylcyanamido bridging ligands. Crystal structure and magnetic properties of Mn^{II} derivatives

Albert Escuer [a,*], Franz A. Mautner [b], Núria Sanz [a], Ramon Vicente [a]

[a] Departament de Química Inorgànica, Universitat de Barcelona, Martí Franqués 1-11, 08028 Barcelona, Spain
[b] Institut für Physikalische und Theoretische Chemie, Technische Universität Graz, A-8010 Graz, Austria

Received 9 January 2004; accepted 20 February 2004
Available online 12 April 2004

Abstract

Several new Mn^{II} compounds with X-phenylcyanamido (Xpcyd) and 1,10-phenantroline (phen) ligands of formula [Mn(3-Clpcyd)(H_2O)(phen)$_2$]$(NO_3)\cdot H_2O$ (**1**), [{Mn(3-Fpcyd)(MeOH)(phen)}$_2$(μ-3-Fpcyd)$_2$] (**2**), [{Mn(3-Fpcyd)(EtOH)(phen)}$_2$(μ-3-Fpcyd)$_2$] (**3**), [{Mn(3-Clpcyd)(MeOH)(phen)}$_2$(μ-3-Clpcyd)$_2$] (**4**) and [{Mn(4-Clpcyd)(EtOH)(phen)}$_2$(μ-4-Clpcyd)$_2$] (**5**) have been synthesised and characterised. Mononuclear compound **1** crystallises in the monoclinic system, $P2_1/c$ space group, dinuclear compounds **2**–**5** crystallise in the monoclinic system, $C2/c$ space group **2**, triclinic system, $P\bar{1}$ space group **3**–**4** and in the monoclinic system, $P2_1/a$ space group **5**. These compounds contain the unusual end-to-end R-cyanamide bridge and give supramolecular one-dimensional networks by means of H-bonds involving the N-amide atoms of the phenylcyanamide ligands. Susceptibility measurements on compounds **2**–**5** reveal moderate AF coupling in all cases. Coupling constants related to the phenylcyanamido bridges are compared with the superexchange model recently proposed for ligands of this kind.
© 2004 Elsevier Ltd. All rights reserved.

Keywords: Manganese; Pheylcyanamide; Magnetic properties; Crystal structures

1. Introduction

Phenylcyanamide ligands (Pcyd) are interesting and practically unexplored ligands from the synthetic and magnetic point of view. Very recently, we have reported the first magnetic measurements on systems with different dimensionality containing the Mn^{II}–$(NCN)_2$–Mn^{II} unit [1,2], the cyanamido group (NCN) being coordinated in the end-to-end mode. In these preliminary works, we demonstrate the ability of this kind of bridge to transmit moderate antiferromagnetic coupling. We propose, on the basis of MO calculations, that the $\mu_{1,3}$-NCN pcyd ligands have an intermediate place between azido and dicyanamido as superexchange mediators [1].

From the synthetic point of view, pcyd ligands offer a wide range of possibilities based on the use of different X-pcyd derivatives which can modify the solubility and crystallinity of the resulting compounds and in the different coordination properties of the two nitrogen atoms: one N-nitrile, (which coordinates preferently) and one N-amide atom, with characteristic bond parameters in each case. Also remarkable is the strong tendency to participate in H-bonded extended networks of X-pcyd ligands by means of the N-amide atom. Exploration of the coordination properties of these kinds of ligands is still a challenge, because most of the work performed with Xpcyd derivatives has been done with Ru^{III} (mainly mononuclear systems) and only a few dinuclear systems derived from other cations such as Ag^{I}, Cu^{I} or Cu^{II} have been reported [3]. The evident relationship with other pseudohalide ligands which in the last few years have provided a great variety of structural topologies and magnetic properties, including ferro, antiferro, (homogeneous or alternating) or in some few cases, ferrimagnetic systems [4–7], encourages us to explore the magnetic properties of pcyd derivatives.

Following our work with this family of ligands, we now report five new Mn^{II}/Xpcyd compounds (using

* Corresponding author. Tel.: +934021264; fax: +934907725.
E-mail addresses: albert.escuer@qi.ub.es (A. Escuer), mautner@ptc.tu-graz.ac.at (F.A. Mautner).

0277-5387/$ - see front matter © 2004 Elsevier Ltd. All rights reserved.
doi:10.1016/j.poly.2004.02.013

3-fluoro, 3-chloro or 4-chlorophenylcyanamide, 3-Fpcyd, 3-Clpcyd or 4-Cl-pcyd, respectively) in combination with the blocking 1,10-phenantroline ligand (phen). The new systems, one mononuclear and four dinuclear molecular derivatives, shows newly how the H-bonds play a central role in generating one-dimensional supramolecular arrangements. Measurement of their magnetic properties adds new data to check the recently proposed coupling model [1].

2. Experimental

2.1. Physical measurements

Magnetic susceptibility measurements were carried out on polycrystalline samples with a DSM8 pendulum susceptometer working in the range 4–300 K, under magnetic fields of approximately 1 T or in a SQUID instrument in the range 2–300 K under an external field of 0.1 T at the Magnetochemistry Service of the University of Barcelona. Diamagnetic corrections were estimated from Pascal Tables. The infrared spectra (4000–400 cm^{-1}) were recorded from KBr pellets on a Nicolet 520 FTIR spectrophotometer. EPR spectra were recorded with a Bruker ES200 spectrometer at X-band frequency. Thermogravimetric measurements were carried out in a Mettler TG 50 instrument at a heating rate of 10 °C min^{-1}.

2.2. Synthesis

Neutral 3-fluoro-, 3-chloro and 4-chlorophenylcyanamide (XpcydH) were prepared in all cases by desulphurization of the corresponding X-phenylthiourea with lead acetate, following the general synthetic procedure described for the haloderivatives of phenylcyanamide [8].

The five compounds were prepared following a common procedure: reaction of a solution of manganese nitrate hexahydrate (1 mmol) and phenantroline (2 mmol for **1** and 1 mmol for **2**–**5**) in 50 mL of methanol (for **1**, **2** or **4**) or ethanol (for **3** and **5**) with a solution of the corresponding XpcydH (2 mmol) in 6 mL of NaOH 0.2 M to deprotonate the ligand, produce yellowish solutions. After filtration of possible impurities, the resulting clear solutions were allowed to evaporate, giving yellowish-orange crystalline compounds suitable for X-ray measurements in one week. Yield for the five compounds around 40%. Elemental *Anal.* Calc. for **1** as $C_{31}H_{24}ClMnN_7O_5$ (665): C, 56.0; H, 3.6; N, 14.7. Found: C, 55.9; H, 3.4; N, 14.7%. Elemental *Anal.* Calc. for **2** as $C_{54}H_{40}F_4Mn_2N_{12}O_2$ (1074.9): C, 60.3; H, 3.7; N, 15.6. Found: C, 59.9; H, 3.7; N 15.9%. Elemental *Anal.* Calc. for **3** as $C_{56}H_{44}F_4Mn_2N_{12}O_2$ (1102.9): C, 61.0; H, 4.0; N, 15.2. Found: C, 61.3; H, 4.0; N, 15.3%. Elemental *Anal.* Calc. for **4** as $C_{54}H_{40}Cl_4Mn_2N_{12}O_2$ (1140.7): C, 56.9; H, 3.5; N, 14.7. Found: C, 56.0; H, 3.5; N, 15.0%. Elemental *Anal.* Calc. for **5** as solvent free **5b** $C_{52}H_{32}Cl_4Mn_2N_{12}$ (1076.6): C, 58.0; H, 3.0; N, 15.6. Found: C, 58.3; H, 3.2; N, 15.6%.

2.3. X-ray data collection for *1*–*5*

The X-ray single-crystal data for [Mn(3-Clpcyd)$(H_2O)(phen)_2$] $(NO_3)\cdot H_2O$ (**1**), [{Mn(3-Fpcyd)(MeOH)(phen)}$_2$(μ-3-Fpcyd)$_2$] (**2**), [{Mn(3-Fpcyd)(EtOH)(phen)}$_2$

Table 1
Crystal data and structure refinement for **1**–**5**

	(1)	(2)	(3)	(4)	(5)
Formula	$C_{31}H_{24}ClMnN_7O_5$	$C_{54}H_{40}F_4Mn_2N_{12}O_2$	$C_{56}H_{44}F_4Mn_2N_{12}O_2$	$C_{54}H_{40}Cl_4Mn_2N_{12}O_2$	$C_{56}H_{44}Cl_4Mn_2N_{12}O_2$
Formula weight	664.96	1074.86	1102.91	1140.66	1168.71
Space group	$P2_1/c$	$C2/c$	$P\bar{1}$	$P\bar{1}$	$P2_1/a$
a (Å)	12.798(3)	15.994(7)	9.921(3)	10.175(3)	10.588(4)
b (Å)	11.944(3)	13.853(5)	10.660(3)	11.549(4)	22.866(8)
c (Å)	20.039(5)	22.268(7)	11.750(3)	11.772(4)	11.338(4)
α (°)	90	90	99.57(2)	77.33(2)	90
β (°)	104.58(2)	94.78(3)	94.05(2)	73.23(2)	102.28(3)
γ (°)	90	90	90.25(2)	76.37(2)	90
V ($Å^3$)	2964(1)	4917(3)	1222.1(6)	1270.1(7)	2682(2)
Z	4	4	1	1	2
T (K)	298(2)	87(2)	87(2)	87(2)	87(2)
λ (Mo Kα) (Å)	0.71069	0.71069	0.71069	0.71069	0.71069
ρ_{calc} ($g\,cm^{-3}$)	1.490	1.452	1.499	1.491	1.447
μ (Mo Kα) (mm^{-1})	0.590	0.585	0.591	0.764	0.725
Collected data	4718	5616	6184	6413	5753
Independent data	3882	4824	5386	5589	4720
R_{int}	0.0183	0.0323	0.0376	0.0320	0.0507
Refined parameters	432	339	358	339	348
R^a [$I > 2s(I)$]	0.0352	0.0657	0.0456	0.0500	0.0605
ωR^{2b}	0.0793	0.1901	0.1043	0.1236	0.1614

[a] $R(F_o) = \sum ||F_o| - |F_c|| / \sum |F_o|$.
[b] $\omega R(F_o)^2 = \{\sum[\omega((F_o)^2 - (F_c)^2)^2] / \sum[\omega(F_o)^4]\}^{1/2}$.

(μ-3-Fpcyd)$_2$] (**3**), [{Mn(3-Clpcyd)(MeOH)(phen)}$_2$(μ-3-Clpcyd)$_2$] (**4**) and [{Mn(4-Clpcyd)(EtOH)(phen)}$_2$(μ-4-Clpcyd)$_2$] (**5**) were collected on a modified STOE four-circle diffractometer. The crystallographic data, conditions retained for the intensity data collection, and some features of the structure refinement are listed in Table 1. Graphite-monochromatized MoKα radiation ($\lambda = 0.71069$ Å) with the ω-scan technique was used to collect the data sets. Corrections were applied for Lorentz-polarisation effects and intensity decay. The structures were solved by direct methods using the SHELX-86 computer program [9], and refined by full-matrix least-squares methods on F^2, using the SHELXS-93 program [10] incorporated in the SHELXTL/PC package [11] and PLUTON-92 [12] program. All non-hydrogen atoms were refined anisotropically. Hydrogen atoms bonded to C-atoms were located on calculated positions by use of the HFIX utility of the SHELXS-93 program whereas the remaining hydrogen atoms were located from difference Fourier maps and included in the final refinement cycles by use of O–H distance restraints. For compounds **1** and **3** the occupancy of disordered atoms Cl(1)/Cl(2) and F(2)/F(12) was refined as 0.564(2)/0.436(2) and 0.827(5)/0.173(5), respectively. IR Xpcyd main absorptions: 2136 cm^{-1} **1**, 2170, 2143 cm^{-1} **2** and **3**, 2170, 2140 cm^{-1} **4** and 2149 cm^{-1} **5b**.

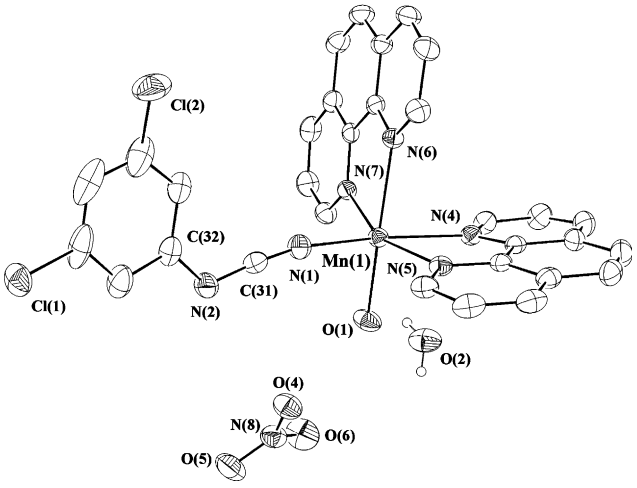

Fig. 1. ORTEP labelled plot (probability 30%) for compound **1**. For the sake of clarity, only the labels for the coordination sphere of the Mn^{II} cations and the NCN groups are shown. Cl(1)/Cl(2) atoms correspond to the disordered Cl atom of the 3-Clpcyd ligand.

3. Results and discussion

3.1. Description of the structures

3.1.1. Crystal structure of [Mn(3-Clpcyd)(H$_2$O)(phen)$_2$](NO$_3$)·H$_2$O (1)

The structure consists of mononuclear [Mn(3-Clpcyd)(H$_2$O)(phen)$_2$]$^+$ units and nitrate counterions. Hexacoordination of the Mn^{II} atoms is completed by two phenantroline ligands and one N-nitrile atom from the 3-Clpcyd$^-$ ligand and one water molecule, Fig. 1. Selected bond parameters are listed in Table 2.

Table 2
Selected bond lengths (Å) and angles (°) for **1**

Manganese environment				
Bond lengths				
Mn(1)–O(1)	2.149(3)	Mn(1)–N(1)	2.119(3)	
Mn(1)–N(4)	2.300(2)	Mn(1)–N(6)	2.319(3)	
Mn(1)–N(5)	2.305(2)	Mn(1)–N(7)	2.301(3)	
Bond angles				
O(1)–Mn(1)–N(6)	164.5(1)	N(6)–Mn(1)–N(1)	97.5(1)	
O(1)–Mn(1)–N(1)	92.2(1)	N(6)–Mn(1)–N(7)	72.1(1)	
O(1)–Mn(1)–N(7)	94.1(1)	N(6)–Mn(1)–N(4)	84.0(1)	
O(1)–Mn(1)–N(4)	89.6(1)	N(6)–Mn(1)–N(5)	93.4(1)	
O(1)–Mn(1)–N(5)	98.0(1)	N(7)–Mn(1)–O(4)	91.3(1)	
N(1)–Mn(1)–N(7)	102.6(1)	N(7)–Mn(1)–N(5)	159.5(1)	
N(1)–Mn(1)–N(4)	165.8(1)	N(4)–Mn(1)–N(5)	72.3(1)	
N(1)–Mn(1)–N(5)	93.5(1)			
3-Clpcyd ligand				
Bond lengths				
N(1)–C(31)	1.165(4)	C(31)–N(2)	1.287(5)	
N(2)–C(32)	1.399(5)			
Bond angles				
Mn(1)–N(1)–C(31)	168.3(2)	N(1)–C(31)–N(2)	174.4(3)	
C(31)–N(2)–C(32)	120.1(3)			
H-bonds				
	O–H	H···O	O···O/N	Angle
O(1)–H(31)–O(4)	0.82(3)	1.96(3)	2.779(4)	178(2)
O(1)–H(32)–O(2)	0.81(3)	1.83(3)	2.664(4)	179(4)
O(2)–H(33)–N(2)	0.81(3)	2.03(3)	2.826(4)	167(5)
O(2)–H(34)–O(4)	0.82(5)	2.16(5)	2.960(4)	165(5)

The coordination polyhedron is strongly distorted as result of placement of the phen ligands, which impose two N–Mn–N bond angles around 72°, and consequently several bond angles are strongly deviated from the regular 90° value. Bond distances are also asymmetric, with two short distances Mn(1)–O(1) and Mn(1)–N(1) of 2.149(3) and 2.119(3) Å, respectively, whereas the four Mn–N(phen) bond distances are larger than 2.300 Å. Coordination of the 3-Clpcyd ligand is close to linearity with a Mn(1)–N(1)–C(31) bond angle of 168.3(2)°.

Mononuclear units form a supramolecular structure by means of H-bonds involving the N-amide (3-Clpcyd), the coordinated water molecule, the nitrate counterion and the crystallization water molecule, giving a one-dimensional double chain arrangement along *b* crystallographic axis, Fig. 2. Shorter Mn···Mn distance is 8.465(1) Å.

*3.1.2. Common remarks on crystal structure of the dinuclear compounds **2**–**5***

The four structures show common features that permit a general description. In all cases the system consists of dinuclear centrosymmetric entities, with double Xpcyd bridge. In addition to the N-amide and N-nitrile atoms from the bridging ligands, coordination polyhedron around Mn^{II} atoms is completed with one bidentate phenantroline ligand, one terminal Xpcyd ligand and one solvent (MeOH or EtOH) molecule in *trans* position with respect to the N-amide atom of the bridging Xpcyd.

Also, for all of them, coordination polyhedra are strongly distorted as a consequence of the coordination of phen ligands that gives N–Mn–N bond angles close to 72°. Bond distances in the bridging region show as common features large Mn–N(amide) bond distances, greater than 2.300 Å, short Mn–N-nitrile bond distances around 2.150 Å and intermediate Mn–O(solvent) bond distances around 2.200 Å.

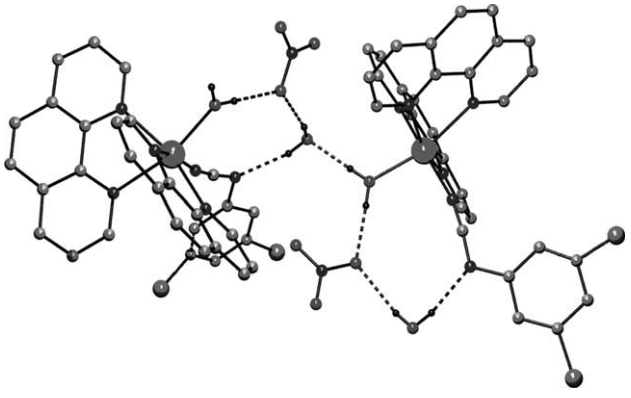

Fig. 2. One-dimensional H-bond network for compound **1**. H-bonds (dashed lines) involve the N-amide atoms of terminal 3-Clpcyd ligands, the coordinated water molecule, the O(4) atom from nitrate anion and the crystallization water molecule present in the structure. The two positions for the disordered Cl atom of the 3-Clpcyd ligand are shown in the plot.

In a similar fashion to previously reported dinuclear systems with similar arrangement [1,2], the R–OH coordinated solvent forms H-bonds with the N-amide atom of the neighbouring terminal X-pcyd ligand, giving double H-bond bridges and a one-dimensional arrangement of the dinuclear units, in which the intramolecular Mn···Mn distance is always 1–2 Å shorter than the intermolecular Mn···Mn. As example, Fig. 3 show one of these H-bond one-dimensional arrays.

Description of relevant details of the bond parameters of the bridging ligands will be set out separately below.

*3.1.3. Crystal structure of [{Mn(3-Fpcyd)(MeOH)(phen)}$_2$(μ-3-Fpcyd)$_2$] (**2**)*

Selected bond parameters are given in Table 3 and a labelled ORTEP plot of the dinuclear unit is shown in Fig. 4.

Bond angles in the bridging region follow the general trends of this kind of bridges, that is to say, a large Mn(1A)–N(1)–C(1) (nitrile) bond angle of 157.7(3)° and a closed Mn(1)–N(2)–C(1) (amide) bond angle of 114.4(2)°. Mn–$(NCN)_2$–Mn ring shows a chair distortion which may be evaluated from the dihedral angle (named δ) between the $(NCN)_2$ plane and the N(1)–Mn(1)–N(2A) plane as 12.6(1)°. The bridging 3-Fpcyd ligand is practically coplanar with the main $(NCN)_2$ plane, the angle between the direction C(2)–N(2) and this plane being only 4.8(2)°. Intramolecular Mn···Mn distance is 5.498(1) Å whereas the intermolecular Mn···Mn distance trough the H-bonds direction is 6.690 Å.

*3.1.4. Crystal structure of [{Mn(3-Fpcyd)(EtOH)(phen)}$_2$(μ-3-Fpcyd)$_2$] (**3**)*

Selected bond parameters are given in Table 4 and a labelled ORTEP plot of the dinuclear unit is shown in Fig. 5.

This compound is analogous to **2** with EtOH instead the coordinated MeOH. Therefore, this minor variation in the coordinated solvent introduce important differ-

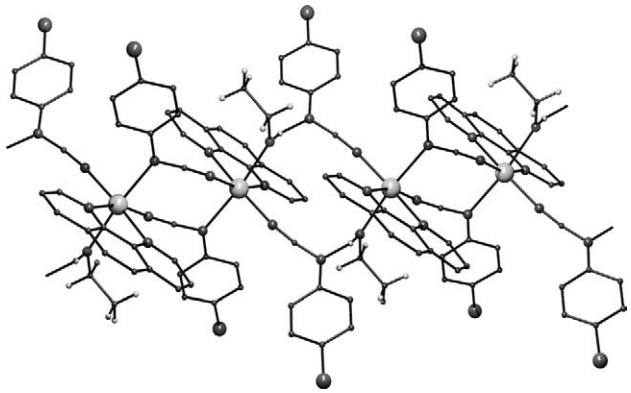

Fig. 3. H-bonds involving the N-amide and the –OH group of the coordinated solvent that allow to one-dimensional extended arrays for **2**–**5**. As example, in the figure is shown compound **4**.

Table 3
Selected bond lengths (Å) and angles (°) for compound **2**

Manganese environment				
Bond lengths				
Mn(1)–O(1)	2.228(3)	Mn(1)–N(3)	2.129(3)	
Mn(1)–N(2)	2.293(3)	Mn(1)–N(5)	2.284(3)	
Mn(1)–N(1A)	2.165(2)	Mn(1)–N(6)	2.303(3)	
Bond angles				
O(1)–Mn(1)–N(2)	177.5(1)	N(2)–Mn(1)–N(1A)	88.5(1)	
O(1)–Mn(1)–N(1A)	89.4(1)	N(2)–Mn(1)–N(3)	91.1(1)	
O(1)–Mn(1)–N(3)	88.4(1)	N(2)–Mn(1)–N(6)	105.0(1)	
O(1)–Mn(1)–N(6)	77.4(1)	N(2)–Mn(1)–N(5)	94.0(1)	
O(1)–Mn(1)–N(5)	87.1(1)	N(3)–Mn(1)–N(6)	92.3(1)	
N(1A)–Mn(1)–N(3)	103.0(1)	N(3)–Mn(1)–N(5)	164.5(1)	
N(1A)–Mn(1)–N(6)	160.6(1)	N(6)–Mn(1)–N(5)	72.2(1)	
N(1A)–Mn(1)–N(5)	91.8(1)			
3-Fpcyd ligands				
Bond lengths				
N(1)–C(1)	1.162(5)	N(3)–C(9)	1.167(5)	
C(1)–N(2)	1.295(5)	C(9)–N(4)	1.286(5)	
N(2)–C(2)	1.411(5)	N(4)–C(10)	1.402(5)	
Bond angles				
Mn(1A)–N(1)–C(1)	157.7(3)	Mn(1)–N(3)–C(9)	157.2(3)	
N(1)–C(1)–N(2)	176.0(4)	N(3)–C(9)–N(4)	178.1(5)	
C(1)–N(2)–Mn(1)	114.2(2)	C(9)–N(4)–C(10)	116.2(3)	
Mn(1)–N(2)–C(2)	128.5(2)			
C(1)–N(2)–C(2)	117.2(3)			
H-bonds				
	O–H	H···N	O···N	Angle
O(1)–H(1)–N(4)	0.80(3)	1.99(3)	2.773(4)	163(5)

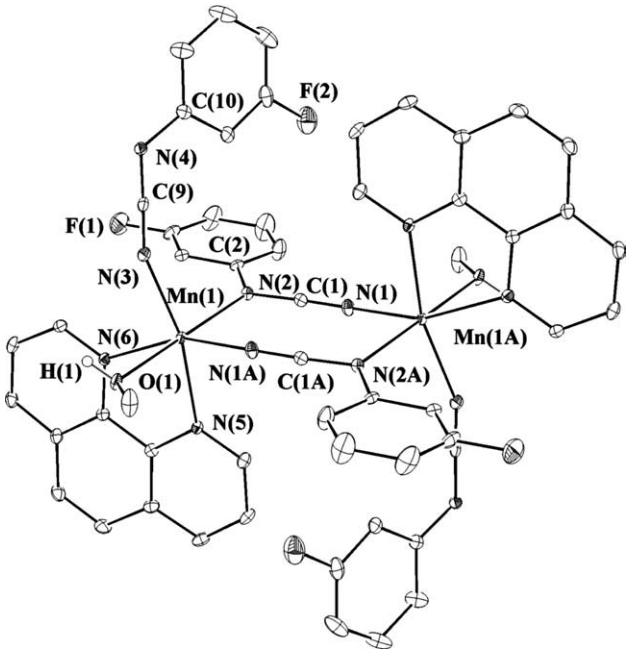

Fig. 4. ORTEP labelled plot (probability 30%) for compound **2**.

ences in the bond parameters of the compound. Mn(1)–N(1A)–C(1A) (nitrile) bond angle is only of 140.8(2)° and also Mn(1)–N(2)–C(1) (amide) bond angle reduces to 110.6(2)°. Mn–$(NCN)_2$–Mn ring show a greater chair distortion, being the dihedral angle δ between the $(NCN)_2$ plane and the N(1A)–Mn(1)–N(2) plane 37.6(1)°.

In this case, the 3-Fpcyd ligand is not coplanar with the main $(NCN)_2$ plane, being the angle of the C(2)–N(2) vector with this plane of 22.9(1)°. Intramolecular Mn···Mn distance is 5.233(1) Å and the intermolecular Mn···Mn distance trough the H-bonds direction is 7.115(1) Å.

*3.1.5. Crystal structure of [{Mn(3-Clpcyd)(MeOH)(phen)}$_2$(μ-3-Clpcyd)$_2$] (**4**)*

Selected bond parameters are given in Table 5 and a labelled ORTEP plot of the dinuclear unit is shown in Fig. 6.

Mn(1)–N(1A)–C(1A) (nitrile) bond angle is only of 154.0(2)° and Mn(1)–N(2)–C(1) (amide) bond angle is 111.7(2)°. Mn–$(NCN)_2$–Mn ring shows an intermediate chair distortion, being the dihedral angle δ between the $(NCN)_2$ plane and the N(1A)–Mn(1)–N(2) plane 17.2(1)°.

In this case, the 3-Clpcyd ligands are strongly deviated from planarity with the main $(NCN)_2$ plane, the angle of the C(2)–N(2) vector with this plane being 34.5(1)°. Intramolecular Mn···Mn distance is 5.430(1) Å and the intermolecular Mn···Mn distance trough the H-bonds direction is 6.517(1) Å.

Table 4
Selected bond lengths (Å) and angles (°) for compound **3**

Manganese environment				
Bond lengths				
Mn(1)–O(1)	2.250(2)	Mn(1)–N(3)	2.128(2)	
Mn(1)–N(2)	2.291(2)	Mn(1)–N(5)	2.259(2)	
Mn(1)–N(1A)	2.158(2)	Mn(1)–N(6)	2.318(2)	
Bond angles				
O(1)–Mn(1)–N(2)	170.6(1)	N(2)–Mn(1)–N(1A)	90.1(1)	
O(1)–Mn(1)–N(1A)	90.8(1)	N(2)–Mn(1)–N(3)	97.1(1)	
O(1)–Mn(1)–N(3)	91.9(1)	N(2)–Mn(1)–N(6)	86.1(1)	
O(1)–Mn(1)–N(6)	84.5(1)	N(2)–Mn(1)–N(5)	92.3(1)	
O(1)–Mn(1)–N(5)	84.4(1)	N(3)–Mn(1)–N(6)	166.1(1)	
N(1A)–Mn(1)–N(3)	100.6(1)	N(3)–Mn(1)–N(5)	93.8(1)	
N(1A)–Mn(1)–N(6)	92.9(1)	N(6)–Mn(1)–N(5)	72.5(1)	
N(1A)–Mn(1)–N(5)	165.0(1)			
3-Fpcyd ligands				
Bond lengths				
N(1)–C(1)	1.172(3)	N(3)–C(10)	1.167(3)	
C(1)–N(2)	1.292(3)	C(10)–N(4)	1.286(3)	
N(2)–C(2)	1.406(3)	N(4)–C(11)	1.398(3)	
Bond angles				
Mn(1A)–N(1)–C(1)	140.8(2)	Mn(1)–N(3)–C(10)	163.6(2)	
N(1)–C(1)–N(2)	173.9(3)	N(3)–C(10)–N(4)	174.6(3)	
C(1)–N(2)–Mn(1)	110.6(2)	C(10)–N(4)–C(11)	119.8(2)	
Mn(1)–N(2)–C(2)	132.4(2)			
C(1)–N(2)–C(2)	117.1(2)			
H-bonds				
	O–H	H···N	O···N	Angle
O(1)–H(1)–N(4)	0.87(3)	1.84(3)	2.701(3)	174(4)

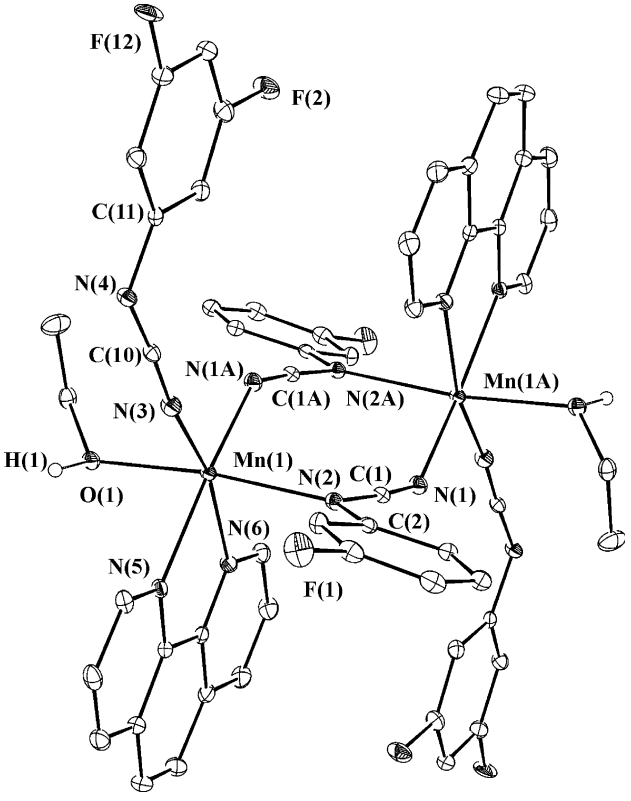

Fig. 5. ORTEP labelled plot (probability 30%) for compound **3**. The two positions for the disordered F atom of the 3-Fpcyd ligand are shown in the plot.

*3.1.6. Crystal structure of [{Mn(4-Clpcyd)(EtOH)(phen)}$_2$(μ-4-Clpcyd)$_2$] (**5**)*

Selected bond parameters are given in Table 6 and a labelled ORTEP plot of the dinuclear unit is shown in Fig. 7.

Mn(1A)–N(1)–C(1) (nitrile) bond angle is only of 148.4(4)° and Mn(1)–N(2)–C(1) (amide) bond angle is 110.5(3)°. Mn–(NCN)$_2$–Mn ring shows a strong chair distortion, the dihedral angle δ between the (NCN)$_2$ plane and the N(1A)–Mn(1)–N(2) plane being 26.6(1)°.

The 4-Clpcyd ligands are close to co-planarity with the main (NCN)$_2$ plane, the angle of the C(2)–N(2) vector with this plane being 5.8(3)°. Intramolecular Mn···Mn distance is 5.319(1) Å and the intermolecular Mn···Mn distance trough the H-bonds direction is 6.258(1) Å.

3.2. Thermal behaviour

Crystals of dinuclear compounds **2**–**5** degraded more or less slowly if they are maintained in open air, due to the loss of coordinated solvent. Structural determination was performed at low temperature on crystals just extracted from the mother solutions. In order to characterise the reason for this behaviour, thermogravimetric measurements on fresh crystals or freshly powdered crystalline samples.

For compounds **2**–**4** the measurements reveal a reasonable stability, with loss of coordinated solvent at

Table 5
Selected bond lengths (Å) and angles (°) for compound **4**

Manganese environment				
Bond lengths				
Mn(1)–O(1)	2.216(2)	Mn(1)–N(3)	2.124(3)	
Mn(1)–N(2)	2.310(2)	Mn(1)–N(5)	2.309(2)	
Mn(1)–N(1A)	2.154(2)	Mn(1)–N(6)	2.286(3)	
Bond angles				
O(1)–Mn(1)–N(2)	177.2(1)	N(2)–Mn(1)–N(1A)	89.8(1)	
O(1)–Mn(1)–N(1A)	87.1(1)	N(2)–Mn(1)–N(3)	90.0(1)	
O(1)–Mn(1)–N(3)	91.3(1)	N(2)–Mn(1)–N(6)	100.6(1)	
O(1)–Mn(1)–N(6)	81.8(1)	N(2)–Mn(1)–N(5)	94.4(1)	
O(1)–Mn(1)–N(5)	84.9(1)	N(3)–Mn(1)–N(6)	93.1(1)	
N(1A)–Mn(1)–N(3)	102.3(1)	N(3)–Mn(1)–N(5)	165.7(1)	
N(1A)–Mn(1)–N(6)	161.4(1)	N(6)–Mn(1)–N(5)	72.7(1)	
N(1A)–Mn(1)–N(5)	91.4(1)			
3-Clpcyd ligands				
Bond lengths				
N(1)–C(1)	1.167(3)	N(3)–C(9)	1.161(3)	
C(1)–N(2)	1.295(3)	C(9)–N(4)	1.289(3)	
N(2)–C(2)	1.416(3)	N(4)–C(10)	1.401(4)	
Bond angles				
Mn(1A)–N(1)–C(1)	154.0(2)	Mn(1)–N(3)–C(9)	164.4(3)	
N(1)–C(1)–N(2)	175.6(3)	N(3)–C(9)–N(4)	173.3(3)	
C(1)–N(2)–Mn(1)	111.7(2)	C(9)–N(4)–C(10)	119.7(2)	
Mn(1)–N(2)–C(2)	124.1(2)			
C(1)–N(2)–C(2)	116.7(2)			
H-bonds				
	O–H	H···N	O···N	Angle
O(1)–H(1)–N(4)	0.87(3)	1.83(3)	2.685(4)	170(3)

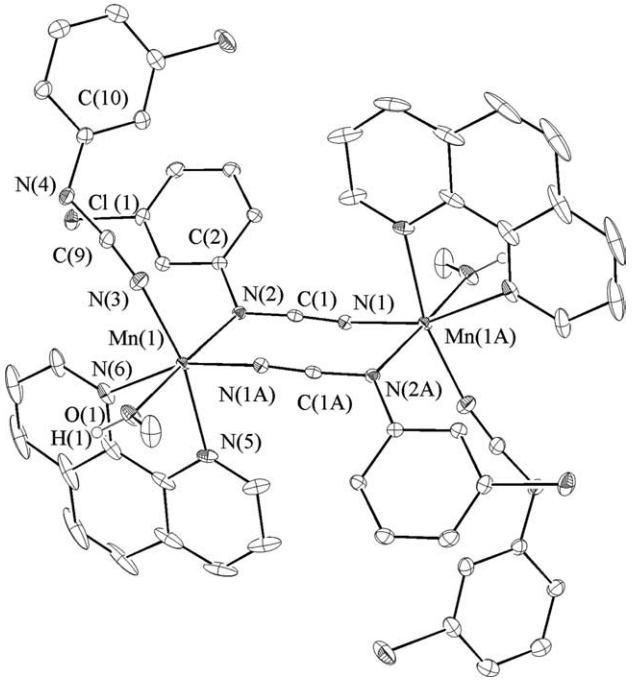

Fig. 6. ORTEP labelled plot (probability 30%) for compound **4**.

similar temperatures (120, 130, and 135 °C). The three compounds start to decompose at temperatures greater than 250 °C. The loss of weight agrees with the alcohol molecules present in the structure, 5.6% for **2** (theoretical 5.95%) and 6.6% for **3** (theoretical 8.3%) and 5.6% for **4** (theoretical 5.62%). In contrast, compound **5** does not show relevant loss of weight until 250 °C, corresponding to the decomposition of the complex. For **5**, the loss of coordinated ethanol is very fast and becomes practically total in the time of preparation of the sample under a dry nitrogen atmosphere. On the basis of these data, compounds **2**–**4** can be studied magnetically as the dinuclear entities structurally characterized. But compound **5** should be assumed to be a homogeneous chain with double 4-Clpcyd bridge with formula $[Mn(phen)(\mu\text{-}4\text{-}Clpcyd)_2]_n$ (**5b**). This assumption is reasonable on the basis of the arrangement of the H-bonds and the vicinity of the N-amide atoms of the terminal 4-Clpcyd ligands to the corresponding Mn^{II} atom of the neighbour dinuclear molecule and agree with the analytical data and the single IR absorption in the nitrile region at 2149 cm^{-1}. As corroborated by the EPR and susceptibility measurements, as is shown in the next section, $[Mn(phen)(\mu\text{-}4\text{-}Clpcyd)_2]_n$ (**5b**) formulation should be assumed for the solvent-free powdered compound.

3.3. Susceptibility measurements and powder EPR spectrum

Susceptibility measurements performed on freshly powdered samples for the four **2**–**5** compounds reveals

Table 6
Selected bond lengths (Å) and angles (°) for compound **5**

Manganese environment				
Bond lengths				
Mn(1)–O(1)	2.238(3)	Mn(1)–N(3)	2.112(5)	
Mn(1)–N(2)	2.312(4)	Mn(1)–N(5)	2.334(5)	
Mn(1)–N(1A)	2.146(4)	Mn(1)–N(6)	2.268(4)	
Bond angles				
O(1)–Mn(1)–N(2)	171.7(1)	N(2)–Mn(1)–N(3)	92.8(2)	
O(1)–Mn(1)–N(3)	93.3(2)	N(2)–Mn(1)–N(1A)	91.4(2)	
O(1)–Mn(1)–N(1A)	88.6(2)	N(2)–Mn(1)–N(5)	86.0(2)	
O(1)–Mn(1)–N(5)	85.7(1)	N(2)–Mn(1)–N(6)	95.9(2)	
O(1)–Mn(1)–N(6)	82.1(1)	N(1A)–Mn(1)–N(5)	92.9(2)	
N(3)–Mn(1)–N(1A)	101.4(1)	N(1A)–Mn(1)–N(6)	163.4(2)	
N(3)–Mn(1)–N(5)	165.7(1)	N(5)–Mn(1)–N(6)	72.8(2)	
N(3)–Mn(1)–N(6)	93.2(1)			
4-Clpcyd ligands				
Bond lengths				
N(1)–C(1)	1.172(6)	N(3)–C(8)	1.179(6)	
C(1)–N(2)	1.294(6)	C(8)–N(4)	1.295(6)	
N(2)–C(2)	1.408(6)	N(4)–C(9)	1.390(6)	
Bond angles				
Mn(1A)–N(1)–C(1)	148.4(4)	Mn(1)–N(3)–C(8)	171.9(4)	
N(1)–C(1)–N(2)	175.7(5)	N(3)–C(8)–N(4)	172.9(5)	
C(1)–N(2)–Mn(1)	110.5(3)	C(8)–N(4)–C(9)	120.1(4)	
Mn(1)–N(2)–C(2)	130.3(3)			
C(1)–N(2)–C(2)	118.0(4)			
H-bonds				
	O–H	H···N	O···N	Angle
O(1)–H(1)–N(4)	0.88(5)	1.87(5)	2.728(5)	167(5)

more or less weak antiferromagnetic coupling. In all cases, the $\chi_M T$ value at room temperature is slightly lower than the 4.375 $cm^3\,K\,mol^{-1}$ value by Mn^{II} atom, corresponding to the isolated isotropic Mn^{II} ions. On cooling, $\chi_M T$ decreases, tending to zero at low temperature. $\chi_M T$ versus T plots, Fig. 8, show susceptibility maxima at 11 K (**2**), 15.2 K (**4**) and 15 K for **5b**. In contrast, compound **3** does not reach maximum in the susceptibility plot, indicating a much less weak AF coupling. As explained above, due to the fast loss of coordinated solvent for **5**, this compound was assumed as the homogeneous $[Mn(phen)(\mu\text{-}4\text{-}Clpcyd)_2]_n$ one-dimensional **5b** system and compounds **2**–**4** as dinuclear entities. Then, the susceptibility data were fitted to the expression derived from the Hamiltonian $H = -JS_1S_2$ for an isotropic $S = 5/2$ dinuclear system and in the case of compound **5** with the expression derived from $H = \Sigma - JS_iS_{i+1}$ for an isotropic $S = 5/2$ uniform one-dimensional chain [13]. The best fit parameters obtained for the reported compounds were $J = -3.34$ cm^{-1}, $g = 2.01$ for **2**, $J = -0.41$ cm^{-1}, $g = 2.01$ for **3**, $-2.89\,cm^{-1}$ $g = 2.01$ for **4** and $-2.60\,cm^{-1}$ $g = 2.00$ for the one-dimensional system **5**.

Powder EPR spectra also confirm the dimensionality of the above compounds. In all cases, the spectra at room temperature consist of an isotropic absorption centred at $g = 2.00$; on cooling, weak half field signals may be observed, but the main $g = 2.00$ absorption remains constant. Peak-to-peak linewidth for the dinuclear systems **2**–**4** are 282, 303 and 255 G. In contrast, compound **5** exhibits a sharp isotropic signal centred at $g = 2.00$ with a linewidth of only 66 G in good agreement with similar one-dimensional pseudohalide or X-pcyd systems [1,14], giving a complementary confirmation of the $[Mn(phen)(\mu\text{-}4\text{-}Clpcyd)_2]_n$ (**5b**) formula for the powdered **5** compound.

X-Pcyd ligands introduce a large number of variable parameters in the coordination sphere of the metallic ion and in the bridging region. Structural parameters for compound **5** cannot be used for the solvent-free 5b; thus, useful magneto-structural data is only available for **2**–**4**. Previous MO calculations show that the factors favouring the greatest AF coupling are mainly related to the distortions in the Mn–$(NCN)_2$–Mn region: greater AF coupling is expected for systems in which the bridging region is not chair-distorted or in which the NCN-pcyd mean plane lies coplanar to the $(NCN)_2$ plane [1]. As a minor effect, for similar distortions, the ligands with the X-atom in *para* position (4-Xpcyd) should be more AF than pcyd or 3-Xpcyd ligands. In our case, compounds **2**–**4**, with 3-Xpcyd (X = F, Cl) and the same phen terminal ligand permit a good comparison of the general rules for these kinds of compounds. Compound **2** shows the minor distortion in all parameters, with a δ chair distortion of only 12.6° and shows the 3-Fpcyd ligands

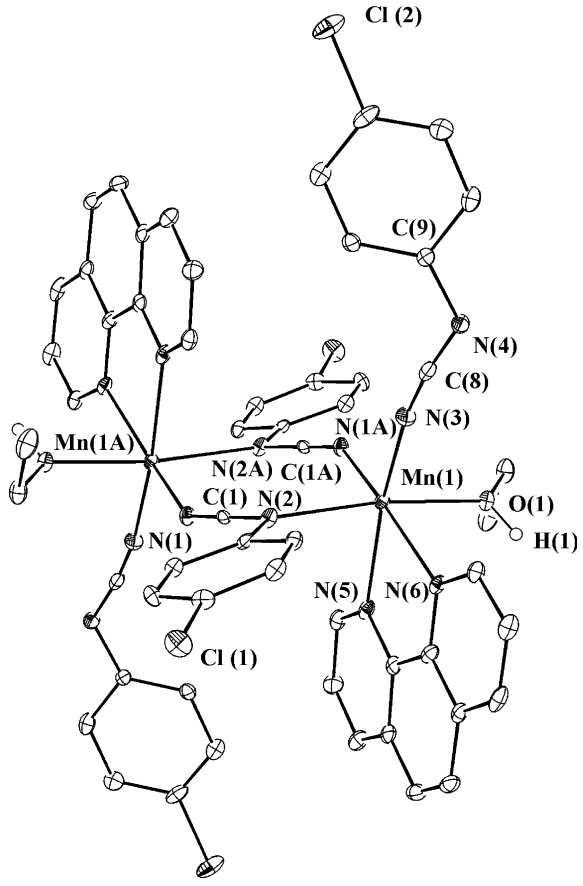

Fig. 7. ORTEP labelled plot (probability 30%) for compound **5**.

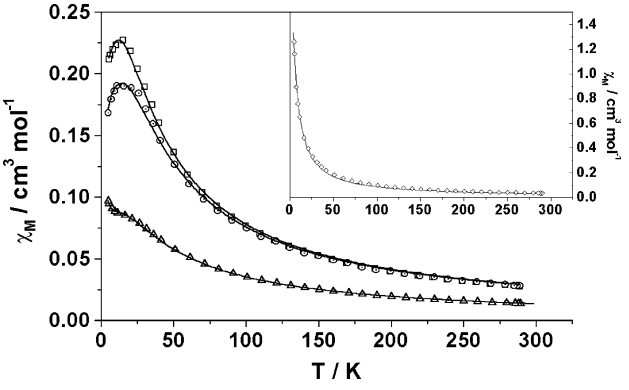

Fig. 8. Susceptibility data for compounds **2** (○), **3** (inset), **4** (□) and **5** (△). Solid lines correspond to the best fit indicated in the text.

practically coplanar with the main Mn–$(NCN)_2$–Mn plane, exhibits greater AF coupling. On the other hand, the highly distorted compound **3** (δ of 37.6° and phenyl rings 22.9° out of the mean Mn–$(NCN)_2$–Mn plane) shows a very weak AF coupling. In good accordance with the general rules, compound **4**, with chair distortion closer to **2** and greater out-of-plane deviation of the phenyl rings, shows a J value closer to **2**.

Therefore, it should be taken into account that correlations for ligands of this kind are multiparameter and only the extreme data, between comparable compounds, is reliable.

4. Supplementary material

Crystallographic data in CIF format have been deposited at the Cambridge Crystallographic data centre with CCDC reference numbers CCDC 216085–216089 for **1**–**5**, respectively. Copies of this information may be obtained free of charge from the Director, CCDC, 12 Union Road, Cambridge CB2 1EZ, UK (fax: +44-1223-336033; E-mail: deposit@ccdc.cam.ac.uk or www: http://www.ccdc.cam.ac.uk).

Acknowledgements

A.E., R.V., and N.S. thank the Ministerio de Ciencia y Tecnología (Spain), Project BQU2003/0538, for financial support of this research. F. M. thanks Prof. Belaj and Prof. Kratky (University of Graz) for the use of experimental equipment and OENB (Project 7967) for financial support.

References

[1] A. Escuer, N. Sanz, R. Vicente, F.A. Mautner, Inorg. Chem. 42 (2003) 541.
[2] A. Escuer, N. Sanz, R. Vicente, F.A. Mautner, Dalton Trans. (2003) 2121.
[3] R.J. Crutchley, Coord. Chem. Rew. 219–221 (2001) 125.
[4] J. Ribas, A. Escuer, M. Monfort, R. Vicente, R. Cortés, L. Lezama, T. Rojo, Coord. Chem. Rev. 193–195 (1999) 1027.
[5] P.M. Van der Werff, S.R. Batten, P. Jensen, B. Moubaraki, K.S. Murray, Inorg. Chem. 40 (2001) 1718.
[6] J.W. Raebiger, J.L. Manson, R.D. Sommer, U. Geiser, A.L. Rheingold, J.S. Miller, Inorg. Chem. 40 (2001) 2578.
[7] B. Vangdal, J. Carranza, F. Lloret, M. Julve, J. Sletten, J. Chem. Soc., Dalton Trans. (2002) 566, and references therein.
[8] B.R. Hollebone, R.S. Nyholm, J. Chem. Soc. (A) (1971) 332.
[9] G.M. Sheldrick, SHELXS-86, Program for the Solution of Crystal Structure, University of Gottingen, Germany, 1986.
[10] G.M. Sheldrick, SHELXL-93, Program for the Refinement of Crystal Structure, University of Gottingen, Germany, 1993.
[11] SHELXTL 5.03 (PC-Version), Program library for the Solution and Molecular Graphics. Siemens Analytical Instruments Division, Madison, WI, 1995.
[12] A.L. Spek, PLUTON-92, University of Utrecht, Utrecht, The Netherlands, 1992.
[13] O. Kahn, Molecular Magnetism, VCH, New York, 1993.
[14] M.A.M. Abu-Youssef, A. Escuer, D. Gatteschi, M.A.S. Goher, F.A. Mautner, R. Vicente, Inorg. Chem. 38 (1999) 5716.

Available online at www.sciencedirect.com
SCIENCE DIRECT®
Polyhedron 23 (2004) 1419–1426
POLYHEDRON
www.elsevier.com/locate/poly

Reactions of [{bis(2-pyridylmethyl)amine}trichloroiron(III)] with $(HOCH_2)_3CNHCO(CH_2)_nCONHC(CH_2OH)_3$ ($n = 0 - 2$): crystal structures of (μ-oxo)bis{(oxalato){[bis(pyridylmethyl)amine]iron(III)} and $(HOCH_2)_3CNHCO(CH_2)_2CONHC(CH_2OH)_3$

Christiane Fernandes [a,*], James L. Wardell [b], Adolfo Horn Jr. [a], Janet M.S. Skakle [c], Valderes Drago [d]

[a] *Laboratório de Ciências Químicas, Universidade Estadual do Norte Fluminense, 28013 602, Campos dos Goytacazes, RJ, Brazil*
[b] *Departamento de Química Inorgânica, Instituto de Química, Universidade Federal do Rio de Janeiro, 21945-970 Rio de Janeiro, RJ, Brazil*
[c] *Department of Chemistry, University of Aberdeen, Meston Walk, Old Aberdeen, AB24 3UE Scotland, UK*
[d] *Departamento de Física, Universidade Federal de Santa Catarina, 88040-900 Florianópolis, SC, Brazil*

Received 1 July 2003; accepted 22 February 2004
Available online 9 April 2004

Dedicated to Prof. Wilson A. Gazotti Jr. in memoriam

Abstract

The crystal structure and Mössbauer spectrum of the dinuclear complex $[(ox)(BMPA)Fe^{III}(\mu\text{-}O)Fe^{III}(BMPA)(ox)]\cdot 5H_2O$ (**4**), isolated from the reactions between $[(BMPA)FeCl_3]$ and $(HOCH_2)_3CNHCO(CH_2)_nCONHC(CH_2OH)_3$, (**1**: $n = 0$) or HO_2CCO_2H in basic media, are reported: BMPA = bis-(2-pyridylmethyl)amine; ox = oxalato. Each iron centre in **4** is coordinated to all three nitrogen atoms of a BMPA ligand, to two oxygen atoms from a chelating oxalato ligand and to a bridging oxide linking the two metals. The central Fe–O–Fe bond in centrosymmetric **4** is linear. The Fe(III) centres have distorted octahedral geometries with the three oxygen donor centers *trans* to nitrogen centres. Molecules of **4** are linked mainly via the water solvate molecules into a supramolecular network by an extensive array of hydrogen bonds, involving both strong O–H···O interactions as well as weaker C–H···O interactions. The amido NH group only takes part in an intramolecular interaction with a carbonyl oxygen of the oxalate ligand. Reactions of $(HOCH_2)_3CNHCO(CH_2)_nCONHC(CH_2OH)_3$, (**2**: $n = 1$: **3**: $n = 2$) with BMPA led to no identifiable products. The crystal structure and supramolecular arrangement in **3** are reported and are compared with those of **1** and **2**. Compounds, **1**–**3**, have elaborate, but different, H-bonding networks.
© 2004 Elsevier Ltd. All rights reserved.

Keywords: Iron; (μ-O)di-iron complex; Bis-(2-pyridylmethyl)amine; Oxalato; Hydrogen bonding; Mössbauer spectra

1. Introduction

Polyhydroxy-organic compounds attract attention for various reasons. The major interests, especially of carbohydrate derivatives, are their biological activities. However, considerable attention has also been paid to other aspects such as interactions with inorganic and organometallic species [1,2].

Our work with polyhydroxy compounds, such as the hexahydroxydiamido compounds, $(HOCH_2)_3CNHCO(CH_2)_nCONHC(CH_2OH)_3$, (**I**), [3–6] is concerned with interactions with inorganic/organometallic compounds, supramolecular arrangements in the solid state and uses

* Corresponding author.
E-mail address: chrisf@uenf.br (C. Fernandes).

0277-5387/$ - see front matter © 2004 Elsevier Ltd. All rights reserved.
doi:10.1016/j.poly.2004.02.027

as dendrimer precursors. We have previously reported the crystal structures and supramolecular arrangements of *N*,*N*′-bis[tris(hydroxymethyl)methyl]ethanediamide **1** [3] and *N*,*N*′-bis[tris(hydroxymethyl)methyl]malonamide, **2** [4], formed from $(HOCH_2)_3CNH_2$ with EtO_2CCO_2Et [7] and $EtO_2CCH_2CO_2Et$, respectively, as well as the formation of derivatives of **1**, including organotin and mercury derivatives [5,6].

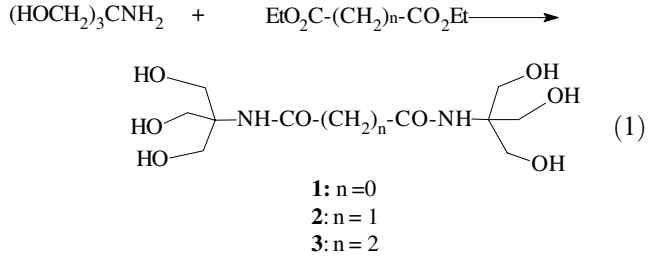

(1)

We now wish to report the synthesis and crystal structure of a further member of the series **I**, namely *N*,*N*′-bis[tris(hydroxymethyl)methyl]succinamide, **3**, as well as reactions of **1**–**3** with [Fe(BMPA)Cl_3] [BMPA = bis-(2-pyridylmethyl)amine]. Unexpectedly, one of the products isolated from the reaction with **1** was (μ- oxo)bis{(oxalato){[bis(pyridylmethyl)amine] iron(III)}, **4**. (μ-Oxo)di-iron complexes [8–11] are of interest due to the presence of complexes with (μ-oxo) diiron cores in metalloproteins, such as hemerythrin [12,13], ribonucleotide reductase [14,15] and methane mono-oxygenase [16,17].

2. Experimental

2.1. General information

Aminotris(hydroxymethyl)methane, $(HOCH_2)_3CNH_2$ (TRIS), dimethyl oxalate, diethyl malonate and diethyl succinate were purchased from Aldrich Chemical Co. and were used as received. Compounds, bis(2-pyridylmethyl)amine [18] and [{bis(2-pyridylmethyl)amino}trichloroiron(III)], [Fe(BMPA) Cl_3] [19] were synthesized according to literature procedures. Elemental (C, H, N) analyses were performed on a Perkin–Elmer 2400 CHN analyzer. Infrared spectra were recorded in KBr or CsI disks or polyethylene films on a Nicolet-Magna IR 760 instrument. Mössbauer spectra were obtained at 298 and 115 K using a Wissel instrument in the constant acceleration mode with transmission geometry where the WEB Research 20 mCi ^{57}Co/Rh source was maintained at room temperature. The resultant spectra where least square fitted to Lorentzian-shaped lines using the NORMOS software (Wissel company). Metallic iron was used for energy calibration and also as a reference for the isomer shift (δ) scale.

2.2. Synthesis of *1*, *2* and *3*

N,*N*′-bis[tris(hydroxymethyl)methyl]ethanediamide (**1**) [3,7] and *N*,*N*′-bis[tris(hydroxymethyl)methyl]malonamide (**2**) [4] were prepared according to published procedures.

2.2.1. Compound *1*

IR(KBr, cm^{-1}): 3700–2500br (max at 3412, 3338, 3223, 2956, 2916, 2878) 1667(CO), 1515(CN). ^1H (NMR (Me_2SO-d_6): δ: 3.51(d, 12H, CH_2OH), 4.76(t, 6H, OH), 7.78(s, 2H, NH). ^{13}C (NMR (Me_2SO-d_6): δ: 60.0(CH_2OH), 62.2(C_{quart}), 160.0(CO).

2.2.2. Compound *2*

IR(KBr, cm^{-1}): 3700–2500br (max at 3361, 3308, 3218, 2953, 2883, 2740), 1650(CO), 1561(CN). ^1H (NMR (Me_2SO-d_6): δ: 3.15(s, 2H, CH_2C)), 3.54(d, 12H, CH_2OH), 4.63(t, 6H, OH), 7.55(s, 2H, NH). ^{13}C (NMR (Me_2SO-d_6): δ: 44.4(CH_2CH_2), 60.6(CH_2OH), 62.9(C_{quart}), 168.8(CO).

2.2.3. Synthesis of *N,N′-bis[tris(hydroxymethyl)methyl]succinamide (3)*

A mixture of diethyl succinate (0.0226 mol) and $(HOCH_2)_3CNH_2$ (0.0451 mol) in methanol (40 ml) was refluxed for 5 h. On cooling, colorless crystals of **3** slowly formed, yield 90%, m.p. 224–225 °C. The product was recrystallised from EtOH for the X-ray diffraction study. IR(KBr, cm^{-1}): 3700–2500br (max at 3515, 3264, 3099, 2964, 2942, 2887), 1633(CO), 1574(CN). ^1H (NMR (Me_2SO-d_6): δ: 2.36(s, 4H, CH_2CH_2), 3.52(d, 12H, CH_2OH), 4.64(t, 6H, OH), 7.15(s, 2H, NH).

^{13}C (NMR (Me_2SO-d_6): δ: 31.6(CH_2CH_2), 60.4(CH_2OH), 62.2(C_{quart}), 172.9(CO).

2.3. General reactions between *[Fe(BMPA)Cl3]* and *1*–*3*

Reactions of the hexahydroxydiamides, **1**–**3** (ca. 1.0 mmol), with [Fe(BMPA)Cl_3] (ca. 2.1 mmol) were carried out in the presence of Et_3N in refluxing methanol. Interactions in all cases were evident from the formation of deep red-colored solutions. However, it was only possible to characterize products from the reaction with **1**.

2.4. Reaction between *[Fe(BMPA)Cl3]* and formation of *4* and *5*

Solutions of [Fe(BMPA)Cl_3] (750 mg, 2.08 mmol) in methanol (20 cm^3) and **1** (280 mg, 0.9 mmol) in methanol (50 cm^3) were mixed and Et_3N was added until pH 6. The reaction mixture was refluxed for 4 h and then left at room temperature. Dark-red crystals of $[(ox)(BMPA)Fe^{III}(\mu\text{-}O)Fe^{III}(BMPA)(ox)]\cdot 5H_2O$ (**4**) slowly formed. The crystals were collected after one week, yield: 35%. *Anal.* Calc. for $C_{28}H_{32}Fe_2N_6O_{14}$: C,

44.47; H, 4.26; N, 11.11. Found: C, 44.34; H, 4.23; N, 11.15%. IR (KBr, CsI or polyethylene, cm^{-1}): *v*: 3500–2500br (max at 3508, 3431, 3214, 3111, 3076, 3034, 2946, 2916), 1708, 1678 and 1642(all C=O), 1606, 1572, 1487, 1439, 1397, 1362, 1288, 1264, 1225, 1167, 1101, 1056, 1023, 1009, 984, 930, 897, 832, 810, 783, 724, 649, 631, 571, 519, 485, 418, 341, 310, 292, 265, 237. The bands in the OH region were relatively much less intense than those observed for **1**.

The filtrate yielded on concentration and further standing a deep brown solid, **5**. *Anal*. Calc. for $C_{22}H_{35}FeN_5O_9Cl_3$: C, 39.10; H, 5.22; N, 10.36. Found: C, 39.05; H, 5.34; N, 10.44%. IR(KBr, cm^{-1}) *v* 3500–2000br (max at 3103, 3080, 3038, 2899), 1632 (C=O), 1597, 1566, 1475, 1464, 1362, 1291, 1262, 1245, 1171, 1154, 1114, 1094, 1047, 1025, 987, 900, 855, 831, 794, 769, 738, 692, 673, 692, 673, 649, 625, 581, 542, 443, 334, 312, 287, 271, 241, 229.

2.5. Direct synthesis of *4*

Solutions of [Fe(BMPA)Cl_3] (360 mg, 1.00 mmol) in methanol (20 mL) and oxalic acid (90 mg, 1.0 mmol) in methanol (20 mL) were mixed and Et_3N was added until pH 6. The reaction mixture was refluxed for 5 h and then left at room temperature. Dark-red crystals of **4** slowly formed and were collected after one week, yield: 55%. Physical and spectral properties were identical with the product formed from **1**.

2.6. Crystal structure determination and refinement

Intensity data were collected on a Nonius Kappa CCD area detector by the EPSRC X-ray crystallographic service at the University of Southampton, UK. The entire processes of data collection, cell refinement and data reduction were accomplished by means of the programs, DENZO [20] and COLLECT [21]. Correction for absorption was achieved by a semi-empirical method based upon the variation in intensity of equivalent reflections with the program SORTAV [22,23]. The structure was solved by direct methods in SHELXS 97 [24] within the OSCAIL suite of programs [25] and refined in SHELXL 97 [26]. In the final stages of refinement H atoms were placed in calculated positions and refined with a riding model. PLATON was used for the analysis of the hydrogen bonding [27]. The program ORTEP-3 for windows [28] was used to obtain the figures. Crystal data and structure refinement for **3** and **4** are shown in Table 1.

Table 1
Crystal data and structure refinement for **3** and **4**

Compound	**3**	**4**
Empirical formula	$C_6H_{12}NO_4$	$C_{28}H_{38}Fe_2N_6O_{14}$
Formula weight	162.17	792.33
Temperature (K)	120(2)	120(2)
Wavelength (Å)	0.71073	0.71073
Crystal system	monoclinic	monoclinic
Space group	$P2(1)/n$	$C2/c$
Unit cell dimensions		
a (Å)	6.4487(2)	11.2203(10)
b (Å)	6.1087(2)	15.7311(13)
c (Å)	19.2031(8)	19.3048(18)
α (°)	90	90
β (°)	98.4964(17)	106.514(3)
γ (°)	90	90
Volume ($Å^3$)	748.17(5)	3266.9(5)
Z, D_{calc} (Mg/m^3)	4, 1.440	4, 1.611
Absorption coefficient (mm^{-1})	0.121	0.967
$F(000)$	348	1640
Crystal size (mm)	$0.20 \times 0.10 \times 0.04$	$0.10 \times 0.10 \times 0.05$
θ range for data collection (°)	3.22–27.50	3.40–27.52
Index ranges	$-8 \leqslant h \leqslant 8$	$-14 \leqslant h \leqslant 14$
	$-7 \leqslant k \leqslant 7$	$-19 \leqslant k \leqslant 20$
	$-24 \leqslant l \leqslant 24$	$-25 \leqslant l \leqslant 20$
Reflections collected/unique	3200/1715 [$R_{int} = 0.0297$]	7986/3128 [$R_{int} = 0.1377$]
Completeness to 2θ (%)	27.50 (99.6)	27.52 (40)
Absorption correction	empirical	empirical
Maximum and minimum transmission	0.90768 and 0.87506	1.04233 and 0.94779
Refinement method	full least-squares on F^2	full least-squares on F^2
Data/restraints/parameters	1715/0/103	3128/0/246
Goodness-of-fit on F^2	1.214	1.044
Final R indices [$I > 2\sigma(I)$]	$R_1 = 0.0856$, $wR_2 = 0.2526$	$R_1 = 0.0699$, $wR_2 = 0.1646$
R indices (all data)	$R_1 = 0.0996$, $wR_2 = 0.2599$	$R_1 = 0.1216$, $wR_2 = 0.1909$
Largest difference peak and hole ($Å^3$)	0.663 and −0.470	0.462 and −0.570

Data collection for **4** was hampered by the quality of the crystals, as evidenced by the high R_{int}, low completeness (83%) and poor ellipsoidal shapes; however, of data collections from several crystals, this represents the best possible, and results were consistent between crystals. Therefore, we believe that this is a good representation of the crystal structure within the limits of the available material.

3. Results and discussion

3.1. Compound 3

Compound **3** was obtained as a crystalline colorless solid from reactions of TRIS with $EtO_2C(CH_2)_2CO_2Et$ in refluxing methanol, by a similar reaction used to prepare **1** and **2**, Eq. (1).

3.2. Crystal structure of 3

Selected bond lengths and angles are listed in Table 2. An extensive array of H-bonds is present in the crystal, see Fig. 1 and Table 3. The molecule of **3**, which lies across an inversion plane, see Fig. 1(a), are linked into dimers and an $R_2^2(10)$ motif, via N(1)–H(1)···O(13)^{ii} H-bonds [ii $= -x, 1-y, -z$], Fig. 1(b). The supramolecular arrangements are completed by (a) H-bonds, O(12)–H(12)···O(1)^{iii}, which provide C(7) chains along *a* and by (b) H-bonds, O(13)–H(13)···O(12)^{iv}, which lead to C(6) chains along *b*. For the graph set notations, $R_m^n(X)$, C(*Y*) and S(*Z*), see [29]. These H-bonds combine to give $R_4^4(22)$ rings, [iii $= 1+x, y, z$; iv $= x, 1+y, z$], see

Table 2
Selected bond lengths (Å) and angles (°) for **3**

Bond lengths			
C(1)–N(1)	1.478(5)	C(1)–C(13)	1.533(5)
C(1)–C(12)	1.534(6)	C(1)–C(11)	1.538(5)
C(11)–O(11)	1.419(5)	C(12)–O(12)	1.430(5)
C(13)–O(13)	1.425(5)	N(1)–C(2)	1.320(5)
N(1)–C(2)	1.320(5)	C(2)–O(1)	1.259(5)
C(2)–C(3)	1.510(5)	C(3)–C(3)^{i}	1.534(8)
Bond angles			
N(1)–C(1)–C(13)	106.4(3)	N(1)–C(1)–C(12)	110.0(3)
C(13)–C(1)–C(12)	108.9(3)	C(13)–C(1)–C(12)	108.9(3)
N(1)–C(1)–C(11)	109.7(3)	C(13)–C(1)–C(11)	109.9(3)
C(12)–C(1)–C(11)	111.9(3)	O(11)–C(11)–C(1)	109.9(3)
O(12)–C(12)–C(1)	111.3(3)	O(13)–C(13)–C(1)	112.1(3)
C(2)–N(1)–C(1)	126.5(3)	O(1)–C(2)–N(1)	124.1(4)
O(1)–C(2)–C(3)	119.5(3)	N(1)–C(2)–C(3)	116.5(3)
C(2)–C(3)–C(3)^{i}	111.3(4)		

Symmetry transformations used to generate equivalent atoms: i, $-x-1, -y, -z$.

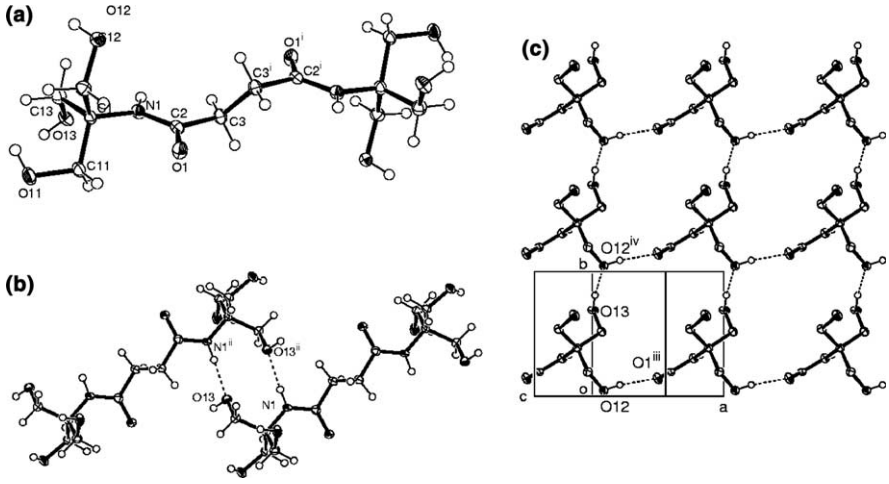

Fig. 1. (a) Atom arrangements and numbering scheme for a molecule of **3**: symmetry operation: i, $-x-1, -y, -z$; (b) Formation of dimers and $R_2^2(10)$ rings, generated by N(1)–H1···O13^{ii}: symmetry operation: ii, $-x, 1-y, -z$; (c) sheets, and $R_4^4(22)$ rings, formed from further O–H···O hydrogen bonds: O12–H12···O1^{iii} [leading to C(7) chains along *a*] and O13–H13···O12^{iv} [leading to C(6) chains along *b*]: only the symmetry related half of each molecule is omitted for clarity: symmetry operations: iii, $1+x, y, z$; and iv $= x, 1+y, z$. Ellipsoids drawn at the 50% level.

Table 3
Parameters (Å) and (°) for hydrogen bonds in **3**

D–H···A	*d*(D–H)	*d*(H···A)	*d*(D···A)	D–H···A (°)
N(1)–H(1)···O(13)^{ii}	0.88	2.03	2.886(4)	162.6
O(12)–H(12)···O(1)^{iii}	0.84	1.89	2.725(4)	171.3
O(13)–H(13)···O(12)^{iv}	0.84	1.82	2.653(4)	170.2
C(11)–H(11B)···O(1)	0.99	2.49	3.033(5)	114.5
C(13)–H(13B)···O(12)	0.99	2.55	2.930(5)	102.5

i, $-x-1,-y,-z$; ii, $-x,-y+1,-z$; iii, $x+1,y,z$; iv, $x,y+1,z$.

Fig. 1(b) and (c), in which only half of each molecule is shown for purposes of clarity. Altogether, the H-bonds form a sheet in (1 1 0), i.e., perpendicular to (0 0 1). The dimers have the effect of doubling the thickness of this sheet.

The different number of methylene groups in **1**–**3** results in significant differences between the structures. All three compounds have elaborate, but different, H-bonding networks. Molecules of near centro-symmetric **1** are linked into a two-dimensional structure, made up of distinct ring motifs: S(7), $R_3^3(10)$ and $R_2^2(22)$. Molecules of **2** lie about a twofold axis and are linked into a three-dimensional framework, formed from C(5) C(7) and C(12) chains, and $R_2^2(18)$, $R_2^2(12)$, $R_4^4(8)$, $R_2^2(8)$ and $R_2^2(13)$ rings.

As in **3**, the amido NH groups in **2** form intermolecular H-bonds with HO groups in adjacent molecules, but in contrast, the amido NH units in **1** take no part in the supramolecular aggregation, and are only involved in intramolecular bonding with the adjacent carbonyl atoms.

3.3. Spectra of *1*–*3*

There are some significant spectral shifts for the amido group in going from **1** to **3**. For example, the sequences of values for: (i) ν(CO) in the IR spectra in KBr disks are 1667, 1647 and 1633 cm^{-1}, for (ii) δ ^{1}H (NH) values in the ^{1}H NMR spectra are 7.78, 7.55 and 7.15 ppm and (iii): δ^{13}C (CO) values in the ^{13}C NMR spectra are 160.0, 168.8 and 172.9 ppm, all for **1**–**3**.

3.4. Reactions of *1*–*3* with *[Fe(BMPA)Cl$_3$]*

The reactions between **1**–**3** and [Fe(BMPA)Cl$_3$] were carried out with the expectation of obtaining mono- and bis-metallated complexes, such as **6** and **7**, see Fig. 2. However, in no case were there any indications that such complexes were formed. Moreover, while some reactions occurred between **1** and **3** with [Fe(BMPA)Cl$_3$], as shown by the color change of the solutions, solid products were only characterized from the reaction with

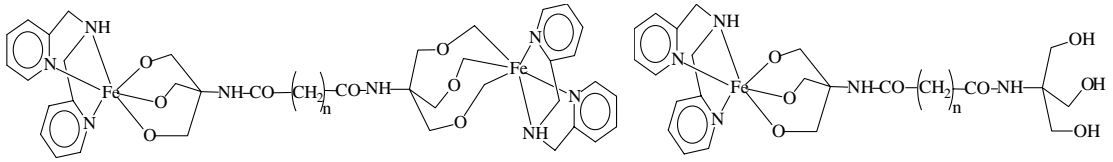

6 **7**

Fig. 2. Target products of reaction between **1**–**3** and [Fe(BMPA)Cl$_3$.

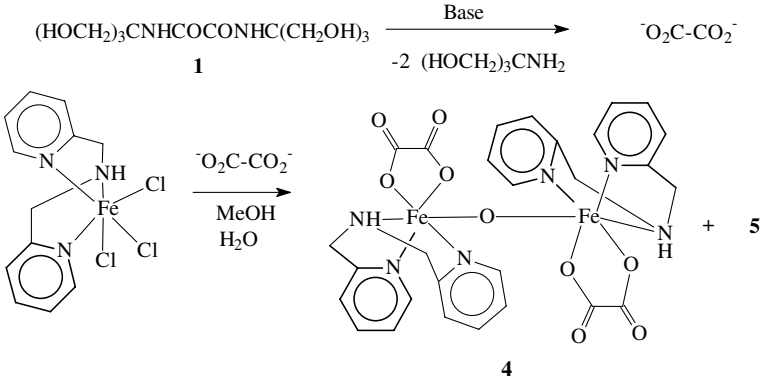

4

Scheme 1. Reaction of **1** with [Fe(BMPA)Cl$_3$].

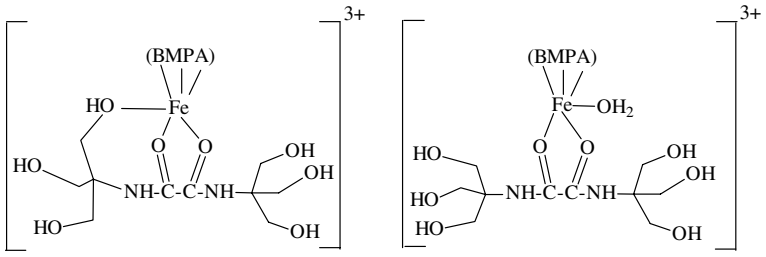

Fig. 3. Possible structures of the cation of **5**.

1. The residues extracted from reactions with **2** and **3** were inseparable oily-solid mixtures of compounds.

As indicated in Section 2, two products were obtained from reaction of **1** and [Fe(BMPA)Cl_3]: a crystalline material, **4**, which was confirmed by X-ray crystallography to be {[(ox)(BMPA)Fe(μ-O)Fe(BMPA)(ox)]·$5H_2O$}, and an amorphous material, **5**, see Scheme 1.

The formation of **4** proceeded via the base hydrolysis of the bis-amide, **1**, to the oxalato dianion, which then underwent reaction with [Fe(BMPA)Cl_3], Scheme 1. Base hydrolysis of an ester to a carboxylate anion and an alcohol is a well-known process. From subsequent study, **4** was obtained directly from [Fe(BMPA)Cl_3] and oxalic acid in basic medium.

3.5. Compound 5

Suitable crystals of **5** could not be grown and its structure remains uncertain. However, a combination of C,H,N analysis, IR and Mössbauer spectra indicated possible structures, such as [(BMPA)(**1**)Fe(OH_2)]Cl_3 or [(BMPA)(**1**)Fe]$Cl_3 \cdot H_2O$, in which an intact ligand, **1**, is chelated to Fe(III) via the carbonyl groups, with the hexacoordination of Fe(III) completed by the tridentate BMPA and an aqua ligand or a hydroxyl group, see Fig. 3. The broad and intense absorptions in the IR spectrum of **5** in the 2000–3500 cm^{-1} region pointed to the presence of several hydroxyl groups, while (CO) = 1632 and the combined NH deformation + C–N stretching band at 1597 cm^{-1} (compared to the values of 1660 and 1515 cm^{-1} in free **1**) indicated complexation had occurred with the amido groups. Relatively strong bands in the far IR were observed at 443 and 334 cm^{-1}. The Mössbauer spectral data for **5**, $\delta = 0.34$ and $\Delta E_Q = 0.84$ mm/s, at 298 K, were as expected for a distorted octahedral Fe(III) complex with 3N and 3O donor atoms [30]. Some changes in the Mössbauer spectral parameters occurred on cooling to 115 K, the values at the lower temperature being $\delta = 0.44$ and $\Delta E_Q = 0.66$ mm/s. The ΔE_Q values exclude the possibility of **5** being a (μ-oxo)di-iron species as such compounds are known to have ΔE_Q values near 1.5 mm/s [31,32].

3.6. Compound 4

X-ray crystallography revealed **4** to be a penta-hydrated centrosymmetric dinuclear complex, in which each iron centre is coordinated to all three nitrogen at-

Table 4
Selected bond lengths (Å) and angles (°) for **4**

Bond lengths			
Fe(11)–O(1)	1.7885(7)	Fe(11)–O(3)	2.019(4)
Fe(11)–O(2)	2.036(4)	Fe(11)–N(3)	2.122(5)
Fe(11)–N(1)	2.124(4)	Fe(11)–N(2)	2.213(4)
O(2)–C(13)	1.288(7)	O(3)–C(14)	1.239(9)
C(13)–O(5)	1.206(9)	C(14)–O(4)	1.244(8)
O(1)–Fe(11)^{i}	1.7885(7)		
Bond angles			
O(1)–Fe(11)–O(3)	100.12(11)	Fe(11)–O(1)–Fe(11)^{i}	180.0
O(3)–Fe(11)–O(2)	79.3(2)	O(1)–Fe(11)–O(2)	99.51(11)
O(3)–Fe(11)–N(3)	88.0(2)	O(1)–Fe(11)–N(3)	96.83(13)
O(1)–Fe(11)–N(1)	96.70(11)	O(2)–Fe(11)–N(3)	160.81(17)
O(2)–Fe(11)–N(1)	91.44(15)	O(3)–Fe(11)–N(1)	161.89(16)
O(1)–Fe(11)–N(2)	169.30(18)	N(3)–Fe(11)–N(1)	96.58(17)
O(2)–Fe(11)–N(2)	89.1(2)	O(3)–Fe(11)–N(2)	87.68(18)
N(1)–Fe(11)–N(2)	76.57(16)	N(3)–Fe(11)–N(2)	76.0(2)
C(1)–N(1)–Fe(11)	122.9(3)	C(14)–O(3)–Fe(11)	116.6(4)
C(7)–N(2)–Fe(11)	111.2(4)	C(5)–N(1)–Fe(11)	119.1(4)
C(12)–N(3)–Fe(11	123.6(4)	C(6B)–N(2)–Fe(11)	110.8(6)
C(8)–N(3)–Fe(11)	117.1(5)	C(6A)–N(2)–Fe(11)	111.6(5)
		C(13)–O(2)–Fe(11)	116.2(4)

Symmetry transformations used to generate equivalent atoms: i, $-x+2, -y, -z+1$.

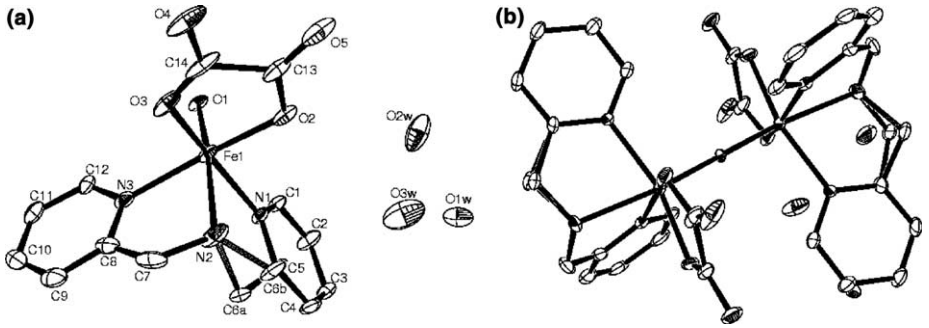

Fig. 4. (a) Atom arrangements and numbering scheme for the asymmetric unit of $[(Ox)(BMPA)Fe(\mu\text{-}O)Fe(BMPA)(Ox)]\cdot 5H_2O$ **4**. (b) Molecular structure of **4**. Hydrogen atoms have been omitted for clarity. Ellipsoids drawn at the 30% level.

oms of a BMPA ligand, to two oxygen atoms from a chelating oxalate ligand, ox, and to a bridging oxide linking the two metals. Selected bond lengths and angles are listed in Table 4. The asymmetric unit is made up of a [(ox)(BMPA)Fe] moiety, two and half water solvate molecules and half the bridging O, see Fig. 4(a). The complete molecule is shown in Fig. 4(b). Atom C(6) was best modeled by disordering the atom over two sites, as shown in Fig. 4(a). The $Fe\text{–}O_{bridge}$ bond length, 1.7885(7)Å, is in the region normally found for other oxygen bridged di-iron compounds [33]: all other Fe–O and the Fe–N bond lengths are also in the expected regions. All three oxygen donor centers are *trans* to nitrogen centres in **4**: the bridging oxide, O1, is *trans* to the aliphatic amine, N(2) [O(1)–Fe(1)–N(2) = 169.30(18)°] and oxalato O *trans* to pyridinyl N [N(3)–Fe(1)–O(2) = 160.81(17)° and O(3)–Fe(1)–N(1) = 161.89(16)°]. The bite angles of the bidentate oxalato ligands [O(3)–Fe(1)–O(2) = 79.3(3)°] and two of the three bite angles of the tridentate bis(2-pyridylmethyl)amine [N(1)–Fe(1)–N(2) = 76.57(17)° and N(2)–Fe(1)–N(3) = 76.0(2)°] are considerable less than the ideal *cis* 90° angles. The third bite angle of the BMPA ligand, N(3)–Fe(1)–N(1), is much larger at 96.58(17)°. The BMPA ligand is a very flexible tridentate ligand as shown by the variation in its bite angles in different iron complexes. For example, the bite angles in two independent molecules of $[(BMPA)Fe(\mu\text{-}O)(\mu\text{-}O_2CCH_3)_2Fe(BMPA)][ClO_4]_2\cdot 0.9Me_2CO$ (**8**) [34], are 77.1(2)°, 77.2(2)° and 83.8(2)°, and 76.7(2)°, 77.3(2)° and 89.4(2)°], while in orthorhombic $[(BMPA)FeCl_3]$, all three BMPA bite angles are between 75.8(2)° and 79.9(2)° [19b].

The crystallographic symmetry imposes an 180° angle on the Fe(1)–O(1)–Fe(1)^{i} bond $(i: -x+2, -y, -z+1)$ and consequently a Fe(1)···Fe(1)^{i} separation of twice the $Fe\text{–}O_{bridge}$ bond length of 1.7885(7) Å. A wide range of Fe–O–Fe bond angles (from ca. 115° to 180°) have been reported for (μ-O)di-iron species [33]. A 180° angle is also present, for example, in $[(H_2O)_2(Cl\text{-}pdc)Fe(\mu\text{-}O)Fe(Cl\text{-}pdc)(H_2O)_2]$ [35]: Cl-pdc = 2,6-($^{-}O_2C$)$_2$-4-Cl-pyridine), while in **8**, the Fe–O–Fe angle is one of the smallest reported at 116.2(2)° [34]. A further difference between **4** and **8** was found with the bonding modes of the carboxylate ligands: in **4**, the dicarboxylato ligands are chelating while in **8** the mono-carboxylate groups are bridging [34].

The molecules of **4** are linked mainly via the water solvate molecules into a supramolecular network by an extensive array of hydrogen bonds, involving both

Table 5
Parameters (Å, °), of hydrogen-bonds in **4**

D–H···A	*d*(D–H)	*d*(H···A)	*d*(D···A)	∠(DHA)
N(2)–H(2A)···O(4)	0.93	1.97	2.866(8)	160.8
O(1W)–H(1WA)···O(2W)	0.91	2.35	2.865(6)	115.4
O(1W)–H(1WB)···O(2W)^{iii}	0.90	2.02	2.865(6)	156.5
O(2W)–H(2WA)···O(3W)	0.96	2.28	2.919(10)	123.7
O(2W)–H(2WB)···O(2)	0.96	1.93	2.879(6)	170.3
O(3W)–H(3WA)···O(2W)	0.96	2.20	2.919(10)	130.7
O(3W)–H(3WB)···O(3W)^{iii}	0.96	1.97	2.813(11)	145.0
C(1)–H(1)···O(3)^{i}	0.95	2.40	3.328(6)	164.3
C(6B)–H(6B2)···O(3W)	0.99	2.44	3.40(2)	164.7
C(7)–H(7A)···O(5)^{ii}	0.99	2.37	3.330(8)	162.2
C(7)–H(7B)···O(1W)^{iv}	0.99	2.51	3.373(7)	146.1
C(10)–H(10)···O(3)^{v}	0.95	2..50	3.302(9)	142.1
C(12)–H(12)···O(2)^{i}	0.95	2.37	3.314(8)	174.6

Symmetry transformations used to generate equivalent atoms: i, $-x+2, -y, -z+1$; ii, $-x+3/2, -y+1/2, -z+1$; iii, $-x+1, y, -z+1/2$; iv, $x+1/2, y+1/2, z$; v, $-x+5/2, -y+1/2, -z+1$.

strong O–H···O interactions as well as weaker C–H···O interactions. The amido NH group only takes part in an intramolecular interaction with a carbonyl oxygen of the oxalato ligand (see Table 5).

3.7. Spectra of **4**

Selected IR frequencies associated with the chelating oxalate groups in $K_3[Fe(oxalato)_3]\cdot 3H_2O$ have been reported to be 1712, 1688 and 1647 [ν(C=O)], 1390, 1270 and 1255 [ν(C–O)], 892 [ν(C–C)], 803 and 790 [δ(O–C–O)], 580 and 532 [ν(Fe–O)] [36]. Corresponding frequencies in **4** are considered to be 1708, 1678 and 1642 [ν(C=O)], 1397, 1288 and 1264[ν(C–O)], 810 and 783 [ν(C–C)], and 571 and 518[ν(Fe–O)]. Sanders-Loehr et al. [33] reported a correlation between the Fe–O–Fe bond angle and values of IR active ν_{as}(Fe–O–Fe) and Raman active ν_s(Fe–O–Fe) in various oxo-bridged dinuclear iron species. For a Fe–O–Fe bond angle of 180°, as in **4**, ν_{as}(Fe–O–Fe) is expected to be near 885 cm^{-1}. The IR spectrum of **4** in fact contained a weak band at 897 cm^{-1}.

The Mössbauer parameters at 298 K for **4** were $\delta = 0.25$ and $\Delta E_Q = 1.47$ mm/s, which are in the regions consistent with a substantial distorted octahedral high-spin Fe(III) compound, with a (μ-O)di-iron core [31,32].

4. Supplementary material

Crystallographic data for the structural analysis have been deposited with the Cambridge Crystallographic Data Centre, CCDC 212024 and 212025, for **3** and **4**, respectively. Copies of this information may be obtained free of charge from The Director, CCDC, 12 Union Road, Cambridge CB2 1EZ, UK (fax: +44-1223-336033; e-mail: deposit@ccdc.cam.ac.uk or www: http://www.ccdc.cam.ac.uk).

Acknowledgements

C.F., A.H.Jr. and J.L.W. thank CNPq, FAPERJ and FUJB (Brazil) for support. The EPSRC X-ray diffraction service at the University of Southampton, UK, is thanked for the data collection for compounds **3** and **4**.

References

[1] L. Pellerito, L. Nagy, Coord. Chem. Rev. 224 (2002) 111.
[2] B. Gyurcsik, L. Nagy, Coord. Chem. Rev. 203 (1999) 81.
[3] J.N. Ross, J.N. Low, C. Fernandes, J.L. Wardell, C. Glidewell, Acta Crystallogr., Sect. C 57 (2001) 1.
[4] C. Fernandes, J.L. Wardell, J.M.S. Skakle, Acta Crystallogr., Sect. C 58 (2002) 499.
[5] J.-N. Ross, J.L. Wardell, J.N. Low, G. Ferguson, Acta Crystallogr., Sect. C 52 (1996) 228.
[6] J.N. Low, B.F. Milne, J.-N. Ross, J.L. Wardell, Braz. J. Chem. Soc. 13 (2002) 207.
[7] G.E. Dubois, B. Zhi, G.M. Roy, S.Y. Stevens, M. Yalpani, J. Chem. Soc., Chem. Commun. (1992) 1604.
[8] S.J. Lippard, Chem. Br. 16 (1986) 222.
[9] J.H. Satcher, M.M. Olmstead, M.W. Droege, S.R. Parkin, B.C. Noll, L. May, Inorg. Chem. 37 (1998) 6751.
[10] C. Fernandes, A. Neves, I. Vencato, A.J. Bordoluzzi, V. Drago, T. Weyhermüller, E. Rentschler, Chem. Lett. (2000) 540.
[11] Y. Hayashi, T. Kayatani, H. Sugimoto, M. Suzuki, K. Inomata, A. Uehara, Y. Mizutani, T. Kitagawa, Y. Maeda, J. Am. Chem. Soc. 117 (1995) 11220.
[12] L. Que Jr., A.E. True, Prog. Inorg. Chem. 38 (1990) 97.
[13] J.B. Vincent, G.L. Olivier-Lilley, B.A. Averill, Chem. Rev. 90 (1990) 1447.
[14] P. Norlund, B.M. Sjöberg, H. Eklund, Nature 345 (1990) 593.
[15] J.B. Lynch, C. Juarez-Garcia, E. Münck, L. Que Jr., Biol. Chem. 264 (1989) 8091.
[16] J. Uppenberg, F. Lindqvist, C. Svensson, B. Ek-Rylander, G. Anderson, J. Mol. Biol. 290 (1999) 201.
[17] A.L. Feig, S.J. Lippard, Chem. Rev 94 (1994) 759.
[18] A Neves, M.A de Brito, V. Drago, K. Griesar, W. Haase, Inorg. Chim. Acta 237 (1995) 131.
[19] (a) R. Viswanathan, M. Palaniandavar, T. Balasubramanian, P.T. Muthiah, J. Chem. Soc., Dalton Trans. (1996) 2519;
(b) K.R.J. Thomas, M. Velusamy, M. Palaniandavar, Acta Crystrallogr., Sect. C 54 (1998) 741.
[20] Z. Otwinowski, W. Minor, in: C.W. Cater, R.M. Sweet (Eds.), Methods in Enzymology: Macromolecular Crystallography, part A, vol. 276, Academic Press, New York, 1997, pp. 307–326.
[21] R. Hooft, COLLECT, Nonius BV, Delft, The Netherlands, 1998.
[22] R.H. Blessing, Acta Crystallogr., Sect. A 51 (1995) 33.
[23] R.H. Blessing, J. Appl. Crystallogr. 30 (1997) 421.
[24] G.M. Sheldrick, SHELXS 97. Program for the Solution of Crystal Structures, University of Göttingen, Germany, 1997.
[25] P. McArdle, OSCAIL for windows, National University of Ireland, Galway, Ireland, 2000.
[26] G.M. Sheldrick, SHELXL 97. Program for the Refinement of Crystal Structures, University of Göttingen, Germany, 1997.
[27] A.L. Spek, PLATON. Version of 2002, University of Utrecht, The Netherlands, 2002.
[28] L.J. Farrugia, J. Appl. Crystallogr. 30 (1997) 565.
[29] J. Bernstein, R.E. Davis, L. Shimoni, N.-L. Chang, Angew. Chem., Int. Ed. Engl. 34 (1995) 1555.
[30] D.P.E. Dickson, F.J. Berry, Mössbauer Spectrsocopy, London, 1986.
[31] S. Yan, D.D. Cox, L.L. Pearce, C. Juárez-Garcia, L. Que Jr., J.H. Zhang, C.J. O' Connor, Inorg. Chem. 28 (1989) 2509.
[32] R.E. Norman, S. Yan, L. Que Jr., G. Backes, J. Ling, J. Sanders-Loehr, J.H. Zhang, C.J. O' Connor, J Am. Chem. Soc. 112 (1990) 1554.
[33] J. Sanders-Loehr, W.D. Wheeler, A.K. Shiemke, B.A. Averill, T.M. Loehr, J. Am. Chem. Soc. 111 (1989) 8084.
[34] R.J. O'Brien, J.F. Richardson, R.M. Buchanan, Acta Crystrallogr., Sect. C 47 (1991) 2307.
[35] C.C. Ou, R.G. Wollmann, D.N. Hendrickson, J.A. Potenza, H.J. Schugar, J. Am. Chem. Soc. 100 (1978) 4717.
[36] M. Jaber, F. Bertini, G. Thomas-David, Can. J. Chem. 58 (1980) 1220.

Available online at www.sciencedirect.com
SCIENCE DIRECT®
Polyhedron 23 (2004) 1427–1439
POLYHEDRON
www.elsevier.com/locate/poly

Synthesis and electronic properties of mononuclear osmium(II) and rhenium(I) complexes containing ligands derived from [2,3-a:3′,2′-c]dipyridophenazine (ppb)

Matthew I.J. Polson [a], Sarah L. Howell [a], Amar H. Flood [a], Anthony K. Burrell [b], Allan G. Blackman [a,*], Keith C. Gordon [a,*]

[a] *Department of Chemistry, University of Otago, P.O. Box 56, Dunedin, New Zealand*
[b] *Los Alamos National Laboratory, Los Alamos, NM 87544, USA*

Received 22 January 2004; accepted 23 February 2004
Available online 12 April 2004

Abstract

An improved method for the synthesis of the polypyridyl ligand [2,3-a:3′,2′-c]dipyridophenazine (ppb) is reported. In addition, the syntheses of the new ppb-based ligands L (L = [2,3-a:3′,2′-c]dipyridophenazine, [2,3-a:3′,2′-c]dipyrido-6,7-dimethylphenazine, [2,3-a:3′,2′-c]dipyrido-6,7-dichlorophenazine, [2,3-a:3′,2′-c]dipyrido[1,2-e]benzophenazine, [2,3-a:3′,2′-c:3″,2″-e]tripyridoquinoxaline and [2,3-a:3′,2′-c]dipyrido-5-methylphenazine) are detailed. The complexes $[Os(ppb)(bpy)_2]^{2+}$ and $[Os(L)(bpy)_2]^{2+}$ have been synthesised and their electrochemical, electronic absorption and UV–Vis spectrochemical properties measured. Syntheses of the rhenium(I) complexes *fac*-$[Re(L'')(CO)_3Cl]$ (L″ = [2,3-a:3′,2′-c]dipyridophenazine, [2,3-a:3′,2′-c]dipyrido-6,7-dimethylphenazine, [2,3-a:3′,2′-c]dipyrido-6,7-dichlorophenazine, [2,3-a:3′,2′-c]dipyrido[1,2-e]benzophenazine) are also reported. The osmium(II) complexes $[Os(L')(bpy)_2]^{2+}$ (L′ = 2,3-di-(2-pyridyl)quinoxaline, 6,7-dimethyl-2,3-di-(2-pyridyl)quinoxaline, 6,7-chloro-2,3-di-(2-pyridyl)quinoxaline, 2,3-di-(2-pyridyl)benzo[g]quinoxaline, 4-methyl-di-(2-pyridyl)quinoxaline) have also been prepared and studied. The electronic spectra of the Os and Re complexes are dominated by strong MLCT transitions. The lowest energy MLCT transitions correlate linearly with the first reduction potential for the $[Os(L)(bpy)_2]^{2+}$ series. Electrochemical oxidation of the $[Os(L)(bpy)_2]^{2+}$ and $[Os(L')(bpy)_2]^{2+}$ complexes results in the appearance of LMCT transitions in the visible region while reduction of the $[Os(L)(bpy)_2]^{2+}$ complexes produces complex electronic spectra. Comparison with the reduced *fac*-$[Re(L'')(CO)_3Cl]$ complexes allows assignment of $L''^{\cdot-}$ $\pi \rightarrow \pi^*$ transitions in the NIR (1200–1000 nm) and red (850–700 nm) regions. The nonsymmetrical ligands [2,3-a:3′,2′-c:3″,2″-e]tripyridoquinoxaline and [2,3-a:3′,2′-c]dipyrido-5-methylphenazine both coordinate to the $[Os(bpy)_2]^{2+}$ unit in a stereospecific manner to give a single geometric isomer. The crystal structure of $[Re(CO)_3(ppb)Cl]$ is reported, in which the polypyridyl ligand deviates significantly from planarity.
© 2004 Elsevier Ltd. All rights reserved.

Keywords: Osmium; Rhenium; Polypyridyl; Synthesis; Spectroscopy

1. Introduction

There has been a considerable amount of research into the use of polypyridyl ligands that can act as bridging units in the formation of supramolecular arrays and grids [1–5] and large multinuclear complexes [6–9]. Such complexes may be used in photocatalysis [10], CO_2 remediation [11], solar energy systems [12–14], molecular electronics [6–8,15] and light-emitting diodes [16–24]. In this paper we report the syntheses and electronic properties of mononuclear Os(II) and Re(I) complexes containing a series of rigid ligands L based on the potential bridging ligand [2,3-a:3′,2′-c]dipyridophenazine (ppb, **21**, Fig. 1) and these are compared to analogous complexes containing the more flexible ligands L′ (**11-14**, **16**, Fig. 1) [25–29]. We also report a synthesis of **21** which utilises less forcing conditions than the previously

* Corresponding authors. Tel.: 64-3-479-7931; fax: 64-3-479-7906.
E-mail addresses: blackman@alkali.otago.ac.nz (A.G. Blackman), kgordon@alkali.otago.ac.nz (K.C. Gordon).

0277-5387/$ - see front matter © 2004 Elsevier Ltd. All rights reserved.
doi:10.1016/j.poly.2004.02.012

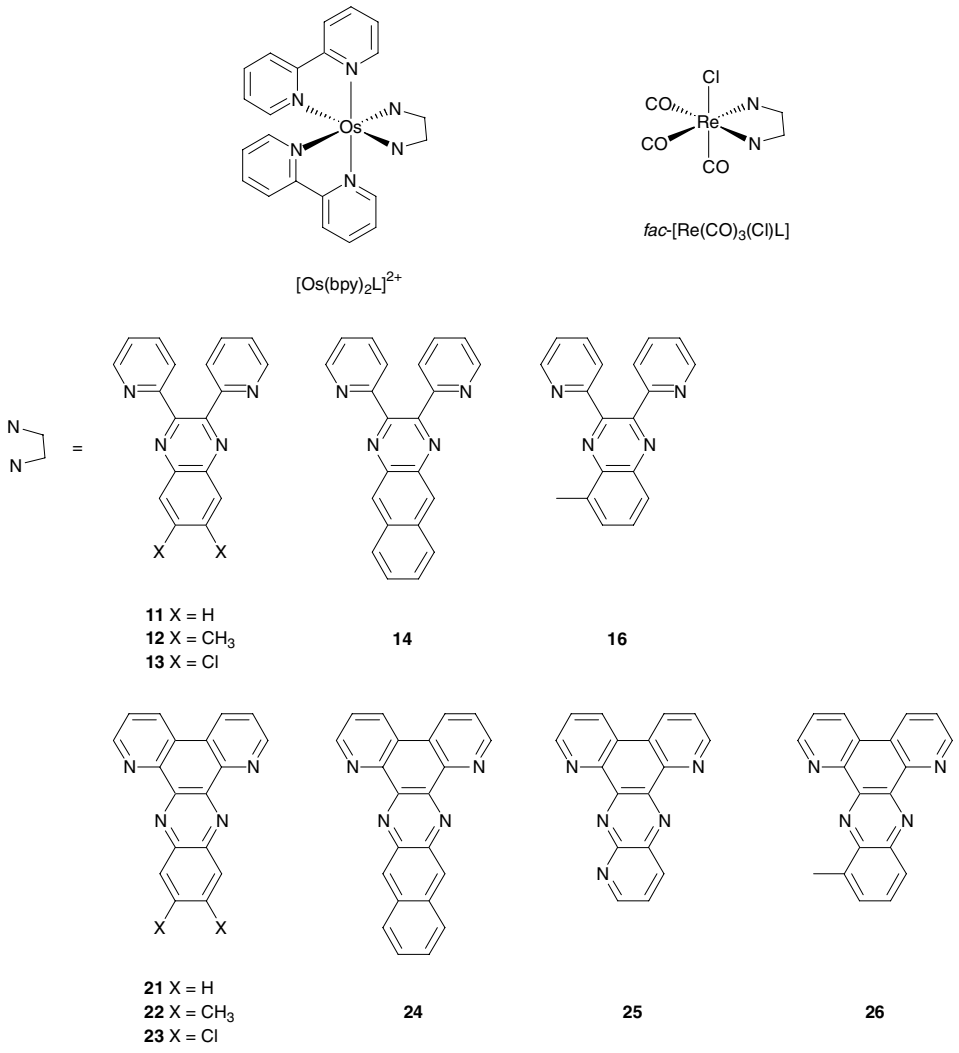

Fig. 1. Structures of the polypyridyl ligands.

reported method [30] and which was adapted to prepare the series of ligands L (**22–26**). The metal-containing moieties $[Os(bpy)_2]^{2+}$, $[Os(phen)_2]^{2+}$ and *fac*-$[Re(CO)_3Cl]$ were chosen in order to influence the electronic properties of the ligand [31]. Complexation of polypyridyl ligands to the *fac*-$[Re(CO)_3Cl]$ moiety simplifies the electronic absorption properties of the resulting compounds by removing the chromophores associated with the 2,2′-bipyridine or 1,10-phenanthroline ancillary ligands from the coordination sphere, thus allowing easier assignment of the observed absorptions [32,33].

2. Results and discussion

2.1. Ligand synthesis

The ligands **21**–**26** were synthesised in a four step process modified from that used previously for ppb [30] (Scheme 1). Acetylation of 2-methoxyphenylene-1,4-diamine (**1**) using pyridine/acetic anhydride gave **2** in reasonable yield. **2** was found to react less vigorously than **1** in the subsequent exothermic Skraup reaction and gave a good yield of product. Addition of acetic acid also helped to moderate this reaction.

The published synthesis of **3** requires two separate Skraup reactions, an additional step involving the reduction of the nitro-substituted starting material to an amine, and the use of As_2O_5 as an oxidant to lower the amount of reduction during the first Skraup reaction [30]. The synthesis reported herein produces **3** under milder conditions, in a higher overall yield and in fewer steps than the published procedure. The attempted oxidation of **3** to 4,7-phenanthroline-5,6-dione was carried out following the published procedure [30] by use of a mixture of fuming nitric acid and concentrated sulfuric acid. However, the product isolated was the bis-methyl hemiacetal **4**, and not the free diketone as reported [30]. However, Schiff-base condensation [34] of **4** with the appropriately substituted phenylenediamine in slightly

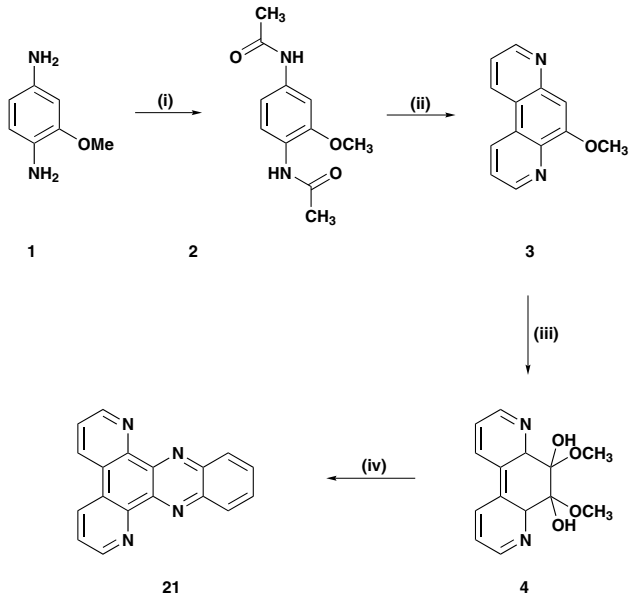

Scheme 1. The synthesis of [2,3-a:3′,2′-c]dipyridophenazine (ppb). Ligands **22**–**26** were prepared in analogous fashions by the use of the appropriate diamine in step (iv): (i) acetic anhydride, pyridine; (ii) ethylene glycol, conc. H_2SO_4, acetic acid, $Fe_2(SO_4)_3$; 120 °C 1 h, 140 °C 1 h; (iii) fuming HNO_3, conc. H_2SO_4; 120 °C, 2 h; (iv) phenylene-1,2-diamine, methanol, dilute HCl; reflux 30 min.

acidic methanol gave the series of ligands L outlined in Fig. 1.

2.2. Synthesis of metal complexes

The Os(II) complexes were prepared by refluxing $[Os(bpy)_2Cl_2]$ or $[Os(phen)_2Cl_2]$ with a 2-fold excess of the appropriate ligand in ethylene glycol. Purification was achieved by column chromatography on Sephadex SP-C25 resin using sodium *p*-tolylsulfonate as eluent [35] and the complexes were isolated as PF_6^- salts following addition of NH_4PF_6. The Re(I) complexes were prepared by heating $[Re(CO)_5Cl]$ with a slight excess of ligand under reflux in methanol under argon. Chromatography on silica separated the desired mononuclear species from some binuclear impurities. Satisfactory elemental analyses were obtained for all metal complexes reported herein.

Bidentate coordination of the asymmetric ligands **16**, **25** and **26** to a single metal centre can result in the formation of geometric isomers having the metal disposed either *syn* or *anti* with respect to the nitrogen atom or methyl substituent of the terminal phenazine ring (Fig. 2).

The ^1H (2.35 ppm) and ^{13}C NMR (17.7 ppm) spectra of $[Os(bpy)_2(\mathbf{26})](PF_6)_2$ both show only one methyl resonance. This can be compared to the corresponding dimethyl complex $[Os(bpy)_2(\mathbf{22})](PF_6)_2$ which displays two ^1H peaks (2.36 and 1.98 ppm) and two ^{13}C peaks (19.8 and 18.9 ppm) in the methyl region. The complex

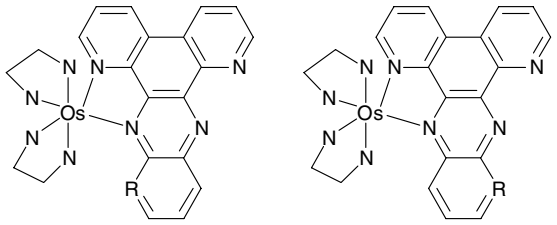

Fig. 2. The two geometric isomers of $[Os(bpy)_2L]^{2+}$ (L = **25** (R = N) and **26** (R = C–CH_3)).

$[Os(bpy)_2(\mathbf{16})](PF_6)_2$ also displays only one methyl resonance in both the ^1H (3.17 ppm) and ^{13}C NMR (16.6 ppm) spectra. These observations are consistent with the formation of only one isomer, which we assign as that in which the sterically demanding methyl group points away from the metal centre. Despite the fact that ligand **25** is sterically only slightly different from **21**, neither the ^1H nor ^{13}C NMR spectra of $[Os(bpy)_2(\mathbf{25})](PF_6)_2$ show any evidence of an isomeric mixture. Likewise, the COSY spectrum of $[Os(bpy)_2(\mathbf{25})](PF_6)_2$ showed no evidence of any ''hidden'' proton signals attributable to a second isomer. Nuclear Overhauser effect (nOe) experiments were carried out to allow complete assignment of the ^1H spectrum of $[Os(bpy)_2(\mathbf{25})](PF_6)_2$. Linked pyridine rings of the bpy ligands were identified through interactions between the 3 and 3′ protons. Irradiation of the 6 and 6′ protons of the 2,2′-bipyridine ligand was used to determine the orientation of ligand **25** with respect to the bpy ligands. No interaction between any of the 6 or 6′ protons and the proton on **25** *para* to the terminal ring nitrogen was observed, and this suggests that the nitrogen of the terminal ring is *syn* to the osmium centre.

The formation of only a single isomer in both cases is surprising. There is a possibility that the other isomer was lost during workup, either through irreversible binding to the Sephadex SP-C25 resin or through differences in solubility during the precipitation process, but we believe any such losses to be small. In the case of $[Os(bpy)_2(\mathbf{25})]^{2+}$, the observed selectivity may possibly be due to the decreased steric requirements of **25** as compared to ppb; the absence of a proton attached to the nitrogen in the terminal ring of **25** may result in reduced steric interactions with the *cis* bpy ligand. The positioning of the terminal ring nitrogen atom *syn* to the metal ion may also assist in pre-organisation of the metal–ligand assembly, resulting in the observed stereochemistry.

2.3. Crystallography

Selected bond lengths and angles for *fac*-[Re(**21**)$(CO)_3Cl$] are given in Table 1, and ORTEP diagrams of the complex are given in Fig. 3.

Table 1
Selected bond lengths (Å) and angles (°) for *fac*-[Re(**21**)$(CO)_3$Cl]

Bond lengths	
Re(1)–C(21)	1.933(6)
Re(1)–C(22)	1.928(6)
Re(1)–C(23)	1.925(6)
Re(1)–N(1)	2.206(4)
Re(1)–N(2)	2.163(4)
Re(1)–Cl(1)	2.4794(12)
O(1)–C(21)	1.125(6)
O(2)–C(22)	1.144(7)
O(3)–C(23)	1.148(6)
Bond angles	
C(23)–Re(1)–C(22)	85.4(2)
C(23)–Re(1)–C(21)	91.1(2)
C(22)–Re(1)–C(21)	92.0(2)
C(23)–Re(1)–N(2)	97.22(19)
C(22)–Re(1)–N(2)	172.80(19)
C(21)–Re(1)–N(2)	94.69(19)
C(23)–Re(1)–N(1)	171.82(18)
C(22)–Re(1)–N(1)	101.69(19)
C(21)–Re(1)–N(1)	92.73(19)
N(2)–Re(1)–N(1)	75.27(14)
C(23)–Re(1)–Cl(1)	92.08(16)
C(22)–Re(1)–Cl(1)	89.69(17)
C(21)–Re(1)–Cl(1)	176.51(17)
N(2)–Re(1)–Cl(1)	83.52(10)
N(1)–Re(1)–Cl(1)	83.93(10)
O(1)–C(21)–Re(1)	178.8(5)
O(2)–C(22)–Re(1)	177.7(5)
O(3)–C(23)–Re(1)	179.0(5)

The structure consists of a rhenium(I) ion coordinated to the carbon atoms of three facially disposed carbonyl ligands, a chloride ligand and two nitrogen atoms of the chelating ppb ligand. The Re–Cl, Re–C and Re–N bond distances are comparable to those previously found in *fac*-[Re(L)$(CO)_3$Cl] complexes containing bidentate polypyridyl ligands [33,36–39]. The severely distorted octahedral geometry of the metal ion results from the small bite angle of the ppb ligand, with the angle N1–Re1–N2 being 75.27(14)°. The distorted environment of the metal ion is further evidenced by the fact that Re(1) lies 0.0917 Å above the least-squares plane of the four equatorial ligand donor atoms N1, N2, C22 and C23. The ppb ligand is extremely distorted and exhibits remarkable curvature in the complex, with both C9 and C10 lying ~2.8 Å below the C22–Re1–C23 plane and C16 1.21 Å above it. Similar but less pronounced distortions have been observed previously in *fac*-[Re(L)$(CO)_3$Cl] complexes [36–39], and may possibly be due, in part, to a destabilising steric interaction between the equatorial carbonyl groups and the protons *ortho* to the nitrogen donor atoms. In this case, there is an additional destabilising steric interaction between the carbonyl carbon C22 and H17A, which lie only 2.425 Å apart, and which would be significantly closer if the ligand was coplanar with the carbonyl ligands. This argument is supported by the observation that the dichloro ppb ligand in $[(PPh_3)_2Cu(\mathbf{23})Cu(PPh_3)_2](BF_4)_2 \cdot 4H_2O \cdot CH_2Cl_2$ [40], the only other structurally characterised ppb complex, is planar; the tetrahedral geometry about the Cu(I) ions means that there are no potentially destabilising interactions between the PPh_3 ligands and protons of the ppb ligand [40].

2.4. Electrochemistry

The electrochemistry of the ligands **11–14**, **16** and **21–26** and of the complexes of these ligands was investigated using cyclic voltammetry (Table 2). Ligands **21–26** display a reversible single electron reduction over the range −0.95 to −1.31 V versus SHE. The reduction potentials are more anodic than those found for the corresponding **11–14** and **16** species due to the comparatively extended conjugation of the π systems of **21–26**. The ligands display shifts in their reduction potential commensurate with the electron donating or withdrawing character of the substituent [7,41] and the substituent effects for **21–26** are maintained upon coordination to the $[Os(bpy)_2]^{2+}$, $[Os(phen)_2]^{2+}$ or *fac*-[Re$(CO)_3$Cl] moieties.

In addition to the ligand-based reduction process, an oxidation at a potential typical of the Os(II)/(III) couple

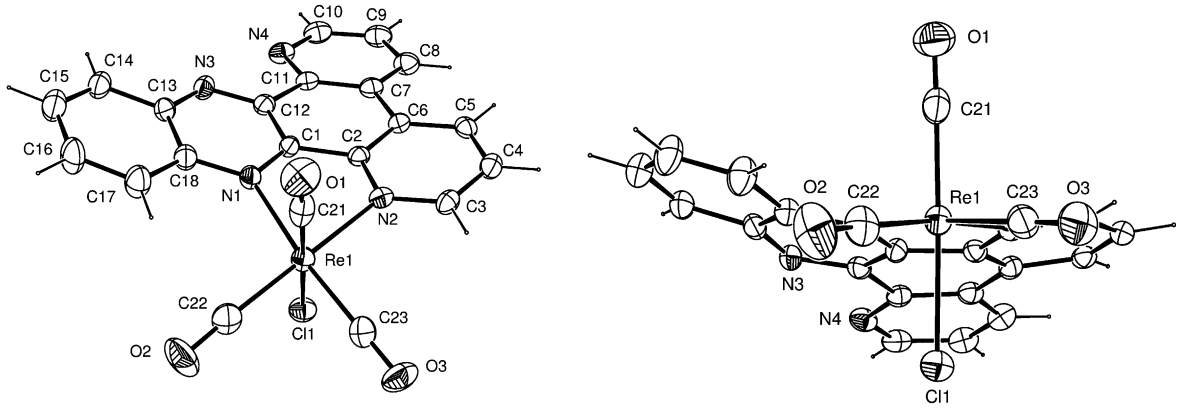

Fig. 3. ORTEP diagrams of *fac*-[Re$(CO)_3$(**21**)Cl]. The right-hand diagram emphasises the distortion of the ligand **21**.

Table 2
Electrochemical data for the ligands **11**–**14**, **16** and **21**–**26** and complexes containing these ligands

	E (V) vs. SHE		
	Oxidation	Reduction 1	Reduction 2
(**11**)		−1.56	
(**12**)		−1.69	
(**13**)		−1.36	
(**14**)		−1.28	
(**16**)		−1.29	
(**21**)		−1.27	
(**22**)		−1.31	
(**23**)		−1.05	
(**24**)		−0.95	
(**25**)		−1.04	
(**26**)		−1.29	
$[Os(bpy)_2(\mathbf{11})]^{2+}$	1.00	−0.89	
$[Os(bpy)_2(\mathbf{12})]^{2+}$	0.98	−0.85	
$[Os(bpy)_2(\mathbf{13})]^{2+}$	1.05	−0.61	
$[Os(bpy)_2(\mathbf{14})]^{2+}$	1.03	−0.61	
$[Os(bpy)_2(\mathbf{16})]^{2+}$	0.98	−0.81	
$[Os(phen)_2(\mathbf{11})]^{2+}$	1.04	−0.64	
$[Os(bpy)_2(\mathbf{21})]^{2+}$	1.07	−0.51	
$[Os(bpy)_2(\mathbf{22})]^{2+}$	1.06	−0.63	
$[Os(bpy)_2(\mathbf{23})]^{2+}$	1.12	−0.42	
$[Os(bpy)_2(\mathbf{24})]^{2+}$	1.05	−0.43	
$[Os(bpy)_2(\mathbf{25})]^{2+}$	1.00	−0.47	
$[Os(bpy)_2(\mathbf{26})]^{2+}$	1.07	−0.59	
$[Os(phen)_2(\mathbf{21})]^{2+}$	1.07	−0.58	
$[Re(CO)_3(\mathbf{21})Cl]$		−0.68	−1.35qr
$[Re(CO)_3(\mathbf{22})Cl]$		−0.74	−1.40qr
$[Re(CO)_3(\mathbf{23})Cl]$		−0.49	−1.22qr

Conditions used for the cyclic voltammograms: **11**–**16** (Pt w.e., MeCN, SCE); **21**–**26** (Pt w.e., 200 $mV\,s^1$, CH_2Cl_2, Fc internal calibrant); Os(II) complexes (Pt w.e., 200 $mV\,s^{-1}$, MeCN, Fc internal calibrant); Re(I) complexes (Pt w.e., 200 $mV\,s^{-1}$, CH_2Cl_2, Fc internal calibrant); qr = quasi-reversible.

[29] is also observed for the Os(II) complexes. Little variation in the oxidation potential is observed as the ligand is changed, supporting the Os(II)/(III) assignment. The modest variation that is observed may be attributed to the ability of the ligand to tune the metal orbital energies.

2.5. Electronic absorption

The electronic absorption spectra of ligands **21–23** are similar, with three absorption bands observed in the UV region (Table 3). These bands are ligand-centred (LC) with band maxima at ~385, 310 and 270 nm, respectively, and are assigned as $\pi \rightarrow \pi^*$ electronic transitions.

The spectral profiles of the four *fac*-$[Re(L'')(CO)_3Cl]$ complexes are similar. Four absorption bands are present, three in the UV and one in the visible region. The UV bands are correlated to the LC transitions of the free ligands and are similarly assigned as $\pi \rightarrow \pi^*$ transitions. The LC features show little change upon complexation. The lowest energy transition at ~ 470 nm ($\varepsilon \sim 4000\ M^{-1}\,cm^{-1}$) is responsible for the red colour of the mononuclear complexes. This electronic absorption band is assigned to a $Re(d\pi) \rightarrow L''(\pi^*)$ MLCT transition by comparison with assignments made for similar complexes, and exhibits band shifts that correlate with the electron-donating/withdrawing nature of the ligand substituents.

The electronic absorption spectra of the Os(II) complexes are summarised in Table 3. LC $\pi \rightarrow \pi^*$ transitions are observed for the $[Os(bpy)_2(L)]^{2+}$ and $[Os(bpy)_2(L')]^{2+}$ complexes in the UV region. These have been assigned in the literature [31] as corresponding to two bpy $\pi \rightarrow \pi^*$ transitions (250 and 280 nm) and a π–π^* transition (350 nm for L′ and 360 nm for L). Substitution on the ligand L or L′ has little effect on the energy of either bpy transition. The UV–Vis spectra of $[Os(bpy)_2(\mathbf{21})]^{2+}$ and $[Os(phen)_2(\mathbf{21})]^{2+}$ support these assignments as the transition attributed to **21** at 360 nm is common to both complexes.

The energies of the lowest energy MLCT transitions for $Os(II) \rightarrow L$ and $Os(II) \rightarrow L'$ can be related to the nature of the acceptor ligand and the electrochemical properties of the complexes. In the case of the Os(II) complexes a plot of ΔE_{red-ox}, the thermodynamic energy gap ($\Delta E_{red-ox} = E_{first\ oxidation} - E_{first\ reduction}$), versus the transition energy, ΔE_{op} (eV), is linear (Fig. 4) [31]. This holds for the energies of both the ^{1}MLCT and ^{3}MLCT transitions in the Os(II) complexes.

2.6. Electronic absorption spectroelectrochemistry

Spectroelectrochemical data for the oxidation and reduction processes of the Os and Re complexes are summarised in Tables 4 and 5, respectively.

Upon oxidation of the Os(II) complexes the MLCT features in the visible region are bleached, leaving two weak transitions in the visible region. The low intensity of the new transitions is consistent with oxidation of the metal as the resulting LMCT transitions have generally lower oscillator strengths than their MLCT counterparts [42]. The variation in wavelength and extinction coefficient observed for the LMCT transitions suggests that they are associated with the non-ancillary ligands, i.e. L,L′ or L″.

The UV region shows bpy features characteristic of a Os(III)-bpy complex [21], supporting the assignment of the first oxidation as being metal-based; the intense $\pi \rightarrow \pi^*$ transition of the Os(II) complexes at 285 nm is split into two bands at 305 and 315 nm, as is also found for $[Os(bpy)_3]^{3+}$.

Electrochemical reduction of the *fac*-$[Re(L'')(CO)_3Cl]$ and $[Os(L)(bpy)_2]^{2+}$ complexes gives spectral changes throughout the visible and NIR regions (Table 5). The UV–Vis spectra corresponding to the first reduction process associated with the *fac*-$[Re(L'')(CO)_3Cl]$ complexes show a bleach of the ground state features and the

Table 3
Electronic absorption data for the polypyridyl ligands (CH_2Cl_2), their Os(II) complexes (CH_3CN) and Re(I) complexes (CH_2Cl_2)

	λ (nm) [ε (10^3 M^{-1} cm^{-1})]							
	^{3}MLCT Os–L	^{1} MLCT M–L	^{1}MLCT Os–bpy, Os–phen	π–π* L	π–π* L	π–π* bpy, phen	π–π* L	π–π* bpy, phen
(**21**)				375(8.0)	307(16.0)		270(39.0)	
(**22**)				383(12.0)	312(17.0)		274(53.0)	
(**23**)				388(10.0)	311(18.5)		270(37.4)	
(**24**)				391(12.0)	305(25.4)		274(43.0)	
(**25**)				412(11.1)	319(18.5)		308(63.1)	
(**26**)				383(12.0)	311(20.0)		274(58.7)	
$[Os(bpy)_2(\mathbf{11})]^{2+}$	765(1.2)	531(7.5)	432(7.2)	350(14.6)		286(54.7)		250(24.0)
$[Os(bpy)_2(\mathbf{12})]^{2+}$	765(1.7)	529(10.2)	442(9.4)	352(20.8)		285(49.3)		253(32.2)
$[Os(bpy)_2(\mathbf{13})]^{2+}$	824(1.4)	553(10.5)	436(8.4)	361(19.9)		285(64.6)		254(32.8)
$[Os(bpy)_2(\mathbf{14})]^{2+}$	831(1.0)	569(8.7)	443(8.9)	322(32.0)		288(56.7)		243(36.7)
$[Os(bpy)_2(\mathbf{16})]^{2+}$	776(1.6)	535(11.3)	427(10.0)	349(20.5)		287(75.4)		254(31.0)
$[Os(phen)_2(\mathbf{11})]^{2+}$	799(1.9)	553(11.3)	444(8.1)	361(20.9)		284(73.0)		250(49.1)
$[Os(bpy)_2(\mathbf{21})]^{2+}$	817(2.0)	557(13.0)	442(9.0)	360(21.3)		284(75.3)		252(47.2)
$[Os(bpy)_2(\mathbf{22})]^{2+}$	789(2.0)	550(12.5)	447(9.3)	366(23.4)		284(75.2)		247(39.5)
$[Os(bpy)_2(\mathbf{23})]^{2+}$	866(2.2)	579(14.0)	442(9.4)	369(28.4)		286(84.7)		256(52.0)
$[Os(bpy)_2(\mathbf{24})]^{2+}$	905(2.0)	608(13.0)	446(9.6)	322(45.5)		286(60.2)		249(52.0)
$[Os(bpy)_2(\mathbf{25})]^{2+}$	902(2.1)	589(14.1)	436(8.6)	358(26.0)		285(62.4)		249(56.9)
$[Os(bpy)_2(\mathbf{26})]^{2+}$	802(2.1)	555(13.4)	437(9.4)	358(20.9)		285(73.7)		250(47.3)
$[Os(phen)_2(\mathbf{21})]^{2+}$	811(2.8)	557(17.9)	436(14.3)	360(25.9)		263(108.9)		220(93.1)
$[Re(CO)_3(\mathbf{21})Cl]$		476(3.2)		391(11.0)	301(22.0)		271(42.0)	
$[Re(CO)_3(\mathbf{22})Cl]$		463(3.5)		398(16.0)	309(25.0)		277(40.0)	
$[Re(CO)_3(\mathbf{23})Cl]$		501(3.3)		407(18.0)	308(23.0)		274(46.0)	

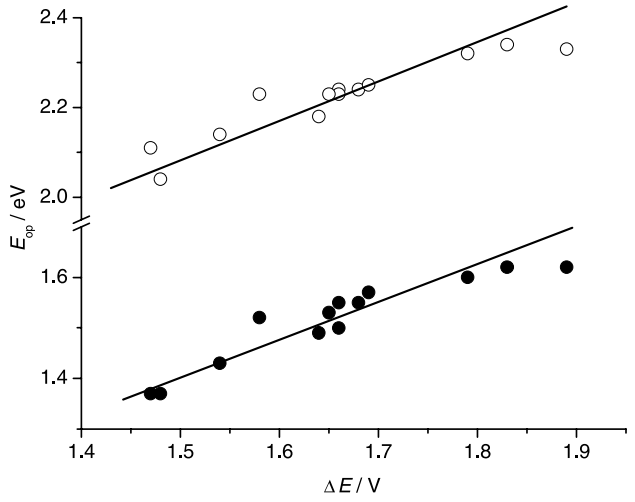

Fig. 4. Plot of the energy of the two lowest energy electronic absorptions vs. the electrochemical difference between the oxidation and the reduction potentials for the $[Os(bpy)_2(L'')]^{2+}$ and $[Os(bpy)_2(L)]^{2+}$ complexes. Open circles denote transitions assigned as ^{1}MLCT. Closed circles denote transitions assigned as ^{3}MLCT. The relationship for the ^{1}MLCT transition energies follows: $E_{op} = 0.66 \times \Delta E + 1.12$, $R^2 = 0.88$; for the ^{3}MLCT transitions the relationship is: $E_{op} = 0.62 \times \Delta E + 0.86$, $R^2 = 0.89$.

concomitant growth of new features of lower intensity at longer wavelengths. These spectra are consistent with the formation of the ligand radical anion species *fac*-$[Re(L'')(CO)_3Cl]^{\cdot -}$ with four features present at ~1100, 530, 400 and 330 nm (Table 5).

In the $[Os(bpy)_2(L')]^{2+}$ series the new features displayed upon reduction are assigned as π^*–π^* transitions of the radical anion $L'^{\cdot -}$. Similar bands are seen in the electronic absorption spectrum of the radical anions of **11–14** and **16** and of Re(I) complexes with similar ligands [43]. The spectra of the electrochemically reduced $[Os(bpy)_2(L)]^+$ complexes display bands in the visible region that are associated with the radical anion $L^{\cdot -}$. The reduced forms of the *fac*-$[Re(CO)_3(L'')Cl]$ complexes show similar transitions.

The MLCT (Os(II) → bpy) bands of the reduced Os(II) species are slightly red-shifted with respect to the parent complexes. This is consistent with the electron being localised mainly on the ligand moiety. The red-shift is caused by electron donation from the ligand π^* orbital to the metal dπ orbital which is thus destabilised.

3. Conclusions

We have developed a method for the synthesis of rigid polypyridyl bridging ligands based on ppb. The electrochemical properties of the ppb-ligands (**21–26**) are consistent with the electron withdrawing and donating effects of the substituents, and the electrochemical and electronic absorption properties of the complexes mirror these substituent effects.

The Os(II) complexes have strong MLCT transitions in the visible region that are singlet and triplet in nature. For these complexes the ^{1}MLCT and ^{3}MLCT bands show a linear correlation with the electrochemical properties of the complexes. This strengthens the assignment of these bands as involving the non-ancillary ligands.

Spectroelectrochemical studies reveal that the first oxidation for the Os(II) complexes is metal-based, with the strong MLCT bands being bleached and weaker LMCT transitions growing in. Electrochemical reduction is based on the non-ancillary ligands, as evidenced by the spectroelectrochemical behaviour of the Re(I) complexes.

The present study provides a method for the synthesis of a new group of complexes containing polypyridyl ligands based on ppb. These have already been shown to possess very interesting photophysical properties and

Table 4
Electronic absorption data for the oxidised Os(II) complexes

	λ (nm) [ε (10^3 M^{-1} cm^{-1})]					
	LMCT L–Os	LMCT L–Os	π–π^* L	π–π^* L	π–π^* bpy, phen	π–π^* bpy, phen
$[Os(bpy)_2(\mathbf{11})]^{3+}$	590(1.3)	394(7.6)		369(8.8)	315(30.9)	302(35.9)
$[Os(bpy)_2(\mathbf{12})]^{3+}$	566(0.7)	388(13.0)			316(46.5)	306(48.2)
$[Os(bpy)_2(\mathbf{13})]^{3+}$	603(0.7)	404(12.9)			316(39.3)	304(44.8)
$[Os(bpy)_2(\mathbf{14})]^{3+}$	519(1.8)	412(10.5)		347(2.8)	316(43.7)	304(40.9)
	667s	434(10.0)				
$[Os(bpy)_2(\mathbf{16})]^{3+}$	555(1.2)	438(5.0)		375(1.3)	316(39.1)	300(37.3)
$[Os(phen)_2(\mathbf{11})]^{3+}$	563(1.0)	453(3.0)		394(9.7)	314(31.8)	305(33.7)
$[Os(bpy)_2(\mathbf{21})]^{3+}$	574(1.2)	453(2.8)	391(13.8)	376(14.1)	315(55.1)	305(58.1)
$[Os(bpy)_2(\mathbf{22})]^{3+}$	587(1.7)	462(4.3)	407(11.7)		316(40.1)	307(40.4)
$[Os(bpy)_2(\mathbf{23})]^{3+}$	585(2.5)	458(3.3)	411(12.6)	390(8.9)	317(46.7)	307(47.9)
$[Os(bpy)_2(\mathbf{24})]^{3+}$	656(2.6)	522(0.5)	435(9.6)	414(9.8)	335(42.6)	316(50.0)
$[Os(bpy)_2(\mathbf{25})]^{3+}$	553(1.6)	449(4.0)	389(13.1)	378(12.8)	315(34.8)	304(35.7)
$[Os(bpy)_2(\mathbf{26})]^{3+}$	573(1.0)	460(3.8)	393(11.0)	376(11.4)	317(44.9)	306(49.2)
$[Os(phen)_2(\mathbf{21})]^{3+}$	576(11.6)	448(5.3)	393(14.4)	375(16.3)	318(39.2)	307(47.2)

Data recorded from 1 mM CH_3 CN solutions containing 0.1 M $TBAPF_6$ supporting electrolyte.

Table 5
Electronic absorption data for the reduced forms of the Os(II) and Re(I) complexes

	λ (nm) [ε (10^3 M^{-1} cm^{-1})]						
	π^*–π^* L$^{\cdot-}$	π^*–π^* L$^{\cdot-}$	^{1}MLCT MOs–L$^{\cdot-}$	π^*–π^* L$^{\cdot-}$	^{1}MLCT Os–bpy, Os–phen	π–π^* L$^{\cdot-}$	π–π^* bpy, phen
[Os(bpy)$_2$(**11**)]$^+$		742(0.9)	579(3.6)s	488(7.9)	460(7.3)	345(12.6)	294(47.3)
[Os(bpy)$_2$(**12**)]$^+$		763(2.3)	578(8.7)	486(13.3)	457(9.5)	349(18.0)	293(55.4)
[Os(bpy)$_2$(**13**)]$^+$	1072(1.1)	759(2.3)	576(6.5)	481(11.3)	451(11.0)	362(18.7)	293(61.9)
[Os(bpy)$_2$(**14**)]$^+$		858(2.8)	672(4.8)	490(10.7)	456(11.0)	374(23.8)	293(61.3)
						338(25.1)	
[Os(bpy)$_2$(**16**)]$^+$	1073(1.8)	709(3.7)	569(7.2)	481(13.3)	457(13.0)	348(23.2)	292(37.3)
[Os(phen)$_2$(**11**)]$^+$	1213(1.0)	767(2.1)	589(5.1)	482(8.9)	451(8.4)	376(15.6)	292(44.4)
[Os(bpy)$_2$(**21**)]$^+$	1200(2.0)	707(4.0)	571(7.2)	487(14.3)	453(11.2)	361(21.5)	291(75.3)
[Os(bpy)$_2$(**22**)]$^+$		726(4.1)	578(3.8)	493(11.2)	454(8.3)	372(17.6)	292(50.0)
[Os(bpy)$_2$(**23**)]$^+$	1200(1.2)	778(2.5)	594(4.4)	488(11.4)	452(10.0)	376(18.4)	291(67.9)
[Os(bpy)$_2$(**24**)]$^+$		838(4.3)	702(4.2)	492(11.5)	451(9.8)	369(30.2)	291(75.3)
[Os(bpy)$_2$(**25**)]$^+$	1170(2.0)	791(4.2)	598(7.6)	494(12.0)	452(11.9)	369(19.6)	290(55.1)
[Os(bpy)$_2$(**26**)]$^+$	1030(1.7)	693(3.5)	582(5.4)	495(14.3)	448(13.4)	366(20.7)	292(58.3)
	1280(1.3)						
[Os(phen)$_2$(**21**)]$^+$	1240(3.0)	743(4.9)	583(7.1)	487(18.7)	446(15.4)	364(18.7)	263(87.2)
[Re(CO)$_3$(**21**)Cl]$^-$	1166(0.9)			523(5.0)		391(8.9)	
[Re(CO)$_3$(**22**)Cl]$^-$	1200(1.0)			529(4.8)		398(11.0)	
[Re(CO)$_3$(**23**)Cl]$^-$	1111(1.0)			549(4.9)		403(10.0)	

Data recorded from 1 mM solutions with 0.1 M $TBAPF_6$ supporting electrolyte for Os(II) complexes (CH_3CN) and Re(I) complexes (CH_2Cl_2).

rich electronic spectral properties. The utility of these materials as photosensitisers in solar cells [44] and as electroluminescent emitting materials [45] is currently underway in our laboratory.

4. Experimental

Synthetic reagents were LR or AR grade and were used without further purification unless otherwise specified. All solvents used for spectroscopic and electrochemical measurements were Aldrich spectroscopic or HPLC grade and were used without further purification. [Os(bpy)$_2$Cl$_2$] was prepared by literature methods [29]. [Re(CO)$_5$Cl] was prepared from [Re$_2$(CO)$_{10}$] (Aldrich) according to literature methods [46]. DMF (HPLC grade) was dried by stirring over CaH_2 with subsequent vacuum distillation. Tetrabutylammonium hexafluorophosphate (TBAPF) was metathesised from tetrabutylammonium hydroxide (TBAH) and hexafluorophosphoric acid, recrystallised twice from dry methanol and stored in a vacuum desiccator. NaI solutions used as eluents were prepared as required due to the air oxidation of I^- to I_2. 1 M solutions of sodium *p*-tolylsulfonate were prepared by the basification of a *p*-tolylsulfonic acid solution with an equimolar amount of solid NaOH. The resulting solution was filtered to remove a brown impurity and diluted as required.

4.1. Instrumentation

Electronic absorption spectra were recorded on a Perkin–Elmer Lambda-19 UV–Vis–NIR spectrophotometer using Perkin–Elmer UVDM software. Extinction coefficients were calculated by linear regression of the absorbance of a number of parallel-diluted solutions ($\varepsilon \pm 10\%$). Solid-state IR spectra were recorded as KBr discs using a Perkin–Elmer BX FTIR spectrometer and Perkin–Elmer Spectrum v2.00 software. Solution IR spectra were collected on the same instrument in a 0.50 mm path-length solution cell with NaCl windows, against a background of the pure solvent. Post-acquisition data treatment was performed using Galactic Grams/32 version 5.05. Cyclic voltammograms and square-wave voltammograms were recorded on an EG&G PAR Model 273A Potentiostat with Model 270 software. Typically the samples were at 1 mM concentration with 0.1 M TBAPF electrolyte. The scans were recorded at 200 mV s^{-1} and referenced to silver wire, which was itself referenced to the ferrocene/ferrocenium couple (0.40V versus NHE). The reversibility of a process was defined by comparison of the peak separation in the cyclic voltammogram to an internal ferrocene reference (typically $\Delta E_p \approx 0.100$ V for the cell used).

4.2. X-ray crystallography

Single crystals of *fac*-[Re(CO)$_3$(**21**)Cl] were grown by slow diffusion of diethyl ether into a dichloromethane solution of the complex. Single crystal data were collected using a Bruker SMART CCD system (Mo Kα radiation, 0.71073 A). The structure was solved by direct methods using SHELXS-97 [47] running within the WinGX [48] package and weighted full-matrix refinement on F^2 was carried out using SHELXL-97 [49], with all non-hydrogen atoms being refined anisotropically.

Hydrogen atoms were included in calculated positions and were refined as riding atoms with individual isotropic displacement parameters. The maximum and minimum peaks on the final difference Fourier maps corresponded to 1.650 and −1.214 e Å^{-3}.

4.3. Ligand precursor synthesis

4.3.1. N,N′-Diacetyl-2-methoxy-1,4-phenylenediamine (2)

2-Methoxyphenylene-1,4-diamine (25 g) was suspended in pyridine (75 ml) and stirred vigorously. Acetic anhydride (100 ml) was added slowly. No attempt was made to control the temperature of the strongly exothermic reaction. The solution was cooled, poured onto ice, and the crude product collected by filtration. The crude product was purified by recrystallisation from ethanol. A second crop of product was collected by concentration of the combined filtrates followed by recrystallisation from ethanol. Yield (18.52 g, 46%). Found: C, 59.34; H, 6.45; N, 12.76%. $C_{11}H_{14}N_2O_3$ requires: C, 59.45; H, 6.35; N, 12.60. δ_H (200 MHz, $CDCl_3$) 8.24 (1H, d, $J^d = 8.5$ Hz), 7.65 (2H, d, $J^d = 2.0$ Hz), 7.20 (1H, br s) 6.63 (1H, dd, $J^{d1} = 8.5$ Hz, $J^{d2} = 2.0$ Hz), 3.80 (3H, s), 2.19 (3H, s), 2.17 (3H, s). δ_C (50 MHz, $CDCl_3$) 143.8, 137.5, 136.9, 119.8, 111.7, 111.3, 103.1, 103.1, 55.9, 24.9, 24.7.

4.3.2. 5-Methoxy-4,7-phenanthroline (3)

N,*N*′-Diacetyl-2-methoxy-1,4-phenylenediamine (5 g), glacial acetic acid (100 ml) and conc. H_2SO_4 (30 ml) were added to a suspension of $Fe_2(SO_4)_3 \cdot xH_2O$ (45 g) in conc. H_2SO_4 (37 ml). Glycerol (10 g) was added and the reaction heated to 120 °C for 2 h in an open round bottomed flask, before being raised to 140 °C for a further 2 h. On cooling, the reaction mixture was carefully poured onto ice and the pH adjusted to ≈10 with 10 M KOH. The resulting black/brown solid was removed by filtration with the aid of celite and retained. The filtrate was extracted 3 times with $CHCl_3$ (200 ml) and discarded. The solid/celite mixture was boiled three times with $CHCl_3$ (500 ml), each time being filtered through additional celite. The combined $CHCl_3$ extracts were concentrated and purified by column chromatography on neutral alumina ($CHCl_3$ eluant). Yield (4.40 g, 93%). Found: C, 74.47; H, 4.96; N, 13.05%. $C_{13}H_{10}N_2O$ requires: C, 74.27; H, 4.79; N, 13.32. δ_H (200 MHz, $CDCl_3$) 8.95 (1H, d, $J^d = 3.0$ Hz), 8.79 (1H, d, $J^d = 4.0$ Hz), 8.69 (1H, d, $J^d = 7.5$ Hz), 8.59 (1H, d, $J^d = 8.5$ Hz), 7.56 (1H, dd, $J^{d1} = 4.5$ Hz, $J^{d2} = 8.0$ Hz), 7.38 (1H, dd, $J^{d1} = 4.5$ Hz, $J^{d2} = 8.5$ Hz), 7.33 (1H, s), 4.15 (3H, s). δ_C (50 MHz, $CDCl_3$) 155.8, 149.6, 149.1, 147.9, 140.6, 130.5, 130.1, 124.7, 122.1, 119.2, 119.8, 106.2, 55.6.

4.3.3. 5,6-Dimethoxy-5,6-dihydro-[4,7]phenanthroline-5,6-diol (4)

To a solution of 5-methoxy-4,7-phenanthroline (4.70 g) in conc. H_2SO_4 (25.0 ml) at −10 °C (ice/NaCl bath) was slowly added fuming nitric acid (15.0 ml, $d = 1.51$). The mixture was then heated to 120 °C for 2 h in a dry reflux apparatus. On cooling, the reaction mixture was poured carefully onto ice and was adjusted to pH 7 with 10 M NaOH, care being taken to not let the solution change from yellow to blue/black (at pH >7). After standing for 2 h at 4 °C, the crude precipitate was collected by filtration. The pure product was collected by filtration following recrystallisation from methanol. Yield (2.48 g, 40%). Found: C, 61.09; H, 5.19; N, 10.21%. $C_{14}H_{14}N_2O_4$ requires: C, 61.31; H, 5.15; N, 10.21. δ_H (200 MHz, $CDCl_3$) 8.54 (2H, dd, $J^{d1} = 1.5$ Hz, $J^{d2} = 5.0$ Hz), 8.08 (2H, dd, $J^{d1} = 1.5$ Hz, $J^{d2} = 8.0$ Hz), 7.45 (2H, dd, $J^{d1} = 5.0$ Hz, $J^{d2} = 8.0$ Hz), 6.09 (2H, s) 3.04 (6H, s). δ_C (50 MHz, $CDCl_3$) 153.5, 147.3, 131.9, 125.9, 124.6, 95.5, 50.0.

4.4. Synthesis of ligands 21–26

5,6-Dimethoxy-5,6-dihydro-[4,7]phenanthroline-5,6-diol (300 mg, 1.0 mmol) and an equimolar amount of the appropriate diamine were gently heated in 50 ml of methanol until all of the solids dissolved. Two drops of 2 M HCl were added and the mixture rapidly heated to reflux. After 30 min, 50 ml of water was added to the solution and the crude products were collected by filtration and washed with ice cold methanol and copious amounts of ether. The individual products were purified by chromatography on a short (3 cm) plug of silica gel with $CHCl_3$ as eluent. The products crystallised on evaporation of the $CHCl_3$ solution.

4.4.1. [2,3-a:3′,2′-c]dipyridophenazine (21)

Yield (271 mg, 90%). Found: C, 76.86; H, 3.81; N, 19.69%. $C_{18}H_{10}N_4$ requires: C, 76.58; H, 3.57; N, 19.85. δ_H (200 MHz, $CDCl_3$) 9.30 (2H, dd, $J^{d1} = 1.5$ Hz, $J^{d2} = 4.5$ Hz), 8.91 (2H, dd, $J^{d1} = 1.5$ Hz, $J^{d2} = 8.5$ Hz), 8.69 (2H, dd, $J^{d1} = 6$ Hz, $J^{d2} = 3$ Hz), 8.00 (2H, AA′BB′, $J = 3.5$ Hz), 7.82 (2H, dd, $J^{d1} = 4.5$ Hz, $J^{d2} = 8.5$ Hz). δ_C (50 MHz, $CDCl_3$) 151.5, 146.1, 143.4, 143.2, 131.5, 131.4, 127.9, 126.6, 124.8.

4.4.2. [2,3-a:3′,2′-c]dipyrido-6, 7-dimethylphenazine (22)

Yield (327 mg, 74%). Found: C, 69.23; H, 5.03; N, 16.14%. $C_{20}H_{14}N_4 \cdot 2H_2O$ requires: C, 69.34; H, 5.24; N, 16.18. δ_H (200 MHz, $CDCl_3$) 9.27 (2H, dd, $J^{d1} = 1.5$ Hz, $J^{d2} = 4.5$ Hz), 8.88 (2H, dd, $J^{d1} = 1.5$ Hz, $J^{d2} = 8.5$ Hz), 8.40 (2H, s), 7.78 (2H, dd, $J^{d1} = 4.5$ Hz, $J^{d2} = 8.0$ Hz), 2.62 (6H, s). δ_C (50 MHz, $CDCl_3$) 151.3, 146.2, 142.7, 142.5, 142.4, 131.3, 129.0, 125.1, 124.4, 20.9.

*4.4.3. [2,3-a:3′,2′-c]dipyrido-6,7- dichlorophenazine (**23**)*

Yield (466 mg, 93%). Found: C, 55.68; H, 2.75; N, 14.55%. $C_{18}H_8N_4Cl_2 \cdot 2H_2O$ requires: C, 55.83; H, 3.12; N, 14.47%. δ_H (200 MHz, $CDCl_3$) 9.28 (2H, dd, $J^{d1} = 1.5$ Hz, $J^{d2} = 4.5$ Hz), 8.90 (2H, dd, $J^{d1} = 1.5$ Hz, $J^{d2} = 8.5$ Hz), 8.79 (2H, s), 7.84 (2H, dd, $J^{d1} = 4.5$ Hz, $J^{d2} = 8.5$ Hz). δ_C (50 MHz, $CDCl_3$) 151.6, 145.5, 143.9, 141.8, 136.5, 131.5, 130.7, 126.9, 125.3.

*4.4.4. [2,3-a:3′,2′-c]dipyrido[1,2-e]benzophenazine (**24**)*

Yield (394 mg, 83%). Found: C, 74.07; H, 3.88; N, 15.64%. $C_{22}H_{12}N_4 \cdot 1.5H_2O$ requires: C, 74.45; H, 4.12; N, 15.80. δ_H (200 MHz, $CDCl_3$) 9.30 (2H, s), 9.29 (2H, dd, $J^{d1} = 1.5$ Hz, $J^{d2} = 4.5$ Hz), 8.86 (2H, dd, $J^{d1} = 1.5$ Hz, $J^{d2} = 8.0$ Hz), 8.24 (2H, AA′BB′, $J = 3.5$ Hz), 7.81 (2H, dd, $J^{d1} = 4.5$ Hz, $J^{d2} = 8.5$ Hz), 7.64 (2H, AA′BB′, $J = 3.0$ Hz). δ_C (50 MHz, $CDCl_3$) 151.5, 150.4, 143.4, 142.7, 139.4, 134.9, 131.4, 129.0, 128.9, 127.4, 125.0.

*4.4.5. [2,3-a:3′,2′-c:2″, 3″-e]tripyridoquinoxaline (**25**)*

Yield (252 mg, 86%). Found: C, 72.21; H, 3.35; N, 24.92%. $C_{17}H_9N_4$ requires: C, 72.08; H, 3.20; N, 24.78. δ_H (200 MHz, $CDCl_3$) 9.47 (1H, dd, $J^{d1} = 2.0$ Hz, $J^{d2} = 4.0$ Hz), 9.31 (2H, m), 9.01 (1H, dd, $J^{d1} = 2.0$ Hz, $J^{d2} = 8.5$ Hz), 8.92 (2H, m), 7.92 (1H, dd, $J^{d1} = 4.0$ Hz, $J^{d2} = 8.5$ Hz), 7.84 (2H, m). δ_C (50 MHz, $CDCl_3$) 156.6, 153.4, 151.5, 151.4, 145.4, 145.3, 143.9, 140.3, 139.0, 131.5, 131.2, 128.5, 126.9 (2C), 126.3, 125.3, 125.2.

*4.4.6. [2,3-a:3′,2′-c]dipyrido-5-methylphenazine (**26**)*

Yield (327 mg, 77%). δ_H (200 MHz, $CDCl_3$) 9.25 (2H, m), 8.86 (2H, d, $J^d = 7.0$ Hz), 8.49 (1H, d, $J^d = 8.0$ Hz), 7.9-7.7 (4H, m), 3.17 (3H, s). δ_C (50 MHz, $CDCl_3$) 151.3, 151.2, 146.2, 146.0, 143.4, 142.6 (2C), 141.9, 138.6, 131.3 (2C), 131.1, 128.3, 128.1, 126.4, 126.3, 124.5, 124.4, 17.8.

4.5. Synthesis of Os(II) complexes

$[Os(bpy)_2Cl_2]$ (100 mg) or $[Os(phen)_2Cl_2]$ (110 mg) and a 2-fold excess of the appropriate ligand were gently heated in ethylene glycol (50 ml) until completely dissolved. The solution was then heated to reflux for 2 h. On cooling, dichloromethane (100 ml) and water (200 ml) were added. The organic layer was separated and discarded and the aqueous layer again extracted with dichloromethane (100 ml). The water layer was diluted and loaded on to a Sephadex SP-C25 column (10 cm × 2 cm diameter) and washed well with water and 0.05 M sodium *p*-tolylsulfonate to remove uncharged species. The mononuclear complex was eluted with 0.1–0.2 M sodium *p*-tolylsulfonate and was separated from the eluent by precipitation with solid NH_4PF_6 (1 g) followed by extraction with 5 × 100 ml of dichloromethane. The resulting intensely coloured organic solution was reduced to dryness (rotavap), dissolved in a minimum volume of acetonitrile and reprecipitated by addition to an aqueous solution of NH_4PF_6. The solid was collected by filtration, dissolved in acetonitrile and reprecipitated by addition to ether.

*4.5.1. [Os(bpy)$_2$(**21**)](PF$_6$)$_2$*

Yield (140 mg, 70%) Found: C, 41.10; H, 2.83; N, 9.89%. $C_{38}H_{26}N_8OsP_2F_{12} \cdot 2H_2O$ requires: C, 41.09; H, 2.72; N, 10.09. δ_H (200 MHz, d_3-MeCN) 9.14 (2H, m), 8.94 (1H, dd, $J^{d1} = 8.5$ Hz, $J^{d2} = 1.5$ Hz), 8.64 (1H, d, $J^d = 8.0$ Hz), 8.57 (1H, d, $J^d = 8.0$ Hz), 8.36 (1H, dd, $J^{d1} = 8.5$ Hz, $J^{d2} = 1.0$ Hz), 8.00 (4H, m), 7.88 (2H, m), 7.77 (5H, m), 7.49 (6H, m), 7.09 (3H, m). *m/z* 931 ({M-PF_6}$^+$).

*4.5.2. [Os(bpy)$_2$(**22**)](PF$_6$)$_2$*

Yield (90 mg, 45%). Found: C, 43.27; H, 3.30; N, 10.05%. $C_{40}H_{30}N_8OsP_2F_{12} \cdot 0.5H_2O$ requires: C, 43.21; H, 2.81; N, 10.08. δ_H (200 MHz, d_3-MeCN) 9.09 (1H, dd, $J^{d1} = 8.5$ Hz, $J^{d2} = 1.5$ Hz), 8.95 (1H, dd, $J^{d1} = 4.5$ Hz, $J^{d2} = 1.5$ Hz), 8.90 (1H, dd, $J^{d1} = 8.5$ Hz, $J^{d2} = 1.0$ Hz), 8.64 (1H, d, $J^d = 8.0$ Hz), 8.58 (1H, d, $J^d = 8.0$ Hz), 8.56 (1H, d, $J^d = 8.0$ Hz), 8.40 (1H, d, $J^d = 8.0$ Hz), 7.95 (7H, m), 7.75 (2H, m), 7.59 (3H, m), 7.45 (1H, ddd, $J^{d1} = 7.5$ Hz, $J^{d2} = 6.0$ Hz, $J^{d3} = 1.3$ Hz), 7.11 (4H, m), 2.36 (3H, s), 1.98 (3H, s). *m/z* 959 ({M-PF_6}$^+$).

*4.5.3. [Os(bpy)$_2$(**23**)](PF$_6$)$_2$*

Yield (110 mg, 56%). Found: C, 40.11; H, 2.38; N, 9.77%. $C_{38}H_{24}N_8OsP_2F_{12}Cl_2$ requires: C, 39.91; H, 2.12; N, 9.80. δ_H (200 MHz, d_3-MeCN) 9.48 (1H, d, $J^d = 6.5$ Hz), 9.03(1H, d, $J^d = 8.0$ Hz), 8.91 (1H, dd, $J^{d1} = 7.5$ Hz, $J^{d2} = 1.0$ Hz), 8.91 (1H, d, $J^d = 8.5$ Hz), 8.73 (1H, d, $J^d = 8.5$ Hz), 8.61 (1H, d, $J^d = 8.0$ Hz), 7.95 (5H, m), 7.83 (3H, m), 7.65 (4H, m), 7.39 (4H, m), 7.12 (2H, m). *m/z* 999 ({M-PF_6}$^+$).

*4.5.4. [Os(bpy)$_2$(**24**)](PF$_6$)$_2$*

Yield (70 mg, 35%). Found: C, 43.54; H, 1.81; N, 9.71%. $C_{42}H_{28}N_8OsP_2F_{12} \cdot 2H_2O$ requires: C, 43.45; H, 2.78; N, 9.65. δ_H (200 MHz, d_3-MeCN) 9.20 (2H, m), 8.90 (3H, m), 8.50 (2H, m), 8.33 (1H, d, $J^d = 8.5$ Hz), 7.90 (5H, m), 7.73 (4H, m), 7.51 (7H, m), 7.09 (3H, m), 7.02 (1H, dd, $J^{d1} = 8.5$ Hz, $J^{d2} = 1.0$ Hz). *m/z* 981 ({M-PF_6}$^+$).

*4.5.5. [Os(bpy)$_2$(**25**)](PF$_6$)$_2$*

Yield (120 mg, 60%). Found: C, 40.09; H, 2.45; N, 11.63%. $C_{37}H_{25}N_9OsP_2F_{12} \cdot 2H_2O$ requires: C, 39.97; H, 2.63; N, 11.34. δ_H (500 MHz, d_3-MeCN) 9.23 (1H, dd, $J^{d1} = 4.0$ Hz, $J^{d2} = 1.5$ Hz, p6′), 9.20 (1H, dd, $J^{d1} = 8.5$ Hz, $J^{d2} = 1.5$ Hz, p4′), 8.91 (1H, dd, $J^{d1} = 8.5$ Hz, $J^{d2} = 1.0$ Hz, p4″), 8.64 (2H, m, p2, bB3), 8.50 (1H, d, $J^d = 8.0$ Hz, bB3′), 8.46 (1H, d, $J^d = 8.5$ Hz, bA3′), 8.36 (1H, d, $J^d = 7.5$ Hz, bA3), 8.33 (1H, dd, $J^{d1} = 2.5$ Hz, $J^{d2} = 2.0$ Hz, p4), 8.14 (1H, dd, $J^{d1} = 5.5$ Hz, $J^{d2} = 1.0$

Hz, p6″), 8.02 (2H, m, p5′, bB4), 7.94 (1H, ddd, $J^{d1} = 8.5$ Hz, $J^{d2} = 7.5$ Hz, $J^{d3} = 1.5$ Hz, bA4′), 7.83(2H, m, bB4′, bA4), 7.77 (1H, dd, $J^{d1} = 8.5$ Hz, $J^{d2} = 6.0$ Hz, p5″), 7.71 (1H, dd, $J^{d1} = 8.5$ Hz, $J^{d2} = 4.0$ Hz, p3), 7.68 (1H, d, $J^{d} = 5.0$ Hz, bA6′), 7.64 (1H, d, $J^{d} = 5.0$ Hz, bB6), 7.53 (1H, ddd, $J^{d1} = 7.5$ Hz, $J^{d2} = 6.0$ Hz, $J^{d3} = 1.5$ Hz, bB5), 7.48 (1H, d, $J^{d} = 5.5$ Hz, bB6′), 7.42 (1H, ddd, $J^{d1} = 6.5$ Hz, $J^{d2} = 5.5$ Hz, $J^{d3} = 1.5$ Hz, bA5′), 7.21 (1H, d, $J^{d} = 5.5$ Hz, bA6), 7.07 (1H, ddd, $J^{d1} = 6.5$ Hz, $J^{d2} = 5.5$ Hz, $J^{d3} = 1.5$ Hz, bA5), 7.03 (1H, ddd, $J^{d1} = 6.5$ Hz, $J^{d2} = 5.5$ Hz, $J^{d3} = 1.5$ Hz, bB5′). *m/z* 932 ({M-PF_6}$^+$).

4.5.6. [Os(bpy)$_2$(**26**)](PF$_6$)$_2$

Yield (180 mg, 90%). Found: C, 42.61; H, 3.02; N, 10.33%. $C_{39}H_{28}N_8OsP_2F_{12} \cdot H_2O$ requires: C, 42.32; H, 2.73; N, 10.12. δ_H (200 MHz, d_3-MeCN) 9.44 (1H, dd, $J^{d1} = 6.5$ Hz, $J^{d2} = 0.5$ Hz), 9.09 (1H, dd, $J^{d1} = 8.5$ Hz, $J^{d2} = 1.5$ Hz), 8.63 (3H, m), 8.52 (1H, d, $J^{d} = 8.0$ Hz), 8.36 (3H, m), 8.00 (7H, m), 7.89 (4H, m), 7.71 (4H, m), 7.23 (1H, d, $J^{d} = 8.0$ Hz), 2.35 (3H, s). *m/z* 945 ({M-PF_6}$^+$).

4.5.7. [Os(phen)$_2$(**21**)](PF$_6$)$_2$

Yield (160 mg, 80%). Found: C, 41.44; H, 2.81; N, 9.84%. $C_{42}H_{26}N_8OsP_2F_{12} \cdot 2H_2O$ requires: C, 41.53; H, 2.61; N, 9.67%. δ_H (200 MHz, d_3-MeCN) 9.26 (1H, d, $J^{d} = 8.0$ Hz), 8.89 (1H, d, $J^{d} = 8.0$ Hz), 8.69 (1H, d, $J^{d} = 7.5$ Hz), 8.51 (3H, m), 8.46 (1H, dd, $J^{d1} = 8.0$ Hz, $J^{d2} = 1.5$ Hz), 8.00 (7H, m), 7.82 (5H, m), 7.72 (4H, m), 7.41 (2H, m), 7.18 (1H, dd, $J^{d1} = 7.0$ Hz, $J^{d2} = 6.5$ Hzz). *m/z* 979 ({M-PF_6}$^+$).

4.5.8. [Os(bpy)$_2$(**11**)](PF$_6$)$_2$

Yield (125 mg, 66%). Found: C, 42.59; H, 2.66; N, 10.52%. $C_{38}H_{28}N_8OsP_2F_{12}$ requires: C, 42.39; H, 2.62; N, 10.40. δ_H (200 MHz, d_3-MeCN) 8.69 (3H, m), 8.26 (2H, m), 8.19 (1H, dd, $J^{d1} = 7.5$ Hz, $J^{d2} = 1.5$ Hz), 8.08 (2H, m), 7.90 (2H, d, $J^{d} = 6.5$ Hz), 7.81 (5H, m), 7.66 (1H, ddd, $J^{d1} = 5.0$ Hz, $J^{d2} = 4.5$ Hz, $J^{d3} = 1.5$ Hz), 7.58 (2H, m), 7.48 (4H, m), 7.39 (4H, m), 7.26 (1H, ddd, $J^{d1} = 6.5$ Hz, $J^{d2} = 6.0$ Hz, $J^{d3} = 1.5$ Hz), 7.13 (1H, ddd, $J^{d1} = 7.5$ Hz, $J^{d2} = 6.0$ Hz, $J^{d3} = 1.5$ Hz).

4.5.9. [Os(bpy)$_2$(**12**)](PF$_6$)$_2$

Yield (156 mg, 81%). Found: C, 42.36; H, 3.22; N, 9.92%. $C_{40}H_{32}N_8OsP_2F_{12} \cdot 2H_2O$ requires: C, 42.11; H, 3.18; N, 9.82. δ_H (200 MHz, d_3-MeCN) 8.67 (2H, m), 8.33 (1H, d, $J^{d} = 8.5$ Hz), 8.23 (1H, d, $J^{d} = 8.0$ Hz), 8.17 (2H, m), 8.00 (3H, m), 7.85 (5H, m), 7.61 (2H, m), 7.49 (3H, m), 7.4-7.1 (7H, m), 2.42 (3H, s), 2.01 (3H, s).

4.5.10. [Os(bpy)$_2$(**13**)](PF$_6$)$_2$

Yield (118 mg, 59%). Found: C, 39.00; H, 2.24; N, 9.53%. $C_{38}H_{26}N_8OsP_2F_{12}Cl_2 \cdot H_2O$ requires: C, 39.22; H, 2.43; N, 9.62%. δ_H (200 MHz, d_3-MeCN) 8.70 (3H, m), 8.38 (1H, d, $J^{d} = 7.5$ Hz), 8.30 (1H, s), 8.28 (1H, d, $J^{d} = 9.0$ Hz), 8.19 (2H, m), 8.03 (2H, m), 7.91 (4H, m), 7.68 (2H, m), 7.53 (5H, m), 7.49 (1H, s), 7.37 (2H, m), 7.26 (1H, ddd, $J^{d1} = 7.5$ Hz, $J^{d2} = 6.0$ Hz, $J^{d3} = 1.5$ Hz), 7.15 (1H, ddd, $J^{d1} = 7.5$ Hz, $J^{d2} = 6.0$ Hz, $J^{d3} = 1.5$ Hz).

4.5.11. [Os(bpy)$_2$(**14**)](PF$_6$)$_2$

Yield (100 mg, 50%). Found: C, 43.62; H, 3.06; N, 9.71%. $C_{42}H_{30}N_8OsP_2F_{12} \cdot 2H_2O$ requires: C, 43.37; H, 2.96; N, 9.62. δ_H (200 MHz, d_3-MeCN) 8.72 (4H, m), 8.22 (2H, m), 8.15 (2H, m), 8.00 (4H, m), 7.91 (1H, s), 7.84 (2H, m), 7.75 (1H, dd, $J^{d1} = 6.0$ Hz, $J^{d2} = 1.5$ Hz), 7.69-7.35 (12H, m), 7.18 (1H, ddd, $J^{d1} = 9.5$ Hz, $J^{d2} = 6.0$ Hz, $J^{d3} = 1.5$ Hz), 7.14 (1H, ddd, $J^{d1} = 9.5$ Hz, $J^{d2} = 6.5$ Hz, $J^{d3} = 1.5$ Hz).

4.5.12. [Os(bpy)$_2$(**16**)](PF$_6$)$_2$

Yield (185 mg, 93%). Found: C, 42.05; H, 3.11; N, 10.23%. $C_{38}H_{30}N_8OsP_2F_{12}$ requires: C, 42.30; H, 2.80; N, 10.39. δ_H (200 MHz, d_3-MeCN) 9.26 (1H, dd, $J^{d1} = 6.5$ Hz, $J^{d2} = 1.0$ Hz), 9.16 (1H, d, $J^{d} = 4.5$ Hz), 8.94 (1H, dd, $J^{d1} = 8.0$ Hz, $J^{d2} = 1.0$ Hz), 8.69 (2H, m), 8.63 (1H, d, $J^{d} = 7.0$ Hz), 8.57 (1H, d, $J^{d} = 8.0$ Hz), 8.36 (1H, dd, $J^{d1} = 8.5$ Hz, $J^{d2} = 1.0$ Hz), 8.11 (6H, m), 7.94 (4H, m), 7.49 (7H, m), 7.28 (2H, m), 2.30 (3H, s).

4.5.13. [Os(phen)$_2$(**11**)](PF$_6$)$_2$

Yield (130 mg, 65%). Found: C, 43.97; H, 2.27; N, 10.13%. $C_{42}H_{28}N_8OsP_2F_{12} \cdot H_2O$ requires: C, 44.14; H, 2.64; N, 9.80. δ_H (200 MHz, d_3-MeCN) 9.19 (2H, m), 8.81 (1H, dd, $J^{d1} = 8.0$ Hz, $J^{d2} = 1.0$ Hz), 8.75 (1H, d, $J^{d} = 7.0$ Hz), 8.51(2H, m), 8.05 (3H, m), 7.98 (3H, m), 7.76 (3H, m), 7.64 (5H, m), 7.49 (5H, m), 7.09 (2H, m), 6.97 (1H, dd, $J^{d1} = 7.0$ Hz, $J^{d2} = 6.5$ Hz).

4.6. Synthesis of Re(I) complexes

[$Re(CO)_5Cl$] (149 mg) and a 1.5-fold excess of the appropriate ligand were refluxed in methanol (50 ml) under an argon atmosphere for 2.5 h, to give a dark red solution. This was left to cool and the resulting precipitate was collected by filtration. The crude solid was washed with methanol, diethyl ether and finally pentane, then dissolved in dichloromethane (~1000 ml) and any remaining solid removed by filtration. The dilute solution was loaded onto a partially deactivated (10% v/v H_2O) silica gel column (25 cm × 5 cm diameter, 200–400 mesh, 0.040–0.063 mm) and a 4:1 ratio of dichloromethane:ethyl acetate eluted the purple binuclear complex. The desired mononuclear complex eluted as an orange band using a 1:4 dichloromethane:ethyl acetate mixture. Removal of solvent (rotavap) afforded the pure complex.

4.6.1. fac-[Re(CO)$_3$(**21**)Cl]

Yield (126 mg, 52%). Found: C, 42.71; H, 1.41; N, 9.24%. $C_{21}H_{10}N_4O_3ClRe$ requires: C, 42.89; H, 1.71; N,

9.53. δ_H (300 MHz, $CDCl_3$) 9.56 (1H, dd, $J^{d1} = 4.8$ Hz, $J^{d2} = 0.9$ Hz), 9.43(1H, dd, $J^{d1} = 4.2$ Hz, $J^{d2} = 1.5$ Hz), 9.14 (two overlapping doublets, 2H, $J = 8.1$ Hz), 8.97 (1H, dd, $J^{d1} = 8.1$ Hz, $J^{d2} = 1.5$ Hz), 8.84 (1H, dd, $J^{d1} = 8.7$ Hz, $J^{d2} = 1.2$ Hz), 8.30-8.19 (2H, m), 8.04 (1H, dd, $J^{d1} = 7.8$ Hz, $J^{d2} = 5.4$ Hz), 7.96 (1H, dd, $J^{d1} = 7.8$ Hz, $J^{d2} = 4.5$ Hz). *m/z* 589 ($\{MH\}^+$), 553 ($\{MH\text{-}HCl\}^+$).

4.6.2. *fac*-[Re(CO)$_3$(**22**)Cl]

Yield (151 mg, 60%). Found: C, 44.93; H, 2.25; N, 9.11%. $C_{23}H_{14}N_4O_3ClRe$ requires: C, 44.84; H, 2.29; N, 9.09. δ_H (300 MHz, $CDCl_3$) 9.54 (1H, dd, $J^{d1} = 5.3$ Hz, $J^{d2} = 1.4$ Hz), 9.41 (1H, dd, $J^{d1} = 4.5$ Hz, $J^{d2} = 1.5$ Hz), 9.12 (dd, 1H, $J^{d1} = 8.9$ Hz, $J^{d2} = 1.4$ Hz), 8.95 (1H, dd, $J^{d1} = 8.7$ Hz, $J^{d2} = 1.5$ Hz), 8.92 (1H, s), 8.57 (1H, s), 8.07 (1H, dd, $J^{d1} = 8.4$ Hz, $J^{d2} = 5.1$ Hz), 7.92 (1H, dd, $J^{d1} = 8.3$ Hz, $J^{d2} = 4.4$ Hz), 2.77 (3H, s), 2.70 (3H, s). *m/z* 617 ($\{MH\}^+$), 589 ($\{MH\text{-}CO\}^+$), 581 ($\{MH\text{-}HCl\}^+$), 560 ($\{MH\text{-}HC_2O_2\}^+$).

4.6.3. *fac*-[Re(CO)$_3$(**23**)Cl]·0.5CH_2Cl_2

Yield (202 mg, 70%). Found: C, 36.75; H, 1.27; N, 7.91%. $C_{21.5}H_9N_4O_3Cl_4Re$ requires: C, 36.87; H, 1.30; N, 8.00. δ_H (300 MHz, $CDCl_3$) 9.55 (1H, dd, $J^{d1} = 5.1$ Hz, $J^{d2} = 1.2$ Hz), 9.42 (1H, dd, $J^{d1} = 4.5$ Hz, $J^{d2} = 1.5$ Hz), 9.29 (s, 1H), 9.15 (1H, dd, $J^{d1} = 8.4$ Hz, $J^{d2} = 1.2$ Hz), 8.97 (1H, dd, $J^{d1} = 8.3$ Hz, $J^{d2} = 1.4$ Hz), 8.97 (1H, s), 8.07 (1H, dd, $J^{d1} = 8.1$ Hz, $J^{d2} = 5.4$ Hz), 7.98 (1H, dd, $J^{d1} = 8.3$ Hz, $J^{d2} = 4.4$ Hz). *m/z* 657 ($\{MH\}^+$), 621 ($\{MH\text{-}HCl\}^+$).

5. Supplementary material

$C_{21}H_{10}ClN_4O_3Re$, $M = 587.98$, monoclinic, $a = 15.3346(2)$, $b = 9.42610(10)$, $c = 13.02640(10)$ Å, $\beta = 92.7560(10)°$, $U = 1880.73(3)$ Å^3, $T = 203(2)$ K, space group $P2_1/c$ (no. 14), $Z = 4$, μ(Mo Kα) = 6.636 mm^{-1}, 11 223 reflections measured, 4151 unique ($R_{int} = 0.0292$) which were used in all calculations. The final $wR(F^2)$ was 0.0782 (all data).

Crystallographic data for *fac*-[Re(CO)$_3$(**21**)Cl] (CCDC 226823) have been deposited with the Cambridge Crystallographic Data Centre. A copy of this information may be obtained free of charge from The Director, CCDC, 12 Union Road, Cambridge, CB2 1EZ, UK (fax: +44-1223-3360333; e-mail: deposit@ccdc.cam.ac.uk; www: http://www.ccdc.cam.ac.uk).

References

[1] M. Fujita, K. Umemoto, M. Yoshizawa, N. Fujita, T. Kusukawa, K. Biradha, Chem. Commun. (2001) 509.
[2] S.R. Seidel, P.J. Stang, Acc. Chem. Res. 35 (2002) 972.
[3] R.V. Slone, J.T. Hupp, C.L. Stern, T.E. Albrecht-Schmitt, Inorg. Chem. 35 (1996) 4096.
[4] J. Rojo, F.J. Romero-Salguero, J.M. Lehn, G. Baum, D. Fenske, Eur. J. Inorg. Chem. (1999) 1421.
[5] P. Ceroni, A. Credi, V. Balzani, S. Campagna, G.S. Hanan, C.R. Arana, J.M. Lehn, Eur. J. Inorg. Chem. (1999) 1409.
[6] M. Venturi, S. Serroni, A. Juris, S. Campagna, V. Balzani, Top. Curr. Chem. 197 (1998) 193.
[7] R. Ziessel, M. Hissler, A. El-Ghayoury, A. Harriman, Coord. Chem. Rev. 180 (1998) 1251.
[8] A. Harriman, R. Ziessel, Coord. Chem. Rev. 171 (1998) 331.
[9] F. Scandola, R. Argazzi, C.A. Bignozzi, C. Chiorboli, M.T. Indelli, M.A. Rampi, in: V. Balzani, L. DeCola (Eds.), Supramolecular Chemistry, Kluwer Academic Publishers, Dordrecht, 1992.
[10] F. Scandola, M.T. Indelli, C. Chiorboli, C.A. Bignozzi, Top. Curr. Chem. 158 (1990) 73.
[11] H.M. Sung-Suh, D.S. Kim, C.W. Lee, S.E. Park, Appl. Organomet. Chem. 14 (2000) 826.
[12] M.K. Nazeeruddin, A. Kay, I. Rodicio, R. Humphrybaker, E. Muller, P. Liska, N. Vlachopoulos, M. Grätzel, J. Am. Chem. Soc. 115 (1993) 6382.
[13] K. Kalyanasundaram, M. Gratzel, Coord. Chem. Rev. 177 (1998) 347.
[14] C.A. Bignozzi, J.R. Schoonover, F. Scandola, Prog. Inorg. Chem. 44 (1997) 1.
[15] V. Balzani, M. Gomez-Lopez, J.F. Stoddart, Acc. Chem. Res. 31 (1998) 405.
[16] H. Szmacinski, Q. Chang, Appl. Spectrosc. 54 (2000) 106.
[17] J.H. Yang, K. Gordon, B.H. Robinson, Synth. Met. 137 (2003) 999.
[18] J.K. Lee, D.S. Yoo, E.S. Handy, M.F. Rubner, Appl. Phys. Lett. 69 (1996) 1686.
[19] C.H. Lyons, E.D. Abbas, J.K. Lee, M.F. Rubner, J. Am. Chem. Soc. 120 (1998) 12100.
[20] E.S. Handy, A.J. Pal, M.F. Rubner, J. Am. Chem. Soc. 121 (1999) 3525.
[21] A. Wu, D. Yoo, J.K. Lee, M.F. Rubner, J. Am. Chem. Soc. 121 (1999) 4883.
[22] H. Rudmann, S. Shimada, M.F. Rubner, J. Am. Chem. Soc. 124 (2002) 4918.
[23] M. Li, J. Yu, Z.J. Chen, K. Totani, T. Watanabe, S. Miyata, Jpn. J. Appl. Phys. 39 (2000) L1171.
[24] F.G. Gao, A.J. Bard, J. Am. Chem. Soc. 122 (2000) 7426.
[25] J.R. Sherborne, S.E. Page, A. Flood, M.I.J. Polson, K.C. Gordon, Asian J. Spectrosc. 6 (2002) 169.
[26] J. Sherborne, S.M. Scott, K.C. Gordon, Inorg. Chim. Acta 260 (1997) 199.
[27] S.M. Scott, K.C. Gordon, Inorg. Chim. Acta 254 (1997) 267.
[28] J.A. Treadway, B. Loeb, R. Lopez, P.A. Anderson, F.R. Keene, T.J. Meyer, Inorg. Chem. 35 (1996) 2242.
[29] M.M. Richter, K.J. Brewer, Inorg. Chim. Acta 180 (1991) 125.
[30] K. Kloc, J. Mlochowski, Z. Szulc, J. Prakt. Chem. 319 (1977) 959.
[31] E.S. Dodsworth, A.B.P. Lever, in: E.I. Solomon, A.B.P. Lever (Eds.), Inorganic Electronic Structure and Spectroscopy 2, Wiley, New York, 1999.
[32] A. Flood, R.B. Girling, K.C. Gordon, R.E. Hester, J.N. Moore, M.I.J. Polson, J. Raman Spectrosc. 33 (2002) 434.
[33] M.R. Waterland, T.J. Simpson, K.C. Gordon, A.K. Burrell, J. Chem. Soc., Dalton Trans. (1998) 185.
[34] H. Goodwin, F. Lions, J. Am. Chem. Soc. 81 (1959) 6415.
[35] N.C. Fletcher, F.R. Keene, J. Chem. Soc., Dalton Trans. (1999) 683.
[36] V.W.W. Yam, V.C.Y. Lau, K.K. Cheung, Organometallics 14 (1995) 2749.
[37] X.Y. Chen, F.J. Femia, J.W. Babich, J.A. Zubieta, Inorg. Chem. 40 (2001) 2769.
[38] X.Y. Chen, F.J. Femia, J.W. Babich, J. Zubieta, Inorg. Chim. Acta 316 (2001) 33.

[39] J.R. Kirchhoff, K. Kirschbaum, Polyhedron 17 (1998) 4033.
[40] S.L. Howell, B.J. Matthewson, M.I.J. Polson, A. Flood, A.K. Burrell, K.C. Gordon, Inorg. Chem., in press.
[41] A. Juris, S. Campagna, I. Bidd, J.M. Lehn, R. Ziessel, Inorg. Chem. 27 (1988) 4007.
[42] M.K. Nazeeruddin, S.M. Zakeeruddin, K. Kalyanasundaram, J. Phys. Chem. 97 (1993) 9607.
[43] A.S. Ichimura, L.P. Szajek, Q.S. Xie, R.H. Huang, S.Z. Huang, M.J. Wagner, J.L. Dye, J.E. Jackson, J. Phys. Chem. B 102 (1998) 11029.
[44] N.W. Duffy, K.D. Dobson, K.C. Gordon, B.H. Robinson, A.J. McQuillan, Chem. Phys. Lett. 266 (1997) 451.
[45] J.H. Yang, K.C. Gordon, Chem. Phys. Lett. 372 (2003) 577.
[46] S.P. Schmidt, W.C. Trogler, F. Basolo, Inorg. Synth. 28 (1990) 160.
[47] G.M. Sheldrick, SHELXS-97, Program for the Solution of Crystal Structures, University of Göttingen, 1997.
[48] L.J. Farrugia, J. Appl. Cryst. 32 (1999) 837.
[49] G.M. Sheldrick, SHELXL-97, Program for the Refinement of Crystal Structures, University of Göttingen, 1997.

Available online at www.sciencedirect.com
SCIENCE DIRECT®
Polyhedron 23 (2004) 1441–1446
POLYHEDRON
www.elsevier.com/locate/poly

$[(\eta^5\text{-}C_5H_5)Fe(CO)_2](Fp)$-complexes of the parabanic acid mono- and dianion: synthesis, X-ray structures and reactivity of the heterocyclic ligand

Konrad Kowalski [a], Janusz Zakrzewski [a,*], Agnieszka Rybarczyk-Pirek [b]

[a] *Department of Organic Chemistry, University of Łódź, 90-136- Łódź, Narutowicza 68, Poland*
[b] *Department of Crystallography, University of Łódź, 90-236 Łódź, Pomorska 149/153, Poland*

Received 6 December 2003; accepted 26 February 2004
Available online 12 April 2004

Abstract

$[(\eta^5\text{-}C_5H_5)Fe(CO)_2](Fp)$-complexes of the parabanic acid mono- and dianion have been synthesised in a photochemical reaction of FpI with parabanic acid and diisopropylamine in benzene. The former contains a reactive *N(3)*–H bond and can be readily thallated with TlOEt. Reaction of the thallated complex with Ph_3PAuCl, benzyl chloride and ethyl bromoacetate in DMF gave *N(3)*-aurated, *N(3)*-benzyl and *N(3)*-carboethoxymethyl complex, respectively. The structures of these complexes were confirmed by X-ray diffraction. The ester function in the *N(3)*-carboethoxymethyl complex was hydrolysed to afford air-stable, water-soluble acid, a potential metallocarbonyl labelling reagents for proteins.
© 2004 Elsevier Ltd. All rights reserved.

Keywords: Parabanic acid; Iron; Cyclopentadienyl; Carbonyl; Thallium; Gold (I) complex; Alkylation

1. Introduction

The $[(\eta^5\text{-}C_5H_5)Fe(CO)_2](Fp)$-moiety forms neutral and cationic complexes with a variety of nitrogen ligands [1–5]. In this laboratory, we have elaborated a way to Fp-complexes of anions of N–H acids by the photochemical substitution of iodide in FpI (Eq. (1)), where X and/or Y are electron-withdrawing groups and dipa stands for diisopropylamine [6–14]:

$$\mathrm{FpI} + \mathrm{HN(X)(Y)} + \mathrm{dipa} \xrightarrow{h\nu} \mathrm{FpN(X)(Y)} + \mathrm{dipaH^+I^-} \quad (1)$$

We have synthesised using this approach Fp-complexes of anions of a variety of NH acids, e.g., pyrroles, indoles, cyclic imides, sulfonamides, sulfamates, hydantoins and barbiturates. Some of these compounds proved useful metallocarbonyl labelling reagents of biomolecules [12–15].

In this paper, we report on synthesis of the Fp-complexes derived from parabanic acid **1** (Scheme 1). It is a dibasic acid forming mono- and bis-anion. Therefore, one can expect formation of its mono- and bis-Fp complexes. The former will contain a reactive imide N(3)–H bond, providing a possibility of further fuctionalisation. We thought that it would be of interest to check if it is possible to alkylate or metallate N(3) without affecting rather labile Fp group because this would open a way to substituted or binuclear complexes.

2. Results and discussion

All reactions described in this work are presented in Schemes 1 and 2.

Photolysis of FpI with **1** in benzene containing diisopropylamine yielded a mixture of mono-Fp and bis-Fp complexes (**2** and **3**, respectively).

Previous experiments have shown that the best solvent for photochemical reactions of FpI with NH-acids and diisopropylamine is benzene. Unfortunately, **1** is

* Corresponding author. Tel.: 4842-678-4731; fax: 4842-678-6583.
E-mail address: janzak@uni.lodz.pl (J. Zakrzewski).

0277-5387/$ - see front matter © 2004 Elsevier Ltd. All rights reserved.
doi:10.1016/j.poly.2004.02.015

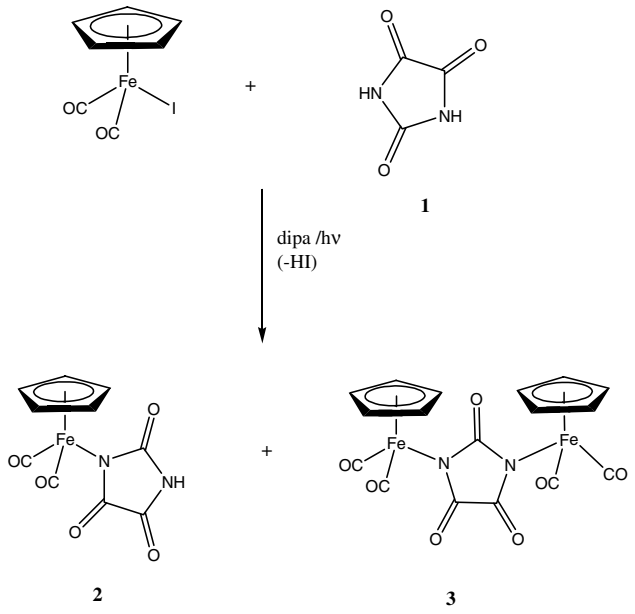

Scheme 1.

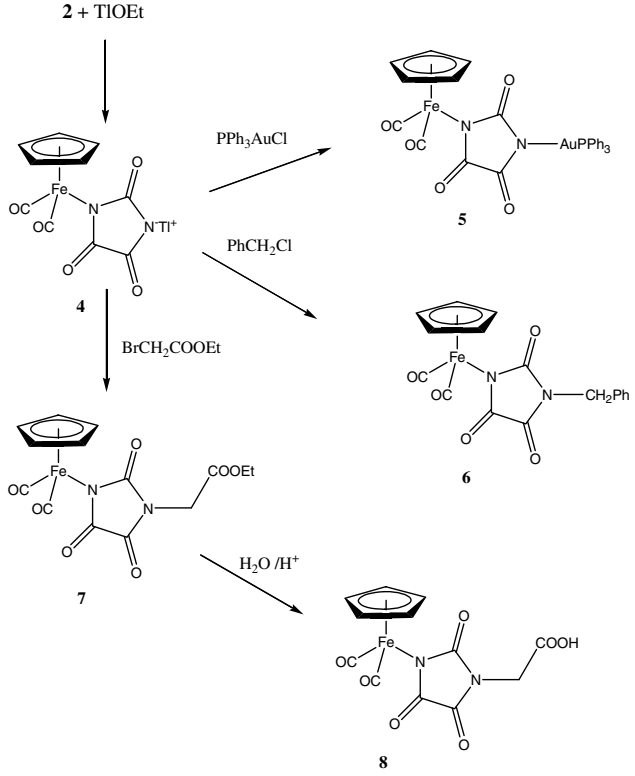

Scheme 2.

only scarcely soluble in this solvent and we had to photolyse solutions of FpI in benzene containing diisopropylamine and suspended **1**. However, hopefully, it has been found that a small solubility of **1** in benzene is sufficient for a substitution of iodide in FpI by the anion of **1** to take place quite efficiently. Regardless of the ratio FpI to **1**, both mono-Fp (**2**) and bis-Fp (**3**) products were formed. They were separated by column chromatography and their structure confirmed by spectral and analytical data as well as by X-ray diffraction (vide infra). At the molar ratio of FpI to **1** equals 0.25, the isolated yields of **2** and **3** were 40% and 17%, respectively, whereas at the FpI to **1** ratio equals 2.3, these yields were 5% and 27%, respectively. The bis-Fp product **3** was therefore formed even when an excess of **1** was used. This may be explained by the fact that **2** is much better soluble in benzene than **1** and therefore efficiently competes with this compound in the photoreaction with FpI. Another interesting fact is also worth noting. It has been found that irradiation with visible light of **3** in the presence of **1** and diisopropylamine leads to the formation of **2** (via Fp^+ dissociation?).

Compound **2** contains an imide N–H bond, offering a possibility of N-alkylation or N-metallation of the heterocyclic ligand. However, since it has been found that Fp-complexes with *N*-imidato ligands decompose in alkaline media [15] we wanted to avoid generation of alkaline metal *N*-anions. We have decided to try to transform **2** into thallium(I) salt **4** (Scheme 2), which was expected to react under mild conditions with reactive organic halides or compounds having metal–halogen bonds with formation of nitrogen–carbon or nitrogen–metal bonds, respectively.

In fact, it is known that pyrrylthallium(I) reacts with alkyl halides to afford 1-alkylpyrroles [16], and reaction of succinimidylthallium(I) with $Mn(CO)_5Br$ leads to $Mn(CO)_5$ (η^1-*N*-succinimidato) [17].

The treatment of **2** with thallium(I) ethoxide in ethanol at 0–5 °C brings about precipitation of a rather unstable pale-yellow solid, for which we suggest the structure **4** (Scheme 2). This material has been filtered off, dried and used without additional purification or analyses in further syntheses. It has been found that reaction of **4** Ph_3PAuCl in DMF at r.t. leads to the heterobinuclear complex **5** isolated in 50% yield. The coordinated triphenylphosphane ligand in this compound gives the ^{31}P NMR signal at 31.7 ppm, which is close to the value reported for the PPh_3-Au bound to the *N*-anion of hydantoin, 32.7 ppm [18].

Reaction of **4** with benzyl chloride and ethyl bromoacetate proceeded smoothly in DMF at r.t. to afford the *N*-alkylated complexes **6** and **7** in 53% and 88% yield, respectively. The structures of these compounds have been confirmed by spectral and analytical data and for **5** and **6** also by X-ray diffraction (vide infra). A careful acid hydrolysis of **7** in 0.1 M aqueous HCl at 50 °C gave acid **8** in 55% yield. This complex is air-stable, water-soluble, yellow crystalline solid. It can be regarded as a metallocarbonyl derivative of the simplest aminoacid, glycine. Its stability and solubility in water make it interesting for bioorganometallic applications (e.g., as an IR-detectable marker for biomolecules).

The aforementioned reactions demonstrate that chemical modification of the parabanic acid ligand in **2** using its Tl(I) salt **4** is feasible and can proceed with formation of either N–C or N–metal bond. This opens a new entry to complexes of *N*-substituted parabanic acids and to bimetallic complexes.

The infrared data for synthesised compounds provide an evidence that the electronic properties of the Fp-moiety bound to N(1) are influenced by the substitution at N(3) (Table 1).

It is seen that replacement of the N–H nitrogen in **2** by a metal centre results in diminution of the $\nu_{(C\equiv O)}$ frequencies of the Fp moieties. This means that there is stronger backbonding from nitrogen to iron caused by the second electron-donating metal centre. On the other hand benzylation of N(3) practically does not influence these frequencies.

Table 1
The $\nu_{(C\equiv O)}$ frequencies measured in $CHCl_3$ solutions

Compound	$\nu_{(C\equiv O)}$ (cm^{-1})
2	2062, 2015
3	2056, 2011
5	2056, 2009
6	2061, 2014

Table 2
Crystallographic data and structure refinement details

	2	**3**	**5**	**6**
Crystal data				
Formula	$C_{10}H_6FeN_2O_5$	$C_{17}H_{10}Fe_2N_2O_7$	$C_{28}H_{22}AuFeN_2O_6P$	$C_{17}H_{12}FeN_2O_5$
Formula weight	290.02	465.97	766.26	380.14
Crystal description	yellow plate	yellow plate	yellow prism	yellow needle
Crystal size (mm)	$0.6\times0.25\times0.05$	$0.2\times0.1\times0.05$	$0.3\times0.1\times0.1$	$0.5\times0.05\times0.05$
Space group	$Pca2_1$	$Pbcn$	$P\bar{1}$	$P2_1/c$
a (Å)	7.434(2)	6.692(2)	9.714(1)	12.913(5)
b (Å)	11.041(3)	22.778(1)	12.463(1)	6.278(3)
c (Å)	26.402(3)	11.404(1)	12.926(2)	20.151(2)
α (°)	90	90	72.96(1)	90
β (°)	90	90	93.58(1)	100.69(2)
γ (°)	90	90	104.55(1)	90
V (Å^3)	2167(1)	1739(1)	1449(1)	1605(1)
Z	8	4	2	4
d_x (g/cm^3)	1.778	1.781	1.757	1.573
Data collection				
Diffractometer	Rigaku AFC5S			
Radiation type/λ (Å)	Cu Kα/1.54178			
μ (mm^{-1})	11.358	13.809	14.293	7.825
Temperature	293(2)			
Index ranges	$0\leqslant h\leqslant 8$, $0\leqslant k\leqslant 13$, $0\leqslant l\leqslant 31$	$-7\leqslant h\leqslant 7$, $-13\leqslant k\leqslant 27$, $-7\leqslant l\leqslant 13$	$-11\leqslant h\leqslant 11$, $0\leqslant k\leqslant 14$, $-14\leqslant l\leqslant 15$	$0\leqslant h\leqslant 14$, $0\leqslant k\leqslant 7$, $-24\leqslant l\leqslant 23$
Number of reflections collected	1953	2900	5303	2867
Number of independent reflections	1953	1546	5054	2736
Number of reflections with $I>2\sigma(I)$	1143	680	3805	1794
Solution and refinement				
Solution	direct methods			
Refinement method	full-matrix least-squares on F^2			
H atoms treatment	constrained			
Number of parameters	328	128	356	226
$R(F)$[a] for $I>2\sigma(I)$	0.0416	0.0591	0.0578	0.0497
$R(F)$[a]	0.0960	0.1474	0.0765	0.2162
$wR(F^2)$[b] for $I>2\sigma(I)$	0.0972*	0.1539**	0.1572****	0.1130***
$wR(F^2)$[b]	0.1068*	0.1763**	0.1578****	0.1466***
$(\Delta/\sigma)_{max}$	0.000	0.002	0.000	0.000
Largest difference peak/hole (e Å^{-3})	0.406/−0.429	0.491/−0.592	2.237/−2.346	0.269/−0.356
Flack parameter	0.094			

[a] $R(F)=\sum(|F_o-F_c|)/\sum|F_o|$.
[b] $wR(F^2)=[\sum w(|F_o-F_c|)^2/\sum|F_o|^2]^{1/2}$.
* $w=\exp[(\sin\theta/\lambda)^2]/[\sigma^2(F_o^2)+(0.0590P^2)]$, where $P=[(F_o^2)+2(F_c^2)]/3$.
** $w=\exp 0.9[(\sin\theta/\lambda)^2]/[\sigma^2(F_o^2)+(0.1010P)^2]$.
*** $w=\exp 4.7[(\sin\theta/\lambda)^2]/[\sigma 2(F_o^2)+(0.0542P)^2]$.
**** $w=1/[\sigma^2(F_o^2)+(0.1090P)^2]$.

3. X-ray crystal structures of 2, 3, 5, 6

The structures of compounds **2**, **3**, **5**, **6** were determined by single-crystal X-ray diffraction (Table 2 and Figs. 1–4).

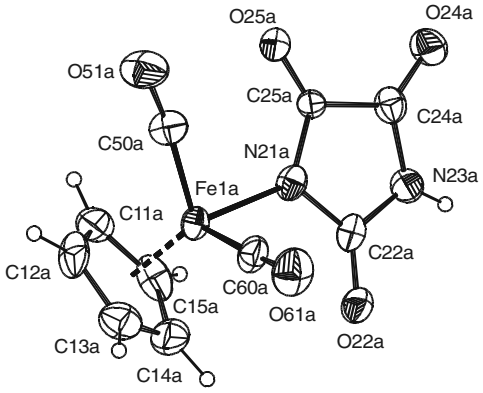

Fig. 1. Molecular drawing of compound **2** (molecule **a**). Displacement ellipsoids are shown at 30% probability level. The Fe–N distances: 1.955 (6) Å (**2a**) and 1.976 (6) Å (**2b**).

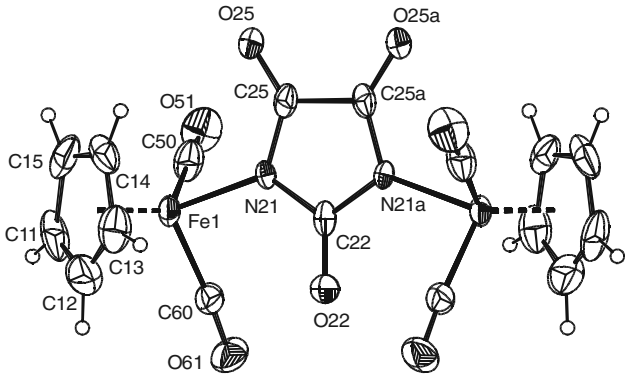

Fig. 2. Molecular drawing of compound **3**. Displacement ellipsoids are shown at 30% probability level. The Fe–N distance 1.959 (6) Å.

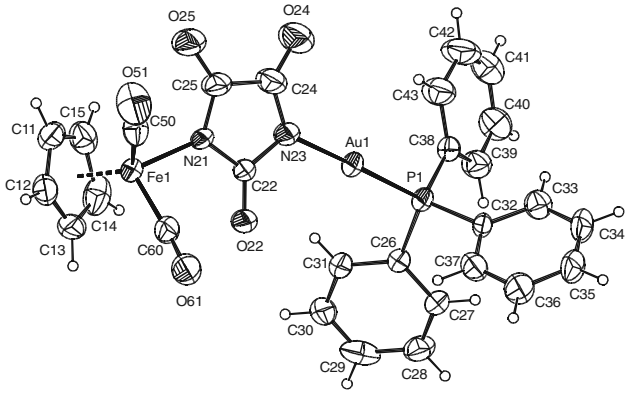

Fig. 3. Molecular drawing of compound **5**. Displacement ellipsoids are shown at 30% probability level. The Fe–N distance 1.961 (6) Å.

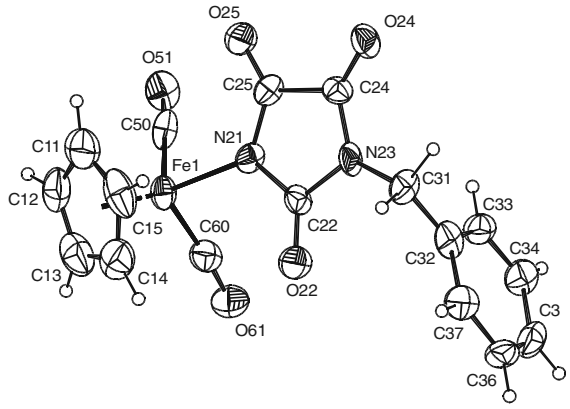

Fig. 4. Molecular drawing of compound **6**. Displacement ellipsoids are shown at 30% probability level. The Fe–N distance 1.958 (6) Å.

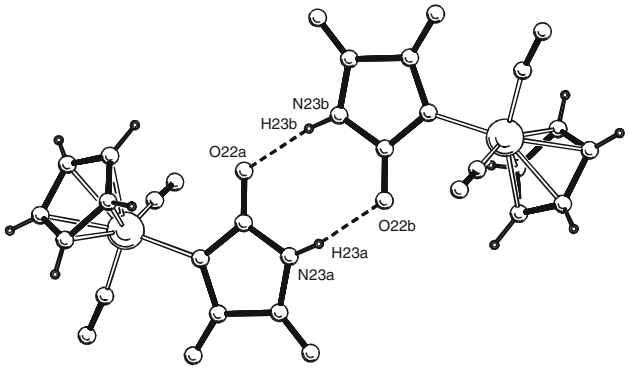

Fig. 5. Scheme of hydrogen bonding in crystal structure of **2**.

Table 3
Geometry of hydrogen bonding in dimers of **2**

	D–H (Å)	H···A (Å)	D···A (Å)	D–H···A (°)
N23a–H23a···O22b[a]	0.86	1.984	2.833(4)	169
N23b–H23b···O22a[b]	0.86	1.987	2.840(4)	171

[a] symmetry codes: $x-1, y, z$.
[b] symmetry codes: $x+1, y, z$.

They confirm in all the cases the η^1-*N*-coordination. In the solid state compound, **2** forms dimers through intermolecular N–H···O bonds (Fig. 5 and Table 3).

The Fe–N bonding distances in the investigated complexes are the same within experimental error (~1.962(8) Å) and similar to that found in 1-Fp-5,5-diphenylhydantoin, 1.949(3) Å [12]. Therefore, the length of this bond does not seem to be sensitive to electronic or steric factors in the heterocyclic ligand.

4. Conclusion

We have synthesised Fp-complexes of parabanic acid mono- and dianion. The mono-Fp complex has proven

useful staring material in syntheses of N(3)-substituted and metallated complexes.

5. Experimental

All reactions were carried our under argon. Benzene was distilled over sodium-benzophenone. Other solvents and reagents were reagent grade and were used without prior purification. Chromatographic separations were carried out using silica gel 60 (Merck, 230–400 mesh ASTM). NMR spectra were recorded in $CDCl_3$ on a Varian Gemini 200BB (200 MHz for ^1H) spectrometer. IR spectra were recorded in $CHCl_3$ on a Biorad 175C apparatus.

5.1. Synthesis of 2 and 3

A magnetically stirred solution of FpI (151 mg, 0.5 mmol) in benzene (15 ml) and diisopropylamine (1 ml), containing suspended parabanic acid (112 mg, 2 mmol) was photolysed (4×150 W tungsten lamp and external cooling with ice-water) for 2 h. The solid residue was filtered off and washed with benzene. The solvent was evaporated from the filtrate and the residue dissolved in chloroform–methanol (25:1) and chromatographed using the same solvent mixture as eluent. Two yellow fractions were collected: the first one containing **3** and the second containing **2**. Analytical samples were prepared by crystallisation from chloroform–hexane. Yields: **3**: 20 mg (17%); **2**: 56 mg (40%).

3. ^1H NMR (δ, ppm): 5.08 (s, Cp) IR (cm^{-1}): 2056, 2011, 1651, 1633. Elemental *Anal.* Calc. for $C_{17}H_{10}O_7FeN_2$: C, 43.82; H, 2.16; N, 6.01. Found: C, 43.94; H, 2.30; N, 6.07%.

2. ^1H NMR (δ, ppm): 7.97 (bs, 1H, NH), 5.15 (s, 5H,Cp). IR (cm^{-1}): 2062, 2015, 1701, 1682. Elemental *Anal*. Calc. for $C_{10}H_6O_5FeN_2$: C, 41.42; H, 2.09; N, 9.66. Found: C, 41.80; H, 2.14; N, 9.60%.

5.2. Synthesis of 4

Thallium(I) ethoxide (45 μl, 0.63 mmol) was added to a stirred solution of **2** (98 mg, 0.33 mmol) in ethanol (12 ml) at 0–5 °C. After 30 min strirring at this temperature the pale yellow solid was filtered off, washed with ethanol and dried under vacuum. Yield: 170 mg (100%).

5.3. Synthesis of 5

$(PPh_3)AuCl$ (198 mg, 0.40 mmol) was added to the solution of **4** (190 mg, 0.38 mmol) in DMF (15 ml) at r.t. After 1.5 stirring the colorless precipitate of TlCl was filtered off and the solvent evaporated under vacuum. Column chromatography (eluent-chloroform) afforded **5** as a yellow crystalline solid. Yield: 130 mg (48%).

^1H NMR (δ, ppm): 7.5 (m, 15H, Ph), 5.11 (s, 5H, Cp). ^{31}P NMR (δ, ppm): 31.7. IR (cm^{-1}): 2056, 2009, 1657, 1635. Elemental *Anal.* Calc. for $C_{28}H_{22}AuFeN_2PO_6$ (monohydrate): C, 43.89; H, 2.89; N, 3.66. Found: C, 43.60; H, 2.66; N, 3.59%.

5.4. Synthesis of 6

Benzyl chloride (43 μl, 0.37 mmol) was added to the solution of **4** (77 mg, 0.15 mmol) in DMF (10 ml) at r.t. After 30 min stirring the colourless precipitate of TlCl was filtered off and the solvent evaporated under vacuum. Column chromatography (eluent-chloroform) afforded **6** as a yellow crystalline solid. Analytical sample was recrystallized from chloroform–hexane. Yield: 30 mg (53%).

^1H NMR (δ, ppm): 7.26–7.36 (m, 5H, Ph), 5.11 (s, 5H, Cp), 4.69 (s, 2H, CH_2). IR ($CHCl_3$, cm^{-1}): 2061, 2014, 1658, 1637. Elemental *Anal.* Calc. for $C_{17}H_{12}FeN_2O_5$: C, 53.71; H, 3.18; N, 7.37. Found: C, 53.40; H, 3.00; N, 7.34%.

5.5. Synthesis of 7

Ethyl bromoacetate (113 μl, 1 mmol) was added to the solution of **4** (254 mg, 0.5 mmol) in DMF (15 ml) at r.t. After 30 min stirring the colourless precipitate of TlBr was filtered off and the solvent evaporated under vacuum. Column chromatography (eluent-chloroform) afforded **7** as an yellow oil. Yield: 165 mg (88%).

^1H NMR (δ, ppm): 5.21 (s, 5H, Cp), 4.26 (s, 2H, CH_2), 4.18 (t, $J = 8$ Hz, 2H, CH_2 in Et), 1.25 (t, $J = 8$ Hz, 3H, CH_3 in Et). IR (cm^{-1}): 2062, 2015, 1749, 1657, 1637. Elemental *Anal.* Calc. for $C_{14}H_{12}FeN_2O_7$: C, 44.71; H, 3.22; N, 7.45. Found: C, 44.77; H, 3.31; N, 7.40%.

5.6. Synthesis of 8

Compound **7** (169 mg, 0.44 mmol) was dissolved in 50 ml of 0.1 M aq. HCl and heated to 50 °C for 5 h. Extraction with CH_2Cl_2 and chromatography (SiO_2, $CHCl_3$–methanol 10:3 v/v) afforded **8** as an yellow solid. Yield: 93 mg (55%).

^1H NMR (δ, ppm): 5.21 (s, 5H, Cp), 4.01 (s, 2H, CH_2). IR (cm^{-1}): 3424, 2051, 2001, 1742, 1683, 1617. Elemental *Anal.* Calc. for $C_{12}H_8FeN_2O_7 \cdot 2H_2O$: C, 37.50; H, 3.15; N, 7.29. Found: C, 37.25; H, 3.19; N, 7.01%.

6. X-ray structure determinations

X-ray data were collected on Rigaku AFC5S difractometer [19] using Cu Kα X-ray source and graphite monochromator. For all the crystals procedure of

measurement, structure solution and refinemnt was the same. The unit cell dimensions were obtained from least-squares fit to setting angles of 25 reflections. Monitoring of three standard reflections during data collections show no significant change of intensities under X-ray radiation. Reflection intensities were corrected for Lorentz and polarization effects and analytical absorption corrections were applied [20]. A summary of X-ray details is given in Table 2. The crystal structures were solved using SHELXS86 [21] program and refined using full-matrix least squares calculation using SHELXL97 [22]. In the final step of refinement procedure, all non-hydrogen atoms were refined with anisotropic themal displacement parametrs. Hydrogen atoms were included in calculated positions with ideal geometry using rigid body model. They were given isotropic displacement parametrs equal to 1.2 (for aromatic C parent atoms) or 1.5 (in the other cases) of the equivalent displacement parameters of the atoms to which they are attached. The molecular geometry was calculated by SHELXL and the plots were made by PLATON [23].

There are two independent molecules (molecule **a** and molecule **b**) in the asymmetric unit for compound **2**. As no significant differences in their geometry are observed these molecules were refined using SAME instruction with default parameters. Molecules of compound **5** were found to cocrystalize with one water molecule. In the molecular drawing of this compound the water molecule is omitted for clarity.

7. Supplementary material

Full crystallographic data (CCDC No. 207091 for compound **2**, CCDC No. 207092 for compound **3**, CCDC No. 207093 for compound **5** and CCDC No. 207094 for compound **6**) have been deposited at the Cambridge Crystallographic Data Centre and are available on request from the Director, CCDC, 12 Union Road, Cambridge CB2 1EZ, UK (fax: +44-1223-336-033; Email:deposit@ccdc.cam.ac.uk or http://www.ccdc.cam.ac.uk).

Acknowledgements

Support of this work by the Polish State Committee for Scientific Research (KBN, Grant PBZ-KBN 15/09/T09/99/01) is thankfully acknowledged.

References

[1] P.L. Pauson, A.R. Quazi, J. Organomet. Chem. 7 (1967) 321.
[2] A.N. Nesmeyanov, Yu. A. Belousov, V.N. Babin, G.G. Aleksandrov, Yu. T. Struchkov, Inorg. Chim. Acta 23 (1977) 155.
[3] M.Yu. Antipin, G.G. Aleksandrov, Yu.T. Struchkov, Yu. A. Belousov, V.N. Babin, N.S. Kochetkov, Inorg. Chim. Acta 68 (1983) 229.
[4] H. Schumann, M. Speis, W.P. Bosman, J.M.M. Smits, P.T. Beurkens, J. Organomet. Chem. 403 (1991) 165.
[5] A. Palazzi, S. Stagni, S. Bordoni, M. Monazi, S. Selva, Organometallics 21 (2002) 3774.
[6] J. Zakrzewski, J. Organomet. Chem. 327 (1987) C41.
[7] J. Zakrzewski, J. Organomet. Chem. 359 (1989) 215.
[8] M. Bukowska-Strzyzewska, A. Tosik, D. Wodka, J. Zakrzewski, Polyhedron 13 (1994) 1689.
[9] J. Zakrzewski, A. Tosik, M. Bukowska-Strzyżewska, J. Organomet. Chem. 495 (1995) 83.
[10] A. Kłys, J. Zakrzewski, C. Giannotti, J. Organometal. Chem. 531 (1997) 91.
[11] J. Zakrzewski, M. Pawlak, J. Organomet. Chem. 568 (1998) 171.
[12] A. Vessierès, K. Kowalski, J. Zakrzewski, A. Stepien, M. Grabowski, G. Jaouen, Bioconjugate Chem. 10 (1999) 379.
[13] B. Rudolf, J. Zakrzewski, Tetrahedron Lett. 35 (1994) 9611.
[14] A. Kazimierczak, J. Zakrzewski, M. Salmain, G. Jaouen, Bioconjugate Chem. 8 (1997) 489.
[15] B. Rudolf, J. Zakrzewski, M. Salmain, G. Jaouen, New J. Chem. (1998) 813.
[16] C.F. Candy, R.A. Jones, J. Org. Chem. 36 (1971) 3993.
[17] H. Adams, N.A. Bailey, T.N. Briggs, J.A. McCleverty, H.M. Colqohoun, D.J. Williams, J. Chem. Soc., Dalton Trans. (1986) 813.
[18] D. Koch, K. Sünkel, W. Beck, Z. Naturforsch 54b (1999) 96.
[19] MSC/AFC Diffractometer Control Software, Molecular Structure Corporation, The Woodlands, TX, 1989.
[20] J. de Meulenaer, H. Tompa, Acta Crystallogr., Sect. A 19 (1965) 1014.
[21] G.M. Sheldrick, SHELXS86 Program for Crystal Structure Solution, University of Göttingen, Germany, 1990.
[22] G.M. Sheldrick, SHELXL97 Program for the Refinement of Crystal Structures, University of Göttingen, Germany, 1997.
[23] A.L. Spek, PLATON Molecular Geometry Program, University of Utrecht, The Netherlands, 1990.

Available online at www.sciencedirect.com
SCIENCE DIRECT®
Polyhedron 23 (2004) 1447–1451
POLYHEDRON
www.elsevier.com/locate/poly

Copper(I) and palladium(II) complexes of 4,5-bis(methylthio)-1,3-dithiole-2-thione, coordination and S···S contact assembled ribbon structures ☆

Jie Dai [a,b,*], Wei Yang [a], Zhi-Gang Ren [a], Qin-Yu Zhu [a], Ding-Xian Jia [a]

[a] *Department of Chemistry and Chemical Engineering, Suzhou University, Shizi Street, Suzhou 215006, PR China*
[b] *State Key Laboratory of Coordination Chemistry, Nanjing University, Nanjing 210093, PR China*

Received 16 December 2003; accepted 27 February 2004
Available online 9 April 2004

Abstract

Two complexes of 4,5-bis(methylthio)-1,3-dithiole-2-thione ($C_5H_6S_5$), $C_5H_6S_5CuI$ (**1**) and $(C_5H_6S_5)_2PdI_2$ (**2**), have been synthesized and characterized crystallographically. They are assembled into ribbon structures by coordination bonds and S···S contacts. There are very short S···S contacts (3.268 Å) between the ribbons of complex **1**. The contacts are arranged parallel to the heterocycle plane with one C–S···S–C grouping close to linear. The results of the synthetic reactions and crystal structures indicate that the planar coordination of the thiocarbonyl sulfur with Pd(II) is more efficient than the tetrahedral coordination of Cu(I) and the preferential coordination site to Cu(I) and Pd(II) is the S in thiocarbonyl group not the methylthio group.
© 2004 Elsevier Ltd. All rights reserved.

Keywords: Crystal structure; Molecular assembly; 1,3-Dithiole-2-thione; Complex

1. Introduction

In order to achieve the goals of developing advanced materials, for chemists, the past 10 years have brought a blossoming of a large field of supramolecular chemistry [1,2]. Intermolecular interactions such as hydrogen bonds, S···S contacts and π···π stacking are efficient organizing forces in supramolecular architecture and design of new solid-state materials for applications. Many research groups have succeeded in the strategy to control organic molecular aggregation by hydrogen bonding [3,4], and to synthesize organic conductors assembled by π···π stacking [5–7] or S···S contacts [8–12]. The unique physical properties of these compounds not only depend on the specific properties of the individual components, but also are strongly influenced by the arrangement of molecules within the crystal lattice. In sulfur-rich compounds, such as tetrathiafulvalene (TTF) and its derivatives [13–15], and 4,5-disulfanyl-1,3-dithio-2-thionate (dmit) complexes $[M(C_3S_5)_2]^{n-}$ [11,12], short S···S contacts were found to play an important role in their electric conductivity.

We have reported a series of complexes of 4,5-ethylenedithio-1,3-dithiole-2-thione ($C_5H_4S_5$). $C_5H_4S_5$ is a derivative of dmit and has a structure similar to half of BEDT-TTF. Up to now, three silver(I) [16,17], one copper(I) [18] and one mercury(II) [19] complex of $C_5H_4S_5$ have been synthesized and crystallographically characterized. They display a variety of one- to three-dimensional frameworks based on the coordination bonds as well as intermolecular S···S contacts. Our recent interest is still focused on the construction of this kind of supramolecular frameworks. The ligand used in this work is 4,5-bismethylthiol-1,3-dithiole-2-thione ($C_5H_6S_5$), a derivative of dmit. It is also an electron donor and shows some common features to $C_5H_4S_5$, but the 4,5-ethylenedithio group is replaced by 4,5-bis(methylthio) groups. In this paper, we report the synthesis and new structures of the copper(I) and

☆ Supplementary data associated with this article can be found, in the online version, at doi:10.1016/j.poly.2004.03.002.

* Corresponding author. Tel./fax: +86-512-65224783.
E-mail address: daijie@suda.edu.cn (J. Dai).

0277-5387/$ - see front matter © 2004 Elsevier Ltd. All rights reserved.
doi:10.1016/j.poly.2004.03.002

palladium(II) complexes of $C_5H_6S_5$ with short S···S contacts.

2. Experimental

2.1. General comments

$C_5H_6S_5$ was prepared using a literature method [20] and characterized. Acetonitrile was dried and distilled by a standard method before use. All other chemicals were obtained from commercial sources and used without further purification. Infrared spectra were measured as KBr discs on a Nicolet Magna 550 FT-IR Spectrometer and elemental analysis was recorded on an EA-1110 analytical instrument.

2.2. Preparation of the complexes of $C_5H_6S_5$

2.2.1. $C_5H_6S_5CuI$ (1)

A solution of CuI (38.0 mg, 0.2 mmol) in acetonitrile (4 ml) was added to a solution of $C_5H_6S_5$ (22.6 mg, 0.1 mmol) in acetonitrile (4 ml) at room temperature under argon atmosphere. An orange precipitate was formed immediately and the mixture was stirred for 30 min. The precipitate was filtered, washed with acetonitrile and dried in argon (yield: 73%). Orange crystals for X-ray measurement were obtained by slow evaporation of the filtrate. *Anal.* Calc.: C, 14.41; H, 1.45. Found: C, 14.11; H, 1.42%. IR (cm^{-1}), 2905vw, 1451m, 1420w, 1034vs, 968w, 538w, 463w.

2.2.2. $(C_5H_6S_5)_2PdI_2$ (2)

A solution of $Pd(CH_3CN)_2Cl_2$ (22 mg, 0.086 mmol) in dichloromethane (50 ml) was added to a solution of $C_5H_6S_5CuI$ (36 mg, 0.086 mmol) in acetonitrile (50 ml) at room temperature. The solution was stirred for 30 min and then it was filtered. Dark-red crystals for X-ray measurement were obtained by slow evaporation of the red filtrate (yield: 51%). *Anal.* Calc.: C, 14.77; H, 1.49. Found: C, 14.53; H, 1.39%. IR (cm^{-1}), 2904vw, 1467m, 1424w, 1035vs, 967w, 538w, 464w.

2.3. X-ray crystallography

X-ray diffraction experiments were made on a Rigaku Mercury CCD area detector with graphite monochromated Mo Kα radiation. The data were collected at a temperature of -80 ± 1 °C to a maximum 2θ value of 55.0° by using the ω-scan method. For complex **1**, a total of 4254 reflections were collected, in which 2411 were unique; for complex **2**, a total of 4520 reflections were collected, in which 2409 were unique. An empirical absorption correction was applied for both **1** and **2**, which resulted in transmission factors ranging from 0.64 to 1.00. The data were corrected for Lorentz and polarization effects.

The structures were solved by direct methods [21] and expanded using Fourier techniques [22]. The non-hydrogen atoms were refined anisotropically. Hydrogen atoms were refined using the riding model. All calculations were performed using the Crystal Structure [23,24] crystallographic software package.

3. Results and discussion

3.1. Crystal structure of $[C_5H_6S_5CuI]_\infty$ (1)

An ORTEP view of the unit of $[C_5H_6S_5CuI]_\infty$ (**1**) with selected atom labelling is shown in Fig. 1. The crystallographic data are listed in Table 1 and the selected bond distances and angles are listed in Table 2. The geometry around the copper atom is a distorted tetrahedron with three bridging iodide ions and a thiocarbonyl sulfur atom from the ligand. This is different from the structure of $[Cu_4I_4(C_5H_4S_5)_4]$ [18], although the difference for $C_5H_6S_5$ and $C_5H_4S_5$ is only the replacement of an ethylenedithio group by a bis(methylthio) group at sites 4 and 5. In the $C_5H_4S_5$ case, the ligand displays a bidentate coordination mode through the sulfur atoms of both the thioether and the thiocarbonyl groups. The Cu–S (thiocarbonyl sulfur) distance of 2.284(1) Å and the S(1)=C(1) distance of 1.667(3) Å for **1** are close to those for $[Cu_4I_4(C_5H_4S_5)_4]$ [18]. The Cu–I distances are within the expected values for these kinds of sulfur-rich ligands.

The most striking feature of complex **1** is that the $C_5H_6S_5CuI$ unit forms a poly structure in the solid state. The central part of this structure is a zig-zag ladder-like ribbon (or chain, Fig. 2), which is formed by the Cu and

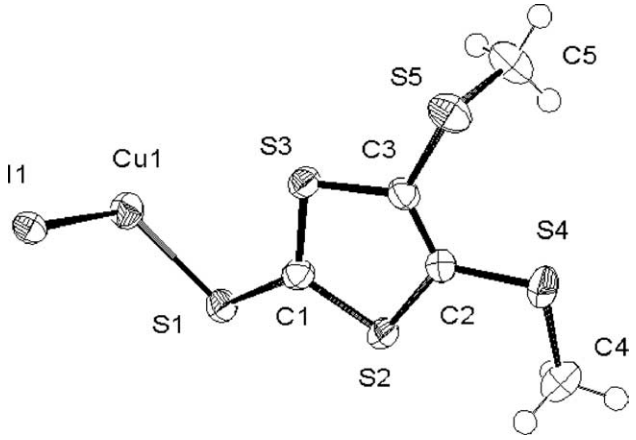

Fig. 1. ORTEP view of the unit of $[C_5H_6S_5CuI]_\infty$ (**1**) showing the atom labelling scheme. Non-H atoms are shown as 50% probability displacement ellipsoids.

Table 1
Crystal data of complexes **1** and **2**

	1	**2**
Empirical formula	$C_5H_6S_5CuI$	$C_{10}H_{12}S_{10}PdI_2$
Formula weight	416.85	813.01
Crystal color	orange	dark-red
Habit	prism	platelet
Crystal size (mm)	0.18×0.35×0.05	0.40×0.20×0.04
Crystal system	triclinic	triclinic
Lattice type	primitive	primitive
Space group	$P\bar{1}$ (No. 2)	$P\bar{1}$ (No. 2)
a (Å)	4.388(2)	8.082(5)
b (Å)	11.856(5)	8.277(6)
c (Å)	11.482(5)	9.284(7)
α (°)	74.795(11)	89.89(3)
β (°)	81.55(1)	67.19(2)
γ (°)	77.453(13)	81.42(3)
V (Å^3)	560.1(4)	565.0(7)
Z	2	1
D_{calc} (g cm^{-3})	2.471	2.389
$F(000)$	396.00	384.00
μ (cm^{-1})	55.82	44.72
Reflections collected	4254	4520
Unique reflections	2411	2409
Observations	2142	2148
R_1 [$I > 2.00\sigma(I)$]	0.025	0.049
R_w [$I > 2.00\sigma(I)$]	0.072	0.182
Goodness-of-fit	0.99	1.03

Table 2
Selected bond distances (Å) and angles (°) of **1**

Bond distances			
I(1)–Cu(1)	2.6680(10)	Cu(1)–S(1)	2.2840(10)
S(1)–C(1)	1.667(3)	S(2)–C(1)	1.729(3)
S(2)–C(2)	1.739(3)	S(3)–C(1)	1.712(3)
S(3)–C(3)	1.745(3)	S(4)–C(2)	1.741(3)
S(4)–C(4)	1.792(4)	S(5)–C(3)	1.755(3)
S(5)–C(5)	1.812(4)	C(2)–C(3)	1.350(4)
Bond angles			
I(1)–Cu(1)–S(1)	108.74(4)	Cu(1)–S(1)–C(1)	108.08(10)
C(1)–S(2)–C(2)	97.1(1)	C(1)–S(3)–C(3)	97.1(1)
C(2)–S(4)–C(4)	103.3(2)	C(3)–S(5)–C(5)	102.6(2)
S(1)–C(1)–S(2)	121.1(2)	S(1)–C(1)–S(3)	125.2(2)
S(2)–C(1)–S(3)	113.7(2)	S(2)–C(2)–S(4)	121.9(2)
S(2)–C(2)–C(3)	115.9(2)	S(4)–C(2)–C(3)	122.1(2)
S(3)–C(3)–S(5)	119.6(2)	S(3)–C(3)–C(2)	116.2(2)
S(5)–C(3)–C(2)	124.3(2)		

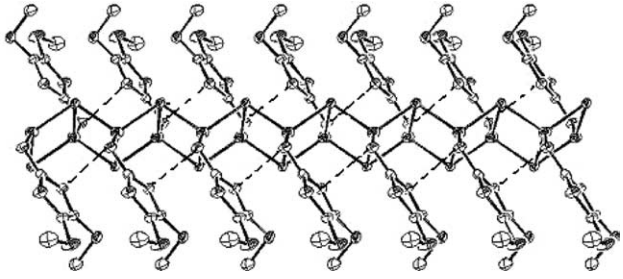

Fig. 2. Part of a zig-zag ladder-like ribbon in which the intrachain S···S contacts are showed by dashed lines.

I atoms and propagated in the direction of the a-axis. A similar structure has been reported in $[Cu(C_6H_4OS_5)I]_\infty$ ($C_6H_4OS_5$ = 2-thioxo-5H-1,3-dithiolo[4,5-b][1,4]di-thiepin-6(7H)-one) [25]. The Cu···Cu separation of 2.929 Å in the complex is longer than that in $[Cu_4I_4(C_5H_4S_5)_4]$ (2.789 Å) [18]. The short intra-ribbon S···S contacts occurs between S(1) and S(3′) (3.578 Å), which is smaller than the sum of the van der Waals radii of two S atoms (3.70 Å). The shortest inter-ribbon contacts of 3.268 Å between S(4) and S(4′) indicate that there are strong interactions between two neighboring polymeric units. This gives rise to a novel two-dimensional network. Fig. 3 shows the molecular packing and the intermolecular S···S contacts.

S···S contacts with distances below 3.30 Å are rarely found in the crystals of sulfur-rich compounds and in general the contacts are in the range 3.35–3.70 Å. An example having an unusually short contact is $[Cu_4I_4(C_5H_4S_5)_4]$ [18], in which the S···S contact (3.257 Å) is between thioether and thiocarbonyl sulfur atoms (head to tail), but in the present case, the contacts are between two thioether sulfur atoms (tail to tail). Another example of an unusually short contact, with a S···S distance of 3.251 Å, is an organic compound [26]. The arrangement of the unusual S···S contact of **1** is shown in Fig. 3(b), which is similar to the case reported in [26]. The contacts are arranged parallel to the heterocycle plane with a center inversion. It is known that the contacts where one C–S···S–C grouping is close to linear are shorter than those where the S···S vector is perpendicular to the plane of the sulfides [26,27].

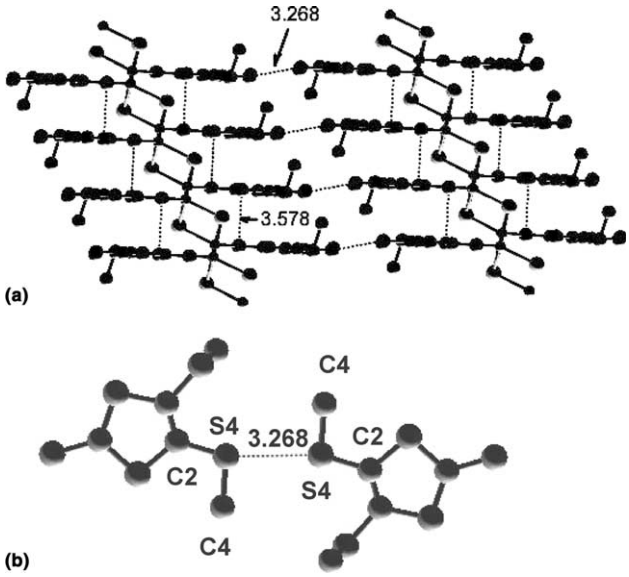

Fig. 3. The molecular packing and the two-dimensional assembly (a) and the unusually short intermolecular S···S contact (b).

3.2. Crystal structure of $(C_5H_6S_5)_2PdI_2$ (2)

An ORTEP view of complex **2** together with the atomic labelling scheme is given in Fig. 4. The selected bond lengths and angles are given in Table 3. The palladium atom is four-coordinated with two iodide atoms and two thiocarbonyl sulfur atoms. The geometry around Pd(II) is square planar. The Pd(II) ion and the two ligands, except the methyl groups, are basically coplanar. The Pd–S and Pd–I distances are 2.330 and 2.602 Å, respectively. The C(1)═S(1) distance of 1.676 Å is similar to that in the CuI complex (1.667 Å), in accordance with the results of the IR measurements. The C═S IR stretching frequencies of **1** and **2** are essentially same, 1034 cm^{-1} for **1** and 1035 cm^{-1} for **2** (1057 cm^{-1} for the free ligand). The complexes are further self-assemble to a one-dimensional network by short contacts of 3.539 Å between S(1) and S(2′). The ribbon structure is shown in Fig. 5.

It is notable that there is a significant difference between the bond lengths of C(1)–S(3) and C(1)–S(2) for both compounds **1** and **2** (see Tables 2 and 3). The former bond is shorter in both cases and *cis* to the S–metal bond. It is unclear for this phenomena, but we found it might be related to the torsion angles of M–S(1)–C(1)–S(3). The torsion angles of **1** and **2** are 0.91° and 0.79°, in other words, the M–S(1) bond is within the plane defined by S(1)–S(3) and C(1)–C(3). The bond lengths of C(1)–S(3) and C(1)–S(2) tend to equivalence when the torsion angle is increased [17,19].

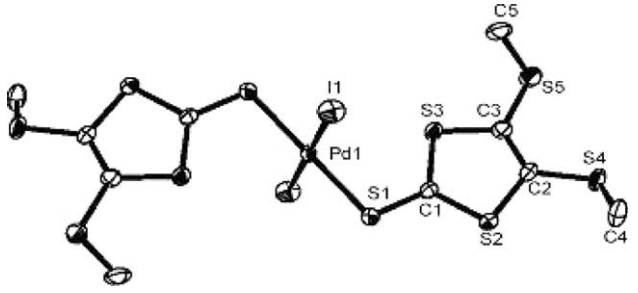

Fig. 4. ORTEP view of $(C_5H_6S_5)_2PdI_2$ (**2**) showing the atom labelling scheme. Non-H atoms are shown as 50% probability displacement ellipsoids.

Table 3
Selected bond distances (Å) and angles (°) of **2**

Bond distances			
I(1)–Pd(1)	2.602(2)	Pd(1)–S(1)	2.330(2)
S(1)–C(1)	1.676(6)	S(2)–C(1)	1.721(6)
S(2)–C(2)	1.745(6)	S(3)–C(1)	1.697(6)
S(3)–C(3)	1.742(6)	S(4)–C(2)	1.737(6)
S(4)–C(4)	1.801(7)	S(5)–C(3)	1.748(6)
S(5)–C(5)	1.804(8)	C(2)–C(3)	1.365(8)
Bond angles			
I(1)–Pd(1)–S(1)	90.81(9)	Pd(1)–S(1)–C(1)	103.6(2)
C(1)–S(2)–C(2)	97.0(3)	C(1)–S(3)–C(3)	97.4(3)
C(2)–S(4)–C(4)	101.8(3)	C(3)–S(5)–C(5)	100.0(3)
S(1)–C(1)–S(2)	122.8(3)	S(1)–C(1)–S(3)	122.9(4)
S(2)–C(1)–S(3)	114.3(3)	S(2)–C(2)–S(4)	120.1(3)
S(2)–C(2)–C(3)	115.2(5)	S(4)–C(2)–C(3)	124.7(5)
S(3)–C(3)–S(5)	119.0(4)	S(3)–C(3)–C(2)	115.9(5)
S(5)–C(3)–C(2)	125.1(5)		

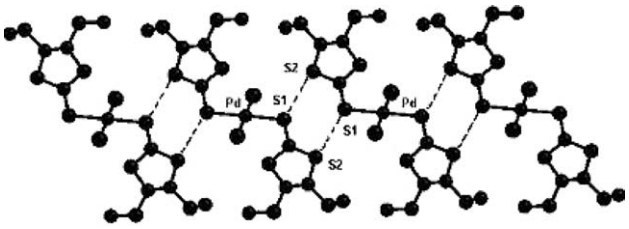

Fig. 5. Part of the band-like structure of **2**, the intermolecular S···S contacts are showed by dashed lines.

The complex **2** is an unexpected product. The goal for the synthesis is a hetero nuclear polymer. Because the bis(methylthio)-ethylene moiety is a well-known chelate for soft metals, such as Ag(I), Cu(I) and Pd(II) [8,28–30], and a palladium complex with tetrakis(methylthio)-ethylene $[Pd(TMTE)Cl_2]$ has been prepared recently by our group [30], it seems reasonable to prepare a hetero-nuclear coordination compound by introducing Pd(II) to complex **1**. However, the result is that the Cu(I) of **1** is completely replaced by Pd(II) in the reaction

$$2[(C_5H_6S_5)CuI] + PdCl_2 \xrightarrow{\text{inacetonitrile}} [PdI_2(C_5H_6S_5)_2] + 2CuCI \quad (1)$$

It reveals that the planar coordination of the thiocarbonyl sulfur with Pd(II) is more efficient than the tetrahedral coordination of Cu(I), although the bond strengths of M–S(1) in **1** and **2** are similar. On the other hand, the coordination ability of the thioether sulfur (methylthio group) is weaker than that of the thiocarbonyl group, thus the preferential coordination site is the S of the C═S group not the methylthio group.

4. Conclusion

As sequential work in the study of the structures of a series of complexes of 4,5-ethylthiol-1,3-dithiole-2-thione, $C_5H_4S_5$, we have now succeeded in the synthesis and characterization of two new complexes of 4,5-bis(methylthio)-1,3-dithiole-2-thione, $C_5H_6S_5$. With the co-operation of coordination bonds and S···S contacts, the complexes are assembled to form two- and one-dimensional supermolecules. The unusual shortest S···S contacts 3.268 Å found for **1** indicates that the molecular assembly of organic donors with coordination linkage in metal complexes can be expected to enhance the intra- or inter-molecular interactions, which may be an important strategy in the search for new materials in crystal engineering.

5. Supplementary material

Crystallographic data for the structural analysis have been deposited with the Cambridge Crystallographic Data Centre, CCDC reference numbers 226839 and 226840. Copies of this information may be obtained free of charge from The Director, CCDC, 12 Union Road, Cambridge CB2 1EZ, UK (fax: +44-1233-336033; e-mail: deposit@ccdc.cam.ac.uk or http://www.ccdc.cam.ac.uk).

Acknowledgements

This work is supported by the National Natural Science Foundation, PR China (20071024 and 20371033). The authors are also grateful to the Key Laboratory of Organic Synthesis of Jiangsu Province, Suzhou University, for financial support.

References

[1] J.-M. Lehn, Supramolecular Chemistry, VCH, Weinheim, 1995.
[2] J.-M. Lehn, Angew. Chem., Int. Ed. Engl. 29 (1990) 1304.
[3] J.C. MacDonald, G.M. Whitesides, Chem. Rev. 94 (1994) 2383.
[4] C.B. Aakeroy, K.R. Seddon, Chem. Soc. Rev. 22 (1993) 397.
[5] M. Kato, K. Sasano, C. Kosuge, M. Yamazaki, S. Yano, M. Kimura, Inorg. Chem. 35 (1996) 116.
[6] M. Munakata, T. Kuroda-Sowa, M. Maekawa, M. Nakamura, S. Akiyama, S. Kitagawa, Inorg. Chem. 33 (1994) 1284.
[7] M. Munakata, J. Dai, M. Maekawa, T. Kuroda-Sowa, J. Fukui, J. Chem. Soc., Chem. Commun. (1994) 2331.
[8] M. Munakata, T. Kuroda-Sowa, M. Maekawa, A. Hirota, S. Kitagawa, Inorg. Chem. 34 (1995) 2705.
[9] J.M. Williams, H.H. Wang, T.J. Emge, U. Geiser, M.A. Beno, P.C.W. Leung, K.D. Carlson, R.J. Thorn, A.J. Schultz, M. Whangbo, Prog. Inorg. Chem. 35 (1987) 1.
[10] M.R. Bryce, Chem. Soc. Rev. 20 (1991) 355.
[11] R.M. Olk, B. Olk, W. Dietzsch, R. Kirmse, E. Hoyer, Coord. Chem. Rev. 117 (1992) 99.
[12] P. Cassoux, L. Valade, H. Kobayashi, A. Kobayashi, R.A. Clark, A.E. Underhill, Coord. Chem. Rev. 110 (1991) 115.
[13] B.A. Scott, S.J.L. Laca, J.B. Torrance, B.D. Silverman, B. Welber, J. Am. Chem. Soc. 99 (1977) 6631.
[14] C.K. Johnson, C.R. Watson, J. Chem. Phys. 64 (1976) 2271.
[15] H. Mori, S. Tanaka, T. Mori, Y. Maruyama, Bull. Chem. Soc. Jpn. 68 (1995) 1136.
[16] J. Dai, T. Kuroda-Sowa, M. Munakata, M. Maekawa, Y. Suenaga, Y. Ohno, J. Chem. Soc., Dalton Trans. (1997) 2363.
[17] J. Dai, M. Munakata, T. Kuroda-Sowa, Y. Suenaga, L.P. Wu, M. Yamamoto, Inorg. Chim. Acta 255 (1997) 163.
[18] J. Dai, M. Munakata, L.P. Wu, T. Kuroda-Sowa, Y. Suenaga, Inorg. Chim. Acta 258 (1997) 65.
[19] J. Dai, M. Munakata, G.Q. Bian, Q.F. Xu, T. Kuroda-Sowa, M. Maekawa, Polyhedron 17 (1998) 2267.
[20] G. Teimecke, H.J. Sieler, R. Kirmse, E. Hoyer, Phosphone Sulfur 6 (1979) 49.
[21] SIR-97: A. Altomare, M. Burla, M. Camalli, G. Cascarano, C. Giacovazzo, A. Guagliardi, A. Moliterni, G. Polidori, R. Spagna, J. Appl. Crystallogr. 32 (1999) 115.
[22] DIRDIF-99: P.T. Beurskens, G. Admiraal, G. Beurskens, W.P. Bosman, R. de Gelder, R. Israeland, J.M.M. Smits, The DIRDIF-99 Program System: Technical Report of the Crystallography Laboratory, University of Nijmegen, The Netherlands, 1999.
[23] Crystal Structure 3.10: Crystal Structure Analysis Package, Rigaku and Rigaku/MSC (2000–2002).
[24] D.J. Watkin, C.K. Prout, J.R. Carruthers, P.W. Betteridge, CRYSTALS Issue 10, Chemical Crystallography Laboratory, Oxford, UK.
[25] T. Jørgensen, T.K. Hansen, J. Becher, J. Chem. Soc. Rev. (1994) 41.
[26] R.E. Rosenfield, R. Parthasarathy, J. Am. Chem. Soc. 96 (1974) 1925.
[27] R.E. Rosenfield, R. Parthasarathy, J.D. Dunitz, J. Am. Chem. Soc. 99 (1977) 4860.
[28] L.-P. Wu, J. Dai, M. Munakata, T. Kuroda-Sowa, M. Maekawa, Y. Suenaga, Y. Ohno, J. Chem. Soc., Dalton Trans. (1998) 3255.
[29] C. Jia, D. Zhang, C.-M. Liu, W. Xu, H. Hu, D. Zhu, New J. Chem. 26 (2002) 490.
[30] X. Wang, G.-Q. Bian, J. Dai, Q.-Y. Zhu, K.-B. Yu, Chin. J. Struct. Chem. 21 (2002) 264.

Available online at www.sciencedirect.com
SCIENCE DIRECT®
Polyhedron 23 (2004) 1453–1460
POLYHEDRON
www.elsevier.com/locate/poly

X-ray and spectroscopic characterisation of cobalt(III) and nickel(II) complexes with 2-(2-pyridyl)iminotetrahydro-1,3-thiazine hydrochloride · water (1/2) (PyTzHCl · $2H_2O$) in the solid state and study of its interaction with cobalt(II) and nickel(II) in aqueous solution

F.J. Barros-García, Alvaro Bernalte-García *, Fransisco J. Higes-Rolando, F. Luna-Giles, R. Pedrero-Marín

Departamento de Química Inorgánica, Facultad de Ciencias, Universidad de Extremadura, E06071 Badajoz, Spain

Received 22 January 2004; accepted 27 February 2004
Available online 12 April 2004

Abstract

We have carried out the study of the interaction of cobalt(II) and nickel(II) chloride salts with 2-(2-pyridyl)iminotetrahydro-1,3-thiazine hydrochloride · water (1/2) (PyTzHCl · $2H_2O$) in order to determine what complex species can be formed, with the aim of evaluating the different behaviour of the complexes with respect to the free ligand. The compounds carbonato-κ^2O,O'-bis[2-(2-pyridyl-κN)amino-5,6-dihydro-4H-1,3-thiazine-κN]cobalt(III) chloride · water (1/6.6), $[Co(CO_3)(PyTz)_2]Cl \cdot 6.6H_2O$, and diaqua-bis[2-(2-pyridyl-κN)amino-5,6-dihydro-4H-1,3-thiazine-κN]nickel(II) chloride · water (1/6), $[Ni(PyTz)_2(H_2O)_2]Cl_2 \cdot 6H_2O$, have been isolated and their crystal and molecular structure determined by X-ray diffraction. Both complex cations show a distorted octahedral geometry. The solid phases were also characterized through elemental analysis, magnetic susceptibility, UV–Vis–NIR (UV–Visible–Near IR) diffuse reflectance and infrared spectroscopy. Likewise, the equilibria study of PyTzHCl · $2H_2O$ with Co(II) and Ni(II) at 298 K and 0.1 M ionic strength in aqueous solution was performed by means of potentiometric titration.
© 2004 Elsevier Ltd. All rights reserved.

Keywords: Crystal structure; Thiazine; Cobalt(III) complex; Nickel(II) complex; Pyridine

1. Introduction

In recent years, the investigation on thiazine derivatives coordination chemistry has undergone a considerable increase, due to the potential pharmacological and medical applications of these compounds.

Siderophore analogues constitute a clear example of this development, since they are prototypes for the synthesis of chelating agents employed for clinical use [1]. The research on this area will lead to the design of new clinical drugs for certain metal detoxification [2]. There have been characterized siderophores containing thiazine or thiazoline rings, as the desferrithiocin analogue DL-2-(3-hydroxipyridin-2-yl))-4H-5,6-dihydro-1,3-thiazine-4-carboxilic acid [3].

Taking into account the aforementioned, as well as their interest as potential antibiotic and anti-tumour agents [4], during last years we have carried out a systematic investigation on the coordination chemistry of thiazine derivatives with ions from the transition elements [5]. As a continuation of this research, we report here the study of the interactions between PyTzHCl · $2H_2O$ and the metal ions cobalt(II) and nickel(II).

* Corresponding author. Tel.: +34-924-289394; fax: +34-924-289395.
E-mail address: alberga@unex.es (A. Bernalte-García).
Abbreviations: PyTz, 2-(2-pyridyl)iminotetrahydro-1,3-thiazine; PyTzHCl · $2H_2O$, 2-(2-pyridyl)iminotetrahydro-1,3-thiazine hydrochloride · water (1/2); btz, 2,2′-bis(4,5-dihydro-6H-1,3-thiazine).

0277-5387/$ - see front matter © 2004 Elsevier Ltd. All rights reserved.
doi:10.1016/j.poly.2004.02.024

The reactions between PyTz and the metal ions Co(II) and Ni(II) have afforded the complexes $[Co(CO_3)(PyTz)_2]Cl \cdot 6.6H_2O$ and $[Ni(PyTz)_2(H_2O)_2]Cl_2 \cdot 6H_2O$, respectively. During the reaction of the first complex, the cobalt(II) ion has been oxidized to cobalt(III). The coordination behaviour of PyTz in these complexes is analogous to that exhibited towards copper(II) [5], as was to be expected, acting in both cases as didentate ligand. The solid phases obtained by these reactions were isolated and characterized through elemental analyses, UV–Vis–NIR (UV–Visible–Near IR) diffuse reflectance, infrared spectroscopy, magnetic susceptibility measurement and X-ray diffraction. Likewise, the equilibria study of $PyTzHCl \cdot 2H_2O$ with Co(II) and Ni(II) was performed in aqueous solution at 298 K and 0.1 M ionic strength in $NaClO_4$, yielding several complex species different from those obtained as solid phases.

2. Experimental

2.1. Reagents

Nickel(II) and cobalt(II) stock solutions were prepared in doubly distilled freshly boiled water from its chloride and their concentrations were determined by titration against NaOH. The ionic strength of the solutions was adjusted to a perchlorate concentration of 0.1 M by the addition of sodium perchlorate. Sodium hydroxide stock solutions were prepared by dilution of a concentrated solution of sodium hydroxide, according to Kolthoff et al. [6]. These solutions were kept under a CO_2-free atmosphere and standardized by titration against potassium hydrogen phthalate.

2.2. Preparation of $[Co(CO_3)(PyTz)_2]Cl \cdot 6.6H_2O$

The cobalt(III) complex was isolated from a freshly prepared aqueous solution of cobalt(II) chloride (106.4 mg, 0.447 mmol) that was added to an aqueous solution of $PyTzHCl \cdot 2H_2O$ (106.3 mg, 0.400 mmol). The pH of the whole solution was adjusted by dropwise addition of NaOH, to an appropriate pH according to the titration curves (pH 8). The solution was allowed to evaporate slowly at room temperature and after a few days, red crystals were isolated from the solution (68%, 100 mg). During the course of the reaction, the cobalt ion has been oxidized from its starting 2+ to state 3+ in the complex. *Anal.* Calc. for $C_{19}H_{35}ClCoN_6O_{9.6}S_2$: C, 34.59; H, 5.38; N, 12.73; S, 9.72. Found: C, 34.54; H, 5.26; N, 12.66; S, 9.11%.

2.3. Preparation of $[Ni(PyTz)_2(H_2O)_2]Cl_2 \cdot 6H_2O$

The nickel(II) complex was obtained by addition of a freshly prepared aqueous solution of nickel(II) chloride (58.4 mg, 0.246 mmol) to an aqueous solution of $PyTzHCl \cdot 2H_2O$ (115.1 mg, 0.433 mmol) and adjusting the pH of the mixture, by dropwise addition of NaOH, to an appropriate value according to the potentiometric titration curves (pH 8). The solution was allowed to evaporate slowly at room temperature for a few days, being isolated blue crystals (83%, 121 mg). *Anal.* Calc. for $C_{18}H_{38}Cl_2NiN_6O_8S_2$: C, 32.74; H, 5.80; N, 12.72; S, 9.71. Found: C, 32.87; H, 5.64; N, 12.85; S, 8.51%.

2.4. Instrumental procedures

Chemical analyses of carbon, hydrogen, nitrogen and sulfur were performed by means of microanalytical methods using a Leco CHNS-932 microanalyser. A UV–Vis–NIR reflectance spectrum of each complex in the 200–1000 nm range was obtained from a pellet of the sample, using a Shimadzu UV-3101 PC spectrophotometer and $BaSO_4$ as a reference. IR spectra were recorded on a Perkin–Elmer FT-IR 1720 spectrophotometer, from KBr pellets in the 4000–370 cm^{-1} range and on a Perkin–Elmer FT-IR 1700X spectrophotometer, from polyethylene pellets in the 500–150 cm^{-1} range. Magnetic susceptibility measurements were performed on powdered samples in the temperature range 2–290 K using a magnetometer with pendulum MANICS DSM8, equipped with helium continuous-flow cryostat and a electromagnetometer DRUSCH EAF 16 UE. Data were corrected for temperature-independent paramagnetism and diamagnetic contributions, which were estimated from the Pascal constants.

Potentiometric measurements were carried out with a Metrohm 702 SM Titrino equipped with a combined pH glass electrode. The electrode system was calibrated in terms of hydrogen ion concentration by performing strong acid versus strong base titrations [7]. The ligand concentration of the samples was always 2×10^{-3} M, and metal complex formation curves were obtained at different ligand-to-metal ratios from 1:1 to 3:1. Sample solutions were titrated in a double-walled vessel maintained at 298 ± 0.1 K by circulating water and stirred magnetically under a continuous flow of nitrogen. The ionic strength was fixed to 0.1 M by addition of appropriate amount of $NaClO_4 \cdot H_2O$. The numerical analysis of all the experimental e.m.f. data was carried out with the computer program SUPERQUAD [8]. All calculations were performed on a PC.

2.5. Crystal structure determinations

Crystal data, data collection and refinement details for $[Co(CO_3)(PyTz)_2]Cl \cdot 6.6H_2O$ and $[Ni(PyTz)_2(H_2O)_2]Cl_2 \cdot 6H_2O$ are given in Table 1. The first 50 frames were recollected at the end of data collection to monitor for decay.

Table 1
Crystal data, data collection and refinement details for $[Co(CO_3)(PyTz)_2]Cl \cdot 6.6H_2O$ and $[Ni(PyTz)_2(H_2O)_2]Cl_2 \cdot 6H_2O$

	$[Co(CO_3)(PyTz)_2]Cl \cdot 6.6H_2O$	$[Ni(PyTz)_2(H_2O)_2]Cl_2 \cdot 6H_2O$
Crystal shape	prism	prism
Size (mm)	$0.32 \times 0.20 \times 0.18$	$0.32 \times 0.20 \times 0.18$
Chemical formula	$C_{19}H_{35}ClCoN_6O_{9.6}S_2$	$C_{18}H_{38}Cl_2NiN_6O_8S_2$
Formula weight	658.03	660.27
Crystal system	triclinic	monoclinic
Space group	$P\bar{1}$	$I2/a$
Unit cell dimensions		
a (Å)	9.6837(2)	12.1987(2)
b (Å)	12.4467(2)	16.1952(2)
c (Å)	13.8316(1)	15.8900(2)
α (°)	63.3660(10)	
β (°)	84.7740(10)	106.5800(1)
γ (°)	72.6430(10)	
Cell volume (Å^3)	1420.59(4)	3008.71(7)
Z	2	4
D_{calc} (g cm^{-3})	1.538	1.458
μ (cm^{-1})	0.904	1.010
$F(000)$	686	1384
Diffractometer	Bruker SMART CCD	Bruker SMART CCD
Radiation	Mo Kα ($\lambda = 0.71073$ Å)	Mo Kα ($\lambda = 0.71073$ Å)
T (K)	293(2)	293(2)
Collection method	$\phi - \omega$	$\phi - \omega$
2θ range	3.3–56.6	3.7–56.3
Index ranges	$-9 \leqslant h \leqslant 12$, $-15 \leqslant k \leqslant 16$	$-16 \leqslant h \leqslant 9$, $-21 \leqslant k \leqslant 21$
	$-18 \leqslant l \leqslant 18$	$-20 \leqslant l \leqslant 21$
Total No. of measured reflections	9546	10 272
Independent reflections	6803 [$R_{int} = 0.0258$]	3685 [$R_{int} = 0.0382$]
Absorption correction	empirical	empirical
Maximum and minimum transmission	0.8542/0.7608	0.8391/0.7381
Observed reflections	5243 [$F > 4.0\sigma(F)$]	2726 [$F > 4.0\sigma(F)$]
Data/restraints/parameters	6803/15/402	3685/0/200
Final R indices [$I > 2\sigma(I)$]	$R_1 = 0.061$	$R_1 = 0.0459$
	$wR_2 = 0.1435$	$wR_2 = 0.1225$
R indices (all data)	$R_1 = 0.086$	$R_1 = 0.0687$
	$wR_2 = 0.1605$	$wR_2 = 0.1356$
Goodness-of-fit on F^2	1.033	0.997
ρ_{max}, ρ_{min} (e Å^{-3})	1.617, −0.927	0.489, −0.475

All intensity data were corrected for Lorentz and polarization effects. Moreover, data were also corrected for absorption effects using an empirical method based on azimuthal scan data. The structures were solved by direct methods and subsequent Fourier differences using the WINGX package [9] and refined by full-matrix least-squares. The H-atoms were located from a differential Fourier synthesis and included in the calculation with estimated isotropic displacement parameters without refinement (riding model).

3. Results and discussion

3.1. Potentiometric studies

As we described in a previous paper [5], the analysis of $PyTzHCl \cdot 2H_2O$ potentiometric titration curves by SUPERQUAD [8] computer method led to the establishment of the ligand ionization constant, whose value is essential for the later determination of possible complex stability constants.

In the present report, the titration curves for the $PyTzHCl \cdot 2H_2O$/Ni(II) and $PyTzHCl \cdot 2H_2O$/Co(II) systems were obtained for duplicate in the 5–11 pH range. They are studied using SUPERQUAD program in order to determine what complex species are formed and their stability constants, designed as β_{pqrs}, where the subscripts p, q, r, s make reference to the complex stoichiometry in the metal, ligand, hydrogen ion, chloride order.

The more probable complex species, together with formation constants and statistical parameters σ and χ^2, are reported in Table 2.

Metal hydroxides and cobalt chlorocomplexes formation constants are considered in calculations, but not the presence of nickel chlorocomplexes in accordance with the bibliography related with the formation of these species [10,11].

Table 2
Formation constants ($\log\beta$) at 298 K and $I = 0.1$ M ($NaClO_4$)

System	Species	$\log\beta$	χ^2	σ
$PyTzH^+/Co^{2+}$ (1/1)	$[Co(PyTz)]^{2+}$	13.80(0)	11.04	2.46
$PyTzH^+/Co^{2+}$ (2/1)	$[Co(PyTz)]^{2+}$	13.76(1)	3.33	2.00
	$[Co(PyTz)_2]^{2+}$	17.77(1)		
$PyTzH^+/Co^{2+}$ (3/1)	$[Co(PyTz)]^{2+}$	13.73(3)	3.87	1.24
	$[Co(PyTz)_2]^{2+}$	17.11(13)		
$PyTzH^+/Ni^{2+}$ (1/1)	$[Ni(PyTz)]^{2+}$	17.80(1)	5.00	2.96
$PyTzH^+/Ni^{2+}$ (2/1)	$[Ni(PyTz)]^{2+}$	18.32(6)	2.21	2.47
	$[Ni(PyTz)_2]^{2+}$	23.81(10)		
$PyTzH^+/Ni^{2+}$ (3/1)	$[Ni(PyTz)]^{2+}$	17.46(2)	4.37	3.32
	$[Ni(PyTz)_3]^{2+}$	26.05(7)		

As it can be observed, in the case of a 1:1 ligand/metal ratio, a complex specie was detected for $PyTzHCl \cdot 2H_2O$/Ni(II) system, and the best fit between experimental and theoretical potentiometric titration curves was found for the model considering the specie ML. Likewise, in the titration curve with 2:1 ligand/metal ratio it was found that the species ML and ML_2 satisfied the experimental data, while in the titration curve with a 3:1 ligand/metal ratio, a new model formed by the combination of complex ML and ML_3 resulted in a satisfactory numerical and graphical fit.

With regard to $PyTzHCl \cdot 2H_2O$/Co(II) system, the 1:1 ligand/metal ratio titration curves study provided the specie ML, whereas for 2:1 and 3:1 ligand/metal proportions, the model that gave a satisfactory fit to the experimental data was that which considers the species ML and ML_2 in both cases.

In an analogous way to its behaviour towards copper [5], the ligand acts as unprotonated form in all detected species.

Every proposed hydroxide and chlorinated complexes have been rejected by SUPERQUAD species selection [8], generating a new model that did not include them.

Finally, it can be said that the reported global formation constants are reproducible and the statistical parameters acceptable.

3.2. Description of the structures

The structure of the red cobalt(III) complex is built up by $[Co(CO_3)(PyTz)_2]^+$ cations, chloride anions and water molecules of crystallization. Fig. 1 shows the molecular structure of the complex cation. Selected bond lengths, angles and hydrogen-bond parameters are listed in Table 3.

The environment around the cobalt(III) atom may be described as a distorted octahedral geometry with the ligand–metal–ligand bite angles varying between 68.9(1)° [O(1)–Co–O(2)] and 98.9(1)° [O(1)–Co–N(3)], and the metallic atom coordinated to two carbonato

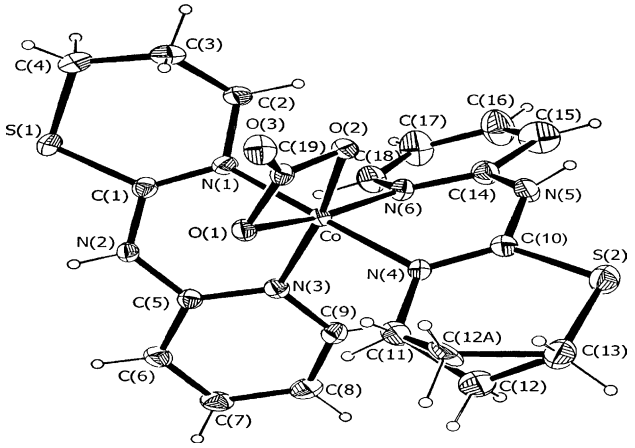

Fig. 1. Molecular structure of the $[Co(CO_3)(PyTz)_2]^+$ cation, showing the atom-numbering scheme. The thermal ellipsoids are drawn at a 50% level.

oxygen atoms [av. Co–O = 1.913 Å], two thiazine nitrogen atoms [av. Co–N = 1.933 Å] and two pyridine nitrogen atoms [av. Co–N = 1.936 Å]. This compound is the first structurally characterized compound having a 1,3-thiazine link to cobalt(III). The whole molecule exhibits pseudo-C_2 symmetry with the C_2 axis passing through the C(19)–O(3) bond.

The Co–O bond lengths are similar and comparable to the calculated average value [1.913(16) Å] for 35 octahedral cobalt(III) carbonato complexes with a chromophore group CoN_4O_2 obtained from the Cambridge Structural Database (CSD) [12]. Likewise, the Co^{III}–$N_{(pyridine)}$ distances are in good agreement with the mean value [1.946(33) Å] calculated using the data of 19 six-coordinate cobalt(III) complexes obtained from CSD.

The two six-membered chelate rings show an intermediate form between boat and half-boat conformations with the atoms Co and N(2) [or N(5)] deviating ~ 0.80 and ~0.25 Å, respectively, above the plane formed by N(1), C(1), N(3), C(5) [or N(4), C(10), N(6), C(14)]. These geometries are proved by the puckering parameters [$Q = 0.587$ Å; $\phi = 179.1°$; $\theta = 110.1°$] for the chelate ring Co–N(1)–C(1)–N(2)–C(5)–N(3) and [$Q = 0.607$ Å; $\phi = 177.1°$; $\theta = 108.8°$] for the chelate ring Co–N(4)–C(10)–N(5)–C(14)–N(6), both of them calculated according to Cremer and Pople [13].

The chelate ring Co–O(1)–C(19)–O(2) is essentially planar with maximum mean plane deviation for O(3) (0.003 Å).

In a similar way to that observed in the previously reported copper(II) complex [5], the analysis of bond lengths and angles shows that the organic ligands present an amino-5,6-dihydro-4H-1,3-thiazine form instead the imino-tetrahydro-1,3-thiazine form, detected for PyTz as free ligand.

The thiazine ring S(1)–C(1)–N(1)–C(2)–C(3)–C(4) presents an intermediate form between half-boat conformation with the apex at C(2) and twist boat confor-

Table 3
Selected bond lengths (Å), angles (°) and hydrogen-bond parameters for $[Co(CO_3)(PyTz)_2]Cl \cdot 6.6H_2O$

Bond lengths			
Co–O(1)	1.919(2)	Co–O(2)	1.907(2)
Co–N(1)	1.926(3)	Co–N(3)	1.936(3)
Co–N(4)	1.940(3)	Co–N(6)	1.936(3)
S(1)–C(1)	1.748(4)	S(1)–C(4)	1.823(5)
S(2)–C(10)	1.741(4)	S(2)–C(13)	1.785(4)
N(4)–C(10)	1.292(4)	N(4)–C(11)	1.474(5)
C(1)–N(1)	1.291(4)	N(1)–C(2)	1.484(4)
N(3)–C(9)	1.368(5)	N(3)–C(5)	1.337(4)
N(6)–C(14)	1.336(5)	N(6)–C(18)	1.370(5)
Bond angles			
O(2)–Co–O(1)	68.9(1)	O(2)–Co–N(1)	89.2(1)
O(1)–Co–N(1)	88.6(1)	O(2)–Co–N(6)	98.3(1)
O(1)–Co–N(6)	167.2(1)	N(1)–Co–N(6)	92.0(1)
O(2)–Co–N(3)	167.7(1)	O(1)–Co–N(3)	98.9(1)
N(1)–Co–N(3)	89.3(1)	N(6)–Co–N(3)	93.9(1)
O(2)–Co–N(4)	88.2(1)	O(1)–Co–N(4)	89.3(1)
N(6)–Co–N(4)	89.7(1)	N(3)–Co–N(4)	93.0(1)
N(4)–C(10)–N(5)	121.7(3)	N(4)–C(10)–S(2)	128.1(3)
N(5)–C(10)–S(2)	110.2(2)	C(2)–N(1)–Co	120.3(2)
C(1)–N(2)–C(5)	125.3(3)	C(18)–N(6)–Co	121.1(2)
C(14)–N(5)–C(10)	124.9(3)	N(6)–C(14)–N(5)	120.1(3)
C(1)–S(1)–C(4)	103.5(2)	C(10)–S(2)–C(13)	102.6(2)
C(10)–N(4)–C(11)	120.2(3)	C(10)–N(4)–Co	120.1(3)
C(11)–N(4)–Co	118.7(2)	C(5)–N(3)–Co	120.1(2)
C(9)–N(3)–Co	120.7(2)	C(1)–N(1)–C(2)	117.7(3)
C(1)–N(1)–Co	121.0(2)	C(2)–N(1)–Co	120.3(2)
N(1)–C(1)–N(2)	121.6(3)	N(1)–C(1)–S(1)	126.8(3)
N(2)–C(1)–S(1)	111.6(2)	C(14)–N(6)–Co	119.3(3)
N(3)–C(5)–N(2)	120.0(3)	N(6)–C(14)–N(5)	120.1(3)
C(13)–C(12A)–C(11)	124.8(11)	C(11)–C(12)–C(13)	112.5(5)
N(2)–C(1)–S(1)	111.6(2)	C(14)–N(6)–Co	119.3(3)
Bond A···H–D	Position of D	A···D (Å)	A···H–D (°)
O(3W)···H(2W)–O(1W)	x, y, z	2.831(8)	171(4)
O(1W)···H(3W)–O(2W)	x, y, z	2.861(6)	161(4)
O(6W1)···H(6W)–O(3W)	x, y, z	2.780(10)	169(1)
Cl···H(10W)–O(5W)	x, y, z	3.093(9)	163(4)
O(2W)···H(9W)–O(5W)	x, y, z	2.817(8)	168(2)
O(3W)···H(5)–N(5)	x, y, z	2.844(6)	157.1(3)
O(3W)···H(2W)–O(1W)	$-x, -1+y, -2+z$	2.790(5)	162(2)
O(4W)···H(4W)–O(2W)	$-1+x, -1+y, -1+z$	2.881(2)	168(5)
Cl···H(5W)–O(3W)	$-1+x, -1+y, -1+z$	3.031(7)	156(4)
O(4W)···H(7W)–O(4W)	$-1+x, -1+y, -1+z$	2.709(2)	156(5)
Cl···H(8W)–O(4W)	$-1+x, -1+y, -1+z$	3.164(7)	164(3)
O(1)···H(2)–N(2)	$-1-x, -2+y, -2+z$	2.838(4)	172.4(2)

mation with S(1) and C(2) above and C(1) and C(3) below the atoms N(1) and C(4). This geometry is proved by the puckering parameters [$Q = 0.596$ Å; $\phi = 26.4°$; $\theta = 112.1°$], calculated according to Cremer and Pople [13].

The other thiazine ring shows a dynamic disorder affecting C(12) and C(12A) atoms, each one with a 50% of occupancy, which give rise to two extreme conformations. One of them shows an intermediate form between half-chair and half-boat, with the C(12) and C(13) atoms deviating −0.578 and 0.106 Å, respectively, from the plane formed by S(2), C(10), N(4) and C(11) [$Q = 0.480$ Å; $\phi = 251.8°$; $\theta = 50.7°$]. On the contrary, the second conformation is near to half-boat, with the apex at C(12A). This atom is 0.385 Å out of the plane formed by S(2), C(10), N(4), C(11) and C(13) [$Q = 0.292$ Å; $\phi = 51.3°$; $\theta = 122.9°$].

Moreover, the crystal structure shows static disorder that involves some of the crystallization water molecules. Specifically, it is observed a partial substitution of a pair H_2 (O6W1)···H_2 (O6W3) for a molecule H_2 (O6W2) that is located on a halfway position between both members of the pair, in such a way that the occupation degree for the first pair component is ~55%, while for the second one is ~45%.

Likewise, the crystal structure presents an extensive hydrogen-bond network, in which atoms O(1) and O(2)

and chloride anions act as acceptors of hydrogen, amino nitrogen atoms act as donors and crystallization water molecules act on both ways.

The X-ray study of the nickel(II) complex revealed that the crystals are made up of monoclinic unit cells, each one containing four $[Ni(PyTz)_2(H_2O)_2]^{2+}$ cations, eight chloride anions and 24 crystallization water molecules. Therefore, the complex salt may be formulated as $[Ni(PyTz)_2(H_2O)_2]Cl_2 \cdot 6H_2O$. A diagram of the molecular structure of the complex cation is shown in Fig. 2, and selected bond lengths, angles and hydrogen-bond parameters are given in Table 4.

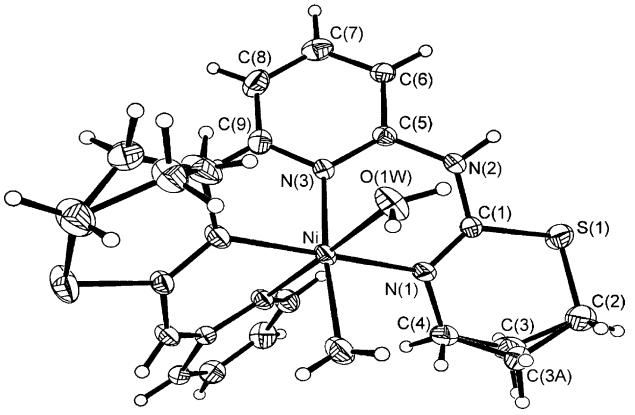

Fig. 2. Molecular structure of the $[Ni(PyTz)_2(H_2O)_2]^{2+}$ cation, showing the atom-numbering scheme. The thermal ellipsoids are drawn at a 50% level.

The complex cation possesses a crystallographic C_2 symmetry, with the twofold axis being coincident with the bisector of the angle formed by the two oxygen atoms and the central cation.

The environment around the nickel(II) atom may be described as a distorted octahedral geometry with the metal coordinated to two water molecules [Ni–O(1W) = 2.119(2) Å], two thiazine nitrogen atoms [Ni–N(1) = 2.075(2) Å] and two pyridine nitrogen atoms [Ni–N(3) = 2.082(2) Å]. The ligand–metal–ligand bite angles differ from the ideal value of 90°, varying between 86.0(1)° and 94.2(1)°. Likewise, this compound is the first structurally characterized compound having a 1,3-thiazine link to nickel(II).

In this complex, the bond length Ni–O(1W) is similar to the average value [2.120(64) Å] calculated using 104 octahedral Ni(II) aquacomplexes with a chromophore group NiN_4O_2 collected in CSD. The $Ni–N_{pyridine}$ bond distance is comparable with the mean value [2.104(33) Å] calculated from the data of 19 octahedral Ni(II)

Table 4
Selected bond lengths (Å) and angles (°) for $[Ni(PyTz)_2(H_2O)_2]Cl_2 \cdot 6H_2O$

Bond lengths			
Ni–N(1)	2.075(2)	Ni–N(3)	2.082(2)
Ni–O(1W)	2.119(2)	S(1)–C(1)	1.756(3)
S(1)–C(4)	1.794(4)	N(2)–C(1)	1.373(3)
N(2)–C(5)	1.391(3)	N(1)–C(1)	1.291(3)
N(1)–C(2)	1.465(4)	N(3)–C(5)	1.337(3)
N(3)–C(9)	1.361(3)		
Bond angles			
N(1)–Ni–N(3)	86.0(1)	N(3)–Ni–O(1W)	89.4(1)
N(1)–Ni–N(3a)	94.2(1)	N(3)–Ni–N(3a)	93.9(1)
N(1)–Ni–O(1W)	89.2(1)	Ni(1a)–Ni–O(1W)	90.6(1)
O(1W)–Ni–O(1Wa)	87.7(1)	C(1)–S(1)–C(4)	103.2(2)
C(1)–N(2)–C(5)	127.9(2)	C(1)–N(1)–C(2)	117.7(2)
C(1)–N(1)–Ni	120.9(2)	C(2)–N(1)–Ni	120.9(2)
C(5)–N(3)–C(9)	117.4(2)	C(5)–N(3)–Ni	121.1(2)
C(9)–N(3)–Ni	120.3(2)	C(2)–C(3)–C(4)	122.6(8)
C(2)–C(3A)–C(4)	114.9(5)	N(1)–C(1)–N(2)	122.8(2)
N(1)–C(1)–S(1)	126.3(2)	N(2)–C(1)–S(1)	110.8(2)
N(3)–C(5)–N(2)	120.0(2)		
Bond A···H–D	Position of D	A···D (Å)	A···H–D (°)
O(2)···H(2W)–O(1W)	x, y, z	2.793(3)	168.3(2)
O(1)···H(1W)–O(1W)	$1+x, y, z$	2.811(3)	167.9(2)
Cl(1)···H(5)–N(2)	$-x, 1-y, 1-z$	3.177(2)	175.4(2)
O(4)···H(3W)–O(2)	$x, -1+y, z$	2.729(1)	172.6(4)
Cl(2)···H(3W)–O(2)	$x, 1-y, z$	3.283(4)	149.3(2)
Cl(1)···H(4W)–O(2)	$-1/2+x, 1-y, z$	3.294(4)	155.5(2)
O(3)···H(4W)–O(2)	$-1/2+x, 1-y, z$	2.670(9)	158.4(4)
Cl(1)···H(5W)–O(1)	$-1/2+x, 1-y, z$	3.270(3)	168.0(6)
O(3)···H(6W)–O(1)	$-1+x, -1+y, z$	2.796(9)	172.0(6)
Cl(2)···H(6W)–O(1)	$-1+x, -1+y, z$	3.240(4)	143.0(5)

diaquacomplexes with a chromophore group NiN_4O_2 using CSD.

The chelate ring [$Q = 0.594$ Å; $\phi = 0.6°$; $\theta = 69.0°$] shows an intermediate conformation between half-boat and boat, with the atoms Ni and N(2) deviating 0.832 and 0.234 Å, respectively, above the plane formed by N(1)–C(1)–C(5)–N(3).

The organic moiety shows an amino-5,6-dihydro-4H-1,3-thiazine form, like in the cobalt(III) complex. Likewise, the thiazine ring also shows a dynamic disorder affecting C(3) atom, which give rise to two extreme conformations. One of them is near to half-boat [$Q = 0.499$ Å; $\phi = 297.5°$; $\theta = 57.5°$], with C(4) deviating 0.637 Å from the plane formed by S(1)–C(1)–N(1)–C(2)–C(3). The second conformation is intermediate between half-boat [$Q = 0.505$ Å; $\phi = 17.6°$; $\theta = 109.1°$] with the apex at C(2), and twist boat with S(1) and S(2) above and C(1) and C(3) below the atoms N(1) and C(4).

There are two kinds of chloride anions in the crystal structure, named as Cl(1) and Cl(2). The Cl(1) ions are located on the twofold axis of symmetry, as the nickel atom. However, the Cl(2) ions are situated in a general position, which lead to a Cl(2) occupation degree of 50%, in order to reach neutrality. Because of this, a static disorder takes place in the structure in such a way that the holes left by the Cl(2) ions are occupied by two water molecules: $H_2O(3)$ and $H_2O(4)$, each one with an occupation degree of 50%.

The crystal structure is stabilized by a wide network of hydrogen-bonds, in which the coordination water molecules and the exocyclic nitrogen atoms act as hydrogen donors, the chloride ions act as acceptors and the crystallization water molecules act on both ways.

3.3. Magnetic studies

The observed molar magnetic susceptibility for $[Ni(PyTz)_2(H_2O)]Cl_2 \cdot 6H_2O$ was corrected for diamagnetism and temperature-independent paramagnetism to provide the fully corrected magnetic moment at room temperature ($\mu = 3.23$ MB). This value is consistent with the octahedral environment around nickel(II) [14].

3.4. Spectroscopic studies

The electronic spectrum of the isolated cobalt(III) complex in the Vis–near UV region exhibits the presence of only two absorption bands due to the d–d transitions in the octahedral CoN_4O_2 crystal field. The higher energy band at 395 nm (25 320 cm^{-1}) is found as a shoulder covered by the charge transfer transition. This d–d absorption is assigned to the $^1A_{1g}(I) \rightarrow {}^1T_{2g}(I)$ transition. Therefore, a Gaussian-shaped band is found at 532 nm (18 800 cm^{-1}), which can be assigned to the $^1A_{1g}(I) \rightarrow {}^1T_{1g}(I)$ transition. This shape and its intensity suggest that the compound has a *cis* octahedral geometry, which is supported by the X-ray structural determination for this carbonato complex.

The bands of more intensity at 305 nm (32 800 cm^{-1}) and 239 nm (41 300 cm^{-1}) can be assigned to the $\pi \rightarrow \pi^*$ transitions of the organic ligand, whereas the band at 328 nm (30 500 cm^{-1}) is assigned to charge transfer absorption involving the imine function.

Using the frequencies of the d–d transitions, we have calculated the values of 10 Dq and the Racah interelectronic repulsion parameters B and C by means of the Tanabe–Sugano diagram and the equations proposed by Lever [15]:

$$E[^1A_{1g}(I) \rightarrow {}^1T_{1g}(I)] = 10\ Dq - C$$

$$E[^1A_{1g}(I) \rightarrow {}^1T_{2g}(I)] = 10\ Dq + 16B - C$$

The calculated values of the ligand field parameters 10 Dq = 19 700 cm^{-1}, $B = 408$ cm^{-1} and $C = 880$ cm^{-1} are consistent with the presence of the chromophore group $[Co^{III}N_4O_2]$ in several carbonato complexes [16].

In the nickel(II) complex, the electronic spectrum shows two intense bands at 296 nm (33 780 cm^{-1}) and 246 nm (40 630 cm^{-1}), which are assigned to the $\pi \rightarrow \pi^*$ transitions of the organic ligand. Moreover, the spectrum exhibits absorption bands at 948 nm (10 550 cm^{-1}) and 587 nm (17 030 cm^{-1}), both of low intensity. These bands may be assigned to: $^3A_{2g}(F) \rightarrow {}^3T_{2g}(F)$ (10 550 cm^{-1}) and $^3A_{2g}(F) \rightarrow {}^3T_{1g}(F)$ (17 030 cm^{-1}) transitions in an idealized O_h symmetry. The position of the observed d–d transitions permits to calculate the ligand field parameters 10 Dq and B, using the following known relationships:

$$E[^3A_{2g}(F) \rightarrow {}^3T_{2g}(F)] = 10\ Dq$$

$$E[^3A_{2g}(F) \rightarrow {}^3T_{1g}(F)] = (1/2)(15B + 30\ Dq) - (1/2)[(15B - 10\ Dq)^2 + 12B.10\ Dq]^{1/2}$$

The calculated values of the ligand field parameters 10 Dq = 10 550 cm^{-1} and $B = 900$ cm^{-1} are consistent with the presence of the chromophore group $[Ni^{II}N_4O_2]$ [17].

The IR spectrum of both complexes in the 4000–370 cm^{-1} region shows the presence of bands due to the in plane thiazine ring vibrations at 1636, 954, 856, 790, 776, 630 and 602 cm^{-1} for the cobalt(III) complex, and at 1630, 944, 876, 778, 700, 626 and 595 cm^{-1} for the nickel(II) complex, whereas the out of plane thiazine ring vibrations are detected at 530 and 435 cm^{-1} for the former and at 524 and 430 cm^{-1} for the latter.

Likewise, characteristic bands of pyridine ring vibrations are registered at 1601(8a), 1530(8b), 1485(19a), 1428(19b), 653(4) and 417(16b) cm^{-1} for the cobalt(III) complex and at 1603(8a), 1520(8b), 1485(19a), 1423(19b), 1015(1), 638(6b) and 653(4) cm^{-1} for the nickel(II) complex.

The spectra exhibit other relevant bands at 3269, 3242, 3195, 3177 and 3137 cm^{-1}, corresponding to the bridging amino group stretching vibrations [18], 1293 cm^{-1} [ν(C–N)] and 3410 cm^{-1} [$\nu(H_2O)$] for the cobalt(III) complex and at 3192 and 3148 cm^{-1} [ν(N–H)] [16], 1291 cm^{-1} [ν(C–N)] and 3392 cm^{-1} [$\nu(H_2O)$] [19] for the nickel(II) complex.

Due to the presence of the carbonato group, the cobalt(III) complex spectrum shows several bands at 2052, 1658, 1267, 987, 842 and 733 cm^{-1}, that are in accord with the available bidentate carbonato ligands bibliography [20–24].

In the far infrared region, the C_2 symmetry of both complex cations predicts the existence of six bands [20,25] in the $[Co(CO_3)(PyTz)_2]Cl \cdot 6.6H_2O$ and $[Ni(PyTz)_2(H_2O)_2]Cl_2 \cdot 6H_2O$ spectra, which takes place for the first complex, but not for the second one.

Thus, the Co(III) spectrum shows six bands at 486, 464 cm^{-1} [$\nu(Co–OCO_2)$] [19,20], 376, 337 cm^{-1} [$\nu(Co–N_{pyridine})$] [20], 293 and 249 cm^{-1} [$\nu(Co–N_{thiazine})$] [26], whereas for Ni(II) complex, only two bands are detected at 370 cm^{-1}, corresponding to a $\nu(Ni–OH_2)$ vibration [19,27], and at 280 cm^{-1}, which could be assigned to a $\nu(Ni–N_{thiazine})$ vibration, registered at 270 cm^{-1} for $[Ni(btz)_3](ClO_4)_2$ [26], or to a $\nu(Ni–N_{pyridine})$ vibration, according to the consulted bibliography for several octaedrical nickel(II) complexes [20,21,28,29].

4. Supplementary material

CCDC 223482 ($[Co(CO_3)(PyTz)_2]Cl \cdot 6.6H_2O$) and CCDC 223483 ($[Ni(PyTz)_2(H_2O)_2]Cl_2 \cdot 6H_2O$) contain the supplementary crystallographic data for this paper. These data can be obtained free of charge via www.ccdc.cam.ac.uk/conts/retrieving.html (or from the CCDC, 12 Union Road, Cambridge CB2 1EZ, UK; fax: +44 1223 336033; e-mail: deposit@ccdc.cam.ac.uk).

Acknowledgements

We thank the Spanish Ministerio de Ciencia y Tecnología [under the Project BQ01-0374], Junta de Extremadura (Consejería de Educación, Ciencia y Tecnología, Dirección General de Enseñanzas Universitarias e Investigación) and FEDER [under the Projects IPR00A028 and 2PR02A098] for financial support.

References

[1] M.L. Guerinot, Annu. Rev. Microbiol. 48 (1994) 743.
[2] K. Langemann, D. Heineke, S. Rupprecht, K.N. Raymond, Inorg. Chem. 35 (1996) 5663.
[3] R.J. Bergeron, C.Z. Liu, J.S. Mcmanis, M.X.B. Xia, S.E. Algee, J. Wiegand, J. Med. Chem. 37 (1994) 1411.
[4] A. Korolkovas, J.H. Burckhalter, in: Compendio Esencial de Química Farmacéutica, Reverté, Barcelona, 1978.
[5] A. Bernalte García, F.J. García Barros, F.J. Higes Rolando, F. Luna Giles, R. Pedrero Marín, J. Inorg. Biochem. 98 (2004) 15.
[6] I.M. Kolthoff, E.B. Sandell, E.J. Meehan, S. Bruckenstein, in: Quantitative Chemical Analysis, Collier-Macmillan Canada Ltd., Toronto, 1969.
[7] P.W. Linder, R.G. Torrington, D.R. Williamsin, Analysis Using Glass Electrodes, Open University Press, Milton Keynes, 1984.
[8] P. Gans, A. Sabatini, A. Vacca, J. Chem. Soc., Dalton Trans. (1985) 1195.
[9] L.J. Farrugia, J. Appl. Crystallogr. 32 (1999) 837.
[10] F.A. Cotton, G. Wilkinson, C.A. Murillo, M. Bochman, in: Advanced Inorganic Chemistry, 6th ed., Wiley Interscience, New York, 1999.
[11] G. Wilkinson, R.D. Gillard, J.A. McCleverty, in: Comprehensive Coordination Chemistry, vol. 5, Pergamon Press, Oxford, 1987.
[12] Cambridge Structural Database, Cambridge Crystallographic Data Centre, Cambridge, 2002.
[13] D. Cremer, J.A. Pople, J. Am. Chem. Soc. 97 (1975) 1354.
[14] J. Reedijk, P.W.N.M. Van Leenwen, W.L. Groeneveld, Rec. Trav. Chim. Pays-Bas 87 (1968) 129.
[15] A.B.P. Lever, in: Inorganic Electronic Spectroscopy, Elsevier, Amsterdam, 1984.
[16] E.C. Niederhoffer, A.E. Martell, P. Rudolf, A. Clearfield, Inorg. Chem. 21 (1982) 3734.
[17] L. Sacconi, Trans. Met. Chem. 4 (1968) 199.
[18] R.T. Conley, in: Espectroscopía Infrarroja, Alhambra, Madrid, 1979.
[19] M. Arshad Ali Beg, S. Ashfaq Husain, Polyhedron 2 (1983) 881.
[20] K. Nakamoto, in: Infrared and Raman Spectra of Inorganic and Coordination Compounds, 5th ed., Wiley, New York, 1997.
[21] J.R. Ferraro, in: Low-Frequency Vibrations of Inorganic and Coordination Compounds, Plenum Press, New York, 1971.
[22] B.N. Gatehouse, S.E. Livingstone, R.S. Nyholm, J. Chem. Soc. (1957) 4222.
[23] K. Nakamoto, J. Fujita, S. Tamaka, M. Kobayashi, J. Am. Chem. Soc. 79 (1957) 4904.
[24] A.M. Greenaway, T.P. Dasgupta, K.C. Koshy, G.G. Sadler, Spectrochim. Acta 42A (1986) 949.
[25] W.G. Fateley, F.R. Dollish, N.T. McDevitt, F.F. Bentley, in: Infrared and Raman Selection Rules for Molecular and Lattice Vibrations: The Correlation Method, Wiley, New York, 1972.
[26] J. Nelson, S.M. Nelson, W.D. Perry, J. Chem. Soc. (1976) 1282.
[27] A. Bernalte García, F.J. García Barros, F.J. Higes Rolando, A.M. Pizarro Galán, C. Valenzuela Calahorro, Thermochim. Acta 339 (1999) 95.
[28] D.A. Thornton, Coord. Chem. Rev. 104 (1990) 251.
[29] N. Saha, A. Saha, S. Chaudhuri, T.C.W. Mak, T. Banerjee, P. Roychoudhury, Polyhedron 11 (1992) 2341.

Available online at www.sciencedirect.com
SCIENCE DIRECT®
Polyhedron 23 (2004) 1461–1466
POLYHEDRON
www.elsevier.com/locate/poly

Assembly of superanion capsules of *p*-sulfonatothiacalix[4]arenes with transition metal ions and diaza-crown ether

Qian-Ling Guo, Wen-Xiang Zhu *, Shu-Lan Ma, Shu-Jing Dong, Miao-Qiong Xu

Department of Chemistry, Beijing Normal University, Xinjekou Waidajie Street 19, Beijing 100875, China

Received 17 December 2003; accepted 29 February 2004
Available online 12 April 2004

Abstract

The reaction of tetrasodium *p*-sulfonatothiacalix[4]arene and transition metal ions (Co^{2+}, Ni^{2+} and Cu^{2+}) in the presence of 4,13-diaza-18-crown-6 gives two types of crystalline complex: (4,13-diaza-18-crown-6)$_2$[$M(H_2O)_6^{2+}$]{(4,13-diprotodiaza-18-crown-6) $\subset$ [$M(H_2O)_3^{2+}$(*p*-sulfonatothiacalix[4]arene)$^{4-}$]$_2$} $\cdot$ nH_2O ($M^{2+} = Co^{2+}$, Ni^{2+}, $n = 12$ for Co^{2+} and 14 for Ni^{2+}) (**1**) and (4,13-diprotodiaza-18-crown-6)$_2$[$Cu(H_2O)_6^{2+}$] [$Cu(H_2O)_2^{2+}$(*p*-sulfonatothiacalix[4]arene-H^+)$^{5-}$]$_2$ $\cdot$ $12H_2O$ (**2**). Both complexes feature slipped capsule assemblies with the diprotonated diaza-18-crown-6 shrouded by two head-to-head thiacalixarenes to form a bi-layer structure in which an exo-capsule diaza-18-crown-6 traverses the hydrophobic layer of the thiacalixarenes and a hexa-aqua metal ion occupies the hydrophilic layer. In complex **1**, each thiacalixarene coordinates to a metal ion through two deprotonated phenolic groups and a bridging sulfur atom, and an exo-capsule crown ether is located in the hydrophilic equator. However, in complex **2**, a coordination dimer is formed with the metal ion bound to a sulfonato group of one thiacalixarene as well as a deprotonated phenolic group and a bridging sulfur atom of an adjacent thiacalixarene.
© 2004 Elsevier Ltd. All rights reserved.

Keywords: Sulfonatothiacalixarene; Capsules; Diaza-Crown ether; Transition metal ions; Assembly

1. Introduction

Certain rigid, non-planar molecules with curved or bowl-shaped micro-environments have the extraordinary ability to assemble into capsules or cage molecules or ions [1–7]. These species may form nano-structures of relevance to materials and biological science, and their encapsulation of guest molecules has implications for drug delivery and catalysis [8]. The hydrophobic, bowl-shaped motif of calixarenes and related resorcinarenes make them inherently versatile building blocks for the construction of ionic or molecular capsules. Capsules based on two *p*-sulfonatocalix[*n*]arenes shrouding other molecules including crown ethers [9–11], tetra-protonated cyclam [12], di-protonated [2,2,2] cryptand ($n = 4$) [13] and H_2SO_4 ($n = 5$) [14] have recently been established. The use of the large water soluble, highly charged sulfonated calix[*n*]arenes to gain access to novel capsules relies on a combination of supramolecular interactions, notably coordination, hydrogen bonding, electrostatic and van der Waals, where there is size, shape and electronic complementarity between the molecular components [9].

In 1997, soon after the discovery of the practical method for the synthesis of *p*-tert-butylthiacalix[4]arene [15], thiacalix[4]arene tetrasulfonate, a new water-soluble host molecule, was obtained [16]. Similar to *p*-sulfonatocalixarenes, Na_4[thiacalix[4]arene tetrasulfonate] $\cdot$ ethanol $\cdot$ $8H_2O$ also shows a bi-layer structure in the solid state [17] in which the thiacalixarene unit adopts the cone configuration. Herein, we report the formation of new ionic capsules, where the di-protonated 4,13-diaza-18-crown-6 is shrouded by two *p*-sulfonatothiacalix[4]arenes in the presence of transition metal ions, and a new type of intercalation within the thiacalixarene bi-layer system showing that amphiphilic macrocyclic compounds without aromatic rings, in this case

* Corresponding author. Tel.: +86-10-62-207838; fax: +86-10-62-200567.
E-mail address: wx-zhu@263.net (W.-X. Zhu).

0277-5387/$ - see front matter © 2004 Elsevier Ltd. All rights reserved.
doi:10.1016/j.poly.2004.02.025

diaza-crown ethers or di-protonated diaza-crown ether cations, can span the hydrophobic layers.

2. Experimental

2.1. Materials and methods

4,13-Diaza-18-crown-6 [18] and tetrasodium *p*-sulfonatothiacalix[4]arene [17] were synthesized by literature methods. All other reagents were commercially available and used without further purification.

Elemental analyses were performed with an Elementar Vario EL analyser. The IR spectra were recorded on a Nicolet Avatar 360 FT-IR spectrometer using the KBr pellet technique in the 400–4000 cm^{-1} region.

2.2. Synthesis of (4,13-diaza-18-crown-6)$_2$[M(H$_2$O)$_6^{2+}$] {(4,13-diaza-18-crown-6+2H$^+$) ⊂ [M(H$_2$O)$_3^{2+}$(p-sulfonatothiacalix[4]arene)$^{4-}$]$_2$ · nH$_2$O} ($M^{2+} = Co^{2+}$, Ni^{2+}, $n = 12$ for Co^{2+} and 14 for Ni^{2+}), (**1**)

4,13-Diaza-18-crown-6 (39 mg, 0.15 mmol) and tetrasodium *p*-sulfonatothiacalix[4]arene (90 mg, 0.1 mmol) were dissolved in deionized water (5 mL). The solution was adjusted to pH ≈ 2 with perchloric acid and 0.15 mmol of the corresponding M^{2+} nitrate ($M^{2+} = Co^{2+}$, Ni^{2+}) was added. After several days, large crystals suitable for X-ray diffraction analysis were formed, yield = 32 mg (21%, for the Co^{2+} complex) and 40 mg (26%, for the Ni^{2+} complex). The crystals quickly cracked when removed from the mother liquor. IR: sulfonate absorptions: $v = 1222$, 1181, 1146, 1037 cm^{-1} (for the Co^{2+} complex), $v = 1220$, 1174, 1141, 1034 cm^{-1} (for the Ni^{2+} complex). Elemental analysis (%): *Anal.* Calc. for $C_{42}H_{76}Co_{1.5}N_3O_{34}S_8$: C, 33.36; H, 5.08; N, 2.78. Found: C, 33.21; H, 4.78; N, 2.61%; *Anal.* Calc. for $C_{42}H_{76}N_3Ni_{1.5}O_{34}S_8$: C, 33.36; H, 5.08; N, 2.78. Found: C, 33.13; H, 4.71; N, 2.64% (the analytical data is only for samples having lost one water molecules during transport).

2.3. Synthesis of (4,13-diaza-18-crown-6+2H$^+$)$_2$[Cu(H$_2$O)$_6^{2+}$] [Cu(H$_2$O)$_2^{2+}$(p-sulfonatothiacalix[4]arene-H$^+$)$^{5-}$]$_2$ · 12H$_2$O, (**2**)

4,13-Diaza-18-crown-6 (26 mg, 0.1 mmol) and tetrasodium *p*-sulfonatothiacalix[4]arene (90 mg, 0.1 mmol) were dissolved in deionized water (5 mL). The solution was adjusted to pH ≈ 2 with perchloric acid and 0.15 mmol of Cu^{2+} nitrate was added. Yellow green crystals formed after several days, yield = 80 mg (29%). The crystals quickly cracked if removed from the mother liquor. IR: sulfonate absorptions: $v = 1220$, 1183, 1145, 1036 cm^{-1}, Elemental analysis (%): *Anal.* Calc. for $C_{72}H_{108}Cu_3N_4O_{55}S_{16}$: C, 33.09; H, 4.17; N, 2.14. Found: C, 32.79; H, 3.89; N, 2.01% (the analytical data is only for samples having lost seven water molecules during transport).

2.4. X-ray crystallography

X-ray data were collected at 293 (2) K on a Bruker SMART 1000 CCD diffractometer using Mo Kα radiation ($\lambda = 0.71073$ Å). The crystals were mounted in a glass capillary with a drop of mother liquor in order to

Table 1
Summary of data collection and crystal parameters for complexes **1** and **2**

	1		**2**
Formula	$C_{42}H_{76}Co_{1.5}N_3O_{34}S_8$	$C_{42}H_{78}N_3Ni_{1.5}O_{35}S_8$	$C_{72}H_{122}Cu_3N_4O_{62}S_{16}$
M_r (g/mol)	1511.94	1529.62	2739.32
Crystal system	triclinic	triclinic	triclinic
Space group	$P\bar{1}$	$P\bar{1}$	$P\bar{1}$
a (Å)	14.358(5)	14.224(5)	14.664(3)
b (Å)	16.151(6)	16.049(6)	15.211(3)
c (Å)	16.770(6)	16.657(5)	16.848(3)
α (°)	112.012(7)	111.756(5)	111.057(8)
β (°)	93.288(7)	93.261(6)	110.260(9)
γ (°)	111.422(7)	111.329(6)	100.571(9)
V (Å^3)	3270(2)	3208(2)	3080(1)
Z	2	2	1
ρ_{calc} (g/cm^3)	1.533	1.584	1.477
μ (mm^{-1})	0.732	0.800	0.878
θ range (°)	2.30–25.03	1.96–26.39	1.55–25.00
Reflections collected	13 301	15 081	15 422
Unique reflections	11 245	11 875	10 620
R_{int}	0.0579	0.0208	0.0766
Observed reflections	5831	8151	4708
Final R indices	$R_1 = 0.0842$	$R_1 = 0.0543$	$R_1 = 0.0758$
$[I > 2\sigma(I)]$	$\omega R_2 = 0.1595$	$\omega R_2 = 0.1299$	$\omega R_2 = 0.1466$

prevent deterioration of the crystal owing to solvent loss. The structures were solved by direct methods and refined by full-matrix least-square techniques on F^2 using the SHELXL 97 program. All non-hydrogen atoms were refined anisotropically. The hydrogen atoms on the crown ether and the thiacalixarene were placed at their calculated positions and assigned with isotropic displacement parameters. The hydrogen atoms of the water molecules could not be located. A number of lattice water molecules were disordered and given partial occupancies. Experimental details for X-ray data collection of the complexes are presented in Table 1.

3. Results and discussion

The complexes were prepared by mixing the corresponding transition metal ion (II) nitrates, 4,13-diaza-18-crown-6 and tetrasodium *p*-sulfonatothiacalix[4]arene in an aqueous solution, with the pH adjusted to 2 (see Scheme 1).

The structure of complex **1**, as shown in Fig. 1, consists of several structural components: the superanion capsule {(4,13-diprotodiaza-18-crown-6) ⊂ $[M(H_2O)_3{}^{2+}$ (*p*-sulfonatothiacalix[4]arene)$^{4-}]_2$}, one hexa-aqua metal ion(II) and two types of exo-capsule diaza-crown ethers.

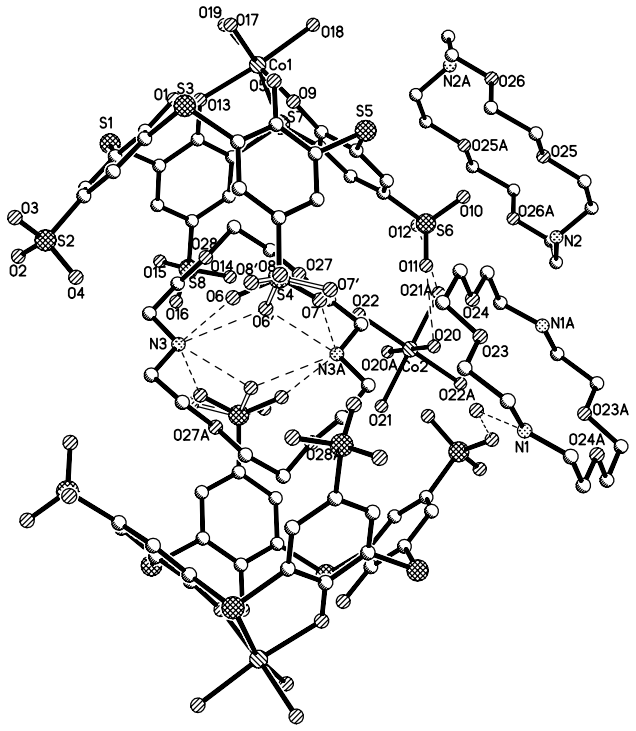

Fig. 1. An 'ionic capsule' in complex **1**, M = Co^{2+}, dashed lines indicate hydrogen bonds (hydrogen atoms and crystal water molecules have been omitted for clarity).

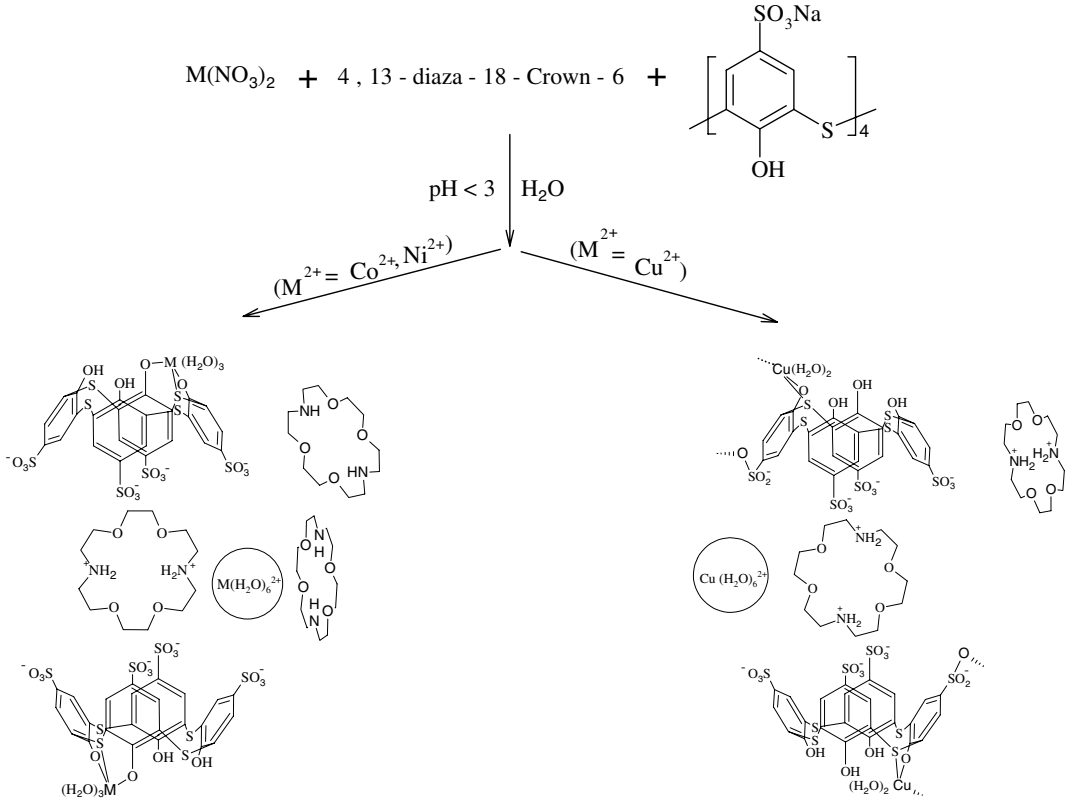

Scheme 1.

There are also several lattice water molecules and some of them are disordered and given partial occupancies.

A di-protonated diaza-crown ether is sandwiched by two thiacalixarenes in an 'up–down' fashion to create a capsule. Two phenolic groups of each thiacalixarene are deprotonated and coordinate to a M^{2+} at the base of the thiacalixarene. A bridging sulfur atom of this thiacalixarene and three aqua ligands also coordinate to M^{2+}, which is ligated in a distorted octahedral manner with average M–O (phenolic) bond distances of 2.019 Å (Ni^{2+}), 2.040 Å (Co^{2+}), M–OH_2 of 2.078 Å (Ni^{2+}), 2.139 Å (Co^{2+}) and M–S of 2.427 Å (Ni^{2+}), 2.502 Å (Co^{2+}). Two of the four sulfonato groups of each thiacalixarene are necessarily protonated to achieve overall charge balance. These protons were not found crystallographically and the hydrogen bonding network is implied through the numerous close N···O contacts. Some sulfonato groups are disordered (three for the Ni^{2+} complex and one for the Co^{2+} complex). The di-protonated nitrogen atoms of the crown ether are hydrogen-bonded to the sulfonato groups of the two thiacalixarenes in the 'ionic capsule' with N···O distances from 2.821 to 3.021 Å. There are also hydrogen bonds from the lattice water molecules to the sulfonato groups of these two thiacalixarenes with O···O distances from 2.741 to 2.986 Å. In addition to the H-bonding interactions, the crown ether cation interacts with the two thiacalixarenes through a non-classical H-bond (C–H···aromatic ring; a methylene hydrogen atom points to the centre of one of the aromatic rings of each thiacalixarene, with a C···ring centroid distance 3.621 Å (for the Ni^{2+} complex) or 3.596 Å (for the Co^{2+} complex)). The capsule is an example of a slipped capsule, with the two bowl thiacalixarene cavities offset relative to each other. Similar capsules have been observed in [{cyclamH_4^{4+}} ⊂ {(*p*-O_3S- calix[4]arene)$_2$}]$^{4-}$ [12]. Complementarity of curvature of the crown ether with that of the thiacalixarene is achieved by the splaying of two opposite phenol rings. The dihedral angles between the two aromatic rings and the plane of the four phenolic oxygens are 140° and 135.8°. The dihedral angles between other two aromatic rings and the plane of the four phenolic oxygens are 103.9° and 122.2°. The conformation of the thiacalixarene is less symmetrical than that of the 'classical' calixarene in the ionic capsules[11]. This may be due to the coordination of two phenolic groups to one M^{2+} ion.

In addition to the M^{2+} ion coordinated by the thiacalixarene, there is another type of M^{2+} ion, which is not coordinated by the thiacalixarene but exists simply as a hexa-aqua cation [M $(H_2O)_6^{2+}$] in the hydrophilic layer and forms part of the second coordination sphere through hydrogen bonding of the aqua ligands to the sulfonato groups of two thiacalixarenes which belong to different capsules.

There are two types of non-protonated crown ethers, which are not involved in the capsules. One crown ether molecule is located at the hydrophilic equator of the superanion through lattice water molecules bridging the nitrogen atoms and sulfonato groups, with N···OH_2 and H_2O···OS distances ranging from 2.754 to 2.790 Å. The other crown ether is intercalated into the hydrophobic layer. The nitrogen atoms of the crown ether are weakly hydrogen-bonded to the sulfonato groups of two adjacent 'up' and 'down' thiacalixarenes, with N···OS distances from 3.069 to 3.155 Å. The crown ether is seen to traverse the hydrophobic layer with one NH group directed towards the sulfonato groups of the 'up' thiacalixarene and the other NH group directed towards the sulfonato groups of the 'down' one.

A particular bi-layer structure forms in the present structure because exo-capsule crown ethers are interspersed between columns of 'up'/'down' thiacalixarenes (see Fig. 2). An 'up' thiacalixarene is surrounded by three 'down' thiacalixarenes. The 'up' thiacalixarene interacts with only one of these 'down' thiacalixarenes through aromatic ring π-stacking (the distances between two adjacent parallel aromatic ring planes are 3.525 Å (for the Co^{2+} complex) and 3.573 Å (for the Ni^{2+} complex)), but is staggered to the other two 'down' thiacalixarenes and linked to them through H-bonds between sulfonato groups and the ligated water molecules of the M^{2+} ions, or H-bonds between sulfonato groups and lattice water molecules. It also links an exo-capsule crown ether which traverses the hydrophobic layer.

The structure of complex **2** (Fig. 3) consists of several structural components: the superanion capsule, the coordination dimer $[Cu(H_2O)_2^{2+}$(*p*-sulfonatothiacalix[4]arene – $H^+)^{5-}]_2$, one hexa-aqua copper ion(II) and one exo-capsule diprotonated diaza-crown ether. There are also several lattice water molecules and some of them are disordered and given partial occupancies.

Each copper ion (Cu2 and Cu2A) in the dimer is coordinated by four oxygen and one sulfur donor forming a distorted square pyramid: two coordinated water molecules occur at an average Cu–O bond distance of 1.983 Å, a sulfonato group of one thiacalixarene at a distance of Cu–OSO_2 2.297 Å as well as a deprotonated phenolic group and a bridging sulfur atom of an adjacent thiacalixarene *cis* to the sulfonato group at a Cu–O distance of 1.937 Å and at a Cu–S distance of 2.451 Å.

This is another example of slipped ionic capsules in which a di-protonated diaza-18-crown-6 is at the core. The supramolecular assembly is primarily stabilized by van der Waals forces associated with complementary curvature. The dihedral angles between the two splaying aromatic rings and the plane of the four phenolic oxygens are 147° and 122.7°. The dihedral angles between the other two aromatic rings and the plane of the four phenolic oxygens are 107.1° and 116.8°. The nitrogen atoms of the crown ether in the cavity are surrounded by

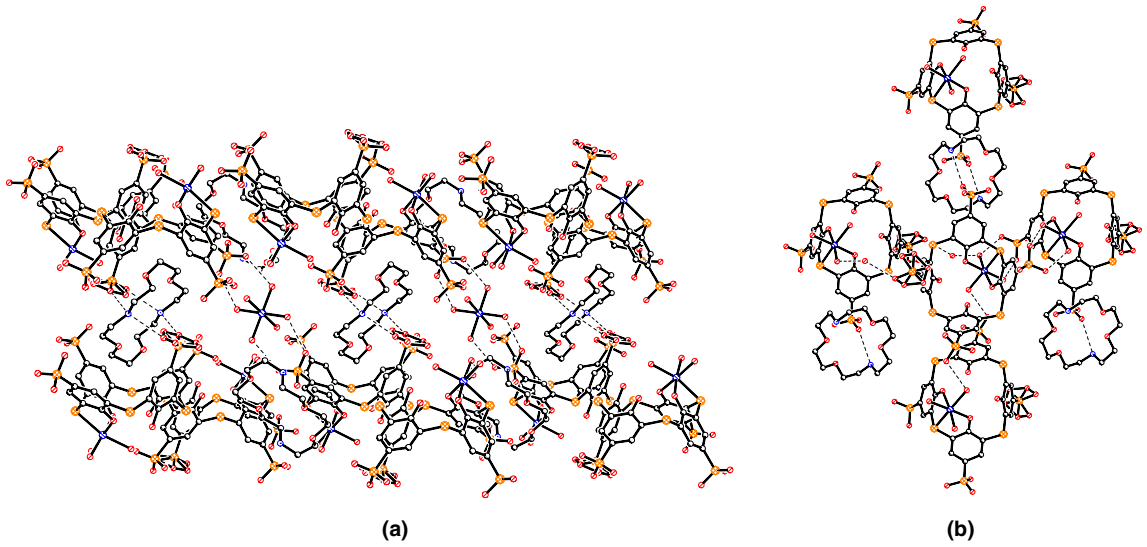

Fig. 2. Projection of the structure of complex **1**, M = Co^{2+}: (a) showing the bi-layer arrangement in which the crown ether molecules span the hydrophobic layer (the exo-capsules crown ethers in the hydrophilic layer have been omitted for clarity) and (b) the interactions of the adjacent thiacalixarenes and the crown ether in the hydrophobic layer.

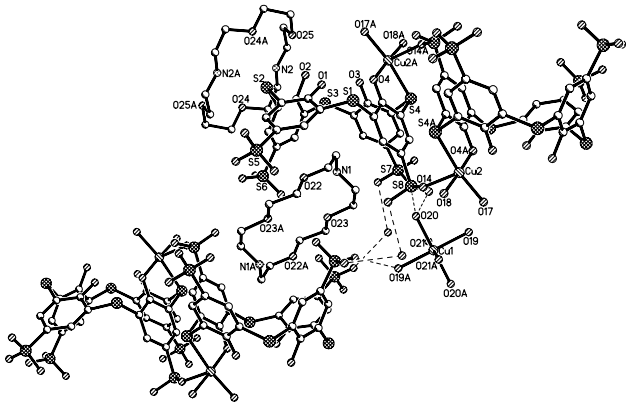

Fig. 3. The 'ionic capsule' in complex **2**, showing the coordination spheres of coordination dimer and the interactions around the 'ionic capsule'; dashed lines indicate hydrogen bonds (hydrogen atoms and crystal water molecules have been omitted for clarity).

the sulfonato groups of the two thiacalixarenes. This presumably maximizes the electrostatic interaction between the sulfonato and the NH_2^+ groups. There are also hydrogen bonds from the lattice water molecules to the sulfonato groups of these two thiacalixarenes with O···O distances from 2.877 to 3.030 Å.

There is also a $[M(H_2O)_6^{2+}]$ moiety in the hydrophilic layer. The hexa-aqua copper(II) ion takes the shape of a flattened octahedron. In addition, there are extensive hydrogen bonds from two aqua ligands to the sulfonato groups of the two thiacalixarenes that form the shell of the 'ionic capsule' with MO···OS distances ranging from 2.826 to 2.923 Å. Other aqua ligands are also hydrogen-bonded to the sulfonato groups of thiacalixarenes from neighbouring capsule with similar MO···OS distances.

A particular bi-layer structure similar to that in complex **1** also forms, in which the exo-capsule diprotonated

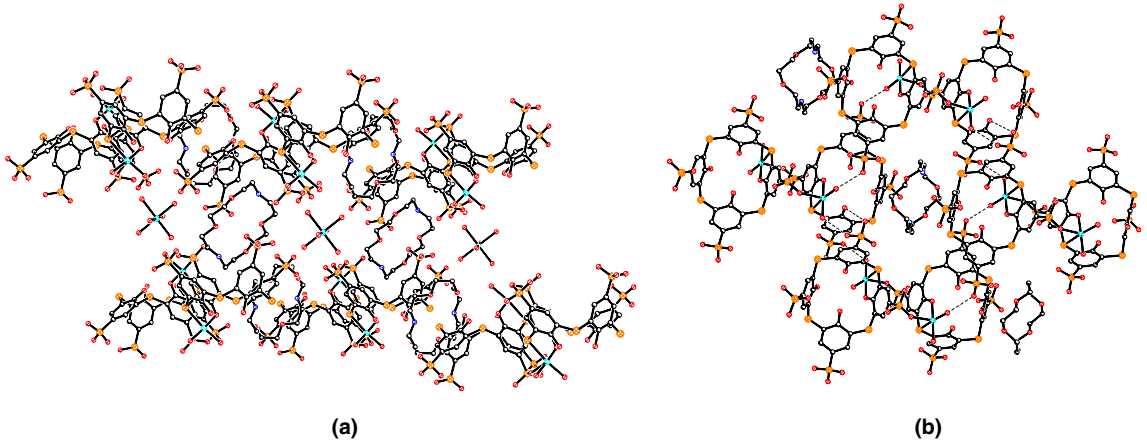

Fig. 4. Projection of the structure of complex **2**: (a) showing the bi-layer arrangement in which the crown ether cations span the hydrophobic layer and (b) the interactions of the adjacent thiacalixarenes and the crown ether in the hydrophobic layer.

diaza-crown ethers intersperse into hydrophobic layers (see Fig. 4). An 'up' thiacalixarene is also surrounded by three 'down' thiacalixarenes, but the interactions with adjacent thiacalixarenes are different from those of complex **1**. In this structure, the adjacent thiacalixarenes are interconnected through π-stacking (the distances between two adjacent parallel aromatic ring planes are in the range 3.380–3.561 Å). H-bonds between sulfonato groups and the aqua ligands of the M^{2+} ions coordinated by the adjacent thiacalixarene (with MO···OS distances ranging from 2.779 to 2.854 Å) and H-bonds between sulfonato groups and the phenolic groups of the adjacent thiacalixarene (with a HO···OS distance of 2.930 Å) should also exist. This 'up' thiacalixarene also links an exo-capsule crown ether cation not through H-bonds but through shape complementarity. The crown ether spans the hydrophobic layer with NH_2^+ groups located in the middle section.

4. Conclusion

In complexes **1** and **2**, 4,13-diaza-18-crown-6 is shrouded by two thiacalixarenes in the presence of transition metal ions and forms an ionic capsule. The thiacalixarene coordinates to the transition metal ion through phenolic hydroxyl groups and a bridging sulfur atom at the base. This may be attributed to the fact that the bridging sulfur atom tends to bind the transition metal ions. Due to the Jahn–Teller effect, the copper(II) ion has a flexible coordination manner. So in complex **2**, the copper ion can be coordinated by the sulfonato group of the adjacent thiacalixarene forming a coordination dimer. In addition to forming 'ionic capsules', the diaza-crown ethers can also insert into the hydrophobic layers and the hydrophilic layers via a variety of supramolecular interactions (hydrogen bonding, shape complementarity).

5. Supplementary data

CCDC-218691 (Co complex), CCDC-218692 (Ni complex) and CCDC-218693 (complex **2**) contains the supplementary crystallographic data for this paper. These data can be obtained free of charge at www.ccdc.cam.ac.uk/conts/retrieving.html or from the Cambridge Crystallographic Data Centre, 12, Union Road, Cambridge, CB2 1EZ, UK [fax: (internat.) +44-1223/336-033; e-mail: deposit@ccdc.cam.ac.uk].

Acknowledgements

We are grateful to the Municipal Natural Science Foundation of Beijing (No. 2022011).

References

[1] J. Kang, J. Santamaria, G. Hilmersson, J. Rebek, J. Am. Chem. Soc. 120 (1998) 7389.
[2] K.N. Rose, L.J. Barbour, G.W. Orr, J.L. Atwood, Chem. Commun. (1998) 407.
[3] O. Mogek, M. Pons, V. Bohmer, W. Vogt, J. Am. Chem. Soc. 119 (1997) 5706.
[4] K. Nakamura, C. Sheu, A.E. Keating, K.N. Houk, J.C. Sherman, R.G. Chapman, W.L. Jorgensen, J. Am. Chem. Soc. 119 (1997) 4321.
[5] K. Murayama, K. Aoki, Chem. Commun. (1998) 607.
[6] F. Ibukuro, T. Kusukawa, M. Fujita, J. Am. Chem. Soc. 120 (1998) 8561.
[7] T.N. Parac, D.L. Caulder, K.N. Raymond, J. Am. Chem. Soc. 120 (1998) 8003.
[8] T. Douglas, M. Young, Nature 393 (1998) 152.
[9] M.J. Hardie, C.L. Raston, J. Chem. Soc., Dalton Trans. (2000) 2483.
[10] H.R. Webb, M.J. Hardie, C.L. Raston, Chem. Eur. J. 7 (2001) 3616.
[11] S.J. Dalgarno, C.L. Raston, J. Chem. Soc., Dalton Trans. (2003) 287.
[12] S. Airey, A. Drljaca, M.J. Hardie, C.L. Raston, Chem. Commun. (1999) 1137.
[13] S.J. Dalgarno, C.L. Raston, Chem. Commun. (2002) 2216.
[14] M.J. Hardie, M. Makha, C.L. Raston, Chem. Commun. (1999) 2409.
[15] H. Kumagai, M. Hasegawa, S. Miyanari, Y. Sugawa, Y. Sato, T. Hori, S. Ueda, H. Kamiyama, S. Miyano, Tetrahedron Lett. 38 (1997) 3971.
[16] N. Iki, T. Fujimoto, S. Miyano, Chem. Lett. (1998) 625.
[17] D. Yuan, W.-X. Zhu, S. Ma, X. Yan, J. Mol. Struct. 616 (2002) 241.
[18] S. Kulstad, L.A. Malmaston, Acta Chem. Scand. B33 (1979) 469.

Available online at www.sciencedirect.com
SCIENCE DIRECT®
Polyhedron 23 (2004) 1467–1472
POLYHEDRON
www.elsevier.com/locate/poly

Synthesis, characterisation and thermal decomposition study of cerium(IV) 2-(2′-hydroxyphenyl)-2-oxazoline derivatives

Hervé Guillon [a], Stéphane Daniele [a], Liliane G. Hubert-Pfalzgraf [a,*], J.M. Letoffe [b]

[a] Université Claude Bernard Lyon I, IRC, 2 avenue A. Einstein, 69626 Villeurbanne Cedex, France
[b] Université Claude Bernard Lyon I, LMI-UMR 5615, 43 boulevard du 11 Novembre 1918, 69622 Villeurbanne Cedex, France

Received 2 February 2004; accepted 4 March 2004
Available online 13 April 2004

Abstract

Cerium(IV) oxazoline derivatives $Ce(Me_2oxaz)_4$ (**1**) [Me_2oxazH = 2-(2′-hydroxyphenyl)-4-dimethyl)oxazoline] and $Ce(Pr^iHoxaz)_4$ (**2**) [$Pr^iHoxazH$ = 2-(2′-hydroxyphenyl)-4-isopropyl)oxazoline] were prepared in high yields by ligand exchange reactions between $Ce_2(OPr^i)_8(Pr^iOH)_2$ and the corresponding 2-(2′-hydroxyphenyl)-2-oxazolines. Characterisation was achieved by elemental analysis, FT-IR, ^1H NMR and mass spectroscopy (MS). **2** was also characterized by polarimetric measurement. Their thermal decomposition pathways under nitrogen were studied by TGA and coupled TGA-CG/MS experiments.
© 2004 Elsevier Ltd. All rights reserved.

Keywords: Cerium; Oxazolines; Chiral; Thermal decomposition; MOCVD; β-ketoesterates

1. Introduction

Cerium dioxide films find use in numerous applications such as corrosion protection coating alternative to chromate films, electrode in solid oxide fuel cell (SOFC), photocatalysts and buffer layers for superconducting electronics [1,2]. Indeed, ceria displays a relative lattice misfit to $YBa_2Cu_3O_{7-x}$ of only 0.6% and ceria or ceria doped with Gd_2O_3 has thus been, with YSZ (yttrium stabilized zirconia) films, one of the most investigated buffer layers for high T_c superconductors [3]. Films of CeO_2 have been deposited by physical or chemical techniques such as sputtering, sol–gel methods [4], metal–organic deposition (MOD) [3] or metal–organic chemical vapour deposition (MOCVD) [5,6]. MOCVD offers a number of advantages including easy scale-up, conformational deposition on a variety of complex substrates, access to multilayer architectures, rapid growth rates, epitaxial layers. If deposition can be achieved in the absence of an oxygen atmosphere, deposition on substrates sensitive to oxidation such as silicon becomes possible. MOCVD relies on the availability of appropriate volatile precursors [7,8]. Easy to handle, fluorine free precursors allowing deposition of CeO_2 at low temperature are desirable. Fluorinated and non-fluorinated-diketonates have been the most investigated [9–12] although fluorinated alkoxide complexes [13] or β-ketoiminates [14,15] have also been used as CVD sources and volatile Ce(IV) β-ketoesterates have been developed [16].

The use of oxazoline type ligands as chirality-transfer auxiliaries has been largely developed in the recent years for a broad range of catalytic reactions based on a variety of metals [17–19]. The oxazoline fragment is easily accessible by reaction between commercially available starting materials namely aminoalcohols and nitriles and the nature of the substituents can thus be modified for a fine tuning of the properties. Such chelating N,O ligands were attractive to us for MOCVD applications. 2-(2′-hydroxyphenyl)-2-oxazoline related ligands for instance should favor monomeric structures due to the rigidity of the ligand (the two cycles are in a same plane), a favorable feature for volatility and for kinetically inert complexes. Hydrolytic stability is also of interest either for conventional MOCVD or for MOCVD by liquid

* Corresponding author. Tel.: +33-4-72-43-15-70; fax: +33-4-72-43-15-68.
E-mail address: Hubert@univ-lyon1.fr (L.G. Hubert-Pfalzgraf).

0277-5387/$ - see front matter © 2004 Elsevier Ltd. All rights reserved.
doi:10.1016/j.poly.2004.03.006

injection (PI-MOCVD) where precursors might be mixed in an unique reactor for access to multimetallic materials.

We wish to report herein the synthesis, the characterisation of cerium(IV) hydroxyphenyl oxazoline derivatives and how a small modifications of the ligand can generate different thermal behaviours.

2. Experimental

All reactions were achieved under inert atmosphere using Schlenk tube techniques. Solvents were dried and purified by distillation by standard methods. $Ce_2(OPr^i)_8(Pr^iOH)_2$ [20], Me_2oxazH and (S)-Pr^iHoxazH were obtained according to the literature.[21,22] ^{1}H NMR and FT-IR spectra were run on Bruker AC-200 and IR-FTS 45 spectrometers, respectively. IR spectra were obtained as Nujol mulls. Polarimetric measurements were carried out on a Ameria AA-10 apparatus (26 °C, 589 nm). Analyses were obtained from the Centre de Microanalyses du CNRS. Mass spectrometry (Electronic Impact) experiments were achieved on a Thermofinnigan MAT95XL spectrometer. TGA and TGA-CG/MS analyses were carried out on a Mettler-Toledo TGA 851^e thermobalance coupled with an GC(6890)/MS(5973) Agilent Technologies system using a temperature ramp of 10 °C/mn.

2.1. Synthesis of $Ce(Me_2oxaz)_4$ (1) and $Ce(Pr^iHoxaz)_4$ (2)

6.92 mmol of hydroxyphenyloxazoline in 5 ml of THF was added to a solution of 0.75 g of $Ce_2(OPr^i)_8(Pr^iOH)_2$ (0.86 mmol) in 30 ml of THF. The colour of the solution turned immediatly from yellow to dark red. Crystallisation yielded dark red crystals of $Ce(Me_2oxaz)_4$ (**1**) and $Ce(Pr^iHoxaz)_4$ (**2**) (1.40 g, 90% and 1.56 g, 95%, respectively). **1** and **2** were volatile (195–200 °C and 175–180 °C, respectively, under 4×10^{-4} Torr) and soluble in chloroform, toluene, THF and diglyme.

2 could also be obtained from $(NH_4)_2Ce(NO_3)_6$; 2.73 mmol of Pr^iHoxazH and Et_2NH in 5 ml of THF were added to 0.37g of $(NH_4)_2Ce(NO_3)_6$ (0.68 mmol) in 10 ml of THF. The colour of the solution changed from yellow to dark red. The solvent was evaporated after 19 h and the solid obtained was dissolved in toluene. After filtration, crystallisation yielded **2** (0.58 g, 90%).

1: *Anal*. found: C, 58.12; H, 5.37, calc. for $C_{44}H_{48}O_8N_4Ce$: C, 58.64; H, 5.32%. FT-IR (cm^{-1}): 1643w, 1617s, 1589w, 1558m, 1475s, 1440m (νC = N, νC=C); 1362m, 1330m, 1310s, 1262s, 1250m; 1211w, 1156m, 1129w, 1060s, 1035m, 1001w (νC–O); 968w, 934w, 877m, 847m, 822w, 768w, 754s, 692m, 664m; 623w, 595m, 541w, 547w, 422w (νM–O, νM–N). ^{1}H NMR (C_6D_6): 8.10 (d, $J = 7.0$ Hz, 2H, Ph); 7.71 (d, $J = 7.4$ Hz, 2H, Ph); 7.15 (m, 4H, Ph); 6.50 (m, 4H, Ph); 6.34 (m, 4H, Ph); 3.67 (s, 8H,CH_2); 1.61 (s, 12H, Me); 1.41 (s, 6H, Me); 1.10(s, 6H, Me). TGA (N_2, 1 atm) 200–320 °C (−19%); 320– 450 °C (−40%); 450–600 °C (−5%). MS (m/z^+, %): 710 (5) [$Ce(Me_2oxaz)_3$]; 638 (11) [$Ce(Me_2oxaz)_2(OC_6H_4CN)$]; 566 (8) [$Ce(Me_2oxaz)(OC_6H_4CN)_2$]; 519 (2) [$CeH(Me_2oxaz)_2$]; 494 (16) [$Ce(OC_6H_4CN)_3$]; 448 (11) [$HCe(Me_2oxaz)(OC_6H_4CN)$]; 376 (100) [$HCe(OC_6H_4CN)_2$]; 284 (6); 274 (5); 247 (11); 191 (7) [Me_2oxaz]; 188 (11); 156 (6); 119 (17) [HOC_6H_4CN]; 91 (10) [HOC_6H_5].

2: *Anal*. found: C, 60.06; H, 5.95, calc. for $C_{48}H_{56}O_8N_4Ce$: C, 60.22; H, 5.85%. FT-IR (cm^{-1}): 1614s, 1586w, 1551w, 1496w, 1477m, 1440s (νC=N, νC=C); 1369m, 1336w, 1325s, 1304w, 1266m,; 1232m, 1208w, 1175w, 1153w, 1137w, 1126w, 1115w, 1061m, 1049w, 1031w (νC–O); 986w, 958w, 951w, 872w, 854s, 804w, 777w, 754s, 690m, 664m; 593s, 543m, 524w, 501w, 465w (νM–O, νM–N). ^{1}H NMR ($CDCl_3$): 7.61 (dd, $J = 1.7$ Hz; 7.8 Hz, 4H, Ph); 7.40 (m, 4H, Ph); 6.58 (m, 8H, Ph); 4.73 (d, $J = 8.1$ Hz, 4H, CH_2); 4.01 (dd, $J = 2.8$ Hz; 8.1 Hz, 4H, CH_2); 2.97 (m, 4H, NCH); 2.37 [m, 4H, $CH(Pr^i)$]; 0.79 (d, $J = 7.0$ Hz, 12H, Me); 0.40 (d, $J = 6.9$ Hz, 12H, Me). $[\alpha]_{589}^{26} = 1150$ ($C = 2 \times 10^{-2}$ moll^{-1}, $CHCl_3$). TGA (N_2, 1 atm): 100–200 °C (−8%); 200–380 °C (−68%); 380–450 °C (−4%). MS (m/z^+, %) : 752 (100) [$Ce(Pr^iHoxaz)_3$]; 666 (33) [$Ce(Pr^iHoxaz)_2(OC_6H_4CN)$]; 580 (3) [$CeH(Pr^iHoxaz)(OC_6H_4CN)_2$]; 548 (87) [$Ce(Pr^iHoxaz)_2$]; 462 (61) [$HCe(Pr^iHoxaz)(OC_6H_4CN)$]; 418 (39) [$HCe(Pr^iHoxaz)(OCHNCHCH_2)$]; 376 (100) [$HCe(OC_6H_4CN)_2$]; 284 (8); 274 (13); 204 (34) [Pr^iHoxaz]; 162 (64); 134 (42) [2-methylbenzofuran]; 120 (18) [HOC_6H_4CN]; 107 (35) [HOC_6H_4Me]; 91 (18) [HOC_6H_5].

3. Results and discussion

3.1. Syntheses and characterisation

Two 2-(2′-hydroxyphenyl)-2-oxazoline ligands were selected in view of their easy synthesis and purification as well as simplicity of their NMR pattern. These were based on R_1 and R_2 substituents with $R_1 = R_2 = Me$ and $R_1 = H$, $R_2 = {}^i$Pr and abbreviated as Me_2oxazH and Pr^iHoxazH respectively. Methylpivaloylacetate (mpaH) [16] was also used as a ligand for Ce(IV) in similar conditions [17–19] and the data compared with those obtained with the hydroxyphenyl oxazolines.

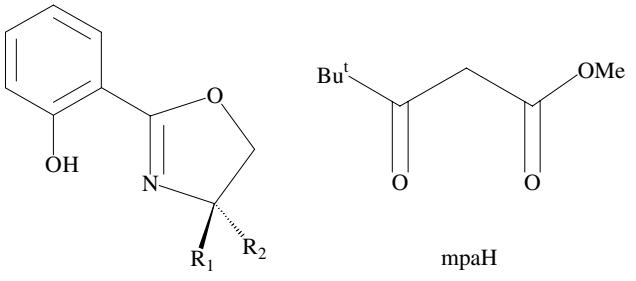

The reactions between $Ce_2(OPr^i)_8(Pr^iOH)_2$ and Me_2oxazH or Pr^iHoxazH in THF (1:8 stoichiometry) at r.t. afforded dark red microcrystals of $Ce(Me_2oxaz)_4$ (**1**) and $Ce(Pr^iHoxaz)_4$ (**2**) which were isolated with yields higher that 90%. These compounds are air stable as solids and were characterized by elemental analyses, FT-IR, NMR and MS. Their diamagnetic character confirms oxidation state IV for cerium and thus that the four 2-(2′-hydroxyphenyl)-2-oxazoline acts as anionic ligands. FT-IR spectra show the absence of υOH and δOH absorption bands. These spectra display essentially the absorption bands due to the C=N stretching vibrations between 1643 and 1550 cm^{-1} and those of the C–O bonds around 1230–1000 cm^{-1}. Absorption bands between 600 and 400 cm^{-1} account for the Ce–O and Ce–N vibrations.

Despite numerous attempts, no single crystals suitable for X-ray studies could be grown for either **1** nor **2**. Structural information was thus gained by ^{1}H NMR. All ligands are magnetically equivalent for **2** but the diastereotopy of the methyl of the isopropyl groups is enhanced by complexation and they appear as two doublets at 0.79 and 0.40 ppm, respectively. The compound is chiral with an optical activity of $[\alpha]_{589}^{26}$ in chloroform (concentration 2×10^{-2} moll^{-1}). **1** and **2** are likely to be monomeric (as shown by MS) and cerium is thus octacoordinated (Fig. 1). Such a coordination number was observed for instance for $Ce(thd)_4$ [9–12] or $Ce(salphen)_2$ [salphen = *N*,*N*′-1,2-diphenylethylene-bis(salicyldeimine)] [23] whose structures were determined by X-ray diffraction. In contrast, the ^{1}H NMR spectrum of **1** at r.t. shows two types of magnetically non-equivalent ligands in a 1:1 ratio. The two types of ligands are differentiated by their methyl groups as well as by two hydrogens of the aromatic ring which are quite deshielded (8.10 ppm). These observations suggest that the coordination sphere of **1** is more distorted than that of **2** with two types of Ce–O and Ce–N bond distances. Molecular modelling (Hyperchem V) confirms this hypothesis since the steric interactions between the ligands are best released (lowest energy) with a structure in which the Ce–O distances have values of 2.27 and 2.29 Å. A first set of two ligands would form a square with the ligands in trans position in order to minimize steric hindrance [as observed for the solid state structure of $Cu(\eta^2\text{-}Me_2oxaz)_2$ [16,24] and could account for the resonances at 1.61 ppm (four equivalent Me groups) and at 8.1 ppm (two aromatic protons in ortho position). For the two other ligands, the methyl groups are non-equivalent (1.41 and 1.10 ppm) and the H in ortho position are less deshielded (7.71 ppm).

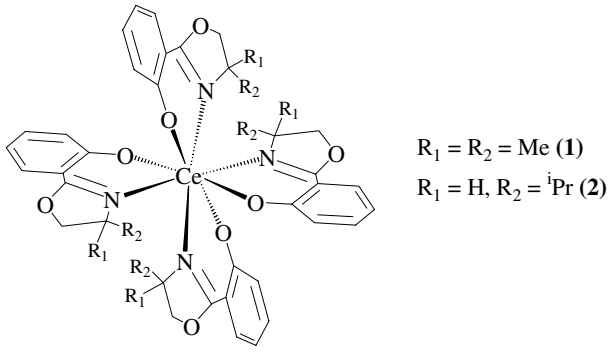

Fig. 1. Proposed structure of complexes **1** and **2**.

3.2. Physicochemical properties

Liquid injection MOCVD is a promising alternative to conventional MOCVD especially for metal oxide thin films whose sources are mostly solids, thus generating a number of problems such as modification of the surface properties, and thus of transport properties over time. Solubility, stability in solution, clean deposition are important requirements for control of the material properties [7,8]. Both novel cerium compounds as well as $Ce(mpa)_4$ are air stable as solids. However, the structural differences between **1** and **2** in solution as shown by ^{1}H NMR result in a difference in stability toward hydrolysis. By contrast to **2**, **1** is hydrolysed after two days in a solution open to air. This difference in hydrolytic susceptibility explains why **1**, by contrast with **2**, could not be prepared by starting from ammonium cerium(IV) nitrate. **1** and **2** are both volatile but less than $Ce(thd)_4$, $Ce(mpa)_4$ or the adducts of the fluoroisopropoxides such as $Ce(hfip)_4$(diglyme) (hfip = $OCH(CF_3)_2$ despite the fact that they have similar molecular weight (Table 1). The lower volatility of the oxazoline compounds is probably due to some intermolecular π interactions due to the phenyl substituent. Such effect has been pointed out to reduce the volatility of copper β-diketonates $Cu(bac)_2$ (bacH = 1-phenyl propane-1,3-dione) and $Cu(dbzm)_2$

Table 1
Solubilities and temperatures of sublimation of various Ce(IV) complexes

Complexes	MW (g/mol)	Solubility In diglyme (moll^{-1})	T_{sub} (°C/mbar)	Reference
$Ce(thd)_4$	873.24	1.5×10^{-2}	$135–140/1.3 \times 10^{-3}$	[6,16b]
$Ce(Me_2oxaz)_2$ (**1**)	901.16	2.0×10^{-2}	$195–200/4.0 \times 10^{-4}$	This work
$Ce(Pr^iHoxaz)_4$ (**2**)	957.28	1.6×10^{-2}	$175–180/4.0 \times 10^{-4}$	This work
$Ce(mpa)_4$	768.90	3.0×10^{-1}	$100–110/1.3 \times 10^{-4}$	[16b]
$Ce(hfip)_4$(diglyme)	837	1.5×10^{-2}	$70/10^{-4}$	[13b]

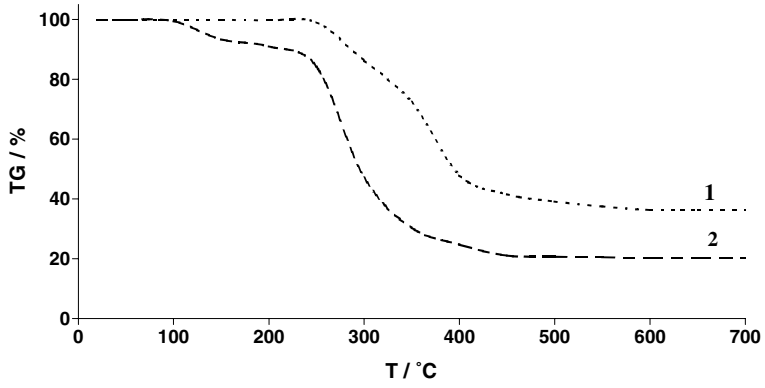

Fig. 2. TGA patterns of $Ce(Me_2oxaz)_4$ (**1**) and $Ce(Pr^iHoxaz)_4$ (**2**) (under 1 atm of dinitrogen).

(dbzmH = 1,3-diphenyl propane-1,3-dione) compared to $Cu(acac)_2$ [25,26].

MOCVD liquid delivery techniques are a way to overcome problems related to limited volatility and/or stability of solid precursors. However, since reasonable growth rates are required for applications, high solubility properties in a solvent appropriate for injection or aerosol assisted techniques are needed in order to minimize the influence of the volatiles issued from solvent decomposition. The solubility of **1** and of **2** was compared to that of $Ce(thd)_4$ which remains the precursor commonly used for access to CeO_2 by MOCVD techniques. They are slightly more soluble in diglyme than thd analogs but much less than $Ce(mpa)_4$ (Table 1). No complexation was observed in diglyme for **1** or **2** as indicated by UV–Vis spectroscopy. Hydrocarbons such as hexane or octane are better solvents than diglyme for the isopropoxide adducts and for $Ce(thd)_4$.

The thermal behaviour of **1** and **2** was investigated under dinitrogen (1 atm) by TGA up to 700 °C (Fig. 2). Although the general patterns are similar, they are drastically dependent on the R_1 and R_2 substituents since the Pr^i derivative **2** decomposes into ceria whereas decomposition remains partial for the Me derivative. **2** starts also to decompose 100 °C lower than **1**. Its first weight loss (100–200 °C) corresponds to a partial decomposition (−8%) of the oxazoline ligand and the second one (200–380 °C) to a weight loss of 68%. The last thermal event (−4%) between 380 and 450 °C leads to cerium oxide. In the case of $Ce(Me_2oxaz)_4$, only three hydroxyphenyloxazoline ligands are removed totally between 200–450 °C. Decomposition of the last one remains incomplete leading thus to a black residue (≃36%)

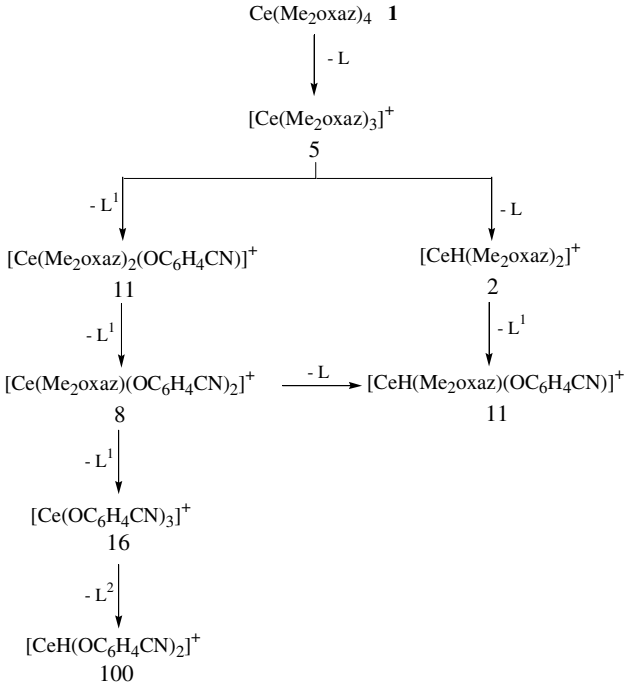

Scheme 1. Fragmentation pathway of **1** (with relative intensities) [L = Me_2oxaz, $L^1 = R_1R_2CHCHO$, $L^2 = OC_6H_4CN$].

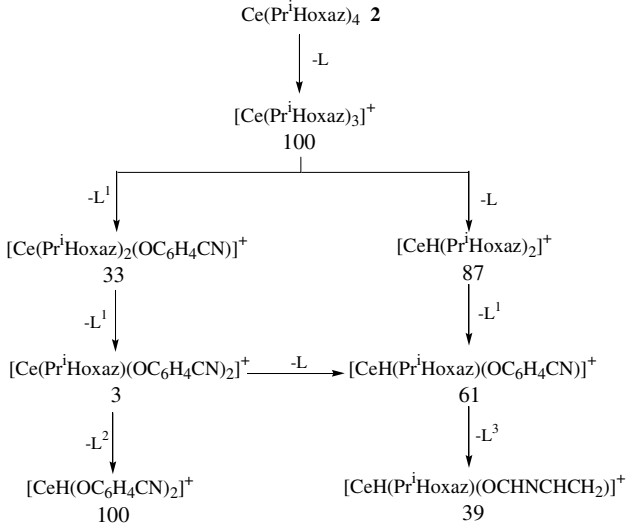

Scheme 2. Fragmentation pathway of **2** (with relative intensities) [L = Pr^iHoxaz, $L^1 = R_1R_2CHCHO$, $L^2 = OC_6H_4CN$, L^3 = 2-methylbenzofuran].

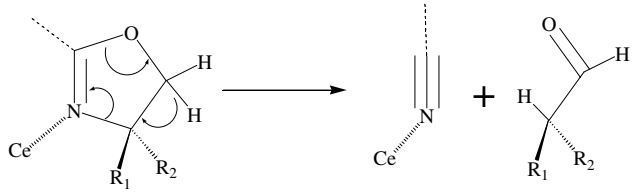

Scheme 3. Proposed degradation pathway of the oxazoline moiety of **1** and **2** mediated by cerium.

containing organics (as evidenced by FT-IR) and no CeO_2 is obtained up to 1000 °C under dinitrogen.

Mass spectrometry (IE) and coupled TGA-GC/MS experiments were carried out in order to get insight into the decomposition pathways of **1** and **2** (analyses of the volatiles by FT-IR or ^{1}H NMR was uninformative due to the presence of large amounts of oxazoline). Those are summarised in Schemes 1 and 2, respectively. For both compounds, the first fragment corresponds to $[CeL_3]^+$ (L = Me_2oxaz or Pr^iHoxaz) and the most intense one (m/z 376) corresponds to $[CeH(OC_6H_4CN)_2]^+$ (OC_6H_4CN = cyanophenoxo). These results indicate that steric hindrance favours the loss of one of the hydroxyphenyloxazoline ligand and that oxazoline moieties are easily degraded (Scheme 3). Indeed, fragments at m/z 638 and 666, for **1** and **2**, respectively, confirm the decomposition of the oxazoline ligands giving $[CeL_2(OC_6H_4CN)]^+$. The same process is repeated giving successively the $[CeHL_2]^+$ and $[CeHL(OC_6H_4CN)]^+$ fragments for both **1** and **2**. This was also confirmed by analysing the volatiles by TGA-GC/MS. Between 200 and 350 °C, 2-methyl 1-propene was detected for **1** whereas 2-methylpropanal and 2-methyl 2-propenal were obtained for **2**. At higher temperature, ≈400 °C, acetone and aromatics such as phenol and 2-methylbenzofuran were detected for **2** while only C4 and C5 alkenes and ketones could be found for **1**. Two main differences are observed in the mass spectra: (i) the very low intensity for all fragments derived from **1** except that at m/z 376 and (ii) the presence for **2** of the fragment m/z 418 resulting from the degradation of the phenoxo moiety. Loss of 2-methylbenzofuran explains the fragments at m/z 418 and 134 for **2**. The overall data suggest that the degradation of **1** is mainly directed by the decomposition of the oxazoline moiety giving a stable $[CeH(OC_6H_4CN)_2]^+$ species. By contrast, the phenoxo moiety can be significantly degraded for **2**. Hence, in order to get CeO_2, the last phenoxo group has to be removed but oxygen atoms are also needed. This can be afforded for **2** since the lower steric hindrance might permit the rotation around the phenoxo-oxazoline bond to link the oxygen of the oxazoline moiety with cerium. The opening of the oxazoline moiety leads to compound **A** stabilised by electronic delocalisation and subsequent cleavage reactions can give the expected organics (Scheme 4). Indeed decomposition of **1** under

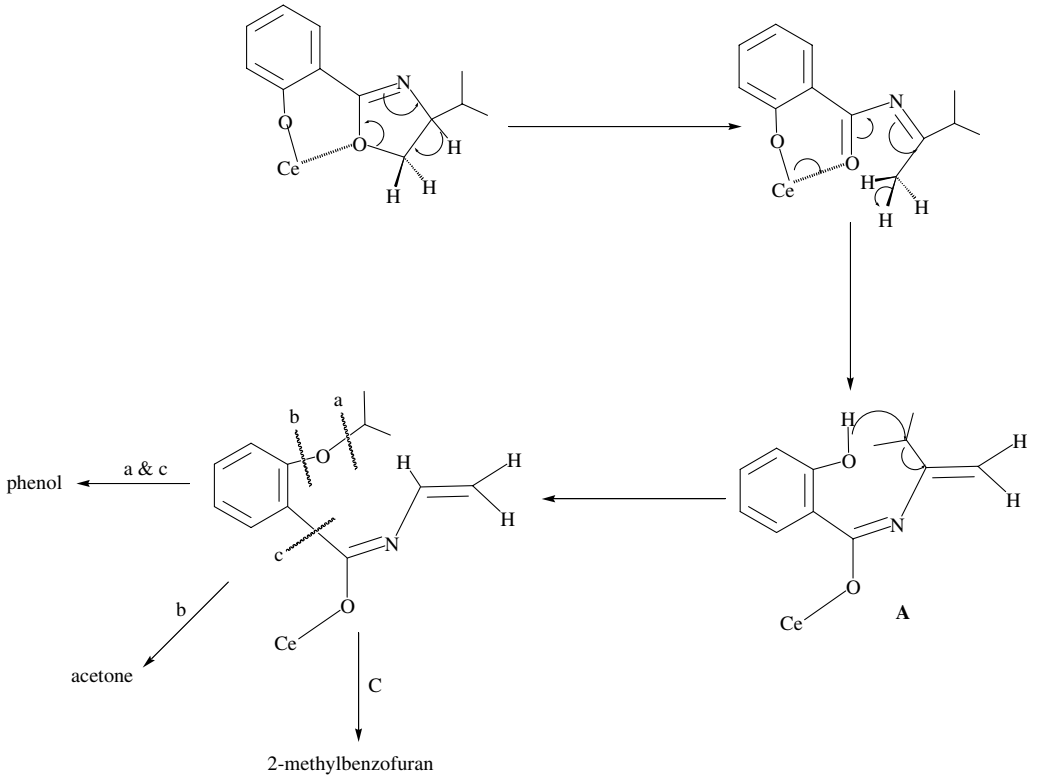

Scheme 4. Proposed degradation pathway of **2**.

air afforded CeO_2 at 450 °C, thus at a temperature similar to that observed for **2** or $Ce(mpa)_4$, which both can be converted into ceria in the absence of additional oxygen.

These results show how small modifications at the ligand can affect decomposition pathways. Ligands containing phenyl substituents favour monomers, improve stability toward moisture but might lead to high sublimation temperatures due to a higher MW as well as high decomposition temperatures especially under inert atmosphere. **2** can be a potential precursor for CeO_2 deposits on oxidation sensitive substrates, thus under inert atmosphere, whereas **1** is an unsuitable precursor in non-oxidative conditions.

Acknowledgements

Financial support by the EEC (BRE2-CT94-0742) is acknowledged. The authors are grateful to Mr R. Astier (Université Montpellier II) for the mass spectra.

References

[1] G. Blasse, Chem. Mater. 6 (1994) 1465.
[2] S. Guo, H. Arwin, S.N. Jacobson, K. Jarrendahl, V. Helmersson, J. Appl. Phys. 77 (1995) 1829.
[3] S. Morlens, I.A. Enesca, D. Charrier, L. Ortega, S. Phok, L.G. Hubert-Pfalzgraf, P. Odier, Eucas Proc. (2004) 0000.
[4] F. Cerwinski, J.A. Szpunar, J. Sol–Gel Sci. Technol. 9 (1997) 103.
[5] P. O'Brien, N.L. Pickett, D.J. Otway, Chem. Vap. Dep. 8 (2002) 273.
[6] K.D. Pollard, H.A. Jenkins, R.J. Puddephatt, Chem. Mater. 12 (2000) 701.
[7] L.G. Hubert-Pfalzgraf, Coord. Chem. Rev. 177–178 (1999) 967.
[8] Inorg. Chem. Commun. 6 (2003) 102.
[9] M. Becht, T. Gerfin, K.H. Dahmen, Chem. Mater. 5 (1993) 137.
[10] J. McAleese, J.A. Darr, B.C.H. Steele, Thin Solid Films 280 (1996) 152.
[11] I. Baxter, J.A. Darr, M.B. Hursthouse, K.M.A. Malik, J. Mc Aleese, D.M.P. Mingos, Polyhedron 12 (1998) 1329.
[12] G. Malandrino, R. La Nigro, C. Benelli, F. Castelli, I.L. Fragala, Chem. Vap. Dep. 6 (2000) 233.
[13] (a) S. Daniele, L.G. Hubert-Pfalzgraf, M. Perrin, Polyhedron 21 (2002) 1985;
(b) V. Abada, L.G. Hubert-Pfalzgraf, J. Vaissemann, Dalton (1998) 1437.
[14] N.L. Edleman, A. Wang, J.A. Belot, A.W. Metz, J.R. Babcock, A.M. Kawaoka, J. Ni, M.V. Metz, C.J. Flascherein, C.L. Stern, L.M. Liable-Sands, A.L. Rheingold, P.R. Markworth, R.P.H. Chang, M.P. Chudzik, C.R. Kannenwurf, T.J. Marks, Inorg. Chem. 41 (2002) 5005.
[15] Y.L. Tung, W.C. Tseng, C.Y. Lee, P.F. Hsu, Y. Chi, S.M. Peng, G.H. Lee, Organometallics 18 (1999) 864.
[16] (a) H. Guillon, S. Daniele, L.G. Hubert-Pfalzgraf, C. Bavoux, Inorg. Chim. Acta 304 (2000) 99;
(b) L. Hubert-Pfalzgraf, unpublished results; H. Guillon, Ph.D. Thesis, Université de Nice Sophia-Antipolis, 1998.
[17] M. Gomez, G. Muller, M. Rocamora, Coord. Chem. Rev. 193–195 (1999) 769.
[18] M. Gomez-Simon, S. Jansat, G. Muller, D. Panyella, M. Font-Badia, X. Solans, J. Chem. Soc., Dalton Trans. (1997) 3755.
[19] H.R. Hoveyda, V. Karunaratne, S.J. Rettig, C. Orvig, Inorg. Chem. 31 (1992) 5408.
[20] B.A. Vaarstra, J.C. Huffman, P.S. Gradeff, L.G. Hubert-Pfalzgraf, J.C. Daran, S. Parraud, K. Yunlu, K.G. Caulton, Inorg. Chem. 29 (1990) 3126.
[21] P.G. Cozzi, E. Gallo, C. Floriani, Organometallics 14 (1995) 4994.
[22] P.G. Cozzi, C. Floriani, A. Chiesi-Villa, C. Rizzoli, Inorg. Chem. 34 (1995) 2921.
[23] A. Terzis, D. Mentzafos, H.A. Tajmir-Riahi, Inorg. Chim. Acta 84 (1984) 187.
[24] G. Mugesh, H. Singh, R.J. Butcher, Eur. J. Inorg. Chem. (2001) 669.
[25] S.I. Trojanov, N.P. Kuzmina, I.E. Soboleva, N.V. Chugarov, in: Fourteenth International Conference on Chemical Vapor Deposition and EUROCVD-11/1997.
[26] M.D. Allendorf, C. Bernard, (Eds.), The Electrochemical Society Proceeding Series, PV 97-25, Pennington, NJ, 1997, p. 886.

Available online at www.sciencedirect.com
SCIENCE DIRECT®
Polyhedron 23 (2004) 1473–1478
POLYHEDRON
www.elsevier.com/locate/poly

Synthesis, structural characterization and catalysis of ethyl-substituted indenylnickel(II) halides

Wan-Fei Li [a,b], Hong-Mei Sun [a,b], Qi Shen [a,b,*], Yong Zhang [a], Kai-Bei Yu [c]

[a] College of Chemistry and Chemical Engineering, Suzhou University, Suzhou 215006, PR China
[b] The Key Laboratory of Organic Synthesis of Jiangsu Province, Suzhou University, Suzhou 215006, PR China
[c] Chengdu Institute of Organic Chemistry, Chinese Academy of Sciences, Chengdu 610043, PR China

Received 11 February 2004; accepted 5 March 2004
Available online 9 April 2004

Abstract

The reaction of (1-Et-Ind)Li (1-Et-Ind = 1-ethylindenyl) with 1.81 equivalent of $Ni(PPh_3)_2Cl_2$ in ether, followed by crystallization from CH_2Cl_2/hexane, affords (1-Et-Ind)$Ni(PPh_3)Cl$ (**1**) in 58% yield. Similar reaction of (1-Et-Ind)Li with 1.81 equivalent of $Ni(PPh_3)_2Br_2$ in 1,2-dimethoxyethane (DME) affords (1-Et-Ind)$Ni(PPh_3)Br$ (**2**) in 60% yield. The reaction of complex **1** with KI in THF/acetone affords (1-Et-Ind)$Ni(PPh_3)I$ (**3**) quantitatively. Crystal structure analysis revealed that **2** and **3** are isomorphous. The hapticities of the indenyl ligand in these complexes are very similar and significantly distorted from an idealized η^5 mode to an unsymmetrical η^3 mode. The complexes are inert toward the insertion of styrene, but are able to catalyze the polymerization of styrene effectively in the presence of PPh_3 and $NaBPh_4$.
© 2004 Elsevier Ltd. All rights reserved.

Keywords: Synthesis; Crystal structures; Indenyl ligand; Nickel complex; Catalysis

1. Introduction

In recent years, the use of Ind (Ind = indenyl anion and its substituted derivatives) as supporting ligand systems in transition metal coordination chemistry has attracted considerable attention [1–5]. In comparison to their Cp analogues (Cp = cyclopentadienyl anion and its substituted derivatives), many transition metal Ind complexes possess greater reactivity owing to the so-called "indenyl effect". The Ind ligands can be tuned spontaneously to coordinated to the center metal from η^1 to η^5 via relatively facile "ring slippage", thus leading to better stabilization of transition states or reaction intermediates. However, their application in regard to group 10 metal complexes remains relatively poorly explored [6–9]. Recently, Zargarian reported that (Ind)$(PR_3)Ni$–X (Ind = indenyl anion and its substituted derivatives; R = Ph, Me, Cy, Bu; X = halide, alkyl, alkynyl, imidate, thiolate) [10] could act as effective pre-catalysts in a number of reactions, such as the oligomerization or polymerization of ethylene [11–15], styrene [16] and phenylacetylene [17]. Preliminary studies have implied that the in situ generated cationic species $[Ind(PPh_3)Ni]^+$ might be the active centers for these reactions, which is in evidence by styrene reactions catalyzed by in situ generated cations from (η^3, η^0-Ind–$CH_2CH_2NMe_2$)$(PPh_3)Ni$–Cl [16]. However, detailed knowledge about the structure–activity relationships of indenyl nickel complexes seems still insufficient.

Recently, we have found that simple alkyl-substituted indenylnickel complexes [(1-R-Ind)$Ni(PPh_3)Cl$, R = cyclopentyl, and benzyl] can efficiently initiate the polymerization of styrene in the presence of PPh_3 and $NaBPh_4$, and the alkyl substituent has a manifest effect on the catalytic activity of these complexes [18]. As an extension, we report herein the synthesis and characterization of a series of indenylnickel complexes containing different halogen atom with the general formula (1-Et-Ind)$Ni(PPh_3)X$ [1-Et-Ind = 1-ethylindenyl; X = Cl (**1**), Br (**2**) and I (**3**)], together with the initial

* Corresponding author. Tel.: +86-512-65112513; fax: +86-512-65112371.
E-mail address: qshen@suda.edu.cn (Q. Shen).

0277-5387/$ - see front matter © 2004 Elsevier Ltd. All rights reserved.
doi:10.1016/j.poly.2004.03.001

investigation of their catalytic activities in the polymerization of styrene.

2. Results and discussion

2.1. Synthesis

The indenylnickel complexes **1** and **2** were synthesized by the reaction of the corresponding $Ni(PPh_3)_2Cl_2$ or $Ni(PPh_3)_2Br_2$ with (1-Et-Ind)Li (1-Et-Ind = 1-ethylindenyl), respectively (Scheme 1). Because the reaction of 1-Et-Ind with an equimolar amount of *n*-BuLi in Et_2O gave a quantitative yield of (1-Et-Ind)Li, so freshly prepared solution of indenyl lithium was directly used in the following metathesis reaction. Thus, 1-Et-Ind reacted with *n*-BuLi in Et_2O for half an hour at 0 °C, and the resultant solution was added dropwise into a stirring suspension of $Ni(PPh_3)_2Cl_2$ in Et_2O, or a solution of $Ni(PPh_3)_2Br_2$ in 1,2-dimethoxyethane (DME), in 1:1.8 molar ratio at 0 °C. After workup, the expected complexes (1-Et-Ind)$Ni(PPh_3)X$ [X = Cl (**1**), Br (**2**)] were isolated as dark red crystals in 58% (**1**) or 60% (**2**) yield, as substantiated by elemental analysis and ^1H NMR spectroscopy. Suitable crystals of **1** and **2** for X-ray diffraction studies were grown from Et_2O/hexane at 0 °C. It is noteworthy that the reaction conditions, such as concentration, temperature, and especially the rate of the addition of (1-Et-Ind)Li, have an obvious effect on the formation of indenylnickel complexes. It is of benefit to prepare these complexes by the dropwise addition of a dilute solution of (1-Et-Ind)Li to a dilute suspension of $Ni(PPh_3)_2Cl_2$ in Et_2O, or a dilute solution of $Ni(PPh_3)_2Br_2$ in DME, at 0 °C, since such conditions could efficiently suppress the formation of the byproducts, i.e., the Ni(I) species and 1,1′-biindene [19].

The reaction of complex **1** with KI in THF/acetone at 50 °C afforded the product (1-Et-Ind)$Ni(PPh_3)I$ (**3**) quantitatively. After workup, the red microcrystals were obtained in high yield as identified by elemental analysis and ^1H NMR spectroscopy. Suitable crystals of **3** for X-ray diffraction studies were grown from Et_2O/hexane at 0 °C.

Complexes **1**, **2**, and **3** are soluble in dichloromethane, toluene, DME, THF and diethyl ether. However, complex **1** is completely insoluble in hexane, while complex **2** and **3** have a little solubility in hexane. Due to their good solubility in CH_2Cl_2 or Et_2O and sparing solubility in hexane, they can be crystallized from CH_2Cl_2/hexane (or Et_2O/hexane) in high yield. Notably, their solubility in organic solvents is evidently better than that of bis(triphenylphosphine)halides, e.g., $Ni(PPh_3)_2Cl_2$.

As expected, among these complexes, **1** has the best thermal stability, while **3** has the relatively lower thermal stability. For example, the color of complex **1** remains unchanged at 301–302 °C (its melt point); however, the decomposition of complex **3** is observed at 165–167 °C. Furthermore, complex **1** is slightly sensitive to air and moisture, while both **2** and **3** are sensitive, especially the later one, and can be kept for only a few minutes in open air. However, all of them are relatively more sensitive to air and moisture as compared to the corresponding bis(triphenylphosphine)halides.

2.2. Crystal structures of (1-Et-Ind)$Ni(PPh_3)X$ [X = Cl (**1**), Br (**2**) and I (**3**)]

Since structural data for indenylnickel halides (1-R-Ind)$Ni(PPh_3)X$ have seldom been reported [10], the crystal structures of **1**, **2** and **3** were determined in order to assess the influence of the halogen on the structures of these complexes. Complex **2** and **3** are isomorphous, and the molecular structures of **1** and **2** are presented in Figs. 1 and 2, respectively. The crystallographic data and selected bond lengths and angles for **1**, **2** and **3** are listed in Tables 1 and 2, respectively. The coordination geometries around nickel atoms in **1**, **2** and **3** are similar, i.e., each Ni in these complexes is bound to X, P, C1, C2, and C9 based on the bond distances of Ni to these atoms, while the bond distances of the other two carbon atoms of the five-membered ring, i.e., C3 and C8, to Ni are significantly longer. Inspection of the C–C and Ni–C bond distances for these complexes revealed that the geometry of these complexes around Ni can be described as a distorted square planar with C1=C9 occupying a single coordination site (reflected by a shorter C1–C9 bond relative to C1–C2 bond) (Table 2). In all of these structures, the Ind ligand is significantly distorted away from an idealized η^5 mode toward a fairly unsymmetric η^3 coordination, which is common in this family of complexes [10]. Such distortions can be mainly attributed to the tendency of Ni(II) to avoid forming an 18-electron configuration and the unequal trans influences of the PPh_3 and X (Cl, Br and I) groups [20]. Somewhat to our surprise, except for the Ni–X bond distance, the halogen atom has little effect on the structures of these complexes. For instance, almost the same Ni–Ind interaction occurred in present case. According to the literature [20], the Ni–Ind interaction can be compared

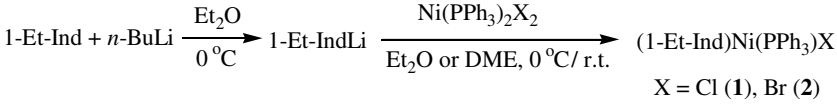

Scheme 1.

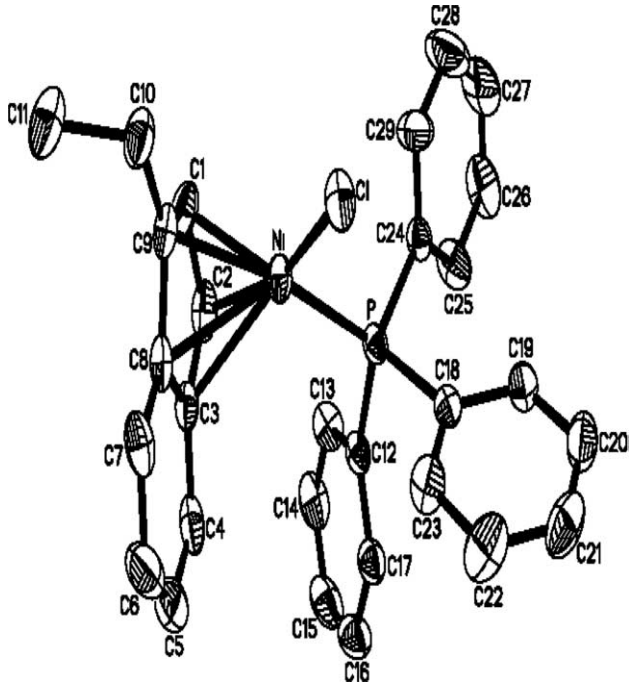

Fig. 1. Molecular structure of complex **1**.

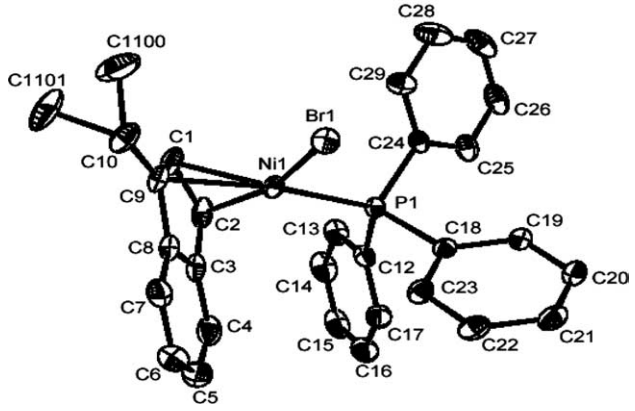

Fig. 2. Molecular structure of complex **2**.

quantitatively by calculating geometrical parameters such as the slip value (ΔM–C) = [M–C_{av} (for C_1, C_5)] – [M–C_{av} (for C_2, C_4)]. In **1**, ΔM–C = 0.256, meanwhile the values of **2** and **3** are 0.250 and 0.246, respectively (Table 2), indicating almost the same slip-fold distortion of the Ind ligand in these complexes. Furthermore, as the observed values of the C1–C9, C1–C2, Ni–C2 and Ni–C9 bond lengths reflect the delocalization of the allyl moiety of Ind ligand, so the local symmetry in the coordination of the allyl moiety are also very similar in **1**, **2** and **3**, and indicate an unsymmetrical η^3 mode Ni–Ind interaction in these complexes. Additionally, the difference among the Ni–P bond distance in these complexes is rather small, and just a bit longer bond distance is observed in **3** [2.1805(9)] as compared to that of in **1** [2.179(1)] or **2** [2.178(1)]. Thus, both Ni–Ind interaction and Ni–P interaction are very similar among these complexes, indicating that the halogen atom play a slight role on these interactions in the indenylnickel halide, which is quite different from the role of the alkyl substituent on indenyl ring [18]. On the other hand, as expected, apparent difference among the Ni–X bond distance in these complexes is observed, i.e., Ni–I > Ni–Br > Ni–Cl (Table 2).

Since the nature of the Ni–Ind interaction in solution is believed to be able to influence substantially the reactivity of Ind complexes, it is important to understand Ind hapticity in solution. Zargarian's group [20] had reported that, for (1-Me-Ind)Ni(PPh_3)Cl (**4**) and its methyl derivative, the ^{1}H NMR resonances for the symmetry-related pairs of protons (H2/H9, H4/H7, and H5/H6) could be used as a convenient indicator of Ind hapticity. Accordingly, they concluded that the solid state structures of these complexes were maintained in the solution. Herein, the same conclusion could also be reached from the paired comparisons of the ^{1}H NMR spectra of these complexes (i.e., **1/4**, **2/4**, and **3/4**), as their ^{1}H NMR spectra are very similar in pairs. For example, the H2 resonance in **1** (3.37 ppm) or in **2** (3.61 ppm) is very close to the corresponding resonance for **4** (3.37 ppm).

*2.3. The catalysis of (1-Et-Ind)Ni(PPh_3)X [X = Cl (**1**), Br (**2**) and I (**3**)] in styrene polymerization*

To the best of our knowledge, the catalytic activity of indenyl nickel complexes for styrene reactions has been reported only by Zargarian's group, a chelating amino-indenyl cationic nickel complex in situ generated from the reaction of (η^3, η^0-Ind–$CH_2CH_2NMe_2$)Ni(PPh_3)Cl and $AgBPh_4$ (or $AgBF_4$) for styrene polymerization or a [(1-Me-Ind)Ni(PPh_3)Cl/$AgBF_4$ system for oligomerization of styrene[16]. Recently, we have found that simple alkyl-substituted indenylnickel complexes [(1-R-Ind)Ni(PPh_3)Cl, R = cyclopentyl and benzyl] could also efficiently initiate the polymerization of styrene in the presence of PPh_3 and $NaBPh_4$, and the alkyl substituent has a manifest effect on the catalytic activity of these complexes [18]. The purpose of $NaBPh_4$ is to abstract the Cl^- ligand from these complexes and facilitate the formation of cationic species [16], while the addition of moderate PPh_3 is of benefit to suppress the decomposition of the cationic species [18]. In the present case, the catalytic activity of (1-Et-Ind)Ni(PPh_3)X [X = Cl (**1**), Br (**2**), I(**3**)] in styrene polymerization has been preliminarily investigated. It is observed that complex **1** or **2** or **3** without $NaBPh_4$ is inert toward the insertion of styrene, however, together with $NaBPh_4$ and PPh_3, they show highly catalytic activity for the polymerization of styrene, and the halogen atom of (1-R-Ind)Ni(PPh_3)X possess an significantly effect on their catalytic activity. For example, when styrene polymerization was carried

Table 1
Crystal data and experimental parameters for **1**, **2** and **3**

	1	**2**	**3**
Empirical formula	$C_{29}H_{26}ClNiP$	$C_{29}H_{26}BrNiP$	$C_{29}H_{26}INiP$
Formular weight	499.63	544.10	591.10
T (K)	291(2)	193(2)	193(2)
λ (Mo Kα) (Å)	0.71073	0.71070	0.71070
Crystal system	monoclinic	triclinic	triclinic
Space group	$P2(1)/n$	$P\bar{1}$	$P\bar{1}$
Unit cell dimensions			
a (Å)	9.731 (2)	9.011(4)	9.145(1)
b (Å)	28.572(8)	10.339(5)	10.613(1)
c (Å)	9.750(2)	14.583(7)	14.227(3)
α (°)	90	83.31(1)	85.00(1)
β (°)	113.42(2)	86.94(1)	89.08(1)
γ (°)	90	64.598(7)	64.821(7)
V (Å^3)	2487.5(10)	1219(1)	1244.5(3)
Z	4	2	2
D_{calc} (g/cm^3)	1.334	1.482	1.577
Absorption cofficent (mm^{-1})	0.966	2.520	2.099
$F(000)$	1040	556	592
Crystal size (mm)	0.50×0.32×0.22	0.60×0.30×0.11	0.09×0.49×0.35
$2\theta_{max}$ (°)	50.0	55.0	55.0
Reflections collected	4199	12 108	28 068
Independent reflections	4381	5447	5604
Goodness-of-fit on F^2	0.845	1.02	1.004
Final R indices [$I > 2\sigma(I)$]	0.0740	0.035	0.030
Parameters refined	291	382	316
R_w	0.074	0.100	0.076

Table 2
Selected bond distances (Å) and angles (°) in **1**, **2** and **3**

	1	**2**	**3**
Bond distances			
Ni–P	2.179(1)	2.178(1)	2.1805(9)
Ni–X	2.185(1)	2.319(1)	2.4971(6)
Ni–C1	2.048(4)	2.072(5)	2.064(4)
Ni–C2	2.022(4)	2.032(5)	2.031(5)
Ni–C3	2.303(4)	2.315(5)	2.310(4)
Ni–C8	2.373(4)	2.351(5)	2.340(4)
Ni–C9	2.142(4)	2.135(6)	2.126(3)
C1–C2	1.418(5)	1.424(5)	1.411(6)
C1–C9	1.398(5)	1.401(4)	1.402(4)
C2–C3	1.440(5)	1.454(5)	1.463(5)
C3–C8	1.417(5)	1.425(4)	1.415(4)
C8–C9	1.469(5)	1.462(4)	1.462(5)
P–C12	1.837(4)	1.828(5)	1.823(4)
P–C18	1.820(4)	1.828(5)	1.833(4)
P–C24	1.814(4)	1.823(5)	1.818(3)
Bond angles			
C2–Ni–C9	66.58(15)	66.64(2)	66.5(1)
C2–Ni–P	100.11(12)	100.10(2)	99.7(1)
C9–Ni–P	166.42(10)	166.40(2)	166.1(1)
X–Ni–P	97.70(4)	95.33(5)	99.27(3)
ΔM–C (Å)	0.256	0.250	0.246

out in toluene at 80 °C with $NaBPh_4$/**1**/PPh_3 = 7:1:4 (mole ratio), [styrene]/[**1**] = 300 (mole ratio), the polymer yield could reached 100% after 24 h, but only 84% for **2** and 41% for **3** under the same conditions. The obtained polystyrene is soluble in THF with $M_n = 18\,000$ ($M_w/M_n = 2.1$) for **1**, $M_n = 12\,000$ ($M_w/M_n = 2.6$) for **2**, and $M_n = 9000$ ($M_w/M_n = 1.8$) for **3**. The differences among their catalytic activities are probably due to the different Ni–X distance together with the different thermal stability of these complexes at the polymerization temperature. By the way, some experimental results are in the negative of a radical pathway. Careful experiments showed that the addition of varying amounts of 2,2,6,6-tetramethyl-1-piperidinyloxy (TEMPO), a strong and efficient radical scavenger, only partly reduced the speed of the present styrene polymerization. For instance, when 1% or 2% (referred to monomer weight) amounts of TEMPO were added into $NaBPh_4$/**1**/PPh_3 (in large excess to 1 mol) at the beginning of the polymerization, the polymer yield still remained at 75% (no adding TEMPO, yield is 100%). Meanwhile, styrene polymerization initiated by azobis(isobutyronitrile) (AIBN; conditions are the same as **1**), which is a classical radical initiator, was completely hindered by adding the same amount of TEMPO. Thus, combination with the reported results [16,18] indicate that the present styrene polymerization mainly also be catalyzed by the in situ generated cationic species [1-Et-Ind(PPh_3)Ni(PPh_3)]$^+$, which produced from the reaction of (1-Et-Ind)Ni(PPh_3)X and $NaBPh_4$ in the presence of PPh_3. Further investigations focusing on the detailed structure–activity relationships and mechanistic aspects of the polymerization using these complexes are now in progress.

3. Experimental

All manipulations were performed under pure argon with rigorous exclusion of air and moisture using standard Schlenk techniques. Solvents were distilled from Na/benzophenone ketyl prior to use. 2,2,6,6-Tetramethyl-1-piperidinyloxy (TEMPO) (Aldrich) was used as received. Azobis(isobutyronitrile) (AIBN) were recrystallized from 95% ethanol. Indene (Fluka) (dried over 4 Å molecular sieves) and styrene (dried over CaH_2) were distilled before use. $(PPh_3)_2NiCl_2$ [21] and $(PPh_3)_2NiBr_2$ [22] were prepared by published methods. 1-Ethylindene was prepared according to the literature method [23]. Melting points were determined in sealed Ar-filled capillaries and are uncorrected. Carbon and hydrogen analyses were performed by direct combustion on a Carlo Erba-1110 instrument; quoted data are the average of at least two independent determinations. ^1H NMR (C_6D_6) spectra were measured on a Unity Inova-400 spectrometer. Molecular weight and molecular weight distributions were determined against polystyrene standard by gel permeation chromatography (GPC) on a Waters 1515 apparatus with three HR columns (HR-1, HR-3 and HR-4); THF was used as an eluent at 30 °C.

3.1. Synthesis of (1-Et-Ind)Ni(PPh_3)Cl (1)

A Schlenk flask was charged with 1-Et-Ind (0.43 g, 3 mmol), Et_2O (30 ml) and a stir bar. To this solution was added a solution of *n*-BuLi in hexane (2.3 ml, 3 mmol) dropwise via syringe at 0 °C. The solution was stirred for 30 min and then added slowly to a stirring suspension of $Ni(PPh_3)_2Cl_2$ (3.53 g, 5.4 mmol) in Et_2O (60 ml) at 0 °C. The color of the solution immediately changed to red. The resultant solution was then stirred for another 40 min at room temperature, filtered, and evaporated to dryness. The residue was washed with hexane (3× ca. 20 ml) to remove PPh_3 and other byproducts and recrystalized from CH_2Cl_2/hexane at −30 °C to give the product as a dark red needle crystals (869 mg, 58%) suitable for elemental analysis, m.p. 301–302 °C. *Anal.* Calc. for $C_{29}H_{26}$ ClNiP: C, 69.74; H, 5.21. Found: C, 69.65; H, 5.25%. ^1H NMR (400 MHz, C_6D_6): 7.80 (t, 1H, H6), 7.69 (m, 5H, P*Ph*$_3$), 7.40 (m, 1H, H7), 7.02 (m, 10H, P*Ph*$_3$), 6.89 (t, 1H, H5), 6.42 (br s, 1H, H2), 6.16 (d, 1H, H4), 3.37 (br s, 1H, H1), 1.80 (m, 2H, *CH*$_2$), 1.39 (d, 3H, *CH*$_3$). Crystals suitable for X-ray diffraction studies were obtained by recrystallization from Et_2O/hexane at 0 °C.

3.2. Synthesis of (1-Et-Ind)Ni(PPh_3)Br (2)

The synthesis of compound **2** was carried out as described for **1**, but a solution of $Ni(PPh_3)_2Br_2$ (4.01 g, 5.4 mmol) in DME (60 ml) was used in place of the solution of $Ni(PPh_3)_2Cl_2$ (3.53 g, 5.4 mmol) in Et_2O. The dark red product was obtained by recrystallization from CH_2Cl_2/hexane at −30 °C (979 mg, 60%), m.p. 285–287 °C. *Anal.* Calc. for $C_{29}H_{26}BrNiP$: C, 63.31; H, 4.68. Found: C, 64.02; H, 4.82%. ^1H NMR (400 MHz, C_6D_6): 7.68 (m, 5H, P*Ph*$_3$), 7.40 (t, 1H, H6), 7.14 (m, 1H, H7), 7.02 (m, 10H, P*Ph*$_3$), 6.90 (t, 1H, H5), 6.35 (br s 1H, H2), 6.17 (d, 1H, H4), 3.61 (br s, 1H, H1), 2.01 (m, 1H, *CH*$_2$), 2.47 (m, 1H, *CH*$_2$), 1.37(t, 3H, *CH*$_3$). Crystals suitable for X-ray diffraction studies were obtained by recrystallization from Et_2O/hexane at 0 °C.

3.3. Synthesis of (Et-Ind)Ni(PPh_3)I (3)

A Schlenk flask was charged with a solution of **1** (499 mg, 1 mmol) in THF (20 ml) and a stir bar. To this solution, a solution of KI (200 mg, 1.2 mmol) in acetone (10 ml) was added. The resultant mixture was stirred for 12 h at 50 °C, evaporated to dryness and extracted with Et_2O. The product was obtained by evaporization of the solvent as a red solid (ca. quantitative yield), m.p. 165–167 °C (dec.). *Anal.* Calc. for $C_{29}H_{26}INiP$: C, 58.92; H, 4.43. Found: C, 58.54; H, 4.53%. ^1H NMR(400 MHz, C_6D_6): 7.66 (m, 5H, P*Ph*$_3$), 7.41 (t, 1H, H6), 7.14 (m, 1H, H7), 7.03 (m, 10H, P*Ph*$_3$), 6.94 (t, 1H, H5), 6.35 (br s 1H, H2), 6.17 (d, 1H, H4), 3.93 (br s, 1H, H1), 2.87 (m, 1H, CH_2), 2.46 (m, 1H, *CH*$_2$), 1.37 (t, 3H, *CH*$_3$). Crystals suitable for X-ray diffraction studies were obtained by recrystallization from Et_2O/hexane at 0 °C.

3.4. A typical procedure for polymerization of styrene

A typical polymerization reaction is as follows. Under dry argon, the solid initiator **1** (10 mg, 0.02 mmol), PPh_3 (21 mg, 0.08 mmol), $NaBPh_4$ (48 mg, 0.14 mmol), toluene (0.2 ml) and styrene (1.2 ml, 0.01 mol) were added into a dry glass ampule in turn. Then, the sealed ampule was placed in a water bath held at 80 °C. After a definite reaction time, the polymerization was stopped by adding 1 ml of 5% HCl/ethanol. After evaporation of solvent and unreacted monomer, the resulted polymer was dissolved in THF, followed by precipitation in 95% ethanol. After filtration, the white polymer was dried in vacuum at room temperature overnight. The polymer yield was determined gravimetrically.

3.5. X-ray structural determination of 1, 2 and 3

Suitable single crystals of complex **1**, **2** and **3** were each sealed in a thin-walled glass capillary for X-ray structural analysis. Diffraction data were collected on a Siemens SMART CCD area detector using theta scans for **1**, or a Rigaku Mercury CCD area detector using omega scans for **2** and **3**. The crystal structures of **1** and **3** were solved by direct methods using the SHELXS-97 program, and the crystal structures of **2** was solved by

Patterson methods using the CRYSTALSTRUCTURE program. All the non-hydrogen atoms were refined anisotropically. Hydrogen atoms were treated as idealized contributions.

4. Supplementary data

Crystallographic data for the structural analysis have been deposited with the Cambridge crystallographic data Center, CCDC Nos. 225155, 223964 and 227411 for complexes **1**, **2** and **3**, respectively. Copies of this information may be obtained free of charge from the Director, CCDC, 12 Union Road, Cambridge CB2 1EZ, UK (fax: +44-1223-336033; e-mail: deposit@ccdc.cam.ac.uk or www: http://www.ccdc.cam.ac.uk).

Acknowledgements

We thank the Chinese National Natural Science Foundation (20272040), the Department of Education of Jiangsu Province (02KJB150002) and the Key Laboratory of Organic Chemistry of Jiangsu Province for the financial support.

References

[1] M.E. Stoll, P. Belanzoni, M.J. Calhorda, M.G.B. Drew, V. Félix, W.E. Geiger, C.A. Gamelas, I.S. Goncalves, C.C. Romão, L.F. Veiros, J. Am. Chem. Soc. 123 (2001) 10595, and references cited therein.
[2] J.A. Ewen, J. Am. Chem. Soc. 106 (1984) 6355.
[3] W. Kaminsky, Makromol. Chem. Macromol. Symp. 47 (1991) 83.
[4] R.L. Halterman, Chem. Rev. 92 (1992) 965.
[5] H. Schumann, D.F. Karasiak, S.H. Mühle, W. Kaminsky, U. Weingarten, J. Organomet. Chem. 636 (2001) 31, and references cited therein.
[6] H. Lehmkuhl, J. Näser, G. Mehler, T. Keil, F. Danowski, R. benn, R. Mynott, G. Schroth, B. Gabor, C. KrÜger, P. Betz, Chem. Ber. 124 (1991) 441.
[7] K. Nakasuji, M. Yamaguchi, I. Murata, K. Tatsumi, A. Nakamura, Organometallics 3 (1984) 1257.
[8] T. Tanase, T. Nomura, T. Fukushima, Y. Yamamoto, K. Kobayashi, Inorg. Chem. 32 (1993) 4587.
[9] D. O'Hare, Organometallics 6 (1987) 1766.
[10] D. Zargarian, Coord. Chem. Rev. (2002) 233, and references cited therein.
[11] R. Vollmerhaus, F. Bélanger-Gariépy, D. Zargarian, Organometallics 16 (1997) 4762.
[12] M.-A. Dubois, R. Wang, D. Zargarian, J. Tian, R. Vollmerhaus, Z. Li, S. Collins, Organometallics 20 (2001) 663.
[13] L.F. Groux, D. Zargarian, L.C. Simon, J.B.P. Soares, J. Mol. Catal. A 3781 (2002) 1.
[14] R. Wang, L.F. Groux, D. Zargarian, Organometallics 21 (2002) 5531.
[15] L.F. Groux, D. Zargarian, Organometallics 22 (2003) 3124.
[16] L.F. Groux, D. Zargarian, Organometallics 20 (2001) 3811.
[17] R. Wang, F. Bélanger-Gariépy, D. Zargarian, Organometallics 18 (1999) 5548.
[18] H.M. Sun, W.F. Li, X.Y. Han, Q. Shen, Y. Zhang, J. Organomet. Chem. 688 (2003) 132.
[19] T.A. Huber, F. Bélanger-Gariépy, D. Zargarian, Organometallics 14 (1995) 4997.
[20] T.A. Huber, M. Bayrakdarian, S. Dion, I. Dubuc, F. Bélanger-Gariépy, D. Zargarian, Organometallics 16 (1997) 5811, and references cited therein.
[21] L.M. Venanzi, J. Chem. Soc. (1958) 719.
[22] H. Uegaki, Y. Kotani, M. Kamigaito, M. Sawamoto, Macromolecules 30 (1997) 2249.
[23] N.E. Grimmer, N.J. Coville, C.B. Koning, J.M. Smith, L.M. Cook, J. Organomet. Chem. 616 (2000) 112.

Available online at www.sciencedirect.com
SCIENCE DIRECT®
Polyhedron 23 (2004) 1479–1504
POLYHEDRON
www.elsevier.com/locate/poly

Polyhedron Report No. 70

Structures of alkali and alkaline earth metal clusters with oxygen donor ligands

Katharina M. Fromm [a,*], Estelle D. Gueneau [b]

[a] Department of Chemistry, University of Basel, Spitalstrasse 51, CH-4056 Basel, Switzerland
[b] University of Geneva, CH-1211 Geneva, Switzerland

Received 20 February 2004; accepted 1 April 2004

Abstract

This review based on 169 references gives an actual overview on group 1 and 2 clusters with oxygen donor ligands. A first part deals with alkali metal compounds of which synthesis and the most important structurally characterized examples a presented in detail. Homo- and heterometallic aggregates of group 1 metals as well as mixed group 1 and 2 compounds are classified with respect to the ligand type. Finally, alkaline earth metal clusters are treated, starting with Mg-compounds, then pursuing with the heavier homologues. This chapter also contains a brief description of CVD and sol-gel methods.
© 2004 Elsevier Ltd. All rights reserved.

Keywords: Alkoxides; Enolates; β-Diketonates; Carboxylates; Alkali metals; Alkaline earth metals; Cluster compounds

1. Introduction

During the past years, two major tendencies are found for the motivations of doing research in s-block chemistry. The first one is based on the formation of polymetallic complexes with alkali and/or alkaline earth metals mainly based on organic oxygen or nitrogen donor ligands. These organo-heterometallic compounds are of interest due to their enhanced reactivity compared to their homometallic homologues. This higher reactivity induces an important role in synthetic chemistry, especially based on the superbasic character of such species. The second motivation is related to the application of alkali and alkaline earth metals in materials. The oxides and halides of s-block elements occupy an especially important place. They can act as material themselves with a proper functionality or else as precursor for more complicated materials such as superconductors. The high temperature synthesis of such oxide materials is generally more complicated for s-block elements due to the ionic character of their oxides, the hygroscopy of the compounds, and the reactivity of s-block metal oxides towards carbon dioxide in order to form carbonates. This is why an alternative had to be found for the controlled elaboration of these compounds during the past 15 years. So in parallel, a molecular route was tested, compared to the traditional solid-state synthesis, evidencing more flexible synthetic methods such as metal-organic chemical vapor deposition (MO-CVD) or sol–gel techniques.

This review will deal with the recent developments of ''organo-metallic'' compounds of s-block elements, with a focus on the synthesis and characterization of polymetallic compounds with mainly M–O bonds. It is meant to give an overview on the most significant clusters containing O-donor ligands such as alkoxides/aryloxides, enolates, β-diketonates or carboxylates. The compounds are regrouped by the type of ligands, first the pure group 1 metals, then mixed alkali and alkaline earth metal compounds, and finally group 2 metals. They are chosen for their originality and variety in structure and synthesis. The recent results in this field,

* Corresponding author. Tel.: +41-61-267-1004; fax: +41-61-267-1021.
E-mail address: katharina.fromm@unibas.ch (K.M. Fromm).

0277-5387/$ - see front matter © 2004 Elsevier Ltd. All rights reserved.
doi:10.1016/j.poly.2004.04.014

presented in this review, give rise to high expectations as to new compounds and structural varieties, which are yet to be discovered.

The polymetallated compounds that are dealt with in this review will be called "clusters" in the sense of aggregates of two or more metal atoms with bridging ligands, not necessarily implying that metal–metal bonds are present (which is a more strict definition of the term "cluster" in transition metal chemistry).

2. Alkali metal clusters

2.1. General introduction

Historically, a great number of alkali metal clusters was merely discovered by serendipity as secondary products using superbases [1] or metallation agents [2] in organic synthesis. However, many of the structures as well as the formation mechanisms for these species remain to be investigated. The so far characterized clusters possess very interesting structures, such as tetramers, hexamers, nonamers or decamers, which might explain their reactivity. Indeed, larger aggregates seem to exhibit an enhanced reactivity compared to more simple compounds.

Organo-lithium compounds show some typical properties known for covalent species: solubility in non-polar solvents and volatility. Thus, the lithium clusters were among the first discovered ones, as unexpected intermediates or secondary products during metallation reactions. Some of them are now used as reagents in organic synthesis and possess fascinating structures. They are known for their formation of aggregates in solution, the gas phase, and the solid state [3]. Small alkali metal cations have been found to form cage structures, whereas clusters of the heavier homologues are almost unknown [4].

The reactivity of organometallic compounds MR in general can be increased considerably by addition of Lewis bases, such as amines or alkoxides M′OR′. This important effect is based on the formation of mixed aggregates of for instance [(MR)(M′OR′)], yielding a "superbase". A better solubility in organic solvents is observed, which is reflected in higher reactivity as well.

Since many of these compounds are air and/or moisture sensitive, the single crystal structure resolution is usually delicate. However, the great interest in alkoxides and enolates of alkali metals pushed forward the investigations of these compounds.

2.2. Homo-ligand homo-metallic clusters

2.2.1. Alkoxides

The use of alkoxides as reagents or building blocks in organometallic synthesis often depends on their solubility, a property derived from their structure [5]. The regain in interest of alkali alkoxides also resides in the discovery of high-temperature superconducting compounds which has generated a great interest in the formation of oxide materials and other ceramics. Soluble alkoxides can thus serve as valuable precursors for making metal oxides under rather mild conditions as encountered by sol–gel methods or chemical vapor deposition (CVD) [6,7].

2.2.1.1. General synthesis of $M(OR)_x$ for cluster formation. Compounds of the type $M(OR)_n$ and $L_xM(OR)_y$ (R = alkyl or aryl, L_x = other neutral or anionic ligands, n, y = integers) are accessible via several synthetic procedures of which the most relevant are listed below. The methods of preparation are often chosen as a function of the electronegativity of the metal [8].

Alkoxides and phenoxides can be obtained by direct reactions of the crude metal which is dissolved in the corresponding alcohol, following the reaction:

$$M + ROH \rightarrow MOR + 1/2\,H_2 \quad (1)$$

The interest in this reaction clearly relies on the fact that the secondary product, hydrogen, is volatile, allowing easy purification of the product. This method is limited to the more electropositive metals (group 1) due to the high pK_a values of the most common alcohols and phenols. For the less electropositive metals, a catalyst is necessary to start the reaction, in general I_2 or HgX_2.

Alkali metal alkoxides and phenoxides can also be prepared by a reaction of the metal hydroxide with the alcohol:

$$MOH + ROH \rightarrow MOR + H_2O \quad (2)$$

The water formed during this reaction has to be eliminated by azeotropic distillation, for instance with NaOH dissolved in a mixture ethanol/benzene under reflux. The more acidic phenols allow formation of the group 1 phenoxides more readily by simple heating of the hydroxide in dried ethanol, followed by recrystallization. Magnesium phenoxide is obtained commercially by a reaction of MgO with phenol.

Finally, beryllium and magnesium form mixed compounds of the type RMOR′ which are obtained by reaction of an organometallic compound MR_2 (R = alkyl or H) with the alcohol R′OH. The carbanion or the hydride reacts then with R′OH to give R′OM in good yield. The secondary product is usually volatile (hydrogen or alkane) [9,10].

2.2.1.2. Physical and spectroscopic properties. Given the strong electronegative character of oxygen, mainly ionic character for the metal–oxygen bond can be expected. However, most of the alkoxides present properties such as solubility in non-polar solvents and volatility due to their hydrophobic envelope formed by more or less

sterically demanding alkyl chains. Many alkali metal monoalkoxides are neither volatile nor soluble and decompose when heated. They possess a very ionic character and form polymers. Li*O*t*Bu* is an exception to this rule as it can be sublimed at 110 °C and a pressure of 1.1 torr and is soluble in most organic solvents, such as cyclohexanes and benzene.

2.2.1.3. Structural varieties. (a) *Non-solvated pure alkoxides.* The progress made during the last 15 years in the techniques of single crystal data acquisition allowed the screening of the structures of a large number of organometallic group 1 and magnesium compounds. They show a variety of possible structure types, such as cycles, hetero-cubanes, chains, layers, etc.) (Fig. 1). These structural types can be applied to carbanions as well as amides, imides, halides, and oxygen-donor ligands such as alkoxides, phenoxides, and enolates. The first monographies by Bradley in 1978 and Malhotra in 1982 show, however, that the investigations of alkoxide and phenoxide compounds are more recent than the ones on organometallic compounds [11,12].

The geometry of the structures depends very much on the steric demand of the group R. Since the classical synthesis is carried out in organic solvents, uncoordinating solvents will lead to solvent-free structures, whereas coordinating solvents may lead to the formation of other structures.

The unsolvated group 1 methoxides of type MOMe (M = Li–Cs) and some iso-propanolates M*O*^{i}*Pr* (M = K–Cs) form sheet-like infinite structures [13–19]. So do some of the methoxides of the alkaline earths Ca, Sr, and Ba [20–22]. The alkoxide groups of these structures are oriented toward the outside of the layers, whereas the cations are distributed inside the structure on one (Li, Na, Ca, Sr, and Ba) or two different sites (K, Rb, and Cs), depending on their charge and radius. Due to their polymer arrangement in layers, these compounds are neither volatile nor soluble in organic compounds.

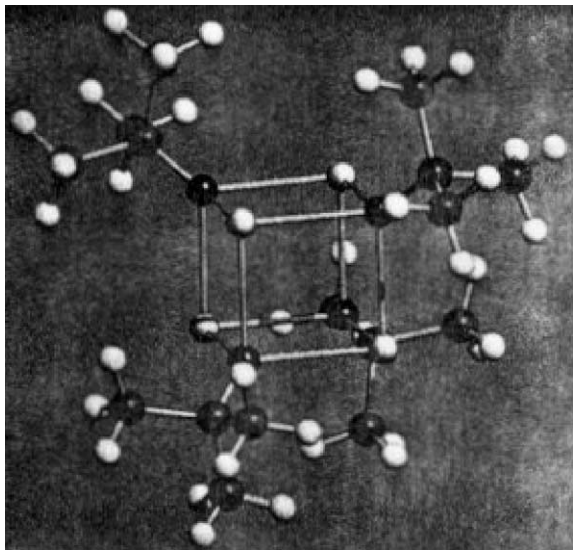

Fig. 2. The cubane structure of (KO*t*Bu)$_4$. Isotypic structures include [MO*t*Bu]$_4$ (M = Rb, Cs) and [MOSiMe$_3$]$_4$ (M = K, Rb, Cs) [23–26].

The formation of layers is not possible any more with sterically more demanding groups R. Then, spherical or cyclic structures are built and molecular compounds are obtained. This is the case for *tert*-butoxides. The first ones to be discovered, (MO^{t}*Bu*)$_4$, M = K, Rb, Cs [23–26], are all tetrameric and build cubane structures (Fig. 2).

The metal and the oxygen atoms sit on alternating corners of a distorted cube. The compounds are soluble and volatile due to their structures where the shell of the

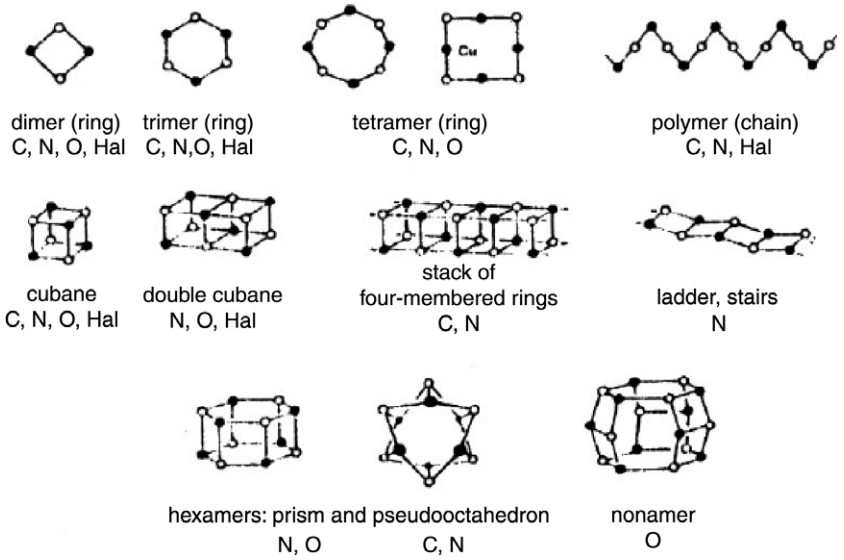

Fig. 1. Important idealized coordination types for ion aggregates of the alkali metals (•) with C, N, O, and halogen anions (○) [11,12].

structure exhibits a highly hydrophobic character. The determination of molar masses in solution by colligative methods and in aprotic solvents usually indicates a similar state of aggregation as in the solid state [27]. The structures are also maintained in the gas phase as can be deduced from the mass spectrum of $(KO^tBu)_4$ [28,29].

The structure of the lighter homologue, sodium, is particularly interesting as in the unit cell, two types of aggregates coexist. Hexamers $(NaO^tBu)_6$ and nonamers $(NaO^tBu)_9$ are found in the solid state (Figs. 3(a) and (b)) [23–26]. Whereas the cubane structure can be interpreted as a stacking of two dimers M_2O_2 to give a ring, the trigonal prismatic structure of the hexamer can be seen as stacking of three entities M_2O_2 arranged to a ring. The nonamer can then be interpreted as fusion of three deformed cycles of M_3O_3.

For many years, several attempts have been made to solve the crystal structure of Li*O*t*Bu*. The structure has been confirmed to be hexameric in the gas phase as well as in solution [28–30]. Only recently, in 1998, a non-solvated hexamer was described from an octane solution [31]. Very recently has the crystal structure been obtained by the authors' group as well as by Olbrich and co-workers [32,33]. As for the sodium homologue, two independent molecules are found in the unit cell. In contrast to the sodium compound, both are hexamers. They are different insofar as they possess different symmetry. The oxygen atoms of the O*t*Bu groups form a regular octahedron. The six lithium atoms are then delocalized over the eight equivalent triangular faces of the octahedron. This is why disorder is so great in this structure and structure solution was problematic (Fig. 4).

This type of coordination is also found in the copper compound $[Li_7(OtBu)_6][Cu_2(Si(SiMe_3)_3)_3]$ in which the hexagonal prism of $(LiOtBu)_6$ is capped on one side by a Li^+ (Fig. 5) [34].

(b) *Superbasic compounds of type [(RM)(MOR′)] (R, R′ = alkyl)*. The lithiated compound $[(n\text{BuLi})(LiOtBu)]_4$ is an example for a superbasic compound with a tetrameric structure containing a core Li_8O_4 which builds a structure of three stacked hetero-cubanes as shown in Fig. 6 [35]. The four central lithium ions are

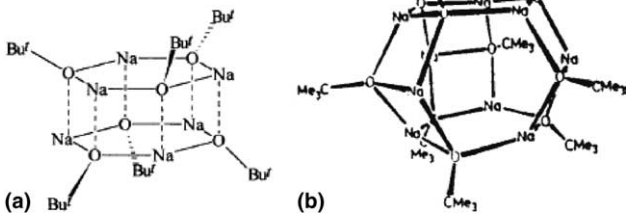

Fig. 3. (a) Structure of the hexameric $(NaOtBu)_6$ [23–26]. (b) Structure of the nonameric (NaO *t*Bu)$_9$ [23–26].

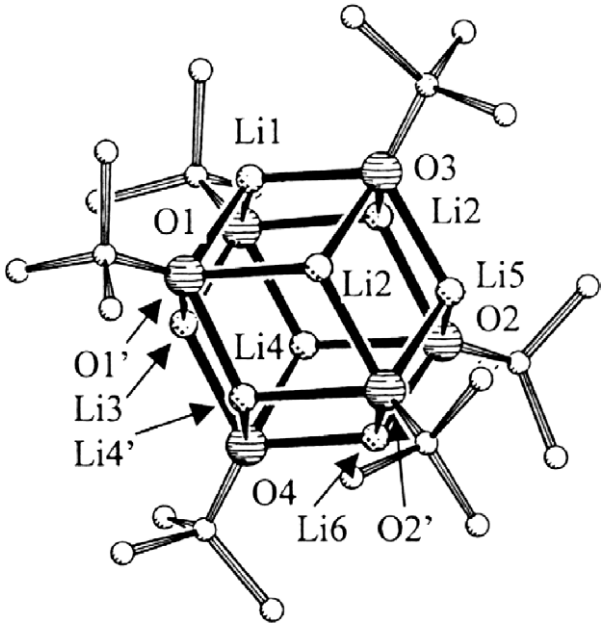

Fig. 4. Structure of one molecule of the asymmetric unit of $(LiOtBu)_6$.

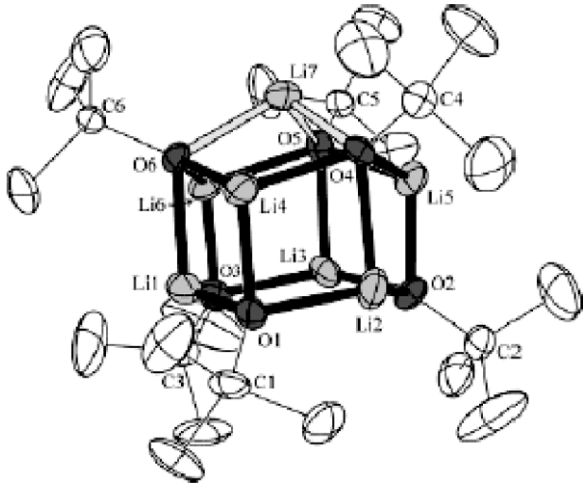

Fig. 5. ORTEP structure of the cationic species $[Li_7(OtBu)_6]^+$ [34].

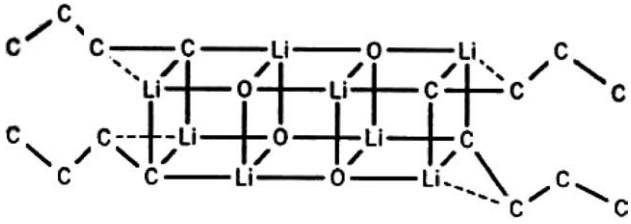

Fig. 6. Schematic drawing of $[(LinBu)(LiOtBu)]_4$ [35].

coordinated by one carbon atom of the *n*Bu groups and three oxygen atoms of the anions O*t*Bu. The four outer lithium cations are linked to one oxygen atom, two α-

carbon atoms, and one β-carbon of *n*Bu groups. This compound is soluble in apolar and aprotic solvents as benzene.

(c) *Superbasic compounds of type [(ROM)(MOH)].* The alkoxide LiO*t*Bu can also be built into a larger aggregate structure, as can be seen from the following example of a mixed anion compound, which can be written as $(LiOtBu)_{10}(LiOH)_6$ and was described in 1995 [36]. This compound was simply obtained by partial hydrolysis in air of a solution of LiO*t*Bu, as described by the following reaction scheme:

$$16LiOtBu + 6H_2O \rightarrow (LiOR)_{10}(LiOH)_6 + 6HOR \quad (3)$$

Complete hydrolysis leads to the formation of the alcohol and precipitation of LiOH. The single crystal structure of the above compound can be described as a centrosymmetric dimer of hexagonal prismatic moieties of $Li_6(OtBu)_5(OH)$, which themselves are linked by a crossed ladder-type arrangement of LiOH-units (Fig. 7). The latter structural motif is also often found in lithium amide chemistry for $LiNR_2$-compounds.

(d) *Solvated compounds.* The larger the organic ligand R is, and the more sterically hindering it is, the smaller the clusters which are formed. Thus, compounds with an extremely low coordination number for the metal ions can be realized. This is the case for the dimer $[Li(OCtBu_3)]_2$ which was characterized in solution as well as in the solid state. The crystals are obtained at −25 °C after a room temperature reaction of *n*BuLi with the corresponding alcohol [37]. A solvated form of this compound was isolated as $[\{Li(OCtBu_3)(thf)_2\}]$ where two THF-molecules complete the coordination spheres of the lithium ions which reach a coordination number of 3 [38]. The Li–O distances are therefore also longer than in the non-solvated compound (1.83–1.85 Å). The sterical hindering of the ligand is so important that dimerisation is impossible, avoiding therefore the formation of the typical and more often encountered heterocubane structure, even though the coordination numbers of the metal atoms are rather low.

(e) *Compounds of type $[(ROM)_x(HOR)_y]$.* The alkoxides which are solvated by their parent alcohol are mostly known for the first elements of a series of the periodic table of elements, and only few structures are described, i.e. $[(KOtBu)(tBuOH)]$ [39–42]. For $x = 1$ and $y = 2$, $[Li(OMe)(MeOH)_2]$ can be found as an example; it possesses a tetramer unit of $[Li_4(\mu\text{-}OMe)_4(\mu\text{-}MeOH)_2(MeOH)_4]\cdot 2MeOH$. The structure can be described as two distorted squares of $[Li_2(OMe)(MeOH)]$ linked by bridging methoxy ligands and hydrogen bonds (Fig. 8) [43]. This compound easily looses the solvating molecules of alcohol to give the polymeric structure of LiOMe described before.

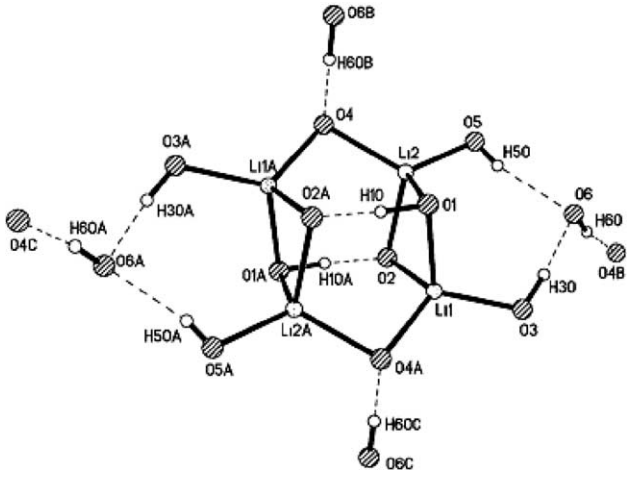

Fig. 8. Structure of $[Li_4(\mu\text{-}OMe)_4(\mu\text{-}MeOH)_2(MeOH)_4]\cdot 2MeOH$ [43].

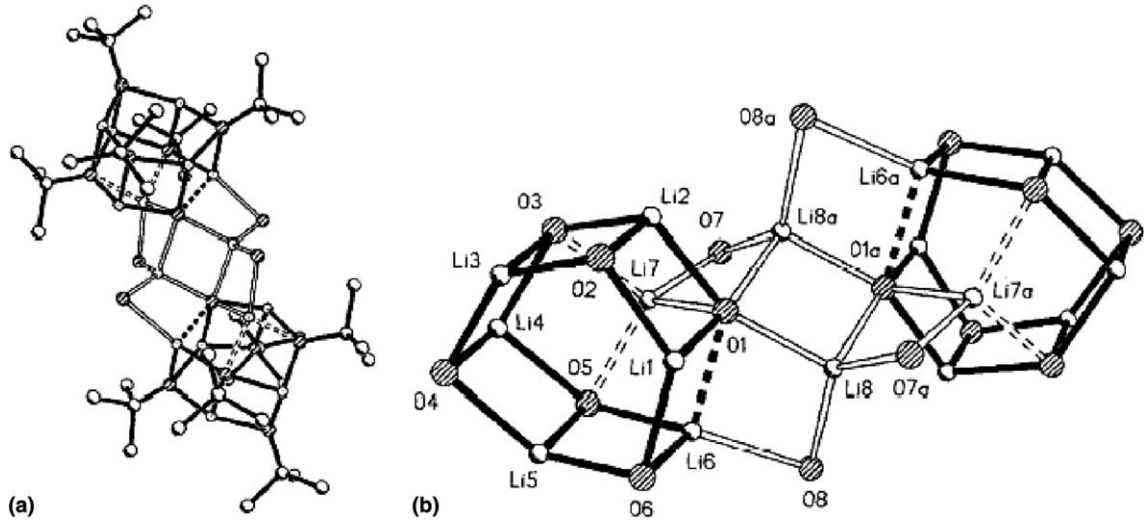

Fig. 7. Structural arrangement in $(LiOtBu)_{10}(LiOH)_6$: (a) of the molecule, (b) of the core [36].

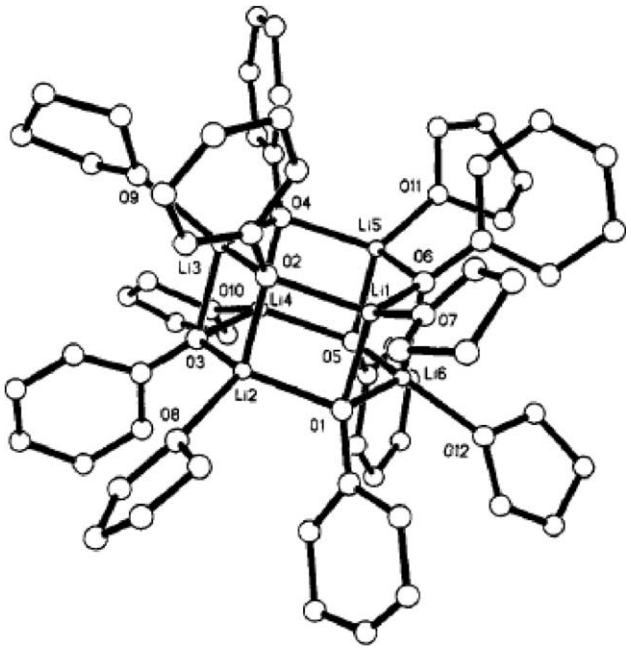

Fig. 9. Structure of $[Li(\mu_3\text{-}OPh)(thf)]_6$ [44].

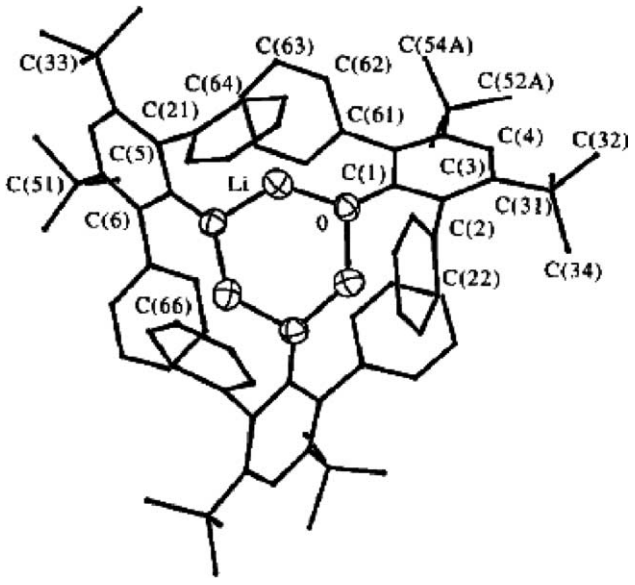

Fig. 10. ORTEP structure of [{Li(μ-OAr)}$_3$](2,6-diphenyl-3,5-di-*tert*-butylphenoxide = OAr) [45].

2.2.2. Aryloxides

The lithium aryloxides can be prepared similar to the methods encountered before for the alkoxides. The degree of aggregation depends also on the steric demand of the phenoxide and on the presence or absence of a Lewis base. Thus, the simple lithium phenoxide forms a hexameric structure of $[Li(\mu_3\text{-}OPh)(thf)]_6$ at the solid state as well as in solution (Fig. 9) [44], whereas the sterically more demanding ortho-substituted lithium 2,6-di-*tert*-butylphenoxide builds dimers of composition $[Li(\mu\text{-}OC_6H_3{}^tBu\text{-}2,6)(thf)]_2$.

In the case of aryloxides, substitution in meta-positions reduces the tendency to form cyclic anti-prismatic aggregates. Thus, the sterically important alcohol 2,6-diphenyl-3,5-di-*tert*-butylphenoxide (HOAr) reacts with *n*BuLi in toluene to give a lithiated trinuclear species [{Li(μ-OAr)}$_3$][45]. A six-membered ring is formed, alternating Li and O, with the phenyl groups of the ligand pointing alternatingly up and down of the ring plane. Due to this bulk, fusion of two rings to yield the hexagonal anti-prism is inhibited (Fig. 10).

Basic adducts of alkoxides and phenoxides are formed from alkoxides as well as organometallic compounds. Those with alkoxides are rare. Apart from alkali metal enolates, two examples found in the literature are the dimers of phenoxides, $[Li(p\text{-}OC_6H_4Br)(tmeda)]_2$ and $[Na(OPh)(pmdeta)]_2$ [46,47]. The lithium has a coordination number of 4, sodium of 5, and in both structures dimers of M_2O_2 are found [46,47]. Only a few more substituted phenoxides possess cyclic structures as well, such as $[Li(OC_6H_3\text{-}tBu_2\text{-}2,6)(OEt_2)]_2$ and $[Li(OC_6H_2Me\text{-}4\text{-}tBu_2\text{-}2,6)(OEt_2)]_2$ [48], and $[Na(OC_6H_2(CF_3)_3\text{-}2,4,6)(thf)_2]_2$ [49], which are also arranged in dimers M_2O_2. The compound $[Li\{OC_6H_2\text{-}2,6\text{-}(CH_2NMe_2)_2\text{-}4\text{-}Me\}]_3$ is a special case where a cyclic trimer $(LiOR)_3$ is formed by internal solvation by the two amino substituents [50]. In these compounds, lithium usually has the coordination number of 4.

With bulky ligands as in $[Li(OC_6H_2Me\text{-}4\text{-}tBu_2\text{-}2,6)(OEt_2)]_2$ [48], the lithium ion adopts a coordination number of three, the overall compound possessing an almost spherical structure with the alkyl groups pointing

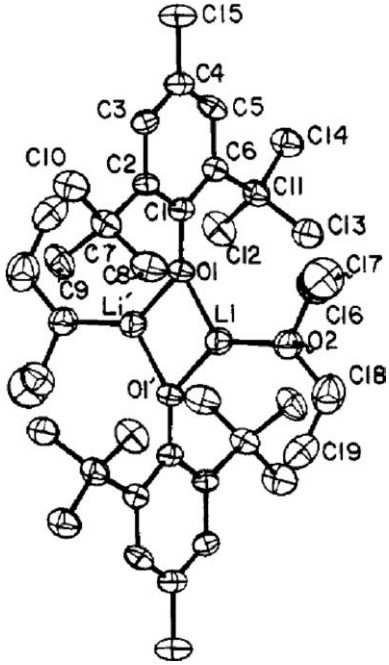

Fig. 11. ORTEP structure of $[Li(OC_6H_2Me\text{-}4\text{-}tBu_2\text{-}2,6)(OEt_2)]_2$ [48].

to the surface of the sphere. Hence, it possesses unexpectedly good solubility in hydrocarbons (Fig. 11).

$$2n\mathrm{BuLi} + 2\mathrm{ArOH} \overset{\mathrm{OEt_2}}{\rightarrow} (\mathrm{LiOAr} \cdot \mathrm{OEt_2})_2 + 2\mathrm{C_4H_{10}} \qquad (4)$$

2.2.3. Enolates

The enolate anions are other widely used ligands in the construction of clusters. An enolate is a nucleophilic reagent through the carbon as well as the oxygen atom and is very useful in organic synthesis.

Seebach [51] has shown that the chemistry of lithium enolates is well developed. The aggregates generally form dimers, tetramers or hexamers. The cited examples show that the degree of aggregation depends less on the structure of the enolate but on the otherwise present complexing agents [52]. Thus, dimers are more readily formed in the presence of polydentate ligands, i.e., ethylene diamine and its derivatives, whereas tetramers are obtained with ether ligands such as THF [51,53]. In solution, aggregates are formed as well, as for instance the lithiated derivative of isobutyrophenone which exists as a tetramer with a heterocubane structure, oxygen and lithium alternating on the corners of the cube [54,55].

In 1981, reports of two lithium enolates derived from pinacolone and cyclopentanone were published. Already identified in solution, they also form tetramers in the solid state, their structure being based on the heterocubane Li_4O_4 moiety, with the lithium atoms also solvated by one THF each [56]. In 1985, Williard and Carpenter [57] described the structure of the unsolvated lithiated pinacolone, which forms a hexamer. With sodium and potassium, the corresponding pinacolones

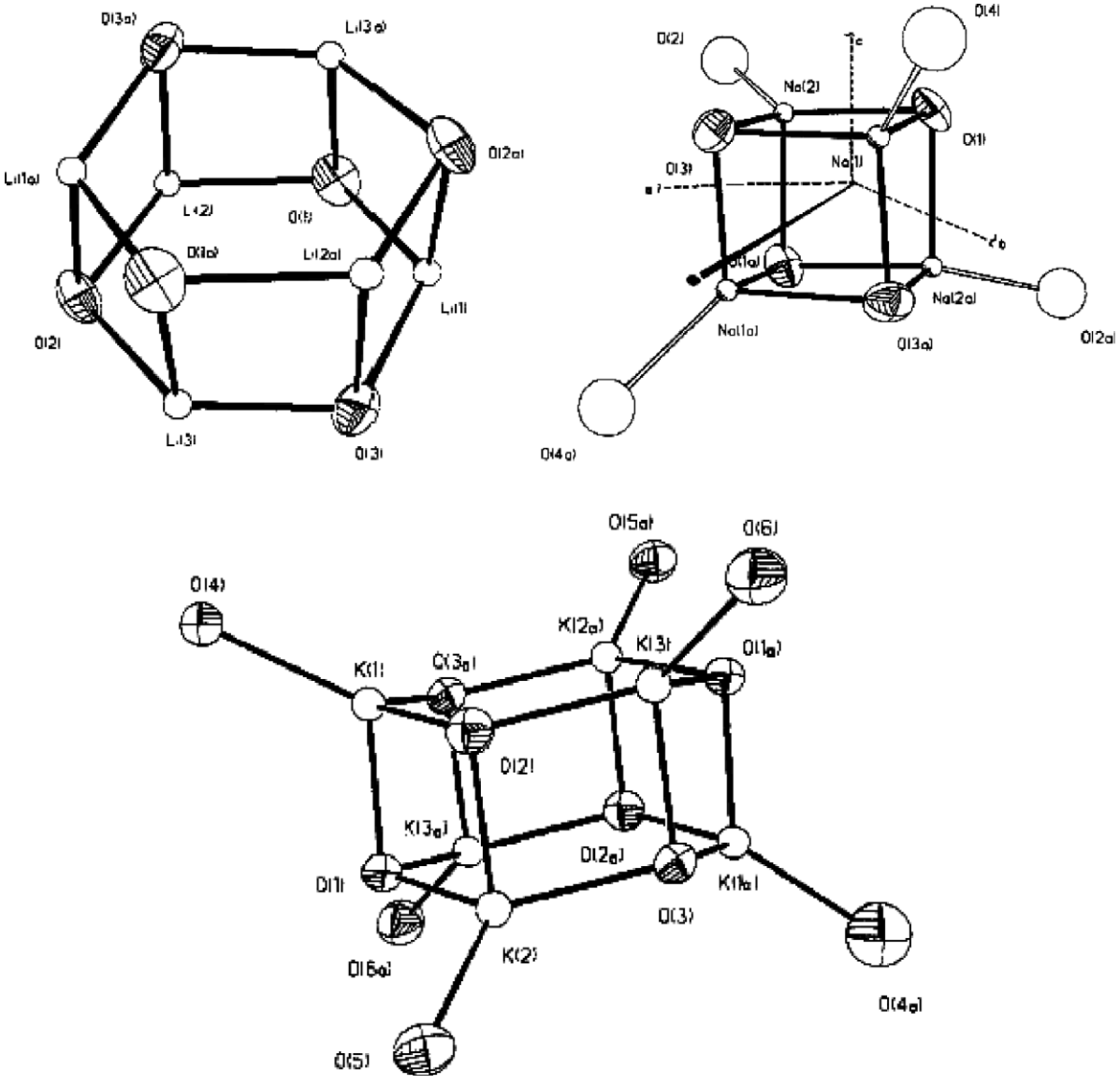

Fig. 12. ORTEP structure comparison for metallated pinacolone with Li, Na, and K, solvated and un-solvated structures [57,58].

were also obtained by reaction of the metal amide with pinacolone [58]. This allows comparison of the structures as a function of the cation size (Fig. 12). Thus, the tetrameric enolate of sodium, solvated by pinacolone, $[NaOC(=CH_2)(t\text{Bu})\{O=C(Me)(t\text{Bu})\}]_4$ presents similarities with the cubane structure of the lithiated compound solvated by THF, $[LiOC(=CH_2)(t\text{Bu})(thf)]_4$. The non-solvated lithiated pinacolone $[LiOC(=CH_2)(t\text{Bu})]_6$ forms a hexamer in which the presence of π interactions of the $=CH_2$ groups and the lithium cations inhibits the stacking of the Li_3O_3 cycles [58]. For the potassium compound, the stacking is inhibited by solvating THF molecules, so that a hexamer, $[KOC(=CH_2)(t\text{Bu})(thf)]_6$, is obtained [57].

This solvated potassium structure can be compared to the tetrameric sodium compound described earlier. The size of the aggregate has been found to apparently augment with the size of the cation, which is the inverse tendency, observed for non-solvated M*O*t*Bu*. The unsolvated lithium derivative has the same structure as the solvated higher homologues, so that solvation generally leads to smaller clusters and inhibits aggregation. Comparing the hexameric structures reveals that the larger potassium ion is displaced out of the hexameric prism, whereas the lithium resides more inside of the prism. The differences in structure are also probably responsible for the differences in reactivity. With a sterically more important Lewis base, the lithium pinacolone forms dimeric units, $[LiOC(=CH_2)(t\text{Bu})(tmeda)]_2$, [59] with the typical M_2O_2 rings and a coordination number of four for the lithium ions.

2.3. Homo-metallic hetero-ligand clusters

In 1995, Williard et al. described a homo-metallic dimer which was obtained from a mixture of anionic ligands, one alkoxide and one amide. $[\{Pr_2NLi\}\{(Me_2NCH_2)_2CHOLi\}]_2$ was obtained by reaction of *n*BuLi on di-isopropylamine and 1,3-bis(dimethylamino)-2-propanol in hexanes [60]. The structure consists of two four-membered cycles [LiNLiO], which are linked together via a $[LiO]_2$ unit in order to give a ladder-like motif (Fig. 13). This structure has been confirmed by ^{6}Li NMR in solution.

With sodium, homo-metallic hetero-ligand clusters exist as well. Thus, Bock et al. [61] have recently described a cluster with 14 sodium ions, $[(Na_8O)Na_6(bpy)_6(tmeda)_6]$, which compares well to the general structure that transition metal clusters adopt with the metal atoms in the cluster core, protected by bulky ligands. Two types of ligands act as protecting ligands: one with oxygen and the other with nitrogen donor atoms (Fig. 14).

2.4. Hetero-metallic hetero-ligand clusters

As described above, the organo-lithiated compounds MR, (alkyls, amides or enolates) with alkali metal alkoxides M′OR′ (M = Na, K, Rb, Cs; R′ = O*t*Bu), for instance BuLi/KO *t*Bu, are known as superbases. These reagents with enhanced reactivity are capable of chemo-, region- or stereo-selective reactions compared to the all-lithiated compounds [1]. The increase in reactivity of the obtained mixtures of RLi/MOR′ seems to be due to metal ion exchange, yielding RM/LiOR′. Electrostatically, the interaction of the small and hard cation Li^+

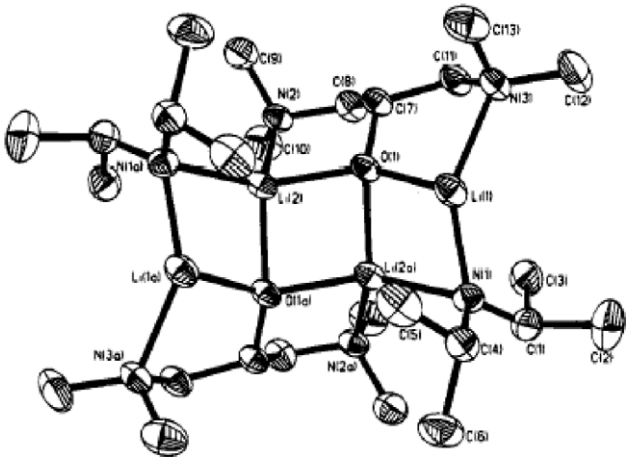

Fig. 13. Ladder ORTEP structure of $[\{Pr_2NLi\}\{(Me_2NCH_2)_2CHOLi\}]_2$ [60].

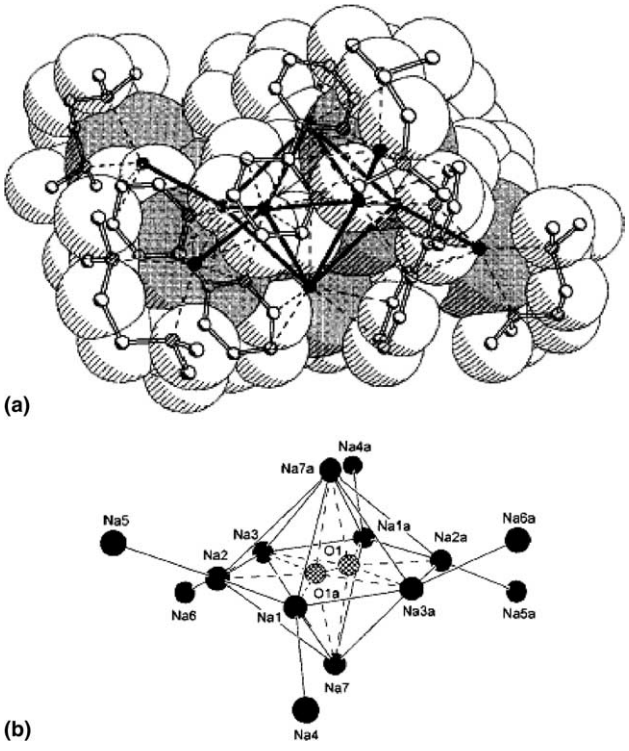

Fig. 14. Space filling model (a) and cluster core (b) of $[(Na_8O)Na_6(bpy)_6(tmeda)$ textsubscript6] [61].

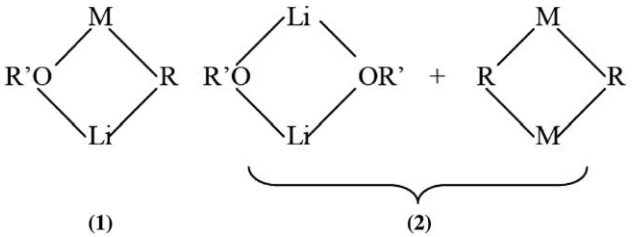

Scheme 1. Formation of superbases.

with the hard oxygen anion is favorable. In addition to this, these compounds form aggregates in solution as well as in the solid state [62–64]. The aggregates can exist either as mixed aggregates of monomers RM and R′OM (1) or as separate aggregates RM and R′OLi (2), as shown in Scheme 1.

The crystallization of such clusters is extremely difficult, as generally a simple mixture of compounds leads to the precipitation of homo-metallic species. This does however not exclude the existence of the mixed metal compounds in solution, as these precipitates simply correspond to the less well soluble species [65,66].

Mixed-metal hetero-ligand compounds were, for instance, obtained by heating to reflux an equimolar mixture of sodium 2,4,6-trimethyl-phenoxide with *n*BuLi in hexanes under an inert atmosphere [67]. The single crystal structure of the obtained compound can be described as a tetrameric aggregate of the composition $[Li(OC_6H_2\text{-}4,6\text{-}Me_2\text{-}2\text{-}CH_2Na)(tmeda)]_4$, and it is the very first example of a mixed aggregate between an organo-sodium compounds and a lithium alkoxide. The ligand plays the role of both R and R′ (Fig. 15).

In 1989, the group of Williard et al. co-crystallized at low temperature the *tert*-butoxides of lithium or potassium with the pinacolates of lithium or potassium in THF. They obtained the first hetero-metal (Li/K) hetero-ligand (alkoxide/enolate) compound $[Li_4\{OC(=CH_2)(t\text{Bu})\}_4K_4(O t\text{Bu})_4(KOH)(thf)_5]$ [68]. The cations and oxygen atoms form a dome (Fig. 16), protected by the diverse ligands.

The same group has also described the first example of a hetero-metallic enolate which contains a protic ligand, a secondary amide, in its structure. Thus, the deprotonation reaction of pinacolone with LDA/NDA leads to the formation of a cluster with six metal ions, $[Li_2Na_4\{C(=CH_2)(t\text{Bu})\}_6(HNiPr_2)_2]$ [69]. It has an open hetero-cubane structure, where two $[LiNa_3O_4]$ cubes with one open edge are fused together via a $[Na_2O_2]$ face. It can also be described as partially open ring-stacking structure where two $[LiO_2Na]$ rings sandwich a $[Na_2O_2]$ ring (Fig. 17).

Two of the sodium ions are pushed slightly out of the cubanes due to their larger size compared to lithium and their interaction with the di-isopropylamine molecules.

Following this result, sodium was introduced in many other organo-lithium compounds in order to obtain more basic and nucleophilic reagents which are more performing than the simple lithiated homologues. With the same aim to increase reactivity and selectivity, the first trimetallic alkali metal clusters were synthesized, following the reaction below [70]

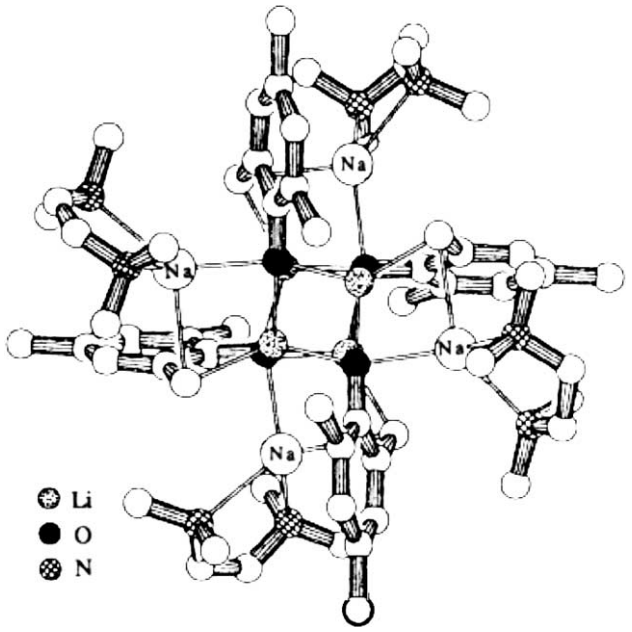

Fig. 15. Structure of $[Li(OC_6H_2\text{-}4,6\text{-}Me_2\text{-}2\text{-}CH_2Na)(tmeda)]_4$ [67].

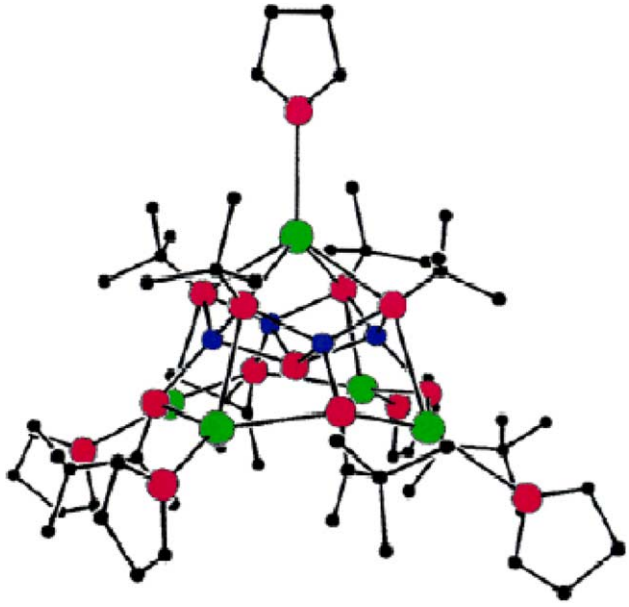

Fig. 16. Structure of $[Li_4\{OC(=CH_2)(t\text{Bu})\}_4K_4(O t\text{Bu})_4(KOH)(thf)_5]$ [68].

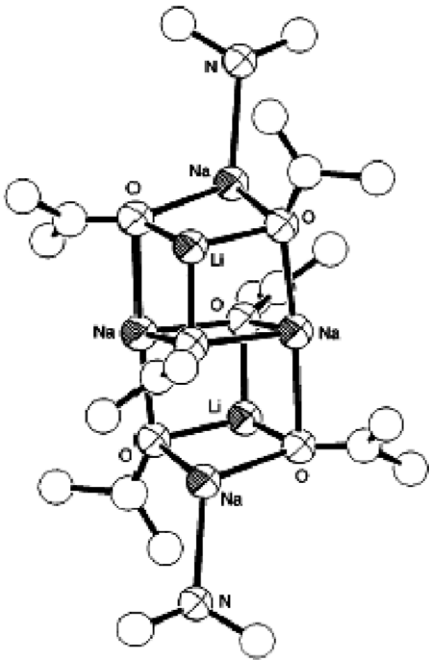

Fig. 17. ORTEP structure of $[Li_2Na_4\{OC(=CH_2)(t\text{Bu})\}_6(HNiPr_2)_2]$ [69].

$$2RN(H)Li + {}^{t}BuONa + {}^{t}BuOK + 2tmeda \xrightarrow{\text{hexane}} 1/2(\{[RN(H)]_2({}^{t}BuO)LiNaK(tmeda)_2\}) \quad (R = Ph \text{ or } p\text{-}CH_3C_6H_4\}) \quad (5)$$

These clusters, derived from the parent (*n*BuLi) (*t*BuOK), contain a mixture of alkali metal ions as well as anions, alkoxides, and amides. The two compounds presented here, which are formed from *p*-toluidine and lithiated anilide, are isostructural [71]. The compound $[\{[PhN(H)]_2(t\text{BuO})LiNaK(tmeda)_2\}_2]$ is one of the first examples combining two distinct anions, amide and alkoxide. It is obtained from a reaction containing lithium anilide, NaO*t*Bu and KO*t*Bu in the presence of tmeda in hexanes. The cluster crystallizes in a centrosymmetric space group, where four out of the six cations, two Li and two Na, possess a distorted tetrahedral coordination, and the larger potassium ions have a coordination number of six resulting from a distorted octahedral environment. Whereas the sodium ions are only linked to nitrogen atoms of the amide or tmeda, Li^+ and K^+ interact with nitrogen and oxygen donor atoms of the ligands (Fig. 18). This cluster can also be described as assembly of two hetero-metallic cycles of [NaNLiN] with the homometallic cycle K_2O_2, linked perpendicularly (Scheme 2).

Considering this structure as a model for superbases as far as their reactivity is concerned, it is probable that the amides, which are responsible for deprotonation of the protic substrate, probably form a σ-bond to the lithium cation and two more elongated, and therefore less strong bonds, to the sodium and potassium ions.

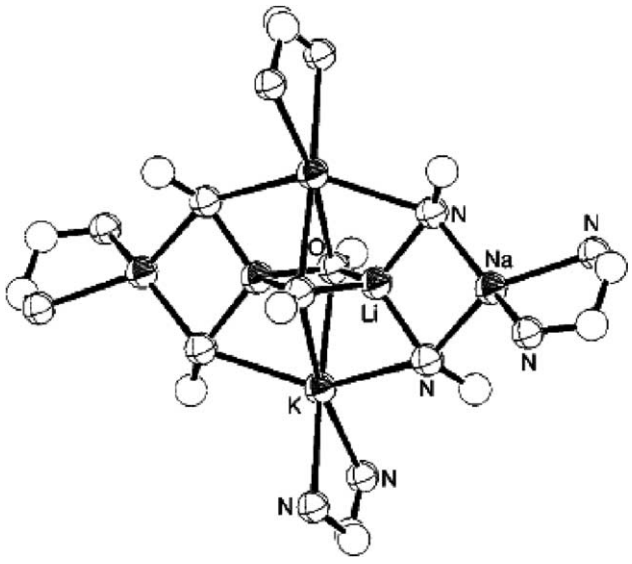

Fig. 18. ORTEP structure of $[\{[PhN(H)]_2(t\text{BuO})LiNaK(tmeda)_2\}_2]$ [71].

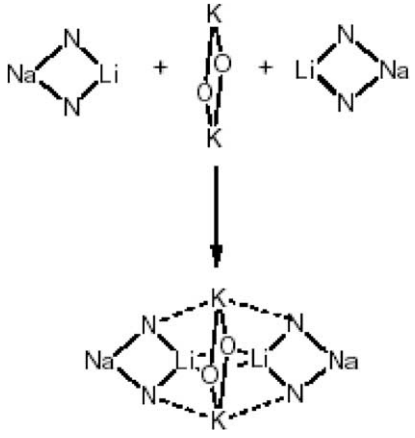

Scheme 2. Possible formation of $[\{[PhN(H)]_2(t\text{BuO})LiNaK(tmeda)_2\}_2]$ [71].

This could render the amides more cleavable and, therefore, more reactive than if they were linked to the same metal ion, as it is the case in the lithium amides where ladder-type, polymeric structures are observed.

2.5. Homo- and hetero-metallic clusters with diverse ligands

Other anions can intervene as well in the constructions of clusters, such as hydrides, oxo, peroxo, and hydroxyl-groups and they can be considered as models for superbases as well. Thus, the largest lithium cluster ever registered so far contains 33 lithium ions and is based on *tert*-butoxide and hydride, $[Li_{33}H_{17}(Ot\text{Bu})_{16}]$ [72]. It has been obtained by photolysis of a 7:3 mixture of *t*BuOLi/*t*BuLi, a synthetic method which has not been explored very much so far. The structure consists of

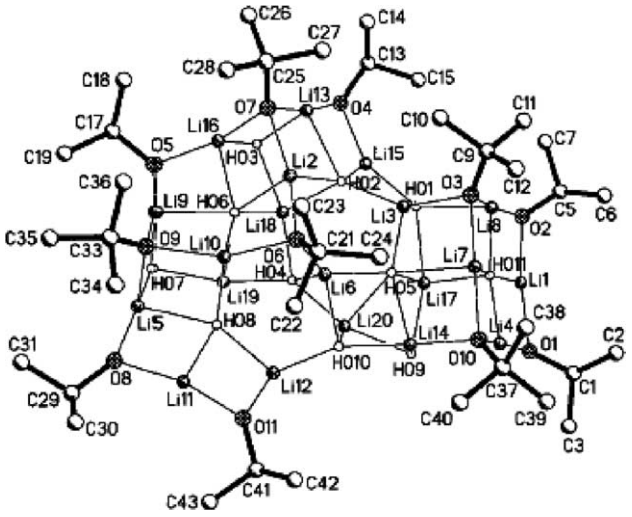

Fig. 19. Structure of $[Li_{33}H_{17}(OtBu)_{16}]$ [72].

several fused cubes of lithium hydride whose expansion into infinity is limited by the presence of bulky O*t*Bu groups at the periphery of the cluster. The latter are also responsible for the good solubility of the cluster in non-polar solvents (Fig. 19).

Homo- and hetero-alkali metal clusters with amino-alkoxide anions, $[Me_2N(CH_2)_2OLi]_8$ and $[\{Me_2N(CH_2)_2O\}_2Li_8K_6]O$, have been obtained only recently [73]. They are obtained from the reaction of *n*BuLi, respectively, *n*BuLi/*n*BuK on DMAEH ($=N,N'$-dimethyl amino ethanol), and their structures are shown below (Fig. 20).

Both form cage-type structures. The lithium compound is reminiscent of a trimer $(LiO)_3$ in form of a hexagonal anti-prism to which a dimer $(LiO)_2$ has been fused. The hetero-metallic cluster is comprised of a quasi spherical structure, incorporating an oxo-anion in the center of the structure, the remainder of traces of water during the reaction.

A decanuclear compound, $[Li_8K_2(O)(OtBu)_8(tmeda)_2]$, was also characterized in the solid state. It forms a polyhedron with 16 vertices (Li_8O_8) which are constructed around a central oxo-anion. This polyhedron can also be described as superposition of two $(LiO)_4$ rings. The potassium ions are then linked at the outside of the polyhedron and chelated by the tmeda molecules (Fig. 21) [74]. Again, the product is obtained by serendipity in the presence of traces of water during the reaction of *t*BuNHLi with KO*t*Bu in the presence of tmeda.

The heterometallic compound $[\{tBuOLi)_5(tBuORb)_4(Li_2O_2)(tmeda)_2\}_\infty$ [75] has oxo, alkoxide, and N-donor ligands and possesses a cage-like structure with 11 metal ions. The clusters are linked via the tmeda molecules, leading to a polymeric chain of clusters (Fig. 22).

In order to synthesize a compound similar to the previous one but without oxo-anions, Mulvey et al. obtained the mixed-metal cluster $[Li_4K_4(OtBu)_8]$ from a toluene solution of the two starting products in equimolar proportions. An empty cage structure is built (Fig. 23) [76]. The cluster is formed of fused M_2O_2 rings.

Another octanuclear compound is obtained with a mixture of anions when KO*t*Bu is reacted with

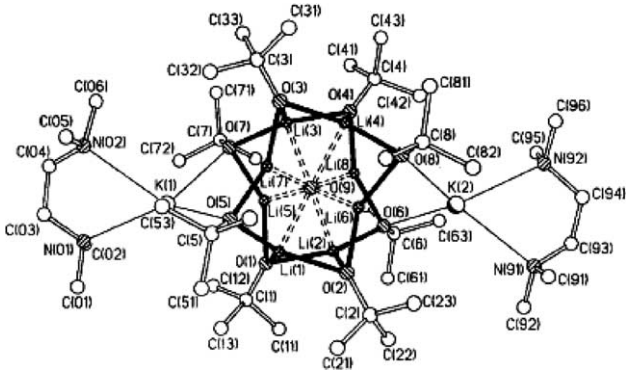

Fig. 21. Structure of $[Li_8K_2(O)(OtBu)_8(tmeda)_2]$ [74].

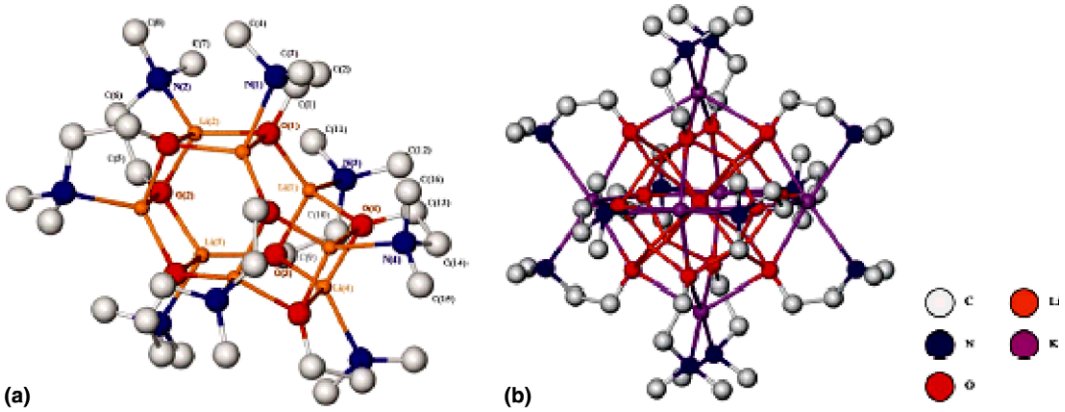

Fig. 20. Structures of $[Me_2N(CH_2)_2OLi]_8$ (a) and $[\{Me_2N(CH_2)_2O\}_{12}Li_8K_6]O$ (b) have been obtained only recently [73].

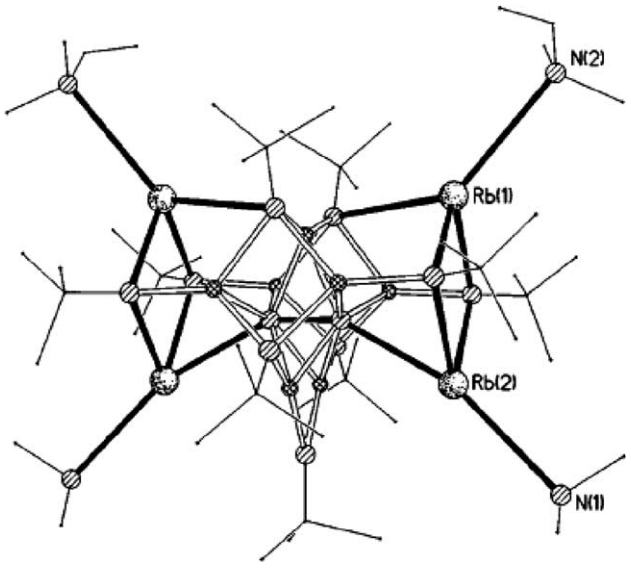

Fig. 22. Structure of $[\{t\text{BuOLi})_5(t\text{BuORb})_4(Li_2O_2)(tmeda)_2\}_\infty]$ [75].

*t*BuNHLi in benzene [77]. Again, the structure is formed of rings, (M-heteroatom)$_2$, this time two (Li_2N_2) and two (K_2O_2) rings are oriented quasi-perpendicular to each other. The rings are attached to each other via rather short Li–O contacts (1.872 Å) compared to the ones in Li*O*t*Bu (1.96 Å) [78]. Identical rings are parallel to each other. Benzene molecules act as η^6 and η^3-ligands toward potassium ions, linking the clusters to infinite chains by this type of π-interaction (Fig. 24).

Nonanuclear compounds of group I metals have recently been obtained, based on alkoxides, amides, and hydroxide. The compound $[Li_4Na_4(t\text{BuO})_4\{PhN(H)\}_4(NaOH)(4\text{-Me-py})_4]$ was obtained either by reaction of lithium anilide with Na*O*t*Bu or vice versa from the sodium anilide with Li*O*t*Bu, both in the presence of the substituted pyridine ring [79].

The structure is composed of a dome-like arrangement with 17 summits, based on a tetrameric ring (Na–N)$_4$. Above this ring, another ring of (Li–O)$_4$ is placed which is capped by a fifth sodium ion in apical position. The OH group is found in the centre of the dome (Fig. 25a).

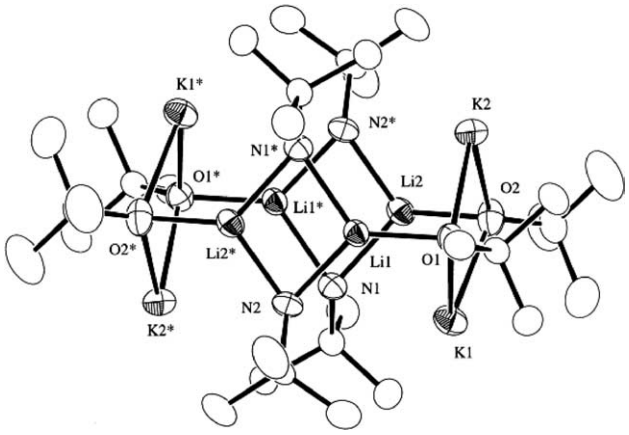

Fig. 24. ORTEP structure of $[LiK(Ot\text{Bu})(NHt\text{Bu})]_4$ [77].

This structure resembles very much the one obtained for the mixed metal cluster obtained by Williard and MacEwan [68] $[Li_4K_4(t\text{Bu})_4(C_6H_{11}O)_4(KOH)(thf)_5]$ (Fig. 25b). It was the first compound combining alkoxide ligands and enolates within such a cluster structure. The enolates form with the potassium ions the lower rim of the cluster, followed in the layer above by the tetrameric LiOR-unit in one plane, which is finally capped by one potassium ion. The latter carries additionally one THF-ligand. The encapsulation of hydroxide is explained by traces of water being present during the reaction.

2.6. Hetero-metallic compounds of group I and II with diverse ligands

The two structures described above possess OH groups in their structure derived from NaOH and KOH.

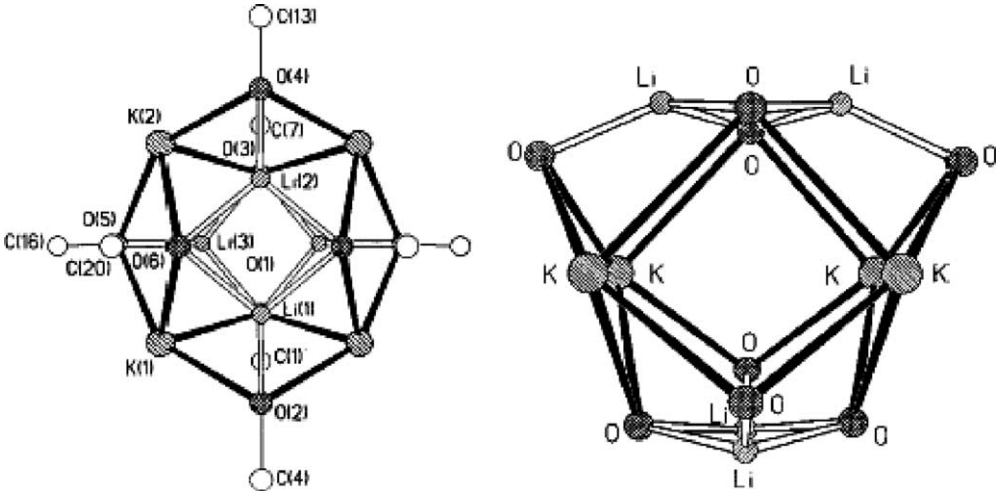

Fig. 23. Structure and core of $[Li_4K_4(Ot\text{Bu})_8]$ [76].

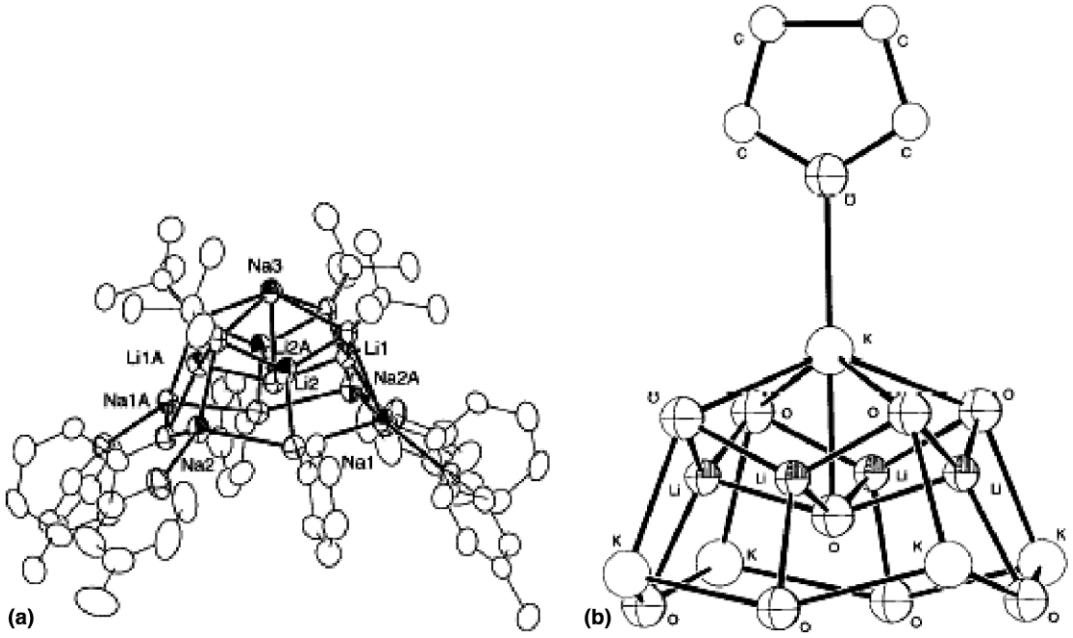

Fig. 25. ORTEP structure of $[Li_4Na_4(t\text{BuO})_4\{PhN(H)\}_4(NaOH)(4\text{-Me-py})_4]$ (a) [79] and $[Li_4K_4(t\text{Bu})_4(C_6H_{11}O)_4(KOH)(thf)_5]$ (b) [68].

Very recently, penta nuclear clusters with group I and group II metals as well as mixed ligands of type $[IM(\text{-LiO}t\text{Bu})_4(OH)(thf)_4]$, M = Sr, Ba, have been reported by the authors' group (Fig. 26) [32,33,80]. The structure resembles the former two compounds and is to our knowledge the first one incorporating a IM(OH) entity. Similar to the other two structures described above, the structure contains a square anti-prismatic arrangement of lithium and oxygen atoms of a $(\text{LiO}t\text{Bu})_4$ tetramer. Instead of a capping alkali metal, Na^+ or K^+, this has been replaced by an isoelectronic fragment, $(MI)^+$, M = Sr, Ba. Furthermore the lower rim of the dome, consisting either of $(NR)_4$- or $(KO)_4$-units, has been removed. However, adding such a reagent to the reaction mixture in order to obtain a much larger group I/II mixed metal cluster should be possible.

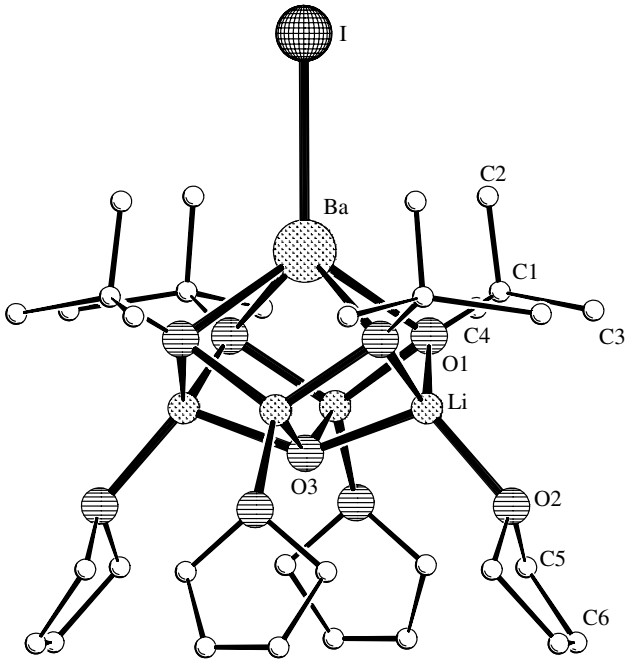

Fig. 26. Structure of $[IM(\text{LiO}t\text{Bu})_4(OH)(thf)_4]$, M = Sr, Ba, H-atoms omitted [32,33,80].

Mixed-anion group I/II metal clusters as described above are rather rare. One example is the $[Ba_6Li_3O_2(Ot\text{Bu})_{11}(thf)_3]$ [81]. The synthesis is successful when using metallic barium which reacts with *tert*-butanol in the presence of *n*BuLi in hexanes. The structure of the $Ba_6Li_3O_2$-core of the cluster contains two oxo-anions, one of which is surrounded by six barium cations in form of an octahedron and the other by a prism of three barium and three lithium ions. Both structural features are fused via the triangular Ba_3-face of both polyhedra. The cluster core is charged 11+, which is neutralized by the O*t*Bu groups, which form a lipophilic mantle around the core assuring the kinetic stability of the compound (Fig. 27).

The following series of compounds give an example of how a central anion such as the oxo or peroxo ion can be integrated under controlled conditions, not only by serendipity. Metallation of the N-donor ligand 2,2,6,6-tetramethylpiperidine $Me_2C(CH_2)_3CMe_2NH$ yields the homometallated lithiated compound $[\{Me_2C(CH_2)_3CMe_2NLi\}_4]$, which adopts a cyclic structure (Fig. 28) [82].

Two of the lithium ions can then be substituted by two Mg^{2+}, which possess a similar size to give a 2+ charged complex. The additional charge will then be

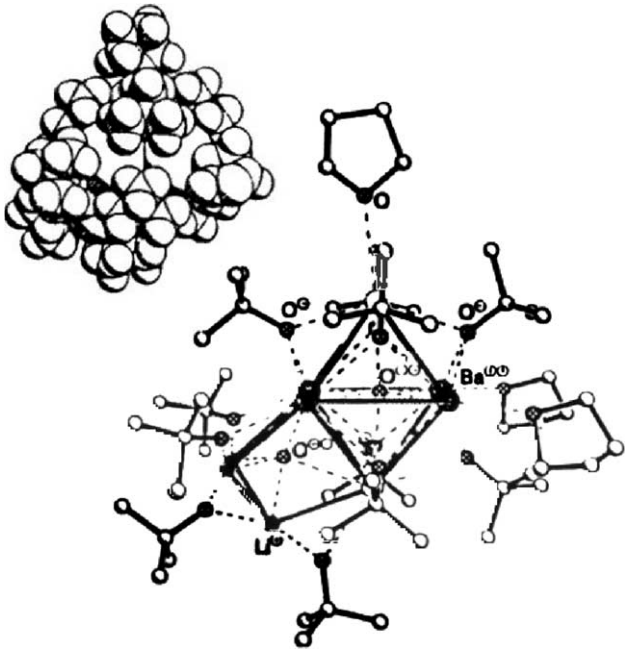

Fig. 27. Structure of $[Ba_6Li_3O_2(OtBu)_{11}(thf)_3]$ [81].

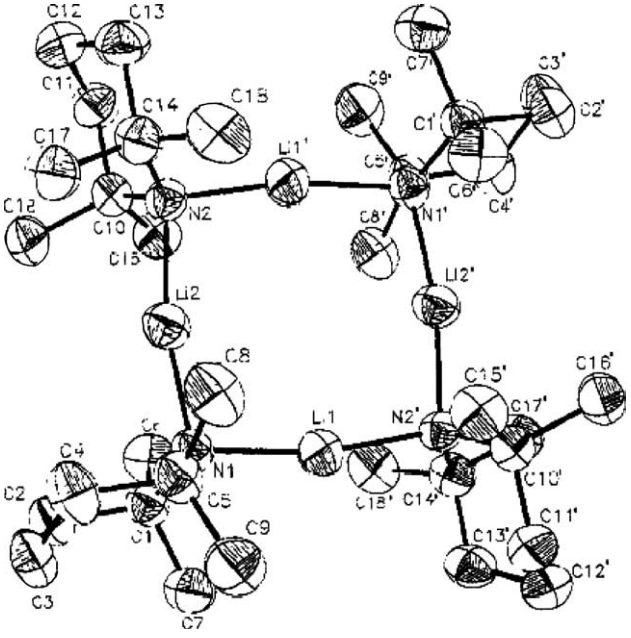

Fig. 28. ORTEP structure of $[\{Me_2C(CH_2)_3CMe_2NLi\}_4]$ [82].

compensated by introducing an oxo anion in the centre of the structure (Scheme 3) [71].

Similarly, the compound $[\{(Me_3Si)_2N\}_4Li_2Mg_2(O_2)]$ was obtained, and this time the resulting compound possesses a central peroxo-anion (Fig. 29) [83].

This type of compound can be classified as a molecular oxide as well as an intermetallic amide, and their possible applications in the synthesis of new materials or in organic synthesis remain promising and need to be studied. Thus, the performances of such compounds can be improved when certain alkali metal amides are paired with the corresponding magnesium bis-amides [84]. The obtained basicity can then be useful to polymetallate a metallocene [85]. Therefore, this chemistry has been developed recently and mixed metal lithium–sodium–magnesium alkoxides/di-idopropyl-amides, $[\{MMg(NiPr_2)_2OR\}_2]$, M = Li, Na; R = *n*Bu or *n*Oct, have been obtained by reaction of a mixture of the amides with the appropriated alcohol [86]. The characterized structures of these compounds can be attributed to the ones called "inverse crowns" due to their inversed topology compared to the classical crown ethers. Thus, the cations are found in the host part of the structure

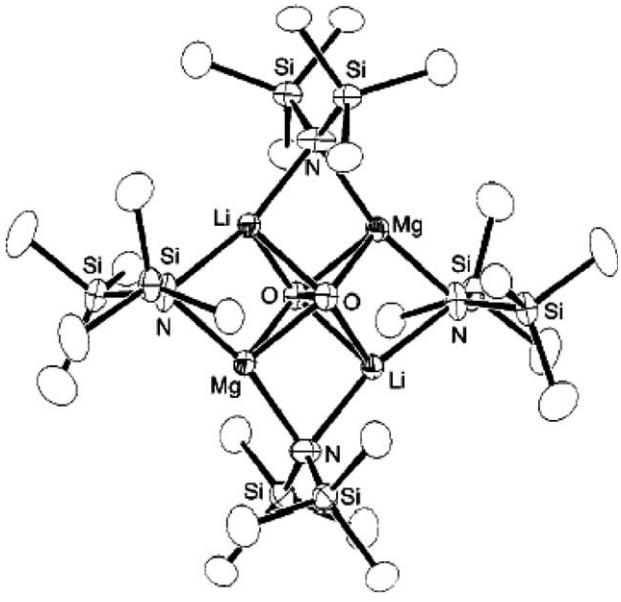

Fig. 29. ORTEP structure of $[\{(Me_3Si)_2N\}_4Li_2Mg_2(O_2)]$ [83].

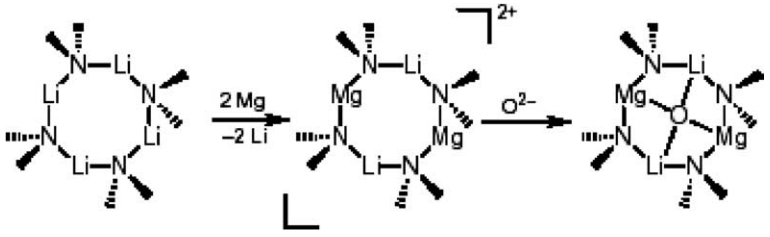

Scheme 3. Formal substitution of two Li^+ by $(Mg_2O)^{2+}$ [71].

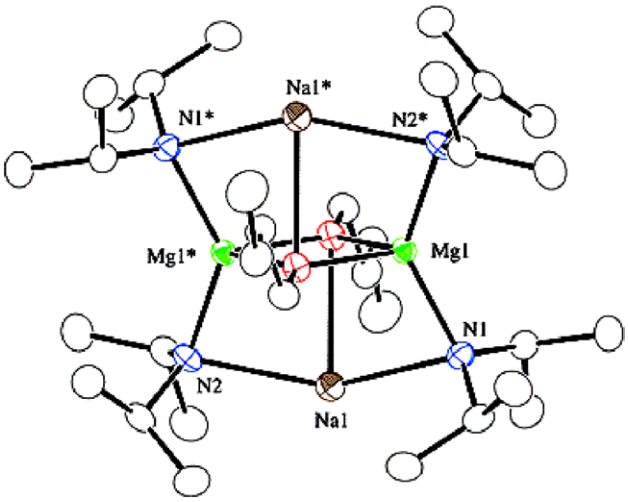

Fig. 30. ORTEP structure of [{MMg(N*i*Pr$_2$)$_2$OR}$_2$]for M = Na, R = *n*Bu [86].

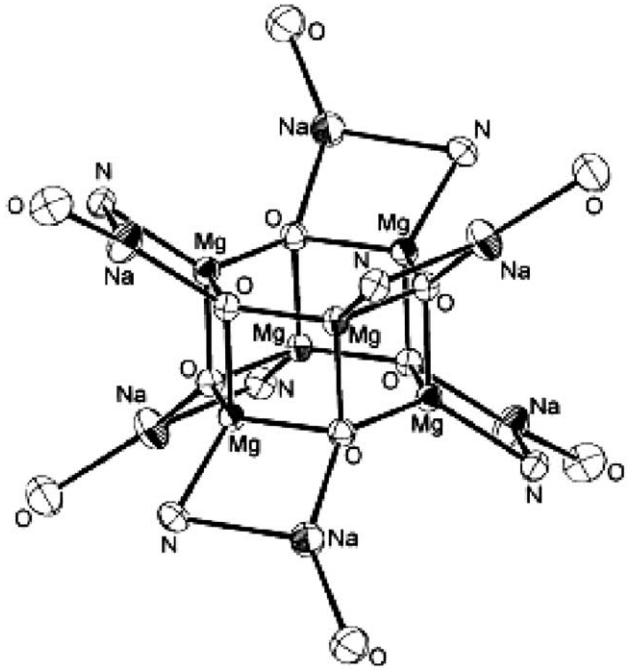

Fig. 31. ORTEP structure of [{NaMg(N*i*Pr)(O)(thf)}$_6$] with 12 metal ions in total [87].

whereas the oxo or peroxo anion is considered as guest (Fig. 30).

Some examples of inverse crown ethers are given in Scheme 4. The larger ones do, however, not contain

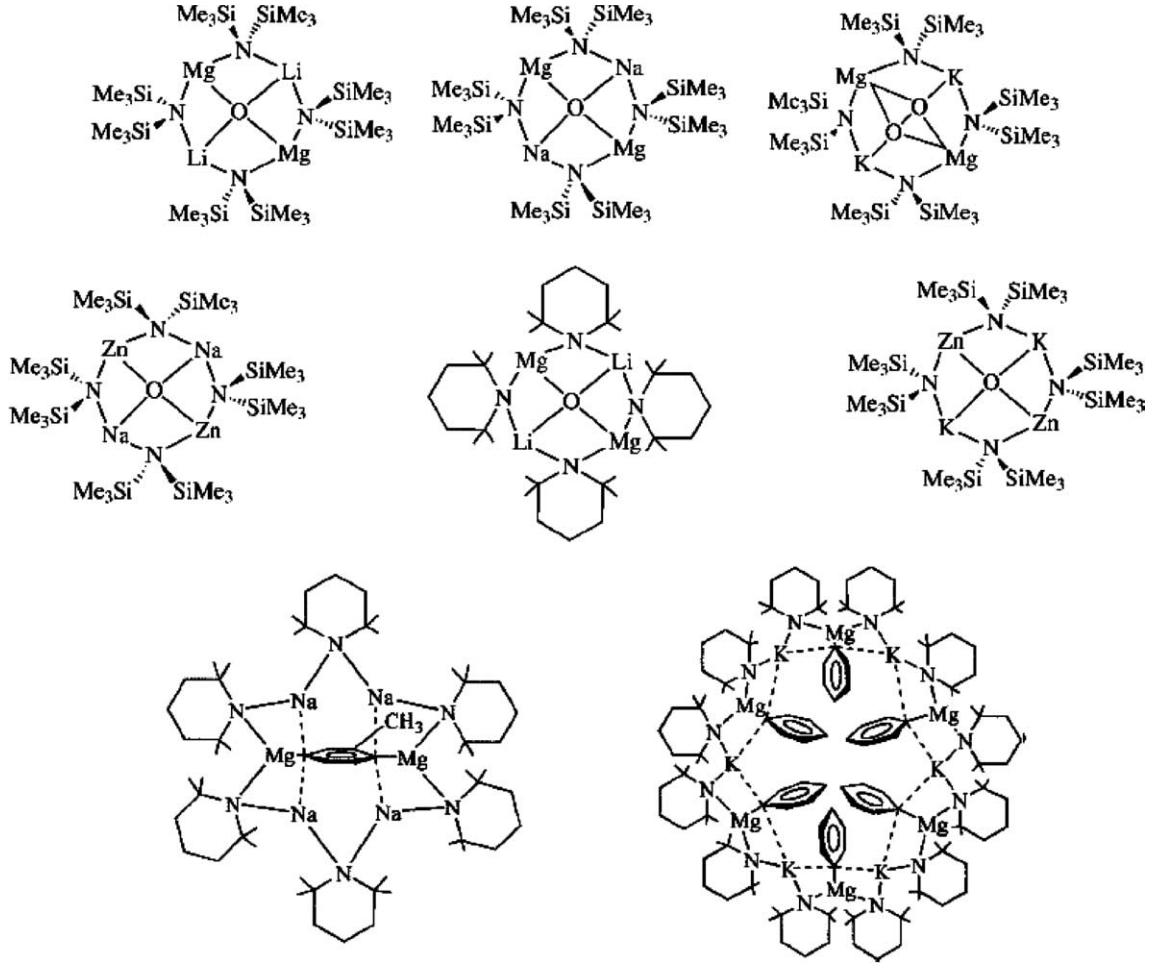

Scheme 4. Examples of inverse crown ethers.

oxygen atoms in their center and will, therefore, not be further discussed in this review.

One of the largest aggregates of this type containing oxygen is to our knowledge the hexameric $[\{NaMg(NiPr)(O)(thf)\}_6]$ with 12 metal ions in total [87]. Six magnesium ions combine with six oxo anions to form a hexagonal prism, which is capped by three sodium ions on either rim (Fig. 31).

3. Clusters of alkaline earth metals

3.1. Introduction and properties of alkaline earth metals

Some alkaline earth metal compounds were already encountered in the previous section when discussing group I/II heterometallic clusters of the superbasic type. Pure alkaline earth metal compounds are often also used as precursors for metal oxides with a view to applications in CVD [88] or for sol–gel processes [6,7], and the compounds of the heavier homologues have especially regained in interest in this context [89].

The utilization of sterically important ligands allows the heavier alkaline earth metal compounds to get out of the shadow of the beforehand studied compounds of magnesium, i.e., the well-studied Grignard reagents. As for the alkali metals, the number of examples of alkoxides is smaller than the better studied carbanionic species.

Concerning coordination, except for Mg^{2+}, the heavier group 2 ions have a non-saturated coordination sphere with medium sized ligands, such as ethyl, methoxy or Cp. In order to compensate for their higher coordination numbers (8–12, growing in the order Ca < Sr < Ba), irreversible formation of oligomers/polymers in the solid state or decomposition of the species occurs. The polarizability of the cations grows toward the heavier homologues, which renders the organic groups of these simple ligands more nucleophilic.

Monovalent species can be stabilized in gas matrices and at low temperatures. The radical species of organometallics have been shown to exist in the gas phase, i.e., $CpCa^{\cdot}$, $CH_3Ca^{\cdot}$, $HCCSr^{\cdot}$, etc. [90]. Apart from these examples, the alkaline earth metal ions have their oxidation state of 2^+. No redox chemistry is known as for transition metals. Usually, they form species like MLL′ or ML″, where the ligands are negatively charged, 1- or 2-, respectively. Anionic complexes with alkaline earth metal ions are quite rare, such as $K_2[(C_8H_8)_2Ca(dme)_2]$ [91] and $Li[Cp_2{*}BaR(thf)_2]$ [92]. The missing valence electrons lead to a kinetic lability of the ligands which are therefore generally easily split off.

As far as their relation between charge and size is concerned, the alkaline earth metal ions are similar to the alkali metal ions. They are rather hard and weakly polarizable [93,94]. The M–C bonds are usually polar and sensitive to humidity and oxygen. The alkaline earth metal compounds are in general ionic and soluble in water and polar solvents such as DMSO, ethers or amines. Organobarium compounds often exist as ion pairs, even in THF and pyridine. Coordinating solvents will generally lead to solvated ion pairs [95,96].

The influence of the ligand on the compound will be to avoid oligomerisation in the solid state as well as in solution, and to stabilize the Lewis base/acid adducts.

3.2. Magnesium compounds

3.2.1. Grignard-type reagents

Before describing the magnesium clusters obtained with alkoxides and aryloxides, one has to mention the Grignard reagents of the type RMgX, (R = Alkyl, X = halide), which were discovered in the early 20th century. Their use in organic synthesis is so important that they can be considered among the most important organometallic compounds. The Grignard reagents are generally synthesized by the reaction of a lithium organyl with a magnesium halide salt, following the equation:

$$LiR + MgX_2 \rightarrow RMgX + LiX \quad (6)$$

Even though they are mainly prepared and directly used in solution, the knowledge of their structure is important because it gives hints about possible coordination numbers and geometries, aggregates that might be formed in solution, as well as basic information for theoretical investigations of the compounds. In solution, the Schlenk equilibrium can be observed:

$$2RMgX(solvent)_x \rightleftarrows MgR_2(solvent)_y + MgX_2(solvent)_z \quad (7)$$

In ethers and other Lewis basic solvents, the compounds probably have similar coordination numbers than in the solid state.

3.2.2. Organomagnesium alkoxides, aryloxides, and carboxylates

The first synthesis of magnesium alkoxides dates back to the beginning of the 20th century [97–99], but only for the past 15–20 years have they found an application in organic chemistry, either as reagents or precursors for catalytic reactions [100–102]. Meanwhile, a few of the alkoxides could be isolated and characterized. For instance, the magnesium methoxide $[Mg(OMe)_2(MeOH)_{3.5}]$ possesses a molecular formula which can be written as $[Mg_4(\mu_3\text{-}OMe)_4(OMe)_4(MeOH)_8]$ (Fig. 32). Other examples are the tetrameric aggregates $[Mg_4(OCH_2CH(CH_2)_3O)_6Cl_2]$ and $[Mg(OCH(CH_3)CH_2OCH_3)_2]_4$ [40,103].

These compounds have been described as intermediates for the synthesis of polymerization catalysts for

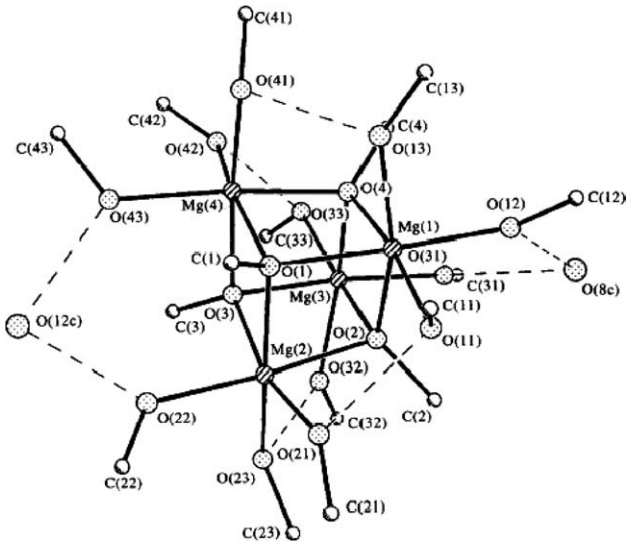

Fig. 32. Structure of $[Mg_4(\mu_3\text{-}OMe)_4(OMe)_4(MeOH)_8]$ [40,103].

alkenes. Based on the idea to have polymers of a certain form, one can build pro-catalysts of the same form with a good productivity and selectivity. Knowing that the compound $[Mg_4(OMe)_6(MeOH)_{10}]$ already exists [104], one can aim to synthesize a new cluster of Mg incorporating alcoxo species such as the bidentate 2-tetrahydro furfuroxo [105]. Such a compound would then be a good starting material for the preparation of polyalkene catalysts. This is the case with $[Mg_4\{OCH_2CH(CH_2)_3O\}_6Cl_2]$ (Fig. 33), which was obtained from the reaction of $Mg(OCH_2CH(CH_2)_3O]_2$ with $MgCl_2$ in CH_2Cl_2.

The structure consists of an almost regular rhombus of four Mg ions, with bridging oxygen atoms. Two types of Mg-ions are present: one of which is coordinated by six oxygen atoms quasi octahedrally and the other in a trigonal bipyramid of MgO_4Cl with a coordination number of 5.

With aryloxide ligands, dimers such as $[Mg(OAr)_2]_2$, ($OAr = OC_6H_2(CMe_3)_2Me = BHT$, and $OC_6H_3(CMe_3)_2 = BHB$), prepared by Ittel and coworkers [106], or the fluorinated species, $[Mg\{OC_6H_2(CF_3)_3\}_2(thf)_3]$ have been described [107]. Recently, a number of new compounds were obtained by reacting $MgBu_2$ with several derivatives of bulky phenols, such as 2,6-dimethyl-, 2,6-diisopropyl-, and 2,4,6-trichlorophenol, Hdmp, Hdip, and Htcp, respectively [108]. These ligands were chosen as they can increase the solubility of the product and are easily deprotonated. Depending on the Lewis bases present, monomeric compounds of type $[MgL_2(solvent)_3]$ with a trigonal bipyramidal arrangement around the metal ion are obtained. In the absence of a Lewis basic solvent, trimeric species are isolated in which the metal ions are arranged linearly with a coordination number of 4 for the central metal ions and 3 for the outer ones (Fig. 34). These structures have been determined spectroscopically.

With carboxylates, carbamato, and carbonato ligands, a large variety of Mg-clusters could be obtained, mainly hexameric ones in which the six magnesium ions adopt ring-like structures in boat or chair conformations, or rather build cage-like clusters as soon as an oxo-anion is incorporated (Fig. 35) [109].

3.2.3. Magnesium enolates

The enolates were generally obtained by reaction of an organometallic base, such as lithium amide or magnesium amide, on the ketone. In 1998, a new synthetic route was discovered, using halogenated bases such as R_2NMgX (Hauser bases), iPr_2NMgCl or iPr_2NMgBr, which allows the preparation of aggregates of magnesium enolates [110].

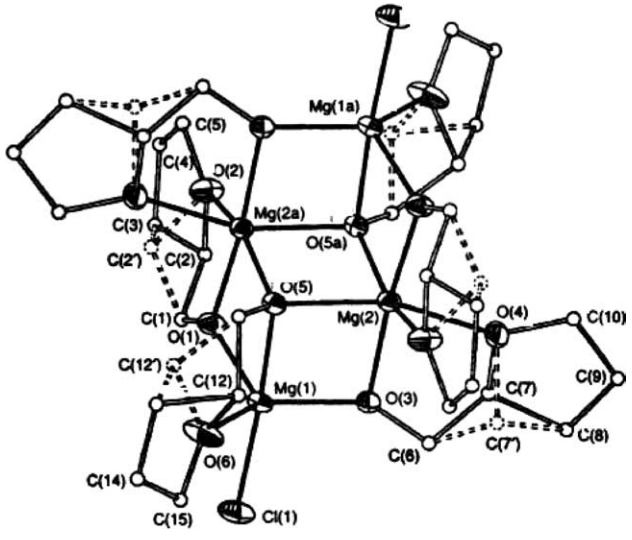

Fig. 33. ORTEP structure of $[Mg_4\{OCH_2CH(CH_2)_3O\}_6Cl_2]$ [105].

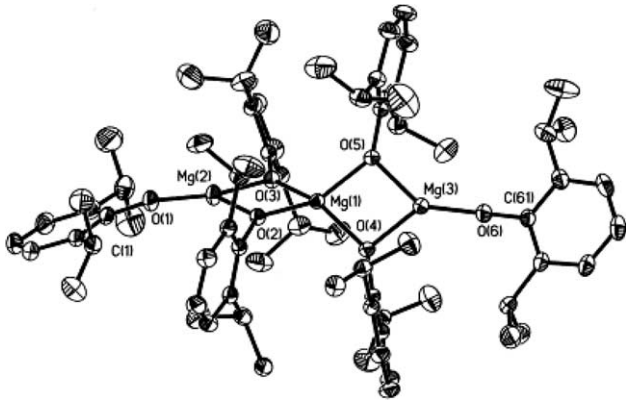

Fig. 34. ORTEP structure of $[MgL_2(solvent)_3]$ for L = 2,6-dimethylphenol [108].

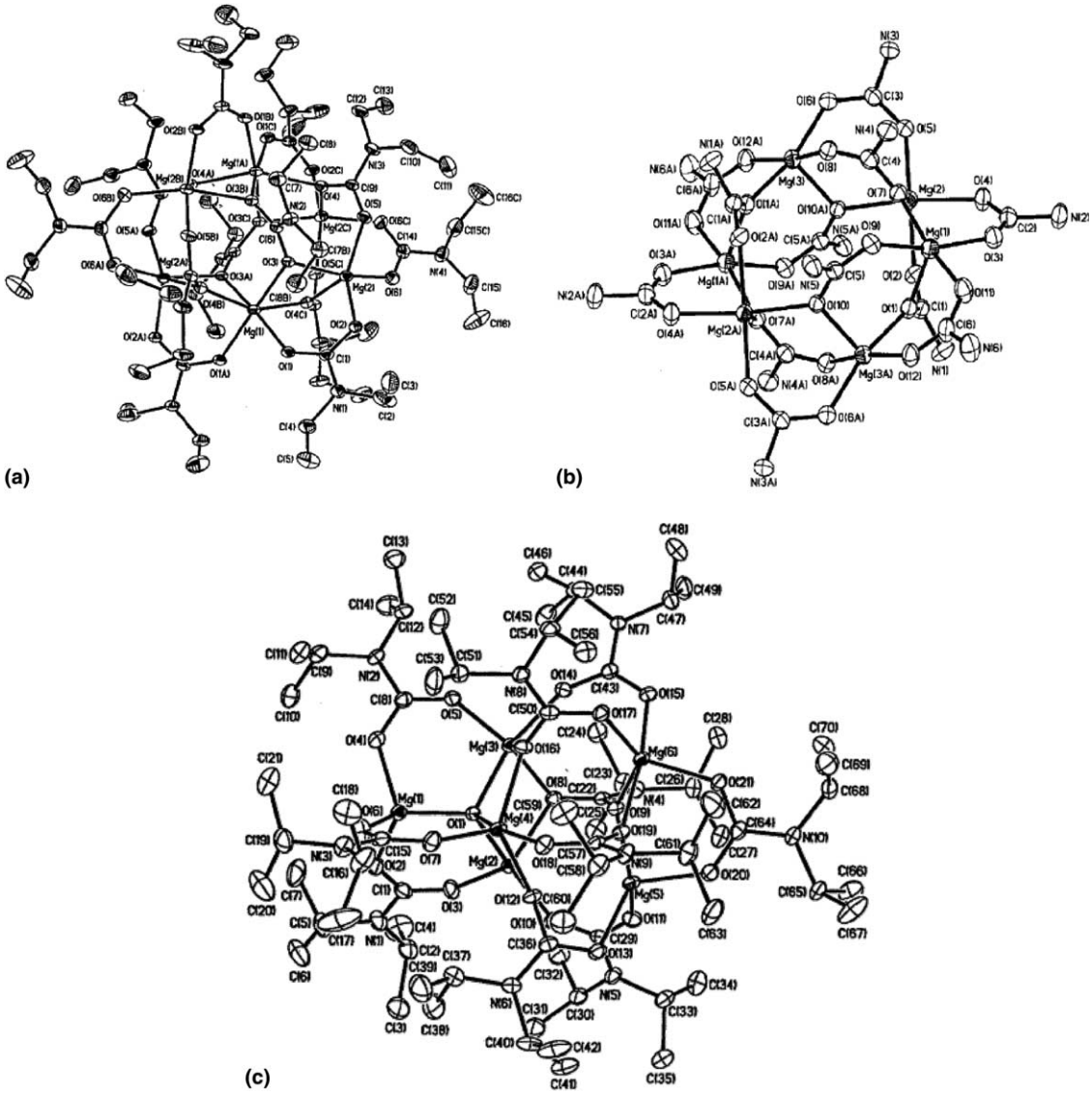

Fig. 35. ORTEP structure of: (a) $[Mg_6(O_2CNEt_2)_{12}]$, (b) $[Mg_6(O_2CNPh_2)_{12}]$, and (c) $[Mg_6(\mu_4\text{-}O)(O_2CN\mathit{i}Pr_2)_{10}]$ [109].

$$R_2NH + EtMgX \rightarrow R_2NMgX + EtH \quad (8)$$

$$R_2NMgX + R'CH_2C(=O)R'' \rightarrow R''(R'CH=)COMgX + R_2NH \quad (9)$$

Thus, the two compounds $[\{t\text{BuC}(=CH_2)\text{OMgBr(hmpa)}\}_2]$ and $[Me_2CHC(=CMe_2)O\text{-MgBr(hmpa)}]$ have been obtained from pinacolone, respectively, from di-isopropylketone, in ether. In both cases, the cations possess a coordination number of 4. Only the first one forms a dimeric structure (Fig. 36), whereas the ligand of the second compound is too bulky to allow oligomerization.

Non-solvated enolates exist also as trimers, as for instance in $[Mg_3(acac)_6]$ or its derivative $[Mg_3\{(Et_2O)_2P(O)CHC(O)Me\}_6]$ [52]. As the dications usually prefer an octahedral coordination sphere, MO_6-units with

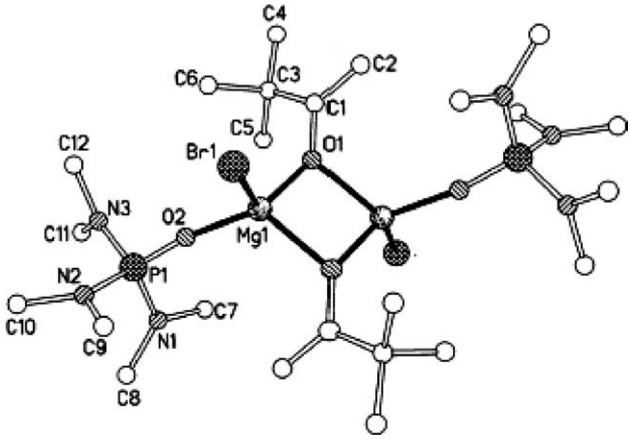

Fig. 36. Structure of $[\{t\text{BuC}(=CH_2)\text{OMgBr(hmpa)}\}_2]$ [110].

common faces similar to the ones found in transition metal enolates such as $[Zn_3(acac)_6]$ or $[Ni_3(acac)_6]$ are present in the structures [111,112]. Recently, the dimeric $[\{HC(C(Me)=N\text{-}2,6\text{-}iPr_2C_6H_3)_2\}Mg(\mu\text{-}OC(=CH_2)\text{-}2,4,6\text{-}Me_3C_6H_2)]_2$ was described. It forms an eight-membered ring MgOCCMgOCC and is an excellent catalyst for the syndioselective polymerization of methyl methacrylate [113].

3.3. Compounds of the heavier alkaline earth metals

Recently after the discovery of Grignard compounds in 1900, their heavier homologues appeared in the literature [114]. Even though they were intensely studied by Gilman et al. [115,116], these compounds could not be used in a similar fashion to the Grignards, because of the difficult synthesis of RMX, their thermal instability, and their insolubility in organic solvents compared to their magnesium homologues.

Only the synthesis of high temperature superconductors containing alkaline earth metal oxide has revived the interest in group II compounds [117–120]. They could be molecular precursors [11,121] for compounds such as $YBa_2Cu_3O_7$ [122–124] or for the deposition in thin films of catalysts, for instance ABO_3, A = Ca, Sr, Ba and B = Ti, Zr, Ce [125,126].

3.3.1. Principles of CVD and sol–gel methods

The technique of CVD in general is based on the decomposition/thermolysis of organometallic volatile precursors. The precursors must be volatile at low temperatures, easy to synthesize and handle, and void of impurities which might influence the epitaxy of the deposits as thin layers or powders [127,128]. In order to make superconductors as described above [122–124], several precursors are generally processed together in order to obtain a mixture of oxides, which is then annealed. As single molecule precursors are unknown for this type of mixed metal compounds, usually the alkoxides or β-diketonates of the metals are used. Whereas the ones for transition metals are well studied and suitable for CVD, many alkaline earth metal precursors of this type show a tendency to decompose or oligomerize under the physical conditions of CVD. This makes a quantitative deposition of the group II compounds more difficult.

The disadvantages of CVD are the great technological requirements such as high vacuum, so other techniques have been developed based on sol–gels. As ceramics generally require high temperatures for annealing in order to obtain a superconducting material [87], they can be made by the sol–gel process as well. The sol–gel synthesis is based on compounds with hydrolysable metal–ligand bonds in order to control the stoichiometries as well as the size of the formed particles [129]. Hydrolysis then leads to polycondensation of the molecules to yield a sol or a gel of a mixture of compounds. By gentle thermal treatment, the volatile building blocks are eliminated to give the (mixed) oxide in the end. Barium amides, such as $[\{BaNP(NMe_2)_2NP(NMe_2)_2NSiMe_3\}_4]$ which is based on a hetero-cubane structure, for instance have been shown to lead to a gel of composition $Ba(OH)_2(H_2O)_x$ [130]. Research has of course also focused on oxygen donor ligands as described below.

3.3.2. Alkoxides and aryloxides

Whereas many precursors have been studied for copper [131] and lanthanides [132] as common ingredients for oxide materials, relatively few results are known for alkoxides of alkaline earth metals, probably due to their low solubility, as for instance for $Sr(OMe)_2$ (which is polymeric) [20–22].

Recently, two strontium compounds, $[Sr(\mu\text{-}ONc)_2(HONc)_4]_2$ and $[Sr_5(\mu_4\text{-}O)(\mu_3\text{-}ONep)_4(\mu\text{-}ONep)_4(HONep)(solvent)_4]$, ONc = $O_2CCH_2CMe_3$; Nep = neopentyl; solvent = THF or 1-methyl-imidazole) have been synthesized [133]. They are more soluble than the commercially available precursors $Sr(Oac)_2$ and $Sr(OiPr)_2$, which are used in solution to synthesize thin films of ceramics such as $SrBi_2Ta_2O_9$ or $Ba_{1-x}Sr_xTiO_3$ [134].

The first isolated alkoxides of Ca, Sr, and Ba were obtained by desolvation of $M(OR)_2 \cdot 4ROH$ and contain compact groups such as OMe, OEt, etc. They form oligomers or polymers of type $[M(OR)_2]_n$ with a three-dimensional structure of the CdI_2-type. They are neither volatile nor soluble in organic solvents [11,12]. However, in aprotic solvents, alkaline earth metal alkoxides may form molecular aggregates, as shown by Turova et al. They have described a cluster $[Ca_6(O)_2(OEt)_8](OEt_2)_{14}$, which was obtained after refluxing $Ca(OEt)_2$ in ethanol [39–42]. The structure consists of two hetero-cubanes $[Ca_4O_4]$ fused via a $[Ca_2O_2]$-face containing the oxo groups.

Among the pure alkoxide compounds, $[Ca_9(OCH_2CH_2OMe)_{18}(HOC_2H_4OMe)_2]$ is with its nine metal atoms the largest calcium cluster so far described and build an excerpt of a sheet structure (Fig. 37) [135]. The central core adopts also the CdI_2-type structure, but the bidentate ligands reduce the tendency to polymerize and allow formation of a molecular structure.

Whereas the preceding example has a sheet-like arrangement, more spherical clusters can also be obtained with smaller oxygen donor ligands such as OH. Thus, in the author's group, the aggregate $Li[\{Ca_7(\mu_3\text{-}OH)_8I_6(thf)_{12}\}_2(\mu\text{-}I)](thf)_3$ has been synthesized [136]. It consists of a dumb bell arrangement of two Ca_7-units which are built by two $[Ca_4O_4]$-hetero-cubanes linked via one calcium ion (Fig. 38).

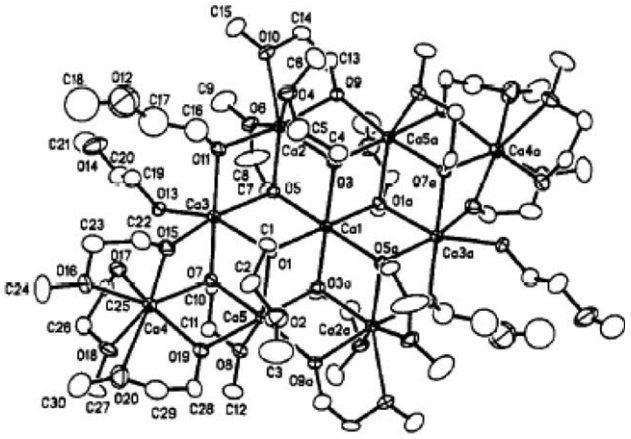

Fig. 37. ORTEP structure of $[Ca_9(OCH_2CH_2OMe)_{18}(HOC_2H_4OMe)_2]$, the largest calcium cluster so far described [135].

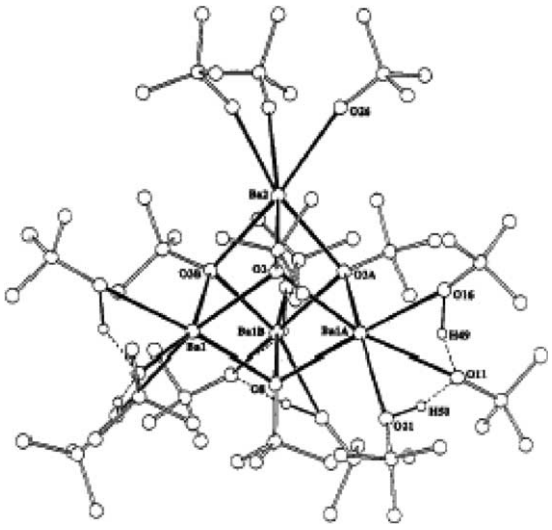

Fig. 39. Structure of $[Ba(\mu_3\text{-}OtBu)(OtBu)(HOtBu)_2]_4$ consisting of a distorted heterocubane $[Ba_4O_4]$ [42].

A similar structural motif is found in the cluster $[Ba(\mu_3\text{-}OtBu)(OtBu)(HOtBu)_2]_4$ which consists of a distorted heterocubane $[Ba_4O_4]$ (Fig. 39) [42].

This compound is the first homoleptic alkoxide of barium with this structural motif and it is obtained upon alcoholysis of $[Ba\{N(SiMe_3)_2\}_2]_2(thf)_2$.

Controlling the structure of an alkoxide is possible by introducing sterically important groups such as BHT (OC_6H_2-tBu_2-2,6-Me-4) and clox ($OC(Ph)_2CH_2C_6H_4$-Cl-4), with which lipophilic species such as $[M(BHT)_2(thf)_n]$ ($M = Ca$, $n = 3$; Ba, $n = 4$) or $[\{Ca(m\text{-clox})(clox)(thf)\}_2]$. They possess trigonal or tetragonal bipyramidal arrangements [137,138]. The monomeric compounds $[M(OAr)_2(thf)_3]$ ($OAr = BHT$ or clox) are isostructural. Other monomers, solvated or not, are also formed with other bulky ligands, such as $[Sr(OC_6H_2(tBu)_3)_2(thf)_3]$ [139], $[Ca\{OC_6H_3\text{-}(NO_2)_2\text{-}2,4\}_2]$ and $[Ba\{OC_6H_2\text{-}(NO_2)_3\text{-}2,4,6\}_2]$ [140,141], $[Ba(2,6\text{-}tBu_2C_6H_3O)_2(HOCH_2CH_2NMe_2)_4]$ which is bonded by hydrogen bonds, [117–120] and the alkoxides $[Ba\{(OC_2H_4)[N(C_2H_4OH)_2]\}_2(EtOH)_2]$, and $[Ba_2(OCPh_3)_4(thf)_3]$ [146–148].

In the compound $[Sr_4(OPh)_8(PhOH)_2(thf)_6]$ [142], the simple combination of the solvent with the metal ion and phenol is enough to produce a soluble molecular aggregate in which the cation possesses a pseudo-octahedral environment. The THF present in the structure is on one hand responsible for avoiding polymerization and on the other hand labile enough to yield a volatile species.

As barium is present in many superconducting cuprates [143,144], some authors have chosen to use simple aryloxides in the presence of bulky ligands, i.e., hmpa ($= [NMe_2]_3PO$). A homo-metallic species, $[H_2Ba_8(\mu_5\text{-}O)_2(OPh)_{14}(hmpa)_6]$ and a mixed-metal cluster with Sr and Ba are obtained [145]. Thus, a first intermediate $[Sr_3(OPh)_6(hmpa)_5]$ has been characterized before reaction with barium metal and phenol to yield $[H_2Sr_6Ba_2(\mu_5\text{-}O)_2(OPh)_{14}(hmpa)_6]$. Both structures

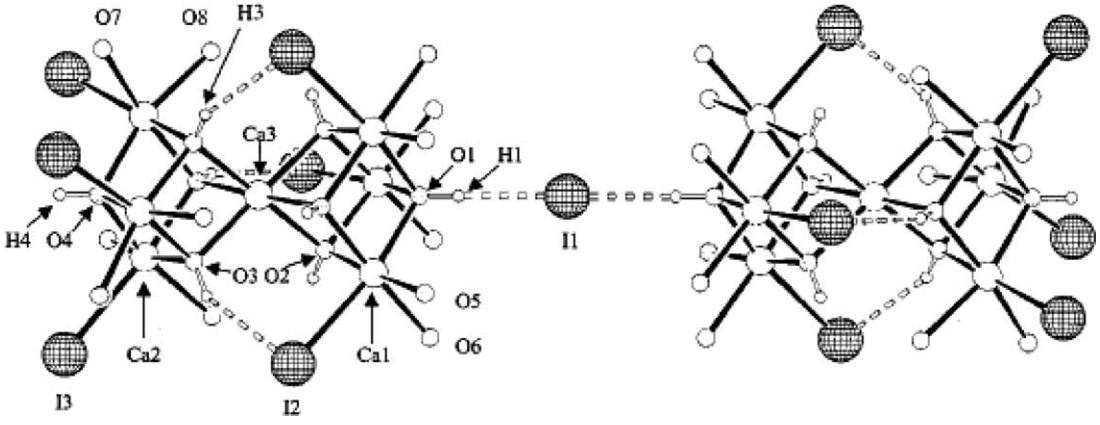

Fig. 38. Structure of $Li[\{Ca_7(\mu_3\text{-}OH)_8I_6(thf)_{12}\}_2(\mu\text{-}I)(thf)_3]$ [136].

consist of two edge-fused square pyramids with the oxo-anions in the center of the square plane of metal atoms (Fig. 40).

Oxo-free derivatives of silyloxides, alkoxides, and aryloxides have been described before [146–148], but they seldom have more than three metal atoms, except for $[Ba_6(OPh)_{12}(tmeda)_4]$. The presence of oxo-anions introduced upon hydrolysis by traces of humidity augments the nuclearity, as shown for instance in $[H_4Ba_6(O)(OCH_2CH_2OCH_3)_{14}]$ and $[Ba_6(O)(OCH_2CH_2OMe)_{10}(HOCH_2CH_2OMe)_4]$ [117–120], $[H_3Ba_6(O)(O\mathit{t}Bu)_{11}(OCEt_2CH_2O)(thf)_3]$ and $[Ba_4(O)(\mu_2\text{-}OC_6H_2(CH_2NMe_2)_3\text{-}2,4,6)_6]$ [146–148], $[HBa_5(O)(OPh)_9(thf)_8]$ and $[H_2Ba_8(O)_2(OPh)_{14}(hmpa)_6]$ [145]. In general, the higher the nuclearity of the cluster, the lower the volatility, and the less they are useful as precursors in CVD.

3.3.3. β-Diketonates

The β-diketonates of metals in general and more precisely alkaline earth metals are among the best studied systems [149]. The coordination modes are very flexible. The metallacycles are six-membered and therefore rather stable when coordinating in the anionic enol form [150,151]. Not only the structure, but also the physical properties depend strongly on the ligand type. For main group and transition metals, the volatility is good when alkoxides are used [152,153], whereas for group II metal ions, the β-diketonates are the best ligands so far as volatility and stability are concerned. The barium derivatives have been extensively studied. The volatility depends on the degree of oligomerization, and the latter depends on the ligand size. 2,2,6,6-Tetramethylheptane-3,5-dionate (thd) has turned out to be

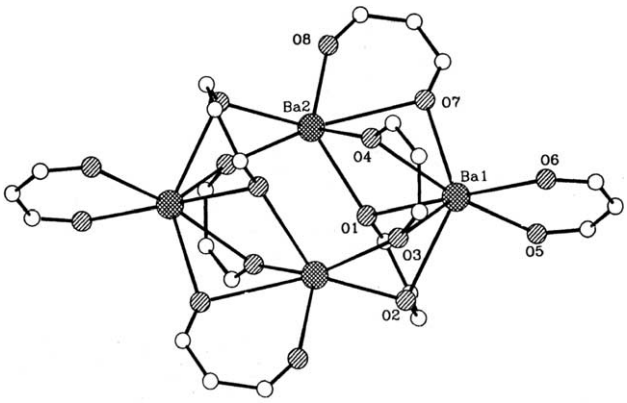

Fig. 41. Structure of $[Ba_4(thd)_8]$ [154,155].

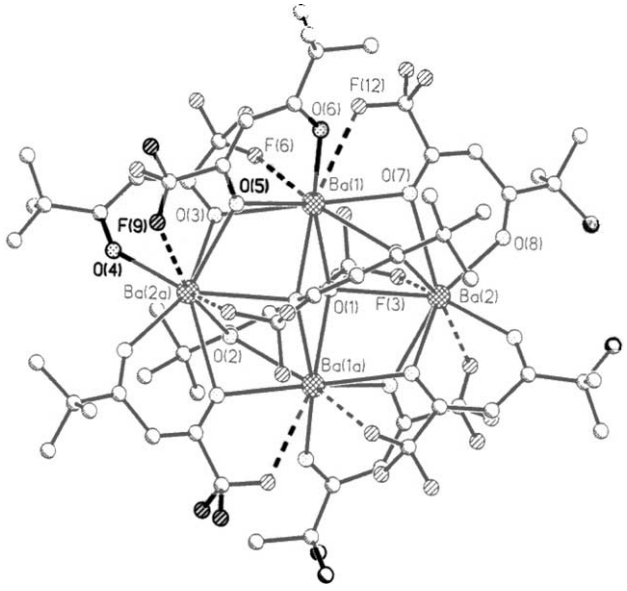

Fig. 42. Structure of $[Ba_4(pta)_8]$ [159].

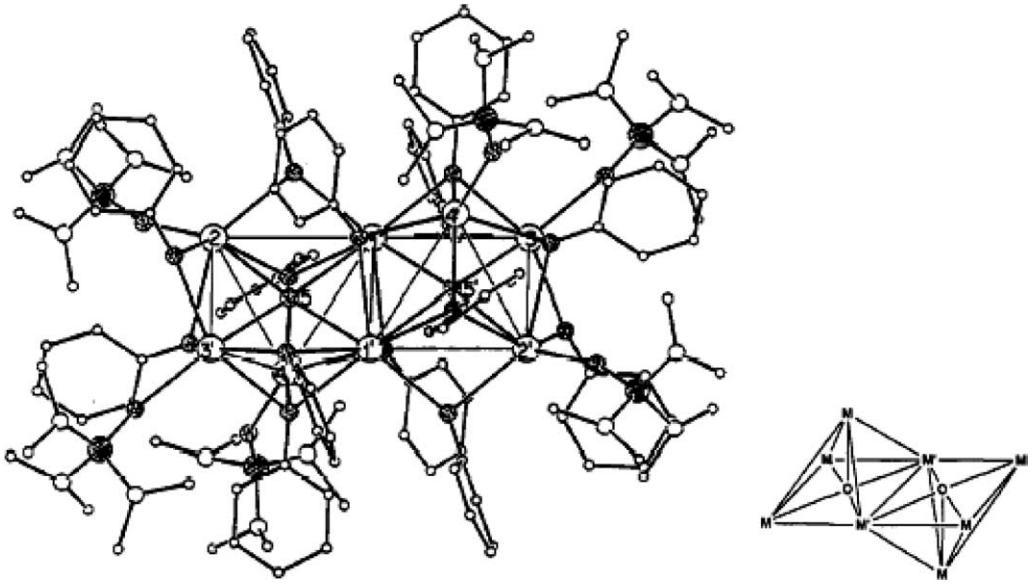

Fig. 40. Structure of $[H_2Sr_6Ba_2(\mu_5\text{-}O)_2(OPh)_{14}(hmpa)_6]$ [145].

a suitable ligand and forms the tetrameric compound $[Ba_4(thd)_8]$ with barium (Fig. 41) [154,155].

More volatility was expected by introducing the fluorinated ligand 1,1,1,5,5,5-hexafluoropentane-2,4-dionate (hfa), which forms however a polymer Ba-compound $[Ba(hfa)_2]$. The latter is therefore less volatile, whereas the tetramer sublimes under mild conditions [156,157].

Upon hydrolysis of $[Ba_4(thd)_8]$ in air, the compound $[Ba_6(thf)_{10}(O_2)(H_2O)]$ is obtained [158]. It consists of a hexanuclear octahedral Ba_6-cluster surrounding a peroxo anion. Such systems have also been studied with the ligand pivaloyltrifluoro acetone (Hpta), containing *t*Bu groups as well as terminal trifluoromethane units [159]. The compound $[Ba(pta)_2(H_2O)]$, which is obtained from a mixture of water and methanol, can be heated gently to give $[Ba_4(pta)_8]$ upon sublimation. Whereas the precursor forms infinite chains, the final product is made of tetrameric units (Fig. 42).

Even though $[Ba_4(thd)_8]$ is frequently used as CVD-precursor for the preparation of oxide materials, the research for more volatile species continues. The ligand 2-methoxy-2,6,6-trimethylheptane-3,5-dionate (HL) gives with metallic barium the compound $[Ba_2L_4(H_2O)_{1.81}]$ [160]. In this dinuclear product, the distance Ba–Ba is the shortest ever observed so far with 3.910(1) Å.

The alkaline earth metal ethoxides $[\{M(OEt)_2(EtOH)_4\}_n]$ react with β-diketonates such as 2,2,6,6-tetramethylheptane-3,5-dione (Htmhd) to give volatile complexes of the type $[Sr_3(tmhd)_6(Htmhd)]$ or $[Ba_4(tmhd)_8]$, following the general reaction scheme [161]:

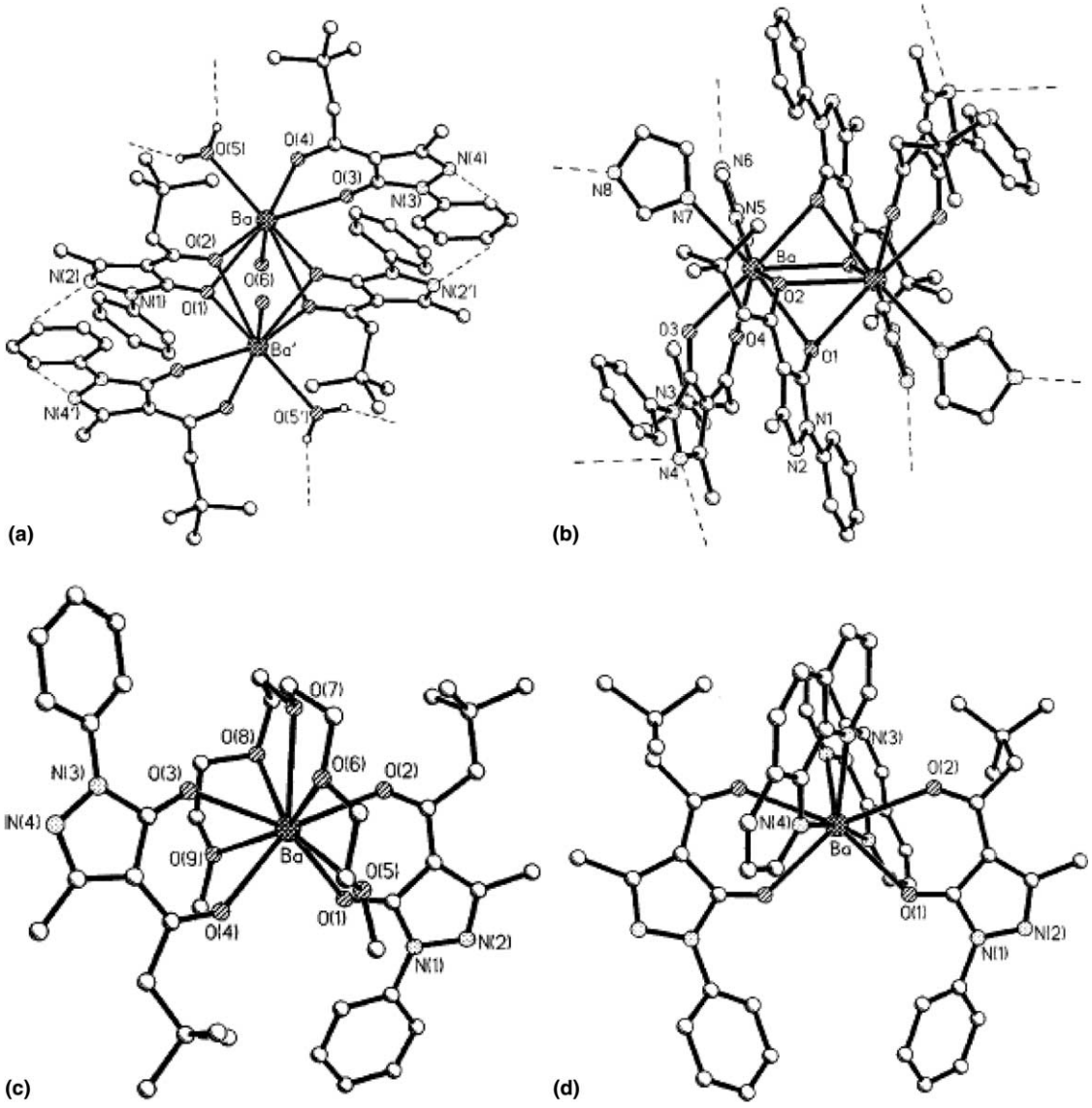

Fig. 43. Structures of $[\{BaQ_2(H_2O)_2\}_2]$, $[Ba_2Q_4(Him)_4]$, $[BaQ_2(tetraglyme)$, and $[BaQ_2(phen)_2]$ (Q = 4-*tert*-butylacetyl-3-methyl-1-phenylpyrazol-5-onate) [164].

$$[M(OEt)_2(EtOH)_4] + 2Htmhd \rightarrow [\{M(tmhd)_2\}_n] + 6EtOH \quad (10)$$

Some difficulties remain when it comes to synthesizing homoleptic β-diketonates of Sr and Ba with Htmhd or Hhfa, $[M(L)_2]$, due to their tendency to decompose and their sensitivity toward humidity and O_2 as well as the facile incorporation of coordinating solvent molecules. With the aim to make new single source precursors for CVD, mixed-ligand mixed-metal compounds were studied and were obtained for the combinations Ba/Cu and Ba/Y with β-diketonates and alkoxides as well as Lewis base solvent molecules as ligands [162,163].

Parallel to this, the chemistry of hetero-cyclic β-diketonates has only been poorly developed [164]. However, they generally possess a good solubility in organic solvents. The anionic ligand 4-*tert*-butylacetyl-3-methyl-1-phenylpyrazol-5-onate (Q^-) was used to obtain different products, depending on the coordinating solvent used. These are $[\{BaQ_2(H_2O)_2\}_2]$, $[Ba_2Q_4(Him)_4]$, $[BaQ_2(tetraglyme)]$, and $[BaQ_2(phen)_2]$ (Fig. 43).

Even though the interest is great in alkaline earth metal β-diketonates, little effort has been made to correlate their structure to the volatility [89]. Many solid state structures of compounds used in CVD are unknown, and the composition of them can vary from case to case depending on the preparation. For instance, traces of humidity can transform the compound $[Ba(tmhd)_2]$ [165] into the cluster compound $[Ba_5(tmhd)_9(H_2O)_3(OH)]$ [166].

The sublimation temperatures of a series of alkoxides and fluoroalkoxides have been monitored as a function of their molecular weight. The more bulky the ligand is, the less it forms oligomers, and the lower its sublimation temperature.

3.3.4. Carboxylates

For several years now the carboxylates have taken a place as possible precursors in CVD. Even though the preparation is similar to the alkoxides, few examples of polyether carboxylates (Scheme 5) with electron poor metal ions are known to date. The most efficient procedure is reaction of the metal hydroxide with the acid in water. After elimination of water, the carboxylates can be isolated generally in high yields, following the reaction

$$M(OH)_2 + (2/n)R(COOH)_n \rightarrow M(OOCR)_{2/n}(H_2O)_m + 2H_2O \quad (11)$$

(M = Ca, Sr, Ba; R = see Scheme 5).

Some calcium-containing compounds have been isolated as structural models for intermediates in biological systems, such as $[Ca_2\{2\text{-}OCO\text{-}3\text{-}CH_3C_6H_3NHCO)_2\text{-}C(CH_3)_2\}_2(CH_3OH)_6]$ (Fig. 44) [168].

The structure of this compound is stabilized by the presence of four hydrogen bonding interactions between the amide groups and the oxygen of a carboxylate anion (NH···O) [169,167]. Polymeric structures can thus be obtained by bridging oxygen atoms.

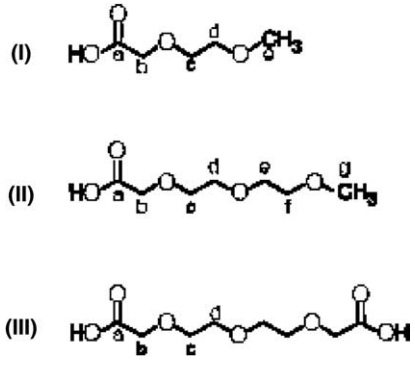

Scheme 5. Polyether carboxylates.

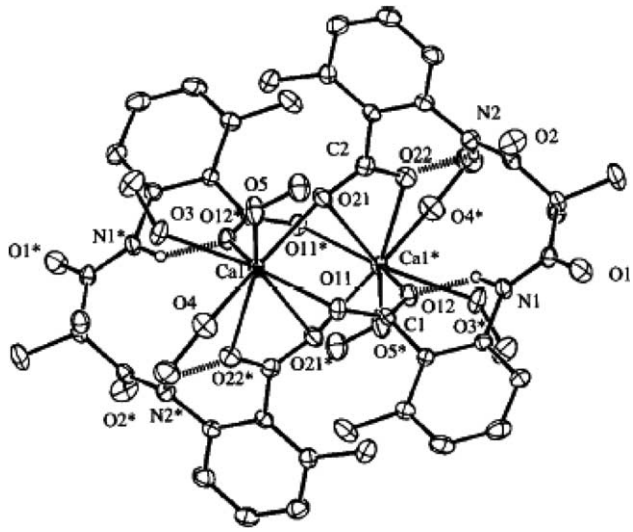

Fig. 44. ORTEP structure of $[Ca_2\{2\text{-}OCO\text{-}3\text{-}CH_3C_6H_3NHCO)_2C(CH_3)_2\}_2(CH_3OH)_6]$ [168].

4. Conclusions

In the chemistry of alkali and alkaline earth metal compounds, the pure organo-metallic compounds with metal–C bonds have dominated for a long time, and a number of review articles report on the importance of these compounds in synthesis and catalysis. Only recently have the compounds with metal–O bonds been investigated, as analogues to the organo-metallics, and several papers review either one group of metals or one single family of oxygen donating ligands. The purpose of this review was to regroup some of these results. The compounds described herein were chosen for their original structures and are presented also as examples of

synthesis. Their structures reflect the huge variety of geometric arrangements possible for alkali and alkaline earth metal aggregates, of which tetramers and hexamers with hetero-cubane, respectively, hexagonal prismatic structures are among the most common so far. Recent results, however, suggest that many structural varieties remain to be discovered in this field. Therefore, with the revival of research in this area, the improved techniques of controlled synthesis in non-aqueous solvents, and the routine single crystal analysis available today, many more advances are to be expected.

References

[1] L. Lochmann, Eur. J. Inorg. Chem. 6 (2000) 1115.
[2] M. Geissler, J. Kopf, B. Schubert, E. Weiss, W. Neugebauer, Angew. Chem. 99 (1987) 569.
[3] B.J. Wakefield, The Chemistry of Organolithium Compounds, Pergamon Press, Oxford, 1974.
[4] M. Veith, Chem. Rev. 90 (1990) 3.
[5] D.E. Pearson, C.A. Buehler, Chem. Rev. 74 (1974) 45.
[6] D.C. Bradley, Chem. Rev. 89 (1989) 1317.
[7] K.G. Caulton, L.G. Hubert-Pfalzgraf, Chem. Rev. 90 (1990) 969.
[8] M.H. Chisholm, I.P. Rothwell, in: G. Wilkinson, R.D. Gillard, J.A. McCleverty (Eds.), Comprehensive Coordination Chemistry, vol. 2, Pergamon, London, UK, 1987, p. 335.
[9] G.E. Coates, A.H. Fishwick, J. Chem. Soc. (A) (1968) 477.
[10] R.A. Anderson, G.E. Coates, J. Chem. Soc., Dalton Trans. (1972) 2153.
[11] D.C. Bradley, R.C. Mehrotra, D.P. Gaur, Metal Alkoxides, Academic Press, London, 1978.
[12] K.C. Malhotra, R.L. Martin, J. Organomet. Chem. 239 (1982) 159.
[13] P.J. Wheatley, J. Chem. Soc. (1960) 4270.
[14] H. Dunken, J. Krausse, Z. Chem. 1 (1961) 27.
[15] E. Weiss, Z. Anorg. Allg. Chem. 332 (1964) 197.
[16] E. Weiss, W. Büchner, Angew. Chem., Int. Ed. Engl. 3 (1964) 152.
[17] E. Weiss, Helv. Chim. Acta 46 (1963) 2051.
[18] E. Weiss, H. Alsdorf, Z. Anorg. Allg. Chem. 372 (1970) 206.
[19] T. Greiser, E. Weiss, Chem. Ber. 112 (1979) 844.
[20] H. Staeglich, E. Weiss, Chem. Ber. 111 (1978) 901.
[21] N.J. Turowa, B.A. Popowkin, A.W. Nowoselowa, Z. Anorg. Allg. Chem. 365 (1969) 100.
[22] H.D. Lutz, Z. Anorg. Allg. Chem. 353 (1967) 207.
[23] T. Greiser, E. Weiss, Chem. Ber. 110 (1977) 3388.
[24] J.E. Davies, J. Kopf, E. Weiss, Acta Crystallogr., Sect. B 38 (1982) 2251.
[25] E. Weiss, H. Alsdorf, H. Kühr, Angew. Chem., Int. Ed. Engl. 6 (1967) 801.
[26] E. Weiss, H. Alsdorf, H. Kühr, H.F. Grützmacher, Chem. Ber. 101 (1968) 3777.
[27] V. Halaska, L. Lochmann, D. Lim, Collect. Czech. Chem. Commun. 33 (1968) 3245.
[28] G.E. Hartwell, T.L. Brown, Inorg. Chem. 5 (1966) 1257.
[29] G.E. Hartwell, A. Allerhand, J. Am. Chem. Soc. 93 (1971) 4415.
[30] H. Huml, Czech. J. Phys. B 15 (1965) 699.
[31] R.D. Thomas, S.G. Bott, P.W. Gravelle, H.D. Nguyen, Book of Abstracts, 215th ACS National Meeting, 1998, INOR-291.
[32] K.M. Fromm, E.D. Gueneau, G. Bernardinelli, H. Goesmann, J. Weber, M.-J. Mayor-López, P. Boulet, H. Chermette, J. Am. Chem. Soc. 125 (12) (2003) 3593.
[33] H. Nekola, F. Olbrich, U. Behrens, Z. Anorg. Allg. Chem. 628 (9, 10) (2002) 2067.
[34] K.W. Klinkhammer, Z. Anorg. Allg. Chem. 626 (2000) 1217.
[35] M. Marsch, K. Harms, L. Lochmann, G. Boche, Angew. Chem., Int. Ed. Engl. 29 (1990) 308.
[36] C. Lambert, F. Hampel, P.v.R. Schleyer, M.G. Davidson, R. Snaith, J. Organomet. Chem. 487 (1995) 139.
[37] G. Beck, P.B. Hitchcock, M.F. Lappert, I.A. MacKinnon, J. Chem. Soc., Chem. Commun. (1989) 1312.
[38] J. Hvoslef, H. Hope, B.D. Murray, P.P. Power, J. Chem. Soc., Chem. Commun. (1983) 1438.
[39] M.H. Chisholm, S.R. Drake, A.A. Naiini, W.E. Streib, Polyhedron 10 (1991) 337.
[40] Z.A. Starikova, A.I. Yanovsky, E.P. Turevskaya, N.Y. Turova, Polyhedron 16 (1997) 967.
[41] N.Y. Turova, E.P. Turevskaya, V.G. Kessler, A.I. Yanovsky, Y.T. Struchkov, J. Chem. Soc., Chem. Commun. (1993) 21.
[42] B. Borup, J.A. Samuels, W.E. Streib, K.G. Caulton, Inorg. Chem. 33 (1994) 994.
[43] Z.A. Starikova, E.P. Turevskaya, N.Y. Turova, A.I. Yanovsky, J. Chem. Soc., Dalton Trans. (2000) 3237.
[44] L.M. Jackman, D. Cizmeciyan, P.G. Williard, M.A. Nichols, J. Am. Chem. Soc. 115 (1993) 6262.
[45] J.S. Vilardo, P.E. Fanwick, I.P. Rothwell, Polyhedron 17 (1998) 769.
[46] M. Geissler, E. Weiss, unpublished work.
[47] M. Geissler, Dissertation, Hamburg, 1987.
[48] B. Cetinkaya, I. Gümrükçü, M.F. Lappert, J.L. Atwood, R. Shakir, J. Am. Chem. Soc. 102 (1980) 2086.
[49] S. Brooker, F.T. Edelmann, T. Kottke, H.W. Roesky, G.M. Sheldrick, D. Stalke, K.H. Whitmire, J. Chem. Soc., Chem. Commun. (1991) 144.
[50] P.A. van der Schaaf, M.P. Hogerheide, D.M. Grove, A.L. Spek, G. van Koten, J. Chem. Soc., Chem. Commun. (1992) 1703.
[51] D. Seebach, Angew. Chem., Int. Ed. Engl. 27 (1988) 1624.
[52] E. Weiss, J. Kopf, T. Gardein, S. Corbelin, U. Schümann, M. Kirilov, G. Petrov, Chem. Ber. 118 (1985) 3529.
[53] G. Boche, Angew. Chem., Int. Ed. Engl. 28 (1989) 277.
[54] L.M. Jackman, B.C. Lange, J. Am. Chem. Soc. 103 (1981) 4494.
[55] L.M. Jackman, B.C. Lange, Tetrahedron 33 (1977) 2737.
[56] R. Amstutz, W.B. Schweizer, D. Seebach, J.D. Dunitz, Helv. Chim. Acta 64 (1981) 2617.
[57] P.G. Williard, G.B. Carpenter, J. Am. Chem. Soc. 107 (1985) 3345.
[58] P.G. Williard, G.B. Carpenter, J. Am. Chem. Soc. 108 (1986) 462.
[59] T. Laube, J.D. Dunitz, D. Seebach, Helv. Chim. Acta 68 (1985) 1373.
[60] K.W. Henderson, D.S. Walther, P.G. Williard, J. Am. Chem. Soc. 117 (1995) 8680.
[61] H. Bock, J.M. Lehn, J. Pauls, S. Holl, V. Krenzel, Angew. Chem., Int. Ed. Engl. 38 (1999) 952.
[62] W. Setzer, P. von R. Schleyer, Adv. Organomet. Chem. 24 (1985) 353.
[63] C. Schade, P. von R. Schleyer, Adv. Organomet. Chem. 27 (1987) 169.
[64] W. Bauer, D. Seebach, Helv. Chim. Acta 67 (1984) 1972.
[65] L. Lochmann, D. Lím, J. Organomet. Chem. 28 (1971) 153.
[66] R. Pi, W. Bauer, P. von R. Schleyer, J. Organomet. Chem. 306 (1986) C1.
[67] S. Harder, A. Streitwieser, Angew. Chem., Int. Ed. Engl. 32 (1993) 1066.
[68] P.G. Williard, G.J. MacEwan, J. Am. Chem. Soc. 111 (1989) 7671.
[69] K.W. Henderson, P.G. Williard, P.R. Bernstein, Angew. Chem., Int. Ed. Engl. 34 (1995) 1117.

[70] F.M. Mackenzie, R.E. Mulvey, W. Clegg, L. Horsburgh, J. Am. Chem. Soc. 118 (1996) 4721.
[71] W. Clegg, A.R. Kennedy, R.E. Mulvey, R.B. Rowlings, unpublished results, see [70].
[72] D. Hoffman, T. Kottke, R.J. Lagow, R.D. Thomas, Angew. Chem., Int. Ed. 37 (1998) 1537.
[73] P.C. Andrews, J.G. MacLellan, R.E. Mulvey, P.J. Nichols, J. Chem. Soc., Dalton Trans. 8 (2002) 1651.
[74] F.M. Mackenzie, R.E. Mulvey, W. Clegg, L. Horsburgh, Polyhedron 17 (1998) 993.
[75] W. Clegg, A.M. Drummond, R.E. Mulvey, S.T. Liddle, Chem. Commun. 21 (1998) 2391.
[76] W. Clegg, S.T. Liddle, A.M. Drummond, R.E. Mulvey, A. Robertson, Chem. Commun. 16 (1999) 1569.
[77] A.R. Kennedy, J.G. MacLellan, R.E. Mulvey, Angew. Chem., Int. Ed. 40 (2001) 3245.
[78] P. Jetter, A.R. Kennedy, R.E. Mulvey, unpublished results, see [77].
[79] A.R. Kennedy, J.G. MacLellan, R.E. Mulvey, A. Robertson, J. Chem. Soc., Dalton Trans. 22 (2000) 4112.
[80] K.M. Fromm, E.D. Gueneau, H. Goesmann, Chem. Commun. (2000) 2187.
[81] H. Bock, T. Hauck, C. Näther, N. Rösch, M. Staufer, O.D. Häberlen, Angew. Chem., Int. Ed. Engl. 34 (1995) 1353.
[82] M.F. Lappert, M.J. Slade, A. Singh, J.L. Atwood, R.D. Rogers, R. Shakir, J. Am. Chem. Soc. 105 (1983) 302.
[83] R.E. Mulvey, Chem. Soc. Rev. 27 (1998) 339.
[84] R.E. Mulvey, Chem. Commun. (2001) 1049.
[85] W. Clegg, K.W. Henderson, A.R. Kennedy, R.E. Mulvey, C.T. O'Hara, R.B. Rowlings, D.M. Tooke, Angew. Chem., Int. Ed. Engl. 40 (2001) 3902.
[86] K.J. Drewette, K.W. Henderson, A.R. Kennedy, R.E. Mulvey, C.T. O'Hara, R.B. Rowlings, Chem. Commun. (2002) 1176.
[87] A.M. Drummond, L.T. Gibson, A.R. Kennedy, R.E. Mulvey, C.T. O'Hara, R.B. Rowlings, T. Weightman, Angew. Chem., Int. Ed. 41 (2002) 2382.
[88] J.V. Mantese, A.B. Catalan, A.H. Hamdi, A.L. Micheli, Appl. Phys. Lett. 52 (1988) 1741.
[89] T.P. Hanusa, Chem. Rev. 93 (1993) 1023.
[90] P.F. Bernath, Science 254 (1991) 665.
[91] S.A. Kinsley, A. Streitwieser Jr., A. Zalkin, Organometallics 4 (1985) 52.
[92] S.C. Sockwell, T.P. Hanusa, J.C. Huffman, J. Am. Chem. Soc. 114 (1992) 3393.
[93] T.P. Hanusa, J. Chem. Educ. 64 (1987) 686.
[94] R.G. Pearson, Hard and Soft Acids and Bases, Dowden, Hutchinson & Ross, Stroudsburg, PA, 1973.
[95] C. Mathis, B. François, J. Smid, J. Organomet. Chem. 217 (1981) 291.
[96] S.R. Drake, D.J. Otway, Polyhedron 11 (1992) 745.
[97] V. Cerchez, Bull. Soc. Chim. 43 (1928) 762.
[98] H. Lund, J. Bjerrum, Chem. Ber. B 64 (1931) 210.
[99] D.C. Bradley, R.C. Mehrotra, D.P. Gaur, Metal Alkoxides, Academic Press, New York, 1978.
[100] E.P.J. Moore, Polypropylene Handbook, Hanser/Gardner Publications, Cincinnati, OH, 1996.
[101] S.G. Hegde, D.C. Myles, Synth. Commun. 27 (1997) 2111.
[102] S. Kanemasa, M. Nishiuchi, E. Wada, Tetrahedron Lett. 33 (1992) 1357.
[103] L. Albaric, N. Hovnanian, A. Julbe, C. Guizard, A. Alvarezlarena, J.F. Piniella, Polyhedron 16 (1997) 587.
[104] N. Ya Turova, E.P. Turevskaya, J. Organomet. Chem. 42 (1972) 9.
[105] P. Sobota, J. Utko, Z. Janas, S. Szafert, Chem. Commun. (1996) 1923.
[106] J. Calabrese, M.A. Cushing, S.D. Ittel, Inorg. Chem. 27 (1988) 867.
[107] H.W. Roesky, M. Scholz, M. Noltmeyer, Chem. Ber. 123 (1990) 2303.
[108] C.A. Zechmann, T.J. Boyle, M.A. Rodriguez, R.A. Kemp, Polyhedron 19 (2000) 2557.
[109] K.-C. Yang, C.-C. Chang, C.-S. Yeh, G.-H. Lee, S.-M. Peng, Organometallics 20 (2001) 126.
[110] J.F. Allan, W. Clegg, K.W. Henderson, L. Horsburgh, A.R. Kennedy, J. Organomet. Chem. 559 (1998) 173.
[111] M.J. Bennett, F.A. Cotton, R. Eiss, R.C. Elder, Nature 213 (1967) 174.
[112] G.J. Bullen, R. Mason, P. Pauling, Inorg. Chem. 4 (1965) 456.
[113] A.P. Dove, V.C. Gibson, E.L. Marshall, A.J.P. White, D.J. Williams, Chem. Commun. 11 (2002) 1208.
[114] E. Beckman, Chem. Ber. 38 (1905) 904.
[115] H. Gilman, F. Schulze, J. Am. Chem. Soc. 48 (1926) 2463.
[116] H. Gilman, A.H. Haubein, G. O'Donnell, L. Woods, J. Am. Chem. Soc. 65 (1943) 268.
[117] K.G. Caulton, M.H. Cisholm, S.R. Drake, K. Folting, J. Chem. Soc., Chem. Commun. (1990) 1349.
[118] K.G. Caulton, M.H. Cisholm, S.R. Drake, J.C. Huffman, J. Chem. Soc., Chem. Commun. (1990) 1498.
[119] K.G. Caulton, M.H. Cisholm, S.R. Drake, K. Folting, Inorg. Chem. 30 (1991) 1500.
[120] K.G. Caulton, M.H. Cisholm, S.R. Drake, W.E. Streib, Angew. Chem., Int. Ed. Engl. 29 (1990) 1483.
[121] L.G. Hubert-Pfalzgraf, New J. Chem. 11 (1987) 663.
[122] A.D. Berry, R.T. Gaskill, E.J. Holm, R. Cukauskas, R. Kaplan, R.L. Henry, Appl. Phys. Lett. 52 (1988) 1743.
[123] A.J. Panson, R.G. Charles, D.N. Schmidt, J.R. Szedon, G.J. Machiko, A.I. Braginski, Appl. Phys. Lett. 53 (1988) 1756.
[124] D.S. Richeson, L.M. Tonge, J. Zhao, J. Zhang, H.O. Marcy, T.J. Matks, B.W. Wessels, C.R. Kannewurf, Appl. Phys. Lett. 54 (1989) 2154.
[125] H. Nagamoto, K. Amanuma, H. Nobutomo, H. Inoue, Chem. Lett. 2 (1988) 237.
[126] P. Pereira, S.H. Lee, G.A. Somorjai, H. Heinemann, Catal. Lett. 6 (1990) 255.
[127] A. Gupta, E.I. Jagannathan, E.A. Cooper, E.A. Giess, J.I. Landman, B.W. Hussey, Appl. Phys. Lett. 52 (1988) 2077.
[128] M. Veith, J. Chem. Soc., Dalton Trans. (2002) 2405.
[129] L.L. Hench, J.K. West, Chem. Rev. 90 (1990) 33.
[130] S.K. Pandey, A. Steiner, H.W. Roesky, D. Stalke, Angew. Chem., Int. Ed. 32 (1993) 596.
[131] S.C. Goel, K.S. Kramer, M.Y. Chiang, W.E. Buhro, Polyhedron 9 (1990) 611.
[132] W.J. Ewans, J.M. Olofson, J.W. Ziller, J. Am. Chem. Soc. 112 (1990) 2308.
[133] T.J. Boyle, C.J. Tafoya, B.L. Scott, J.W. Ziller, J. Coord. Chem. 51 (2000) 361.
[134] T.J. Boyle, H.N. Al-Shareef, C.D. Buchheit, R.T. Cygan, D. Dimos, M.A. Rodriguez, B. Scott, J.W. Ziller, Integr. Ferroelectr. 18 (1997) 231.
[135] S.C. Goel, M.A. Matchett, M.Y. Chiang, W.E. Buhro, J. Am. Chem. Soc. 113 (1991) 1844.
[136] K.M. Fromm, Chem. Commun. 17 (1999) 1659.
[137] K.F. Tesh, T.P. Hanusa, J.C. Huffman, C.J. Huffman, Inorg. Chem. 31 (1992) 5572.
[138] P.B. Hitchcock, M.F. Lappert, G.A. Lawless, B. Royo, J. Chem. Soc., Chem. Commun. (1990) 1141.
[139] S.R. Drake, D.J. Otway, M.B. Hursthouse, K.M. Abdul Malik, Polyhedron 11 (1992) 1995.
[140] L.B. Cole, E.M. Holt, J. Chem. Soc., Perkin Trans. 2 (1986) 1997.
[141] D.L. Hugues, J.N. Wingfield, J. Chem. Soc., Chem. Commun. (1977) 804.
[142] S.R. Drake, W.E. Streib, M.H. Chisholm, K.G. Caulton, Inorg. Chem. 29 (1990) 2707.

[143] R.J. Cava, Science 247 (1990) 656.
[144] S.N. Putlin, E.V. Antipov, O. Chmaissem, M. Marezio, Nature 362 (1993) 226.
[145] K.G. Caulton, M.H. Chisholm, S.R. Drake, K.J. Folting, J.C. Huffman, Inorg. Chem. 32 (1993) 816.
[146] S.R. Drake, W.E. Streib, K.J. Folting, M.H. Chisholm, K.G. Caulton, Inorg. Chem. 31 (1992) 3205.
[147] K.G. Caulton, M.H. Chisholm, S.R. Drake, K.J. Folting, J.C. Huffman, W.E. Streib, Inorg. Chem. 32 (1993) 1970.
[148] O. Poncelet, L.G. Hubert-Pfalzgraf, L. Toupet, J.-C. Daran, Polyhedron 10 (1991) 2045.
[149] R.C. Mehrotra, R. Bohra, D.P. Gaur, Metal β-Diketonates and Allied Derivatives, Academic Press, London, 1978.
[150] L.G. Hubert-Pfalzgraf, Appl. Organomet. Chem. 6 (1992) 627.
[151] A.R. Barron, W.S. Rees Jr., Adv. Mater. Opt. Electron. 2 (1993) 271.
[152] D.C. Bradley, Polyhedron 13 (1994) 1121.
[153] J. Aarik, A. Aidla, A. Jaek, M. Leskela, L. Niinisto, J. Mater. Chem. 4 (1994) 1299.
[154] A.A. Drozdov, S.I. Troyanov, Polyhedron 11 (1992) 2877.
[155] A. Drozdov, S. Troyanov, A. Pisarevsky, Yu. Struchkov, Polyhedron 13 (1994) 2459.
[156] D. Bradley, M. Hasan, M. Hursthouse, M. Motevalli, O.F.Z. Khan, R. Pritchard, J. Williams, J. Chem. Soc., Chem. Commun. (1992) 575.
[157] A. Drozdov, S. Troyanov, J. Chem. Soc., Chem. Commun. (1993) 1619.
[158] A. Drozdov, S. Troyanov, Polyhedron 15 (1996) 1747.
[159] A. Drozdov, A. Pozhitkov, S. Troyanov, A. Pisarevsky, Polyhedron 15 (1996) 1731.
[160] S. Ivanov, N. Snezko, A. Ilyukhin, V. Sergienko, Polyhedron 16 (1997) 2527.
[161] S.R. Drake, M.B. Hurthouse, K.M. Abdul Malik, D.J. Otway, J. Chem. Soc., Dalton Trans. (1993) 2883.
[162] V.G. Kessler, L.G. Hubert-Pfalzgraf, S. Daniele, A. Gleizes, Chem. Mater. 6 (1994) 2336.
[163] F. Labrize, L.G. Hubert-Pfalzgraf, J. Vaissermann, C.B. Knobler, Polyhedron 15 (1996) 577.
[164] C. Pettinari, F. Marchetti, A. Cingolani, D. Leonesi, S. Troyanov, A. Drozdov, J. Chem. Soc., Dalton Trans. (1999) 1555.
[165] A. Gleizes, S. Sans-Lenain, D. Medus, C. R. Acad. Sci. Paris 313 (1991) 761.
[166] S.B. Turnipseed, R.M. Barkley, R.E. Sievers, Inorg. Chem. 30 (1991) 1164.
[167] A.M. Bahl, S. Krishnaswamy, N.G. Massand, D.J. Burkey, T.P. Hanusa, Inorg. Chem. 36 (1997) 5413.
[168] N. Ueyama, J. Takeda, Y. Yamada, A. Onoda, T. Okamura, Inorg. Chem. 38 (1999) 475.
[169] C.J. Carrell, H.L. Carrell, J. Erlebacher, J.P. Glusker, J. Am. Chem. Soc. 110 (1988) 8651.

Available online at www.sciencedirect.com
SCIENCE DIRECT®
Polyhedron 23 (2004) 1505–1518
POLYHEDRON
www.elsevier.com/locate/poly

Solid state coordination chemistry of mononuclear mixed-ligand complexes of Ni(II), Cu(II) and Zn(II) with α-hydroxycarboxylic acids and imidazole ☆

R. Carballo [a,*], A. Castiñeiras [b], B. Covelo [a], E. García-Martínez [a], J. Niclós [c], E.M. Vázquez-López [a]

[a] *Departamento de Química Inorgánica, Facultade de Ciencias-Quimica, Universidade de Vigo, E-36200 Vigo, Galicia, Spain*
[b] *Departamento de Química Inorgánica, Facultade de Farmacia, Universidade de Santiago de Compostela, E-15706 Santiago de Compostela, Galicia, Spain*
[c] *Departamento de Química Inorgánica, Facultad de Farmacia, Universidad de Granada, E-18071 Granada, Spain*

Received 19 November 2003; accepted 27 February 2004
Available online 27 April 2004

Abstract

Nine mononuclear metal complexes of monoanionic α-hydroxycarboxylates (HL′) with imidazole as a co-ligand have been synthesised and structurally characterized by X-ray diffraction. The nickel(II) complexes can be described by two formulae: $[Ni(HL')_2(Im)_2]$, HL′ = 2-methyllactate (HmL) (**1**) or mandelate (HM) (**2**), and $[Ni(HB)_2(Im)_3]$, HB = benzylate (**3**). In these compounds the nickel atom is in a distorted octahedral environment. The copper(II) complexes of the general formula $[Cu(HL')_2(Im)]$, HL′ = glycolate (HG) (**4**), lactate (HL) (**5**) or 2-methyllactate (HmL) (**6**) presents a square pyramidal coordination geometry with a distortion evaluated in terms of the τ parameter. The zinc(II) complexes have the general formula $[Zn(HL')_2(Im)_2]\cdot xH_2O$, HL′ = lactate (HL) and $x = 1/2$ (**7**), 2-methyllactate (HmL) and $x = 0$ (**8**) and display a distorted octahedral geometry. However, the reaction with H_2B afforded the imidazole complex $[Zn(Im)_6](HB)_2$, HB = benzylate (**9**), which has two uncoordinated benzylate units. In most of the complexes the α-hydroxycarboxylato ligands behave as bidentate monoanionic systems, apart from in **3**, where one ligand is monodentate. All of the complexes are extended into 2D or 3D frameworks through hydrogen bonding. The complexes were also characterized by elemental analysis, FT-IR and UV/Vis spectroscopy. The nickel and copper compounds were also studied by room temperature magnetic susceptibility and room temperature ESR spectra were obtained for the copper compounds. Finally, the thermal behaviour of all the compounds was investigated.
© 2004 Elsevier Ltd. All rights reserved.

Keywords: Nickel; Copper; Zinc; Imidazole; α-Hydroxycarboxylato complexes; Thermal behaviour; Crystal structures

1. Introduction

An important group of biogenic ligands is represented by the anions of α-hydroxycarboxylic acids. These anions take part in many fundamental biochemical processes, e.g., in the Krebs cycle (malate, citrate, isocitrate), Cory cycle (lactate), photorespiration (glycolate) and others. Elsewhere, α-hydroxycarboxylates, by virtue of their hydroxy and carboxylate functionalities, may also mimic more complex biogenic ligands, e.g., sugars. The imidazole ring, as a histidine moiety, is also present as a ligand toward transition metal ions in a variety of biologically important molecules including non-heme systems and several metalloproteins. These two ligands can simultaneously coordinate metal ions and provide potential intermolecular interactions that allow the formation of supramolecular arrays. Together with the use of these ligands, a selection of individual metal ions with different coordination properties can be a useful tool to generate networks of different dimensionality.

☆ Supplementary data associated with this article can be found, in the online version, at doi:10.1016/j.poly.2004.02.028.

* Corresponding author. Tel.: 34-986-812273; fax: 34-986812556.
E-mail address: rcrial@uvigo.es (R. Carballo).

0277-5387/$ - see front matter © 2004 Elsevier Ltd. All rights reserved.
doi:10.1016/j.poly.2004.02.028

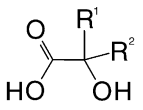

		R^1	R^2
Glycolic acid	H_2G	H	H
Lactic acid	H_2L	H	CH_3
2-Methyllactic acid	H_2mL	CH_3	CH_3
Mandelic acid	H_2M	H	Ph
Benzylic acid	H_2B	Ph	Ph

Scheme 1.

The present paper includes a detailed structural study on the solid state of nickel(II), copper(II) and zinc(II) mixed-ligand complexes with biologically relevant ligands such as α-hydroxycarboxylates and imidazole. For this study, five α-hydroxycarboxylic acids with different levels of bulkiness (Scheme 1) were selected: Glycolic (H_2G), Lactic (H_2L), 2-methyllactic (H_2mL), Mandelic (H_2M) and Benzylic (H_2B) acids.

Previous work in this field has been undertaken by our group and involved the study of mixed-ligand complexes of copper(II) with *N*,*N*-chelating aromatic amines such as 1,10-phenanthroline [1,2] and 2,2′-bipyridine [3,4]. In most of these complexes a pentacoordinated copper(II) ion in a distorted square pyramidal environment is present, but there are also some complexes with an octahedral coordination geometry. The behaviour of the α-hydroxycarboxylic acids in these complexes is very diverse and includes: bidentate monoanion, bidentate dianion, bidentate bridging by the hydroxyl oxygen, monodentate monoanion, monoanionic counterion and also as a neutral molecule in the outer coordination sphere. However, structural studies of first-row transition metal complexes of α-hydroxycarboxylates with monodentate N-donor ligands are not common. To the best of our knowledge the only structural reports in this area concern the glycolate ligand and NH_3 or pyridine as monodentate N-donor ligands: $[Ni(HG)_2(py)_2]\cdot 2H_2O$ [5], $[Cu(HG)_2(NH_3)_2]$ and $[Cu(HG)_2(py)_2]$ [6] contain bidentate monoanionic ligands and the dinuclear copper compound $[Cu_2G_2(py)_2]$ ethane-1,2-diol solvate [7], which contains a bridging bidentate dianionic glycolate ligand.

2. Results and discussion

Reaction of the α-hydroxycarboxylic acids and imidazole in EtOH and/or H_2O with $Ni(AcO)_2\cdot 4H_2O$, $CuCO_3\cdot Cu(OH)_2\cdot 1/2H_2O$ and $ZnCO_3$ led to the isolation of the crystalline products **1**–**9** after slow evaporation of the mother liquors (compounds **2**, **4** and **9**) or after the redissolution of oils or powders obtained in the reactions in MeOH/*i*PrOH (compounds **1**, **3**, **5**, **6** and **8**) or in MeOH/acetone (compound **7**). The yields are high for **1** and **2**, around 50% for **4**–**7** and low for **3**, **8** and **9**. The complexes are air-stable, with melting or decomposition points above 250 °C (**1, 2**), around 200 °C (**4**–**6**) and slightly above 100 °C for the zinc compounds. The complexes are soluble in water, methanol, ethanol and slightly soluble in chlorinated solvents.

2.1. Crystal structures

Metal–ligand bond distances and angles are listed in Table 1. Figs. 1–7 show drawings of the molecular structures together with the atom-numbering schemes used.

The Ni(II) compounds **1** and **2** (Fig. 1 shows compound **2**) and the Zn(II) compounds **7** (Fig. 2) and **8** (Fig. 3) have structures based on neutral complexes $[M(HL')_2(Im)_2]$, where HL′ is a monoanionic *O*,*O*′-bidentate α-hydroxycarboxylato ligand (2-methyllactato for **1** and **8**, lactato for **7** and mandelato for **2**) that chelates the M^{2+} ion through the carboxylato and the hydroxyl oxygen atoms to form a five-membered chelate ring. In this chelate ring the two imidazole ligands are *cis* to each other and *trans* to the hydroxyl oxygen atoms when the metal ion is nickel, but *trans* to the carboxylato oxygen atom in the zinc compound **8**. In compounds **1** and **2** the hydroxyl groups of the two ligands are mutually *cis*, but in **8** they are mutually *trans* in a similar way to the aqua-complex $[Zn(HmL)_2(H_2O)_2]$ [8]. In compound **7** an *all cis* configuration is found. The structure of the nickel compound **3** (Fig. 4) corresponds to neutral molecules $[Ni(HB)_2(Im)_3]$ with a *fac*-disposition of the ligands. In this arrangement one HB ligand acts as a monoanionic *O*,*O*′-bidentate chelating system but the other HB ligand is monoanionic unidentate, so the coordination of the hydroxyl group of one HB ligand is replaced by the coordination of a third imidazole molecule. It therefore appears that the steric requirements of this ligand favour the coordination of a small monodentate ligand like imidazole over the stabilization provided by chelate formation. In all of these complexes, the coordination polyhedra are distorted octahedral with the main deviations from regularity affecting the chelating angles $O_{hydroxyl}$–M–$O_{carboxy}$ [in the range 76.37°–77.95° for the nickel compounds and 74.68°–76.85° for **7** and **8**]. The Ni–N bond lengths are in the range 2.031–2.077 Å, which is only slightly shorter than that found in the pyridine complex $[Ni(HG)_2(py)_2]\cdot 2H_2O$ [5]. The Ni–$O_{hydroxyl}$ distances (Table 1) increase slightly on going from **1** (containing the less bulky hydroxycarboxylato ligand) to **3** (with the more bulky ligand) and are longer than those in the nickel(II) pyridine compound with the glycolato ligand [5]. The Ni–$O_{carboxy}$ distances are in the range 2.027–2.0466 Å

Table 1
Selected bond lengths (Å) and angles (°)

Compound	**1**[*]	**2**	**3**	**4** ($\tau = 0.04$)	**5** ($\tau = 0.03$)	**6** ($\tau = 0.29$)	**7**	**8**[**]	**9**[***]
Bond lengths									
M–O11	2.0466(15)	2.029(3)	2.034(4)	1.962(4)	1.952(4)	1.932(3)	2.098(2)	2.117(2)	
M–O21		2.027(4)	2.155(4)	1.945(4)	1.920(4)	1.956(3)	2.079(2)		
M–N1	2.0632(17)	2.034(4)	2.054(5)	1.958(5)	1.944(5)	1.973(3)	2.115(3)	2.094(3)	2.183(2)
M–N3		2.031(4)	2.058(5)				2.077(3)		2.190(2)
M–N5			2.077(5)						2.203(2)
M–O13	2.1084(15)	2.122(4)	2.135(4)	2.383(5)	2.284(5)	2.256(3)	2.106(2)	2.113(2)	
M–O23		2.109(4)		1.993(5)	1.969(4)	1.951(3)	2.257(2)		
Bond angles									
O11–M–O11^{i}/O21	172.85(8)	169.40(14)	89.84(15)	173.74(19)	171.22(19)	88.99(11)	87.45(9)	92.09(14)	
O11–M–N1	93.79(6)	94.03(17)	90.52(17)	93.45(19)	94.56(18)	94.54(12)	170.74(10)	88.44(10)	
O11–M–N1^{i}/N3	91.19(6)	93.24(17)	88.36(17)				94.95(10)	170.40(10)	
O11–M–O13	76.41(5)	76.31(14)	77.95(15)	76.14(16)	77.09(17)	76.64(10)	76.85(8)	74.68(9)	
O11–M–O13^{i}/O23	98.33(6)	94.26(15)		91.76(18)	91.08(17)	169.96(11)	87.50(9)	91.55(9)	
O11–M–N5			171.23(18)						
N1–M–N1^{i}/N3	91.79(10)	90.92(19)	92.90(19)				92.94(10)	92.63(16)	90.35(9)
N1–M–O13	91.70(7)	90.90(17)	91.34(18)	95.42(19)	96.2(2)	109.81(12)	86.99(10)	97.83(11)	
N1–M–O13^{i}/O23	167.31(6)	171.15(18)		171.2(2)	169.4(2)	95.18(3)	85.47(10)	95.73(10)	
N1–M–N5			94.61(19)						88.76(9)
O13–M–O13^{i}/O23	87.53(9)	88.04(15)		92.66(19)	93.8(2)	102.35(11)	88.92(9)	160.32(14)	
O21–M–N3		93.05(18)	87.79(17)				96.40(10)		
O21–M–N1		94.40(17)	179.23(17)	92.56(19)	92.14(19)	152.45(12)	96.48(10)		
O21–M–O23		77.03(15)		82.06(18)	81.44(18)	81.22(11)	74.81(8)		
O21–M–O13		97.12(14)	88.07(16)	105.03(18)	107.83(18)	97.60(10)	157.93(9)		
N3–M–O23		91.71(18)					170.79(10)		
N3–M–O13		169.49(19)	165.70(17)				100.28(11)		
N3–M–N5			98.46(19)						91.38(9)
N5–M–O13			94.80(17)						
N5–M–O21			84.96(17)						
N1–M–N3^{i}									89.65(9)
N1–M–N5^{i}									91.24(9)
N3–M–N5^{i}									88.62(9)

[*] $i = -x, y, -z + 1/2$.
[**] $I = -y + 1, -x + 1, -z + 1/2$.
[***] $i = -x + 1, -y + 1, -z$.

when the α-hydroxycarboxylato ligand is a bidentate chelate but in **3**, where one HB ligand acts in a monodentate manner, this bond length has a larger value (2.155 Å). In the nickel compounds, however, when the anionic ligand acts as a chelating system, the Ni–$O_{hydroxyl}$ bonds are longer than the Ni–$O_{carboxy}$ bonds. In **7** and **8** the Zn–N bond lengths are shorter than those observed in hexakis-substituted imidazole complexes (compound **9** in this work and [9]) but slightly longer than those found in other bis-substituted systems [10–12]. The Zn–$O_{hydroxyl}$ and Zn–$O_{carboxy}$ distances are longer than the corresponding distances observed in $[Zn(HmL)_2(H_2O)_2]$ [8].

In compounds **4**–**6** the asymmetric unit is composed of the neutral complex $[Cu(HL')_2(Im)]$ where HL′ = HG (**4**), L = HL (**5**) and L = HmL (**6**). In these three compounds the copper atom is pentacoordinated and the α-hydroxycarboxylato ligands acts as monoanionic *O*,*O*′-bidentate chelate systems. The resulting coordination polyhedra are square pyramids, which are almost perfect for **4** and **5** (Fig. 5 shows compound **5**) but with a slight deviation towards a trigonal bipyramid in **6** (Fig. 6) (Addison's τ value [13] is 0.04 in **4**, 0.03 in **5** and 0.29 in **6**). The hydroxyl group (O13) of one of the anionic ligands is located at the apex of the square pyramid and there is a correlation between this apical Cu–O distance (Table 2) and the value of the tetragonality parameter *T* (ratio between the mean of the four shortest and largest distances: 0.82 for **4**, 0.85 for **5** and 0.87 for **6**). In the basal plane of **4** and **5** the carboxylato oxygen atoms are mutually *trans* but in **6**, where the ligand is 2-methyllactato, they are mutually *cis*. The chelate angles $O_{carboxy}$–Cu–$O_{hydroxyl}$ (range 76.14°–77.09°) have similar values to those observed in the nickel complexes. The Cu–N bond lengths agree with those reported for other copper(II) complexes with imidazole [14,15]. Both the apical and the basal Cu–$O_{hydroxyl}$ distances decrease on going from **4** to **6** and as usual in square pyramidal copper complexes, the Cu–apex distance Cu–O13 is longer than the bond lengths in the base. The apical Cu–$O_{hydroxyl}$ distances are similar to the Cu–$O_{hydroxyl}$ distances found in hexacoordinated copper(II) α-hydroxycarboxylato complexes with 4,4′-bipyridine [16] or 2,2′-bipyridine [3]. In **6** the basal

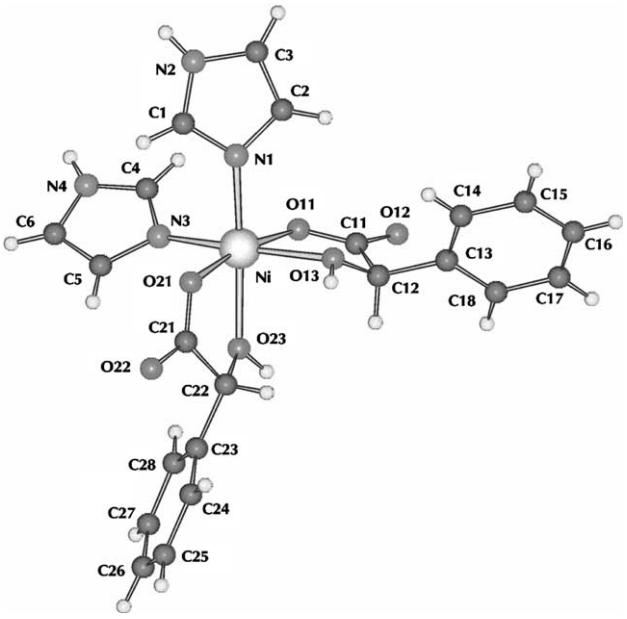

Fig. 1. Molecular structure of $[Ni(HM)_2(Im)_2]$ (**2**), showing the atom numbering scheme.

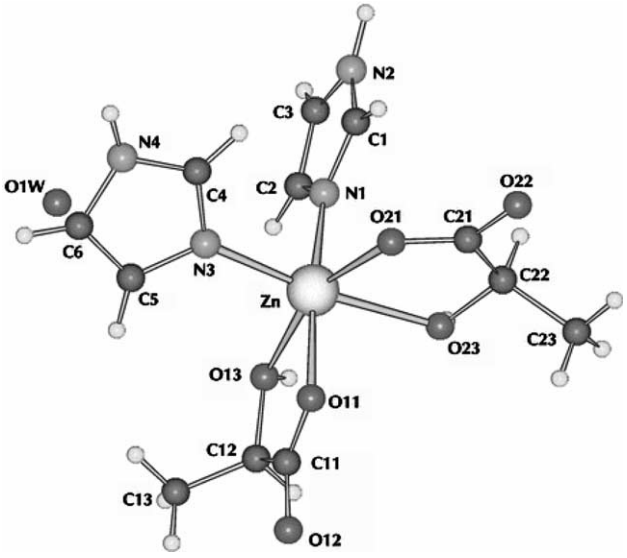

Fig. 2. Molecular structure of *all cis*-$[Zn(HL)_2(Im)_2] \cdot 1/2H_2O$ (**7**).

$Cu–O_{hydroxyl}$ distance is slightly shorter than the $Cu–O_{carboxy}$ distance (belonging the two oxygen atoms of the same ligand). The $Cu–O_{carboxy}$ distances fall within the range usually observed in other copper(II) α-hydroxycarboxylato complexes with N-donor ligands [1–4,16].

The structure of compound **9** is shown in Fig. 7. The zinc ion (located on an inversion centre, d position in the Wyckoff notation) is coordinated to six imidazole ligands and the α-hydroxycarboxylato (benzylato) is present as a monoanionic counterion. Numerous structural reports have been published on octahedral hexakis(imidazole) complexes with first-row transition metals such as Mn(II), Ni(II), Co(II) and Cu(II) but, to the best of our knowledge, only one structure has been reported for a hexakis-substituted complex with Zn(II): $[Zn(Im)_6]Cl_2 \cdot 4H_2O$ [9]. As required by symmetry, the imidazole rings in a *trans* arrangement are coplanar and the metal ion also lies in this plane. The Zn–N distances (Table 1) are similar to those found in $[Zn(Im)_6]Cl_2 \cdot 4H_2O$ [9].

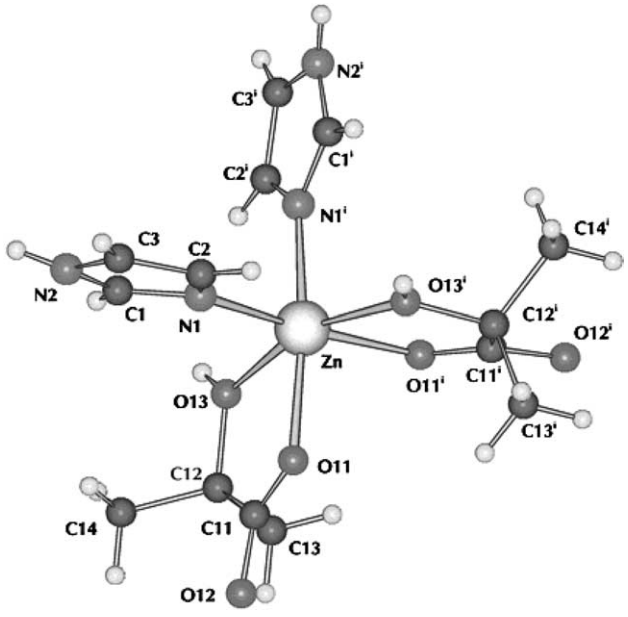

Fig. 3. Molecular structure of $[Zn(HmL)_2(Im)_2]$ (**8**).

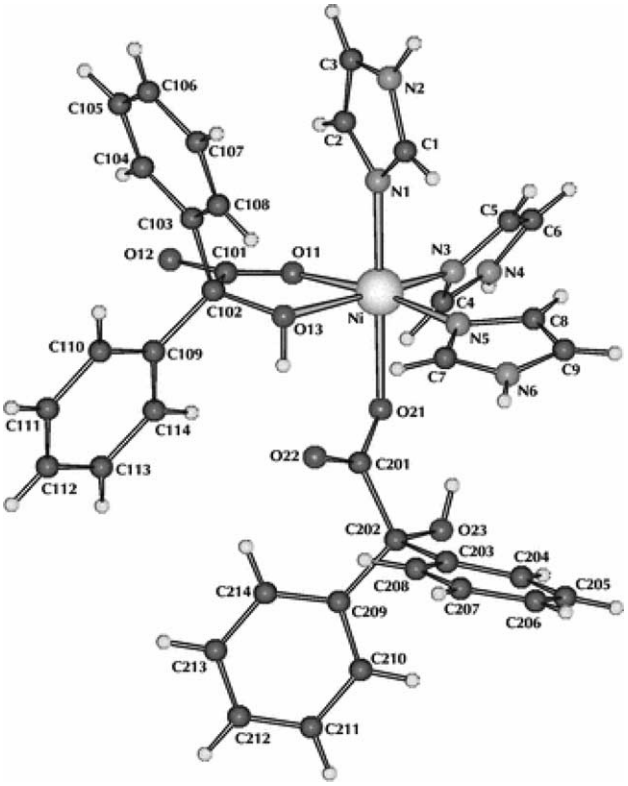

Fig. 4. Molecular structure of *fac*-$[Ni(HB)_2(Im)_3]$ (**3**).

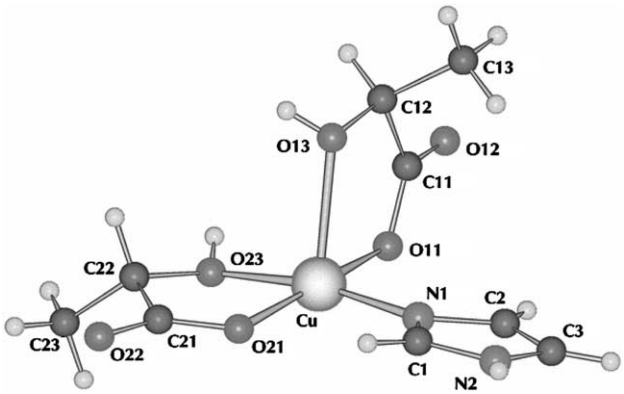

Fig. 5. Molecular structure of $[Cu(HL)_2(Im)]$ (**5**).

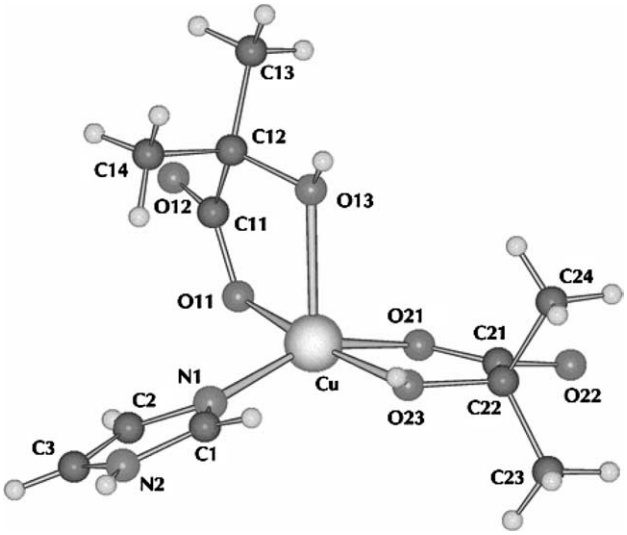

Fig. 6. Molecular structure of $[Cu(HmL)_2(Im)]$ (**6**).

The nature of the imidazole and α-hydroxycarboxylato ligands allows the formation of supramolecular architectures based on hydrogen bonding (Table 2). In most cases, an infinite two-dimensional network is obtained and the 2D structure for **5** is shown in Fig. 8. In complex **3** (Fig. 9), the presence of three imidazole ligands in a *fac*-disposition gives rise to a 3D structure. In all compounds the shortest and most linear intermolecular hydrogen bonds are those between the hydroxyl groups and/or the –NH groups as donors and the uncoordinated oxygen atoms of the carboxylato groups of adjacent molecules as acceptors (O...O range 2.50–2.76 Å and N...O range 2.72–2.95 Å). In addition, other types of intermolecular hydrogen bonds are present in some complexes, where the coordinated $O_{carboxy}$ atom acts as an acceptor and the donors are the –NH groups of the imidazoles (nickel compounds **1** and **3**, N...O distances = 3.004 and 3.191 Å; zinc compound **7**, N...O = distance: 2.799 Å) or the –OH group (copper complexes **5** and **6**, O...O distances = 2.827 and 3.226 Å; zinc compound **7**, O...O distance = 2.785 Å). An interaction between the –NH group and the –OH group acting as an acceptor is also observed in the nickel compound **3** (N...O distance = 2.814 Å) and the zinc compound **9,** where HB acts as a counterion (N...O distance = 3.218 Å). In **4** and **8** there are also C–H...O bonds, which involve imidazole carbons and uncoordinated $O_{carboxy}$ atoms. The values of C...O distances (3.215 and 3.346 Å) and C–H...O angles (152.3° and 161.2°) provide evidence for a significant interaction [17]. This latter bond leads to the formation of 3D networks in **4** (Fig. 10 shows the 2D sheets linked by C–H...O bonds) and in **8** (Fig. 11). In **9** each imidazole ligand participates

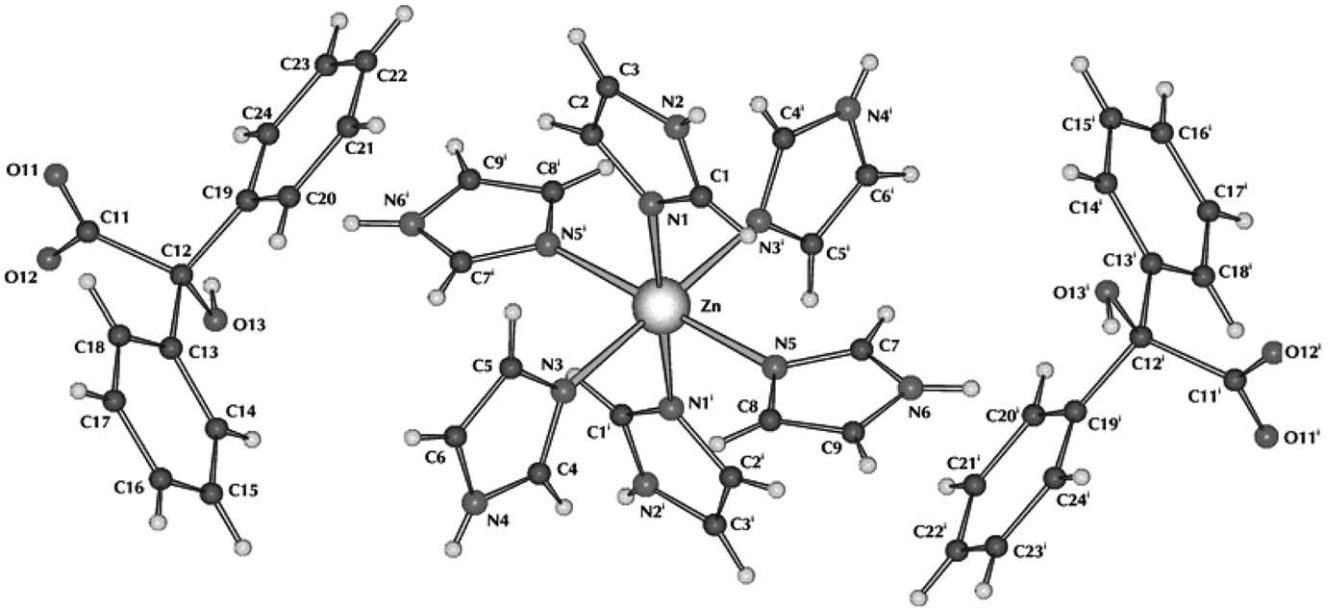

Fig. 7. Molecular structure of $[Zn(Im)_6](HB)_2$ (**9**).

Table 2
Main hydrogen bonds [Å, °]

D–H...A	*d*(D–H)	*d*(H...A)	*d*(D...A)	∠(DHA)
Compound **1** (2D) $i = x, -y+1, z-1/2; ii = x, -y+2, z-1/2$				
N2–H20...O11^{i}	0.874(18)	2.18(2)	3.004(3)	158(3)
N2–H20...O12^{i}	0.874(18)	2.39(3)	3.141(3)	145(3)
O13–H13...O12^{ii}	0.832(17)	1.886(17)	2.716(2)	175(3)
Compound **2** (2D)				
$i = -x, -y, -z+1; ii = -x, -y+1, -z+1; iii = -x+1, -y, -z+1;$				
$iv = -x+1, -y+1, -z+1$				
N2–H20...O22^{iii}	0.86	2.00	2.812(6)	158.2
N4–H40...O12^{iv}	0.86	1.99	2.827(5)	163.3
O13–H13...O22^{i}	0.876(19)	1.77(2)	2.620(5)	162(5)
O23–H23...O12^{ii}	0.906(19)	1.72(2)	2.621(5)	173(5)
Compound **3** (3D)				
$i = -x+1, -y, -z+1; ii = x-1/2, -y+1/2, z+1/2; iii = x-1, y, z$				
N2–H20...O12^{ii}	0.99(8)	1.78(8)	2.763(7)	172(7)
N4–H40...O23^{i}	0.89(6)	1.93(6)	2.814(7)	168(6)
N6–H60...O11^{iii}	0.81(7)	2.48(7)	3.191(7)	146(6)
N6–H60...O12^{iii}	0.81(7)	2.25(7)	2.953(8)	145(6)
Compound **4** (3D)				
$i = -x+1, -y+1, -z; ii = -x+2, -y, -z+1; iii = x-1, y, z;$				
$iv = x+1, y+1, z$				
N2–H20...O22^{i}	0.88(6)	1.91(6)	2.787(7)	174(6)
O13–H13...O12^{iii}	0.81(6)	1.98(7)	2.760(6)	161(6)
O23–H23...O12^{ii}	0.71(6)	1.94(7)	2.648(6)	170(7)
C3–H3...O22^{iv}	0.93	2.36	3.215(7)	152.3
Compound **5** (2D) $i = x-1, y, z; ii = -x+1, -y, -z; iii = -x, -y+1, -z$				
N2–H20...O22^{iii}	0.988(5)	1.783(4)	2.721(7)	157.3(3)
O13–H13...O11^{i}	0.823(19)	2.56(4)	3.226(6)	138(6)
O13–H13...O12^{i}	0.823(19)	1.94(3)	2.727(6)	159(7)
O23–H23...O12^{ii}	0.781(19)	1.90(3)	2.642(6)	160(5)
Compound **6** (2D) $i = x+1/2, -y+3/2, z+1/2; ii = x+1, y, z$				
N2–H20...O22^{ii}	0.96(4)	1.82(4)	2.759(5)	166(4)
O23–H23...O12^{i}	0.94(4)	1.67(4)	2.597(4)	166(3)
O13–H13...O21^{i}	0.93(4)	1.91(4)	2.827(4)	167(3)
Compound 7 (2D)				
$i = -x+3/2, -y+1/2, z+1/2; ii = -x+3/2, y+1/2, z : iii = x, -y, z+1/2$				
N2–H20...O11^{i}	0.96(4)	1.86(4)	2.799(4)	167(4)
O13–H13...O22^{ii}	0.79(4)	1.81(4)	2.587(3)	168(4)
O23–H23...O21^{ii}	0.86(4)	1.94(4)	2.785(3)	165(3)
N4–H40...O12^{iii}	0.85(3)	1.92(3)	2.729(4)	160(3)
Compound **8** (3D)				
$i = -x+1/2, y+1/2, -z+3/4; ii = -y+1/2, x+1/2, z-1/4;$				
$iii = -y, -x+1, -z+1/2$				
N2–H20...O12^{iii}	0.84(5)	1.93(5)	2.737(4)	160(4)
O13–H13...O12^{ii}	0.98(6)	1.65(6)	2.623(3)	173(5)
C2–H2...O12^{i}	0.93	2.45	3.346(5)	161.2
Compound **9** (3D)				
$i = -x, -y, -z; ii = -x, -y+1, -z; iii = -x+1, y+1/2, -z+1/2;$				
$iv = x+1, y+1, z$				
N2–H20...O11^{iii}	0.78(4)	1.99(4)	2.762(4)	171(4)
N4–H40...O13^{ii}	0.76(4)	2.54(4)	3.218(4)	150(4)
N4–H40...O12^{ii}	0.76(4)	2.38(4)	3.041(4)	145(4)
N6–H60...O12^{iv}	0.90(3)	1.90(4)	2.793(3)	172(3)
O13–H13...O12^{i}	0.82	2.11	2.918(3)	170.1
C24–H24...O12^{i}	0.93	2.49	3.329(4)	149.8

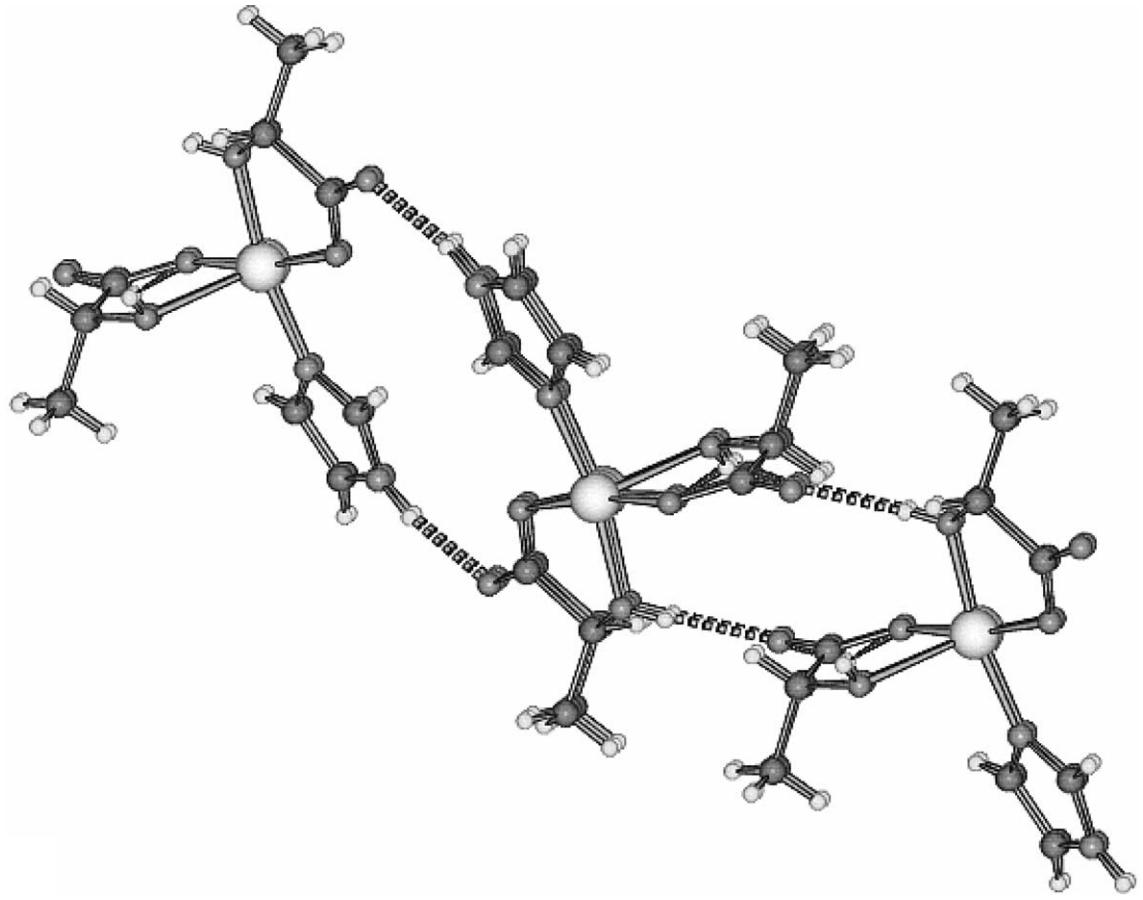

Fig. 8. View of the 2D crystal packing through hydrogen bonding in $[Cu(HL)_2(Im)]$ (**5**).

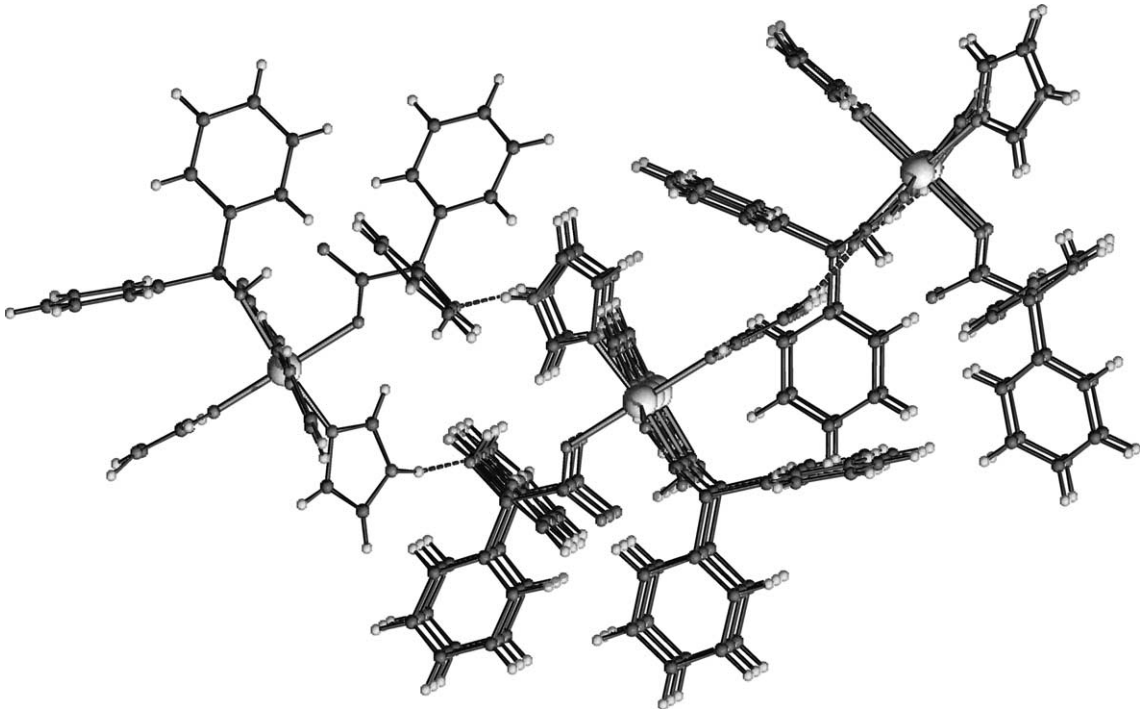

Fig. 9. Crystal packing diagram running along the *a*-axis for $[Ni(HB)_2(Im)_3]$ (**3**).

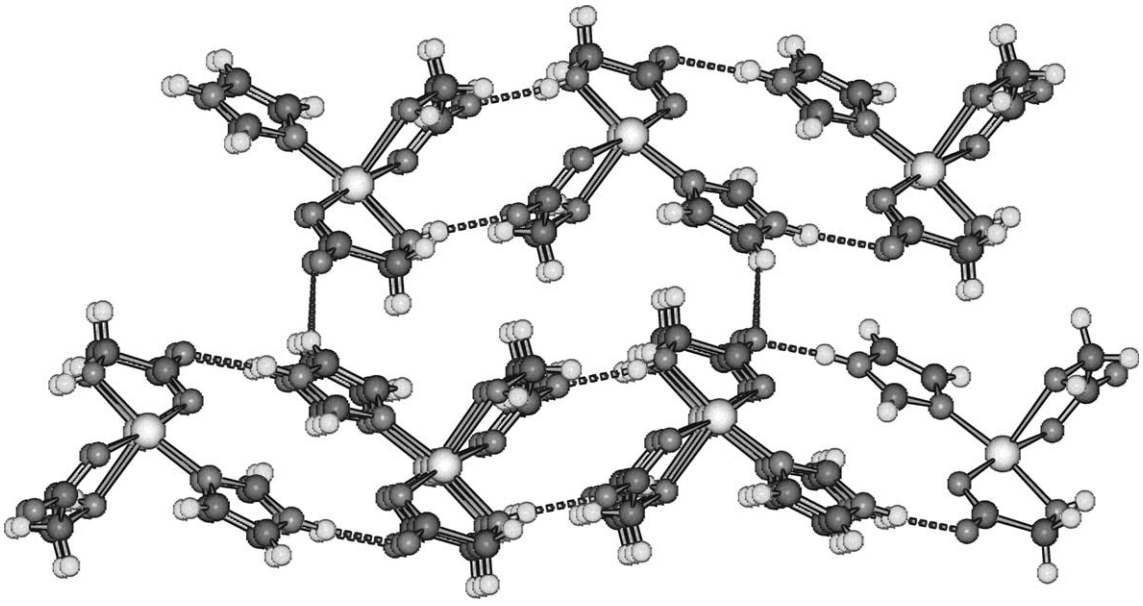

Fig. 10. View of the packing in $[Cu(HG)_2(Im)]$ (**4**) showing the linkage by C–H...O hydrogen bonds of the 2D sheets.

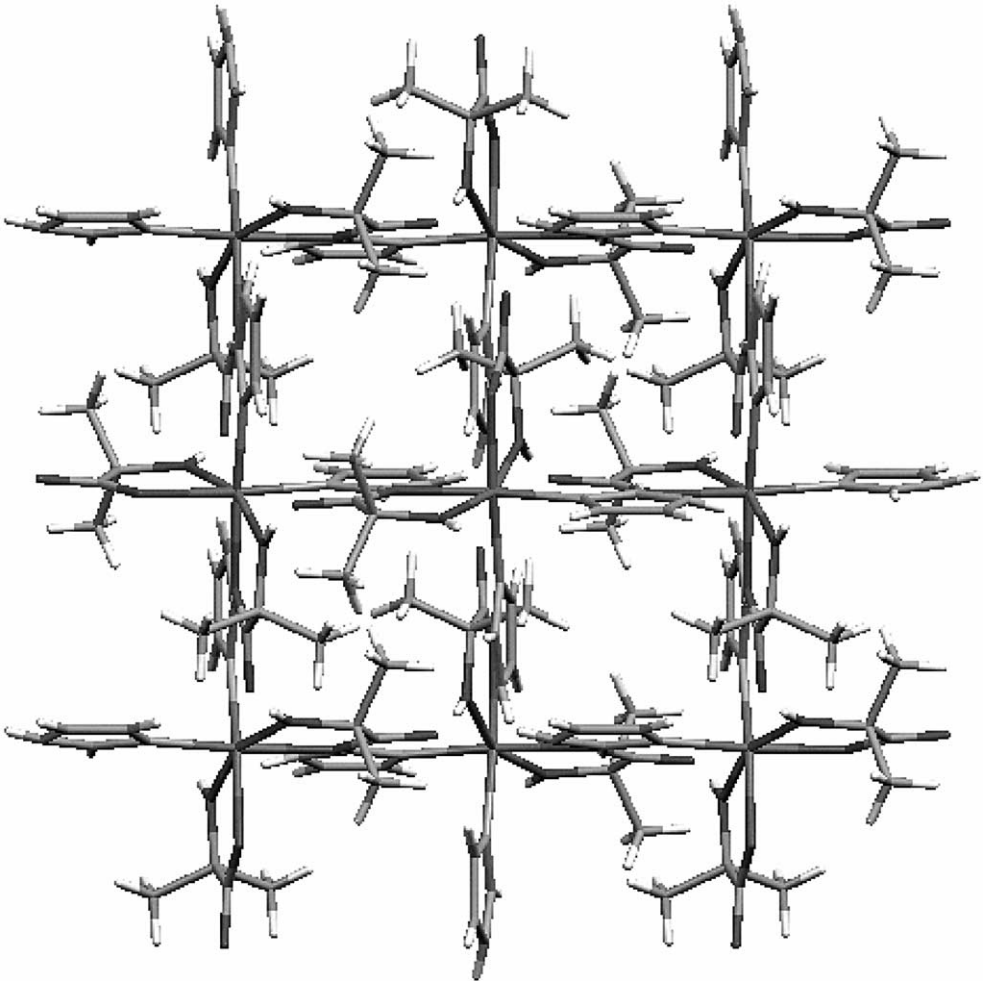

Fig. 11. View of the 3D crystal packing in $[Zn(HmL)_2(Im)_2]$ (**8**) in the ab plane.

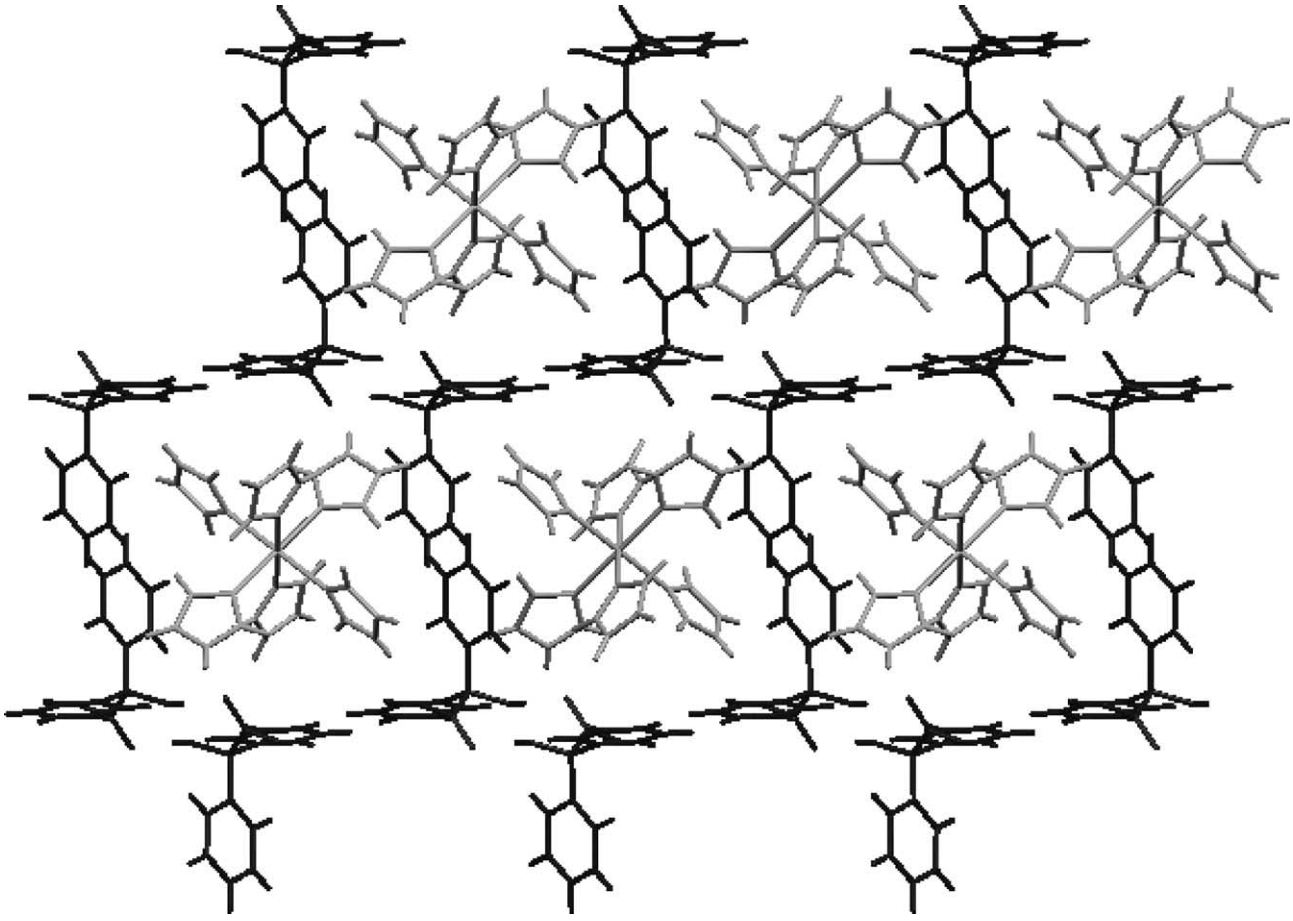

Fig. 12. A fragment of the infinite 3D network through hydrogen bonds of $[Zn(Im)_6](HB)_2$ (**9**) showing the close-packing in the plane *ac*.

in hydrogen bonds with HB molecules, meaning that each cation $[Zn(Im)_6]^{2+}$ is surrounded by six HB molecules and each HB molecule interacts with three cationic species to generate a 3D network (Fig. 12).

All compounds crystallize without solvent molecules in their structures apart from **7**, which contains one water molecule located on a twofold axis (Wyckoff position 4c). This water molecule is not involved in hydrogen bonding.

There are also a number of stacking interactions that involve the imidazole rings. The shortest centroid-to-centroid distances are observed in compounds **4** and **5** (3.581 and 3.571 Å, respectively) with an interplanar dihedral angle α of 0.00° (indicating Im/Im parallelism) and slipping angles β and γ of approximately 24°, revealing a moderate slipping of the stacked rings [18]. Edge-to-face C–H$\ldots\pi$ interactions are also observed in some cases. The main interactions are found in **9** [with an intramolecular C–H(Im)...imidazole centroid of 3.59 Å] and intermolecular interactions in **2** [C–H(Im)... phenyl centroid, 3.52 Å], **4** [C–H(methyl group)... imidazole centroid, 3.49 Å], **5** [C–H(Im)...imidazole centroid, 3.30 Å], **6** [C–H(methyl group)...imidazole centroid,3.67 Å] and **7** [C–H(Im)...imidazole centroid, 3.49 Å].

2.2. Thermal behaviour

Thermogravimetric analysis (TGA) was performed to investigate the thermal stability of compounds **1**–**9**. A summary of the results is given in Table 3. The species were investigated by monitoring the evolved gases by IR spectroscopy. The thermal behaviour of most of the compounds is very similar and generally shows two steps, with the exception of **2** and **9** (three steps) and **7**, which contains water of crystallization (four steps). The nickel and copper compounds are stable up to 170–200 °C and the zinc compounds to 120–150 °C. In **7** the first step corresponds to the loss of the non-coordinated water (75–150 °C). In most of the compounds, however, the first mass loss corresponds to pyrolysis of the α-hydroxycarboxylato ligands followed, in a second step, by the loss of imidazole. Finally, the complexes give residues of NiO at 375–500 °C (nickel compounds), CuO at 425–450 °C (copper compounds) and ZnO or $Zn(OH)_2$ at 475–550 °C (zinc compounds).

Table 3
Summary of thermal, spectral and magnetic properties ($^*\Delta v = v_{as}(OCO) - v_s(OCO)$)

Compound	1	2	3	4	5	6	7	8	9
TG analysis									
Number of steps	2	3	2	2	2	2	4	2	3
T (°C)	200–500	215–400	175–375	200–450	170–450	200–425	75–475	150–550	120–500
1st step loss	HmL	HM	Im	HG	HL	HmL	H_2O	HmL	HB
Other steps loss	Im	Im	HB	Im	Im	Im	HmL, Im	Im	Im
Final residue	NiO	NiO	NiO	CuO	CuO	CuO	ZnO	$Zn(OH)_2$	ZnO
IR data (cm^{-1})									
ν(OH)/ν(NH)	3140 overlap	3240/3139	3400/3178	3230/3137	3399/3169	3279/3142	3388, 3149	3400-3100 overlap	3391, 3216/3133
ν_{as}(OCO)/Im I band	1579/1640	1597 overlap	1599/1620	1597 overlap	1610 overlap	1571/1643	1597 overlap	1589 overlap	1598 overlap
ν_s(OCO)	1401	1379	1362	1377	1380	1379	1388	1362	1367
$\Delta\nu^*$	178	~218	237	~220	~230	192	~209	~227	~231
Electronic spectrum (cm^{-1})	9090 (ν_1), 15 480 (ν_2), 26 740 (ν_3)	9415 (ν_1), 15 200 (ν_2), 25 900 (ν_3)	9900 (ν_1), 15 825 (ν_2), 26 740 (ν_3)	13 850	13 440	12 315			
μ (BM) *at 293 K*	3.21	3.36	2.96	1.86	1.75	2.25			
ESR type				axial	axial	quasi-iso			
$g_{\|}$, $g_{\perp}$				2.31, 2.06	2.31, 2.05				
$g_{average}$						2.13			

2.3. Infrared spectra

The IR spectra of most of the complexes (Table 3) show sharp bands in the 3100–3200 cm^{-1} region, which are assigned to the NH stretching frequency. Complexes **1** and **8** show broad bands in the 3100–3200 cm^{-1} region including ν(OH) and ν(NH) and the remaining complexes show broad bands in the 3200–3400 cm^{-1} region, which correspond to ν(OH). The intense bands appearing around 1600 cm^{-1}, which in most cases overlap with bands associated with the imidazole I band, are assigned to the asymmetric COO^- vibration. The bands found between 1360 and 1400 cm^{-1} are assigned to ν_s(COO). The estimated values around 200 cm^{-1} for $\Delta\nu = \nu_{as}(OCO) - \nu_s(OCO)$ are typical of monodentate carboxylato groups [19]. In compounds **1**–**8** a band is observed in the 420–450 cm^{-1} region and this is attributed to ν(MO) [20].

2.4. Electronic spectra

The reflectance spectra of the nickel and copper complexes in the solid state were recorded in the range 250–1500 nm. The spectra of compounds **1**–**3** (Table 3) are typical of Ni(II) [ground state $^3A_{2g}(F)$] octahedral complexes. The band found between 9090 and 9900 cm^{-1} can be assigned to the $^3T_{2g}(F) \leftarrow {}^3A_{2g}(F)$ (ν_1) transition, that observed around 15 000 cm^{-1} to the $^3T_{1g}(F) \leftarrow {}^3A_{2g}(F)$ (ν_2) transition and the band close to 26 000 cm^{-1} to the $^3T_{1g}(P) \leftarrow {}^3A_{2g}(F)$ (ν_3) transition. The spectra of the copper(II) complexes **4**–**6** all exhibits a broad band, centred at around 13 500 cm^{-1} for **4** and **5** and at 12 300 cm^{-1} for **6**. These bands are characteristic of a copper(II) d–d transition [21] in a tetragonal field in which the copper(II) atom is in a distorted square-based pyramidal coordination environment.

2.5. Magnetic properties

For the nickel complexes (**1**–**3**) the magnitude of the effective magnetic moments between 2.96 and 3.36 BM at room temperature are as one would expect for octahedral symmetry but larger than the spin-only value (2.83 BM) expected for the two unpaired electrons of the Ni(II) cation with a d^8 configuration [22]. For the copper complexes (**4**–**6**), μ_{eff} at room temperature varies from 1.75 to 2.25 BM and these values lie in the range expected for pentacoordinated complexes of copper(II) [23] and are also larger than the spin-only value for an uncoupled Cu(II) ion (1.73 BM).The ESR spectra at room temperature are of the axial type for compounds **4** and **5** ($g_{\|} = 2.31 > g_{|} = 2.06$–$2.05$) and quasi-isotropic or near isotropic ($g_{av} \sim 2.13$) for **6**. These spectra are in accordance with a $d_{x^2-y^2}$ ground state for copper(II), as one would expect for an elongated square-based pyramidal coordination polyhedron.

3. Experimental

3.1. Materials and physical measurements

All reagents and solvents were obtained commercially and were used as supplied.

Microanalyses (C, H, N) were carried out with a FISONS EA-1108 elemental analyser. Melting points (m.p.) were measured with a Gallenkamp MBF-595 apparatus. FT-IR spectra in the 4000–400 cm^{-1}region were recorded from KBr pellets on a Bruker VECTOR 22 spectrophotometer. A Shimadzu UV-3101PC spectrophotometer was used to obtain the electronic spectra in the region 250–1500 nm. ESR spectra of polycrystalline samples were recorded without magnetic dilution using a Bruker ESP 300E spectrophotometer (X band) at room temperature. Magnetic susceptibility measurements were performed at 25 °C using a Johnson Matthey Alfa MSB-MKI Gouy balance. TG/DTG analysis profiles (pyrolysis, 300–1000 K, with IR and MS investigation of evolved gases) were recorded under a 100 mL min^{-1} air flow using a Shimadzu TGA-DTG-50H Thermobalance coupled to a Nicolet Magma 550 FT-IR apparatus and a Fisons Thermolab mass spectrometer.

3.2. Synthesis and crystallisation of the complexes

3.2.1. Nickel(II) Compounds

Compounds **1** and **2** were synthesised by reacting $Ni(AcO)_2 \cdot 4H_2O$ (1 mmol) with 2-methyllactic acid (H_2mL) and mandelic acid (H_2M) (2 mmol), respectively, and Im (2 mmol) in EtOH (30 mL). The mixture was refluxed for 2 h and was then left to cool to room temperature, after which stirring was maintained for 7 days. The light blue powders of **1** and **2** were filtered off. When the reactions were carried out in the molar ratio 1:2:1, the resulting products were respectively: $[Ni(HmL)_2(OH_2)_2]$ (~50%) and **1** (~50%); $[Ni(HM)_2(OH_2)_2]$. H_2O (~50%) and **2** (~50%).

Data for *[Ni(HmL)$_2$(OH$_2$)$_2$]*: m.p.>250 °C. *Anal.* Calc. for $C_8H_{18}O_8Ni$ (300.92): C, 31.9; H, 6.5. Found: C, 32.0; H, 6.2%. IR (ν cm^{-1}): 3448 s, 3193 s, 1624 s, 1487 s, 1174 s. UV–Vis (ν, cm^{-1}): 25 250, 13 625, 8700.

Data for *[Ni(HM)$_2$(OH$_2$)$_2$]·H$_2$O*: m.p.>250 °C. *Anal.* Calc. for $C_{16}H_{20}O_9Ni$ (415.02): C, 46.3; H, 4.9. Found: C, 45.7; H, 4.8%. IR (ν cm^{-1}): 3391 s, 3100 s, 1610 s, 1395 m, 1028 m. UV–Vis (ν, cm^{-1}): 25 640, 13 660, 8350.

*3.2.1.1. [Ni(HmL)$_2$(Im)$_2$] (**1**).* Yield: 81%; m.p. >250 °C. *Anal.* Calc. for $C_{14}H_{22}N_4O_6Ni$ (401.07): C, 41.9; H, 5.1; N, 13.1. Found: C, 41.1; H, 6.1; N, 12.4%. IR (ν cm^{-1}): 3140 vs b, 2975 vs, 1640 vs, 1579 vs, 1491 s, 1401 s, 1175 s, 1073 s, 966 m, 925 s, 824 m, 730 s, 623 m, 432 m.

Recrystallisation from MeOH/*i*PrOH (1:1) of the light blue oil resulting from the slow evaporation of the mother liquor yielded single crystals of **1**.

*3.2.1.2. [Ni(HM)$_2$(Im)$_2$] (**2**).* Yield: 73%; m.p.> 250 °C. *Anal.* Calc. for $C_{22}H_{22}N_4O_6Ni$ (497.15): C, 53.2; H, 4.5; N, 11.3. Found: C, 53.0; H, 4.0; N, 11.0%. IR (ν cm^{-1}): 3240 s, 3139 s, 2956 s, 1597 vs, 1419 s, 1379 s, 1066 s, 944 m, 802 s, 741 s, 698 s, 576 s, 444 m.

Single crystals of **2** were obtained by slow evaporation at room temperature of the filtrate.

*3.2.1.3. [Ni(HB)$_2$(Im)$_3$] (**3**).* Compound **3** was obtained by a similar procedure, but in this case only when the molar ratio 1:2:1 was used was it possible to identify the resulting products. Firstly, a green powder of formula $[Ni(HB)_2(OH_2)_2]$ was isolated from the resulting suspension. Secondly, recrystallisation from MeOH/*i*PrOH (1:1) of the green oil obtained after the slow evaporation of the mother liquor allowed the isolation of single crystals of **3**.

Data for *[Ni(HB)$_2$(OH$_2$)$_2$]*: m.p.>250 °C. *Anal.* Calc. for $C_{28}H_{24}O_8Ni$ (547.18): C, 61.2; H, 4.8. Found: C, 62.1; H, 5.1%. IR (ν cm^{-1}): 3421 s, 1652 s, 1375 m, 1051 m. UV–Vis (ν, cm^{-1}): 23 480, 13 120, 8010.

*[Ni(HB)$_2$(Im)$_3$] (**3**).* Yield: 25%; m.p. 243 °C. *Anal.* Calc. for $C_{37}H_{34}N_6O_6Ni$ (717.41): C, 61.9; H, 4.8; N, 11.7. Found: C, 61.5; H, 4.8; N, 11.5%. IR (ν cm^{-1}): 3400 m b, 3178 s b, 2967 m, 1620 vs, 1599 vs, 1362 s, 1173 m, 1069 s, 942 m, 831 m, 747 s, 699 s, 598 m, 424 w.

3.2.2. Copper(II) compounds

A mixture of $CuCO_3 \cdot Cu(OH)_2 \cdot 1/2H_2O$ (0.5 mmol) and glycolic acid (H_2G) (**4**), lactic acid (H_2L) (**5**) or 2-methyllactic acid (H_2mL) (**6**) (2 mmol) and Im (1 mmol) in H_2O (30 mL) for **4** and in EtOH (30 mL) for **5** and **6** was refluxed for 2 h and then left to cool to room temperature, after which stirring was maintained for several days. The resulting blue solids **4**–**6** were filtered off and dried over $CaCl_2$.

When a molar metal:imidazole ratio of 1:2 was used the same compounds were obtained.

*3.2.2.1. [Cu(HG)$_2$(Im)] (**4**).* Yield: 50%; m.p. 219 °C. Anal. Found: C, 29.7; H, 3.9; N, 9.7. Calcd. for $C_7H_{10}N_2O_6Cu$ (281.71): C, 29.8; H, 3.6; 9.9%. IR (ν cm^{-1}): 3230 m, 3137 m, 2942 m, 1597 vs, 1377 m, 1075 m, 931 w, 841 w, 771 w, 698 w, 550 w, 451 vw.

Single crystals of **4** were obtained by slow concentration of the mother liquor at room temperature.

*3.2.2.2. [Cu(HL)$_2$(Im)] (**5**).* Yield: 56%; m.p. 190 °C. *Anal.* Calc. for $C_9H_{14}N_2O_6Cu$ (309.76): C, 34.9; H, 4.6; N, 9.0. Found: C, 35.1; H, 5.1; N, 9.6%. IR (ν cm^{-1}): 3399 m, 3169 m, 2980 m, 1610 vs, 1380 s, 1102 m, 1077 m, 959 w, 865 m, 769 m, 654 m, 556 m, 425 w.

Table 4
Crystal data and structure refinement

Compound	1	2	3	4	5	6	7	8	9
Empirical formula	$C_{14}H_{22}N_4O_6Ni$	$C_{22}H_{22}N_4O_6Ni$	$C_{37}H_{34}N_6O_6Ni$	$C_7H_{10}N_2O_6Cu$	$C_9H_{14}N_2O_6Cu$	$C_{11}H_{18}N_2O_6Cu$	$C_{12}H_{19}N_4O_{6.5}Zn$	$C_{14}H_{22}N_4O_6Zn$	$C_{46}H_{46}N_{12}O_6Zn$
Formula weight	401.07	497.15	717.41	281.71	309.76	337.81	388.68	407.73	928.32
Crystal system	monoclinic	triclinic	monoclinic	triclinic	monoclinic	monoclinic	orthorhombic	tetragonal	monoclinic
Space group	$C2/c$	$P\bar{1}$	$P2_1/n$	$P\bar{1}$	$P2_1/c$	$P2_1/n$	$Pbcn$	$P4_32_12$	$P2_1/c$
Unit cell dimensions									
a (Å)	19.392(7)	9.170(3)	9.2191(11)	5.528(2)	5.422(3)	9.6623(15)	20.4557(18)	10.7634(9)	12.9507(17)
b (Å)	8.477(3)	10.936(3)	29.972(4)	7.267(3)	13.436(7)	17.630(3)	10.4408(9)	10. 7634(9)	9.0191(11)
c (Å)	11.412(4)	12.717(4)	12.5644(15)	13.626(5)	17.000(9)	9.7978(16)	15. 0918(13)	16.442(3)	22.209(3)
α (°)		106.910(7)		75.045(5)					
β (°)	111.795(7)	110.208(6)	94.428(3)	85.826(6)	92.324(11)	118.748(3)			119.763(6)
γ (°)		90.172(7)		75.613(7)					
Volume (Å^3)	1741.9(11)	1137.4(6)	3461.3(7)	512.2(3)	1237.4(11)	1463.3(4)	3223.2(5)	1904.8(4)	2251.9(5)
Z, ρ_{calc} (g cm^{-3})	4, 1.529	2, 1.452	4, 1.377	2, 1.826	4, 1.663	4, 1.533	8, 1.602	4, 1.422	2, 1.369
$F(000)$	840	516	1496	286	636	700	1608	848	968
Crystal size (mm^3)	$0.25 \times 0.21 \times 0.19$	$0.23 \times 0.07 \times 0.06$	$0.25 \times 0.17 \times 0.16$	$0.15 \times 0.13 \times 0.09$	$0.15 \times 0.08 \times 0.\ 08$	$0.18 \times 0.08 \times 0.08$	$0.35 \times 0.30 \times 0.20$	$0.45 \times 0.38 \times 0.32$	$0.30 \times 0.26 \times 0.23$
Absorption coefficient (mm^{-1})	1.152	0.899	0.616	2.148	1.786	1.518	1.564	1.325	0.608
θ Range (°)	2.26–26.37	1.80–28.03	1.36–28.07	1.55–28.07	1.93–27.98	2.43–28.00	1.99–28.05	2.26–23.25	1.81–28.03
Maximum/minimum transmission	1.0000/0.8297	1.0000/0.7469	1.0000/0.8782	1.0000/0.6652	1.0000/0.7576	1.0000/0.8787	1.0000/0.7300	1.0000/0.9429	1.0000/0.9374
Reflections collected	4760	6291	18394	2335	6303	8121	17452	8295	12 535
Independent reflections (R_{int})	1763 (0.0308)	4405 (0.0628)	7653(0.0885)	1984 (0.0229)	2705 (0.0864)	3293(0.0736)	3852(0.0610)	1366(0.0231)	5094(0.0446)
Final R indices	$R_1 = 0.0317$	$R_1 = 0.0541$	$R_1 = 0.1058$	$R_1 = 0.0675$	$R_1 = 0.0495$	$R_1 = 0.0448$	$R_1 = 0.0401$	$R_1 = 0.0326$	$R_1 = 0.0620$
$[I > 2\sigma(I)]$	$wR_2 = 0.0664$	$wR_2 = 0.0629$	$wR_2 = 0.1619$	$wR_2 = 0.1157$	$wR_2 = 0.0686$	$wR_2 = 0.0511$	$wR_2 = 0.0869$	$wR_2 = 0.0809$	$wR_2 = 0.1013$

The recrystallisation of **5** from a 1:1 mixture of MeOH/*i*PrOH yielded blue single crystals.

*3.2.2.3. [Cu(HmL)$_2$(Im)] (**6**).* Yield: 46%; m.p. 200 °C. *Anal.* Calc. for $C_{11}H_{18}N_2O_6Cu$ (337.81): C, 39.1; H, 5.4; N, 8.3. Found: C, 39.1; H, 5.8; N, 8.3%. IR (ν cm^{-1}): 3279 m b, 3142 s, 2978 s, 1643 vs, 1571 s, 1548 s, 1379 s, 1349 s, 1174 s, 1076 m, 960 m, 817 s, 777 m, 622 m, 527 w, 434 w.

Recrystallisation from MeOH/*i*PrOH (1:1) of the blue oil resulting from the slow evaporation of the mother liquor yielded single crystals.

3.2.3. Zinc(II) compounds

A solution of lactic acid (H_2L) (**7**), 2-methyllactic acid (H_2mL) (**8**) or benzylic acid (H_2B) (**9**) (2 mmol) in ethanol (10 mL) and a solution of Im (2 mmol) in EtOH (10 mL) were added to a suspension of $ZnCO_3$ (1 mmol) in EtOH (10 mL). The mixture was refluxed for 2 h and the resulting white suspension was stirred for several days. The resulting white solids were filtered off and dried. Identification of the solid proved impossible in the reaction with 2-methyllactic acid, but with benzylic acid the solid corresponds to a compound of the formula $[Zn(HB)_2(OH_2)_2]$ and that obtained with lactic acid is consistent with the formula $[Zn(HL)_2(Im)_2]\cdot 1/2H_2O$.

Slow evaporation of the mother liquors of **7** and **8** gave colourless oils, which were dissolved in MeOH/acetone (1:1) for **7** and MeOH/*i*PrOH (1:1) for **8**. Slow solvent evaporation led to the isolation of single crystals of **7** and **8**.

*3.2.3.1. [Zn(HL)$_2$(Im)$_2$]·1/2H$_2$O (**7**).* Yield: 42%; m.p. 104 °C. *Anal.* Calc. for $C_{12}H_{19}N_4O_{6.5}Zn$ (388.68): C, 37.1; H, 4.9; N, 14.4. Found: C, 36.3; H, 4.8; N, 14.1%. IR (ν cm^{-1}): 3388 s b, 3149 s, 2934 m, 1597 vs, 1456 m, 1388 s, 1118 s, 1074 s, 948 m, 831 m, 769 m, 661 s, 557 m, 444 m. ^{1}H NMR (400 MHz, D_2O, ppm): imidazole, 8.15 (s, 1H), 7.32 (s, 2H); lactate, 4.20 (q, 1H), 1.38 (d, 3H).

*3.2.3.2. [Zn(HmL)$_2$(Im)$_2$] (**8**).* Yield: 15%; m.p. 164 °C. *Anal.* Calc. for $C_{14}H_{22}N_4O_6Zn$ (407.73): C, 41.2; H, 5.4; N, 13.7. Found: C, 41.2; H, 5.4; N, 14.1%. IR (ν cm^{-1}): 3400 sh, 3118 vs, 2971 vs, 1589 vs b, 1489 vs, 1362 vs, 1176 vs, 1074 vs, 943 s, 861 s, 731 s, 663 s, 562 m, 432 m. ^{1}H NMR (400 MHz, D_2O, ppm): imidazole, 8.10 (s, 1H), 7.29 (s, 2H); 2-methyllactate, 1.42 (s, 6H).

*3.2.3.3. [Zn(Im)$_6$](HB)$_2$ (**9**).* Yield: 35%; m.p. 130 °C. *Anal.* Calc. for $C_{46}H_{46}N_{12}O_6Zn$ (928.32): C, 59.5; H, 5.0; N, 18.1. Found: C, 59.4; H, 5.0; N, 18.2%. IR (ν cm^{-1}): 3391 s, 3216 s, 3133 s, 2933 s, 1598 vs, 1367 vs, 1146 m, 1098 m, 936 s, 831 s, 773 s, 616 s, 582 m. ^{1}H NMR (400 MHz, D_2O, ppm): imidazole, 7.98 (s, 3H), 7.25 (s, 6H); benzylate, 7.45 (s, 10H).

Slow evaporation of the mother liquor from the reaction with benzylic acid afforded colourless single crystals of **9**.

3.3. X-ray structure determination

Crystallographic data were collected on a Bruker Smart CCD diffractometer at 293 K using graphite-monochromated Mo Kα radiation ($\lambda = 0.71073$ Å). The data were corrected for absorption using the program SADABS [24]. The structures were solved by direct methods using the program SHELXS-97 [25]. All non-hydrogen atoms were refined with anisotropic thermal parameters by full-matrix least-squares calculations on F^2 using the program SHELXL-97 [26]. Hydrogen atoms were inserted at calculated positions and constrained with isotropic thermal parameters, except for those of the hydroxyl groups and of the nitrogen atom in imidazole, which were generally located using a Fourier difference map and refined isotropically. For **8**, which crystallized in the chiral space group $P4_32_12$, the absolute structure parameter of 0.47(3) indicated a twinning by inversion [27] of the crystals. Disorder was observed in some carbon atoms of the phenyl groups in **3** and, consequently, the agreement factors R_1 and wR_2 have unusually high values. Drawings were produced with SCHAKAL [28]. Special computations for the crystal structure discussions were carried out with PLATON for Linux [29]. Crystal data and structure refinement parameters are listed in Table 4.

4. Supplementary material

Crystallographic data for the structural analysis have been deposited with the Cambridge Crystallographic Data Centre, CCDC Nos. 224575–224583. Copies of this information may be obtained free of charge from The Director, CCDC, 12 Union Road, Cambridge, CB2 1EZ, UK (fax: +44-1223-336033; e-mail: deposit@ccdc.cam.ac.uk or www: http://www.ccdc.cam.ac.uk).

Acknowledgements

Financial support from ERDF (EU) and DGI-MCYT (Spain) (research projects BQU2002-03543 and BQU2002-04523) is gratefully acknowledged.

References

[1] R. Carballo, B. Covelo, S. Balboa, A. Castiñeiras, J. Niclós, Z. Anorg. Allg. Chem. 627 (2001) 948.
[2] R. Carballo, B. Covelo, E.M. Vázquez-López, A. Castiñeiras, J. Niclós, Z. Naturforsch. 58b (2003) 151.
[3] R. Carballo, A. Castiñeiras, S. Balboa, B. Covelo, J. Niclós, Polyhedron 21 (2002) 2811.

[4] A. Castiñeiras, S. Balboa, E. Bermejo, R. Carballo, B. Covelo, J. Borrás, J.A. Real, Z. Anorg. Allg. Chem. 628 (2002) 1116.
[5] G. Medina, S. Bernès, A. Martínez, L. Gasque, J. Coord. Chem. 54 (2001) 267.
[6] K. Prout, V.S.B. Mtetwa, F.J.C. Rossotti, Acta Crystallogr. B49 (1993) 73.
[7] M. Lanfranchi, L. Prati, M. Rossi, A. Tiripicchio, J. Chem. Soc., Chem. Commun. (1993) 1698.
[8] R. Carballo, B. Covelo, E. García-Martínez, E.M. Vázquez-López, A. Castiñeiras, J. Niclós, Polyhedron 22 (2003) 1051.
[9] T.P.J. Garret, J.M. Guss, H.C. Freeman, Acta Crystallogr. C39 (1983) 1027.
[10] C.-D. Wu, C.-Z. Lu, D.-M. Wu, H.-H. Zhuang, J.-S. Huang, Inorg. Chem. Commun. 4 (2001) 561.
[11] X.-M. Chen, B.-H. Ye, X.-C. Huang, Z.-T. Xu, J. Chem. Soc., Dalton Trans. (1996) 3465.
[12] W.D. Horrocks Jr., J.N. Ishley, R.R. Whittle, Inorg. Chem. 21 (1982) 3265.
[13] A.W. Addison, T.N. Rao, J. Reedijk, J. Van Rijn, G.C. Verschoor, J. Chem. Soc., Dalton Trans. (1984) 1349.
[14] J. Sanchiz, Y. Rodríguez-Martín, C. Ruiz-Pérez, A. Mederos, F. Lloret, M. Julve, New J. Chem. 26 (2002) 1624.
[15] A.L. Abuhijleh, C. Woods, Inorg. Chem. Commun. 4 (2001) 119.
[16] R. Carballo, A. Castiñeiras, B. Covelo, E.M. Vázquez-López, Polyhedron 20 (2001) 899.
[17] G.R. Desiraju, Acc. Chem. Res. 29 (1996) 441.
[18] C. Janiak, J. Chem. Soc., Dalton Trans. (2000) 3885.
[19] G.B. Deacon, R.J. Phillips, Coord. Chem. Rev. 33 (1980) 227.
[20] K. Nakamoto, Infrared and Raman Spectra of Inorganic and Coordination Compounds, 3rd ed., Wiley, New York, 1978.
[21] M. Melnik, Coord. Chem. Rev. 36 (1981) 287.
[22] E.A. Boudreaux, L.N. Mulay, Theory and Applications of Molecular Paramagnetism, Wiley, New York, 1976.
[23] S.K. Jain, B.S. Garg, Y.K. Bhoon, D.L. Klayman, J.P. Scovill, Spectrochim. Acta 41A (1985) 407.
[24] G.M. Sheldrick, SADABS, a program for absorption correction, University of Göttingen, Germany, 1996.
[25] G.M. Sheldrick, SHELXS-97, a program for the solution of crystal structures from X-ray data, University of Göttingen, Germany, 1997.
[26] G.M. Sheldrick, SHELXL-97, a program for the refinement of crystal structures from X-ray data, University of Göttingen, Germany, 1997.
[27] H.D. Flack, Helv. Chim. Acta 86 (2003) 905.
[28] E. Keller, SCHAKAL-97, a computer program for the graphic representation of molecular and crystallographic models, University of Freiburg, Germany, 1997.
[29] A.L. Spek, Acta Crystallogr. A46 (1990) C34, PLATON, Version 26-05-03.

Available online at www.sciencedirect.com
SCIENCE DIRECT®
Polyhedron 23 (2004) 1519–1526
POLYHEDRON
www.elsevier.com/locate/poly

Electron density distribution, polarizability and bonding in the octahedral clusters $[Mo_6S_8(CN)_6]^{6-}$, $[Re_6S_8(CN)_6]^{4-}$ and $Rh_6(CO)_{16}$

Victor I. Baranovski *, Dimitry V. Korolkov

Chemistry Faculty, St. Petersburg State University, 198504, Universitetskii av. 26, St. Petersburg, Russian Federation

Received 23 November 2003; accepted 27 February 2004
Available online 23 April 2004

Abstract

The geometrical structure and bonding in $[Mo_6S_8(CN)_{12}]^{6-}$, $[Re_6S_8(CN)_6]^{4-}$ and $Rh_6(CO)_{16}$ clusters were studied on the basis of quantum chemical calculations. The main attention was paid to the study of electron density distribution and polarizabilities for these compounds. There is noticeable electron density in the inner part of the M_6 octahedrons as well as on the edges and faces of the M_6S_8 polyhedrons. These observations lead to a model of the electronic structure of the clusters with octahedral cores, in which the mobile electrons are moving in a potential well of spherical symmetry. The resulting one electron states are classified according to the orbital quantum number l (1s, 1p, 1d, 1f and so on). Subsequent crystal field splitting leads to a calculated succession of one electron states of O_h point group symmetry. The high values of the calculated polarizabilities of the compounds under consideration are in accord with the suggested model.
© 2004 Elsevier Ltd. All rights reserved.

Keywords: Clusters; Electron density distribution; Polarizability; Spherical potential well; Finite electric field

1. Introduction

The nature of the bonding in transition metal clusters is of great importance to understand their physical and chemical properties, including stability, reactivity and reaction mechanisms [1–3]. In recent years, special attention has been paid to the study of hexanuclear halcogenide clusters of rhenium and molybdenum of the type $[M_6(\mu_3\text{-}X)_8L_6]^q$ (M = Re, Mo, X = S, Se, L = Cl, Br, I, PR_3, CN^-) [3,4]. The early studies on the electronic structure of such compounds by EHT [5–7] and X_α [8] methods led to the understanding of their molecular orbital energy schemes. The general patterns of these MO schemes were confirmed in recent publications in which more sophisticated quantum chemical methods were used [9–12]. The bonding in these compounds with octahedral metal cores was discussed in terms of the local bonds formed between the ML_4 fragments by the d-orbitals of the metal atoms [3,11].

Electron density distribution is an important manifestation of the nature of the bonding in clusters. The electron density in polyhedral clusters M_n is always significant along the M–M edges; it corresponds to the axial symmetrical M–M σ-bonds. On the other hand, the electron density distribution on the faces and in the cavity of the cluster polyhedron M_n does not directly arise from any characteristics of $M_nX_xY_y$, but can be obtained in the course of special investigations.

Simultaneous information about the electron density distribution on the faces and in the cavity of the cluster polyhedron M_n is important for the theoretical aspect, namely for the comparisons of the main parameters of the electronic structures of $M_nX_xY_y$ with analogous characteristics of the core and polyhedral hydrocarbons C_nH_m and boranes B_nH_m and their numerous derivatives [13]. The quantum chemical study of the geometrical and electronic structure of $[Mo_6S_8(CN)_6]^{6-}$ [12] showed that there is noticeable, almost uniform, electron density in

* Corresponding author. Tel.: +812-4284107; fax: +812-4286939.
E-mail address: baranovs@yandex.ru (V.I. Baranovski).

0277-5387/$ - see front matter © 2004 Elsevier Ltd. All rights reserved.
doi:10.1016/j.poly.2004.03.013

the inner cavity of the Mo_6 octahedron. It was suggested that this effect is to be taken into account in the construction of an appropriate model of the bonding in this compound. This model is based on an assumption that the movement of the electrons takes place in the spherically symmetrical potential with the subsequent splitting of the one-electron energy levels due to the lowering of the symmetry according to the O_h structure of the cluster. The calculated MO levels succession and their symmetry are in accord with this assumption.

In this work, we investigated the relevancy of this model for other transition metal clusters with octahedral metal cores. For this study we have chosen compounds with different metal–ligand bonding: the clusters $[Mo_6S_8(CN)_6]^{6-}$ and $[Re_6S_8(CN)_6]^{4-}$ (with donor ligands but different valence electron counts) and the rhodium $Rh_6(CO)_{16}$ cluster (with π-acid ligands). The electron density distribution over all the complex volume including its inner part suggests the high polarizability of the compounds under consideration. To examine this suggestion, the electron density distribution and polarizability for the clusters of Mo, Re and Rh with octahedral metal cores were calculated and a comparison of these parameters of the three clusters was performed.

2. Method

Quantum chemical calculations were performed by the ab initio SCF method with the 6-31G basis sets for C, N and S atoms. For Mo, Re and Rh atoms, we used SBK (Steven–Bash–Krauss–Jasien) effective core potentials [14] and the corresponding basis sets. Molecular polarizability was calculated with the finite electric field

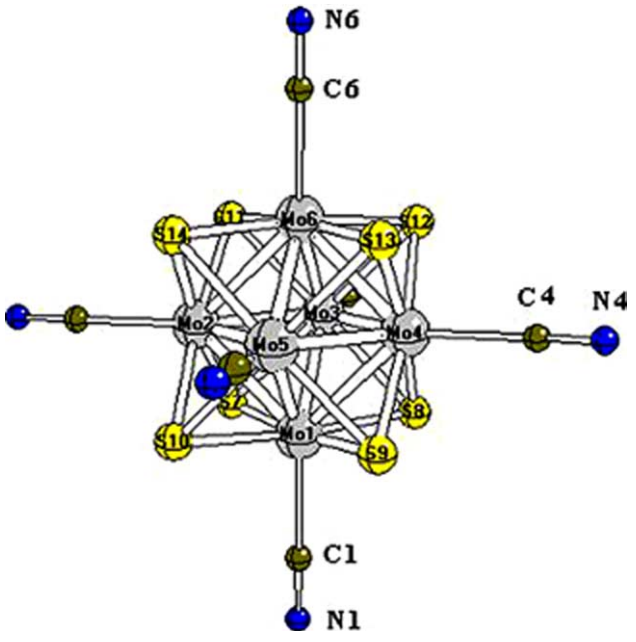

Fig. 1. Molecular structure of the $[Mo_6S_8(CN)_6]^{6-}$ cluster.

Table 1
Average bond lengths for $[M_6S_8(CN)_6]^{n-}$ clusters

Cluster	R(Mo–Mo) (Å)	R(Mo–S) (Å)	R(Mo–C) (Å)
$[Mo_6S_8(CN)_6]^{6-}$	2.725	2.491	2.280
$[Re_6S_8(CN)_6]^{7-}$	2.620	2.400	2.100

method. The bond lengths for the molybdenum cluster were optimized assuming O_h symmetry of this molecule (Fig. 1 and Table 1). For $[Re_6S_8(CN)_6]^{4-}$ and $Rh_6(CO)_{16}$ clusters we used the experimental geometry [4b,15]. The Re complex's bond lengths were obtained by averaging over the data for a number of compounds which contained the $[Re_6S_8(CN)_6]$ fragment, using restrictions imposed according to the symmetry considerations. For the Mo_6S_8 molecule we also performed geometry optimization calculations with a basis which included polarization functions (f-functions for Mo and d-functions for S). All calculations, including electronic density and finite field calculations, were performed with the GAMESS program package [16].

3. One-electron energy levels

The calculated one-electron energy levels diagrams for $[Mo_6S_8(CN)_6]^{6-}$ and $[Re_6S_8(CN)_6]^{4-}$ are shown in Table 2 and for Mo_6S_8 is shown in Table 3. The lowest groups of energy levels (82 in the case of $[M_6S_8(CN)_6]^{6-}$ and 72 in the case of Mo_6S_8) correspond to the molecular orbitals formed by the inner shell atomic orbitals (3d, 4s, 4p for Mo, 1s–2s, 2p and 3s for S and 1s for N and C) and CN molecular orbitals 1σ and 2σ. These molecular orbitals are symmetry adapted linear combinations of the corresponding atomic or CN group molecular orbitals and can be regarded as forming (with the atomic nuclei) the frame for the movement of the remaining valence electrons. Molecular orbitals, corresponding to the upper energy levels (9 t_{2g}–5 t_{2u}), are composed almost totally of the metal and S atomic orbitals. The molecular orbitals that belong to the next large group of MOs (11 a_{1g}–4 t_{2u}) have considerable contributions (up to 83%) from the atomic orbitals of the CN ligand's atoms. In [12], we compare the results of SCF and DFT (B3LYP) calculations of the MO schemes for the $[Mo_6S_8(CN)_6]^{6-}$ cluster. For the upper group of MOs there is good agreement between the results of these calculations. Comparison with the corresponding data for $[Mo_6S_8(CN)_6]^{7-}$ [10] and $Mo_6S_8(PH_3)_6$ [11], obtained in the course of the DV-X_α calculations, shows that in this case there is also general agreement concerning the nature of the nine MOs of the upper group. According to [11], the orbitals of the lower group can be divide into two groups: those composed almost totally of the Mo and S atomic orbitals and those composed by the CN group orbitals. In our case there is substantial mixing of the orbitals of these cluster fragments. The possible reason for such a

Table 2
The molecular orbital energy levels and Mulliken group populations for the $[Re_6S_8(CN)_6]^{4-}$ and $[Mo_6S_8(CN)_{12}]^{6-}$ clusters

$[Re_6S_8(CN)_6]^{4-}$					$[Mo_6S_8(CN)_6]^{6-}$				
ε (eV)	Symmetry	Group population			ε (eV)	Symmetry	Group population		
		6Re	8S	6(CN)			6Mo	8S	6(CN)
−8.08	*10 a_{1g}*	*0.99*	*0.06*	*0.93*	−0.92	*10 a_{1g}*	*0.20*	*0.02*	*1.77*
−7.01	*11 t_{1u}*	*0.42*	*0.09*	*1.47*	−0.81	*7 e_g*	*0.08*	*0.00*	*1.91*
-6.98	*7 e_g*	*0.39*	*0.16*	*1.43*	−0.80	*11 t_{1u}*	*0.11*	*0.01*	*1.87*
−5.17	8 e_g	1.06	0.52	0.40	1.69	11 a_{1g}	0.67	0.00	1.31
−4.89	11 a_{1g}	0.47	0.26	1.26	1.98	12 t_{1u}	0.56	0.26	1.17
−4.85	12 t_{1u}	0.95	0.50	0.53	1.99	8 e_g	0.36	0.35	1.27
−4.53	7 t_{2g}	1.23	0.56	0.19	2.57	7 t_{2g}	1.00	0.46	0.52
−3.82	12 a_{1g}	0.51	1.00	0.47	2.76	13 t_{1u}	0.63	0.46	0.92
−3.66	13 t_{1u}	0.40	0.16	1.42	2.98	12 a_{1g}	0.54	1.37	0.09
−3.61	9 e_g	0.42	0.02	1.54	3.13	*3 t_{2u}*	*0.14*	*0.19*	*1.67*
−3.20	5 a_{2u}	0.71	1.28	0.00	3.26	*3 t_{1g}*	*0.07*	*0.03*	*1.88*
−3.19	*3 t_{2u}*	*0.71*	*0.68*	*0.60*	3.34	9 e_g	0.92	0.64	0.44
−2.55	*3 t_{1g}*	*0.14*	*0.08*	*1.77*	3.43	5 a_{2u}	0.53	1.47	0.00
−2.22	4 t_{2u}	0.70	0.15	1.14	3.53	*14 t_{1u}*	*0.14*	*0.32*	*1.54*
−2.19	*14 t_{1u}*	*0.06*	*0.17*	*1.75*	3.63	8 t_{2g}	0.25	0.37	1.39
−2.11	8 t_{2g}	0.14	0.24	1.61	4.53	4 t_{2u}	0.59	1.13	0.28
−1.42	9 t_{2g}	0.92	1.00	0.06	5.10	9 t_{2g}	0.64	1.31	0.03
−1.41	2 e_u	0.96	1.03	0.00	5.48	2 e_u	0.76	1.23	0.00
−0.77	13 a_{1g}	0.80	0.25	0.94	6.08	13 a_{1g}	1.37	0.12	0.50
−0.37	15 t_{1u}	0.99	0.97	0.03	6.50	15 t_{1u}	0.71	1.27	0.00
0.80	4 t_{1g}	0.43	1.35	0.20	6.85	4 t_{1g}	0.36	1.55	0.08
0.91	5 t_{2u}	1.36	0.39	0.24	6.86	10 t_{2g}	1.14	0.81	0.04
0.92	10 t_{2g}	0.97	0.90	0.11	7.41	16 t_{1u}	1.01	0.88	0.09
1.50	16 t_{1u}	0.74	1.08	0.16	8.16	5 t_{2u}	1.90	0.04	0.05
2.42	10 e_g	1.51	0.51	−0.02					
Virtual orbitals									
10.66	1 a_{2g}				15.15	10 e_g			
10.95	5 t_{1g}				16.02	5 t_{1g}			
11.26	14 a_{1g}				16.11	17 t_{1u}			
11.57	6 t_{2u}				16.69	14 a_{1g}			
11.79	17 t_{1u}				17.46	11 e_g			
12.38	11 e_g								

RHF calculations with the basis set SBK (M)/6-31G (other atoms). The molecular orbitals, which are regarded as mainly localized on the CN groups, are shown in italic.

difference is in the nature of the methods of the calculations used in this work (SCF) and [12] (DFT/B3LYP), on the one hand, and in [10,11] (DV-X_α method), on the other hand. However, even in our case it is possible to distinguish molecular orbitals with negligible contribution from the AO of Mo and S atoms and those with the noticeable CN component.

In the case of the rhodium $Rh_6(CO)_{16}$ cluster there are 88 core and 75 valent orbitals. The molecular orbitals 89–136 are composed mainly of CO atomic orbitals with moderate contribution from the Rh atoms. The upper 27 MOs are mainly the metal core orbitals with a CO orbital contribution of about 10–35%.

4. Electron density distribution

The Mulliken atomic populations are as follows: $[Mo_6S_8(CN)_6]^{6-}$: Mo, −0.13; S, −0.19; C, +0.08 and N, −0.71.

$[Re_6S_8(CN)_6]^{4-}$: Re, −0.55; S, +0.24; C, +0.18 and N, −0.61.

In the rhodium $Rh_6(CO)_{16}$ cluster the effective Rh atoms charges are −0.035 (equatorial atoms) and +0.055 (apex atoms).

In all clusters studied in this work, there are molecular orbitals of a_{1g} symmetry with electron density mainly concentrated inside the metal atoms octahedron (Fig. 2).

The 12 a_{1g} MO is formed mainly by metal s-AOs (with essential contributions from p- and d-AOs) and its density is localized on the edges of the metal octahedron, but it also has a considerable contribution to the density in the inner part of this polyhedron. The next MO of this symmetry, 13 a_{1g}, is constructed from the metal d-orbitals and corresponds to the a_{1g} orbital scheme proposed in [11] (Fig. 8 in [11]). The calculations of the electron density distribution in the clusters under consideration along the edges and planes of the polyhedron showed that the main features are the same for all

Table 3
The molecular orbital energies and Mulliken group populations for the Mo_6S_8 cluster

ε (eV)	Symmetry	Group populations	
		Mo_6	S_8
Occupied orbitals			
−14.58	t_{2g}	1.29	0.70
−14.56	e_g	0.97	1.02
−14.41	t_{1u}	1.11	0.88
−13.87	a_{2u}	0.59	1.40
−13.78	a_{1g}	0.58	1.41
−12.85	a_{1g}	1.92	0. 07
−12.79	t_{2u}	0.74	1.25
−11.75	t_{2g}	0.69	1.30
−11.61	e_u	0.80	1.19
−10.48	t_{1u}	0.77	1.22
−10.17	t_{1g}	0.50	1.49
−10.12	t_{2g}	1.15	0.84
−9.85	t_{1u}	0.99	1.00
−9.02	t_{2u}	1.95	0.04
Virtual orbitals			
−2.03	e_g		
0.01	t_{1g}		
0.26	t_{1u}		
0.87	e_g		

RHF calculations with the basis set the SBK(f) (Mo)/6-31G* (S).

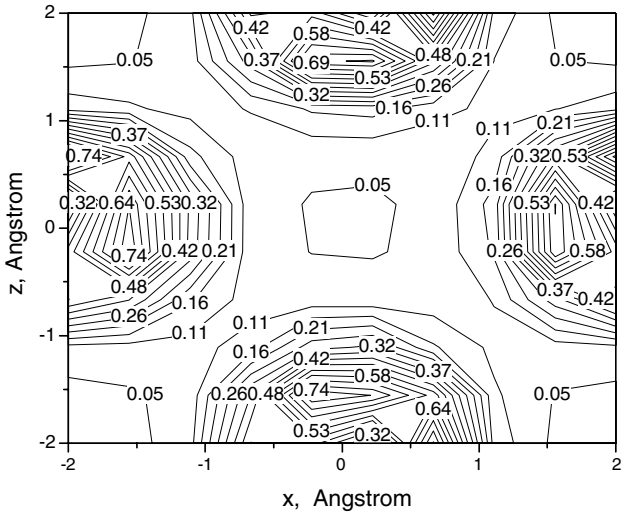

Fig. 3. The electron density distribution in the Re_4 vertical plane (e/a.u.^{3}).

compounds. The electron density distributions in the planes Mo(3)–Mo(4)–Mo(5)–Mo(6), Mo(1)–S–Mo(2), Mo(1)–Mo(3)–Mo(4) are shown in Figs. 3–6 of [12] and on the Re(1)–Re(2)–Re(6)–Re(4) plane – in Fig. 3 of this work. In all cases there is considerable electron density along the edges of the polyhedron; it is never less than 0.08 e/a.u.^{3}. Along the line, connecting the sulfur atom with the center of the metal polyhedrons, there is a small, but distinct maximum near the intersection of this line with the Mo_3 (Re_3) plane. In the central metal octahedral region the density is almost uniform, its value is about 0.04–0.06 e/a.u.^{3} (Fig. 3 of this work and Fig. 5 in [12]). This region can be approximately represented as a sphere with a radius equal to 2 a.u. The effective number of electrons in this volume can be estimated as $0.06 \times \frac{4}{3}\pi R^3 \approx 2$. Besides the electron density from the MOs, mentioned above, some of the density in the center of octahedron comes from the overlap between the other atomic orbitals of the metal atoms.

5. Polarizability calculations

Non-zero electron density inside the M_6S_8 and Rh_6 octahedrons allows to suppose that the polarizability of the cluster compounds under consideration is large. We began the study of this effect from the calculations of the polarizability of the Mo_6S_8 cluster core. To study the influence of the choice of the basis set on the results of polarizability calculations, we performed several RHF calculations for this molecule (Table 4). As can be seen from Table 4, the polarizability of the Mo_6S_8 cluster, calculated in the RHF approximation, increases only by 4% when the basis set is changed from SBK/3-21G (relatively small basis without any polarization and diffuse functions) to the rather extended SBK(f)/6-31+G* basis set. Such a small basis effect on the calcu-

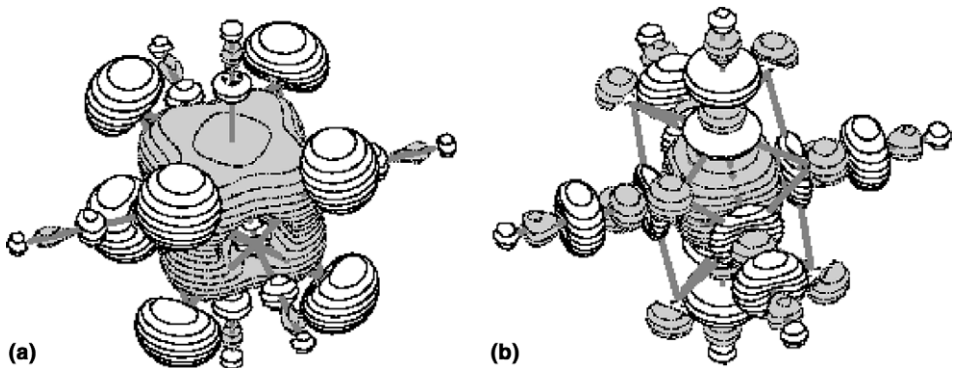

Fig. 2. Molecular orbitals 12 a_{1g} (a) and 13 a_{1g} (b) of the $[Mo_6S_8(CN)_6]^{6-}$ cluster.

Table 4
Results of the RHF polarizability calculations for Mo_6S_8

Basis set Mo/S	Polarizability (Å^3)	
	From energy	From dipole moment
3-21G/3-21G	45.5	45.6
SBK/6-31G*	46.6	46.7
SBK(f)/6-31G*	46.7	46.8
SBK(f)/6-31+G*	47.3	47.4

Geometry optimized with SBK(f)/6-31G* basis set (R(Mo–Mo) = 2.6157 Å, R(Mo–S) = 2.4550 Å).

lated polarizability shows that in the electric field there is electron density displacement through the whole inside volume of the octahedron rather than along chemical bonds and inner atomic spaces.

As in the case of the Mo_6S_8 core, the basis set dependence of the calculated polarizabilities of the clusters is small (Table 5). It is also worth mentioning that in all cases the difference between polarizabilities, calculated from the energy change and from the dipole moment change, is practically negligible. The polarizability of $[Mo_6S_8(CN)_6]^{6-}$ was also calculated according to the additive scheme

$$\alpha_{\parallel}([Mo_6S_8(CN)_6]^{6-}) = \alpha_{\parallel}(Mo_6S_8) + 2\alpha_{\parallel}(CN^-) + 4\alpha_{\perp}(CN^-)$$

with the use of the data for the CN^- group (see Table 5). The results of such an estimation (approximately 56 Å^3) are in good agreement with the results of the straightforward calculations. So the polarization of the CN^- ligands takes place independently (or almost independently) from the main effect – polarization of the inner Mo_6S_8 core.

To examine the electric field effect in more details we performed calculations of the electronic density distribution in the cluster with an electric field (0.01 a.u.) directed along the Mo1–Mo6 axes (Tables 6 and 7). In Fig. 4, the plot of the changes in the electron density distribution due to the inclusion of the electric field is presented. The general trend is a shift of the electronic density in the direction opposite to the direction of the electric field. In accordance with the additivity model, the main effects occur inside the Mo_6S_8 polyhedron. In addition to the main effect there are some more subtle but important effects which do not correspond to the global uniform density shift in the direction opposite to the electric field vector (Fig. 4). In particular, there is a noticeable increase of the electronic density in the outer regions near the Mo6–Mo(equatorial) edges and a pronounced decrease of the electron density in the regions of the Mo1–Mo(equatorial) bonds. This leads to the increase of the Mo6–Mo(equatorial) bond orders and to a decrease of the Mo1–Mo(equatorial) bond orders. There are also

Table 5
Polarizabilities of the CN– group and of the Mo, Re and Rh clusters (Å^3)

Compound	Basis SBK/3-21G		Basis SBK/6-31G	
	From energy	From dipole moment	From energy	From dipole moment
$[Mo_6S_8(CN)_6]^{6-}$	57.0			
$[Re_6S_8(CN)_6]^{4-}$	61.9	61.8	63.6	
$Rh_6(CO)_{16}$	51.3	51.4	53.8	53.9
CN^-				
$\alpha_{\parallel}$	2.53	2.53	3.02	3.02 (4.74)[a]
$\alpha_{\perp}$	1.04	1.04	1.23	1.23 (3.27)[a]

[a] RHF calculation with 6-31+G(3d) basis set [V.I. Baranovski, A.V. Kuteikina-Teplyakova, A.I. Panin, Russ. J. Struct. Chem. 41 (2000) 34].

Table 6
Effective charges (a.u.) on the atoms and CN groups (in parentheses) in $[Mo_6S_8(CN)_6]^{6-}$ (see Fig. 1 for the atom numbering)

Atom	Effective charges on the atoms		
	Without electric field	With electric field (0.01 a.u.)	Optimized in electric field
Mo6	−0.127	0.045	−0.138
Mo4		−0.108	−0.119
Mo1		−0.318	0.221
S11	−0.186	−0.078	−0.040
S7		−0.308	−0.417
C6	0.081	0.006	0.004
C4		0.075	0.071
C1		0.158	0.153
N6	−0.706 (−0.625)	−0.596 (−0.590)	−0.578 (−0.574)
N4		−0.703 (−0.628)	−0.700 (−0.629)
N1		−0.808 (−0.650)	−0.836 (−0.683)

Table 7
Interatomic distances (Å) and bond orders for the $[Mo_6S_8(CN)_6]^{6-}$ cluster

Pairs of atoms	Initial geometry			Geometry, optimized in electric field	
A–B	R(A–B)	W(A–B)	W(A–B)	R(A–B)	W(A–B)
Mo6–Mo4	2.735	0.637	0.785	2.643	0.917
Mo3–Mo4			0.654	2.739	0.703
Mo1–Mo4			0.484	2.975	0.224
Mo6–S11	2.539	0.731	0.733	2.529	0.686
Mo1–S7			0.388	2.637	0.635
Mo6–C6			0.529	2.243	0.577
Mo4–C4	2.305	0.457	0.455	2.297	0.446
Mo1–C1			0.388	2.361	0.419
C6–N6	1.170	2.582	2.636	1.162	2.641
C4–N4			2.585	1.169	2.597
C1–N1			2.503	1.182	2.489

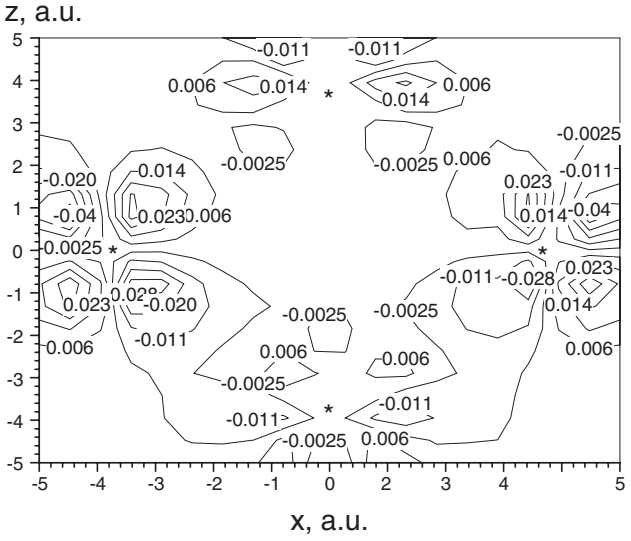

Fig. 4. The changes in electron density distribution in the Re_4 vertical plane due to the electric field effect (e/a.u.^{3}).

analogous changes in the bond orders between the other atoms (Table 7). It is reasonable to expect that such changes in the bond orders lead to the increase or decrease in the corresponding bond lengths in the complex, when placed in an electric field. Optimization of the geometry of $[Mo_6S_8(CN)_6]^{6-}$ in the electric field showed that the changes in the cluster's geometry happen according to the changes in the bond orders in the initial complex with unperturbed geometry (Table 7). However, the effective charges of the Mo atoms (and only the Mo atoms) alter in an unexpected manner, which formally corresponds to the charge flow in the direction of the electric field vector. Possibly this effect reflects the overall reorganization of the bonding in the cluster in the electric field.

6. Discussion

The uniform electron density inside the inner part of the complex reminds us of Thomson's model of the atom with the positively charged atomic nuclei inserted in the electronic jelly. This inspired us to discuss a possible model of the clusters under consideration.

The substantial electron density on the faces and the edges of the metal octahedron resembles a model of the cluster with the electrons distributed on the surface of a sphere. For the description of such a cluster electronic structure, the model of free electrons and simultaneously the theory of tensor surface harmonics (TSH) are used. The TSH theory was developed in framework of the free electron model and uses the theoretical group determination of the nodal structure of cluster molecular orbitals in obvious form [17–20]. According to this theory the atoms M of the cluster M_n are located on the surface of the sphere, and every atom M is described by angle coordinates θ_i and φ_i. The cluster electrons are freely moving on the surface of the sphere that imitates the idealized cluster. The electron wave functions for M_n are the solutions of the Schrödinger equation for the particle on the sphere; these solutions conform to the energy values that depend on their nodal characteristics. So long as the atoms M in the real cluster form a non-spherical polyhedron, the orbitals and energies of the real cluster are determined from the analogous parameters for the spherical cluster using the perturbation theory taking into account the real symmetry of the cluster.

The observation that there is noticeable electron density in the inner parts of the clusters studied in this work, permits the expansion of the above-mentioned model. Let us distinguish two parts in the cluster volume: the inner part consisting of M_6S_8 octahedron and the outer layer of (CN^-) or CO groups. As was shown, the main part of the electron density is localized on the core atomic orbitals and is regarded as fixed inside the corresponding atomic spheres. In our model we also added the electrons on the molecular orbitals with significant contribution from the CN^- or CO ligands to this fixed frame. These electrons together with atomic nuclei generate potential for the movement of the active valence electrons. This potential is approximately a

Table 8
Correlation between the irreducible representation of the spherical symmetry group O(3) and of its subgroup O_h

l	O(3) states	O_h irreducible representation
0	S	a_{1g}
1	P	t_{1u}
2	D	t_{2g}, e_g
3	F	a_{2u}, t_{1u}, t_{2u}
4	G	a_{1g}, e_g, t_{1g}, t_{2g}
5	H	e_u, $2t_{1u}$, t_{2u}
6	I	a_{1g}, a_{2g}, e_g, t_{1g}, $2t_{2g}$

spherical one; moreover, it is almost constant within the inner part of the clusters under consideration. Such a model resembles the state of electrons inside the alkali metal clusters [21]. The solutions of the corresponding Schrödinger equation can be classified as the eigenfunctions of the $\hat{L}^2$ operator (1s, 1p, 1d, etc.). The corresponding one-electron levels are $(2l+1)$-fold degenerated. In the cluster field of the O_h symmetry these levels are split and the new crystal field one electron states are transformed according to the irreducible representations of the O_h point group (see Table 8). So it is possible to arrange a set of nl states taking into account the crystal field splitting and to bring them into correlation with the calculated MO levels. Such a scheme (after deleting from the MO scheme molecular orbitals with substantial contribution from CN^- groups) is the same for the both cyanoclusters, studied in this work (Tables 2 and 3). The tentative correlation of the calculated MOs and the "spherical potential solutions" is presented in Fig. 5. It is worth mentioning that some of the irreducible representations (IRs) are unique: thus, IR a_{2u} is present only in the "f"-subset, IR a_{2g} is present only in the "h"-subset. This facilitates the assignment of the calculated MOs to the different l-subgroups and clarifies the sequence of energies of different O(3) states.

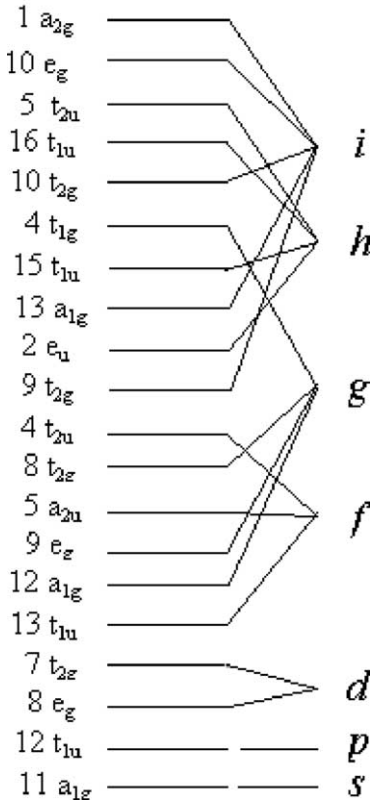

Fig. 5. Tentative correlation between the calculated O_h and suggested O(3) energy levels.

The resulting molecular orbital scheme differs from that of the natrium cluster: the energy goes up with the increasing value of the l quantum number, whereas in the Na_n clusters 2p, 2d and other states appear. The suggested model includes the TSH model as a limiting case with negligible electronic density in the inner part of the cluster.

The results for the clusters embedded in an electric field showed that the structure of such compounds is very flexible and sensitive to external disturbances. The data concerning attachment of new ligands to the clusters [5] or mononuclear complexes [4b] appears to confirm such a suggestion. This problem needs further investigation.

7. Conclusion

The results of the present study demonstrated the common nature of the inner M_6 part of the clusters regardless of the nature of the surrounding ligands. The high (and almost equal) values of the polarizability of the compounds under investigation confirms this thesis and demonstrated the possibility of the strong deformation of their geometrical structure due to the change of the cluster composition or inclusion of the additional ligands.

Acknowledgements

The work was supported by the INTAS Grant 2000-00689. All calculations were performed in the Petrodvoretz Telecommunication Center.

References

[1] D. Mingos, R.L. Johnston, Struct. Bond. 68 (1987) 30.
[2] D.V. Korolkov, Koord. Khimia (Russian) 17 (1991) 1455.
[3] Z. Lin, I.D. Williams, Polyhedron 15 (1996) 3277.
[4] (a) K.A. Brylev, A.V. Virovets, N.G. Naumov, Yu.V. Mironov, D. Fenske, V.E. Fedorov, Russ. Chem. Bull. Int. Ed. 50 (2001) 1; (b) S.B.Artemkina, Coordinational compounds on the base of octahedral cluster halcogenide complexes and metal cations: synthesis and structure, Ph.D. Theses, 2003.

[5] T. Hughbauks, R. Hoffmann, J. Am. Chem. Soc. 105 (1983) 1150.
[6] F.A. Cotton, T.E. Haas, Inorg. Chem. 3 (1964) 10.
[7] R.G. Woolley, Inorg. Chem. 24 (1985) 3519.
[8] L. LeBeuse, M.A. Makhyoun, R. Lissilour, H. Chermett, J. Chem. Phys. 76 (1982) 6060.
[9] Th.G. Gray, C.M. Rudzinski, E.E. Meyer, R.H. Holm, D.G. Nocera, J. Am. Chem. Soc. 125 (2003) 4755.
[10] H. Imoto, personal communication.
[11] H. Imoto, T. Saito, H. Adachi, Inorg. Chem. 34 (1995) 2415.
[12] V.I. Baranovski., D.V. Korolkov, in: A.L. Tchougreeff (Ed.), Proceedings of the 2003 Fock School on Quantum and Computational Chemistry, Int. J. Quantum Chem. (2004), in press.
[13] D.V. Korolkov, O.V. Sizova, Int. J. Quantum Chem. 88 (2002) 606.
[14] W.J. Stevens, H. Basch, M. Krauss, P. Jasien, Can. J. Chem. 70 (1992) 612.
[15] D.H. Farrar, E. Grachova, A. Lough, C.h. Patirana, A. Poe, S.P. Tunik, J. Chem. Soc., Dalton Trans. (2001) 2015.
[16] M.W. Schmidt, K.K. Baldridge, J.A. Boatz, S.T. Elbert, M.S. Gordon, J.H. Jensen, S. Koseki, N. Matsunaga, K. Anguyen, S.J. Su, T.L. Windus, M. Dupuis, J.A. Montgomery, J. Comput. Chem. 14 (1993) 1347.
[17] A.J. Stone, Inorg. Chem. 20 (1981) 563.
[18] A.J. Stone, M. Alderton, Inorg. Chem. 21 (1982) 2297.
[19] A.J. Stone, Polyhedron 3 (1984) 1299.
[20] A.P. Kljagina, Koord. Khimia (Russian) 21 (1995) 612.
[21] W.A. de Heer, Rev. Mod. Phys. 65 (1993) 611.

Available online at www.sciencedirect.com
SCIENCE DIRECT®
Polyhedron 23 (2004) 1527–1533
POLYHEDRON
www.elsevier.com/locate/poly

Complexes of the uranyl ion with bis(diphenylphosphino)methane dioxide

S. Kannan [a,*], N. Rajalakshmi [a], K.V. Chetty [a], V. Venugopal [a], M.G.B. Drew [b,*]

[a] Fuel Chemistry Division, Bhabha Atomic Research Center, Trombay, Mumbai 400085, India
[b] Department of Chemistry, The University of Reading, P.O. Box 224, Whitenights, Reading RG6 6AD, UK

Received 4 February 2004; accepted 8 March 2004
Available online 13 April 2004

Abstract

Bis(diphenylphosphino)methane dioxide compounds of uranyl nitrate and uranyl bis(β-diketonates) have been synthesized and characterized by spectroscopic and X-ray diffraction methods. Monodentate, bidentate chelate and bridging bidentate modes of coordination for this ligand have been established from the single-crystal X-ray diffraction studies of its compounds, $[UO_2(DBM)_2DPPMO]$, $[UO_2(NO_3)_2DPPMO]$ and $[\{UO_2(DBM)_2\}_2DPPMO]$, respectively.
© 2004 Elsevier Ltd. All rights reserved.

Keywords: Bis(diphenylphosphino)methane dioxide; Uranyl nitrate; Uranyl bis(β-diketonates); Monodentate; Bidentate chelate; Bridging bidentate; Coordination modes

1. Introduction

Many multifunctional phosphine oxide (PO) based ligands have been examined for the separation of minor actinides from highly active nuclear waste solution [1–6] and the structures of their lanthanide [7–15] and actinide compounds [16–23] have also been reported. Solvent extraction properties of a variety of bi-functional diphosphine dioxides with actinide and lanthanide ions [24–27] have been examined and some of their lanthanide compounds [28,29] have also been characterized structurally. However, there is no structural study on diphosphine dioxide–actinide compounds, except some IR, molecular weight and conductance data [30–34]. In view of the lack of structural reports on diphosphine dioxide actinide compounds, we felt it important to study such complexes with a relatively simple diphosphine dioxide, e.g., bis(diphenylphosphino)methane dioxide, in order to establish the fundamental structural properties. This ligand can act in three possible modes to bond with the metal ion, as shown in Fig. 1.

The chelating mode of bonding is well established for this ligand in alkali, alkaline earth, main group and lanthanide metal ion compounds [28,29,35–45]. The bridging bidentate mode of bonding is also reported in a few of its compounds [46–49]. However, the monodentate mode of bonding has only been reported in one compound, $[Cl_3LRe(DPPMO)]$, so far [50]. We report herein the compounds of bis(diphenylphosphino)methane dioxide with the uranyl ion, which together show all modes of coordination for this ligand.

2. Experimental

2.1. Materials and measurements

All solvents are analytical grade and used as such without further purification. Bis(diphenylphosphino)methane (DPPM), thenoyl trifluoroacetone (HTTA), benzoyl trifluoroacetone (HBTA), dibenzoyl methane (HDBM) and benzoyl acetone (HBA) were obtained from commercial sources. The starting compounds $[UO_2(OO)_2 \cdot 2H_2O]$ (OO = β-diketonate ligand)

* Corresponding authors. Tel.: +91-22-2559-0643; fax: +91-22-2550-5151.
E-mail addresses: skannan@magnum.barc.ernet.in (S. Kannan), m.g.b.drew@reading.ac.uk (M.G.B. Drew).

0277-5387/$ - see front matter © 2004 Elsevier Ltd. All rights reserved.
doi:10.1016/j.poly.2004.03.008

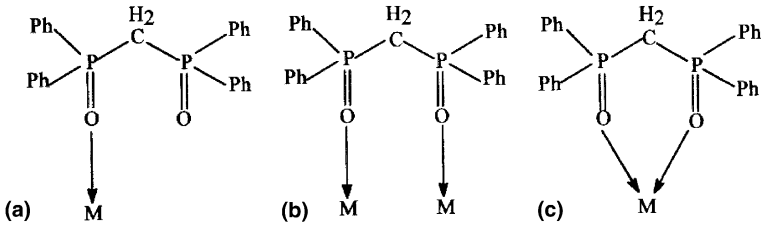

Fig. 1. Different modes of coordination for the DPPMO ligand: (a) monodentate, (b) bridging bidentate, and (c) bidentate chelating.

were prepared according to the reported methods [51]. FT-IR spectra for all compounds were measured on a JASCO FT-IR-610 instrument using Nujol mull. The ^{1}H and $^{31}P\{^{1}H\}$ NMR spectra were recorded on a BRUKER 500 MHz instrument operating at 500 and 202.5 MHz, respectively. The peaks are assigned relative to internal $CHCl_3$ (for ^{1}H) or external 85% H_3PO_4 (for ^{31}P). The Analytical chemistry division of Bhabha Atomic Research Center, Mumbai, performed the carbon, hydrogen and nitrogen analyses.

2.2. Synthesis of $[(C_6H_5)_2P(O)CH_2P(O)(C_6H_5)_2]$ (DPPMO)

To a suspension of bis(diphenylphosphino)methane (DPPM) (10 mg, 0.026 mol) in methanol, H_2O_2 (7 ml of 30% H_2O_2) was added slowly with stirring. The solution became clear on stirring and deposited a white solid. The solvent was removed under vacuum, the resulting solid was extracted with hot methanol and filtered. The hot solution on standing deposited a white crystalline solid (yield, 10.1 mg, 93.5%). *Anal*. Calc. for $C_{25}H_{22}P_2O_2$: C, 72.1; H, 5.3. Found: C, 72.0; H, 5.4%. IR (Nujol mull, KBr, ν cm^{-1}): 1204 (PO). ^{1}H NMR ($CDCl_3$, δ ppm): 3.52 (t, $J(PH) = 15$ Hz, 2H, CH_2); 7.32–7.44 (m, 12H, C_6H_5), 7.71–7.75 (m, 8H, C_6H_5). $^{31}P\{^{1}H\}$ ($CDCl_3$, δ ppm): 23.30 (s).

2.3. Synthesis of $[UO_2(NO_3)_2 \cdot DPPMO]$ (1)

To a hot ethanol solution of DPPMO (200 mg, 0.48 mmol), $[UO_2(NO_3)_2 \cdot 6H_2O]$ in ethanol (241.3 mg, 0.48 mmol) was added and refluxed for 15 min. The resulting solid product was filtered, washed with ethanol and dried. This solid was recrystallized from a methanol/ethanol mixture as a yellow crystalline solid (yield, 370 mg, 95%). *Anal*. Calc. for $C_{25}H_{22}P_2O_{10}N_2U$: C, 37.0; H, 2.7; N, 3.5. Found: C, 37.0; H, 2.5; N, 3.4%. IR (Nujol mull, KBr, ν cm^{-1}): 1523, 1307, 1275 (NO_3); 1139 (PO); 929 (O=U=O). ^{1}H NMR (CD_3COCD_3, δ ppm) : 4.99 (t, $J(PH) = 13$ Hz, CH_2); 7.64–7.67 (t), 7.76–7.79 (t), 8.22–8.26 (m) (C_6H_5, DPPMO). $^{31}P\{^{1}H\}$(CD_3COCD_3, δ ppm): 39. 9 (s).

2.4. Synthesis of $[UO_2(DBM)_2 \cdot DPPMO]$ (2)

To a hot chloroform solution of $[UO_2(DBM)_2 \cdot 2H_2O]$ (250 mg, 0.332 mmol), DPPMO (138.3 mg, 0.332 mmol) was added and refluxed for 3 h. The clear solution was filtered and layered with dodecane. The solution on evaporation yielded a red colored crystalline product. It was filtered, washed with hexane and dried (yield, 350 mg, 93%). *Anal*. Calc. for $C_{55}H_{44}P_2O_8U$: C, 58.3; H, 3.9. Found: C, 57.9; H, 4.1%. IR (Nujol mull, KBr, ν cm^{-1}): 1590 (br, CO, DBM); 1203 (PO, DPPMO); 1140 (PO, DPPMO); 901 (O=U=O). ^{1}H NMR ($CDCl_3$, δ ppm) : 3.89 (br, s, CH_2, DPPMO); 7.18 (s, CH, DBM), 7.22–8.26 (m, br, C_6H_5, DPPMO + DBM). $^{31}P\{^{1}H\}$ ($CDCl_3$, δ ppm): 40.6 (br, s) and 21.30 (br, s).

2.5. Synthesis of $[UO_2(TTA)_2 \cdot DPPMO]$ (3)

To a hot chloroform solution of $[UO_2(TTA)_2 \cdot 2H_2O]$ (200 mg, 0. 267 mmol), DPPMO (111.2 mg, 0.267 mmol) was added and refluxed for 3 h. The clear solution was filtered and layered with dodecane. The solution on evaporation yielded an orange colored product. It was filtered, washed with hexane and dried (yield, 280 mg, 93%). *Anal*. Calc. for $C_{41}H_{30}P_2O_8F_6S_2U$: C, 43.6; H, 2.7. Found: C, 40.5; H, 2.5%. IR (Nujol mull, KBr, ν cm^{-1}): 1612–1593 (br, CO, TTA); 1201 (PO, DPPMO); 1137 (PO, DPPMO); 920 (O=U=O). ^{1}H NMR ($CDCl_3$, δ ppm): 4.15 (br, s, CH_2, DPPMO); 5.10 (br, s, CH_2, DPPMO)*; 6.80, 6.88 (s, CH, TTA), 7.19–8.34 (m, br, C_6H_5 of DPPMO + C_4H_3S of TTA). $^{31}P\{^{1}H\}$ ($CDCl_3$, δ ppm): 42.14 (s)*, 41.87 (br, s)*, 41.59 (br, s), 41.31 (br, s) and 22.30 (br, s) (* due to the dinuclear compound **6**).

2.6. Synthesis of $[UO_2(BTA)_2 \cdot DPPMO]$ (4)

To a chloroform solution of $[UO_2(BTA)_2 \cdot 2H_2O]$ (250 mg, 0.3396 mmol), DPPMO (141.3 mg, 0.3396 mmol) was added and refluxed for 3 h. The clear solution was filtered and layered with dodecane. The solution on evaporation yielded a yellow colored product. It was filtered, washed with hexane and dried (yield, 350 mg, 92%). *Anal*. Calc. for $C_{45}H_{34}P_2O_8F_6U$: C, 48.4; H, 3.0. Found: C, 46.4; H, 2.7%. IR (Nujol mull, KBr, ν cm^{-1}): 1606–1572 (br, CO, BTA); 1202 (PO, DPPMO); 1141 (PO, DPPMO); 921 (O=U=O). ^{1}H NMR ($CDCl_3$, δ ppm): 4.14 (br, s, CH_2, DPPMO); 5.13 (br, s, CH_2, DPPMO)*; 6.97, 7.04 (s, CH, BTA), 7.04–8.6 (m, br, C_6H_5 of DPPMO + BTA). $^{31}P\{^{1}H\}$ ($CDCl_3$, δ ppm): 42.4 (br, s)*, 41.42 (br, s)* and 22. 29 (s) (* due to the

mixture of mononuclear compound **4** and dinuclear compound **7**).

2.7. Synthesis of $[\{UO_2(DBM)_2\}_2 \cdot DPPMO]$ (**5**)

To a hot chloroform solution of $[UO_2(DBM)_2 \cdot 2H_2O]$ (400 mg, 0.544 mmol), DPPMO (113.3 mg, 0. 272 mmol) was added and refluxed for 3 h. The clear solution was filtered and layered with dodecane. The solution on evaporation yielded a red colored crystalline product. It was filtered, washed with hexane and dried (yield, 470 mg, 96%). *Anal*. Calc. for $C_{85}H_{66}P_2O_{14}U_2$: C, 55.2; H, 3.6. Found: C, 55.8; H, 3.8%. IR (Nujol mull, KBr, ν cm^{-1}): 1590 (br, CO, DBM); 1152 (PO, DPPMO); 905 (O=U=O). ^{1}H NMR ($CDCl_3$, δ ppm): 4.64 (br, s, CH_2, DPPMO); 6.97 (s, CH, DBM), 7.16–8.66 (m, br, C_6H_5 of DPPMO + DBM). $^{31}P\{^1H\}$ ($CDCl_3$, δ ppm): 38.73 (s).

2.8. Synthesis of $[\{UO_2(TTA)_2\}_2 \cdot DPPMO]$ (**6**)

To a hot chloroform solution of $[UO_2(TTA)_2 \cdot 2H_2O]$ (200 mg, 0.267 mmol), DPPMO (55.6 mg, 0.133 mmol) was added and refluxed for 3 h. The clear solution was filtered and layered with dodecane. The solution on evaporation yielded a red colored product. It was filtered, washed with hexane and dried (yield, 230 mg, 93%). *Anal*. Calc. for $C_{57}H_{38}P_2O_{14}F_{12}S_4U_2$: C, 37.2; H, 2.1. Found: C, 37.6; H, 2.4%. IR (Nujol mull, KBr, ν cm^{-1}): 1612–1594 (br, CO, DBM); 1137 (PO, DPPMO); 921 (O=U=O). ^{1}H NMR ($CDCl_3$, δ ppm): 5.10 (t, CH_2, DPPMO); 6.81, 6.85 (s, CH, TTA), 7.18–8.32 (m, br, C_6H_5 of DPPMO and C_4H_3S of TTA). $^{31}P\{^1H\}$ ($CDCl_3$, δ ppm): 42.13 (s) and 41.87 (s).

2.9. Synthesis of $[\{UO_2(BTA)_2\}_2 \cdot DPPMO]$ (**7**)

To a chloroform solution of $[UO_2(BTA)_2 \cdot 2H_2O]$ (250 mg, 0.3396 mmol), DPPMO (70.65 mg, 0.1698 mmol) was added and refluxed for 3 h. The clear solution was filtered and layered with dodecane. The solution on evaporation yielded a yellow colored crystalline product. It was filtered, washed with hexane and dried (yield, 300 mg, 92.6%). *Anal*. Calc. for $C_{65}H_{46}P_2O_{14}F_{12}U_2$: C, 43.0; H, 2.5. Found: C, 43.1; H, 2.4%. IR (Nujol mull, KBr, ν cm^{-1}): 1606–1573 (br, CO, DBM); 1148 (PO, DPPMO); 921 (O=U=O). ^{1}H NMR ($CDCl_3$, δ ppm): 5.12 (t, $J(PH) = 15$ Hz, CH_2, DPPMO); 6.92 (br, s, CH, BTA), 7.03–7.98 (m, br, C_6H_5 of DPPMO), 8.58 (m, br, C_6H_6 of BTA). $^{31}P\{^1H\}$ ($CDCl_3$, δ ppm): 42.41 (s) and 41.40 (s).

2.10. Synthesis of $[\{UO_2(BA)_2\}_2 \cdot DPPMO]$ (**8**)

To a hot chloroform solution of $[UO_2(BA)_2 \cdot 2H_2O]$ (300 mg, 0.477 mmol), DPPMO (99.36 mg, 0.2388 mmol) was added and refluxed for 3 h. The clear solution was filtered and layered with dodecane. The solution on evaporation yielded an orange colored product. It was filtered, washed with hexane and dried (yield, 325 mg, 85%). *Anal*. Calc. for $C_{65}H_{58}P_2O_{14}U_2$: C, 48.7; H, 3.6. Found: C, 48.3; H, 3.4%. IR (Nujol mull, KBr, ν cm^{-1}): 1590 (br, CO, BA); 1148 (PO, DPPMO); 908 (O=U=O). ^{1}H NMR ($CDCl_3$, δ ppm): 2.22 (s, br, CH_3); 2.79 (s, br, CH_3); 4.92 (s, br, CH_2, DPPMO); 6.55 (br, s, CH, BA), 7.21–8.5 (m, br, C_6H_5 of DPPMO + BA). $^{31}P\{^1H\}$ ($CDCl_3$, δ ppm): 38.45 (s) and 38.07 (s).

2.11. Crystal structure determination

Data for all three crystals **1**, **2** and **5** were measured with Mo Kα radiation ($\lambda = 0.71073$ Å) using the MARresearch Image Plate System. The crystals were positioned at 70 mm from the Image Plate. One hundred frames were measured at 2° intervals with a counting time of 2 min. Data analysis was carried out with the

Table 1
The crystal and refinement details for **1**, **2** and **5**

	1	**2**	**5**
Empirical formula	$C_{25}H_{22}N_2O_{10}P_2U$	$C_{55}H_{44}O_8P_2U$	$C_{85}H_{66}O_{14}P_2U_2$
Formula weight	810.42	1132.82	1849.36
Crystal system	monoclinic	monoclinic	monoclinic
Space group	$P2_1/n$	$P2_1/n$	$C2/c$
a (Å)	10.358(12)	19.23(2)	24.33(3)
b (Å)	24.88(3)	12.854(14)	18.713(19)
c (Å)	11.571(14)	19.81(2)	19.57(2)
β (°)	100.23(1)	92.28(1)	105.18(1)
V (Å^3)	2934	4893	8602
Z	4	4	4
ρ_{calc} (Mg m^{-3})	1.834	1.537	1.459
Absorption coefficient (mm^{-1})	5.696	3.439	3.858
Reflections collected	13740	30601	17228
Unique data/restrains/parameters	5305/0/361	9220/0/596	6157/0/490
Final R indices [$I > 2\sigma(I)$] R_1, wR_2	0.0939, 0.1744	0.0869, 0.1573	0.1103, 0.2818
R indices (all data)	0.1185, 0.1832	0.1146, 0.1671	0.1668, 0.3213
Largest difference peak and hole (e Å^{-3})	2.415 and −2.604	1.780 and −2.751	2.078 and −1.392

XDS program [52]. The structures were solved using direct methods with the SHELX-86 program [53]. The non-hydrogen atoms were refined with anisotropic thermal parameters in all cases. The hydrogen atoms bonded to carbon atoms were included in geometric positions and given thermal parameters equivalent to 1.2 times those of the atoms to which they were attached. Empirical absorption corrections were carried out using the DIFABS program [54]. The structures were refined to convergence on F^2 using SHELXL [55]. Selected crystallographic data for all the compounds are summarized in Table 1.

3. Results and discussion

3.1. Uranyl nitrate–DPPMO compound [$UO_2(NO_3)_2 \cdot DPPMO$] (1)

The reaction of $[UO_2(NO_3)_2 \cdot 6H_2O]$ with bis(diphenylphosphino)methane dioxide in ethanol yielded **1**. The IR spectrum of **1** shows that the water molecules from the starting compound $[UO_2(NO_3)_2 \cdot 6H_2O]$ are replaced completely by the DPPMO ligand. It suggests further that the ligand coordinates through both the phosphine oxide oxygen atoms to the uranyl group ($\Delta\nu_{PO} = 65$ cm^{-1}). The $^{31}P\{^1H\}$ NMR of **1** shows a single resonance at 39.9 ppm which is deshielded by ca. 16 ppm with respect to the free ligand. The ^1H NMR spectrum of **1** shows that the CH_2 protons of the DPPMO ligand are deshielded by ca. 1.42 ppm with respect to the free ligand. It supports further the coordination of both the phosphine oxide oxygen atoms to the uranyl group. The carbon, hydrogen and nitrogen analysis revealed that the ratio of $UO_2(NO_3)_2$ to DPPMO is 1:1 in **1**. The molecular weight determination on similar type of compounds $[UO_2(NO_3)_2X]$ (where X = EBDPM or CHDPH) reported earlier, revealed a monomeric structure [32] with bis(phosphine) oxide, acting as a chelating ligand. By comparison, the viscosity measurements revealed a polymeric structure [32] with bis(phosphine) oxide acting as a bridging bidentate ligand. The structure of **1** was determined by the X-ray diffraction method and confirms the chelating mode of coordination for this ligand.

3.2. Molecular structure of [$UO_2(NO_3)_2DPPMO$] (1)

The molecular structure of **1** is shown in Fig. 2 and selected interatomic bond distances and angles are given in Table 2. The structure shows that the uranium atom is surrounded by eight oxygen atoms in a hexagonal bipyramidal geometry. The four oxygen atoms of the nitrate groups and two oxygen atoms of DPPMO forms a planar hexagon and these six oxygen atom atoms are coplanar to within 0.07 Å. The observed (average) bond distances between U–$O_{(uranyl)}$ (1.775(11) Å) U–$O_{(nitrate)}$ (2.5398(12) Å) and U–$O_{(DPPMO)}$ (2.386(9) Å) agree well with the earlier reported uranyl nitrate, phosphine oxide compound $[UO_2(NO_3)_2(PPh_3O)_2]$ [56]. In $[UO_2(NO_3)_2(PPh_3O)_2]$ all the groups are *trans* to each other, i.e., phosphine oxide *trans* to phosphine oxide and nitrate *trans* to nitrate group. However, in **1** the phosphine

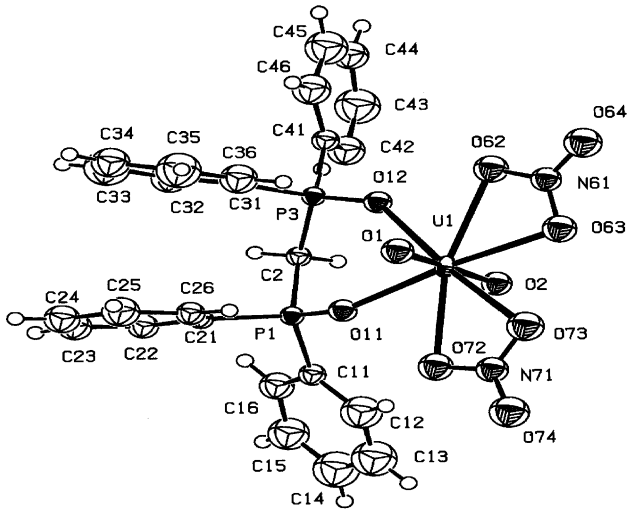

Fig. 2. Molecular structure of $[UO_2(NO_3)_2$ DPPMO] with ellipsoids at 50% probability.

Table 2
Selected bond distances (Å) and angles (°) for **1**, **2** and **5**

Compound ***1***			
U(1)–O(1)	1.768(11)	O(1)–U(1)–O(2)	178.4(5)
U(1)–O(2)	1.781(11)	O(11)–U(1)–O(12)	71.5(4)
U(1)–O(11)	2.370(9)	O(73)–U(1)–O(72)	50.0(4)
U(1)–O(12)	2.402(10)	O(73)–U(1)–O(63)	60.0(4)
U(1)–O(72)	2.515(12)	O(62)–U(1)–O(63)	49.9(4)
U(1)–O(73)	2.541(12)	O(63)–N(61)–O(62)	115.9(12)
U(1)–O(62)	2.549(12)	O(73)–N(71)–O(72)	115.7(14)
U(1)–O(63)	2.554(12)	P(3)–C(2)–P(1)	111.7(7)
Compound ***2***			
U(1)–O(1)	1.776(7)	O(1)–U(1)–O(2)	178.7(4)
U(1)–O(2)	1.779(8)	O(55)–U(1)–O(51)	70.2(3)
U(1)–O(51)	2.348(8)	O(1)–U(1)–O(11)	89.5(3)
U(1)–O(55)	2.344(8)	O(51)–U(1)–O(81)	146.8(3)
U(1)–O(81)	2.385(8)	O(55)–U(1)–O(85)	72.9(3)
U(1)–O(85)	2.388(7)	O(81)–U(1)–O(85)	70.1(3)
U(1)–O(11)	2.384(7)	P(1)–C(2)–P(3)	119.0(5)
P(1)–O(21)	1.471(9)	P(3)–O(11)–U(1)	146.9(4)
Compound ***5***			
U(1)–O(1)	1.80(2)	O(1)–U(1)–O(2)	178.8(9)
U(1)–O(1)	1.822(17)	O(2)–U(1)–O(15)	92.5(7)
U(1)–O(71)	2.352(19)	O(71)–U(1)–O(15)	69.7(6)
U(1)–O(75)	2.49(2)	O(15)–U(1)–O(11)	71.2(5)
U(1)–O(11)	2.392(18)	O(11)–U(1)–O(41)	74.9(5)
U(1)–O(15)	2.393(15)	O(41)–U(1)–O(75)	73.9(6)
U(1)–O(41)	2.418(15)	P(42)–O(41)–U(1)	154.7(11)

oxide and nitrate groups are *cis* to each other, due to the chelating nature of the DPPMO ligand. The six membered metallocyclic ring formed by the DPPMO ligand is severely folded with an angle of 52.8° between the plane of U(1), O(11), O(12) and of the P(1), C(2) and P(3) atoms. The bond angles and lengths around the phosphine oxide part of the molecule agree well with earlier reported lanthanide DPPMO compounds [28,29].

3.3. Mononuclear compound $[UO_2(DBM)_2DPPMO]$ (2)

The 1:1 reaction of $[UO_2(DBM)_2 \cdot 2H_2O]$ with DPPMO in chloroform yielded **2**. The IR spectrum of **2** shows that the water molecules from the starting compound are completely replaced by the DPPMO ligand. It suggests further, that the DPPMO ligand coordinates through one of the phosphine oxide oxygen atoms to the uranyl group and the other one is free. This observation is further supported by the $^{31}P\{^1H\}$ NMR spectrum, which displayed two resonances with equal intensities, with one deshielded by ca. 15 ppm and other with very little change with respect to the free ligand. The ^1H NMR of **2** showed a single resonance for the CH_2 protons of DPPMO and is deshielded by 0.37 ppm with respect to the free ligand. The deshielding of CH_2 protrons in **2** is much smaller as compared to **1**, where the DPPMO is bonded through both PO oxygen atoms to the uranyl group. The structure of **2** was determined by single-crystal X-ray diffraction methods and confirms the spectral interpretation.

3.4. Molecular structure of $[UO_2(DBM)_2\ DPPMO]$

The molecular structure of **2** is shown in Fig. 3 and selected interatomic bond distances and angles are given in Table 2. The structure shows that the uranium atom is surrounded by seven oxygen atom in a pentagonal bipyramidal geometry. The four oxygen atoms of DBM and one oxygen of DPPMO form a planar pentagon and these oxygen atoms are coplanar to within 0.06 Å. The structure shows clearly that the DPPMO is acting as a monodentate ligand and is bonded through one of the phosphine oxide oxygen atoms (O11) to the uranyl group, and the other oxygen atom is free (O21). The observed average bond lengths for $U–O_{(uranyl)}$ (1.778(7) Å) [56–61], $U–O_{(DBM)}$ (2.3663(8) Å) [58–60] and $U–O_{(DPPMO)}$ (2.384(7) Å) [56,60,61] agree well with earlier reported values. The bond lengths and angles around the DPPMO part of the molecule agree well with an earlier reported rhenium–DPPMO compound $[Cl_3LRe(DPPMO)]$ [50].

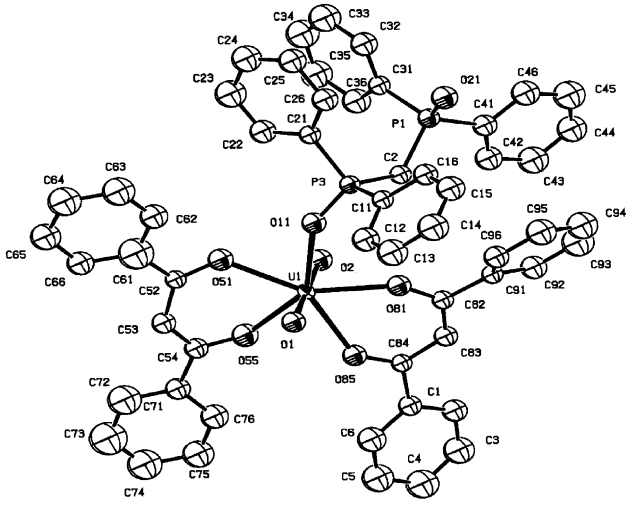

Fig. 3. Molecular structure of $[UO_2(DBM)_2DPPMO]$ with ellipsoids at 50% probability.

Attempts to prepare (pure) 1:1 compounds of $[UO_2(TTA)_2]$ and $[UO_2(BTA)_2]$ with DPPMO (**3** and **4**, similar to **2**), yielded a mixture of mononuclear and dinuclear compounds (similar to **5**–**8**), revealed from ^1H and ^{31}P NMR spectroscopy.

3.5. Dinuclear compounds $[\{UO_2(OO)_2\}_2DPPMO]$ (5–8)

The 2:1 reaction of $[UO_2(OO)_2 \cdot 2H_2O]$ (where, OO = TTA, DBM, BTA or BA) with DPPMO in chloroform yielded **5**–**8**. The IR spectra of **5**–**8** showed that the water molecules from the starting compound are completely replaced by the DPPMO ligand. It suggests further that the DPPMO is coordinating through both the phosphine oxide oxygen atoms to the uranyl group. This observation is further supported by the $^{31}P\{^1H\}$ NMR spectra, which displayed one (DBM) or two (TTA, BTA or BA) resonances, which were deshielded by ca. 13–16 ppm with respect to the free ligand. The presence of two resonances for TTA, BTA or BA show that they are existing as a mixture of two isomeric products, viz., *cis–cis* or *trans–cis* [62]. The ^1H NMR spectra of **5**–**8** showed a single resonance for the CH_2 protons of DPPM which was deshielded by ca. 1.12–1.6 ppm with respect to the free ligand. The deshielding of CH_2 protons in **5**–**8** is much larger as compared to **2**–**4**, where the DPPMO is bonded through one of the PO oxygen atoms and acts as a monodentate ligand. The structure of **5** was determined by single-crystal X-ray diffraction methods and confirms our spectral observations.

3.6. Molecular structure of $[\{UO_2(DBM)_2\}_2DPPMO]$ (5)

The molecular structure of **5** is shown in Fig. 4 and selected interatomic bond distances and angles are given in Table 2. The structure shows a centrosymmetric dimer with the two halves of the $[UO_2(DBM)_2]$ moieties

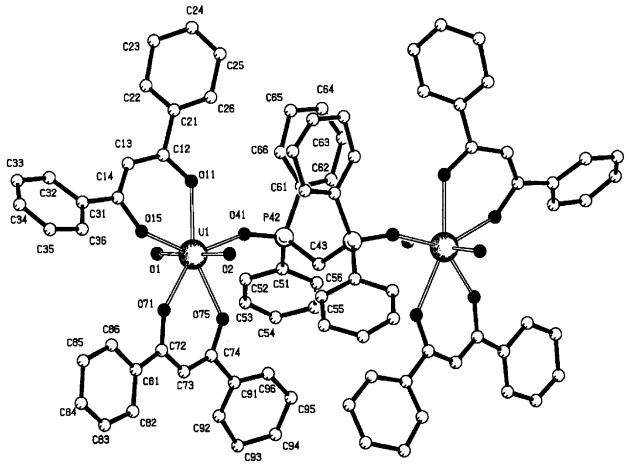

Fig. 4. Molecular structure of $[\{UO_2(DBM)_2\}_2DPPMO]$.

bridged by a DPPMO ligand. The geometry around each individual uranium atom is pentagonal bipyramidal with four oxygen atoms from DBM and one from phosphine oxide forming a planar pentagon, and these oxygen atoms are coplanar to within 0.07 Å. The structure also contains solvent water and methanol molecules with 25% occupancy which are not included in Fig. 4, for clarity. The bond lengths and angles around the uranium atoms are normal [58–60].

It is interesting to note that an attempt to prepare a dinuclear compound $[Cl_3LRe(DPPMO)ReLCl_3]$ from $[Cl_3LRe(DPPMO)]$ (where L = 2-(p-chlorophenyl-azo)-1-methylimidazole), similar to the one that is reported here, was not successful in rhenium compounds [50]. The authors stated that the uncoordinated or free phosphine oxide group in $[Cl_3LRe(DPPMO)]$ is sterically overcrowded [O(2)···P(1) 3.57 Å, O(2)···C(11) 3.55 Å] and therefore it may not allow the second molecule of $ReLCl_3$ to approach to form a dinuclear compound. However, in the present case, the uncoordinated or free phosphine oxide in **2** is relatively much more overcrowded (P(3)···O(21) 3.493 Å, O(21)···C(21) 3.555 Å, O(21)···C(11) 3.77 Å, O(21)···C(21) 3.224 Å) compared to the distances observed in the rhenium compound $[Cl_3LRe(DPPMO)]$ and despite these contacts is still able to form the dinuclear compound **5**. It suggests clearly that the steric crowding around the free phosphine oxide is not an important factor for the formation of the dinuclear compounds as stated in the report of the structure of $[Cl_3LRe(DPPMO)]$.

4. Conclusion

The first structurally characterized bis(phosphine)dioxide compounds of the uranyl ion, **1**, **2** and **5** show that it can act as a bidentate chelating, monodentate or bridging bidentate ligand, depending upon the anions used. Different modes of coordination for the DPPMO ligand can be controlled by suitably selecting the anion and the stoichiometry of the uranyl-bis(β-diketonates) used.

5. Supplementary materials

Crystallographic data may be obtained from the Cambridge Crystallographic Data Center, by quoting the reference numbers CCDC from 229640 to 229642. Copies of this information may be obtained free of charge from The Director, CCDC, 12 Union Road, Cambridge CB2 1EZ, UK (fax: +44-1223-336-033; email: deposit@ccdc.cam.ac.uk or www: http://www.ccdc.cam.ac.uk).

Acknowledgements

We are thankful to The Head Analytical Chemistry Division for the carbon, hydrogen and nitrogen analyses. We are also thankful to the EPSRC and the University of Reading for funding of the image plate system.

References

[1] W.W. Schulz, L.D. McIssac, in: W. Muller, R. Lindner (Eds.), Transplutonium Elements, North-Holland, Amsterdam, 1976, p. 433.
[2] W.W. Schulz, J.D. Navaratil, in: N.W. Li (Ed.), Recent Developments in Separation Science, CRC Press, Boca Raton, FL, 1982, p. 31.
[3] E.P. Horwitz, H. Diamond, D.G. Kalina, in: W.T. Carnall, G.R. Choppin (Eds.), Plutonium Chemistry, ACS Symposium Series, vol. 216, American Chemical Society, Washington, DC, 1983, p. 179.
[4] W.W. Schulz, E.P. Horwitz, Sep. Sci. Technol. 23 (1988) 1191.
[5] J.N. Mathur, M.S. Murali, K.L. Nash, Solvent Extr. Ion Exch. 19 (2001) 357.
[6] K.L. Nash, C. Lavallette, M. Borkowski, R.T. Paine, X. Gan, Inorg. Chem. 41 (2002) 5849.
[7] S.M. Bowen, E.N. Duesler, R.T. Paine, Inorg. Chim. Acta 61 (1983) 155.
[8] S.M. Bowen, E.N. Duesler, R.T. Paine, Inorg. Chem. 22 (1983) 286.
[9] S.M. Bowen, E.N. Duesler, R.T. Paine, Inorg. Chim. Acta 84 (1984) 221.
[10] D.J. McCabe, E.N. Duesler, R.T. Paine, Inorg. Chem. 24 (1985) 4626.
[11] L.J. Caudle, E.N. Duesler, R.T. Paine, Inorg. Chem. 24 (1985) 4441.
[12] B.M. Rapko, E.N. Duesler, P.H. Smith, R.T. Paine, R.R. Ryan, Inorg. Chem. 32 (1993) 2164.
[13] Y.C. Tan, X.M. Gan, J.L. Stanchfield, E.N. Duesler, R.T. Paine, Inorg. Chem. 40 (2001) 2910.
[14] R.T. Paine, Y.C. Tan, X.M. Gan, Inorg. Chem. 40 (2001) 7009.
[15] R.T. Paine, E.M. Bond, S. Parveen, N. Donhart, E.N. Duesler, K.A. Smith, H. Noth, Inorg. Chem. 41 (2002) 444.
[16] S.M. Bowen, E.N. Duesler, R.T. Paine, Inorg. Chem. 21 (1982) 261.

[17] L.J. Caudle, E.N. Duesler, R.T. Paine, Inorg. Chim. Acta 110 (1985) 91.
[18] D.J. McCabe, A.A. Russell, S. Karthikeyan, R.T. Paine, R.R. Ryan, Inorg. Chem. 26 (1987) 1230.
[19] S. Karthikeyan, R.T. Paine, R.R. Ryan, Inorg. Chim. Acta 144 (1988) 135.
[20] S. Karthikeyan, R.R. Ryan, R.T. Paine, Inorg. Chem. 28 (1989) 2783.
[21] D.T. Cromer, R.R. Ryan, S. Karthikeyan, R.T. Paine, Inorg. Chim. Acta (1990) 165.
[22] E.M. Bond, E.N. Duesler, R.T. Paine, M.P. Neu, J.H. Matonic, B.L. Scott, Inorg. Chem. 39 (2000) 4152.
[23] M.W. Peters, E.J. Werner, M.J. Scott, Inorg. Chem. 14 (2002) 1707.
[24] J.E. Mrochek, J.W. O'laughlin, H. Sakurai, C.V. Banks, J. Inorg. Nucl. Chem. 25 (1963) 955.
[25] J.E. Mrochek, C.V. Banks, J. Inorg. Nucl. Chem. 27 (1965) 589.
[26] J.R. Parker, C.V. Banks, J. Inorg. Nucl. Chem. 27 (1965) 631.
[27] T. Yaita, S. Tachimori, Radiochim. Acta 73 (1996) 27.
[28] J. Fawcett, A.W.G. Platt, Polyhedron 22 (2003) 967.
[29] A.M.J. Lees, A.W.G. Platt, Inorg. Chem. 42 (2003) 4673.
[30] T.V. Healy, J.J. Kennedy, J. Inorg. Nucl. Chem. 10 (1959) 128.
[31] J.E. Mrochek, J.W. O'laughlin, C.V. Banks, J. Inorg. Nucl. Chem. (1965) 603.
[32] J.R. Parker, C.V. Banks, J. Inorg. Nucl. Chem. 27 (1965) 583.
[33] A.M. Rozen, Z.I. Nikolotova, N.A. Kartasheva, Dokl. Akad. Nauk. SSSR 22 (1975) 1151.
[34] A.M. Rozen, Z.A. Berkman, Radiokhimiya 18 (1976) 493.
[35] S. Dondi, M. Nardelli, C. Pelizzi, G. Pelizzi, G. Predieri, Organomet. Chem. 308 (1986) 195.
[36] G. Pelizzi, P. Tarasconi, F. Vitali, C. Francesca, Acta Crystallogr., Sect. C (1987) 1505.
[37] E. Bermejo, A. Castineiras, R. Dominguez, C. Schuele, J. Coord. Chem. (1994) 353.
[38] G.R. Willey, M.D. Rudd, C.J. Samuel, M.G.B. Drew, J. Chem. Soc., Dalton Trans. (1995) 759.
[39] I.A. Razak, H.K. Fun, B.M. Bohari, K. Chinnakali, H. Zakaria, N.B. Ismail, Acta Crystallogr., Sect. C 55 (1999) 172.
[40] C.J. Carmatt, L.J. Farrugia, N.C. Norman, Main Group Chem. 1 (1996) 339.
[41] Y. Ding, P.E. Fanwick, A. Richard, Inorg. Chim. Acta 309 (2000) 159.
[42] C. Pettinari, F. Marchetti, A. Cingolani, R. Pettinari, A. Drozdov, S. Troyanov, Inorg. Chim. Acta 312 (2001) 125.
[43] F.J. Arnaiz, R. Aguado, M.R. Maria, J. Mahia, M.A. Maestro, Polyhedron 21 (2002) 1635.
[44] P.K. Baker, M.G.B. Drew, D.S. Moore, J. Organomet. Chem. 664 (2002) 45.
[45] A. Mendia, E. Cerrada, E.J. Fernandez, A. Laguna, M. Laguna, J. Organomet. Chem. 663 (2002) 289.
[46] G.H. Robinson, B. Lee, W.T. Pennington, S.A. Sangokoya, J. Am. Chem. Soc. 110 (1988) 6260.
[47] S.A. Sangokoya, B. Lee, M.F. Self, W.T. Pennington, G.H. Robinson, Polyhedron 8 (1989) 1497.
[48] E.J. Fernandez, P.G. Jones, A. Laguna, A. Mendia, Inorg. Chim. Acta 215 (1994) 229.
[49] Y. Ding, S.S. Lau, P.E. Fanwick, R.A. Walton, Inorg. Chim. Acta 300–302 (2000) 505.
[50] S. Bhattacharyya, I. Chakraborty, B.K. Dirghangi, A. Chakravorty, Chem. Commun. (2000) 1813.
[51] K.M. Abubacker, N.S.K. Prasad, J. Inorg. Nucl. Chem. 16 (1961) 296.
[52] W. Kabsch, J. Appl. Crystallogr. 21 (1988) 916.
[53] G.M. Sheldrick, SHELX-86, Acta Crystallogr., Sect. A 46 (1990) 467.
[54] N. Walker, D. Stuart, Acta Crystallogr., Sect. A 39 (1983) 158.
[55] G.M. Sheldrick, SHELXL: Program for Crystal Structure Refinement, University of Göttingen, Göttingen, Germany, 1983.
[56] N.W. Alcock, M.M. Roberts, D. Brown, J. Chem. Soc., Dalton Trans. (1982) 25.
[57] G. Bombieri, E. Forsellini, J.P. Day, W.I. Azeez, J. Chem. Soc., Dalton Trans. (1978) 677.
[58] S. Kannan, G. Ferguson, Inorg. Chem. 36 (1997) 1724.
[59] S. Kannan, A. Usman, A.Z. Razak, S. Chandrapromma, H.K. Fun, Acta Crystallogr., Sect. C 58 (2002) 368.
[60] S. Alagar, M. Subhananthini, R.V. Krishnakumar, S. Kannan, S. Natarajan, Acta Crystallogr., Sect. E 59 (2003) 524.
[61] C. Panattoni, R. Graziani, G. Bandoli, B. Zarli, G. Bombieri, Inorg. Chem. 8 (1969) 320.
[62] S. Kannan, M.R.A. Pillai, V. Venugopal, P.A. Droege, C.L. Barnes, E.O. Schlember, Polyhedron 15 (1996) 465.

Available online at www.sciencedirect.com
SCIENCE DIRECT®
Polyhedron 23 (2004) 1535–1539
POLYHEDRON
www.elsevier.com/locate/poly

Hydrothermal synthesis and characterization of an organically templated gallophosphate JGP-5 ☆

Yulin Yang, Yunlin Liu, Chao Chen, Wei Wang, Zhuo Yi, Wenqin Pang *

State Key Laboratory of Inorganic Synthesis and Preparative Chemistry, College of Chemistry, Jilin University, Changchun 130023, PR China

Received 17 December 2003; accepted 10 March 2004
Available online 9 April 2004

Abstract

A gallophosphate compound, $[C_6H_{10}(NH_3)_2]Ga_2P_2O_8(OH)_2$ (named JGP-5) has been synthesized hydrothermally by using *trans*-1,4-diaminocyclohexane as the template. It has been characterized by X-ray powder diffraction (XRD), elemental analysis, inductively coupled plasma (ICP) and TGA analysis, and structurally determined by single-crystal X-ray diffraction analysis. JGP-5 crystallizes in the monoclinic, space group *Cc*, with $a = 25.740(5)$, $b = 5.412(1)$, $c = 9.888(2)$ Å, $\beta = 94.32(3)°$, $V = 1373.5(5)$ Å^3 and $Z = 4$. The 2D anionic framework of JGP-5 is built up from vertex linkage of $GaO_4(OH)_2$ octahedra and HPO_4 tetrahedra, forming a gallophosphate sheet with three- and six-membered channels along the *a*-axis direction. The organic amines display a strong templating effect on the inorganic layer.
© 2004 Elsevier Ltd. All rights reserved.

Keywords: Hydrothermal syntheses; Crystal structures; Gallophosphates; Templating effect

1. Introduction

In the past 20 years, the synthesis of new open-framework metal phosphates has attracted considerable attention because of their potential applications in catalysis, adsorption and separation [1–3]. Among the metal phosphates, gallophosphates constitute an important family. Since the discovery of the $GaPO_4$-14 molecular sieves in 1985, many novel gallophosphates with 1D, 2D and 3D structures have been synthesized successfully under hydrothermal or solvothermal conditions [4–6]. The structures of these compounds are built mainly from GaO_4 tetrahedra, GaO_5 trigonal bipyramids, GaO_6 octahedra, or their combination, and PO_4 tetrahedra, but examples of single polyhedra are also known [7–9]. The syntheses typically involve the addition of organic amines. It is proposed that in most cases, the amines act as a structure-directing agent (template) when their shapes are related to the frameworks. Among the various organic amines used, the family of diaminoalkanes is more effective than that of monoaminoalkanes to display a strong templating effect in the formation of gallophosphates with open architecture [10–14].

In recent years, we have devoted efforts toward the synthesis of metal phosphates with novel topologies [15–22]. In the case of gallium, we obtained a new layered gallophosphate with a Ga/P ratio of non-unity [23]. In this paper, we describe the synthesis and structure of a 2D gallophosphate $[C_6H_{10}(NH_3)_2]Ga_2P_2O_8(OH)_2$ (named JGP-5), using *trans*-1,4-diaminocyclohexane as the template.

2. Experimental

JGP-5 is synthesized under hydrothermal conditions. The chemical sources used in the synthesis were an amorphous gallium oxide, which was prepared by heating a gallium oxide hydroxide at 400 °C for 3 h (gallium oxide hydroxide was prepared by direct reaction of gallium metal with water at 220 °C under

☆ Supplementary data associated with this article can be found, in the online version, at doi:10.1016/j.poly.2004.03.004.

* Corresponding author. Tel.: +86-431-8499855; fax: +86-431-5671974.
E-mail address: wqpang@mail.jlu.edu.cn (W. Pang).

0277-5387/$ - see front matter © 2004 Elsevier Ltd. All rights reserved.
doi:10.1016/j.poly.2004.03.004

autogenous pressure for 3 days), phosphoric acid (Beijing Chemical Plant, 85%) and *trans*-1,4-diaminocyclohexane (1,4-DACH, Aldrich).

2.1. Synthesis and characterization

JGP-5 was hydrothermally prepared from a reaction mixture of 1 Ga_2O_3:1 H_3PO_4:0.8 1,4-DACH:185 H_2O (molar ratio, pH 7) with vigorous stirring. The mixture was then aged at room temperature for 1 h, transferred to the Teflon-lined stainless steel autoclave and then heated under autogenous pressure at 180 °C for 3 days. The product was washed with distilled water and dried overnight at 50 °C to give colorless crystals.

The powder X-ray diffraction (XRD) patterns were recorded on a Siemens D5005 diffractometer with Cu Kα radiation ($\lambda = 1.5418$ Å). The elemental analyses were performed on a Perkin–Elmer 2400 elemental analyzer and the inductively coupled plasma (ICP) analysis on a Perkin–Elmer Optima 3300 DV ICP instrument. Thermogravimetric analysis (TGA) was conducted on a Netzsch STA 449C thermogravimetric analyzer with a heating rate of 10 °C min^{-1} in air. IR spectra were recorded on a Nicolet Impact 410 FTIR spectrometer using KBr pellets.

2.2. Determination of crystal structure

A suitable single crystal of JGP-5 was selected for single-crystal XRD analysis. The structural analysis was performed on a Rigaku R-AXIS RAPID IP diffractometer equipped with graphite-monochromated Mo Kα radiation ($\lambda = 0.71073$ Å). The data were collected at a temperature of 193 ± 1 K. Data processing were accomplished with the Process-Auto processing program [24]. The structures were solved by direct methods and refined by full-matrix, least squares based on F^2 using the SHELXTL 5.1 software package [25]. The gallium and phosphorus atoms were first located, and carbon, nitrogen, oxygen atoms and the hydrogen atoms residing in the organic amine molecules were located geometrically. All non-hydrogen atoms were refined anisotropically. The Flack x parameter of JGP-5 was 0.00(6), indicative of correct absolute structure. Crystal data and details of data collection and refinement are given in Table 1.

Table 1
Crystal data and structure refinement for JGP-5

Identification code	JGP-5
Empirical formula	$[C_6H_{10}(NH_3)_2]Ga_2P_2O_8(OH)_2$
Formula weight	479.47
Temperature (K)	193(2)
Wavelength (Å)	0.71073
Crystal system	monoclinic
Space group	*Cc*
Unit cell dimensions	
a (Å)	25.740(5)
b (Å)	5.412(1)
c (Å)	9.888(2)
β (°)	94.32(3)
Volume (Å^3)	1373.5(5)
Z	4
$D_{calc.}$ (Mg/m^3)	1.155
Absorption coefficient (mm^{-1})	2.106
$F(000)$	476
Crystal size (mm)	$0.22 \times 0.12 \times 0.06$
θ Range for data collection (°)	1.59 to 27.47
Limiting indices	$0 \leqslant h \leqslant 33$ $0 \leqslant k \leqslant 7$ $-12 \leqslant l \leqslant 12$
Reflections collected/unique	4777/1702 [$R_{int} = 0.0614$]
Completeness to $\theta = 23.25$	98.7%
Refinement method	full-matrix least-squares on F^2
Data/restraints/parameters	1555/110/199
Goodness-of-fit on F^2	1.009
Final R indices [$I > 2\sigma(I)$]	$R_1 = 0.0462$[a], $wR_2 = 0.1092$[b]
R indices (all data)	$R_1 = 0.0791$[a], $wR_2 = 0.1408$[b]
Largest difference in peak and hole (e Å^{-3})	1.200 and −1.558

[a] $R_1 = \sum ||F_o| - |F_c|| / \sum |F_o|$.
[b] $wR_2 = [\sum[w(F_o^2 - F_c^2)^2] / \sum[w(F_o^2)^2]]^{1/2}$.

3. Results and discussion

3.1. Characterization of JGP-5

The XRD pattern for JGP-5 is entirely consistent with those simulated on the basis of the single-crystal structure. The diffraction peaks in both measured and simulated patterns correspond well to each other in position, indicating the phase purity of the as-synthesized samples. *Anal.* Calc. for JGP-5: Ga, 29.08; (29.15); P, 12.92; (12.99); C, 15.02; (14.97); H, 3.75; (3.80); N, 5.84. Found: Ga, 29.15; P, 12.92; C, 14.97; H, 3.80; N, 5.81%.

The IR spectrum of the JGP-5 compound is assigned as follows: The bands in the 3200–2800 cm^{-1} region are typically attributed to H-bonded O–H and N–H groups. The bands in the 1600–1100 cm^{-1} region are ascribed to vibrations of the 1,4-DACH template. The band at 1130 cm^{-1} is associated with the stretching vibrations of Ga–O groups and the band at 1033 cm^{-1} is attributed to vibration of PO_4 groups.

The thermal behavior of JGP-5 was investigated by TGA thermal analyses. The total weight loss of JGP-5 occurs in two steps. The first weight loss of ca. 24.29% in the range 345–590 °C corresponds to the removal of the template (calc. 24.21%). The second weight loss of ca. 6.84% in the range 590–760 °C corresponds to the removal of the hydroxyl groups (calc. 7.09%). After the removal of the organic templates, XRD analysis indicates that the structure of JGP-5 collapses and recrystallization into a dense phase ($GaPO_4$-quartz) occurs.

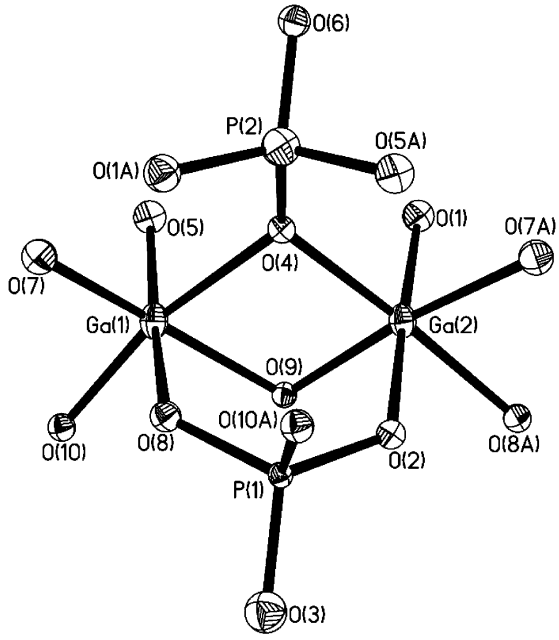

Fig. 1. ORTEP view of the JGP-5 structure showing the atom labelling scheme (50% thermal ellipsoids).

Table 2
Selected bond lengths (Å) and angles (°) for JGP-5

Ga(1)–O(7)	1.826(19)	Ga(2)–O(1)	2.01(2)
Bond lengths			
Ga(1)–O(10)	1.904(18)	Ga(2)–O(8)#1	2.06(2)
Ga(1)–O(9)	1.964(17)	P(1)–O(3)	1.53(2)
Ga(1)–O(5)	1.964(19)	P(1)–O(10)#2	1.56(2)
Ga(1)–O(4)	2.14(2)	P(1)–O(8)	1.57(2)
Ga(1)–O(8)	2.19(2)	P(1)–O(2)	1.57(2)
Ga(2)–O(9)	1.903(18)	P(2)–O(6)	1.480(19)
Ga(2)–O(7)#1	1.90(2)	P(2)–O(5)#2	1.53(2)
Ga(2)–O(2)	2.00(2)	P(2)–O(1)#3	1.54(2)
Ga(2)–O(4)	2.00(2)	P(2)–O(4)	1.58(2)
Bond angles			
O(7)–Ga(1)–O(10)	91.9(7)	O(9)–Ga(2)–O(1)	97.5(8)
O(7)–Ga(1)–O(9)	164.2(4)	O(7)#1–Ga(2)–O(1)	87.1(9)
O(10)–Ga(1)–O(9)	94.3(8)	O(2)–Ga(2)–O(1)	177.3(12)
O(7)–Ga(1)–O(5)	94.7(8)	O(4)–Ga(2)–O(1)	91.9(9)
O(10)–Ga(1)–O(5)	101.3(4)	O(9)–Ga(2)–O(8)#1	95.9(8)
O(9)–Ga(1)–O(5)	98.3(7)	O(7)#1–Ga(2)–O(8)#1	79.5(8)
O(7)–Ga(1)–O(4)	92.9(9)	O(2)–Ga(2)–O(8)#1	87.9(8)
O(10)–Ga(1)–O(4)	165.6(8)	O(4)–Ga(2)–O(8)#1	176.0(10)
O(9)–Ga(1)–O(4)	77.8(8)	O(1)–Ga(2)–O(8)#1	92.0(8)
O(5)–Ga(1)–O(4)	91.8(8)	O(3)–P(1)–O(10)#2	114.7(11)
O(7)–Ga(1)–O(8)	77.8(8)	O(3)–P(1)–O(8)	107.3(11)
O(10)–Ga(1)–O(8)	90.5(8)	O(10)#2–P(1)–O(8)	106.7(11)
O(9)–Ga(1)–O(8)	87.6(8)	O(3)–P(1)–O(2)	109.5(11)
O(5)–Ga(1)–O(8)	166.3(8)	O(10)#2–P(1)–O(2)	106.9(12)
O(4)–Ga(1)–O(8)	77.3(3)	O(8)–P(1)–O(2)	111.8(13)
O(9)–Ga(2)–O(7)#1	173.6(11)	O(6)–P(2)–O(5)#2	104.4(12)
O(9)–Ga(2)–O(2)	85.2(9)	O(6)–P(2)–O(1)#3	113.9(12)
O(7)#1–Ga(2)–O(2)	90.2(9)	O(5)#2–P(2)–O(1)#3	109.8(13)
O(9)–Ga(2)–O(4)	82.7(8)	O(6)–P(2)–O(4)	111.9(12)
O(7)#1–Ga(2)–O(4)	101.6(8)	O(5)#2–P(2)–O(4)	108.9(12)
O(2)–Ga(2)–O(4)	88.3(8)	O(1)#3–P(2)–O(4)	107.9(14)

3.2. Description of the structure

As seen in Fig. 1, the asymmetric unit consists of 22 distinct non-hydrogen atoms, 14 atoms belong to the host atoms or framework atoms consisting of 2 Ga, 2 P and 10 O atoms, and 8 atoms to the guest atoms, being 6 C and 2 N atoms in the structure of JGP-5. Ga(1) and Ga(2) are both octahedrally coordinated and share two tri-bridging hydroxyl groups (–O(4)H and –O(8)H) with adjacent Ga atoms and P atoms (Ga–O: 2.00(2)–2.19(2) Å), two bridging oxygens with adjacent Ga atoms (Ga–O: 1.84(2)–1.96(2) Å), and two bridging oxygen with adjacent P atoms (Ga–O: 1.90(2)–2.01(2) Å). P(1) and P(2) are both tetrahedrally coordinated and share one tri-bridging hydroxyl group with adjacent Ga atoms (P–O: 1.57(2) and 1.58(2) Å, respectively), two bridging oxygen with adjacent Ga atoms (P–O: 1.53(2)–1.57(2) Å) and one shorter P–O bond corresponding to a terminal oxygen moiety (P–O: 1.52(2) and 1.48(2) Å, respectively). In addition, this asymmetric unit also includes one diprotonated *trans*-1,4-DACH. The selected bond lengths and angles are listed in Table 2.

The 2D anionic framework of JGP-5 is built up from vertex linkage of $GaO_4(OH)_2$ octahedra and HPO_4 tetrahedra. This inorganic framework may be viewed as stacking of 1D $[GaO_4(OH)_2]_n$ polyhedra chain, linked by HPO_4 tetrahedra acting as pillars, forming a 2D gallophosphate sheet with three- and six-membered channels along the *a*-axis direction as shown in Fig. 2.

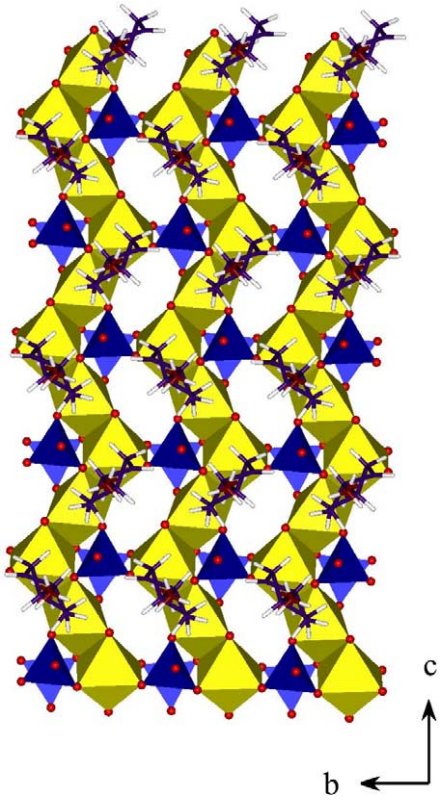

Fig. 2. Polyhedral view of JGP-5 along the *a*-axis direction.

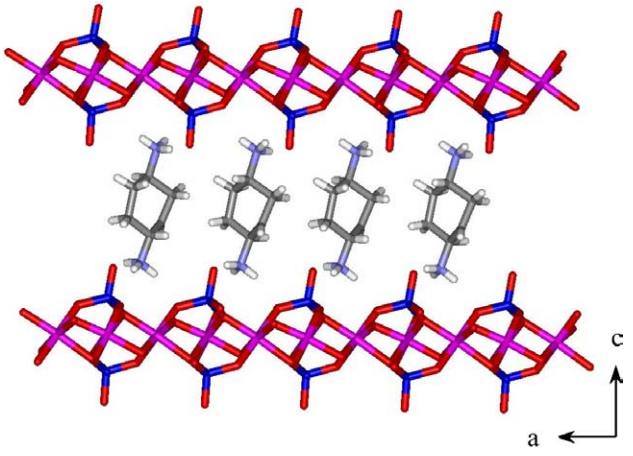

Fig. 3. Stick view of JGP-5 along the *b*-axis direction.

Table 3
Hydrogen bonds for JGP-5 (Å and °)

D–H···A	*d*(H···A)	*d*(D···A)	Angle (D–H···A)
N1–H1A···O5 #1	2.090	2.793	135.19
N1–H1A···O6 #2	2.386	3.235	159.51
N1–H1B···O6 #1	2.014	2.831	151.90
N1–H1C···O1 #1	2.038	2.892	160.69
N2–H2A···O2	2.049	2.849	149.12
N2–H2A···O3	2.643	3.383	141.30
N2–H2B···O3 #3	1.841	2.718	167.95
N2–H2D···O10 #3	2.279	3.068	147.52

Symmetry transformations used to generate equivalent atoms: #1, $x+1/2, y+1/2, z$; #2, $x+1/2, y-1/2, z$; #3, $x, -y, z-1/2$.

This chain is linked by edge-sharing $GaO_4(OH)_2$ octahedra, forming an infinite Ga–O–Ga–O–Ga zigzag chain along the *c*-axis direction. Each common edge is composed of one bridging oxygen and one tri-bridging hydroxyl group. A similar layer structure has also been observed for MIL-35 [26], the difference is that in MIL-35, edge-sharing $GaO_4(OH)_2$ octahedra are linked together via the fluorine atoms, whereas in JGP-5, the linkage corresponds to the oxygen atoms.

The diprotonated *trans*-1,4-DACH are intercalated in the space between the layers and neutralize the negative charge of the inorganic framework (Fig. 3). The 2D framework of JGP-5 is stabilized by the strong hydrogen bonds involving the hydrogen atoms attached to the nitrogen of the *trans*-1,4-DACH and the framework oxygen atoms. Detailed information about the hydrogen bonds is summarized in Table 3.

The organic amines have a strong and definite templating effect on the inorganic layer and exhibit a similar arrangement to the zig–zag chains (Fig. 2). Adjacent amines along the *c*-axis direction are oriented approximately vertically, while those along the *b*-axis direction are parallel to each other. These facts indicate that the guest organic amine molecule possesses a molecular recognition ability for the inorganic host. Perhaps the gallophosphate layer is not formed before the organic amine is incorporated.

4. Conclusion

We have characterized an organically templated gallophosphate JGP-5. JGP-5 exhibits a 2D layered structure intercalating *trans*-1,4-DACH. The organic amines display a strong templating effect on the inorganic layer.

5. Supplementary materials

Crystallographic data for JGP-5 has been deposited with the Cambridge Crystallographic Data Center, CCDC No. 213678. Copies of this information may be obtained free of charge from: The Director, CCDC, 12 Union Road, Cambridge, CB2, IEZ, UK (fax: +44-1233-336-033, e-mail: deposit@ccdc.cam.ac.uk or http//www.ccdc.cam.ac.uk).

Acknowledgements

We are grateful to the National Natural Science Foundation of China (20233030) and the State Basic Research Project (G200077507) for financial support.

References

[1] S.T. Wilson, B.M. Lok, C.A. Messina, T.R. Cannan, E.M. Flanigen, J. Am. Chem. Soc. 104 (1982) 1146.
[2] A.K. Cheetham, G. Férey, T. Loiseau, Angew. Chem., Int. Ed. 38 (1999) 3268.
[3] S.H. Feng, R.R. Xu, Acc. Chem. Res. 34 (2001) 239.
[4] J.B. Parise, J. Chem. Soc., Chem. Commun. (1985) 606.
[5] M. Mrak, U. Kolitsch, C. Lengauer, V. Kaučič, E. Tillmanns, Inorg. Chem. 42 (2003) 598.
[6] L. Beitone, J. Marrot, T. Loiseau, G. Férey, M. Herry, C. Huguenard, A. Gansmuller, F. Taulelle, J. Am. Chem. Soc. 125 (2003) 1912, and references therein.
[7] T.L. Wang, G.D. Yang, S.H. Feng, C.J. Shang, R.R. Xu, J. Chem. Soc., Chem. Commun. (1989) 948.
[8] S.M. Stalder, A.P. Wilkinson, Chem. Mater. 9 (1997) 2168.
[9] F. Taulelle, J.-M. Poblet, G. Férey, M. Bénard, J. Am. Chem. Soc. 123 (2001) 111.
[10] A.M. Chippindale, R.I. Walton, C. Turner, J. Chem. Soc., Chem. Commun. (1995) 1261.
[11] F. Taulelle, A. Samoson, T. Loiseau, G. Férey, J. Phys. Chem. B 102 (1998) 8588.
[12] A. Matijasic, J. Paillaud, J. Patarin, J. Mater. Chem. 10 (2000) 1345.
[13] P. Reinert, B. Marler, J. Patarin, Micro. Meso. Mater. 39 (2000) 509.
[14] A. Matijasic, B. Marler, J.C. Muñoz Acevedo, L. Josien, J. Patarin, Chem. Mater. 15 (2003) 2614.

[15] Y. Zhao, G. Zhu, W. Liu, Y. Zou, W. Pang, Chem. Commun. (1999) 2219.
[16] Y. Zhao, G. Zhu, X. Jiao, W. Liu, W. Pang, J. Mater. Chem. 10 (2000) 463.
[17] W. Liu, Y. Liu, Z. Shi, W. Pang, J. Mater. Chem. 10 (2000) 1451.
[18] Y. Liu, Z. Shi, L. Zhang, Y. Fu, J. Chen, B. Li, J. Hua, W. Pang, Chem. Mater. 13 (2001) 2017.
[19] Y. Guo, Z. Shi, J. Yu, J. Wang, Y. Liu, N. Bai, W. Pang, Chem. Mater. 13 (2001) 203.
[20] Y. Liu, L. Zhang, Z. Shi, H. Yuan, W. Pang, J. Solid State Chem. 158 (2001) 68.
[21] Y. Liu, W. Liu, Y. Xing, Z. Shi, Y. Fu, W. Pang, J. Solid State Chem. 166 (2002) 265.
[22] Y. Xin, Y. Liu, Z. Shi, P. Zhang, Y. Fu, W. Pang, J. Solid State Chem. 163 (2002) 364.
[23] Y. Yang, Y. Liu, Z. Mu, L. Ye, T. Hu, C. Chen, W. Pang, J. Solid State Chem. 177 (2004) 696.
[24] T. Higashi, Program for Absorption Correction, Rigaku Corporation, Tokyo, Japan, 1995.
[25] G.M. Sheldrick, SHELXTL-NT, Version 5.10, Bruker AXS Inc., Madison, WI, 1997.
[26] C. Sassoye, T. Loiseau, G. Férey, J. Fluorine Chem. 107 (2001) 187.

Available online at www.sciencedirect.com
SCIENCE DIRECT®
Polyhedron 23 (2004) 1541–1546
POLYHEDRON
www.elsevier.com/locate/poly

Syntheses and crystal structures of a ferrocene-containing enaminone and its copper complex

Yao-Cheng Shi [a,*], Hua-Mei Yang [a], Hai-Bin Song [b], Yong-Hong Liu [a]

[a] School of Chemistry, Yangzhou University, Yangzhou 225002, PR China
[b] State Key Laboratory of Elemento-Organic Chemistry, Nankai University, Tianjin 300071, PR China

Received 28 January 2004; accepted 10 March 2004
Available online 5 May 2004

Abstract

A new ferrocene-containing enaminone [$C_5H_5FeC_5H_4C(O)CH{=}C\text{-}(NHAr)CH_3$] (**HL**, Ar = 2-$CH_3OC_6H_4$) and its copper(II) complex (**I**, L_2Cu) have been synthesized and characterized by elemental analysis, ^{1}H NMR, IR, UV and X-ray crystallography. The enaminone **HL** in the solid state exists as a mixture of two rotation-constrained conformers. Complex **I** is planar in which the enaminone acts as a monoanionic bidentate ligand and both ferrocenyl groups are anti to each other.
© 2004 Elsevier Ltd. All rights reserved.

Keywords: Ferrocene; Enaminone; Ligand; Copper; Complex; X-ray crystallography

1. Introduction

In the last decade non-metallocene complexes of Group IV metals have attracted much interest as possible alternatives for olefin polymerization catalysts using N_4-macrocycles, porphrins, tripodal amides, mixed cyclopentadienyl-amides and Schiff bases as spectator ligands [1–5]. Because the anions [R′C(O)CHC-(NAr)R]$^-$ generated from enaminones [R′C(O)CHC-(HNAr)R] offer potential isoelectronic alternatives to the cyclopentadienyl-based anion and can be used as good chelating ligands for transition metals, enaminones have been extensively investigated [6–8]. However, owing to very few X-ray diffraction studies, so far the structure of the above enaminones has resulted in inconsistencies and remains uncertain [9–11]. So we have initiated a systematic study on organometallic enaminones, and as part of this work we report on the syntheses and crystal structures of a new ferrocenyl enaminone and its copper complex [12–14].

2. Experimental

2.1. Reagents and general procedures

All chemicals used were of reagent grade. Acetylferrocene was synthesized from ferrocene according to the literature method [15]. Ferrocenoylacetone [$C_5H_5FeC_5H_4C(O)CH_2C(O)CH_3$] was synthesized by acylation of acetylferrocene on the substituted cyclopentadienyl ring using ethyl acetate in THF in the presence of sodium ethoxide [12,16]. Progress of the reactions was monitored by TLC. The ^{1}H NMR spectrum was recorded with a Bruker Avance 500 spectrometer using TMS as an external standard in $CDCl_3$. IR spectra were recorded on a Perkin–Elmer 402 as KBr disks in the range of 400–4000 cm^{-1}. UV spectra were measured with a Shimadzu UV-240 spectrometer using a solution in DMF. C, H and N analyses were performed on an Elementa Vario EL III instrument. Melting points were measured on a Yanagimoto apparatus and are uncorrected.

2.2. Synthesis of enaminone

A solution of ferrocenoylacetone (2.7 g, 10 mmol), 2-methoxyaniline (2.44 g, 20 mmol) and a catalytic trace

* Corresponding author. Tel.: +865147857939; fax: +865147857939.
E-mail address: yzssyc@yzcn.net (Y.-C. Shi).

0277-5387/$ - see front matter © 2004 Elsevier Ltd. All rights reserved.
doi:10.1016/j.poly.2004.04.002

Table 1
Crystallographic data for **HL** and **I**

	HL	**I**
Formula	$C_{21}H_{21}FeNO_2$	$C_{42}H_{40}Fe_2N_2O_4Cu$
Formula weight	375.24	812.03
Crystal size (mm)	$0.30 \times 0.20 \times 0.20$	$0.22 \times 0.20 \times 0.18$
Crystal system	monoclinic	monoclinic
Space group	$P2_1/c$	$P2_1/c$
Unit cell dimensions		
a (Å)	25.800(5)	14.07(1)
b (Å)	12.070(2)	12.277(9)
c (Å)	11.520(2)	9.898(7)
α (°)	90.00	90.00
β (°)	95.53(3)	96.83(1)
γ (°)	90.00	90.00
V (Å^3)	3571(1)	1698(2)
Z	4	2
D_{calc} (g cm^{-1})	1.396	1.588
$F(000)$	1568	838
T (K)	293(2)	293(2)
μ(Mo-Kα) (mm^{-1})	0.858	1.512
Scan mode	$\omega - 2\theta$	$\omega - 2\theta$
θ Range (°)	1.59; 24.97	1.46; 2670
Limiting indices	$-30 \leqslant h \leqslant 30; -14 \leqslant k \leqslant 0; 0 \leqslant l \leqslant 13$	$-16 \leqslant h \leqslant 17; -15 \leqslant k \leqslant 15; -11 \leqslant l \leqslant 12$
Absorption correction	ψ-scan	semi-empirical from equivalents
Reflections collected	6611	12,722
Independent reflections [$I > 2.0\sigma(I)$]	6261	3542
Refinement method	full-matrix least-squares on F^2	full-matrix least-squares on F^2
Number of parameters refined	451	234
Final R indices [$I > 2.0\sigma(I)$]	R_1, 0.0699; wR_2, 0.1583	R_1, 0.0491; wR_2, 0.1190
R indices (all data)	R_1, 0.2108; wR_2, 0.2264	R_1, 0.0702; wR_2, 0.1400
Goodness-of-fit	0.931	1.062
Largest difference peak and hole (e Å^{-3})	0.398 and −0.383	0.904 and −1.000

amount of *p*-TsOH (ca. 10 mg) in 20 ml of toluene was refluxed with a Dean–Stark apparatus to remove water for 2 h. The solvent was evaporated under vacuum, and the residue was recrystallized from petroleum ether (60–90 °C) to afford 2.76 g (90%) of **HL** as a red crystalline solid. M.p. 112.5–113 °C. *Anal*. Calc. for $C_{21}H_{21}NFeO_2$: C, 60.82; H, 5.76; N, 2.29. Found: C, 61.07; H, 5.92; N, 2.11%. IR (KBr disk): ν(C=C) and ν(C=O) 1556, 1562, 1598, 1603 (vs), ν(NH) 3091 (s) cm^{-1}. UV (nm, in DMF): λ_{max} ($\varepsilon \times 10^4$) 261 (3.3) (*B*-band); 366 (1.9) (*K*-band). ^{1}H NMR ($CDCl_3$): δ2.10 (s, 3H, CH_3), 3.88 (s, 3H, OCH_3), 4.19 (s, 5H, C_5H_5), 4.39 (pseudo-singlet, 2H, 2 (H^3, H^4) of C_5H_4 ring), 4.79 (pseudo-singlet, 2H, 2 (H^2, H^5) of C_5H_4 ring), 5.50 (s, 1H, CH), 6.89–6.95, 7.12–7.18 (2m, 4H, C_6H_4), 12.40 (s, 1H, NH).

2.3. Synthesis of copper complex

A solution of 1 mmol of the enaminone ligand (**HL**) in absolute ethanol (10 ml) was added dropwise to a stirred solution of 0.5 mmol of copper acetate monohydrate in the same solvent (10 ml). The mixture was stirred for 24 h at room temperature and then filtered to afford the crude product. The resulting solid was recrystallized from CH_2Cl_2 and petroleum ether (60–90 °C) to give the complex **I** as a brown solid, yield: 0.284 g (70%). M.p. 207–208 °C. *Anal*. Calc. for $C_{42}H_{40}N_2O_4Fe_2Cu$: C, 62.12; H, 4.96; N, 3.45. Found: C, 61.74; H, 4.78; N, 3.21%. IR (KBr disk): ν(C=C) 1513 (vs), ν(C=O) 1565 (m) cm^{-1}. UV (nm, in DMF): λ_{max} ($\varepsilon \times 10^4$) 277 (2.07), 360 (3.42) (*K*-band).

2.4. Crystal structure determinations

Single crystals of enaminone **HL** for X-ray analysis were obtained by slow evaporation of its solution in CH_2Cl_2 and petroleum ether at room temperature. Single crystals of complex **I** for structure determination were obtained by petroleum ether (60–90 °C) diffusion into the CH_2Cl_2 solution at 4 °C. X-ray data were collected on an Enraf-Nonius CAD4 diffractometer for enaminone **HL** and a Bruker SMART CCD area detector diffractometer for complex **I** using graphite-monochromated Mo-Kα radiation ($\lambda = 0.71073$ Å) at 293 K. The intensity data were corrected using PSI-scan for enaminone **HL** and Multi-scan for complex **I**. The structure was solved by direct methods and refined by full-matrix least-squares methods based on F^2 with anisotropic thermal parameters for all non-hydrogen atoms. Hydrogen atoms were placed in their calculated

Table 2
Selected bond distances (Å) and angles (°) for **HL**

Isomer **A**		Isomer **B**	
Bond distances			
O(1)–C(11)	1.25(1)	O(4)–C(33)	1.236(9)
O(2)–C(1)	1.43(1)	O(3)–C(23)	1.42(1)
O(2)–C(2)	1.37(1)	O(3)–C(24)	1.36(1)
N(1)–C(7)	1.42(1)	N(2)–C(29)	1.39(1)
N(1)–C(9)	1.34(1)	N(2)–C(30)	1.35(1)
C(2)–C(7)[a]	1.37 (1)	C(24)–C(29)[a]	1.38(1)
C(8)–C(9)	1.48(1)	C(30)–C(31)	1.50(1)
C(9)–C(10)	1.36(1)	C(30)–C(32)	1.37(1)
C(10)–C(11)	1.42(1)	C(32)–C(33)	1.43(1)
C(11)–C(12)	1.50(1)	C(33)–C(34)	1.49(1)
C(12)–C(16) [b]	1.41(1)	C(34)–C(38)[b]	1.41(1)
C(17)–C(21)[b]	1.40(2)	C(39)–C(43)[b]	1.41(1)
Fe(1)–C(12–16)[c]	2.034(9)	Fe(2)–C(34–38)[c]	2.034(8)
Fe(1)–C(17–21)[c]	2.023(9)	Fe(2)–C(39–43)[c]	2.044(8)
Bond angles			
C(1)–O(2)–C(2)	118.6(8)	C(23)–O(3)–C(24)	116.7(8)
C(7)–N(1)–C(9)	126.5(8)	C(29)–N(2)–C(30)	131.1(8)
N(1)–C(9)–C(8)	118.7(8)	N(2)–C(30)–C(31)	119.1(8)
N(1)–C(9)–C(10)	120.3(8)	N(2)–C(30)–C(32)	121.3(8)
C(8)–C(9)–C(10)	120.9(8)	C(31)–C(30)–C(32)	119.5(8)
C(9)–C(10)–C(11)	123.9(8)	C(30)–C(32)–C(33)	124.2(8)
O(1)–C(11)–C(10)	123.9(9)	O(4)–C(33)–C(32)	122.3(8)
O(1)–C(11)–C(12)	116.5(8)	O(4)–C(33)–C(34)	119.4(8)
C(10)–C(11)–C(12)	119.6(8)	C(32)–C(33)–C(34)	118.2(8)

[a] The mean C–C distance in the benzene ring.
[b] The mean C–C distance in the cyclopentadienyl ring.
[c] The average distance of iron to carbon in the ferrocenyl group.

Table 3
Selected bond distances (Å) and angles (°) for **I**

Bond distances			
Cu–O(1)	1.895(3)	C(1)–C(5)[a]	1.394(7)
Cu–N(1)	1.982(3)	C(6)–C(10)[a]	1.410(5)
O(1)–C(11)	1.272(4)	C(10)–C(11)	1.468(5)
O(2)–C(20)	1.344(5)	C(11)–C(12)	1.350(5)
O(2)–C(21)	1.415(6)	C(12)–C(13)	1.399(5)
N(1)–C(13)	1.310(5)	C(13)–C(14)	1.492(6)
N(1)–C(15)	1.426(5)	C(15)–C(20)[b]	1.372(6)
Fe(1)–C(1–5)[c]	2.016(4)		
Fe(1)–C(6–10)[c]	2.018(4)		
Bond angles			
O(1)–Cu–O(1a)[d]	180.000(1)	C(13)–N(1)–Cu	124.5(3)
O(1)–Cu–N(1)	92.1(1)	C(13)–N(1)–C(15)	115.3(3)
O(1a)–Cu–N(1a)	92.1(1)	C(15)–N(1)–Cu(1)	120.2(2)
O(1a)–Cu–N(1)	87.9(1)	O(1)–C(11)–C(10)	115.8(3)
O(1)–Cu–N(1a)	87.9(1)	O(1)–C(11)–C(12)	124.9(3)
N(1)–Cu–N(1a)	180.000(1)	C(20)–O(2)–C(21)	117.3(4)

[a] The mean C–C distance in the cyclopentadienyl ring.
[b] The mean C–C distance in the benzene ring.
[c] The average distance of iron to carbon in the ferrocenyl group.
[d] Symmetry code: $a, -x+1, -y+1, -z+2$.

positions, assigned fixed isotropic thermal parameters and allowed to ride on their respective parent atoms. All computations were carried out using SHELXS-97 and SHELXL-97 Programs [17]. ORTEP views were made with ORTEP-3 for Windows [18]. Details of the data collection and structure refinement parameters are given in Table 1. Selected bond distances (Å) and angles (°) are listed in Table 2 (enaminone **HL**) and 3 (complex **I**).

3. Results and discussion

3.1. Syntheses of enaminone and its complex

Syntheses of the enaminone and its complex are represented in Schemes 1 and 2. Reaction of ferrocenoylacetone $[C_5H_5FeC_5H_4C(O)CH_2C(O)CH_3]$ and 2-methoxyaniline in the presence of a catalytic trace amount of *p*-toluenesulfonic acid in refluxing toluene via removal of water using a Dean–Stark apparatus affords the enaminone **HL** in a yield of 90%. The enaminone **HL** can react with the copper(II) ion forming the neutral complex **I** with the release of HOAc. TLC analysis of the complex **I** shows that it exists as a single isomer, however that of the enaminone also displays one spot on a silica gel plate.

3.2. Spectra of enaminone and its complex

The ligand **HL** in $CDCl_3$ exhibits the unsubstituted cyclopentadienyl ring proton signal at δ4.19 ppm and substituted cyclopentadienyl ring proton signals at δ4.39 ppm (3,4-position) and δ4.79 ppm (2,5-position). The chemical shift at δ5.50 ppm may be due to the CH proton. The methyl protons of the C(O)CHC(NHAr)CH_3 moiety show a singlet at δ2.10 ppm whereas the absorption of the methoxyl group attached to the benzene ring appears as a singlet at δ3.88 ppm. The proton signal of the NH at δ12.40 ppm disappeared upon deuteration. The downfield position of this signal maybe results mainly from the intramolecular hydrogen bonding. Therefore, the above evidence is in accordance with the proposed structure of the ligand shown in Scheme 1 and further supported by its crystal structure [6,8,12]. As described below, although in the solid state the enaminone **HL** exists as a mixture of isomers **A** and **B**, in solution various rotational isomers can change into each other rapidly at room temperature and therefore in

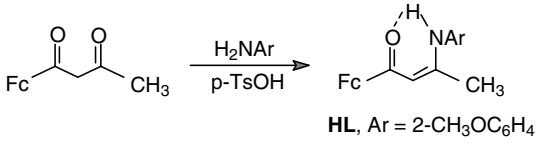

Scheme 1. Synthesis of enaminone **HL**.

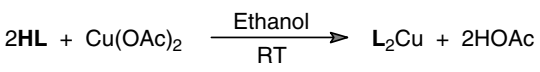

Scheme 2. Synthesis of complex **I**.

its ^{1}H NMR spectrum the enaminone **HL** shows average resonances and the TLC analysis displays one spot as mentioned above.

The complex **I** in its IR spectrum displays significant changes as compared to the ligand. The band at ca. 3080 cm^{-1} in the spectrum of the ligand is due to ν(NH) and does not occur in that of complex **I**. This suggests that the enaminone is coordinated to the copper ion in the monoanionic form. Furthermore, the strong bands assignable to stretching vibrations of the skeleton C=C and C=O groups, which are observed at 1556–1562 and 1598–1603 cm^{-1} in the ligand, are all red-shifted to 1513 and 1565 cm^{-1} in complex **I** [3,8,12]. The spectrum of the ligand in the solid state shows two sets of absorptions of the skeleton C=O and C=C groups and therefore indicates the enaminone **HL** exists as a mixture of two isomers as mentioned above. More interestingly, this has been confirmed by its X-ray crystal structure determination.

In the UV spectra of the enaminone **HL** and complex **I**, the shorter wavelength absorption at 261–277 nm may be assigned to the *B*-band of cyclopentadienyl or benzene rings and the other at 360–366 nm to the *K*-band. The former displays a bathochromic shift whereas the latter shows an inverse shift compared with the free ligand [19]. However, theoretically planar copper complex **I** should exhibit a d–d absorption, in fact, the band of complex **I** is not observed because the weak d–d transition is obscured by other intense absorptions [19,20].

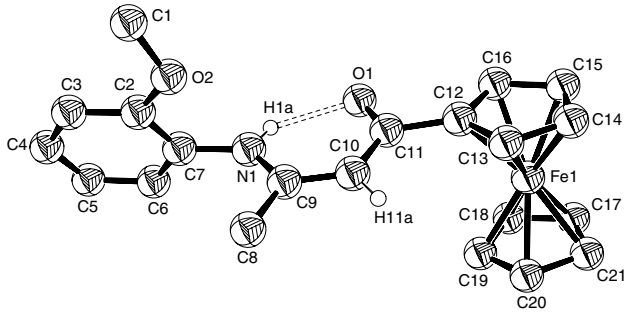

Fig. 1. An ORTEP plot of the isomer **A** in the asymmetric unit of enaminone **HL**. The atoms are drawn with 50% probability ellipsoids.

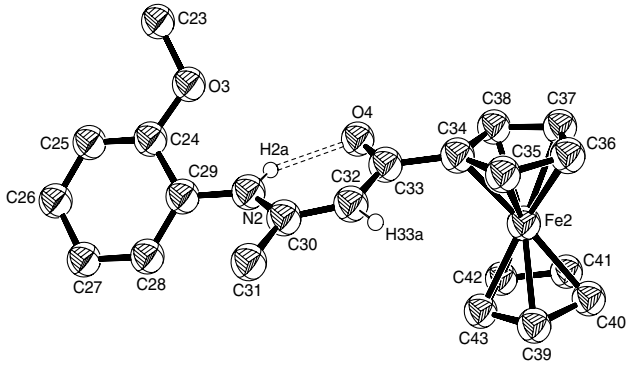

Fig. 2. An ORTEP plot of the isomer **B** in the asymmetric unit of enaminone **HL**. The atoms are drawn with 50% probability ellipsoids.

3.3. Crystal structure of enaminone and its complex

3.3.1. Crystal structure of *HL*

Enaminones with the general formula [R′C(O)CHC(NHAr)R] mentioned above may have the following four isomers: *E*-s-*E*, *E*-s-*Z*, *Z*-s-*E* and *Z*-s-*Z* in which *E* and *Z* refer to two possible geometric arrangements for the carbon–carbon double bond and s-*E* and s-*Z* to both isomerisms about the carbon–carbon single bond between the carbon–carbon and carbon–oxygen double bonds [12,21,22].

The enaminone **HL** crystallizes in the monoclinic space group of $P2_1/c$. In the asymmetric unit are two independent molecules contained, as seen from their ORTEP plots shown in Figs. 1 and 2, the geometry and bonding of them (isomer **A** and isomer **B**) are similar. Main difference results from the different dihedral angles of skeleton O=C–C=C–N and the benzene ring, in other words the different torsion angles of C(6)–C(7)–N(1)–C(9) for isomer **A** and C(24)–C(29)–N(2)–C(30) for isomer **B** (108.29° and 136.24°). Therefore, they belong to conformational isomers which in the solid state are rotation-constrained and the enaminone **HL** exists in the *Z*-s-*Z* form. As indicated by its ^{1}H NMR spectrum and TLC analysis, the two conformers must interconvert so rapidly that they cannot be isolated. Interestingly, the torsion angles C(1)–O(2)–C(2)–C(3) for isomer **A** and C(23)–O(3)–C(24)–C(25) for isomer **B** are −15.20° and 17.93°, indicating the methyl attached to the oxygen atom is not coplanar with the corresponding benzene ring. In order to minimize the steric repulsions, methyl groups attached to oxygen atoms all are bent toward the direction far away from the methyl groups bonded to the skeleton O=C–C=C–N. All atoms in the skeleton O=C–C=C–N can be regarded as sp^2 hybridized. As shown by the comparison of the C=O, C–C, C=C and C–N distances (Table 2) with the corresponding pure double or single bond distances ($C(sp^2)$=O≈1.20, $C(sp^2)$–$C(sp^2)$≈1.48, $C(sp^2)$=$C(sp^2)$≈1.33 and $C(sp^2)$–$N(sp^2)$≈1.44 Å), **HL** exhibits partial delocalization of the O=C–C=C–N system [9,12]. That the H···O distances (1.952 Å for isomer **A** and 1.950 Å for isomer **B**) are significantly shorter than the sum of the van der Waals radii (2.72 Å) indicates the existence of intramolecular hydrogen bonding; this is also in accordance with spectroscopic data [9,23]. The mean C–C distance in the benzene rings is 1.37(1) Å for isomer **A** and 1.38(1) Å for isomer **B**. The mean C–C distances in the cyclopentadienyl rings with and without the side-

chain (1.41(1) and 1.40 (2) Å for isomer **A** and 1.41(1) and 1.41 (1) Å for isomer **B**) are almost equal to the value of 1.41 Å in ferrocene [12]. However, the average distances of iron to carbon in the ferrocenyl group with and without the side-chain (2.034(9) and 2.023(9) Å for isomer **A** and 2.034(8) and 2.044(9) Å for isomer **B**) are slightly shorter than the value of 2.045 Å in ferrocene [12].

3.3.2. Crystal structure of complex *I*

Generally a four-coordinate copper(II) complex may possess eight stereoisomers: planar-*cis*-anti, planar-*cis*-syn, planar-*trans*-anti, planar-*trans*-syn, tetrahedral-*cis*-anti, tetrahedral-*cis*-syn, tetrahedral-*trans*-anti and tetrahedral-*trans*-syn where planar or tetrahedral refers to the coordination geometry of the central metal ion, *cis* or *trans* to isomerism of donor atoms and anti or syn to the two arrangements of both ferrocenyl groups with respect to the mean plane with the central metal ion and donor atoms [12,24,25]. Therefore, to determine its structure, a single-crystal X-ray diffraction analysis on complex **I** was carried out. The molecular structure of complex **I** together with the atomic numbering is shown in Fig. 3. It is worth noting that complex **I** is centrosymmetric. The metal atom displays a planar coordination geometry surrounded by two nitrogen atoms and two oxygen atoms of two deprotonated ligands ($\mathbf{L}^-$), so complex **I** exists only in the planar-*trans*-anti form, which is further supported by the above-described TLC analysis. More interestingly, unlike the complex $[C_5H_5FeC_5H_4C(O)CH{=}C(NC_6H_5)CH_3]_2Cu$, both ferrocenyl groups in complex **I** are anti to each other [12]. In view of the Fe···Fe distance of 10.959 Å, it may be concluded that one ferrocenyl group in complex **I** does not interact sterically with the other and therefore, the anti isomer can be isolated [12,14]. However, up until now the reason that the corresponding syn isomer does not appear is not clear, but doubtless for this, more work needs to be done in the future. As expected, both six-membered chelate rings are planar. In order to decrease the steric strain from the methyl and methoxyl groups, benzene rings are nearly vertical to the above chelate planes (torsion angles of C(13)–N(1)–C(15)–C(16) and Cu(1)–N(1)–C(15)–C(16) are 92.2(5)° and −86.6(4)°). Like the ligand, the torsion angle of C(19)–C(20)–O(2)–C(21) is 4.83°, indicating the methyl group attached to the oxygen atom is not coplanar with the corresponding benzene ring. Angles O(1)–Cu–N(1) and O(1)–Cu–N(1a), which are 92.1(1)° and 87.9(1)(5)°, are slightly smaller than the corresponding values observed in related structures [12,26,27]. Values of angles O(1)–Cu–O(1a) and N(1)–Cu–N(1a) are 180.000(1)° and 180.000(1)°, and therefore, indicate that the coordination geometry about the copper ion is planar as mentioned above [12]. The bonds between the copper atom and the donor sites of the deprotonated ligand (Cu–O(1) = 1.895(3) Å and Cu–N(1) = 1.982(3) Å) are within the range of values normally found for these bonds [26,27]. Unlike the related complex mentioned above, the structural features of two $\mathbf{L}^-$ ions (Table 3) are the same. Each of them exhibits O(1)–C(11), C(11)–C(12), C(12)–C(13) and N(1)–C(13) bond distances of 1.272(4), 1.350(5), 1.399(5) and 1.310(5) Å whereas the corresponding bond distances of **HL** are 1.25(1), 1.42 (1), 1.36(1) and 1.34(1) Å for isomer **A** and 1.236(9), 1.43 (1), 1.37(1) and 1.35(1) Å for isomer **B**. These suggest that the O=C–C=C–N system of complex **I** has more delocalization than that of the free ligand [12]. The mean C–C distance in the benzene rings is 1.372(6) Å and is almost equal to the corresponding distance of **HL**. Similarly, the mean C–C distances in the cyclopentadienyl rings with and without the side-chain are 1.410(5) and 1.394(7) Å, and these are very close to the mean value of 1.41 Å in **HL**. However, the average distances of iron to carbon in the ferrocenyl group with and without the side-chain are 2.018(4) and 2.016(4) Å, and these are shorter than the corresponding distances of **HL** [12].

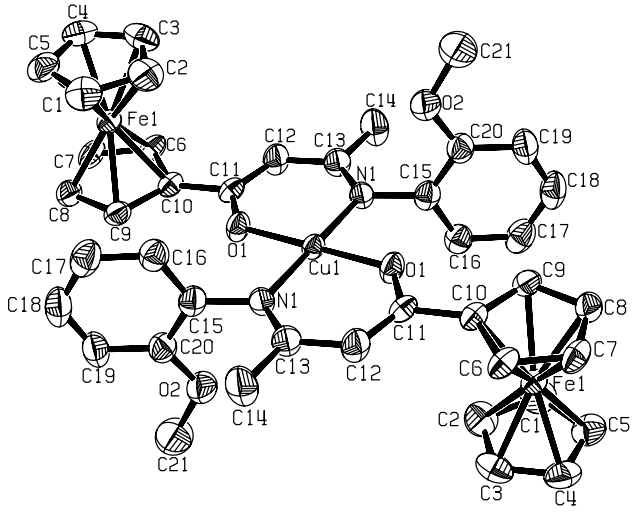

Fig. 3. An ORTEP plot of complex **I**. The atoms are drawn with 50% probability ellipsoids.

4. Conclusion

Reaction of ferrocenoylacetone and *o*-anisidine in the presence of a catalytic amount of *p*-toluenesulfonic acid yields a *Z*-s-*Z* enaminone **HL** $[C_5H_5FeC_5H_4C(O)CH{=}C(NHAr)CH_3]$ (Ar = 2-$CH_3OC_6H_4$). Reaction of enaminone **HL** and copper acetate affords a planar complex **I** in which the enaminone coordinates to the copper ion as a monoanionic bidentate ligand via carbonyl oxygen and enamine nitrogen atoms after deprotonation.

5. Supplementary material

Full crystallographic data (CCDC No. 229432 for enaminone **HL** and CCDC No. 229433 for complex **I**) have been deposited at the Cambridge Crystallographic Database Centre and are available on request from the Director, CCDC, 12 Union Road, Cambridge, CB2 1EZ, UK (fax: +44-1223-336-033; e-mail: deposit@ccdc.cam.ac.uk or http://www.ccdc.cam.ac.uk).

Acknowledgements

Yao-Cheng Shi thanks Yangzhou University (No. D0009107) for financial support of this work.

References

[1] G.J.P. Britovsek, Angew. Chem., Int. Ed. Engl. 38 (1999) 428.
[2] M.J. Bochmann, J. Chem. Soc., Dalton Trans. (1996) 255.
[3] A.A. Osowole, J.A.O. Woods, O.A. Odunola, Synth. React. Inorg. Met.-Org. Chem. 32 (2002) 783.
[4] J. Kim, J.W. Hwang, Y. Kim, M.H. Lee, Y. Han, Y. Do, J. Organomet. Chem. 620 (2001) 1.
[5] S. Doherty, R.J. Errington, N. Housley, J. Ridland, W. Clegg, M.R.J. Elsegood, Organometallics 18 (1999) 1018.
[6] J. Mrosset, C. Floriani, M. Mazzanti, A.C. Villa, C. Guastini, Inorg. Chem. 29 (1990) 3991.
[7] M. Kwiatkowski, A. Olechnowicz, J. Mrozinski, D.M. Ho, E. Deutsch, Inorg. Chim. Acta 158 (1989) 37.
[8] H. Iida, Y. Yuasa, C. Kibayashi, Y. Iitaka, J. Chem. Soc., Dalton Trans. (1981) 2212.
[9] P. Gilli, V. Bertolasi, V. Ferretti, G. Gilli, J. Am. Chem. Soc. 122 (2000) 10405.
[10] L. Kozerski, Tetrahedron 32 (1976) 1299.
[11] G.O. Dudek, G.P. Volpp, J. Am. Chem. Soc. 85 (1963) 2697.
[12] Y.C. Shi, H.M. Yang, W.B. Shen, C.G. Yan, X.Y. Hu, Polyhedron 23 (2004) 15.
[13] Y.C. Shi, H.M. Yang, H.B. Song, C.G. Yan, X.Y. Hu, Polyhedron 23 (2004) 567.
[14] Y.C. Shi, W.B. Shen, H.M. Yang, H.B. Song, X.Y. Hu, Polyhedron 23 (2004) 749.
[15] P.J. Graham, G.W. Parshall, M.L. Peterson, G.M. Whitman, J. Am. Chem. Soc. 79 (1957) 3416.
[16] V. Weinmayr, Naturwiss 45 (1958) 311.
[17] G.M. Sheldrick, SHELXTL 5.01 Software, Bruker Analytical X-ray Systems, Madison, WI, USA, 1996.
[18] L.J. Farrugia, ORTEP-3 for Windows, University of Glasgow, UK, 2003.
[19] Y.C. Shi, Q.B. Song, X.L. Wu, Y.X. Ma, Polyhedron 13 (1994) 2101.
[20] Y.C. Shi, Y.M. Liang, X.L. Wu, Q.B. Song, G.S. Huang, Y.X. Ma, J. Coord. Chem. 33 (1994) 295.
[21] J.V. Greenhill, Chem. Soc. Rev. 6 (1977) 277.
[22] L.F. Tietze, A. Bergmann, G. Brill, K. Brüggemann, U. Hartfiel, E. Voß, Chem. Ber. 122 (1989) 83.
[23] B.E. Douglas, D.H. McDaniel, J.J. Alexander, Concepts and Models of Inorganic Chemistry, Wiley, New York, 1983.
[24] G.E. Gurr, Inorg. Chem. 3 (1964) 614.
[25] R.D. Archer, Inorg. Chem. 2 (1963) 292.
[26] J.P. Costes, J.F. Serra, F. Dahan, J.P. Laurent, Inorg. Chem. 25 (1986) 2790.
[27] M.B. Cingi, A.C. Villa, A.G. Manfredotti, C. Guastini, M. Nardelli, Acta Crystallogr., Sect. B 28 (1972) 1075.

Available online at www.sciencedirect.com
SCIENCE DIRECT®
Polyhedron 23 (2004) 1547–1555
POLYHEDRON
www.elsevier.com/locate/poly

Hydrogen bonding and π–π stacking interaction in the coordination of sulfur and nitrogen donor heterocycle to organotin(IV): syntheses and crystal structures of di- and triorganotin(IV) derivatives with 1-(4-hydroxyphenyl)-1*H*-tetrazole-5-thiol

Chunlin Ma [a,b,*], Jiafeng Sun [a]

[a] *Department of Chemistry, Liaocheng University, Liaocheng 252059, PR China*
[b] *Taishan University, Taian 271021, PR China*

Received 11 February 2004; accepted 10 March 2004
Available online 9 April 2004

Abstract

A series of organotin(IV) complexes with 1-(4-hydroxyphenyl)-1*H*-tetrazole-5-thiol of the type, $R_nSn[S(C_7H_5N_4O)]_{4-n}\cdot L$ ($n=3$, $L=0$: R = Me (**1**), *n*-Bu (**2**), Ph (**3**); $n=3$, $L=0.5C_2H_5OH\cdot 0.5H_2O$, $R=PhCH_2$ (**4**); $n=2$, $L=H_2O$, R = Me (**5**); $n=2$, $L=0$: R = *n*-Bu (**6**), Ph (**7**), $PhCH_2$ (**8**)) have been synthesized. All the complexes **1**–**8** have been characterized by elemental, IR and ^1H NMR analyses. Among them complexes **3**, **4**, **5** and **6** have also been characterized by X-ray crystallography diffraction analyses, which revealed the 1D ribbons of complexes **3** and **5** and the 2D network of complex **6** due to the versatile intermolecular hydrogen bonds O–H···X (X = O, N, S) in the crystallographic structures. Moreover, strong π–π stacking interactions are found in complexes **4** and **5**.
© 2004 Elsevier Ltd. All rights reserved.

Keywords: 1-(4-Hydroxyphenyl)-1H-tetrazole-5-thiol; Organotin(IV); Hydrogen bonding; π–π stacking interaction; Crystal structures; X-ray crystallography

1. Introduction

Increasing investigation of organotin(IV) complexes has been focused on acquiring well-defined solid-state structures to learn the nature of their versatile coordination chemistry [1], especially that of some organotin(IV) derivatives from heterocyclic thionates containing a nitrogen atom (or more) and an adjacent, exocyclic thioketo group [2–4]. In our previous work, we studied the coordination chemistry of two ligands of such kind: 2-mercaptonicotinic acid (Hmnc) and 2,5-dimercapto-1,3,4-thiodiazole (bismuthiol-I), which possess one and two deprotonated heterocyclic thioamide group $(N–C–S)^-$, respectively. The X-ray analyses revealed that the former act as thiol form but the primary bond of the latter to the tin atom varies dramatically according to distinct R of the precursor R_nSnCl_{4-n} [5,6]. These results indicate there are several factors can influence the topologies of the organotin derivatives from heterocyclic thionates such as the special geometries of ligand, the spacial resistant from R, etc. To continue our studies in this field, we choose another fascinating heterocyclic thionate: 1-(4-Hydroxyphenyl)-1*H*-tetrazole-5-thiol, which possesses one –SH and one –OH group, through which primary bonds to tin atoms are likely formed. Moreover, the three potential coordination nitrogen atoms of tetrazole make the ligand act as a fulcrum about which lattice construction is orchestrated in one or more dimensions.

* Corresponding author. Tel.: +866358238121; fax: +866358238274.
E-mail address: macl@lctu.edu.cn (C. Ma).

0277-5387/$ - see front matter © 2004 Elsevier Ltd. All rights reserved.
doi:10.1016/j.poly.2004.03.003

In this paper, we report some details of the syntheses and characterizations of a series of organotin(IV) complexes with the ligand of the type $R_nSn[S(C_7H_5N_4O)]_{4-n}\cdot L$ ($n = 3$, $L = 0$: $R = Me$ (**1**), *n*-Bu (**2**), Ph (**3**); $n = 3$, $L = 0.5C_2H_5OH\cdot 0.5H_2O$, $R = PhCH_2$ (**4**); $n = 2$, $L = H_2O$, $R = Me$ (**5**); $n = 2$, $L = 0$: $R = n$-Bu (**6**), Ph (**7**), $PhCH_2$ (**8**)). X-ray crystallography of complexes **3**, **4**, **5** and **6** show that all the complexes contain the thiol form of the ligand, i.e. the ligand is linked to the organometal moiety primarily through sulfur, resembling as Hmnc and 1-phenyl-1*H*-tetrazole-5-thiol [5,7]. Interestingly, the versatile hydrogen bonding, O–H···X (X = O, N, S), and strong π–π stacking interactions are found.

2. Experimental

2.1. Materials and measurements

Trimethyltin chloride, tri-*n*-butyltin chloride, triphenyltin chloride, dimethyltin dichloride, di-*n*-butyltin dichloride, diphenyltin dichloride and 1-(4-hydroxyphenyl)-1*H*-tetrazole-5-thiol were commercially available, and they were used without further purification. Tribenzyltin chloride and dibenzyltin chloride were prepared by a standard method reported in the literature [8]. The melting points were obtained with Kofler micro melting point apparatus and are uncorrected. Infrared-spectra were recorded on a Nicolet-460 spectrophotometer using KBr disks and sodium chloride optics. ^{1}H NMR spectra were obtained on a JEOL-FX-90Q spectrometer, chemical shifts were given in ppm relative to Me_4Si in $CDCl_3$ solvent. Elemental analyses were performed with a PE-2400II apparatus.

2.2. Syntheses of the complexes **1**–**8**

2.2.1. $Me_3Sn[S(C_7H_5N_4O)]$ (**1**)

The reaction was carried out under nitrogen atmosphere. The 1-(4-hydroxyphenyl)-1*H*-tetrazole-5-thiol (0.194 g, 1 mmol) was added to the solution of ethanol 20 ml with sodium ethoxide (0.068 g, 1 mmol), and the mixture was stirred for 10 min, then add Me_3SnCl (0.199 g, 1 mmol) to the mixture, continuing the reaction for 12 h at 45 °C. After cooling down to the room temperature, the solution was filtered. The solvent of the filtrate was gradually removed by evaporation under vacuum until solid product was obtained. The solid was then recrystallized from ether. White crystal was formed. Yield, 65%. m.p. 118–120 °C. *Anal*. Calc. for $C_{10}H_{14}N_4OSSn$: C, 33.64; H, 3.95; N, 15.69. Found: C, 33.68; H, 3.95; N, 15.70%. ^{1}H NMR (90 MHz, $CDCl_3$): δ 7.23–7.38 (m, 4H,C_6H_4–N), 0.75 (s, 9H, Sn–CH_3) ppm. IR (KBr, cm^{-1}): ν(C=N) 1600, $\nu(Sn–C)_{as}$ 536, $\nu(Sn–C)_s$ 504, ν(Sn–S) 312.

2.2.2. $(n\text{-}Bu)_3Sn[S(C_7H_5N_4O)]$ (**2**)

The synthesis procedure was the same as **1**. 1-(4-Hydroxyphenyl)-1*H*-tetrazole-5-thiol (0.194 g, 1 mmol), sodium ethoxide (0.068 g, 1 mmol) and (n-Bu)$_3$SnCl (0.326 g, 1 mmol), reaction time 12 h, temperature 45 °C. Recrystallized from ether–petroleum. White crystal was formed. Yield, 74%. m.p. 67–69 °C. *Anal*. Calc. for $C_{19}H_{32}N_4OSSn$: C, 47.22; H, 6.67; N, 11.59. Found: C, 47.26; H, 6.57; N, 11.70%. ^{1}H NMR (90 MHz, $CDCl_3$): δ 7.25–7.38 (m, 4H,C_6H_4–N), 0.84–1.71 (m, 27H, Sn–C_4H_9) ppm. IR (KBr, cm^{-1}): ν(C=N) 1601, $\nu(Sn–C)_{as}$ 445, $\nu(Sn–C)_s$ 425, ν(Sn–S) 309.

2.2.3. $Ph_3Sn[S(C_7H_5N_4O)]$ (**3**)

The synthesis procedure was the same as **1**. 1-(4-Hydroxyphenyl)-1*H*-tetrazole-5-thiol (0.194 g, 1 mmol), sodium ethoxide (0.068 g, 1 mmol) and Ph_3SnCl (0.385 g, 1 mmol), reaction time 12 h, temperature 45 °C. Recrystallized from hexane-dichloromethane. White crystal was formed. Yield, 72%. m.p. 184–186 °C. *Anal*. Calc. for $C_{25}H_{20}N_4OSSn$: C, 55.27; H, 3.71; N, 10.31. Found: C, 55.31; H, 3.76; N, 10.32%. ^{1}H NMR (90 MHz, $CDCl_3$): δ 7.18–7.37 (m, 4H,C_6H_4–N), 7.46–7.79 (m, 15H, Sn–C_6H_5) ppm. IR (KBr, cm^{-1}): ν(C=N) 1599, $\nu(Sn–C)_{as}$ 444, $\nu(Sn–C)_s$ 409, ν(Sn–S) 310.

2.2.4. $(PhCH_2)_3Sn[S(C_7H_5N_4O)]\cdot 0.5C_2H_5OH\cdot 0.5H_2O$ (**4**)

The synthesis procedure was the same as **1**. 1-(4-Hydroxyphenyl)-1*H*-tetrazole-5-thiol (0.194 g, 1 mmol), sodium ethoxide (0.068 g, 1 mmol) and $(PhCH_2)_3SnCl$ (0.427 g, 1 mmol), reaction time 12 h, temperature 45 °C. Recrystallized from dichloromethane. White crystal was formed. The crystal suitable for X-ray diffraction was grown from ethanol (95%). Yield, 78%. m.p. 124–126 °C. *Anal*. Calc. for $C_{29}H_{30}N_4O_2SSn$: C, 56.42; H, 4.90; N, 9.08. Found: C, 56.47; H, 4.86; N, 9.14%. ^{1}H NMR (90 MHz, $CDCl_3$): δ 7.30 (m, 4H,C_6H_4–N), 6.88–7.15 (m, 15H, Sn–$CH_2C_6H_5$), 3.74 (m, 1H, CH_3CH_2-OH), 2.78 (s, 6H, Sn–$CH_2C_6H_5$), 1.25 (t, 1.5H, CH_3CH_2 OH) ppm. IR (KBr, cm^{-1}): ν(C=N) 1599, $\nu(Sn–C)_{as}$ 450, $\nu(Sn–C)_s$ 427, ν(Sn–S) 309.

2.2.5. $Me_2Sn[S(C_7H_5N_4O)]_2\cdot H_2O$ (**5**)

The synthesis procedure was the same as **1**. 1-(4-Hydroxyphenyl)-1*H*-tetrazole-5-thiol (0.388 g, 2 mmol), sodium ethoxide (0.136 g, 2 mmol) and Me_2SnCl_2 (0.220 g, 1 mmol), reaction time 12 h, temperature 45 °C. Recrystallized from ether–petroleum. White crystal was formed. The crystal suitable for X-ray diffraction was grown from ethanol (95%). Yield, 70%. m.p. 126–128 °C. *Anal*. Calc. for $C_{16}H_{18}N_8O_3S_2Sn$: C, 34.74; H, 3.28; N, 20.26. Found: C, 34.84; H, 3.23; N, 20.07%. ^{1}H

NMR (90 MHz, $CDCl_3$): δ 7.26–7.40 (m, 8H,C_6H_4–N), 1.42 (s, 6H, Sn–CH_3) ppm. IR (KBr, cm^{-1}): ν(C=N) 1600, $\nu(Sn–C)_{as}$ 476, $\nu(Sn–C)_s$ 450, ν(Sn–S) 310.

*2.2.6. (n-Bu)$_2$Sn[S(C$_7$H$_5$N$_4$O)]$_2$ (**6**)*

The synthesis procedure was the same as **1**. 1-(4-Hydroxyphenyl)-1*H*-tetrazole-5-thiol (0.388 g, 2 mmol), sodium ethoxide (0.136 g, 2 mmol) and $(n\text{-}Bu)_2SnCl_2$ (0.304 g, 1 mmol), reaction time 12 h, temperature 45 °C. Recrystallized from ether–petroleum. White crystal was formed. Yield, 76%. m.p. 128–130 °C. *Anal*. Calc. for $C_{22}H_{28}N_8O_2S_2Sn$: C, 42.66; H, 4.56; N, 18.09. Found: C, 42.75; H, 4.49; N, 18.20%. ^{1}H NMR (90 MHz, $CDCl_3$): δ 7.20–7.37 (m, 8H,C_6H_4–N), 0.86–2.12 (m, 18H, Sn–C_4H_9) ppm. IR (KBr, cm^{-1}): ν(C=N) 1600, $\nu(Sn–C)_{as}$ 441, $\nu(Sn–C)_s$ 425, ν(Sn–S) 315.

*2.2.7. Ph$_2$Sn[S(C$_7$H$_5$N$_4$O)]$_2$ (**7**)*

The synthesis procedure was the same as **1**. 1-(4-Hydroxyphenyl)-1*H*-tetrazole-5-thiol (0.388 g, 2 mmol), sodium ethoxide (0.136 g, 2 mmol) and Ph_2SnCl_2 (0.344 g, 1 mmol), reaction time 12 h, temperature 50 °C. Recrystallized from ether–petroleum. White crystal was formed. Yield, 67%. m.p. 168–170 °C. *Anal*. Calc. for $C_{26}H_{20}N_8O_2S_2Sn$: C, 47.36; H, 3.06; N, 17.00. Found: C, 47.48; H, 2.91; N, 17.12%. ^{1}H NMR (90 MHz, $CDCl_3$): δ 7.20–7.33 (m, 8H,C_6H_4–N), 7.46–7.79 (m, 10H, Sn–C_6H_5) ppm. IR (KBr, cm^{-1}): ν(C=N) 1601, $\nu(Sn–C)_{as}$ 444, $\nu(Sn–C)_s$ 415, ν(Sn–S) 309.

*2.2.8. (PhCH$_2$)$_2$Sn[S(C$_7$H$_5$N$_4$O)]$_2$ (**8**)*

The synthesis procedure was the same as **1**. 1-(4-Hydroxyphenyl)-1*H*-tetrazole-5-thiol (0.388 g, 2 mmol), sodium ethoxide (0.136 g, 2 mmol) and $(PhCH_2)_2SnCl_2$ (0.372 g, 1 mmol), reaction time 12 h, temperature 45 °C. Recrystallized from ether–petroleum. White crystal was formed. Yield, 79%. m.p. 112–114 °C. *Anal*. Calc. for $C_{28}H_{24}N_8O_2S_2Sn$: C, 48.92; H, 3.52; N, 16.30. Found: C, 49.02; H, 3.59; N, 16.39%. ^{1}H NMR (90 MHz, $CDCl_3$): δ 7.17–7.42 (m, 8H, C_6H_4–N), 6.82–7.05 (m, 10H, Sn–$CH_2C_6H_5$), 3.52 (s, 4H, Sn–$CH_2C_6H_5$) ppm. IR (KBr, cm^{-1}): ν(C=N) 1600, $\nu(Sn–C)_{as}$ 440, $\nu(Sn–C)_s$ 421, ν(Sn–S) 310.

2.3. X-ray crystallographic studies of complexes **3**, **4**, **5** and **6**

Crystals were mounted in Lindemann capillaries under nitrogen. All X-ray crystallographic data were collected on a Bruker SMART CCD 1000 diffractometer with graphite monochromated Mo Kα radiation ($\lambda = 0.71073$ Å) at 298(2) K. A semi-empirical absorption correction was applied to the data. The structure was solved by direct methods using SHELXL-97 and refined against F^2 by full-matrix least-squares using SHELXL-97. Hydrogen atoms were placed in calculated positions. Crystal data and experimental details of the structure determinations are listed in Table 1.

Table 1
Crystal data and structure refinement parameters for complex **3**, **4**, **5** and **6**

Complexes	**3**	**4**	**5**	**6**
Empirical formula	$C_{25}H_{20}N_4OSSn$	$C_{29}H_{30}N_4O_2SSn$	$C_{16}H_{18}N_8O_3S_2Sn$	$C_{22}H_{28}N_8O_2S_2Sn$
Formula weight	543.20	617.32	553.19	619.33
Crystal system	triclinic	triclinic	orthorhombic	monoclinic
Space group	$P\bar{1}a$	$P\bar{1}$	*Pnma*	$P2_1/n$
Unit cell dimensions				
a (Å)	9.517(5)	10.533(5)	7.223(13)	14.964(12)
b (Å)	14.348(8)	12.313(6)	22.09(4)	9.548(8)
c (Å)	18.953(11)	24.147(11)	16.76(3)	20.233(16)
α (°)	107.796(8)	86.956(6)	90	90
β (°)	100.726(8)	88.200(7)	90	111.703(9)
γ (°)	102.442(8)	71.827(6)	90	90
V (Å^3)	2316(2)	2971(2)	2674(8)	2686(4)
Z	4	4	4	4
D_c (Mg m^{-3})	1.558	1.380	1.374	1.532
Absorption coefficient (mm^{-1})	1.218	0.961	1.140	1.142
$F(000)$	1088	1256	1104	1256
Crystal size (mm)	$0.32 \times 0.15 \times 0.11$	$0.55 \times 0.33 \times 0.25$	$0.29 \times 0.23 \times 0.16$	$0.41 \times 0.35 \times 0.09$
θ range (°)	1.56–25.03	1.69–25.03	1.84–25.02	2.39–25.02
Independent reflections	8093 ($R_{int} = 0.0281$)	10345 ($R_{int} = 0.0254$)	2323 ($R_{int} = 0.1932$)	4652 ($R_{int} = 0.0462$)
Data/restraints/parameters	8093/0/577	10345/5/675	2323/3/147	4652/0/316
Goodness-of-fit on F^2	0.925	1.063	0.904	0.956
Final R indices [$I > 2\sigma(I)$]	$R_1 = 0.0408$, $wR_2 = 0.0937$	$R_1 = 0.0413$, $wR_2 = 0.0981$	$R_1 = 0.0706$, $wR_2 = 0.1319$	$R_1 = 0.0537$, $wR_2 = 0.1317$
R indices (all data)	$R_1 = 0.0704$, $wR_2 = 0.1143$	$R_1 = 0.0662$, $wR_2 = 0.1139$	$R_1 = 0.1526$, $wR_2 = 0.1563$	$R_1 = 0.0838$, $wR_2 = 0.1492$

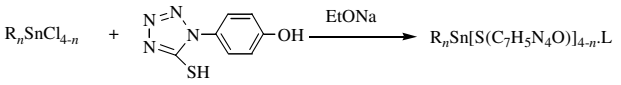

(n = 3, L = 0: R = Me **1**, n-Bu **2**, Ph **3**; n = 3, L = 0.5C_2H_5OH 0.5H_2O, R = $PhCH_2$ **4**; n = 2, L = H_2O, R = Me **5**; n = 2, L = 0: R = n-Bu **6**, Ph **7**, $PhCH_2$ **8**)

Scheme 1.

3. Results and discussion

3.1. Syntheses of the complexes *1–8*

The synthesis procedure is given in Scheme 1.

3.2. IR spectroscopic studies of the complexes *1–8*

The explicit feature in the IR spectra of the eight complexes **1–8** is the absence of the band in the region 2550–2430 cm^{-1}, which appears in the free ligand as the ν(S–H) vibration, thus indicating metal–ligand bond formation through this site. In the far-IR spectra, the absorption about 310 cm^{-1} region for all complexes **1–8**, which is absent in the spectrum of the ligand, is assigned to the Sn–S stretching mode of the vibration and all the values are located within the range for Sn–S vibration observed in common organotin derivatives of thiolate (300–400 cm^{-1}) [9,10]. In organotin compounds, the IR spectra can provide useful information concerning the geometry of the SnC_n moiety [11]. In the case of our compounds, for both di- and triorganotin(IV) derivatives, two bands were assigned to asymmetric and symmetric Sn–C vibrations. Thus suggesting nonlinear SnC_2 units for diorganotins and non-planar SnC_3 fragments for triorganotins, respectively. The middle intensity bands observed at about 1600 cm^{-1} in the spectra of all complexes have been assignable to ν(C=N) according to literatures [12,13], which suggested the coordinates of free ligand to these complexes is through sulfur atoms via thiol form.

3.3. ^1H NMR data of the complexes *1–8*

^1H NMR data showed that the signal of the –SH proton in the spectrum of the ligand is absent in all of the complexes, indicating the removal of the –SH proton and the formation of Sn–S bonds. The formation accords well with what the IR data have revealed. Moreover, the ^1H NMR spectra show that the chemical shifts of the phenyl group (Sn–C_6H_5) in complexes **3** and **7**, 7.46–7.79 ppm, and those of methylene connected directly with tin in complexes **2**, **4**, **6** and **8**, 1.71–3.52 ppm, upfield shift as compared with those of their corresponding precursors. All these data are similar to those cases appear in literature [14], indicating there may exist novel coordination of the ligand to tin atom for all the eight complexes **1–8**. In addition, the resonance of the phenyl group connected with nitrogen atom and hydroxyl group (N–C_6H_4–OH) appears at 7.17–7.42 ppm for all complexes **1–8**.

3.4. Crystal structures of complexes *3, 4, 5* and *6*

3.4.1. $Ph_3Sn[S(C_7H_5N_4O)]$ (*3*)

For complex **3**, the asymmetric unit contains two monomers A and B (Fig. 1), which are crystallographically nonequivalent. The conformations of the two independent molecules A and B are almost the same, with only small differences in bond lengths and bond angles (see Table 2). The compound is formed by discrete molecules in which the tin atom is indeed bound to the sulfur atom of the tetrazolate, which together with the phenyl groups defines a distorted tetrahedron around

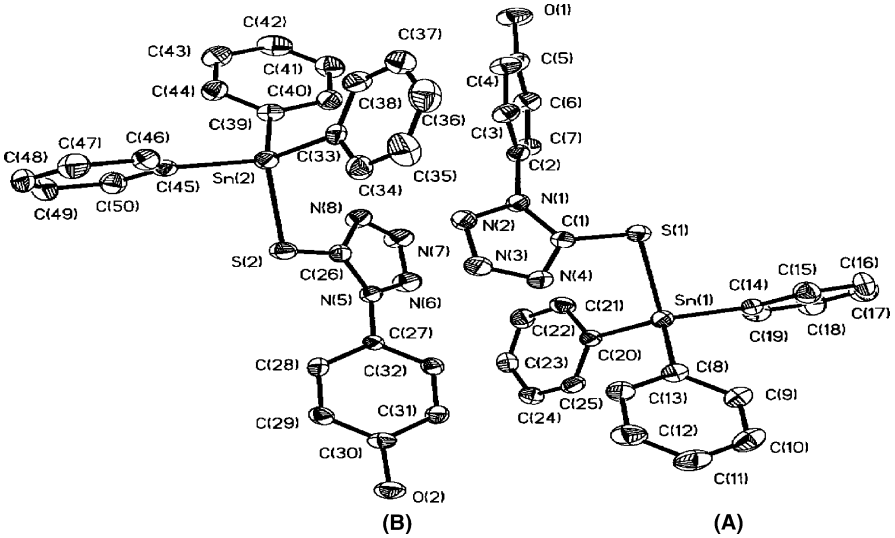

Fig. 1. Molecular structure of the complex **3**.

Table 2
Selected bond lengths (Å) and bond angles (°) for complex **3**

Molecule A		Molecule B	
Bond lengths			
Sn(1)–C(8)	2.128(6)	Sn(2)–C(39)	2.122(6)
Sn(1)–C(20)	2.136(6)	Sn(2)–C(45)	2.129(5)
Sn(1)–C(14)	2.152(5)	Sn(2)–C(33)	2.138(6)
Sn(1)–S(1)	2.4760(17)	Sn(2)–S(2)	2.4726(17)
Sn(1)···N(4)	3.330(6)	Sn(2)···N(8)	3.487(6)
N(4)–C(1)	1.313(7)	N(8)–C(26)	1.315(7)
S(1)–C(1)	1.740(5)	S(2)–C(26)	1.727(6)
Bond angles			
C(8)–Sn(1)–C(20)	112.4(2)	C(39)–Sn(2)–C(45)	112.1(2)
C(8)–Sn(1)–C(14)	110.1(2)	C(45)–Sn(2)–C(33)	110.3(2)
C(20)–Sn(1)–C(14)	111.9(2)	C(39)–Sn(2)–C(33)	111.2(2)
C(8)–Sn(1)–S(1)	119.28(15)	C(39)–Sn(2)–S(2)	119.55(15)
C(20)–Sn(1)–S(1)	104.81(15)	C(33)–Sn(2)–S(2)	108.24(16)
C(14)–Sn(1)–S(1)	97.31(15)	C(45)–Sn(2)–S(2)	94.07(14)
C(1)–S(1)–Sn(1)	99.83(18)	C(26)-S(2)–Sn(2)	105.8(2)
N(4)–C(1)–S(1)	126.9(4)	N(8)–C(26)–S(2)	126.9(4)

the tin atom. There is also an intramolecular tin–nitrogen short contact (Sn(1)···N(4) 3.330(6) Å for A and Sn(2)···N(8) 3.487(6) Å for B), shorter than the sum of the van der Waals radii (3.75 Å) [15]. The C–Sn–C bond angles are close to the theoretical tetrahedral angle but the C–Sn–S bond angles more acute or obtuse than it, largest deviations occurring in C(8)–Sn(1)–S(1) 119.28(15)° for A and C(39)–Sn(2)–S(2) 119.55(15)° for B; C(14)–Sn(1)–S(1) 97.31(15)° for A and C(45)–Sn(2)–S(2) 94.07(14)° for B. This is possibly due to the secondary interaction (Sn(1)···N(4) for A and Sn(2)···N(8) for B). The Sn–S bond length (Sn(1)–S(1) 2.4760(17) Å for A and Sn(2)–S(2) 2.4726(17) Å for B) lies toward the middle of the range reported for triphenyltin heteroarenethiolates (2.405–2.481 Å) [16,17] and approach the sum of the covalent radii of tin and sulfur (2.42 Å) [18]. In the tetrazolate, the C–S bond distance (C(1)–S(1) 1.740(5) Å for A and C(26)–S(2) 1.727(6) Å for B) lies between the average value for the double C=S bond in thioureas (1.681 Å) and the single C–S bond in the C–S–Me fragment (1.789 Å) [19], suggesting that the C–S bond has some double-bond character in the deprotonated tetrazole.

Moreover, the discrete molecules of complex **3** associate in a 1D ribbon by hydrogen bonds (O(1)–H(1)···N(3) 2.911 Å, O(1)–H(1)–N(3) 157.88° for A; O(2)–H(2)···N(7) 2.857 Å, O(1)–H(1)–N(3) 148.77° for B). A view of the extended ribbon is shown in Fig. 2.

3.4.2. $(PhCH_2)_3Sn[S(C_7H_5N_4O)]\cdot 0.5C_2H_5OH\cdot 0.5H_2O$ (**4**)

The X-ray diffraction investigation of complex **4** has shown two independent molecules in the unit cell, which are alternatively associated in a polymeric chain through intermolecular dative N → Sn bonds. The differences in the bond lengths and angles within the two molecules might be the result of packing effects in the crystal. The molecular structure of complex **4** is shown in Fig. 3. Selected bond lengths and angels are listed in Table 3.

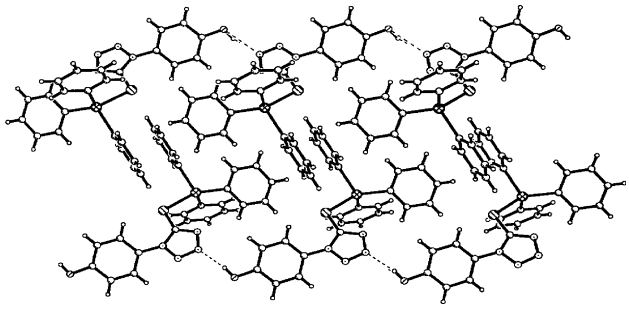

Fig. 2. perspective view showing the 1D ribbon of the complex **3**.

In the monomeric units the tetrazolethiolato ligand is primarily coordinated through the sulfur atom: Sn(1)–S(1) 2.5812(14) Å, Sn(2)–S(2) 2.6260(15) Å. They are slightly longer than the sum of the covalent radii (2.42 Å) [18]. This is consistent with the thiol form of the ligand in the previously reported molecular structure of Bz_3SnSCN_4Ph [7c], and in contrast to the primary coordination suggested on the basis of IR data. It is similar to the complex **3**, there are also secondary intramolecular tin–nitrogen short contacts (Sn(1)···N(4) 3.289(4) Å and Sn(2)···N(8) 3.311(4) Å), shorter than the sum of the van der Waals radii (3.75 Å) [15]. In the crystal, the molecules of complex **3** associated in polymeric chains through intermolecular, dative tin–nitrogen bonds (Sn(1)–N(7A) 2.604(4) Å and Sn(2)–N(3) 2.557(4) Å). This leads to an increase in the tin coordination number to 5. The coordination polyhedron around the central tin atom can be described as distorted trigonal bipyramidal. The methylene carbons are in equatorial positions and the axial ones are occupied by the sulfur atom of the ligand and a nitrogen atom of a neighboring molecule, respectively.

The component $(PhCH_2)_3Sn[S(C_7H_5N_4O)]$ crystallizes with 0.5 molecules of ethanol and 0.5 molecules of water while the water molecule shows no short contacts, the ethanol is involved in two hydrogen bonds, both as a donor (O(3)–H(3A)···O(2) 2.735 Å, O(3)–H(3A)–O(2) 169.33°) and as an acceptor (O(2)–H(33)···O(3) 2.735 Å, O(2)–H(33)–O(3) 168.41°). Moreover, the polymeric chain in the unit cell associates in a dimeric form with another chain through the O(1)–H(5)···S(1) (O(1)···S(1) 3.338 Å, O(1)–H(5)–S(1) 155.93°) hydrogen bond. The crystal structure of **4** shows ring-stacking interactions, each hydroxyphenyl group involved O–H···S hydrogen bond is arrange face-to-face at a distance of 3.744 Å and shows significant π–π stacking interactions, as reported in the literatures [20]. A view of the unit cell of **4** showing hydrogen bonds and π–π stacking interactions is given in Fig. 4.

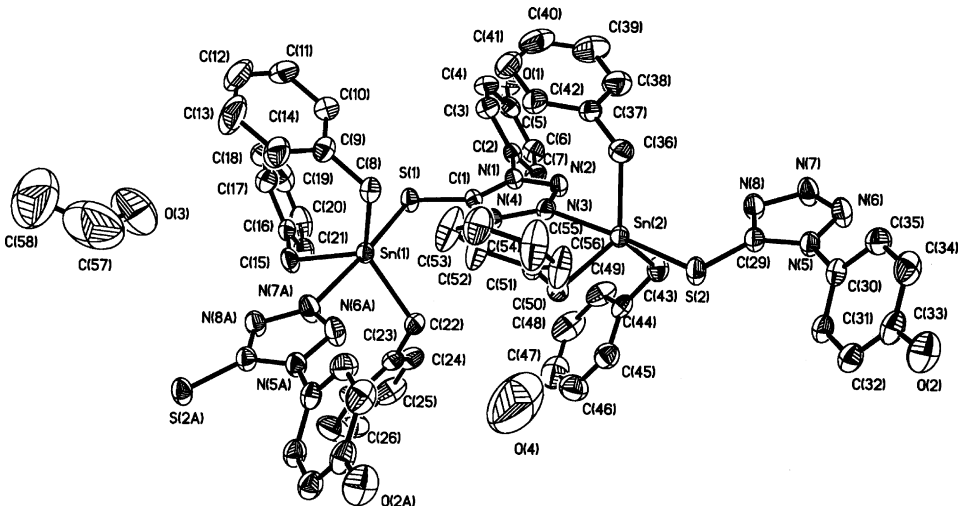

Fig. 3. Molecular structure of the complex **4**.

Table 3
Selected bond lengths (Å) and bond angles (°) for complex **4**

Intramolecular			
Bond lengths			
Sn(1)–C(8)	2.144(5)	Sn(2)–C(36)	2.154(5)
Sn(1)–C(15)	2.149(4)	Sn(2)–C(43)	2.159(5)
Sn(1)–C(22)	2.166(5)	Sn(2)–C(50)	2.163(5)
Sn(1)–S(1)	2.5812(14)	Sn(2)–S(2)	2.6260(15)
Sn(1)···N(4)	3.289(4)	Sn(2)···N(8)	3.311(4)
N(4)–C(1)	1.326(5)	N(8)–C(29)	1.327(6)
S(1)–C(1)	1.729(4)	S(2)–C(29)	1.706(5)
Bond angles			
C(8)–Sn(1)–C(15)	116.3(2)	C(36)–Sn(2)–C(43)	127.6(2)
C(8)–Sn(1)–C(22)	124.16(19)	C(36)–Sn(2)–C(50)	116.0(2)
C(15)–Sn(1)–C(22)	114.9(2)	C(43)–Sn(2)–C(50)	115.2(2)
C(8)–Sn(1)–S(1)	96.32(15)	C(36)–Sn(2)–S(2)	94.09(14)
C(15)–Sn(1)–S(1)	95.73(14)	C(43)–Sn(2)–S(2)	97.19(15)
C(22)–Sn(1)–S(1)	99.43(14)	C(50)–Sn(2)–S(2)	89.04(14)
C(1)–S(1)–Sn(1)	98.41(15)	C(29)–S(2)–Sn(2)	100.00(16)
N(4)–C(1)–S(1)	128.0(3)	N(8)–C(29)–S(2)	126.1(4)
Intermolecular			
Bond lengths			
Sn(1)–N(7A)	2.604(4)	Sn(2)–N(3)	2.557(4)
Bond angles			
N(7A)–Sn(1)–C(8)	85.04(18)	N(3)–Sn(2)–C(36)	87.85(17)
N(7A)–Sn(1)–C(15)	80.05(17)	N(3)–Sn(2)–C(43)	83.69(17)
N(7A)–Sn(1)–C(22)	83.06(17)	N(3)–Sn(2)–C(50)	87.72(16)
N(7A)–Sn(1)–S(1)	175.73(10)	N(3)–Sn(2)–S(2)	176.71(9)

*3.4.3. $Me_2Sn[S(C_7H_5N_4O)]_2 \cdot H_2O$ (**5**) and $(n\text{-}Bu)_2Sn[S(C_7H_5N_4O)]_2$ (**6**)*

Selected bond lengths and bond angles for **5** and **6** are given in Tables 4 and 5, respectively. The molecular structures of **5** and **6** are shown in Figs. 5 and 6. In contrast with the triorganotin derivatives mentioned above, the coordination of diorganotin derivatives is different. In both complexes **5** and **6**, the tin atom establishes covalent bonds with the two heterocyclic sulfur atoms, apart from the two methyl or methylene carbons, and interacts intramolecularly with the unsubstituted nitrogen atoms of the ring thioamide moiety (N(4), N(4A) for **5** and N(4), N(8) for **6**). The Sn–C bond lengths (2.050(15) and 2.111(14) Å in **5**; 2.134(6) and 2.150(7) Å in **6**) are quite close to those previously described in the literature [6]. The Sn–S bond distances (2.505(4) Å in **5**; 2.4740(19) and 2.4716(19) Å in **6**) are very close to the sum of the corresponding covalent radii

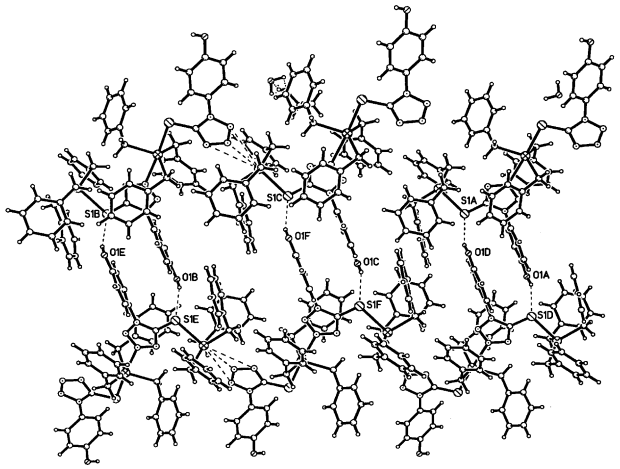

Fig. 4. Packing diagram of complex **4**, showing hydrogen bonds and π–π stacking interactions.

Table 4
Selected bond lengths (Å) and bond angles (°) for complex **5**

Bond lengths			
Sn(1)–C(9)	2.050(15)	Sn(1)–N(4)	2.704(8)
Sn(1)–C(8)	2.111(14)	N(4)–C(1)	1.287(10)
Sn(1)–S(1)	2.505(4)	S(1)–C(1)	1.724(9)
Bond angles			
C(9)–Sn(1)–C(8)	134.8(6)	S(1A)–Sn(1)–N(4)	151.95(16)
C(9)–Sn(1)–S(1)	103.6(3)	S(1)–Sn(1)–N(4)	60.59(18)
C(8)–Sn(1)–S(1)	107.5(3)	C(1)–N(4)–Sn(1)	89.9(5)
S(1A)–Sn(1)–S(1)	91.50(17)	C(1)–S(1)–Sn(1)	88.1(3)
C(9)–Sn(1)–N(4)	87.0(2)	N(4)–C(1)–S(1)	121.3(6)
C(8)–Sn(1)–N(4)	80.72(19)		

Table 5
Selected bond lengths (Å) and bond angles (°) for complex **6**

Bond lengths			
Sn(1)–C(15)	2.134(6)	Sn(1)–N(8)	3.175(5)
Sn(1)–C(19)	2.150(7)	N(4)–C(1)	1.324(6)
Sn(1)–S(2)	2.4716(19)	N(8)–C(8)	1.318(6)
Sn(1)–S(1)	2.4740(19)	S(1)–C(1)	1.732(5)
Sn(1)–N(4)	3.154(5)	S(2)–C(8)	1.743(5)
Bond angles			
C(15)–Sn(1)–C(19)	129.2(3)	C(19)–Sn(1)–N(8)	92.63(17)
C(15)–Sn(1)–S(2)	108.55(17)	S(2)–Sn(1)–N(8)	56.27(9)
C(19)–Sn(1)–S(2)	109.64(17)	S(1)–Sn(1)–N(8)	140.61(8)
C(15)–Sn(1)–S(1)	107.78(18)	N(4)–Sn(1)–N(8)	161.87(11)
C(19)–Sn(1)–S(1)	107.83(17)	C(1)–N(4)–Sn(1)	79.3(3)
S(2)–Sn(1)–S(1)	84.87(8)	C(8)–N(8)–Sn(1)	79.7(3)
C(15)–Sn(1)–N(4)	86.88(17)	N(4)–C(1)–S(1)	96.92(17)
C(19)–Sn(1)–N(4)	83.52(17)	C(8)–S(2)–Sn(1)	97.88(17)
S(2)–Sn(1)–N(4)	141.56(8)	N(4)–C(1)–S(1)	126.9(4)
S(1)–Sn(1)–N(4)	56.73(9)	N(8)–C(8)–S(2)	126.0(4)
C(15)–Sn(1)–N(8)	81.85(17)		

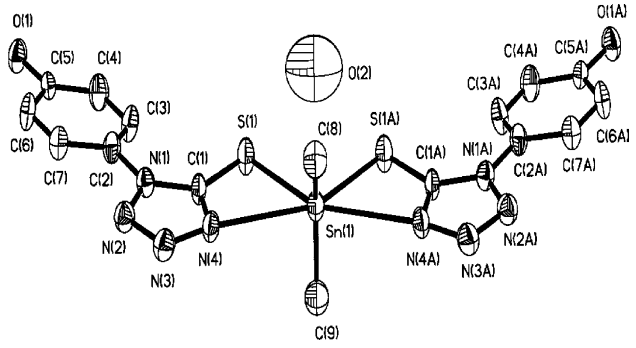

Fig. 5. Molecular structure of the complex **5**.

(2.42 Å) [18], and is similar to the distances found in other Sn(IV) complexes of the terazolethiolato with metal–sulfur primary bonds, viz. 2.474(3)–2.614(5) Å. It is worth noting that in complex **5** the Sn–N bond length is shorten (2.704(8) Å) than those reported in analogous diorganotin derivatives of 1-phenyl-1*H*-tetrazole-5-

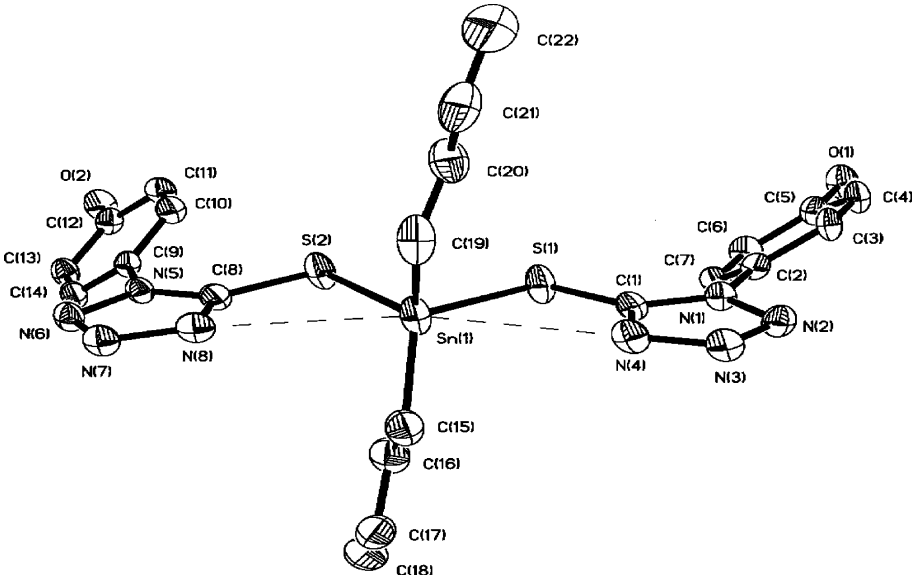

Fig. 6. Molecular structure of the complex **6**.

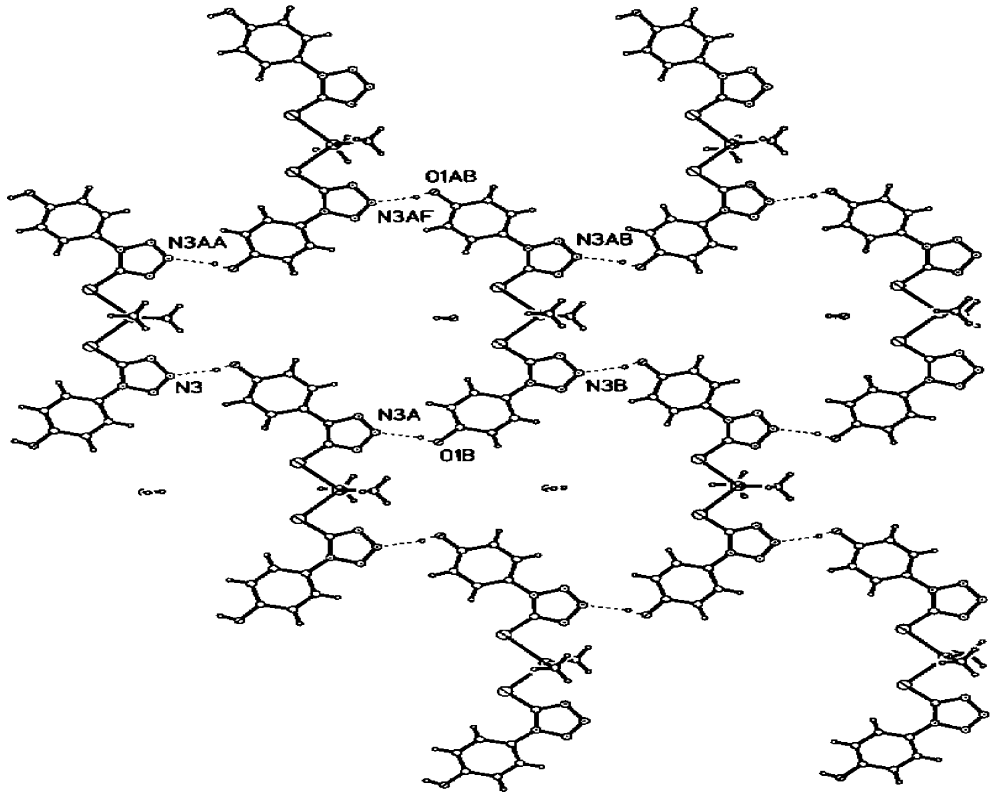

Fig. 7. perspective view showing the 2D network of the complex **5**.

thilato (2.975(5) [7a] and 2.947(4) Å [7b]). But in complex **6** the Sn–N bond lengths are longer (3.154(5) Å and 3.175(5) Å), although they all lie within the sum of their respective van der Walls radii (3.75 Å).

The establishment of such intramolecular tin–nitrogen interactions brings the present structure rather far from a regular tetrahedron, i.e. despite the fact that the complexes' core angles (S(1)–Sn(1)–C(9) 103.6(3)° and S(1)–Sn(1)–C(8) 107.5(3)° for **5**; S(1)–Sn(1)–C(15) 107.78(18)°, S(1)–Sn(1)–C(19) 107.83(17)°, S(2)–Sn(1)–C(15) 108.55(17)° and S(2)–Sn(1)–C(19) 109.64(17)° for **6**) are close the expected tetrahedral value, the C–Sn–C angle (134.8(6)° for **5** and 129.2(3)° for **6**) is more obtuse due to the occurrence of the Sn–N secondary interactions in a plane bisecting it, with the concomitant decrease of the S–Sn–S angle (91.50(17)° for **5** and 84.87(8)° for **6**). The geometry around the metal may thus be viewed, alternatively, as a distorted trapezoidal bipyramid, with the two methyl or methylene carbons in bent axial positions and the trapezoidal plane being defined by the two Sn–S covalent bonds and the two Sn–N secondary interactions.

In the complex **5**, the hydrogen bonding between the hydroxyl of ligand and nitrogen atom adjacent molecule (O(1)–H(1)···N(3) 2.750 Å, O(1)–H(1)–N(3) 167.89°) is recognized, which contributes to construct the 2D network of **5** (see Fig. 7). It is worthy noting that no short contacts have been found though the main component $Me_2Sn[S(C_7H_5N_4O)]_2$ crystallizes with one water molecule. Moreover, ring-stacking interactions are shown in the complex **5**. The orientation is such that the phenyl ring substituents 'face' other phenyl ring on neighboring layer at a distance of 3.677 Å and show significant π–π stacking interactions [20]. A view of the crystal packing along the *a* axis is shown in Fig. 8. As for **6**, the hydrogen bonds are also found (O(1)–H(1)···N(3) 2.892 Å, O(1)–H(1)–N(3) 138.73° and O(2)–H(2)···N(7) 2.886 Å, O(1)–H(1)–N(3) 139.08°) and its discrete molecules are

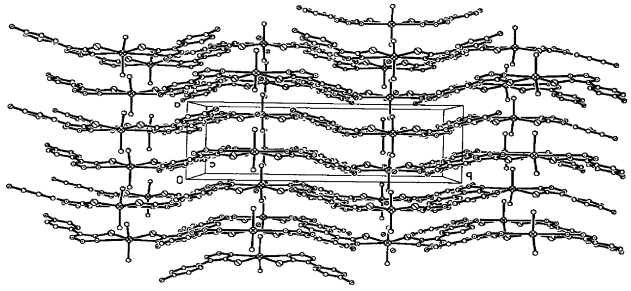

Fig. 8. Packing diagram of complex **5**, showing π–π stacking interactions.

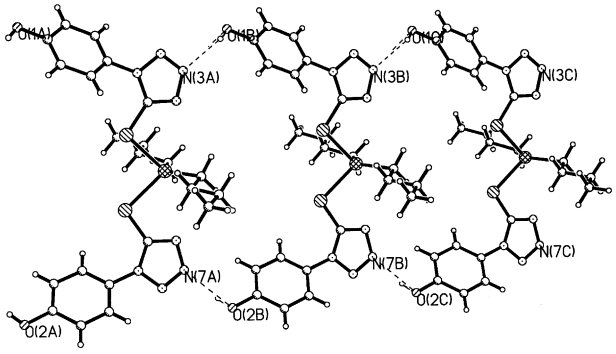

Fig. 9. perspective view showing the 1D ribbon of the complex **6**.

connected to 1D ribbon through hydrogen bonding (see Fig. 9).

4. Conclusions

A series of organotin(IV) complexes based on 1-(4-hydroxyphenyl)-1*H*-tetrazole-5-thiol have been synthesized and characterized. Detailed studies on the structures and spectra of these complexes indicate that there exist such an inclination that the structures of those dialkyltin complexes are likely to construct distorted trapezoidal bipyramidal geometry and those trialkyltin complexes are apt to have diverse geometry. The complex **3** is formed by discrete molecules but the molecules of complex **4** associates in polymeric chains through intermolecular, dative $N \rightarrow Sn$ bonds. Such differences may attribute to the fact that the stereo-constraints of $PhCH_2$-groups are smaller than that of Ph-groups. Consequently, it can be concluded that the decrease of stereo-constraints may benefit the coordination of nitrogen atoms.

5. Supplementary material

Crystallographic data (excluding structure factors) for the structure reported in this paper have been deposited with the Cambridge Crystallographic Data Center as Supplementary Publication Nos. CCDC-220182, 222015, 222017, 220175. Copies of the data can be obtained free of charge on application to the Director, CCDC, 12 Union Road, Cambridge CB2 1EZ, UK (fax: +44-1223-336033; e-mail: deposit@ccdc.cam.ac.uk or http://www.ccdc.cam.ac.uk).

Acknowledgements

We thank the National Natural Science Foundation of China (20271025) and the Natural Science Foundation of Shandong Province for financial support.

References

[1] L. Pellerito, L. Nagy, Coordin. Chem. Rev. 224 (2002) 111.
[2] J.A. Deiters, R.R. Holmes, J. Am. Chem. Soc. 109 (1987) 1686.
[3] K.C. Molloy, S.J. Blunden, R. Hill, J. Chem. Soc., Dalton Trans. (1988) 1259.
[4] S. Bhandari, M.F. Mahon, J.G. Mc Ginley, K.C. Molloy, C.E.E. Roper, J. Chem. Soc., Dalton Trans. (1998) 3425.
[5] C.L. Ma, Q. Jiang, R.F. Zhang, J. Organomet. Chem. 678 (2003) 148.
[6] C.L. Ma, F. Li, Q. Jiang, R.F. Zhang, J. Organomet. Chem. 689 (2004) 96.
[7] (a) R.J. Deeth, K.C. Molloy, M.F. Mahon, S. Whittaker, J. Organoment. Chem. 430 (1992) 25;
(b) O. Jiménez-Sandoval, R. Cea-Olivares, S. Hernández-Ortega, Polyhedron 16 (1997) 4129;
(c) R. Cea-Olivares, O. Jiménez-Sandoval, G. Espinosa-Pérez, C. Silvestru, Polyhedron 13 (1994) 2809;
(d) J. Bravo, M.B. Cordero, J.S. Casas, A. Sánchez, J. Sordo, E.E. Castellano, J. Zukerman-Schpector, J. Organoment. Chem. 482 (1994) 147;
(e) R. Cea-Olivares, O. Jiménez-Sandoval, G. Espinosa-Pérez, C. Silvestru, J. Organoment. Chem. 484 (1994) 33.
[8] K. Sisido, Y. Takeda, Z. Kinugawa, J. Am. Chem. Soc. 83 (1961) 538.
[9] T.A. Geoge, J. Organomet. Chem. 31 (1971) 233.
[10] J.R. May, W.R. Mc Whinnie, R.C. Poller, Spectrochim. Acta A 27 (1971) 969.
[11] R.C. Poller, The Chemistry of Organotin Compounds, Logos Press, London, 1970.
[12] C.L. Ma, Q. Jiang, R.F. Zhang, Can. J. Chem. 81 (2003) 825.
[13] C.L. Ma, Q. Jiang, R.F. Zhang, Appl. Organometal. Chem. 17 (2003) 623.
[14] Y. Ye, Q. Zeng, L.Z. Liu, Synth. Commun. 31 (2001) 2373.
[15] A. Bondi, J. Phys. Chem. 68 (1964) 441.
[16] B.D. James, R.J. Magee, W.C. Patalinghug, B.W. Skelton, A.H. White, J. Organomet. Chem. 467 (1994) 51.
[17] J.S. Casas, A. Castineiras, E.G. Martinez, A.S. González, A. Sánchez, J. Sordo, Polyhedron 16 (1997) 795.
[18] J.E. Huheey, Inorganic Chemistry, 3rd ed., Harper Int., Cambridge, 1983.
[19] F.H. Allen, O. Kennard, D.G. Watson, L. Brammer, A.G. Orpen, R. Taylor, J. Chem. Soc., Perkin Trans. II S1 (1987).
[20] (a) T. Steiner, B. Lutz, J. van der Mass, A.M.M. Schreurs, J. Kroon, M. Tamm, Chem. Commun. (1998) 171;
(b) M.C. Etter, Acc. Chem. Res. 23 (1990) 120;
(c) B.-H. Ye, X.-M. Chen, G.-Q. Xue, L.-N. Ji, J. Chem. Soc., Dalton Trans. (1998) 2827.

Available online at www.sciencedirect.com
SCIENCE DIRECT®
Polyhedron 23 (2004) 1557–1565
POLYHEDRON
www.elsevier.com/locate/poly

High-temperature synthesis of polynuclear iron oxo-hydroxy complexes

Andrew A. Smith [a], Robert A. Coxall [b], Andrew Harrison [b], Madeleine Helliwell [a], Simon Parsons [b], Richard E.P. Winpenny [a,*]

[a] Department of Chemistry, The University of Manchester, Oxford Road, Manchester M13 9PL, UK
[b] School of Chemistry, The University of Edinburgh, Joseph Black Building, West Mains Road, Edinburgh EH9 3JJ, UK

Received 19 January 2004; accepted 11 March 2004
Available online 23 April 2004

Abstract

Four polymetallic iron complexes have been synthesised by a high-temperature route. Two complexes have a $[Fe_6O_2(OH)_2]^{12+}$ core, one containing benzoate ligands and the other pivalates. The other two have a $[Fe_{11}O_6(OH)_6]^{15+}$ core, with benzoate or *t*-butylacetate bridging ligands, respectively. These complexes have been characterised by X-ray crystallography, elemental analysis and magnetochemistry. All four complexes consist of Fe^{III} ions, and anti-ferromagnetic exchange between the metal centres lead to low spin ground states.
© 2004 Elsevier Ltd. All rights reserved.

1. Introduction

Interest in transition metal polynuclear complexes has developed rapidly over the past decade due to the interesting magnetic properties of some of these complexes, e.g., $[Mn_{12}O_{12}(O_2CCH_3)_{16}(H_2O)_4]$ shows slow relaxation of magnetisation at low temperatures [1]. Our research group is interested in developing routes to these types of complexes. We have been investigating a procedure that involves heating simple transition metal carboxylates under an inert atmosphere at temperatures ranging from 200 to 400 °C. This method was first employed by Gerbeleu and co-workers [2] who synthesised a dodecanuclear Cr^{III} complex, $[Cr_{12}O_9(OH)_3(O_2CC(CH_3)_3)_{15}]$, by heating a Cr^{III} trimethylacetate starting material in a furnace to 400 °C. Our research group has adopted this technique and have reported the preparation of five Cr^{III} polynuclear complexes, $[Cr_8(OH)_8(O_2CC_6H_5)_{16}]$ [3], $[Cr_8O_4(O_2CC_6H_5])_6]$ [3], $[Cr_{12}O_8(O_2CCH(CH_3)_2)_{20}(H_2O)_4]$ [4], $[Cr_6O_2(OH)_2(O_2CC(CH_3)_3)_{11}][Cr_6O_4(O_2CC(CH_3)_3)_{11}]$ [5], $[Cr_8$- $(OH)_8(O_2CC_6H_4Cl)_{16}]$ [5], and a one-dimensional Mn polymer, $[Mn_4(O_2CC_6H_5)_8(CH_3CH_2OH)_6]_n$ [5]. We have also re-made the dodecanuclear chromium cage and studied its magnetic and spectroscopic behaviour in detail [6].

Further exploitation of this technique using simple Fe carboxylates has resulted in the formation of four Fe^{III} polynuclear complexes; $[Fe_6O_2(OH)_2(O_2CC(CH_3)_3)_{12}(THF)_2]$ (**1**), $[Fe_6O_2(OH)_2(O_2CC_5H_6)_{12}(H_2O_2)_2]$ (**2**), $[Fe_{11}O_6(OH)_6(O_2CC_5H_6)_{15}]$ (**3**) and $[Fe_{11}O_6(OH)_6(O_2CCH_2C(CH_3)_3)_{15}]$ (**4**). The syntheses, X-ray crystal structures and magnetic properties of each of these complexes are discussed.

2. Experimental

2.1. Synthesis

2.1.1. $[Fe_6O_2(OH)_2(O_2CC(CH_3)_3)_{12}(THF)_2]\cdot 2THF$ (1)

A mixture of H_2O (125 cm^3), KOH (5.05 g, 0.09 mol) and $(CH_3)_3CCO_2H$ (18.4 g, 0.18 mol) was heated, with stirring, to 80 °C. Small portions of $FeCl_2\cdot 4H_2O$ (9.00 g, 0.05 mol) were added and an orange precipitate formed. The mixture was cooled to room temperature and the precipitate was filtered, washed with hot H_2O

* Corresponding author. Tel.: +44-162754653; fax: +44-1612754598.
E-mail address: richard.winpenny@man.ac.uk (R.E.P. Winpenny).

0277-5387/$ - see front matter © 2004 Elsevier Ltd. All rights reserved.
doi:10.1016/j.poly.2004.03.012

and dried in vacuo. The precipitate, likely to be crude $[Fe_3O(O_2CC(CH_3)_3)_6(H_2O)_3]$, (4.30 g) was heated to 300 °C for 5 min in a tube furnace under N_2. The brown solid that results (1.69 g) was dissolved in THF (40 cm^3) and red crystals of **1** formed by slow evaporation after 5 days in 9% yield. *Anal.* Calc. (Found) for **1**: C, 46.44 (46.53); H, 7.22 (7.18); N, 0(0)%.

2.1.2. $[Fe_6O_2(OH)_2(O_2CC_6H_5)_{12}(H_2O)_2]\cdot C_6H_5CO_2H\cdot 4.33CH_2Cl_2$ (**2**)

$[Fe_3O(O_2CC_6H_5)_6(\ _2O)_2(MeCN)]$ (2.53 g, 2.56 mmol) was first synthesised by the literature procedure [7], and then heated to 300 °C for 5 min in a tube furnace under N_2. The dark brown crude product (1.83 g) was dissolved in CH_2Cl_2 (50 cm^3) and red crystals of **2** formed by slow evaporation after 9 days in 17% yield. *Anal.* Calc. (Found) for $\mathbf{2}\cdot C_6H_5CO_2H.CH_2Cl_2$: C, 52.68 (52.04); H, 3.56 (3.62); N, 0 (0)%.

2.1.3. $[Fe_{11}O_6(OH)_6(O_2CC_6H_5)_{15}]\cdot 13MeCN$ (**3**)

Crude $[Fe_3O(O_2CC_6H_5)_6(H_2O)_3](NO_3)$ was prepared by slowly adding $Fe(NO_3)_3\cdot 9H_2O$ (0.06 mol, 24.24 g) to a mixture of H_2O (75 cm^3), EtOH (75 cm^3), KOH (0.12 mol, 6.73 g) and $C_6H_5CO_2H$ (0.12 mol, 14.66 g). The resulting orange precipitate was filtered and dried in vacuo, yield 94%.

The crude $[Fe_3O(O_2CC_6H_5)_6(H_2O)_3](NO_3)$ (2.14 g, 2.09 mmol) was heated to 300 °C for 5 min in a tube furnace under N_2. The red/orange solid crude product (1.32 g) was dissolved in MeCN (35 cm^3) and red crystals of **3** formed by slow evaporation after 4 days in 21% yield. *Anal.* Calc. (Found) for $\mathbf{3}\cdot$MeCN: C, 48.13 (49.54); H, 3.17 (3.18); N, 0.52 (0.49)%.

2.1.4. $[Fe_{11}O_6(OH)_6(O_2CCH_2C(CH_3)_3)_{15}]\cdot 2.5MeCN$ (**4**)

A mixture of H_2O (125 cm^3), KOH (5.05 g, 0.09 mol) and $(CH_3)_3CCH_2CO_2H$ (10.45 g, 0.18 mol, 11.46 cm^3) was heated, with stirring, to 80 °C in a round bottom flask. Small portions of $FeCl_2\cdot 4H_2O$ (9.00 g, 0.05 mol) were added and an orange precipitate formed. The mixture was cooled to room temperature and the precipitate was filtered, washed with hot H_2O and dried in vacuo. The precipitate, likely to be crude $[Fe_3O(O_2CCH_2C(CH_3)_3)_6(H_2O)_3]$, (3.50 g) was heated to 300 °C for 15 min in a tube furnace under N_2. The brown solid product (1.47 g) was dissolved in acetone (40 cm^3) and red crystals of **4** formed when MeCN (10 cm^3) was diffused into this solution after 2 days in 14% yield. *Anal.* Calc. (Found) for **4**: C, 42.56 (43.00); H, 6.79 (6.76); N, 0 (0)%.

2.2. Crystal structures

Data for **1** and **3** were collected on a Stoe Stadi-4 four-circle diffractometer and for **2** and **4** on a Bruker Smart APEX CCD area detector. Both diffractometers were fitted with an Oxford Cryosystems low-temperature device [8] and used graphite monochromated Mo Kα radiation with ω–θ scans for **1** and **3** and ω-scans for **2** and **4**. Crystallographic data (excluding structure factors) for the structures reported in this paper have been deposited with the Cambridge Crystallographic Data Centre as supplementary publication nos. CCDC 228440–228443. All refinements were against F^2 and used SHELXL-PC [9].

3. Results and discussion

3.1. Synthesis

Four Fe^{III} polynuclear complexes have been synthesised by heating simple Fe carboxylates in a tube furnace under inert conditions. Heating a crude solid sample of $[Fe_3O(O_2CC(CH_3)_3)_6(H_2O)_3]$ to 300 °C followed by crystallisation from THF has produced a hexanuclear Fe^{111} complex, $[Fe_6O_2(OH)_2(O_2CC(CH_3)_3)_{12}(THF)_2]$ (**1**). This complex has the same $[Fe_6O_2(OH)_2]^{12+}$ core as $[Fe_6O_2(OH)_2(O_2CC(CH_3)_3)_{12}]$ prepared by Gerbeleu et al. [10], and $[Fe_6O_2(OH)_2(O_2CC_6H_5)_{12}(C_4H_8O_2)(H_2O)]$ synthesised by Micklitz and Lippard [11]. Using the same procedure used in the formation of **1**, another hexanuclear complex has been prepared with the $[Fe_6O_2(OH)_2]^{12+}$ core. $[Fe_6O_2(OH)_2(O_2CC_6H_5)_{12}(H_2O)_2]$ (**2**) was synthesised by heating a solid sample of $[Fe_3O(O_2CC_6H_5)_6(H_2O)_2(MeCN)]$ to 300 °C and crystals of **2** were obtained from CH_2Cl_2.

Two undecanuclear complexes $[Fe_{11}O_6(OH)_6(O_2CC_6H_5)_{15}]$ (**3**) and $[Fe_{11}O_6(OH)_6(O_2CCH_2C(CH_3)_3)_{15}]$ (**4**) have also been prepared via the high-temperature route. **3** was first synthesised by Lippard and co-workers [12,13] who dissolved $(Et_4N)_2[Fe_2OCl_6]$ in MeCN and added sodium benzoate. To obtain crystals they then allowed water to diffuse into the solution. We have produced the same complex by heating a crude solid sample of $[Fe_3O(O_2CC_6H_5)_6(H_2O)_3](NO_3)$ to 300 °C and subsequently crystallising from MeCN. Synthesis of **4** was achieved by heating $[Fe_3O(O_2CCH_2C(CH_3)_3)_6(H_2O)_3]$ to 300 °C followed by dissolving the product in acetone and allowing MeCN to diffuse into the solution.

3.2. Structure descriptions

3.2.1. $[Fe_6O_2(OH)_2(O_2CC(CH_3)_3)_{12}(THF)_2]\cdot 2THF$ (**1**)

A SCHAKAL [14] representation of the structure of **1** is shown in Fig. 1. Tables of the crystallographic data and selected bond lengths and bond angles for **1** are given in Tables 1 and 2, respectively. There are two oxo-centred trimer units linked by two μ_2 hydroxide ligands

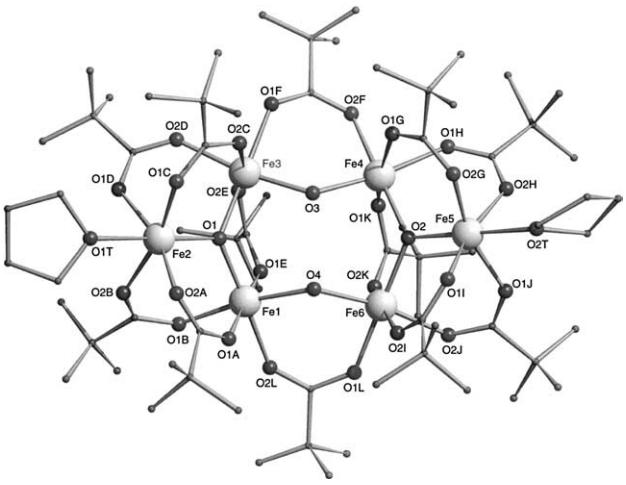

Fig. 1. The structure of **1** in the crystal.

O3 and O4, and two 1,3-bridging trimethylacetate ligands. The first trimer unit comprises Fe1, Fe2 and Fe3, and the second Fe4, Fe5 and Fe6. Coordination around Fe2 and Fe5 is the same, with terminal THF ligands attached to both. Fe2 is linked to Fe1 and Fe3 through a μ_3-oxo atom O1 and Fe5 bridges to Fe4 and Fe6 in the same fashion through O2. There are two 1,3-bridging trimethylacetate on each edge of the triangles, i.e., Fe2···Fe1, Fe2···Fe3, Fe4···Fe5 and Fe5···Fe6. All of the Fe atoms in this complex are in the +3 oxidation state and have distorted octahedral geometry.

Examination of the bond lengths between the Fe atoms and the μ_3-oxo atoms of **1** reveals that each of the trimer units is asymmetric. The bond length of Fe2–O1 is 1.8561(15) Å and Fe5–O2 is 1.8640(16) Å. These bond lengths are much shorter than the other bonds involving the μ_3-oxide (av. 1.96 Å). This may be related to the bond length of Fe2–O1T and Fe5–O2T, both of which are longer than expected at 2.2306(18) and 2.1887(19) Å, respectively.

3.2.2. $[Fe_6O_2(OH)_2(O_2CC_6H_5)_{12}(H_2O)_2]\cdot C_6H_5CO_2H\cdot 4.33CH_2Cl_2$ (**2**)

Fig. 2 shows a SCHAKAL [14] representation of the structure of **2**. Crystallographic data for **2** is given in Table 1 and selected bond lengths and bond angles for **2** are given in Table 3. The structure and connectivity of **2** is the same as **1** with H_2O replacing the THF ligands coordinated to Fe2 and Fe5, and the trimethylacetate ligands are replaced by benzoate ligands. Just like **1**, the Fe atoms are all in the +3 oxidation state and have octahedral geometry. Again, each of the trimer units is asymmetric due to the short Fe2–O1 and Fe5–O2 bonds. These bond lengths are comparable with those observed for **1**. The Fe–O(H_2O) bond lengths are slightly elongated at 2.1027(19) Å for Fe2–O1 W and 2.1456(17) Å for Fe5–O2W.

3.2.3. $[Fe_{11}O_6(OH)_6O_2CC_6H_5)_{15}]\cdot 13MeCN$ (**3**)

The structure of **3** is depicted in Fig. 3 by a SCHAKAL representation [14]. Table 1 contains the, crystallographic data for **3** and Table 4 displays selected bond lengths and angles for **3**. Alone, the Fe atoms in **3** form a distorted pentacapped trigonal prism with Fe1, Fe7 and Fe9 forming one of the triangular faces of the trigonal prism and Fe3, Fe6 and Fe10 forming the other triangular face. Fe2, Fe4 and Fe11 cap the rectangular faces and Fe5 and Fe8 cap the triangular faces of the trigonal prism. This structure has non-crystallographic D_3 symmetry with a C_3 axis along Fe5 and Fe8 and three C_2 axes formed by Fe2, Fe4 and Fe11 bisecting the C_3 axis.

Table 1
Crystallographic data for compounds **1**–**4**

Compound	**1**	**2**	**3**	**4**
Formula	$C_{76}H_{142}Fe_6O_{32}$	$C_{95.33}H_{80.66}Cl_{8.66}Fe_6O_{32}$	$C_{131}H_{120}Fe_{11}N_{13}O_{42}$	$C_{95}H_{178.5}Fe_{11}N_{2.5}O_{42}$
Formula weight (g mol^{-1})	1903.00	2380.50	3162.75	2642.22
Crystal system	triclinic	triclinic	triclinic	monoclinic
Space group	$P\bar{1}$	$P\bar{1}$	$P\bar{1}$	$P2_1/n$
Unit cell dimensions				
a (Å)	13.678(4)	14.630(4)	16.454(5)	17.4380(9)
b (Å)	15.051(4)	15.086(4)	19.288(5)	23.4422(13)
c (Å)	25.750(7)	26.903(8)	22,434(6)	32.0369(17)
α (°)	90.350(5)	78.637(5)	80.931(5)	90
β (°)	97.719(4)	78.575(5)	85.284(5)	95.9510(10)
γ (°)	113.067(4)	66.479(5)	86.458(5)	90
V (Å^3)	4823	5290	6999	13025.6
Z	2	2	2	4
T (°C)	−123	−123	−123	−173
λ (Å)	0.71073	0.71073	0.71073	0.71073
ρ_{calc} (g cm^{-3})	1.310	1.494	1.501	1.344
R (%)	4.09	3.92	6.37	5.90
R_w	12.26	10.18	15.88	14.77

Table 2
Selected bond lengths (Å) and bond angles (°) for **1**

Bond lengths			
Fe1–O1	1.9544(16)	Fe4–O2	1.9717(16)
Fe1–O4	1.9550(17)	Fe4–O3	1.9324(17)
Fe1–O1A	2.0193(18)	Fe4–O2F	1.9982(17)
Fe1–O1B	2.0322(19)	Fe4–O1G	2.0306(19)
Fe1–O1E	1.991(2)	Fe4–O1H	2.0539(18)
Fe1–O2L	2.0246(17)	Fe4–O1K	2.0129(19)
Fe2–O1	1.8561(15)	Fe5–O2	1.8640(16)
Fe2–O2A	2.0261(17)	Fe5–O2G	2.0191(19)
Fe2–O2B	2.0258(18)	Fe5–O2H	2.0118(19)
Fe2–O1C	2.0262(19)	Fe5–O1I	2.0261(19)
Fe2–O1D	2.0221(19)	Fe5–O1J	1.998(2)
Fe2–O1T	2.2306(18)	Fe5–O2T	2.1887(19)
Fe3–O1	1.9744(16)	Fe6–O2	1.9588(16)
Fe3–O3	1.9252(18)	Fe6–O4	2.0048(17)
Fe3–O2C	2.031(2)	Fe6–O2I	2.0167(19)
Fe3–O2D	2.041(2)	Fe6–O2J	2.0449(18)
Fe3–O2E	1.999(2)	Fe6–O2K	1.9872(19)
Fe3–O1F	2.0258(18)	Fe6–O1L	2.0099(17)
Bond angles			
O1–Fe1–O4	94.41(7)	O2–Fe4–O3	92.73(7)
O1–Fe1–O1A	94.29(7)	O2–Fe4–O2F	176.12(7)
O1–Fe1–O1B	93.11(7)	O2–Fe4–O1G	95.47(7)
O1–Fe1–O1E	92.13(7)	O2–Fe4–O1H	94.11(7)
O1–Fe1–O2L	177.08(7)	O2–Fe4–O1K	90.49(7)
O4–Fe1–O1A	88.60(8)	O3–Fe4–O2F	88.78(7)
O4–Fe1–O1B	172.18(7)	O3–Fe4–O1G	90.35(8)
O4–Fe1–O1E	95.15(9)	O3–Fe4–O1H	171.41(8)
O4–Fe1–O2L	88.46(7)	O3–Fe4–O1K	100.66(9)
O1A–Fe1–O1B	88.73(6)	O2F–Fe4–O1G	88.10(8)
O1A–Fe1–O1E	172.29(8)	O2F–Fe4–O1H	84.72(7)
O1A–Fe1–O2L	86.26(8)	O2F–Fe4–O1K	85.72(8)
O1B–Fe1–O1E	86.67(9)	O1G–Fe4–O1H	83.83(9)
O1B–Fe1–O2L	84.03(7)	O1G–Fe4–O1K	167.23(9)
O1E–Fe1–O2L	87.10(8)	O1H–Fe4–O1K	84.48(9)
O1–Fe2–O2A	99.63(7)	O2–Fe5–O2G	99.10(7)
O1–Fe2–O2B	98.25(7)	O2–Fe5–O2H	98.91(7)
O1–Fe2–O1C	98.51(7)	O2–Fe5–O1I	97.29(7)
O1–Fe2–O1D	99.09(7)	O2–Fe5–O1J	99.86(8)
O1–Fe2–O1T	179.34(7)	O2–Fe5–O2T	178.64(7)
O2A–Fe2–O2B	86.02(7)	O2G–Fe5–O2H	89.21(9)
O2A–Fe2–O1C	95.01(8)	O2G–Fe5–O1I	89.70(9)
O2A–Fe2–O1D	160.27(7)	O2G–Fe5–O1J	161.02(8)
O2A–Fe2–O1T	80.25(7)	O2G–Fe5–O2T	80.13(8)
O2B–Fe2–O1C	162.79(7)	O2H–Fe5–O1I	163.74(8)
O2B–Fe2–O1D	85.18(9)	O2H–Fe5–O1J	87.04(9)
O2B–Fe2–O1T	82.40(8)	O2H–Fe5–O2T	82.22(7)
O1C–Fe2–O1D	88.34(9)	O1I–Fe5–O1J	88.74(9)
O1C–Fe2–O1T	80.86(7)	O1I–Fe5–O2T	81.60(8)
O1D–Fe2–O1T	81.10(8)	O1J–Fe5–O2T	80.93(8)
O1–Fe3–O3	93.82(7)	O2–Fe6–O4	93.75(7)
O1–Fe3–O2C	91.74(7)	O2–Fe6–O2I	94.72(7)
O1–Fe3–O2D	94.66(7)	O2–Fe6–O2J	94.84(7)
O1–Fe3–O2E	91.73(8)	O2–Fe6–O2K	90.20(7)
O1–Fe3–O1F	177.91(7)	O2–Fe6–O1L	176.96(7)
O3–Fe3–O2C	93.22(9)	O4–Fe6–O2I	86.69(8)
O3–Fe3–O2D	171.18(8)	O4–Fe6–O2J	168.70(8)

The triangular faces of the trigonal prism are twisted. This twist angle can be calculated by measuring the dihedral angle between the Fe atoms at the corners of the two triangular faces of the prism that represent one edge

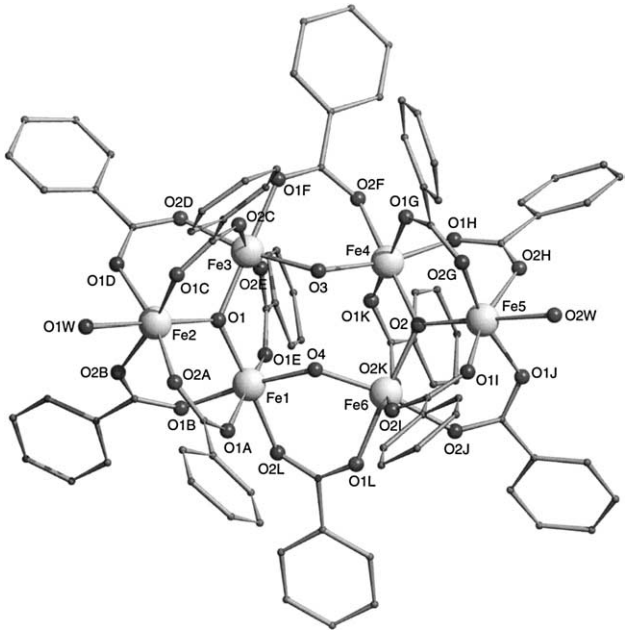

Fig. 2. The structure of **2** in the crystal.

of the rectangular faces and the two Fe atoms on the C_3 axis. For Fe1, Fe8, Fe5 and Fe3 the dihedral angle is 15.97°, for Fe6, Fe5, Fe8 and Fe7 it is 16.86° and for Fe9, Fe8, Fe5 and Fe10 it is 20.06°.

Fe1, Fe3, Fe6, Fe7, Fe9 and Fe10 have the same coordination environment. Each of which is linked to another Fe atom of the trigonal prism along the edge of the rectangular face by one 1,3-bridging benzoate ligand and two μ_3-hydroxide ligands. For example Fe1 bridges to Fe3 through the benzoate ligand F and the μ_3-hydroxide ligands O6 and O7. There is one μ_3-oxo ligand connecting each of the trigonal prism Fe atoms to one rectangular face capping Fe atom and one triangular face capping Fe atom. There are also two 1,3-bridging benzoate ligands, which join the Fe atom of the trigonal prism to the two different capping Fe atoms. For example Fe1 is connected to Fe2 and Fe8 through the μ_3-oxo ligand O2 and Fe1 is linked to Fe2 via the benzoate ligand A and to Fe8 through the benzoate ligand C. All of the Fe atoms have distorted octahedral geometry and are in the +3 oxidation state.

Fe–O($O_2CC_6H_5$) bond lengths range from 1.946 to 2.122 Å, Fe–O(OH) bond lengths range from 2.044 to 2.143 Å and Fe–O(O) bond lengths range from 1.877 to 1.945 Å. The difference between the Fe–O(OH) and Fe–O(O) ranges clearly shows that the O atoms O1, O4, O6, O7, O9 and O11 are OH ligands. There are four MeCN molecules hydrogen bonded to four μ_3-OH ligands, O1, O6, O7 and O9. These O(H)–N hydrogen bond lengths range from 2.820 to 2.943 Å. This gives confirmation to the presence of the H atom attached to the O atom at these sites.

Table 3
Selected bond lengths (Å) and bond angles (°) for **2**

Bond lengths			
Fe1–O1	1.9538(17)	Fe4–O2	1.9612(17)
Fe1–O4	1.9424(16)	Fe4–O3	2.0081(16)
Fe1–O1A	2.0547(19)	Fe4–O2F	1.9991(18)
Fe1–O1B	2.0522(17)	Fe4–O1G	2.0361(17)
Fe1–O1E	1.9974(19)	Fe4–O1H	2.0145(17)
Fe1–O2L	2.0500(18)	Fe4–O1K	1.9754(17)
Fe2–O1	1.8767(16)	Fe5–O2	1.8611(15)
Fe2–O2A	2.024(2)	Fe5–O2G	2.0160(19)
Fe2–O2B	2.0322(18)	Fe5–O2H	2.0409(18)
Fe2–O1C	2.0097(18)	Fe5–O1I	1.9880(19)
Fe2–O1D	2.0197(19)	Fe5–O1J	2.0843(18)
Fe2–O1W	2.1027(19)	Fe5–O2W	2.1456(17)
Fe3–O1	1.9632(17)	Fe6–O2	1.9609(17)
Fe3–O3	2.0254(16)	Fe6–O4	1.9268(16)
Fe3–O2C	2.0282(17)	Fe6–O2I	2.0432(19)
Fe3–O2D	1.9937(17)	Fe6–O2J	2.0429(17)
Fe3–O2E	1.9709(17)	Fe6–O2K	2.0487(19)
Fe3–O1F	2.0625(17)	Fe6–O1L	2.0166(18)
Bond angles			
O1–Fe1–O4	92.90(7)	O2–Fe4–O3	95.13(7)
O1–Fe1–O1A	96.66(7)	O2–Fe4–O2F	176.73(7)
O1–Fe1–O1B	93.05(7)	O2–Fe4–O1G	93.76(7)
O1–Fe1–O1E	94.10(7)	O2–Fe4–O1H	93.40(7)
O1–Fe1–O2L	177.19(6)	O2–Fe4–O1K	89.59(7)
O4–Fe1–O1A	91.62(7)	O3–Fe4–O2F	87.39(7)
O4–Fe1–O1B	173.76(7)	O3–Fe4–O1G	84.73(7)
O4–Fe1–O1E	96.78(7)	O3–Fe4–O1H	170.07(7)
O4–Fe1–O2L	89.91(7)	O3–Fe4–O1K	97.64(7)
O1A–Fe1–O1B	85.83(8)	O2F–Fe4–O1G	88.53(8)
O1A–Fe1–O1E	165.99(7)	O2F–Fe4–O1H	84.28(7)
O1A–Fe1–O2L	83.23(7)	O2F–Fe4–O1K	88.01(8)
O1B–Fe1–O–O1E	84.66(7)	O1G–Fe4–O1H	89.65(7)
O1B–Fe1–O2L	84.14(7)	O1G–Fe4–O1K	175.71(8)
O1E–Fe1–O2L	85.58(7)	O1H–Fe4–O1K	87.49(7)
O1–Fe2–O2A	96.48(7)	O2–Fe5–O2G	95.75(7)
O1–Fe2–O2B	96.96(7)	O2–Fe5–O2H	100.66(7)
O1–Fe2–O1C	95.81(7)	O2–Fe5–O1I	96.32(7)
O1–Fe2–O1D	100.17(7)	O2–Fe5–O1J	98.65(7)
O1–Fe2–O1W	178.62(8)	O2–Fe5–O2W	177.01(7)
O2A–Fe2–O2B	91.00(8)	O2G–Fe5–O2H	90.90(7)
O2A–Fe2–O1C	87.22(9)	O2G–Fe5–O1I	89.67(8)
O2A–Fe2–O1D	163.34(7)	O2G–Fe5–O1J	165.55(7)
O2A–Fe2–O1W	82.25(8)	O2G–Fe5–O2W	82.81(7)
O2B–Fe2–O1C	167.22(7)	O2H–Fe5–O1I	162.86(7)
O2B–Fe2–O1D	87.71(8)	O2H–Fe5–O1J	85.31(7)
O2B–Fe2–O1W	83.60(8)	O2H–Fe5–O2W	82.01(7)
O1C–Fe2–O1D	90.38(8)	O1I–Fe5–O1J	89.90(7)
O1C–Fe2–O1W	83.62(8)	O1I–Fe5–O2W	81.07(7)
O1D–Fe2–O1W	81.10(8)	O1J–Fe5–O2W	82.85(7)
O1–Fe3–O3	93.54(7)	O2–Fe6–O4	96.05(7)
O1–Fe3–O2C	94.84(7)	O2–Fe6–O2I	92.64(7)
O1–Fe3–O2D	95.79(7)	O2–Fe6–O2J	93.84(7)
O1–Fe3–O2E	92.85(7)	O2–Fe6–O2K	88.50(7)
O1–Fe3–O1F	179.31(7)	O2–Fe6–O1L	174.02(7)
O3–Fe3–O2C	82.81(7)	O4–Fe6–O2I	91.39(7)
O3–Fe3–O2D	169.11(7)	O4–Fe6–O2J	169.90(7)
O3–Fe3–O2E	95.87(7)	O4–Fe6–O2K	99.70(7)
O3–Fe3–O1F	86.49(7)	O4–Fe6–O1L	87.39(7)
O2C–Fe3–O2D	90.79(8)	O2I–Fe6–O2J	86.09(7)
O2C–Fe3–O2E	172.26(7)	O2I–Fe6–O2K	168.68(7)
O2C–Fe3–O1F	85.85(7)	O2I–Fe6–O1L	92.17(7)
O2D–Fe3–O2E	89.29(7)	O2J–Fe6–O2K	82.59(8)
O2D–Fe3–O1F	84.25(7)	O2J–Fe6–O1L	82.94(7)
O2E–Fe3–O1F	86.46(7)	O2K–Fe6–O1L	86.09(8)

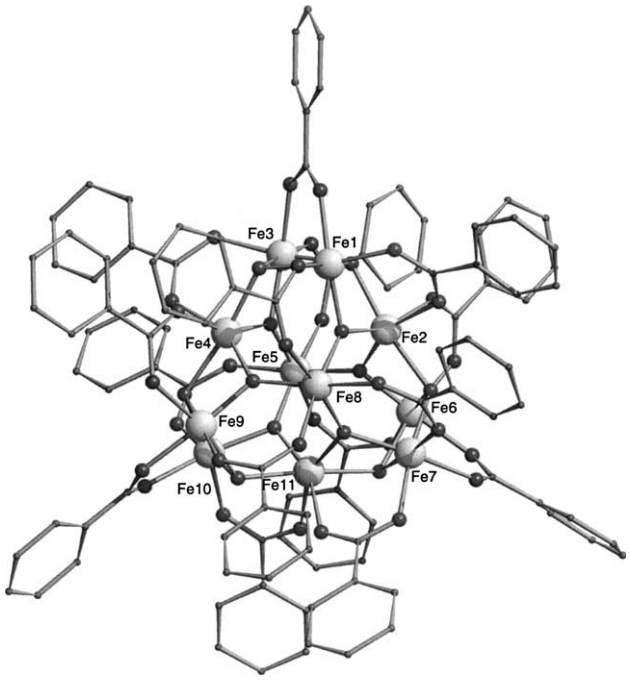

Fig. 3. The structure of **3** in the crystal.

3.2.4. $[Fe_{11}O_6(OH)_6(O_2CCH_2C(CH_3)_3)_{15}]\cdot 2.5MeCN$ (**4**)

Shown in Fig. 4 is a SCHAKAL representation [14] of **4**. Crystallographic data for **4** is listed in Table 1 and the selected bond lengths and angles are given in Table 5. The structure and connectivity of **4** is the same as **3** with *t*-butylacetate replacing the benzoate ligands. The Fe atoms are in the +3 oxidation state and have distorted octahedral geometry. Fe–O(O_2CR) bond lengths range from 1.937 to 2.156 Å, Fe–O(OH) bond lengths range from 2.044 to 2.153 Å and Fe–O(O) bond lengths range from 1.893 to 1.932 Å. These ranges are in good agreement with the equivalent ranges for **3**. As was seen in **3** the difference between the Fe–O(OH) and Fe–O(O) bond length ranges shows that the O atoms O1, O2, O7, O8, O9 and O10 are OH ligands. The Fe atoms of **4** also form a twisted trigonal prism and the twist angles are 18.03°, 18.07° and 18.19°. There is only one MeCN molecule hydrogen bonded to a μ_3-OH ligand, O2. The O(H)–N hydrogen bond length is 2.822 Å.

3.3. Structural comparisons

$[Fe_6O_2(OH)_2(O_2CC_6H_5)_{12}(H_2O)(C_4H_8O_2)]$ by Micklitz and Lippard [11] has an almost identical structure to **1** and **2**. The only differences being the carboxylate and the coordinated solvent present. There is another similar hexanuclear Fe complex, $[Fe_6O_2(OH)_2(O_2CC(CH_3)_3)_{12}]$ synthesised by Gerbeleu et al. [10], that makes use of the same carboxylate as **1** but has a different connectivity. $[Fe_6O_2(OH)_2(O_2CC(CH_3)_3)_{12}]$ has two oxo-centred

Table 4
Selected bond lengths (Å) and bond angles (°) for **3**

Bond lengths			
Fe1–O2	1.916(4)	Fe6–O2G	2.003(4)
Fe1–O6	2.114(4)	Fe6–O1H	2.032(4)
Fe1–O7	2.090(4)	Fe6–O20	1.972(4)
Fe1–O1A	2.001(4)	Fe7–O1	2.044(4)
Fe1–O2E	1.955(4)	Fe7–O3	1.919(3)
Fe1–O2F	2.038(4)	Fe7–O4	2.138(4)
Fe2–O1	2.079(4)	Fe7–O2B	1.981(4)
Fe2–O2	1.932(3)	Fe7–O2C	1.995(4)
Fe2–O5	1.945(4)	Fe7–O2H	2.084(3)
Fe2–O6	2.060(4)	Fe8–O2	1.898(4)
Fe2–O2A	2.111(4)	Fe8–O3	1.909(3)
Fe2–O1G	2.071(4)	Fe8–O8	1.936(3)
Fe3–O6	2.089(4)	Fe8–O1B	2.083(4)
Fe3–O7	2.133(4)	Fe8–O1D	2.122(4)
Fe3–O12	1.922(4)	Fe8–O1E	2.111(4)
Fe3–O1F	2.030(4)	Fe9–O8	1.888(3)
Fe3–O2M	1.998(4)	Fe9–O9	2.112(4)
Fe3–O2N	1.958(4)	Fe9–O11	2.135(4)
Fe4–O7	2.053(4)	Fe9–O2D	1.946(4)
Fe4–O8	1.926(4)	Fe9–O2K	2.045(4)
Fe4–O11	2.103(4)	Fe9–O2L	2.018(4)
Fe4–O12	1.910(4)	Fe10–O9	2.137(4)
Fe4–O1L	2.065(4)	Fe10–O10	1.909(3)
Fe4–O1M	2.095(4)	Fe10–O11	2.085(4)
Fe5–O5	1.932(3)	Fe10–O2I	1.961(4)
Fe5–O10	1.939(4)	Fe10–O1J	1.976(4)
Fe5–O12	1.904(4)	Fe10–O1K	2.086(4)
Fe5–O1I	2.063(4)	Fe11–O3	1.929(4)
Fe5–O1N	2.093(4)	Fe11–O4	2.085(3)
Fe5–O10	2.104(4)	Fe11-09	2.095(3)
Fe6–O1	2.143(4)	Fe11–O10	1.930(4)
Fe6–O4	2.138(4)	Fe11–O1C	2.106(4)
Fe6–O5	1.877(3)	Fe11–O2J	2.090(4)
Bond angles			
O2–Fe1–O6	77.56(14)	O4–Fe6–O20	86.94(15)
O2–Fe1–O7	92.55(14)	O5–Fe6–O2G	97.22(15)
O2–Fe1–O1A	94.98(15)	O5–Fe6–O1H	163.86(16)
O2–Fe1–O2E	102.17(16)	O5–Fe6–O20	104.42(16)
O2–Fe1–O2F	164.10(16)	O2G–Fe6–O1H	87.26(15)
O6–Fe1–O7	83.27(14)	O2G–Fe6–O20	97.21(16)
O6–Fe1–O1A	95.72(15)	O1H–Fe6–O20	90.30(16)
O6–Fe1–O2E	171.40(15)	O1–Fe7–O3	93.20(14)
O6–Fe1–O2F	86.56(15)	O1–Fe7–O4	83.86(14)
O7–Fe1–O1A	172.00(15)	O1–Fe7–O2B	91.67(15)
O7–Fe1–O2E	88.16(15)	O1–Fe7–O2C	170.05(15)
O7–Fe1–O2F	84.74(15)	O1–Fe7–O2H	83.88(14)
O1A–Fe1–O2E	92.86(16)	O3–Fe7–O4	76.69(14)
O1A–Fe1–O2F	87.28(16)	O3–Fe7–O2B	101.67(15)
O2E–Fe1–O2F	93.42(16)	O3–Fe7–O2C	95.38(15)
O1–Fe2–O2	107.57(15)	O3–Fe7–O2H	163.51(15)
O1–Fe2–O5	78.19(14)	O4–Fe7–O2B	175.11(16)
O1–Fe2–O6	171.36(14)	O4–Fe7–O2C	93.21(15)
O1–Fe2–O2A	81.10(14)	O4–Fe7–O2H	86.85(14)
O1–Fe2–O1G	90.21(14)	O2B–Fe7–O2C	91.52(16)
O2–Fe2–O5	107.98(15)	O2B–Fe7–O2H	94.66(15)
O2–Fe2–O6	78.54(15)	O2C–Fe7–O2H	86.47(15)
O2–Fe2–O2A	87.44(14)	O2–Fe8–O3	94.34(15)
O2–Fe2–O1G	157.07(15)	O2–Fe8–O8	93.53(15)
O5–Fe2–O6	106.08(15)	O2–Fe8–O1B	89.17(15)
O5–Fe2–O2A	157.13(15)	O2–Fe8–O1D	170.76(15)
O5–Fe2–O1G	89.43(15)	O2–Fe8–O1E	96.12(15)
O6–Fe2–O2A	93.26(15)	O3–Fe8–O8	97.67(15)
O6–Fe2–O1G	82.40(15)	O3–Fe8–O1B	93.93(15)

Table 4 (*continued*)

Bond angles			
O2A–Fe2–O1G	81.00(15)	O3–Fe8–O1D	87.04(15)
O6–Fe3–O7	82.85(14)	O3–Fe8–O1E	169.14(15)
O6–Fe3–O12	91.90(14)	O8–Fe8–O1B	167.85(15)
O6–Fe3–O1F	84.06(15)	O8–Fe8–O1D	95.34(15)
O6–Fe3–O2M	169.85(15)	O8–Fe8–O1E	84.64(15)
O6–Fe3–O2N	90.19(15)	O1B–Fe8–O1D	81.62(15)
O7–Fe3–O12	77.05(14)	O1B–Fe8–O1E	83.30(14)
O7–Fe3–O1F	86.18(15)	O1D–Fe8–O1E	82.17(15)
O7–Fe3–O2M	91.63(15)	O8–Fe9–O9	90.91(14)
O7–Fe3–O2N	173.04(15)	O8–Fe9–O11	77.39(14)
O12–Fe3–O1F	163.12(16)	O8–Fe9–O2D	103.86(16)
O12–Fe3–O2M	95.18(15)	O8–Fe9–O2K	165.52(16)
O12–Fe3–O2N	103.21(16)	O8–Fe9–O2L	99.48(15)
O1F–Fe3–O2M	87.08(16)	O9–Fe9–O11	82.88(14)
O1F–Fe3–O2N	93.21(16)	O9–Fe9–O2D	91.18(15)
O2M–Fe3–O2N	95.26(16)	O9–Fe9–O2K	84.48(14)
O7–Fe4–O8	106.18(15)	O9–Fe9–O2L	166.82(15)
O7–Fe4–O11	172.40(14)	O11–Fe9–O2D	173.97(15)
O7–Fe4–O12	79.29(15)	O11–Fe9–O2K	88.40(15)
O7–Fe4–O1L	81.67(15)	O11–Fe9–O2L	91.45(15)
O7–Fe4–O1M	95.16(15)	O2D–Fe9–O2K	89.99(16)
O8–Fe4–O11	77.41(14)	O2D–Fe9–O2L	94.13(16)
O8–Fe4–O12	109.10(15)	O2K–Fe9–O2L	83.48(15)
O8–Fe4–O1L	90.22(15)	O9–Fe10–O10	78.24(14)
O8–Fe4–O1M	154.42(15)	O9–Fe10–O11	83.49(14)
O11–Fe4–O12	106.09(15)	O9–Fe10–O2I	172.25(15)
O11–Fe4–O1L	91.71(14)	O9–Fe10–O1J	93.00(15)
O11–Fe4–O1M	79.84(15)	O9–Fe10–O1K	84.78(14)
O12–Fe4–O1L	155.95(15)	O10–Fe10–O11	92.19(14)
O12–Fe4–O1M	88.30(15)	O10–Fe10–O2I	104.94(16)
O1L–Fe4–O1M	78.88(15)	O10–Fe10–O1J	96.70(15)
O5–Fe5–O10	93.70(15)	O10–Fe10–O1K	162.97(16)
O5–Fe5–O12	93.77(15)	O11–Fe10–O2I	89.29(15)
O5–Fe5–O1I	95.16(15)	O11–Fe10–O1J	169.59(15)
O5–Fe5–O1N	87.61(15)	O11–Fe10–O1K	84.44(14)
O5–Fe5–O10	172.07(15)	O2I–Fe10–O1J	93.62(16)
O10–Fe5–O12	96.15(15)	O2I–Fe10–O1K	91.74(15)
O10–Fe5–O1I	86.50(15)	O1J–Fe10–O1K	85.48(15)
O10–Fe5–O1N	169.43(16)	O3–Fe11–O4	77.74(14)
O10–Fe5–O10	93.84(15)	O3–Fe11–O9	105.67(14)
O12–Fe5–O1I	170.50(16)	O3–Fe11–O10	107.51(15)
O12–Fe5–O1N	94.22(16)	O3–Fe11–O1C	87.48(15)
O12–Fe5–O10	87.84(15)	O3–Fe11–O2J	155.20(14)
O1I–Fe5–O1N	82.94(16)	O4–Fe11–O9	175.16(15)
O1I–Fe5–O10	82.88(15)	O4–Fe11–O10	103.57(14)
O1N-Fe5–O10	84.53(15)	O4–Fe11–O1C	94.22(14)
O1–Fe6–O4	81.54(13)	O4–Fe11–O2J	82.03(14)
O1–Fe6–O5	78.07(14)	O9–Fe11–O10	78.84(14)
O1–Fe6–O2G	93.77(15)	O9–Fe11–O1C	82.61(14)
O1–Fe6–O1H	86.19(15)	O9–Fe11–O2J	93.78(14)
O1–Fe6–O20	168.29(15)	O10–Fe11–O1C	158.69(15)
O4–Fe6–O5	91.31(14)	O10–Fe11–O2J	91.01(15)
O4–Fe6–O2G	169.23(14)	O1C–Fe11–O2J	79.80(14)
O4–Fe6–O1H	82.77(14)		

trimer units that are joined by two μ_3-hydroxide ligands and four 1,3-bridging trimethylacetate ligands. In **1** and **2**, Fe2 and Fe5 have solvent ligands coordinated. The corresponding Fe atoms in $[Fe_6O_2(OH)_2(O_2CC(CH_3)_3)_{12}]$ are five coordinate with trigonal bipyramidal geometry.

Lippard and co-workers [12,13] prepared two crystal forms of **3** using a completely different technique. In one

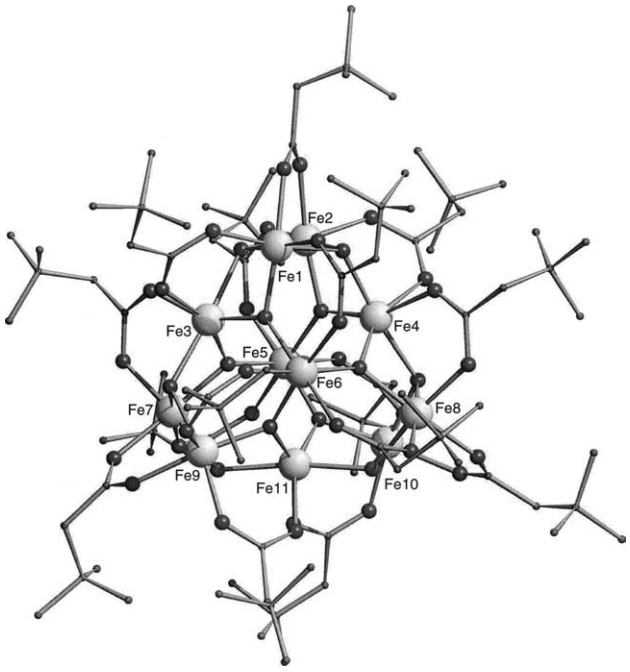

Fig. 4. The structure of **4** in the crystal.

of the crystal forms that was synthesised by Lippard and co-workers, MeCN is present. This would suggest that the unit cell for **3** should be the same but there is a subtle difference, **3** has an additional five molecules of MeCN per molecule of **3**. This has made the unit cell for **3** slightly bigger than the unit cell for the same complex produced by Lippard and co-workers. They also observed that four MeCN were hydrogen bonded to four of the μ_3-OH ligands. The O(H)–N hydrogen bond lengths range from 2.82 to 2.91 Å. This is the same as was observed for **3** and **4**. Bond length ranges are also similar to what was seen in **3** and **4**; Fe–O($O_2CC_6H_5$) are between 1.93 and 2.13 Å, Fe–O(OH) are 2.03–2.16 Å and Fe–O(O) are 1.88–1.94 Å. Lippard and co-workers also found that the Fe atoms formed a twisted prism and the twist angles they have recorded are 16.2°, 16.9° and 19.9°, this compliments our own findings for **3**.

In the other crystal form synthesised by Lippard and co-workers the cell is rhombohedral and has crystallographic D_3, symmetry. There are six THF molecules hydrogen bonded to each of the six μ_3-OH ligands with a O(H)–O distance of 2.78 Å. Fe–O($O_2CC_6H_5$) bond lengths range from 1.967 to 2.106 Å, Fe–O(OH) range from 2.061 to 2.078 Å and Fe–O(O) from 1.826 to 1.926 Å. Again these ranges are comparable with those seen in **3** and **4**. The symmetry of this crystal form means there is only one twist angle of 17.4°, which is similar to the angles observed in **3** and **4**.

A further pentacapped trigonal prism of Fe^{III} centres has been reported by Frey et al. [15], featuring a keto-carboxylate ligand. In that molecule, the ketone func-

Table 5
Selected bond lengths (Å) and bond angles (°) for **4**

Bond lengths			
Fe1–O1	2.077(3)	Fe6–O2A	2.104(3)
Fe1–O2	2.106(2)	Fe6–O2H	2.083(3)
Fe1–O4	1.899(3)	Fe6–O2L	2.156(3)
Fe1–O1A	1.944(3)	Fe7–O6	1.902(3)
Fe1–O1B	2.041(3)	Fe7–O8	2.125(2)
Fe1–O1D	1.974(3)	Fe7–O10	2.101(3)
Fe2–O1	2.151(3)	Fe7–O2F	1.986(3)
Fe2–O2	2.064(3)	Fe7–O2I	2.020(3)
Fe2–O3	1.903(2)	Fe7–O1K	1.957(3)
Fe2–O2B	2.031(3)	Fe8–O5	1.893(3)
Fe2–O1C	1.988(3)	Fe8–O7	2.134(3)
Fe2–O1E	1.937(3)	Fe8–O9	2.086(3)
Fe3–O2	2.081(3)	Fe8–O2G	1.986(3)
Fe3–O4	1.923(3)	Fe8–O1J	2.040(3)
Fe3–O6	1.931(3)	Fe8–O1L	1.944(3)
Fe3–O8	2.072(3)	Fe9–O8	2.061(3)
Fe3–O2D	2.075(3)	Fe9–O10	2.153(3)
Fe3–O1F	2.065(3)	Fe9–O12	1.893(2)
Fe4–O1	2.058(3)	Fe9–O1H	1.951(3)
Fe4–O3	1.918(2)	Fe9–O1I	2.039(3)
Fe4–O5	1.921(3)	Fe9–O2P	2.005(3)
Fe4–O7	2.077(2)	Fe10–O7	2.080(3)
Fe4–O2C	2.087(3)	Fe10–O9	2.128(2)
Fe4–O1G	2.121(3)	Fe10–O11	1.896(3)
Fe5–O3	1.924(3)	Fe10–O2J	2.065(3)
Fe5–O6	1.916(3)	Fe10–O1M	1.989(3)
Fe5–O11	1.929(3)	Fe10–O2N	1.945(3)
Fe5–O2E	2.112(3)	Fe11–O9	2.054(2)
Fe5–O2K	2.122(3)	Fe11–O10	2.044(3)
Fe5–O1N	2.120(3)	Fe11–O11	1.927(3)
Fe6–O4	1.914(3)	Fe11–O12	1.922(2)
Fe6–O5	1.923(3)	Fe11–O2M	2.118(3)
Fe6–O12	1.932(2)	Fe11–O1P	2.100(3)
Bond angles			
O1–Fe1–O2	82.96(10)	O5–Fe6–O2L	94.35(11)
O1–Fe1–O4	91.62(11)	O12–Fe6–O2A	169.53(11)
O1 -Fe1–O1 A	89.60(11)	O12–Fe6–O2H	93.68(11)
O1–Fe1–O1B	84.32(11)	O12–Fe6–O2L	91.10(10)
O1–Fe1–O1D	171.49(12)	O2A–Fe6–O2H	83.34(11)
O2–Fe1–O4	78.73(11)	O2A–Fe6–O2L	78.56(11)
O2–Fe1–O1A	172.32(11)	O2H–Fe6–O2L	82.06(11)
O2–Fe1–O1B	87.03(11)	O6–Fe7–O8	77.92(11)
O2–Fe1–O1D	94.40(11)	O6–Fe7–O10	91.40(11)
O4–Fe1–O1A	103.46(12)	O6–Fe7–O2F	94.84(12)
O4–Fe1–O1B	165.58(12)	O6–Fe7–O2I	164.27(11)
O4–Fe1–O1D	95.81(11)	O6–Fe7–O1K	105.58(12)
O1A–Fe1–O1B	90.37(12)	O8–Fe7–O10	82.23(10)
O1A–Fe1–O1D	92.69(12)	O8–Fe7–O2F	98.37(11)
O1B–Fe1–O1D	87.47(12)	O8–Fe7–O2I	86.54(11)
O1–Fe2–O2	82.15(10)	O8–Fe7–O1K	169.00(11)
O1–Fe2–O3	77.72(10)	O10–Fe7–O2F	173.72(11)
O1–Fe2–O2B	86.33(11)	O10–Fe7–O2I	83.99(11)
O1–Fe2–O1C	90.17(12)	O10–Fe7–O1K	87.22(11)
O1–Fe2–O1E	175.50(12)	O2F–Fe7–O2I	89.80(12)
O2–Fe2–O3	93.81(11)	O2F–Fe7–O1K	91.78(11)
O2–Fe2–O2B	85.04(11)	O2I–Fe7–O1K	89.26(11)
O2–Fe2–O1C	166.75(13)	O5–Fe8–O7	77.81(10)
O2–Fe2–O1E	93.55(12)	O5–Fe8–O9	91.43(10)
O3–Fe2–O2B	164.01(11)	O5–Fe8–O2G	96.67(12)
O3–Fe2–O1C	95.09(11)	O5–Fe8–O1J	164.76(11)
O3–Fe2–O1E	104.02(12)	O5–Fe8–O1L	103.94(11)
O2B–Fe2–O1C	83.70(12)	O7–Fe8–O9	82.43(9)
O2B–Fe2–O1E	91.97(12)	O7–Fe8–O2G	92.91(11)

Table 5 (*continued*)

Bond angles			
O1C–Fe2–O1E	93.79(14)	O7–Fe8–O1J	87.09(10)
O2–Fe3–O4	78.83(10)	O7–Fe8–O1L	172.69(11)
O2–Fe3–O6	104.07(11)	O9–Fe8–O2G	169.61(11)
O2–Fe3–O8	175.25(9)	O9–Fe8–O1J	84.50(10)
O2–Fe3–O2D	93.74(11)	O9–Fe8–O1L	90.40(10)
O2–Fe3–O1F	81.02(11)	O2G–Fe8–O1J	86.00(12)
O4–Fe3–O6	107.56(9)	O2G–Fe8–O1L	93.93(11)
O4–Fe3–O8	104.23(10)	O1J–Fe8–O1L	90.80(11)
O4–Fe3–O2D	89.01(11)	O8–Fe9–O10	82.50(10)
O4–Fe3–O1F	156.78(11)	O8–Fe9–O12	93.24(11)
O6–Fe3–O8	78.62(10)	O8–Fe9–O1H	94.52(11)
O6–Fe3–O2D	157.56(11)	O8–Fe9–O1I	84.98(10)
O6–Fe3–O1F	88.43(11)	O8–Fe9–O2P	166.55(11)
O8–Fe3–O2D	82.74(11)	O10–Fe9–O12	77.44(10)
O8–Fe3–O1F	95.22(11)	O10–Fe9–O1H	177.01(12)
O2D–Fe3–O1F	80.88(10)	O10–Fe9–O1I	85.84(10)
O1–Fe4–O3	79.75(10)	O10–Fe9–O2P	89.69(11)
O1–Fe4–O5	104.75(11)	O12–Fe9–O1H	102.68(11)
O1–Fe4–O7	173.75(10)	O12–Fe9–O1I	163.27(10)
O1–Fe4–O2C	93.73(11)	O12–Fe9–O2P	95.73(10)
O1–Fe4–O1G	79.82(11)	O1H–Fe9–O1I	94.04(11)
O3–Fe4–O5	109.90(11)	O1H–Fe9–O2P	93.26(12)
O3–Fe4–O7	104.21(10)	O1I–Fe9–O2P	83.54(11)
O3–Fe4–O2C	90.28(11)	O7–Fe10–O9	82.71(10)
O3–Fe4–O1G	155.76(11)	O7–Fe10–O11	91.83(10)
O5–Fe4–O7	78.62(10)	O7–Fe10–O2J	84.34(10)
O5–Fe4–O2C	154.54(12)	O7–Fe10–O1M	168.05(11)
O5–Fe4–O1G	87.88(11)	O7–Fe10–O2N	92.06(11)
O7–Fe4–O2C	81.51(11)	O9–Fe10–O11	78.03(10)
O7–Fe4–O1G	95.17(11)	O9–Fe10–O2J	86.61(10)
O2C–Fe4–O1G	78.18(12)	O9–Fe10–O1M	92.10(11)
O3–Fe5–O6	94.42(11)	O9–Fe10–O2N	174.72(11)
O3–Fe5–O11	94.72(10)	O11–Fe10–O2J	164.54(11)
O3–Fe5–O2E	93.52(11)	O11–Fe10–O1M	97.64(11)
O3–Fe5–O2K	169.16(12)	O11–Fe10–O2N	102.98(11)
O3–Fe5–O1N	91.25(10)	O2J–Fe10–O1M	84.61(11)
O6–Fe5–O11	94.20(11)	O2J–Fe10–O2N	92.15(11)
O6–Fe5–O2E	89.76(11)	O1M–Fe10–O2N	92.90(11)
O6–Fe5–O2K	94.66(11)	O9–Fe11–O10	172.72(10)
O6–Fe5–O1N	170.27(10)	O9–Fe11–O11	79.21(10)
O11–Fe5–O2E	170.56(11)	O9–Fe11–O12	104.69(10)
O11–Fe5–O2K	90.49(1 1)	O9–Fe11–O2M	94.10(11)
O11–Fe5–O1N	93.19(11)	O9–Fe11–O1P	81.88(10)
O2E–Fe5–O2K	80.63(11)	O10–Fe11–O11	104.94(10)
O2E–Fe5–O1N	82.01(10)	O10–Fe11–O12	79.54(10)
O2K–Fe5–O1N	78.95(11)	O10–Fe11–O2M	80.23(11)
O4–Fe6–O5	94.98(11)	O10–Fe11–O1P	92.35(11)
O4–Fe6–O12	95.95(11)	O11–Fe11–O12	111.70(11)
O4–Fe6–O2A	93.96(11)	O11–Fe11–O2M	87.70(11)
O4–Fe6–O2H	87.67(11)	O11–Fe11–O1P	154.76(11)
O4–Fe6–O2L	167.90(11)	O12–Fe11–O2M	154.97(11)
O5–Fe6–O12	93.77(10)	O12–Fe11–O1P	89.16(10)
O5–Fe6–O2A	88.72(11)	O2M–Fe11–O1P	77.10(10)
O5–Fe6–O2H	171.78(11)		

tions are found H-bonded to the surface hydroxide groups of the $\{Fe_{11}\}$ cage.

3.4. Magnetism

Variable temperature magnetic susceptibilities of powdered samples of **1** and **2** were measured between 1.8 and 300 K in a magnetic field of 100 G (Fig. 5). At room temperature $\chi_m T$ for **1** is 8.62 emu K mol^{-1}, which is similar to the value obtained for **2** of 8.34 emu K mol^{-1}. The expected room temperature $\chi_m T$ value, with $g = 2.00$, for both complexes is 26.25 emu K mol^{-4}. This suggests that there is a very strong anti-ferromagnetic exchange between the Fe^{III} centres. $\chi_m T$ decreases as the temperature is decreased and **1** reaches 1.71 emu K mol^{-1} at 1.8 K and **2** goes to 0.23 emu K mol^{-1} at 1.8 K. The curves for **1** and **2** are similar in shape and the curve for **1** has a sharp down turn at 1.8 K which appears to be heading for 0 emu K mol^{-1} at 0 K. Both **1** and **2** have an $S = 0$ ground state. $[Fe_6O_2(OH)_2(O_2CC_6H_5)_{12}(H_2O)(C_4H_8O_2)]$ also shows anti-ferromagnetic exchange and has a room temperature magnetic moment

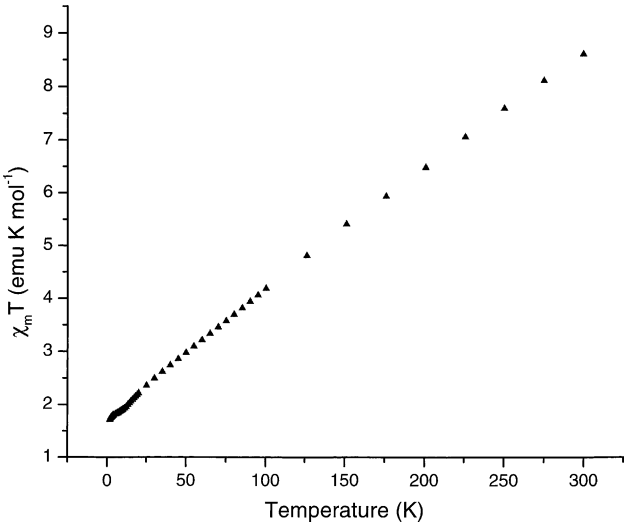

Fig. 5. Variable temperature magnetic behaviour of **1**, illustrated as a plot of $\chi_m T$ against T. The behaviour of **2** is very similar.

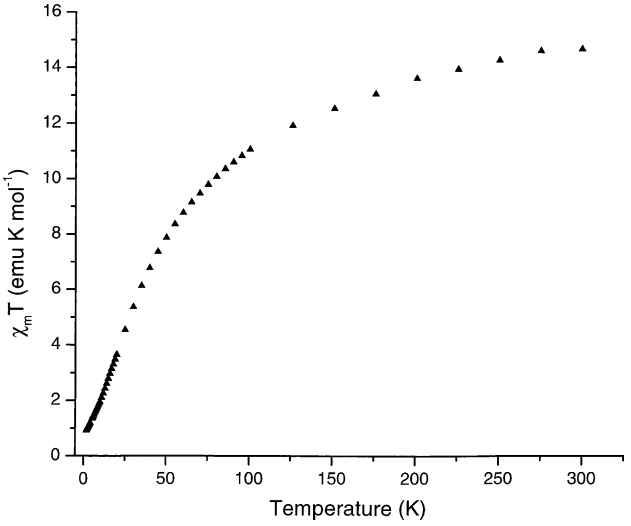

Fig. 6. Variable temperature magnetic behaviour of **3**, illustrated as a plot of $\chi_m T$ against T.

of 7.33 μ_B which decreases to 0.62 μ_B at 2 K [11]. Room temperature magnetic moments for **1** and **2** are 8.30 and 8.17 μ_B, respectively. These values decrease to 3.70 μ_B for **1** and 1.35 μ_B for **2** at 2 K.

Fig. 6 shows the variable temperature magnetic susceptibility of a powdered sample of **3**. This was measured in a magnetic field of 100 G between 1.8 and 300 K. Room temperature value for $\chi_m T$ is 14.71 emu K mol^{-1}. This decreases as the temperature decreases to 0.92 emu K mol^{-1} at 1.8 K. The expected room temperature value for 11 non-interacting Fe^{III} centres with $g = 2.00$ is 48.13 emu K mol^{-1}. There is a large difference between the theoretical and experimental room temperature value of $\chi_m T$. This suggests that there are very strong anti-ferromagnetic exchanges between the Fe centres. Lippard and co-workers [13] found that the magnetic moment of their product crystallised from THF at 298 K was 13.92 μ_B, and that this decreases to 3.32 μ_B at 2.6 K. **3** has a magnetic moment of 10.85 μ_B at 300 K and 2.71 μ_B at 1.8 K.

4. Conclusions

The high-temperature method used in the preparation of complexes **1**, **2**, **3** and **4** is an alternative to the usual methods that are employed in the synthesis of complexes of this nature. Unfortunately, where for chromium new clusters resulted [3–5], for iron only cages closely related to known compounds have resulted. This probably reflects the fact that much more cluster chemistry is known for Fe^{III} than was known for Cr^{III} when we began this project. Complexes **1** and **2** are new additions to the family of structures with the $[Fe_6O_2(OH)_2]^{12+}$ core, while **3** and **4** join the family of undecanuclear iron cages based on pentacapped trigonal prisms. This core is very similar to that found in the dodecanuclear chromium cage $[Cr_{12}O_9(OH)_3(O_2CC(CH_3)_3)_{15}]$, the difference being that the chromium cage has a central Cr^{III} centre.

As similar structures to **1**–**4** have been reported previously, it is debatable whether the high temperature employed in the synthesis is a requirement for the synthesis. However, the undecanuclear complexes are difficult to make in good yield [7], therefore there is some merit in this new approach. **3** and **4** cannot be made by refluxing the substrates in the recrystallisation solvents. The yields we find are poor to moderate, in the range 10–20%, and alternate routes to the complexes could be higher yielding. It is doubtful that the complexes are sufficiently interesting that they merit studies to optimise yields.

References

[1] (a) R. Sessoli, H. Tsai, A.R. Schake, S. Wang, J.B. Vincent, K. Foiling, D. Gatteschi, G. Christou, D.N. Hendrickson, J. Am. Chem. Soc. 115 (1993) 1804;
(b) R. Sessoli, D. Gatteschi, A. Caneschi, M.A. Novak, Nature 365 (1993) 141.

[2] A.S. Batsanov, G.A. Timco, Yu.T. Struchkov, N.V. Gerbeleu, K.M. Indrichan, Koord. Khim. 17 (1991) 662.

[3] I.M. Atkinson, C. Benelli, M. Murrie, S. Parsons, R.E.P. Winpenny, Chem. Commun. (1999) 285.

[4] S. Parsons, A.A. Smith, R.E.P. Winpenny, Chem. Commun. (2000) 579.

[5] R.A. Coxall, A. Parkin, S. Parsons, A.A. Smith, G.A. Timco, R.E.P. Winpenny, J. Solid State Chem. 159 (2001) 321.

[6] D. Collison, M. Murrie, V.S. Oganesyan, S. Piligkos, N.R.J. Poolton, G. Rajaraman, G.M. Smith, A.J. Thomson, G.A. Timco, W. Wernsdorfer, R.E.P. Winpenny, E.J.L. McInnes, Inorg. Chem. 42 (2003) 5293.

[7] W. Micklitz, V. McKee, R.L. Rardin, L.E. Pence, G.C. Papaefthymiou, S.G. Bott, S.J. Lippard, J. Am. Chem. Soc. 116 (1994) 8061.

[8] J. Cosier, A.M. Glazer, J. Appl. Cryst. 19 (1986) 105.

[9] SHELXL-PC Package, Bruker Analytical X-ray Systems, Madison, WI, 1998.

[10] N.V. Gerbeleu, A.S. Batsanov, G.A. Timco, Yu.T. Struchkov, K.M. Indrichan, G.A. Popovich, Dokl. Akad. Nauk. SSSR 293 (1987) 364.

[11] W. Micklitz, S.J. Lippard, Inorg. Chem. 27 (1988) 3067.

[12] S.M. Gorun, S.J. Lippard, Nature 319 (1986) 666.

[13] S.M. Gorun, G.C. Papaefthymiou, R.B. Frankel, S.J. Lippard, J. Am. Chem. Soc. 109 (1987) 3337.

[14] E. Keller, SCHAKAL-99: Program for Representation of Crystallographic Models, University of Freiburg, 1999.

[15] M. Frey, S.G. harris, J.M. Holmes, D.A. Nation, S. Parsons, P.A. Tasker, R.E.P. Winpenny, Chem. Eur. J. 6 (2000) 1407.

Available online at www.sciencedirect.com
SCIENCE DIRECT®
Polyhedron 23 (2004) 1567–1572
POLYHEDRON
www.elsevier.com/locate/poly

Synthesis and characterization of cyclopentadienylruthenium(II) complexes containing *N*,*N*′-donor Schiff base ligands: crystal and molecular structure of $[(\eta^5\text{-}C_5H_5)Ru(C_5H_4N\text{-}2\text{-}CH{=}N\text{–}C_6H_4\text{–}p\text{-}OCH_3)(PPh_3)]PF_6$ ☆

P. Govindaswamy [a], Yurij A. Mozharivskyj [b], Mohan Rao Kollipara [a,*]

[a] *Department of Chemistry, North-Eastern Hill University, Shillong 793 022, India*
[b] *Ames Laboratory, Iowa State University of Science and Technology, Ames, IA 50011, USA*

Received 27 February 2004; accepted 15 March 2004
Available online 20 April 2004

Abstract

Complexes of the formulae $[(\eta^5\text{-}C_5H_5)Ru(PPh_3)(C_5H_5N\text{-}2\text{-}CH{=}N\text{–}C_6H_4\text{–}p\text{-}X)]^+$ [X = H (**2a**), CH_3 (**2b**), OCH_3 (**2c**), Cl (**2d**), NO_2 (**2e**)] and $[(\eta^5\text{-}C_5H_5)Ru(PPh_3)(C_5H_5N\text{-}2\text{-}CH{=}N\text{–}C_6H_{11})]^+$ (**3**) were prepared by reacting *para*-substituted *N*-(pyrid-2-ylmethylene)-phenylamines (**2-PP**) and *N*-(pyrid-2-ylmethylene)cyclohexylamine (**2-PC**) with $[(\eta^5\text{-}C_5H_5)Ru(PPh_3)_2Cl]$ (**1**) in methanol. These complexes have been isolated as hexa-fluorophosphate salts. Representative complex **2c** has been established by single crystal X-ray diffraction analysis. Complex **2c** crystallizes in the orthorhombic space group P_{bcn}, with $a = 21.1560$ (11) Å, $b = 18.3972$ (9) Å and $c = 17.5130$ (9) Å, $V = 6816.3$ (6) Å^3 and $z = 8$. All these complexes were characterized by FT-IR, ^{1}H NMR and ^{31}P{^{1}H} NMR spectroscopy.
© 2004 Elsevier Ltd. All rights reserved.

Keywords: Cyclopentadienyl; Schiff bases; Pyridine-2-carboxaldehyde; Ruthenium

1. Introduction

As a part of our continuing investigation of the complexes of η^5-cyclopentadienyl-ruthenium(II) [1], η^5-indenylruthenium(II) [2], η^5-cyclopentadienylosmium(II) [3] and η^6-areneruthenium(II) [4] with a variety of nitrogen-based ligands, we here report the syntheses of complexes of the cyclopentadienylruthenium(II) system with some chelating Schiff base ligands. Considerable interest has arisen in the chemistry of ruthenium (II) complexes having Schiff bases [5] or chelating nitrogen heterocyclic ligands [6] because of their photochemical and catalytic activities [7]. Steric factors play an important role compared to electronic factors in the structure and chemistry of these complexes. We had earlier reported the reaction of η^5-indenylruthenium(II) [8] and η^6-arene-ruthenium(II) [9] with Schiff base ligands. During the reactions involving the analogous pentamethylcyclopentadienyl or indenyl systems, the products did not show evidence of binding of these organic ligands, simple coordination compounds being formed instead. Although these groups can provide more electron density to the metal for binding, their large bulk compared to the cyclopentadienyl ligand prevents effective binding. This observation indicates steric factors playing a major role compared to electronic factors. However, relatively fewer reports are available in the literature for the analogous cyclopentadienylruthenium(II) Schiff base complexes [10]. We report here the synthesis and characterization of new cationic cyclopentadienylruthenium(II) complexes with *N*,*N*′-donor Schiff base ligands, viz., various

☆ Supplementary data associated with this article can be found, in the online version, at doi: 10.1016/j.poly.2004.03.007.

* Corresponding author. Tel.: +91-364-272-2620; fax: +91-364-272-1000.
E-mail addresses: kmrao@nehu.ac.in, mrkollipara@yahoo.com (M. Rao Kollipara).

0277-5387/$ - see front matter © 2004 Elsevier Ltd. All rights reserved.
doi:10.1016/j.poly.2004.03.007

para-substituted *N*-(pyrid-2-ylmethylene) phenylamines (**2-PP**) and *N*-(pyrid-2-ylmethylene)cyclohexylamine (**2-PC**). The molecular structure of the complex $[(\eta^5\text{-}C_5H_5)Ru(C_5H_4N\text{-}2\text{-}CH{=}N\text{–}C_6H_4\text{–}p\text{-}OCH_3)(PPh_3)]PF_6$ as solved by X-ray crystallography is reported here as well.

2. Experimental

2.1. General remarks

All reactions were carried out in distilled and dried solvents under a dry nitrogen atmosphere. $RuCl_3 \cdot 3H_2O$ was purchased from Arora Matthey Ltd. and used as such. Pyridine-2-carboxaldehyde (Fluka) was purchased and used as received. All liquid amines were reagent grade and distilled prior to use, while solid amines were used as such. Elemental analyses were performed in a Perkin–Elmer-2400 CHN/O analyzer. Infrared spectra were recorded on a Perkin–Elmer-model 983 spectrophotometer with the sample prepared as KBr pellets. Electronic spectra were recorded on a Hitachi-300 spectrophotometer. Conductivity measurements were performed in Wayne Kerr automatic precision bridge B-905. The ^1H NMR spectra were recorded in $CDCl_3$ solvent (with tetramethylsilane as the internal standard) on a Bruker ACF-400 MHz spectrometer, coupling constants J being given in hertz (hz). $^{31}P\{^1H\}$ NMR chemical shifts were recorded relative to H_3PO_4 (85%). The ligands $C_5H_4N\text{-}2\text{-}CH{=}C_6H_4\text{–}p\text{-}X$ (where X = H, CH_3, OCH_3, Cl, NO_2) [11], and the precursor complex $[(\eta^5\text{-}C_5H_5)Ru(PPh_3)_2Cl]$ (**1**) [12] were prepared following literature methods.

2.2. Preparation of $[(\eta^5\text{-}C_5H_5)Ru(PPh_3)(C_5H_5N\text{-}2\text{-}CH{=}N\text{–}C_6H_4\text{–}p\text{-}X)]PF_6$ (**2a**–**e**), (X = H (**2a**), CH_3 (**2b**), OCH_3 (**2c**), Cl (**2d**), NO_2 (**2e**)

The following general procedure was used for preparation of these five complexes:

The mixture of the starting complex $[(\eta^5\text{-}C_5H_5)Ru(PPh_3)_2Cl]$ (0.1 g, 0.110 mmol), the appropriate Schiff base ligand **2-PP** (0.165 mmol) and NH_4PF_6 (0.165 mmol) was refluxed in methanol (40 ml) whereby the orange color suspension gradually changed to a dark brown solution. It was refluxed for 6 h, and the solvent then rotary evaporated. The residue was dissolved in dichloromethane and filtered through a short silica gel column to remove insoluble material. The filtrate was again concentrated to about 2 ml, whereupon addition of excess hexane gave the desired complexes (**2a**–**e**) as dark brown solids. The solid was washed with diethyl ether and dried under vacuum to afford an 80–85% yield of the complexes.

2.3. Preparation of $[(\eta^5\text{-}C_5H_5)Ru(PPh_3)(\mathbf{2\text{-}PC})]PF_6$ (**3**)

This complex was prepared in a similar manner to that of the preparation of (**2a**–**e**), except that the ligand **2-PC** was used instead of **2-PP** to yield the dark brown solid complex in 80% yield.

3. Structure analysis and refinement

X-ray quality crystals of the complex **2c** were grown by slow diffusion of hexane into a dichloromethane solution. A brown crystal of complex **2c** was mounted on a Bruker Apex CCD diffractometer in a full reciprocal sphere equipped with CCD detector and used for data collection. X-ray intensity data were collected with graphite mono-chromated Mo Kα radiation at 293(2) K, with 0.3° scans in ω scan mode and 10-s exposure time per frame. The intensity data were corrected for Lorentz and polarization effects through the SAINT program [13]. A summary of the crystal data, data collection parameters and convergence results are compiled in Table 3. An empirical absorption correction was made by modeling a transmission surface by spherical harmonics employing equivalent reflections with $I > 3\sigma(I)$ (program SADABS) [14]. The structure was solved by direct methods [15]. All the non-hydrogen atoms were refined anisotropically using the full-matrix least-squares technique on F^2 using the SHELXL 97 software [16]. All the hydrogen atom positions were found from difference Fourier synthesis after four cycles of anisotropic refinement and as ''riding'' model. Fig. 1 is the ORTEP [17] representation of the molecules with 50% probability thermal ellipsoids displayed. Refinement coverage at a final value of $R_1 = 0.0462$ (for observed data F) and at value of $wR_2 = 0.1192$, respectively (for unique data F^2).

4. Results and discussion

The synthetic reaction of the cyclopentadienyl complex **1** with excess of *N*,*N*′-donor Schiff base ligands, viz., **2-PP** and **2-PC**, in methanol under refluxing condition resulted in the formation of brown colored and air-stable cationic complexes of the type **2** (Scheme 1) by dissociation of one of the triphenylphosphines and chloride ligand. Here, we would like to point out that when similar reactions were carried out with complexes bearing the substituted analogue Cp^* and the indenyl group instead, the resulting complexes had no organic groups bound to the metal.

These complexes are highly soluble in polar solvents such as chloroform, dichloromethane, etc., but insoluble in non-polar solvents such as hexane, pentane, etc.

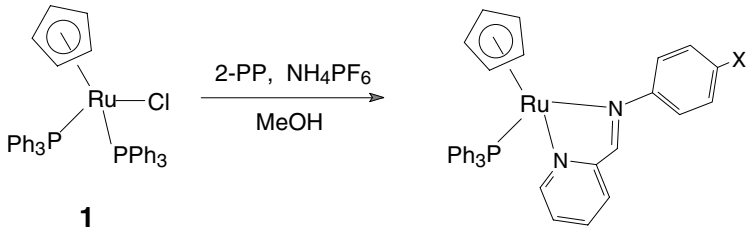

1

X = H, CH_3, OCH_3, Cl, NO_2 (2a-e)

2-PP = N-(pyrid-2-ylmethylene)phenylamine

Scheme 1.

These complexes were characterized by using analytical, IR, ^{1}H and ^{31}P NMR spectroscopic techniques. The data, as presented in Table 1, support the formation of these complexes. The X-ray structure of the representative complex **2c** was determined to confirm the structure of the complex. The IR spectra of these complexes show a strong band in the range of 1602–1584 cm^{-1} due to the $\nu_{C=N}$ group of the Schiff base ligand. In addition, the IR spectra contain strong bands due to the phenyl groups of triphenylphosphine and a strong band at 840 cm^{-1} due to the ν_{P-F} of the PF_6 group. Complex **2e** shows the characteristic bands for ν_{NO2} (asymmetric stretch at 1523 cm^{-1} and symmetric stretch 1346 cm^{-1}).

In the ^{1}H NMR spectra of these complexes, the cyclopentadienyl ring protons display a sharp singlet at 4.7 ppm. The presence of η-Cp, PPh_3 and **2-PP** or **2-PC** in a 1:1:1 ratio is inferred from the areas obtained upon peak integration of the ^{1}H NMR spectra. The resonance of the *ortho* proton of the pyridine ring of the ligand is observed as a doublet in the range 9.28–8.45 ppm in these complexes. The multiplet observed in the range 8.13–6.76 ppm is due to the phenyl protons of the triphenylphosphine moiety, the amine group and the *N*-heterocyclic ring of the ligands (**2-PP** or **2-PC**). The ^{31}P NMR spectra of the complexes **2** and **3** exhibit a single sharp resonance for triphenylphosphine around 47 ppm, whereas the starting complex [(η^5-Cp)Ru(PPh_3)$_2$Cl] (**1**) exhibits it at 42 ppm for both triphenylphosphines indicating the cationic nature of these complexes. The ionic nature of these complexes was confirmed by carrying out conductivity measurements (Table 2).

The electronic spectra and conductivity data of these complexes are shown in Table 2. The electronic spectra of these complexes in dichloromethane exhibit bands in the range of 428–461 nm. This low-energy absorption is assigned to a Ru dπ to ligand π* metal-to-ligand charge transfer (MLCT) transition. The molar conductivity of the complexes in acetonitrile solvent ranges from 123.0 to 150.0 S cm^2 mol^{-1}, suggesting that these complexes are ionically dissociated in the ratio of 1:1 [18].

Table 1
Analytical[a], FT IR, ^{1}H NMR[b] and ^{31}P NMR of the complexes **2a–e** and **3**

Complex	Analyses %			IR (KBr Pellets, cm^{-1})	^{1}H NMR δ [multiplicity, nH, J (Hz)]	^{31}P NMR (δ)
	C	H	N			
2a	55.6 (56.0)	4.0 (4.3)	3.7 (3.4)	1587($\nu_{C=N}$) 839(ν_{P-F})	9.28 (d, 1H, 5.48); 8.26 (d, 1H); 7.69–6.96 (m, 23H); 4.66 (s, 5H, Cp).	46.91
2b	56.1 (56.6)	4.1 (4.3)	3.6 (2.9)	1602($\nu_{C=N}$) 840(ν_{P-F})	9.26 (d, 1H, 2.96); 8.23 (d, 1H); 7.65–6.91 (m, 22H); 4.67 (s, 5H, Cp); 2.36 (s, 3H).	47.09
2c	55.0 (55.5)	4.1 (4.5)	3.6 (3.2)	1598($\nu_{C=N}$) 837(ν_{P-F})	9.20 (d, 1H, 5.56); 8.23 (d, 1H); 7.69–6.76 (m, 22H); 4.68 (s, 5H, Cp); 3.84 (s, 3H)	47.25
2d	53.2 (53.8)	3.7 (3.2)	3.5 (2.9)	1586($\nu_{C=N}$) 837(ν_{P-F})	9.21 (d, 1H, 5.44); 8.31 (d, 1H); 7.73–6.96 (m, 22H); 4.68 (s, 5H, Cp)	46.24
2e	52.5 (52.4)	3.6 (3.9)	5.3 (5.7)	1589($\nu_{C=N}$) 840(ν_{P-F})	8.45 (d, 1H, 2.96); 8.11 (d, 1H); 7.83–6.93 (m, 22H); 4.69 (s, 5H, Cp)	46.70
3	55.3 (55.1)	4.6 (4.2)	3.7 (3.9)	1589($\nu_{C=N}$) 839(ν_{P-F})	9.06 (d, 1H, 7.04); 8.23 (d, 1H); 8.14–7.04 (m, 18H); 4.65 (s, 5H, Cp); 1.12–2.10 (m, 10H).	47.35

[a] Calculated values are in parentheses.
[b] In $CDCl_3$; s singlet; d, doublet; m, multiplet; $J_{(H-H)}$ in Hz.

Table 2
UV–Vis and conductivity data of the complexes at room temperature

S. no.	Complexes	λ_{max} (nm)	Conductivity, Λ_m ($S\,cm^2\,mol^{-1}$)
2a	$[(\eta^5\text{-}C_5H_5)Ru(PPh_3)(C_5H_4N\text{-}2\text{-}CH{=}N\text{–}C_6H_4\text{–}p\text{-}H)]PF_6$	454	150.00
2b	$[(\eta^5\text{-}C_5H_5)Ru(PPh_3)(C_5H_4N\text{-}2\text{-}CH{=}N\text{–}C_6H_4\text{–}p\text{-}CH_3)]PF_6$	452	126.02
2c	$[(\eta^5\text{-}C_5H_5)Ru(PPh_3)(C_5H_4N\text{-}2\text{-}CH{=}N\text{–}C_6H_4\text{–}p\text{-}CH_3)]PF_6$	454	143.90
2d	$[(\eta^5\text{-}C_5H_5)Ru(PPh_3)(C_5H_4N\text{-}2\text{-}CH{=}N\text{–}C_6H_4\text{–}p\text{-}Cl)]PF_6$	458	137.91
2e	$[(\eta^5\text{-}C_5H_5)Ru(PPh_3)(C_5H_4N\text{-}2\text{-}CH{=}N\text{–}C_6H_4\text{–}p\text{-}NO_2)]PF_6$	461	136.79
3	$[(\eta^5\text{-}C_5H_5)Ru(PPh_3)(C_5H_4N\text{-}2\text{-}CH{=}N\text{–}C_6H_{11})]PF_6$	428	123.80

Table 3
Summary of structure determination of complex $[(\eta^5\text{-}C_5H_5)Ru(C_5H_4N\text{-}2\text{-}CH{=}N\text{–}C_6H_4\text{–}p\text{-}OCH_3)]PF_6$ (**2c**)

Formula	$C_{36}H_{32}F_6N_2OP2Ru$
Formula weight	785.65
Crystal system	orthorhombic
Space group	*Pbcn*
Unit cell dimensions	
a (Å)	21.1560(11)
b (Å)	18.3972(9)
c (Å)	17.5130(3)
V (Å^3)	6816.3(6)
Z	8
Crystal size (mm)	$0.3 \times 0.3 \times 0.6$
D_{calc} ($g\,cm^{-3}$)	1.531
F(0 0 0)	3184
θ range for data collection (°)	1.87–28.30
Index ranges	$-28 \leqslant h 27$, $-23 \leqslant k \leqslant 24$, $-23 \leqslant l \leqslant 23$
Reflections collected	57 254
Independent reflections	8285 [$R_{int} = 0.0354$]
Absorption coefficient (mm^{-1})	0.619
Absorption correction	empirical (SADABS)
Refinement method	full-matrix least-squares on F^2
Data/restraints/parameters	8285/0/356
Goodness-of-fit on F^2	1.006
Final *R* indices [$I > 2\sigma(I)$]	$R_1 = 0.0462$, $wR_2 = 0.1192$
R indices (all data)	$R_1 = 0.0594$, $wR_2 = 0.1286$
Largest difference peak and hole ($e\,Å^{-3}$)	0.896 and −0.530

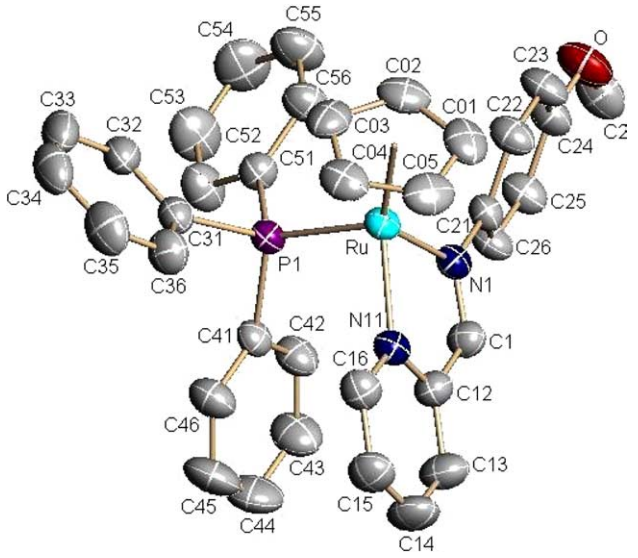

Fig. 1. ORTEP drawing of compound **2c** with 50% probability thermal ellipsoids. Hydrogen atoms and PF_6 omitted for clarity.

5. Crystal structure of 2c

The structure of complex **2c** is shown in Fig. 1. Representative bond length and bond angle values are listed in Table 4. The ruthenium atom is coordinated to two nitrogen atoms of the Schiff base ligand, one triphenylphosphine ligand and a pentahapto-bound cyclopentadienyl ligand. The geometry around the metal atom can be regarded as distorted octahedral if the η^5-cyclopentadienyl group is assumed to occupy three facial coordinated positions.

The $[(\eta^5\text{-}C_5H_5)Ru(PPh_3)(C_5H_5N\text{-}2\text{-}CH{=}N\text{–}C_6H_4\text{–}p\text{-}OCH_3)]PF_6$ complex crystallizes in the orthorhombic space group P_{bcn}. The cyclopentadienyl group is clearly bonded in a pentahapto fashion to the metal. Three of the Ru–C bond lengths, viz., those involving the C(03), C(04) and C(05), are shorter (2.191, 2.182 and 2.196 Å) than the other two bonds involving the C(01) and C(02) carbon atoms (2.214 and 2.211 Å). The average Ru–C distance is 2.199 Å, whereas the distance between the ruthenium atom and the centroid of the ring is 1.837 Å at the axis $x = 0.0947$, $y = 0.0534$ and $z = 0.4796$. The Ru–P bond length is 2.3100 Å, which is within the usual range of Ru–P bond distances (2.20–2.43 Å) [19]. The ruthenium atom is directly coordinated to two nitrogen atoms of the Schiff base ligand with an average distance of 2.090 Å. The bite angle of the chelating ligand is 76.42(8°), not very different from that in other related complexes [20]. The geometry of the complex is octahedral (of the piano-stool type) with the cyclopentadienyl moiety occupying three coordination sites. This is evident in the nearly 90° values for the bond angle N(1)–Ru–P(1) between the non-cyclopentadienyl ligands (90.39(6)°) and for the bond angle N(11)–Ru–P(1) (92.67(6)°) at the metal centre. The orientation of the phenyl group of the amine is similar to the observed mutually perpendicular orientation found for similar types of ligand in arene ruthenium complexes [9].

Table 4
Selected bond lengths (Å) and bond angles (°) for [CpRu(PPh_3)(C_5H_5N-2-CH=N–C_6H_4–*p*-OCH_3)]PF_6 (**2c**)

Bond lengths					
Ru(1)–N(11)	2.0801(13)	Ru(1)–N(1)	2.110(2)	Ru(1)–P(1)	2.3100(8)
Ru(1)–C(01)	2.214(2)	Ru(1)–C(02)	2.211(2)	Ru(1)–C(03)	2.191(2)
Ru(1)–C(04)	2.182(2)	Ru(1)–C(05)	2.196(2)	P(1)–C(51)	1.8357(12)
P(1)–C(31)	1.8570(12)	P(1)–C(41)	1.8363(12)	N(1)–C(1)	1.296(4)
N(1)–C(21)	1.438(3)	N(11)–C(12)	1.3900	N(11)–C(16)	1.3900
Ru–Cp[a]	1.837				
Bond angles					
N(11)–Ru–N(1)	76.42(8)	N(11)–Ru–P(1)	92.67(6)		
N(1)–Ru–P(1)	90.39(6)				

[a] Ruthenium to centroid of Cp.

6. Conclusion

We have observed interesting phenomena in the case of the cyclopentadienyl complex **1**, which distinguish it from the analogous pentamethylcyclopentadienyl or indenyl ruthenium systems. Unlike the case of the complex **1**, the reactions of Schiff bases with the [(η^5-Cp*)Ru(PPh_3)$_2$Cl] and [(η^5-ind.)Ru(PPh_3)$_2$Cl] systems yield complexes without any organic group. We suggest that in order to obtain complexes bound to organic ligands for these cases, one has to start from acetonitrile complexes. The reactions of [(η^5-Cp)Ru(PPh_3)$_2$Cl] with Schiff base ligands, viz, *para*-substituted *N*-(pyrid-2-yl methylene)phenylamines and *N*-(pyrid-2-ylmethylene)-cyclohexylamine, in methanol yielded complexes **2a**–**e** of the type [[(η^5-Cp)Ru(PPh_3)(**2-PP**)]X and [(η^5-Cp)Ru (PPh_3)(**2-PC**)]X]. The molecular structure of the representative complex **2c** has been characterized by single crystal X-ray diffraction analysis.

7. Supplementary material

Crystallographic data for the structural analysis have been deposited at the Cambridge Crystallographic Data Centre (CCDC), CCDC No. 231959 for complex **2c**. Copies of this information may be obtained free of charge from the Director, CCDC, 12 Union Road, Cambridge, CB2 1EZ, UK (fax: +44-1223-336033; e-mail: deposit@ccdc.cam.ac.uk; website: www: http://www.ccdc.cam.ac.uk).

Acknowledgements

We thank Professor R.H. Duncan Lyngdoh for his help in preparing the manuscript. K.M.R. and P.G. thank the Sophisticated Instruments Facility (SIF), Indian Institute of Science, Bangalore, for providing the NMR facility.

References

[1] (a) M.R. Kollipara, C.R.K. Rao, P.S. Zacharias, Polyhedron 16 (1997) 2369;
(b) R. Lalrempuia, P. Govindaswamy, Y.A. Mozharivskyj, M.R. Kollipara, Polyhedron 23 (2004) 1069;
(c) M.R. Kollipara, L. Mishra, U.C. Agarwala, Polyhedron 6 (1987) 1383.
[2] M.R. Kollipara, E.K. Rymmai, Polyhedron 22 (2003) 307.
[3] (a) R. Lalrempuia, P.J. Carroll, M.R. Kollipara, Polyhedron 22 (2003) 1391;
(b) R. Lalrempuia, Hemant Yennawar, Y.A. Mozharivskyj, M.R. Kollipara, J. Organomet. Chem. 689 (2004) 539.
[4] (a) R. Lalrempuia, M.R. Kollipara, Polyhedron 22 (2003) 3155;
(b) M.R. Kollipara, P. Sarkhel, S. Chakraborty, R. Lalrempuia, J. Coord. Chem. 56 (2003) 1085;
(c) Lalrempuia, P.J. Carroll, M.R. Kollipara, J. Coord. Chem. 56 (2003) 1499.
[5] S.A. Serron, C.M. Haar, S.P. Nolan, Organometallics 16 (1997) 5120.
[6] (a) C.W. Chang, G.H. Lee, Organometallics 22 (2003) 3107;
(b) M.R. Kollipara, E.K. Rymmai, Polyhedron 22 (2003) 307.
[7] (a) C.S. Hauser, C. Slugove, K. Mereiter, R. Schmid, K. Kirchner, L. Xiao, W. Weissensteiner, J. Chem. Soc., Dalton Trans. (2001) 2989;
(b) U. Karllson, G.Z. Wang, J.-E. Backvall, J. Org. Chem. 59 (1994) 1196;
(c) C. Ruppin, P.H. Dixneuf, S. Lewlier, Tetrahedron Lett. 20 (1998) 5365;
(d) B. Seiller, C. Bruneau, P.H. Dixneuf, J. Chem. Soc., Chem. Commun. 493 (1994);
(e) V. Rotleng, R. Bertani, M. Pfeffer, C. Sirlin, J. Hirschinges, Inorg. Chem. 40 (2001) 5117;
(f) C.A. Merlic, M.E. Pauly, J. Am. Chem. Soc. 18 (1996) 11319.
[8] S.S. Keisham, Y.A. Mozharivskyj, P.J. Carroll, M.R. Kollipara, J. Organomet. Chem. 689 (2004) 1249.
[9] R. Lalrempuia, M.R. Kollipara, P.J. Carroll, Polyhedron 22 (2003) 605.
[10] S.K. Mandal, A.R. Chakravarty, Polyhedron 10 (1991) 2483.
[11] (a) R.N. Dominey, B. Hauser, J. Habbard, J. Dunham, Inorg. Chem. 30 (1991) 4754;
(b) E.V. Dose, L.J. Wilson, Inorg. Chem. 17 (1978) 2660.
[12] M.I. Bruce, N.J. Windsor, Aust. J. Chem. 30 (1977) 1601.
[13] D. Becke, J. Chem. Phys. 98 (1993) 5648.
[14] XRD Single Crystal Software; Bruker Analytical X-ray systems, Madison, WI, 2002.
[15] G.M. Sheldrick, SHELXS 86, Program for Crystal Structure Solution, University of Göttingen, Göttingen, Germany, 1986.
[16] M. Sheldrick, SHELXS 97, Program for Crystal Structure Refinement, University of Göttingen, Göttingen, Germany, 1997.

[17] C.K. Johnson, ORTEP II: A Fortran Thermal Ellipsoid Plot Program for Crystal Structure Illustrations, ORNL-5138, 1976.
[18] J. Geary, Coord. Chem. Rev. 7 (1971) 81.
[19] L.J. Guggenberger, Inorg. Chem. 12 (1973) 1317.
[20] S.K. Mandal, A.R. Chakravarty, Polyhedron 11 (1992) 823.

Available online at www.sciencedirect.com
SCIENCE DIRECT®
Polyhedron 23 (2004) 1573–1578
POLYHEDRON
www.elsevier.com/locate/poly

Syntheses and study on nickel(II) complexes with thiodiglycolic acid and nitrogen-donor ligands. X-ray structures of $[Ni(bpy)(tdga)(H_2O)]\cdot 4H_2O$ and $[(en)Ni(\mu\text{-}tdga)_2Ni(en)]\cdot 4H_2O$ ($tdgaH_2$ = thiodiglycolic acid)

Pavel Kopel [a,*], Zdeněk Trávníček [a], Jaromír Marek [b], Jerzy Mrozinski [c]

[a] Department of Inorganic Chemistry, Faculty of Science, Palacký University, Křížkovského 10, CZ-771 47 Olomouc, Czech Republic
[b] Laboratory of Functional Genomics and Proteomics, Faculty of Science, Masaryk University, Kotlářská 2, CZ-611 37 Brno, Czech Republic
[c] Faculty of Chemistry, University of Wroclaw, 14 F. Joliot-Curie, PL-50 383 Wroclaw, Poland

Received 6 January 2004; accepted 16 March 2004
Available online 20 April 2004

Abstract

Mixed-ligand Ni(II) complexes involving thiodiglycolate(2−) anion (tdga) and nitrogen-donor ligands in the coordination sphere have been prepared. The complexes of composition $[Ni(bpy)(tdga)(H_2O)]\cdot 4H_2O$ (**1**), $[(en)Ni(\mu\text{-}tdga)_2Ni(en)]\cdot 4H_2O$ (**2**), $[Ni(phen)(tdga)(H_2O)]$ (**3**), $[Ni(1,8\text{-}dan)(tdga)(H_2O)]$ (**4**), $[Ni(nphen)(tdga)(H_2O)]\cdot H_2O$ (**5**), $[Ni(ampy)(tdga)(H_2O)]$ (**6**), where bpy = 2,2′-bipyridine, en = ethylenediamine, phen = 1,10-phenanthroline, 1,8-dan = 1,8-diaminonaphthalene, nphen = 5-nitro-1,10-phenanthroline and ampy = 2-(aminomethyl)-pyridine, have been characterized by elemental analysis, IR and UV–Vis spectroscopies, and magnetic susceptibility measurements. Room temperature effective magnetic moments for **1**–**6** are ranging from 3.06 to 3.28 μ_{eff}/μ_B. and thus indicating that nickel atoms are six-coordinated in a deformed octahedral arrangement in all the prepared complexes. This conclusion has been confirmed by single-crystal X-ray analysis of $[Ni(bpy)(tdga)(H_2O)]\cdot 4H_2O$ (**1**). A binuclear structure of complex $[(en)Ni(\mu\text{-}tdga)_2Ni(en)]\cdot 4H_2O$ (**2**) has been anticipated in connection with study of its magnetic properties over the 1.8–300 K temperature range ($J = -4.35$ cm^{-1}, $D = 5.53$ cm^{-1}, $zJ = -0.94$ cm^{-1} for $g = 2.00$) and unambiguously proved by a single-crystal X-ray analysis.
© 2004 Elsevier Ltd. All rights reserved.

Keywords: Nickel(II); Thiodiglycolic acid complexes; X-ray structures; Magnetic properties

1. Introduction

Transition metal complexes of carboxylic acids are in the interests of many research workers for many years. The complexes are often studied not only for their interesting magnetic properties but also for their biological occurrence in living organisms in metalloenzymes. It is well known that there are many possibilities for bonding of carboxylato group including also bridging properties [1,2]. More complicated systems are obtained in the case of polycarboxylic acids in comparison with monocarboxylic ones. For instance, thiodiglycolic acid belongs to dicarboxylic acids and moreover, it contains sulfur atom which can also takes part in coordination to central atom. To date, some transition metal complexes involving thiodiglycolic acid were characterized by single-crystal X-ray analysis, e.g. Cd(II), Zn(II), Ni(II), Cu(II) and Nd(III) [3–9]. From the X-ray study follows that the compounds can be either mononuclear, with one- or two-coordinated carboxylato groups, or polynuclear with tdga mostly forming linear chains having uncoordinated sulfur atom. The coordination sphere of a central atom in these systems may be completed by coordination of water molecules and/or nitrogen-donor ligands.

In our recent work, we have prepared and studied binuclear copper(II) complexes of the composition

* Corresponding author. Tel.: +420-58-563-4354; fax: +420-58-522-5737.
E-mail address: kopel@risc.upol.cz (P. Kopel).

0277-5387/$ - see front matter © 2004 Elsevier Ltd. All rights reserved.
doi:10.1016/j.poly.2004.03.005

$[(phen)_2Cu(\mu\text{-tdga})Cu(phen)](NO_3)_2 \cdot 5H_2O$ and $[(H_2O)(pmdien)Cu(\mu\text{-tdga})Cu(pmdien)(H_2O)](ClO_4)_2$, where pmdien = *N*,*N*,*N*′,*N*″,*N*″-pentamethyldiethylenetriamine. It has been proved by single-crystal X-ray analysis that the complexes are bridged by thiodiglycolate dianion in different coordination modes. Magnetic susceptibility measurements over the 1.9–300 K temperature range revealed weak antiferromagnetic interactions between copper atoms in both complexes [10]. Our effort to prepare Mn(II) complex with tdga bridge has led to the synthesis of $[Mn(phen)_2(H_2O)_2][Mn(phen)_2(tdga)](tdga) \cdot 13H_2O$. Its crystal and molecular structure proved coordination of tdga to one Mn(II) center by two oxygens of both carboxylato groups leading to the formation of an eight-membered ring. A sulfur atom is not coordinated to Mn(II) ion in the case and one uncoordinated tdga dianion is also present in the structure [11].

In this paper, we report the results of study on mixed-ligand nickel(II) complexes involving a combination of the thiodiglycolate(2−) anion (tdga) and nitrogen-donor ligands in the coordination sphere. The aim of the present work was also to prove a coordination mode of thiodiglycolic acid to nickel centers and to compare our findings with published results. We have decided to use bidentate aromatic as well as aliphatic nitrogen-donor ligands for the replacement of coordinated water molecules in the starting $[Ni(tdga)(H_2O)_3]$ complex. Molecular structures of two complexes were determined by single-crystal X-ray analysis. Surprisingly, the complex **2** is dinuclear with bridging thiodiglycolato dianion having composition of $[(en)Ni(\mu\text{-tdga})_2Ni(en)] \cdot 4H_2O$.

2. Experimental

2.1. Materials and methods

The C, H, N, S analyses were carried out on an EA 1108 instrument (Fisons). IR and diffuse-reflectance spectra in Nujol mulls were recorded on a Specord M 80 and on a Specord M 40 (Carl Zeiss, Jena), respectively. Magnetochemical data for **1**–**6** were obtained by Faraday method at 293 K using a Sartorius M-25D electrobalance. $Hg[Co(SCN)_4]$ was used as a calibrant. The correction for diamagnetism was calculated using Pascal's constants [12]. The magnetic susceptibility of the powdered sample **2** was measured over the temperature range 1.8–300 K using a Quantum Design SQUID-based MPMSXL-5-type magnetometer. The superconducting magnet was generally operated at a field strength ranging from 0 to 5 T. Magnetization was made at magnetic field 0.5 T. The SQUID magnetometer was calibrated with a palladium rod sample for which the gram magnetic susceptibility was taken as 5.30×10^{-6} cm^3 g^{-1} at $T = 293.1$ K. Diamagnetic correction is based on substracting the sample-holder signal and the contribution χ_{dia} estimated from the Pascal constants as -289×10^{-6} cm^3 mol^{-1}. The temperature independent paramagnetism of the Ni^{2+} centers

$$\chi_{tip} = \frac{8N\beta^2}{10\,Dq},$$

was used as $+215 \times 10^{-6}$ cm^3 mol^{-1}.

2.2. Syntheses

2.2.1. $[Ni(tdga)(H_2O)_3]$

A solution of $tdgaH_2$ (1.5 g, 10 mmol) dissolved in water (20 cm^2) was added to a well-stirred suspension of $NiCO_3 \cdot 2Ni(OH)_2 \cdot 4H_2O$ (3.76 g, 10 mmol) in water (100 cm^2). The reaction mixture was stirred and heated at 80 °C for 3 h. A small amount of insoluble nickel salt was filtered off. The solution was left for crystallization at ambient temperature. After two weeks thick green needles were filtered off and washed several times with small amount of cold water, and dried in air. Yield: 68%. *Anal.* Calc.: C, 18.4; H, 3.9; S, 12.3. Found: C, 18.8; H, 3.9; S, 12.0%.

2.2.2. General preparation of $[Ni(bpy)(tdga)(H_2O)] \cdot 4H_2O$ (**1**), $[(en)Ni(\mu\text{-tdga})_2Ni(en)] \cdot 4H_2O$ (**2**), $[Ni(phen)(tdga)(H_2O)]$ (**3**), $[Ni(1,8\text{-dan})(tdga)(H_2O)]$ (**4**), $[Ni(nphen)(tdga)(H_2O)] \cdot H_2O$ (**5**), $[Ni(ampy)(tdga)(H_2O)]$ (**6**)

The complexes were prepared by reaction of $[Ni(tdga)(H_2O)_3]$ (0.26 g, 1 mmol) with appropriate bidentate ligand (1.2 mmol). $[Ni(tdga)(H_2O)_3]$ was dissolved in 50 cm^3 of water and then, ligands dissolved in ethanol were added during stirring. A change in color of solution was observed. The reaction mixture was heated at 80 °C for 30 min. and left for crystallization at ambient temperature. Crystals or crystalline solids were obtained approximately after a week. These were filtered off and washed with small amounts of cold water and dried in air.

2.2.2.1. $[Ni(bpy)(tdga)(H_2O)] \cdot 4H_2O$ (**1**). Color: blue. Yield: 82%. *Anal.* Calc.: C, 44.1; H, 3.7; N, 7.4; S, 8.4. Found: C, 43.9; H, 3.6; N, 7.2; S, 7.8%. UV–Vis (nm): λ_{max} 300, 585. IR (cm^{-1}): 1620 m (ν_{as}COO), 1384 s (ν_{sym}COO). $\mu_{eff}/\mu_B = 3.20$.

2.2.2.2. $[(en)Ni(\mu\text{-tdga})_2Ni(en)] \cdot 4H_2O$ (**2**). Color: blue. Yield: 86%. *Anal.* Calc.: C, 23.8; H, 5.3; N, 9.2; S, 10.6. Found: C, 23.9; H, 5.3; N, 9.1; S, 10.4%. UV–Vis (nm): λ_{max} 255, 365, 585. IR (cm^{-1}): 1600 m (ν_{as}COO), 1380 s (ν_{sym}COO). $\mu_{eff}/\mu_B = 3.06$.

2.2.2.3. $[Ni(phen)(tdga)(H_2O)]$ (**3**). Color: blue. Yield: 78%. *Anal.* Calc.: C, 47.4; H, 3.5; N, 6.9; S, 8.8. Found: C, 47.1; H, 3.3; N, 6.5; S, 7.3%. UV–Vis (nm): λ_{max} 295, 350, 605. IR (cm^{-1}): 1586 m (ν_{as}COO), 1376 s (ν_{sym}COO). $\mu_{eff}/\mu_B = 3.28$.

*2.2.2.4. [Ni(1,8-dan)(tdga)(H$_2$O)] (**4**).* Color: brown. Yield: 70%. *Anal.* Calc.: C, 46.1; H, 3.9; N, 7.7; S, 8.8. Found: C, 45.5; H, 4.2; N, 7.3; S, 8.4%. UV–Vis (nm): λ_{max} 325, 355, 585. IR (cm^{-1}): 1606 m (ν_{as}COO), 1372 s (ν_{sym}COO). $\mu_{eff}/\mu_B = 3.16$.

*2.2.2.5. [Ni(nphen)(tdga)(H$_2$O)]·H$_2$O (**5**).* Color: green. Yield: 65%. *Anal.* Calc.: C, 41.1; H, 3.2; N, 9.0; S, 6.8. Found: C, 41.1; H, 3.2; N, 8.9; S, 6.4%. UV–Vis (nm): λ_{max} 275, 585. IR (cm^{-1}): 1580 m (ν_{as}COO), 1384 s (ν_{sym}COO). $\mu_{eff}/\mu_B = 3.23$.

*2.2.2.6. [Ni(ampy)(tdga)(H$_2$O)] (**6**).* Color: blue. Yield: 75%. *Anal.* Calc.: C, 36.1; H, 4.2; N, 8.4; S, 9.6. Found: C, 36.3; H, 4.3; N, 8.3; S, 9.5%. UV–Vis (nm): λ_{max} 270, 585. IR (cm^{-1}): 1570 m (ν_{as}COO), 1374 s (ν_{sym}COO). $\mu_{eff}/\mu_B = 3.12$.

2.3. Crystal structure determinations

Crystals of **1** and **2** were obtained by slow evaporation of water solutions of the complexes. The all X-ray data were collected on a four-circle κ-axis KUMA KM-4 diffractometer (KUMA Diffraction, Wroclaw) equipped with an Oxford Cryostream cooler. X-ray data of **1** were collected at 150 K using graphite-monochromated Mo Kα radiation, a scintillation point detector and ω–2θ scan technique. Data reduction was performed using DataredC (KUMA Diffraction, Wroclaw) software. X-ray data of **2** were collected at 120 K using Mo Kα radiation monochromated by monochromator Enhance (Oxford Diffraction Ltd.), a CCD area detector and rotation method with ω-scan. The CrysAlis (Oxford Diffraction Ltd.) software was used for data reduction. The structures were solved using the direct methods (SHELXS-97) [13]. Both structures were refined anisotropically on F^2 using full-matrix least-squares procedure (SHELXL-97) [14]. H atoms attached to C and N atoms were positioned geometrically, with U_{iso} values derived from U_{eq} values of the corresponding C and N atoms. H atoms attached to O atoms were refined with a DFIX (SHELXL-97, [14]) restraint of 0.95(2) Å and free variables were used to describe the U_{iso}(H) values of H atoms attached at individual water molecules. Crystal data and structure refinements for **1** and **2** are given in Table 1.

3. Results and discussion

3.1. Physical techniques

Our initial attempts to obtain bridged nickel(II)–thiodiglycolate complexes by reaction of nickel(II) nitrate

Table 1
Data collection and refinement parameters for [Ni(bpy)(tdga)(H$_2$O)]·4H$_2$O (**1**) and [(en)Ni(μ-tdga)$_2$Ni(en)]·4H$_2$O (**2**)

Complex	**1**	**2**
Empirical formula	$C_{14}H_{22}N_2NiO_9S$	$C_6H_{16}NiN_2O_6S$
Formula weight	453.11	302.98
T (K)	150(2)	120(2)
Wavelength (Å)	0.71073	0.71073
Crystal system	triclinic	orthorhombic
Space group	$P\bar{1}$	*Pbca*
Unit cell dimensions		
a (Å)	9.019(4)	14.3454(7)
b (Å)	10.574(5)	9.0441(4)
c (Å)	11.432(3)	17.9272(9)
α (°)	101.91(3)	
β (°)	103.64(3)	
γ (°)	113.63(4)	
V (Å^3)	913.5(6)	2325.90(19)
Z	2	8
D_{calc} (Mg/m^3)	1.647	1.730
Absorption coefficient (mm^{-1})	1.228	1.863
$F(000)$	472	1264
Crystal size (mm)	0.50×0.50×0.50	0.40×0.30×0.15
Index ranges	$-9 \leqslant h \leqslant 9$, $-11 \leqslant k \leqslant 11$, $0 \leqslant l \leqslant 12$	$-15 \leqslant h \leqslant 17$, $-10 \leqslant k \leqslant 10$, $-21 \leqslant l \leqslant 20$
Reflections collected	3072	8417
Independent reflections (R_{int})	2927 (0.0393)	2041 (0.0539)
Refinement method	full-matrix least-squares on F^2	full-matrix least-squares on F^2
Data/restraints/parameters	2927/8/328	2041/4/165
Goodness-of fit on F^2	1.022	0.974
Final R indices [$I > 2\sigma(I)$]	$R_1 = 0.0428$, $wR_2 = 0.1200$	$R_1 = 0.0297$, $wR_2 = 0.0757$
R indices (all data)	$R_1 = 0.0473$, $wR_2 = 0.1245$	$R_1 = 0.0325$, $wR_2 = 0.0780$
Largest difference peak and hole (e Å^{-3})	0.970 and −1.005	0.672 and −0.352

or perchlorate with amines and sodium salt of thiodiglycolic acid were unsuccessful. We have obtained viscous substances only. These have been treated with acetone or diethylether to receive powder material but samples thus obtained were hygroscopic and not suitable for performing of elemental analysis. That is why we have changed a manner of synthesis. We have used $[Ni(tdga)(H_2O)_3]$ as a starting material and we have tried to perform substitution of coordinated water molecules by a bidentate N-donor ligand. Thus we have succeeded in preparation of complexes **1**–**6** and characterized them by elemental analyses (see Section 2), IR and diffuse reflectance spectra and by magnetochemical measurement. Moreover, our findings were confirmed by complete X-ray analyses of two complexes.

The characteristic bands of carboxylate and nitrogen ligands are present in the IR spectra of the complexes and in comparison with the free ligands they are mostly shifted to lower frequencies. However, possible overlapping of main characteristic bands of the ligands complicates a detailed interpretation of the IR spectra. The IR spectra of all complexes contain very strong peaks at ca. 1580 cm^{-1} attributable to $\nu_{as}(COO^-)$, whereas peaks observed in 1384–1372 cm^{-1} range may be assigned to $\nu_s(COO^-)$. However, in the same range (1655–1430 cm^{-1}) peaks attributable to the C=C and C=N ring stretching vibrations of heterocycles occur. The $\Delta\nu$ value of carboxylate vibrations of approximatelly 200 cm^{-1} indicates that COO^- groups behave as a monodentate ligand [15]. The ν(N–H) bands extend from 3450–3250 cm^{-1} and appear in the spectra of the complexes (**2**, **4**, **6**) containing amine ligands [16].

All the nickel complexes have their magnetic moments in the range of 3.06–3.28 μ_{eff}/μ_B. These values are typical for deformed octahedrally coordinated nickel(II) ion. Moreover, the positions of bands found in diffusion-reflection spectra of the complexes are in good agreement with this assumption. In general, the spectra of the complexes are very similar. One set of bands attributable to the $^3A_{2g} \rightarrow {}^3T_{1g}(F)$ transition was observed in the 605–585 nm region, whereas the bands at 370–350 nm are probably due to the $^3A_{2g} \rightarrow {}^3T_{1g}(P)$ transition. However, the bands in the latter region can be also assigned to the π–π^* transition. The bands observed in the range 325–255 nm can be connected with CT or π–π^* transitions [17].

3.2. Crystal structures of $[Ni(bpy)(tdga)(H_2O)]\cdot 4H_2O$ (*1*) and $[(en)Ni(\mu\text{-}tdga)_2Ni(en)]\cdot 4H_2O$ (*2*)

Molecular structures of **1** and **2** are depicted in Figs. 1 and 2, respectively, while selected bond lengths and angles are listed in Tables 2 and 3. The structure of $[Ni(bpy)(tdga)(H_2O)]\cdot 4H_2O$ (**1**) consists of an electroneutral nickel complex and four crystal water molecules. The coordination polyhedron around the nickel atom

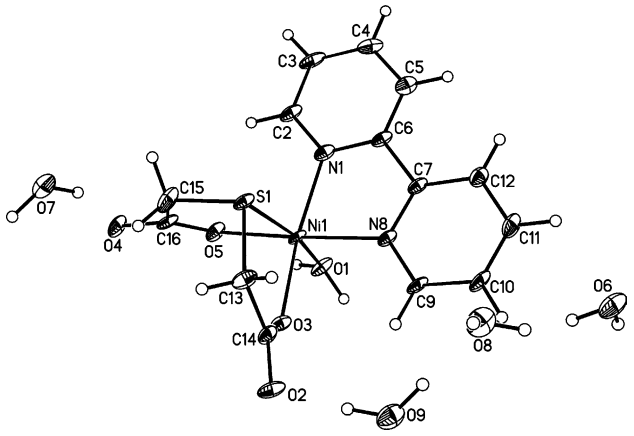

Fig. 1. The structure of $[Ni(bpy)(tdga)(H_2O)]\cdot 4H_2O$ (**1**) (ORTEPIII, [19]). Displacement ellipsoids are drawn at the 50% probability level and H atoms are shown as small spheres of arbitrary radii.

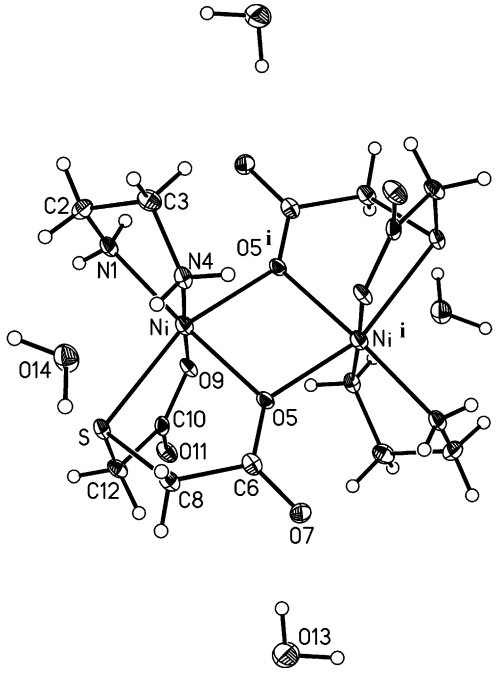

Fig. 2. The structure of centrosymmetric dimer $[(en)Ni(\mu\text{-}tdga)_2Ni(en)]\cdot 4H_2O$ (**2**). Displacement ellipsoids are drawn at the 50% probability level and H atoms are shown as small spheres of arbitrary radii. Symmetry code: (i) $-x+1, -y, -z+1$.

can be described as a deformed octahedron with a NiN_2SO_3 chromophore. Thus, nickel is coordinated by two nitrogen atoms of bpy, oxygen atoms of water molecule and thiodiglycolate dianion. The dianion is coordinated via sulfur atom and two oxygens from two carboxylato groups. The structure is very similar to that found for $[Zn(bpy)(tdga)(H_2O)]\cdot 4H_2O$ [5].In $[(en)Ni(\mu\text{-}tdga)_2Ni(en)]\cdot 4H_2O$ (**2**), two oxygen atoms of the tdga ligands form bridges between two Ni(II) ions. Each of two tdga anions is coordinated to nickel via one sulfur atom and two oxygens of different carboxylato groups. The remaining coordination positions on each of two

Table 2
Selected bond lengths (Å) and angles (°) for [Ni(bpy)(tdga)(H_2O)]·$4H_2O$ (**1**)

Bond lengths			
Ni(1)–O(5)	2.016(2)	Ni(1)–O(1)	2.046(2)
Ni(1)–O(3)	2.036(2)	Ni(1)–N(8)	2.071(3)
Ni(1)–N(1)	2.042(3)	Ni(1)–S(1)	2.4226(16)
C(14)–O(2)	1.235(4)	C(16)–O(4)	1.249(4)
C(14)–O(3)	1.267(4)	C(16)–O(5)	1.248(4)
Bond angles			
O(5)–Ni(1)–O(3)	92.38(10)	N(1)–Ni(1)–N(8)	79.06(11)
O(5)–Ni(1)–N(1)	97.18(11)	O(1)–Ni(1)–N(8)	92.39(11)
O(3)–Ni(1)–N(1)	169.46(10)	O(5)–Ni(1)–S(1)	83.63(8)
O(5)–Ni(1)–O(1)	85.33(10)	O(3)–Ni(1)–S(1)	83.57(8)
O(3)–Ni(1)–O(1)	94.42(10)	N(1)–Ni(1)–S(1)	93.07(9)
N(1)–Ni(1)–O(1)	90.78(11)	O(1)–Ni(1)–S(1)	168.68(7)
O(5)–Ni(1)–N(8)	175.59(10)	N(8)–Ni(1)–S(1)	98.79(8)
O(3)–Ni(1)–N(8)	91.55(10)		

Table 3
Selected bond lengths (Å) and angles (°) for [(en)Ni(μ-tdga)$_2$Ni(en)]·$4H_2O$ (**2**)

Bond lengths			
Ni–O(9)	2.0453(17)	O(5)–Ni#1	2.0857(16)
Ni–N(1)	2.059(2)	O(5)–C(6)	1.281(3)
Ni-N(4)	2.065(2)	C(6)–O(7)	1.236(3)
Ni–O(5)	2.0679(16)	O(9)–C(10)	1.268(3)
Ni–O(5)#1	2.0857(16)	C(10)–O(11)	1.246(3)
Ni–S	2.4353(6)		
Bond angles			
O(9)–Ni–N(1)	96.40(8)	O(9)–Ni–O(5)#1	88.61(7)
O(9)–Ni–N(4)	178.12(7)	N(1)–Ni–O(5)#1	98.68(7)
N(1)–Ni–N(4)	84.48(8)	N(4)-Ni–O(5)#1	89.61(7)
O(9)–Ni–O(5)	88.25(7)	O(5)–Ni–O(5)#1	79.04(7)
N(1)–Ni–O(5)	174.79(7)	N(4)–Ni–S	96.94(6)
N(4)–Ni–O(5)	90.81(7)	O(5)–Ni–S	82.96(5)
O(9)–Ni–S	84.56(5)	O(5)#1–Ni–S	160.93(5)
N(1)–Ni–S	99.76(6)		

Symmetry transformations used to generate equivalent atoms: #1: $-x+1, -y, -z+1$.

nickel atoms are occupied by two nitrogens from ethylenediamine. The coordination geometry around the nickel atoms is distorted octahedron with a N_2O_3S donor arrangement.

3.3. Temperature dependence of magnetic susceptibility of 2

The effective magnetic moment of **2**, calculated from $\mu_{\text{eff}} = 2.83\ (\chi_{\text{Ni}^{2+}})^{1/2}$ (BM), decreases from 3.06 BM at 300 K to 0.26 BM at 1.8 K (see Fig. 3). The μ_{eff} value at room temperature is characteristic for nickel(II) complexes in distorted octahedral coordination sphere. In the temperature range 50–300 K, susceptibility data obey Curie–Weiss law $[1/\chi_{\text{M}} = C(T-\theta)]$ with $C = 1.217$ cm^3 K mol^{-1} and $\theta = -1.17$ K, respectively.

For the description of the magnetic susceptibility data the equation, obtained by Ginsberg et al. [18] and the Hamiltonian, was employed

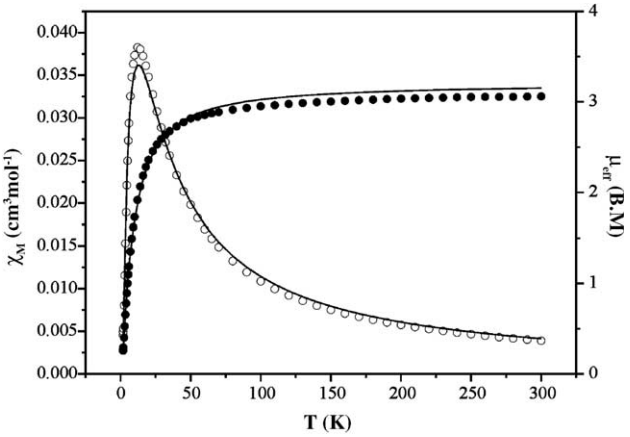

Fig. 3. Plot of the magnetic data for (**2**), χ_{M} {experimental (○) and calculated data (full line)} vs. temperature (K) and temperature dependence of μ_{eff} for (**2**) {experimental (●) and calculated data (full line)} using results from Ginsberg equation.

$$H = -2J\hat{S}_1\hat{S}_2 - D\left(\hat{S}_1Z^2 + \hat{S}_2Z^2\right) - 2zJ'\hat{S}_i\langle\hat{S}_i\rangle - g_iBH\hat{S}_i.$$

The symbols have their usual meanings. The magnetic susceptibility of the polycrystalline sample per gram-atom of Ni^{2+} is

$$\chi_{\text{A}} = \frac{Ng^2\beta^2}{3k}\left\{\frac{F_1(J,D,T)}{T - 4Z'J'F_1(J,D,T)} + \frac{2F'(J,D,T)}{1 - 4Z'J'F'(J,D,T)}\right\} + N\alpha,$$

where

$$F'(J,D,T) = \frac{1}{D}F_2(J,D,T) + \frac{3C_2^2}{3J-\delta}F_3(J,D,T) + \frac{3C_1^2}{3J+\delta}F_4(J,D,T),$$

$$F_1(J,D,T) = \frac{1 + e^{4J/kT} + 4e^{4J/kT}e^{D/kT}}{2 + e^{D/kT} + e^{J/kT}e^{-\delta/kT} + e^{J/kT}e^{\delta/kT} + 2e^{4J/kT} + 2e^{4J/kT}e^{D/kT}},$$

$$F_2(J,D,T) = \frac{2e^{4J/kT}e^{D/kT} + e^{D/kT} - 1 - 2e^{4J/kT}}{2 + e^{D/kT} + e^{J/kT}e^{-\delta/kT} + e^{J/kT}e^{\delta/kT} + 2e^{4J/kT} + 2e^{4J/kT}e^{D/kT}},$$

$$F_3(J,D,T) = \frac{e^{4J/kT} - e^{J/kT}e^{\delta/kT}}{2 + e^{D/kT} + e^{J/kT}e^{-\delta/kT} + e^{J/kT}e^{\delta/kT} + 2e^{4J/kT} + 2e^{4J/kT}e^{D/kT}},$$

$$F_4(J,D,T) = \frac{e^{4J/kT} - e^{J/kT}e^{-\delta/kT}}{2 + e^{D/kT} + e^{J/kT}e^{-\delta/kT} + e^{J/kT}e^{\delta/kT} + 2e^{4J/kT} + 2e^{4J/kT}e^{D/kT}},$$

$$\delta = [(3J+D)^2 - 8JD]^{1/2},$$

$$C_1 = 2\sqrt{2D}\Big/\left[(9J - D + 3\delta)^2 + 8D^2\right]^{1/2},$$

$$C_2 = (9J - D + 3\delta) \Big/ \left[(9J - D + 3\delta)^2 + 8D^2\right]^{1/2}.$$

The values of exchange parameters were determined by least-square procedure and the minimization of the function R was the criterion used to determine the best fit

$$R = \sqrt{\frac{\sum_{i=1}^{n}\left[(\chi_M)_i^{exp} - (\chi_M)_i^{calc}\right]^2 \Big/ \left[(\chi_M)_i^{exp}\right]^2}{n}}.$$

Least-square fits to the experimental data were obtained for $J = -4.35$ cm^{-1}, $D = 5.53$ cm^{-1}, $zJ' = -0.94$ cm^{-1}, $g = 2.00$ and $R = 4.41 \times 10^{-2}$.

However, it can be noticed, that in the higher temperature range, the fitting of theoretical and experimental data was not satisfactory.

4. Supplementary material

Crystallographic data for the structural analysis have been deposited with the Cambridge Crystallographic Data Center, CCDC Nos. 212990 and 212991 for complexes **1** and **2**, respectively. Copies of this information may be obtained free of charge from The Director, CCDC, 12 Union Road, Cambridge CB2 1EZ, UK (fax: +44-1223-336033; e-mail: deposit@ccdc.cam.ac.uk or www: http://www.ccdc.cam.ac.uk).

Acknowledgements

Authors thank the Grant Agency of the Czech Republic (GACR 203/02/0436) and the Ministry of Education of the Czech Republic (MSMT 143100008) for support of crystallographic part of this work and the Polish State Committee for Scientific Research a Grant No. 4T09A 11523. Authors thank Mr. Martin Biler for room temperature magnetochemical data collection.

References

[1] D. Gatteschi, O. Kahn, R.D. Willet, Magneto-Structural Correlations in Exchange Coupled Systems, Reidel, Dordrecht, 1984, p. 1.
[2] O. Kahn, Molecular Magnetism, VCH, New York, 1993, p. 103.
[3] S.H. Whitlow, Acta Crystallogr., Sect. B 31 (1975) 2531.
[4] M.G.B. Drew, D.A. Rice, C.W. Timewell, J. Chem. Soc., Dalton Trans. (1975) 144.
[5] R. Baggio, M. Perec, M.T. Garland, Acta Crystallogr., Sect. C 52 (1996) 2457.
[6] J. Delaunay, C. Kappenstein, R. Hugel, Acta Crystallogr., Sect. B 32 (1976) 2341.
[7] J. Delaunay, C. Kappenstein, R. Hugel, J. Chem. Res. 48 (1978) 801.
[8] P.B. Bonomo, E. Rizzarelli, N. Bresciani-Pahor, G. Nardin, J. Chem. Soc., Dalton Trans. (1982) 681.
[9] C.J. Kepert, B.W. Skelton, A.H. White, Aust. J. Chem. 52 (1999) 617.
[10] P. Kopel, Z. Trávníček, J. Marek, M. Korabik, J. Mrozinski, Polyhedron 22 (2003) 411.
[11] J. Marek, Z. Trávníček, P. Kopel, Acta Crystallogr., Sect. C 59 (2003) m429.
[12] E. König, Magnetic Properties of Coordination and Organometallic Transition Metal, Springer, Berlin, 1966, p. 1.
[13] G.M. Sheldrick, SHELXS-97: enhanced version of SHELX-S, Acta Crystallogr., Sect. A 46 (1990) 467.
[14] G.M. Sheldrick, SHELXL-97: Program for Crystal Structure Refinement, University of Göttingen, Göttingen, Germany, 1997.
[15] K. Nakamoto, Infrared and Raman Spectra of Inorganic and Coordination compounds, Wiley, New York, 1997, p. 59.
[16] C.J. Pouchert, The Aldrich Library of Infrared Spectra, third ed., Aldrich Chemical Company, Milwaukee, WI, 1981, p. 163.
[17] A.B.P. Lever, Inorganic Electronic Spectroscopy, Elsevier, Amsterdam, 1984.
[18] A.P. Ginsberg, R.L. Martin, R.W. Brookes, R.C. Sherwood, Inorg. Chem. 11 (1972) 2884.
[19] C.K. Johnson, M.N. Burnett, ORTEP-III: Oak Ridge Thermal Ellipsoid Plot Program for Crystal Structure Illustrations, Report ORNL-6895, Oak Ridge National Laboratory, Oak Ridge, TN, 1996.

Available online at www.sciencedirect.com
SCIENCE DIRECT®
Polyhedron 23 (2004) 1579–1586
POLYHEDRON
www.elsevier.com/locate/poly

Rational approach of the stoichiometries of lanthanide complexes with α_2-$[P_2W_{17}O_{61}]^{10-}$ heteropolytungstate in aqueous solution ☆

Yu-Wei Lu *, Bineta Keita, Louis Nadjo

Laboratoire de Chimie Physique, UMR 8000, CNRS, Electrochimie et Photoèlectrochimie, Université Paris-Sud, Bâtiment 420, 91405 Orsay Cedex, France

Received 5 November 2003; accepted 18 March 2004
Available online 22 April 2004

Abstract

An extended series of lanthanides (Ln) in their Ln^{III} oxidation state was reacted with $[\alpha_2\text{-}P_2W_{17}O_{61}]^{10-}$ (HPA) and the formation constants were determined for the complexes. The technique was the competition between this lacunary heteropolyanion and Arsenazo III for complexation of the same lanthanide. Unlike the usually featureless spectra of the Ln–HPA derivative, the visible spectra of the Arsenazo III complexes, in the presence of HPA, remain sharp, well-defined and could be recorded without interference from the Ln:HPA complexes formed simultaneously. These spectra were compared to those obtained with the same concentration of lanthanide in the absence of the heteropolyanion. Previous knowledge of the formation constants for Arsenazo III complexes with each lanthanide was necessary, so that those pertaining to the heteropolyanion complexes were left as the only unknowns in the set of equations. The 1:1 and 1:2 types of Ln:HPA complexes were found to coexist easily. Typically, values of $\log\beta_1 = 9.66$ and $\log\beta_2 = 16.26$ were found for the apparent formation constants corrected for acidity and other complexation effects in the case of the Ce^{3+} cation. Such values explain the coexistence of the two types of complexes in dilute solutions, with the possibility to keep a majority of a single species in solution under drastic concentration conditions. The same observation holds for all the series of Ln^{III} species examined in this work, because the formation constants are close from one lanthanide to the next. The comparison with the few values of formation constants available in the literature is satisfactory.
© 2004 Elsevier Ltd. All rights reserved.

Keywords: Dawson lacunary heteropolyanion; Complex formation constants; Lanthanides; Arsenazo III

1. Introduction

The diversity of the properties of polyoxometalates and of the associated applications maintains the study of these chemicals at a high level [1–10]. Part of their interest, which is emphasized in the following, must be traced to their ability to generate lacunary species and then metal cation substituted derivatives. Much impetus was triggered by the pioneering remark by Baker [11] that monosubstituted heteropolyanions can be considered as the analogues of metallated porphyrins, and used in catalytic processes with the advantage over their organic counterparts of thermal stability, robustness and inertness toward oxidizing environments. A primary direction, not necessarily aimed at catalysis, had also received extensive attention: it concerns the use of lacunary polyoxometalates in the sequestration and/or separation of ions, particularly in nuclear waste treatment [10,12–42]. Peacock and Weakley [39] were the first to demonstrate that rare-earth cations are easily complexed by lacunary heteropolyanions. More specifically, the monovacant Dawson anion α_1- and α_2-$[P_2W_{17}O_{61}]^{10-}$ isomers are known to be obtained by removal of one $[WO]^{4+}$ group from the saturated anion $[P_2W_{18}O_{62}]^{6-}$. They were shown to function

☆ Supplementary data associated with this article can be found, in the online version, at doi:10.1016/j.poly.2004.03.014.

* Corresponding author. Tel.: +33-1-69-15-47-28; fax: +33-1-69-15-43-28.
E-mail address: yuwei.lu@lcp.u-psud.fr (Y.-W. Lu).

0277-5387/$ - see front matter © 2004 Elsevier Ltd. All rights reserved.
doi:10.1016/j.poly.2004.03.014

as strong tetradentate ligands, [10,12–16,23–25,42] with high formation constants with transition metal and rare-earth ions [12,15,17–22]. Cerium appears as a favorite among lanthanide (Ln) studies and its heteropolyanion complexes are numerous [14,15,39–46]. Despite continuous efforts since the work of Peacock and Weakley [39], only recently were the problems of stoichiometry, structures and stabilities talked about for their own interest, and are beginning to receive satisfactory and complete solutions. Taking more specifically α_2-$[P_2W_{17}O_{61}]^{10-}$ as a representative ligand, the existence of 1:1 and 1:2 (Ln:heteropolyanion) complexes has long been noted [39]. Mostly, these species were detected and characterized by spectroscopic and electrochemical methods [15,42]. However, most attempts to isolate a solid from an equimolar mixture of $Ce(NO_3)_3$ and α_2-$K_{10}[P_2W_{17}O_{61}]$ yielded salts of the 1:2 complexes. To our knowledge, only in one case [15] was reported the successful isolation of the 1:1 complex, until the recent work by Pope et al. [46] indicating that the use of a threefold excess of Ce^{3+} has permitted this complex to be obtained as a pure crystalline ammonium salt. The structural analysis of the latter reveals a dimeric head-to-head anion, thus featuring a 2:2 complex in the solid state. Characterization of this complex in water by ^{31}P NMR, also supported by ^{183}W NMR data, reveals a complicated overall "monomer–dimer" equilibrium in solution [46]. Recently, 1:1 Ln:$[\alpha_2$-$P_2W_{17}O_{61}]^{10-}$ complexes were isolated for a series of lanthanides [47]. In slight contrast with the aforementioned Ce^{3+} complex in the solid state, the X-ray structure of the Eu^{3+} analogue revealed two identical [Eu-$(H_2O)_3(\alpha_2$-$P_2W_{17}O_{61})]^{7-}$ moieties, connected through two Eu–O–W bonds, one from each polyoxometalate unit, but which were not head-to-head. The solution studies indicated, however, that the molecules dissociate in solution to form the monomeric $[Ln(H_2O)_4(\alpha_2$-$P_2W_{17}O_{61})]^{7-}$ species.

With the aim to get a further understanding of the lability of such complexes in solution, the present paper describes the determination of formation constants of the various complexes of an extended series of lanthanide cations, including Ce^{3+}, with α_2-$[P_2W_{17}O_{61}]^{10-}$.

2. Experimental

2.1. Apparatus

UV–visible spectra were recorded on Perkin–Elmer Lambda 19 spectrophotometer coupled to a computer. The spectra were recorded from 800 to 400 nm using 1.000-cm quartz cuvettes.

All pH measurements were made on a Tacussel LPH 430T pH meter with a Tacussel combination pH glass electrode. Calibration of the pH meter was checked at regular intervals.

2.2. Reagents

Pure water was used throughout. It was obtained by passing through a Millipore RiOs unit and subsequently through a Millipore Q water purification set. All the chemicals were of high-purity grade and were used as received. Arsenazo III as a disodium salt (98%) and monochloroacetic acid (99+%) were obtained from Aldrich and sodium hydroxide from Prolabo. All the lanthanides were obtained as nitrate salts from Alfa Aesar (99.99%). The α_2 isomer, $K_{10}[\alpha_2$-$P_2W_{17}O_{61}]$, was prepared following literature methods [12]. It was standardized as described in the literature [14]. The pH 3.50 electrolyte was usually made up of 0.1 M $CH_2ClCOONa$ + $CH_2ClCOOH$.

Experiments were performed at the laboratory temperature.

2.3. Procedure

The general procedure was the competition between α_2-$[P_2W_{17}O_{61}]^{10-}$ (HPA) and Arsenazo III (Ar) for complexation of the same lanthanide. Arsenazo III is the common designation of {3,6-bis[(2-arsonophenyl)-azo]-4,5-dihydroxy-2,7-naphthalenedisulfonic acid}; the overall formula of the disodium salt reads: $C_{22}H_{16}As_2Na_2N_4O_{14}S_2$ (the anion is abbreviated as Ar in the following). This bis-azo derivative of chromotropic acid forms stable complexes with a large variety of ions over a wide pH range [48]. Specifically, it is extensively used for spectrophotometric biomedical analysis of various ions including Ca^{2+} and Al^{3+}.

The Arsenazo III solutions were standardized by means of spectrophotometric titration with a standard solution of $FeCl_3$ and lanthanide solutions with EDTA as described in detail elsewhere [49]. The concentrations of Arsenazo III stock solutions in the pH 3.5 buffer ranged from 4.00×10^{-5} to 4.73×10^{-5} M. Typically, the following concentrations were determined for lanthanide solutions: Nd, 1.45×10^{-3} M; La, 1.55×10^{-3} M; Dy, 2.23×10^{-3} M; Sm, 1.07×10^{-3} M; Eu, 1.24×10^{-3} M; Gd, 2.34×10^{-3} M; Ho, 2.12×10^{-3} M; Tb, 1.45×10^{-3} M; Yb, 2.20×10^{-3} M; Ce, 1.60×10^{-3} M; Pr, 2.00×10^{-3} M.

Finally, in a representative experiment, the quartz cuvette contained 1.5 or 2 mL of the Arsenazo III solution, 1.5 or 1 mL of the pH 3.50 buffer and 10–100 μL of the HPA solution, depending on the initial concentration of the corresponding stock solution. The initial concentration of HPA in the cuvette thus ranges from 1×10^{-5} to 2.34×10^{-5} M. Aliquots of 4 or 5 μL of lanthanide solution were added and the absorbance of Arsenazo III and its complexes were recorded after each addition. The experiments were stopped when the absorbances no longer varied.

Calculations of the apparent formation constants were then carried out as explained in the following.

3. Results and discussion

3.1. Formation constants of Ln:HPA and Ln:HPA$_2$ complexes

The determination of formation constants was carried out by UV–visible spectrometry. The following reason dictated this choice: it was desirable to apply the same technique to a large selection of lanthanide cations. As most of them were not expected to present easily tractable redox properties, potentiometric measurements appear limited to only few examples. One spectrophotometric possibility was exemplified previously [15] by the study of the competition between Ce^{3+} and Zn^{2+} or Co^{2+} for complexation by α_2-$[P_2W_{17}O_{61}]^{10-}$. In the present work, the selected technique consists of studying the competition between two ligands for the complexation of the same Ln cation. It is assumed that the complex formation constants with the reference ligand are known from separate experiments; also it is desirable that the formation constants with the new ligand be sufficiently close to those of the reference ligand, in order that good accuracy could be achieved in the determination of the unknown values. With these guidelines and literature indications [49–52], Arsenazo III was selected as the reference ligand. Its interactions with lanthanides were investigated in some detail [49–52]. In particular, Arsenazo III was shown to build up the same type of complex with lanthanides, a very useful remark to minimize modelization time in the series. Furthermore, the literature values for formation constants with lanthanides [49,50] are in the range expected for Ln:HPA complexes, with regard to the very few published constants for the latter [15,17,53]. Also, the chromophore groups in the ligand facilitate the spectrophotometric study in the visible domain. Finally, we have checked that Arsenazo III is stable in acidic solution.

3.1.1. Formation constants of Ln:Ar complexes: a reevaluation [49]

Published formation constant values for Ln:Ar complexes [50] were obtained with solutions containing at the utmost 5.68×10^{-6} M Arsenazo III. The conclusion was that dilute solutions of this ligand react in a 1:1 ratio with the lanthanides at pH 3.5 with formation constants ranging from 2×10^7 to 8×10^7 M^{-1}. Completeness of the reaction is an important assumption behind these results. For larger concentrations of Arsenazo III, a new determination of these formation constants, without any a priori assumption, was warranted, at least as a cross-check of previous conclusions. Actually, it turns out that three Ln:Ar complexes are currently formed in equilibrium, with a definite tendency to obtain the 1:1 and 2:2 complexes in the presence of a slight excess of Ln. The apparent formation constants for the three complexes were published elsewhere [49] and are gathered here in Table 1, for use in the following.

Table 1
Formation constants of Arsenazo III–lanthanide complexes calculated by the Taylor expansion method

Lanthanide	$\log K_{11}$	$\log K_{12}$	$\log K_{22}$
La	5.06	9.73	14.97
Ce	5.19	9.87	15.27
Pr	4.88	9.56	14.58
Nd	5.32	9.90	15.37
Sm	5.15	10.00	15.47
Eu	5.15	9.98	15.43
Gd	5.08	9.93	15.35
Tb	4.97	9.68	14.87
Dy	5.13	9.93	15.37
Ho	5.12	9.97	15.45
Yb	5.11	9.92	15.33

For further details, see text and reference [49].

3.1.2. Formation constants of Ln:HPA complexes

It is worth noting that Ln:HPA complexes are colorless. Therefore, during the competition of HPA and Arsenazo III for complexation of a common Ln, the spectrum in the visible wavelength domain pertains essentially to Arsenazo III and its complexes. Typically, Fig. 1 illustrates this point by showing the two spectra obtained with a selected initial concentration of Arsenazo III and the addition of the same amount of lanthanide, but with the presence of HPA in one of the experiments. However, possible interference in the observed spectrum arising from a mixed complex deserves

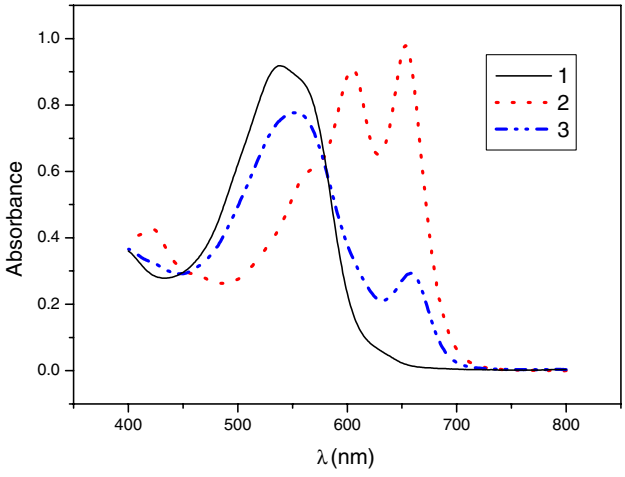

Fig. 1. Selected spectra associated with the titration of Arsenazo III with La^{3+} at pH 3.50, in the absence and presence of HPA; [Arsenazo III] = 2.67×10^{-5} M. 1, Arsenazo III alone; 2, Arsenazo III without HPA, $V_{La^{3+}} = 45$ μL; 3, Arsenazo III with HPA, [HPA] = 2.08×10^{-5} M, $V_{La^{3+}} = 45$ μL.

consideration. As a matter of fact, the possibility exists that a mixed Ar:Ln:HPA complex be formed in solution. Spectral deconvolution of the spectra before and during the competition was helpful to answer this question.

Spectral deconvolution. To illustrate the procedure, Fig. 2 shows the spectrum of Arsenazo III in the presence of α_2-$[P_2W_{17}O_{61}]^{10-}$ and an example of its evolution upon addition of La^{3+}. A detailed description of the procedure, based on the additivity of Beer–Lambert's law, has been given elsewhere [49]. Free Arsenazo III has a spectrum consisting of a broadband peaking around 540 nm. The spectrum of the La^{3+}-complex displays two sharp peaks at 606 nm and 654 nm for La_2Ar_2 and $LaAr_2$, respectively, and a broadband peaking around 601 nm for LaAr [49]. The concentrations of the various species in solution are needed for the determination of the complex formation constants.

Each spectrum can be decomposed into a sum of several Gaussian-type spectra. The software Origin 5.0 was used for this purpose. The following criteria were taken as guides: for the fitting accuracy to the experimental spectra, the correlation coefficient must be larger than 0.995; for significance of the deconvolution, each Gaussian component is characterized by its peak wavelength and its half-peak width: in favorable cases, the peak wavelength identifies a species in solution; whenever these characteristics reach stable values during a deconvolution process, the absorbance at the peak of the Gaussian component might be considered to represent the concentration of the species actually present in the reaction mixture through Beer-Lambert's law.

These guidelines were followed to generate the deconvolution shown in Fig. 2. Other pertinent details can be found in the reference cited [49]. Fig. 3(a) shows the overall absorbance variations observed for Arsenazo III at 538 nm and for a new peak at 654 nm. However, these

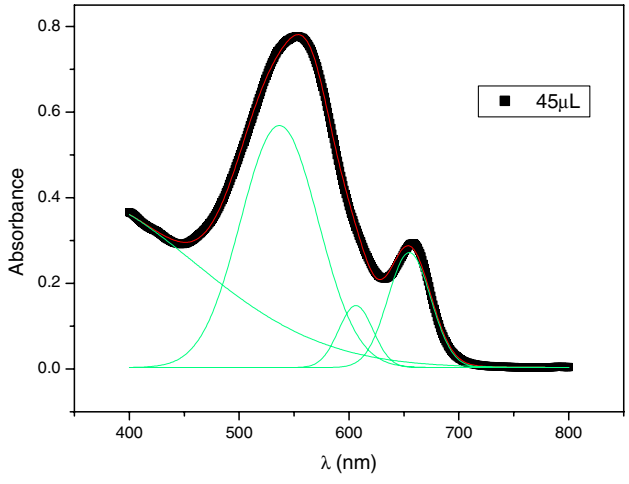

Fig. 2. Deconvolution into Gaussians of spectrum 3 of Fig. 1.

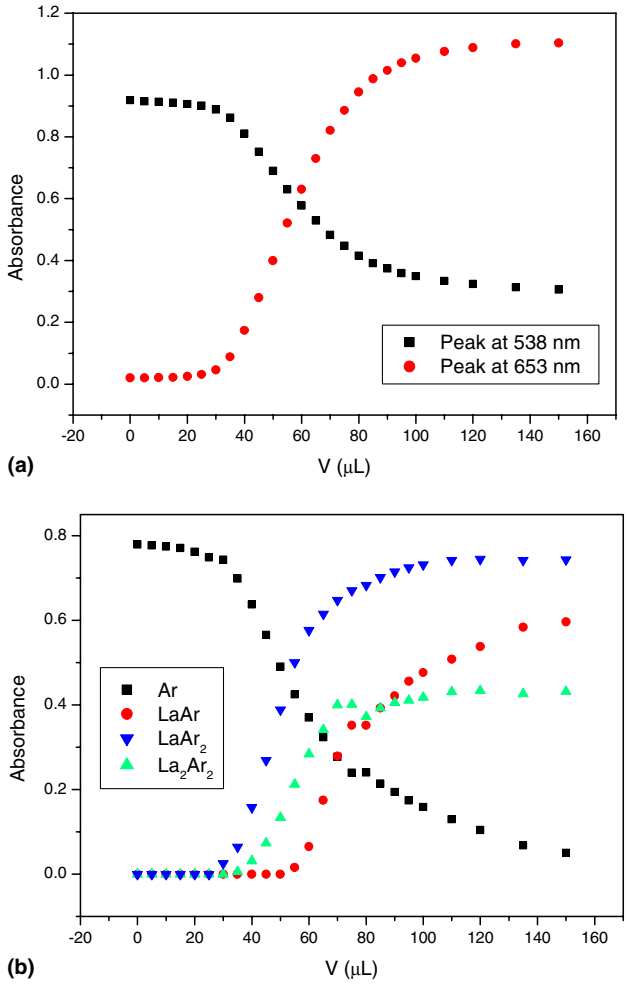

Fig. 3. Variations of the peak absorbances during the titration of Arsenazo III as a function of the added volume of a 1.55×10^{-3} M solution of La^{3+} at pH 3.50; [Arsenazo III] $= 2.67 \times 10^{-5}$ M and [HPA] $= 2.05 \times 10^{-5}$ M: (a) before the spectral deconvolution and (b) variations of the absorbance peaks of the Gaussians after the deconvolution.

experimental points represent overlapping spectra. Fig. 3(b) gives detailed variations of absorbances measured from Gaussian-type deconvoluted spectra from which accurate calculations could be undertaken.

Such spectral deconvolution was carried out for La through Yb, with the exception of Er. It was observed (see Tables S1 and S2 in the Supplementary Materials) that the peak wavelength locations and the half-peak widths for the various Gaussian deconvoluted spectra do not vary in the absence or presence of HPA; they also remain constant during the competition process of the two ligands for complexation of Ln up to its completion. The same remark is valid for Ln:Arsenazo III complexes in the absence or presence of HPA. Importantly, it is also observed that, during the competition process, no new peak appeared in the system of deconvoluted spectra, which would have indicated the build up of a

new complex. These observations, together, rule out any significant formation of a mixed complex, Ar:Ln:HPA. Therefore, the conditions are fulfilled for a quantitative analysis of the competition process between Arsenazo III and HPA for complexation of lanthanides.

Apparent formation constants of the various Ln:HPA complexes. In agreement with experimental evidence firmly established in the pertinent literature, two main equilibria must be considered (overall charges of the species are omitted in the equations):

$$\mathrm{HPA} + \mathrm{Ln} \leftrightarrows \mathrm{LnHPA} \quad \text{apparent formation constant } \beta'_1, \tag{1}$$

$$2\mathrm{HPA} + \mathrm{Ln} \leftrightarrows \mathrm{LnHPA_2} \quad \text{apparent formation constant } \beta'_2. \tag{2}$$

These equilibria are in competition with the simultaneous consumption of Ln by Arsenazo III.

$$\mathrm{Ar} + \mathrm{Ln} \rightleftarrows \mathrm{LnAr} \quad \text{apparent formation constant } K_{11},$$

$$2\mathrm{Ar} + \mathrm{Ln} \rightleftarrows \mathrm{LnAr_2} \quad \text{apparent formation constant } K_{12},$$

$$2\mathrm{Ar} + 2\mathrm{Ln} \rightleftarrows \mathrm{Ln_2Ar_2} \quad \text{apparent formation constant } K_{22}$$

for which the apparent formation constants were determined previously [49] and recalled in Table 1.

The set of equations from which the values of β'_1 and β'_2 are extracted was solved with the matter conservation equations and the necessary conditions for the equilibria relationships (see Appendix A). An example of the solution is illustrated by the representative case of La^{3+} complexes with HPA. Obviously, the relevant concentrations for this calculation are those pertaining to the domain where the consumption of La^{3+} by Arsenazo III or by both ligands is realized. Therefore, we found that the absorbance profile for Arsenazo III during the complexation process can be fitted to a Maclaurin polynomial series of the general form:

$$y = p_0 + p_1(x - x_0) + p_2(x - x_0)^2 + p_3(x - x_0)^3 + p_4(x - x_0)^4 + \cdots$$

The parameters p_0–p_5 were calculated using the Origin 5.0 software. The results are shown in Fig. 4. It is worth noting the very good correlation coefficient for this fitting.

Finally, the relevant set of equations to be solved are presented in Appendix A. The apparent formation constants in our experimental conditions ensue. These values are designated by β'_1 and β'_2, respectively, and are gathered in Table 2.

3.2. Corrections of apparent formation constant values

Corrections for acidity and complexation of HPA by other cations are needed. As a matter of fact, α_2-$[P_2W_{17}O_{61}]^{10-}$ has three acidity constants, and is also complexed by alkaline cations [54].

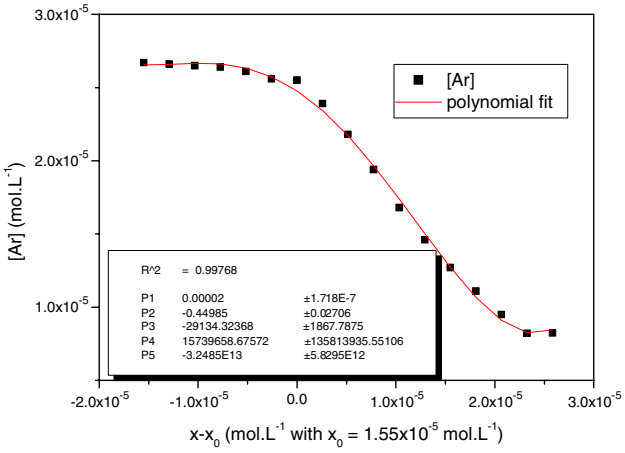

Fig. 4. Maclaurin polynomial fitting of the concentration of Ar as a function the operational concentration ($x - x_0$).

Table 2
Apparent formation constants of Ln:HPA complexes calculated by the Maclaurin expansion method before corrections

Lanthanide	β'_1	β'_2	$\log \beta'_1$	$\log \beta'_2$
La	3.41E + 07	9.28E + 12	7.53	12.97
Ce	7.15E + 07	4.34E + 12	7.85	12.64
Pr	1.90E + 08	5.67E + 12	8.28	12.75
Nd	8.34E + 07	2.65E + 12	7.92	12.42
Sm	1.44E + 07	4.35E + 12	7.16	12.64
Eu	1.11E + 08	3.89E + 14	8.05	14.59
Gd	6.94E + 07	2.77E + 13	7.84	13.44
Tb	1.06E + 08	1.18E + 14	8.03	14.07
Dy	1.77E + 08	9.72E + 14	8.25	14.99
Ho	1.08E + 09	2.35E + 14	9.03	14.37
Yb	8.47E + 07	2.02E + 14	7.93	14.31

For further details, see text.

$$\mathrm{HPA} + \mathrm{H^+} \rightleftarrows \mathrm{HPAH}, \quad K_1 = \frac{[\mathrm{HPAH}]}{[\mathrm{HPA}][\mathrm{H^+}]}, \quad \log K_1 = 4.49,$$

$$\mathrm{HPAH} + \mathrm{H^+} \rightleftarrows \mathrm{HPAH_2}, \quad K_2 = \frac{[\mathrm{HPAH_2}]}{[\mathrm{HPAH}][\mathrm{H^+}]}, \quad \log K_2 = 3.75,$$

$$\mathrm{HPAH_2} + \mathrm{H^+} \rightleftarrows \mathrm{HPAH_3}, \quad K_3 = \frac{[\mathrm{HPAH_3}]}{[\mathrm{HPAH_2}][\mathrm{H^+}]}, \quad \log K_3 = 2.00,$$

$$\mathrm{HPA} + \mathrm{Na^+} \rightleftarrows \mathrm{HPANa}, \quad K_{\mathrm{Na}} = \frac{[\mathrm{HPANa}]}{[\mathrm{HPA}][\mathrm{Na^+}]}, \quad \log K_{\mathrm{Na}} = 2.55,$$

$$\begin{aligned}[\mathrm{HPA}]^{\mathrm{app}} &= [\mathrm{HPA}] + [\mathrm{HPAH}] + [\mathrm{HPAH_2}] + [\mathrm{HPAH_3}] \\ &\quad + [\mathrm{HPANa}] \\ &= [\mathrm{HPA}](1 + K_1[\mathrm{H^+}] + K_1K_2[\mathrm{H^+}]^2 \\ &\quad + K_1K_2K_3[\mathrm{H^+}]^3) + [\mathrm{HPA}](1 + K_{\mathrm{Na}}[\mathrm{Na^+}]) \\ &\quad - [\mathrm{HPA}] \\ &= [\mathrm{HPA}](\alpha_{\mathrm{HPA(H)}} + \alpha_{\mathrm{HPA(Na)}} - 1),\end{aligned}$$

Table 3
Formation constants of complexes between Lanthanides and α_2-$[P_2W_{17}O_{61}]^{10-}$

Lanthanide	This work		Reference 53		Reference 17	
	$\log\beta_1$	$\log\beta_2$	$\log\beta_1$	$\log\beta_2$	$\log\beta_1$	$\log\beta_2$
La	9.34	16.59	8.25			
Ce	9.66	16.26			11.5–12.2	
Pr	10.09	16.37				
Nd	9.73	16.04	9.30	16.49	10.7–12.7	
Sm	8.97	16.26				
Eu	9.86	18.21	9.91	17.45	10.35	18.4
Gd	9.65	17.06				
Tb	9.84	17.69				
Dy	10.06	18.61				
Ho	10.84	17.99				
Er			9.55	17.79		
Yb	9.74	17.93	9.59			

Comparison with the few published literature values. For further details, see text.

where $[HPA]^{app}$ is the apparent concentration, [HPA] represents the effective concentration, $\alpha_{HPA(H)}$ the protonation coefficient, $\alpha_{HPA(Na)}$ the complexation coefficient by Na^+. These αs are known as Ringböm coefficients.

These values indicate that the HPA is partly protonated and also complexed at pH 3.5 and 0.1 M Na^+ medium where the complexation by lanthanides is carried out. Then the apparent formation constants defined previously actually read:

$$HPA + Ln \rightleftarrows LnHPA, \quad \beta_1' = \frac{[LnHPA]^{app}}{[HPA]^{app}[Ln^{3+}]^{app}},$$

$$2HPA + Ln^{3+} \rightleftarrows LnHPA_2, \quad \beta_2' = \frac{[LnHPA_2]^{app}}{([HPA]^{app})^2[Ln^{3+}]^{app}}.$$

If it is assumed that the effective concentrations of LnHPA, $LnHPA_2$ and Ln are equal to their respective apparent concentrations, then the relationship for $[HPA]^{app}$ leads to:

$$\beta_1 = \beta_1'(\alpha_{HPA(H)} + \alpha_{HPA(Na)} - 1)$$

and

$$\beta_2 = \beta_2'(\alpha_{HPA(H)} + \alpha_{HPA(Na)} - 1)^2.$$

In our experimental conditions, pH 3.5 and $[Na^+] = 0.1$ M, $\alpha_{HPA(H)} + \alpha_{HPA(Na)} - 1 = 64.18$. The final results, after these corrections, are gathered in Table 3. In the same Table, the few values available in the literature are gathered for comparison. No corrections were made for the values already extrapolated to zero ionic strength [17]. Corrections from medium effects were carried out in the case where a pH 6 and 1.0 M Na^+ medium was used [53]. The correction coefficient is: $\alpha_{HPA(H)} + \alpha_{HPA(Na)} - 1 = 355.8$. The comparison turns out to be satisfactory in the cases where it is possible.

4. Concluding remarks

The lability of 1:1 and 1:2 Ln:HPA complexes in solution and, in several examples, the intriguing isolation of only one of these two complexes in the solid state can be rationalized with the knowledge of their formation constants. In the present work, such values were determined for an extended series of lanthanides in the presence of the lacunary heteropolyanion α_2-$[P_2W_{17}O_{61}]^{10-}$. Even though appropriate corrections could be carried out to obtain absolute formation constant values, apparent constants might suffice as significant guides when particular experimental conditions are selected. Then, the relative closeness of the formation constants for 1:1 and 1:2 complexes would explain readily the difficulty in avoiding the monomer–dimer equilibria in solution. As expected, calculations confirm easily that this shortcoming is particularly sensitive when a pure 1:2 complex, dissolved in micromolar and submicromolar concentrations in solution, is very significantly reversed to the corresponding monomer. Another conclusion concerns the methodology. The satisfactory comparison with the few values available in the literature and obtained by completely different methods, supports the present way of handling the data. In particular, it is confirmed that only a few accurate and appropriately selected experimental points are sufficient to evaluate the formation constants of Ln/HPA complexes.

Finally, the problem remains as to the actual catalytic species in electrocatalytic processes based on necessarily dilute solutions of these complexes. Work in progress will discuss this problem.

Acknowledgements

This work was supported by the CNRS (UMR 8000) and the University Paris XI. The participation of

G. Laurent and H. Pereira in the early parts of this work is thankfully acknowledged.

Appendix A

For the sake of clarity, the following notations are used: Ar designates Arsenazo III; HPA stands for the lacunary heteropolyanion α_2-$[P_2W_{17}O_{61}]^{10-}$ and Ln stands for any lanthanide; the overall concentration of Arsenazo III reads C_{Ar}, that of HPA C_{HPA} and that of any lanthanide C_{Ln}, the corresponding equilibrium concentrations will be noted: [Ar], [HPA] and [Ln], respectively. The other equilibrium concentrations of the various complexes read respectively: [LnAr]; [$LnAr_2$]; [Ln_2Ar_2]; [LnHPA] and [$LnHPA_2$].

The following relationships hold:

Matter conservation.

$$C_{Ar} = [Ar] + [LnAr] + 2[LnAr_2] + 2[Ln_2Ar_2],$$

$$C_{Ln} = [Ln] + [ArLn] + [LnAr_2] + 2[Ln_2Ar_2] + [LnHPA] + [LnHPA_2],$$

$$C_{HPA} = [HPA] + [HPALn] + 2[LnHPA_2],$$

Equilibrium constants

$$K_{11} = \frac{[LnAr]}{[Ar][Ln]},$$

$$K_{12} = \frac{[LnAr_2]}{[Ar]^2[Ln]},$$

$$K_{22} = \frac{[Ln_2Ar_2]}{[Ar]^2[Ln]^2},$$

$$\beta_1 = \frac{[LnHPA]}{[Ln][HPA]},$$

$$\beta_2 = \frac{[LnHPA_2]}{[Ln][HPA]^2}.$$

The first derivatives with respect to C_{Ln} are necessary and read:

$$0 = \frac{d[Ar]}{dC_{Ln}} + \frac{d[LnAr]}{dC_{Ln}} + 2\frac{d[LnAr_2]}{dC_{Ln}} + 2\frac{d[Ln_2Ar_2]}{dC_{Ln}},$$

$$1 = \frac{d[Ln]}{dC_{Ln}} + \frac{d[LnAr]}{dC_{Ln}} + \frac{d[LnAr_2]}{dC_{Ln}} + 2\frac{d[Ln_2Ar_2]}{dC_{Ln}} + \frac{d[LnHPA]}{dC_{Ln}} + \frac{d[LnHPA_2]}{dC_{Ln}},$$

$$0 = \frac{d[HPA]}{dC_{Ln}} + \frac{d[LnHPA]}{dC_{Ln}} + 2\frac{d[LnHPA_2]}{dC_{Ln}},$$

$$\frac{d[LnAr]}{dC_{Ln}} = K_{11}\left([Ln]\frac{d[Ar]}{dC_{Ln}} + [Ar]\frac{d[Ln]}{dC_{Ln}}\right),$$

$$\frac{d[LnAr_2]}{dC_{Ln}} = K_{12}\left(2[Ar][Ln]\frac{d[Ar]}{dC_{Ln}} + [Ar]^2\frac{d[Ln]}{dC_{Ln}}\right),$$

$$\frac{d[Ln_2Ar_2]}{dC_{Ln}} = 2K_{22}\left([Ar][Ln]^2\frac{d[Ar]}{dC_{Ln}} + [Ar]^2[Ln]\frac{d[Ln]}{dC_{Ln}}\right),$$

$$\frac{d[LnHPA]}{dC_{Ln}} = \beta_1\left([Ln]\frac{d[HPA]}{dC_{Ln}} + [HPA]\frac{d[Ln]}{dC_{Ln}}\right),$$

$$\frac{d[LnHPA_2]}{dC_{Ln}} = \beta_2\left(2[HPA][Ln]\frac{d[HPA]}{dC_{Ln}} + [HPA]^2\frac{d[Ln]}{dC_{Ln}}\right).$$

Using the Maclaurin expansion, the already known values are: [Ar], $d[Ar]/dC_{Ln}$, C_{Ar}, C_{Ln}, C_{HPA}, K_{11}, K_{12} and K_{22}. Then, [Ln] and $d[Ln]/dC_{Ln}$ are calculated through the following equalities:

$$[Ln] = \Big\{ -(2K_{12}[Ar] + K_{11}) + \sqrt{(2K_{12}[Ar] + K_{11})^2 - 8K_{22}([Ar] - C_{Ar})} \Big\} \Big/ \{2K_{22}[Ar]\},$$

$$\frac{d[Ln]}{dC_{Ln}} = \Big\{ -(1 + K_{11}[Ln] + 4K_{12}[Ln][Ar] + 4K_{22}[Ln]^2[Ar])\frac{d[Ar]}{dC_{Ln}} \Big\} \Big/ \Big\{K_{11}[Ar] + 2K_{12}[Ar]^2 + 4K_{22}[Ln][Ar]^2\Big\}.$$

Putting o and p to designate the following expressions:

$$o = 2K_{22}[Ar]^2[Ln]^2 + (K_{12}[Ar]^2 + K_{11}[Ar] + 1)[Ln]$$

and

$$p = (1 + K_{11}[Ar] + K_{12}[Ar]^2 + 4K_{22}[Ln][Ar]^2)\frac{d[Ln]}{dC_{Ln}} + (K_{11}[Ln] + 2K_{12}[Ln][Ar] + 4K_{22}[Ln]^2[Ar])\frac{d[Ar]}{dC_{Ln}}$$

the set of equations to solve reads:

$$[HPA] + \beta_1[HPA][Ln] + 2\beta_2[HPA]^2[Ln] = C_{HPA},$$

$$\beta_1[HPA][Ln] + \beta_2[HPA]^2[Ln] + o = C_{Ln},$$

$$(1 + \beta_1[Ln] + 4\beta_2[Ln][HPA])\frac{d[HPA]}{dC_{Ln}} + (\beta_1[HPA] + 2\beta_2[HPA]^2)\frac{d[Ln]}{dC_{Ln}} = 0,$$

$$(\beta_1[\mathrm{ln}] + 2\beta_2[\mathrm{ln}][\mathrm{HPA}])\frac{\mathrm{d}[\mathrm{HPA}]}{\mathrm{d}C_{\mathrm{Ln}}} + (\beta_1[\mathrm{HPA}] + \beta_2[\mathrm{HPA}]^2)\frac{\mathrm{d}[\mathrm{Ln}]}{\mathrm{d}C_{\mathrm{Ln}}} + p = 1.$$

The apparent formation constants gathered in Table 2 ensue.

References

[1] C.L. Hill (Guest Ed.) Chem. Rev. 98 (1998) 1.
[2] M.T. Pope, Heteropoly and Isopoly Oxometalates, Springer-Verlag, Berlin, 1983.
[3] M.T. Pope, A. Muller (Eds.), Polyoxometalates: From Platonic Solids to Antiretroviral Activity, Kluwer Academic Publications, Dordrecht, 1994.
[4] M. Sadakane, E. Steckhan, Chem. Rev. 98 (1998) 219.
[5] A. Belhouari, B. Keita, L. Nadjo, R. Contant, New J. Chem. (1998) 83.
[6] R. Contant, M. Abbessi, J. Canny, A. Belhouari, B. Keita, L. Nadjo, Inorg. Chem. 36 (1997) 4961.
[7] B. Keita, L. Nadjo, R. Contant, J. Electroanal. Chem. 443 (1998) 168.
[8] R. Contant, M. Abbessi, J. Canny, B. Keita, A. Belhouari, L. Nadjo, Eur. J. Inorg. Chem. (2000) 567.
[9] B. Keita, Y.W. Lu, L. Nadjo, R. Contant, M. Abbessi, J. Canny, M. Richet, J. Electroanal. Chem. 477 (1999) 146.
[10] B. Keita, F. Girard, L. Nadjo, R. Contant, J. Canny, M. Richet, J. Electroanal. Chem. 478 (1999) 76.
[11] L.C. Baker, Plenary Lecture. in: Proceedings of the XV International Conference of Coordination Chemistry, Moscow, 1973.
[12] D.K. Lyon, W.K. Miller, T. Novet, P.J. Domaille, E. Evitt, D.C. Johnson, R.G. Finke, J. Am. Chem. Soc. 113 (1991) 7209.
[13] D. Mansuy, J.F. Bartoli, P. Battioni, D.K. Lyon, R.G. Finke, J. Am. Chem. Soc. 113 (1991) 7222.
[14] J. Bartis, M. Dankova, J.J. Lessmann, Q.-H. Luo, W. Horrocks Jr., L.C. Francesconi, Inorg. Chem. 38 (1999) 1042.
[15] J.P. Ciabrini, R. Contant, J. Chem. Res. (1993) (S)391 (M) 2720.
[16] T.L. Jorris, M. Kozik, N. Casan-Pastor, P.J. Domaille, R.G. Finke, W.K. Miller, L.C.W. Baker, J. Am. Chem. Soc. 109 (1987) 7402.
[17] L. Bion, F. Mercier, P. Decambox, P. Moisy, Radiochim. Acta 87 (1999) 161.
[18] L. Bion, P. Moisy, F. Vaufrey, S. Meot-Reymond, E. Simoni, C. Madic, Radiochim. Acta 78 (1997) 73.
[19] J. Bartis, Y. Kunina, M. Blumenstein, L.C. Francesconi, Inorg. Chem. 35 (1996) 1497.
[20] M.L. Hamlaoui, K. Vlassenko, D. Messadi, C. R. Acad. Sci. Ser. II 311 (1990) 795.
[21] K. Nomiya, M. Miwa, Polyhedron 4 (1985) 89.
[22] V.I. Spitsyn, M.M. Orlova, N.N. Krot, A.S. Saprykin, Russ. J. Inorg. Chem. 23 (1978) 677.
[23] A. Venturelli, M.J. Nilges, A. Smirnov, R.L. Bedford, L.C. Francesconi, J. Chem. Soc., Dalton Trans. (1999) 301.
[24] L. Qu, S. Wang, J. Peng, Y. Chen, G. Wang, Polyhedron 11 (1992) 2645.
[25] A.B. Yusov, V.P. Shilov, Sov. Radiochem. 41 (1999) 1.
[26] L. Bion, P. Moisy, C. Madic, Radiochim. Acta 69 (1995) 251.
[27] M. Kamoshida, T. Fukasawa, F. Kawamura, J. Nucl. Sci Technol. 35 (1998) 185.
[28] D.A. Malikov, M.S. Milyukova, B.F. Myasoedov, Sov. Radiochem. 31 (1989) 425.
[29] D.A. Malikov, M.S. Milyukova, E.V. Kuzovkina, B.F. Myasoedov, Sov. Radiochem. 35 (1993) 465.
[30] M.S. Milyukova, N.S. Varezhkina, B.F. Myasoedov, J. Radioanal. Nucl. Chem. 105 (1986) 249.
[31] M.S. Milyukova, N.S. Varezhkina, B.F. Myasoedov, J. Radioanal. Nucl. Chem. 121 (1988) 403.
[32] M.S. Milyukova, N.S. Varezhkina, B.F. Myasoedov, Sov. Radiochem. 32 (1990) 361.
[33] N.S. Varezhkina, M.S. Milyukova, B.F. Myasoedov, J. Radioanal. Nucl. Chem. 135 (1989) 67.
[34] A.S. Saprykin, V.P. Shilov, V.I. Spitsyn, N.N. Krot, Dokl. Chem. 226 (1976) 114.
[35] B.F. Myasoedov, I.A. Lebedev, Sov. Radiochem. 19 (1977) 69.
[36] V.N. Kosyakov, G.A. Timofeev, E.A. Erin, V.I. Andreev, V.V. Kopitov, G.A. Simakin, Sov. Radiochem. 19 (1977) 418.
[37] E.A. Erine, A.A. Baranov, V.A. Yu, V.M. Chistyakov, G.A. Timofeev, J. Alloys, Compds. 271 (1998) 782.
[38] V.M. Chistyakov, A.A. Baranov, P.N. Karbovnichii, E.A. Erine, G.A. Timofeev, Sov. Radiochem. 32 (1990) 334.
[39] R.D. Peacock, T.J.R. Weakley, J. Chem. Soc. A (1971) 1836.
[40] J. Bartis, M. Dankova, E. Kraft, R. Kronzon, M. Blumenstein, L.C. Francesconi, J. Alloys Compds. 249 (1997) 56.
[41] J. Bartis, S. Sukal, M. Dankova, E. Kraft, R. Kronzon, M. Blumenstein, L.C. Francesconi, J. Chem. Soc., Dalton Trans. (1997) 1937.
[42] N. Haraguchi, Y. Okaue, T. Isobe, Y. Matsuda, Inorg. Chem. 33 (1994) 115.
[43] M. Sadakane, M.H. Dickman, M.T. Pope, Angew. Chem., Int. Ed. 39 (2000) 2914.
[44] Q.-H. Luo, R.C. Howell, M. Dankova, J. Bartis, C.W. Williams, W. DeW. Horrocks Jr., V.G. Young Jr., A.L. Rheingold, L.C. Francesconi, M.R. Antonio, Inorg. Chem. 40 (2001) 1894.
[45] M. Sadakane, M.H. Dickman, M.T. Pope, Inorg. Chem. 40 (2001) 2715.
[46] M. Sadakane, A. Ostuni, M.T. Pope, J. Chem. Soc., Dalton Trans. (2002) 63.
[47] Q. Luo, R.C. Howell, J. Bartis, M. Dankova, W. deW. Horrocks Jr., A.L. Rheingold, L.C. Francesconi, Inorg. Chem. 41 (2002) 6112.
[48] N.N. Basargin, V.M. Ivanov, V.V. Kuznetsov, A.V. Mikhailova, J. Anal. Chem. 55 (2000) 204.
[49] Y.W. Lu, G. Laurent, H. Pereira, Talanta 62 (2004) 959.
[50] H. Rohwer, N. Collier, E. Hosten, Anal. Chim. Acta 314 (1995) 219.
[51] E. Hosten, H. Rohwer, Anal. Chim. Acta 345 (1997) 227.
[52] H. Rohwer, E. Hosten, Anal. Chim. Acta 345 (1997) 271.
[53] C.E. VanPelt, W.J. Crooks III, G.R. Choppin, Inorg. Chim. Acta 340 (2002) 1.
[54] R. Contant, J.P. Ciabrini, J. Chem. Res. (Synopsis) (1982) 50 (Miniprint) 0641-0660.

Available online at www.sciencedirect.com
SCIENCE DIRECT®
Polyhedron 23 (2004) 1587–1594
POLYHEDRON
www.elsevier.com/locate/poly

Pyridineenolato and pyridineenamido complexes of zirconium, titanium and aluminum

Ui Gab Joung [a], Tae Ho Kim [a], Dae June Joe [a], Bun Yeoul Lee [a,*], Dong Mok Shin [b], Young Keun Chung [b]

[a] Department of Molecular Science and Technology, Ajou University, San 5, Wonchondong, Suwon 442-749, Republic of Korea
[b] School of Chemistry and Center for Molecular Catalysis, Seoul National University, Seoul 151-747, Republic of Korea

Received 11 February 2004; accepted 8 March 2004
Available online 15 April 2004

Abstract

Deprotonation of 2-acetylpyridine with KH in THF afford a potassium enolate compound (**2**) which reacts with $Zr(NEt_2)_2Cl_2(THF)_2$ and $Ti(NMe_2)_2Cl_2$ to yield $[CH_2{=}C(C_5H_4N)O\text{-}\kappa^2N,O]_2M(NR_2)_2$ (M = Zr, R = Et, **3**; M = Ti, R = Me, **4**) in 84% and 76% yield, respectively. Deprotonation of imines derived from 2-acetylpyridine, $(2,6\text{-}Me_2C_6H_3)N{=}C(C_5H_4N)(CH_3)$ (**5**) and $(2,6\text{-}i Pr_2C_6H_3)N{=}C(C_5H_4N)(CH_3)$ (**6**), affords potassium enamides, $K[(2,6\text{-}Me_2C_6H_3)N\text{–}C(C_5H_4N)(=CH_2)]$ (**7**) and $K[(2,6\text{-}iPr_2C_6H_3)N\text{-}(C_5H_4N)(=CH_2)]$ (**8**). Reactions of the potassium salt **7** with $Zr(NEt_2)_2Cl_2(THF)_2$ and $Ti(NMe_2)_2Cl_2$ afford pyridineenamido complexes, $[(2,6\text{-}Me_2C_6H_3)NC(C_5H_4N)(=CH_2)\text{-}\kappa^2N,N]_2M(NR_2)_2$ (M = Zr, R = Et, **9**; M = Ti, R = Me, **10**). Reaction of **8** with $Zr(NEt_2)_2Cl_2(THF)_2$ affords $[(2,6\text{-}iPr_2C_6H_3)NC(C_5H_4N)(=CH_2)]_2Zr(NEt_2)_2$ (**11**) but the reaction of **8** with $Ti(NMe_2)_2Cl_2$ yields $[(2,6\text{-}iPrC_6H_3)NC(C_5H_4N)(=CH_2)]TiCl(NMe_2)_2$ (**12**). Addition of excess $AlMe_3$ to **3** or **4** results in transmetallation of Zr or Ti to Al to afford an aluminum enolate complex, $[CH_2{=}C(C_5H_4N)(OAlMe_3)\text{-}\kappa^2N,O]AlMe_2$ (**13**). Addition of $AlMe_3$ to **12** results in the formation of a transmetallated complex, $[(2,6\text{-}iPr_2C_6H_3)NC(C_5H_4N)(=CH_2)]AlMe_2$ (**14**). The solid structures of **4, 11, 13** and **14** were determined by X-ray crystallography.
© 2004 Elsevier Ltd. All rights reserved.

Keywords: Enolato; Enamido; Zirconium; Titanium; Aluminum

1. Introduction

A great deal of effort has been devoted in developing single site polymerization catalysts in both academic and industrial fields [1]. Metal complexes beyond metallocenes using various ligand systems including chelating diamido [2] and phenoxy-imine [3–5] have been developed and expansion from group 4 metal complexes to complexes based on the late transition metals [6] has been achieved. Bazan and Lee have described some metal complexes based on carboxylato [7], carboxamido [8] and enamido ligands [9]. The complexes are characteristic since the ligands have an electron-rich atom to which a Lewis acidic cocatalyst can bind to afford zwitterionic active complexes (Eq. (1)). A novel activation reaction was successfully applied to nickel complexes and recently it was expanded to the early transition metal complexes with an enamido ligand [10]. Herein, we report preparation of pyridineenolato and pyridineenamido complexes of titanium, zirconium and aluminum. The complexes have an electron-rich methylene carbon to which a Lewis acidic cocatalyst can bind.

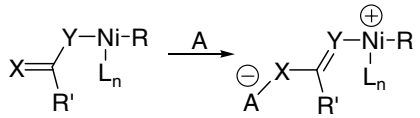

(1)

* Corresponding author. Tel.: +82-31-219-1844; fax: +82-31-219-1592.
E-mail address: bunyeoul@ajou.ac.kr (B.Y. Lee).

0277-5387/$ - see front matter © 2004 Elsevier Ltd. All rights reserved.
doi:10.1016/j.poly.2004.03.009

2. Results and discussion

2.1. Synthesis and characterization

Deprotonation of 2-acetylpyridine is successfully conducted by KH in THF (Eq. (2)). Addition of $Zr(NEt_2)_2Cl_2(THF)_2$ and $Ti(NMe_2)_2Cl_2$ to the potassium enolate salt **2** results in clean formation of the desired enolato complexes, $[CH_2{=}C(C_5H_4N)O\text{-}\kappa^2N,O]_2M(NR_2)_2$ (M = Zr, R = Et, **3**; M = Ti, R = Me, **4**) in 84% and 76% yield, respectively (Eq. (2)). The characteristic methylene proton signals are observed at 4.99 and 4.82 ppm for **3** and at 4.99 and 4.78 ppm for **4** as singlets in the ^1H NMR spectra (C_6D_6). The $=CH_2$ carbon signals are observed at 87.63 and 85.48 ppm for **3** and **4,** respectively, in the ^{13}C NMR spectra (C_6D_6). Single crystals of **4** suitable for X-ray crystallography were obtained by recrystallization in toluene and the solid structure was confirmed.

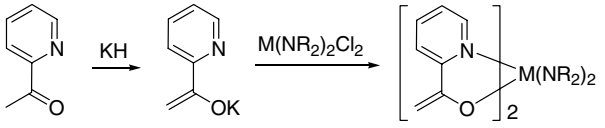

(2)

Syntheses of the imine compounds **5** [11] and **6** [12] have been reported. The deprotonation is carried out cleanly by KH in THF (Eq. (3)). The potassium salts are readily soluble in a cosolvent of benzene and THF (v/v, ~5:1) and are characterized by the ^1H and ^{13}C NMR spectra. Reaction of the potassium salts with $Zr(NEt_2)_2Cl_2(THF)_2$ and $Ti(NMe_2)_2Cl_2$ yields the desired pyridineenamido complexes **9**–**11** (Eq. (3)). The complexes were isolated by recrystallization in toluene.

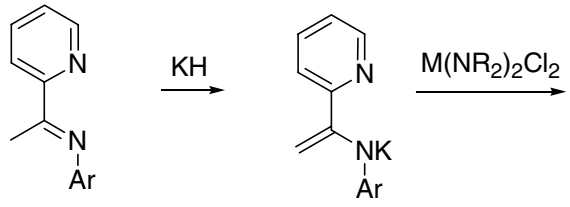

(3)

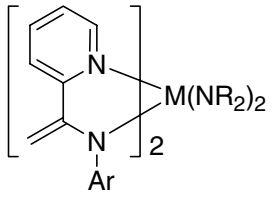

The enamido ligand is ambiphilic. Either nitrogen or methylene carbon can coordinate to the metal center [9]. Observation of two singlet signals at 4.8–3.7 ppm in the ^1H NMR spectra (C_6D_6) and observation of a signal at 79–89 ppm in the ^{13}C NMR spectra support that the nitrogen coordinates as depicted in Eq. (3). If two pyridineenamido ligands and two dialkylamido ligands coordinate to the metal center to form an octahedral complex, eight stereochemical structures are possible as the case in the phenoxy-imine complexes [4]. In case of the phenoxy-imine complexes, the most stable isomer was calculated to have the structure shown below and actually only the most stable complex was obtained. X-ray crystallographic studies of a single crystal of **11** obtained by recrystallization in toluene reveal that the complex has similar stereochemical structure as observed for the phenoxy-imine complexes, with a *cis*-relationship between the two dialkylamide ligands and a *trans*-relationship between the two amido nitrogen atoms. Since similar signal patterns are observed for **9** and **10** in the ^1H and ^{13}C NMR spectra, we presume they have a similar stereochemical structure as observed for **11**.

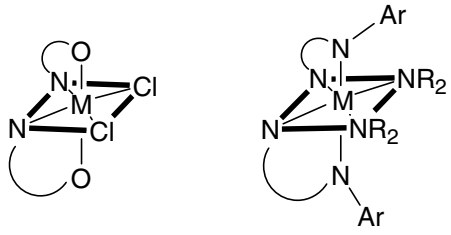

In the case of the reaction of potassium salt **8** with $Ti(NMe_2)_2Cl_2$, the desired complex is not obtained. The major product isolated by recrystallization in toluene can be assigned to the structure **12** by the analysis of the ^1H NMR spectrum. The relative intensity of the dimethylamido methyl signal is twice that observed for **10** and only one broad septet isopropyl CH signal and two doublet isopropyl CH_3 signals are observed. In the ^1H NMR spectrum of **11,** two septet isopropyl CH signals and four doublet isopropyl CH_3 signals are observed.

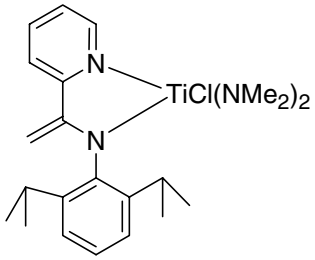

12

Transformation of the bis(dialkylamido) complex to the dichloro or dialkyl complex is desired because the latter is effectively activated with a common cocatalyst such as MAO or $B(C_6F_5)_3$. When chlorinating reagent,

Me_3SiCl or Me_2SiCl_2, is reacted with **3**–**4** and **9**–**11,** a complex mixture of products is observed in the ^1H NMR spectra. When alkylating reagent, $AlMe_3$ (10 equivalents) is reacted with the enolate complex **3**, aiming to obtain the dimethyl zirconium complex, the ^1H NMR spectrum indicates that a complex is formed cleanly. The complete set of signals for the pyridineenolate ligand is observed in the ^1H NMR spectra but two methyl signals are observed at −0.04 and −0.27 ppm with integration values of 9 and 6. The ^1H and ^{13}C NMR spectra of the reaction product between **4** and $AlMe_3$ are exactly the same as those observed for the reaction product of **3**. Single crystals suitable for X-ray crystallography were obtained by recrystallization in pentane at −30 °C and the molecular structure was determined. The product is an $AlMe_3$-coordinated enolatodimethylaluminum complex (Eq. (4)).

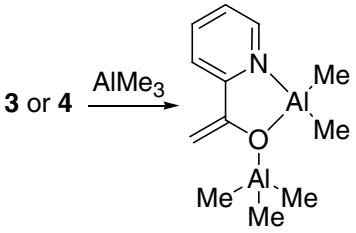

13 (4)

Several sets of signals are observed in the ^1H NMR spectrum when sterically hindered complex **11** is reacted with $AlMe_3$. The main product is deposited from pentane solution at −30 °C as single crystals, which are suitable for X-ray crystallography. The X-ray crystallographic studies of the product reveal that the main product is a transmetallated aluminum complex as shown in Eq. (5).

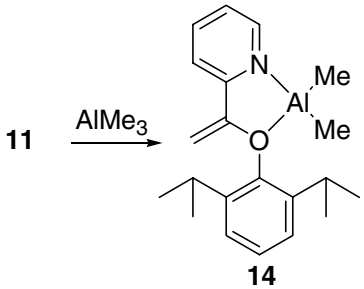

14 (5)

2.2. X-ray crystallographic studies

The solid structure of **4** and selected bond distances and angles are shown in Fig. 1. It shows a distorted octahedral structure with a *trans*-relationship between the two oxygen atoms and a *cis*-relationship between the two dimethylamido ligands. All atoms in the pyridineenolate ligand and the titanium atom are situated in a plane and hence the dihedral angle of C(8)–C(13)–O(2)–Ti(1), C(11)–C(12)–N(2)–Ti(1) and C(9)–C(8)–C(13)–O(2) are measured to be 1.9°, −179.4° and −179.7°, respectively. The C(6)–C(7) distance (1.335(4) Å) and the C(13)–C(14) distance (1.324(4) Å) are indicative of a double bond between these two atoms. The O(1)–C(6) distance (1.327(4) Å) and the O(2)–C(13) distance (1.336(4) Å) are indicative of a shortened single bond by resonance. The dimethylamido nitrogen atoms are almost trigonal planar (sum of bonding angles, 359.8° and 357.1°) indicating π-electron donation to the titanium metal.

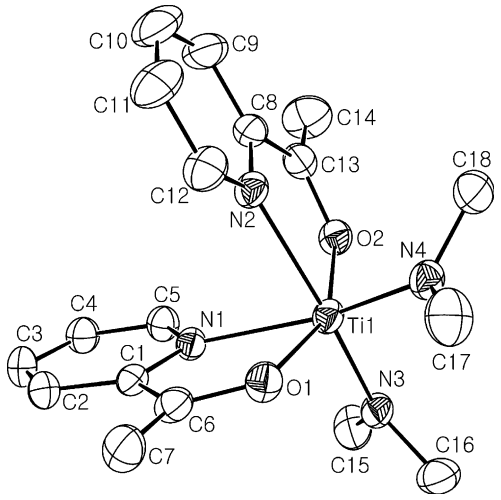

Fig. 1. Thermal ellipsoid plot (30% probability level) of the structure of **4**. Selected bond distances (Å) and angles (°): Ti(1)–O(1), 1.949(2); Ti(1)–O(2), 1.923(2); Ti(1)–N(1), 2.282(2); Ti(1)–N(2), 2.269(2); Ti(1)–N(3), 1.929(2); Ti(1)–N(4), 1.914(3); O(1)–C(6), 1.327(4); O(2)–C(13), 1.336(4); C(6)–C(7), 1.335(4); C(13)–C(14), 1.324(4); O(2)–Ti(1)–O(1), 154.51(9); N(4)–Ti(1)–N(1), 159.75(10); N(3)–Ti(1)–N(2), 164.92(10); C(6)–O(1)–Ti(1), 126.10(18); C(13)–O(2)–Ti(1), 126.12(19).

The solid structure of **11** and selected bond distances and angles are shown in Fig. 2. It also shows a distorted octahedral structure. The two amido nitrogen atoms are in a *trans*-relationship and the two dimethylamido ligands are situated in a *cis*-relationship. The Zr–N distances are in the order of Zr–NEt_2 (2.078(3) and 2.058(3) Å) <Zr–N(amido) (2.278(3) and 2.279(2) Å) <Zr–N(pyridine) (2.420(3) and 2.429(3) Å). A ring, (Zr(1)–N(3)–C(20)–C(25)–N(4)), formed by chelation is coplanar (dihedral angles of N(3)–C(20)–C(25)–N(4) and C(20)–C(25)–N(4)–Zr(1) are 1.6° and −0.3°, respectively) while the other ring (Zr(1)–N(1)–C(1)–C(6)–N(2)) is slightly out of coplanarity (dihedral angles of N(1)–C(1)–C(6)–N(2) and C(1)–C(6)–N(2)–Zr(1) are 11.3° and −19.1°, respectively). The aryl rings are almost perpendicular to the plane formed by chelation (dihedral angles of C(6)–N(2)–C(8)–C(9) and C(25)–N(4)–C(27)–C(28) are −76.4° and 78.5°, respectively). The C(6)–C(7) distance (1.366(5) Å) and the C(25)–C(26) distance (1.347(4) Å) are indicative of a double bond although they are slightly longer than the corresponding distances observed for the enolate complex **4**. All the diethylamido nitrogens and amido nitrogens show trigonal planar

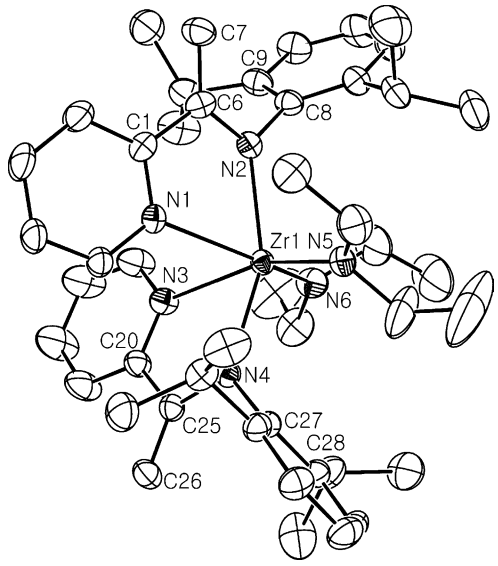

Fig. 2. Thermal ellipsoid plot (30% probability level) of the structure of **11**. Selected bond distances (Å) and angles (°): Zr(1)–N(1), 2.420(3); Zr(1)–N(2), 2.278(3); Zr(1)–N(3), 2.429(3); Zr(1)–N(4), 2.279(2); Zr(1)–N(5), 2.078(3); Zr(1)–N(6), 2.058(3); N(2)–C(6), 1.390(4); N(4)–C(25), 1.391(4); C(6)–C(7), 1.366(5); C(25)–C(26), 1.347(4); N(2)–Zr(1)–N(4), 155.95(9); N(6)–Zr(1)–N(1), 147.50(12); N(5)–Zr(1)–N(3), 158.64(10); C(25)–N(4)–Zr(1), 123.20(19); C(6)–N(2)–Zr(1), 120.5(2).

structure and hence the sum of bonding angles around N(2), N(4), N(5) and N(6) are calculated to be 359.9°, 359.6°, 359.7° and 359.9°, respectively.

The solid structure of **13** and selected bond distances and angles are shown in Fig. 3. Two aluminum atoms show a distorted tetrahedral structure. All the atoms on the pyridineenamide ligand and the two aluminum atoms are almost situated in a plane (dihedral angles of C(4)–C(5)–N(1)–Al(1) and C(5)–N(1)–Al(1)–Al(2) are −178.2° and 177.7°, respectively). The oxygen atom

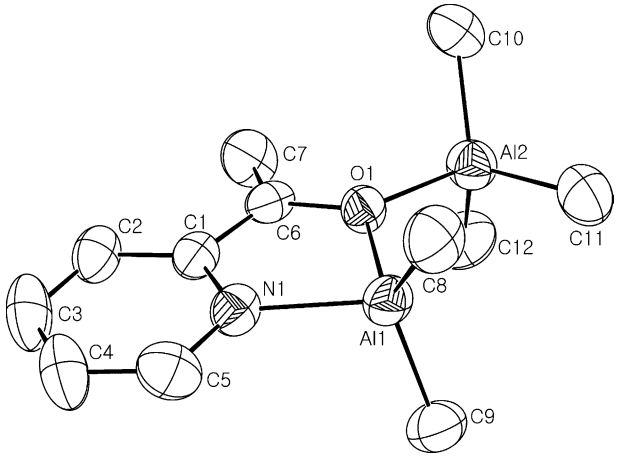

Fig. 3. Thermal ellipsoid plot (30% probability level) of the structure of **13**. Selected bond distances (Å) and angles (°): Al(1)–O(1), 1.847(6); Al(1)–N(1), 1.980(8); Al(1)–C(8), 1.941(9); Al(1)–C(9), 1.929(9); Al(2)–O(1), 1.934(6); Al(2)–C(10), 1.951(10); Al(2)–C(11), 1.962(11); Al(2)–C(12), 1.972(11); O(1)–C(6), 1.390(10); C(6)–C(7), 1.306(11); C(6)–O(1)–Al(1), 117.0(6); C(6)–O(1)–Al(2), 124.1(6); Al(1)–O(1)–Al(2), 116.9(3).

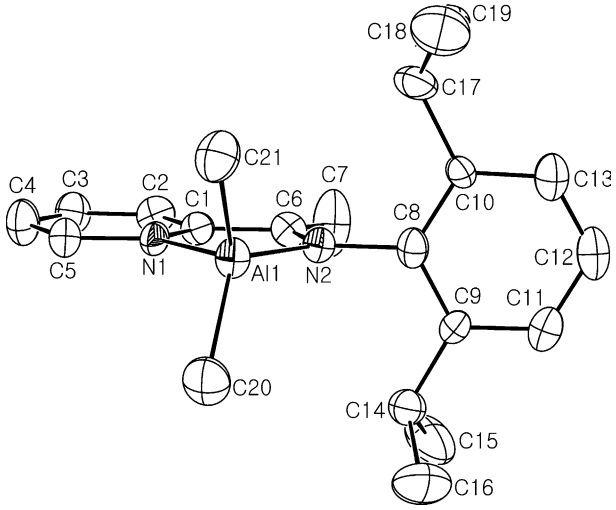

Fig. 4. Thermal ellipsoid plot (30% probability level) of the structure of **14**.

shows almost a trigonal planar structure (sum of bonding angle, 358.0°). The Al(1)–O(1) distance (1.847(6) Å) is shorter than the Al(2)–O(1) distance (1.934(6) Å) and the Al(1)–C distances (1.941(9) and 1.929(9) Å) are shorter as well than the Al(2)–C distances (1.951(10), 1.962(11) and 1.972(11) Å).

The solid structure of **14** is shown in Fig. 4. The final R indices for the refinement are too high ($R_1 = 0.1573$, $wR_2 = 0.3676$) to do quantitative analysis for the bond distances and angles, but it can be seen that Al(1), C(6), N(2) and all the atoms in the pyridine ring are coplanar and the 2,6-diisopropyl benzene ring is perpendicular to the plane.

3. Experimental

3.1. General considerations

All manipulations were performed under an inert atmosphere using standard glove box and Schlenk techniques. Toluene, pentane, THF and C_6D_6 were distilled from benzophenone ketyl. $Zr(NEt_2)_2Cl_2(THF)_2$ [13] and $Ti(NMe_2)_2Cl_2$ [14] were prepared according to the literature method. ^1H NMR (400 MHz) and ^{13}C NMR (100 MHz) spectra were recorded on a Varian Mercury plus 400. Elemental analyses were carried out on a Perkin–Elmer 2400 CHN microanalyzer.

3.2. Synthesis of $CH_2{=}C(C_5H_4N)OK$ (**2**)

2-Acetylpyridine (1.00 g, 8.25 mmol) and KH (0.331 g, 8.25 mmol) were weighed in a flask and cold THF (10 ml, −30 °C) was added. The solution was stirred for 4 h at room temperature. The precipitated solid was filtered and washed with THF to give a white solid (1.13 g, 86%). The solid was not soluble in pyridine, benzene or THF.

3.3. Synthesis of $[CH_2{=}C(C_5H_4N)O\text{-}\kappa^2N,O]_2Zr(NEt_2)_2$ (**3**)

$ZrCl_2(NEt_2)_2(THF)_2$ (1.41 g, 3.14 mmol) was dissolved in THF (20 ml) and solid **2** (1.00 g, 6.28 mmol) was added in one portion at room temperature. The solution was stirred overnight. Solvent was removed by vacuum. The product was extracted with toluene (15 ml × 2) and the toluene was removed by vacuum to give a yellow solid (1.25 g, 84%) which was analytically pure. ^{1}H NMR (C_6D_6): δ 8.51 (dt, $J = 5.6$, 1.2 Hz, 1H, py-H^6), 7.01 (d, $J = 8.0$ Hz, 1H, py-H^3), 6.60 (ddd, $J = 8.0$, 7.2, 1.2 Hz, 1H, py-H^4), 6.29 (ddd, $J = 7.2$, 5.6, 1.2 Hz, 1H, py-H^5), 4.99 (s, 1H, =CH$_2$), 4.82 (s, 1H, =CH$_2$), 3.73 (q, $J = 6.8$ Hz, 4H, C*H*$_2$CH$_3$), 1.21 (t, $J = 6.8$ Hz, 6H, CH$_2$C*H*$_3$) ppm. ^{13}C{^{1}H}NMR (C_6D_6) δ 162.31, 157.90, 146.68, 137.33, 122.37, 119.86, 87.63 (=*C*H$_2$), 44.54 (*C*H$_2$CH$_3$), 16.11 (CH$_2$*C*H$_3$) ppm. *Anal.* Calc. ($C_{22}H_{32}N_4O_2Zr$): C, 55.54; H, 6.78; N, 11.78. Found: C, 55.72; H, 6.53; N, 11.38%.

3.4. Synthesis of $[CH_2{=}C(C_5H_4N)O\text{-}\kappa^2N,O]_2Ti(NMe_2)_2$ (**4**)

The complex was synthesized using the same procedure and conditions as for **3,** but with $TiCl_2(NMe_2)_2$ (0.500 g, 2.42 mmol) and the potassium salt **2** (0.770 g, 4.84 mmol). The analytically pure red solid was isolated by extraction with toluene (0.690 g, 76%). Single crystals suitable for X-ray crystallography were obtained by recrystallization in toluene at −30 °C. ^{1}H NMR (C_6D_6): δ 8.57 (dt, $J = 5.6$, 1.2 Hz, 1H, py-H^6), 7.01 (dd, $J = 6.8$, 1.2 Hz, 1H, py-H^3), 6.64 (ddd, $J = 8.8$, 6.8, 1.2 Hz, 1H, py-H^4), 6.34 (ddd, $J = 7.2$, 5.6, 1.2 Hz, 1H, py-H^5), 4.99 (s, 1H, =CH$_2$), 4.78 (s, 1H, =CH$_2$), 3.57 (s, 6 H, CH$_3$) ppm. ^{13}C{^{1}H}NMR (C_6D_6) δ 163.88, 157.12, 146.39, 136.99, 122.34, 119.47, 85.48 (=CH$_2$), 48.20 (CH$_3$) ppm. *Anal.* Calc. ($C_{18}H_{24}N_4O_2Ti$): C, 57.46; H, 6.43; N, 14.89. Found: C, 57.03; H, 6.73; N, 14.59%.

3.5. Synthesis of $K[(2,6\text{-}Me_2C_6H_3)N\text{–}C(C_5H_4N)(=CH_2)]$ (**7**)

A solution of **5** (1.20 g, 5.35 mmol) in THF (20 ml) was added to a slurry of KH (0.429 g, 1.07 mmol) in THF (5.0 ml) and the resulting mixture was stirred for one day at room temperature. The dark brown solution was filtered and solvent was removed under vacuum. The residue was triturated in pentane to give a greenish yellow solid. The yield was 1.15 g (82%). ^{1}H NMR (C_6D_6:THF-d_8, 5:1): δ 7.95 (d, $J = 8.0$ Hz, 1H, py-H^6), 7.44 (d, $J = 5.2$ Hz, 1H, py-H^3), 7.24 (d, $J = 7.2$ Hz, 2H, ph-H$^{3\text{ and }5}$), 7.13 (td, $J = 8.0$, 1.6 Hz, 1H, py-H^5), 6.95 (t, $J = 7.2$ Hz, 1H, ph-H^4), 6.62 (dd, $J = 7.2$, 5.2 Hz, 1H, py-H^4), 4.11 (s, 1H, =CH$_2$), 3.29 (s, 1H, =CH$_2$), 2.30 (s, 6H, CH$_3$) ppm. ^{13}C{^{1}H}NMR (C_6D_6:THF-d_8, 5:1) δ 169.57, 158.59, 154.57, 148.16, 135.32, 131.75, 128.65, 121.93, 120.77, 118.79, 69.40 (=CH$_2$), 19.21 (CH$_3$) ppm.

3.6. Synthesis of $K[(2,6\text{-}iPr_2C_6H_3)N(C_5H_4N)(=CH_2)]$ (**8**)

This salt was synthesized using the same procedure and conditions for **7,** but with **6** (1.61 g, 5.74 mmol) and KH (0.461 g, 11.5 mmol). The mixture was stirred for two days. The yield was 1.61 g (88%). ^{1}H NMR (C_6D_6:THF-d_8, 5:1): δ 7.99 (d, $J = 8.0$ Hz, 1H, py-H^6), 7.70 (d, $J = 5.2$ Hz, 1H, py-H^3), 7.33 (d, $J = 7.2$ Hz, 2H, ph-H$^{3\text{ and }5}$), 7.20 (t, $J = 7.2$ Hz, 1H, ph-H^4), 7.12 (td, $J = 8.0$, 1.6 Hz, 1H, py-H^5), 6.64 (td, $J = 8.0$, 1.2 Hz, 1H, py-H^4), 4.15 (s, 1H, =CH$_2$), 3.52 (septet, $J = 7.2$ Hz, 2H, C*H*(CH$_3$)$_2$), 3.26 (s, 1H, =CH$_2$), 1.51 (d, $J = 7.2$ Hz, 6H, CH(C*H*$_3$)$_2$), 1.16 (d, $J = 7.2$ Hz, 6H, CH(C*H*$_3$)$_2$) ppm. ^{13}C{^{1}H}NMR (C_6D_6:THF-d_8, 5:1) δ 164.24, 157.92, 155.83, 147.85, 142.87, 135.49, 123.54, 122.45, 120.84, 119.90, 71.60 (=CH$_2$), 27.81 (CH(*C*H$_3$)$_2$), 26.75 (CH(*C*H$_3$)$_2$), 26.02 (*C*H(CH$_3$)$_2$) ppm.

3.7. Synthesis of $[(2,6\text{-}Me_2C_6H_3)NC(C_5H_4N)(=CH_2)\text{-}\kappa^2N,N]_2Zr(NEt_2)_2$ (**9**)

$ZrCl_2(NEt_2)_2(THF)_2$ (0.523 g, 1.16 mmol) and potassium salt **7** (0.609 g, 2.32 mmol) were weighed in a flask and THF (30 ml) was added. The resulting solution was stirred for two days. Solvent was removed under vacuum to give a black residue which was dissolved in toluene (40 ml). The solution was filtered and solvent was reduced to ~10 ml, at which point yellow solids precipitated. The deposited solid was collected by filtration (0.486 g, 61%). ^{1}H NMR (C_6D_6): δ 8.80 (br d, $J = 4.8$ Hz, 1H, py-H^6), 7.41 (d, $J = 8.4$ Hz, 1H, py-H^3), 7.20 (d, $J = 7.2$ Hz, 1H, ph-H$^{3\text{ or }5}$), 7.14 (d, $J = 7.2$ Hz, 1H, ph-H$^{3\text{ or }5}$), 7.03 (t, $J = 7.2$ Hz, 1H, ph-H^4), 6.71 (br t, $J = 7.2$ Hz, 1H, py-H^5), 6.23 (br t, $J = 6.0$ Hz, 1H, py-H^4), 4.60 (s, 1H, =CH$_2$), 3.89 (s, 1H, =CH$_2$), 3.22 (dq, $J = 14$, 7.2 Hz, 2H, NC*H*$_2$CH$_3$), 2.75 (dq, $J = 14$, 7.2 Hz, 2H, NC*H*$_2$CH$_3$), 2.64 (s, 3H, CH$_3$), 2.51 (s, 3H, CH$_3$), 0.71 (t, $J = 7.2$ Hz, 6H, CH$_2$C*H*$_3$). ^{13}C{^{1}H}NMR (C_6D_6) δ 158.77, 153.27, 151.58, 147.79, 137.10, 136.59, 134.97, 129.32, 128.80, 124.06, 121.19, 120.98, 83.30 (=*C*H$_2$), 42.07 (CH$_2$*C*H$_3$), 22.36 (CH$_3$), 20.46 (CH$_3$), 13.36 (*C*H$_2$CH$_3$) ppm. *Anal.* Calc. ($C_{38}H_{50}N_6Zr$): C, 66.92; H, 7.39; N, 12.32. Found: C, 67.23; H, 7.45; N, 12.11%.

3.8. Synthesis of $[(2,6\text{-}Me_2C_6H_3)NC(C_5H_4N)(=CH_2)\text{-}\kappa^2N,N]_2Ti(NMe_2)_2$ (**10**)

The complex was synthesized using the same procedure and conditions for **9,** but with $TiCl_2(NMe_2)_2$ (0.174 g, 0.840 mmol) and the potassium salt **7** (0.440 g,

1.68 mmol). The solution was stirred for two days at 50 °C. The complex was purified by recrystallization in toluene at −30 °C. The yield was 0.140 g (29%). ^{1}H NMR (C_6D_6): δ 8.70 (d, $J = 4.8$ Hz, 1H, py-H^6), 7.48 (d, $J = 8.4$ Hz, 1H, py-H^3), 7.23 (d, $J = 7.6$ Hz, 1H, ph-H$^{3\text{ or }5}$), 7.15 (d, $J = 7.6$ Hz, 1H, ph-H$^{3\text{ or }5}$), 7.04 (t, $J = 7.2$ Hz, 1H, ph-H^4), 6.74 (td, $J = 7.6$, 2.0 Hz, 1H, py-H^5), 6.21 (td, $J = 6.4$, 0.8 Hz, 1H, py-H^4), 4.50 (s, 1H, =CH_2), 3.89 (s, 1H, =CH_2), 2.63 (s, 6H, CH_3), 2.45 (s, 3H, CH_3). ^{13}C{^{1}H}NMR (C_6D_6) δ 158.09, 153.88, 153.69, 147.67, 136.45, 135.68, 134.51, 129.56, 129.02, 123.73, 121.13, 120.83, 78.95 (=CH_2), 48.13 (NCH_3), 23.21 (CH_3), 20.13 (CH_3) ppm. *Anal.* Calc. ($C_{34}H_{42}N_6Ti$): C, 70.09; H, 7.27; N, 14.42. Found: C, 69.71; H, 7.52; N, 14.11%.

3.9. Synthesis of [(2,6-iPr$_2$C$_6$H$_3$)NC(C$_5$H$_4$N)(=CH$_2$)]$_2$Zr(NEt$_2$)$_2$ (11)

The complex was synthesized using the same procedure and conditions for **9,** but with $ZrCl_2(NEt_2)_2(THF)_2$ (0.707 g, 1.57 mmol) and the potassium salt **8** (1.00 g, 3.14 mmol). The solution was stirred for one day at room temperature. The crystals, which were analytically pure and suitable for X-ray crystallography, were obtained by recrystallization in toluene at −30 °C. The yield was 0.742 g (60%). ^{1}H NMR (C_6D_6): δ 8.70 (d, $J = 5.6$ Hz, 1H, py-H^6), 7.50–7.24 (m, 4H), 6.76 (td, $J = 7.2$, 1.2 Hz, 1H, py-H^5), 6.44 (t, $J = 6.4$ Hz, 1H, py-H^4), 4.79 (s, 1H, =CH_2), 4.11 (septet, $J = 6.8$ Hz, 2H, C*H*(CH_3)$_2$), 3.78 (s, 1H, =CH_2), 3.43 (septet, $J = 6.8$ Hz, 2H, C*H*(CH_3)$_2$), 3.33 (dq, $J = 14$, 6.8 Hz, 2H, NCH_2), 2.77 (dq, $J = 14$, 6.8 Hz, 2H, NCH_2), 1.50 (d, $J = 6.8$ Hz, 3H, CH(C*H*$_3$)$_2$), 1.48 (d, $J = 6.8$ Hz, 3H, CH(C*H*$_3$)$_2$), 1.44 (d, $J = 6.8$ Hz, 3H, CH(C*H*$_3$)$_2$), 1.34 (d, $J = 6.8$ Hz, 3H, CH(C*H*$_3$)$_2$), 0.70 (t, $J = 7.2$ Hz, 6H, NCH_2CH_3) ppm. ^{13}C{^{1}H}NMR (C_6D_6) δ 159.15, 156.34, 151.30, 147.61, 146.28, 144.65, 137.20, 124.96, 124.70, 124.19, 121.01, 120.85, 89.13 (=CH_2), 43.42 (NCH_2), 29.03, 28.00, 27.79, 27.43, 25.76, 24.65, 14.15 (NCH_2CH_3) ppm. *Anal.* Calc. ($C_{46}H_{66}N_6Zr$): C, 69.56; H, 8.38; N, 10.58. Found: C, 69.43; H, 8.42; N, 10.21%.

3.10. Synthesis of [(2,6-iPr$_2$C$_6$H$_3$)NC(C$_5$H$_4$N)(=CH$_2$)]TiCl(NMe$_2$)$_2$ (12)

The complex was synthesized using the same procedure and conditions for **9,** but with $TiCl_2(NMe_2)_2$ (0.325 g, 1.57 mmol) and the potassium salt **8** (1.00 g, 3.14 mmol). The solution was stirred for one day at room temperature. The single crystals, which were analytically pure, were obtained by recrystallization in toluene at −30 °C. The yield was 0.445 g (63%). ^{1}H NMR (C_6D_6): δ 8.52 (d, $J = 5.2$ Hz, 1H, py-H^6), 7.28–7.10 (m, 4H), 6.87 (td, $J = 7.2$, 0.8 Hz, 1H, py-H^5), 6.49 (t, $J = 6.0$ Hz, 1H, py-H^4), 4.56 (s, 1H, =CH_2), 3.75 (s, 1H, =CH_2), 3.29 (br septet, $J = 6.8$ Hz, 2H, C*H*(CH_3)$_2$), 3.01 (s, 12H, NCH_3), 1.26 (d, $J = 7.2$ Hz, 6H, CH(C*H*$_3$)$_2$), 1.25 (d, $J = 7.2$ Hz, 6H, CH(C*H*$_3$)$_2$) ppm. ^{13}C{^{1}H}NMR (C_6D_6) δ 156.52, 155.44, 149.01, 147.40, 142.84, 137.12, 125.56, 123.64, 122.55, 119.61, 87.96 (=CH_2), 47.2 (br NCH_3), 28.86 (*C*H(CH_3)$_2$), 27.20 (CH(*C*H$_3$)$_2$), 24.18 (CH(*C*H$_3$)$_2$) ppm. *Anal.* Calc. ($C_{23}H_{35}N_4ClTi$): C, 61.27; H, 7.84; N, 12.43. Found: C, 60.88; H, 7.89; N, 12.33%.

3.11. Synthesis of [CH$_2$=C(C$_5$H$_4$N)(OAlMe$_3$)-κ^2N,O]AlMe$_2$ (13)

Complex **3** (0.100 g, 0.210 mmol) was dissolved in benzene (3.0 ml) and $AlMe_3$ (0.15 g, 2.10 mmol) was added. The solution was stirred at room temperature overnight. All volatiles were completely removed under high vacuum at room temperature. Pentane was added and the solution was filtered over celite. White crystals were deposited when the solution was stored at −30 °C. The yield was 45 mg (43%). ^{1}H NMR (C_6D_6): δ 7.17 (d, $J = 6.8$ Hz, 1H, py-H^6), 6.72 (td, $J = 6.8$, 0.8 Hz, 1H, py-H^4), 6.62 (d, $J = 8.8$ Hz, 1H, py-H^3), 6.31 (t, $J = 6.4$ Hz, 1H, py-H^5), 5.56 (d, $J = 3.6$ Hz, 1H, =CH_2), 4.86 (d, $J = 3.6$ Hz, 1H, =CH_2), −0.04 (s, 9H, $AlCH_3$), −0.27 (s, 6H, $AlCH_3$) ppm. ^{13}C{^{1}H}NMR (C_6D_6) δ 151.54, 150.37, 142.53, 140.59, 124.40, 120.30, 97.94 (=*C*H$_2$), −6.20 (br, AlC), −7.87 (br, AlC) ppm. *Anal.* Calc. ($C_{12}H_{21}NOAl_2$): C, 57.82; H, 8.51; N, 5.62. Found: C, 57.55; H, 8.15; N, 5.33%.

3.12. Synthesis of [(2,6-iPr$_2$C$_6$H$_3$)NC(C$_5$H$_4$N)(=CH$_2$)]AlMe$_2$ (14)

The complex was synthesized using the same procedure and conditions for **13,** but with **11** (0.100 g, 0.126 mmol) and $AlMe_3$ (0.024 ml, 0.252 mmol) in benzene (1.0 ml). The solvent was removed by vacuum and the residue was extracted with pentane. Light yellow single crystals were deposited when the pentane solution was stored at −30 °C overnight (20 mg, 24%).

^{1}H NMR (C_6D_6): δ 7.46 (d, $J = 5.6$ Hz, 1H, py-H^6), 7.19 (t, $J = 8.4$ Hz, 1H, py-H^3), 6.70 (ddd, $J = 8.0$, 7.2, 1.2 Hz, 1H, py-H^5), 6.26 (ddd, $J = 7.2$, 5.2, 1.2 Hz, 1H, py-H^4), 4.55 (d, $J = 1.2$ Hz, 1H, =CH_2), 3.86 (d, $J = 1.2$ Hz, 1H, =CH_2), 3.58 (septet, $J = 7.2$ Hz, 2H, C*H*(CH_3)$_2$), 1.39 (d, $J = 7.2$ Hz, 6H, CH(C*H*$_3$)$_2$), 1.36 (d, $J = 7.2$ Hz, 6H, CH(C*H*$_3$)$_2$), −0.28 (s, 8H, $AlCH_3$) ppm. ^{13}C{^{1}H}NMR (C_6D_6) δ 156.28, 150.26, 147.22, 142.68, 139.13, 126.24, 124.48, 122.90, 120.87, 84.26 (=*C*H$_2$), 28.35, 26.41, 25.21, −8.49 (AlC) ppm. *Anal.* Calc. ($C_{21}H_{29}N_2Al$): C, 74.96; H, 8.71; N, 8.33. Found: C, 74.62; H, 8.52; N, 8.45%.

Table 1
Crystallographic parameters of **4**, **11**, **13** and **14**[a]

	4	**11**	**13**	**14**
Formula	$C_{18}H_{24}N_4O_2Ti$	$C_{46}H_{66}N_6Zr$	$C_{12}H_{21}Al_2NO$	$C_{21}H_{29}AlN_2$
F_w	376.31	794.27	249.26	336.44
Color	dark brown	yellow	pale yellow	pale yellow
Size (mm)	$0.3 \times 0.3 \times 0.15$	$0.20 \times 0.20 \times 0.15$	$0.20 \times 0.15 \times 0.15$	$0.30 \times 0.30 \times 0.20$
a (Å)	8.3150(10)	12.6440(10)	8.865(3)	14.5650(10)
b (Å)	13.9490(10)	17.6100(10)	9.262(3)	8.617(2)
c (Å)	17.1270(10)	20.0200(10)	10.200(2)	17.395(2)
α (°)	90	90	78.869(17)	90
β (°)	97.476(3)	90	88.652(18)	106.349(6)
γ (°)	90	90	73.658(10)	90
V (Å^3)	1969.6(3)	4457.7(5)	788.1(4)	2094.9(6)
Crystal system	monoclinic	orthorhombic	triclinic	monoclinic
Space group	$P21/c$	$P2_12_12_1$	$P\bar{1}$	$P21/N$
D_{calc} (g cm^{-3})	1.269	1.184	1.050	1.067
Z	4	4	2	4
μ (mm^{-1})	0.452	0.283	0.168	0.101
Number of data collected	8080	10,110	2699	8672
Number of unique data	4418	10,110	1643	3115
Number of variables	230	491	151	224
R (%)	0.0587	0.0442	0.0811	0.1573
R_w(%)	0.1029	0.0942	0.2321	0.3676
Goodness-of-fit	1.010	1.029	1.329	1.230

[a] Data collected at 293(2) K with Mo Kα radiation (λ (Kα) = 0.7107), $R(F) = \sum ||F_o| - |F_c|| / \sum |F_o|$ with $F_o > 2.0\sigma(I)$, $R_w = [\sum[w(F_o^2 - F_c^2)^2] / \sum[w(F_o^2)^2]]^{1/2}$ with $F_o > 2.0\sigma(I)$.

3.13. Crystallographic studies

Crystals of **4, 11, 13** and **14** coated with grease (Apiezon N) were mounted inside a thin glass tube with epoxy glue and placed on an Enraf-Nonius CCD single crystal X-ray diffractometer. The structures were solved by direct methods (SHELXS-97) [15] and refined against all F^2 data (SHELXS-97). All non-hydrogen atoms were refined with anisotropic thermal parameters. The hydrogen atoms were treated as idealized contributions. The crystal data and refinement results are summarized in Table 1.

4. Supplementary material

Crystallographic data for the structural analyses have been deposited with the Cambridge Crystallographic Data Center (**4**: CCDC no. 230878; **8**: CCDC no. 230879; **13**: CCDC no. 230880; **14**: CCDC no. 230881). Copies of this information may be obtained free of charge from The Director, CCDC, 12 Union Road, Cambridge CB2 1EZ, UK (fax: +44-1223-336033: e-mail: deposit@ccdc.cam.ac.uk or www: http://www.ccdc.cam.ac.uk).

Acknowledgements

This work was supported by grant No. (R05-2002-000155-0) from the Basic Research Program of the Korea Science and Engineering Foundation.

References

[1] (a) Review: H.H. Brintzinger, D. Fischer, R. Mülhaupt, B. Rieger, R.M. Waymouth, Angew. Chem. Int. Ed. 34 (1995) 1143;
(b) A. Togni, R.L. Halterman (Eds.), Metallocenes, Wiley-VCH, New York, 1998;
(c) G.J.P. Britovsek, V.C. Gibson, D.F. Wass, Angew. Chem. Int. Ed. 38 (1999) 429;
(d) H.G. Alt, A. Köpple, Chem. Rev. 100 (2000) 1205;
(e) G.W. Coates, Chem. Rev. 100 (2000) 1223;
(f) L. Resconi, L. Cavallo, A. Fait, F. Piemontesi, Chem. Rev. 100 (2000) 1253;
(g) E.Y.-X. Chen, T.J. Marks, Chem. Rev. 100 (2000) 1391;
(h) G.W. Coates, J. Chem. Soc. Dalton Trans. (2002) 467;
(i) G.W. Coates, P.D. Hustad, S. Reinartz, Angew. Chem. Int. Ed. 41 (2002) 2236.

[2] (a) J.D. Scollard, D.H. McConville, J. Am. Chem. Soc. 118 (1996) 10008;
(b) J.D. Scollard, D.H. McConville, N.C. Payne, J.J. Vittal, Macromolecules 29 (1996) 5241;
(c) P.N. O'Shaughnessy, K.M. Gillespie, C. Morton, I. Westmoreland, P. Scott, Organometallics 19 (2002) 4496;
(d) C.H. Lee, Y.-H. La, J.W. Park, Organometallics 19 (2000) 344;
(e) L.-C. Liang, R.R. Schrock, W.M. Davis, Organometallics 19 (2000) 2526;
(f) Y.-M. Jeon, J. Heo, W.M. Lee, T. Chang, K. Kim, Organometallics 18 (1999) 4107.

[3] (a) S. Matsui, T. Fujita, Catal. Today 66 (2001) 63;
(b) M. Mitani, R. Furuyama, J. Mohri, J. Saito, S. Ishii, H. Terao, N. Kashiwa, T. Fujita, J. Am. Chem. Soc. 124 (2002) 7888;
(c) M. Mitani, J. Mohri, Y. Yoshida, J. Saito, S. Ishii, K. Tsuru, S. Matsui, R. Furuyama, T. Nakano, H. Tanaka, S.-i. Kojoh, T. Matsugi, N. Kashiwa, T. Fujita, J. Am. Chem. Soc. 124 (2002) 3327;
(d) J. Tian, G.W. Coates, Angew. Chem. Int. Ed. 39 (2000) 3626.

[4] S. Matsui, M. Mitani, J. Saito, Y. Tohi, H. Makio, N. Matsukawa, Y. Takagi, K. Tsuru, M. Nitabaru, T. Nakano, H. Tanaka, N. Kashiwa, T. Fujita, J. Am. Chem. Soc. 123 (2001) 6847.
[5] (a) T.R. Younkin, E.F. Connor, J.I. Henderson, S.K. Friedrich, R.H. Grubbs, D.A. Banselben, Science 287 (2000) 460;
(b) C. Wang, S. Friedrich, T.R. Younkin, R.T. Li, R.H. Grubbs, D.A. Bansleben, M.W. Day, Organometallics 17 (1998) 3149;
(c) E.F. Connor, T.R. Younkin, J.I. Henderson, A.W. Waltman, R.H. Grubbs, Chem. Commun. (2003) 2272.
[6] (a) V.C. Gibson, S.K. Spitzmesser, Chem. Rev. 103 (2003) 283;
(b) S. Mecking, A. Held, F.M. Bauer, Angew. Chem. Int. Ed. 41 (2002) 544;
(c) S.D. Ittel, L.K. Johnson, M. Brookhart, Chem. Rev. 100 (2000) 1169;
(d) S. Mecking, Coord. Chem. Rev. 203 (2000) 325.
[7] (a) Z.J.A. Komon, X. Bu, G.C. Bazan, J. Am. Chem. Soc. 122 (2000) 1830;
(b) Z.J.A. Komon, X. Bu, G.C. Bazan, J. Am. Chem. Soc. 122 (2000) 12379;
(c) B.Y. Lee, Y.H. Kim, H.J. Shin, C.H. Lee, Organometallics 21 (2002) 3481;
(d) Z.J.A. Komon, G.M. Diamond, M.K. Leclerc, V. Murphy, M. Okazaki, G.C. Bazan, J. Am. Chem. Soc. 124 (2002) 15280;
(e) C.B. Shim, Y.H. Kim, B.Y. Lee, Y. Dong, H. Yun, Organometallics 22 (2003) 4272.
[8] (a) B.Y. Lee, G.C. Bazan, J. Vela, Z.J.A. Komon, X. Bu, J. Am. Chem. Soc. 123 (2001) 5352;
(b) B.Y. Lee, X. Bu, G.C. Bazan, Organometallics 20 (2001) 5425;
(c) C.B. Shim, Y.H. Kim, B.Y. Lee, D.M. Shin, Y.K. Chung, J. Organomet. Chem. 675 (2003) 72.
[9] Y.H. Kim, T.H. Kim, B.Y. Lee, D. Woodmansee, X. Bu, G.C. Bazan, Organometallics 21 (2002) 3082.
[10] (a) Y.H. Kim, T.H. Kim, N.Y. Kim, E.S. Cho, B.Y. Lee, D.M. Shin, Y.K. Chung, Organometallics 22 (2003) 1503;
(b) Y. Zhang, D.A. Kissounko, J.C. Fettinger, L.R. Sita, Organometallics 22 (2003) 21.
[11] A. Koppl, H.G. Alt, J. Mol. Catl. A: Chem. 154 (2000) 45.
[12] T.V. Laine, U. Piironen, K. Lappalainen, M. Klinga, E. Aitola, M. Leskela, J. Organomet. Chem. 606 (2000) 112.
[13] S. Brenner, R. Kempe, P. Arndt, Z. Anorg. Allg. Chem. 621 (1995) 2021.
[14] E. Benzing, W. Kornicker, Chem. Ber. 94 (1961) 2263.
[15] G.M. Sheldrick, SHELXL-97 Program for the Refinement of Crystal Structures, University of Göttingen, Germany, 1997.

Available online at www.sciencedirect.com
SCIENCE DIRECT®
Polyhedron 23 (2004) 1595–1603
POLYHEDRON
www.elsevier.com/locate/poly

Synthesis, characterization and crystal structure of oxomolybdenum (VI) and (IV) complexes of some tridentate ONS donor ligands

Nikhil Ranjan Pramanik [a], Saktiprosad Ghosh [b], Tapas Kumar Raychaudhuri [a], Sibdas Ray [a], Ray J. Butcher [c], Sudhanshu Sekhar Mandal [a,*]

[a] *Department of Chemistry, University College of Science, 92, Acharya Prafulla Chandra Road, Kolkata 700009, India*
[b] *Department of Inorganic Chemistry, Indian Association for the Cultivation of Science, Kolkata 700032, India*
[c] *Department of Chemistry, Howard University, 2400 Sixth Street, N.W. Washington, DC 20059, USA*

Received 6 November 2003; accepted 8 March 2004
Available online 20 April 2004

Abstract

A number of oxomolybdenum (VI) and (IV) complexes with potentially tridentate ONS donor Schiff bases of S-benzyl and S-methyl dithiocarbazates with salicylaldehyde have been synthesized. The Mo(VI) complexes are *cis*-dioxo, MoO_2L (where L = H_2L^1 and H_2L^2) with one coordination site available for substrate binding. The Mo(IV) complexes, MoOL, are derived from the corresponding Mo(VI)-dioxo complexes by oxo abstraction with PPh_3. The complexes were characterized by elemental analysis, UV, IR and ^1H NMR spectroscopy, magnetic susceptibility measurement, molar conductivities in solution and by cyclic voltammetry. Two of the complexes MoO_2L^1 and MoO_2L^2 were crystallographically characterized. The structures reveal that the molybdenum acceptor center is present in a distorted octahedral NO_4S donor environment.
© 2004 Published by Elsevier Ltd.

Keywords: Dioxomolybdenum (VI) and oxomolybdenum (IV) complexes; Dithiocarbazate; Schiff bases; X-ray structures

1. Introduction

Chemistry of higher valent molybdenum ligated to mixed hard–soft nitrogen–sulfur donor ligands is a field of current interest. Interest of inorganic and bioinorganic chemists increased manifold with the revelation that some oxido-reductases, hydrogenase, xanthine oxidase, DMSO reductase and other oxo-transferases containing Mo(VI) and Mo(IV) as their prosthetic groups are ligated to a multidentate ligand framework through NS/NSO donor points [1–4]. Also sulfur donor centers in a mixed hard–soft ligand system are known to stabilize uncommon oxidation states to generate less familiar coordination numbers and to participate in diverse types of chemical and electrochemical reactions [5–13].

Several oxomolybdenum (VI), (V) and (IV) complexes with various bi-, tri- and tetradentate NS, SS and ONS donor systems have been reported [14–22] to simulate many characteristic properties of the active sites of molybdoenzymes. However, a survey of the relevant literature has failed to locate any study on oxomolybdenum complexes of Schiff bases derived by the condensation of salicylaldehyde with S-benzyl and S-methyl dithiocarbazates, acting as diacidic tridentate ONS donor ligands.

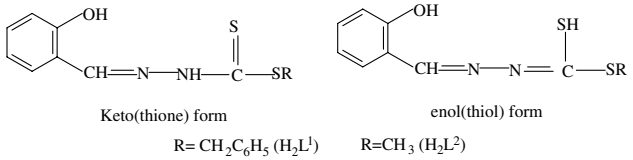

Keto(thione) form R= $CH_2C_6H_5$ (H_2L^1)

enol(thiol) form R=CH_3 (H_2L^2)

* Corresponding author. Tel.: +91-33-2350-8386; fax: +91-33-2351-9755.
E-mail address: ssmandal2000@yahoo.com (S.S. Mandal).

0277-5387/$ - see front matter © 2004 Published by Elsevier Ltd.
doi:10.1016/j.poly.2004.03.010

Our main aim is to study the chemistry of oxometal cations bonded to mixed hard–soft NS donors in general and modeling of the active sites of molybdoenzymes in particular. It is to be noted that our work is one of the few instances of the use of substituted thiocarbazate ligands in the modeling of the molybdenum binding site of the molybdenum cofactors. We report here a set of Mo(VI)-dioxo and Mo(IV)-oxo complexes of the above ligands. Such tridentate chelating ligands form complexes like MoO_2L or MoOL, possessing one or two "open" coordination sites that can be utilized for substrate binding. In this work we report on the synthesis of Mo(VI) complexes of the type MoO_2L and $MoO_2L \cdot B$ (where B is a neutral monodentate Lewis base) and also of Mo(IV) complexes of the type MoOL and MoOL(N–N) (where N–N is a neutral bidentate donor like bipy or *o*-phen). Oxo abstraction from Mo(VI)-dioxo complexes with the help of PPh_3 has been successfully carried out to generate the corresponding Mo(IV) species. All the complexes have been characterized by elemental analysis, magnetic susceptibility measurement in the solid state, molar conductivity in solution and various spectroscopic (NMR, IR, UV–Vis) methods. Electrochemical characteristics of the complexes were examined by cyclic voltammetry at a platinum disc electrode in DMF solution with TEAP as supporting electrolyte. All the complexes are found to be diamagnetic and non-electrolytic in nature. Crystal and molecular structures of two complexes MoO_2L^1 and $MoO_2L^2 \cdot H_2O$ have been determined by the single crystal X-ray diffraction technique.

2. Results and discussion

2.1. Synthesis and characterization of the ligand

The Schiff base ligands (H_2L^1 and H_2L^2) were prepared by condensing S-benzyl and S-methyl dithiocarbazates [23] with salicylaldehyde in ethanol. The ligands have been satisfactorily characterized by elemental analysis (Table 1), IR and ^1H NMR data.

2.2. Synthesis and characterization of molybdenum (VI) and (IV) complexes

Dioxo molybdenum (VI) complexes (**1a** and **1b**) of formula MoO_2L^1 and $MoO_2L^2 \cdot H_2O$ were prepared [7a] by refluxing $MoO_2(acac)_2$ with the appropriate ligand in 1:1 molar proportion using methanol as solvent. The Mo(VI) complexes (**1c**–**1j**) of general formula MoO_2LB (where B = γ-picoline, imidazole, thiophene and THF) were also prepared by refluxing **1a** and **1b** with the corresponding neutral monodentate Lewis base in methanol medium. The base B is coordinated in the sixth coordination position. All the compounds are orange-red crystalline solids. Oxomolybdenum (IV) complexes (**2a** and **2b**) of general formula MoOL, dark brown solids, and the complexes (**2c**–**2f**) of general formula MoOL(bipy/*o*-phen), dark green solids, were prepared by oxo-abstraction reaction of **1a** and **1b** with PPh_3in the presence of bipy/*o*-phen in CH_2Cl_2 medium, respectively. All the compounds are air-stable, insoluble in water and are diamagnetic in nature [24]. All of them are readily soluble in polar solvents like CH_2Cl_2,

Table 1
Elemental analyses for the ligands and complexes

Compounds	Analysis found (Calc.) (%)			
	C	H	N	Mo
H_2L^1	59.71 (59.60)	4.80 (4.64)	9.43 (9.30)	
H_2L^2	48.12 (47.79)	4.39 (4.42)	12.53 (12.39)	
MoO_2L^1 (**1a**)	41.50 (42.05)	3.0 (2.80)	6.32 (6.54)	21.98 (22.42)
$MoO_2L^2 \cdot H_2O$ (**1b**)	30.05 (29.19)	2.54 (2.70)	7.69 (7.57)	26.38 (25.95)
MoO_2L^1(γ-pic) (**1c**)	47.94 (48.36)	3.64 (3.64)	7.89 (8.06)	18.23 (18.42)
MoO_2L^2(γ-pic) (**1d**)	39.88 (40.44)	3.34 (3.37)	9.22 (9.44)	22.52 (21.57)
MoO_2L^1(imz) (**1e**)	43.31 (43.54)	3.18 (3.22)	11.14 (11.29)	18.85 (19.35)
MoO_2L^2(N-meimz) (**1f**)	36.12 (35.94)	3.10 (3.23)	12.95 (12.90)	22.46 (22.12)
MoO_2L^1(thiophene) (**1g**)	44.10 (44.53)	3.21 (3.13)	5.12 (5.47)	18.85 (19.35)
MoO_2L^2(thiophene) (**1h**)	36.0 (35.78)	2.63 (2.75)	6.51 (6.42)	21.87 (22.01)
MoO_2L^1(THF) (**1i**)	44.82 (45.60)	3.85 (4.0)	5.80 (5.60)	18.89 (19.20)
MoO_2L^2(THF) (**1j**)	35.90 (36.79)	3.52 (3.77)	6.52 (6.60)	22.15 (22.64)
$MoOL^1$ (**2a**)	43.35 (43.69)	2.95 (2.91)	6.59 (6.79)	22.78 (23.30)
$MoOL^2$(**2b**)	31.92 (32.14)	2.31 (2.38)	8.20 (8.33)	27.56 (28.57)
$MoOL^1$(bipy) (**2c**)	51.74 (52.82)	3.49 (3.52)	9.62 (9.86)	16.32 (16.90)
$MoOL^2$(bipy) (**2d**)	45.31 (46.34)	3.19 (3.25)	11.20 (11.38)	20.12 (19.51)
$MoOL^1$(*o*-phen) (**2e**)	53.64 (54.73)	3.43 (3.38)	9.22 (9.46)	16.20 (16.22)
$MoOL^2$(*o*-phen) (**2f**)	47.62 (48.83)	3.0 (3.10)	10.22 (10.85)	18.73 (18.60)

Table 2
Cyclic voltammetric peak potential data (V vs. SCE) in DMF solution at 298 K

Compound	Cathodic peak potential		Anodic peak potential E_A (in V)
	E_{C_I} (in V)	$E_{C_{II}}$ (in V)	
MoO_2L^1	−0.20	−1.01	
$MoO_2L^2 \cdot H_2O$	−0.16	−1.13	
$MoOL^1$		−0.99	+0.48
$MoOL^2$		−1.02	+0.45

Solvent: DMF (dry,d egassed); supporting electrolyte: 0.1 M TEAP; solution strength 10^{-3} M; electrode: platinum; reference electrode: SCE; scan rate: 200 mV s^{-1}.

CH_3CN and DMF, etc. Molar conductivity data in 10^{-3}(M) CH_2Cl_2 solution indicate that they are non-electrolytes. Electronic spectra of all the complexes were recorded in CH_2Cl_2 and cyclic-voltammograms of some representative compounds were recorded in DMF (Table 2).

2.3. Crystal structure of the complexes *1a* and *1b*

The molecular structure and atom-numbering schemes of the complexes **1a** and **1b** are shown in Figs. 1–3. Experimental details are given in Table 3 and selected bond lengths and bond angles are in Tables 4 and 5. In both complexes **1a** and **1b** the ligands H_2L^1 and H_2L^2 behave in a dianionic tridentate manner, the donor points O(3), N (1), S (1) occupying a meridonial plane [25,26] and N(1) is situated *trans* to the oxo-oxygen O(1). As the structures of the two complexes are quite similar, that of complex **1a** is discussed in detail and the points of differences are pointed out at the end. Along with the two oxo-oxygens, O(1) and O(2), the three ONS donor points of the ligand complete the five coordinate environment around the Mo(VI) acceptor center in complex **1a**, the disposition of the donor points being roughly square pyramidal. The sixth coordination site, *trans* to the oxo-oxygen O(2), is occupied by an oxo-oxygen O(2A) of the next neighboring complex molecule and this pattern is repeated leading to a chain of MoO_2L molecules (Fig. 2). The dianionic tridentate ligand is found to form 1 five-membered and 1 six-membered metallocycle involving the MoO_2^{2+}core, the bite angles N(1)MoS(1) and N(1)MoO(3) being 76.2(3)° and 84.9(4)°, respectively.

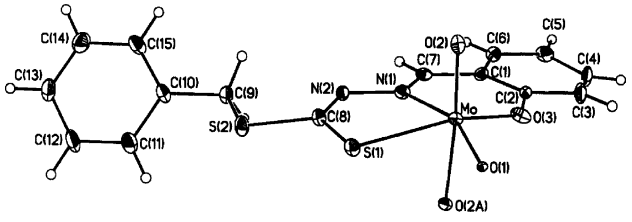

Fig. 1. ORTEP plot of complex **1a** [MoO_2L^1].

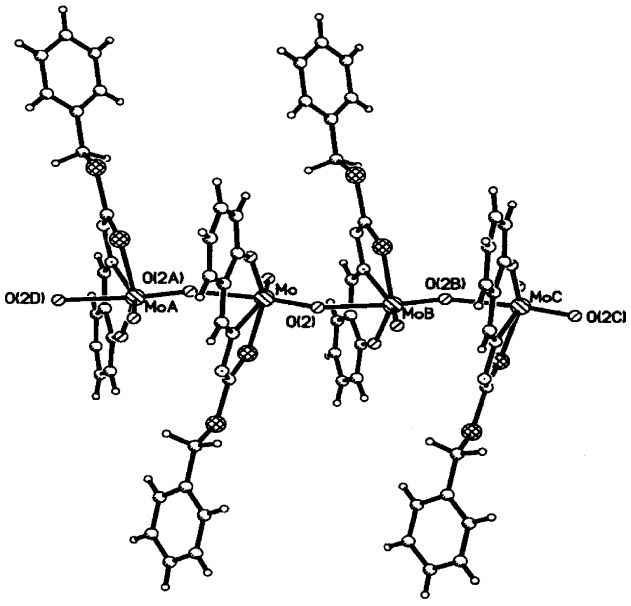

Fig. 2. Stacking diagram of complex **1a**.

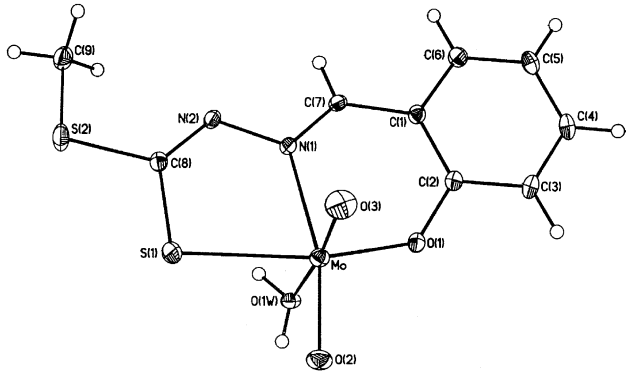

Fig. 3. ORTEP plot of complex **1b** [MoO_2L^2, H_2O].

The overall coordination geometry around the Mo(VI) acceptor can be described as distorted octahedral. The Schiff-base ligand is bonded to the MoO_2^{2+} core in a planar fashion involving the *xy*-plane through the phenolate oxygen O(3), the thioenolate sulfur S(1) and the imine nitrogen N(1), the oxo group O(1) lying *trans* to N(1). The oxo-oxygen O(2) is found to occupy one apical position while other apex is occupied by an oxo-oxygen O(2A) of the nearest neighbor complex molecule, the O(2)–Mo–O(2A) angle being 169.46(16)°. This may be visualized as an effect of stacking of the complex molecules along the *z*-axis. The length of the Mo–O(2A) bond (2.32 Å) is considerably longer than the other Mo–O bonds, the longest of which [Mo–O(3)] is 1.956(10) Å. This is indicative of weaker coordination by the oxo-oxygen O(2A) and suggests that this is expected to be the point of maximum reactivity of the complex. This structural feature points to a reactivity pattern in which this Mo–O(2A) bond can be broken on

Table 3
Crystallographic data for complexes **1a** and **1b**

	Complex**1a**	Complex **1b**
Chemical formula	$C_{15}H_{12}MoN_2O_3S_2$	$C_9H_{10}MoN_2O_4S_2$
Formula weight (M)	428.33	370.25
Crystal system	monoclinic	orthorhombic
a (Å)	16.417(7)	6.1250(13)
b (Å)	7.848(3)	11.702(2)
c (Å)	13.612(6)	17.425(3)
β (°)	111.173(5)	
V (Å^3)	1635.3(12)	1248.9(4)
Temperature (K)	158 (2)	293(2)
Z	4	4
Space group	$P2_1/c$	$P2_12_12_1$
μ (Mo Kα) (mm^{-1})	1.072	1.391
Goodness of-fit	1.143	1.080
Number of data/restraints/parameter	3212/12/220	1668/0/181
Final R indices $[I > 2\sigma(I)]$	$R_1 = 0.1077$, $wR_2 = 0.2638$	$R_1 = 0.0228$, $wR_2 = 0.0596$
R indices (all data)	$R_1 = 0.1403$, $wR_2 = 0.2965$	$R_1 = 0.0239$, $wR_2 = 0.0601$
Largest difference peak and hole (e Å^{-3})	4.392 and −2.468	0.320 and −0.483

Table 4
Selected bond lengths (Å) for complexes **1a** and **1b**

Bond lengths	Complex **1a**	Bond lengths	Complex **1b**
Mo–O(1)	1.659(7)	Mo–O(2)	1.698(3)
Mo–O(2)	1.721(10)	Mo–O(3)	1.697(3)
Mo–O(3)	1.956(10)	Mo–O(1)	1.929(2)
Mo–O(2A)	2.320(10)	Mo–O(1W)	2.321(3)
Mo–N(1)	2.260(10)	Mo–N(1)	2.283(3)
Mo–S(1)	2.439(4)	Mo–S(1)	2.438(10)
C(2)–O(3)	1.363(14)	C(2)–O(1)	1.339(4)
C(1)–C(2)	1.388(16)	C(1)–C(2)	1.396(5)
C(1)–C(7)	1.439(18)	C(1)–C(7)	1.439(4)
C(1)–C(6)	1.444(19)	C(1)–C(6)	1.404(5)
N(1)–C(7)	1.316(17)	N(1)–C(7)	1.290(4)
N(1)–N(2)	1.420(15)	N(1)–N(2)	1.420(4)
N(2)–C(8)	1.311(16)	N(2)–C(8)	1.294(4)
S(1)–C(8)	1.729(13)	S(1)–C(8)	1.737(4)
S(2)–C(8)	1.781(13)	S(2)–C(8)	1.738(3)

Table 5
Selected angles (°) for complexes **1a** and **1b**

Angles	Complex **1a**	Angles	Complex **1b**
O(1)–Mo–O(2)	106.0(4)	O(2)–Mo–O(3)	105.85(15)
O(1)–Mo–O(2A)	84.6(4)	O(2)–Mo–O(1W)	84.00(11)
O(1)–Mo–O(3)	102.4(4)	O(2)–Mo–O(1)	103.80(12)
O(1)–Mo–N(1)	156.2(4)	O(2)–Mo–N(1)	158.63(12)
O(1)–Mo–S(1)	88.5(3)	O(2)–Mo–S(1)	91.26(10)
O(2)–Mo–O(2A)	169.46(16)	O(3)–Mo–O(1W)	170.06(12)
O(2)–Mo–O(3)	100.7(4)	O(3)–Mo–O(1)	99.58(13)
O(2)–Mo–N(1)	94.6(4)	O(3)–Mo–N(1)	92.84(13)
O(2)–Mo–S(1)	99.5(3)	O(3)–Mo–S(1)	97.34(11)
O(3)–Mo–O(2A)	77.3(4)	O(1)–Mo–O(1W)	78.90(10)
O(3)–Mo–N(1)	84.9(4)	O(1)–Mo–N(1)	82.70(10)
O(3)–Mo–S(1)	153.3(3)	O(1)–Mo–S(1)	153.22(8)
N(1)–Mo–S(1)	76.2(3)	N(1)–Mo–S(1)	75.85(7)
N(1)–Mo–O(2A)	74.9(4)	N(1)–Mo–O(1W)	77.23(10)
S(1)–C(8)–S(2)	113.1(7)	S(1)–C(8)–S(2)	111.57(19)

treatment with a monodentate heterocyclic Lewis base which will coordinate at this point. This expectation is realized in the facile formation of the complexes $MoO_2L \cdot B$, where B is a neutral monodentate Lewis base like imidazole, picoline, THF, thiophene, etc.

The O(2)=Mo=O(1) bond angle of 106.0(4)° and the Mo=O bond lengths Mo=O(1) = 1.659(7), Mo=O(2) = 1.721(10) Å are unexceptional [27–30]. The imine nitrogen N(1) is *trans* to the oxo-oxygen O(1) and the Mo–N(1) bond length of 2.260(10) Å is rather long due to *trans* effect. The C(8)–N(2) length [1.311(16) Å] is close to usual C=N bond length [31,32]. The Mo–S distance of 2.438(4) Å is very near to the values observed in the case of similar molybdenum complexes [26,33,34].

Careful analysis of the bond length and bond angles data leads to the overall conclusion that complex **1a** has a highly distorted octahedral coordination around the Mo(VI) acceptor center with the Mo center slightly displaced from the median square plane described by N(1), O(3), O(1), S(1) towards the apical oxo-oxygen O(2). The sixth position in the coordination octahedron of the Mo(VI) center is taken up by one of the oxo-oxygen O(2A) of the immediate neighbor complex **1a** and a type of chain is formed by the stacking of the complex **1a** molecules along the z-axis. The unusually longer Mo–O(2A) bond length identifies it as the potential center of reactivity.

A rather unusual but noteworthy feature of complex **1a** is the length of the bridging Mo–O(2A) bond. Though it is a molybdenum–oxygen double bond it has been lengthened considerably [2.32(10) Å] from its usual value of around ~1.70 Å. It is also to be noted that it is practically equal to the Mo–O(1W) single bond length in the complex **1b** [29] (Fig. 3). The coordinated water molecule in complex **1b** is found to take part in inter molecular hydrogen bonding involving four molecules

of the unit cell and is expected to increase the stability of the complex system. TG data of the two complexes bear out this connection.

In both the complexes **1a** and **1b**, the molybdenum (VI) acceptor center is present in a distorted octahedral NO_4S donor surrounding, the points of difference being, in complex **1a**, one among the four oxygen atoms is a Mo=O oxygen of the immediate neighbor molecule while in complex **1b** this oxygen is from a coordinated water. Almost all the comparable bond lengths and bond angles are closely similar and the center of reactivity in both the complexes is detected as the point *trans* to one oxo-oxygen. Experiments on activity towards neutral monodentate Lewis bases have led to similar products.

2.4. IR and ^1H NMR studies

A few characteristic infrared absorption frequencies of both the ligands and their complexes are given in Sections 3.3 and 3.4. All physico-chemical properties of the complexes support dianionic tridentate SNO chelation of the ligands. Both the ligands exhibit two broad IR bands of medium intensity in the 3430–3100 cm^{-1} region, the higher frequency one is due to the ν(O–H) mode while the lower ones are assigned to the ν(N–H) vibrations [35]. The presence of these O–H and N–H hydrogens are also revealed in the X-ray crystal structure of the complexes **1a** and **1b**. Two strong ν(C=N) bands at 1617 and 1619 cm^{-1} for H_2L^1 and H_2L^2 of the free ligands are red-shifted to 1590–1600 and 1592–1604 cm^{-1}, respectively, in the corresponding complexes indicating the coordination of the azomethene nitrogen [36,37] to the metal ion. A strong ν(C=S) band was observed in the 1311–1315 cm^{-1} region for the ligands, which disappeared upon complex formation. A new band in the 634–542 cm^{-1} region was observed for complexes and is assigned to ν(Mo–N) [29,35]. The complexes exhibit a medium intensity band around 374–397 cm^{-1} which may be assigned to ν(Mo–S) [20]. Like most of the *cis*-dioxomolybdenum (VI) complexes, two IR bands are observed in the 979–897 cm^{-1} region, the higher frequency band originating from the anti-symmetric while the lower one from the symmetric stretching mode of the $[MoO_2]^{2+}$ moiety [29,38,39]. In the spectra of the $[Mo^{IV}$(bipy/*o*-phen)] complexes the $(Mo{=}O)_t$ band is located near 970 cm^{-1} and as expected [40], reduction of the oxidation state of molybdenum from VI to IV has the effect of lowering the $(Mo{=}O)_t$ stretch from the value observed in $MoOL^1$ and $MoOL^2$.

^1H NMR data for the ligands and complexes **1a** and **1b** are summarized in Sections 3.3 and 3.4. The relatively broad signal at δ 10.72 and 10.02 in the ^1H NMR spectra corresponding to O–H and N–H of the ligand (H_2L^1), respectively, are found to disappear as a result of complexation. The signal at δ 8.04 of the ligand has shifted downfield to δ 9.00, indicating coordination from the azomethene nitrogen in the NMR spectrum of the complex **1a**. The methylene protons of the ligand and the complex appearing at δ 4.59 and 4.41 indicate that the S-benzyl sulfur is not involved in the coordination. The nine aromatic protons appear as multiplets within the range δ 7.24–7.43 (7 protons) and 6.92–6.98 (2 protons) for the ligand. In complex **1b** with the ligand (H_2L^2) similar changes of the signal positions in the ^1H NMR spectra have been observed. The signals at δ 10.24 and 10.09 for the O–H and N–H protons of the ligand are found to disappear due to complex formation. The methyl protons of the ligand and the complex appear at nearly the same position.

2.5. Electrochemical properties

Dioxomolybdenum (VI) complexes (**1a**–**1d**, **1g**, **1h**): Cyclic voltammograms of the ligands and complexes at a platinum electrode were recorded in dry degassed DMF containing 0.1M TEAP as the supporting electrolyte over a potential range of 0.0 to −1.5 V. The numerical data are given in Table 2 and representative voltammograms are shown in Fig. 4. In the case of complexes $Mo^{VI}O_2L^1$ and $Mo^{VI}O_2L^2 \cdot H_2O$ only one irreversible reductive response could be located in the potential range 0.0 to −1.3 V within the potential window scanned. This response is assigned to a metal-centered $2e^-$ process [31]. Two-electron involvement is established by comparison of the current height with authentic $2e^-$ species. On scan reversal an irreversible oxidative response is located in the −0.16 V to −0.20 V range. This is probably due to the oxidation of the species produced in the range −1.01 to −1.13 V by cathodic reduction followed by chemical reaction with the medium. Cyclic voltammograms of the ligands and their

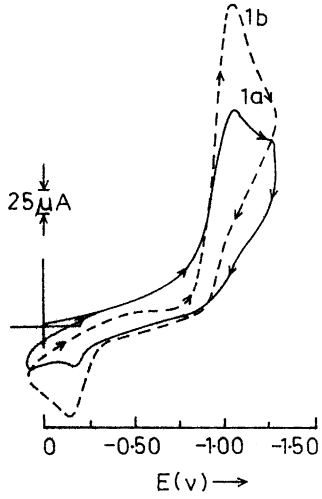

Fig. 4. Cyclic voltammograms for complex **1a** (—) and **1b** (----) in DMF solution.

zinc complexes did not exhibit any reductive response within the potential window scanned. The nature of the voltammograms is found to be independent of scan rate, the normal scan rate being 200 mV/s. The cyclic voltammogram of the $MoO_2L \cdot B$ (where B is a monodentate Lewis base like picoline, imidazole, thiophene, etc.) exhibits little difference from those of the parent complexes and therefore the actual species in solution are $MoO_2L(DMF)$. This is confirmed by recording the electronic spectra of the Mo(VI) complexes and its adducts $MoO_2L.B$ in DMF which exhibit identical spectral features.

Oxomolybdenum (IV) complexes (**2a**, **2b**): Under comparable conditions and in the potential range 0 to +1.3 V the Mo(IV) complexes exhibit one oxidative responses in the 0.45–0.48 V region (Fig. 5). This is assigned to a $2e^-$ oxidation of Mo(IV) to Mo(VI). The $2e^-$ nature of the processes is established by comparing the current height with an authentic $2e^-$system [6,41,42].

2.6. Electronic spectra

Electronic spectra of the Mo(VI) complexes were recorded in dichloromethane solution and the spectral data are presented with the complexes in Section 3.4. The lowest energy absorption maxima are located in the 392–406 nm range and may be assigned [21] to S(pπ)–Mo(dπ) LMCT transition caused by the promotion of an electron from the filled HOMO of the ligand of primarily sulfur pπ character to the empty LUMO of molybdenum dπ character. Other LMCT bands are observed in the region 392–276 nm [6,26,32,41]. These bands may be assigned to the nitrogen to molybdenum and the oxygen to molybdenum charge transfer transitions [21]. The bands appearing below 276 nm are due to intra-ligand transitions. Electronic spectra of Mo(IV) oxo compounds exhibit [33,40] one low-energy charge transfer in the 656–666 nm region.

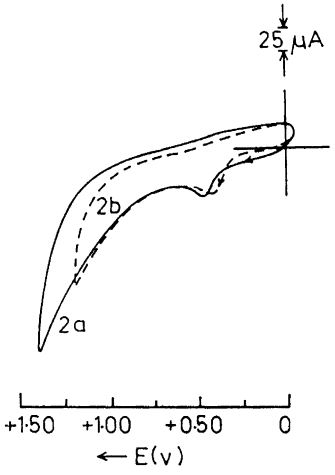

Fig. 5. Cyclic voltammograms for complex **2a** [$MoOL^1$] (—) and **2b** [$MoOL^2$] (----) in DMF solution.

2.7. Study of the reactivity of dioxomolybdenum (VI) and oxomolybdenum (IV) complexes

The dioxomolybdenum (VI) complexes **1a** and **1b** are prepared and isolated from methanol, of which **1a** is found to be oligomeric in the solid state due to weak coordination between the molecules (Fig. 2), while **1b** has a coordinated water molecule. The weak coordination of water is apparent from TG-DTA data of the $MoO_2L^2 \cdot H_2O$ species, which exhibited ready loss of water within the range 120–160 °C. This is substantiated by the facile replacement of the water molecule by a monodentate Lewis base yielding the corresponding MoO_2L^1B and MoO_2L^2B compounds. Again, when these compounds are dissolved in coordinating solvents such as DMF/DMSO the monodentate ligand B is readily replaced by the solvent molecule as is evident from their electronic spectra and electrochemical results. The oxomolybdenum (IV) complexes $MoOL^1$ and $MoOL^2$ have been isolated from CH_3OH/CH_3CN medium, the isolated complexes do not contain any solvent molecules. However, these compounds are found to react readily with 2,2′-bipyridyl/*o*-phenanthrolin to give air stable six-coordinated complexes $MoOL^1$(N–N) and $MoOL^2$(N–N). The complexes $MoO_2L^1$and MoO_2L^2 exhibit oxotransfer to the substrate PPh_3 when reacted with PPh_3 in CH_3OH/CH_3CN medium. It has been observed that a band around 400 nm due to $S(p\pi) \rightarrow Mo(d\pi)$ LMCT transition in the parent complex is shifted to lower energy (~450 nm) and a new band appears around 630 nm. The isolated complexes $MoOL^1$ and $MoOL^2$ have also shown similar spectral features. The oxotransfer reaction may be represented as

$$Mo^{VI}O_2L + PPh_3 \overset{CH_3CN}{\rightarrow} Mo^{IV}OL + OPPh_3$$

which may be considered as a two-electron redox/oxygen atom transfer process. The oxygen atom transfer from the substrate DMSO to the system $MoOL^1$ (**2a**) and $MoOL^2$ (**2b**) has also been studied spectrophotometrically in DMF solution. The parent complex MoOL exhibits a low-energy band around 630 nm with a low ε value and an intense band at ~450 nm. When a drop of DMSO is added to the solution of **2a** and **2b** in DMF, the intensity of the band at ~450 nm is found to decrease slowly and ultimately disappear within 10 min when a new band characteristic of a complex of the type MoO_2L appears around ~400 nm. These observations clearly indicate [43,44] the transfer of an oxygen atom from DMSO to the MoO^{2+} core, leading to the formation of MoO_2^{2+} species and Me_2S. The reaction may be represented as

$$MoOL + DMSO \xrightarrow{DMF} MoO_2L + Me_2S$$

The complexes MoO_2L^1 and MoO_2L^2 are isolated from concentrated DMSO solution of the corresponding MoOL type complexes by adding excess ether. The MoO_2L type complexes precipitated out and are characterized by elemental analysis and spectroscopic techniques.

3. Experimental

3.1. Materials

$[MoO_2(acac)_2]$ was prepared as described in the literature [45]. Reagent grade solvents were dried and distilled prior to use. All other chemicals used for preparative work were of reagent grade and were employed without further purification.

3.2. Physical measurements

Elemental analyses were performed on a Perkin–Elmer 240 C, H, N analyzer. The NMR spectra were recorded on a Bruker 300 L NMR Spectrometer operating at 300 MHz with TMS as internal standard. IR spectra were recorded as KBr pellets on a Perkin–Elmer model 883 Infrared spectrophotometer. Electronic spectra were recorded on a HITACHI U-3501 UV–Vis recording spectrophotometer. Magnetic susceptibility was measured with a PAR model 155 vibrating sample magnetometer with $Hg[Co(SCN)_4]$ as calibrant. Electrochemical data were collected on a BAS CV-27 electrochemical analyzer and a BAS model X-Y recorder at 298 K using a Pt working electrode, Pt auxiliary electrode and Ag/AgCl reference electrode. Voltammograms were recorded in DMF solution of the metal complexes containing 0.1 M TEAP as supporting electroyte.

3.3. Schiff base ligand preparation

3.3.1. S-benzyl-β-N(2-hydroxyphenyl)methylenedithiocarbazate (H_2L^1)

A mixture of 10 ml (0.2 mol) hydrazine hydrate and 11.2 g (0.2 mol) KOH in 70 ml of 90% ethanol was cooled down to −10 °C. 15 ml (0.25 mol) of carbon disulfide was added dropwise with constant stirring. The yellow oil which had formed was separated and dissolved in 60 ml of previously cooled 40% ethanol. To this 23 ml (0.2 mol) of benzyl chloride was added slowly with vigorous stirring. The white product which formed was collected and after re-crystallization from benzene was dissolved in 50 ml of absolute ethanol. To this solution was added 21.5 ml (0.2 mol) of salicylaldehyde in 50 ml ethanol. The resultant mixture was heated on a steam bath for about 10 min. The crystals which settled down were filtered off, washed with ethanol, re-crystallized from benzene and dried in vacuo. Yield ~80%, m.p. ~185 °C.

IR (KBr Pellet), cm^{-1}: $\nu_{(N-H)}$ 3100 (m), $\nu_{(O-H)}$ 3425 (sh), $\nu_{(C=N)}$ 1617 (s), 1604 (s), $\nu_{(C=S)}$ 1311 (s), ^1H NMR(dmso-d_6): (–CH=N–) 8.04 s (1), ($–CH_2–$) 4.59 s (2), (–NH–) 10.02 s, (aromatic –OH) 10.72 b (1), (aromatic proton) 6.92–6.98 m (2), 7.24–7.43 m (7).

3.3.2. S-methyl-β-N(2-hydroxyphenyl)methylenedithiocarbazate (H_2L^2)

This was prepared by following the same procedure only by taking 12.5 ml (0.2 mol) of methyl iodide instead of benzyl chloride. Yield ~80%, m.p. ~210 °C.

IR (KBr Pellet), cm^{-1}: $\nu_{(N-H)}$ 3112 (m), $\nu_{(O-H)}$ 3430 (sh), $\nu_{(C=N)}$ 1619 (s), 1604 (m), $\nu_{(C=S)}$ 1315 (s), ^1H NMR(dmso-d_6): (–CH=N–) 8.01 s (1), ($–CH_2–$) nf, (–NH–) 10.09 s (1), ($–CH_3$) 2.56 s (3), (aromatic –OH) 10.24 b (1), (aromatic proton) 6.93–7.06 m (2), 7.25–7.40 m (2).

3.4. Synthesis of complexes

MoO_2L^1 (**1a**). To a filtered solution of 0.33 g (1.0 mmol) of $MoO_2(acac)_2$ in dry methanol (20 ml) was added 0.302 g (1.0 mmol) of the ligand H_2L^1 in 15 ml of dry methanol. The resulting orange solution was refluxed for 2 h. The volume of the solution was then reduced to about 10 ml on a water bath. The orange compound that separated out was filtered, washed with cold methanol and dried in vacuo over anhydrous $CaCl_2$, yield ~80%. The compound was recrystallized from dry methanol.

IR (KBr Pellet), cm^{-1}: $\nu_{(C=N)}$ 1591(vs), $\nu_{(Mo=O)}$ 946 (s), 981 (m), $\nu_{(Mo-S)}$ 393 (m), $\nu_{(Mo-N)}$ 570 (w) UV–Vis (CH_2Cl_2) [λ_{max}/nm (ε/$dm^3\,mol^{-1}\,cm^{-1}$)]: 300 (70790), 318 (76570), 370 sh (36790), 400 (27650); ^1H NMR(dmso-d_6): (–CH=N–) 9.00 s (1), ($–CH_2–$) 4.41 s (2), (aromatic proton) 6.91–7.10 m (2), 7.23–7.78 m (7).

$MoO_2L^2 \cdot H_2O$ (**1b**) was prepared similarly using 0.226 g (1.0 mmol) of ligand H_2L^2 with a yield of 75%. IR (KBr Pellet), cm^{-1}: $\nu_{(O-H)}$ 3326 (w), $\nu_{(C=N)}$ 1592 (vs), $\nu_{(Mo=O)}$ 976 (s), 913 (m), $\nu_{(Mo-S)}$ 385 (s), $\nu_{(Mo-N)}$ 633 (s); UV–Vis (CH_2Cl_2) [λ_{max}/nm (ε/$dm^3\,mol^{-1}\,cm^{-1}$)]: 243 (78 710), 277 sh (49 950), 306 (51 040), 394 (19 810); ^1H NMR(dmso-d_6): (–CH=N–) 8.92 s (1), ($–CH_3$) 2.71 s (3), (aromatic proton) 6.91–7.06 m (2), 7.50–7.75 m (2).

The compounds **1c**–**1j** were prepared by refluxing the parent compounds **1a** and **1b** with the appropriate monodentate Lewis base such as γ-picoline, imidazole, thiophene, THF in 1:1.2 mole ratio for ~4 h. The orange-red crystalline solids so formed were filtered, washed with dry methanol and dried in vacuo over anhydrous $CaCl_2$. Yield ~75–80%.

MoO_2L^1(γ-pic) (**1c**): IR (KBr Pellet), cm^{-1}: $\nu_{(C=N)}$ 1596 (vs), $\nu_{(Mo=O)}$ 929 (vs), 903 (vs), $\nu_{(Mo-S)}$ 381 (m), $\nu_{(Mo-N)}$ 569 (s); UV–Vis (CH_2Cl_2) [λ_{max}/nm (ε/$dm^3\,mol^{-1}\,cm^{-1}$)]: 239 sh (20 524), 277 sh (12 147), 317 (12 378), 391 (40 820).

MoO_2L^2(γ-pic) (**1d**): IR (KBr Pellet), cm^{-1}: $\nu_{(C=N)}$ 1595 (vs), $\nu_{(Mo=O)}$ 973 (s), 918 (s), $\nu_{(Mo-S)}$ 384 (m), $\nu_{(Mo-N)}$ 630 (s); UV–Vis (CH_2Cl_2) [λ_{max}/nm (ε/$dm^3\,mol^{-1}\,cm^{-1}$)]: 243 (14 644), 277 sh (88 960), 315 (94 390), 398 (30 940).

MoO_2L^1(imz) (**1e**) IR (KBr Pellet), cm^{-1}: $\nu_{(C=N)}$ 1598 (vs), $\nu_{(Mo=O)}$ 918 (vs), 897 (s), $\nu_{(Mo-S)}$ 374 (m), $\nu_{(Mo-N)}$ 542 (m); UV–Vis (CH_2Cl_2) [λ_{max}/nm (ε/$dm^3\,mol^{-1}\,cm^{-1}$)]: 274 sh (12 431), 321 (12 645), 401 (27 210).

MoO_2L^2(N-meimz) (**1f**) IR (KBr Pellet), cm^{-1}: $\nu_{(C=N)}$ 1596 (vs), $\nu_{(Mo=O)}$ 979 (s), 941 (m), $\nu_{(Mo-S)}$ 381 (m), $\nu_{(Mo-N)}$ 612 (s); UV–Vis (CH_2Cl_2) [λ_{max}/nm (ε/$dm^3\,mol^{-1}\,cm^{-1}$)]: 244 (13 571), 277 sh (86 380), 321 (11 378), 406 sh (21 730).

MoO_2L^1(thiophene) (**1g**) IR (KBr Pellet), cm^{-1}: $\nu_{(C=N)}$ 1590 (vs), $\nu_{(Mo=O)}$ 939 (s), 920 (s), $\nu_{(Mo-S)}$ 387 (m), $\nu_{(Mo-N)}$ 570 (m); UV–Vis (CH_2Cl_2) [λ_{max}/nm (ε/$dm^3\,mol^{-1}\,cm^{-1}$)]: 276 (13 462), 306 (12 983), 394 (52 360).

MoO_2L^2(thiophene) (**1h**) IR (KBr Pellet), cm^{-1}: $\nu_{(C=N)}$ 1592 (vs), $\nu_{(Mo=O)}$ 976 (vs), 906 (m), $\nu_{(Mo-S)}$ 386 (s), $\nu_{(Mo-N)}$ 634 (s); UV–Vis (CH_2Cl_2) [λ_{max}/nm (ε/$dm^3\,mol^{-1}\,cm^{-1}$)]: 242 (15 954), 276 (10 192), 304 (10 385), 394 (40 950).

MoO_2L^1(THF) (**1i**) IR (KBr Pellet), cm^{-1}: $\nu_{(C=N)}$ 1596 (vs), $\nu_{(Mo=O)}$ 937 (s), 920 (m), $\nu_{(Mo-S)}$ 387 (m), $\nu_{(Mo-N)}$ 572 (m); UV–Vis (CH_2Cl_2) [λ_{max}/nm (ε/$dm^3\,mol^{-1}\,cm^{-1}$)]: 276 (93 150), 307 (89 730), 394 (36 050).

MoO_2L^2(THF) (**1j**) IR (KBr Pellet), cm^{-1}: $\nu_{(C=N)}$ 1592 (vs), $\nu_{(Mo=O)}$ 975 (vs), 931 (s), $\nu_{(Mo-S)}$ 385 (s), $\nu_{(Mo-N)}$ 634 (s); UV–Vis (CH_2Cl_2) [λ_{max}/nm (ε/$dm^3\,mol^{-1}\,cm^{-1}$)]: 242 (15 074), 276 (96 270), 307 (98 250), 392 (38 550).

All Mo(IV) oxo complexes are prepared under purified dinitrogen.

$MoOL^1$ (**2a**). To a refluxing solution of 0.428 g (1.0 mmol) of MoO_2L^1 in 25 ml dry degassed acetonitrile was added 0.393 g (1.5 mmol) of PPh_3 in 15 ml of degassed acetonitrile. The orange-red solution turned dark brown and a brown compound separated within 10 min. This was filtered and washed well with acetonitrile and dried in vacuo over anhydrous $CaCl_2$. Yield ~80%. IR (KBr Pellet), cm^{-1}: $\nu_{(C=N)}$ 1600 (vs), $\nu_{(Mo=O)}$ 968 (s), $\nu_{(Mo-S)}$ 287 (w), $\nu_{(Mo-N)}$ 626 (m); UV–Vis (CH_2Cl_2) [λ_{max}/nm (ε/$dm^3\,mol^{-1}\,cm^{-1}$)]: 310 (34 550), 411 (28 490), 466 (29 150), 630 (6125).

$MoOL^2$ (**2b**). This compound was prepared by following the methods described above for the preparation of $MoOL^1$ in a yield of 80%. IR (KBr Pellet), cm^{-1}: $\nu_{(C=N)}$ 1600 (vs), $\nu_{(Mo=O)}$ 966 (vs), $\nu_{(Mo-S)}$ 460 (s), $\nu_{(Mo-N)}$ 626 (s); UV–Vis (CH_2Cl_2) [λ_{max}/nm (ε/$dm^3\,mol^{-1}\,cm^{-1}$)]: 239 (15 647), 277 sh (10 103), 307 sh (98 720), 450 (28 630), 629 (6272).

Compounds **2c**–**2f** were prepared by refluxing the parent compounds **1a** and **1b** with bipyridyl and *o*-phenanthrolin and PPh_3 with a mole ratio 1:10:1.5 in dry degassed dichloromethane for ~1–2 h. The green solutions so formed were poured into *n*-hexane whereupon green solids separated out. These were filtered, washed with dichloromethane and dried in vacuo over anhydrous $CaCl_2$. Yield ~70–75%.

$MoOL^1$(bipy) (**2c**). IR (KBr Pellet), cm^{-1}: $\nu_{(C=N)}$ 1600 (vs), $\nu_{(Mo=O)}$ 914 (vs), $\nu_{(Mo-S)}$ 401(m), $\nu_{(Mo-N)}$ 630 (s); UV–Vis (CH_2Cl_2) [λ_{max}/nm (ε/$dm^3\,mol^{-1}\,cm^{-1}$)]: 297 (51 720), 360 (14 930), 436 (17 220), 570 (5860), 685 (7170).

$MoOL^2$(bipy) (**2d**). IR (KBr Pellet), cm^{-1}: $\nu_{(C=N)}$ 1601 (vs), $\nu_{(Mo=O)}$ 940 (vs), $\nu_{(Mo-S)}$ 395(m), $\nu_{(Mo-N)}$ 625 (m); UV–Vis (CH_2Cl_2) [λ_{max}/nm (ε/$dm^3\,mol^{-1}\,cm^{-1}$)]: 287 (17 214), 307 sh (15 262), 341 (10 240), 449 (21 900), 657 sh (7670).

$MoOL^1$ (*o*-phen) (**2e**). IR (KBr Pellet), cm^{-1}: $\nu_{(C=N)}$ 1595 (s), $\nu_{(Mo=O)}$ 940 (s), $\nu_{(Mo-S)}$ 397 (w), $\nu_{(Mo-N)}$ 619 (m); UV–Vis (CH_2Cl_2) [λ_{max}/nm (ε/$dm^3\,mol^{-1}\,cm^{-1}$)]: 265 (10 488), 314 sh (37 010), 464 sh (17 080), 441 (10 900), 626 (8230).

$MoOL^2$(*o*-phen) (**2f**). IR (KBr Pellet), cm^{-1}: $\nu_{(C=N)}$ 1604 (s), $\nu_{(Mo=O)}$ 920 (vs), $\nu_{(Mo-S)}$ 397 (m), $\nu_{(Mo-N)}$ 619 (s); UV–Vis (CH_2Cl_2) [λ_{max}/nm (ε/$dm^3\,mol^{-1}\,cm^{-1}$)]: 267 (60 210), 314 sh (23 420), 360 sh (9220), 444 (10 410), 629 (9250).

3.5. Crystallographic measurements

Complete tabulation of the crystallographic data for complexes **1a** and **1b** were collected on an Enraf-Nonius CAD-4 diffractrometer equipped with graphite-monochromated Mo Kα ($\lambda = 0.71013$ Å) radiation, using ω-scans. Unit-cell dimension and intensity data were measured at 198 and 293 K. The structures were solved by direct methods and refined by full-matrix least-squares based on F^2 with anisotropic displacement parameters of non-hydrogen atoms using XCAD-49 (data reduction) and SHELXTL (absorption correction, structure solution/refinement and molecular graphics). The hydrogen atoms were included in structures factor calculations in their idealized positions. The crystallographic data are summarized in Table 3.

4. Supplementary data

Crystallographic data have been deposited with the CCDC, 12 Union Road, Cambridge, CB2 IEZ, UK (fax: +44-1223-366033; e-mail: deposit@ccdc.cam.ac.uk

or www: http://www.ccdc.cam.ac.uk) and are available on request, quoting the deposition number 159187 and 159188 for the complex **1a** and complex **1b**, respectively.

Acknowledgements

We gratefully acknowledge the help of Dr. S.K. Kar, Department of Chemistry, Calcutta University for recording UV–Vis spectra and also for constant encouragement. Thanks are also due to Dr. C. Sinha, Burdwan University, for providing FT-IR spectral data, Dr. G.C. Mukherjee, Presidency College, Kolkata and Sri A. Hazra for their constant support and interest in this work.

References

[1] (a) A. Muller, B. Kerbs, Sulfur, its significance for Chemistry, for the Geo and Cosmosphere and Technology, in: Studies in Inorganic Chemistry, vol. 5, Elsevier, Amsterdam, 1984;
(b) S.D. Conradsson, B.K. Burgess, W.W. Newton, K.O. Hodgson, J.W. McDonald, J.F. Rubinson, S.F. Gheller, L.E. Mortenson, M.W.W. Adams, P.K. Mascharak, W.A. Armstrong, R.H. Holm, J. Am. Chem. Soc. 107 (1985) 7935;
(c) P.M. Harisson, Metalloproteins, Part 1. Metalloproteins with Redox Roles, Verlag, Chemie, Weinheim, FRG, 1985.
[2] (a) R.H. Holm, J.M. Berg, J. Am. Chem. Soc. 107 (1985) 917;
(b) J.H. Enemark, C.G. Young, Adv. Inorg. Chem. 40 (1993) 1;
(c) L.J. Laughlin, C.G. Young, Inorg. Chem. 35 (1996) 1050;
(d) J. Christiansen, R.C. Tittsworth, B.J. Hales, S.P. Cramar, J. Am. Chem. Soc. 117 (1995) 10017.
[3] R.J. Greenwood, G.L. Wilson, J.R. Pilbrow, A.G. Weed, J. Am. Chem. Soc. 117 (1993) 5385, and references therein.
[4] (a) E.I. Stiefel, D. Coucouvans, W.E. Newton (Eds.), Molybdenum Enzymes Cofactor and Model Systems, ACS Symposium Series, vol. 535, American Chemical Society, Washington, DC, 1993;
(b) G.N. George, R.C. Kipke, R.A. Sunde, J.H. Enemark, Biochem. J. 256 (1988) 307.
[5] (a) H.J. Kruger, G. Peng, R.H. Holm, Inorg. Chem. 30 (1991) 734;
(b) R.H. Holm, Coord. Chem. Rev. 100 (1990) 183.
[6] A.P. Koley, S. Purohit, S. Ghosh, L.S. Prasad, P.T. Manoharan, J. Chem. Soc., Dalton Trans (1998) 2607.
[7] (a) S. Purohit, A.P. Koley, L.S. Prasad, P.T. Manoharan, S. Ghosh, Inorg. Chem. 28 (1998) 3735;
(b) P. Subramanian, J.T. Spence, R. Ortega, J.H. Enemark, Inorg. Chem. 36 (1997) 2938.
[8] A.P. Koley, S. Purohit, L.S. Prasad, S. Ghosh, P.T. Manoharan, Inorg. Chem. 31 (1992) 305.
[9] A.P. Koley, R. Nirmala, L.S. Prasad, S. Ghosh, P.T. Manoharan, Inorg. Chem. 31 (1992) 1764.
[10] M. Maji, S. Ghosh, S.K. Chattopadhyay, T.C.W. Mak, Inorg. Chem. 36 (1997) 2938.
[11] M. Maji, M. Chatterjee, S. Ghosh, S.K. Chattopadhyay, B.M. Wu, T.C.W. Mak, J. Chem. Soc., Dalton Trans. (1999) 135.
[12] M. Maji, S. Ghosh, S.K. Chattopadhyay, Transition Met. Chem. 23 (1998) 81.
[13] M. Hossain, S.K. Chattopadhyay, S. Ghosh, Polyhedron 16 (1997) 143.
[14] J.M. Berg, K.O. Hodgson, S.P. Cramer, J.L. Corbin, A. Elsberry, N. Pariyadath, E.I. Stiefel, J. Am. Chem. Soc. 101 (1979) 2774.
[15] A.J. Wilson, B.R. Penfold, C.J. Wilkins, Acta Crystallogr., Sect. C 39 (1983) 329.
[16] S.P. Cramer, H.B. Gray, K.V. Rajagopalan, J. Am. Chem. Soc. 101 (1979) 2772.
[17] (a) O.A. Rajan, A. Chakravorty, Inorg. Chem. 20 (1981) 660;
(b) J.M. Berg, R.H. Holm, Inorg. Chem. 22 (1983) 1768.
[18] W.-K. Goh, M.-C. Lim, Aust. J. Chem. 37 (1984) 2235.
[19] D.A. Smith, F.A. Schultz, Inorg. Chem. 21 (1982) 3035.
[20] M. Chaudhury, J. Chem. Soc., Dalton Trans. (1984) 115.
[21] M. Chaudhury, Inorg. Chem. 24 (1985) 3011.
[22] A. Rana, R. Dinda, P. Sengupta, S. Ghosh, L.R. Falvello, Polyhedron 21 (2002) 1023.
[23] R. Bose, M. Akbar Ali, J. Inorg. Nucl. Chem. 39 (1977) 265.
[24] E.I. Stiefel, Prog. Inorg. Chem. 22 (1977) 1.
[25] J.A. Craig, E.W. Harlan, B.S. Snyder, M.A. Whitener, R.H. Holm, Inorg. Chem. 28 (1989) 2082.
[26] R. Hahn, U. Kusthardt, W. Scherer, Inorg. Chem. Acta 210 (1993) 177.
[27] J.M. Berg, R.H. Holm, J. Am. Chem. Soc. 106 (1984) 3035.
[28] I. Buchanan, M. Minelli, M.T. Ashby, J.T. King, J.H. Enemark, C.D. Garner, Inorg. Chem. 23 (1984) 495.
[29] S.K. Dutta, D.B. McConville, W.J. Youngs, M. Chaudhury, Inorg. Chem. 36 (1997) 2517.
[30] J. Liimatainen, A. Lehtonen, R. Sillanpaa, Polyhedron 19 (2000) 1133.
[31] C. Bustos, O. Burckhardt, R. Schrebler, D. Carrillo, A.M. Arif, A.H. Cowley, C.M. Nunn, Inorg. Chem. 29 (1990) 3996.
[32] R. Mattes, V. Mikloweit, Inorg. Chem. Acta 122 (1986) L19.
[33] B.B. Kaul, J.H. Enemark, S.L. Merbs, J.T. Spence, J. Am. Chem. Soc. 107 (1985) 2885.
[34] E.I. Steifel, in: G. Wilkinson, J.A. McCleverty, R.D. Gillard (Eds.), Comprehensive Coordination Chemistry, Pergamon Press, Oxford, 1987, p. 1375.
[35] Y.-L. Zhai, X.-X. Xu, X. Wang, Polyhedron 11 (1992) 415.
[36] A. Syamal, K.S. Kale, Inorg. Chem. 4 (1965) 867.
[37] M. Goodgame, P.J. Hayward, J. Chem. Soc. A (1966) 632.
[38] R.H. Holm, E.I. Solomon, Chem. Rev. (1996) 2215.
[39] S. Bhattacharyya, S.B. Kumar, S.K. Dutta, E.R.T. Tiekink, M. Chaudhury, Inorg. Chem. 35 (1996) 1967.
[40] I.W. Boyd, J.T. Spence, Inorg. Chem. 21 (1982) 1602.
[41] S. Purohit, S. Ghosh, J. Chem. Res. (S) (1988) 158.
[42] P. Ghosh, P. Bandyopadhyay, A. Chakravorty, J. Chem. Soc., Dalton Trans. (1983) 401.
[43] K. Yamanouchi, J.H. Enemark, Inorg. Chem. 18 (1979) 1626.
[44] R.H. Holm, J.M. Berg, Pure Appl. Chem. 56 (1984) 1645.
[45] W.C. Fernelius, K. Terada, B.E. Bryant, Inorg. Synth. 6 (1960) 147.

Available online at www.sciencedirect.com
SCIENCE DIRECT®
Polyhedron 23 (2004) 1605–1611
POLYHEDRON
www.elsevier.com/locate/poly

Salts of tetrachloroauric acid with pyridine *N*-oxide having various base/acid ratios of 1/1, 4/3, 3/2 and 2/1: crystal structures, ^{35}Cl NQR and phase transitions

Tetsuo Asaji [a,*], Eigo Akiyama [a], Fukue Tajima [b], Kazuo Eda [b], Masao Hashimoto [b], Yoshihiro Furukawa [c]

[a] *Department of Chemistry, College of Humanities and Sciences, Nihon University, Sakurajosui, Setagaya-ku, 3-25-40, Tokyo 156-8550, Japan*
[b] *Department of Chemistry, Faculty of Science, Kobe University, Nada-ku, Kobe 657-8501, Japan*
[c] *Department of Science Education, Graduate School of Education, Hiroshima University, Kagamiyama, Higashi-Hiroshima 739-8524, Japan*

Received 27 January 2004; accepted 24 March 2004
Available online 30 April 2004

Abstract

We determined crystal structures of $[(PyO)D][AuCl_4]$, $[(PyO)_4D_3][AuCl_4]_3$ and $[(PyO)_3D_2][AuCl_4]_2$ (PyO: pyridine *N*-oxide) at room temperature (1/1, 4/3 and 3/2 D-salts, respectively). The powder X-ray diffraction patterns of these salts (D-salts) were identical to those of the corresponding ones having normal hydrogen (H-salts) unlike the case of $[(PyO)_2D/H][AuCl_4]$. In the crystals of the 4/3 and 3/2 salts, there exist not only the monomer-type protonic adducts of PyO, but also dimer-type adducts in which two PyO units are bridged by a proton. A few types of aggregation of $AuCl_4$ units (sheet and ribbons) were found in these crystals. The variety in the aggregation motif of the anion and that in the structure of the cation seem to be related to the presence of the various salts having several base-to-acid ratios. The isotope effect on the preparation of the salts is discussed. ^{35}Cl NQR and phase transitions of these compounds are also reported.
© 2004 Elsevier Ltd. All rights reserved.

Keywords: Crystal structure; Phase transition; Isotope effect; Hydrogen bond; NQR; Tetrachloroaurate(III)

1. Introduction

It is known that pyridine *N*-oxide (PyO) forms a monomeric hydrogen adduct $[(PyO)H]^+$ in its salts. Examples can be seen in several compounds [1,2]. In addition, PyO has a tendency to form a monovalent diadduct type cation $[(PyO)_2H]^+$, in which the two PyO units are bridged by a proton. This type of cation exists, for instance, in $[(PyO)_2H][AuCl_4]$ [3] and other compounds [4,5]. There is the possibility that both types of cations are incorporated in a salt. In fact, we prepared a compound $[(PyO)_3H_2][AuCl_4]_2$ having a PyO/$HAuCl_4$ ratio of 3/2, which suggests the coexistence of $[(PyO)H]^+$ and $[(PyO)_2H]^+$ in the crystal [4]. Furthermore, we could separate a compound $[(PyO)_4H_3][AuCl_4]_3$ with another PyO/$HAuCl_4$ ratio of 4/3 by controlling the PyO/$HAuCl_4$ ratio in the solution. These findings led us to determine the crystal structures of these compounds to confirm their composition and the structure of the cation.

As a structural change induced by substitution of D for H atom, we recently reported that the structure of the cation $[(PyO)_2D]^+$ in $[(PyO)_2D][AuCl_4]$ and its whole crystal structure itself were dramatically different from those of $[(PyO)_2H][AuCl_4]$ [4]. Since we have been interested in this phenomenon induced by substitution of a hydrogen isotope, a part of this work was devoted to examine the effect of deuteration on the structures of the various salts mentioned above. We also investigated the stability of $[(PyO)_2D][AuCl_4]$ and $[(PyO)_2H][AuCl_4]$ to show that both of them are in stable phases.

The results of DTA/DSC as well as preliminary ^{35}Cl NQR measurements of $[(PyO)_3(H/D)_2][AuCl_4]_2$, $[(PyO)_4H_3][AuCl_4]_3$ and $[(PyO)D][AuCl_4]$ are reported.

* Corresponding author. Tel./fax: +81-3-5317-9739.
E-mail address: asaji@chs.nihon-u.ac.jp (T. Asaji).

0277-5387/$ - see front matter © 2004 Elsevier Ltd. All rights reserved.
doi:10.1016/j.poly.2004.03.022

We briefly discuss the phase transitions in $[(PyO)_3(H/D)_2][AuCl_4]_2$ and $[(PyO)D][AuCl_4]$.

2. Experimental

2.1. Synthesis

The various complex salts $[(PyO)_m(H/D)_n][AuCl_4]_n$ ($m/n = 1/1$, 4/3, 3/2, 2/1) between PyO and (H/D)$AuCl_4$ were prepared by slow evaporation of aqueous solutions (H_2O or D_2O) containing PyO and (H/D)$AuCl_4$ in the molar ratio shown in Table 1. In the text, following abbreviations will be used; $[(PyO)_m(H/D)_n][AuCl_4]_n$: m/n (H/D)-salt. The 4/3 H-salt was not prepared. $DAuCl_4$ was obtained by dissolving Au_2O_3 in a DCl solution in D_2O. Elemental analyses were carried out at the Center for Organic Elemental Microanalysis, Kyoto University. The results of the analyses have already been reported in [4] for $[(PyO)_2D][AuCl_4]$, $[(PyO)_3H_2][AuCl_4]_2$, $[(PyO)H][AuCl_4]$ and $[(PyO)D][AuCl_4]$. In the following, the results of $[(PyO)_3H_2][AuCl_4]_2$, $[(PyO)_3D_2][AuCl_4]_2$ and $[(PyO)_4D_3][AuCl_4]_3$ are reported. *Anal*. Calc. for $[(PyO)_3H_2][AuCl_4]_2$: C, 18.7; H, 1.8; Cl, 29.4; N, 4.4; O, 5.0. Found: C, 18.4; H, 1.8; Cl, 29.2; N, 4.2; O, 4.8%. *Anal*. Calc. for $[(PyO)_3D_2][AuCl_4]_2$: C, 18.6; H/D, 2.0; Cl, 29.3; N, 4.4; O, 5.0. Found: C, 18.5; H/D, 1.9; Cl, 29.4; N, 4.3; O, 4.8%. *Anal*. Calc. for $[(PyO)_4D_3][AuCl_4]_3$: C, 17.1; H/D, 1.9; Cl, 30.3; N, 4.0; O, 4.6. Found: C, 17.2; H/D, 2.0; Cl, 30.4; N, 4.0; O, 4.3%. The extent of the deuteration has been estimated by use of ^2H NMR measurements of the aqueous solution to be H/D = approximately 15/85 for $[(PyO)_3D_2][AuCl_4]_2$, $[(PyO)_4D_3][AuCl_4]_3$ and $[(PyO)D][AuCl_4]$.

The 3/2 (H/D)-salts and the 4/3 D-salt showed an extraordinarily wide temperature range of melting (see Table 1). This is probably due to gradual decompositions of the salts.

2.2. Physical measurements

X-ray powder patterns were recorded by the use of a Rigaku RINT 2100S diffractometer with Cu Kα radiation. Silicon powder was used as an internal standard of the diffraction angle. DTA and DSC measurements were performed using a home-made apparatus and DSC3100S (Bruker AXS), respectively. For the ^2H NMR measurements of the solution, a JEOL JNM-EX270 NMR spectrometer was employed. The density of the crystal at room temperature was determined by a floating method, using a mixture of *o*-xylene and bromoform or benzene and methylene iodide. A pulsed spectrometer based on the Matec gated amplifier 515A was used for the ^{35}Cl nuclear quadrupole resonance (NQR) measurements. The temperature of the NQR sample was controlled in the range 4.2–300 K using an electronic controller (LakeShore 331) and measured with an accuracy of ±0.5 K by use of a gold +0.07% iron versus chromel thermocouple. Solid-state ^1H NMR experiments were carried out by use of a standard pulsed NMR spectrometer at the Larmor frequency of 42.5 MHz.

2.3. Crystallography

A SMART 1000/CCD diffractometer (Bruker) was employed for the diffraction measurements using graphite monochromated Mo Kα radiation. Data collections were carried out at room temperature. Crystal data and the details of the experiments and refinements are given for the 3/2 D-salt, 4/3 D-salt and 1/1 D-salt in Table 2.

The structures were solved by direct methods and refined by full-matrix least-squares calculations based on F_o^2 with absorption correction (SADABS) using SHELXL-97 [6]. Non-hydrogen atoms of each salt were included in the least-squares calculations with anisotropic displacement parameters.

It was found that the monomeric adduct $[(PyO)D]^+$ in the 1/1 D-salt had a mirror plane, being perpendicular to the ring plane and containing the N–O bond, and a C_2-axis, being normal to the mirror plane and passing through the center of the ring (C_{2h} symmetry) indicating an orientational disorder, in which each of the O, N and relevant C (C1) atoms was located on two sites with an equal population. The positions of the N and C1 atoms

Table 1
The complex salts $[(PyO)_m(H/D)_n][AuCl_4]_n$ ($m/n = 1/1$, 4/3, 3/2, 2/1) between PyO and (H/D)$AuCl_4$ obtained from aqueous solutions (H_2O or D_2O)

Chemical formula	Melting point (K)	Molar ratio in crystal PyO:(H/D)$AuCl_4$	Molar ratio in solution PyO:(H/D)$AuCl_4$
$[(PyO)_2H][AuCl_4]$	368–369	2:1	2:1
$[(PyO)_3H_2][AuCl_4]_2$	428–491	3:2 (1.5:1)	1:1
$[(PyO)H][AuCl_4]$	521–528	1:1	1:2 (0.5:1)
$[(PyO)_2D][AuCl_4]$	367–368	2:1	5:1
$[(PyO)_3D_2][AuCl_4]_2$	438–484	3:2 (1.5:1)	2:1[a]
$[(PyO)_4D_3][AuCl_4]_3$	478–497	4:3 (1.3:1)	2:1[a]
$[(PyO)D][AuCl_4]$	517–520	1:1	2:1[a]; 1:1

[a] From the 2:1 solution, three kinds of crystals were obtained case by case.

Table 2
Crystal data and details of the experiments and refinements

Base/acid	1/1	3/2	4/3
Formula	$C_5H_5DONAuCl_4$	$C_{15}H_{15}D_2O_3N_3Au_2Cl_8$	$C_{20}H_{20}D_3O_4N_4Au_3Cl_{12}$
Formula weight	435.87	966.86	1402.73
X-ray radiation	Mo Kα	Mo Kα	Mo Kα
Wavelength (Å)	0.710730	0.710730	0.710730
Crystal system	orthorhombic	monoclinic	triclinic
Space group	*Pbam*	$C2/c$	$P\bar{1}$
a (Å)	7.673(2)	16.46(2)	9.079(2)
b (Å)	8.526(2)	9.038(9)	9.142(2)
c (Å)	7.944(2)	18.65(2)	12.504(2)
α (°)			78.250(3)
β (°)		110.42(2)	85.110(4)
γ (°)			63.438(3)
Cell volume (Å^3)	519.7(2)	2600(5)	908.8(3)
Z	2	4	1
D_c (g cm^{-3})	2.786	2.471	2.564
D_m (g cm^{-3})	2.78 ± 0.02	2.45 ± 0.02	2.55 ± 0.02
μ(Mo Kα)	15.133	12.118	12.994
$F(000)$	396	1784	644
Crystal color	yellow	yellow	yellow
Crystal size (mm)	0.09 × 0.08 × 0.07	0.12 × 0.07 × 0.06	0.08 × 0.07 × 0.06
Temperature	298	298	296
θ range (°)	2.56–27.47	2.61–27.52	1.66–27.48
Index range	$-9 \leqslant h \leqslant 9$, $-10 \leqslant k \leqslant 10$, $-6 \leqslant l \leqslant 9$	$-18 \leqslant h \leqslant 20$, $-11 \leqslant k \leqslant 7$, $-22 \leqslant l \leqslant 18$	$-11 \leqslant h \leqslant 11$, $-11 \leqslant k \leqslant 11$, $-11 \leqslant l \leqslant 16$
Reflections collected	2722	5684	5316
Reflections unique	585	2593	3617
R_{int}	0.0442	0.0593	0.0302
Reflections ($I > 2\sigma(I)$)	433	1639	2422
$R_1(F)(I > 2\sigma(I))$	0.0334	0.0578	0.0423
$wR_2(F^2)$ for all reflection	0.0836	0.1563	0.0971
Number of parameters	44	156	198
Goodness-of-fit for all reflections (F^2)	0.944	1.062	0.919
Weighting scheme	$w^{-1} = (\sigma^2 F_o^2) + (0.0632p)^2 + 0.00p$, $p = (F_o^2 + 2F_c^2)/3$	$w^{-1} = (\sigma^2 F_o^2) + (0.0721p)^2 + 0.00p$, $p = (F_o^2 + 2F_c^2)/3$	$w^{-1} = (\sigma^2 F_o^2) + (0.0443p)^2 + 0.00p$, $p = (F_o^2 + 2F_c^2)/3$
Maximum shift/esd	0.000	0.000	0.001
ρ_{max} (e Å^{-3})	0.960	2.115	2.044
ρ_{min} (e Å^{-3})	−3.152	−2.077	−1.318

were set to be equal. The D and non-disordered H atoms were found from a difference Fourier map and included in the refinement with isotropic displacement parameters (U_{iso}). The H atom attached to C1 was ignored in the refinement.

The asymmetric unit of the 3/2 D-salt contained a $[(PyO)D]^+$ group having a C_2-axis passing through C6 and C9 as shown in Scheme 1 (C_2 symmetry) and a $[PyO–D–PyO]^+$ group having an inversion center (C_i symmetry).

For the latter group, the bridging D atom was fixed at the center of symmetry, and the positions of the H atoms belonging to the PyO moiety were calculated and they were included in the refinement with U_{iso}. The C_2 symmetry of the $[(PyO)D]^+$ group indicates an orientational disorder of the group. In addition, another disorder was found for the group, because the asymmetric unit of the group had two oxygen atoms (O2 and O2′ shown in Scheme 1) with different populations (0.205 and 0.295, respectively). Owing to this disorder of the $[(PyO)D]^+$ group, the N atom was divided into two sites (N2 and N2′), each overlapping C7 and C8, respectively. The position and U_{ij} of C7 were set equal to those of N2, the population of which being that of O2 (0.205). The same treatment was applied to C8 and N2′. The positions of the H atoms attached to C6 and C9 were calculated and they were included in the refinement with U_{iso}. The rest of the H atoms, as well as the D atom were omitted in the refinement.

The asymmetric unit of the 4/3 D-salt was found to include $[(PyO)D]^+$ and $[PyO–D–PyO]^+$ with a center of symmetry. The positions of H atoms belonging to the PyO moieties in the latter unit were calculated and they were included in the refinement with U_{iso}. The bridging D atom was treated in the way same as that described above. The structure of the PyO moiety of the $[(PyO)D]^+$ unit was considerably distorted and the H atoms could not be found on the Fourier maps. The

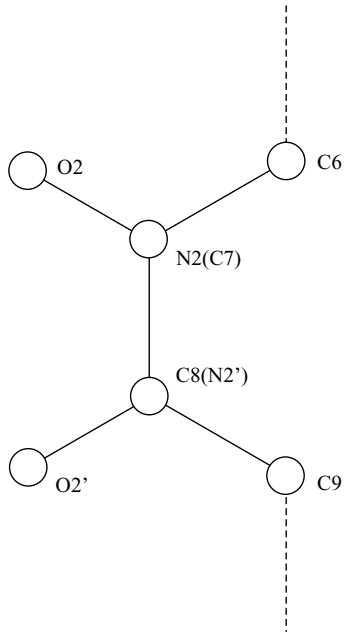

Scheme 1. Asymmetric unit of the disordered $[(PyO)D]^+$ group. The vertical broken line indicates 2-fold axis.

positions of the H atoms were calculated and they were included in the refinement with U_{iso}.

3. Results and discussion

3.1. Effect of deuteration on the crystal structures of the 1/1, 4/3 and 3/2 salts

As an isotope effect on crystal structure, we have reported a novel structural difference between the 2/1 H-salt and the 2/1 D-salt [4]. In relation to this phenomenon, we examined the possibility of such an isotope effect on the crystal structures of the 3/2, 4/3 and 1/1 salts. Their X-ray powder patterns revealed, however, that the deuteration did not change their crystal structures.

Since the quality of the single crystals of the deuterated salts was better than that of the normal ones, X-ray crystal structures of the former salts were determined in the present work.

3.2. Stability of the 2/1 H- and 2/1 D-salts

In order to check the possibility that either of the H- or D-salt is in a meta-stable phase, we carried out DTA measurements to get information on their thermal stability. DTA curves of the two salts measured in the 170–385 K region showed no exothermic heat anomaly corresponding to a monotropic transition of a meta-stable phase. We also examined X-ray powder diffraction patterns measured at room temperature for melt-grown crystals of the H- and D-salts or the crystals annealed at ca. 350 K. The diffraction patterns of the melt-grown or the annealed H- and D-salts were identical to those of the corresponding compounds obtained by crystallization from solutions. These results of the DTA and X-ray experiments strongly suggest that both of the H- and D-salts are in stable phases.

3.3. Crystal structures of the 1/1, 4/3 and 3/2 D-salts at room temperature

The 1/1 D-salt contains only $[(PyO)D]^+$, while there exist both $[(PyO)D]^+$ and $[PyO–D–PyO]^+$ in the crystals of the 4/3 D-salt and the 3/2 D-salt. The molar ratio of the monomeric:dimeric adducts in the crystal is 1:1 in the 3/2 salt and 2:1 in the 4/3 salt. These results are consistent with the chemical compositions of the salts.

The geometries of the monomeric and dimeric adducts are listed in Table 3.

The dimeric adducts in the 4/3 D-salt and the 3/2 D-salt are centrosymmetric (C_i symmetry), while the dimeric adduct in the 2/1 D-salt is non-symmetric (C_1 symmetry) [4]. The O···O distance in the dimeric adduct in the 4/3 D-salt (2.44(1) Å) and that in the 3/2 D-salt (2.41(2) Å) are typical for a symmetric O···H···O

Table 3
Geometries of the dimeric adduct ($[PyO–(H/D)–PyO]^+$) and the monomeric one ($[(PyO)D]^+$)

	$[PyO–(H/D)–PyO]^+$				$[(PyO)D]^+$		
Compounds	2/1 H-salt	2/1 D-salt[a]	3/2 D-salt[b]	4/3 D-salt[b]	3/2 D-salt[c]	4/3 D-salt	1/1 D-salt[c]
N–O distance (Å)	1.362(8)	1.354(9), 1.314(9)	1.32(1)	1.35(1)	–[d]	1.36(1)	1.36(2)
O···O distance (Å)	2.41(1)	2.43(1)	2.41(2)	2.44(1)	–	–	–
N–O···O bond angle (°)	108.24	106.4(5), 116.6(6)	109(1)	106.9(6)	–	–	–
N–O···O–N torsion angle (°)	180	142.7(8)	180	180	–	–	–
References	[3]	[4]	This work	This work	This work	This work	This work

[a] The crystal contains one non-symmetric $[PyO-D-PyO]^+$ in the asymmetric unit.
[b] The crystal contains centrosymmetric $[PyO–D–PyO]^+$.
[c] The monomeric adduct in the crystal is disordered (see text).
[d] The N–O length was not reliable owing to the orientational disorder (see text).

hydrogen bond, being comparable with the corresponding values found, for example, in the 2/1 D-salt [4], 2/1 H-salt [3], $[(PyO)_2H]ClO_4$ [5] and $[(2,6\text{-}(CH_3)_2PyO)_2H]$- $[AuCl_4]$ [7]. The N–O bond lengths of the PyO moiety in $[(PyO)D]^+$ found for the 1/1 and 4/3 D-salts are longer than that of the neutral PyO molecule (1.30 Å) [8]. This observation indicates the hydrogenation of the oxygen atom and/or its participation in the formation of a hydrogen bond.

The crystal of the 1/1 D-salt is built by alternating stacking of the layers of $[(PyO)D]^+$ and $[AuCl_4]^-$ (Fig. 1). $[(PyO)D]^+$ has C_{2h} symmetry to result in its orientational disorder, which can be seen in Fig. 1. It should be mentioned that the $[(PyO)D]^+$ groups in the 1/1 salt form a layer structure as shown in Fig. 2. The short intermolecular O···N contact (3.16(2) Å) suggests a certain interaction between the adjacent $[(PyO)D]^+$ groups. There exists a short intermolecular Cl···Cl contact of 3.391(6) Å, which seems to contribute to connect the layers of $[AuCl_4]^-$. The short intermolecular O1···Cl1 length (3.16(2) Å) indicates possibility of N–O–D···Cl hydrogen bonds.

The crystal structures of the 4/3 D-salt and 3/2 D-salt are depicted in Figs. 3 and 4, respectively. Several aggregation motifs of $[AuCl_4]^-$ ions are found in the 1/1, 4/3, 3/2 and 2/1 D-salts. In the crystal of the 1/1 D-salt, one can recognize a planar sheet structure formed by $[AuCl_4]^-$ ions (Fig. 1). If one takes account of a relatively long Au···Cl contact of 3.509 (3) Å in the sheet structure, the formal coordination number of the Au atom is six and the layer structure is formed by vertex-sharing of the $AuCl_6$ octahedrons. A similar layer structure has been reported for $[EtC(OEt)NH_2][AuCl_4]$ [9].

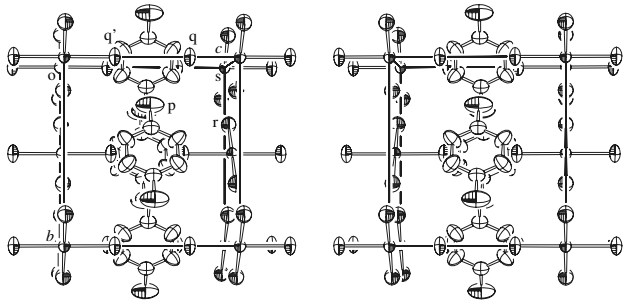

Fig. 1. Crystal structure of the 1/1 D-salt (stereo). Short contacts are Cl1(*q*)···Cl1′(*q*′) (3.391(6) Å), O1···Cl1 (3.16(2) Å) and Cl2···Au (3.509(3) Å). Symbols p, q, q′, r and s denote O1, Cl1, Cl1′, Cl2 and Au, respectively. Symmetry codes: p : $(-x+1.5, y-0.5, -z+1)$; q : $(-x+1, -y+1, -z+1)$; q′ : $(x+1, y-1, z)$; r : $(-x+0.5, y-0.5, -z+1)$ and s : $(x, y-1, z+1)$.

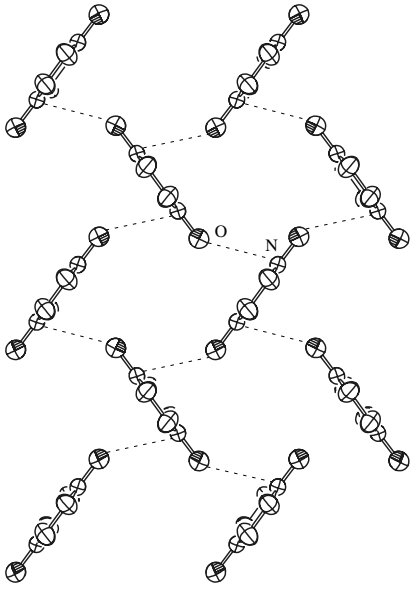

Fig. 2. Layer structure formed by disordered $[(PyO)D]^+$ units in the 1/1 D-salt. The broken lines indicate short O···N contacts of 3.16(2) Å.

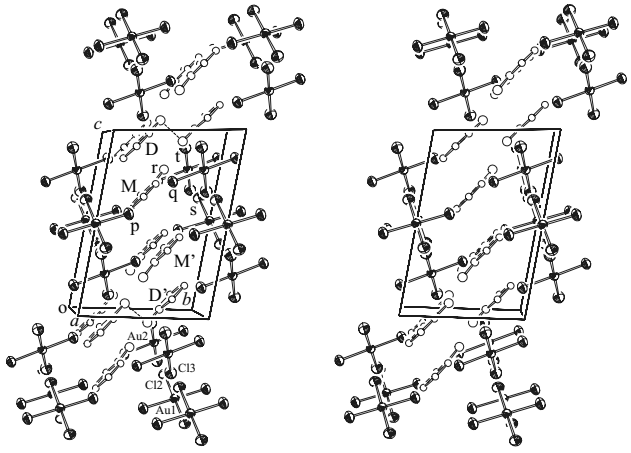

Fig. 3. Crystal structure of the 4/3 D-salt (stereo). D and M indicate $[PyO–D–PyO]^+$ and $[(PyO)D]^+$, respectively. D and D′, M and M′ as well, are related by an inversion center. Symbols p, q, r, s and t are Cl1, Cl4, O1, Cl2 and Cl5, respectively. Symmetry codes: p : $(-x+2, -y+1, -z+1)$; q : (x, y, z); r : (x, y, z); s : $(x-1, y, z)$ and t : $(x-1, y, z)$.

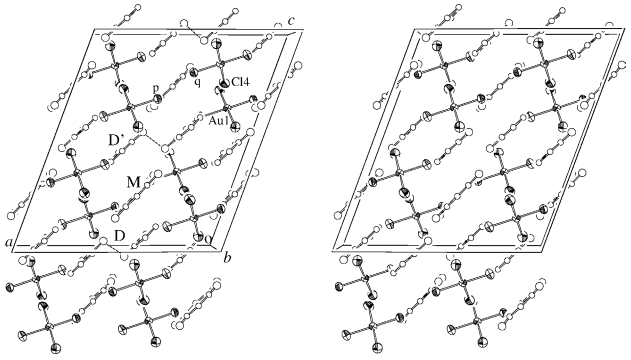

Fig. 4. Crystal structure of the 3/2 D-salt (stereo). D and M denote $[PyO\text{-}D\text{-}PyO]^+$ and $[(PyO)D]^+$ units. Symbols p and q are Cl1 and Cl1′. Symmetry codes: p : $(x+0.5, -y+1.5, z+0.5)$ and q : $(-x+0.5, -y+1.5, -z+1)$.

A ribbon-like aggregation motif of $[AuCl_4]^-$ ions that was found in the 4/3 salt (Fig. 3) can be regarded as a part of the sheet structure observed in the 1/1 D-salt. The Au1···Cl3 and Au2···Cl2 contacts are 3.525(3) and 3.590(3) Å, respectively, being comparable with the Au···Cl contacts found for the chain structures of $[AuCl_4]^-$ ions in [EMIM][$AuCl_4$] and [BMIM][$AuCl_4$] (3.356 and 3.452 Å, respectively) [10]. In the ribbon structure of the 4/3 D-salt, there are six and five coordinations of the Au atom, and vertexes of $AuCl_6$ octahedrons and $AuCl_5$ distorted square pyramids are shared to result in the ribbon.

The crystals of the 3/2 and 2/1 D-salts consist of another type of ribbon structure, each of which can be also regarded formally as a part of the layer structure of the 1/1 salt. The ribbon structure of the 3/2 D-salt has an Au1···Cl4 contact of 3.559(5) Å (Fig. 4). The Au···Cl contact in the 2/1 D-salt amounts to 3.983(2) Å, being comparable to that found for a chain structure of $AuCl_4^-$ ions in $[(H_5O_2)_2$(12-crown-4)$_2][AuCl_4]_2$ (3.845 Å) [11].

In the crystal of the 4/3 D-salt, the ribbons are packed along the crystallographic *a*-axis as shown in Fig. 3. A short Cl···Cl contact (3.612(4) Å of Cl1···Cl4) is observed between the ribbons. A columnar cavity surrounded by four ribbons of $[AuCl_4]_n^-$ is filled by a $[(PyO)D]^+$ (M), a PyO moiety of a $[PyO–D–PyO]^+$ (D) and their inversion-related ones (M′ and D′) as shown in Fig. 3. It is interesting to note that one of the two PyO moieties of a $[PyO–D–PyO]^+$ unit is accommodated in a columnar cavity, while the other one in an adjacent cavity. There are two short intermolecular contacts between the chlorine atoms in the ribbon and an oxygen atom in the PyO group: Cl2···O1 (3.31(1) Å) and Cl5···O1 (3.15(1) Å). The planes of the PyO moieties stack parallel to each other (see Fig. 3).

The crystal structure of the 3/2 D-salt is similar to that of the 4/3 D-salt as can be seen by comparing Figs. 3 and 4. The cavity of the 3/2 D-salt is filled by D, D′ (related to D by 2-fold symmetry axis) and M. The number of the PyO moieties accommodated in a cavity of the 3/2 D-salt is smaller than that of the 4/3 D-salt as a result of the decrease in the width of the ribbon structure. D and M stack almost parallel to each other and M, which is flanked by D and D′, exhibits the disorder mentioned above. There is a short Cl···Cl contact between adjacent ribbons (Cl1···Cl1′ of 3.575(9) Å).

3.4. Characterization of the 1/1, 4/3 and 3/2 D-salts by ^{35}Cl NQR and thermal analysis

For the 4/3 D-salt, we observed the five NQR frequencies (ν) of 29.164, 28.727, 28.625, 28.272 and 27.618 MHz at 77 K. There must be one missing line, since there exist six crystallographically non-equivalent chlorine atoms in the crystal. Previously, we have improperly assigned these frequencies to the 1/1 D-salt [4].

The temperature dependence of the ^{35}Cl NQR frequencies of the 4/3 D-salt is shown in Fig. 5. In the temperature range investigated (77–230 K), ν versus T curves seem to have no anomaly corresponding to a phase transition. The thermal analyses (DTA and DSC) carried out in 150–300 K region also could not detect any anomaly due to a phase transition.

For the 3/2 D-salt, a phase transition was detected at 199 K by the thermal analyses with increasing temperature ($\Delta H = 1.3$ kJ mol^{-1}). For the 3/2 H-salt, it was located at 197 K. The transitions exhibited very slight hysteresis, indicating the first-order nature of the transition. It was suggested from the temperature dependence of the ^{1}H NMR spin–lattice relaxation time of the 3/2 D-salt that at least one of the cationic molecules in the unit cell performs a fast reorientational motion above the phase-transition point. This mobility of the cation shows that the disordered structure found in the crystal structure determination is likely to be a dynamic one. So far, we have found four very broad ^{35}Cl NQR lines at 77 K for the 3/2 D-salt. The crystal structure of the low-temperature phase and details of the NMR/NQR results will be reported in a forthcoming paper.

DTA/DSC curves of the 1/1 D-salt measured in 150–300 K region exhibited a very small thermal anomaly at 273 K (T_{c1}) indicating a phase transition ($\Delta H_{c1} = 0.4$ kJ mol^{-1}). Hysteresis (super-cooling of ca. 30 K) of the transition suggested a first-order nature of the transition. It is very interesting that we could not detect any anomaly in the DTA/DSC curves for the 1/1 H-salt in

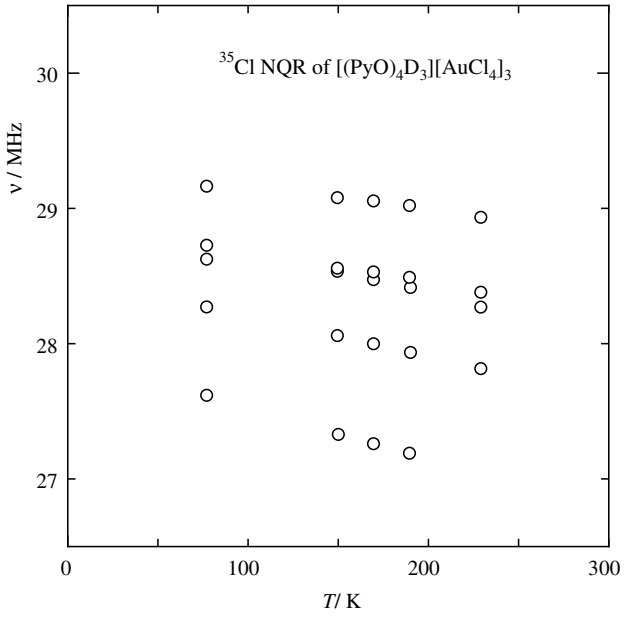

Fig. 5. Temperature dependences of ^{35}Cl NQR frequencies of the 4/3 D-salt.

the temperature range 150–300 K. Such a kind of isotope effect has been reported previously [12,13].

Two ^{35}Cl NQR lines (high- and low-frequency lines) were observed for the 1/1 D-salt at room temperature. When the sample temperature was decreased, the high-frequency line was observed to split drastically into four lines below 70 K (T_{c2}). Thus, from the ^{35}Cl NQR measurements, we have found another phase transition that is more drastic than that at T_{c1}. Moreover, it is interesting that the low-frequency line disappeared before reaching to T_{c2}.

In the region of $T > T_{c2}$, the frequencies (ν) of the two lines decreased monotonously with increasing temperature. No anomaly was detected in the ν versus T curves at T_{c1} within the accuracy of the present frequency measurements. This feature, together with the small value of ΔH_{c1}, indicates quite a subtle structural change at T_{c1}. The presence of the two ^{35}Cl NQR lines is consistent with the crystal structure determined at room temperature having two crystallographically non-equivalent chlorines.

The temperature dependence of the NQR spin–lattice relaxation time T_1 showed an anomalous decrease with decreasing temperature in the region of $T > T_{c2}$. This result suggests a dynamical disorder of the $[(PyO)D]^+$ cations at $T > T_{c2}$, since the ^{35}Cl T_1 behavior can be explained by the relaxation mechanism due to a fluctuation of the electric field gradient caused by reorientational motions between disordered orientations of nearby $[(PyO)D]^+$ cations. The presence of such a motion of the $[(PyO)D]^+$ cation was strongly suggested by the ^{1}H NMR spin–lattice relaxation measurements as well. The details of NMR/NQR measurements will be reported elsewhere.

These conclusions from the NQR and NMR investigations are consistent with the disorder model of the $[(PyO)D]^+$ group proposed in the crystal structure determination. An ordering of the $[(PyO)D]^+$ cation is likely to take place below T_{c2} and hence the transition at T_{c2} seems to be of an order–disorder type.

3.5. Origins of compositional variety and isotope effect on preparation

The present structural analyses revealed that both of the monomeric and dimeric adducts of PyO with proton can be formed in the crystal. In addition, several types of aggregation of $AuCl_4$ units are possible. These structural possibilities found for the cation and anion seem to be a reason why so many salts having different base-to-acid ratio could be formed.

There was a tendency that the base-to-acid molar ratio of the crystal was lower than that of the mother solution in the heavy hydrogen system, while it was found vice versa in the normal hydrogen system (see Table 1). This observation indicates that equilibrium processes in $PyO + (H/D)AuCl_4 + (H/D)_2O$ systems are dependent on the isotopic composition. Similar isotope effects on chemical equilibrium are known, for example, in the enol-enethiol tautomerism of β-thioxoketones [14] and in an acid–base equilibrium [15].

4. Supplementary material

Crystallographic data for the 1/1, 4/3 and 3/2 D-salts have been deposited with the Cambridge Crystallographic Data Centre, CCDC Nos. 219958, 219959 and 219960, respectively. Copies of the information may be obtained free of charge from The Director, CCDC, 12 Union Road, Cambridge, CB2 1EZ, UK (fax: +44-1223-336033; e-mail: deposit@ccdc.cam.ac.uk or www: http://www.ccdc.cam.ac.uk).

Acknowledgements

This work was partially supported by a Grant from the Ministry of Education, Culture, Sports, Science and Technology to promote advanced scientific research.

References

[1] P.G. Tsoucaris, Acta Crystallogr. 14 (1961) 914.
[2] O. Moers, K. Wijaya, T. Hamann, A. Blaschette, P.G. Jones, Z. Naturforsch. 56b (2001) 1052.
[3] M.S. Hussain, E.O. Schlemper, J. Chem. Soc., Dalton Trans. (1982) 751.
[4] T. Asaji, F. Tajima, M. Hashimoto, Polyhedron 21 (2002) 2207.
[5] J. Wasicki, M. Jaskolski, Z. Pajak, M. Szafran, Z. Dega-Szafran, M.A. Adams, S.F. Parker, J. Mol. Struct. 476 (1999) 81.
[6] G.M. Sheldrick, SHELXL-97 Program for the Solution and the Refinement of Crystal Structures, University of Göttingen, Germany, 1997.
[7] M.S. Hussain, Polyhedron 15 (1996) 645.
[8] F.H. Allen, O. Kennard, D.G. Watson, L. Brammer, A.G. Orpen, R. Taylor, J. Chem. Soc., Perkin Trans. II (1987) S1.
[9] R.A. Potts, D.L. Gaj, W.F. Schneider, N.S. Dean, J.W. Kampf, J.P. Oliver, Polyhedron 10 (1991) 1631.
[10] M. Hasan, I.V. Kozhevnikov, M. Rafiq, H. Siddiqui, A. Steiner, N. Winterton, Inorg. Chem. 38 (1999) 5637.
[11] M. Calleja, K. Johnson, W.J. Belcher, J.W. Steed, Inorg. Chem. 40 (2001) 4978.
[12] T. Matsuo, A. Inaba, O. Yamamuro, N. Onoda-Yamamuro, J. Phys.: Condens. Matter 12 (2000) 8595.
[13] T. Gustafsson, M. Ichikawa, I. Olovsson, Solid State Commun. 115 (2000) 473.
[14] B. Andresen, F. Duus, S. Bolvig, P.E. Hansen, J. Mol. Struct. 552 (2000) 45.
[15] S.L.R. Ellison, M.J.T. Robinson, J. Chem. Soc., Chem. Commun. (1983) 745.

Available online at www.sciencedirect.com
SCIENCE DIRECT®
Polyhedron 23 (2004) 1613–1618
POLYHEDRON
www.elsevier.com/locate/poly

Crystal structure of first- and second-sphere complexes of uranyl nitrate with 1,2- and 1,4-diols

Claude Villiers, Pierre Thuéry *, Michel Ephritikhine

CEA/Saclay, DSM/DRECAM/SCM (CNRS URA 331), Bâtiment 125, F91191 Gif-sur-Yvette, France

Received 13 February 2004; accepted 25 March 2004
Available online 15 April 2004

Abstract

2,3-Dimethyl-2,3-butanediol (pinacol, L^1), 2,5-dimethyl-2,5-hexanediol (L^2) and 2,2,7,7-tetramethyl-3,6-di-*tert*-butyl-3,6-octanediol (L^3) were reacted with uranyl nitrate hexahydrate. Whereas L^1 acts as a bidentate chelating ligand, giving the 1/1 anhydrous complex $[UO_2L^1(NO_3)_2]$ in which the nitrate ions are in *cis* geometry, L^2 and L^3 are second-sphere ligands which are hydrogen bonded to the water and nitrate oxygen atoms of the $[UO_2(NO_3)_2(H_2O)_2]$ moiety. In the three cases, hydrogen bonded assemblages, either discrete, two- or three-dimensional, are obtained. The crystal structures of two forms of uncomplexed L^3 are also described.
© 2004 Elsevier Ltd. All rights reserved.

Keywords: Uranyl ions; Diols; Hydrogen bonding; Crystal structures

1. Introduction

The complexation of uranium by 1,2-diols and 1,2-diolates is largely unexplored from a structural viewpoint. To the best of our knowledge, the unique example involving a 1,2-diol is the mononuclear complex *bis*(hydroxylamido)(1,2-ethanediol)dioxouranium(VI), in which the diol is a chelating ligand with both hydroxyl groups bound to the metal atom [1]. Two 1,2-diolate complexes emerged in uranium(IV) chemistry as intermediates in the McMurry reaction [2]. The first one, a tetrahydrofuran solvate of the mononuclear uranium (IV) *bis*(benzopinacolate), $[U(O_2C_2Ph_4)_2(thf)_2]$, resulted from the coupling of benzophenone with UCl_4 in the presence of Na(Hg) [3]; the other one, obtained by treating acetone with the UCl_4–Li(Hg) system, is the uranium(IV) monopinacolate complex $[\{UCl_3(hmpa)_2\}_2(\mu\text{-}OCMe_2CMe_2O)]$, which is a binuclear complex with the pinacolate, in *anti*-conformation, bridging the two metallic centres [4]. The complexation properties of 1,4-diols towards uranyl ions are yet unknown, in contrast with those of acyclic or cyclic (calixarenes) polyphenoxides, which are well documented [5].

We report herein the crystal structures of the air-stable complexes of uranyl nitrate hexahydrate with three aliphatic 1,2- and 1,4-diols: 2,3-dimethyl-2,3-butanediol (pinacol, L^1), 2,5-dimethyl-2,5-hexanediol (L^2) and 2,2,7,7-tetramethyl-3,6-di-*tert*-butyl-3,6-octanediol (L^3), represented in Scheme 1, as well as two crystal structures of L^3, either unsolvated or as a methanol solvate (the crystal structures of L^1 and L^2 have been reported previously [6,7]). In these uranyl complexes, the diol can act as a first- or a second-sphere ligand. In all cases, the propensity of these molecules to form extended hydrogen bonded assemblages is illustrated.

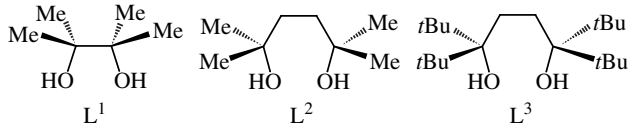

Scheme 1. The diols L^1, L^2 and L^3.

* Corresponding author. Tel.: +33-01-69086329; fax: +33-01-69-08-66-40.
E-mail addresses: villiers@drecam.cea.fr (C. Villiers), thuery@drecam.cea.fr (P. Thuéry), ephri@drecam.cea.fr (M. Ephritikhine).

0277-5387/$ - see front matter © 2004 Elsevier Ltd. All rights reserved.
doi:10.1016/j.poly.2004.03.011

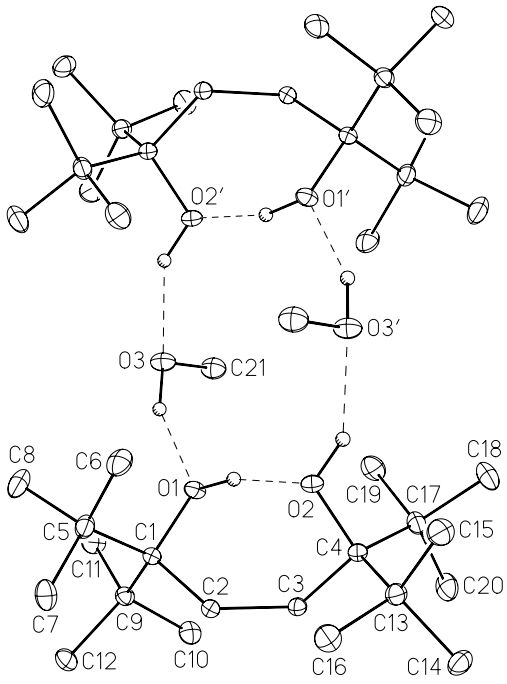

Fig. 1. View of the hydrogen bonded assemblage in compound **1a**. The hydrogen atoms not involved in hydrogen bonding are omitted for clarity. Hydrogen bonds are represented as dashed lines. Displacement ellipsoids are drawn at the 10% probability level. Symmetry code: ′, $1-x,-y,1-z$.

2. Results and discussion

2.1. Uncomplexed diol L^3

Two forms of the 1,4-diol L^3, either as a methanol solvate (**1a**) or unsolvated (**1b**) were obtained by crystallization from methanol and tetrahydrofuran, respectively. The crystal structures differ by the conformation of the diol and the assemblage of molecules through hydrogen bonds. In compound **1a**, the diol is in a *syn*-conformation, with a stabilizing intramolecular hydrogen bond (Fig. 1, Table 1). Moreover, the methanol molecule is both a hydrogen bond donor and acceptor, which results in the formation of a 12-membered, centrosymmetrical ring. The formation of such rings with a "homodromic" arrangement of hydrogen bonds, displaying σ-bond cooperativity and leading to a clustering of polar groups, is a well-known phenomenon [8]. The centrosymmetrical diol in compound **1b** is in the *anti*-conformation (Fig. 2), which favours the formation of intermolecular hydrogen interactions only (the hydroxy protons, necessarily disordered, were not located, but the presence of hydrogen bonds can be inferred from the O···O distances). In contrast with the isolated dimers in **1a**, infinite zigzag chains parallel to the *a*-axis are formed in **1b**, in keeping with the convergent and di-

Table 1
Hydrogen bonding interactions in compounds **1**–**4**: selected distances (Å) and angles (°)

1a	O1···O2	2.791(3)	O1–H1	1.11	H1···O2	1.71	O1–H1···O2	163
	O2···O3′	2.767(3)	O2–H2	0.92	H2···O3′	1.94	O2–H2···O3′	148
	O3···O1	2.772(3)	O3–H3	1.13	H3···O1	1.72	O3–H3···O1	152
1b*	O1···O1″	2.840(6)						
2	O3···O5′	2.829(6)	O3–H3	0.91	H3···O5′	1.93	O3–H3···O5′	169
	O4···O10″	2.782(6)	O4–H4	0.93	H4···O10″	1.92	O4–H4···O10″	153
3	O1A···O5	2.879(6)	O1A–H1A	0.91	H1A···O5	2.02	O1A–H1A···O5	157
	O1B···O1A	2.639(4)	O1B–H1B	0.94	H1B···O1A	1.73	O1B–H1B···O1A	163
	O2···O1B″	2.677(5)	O2–H2	0.91	H2···O1B″	1.80	O2–H2···O1B″	162
	O3···O1B	2.713(5)	O3–H3	0.91	H3···O1B	1.83	O3–H3···O1B	163
4	O3···O1A	2.702(6)	O3–H3A	0.95	H3A···O1A	1.79	O3–H3A···O1A	160
	O3···O1B	2.648(6)	O3–H3B	0.96	H3B···O1B	1.71	O3–H3B···O1B	167
	O4···O1C	2.682(6)	O4–H4A	0.91	H4A···O1C	1.78	O4–H4A···O1C	171
	O4···O1D	2.638(6)	O4–H4B	0.90	H4B···O1D	1.81	O4–H4B···O1D	152
	O1A···O2A	2.705(5)	O1A–H1A	0.96	H1A···O2A	1.83	O1A–H1A···O2A	150
	O1B···O2B	2.696(6)	O1B–H1B	0.94	H1B···O2B	1.82	O1B–H1B···O2B	153
	O1C···O2C	2.697(5)	O1C–H1C	0.87	H1C···O2C	1.84	O1C–H1C···O2C	168
	O1D···O2D	2.693(6)	O1D–H1D	1.02	H1D···O2D	1.74	O1D–H1D···O2D	154
	O2A···O7	3.007(6)	O2A–H2A	0.98	H2A···O7	2.30	O2A–H2A···O7	128
	O2B···O10	3.089(6)	O2B–H2B	1.01	H2B···O10	2.09	O2B–H2B···O10	170
	O2C···O10	3.031(6)	O2C–H2C	0.88	H2C···O10	2.35	O2C–H2C···O10	134
	O2D···O7	3.081(6)	O2D–H2D	1.02	H2D···O7	2.20	O2D–H2D···O7	143

Symmetry codes:
1a: ′, $1-x,-y,1-z$.
1b: ″, $1-x$, $1-y$, $1-z$.
2: ′, $-x,y,0.5-z$; , $0.5-x,y-0.5,0.5-z$.
3: ″, x, $1+y$, z.
* Hydrogen atoms not found.

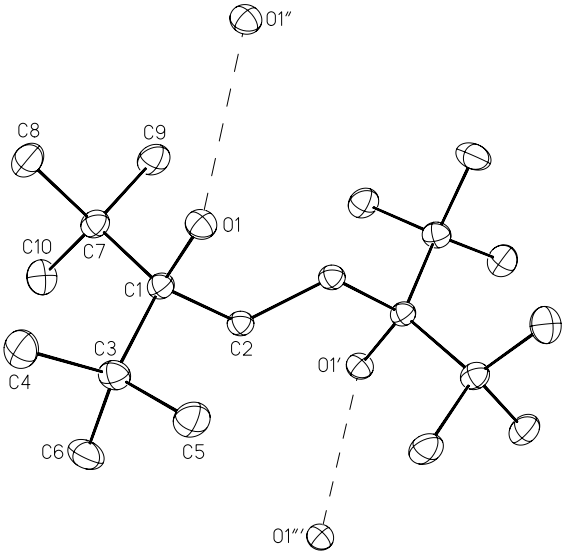

Fig. 2. View of the diol molecule in compound **1b**. Hydrogen atoms are omitted for clarity. Hydrogen bonds are represented as dashed lines. Displacement ellipsoids are drawn at the 10% probability level. Symmetry codes: ′, $-x, 1-y, 1-z$; ″, $1-x, 1-y, 1-z$; ‴, $x-1, y, z$.

vergent positions of the pinacol hydroxy groups in **1a** and **1b**, respectively.

2.2. Uranyl complexes

The uranyl unit in $[UO_2L^1(NO_3)_2]$ (**2**) is bound to two nitrate groups and one L^1 diol in its equatorial plane (Fig. 3), which results in the hexagonal bipyramidal uranium environment usual for small bite bidentate ligands. The diol thus acts as a first-sphere bidentate ligand, as in *bis*(hydroxylamido)(1,2-ethanediol)dioxouranium(VI) [1]. The six donor atoms define a plane with a maximum deviation of 0.179(3) Å, the uranium atom being displaced by 0.023(2) Å from it. The mean U–O(nitrate) bond length is 2.49(2) Å (Table 2), in agreement with the mean value of 2.522(5) Å from the structures involving the $UO_2(NO_3)_2$ group reported in the Cambridge Structural Database [9]. The mean U–O(diol) bond length is 2.449(5) Å, in agreement with the value 2.47(1) Å in *bis*(hydroxylamido)(1,2-ethanediol)dioxouranium(VI). The conformation of the diol is staggered (close to *gauche*) and not *syn*, with a torsion angle O3–C1–C2–O4 of 51.9(9)°. As a result, C1 and C2 are on either side of the mean equatorial plane, with out-of-plane distances of 0.47(1) and −0.37(1) Å, respectively. Each uranyl complex is involved in four intermolecular hydrogen bonds, in which the two OH groups and two NO_3 ligands act as donors and acceptors, respectively. The two hydroxyl groups are bound to oxygen atoms of the nitrate ligands in distinct ways, as shown in Fig. 3: O3 and O3′ are hydrogen bonded to the bridging atoms O5′ and O5, respectively, so as to create a dimer around a binary axis parallel to the *b*-axis. On the other hand, the hydrogen bonds involving O4 and the terminal atom O10 link one molecule to two of its neighbours through the binary screw axis parallel to the *b*-axis, which results in the formation of sheets parallel to the *ab*-plane.

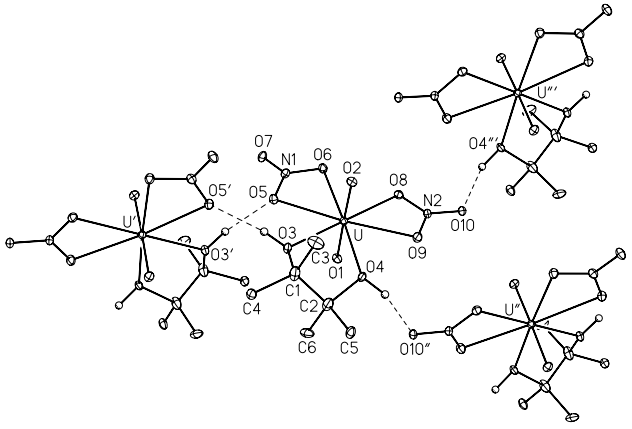

Fig. 3. View of the hydrogen bonding assemblage in complex **2**. The hydrogen atoms not involved in hydrogen bonding are omitted for clarity. Hydrogen bonds are represented as dashed lines. Displacement ellipsoids are drawn at the 20% probability level. Symmetry codes: ′, $-x, y, 0.5-z$; ″, $0.5-x, y-0.5, 0.5-z$; ‴, $0.5-x, 0.5+y, 0.5-z$.

Table 2
Environment of the uranium atom in compounds **2**–**4**: selected bond lengths (Å) and angles (°)

2	U–O1	1.760(4)	O1–U–O2	178.7(2)
	U–O2	1.751(4)	O3–U–O4	62.11(15)
	U–O3	2.445(4)	O3–U–O5	64.48(14)
	U–O4	2.452(4)	O5–U–O6	51.51(14)
	U–O5	2.502(5)	O6–U–O8	65.94(15)
	U–O6	2.488(5)	O8–U–O9	51.35(15)
	U–O8	2.494(4)	O9–U–O4	65.79(15)
	U–O9	2.459(5)		
3	U–O1	1.754(4)	O1–U–O1′	179.9(2)
	U–O2	2.391(6)	O2–U–O4	64.24(9)
	U–O3	2.423(5)	O4–U–O5	50.76(13)
	U–O4	2.505(3)	O5–U–O3	65.03(9)
	U–O5	2.504(3)		
4	U–O1	1.750(4)	O1–U–O2	179.8(2)
	U–O2	1.754(4)	O3–U–O5	64.53(13)
	U–O3	2.411(4)	O5–U–O6	50.50(13)
	U–O4	2.403(4)	O6–U–O4	64.51(13)
	U–O5	2.528(4)	O4–U–O9	64.78(13)
	U–O6	2.519(4)	O9–U–O8	50.37(13)
	U–O8	2.511(4)	O8–U–O3	65.42(13)
	U–O9	2.534(4)	O3–U–O4	179.48(15)

Symmetry code: ′, $1-x, y, 1.5-z$.

A much different situation arises with the 1,4-diol L^2, which gives the *bis*(aquo) complex $[UO_2(NO_3)_2(H_2O)_2]\cdot 2L^2$ (**3**). The separation between the two hydroxyl groups is too large for L^2 to act as a bidentate ligand in a κ^2 fashion. This would imply the formation of a seven-membered ring, which is an unfavourable situation due to entropy loss and for which few examples are to be

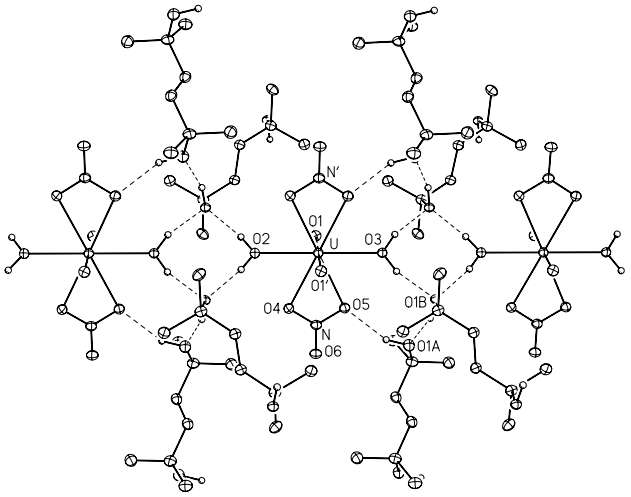

Fig. 4. View of the hydrogen bonded assemblage in compound **3**. The hydrogen atoms not involved in hydrogen bonding are omitted for clarity. Hydrogen bonds are represented as dashed lines. Displacement ellipsoids are drawn at the 20% probability level. Symmetry code: ′, $1-x, y, 1.5-z$.

found in the case of the uranyl ion, most of them with ligands more rigid than the present one [9]. In fact, L^2 is present in **3** as a second-sphere ligand, being hydrogen bonded to the first-sphere nitrate and water molecules (Fig. 4). The uranium atom and the two oxygen atoms of the water molecules (in *trans* positions) are located on the binary axis. The uranium atom is in the usual hexagonal bipyramidal environment, with a mean U–O(nitrate) bond length of 2.505(1) Å and a mean U–O(water) bond length of 2.41(2) Å, in agreement with the mean value of 2.44(3) Å from the Cambridge Structural Database. The uranium and the six equatorial donor oxygen atoms are in a plane with a maximum deviation of 0.031(2) Å. Each complex molecule is surrounded by a hydrogen bonded second-sphere of six L^2 molecules (two molecules A being bound to the nitrate ions and four molecules B to the water ligands). The two protons of each water molecule are involved in hydrogen bonds with two diols related by the binary axis (molecule B and its symmetry equivalent). Since each oxygen atom in molecule B is hydrogen bonded to two water molecules from two distinct complexes, rows of hydrogen bonded complexes along the *b*-axis are formed, which are interconnected by extended B molecules. The eight-membered hydrogen bonded ring formed by the two water and two B molecules is of an "antidromic", non-cooperative nature [8]. Each of the OH groups of molecule B acts in its turn as a donor towards one oxygen atom of another diol (molecule A), the latter being itself a donor towards the nitrate oxygen atom O5, with formation of two other symmetry-related eight-membered rings. An asymmetry is thus introduced in the second-sphere environment of the complex since the nitrate oxygen atom O4 is not involved in hydrogen bonding. Molecules A ensure the linking of the rows in a direction different from that of molecules B, the divergent nature of both diols resulting in a three-dimensional assemblage.

The last complex, $[UO_2(NO_3)_2(H_2O)_2]\cdot 4.5L^3$ (**4**), presents some common features with complex **3**, but differs in the overall assembling mode. The complex core itself is $[UO_2(NO_3)_2(H_2O)_2]$ with a *trans* geometry, as in **3**, but devoid this time of crystallographic symmetry (Fig. 5). The mean U–O(nitrate) and U–O(water) bond lengths, 2.52(1) and 2.407(6) Å, respectively, match those in **3**. The six equatorial donor oxygen atoms are in a plane with a maximum deviation of 0.046(3) Å and an out-of-plane displacement of 0.003(2) Å for the uranium atom. Each water proton is involved in a hydrogen bond with atom O1 of one L^3 molecule. However, since L^3 is not in an extended conformation, the two hydroxyl groups are not divergent as in **3**, but linked one to the other by an intramolecular hydrogen bond. The proton of the second hydroxyl group (O2) is further bound to a terminal nitrate oxygen atom. This gives rise to a circular arrangement with isolated $[UO_2(NO_3)_2(H_2O)_2]\cdot 4L^3$ assemblies held together by eight intermolecular hydrogen bonds, which, with the four intramolecular ones, make an array of twelve successive hydrogen bonds. The hydrogen bonded species thus make a 24-membered ring encircling the central uranyl complex. The second-sphere L^3 molecules, as well as the water protons to which they are bound, are either on one side (A and D) or on the other side (B and C) of the mean equatorial plane. This results in the complex having a pseudo-mirror plane containing the uranyl moiety and

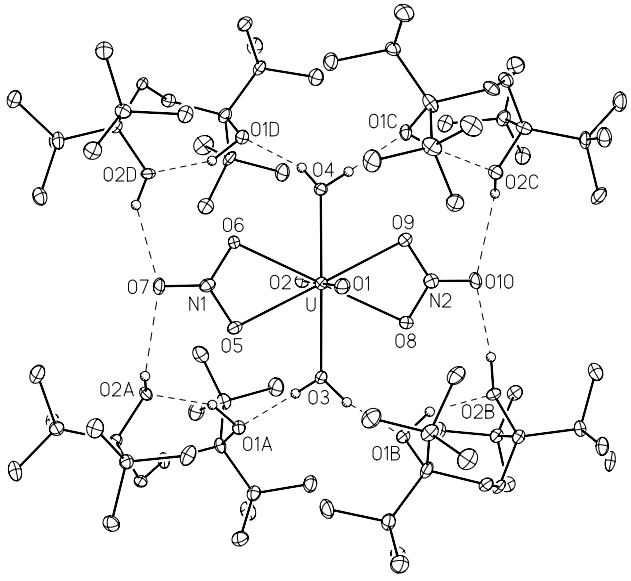

Fig. 5. View of the isolated complex molecule in compound **4**. The hydrogen atoms not involved in hydrogen bonding are omitted for clarity. Hydrogen bonds are represented as dashed lines. Displacement ellipsoids are drawn at the 30% probability level.

Table 3
Crystal data and structure refinement details

	1a	**1b**	**2**	**3**	**4**
Chemical formula	$C_{21}H_{46}O_3$	$C_{20}H_{42}O_2$	$C_6H_{14}N_2O_{10}U$	$C_{16}H_{40}N_2O_{14}U$	$C_{90}H_{193}N_2O_{19}U$
M (g mol^{-1})	346.58	314.54	512.22	722.53	1845.49
Crystal system	monoclinic	triclinic	monoclinic	monoclinic	monoclinic
Space group	$P2_1/n$	$P\bar{1}$	$C2/c$	$C2/c$	$P2_1/c$
a (Å)	11.0873(11)	6.6460(13)	25.0733(15)	18.091(2)	11.4220(6)
b (Å)	15.436(2)	7.893(2)	7.6431(4)	8.5869(12)	26.4338(19)
c (Å)	13.9047(11)	10.208(2)	15.6986(9)	16.9515(18)	33.424(2)
α (°)	90	80.41(3)	90	90	90
β (°)	109.591(5)	82.57(3)	116.199(3)	91.134(8)	97.467(4)
γ (°)	90	70.88(3)	90	90	90
V (Å^3)	2242.0(4)	497.3(2)	2699.4(3)	2632.8(6)	10005.9(11)
Z	4	1	8	4	4
D_{calc} (g cm^{-3})	1.027	1.050	2.521	1.823	1.225
μ(Mo Kα) (mm^{-1})	0.066	0.065	12.074	6.229	1.683
$F(000)$	784	178	1888	1416	3964
T (K)	293(2)	293(2)	100(2)	100(2)	100(2)
Reflections collected	7236	2027	8445	8182	57 452
Independent reflections	3125	899	2544	2492	17 708
"Observed" reflections [$I > 2\sigma(I)$]	1720	503	2199	2203	11 018
R_{int}	0.057	0.082	0.050	0.067	0.107
Number of parameters	218	106	176	155	1063
R_1	0.057	0.070	0.028	0.033	0.060
wR_2	0.141	0.162	0.063	0.073	0.096
S	0.907	1.093	1.048	1.046	1.004
$\Delta\rho_{min}$ (e Å^{-3})	−0.23	−0.15	−0.87	−1.17	−1.02
$\Delta\rho_{max}$ (e Å^{-3})	0.15	0.15	1.39	1.26	0.76

the nitrogen atoms and a pseudo-binary axis containing the uranium and water oxygen atoms (C_{2h} point group). In contrast with the "homodromic" arrangement of hydrogen bonds encountered in compound **1a**, the hydrogen bonds involving the nitrate oxygen atoms are anti-cooperative in **4**, which may explain why they are significantly longer than the other ones, which are cooperative and involve only hydroxy (alcohol or water) groups. The asymmetric unit in compound **4** contains also half a L^3 molecule, the corresponding centrosymmetric diol being surprisingly isolated and not involved in any hydrogen bonding interaction.

3. Conclusion

We have reported herein the synthesis and crystal structures of novel uranyl complexes with 1,2- and 1,4-diols, which display different kinds of complexation. The 1,2-diol L^1 in a staggered conformation acts as a small-bite chelating ligand, whereas the 1,4-diols L^2 and L^3 give second-sphere complexes which both contain the central $[UO_2(NO_3)_2(H_2O)_2]$ motif, with a *trans* arrangement of the ligands in the equatorial plane. A search of the Cambridge Structural Database shows that, in molecular complexes, this moiety is frequently found in association with hydrogen bonded crown ethers, one of them being linked to each water molecule [10]. It is also found in the structure of uranyl nitrate hexahydrate $[UO_2(NO_3)_2(H_2O)_2]\cdot 4H_2O$ [11,12], in which the coordinated water molecules and the nitrate ions are involved in hydrogen bonds with the solvent water molecules, in a way reminiscent of that observed in **3** and **4**. The water molecules being able to be involved in two or three hydrogen bonds, a three-dimensional pattern is generated, as with ligand L^2 in its divergent conformation (compound **3**). The difference between compounds **3** and **4**, both involving 1,4-diols, does not seem to be related in an obvious manner to the difference in the substituents, methyl or *tert*-butyl, of the diols. In spite of synthesis procedures involving identical 1:1 diol/uranyl stoichiometries, the number of diol molecules per complex unit is different in these two compounds. This may be related to solvent effects in solution or packing effects during crystallization. In any case, it indicates that the nature of hydrogen bonded assemblages based on such flexible molecules is hardly predictable.

4. Experimental

4.1. Synthesis

2,3-Dimethyl-2,3-butanediol (pinacol, L^1), 2,5-dimethyl-2,5-hexanediol (L^2), 2,2,4,4-tetramethyl-3-pentanone and Li powder (Aldrich) were used without further purification.

4.1.1. 2,2,7,7-Tetramethyl-3,6-di-tert-butyl-3,6-octanediol (L^3)

2,2,7,7-Tetramethyl-3,6-di-*tert*-butyl-3,6-octanediol (L^3) was prepared by a modified published method [13]. A Schlenk tube equipped with a magnetic stirrer was charged with Li powder (60 mg, 8.7 mmol) in dry tetrahydrofuran (5 ml). 2,2,4,4-Tetramethyl-3-pentanone (1.24 g, 8.7 mmol) was added under argon within 2 min at room temperature and the colour of the solution turned dark brown. Ethylene (1 bar) was then immediately introduced into the Schlenk tube. After stirring for 3 h, the mixture was carefully poured into ice. The organic extract was washed with water and brine, dried with Na_2SO_4, filtered and concentrated under vacuum. The oily residue was purified by column chromatography (SiO_2, *n*-pentane), yielding the colourless 2,2,7,7-tetramethyl-3,6-di-*tert*-butyl-3,6-octanediol (520 mg, 2.9 mmol, 38%); m.p. 116 °C (lit. 115–118 °C [14]); ^{1}H NMR (200 MHz, 23 °C, ^{2}[H_8] thf): δ 0.99 (36H, s), 1.73 (4H, s), 3.01 (2H, s, in exchange with D_2O). Single crystals of $L^3 \cdot$ MeOH (**1a**) and L^3 (**1b**) suitable for X-ray crystallography were obtained by slow evaporation, in air, of solutions of L^3 in methanol and tetrahydrofuran, respectively.

4.1.2. Uranyl complexes

Single crystals of $[UO_2L^1(NO_3)_2]$ (**2**), $[UO_2(NO_3)_2(H_2O)_2] \cdot 2L^2$ (**3**) and $[UO_2(NO_3)_2(H_2O)_2] \cdot 4.5L^3$ (**4**) were obtained by slow evaporation of tetrahydrofuran solutions containing equimolar mixtures of uranyl nitrate hexahydrate and the appropriate diol.

4.2. Crystallography

The data were collected on a Nonius Kappa-CCD area detector diffractometer [15] using graphite-monochromated Mo Kα radiation (λ 0.71073 Å). The crystals were introduced in glass capillaries with a protecting "Paratone-N" oil (Hampton Research) coating. The unit cell parameters were determined from ten frames, then refined on all data. A 180° φ-range was scanned with 2° steps during data collection, with a crystal-to-detector distance fixed to 26 or 28 mm, corresponding to the temperatures of 293 and 100 K, respectively. The data were processed with DENZO-SMN [16]. The structures were solved by direct methods or Patterson map interpretation with SHELXS-97 and subsequent Fourier-difference synthesis and refined by full-matrix least-squares on F^2 with SHELXL-97 [17]. Absorption effects in the uranyl complexes were corrected empirically with the program DELABS from PLATON [18]. The hydrogen atoms bound to oxygen atoms were found on Fourier-difference maps, except those in compound **1b** and that bound to O1E in compound **4**, which is not involved in a hydrogen bond and may be disordered. All the other hydrogen atoms were introduced at calculated positions. All hydrogen atoms were treated as riding atoms with a displacement parameter equal to 1.2 (OH, CH_2) or 1.5 (CH_3) times that of the parent atom. All non-hydrogen atoms were refined with anisotropic displacement parameters. Crystal data and structure refinement parameters are given in Table 3. The molecular plots were drawn with SHELXTL [19]. All calculations were performed on a Silicon Graphics workstation.

5. Supplementary material

Crystallographic data for the structural analysis have been deposited with the Cambridge Crystallographic Data Centre, CCDC nos. 231349–231353 for compounds **1**–**4**, respectively. Copies of this information may be obtained free of charge from The Director, CCDC, 12 Union Road, Cambridge CB2 1EZ, UK (fax: +44-1223-336033; e-mail: deposit@ccdc.cam.ac.uk or www: http://www.ccdc.cam.ac.uk).

References

[1] H.W.W. Adrian, A. Van Tets, Acta Crystallogr. Sect. B 34 (1978) 2632.
[2] M. Ephritikhine, C. Villiers, in: T. Takeda (Ed.), Modern Carbonyl Olefination: Methods and Applications, Wiley-VCH, Weinheim, 2004, pp. 223–285 (Chapter 6).
[3] C. Villiers, R. Adam, M. Lance, M. Nierlich, J. Vigner, M. Ephritikhine, J. Chem. Soc., Chem. Commun. (1991) 1144.
[4] M. Ephritikhine, O. Maury, C. Villiers, M. Lance, M. Nierlich, J. Chem. Soc., Dalton Trans. (1998) 3021.
[5] (a) L. Salmon, P. Thuéry, M. Ephritikhine, B. Masci, Dalton Trans. (2003) 2405, and references therein;
(b) P. Thuéry, M. Nierlich, J. Harrowfield, M. Ogden, in: Z. Asfari, V. Böhmer, J. Harrowfield, J. Vicens (Eds.), Calixarenes 2001, Kluwer Academic Publishers, Dordrecht, 2001, pp. 561–582 (Chapter 30, and references therein).
[6] M. Dahlqvist, R. Sillanpää, J. Mol. Struct. 524 (2000) 141, and references therein.
[7] (a) G.A. Jeffrey, M.S. Shen, J. Chem. Phys. 57 (1972) 56;
(b) R.B. Helmholdt, H. Reynaers, Acta Crystallogr. Sect. B 32 (1976) 2243;
(c) L. Ulicky, V. Kettmann, Chem. Papers 44 (1990) 3.
[8] T. Steiner, Angew. Chem. Int. Ed. 41 (2002) 48.
[9] F.H. Allen, Acta Crystallogr. Sect. B 58 (2002) 380.
[10] P. Thuéry, N. Keller, M. Lance, J.D. Vigner, M. Nierlich, New J. Chem. 19 (1995) 619, and references therein.
[11] D. Hall, A.D. Rae, T.N. Waters, Acta Crystallogr. 19 (1965) 389.
[12] J.C. Taylor, M.H. Mueller, Acta Crystallogr. 19 (1965) 536.
[13] P.D. Bartlett, T.T. Tidwell, W.P. Weber, Tetrahedron Lett. 33 (1970) 2919.
[14] L. Eberson, Acta Chem. Scand. 18 (1964) 1255.
[15] Kappa-CCD Software, Nonius B.V., Delft, The Netherlands, 1998.
[16] Z. Otwinowski, W. Minor, Methods Enzymol. 276 (1997) 307.
[17] G.M. Sheldrick, SHELXS-97 and SHELXL-97, University of Göttingen, Germany, 1997.
[18] A.L. Spek, PLATON, University of Utrecht, The Netherlands, 2000.
[19] G.M. Sheldrick, SHELXTL, Version 5.1, Bruker AXS Inc., Madison, WI, USA, 1999.

Available online at www.sciencedirect.com
SCIENCE DIRECT®
Polyhedron 23 (2004) 1619–1627
POLYHEDRON
www.elsevier.com/locate/poly

Synthesis, structure and norbornene polymerization behavior of neutral palladium complexes ☆

Hua Liang, Jingyu Liu, Xiaofang Li, Yuesheng Li *

State Key Laboratory of Polymer Physics and Chemistry, Changchun Institute of Applied Chemistry, Chinese Academy of Sciences, 5625 Renmin Street, Changchun 130022, China

Received 18 September 2003; accepted 28 March 2004
Available online 27 April 2004

Abstract

A series of neutral palladium(II) complexes bearing non-symmetric bidentate pyrrole-iminato or salicylaldiminato chelate ligands have been synthesized, and the structure of representative complexes (**3a, 4a**, and **5a**) have been confirmed by X-ray crystallographic analysis. These palladium complexes have been investigated as catalysts for the polymerization of norbornene. Using modified methylaluminoxane (MMAO) as a cocatalyst, these complexes display high activities and produce vinyl-addition polynorborenes. Catalytic activity of up to 8.52×10^3 kg/mol$_{Pd}$ h has been observed. Wide-angle X-ray diffraction (WAXD) has been used to investigate the polymer microstructure and it has been found that they are non-crystalline.
© 2004 Elsevier Ltd. All rights reserved.

Keywords: Neutral palladium(II) complex; X-ray crystallography; Catalyst; Methylaluminoxane; Norbornene; Vinylic polymerizaition

1. Introduction

With the boom in transition metal catalysis, there is a rapid development of a wide range of polyolefinic materials. A polymer with a certain microstructure can be easily obtained by employing a certain catalyst. Norbornene is a representative cycloolefin monomer which can be polymerized through ring-opening metathesis polymerization (ROMP), cationic (or radical) and vinylic addition polymerization mechanisms. ROMP yields poly(1,3-cyclopentylenevinylene) which retains one double bond in each polymeric repeat unit [1–3]. Cationic polymerization involves the rearrangement of the norbornene framework and generally produces moderate yields of poly (2,7-bicyclo [2,2,1] hept-2-ene) oligomers [4–7]. Free-radical processes also produce low molecular weight products [3]. In vinylic polymerization, the bicyclic structural unit remains intact and only the double bond is opened. As the vinyl-poly(norbornene) has many unique physical characteristics such as good mechanical strength, heat resistivity, optical transparency and low birefringence [8,9], many interests are focused on this kind of polymerization. The selection of catalysts is the key. Catalysts containing the metals nickel [8–16], chromium [17], titanium [18], zirconium [19–22], cobalt [23,24] and palladium [25–35] are reported in various literatures for the vinyl-type polymerization of nornornene. Nickel and palladium complexes display extremely high catalytic activity and produce high molecular weight polymers with excellent performance. Hence, our interest is keen on the well-defined complexes of nickel and palladium (see Scheme 1).

We found that neutral nickel complexes activated with methylaluminoxane display extremely high activity for the vinylic polymerization of norbornene [14,15], and Novak and co-workers [36] reported that neutral palladium complexes as catalysts for olefin and vinyl monomer polymerizations display excellent activity. This urges us to investigate if neutral palladium(II) complexes have high catalytic activity. Here, we would like to report on the synthesis of novel neutral palladium(II) complexes bearing pyrrole-iminato or

☆ Supplementary data associated with this article can be found, in the online version, at doi:10.1016/j.poly.2004.03.017.

* Corresponding author. Tel.: +86-431-5262124; fax: +86-431-5685653.
E-mail address: ysli@ciac.jl.cn (Y. Li).

0277-5387/$ - see front matter © 2004 Elsevier Ltd. All rights reserved.
doi:10.1016/j.poly.2004.03.017

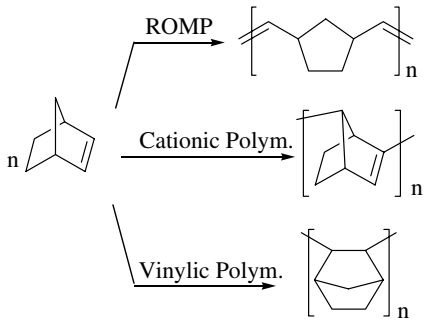

Scheme 1.

salicylaldiminato ligands and the catalysis properties for the vinylic polymerization of norbornene.

2. Experimental

2.1. General procedures and materials

All work involving air and moisture sensitive compounds was carried out using standard Schlenk techniques. NMR data of the ligands and the complexes were obtained on a Varian Unity 300 MHz spectrometer at ambient temperature, with $CDCl_3$ (ligands) or C_6D_6 (complexes) as solvent. IR spectra were recorded on a Bio-Rad FTS-135 spectrophotometer. Single-crystal X-ray diffraction data were received by P4 X-ray crystallography. The wide-angle X-ray diffraction (WAXD) spectrum was measured on a Rigaku D/Max 2500V PC with Cu Kα radiation and a wavelength of 1.54 Å.

Tetrahydrofuran (THF), benzene and diethyl ether were dried over sodium with dibenzophenone as indicator. Chlorobenzene and dichloromethane were refluxed over calcium hydride for two weeks before use. Aniline derivatives were obtained from Acros and purified by distillation before use. Triphenyphosphine, pyrrole-2-carboxaldehyde, sodium tetrachlopalladate-(II) and tetramethyltin were obtained from Aldrich and used without further purification. Pyridine was dried over sodium hydroxide and obtained by reduced distillation. Norbornene from Aldrich was refluxed with sodium, purified by reduced distillation and used as a solution in toluene. Modified methylaluminoxane (MMAO, 7% aluminum in heptane solution) was purchased from Akzo Nobel Chemical Inc. (COD)PdMeCl was prepared by the reaction of $(COD)PdCl_2$ and $SnMe_4$ according to a procedure given by Richard and co-workers [37,38]. Salicylaldehyde derivatives were prepared according to the method of Casiraghi et al. [39], and the salicylaldimines **6a**–**c** were prepared according to the procedure described by Grubbs and co-workers [40]. The pyrrole-imines **1a**–**d** were prepared according to the procedure described previously [15].

2.2. Synthesis of neutral Pd(II) complexes *3a–d, 4a, 5a and 8a–c*

A solution of ligand **1a** (0.45 g, 1.76 mmol) in THF (20ml) was added to NaH (0.12 g, 2.5 mmol). The resulting mixture was stirred at room temperature for 3 h, then filtered and the filtrate was evaporated. The solid residue was dried in vacuum. The sodium salt and (COD)PdMeCl (0.32 g, 1.2 mmol) with PPh_3 (0.32 g, 1.2 mmol) were dissolved in benzene (20 ml) in a 100 ml Schlenk flask and stirred at room temperature for 18 h. The resulting mixture was filtered by cannula filtration. The filtrate should be concentrated in a vacuum to ca. 5 ml, and then pentane (ca. 20 ml) was added. After 24 h, some yellow crystals were obtained from the solution and isolated by cannula filtration to yield 0.55 g (71.9%) of **3a**. The other complexes were prepared by the same procedure with similar yields.

3a: ^{1}H NMR ($CDCl_3$): δ 7.74–7.44 (m, 15 H, PPh–*H*), 7.42 (s,1 H, N=C–*H*), 7.07–6.98 (m, 6 H, Pyrrole-*H* + Ph–*H*), 3.42–3.37 (m, 2 H, C–*H*),1.28–1.19 (m,15 H, *i*-Pr–C*H*$_3$ + Pd–C*H*$_3$). ^{13}C NMR ($CDCl_3$): δ 4.8, 23.0, 25.0, 28.9, 111.6, 118.0, 123.3, 128.6, 128.7, 130.8, 135.1, 135.5, 142.8, 145.0, 161.6.

3b (73.2%): ^{1}H NMR ($CDCl_3$): δ 7.69 (m, 15 H, PPh–*H*), 7.64 (s, 1 H, N=C–*H*), 7.03–7.01 (s, 3 H, Ph–*H*), 6.65–6.45 (s, 3*H,* Pyrrole-*H*), 2.77 (s, 6 H, Ph–C*H*$_3$), 1.07 (s, 3 H, Pd–C*H*$_3$). ^{13}C NMR ($CDCl_3$): δ 15.0, 25.2, 25.5, 111.0, 111.6, 118.2, 126.7, 128.8, 131.6, 132.4, 137.9, 161.5, 161.9.

3c (69.4%): ^{1}H NMR ($CDCl_3$): δ 7.75 (s, 1 H, N=C–*H*), 7.71 (m, 15 H, PPh–*H*), 7.13 (s, 5 H, Ph–*H*), 6.75–

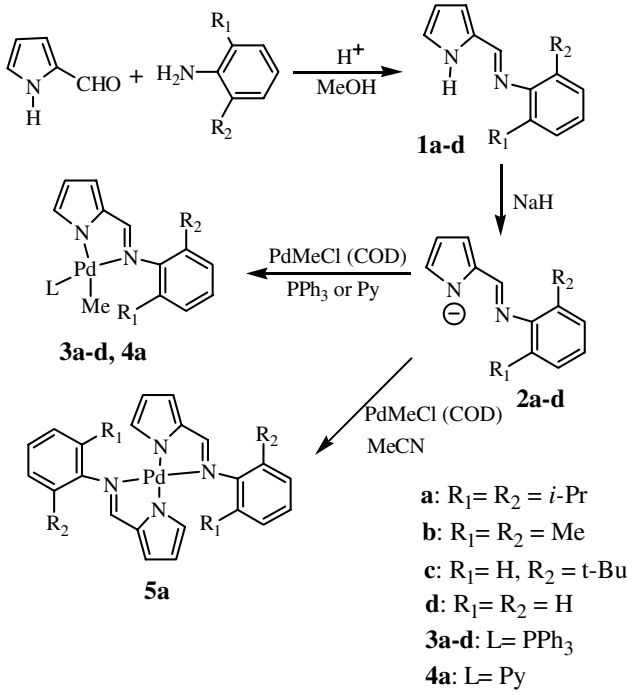

Scheme 2.

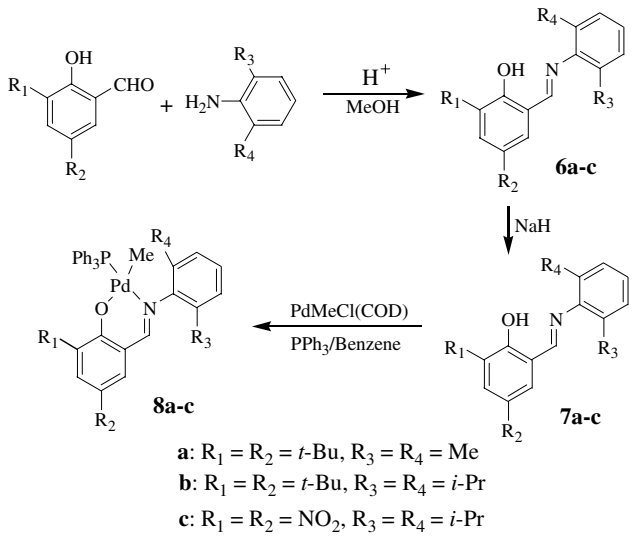

Scheme 3.

6.70 (s, 3*H*, pyrrole-*H*), 0.80 (s, 3 *H*, Pd–CH_3). ^{13}C NMR ($CDCl_3$): δ 5.9, 6.0, 118.7, 118.9, 124.6, 128.6, 130.9, 135.6, 135.3, 137.9, 138.5, 160.8, 161.1.

3d (67.8%): ^{1}H NMR ($CDCl_3$): δ 7.70–7.65 (m, 15 H, PPh–*H*), 7.65 (s, 1 H, N=C–*H*), 7.29–7.18 (s, 4 H, Ph–*H*), 6.76 (s, 3 H, Pyrrole-*H*), 1.34–1.26 (m, 12 H, *t*-Bu–CH_3 + Pd–CH_3). ^{13}C NMR ($CDCl_3$): δ 161.6, 149.9, 143.3, 140.5, 138.3, 135.5, 131.6, 130.2, 127.7, 127.4, 126.5, 125.7, 118.0, 111.5, 36.6, 33.1, 32.3, 31.0, 6.3.

4a (73.0%): ^{1}H NMR ($CDCl_3$): δ 8.16 (d, 2 H, Pydine-*H*), 7.60 (s, 1 H, Pydine-*H*), 7.50 (s, 1 H, C*H*=N), 7.18–6.90 (m, 4 H, Ph–H + Pydine-H), 6.74 (d, 2 H), 6.25 (s, 1 H), 3.34 (m, 2 H), 0.99 (m, 12 H), 0.85 (s, 1 H). ^{13}C NMR ($CDCl_3$): δ 158.7, 151.9, 145.2, 141.4, 125.0, 124.4, 123.3, 117.4, 110.7, 27.9, 24.9, 22.2.

5a (66.3%): ^{1}H NMR ($CDCl_3$): δ 7.38 (s, 2 H, N=C–*H*), 7.17–6.80 (s, 10 H, Ph–*H* + Pyrrole-*H*), 6.36 (s, 2H, Pyrrole-*H*), 3.33 (m, 4H, *i*-Pr–C*H*), 0.95 (t, 24 H, 8CH_3). ^{13}C NMR ($CDCl_3$): δ 164.6, 161.1, 146.9, 143.5, 142.7, 139.6, 137.4, 136.3, 127.5, 126.9, 118.5, 118.0, 28.1, 28.0, 25.7, 24.4, 22.7, 22.3.

8a (71.5%): ^{1}H NMR ($CDCl_3$): δ 7.96 (s, 1 H, N=C–*H*), 7.75 (m, 15 H, PPh–*H*), 7.39 (m, 5 H, Ph–*H*), 2.50 (s, 6H, Ph–CH_3), 1.35–1.25 (s, 21 H, *t*-Bu–CH_3 + Pd–CH_3). ^{13}C NMR ($CDCl_3$): δ 172.9, 172.7, 156.7, 140.8, 140.6, 137.4, 136.6, 133.6, 133.5, 130.6, 130.0, 124.6, 36.9, 35.2, 24.8, 24.3, 7.57, 7.43.

8b (74.0%): ^{1}H NMR ($CDCl_3$): δ 8.22 (s, 1 H, N=C–*H*), 7.98 (m, 15 H, PPh–*H*), 7.2–6.95 (m, 5 H, Ph–*H*), 3.51–3.47 (m, 2 H, C–*H*), 1.27 (s, 12 H, *i*-Pr–CH_3), 1.14 (s, 18 H, *t*-Bu–CH_3), 1.1 (s, 3 H, Pd–CH_3). ^{13}C NMR ($CDCl_3$): δ 167.3, 148.9, 141.8, 135.1, 132.0, 130.9, 130.6, 127.1, 126.3, 125.6, 123.3, 118.4, 35.3, 34.1, 31.9, 29.9, 29.0, 28.2, 25.4, 23.9, 23.3, 3.9.

8c (77.2%): ^{1}H NMR ($CDCl_3$): δ 8.31–8.12 (s, 2 H, Ph–*H*), 7.44 (s, 15 H, PPh_3–*H*), 7.16 (s, 3 H, Ph–*H*), 3.36 (m, 2 H, C–*H*), 1.41–1.01 (m, 15 H, C–CH_3 + Pd–CH_3). ^{13}C NMR ($CDCl_3$): δ 165.2, 162.4, 146.3, 140.5, 140.1, 135.9, 134.9, 134.0, 131.4, 128.1, 124.4, 122.6, 122.4, 29.0, 28.9, 28.2, 24.7, 24.3, 23.0.

2.3. Typical polymerization procedure

1.0 ml of a fresh catalyst solution (chlorobenzene, 0.5 μmol catalyst), 3.0 ml of a solution of norbornene (26.0 mmol, 2.45 g) in chlorobenzene, and 6.5 ml of

Table 1
Crystal data and structure refinements of **3a**, **4a** and **5a**

	3a	**4a**	**5a**
Empirical formula	$C_{36}H_{39}N_2PPd$	$C_{23}H_{29}N_3Pd$	$C_{34}H_{42}N_4Pd$
Formula weight	637.06	453.89	613.12
Crystal system	orthorhombic	monoclinic	monoclinic
Space group	*Pna*2$_1$	*P*2$_1$/*n*	*P*2$_1$/*n*
a (Å)	19.017(8)	8.7190(18)	17.392(3)
b (Å)	12.375(5)	20.457(3)	10.5998(18)
c (Å)	13.986(5)	12.4825(12)	17.800(4)
α (°)	90	90	90
β (°)	90	94.977(13)	108.351(15)
γ (°)	90	90	90
Volume (Å^3)	3291(2)	2218.1(6)	3114.5(9)
ρ_{calc} (Mg m^{-3})	1.286	1.359	1.308
Wavelength (Å)	0.71073	0.71073	0.71703
F(000)	1320	936	1280
θ Range (°)	1.96–26.01	1.92–25.99	1.98–26.00
Independent reflections	3648 (R_{int} = 0.0192)	4363 (R_{int} = 0.0229)	6113 (R_{int} = 0.0242)
Absorption correction	ψ-scan	ψ-scan	ψ-scan
Maximum and minimum transmission	0.4728 and 0.4239	0.4895 and 0.4186	0.5681 and 0.5130
Parameters	366	249	360
Final *R* indices [$I > 2\sigma(I)$]	R_1 = 0.0288, wR_2 = 0.0561	R_1 = 0.0286, wR_2 = 0.0669	R_1 = 0.0392, wR_2 = 0.0519
Goodness-of-fit on F^2	1.026	1.045	0.860
Largest differential peak and hole (e Å^{-3})	0.354 and −0.375	0.209 and −0.629	0.353 and −0.408

chlorobenzene were added under inert gas atmosphere into a Schlenk flask with a mechanical stirrer. The reaction was started by the addition of 0.5 ml of a MMAO solution (1.0 mmol in heptane) at 30 °C. After 10 min, the reaction mixture was poured into 200 ml of acidic ethanol (ethanol/$HCl_{conc.}$ = 50/1). The polymer was isolated by filtration, washed with methanol, and dried under vacuum at 80 °C for 24 h. Total reaction volume was 11 ml, unless otherwise stated. This was achieved by variation of the amount of chlorobenzene if necessary.

3. Results and discussion

3.1. Synthesis and characterization of neutral palladium complexes

Ligands **1a–d** were prepared by the condensation of the corresponding aniline derivatives according to the procedure described previously [15], they were deprotonated using sodium hydride and the anions allowed to react with (COD)PdMeCl in the presence of neutral, two-electron donor ligands to give palladium complexes **3a–d**, and **4a**. The neutral donors ligands are necessary to stabilize the complexes. Different ligands have been used to study their effects on metal catalytic activity. Interestingly, attempts to prepare palladium complex with the acetonitrile ligand have failed and complex **5a** was obtained instead. This shows that the binding strength of the CH_3CN ligand with palladium atom is poorer than that of triphenylphosphine or pyridine, which is in accordance with the results of Novak and coworkers [36]. The general synthetic route for the kind of neutral palladium complex in this study is shown in Scheme 2. Meanwhile we have synthesized neutral palladium complexes **8a–c** bearing salicylaldiminato ligands with a similar method, which is shown in Scheme 3.

Table 2
Selected bond lenths (Å) and angles (°) of **3a**, **4a** and **5a**

3a					
Bond lengths					
Pd–C(1)	2.022(7)	N(1)–C(2)	1.336(8)	P–C(25)	1.819(4)
Pd–N(1)	2.123(6)	N(1)–C(5)	1.354(7)	P–C(19)	1.818(5)
Pd–N(2)	2.121(3)	N(2)–C(6)	1.304(6)	P–C(31)	1.834(5)
Pd–P	2.2279(14)	N(2)–C(7)	1.430(5)		
Bond angles					
C(1)–Pd–N(1)	171.8(2)	C(1)–Pd–P	90.5(2)	C(25)–P–C(19)	106.3(2)
C(1)–Pd–N(2)	93.8(2)	N(1)–Pd–P	96.80(15)	C(25)–P–C(31)	102.3(2)
N(1)–Pd–N(2)	79.12(17)	N(2)–Pd–P	175.23(11)	C(19)–P–C(31)	104.8(2)
C(25)–P–Pd	112.16(15)	C(19)–P–Pd	108.00(15)	C(31)–P–Pd	122.10(16)
4a					
Bond lengths					
Pd–C(1)	2.018(3)	Pd–N(2)	2.004(2)	Pd–N(3)	2.168(2)
N(1)–C(6)	1.325(4)	N(2)–C(10)	1.369(3)	N(3)–C(11)	1.288(3)
N(3)–C(12)	1.436(3)				
Bond angles					
N(2)–Pd–C(1)	94.05(11)	N(2)–Pd–N(1)	174.50(9)	C(1)–Pd–N(1)	90.08(11)
N(2)–Pd–N(3)	79.39(8)	C(1)–Pd–N(3)	172.86(10)	N(1)–Pd–N(3)	96.65(8)
C(6)–N(1)–C(2)	116.9(2)	C(6)–N(1)–Pd	118.7(2)	C(2)–N(1)–Pd	124.4(2)
C(10)–N(2)–Pd	118.7(2)	C(7)–N(2)–C(10)	105.9(2)	C(7)–N(2)–Pd	140.0(2)
C(11)–N(3)–C(12)	121.0(2)	C(11)–N(3)–Pd	110.32(16)	C(12)–N(3)–Pd	128.62(15)
5a					
Bond lengths					
Pd–N(1)	2.026(3)	Pd–N(2)	2.052(3)	Pd–N(3)	2.030(3)
Pd–N(4)	2.052(3)	N(1)–C(1)	1.337(4)	N(1)–C(4)	1.383(4)
N(2)–C(5)	1.298(4)	N(2)–C(6)	1.437(4)	N(3)–C(18)	1.342(4)
N(3)–C(21)	1.384(4)	N(4)–C(22)	1.305(4)	N(4)–C(23)	1.442(4)
Bond angles					
N(1)–Pd–N(3)	179.75(13)	N(1)–Pd–N(2)	80.37(11)	N(2)–Pd–N(3)	99.50(11)
N(1)–Pd–N(4)	99.84(11)	N(3)–Pd–N(4)	80.29(12)	N(2)–Pd–N(4)	179.16(13)
C(1)–N(1)–C(4)	105.8(3)	C(1)–N(1)–Pd	142.0(2)	C(4)–N(1)–Pd	112.3(2)
C(5)–N(2)–C(6)	120.9(3)	C(5)–N(2)–Pd	112.4(2)	C(46)–N(2)–Pd	126.6(2)
C(18)–N(3)–C(21)	106.5(3)	C(18)–N(3)–Pd	141.0(2)	C(21)–N(3)–Pd	112.5(2)
C(22)–N(4)–C(23)	120.7(3)	C(22)–N(4)–Pd	112.3(2)	C(23)–N(4)–Pd	126.9(2)

3.2. Crystal structures of complexes *3a*, *4a* and *5a*

Crystals of **3a**, **4a** and **5a** suitable for X-ray structure determination were grown from a benzene–pentane (volume ratio = 1:2) solution. The data collection and refinement data of the analysis are summarized in Table 1, the selected bond lengths and bond angles are summarized in Table 2, and the molecule structures of **3a**, **4a** and **5a** are shown in Figs. 1–3, respectively.

The Pd atom is at the center of an approximately square-planar arrangement, which is applied to all these three complexes. For **3a**, the bulky 2,6-diisopropylbenzimine filled the position *trans* to the triphenylphosphine ligand with a P–Pd–N2 angle of 175.23(11)°;

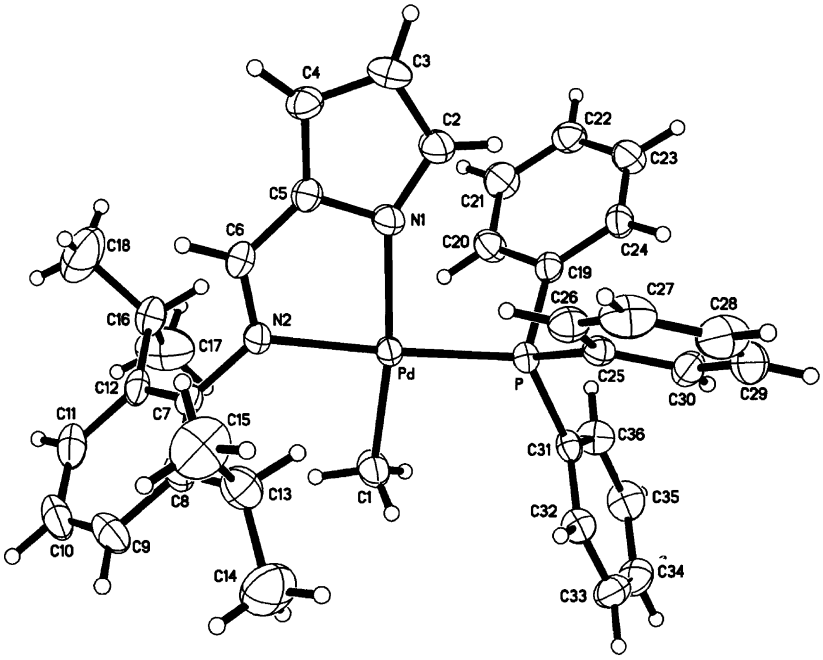

Fig. 1. ORTEP plot of the molecular structure of complex **3a**. Displacement ellipsoids are drawn at the 50% probability level.

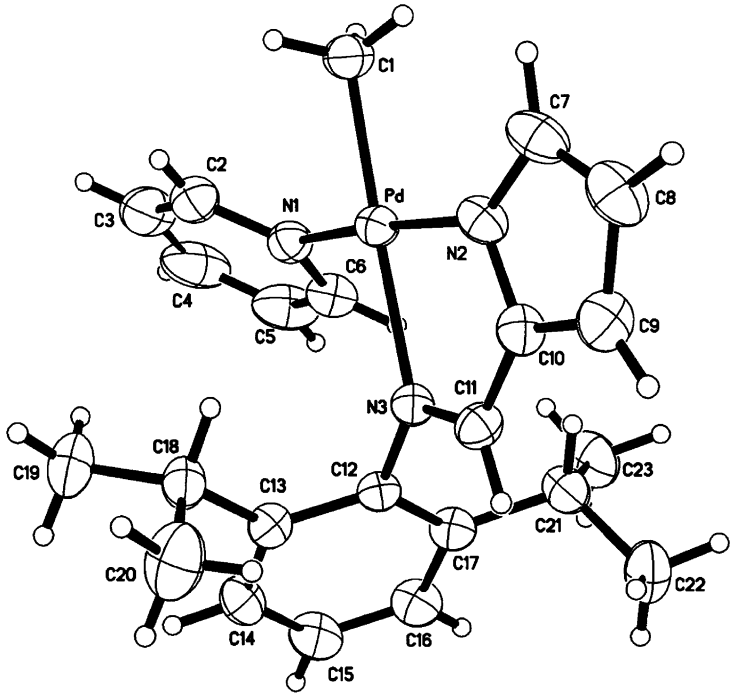

Fig. 2. ORTEP plot of the molecular structure of complex **4a**. Displacement ellipsoids are drawn at the 50% probability level.

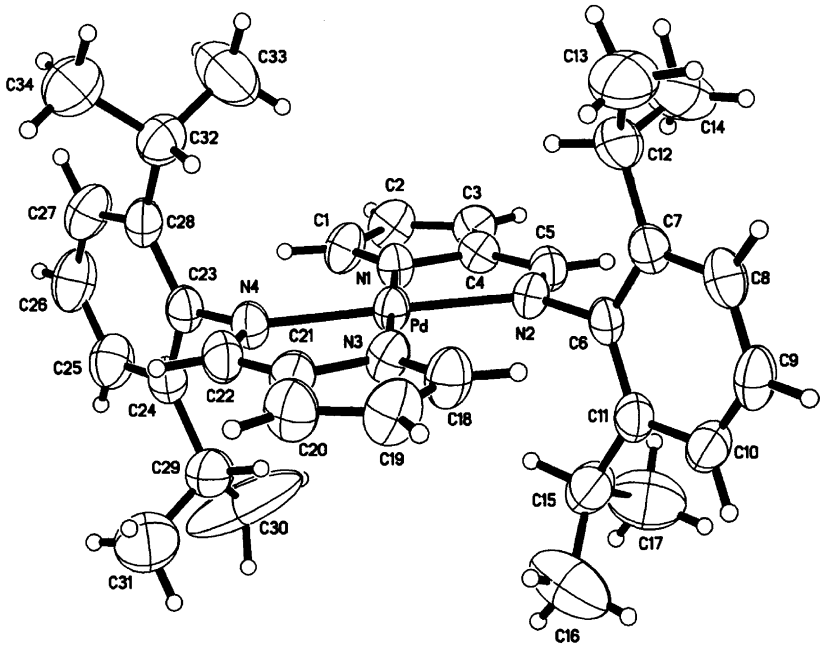

Fig. 3. ORTEP plot of the molecular structure of complex **5a**. Displacement ellipsoids are drawn at the 50% probability level.

the pyrrole group attached to Pd is in the position *trans* to the methyl ligand with a N1–Pd–C1 angle of 171.8(2)°, as shown in Fig. 1. While for **4a**, the 2,6-diisopropylbenzimine is at the position opposite to the methyl ligand with a N3–Pd–C1 angle of 172.86(10)°. The pyridine ligand lies *trans* to the pyrrole ligand through Pd with a N1–Pd–N2 angle of 174.50(9)°, as shown in Fig. 2. For **5a**, the two 2,6-diisopropylbenzimine ligands are *trans* to each other through Pd with a N4–Pd–N2 angle of 179.16(13)°, so are the two pyrrole ligands with a N1–Pd–N3 angle of 179.75(13)°, as shown in Fig. 3. From X-ray structural data by comparison of **3a** and **4a**, the Pd–C1 is sensitive to the nature of the *trans* ligand. The Pd–C1 length of **3a** is 2.022(7) Å and the Pd–C1 length of **4a** is shorter than that of **3a**, being 2.018(3) Å. This shows the ligand 2,6-diisopropylbenzimine has a stronger influence than the pyrrole ligand, according to Abu-Surrah et al. [31].

3.3. Polymerization of norbornene

Our main interest in the study of these complexes is their possible application as catalysts for the polymerization of norbornene and its derivatives. Preliminary experiments indicated that the single-component palladium complexes in the study, like single-component nickel complexes [14,15], are not able to catalyze norbornene polymerization, and MMAO alone is not able to catalyze norbornene polymerization too. From experiments, however, we found that these new neutral palladium complexes display high activities for norbornene polymerization when MMAO is used as a co-catalyst. Yet these catalysts do not work for polymerization of norbornene derivatives, which was not listed in this article.

Catalyst activities and polymer yields depended significantly on the reaction parameters applied to the polymerization of norbornene, as shown in Figs. 4–7. The concentration of norbornene should meet some requirements for good polymerization. In this system when the catalyst concentration reached 0.025 μmol/ml it did well, as shown in Fig. 4. Variation of molar ratio of MMAO to the catalyst **3c**, which is expressed here as the Al/Pd molar ratio, showed considerable effect on the polymerization reaction. When the mole ratio of Al/Pd

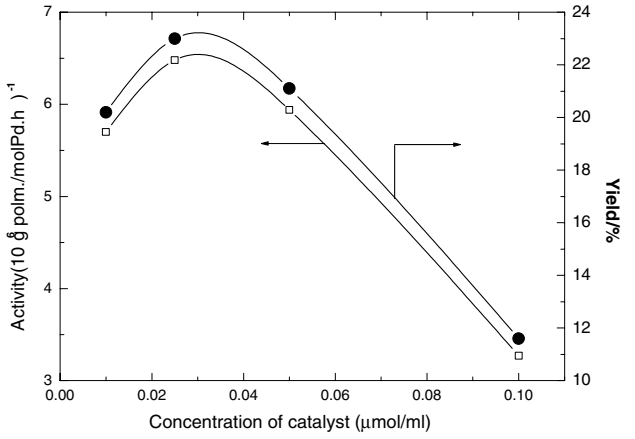

Fig. 4. Plot of polymer yield and catalytic activity versus catalyst concentration. **3a** as catalyst. $V_{total} = 20$ ml, polymerization reaction at 30 °C for 10 min.

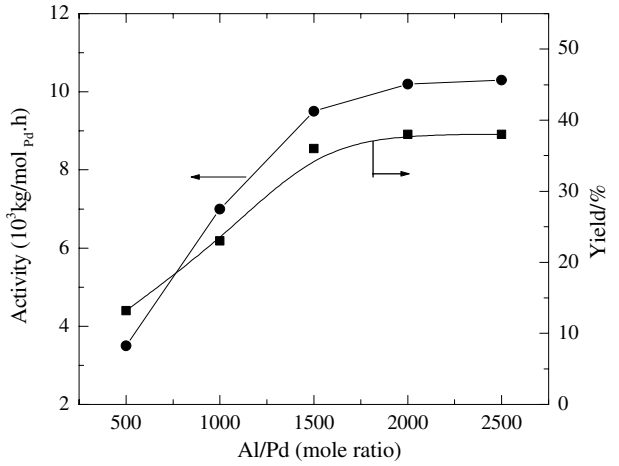

Fig. 5. Plot of polymer yield and catalytic activity versus Al/Pd molar ratio. $V_{total} = 20$ ml, polynorbornene/Pd = 50 000, catalyst (**3a**) = 0.5 μmol, polymerization reaction at 30 °C for 10 min.

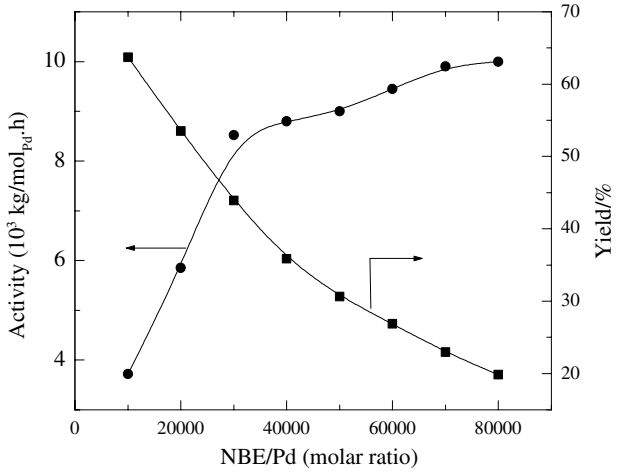

Fig. 6. Plot of polymer yield and catalytic activity versus norbornene/Pd molar ratio. $V_{total} = 20$ ml, catalyst (**3a**) = 0.5 μmol, Al/Pd = 1500, polymerization reaction at 30 °C for 10 min.

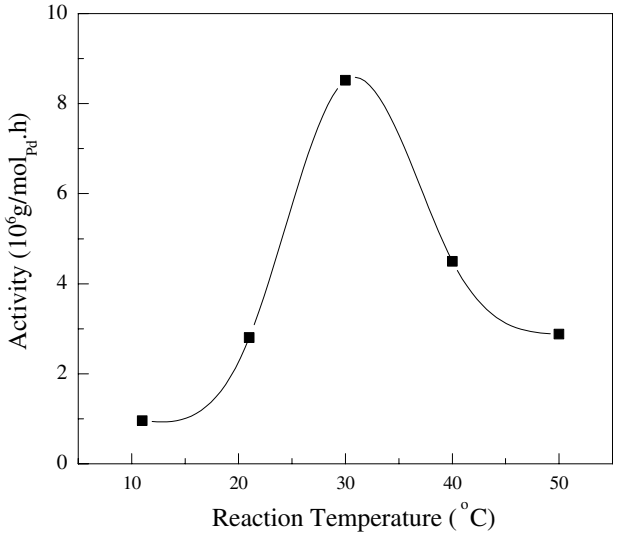

Fig. 7. Plot of polymer yield and catalytic activity versus reaction temperature (°C). $V_{total} = 11$ ml, catalyst (**8a**) = 0.5 μmol, Al/Pd = 2000, norbornene/Pd = 51 900, polymerization reaction at 30 °C for 10 min.

Table 3
Norbornene polymerizations catalysted with different neutral palladium complexes[a]

Entry	Catalyst	Al/Pd (molar ratio)	Yield (g)	Activity (10^6 g/mol$_{Pd}$ h)
1	**3a**	2000	0.14	1.68
2	**3b**	2000	0.23	2.76
3	**3c**	2000	0.22	3.00
4	**3d**	2000	0.25	2.64
5	**4a**	2000	0.32	3.84
6	**5a**	2000	0.13	1.56
7	**8a**	2000	0.71	8.52
8	**8b**	2000	0.47	5.64
9	**8c**	2000	0.26	3.12

[a] 0.5 μmol catalyst, 2.443 g norbornene, $V_{total} = 11$ ml, polymerization reaction for 10 min at 30 °C.

was 1500/1, the catalyst activity reached 1.01×10^7 g polym/mol$_{Pd}$ h, as shown in Fig. 5. On increasing the mole ratio of norbornene/Pd, while other conditions were kept constant, the catalyst activity of the catalyst **3c** grew, reaching 1.0×10^7 g polym/mol$_{Pd}$ h when the mole ratio of norbornene/Pd equalled 70 000, as shown in Fig. 6.

Meanwhile, the catalyst activity of the catalyst **8a** has been examined by varying the polymerization temperature, which is shown in Fig. 7. The catalyst activity first reached a peak and then gradually decreased with the increase of temperature, which means that to get high catalytic activity, polymerization reaction should be at the proper temperature.

The polymerization results using complexes **3a**–**d**, **4a**, **5a** and **8a**–**c** activated with MMAO are summarized in Table 3. From the results, we can see that the neutral palladium complexes bearing salicylaldiminato ligands displayed higher catalytic activities than those bearing pyrrole-imine chelate ligands. According to entries 1–4, with increasing the bulk in the *ortho* position of nitrogen atom of aniline, the polymerization activities decline, which means the bulkier the volumes of the substituents, the harder the insertion of norbornene. This is similar to some neutral nickel complexes [15].

The poly(norbornene)s obtained are insoluble in choloform, benzene, chlorobenzene, 1,2-dichlorobenzene, *N*,*N*-dimethylformamide and *N*,*N*-dimethylacetamide, which is different from polymers got with neutral nickel catalysts [14,15]. The molecular weights of the polymers obtained could not be determined because of their insolubility, which is similar to the result reported by Hu and co-workers [16]. FTIR analyses of the poly(norbornene)s were performed. In the range of 1600–1670 cm^{-1} no absorption is observed which means the catalytic polymerization is via vinyl addition

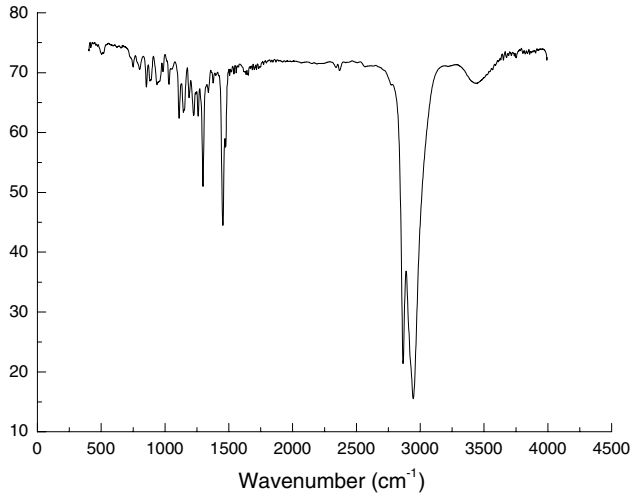

Fig. 8. FTIR spectrum of polynorbornene catalyzed by complex **3d**.

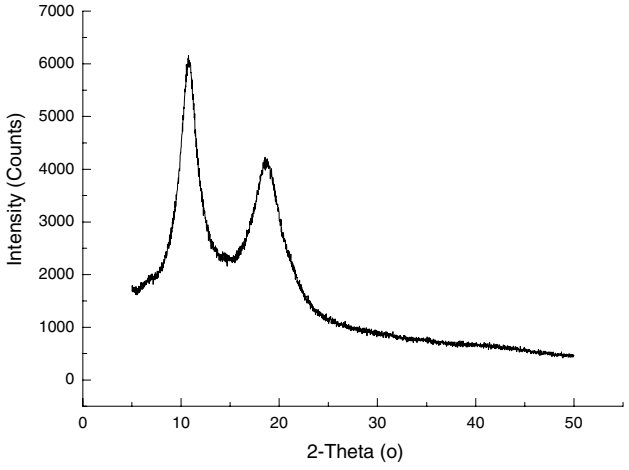

Fig. 9. WAXD plot of polynorbornene catalyzed by the catalyst **3d**.

polymerization, as shown in Fig. 8. WAXD has been employed to get information on the conformation of the polymer obtained. As shown in Fig. 9, we can see two peaks in the figure, 2θ equals 10.759 at peak 1, while 18.899 at peak 2. Haselwender et al. [41] and Zhao et al. [42] reported similar results which mean peak 1 is the reflection of the interchain or intersegment distance of the polymer, while peak 2 is the reflection of the intrachain distance. No traces of Bragg reflection, which is characteristic of a crystalline region were detected. Therefore, the polymer is non-crystalline.

4. Conclusions

In this article, several novel neutral palladium(II) complexes have been synthesized. The crystal structures of some of these complexes have been confirmed by X-ray analysis. High catalytic activities can be reached using these complexes activated with MMAO for vinyl-polymerization of norbornene. The complexes bearing salicylaldiminato ligands have more excellent activity than those bearing pyrrole-imine ligands for norbornene polymerization. IR analysis of the polymers identifies the polymerization is via vinyl addition mechanism. WAXD measurement implies the polymers are non-crystalline.

5. Supplementary material

Crystallographic data for the structures reported in this paper have been deposited at the Cambridge Crystallographic Data Center as supplementary publication numbers CCDC-219639, CCDC-219640 and CCDC-219641. Copies of the data can be obtained on application to: The Director, CCDC, 12 Union Road, Cambridge, CB2 1EZ, UK (fax: +44-1223-336-033; e-mail: deposit@ccdc.cam.ac.uk or www: http://www.ccdc.cam.ac.uk).

Acknowledgements

The authors are grateful for the financial support by Special Funds for Major State Basis Research Projects (No. G1999064801) from Ministry of Science and Technology of China.

References

[1] K.J. Ivin, J.C. Mol, in: Olefin Metathesis and Metathesis Polymerization, Academic Press, San Diego, CA, 1997, p. 407.
[2] R.H. Grubbs, in: Comprehensive Organometallic Chemistry, vol. 8, Pergamon, Oxford, 1982, p. 499.
[3] C. Janiak, P.G. Lassahn, J. Mol. Catal. A: Chem. 166 (2001) 193.
[4] J.P. Kennedy, H.S. Makowski, J. Macromol. Sci. Chem. 1 (1967) 345.
[5] N.G. Gaylord, B.M. Mandal, M. Martan, J. Polym. Sci. Polym. Lett. Ed. 14 (1976) 555.
[6] N.G. Gaylord, A.B. Deshpande, J. Polym. Sci. Polym. Lett. Ed. 14 (1976) 613.
[7] N.G. Gaylord, A.B. Deshpande, B.M. Mandal, M.J. Martan, Macromol. Sci. Chem. 11 (1977) 1053.
[8] F. Peruch, H. Cramail, A. Deffieux, Macromol. Chem. Phys. 199 (1998) 2221.
[9] C. Mast, M. Krieger, K. Dehnicke, A. Greiner, Macromol. Rapid Commun. 20 (1999) 232.
[10] W. Massa, N. Faza, H.C. Kang, C. Focke, W. Heitz, Acta Polym. 48 (1997) 432.
[11] M. Arndt, M. Gosmann, Polym. Bull. 41 (1998) 433.
[12] S. Brorkar, P.K. Saxena, Polym. Bull. 44 (2000) 167.
[13] A.O. Patil, S. Zushma, R.T. Stibrany, S.P. Pucker, L.M. Wheeler, J. Polym. Sci. Part A: Polym. Chem. 41 (2003) 2095.
[14] X.F. Li, Y.S. Li, J. Polym. Sci. Part A: Polym. Chem. 40 (2002) 2680.

[15] Y.S. Li, Y.R. Li, X.F. Li, J. Organomet. Chem. 667 (2003) 185.
[16] X. Mi, Z. Ma, L.Y. Wang, Y.C. Ke, Y.L. Hu, Macromol. Chem. Phys. 204 (2003) 868.
[17] U. Peucker, W. Heitz, Macromol. Rapid Commun. 19 (1998) 159.
[18] Q. Wu, Y.Y. Lu, J. Polym. Sci. Part A: Polym. Chem. 40 (2002) 1421.
[19] W. Kaminsky, A. Bark, M. Arndt, Makromol. Chem. Macromol. Symp. 47 (1991) 83.
[20] W. Kaminsky, A. Noll, Polym. Bull. 31 (1993) 175.
[21] W. Kaminsky, A. Bark, Polym. Int. 28 (1992) 251.
[22] W. Kaminsky, A. Bark, R. Steiger, J. Mol. Catal. 74 (1992) 109.
[23] E.P. Alt, W. Heitz, Macromol. Chem. Phys. 199 (1998) 1951.
[24] E.P. Alt, W. Heitz, Acta Polym. 49 (1998) 477.
[25] C. Tanielian, A. Kiennemann, T. Osparpucu, Can. J. Chem. 57 (1979) 2022.
[26] A. Sen, T.W. Lai, R.R. Thomas, J. Organomet. Chem. 368 (1988) 567.
[27] N. Seehof, C. Meher, S. Breuning, W. Risse, J. Mol. Catal. 76 (1992) 219.
[28] C. Mehler, W. Risse, Macromolecules 25 (1992) 4226.
[29] T.F.A. Haselwaander, W. Heitz, S.A. Krugel, J.H. Wendorff, Macromol. Chem. Phys. 197 (1990) 3435.
[30] B.S. Heinz, E.P. Alt, W. Heitz, Macromol. Rapid Commun. 19 (1988) 251.
[31] S.A. Abu-Surrah, K. Lappalainen, T. Repo, M. Klinga, M. Leskelä, H.A. Hodali, Polyhedron 19 (2000) 1601.
[32] A.S. Abu-Surrah, K. Lapppalainen, M. Kettunen, T. Repo, M. Leskelä, H.A. Hodali, B. Rieger, Macromol. Chem. Phys. 202 (2001) 599.
[33] T.F.A. Haselwander, W. Heitz, M. Maskos, Macromol. Rapid Commun. 18 (1997) 689.
[34] P.G. Lassahn, C. Janiak, J.S. Oh, Macromol. Rapid Commun. 23 (2002) 16.
[35] C. Mehler, W. Risse, Macromol. Rapid Commun. 12 (1991) 255.
[36] G.L. Tian, H.W. Boone, B.M. Novak, Macromolecules 34 (2001) 7656.
[37] L. Chatt, L.M. Vallarino, L.M. Venazi, J. Chem. Soc. (1957) 3413.
[38] E. Richard, R.I.M. Ernsting, A.L. Spek, C.J. Elsevier, P.W.N.M. van Leeuwen, K. Vrieze, Inorg. Chem. 32 (1993) 5769.
[39] G. Casiraghi, G. Casnati, G. Puglia, G. Sartori, G. Terenghi, J. Chem. Soc. Perkin I (1979) 1862.
[40] C. Wang, S. Friedrish, T.R. Younkin, R.H. Grubbs, Organometallics 17 (1998) 3149.
[41] T.F.A. Haselwander, W. Heize, S.A. Krügel, J.H. Wendorff, Macromol. Chem. Phys. 197 (1996) 3435.
[42] C.T. Zhao, M.R. Ribeiro, M.N. Pinho, V.S. Subrahmanyam, C.L. Gil, A.P. Lima, Polymer 42 (2001) 2455.

Available online at www.sciencedirect.com
SCIENCE DIRECT®
Polyhedron 23 (2004) 1629–1639
POLYHEDRON
www.elsevier.com/locate/poly

Molecular aggregates, zig-zag 2D-stairs, -ribbons and 3D-supramolecular networks of cyclic telluranes assisted by intermolecular Te···Cl and Te···Br secondary bonding

Prakash C. Srivastava [a,*], S. Bajpai [a], R. Lath [a], S.M. Bajpai [a], R. Kumar [a], Raymond J. Butcher [b]

[a] Department of Chemistry, Lucknow University, Lucknow 226007, India
[b] Chemistry Department, Howard University, Washington DC, WA 20059, USA

Received 31 December 2003; accepted 29 March 2004
Available online 5 May 2004

Abstract

The metathetical reactions of cyclic telluranes: $C_4H_8TeI_2$, $C_5H_{10}TeI_2$, $C_8H_8TeI_2$, with AgX (X = Cl, Br) yield $C_4H_8TeCl_2$ (**1**), $C_4H_8TeBr_2$ (**2**), $C_5H_{10}TeBr_2$ (**3**), $C_8H_8TeCl_2$ (**4**) and $C_8H_8TeBr_2$ (**5**). Reactions of $C_4H_8TeI_2$ or $C_8H_8TeI_2$ with $[Et_4N]CI$ give X-ray quality crystals of $C_4H_8TeCl_2$ (**1**) and $C_8H_8TeCl_2$ (**4**). The X-ray structures of **1**–**5** reveal that in each case the primary geometry around Te is distorted pseudo trigonal bipyramidal where two Cl or Br atoms are at the axial positions whereas the three equatorial positions are occupied by two $-CH_2-$ groups of the cycle and, apparently, one stereochemically active electron lone pair. The Te···Cl and Te···Br secondary bonds in **1**–**5** act as crystal structure directors yielding zig-zag 2D-stairs in **1** and zig-zag 2D-ribbons in **2**, trimeric molecular aggregates in **3** and 3D-supramolecular networks in **4** and **5**. The supramolecular associations of these cyclic telluranes **1**–**5** are compared with the supramolecular associations in their precursors and in acyclic telluranes.
© 2004 Published by Elsevier Ltd.

Keywords: Cyclic telluranes; Metathetical reactions; Intermolecular; Secondary bonding; Supramolecular networks

The concept of Te···X (X = Cl, Br, I, O, N, S) secondary bonds (non covalent interactions) was first coined by Alcock [1]. King et al. [2] described C–Te···X as 3c–4e bond in organotellurium compounds. The secondary bonds have now become a common place in organotellurium chemistry and the two important organizational tools in supramolecular chemistry are noncovalent interactions [3] and hydrogen bonds [4]. The design of organometallic supramolecular systems that can utilize these forces is a growing field [5]. King et al. [2] reviewed the supramolecular associations in organotellurium complexes formed through Te···S secondary bonds and Drake et al. [6], Dakternieks et al. [7] and others [8] utilized Te···S secondary bonds in the design of supramolecular associations in organotellurium dithio-carbamates, -carbonates and -phosphates. We are developing supramolecular organotellurium chemistry based on Te···X and C–H···O hydrogen bonds and recently we reported supramolecular associations induced by intermolecular Te···O [9] Te···I [10] and C–H···O hydrogen bonds [11] in acyclic and cyclic organotellurium compounds. However supramolecular associations through Te···Cl and Te···Br secondary bonds, to our knowledge, are restricted to only acyclic telluranes [12–16] and there is none on cyclic telluranes. De Matheus et al. [12] reported Te···Cl bonds in *cis*-[(4-$PhOC_6H_4)_2$ $TeCl(\mu\text{-}Cl)]_2$ and Bird et al. [13] reported Te···Br secondary bonds in *cis*- and *trans*-$[ArTeBr(\mu\text{-}Br)]_2$ and $[ArTeBr(\mu\text{-}I)]_2$ (Ar = 4-$MeOC_6H_4$ and 4-$EtOC_6H_4$). Alcock and Harrison [14] reported Te···Cl secondary bonds in Ph_2TeCl_2 and Te···Cl secondary bonds in Me_2TeCl_2 were reported by Ziolo and Troup [15] We reported Te···Br secondary bonds in Me_2TeBr_2 [16] and Chan and Einstein [17] reported corrugated sheets in Me_2TeI_2 through Te···I secondary

* Corresponding author. Tel.: +522-2358473.
E-mail address: pcsrivastava31@rediffmail.com (P.C. Srivastava).

0277-5387/$ - see front matter © 2004 Published by Elsevier Ltd.
doi:10.1016/j.poly.2004.03.019

bonds. We therefore, in the present study report the synthesis of cyclic telluranes $C_4H_8TeCl_2$ (**1**), $C_4H_8TeBr_2$ (**2**), $C_5H_{10}TeBr_2$ (**3**), $C_8H_8TeCl_2$ (**4**) and $C_8H_8TeBr_2$ (**5**) and describe the formation of trimeric molecular aggregates, zig-zag 2D-stairs, -ribbons and 3D-supramolecular networks in **1**–**5** through intermolecular Te···Cl and Te···Br secondary bonds. We also compare the supramolecular associations in **1**–**5** with the supramolecular associations present in their precursors ($C_4H_8TeI_2$, $C_5H_{10}TeI_2$ and $C_8H_8TeI_2$). It is observed that when I is replaced by Cl or Br, more or less, the nature of supramolecular associations remains almost the same. This is in contrast to the drastic modification of the nature of supramolecular associations in these cyclic telluranes when I is replaced by carboxylate groups [9]. We also observe that both cyclic telluranes (**1**–**5**) and acyclic telluranes viz. $(CH_3)_2TeX_2$ (X = Cl,Br,I) contain ordered supramolecular associations [15–17].

1. Results and discussion

The complexes (**1**–**5**) have been synthesized by metathetical reactions of ($C_4H_8TeI_2$ [18], $C_5H_{10}TeI_2$ [19a], $C_8H_8TeI_2$ [20]) with freshly prepared silver salts AgX (X = Cl, Br) or $[Et_4N]Cl$. Metathetical reactions with $[Et_4N]Cl$ have not been so far reported in case of organotellurium iodides. Moreover it is interesting to note that this method affords X-ray quality crystals, which are not obtained when exchange is carried out with silver salts. Previously solids of $C_4H_8TeCl_2$ and $C_4H_8TeBr_2$ have been obtained by the reduction of $C_4H_8TeI_2$ to C_4H_8Te(II) which is a pale yellow oil of repulsive odour and then subsequent reaction of C_4H_8Te(II) with chlorine or bromine [18]. $C_5H_{10}TeBr_2$ was obtained by Morgan and Burgess [19a] as a by-product in the reaction of Aluminium telluride and pentamethylene dibromide at 160–190 °C under 25–30 mm pressure. It was also obtained by Farrar and Gulland [19b] by the reaction of sodium telluride solution with pentamethylene dichloride then by addition of bromine and crystallisation of crude product from pet. ether. Solids of $C_8H_8TeCl_2$ and $C_8H_8TeBr_2$ were obtained by the reduction of $C_8H_8TeI_2$ to C_8H_8Te(II) and its subsequent reaction with SO_2Cl_2 or Br_2 [21]. $C_8H_8TeCl_2$ and $C_8H_8TeBr_2$ have also been synthesised through exchange reactions of $C_8H_8TeI_2$ with AgCl or AgBr and characterized through (^{13}C, ^{125}Te)NMR data only [22]. There is so far no X-ray structural report on these $C_4H_8TeCl_2$ (**1**), $C_4H_8TeBr_2$ (**2**), $C_5H_{10}TeBr_2$ (**3**), $C_8H_8TeCl_2$ (**4**) and $C_8H_8TeBr_2$ (**5**) compounds.

Important bond lengths and bond angles for **1**–**5** are listed in Tables 2–6. The crystal structures of **1**, **2** and **3** are shown in Figs. 1, 3 and 5 and their supramolecular associations are shown in Figs. 2, 4 and 6, respectively. The crystal structures of **4** and **5** are shown in Figs. 7 and 9 and their supramolecular associations are shown in Figs. 8 and 10, respectively.

1.1. Description of the structure of $C_4H_8TeCl_2$ (1)

In telluracyclopentane 1,1-dichloride (Table 2) (Fig. 1), of the four methylene groups in the heterocycle ($C_4H_8TeCl_2$), the two methylene carbon atoms of the C_4H_8 group are bonded to the Te(IV) atom with bond distances and bond angles; Te–C(1) = Te–C(4) = 2.13 Å, C(1)–Te–C(4) = 85.3°. The four closest atoms C(1), C(4), Cl(1), Cl(2) in the molecule provide a distorted trigonal bipyramidal geometry around Te atom with the chlorine atoms in the apical positions [Te–Cl(l) = 2.53 Å, Te–Cl(2) = 2.52 Å]. A stereochemically active electron lone pair apparently occupies the fifth coordination position in the equatorial plane. The Cl(2)–Te–Cl(1) angle of 174.16° deviates from linearity with the chlorine atoms pushed away from the equatorial electron lone pairs [9–11,23–25].

The monomeric unit of the molecule is symmetrically connected to its neighbouring molecule through Te···Cl (3.614 Å) secondary bonds to form the dimers. These dimers are connected together through Te···Cl (3.528 Å) secondary bonds to form zig-zag-2D stairs in b direction (Fig. 2) (Table 7). The Te···Cl distances (3.528, 3.614 Å) are shorter than the sum of van der Waals radii (4.00 Å) [26] and longer than the sum of covalent radii(2.34 Å) [27] and therefore they correspond to secondary bonds [1]. With the Te···Cl, secondary bonds, the alternate tellurium atom is hexa and hepta coordinated with an unshared electron pair at the vertex situated *trans* to one of the $-CH_2$ groups attached to tellurium (the secondary bond itself is in the *trans* position to one of the $-CH_2$ group attached to tellurium). The angles Cl(1A)–Te–C(l) and Cl(lA)–Te–C(4) are 76.4° and 157.0°, respectively, and angles Cl(2B)–Te–C(1) and Cl(2B)–Te–C(4) are 159.5° and 80.7°, respectively, in the molecule. We are not aware of any closely related molecule containing Te···CI secondary bonds responsible for supramolecular associations.

1.2. Description of the structure of $C_4H_8TeBr_2$ (2)

The structure of $C_4H_8TeBr_2$ (Table 3) (Fig. 3) comprises two molecules A and B, which are present as dimers. Of the four methylene groups in the heterocycle of $C_4H_8TeBr_2$, the two methylene carbon atoms of the C_4H_8 group are bonded to the Te(IV) atom with bond distances and bond angles; Te(l)–C(l1) = 2.14 Å, Te(l)–C(14) = 2.13 Å, C(11)–Te(1)–C(14) = 84.3° in molecule A and Te(2)–C(21) = 2.15 Å, Te(2)–C(24) = 2.15 Å, C(21)–Te(2)–C(24) = 85.0° in molecule B. The four closest atoms C(11), C(14), Br(12) and Br(1A) in molecule A and C(21), C(24), Br(22), Br(2A) in molecule B

Table 1
Crystal data and refinement details for compounds **1**–**5**

	1	**2**	**3**	**4**	**5**
Empirical formula	$C_4H_8TeCl_2$	$C_4H_8TeBr_2$	$C_{10}H_{20}Te_2Br_4$	$C_8H_8TeCl_2$	$C_8H_8TeBr_2$
Formula weight	254.60	343.52	715.10	302.64	391.56
Temperature (K)	293(2)	295(2)	296(2)	293(2)	293(2)
Crystal system	monoclinic	monoclinic	monoclinic	orthorhombic	orthorhombic
Space group	$P2_1/c$	$P2_1/n$	$C2/c$	$Fdd2$	$Fdd2$
a (Å)	6.6920(13)	12.2892(14)	17.361(7)	15.4362(16)	15.2871(15)
b (Å)	8.3770(17)	10.1427(12)	22.221(5)	11.2504(9)	11.6377(12)
c (Å)	13.342(3)	13.3238(15)	12.793(5)	11.3289(9)	11.7610(10)
α (°)	90	90	90	90	90
β (°)	90.59(3)	91.699(2)	130.288(18)	90	90
γ (°)	90	90	90	90	90
V (Å^3)	744.9(3)	1660.0(3)	3765(2)	1967.4(3)	2092.4(3)
Z	4	8	8	8	8
μ (mm^{-1})	4.600	13.114	11.570	3.502	10.422
Index ranges	$0 \leqslant h \leqslant 8, 0 \leqslant k \leqslant 10,$ $-17 \leqslant 1 \leqslant 17$	$-16 \leqslant h \leqslant 16, -13 \leqslant k \leqslant 13,$ $-17 \leqslant 1 \leqslant 16$	$0 \leqslant h \leqslant 22, 0 \leqslant k \leqslant 28,$ $-16 \leqslant 1 \leqslant 12$	$-20 \leqslant h \leqslant 20, -13 \leqslant k \leqslant 9,$ $-9 \leqslant 1 \leqslant 13$	$-23 \leqslant h \leqslant 0, -17 \leqslant k \leqslant 0,$ $-17 \leqslant 1 \leqslant 0$
Reflections collected	1847	18185	4452	2253	988
Independent reflections (R_{int})	1706 (0.0467)	4045 (0.0573)	4315 (0.0707)	868 (0.0336)	988 (0.0000)
Final R indices [$I > 2\sigma(I)$]	$R_1 = 0.0327, wR_2 = 0.0805$	$R_1 = 0.0612, wR_2 = 0.1983$	$R_1 = 0.0617, wR_2 = 0.1783$	$R_1 = 0.0293, wR_2 = 0.0783$	$R_1 = 0.0438, wR_2 = 0.0873$
R indices, (all data)	$R_1 = 0.0602, wR_2 = 0.0912$	$R_1 = 0.0956, wR_2 = 0.2161$	$R_1 = 0.1912, wR_2 = 0.2371$	$R_1 = 0.0304, wR_2 = 0.0790$	$R_1 = 0.0775, wR_2 = 0.0986$

Table 2
Important bond lengths (Å) and bond angles (°) for **1**

Bond lengths			
Te–C(l)	2.13(1)	Te–C(4)	2.13(1)
Te–Cl (2)	2.52(2)	Te–Cl(1)	2.53(2)
C(1)–C(2)	1.53(1)	C(2)–C(3)	1.50(1)
C(3)–C(4)	1.51(1)	Te···Cl (2B)	3.528
Te···Cl (1A)	3.614		
Bond angles			
C(1)–Te–C(4)	85.3(3)	C(1)–Te–Cl(2)	87.49(2)
C(4)–Te–Cl (2)	89.04(2)	C(1)–Te–Cl(1)	88.52(2)
C(4)–Te–Cl (1)	86.39(2)	Cl (2)–Te–Cl(1)	174.16(7)
C(2)–C(1)–Te	105.6(4)	C(3)–C(2)–C(1)	109.7(6)
C(2)–C(3)–C(4)	111.0(6)	C(3)–C(4)–Te	104.9(4)
Cl(1A)–Te–C(1)	76.4(2)	Cl(1A)–Te–C(4)	157.0
Cl(2B)–Te–C(1)	159.5(2)	Cl(2B)–Te–C(4)	80.7(2)
Cl(1A)–Te–Cl(1)	106.6(4)	Cl(1A)–Te–Cl (2)	76.6(2)
Cl(2B)–Te–Cl(1A)	112.8(3)	Cl (2B)–Te–Cl (2)	77.5(4)
Cl(2B)–Te–Cl(1)	105.3(2)		

Symmetry transformations used to generate equivalent atoms.

Table 3
Important bond lengths (Å) and bond angles (°) for **2**

Bond lengths			
Te(1)–C(11)	2.14(1)	Te(1)–C(14)	2.13(1)
Te(1)–Br(1A)	2.74(1)	Te(l)–Br(lB)	2.74(1)
Te(1)–Br(12)	2.77(2)	Te(2)–C(21)	2.15(1)
Te(2)–C(24)	2.15(2)	Te(2)–Br(2A)	2.74(1)
Te(2)···Br(22)	2.78(2)	Te(1)–Br(22)	3.656
Te(1A)···Br(12)	3.569	Te(2)···Br(lA)	3.836
Te(2A)···Br(22)	3.628		
Bond angles			
C(11)–Te(1)–C(14)	84.3(6)	C(14)–Te(1)–Br(1A)	95.9(1)
C(11)–Te(1)–Br(1A)	86.1(6)	C(14)–Te(1)–Br(12)	88.0(4)
C(11)–Te(1)–Br(12)	88.9(5)	C(14)–Te(1)–Br(22)	89.0(7)
C(11)–Te(1)–Br(1B)	87.3(5)	Br(1A)–Te(1)–Br(1B)	7.2(7)
Br(1A)–Te(1)–Br(12)	173.3(5)	Br(1B)–Te(1)–Br(12)	175.4(3)
C(24)–Te(2)–C(21)	85.0(6)	C(24)–Te(2)–Br(2A)	94.0(7)
C(21)–Te(2)–Br(2A)	88.0(5)	C(24)–Te(2)–Br(22)	87.3(4)
C(21)–Te(2)–Br(22)	87.9(4)	C(24)–Te(2)–Br(2B)	85.6(9)
C(21)–Te(2)–Br(2B)	88.0(5)	Br(2B)–Te(2)–Br(2A)	8.4(3)
Br(2B)–Te(2)–Br(22)	172.1(7)	Br(2A)–Te(2)–Br(22)	175.5(3)
Te(1A)–Br(12)–Te(1)	97.0(3)	Te(2)–Br(1A)–Te(1)	103.8(4)
Br(22)–Te(1)–C(11)	107.6(4)		

Symmetry transformations used to generate equivalent atoms.

provide a distorted TBP geometry around Te(l) and Te(2) atoms with the bromine atoms in the apical positions [Te(1)–Br(lA) = 2.74 Å, Te(l)–Br(12) = 2.77 Å in molecule A and Te(2)–Br(2A) = 2.74 Å, Te(2)–Br(22) = 2.78 Å in molecule B]. A stereochemically active electron lone pair apparently occupies the fifth coordination position in the equatorial plane. The Br(1A)–Te(l)–Br(12) angle of 173.3° in molecule A and Br (2A)–Te (2)–Br (22) angle of 175.5° in molecule B deviate from linearity with bromine atoms pushed away from the equatorial electron lone pair [9–11,23–25].

Molecule A is symmetrically connected to its neighbouring molecule through Te···Br (3.569 Å) secondary bonds and similarly molecule B is symmetrically connected to its neighbouring molecule through Te···Br (3.628 Å) secondary bonds to form the dimers. These dimers are asymmetrically connected through Te···Br (3.656, 3.836 Å) secondary bonds to form zig-zag ribbon in the a direction (Fig. 4) (Table 7). With the Te–Br secondary bonds, the coordination of each tellurium atom is octahedral with an unshared electron pair at the vertex situated *trans* to one of the $-CH_2$ group attached to tellurium (the secondary bond itself is in the *trans* position to the other $-CH_2$ group attached to tellurium). The angles Br(22)···Te(1)–C(14) and Br(22)···Te(l)–C(ll) are 89.0° and 107.6°, respectively, in molecule A and the angles Br(2B)···Te(2)–C(24) and Br(2B)···Te(2)–C(21) are 85.6° and 88.0°, respectively, in molecule B. Similar coordination environment for tellurium is found in $C_4H_8TeI_2$ [10a] and other organotellurium compounds [9–11,16] in which the unshared electron pair is *trans* to the organic group. The Te···Br distances (3.656, 3.628, 3.569, 3.836 Å) are shorter than the sum of van der Waals radii (4.15 Å) [26] and longer than the sum of covalent radii (2.51 Å) [27] and therefore correspond to secondary bonds [1]. The value of Te···Br secondary bonds is comparable to Te···Br secondary bonds present in 1-thia-4-telluracyclohexane, 4,4-dibromide ($C_4H_8STeBr_2$) [28].

1.3. Description of the structure of $C_5H_{10}TeBr_2$ (**3**)

The structure of $C_5H_{10}TeBr_2$ (Table 4) (Fig. 5) contains two independent molecules A and B. In each molecule the tellurium atom completes a cyclohexane ring with other five carbon atoms. The ring has chair conformation in both molecules due to the staggered situation of C–H bonds on neighbouring carbon atoms. In both molecules tellurium forms two normal bonds with the two neighbouring carbon atoms Te(1)–C(11) = 2.13 Å, Te(1)C(l5) = 2.16 Å, C(11)–Te(l)–C(l5) = 96.5° in molecule A and Te(2)–C(21A) = 2.17 Å, Te(2)–C(25A) = 2.17 Å, C(21A)–Te(2)–C(25A) = 96° in molecule B. Two axial bonds are formed with bromine atoms with bond distances Te(l)–Br(11) = 2.80 Å, Te(l)–Br(12) = 2.74 Å forming bond angle Br(1l)–Te(1)–Br(l2) = 175.93° in molecule A and Te(2)···Br(21) = 2.82 Å, Te(2)–Br(22) = 2.75 Å forming bond angle Br(21)–Te(2)–Br(22) = 176.52° in molecule B. The configuration around tellurium atom in both molecule A and molecule B approximates a distorted trigonal bipyramid with C(11), C(15) and unshared lone pair of electrons in equatorial position and Br(l1) and Br(12) in axial position in molecule A and C(21A), C(25A) and an unshared lone pair of electrons in equatorial positions and Br(21), Br(22) in axial positions in molecule B. The conformations adopted by the cyclohexane rings in the two molecules are same. The average C–C–C angles are 113° and 112.2°, respectively, in molecules A and B. The

Table 4
Important bond lengths (Å) and bond angles (°) for **3**

Bond lengths			
Te(1)–C(11)	2.13(4)	Te(1)–C(15)	2.16(4)
Te(1)–Br(12)	2.74(1)	Te(1)–Br(ll)	2.80(1)
Te(2)–C(21B)	2.17(2)	Te(2)–C(25A)	2.17(2)
Te(2)–C(25B)	2.17(2)	Te(2)–C(21A)	2.17(2)
Te(2)–Br(22)	2.75(5)	Te(2)–Br(21)	2.82(1)
C(11)–C(12)	1.55(4)	C(12)–C(13)	1.54(5)
C(13)–C(14)	1.51(4)	C(14)–C(15)	1.49(5)
C(21A)–C(22A)	1.52(2)	C(22A)–C(23A)	1.52(2)
C(23A)–C(24A)	1.53(2)	C(24A)–C(25A)	1.52(2)
C(21B)–C(22B)	1.52(2)	C(22B)–C(23B)	1.52(2)
C(23B)–C(24B)	1.52(2)	C(24B)–C(25B)	1.52(2)
Te(l)···Br(21)	3.645	Te(2A)···Br(12)	3.778
Bond angles			
C(ll)–Te(1)–C(15)	96.5(1)	C(11)–Te(1)–Br(12)	91.7(11)
C(15)–Te(1)–Br(12)	87.6(1)	C(11)–Te(1)–Br(11)	89.9(11)
C(15)–Te(1)–Br(11)	88.5(1)	Br(12)–Te(1)–Br(11)	175.93(2)
C(21B)–Te(2)–C(25A)	84(2)	C(21B)–Te(2)–C(25B)	94(2)
C(25A)–Te(2)–C(25B)	13(3)	C(21B)–Te(2)–C(21A)	12(2)
C(25A)–Te(2)–C(21A)	96.0(2)	C(25B)–Te(2)–C(21A)	105.2(2)
C(21B)–Te(2)–Br(22)	84(2)	C(25A)–Te(2)–Br(22)	80(3)
C(25B)–Te(2)–Br(22)	90.3(2)	C(21A)–Te(2)–Br(22)	87.8(1)
C(21B)–Te(2)–Br(21)	93(2)	C(25A)–Te(2)–Br(21)	97(3)
C(25B)–Te(2)–Br(21)	87.2(2)	C(2 I A)–Te(2)–Br(21)	90.5(1)
Br(22)–Te(2)–Br(21)	176.52(2)	C(12)–C(11)–Te(1)	115(2)
C(13)–C(12)–C(11)	111(3)	C(14)–C(13)–C(12)	113(3)
C(15)–C(14)–C(13)	116(3)	C(14)–C(15)–Te(1)	114(2)
C(22A)–C(21A)–Te(2)	112(3)	C(23A)–C(22A)–C(21A)	112.8(2)
C(22A)–C(23A)–C(24A)	112.8(2)	C(23A)–C(24A)–C(25A)	112.8(2)
C(24A)–C(25A)–Te(2)	112(3)	C(22B)–C(21B)–Te(2)	124(4)
C(21B)–C(22B)–C(23B)	112.8(2)	C(24B)–C(23B)–C(22B)	112.8(2)
C(23B)–C(24B)–C(25B)	112.8(2)	C(24B)–C(25B)–Te(2)	107(6)

Symmetry transformations used to generate equivalent atoms.

Table 5
Important bond lengths (Å) and bond angles (°) for **4**

Bond lengths			
Te–C(1)#1	2.10(7)	Te–C(1)	2.10(7)
Te–Cl	2.54(1)	Te–Cl(1)#1	2.54(1)
C(1)–C(2)	1.51(1)	C(2)–C(3)	1.39(1)
C(2)–C(2)#1	1.42(1)	C(3)–C(4)	1.38(1)
C(4)–C(4)#1	1.45(2)	Te···Cl	3.495
Bonds angles			
C(1)#1–Te–C(1)	87.5(4)	C(1)#1–Te–Cl	87.2(2)
C(1)–Te–Cl	86.8(2)	C(1)#1–Te–Cl#1	86.8(2)
C(1)–Te–Cl#1	87.2(2)	Cl–Te–Cl#1	171.63(1)
C(2)–C(1)–Te	106.8(4)	C(3)–C(2)–C(2)#1	120.1(5)
C(3)–C(2)–C(1)	120.4(6)	C(2)#1–C(2)–C(1)	119.5(3)
C(4)–C(3)–C(2)	120.4(8)	C(3)–C(4)–C(4)#1	119.5(5)

Symmetry transformations used to generate equivalent atoms.
#1: $-x, -y, z$.

Table 6
Important bond lengths (Å) and bond angles (°) for **5**

Bond lengths			
Te–C(l)	2.13(1)	Te–C(l)#l	2.13(1)
Te–Br	2.70(9)	Te–Br#1	2.70(9)
C(1)–C(2)	1.51(2)	C(2)–C(2)#1	1.40(2)
C(2)–C(3)	1.40(2)	C(3)–C(4)	1.37(2)
C(4)–C(4)#1	1.45(3)	Te···Br	3.547
Bond angles			
C(1)–Te–C(1)#1	86.6(6)	C(1)–Te–Br	88.1(3)
C(l)#1–Te–Br	88.0(3)	C(1)–Te–Br#l	88.0(3)
C(1)#1–Te–Br#1	88.1(3)	Br–Te–Br#1	174.67(5)
C(2)–C(1)–Te	106.1(7)	C(2)#1–C(2)–C(3)	120.4(8)
C(2)# 1–C(2)–C(1)	120.6(5)	C(3)–C(2)–C(1)	119.0(9)
C(4)–C(3)–C(2)	19.7(1)	C(3)–C(4)–C(4)#1	119.8(8)

Symmetry transformations used to generate equivalent atoms.
#1: $-x, -y, z$.

three carbon atoms at the other end of $C_5H_{10}TeBr_2$ cyclohexane ring make an angle C(12)–C(13)–C(14) = 113.3° in molecule A and angle C(22A)–C(23A)–C(24A) = 112.8° in molecule B. The $C_5H_{10}TeBr_2$ in solid state has chair conformation in which part of the ring is flattened and a part is considerably puckered in perfect agreement with the conformation predicted by Lambert and Keske [29] through $R = J_{trans}/J_{cis}$ values (1.5, 3.6) in NMR spectrum of $C_5H_{10}TeBr_2$ in solution.

The Te···Br intermolecular interactions are presented in Fig. 6. Te(l) of molecule A forms secondary bonds with Br(21) of molecule B and Br(12) of the same molecule is connected to the Te(2A) of other adjacent

Table 7
Comparative X-ray structural data and supramolecular associations of precursors and **1–5**

Compound	Te–C	Te–X	Te···X	∠XTeX	∠CTeX	∠CTeC	Supramolecular association	Reference
$C_4H_8TeI_2$	2.14–2.16	2.87–2.97	3.69–3.99	176.48–177.62	88.00–92.00	84.00–84.50	zig-zag 2D-ribbons	[10a]
$C_4H_8TeBr_2$ (**2**)	2.13–2.14	2.74–2.78	3.57–3.84	172.10–175.50	85.60–95.90	84.30–85.00	zig-zag 2D-ribbons	present work
$C_4H_8TeCl_2$ (**1**)	2.13	2.52–2.53	3.53–3.61	174.16	86.39–89.04	85.30	zig-zag 2D-stairs	present work
$C_5H_{10}TeI_2$	2.13–2.16	2.85–3.01	3.87–4.06	176.79–177.66	87.30–91.60	95.30–98.10	trimeric molecular aggregates	[10a]
$C_5H_{10}TeBr_2$ (**3**)	2.13–2.17	2.74–2.82	3.65–3.78	175.93–176.52	80.00–97.00	84.00–105.20	trimeric molecular aggregates	present work
$C_8H_8TeI_2$	2.17	2.90	3.66–3.67	179.49	89.10–90.50	84.70	3D-supramolecular networks	[10a]
$C_8H_8TeBr_2$ (**5**)	2.13	2.70	3.55	174.67	88.00–88.10	86.60	3D-supramolecular networks	present work
$C_8H_8TeCl_2$ (**4**)	2.10	2.54	3.49	171.63	86.80–87.20	87.50	3D-supramolecular networks	present work

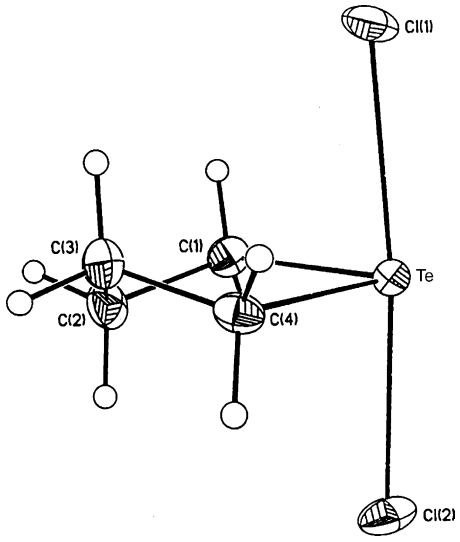

Fig. 1. Crystal structure of **1**.

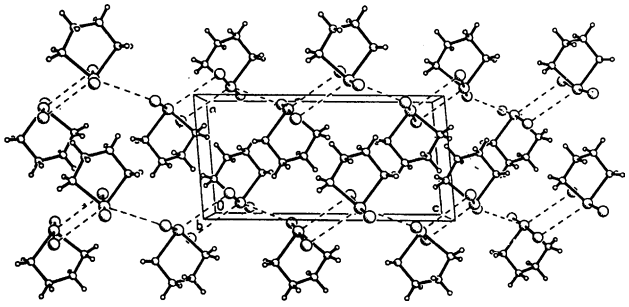

Fig. 2. Zig-zag 2-dimensional stairs for **1** in the b direction linked by Te···Cl secondary bonds.

molecule of $C_5H_{10}TeBr_2$, with bond distances Te(l)–Br(21) = 3.645 Å and Te(2A)–Br(12) = 3.778 Å (Table 4). In this way Te···Br secondary bonds form trimeric molecular aggregates (Table 7).

Despite our repeated crystallizations by varying different solvents and temperatures it was not possible to obtain X-ray quality crystals of $C_5H_{10}TeCl_2$. Among telluracyclohexane derivatives, the X-ray structure of $C_5H_{10}TeBr_2$, in the present investigation, is second one (earlier we reported the first X-ray structure of $C_5H_{10}TeI_2$ [10a] of telluracyclohexane series).

*1.4. Description of the structure of $C_8H_8TeCl_2$ (**4**)*

The X-ray structure analysis of $C_8H_8TeCl_2$ (Table 5) (Fig. 7) reveals it to have a distorted TBP geometry about the Te(IV) atom. Two axial positions are occupied by two chlorine atoms with the same bond length Te–Cl = 2.54 Å. The two methylene carbon atoms are bonded to the tellurium atom with equal Te–C bond lengths of 2.10 Å and bond angles; C(l)#l–Te–C(1) = 87.5°, C(1)#l–Te–Cl = 87.2°, C(1)–Te–Cl = 86.8°

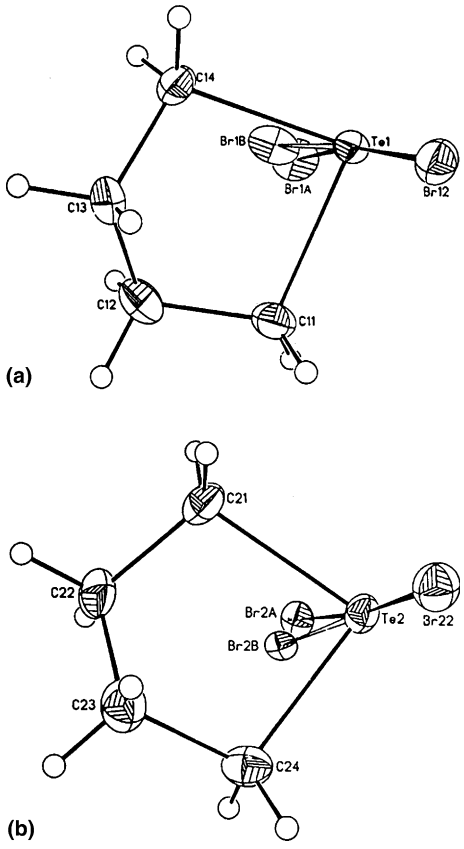

Fig. 3. Crystal structure of **2**.

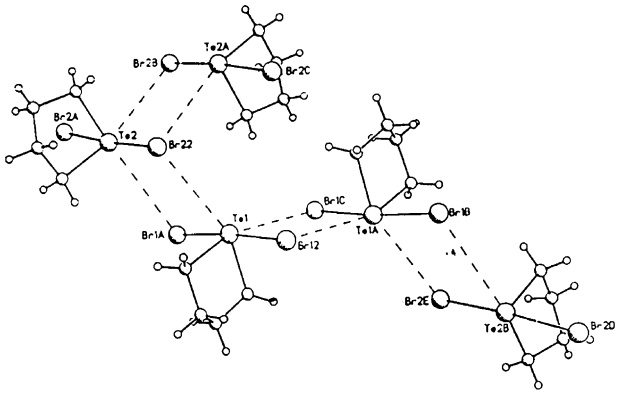

Fig. 4. Zig-zag 2-dimensional ribbon for **2** in the a direction linked by Te···Br secondary bonds.

(Table 5). The fifth coordination position in the equatorial plane is apparently, occupied by a stereochemically active electron lone pair. The bond angle Cl–Te–Cl#1 of 171.63° deviates considerably from linearity with both chlorine atoms pushed away from the equatorial lone pair of electrons [9–11,23–25].

In the unit cell, the molecules of $C_8H_8TeCl_2$ are interlinked through Te···Cl (3.495 Å) secondary bonds and leads to the formation of a three dimensional supramolecular networks in which hexa- and hepta-coordinated telluriums are present. The 3D- supramolecular networks are further assisted by cooperative participation of lesser known weak $C(sp^2)$–H···Cl hydrogen bonds [10b,11,30] (C–H = 0.93 Å, H···Cl = 2.89 Å, C···Cl = 3.802(8) Å, ∠CHCl = 165.9°) (Fig. 8).

*1.5. Description of the structure of $C_8H_8TeBr_2$ (**5**)*

The X-ray structure analysis of $C_8H_8TeBr_2$, (Table 6) (Fig. 9) reveals that the C_8H_8 group is symmetrically bonded to the Te(IV) atom with two same Te–CH_2 bond lengths of 2.13 Å. The coordination geometry formed by the four closest atoms C(1), C(1)#1, Br, Br#1 is approximately trigonal bipyramidal. The Br atoms are at the apical positions with the same Te–Br bond lengths of 2.70 Å and the two carbon atoms in the equatorial plane are bonded through the bond angles C(1)–Te–C(l)#l = 86.6°, C(1)–Te–Br#1 = 88.0°, C(1)–Te–Br = 88.1°. A stereochemically active electron lone pair apparently shares the fifth coordination position, in the equatorial plane. The Br–Te–Br#l angle of 174.67° deviates considerably from linearity with both bromine atoms pushed away from the equatorial tellurium lone pair of electrons [9–11,23–25].

In the unit cell (Fig. 10), the molecules of $C_8H_8TeBr_2$ are interconnected through Te···Br (3.547 Å) secondary bonds and lead to the formation of a three dimensional supramolecular network in which hexa and hepta coordinated tellurium are present.

On comparing the supramolecular associations present in $C_8H_8TeCl_2$, $C_8H_8TeBr_2$ with those present in $C_8H_8TeI_2$ [10a] (Te···I = 3.66–3.67 Å), it is observed that the three dimensional supramolecular networks assisted by Te···Cl, Te···Br and Te···I secondary bonds are present in $C_8H_8TeCl_2$, $C_8H_8TeBr_2$ and $C_8H_8TeI_2$. The Te···X (X = Cl, Br, I) secondary bond lengths follow the order Te···I > Te···Br > Te···CI (Table 7).

We conclude that by the replacement of iodine in the precursors ($C_4H_8TeI_2$, $C_5H_{10}TeI_2$, $C_8H_8TeI_2$) with bromine or chlorine the nature of the the supramolecular association remains almost the same in $C_4H_8TeCl_2$ (**1**), $C_4H_8TeBr_2$ (**2**), $C_5H_{10}TeBr_2$ (**3**), $C_8H_8TeCl_2$ (**4**), $C_8H_8TeBr_2$ (**5**) which is obvious as in all these the crystal structure directors are Te···halogen (X) [X = I, Br, Cl] secondary bonds (Table 7). This is contrary to the earlier perceptions that the intermolecular bonding decreases as one goes from iodides to bromides to chlorides in organotellurium halides [28]. The retention of more or less same type of supramolecular association in **1**–**5** vis a vis the supramolecular associations in their precursors is also in contrast to the drastic modification of supramolecular associations when I is replaced in $C_4H_8TeI_2$ (2D-zig-zag ribbons), $C_5H_{10}TeI_2$ (trimeric molecular aggregates) and $C_8H_8TeI_2$ (3D-supramolecular networks) with $OCOC_6H_5$ group [C_4H_8Te-$(OCOC_6H_5)_2$

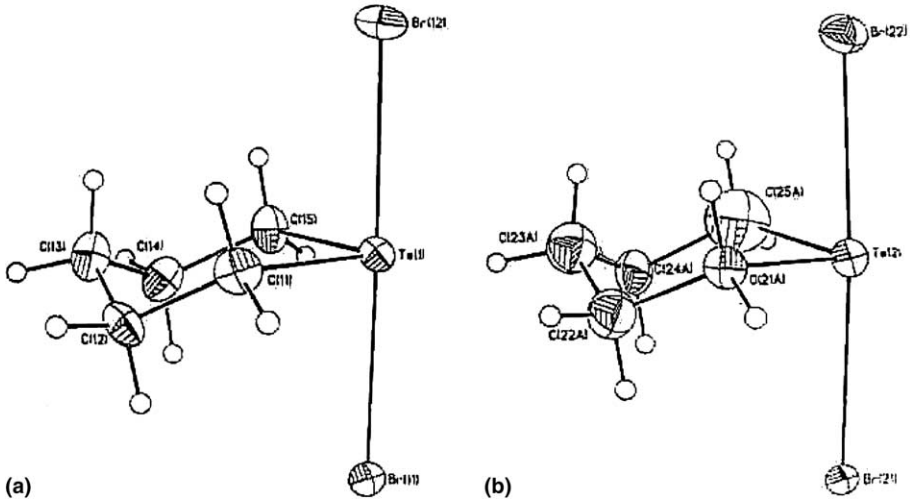

Fig. 5. Crystal structure of **3**.

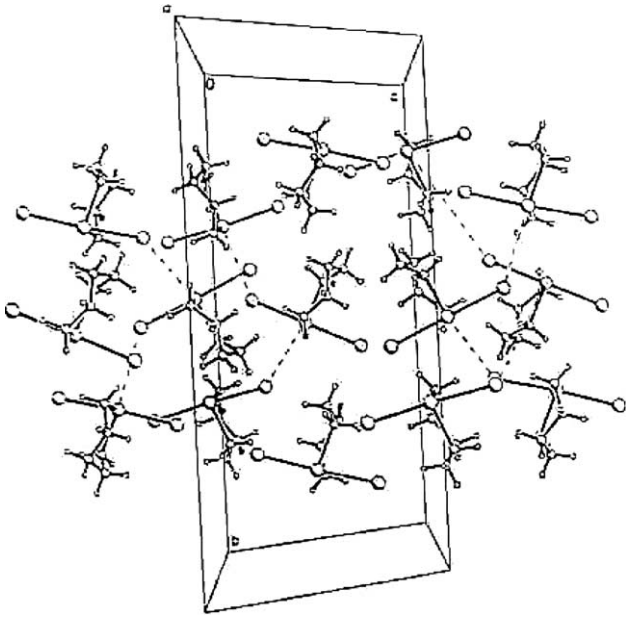

Fig. 6. Trimeric molecular aggregates of **3** linked by Te···Br secondary bonds.

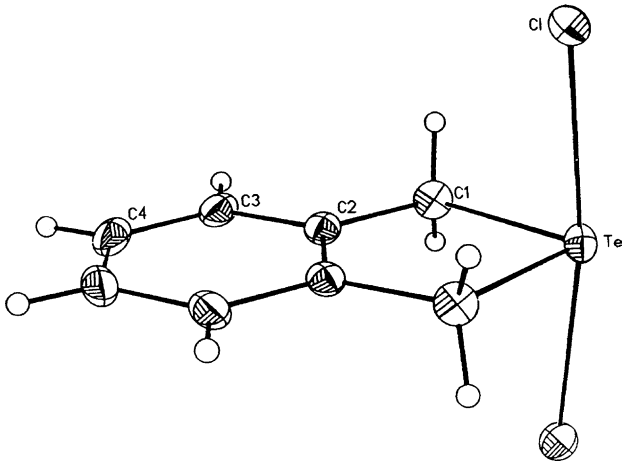

Fig. 7. Crystal structure of **4**.

(polymeric zig-zag chains), $C_5H_{10}Te$- $(OCOC_6H_5)_2$ (polymeric zig-zag chains) and $C_8H_8Te(OCOC_6H_5)_2$ (stairs)] [9a,9c].

1.6. Comparative supramolecular associations in cyclic telluranes and acyclic telluranes

In the past the supramolecular associations in simplest acyclic telluranes viz. Me_2TeI_2, Me_2TeBr_2 and Me_2TeCl_2 were not discussed properly. For example in Me_2TeCl_2 only Te···Cl secondary bonds were discussed [15] and in Me_2TeBr_2 only Te···Br secondary bonds were quoted by us [16] while in Me_2TeI_2 the

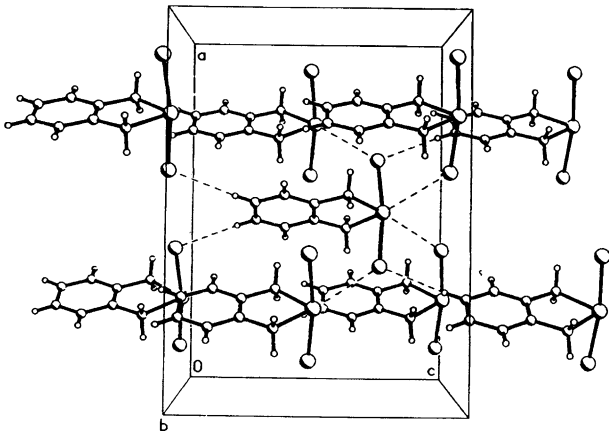

Fig. 8. Dimensional network of **4** linked by Te···Cl secondary bonds and weak $C(sp^2)$–H···Cl hydrogen bonds.

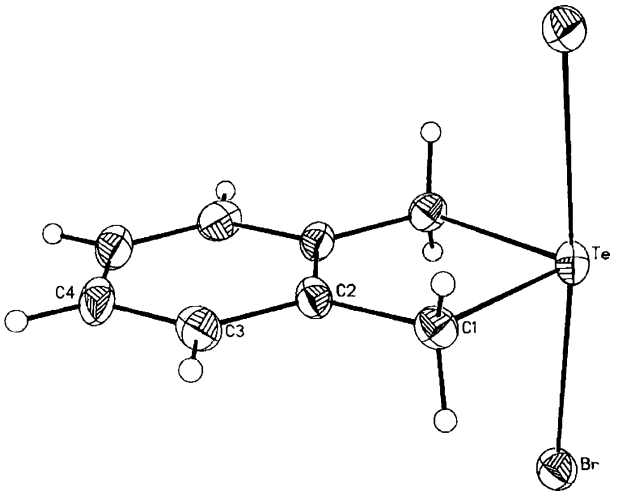

Fig. 9. Crystal structure of **5**.

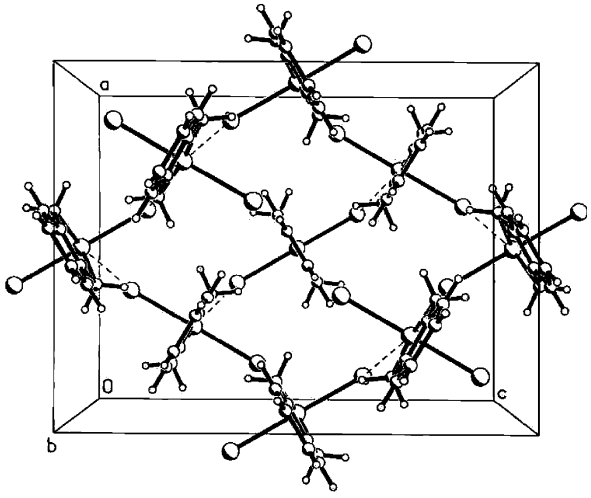

Fig. 10. Dimensional network of **5** linked by Te···Br secondary bonds and weak C(sp^2)–H···Br hydrogen bonds.

Te···I secondary bonds (3.65–4.02 Å) were quoted resulting in corrugated sheets type of supramolecular associations [17]. On the closer look at the X-ray structure of Me_2TeCl_2 [15] and its connectivity with other molecules it is apparent that Me_2TeCl_2 molecules are interconnected through Te···Cl secondary bonds (3.41–3.47 Å) resulting in zig-zag chain type supramolecular associations in Me_2TeCl_2. In our report on Me_2TeBr_2 [16] we did not discuss the supramolecular association in Me_2TeBr_2 but it is evident that Me_2TeBr_2 molecules are interconnected through Te–Br secondary bonds. (3.54–3.62 Å) resulting in dimers and these dimers are interconnected through Te···Br secondary bonds resulting in tetranuclear species (Fig. 11).

In summary, in the present investigation we have, for the first time, been successful in utilizing Te···Cl, Te···Br secondary bonds in the formation of a variety of supramolecular associations in cyclic telluranes (**1**–**5**)

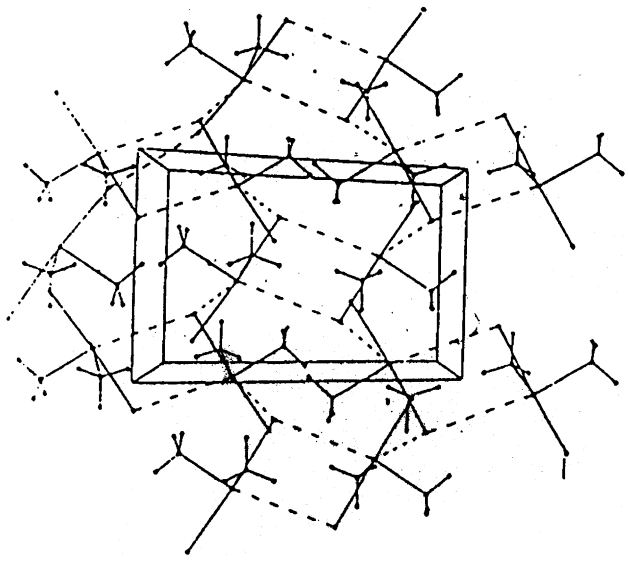

Fig. 11. Tetranuclear species of Me_2TeBr_2 linked by Te···Br secondary bonds.

which they do in almost the same way as Te···I secondary bonds do. Overall Te···X (X = Cl, Br, I) secondary bonds act as crystal structure directors resulting in ordered supramolecular associations in cyclic telluranes. These supramolecuar associations are significantly different from the supramolecular associations in cyclic telluranes where Te···O secondary bonds act as crystal structure directors. When cyclic systems attached to tellurium are changed to acyclic systems while the ligand is halide group, the pattern of the supramolecular association is again changed.

On the basis of the above available data (just about a dozen X-ray structures, considered in the present investigation) it is difficult to make any general comment but it appears that both (a) the organic group attached to tellurium and (b) the ligand attached to tellurium contribute and largely determine the nature and pattern of the supramolecular associations in organotellurium compounds and, for deeper insight into these aspects of supramolecular chemistry, the study prompts further researches in the area.

2. Experimental

1,4-diiodobutane, 1,5-diiodopentane, α,α′-dibromoxylene, Te metal and NaI were procured from Aldrich and used as such. 2-Methoxyethanol, benzene and acetone were purified and dried by standard procedures. The (precursors) cyclic telluranes viz. $C_4H_8TeI_2$ [18] (reaction of 1,4-diiodobutane with Te metal in the temperature range 130–140 °C), $C_5H_{10}TeI_2$ [19a] (reaction of 1,5-diiodopentane with Te metal at 150 °C) and $C_8H_8TeI_2$ [20] (reaction of α,α′-dibromoxylene, Te metal and NaI in 2-methoxyethanol at 100–110 °C) were

prepared by the literature methods. The complexes (**1**–**5**) were synthesized by the metathetical reactions of these cyclic telluranes with freshly prepared AgX(X = Cl, Br) or commercially procured $[Et_4N]Cl$ (Aldrich). The actual experimental work up and characterization data of each complexes (**1**–**5**) is given below.

2.1. Preparation of the compounds

2.1.1. 1,1,2,3,4,5-hexahydro-l,1-dichlorotellurophene, $C_4H_8TeCl_2$ (*1*)

$C_4H_8TeI_2$ (1g, 2.28 mmol) and $[Et_4N]Cl$ (0.76g, 4.56 mmol) were refluxed in dry chloroform (40 cm^3) for 5 h. The insoluble material was filtered off and the filtrate was reduced to ~15 cm^3. To the filtrate was added petroleum ether (60–80 °C). Yellow solid separated which on recrystallisation with acetone: pet. ether (60–80 °C) (1:1) solvent mixture twice gave dull white crystals of $C_4H_8TeCl_2$. [Yield: 0.07 g (12%) based on $C_4H_8TeI_2$], m.p. 120 °C. $C_4H_8Cl_2Te$ (M = 254.60) requires: C, 18.85; H, 3.14; Te, 50.11. Found: C, 18.80; H, 3.12; Te, 50.08%. ^1H NMR spectrum (in $CDCl_3$+DMSO-d_6 at 60 MHz): $\delta = 4.02$ m (4H, $TeCH_2$–); $\delta = 3.22$ m (4H, CCH_2–). The insoluble material on analysis, did not correspond to expected anionic complex $[Et_4N]^+[C_4H_8TeI_2Cl]^-$. The reaction of $C_4H_8TeI_2$ with AgCl (1:2 molar ratio) in chloroform did not give X-ray quality crystals of **1**.

2.1.2. 1,1,2,3,4,5-hexahydro-l,1-dibromotellurophene, $C_4H_8TeBr_2$ (*2*)

To an acetone solution (30 cm^3) of $C_4H_8TeI_2$ (2 g, 4.57 mmol) was added freshly prepared AgBr (1.72 g, 9.15 mmol). The mixture was stirred at room temperature for 2 h and filtered to remove AgI and unreacted AgBr. The filtrate was concentrated to give yellow solid, which on recrystallisation with acetone twice and on slow evaporation after 24 h yielded orange square crystals of $C_4H_8TeBr_2$. Yield: 0.70 g (45%), m.p. 100 °C. $C_4H_8Br_2Te$ ($M = 343.6$) requires: C, 13.96; H, 2.32; Te, 37.13. Found: C, 13.88; H, 2.21; Te, 37.02%. ^1H NMR spectrum (in $CDCl_3$ + DMSO-d_6 at 60 MHz): $\delta = 3.78$ m (4H, $TeCH_2$); $\delta = 2.90$ m (4H, CCH_2–).

2.1.3. 1,1,2,3,4,5,6-heptahydro-1,1-dibromotellurane, $C_5H_{10}TeBr_2$ (*3*)

To an acetone solution (30 cm^3) of $C_5H_{10}TeI_2$ (1.18 g, 2.61 mmol) was added freshly prepared AgBr (0.98 g, 5.25 mmol). The mixture was stirred at room temperature for 3 h and filtered to remove AgI and unreacted AgBr. The filtrate was concentrated under reduced pressure. A layer of petroleum ether (40–60 °C) was laid. Yellow needle shaped crystals were obtained after 24 h, which corresponded to $C_5H_{10}Br_2Te$. Yield: 0.16g (17%), m.p. 72 °C. $C_5H_{10}Br_2Te$ ($M = 357.6$) requires: C, 16.77; H, 2.79; Te, 35.68. Found: C, 16.65; H, 2.75; Te, 35.62% ^1H NMR spectrum (in $CDCl_3$ at 300 MHz): $\delta = 3.66$ t (4H, $TeCH_2$–); $\delta = 2.21$ m (4H, CCH_2–); $\delta = 1.90$ m (2H, CCH_2CH_2).

2.1.4. 1,3-Dihydro-2-λ^4-benzotellurole-2,2-diyl dichloride, $C_8H_8TeCl_2$ (*4*)

$C_8H_8TeI_2$ (2 g, 4.12 mmol) and $[Et_4N]Cl$ (1.36 g, 8.24 mmol) were refluxed in dichloromethane (20 cm^3) for 4 h. The insoluble material was filtered off and filtrate reduced to ~5 cm^3 when pale yellow crystals of $C_8H_8TeCl_2$ (**4**) [Yield: 0.30 g (24%) based on $C_8H_8TeI_2$]; m.p. 180 °C. $C_8H_8Cl_2Te$ ($M = 302.6$) requires: C, 31.72; H, 2.64; Te, 42.16. Found: C, 31.68; H, 2.44; Te, 42.12%. ^1H NMR spectrum (in $CDCl_3$ at 300 MHz): $\delta = 5.07$ m (4H, $TeCH_2$–); $\delta = 7.32$ m (4H, C_6H_4) (and black crystals m.p. 140 °C) appeared. The NMR (^1H, ^{13}C, ^{125}Te) analysis of black crystals in DMSO did not correspond to the expected $[Et_4N]^+[C_8H_8TeI_2Cl]^-$ complex. The reaction of $C_8H_8TeI_2$ with AgCl (1:2 molar ratio) in dichloromethane did not give X-ray quality crystals of **4**.

2.1.5. 1,3-Dihydro-2-λ^4-benzotellurole-2,2-diyl dibromide, $C_8H_8TeBr_2$ (*5*)

$C_8H_8TeI_2$ (2 g, 4.12 mmol) and AgBr (1.56 g, 8.30 mmol) were stirred in acetone (30 cm^3) for 4 h. The precipitated AgI and unreacted AgBr were filtered off and the excess solvent was distilled off to give pale yellow needles of $C_8H_8TeBr_2$. Yield: 0.60 g (37%). m.p. 250 °C dec. $C_8H_8Br_2Te$ ($M = 391.6$) requires: C, 24.51; H, 2.04; Te, 32.58. Found: C, 24.45; H, 2.03; Te, 32.48%. ^1H NMR spectrum (in $CDCl_3$ at 300 MHz): $\delta = 5.40$ m (4H, $TeCH_2$–); $\delta = 7.36$ m (4H, C_6H_4).

2.2. Crystal structure determinations

Crystals (**1**–**5**) were mounted on a Bruker P4 diffractometer using graphite monochromatic Mo Kα (0.71073 Å). The unit cells were determined from 25 randomly selected reflections using the automatic search index and least square refinement. The data were corrected for Lorentz, polarization and absorption effects. The data were monitored by measuring three reflections at every 97 reflections. The structures were solved by the routine heavy atom method SHELXS-97 [31] and Fourier methods and refined by full-matrix least-squares using the SHELXL-97 program [31] with the non-hydrogen atoms anisotropic and hydrogen atoms having fixed isotropic thermal parameters of 0.08 Å (Table 1).

3. Supplementary material

Crystallographic data for the structural analyses have been deposited with the Cambridge Crystallographic Data Centre, CCDC nos. 222539 for $C_4H_8TeCl_2$ (**1**),

226695 for $C_4H_8TeBr_2$ (**2**), 226696 for $C_5H_{10}TeBr_2$ (**3**), 222541 for $C_8H_8TeCl_2$ (**4**) and 222540 for $C_8H_8TeBr_2$ (**5**). Copies of this information may be obtained free of charge from The Director, CCDC, 12 Union Road Cambridge CBZ 1EZ, UK (fax: +44-1223-336033; email deposit@ccdc.cam.ac.uk or www.http//www.ccdc.cam.ac.uk).

Acknowledgements

P.C.S. is thankful to the Department of Science and Technology, Government of India for the financial support.

References

[1] N.W. Alcock, Adv. Inorg. Chem. Radiochem. 15 (1972) 1.
[2] I. Haiduc, R.B. King, M.G. Newton, Chem. Rev. 94 (1994) 301.
[3] J.M. Lehn, Angew. Chem. Int. Ed. Engl. 27 (1988) 89.
[4] (a) D. Braga, F. Grepioni, J. Chem. Soc. Dalton Trans. (1999) 1;
(b) G.R. Desiraju, J. Chem. Soc. Dalton Trans. (2000) 3745.
[5] (a) J.M. Lehn, J.L. Atwood, J.E.D. Davies, D.D. MacNicol, F. Vögtle, Comprehensive Supramolecular Chemistry, Pergamon Press, Oxford, 1996;
(b) I. Haiduc, F.T. Edelmann, Supramolecular Organometallic Chemistry, Wiley-VCH, Weinheim, NY, 1999;
(c) I. Haiduc, J. Zukermann-Schpector, Phosphorus Sulfur Silicon 171 (2001) 171.
[6] (a) J.E. Drake, L.N. Khasrou, A.G. Mislankar, R. Ratnani, Inorg. Chem. 38 (1999) 3994;
(b) J.E. Drake, J. Yang, Inorg. Chem. 36 (1997) 1890;
(c) J.E. Drake, R.J. Drake, L.N. Khasrou, R. Ratnani, Inorg. Chem. 35 (1996) 2831;
(d) J.H.E. Bailey, J.E. Drake, Can. J. Chem. 71 (1993) 42;
(e) J.H.E. Bailey, J.E. Drake, Can. J. Chem. 69 (1991) 1948.
[7] (a) D. Dakternieks, R. Di Giacomo, R.W. Gable, B. Padmanabhan, J. Am. Chem. Soc. 110 (1988) 6753;
(b) D. Dakternieks, R. Di Giacomo, R.W. Gable, B.F. Hoskins, J. Organomet. Chem. 353 (1988) 35;
(c) J.O. Bogason, D. Dakternieks, S. Husebye, K. Maartmann-Moe, H. Zhu, Phosphorus Sulphur Silicon 71 (1992) 13.
[8] (a) S. Husebye, K. Maartmann-Moe, W. Steffenson, Acta Chem. Scand. 44 (1990) 139;
(b) V. G-Montalvo, A. M-Polo, R. Montoya, R.A. Toscano, S. H-Ortlega, R. Cea-Olivares, J. Organomet. Chem. 623 (2001) 74.
[9] (a) P.C. Srivastava, S. Bajpai, R.J. Butcher, J. Organomet. Chem. 586 (1999) 119;
(b) H.W. Roesky, R.J. Butcher, S. Bajpai, P.C. Srivastava, Phosphorus Sulfur Silicon 161 (2000) 135;
(c) P.C. Srivastava, S. Bajpai, R. Lath, C. Ram, M. Srivastava, Sm. Bajpai, R.J. Butcher, M. Zimmer, M. Veith, J. Organomet. Chem. 658 (2002) 34.
[10] (a) P.C. Srivastava, S. Bajpai, R. Lath, R.J. Butcher, J. Organomet. Chem. 608 (2000) 96;
(b) P.C. Srivastava, S. Bajpai, Sm. Bajpai, C. Ram, R. Kumar, J.P. Jasinski, R.J. Butcher, J. Organomet. Chem. 689 (2004) 194.
[11] P.C. Srivastava, S. Bajpai, R. Lath, C. Ram, Sm. Bajpai, R.J. Butcher, M. Zimmer, M. Veith, J. Organomet. Chem. 649 (2002) 70.
[12] M. De Matheus, L. Thorres, J.F. Piniella, J.L. Brianso, C. Miravitles, Acta Crystallogr. C47 (1991) 703.
[13] P.H. Bird, V. Kumar, B.C. Pant, Inorg. Chem. 19 (1980) 2487.
[14] N.W. Alcock, W.D. Harrison, J. Chem. Soc. Dalton Trans. (1982) 251.
[15] R.F. Ziolo, J.M. Troup, J. Am. Chem. Soc. 105 (1983) 229.
[16] P.C. Srivastava, A. Sinha, S. Bajpai, H.G. Schimdt, M. Noltemeyer, J. Organomet. Chem. 575 (1999) 261.
[17] L.Y.Y. Chan, F.W.B. Einstein, J. Chem. Soc. Dalton Trans. (1972) 316.
[18] G.T. Morgan, F.H. Burstall, J. Chem. Soc. (1931) 180.
[19] (a) G.T. Morgan, H. Burgess, J. Chem. Soc. (1928) 321;
(b) W.V. Farrar, J.M. Gulland, J. Chem. Soc. (1945) 11.
[20] T.N. Srivastava, P.C. Srivastava, R. Kumar, Ind. J. Chem. Soc. 59 (1982) 186.
[21] N. Zumbulyadis, H.J. Gysling, J. Organomet. Chem. 192 (1980) 183.
[22] D. Dakternieks, R. Di Giacomo, R.W. Gable, B.F. Hoskins, J. Organomet. Chem. 349 (1988) 95.
[23] N.W. Alcock, W.D. Harrison, C. Howes, J. Chem. Soc. Dalton Trans. (1984) 1709.
[24] N.W. Alcock, J. Culver, S.M. Roe, J. Chem. Soc. Dalton Trans. (1992) 1477.
[25] S.B. Bulgarevich, B.B. Rivkin, N.G. Furmanova, O.O. Exner, D. Ya Movshovich, T.A. Yusman, I.D. Sadekov, V.I. Minkin, Zh. Strukt. Khim. 25 (1984) 97.
[26] F.A. Cotton, G. Wilkinson, Advanced Inorganic Chemistry, Wiley, New York, 1964, p. 104.
[27] F.A. Cotton, G. Wilkinson, Advanced Inorganic Chemistry, Wiley, New York, 1964, p. 93.
[28] C. Knobler, J.D. Mc Cullough, Inorg.Chem. 11 (1972) 3026.
[29] J.B. Lambert, R.G. Keske, Tetrahedron Lett. 47 (1967) 4755.
[30] (a) G.R. Desiraju, Acc. Chem. Res. 24 (1991) 290, 1996 29, 441;
(b) T. Steiner, Chem. Commun. (1997) 727;
(c) T. Steiner, G.R. Desiraju, Chem. Commun. (1998) 891, and references cited therein.
[31] G.M. Sheldrick, SHELXS-86, SHELXS-97 and SHELXL-97, University of Göttingen, 1987, and 1997.

Available online at www.sciencedirect.com
SCIENCE DIRECT®
Polyhedron 23 (2004) 1641–1647
POLYHEDRON
www.elsevier.com/locate/poly

The novel dinuclear doubly and triply bridged copper(II) compound with monoatomic bridges

Sujittra Youngme [a,*], Chatkaew Chailuecha [a], Narongsak Chaichit [b]

[a] Department of Chemistry, Faculty of Science, Khon Kaen University, Khon Kaen 40002, Thailand
[b] Department of Physics, Faculty of Science and Technology, Thammasat University Rangsit, Pathumthani 12121, Thailand

Received 8 January 2004; accepted 29 March 2004
Available online 30 April 2004

Abstract

The planar dihydroxo-bridged $[Cu_2(dpyam)_2(\mu\text{-}OH)_2I_2]\cdot 2H_2O$ **(1)** and the roof-shaped trihydroxo-bridged $[Cu_2(dpyam)_2(\mu\text{-}OH)_3]Cl\cdot 3H_2O$ **(2)** (in which dpyam = di-2-pyridylamine) dinuclear copper(II) compounds have been synthesized and their crystal structures determined by X-ray crystallographic methods. All of compounds are being centrosymmetric molecule. Compound **1** contains a dinuclear $[I(dpyam)Cu(\mu\text{-}OH)_2Cu(dpyam)I]^+$ unit with a strictly planar CuO_2 network, dihedral angle between the CuO_2 planes of 180°. Each copper(II) ion is in a tetrahedrally distorted square pyramidal coordination geometry of the CuN_2O_2I chromophore with a dihedral angle 19.3° between the CuN_2 and CuO_2 planes. In the dinuclear $[(dpyam)Cu(\mu\text{-}OH)_3Cu(dpyam)]^+$ unit of compound **2**, the triply bridged Cu(II) ions show a distorted square pyramidal coordination. The fifth apical ligand is a longer bonded bridging OH^- group, at distance of 2.433(4) Å, which joins the basal CuN_2O_2 planes in a roof-shaped configuration with a dihedral angle of 142.5°. The Cu–Cu distance is 2.803(7) Å.
© 2004 Elsevier Ltd. All rights reserved.

Keywords: Copper(II) complexes; Crystal structure; Dihydroxo-bridged; Roof-shaped; Triply bridged

1. Introduction

In the last three decades, the dinuclear doubly bridged copper(II) compounds with nitrogen donor ligand and monoatomic bridges have been received much attention especially the di-μ-hydroxo-bridged copper(II) systems which have been studied widely both from experimental and theoretical points of view, since the magnetostructural correlations described by Hatfield et al. [1] for the Cu–O–Cu bridging angle and spin coupling constant ($2J$) between the metal centers. More recently, these correlations have been extended by Ruiz et al. [2,3]. However, the structure characterized of the triply bridged copper(II) compounds containing nitrogen donor didentated chelate ligand and monoatomic bridges are less reported. So far only a few closely related structures, $[Cu_2(dpyam)_2(\mu\text{-}OH)_2(\mu\text{-}OH_2)]Cl_2\cdot 2H_2O$ [4], $[Cu_2(dpyam)_2(\mu\text{-}OMe)_2(\mu\text{-}Cl)]Cl\cdot MeOH$ [5] and $[Cu_2(dpyam)_2(\mu\text{-}OH)_2(\mu\text{-}OH_2)]Br_2\cdot 2H_2O$ [6] (in which dpyam = di-2-pyridylamine) are reported in the literature. In order to extend the investigation on this series of compounds an attempt has been made to prepare the novel planar di-μ-hydroxo-bridged copper(II) compound, $[Cu_2(dpyam)_2(\mu\text{-}OH)_2I_2]\cdot 2H_2O$ **(1)**, and the novel dinuclear copper(II) compounds containing three monoatomic bridges with homospecies, $[Cu_2(dpyam)_2(\mu\text{-}OH)_3]Cl\cdot 3H_2O$ **(2)**. Their IR, EPR and electronic spectra have been investigated and discussed, along with structural and spectral comparisons with those of other relevant compounds.

2. Experimental

2.1. Materials and measurements

Di-2-pyridylamine were purchased as commercial chemicals from Aldrich. All reagents are commercial grade

* Corresponding author. Tel.: +66-043-20222241; fax: +66-043-202373.
E-mail address: sujittra@kku.ac.th (S. Youngme).

0277-5387/$ - see front matter © 2004 Elsevier Ltd. All rights reserved.
doi:10.1016/j.poly.2004.03.021

materials and were used without further purification. Elemental analyses (C, H, N) were determined on a Perkin–Elmer PE 2400 CHNS/O Analyzer by Microanalytical Service of Science and Technological Research Equipment Center, Chulalongkorn University.

IR spectra were recorded on a Biorad FTS-7/PC FT-IR and a Perkin–Elmer Spectrum One FT-IR spectrophotometer for compounds **1** and **2**, respectively as KBr disc in the 4000–450 cm^{-1} spectral range. Solid-state (diffuse reflectance) electronic spectra were measured as polycrystalline samples on a Perkin–Elmer Lambda2S spectrophotometer, over the range 8000–18000 cm^{-1}. The X-band powder EPR spectra were obtained on polycrystalline samples at room temperature and 77 K with a JEOL RE2X electron spin resonance spectrometer by Microanalytical Service of Science and Technological Research Equipment Center, Chulalongkorn University.

2.2. Synthesis of compound *1*

2.2.1. $[Cu_2(dpyam)_2(\mu\text{-}OH)_2I_2]\cdot 2H_2O$ (*1*)

The hot aqueous solution (5 ml) of KI (0.166 g, 1.0 mmol) was added to a hot aqueous solution (5 ml) of $Cu(NO_3)_2\cdot 3H_2O$ (0.121 g, 0.5 mmol). Then a hot acetone solution (8 ml) of dpyam (0.086 g, 0.5 mmol) was added to the mixture yielding a green solution. Its color became greenish-blue by slow addition of an aqueous solution (10 ml) of NaOH (0.020 g, 0.5 mmol) and the blue precipitate formed in a few minutes. The precipitate was filtered off and recrystallized in a hot aqueous solution. After two weeks, blue-plate crystals of compound **1** were obtained. *Anal.* Calc. for $C_{20}H_{24}Cu_2I_2N_6O_4$: C, 30.28; H, 3.05; N, 10.59. Found: C, 30.35; H, 3.12; N, 10.40%.

2.3. Synthesis of compound *2*

2.3.1. $[Cu_2(dpyam)_2(\mu\text{-}OH)_3]Cl\cdot 3H_2O$ (*2*)

This compound was prepared by adding a hot acetone solution (10 ml) of dpyam (0.171 g, 1.0 mmol) to a hot aqueous solution (30 ml) of $CuCl_2\cdot 2H_2O$ (0.170 g, 1.0 mmol) yielding a turquoise green solution. Its color became blue by slow addition of an aqueous solution (10 ml) of NaOH (0.039 g, 1.0 mmol). This solution was allowed to evaporate at room temperature. After several days, bluish-purple crystals of compound **2** were obtained which were filtered off, washed with mother liquor and air-dried. *Anal.* Calc. for $C_{20}H_{27}ClCu_2N_6O_6$: C, 41.70; H, 4.72; N, 14.59. Found: C, 41.67; H, 4.81; N, 14.53%.

2.4. Crystallography

The X-ray single-crystal data for two compounds were collected at 298 and 293 K for compounds **1** and **2**, respectively on a 1 K Bruker SMART CCD area-detector diffractometer using graphite monochromated Mo Kα radiation ($\lambda = 0.71073$ Å) at a detector distance of 4.5 cm and swing angle of −35°. A hemisphere of the reciprocal space was covered by combination of three sets of exposures; each set had a different ϕ angle (0°, 88°, 180°) and each exposure of 40 s covered 0.3° in ω. Data reduction and cell refinements were performed using the program SAINT [7]. An empirical absorption correction by using the SADABS [8] program was applied, which resulted in transmission coefficients ranging from 0.741 to 1.000 for compound **1**, 0.752 to 1.000 for compound **2.**

The structures were solved by direct methods and refined by full matrix least-squares method on $(F_{obs})^2$ with anisotropic thermal parameters for all non-hydrogen atoms using the SHELXTL-PC V 6.12 software package [9]. All hydrogen atoms were located geometrically and refined isotropically except those of a hydroxo group and two molecules of lattice water for **2.**

The molecular graphics were created by using SHELXTL-PC [9] package. The crystal and refinement details for compounds **1** and **2** are listed in Table 1. Selected bond lengths and angles are given in Tables 2 and 3.

3. Results and discussion

3.1. Crystal structure of $[Cu_2(dpyam)_2(\mu\text{-}OH)_2I_2]\cdot 2H_2O$ (*1*)

The structure of compound **1** consists of a centrosymmetric dinuclear $[Cu_2(dpyam)_2(\mu\text{-}OH)_2I_2]$ unit and two molecules of lattice water. This unit is depicted in Fig. 1, together with the numbering scheme, with selected distances and angles listed in Table 2. Both copper(II) atoms of the complex are linked through the double hydroxo bridges. Each copper(II) atom has a distorted square pyramidal coordination, $\tau = 0.04$ (the structure index is defined as $\tau = (\beta - \alpha)/60$, where β and α are the largest coordination angles [10,11]), with the basal plane, CuN_2O_2 chromophore, comprised of two nitrogen atoms from a terminal dpyam ligand (Cu(1)–(N1) distance of 2.007(3) and Cu(1)–N(2) distance of 2.006(3) Å) and two oxygen atoms from two hydroxo groups (Cu(1)–O(1) distance of 1.967(2) and Cu(1)–O(1A) distance of 1.960(2) Å). The fifth apical coordination site of each copper(II) atom is occupied by an I atom (Cu–I distance of 3.040 Å) to complete the distorted square pyramidal CuN_2O_2I chromophore. However, the Cu–I distance is too long for even weak semi-coordination. The basal planes are slightly deviated from planarity with a distinct tetrahedral twist, evident from the dihedral angle of 19.3° between CuN_2 and CuO_2 planes. The Cu–Cu separation within the dinuclear unit is 2.988(7) Å, while the bridging Cu(1)–

Table 1
Crystal and refinement data for complexes **1**and **2**

Complex	(**1**)	(**2**)
Molecular formula	$[Cu_2(dpyam)_2(\mu\text{-}OH)_2I_2]\cdot 2H_2O$	$[Cu_2(dpyam)_2(\mu\text{-}OH)_3]Cl\cdot 3H_2O$
Molecular weight	793.33	610.02
T (K)	293(2)	293(2)
Crystal system	triclinic	orthorhombic
Space group	$P\bar{1}$	$Cmc2_1$
a (Å)	9.191	15.690
b (Å)	9.440(2)	8.629
c (Å)	9.472(2)	18.249
α (°)	111.54	90
β (°)	97.08(10)	90
γ (°)	108.84(10)	90
V (Å^3)	695.66(2)	2470.85(5)
Z	1	4
D_{calc} (g cm^{-3})	1.980	1.626
μ (mm^{-1})	3.792	1.877
$F(000)$	402	1228
Crystal size (mm)	$0.05\times0.20\times0.25$	$0.23\times0.45\times0.10$
Number of reflections collected	5226	9012
Number of unique reflections [R_{int}]	3810 [0.0165]	3593 [0.0408]
Data/restraints/parameter	3810/0/219	3593/1/181
Goodness-of-fit	1.012	1.123
Final R indices [$I > 2\sigma(I)$]	$R_1 = 0.0345$, $wR_2 = 0.0824$	$R_1 = 0.0408$, $wR_2 = 0.1386$
R indices (all data)	$R_1 = 0.0483$, $wR_2 = 0.0904$	$R_1 = 0.0453$, $wR_2 = 0.1427$
Largest difference peak and hole (e Å$_3$)	0.963, −1.010	1.539, −0.402

Table 2
Selected bond lengths [Å] and angles [°] with e.s.d.s. in parentheses of $[Cu_2(dpyam)_2(\mu\text{-}OH)_2I_2]\cdot 2H_2O$ **(1)**

Bond lengths				
Cu(1)–N(1)		2.007(3)	Cu(1)–O(1)	1.967(2)
Cu(1)–N(2)		2.006(3)	Cu(1)–O(1A)	1.960(2)
Cu(1)–I(1)		3.040(5)	Cu(1)–Cu(1A)	2.988(7)
Bond angles				
O(1)–Cu(1)–O(1A)		80.93(11)	O(1A)–Cu(1)–I(1)	99.75(9)
O(1)–Cu(1)–N(1)		93.51(10)	N(1)–Cu(1)–N(2)	89.31(11)
O(1)–Cu(1)–N(2)		166.55(12)	N(1)–Cu(1)–I(1)	95.83(8)
O(1)–Cu(1)–I(1)		97.48(8)	N(2)–Cu(1)–I(1)	95.30(9)
O(1A)–Cu(1)–N(1)		164.oo(12)	Cu(1)–O(1)– Cu(1A)	99.07(11)
O(1A)–Cu(1)–N(2)		92.82(10)		
Hydrogen bonds	D-H	H...A	D...A	D-H...A
N(3) – H(5)...O(3)[a]	0.79	2.13	2.9156	173
O(1) – H(10)...O(2)[b]	0.53	2.25	2.7500	157
O(3) – H(13)...O(1)[c]	0.62	2.40	2.8474	130

$A = -x, -y+1, -z$.
[a] $[1-x, 2-y, -z]$.
[b] $[-x, 1-y, -z]$.
[c] $[1-x, 1-y, -z]$.

O(1)–Cu(1A) angle is 99.1(11)°. Each copper atom is displaced toward the apical I atom of 0.243 Å from the basal N_2O_2 plane. The dinuclear unit is exactly planar, a dihedral angle between two CuO_2 planes is 180° and that between the basal N_2O_2 planes is 180° (see Fig. 3). The bite angle of the dpyam ligand N(1)–Cu(1)–N(2) of 89.3(11)° is only slightly less than 90° but the O(1)–Cu(1)–O(1A) angle of 80.9(11)° is significantly less than 90°. The individual pyridine rings are planar, and the dpyam ligand is non-planar, dihedral angle of 27.2° occurs between the individual pyridine rings.

The lattice is further stabilized by a hydrogen bonding between the amine N and the oxygen atom of lattice water molecule with N···O contact of 2.916 Å ; between the oxygen atom of bridging hydroxo group and the oxygen atom of lattice water molecules with O···O contacts of 2.750–2.847 Å.

Table 3
Selected bond lengths [Å] and angles [°] with e.s.d.s. in parentheses of $[Cu_2(dpyam)_2(\mu\text{-}OH)_3]Cl \cdot 3H_2O$ **(2)**

Bond lengths			
Cu(1)–N(1)	1.995(3)	Cu(1)–O(1)	1.942(3)
Cu(1)–N(2)	2.006(3)	Cu(1)–O(2)	1.953(3)
Cu(1)–O(3)	2.433(4)	Cu(1)–Cu(1A)	2.803(7)
Bond angles			
O(1)–Cu(1)–O(2)	81.1(2)	N(1)–Cu(1)–N(2)	91.79(13)
O(1)–Cu(1)–O(3)	78.8(2)	N(1)–Cu(1)–O(3)	102.05(14)
O(1)–Cu(1)–N(1)	174.6(2)	N(2)–Cu(1)–O(3)	104.44(14)
O(1)–Cu(1)–N(2)	93.17(14)	Cu(1)–O(1)–Cu(1A)	92.4(2)
O(2)–Cu(1)–O(3)	76.4(2)	Cu(1)–O(2)–Cu(1A)	91.7(2)
O(2)–Cu(1)–N(1)	93.88(14)	Cu(1)–O(3)–Cu(1A)	70.34(13)
O(2)–Cu(1)–N(2)	174.0(2)		

Hydrogen bonds	D-H	H...A	D...A	D-H...A
N(3) – H(5)...Cl(1)[a]	0.86	2.39	3.2518	176
O(2) – H(11)...Cl(1)[b]	0.63	2.59	3.2283	178
O(3) – H(12)...Cl(1)	0.52	2.66	3.1756	174

$A = -x+2, y, z$.
[a] $[x, -1+y, z]$.
[b] $[1/2+x, -1/2+y, z]$.

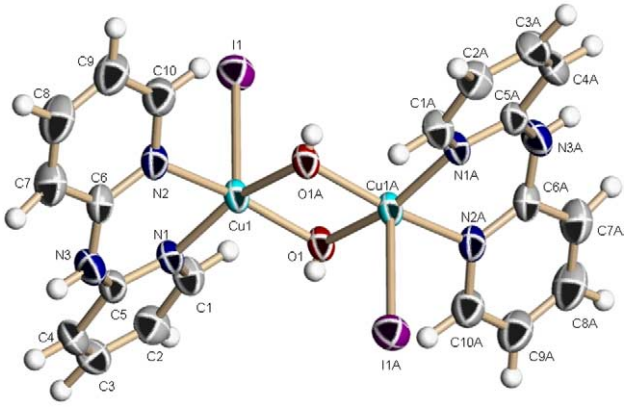

Fig. 1. ORTEP 50% probability plot of the cation in $[Cu_2(dpyam)_2(\mu\text{-}OH)_2I_2] \cdot 2H_2O$ (**1**) Atoms with an "A" are generated by a mirror plane.

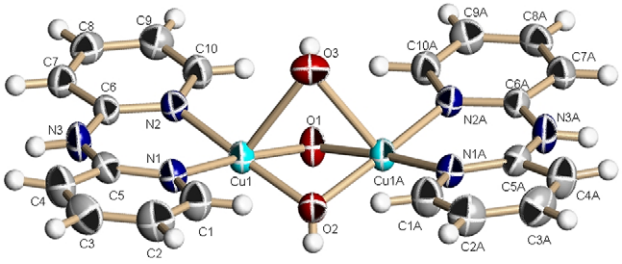

Fig. 2. ORTEP 50% probability plot of the cation in $[Cu_2(dpyam)_2(\mu\text{-}OH)_3]Cl \cdot 3H_2O$ (**2**) Atoms with an "A" are generated by a mirror plane.

3.2. Crystal structure of $[Cu_2(dpyam)_2(\mu\text{-}OH)_3]Cl \cdot 3H_2O$ (2)

The structure of compound **2** is made up of a dinuclear $[Cu_2(OH)_3(dpyam)]^+$ cation, an uncoordinated Cl^- anion and three crystallisation water molecules. This unit is depicted in Fig. 2, together with the numbering scheme, with selected distances and angles listed in Table 3. The cation is located on a mirror plane through the three bridging OH^- groups. The whole cationic unit and the copper environment are the rooftop configuration. Compound **2** involves a triplyhydroxo-bridged structure with a square pyramidal CuN_2O_2O' chromophore, the fifth axial position is occupied by a longer bonded bridging OH^- group with a distance of 2.433(3) Å. The copper atom is displaced from the basal plane towards the apical oxygen by 0.035 Å. The Cu(1)–N(1) and Cu(1)–N(2) distances are

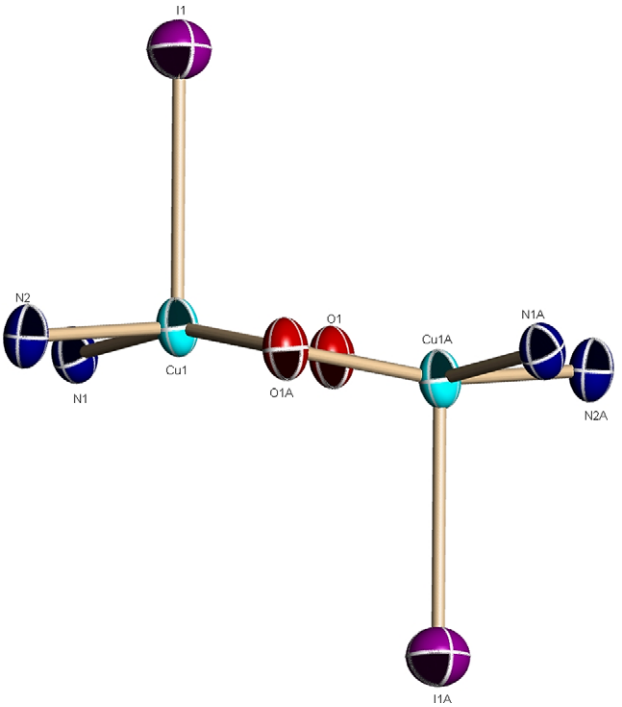

Fig. 3. The chromophore of $[Cu_2(dpyam)_2(\mu\text{-}OH)_2I_2] \cdot 2H_2O$ (**1**).

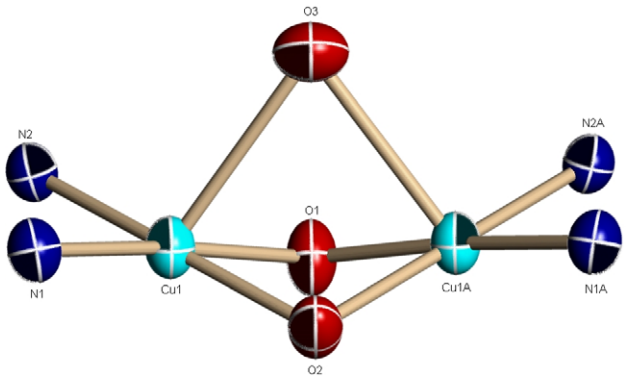

Fig. 4. The chromophore of $[Cu_2(dpyam)_2(\mu\text{-}OH)_3]Cl \cdot 3H_2O$ (**2**).

1.995(3) and 2.006(3) Å, respectively. The average Cu–O (hydroxo bridge) distance of 1.948 Å is slightly shorter and very close to those observed in the corresponding di–hydroxo bridged copper(II) dimers [5,6,12,13]. The CuN_2O_2 chromophore is planar with a slight tetrahedral twist, dihedral angle of 2.8° between the CuN_2 and CuO_2 planes, but the Cu_2O_2 network is not planar, a dihedral angle between the CuO_2 planes is 142.5° (see Fig. 4). The Cu–Cu distance is 2.803(1) Å. The bridging Cu–O(1)–Cu and Cu–O(2)–Cu angles are 92.4(2)° and 91.7(2)°, respectively, which are not in the range normally found for the planar dihydroxo-bridged copper(II) dimers. The dpyam ligand as a whole is nearly planar and involves a dihedral angle of 9.1° between the individual pyridine rings.

The lattice is stabilized by a hydrogen bonding between the amine N and the chloride atom with N···Cl distance of 3.252 Å and between the oxygen atom of bridging hydroxo group and the chloride atom with O···Cl contacts of 3.176–3.228 Å.

3.3. Spectral characterization

The infrared spectra of compounds **1** and **2** show a broad band at 3460 and 3400 cm^{-1}, respectively which can be assigned to the bridging OH vibrations of the hydroxo bridge and/or lattice water.

The electronic diffuse reflectance spectrum of compound **1** shows a broad band centered at 15 120 cm^{-1}. This observed single broad peak is consistent with the tetrahedrally distorted square pyramidal stereochemistry and assigned to be the $d_{z^2}, d_{xy}, d_{xz}, d_{yz}, \rightarrow d_{x^2-y^2}$ transition [14,15]. The reflectance spectrum of **2** displays a broad band and a lower energy shoulder at the frequencies of 17 800 and 14 600(sh) cm^{-1}. The relatively higher energy of this triply bridged dimer is unusual for the square pyramidal geometry. However, they are consistent with those observed for the relevant bipy complexes [16] and the $d_{xy}, d_{yz} \rightarrow d_{x^2-y^2}$ and $d_{xz}, d_{z^2} \rightarrow d_{x^2-y^2}$ transitions are assigned for a broad band and a lower energy shoulder, respectively.

The X-band polycrystalline EPR spectrum of compound **1**, at room temperature, displays a weak signal at ~320 mT ($g_i = 2.078$), while a triplet state signal at ~100–160 mT ($g_i = 6.964$) is not observed properly. The former feature is most certainly from a monomeric Cu(II) impurity, which is always present in dinuclear species. Compound **2** exhibits an intense signal at ~101 mT ($g_i = 6.695$) and a weaker signal at ~307 mT ($g_i = 2.220$). The latter is attributed to the monomeric impurity while the former is usually attributed to intramolecular exchange interaction between copper(II) ions, $\Delta Ms = \pm 2$ transition [17,18].

Compound **1** is planar (dihedral angle of 180° between the CuO_2 planes) and involves the Cu–O–Cu angle of 99.1° expecting a moderate antiferromagnetic coupling ($J = -116$ cm^{-1}) following Hodgson and Hatfield's linear relationship [1,18]. However, the experimental value of singlet-triplet energy gap ($2J$) would be smaller than the predicted value. The difference could be due to the deviation from planarity of the CuN_2O_2 plane with a tetrahedral twist between CuN_2 and CuO_2 planes, which may reduce the orthogonality of the copper(II) $d_{x^2-y^2}$ (or d_{xy}) orbital with the bridging hydroxo groups [4]. The most relevant compound $[Cu_2(dpyam)_2(\mu\text{-}OH)_2Br_2] \cdot 4H_2O$ also involves a double hydroxo bridge and an observed J value of -48.6 cm^{-1}, while the predicted value was as high as -116 cm^{-1} [6]. On the other hand compound **2** has the roof-shaped hydroxo bridge network with a dihedral angle of 142.5° between the CuO_2 planes and the Hatfield's linear relationship, which arises from studies of planar $Cu_2(OH)_2$ cores, is not valid then. The related structure, $[Cu_2(dpyam)_2(\mu\text{-}OH)_2(\mu\text{-}OH_2)]Br_2 \cdot 2H_2O$ compound exhibits $J = -0.6$ cm^{-1}.

3.4. Structure comparison

There are five dihydroxo-bridged copper(II) dimers containing the dpyam ligand: $[Cu_2(dpyam)_2(\mu\text{-}OH)_2Br_2] \cdot 4H_2O$ **(3)**, $[Cu_2(dpyam)_2(\mu\text{-}OH)_2(FBF_3)_2]$ **(4)**, $[Cu_2(dpyam)_2(\mu\text{-}OH)_2(ONO_2)_2]$ **(5)**, $[Cu_2(dpyam)_2(\mu\text{-}OH)_2(\mu\text{-}OH_2)]Cl_2 \cdot 2H_2O$ **(6)** and $[Cu_2(dpyam)_2(\mu\text{-}OH)_2(\mu\text{-}OH_2)]Br_2 \cdot 2H_2O$ **(7)** have been structurally reported [4–6,12]. In the known dimer structures, three copper environments are observed: rhombic coplanar [19], CuN_2O_2, square-based pyramidal, CuN_2O_2X [18,20], and elongated rhombic octahedral [21,22], $CuN_2O_2X_2$. Compounds **1**, **3, 4** and **5** involve the planar dihydroxo-bridged copper(II) dimer, all exhibit the square pyramidal CuN_2O_2X chromophore geometry. Compound **1** involves the square-based pyramidal CuN_2O_2I chromophores which are very comparable to the CuN_2O_2Br, CuN_2O_2F and CuN_2O_2O' chromophores in **3**, **4** and **5**, respectively. The fifth axial distances of 3.040(5) Å in compound **1** are much longer than those of 2.803(2) and 2.804(2), 2.745(7), 2.400(1) and 2.500(1) Å in

compounds **3**, **4** and **5**, respectively. The marked tetrahedral twists of the CuN_2O_2 chromophores in compound **1** and also in compounds **3**, **4** and **5** (dihedral angle of 19.3°, 21.8° and 21.4°, 24.0°, 20.7° and 16.7°, respectively) are less usual. However, the Cu_2O_2 network in these compounds is planar and the planarities of both the CuN_2O_2 chromophore and the Cu_2O_2 unit for each compound are not many different. Consequently, the Cu–Cu separation of 2.988(7) Å in compound **1** is more similar in compounds **3**, **4** and **5** (2.993(2); 2.919(5) and 2.954(2) Å, respectively). The Cu–O–Cu bridging angle of 99.1 Å in compound **1** is comparable to that of compounds **3**, **4** and **5** (98.1° and 100.1°, 99.3°, 99.4° and 98.9°, respectively). There are a significant difference observed in the Cu to N_2O_2 mean plane distances, those of compounds **1** and **3** (0.243, 0.273 Å, respectively) are longer than those of compounds **4** and **5** (0.022; 0.079 and 0.142 Å, respectively) arising from a very weak interaction in the sixth position of the chromophore provided from the other F atom of the BF_4^- group in compound **4** and the other O atom of the NO_3^- group in compound **5**. However, these sixth distances are between 3.0–4.0 Å. The structural data of compounds **1**, **3**, **4** and **5** have revealed that the bigger in the bite N–Cu–N angle (98.3°, 88.6° and 88.9°, 99.3°, 98.9° and 99.4°, respectively), the bigger the bridging Cu–O–Cu angle is observed. Consequently, the Cu–O–Cu angles in the parent dpyam complexes are bigger (>97.5°) than those of the corresponding bipy complexes (<97.5°). This feature is also observed in other corresponding dimers involving the other terminal ligand. This concludes that the terminal ligand other than the anion and solvent molecule influences the magnitude of the Cu–O–Cu angle.

The most interesting and unusual feature in structure of compound **2** is that this is the triply bridged dinuclear compound with a roof-shaped bridge, the dihedral angle between the CuO_2 planes is far from 180°. Each hydroxo group is symmetrically bound, with Cu–O(1) bond slightly shorter than Cu–O(2) bond. The bridging angles in compound **2** are significantly less than those found in the planar dihydroxo-bridged copper (II) dimers and are not in the usual range 95°–105°, normally found for these dimers [23–25]. So far, compound **2** represents the second structurally characterized examples of a triply bridged dinuclear copper(II) compound containing three monoatomic bridges with homospecies. The first one has been pointed out for the known $Cs_3[Cu_2Cl_7\ (H_2O)_2]$ compound [26], containing three Cl^- anions bridging two copper atoms separated by 3.45 Å. The related structures of the roof-shaped dinuclear copper(II) containing three monoatomic bridges are $[Cu_2\ (dpyam)_2(\mu\text{-}OH)_2(\mu\text{-}OH_2)]Cl_2 \cdot 2H_2O$ **(6)** and $[Cu_2\ (dpyam)_2(\mu\text{-}OH)_2(\mu\text{-}OH_2)]Br_2 \cdot 2H_2O$ **(7)** and $[Cu_2(dpyam)_2(\mu\text{-}OMe)_2(\mu\text{-}Cl)]Cl \cdot MeOH$ **(8)**. The cations present in compounds **2**, **6**, **7** and **8** show a similar structure, they exhibit the metal centres in a square pyramidal configuration with in-plane configuration of a dpyam ligand and of two bridging O atoms and involve in similar CuO_2Cu roof-top angles (142.5°, 140.6°, 135.8°, 144.3°, respectively). Also the in-plane Cu–N and Cu–O distances are similar to each other and the Cu–Cu separations are quite comparable (2.803, 2.797, 2.849, 2.792 Å, respectively). The cations differ, however, in the nature of the fifth bridging ligand, which is a hydroxo group in compound **2**, a water molecule in compounds **6** and **7**, and a bigger chloride anion in compound **8**.

4. Conclusion

In comparison to the planar di-μ-hydroxo-bridged complexes significant differences are observed. The dihedral angle between the CuO_2 planes of the dihydroxo-bridged dimers becomes near 180°, while their CuN_2O_2 chromophores are not planar with a distinct tetrahedral twist (except that for the octahedral geometry). On the other hand, the planarity of the square planes for each CuN_2O_2 chromophore with a slight tetrahedral twist is observed in the triply bridged dimers. Due to bending in the molecule, the Cu–Cu distances (2.792–2.849 Å) in the triply bridged complexes are significantly shorter than those of the planar dihydroxo-bridged complexes (2.870–3.000 Å). However, these distances are typical in the range previously observed, 2.80–3.00 Å [1,27]. There is an additional remarkable difference observed, the bridging Cu–O–Cu angles (91.0°–94.7°) in the roof-shaped dimers are significantly smaller than 95.0° while in the planar dihydroxo-bridged dimers, these angles are in the range 95.0°–104.1°.

5. Supplementary material

Crystallographic data (excluding structure factors) for the structures in this paper have been deposited with the Cambridge Crystallographic Data Centre as supplementary publication no.CCDC-223620, 223621, for structures 1 and 2, respectively. Copies of the data can be obtained free of charge on application to CCDC, 12 Union Road, Cambridge CB2 1EZ, UK (fax: (international) +44-1223-336-033, e-mail: deposit@ccdc.cam.ac.uk or www: http://www.ccdc.cam.ac.uk).

Acknowledgements

The authors would like to thank The Thailand Research Fund and Khon Kaen University for research grant. Support of the Postgraduate Education and Research Program in Chemistry is also gratefully acknowledged.

References

[1] V.H. Crawford, H.W. Richardson, J.R. Wasson, D.J. Hodgson, W.E. Hatfield, Inorg. Chem. 15 (1976) 2107.

[2] E. Ruiz, P. Alemany, S. Alvarez, J. Cano, Inorg. Chem. 36 (1997) 3683.

[3] E. Ruiz, P. Alemany, S. Alvarez, J. Cano, J. Am. Chem. Soc. 119 (1997) 1297.

[4] L.P. Wu, M.E. Keniry, B.J. Hathaway, Acta Cryst. C48 (1992) 35.

[5] N. Marsich, A. Camus, F. Ugozzoli, A.M.M. Lanfredi, Inorg. Chim. Acta 236 (1995) 117.

[6] S. Youngme, G.A. van Albada, O. Roubeau, C. Pakawatchai, N. Chaichit, J. Reedijk, Inorg. Chim. Acta 342 (2003) 48.

[7] Siemens. SAINT. 1996, Version4 Software Reference Manual, Siemens Analytical X-Ray Systems, Inc., Madison, WI, USA.

[8] G.M. Sheldrick, SADABS, Program for Empirical Absorption correction of Area Dectector Data, University of Göttingen, Göttingen, Germany, 1996.

[9] Bruker. XSHELL. 1999, Version 6.12 Reference Manual, Bruker AXS, Inc., Madison, WI, USA.

[10] A.W. Addison, T.N. Rao, J. Reedijk, J. van Rijn, G.C. Verschoor, J. Chem. Soc., Dalton Trans. (1984) 1349.

[11] M. Brophy, G. Murphy, C. O'Sullivan, B. Hathaway, B. Murphy, Polyhedron 18 (1999) 611.

[12] S. Youngme, W. Somjitsripunya, K. Chinnakali, S. Chantrapromma, H.K. Fun, Polyhedron 18 (1999) 857.

[13] S. Youngme, G.A. van Albada, H. Kooijman, O. Roubeau, W. Somjitsripunya, A.L. Spek, C. Pakawatchai, J. Reedijk, Eur. J. Inorg. Chem. (2002) 2367.

[14] G. Murphy, C. Murphy, B. Murphy, B. Hathaway, J. Chem. Soc., Dalton Trans. (1997) 2653.

[15] G. Murphy, C. O'Sullivan, B. Murphy, B. Hathaway, Inorg. Chem. 37 (1998) 240.

[16] C.M. Harris, E. Sinn, W.R. Walker, P.R. Woolliams, Aust. J. Chem. 21 (1968) 631.

[17] G. De Munno, M. Julve, F. Lloret, J. Faus, M. Verdaguer, A. Caneschi, Inorg. Chem. 34 (1995) 157.

[18] G.A. van Albada, I. Mutikainen, W.J.J. Smeets, A.L. Spek, U. Turpeinen, J. Reedijk, Inorg. Chim. Acta 327 (2002) 134.

[19] M.F. Charlot, S. Jeannin, Y. Jeannin, O. Kahn, J. Lucrece-Abaul, J. Martin-Frere, Inorg. Chem. 18 (1979) 1675.

[20] J.M. Seco, U. Amador, M.J. González Garmendia, Polyhedron 18 (1999) 3605.

[21] G.A.van Albada, I. Mutikainen, U. Turpeinen, J. Reedijk, Inorg. Chim. Acta 324 (2001) 273.

[22] S. Amani Komaei, G.A. van Albada, J.G. Haasnoot, H. Kooijman, A.L. Spek, J. Reedijk, Inorg. Chim. Acta 286 (1999) 24.

[23] I. Castro, M. Julve, G.D. Munno, G. Bruno, J.A. Real, F. Lloret, J. Faus, J. Chem. Soc., Dalton Trans. (1992) 1739.

[24] I. Castro, M. Julve, G.D. Munno, G. Bruno, J.A. Real, F. Lloret, J. Faus, J. Chem. Soc., Dalton Trans. (1992) 47.

[25] P.J. Hay, J.C. Thibeault, R. Hoffmann, J. Am. Chem. Soc. 97 (1975) 4884.

[26] V.W. Vogt, H. Haas, Acta Cryst., Sect. B. (1971) 1521.

[27] B.J. Hathaway, Comprehensive co-ordination chemistry. in: G. Wilkinson (Editor in Chief), R.D. Gillard, J.A. McCleverty (Executive Editors), The Synthesis, Reactions, Properties and Applications of Co-ordination Compounds, vol. 5, Sec. 53, Pergamon Press, Oxford, 1987; pp. 533–774.

Available online at www.sciencedirect.com
SCIENCE DIRECT®
Polyhedron 23 (2004) 1649–1656
POLYHEDRON
www.elsevier.com/locate/poly

Synthesis, spectroscopy and molecular structures of new salicylketiminato nickel(II) complexes

Mika Kettunen [a], Adnan S. Abu-Surrah [b,*], Hamzeh M. Abdel-Halim [b], Timo Repo [a,*], Markku Leskelä [a], Maarit Laine [a], Ilpo Mutikainen [a], Markku Ahlgren [c]

[a] *Laboratory of Inorganic Chemistry, Department of Chemistry, University of Helsinki, P.O. Box 55, FIN-00014, Finland*
[b] *Department of Chemistry, Hashemite University, P.O. Box 150459, Zarqa 13115, Jordan*
[c] *Department of Chemistry, University of Joensuu, P.O. Box 111, FIN-80101 Joensuu, Finland*

Received 10 February 2004; accepted 29 March 2004
Available online 22 April 2004

Abstract

A series of salicylketimines (2-[(2,6-diisopropylphenylimino)ethyl]phenol, 2-[(2,6-diisopropylphenylimino)ethyl]naphthol and 2-[(2,6-diisopropylphenylimino)(phenyl)-methyl]phenol), and their nickel complexes of general forms [(salicylketiminato)-Ni(PPh_3)(Ph)] and [(salicylketiminato)$_2$Ni] were synthesized and characterized. The formation of monophenyl-nickel(II) complexes versus the corresponding bis(sal)Ni(II) complexes depends on the fine tuning of the reaction work up and is affected by the substituent at the ketimine. Salicylketimines were thus found to form more readily the bis(sal)Ni(II) complexes than salicylaldimines. The molecular structures of the complexes were determined by X-ray crystallography and in all of them Ni has a nearly ideal square-planar coordination sphere.
© 2004 Elsevier Ltd. All rights reserved.

Keywords: Nickel(II) complexes; Schiff bases; Salicylketimine ligands; X-ray crystallography

1. Introduction

Until middle of 1990s, only few reports were introduced utilizing late transition metal complexes as catalyst precursors for polymerization of α-olefins [1]. This could be due to the fact that these catalysts generally exhibited low activities for olefin polyinsertion. In addition, β-hydride elimination steadily competed with the chain growth resulting in the formation of oligomers [2]. However, in 1995 new nickel(II)- and palladium(II)-based catalysts bearing bulky diimine ligands were reported for ethene polymerization, and few years later also iron(II) was successfully applied as a metal centre with bis(imino)pyridine ligands [3]. These complexes, after methylaluminoxane (MAO) activation, produced high molecular weight polymers with a high activity. Moreover, due to their tolerance towards polar functionalities, these systems are viewed as promising alternatives to Ziegler-Natta and metallocene catalysts. By now, late transition metals as olefin polymerization catalysts have been extensively reviewed, and possibilities to apply them even in acrylate polymerization have been demonstrated [4].

The MAO-activated cationic catalysts are, anyhow, electrophilic and hence sensitive to protic solvents and polar monomers. For this reason, there has been a substantial interest in developing new, less oxophilic, catalysts for olefin polymerization [5]. Shell higher olefin process (SHOP) offers an intriguing insight for catalytic activity of neutral nickel catalysts used for ethylene oligomerization [6] and recently novel salicylaldimine based Ni(II) complexes as catalysts for homo and co-polymerization of olefins were described by DuPont [7] and Grubbs and co-workers [8]. The most active systems contain either electron-withdrawing nitro substituents on the aromatic ring or bulky substituents at C-3, a 9-anthracenyl group being the most effective [activity of

* Corresponding authors. Tel.: +962-5-382-6600x4315; fax: +962-5-382-6613 (A.S. Abu-Surrah). Tel.: +358-9191-50228; fax: +358-9191-50198 (T. Repo).
E-mail addresses: asurrah@hu.edu.jo (A.S. Abu-Surrah), timo.repo@helsinki.fi (T. Repo).

0277-5387/$ - see front matter © 2004 Elsevier Ltd. All rights reserved.
doi:10.1016/j.poly.2004.03.018

1.3×10^5 mol ethylene/(mol Ni h)]. It has been reported that the neutral salicylaldiminato nickel(II) complexes work as a single component catalysts or require only a phosphine scavenger such as [Ni(COD)$_2$] (COD: 1,5-cyclooctadiene) to act as catalysts for homo- and copolymerization of ethylene [8]. However, MAO as activator surprisingly turned out to be essential to initiate the homopolymerization of norbornene [9].

Recently, we and other research groups have found that penta-coordinated iron(II) complexes with tridentate ketimine ligands (2,6-bis(imino)pyridyl derivatives) are an order of magnitude more active, as ethylene polymerization catalysts, than their aldimine analogues [3,10]. As an augmentation to our studies upon both the coordination chemistry of heteroatom-containing ligands [11,12] and their catalytic application [4f,10a,13], we now report the synthesis of new nickel(II) complexes with salicylketimine Schiff base ligands. The new compounds were characterized by methods of elemental analysis, IR-, MS-, ^{1}H-, ^{13}C- and ^{31}P-NMR spectroscopy. Furthermore, the complexes were subjects to X-ray structure analysis.

2. Experimental

2.1. Materials

All reactions were carried out under argon by using standard Schlenk techniques. Reagent grade chemicals were purchased from commercial suppliers and used as received unless otherwise stated. *trans*-[(PPh$_3$)$_2$Ni((Ph)Cl] was prepared according to literature [14]. The hydrocarbon and ether solvents were purified by distillation over LiAlH$_4$.

2.2. Physical measurements

Elemental analyses were performed at the Departments of Chemistry of the Universities of Konstanz and Ulm or at the Department of Pharmacy at University of Helsinki with an EA 1110 CHNS-O CE instrument. ^{1}H-, ^{13}C- and ^{31}P-NMR spectra were recorded using a Varian Gemini 200 or a Bruker AMX 400 spectrometer. Infrared spectra were measured on a Perkin–Elmer Spectrum One spectrometer using ATR sampling assessor. Mass spectra were acquired using a JEOL JMS-SX102 mass spectrometer (EI) or Bruker ion trap 3000+ MS equipped with Agilent's AP-MALDI ion source (proto 3).

2.3. Synthesis of ligands

2.3.1. 2-[(2,6-Diisopropylphenylimino)ethyl]phenol (**4**)

A solution of 2-hydroxyacetophenone (3.2 g, 23.9 mmol), 2,6-diisopropylaniline (4.7 g, 23.9 mmol) and five drops of HCOOH in methanol were stirred together with ca. 5 g of Na_2SO_4 at 200 °C in a closed steel autoclave for 24 h. The reaction mixture was then cooled, filtered and the filtrate was evaporated to dryness. The residue was purified with column chromatography on silica with 1:5 mixture of diethylether/hexane as eluent. Yield: 46%. *Anal.* Calc. for $C_{20}H_{25}NO$: C, 81.31; H, 8.53; N, 4.74. Found: C, 81.22; H, 8.54; N, 4.75%. ^{1}H NMR (200 MHz, $CDCl_3$): $\delta = 1.15$ (dd, 12H, $J_{HH} = 1.8$ Hz, $^3J_{HH} = 7.0$ Hz, CHCH_3), 2.19 (s, 3H, N=CCH$_3$), 2.78 (sept, 2H, $^3J = 7.0$ Hz, CHMe$_2$), 6.91 (m, 1H, H–Ar), 7.05 (m, 1H, H–Ar), 7.18 (b, 3H, H–Ar), 7.41 (m, 1H, H–Ar), 7.65 (m, 1H, H–Ar), 14.95 (s, 1H, OH) ppm. ^{13}C NMR (50 MHz, $CDCl_3$): $\delta = 17.6$, 23.1, 23.6, 28.3, 118.0, 118.3, 119.1, 123.2, 125.1, 128.9, 133.1, 138.0, 142.3, 162.4, 172.1 ppm. IR: $\nu = 1608$ cm^{-1} (C=N).

2.3.2. 2-[(2,6-diisopropylphenylimino)ethyl]naphthol (**5**)

The compound was prepared and purified as described above (Section 2.3.1). Yield: 48%. *Anal.* Calc. for $C_{24}H_{27}ON$: C, 83.44; H, 7.87; N, 4.05. Found: C, 83.39; H, 7.88; N, 4.03%. ^{1}H NMR (200 MHz, $CDCl_3$): $\delta = 1.17$ (d, 12H, $^3J_{HH} = 7.0$ Hz, CHCH_3), 2.28 (s, 3H, CCH$_3$), 2.89 (sept, 2H, $^3J = 7.0$ Hz, CHMe$_2$), 7.14 (m, 1H, H–Ar), 7.24 (m, 3H, H–Ar), 7.52 (m, 3H, H–Ar), 7.73 (m, 1H, H–Ar), 8.53 (m, 1H, H–Ar), 17.08 (s, 1H, OH) ppm. ^{13}C NMR (50 MHz, $CDCl_3$): $\delta = 17.2$, 22.8, 23.9, 28.5, 110.56, 115.8, 123.5, 124.7, 126.4, 127.2, 129.1, 136.5, 139.1, 140.6, 167.4, 172.3 ppm. IR: $\nu = 1596$ cm^{-1} (C=N).

2.3.3. 2-[(2,6-diisopropylphenylimino)(phenyl)methyl]-phenol (**6**)

The compound was prepared as described for **4** (Section 2.3.1). The isolated residue was purified with column chromatography using petroleum ether/ethylacetate (8:1) solvent mixture as eluent. Isolated yield: 6%. *Anal.* Calc. for $C_{25}H_{27}ON$: C, 83.99; H, 7.61; N, 3.92. Found: C, 82.29; H, 7.66 N, 3.86%. ^{1}H NMR (200 MHz, $CDCl_3$): $\delta = 1.08$ (d, 6H, $^3J_{HH} = 8.0$ Hz, CHCH_3), 1.17 (d, 6H, $^3J_{HH} = 8.0$ Hz, CHCH_3), 2.97 (sept, 2H, $^3J = 8.0$ Hz, CH Me$_2$), 6.81 (m, 1H, H–Ar), 7.03 (m, 2H, H–Ar), 7.16 (b, 5H, H–Ar), 7.30 (m, 3H, H–Ar), 7.43 (m, 1H, H–Ar), 14.76 (s, 1H, OH). IR: $\nu = 1605$ cm^{-1} (C=N). MS(EI): 357 (M$^+$), 280 (M$^+$ − Ph).

2.4. Synthesis of complexes

2.4.1. {Phenyl)(triphenylphosphine)(2-[(2,6-diisopropylphenylimino) ethyl]phenoxy)}-nickel(II) (**7**)

A solution of ligand **4** (0.65 g, 2.2 mmol) in THF was added to excess amount of NaH (0.18 g, 7.5 mol) at 0 °C. The mixture was stirred for 1 h at room temperature, filtered and evaporated. The pale yellow residue was washed with *n*-pentane and dried. Yield of the sodium salt Na-**4** was 98%. To a solid mixture of

Na-**4** (0.30 g, 0.94 mmol) and *trans*-[$(PPh_3)_2$Ni((Ph)Cl] (0.62 g, 0.90 mmol), 20 ml of benzene was added at 0 °C. The mixture was stirred at room temperature for 6 h and then filtered. After concentrating the filtrate to ca. 3 ml, the product was precipitated as orange powder upon addition of *n*-pentane (30 ml). The solid was isolated by cannula filtration, then washed with pentane and dried. Isolated yield: 30%. *Anal.* Calc. for $C_{44}H_{44}NNiOP$: C, 76.31; H, 6.40; N, 2.02. Found: C, 76.86; H, 6.41; N, 2.04%. ^{1}H NMR (200 MHz, C_6D_6): $\delta = 1.05$ (d, 6H, $^3J_{HH} = 6.8$ Hz, *i*Pr–CH_3), 1.21 (d, 6H, $^3J_{HH} = 6.8$ Hz, *i*Pr–CH_3), 1.83 (s, 3H, N=CCH_3), 3.84 (sept, 2H, $^3J_{HH} = 6.8$ Hz, *i*Pr–CH), 6.29–7.70 (m, 27H, Ar–H). ^{31}P NMR (200 MHz, C_6D_6): $\delta = 23.8$ ppm. IR: $\nu = 1598$ cm^{-1} (C=N).

2.4.2. {Phenyl)(triphenylphosphine)(2-[(2,6-diisopropylphenylimino)ethyl]naphthoxy)}-nickel(II) (*8*)

The sodium salt of the ligand (Na-**5**) and the corresponding complex were prepared following the same procedure used above (Section 2.4.1). The product was purified by recrystallization from 1:5 benzene/*n*-pentane solvent mixture at −20 °C and collected as orange crystals. Isolated yield: 39%. *Anal*. Calc. for $C_{48}H_{46}NNiOP$: C, 77.63; H, 6.24; N, 1.89. Found: C, 77.64; H, 5.90; N, 1.54%. ^{1}H NMR (200 MHz, C_6D_6): $\delta = 1.10$ (d, 6H, $^3J_{HH} = 7.0$ Hz, *i*Pr–CH_3), 1.24 (d, 6H, $^3J_{HH} = 7.0$ Hz, *i*Pr–CH_3), 1.97 (s, 3H, N=CCH_3), 3.89 (sept, 2H, $^3J_{HH} = 7.0$ Hz, *i*Pr–CH), 6.25–7.69 (m, 29H, Ar–H). ^{13}C NMR (50 MHz, $CDCl_3$): $\delta = 23.6$, 24.7, 25.1, 29.4, 114.2, 116.7, 121.8, 124.0, 124.5, 125.8, 126.4, 127.1, 127.3, 127.8, 128.3, 128.5, 128.7, 130.2, 131.7, 131.9, 132.2, 135.0, 135.1, 137.4, 138.7, 140.8, 147.9, 164.2, 169.5 ppm. ^{31}P NMR (200 MHz, C_6D_6): $\delta = 24.3$ ppm. IR: $\nu = 1597$ cm^{-1} (C=N).

2.4.3. Bis[{2-(2,6-diisopropylphenylimino)(phenyl)methyl}phenoxy]nickel(II) (*9*)

The sodium salt of the ligand **6** was prepared as described above (Section 2.4.1). A solution of Na-**6** (0.53 g, 1.40 mmol) in benzene (30 ml) was added to a suspension of *trans*-[$(PPh_3)_2$Ni((Ph)Cl] (0.88 g, 1.27 mmol) in the same solvent (20 ml). The reaction took soon a deep red color and was stirred at room temperature for 6 h and then filtered. After concentrating the filtrate to ca. 3 ml, the product was precipitated upon addition of *n*-pentane (30 ml). The solid was isolated by cannula filtration then washed with *n*-pentane and dried. The isolated product was crystallized from toluene/*n*-hexane 1:5 mixture to give orange crystals suitable for X-ray structure analysis. Isolated yield was 32%. ^{1}H NMR (200 MHz, C_6D_6): $\delta = 1.24$ (d, 12H, $^3J_{HH} = 6.6$ Hz, *i*Pr–CH_3), 2.13 (d, 12H, $^3J_{HH} = 6.6$ Hz, *i*Pr–CH_3), 3.87 (sept, 4H, $^3J_{HH} = 6.6$ Hz, *i*Pr–CH), 5.68 (m, 2H, H–Ar), 6.11 (m, 2H, H–Ar), 6.56–7.20 (m, 10H, H–Ar) ppm. IR: $\nu = 1599$ cm^{-1} (C=N).

2.4.4. Bis[(2-(2,6-diisopropylphenylimino)ethyl)phenoxy]nickel(II) (*10*)

The compound was prepared as described in Section 2.4.3. Crystals suitable for single crystal X-ray analysis were formed upon recrystallization from benzene/*n*-pentane (1:5) solvent mixture. ^{1}H NMR (200 MHz, C_6D_6): $\delta = 1.13$ (d, 12H, $^3J_{HH} = 7.0$ Hz, *i*Pr–CH_3), 1.73 (m, 18H, *i*Pr–CH_3, N=CCH_3), 4.08 (sept, 4H, $^3J_{HH} = 7.0$ Hz, *i*Pr–CH), 5.77 (m, 2H, Ar–H), 6.33 (m, 2H, Ar–H), 6.83–7.25 (m, 10H, Ar–H) ppm. MS(EI): 647 (M^+), 358 ($M^+ - (N \cap O)$). IR: $\nu = 1602$ cm^{-1} (C=N).

2.4.5. Bis[(2-(2,6-diisopropylphenylimino)ethyl)naphtoxy]nickel(II) (*11*)

A solution of Na-**5** (0.52 g, 1.42 mmol) in benzene (30 ml) was added to a suspension of *trans*-[$(PPh_3)_2$Ni((Ph)Cl] (0.88 g, 1.27 mmol) in the same solvent (20 ml). The reaction took soon a deep red color and was stirred at room temperature for 6 h, after which it was treated as in Section 2.4.3. Yield 86%. *Anal.* Calc. for $C_{48}H_{52}N_2O_2Ni$: C, 77.11; H, 7.01; N, 3.74. Found: C, 75.02; H, 6.93; N, 3.65%. ^{1}H NMR (200 MHz, C_6D_6): $\delta = 1.13$ (d, 12H, $^3J_{HH} = 7.0$ Hz, *i*Pr–CH_3), 1.39 (d, 12H, $^3J_{HH} = 7.0$ Hz, *i*Pr–CH_3), 1.72 (s, 3H, N=CCH_3), 4.60 (sept, 2H, $^3J_{HH} = 7.0$ Hz, *i*Pr–CH), 6.14 (m, 2H, H–Ar), 6.76–7.46 (m, 16H, H–Ar) ppm. MS(AP-MALDI): 746 (M^+). IR: $\nu = 1591$ cm^{-1} (C=N).

2.5. X-ray crystal structure determination for the complexes 7–*10*

Single crystals of the compounds were selected for the X-ray measurements and mounted on the glass fibre using the oil drop method [15a]. Data were collected at 120(2) (**7**, **10**) and 173(2) (**8**, **9**) K using Nonius KappaCCD diffractometer. The intensity data were corrected for Lorentz and polarization [15b] effects and for absorption by multi-scan method [16]. The structures were solved by direct methods (SHELXS 97). The refinements and graphics were done using SHELXL 97 and SHELXTL/PC program package, respectively. All non-hydrogen atoms were refined anisotropically. The H atoms were introduced in calculated positions and refined with fixed geometry with respect to their carrier atoms. The cell parameters and the specific data collections parameters are summarized in Table 1.

3. Results and discussion

3.1. Ligand and complex synthesis

The synthesis of the ligands (**4**–**6**) and their nickel complexes (**7**–**11**) are shown in Scheme 1. Preparation of the desired salicylketimines turned out to proceed with

Table 1
Crystal data and structure refinement for **7**–**10**

	7	**8**	**9**	**10**
Formula	$C_{44}H_{44}NNiOP$	$C_{48}H_{46}NNiOP$	$C_{50}H_{52}N_2NiO_2$	$C_{40}H_{48}N_2NiO_2$
Formula weight	692.48	742.54	771.65	647.51
T (K)	120(2)	173(2)	173(2)	120(2)
Crystal system	triclinic	monoclinic	monoclinic	triclinic
Space group	$P\bar{1}$	$P21/c$	$P21/c$	$P\bar{1}$
Unit cell dimensions				
a (Å)	11.6450(1)	14.1440(11)	10.3310(19)	8.36340(10)
b (Å)	11.7285(1)	13.681(2)	11.577(3)	9.9331(2)
c (Å)	14.1484(2)	22.128(4)	19.815(3)	11.5502(2)
α (°)	99.491(1)	90.000(11)	90.000(16)	112.6720(1)
β (°)	96.400(1)	114.726(9)	121.123(15)	100.1010(10)
γ (°)	109.777(1)	90.000(8)	90.000(16)	99.0720(10)
V (Å^3)	1764.13(3)	3889.3(10)	2028.8(8)	844.43(2)
Z	2	4	2	1
D_{calc} (Mg m^{-3})	1.304	1.268	1.263	1.273
Absorption coefficient (mm^{-1})	0.631	0.577	0.521	0.612
Crystal dimensions (mm)	$0.30 \times 0.30 \times 0.10$	$0.25 \times 0.20 \times 0.15$	$0.20 \times 0.20 \times 0.06$	$0.20 \times 0.15 \times 0.05$
θ range (°)	2.13–27.48	5.02–27.50	3.52–27.52	3.96–27.45
Number of data collected	31 239	47 797	139 71	10 310
Number of unique data	8063 [$R_{int} = 0.0437$]	8855 [$R_{int} = 0.0759$]	4622 [$R_{int} = 0.0775$]	3838 [$R_{int} = 0.0293$]
Number of data refined	8063	8855	4622	3838
Number of parameters	438	469	250	210
$R^a[I > 2\sigma(I)]$	0.0366	0.0436	0.0533	0.0317
$wR_2{}^b$	0.0789	0.0828	0.1023	0.0710
Residual density (e A^{-3})	0.369 and −0.437	0.328 and −0.397	0.439 and −0.476	0.282 and −0.313

[a] $R = \sum \|F_o| - |F_c\| / \sum |F_o|$.
[b] $wR_2 = [\sum[w(F_o^2 - F_c^2)^2] / \sum[w(F_o^2)^2]]^{1/2}$.

negligible yields, even with extended refluxing periods. Therefore, ligands **4**, **5** and **6** were prepared in methanol at 200 °C in a closed steel autoclave in the presence of Na_2SO_4 and a catalytic amount of formic acid. After purification by column chromatography, ligands **4** and **5** were isolated with nearly 50% yields, but with only 6% yield for ligand **6**. After deprotonation of the ligands with an excess of NaH in THF, the corresponding sodium salts were allowed to react with *trans*-[$(PPh_3)_2$-Ni((Ph)Cl], either by addition of the reaction solvent (benzene) to a solid mixture of the two reactants at low temperature or by addition of a solution of the corresponding sodium salt to a suspension of the nickel precursor. The former method favours the formation of monophenyl-nickel(II) complexes **7** and **8**, while the latter method leads to the formation of the bis(sal)Ni(II) complexes **9**–**11**.

^{1}H NMR spectra of the ligands are similar to those of the corresponding salicylaldimines [8], except for a singlet (**4** and **5**) which appears at 2.19–2.28 ppm that can be attributed to the ketimine methyl group. Upon complexation, this singlet is shifted upfield to 1.83–1.97 ppm. The septet which is due to CH protons of the isopropyl groups is shifted down field (from that in the spectra of ligands **4** and **5** (2.78 and 2.89 ppm)) to 3.84–3.89 ppm as observed for **7** and **8**. In the case of the bis(sal) complexes, this septet is further shifted to 3.87, 4.08 and 4.60 ppm for **9**, **10** and **11**, respectively. The signals of the triphenylphosphine ligand in the ^{31}P NMR spectra of complexes **7** and **8** are observed at 23.8–24.3 ppm. The IR spectra of **4**, **5** and **6** show bands at 1608, 1596 and 1605 cm^{-1}, respectively, which are ascribed to C=N group. After complexation, these bands are correspondingly found at 1598 and 1597 cm^{-1} for the monophenyl complexes (**7** and **8**) and 1599, 1602 and 1591 cm^{-1} for the bis(sal)-Ni(II) complexes (**9**–**11**), respectively. The IR spectra of all the studied complexes are in good agreement with previous reports of analogous compounds [9].

The reaction of Na-**5** with *trans*-[$(PPh_3)_2$Ni((Ph)Cl] was monitored by ^{1}H NMR. When benzene was added to a solid mixture of the reacting materials, only the monophenyl complex **8** was detected. This complex was purified by recrystallization from 1:5 benzene/*n*-pentane solvent mixture at −20 °C which gave orange crystals. However, when a slight excess of a solution of the sodium salt of **5** in benzene was added to a suspension of nickel precursor at ambient temperature, the bis(sal)-Ni(II) complex **11** was obtained as a major product and only a trace amount of **8** was observed in ^{1}H NMR. Ligand **4** behaved similarly upon complexation, both the monophenyl complex (**7**) and the bis(sal)Ni(II) (**10**) could be isolated.

In its isolated form complex **8** was found to be quite stable in solution at room temperature. According to ^{1}H NMR, no decomposition or transformation to the corresponding bis(sal)–Ni(II) species was detected even after 8 h room temperature and after 50 h the molar ratio of **11**:**8** was found to be 1:15. In the case of the

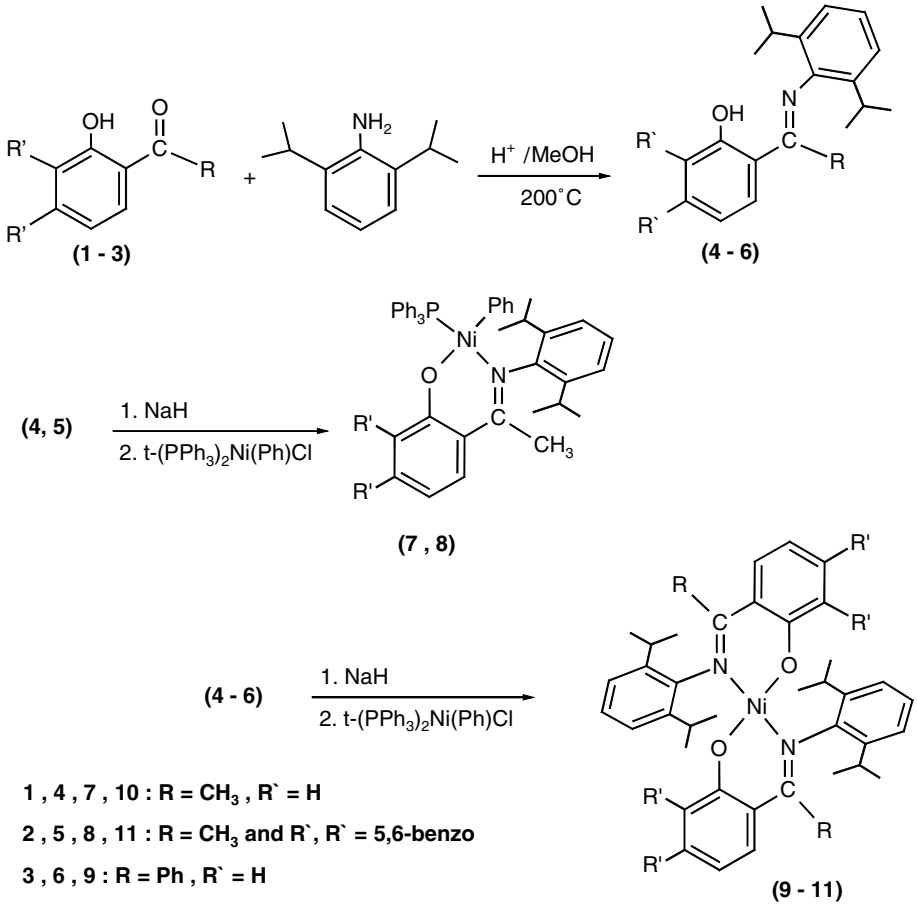

Scheme 1. Synthesis of ligands (**4**–**6**) and complexes (**7**–**11**).

salicylaldimines, the formation of bis(sal)Ni(II) complexes usually require more harsh reaction conditions [17]. In order to form the desired bis(sal)Ni(II) complex [17b], the neutral phenyl substituted salicylaldiminato Ni(II) complex had to be stirred at 50 °C first with vinyl chloride (VC) for four days in toluene and then to continue stirring for another four days in *n*-hexane at 50 °C. The complexation occurred via tetrahedral Ni complex bearing a Cl instead of the Ph ligand, where Cl–Ni bond was formed by 1,2-insertion of VC into Ni–Ph bond followed by β-Cl elimination.

With the salicylketimine ligands, the formation of the bis(sal) complexes can take place spontaneously. Moreover, in the reaction of Na-**6** with *trans*-[$(PPh_3)_2$-Ni((Ph)Cl], the bis(sal)Ni(II) complex (**11**) was the predominant product. It seems that the presence of the phenyl group on the ketimine carbon of the ligand increased the tendency to form a bis(sal) complex. The reason for this particular behaviour remains unclear but it could be due to *trans* influence of the ketimine site, thus allowing a faster dissociation of the second PPh_3 ligand. So, in addition to fine tuning of the reaction conditions, also different substituents on the ketimine carbon may affect on the complexation behaviour of these salicylketimine ligands.

Surprisingly, the monophenyl salicylketiminato based Ni(II) complexes **7** and **8** turned out to be catalytically inactive in homopolymerization of ethene or norbornene when [$Ni(COD)_2$] or BF_3 were applied as phosphine scavengers, even at elevated temperatures (up to 60 °C) and pressures (up to 40 bar).

3.2. Crystal structures of the complexes

For further investigation of structural features of the complexes, crystals of complexes **7** and **8**, suitable for X-ray structure determination, were grown from 1:5 benzene/*n*-pentane mixture at −20 °C and crystals of complexes **9** and **10** were obtained at ambient temperature. The coordination sphere of complex **8** was found to be similar to that of **7**. Also, the coordination spheres of bis(sal)Ni(II) complexes **9** and **10** were found to be alike. Data collection and the refinement of data of **7**–**10** (Figs. 1–4) are summarized in Table 1. [1]

In the solid state, complex **7** has a square-planar geometry. The Ni atom is approximately 0.01 Å out of the

[1] The molecular structure of **11** was also determined. It was found similar to that of **10** and is thus left from discussion here but the data is included in the supplementary material.

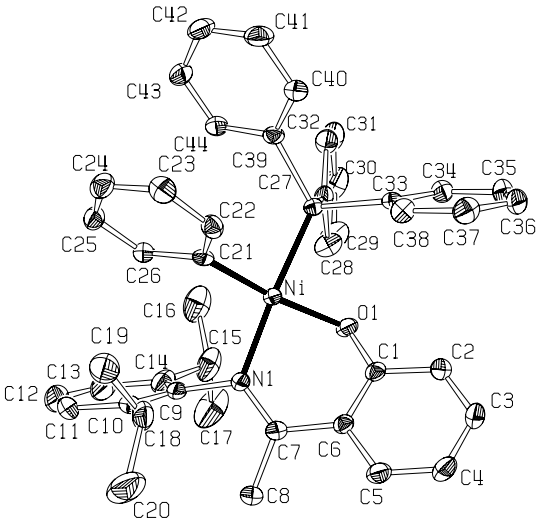

Fig. 1. ORTEP plot of the molecular structure of compound **7**. Displacement ellipsoids are drawn at 50% probability level.

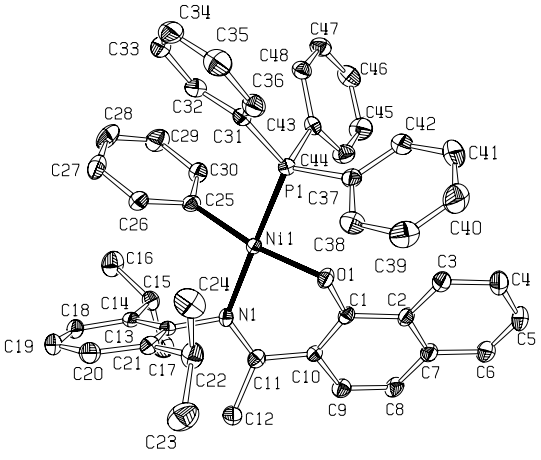

Fig. 2. ORTEP plot of the molecular structure of compound **8**. Displacement ellipsoids are drawn at 50% probability level.

plane of the donor atoms. The bulky 2,6-diisopropylphenylimine occupies the *trans* position to the triphenylphosphine ligand with almost a linear N1–Ni–P1 angle (172.17(5)°) (Table 2). The phenyl group attached to Ni lies in *trans* position to O1 with an O1–Ni–C21 angle of 171.73(7)°. The Ni–O1, Ni–N1 and Ni–C21 bond distances in complex **7** are similar to those for known nickel complexes [18].

The Ni–P1 bond distance (2.185(1) Å) is only a bit longer than those in Grubbs' nickel-based complex (2.172(2) Å) and in Cavell's [Ni(PPh_3)(*o*-tolyl)(N–O)] complexes with N–O bidentate pyridinecarboxylate ligands (*d*(Ni–P) 2.1653(2) Å) [18d]. But, it is clearly shorter than that in nickel(II) salicylaldiminato complexes bearing naphthyl instead of phenyl group *cis* to PPh_3 (2.200(1) and 2.198(2) Å) [9].

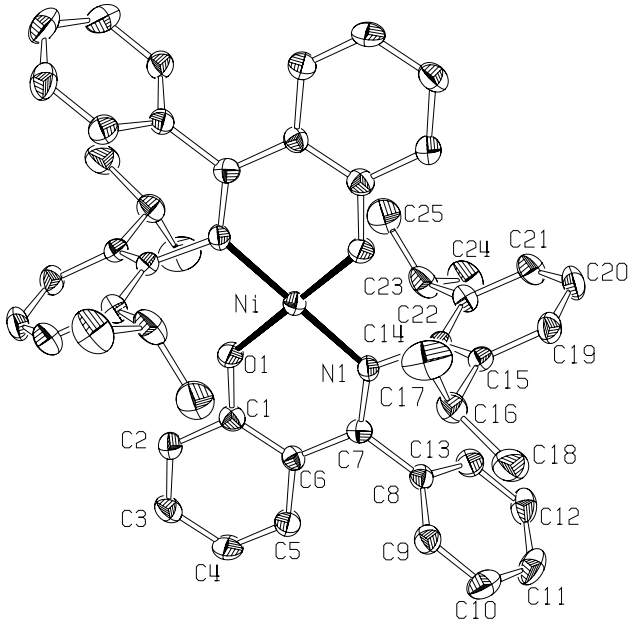

Fig. 3. ORTEP plot of the molecular structure of compound **9**. Displacement ellipsoids are drawn at 50% probability level.

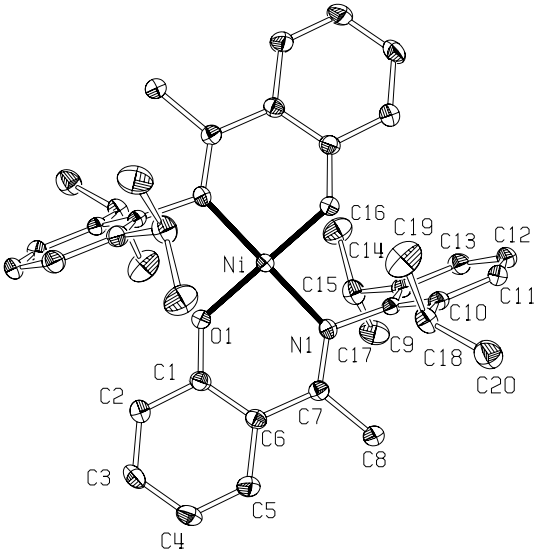

Fig. 4. ORTEP plot of the molecular structure of compound **10**. Displacement ellipsoids are drawn at 50% probability level.

Complex **9** forms a square planar complex, at which nickel lays in the symmetry centre of the molecule and thus in the plane of the four donor atoms (Table 1, Fig. 3). The bond angles and distances are similar to those found for **10** (Table 1, Fig. 4), where the average Ni–O distance (1.808 Å) is somewhat shorter, and the Ni–N distance (1.926) is somewhat longer than those in the bis(salicylaldiminato) complexes which were reported by Jordan and co-workers (Ni–O 1.846 Å, Ni–N 1.899 Å) [17b] and Knoch et al. (1.856, 1.899 Å) [17a].

Table 2
Selected bond lengths (Å) and angles (°) for **7**–**10** (symmetry transformations were used to generate equivalent atoms)

	7 ($x = 21$)	**8** ($x = 26$)	**9**	**10**
Bond lengths				
Ni–C(x)	1.8957(18)	1.905(2)		
Ni–O(1)	1.9050(12)	1.8890(14)	1.809(2)	1.8081(10)
Ni–N(1)	1.9582(15)	1.9498(16)	1.933(2)	1.9262(11)
Ni–P(1)	2.1845(5)	2.1907(7)		
Bond angles				
C(x)–Ni–O(1)	171.73(7)	167.92(8)		
C(x)–Ni–N(1)	95.96(7)	97.00(8)		
O(1)–Ni–N(1)	89.75(6)	90.07(6)	92.04(9)	91.88(5)
O(1)–Ni–P(1)	84.19(4)	87.71(4)		
N(1)–Ni–P(1)	172.17(5)	173.27(5)		
C(x)–Ni–P(1)	90.60(5)	86.31(6)		
O(1A)–Ni–O(1)			180.00(13)	180.00(10)
O(1)–Ni–N(1A)			87.96(9)	88.12(5)
N(1A)–Ni–N(1)			180.000(1)	180.00(10)

4. Conclusions

A method for the synthesis of salicylketimine ligands was developed by condensation of a ketone with an amine in methanol at 200 °C in a closed steel-autoclave. The complexation behaviour of these ligands towards *trans*-[$(PPh_3)_2$Ni((Ph)Cl] was investigated. Two types of Ni(II) complexes could be isolated and characterized, the monophenyl(salicylketimine)Ni(II) complexes and the corresponding bis(salicylketimine) Ni(II) complexes. It was found that salicylketimine ligands form readily the bis(sal)Ni(II) complexes.

5. Supplementary material

Crystallographic data for the structures reported in this paper have been deposited at the Cambridge Crystallographic Data Centre as supplementary publication numbers CCDC 230868 (**7**), CCDC 230869 (**8**), CCDC 230871 (**9**), CCDC 230870 (**10**) and CCDC 230872 (**11**). Copies of the data can be obtained on application to the Director, CCDC, 12 Union Road, Cambridge CB2 1EZ, UK (fax: +44-1223-336-033; e-mail: deposit@ccdc.cam.ac.uk or www:http://www.ccdc.cam.ac.uk).

Acknowledgements

M.K. thanks Fortum foundation for financial support. Academy of Finland is acknowledged for financial support via Centre of Excellence (Bio- and Nanopolymer Research Group, project 77317).

References

[1] A.S. Abu-Surrah, B. Rieger, Angew. Chem., Int. Ed. Engl. 35 (1996) 2475, and references therein.
[2] A. Yamamoto, K. Morifuji, S. Ikeda, T. Saito, Y. Uchia, A. Misono, J. Am. Chem. Soc. 90 (1968) 1878.
[3] (a) L.K. Johnson, C.M. Killian, M. Brookhart, J. Am. Chem. Soc. 117 (1995) 6414;
(b) B.L. Small, M. Brookhart, A.M.A. Bennet, J. Am. Chem. Soc. 120 (1998) 4049;
(c) G.J.P. Britovsek, V.C. Gibson, B.S. Kimberley, P.J. Maddox, S.J. McTavish, G.A. Solan, A.J.P. White, D.J. Williams, Chem. Commun. 7 (1998) 849.
[4] (a) For reviews: A.S. Abu-Surrah, B. Rieger, Top. Catal. 7 (1999) 165;
(b) S.D. Ittel, L.K. Johnson, M. Brookhart, Chem. Rev. 100 (2000) 1169;
(c) L.S. Boffa, B.M. Novak, Chem. Rev. 100 (2000) 1479;
(d) G.W. Coates, P.D. Hustad, S. Reinartz, Angew. Chem., Int. Ed. Engl. 41 (2002) 2236;
(e) V.C. Gibson, S.K. Spitzmesser, Chem. Rev. 103 (1) (2003) 283, For acrylate polymerizations:
(f) P.M. Castro, K. Lappalainen, M. Ahlgrén, M. Leskelä, T. Repo, J. Polym. Sci. Part A: Polym. Chem. 41 (2003) 1380;
(g) G. Tian, H.W. Boone, B.M. Novak, Macromolecules 34 (2001) 7656.
[5] J.C. Jenkins, M. Brookhart, Organometallics 22 (2003) 250.
[6] D. Vogt, in: B. Cornils, W.A. Herrmann (Eds.), Applied Homogeneous Catalysis with Organometallic Compounds, vol. 1, VCH, Weinheim, 1996, pp. 251–258.
[7] L.K. Johnson, A.M.A. Bennett, S.D. Ittel, L. Wang, A. Parthasarathy, E. Hauptman, R.D. Simpson, J. Feldman, E.B. Coughlinm, DuPont Patent WO 9830609.
[8] (a) C. Wang, S. Friedrich, T.R. Younkin, R.T. Li, R.H. Grubbs, D.A. Bansleben, M.W. Day, Organometallics 17 (1998) 3149;
(b) T.R. Younkin, E.F. Connor, J.I. Henderson, S.K. Friedrich, R.H. Grubbs, D.A. Bansleben, Science 287 (2000) 460.
[9] W.-H. Sun, H. Yang, Z. Li, Y. Li, Organometallics 22 (2003) 3678.
[10] (a) A.S. Abu-Surrah, K. Lappalainen, U. Piironen, P. Lehmus, T. Repo, M. Leskela, J. Organomet. Chem. 648 (2002) 55;
(b) G.J.P. Britovsek, M. Bruce, V.G. Gibson, B.S. Kimberley, P.J. Maddox, S. Mastroianni, S.J. McTavish, C. Redshaw, G.A. Solan, S. Strömberg, A.J.P. White, D.J. Williams, J. Am. Chem. Soc. 121 (1999) 8728.
[11] A.S. Abu-Surrah, U. Thewalt, B. Rieger, J. Organomet. Chem. 587 (1999) 58.

[12] A.S. Abu-Surrah, M. Kettunen, K. Lappalainen, U. Piironen, M. Klinga, M. Leskelä, Polyhedron 21 (2002) 27.
[13] (a) A.S. Abu-Surrah, B. Rieger, J. Mol. Catal. A 128 (1998) 239;
(b) M. Kettunen, A.S. Abu-Surrah, T. Repo, M. Leskelä, Polym. Int. 50 (2001) 1223.
[14] M. Hiodai, T. Kashiwagi, T. Ikeuchi, Y. Uchida, J. Organomet. Chem. 30 (1971) 279.
[15] (a) T. Kottke, D. Stalke, J. Appl. Crystallogr. 26 (1993) 615;
(b) Molecular Structure Corporation. TEXSAN, Single Crystal Structure Analysis Software. Version 1.6. MSC, 3200 Research Forest Drive, The Woodlands, TX 77381, USA, 1993.
[16] XPREP in SHELTL version 5.1, Bruker AXS, 1998.
[17] (a) R. Knoch, H. Elias, H. Paulusi, Inorg. Chem. 34 (1995) 4032;
(b) S.R. Foley, R.A. Stockland Jr., H. Shen, R.F. Jordan, J. Am. Chem. Soc. 125 (2003) 4350.
[18] (a) J. Feldman, S.J. McLain, A. Parthasarathy, W.J. Marshall, J.C. Calabrese, S.D. Arthur, Organometallics 16 (1997) 1514;
(b) W. Keim, F.H. Kowaldt, R. Goddard, C. Krüger, Angew. Chem., Int. Ed. Engl. 17 (1978) 466;
(c) U. Klabunde, S.D.J. Ittel, Mol. Catal. 41 (1987) 123;
(d) S.Y. Desjardins, K.J. Cavell, J.L. Hoare, B.W. Skelton, A.N. Sobolev, A.H. White, W. Keim, J. Organomet. Chem. 544 (1997) 163;
(e) F.M. Bauers, S. Mecking, Macromolecules 34 (2001) 1165;
(f) D. Zhang, G.-X. Jin, N. Hu, Chem. Commun. (2002) 574;
(g) L.K. Johnson, A.M.A. Bennett, S.D. Ittel, L. Wang, A. Parthasarathy, E. Hauptman, R.D. Simpson, J. Feldman, E.B. Coughlin, DuPont WO9830609, 1998;
(h) Chem. Abstr. 129 (1998) 149362j;
(i) C. Carlini, M. Martinelli, A.M.R. Galletti, G. Sbrana, Macromol. Chem. Phys. 203 (2002) 1606.

Available online at www.sciencedirect.com
SCIENCE DIRECT®
Polyhedron 23 (2004) 1657–1661
POLYHEDRON
www.elsevier.com/locate/poly

Ruthenium(II) carbonyl complexes containing tertiary phosphine chalcogenide ligands of the type Ph_3PX; X = O, S, Se

Pratap Chutia [a], Nandini Kumari [a], Manab Sharma [a], J. Derek Woollins [b], Alexandra M. Z. Slawin [b], Dipak Kumar Dutta [a,*]

[a] *Material Science Division, Regional Research Laboratory (CSIR), Jorhat 785006, Assam, India*
[b] *Department of Chemistry, University of St. Andrews, St. Andrews KY 16 9ST, UK*

Received 18 February 2004; accepted 29 March 2004
Available online 23 April 2004

Abstract

The reactions of polymeric complex $[Ru(CO)_2Cl_2]_n$ with triphenyl phosphine chalcogenide ligands Ph_3PX; X = O(**a**), S(**b**), Se(**c**) in 1:1 (Ru:L ratio) molar ratio gives five-coordinate complexes of the type $[Ru(CO)_2Cl_2(Ph_3PX)]$(**1a**–**c**) while 1:2 (Ru:2L ratio) molar ratio produces six-coordinate $[Ru(CO)_2Cl_2(Ph_3PX)_2]$(**2a**–**c**) complexes. The complexes **1a**–**c** and **2a**–**c** exhibit two equally intense ν(CO) bands in the range 2059–1989 and 2050–1980 cm^{-1}, respectively, indicating *cis*-disposition of the two terminal carbonyl groups. The values of ν(CO) frequencies irrespective of the complexes, in general, follow the order: $Ph_3PO > Ph_3PS > Ph_3PSe$ which may be ascribed in terms of "Soft–Hard" (Ru(II)–O) and "Soft–Soft" (Ru(II)–S/Se) interactions. The ν(PX) bands of the complexes observed in the range 1173–538 cm^{-1} are 19–41 cm^{-1} lower than those of the corresponding free ligands indicating the formation of Ru–X bonds. The molecular structure of the complex $[Ru(CO)_2Cl_2(Ph_3PS)_2]$ was determined by single X-ray crystallography. The crystal is monoclinic, space group Cc; $a = 11.4990$ Å, $b = 17.3966$ Å, $c = 18.4788$ Å; $\alpha = 90°$, $\beta = 98.160°$, $\gamma = 90°$. In the molecule, the Ru(II) atom occupies the center of a slightly distorted octahedral geometry which consists of two *trans*-S atoms of two Ph_3PS ligands, two *cis*-CO groups and two *cis*-chlorides. The complexes have also been characterized by elemental analysis, ^1H, ^{13}C and ^{31}P NMR spectroscopy.
© 2004 Elsevier Ltd. All rights reserved.

Keywords: Ruthenium(II) carbonyl complexes; Tertiary phosphine chalcogenides; "Soft–Hard" and "Soft–Soft" interactions; X-ray crystal structure; Octahedral structure

1. Introduction

The chemistry of rhodium and ruthenium metal complexes of unsymmetrical chelating phosphines functionalized with chalcogen donors like $Ph_2P(CH_2)_nP(X)Ph_2$ ($n = 1$–4, X = O, S, Se), $Ph_2PC_6H_4COOMe$, $Ph_2P(CH_2)_nOR$ (R = CH_3, C_2H_5) has gained much importance because of their structural novelty, reactivity and catalytic applications [1–7]. In contrast, monodentate tertiary phosphines functionalized with chalcogen donors such as Ph_3PX (X = O, S, Se) received less attention although the chemistry of such ligands is potentially important and well established. There are reports of some complexes with platinum metals [8–15], but to the best of our knowledge, only a few reports [16–21] are there on ruthenium(II) complexes. This prompted us to synthesize, characterize and to study coordination chemistry of ruthenium(II) carbonyl complexes with these chalcogen donors ligands.

In the present communication, we report the synthesis, spectroscopic characterization and structural investigation of some ruthenium(II) carbonyl complexes derived from the reaction of $[Ru(CO)_2Cl_2]_n$ with Ph_3PX; X = O, S, Se and the effect of "Soft–Hard" and "Soft–Soft" nature of the chalcogenide ligands on ν(CO) frequency is discussed. In order to the determine detailed geometry, an X-ray diffraction study was undertaken for one of the sulfide complexes.

* Corresponding author. Tel.: +91-376-237-0081/0147; fax: +91-376-237-0011.
E-mail addresses: dipakkrdutta@yahoo.com, dipdutta49@yahoo.com (D. Kumar Dutta).

0277-5387/$ - see front matter © 2004 Elsevier Ltd. All rights reserved.
doi:10.1016/j.poly.2004.03.016

2. Experimental

2.1. General methods

All the solvents used were distilled under nitrogen prior to use. Carbon and hydrogen analyses were done on a Perkin–Elmer 2400 elemental analyzer. Chloride analyses were performed by standard analytical method [22]. FT-IR spectra of range 4000–400 and 400–200 cm^{-1} were recorded using Perkin–Elmer 2000 and Perkin–Elmer 883 spectrophotometer, respectively, in KBr disc. NMR data were recorded on a Bruker DPX 300 MHz spectrometer and the ^1H and ^{31}P NMR chemical shifts were quoted relative to $SiMe_4$ and 85% H_3PO_4 as internal and external standard, respectively, using $CDCl_3$ and d_6-acetone as solvent. Melting points were determined with a BUCHI B-540 apparatus. $RuCl_3 \cdot 3H_2O$ was purchased from M/s Arrora Matthey Ltd., Kolkata, India. Analytically pure Ph_3P and elemental sulfur, selenium were purchased from M/S Aldrich, USA and used without further purification. The ligands, Ph_3PX, X = O, S, Se were prepared by the literature method [23–25]. The starting complex $[Ru(CO)_2Cl_2]_n$ was prepared by passing CO through a refluxing solution of $RuCl_3 \cdot 3H_2O$ in ethanol for about 24 h [26–29].

2.2. Synthesis of metal complexes

2.2.1. $[Ru(CO)_2Cl_2(Ph_3PX)]$ (**1a**–**c**), X = O, S, Se

0.044 mmol of $[Ru(CO)_2Cl_2]_n$ was dissolved in 10 cm^3 methanol and to this 0.044 mmol of corresponding ligands **a**–**c** in 10 cm^3 dichloromethane was added. The reaction mixture was stirred at room temperature for about 2 h and the solvent was evaporated under vacuum. The solid compound so obtained was washed with diethyl ether and recrystallized from dichloromethane solution.

2.2.2. $[Ru(CO)_2Cl_2(Ph_3PX)_2]$(**2a**–**c**), X = O, S, Se

0.044 mmol of $[Ru(CO)_2Cl_2]_n$ was dissolved in methanol (10 cm^3) and to this 0.088 mmol of corresponding ligands **a**–**c** in 10 cm^3 dichloromethane was added. The reaction mixture was stirred at room temperature for about 2.5 h and the solvent was evaporated under reduced pressure to generate a solid compound which was washed with diethyl ether and finally recrystallized from dichloromethane solution.

Analytical data and physical properties of the complexes are shown in Table 1.

2.3. X-ray crystallography

A crystal of the complex **2b** suitable for X-ray crystallographic analysis was developed from a CH_2Cl_2-hexane solution. Data collection was performed using a Bruker SMART diffractometer, full sphere of data with

Table 2
Crystal data and structure refinement of the complex **2b**

Empirical formula	$C_{38}H_{30}Cl_2O_2P_2RuS_2$
Formula weight	816.65
Temperature (K)	293(2)
Wave length (Å)	0.71073
Crystal system	monoclinic
Space group	Cc
a (Å)	11.4990(11)
b (Å)	17.3966(16)
c (Å)	18.4788(17)
α (°)	90
β (°)	98.160(2)
γ (°)	90
Volume (Å^3)	3659.1(6)
Z	4
D_{calc} (Mg/m^3)	1.482
Absorption coefficient (mm^{-1})	0.809
$F(000)$	1659
Crystal size (mm)	$0.1 \times 0.1 \times 0.02$
θ Range for data collection (°)	2.14–25.40
Index ranges	$-13 \leqslant h \leqslant 12$, $-20 \leqslant k \leqslant 20$, $-22 \leqslant l \leqslant 22$
Reflections collected	12 461
Independent reflections	6304 ($R_{int} = 0.1091$)
Completeness to $\theta = 25.40°$	99.7 %
Absorption correction	MULTISCAN
Maximum and minimum transmission	1.00000 and 0.933609
Refinement method	full-matrix least-squares on F^2
Data/restraints/parameters	6304/2/425
Goodness-of-fit on F^2	0.603
Final R indices [$I > 2\sigma(I)$]	$RI = 0.0475$, $wR_2 = 0.0957$
R indices (all data)	$RI = 0.1495$, $wR_2 = 0.1447$
Absolute structure parameter	0.11(6)
Extinction coefficient	0.00034(14)
Largest differential peak and hole (e Å^{-3})	0.333 and −0.306

Table 1
Analytical data and physical properties of the complexes

Complexes	Yield (%)	Colour	Melting point (°C)	Found (Calc.) (%)		
				C	H	Cl
1a	92	light green	182 (decomposed)	47.44(47.40)	2.93(2.96)	14.00(14.02)
1b	96	red-brown	187	45.91(45.94)	2.89(2.87)	13.56(13.59)
1c	95	dark-brown	173	42.12(42.15)	2.60(2.63)	12.50(12.47)
2a	89	light green	185 (decomposed)	58.09(58.11)	3.80(3.82)	9.03(9.05)
2b	90	red-brown	192	55.83(55.84)	3.66(3.67)	8.71(8.69)
2c	87	dark-brown	176	50.05(50.07)	3.31(3.29)	7.82(7.80)

0.3° slices, room temperature, Mo Kα radiation and empirical absorption corrections. All non-hydrogen atoms were refined anisotropically with the hydrogen atoms being refined in idealized geometries. The structure refinements were done by full matrix least square on F^2 using SHELXTL97 computer program [30]. The crystal data and structure refinement for the complex are listed in Table 2.

3. Results and discussion

Reaction of polymeric $[Ru(CO)_2Cl_2]_n$ with one molar equivalent (Ru:L = 1:1) of the ligands (**a**–**c**) affords five-coordinate 16 electron species of the type $[Ru(CO)_2Cl_2(Ph_3PX)]$(**1a**–**c**) (Scheme 1) where X = O, S, Se. The IR spectra (Table 3) of the complexes show two equally intense *ν*(CO) bands in the range 1980–2060 cm^{-1} attributing *cis*-disposition of the two terminal carbonyl groups [31,32]. The positions of the *ν*(CO) bands lie in the sequence $Ph_3PO > Ph_3PS > Ph_3PSe$. The reason of variation in *ν*(CO) frequency may be explained in terms of "Soft–Hard" and "Soft–Soft" interactions between the metal atom and the chalcogen donors. S and Se donors being "Soft" in complexes **1b** and **1c**, they interact strongly with "Soft" ruthenium(II), in contrast to the "Hard" oxygen in the complex **1a**. Because of the "Soft–Soft" interaction, the electron density increases on the central metal atom which leads to donate more d_π-electrons to the antibonding π^* orbital of the CO [7,32] and consequently reduces the C–O bond order, which in turn lowers the *ν*(CO) frequency. The *ν*(PX) (X = O, S, Se) bands in the complexes **1a**–**c** occur at 1173, 590, 538 cm^{-1}which are 27, 41, 20 cm^{-1} lower than their corresponding free ligands indicating the formation of bonds Ru–O, Ru–S and Ru–Se, respectively [9]. The *cis*-disposition of the two chlorides in the complexes is corroborated by the presence of two *ν*(RuCl) bands in the range 246–330 cm^{-1} [29]. The ^1H NMR spectra of the complexes show a set of multiplets in the *δ*7.26–7.85 ppm range assigned to the phenyl groups of triphenyl chalcogenide ligands. No appreciable shift is observed between coordinated and free ligand proton environment as the protons are remote from the coordinating chalcogen atom. The ^{31}P {H} NMR spectra of the complexes **1a**–**c** (Table 3) exhibit singlet resonance at *δ* 43.88, 48.24, 32.43 ppm, respectively, while their corresponding free ligand values occur at *δ* 30.37, 44.54, 36.53 ppm. Compared to the free ligands, the phosphorus atoms of the complexes show a small down field shift (3.70–13.51 ppm) because the phosphorus atoms are already attached with the chalcogen donor in the ligands. ^{13}C NMR data of the complexes **1a**–**c** are given in Table 3. The principal interest is on the carbonyl carbon and the ^{13}C NMR values are found to be a singlet at 182, 184, 186 ppm of the complexes **1a**–**c** respectively. Similar to the complex $[RuCl_2(PPh_3)_3]$ [33], these 16-electron complexes are assumed to show no steric barrier for H-coordination of a phenyl ring to block the 6th coordination site and the probable structure of the complexes are shown in Fig 1(a), although we could not develop suitable crystal for X-ray study.

Reaction of **1a**–**c** with one molar equivalent of ligands **a**–**c** yields six-coordinate 18 electron species of the type $[Ru(CO)_2Cl_2(Ph_3PX)_2]$(**2a**–**c**) (Scheme 1); X = O, S,

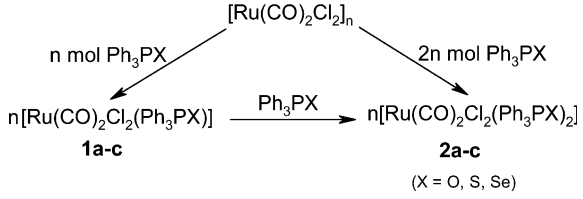

Scheme 1. Synthesis of complexes (**1a**–**c** and **2a**–**c**).

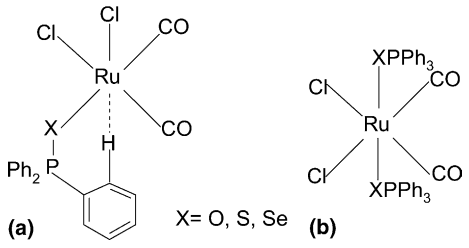

Fig. 1. Proposed structures for complexes **1a**–**c** (a) and **2a**–**c** (b).

Table 3
IR (cm^{-1}) and NMR (ppm) data of the complexes

Complexes	IR			$^{31}P^b$	^1H	^{13}C	
	ν(CO)	*ν*(PX[a]) (X = O, S, Se)	*ν*(RuCl)		C_6H_5	CO	C_6H_5
1a	2059, 1994	1173	330, 257	43.88	7.31–7.85 m	182	128.83–133.81
1b	2054, 1991	590	310, 246	48.24	7.36–7.75 m	184	128.83–132.72
1c	2052, 1989	538	312, 251	32.43	7.26–7.76 m	186	128.86–133.15
2a	2050, 1985	1165	328, 280	43.87	7.27–7.87 m	183	128.81–133.64
2b	2045, 1980	591	314, 281	48.21	7.34–7.81 m	182	128.82–132.72
2c	2043, 1981	539	309, 283	32.46	7.34–7.75 m	184	128.85–133.12

[a] Free Ph_3PO, 1200 cm^{-1}; Ph_3PS, 631cm^{-1}; Ph_3PSe, 558 cm^{-1}.
[b] Free Ph_3PO, 30.37 ppm; Ph_3PS, 44.54 ppm; Ph_3PSe, 36.53 ppm.

Se. The complexes **2a**–**c** can also be synthesized directly by reacting $[Ru(CO)_2Cl_2]_n$ with ligands **a**–**c** in 1:2 molar ratio. As in the complexes **1a**–**c**, the position and nature of ν(CO) and ν(RuCl) IR bands (Table 3) are in agreement with the mutual *cis*-disposition of the terminal carbonyl groups and the two chlorides. Similar to the complexes **1a**–**c**, the ν(PX) (X = O, S, Se) bands in complexes **2a**–**c** also show considerable lower values (19–40 cm^{-1}) suggesting coordination via chalcogen donor sites. The ^{31}P {H } NMR spectra of **2a**–**c** also show one singlet resonance showing a small shift in the range 3.67–13.50 ppm. The ^{13}C NMR spectra (Table 3) of the complexes show characteristics signals for carbonyl and phenyl carbon atoms. Thus on the basis of IR and NMR data, Fig. 1(b) is the most probable structure of the complexes **2a**–**c**.

In order to confirm the structures and to determine the detailed geometry, we tried to grow crystals of the complexes. A good crystal suitable for X-ray structural determination was obtained for the complex **2b**. IR and NMR data are well agreed with this molecular structure of the complex. The arrangements and numbering of the atoms in the crystal are shown in Fig. 2 and the important bond lengths and bond angles are given in Table 4. In the molecule, the ruthenium atom has a slightly distorted octahedral coordination with two Ph_3PS ligands occupying two *trans*-octahedral sites via two sulfur atoms, two *cis* CO groups and two *cis*-chlorides. This atomic arrangement is sterically less hindered and is apparently preferred because both the bonded sulfur atoms of the ligands are *trans* to each other. The bond lengths Ru–Cl "2.432, 2.449 Å", Ru–CO "1.836, 1.865 Å" and Ru–S "2.414, 2.426 Å" are closely similar to those observed previously in $[Ru(CO)_2(BzIPPh_2)Cl_2]$ (Ru–Cl, "2.428, 2.430 Å"; Ru–CO, "1.858, 1.869Å") [34] and $[\eta^6$-$MeC_6H_4Pr^iRu\{\eta^3$-$(SPPh_2)_2CMe$–C,S,S′}]PF_6 (Ru–S, "2.421, 2.449 Å") [35]. The basal Ru–Cl(2) and Ru–C(38) bond lengths are 2.449 and 1.865 Å while their corresponding apical bonds Ru–Cl(1) and Ru–C(37) are little shorter (2.432 and 1.836 Å, respectively). This shortening of the apical bonds may be due to a steric effect [34]. The bond angles for C(37)–Ru–Cl(1), C(38)–Ru–Cl(2) and S(2)–Ru–S(1) are 177.7°, 179° and 163.32°, respectively.

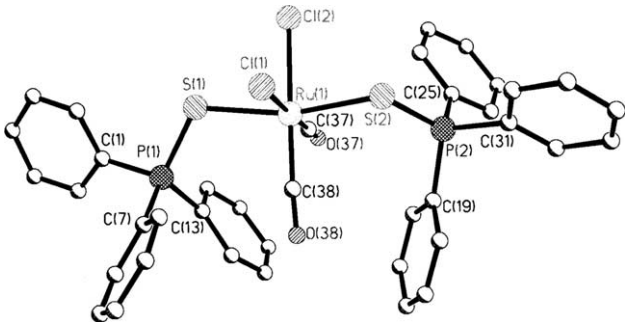

Fig. 2. Molecular structure of $[Ru(CO)_2Cl_2(PPh_3S)_2]$ (**2b**).

Table 4
Selected bond lengths (Å) and bond angles (°) of the complex **2b**

Bond lengths	
Ru–C(37)	1.836(13)
Ru–C(38)	1.865(14)
Ru–S(2)	2.414(3)
Ru–S(1)	2.426(3)
Ru–Cl(1)	2.432(4)
Ru–Cl(2)	2.449(3)
Bond angles	
C(37)–Ru–C(38)	93.2(5)
C(37)–Ru–S(2)	100.5(4)
C(38)– Ru–S(2)	91.2(3)
C(37)– Ru–S(1)	92.0(4)
C(38)–Ru–S(1)	99.2(3)
S(2)–Ru–S(1)	163.32(10)
C(37)–Ru–Cl(1)	177.7(4)
C(38)–Ru–Cl(1)	89.0(4)
S(2)–Ru–Cl(1)	80.17(11)
S(1)–Ru–Cl(1)	86.96(12)
C(37)–Ru–Cl(2)	86.5(4)
C(38)–Ru–Cl(2)	179.0(4)
S(2)–Ru–Cl(2)	87.92(11)
S(1)–Ru–Cl(2)	81.76(10)
Cl(1)–Ru–Cl(2)	91.26(13)

The large deviation from 180° for S(2)–Ru–S(1) is probably due to steric requirement to get a stable structure [36], where the uncoordinated phenyl rings are oriented away from the plane containing chlorides, CO groups and the metal centre. The angles C(37)–Ru–C(38), C(37)–Ru–S(2), C(38)–Ru–S(2), C(37)–Ru–S(1), C(38)–Ru–S(1), C(38)–Ru–Cl(1), S(2)–Ru–Cl(1), S(1)–Ru–Cl(1), C(37)–Ru–Cl(2), S(2)–Ru–Cl(2), S(1)–Ru–Cl(2) and Cl(1)–Ru–Cl(2) exhibit different values in the range 80.17°–100.5° with the deviation from 90° (Table 4). This indicates that there may be significant inter and intra atomic interactions amongst the bonding atoms and with the bulky phenyl rings which cause such deviations.

4. Supplementary material

Supplementary data are available from the CCDC, 12 Union Road, Cambridge CB2 1EZ, UK on request. CCDC deposition number 230409. Copies of this information may be obtained free of charge from the Director, CCDC, 12 Union Road Cambridge, CB2 1EZ, UK (fax: +44-1223-336033; e-mail: deposit@ccdc.cam.ac.uk or www: http://www.ccdc.cam.ac.uk).

Acknowledgements

The authors are grateful to Dr. P.G. Rao, Director, Regional Research Laboratory (CSIR), Jorhat, India, for his kind permission to publish the work. The authors thank Dr. P.C. Borthakur, Head Material Science Division, RRL Jorhat, for his encouragement and support.

The Department of Science and Technology (DST) New Delhi and Oil Industry Development Board (OIDB), Ministry of Petroleum & Natural Gas, New Delhi, are acknowledged for their partial financial grant. The authors N. Kumari and M. Sharma thank CSIR, New Delhi, for the award of Senior Research Fellowship (SRF).

References

[1] D.K. Dutta, J.D. Woollins, A.M.Z. Slawin, D. Konwar, P. Das, M. Sharma, P. Bhattacharyya, S.M. Aucott, J. Chem. Soc., Dalton Trans. (2003) 2674.
[2] P. Chutia, M. Sharma, P. Das, N. Kumari, J.D. Woollins, A.M.Z. Slawin, D.K. Dutta, Polyhedron 22 (2003) 2725.
[3] P. Das, M. Sharma, N. Kumari, D. Konwar, D.K. Dutta, Appl. Organomet. Chem. 16 (2002) 302.
[4] R.W. Wegman, A.G. Abatjoglou, A.M. Harrison, J. Chem. Soc., Chem. Commun. (1987) 1891.
[5] M.J. Baker, M.F. Giles, A.G. Orpen, M.J. Taylor, R.J. Watt, J. Chem. Soc., Chem. Commun. (1995) 197.
[6] T.S. Lobana, in: F.R. Hartley (Ed.), The Chemistry of Organophosphorus Compounds, 2, Wiley, Chichester, 1992, p. 409.
[7] T.S. Lobana, R. Singh, Trans. Met. Chem. 20 (1995) 501.
[8] P. Das, P. Chutia, D.K. Dutta, Chem. Lett. (2002) 766.
[9] P. Das, D. Konwar, P. Sengutta, D.K. Dutta, Trans. Met. Chem. 25 (2000) 426.
[10] G. Bandoli, D.A. Clemente, G. Deganello, G. Carturan, P. Uguagliati, U. Belluco, J. Organomet. Chem. 71 (1974) 125.
[11] M. Hayashi, H. Takezaki, Y. Hashimoto, K. Takaoki, K. Saigo, Tet. Lett. 39 (1998) 7529.
[12] E. Bannister, F.A. Cotton, J. Chem. Soc. (1960) 1959.
[13] Yu.N. Kukushkin, A.V. Iretskii, L.I. Danilina, Koord. Khim. 9 (1983) 1405.
[14] R. Uson, L.A. Oro, M.A. Ciriano, F.J. Lahoj, M.C. Bello, J. Organomet. Chem. 234 (1982) 205.
[15] S.A Dias, A.W. Downs, W.R. McWhinnie, J. Chem. Soc., Dalton Trans. (1975) 162.
[16] A. Araneo, A. Trovati, Inorg. Chim. Acta 3 (1969) 471.
[17] U.C. Aggarwala, S. Datta, Ind. J. Chem. A 20 (1981) 1153.
[18] U.C. Aggarwala, S. Datta, S.K. Shukla, Ind. J. Chem. A 20 (1981) 985.
[19] W. Hieber, P. John, Chem. Ber. 103 (1970) 2161.
[20] P. John, Chem. Ber. 103 (1970) 2178.
[21] C. Claver, F. Gili, J. Vinas, A. Ruiz, Polyhedron 6 (1987) 1329.
[22] A.R. Vogel, In a Text Book of Quantitative Inorganic Analysis Including Elementary Instrumental Analysis, 3rd ed., Longman, London, 1962.
[23] D.H. Williams, R.S. Ward, R.G. Cooks, J. Am. Chem. Soc. 90 (1968) 966.
[24] C. Screttas, A.F. Isbell, J. Org. Chem. 27 (1962) 2573.
[25] G.A. Olah, D. Hehemann, J. Org. Chem. 42 (1977) 2190.
[26] M.L. Berch, A. Davison, J. Inorg. Nucl. Chem. 35 (1973) 3763.
[27] R. Colton, R.H. Farthing, Aust. J. Chem. 20 (1967) 1283.
[28] R.J. Irving, J. Chem. Soc. (1956) 2879.
[29] M.J. Cleare, W.P. Griffith, J. Chem. Soc. A (1969) 372.
[30] G.M. Sheldrick, SHELXTL, Program for Refinement of Crystal Structure, University of Gottingen, Gottingen, Germany, 1997.
[31] L.M. Vallarino, S.W. Sheargold, Inorg. Chim. Acta 36 (1979) 243.
[32] M. Sharma, N. Kumari, P. Das, P. Chutia, D.K. Dutta, J. Mol. Catal. A 188 (2002) 25.
[33] S.J. La Placa, J.A. Ibers, Inorg. Chem. 4 (1965) 778.
[34] L.M. Wilkes, J.H. Nelson, J.P. Mitchener, M.W. Babich, W.C. Riley, B.J. Helland, R.A. Jacobson, M.Y. Cheng, K. Seff, L.B. McCusker, Inorg. Chem. 21 (1982) 1376.
[35] M. Valderrama, R. Contreras, V. Arancibia, P. Munoz, Inorg. Chim. Acta 225 (1997) 221.
[36] Z. Guo, A. Habtemariam, P.J. Sadler, B.R. James, Inorg. Chim. Acta (1998) 221.

Available online at www.sciencedirect.com
SCIENCE DIRECT®
Polyhedron 23 (2004) 1663–1667
POLYHEDRON
www.elsevier.com/locate/poly

Reactions of Mo–Mo singly-bonded complexes $[(\eta^5\text{-}RC_5H_4)_2Mo_2(CO)_6]$ with diphenylditelluride in the presence of $^nBu_4NI$. Crystal structures of complexes $[(\eta^5\text{-}C_5H_5)Mo(CO)_3Te]$ and *cis*/ae-$[(\eta^5\text{-}C_2H_5O_2CC_5H_4)_2Mo_2(\mu\text{-}Te)_2\ (\mu\text{-}TePh)_2]$ ☆

Yao-Cheng Shi *

School of Chemistry, Yangzhou University, 130 XiMenWai Street, Yangzhou 225002, PR China

Received 2 September 2003; accepted 30 March 2004
Available online 5 May 2004

Abstract

Reactions of singly-bonded dimolybdenum complexes $[(\eta^5\text{-}RC_5H_4)_2Mo_2(CO)_6]$ (**I**, R = CH_3CO; **II**, R = C_6H_5CO; **III**, R = CH_3O_2C; **IV**, R = $C_2H_5O_2C$) with diphenylditelluride in the presence of $^nBu_4NI$ were investigated. Although complex **I** reacted with diphenylditelluride in refluxing xylene to give both mononuclear complex **1** $[(\eta^5\text{-}C_5H_5)Mo(CO)_3Te]$ and dinuclear complex **2** *cis*/ae-$[(\eta^5\text{-}CH_3COC_5H_4)_2Mo_2(\mu\text{-}Te)_2(\mu\text{-}TePh)_2]$, reactions of complexes **II**, **III** and **IV** with diphenylditelluride under the same conditions only afforded dinuclear complexes *cis*/ae-$[(\eta^5\text{-}RCC_5H_4)_2Mo_2(\mu\text{-}Te)_2(\mu\text{-}TePh)_2]$ (**3**, R = C_6H_5CO; **4**, R = CH_3O_2C; **5**, R = $C_2H_5O_2C$). All the new complexes have been characterized by elemental analyses, ^1H NMR, ^{13}C NMR and IR spectroscopies. Crystal structures of complexes **1** and **5** have been determined by X-ray diffraction analyses.
© 2004 Elsevier Ltd. All rights reserved.

Keywords: Ph_2Te_2; Metal–metal bond; Molybdenum complex; Mo_2Te_4 complex; Crystal structure

1. Introduction

The chemistry of transition metal complexes containing both Group 6 metals and chalcogenido ligands has been extensively studied not only because of their importance to biology and catalysis [1,2], but also because of their novel structures and widespread use for the synthesis of organometallic compounds, and particularly organometallic clusters, during the last two decades [3–5]. However, considerably less is known about the complex chemistry of the tellurium [6]. Recently, the author has found that triply-bonded dimolybdenum complexes $[(\eta^5\text{-}RC_5H_4)_2Mo_2(CO)_4]$ ($\eta^5\text{-}RC_5H_4$ = parent and substituted cyclopentadienyls) and excess diphenylditelluride in the presence of Cp_2TiX_2 (X = Cl, Br) form novel quadruply-bridged complexes $[(\eta^5\text{-}RC_5H_4)_2Mo_2(\mu\text{-}X)(\mu\text{-}TePh)_3]$ [7,8]. To further extend this methodology, I have investigated the reaction of singly-bonded dimolybdenum complexes $[(\eta^5\text{-}RC_5H_4)_2Mo_2(CO)_6]$ (**I**, R = CH_3CO; **II**, R = C_6H_5CO; **III**, R = CH_3O_2C; **IV**, R = $C_2H_5O_2C$) with diphenylditelluride in the presence of $^nBu_4NI$. Interestingly, unexpectedly this reaction affords a terminal tellurido organomolybdenum complex **1** $[(\eta^5\text{-}C_5H_5)Mo(CO)_3Te]$ and quadruply-bridged dimolybdenum complexes **2**–**5** *cis*/ae-$[(\eta^5\text{-}RC_5H_4)_2Mo_2(\mu\text{-}Te)_2(\mu\text{-}TePh)_2]$. To my knowledge, these complexes are the unprecedented examples [9–12], herein I wish to report on such an unexpected reaction.

2. Experimental

All reactions were carried out under purified dinitrogen atmosphere using standard Schlenk techniques. Xylene was distilled from Na/benzophenone under

☆ Supplementary data associated with this article can be found, in the online version, at doi:10.1016/j.poly.2004.03.015.

* Tel./fax: +86-514-7857939.
E-mail address: yzssyc@yzcn.net (Y.-C. Shi).

0277-5387/$ - see front matter © 2004 Elsevier Ltd. All rights reserved.
doi:10.1016/j.poly.2004.03.015

dinitrogen atmosphere. Singly-bonded dimolybdenum complexes $[(\eta^5\text{-}RC_5H_4)_2Mo_2(CO)_6]$ (**I**, R = CH_3CO; **II**, R = C_6H_5CO; **III**, R = CH_3O_2C; **IV**, R = $C_2H_5O_2C$) and Ph_2Te_2 were prepared according to the literature methods [13,14]. Progress of the reactions was monitored periodically by TLC. The products were separated by preparative TLC (silica gel H, 10–40 μm) and further recrystallized from deoxygenated solvents (CH_2Cl_2/petroleum ether). NMR spectra were determined on a Bruker Avance 300 spectrometer using TMS as an external standard in $CDCl_3$. IR spectra were recorded on a Perkin–Elmer 402 as KBr disks in the range of 400–4000 cm^{-1}. Analyses for C and H were performed on an Elementa Vario EL III instrument. Melting points were measured on a Yanagimoto apparatus.

2.1. Syntheses of complexes *1* and *2*

A 100 ml Schlenk flask fitted with a magnetic stir-bar, a rubber septum and a reflux condenser topped with a nitrogen inlet tube was charged with 0.574 g (1 mmol) of complex **I** $[(\eta^5\text{-}CH_3COC_5H_4)_2Mo_2(CO)_6]$ and 0.819 g (2 mmol) of Ph_2Te_2 in 40 ml of xylene. The mixture was stirred at 110 °C for 1 h, then 0.739 g (2 mmol) of $^nBu_4NI$ was added and further refluxed for 4 h. The resulting brown mixture was evaporated to dryness under vacuum, the residue obtained thus was subjected to preparative TLC using CH_2Cl_2 as an eluant. The first main band afforded 0.173 g (23.2%) of complex **1** as a brown solid; m.p. 110–113 °C. *Anal.* Calc. for $C_8H_5MoO_3Te$: C, 25.78; H, 1.35. Found: C, 25.80; H, 1.56%. IR (KBr disk): terminal carbonyl 2036.38 (vs), 1962.42 (vs, sh), 1939.75 (vs) cm^{-1}. ^1H NMR ($CDCl_3$): δ 5.615 (s, 5H, C_5H_5). ^{13}C NMR (300MHz, $CDCl_3$): δ 236.030, 219.876 (CO); 93.889 (C_5H_5). The second main band gave 0.487 g (45.5%) of complex **2** as a brown solid; m.p. 148 °C. *Anal.* Found: C, 29.31; H, 2.24. Calc. for $C_{26}H_{24}Mo_2O_2Te_4$: C, 29.17; H, 2.26%. IR (KBr disk): acetyl carbonyl 1659.21 (vs) cm^{-1}. ^1H NMR ($CDCl_3$): δ 7.024–7.070 (2m, 10H, $2C_6H_5$); 5.522, 5.582, 5.717, 5.911 (4s, 4× 2H, $2C_5H_4$); 2.135 (s, 6H, $2CH_3$). ^{13}C NMR ($CDCl_3$): δ 199.049 (CO); 138.292, 127.864, 127.284 (TeC_6H_5); 93.880, 92.086, 86.119, 85.579, 79.503 (C_5H_4); 26.590 (CH_3).

2.2. Synthesis of complex *3*

The similar reaction of 0.698 g (1 mmol) of complex **II** $[(\eta^5\text{-}C_6H_5COC_5H_4)_2Mo_2(CO)_6]$, 0.819 g (2 mmol) of Ph_2Te_2 and 0.739 g (2 mmol) of $^nBu_4NI$ in 40 ml of xylene furnished 0.514 g (43%) of complex **3** as a brown solid; m.p. 160 °C. *Anal.* Found: C, 36,27; H, 2.41. Calc. for $C_{36}H_{28}Mo_2O_2Te_4$: C, 36.19; H, 2.36%. IR (KBr disk): benzoyl carbonyl 1629.57 (vs) cm^{-1}. ^1H NMR ($CDCl_3$): δ 6.938–7.464 (3m, 20H, $4C_6H_5$); 5.514, 5.587, 5.911, 6.028 (4s, 4× 2H, $2C_5H_4$). ^{13}C NMR ($CDCl_3$): δ 194.844 (CO); 139.120, 138.240, 138.070, 131.187, 127.951, 127.633, 127.580, 127.244 (TeC_6H_5); 93.009, 91.736, 87.331, 85.111, 79.620 (C_5H_4).

2.3. Synthesis of complex *4*

The similar reaction of 0.610 g (1 mmol) of complex **III** $[(\eta^5\text{-}CH_3O_2CC_5H_4)_2Mo_2(CO)_6]$, 0.819 g (2 mmol) of Ph_2Te_2 and 0.739 g (2 mmol) of $^nBu_4NI$ in 40 ml of xylene furnished 0.527 g (47.8%) of complex **4** as a brown solid using CH_2Cl_2 as an eluant; m.p. 146–148 °C. *Anal.* Calc. for $C_{26}H_{24}Mo_2O_4Te_4$: C, 28.32; H, 2.19. Found: C, 28.44; H, 2.43%. IR (KBr disk): ester carbonyl 1707.19 (vs) cm^{-1}. ^1H NMR ($CDCl_3$): δ 7.211–7.634 (m, 10H, $2C_6H_5$); 5.699–6.084 (m, 8H, $2C_5H_4$); 3.678 (s, 6H, $2CH_3$). ^{13}C NMR ($CDCl_3$): δ 169.709 (CO); 138.447, 127.984, 127.647, 127.133 (TeC_6H_5); 91.800, 87.008, 85.837, 84.931, 79.985 (C_5H_4); 51.569 (CH_3).

2.4. Synthesis of complex *5*

The similar reaction of 0.638 g (1 mmol) of complex **IV** $[(\eta^5\text{-}C_2H_5O_2CC_5H_4)_2Mo_2(CO)_6]$, 0.819 g (2 mmol) of Ph_2Te_2 and 0.739 g (2 mmol) of $^nBu_4NI$ in 40 ml of xylene furnished 0.505 g (44.7%) of complex **5** as a brown solid using CH_2Cl_2/petroleum ether (2:1) as an eluant; m.p. 174–176 °C. *Anal.* Calc. for $C_{28}H_{28}Mo_2O_4Te_4$: C, 29.74; H, 2.50. Found: C, 29.49; H, 2.47%. IR (KBr disk): ester carbonyl 1709.26 (vs) cm^{-1}. ^1H NMR ($CDCl_3$): δ 7.293–7.629 (2m, 10H, $2C_6H_5$); 5.743–6.015 (3m, 8H, $2C_5H_4$); 4.163 (q, $^3J_{HH} = 6.9$ Hz, 4H, $2CH_2$); 1.201 (t, $^3J_{HH} = 6.9$ Hz, 6H, $2CH_3$). ^{13}C NMR ($CDCl_3$): δ 169.42 (CO); 138.15, 137.33, 128.73, 128.05, 126.83 (TeC_6H_5); 94.74, 89.30, 87.22, 82.15 (C_5H_4); 60.71 (CH_2); 15.28 (CH_3).

2.5. Crystal structure determination

Dark-brown single crystals for X-ray determination were obtained by slow evaporation of the solutions from $CH_2Cl_2$and petroleum ether of complexes **1** and **5** at ca. 5 °C. For each of complexes **1** and **5**, a selected single crystal was mounted on a glass fibre with epoxy resin. Measurements of diffraction intensity of single crystals of complexes **1** and **5** were carried out on an Enraf-Nonius CAD4 diffractometer. The data were collected using the $\omega - 2\theta$ scan mode. The structures were solved by direct methods and refined by full-matrix least-squares refinement with anisotropic thermal parameters for all non-hydrogen atoms. Hydrogen atoms were placed in their calculated positions, assigned fixed isotropic thermal parameters and allowed to ride on their respective parent atoms. All computations were carried out using the SHELEXTL PC Program Package [15]. Crystal data and details of data collection and structure refinement are summarized in Table 3.

3. Results and discussion

3.1. Syntheses of complexes 1–5

It was found that reaction of singly-bonded dimolybdenum complexes $[(\eta^5\text{-}RC_5H_4)_2Mo_2(CO)_6]$ (**I**, R = CH_3CO; **II**, R = CH_3O_2C; **III**, R = CH_3O_2C; **IV**, R = $C_2H_5O_2C$) and two molar amount of diphenylditelluride in the presence of $^nBu_4NI$ in refluxing xylene for 4 h resulted in complete disappearance of the singly-bonded material and the formation of products as shown by TLC analysis. After the solvent had been removed, the residue was subjected to preparative TLC to afford the corresponding complexes $[(\eta^5\text{-}C_5H_5)Mo(CO)_3\text{-}Te]$ (**1**) and *cis*/ae-$[(\eta^5\text{-}RC_5H_4)_2Mo_2(\mu\text{-}Te)_2(\mu\text{-}TePh)_2]$ (**2**, R = CH_3CO; **3**, R = C_6H_5CO; **4**, R = CH_3O_2C; **5**, R = $C_2H_5O_2C$) as dark brown crystalline solids in 23–48% yield. All the new complexes have been characterized by elemental analyses, ^1H NMR, ^{13}C NMR and IR spectroscopies, especially by single crystal X-ray diffraction crystallography. Therefore, the reaction undoubtedly provides a useful method for synthesizing Mo_2Te_4 core-containing complexes.

3.2. Spectroscopies of complexes 1–5

The ^1H NMR spectrum of complex **1** displays a singlet at 5.615 ppm for its cyclopentadienyl ring, its ^{13}C NMR spectrum shows the corresponding absorption at 93.889 ppm for the cyclopentadienyl ring and 219.876 and 236.030 ppm for the terminal carbonyls.

The ^1H NMR spectra of complexes **2** and **4** exhibit one singlet at 2.135 and 3.678 ppm for their methyl groups, whereas that of complex **5** displays one triplet at 1.201 ppm and one quartet at 4.163 ppm for its ethyl group ($^3J_{HH} = 6.9$ Hz). The ^1H NMR spectrum of complex **3** displays four broad singlets in the range of 5.514–6.028 ppm for the cyclopentadienyl ring and three multiplets in the range of 6.938–7.464 ppm for the benzene rings. In addition, complexes **4** and **5** show one to three multiplets in the range of 5.743–7.634 ppm for the substituted cyclopentadienyl rings and the phenyl groups, whereas complex **2** displays four singlets in the range of 5.522–5.911 ppm for the substituted cyclopentadienyl rings. ^{13}C NMR spectra of complexes **2** and **4** exhibit one absorption at 26.590 and 51.569 ppm assigned to their methyl groups, respectively, whereas that of complex **5** displays two absorptions at 15.280 and 60.710 ppm due to its ethyl group. The complexes except complex **1** show four to five absorptions in the range of 79.503–94.740 ppm for the substituted cyclopentadienyl rings and the phenyl groups in the range of 127.133–139.120 ppm. In addition, these also display the corresponding absorption for their ketonic (199.049 and 194.844 ppm) or ester carbonyls (169.709 and 169.420 ppm).

The IR spectrum of complex **1** displays three strong absorption bands at 1939.75, 1962.42 (sh) and 2036.38 cm^{-1}, while those of complexes **2**–**4** exhibit one respective absorption band in the range of 1629.57–1709.26 cm^{-1} for their ketonic or ester carbonyls.

3.3. Crystal structures of complexes 1 and 5

To determine the two types of structures mentioned above, the author carried out single crystal X-ray diffraction analyses for complexes **1** and **5**. Crystal structures

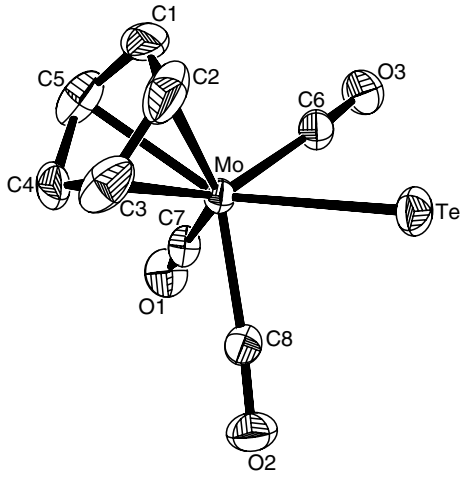

Fig. 1. Molecular structure of complex **1**. The atoms are drawn with 30% probability ellipsoids. Hydrogen atoms are omitted for clarity.

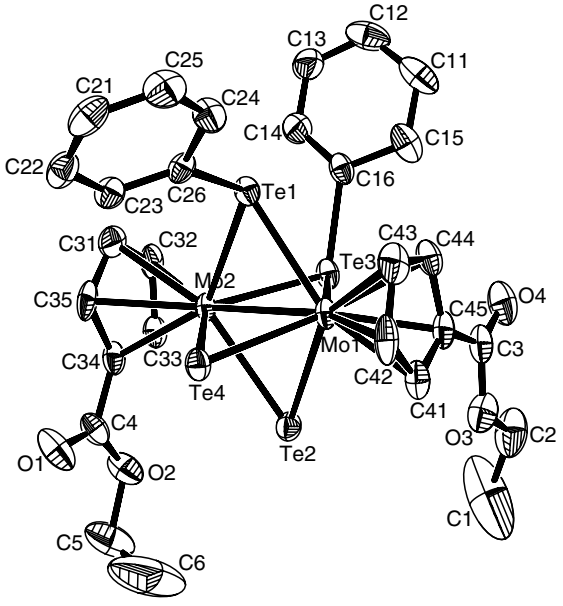

Fig. 2. Molecular structure of complex **5**. The atoms are drawn with 30% probability ellipsoids. Hydrogen atoms are omitted for clarity.

Table 1
Selected bond lengths [Å] and angles [°] for complex **1**

Bond lengths		Bond angles	
Te–Mo	2.832(1)	O(1)–C(7)–Mo	179.7(8)
Mo–C(6)	2.028(9)	O(2)–C(8)–Mo	176.5(7)
Mo–C(7)	1.977(9)	O(3)–C(6)–Mo	176.6(8)
Mo–C(8)	1.992(8)	C(6)–Mo–Te	75.8(3)
O(1)–C(7)	1.13(1)	C(7)–Mo–Te	129.2(2)
O(2)–C(8)	1.15(1)	C(8)–Mo–Te	76.0(2)
O(4)–C(6)	1.12(1)		

Table 2
Selected bond lengths [Å] and angles [°] for complex **5**

Bond lengths			
Mo(1)–Mo(2)	2.731(1)	Mo(2)–C(35)	2.314(9)
Mo(1)–Te(1)	2.740(1)	Te(1)–C(26)	2.132(9)
Mo(1)–Te(2)	2.817(1)	Te(3)–C(16)	2.13(1)
Mo(1)–Te(3)	2.739(1)	O(1)–C(4)	1.19(1)
Mo(1)–Te(4)	2.784(1)	O(2)–C(4)	1.32(2)
Mo(2)–Te(1)	2.720(1)	O(2)–C(5)	1.46(2)
Mo(2)–Te(2)	2.830(1)	O(3)–C(3)	1.34(2)
Mo(2)–Te(3)	2.742(1)	O(4)–C(3)	1.17(2)
Mo(2)–Te(4)	2.805(1)	O(3)–C(2)	1.49(2)
Mo(1)–C(44)	2.24(1)	C(1)–C(2)	1.37(4)
Mo(1)–C(45)	2.23(1)	C(5)–C(6)	1.47(3)
Mo(2)–C(34)	2.24(1)	C(4)–C(34)	1.47(2)
Bond angles			
Te(1)–Mo(1)–Te(2)	120.71(4)	Mo(1)–Te(1)–C(26)	113.6(3)
Te(1)–Mo(1)–Te(3)	75.74(4)	Mo(2)–Te(1)–C(26)	112.5(3)
Te(1)–Mo(1)–Te(4)	80.40(3)	Mo(1)–Te(3)–C(16)	109.7(3)
Te(1)–Mo(1)–Mo(2)	59.62(3)	Mo(2)–Te(3)–C(16)	112.1(3)
Te(2)–Mo(1)–Mo(2)	61.32(3)	Te(1)–Mo(1)–C(45)	130.7(3)
Te(3)–Mo(1)–Mo(2)	60.18(3)	Te(1)–Mo(2)–C(34)	142.0(3)
Te(4)–Mo(1)–Mo(2)	61.14(3)	Te(1)–Mo(1)–C(45)	130.7(3)
Mo(1)–Te(1)–Mo(2)	60.02(3)	O(1)–C(4)–C(34)	125(1)
Mo(1)–Te(2)–Mo(2)	57.84(3)	O(1)–C(4)–O(2)	124(1)
Mo(1)–Te(3)–Mo(2)	59.78(3)	O(2)–C(4)–C(34)	111(1)
Mo(1)–Te(4)–Mo(2)	58.50(3)	C(4)–O(2)–C(5)	116(1)

of complexes **1** and **5** are shown in Figs. 1 and 2, whereas the selected bond lengths and angles of complexes **1** and **5** are listed in Tables 1 and 2.

As seen from Fig. 1, complex **1** is monomeric and displays the commonly observed piano-stool conformation with the corresponding angles 75.8(3) (C(6)–Mo–Te), 129.2(2) (C(7)–Mo–Te), 76.0(2) (C(8)–Mo–Te), 77.3(3) (C(6)–Mo–C(7)), 112.8(3) (C(6)–Mo–C(8)) and 76.0(3)° (C(7)–Mo–C(8)). The distance of center of Cp to Mo is 1.98 Å which is close to that of $[(\eta^5\text{-}C_5H_5)Mo(CO)_3SeCH_2Ph]$ [16]. The Mo–Te bond length (2.832(1) Å) indicates an Mo–Te single bond, comparable with the corresponding bond length (2.811(2)–2.829(2) Å) in the complex $[(\eta^5\text{-}CH_3O_2CC_5H_4)_2Mo_2(CO)_4(\mu\text{-}TePh)_2]$ [8], which is also supported by the crystal structure of complex **5** (Tables 1 and 2). Against expectations, although complex **1** has a monovalent terminal telluride, it is extremely stable, it melts at 110 °C without decomposition!

Table 3
Crystallographic data and structure refinements for complexes **1** and **5**

	1	**5**
Formula	$C_8H_5MoO_3Te$	$C_{28}H_{28}Mo_2O_4Te_4$
Formula weight	372.66	1130.78
Crystal size (mm)	$0.5 \times 0.4 \times 0.4$	$0.4 \times 0.4 \times 0.3$
Crystal system	monoclinic	monoclinic
Space group	$P2_1n$	$C2/c$
Unit cell dimensions		
a (Å)	10.500(2)	28.020(6)
b (Å)	7.880 (2)	14.100(3)
c (Å)	12.250(3)	18.530(4)
α (°)	90.00	90.00
β (°)	90.06(3)	120.76(3)
γ (°)	90.00	90.00
V (Å^3)	1013.6(4)	6291(2)
Z	4	8
D_c (g cm^{-1})	2.442	2.380
$F(000)$	684	4146
T (K)	293(2)	293(2)
μ(Mo Kα) (mm^{-1})	4.086	4.464
Scan mode	$\omega - 2\theta$	$\omega - 2\theta$
θ Range (°)	2.55; 25.08	1.67; 25.00
Limiting indices	$-12 \leqslant h \leqslant 0$, $-9 \leqslant k \leqslant 0$, $-14 \leqslant l \leqslant 14$	$0 \leqslant h \leqslant 33$, $0 \leqslant k \leqslant 16$, $-22 \leqslant l \leqslant 18$
Reflections collected	1903	5644
Independent reflections [R_{int}]	1800 [0.0363]	5523 [0.0297]
Number of parameters refined	119	343
Final R indices [$I > 2.0\sigma(I)$]	$R = 0.0334$, $Rw = 0.1238$	$R = 0.0413$, $Rw = 0.1299$
R indices (all data)	$R = 0.0397$, $Rw = 0.1378$	$R = 0.0646$, $Rw = 0.1485$
Goodness-of-fit	0.937	0.976
Maximum peak and hole (e Å^{-3})	0.808 and −0.564	1.219 and −1.209

For convenience, the stereoisomers of $[(\eta^5\text{-}RC_5H_4)_2M_2(\mu\text{-}E)_2(\mu\text{-}E'R')_2]$ (E, E′ = S, Se, Te; M = Cr, Mo, W) may be described by the following terminologies. The *trans* and *cis* refer to the two naked E atoms or the two E′ atoms with substituents (R′) with respect to the M–M vector, *anti* and *syn* refer to the mutual orientations of the two substituents (R′) with respect to their attached planar $M_2E'_2$ ring, whereas a and e refer to the mutual orientations of the two substituents (R′) with respect to their attached butterfly $M_2E'_2$ skeleton. Accordingly, bridged complexes with the above general formula may have five isomers, viz. *trans*/*anti*, *trans*/*syn*, *cis*/aa, *cis*/ae and *cis*/ee. The X-ray analysis has revealed that complex **5** is a *cis*/ae isomer as shown in Fig. 2. The four bridged atoms in complex **5** form a plane, which is parallel to the two substituted cyclopentadienyl ring planes and bisects the Mo–Mo vector perpendicularly. The non-bonding distances between the bridged atoms are 3.248, 3.363, 3.469 and 3.566 Å. These distances fall in the range of the sum of van der waals radii of two Te atoms (4.4 Å) and indicate a weak interation between the bridging atoms [7,8]. Complex **5** is a d^2–d^2 dimer and would have a $\sigma^2\delta^2$ electronic configuration [17]. This suggests a double bond present between the two Mo(IV) atoms, which is consistent with the 18 valence-electron rule. It is worth noting that the Mo–Mo bond length of 2.731(1) Å in complex **5** is greater than that in the complex *trans*/*syn*-$[(\eta^5\text{-}C_5H_5)_2Mo_2(\mu\text{-}Se)_2(\mu\text{-}SePh)_2]$ (2.653(2) Å) [16] and very close to the Mo–Mo single bond length in $[(\eta^5\text{-}CH_3O_2CC_5H_4)_2Mo_2(\mu\text{-}Cl)(\mu\text{-}TePh)_3]$ (2.735(1)–2.756(3) Å) [8,9]. The Mo–Te bond lengths differ greatly because of the different coordination numbers of tellurium. In the case of the tellurido bridge, the values are 2.817(1) (Mo(1)–Te(2)) and 2.830(1) Å (Mo(2)–Te(2)), whereas the corresponding Mo–TePh bond lengths are 2.740(1) (Mo(1)–Te(1)) and 2.720(1) Å (Mo(2)–Te(1)). Therefore, the bonding situation is different from complexes *trans*/*syn*-$[(\eta^5\text{-}C_5H_5)_2Mo_2(\mu\text{-}Se)_2(\mu\text{-}SePh)_2]$, *trans anti*- and *trans*/*syn*-$[(\eta^5\text{-}C_2H_5O_2CC_5H_5)_2Mo_2(\mu\text{-}Se)_2(\mu\text{-}SeCH_2Ph)_2]$ in which the Mo–Se (naked) bond lengths are shorter than those of the Mo–Se (selenolato) bonds [9,11,16]. The phenyltellurolato Te atoms display almost tetrahedral bond angles (Mo(1)–Te(3)–C(16), 109.7(3)° and Mo(2)–Te(3)–C(16), 112.1(3)°), whereas the angles belonging to the Mo_2Te_4 core are acute (Mo(1)–Te(1)–Mo(2), 60.02(3)° and Mo(1)–Te(2)–Mo(2), 57.84(3)°) (Table 2). In addition, the two phenyl groups bonded to Te atoms are all bent toward the directions far away from the $C_2H_5O_2C$ substituents in order to minimize the steric repulsions between them.

4. Supplementary material

Full crystallographic data (CCDC 216750 for complex **1** and CCDC 216751 for complex **5**) have been deposited at the Cambridge Crystallographic Database Centre and are available on request from the Director, CCDC, 12 Union Road, Cambridge, CB2 1EZ, UK (fax: +44-1223-336033; e-mail: deposit@ccdc.cam.ac.uk or http//www.ccdc.cam.ac.uk).

Acknowledgements

Y.-C. Shi thanks Mr. Wang Huaqin for crystallographic data collections. This work was supported by the Yangzhou University (D0009107).

References

[1] R.H. Holm, Chem. Soc. Rev. 10 (1981) 455.
[2] B.C. Wiegand, C.M. Friend, Chem. Rev. 92 (1992) 491.
[3] P. Schollhammer, F.Y. Petillon, R. Pichon, S. Poder-Guillou, J. Talarmin, K.M. Muir, L. Manojlovic-Muir, Organometallics 14 (1995) 2277.
[4] P. Li, M.D. Curtis, Inorg. Chem. 29 (1990) 1242.
[5] P. Mathur, Md.M. Hossain, S.B. Umbarkar, C.V.V. Satyanarana, A.L. Rheingold, L.M. Liable-Sands, G.P.A. Yap, Organometallics 15 (1996) 1898.
[6] U. Siemeling, Angew. Chem. Int. Ed. Engl. 32 (1993) 67.
[7] L.C. Song, Y.C. Shi, Q.H. Hu, Y. Chen, J. Sun, J. Organomet. Chem. 626 (2001) 192.
[8] L.C. Song, Y.C. Shi, W.F. Zhu, Q.M. Hu, X.Y. Huang, F. Du, X.A. Mao, Organometallics 19 (2000) 56.
[9] H. Rakoczy, M. Schollenberger, B. Nuber, M.L. Ziegler, J. Organomet. Chem. 467 (1994) 217.
[10] L.C. Song, J.Q. Wang, X.Y. Huang, Polyhedron 17 (1998) 3759.
[11] L.C. Song, Y.C. Shi, W.F. Zhu, Q.M. Hu, L.H. Weng, J. Organomet. Chem. 613 (2000) 42.
[12] (a) P. Jaitner, W. Wohlgenannt, Inorg. Chim. Acta 101 (1985) L43; (b) P. Jaitner, W. Wohlgenannt, A. Gieren, H. Betz, T. Nübner, J. Organomet. Chem. 297 (1985) 281.
[13] L.C. Song, J.Y. Sun, Chem. J. Chin. Univ. 13 (1992) 1227.
[14] W.S. Haller, K.J. Irgolic, J. Organomet. Chem. 38 (1972) 97.
[15] G.M. Sheldrick, SHELXTL 5.01 Software, Bruker Analytical X-ray Systems, Madison, WI, USA, 1996.
[16] C. Thöne, P.G. Jones, J. Laube, Acta Crystallogr. C 53 (1997) 1539.
[17] N.G. Connelly, L.F. Dahl, J. Am. Chem. Soc. 92 (1970) 7470.

Available online at www.sciencedirect.com
SCIENCE DIRECT®
Polyhedron 23 (2004) 1669–1676
POLYHEDRON
www.elsevier.com/locate/poly

2D Extended supramolecular structures via π–π interactions of 1D coordination polymers of cadmium(II) complexes of arylazoimidazole using azido and thiocyanato bridging ligands

Brojogopal Chand [a], Umasankar Ray [a], Golam Mostafa [b], Tian-Huey Lu [b], Chittaranjan Sinha [a,*]

[a] *Department of Chemistry, The University of Burdwan, Burdwan 713104, India*
[b] *Department of Physics, National Tsing-Hua University, Hisnchu 300, Taiwan, ROC*

Received 13 November 2003; accepted 16 February 2004
Available online 25 May 2004

Abstract

Two new one-dimensional polymeric azido- and thiocyanato-bridged cadmium (II) complexes of 1-alkyl-2-(arylazo)imidazoles [RaaiR′ (where R = H (**a**), Me (**b**); R′ = Me (**1/3/5**), Et (**2/4/6**)] are described in this work. The 1D chain structures of these complexes have been confirmed by X-ray diffraction studies of $[Cd(HaaiEt)(N_3)_2]_n$ (**4a**) and $[Cd(MeaaiEt)(SCN)_2]_n$ (**6b**). The azide (N_3^-) acts as end-on (μ-1,1; EO) and the thiocyanate (SCN^-) as end-to-end (μ-1,3; EE) double bridging agents, respectively. The π–π interactions amongst inter-chain aromatic-heterocycles generate a uniform sheet. The coordination environment of the cadmium in all these complexes is distorted octahedral. The ligand, RaaiR′, is an unsymmetric N,N′-chelator and the distortion in the octahedral geometry is mainly due to the small chelate bite angle.
© 2004 Elsevier Ltd. All rights reserved.

Keywords: Arylazoimidazoles; Cadmium(II) complexes; End-on and end-to-end bridging; X-ray structure; 1D chain; Sheet structure

1. Introduction

Supramolecular metal complexes formed by self-assembly are a frontier field in research because of their potential applications in catalyses, molecular recognition, molecular electronics and photonic materials etc. Weak forces such as hydrogen bonding, π-stacking, dipole-dipole attractions and van der Waals forces are used to assemble molecular components selectively into complex structural motifs [1–4]. For this purpose, a metal template, appropriate organic blocker and a bridging agent are necessary. The pseudohalides, especially, azide [5,6] and ambidentate thiocyanate [7] are interesting bridging agents which form a variety of networks with various transition and non-transition metals. In transition metal complexes the structural and electronic versatility of these bridgers have been used to explore magnetic materials, photo-devices, liquid crystals, catalysts and other functional materials [8–13]. However, the corresponding non-transition metal complexes are still few [14–20]. The majority of the development in the non-transition metals are with the Group 12 metals: zinc, cadmium and mercury. Because of border-line acidity, cadmium(II) prefers to bind both hard and soft donors which thus widens its scope to study crystal engineering [7,14–20].

Apparently the organic blocker has little role relative to bridging agents in the influence of physical, chemical and magnetic properties of the coordination polymer. However, subtle change in steric and electronic effects of the blocking agent significantly influence the structure, geometry and properties of the polymer [14–23]. So, choice of blocking agent is equally important with the bridging group in the network construction and thereof

* Corresponding author. Tel.: +91-342-557-683; fax: +91-342-253-0452.
E-mail address: c_r_sinha@yahoo.com (C. Sinha).

0277-5387/$ - see front matter © 2004 Elsevier Ltd. All rights reserved.
doi:10.1016/j.poly.2004.02.029

the properties of the molecules. The use of different heterocyclic-N donor ligands such as pyridine, polypyridine and their substituted derivatives are well established [17–24], but no such work has been initiated with unsymmetrical ligands having azo-N and heterocyclic-N donor centers. Here arylazoheterocycles function as organic end-capping chelators.

For the last few years this group has been engaged in exploring the chemistry of such a ligand system with transition and non-transition metal ions. Major growth has been directed in the field of transition metal chemistry [25–28]. Non-transition metal complexes of arylazoimidazoles have also been reported from our group [29–34]. In this article we describe the syntheses and characterization of new polynuclear cadmium(II) azido and thiocyanato bridged complexes with 1-alkyl-2-(arylazo)imidazole (RaaiR′) ligands.

2. Experimental

2.1. Materials

Imidazole was purchased from Aldrich. Cd(II) acetate dihydrate, sodium azide and ammonium thiocyanate were obtained from Loba Chemicals, Bombay, India. All other chemicals and solvents were reagent grade and used as received. 2-(Arylazo)-imidazole (RaaiR′) was prepared by the reported procedure [25].

Warning: Cadmium and its compounds are toxic [35,36], and sodium azide is a potential explosive. Only small amounts should be prepared and handled with due care.

2.2. Physical measurements

Microanalytical (C,H,N) data were obtained from a Perkin–Elmer 2400 CHNS/O elemental analyzer. Spectroscopic data were obtained using the following instruments: UV–Vis and reflectance spectra, JASCO UV/Vis/NIR model V-570; IR (KBr disk, 4000–200 cm^{-1}), JASCO FT-IR model 420 spectrophotometer, and ^1H NMR, Bruker 400 MHz FT-NMR spectrometer.

2.3. Synthesis of $[Cd(HaaiEt)(N_3)_2]_n$ (**4a**)

1-Ethyl-2-(phenylazo)imidazole (0.05 g, 0.25 mmol) in MeOH (10 ml) was added dropwise to a stirred methanolic solution (10 ml) of $Cd(OAc)_2 \cdot 2H_2O$ (0.065 g, 0.25 mmol) at room temperature (298 K). To the resulting mixture a methanolic solution of NaN_3 (0.033 g, 0.50 mmol) was added very slowly. The orange-red solution was left undisturbed for two weeks. Bright orange-red crystals were obtained which were then washed with water and finally dried in vacuo. The yield was 0.10 g (65%).

All other complexes were prepared by the same procedure. The yields varied from 60% to 65%.

2.4. Synthesis of $[Cd(MeaaiEt)(SCN)_2]_n$ (**6b**)

The complex was prepared by the addition of a methanolic solution (10 ml) of 1-ethyl-2-(*p*-tolylazo)imidazole (0.054 g, 0.25 mmol) to a methanolic solution (10 ml) of $Cd(OAc)_2 \cdot 2H_2O$ (0.065 g, 0.25 mmol) at room temperature (298 K). To the resulting solution a methanolic solution (10 ml) of NH_4SCN (0.038 g, 0.50 mmol) was added in drops. The orange-red solution was left undisturbed for two weeks. Bright orange-red crystals were obtained which were then washed with water and finally dried in vacuo. The yield was 0.11 g (65%).

All other complexes were prepared by the same procedure. The yields varied from 60% to 65%.

2.5. X-ray diffraction study

Suitable single crystals of complexes **4a** and **6b** were mounted on a Siemens CCD diffractometer equipped with graphite monochromated Mo Kα ($\lambda = 0.711073$ Å)

Table 1
Summarized crystallographic data for $[Cd(HaaiEt)(N_3)_2]_n$ (**4a**) and $[Cd(MeaaiEt)(SCN)_2]_n$ (**6b**)

	$[Cd(HaaiEt)(N_3)_2]_n$ (**4a**)	$[Cd(MeaaiEt)(SCN)_2]_n$ (**6b**)
Empirical formula	$C_{11}H_{12}CdN_{10}$	$C_{14}H_{14}CdN_6S_2$
Formula weight	396.72	442.86
Temperature (K)	293(2)	293(2)
Crystal system	triclinic	triclinic
Space group	$P\bar{1}$	$P\bar{1}$
a (Å)	6.7777(5)	10.2524(6)
b (Å)	10.1673(8)	10.3399(6)
c (Å)	11.8393(9)	10.5488(7)
α (°)	104.319(2)	63.8500(10)
β (°)	95.059(2)	63.5550(10)
γ (°)	102.4170(10)	81.5300(10)
V (Å)^3	763.36(10)	897.10(9)
Z	2	2
λ (Å)	0.71073	0.71073
μ (Mo Kα) (mm^{-1})	1.444	1.456
2θ range (°)	4.26 −55.02	4.4 −56.2
D_{calc} ($Mg\,m^{-3}$)	1.726	1.640
Refined parameters	208	208
Reflection number total	4887	8809
Unique reflections	3396	3930
Observed data $[I > 2\sigma(I)]$	2672	3484
R[a]	0.0358	0.0261
wR_2[b]	0.0756	0.0713
Goodness-of-fit[c]	1.016	1.034

[a] $R = \sum ||F_o| - |F_c|| / \sum |F_o|$.

[b] $wR_2 = [\sum w(F_o^2 - F_c^2)^2 / \sum w(F_o^2)^2]^{1/2}$, $w = 1/[\sigma^2(F_o^2) + (xP)^2 + yP]$, $P = (F_o^2 + 2F_c^2)/3$, where $x = 0.0250$ for (**4a**), 0.0402 for (**6b**); $y = 0$ for **4a** and 0.2684 for **6b**.

[c] Goodness-of-fit is defined as $[w(F_o - F_c)/(n_o - n_v)]^{1/2}$, where n_o and n_v denote the number of data and variables, respectively.

radiation. The crystallographic data are listed in Table 1. The unit cell parameters and crystal-orientation matrices were determined for the two complexes by least squares refinements of all reflections. The intensity data were corrected for Lorentz and polarisation effects and an empirical absorption correction were also employed using the SAINT program for both complexes. Reflection data were assumed applying the condition $I > 2\sigma(I)$ for the complexes. The structures were solved by direct methods and followed by successive Fourier and difference Fourier syntheses. Full-matrix least-squares refinements on F_0^2 were carried out using SHELXL-97 with anisotropic displacement parameters for all non-hydrogen atoms. During refinement, the pendant C11 atom of the ethyl group of the imidazole moiety was found to be disordered over two positions (C11A/C11B) with the occupancy ratio 0.6/0.4. Hydrogen atoms were constrained to ride on the respective carbon or nitrogen atoms with isotropic displacement parameters equal to 1.2 times the equivalent isotropic displacement of their parent atom in all cases. All calculations were carried out using SHELXS97 [37], SHELXL97 [38], PLATON99 [39], ORTEP-3 [40] programs.

3. Results and discussion

3.1. Synthesis and spectral characterisation

Four 1-alkyl-2-(arylazo)imidazole ligands (RaaiR′, where R = H (**a**), Me (**b**); R′ = Me (**1**), Et (**2**)) are used in this work. They are unsymmetrical N,N′-bidentate chelator where N and N′ refer to N(imidazole) and N(azo) donor centers, respectively. Upon reaction of a methanolic solution of $Cd(OAc)_2 \cdot 2H_2O$, RaaiR′ and NaN_3 in 1:1:2 mole proportion, red-orange crystalline products of composition $[Cd(RaaiR')(N_3)_2]_n$ have been isolated. $[Cd(RaaiR')(SCN)_2]_n$ complexes were synthesized by the same procedure using ammonium thiocyanate in methanol. Microanalytical data support the composition of the complexes (Table 2) and in two cases the structures have been established by single crystal X-ray diffraction studies.

The complexes are insoluble in non-polar solvents and common polar solvents indicating their polymeric nature, but they are fairly soluble in DMSO and DMF. The complexes are non-conducting. The solution electronic spectra in DMSO exhibit three major transitions at 450–465, 380–390 and 355–375 nm. The reflectance spectra show only two broad absorptions at 450–470 and 360–390 nm. Free ligands show absorption below 400 nm and are assigned to intraligand charge transfer transitions [26]. Thus longer wavelength absorption is related to metal-to-ligand charge transfer transitions. Cadmium(II), a $3d^{10}$ metal ion, and RaaiR′, π-acidic ligands with low-lying vacant orbitals dominated by the

Table 2
Microanalytical[a], IR[b], solution[c] and reflectance spectral data

Compound	Anal. found (Calc.) (%)			IR data (cm^{-1})				Solution spectral data	Reflectance data
	C	H	N	$\nu(N_3)$	$\nu(CN)$	$\nu(C{=}N)$	$\nu(N{=}N)$	(λ_{max}/nm)(10^{-3} ε/M^{-1} cm^{-1})	(λ_{max}/nm)
[Cd(HaaiMe)$(N_3)_2$] (**3a**)	31.30 (31.38)	2.53 (2.62)	36.52 (36.61)	2031, 2070		1578	1438	464 (1.07), 382 (13.65), 368 (14.48)	454, 381
[Cd(HaaiEt)$(N_3)_2$] (**3b**)	33.25 (33.30)	2.91 (3.03)	35.25 (35.32)	2040, 2061		1578	1435	460 (1.49), 382 (17.44), 372 (18.10)	458, 377
[Cd(MeaaiMe)$(N_3)_2$] (**4a**)	33.22 (33.30)	3.10 (3.03)	35.21 (35.32)	2035, 2067		1596	1443	470 (2.20), 386 (27.50), 372 (18.75)	464, 360
[Cd(MeaaiEt)$(N_3)_2$] (**4b**)	35.18 (35.09)	3.48 (3.41)	34.00 (34.11)	2040, 2068		1599	1445	464 (2.02), 390 (23.48), 372 (25.42)	467, 391
[Cd(HaaiMe)$(SCN)_2$] (**5a**)	34.68 (34.75)	2.33 (2.41)	20.36 (20.27)		2076, 2112	1583	1429	450 (3.0), 384 (26.74), 364 (29.08)	453, 382
[Cd(HaaiEt)$(SCN)_2$] (**5b**)	36.37 (36.41)	2.86 (2.80)	19.55 (19.60)		2078, 2113	1582	1435	462 (1.21), 384 (7.88), 358 (23.50)	454, 378
[Cd(MeaaiMe)$(SCN)_2$] (**6a**)	36.33 (36.41)	2.70 (2.80)	19.51 (19.60)		2098, 2066	1596	1434	450 (3.47), 388 (24.37), 366 (24.67)	462, 358
[Cd(MeaaiEt)$(SCN)_2$] (**6b**)	37.90 (37.97)	3.21 (3.16)	18.87 (18.99)		2065, 2110	1580	1434	450 (1.58), 384 (16.69), 372 (14.01)	467, 362

[a] Calculated values are in parentheses.
[b] In KBr disk.
[c] In DMSO solution.

azo (N=N) group [31], may involved in metal-to-ligand charge transfer transitions. Data in Table 2 reveal that $[Cd(RaaiR')(SCN)_2]_n$ (**5**, **6**) absorb at higher energy (450–460 nm) relative to $[Cd(RaaiR')(N_3)_2]_n$ (**3**, **4**) (460–470 nm). This is reasonable because of the strong preference of Cd(II) for the S donor center of the thiocyanate group.

Infra-red spectra of the complexes are very informative. The IR spectra of **3/4** exhibit a strong doublet corresponding to $\nu_{as}(N_3)$ at 2060–2070 and 2030–2040 cm^{-1}. The IR spectra of the thiocyanato compounds, $[Cd(RaaiR')(SCN)_2]_n$ (**5/6**), show a sharp strong band at 2070–2090 cm^{-1} and weak diffused shoulders at 2100–2120 cm^{-1}. These are referred to ν(CN) of bonded SCN. Medium to strong bands observe at 775–785 and 655–765 cm^{-1} have been assigned to ν(CS). The band position and splitting pattern are corroborated with bridging N,S-thiocyanato groups [19]. The ν(NCS) appear at 450 and 400 cm^{-1}.

The ^{1}H NMR spectra of the complexes have been used to determine the coordination mode of RaaiR′. The spectra are assigned (Table 3) on the basis of spin–spin interaction, effect of substituents and on comparing with free ligand values. The spectra are recorded in DMSO-d_6 and the atom numbering pattern is shown in Scheme 1. Imidazole protons 4-H and 5-H appear as singlet that may be due to rapid proton exchange in DMSO. The protons are in general downfield shifted indicating the coordination to Cd(II). The 4-H proton suffers significant downfield shifting ($\Delta\delta = 0.4$–0.5 ppm) with reference to the free ligand value [25,26]. This indicates preferential binding of imidazole-N to Cd(II) (which is also supported from Cd–N bond distance data, vide infra). 4-H is closer to the azo group which is an electron withdrawing agent. Thus 4-H is downfield shifted. Aryl-H (7-H–11-H) signals appear in their usual positions: 7,11-H appear at the most downfield position because of their closeness to the electron withdrawing azo function and 8,10-H suffer significant upfield shifting by the substitution of an electron donating –Me group [26].

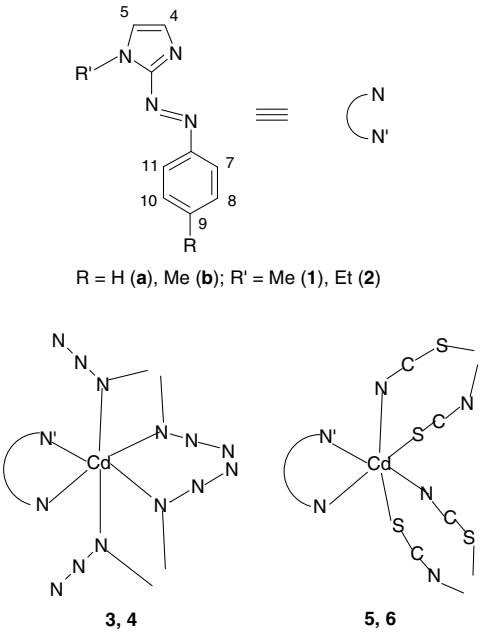

Scheme 1.

3.2. Molecular structures

3.2.1. [Cd(HaaiEt)(N$_3$)$_2$]$_n$ (**4a**)

A perspective view of **4a** is shown in Fig. 1 and selected bond parameters are listed in Table 4. The cadmium atom is in a distorted octahedral environment with CdN_6 coordination. HaaiEt acts as an unsymmetric N,N′ chelating ligand. Azido (N_3) groups act as end-on (μ-1,1 EO) double bridging agent with two neighbouring cadmium atoms. The bridging Cd_2N_2 unit constitutes a parallelogram unit with bond length Cd(1)–N(8), 2.290(3), Cd(1)–

Table 3
^{1}H NMR spectral data in DMSO-d_6

Compound	δ/ppm (J/Hz)							
	4-H[a]	5-H[a]	7,11-H[b]	8,10-H	N(1)–Me	N(1)CH_2[c]	[N(1)–CH_2]CH_3[d]	9-Me
3a	7.68	7.26	7.98 (8.0)	7.59[e]	4.03			
3b	7.61	7.26	7.94 (8.0)	7.58[e]		4.47 (12.0)	1.43 (8.0)	
4a	7.62	7.22	7.81 (8.0)	7.35 (8.0)[b]	4.00			2.40
4b	7.58	7.20	7.78 (8.0)	7.33 (8.0)[b]		4.42 (14.0)	1.41 (8.0)	2.37
5a	7.63	7.25	7.92 (8.0)	7.60[e]	4.01			
5b	7.75	7.26	7.92 (8.0)	7.60[e]		4.46 (14.0)	1.43 (8.0)	
6a	7.57	7.21	7.81 (8.0)	7.39 (8.0)[b]	3.98			2.40
6b	7.64	7.22	7.80 (8.0)	7.39 (8.0)[b]		4.43 (15.0)	1.41 (9.0)	2.40

[a] Singlet.
[b] Doublet.
[c] Quartet.
[d] Triplet.
[e] Multiplet and includes δ(9-H).

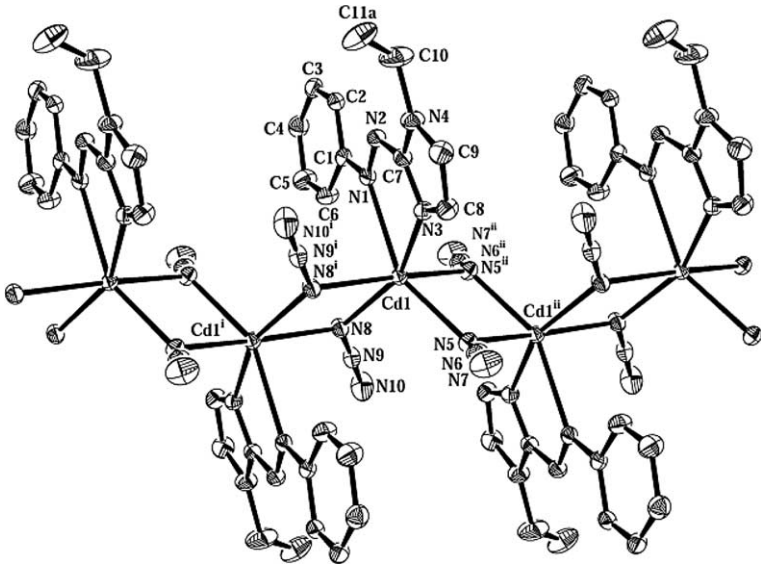

Fig. 1. A fragment of the perspective view along the a-direction of a 1D chain in $[Cd(HaaiEt)(N_3)_2]_n$ (**4a**). Symmetry code: $i = 1 - x, 2 - y, -z$; $ii = -x, 2 - y, -z$.

Table 4
Selected bond distances (Å) and angles (°) for $[Cd(HaaiEt)(N_3)_2]_n$ (**4a**)

Bond distance		Bond angle	
Cd(1)–N(1)	2.551(3)	N(1)–Cd(1)–N(3)	67.41(11)
Cd(1)–N(3)	2.314(3)	N(1)–Cd(1)–N(5)	151.67(11)
Cd(1)–N(8)	2.290(3)	N(1)–Cd(1)–N(8)	101.60(11)
Cd(1)–N(5)^{ii}	2.344(3)	N(1)–Cd(1)–N(5)^{ii}	90.60(10)
Cd(1)–N(8)^{i}	2.398(3)	N(1)–Cd(1)–N(8)^{i}	87.96(10)
N(1)–N(2)	1.259(5)	N(3)–Cd(1)–N(5)	91.53(11)
N(8)–N(9)	1.188(4)	N(3)–Cd(1)–N(8)	154.89(11)
N(9)–N(10)	1.147(4)	N(3)–Cd(1)–N(5)^{ii}	107.15(11)
Cd(1)–N(5)	2.329(3)	N(3)–Cd(1)–N(8)^{i}	84.12(10)
Cd(1)–Cd(1)^{i}	3.649(5)	N(5)–Cd(1)–N(8)	104.89(12)
Cd(1)–Cd(1)^{ii}	3.649(5)	N(5)–Cd(1)–N(5)^{ii}	77.31(12)
N(5)–N(6)	1.193(5)	N(5)–Cd(1)–N(8)^{i}	109.32(11)
N(6)–N(7)	1.151(5)	N(5)^{ii}–Cd(1)–N(8)	95.09(11)
N(5)–Cd(1)^{ii}	2.344(3)	N(8)–Cd(1)–N(8)^{i}	72.66(12)
N(8)–Cd(1)^{i}	2.398(3)	N(5)^{ii}–Cd(1)–N(8)^{i}	167.08(11)
		Cd(1)–N(5)–Cd(1)^{ii}	102.69(12)
		Cd(1)–N(8)–Cd(1)^{i}	107.34(12)
		Cd(1)^{i}–Cd(1)–Cd(1)^{ii}	131.72(4)
		N(5)–N(6)–N(7)	179.10(5)
		N(8)–N(9)–N(10)	178.10(4)
		Cd(1)–N(1)–N(2)	115.80(3)
		Cd(1)–N(5)–N(6)	122.80(3)
		Cd(1)^{i} i–N(5)–N(6)	125.20(3)
		Cd(1)–N(8)–N(9)	127.80(3)
		Cd(1)^{i}–N(8)–N(9)	121.00(2)

Symmetry code: $i = 1 - x, 2 - y, -z$; $ii = -x, 2 - y, -z$.

N(8)^{i}, 2.398(3) Å and bond angles, Cd(1)–N(8)–Cd(1)^{i}, 107.34(12)°, N(8)–Cd(1)–N(8)^{i}, 72.66(12)° ($i = 1 - x$, $2 - y, -z$; $ii = -x, 2 - y, -z$). The small chelate angle (∠N(1)–Cd(1)–N(3), 67.41(11)°) may cause the structural distortion. The bridge angles (e.g., ∠Cd(1)–N(5)–Cd(1)^{ii}, 102.69(12)°; Cd(1)–N(8)–Cd(1)^{i}, 107.34(12)°) lie in the reported angular range [7]. A 1D neutral chain is running along the a-direction by repeating the Cd_2N_2 unit. Each chelating ligand per metal ion in two adjacent Cd centers coordinates in two different ways. Two N′ (N(azo)) approach closer together or away from each other. The distortion in the CdN_6 coordination is supported by six unequal Cd–N bond distances. The longest distance is Cd–N(azo) (Cd–N(1), 2.551(3) Å) which is less than the sum of the van der Waals radii of N(azo) and Cd(II), indicating the existence of covalent interaction between Cd(II) and N(azo) [41]. The shortest distance is 2.290(3) Å and is observed for one of the Cd–N(azido) [Cd(1)–N(8)], bonds (Table 4). The N=N bond length is 1.259(5) Å which is slightly elongated ($\Delta d \sim 0.01$ Å) compared to that of the free ligand value [42]. Two neighbouring Cd-centres are in an angular arrangement with the central Cd atom and make an angle of 131.72(2)°.

3.2.2. *[Cd(MeaaiEt)(SCN)$_2$]$_n$ (**6b**)*

A perspective view of **6b** is shown in Fig. 2 and selected bond parameters are listed in Table 5. The structure consists of neutral chains of cadmium atoms linked by four SCN bridges. The octahedral coordination around Cd consists of a chelate ring from MeaaiEt, Cd(N,N′) type (MeaaiEt is an unsymmetric N,N′-chelator 1-ethyl-2-(*p*-tolylazo)imidazole), and four SCN bridges. Thiocyanate (SCN) acts as a μ-1,3 N,S-type double bridging agent with two neighbouring cadmium centres. Thus, each complex molecular fragment shows an octahedral CdN_4S_2 coordination arrangement. Thiocyanate (SCN) is an ambidentate ligand and has a schizophrenic preference to Cd(II) exhibiting both S and N bonding modes [43]. Out of four SCN groups around the Cd centre two are S-bonded and two are N-bonded. Thus double bridged NCS forms an eight membered puckered ring structure. Each Cd centre is associated

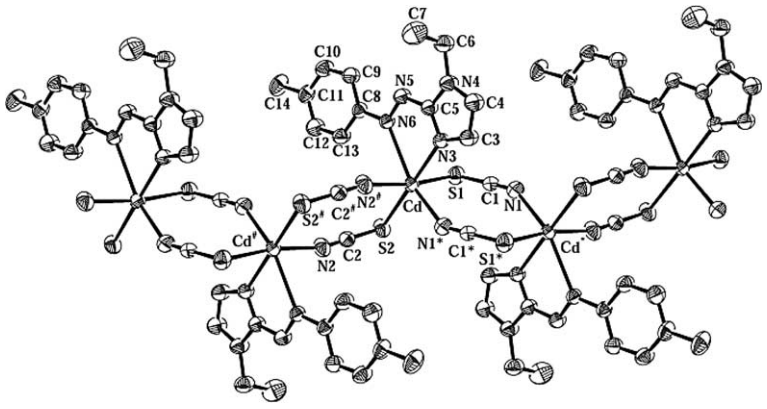

Fig. 2. A fragment of the perspective view along the b-direction of a 1D chain in $[Cd(MeaaiEt)(SCN)_2]_n$ (**6b**). Symmetry code: $* = -x, 1-y, 1-z$; $\# = -x, -y, 1-z$.

Table 5
Selected bond distances (Å) angle (°) for $[Cd(MeaaiEt)(SCN)_2]_n$ (**6b**)

Bond distance		Bond angle	
Cd–S(1)	2.7249(8)	S(1)–Cd–S(2)	82.51(2)
Cd–S(2)	2.6520(7)	S(1)–Cd–N(3)	89.97(6)
Cd–N(3)	2.293(2)	S(1)–Cd–N(6)	88.57(5)
Cd–N(6)	2.615(2)	S(1)–Cd–N(1)*	98.76(7)
Cd–N(1)*	2.296(2)	S(1)–Cd–N(2)#	166.89(7)
Cd–N(2)#	2.292(2)	S(2)–Cd–N(3)	171.45(6)
S(1)–C(1)	1.650(3)	S(2)–Cd–N(6)	108.60(5)
S(2)–C(2)	1.645(3)	S(2)–Cd–N(1)*	96.42(7)
N(1)–C(1)	1.142(3)	S(2)–Cd–N(2)#	93.63(6)
N(2)–C(2)	1.145(4)	N(3)–Cd–N(6)	66.95(7)
N(5)–N(6)	1.267(3)	N(1)*–Cd–N(3)	88.72(8)
Cd–Cd(*)	5.4770(5)	N(2)#–Cd–N(3)	92.81(8)
Cd–Cd(#)	5.8426(5)	N(1)*–Cd–N(6)	154.68(8)
N(1)–Cd(*)	2.296(2)	N(2)#–Cd–N(6)	80.76(8)
N(2)–Cd(#)	2.292(2)	N(1)*–Cd–N(2)#	94.11(10)
		S(1)–C(1)–N(1)	179.3(2)
		S(2)–C(2)–N(2)	178.4(2)
		Cd(*)–Cd–Cd(#)	131.94(1)
		Cd–N(3)–C(5)	116.30(17)
		Cd–N(6)–N(5)	114.48(15)
		Cd–S(2)–C(2)	99.12(9)
		Cd–S(1)–C(1)	92.28(9)
		Cd(*)–N(1)–C(1)	147.40(2)
		Cd(#)–N(2)–C(2)	163.80(2)
		C(5)–N(5)–N(6)	113.80(2)

Symmetry code: $* = -x, 1-y, 1-z$; $\# = -x, -y, 1-z$.

with two eight membered rings and one five membered chelate ring from MeaaiEt. The two eight membered rings are not equivalent; one of them suffers severe distortion in which Cd is deviated from planarity by 0.27 Å, the S and N are deviated by −0.27 and 0.34 Å, respectively, from the mean plane. These two rings make a dihedral angle of 55.74(7)°. The chelate ring is a good plane and the pendant phenyl ring is almost planar with the chelate ring (dihedral 3.62(14)°).

The two sets of μ-(N,S)-thiocyanato bridges are not equivalent which is evident from their bond parameters data (Table 5). The two Cd–S bond distances differ by 0.073 Å while the two Cd–N distances differ insignificantly (0.004 Å). The Cd–S(2) bond *trans* to the Cd–N(imidazole) (Cd–N(3)) is shorter than the second Cd–S(1) bond length. Other distances about SCN (C–N, C–S) differ only by 0.003–0.006 Å. The bridging SCN does not show deviation from linearity (∠S–C–N, av. 178.8°). MeaaiEt forms a strained chelate ring around cadmium; the chelate angle is 66.95(7)°. The Cd–N(MeaaiEt) distances differ significantly. Because of matching softness character of Cd(II) and imidazole-N, the Cd–N(imidazole) (Cd–N(3), 2.293(2) Å) bond length is substantially lower than the Cd–N(azo) (Cd–N(6), 2.615(2) Å) length and the difference is 0.32 Å. The azo N=N bond length, 1.267(3) Å, is slightly elongated from that of the free ligand value (1.250(1) Å) [42]. The chelate ring strain may be the reason for the inequivalence of the two μ-(N,S)-thiocyanato group double bridges about Cd(II). Two neighbouring Cd centers in the bridging head of one Cd are not in the same phase and these three Cd centers extend an angular arrangement of 131.94(1)°. The versatile bridging nature of the SCN ligands gives a 1D polymeric chain along the *b*-axis. The Cd–Cd separations are 5.4770(5) and 5.8426(5) Å.

3.2.3. Supramolecular sheet

The 1D chains are self-assembled into molecular sheets via π–π interactions between aromatic rings and are described in Figs. 3 and 4. The chelated arylazoimidazole in the molecular unit of each chain is projected into the space provided by two neighbouring molecular units of adjacent chains. This natural penetration is meaningful and we find some π–π interaction with the aromatic rings. The aryl ring (Ar) of one chelated molecule in one 1D chain interacts with imidazole ring (Imz) from the adjacent molecule of a neighbouring chain. Thus, Imz(A)–Ar(B) (A stands for one 1D chain and B stands for the adjacent 1D chain) are separated by 4.34 Å for $[Cd(HaaiEt)(N_3)_2]_n$ and 4.05 Å for $[Cd(MeaaiEt)(SCN)_2]_n$. The Ar rings are also under π–π interaction and their separations are 3.95 and 3.94 Å for $[Cd(HaaiEt)(N_3)_2]_n$ and $[Cd(MeaaiEt)(SCN)_2]_n$, respec-

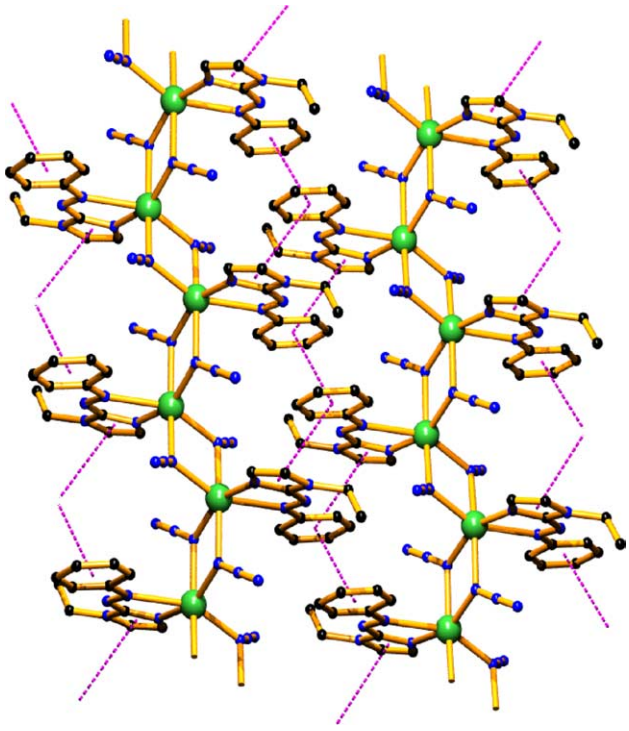

Fig. 3. Supramolecular sheet via π–π interaction in $[Cd(HaaiEt)(N_3)_2]_n$ (**4a**).

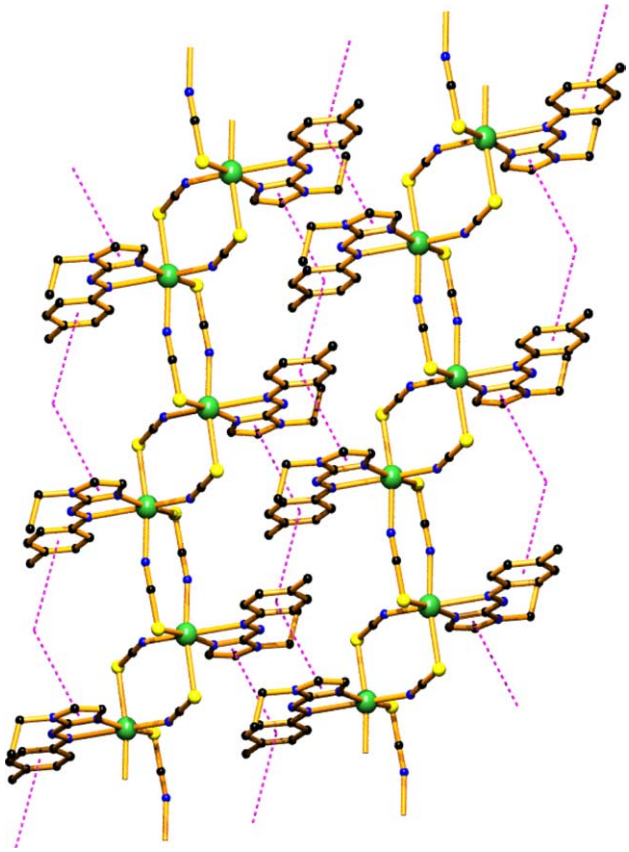

Fig. 4. Supramolecular sheet via π–π interaction in **6b**.

tively. The non-covalent interaction is thus associated with –Imz(A)–Ar(B)–Ar′(A)–Imz′(B)– [′ refers to the second molecule in the respective chain] and thus adjacent chains generate a sheet. The Ar–Ar interaction is stronger than the Imz–Ar interaction as is evident from the Cg–Cg distance data. However, the strength of the π–π interaction is about to same between the Ar–Ar system in the two classes of molecules irrespective of the substituent in the rings, while Imz–Ar interaction is stronger in $[Cd(MeaaiEt)(SCN)_2]_n$ than $[Cd(HaaiEt)(N_3)_2]_n$. The reason is unclear at present and may be due to a difference in their bridge pattern (EO in the azido compound and EE in the thiocyanato system) and the strain in the bridged motif (four membered ring in Cd-azido and eight membered in the Cd-SCN system).

4. Supplementary material

Crystallographic data for the structural analysis have been deposited with the Cambridge Crystallographic Data Centre, CCDC No. 216059 for $[Cd(HaaiEt)(N_3)_2]_n$ (**4a**) and CCDC No. 216060 for $[Cd(MeaaiEt)(SCN)_2]_n$ (**6b**). Copies of this information may be obtained free of charge from the Director, CCDC, 12 Union Road, Cambridge, CB2 1FZ, UK (fax: +44-1223-336033; E-mail: deposit@ccdc.cam.ac.uk or www: http://www.ccdc.cam.ac.uk).

Acknowledgements

Financial support (C.S.) and fellowship (U.S.R.) from the University Grants Commission, New Delhi is gratefully acknowledged.

References

[1] R.H. Holm, J.A. Ibers, Science 209 (1980) 223.
[2] Special issue on Focus on Self-assembly, Acc. Chem. Res. 32 (1999) 4.
[3] B.J. Holliday, C.A. Mirkin, Angew. Chem. Int. Ed 40 (2001) 2022.
[4] D. Braga, L. Maini, M. Polito, L. Scaccianoce, G. Cojazzi, F. Grepioni, Coord. Chem. Rev. 216–217 (2001) 225.
[5] D.A. Buckingham, Coord. Chem. Rev. 587 (1994) 135.
[6] Z. Dori, R.F. Ziolo, Chem. Rev. 73 (1973) 247.
[7] H. Zhang, X. Wang, K. Zhang, B.K. Teo, Coord. Chem. Rev. 183 (1999) 157.
[8] A.M. Golub, H. Kohler, V.V. Skopenko, Chemistry of Pseudohalides, Elsevier, Amsterdam, 1986.
[9] J. Ribas, M. Monfort, B.K. Ghosh, X. Solans, M.F. Bardia, J. Chem. Soc., Chem. Commun. (1995) 2375.
[10] E. Ruiz, J. Cano, S. Alvarez, P. Alemany, J. Am. Chem. Soc. 120 (1998) 11122.
[11] A. Hagfelot, M. Gratzel, Acc. Chem. Res. 33 (2003) 269.
[12] S. Chandrasekhar, Liquid Crystals, 2nd ed., Cambridge University Press, Cambridge, 1992.
[13] C.L. Bowes, G.A. Ogin, Adv. Mater. 8 (1996) 13.

[14] A. Mondal, G. Mostafa, A. Ghosh, I.R. Laskar, N. Ray Chaudhuri, J. Chem. Soc., Dalton Trans (1999) 9.
[15] A. Mondal, G. Mostafa, A. Ghosh, N. Ray Chaudhuri, J. Chem. Res. (S) (1998) 570.
[16] H. Zhang, X. Wang, K. Zhang, B.K. Teo, Inorg. Chem. 37 (1998) 3490.
[17] M.A.S. Goher, F.A. Mautner, M.A.M. Abu-Youssef, A.K. Hafez, A.M.-A. Badar, J. Chem. Soc., Dalton Trans (2002) 3309.
[18] H.-J. Chen, X.-M. Chen, Inorg. Chim. Acta 329 (2002) 13.
[19] M.A.S. Goher, F.A. Mautner, A.K. Hafez, M.A.M. Abu-Youssef, C. Gspan, A.M.-A. Badar, Polyhedron 22 (2003) 975.
[20] N. Mondal, M.K. Saha, S. Mitra, V. Gramlich, J. Chem. Soc., Dalton Trans. (2000) 3218.
[21] J.-C. Dai, X.-T. Wu, Z.-Y. Fu, S.-M. Hu, W.-X. Du, C.-P. Cui, L.-M. Wu, H.-H. Zhang, R.-Q. Sun, Chem. Commun. (2002) 12.
[22] M.B. Francis, E.N. Jacobson, Angew Chem. Int. Ed. 38 (1999) 937.
[23] R. Sekiya, S. Nishikiori, Chem. Commun. (2001) 2612.
[24] M.I. Scudder, H.A. Goodwin, I.G. Dance, New J. Chem. 23 (1999) 695.
[25] T.K. Misra, D. Das, C. Sinha, P.K. Ghosh, C.K. Pal, Inorg. Chem. 37 (1998) 1672.
[26] T.K. Misra, D. Das, C. Sinha, Polyhedron 16 (1997) 4163.
[27] S. Pal, D. Das, C. Sinha, C.-H.L. Kennard, Inorg. Chim. Acta 21 (2001) 313.
[28] P. Byabartta, S. Pal, T.K. Misra, C. Sinha, F.-L. Liao, K. Panneersalvam, T.-H. Lu, J. Coord. Chem. 55 (2002) 479, and references therein.
[29] J.K. Nag, P.K. Santra, C. Sinha, F.-L. Liao, T.-H. Lu, Polyhedron 20 (2001) 2253.
[30] B.G. Chand, U.S. Ray, P.K. Santra, G. Mostafa, T.-H. Lu, C. Sinha, Polyhedron 22 (2003) 1205.
[31] J. Dinda, K. Bag, C. Sinha, G. Mostafa, T.-H. Lu, Polyhedron 22 (2003) 1367.
[32] B.G. Chand, U.S. Ray, J. Cheng, T.-H. Lu, C. Sinha, Polyhedron 22 (2003) 1213.
[33] K. Bag, T.K. Misra, C. Sinha, J. Indian Chem. Soc. 75 (1998) 421.
[34] K. Bag, N.K. De, B.R. De, C. Sinha, Proc. Indian Acad. Sci. (Chem. Sci.) 109 (1997) 159.
[35] Cadmium in the environment and its significance to man, Pollution paper No.17, Her Majesty's Stationery Office, London, 1980.
[36] R.M. Izatt, J.J. Christensen, J.H. Rytting, Chem. Rev. 71 (1971) 439.
[37] G.M. Sheldrick, SHELXS 97, Program for the Solution of Crystal Structures, University of Göttingen, Germany, 1997.
[38] G.M. Sheldrick, SHELXL 97, Program for the Refinement of Crystal Structures, University of Göttingen, Germany, 1997.
[39] A.L. Spek, PLATON, Molecular Geometry Program, University of Utrecht, The Netherlands, 1999.
[40] L.J. Farrugia, J. Appl. Cryst. 30 (1997) 565.
[41] A.G. Orpen, L. Brammar, F.H. Allen, O. Kennard, D.G. Watson, R. Taylor, J. Chem. Soc., Dalton Trans. (1989) SI.
[42] D. Das, Ph.D. Thesis, Burdwan University, Burdwan, India, 1998.
[43] J.L. Burmeister, in: A.A. Newmann (Ed.), The Chemistry and Biochemistry of Thiocyanic Acid and Its Derivatives, Academic Press, New York, 1975 (Chapter 2).

Available online at www.sciencedirect.com
SCIENCE DIRECT®
Polyhedron 23 (2004) 1677–1683
POLYHEDRON
www.elsevier.com/locate/poly

Hydrocarboxylation and stepwise alternating oligomerization of carbon monoxide and ethylene catalyzed by *cis*-[$Rh(CO)_2(amine)_2$](PF_6) complexes in a wet liquid tetrabutylammonium hydrogensulfate

Alvaro J. Pardey [a,*], Clementina Longo [b], Tiziana Funaioli [c], Giuseppe Fachinetti [c]

[a] *Centro de Equilibrios en Solución, Escuela de Química, Facultad de Ciencias, Universidad Central de Venezuela, Caracas, Venezuela*
[b] *Centro de Investigación y Desarrollo de Radiofármacos, Facultad de Farmacia, Universidad Central de Venezuela, Caracas, Venezuela*
[c] *Dipartimento di Chimica e Chimica Industriale, Università de Pisa, via Risorgimento 35, I-56126, Pisa, Italy*

Received 10 October 2003; accepted 19 March 2004
Available online 1 June 2004

Abstract

In aqueous solution with tetrabutylammonium hydrogensulfate cocatalyst, rhodium complexes like *cis*-[$Rh(CO)_2(amine)_2$](PF_6) (amine = 4-picoline, 3-picoline, 2-picoline, pyridine, or 2,6-lutidine) promote the oligomerization and, to a lesser extent, the hydrocarboxylation of CO/ethylene. Higher rates for both the production of alternating polyketones and propionic acid are observed in wet tetrabutylammonium hydrogensulfate medium. An in situ FT-IR spectroscopy study confirms that five coordinated rhodium species of the type *trans*-[$Rh(CO)_3(amine)_2$]$^+$ are formed under catalytic conditions. The data are discussed in terms of a potential catalytic cycle, and the formation of propionic acid and ketones is determined to come from the hydrolysis and hydrogenolysis of the Rh-acyl intermediates formed under the catalytic conditions.
© 2004 Elsevier Ltd. All rights reserved.

Keywords: Hydrocarboxylation; Oligomerization; Catalysis; Rhodium complexes; Ethylene; Carbon monoxide

1. Introduction

Catalytic hydrocarboxylation of ethylene (Eq. (1)) and higher olefins under CO/water to carboxylic acids catalyzed by cobalt pyridine complexes [1–4], the co-oligomerization of CO/ethylene to polyketones (Eq. (2)) catalyzed by palladium complexes bearing nitrogen and phosphorous donor ligands [5–9] and palladium-promoted copolymerization in water [10–14] have been studied in detail. On the other hand, the use of water in some of the above described processes is due to its environmental friendly characteristic, cheapness and for its promoting effect, which has been related to the formation of active metal-hydride species [15], an important first step in the catalytic cycle, via a reaction closely related to the water gas shift reaction [16]. Also, in the literature exist few examples of CO/ethylene co-oligomerization [17–20] and copolymerization [21] reaction promoted by a rhodium system and an example of homogeneous catalytic carboxylation reaction carried out in salty medium [22]. However, little is known about the hydrocarboxylation or the co-oligomerization of CO/ethylene promoted in aqueous media by rhodium complexes bearing nitrogen donor ligands. We wish to report our preliminary observations on the reaction of carbon monoxide and ethylene by the rhodium(I) complexes *cis*-[$Rh(CO)_2(amine)_2$](PF_6) (amine = 4-picoline, 3-picoline, 2-picoline, pyridine, or 2,6-lutidine) in water with tetrabutylammonium hydrogensulfate (40/2.5, w/w) cocatalyst and, by comparison, in wet, liquid, tetrabutylammonium hydrogensulfate/H_2O (80/40, w/w).

$$C_2H_4 + CO + H_2O \rightarrow C_2H_5COOH \quad (1)$$

* Corresponding author. Tel.: +5-58-2-481-8723; fax: +58212-605-1225/+5-582-605-2707.
E-mail address: apardey@strix.ciens.ucv.ve (A.J. Pardey).

0277-5387/$ - see front matter © 2004 Elsevier Ltd. All rights reserved.
doi:10.1016/j.poly.2004.03.023

$$n(CH_2{=}CH_2) + nCO{+} \rightarrow H(-CH_2CH_2CO-)_nCH_2CH_3 \quad (2)$$

2. Experimental

2.1. Materials

Pyridine (py), methyl pyridines (4-picoline (4-pic), 3-picoline (3-pic) and 2-picoline (2-pic)) and dimethyl pyridine (2,6-lutidine (2,6-lut)) were obtained from Aldrich and distilled over KOH. Tetrabutylammonium hydrogensulfate ($(CH_3(CH_2)_3)_4N(HSO_4)$, 97%) from Aldrich was used as received. Water was distilled. CaO containing ethyl violet as indicator from Carlo Erba was used as received. CO (Rivoira) and ethylene (Praxair) were used as received. The complexes of the type *cis*-$[Rh(CO)_2(amine)_2](PF_6)$ (amine = 4-picoline, 3-picoline, 2-picoline, pyridine, or 2,6-lutidine) were synthesized and characterized as reported by Denise and Pannetier [23] and their IR spectra in chloroform demonstrated their identity and purity (two strong bands in the $\nu_{(CO)}$ region at 2095 and 2020 cm^{-1}).

2.2. Instrumentation

Organic products were analyzed on a Dani Model 8400 gas chromatograph (equipped with a flame ionization detector and a 2 m × 1/8 in. Carbowax W (80–100 mesh) packed column, using He (Rivoira) as carrier gas) on a Hewlett-Packard 6890/5973 GC/MS coupled system (fitted with a 5% phenylmethyl siloxane column (30 m × 25 μm × 0.25 m) using He as carrier gas (1 mL/min)) on a Varian Gemini 200 ^1H NMR, on a Perkin–Elmer Model FT-IR 1725-X and on a Paragon 500 FT-IR instruments. The potentiometric titrations and determinations of pH were performed on a Crison model 2001 pH-meter.

2.3. Catalyst testing

Catalytic runs were carried out in a 400 mL mechanically stirred stainless steel autoclave charged with 40.0 g of H_2O (2.22 mol), 1.5×10^{-4} mol of the rhodium complex and tetrabutylammonium hydrogensulfate in the range 2.52 g (7.4 mmol)–80.00 g (235.6 mmol). The reaction vessel was charged firstly with 20.0 g of ethylene and then with 20.0 g of CO (total pressure = 88 atm) and warmed at 150 ± 1 °C by mean of a circulating oil bath. These pressure and temperature were chosen in order to average the previous reported systems based on $Rh_4(CO)_{14}$/organic solvents [16–20]. At the end of the reaction time, the amounts of formed CO_2 and propionic acid were determined by the increase in weight of a glass column packed with CaO where the pre-dried gases of the reaction were passed through and by potentiometric titration of an aliquot of the yielded catalytic mixture with NaOH (0.1 M), respectively. For the potentiometric titration, an aliquot (typically, 2.0 g) of the previously shacked catalytic mixture was diluted in 10 mL of water and then titrated with a 0.1 M NaOH solution. Two inflection points were observed, the first corresponding to $[(CH_3(CH_2)_3)_4NHSO_4]$ (pH range 2–4) and the second corresponding to propionic acid (pH range 7–11). Propionic acid concentration ([propionic acid] (mol)) was calculated by the following expression [propionic acid] = [(volume (L) of NaOH consumed until the second inflection point of titration curve) − (volume (L) of NaOH consumed until the first inflection point)]*([NaOH] (mol/L))*[(total weight (g) of the catalytic mixture)/(weight (g) of the titration aliquot)]. The other organic products were extracted with diethyl ether and subjected to column chromatography on silica gel with diethyl ether/*n*-hexane 9:1. The three major separated fractions were penta-3-one, octane-3,6-dione and undecane-3,6,9-trione which were identified by ^1H NMR, IR and GC-MS [24,25]. The extent of the co-oligomerization was established on the base of produced CO_2 (Eq. (3)), while the amount of single ketones were not quantitatively determined.

3. Results and discussion

3.1. Catalysis studies

The *cis*-$[Rh(CO)_2(amine)_2][PF_6]$ (amine = 3-picoline, 2-picoline, pyridine, or 2,6-lutidine) complexes were investigated as precursors for catalytic CO/ethylene reactions in water containing 6% of tetrabutylammonium hydrogensulfate. All the complexes were active for both ethylene hydrocarboxylation (Eq. (1)) and ethylene/CO co-oligomerization (Eq. (3)). The relative extent of the two competing catalytic reactions can be established by the TOF(C_2H_5COOH) and the TOF(CO_2) (TOF = moles of product/moles of rhodium/24 h). The results are shown in Table 1. All the five solutions left after cooling the reactor show two liquids phases. The upper organic phase is dark-red, and the aqueous phase has a pale-yellow color. Also, control experiments show that the activity toward the hydrocarboxylation and hydrocarbonylation of ethylene under CO was not observed when the same aqueous solution of tetrabutylammonium hydrogensulfate was tested under similar experimental conditions in the absence of any of the carbonylaminerhodium(I) complexes.

$$n(CH_2{=}CH_2) + nCO + H_2O \rightarrow CH_3{-}CH_2{-}C(O){-}\mathbf{R} + CO_2 \quad (3)$$

Table 1
The catalytic hydrocarboxylation and co-oligomerization of CO/ethylene promoted by *cis*-$[Rh(CO)_2(amine)_2](PF_6)$

Run	Amine (pK_a)	Wt. CO_2 (g)	TOF(CO_2)[b](% of CO conversion to CO_2)	Mol of propionic acid (selectivity, %)	TOF (propionic acid)[b] (yield %)
1	2,6-Lut[c] (6.75)	0.53	305 (2)	0.006 (33)	152 (1)
2	4-Pic[c] (6.00)	2.55	1473 (8)	0.022 (27)	558 (3)
3	2-Pic[c] (5.97)	2.17	1252 (7)	0.013 (21)	330 (2)
4	3-Pic[c] (5.52)	2.35	1356 (7)	0.014 (21)	356 (2)
5	Py[c] (5.27)	2.10	1211 (7)	0.014 (23)	356 (2)
6	3-Pic[d] (5.52)	5.03	19 878 (16)	0.193 (63)	33 565 (27)

[a] $Rh = 1.5 \times 10^{-4}$ mol; $H_2O = 40.0$ g; $CO = C_2H_4 = 20.0$ g (88 atm); $T = 150 \pm 1$ °C for 6.3 h.
[b] TOF(product) = mol product/mol Rh/24 h.
[c] $[(CH_3(CH_2)_3)_4N][HSO_4] = 2.52$ g (7.4 mmol).
[d] $[(CH_3(CH_2)_3)_4N][HSO_4] = 80.00$ g (235.6 mmol); 0.92 h.

for $n = 2$, $\mathbf{R} = CH_2–CH_3$; (penta-3-one).
for $n = 3$, $\mathbf{R} = CH_2–CH_2–C(O)–CH_2–CH_3$; (octane-3,6-dione).
for $n = 4$, $\mathbf{R} = CH_2–CH_2–C(O)–CH_2–CH_2–C(O)–CH_2–CH_3$; (undecane-3,6,9-trione).

The ketones products penta-3-one, octane-3,6-dione and undecane-3,6,9-trione come from the catalytic stepwise co-oligomerization of the CO/ethylene mixture (Eq. (3)). No attempts were made to quantify separately the yields of the each ketone. However, a 65% of penta-3-one and 35% of octane-3,6-dione was observed in one of the fractions (which contained only these two ketones), based on ^1H NMR signals.

In aqueous solution containing 5.9% of hydrogensulfate salt, the TOF(CO_2) followed the order: 3-pic (1356) > 2-pic (1252) > py (1211) > 2,6-lut (305) under the same catalytic conditions, based on CO_2 produced (Table 1).

Further, propionic acid (Eq. (1)) was separated after a treatment of the resulting aqueous phase of the catalytic solution, first with diethyl ether/H_2O, later with K_2SO_3/H_2O and finally with H_2SO_4/diethyl ether. The ^1H NMR δ_H ($CDCl_3$) = 0.949 (t, 3H, CH_3), 2.254 (q, 2H, CH_2Me) and 4.667 ppm (s, 1H, OH), and the GC-MS (molecular ion peak and base peak at $m/e = 74$) of this fraction are similar to a pure sample of propionic acid. The amount of propionic acid formed was determined by potentiometric titration.

The reactivity toward propionic acid formation for this Rh/amine system proved also to be dependent on the nature of the heterocyclic nitrogen ligand coordinated to the rhodium center (Table 1), for example the TOF(propionic acid) (24 h^{-1}) values for these carbonyl rhodium complexes followed the order: 3-pic (356) = py (356) > 2-pic (330) > 2,6-lut (152) under the same catalytic conditions.

The results show the positive effect of amine basicity on the ketones and to a lesser extent on propionic acid production, which increases with pK_a augmentation of the amine ligand in absence of steric effect (present in the 2-picoline and 2,6-lutidine); namely, 3-picoline displays the highest activity. However, reaction rates decreased markedly with increasing steric hindrance of the coordinated amine as shown by the lower activity of 2-picoline and 2,6-lutidine. These results suggest a critical steric parameter, which can be viewed as the effect of competition for binding to the catalytic center, which is more affected by steric constraints than by electronic effects. For example, the coordination of the ethylene to the rhodium center is a crucial step [17], and it can be inhibited in some degree by the effective block of methyl groups in *ortho* position to nitrogen atom of the aromatic ring and consequently decreasing the catalytic activity. Also, the blocking effect can prevent or decrease the rate of other elementary reactions of the catalytic cycle, which require an open coordination site on the metal center. This kind of blocking has been illustrated by Vallarino and Sheargold [26] on the solid state isomerism and intermetallic interactions in the square planar rhodium(I), $[RhX(CO)_2(amine)]$ (X = Cl, Br, amine = 2-picoline, 2,6-lutidine, etc.) complexes, that can be rationalized in terms of the steric hindrance of the amino ligand which effectively prevent interactions between adjacent Rh(I) centers. The methyl group of these ligands when coordinated to the metal ion effectively blocks the axial position of the square planar environment. For example, complexes in which the amine ligand has a highly hindered N-donor atom are obtained in the non-stack form while the stacked form is common for non-hindered ligands.

A test was performed by using as a catalytic precursor the complex *cis*-$[Rh(CO)_2(4\text{-pic})_2](PF_6)$ (bearing a less crowed 4-picoline ligand) to confirm this hypothesis. Under similar reactions conditions the TOF(CO_2) and TOF(propionic acid) values for this R(4-pic) system are 1473 and 558 (24 h^{-1}), respectively. It can be observed that overall TOF (TOF(CO_2) plus TOF(propionic acid)) of the Rh(4-pic) system (2031 (24 h^{-1})) is 4.4 times more active than the Rh(2,6-lut) system (457 (24 h^{-1})) and 1.3 times more active than the Rh(2-pic) system (1582 (24 h^{-1})). A plot of total TOF/day values vs. pK_a of the protonated base for the sterically and non-sterically

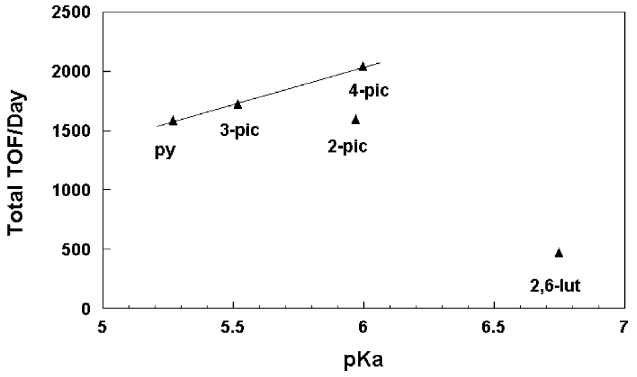

Fig. 1. Plot of total TOF/day vs. pK_a (BH^+) of pyridines and substituted pyridines. (Line drawn for illustrative purposes only.)

hindered pyridines used is shown in Fig. 1. The total TOF day values followed as 4-pic (2031) > 3-pic (1712) > 2-pic (1582) > py (1567) > 2,6-lut (457). Apparently the catalytic activity observed in these systems is the consequence of a fine balance between electronic and sterical factors. However, it can be seen that the sterical factor predominates over the electronic influence.

In these studies it was observed that all the catalytic solutions have undergone some pH changes. For example, the freshly prepared solution from *cis*-[Rh(CO)$_2$(amine)$_2$](PF$_6$)/aqueous tetrabutylammonium hydrogensulfate (0.2 M) gave a pH value of 1.29, while the catalytic solutions formed under a continuous heating (6.3 h), at 150 °C under CO/ethylene atmosphere gave a pH value of 1.49–1.56.

A remarkable result related to the ketone and propionic acid formations catalyzed by the Rh/3-pic system is observed when the concentration of the [$(CH_3(CH_2)_3)_4NHSO_4$] salt increased from 2.52 g (5.9%) to 80 g (66.7%). As observed in Table 1, the TOF(CO_2) and TOF(propionic acid) reaches the highest values of 19 878 (16% conversion in 6.3 h) and 33 565 (24 h)$^{-1}$ (selectivity ca. 63% at 27% conversion in 6.3 h), respectively, under a wet liquid tetrabutylammonium hydrogensulfate medium. These results suggested that the salty medium stabilize the ionic Rh catalytic species formed under the reaction conditions, therefore enhancing the reactivity. The approach related to the use of salty medium can constitute an alternative reaction media in comparison to the more recently reported ionic liquid [27]. Furthermore, the evaluation with the Rh/3-pic system in wet liquid tetrabutylammonium hydrogensulfate was made long before the discovery for us of the most active Rh/4-pic system. No attempt was made to evaluate the Rh/4-pic system in wet liquid tetrabutylammonium hydrogensulfate.

3.2. FT-IR characterization studies

The FT-IR spectra of recently prepared KBr pellets of *cis*-[Rh(CO)$_2$(amine)$_2$](PF$_6$) (amine = 4-picoline, 3-picoline, 2-picoline, pyridine, or 2,6-lutidine) show two strong bands in the ν_{CO} region before being exposed to CO in agreement to the results reported by Denise and Pannetier [23]. On the contrary, the in situ FT-IR spectrum of the active Rh(amine)$_2$/R_4NHSO_4 catalyst solution, after being exposed to CO/ethylene, displays one strong band and a weak satellite at higher frequency in the ν_{CO} region (Table 2). Probably, under the catalytic conditions at high pressure a CO molecule is coordinated to starting *cis*-dicarbonyl rhodium complex forming the *trans*-[Rh(CO)$_3$(amine)$_2$]$^+$ (Eq. (4)), where both amine ligands are in *trans*-position. This ν_{CO} spectrum is typical for M(CO)$_3$L$_2$ system with D_3h form on the grounds of selection rules [28]. The single strong band in the *trans* complex is assigned the e' mode and the weak shoulder is probably the a_1' mode made weakly infrared-active by asymmetry of the ligands. Attempts to isolate and characterize the rhodium products after a catalytic run were unsuccessful due to the unstable nature of the rhodium catalytic species. The Rh species are only stable under the catalytic conditions.

$$\textit{cis}\text{-}[Rh(CO)_2(amine)_2]^+ + CO \rightarrow \textit{trans}\text{-}[Rh(CO)_3(amine)_2]^+ \quad (4)$$

3.3. Mechanistic consideration

The products of these reactions may be explained by the mechanism illustrated in Schemes 1 and 2. The overall mechanism is similar to the one proposed by Bianchini et al. [12] for the CO/ethylene alternating copolymerization and terpolymerization catalyzed by water soluble Pd(II)–Na_2DPPPDS catalyst. However, there are some important differences. First, Bianchini

Table 2
IR data for *cis*-[Rh(CO)$_2$(amine)$_2$](PF$_6$) and catalytic solutions

Amine	Solid sample ν_{CO} (cm^{-1})[a]	Catalytic solution ν_{CO} (cm^{-1})[a]
4-Picoline	2095 (vs) and 2020 (vs)	2036 (sh) and 2012 (vs)
3-Picoline	2101 (vs) and 2041 (vs)	2038 (sh) and 2012 (vs)
2-Picoline	2095 (vs) and 2020 (vs)	2044 (sh) and 2012 (vs)
Pyridine	2095 (vs) and 2020 (vs)	2040 (sh) and 2012 (vs)

[a] vs, very strong and sh, shoulder.

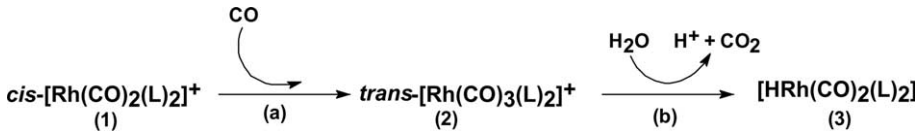

Scheme 1.

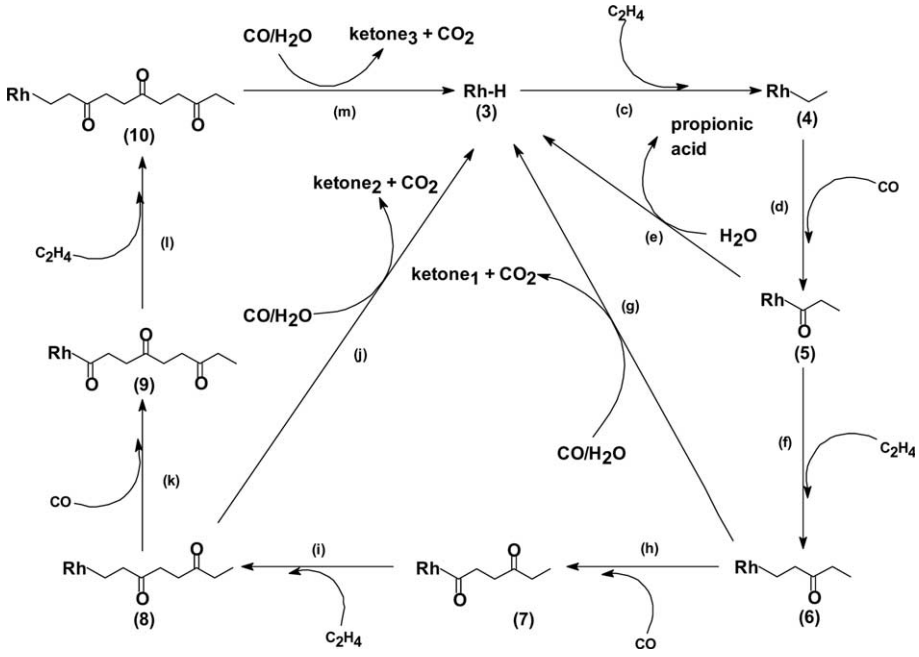

Scheme 2. Ketone$_1$ = penta-3-one; ketone$_2$ = octane-3,6-dione; ketone$_3$ = undecane-3,6,9-trione.

et al. did not observe in their system formation of propionic acid. The formation of propionic acid implies the hydrolysis of Rh–C bonds in the propagation unit Rh–$C(O)CH_2CH_3$ as one of the termination steps. Second, they suggested that the production of CO_2 goes via insertion of CO into Pd–OH bonds to give Pd–COOH. Proposed here is that the production of free CO_2 goes via decarboxylation of Rh-hydroxycarbonyl species formed by nucleophilic attack of water on coordinated CO under water gas shift reactions (WGSR) conditions [29]. The results of the TOF values (Table 1) suggest that termination steps by hydrolysis affording propionic acid are faster than the termination step by in situ hydrogenolysis to affording ketones by factor range of 2.0–3.8.

The catalytic precursors *cis*-$[Rh(CO)_2(L)_2]^+$ (**1**, L = amine) suffer diverse transformations before forming the catalytic $[HRh(CO)_2(L)_2]$ species (**3**). Namely, their reaction with CO to form the tricarbonyl-rhodium *trans*-$[Rh(CO)_3(L)_2]^+$ complex (Eq. (4)), which under CO/H_2O is gradually transformed (steps a–b) in the neutral complex Rh–H (**3**) (Scheme 1). The characterization by in situ ^1H NMR spectroscopic studies of rhodium hydride intermediates (Rh–H) formed by the transformation of the rhodium(I) complex, *cis*-$[Rh(CO)_2(py)_2](PF_6)$ dissolved in aqueous pyridine, under water gas shift reaction conditions has been reported [30].

In Scheme 2, the CO and amine ligands of the starting rhodium complex (**3**) are omitted for clarity. The propionic acid formation (step e) and ketones (steps g, j and m) arise by hydrolysis and hydrogenolysis, of the Rh-acyl intermediates, respectively. The oligomerization may proceed by a single mode of chain growth involving alternate insertion of CO and ethylene (C_2H_4) forming intermediate Rh-acyls [20]. The Rh-acyl species are terminated by reaction with the CO/H_2O couple affording CO_2 and the corresponding ketones. The formation of propionic acid may be facilitated by the coordinated pyridine. It has been proposed that pyridine has vacant antibonding π-orbitals, capable of accepting the electrons coming from rhodium-back donation, lowering the electron density on the Rh center [17,31]. Accordingly, the pyridine coordinated σ-acyl complex (**5**) may be easily attacked by nucleophillic OH^- group (coming from H_2O) given propionic acid (step e). The hydrogenolysis of the Rh-acyl intermediates, which leads to ketone formation (steps g, j and m), comes probably from *intra*-hydrogen transfer from Rh–H species formed under conditions similar to the WGSR [30]. Namely, nucleophilic attack by OH^- on a

coordinated carbonyl ligand of the $[Rh(CO)_2(L)_2(acyl)]$ complexes (**6**, **8** and **10**) would afford the anionic rhodium hydroxycarbonyl $[Rh(CO)_2(CO_2H)(L)_2(acyl)]^-$ complexes and a H^+ (Eq. (5)).

$$[Rh(CO)_2(L)_2(acyl)] + H_2O \rightarrow Rh(CO)(CO_2H)(L)_2(acyl)]^- + H^+ \quad (5)$$

Decarboxylation of rhodium hydroxycarbonyl intermediate would generate a rhodium hydride complex $[HRh(CO)(L)_2(acyl)]^-$ and CO_2 (Eq. (6)).

$$[Rh(CO)(CO_2H)(L)_2(acyl)]^- \rightarrow [HRh(CO)(L)_2(acyl)]^- + CO_2 \quad (6)$$

Reductive elimination of hydride-acyl complex affords the corresponding ketones and the coordinative unsaturated $[Rh(CO)(L)_2]_-$ complex according to Eq. (7). The accumulate negative charge on the hydride-acyl complex favors the migration of the coordinate H to the Rh–C bonds.

$$[HRh(CO)(L)_2(acyl)]^- \rightarrow [Rh(CO)(L)_2]^- + \text{ketone} \quad (7)$$

Protonation of the later anionic complex by H^+ (coming from Eq. (5)) and carbonylation by CO (Eq. (8)) would give the starting $[HRh(CO)_2(L)_2]$ complex (**3**) to get catalytic cycle closed.

$$[Rh(CO)(L)_2]^- + H^+ + CO \rightarrow [HRh(CO)_2(L)_2] \quad (8)$$

All the last four reactions, (5)–(8) lead to the formation of the starting (**3**) complex, CO_2, and ketones (Eq. (9)).

$$[Rh(CO)_2(L)_2(acyl)] + CO + H_2O \rightarrow [HRh(CO)_2(L)_2] + CO_2 + \text{ketone} \quad (9)$$

The electronic and steric effects of the coordinate amine can control all or some of these catalytic key steps.

Finally, analyses of the effects of varying the CO pressure, Rh concentration and temperature on the activity of these complexes, which are important parameters for the carbonylation reaction are in progress, and they will be reported elsewhere.

4. Conclusions

In this study, propionic acid and the ketones (penta-3-one, octane-3,6-dione and undecane-3,6,9-trione) were synthesized by a hydrocarboxylation of ethylene and by a stepwise alternating co-oligomerization of CO/ethylene, respectively. Both reactions were catalyzed by *cis*-$[Rh(CO)_2(amine)_2](PF_6)$ complexes in a salty medium of tetrabutylammonium hydrogensulfate. It can be seen a remarkable increment on the ketone and propionic acid formations catalyzed by the Rh/3-pic system when the concentration of the tetrabutylammonium hydrogensulfate salt increased. On the other hand, the reaction rates decreased markedly with increasing steric hindrance of the coordinated amine. Our approach related to the use of salty medium can constitute another alternative reaction media to propionic acid and ketones synthesis. Such a catalytic system contains a high concentration of the *trans*-$[Rh(CO)_3(amine)_2]^+$ complex, characterized by IR, which is formed by coordinative addition of one CO molecule to the starting *cis*-$[Rh(CO)_2(amine)_2]^+$ complex, under the catalytic reaction conditions.

Acknowledgements

This work was supported by CDCH-UCV (03.12.4957.02). The authors thank Mr. F. Del Cima for skilful technical assistance. C.L. and A.J.P. thank CDCH-UCV for the sabbatical leave scholarship.

References

[1] P. Pino, F. Piacenti, M. Bianchi, in: M. Wender, P. Pino (Eds.), Organic Synthesis via Metal Carbonyls, vol. 2, Wiley, New York, 1977, pp. 233–296.
[2] N.S. Imyanitov, D.M. Rudkovsky, J. Russ, J. Org. Chem. 2 (1966) 231 (in Russian); Chem. Abstr. 71 (1969) 21650.
[3] V.A. Ribakov, A.M. Nalimov, S.K. Ogorodnikov, Kinet. Catal. 18 (1977) 404 (in Russian).
[4] Y.T. Vigranenko, V.A. Ribakov, V.V. Kashina, B.P. Tarasov, Kinet. Catal. 37 (1996) 558 (in Russian).
[5] C. Bianchini, A. Meli, Coord. Chem. Rev. 225 (2002) 35.
[6] R. Van Asselt, E.G.C. Gielens, E.R. Rulke, K. Vrieze, C.J. Elsevier, J. Am. Chem. Soc. 116 (1994) 977.
[7] C. Rix, M. Brookhart, P.S. White, J. Am. Chem. Soc. 118 (1996) 4746.
[8] E. Drent, P.H. Budzelaar, Chem. Rev. 96 (1996) 663.
[9] E. Drent, J.A.M. Van Broekhoven, M.J. Doyle, J. Organomet. Chem. 417 (1991) 235.
[10] Z. Jiag, A. Sen, Macromolecules 27 (1994) 7215.
[11] G. Verspui, G. Papadogianakis, R.A. Sheldon, Chem. Commun. (1998) 401.
[12] C. Bianchini, H.M. Lee, A. Meli, S. Monetti, V. Patinec, G. Petruicci, F. Vizza, Macromolecules 32 (1999) 3859.
[13] E. Linder, M. Schmid, J. Wald, J.A. Queisser, M. Geprägs, P. Wegner, C. Nachtigal, J. Organomet. Chem. 602 (2000) 173.
[14] A. Held, L. Kolb, M. Zuideveld, R. Thomas, S. Mecking, M. Schmid, R. Pietruscka, E. Linder, M. Khanfar, M. Sunjuk, Macomolecules 35 (2002) 3342.
[15] A. Vavasori, L. Toniolo, J. Mol. Catal. 110 (1996) 13.
[16] P.C. Ford, A. Rokicki, Adv. Organomet. Chem. 28 (1988) 139.
[17] Y. Iwashita, M. Sakuraba, Tetrahedron Lett. 26 (1971) 2409.
[18] P. Hong, H. Yamazaki, Chem. Lett. (1979) 1335.
[19] P. Hong, H. Yamazaki, J. Mol. Catal. 26 (1984) 297.
[20] A. Sen, J.S. Brumbaugh, J. Organomet. Chem. 279 (1985) C5.
[21] G. Consiglio, B. Studer, F. Oldani, P. Pino, J. Mol. Catal. 58 (1990) L9.
[22] G.W. Parshall, J. Am. Chem. Soc. 94 (1972) 8716.
[23] B. Denise, G. Pannetier, J. Organomet. Chem. 28 (1973) 423.

[24] A.G. Davies, L. Julia, S.N. Yazdi, Chem. Soc., Perkin Trans. II (1989) 239.
[25] R. Ballini, M. Petrini, E. Marcantoni, G. Rosini, Synthesis 231 (1988).
[26] L.M. Vallarino, S.W. Sheargold, Inorg. Chim. Acta 36 (1979) 243.
[27] T. Welton, Chem. Rev. 99 (1999) 2071.
[28] A. Reckziel, M. Birgorgne, J. Organomet. Chem. 3 (1965) 341.
[29] C. Longo, J. Alvarez, M. Fernández, A.J. Pardey, S.A. Moya, P. Baricelli, M.M. Mdleleni, Polyhedron 19 (2000) 487.
[30] A.J. Pardey, P.C. Ford, J. Mol. Catal. 53 (1989) 247.
[31] P.A. Lay, Inorg. Chem. 23 (1984) 4775.

Available online at www.sciencedirect.com
SCIENCE DIRECT®
Polyhedron 23 (2004) 1685–1694
POLYHEDRON
www.elsevier.com/locate/poly

The crystal structure and electronic properties of a *cis*-distorted octahedral CuN_4O_2 chromophore: $[Cu(dpyam)_2(OXO)]^+$, OXO = ONO^-, O_2CH^- and ONO_2^-

Sujittra Youngme [a,*], Pongthipun Phuengphai [a], Saksit Booncoon [a], Narongsak Chaichit [b]

[a] *Department of Chemistry, Faculty of Science, Khon Kaen University, Khon Kaen 40002, Thailand*
[b] *Department of Physics, Faculty of Science and Technology, Thammasat University Rangsit, Pathumthani 12121, Thailand*

Received 19 February 2004; accepted 29 March 2004
Available online 18 May 2004

Abstract

The crystal structures of three bis(dpyam)copper(II) complexes, $[Cu(dpyam)_2(NO_2)](NO_2)$ (**I**) and $[Cu(dpyam)_2(O_2CH)](ClO_4)$ (**II**) and $[Cu(dpyam)_2(ONO_2)](BF_4)$ (**III**) have been determined by X-ray analysis. In **I**, the copper atom and the asymmetrically bonded nitrito group lie on a crystallographic C_2-axis. The nitrito group is clearly disordered about the C_2-axis giving a square pyramidal *cis*-distorted octahedral ($4 + 1 + 1^*$) chromophore rather than a pseudo-regular *cis*-distorted octahedral chromophore. In **II** and **III**, a distortion of the *cis*-distorted CuN_4O_2 chromophore towards a square pyramidal ($4 + 1 + 1^*$) stereochemistry is also present. The polycrystalline EPR spectra of **I**–**III** together with the high asymmetry in geometry of the CuN_4O_2 chromophores are suggesting that all complexes appear to be near the static distortion limit of the fluxional CuN_4O_2 chromophore geometry. The electronic reflectance spectra of the three complexes involve two bands at the same intensity corresponding to a *cis*-distorted octahedral geometry.
© 2004 Elsevier Ltd. All rights reserved.

Keywords: Copper complexes; Di-2-pyridylamine; Nitrito complexes; Plasticity effect; *cis*-Distorted octahedron; Fluxional behaviour

1. Introduction

The molecular structures of the [Cu(II)(chelate)$_2$(OXO)]Y complex (chelate is 2,2′-bipyridyl (bpy) and 1,10-phenanthroline (phen) and OXO is a bidentate oxoanion such as ONO^-, ONO_2^-, $CH_3CH_2CO_2^-$, $CH_3CO_2^-$ or HCO_2^-) were classified as *cis*-distorted octahedral [1] and well characterized as fluxional copper(II) geometries [2–4]. The temperature variability in EPR spectra and in the chemical bond parameters of the CuN_4O_2 chromophore strongly evidence that vibronic coupling is operative in these complexes [5,6]. The symmetric structures with average C_2 symmetries (not static C_2 symmetries) found in the [Cu(chelate)$_2$(OXO)]Y complexes actually represent the superposition of two interconverting asymmetric structures (a 'dynamic pseudo-Jahn–Teller effect' at least at room temperature) with equally relative thermal populations of the two conformers [6,7]. The corresponding complexes of this series with the more flexible dpyam (di-2-pyridylamine) ligand have been amply characterized and investigated concerning apparent structural distortions and electronic properties in the context of the fluxional behaviour. Only four crystal structures of $[Cu(dpyam)_2(ONO)]^+$ cation distortion isomers involving the counter anions, BF_4^-, NO_3^-, ClO_4^- and NO_2^- have been reported [8,9]. The last one, $[Cu(dpyam)_2(ONO)](NO_2)$ is in surprisal, as its structure reported by Hathaway and co-workers [8] involves a regular *cis*-distorted octahedral geometry, but with unreasonable O–N–O bond angle. This unusual feature encourages us to reprepare this compound and the detailed structure redetermined. For the corresponding nitrate complex, no examples are known for a

* Corresponding author. Tel.: +66-43-20222241; fax: +66-43-202373.
E-mail address: sujittra@kku.ac.th (S. Youngme).

0277-5387/$ - see front matter © 2004 Elsevier Ltd. All rights reserved.
doi:10.1016/j.poly.2004.03.020

cis-distorted octahedral structure in [Cu(chelate)$_2$-(ONO$_2$)]Y type complexes. Only the complex [Cu-(dpyam)$_2$(O$_2$CH)]- (BF$_4$) [10] has been reported for the corresponding dpyam complex with the formate oxoanion.

In the present paper, we report the synthesis, crystal structures and spectroscopic properties of three further examples of the [Cu(dpyam)$_2$(OXO)]Y complexes, [Cu(dpyam)$_2$(NO$_2$)](NO$_2$) (**I**) and [Cu(dpyam)$_2$(O$_2$CH)]-(ClO$_4$) (**II**) and [Cu(dpyam)$_2$(ONO$_2$)](BF$_4$) (**III**) which consist of NO_2^-, O_2CH^- and NO_3^- oxoanions. Complex **III** is very rare case found with the nitrate oxoanion involved in the *cis*-distorted octahedral of this series and the purpose of this paper is to examine the electronic properties of this dpyam series in the context of fluxional behaviour [11].

2. Experimental

All reagents were commercial grade materials and were used without further purification. Elemental analyses (C, H and N) were performed by the Microanalytical Service of Science and Technological Research Equipment Centre, Chulalongkorn University on a Perkin–Elmer PE2400 CHNS/O Analyzer. The infrared spectra were recorded on a Spectrum One Perkin–Elmer FT-IR spectrophotometer as KBr pellets in the 4000–450 cm^{-1} region. Solid-state (diffuse reflectance) electronic spectra were recorded as polycrystalline samples on a Perkin–Elmer Lambda2S spectrophotometer over the range 8000–18 000 cm^{-1}. The X-band EPR spectra were recorded on polycrystalline samples at room temperature (r.t.) and liquid nitrogen temperature (77 K) with a JEOL EPR JES-RE2X spectrometer (operating at the X-band) by the service of Scientific and Technological Research Equipment Centre, Chulalongkorn University.

2.1. Preparation

2.1.1. Preparation of [Cu(dpyam)$_2$(ONO)](NO$_2$) (*I*)

2.1.1.1. Method a. An aqueous solution (10 ml) of Cu(O$_2$CCH$_3$)$_2$ · H$_2$O (0.090 g, 0.5 mmol) was added to a solution of dpyam (0.171 g, 1.0 mmol) in methanol (5 ml), followed by an aqueous solution (10 ml) of KNO$_2$ (0.085 g, 1.0 mmol) resulting green solution. On standing for a week, green crystals of **I** were formed. They were filtered off, washed with mother liquor and air-dried. Yield approximately 90%. *Anal.* Calc. for C$_{20}$H$_{18}$N$_8$CuO$_4$: C, 48.24; H, 3.64; N, 22.50. Found: C, 48.35; H, 3.54; N, 22.53%.

2.1.1.2. Method b. The aqueous solution (40 ml) of Cu(dpyam)(NO$_2$)$_2$] (0.33 g, 1.0 mmol) was refluxed with ca. 1 g copper metal sheet and extra dpyam (0.34 g, 2.0 mmol) under an atmosphere for 8 h. After evaporation at room temperature, green crystals of **I** were obtained as the reoxygenation product of copper metal reduction. Yield approximately 88%. The complex [Cu(dpyam)-(NO$_2$)$_2$] was prepared following the previous method [12].

2.1.2. Preparation of [Cu(dpyam)$_2$(O$_2$CH)](ClO$_4$) (*II*)

The complex **II** was prepared by adding an aqueous solution (10 ml) of Cu(ClO$_4$)$_2$ · 6H$_2$O (0.370 g, 1.0 mmol) to a solution of dpyam (0.171 g, 1.0 mmol) in methanol (20 ml) after which solid HCOONa (0.035 g, 0.5 mmol) was added. The green solution was slowly evaporated at room temperature. Green crystals of **II** were deposited after several days. Yield approximately 85%. *Anal.* Calc. for C$_{21}$H$_{19}$N$_6$CuO$_6$Cl: C, 45.82; H, 3.48; N, 15.27. Found: C, 45.75; H, 3.56; N, 15.22%.

2.1.3. Preparation of [Cu(dpyam)$_2$(ONO$_2$)](BF$_4$) (*III*)

A solution of dpyam (0.272 g, 2.0 mmol) in methanol (20 ml) was slowly added to an aqueous solution (20 ml) of Cu(NO$_3$)$_2$ · 2.5H$_2$O (0.232 g, 1.0 mmol) after which solid NaBF$_4$ (0.163 g, 1.5 mmol) was added resulting green solution. Dark green needle crystals of **III** were deposited after several days. Yield approximately 90%. *Anal.* Calc. for C$_{20}$H$_{18}$N$_7$CuO$_3$BF$_4$: C, 43.30; H, 3.27; N, 17.67. Found: C, 43.24; H, 3.20; N, 17.56%.

2.2. Crystallography

Reflection data for complexes **I**–**III** were collected at 293 K on a 1K Bruker SMART CCD area-detector diffractometer using graphite monochromated Mo Kα radiation ($\lambda = 0.71073$ Å) at a detector distance of 4.5 cm and swing angle of −35°. A hemisphere of the reciprocal space was covered by combination of three sets of exposures; each set had a different ϕ angle (0°, 88° and 180°) and each exposure of 30, 30 and 30 s for **I**, **II** and **III**, respectively, covered 0.3° in ω. Data reduction and cell refinements were performed using the program SAINT [13]. An empirical absorption correction by using the SADABS [14] program was applied, which resulted in transmission coefficients ranging from 0.793 to 1.000 for **I**, 0.807 to 1.000 for **II** and 0.827 to 1.000 for **III**. The structures were solved by direct methods and refined by full-matrix least-squares method on F^2_{obs} with anisotropic thermal parameters for all non-hydrogen atoms using the SHELXTL-PC V 6.12 [15] software package. All hydrogen atoms in **I**–**III** were located by difference synthesis and refined isotropically. All non-H atoms were refined anisotropically except the perchlorate, O(4A) atom in **II** and the tetrafluoroborate, F(3) atom in **III**. The nitrite anions in **I** and the perchlorate groups in **II** are disordered with site occupancies of 0.50, for both conformers. The tetrafluoroborate groups in **III** are also disordered with site occupancies of 0.45 and

0.55 for both conformers. The molecular graphics were created by using SHELXTL-PC. The crystal and refinement details for complexes **I**–**III** are listed in Table 1. Selected bond lengths and angles are given in Tables 2–4. Figs. 1, 2 and 3 illustrate the structures of **I**, **II** and **III**, respectively, and the atom numbering scheme used.

3. Results and discussion

3.1. Crystal structures

The crystal structures of **I**–**III** consist of discrete $[Cu(dpyam)_2(ONO)]^+$, $[Cu(dpyam)_2(O_2CH)]^+$ and

Table 1
Crystal and refinement data for complexes **I**–**III**

Complex	**I**	**II**	**III**
Molecular formula	$[Cu(dpyam)_2(NO_2)](NO_2)$	$[Cu(dpyam)_2(O_2CH)](ClO_4)$	$[Cu(dpyam)_2(NO_3)](BF_4)$
Molecular weight	497.96	550.41	554.76
Temperature (K)	293(2)	293(2)	293(2)
Crystal system	orthorhombic	monoclinic	monoclinic
Space group	*Pccn*	$P2_1/c$	$P2_1/n$
a (Å)	11.28770(10)	13.8098(2)	17.4776(7)
b (Å)	12.47520(10)	7.70320(10)	7.7996(3)
c (Å)	15.0005(2)	22.3382(2)	18.1696(8)
α (°)	90	90	90
β (°)	90	95.59	104.1420(10)
γ (°)	90	90	90
V (Å^3)	2112.31(4)	2365.04(5)	2401.78(17)
Z	4	4	2
D_{calc} (g cm^{-3})	1.566	1.546	0.767
Absorption coefficient (mm^{-1})	1.081	1.086	0.489
$F(000)$	1020	1124	562
Crystal size (mm)	$0.45 \times 0.48 \times 0.20$	$0.08 \times 0.20 \times 0.25$	$0.16 \times 0.43 \times 0.09$
θ range (°)	2.79–30.50	1.48–30.44	1.45–30.53
Number of reflection collected	14 651	16 882	17 150
Number of unique reflections	3119	6758	6903
Number of observed reflection	2508	4836	4018
T_{max} and T_{min}	1.0000 and 0.793000	1.0000 and 0.806806	1.0000 and 0.827379
Data/restraints/parameter	3119/0/206	6758/0/416	6903/0/434
Goodness of fit	1.051	1.032	1.080
Final R indices [$I > 2s(I)$]	$R_1 = 0.0310$ and $wR_2 = 0.0816$	$R_1 = 0.0404$ and $wR_2 = 0.1004$	$R_1 = 0.0606$ and $wR_2 = 0.1124$
R indices (all data)	$R_1 = 0.0411$ and $wR_2 = 0.0879$	$R_1 = 0.0649$ and $wR_2 = 0.1144$	$R_1 = 0.1204$ and $wR_2 = 0.1350$
Largest difference peak and hole (e Å^{-3})	0.255 and −0.424	0.457 and −0.443	0.529 and −0.414

$R = \sum ||F_o| - |F_c|| / \sum |F_o|$ and $R_w = [\sum w\{|F_o| - |F_c|\}^2 / w|F_o|^2]^{1/2}$.

Table 2
Selected bond lengths (Å) and angles (°) with e.s.d.s. in parentheses of $[Cu(dpyam)_2(NO_2)](NO_2)$ (**I**)

Bond lengths			
Cu–N(1)	2.132(12)	Cu–N(5)	2.097(2)
Cu–O(1)	2.075(4)	Cu–O(2)	2.487(2)
N(7)–O(1)	1.273(6)	N(7)–O(2)	1.237(8)
Bond angles			
N(1)–Cu–N(4)	172.3(2)	N(4)–Cu–O(1)	86.5(2)
N(1)–Cu–O(1)	87.1(2)	N(4)–Cu–N(5)	87.3(2)
N(1)–Cu–N(5)	97.4(2)	N(5)–Cu–O(1)	96.3(2)
N(1)–Cu–N(2)	87.3(2)	N(4)–Cu–N(2)	97.4(2)
O(1)–Cu–N(2)	162.2(2)	N(5)–Cu–N(2)	101.0(2)
O(2)–Cu–N(1)	86.3(2)	O(2)–Cu–N(2)	109.8(2)
O(2)–Cu–N(4)	86.5(2)	O(2)–Cu–N(5)	149.0(2)
O(2)–Cu–O(1)	52.9(2)	O(1)–N(7)–O(2)	110.9(8)
Cu–O(1)–N(7)	107.7(6)	Cu–O(2)–N(7)	88.3(3)

Symmetry code: #1: $-x+3/2$, $-y+1/2$, z; #2: $-x+3/2$, $-y+3/2$, z; N(1)≡[N(1)#1], N(2)≡[N(5)], N(4)≡[N(1)], N(5)≡[N(5)#1], O(2)≡[O(2A)#1].

Table 3
Selected bond lengths (Å) and angles (°) with e.s.d.s. in parentheses of $[Cu(dpyam)_2(O_2CH)](ClO_4)$ (**II**)

Bond lengths			
Cu–N(1)	2.000(3)	Cu–N(2)	2.034(3)
Cu–N(4)	2.013(3)	Cu–N(5)	2.167(3)
Cu–O(1)	2.013(3)	Cu–O(2)	2.892(3)
C(21)–O(1)	1.263(3)	C(21)–O(2)	1.215(3)
Bond angles			
N(1)–Cu–N(4)	170.5(2)	N(1)–Cu–N(2)	88.1(2)
N(4)–Cu–N(2)	91.5(2)	N(1)–Cu–N(5)	100.7(2)
N(4)–Cu–N(5)	88.7(2)	N(2)–Cu–N(5)	98.1(2)
N(1)–Cu–O(1)	89.0(2)	N(4)–Cu–O(1)	88.6(2)
N(2)–Cu–O(1)	162.8(2)	N(5)–Cu–O(1)	99.1(2)
O(2)–Cu–N(1)	78.3(3)	O(2)–Cu–N(2)	113.1(3)
O(2)–Cu–N(4)	93.2(3)	O(2)–Cu–N(5)	148.6(3)
O(2)–Cu–O(1)	49.7(3)	O(1)–C(21)–O(2)	126.3(3)
Cu–O(1)–C(21)	112.5(3)	Cu–O(2)–C(21)	71.3(3)

Table 4
Selected bond lengths (Å) and angles (°) with e.s.d.s. in parentheses of $[Cu(dpyam)_2(ONO_2)](BF_4)$ (**III**)

Bond lengths			
Cu–N(1)	1.975(3)	Cu–N(2)	2.003(3)
Cu–N(4)	1.991(3)	Cu–N(5)	2.100(3)
Cu–O(1)	2.151(3)	Cu–O(2)	2.659(3)
N(7)–O(1)	1.279(4)	N(7)–O(2)	1.228(4)
N(7)–O(3A)	1.240(5)	N(7)–O(3B)	1.229(5)
Bond angles			
N(1)–Cu–N(4)	168.0(2)	N(1)–Cu–N(2)	88.6(2)
N(4)–Cu–N(2)	94.3(2)	N(1)–Cu–N(5)	101.4(2)
N(4)–Cu–N(5)	89.0(2)	N(2)–Cu–N(5)	106.1(2)
N(1)–Cu–O(1)	87.6(2)	N(4)–Cu–O(1)	85.2(2)
N(2)–Cu–O(1)	157.3(2)	N(5)–Cu–O(1)	96.6(2)
O(2)–Cu–N(1)	79.1(2)	O(2)–Cu–N(2)	105.7(2)
O(2)–Cu–N(4)	88.9(2)	O(2)–Cu–N(5)	148.2(2)
O(2)–Cu–O(1)	51.6(2)	O(1)–N(7)–O(2)	117.5(2)
O(3A)–N(7)–O(2)	112.2(11)	O(1)–N(7)–O(3A)	129.5(11)
Cu–O(1)–N(7)	106.9(2)	Cu–O(2)–N(7)	83.7(2)

$[Cu\text{-}(dpyam)_2(ONO_2)]^+$ cations and a NO_2^-, ClO_4^- or BF_4^- anion, respectively.

The $[Cu(dpyam)_2(ONO)]^+$ cation in **I**, $[Cu(dpyam)_2(O_2CH)]^+$ in **II** and $[Cu(dpyam)_2(ONO_2)]^+$ cation in **III** involve a *cis*-distorted octahedral CuN_4O_2 chromophore with an asymmetrically coordinated nitrito group, formato group and nitrato group, respectively. The copper atom in all complexes is surrounded by four nitrogen atoms from two dpyam ligands and two oxygen atoms from the coordinated anion. A terminal nitrogen of each dpyam ligand occupies the axial direction while the remaining nitrogen atoms and the oxygen atoms from OXO^- anion occupies the equatorial positions. The CuN_4O_2 chromophore in **I** has a C_2-axis of symmetry bisecting the O(1)–Cu–O(2) and N(2)–Cu–N(5) angles, but with disorder of the coordinated nitrito group. Two conformers of the asymmetrically coordinated nitrito group in **I** retain site occupancies of 0.5. Compound **I** is the second example of [Cu(chelate)$_2$(OXO)]Y complexes, where chelate = 2,2′-bipyridyl, 1,10-phenanthroline and di-2-pyridylamine, and OXO^- = nitrito, formate, acetate and propionate, reported to involve an asymmetric *cis*-distorted octahedral CuN_4OO' chromophore, although there is a crystallographic C_2 symmetry present. The first one was found recently for the corresponding dpyam complex $[Cu(dpyam)_2(ONO)](NO_3)$ [9]. This was resulted from the marked disorder of the nitrito group, compared with the previous reported pseudo-regular *cis*-distorted octahedral CuN_4O_2 chromophore of the bpy and phen ligands [6,7,16] in which the ellipsoids of the oxoanion atoms represent the superposition of one asymmetric structure with relative contributions ranging from 1:1 for the 'symmetric' structures (i.e., those with average C_2 symmetries) to approximately 1:0 for the very asymmetric structures. This has demonstrated the nature of chelate ligands on the geometric distortion and consequently, on the fluxional behaviour of the copper chromophore.

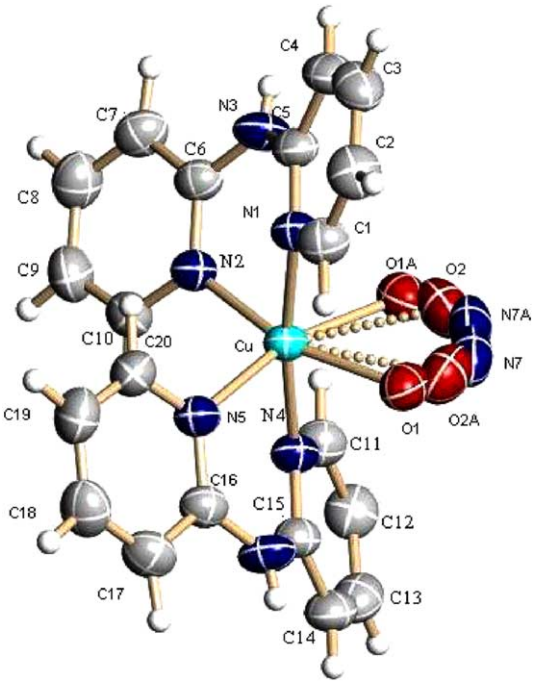

Fig. 1. The molecular structure of $[Cu(dpyam)_2(NO_2)](NO_2)$ (**I**).

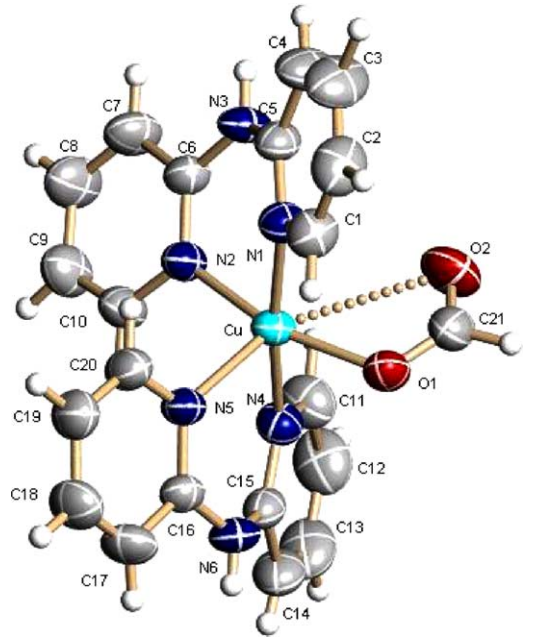

Fig. 2. The molecular structure of $[Cu(dpyam)_2(O_2CH)](ClO_4)$ (**II**).

The geometry of the CuN_4O_2 chromophore in **I**–**III** is basically five-coordinate with a second oxygen of the OXO^- anion occupying a sixth coordinating position at distance greater than 2.4 Å [2.487(2) Å for **I**, 2.892(3)Å for **II** and 2.659(3) Å for **III**] to give a $(4 + 1 + 1^*)$-type coordination.

The large O(1)–Cu–N(2) angles of 162.2(2)°, 162.8(2)° and 157.3(2)° for **I**, **II** and **III**, respectively, are

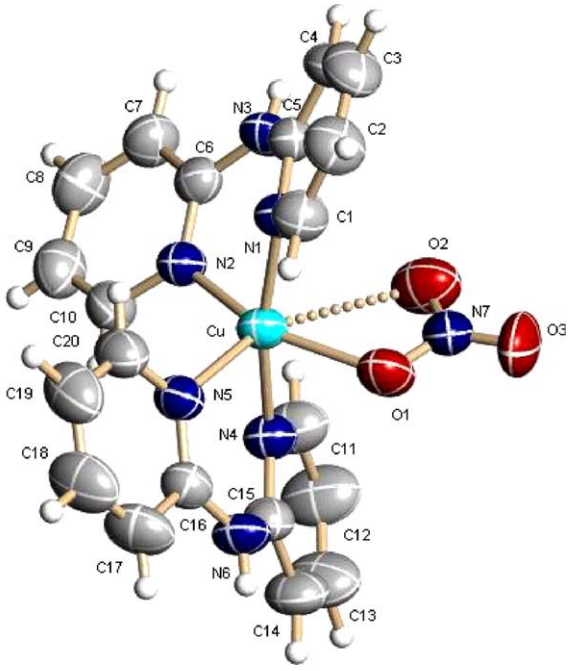

Fig. 3. The molecular structure of $[Cu(dpyam)_2(ONO_2)](BF_4)$ (**III**).

opposite the elongated Cu–N(5) direction. This could be taken as the basal angle of a square-based pyramidal geometry with elongation in the Cu–N(5) direction [17]. However, an exception case in the shorter Cu–N(5) distance compared to those of the basal plane is found in **I**. The Cu atom is displaced from the basal plane by 0.19 Å in **I**, 0.23 Å in **II** and 0.29 Å in **III**, in the direction of N(5) atom. The basal planes of three complexes also show a slight tetrahedral distortion from planarity (r.m.s.d 0.1102, 0.0685 and 0.1104 Å for **I**, **II** and **III**, respectively). The τ values ($\tau = [\{N(1)–Cu–N(4)\} - \{N(2)–Cu–O(1)\}]/60$) [18] are 0.16, 0.13 and 0.18 for **I**, **II** and **III**, respectively. All relatively close to that of a regular square pyramidal CuN_3ON' chromophore, $\tau = 0$. Hence, all structures are best described as a square pyramidal *cis*-distorted octahedral $(4 + 1 + 1^*)$, but being different in significant angular distortions. As the $\Delta O_{1,2}$ value of 0.879 Å in **II** is larger than that of 0.412 Å in **I** and 0.508 Å in **III**, **II** is more closely related to the static structure than **I** and **III**. The axial N–Cu–N angles in **I**, **II** and **III** are almost linear, 172.3(2)°, 170.5(3)° and 168.0(2)°, respectively.

The pyridine rings form dihedral angles of 28.7° in **I**, 26.2° and 25.2° in **II**, and 32.1° and 22.9° in **III** for the ligands defined by N(1)/N(2) and N(4)/N(5), respectively; the dpyam bite angles are 87.3(2)° for **I**, 88.1(2)° and 88.7(2)° for **II** and 88.6(2)° and 89.0(2)° for **III**.

The asymmetric bidentate nitrito group in **I** has no unusual bond lengths and angles, the N–O(1) distance (1.273(6) Å) involving the stronger Cu···O(1) interaction is longer than the N–O(2) distance (1.237(8) Å) involving the weaker Cu···O(2) interaction, consistent

with the more single-bond character in the N–O(1) distance. The mean N–O distance of 1.255 Å in **I**, of the nitrite group is not significant different from the 1.236 Å for the free nitrite ion, but O(1)–N–O(2) angle of 110.9(8)° in **I** is significant smaller than the 115.4° of the free ion [8,19]. The O(1)–Cu–O(2) bond angle of 52.9(2)° in **I**, agrees well with the value previously reported for the bite angle of the coordinated nitrito group found in the [Cu(chelate)$_2$(ONO)]Y complexes [20]. The Cu–O(1)–N(7) angle (107.7(6)° for **I**) is also between the value of 119.5° for the purely monodentate nitrite [21] and 93°–100° for the purely bidentate nitrite [22]. The binding mode of the nitrito group in this complex system was well investigated [20] and found that the O(1)–Cu–O(2) and O(1)–N–O(2) angles are effectively independent of the nitrito coordination mode, but clearly

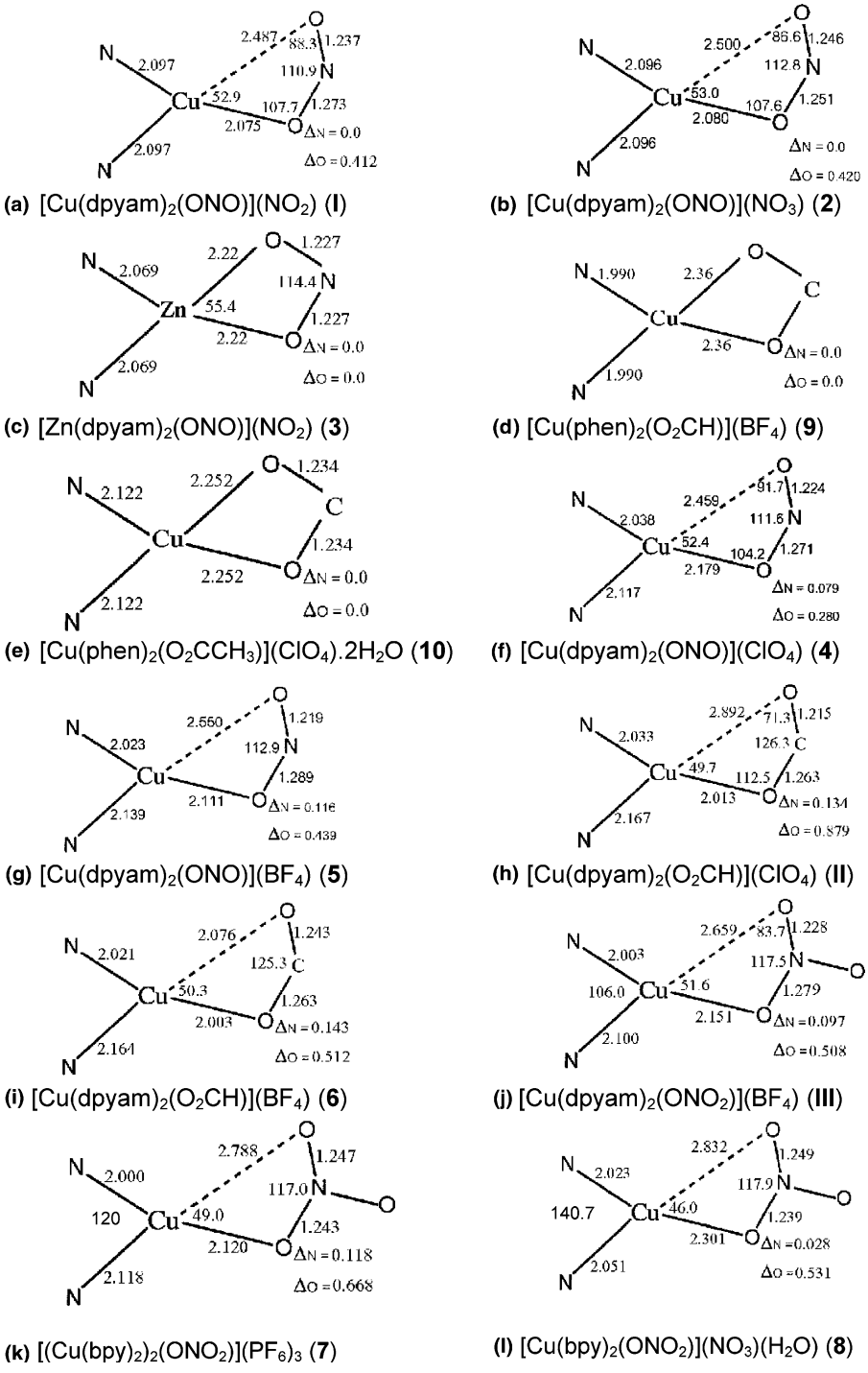

Fig. 4. Comparison of [M(chelate)$_2$(OXO)]$^+$ coordination geometries.

dependent to the Cu–O(1)–N angle. By using the correlations applied for **I**, the binding mode of the nitrito group in this complex is intermediate between monodentate and bidentate coordination.

The coordinated formato group for **II** gives asymmetric C–O distances with the C(21)–O(1) and C(21)–O(2) values of 1.263(3) and 1.215(3) Å, respectively, this is not significant different from the previous reported for coordinated carboxylato group having the C–O distance of 1.236–1.286 Å. The O–C–O angle of 126.3(3)° is usually observed in the previous reported (ranging 122.2°–126.2°) [10,23–25].

The rarely found, coordinated nitrato group in the *cis*-distorted octahedral geometry in **III** involves reasonable N–O bond lengths, mean 1.253 Å with considerable disorder in an uncoordinated O(3) atom to give a slight distortion of the N(7)–O(3A) and N(7)–O(3B) distances of 1.240(5) and 1.229(5) Å, respectively. The N–O distances of 1.279(4) and 1.228(4) Å and the O–N–O angle of 117.5(3)° which involve the coordinated O atoms are in good agreement with the values of 1.245 Å and 119.9° generally quoted for the free nitrate ion [26]. The N(7)–O(1) distance is longer than N(7)–O(2), consistent with the stronger Cu–O(1) than the Cu–O(2) bond. There is however, a significant deviation of the uncoordinated O–N–O angles from those usually found for the unsymmetrically coordinated [27] or free nitrate group [9,26]. This arises due to disorder in an uncoordinated O atom and the involvement of this uncoordinated O atom in the hydrogen bonding.

The lattice structures are stabilized by moderate to weak hydrogen bonding N–H···O(NO_2) and N–H···N(NO_2) hydrogen bonds in **I**; N–H···O(HCO_2) and N–H···O(ClO_4) hydrogen bonds in **II** and N–H···O(NO_3) and N–H···F(BF_4) hydrogen bonds in **III**]. Details of the hydrogen bondings are given in Table 6.

3.2. Structure comparison

The structures of **I**–**III** are clearly different from the equally elongated rhombic-octahedral (4 + 2) chromophore in [Cu(bpy)$_2$(S_3O_6)] [28] and [Cu(bpy)$_2$(S_4O_6)] [29] and the unequally elongated rhombic-octahedral (4 + 1 + 1*) chromophore of [Cu(bpy)$_2$(O_2ClO_2)](ClO_4) [30]. There is some similarity to the pseudo-symmetric *cis*-distorted octahedral geometries of [Cu(phen)$_2$-(O_2CMe)]Y, Y = $ClO_4^- \cdot 2H_2O$, $BF_4^- \cdot 2H_2O$ [6,7] and [Cu(phen)$_2$(HCO_2)]Y, Y = BF_4^- and ClO_4^- [2,16] with two Cu–O distances of 2.26–2.36 Å, Figs. 4(d) and (e). This geometry is typical for this complex system involving C_2 symmetric OXO group. There is a closer similarity to the [Cu(dpyam)$_2$(OXO)]$^+$ cations, where OXO^- = formate [10], acetate [10,25], propionate [31,32] and nitrite [8,9,31], all of which having a (4 + 1 + 1*)-

Table 5
Molecular dimension of the complexes [M(chelate)$_2$(OXO)]Y

Complexes	**I**	**1**	**2**	**3**	**4**	**5**	**II**	**6**	**III**	**7**	**8**
M	Cu	Cu	Cu	Zn	Cu	Cu	Cu	Cu	Cu	Cu	Cu
Chelate	dpyam	dpyam	dpyam	dpyam	dpyam	dpyam	dpyam	dpyam	dpyam	bpy	bpy
OXO	NO_2	NO_2	NO_2	NO_2	NO_2	NO_2	O_2CH	O_2CH	NO_3	NO_3	NO_3
Y	NO_2	NO_2	NO_3	NO_2	ClO_4	BF_4	ClO_4	BF_4	BF_4	PF_6	$NO_3 \cdot H_2O$
Reference	this work	[8]	[9]	[20]	[9]	[8]	this work	[10]	this work	[35]	[36]
M–N(1)	2.132	2.008(8)	2.009(2)	2.163	1.979(2)	1.986	2.000	1.999	1.975	2.012(5)	1.986(5)
M–N(2)	2.097	2.095(9)	2.096(2)	2.069	2.038(3)	2.023	2.033	2.021	2.003	2.000(6)	2.023(5)
M–N(4)	2.132	2.008(8)	2.009(2)	2.163	2.001(3)	2.012	2.013	2.015	1.991	1.988(6)	1.973(5)
M–N(5)	2.097	2.095(9)	2.096(2)	2.069	2.117(3)	2.139	2.167	2.164	2.100	2.118(6)	2.051(5)
M–O(1)	2.075	2.074(16)	2.080(8)	2.22	2.179(3)	2.111	2.013	2.003	2.151	2.120(5)	2.301(5)
M–O(2)	2.487	2.551(26)	2.500(2)	2.22	2.459(3)	2.550	2.892	2.076	2.659	2.788(6)	2.832(5)
X–O(1)	1.273	1.262(40)	1.246(3)	1.227	1.272(4)	1.289	1.263	1.263	1.279	1.243(7)	1.239(5)
X–O(2)	1.237	1.228(40)	1.251(3)	1.227	1.224(4)	1.219	1.217	1.243	1.228	1.247(8)	1.249(5)
O(1)–X–O(2)	110.9	118.6	112.8(2)	114.4	111.6(2)	112.9	126.3	125.3	118.7	117	117.9
O(1)–M–O(2)	52.9	54.0	53.0(2)	55.4	52.4(3)	-	49.7	50.3	51.6	49.0(2)	46.0
$\Delta N_{1,4}$	0.0	0.0	0.0	0.0	0.022	0.026	0.013	0.016	0.016	0.016	0.013
$\Delta N_{2,5}$	0.0	0.0	0.0	0.0	0.079	0.116	0.134	0.143	0.097	0.118	0.028
ΔO	0.412	0.477	0.420	0.0	0.280	0.439	0.879	0.873	0.508	0.668	0.531

Table 6
Hydrogen bond details, distances (Å) and angles (°)

Donor–H···Acceptor	[ARU]	D–H	H···A	D···A	D–H···A
*[Cu(dpyam)$_2$(NO$_2$)](NO$_2$) (**I**)*					
N(3)–H(5)···O(4)	$[x, y-1, z]$	0.70	2.38	171	3.080
N(3)–H(5)···N(8)	$[x, y-1, z]$	0.70	2.49	172	3.187
N(3)–H(5)···O(3)	$[x, y-1, z]$	0.70	2.58	144	3.186
*[Cu(dpyam)$_2$(HCO$_2$)](ClO$_4$) (**II**)*					
N(3)–H(5)···O(2)	$[1-x, 1/2+y, 1/2+-z]$	0.84	2.02	170	2.850
N(6)–H(15)···O(5)	$[1-x, -y, -z]$	0.76	2.14	164	2.879
N(6)–H(15)···O(5A)	$[1-x, -y, -z]$	0.76	2.32	168	3.071
*[Cu(dpyam)$_2$(ONO$_2$)](BF$_4$) (**III**)*					
N(3)–H(5)···F(2A)	$[1/2-x, 1/2+y, 1/2-z]$	0.75	2.14	175	2.889
N(3)–H(5)···F(3A)	$[1/2-x, 1/2+y, 1/2-z]$	0.75	2.51	138	3.101
N(6)–H(15)···O(1)	$[-x+2, -y+1, -z]$	0.79	2.33	157	3.067
C(10)–H(10)...O(3A)	$[x, -1+y, z]$	0.98	2.51	162	3.454
C(17)–H(17)...O(3A)	$[1-x, 2-y, 1-z]$	0.89	2.41	162	3.271
C(17)–H(17)...O(3B)	$[1-x, 2-y, 1-z]$	0.89	2.58	150	3.381

type coordination of the square pyramidal *cis*-distorted octahedral CuN_4OO' chromophore with the Cu–O(2) > 2.4 Å and the ΔO > 0.4 Å. From these dpyam complexes, the [Cu(dpyam)$_2$(ONO)](NO$_3$) (**2**) [9], with ΔO = 0.420 Å, Fig. 4 and Table 5, has the most similarity in distorted geometry to that of **I**, ΔO = 0.412 Å, while [Cu(dpyam)$_2$(O$_2$CH)](BF$_4$) (**6**) [10], with ΔO = 0.873 Å, Fig. 4 and Table 5, has the most similarity in distorted geometry to that of **II**, ΔO = 0.879 Å. The structure of **1**, Table 5, was first determined by Hathaway and co-workers [33,34] (1980, room temperature, visually estimated intensities) involving an average C_2 symmetry. The structure was classified as regular *cis*-distorted octahedral of fluxional CuN_4O_2 chromophore, but with an unsymmetrically coordinated nitrito group and an unacceptable high value of the O–N–O angle of 118.6° [8,20]. The detailed structural data for this compound have not been reported in the literature. Hence, the structural redetermination and a closer examination in the present work as compound **I** have confirmed that this structure should be described as a nearly static structure of an asymmetric *cis*-distorted octahedral geometry, comparable to that of **2** with ΔO = 0.420 Å, both of which involve disorder of the coordination ONO group with the static C_2 symmetry.

The nitrate complex **III** is unique and found to be the first example for the [Cu(chelate)$_2$(ONO$_2$)]Y type complex adopting an asymmetric *cis*-distorted octahedral $4+1+1^*$ geometry. When compared with the other $4+1+1^*$ distorted complexes [6,8], the present chromophore in **III** is in good agreement to that of the *cis*-distorted octahedral geometry having [Cu(chelate)$_2$(OXO)]$^+$ cation [2].The N(2)–Cu–N(5) angle of 106.1(2)° and O(1)–Cu–O(2) angle of 51.6(2)° are in usual range of 96°–113° and 50–54° found in this type of complexes, Fig. 4 and Table 5. There are only two other related nitrate complexes, [(Cu(bpy)$_2$)$_2$(ONO$_2$)](PF$_6$)$_3$ (**7**) [35] and [Cu(bpy)$_2$(ONO$_2$)](NO$_3$)(H$_2$O) (**8**) [36] previously studied, are known in the [Cu(chelate)$_2$(ONO$_2$)]Y type complexes. However, the latter adopts an asymmetrical bicapped square-pyramidal structure while the former exhibits an intermediate geometry between the asymmetric *cis*-distorted octahedral $4+1+1^*$ and the asymmetrical bicapped square-pyramidal structure, indicated following the classification of Hathaway, which based on the types of distortion from the regular *cis*-distorted geometry [36]. These complexes involve the N(2)–Cu–N(5) angle remarkably larger than 113° (140.7° for **8** and 120° for **7**) and the O(1)–Cu–O(2) angle smaller than 50° (46.0° for **8** and 49.0° for **7**).

In conclusion, the series of complexes **I**, **4**, **2**, **5** and **1**, Fig. 4 and Table 5, represent a sequence of cation distortion isomers of increasing asymmetry. The CuN_4O_2 chromophore in **I** shows significant differences from the ordered [Zn(dpyam)$_2$(ONO)]$^+$ cation of **3** [8,20], Fig. 4 and Table 5, which has static C_2 symmetry. The coordination geometries of the corresponding [Cu(chelate)$_2$(OXO)]$^+$ cations, where chelate = bpy, phen or dpyam are compared with those of the title complexes as in Fig. 4.

3.3. Spectroscopic properties

3.3.1. EPR spectra

The polycrystalline EPR spectra of **I** are isotropic at both room temperature and liquid nitrogen temperature (77 K) with $g_i = 2.165$ and 2.163, respectively, giving no information regarding to the electronic ground state and no information indicative to the fluxional behaviour [1], due to the misalignment of the CuN_4OO' chromophore. In **II**, the room temperature spectrum is isotropic with $g_i = 2.132$, with lowering the temperature to liquid nitrogen temperature the spectrum is more resolved and found to be axial [1] with $g_{\|} \approx 2.417$ and $g_{\perp} = 2.078$. In

III, the room temperature spectrum is nearly axial [1] with $g_{\|} \approx 2.314$ and $g_{\perp} = 2.093$, with decreasing the temperature to liquid nitrogen temperature the spectrum is more resolved and found to be nearly rhombic with $g_1 \approx 2.012$, $g_2 = 2.089$ and $g_3 = 2.228$, consistent with the $d_{x^2-y^2}$ ground state of a square-pyramidal *cis*-distorted octahedral CuN_4O_2 chromophore present for both complexes [2,23,37]. However, a change in EPR spectra of **II** and **III** arises due to the more resolved feature at low temperature, not due to the fluxional behaviour observed. Moreover, these complexes exhibit the high asymmetry in geometry. These suggest that a nearly static CuN_4O_2 chromophore is favourable for all three complexes.

This suggestion is supported by the non-variable-temperature (at room temperature and liquid nitrogen temperature) EPR spectra of the corresponding complexes **6**, **2** and **4** complexes [9,25] in which their structures were suggested to be near static distortion limit of the fluxional CuN_4O_2 chromophore. However, although the EPR spectra seemed to support a nearly static and a very asymmetric *cis*-distorted octahedral geometry in this dpyam system, single-crystal X-ray diffraction studies carried out at very much low temperatures are needed for the $[Cu(dpyam)_2(OXO)]Y$ complexes to prove significant changes in the bond lengths of the fluxional CuN_4O_2 chromophore, especially for the more symmetrical structures. As the more symmetrical structure is actually interconverting asymmetric structures give average, not static, C_2 structure [2]. The sensitivity of the coordination mode to temperature suggests the small difference in energy between the two conformers (extreme geometries) [2].

3.3.2. Electronic spectra

The electronic spectra of complexes **I**–**III** consist of two clearly resolved peaks with almost equal intensity at approximately 14 570 and 10 000 cm^{-1} for **I**, 14 450 and 10 050 cm^{-1} for **II** and 14 950 and 10 200 cm^{-1} for **III**, similar to those previously reported for $[Cu(chelate)_2(OXO)]Y$ complexes involving the *cis*-distorted octahedral CuN_4O_2 chromophore. The slight difference in electronic spectra of this series is due to the nearly comparable distortion of the extreme stereochemistries of the underlying static $(4 + 1 + 1^*)$ CuN_4O_2 chromophores in **I**–**III**. This arises due to the different lattice environments of the $[Cu(dpyam)_2(OXO)]^+$ cations in this series, as a consequence of the 'plasticity effects' [38,39]. The one electron energy sequence of the Cu(II) ion in the asymmetrically distorted CuN_4O_2 geometry of **I**–**III** is approximately the same as that predicted for the square-based pyramidal geometry, namely $d_{x^2-y^2} > d_{z^2} > d_{xy} > d_{xz} \approx d_{yz}$. The highest energy bands at 14 570 cm^{-1} for **I**, 14 450 cm^{-1} for **II** and 14 950 cm^{-1} for **III** may be tentatively assigned as the d_{xy}, $d_{yz} \approx d_{zx} \rightarrow d_{x^2-y^2}$ and the bands at 10 000 cm^{-1} for **I**, 10 050 cm^{-1} for **II** and 10 200 cm^{-1} for **III** as $d_{z^2} \rightarrow d_{x^2-y^2}$ transitions.

3.3.3. Infrared spectra

The most relevant feature of the infrared spectra in **I** is the evidence for the chelating nitrito coordination. It is clear that the position of IR bands distinguishes between nitro and nitrito coordination [40], but it is not possible to distinguish the symmetrical from asymmetrical bidentate nitrito coordination present in these complexes. On the basis of the structure found and a comparison with spectra of related complexes, the IR spectra of **I**–**III** have been tentatively assigned. The IR spectrum of the nitrito group in **I** appears at 1365, 1150 and 840 cm^{-1} corresponding to the $\nu_{as}(NO_2)$, $\nu_s(NO_2)$ and $\delta(NO_2)$ absorption bands, respectively. That of **II** shows bands at 1585_s and 1420, $\nu_{as}(COO)$ and $\nu_s(COO)$, respectively, a medium intensity band at 1090 and 1120 cm^{-1} is masked by a broad and strong band of ClO_4^- ion [9]. The IR spectrum of **III** shows bands at 1386_m, $\nu_{as}(NO_3)$; 1310_m, $\nu_s(NO_3)$ and 650_w, $\delta(NO_3)$, a medium intensity band at 1096 and 1020 cm^{-1} is masked by a broad and strong band of BF_4^- ion [2,7,9].

4. Supplementary material

Crystallographic data (excluding structure factors) for the structures in this paper have been deposited with the Cambridge Crystallographic Data Centre as supplementary publication nos. CCDC-230772–230774 for structures **I**–**III**, respectively. Copies of the data can be obtained free of charge on application to CCDC, 12 Union Road, Cambridge CB2 1EZ, UK [fax: (internat.) +44-1223-336-033, E-mail: deposit@ccdc.cam.ac.uk or www: http://www.ccdc.cam.ac.uk].

Acknowledgements

The authors thank The Thailand Research Fund and Khon Kaen University for research grant. Support of the Postgraduate Education and Research Program in Chemistry is also gratefully acknowledged.

References

[1] B.J. Hathaway, Struct. Bonding (Berl.) 57 (1984) 55.
[2] C.J. Simmons, B.J. Hathaway, K. Amornjarusiri, B.D. Santarsiero, A. Clearfield, J. Am. Chem. Soc. 109 (1987) 1947, and references therein.
[3] W. Fitzgerald, B. Murphy, S. Tyagi, B. Walsh, A. Walsh, B.J. Hathaway, J. Chem. Soc., Dalton Trans. (1981) 2271.
[4] I.M. Procter, B.J. Hathaway, D.E. Billing, R. Dudley, P. Nicholls, J. Chem. Soc., Sect. A (1969) 1192.
[5] C.J. Simmons, K. Seff, F. Clifford, B.J. Hathaway, Acta Crystallogr., Sect. C 39 (1983) 1360.

[6] W. Fitzgerald, B.J. Hathaway, C.J. Simmons, J. Chem. Soc., Dalton Trans. (1985) 141.
[7] F. Clifford, E. Counihan, W. Fitzgerald, K. Seff, C. Simmons, S. Tyagi, B.J. Hathaway, J. Chem. Soc., Chem. Commun. (1982) 196.
[8] A. Walsh, B. Walsh, B. Murphy, B.J. Hathaway, Acta Crystallogr., Sect. B 37 (1981) 1512.
[9] S. Youngme, N. Chaichit, N. Koonsaeng, Inorg. Chim. Acta 335 (2002) 36.
[10] S. Aduldecha, M.E. Keniry, P. Akhter, S. Tyagi, B.J. Hathaway, Acta Crystallogr., Sect. C 47 (1991) 1378.
[11] B.J. Hathaway, M. Duggan, A. Murphy, J. Mullane, C. Power, A. Walsh, B. Walsh, Coord. Chem. Rev. 36 (1981) 271.
[12] S. Youngme, S. Tonpho, K. Chinnakali, S. Chantrapromma, H.K. Fun, Polyhedron 18 (1999) 851.
[13] Siemens, SAINT, Version 4, Software Reference Manual, Siemens Analytical X-Ray Systems, Inc., Madison, WI, USA, 1997.
[14] G.M. Sheldrick, SADABS, Program for Empirical Absorption correction of Area Dectector Data, University of Göttingen, Göttingen, Germany, 1997.
[15] Siemens. SHELXTL, Version 6.12, Reference Manual, Siemens Analytical X-Ray Systems, Inc., Madison, WI, USA, 1997.
[16] C. Escobar, O. Wittke, Acta Crystallogr., Sect. C 39 (1983) 1643.
[17] B.J. Hathaway, Struct. Bonding (Berl.) 14 (1973) 49.
[18] A.W. Addison, T. Nageswara Rao, J. Reedijk, J. van Run, G.C. Verschoor, J. Chem. Soc., Dalton Trans. (1984) 1340.
[19] G.B. Carpenter, Acta Crystallogr. 8 (1955) 852.
[20] S.J. Hill, P. Hubberstey, W.S. Li, Polyhedron 16 (1997) 2447.
[21] M.G.B. Drew, D.M.L. Goodgame, M.A. Hitchman, D. Rogers, Proc. Chem. Soc. (1964) 363.
[22] (a) I.M. Procter, F.S. Stephens, J. Chem. Soc., Sect. A (1969) 1248;
(b) M.G.B. Drew, D. Rogers, Chem. Commun. (1965) 476.
[23] W. Fitzgerald, B.J. Hathaway, J. Chem. Soc., Dalton Trans. 178 (1978) 567.
[24] B.J. Hathaway, N. Ray, D. Kennedy, N. O'Brien, B. Murphy, Acta Crystallogr., Sect B 36 (1980) 1360.
[25] S. Youngme, C. Pakawatchai, W. Somjitsripunya, K. Chinnakali, H.K. Fun, Inorg. Chim. Acta 303 (2000) 181.
[26] C.C. Addison, N. Logan, S.C. Wallwork, C.D. Garner, Q. Rev. Chem. Soc. 25 (1971) 289.
[27] S. Youngme, N. Chaichit, K. Damatara, Polyhrdron 21 (2002) 943.
[28] M.B. Ferrari, G.G. Fava, C. Pelizzi, J. Chem. Soc., Chem. Commun. (1977) 8.
[29] W.D. Harrison, B.J. Hathaway, Acta Crystallogr., Sect. B 34 (1978) 2843.
[30] (a) H. Nakai, Bull. Chem. Soc. Jpn. 44 (1971) 2412;
(b) J. Foley, D. Kennefick, D. Phelan, S. Tyagi, B.J. Hathaway, J. Chem. Soc., Dalton Trans. (1983) 2333.
[31] S. Youngme, K. Chandavong, C. Pakawatchai, Z.Y. Zhou, H.K. Fun, Acta Crystallogr., Sect. C 54 (1998) 199.
[32] S. Youngme, K. Poopasit, H.K. Fun, K. Chinnakali, I.A. Razak, S. Chantrapromma, Acta Cryastallogr., Sect. C 54 (1998) 1221.
[33] (a) V. Kasempimolporn, S. Tyagi, B.J. Hathaway, 1980, unpublished data;
(b) P.C. Power, B.J. Hathaway, 1980, unpublished data;
(c) H.A. Chen, J.P. Fackler, 1980, private communication.
[34] V. Koonsaeng, Ph.D. Thesis, University College Cork, Ireland, 1989.
[35] J. Sletten, A. Sorenen, Acta Chim. Scand. 44 (1990) 1018.
[36] (a) R.J. Fereday, P. Hodgson, S. Tyagi, B.J. Hathaway, J. Chem. Soc., Dalton. Trans (1981) 2070;
(b) R.J. Fereday, P. Hodgson, S. Tyagi, B.J. Hathaway, Inorg. Nucl. Chem. Lett. 17 (1981) 243.
[37] B.J. Hathaway, Comprehensive coordination chemistry, in: G. Wilkinson, R.D. Gillard, J.A. McCleverty (Eds.), The Synthesis, Reactions, Properties and Applications of Coordination Compounds, vol. 5, Pergamon Press, Oxford, 1987, pp. 533–774, Section 53.
[38] E.L. Muetterties, Inorg. Chem. 4 (1965) 795.
[39] J. Gazo, I.B. Bersuker, J. Garaj, M. Kabesova, J. Kohout, M. Langfelderova, M. Melnik, M. Seraton, F. Valach, Coord. Chem. Rev. 11 (1976) 253.
[40] K. Nakamoto, Infrared and Raman Spectra of Inorganic and Coordination Compounds, Part B, 5th ed., Wiley, New York, 1997.

Available online at www.sciencedirect.com
SCIENCE DIRECT®
Polyhedron 23 (2004) 1695–1700
POLYHEDRON
www.elsevier.com/locate/poly

Synthesis, spectroscopic, magnetic and EPR results and crystal structure of di-μ-(*N*-methyl-*N*-methoxy-2-pyridinamine) bis[(2,2′-bipyridine)copper(II)]hexaflourophosphate

Montserrat Barquín [a], María J. González Garmendia [a,*], Sergio Pacheco [a], Elena Pinilla [b,c], José M. Seco [a], María R. Torres [b]

[a] *Grupo de Química Inorgánica, Facultad de Ciencias Químicas, Universidad del País Vasco, UPV/EHU, Apartado 1072, E-20080 San Sebastián, Spain*
[b] *Laboratorio de Difracción de Rayos-X, Facultad de Ciencias Químicas, Universidad Complutense, 28040 Madrid, Spain*
[c] *Departamento de Química Inorgánica, Facultad de Ciencias Químicas, Universidad Complutense, 28040 Madrid, Spain*

Received 22 October 2003; accepted 1 April 2004
Available online 4 May 2004

Abstract

A new binuclear complex $[\{Cu(bipy)\}_2\{\mu\text{-}Me(OCH_2)Npy\}_2](PF_6)_2$, where bipy = 2,2′-bipyridine and $Me(OCH_2)Npy$ = *N*-methyl-*N*-methoxy-2pyridinamine, has been synthesized and characterized by chemical analysis, conductance measurements and IR and electronic spectroscopies. The X-ray crystal structure shows a distorted square-planar pyramidal coordination for Cu(II), determinated by two nitrogen atoms of bipy and two methoxo oxygen atoms in the equatorial plane and the pyridinic nitrogen atom of the ligand in the axial position. Magnetic susceptibility measurements (in the 2–290 K range) reveal a slightly antiferromagnetic character ($2J = -3.6$ cm^{-1}). In the Q-band EPR spectrum signals of triplet ($D > hv$) are observed.
© 2004 Elsevier Ltd. All rights reserved.

Keywords: Copper dimer; Magnetic properties; Antiferromagnetic dimer; Crystal structure

1. Introduction

The magnetic aspects of dinuclear Cu(II) complexes, $[\{Cu(NN)(\mu\text{-}OH)\}_2]X_2$, with NN = bidentate nitrogen ligand, have been intensively studied since the magnetostructural correlations described by Hatfield et al. [1] for planar dimers of Cu(II) with the Cu_2O_2 group. More recently, these correlations have been extended and theoretically justified by Ruiz et al. [2,3].

The 2-anilinopyridine, (*N*-phenyl-2-pyridinamine, PhNHpy), is an asymmetric ligand, with two nitrogen atoms in 1,3 positions, which can coordinate as monodentate or bidentate. As monodentate ligand the coordination is established through the pyridinic nitrogen and as anionic bidentate through both nitrogen atoms [4,5].

In previous papers, we described the interaction between $[\{Cu(bipy)\}_2(\mu\text{-}OH)_2]X_2 \cdot xH_2O$ dimers, where $X^- = PF_6^-$, ClO_4^-, and the ligand PhNHpy. With the hexaflourophosphate complex, the compound $[\{Cu(bipy)(PhNHpy)\}_2(\mu\text{-}OH)_2](PF_6)_2$ was formed [6]. Each PhNHpy molecule was coordinated to a copper atom through the piridinic nitrogen atom and the hydrogen bonded to the anilinic nitrogen is involved in an hydrogen bond with the oxygen atom of a bridging OH group. In the case of the perchlorate compound, a methylene group was inserted between the anilinic nitrogen atom of the ligand and the bridging oxygen, and the $[\{Cu(bipy)\}_2\{\mu\text{-}Ph(OCH_2)Npy\}_2](ClO_4)_2$ was formed [7].

In the present work, we describe the interaction between MeNHpy and the $[\{Cu(bipy)\}_2(\mu\text{-}OH)_2](PF_6)_2 \cdot 2H_2O$ dimer. In this case, unlike the result obtained with PhNHpy and the hexafluorophosphate, the

* Corresponding author. Fax: 34-43-015270.
E-mail address: qppgogam@sq.ehu.es (M.J. González Garmendia).

0277-5387/$ - see front matter © 2004 Elsevier Ltd. All rights reserved.
doi:10.1016/j.poly.2004.04.013

methylene group is also inserted, and the $[\{Cu(bipy)\}_2\{\mu\text{-}Me(OCH_2)Npy\}_2](PF_6)_2$ is obtained.

2. Experimental

2.1. Synthesis

$[\{Cu(bipy)\}_2(\mu\text{-}OH)_2](PF_6)_2 \cdot 2H_2O$ was prepared according to Harris et al. [8]. The anionic form of MeNHpy was prepared, in situ. The ligand was dissolved in abs ethanol (5 ml) and metallic sodium, in stoichiometric proportion, was added. The mixture was allowed to stand 10 m before using it [9].

$[\{Cu(bipy)\}_2\{\mu\text{-}Me(OCH_2)Npy\}_2](PF_6)_2$: a solution of $MeNpy^-$ (0.1 ml, 1 mmol) in abs ethanol (5 ml) was slowly added to a solution of $[\{Cu(bipy)\}_2(\mu\text{-}OH)_2](PF_6)_2 \cdot 2H_2O$ (0.2 g, 0.25 mmol) in methanol (80 ml). The brown mixture was refluxed during 3 h. After a time of stirring without heating until cooling to room temperature, it was again refluxed for 3 h. This process was repeated until the solution becomes green in colour. The solution was concentrated and a blue precipitate was filtered off. The green filtrate was evaporated until the formation of green crystals. These were filtered off and washed with ether. The compound was soluble in acetonitrile, methanol and nitromethane.

Yield: 25%. Elemental *Anal.* Calc. for $C_{34}Cu_2F_{12}H_{34}N_8O_2P_2$: C, 40.7; H, 3.4; N, 11.2. Found: C, 40.6; H, 3.9; N, 11.0%.

2.2. Physical measurements

C, H and N were analysed in a Leco 932-CHNS Elemental Analyzer. Conductivity measurements were made using a Metrhom E518 conductimeter. IR spectra were recorded on a Nicolet FT-IR 510 spectrometer in the range 4000–400 cm^{-1} using KBr pellets. Electronic spectra were recorded on a Schimadzu UV-265 FW spectrophotometer.

Magnetic measurements were carried out in the 300–2 K range with a magnetometer SQUID MPMS XL (Quantum Design). Diamagnetic corrections have been applied [10]. The EPR spectra were recorded on a Bruker ESP 300 spectrometer with a Bruker ER 035 M gaussmeter, Oxford ITC4 cryostat and HP 5325B frequency counter.

2.3. Crystal structure determination

The X-ray diffraction data for $[\{Cu(bipy)\}_2\{\mu\text{-}Me(OCH_2)Npy\}_2](PF_6)_2$ were collected for a prismatic green crystal on a Bruker Smart CCD diffractometer, with graphite-monochromated Mo Kα ($\lambda = 0.71073$ Å) radiation, at 296 K. A summary of the fundamental crystal data and refinement parameters are given in Table 1. Data were collected over an hemisphere of the reciprocal space by combination of the three exposure sets. Each exposure of 20 covered 0.3 in ω. The first 50 frames were recollected at the end of the data collection to monitor crystal decay. No appreciable drop in the intensities of standard reflections was observed.

Table 1
Crystallographic and structure refinement data for $[\{Cu(bipy)\}_2\{\mu\text{-}Me(OCH_2)Npy\}_2](PF_6)_2$

Formula	$[C_{17}H_{17}N_4OCu]_2(PF_6)_2$
Formula weight	1003.71
T (K)	296(2)
λ (Å)	0.71073
Crystal system	triclinic
Space group	$P\bar{1}$
a (Å)	10.131(1)
b (Å)	14.172(1)
c (Å)	15.154(1)
α (°)	79.369(2)
β (°)	74.327(1)
γ (°)	70.369(1)
Z	2
V (Å^3)	1962.6(2)
D_{calc} (g cm^{-3})	1.698
Absorption coefficient, μ (mm^{-1})	1.267
Scan technique	φ and ω
$F(000)$	1012
Crystal size (mm)	$0.12\times0.20\times0.40$
θ range for data collection (°)	1.40–25.00
Index ranges	$-12 \leqslant h \leqslant 12$, $-10 \leqslant k \leqslant 16$, $-15 \leqslant l \leqslant 18$
Reflections collected	10 254
Independent reflections (R_{int})	6797 (0.0433)
Completeness to $\theta = 25.00°$ (%)	98.5
Absorption correction	none
Data/restraints/parameters	6797/0/469
Goodness-of-fit on F^2	1.018
Final R^a indices [$I > 2\sigma(I)$]	$R_1 = 0.0575$ (4261 observed reflections)
R^b indices (all data)	$wR_2 = 0.1694$

[a] $R_1 = \sum ||F_o| - |F_c|| / \sum |F_o|$.
[b] $wR_2 = \{\sum[w(F_o^2 - F_c^2)^2] / \sum[w(F_o^2)^2]\}^{1/2}$.

The structure was solved by Patterson (Cu atoms) and conventional Fourier techniques and refined by full-matrix least-squares on F^2 [11]. The fluoro atoms of the hexafluorophosphate groups were refined only two cycles anisotropically and in the last cycle the thermal factors has been fixed. The rest of the non-hydrogen atoms were refined anisotropically. Hydrogen atoms were included in calculated positions and refined riding on the respective carbon atoms.

3. Results and discussion

3.1. Characterization

The molar conductivity of the complex in acetonitrile (285.7 Ω^{-1} cm^2 mol^{-1}) corresponds to a 2:1 elec-

trolyte [12], according to the dimeric character of the cations.

Unlike the $[\{Cu(bipy)(PhNHpy)\}_2(\mu\text{-}OH)_2](PF_6)_2$ complex [6], the IR spectrum does not show the stretching ν(O–H) and ν(N–H) bands. The ν(Cu–O) band shifts to higher frequency (491 cm^{-1}) to the original dimer $[\{Cu(bipy)\}_2(\mu\text{-}OH)_2](PF_6)_2 \cdot 2H_2O$ (487 cm^{-1}) [13].

The electronic spectra of the solution in acetonitrile exhibits, besides the ligands bands, the d-d band of Cu(II) at 638 nm ($\varepsilon_{max} = 1451$ cm^{-1} mol^{-1}).

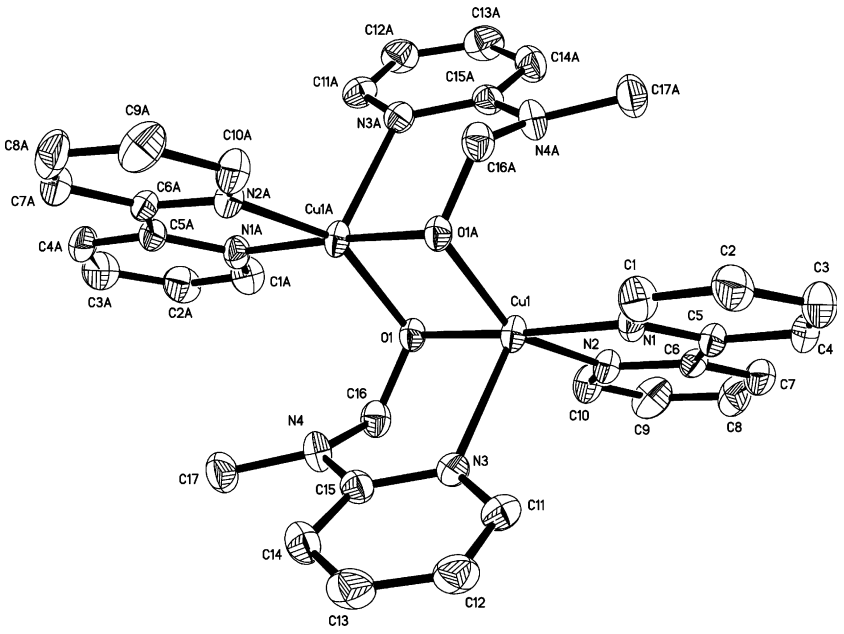

Fig. 1. ORTEP view of the $[\{Cu(bipy)\}_2\{\mu\text{-}Me(OCH_2)Npy\}_2]^{2+}$ cation (dimer 1).

Table 2
Selected interatomic distances (Å) and angles (°) for $[\{Cu(bipy)\}_2\{\mu\text{-}Me(OCH_2)Npy\}_2](PF_6)_2$

Interatomic distances			
Dimer 1		Dimer 2	
Cu(1)–O(1)	1.926(3)	Cu(2)–O(2)	1.932(3)
Cu(1)–O(1A)	1.984(3)	Cu(2)–O(2A)	2.007(3)
Cu(1)–N(1)	1.987(4)	Cu(2)–N(6)	1.989(4)
Cu(1)–N(2)	2.018(4)	Cu(2)–N(5)	2.032(4)
Cu(1)–N(3)	2.296(5)	Cu(2)–N(7)	2.253(5)
Cu(1)···Cu(1A)	2.923(1)	Cu(2)···Cu(2A)	2.948(1)
O(1)···O(1A)	1.984(3)	O(2)···O(2A)	2.612(7)
O(1)–C(16)	1.392(6)	O(2)–C(33)	1.407(7)
N(4)–C(16)	1.452(7)	N(8)–C(33)	1.460(8)
N(4)–C(15)	1.362(7)	N(8)–C(32)	1.382(8)
N(4)–C(17)	1.463(7)	N(8)–C(34)	1.443(8)
Interatomic angles			
Dimer 1		Dimer 2	
O(1)–Cu(1)–N(2)	96.9(2)	O(2)–Cu(2)–N(5)	96.6(2)
N(1)–Cu(1)–N(2)	80.8(2)	N(5)–Cu(2)–N(6)	80.2(2)
N(1)–Cu(1)–O(1A)	96.5(2)	N(6)–Cu(2)–O(2A)	97.3(2)
O(1)–Cu(1)–O(1A)	83.3(2)	O(2)–Cu(2)–O(2A)	83.1(1)
O(1)–Cu(1)–N(1)	175.0(2)	O(2)–Cu(2)–N(6)	174.3(2)
N(2)–Cu(1)–O(1A)	149.1(2)	N(5)–Cu(2)–O(2A)	149.3(2)
N(3)–Cu(1)–N(1)	96.3(2)	N(7)–Cu(2)–N(6)	93.5(2)
N(3)–Cu(1)–N(2)	110.7(2)	N(7)–Cu(2)–N(5)	107.4(2)
N(3)–Cu(1)–O(1)	88.6(2)	N(7)–Cu(2)–O(2)	92.0(2)
N(3)–Cu(1)–O(1A)	100.3(2)	N(7)–Cu(2)–O(2A)	103.3(2)
Cu(1)–O(1)–Cu(1A)	96.8(2)	Cu(2)–O(2)–Cu(2A)	96.9(1)

Symmetry transformations used to generate equivalent atoms A: dimer 1, $-x, -y+1, -z+2$; dimer 2, $-x+1, -y+2, -z+1$.

3.2. Crystal structure

The compound $[\{Cu(bipy)\}_2\{\mu\text{-}Me(OCH_2)Npy\}_2](PF_6)_2$ consists of $[\{Cu(bipy)\}_2\{\mu\text{-}Me(OCH_2)Npy\}_2]^{2+}$ divalent cationic dimers and $(PF_6)^-$ anions. The asymmetrical units contains two chemically identical, but crystallographically different, dimers with very slight differences. The centrosymmetric dimers consist of two sections, composed each of them, by a slightly bent bipy molecule and a $[Me(OCH_2)Npy]^-$ group bonded to a copper atom through the pyridinic nitrogen atom and to the both copper atoms through the oxygen atom. Two of such sections are linked together by the two oxygen bridges, across a centre of symmetry. Fig. 1 shows an ORTEP view of the geometry of one cation (dimer 1) with 35% probability ellipsoids. The $(PF_6)^-$ group and hydrogen atoms have been omitted for clarity. Selected interatomic distances and angles are listed in Table 2 for the two dimers.

Each copper atom has a distorted square-planar pyramidal coordination (trigonality index [14], $\tau = 0.42$) with Cu(1)–O(1) and Cu(1)–O(1A) distances of 1.926(3) and 1.984(3) Å; Cu(1)–N(1) and Cu(1)–N(2) distances of 1.987(4) and 2.018(4) Å. The fifth distance, Cu(1)–N(3), is larger, 2.296(5) Å . The copper atom rises from the basal plane to the apical N(3) by 0.308(2) Å . The Cu_2O_2 group is planar, with average angles for the two dimers of 83.2(2)° in Cu and 96.9(2)° in O atom. The Cu–O distances are asymmetrical, being the shortest that which closes the CuNCNCO ring. The Cu(1)···Cu(1A) and O(1)···O(1A) separation are 2.923(1) and 1.984(3) Å . All these results are very similar to those found for $[\{Cu(bipy)\}_2\{\mu\text{-}Ph(OCH_2)Npy\}_2](ClO_4)_2$ [7]. The bipyridine molecule are slightly bent; the angle formed by the two planar pyridyl groups being significatively different in the two dimers: 1.3° in dimer 1 and 6.4° in dimer 2.

As in $[\{Cu(bipy)\}_2\{\mu\text{-}Ph(OCH_2)Npy\}_2](ClO_4)_2$, the nitrogen atom of the reaction ligand, MeNHpy in this case, bonded to the copper atom is that belonging to the pyridine ring, N(3), and the nitrogen atom, N(4) (bonded to a methyl and to a pyridine groups) has lost its hydrogen atom to form a N–C bond with C(16). This C(16) atom is bonded to the bridging oxygen atom,

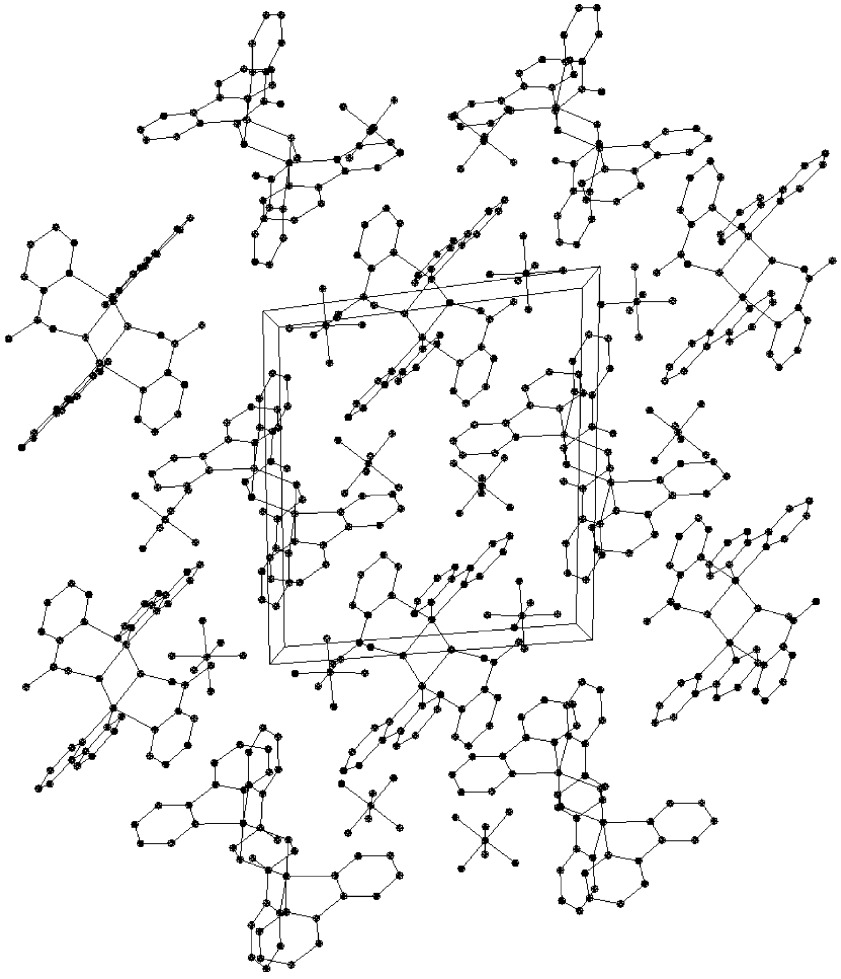

Fig. 2. Crystal structure of $[\{Cu(bipy)\}_2\{\mu\text{-}Me(OCH_2)Npy\}_2](PF_6)_2$ viewed along the *a*-axis.

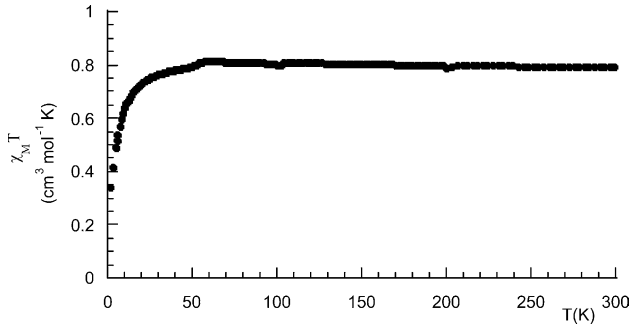

Fig. 3. Plot of $\chi_M T$ vs. T for [{Cu(bipy)}.

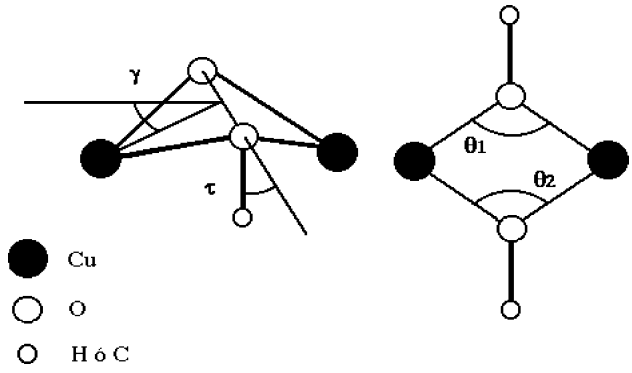

Fig. 4. θ, τ and γ angles in the Cu_2O_2 group.

O(1). A CH_2 group is inserted between N and O. The N(4)–C(16) and C(16)–O(1) distances agree with the bond length for simple covalent bonds between these elements.

Fig. 2 shows the crystal structure of the complex viewed along the *a*-axis.

3.3. Magnetic results

The variable temperature magnetic susceptibility data have been measured in the 2–300 K temperature range. The plot of $\chi_M T$ per 2Cu(II) versus temperature is shown in Fig. 3. The $\chi_M T$ value is approximately constant (0.80 cm^3 K mol^{-1}; $\mu_{eff} = 1.79\ \mu_B$) in the range 300–50 K. Below this temperature, $\chi_M T$ decreases until 0.34 cm^3 K mol^{-1} at 2 K ($\mu_{eff} = 1.17\ \mu_B$), indicating an antiferromagnetic intradimeric interaction. The data were fitted to the Bleaney–Bowers equation modified by the inclusion of the fraction of monomeric impurity [15]: $\chi_M = [C e^x(1-\rho)/(1+3e^x)] + C\rho/4$, where $C = Ng^2\beta^2/kT$, $x = 2J/kT$, ρ is the fraction of monomeric impurity.

The fitting results were $2J = -3.6$ cm^{-1}, $g = 2.07$ and $\rho = 0.025$. This slight antiferromagnetism is intermediate between the ferromagnetism ($2J = 10$ cm^{-1}) of [{Cu(bipy)}$_2${μ-Ph(OCH$_2$)Npy}$_2$](ClO$_4$)$_2$ and the antiferromagnetism ($2J = -98$ cm^{-1}) of [{Cu(phen)}$_2${μ-Ph(OCH$_2$)Npy}$_2$](ClO$_4$)$_2$ [7]. The magnetic results and significant structural data of these compounds are collected in Table 3.

The correlation deduced by Hatfield et al. [1] between $2J$ and θ (bridging angle CuOCu) for di-μ-hydroxo planar copper dimers: $2J$ (cm^{-1}) $= -74.53\theta + 7270$ predicts ferromagnetism for $\theta < 97.5°$ and antiferromagntism for $\theta > 97.5°$. Ruiz et al. [2,3] studied the effect of other structural parameters for copper dimers with hydroxo and alkoxo bridges. These are, besides θ, the angle τ, formed between the O–O direction and the hydrogen or carbon atom bounded to the bridging oxygen atom, and the non-planarity of the Cu_2O_2 group, measured by γ (Fig. 4). High τ values are associated with lower values of θ and correspond to $2J$ more positive (ferromagnetism). For $\theta < 97.5°$ and $\tau > 40°$ a ferromagnetic effect is to be expected. The non-planarity of the Cu_2O_2 group (γ) reduces the antiferromagnetic character and enhances the influence of τ.

The data collected in Table 3 indicate that the magnetostructural correlations for copper dimers with hydroxo and alkoxo bridges are not directly applicable to theses complexes where the Cu_2O_2 group is altered by the coordinated ligand which closes a ring CuNCNCO. They are variations in the structural factors near the limit between ferro- and antiferromagnetic interaction.

3.4. EPR spectra

The X-band EPR spectrum of the powdered sample shows four signals: three derived from the triplet state

Table 3
Magnetic results and significant structural data

	Compound **1**	Compound **2**	Compound **3**
$2J$ (cm^{-1})	−3.6	10	−98
d_{Cu-Cu} (Å)	2.935	2.974	2.952
$d_{Cu-basal\ plane}$ (Å)	0.308	0.305	0.357
θ (°)	96.9	97.8	98.3
τ (°)	61.5	62.0	48.7
γ (°)	0	0	0
$2J(\theta)$[a] (cm^{-1})	48	−19	−56

Compound **1**: [{Cu(bipy)}2{μ-Me(OCH$_2$)Npy}$_2$](PF$_6$)$_2$ (this work). Compound **2**: [{Cu(bipy)}$_2${μ-Ph(OCH$_2$)Npy}$_2$](ClO$_4$)$_2$ [7]. Compound **3**: [{Cu(phen)}$_2${μ-Ph(OCH$_2$)Npy}$_2$](ClO$_4$)$_2$ [7].

[a] Calculated from $2J(\theta) = (-74.53\theta + 7270)$ cm^{-1}.

($H = 1715$, 6333 and 8285 G) and one ($H = 3315$ G) connected with the noncoupled copper.

The spectrum is similar to those observed for other copper dimers with $D > h\nu$ (D is the zero field splitting parameter) [6,7]. As it is observed for some cases, is not possible to analyse the spectra with the Wasserman et al. [16] equations for triplet state; it is not possible to do assignations corresponding to reasonable values of parameter g.

At Q-band an absorption at zero field is observed, in agreement with the condition $D > h\nu$ ($D > 1.14$ cm^{-1}).

4. Supplementary material

Further structural data have been deposited with the Cambridge Crystallographic Data Centre, CCDC 215374. Copies of this information may be obtained free of charge from the CCDC, 12 Union Road, Cambridge CB2 1EZ, UK (fax: +44-1233-336033; e-mail: deposit@ccdc.cam.ac.uk or www: http://www.ccdc.cam.ac.uk).

Acknowledgements

The authors thank Prof. Dr. L. Lezama for recording the EPR spectra. Finantial support from the ''Diputación Foral de Gipuzkoa'', the ''Universidad del País Vasco-Euskal Herriko Unibertsitatea'' and the Ministerio de Ciencia y Tecnología (Project BQU2002-00129) is gratefully acknowledged.

References

[1] Van H. Crawford, H.W. Richardson, J.R. Wasson, D.J. Hodgson, W.E. Hatfield, Inorg. Chem. 15 (1976) 2107.
[2] E. Ruiz, P. Alemani, S. Alvarez, J. Cano, Inorg. Chem. 36 (1997) 3683.
[3] E. Ruiz, P. Alemani, S. Alvarez, J. Cano, J. Am. Chem. Soc. 119 (1997) 1297.
[4] A.R. Chakravarty, F.A. Cotton, Inorg. Chim. Acta 105 (1985) 19.
[5] D. Barr, W. Clegg, R.E. Mulvey, R. Snaith, J. Chem. Soc., Chem. Commun. (1984) 469.
[6] J.M. Seco, U. Amador, M.J. González Garmendia, Polyhedron 18 (1999) 3605.
[7] J.M. Seco, U. Amador, M.J. González Garmendia, Inorg. Chim. Acta 303 (2000) 256.
[8] C.M. Harris, E. Sinn, W.R. Walker, P.R. Woolliams, Aust. J. Chem. 21 (1968) 631.
[9] D.A. Tocher, J.H. Tocher, Polyhedron 25 (1986) 1615.
[10] R.L. Carlin, Magnetochemistry, Springer, Berlin, 1986.
[11] G.M. Sheldrick, SHELXL-97: A Program for Refinement of Crystal Structure, University of Göttingen, Göttingen, Germany, 1997.
[12] W.J. Geary, Coord. Chem. Rev. 7 (1971) 81.
[13] J.R. Ferraro, W.R. Walker, Inorg. Chem. 4 (1965) 1382.
[14] A.W. Addison, T.N. Rao, J. Reedjik, J. van Rijn, G.C. Verschoor, J. Chem. Soc., Dalton Trans. (1984) 1349.
[15] M. Nakashima, M. Mikuriya, Y. Muto, Bull. Chem. Soc. Jpn. 58 (1985) 968.
[16] E. Wasserman, L.C. Snyder, W.A. Yager, J. Chem. Phys. 41 (1964) 1763.

Available online at www.sciencedirect.com
SCIENCE DIRECT®
Polyhedron 23 (2004) 1701–1707
POLYHEDRON
www.elsevier.com/locate/poly

Synthesis and structural characterization of zinc(II) and cadmium(II) complexes with 2-oxo-1,3-dithiole-4,5-dithiolate and 1,10-phenanthroline

Wenyong Guo, Zhenghe Peng *, Daocong Li, Yunhong Zhou

Department of Chemistry, Wuhan University, Wuhan 430072, PR China

Received 13 November 2003; accepted 17 March 2004
Available online 23 April 2004

Abstract

Isomorphous complexes Zn(dmid)(phen)$_2$ (**1**) and Cd(dmid)(phen)$_2$ (**2**) have been synthesized through a ligand substitute reaction. Their structures and properties have been characterized by elemental analysis, IR, UV–Vis, fluorescence and single-crystal X-ray analysis. The octahedral N_4S_2 coordination geometry, bonding, electronic structure and IR spectra of the Zn(dmid)(phen)$_2$ molecule were studied in detail using DFT and INDO/S methods. In the crystal packing, there exists a strong π–π interaction between two parallel 1,10-phenanthrolines of adjacent molecules. Complex **1** (or **2**) in the solid state exhibits an intensive fluorescence band at 539.5 nm (or 536 nm) when the excitation wavelength is 371 nm (or 370.5 nm) at room temperature.
© 2004 Elsevier Ltd. All rights reserved.

Keywords: Zinc complex; Cadmium complex; 2-Oxo-1,3-dithiole-4,5-dithiolate; Synthesis; Crystal structure; Density functional calculation

1. Introduction

Over the past decade, dithiolene metal complexes of multi-sulfur donor ligands have attracted much interest because of their potential applications as molecular conductors, superconductors and molecular photo-devices [1,2]. Among them, metal complexes of dmit (dmit = 1,3-dithiole-2-thione-4,5-dithiolate) have been extensively investigated [3]. Through converting the thione group of the dmit ligand into a ketone group, dmid (2-oxo-1,3-dithiole-4,5-dithiolate) can be obtained. The replacement of sulfur atoms by oxygen atoms on the periphery of the ligand changes the properties of the complexes in two ways [4]: (1) the change in intermolecular interactions due to the replacement of S···S by O···O, (2) the change of electron distribution in the HOMO due to the more electronegative oxygen atoms, which do affect the intermolecular bonding and intermolecular interactions. However, metal complexes with dmid have not been studied so widely in comparison with dmit complexes, although the former have been shown to exhibit some unique properties such as electrical switching and memory function [5].

In our laboratory complexes containing both dmid and phen ligands are studied in an effort to prepare complexes with unique geometries and special physical properties. As examples of such complexes, Zn(dmid)(phen)$_2$ (**1**) and Cd(dmid)(phen)$_2$ (**2**) have been synthesized, and their crystal structures, IR spectra, UV–Vis and fluorescence are investigated in this work. To the best of our knowledge, **1** and **2** are the first two examples of mixed-ligand neutral complexes of dmid.

2. Experimental

All solvents were dried and distilled using standard methods. Reagents were obtained from commercial sources and were used without further purification. Complexes $(NEt_4)_2[Zn(dmid)_2]$ and $(NEt_4)_2[Cd(dmid)_2]$ were synthesized according to the literature procedure [6].

* Corresponding author. Tel.: +86-278-866-2668; fax: +86-278-766-7617.
E-mail addresses: gwy64@126.com (W. Guo), pengzh@chem.whu.edu.cn (Z. Peng).

0277-5387/$ - see front matter © 2004 Elsevier Ltd. All rights reserved.
doi:10.1016/j.poly.2004.04.003

Elemental analysis was carried out on a Perkin–Elmer 2400|CHNSO elemental analyzer. The contents of Zn and Cd were measured through EDTA titration. The thermal analyses were performed with a Perkin–Elmer TGS-Z thermogravimetril analyzer in the range of 40–830 °C. The IR spectra were recorded with a Nicolet 170SX FT-IR spectrometer in the region 400–4000 cm^{-1} (KBr pellets). Electronic spectra were performed on a Shimadzu UV-240 spectrometer over the range of 200–700 nm. The spectra of fluorescent emission were performed on Perkin–Elmer LS 55 luminescence spectrometer in the range of 200–700 nm.

2.1. Synthesis

2.1.1. Zn(dmid)(phen)$_2$ (**1**)

Complex **1** was prepared through a ligand substitute reaction according to the following procedure. A solution of $(NEt_4)_2[Zn(dmid)_2]$ (1 mmol, 0.686 g) in 30 ml acetone was added cautiously to a solution of phen (3 mmol) in 30 ml DMF to form two clear layers in a test tube. The test tube was then allowed to stand undisturbed at room temperature for seven days without illumination, and then the red crystals of Zn(dmid)(phen)$_2$ suitable for single-crystal X-ray diffraction were obtained (0.560 g, 92% based on $(NEt_4)_2[Zn(dmid)_2]$). *Anal*. Calc. for $C_{27}H_{16}N_4OS_4Zn$: C, 53.51; H, 2.66; N, 9.24; Zn, 10.79. Found: C, 53.78; H, 2.66; N, 9.15; Zn, 10.88%. IR (KBr pellets, cm^{-1}): 1786(w), 1654(s), 1608(vs), 1512(s), 1492(w), 1446(s), 1422(vs), 1341(m), 1321(w), 1302(w), 1220(w), 1140(m), 1099(m), 974(w), 894(m), 865(m), 846(vs), 770(m), 728(s), 636(m).

2.1.2. Cd(dmid)(phen)$_2$ (**2**)

The crystals of complex **2** were prepared as described for **1** except using $(NEt_4)_2[Cd(dmid)_2]$ instead of $(NEt_4)_2[Zn(dmid)_2]$ (yield: 94%, based on $(NEt_4)_2[Cd(dmid)_2]$). *Anal*. Calc. for $C_{27}H_{16}CdN_4OS_4$: C, 49.66; H, 2.47; N, 8.57; Cd, 17.21. Found: C, 49.97; H, 2.48; N, 8.53; Cd, 17.52%. IR (KBr pellets, cm^{-1}): 1788(w), 1656(s), 1610(vs), 1512(s), 1493(w), 1441(s), 1424(vs), 1340(m), 1319(w), 1300(w), 1219(w), 1142(m), 1098(m), 968(w), 895(m), 846(vs), 771(m), 728(s), 636(m).

2.2. Theoretical calculation

All theoretical calculations were performed on a Pentium IV 1.72 GHz (80 GB, 512 MB) computer. The calculations of geometry optimization and vibrational frequencies of the gaseous Zn(dmid)(phen)$_2$ were carried out by using the B3LYP method of density functional theory with the 6-31G* basis set in GAUSSIAN-98 [7]. The calculations of electronic absorption spectra of Zn(dmid)(phen)$_2$ in the gaseous state were performed using the configuration interaction (CI) by the INDO/S method in HYPERCHEM [8]. The configuration number of CI was established by the numbers of the HOMO ($n_{OO} = 8$) and LUMO ($n_{UO} = 12$).

2.3. Crystal structure determination

The crystal data, structure solution and refinement details for the two structures determined are presented in Table 1. Relevant bond distances and bond angles for **1** and **2** are collected in Tables 2 and 3. Suitable single

Table 1
Crystal data and structural refinement of the complexes **1** and **2**

	1	**2**
Empirical formula	$C_{27}H_{16}N_4OS_4Zn$	$C_{27}H_{16}CdN_4OS_4$
Formula weight	606.05	653.08
T (K)	273(2)	291(2)
Crystal system	triclinic	triclinic
Space group	$P\bar{1}$	$P\bar{1}$
Crystal size (mm)	0.26×0.20×0.16	0.20×0.20×0.18
Unit cell dimensions		
a (Å)	10.988(2)	11.134(2)
b (Å)	12.922(3)	13.011(3)
c (Å)	9.520(2)	9.681(2)
α (°)	97.13(3)	97.51(3)
β (°)	112.49(3)	112.85(3)
γ (°)	112.49(3)	85.48(3)
V (Å^3)	1239.2(4)	1280.5(4)
Z	2	2
θ Range (°)	1.59–27.53	1.58–27.50
D_{calc} (Mg m^{-3})	1.624	1.694
Absorption correction	none	none
Reflections collected/unique	3850/3850	4112/4112
Data/restraints/parameters	3850/0/335	4112/0/335
Final R indices [$I > 2\delta(I)$]	$R_1 = 0.0411$, $wR_2 = 0.0809$	$R_1 = 0.0547$, $wR_2 = 0.1286$
Goodness-of-fit	1.057	1.048
Largest difference peak and hole (e Å^{-3})	0.366 and −0.344	1.149 and −1.455

Table 2
Selected bond lengths (Å) for complexes **1** and **2**

Bond	Bond length		Bond	Bond length	
	1 (M = Zn)	**2** (M = Cd)		**1** (M = Zn)	**2** (M = Cd)
M–N1	2.200(2)	2.406(5)	M–S2	2.463(1)	2.548(2)
M–N2	2.238(3)	2.462(5)	O–C27	1.207(5)	1.213(9)
M–N3	2.305(3)	2.411(5)	S1–C25	1.739(4)	1.748(7)
M–N4	2.226(3)	2.383(5)	S2–C26	1.743(4)	1.753(7)
M–S1	2.406(6)	2.601(2)	C25–C26	1.362(5)	1.358(9)

Table 3
Selected bond angles (°) of complexes **1** and **2**

Bond angle	Numerical value		Bond angle	Numerical value	
	1 (M = Zn)	**2** (M = Cd)		**1** (M = Zn)	**2** (M = Cd)
N1–M–N2	75.22(1)	68.2(2)	N1–M–S2	100.86(8)	101.5(1)
N1–M–N3	87.13(1)	92.8(2)	N2–M–S1	171.47(7)	166.0(1)
N1–M–N4	156.09(1)	150.1(2)	N2–M–S2	89.38(8)	96.6(1)
N2–M–N3	87.19(1)	86.7(2)	N3–M–S1	93.22(8)	92.0(1)
N2–M–N4	90.24(1)	86.5(2)	N3–M–S2	170.21(7)	165.6(1)
N3–M–N4	73.07(1)	69.3(2)	N4–M–S1	98.03(9)	106.1(1)
N1–M–S1	96.29(8)	97.9(3)	N4–M–S2	97.80(9)	96.8(1)
S1–M–S2	91.53(4)	88.2(6)			

crystals were mounted for data collection on a Rigaku R-axis IV equipped with Mo Kα radiation ($\lambda = 0.71073$ Å). The structures were solved by direct methods and refined by a full-matrix least-squares technique procedure using anisotropic displacement parameters. All hydrogen atoms were located from difference Fourier maps, placed at calculated positions (C–H: 0.93–0.97 Å) and refined isotropically using a riding model.

3. Results and discussion

3.1. Crystal and molecular structures

Complex **1** consists of discrete molecules with a N_4S_2 six-coordinate zinc center with octahedral geometry. The metal atom is coordinated to four nitrogen atoms from two phen, and two sulfur atoms from dmid (Fig. 1). Both of the phen and dmid ligands are quite planar. The planes of the two phen ligands in complex **1** are nearly perpendicular to each other with a dihedral angle of 89.8°. The dihedral angles between the plane of dmid and the plane of phen1 (C1–C12) and of phen2 (C13–C24) are 91.5° and 105°, respectively. There are no abnormal carbon–nitrogen, carbon–sulfur or carbon–carbon bond lengths.

Through an inversion center, the plane of the phen1 (C1–C12) ligand overlaps with that of another phen1 ligand on an adjacent molecule, while the plane of the phen2 (C13–C24) ligand overlaps with that of another phen2 ligand on the other adjacent molecule. The planes of phen1 overlap through the outer-ring of phen. The distance separating the two ligands is 3.2296 Å. The planes of phen2 overlap through the middle-ring of phen. The separating distance between the two ligands is 3.4886 Å. The separation between the planes of phen indicates that the parallel phens have a strong π–π interaction [9]. The planes of dmid in **1** are different from the planes of dmid in $[Cp_2Mo(dmid)][TCNQF_4]$ and $[Cp_2W(dmid)][TCNQF_4]$ [10] which form dimers held together by dmid/dmid overlap interactions to give spin ladders. They have no apparent contact with each other just like in $(NBu_4)_2[(dmid)Ni(tto)Ni(dmid)]$ [11]. The distance separating the O atom of dmid and the plane of phen1 on an adjacent molecule is about 3.1 Å. They contact apparently through n–π interactions [9]. These two types of interaction create a three-dimensional packing system (Fig. 2).

The crystal structure of **2** is isomorphous with that of **1**. The dihedral angles between the two phen ligands, phen1 (C1–C12) and dmid, phen2 (C13–C24) and dmid are 94.2°, 106.9° and 93°, respectively. The distances of overlapping adjacent phen ligands are 3.2651 and 3.4699 Å for phen1 and phen2, respectively. The distance between the O atom of dmid and the adjacent phen1 is about 3.0 Å.

3.2. Thermal analyses

To study the thermal stability of compounds **1** and **2**, thermogravimetric analysis (TGA) was performed on the single-crystal samples. The TGA curves of the two compounds indicate that they are stable below 210 °C and one striking weight loss step occurred from 213.8 to 273.9 °C (loss 66%) for **1** and from 212.3 to 280 °C (loss

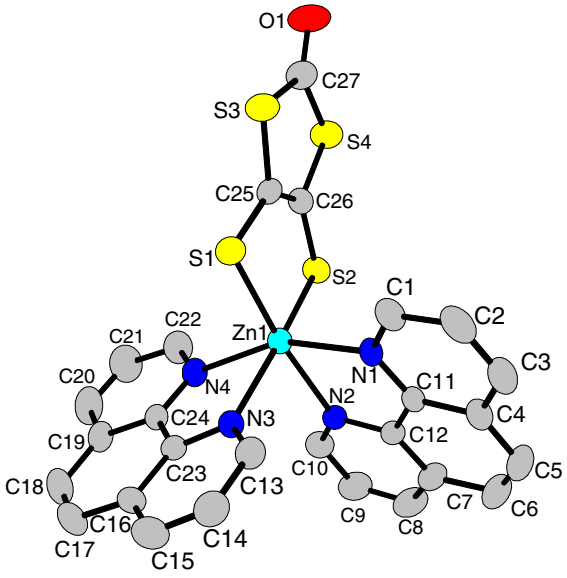

Fig. 1. Molecular structure of Zn(dmid)(phen)$_2$.

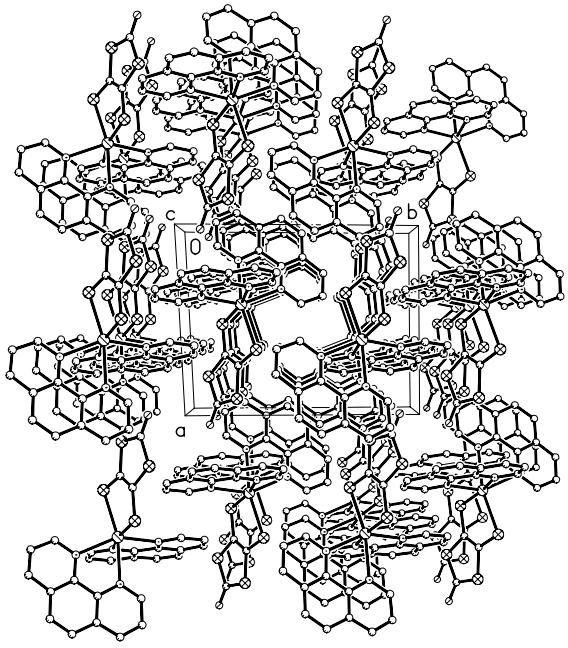

Fig. 2. The crystal packing of complex **1** facing the *ab*-plane.

64%) for **2**. The two isomorphous complexes have nearly the same thermal stability.

3.3. Infrared spectra

The IR spectra of complexes **1** and **2** are very similar to each other, except for a small shift of absorption bands. In order to explain these data, the vibrational properties of gaseous Zn(dmid)(phen)$_2$ were calculated. The geometry optimization calculations showed the molecular structure of gaseous Zn(dmid)(phen)$_2$ was similar to that of **1**, except for a C_2 symmetry. Some selected bond distances and bond angles for gaseous Zn(dmid)(phen)$_2$ are collected in Table 4. The atomic labels of Zn(dmid)(phen)$_2$ in the gaseous state were the same as complex **1**. In the band assignment, a scientific method was adopted [12]. The essentiality of this method was to give main fixed points and the crucial vibrations for each vibration mode. For example, the vibrations of S–C from dmid at 980.3 cm^{-1} are not simple stretching of S–C bonds. The C^{25}–C^{26} bond rocks in the plane of dmid while the S–C bonds stretch. So the absorption at 968 cm^{-1} observed for complex **1** could not simply be assigned to S–C stretching. The absorption at 463 cm^{-1} also could not be attributed to S–Zn stretching only. Some characteristic IR spectral data of complex **1** and the results of the calculation are presented in Table 5. Compared with the IR spectra of Zn(NCS)$_2$(phen)$_2$ [13], the observed frequencies of dmid listed in Table 5 were not found in the IR spectra of Zn(NCS)$_2$(phen)$_2$. The calculation results are in good agreement with the observed absorption frequencies.

Table 4
Selected bond lengths (Å) and angles (°) for Zn(dmid)(phen)$_2$ in the gaseous state (calculated)

Bond lengths			
Zn1–N1	1.915	Zn1–S1	2.355
Zn1–N2	2.201	Zn1–S2	2.355
Zn1–N3	2.201	S2–C26	1.772
Zn1–N4	1.915	S1–C25	1.772
O1–C27	1.228	C25–C26	1.361
Bond angles			
N1–Zn1–N2	77.52	N1–Zn1–S2	102.98
N1–Zn1–N3	77.78	N2–Zn1–S1	177.26
N1–Zn1–N4	144.60	N2–Zn1–S2	87.02
N2–Zn1–N3	90.59	N3–Zn1–S1	87.02
N2–Zn1–N4	77.78	N3–Zn1–S2	177.26
N3–Zn1–N4	77.52	N4–Zn1–S1	102.98
N1–Zn1–S1	100.64	N4–Zn1–S2	100.64
S1–Zn1–S2	94.59		

3.4. Electronic absorption spectra

The electronic absorption bands measured in DMF and DMSO in the range of 190-700 nm occur at 266, 325 (shoulder), 376 and 400 nm for **1** in DMF, and at 266, 320 (shoulder), 362 and 393 nm for **1** in DMSO. The bands in the range of 300–400 nm show that they are solvent dependent and shift to higher energy with increasing solvent polarity (DMSO > DMF) [14]. They are the solvatochromic bands and support the LL′CT assignment [15]. The results of the calculation of electronic absorption spectra of gaseous Zn(dmid)(phen)$_2$ are consistent with the experimental data of electronic absorption spectra for **1** (Table 6), while the oscillator strength of the calculation is consistent with the experimental results. The theoretical spectra differ slightly

Table 5
Observed absorption bands of complex **1** and calculated vibrational spectra (normal mode frequencies in cm^{-1}) in the gaseous state of $Zn(dmid)(phen)_2$

Observed frequency (transparency (%))	Calculated			Assignment	
	Symmetry	Frequency	Intensity	Fixed point	Vibration
	14 *A*	309.3	35.7540	O, phen	$\nu_s(S^1–Zn, S^2–Zn)$, $\delta_s(S^1–C^{25}, S^2–C^{26})$
463 (31)	18 *A*	464.4	26.3680	O, Zn, phen	$[\nu_s(S^3–C^{25}, S^4–C^{26}), \nu_s(S^1–C^{25}, S^2–C^{26})]_s$, $[\nu_s(S^3–C^{27}, S^4–C^{27}), \delta_s(S^1–Zn, S^2–Zn)]$
895 (27.5)	34 *A*	862.5	54.9115	O, Zn, phen, S^i, C^{27}, $M(C^{25}–C^{26})$	$\eta(C^{25}–C^{26})$ on C_2
968 (36.1)	40 *B*	980.3	2.2491	O, Zn, phen, S^i, C^{27}, $M(C^{25}–C^{26})$	$[\nu_{as}(S^1–C^{25}, S^2–C^{26}), \nu_{as}(S^3–C^{25}, S^4–C^{26})]_{AS}$, $\rho_t(C^{25}–C^{26})$
1610 (7.97)	69 *B*	1652.3	16.6627	Zn, dmid, N^i	$[\nu_s(C^5–C^6, C^{11}–C^{12}), \nu_s(C^{17}–C^{18}, C^{23}–C^{24})]_{AS}$
1660 (10.4)	68 *A*	1670.2	432.2952	Zn, phen, S^i	$[\nu(C^{27}–O), \nu_s(S^3–C^{27}, S^4–C^{27})]_{AS}$
3040 (40.7)	70 *B*	3140.6	60.0326	Zn, dmid, N^i, $C^2–C^{23}$, $H^2–H^{23}$	$\nu_{as}(H^1–C^1, H^{24}–C^{24})$
3040 (40.7)	69 *A*	3140.9	51.4904	Zn, dmid, N^i, $C^2–C^{23}$, $H^2–H^{23}$	$\nu_{as}(H^1–C^1, H^{24}–C^{24})$

ν, stretching; δ, bending or waggling in-plane; ρ_r, rocking in-plane; η, heaving along the specified direction; s, symmetry; as, asymmetry; M, midpoint (center) of a bond or unit.

Table 6
Calculated electronic spectra in the gaseous state of $Zn(dmid)(phen)_2$ and observed absorption bands of **1** in DMF and in DMSO

Calcd. (CI, $n_{OO} = 18$, $n_{UO} = 20$)			Obsd., λ_{max}/nm (intensity)	
λ_{max} (nm)	State dipole (Debye)	Oscillator strength	DMF	DMSO
422.8	2.5883	0.0001	400.0 (0.02377)	393.0 (0.03299)
379.3	26.5539	0.0001	376.0 (0.02576)	362.0 (0.03312)
363.2	25.1469	0.0007		
313.2	24.8205	0.0178	325.0 (0.04834)	320.0 (0.1153)
289.2	11.0580	0.0112		
270.6	25.3915	0.4123	266.0 (1.2176)	266.0 (1.4630)
259.0	25.9120	1.8391		

from the experimental results because the effect of the solvent has been neglected and the multiple states from the electronic repulsion and spin–orbital coupling interactions have not been taken into account in the course of the calculation. The calculation showed that the HOMO was mainly composed of the orbitals of dmid and d(Zn) atomic orbitals and the LUMO was almost exclusively orbitals of phen (Figs. 3 and 4). Like other related complexes with dithiolate and diimine ligands [16], the high-energy bands at 266 nm for **1** and **2** are assigned to the intraligand diimine transition [π (phen)–π* (phen)] and lower energy bands 300-400 nm likely involve a ligand-to-ligand charge transfer [LL′CT, π (dmid)–π* (phen)] character and the LL′CT dominates for **1** and **2**. These assignments are supported by the calculation of electronic absorption spectra.

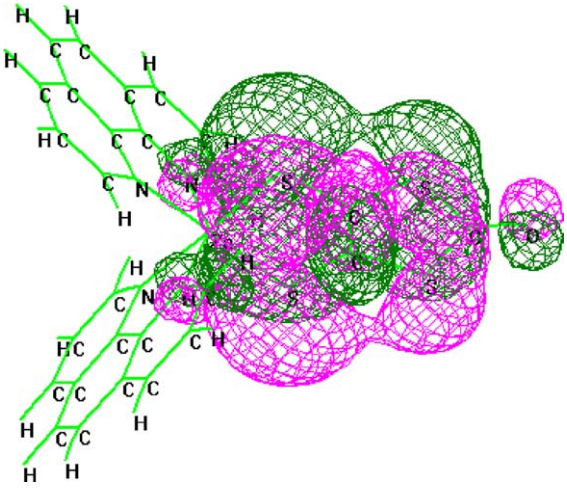

Fig. 3. HOMO, 33*b*, −7.1326 eV.

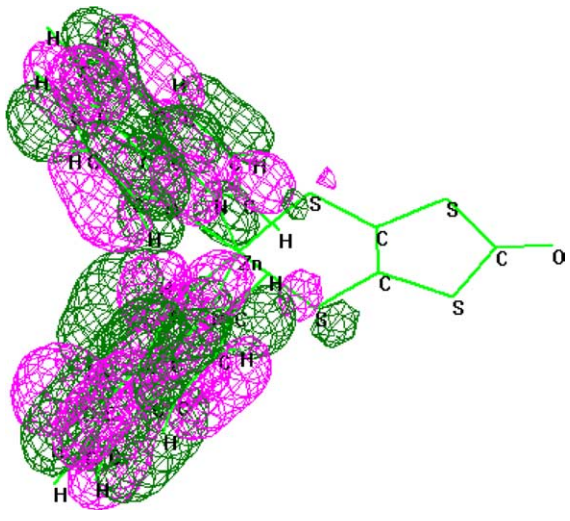

Fig. 4. LUMO, 34*b*, −1.9673 eV.

3.5. Fluorescence spectra

The fluorescent emission spectra of complexes **1** and **2** in solutions are showed in Figs. 5–7. The emissions at 417 and 435 nm in DMSO, at 407 (shoulder) and 428 nm in DMF, at 408 (shoulder) and 422.5 nm in pyridine were observed for **1**. Under the same conditions, complex **2** exhibited almost the same fluorescent emission spectrum as those of **1**, except for lower intensity. The intensity of emissions of **1** and **2** was much higher in pyridine than in DMF and in DMSO. The excitation and emission spectrum shifted to longer wavelength as the polarity of the solvent increased (DMSO > DMF > pyridine) [14]. Since the excitation wavelengths were at 351–390 nm, the emissions spectrum of **1** and **2** can be assigned to the π^*–π transition of the phen ligand to dmid ligand according to the calculation of the electronic absorption spectra. The emission behaviors of the complexes in the solid state (Fig. 8) differed from those in solution. The emissions at 484 and 538 nm were observed for both of them in the solid state. Compared with those in solution, the emissions showed large red-shifts, which were ascribed to the exciplex emissions [17]. The large red-shift revealed the strong interactions between molecules, resulting from the strong π–π stacking of the aromatic rings (Fig. 2).

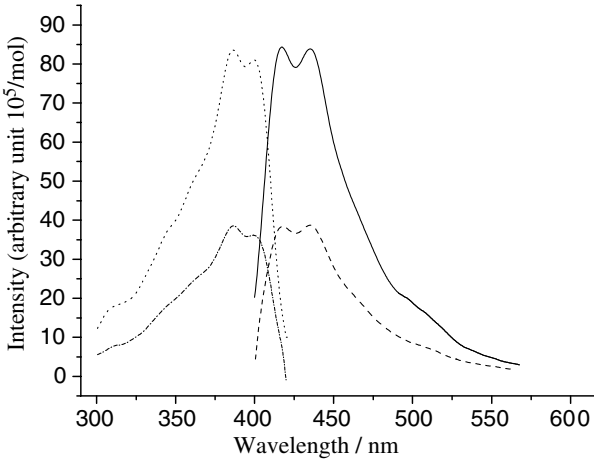

Fig. 5. Fluorescence spectra of **1** and **2** in DMSO. $Zn(dmid)(phen)_2$: – Em with Ex = 386.5 nm, ··· Ex for Em = 435 nm, Ex = 386.5 nm, Em = 417 nm, 435 (nm); $Cd(dmid)(phen)_2$: --- Em with Ex = 386.5 nm, –·– Ex for Em = 435 nm (Ex = 386.5 nm, Em = 417 nm, 435 nm).

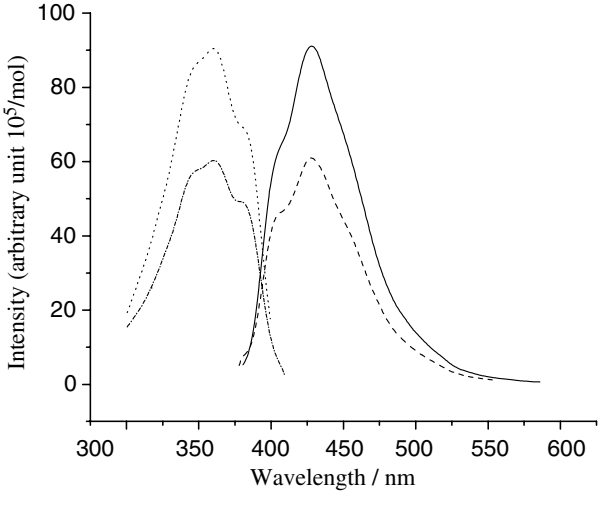

Fig. 6. Fluorescence spectra of **1** and **2** in DMF. $Zn(dmid)(phen)_2$: – Em with Ex = 360 nm, ··· Ex for Em = 428 nm, [Ex = 360 nm, Em = 407 (shoulder) nm, 428 nm]; $Cd(dmid)(phen)_2$: --- Em with Ex = 360 nm, –·– Ex for Em = 428 nm, (Ex = 360 nm, Em = 407 (shoulder) nm, 428 nm).

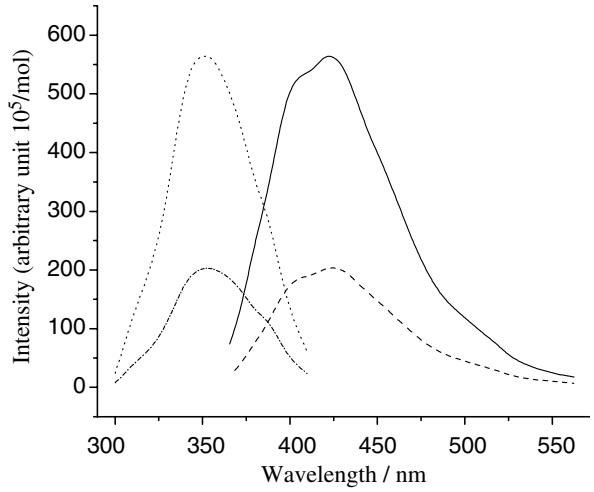

Fig. 7. Fluorescence spectra of **1** and **2** in pyridine. $Zn(dmid)(phen)_2$: – Em with Ex = 351 nm, ··· Ex for Em = 422.5 nm,[Ex = 351 nm, Em = 408 (shoulder) nm, 422.5 nm]; $Cd(dmid)(phen)_2$: --- Em with Ex = 353 nm, –·– Ex for Em = 424.5 nm, [Ex = 353 nm, Em = 410 (shoulder) nm, 424.5 nm].

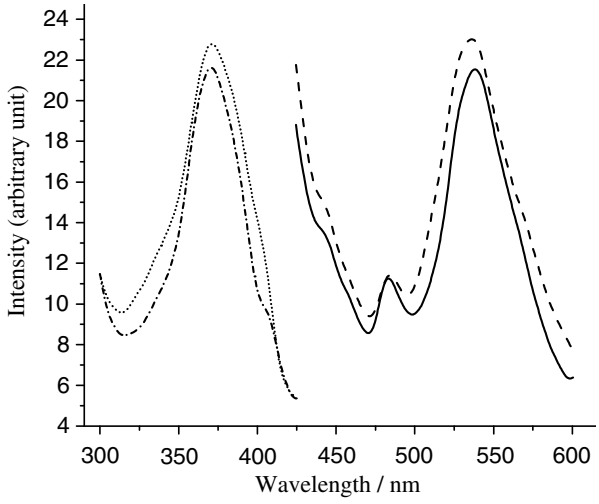

Fig. 8. Solid fluorescence spectra of **1** and **2**. $Zn(dmid)(phen)_2$: – Em with Ex = 370.5 nm, ··· Ex for Em = 539.5 nm, (Ex = 370.5 nm, Em = 539.5 nm, 483.5 nm); $Cd(dmid)(phen)_2$: --- Em with Ex = 371 nm, –·– Ex for Em = 536 nm, (Ex = 371 nm, Em = 536 nm, 484.5 nm).

4. Supplementary material

Crystallographic data for the structural analyses have been deposited with the Cambridge Crystallographic Data Center (CCDC No. 206969 for Zn(dmid)(phen)$_2$, CCDC No. 206970 for Cd(dmid)(phen)$_2$). That information is available from the Director, CCDC, 12 Union Road, Cambridge CB2 1EZ, UK (fax: +44-1223-336-033; e-mail: deposit@ccdc.cam.ac.uk or http://www.ccdc.cam.ac.uk).

Acknowledgements

We gratefully acknowledge the financial support from the National Nature Science Foundation of China (Nos. 29833090 and 29771025).

References

[1] N. Roertson, L. Cronin, Coord. Chem. Rev. 227 (2002) 93.
[2] M. Hissler, J.E. McGarrah, W.B. Connick, D.K. Geiger, S.D. Curmmings, R. Eisenberg, Coord. Chem. Rev. 208 (2000) 115.
[3] E.P. Anthony, R.-M. Olk, Coord. Chem. Rev. 188 (1999) 211.
[4] I. Hawkins, R.A. Clark, C.E. Hainwright, A.E. Underhill, Mol. Cryst. Liq. Cryst. 181 (1990) 209.
[5] S.G. Liu, P.J. Wu, Y.Q. Liu, D.B. Zhu, Mol. Cryst. Liq. Cryst. 275 (1996) 211.
[6] S. Ikegawa, T. Nogami, Y. Shirota, Bull. Chem. Soc. Jpn. 63 (1990) 262.
[7] M.J. Frisch, G.W. Trucks, H.B. Schlegel, G.E. Scuseria, M.A. Robb, J.R. Cheeseman, V.G. Zakrzewski, J.A. Montgomery, J.R.E. Stratmann, J.C. Burant, S. Dapprich, J.M. Millam, A.D. Daniels, K.N. Kudin, M.C. Strain, O. Farkas, J. Tomasi, V. Barone, M. Cossi, R. Cammi, B. Mennucci, C. Pomelli, C. Adamo, S. Clifford, J. Ochterski, G.A. Petersson, P.Y. Ayala, Q. Cui, K. Morokuma, D.K. Malick, A.D. Rabuck, K. Raghavachari, J.B. Foresman, J. Cioslowski, J.V. Ortiz, B.B. Stefanov, G. Liu, A. Liashenko, P. Piskorz, I. Komaromi, R. Gomperts, R.L. Martin, D.J. Fox, T. Keith, M.A. Al-Laham, C.Y. Peng, A. Nanayakkara, C.Gonzalez, M. Challacombe, P.M.W. Gill, B. Johnson, W. Chen, M.W. Wong, J.L. Andres, C. Gonzalez, M. Head-Gordon, E.S. Replogle, J.A. Pople, Gaussian, Inc., Pittsburgh, PA, 1998.
[8] HYPERCHEM. Release 7.01 for Windows, Molecular Modelling System, Hypercube, Inc., 2002.
[9] C.A. Hunter, J.K. Sanders, J. Am. Chem. Soc. 112 (1990) 5525.
[10] M. Fourmigue, B. Domercq, I.V. Jourdain, P. Molinie, F. Guyon, J. Amaudrut, Chem. Eur. J. 4 (1998) 1714.
[11] A.S. Batsanov, M.R. Bryce, A.S. Dhindsa, J.A.K. Howard, A.E. Underhill, Polyhedron 20 (2001) 537.
[12] L.-F. Yang, Z.-H. Peng, X.-M. Ren, G.-Z. Cheng, P. Cai, Spectrochim. Acta A 57 (2001) 2745.
[13] A.A. Schilt, K. Fritsch, J. Inorg. Nucl. Chem. 28 (1966) 2677.
[14] N.S. Isaacs, Physical Organic Chemistry, Longman Scientific & Technical, London, 1990.
[15] A. Vogler, H. Kunkely, J. Am. Chem. Soc. 103 (1981) 1559.
[16] J.A. Zuleta, J.M. Bevilacqua, D.M. Proserpio, P.D. Harvey, R. Eisenberg, Inorg. Chem. 31 (1992) 2396.
[17] N. Tamai, T. Yamazaki, I. Yamazaki, J. Phys. Chem. 91 (1987) 841.

Available online at www.sciencedirect.com
SCIENCE DIRECT®
Polyhedron 23 (2004) 1709–1717
POLYHEDRON
www.elsevier.com/locate/poly

Copper amino-acid complexes – towards encapsulated metal centres

Diane L. Stone, David K. Smith *, Adrian C. Whitwood

Department of Chemistry, University of York, Heslington, York, YO10 5DD, UK

Received 22 January 2004; accepted 2 April 2004
Available online 27 April 2004

Abstract

This article reports the synthesis of two novel amino-acid derivatives in which the side chain of glutamic acid (Glu) is coupled with different amines – *tert*-butylamine (ligand **A**) or a first generation 'Newkome' type dendron (ligand **B**). Consequently, ligand **B** possesses a bulkier branch than ligand **A**. Ligands **A** and **B** bind Cu^{2+} ions in solution, generating copper complexes **A–Cu** ($M_r = 508$) and **B–Cu** ($M_r = 1077$). These complexes were fully characterised and, in particular, have been investigated by electrochemical and electron spin resonance techniques to determine the extent of encapsulation of the copper ions. There were significant differences between the two complexes, indicating that Cu^{2+} may be more deeply encapsulated by ligand **B** and hence less able to interact with its surroundings. This indicates that metal ions can be sensitive reporters of even relatively small amounts of organic functionality, and emphasises the important role which protein superstructures can play in modulating the function of active metal ions.
© 2004 Elsevier Ltd. All rights reserved.

Keywords: Amino acid; Copper; Dendrimers; Electrochemistry; Electron spin resonance; Ligand

1. Introduction

Metal ions play a dominant role in controlling the behaviour of many biologically important macromolecules [1]. By changing the metal ion, biological systems are able to achieve a wide range of different functions. However, it is also clear that a metal ion alone is not sufficient to achieve the required range of functions. It is only by carefully tuning the ligands employed, and the surrounding organic functional groups within the protein superstructure that biology can achieve selective function. Many active sites are deeply encapsulated within protein and enzyme superstructures, and this has profound effects on factors such as the microenvironmental dielectric constant experienced by the metal and its accessibility to different substrates [2].

There is currently great interest in mimicking biological systems [3], and recently, encapsulation of an active unit has been probed using dendritic molecules, in which a branched superstructure surrounds a central metal ion, with the effect of this on function being investigated [4]. There have, for example, been many studies of the effect of a dendritic microenvironment on the optical [5], redox [6–8] or catalytic [9] properties of an encapsulated active site. On encapsulation of a redox active unit, it is well-known that the electron transfer kinetics are significantly slower – a feature also observed in redox-active proteins. Furthermore, cytochromes and their dendritic mimics indicate that the encapsulated micro-environment is significantly different to that of the surrounding bulk solvent/electrolyte, leading to modification of the redox potential of the metal ion [7].

Copper complexes have considerable biological importance, but encapsulated copper centres are less well studied than encapsulated iron. Aida and co-workers reported a dendrimer capable of ligating a copper ion at its focal point, and showed that this dendrimer could react with oxygen to form a bridged bis-copper complex [10]. Multiple copper ions bound within a spherical dendrimer have also been used for O_2 binding [11]. Chow and co-workers [12] used a dendritic bis(oxazoline) ligand to bind to copper triflate and then used the

* Corresponding author. Tel.: +44-0-1904-434181; fax: +44-0-1904-432516.
E-mail address: dks3@york.ac.uk (D.K. Smith).

0277-5387/$ - see front matter © 2004 Elsevier Ltd. All rights reserved.
doi:10.1016/j.poly.2004.04.001

complex in Diels–Alder catalysis, while recently, functionalised bipyridine and phenanthroline ligands have been used to achieve effective encapsulation of copper ions and generate a wide range of interesting molecular architectures [13].

The coordination of amino acids to metal ions is well-known [14], with strong binding to transition metals occurring via a chelate binding mode involving both carboxylate and amine groups (Fig. 1). We therefore reasoned that the side chain of an amino acid offered a suitable point to attach functionality capable of encapsulating the bound metal ion. For this reason, we became interested in the development of synthetic amino-acid derivatives with bulky side chains. Whilst this work was in progress, Krishna and Jayaraman [15] reported some different modified amino-acid ligands and described their ability to bind and encapsulate cobalt ions.

In this paper, we report amino-acid derivatives functionalised with small, flexible branches, and illustrate their ability to bind Cu^{2+} ions. Using electrochemical and electron spin resonance (ESR) methods, we have investigated the metal complexes in order to probe the degree of isolation of the Cu^{2+} ion. We report that the copper ions were surprisingly sensitive reporter units, with their properties being modified even by the small amounts of branching used in this case. These preliminary results have significance for biological chemists interested in the role played by the organic superstructure in shielding the active sites of metalloproteins and enzymes.

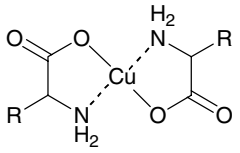

Fig. 1. Amino acids bind to copper(II) in a chelate binding mode.

2. Results and discussion

2.1. Synthesis and characterisation of ligands *A* and *B*

Ligand **A** was prepared using standard protecting group and peptide coupling methodology (Scheme 1). The side chain of *N*-Boc, *tert*-butyl ester protected glutamic acid (**1**) was coupled with *tert*-butylamine (**2**) using 1,3-dicyclohexylcarbodiiimide (DCC), 1-hydroxybenzotriazole (HOBt) and triethylamine in CH_2Cl_2 to yield compound **3** After purification of the product by flash chromatography on silica, the product was obtained in 50% yield. The amino-acid protecting groups were then removed simultaneously. Previous literature indicated that a mild organic acid such as CF_3COOH should be sufficient, but even after stirring for 18 h the reaction was incomplete. Harsher conditions (45% HBr in acetic acid) were therefore employed and after stirring for 2 min, deprotection was complete in near quantitative yield to provide ligand **A**. This ligand was used for the synthesis of copper(II) complexes without isolation (although NMR characterisation of the ligand was achieved by performing the deprotection on one occasion in D_2O).

Initially, the synthesis of ligand **B** was attempted using the same approach (Scheme 1). The DCC/HOBt mediated coupling of first generation 'Newkome' type dendritic branch **4** to the protected glutamic acid **1** was very successful, providing compound **5** in 93% yield. Once again, however, CF_3COOH would not fully deprotect the amino-acid group, even on heating (the Boc group was rapidly removed but the *t*-butyl ester would not come off). Unfortunately, the alternative conditions

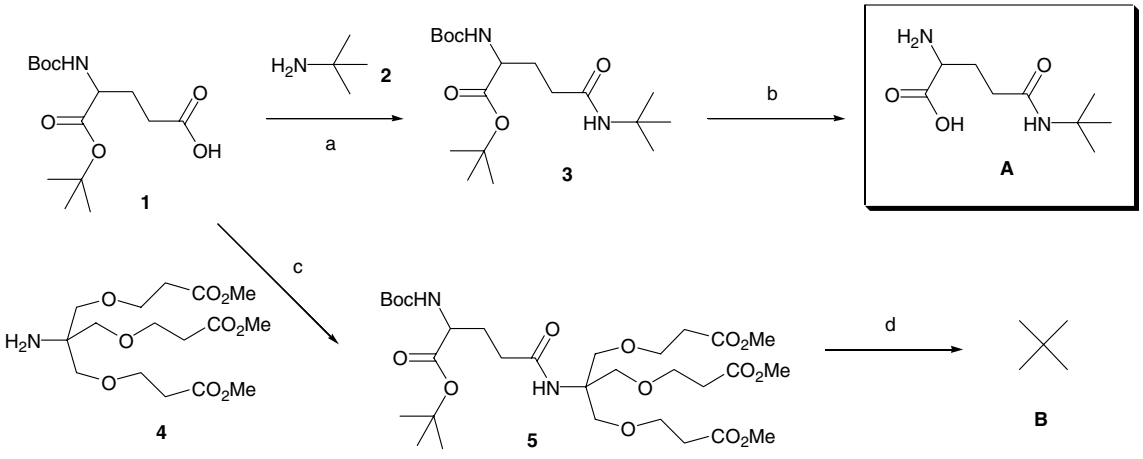

Scheme 1. Synthesis of **A** and attempted synthesis of **B** using Boc/*tert*-butyl ester protecting group methodology. Reagents and conditions: (a) DCC, HOBt, NEt_3, CH_2Cl_2, 50%, (b) HBr/CH_3COOH, 2 min, quant., (c) DCC, HOBt, NEt_3, CH_2Cl_2, 93%, (d) HBr/CH_3COOH, 2 min, 0%.

using HBr/CH_3COOH were too harsh, and NMR analysis of the product indicated that the methyl ester units on the branch had also been removed by acid catalysed hydrolysis (peak at $\delta = 3.65$ ppm disappeared).

An alternative strategy was therefore developed in which the amino-acid protecting groups were removed non-hydrolytically. Consequently, *N*-CBz, benzyl ester protected glutamic acid (**6**) was used as the starting material (Scheme 2). DCC/HOBt coupling of this with first generation 'Newkome' type branch **4** was performed and product **7** was purified using gel permeation chromatography (Biobeads SX-1, CH_2Cl_2). This compound was obtained in 60% yield and fully characterised. Simultaneous deprotection of the two amino-acid groups was then attempted using Pd/C under H_2 in ethanol. The reaction had to be stopped after just 30 min, because over longer time-scales, mass spectral and NMR analysis indicated that (unusually) the benzyl ester had been transesterified to an ethyl ester. We do not have a good explanation for this side-reaction, which is unexpected (EtOH is indeed normally the solvent of choice for the deprotection of benzyl esters). Nonetheless, by employing a 30-min reaction time, ligand **B** could be obtained in 93% yield and was fully characterised.

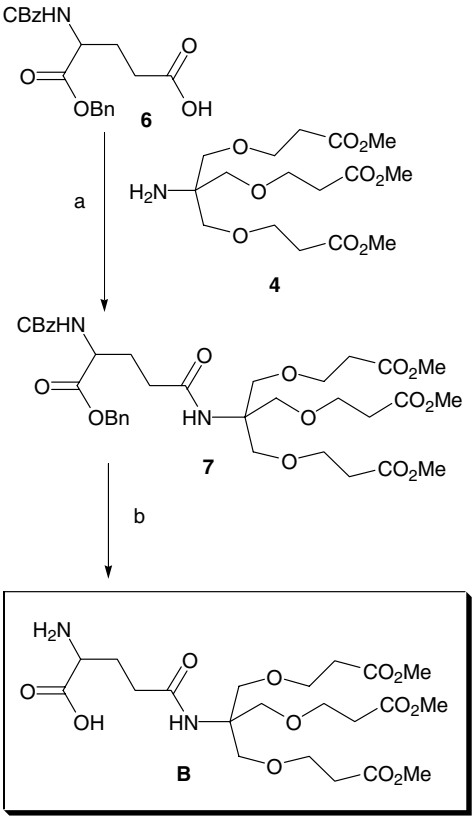

Scheme 2. Synthesis of **B** using CBz/benzyl ester protecting group methodology. Reagents and conditions: (a) DCC, HOBt, NEt_3, CH_2Cl_2, 60%, (b) H_2, 10% Pd/C, EtOH, 30 min, quant.

2.2. Synthesis and characterisation of copper complexes *A–Cu* and *B–Cu*

The usual literature technique for the preparation of copper complexes is to dissolve both the ligand and a copper salt in water, and to encourage complexation by the addition of base. This is normally followed by spontaneous precipitation or recrystallisation of the complex. For the synthesis of **A–Cu**, ligand **A** was dissolved in water which had been basified with 10% NaOH. Copper carbonate was added and the mixture stirred for 2 h. On cooling, a light blue precipitate of complex **A–Cu** was obtained in 45% yield (see Fig. 2).

The complex was analysed using electrospray mass spectrometry (ESMS) and a peak corresponding to $[M + Na]^+$ was observed at m/z 488, with an isotope peak at m/z 490. A peak was also observed at m/z 953, corresponding to $[2M + Na]^+$, with isotope peaks at m/z 955 and 957. These higher mass peaks were not,

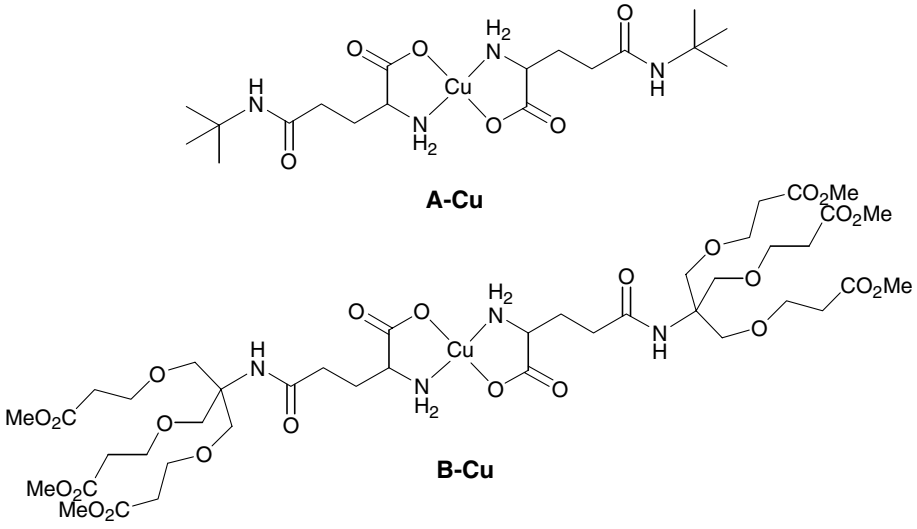

Fig. 2. Structures of complexes **A–Cu** and **B–Cu**.

however, observed by MALDI-TOF mass spectrometry. These peaks could indicate dimerisation of the complex in solution, or could alternatively be an artefact of the electrospray ionisation process – aggregation with Na^+ ions in ESMS is not uncommon. Infra red spectroscopy of the complex showed the expected ligand peaks. Elemental analysis provided a good match for the composition of the complex.

Initial attempts to synthesise complex **B–Cu** used the procedure described above. Although the reaction changed colour (from pale green to deep blue) indicating complexation may have occurred, no precipitate was formed on cooling. Attempts at recrystallisation from the liquor failed and the procedure was therefore modified. Copper carbonate and ligand **2** were dissolved in methanol and one equivalent of solid sodium hydroxide (relative to the ligand) was added to the mixture. The mixture was stirred for 6 days and a gradual colour change was observed. The product was purified by gel permeation chromatography (Sephadex LH-20, methanol). A blue band was collected from the column and evaporated to give a blue oil in 19% yield.

Complex **B–Cu** was characterised by electrospray mass spectrometry, with the major peak in the mass spectrum being observed at m/z 1100 $[M + Na]^+$, and the correct intensity isotope peak being observed at m/z 1102. Peaks corresponding to $[2M + Na]^+$ were not observed in this case. Infra red spectroscopy of the complex showed the expected ligand peaks. Elemental analysis provided a reasonable match for the composition of the complex.

2.3. Electrochemistry of copper complexes *A–Cu* and *B–Cu*

As stated in the introduction, electrochemistry is a widely used method for probing the microenvironment experienced by encapsulated redox active units [6–8]. Copper(II) is a biologically important redox active metal, with the Cu(II)/Cu(I) redox couple being implicated in the function of a wide range of enzymes. Furthermore, Cu(II) can also be oxidised to Cu(III) under very oxidising conditions. The electrochemical properties of complexes **A–Cu** and **B–Cu** were therefore investigated using cyclic voltammetry in dimethylformamide (DMF) solution.

Complex **A–Cu** was investigated at different scan rates (Fig. 3). Initially the solution was swept in the reducing direction and then subsequently swept to oxidising potentials. In each case the same components were observed in the cyclic voltammogram. The reduction peak which is tentatively assigned to the Cu(II) to Cu(I) transition was observed at a peak potential ca. −990 mV. Re-oxidation was then observed at ca. −140 mV. The large peak to peak separation and the broad reduction and oxidation peaks indicate a quasi-

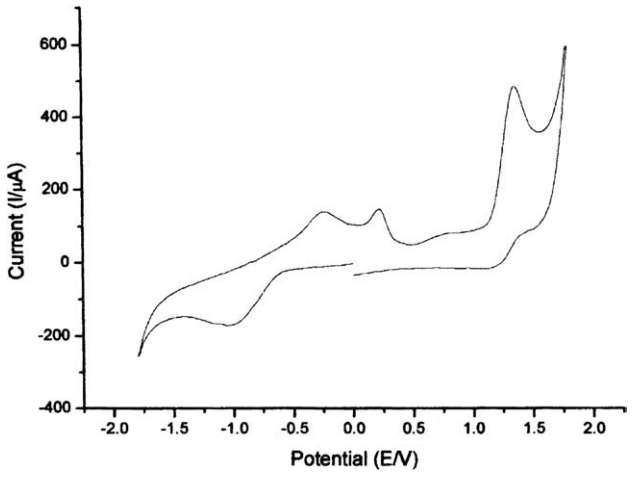

Fig. 3. Cyclic voltammogram of complex **A–Cu** (2 mM) in DMF solution with a supporting electrolyte of 0.1 M $[Bu_4N]^+[BF_4]^-$. Scan rate = 200 mV s^{-1}.

reversible process. On continued oxidation (scan rate: 200 mV s^{-1}) a sharp peak was observed at +210 mV, probably a stripping peak. Stripping peaks are typically observed following electrodeposition of metals (e.g., Cu(0) from disproportionation of decomplexed Cu(I) ion). In fact, on decreasing the scan rate to 50 mV s^{-1} the relative peak current of this peak increased significantly, while on increasing the scan rate to 500 mV s^{-1}, this stripping peak disappeared, in agreement with the above analysis. On continuing the sweep in the oxidative direction an oxidation peak was observed at ca. 1310 mV. This could correspond to the oxidation of Cu(II) to Cu(III), however, given the peak height, it is possible that ligand oxidation is also occurring. This process was irreversible. It is well-known that very robust ligands would be required if Cu(III) were to be observed as a stable species [16].

Complex **B–Cu** was then investigated using cyclic voltammetry under the same conditions of solvent and scan rate (Fig. 4). Interestingly, the Cu(II)/Cu(I) couple was significantly more reversible than for **A–Cu**. At a scan rate of 50 mV s^{-1}, the peak to peak separation was only 150 mV (rather than ca. 850 mV as observed for **A–Cu**). Furthermore, the stripping peak (observed for **A–Cu** at +210 mV) was absent. These observations indicate that the steric bulk of ligand **B** enhances the stability of the reduced complex, hence preventing the release of Cu(I) ion and its subsequent disproportionation. Complex **B–Cu** has an additional oxidation peak at ca. 1.0 V, which can tentatively be assigned to oxidation of the ligand framework. The other oxidation peak was now observed at +1370 mV, which compares with +1310 mV for complex **A–Cu**. This might reflect differences between the oxidation of the ligand structures in these two complexes although it may also indicate that the oxidation of Cu(II) to Cu(III) is thermodynamically more

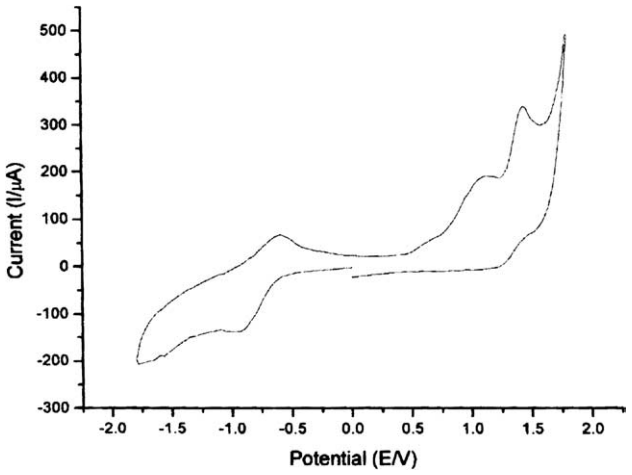

Fig. 4. Cyclic voltammogram of complex **B–Cu** (2 mM) in DMF solution with a supporting electrolyte of 0.1 M $[Bu_4N]^+[BF_4]^-$. Scan rate = 200 mV s^{-1}.

difficult for **B–Cu** than **A–Cu**. This would be in agreement with our previous observations of dendritic effects which have indicated that charge build up is disfavoured when the redox active unit is encapsulated within an organic shell, and is hence more distant from bulk solvent/electrolyte [8a,8b]. Interestingly, the comparison between **A–Cu** and **B–Cu** indicates that even relatively small amounts of organic functionalisation appear to have significant effects on the kinetics and thermodynamics of redox processes.

2.4. Electron spin resonance of copper complexes *A–Cu* and *B–Cu*

As a d^9 paramagnetic species, copper(II) is appropriate for characterisation by ESR experiments. This technique has frequently been applied for the analysis of copper complexes as well as copper ions in biological systems [17], and is a useful method of determining the geometry of a copper centre when X-ray quality crystals cannot be obtained. For a mononuclear copper(II) complex, the nuclear spin $(I = 3/2)$ means that four lines would be expected in the hyperfine splitting pattern in solution. In the case of the actual axial symmetry, the spectrum is characterised by $a_{\|}$ (G), $a_{\perp}$ (G), $\langle a \rangle$ (G), $g_{\perp}$, $g_{\|}$, $\langle g \rangle$ values, which can be obtained from the splitting pattern of the spectrum and compared with values for complexes of known geometry in order to define the composition of the equatorial coordination of the complex [18a].

ESR experiments were performed on 1 mM frozen solution of the complexes in methanol. The ESR spectrum of **A–Cu** shows the expected approximate four line hyperfine splitting (Fig. 5) The values derived from the analysis of this spectrum were $g_{\|} = 2.258$, $a = 170$ G and $g_{\perp} = 2.063$. These values are consistent with complex **A–Cu** having Jahn-Teller distorted octahedral geometry. It would be expected that the amino-acid ligands will be bound in the equatorial positions in a chelate mode, whilst there will be two more distant axial ligands.

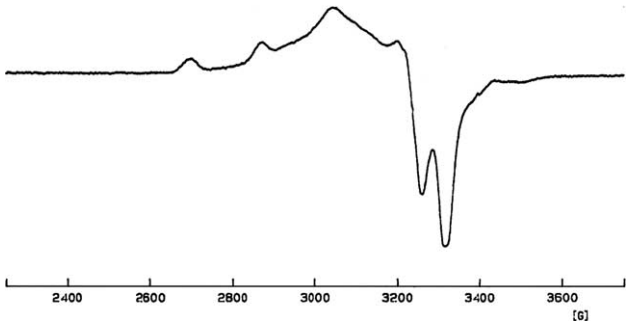

Fig. 5. ESR spectrum of complex **A–Cu** (1 mM) in frozen methanol solution.

The ESR spectrum of complex **B–Cu** was then measured (Fig. 6). The values derived from the analysis of this spectrum were $g_{\|} = 2.260$, $a = 171$ G and $g_{\perp} = 2.057$. These values are very similar to those obtained for **A–Cu** and indicate once again, an equivalent Jahn-Teller distorted octahedral geometry. This indicates that the additional steric hindrance of ligand **B** does not manifest itself through a change in coordination geometry.

Most interesting, however, was the fact that the spectrum of **B–Cu** was much sharper than that of **A–Cu**. The broadening in the ESR spectrum of **A–Cu** could possibly be caused by interaction between Cu^{2+} ions. This ESR evidence indicates that interaction between copper(II) ions may be occurring for **A–Cu**. It is well-known, for example, that carboxylate ligands can act as bridging ligands connecting two copper centres [18]. On the other hand, for complex **B–Cu**, where a more ideal ESR sepctrum with sharp well-defined peaks is observed, the copper centre will be more shielded from other copper nuclei by the ligand bulk, hence preventing copper–copper interactions.

The mediation of copper–copper interactions is of key importance in biological chemistry [19], and these

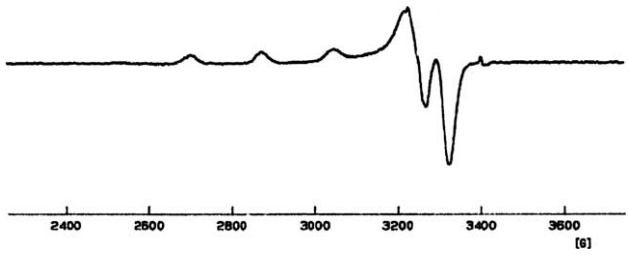

Fig. 6. ESR spectrum of complex **B–Cu** (1 mM) in frozen methanol solution.

results indicate that relatively small amounts of steric bulk (complex **B–Cu** only has approximately twice the molecular mass of complex **A–Cu**) can have a marked effect on the isolation of metal ions. The use of an organic shell to protect copper ions in this way is an important strategy in biological chemistry, and it appears that it is possible to mimic such an effect in a relatively simple manner. Work is now ongoing to extend the extent of functionalisation of these amino-acid ligands to achieve even more effective encapsulation of copper ions.

3. Conclusions

This article describes the synthesis of two novel amino-acid ligands and their characterisation. Furthermore, these ligands have been used in the assembly of two novel copper(II) complexes with different degrees of steric bulk at the periphery. These complexes have been fully characterised and subsequently investigated using electrochemical and ESR methods. The results indicate that even for these relatively small molecules, the differential encapsulation experienced by the metal ion in the two complexes is significant. This emphasises the important role which an organic superstructure can play (even in relatively small quantities) to shield and modify the properties of metal ions within metalloproteins and enzymes. Modelling the role played by the organic superstructure of metalloproteins remains a real challenge for bioinorganic chemists in the attempt to mimic the remarkable levels of function which can be obtained by highly evolved natural systems.

4. Experimental

4.1. Materials and methods

All ^{1}H and ^{13}C NMR spectra were determined either on a Jeol-E270 (270 MHz) or a Bruker AMX 500 (500 MHz) instrument, according to requirements and referenced to residual solvent. Neat IR, carried out on oil-like compounds, were measured on a Mattson Genesis Series FTIR spectrometer, whereas solid IR using KBr disks were performed using a Mattson Sirius Research FTIR spectrometer. Electrospray mass spectrometry was carried out on a Finnigan LCQ. MALDI-TOF mass spectrometry was performed at Central Science Laboratories, York. Silica column chromatography was carried out using silica gel provided by Fluorochem Ltd. (35–70 μm). Thin layer chromatography was performed on commercially available Merck aluminium backed silica plates. Preparative gel permeation chromatography was carried out using a 2 m glass column packed with Biobeads SX-1 (Biorad) eluted with CH_2Cl_2 or using standard (ca. 50 cm) columns packed with Sephadex LH-20 and eluted using MeOH. The electrochemical studies were carried out on an EG & G Princeton Applied Research potentiostat/galvanostat model 273 with a standard 3 electrode configuration, consisting of platinum working (0.5 mm diameter disk) and counter electrodes and an Ag/AgCl reference electrode. Each compound was studied at a concentration of 2 mM in a supporting electrolyte of 0.1 M $[Bu_4N]^+[BF_4]^-$ using scan rates of 50–500 mV s^{-1}. ESR experiments were performed using a Bruker ESP300 spectrometer. Elemental analysis was performed by the microanalytical lab at The University of Manchester.

4.2. Synthesis and characterisation

All protected amino acids were purchased commercially, and first generation 'Newkome' type branches were prepared according to literature methodology [20].

4.2.1. *N-(tert-Butoxycarbonyl)-L-glutamic acid 1-tert-butyl ester, 5-tert-butylamide, compound **3***

N-(*tert*-Butoxycarbonyl)-L-glutamic acid 1-*tert*-butyl ester (1.0 g, 3.3 mmol), DCC (0.68 g, 3.3 mmol) and HOBt (0.44 g, 3.3 mmol) were dissolved in dry CH_2Cl_2 (10 ml) and stirred at room temperature for 10 min. Then NEt_3 (1 ml, 7.18 mmol) and *tert*-butylamine (0.64 g, 3.3 mmol) were added as a mixture in dry CH_2Cl_2 (5 ml). The reaction was stirred under N_2 at room temperature for 2 d. After this period, CH_2Cl_2 (30 ml) was added to the mixture, which was then filtered into a separating funnel, and washed with sat. aq. $NaHCO_3$ (2×50 ml) and H_2O (2×50 ml). The organic phase was dried over $MgSO_4$, filtered and evaporated to give the crude product. This was purified by silica gel chromatography (CH_2Cl_2:MeOH, 98:2) to yield the pure product (0.591 g, 1.65 mmol, 50%). White solid; R_f 0.45 (CH_2Cl_2–MeOH 98:2); ν_{max} (KBr disk) 3338 m (NH), 2979 m and 2933 m (alkyl), 1721 m, and 1655 m (C=O), 1543 m, 1456 m, 1366 m, 1277 m and 1153 m, 1051 m, 848 s; $\delta_H(CDCl_3)$ 1.35 (9H, s, $NHC(CH_3)_3$), 1.44 and 1.46 (18H, 2s, $OC(CH_3)_3$), 1.86 (2H, m, CH_2CH_2CO), 2.15 (2H, m, CH_2CH_2CO), 4.13 (1H, t, $J = 8.5$, $CHCH_2$), 5.16 and 5.20 (1H, d, $J = 10.0$, $NHCHCH_2$), 5.80 (1H, bs, $NHC(CH_3)_3$); $\delta_C(CDCl_3)$ 28.7, 28.3, 28.0 (CCH_3), 29.3 (CH_2CH_2CONH), 33.8 (CH_2CONH), 51.2 ($NHC(CH_3)_3$), 53.6 (NHCH), 79.8 and 82.1 ($CO_2C(CH_3)_3$), 155.8 (CONH), 171.5 and 171.4 ($CO_2C(CH_3)_3$); m/z (Electrospray) $[M + Na]^+$ requires 381, found 381 (100%), 382 (19%); HRMS (CI+) ($C_{18}H_{34}N_2O_5$): found 359.2552, calculated 359.2546.

4.2.2. *L-Glutamic acid 5-tert-butylamide, ligand **A***

N-(*tert*-Butoxycarbonyl)-L-glutamic acid 1-*tert*-butyl ester, 5-*tert*-butylamide (**3**) was dissolved in hydrobromic acid (45% in acetic acid) and stirred at r.t. for 2 min.

The mixture was then added to ice water (20 ml), stirred for 10 min and evaporated to dryness. The resulting product was used without further purification for complex formation. R_f 0.0 (CH_2Cl_2–MeOH 90:10); $\delta_H(CD_3OD)$ 1.33 (9H, s, NHC(CH_3)$_3$), 2.17 (2H, m, CHCH_2CH$_2$), 2.47 (2H, t, $J = 7.0$, CHCH$_2$CH_2), 4.06 (1H, m, CHCH$_2$CH$_2$); $\delta_C(CD_3OD)$ 28.8 (C(CH_3)$_3$), 30.2 (CHCH_2), 33.2 (CH_2CONH), 52.3 (C(CH$_3$)$_3$), 53.6 (CHCH$_2$), 170.6 (CONH), 173.5 (CO_2H); m/z (Electrospray) $[M + H]^+$ requires 203, found 203 (100%).

4.2.3. Compound 5

N-(*tert*-Butoxycarbonyl)-L-glutamic acid 1-*tert*-butyl ester (**1**) (0.72 g, 2.37 mmol) was dissolved in dry CH_2Cl_2 (5 ml) then DCC (0.49 g, 2.37 mmol) and HOBt (0.32 g, 2.37 mmol) were added. The reaction was stirred under N_2 at r.t. for 5 min. Next, NEt_3 (0.5 ml, 3.59 mmol) and the first generation 'Newkome' type branch **2** (0.9 g, 2.37 mmol) in dry CH_2Cl_2 (5 ml) were added, and the mixture was stirred at r.t. under N_2 for 2 d. After this period, CH_2Cl_2 (30 ml) was added to the mixture, which was then filtered into a separating funnel and washed with sat. aq. $NaHCO_3$ (2×50 ml) and H_2O (2×50 ml). The organic phase was dried over $MgSO_4$, filtered and evaporated to give product **5** (1.47 g, 2.21 mmol, 93%). Colourless oil; R_f 0.61 (CH_2Cl_2–MeOH 90:10); ν_{max} (neat) 3370 w (NH), 2977 m and 2897 m (alkyl), 1740 s and 1675 s (C=O), 1518 s, 1438 s, 1367 s, 1254 s, 1175 s, 1112 s, 848 w; $\delta_H(CDCl_3)$ 1.41 and 1.43 (18H, 2s, C(CH_3)$_3$), 1.66 (2H, m, CHCH_2CH$_2$CO), 1.87 (2H, m, CHCH$_2$CH_2CO), 2.53 (6H, t, $J = 6.5$, CH_2CO$_2$Me), 3.67 (21H, m, CH_2OCH_2 and CO$_2$CH_3), 4.10 (1H, m, CHCH$_2$), 6.16 (1H, s, CONH); $\delta_C(CDCl_3)$ 27.9, 28.3 (OC(CH_3)$_3$), 28.7 (CHCH_2), 33.3 and 34.7 (CH_2CONH and CH_2CO_2), 53.8 (CH), 57.7 (CO_2CH_3), 59.7 (NHC(CH$_2$)$_3$), 66.7, 69.1 (CH_2OCH_2), 79.5, 81.8 (OC(CH$_3$)$_3$), 155.7 (CONH), 171.6, 172.1, 172.3 (CO_2); *m/z* (Electrospray) $[M + Na]^+$ requires 687, found 687 (100%), 688 (32%); HRMS (FAB) ($C_{30}H_{52}N_2O_{14}$): found 687.3313, calculated 687.3316.

4.2.4. Compound 7

N-(Benzyloxycarbonyl)-L-glutamic acid 1-benzyl ester (**6**) (1.00 g, 2.7 mmol) was dissolved in dry THF (10 ml), followed by the 'Newkome' type branch **4** (1.50 g, 4.0 mmol) in dry THF (10 ml). To it was added NEt_3 (1 ml, 7.0 mmol) followed by DCC (0.84 g, 4.1 mmol) and HOBt (0.54 g, 4.1 mmol) in dry THF (5 ml). The reaction was stirred under N_2 at r.t. for 72 h. The solvent was removed by evaporation and CH_2Cl_2 (50 ml) was added. The mixture was filtered, then washed with saturated aqueous $NaHCO_3$ (2×50 ml) and H_2O (2×50 ml). The organic phase was dried over $MgSO_4$ for 1 h, filtered and evaporated to give the crude product (2.684 g). The crude mixture was separated on a Biobeads gel column, and the pure product **7** was isolated (1.195 g, 1.63 mmol, 60%). Colourless oil; R_f 0.7 (CH_2Cl_2–MeOH 90:10); ν_{max} (neat) 3358 s (NH), 2952 s and 2879 s (alkyl), 1797 m, 1735 s and 1674 m (C=O), 1524 m, 1456 m, 1260 s, 1197 s, 1111 m, 744 m, 699 m; $\delta_H(CDCl_3)$ 1.98 and 2.21 (4H, m, CHCH_2CH_2), 2.50 (6H, t, $J = 6.5$ Hz, CH_2CO$_2$Me), 3.63 (21H, m, CH_2OCH_2, CO$_2$(CH_3)$_3$), 4.36 (1H, m, NHCHCH$_2$), 5.07 and 5.15 (2H and 2H, 2s, PhCH_2O), 5.84 and 5.87 (1H, d, $J = 7.5$ Hz, NHCHCH$_2$), 6.15 (1H, s, CONH), 7.31 (10H, s, C$_6H_5$CH$_2$); $\delta_C(CDCl_3)$ 27.8 (CHCH_2), 32.9 (CH_2CONH), 34.6 (CH_2CO_2Me), 51.6 (CO_2CH_3), 53.8 (CHCH$_2$), 59.6 (NHC(CH$_2$)$_3$), 66.6, 66.8, 67.1 and 69.0 (CH_2OCH_2 and OCH_2Ph), 128.0, 128.0, 128.2, 128.3, 128.4 and 128.5 (Aryl *C*H), 135.3 and 136.2 (Aryl *C*), 156.2 (CH_2CONH), 171.9, 172.1 and 172.1 (CO_2Me and CO_2CH_2); m/z (Electrospray) $[M + Na]^+$ requires 755, found 755 (100), 756 (36); HRMS (FAB) ($C_{36}H_{48}N_2O_{14}Na$): found 755.3009, calculated 755.3003.

4.2.5. Ligand B

Compound **7** (174 mg, 0.24 mmol) was dissolved in EtOH (10 ml) and 10% Pd-C (60 mg) was added. The reaction was stirred under H_2 for 30 min, and the reaction followed by TLC (90:10 CH_2Cl_2–MeOH). The mixture was filtered through Celite, and evaporated to give the product in near quantitative yield (113 mg, 0.22 mmol, 93%). Colourless oil; R_f 0.0 CH_2Cl_2–MeOH 90:10; ν_{max} (neat) 3362 w and 3261 w (NH and NH_2), 3069 w, 2953 w and 2879 w (alkyl), 1737 s and 1654 m (C=O), 1543 w, 1438 w, 1364 w, 1266 w, 1198 m, 1178 m, 1109 m, 1075 m; $\delta_H(CD_3OD)$ 2.07 (2H, m, CHCH_2CH$_2$), 2.44 (2H, m, CHCH$_2$CH_2), 2.56 (6H, t, $J = 6.0$ Hz, CH_2CO$_2$Me), 3.69 (22H, m, CO$_2$CH_3, CH_2OCH_2, CHCH$_2$); $\delta_C(CD_3OD)$ 27.2 (CHCH_2CH$_2$), 33.2 (CHCH$_2$$CH_2$), 34.8 ($CH_2CO_2$Me), 51.4 ($CH_2CO_2CH_3$), 54.9 $CHCH_2CH_2$), 60.7 (NHC(CH$_2$)$_3$), 67.2 and 68.8 (CH_2OCH_2), 127.4 (CONH), 173.2 (CO_2Me), 174.5 (CO_2H); m/z (Electrospray) $[M - H]^-$ requires 507, found 507 (100%), 508 (16%).

4.2.6. Complex A–Cu

Ligand **A** (144 mg, 0.828 mmol) was dissolved in H_2O (20 ml) and $CuCO_3$ (51 mg, 0.414 mmol) was added. The pH was measured and NaOH soln (10%) was added dropwise with stirring, until pH 11 was reached. The solution was stirred for 2 h, and a blue precipitate was formed. The solution was placed in an ice bath for 1 h and the precipitate was then collected by filtration to give complex **A–Cu** (72 mg, 0.15 mmol, 39%). Blue powder; ν_{max} (solid KBr) 3434 s and 3296 s (NH), 2968 m and 2933 m (alkyl), 1648 s (C=O), 1456 m, 1365 s, 1226 s, 1091 s; m/z (Electrospray) $[M + Na]^+$ requires 488, found 488 (90%), 490 (36%), 953 $[2M + Na]^+$ (87%), 955 (100%), 957 (34%); HRMS (FAB) ($C_{18}H_{35}N_4O_6Cu$): found 466.1851, calculated 466.1853;

Elemental analysis $C_{18}H_{34}N_4O_6Cu \cdot 2H_2O$ requires C, H, N: 43.06, 7.63, 11.16; found 43.62, 7.38, 11.10.

4.2.7. Complex *B*–Cu

Ligand **B** (305 mg, 0.60 mmol) was dissolved in MeOH (10 ml) and $CuCO_3$ (23 mg, 0.19 mmol) was added, followed by solid NaOH (22 mg, 0.60 mmol). The reaction was stirred at r.t. for 14 d. The resulting blue/green mixture was filtered twice and reduced in volume by rotary evaporation. The product was then purified over a Sephadex (LH-20) gel column with MeOH as eluent. The blue band was collected from the column and evaporated to dryness to give a blue oil (38 mg, 0.035 mmol, 19%). Blue viscous oil; ν_{max} (neat) 3297 w (NH), 2954 w, 2924 w, and 2879 w (alkyl), 1739 m and 1652 m (C=O), 1559 w, 1439 w, 1370 w, 1261 w, 1176 m; m/z (Electrospray) $[M + Na]^+$ requires 1100, found 1100 (100%), 1102 (55%), 1006 (50%); Elemental analysis $C_{42}H_{70}N_4O_{24}Cu \cdot 2H_2O$ requires C, H, N: 45.26, 6.69, 5.03; found 44.77, 6.13, 4.92.

Acknowledgements

We are grateful for funding through the CASE award scheme from EPSRC and Cytec Engineered Materials (D.L.S.).

References

[1] (a) J.J.R. Fraústo da Silva, R.J.P. Williams, The Biological Chemistry of the Elements: The Inorganic Chemistry of Life, Oxford University Press, Oxford, 2001;
(b) S. Lippard, J.M. Berg, Principles of Bioinorganic Chemistry, University Science Books, 1994;
(c) P.C. Wilkins, R.G. Wilkins, Inorganic Chemistry in Biology, Oxford University Press, Oxford, 1997.

[2] (a) For recent papers discussing the effect of encapsulation (and the microenvironments generated) on the behaviour of biological systems see:. E.L. Mehler, M. Fuxreiter, I. Simon, E.B. Garcia-Moreno, Proteins: Struct. Funct. Gen. 48 (2002) 283;
(b) L. Avila, M. Wirtz, R.A. Bunce, M. Rivera, J. Biol. Inorg. Chem. 4 (1999) 664;
(c) F. Hollfelder, A.J. Kirby, D.S. Tawfik, K. Kikuchi, D. Hilvert, J. Am. Chem. Soc. 122 (2000) 1022;
(d) X. Barril, C. Aleman, M. Orozco, F.J. Luque, Proteins: Struct. Funct. Gen. 32 (1998) 67;
(e) M. Rivera, R. Seetharaman, D. Girdhar, M. Wirtz, X.J. Zhang, X.Q. Wang, S. White, Biochemistry 37 (1998) 1485;
(f) J. Clarkson, P.J. Tonge, K.L. Taylor, D. Dunaway-Mariano, P.R. Carey, Biochemistry 36 (1997) 10192.

[3] (a) H.B. Gray, Proc. Natl. Acad. Sci. USA 100 (2003) 3563;
(b) C.J. Elsevier, J. Reedijk, P.H. Walton, M.D. Ward, Dalton Trans. (2003) 1869.

[4] (a) For reviews focussing on the effect of dendritic encapsulation see: D.K. Smith, F. Diederich, Chem. Eur. J. 4 (1998) 1353;
(b) C.B. Gorman, J.C. Smith, Acc. Chem. Res. 34 (2001) 60;
(c) S. Hecht, J.M.J. Fréchet, Angew. Chem. Int. Ed 40 (2001) 74.

[5] (a) C.J. Hawker, K.L. Wooley, J.M.J. Fréchet, J. Am. Chem. Soc. 115 (1993) 4375;
(b) J. Issberner, F. Vögtle, L. De Cola, V. Balzani, Chem. Eur. J. 3 (1997) 706;
(c) C. Devadoss, P. Bharathi, J.S. Moore, Angew. Chem. Int. Ed. Engl. 36 (1997) 1633;
(d) F. Vögtle, M. Plevoets, M. Nieger, G.C. Azzellini, A. Credi, L. de Cola, V. de Marchis, M. Venturi, V. Balzani, J. Am. Chem. Soc. 121 (1999) 6290;
(e) D.-L. Jiang, T. Aida, Nature 388 (1997) 454;
(f) M. Kawa, J.M.J. Fréchet, Chem. Mater. 10 (1998) 286;
(g) G.M. Dykes, L.J. Brierley, D.K. Smith, P.T. McGrail, G.J. Seeley, Chem. Eur. J. 7 (2001) 4730;
(h) S.A. Vinogradov, D.F. Wilson, Chem. Eur. J. 6 (2000) 2456;
(i) S. Koenig, L. Müller, D.K. Smith, Chem. Eur. J. 7 (2001) 979;
(j) V. Vicinelli, P. Ceroni, M. Maestri, V. Balzani, M. Gorka, F. Vogtle, J. Am. Chem. Soc. 124 (2002) 6461;
(k) E.M. Harth, S. Hecht, B. Helms, E.E. Malmstrom, J.M.J. Frechet, C.J. Hawker, J. Am. Chem. Soc. 124 (2002) 3926.

[6] (a) For selected examples of dendritic encapsulation affecting redox properties see: G.R. Newkome, R. Güther, C.N. Moorefield, F. Cardullo, L. Echegoyen, E. Pérez-Cordero, H. Luftmann, Angew. Chem. Int. Ed. Engl. 34 (1995) 2023;
(b) H.F. Chow, I.Y-.K. Chan, D.T.W. Chan, R.W.M. Kwok, Chem. Eur. J. 2 (1996) 1085;
(c) K.W. Pollak, J.W. Leon, J.M.J. Fréchet, M. Maskus, H.D. Abruña, Chem. Mater. 10 (1998) 30;
(d) F. Vögtle, M. Plevoets, M. Nieger, G.C. Azzellini, A. Credi, L. De Cola, V. De Marchis, M. Venturi, V. Balzani, J. Am. Chem. Soc. 121 (1999) 6290;
(e) H.F. Chow, I.Y.K. Chan, P.S. Fung, T.K.K. Mong, M.F. Nongrum, Tetrahedron 57 (2001) 1565.

[7] (a) For dendritic cytochrome mimics see: P.J. Dandliker, F. Diederich, M. Gross, C.B. Knobler, A. Louati, E.M. Sanford, Angew. Chem. Int. Ed. Engl. 33 (1994) 1739;
(b) P.J. Dandliker, F. Diederich, J.-P. Gisselbrecht, A. Louati, M. Gross, Angew. Chem. Int. Ed. Engl. 34 (1995) 2725;
(c) P.J. Dandliker, F. Diederich, A. Zingg, J.-P. Gisselbrecht, M. Gross, A. Louati, E. Sanford, Helv. Chim. Acta 80 (1997) 1773;
(d) P. Weyermann, J.-P. Gisselbrecht, C. Boudon, F. Diederich, M. Gross, Angew. Chem. Int. Ed. 38 (1999) 3215;
(e) P. Weyermann, F. Diederich, Helv. Chim. Acta 85 (2002) 599.

[8] (a) For dendritic ferrocenes as probes of an encapsulated microenvironment see: D.L. Stone, D.K. Smith, P.T. McGrail, J. Am. Chem. Soc. 124 (2002) 856;
(b) D.L. Stone, D.K. Smith, Polyhedron 22 (2003) 763;
(c) D.K. Smith, J. Chem. Soc. Perkin Trans. 2 (1999) 1563;
(d) C.M. Cardona, A.E. Kaifer, J. Am. Chem. Soc. 120 (1998) 4023;
(e) Y. Wang, C.M. Cardona, A.E. Kaifer, J. Am. Chem. Soc. 121 (1999) 9756;
(f) C.M. Cardona, T.D. McCarley, A.E. Kaifer, J. Org. Chem. 65 (2000) 1857.

[9] For a good recent review of this topic see: L.J. Twyman, A.S.H. King, I.K. Martin, Chem. Soc. Rev. 31 (2002) 69.

[10] M. Enomoto, T. Aida, J. Am. Chem. Soc. 121 (1999) 874.

[11] R.J.M.K. Gebbink, A.W. Bosman, M.C. Feiters, E.W. Meijer, R.J.M. Nolte, Chem. Eur. J. 5 (1999) 65.

[12] (a) H.F. Chow, C.C. Mak, J. Org. Chem. 62 (1997) 5116;
(b) C.C. Mak, H.F. Chow, Macromolecules 30 (1997) 1228.

[13] (a) J.-F. Nierengarten, D. Felder, J.F. Nicoud, Tetrahedron Lett. 40 (1999) 273;
(b) N. Armaroli, C. Boudon, D. Felder, J.-P. Gisselbrecht, M. Gross, G. Marconi, J.F. Nicoud, J.-F. Nierengarten, V. Vicinelli, Angew. Chem. Int. Ed. 38 (1999) 3730;
(c) R. Roy, J.M. Kim, Tetrahedron 59 (2003) 3881;
(d) B.Y. Yang, X.M. Chen, G.J. Deng, Y.L. Zhang, Q.H. Fan, Tetrahedron Lett. 44 (2003) 3535.

[14] (a) H.C. Freeman, in: E.L. Eichhorn (Ed.), Inorganic Biochemistry, Elsevier, Amsterdam, 1973;
(b) K. Severin, R. Bergs, W. Becks, Angew. Chem. Int. Ed. Engl. 37 (1998) 1635;
(c) P. Manikandan, B. Epel, D. Goldfarb, Inorg. Chem. 40 (2001) 781, and references therein.
[15] T.R. Krishna, N. Jayaraman, J. Chem. Soc. Perkin Trans. 1 (2002) 746.
[16] T.J. Collins, K.L. Kostka, E.S. Uffelman, T.L. Weinberger, Inorg. Chem. 30 (1991) 4204.
[17] (a) J. Peisach, W.E. Blumberg, Arch. Biochem. Biophys. 165 (1974) 691;
(b) F.A. Taiwo, Spectr. Int. J. 17 (2003) 53.
[18] (a) E. Colacio, M. Ghazi, R. Kivekas, J.M. Moreno, Inorg. Chem. 39 (2000) 2882;
(b) J.M. Schveigkardt, A.C. Rizzi, O.E. Piro, E.E. Castellano, R.C. de Santana, R. Calvo, C.D. Brondino, Eur. J. Inorg. Chem. (2002) 2913.
[19] R. Calvo, E.C. Abresch, R. Bittl, G. Feher, W. Hofbauer, W. Lubitz, M.L. Paddock, J. Am. Chem. Soc. 122 (2000) 7327.
[20] (a) G.R. Newkome, X.F. Lin, Macromolecules 24 (1991) 1443;
(b) G.R. Newkome, X.F. Lin, C.D. Weis, Tetrahedron: Asymmetry 2 (1991) 957;
(c) J.K. Young, G.R. Baker, G.R. Newkome, K.F. Morris, C.S. Johnson Jr., Macromolecules 27 (1994) 3464;
(d) J.-F. Nierengarten, T. Habicher, R. Kessinger, F. Cardullo, F. Diederich, V. Gramlich, J.-P. Gisselbrecht, C. Boudon, M. Gross, Helv. Chim. Acta 80 (1997) 2238.

Available online at www.sciencedirect.com
SCIENCE DIRECT®
Polyhedron 23 (2004) 1719–1729
POLYHEDRON
www.elsevier.com/locate/poly

Synthesis, characterization and X-ray crystallography of a metallacrown ether complex containing a $Ru^{II}(bpy)_2^{2+}$ chromophore and its $Mo(CO)_4$ analog ☆

Jennifer M. Butler, Gary M. Gray *, Juan Pablo Claude *

Department of Chemistry, University of Alabama at Birmingham, 901, 14th Street South, Birmingham, AL 35294-1240, USA

Received 29 September 2003; accepted 3 April 2004
Available online 19 May 2004

Abstract

The chelating ligand (2,2′-$C_{12}H_8O_2$)$P(CH_2CH_2O)_4P$(2,2′-$O_2C_{12}H_8$) reacts with both $Ru(bpy)_2(O_3SCF_3)_2$ and $Mo(CO)_4(C_7H_8)$ to form the new metallacrown ether complexes *cis*-[$Ru(bpy)_2$((2,2′-$C_{12}H_8O_2$)$P(CH_2CH_2O)_4P$(2,2′-$O_2C_{12}H_8$))]$(O_3SCF_3)_2$ (**1**) and *cis*-[$Mo(CO)_4$((2,2′-$C_{12}H_8O_2$)$P(CH_2CH_2O)_4P$(2,2′-$O_2C_{12}H_8$))] (**2**). The X-ray crystal structures for both complexes indicate that the metallacrown ether ring oxygen atoms point their lone pairs towards the cavity in the *cis*-metallacrown ether ring. The effect of interactions of the metallacrown ether complex with selected monoatomic cations (Li^+, Na^+ and Hg^{2+}) on the emissive properties of the $Ru(bpy)_2^{2+}$ chromophore were studied by steady-state and time-dependent emission spectroscopy. Our results suggest that complex **1** interacts weakly with Li^+, Na^+ and Hg^{2+}, and subtle changes are observed in its photophysical properties. These changes are discussed in terms of excited-state parameters obtained from a Franck–Condon analysis of the emission spectra.
© 2004 Elsevier Ltd. All rights reserved.

Keywords: Ruthenium; Fluoroionophore; X-ray; Metallacrown

1. Introduction

The coupling of a cation binding center to a luminescent group has been successfully exploited in the past to synthesize fluoroionophores, whose emission characteristics are modulated by association with specific metal cations [1,2]. The modulation of the emissive properties of the fluoroionophore upon cation binding can originate through several mechanisms. These mechanisms include structural effects [3], exciplex formation [4], electron transfer quenching [5–7], and changes in dipole moments and π-delocalization [8]. Within the several structural families of fluoroionophores, those in which a crown ether cation receptor is attached to an organic dye are quite common [1,2]. Crown ether rings attached to inorganic fluorophores are much less frequent. Only two examples of such molecules ave been reported, one with a crown ether attached to a *fac*-[(bpy)$Re^I(CO)_3L]^+$ group [6], and the other with a crown ether attached to a $[Ru(bpy)_3]^{2+}$ center [7]. Both of these examples achieve enhanced emission quantum yields upon cation binding by suppressing electron transfer quenching of the luminescent Re(I) or Ru(II) centers.

One class of molecules that could be potentially useful inorganic fluoroionophores is metallacrown ethers. These molecules are formed by chelation of α, ω-bis(phosphorus-donor)polyether ligands to transition metals [9–21] and can bind hard metal cations or small molecules analogously to traditional organic crown ethers [22–25]. The close proximity between the binding site and the transition metal center in metallacrown ethers suggests that the spectroscopic properties of the transition metal could be strongly coupled to the binding state of the metallacrown ether.

☆ Supplementary data associated with this article can be found, in the online version, at doi:10.1016/j.poly.2004.04.004.

* Corresponding authors. Tel.: +1-205-975-2478/934-4747; fax: +1-205-934-2543.
E-mail addresses: gmgray@uab.edu (G.M. Gray), jpclaude@uab.edu (J.P. Claude).

0277-5387/$ - see front matter © 2004 Elsevier Ltd. All rights reserved.
doi:10.1016/j.poly.2004.04.004

None of the metallacrown ethers that have been studied to date have incorporated transition metal chromophores that could function as spectroscopic probes for binding. An obvious candidate for a transition metal chromophore embedded in a metallacrown ether is bis(2,2′-bipyridine)ruthenium(II), $Ru(bpy)_2^{2+}$. Tris(2,2′-bipyridine)ruthenium(II), $Ru(bpy)_3^{2+}$, and its derivatives have been of fundamental importance in developing the understanding of electron and energy transfer reactions [26–28], and in probing medium effects [26,29–32]. The popularity of $Ru(bpy)_3^{2+}$ and derived complexes in photophysical and photoinduced electron and energy transfer studies stems from their easily measured spectroscopic characteristics, long-lived emissive excited states, greatly enhanced excited-state redox potentials and well-developed synthetic chemistry. The available synthetic methodology currently allows predictable fine-tuning of the electronic characteristics of these complexes [26,33,34]. In addition, ruthenium(II) is a low-spin, d^6 transition metal and thus inert to ligand exchange. Previous work with molybdenum(0), another low-spin d^6 transition metal, has demonstrated that stable molecular metallacrown ethers can be readily formed in high yields with such transition metals [9–19].

In this paper, we report the syntheses of the first metallacrown ether containing a $Ru(bpy)_2^{2+}$ chromophore, *cis*-[$Ru(bpy)_2(C_{12}H_8O_2P(OCH_2CH_2)_4OPO_2C_{12}H_8)$]$(CF_3SO_3)_2$ (**1**), and of the closely related *cis*-[$Mo(CO)_4(C_{12}H_8O_2P(OCH_2CH_2)_4OPO_2C_{12}H_8)$] (**2**), metallacrown ether. These metallacrown ethers have been characterized by multinuclear NMR spectroscopy and X-ray crystallography. Cation binding to **2** has been evaluated using standard NMR techniques. Finally, the luminescent properties of **1** in the presence and absence of metal cations have been studied to determine if it can be used as a probe for cation binding.

2. Experimental

All reactions and purification procedures were carried out under high-purity nitrogen. All starting materials were reagent grade and were used as received. Tetrahydrofuran (THF) was distilled from sodium/benzophenone and both acetonitrile and triethylamine were distilled from calcium hydride prior to use. Deuterated NMR solvents (chloroform-d, dichloromethane-d_2) were opened and handled under a nitrogen atmosphere at all times. The *cis*-$Mo(CO)_4$(nbd) [35], 2,2′-biphenylylenephosphochloridite ester [36], and bis(2,2′-bipyridine)bis(trifluoromethanesulfonato)ruthenium(II) [37] were synthesized using the literature procedures. $[Ru(bpy)_3](PF_6)_2$ was prepared by treating an aqueous solution of $[Ru(bpy)_3]Cl_2$ (purchased from Aldrich) with concentrated aqueous ammonium hexafluorophosphate. The $[Ru(bpy)_3](PF_6)_2$ precipitate was collected by vacuum filtration, rinsed with water and dried under vacuum.

All one-dimensional $^{31}P\{^1H\}$, $^{13}C\{^1H\}$ and ^1H NMR spectra of the ligands and complexes were recorded using a Bruker ARX-300 NMR spectrometer with a quad (^1H, ^{13}C, ^{19}F, ^{31}P) 5 mm probe. The $^{31}P\{^1H\}$ NMR spectra were referenced to external 85% phosphoric acid, and both the ^{13}C and the ^1H NMR spectra were referenced to internal $SiMe_4$.

Elemental analyses were performed by Atlantic Microlabs, Norcross, GA. A solvent of crystallization is included in a calculated analysis only if the solvent was observed in the ^1H NMR spectrum of the analytical sample.

2.1. $(2,2'\text{-}C_{12}H_8O_2)P(CH_2CH_2O)_4P(2,2'\text{-}O_2C_{12}H_8)$

A solution of 10.0 g (40.0 mmol) of 2,2′-biphenylylenephosphochloridite ester in 30 ml of freshly distilled THF was added dropwise to a solution of 3.88 g (20.0 mmol) of tetraethylene glycol and 5.58 ml (40.0 mmol) triethylamine in 100 ml of tetrahydrofuran, and was stirred under nitrogen for 1 h. The solution was filtered through Celite®, under nitrogen, and evaporated to dryness to yield 12.2 g (68.2%) of crude (2,2′-$C_{12}H_8O_2$)$P(CH_2CH_2O)_4P$(2,2′-$O_2C_{12}H_8$) as a viscous, colorless oil. $^{31}P\{^1H\}$ NMR (chloroform-d): δ 140.39 (s). ^1H NMR (chloroform-d): δ 7.34 (m, 16H, Ar), 4.08 (m, 4H, CH_2), 3.66 (m, 12H, CH_2).

2.2. cis-$[Ru(bpy)_2((2,2'\text{-}C_{12}H_8O_2)P(CH_2CH_2O)_4P(2,2'\text{-}O_2C_{12}H_8))](O_3SCF_3)_2$ (**1**)

Solutions of 0.220 g (3.09 mmol) of $Ru(bpy)_2(O_3SCF_3)_2$ in 50 ml of degassed dichloromethane [1] and 0.192 g (3.09 mmol) of (2,2′-$C_{12}H_8O_2$)$P(CH_2CH_2O)_4P$(2,2′-$O_2C_{12}H_8$) in 50 ml of degassed dichloromethane were added simultaneously and dropwise to 125 ml of degassed dichloromethane over a 2 h period. This mixture was stirred for three days. The clear, red solution was then evaporated to dryness, and the residue was triturated with ether to yield an orange solid. Yield: 0.377 g (92.2%). *Anal.* Calc. for $C_{54}H_{48}F_6O_{15}S_2N_4P_2Ru$ (with four mole H_2O): C, 46.12; H, 3.98; N, 3.99; F, 8.11%. Found: C, 46.12; H, 3.78; N, 4.09; F, 8.31%. $^{31}P\{^1H\}$ NMR (dichloromethane-d_2): δ 142.85 (s).

[1] The Ru precursor was not completely soluble in the dichloromethane. However, the insoluble portion remained suspended in the solution and was efficiently added to the reaction mixture. The suspended solid gradually disappeared during the three days that the reaction mixture was stirred at ambient temperature.

2.3. cis-[Mo(CO)$_4$((2,2′-C$_{12}$H$_8$O$_2$)P(CH$_2$CH$_2$O)$_4$P(2,2′-O$_2$C$_{12}$H$_8$))] (2)

Solutions of 0.829 g (2.77 mmol) of Mo(CO)$_4$(C$_7$H$_8$) in 100 ml of degassed dichloromethane and 1.72 g (2.77 mmol) of (2,2′-C$_{12}$H$_8$O$_2$)P(CH$_2$CH$_2$O)$_4$P(2,2′-O$_2$C$_{12}$H$_8$) in 100 ml of degassed dichloromethane were added simultaneously and dropwise to 200 ml of degassed dichloromethane over a 2 h period. This mixture was stirred for 15 min. The clear, colorless solution was then evaporated to dryness and washed with hexane to yield a white powder upon filtration. Yield: 2.10 g (88.3%). *Anal.* Calc. for C$_{36}$H$_{32}$O$_{13}$P$_2$Mo: C, 52.09; H, 3.89%. Found: C, 52.18; H, 3.95%. ^{31}P{^{1}H} NMR (chloroform-d): δ 170.09 (s). ^{1}H NMR (chloroform-d): δ 7.43 (m, 2H, Ar), 7.24 (m, 14H, Ar), 4.09 (m, 4H, CH$_2$), 3.65 (m, 12H, CH$_2$). ^{13}C NMR (chloroform-d): δ 71.07 (s, C4 and C5), 70.86 (s, C3 and C6), 70.35 (bt, C2 and C7), 66.76 (bt, C1 and C8).

2.4. X-ray data collection and solution

Suitable single crystals of **1** and **2** were mounted on glass fibers with epoxy cement and aligned upon an Enraf Nonius CAD4 single-crystal diffractometer under aerobic conditions. Standard peak search and automatic indexing routines followed by least squares fits of 25 accurately centered reflections resulted in reliable unit cell parameters. These unit cell parameters indicated that both crystals belonged to the monoclinic crystal system. Systematic absences indicated that the space groups for **1** and **2** were $C2/c$ and $P2(1)/n$, respectively. In both cases, the analytical scattering factors of the complexes were corrected for both $\Delta f'$ and $i\Delta f''$ components of anomalous dispersion. The metal and phosphorus positions were located using Patterson functions, and the other non-hydrogen atoms were located in difference Fourier maps. Positional and anisotropic displacement parameters for all non-hydrogen atoms were

Table 1
Crystal data and structure refinement for **1** and **2**

	Compound **1**	Compound **2**
Empirical formula	C$_{54}$H$_{52}$F$_6$N$_2$O$_{15}$P$_2$RuS$_2$	C$_{36}$H$_{32}$MoO$_{13}$P$_2$
Formula weight	1310.11	830.50
T (K)	293(2)	293(2)
λ (Å)	0.71073	0.71073
Crystal system	monoclinic	monoclinic
Space group	$C2/c$	$P2(1)/n$
Unit cell dimensions		
a (Å)	24.451(5)	13.025(3)
b (Å)	14.698(3)	15.791(3)
c (Å)	17.083(3)	18.174(4)
α (°)	90	90
β (°)	115.03(3)	97.27(3)
γ (°)	90	90
V (Å^3)	5562.3(19)	3708.1(13)
Z	4	4
D_{calc} (Mg/m^3)	1.564	1.488
Absorption coefficient (mm^{-1})	0.504	0.504
$F(000)$	2680	1696
Crystal size (mm)	0.32×0.19×0.12	0.21×0.19×0.19
θ Range for data collection (°)	2.35–22.48	2.04–22.48
h_{max}, h_{min}	26, −18	14, −13
k_{max}, k_{min}	15, 0	16, 0
l_{max}, l_{min}	18, −17	0, −19
Reflections collected	3946	4995
Independent reflections (R_{int})	3630 (0.0257)	4821 (0.0129)
Completeness to $\theta = 22.48°$ (%)	99.9	99.9
Absorption correction	empirical	none
Maximum and minimum transmission	0.3305 and 0.3055	
Refinement method	full-matrix least-square on F^2	full-matrix least-square on F^2
Data/restraints/parameters	3630/0/385	4821/0/471
Goodness-of-fit on F^2	1.050	1.074
Final R indices [$I > 2\sigma(I)$]	$R_1 = 0.0538$, $wR_2 = 0.1396$	$R_1 = 0.0307$, $wR_2 = 0.0779$
R indices (all data)	$R_1 = 0.0856$, $wR_2 = 0.1557$	$R_1 = 0.0489$, $wR_2 = 0.0869$
Extinction coefficient	0.00067(14)	0.0070(3)
Largest difference peak and hole (e Å^{-3})	1.608 and −0.644	0.562 and −0.257

refined. Hydrogen atoms were not located directly but were input in calculated positions with d(C–H) = 0.96 Å. The isotropic displacement parameter of each hydrogen atom was set equal to 1.2 times the U_{eq} value of the carbon atom to which it was bonded. The Siemens SHELXTL-PC® program package was used for all crystallographic calculations [38]. The experimental details of the data collection and refinement are summarized in Table 1. Selected bond lengths and angles are given in Table 2 and selected torsion angles are given in Table 3 for each complex. ORTEP drawings of the molecules are given in Figs. 1 and 2 and ORTEP drawings of the metallacrown ether rings are shown in Fig. 3.

2.5. Optical spectroscopy

UV–Vis spectra were obtained with a Hewlett–Packard model 8453 diode array spectrophotometer. Samples of **1** for the emission studies were 3×10^{-3} M acetonitrile solutions, placed in 1.0 cm path length quartz cuvettes and bubble degassed with dry nitrogen for a minimum of 20 min. Samples with cations contained 1.1 equivalents

Table 2
Selected bond lengths (Å) and angles (°) for **1** and **2**

Compound **1**		Compound **2**			
Bond lengths					
Ru–P	2.2558(17)	Mo–P1	2.4447(11)	Mo–P2	2.4421(11)
Ru–N1	2.088(4)	C33–Mo	2.006(4)	C35–Mo	2.044(5)
Ru–N2	2.188(5)	C34–Mo	2.003(4)	C36–Mo	2.038(5)
O4–P	1.607 (4)	O6–P1	1.616(2)	O8–P2	1.609(2)
O5–P	1.614(4)	O7–P1	1.621(2)	O9–P2	1.631(2)
O1–P	1.566(4)	O1–P1	1.575(3)	O5–P2	1.574(3)
C1–O1	1.462(7)	C1–O1	1.454(4)	C8–O5	1.436(4)
C1–C2	1.485(10)	C1–C2	1.475(5)	C7–C8	1.495(5)
C2–O2	1.390(9)	C2–O2	1.392(5)	C7–O4	1.402(5)
C3–O2	1.308(10)	C3–O2	1.425(5)	C6–O4	1.423(5)
C3–C4	1.403(14)	C3–C4	1.498(6)	C5–C6	1.490(6)
C4–O3	1.397(15)	C4–O3	1.409(5)	C5–O3	1.396(5)
C4–O3A	1.481(15)				
Bond angles					
P–Ru–P A	88.89(9)	P2–Mo–P1	91.21(3)		
N1–Ru–N2	77.84(17)	C33–Mo–P1	178.10(13)	C33–Mo–P2	88.07(12)
P–Ru–N1	103.11(13)	C34–Mo–P1	87.39(11)	C34–Mo–P2	173.83(12)
P–Ru–N2	176.80(13)	C35–Mo–P1	92.25(11)	C35–Mo–P2	97.88(12)
		C36–Mo–P1	89.74(12)	C36–Mo–P2	84.69(12)
O4–P–Ru	107.86(16)	O6–P1–Mo	110.81(9)	O8–P2–Mo	114.52(9)
O5–P–Ru	121.23(17)	O7–P1–Mo	123.37(10)	O9–P2–Mo	123.82(9)
O1–P–Ru	117.17(17)	O1–P1–Mo	114.06(10)	O5–P2–Mo	109.61(10)
P–O1–C1	127.0(4)	P1–O1–C1	125.2(3)	P2–O5–C8	128.3(2)
O1–C1–C2	108.9(6)	O1–C1–C2	109.0(3)	O5–C8–C7	107.5(3)
C1–C2–O2	110.2(7)	C1–C2–O2	110.7(3)	C8–C7–O4	114.0(3)
C2–O2–C3	120.5(8)	C2–O2–C3	113.4(3)	C7–O4–C6	113.3(3)
O2–C3–C4	120.8(10)	O2–C3–C4	115.6(3)	O4–C6–C5	108.5(4)
C3–C4–O3	104.8(10)	C3–C4–O3	108.8(3)	C5–C6–O3	110.0(4)
C3–C4–O3A	124.3(9)				
C4–O3–C4A	110.5(10)	C4–O3–C5	114.8(3)		

Table 3
Torsion angles (°) for the metallacrown ether rings in **1** and **2**

Compound **1**		Compound **2**			
P1–Ru–P–O1	−60.4(2)	P2–Mo–P1–O1	−66.59(12)	P1–Mo–P2–O5	−115.70(11)
Ru–P–O1–C1	−160.1(5)	Mo–P1–O1–C1	−180.0(3)	Mo–P2–O5–C8	169.4(3)
P–O1–C1–C2	−152.5(5)	P1–O1–C1–C2	−161.2(3)	P2–O5–C8–C7	164.2(3)
O1–C1–C2–O2	72.1(8)	O1–C1–C2–O2	73.8(4)	O5–C8–C7–O4	−66.1(4)
C1–C2–O2–C3	151.7(10)	C1–C2–O2–C3	170.9(3)	C8–C7–O4–C6	−89.8(4)
C2–O2–C3–C4	179.4(11)	C2–O2–C3–C4	77.0(5)	C7–O4–C6–C5	172.9(3)
O2–C3–C4–O3	−60.0(16)	O2–C3–C4–O3	63.3(5)	O4–C6–C5–O3	−74.2(5)
O2–C3–C4–O3A	1(2)				
C3–C4–O3–C4A	157.0(11)	C3–C4–O3–C5	168.0(4)	C6–C5–O3–C4	172.5(4)
C3–C4–O3A–C4A	−126(2)				
C5–C10–C11–C16	44.3(9)	C9–C14–C15–C20	−44.8(5)	C21–C26–C27–C32	−42.5(5)

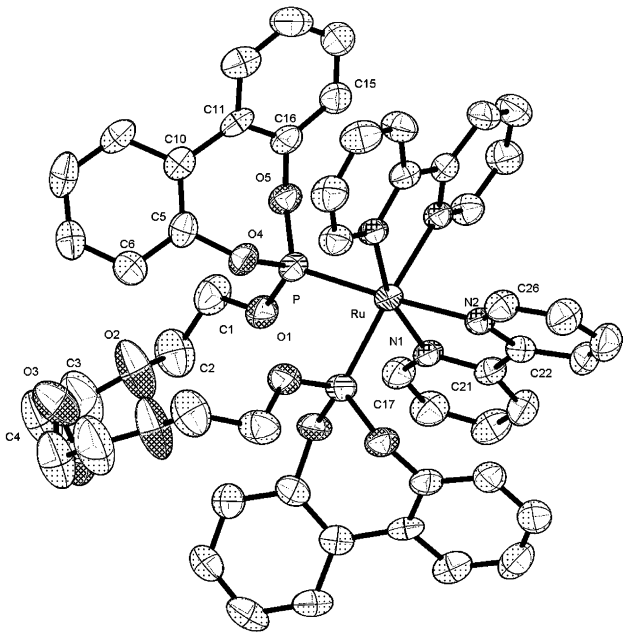

Fig. 1. Molecular structure of *cis*-[Ru(bpy)$_2$((2,2′-$C_{12}H_8O_2$) P(CH_2-$CH_2O)_4$P(2,2′-$O_2C_{12}H_8$))](O_3SCF_3)$_2$ (**1**) shown without triflate anions.

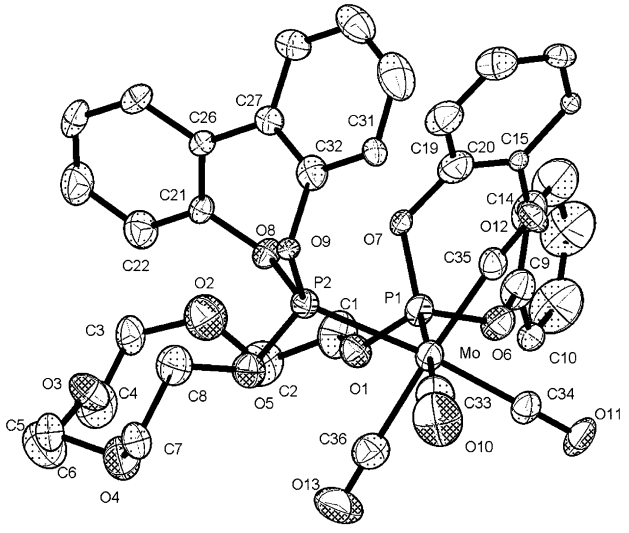

Fig. 2. Molecular structure of *cis*-[Mo(CO)$_4$((2,2′-$C_{12}H_8O_2$) P($CH_2CH_2O)_4$P(2,2′-$O_2C_{12}H_8$))] (**2**).

of $LiBF_4$, $NaBPh_4$ or $HgCl_2$, and were prepared by adding 100 μl of 0.132 M salt solution in acetonitrile to 4.0 ml of the solution of **2** in the fluorescence cell before bubble degassing. All samples were optically dilute, with absorbances below 0.65 at the excitation wavelength.

Steady-state emission spectra were recorded using a Spex Fluorolog FL3-22 fluorometer with double grating excitation and emission monochromators and a thermoelectrically cooled Hamamatsu R-928 photomultiplier tube running in photon counting mode. Emission spectra were corrected for instrument response with

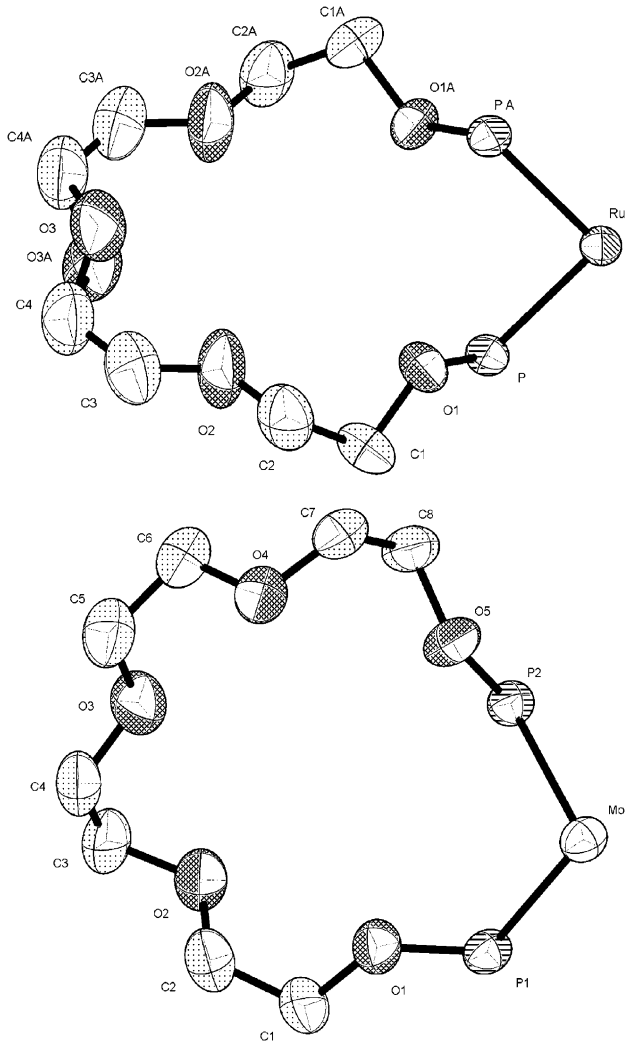

Fig. 3. Orientation of oxygen atoms suggest that the crown ether rings in both **1** and **2** are in an acceptable conformation for cation binding.

factors collected using a NIST standard lamp. All samples were excited at 400 nm. Cutoff filters were used to remove scattered excitation light when required, with cutoff wavelengths chosen well below the data collection range. Emission quantum yields were measured relative to [Ru(bpy)$_3$](PF_6)$_2$ in acetonitrile and calculated using the following equation:

$$\phi_u = \phi_s \left(\frac{I_u}{I_s}\right)\left(\frac{A_s}{A_u}\right),$$

where ϕ is the emission quantum yield, I is the integrated emission intensity, A is the sample absorbance at the excitation wavelength, and the subscripts 's' and 'u' refer to the standard and unknown samples, respectively [39].

Emission lifetimes were measured using a PTI GL3300 pulsed nitrogen laser with an attached GL301 tunable dye head. The samples were excited at 387 nm using BBQ dye (Exciton) in *p*-dioxane, and the decay was monitored at the emission maximum. Emission decays were col-

lected at a right angle to the excitation, using a McPherson 272 monochromator with a holographic grating, and a thermoelectrically cooled (−20 °C) Hamamatsu R-928 photomultiplier tube. A 400 MHz Tektronix TDS 380 oscilloscope was used to digitize the data. All lifetimes were averages of 256 laser pulses. Decay rates were determined by fitting the data to a single or double exponential model using a least-squares routine.

2.6. Emission spectral fitting

Emission spectra were fit by a one-mode Franck–Condon analysis using the following equation [39–45]:

$$I(\bar{\nu}) = \sum_{\upsilon_M=0}^{5} \left\{ \left(\frac{E_0 - \upsilon_M \hbar\omega_M}{E_0} \right)^3 \left(\frac{S_M^{\upsilon_M}}{\upsilon_M!} \right) \times \exp\left[-4\ln(2) \left(\frac{\bar{\nu} - E_0 + \upsilon_M \hbar\omega_M}{\Delta\bar{\nu}_{0,1/2}} \right)^2 \right] \right\},$$

where $I(\bar{\nu})$ is the emitted light intensity at the energy $\bar{\nu}$ in cm^{-1}, relative to the intensity of the $0 \rightarrow 0$ transition. E_0 is the energy gap between the zeroth vibrational levels of the ground and excited states. $\hbar\omega_M$ is the quantum spacing for averaged coupled vibrational modes of medium frequency. S_M is the Huang–Rhys factor reflecting nuclear distortion along the medium frequency quantum mode [46]. The relationship between the S and Q (internal) coordinates is given below, where M is the reduced mass of the vibrating system, ω is the frequency of vibration, and ΔQ is the nuclear displacement

$$S = \frac{1}{2}\left(\frac{M\omega}{\hbar}\right)(\Delta Q)^2,$$

where $\Delta\bar{\nu}_{0,1/2}$ is the full-width at half-maximum for individual vibronic lines, and it includes contributions from solvent librations and low frequency molecular modes treated classically. The parameters E_0, S_M, $\hbar\omega_M$ and $\Delta\bar{\nu}_{0,1/2}$ were optimized with a least squares minimization routine using a simplex algorithm [43]. The variance-covariance matrix, correlation matrix and standard deviations for the individual parameters were computed by means of a quadratic extrapolation at the minimum [43].

2.7. Other fits

An estimation of the cavity size of the metallacrown ether ring in complex **1** was obtained by finding the sphere that minimizes the distance between its surface and the center of all six oxygen atoms in the ring. The center coordinates (x_0, y_0, z_0 in Cartesian coordinates) and the radius (r) of the sphere were optimized by minimizing the objective function

$$ssq = \sum_{j=1}^{6} \left(\sqrt{(x_j - x_0)^2 + (y_j - y_0)^2 + (z_j - z_0)^2} - r \right)^2,$$

where x_j, y_j and z_j are the Cartesian coordinates of the jth oxygen atom of the metallacrown ring. The objective function *ssq* was minimized using Mathematica 4.2. Other non-linear fits throughout the manuscript were performed with a Gauss–Newton algorithm included in the JMP Statistical Discovery Software published by the SAS Institute.

3. Results and discussion

3.1. Syntheses of the bis(phosphepin)polyether ligand and the metallacrown ether complexes

The unsymmetrical bis(phosphepin)polyether ligand, (2,2′-$C_{12}H_8O_2$)P(CH_2CH_2O)$_4$P(2,2′-$O_2C_{12}H_8$), was prepared by the reaction of 2,2′-biphenylylenephosphochloridite ester with tetraethyleneglycol in the presence of triethylamine as shown in Fig. 4. The reaction is quantitative if dry reagents are used, as indicated by the presence of a singlet in the $^{31}P\{^1H\}$ NMR spectrum and by the correct integration ratio of aliphatic and aromatic resonances in the ^1H NMR spectra of the crude ligand. In addition, no unexplained resonances should be present in the ^1H NMR spectra of the crude ligand.

The metallacrown ethers, *cis*-[Ru(bpy)$_2$((2,2′-$C_{12}H_8O_2$)P(CH_2CH_2O)$_4$P(2,2′-$O_2C_{12}H_8$))](O_3SCF_3)$_2$ (**1**) and *cis*-[Mo(CO)$_4$((2,2′-$C_{12}H_8O_2$)P(CH_2CH_2O)$_4$P(2,2′-O_2-

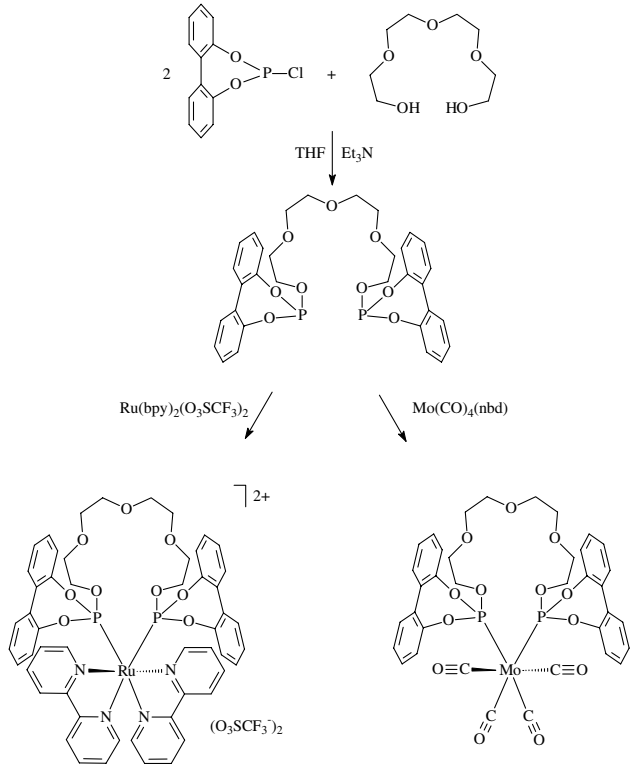

Fig. 4. Synthesis of the bis(phosphepin)polyether ligand and metallacrown ethers.

$C_{12}H_8$))] (**2**), were prepared by the reactions of the ligand with the appropriate metal precursors at moderate dilutions as shown in Fig. 4. Only the monomeric metallacrown ethers were obtained, as indicated by the presence of a singlet in the $^{31}P\{^1H\}$ NMR spectrum of each complex, and these complexes were obtained in high yields. As is the case in previously studied [1,3,2]-dioxaphosphepin ligands derived from 2,2′-biphenol, the single $^{31}P\{^1H\}$ NMR resonance for each metallacrown ether suggests that the enantiomers of the [1,3,2]-dioxaphosphepin rings are rapidly interconverting at ambient temperature [47,48].

3.2. X-ray crystal structures of *1* and *2*

The X-ray crystal structures of **1** and **2** have been determined. An ORTEP drawing of **1** (without the triflate anions) is shown in Fig. 1 and an ORTEP drawing of **2** is shown in Fig. 2. A comparison of the metallacrown ether rings in the two complexes is shown in Fig. 3.

The coordination environment of the metal in each complex is a distorted octahedron. The distortions from the ideal octahedral coordination geometry are more severe in **1** due to the small bite angle of the 2,2′-bipyridine ligand (77.84(17)°). The distortions from octahedral coordination geometry in **2** are much smaller, and they are similar to those previously observed in other metallacrown ethers containing α,ω-bis(phosphite)polyether ligands [15,19].

The [1,3,2]-dioxaphosphepin ligands in **1** and **2** are enantiomeric due to the twist of the 2,2′-biphenoxy groups [48]. The chirality of the ligands can be determined from the torsion angles about the C–C bonds of the 2,2′-biphenoxy groups, given in Table 3. When both torsion angles have the same sign, as is required by the C_2 molecular symmetry in **1** and is also observed for **2**, the enantiomer is either the *R***R** or *S***S** diastereomer. [2] Because both metallacrown ethers crystallize in centrosymmetric space groups, both the *R***R** and *S***S** diastereomers are present in each crystal.

An interesting aspect of the structures of **1** and **2** is the conformation of the metallacrown ether ring. The metallacrown ether rings in both molecules are relatively planar as shown in Figs. 1 and 2. However, the C_2 molecular symmetry in **1** means that the two halves of the ring (split at Ru and O3/O3A) have the same torsion angles. This is not the case for the metallacrown ether ring in **2**. The torsion angles of all but three of the chemically equivalent bonds in **2** (the exceptions are P2–Mo–P1–O1 and P1–Mo–P2–O5; C1–C2–O2–C4 and C8–C7–O4–C6; C2–O2–C3–C4 and C7–O4–C6–C5) are of the same magnitude but differ in sign. This indicates that the metallacrown ether ring in **2** is close to having mirror symmetry with the mirror plane passing through Mo and O3 and perpendicular to the plane of the metallacrown ether rings. This suggests that, as expected, a variety of conformations are available for metallacrown ether rings formed by cis-coordination of the bis(phosphepin)/polyether ligand in **1** and **2**.

The planar, open conformations of the metallacrown ether rings in both **1** and **2** and the orientations of the ether oxygens into the rings, shown in Fig. 3, suggest that the solid-state conformations may not be significantly different from those that could exist in complexes with hard metal cations. To determine the types of cations that could be bound by these metallacrown ethers, a non-linear least-squares optimization was used to estimate the size of a sphere that would fit into the cavity of the metallacrown ether ring in **1**. This calculation demonstrated that the oxygen atoms are relatively evenly distributed about the centroid of the ring (sphere radius = 2.64 Å; deviations: O1 = 0.094 Å, O2 = −0.29 Å, O3 = 0.20 Å) and that the distance between the center of the nearest oxygens and the center of the sphere is 2.35 Å. This distance suggests that Li^+ cations should easily fit into the cavity but that the cavity is marginally too small for a Na^+ cation [10,49] and significantly too small for a Hg^{2+} cation [10].

3.3. Cation complexation by *1* and *2*

The X-ray crystallography results suggest that both **1** and **2** should be able to bind Li^+ cations but that the binding of Na^+ and Hg^{2+} cations is less likely. These results are consistent with those reported by Powell et al. [50,51] for the closely related *cis*-$Mo(CO)_4(Ph_2PO(CH_2CH_2O)_4PPh_2)$ metallacrown ether, which was reported to bind Li^+ but not Na^+ cations. However, when either $LiBPh_4 \cdot 3dme$ (dme = dimethoxyethane) or $NaBPh_4$ are added to a solution of **2** in chloroform-d, no change is observed in either the $^{31}P\{^1H\}$ or ^1H NMR spectra of the solution. This suggests that either strong binding is not occuring or that binding of the cations does not have a measurable effect on either the $^{31}P\{^1H\}$ or ^1H NMR spectra [12].

To further probe cation binding by **2**, a catalytic amount of solid $HgCl_2$was added to a chloroform-d solution of **2**. In all previous studies, this addition has caused a rapid *cis–trans* isomerization of the *cis*-$Mo(CO)_4$(phosphorous-donor ligand)$_2$ center [18]. However, in case of **2**, no isomerization is observed even after several days at ambient temperature. This behavior is unprecedented and suggests that the cation binding abilities of metallacrown ethers derived from

[2] Throughout this paper, *R** and *S** are used to refer to the relative conformations of the 2,2′-biphenyl groups. The first conformation referred to in a molecule is designated *R** by convention.

(2,2′-$C_{12}H_8O_2$)P(CH_2CH_2O)$_4$P(2,2′-$O_2C_{12}H_8$) are quite different from those of other metallacrown ethers, even those derived from $Ph_2P(CH_2CH_2O)_4PPh_2$ that have the same ring size and number of oxygens.

3.4. Photophysical properties of cis-[Ru(bpy)$_2$((2,2′-$C_{12}H_8O_2$)P(CH_2CH_2O)$_4$P(2,2′-$O_2C_{12}H_8$))](O$_3$SCF$_3$)$_2$ (1)

Because the $Ru^{II}(bpy)_2$ chromophore group in complex **1** is an integral part of the metallacrown ring, we expected that its excited state properties could be dependent on the binding state of the ring. The modulation of the excited state parameters of **1** through interactions with cations was assessed by measuring the steady-state and time-dependent emissive characteristics of **1** and of mixtures of **1** and either $LiBF_4$, $NaBPh_4$ or $HgCl_2$ in acetonitrile.

Fig. 5 shows the UV–Vis absorption spectrum of **1** in acetonitrile. As can be seen in the inset in Fig. 5, the lowest energy absorption is a shoulder at about 350 nm. This transition probably corresponds to the $d\pi(Ru) \rightarrow \pi^*(bpy)$ metal-to-ligand (MLCT) transition of the $Ru^{II}(bpy)_2^{2+}$ group. This absorption is blue-shifted by 100 nm with respect to the equivalent MLCT transition in $Ru(bpy)_3^{2+}$ and it is significantly weaker (MLCT at 450 nm, $\varepsilon \approx 10^4$ M^{-1} cm^{-1}) [26,52]. The increased energy gap between the ground and the bpy-based MLCT excited states is probably due to the π-acidic character of the phosphepin groups attached to Ru(II) in **1**. The π-backbonding interaction between the Ru and P atoms decreases the energy of the dπ(Ru) orbitals relative to the π*(bpy) orbitals, increasing the energy required for the transition. The energy gap between the ground and bpy MLCT excited states, E_0, can be obtained from the emission spectrum of **1** and the Franck–Condon analysis of its profile as described in Section 2 (see Fig. 6). The E_0 value for **1** in acetonitrile is 17 290 cm^{-1} (Table 4) and is significantly larger than the corresponding E_0 value of 16 360 cm^{-1} for $Ru(bpy)_3^{2+}$.

Another important difference between complex **1** and $Ru(bpy)_3^{2+}$ is the significantly smaller quantum yield of emission, ϕ_{em} for **1**. In fact, as seen on Table 4, ϕ_{em} for **1** is about 18 times smaller for complex **1**. A reason for this difference is the much weaker absorption cross-section for the MLCT transition in **1**, compared to $Ru(bpy)_3^{2+}$. A decreased absorption cross-section is the consequence of a smaller transition probability for the absorption, **B**, which is proportional to the radiative decay rate, as indicated by the following equation [40,53]:

$$k_r = 8\pi\hbar c n^3 \langle \bar{\nu}^{-3} \rangle^{-1} \mathbf{B}, \quad (1)$$

where k_r is the radiative decay rate, n is the refractive index of the medium, $\bar{\nu}$ is the emission energy in wavenumbers, and $\langle \bar{\nu}^{-3} \rangle^{-1}$ is the inverse of the average value of $\bar{\nu}^{-3}$ for the emission spectrum. The value of $\langle \bar{\nu}^{-3} \rangle^{-1}$ can be calculated using Eq. (2), where I is the emission intensity in units of number of quanta per energy interval per second [40,53]

$$\langle \bar{\nu}^{-3} \rangle^{-1} = \frac{\int I(\bar{\nu})\, d\bar{\nu}}{\int I(\bar{\nu}) \bar{\nu}^{-3}\, d\bar{\nu}}. \quad (2)$$

As the emission quantum yield is the ratio of the observed radiative rate to the sum of all radiative and non-radiative decay channels (Eq. (3)), a decrease in k_r results in a decrease in ϕ_{em}

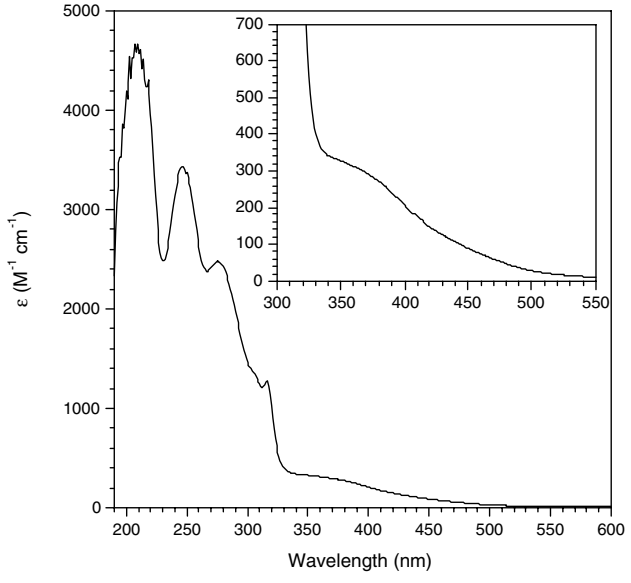

Fig. 5. UV–Vis absorption spectrum of *cis*-[Ru(bpy)$_2$((2,2′-$C_{12}H_8O_2$)P(CH_2CH_2O)$_4$P(2,2′-$O_2C_{12}H_8$))](O$_3$SCF$_3$)$_2$ (**1**) in acetonitrile. The inset shows a magnification of the lowest energy transition.

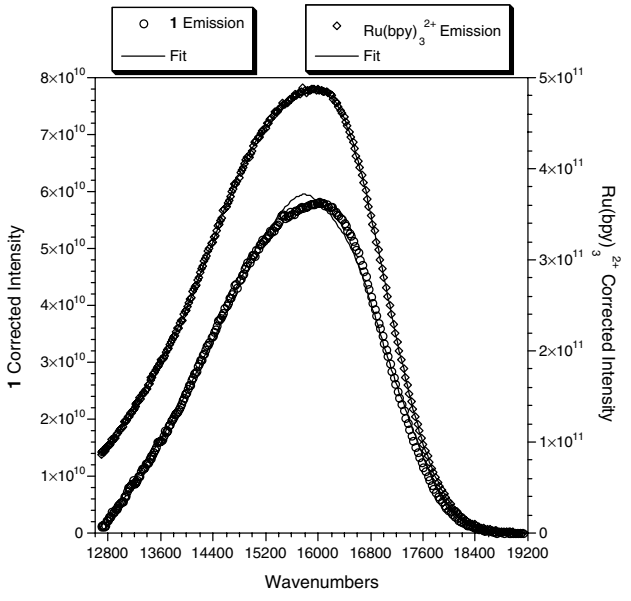

Fig. 6. Emission spectra of *cis*-Ru(bpy)$_3$(PF$_6$)$_2$ and [Ru(bpy)$_2$((2,2′-$C_{12}H_8O_2$)P(CH_2CH_2O)$_4$P(2,2′-$O_2C_{12}H_8$))](O$_3$SCF$_3$)$_2$ (**1**) in acetonitrile with excitation at 400 nm. The solid lines correspond to the Franck–Condon fits (see text).

Table 4
Photophysical properties for $Ru(bpy)_3^{2+}$ and complex **1** in acetonitrile at 25 °C with different ions added (1.1 equivalents)

Complex, ion	A_1[a]	τ_1 (ns)	A_2[a]	τ_2 (ns)	ϕ_{em}[b]	E_0 (cm^{-1})	S_M	$\hbar\omega_M$ (cm^{-1})	$\Delta\bar{\nu}_{0,1/2}$ (cm^{-1})
$Ru(bpy)_3^{2+}$, none		855[c]			0.062[c]	16 360	1.1	1350	1740
1, none	1.0	974	2.2	43	0.0035	17 290	2.8	760	1020
1, Na^+	1.0	950	5.0	32	0.0031	17 340	2.9	700	930
1, Li^+	1.0	938	8.5	28	0.0032	17 330	2.9	720	950
1, Hg^{2+}	1.0	907	1.8	43	0.0030	17 330	2.9	700	940

[a] A_1 and A_2 are the pre-exponential parameters for the emission lifetime fits, see Eq. (4). Their values have been normalized to A_1.
[b] ϕ_{em} is the emission quantum yield.
[c] Data taken from [39].

$$\phi_{em} = \frac{k_r}{\sum k_r + \sum k_{nr}}. \quad (3)$$

The emission decay observed for complex **1** was not single exponential but could be satisfactorily fit to the double exponential function in Eq. (4). The fit parameters A_n and τ_n are listed in Table 4

$$D(t) = A_1 \exp\left(-\frac{t}{\tau_1}\right) + A_2 \exp\left(-\frac{t}{\tau_2}\right). \quad (4)$$

The principal lifetime for **1**, $\tau_1 = 974$ ns is quite comparable to the excited state lifetime of 855 ns for $Ru(bpy)_3^{2+}$. [3] The minor lifetime for **1**, $\tau_2 = 43$ ns is probably associated with a weak and broad emission observable at about 500 nm in Fig. 7. We are currently uncertain regarding the origin of this emission, but as can be observed in Fig. 7, its intensity is sharply dependent on the addition of cations to the solution of complex **1**. This emission may possibly originate from the biphenol groups of the phosphepin groups in complex **1**, as discussed below.

The results from the Franck–Condon profile analysis of the emission spectra are listed in Table 4. There are some very striking differences in the parameters obtained for complex **1** and $Ru(bpy)_3^{2+}$. As can be seen in Fig. 6, the quality of the fit for the emission spectrum of $Ru(bpy)_3^{2+}$ is higher than for the emission spectrum of **1**. We believe that this is due to the overlap of the short-lived emission, discussed above, with the major emission component at 620 nm. Due to this problem, the fit parameters for **1** may contain systematic errors and correlations and should be interpreted carefully. However, the difference in the parameters for **1** and $Ru(bpy)_3^{2+}$ are too large to be explained by fitting problems. As indicated earlier, the energy gap (E_0) for complex **1** is 930 cm^{-1} larger than for $Ru(bpy)_3^{2+}$ due to the π-acid nature of the phosphepin groups. Unexpectedly, the vibrational spacing for the average, medium-frequency coupled vibrational mode ($\hbar\omega_M$) for **1** is nearly half the value seen for $Ru(bpy)_3^{2+}$. $\hbar\omega_M$ is an average of all the molecular vibrational modes coupled to the electronic transition from the excited state to the ground state. The degree of participation of an individual vibrational mode into this average is gauged by the amount of distortion (S) that the molecule undergoes along that mode as a result of the electronic transition, as seen in the following equation:

$$\hbar\omega_M = \frac{\sum_j S_j \hbar\omega_j}{\sum_j S_j}. \quad (5)$$

The 1350 cm^{-1} value of $\hbar\omega_M$ observed for $Ru(bpy)_3^{2+}$ is largely dominated by medium-frequency breathing modes of the bpy ligands, as the occupancy of the π^*(bpy) orbitals changes during the electronic transition. The 760 cm^{-1} value of $\hbar\omega_M$ observed for **1** suggests that bpy breathing modes are much less important in the deactivation of the excited state and lower frequency

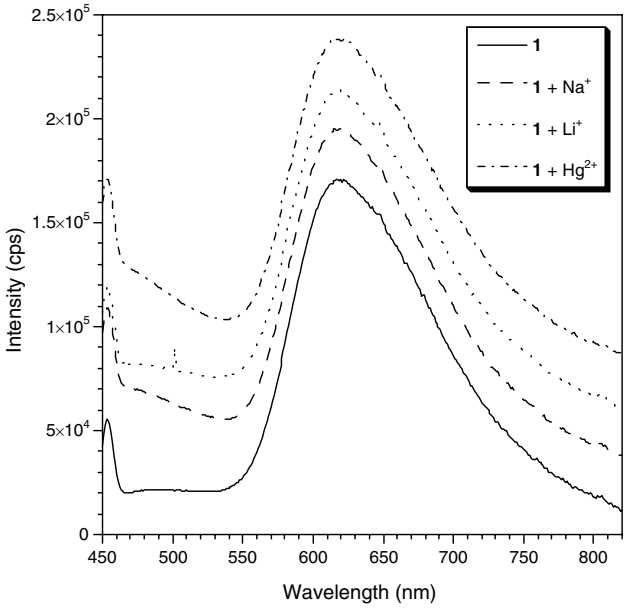

Fig. 7. Emission spectra of *cis*-$[Ru(bpy)_2((2,2'\text{-}C_{12}H_8O_2)P(CH_2CH_2O)_4P(2,2'\text{-}O_2C_{12}H_8))](O_3SCF_3)_2$ (**1**) in acetonitrile with different cations added (1.1 equivalents). The spectra have been offset for clarity. The sharp peaks at 455 nm are water Raman signals.

[3] We estimated the participation of a given component in the double exponential decay by integrating $D(t)$. The integral for a given component is the product of the pre-exponential factor (A) and the lifetime (τ), and it is proportional to the number of photons emitted through that channel.

modes are dominating. These lower frequency modes could involve bending motions of the polyether ring and the phosphepin groups. This significant difference in the value of of $\hbar\omega_M$ could also indicate that the nature of the lowest-lying excited state for **1** is not purely a bpy-based MLCT state, but that the bis(phosphite) ligand may have a significant participation as well. The much larger value of S_M observed for **1** implies a larger degree of excited state distortion and a larger inner-sphere reorganizational energy ($\lambda_i = S_M\hbar\omega_M$; $\lambda_i = 2130$ cm^{-1} for **1** and 1490 cm^{-1} for $Ru(bpy)_3^{2+}$). Finally, the bandwidth for a vibronic line, $\Delta\bar{\nu}_{0,1/2}$, is 720 cm^{-1} smaller for **1** that it is for $Ru(bpy)_3^{2+}$. The reduced value of $\Delta\bar{\nu}_{0,1/2}$ observed for **1** may be a reflection of of a decreased outer-sphere reorganizational energy (λ_o). Ruling out specific solvent effects, a decrease in λ_o may be caused by a decrease in the dipole moment difference between the ground and excited states in **1**. All of the differences in the spectral fitting parameters between **1** and $Ru(bpy)_3^{2+}$ discussed above are consistent with a significantly different electronic and vibrational structure for the lowest-lying excited state of **1**.

When adding different ions to an acetonitrile solution of **1**, subtle changes are observed in the emission spectrum and the excited state lifetime. The results are summarized on Table 4. In general, the long-lived and short-lived components of the emission decay become shorter as cations are introduced into the solution. Also, the emission quantum yield is slightly decreased, by an average of 11%, upon addition of cations. The observed changes are overall small and not particularly specific to the identity or charge of the cation added to the solution. However, the changes in the emission properties of **1** are observable, despite the fact that the interactions between the complex and cations appear to be very weak. Considering the spectral fitting parameters on Table 4, it appears that the presence of the cations produces a slight increase in the energy gap (E_0). Such a change is plausible if the interaction of a cation with the metallacrown ether increases the overall π-acidity of the diphosphite ligand. The vibrational spacing ($\hbar\omega_M$) also shows a tendency to decrease as cations are added to the sample. Again, this could be caused by a weak interaction between the cation and the metallacrown ether. If, as argued above, the metallacrown ether vibrational modes are coupled to the electronic transition, a structural change caused by an interaction with a cation could alter the value of $\hbar\omega_M$ through changes in both vibrational frequencies and excited-state distortions (see Eq. (5)). Another interesting change is the reduction of the bandwidth, $\Delta\bar{\nu}_{0,1/2}$, upon addition of cations to the sample of **1**. A decrease in $\Delta\bar{\nu}_{0,1/2}$ would indicate a reduction in λ_o due to either a loss of specific solvent effects, or a decrease in the dipole moment change during the electronic transition. Another possibility that cannot be ruled out is the change in ionic strength of the medium.

The emission spectra for **1** with different cations added, shown in Fig. 7, exhibit a secondary emission between 450 and 550 nm. This emission is dependent on the identity of the cation added to **1**, and appears to be most intense for Na^+ and Hg^{2+}, and weakest in the absence of a cation. We believe that this emission corresponds to the τ_2 component of the emission decay, and because of its high energy, it could correspond to an emission from the biphenol moieties of the phosphepin groups of **1**. If this is indeed the origin of this emission, its dependence on the presence and nature of the cations added to the sample could arise from structural changes in the metallacrown ether. As the metallacrown ether ring distorts to interact with a cation, the planarity of the biphenol group could be increased, lowering the energy of its emission. This interpretation for the secondary emissions seen in Fig. 7 is still speculative, and they will be studied in more detail in the near future due to their dependency on the presence and nature of cations.

4. Conclusions

This manuscript demonstrates how a chromophoric group, $Ru^{II}(bpy)_2^{2+}$, can be easily incorporated into a metallacrown ether ring. The interactions between the metallacrown ether ring and monoatomic cations in this type of compound could be exploited for sensing applications, as the coordination of the cation can modulate the photophysical properties of the neighboring chromophore. Unfortunately, complex **1** described here seems to interact only weakly with the selected cations, and its emission appears to be *quenched* by interacting with them. Ideally, a cation sensor should be specific, have a large equilibrium constant for the formation of the metallacrown ether–cation complex, and be luminescent in the complexated form. However, as a first example of a $Ru^{II}(bpy)_2^{2+}$-containing metallacrown ether, complex **1** provides important insight into the design of more effective cation sensors. First, specificity and metallacrown ether–cation complex stability issues can be addressed by systematically varying the length of the polyether portion of the metallacrown ring, and by changing the linkage to the phosphorus atoms. Both phosphite and phosphine linkages are possible in designing the chelating ligand. Second, the detailed nature of the emitting state in the metallacrown ether complex must be understood. We are currently planning on deleting the biphenol groups on the chelating ligand to eliminate their possible emission and simplify the spectroscopic measurements. Concurrently, we are also planning on exploiting the cation dependence of the putative biphenol emission in related complexes. Finally, we believe that chromophore-containing metallacrown ethers have great potential for sensing

applications due to their synthetic versatility and their possibilities for chromophore–host interactions.

5. Supplementary material

Tables of complete crystallographic information for compounds **1** and **2**. This material is available free of charge via the Internet at http://pubs.acs.org.

References

[1] H.-G. Löhr, F. Vögtle, Acc. Chem. Res. 18 (1985) 65.
[2] Ç. Erk, Ind. Eng. Chem. Res. 39 (2000) 3582.
[3] K. Rurack, M. Kollmannsberger, U. Resch-Genger, J. Daub, J. Am. Chem. Soc. 122 (2000) 968.
[4] A. Yamauchi, T. Hayashita, S. Nishizawa, M. Watanabe, N. Teramae, J. Am. Chem. Soc. 121 (1999) 2319.
[5] H. He, M.A. Mortellaro, M.J.P. Leiner, S.T. Young, R.J. Fraatz, J.K. Tusa, Anal. Chem. 75 (2003).
[6] D.B. MacQueen, K.S. Schanze, J. Am. Chem. Soc. 113 (1991) 6108.
[7] L.J. Charbonnière, R.F. Ziessel, C.A. Sams, A. Harriman, Inorg. Chem. 42 (2003) 3466.
[8] S. Fery-Forgues, M.-T. Le Bris, J.-P. Guetté, B. Valeur, J. Phys. Chem. 92 (1988) 6233.
[9] G.M. Gray, Comments Inorg. Chem. 17 (1995) 95.
[10] G.M. Gray, C.H. Duffey, Organometallics 14 (1995) 238.
[11] G.M. Gray, C.H. Duffey, Organometallics 14 (1995) 245.
[12] G.M. Gray, F.P. Fish, C.H. Duffey, Inorg. Chim. Acta 246 (1996) 229.
[13] P.J. Stang, D.H. Cao, K. Chen, G.M. Gray, D.C. Muddiman, R.D. Smith, J. Am. Chem. Soc. 119 (1997) 5163.
[14] C.H. Duffey, C.H. Lake, G.M. Gray, Organometallics 17 (1998) 3550.
[15] M. Hariharasarma, C.H. Lake, C.L. Watkins, G.M. Gray, J. Organomet. Chem. 580 (1998) 328.
[16] H. Maheswaran, C.L. Watkins, G.M. Gray, Organometallics 19 (2000) 1232.
[17] G.M. Gray, D.C. Smith Jr., C.H. Duffey, Inorg. Chim. Acta 300–302 (2000) 581.
[18] C.H. Duffey, C.H. Lake, G.M. Gray, Inorg. Chim. Acta 317 (2001) 199.
[19] J.M. Butler, M.J. Jablonski, G.M. Gray, Organometallics 22 (2003) 1081.
[20] D.C. Smith Jr., G.M. Gray, Inorg. Chem. 37 (1998) 1791.
[21] D.C. Smith Jr., G.M. Gray, J. Chem. Soc., Dalton Trans. (2000) 677.
[22] F. Vogtle, Host Guest Complexes Chemistry II, Springer, Berlin, 1982.
[23] L.F. Lindoy, The Chemistry of Macrocyclic Ligand Complexes, Cambridge University Press, Cambridge, 1989.
[24] F.V.J.M. van Veggel, W. Verboom, D.N. Reinhoudt, Chem. Rev. 94 (1994) 279.
[25] B.R. Cameron, S.S. Corrent, S.J. Loeb, Angew. Chem., Int. Ed. Engl. 34 (1995) 23.
[26] A. Juris, V. Balzani, F. Barigelletti, S. Campagna, P. Belser, A. Von Zelewsky, Coord. Chem. Rev. 84 (1988) 85.
[27] F. Barigelletti, L. Flamigni, V. Balzani, J.P. Collin, J.P. Sauvage, A. Sour, E.C. Constable, A. Thompson, Coord. Chem. Rev. 132 (1994) 209.
[28] V. Balzani, A. Juris, M. Venturi, S. Campagna, S. Serroni, Chem. Rev. 96 (1996) 759.
[29] P.Y. Chen, T.J. Meyer, Chem. Rev. 98 (1998) 1439.
[30] C. Creutz, Prog. Inorg. Chem. 30 (1983) 1.
[31] T.J. Meyer, H. Taube, in: G. Wilkinson, R.D. Gillard, J.A. McCleverty (Eds.), Comprehensive Coordination Chemistry, Pergamon Press, London, 1987, p. 331.
[32] N. Sutin, B.S. Brunschwig, C. Creutz, J.R. Winkler, Pure Appl. Chem. 60 (1988) 1817.
[33] M.J. Cook, A.P. Lewis, G.S.G. McAuliffe, V. Skarda, A.J. Thompson, J.L. Glasper, D.J. Robbins, J. Chem. Soc., Perkin Trans. 2 (1984) 1293.
[34] M.J. Cook, A.P. Lewis, G.S.G. McAuliffe, V. Skarda, A.J. Thompson, J.L. Glasper, D.J. Robbins, J. Chem. Soc., Perkin Trans. 2 (1984) 1303.
[35] W. Ehrl, R. Ruck, H. Vahrenkamp, J. Organomet. Chem. 56 (1973) 285.
[36] L.V. Verizhnikov, P.A. Kirpichnikov, Zh. Obshch. Khim. 37 (1966) 1355.
[37] M.J. Ridd, D.J. Gakowski, G.E. Sneddon, R.F. Keene, J. Chem. Soc., Dalton Trans. (1992) 1949.
[38] G.M. Sheldrick, SHELXTL-NT ver. 510, Bruker AXS, Inc., Madison, WI, 1999.
[39] J.V. Caspar, T.J. Meyer, J. Am. Chem. Soc. 105 (1983) 5583.
[40] E.M. Kober, J.V. Caspar, R.S. Lumpkin, T.J. Meyer, J. Phys. Chem. 90 (1986) 3722.
[41] J.V. Caspar, Ph.D. Thesis, University of North Carolina at Chapel Hill, 1982.
[42] R.S. Lumpkin, Ph.D. Thesis, University of North Carolina at Chapel Hill, 1987.
[43] J.P. Claude, Ph.D. Thesis, University of North Carolina at Chapel Hill, 1995.
[44] J.P. Claude, T.J. Meyer, J. Phys. Chem. 99 (1995) 51.
[45] J.V. Caspar, T.J. Meyer, Inorg. Chem. 22 (1983) 2444.
[46] K. Huang, A. Rhys, Proc. R. Soc. A 204 (1950) 406.
[47] M. Hariharasarma, C.H. Lake, C.L. Watkins, G.M. Gray, Organometallics 18 (1999) 2593.
[48] H. Byrd, J.D. Harden, J.M. Butler, M.J. Jablonsky, G.M. Gray, Organometallics 22 (2003) 4198.
[49] A.L. Bajaj, N.S. Poonia, Coord. Chem. Rev. 87 (1988) 55.
[50] J. Powell, A. Kuskis, C.J. May, S.C. Nyburg, S.J. Smith, J. Am. Chem. Soc. 103 (1981) 5941.
[51] J. Powell, M.R. Gregg, A. Kuskis, C.J. May, S.J. Smith, Organometallics 8 (1989) 2918.
[52] O. Horváth, K.L. Stevenson, Charge Transfer Photochemistry of Coordination Compounds, VCH, New York, 1993.
[53] S.J. Strickler, R.A. Berg, J. Chem. Phys. 37 (1962) 814.

Available online at www.sciencedirect.com
SCIENCE DIRECT®
Polyhedron 23 (2004) 1731–1737
POLYHEDRON
www.elsevier.com/locate/poly

Synthesis and structure of Mn(II), Cu(II) and Zn(II) complexes containing bis-imidazole ligands

Suaad Abuskhuna [a], Malachy McCann [a,*], John Briody [a], Michael Devereux [b], Vickie McKee [c]

[a] Department of Chemistry, St. Patrick's College, National University of Ireland Maynooth, Maynooth, Co. Kildare, Ireland
[b] Dublin Institute of Technology, Cathal Brugha Street, Dublin, Ireland
[c] Chemistry Department, Loughborough University, Loughborough, Leics LE11 3TU, UK

Received 9 December 2003; accepted 5 April 2004

Abstract

A family of bis-imidazole ligands based on the parent bis(imidazol-2-yl)methane structure, and which can mimic multi-histidine coordination in biological systems, have been complexed to Mn(II), Cu(II) and Zn(II) centres. Five complexes were characterised by X-ray crystallography. A common structural feature of the ligands is that the two imidazole rings, which have a single spacer tetrahedral carbon atom between them, form stable, six-membered *N*,*N*′ chelate rings with the metals.
© 2004 Elsevier Ltd. All rights reserved.

Keywords: Bis-imidazole; Metal complexes; X-ray structures; Manganese(II); Copper(II); Zinc(II)

1. Introduction

The imidazole function of histidine is a ubiquitous ligand in Zn(II) and Cu(II) metalloproteins. In these enzymes the three-dimensional structure of the peptide chains effectively brings together two or more distant imidazole moieties close enough to simultaneously bind the central metal ion. Thus, there is great interest in bis-imidazole ligands which can mimic multi-histidine co-ordination in biological systems [1,4]. The present study centres on the synthesis and structural characterisation of Mn(II), Cu(II) and Zn(II) complexes of the *N*,*N*′ chelating ligands, bis(imidazol-2-yl)methane (2-BIM), bis(-1-methyl-1H-imidazol-2-yl)methane (2-BIM(Me)), bis(1-benzyl-1H-imidazol-2-yl)methanol (2-BIM(Bz)OH), 3-(2-{[1-(2-cyanoethyl)-1H-imidazol-2-yl]methyl}-1H-imidazol-1-yl)propanenitrile (2-BIM(CN)) and 1-(2,4-dichlorobenzyl)-2-{[1-(2,4-dichlorobenzyl)-1H-imidazol-2- yl] methyl}-1H-imidazole (2-BIM(ClBz)) (Fig. 1). A common structural feature of the ligands is that the two imidazole rings have a single spacer tetrahedral carbon atom and are able to form a stable six-membered chelate ring to the metal centre. Although a number of metal complexes of 2-BIM and a few of its derivatives have already been reported [1–18], relatively few of these [1,8,9,14,16,17] have been structurally characterised.

2. Results and discussion

In general, the Mn(II), Cu(II) and Zn(II) complexes were all prepared in a similar manner with the particular metal perchlorate salt being reacted with the bis-imidazole ligand in either a 1:2 or 1:3 molar ratio. All of the complexes were essentially insoluble in water. The X-ray crystal structure of $[Zn(2\text{-}BIM)_2](ClO_4)_2$ is shown in Fig. 2 and important bond lengths and angles are given in Table 1. The Zn(II) ion sits on a 2-fold axis (site symmetry 2) and the geometry is significantly distorted from regular tetrahedral. The Zn–N1–N4 plane is inclined at 66.50(5)° to the Zn–N1A–N4A plane and within each 2-BIM ligand the five-membered rings are inclined at 16.8(1)° to each other. Hydrogen-bonding involving the

* Corresponding author. Tel.: +353-1-7083767; fax: +353-1-7083815.
E-mail address: mmcann@may.ie (M. McCann).

0277-5387/$ - see front matter © 2004 Elsevier Ltd. All rights reserved.
doi:10.1016/j.poly.2004.04.015

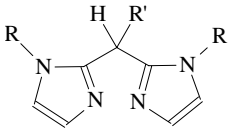

	R	R'
2-BIM	H	H
2-BIM(Me)	Me	H
2-BIM(Bz)OH	$PhCH_2$	OH
2-BIM(CN)	$NC(CH_2)_2$	H
2-BIM(ClBz)	Cl_2PhCH_2	H

Fig. 1. Ligand symbols and structures.

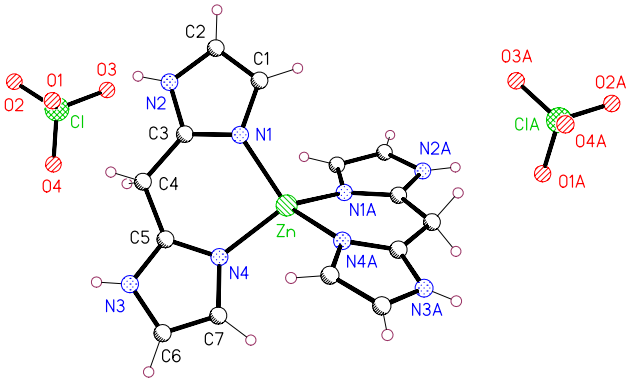

Fig. 2. X-ray crystal structure of $[Zn(2\text{-}BIM)_2](ClO_4)_2$.

Table 1
Selected bond lengths (Å) and angles (°) for $[Zn(2\text{-}BIM)_2](ClO_4)_2$

Bond lengths	
Zn–N(1)	1.9911(13)
Zn–N(4)	1.9911(13)
Bond angles	
N(1)#1–Zn–N(1)	105.39(8)
N(1)–Zn–N(4)#1	132.68(6)
N(1)–Zn–N(4)	94.06(5)
N(4)#1–Zn–N(4)	103.70(8)

Symmetry transformations used to generate equivalent atoms: #1 $-x, y, -z + 3/2$.

perchlorate anion and the amine groups of the cation link the ions into puckered two-dimensional sheets (Fig. 3). The bidentate coordination mode of the 2-BIM ligands in the complex is the same as that found in the structurally characterized Cu(II) analogue $[Cu(2\text{-}BIM)_2(ClO_4)_2]$ [1] in which the metal sits in a square plane of 4N and with weak bonding interactions with an oxygen atom from each of the apical perchlorate ions. As expected, the mean metal–N bond distances in $[Zn(2\text{-}BIM)_2](ClO_4)_2$ and $[Cu(2\text{-}BIM)_2(ClO_4)_2]$ are very similar.

Mn(II), Cu(II) and Zn(II) complexes containing the ligand 2-BIM(Me) were synthesised and the latter two structurally characterised (Figs. 4 and 5, and Tables 2 and 3). $[Cu(2\text{-}BIM(Me))_2](ClO_4)_2$ and $[Zn(2\text{-}BIM(Me))_2](ClO_4)_2$ are isomorphous. The metal ion (site symmetry 222) lies at the intersection of three two 2-fold axes, one passing through the methylene carbon atoms, one bisecting the N1–N1b and N1a–N1c vectors and one

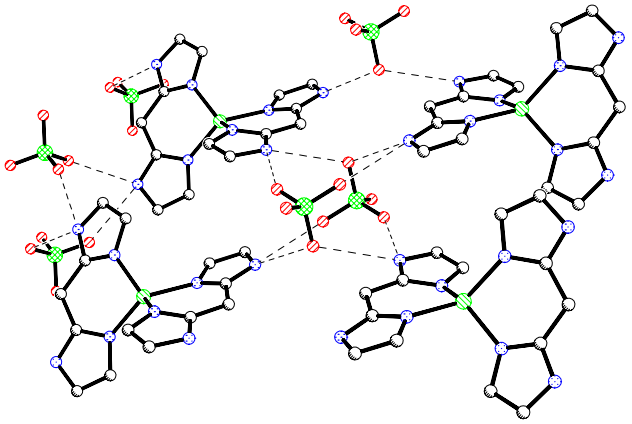

Fig. 3. H-bonding in $[Zn(2\text{-}BIM)_2](ClO_4)_2$.

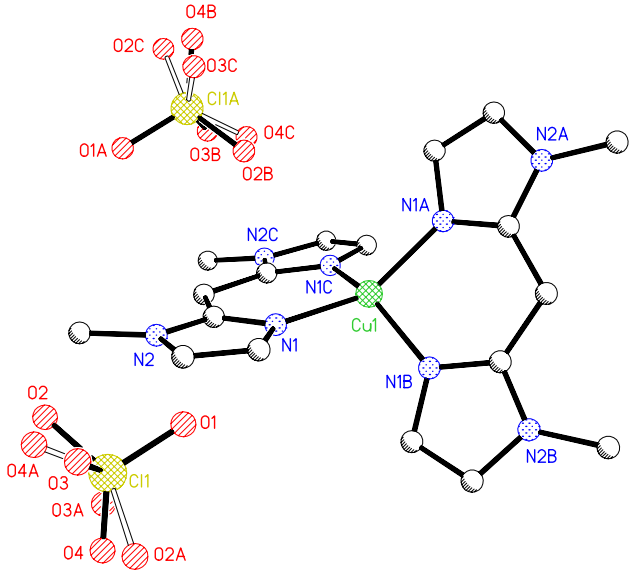

Fig. 4. X-ray crystal structure of $[Cu(2\text{-}BIM(Me))_2](ClO_4)_2$.

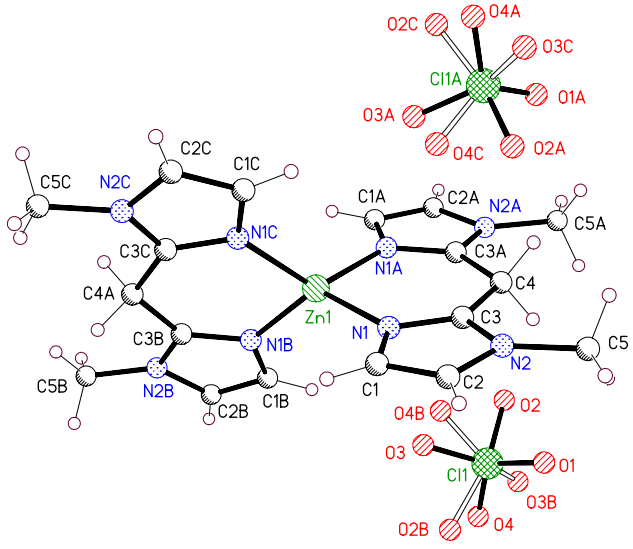

Fig. 5. X-ray crystal structure of $[Zn(2\text{-}BIM(Me))_2](ClO_4)_2$.

Table 2
Selected bond lengths (Å) and angles (°) for $[Cu(2\text{-}BIM(Me))_2](ClO_4)_2$

Bond lengths	
Cu(1)–N(1)	1.9407(17)
Bond angles	
N(1)#1–Cu(1)–N(1)	97.97(10)
N(1)–Cu(1)–N(1)#2	93.19(10)
N(1)–Cu(1)–N(1)#3	143.67(10)

Symmetry transformations used to generate equivalent atoms: #1 $y-1/4, x+1/4, -z+1/4$; #2 $-y+5/4, -x+5/4, -z+1/4$; #3 $-x+1, -y+3/2, z+0$.

Table 3
Selected bond lengths (Å) and angles (°) for $[Zn(2\text{-}BIM(Me))_2](ClO_4)_2$

Bond lengths	
Zn(1)–N(1)	1.969(2)
Bond angles	
N(1)#1–Zn(1)–N(1)	129.32(11)
N(1)–Zn(1)–N(1)#2	95.54(11)
N(1)–Zn(1)–N(1)#3	105.65(12)

Symmetry transformations used to generate equivalent atoms: # 1 $-x+0, -y+1/2, z+0$; #2 $-y+1/4, -x+1/4, -z+1/4$; #3 $y-1/4, x+1/4, -z+1/4$.

bisecting N1–N1c and N1a–N1b. Each ligand is essentially planar but the two structures differ in the interplanar angle between the two ligands. The value for the zinc complex (64.02(2)°) shows it is further along the path from square planar to tetrahedral than the copper analogue (59.22(2)°).

For the 2-BIM(CN) ligand Mn(II), Cu(II) and Zn(II) complexes were prepared and the latter was structurally characterized. The X-ray crystal structure of $[Zn(2\text{-}BIM(CN))_2](ClO_4)_2 \cdot 0.5MeCN$ (Fig. 6 and Table 4) shows the asymmetric unit to contain two independent

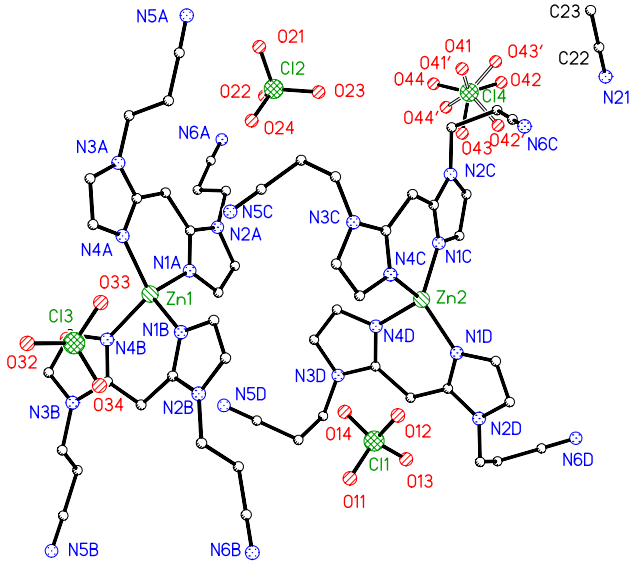

Fig. 6. X-ray crystal structure of $[Zn(2\text{-}BIM(CN))_2](ClO_4)_2 \cdot 0.5MeCN$.

Table 4
Selected bond lengths (Å) and angles (°) for $[Zn(2\text{-}BIM(CN))_2](ClO_4)_2 \cdot 0.5MeCN$

Bond lengths	
Zn(1)–N(1B)	1.975(2)
Zn(1)–N(4A)	1.976(2)
Zn(1)–N(1A)	1.982(2)
Zn(1)–N(4B)	1.984(2)
Zn(2)–N(1D)	1.972(2)
Zn(2)–N(1C)	1.981(2)
Zn(2)–N(4C)	1.989(2)
Zn(2)–N(4D)	2.012(2)
Bond angles	
N(1B)–Zn(1)–N(4A)	123.14(9)
N(1B)–Zn(1)–N(1A)	113.43(9)
N(4A)–Zn(1)–N(1A)	94.86(8)
N(1B)–Zn(1)–N(4B)	95.09(8)
N(4A)–Zn(1)–N(4B)	113.75(8)
N(1A)–Zn(1)–N(4B)	118.48(8)
N(1D)–Zn(2)–N(1C)	128.15(9)
N(1D)–Zn(2)–N(4C)	121.15(9)
N(1C)–Zn(2)–N(4C)	94.76(9)
N(1D)–Zn(2)–N(4D)	94.59(9)
N(1C)–Zn(2)–N(4D)	111.53(9)
N(4C)–Zn(2)–N(4D)	105.47(9)

$[Zn(2\text{-}BIM(CN))_2]^{2+}$ cations, four perchlorate anions and one molecule of acetonitrile solvate. The two cations differ principally in the orientation of the "tails"; these are *anti* on both ligand molecules bonded to Zn2 but one ligand bonded to Zn1 has the tail *syn*. The geometry at the metal ion in each case is approaching tetrahedral but the small bite angle of the ligand leads to significant distortion. One of the perchlorate anions is disordered and this has been modelled as 50% occupancy of two sites related by rotation about one of the Cl–O bonds.

The X-ray crystal structure of $[Cu(2\text{-}BIM(Bz)OH)_2(H_2O)_2](ClO_4)_2$ (Fig. 7 and Table 5) shows the cation to be centrosymmetric with the Cu(II) ion having tetragonal geometry and site symmetry $\bar{1}$, being coordinated by

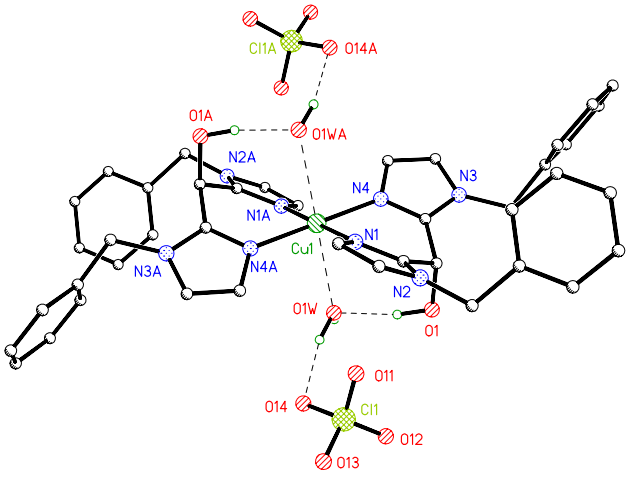

Fig. 7. X-ray crystal structure of $[Cu(2\text{-}BIM(Bz)OH)_2(H_2O)_2](ClO_4)_2$.

Table 5
Selected bond lengths (Å) and angles (°) for $[Cu(2\text{-}BIM(Bz)OH)_2(H_2O)_2](ClO_4)_2$

Bond lengths	
Cu(1)–N(4)	1.9871(14)
Cu(1)–N(1)	1.9899(14)
Cu(1)–O(1W)	2.6307(14)
Bond angles	
N(4)–Cu(1)–N(1)	86.75(6)
N(4)–Cu(1)–O(1W)	92.04(5)
N(1)–Cu(1)–O(1W)	88.09(5)

Symmetry transformations used to generate equivalent atoms: #1 $-x+1, -y+1, -z+1$.

the 4N atoms from the two bidentate 2-BIM(Bz)OH ligands and two axial water molecules. The alcohol groups of the 2-BIM(Bz)OH ligands are each hydrogen-bonded to one of the coordinated water molecules and these have further hydrogen bonds to the perchlorate anion and to the alcohol group of a neighboring cation. The H-bonding links the complexes into one-dimensional chains (parallel to the *a*-axis) and there are additional H-bonding interactions between the chains.

Although the Mn(II), Cu(II) and Zn(II) complexes of the 2-BIM(ClBz) ligand were synthesised and characterised using IR and microanalytical data none of these provided crystals suitable for X-ray crystallographic analysis.

Prompted by the antitumor activity reported for the Pt(II) complex $[Pt(2\text{-}BIM(Me)OH)Cl_2]$ [16] and the use of the diiron(II) complex $[Fe_2(HCO_2)_4\{\text{-}BIM(Me)OMe(Ph)\}_2]$ to model features of polyiron-oxo proteins [18] we have already initiated the next phase of our studies with the bis-imidazole ligands. A number of the ligands have been complexed to silver(I) to give novel dimeric complexes and these have been shown to exhibit good antimicrobial activity in vitro [19].

3. Experimental

Chemicals were purchased from commercial sources and, unless specified, were used without further purification. Literature methods were used to prepare 2-BIM [20,21], 2-BIM(Me) [22], BIM(Bz)OH [23], 2-BIM(CN) [19] and 2-BIM(ClBz) [19]. Infrared spectra of solids (in a KBr matrix) were recorded in the region 4000–400 cm^{-1} on a Nicolet FT-IR Impact 400D infrared spectrometer and ^1H NMR spectra were run on a Bruker Avance 300 MHz instrument. Microanalytical data were provided by the Microanalytical Laboratory, National University of Ireland, Cork, Ireland.

3.1. $[Zn(2\text{-}BIM)_2](ClO_4)_2$

A solution of $Zn(ClO_4)_2 \cdot 6H_2O$ (0.62 g, 1.67 mmol) in methanol (5 cm^3) was added to a stirred solution of 2-BIM (0.5 g, 3.37 mmol) in methanol (15 cm^3). The resulting clear solution was stirred for 1 h and then sat aside to slowly evaporate at room temperature. The product formed as colourless crystals. The solid was filtered off, washed with methanol and allowed to air dry. Yield: 0.2 g (21%). The complex was soluble in acetonitrile and methanol and was insoluble in water. *Anal*. Calc.: C, 30.4; H, 2.88, N, 20.00. Found: C, 30.00; H, 2.82; N19.91%. IR: 3215, 1632, 1574, 1498, 1402, 1281, 1095, 932, 868, 746, 624 cm^{-1}. ^1H NMR (ppm DMSO): 12.88 (4H, s), 7.30 (4H, s), 6.75 (4H, s), 4.39 (4H, s).

3.2. $[Mn(2\text{-}BIM(Me))_3](ClO_4)_2 \cdot 2H_2O$

A solution of $Mn(ClO_4)_2 \cdot 6H_2O$ (0.137 g, 0.38 mmol) in methanol (3 cm^3) was added to a solution of 2-BIM(Me) (0.2 g, 1.14 mmol) in methanol (10 cm^3) and the mixture stirred for 1 h at room temperature. The precipitated white solid was filtered off, washed with methanol and dried in air. Yield: 0.18 g (58%). The complex was soluble in acetonitrile and hot acetone and was insoluble in water. *Anal*. Calc.: C, 39.61; H, 4.92; N, 20.53. Found: C, 39.52; H, 4.48; N, 20.69%. IR: 3432, 2927, 1640, 1510, 1406, 1289, 1092, 956, 898, 812, 763, 658, 624, 461 cm^{-1}.

3.3. $[Cu(2BIM(Me))_2](ClO_4)_2 \cdot H_2O$ and $[Cu(2\text{-}BIM(Me))_2](ClO_4)_2$

A solution of $Cu(ClO_4)_2 \cdot 6H_2O$ (0.21 g, 0.57 mmol) in methanol (3 cm^3) was added to a solution of 2-BIM(Me) (0.2 g, 1.14 mmol) in methanol (10 cm^3) and the mixture stirred for 1 h at room temperature. The precipitated blue solid $[Cu(2\text{-}BIM(Me))_2](ClO_4)_2 \cdot H_2O$ was filtered off, washed with MeOH and diethyl ether and then air-dried. Yield: 0.3 g (57%). The complex was soluble in acetonitrile and was insoluble in water. *Anal*. Calc.: C, 34.15; H, 4.14; N, 17.70. Found: C, 34.08; H, 3.61; N, 17.29%. IR: 3511, 3138, 1529, 1415, 1300, 1108, 980, 811, 766, 628, 483 cm^{-1}. A sample of the anhydrous complex $[Cu(2\text{-}BIM(Me))_2](ClO_4)_2$ suitable for X-ray analysis was obtained following the same method above except replacing the solvent MeOH with MeCN. Bright blue crystals of the product formed when the reaction solution was allowed to slowly evaporate in air.

3.4. $[Zn(2\text{-}BIM(Me))_2](ClO_4)_2$

A solution of $Zn(ClO_4)_2 \cdot 6H_2O$ (0.21 g, 0.56 mmol) in methanol (3 cm^3) was added to a stirred solution of 2-BIM(Me) (0.2 g, 1.14 mmol) in methanol (10 cm^3). The mixture was stirred for 1 h at room temperature and the white product was filtered off, washed with methanol and allowed to air dry. The solid was recrystallised from a 1:1 acetonitrile:acetone mixture. Yield: 0.19 g (54%).

The complex was soluble in acetonitrile and hot acetone and was insoluble in water. *Anal.* Calc.: C, 35.04; H, 3.89; N, 18.17. Found: C, 34.70; H, 3.92; N, 17.99%. IR: 3460, 3138, 2958, 1529, 1421, 1338, 1300, 1102, 981, 936, 772, 627, 477 cm^{-1}. ^1H NMR (ppm DMSO): 7.23 (4H, s), 6.58 (4H, s), 4.32 (4H, s), 3.65 (12H, s).

3.5. $[Cu(2BIM(Bz)OH)_2(H_2O)_2](ClO_4)_2$

A solution of $Cu(ClO_4)_2 \cdot 6H_2O$ (0.21 g, 0.57 mmol) in methanol (3 cm^3) was added to a stirred solution of 2-BIM(Bz)OH (0.4 g, 1.16 mmol) in methanol (10 cm^3). The mixture was stirred for 4 h at room temperature, giving a purple solid product. The solid was filtered off, washed with methanol and air-dried. The complex was recrystallised from acetonitrile. Yield: 0.38 g (65%). The complex was soluble in acetonitrile and was insoluble in water. *Anal.* Calc.: C, 51.09; H, 4.49; N, 11.35. Found: C, 51.01; H, 4.47; N, 11.43%. IR: 3344, 3138, 1714, 1504, 1459, 1364, 1287, 1114, 968, 926, 836, 714, 628 cm^{-1}.

3.6. $[Mn(2\text{-}BIM(CN))_3](ClO_4)_2 \cdot 2H_2O$

$Mn(ClO_4)_2 \cdot 6H_2O$ (0.14 g, 0.39 mmol) in methanol (3 cm^3) was added to a solution of 2-BIM(CN) (0.3 g, 1.18 mmol) in methanol (7 cm^3) and the mixture stirred for 1 h at room temperature. The resulting white precipitate was filtered off, washed with methanol and then dried in air. Yield: 0.21 g (51%). The complex was soluble in acetonitrile and hot acetone and was insoluble in water. *Anal.* Calc.: C, 44.49; H, 4.40; N, 23.95. Found: C, 44.85; H, 4.02; N, 23.58%. IR: 3447, 3138, 2264, 1542, 1510, 1421, 1293, 1108, 958, 916, 756, 627 cm^{-1}.

3.7. $[Cu(2\text{-}BIM(CN))_2](ClO_4)_2 \cdot 2H_2O$

$Cu(ClO_4)_2 \cdot 6H_2O$ (0.14 g, 0.39 mmol) in methanol (3 cm^3) was added to a solution of 2-BIM(CN) (0.2 g, 0.79 mmol) in methanol (7 cm^3) and the mixture was stirred for 1 h at room temperature. The precipitated purple solid was filtered off, washed with methanol and then dried in air. Yield: 0.21 g (66%). The complex was soluble in acetonitrile and was insoluble in water. *Anal.* Calc.: C, 38.49; H, 3.97; N, 20.72. Found: C, 39.35; H, 3.44; N, 20.52%. IR: 3434, 3151, 2984, 2264, 1708, 1632, 1511, 1427, 1376, 1294, 1096, 974, 919, 753, 627 cm^{-1}.

3.8. $[Zn(2\text{-}BIM(CN))_2](ClO_4)_2 \cdot H_2O$ and $[Zn(2BIM(CN))_2](ClO_4)_2 \cdot 0.5MeCN$

$Zn(ClO_4)_2 \cdot 6H_2O$ (0.21 g, 0.56 mmol) in methanol (3 cm^3) was added to a solution of 2-BIM (CN) (0.3 g, 1.18 mmol) in methanol (10 cm^3) and the reaction mixture stirred at room temperature for 1 h. The white precipitate of $[Zn(2\text{-}BIM(CN))_2](ClO_4)_2 \cdot H_2O$ was filtered off, washed with methanol and then air dried. Yield = 0.33 g (70%). The complex was soluble in acetonitrile and was insoluble in water. *Anal.* Calc.: C, 39.48; H, 3.83; N, 21.26. Found: C, 39.62; H, 3.33; N, 20.49%. IR: 3524, 3151, 2984, 2264, 1632, 1517, 1421, 1357, 1300, 1102, 981, 919, 820, 759, 628, 474 cm^{-1}. ^1H NMR (ppm DMSO): 7.47 (4H, s), 6.78 (4H, s), 4.56 (8H, t), 4.5 (4H, s), 3.17 (8H, t). Recrystallising $[Zn(2\text{-}BIM(CN))_2](ClO_4)_2 \cdot H_2O$ from acetonitrile afforded crystals of $[Zn(2\text{-}BIM(CN))_2](ClO_4)_2 \cdot 0.5MeCN$ suitable for X-ray studies.

3.9. $[Mn(2\text{-}BIM(ClBz))_2](ClO_4)_2 \cdot 5H_2O$

$Mn(ClO_4)_2 \cdot 6H_2O$ (0.05 g, 0.14 mmol) was added to a solution of 2-BIM(ClBz) (0.2 g, 0.43 mmol) in methanol (7 cm^3) and the mixture stirred for 1 h. The resulting white precipitate was filtered off, washed with methanol and then air-dried. Yield: 0.16 g (89%). The complex was soluble in hot acetonitrile and insoluble in water. *Anal.* Calc.: C, 39.53; H, 3.32; N, 8.78. Found: C, 39.57; H, 2.73; N, 8.59%. IR: 3445, 1590, 1480, 1393, 1276, 1116, 1012, 953, 864, 830, 744, 701, 627, 556, 507 cm^{-1}.

3.10. $[Cu(2\text{-}BIM(ClBz))_2](ClO_4)_2 \cdot H_2O$

A solution of $Cu(ClO_4)_2 \cdot 6H_2O$ (0.08 g, 0.22 mmol) in methanol (3 cm^3) was added to a stirred solution of 2-BIM(ClBz) (0.2g, 0.43 mmol) in methanol (10 cm^3). The mixture was stirred for 1 h at room temperature, giving a blue solid product. The solid was filtered off, washed with methanol and air-dried. Yield: 0.08 g (31%). The complex was soluble in hot acetonitrile and was insoluble in water. *Anal.* Calc.: C, 41.58; H, 2.80; N, 9.24. Found: C, 41.63; H, 2.52; N, 8.99%. IR: 3461, 2923, 1595, 1560, 1517, 1482, 1448, 1390, 1351, 1297, 1102, 977, 862, 843, 821, 752, 625, 554 cm^{-1}.

3.11. $[Zn(2\text{-}BIM(ClBz))_2](ClO_4)_2$

A solution of $Zn(ClO_4)_2 \cdot 6H_2O$ (0.08 g, 0.21 mmol) in methanol (3 cm^3) was added to a stirred solution of 2-BIM(ClBz) (0.2 g, 0.43 mmol) in methanol (7 cm^3). The mixture was stirred for 1 h at room temperature and the white product was filtered off, washed with methanol and allowed to air dry. Yield: 0.17 g (65%). The complex was soluble in hot acetonitrile and was insoluble in water. *Anal.* Calc.: 42.14; H, 2.67; N, 9.36. Found: C, 42.05; H, 2.57; N, 9.08%. IR: 3119, 1590, 1560, 1517, 1478, 1395, 1351, 1302, 1107, 980, 862, 843, 816, 755, 625, 554 cm^{-1}. ^1H NMR (ppm DMSO): 7.87 (4H, d, 2.0 Hz), 7.51–7.53 (8H, m), 6.86–6.95 (8H, m), 5.60 (8H, s), 4.43 (4H, s).

3.12. X-ray crystallography

All of the data were collected at 150 K on a Bruker SMART 1000 diffractometer using Mo Kα radiation

Table 6
X-ray crystallographic data

Identification code	$[Zn(2\text{-}BIM)_2](ClO_4)_2$	$[Cu(2\text{-}BIM(Me))_2](ClO_4)_2$	$[Zn(2\text{-}BIM(Me))_2](ClO_4)_2$	$[Zn(2\text{-}BIM(CN))_2](ClO_4)_2 \cdot 0.5MeCN$	$[Cu(2\text{-}BIM(Bz)OH)_2(H_2O)_2](ClO_4)_2$
Empirical formula	$C_{14}H_{16}Cl_2N_8O_8Zn$	$C_{18}H_{24}Cl_2CuN_8O_8$	$C_{18}H_{24}Cl_2N_8O_8Zn$	$C_{27}H_{29.50}Cl_2N_{12.50}O_8Zn$	$C_{42}H_{44}Cl_2CuN_8O_{12}$
Formula weight	560.62	614.89	616.72	793.40	987.29
Crystal system	monoclinic	tetragonal	tetragonal	triclinic	triclinic
Space group	C_2/c	$I4_1/acd$	$I4_1/acd$	$P\bar{1}$	$P\bar{1}$
a (Å)	12.919(2)	13.8156(6)	13.7996(7)	14.4356(5)	8.0216(6)
b (Å)	8.3062(16)	13.8156(6)	13.7996(7)	15.4525(6)	10.5415(8)
c (Å)	18.932(4)	26.2402(15)	26.566(2)	16.2410(6)	12.4771(10)
α (°)	90	90	90	100.4290(10)	94.1480(10)
β (°)	97.064(3)	90	90	97.5650(10)	91.0350(10)
γ (°)	90	90	90	103.7460(10)	92.8650(10)
Volume (Å^3)	2016.1(7)	5008.5(4)	5059.0(5)	3402.6(2)	1050.73(14)
Z	4	8	8	4	1
$F(000)$	1136	2520	2528	1628	511
Crystal size (mm)	$0.38 \times 0.31 \times 0.21$	$0.41 \times 0.37 \times 0.13$	$0.49 \times 0.40 \times 0.13$	$0.28 \times 0.20 \times 0.19$	$0.45 \times 0.20 \times 0.11$
θ Range for data collection (°)	2.17–28.64	2.60–24.99	2.59–25.00	1.68–25.00	1.64–28.75
Reflections collected	8362	16 320	16 592	24 624	9129
Independent reflections [R_{int}]	2377 [0.0166]	1111 [0.0224]	1123 [0.0284]	11923 [0.0133]	4766 [0.0118]
Completeness to $\theta = 25°$ (%)	100	100.0	100.0	99.5	99.5
Absorption correction	multiscan	multiscan	multiscan	multiscan	multiscan
Maximum and minimum transmission	1.000 and 0.909	1.000 and 0.874	1.000 and 0.773	1.000 and 0.961	1.000 and 0.884
Data/restraints/parameters	2377/0/156	1111/0/101	1123/0/101	11923/62/938	4766/0/295
R_1, wR_2 [$I > 2\sigma(I)$]	0.0241, 0.0613	0.0272, 0.0753	0.0315, 0.0887	0.0352, 0.0916	0.0330, 0.0860
R_1, wR_2 (all data)	0.0268, 0.0628	0.0310, 0.0789	0.0372, 0.0954	0.0424, 0.0964	0.0386, 0.0897

($\lambda = 0.71073$Å) (Table 6). The structures were solved by direct methods and refined by full-matrix least-squares on F^2 using all the reflections [24]. All non-hydrogen atoms were refined with anisotropic atomic displacement parameters and hydrogen atoms bonded to carbon were inserted at calculated positions. In $[Zn(2\text{-}BIM)_2](ClO_4)_2$ the hydrogen bonded to nitrogen was located and refined with a fixed isotropic thermal parameter; in $[Cu(2\text{-}BIM(Bz)OH)_2(H_2O)_2](ClO_4)_2$ hydrogen atoms bound to oxygen were located from difference maps and not further refined. $[Cu(2\text{-}BIM(Me))_2](ClO_4)_2$ and $[Zn(2\text{-}BIM(Me))_2](ClO_4)_2$ are isomorphous and in each case the perchlorate ion is disordered about a 2-fold axis passing through the chlorine and one oxygen atom. The asymmetric unit of $[Zn(2\text{-}BIM(CN))_2](ClO_4)_2 \cdot 0.5CH_3CN$ contains two independent $[Zn(2\text{-}BIM(CN))_2]^{2+}$ cations, four perchlorate anions and a single acetonitrile solvate; one of the perchlorate ions is disordered and this has been modelled as 50% occupancy of two sites related by rotation about one of the Cl–O bonds.

4. Supplementary data

X-ray supplementary data for $[Zn(2\text{-}BIM)_2](ClO_4)_2$, $[Cu(2\text{-}BIM(Me))_2](ClO_4)_2$, $[Zn(2\text{-}BIM(Me))_2](ClO_4)_2$, $[Zn(2\text{-}BIM(CN))_2](ClO_4)_2 \cdot 0.5MeCN$ and $[Cu(2\text{-}BIM(Bz)OH)_2(H_2O)_2](ClO_4)_2$ are available from the Cambridge Crystallographic Data Centre, 12 Union Road, Cambridge CB2 1EZ, England (fax: +44-1223-336033, E-mail: deposit@ccdc.cam.ac.uk or www: http://www.ccdc.cam.ac.uk), on request quoting the deposition numbers CCDC 218894, CCDC 218895, CCDC 218896, CCDC 218897 and CCDC 218898, respectively.

Acknowledgements

S. Abuskhuna acknowledges financial support from the Libyan Higher Education Department.

References

[1] C. Place, J.-L. Zimmermann, E. Mulliez, G. Guillot, C. Bois, J.-C. Chottard, Inorg. Chem. 37 (1998) 4030.
[2] K. Várnagy, I. Sóvágó, K. Ágoston, Z. Likó, H. Süli-Vargha, D. Sanna, G. Micera, J. Chem. Soc. Dalton Trans. (1994) 2939.
[3] E.A. Kesicki, M.A. DeRosch, L.H. Freeman, C.L. Walton, D.F. Harvey, W.C. Trogler, Inorg. Chem. 32 (1993) 5851.
[4] M.S. Mohan, Indian J. Chem. 20A (1981) 252.
[5] G. Guillot, E. Mulliez, P. Leduc, J.-C. Chottard, Inorg. Chem. 29 (1990) 577.

[6] B.J. Parsons, S. Navaratnam, Z. Zhao, L. Chen, J. Chem. Soc. Faraday Trans. 90 (1994) 2467.
[7] A.J. Canty, L.A. Titcombe, B.W. Skelton, A.H. White, J. Chem. Soc. Dalton Trans. (1988) 35.
[8] S. Elgafi, B.A. Messerle, T.W. Hambley, P. Turner, J. Chem. Soc. Dalton Trans. (1997) 2341.
[9] R. Bhalla, M. Helliwell, C.D. Garner, J. Chem. Soc. Chem. Commun. (1996) 921.
[10] K. Õsz, K. Várnagy, H. Süli-Vargha, D. Sanna, G. Micera, I. Sóvágó, Inorg. Chim. Acta 339 (2002) 373.
[11] K. Prasad, M.S. Mohan, H.B. Bathina, J. Coord. Chem. 17 (1988) 63.
[12] A. Koteswar, P. Venkataiah, M.S. Mohan, H.B. Bathina, J. Coord. Chem. 20 (1989) 69.
[13] F. Bachechi, A. Burini, R. Galassi, B.R. Pietroni, M. Severini, J. Organomet. Chem. 575 (1999) 269.
[14] X.-M. Chen, Z.-T. Xu, T.C.W. Mak, Polyhedron 14 (1995) 319.
[15] H. Sigel, A. Saha, N. Saha, P. Carloni, L.E. Kapinos, R. Griesser, J. Inorg. Biochem. 78 (2000) 129.
[16] M.J. Bloemink, H. Engelking, S. Karentzopoulos, B. Krebs, J. Reedijk, Inorg. Chem. 35 (1996) 619.
[17] M. Grehl, B. Krebs, Inorg. Chem. 33 (1994) 3877.
[18] W.B. Tollman, S. Liu, J.G. Bentsen, S.J. Lippard, J. Am. Chem. Soc. 113 (1991) 152.
[19] S. Abuskhuna, J. Briody, M. McCann, M. Devereux, K. Kavanagh, J. Barreira Fontecha, V. McKee, Polyhedron 23 (2004) 1249.
[20] M. Joseph, T. Leigh, M.L. Swain, Synthesis 7 (1977) 459.
[21] R.S. Brown, R.G. Clewely, J. Org. Chem. 52 (1987) 1216.
[22] B.P. Cantwell, Ph.D. Thesis, NUI Maynooth, 1992.
[23] A.M. Roe, J. Chem. Soc. (1963) 2195.
[24] G.M. Sheldrick, SHELXTL version 6.12, Bruker AXS, Madison, WI, USA, 2001.

Available online at www.sciencedirect.com
SCIENCE DIRECT®
Polyhedron 23 (2004) 1739–1747
POLYHEDRON
www.elsevier.com/locate/poly

Structurally characterized magnesium carboxylates with tuned melting points

Eric N. Coker *, Timothy J. Boyle *, Mark A. Rodriguez, Todd M. Alam

Advanced Materials Laboratory, Sandia National Laboratories, 1001 University Boulevard SE, Albuquerque, NM 87106, USA

Received 8 January 2004; accepted 5 April 2004
Available online 4 May 2004

Abstract

A novel family of carboxylic acid modified Mg species has been synthesized through the reaction of $Mg(OEt)_2$ with a series of sterically varied carboxylic acids (HORc) where HORc = HO_2CMe (HOAc), HO_2CCHMe_2 (HOPc), HO_2CCMe_3 (HOBc) and $HO_2CCH_2CMe_3$ (HONc). The resultant products were isolated as $[Mg(OAc)_2]_3(HOAc)_2(H_2O)_2 \cdot 2(HOAc)$ (**1**), $[Mg(OPc)_2(HOPc)]_6$ (**2**), $Mg(OBc)_2(HOBc)_4$ (**3**) and $[Mg(ONc)_2(HONc)]_6$ (**4**). Compound **1** is trinuclear wherein the two terminal octahedral (Oh) bound Mg metal centers possess one terminal water, one terminal, one unidentate bridging and two bidentate bridging OAc ligands that symmetrically bind to the central Oh bound Mg cation. The water in **1** is believed to be generated in situ through an esterification process. In contrast, each of the six Mg atoms of **2** or **4** adopt a trigonal bipyramidal geometry by coordinating one terminal and four bidentate bridging ORc ligands that yield a ring (diameter 6.54 Å for **2** and 6.57 Å for **4**) of bridging ORc ligands. Compound **3** binds two terminal OBc ligands and four terminal HOBc ligands to yield a monomeric complex with no water present. Standard analytical data were obtained but did not add significant amounts of information concerning the bulk properties of **1**–**4**. Differential scanning calorimetry and thermal analysis indicated the melting point of these species was tunable.
© 2004 Elsevier Ltd. All rights reserved.

Keywords: Magnesium carboxylate; Meltable; Dispersion processing; Thermal properties

1. Introduction

Magnesium alkoxides ($Mg(OR)_2$) have been available for study since the early 1900s [1–3] and have found use in several applications, such as Ziegler-Natta catalyst support precursors [4] and reagents for organic synthesis [5,6]. Although they are widely used, only a handful of structurally characterized $Mg(OR)_2$ complexes had been reported. Therefore, we synthesized and characterized a novel family of sterically hindering aryloxide derivatives "$Mg(OAr)_2(solv)_x$" (OAr = series of substituted phenoxides [13] and phenyl bearing alkoxide ligands [14]). The nuclearity of these compounds was controlled by altering the steric bulk of the substituents and the Lewis basicity of the solvent. The tailoring of other properties of these compounds was of interest. In particular, we were concerned with synthesizing low melting point Mg species to generate controlled mono-dispersed, spherical particles through dispersion routes. The previously investigated "$Mg(OR)_2(solv)_x$" species decompose prior to melting and thus were of no use for dispersion investigations [7–14].

We have previously reported a highly soluble, low-melting carboxylic acid (HORc)-modified Sr precursor, $[Sr(ONc)_2(HONc)_4]_2$ [15] (HONc = $HO_2CCH_2CMe_3$, *tert*-butyl acetic acid). This phenomenon was attributed to the excess bound HONc which upon heating, yielding a pool of solvent from the free HONc, which could dissolve the remaining species. Therefore, it was of interest to investigate the utility of this approach to generate low melting point "$Mg(ORc)_2$" precursors. While a number of these compounds have been reported in the literature, the majority possess coordinated H_2O [16–36], with few systematic structural variations present that could be used to discern structure-property relationships. For this

* Corresponding authors. Tel.: +1-505-272-7593; fax: +1-505-272-7304.
E-mail addresses: encoker@sandia.gov (E.N. Coker), tjboyle@sandia.gov (T.J. Boyle).

0277-5387/$ - see front matter © 2004 Elsevier Ltd. All rights reserved.
doi:10.1016/j.poly.2004.04.005

family of compounds, the ORc ligand has been observed to bind in a number of different manners, some of which are shown in Fig. 1.

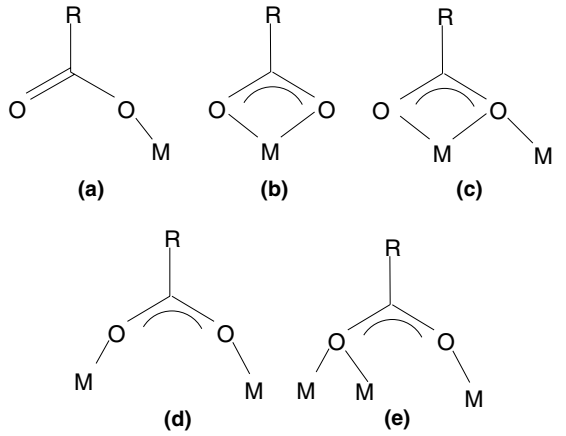

Fig. 1. Schematic representation of select binding modes of carboxylate ligands: (a) terminal, (b) unidentate, (c) unidentate bridging, (d) bidentate bridging, (e) unidentate, bidentate bridging.

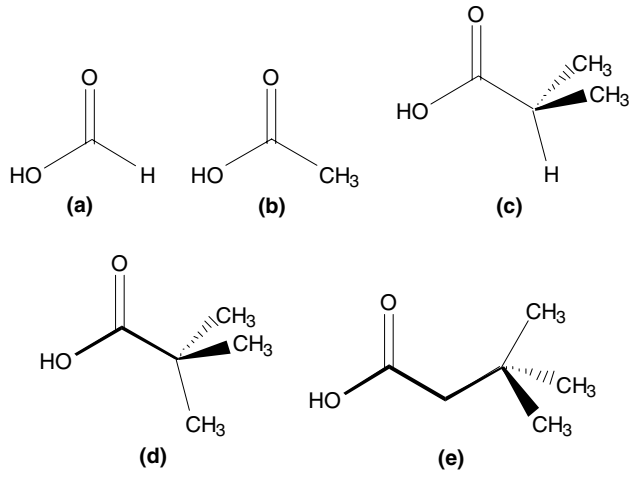

Fig. 2. Schematic representation of the sterically varied carboxylate ligands investigated: (a) formic acid (HOFc), (b) acetic acid (HOAc), (c) *iso*-butyric acid (HOPc), (d) trimethyl acetic acid (HOBc) and (e) *tert*-butyl acetic acid (HONc).

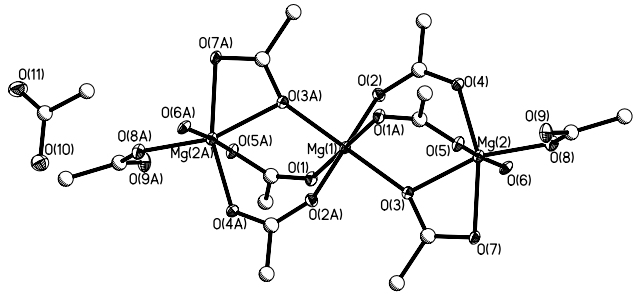

Fig. 3. Structural plot of **1**. Thermal ellipsoids for Mg and O drawn at 30%.

Therefore, we chose to synthesize a series of $Mg(ORc)_2$ compounds using simple organic carboxylate modifiers that systematically increased in steric bulk: formic acid (HO_2CH, HOFc), acetic acid (HO_2CCH_3, HOAc), *iso*-butyric acid (HO_2CCHMe_2, HOPc), trimethyl acetic acid (HO_2CCMe_3, (HOBc) and *tert*-butyl acetic acid ($HO_2CCH_2CMe_3$, HONc). A schematic representation of the HORc compounds is shown in Fig. 2. The $Mg(ORc)_2$ compounds were synthesized through the modification of $Mg(OEt)_2$ with excess HORc, as shown in Eq. (1). The reaction was run neat to minimize any solvent influences on the final structures. The following novel species were isolated:

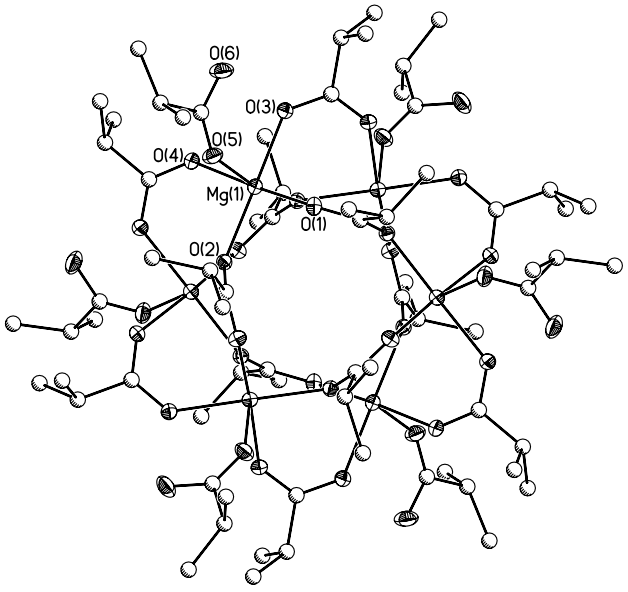

Fig. 4. Structural plot of **2**. Thermal ellipsoids for Mg and O drawn at 30%.

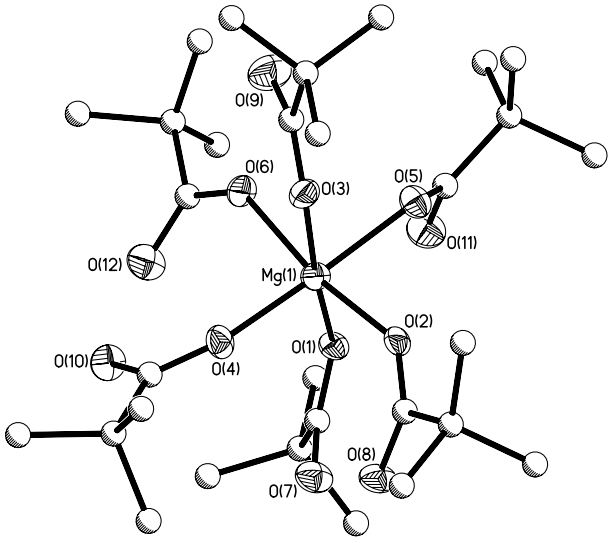

Fig. 5. Structural plot of **3**. Thermal ellipsoids for Mg and O drawn at 30%.

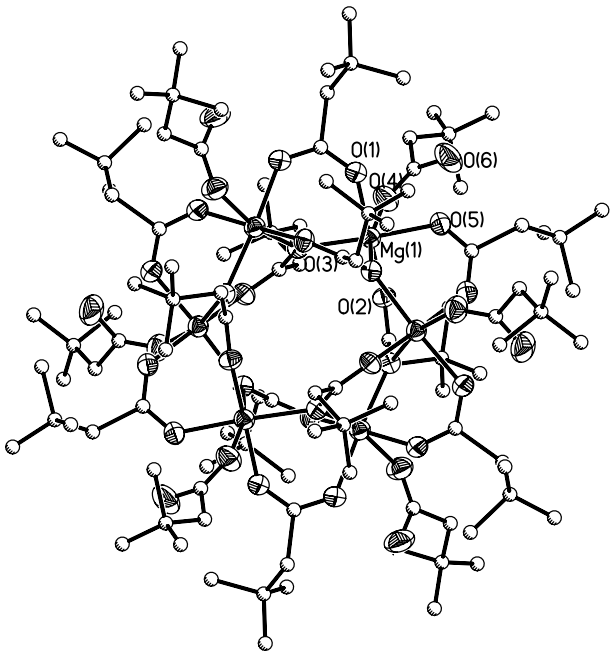

Fig. 6. Structural plot of **4**. Thermal ellipsoids for Mg and O drawn at 30%.

$[Mg(OAc)_2]_3(HOAc)_2(H_2O)_2$2(HOAc) (**1**), $[Mg(OPc)_2(HOPc)]_6$ (**2**), $Mg(OBc)_2(HOBc)_4$ (**3**) and $[Mg(ONc)_2(HONc)]_6$ (**4**) and these are shown in Figs. 3–6, respectively. The structure of the formic acid derivative, $[Mg(OFc)_2(H_2O)_2]_n$, has been reported in the literature [30,42,43], and will not be discussed further here.

$$Mg(OEt)_2 + (xs)HORc \rightarrow Mg(ORc)_2 \cdot nHORc + 2HOEt \quad (1)$$

The synthesis and characterization of **1**–**4** will be discussed in detail. The utility of these compounds in melt-dispersion processing for the control of particle morphology is currently under investigation.

2. Experimental

All compounds described below were handled with rigorous exclusion of air and water using standard Schlenk line and glove box techniques. HOFc (Aldrich) and HOAc (Fisher) were freshly distilled from the appropriate drying agents immediately prior to use [37]. The following chemicals were used as received (Aldrich): $Mg(OEt)_2$, HOPc, HOBc, HONc.

FT-IR data were obtained on a Bruker Vector 22 Instrument using KBr pellets under an atmosphere of flowing nitrogen. Elemental analysis was performed on a Perkin–Elmer 2400 CHN-S/O Elemental Analyzer. Differential scanning calorimetry (DSC) profiles were recorded on a Perkin–Elmer DSC 7 calorimeter. Samples were heated at a rate of 10 °C min^{-1} from 25 to 500 °C under a flow of 25 ml min^{-1} dry nitrogen or dry air. Thermal gravimetric analysis/differential thermal analysis (TGA/DTA) profiles were recorded on a TA Instruments SDT 2960 Simultaneous DTA-TGA balance. Samples were heated at a rate of 5 °C min^{-1} from 25 to 650 °C under a flow of 100 ml min^{-1} dry air and then held at 650 °C for 30 min. Visual confirmation of melting points (below 350 °C) were made using a bench top Electrothermal® melting point apparatus.

All NMR samples were prepared from dried crystalline materials that were handled and stored under an argon atmosphere. The $^{13}C\{^1H\}$ solid state cross-polarized magic angle spinning (CP-MAS) NMR spectra were obtained on a Bruker AMX400 spectrometer, at a frequency of 100.63 MHz using a 4 mm broadband probe spinning at 4 kHz. The CP-MAS spectra were acquired using a standard CP sequence with high power ^1H decoupling, 10 s recycle delay, a 1 ms contact time and 64–256 scan averages.

For the solution NMR spectra, **1** was dissolved in D_2O, while **2**–**4** were dissolved in toluene-d_8 at saturated solution concentrations. All solution NMR spectra were obtained on a Bruker DRX400 spectrometer at 399.87 and 100.54 MHz for ^1H and ^{13}C experiments, respectively. A 5 mm broadband probe was used for all experiments. ^1H NMR spectra were obtained using a direct single pulse excitation with a 10 s recycle delay and 8 scan average. The $^{13}C\{^1H\}$ NMR spectra were obtained using a WALTZ-16 composite pulse ^1H decoupling, a 5 s recycle delay and a $\pi/4$ pulse excitation.

Due to the similarity of synthetic procedures, a general description is presented for each reaction with individual variations noted in the respective section. To a pre-weighed sample of $Mg(OEt)_2$, the appropriate HORc was added until the majority of $Mg(OEt)_2$ was dissolved. The reaction was then heated with stirring until the solution became clear and then was allowed to cool to room temperature and sit until crystals formed. If crystal growth did not occur, some of the volatile fraction was removed via rotary evaporation and the reaction allowed to stand at room temperature. This process was repeated as often as necessary until X-ray quality crystals formed. All other characterizations were carried out on the bulk powder materials.

$[Mg(OFc)_2(H_2O)_2]_n$. Used $Mg(OEt)_2$ (0.234 g, 2.04 mmol) and HOFc (11.2 g, 243 mmol). Yield: 0.27 g (100%). FTIR (KBr pellet, cm^{-1}) 3386(m, br), 2934(w), 2906(w), 2882(w), 1678(m), 1639(s), 1612(s), 1418(m), 1407(m), 1352(s), 1069(w), 796(m). ^1H NMR (399.9 MHz, D_2O) δ 8.25 (1 H, s, OOC*H*,), 4.65 (s, O*H*$_2$). $^{13}C\{^1H\}$ NMR (100.54 MHz, D_2O) δ 170.2 (O_2*C*H). Elemental Analysis calc. for $C_2H_6MgO_6$: C, 15.97; H, 4.02. Found: C, 19.80; H, 2.54%.

$[Mg(OAc)_2]_3(HOAc)_2(H_2O)_2 \cdot 2(HOAc)$ (**1**). Used $Mg(OEt)_2$ (0.220 g, 1.92 mmol) and HOAc (5.184 g, 86.3 mmol). Yield: 0.454 g (100%). FTIR (KBr pellet, cm^{-1}) 3019 (w, br), 2936 (w), 1716 (m), 1601 (s), 1421 (s), 1344

(m), 1230 (w), 1054 (m), 1028 (m), 672 (m), 621 (m). ^{1}H NMR (399.9 MHz, D_2O) δ 1.78 (s, OOCCH_3), 4.65 (s, OH_2). ^{13}C{^{1}H} NMR (100.54 MHz, D_2O) δ 178.9 (O_2CCH_3), 21.5 (O_2CCH_3). Elemental Analysis calc. for $C_{20}H_{38}Mg_3O_{22}$: C, 34.15; H, 5.44. Found: C, 34.23; H, 4.71%.

[Mg(OPc)$_2$(HOPc)]$_6$ (**2**). Used Mg(OEt)$_2$ (0.214 g, 1.87 mmol) and HOPc (5.070 g, 57.5 mmol). Yield: 0.373 g (69%). FTIR (KBr pellet, cm^{-1}) 2972 (m), 2931 (w), 2874 (w), 1697 (w), 1591 (m), 1473 (m), 1427 (m), 1374 (w), 1361 (w), 1308 (w), 1256 (w), 1163 (w), 1098 (m), 782 (w), 657 (w), 558 (w). ^{1}H NMR (399.9 MHz, toluene-d$_8$) δ 8.82 (5.7H br s, $HO_2CCH(CH_3)_2$), 2.00 (6.6H, br s, $O_2CCH(CH_3)_2$), 1.92, 1.88 (9.7H, br s, $O_2CCH(CH_3)_2$). ^{13}C{^{1}H} NMR (100.54 MHz, toluene-d$_8$) δ 184.9 ($O_2CCH(CH_3)_2$), 35.3 ($O_2CCH(CH_3)_2$), 20.2 ($O_2CCH(CH_3)_2$). Elemental Analysis calc. for $C_{12}H_{22}MgO_6$: C, 50.30; H, 7.74. Found: C, 49.55; H, 7.34%.

Mg(OBc)$_2$(HOBc)$_4$ (**3**). Used Mg(OEt)$_2$ (0.214 g, 1.87 mmol) and HOBc (4.830 g, 47.3 mmol). Yield: 0.650 g (55%). FTIR (KBr pellet, cm^{-1}) 2969 (s), 2933 (w), 2874 (w), 2588 (w, br), 1686 (s), 1647 (s), 1479 (s), 1453 (w), 1400 (s), 1354 (s), 1210 (s), 1091 (w), 1026 (w), 874 (m), 795 (m), 604 (w), 501 (w), 532 (m). ^{1}H NMR (399.87 MHz, toluene-d$_8$) δ 13.1 (2.6H, s, br, $HO_2CC(CH_3)_3$), 1.18 (55H, mult., $O_2CC(CH_3)_3$). ^{13}C{^{1}H} NMR (100.54 MHz, toluene-d$_8$) δ 186.8 ($O_2CC(CH_3)_3$), 39.3 ($O_2CC(CH_3)_3$), 27.6 ($O_2CC(CH_3)_3$). Elemental Analysis calc. for $C_{30}H_{58}MgO_{12}$: C, 56.74; H, 9.21. Found: C, 56.31; H, 8.66%.

[Mg(ONc)$_2$(HONc)]$_6$ (**4**). Used Mg(OEt)$_2$ (0.202 g, 1.77 mmol) and HONc (5.304 g, 45.7 mmol). Yield: 0.689 g (39%). X-ray quality crystals were grown from hot dodecane. FTIR (KBr pellet, cm^{-1}) 2960 (s), 2914 (w), 2875 (m), 1703 (m), 1604 (s), 1466 (m), 1440 (m), 1387 (m), 1367 (m), 1302 (w), 1275 (w), 1236 (w), 1196 (w), 1144 (w), 1047 (w, br), 815 (m), 736 (m), 643 (m). ^{1}H NMR (399.87 MHz, toluene-d$_8$) δ 12.3 (v-br, $HO_2CCH_2C(CH_3)_3$), 2.04 (6H, multiplet, $O_2CCH_2C(CH_3)_3$, $J_{H-H} = 2.2$ Hz), 1.05 (27H, $O_2CCH_2C(CH_3)_3$). ^{13}C{^{1}H} NMR (100.54 MHz, toluene-d$_8$) δ 182.3, 180.4 ($O_2CCH_2C(CH_3)_3$), 51.2, 50.2 ($O_2CCH_2C(CH_3)_3$), 31.3, 30.8 ($O_2CCH_2C(CH_3)_3$), 30.4, 30.1 ($O_2CCH_2C(CH_3)_3$). Elemental Analysis calc. for $C_{18}H_{34}MgO_6$: C, 58.4; H, 9.2. Found: C, 58.5; H, 9.6%.

General X-ray crystal structure information [38]. Each crystal was mounted onto a thin glass fiber from a pool of Fluorolube^{TM} and immediately placed under a liquid N_2 boil-off stream, on a Bruker AXS diffractometer. The radiation used was graphite monochromatized Mo Kα radiation ($\lambda = 0.7107$ Å). The lattice parameters were optimized from a least-squares calculation on carefully centered reflections. The final crystal determination was solved using SMART Version 5.054 software, SAINT+ 6.04 (1/19/01), SHELXTL 5.1 (10/29/98), XSHELL 4.1 (11/08/2000) and SADABS (Ver. 2.03) software.

Each structure was solved using direct methods. This procedure yielded the heavy atoms, along with a number of the C atoms. Subsequent Fourier synthesis yielded the remaining C atom positions. The hydrogen atoms were fixed in positions of ideal geometry and refined within the XSHELL software. For H atoms on OH groups, the H atoms were located via difference Fourier mapping. These H atoms had their positions and

Table 1
Data collection parameters for **1**–**4**

Compound	**1**	**2**	**3**	**4**
Chemical formula	$C_{20}H_{38}Mg_3O_{22}$	$C_{72}H_{132}Mg_6O_{36}$	$C_{30}H_{58}MgO_{12}$	$C_{108}H_{204}Mg_6O_{36}$
Formula weight	703.43	1719.64	635.07	2224.57
T (K)	168(2)	168(2)	168(2)	298(2)
Crystal system	triclinic	rhombohedral	monoclinic	rhombohedral
Space group	$P\bar{1}$	$R\bar{3}$	$P2(1)/c$	$R\bar{3}$
a (Å)	6.9809(10)	26.499(5)	17.240(7)	29.420(18)
b (Å)	8.9748(13)	26.499(5)	10.618(4)	29.240(18)
c (Å)	13.023(2)	11.954(3)	21.067(9)	14.089(12)
α (°)	85.082(3)			
β (°)	77.344(3)		104.688(7)	
γ (°)	83.514(3)	120		120
V (Å^3)	789.4(2)	7270(3)	3730(3)	10561(13)
Z	1	3	4	3
D_{calc} (Mg/m^3)	1.480	1.178	1.131	1.049
μ (mm^{-1}) (Mo Kα)	0.185	0.127	0.100	0.100
R_1 (%)	5.22	7.51	7.96	8.47
wR_2 (%) [$I > 2\sigma(I)$]	11.58	17.80	18.27	20.46
R_1 (%, all data)	9.59	22.84	28.26	17.45
wR_2 (%, all data)	13.74	28.14	24.36	26.30

$R_1 = \sum ||F_o| - |F_c|| / \sum |F_o| \times 100$.
$wR_2 = [\sum w(F_o^2 - F_c^2)^2 / \sum (w|F_o|^2)^2]^{1/2} \times 100$.

isotropic displacement parameters refined. These idealized hydrogen atoms had their isotropic temperature factors fixed at 1.2 or 1.5 times the equivalent isotropic U of the C atoms to which they were bonded. The final refinement of each compound included anisotropic thermal parameters on all non-hydrogen atoms. Data collection parameters for **1**–**4** are given in Table 1.

The maximum θ angle for dataset integration was selected to optimize the data/parameter ratio, completeness of dataset coverage and reasonable residual errors during refinement. Although the data are not of the highest quality, the general usefulness concerning the connectivity of the structures can prove valuable and is the main focus of this paper. The problems associated with the structures are mainly due to difficulties in obtaining statistically useful data at higher θ angles (above 23°). Any variations in the handling of the individual crystals are described below.

$Mg(OBc)_2(HOBc)_4$ (**3**). Due to the instability of the refinement, all C atoms were refined with isotropic temperature factors only. Additionally, SADI bond length restraints were placed on all O–C and C–C bonds to force them to be equal ($\sigma = 0.04$ Å). Disordering of one of the acid groups (O6/O12, C26, C27, C28/C29/C30) was modelled by reducing the occupancies of the methyl carbons C28/C29/C30 to 0.5 and locating additional methyl carbons C28′/C29′/C30′, which were also fixed at 0.5 site occupancy. Due to the complication of the disorder, the hydrogens were left off this disordered acid group but counted in the chemical formula. In order to achieve charge balance, it is assumed that two of the acid groups are deprotonated. Since the H atoms could not be located they were not included in the figure but were included in the final chemical formula. Due to the uncertainties in structure refinement, the conformation of **3** given in Table 1 has a relatively large margin of error; therefore, we will only discuss the connectivity, which is unequivocally established.

$[Mg(ONc)(HONc)]_6$ (**4**). Data for compound **4** was collected under ambient nitrogen atmosphere since any cooling under the liquid nitrogen purge caused the crystal to crack.

3. Results and discussion

We have characterized several novel HORc-modified Mg compounds (**1**–**4**) that are unusual in comparison to existing members of this family of compounds. The synthesis, solid state and solution state characteristics of **1**–**4** are described below. The binding modes available and the carboxylate ligands that were used are shown in Figs. 1 and 2, respectively. The investigation of structure-property as it applies to the melting point of these compounds was also explored.

3.1. Synthesis

The HORc-derivatives of Mg were synthesized by dissolving $Mg(OEt)_2$ in an excess of the appropriate HORc (Eq. (1)). These reactions were stirred with heating, if necessary, until a clear solution resulted. The mixtures were allowed to sit until crystals formed. If a solution did not yield crystals, part of the volatile portion was removed by rotary evaporation and again the reaction mixture was allowed to sit. X-ray quality crystals were isolated for **1**–**4** and their structures are shown in Figs. 3–6, respectively. For each, there were no alkoxide ligands present in the final material. A number of these species did retain water that is believed to be formed through an esterification reaction pathway. Surprisingly, no oxo species were generated from the water by-product, as is often observed for HORc-modified metal alkoxide species [39,40].

3.2. Solid state

While a great deal of research has been conducted involving $Mg(ORc)_2$ complexes, no systematic structural studies of these "simple" compounds has been proffered. A series of furan-substituted carboxylate structures were reported forming dimeric and polymeric structures dependant on the orientation of the furan ring [16]. Monomeric $Mg(ORc)_2 \cdot (H_2O)_{n.}$ species were isolated using mandelic acid [17], malonic acid [18,19] or aromatic substituted carboxylates (ORc-OAr) [20–26] (a polymeric $[Mg(ORc\text{-}OAr)_2(H_2O)_2]_\infty$ species was also isolated) [27]. Salt species were isolated for the polycarboxylates such as oratic acid (H-Or) $[Mg(H_2O)_6^{+2}][Mg(Or)^{-1}]_2$ [28] and citric acid (H-OCit) $\{[Mg(H_2O)_6^{+2}][Mg(OCit)^{-1}]_2 \cdot 2H_2O\}_n$ [29]. A few structures of simple organic carboxylic acid derivatised Mg species have been reported including $[Mg(OFc)_2(H_2O)_2]_n$ [30], $Mg(OAc)_2 \cdot 4H_2O$ [31–34], $[Mg(O\text{-}n\text{-}Bc)_2(H_2O)_4]_2 \cdot HO\text{-}n\text{-}Bc$ where O-*n*-Bc = $O_2C(CH_2)_2(CH_3)$ [36], and $[Mg(OPyn)_2(H_2O)]_n$, where OPyn = O_2CCCH. Interestingly, until recently with the isolation of $Mg_3(OPc)_6(solv)_2$ (solv = THF or HMPA) [35], $Mg_3(O_2CC{\equiv}CPh)_6(THF)_2$ [35], and $Mg_3(O_2C{\equiv}CSiMe_3)_6(HMPA)_4$ [41], where THF = tetrahydrofuran and HMPA = hexamethyl phosphoramide, water was found coordinated to the Mg metal centers for each carboxylate species reported independent of the solvent utilized.

Therefore, crystal structures of the simple carboxylates generated from solvent free environment were obtained to elucidate the structural arrangements unhindered by solvent, polydentate ligands or other complexing agents. The thermal ellipsoid plots of **1**–**4** are shown in Figs. 3–6, respectively. Table 1 lists the data parameters for **1**–**4**.

The compound $[Mg(OFc)_2(H_2O)_2]_n$ [30,42,43] is a polymeric structure wherein there are two unique

octahedrally (Oh) bound Mg metal centers. The equatorial OFc ligands bridge from one Mg(1) to four individual Mg(1′) metal centers. The two axial Mg(1) OFc ligands bridge to different Mg(2) metal centers that are shifted 1/2 unit cell along the b-axis. Mg(2) is equatorially bound by OFc ligands from Mg(1) cations and fills its coordination sphere by binding four water molecules. Due to the bite angle of the OFc ligand, the Mg(2) cations are tilted in opposite orientations relative to each other which leads to an AB/AB/AB packing.

In contrast to $[Mg(OFc)_2(H_2O)_2]_n$, compound **1** is trinuclear with a C_2 axis of symmetry. All of the Mg metal centers are six-coordinated in a psuedo-Oh geometry binding a variety of ligands. Each terminal Mg coordinates one H_2O and one terminally bound HOAc molecule. In addition, there are two bidentate-bridging and one unidentate-bridging OAc ligands (Fig. 1) that bridge to the central Mg. This structure is similar in arrangement as was noted for the HMPA adduct of $Mg_3(ORc)_6(HMPA)_2$ where $ORc = O_2CC{\equiv}CSiMe_3$ [41] or OPc [35]; however, for **1** HOAc solvent molecules are used to fill the coordination sphere of the terminal Mg. Two additional molecules of HOAc are located in the unit cell (only one is shown in Fig. 3).

Surprisingly, by increasing the steric bulk on the pendant hydrocarbon chain of the carboxylic acid, the species isolated, **2**, was not isostructural with the previously isolated trinuclear species [35]. Instead, a hexanuclear species was isolated that does not incorporate any H_2O. Each Mg adopts a trigonal biplanar (TBP) geometry coordinating one terminal HOPc and four OPc ligands to form a six-membered ring (Fig. 4). The carboxylate ligands bridge equally between adjacent and alternating Mg metal centers forming a ring with a diameter of 6.54 Å. The depth of the ring is about 1/2 the *c*-axis or ~6 Å, forming a cubic volume of ~805 Å^3. A hexanuclear structure was previously observed for the carbamide complex, $Mg_6(O_2CNEt_2)_{12}$ which indicates there are more similarities between these ligands than was previously expected [35,44]. An identical structural arrangement was noted for **4** with a central ring diameter of 6.57 Å.

Further increases in the steric bulk of the ORc ligand yielded the mononuclear Mg species **3**. Each metal center of **3** is Oh bound by monodentate HOBc and OBc ligands (Fig. 5). Again, *no* H_2O was found bound to the metal centers and *none* of the ligands are present in a bidentate manner. While there are numerous monomeric $Mg(ORc)_2$ species present in the literature, the majority of these utilize water to stabilize the structure [20–23,33,34] (e.g., $Mg(OAc)_2(H_2O)_4$) [33,34] or combine polydentate ORc ligands with coordinated H_2O [17,25,26] (e.g., Mg(1,2-dioxydiacetato-O,O′,O″,O‴-benzene)$(H_2O)_3$) [25].

Compound **4**, shown in Fig. 6, was isostructural with **2**.

Metrical data of **1**–**4** are consistent with each other and the literature values [16–36]. The Mg – Mg distances are av. 3.53 Å, the O–C–O range from 121.0 to 126.7° for both bridging and terminal ORc ligands. The unidentate bridging OAc ligand of **2** has the smallest angle of 118.2° due to the constrained bite angle. The Mg–O distances are within a relatively small range (2.00–2.25 Å) when the variety of ligands and binding types are taken into consideration. The angles are slightly distorted from ideal Oh or TBP due to the constraints of the ORc ligands.

Attempts to demonstrate that the bulk powders were uniform and a single product were complicated by the inclusion of the free HORc, which makes complete characterization of these compounds difficult since the ligands and bound acid are difficult to distinguish from each other. Elemental analyses of **1**–**4** were consistent with the empirical formula of the single crystal structures. Since each of these samples were handled in the ambient atmosphere, it appears that **1**–**4** are relatively air stable.

For each sample, the FT-IR spectra of **1**–**4** reveal OH peaks around 3000 cm^{-1} due to the bound HORc and in some instances the H_2O. For the aqueous species, this peak is much broader than the HORc bound compounds. For each sample, the bound acids have a shift of ~200 cm^{-1} in comparison to the free HORc and much stronger stretches, indicative of coordination to the Mg metal center. There was no specific stretch that was conclusively associated with Mg–O.

CP-MAS ^{13}C NMR data was collected on the bulk samples of **1**–**4** to verify that the bulk powder was identical to the single crystal. Table 2 lists the resonances observed for the various samples. Compounds **1** and **4** have the same general structure type wherein each has two non-equivalent bridging and one terminal ORc indicating two types of carboxylate species that can be observed in the solid state. For **1**, four types of OAc ligands were observed whereas for **4**, three types of ONc ligands were recorded. The variations in the crystal structure and observed ^{13}C CP-MAS NMR data for **1** can be attributed to increased asymmetry of the crystalline material due to the reduction in averaging typi-

Table 2
CP MAS NMR data for **1**–**4**

Compound	^{13}C (δ ppm)
1	186.1, 184.2, 179.7, 178.5 ($O_2\mathit{C}CH_3$)
	23.61, 22.82, 21.25, 20.86 ($O_2C\mathit{C}H_3$)
2	186.9, 182.9 ($O_2\mathit{C}CH(CH_3)_2$)
	36.2, 34.7 ($O_2C\mathit{C}H(CH_3)_2$)
	22.8, 20.5, 19.1 ($O_2CCH(\mathit{C}H_3)_2$)
3	186.0 ($O_2\mathit{C}C(CH_3)_3$)
	39.5, 38.8 ($O_2C\mathit{C}(CH_3)_3$)
	28.4, 27.8 ($O_2CC(\mathit{C}H_3)_3$)
4	183.8, 182.9, 179.9 ($O_2\mathit{C}CH_2C(CH_3)_3$)
	52.1, 49.4 ($O_2C\mathit{C}H_2C(CH_3)_3$)
	31.8 ($O_2CCH_2\mathit{C}(CH_3)_3$)
	30.6, 29.6 ($O_2CCH_2C(\mathit{C}H_3)_3$)

cally noted for solution species. For **2**, two quaternary and methylene, but three types of methyl resonances were observed. The observance of two complete sets of resonances is consistent with the terminal and bridging OPc ligands. The multiple resonances noted in the methyl region are most likely due to inequivalencies of "locked out" methyl groups of the OPc ligand. As expected for **3**, only one set of resonances were observed for the OBc derivative; however, each resonance was present as a multiplet. Again, packing inequivalancies associated with the OBc/HOBc ligands would account for the multiple resonances. In general, it appears that the solid state powders were consistent with the single crystal structures collected.

3.3. Solution phase NMR

Dried crystals of **1** were dissolved in D_2O, while **2**–**4** were dissolved in toluene-d_8 to determine the solution behavior of these compounds. In the ^1H NMR spectrum of **1** only one set of sharp peaks for the ligands was observed. For **2**–**4**, resonances associated with the bound HORc and ORc ligands were observed. The ^{13}C NMR spectra for **1**–**4** show little information except for the carboxylic acid region wherein for each sample the number of carboxylates is directly related to the solid state structure. From these data, little information pertaining to the structure of these compounds is readily obtained except for the presence of the various ligands.

3.4. Thermal properties

The thermal decompositions of $[Mg(OFc)_2(H_2O)_2]_n$, and **1**–**4** were investigated by TGA/DTA (25–650 °C, air) and DSC (25–500 °C, air or N_2). The DSC data were consistent with the TGA/DTA data for each sample. Table 3 tabulates some of the thermal data obtained on these compounds.

For the H_2O coordinated species ($[Mg(OFc)_2(H_2O)_2]_n$ and **1**), the loss of both the coordinated species (water and HORc) and the bound ORc were easily observed. The bulk powder form of $[Mg(OFc)_2(H_2O)_2]_n$ exhibited a total weight loss in the TGA of 69.5%, which is clearly delineated into the loss of one water molecule per Mg center below 150 °C and loss of two formate groups per Mg between 330 and 440 °C. The loss of a water molecule was accompanied by a broad endotherm in the DTA, centered at 135 °C, concomitant with a desorption process, and the loss of OFc was accompanied by a sharp exotherm peaking at 430 °C. For **1**, a total weight loss of 82.4% was observed with the stepwise loss of solvating HOAc (<90 °C), coordinated water and HOAc (90–130 °C) and finally the loss of coordinated OAc in three stages: one OAc (per 3 Mg unit cell) at 315–320 °C, four OAc at 325–345 °C and one OAc at 360–420 °C. Each of the weight losses was associated with a thermal event; coordinated solvents revealed small endotherms and the bound OAc ligands produced sharp exothermic peaks in the 300–440 °C range.

Table 3
Thermophysical properties of $[Mg(OFc)_2(H_2O)_2]_n$ and **1**–**4**

Compound	Wt. loss[a] (%)	Melting point[b] (°C)
$[Mg(OFc)_2(H_2O)_2]_n$	69.5	440
1	82.4	322
2	90.5	129
3	98.4	140
4	93.8	198

[a] Temperature range 25–600 °C.
[b] Determined by Differential scanning calorimetry (DSC) under N_2.

For the non-aqueous species (**2**–**4**), the loss of HORc versus ORc were less clearly distinguished. On heating of **2**, the coordinated HOPc was lost in several steps up to 365 °C in the TGA, accompanied by a broad endotherm in the DTA. This process also initiated the loss of OPc ligands, which were completely removed by 430 °C, accompanied by a large exotherm. Compound **3** displayed a loss of coordinated HOBc in the range before 160 °C, as evidenced by a weight loss and corresponding endotherm. Above 300 °C, a second sharp weight loss occurred, which was assigned to the loss of ligated OBc and was accompanied by a broad exotherm. No further weight loss or thermal events were observed above 430 °C. The low temperature region of the DSC trace of **3**, recorded under N_2, is shown in Fig. 7(a). The material initially melts at approximately 140 °C (small endotherm), then exhibits three further sharp endothermic events above 190 °C. Note that the boiling point of HOBc is 163 °C, thus the latter three peaks are assigned to melting points of $Mg(OBc)_2.nHOBc$ species where $n < 4$ as the amount of "solvating" HOBc decreases steadily due to vaporization above 163 °C. Multiple melting points were also observed visually in an Electrothermal Melting Point Apparatus, but could not be resolved satisfactorily. Fig. 7(b) indicates the cyclability of melting **3** (provided the boiling point of HOBc is not exceeded), where **3** was subjected to three heating/cooling cycles between 120 and 150 °C. Note that the endotherm representing melting shows little change in intensity or peak position on repeated melting/solidifying. This result shows that **3** may be subjected to fusion/solidification processing without loss of meltability. Attempts to cycle the melting event above 163 °C were unsuccessful, as HOBc vaporized too easily. For **4**, loss of coordinated HONc was observed over the range of 50–170 °C (endothermic) while between 300 and 440 °C, a sharp exotherm accompanied the combustion of the remaining ONc groups. No further weight loss or thermal events were observed above 400 °C. In general, the compounds appear to be relatively thermally stable and should initiate a melt prior to decomposition, as was observed (Table 3). The total weight loss observed in the

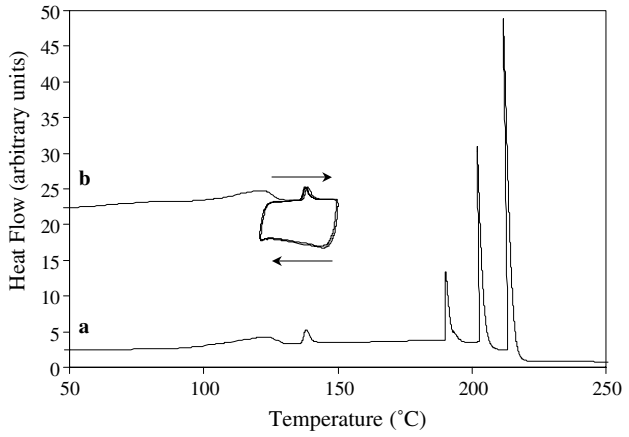

Fig. 7. Differential scanning calorimetry trace of **3** under N_2: (a) low temperature region; (b) initial melting point cycled three times. Arrows indicate heating and cooling cycles. Positive heat flow = endothermic event.

TGA up to 600 °C for **3** and **4** approximated 100%, indicating that the Mg-carboxylates were volatile which may be exploitable for metallo-organic chemical vapor deposition (MOCVD) processes.

4. Summary and conclusion

We have characterized a novel family of $Mg(ORc)_2$ complexes, the structural aspects of which are dictated by the changes in the steric bulk of the pendant hydrocarbon chain along with the rapidity with which the acids undergo esterification. The structures vary from organized polymeric complexes ($[Mg(OFc)_2(H_2O)_2]_n$), short oligomeric chains (**1**), hexanuclear rings (**2** and **4**), to monomeric species (**3**). The nuclearity of the resultant molecule appears to diminish with increased steric bulk; however, the presence of water and free HORc complicate the final structures observed by filling potential oligomerization sites. The water is thought to be generated by an esterification mechanism that is often observed when HORc are mixed with $M(OR)_x$. The expanded structural types observed for this new family of compounds are in line with carbamato derivatives and allow for more direct comparison between the two sets of precursors. The melting point properties of these compounds have been altered mainly due to the presence of the free acids bound to the metal centers, which act as a pool of solvent to aid in dissolution. This tailored property is being exploited to generate size-tunable spherical particles through a simple fluid dispersion processing method. These results will be published separately.

5. Supplementary material

CCDC 228261–228265 contain the supplementary crystallographic data for this paper. These data can be obtained free of charge via www.ccdc.cam.ac.uk/conts/retrieving.html, by emailing data_request@ccdc.cam.ac.uk, or by contacting The Cambridge Crystallographic Data Centre, 12, Union Road, Cambridge CB2 1EZ, UK; fax: +44-1223-336033.

Acknowledgements

For support of this research, the authors thank the Office of Basic Energy Sciences of the Department of Energy, Union Carbide Corporation, a subsidiary of The Dow Chemical Company, and the United States Department of Energy under contract DE-AC04-94AL85000. Sandia is a multiprogram laboratory operated by Sandia Corporation, a Lockheed Martin Company, for the United States Department of Energy.

References

[1] V. Cerchez, Bull. Soc. Chim. 43 (1928) 762.
[2] H. Lund, J. Bjerrum, Chem. Ber. B 64 (1931) 210.
[3] D.C. Bradley, R.C. Mehrotra, D.P. Gaur, Metal Alkoxides, Academic Press, New York, 1978.
[4] E.P.J. Moore, Polypropylene Handbook, Hanser/Gardner Publications, Inc, Cincinnati, OH, 1996.
[5] S.G. Hegde, D.C. Myles, Synth. Commun. 27 (1997) 2111.
[6] S. Kanemasa, M. Nishiuchi, E. Wada, Tetrahedron Lett. 33 (1992) 1357.
[7] Z.A. Starikova, A.I. Yanovsky, E.P. Turevskaya, N.Y. Turova, Polyhedron 16 (1997) 967.
[8] P. Sobota, J. Utko, Z. Janas, S. Szafert, Chem. Commun. (1996) 1923.
[9] L. Albaric, N. Hovnanian, A. Julbe, C. Guizard, A. Alvarezlarena, J.F. Piniella, Polyhedron 16 (1997) 587.
[10] A. Klemp, H.W. Roesky, H.-G. Schmidt, H.S. Par, M. Noltemeyer, Organometallics 17 (1998) 5225.
[11] J. Calabrese, M.A.J. Cushing, S.D. Ittel, Inorg. Chem. 27 (1988) 867.
[12] H.W. Roesky, M. Scholz, M. Noltemeyer, Chem. Ber. 123 (1990) 2203.
[13] C.A. Zechmann, T.J. Boyle, M.A. Rodriguez, R.A. Kemp, Polyhedron 19 (2000) 2557.
[14] C.A. Zechmann, T.J. Boyle, M.A. Rodriguez, R.A. Kemp, Inorg. Chim. Acta 319 (2001) 137.
[15] T.J. Boyle, C.J. Tafoya, B.L. Scott, J.W. Ziller, J. Coord. Chem. 51 (2000) 361.
[16] B. Paluchowska, J.K. Maurin, J. Leciejewics, J. Chem. Cryst. 27 (1997) 177.
[17] M. Schmidt, A. Schier, H. Schmidbaur, Z. Naturforsch., Teil B 53 (1998) 1098.
[18] L. Walter-Levy, J. Perrotey, J.W. Visser, C. R. Acad. Sci. C 277 (1973) 1351.
[19] B. Briggman, A. Oskarsson, Acta Crystallogr., Sect. B 34 (1978) 3357.
[20] L.B. Cole, E.M. Holt, Inorg. Chim. Acta 160 (1999) 195.
[21] S.R. Drake, K.D. Sanderson, M.B. Hursthouse, K.M.A. Malik, Inorg. Chem. 32 (1993) 1041.
[22] B.M. Kariuki, J.B. Valim, W. Jones, J. King, Acta Crystallogr., Sect. C 51 (1995) 1051.
[23] G. Smith, E.J. O'Reilly, C.H.L. Kennard, Cryst. Struct. Commun. 10 (1981) 1397.
[24] C.H.L. Kennard, E.J. O'Reilly, S. Schiller, G. Smith, A.H. White, Aust. J. Chem. 39 (1986) 1823.

[25] G. Smith, E.J. O'Reilly, C.H.L. Kennard, Polyhedron 6 (1987) 871.
[26] C.H.L. Kennard, G. Smith, E.J. O'Reilly, B.J. Reynolds, T.C.W. Mak, J. Chem. Soc., Dalton Trans. (1988) 2357.
[27] G. Smith, E.J. O'Reilly, C.H.L. Kennard, J. Chem. Soc., Dalton Trans. (1980) 2462.
[28] I. Bach, O. Kumerger, H. Schmidaur, Chem. Ber. 123 (1990) 2267.
[29] C.K. Johnson, Acta Crystallogr. 18 (1965) 1004.
[30] C. Malard, H. Pezerat, P. Herpin, P. Toledano, J. Solid State Chem. 41 (1982) 67.
[31] J. Shankar, P.G. Khubchandani, V.M. Padmanabhan, Proc. Indian Acad. Sci. A 45 (1957) 117.
[32] A.C. Padmanabhan, R. Srinivasan, Indian J. Pure Appl. Phys 11 (1973) 404.
[33] V.K. Trunov, N.O. Endeladze, Zh. Strukt. Khim. 27 (1986) 151.
[34] D.E. Irish, J. Semmler, N.J. Taylor, G.E. Toogood, Acta Crystallogr., Sect. C 47 (1991) 2322.
[35] K.-C. Yang, C.-C. Chang, C.-S. Yeh, G.-H. Lee, S.-M. Peng, Organometallics 20 (2001) 126.
[36] T.A. Mimaya, A.P. Polishchuk, A.S. Tolochko, S.V. Volkov, Kristallografiya 38 (1993) 49.
[37] D.D. Perrin, W.L.F. Armarego, Purification of Laboratory Chemicals, 3rd ed., Pergamon Press, New York, 1988.
[38] The listed versions of SAINT, SMART, XSHELL, and SADABS Software from Bruker Analytical X-Ray Systems Inc., 6300 Enterprise Lane, Madison, WI 53719, were used in analysis.
[39] T.J. Boyle, R.P. Tyner, T.M. Alam, B.L. Scott, J.W. Ziller, B.G.J. Potter, J. Am. Chem. Soc. 121 (1999) 12104.
[40] T.J. Boyle, T.M. Alam, C.J. Tafoya, B.L. Scott, Inorg. Chem. 37 (1998) 5588.
[41] K.-C. Yang, C.-C. Chang, C.-S. Yeh, G.-H. Lee, Y. Wang, Organometallics 21 (2002) 1296.
[42] K. Osaki, Y. Nakai, T. Watanabe, J. Phys. Soc. Jpn. 19 (1964) 717.
[43] G. de With, S. Harkema, G.J. van Hummel, Acta Crystallogr., Sect. B 32 (1976) 1980.
[44] M.T. Caudle, R.A. Nieman, V.G. Yound, J. Inorg. Chem. 40 (2001) 1571.

Available online at www.sciencedirect.com
SCIENCE DIRECT®
Polyhedron 23 (2004) 1749–1767
POLYHEDRON
www.elsevier.com/locate/poly

Intramolecular NH–π and π–π interactions in ternary cobalt(III) complexes of aromatic aminoacids: a structural and NMR study ☆

Paul Emseis [a], Timothy W. Failes [b], David E. Hibbs [b,*], Peter Leverett [a,*], Peter A. Williams [a,*]

[a] School of Science, Food and Horticulture, University of Western Sydney, Locked Bag 1797, Penrith South DC NSW 1797, Australia
[b] School of Chemistry, Building F11, University of Sydney, NSW 2006, Australia

Received 7 January 2004; accepted 7 April 2004

Abstract

The synthesis and characterization of a series of ternary Co(III) complexes which could act as simple model systems for the study of non-covalent interactions involving aromatic residues is reported. Such interactions are important to the discriminatory processes associated with molecular recognition in chemical and biochemical systems, but are relatively poorly understood due to the inherent complexity of the majority of systems. The species reported in this paper are Λ-β$_1$-[Co(*R*,*R*-picchxn)(*S*-trp)]$^{2+}$ (picchxn = *N*, *N*′-di(2-picolyl)-1,2-diaminocyclohexane; trp = the anion of tryptophan) and Δ-α-, Λ-β$_1$- and Λ-β$_2$-[Co(*R*,*R*-picchxn)(*R*-trp)]$^{2+}$. A single-crystal X-ray study of the Δ-α- and Λ-β$_2$-*R*-trp complexes has demonstrated that the molecular cation of each adopts a conformation where intramolecular π–π interactions involving the indole group and a pyridyl ring occur in the solid state. 2D-ROESY and ^{1}H NMR experiments of these diamagnetic complexes have established that these interactions persist in solution, as is also the case with the Λ-β$_1$-*S*-trp cation. Except for the Λ-β$_2$-*R*-trp species, all possess various combinations of NH–π interactions as well, and these too serve to influence markedly the rotamer distributions in several instances. Equilibrium rotamer populations determined using NMR have enabled the energetics of the system to be evaluated. NMR measurements also show that the rotamer populations are relatively unchanged at elevated temperatures, and that the non-covalent interactions which dictate both the solid state and solution configurations of these complexes persist in a variety of solvents. It is shown for *R*-trp that combined NH–π and π–π interactions provide the driving force for octahedral inversion of both Λ-β$_1$ and Λ-β$_2$ diastereoisomers to the Δ-α form. The unprecedented stabilization of this species is rationalized in terms of a hierarchy of competing non-covalent aromatic interactions.
© 2004 Elsevier Ltd. All rights reserved.

Keywords: Aromatic aminoacidate; Cobalt(III); Non-covalent interactions; Octahedral inversion; Tetradentate ligands; NMR

1. Introduction

Weak, non-covalent bonding interactions, which include classical and non-classical hydrogen bonding [1], hydrophobic association [2], aromatic ring stacking [3], π-facial [4] and electrostatic interactions [5], are often overlooked when describing the structure and reactivity of molecules. During the past decade, a consistent picture of their importance to the discriminatory processes associated with molecular recognition and self-assembly in chemical and biochemical systems has emerged [6]. What is yet to be drawn is a consistent picture of these relatively poorly understood attractive forces [2a,5,7]. This is understandable taken in the context of biochemical systems, where non-covalent interactions play vital roles in processes such as protein–ligand recognition [8], enzymatic activity [9], antigen–antibody binding [10], and the determination of three-dimensional structure [11]. Such systems are inherently complex, with

☆ Supplementary data associated with this article can be found, in the online version, at doi:10.1016/j.poly.2004.04.016.

* Corresponding authors. Tel.: +61-2-9685-9977; fax: +61-2-9685-9915.
E-mail address: p.williams@uws.edu.au (P.A. Williams).

0277-5387/$ - see front matter © 2004 Elsevier Ltd. All rights reserved.
doi:10.1016/j.poly.2004.04.016

multiple weak interactions acting in synergy to facilitate discrimination. This in turn gives rise to a need for simple model systems suitable for studying these interactions.

We have chosen to focus our study on NH–π [4a,8,12] and π–π interactions [2,3], as their wider significance to the molecular recognition and stabilization of molecular structures has been recognized [13]. In this paper, we report the synthesis and characterization of a series of ternary Co(III) complexes which could act as simple model systems for studying these interactions. An important feature of the model complexes is that they possess manageable numbers of non-covalent interactions and can be studied in detail. The molecular design rationale of the reported complexes is based on a previous exploration of the stereochemistry and stability of ternary Co(III) complexes containing ligands based on *picen* (**1**, 1,6-di(2-pyridyl)-2,5-diazahexane) [14]. A chiral analogue of this ligand, *picchxn* (**2**, *N*,*N*′-di(2-picolyl)-1,2-diaminocyclohexane) has been singled out for focused studies [15] concerning chiral inductions during the reactions of other coordinated ligands, the resolution of amino acids, and aspects of stereospecific coordination behaviour. *N*,*N*′-Dimethylated analogues of these ligands enforce α geometry (Fig. 1) at Co(III) [16], but ligand **2** has been supposed to form more stable β complexes (Fig. 2) with Co(III), on the basis of the isolation of many β Co(III) complexes of *R*,*R*-picchxn containing a wide variety of bidendates [17].

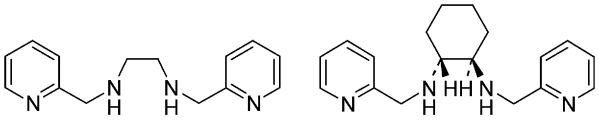

1 **2**

Indeed, the isolation of an α complex, Δ-α-[Co(*R*,*R*-picchxn)(AbuH)]$^{2+}$, $AbuH_2$ = 2-amino-2-butylpropandioic acid, was attributed to kinetic effects in that it was shown to quickly epimerize in DMSO solution to the corresponding Λ-β_1 diastereoisomer [18]. In related complexes containing aromatic amino acids, intramolecular π–π interactions between the amino acid side-chain and a pyridyl ring of the tetradentate have been identified for certain stereochemical combinations. A first example was found [19] in the structure of Λ-β_1-[Co(*R*,*R*-picchxn)(*R*-ABzH)]$^{2+}$, $ABzH_2$ = 2-amino-2-benzylpropandioic acid, in which the π–π interaction was seen to stabilize the transition state involved in the decarboxylation of the substituted aminomalonic acid to yield phenylalanine. Subsequently, in an exploration of ternary Co(III) complexes containing phenylalanine and *N*,*N*′-dimethyl analogues of **1**, **2** and related ligands, it was shown [20] that such π–π interactions are quite general in the solid state, as revealed by a series of single-crystal X-ray structures, and, more intriguingly, the interactions persisted in solution. In the case of Λ-β_1-[Co(*R*,*R*-picchxn)(*R*-ABzH)]$^{2+}$, the unusual situation of an NH proton of the aminoacidate lying between the interacting aromatic rings was noted in terms of chemical shift effects in the NMR, but it was not apparent at the time that the fragment was not innocent with respect to its bonding contribution [19]. A similar combination of π–π and bifurcated NH–π interactions is also evident in the analogous ternary complex containing α-methyl-*S*-tryptophan [21], and in other related complexes [20].

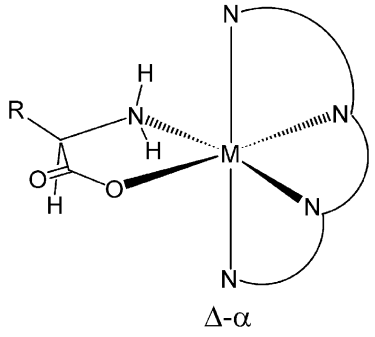

Δ-α

Fig. 1. Representation of the Δ-α coordination topology for octahedral complexes of *R*,*R*-picchxn containing a bidentate aminoacidate ligand.

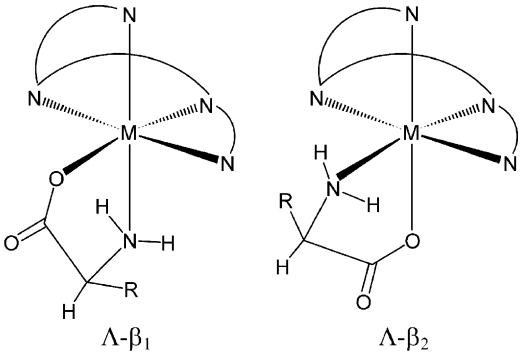

Λ-β_1 Λ-β_2

Fig. 2. The two kinds of octahedral β distereoisomers, β_1 or β_2 are illustrated for the Λ-complex of *R*,*R*-picchxn.

We now recognize the fact that NH–π interactions also represent important stabilizing forces in this class of molecules, and have explored this in a series of coordination complexes of Co(III), *R*,*R*-picchxn and *R*- or *S*-tryptophan. These NH–π bonds are strong enough to stabilize α isomers of *R*,*R*-picchxn with Co(III), resulting in the isolation of an unprecedented stable α complex with *R*-tryptophan, as reported in this work. Further, we have been able to estimate the energetic contributions of the interactions to bonding by a combination of structural and solution studies, described below. It is concluded that in an appropriate environment [8,22], NH–π bonds can be much stronger than attractive π–π interactions in these complexes and can be as strong as normal hydrogen bonds.

2. Experimental

2.1. General procedures

NMR studies were carried out with Varian Unity*inova*-500 (500 MHz), *Mercury*-400 (400 MHz) and Unity*plus*-300 (300 MHz) spectrometers with DMSO-d_6 (98.5%), D_2O (99.9%), benzene-d_6 (99.6%) and pyridine-d_5 (99%) as solvents. Chemical shifts (δ) are given in ppm relative to TMS (DMSO) and TSP sodium salt (D_2O) as internal standards for ^1H and ^{13}C spectra. Chemical shifts are positive if the signal was shifted to higher frequencies than the standard. Unless otherwise indicated, all experiments were performed at 25 °C. Electronic spectra were recorded on a Perkin–Elmer Lambda EZ-210 spectrophotometer and circular dichroism spectra (CD) on a Jasco J-810 spectropolarimeter. Λ-β-[Co(*R*,*R*-picchxn)Cl_2]$ClO_4 \cdot 0.5H_2O$ was synthesized as previously described [23]. Crystals of the three salts of the complexes containing the *R*-aminoacidate that were obtained were suitable for X-ray analysis.

2.2. Caution

Perchlorate salts are potentially explosive and should be handled with care. However, we have not experienced any problems with the synthesis and manipulation of these compounds.

2.3. Λ-β_1-[Co(*R*,*R*-picchxn)(*S*-trp)]$(ClO_4)_2 \cdot NaClO_4 \cdot 2H_2O$ (**3**)

It is preferable, to increase yields, to carry out the synthesis in the dark. Λ-β_1-[Co(*R*,*R*-picchxn)Cl_2]$(ClO_4) \cdot 0.5H_2O$ (0.50 g, 0.94 mmol) and *S*-trpH (0.96 g, 4.72 mmol) were stirred in water at 60 °C until the solids had dissolved. Aqueous NaOH (1 ml, 1 M) was added dropwise and the mixture cooled to room temperature. The orange solution was diluted fivefold with water and applied to a column (40×2 cm) of CM-Sephadex® C25 in the Na^+ cycle. Elution with 0.3 M aqueous NaCl resulted in a slow-moving orange band that was collected in fractions. Electronic spectroscopy showed that a single isomer was present. Solid $NaClO_4 \cdot xH_2O$ (ca. 0.15 g) was added to each fraction and the fractions stored over silica gel at room temperature under reduced pressure. After some four weeks, the complex was recovered as a microcrystalline powder from the majority of the fractions by filtration at the pump, then washing with a minimum of ice-cold water and air-drying. Yield: 0.18 g. *Anal*. Calc. for $C_{29}H_{39}Cl_3CoN_6NaO_{16}$: C, 38.03; H, 4.29; N, 9.18. Found: C, 38.21; H, 4.44; N, 9.04%. Electronic spectrum: λ_{max}/nm (H_2O) 349 (ε/M^{-1} cm^{-1} 4120), 472 (2710). CD spectrum: λ_{max}/nm (H_2O) 306 ($\Delta\varepsilon/M^{-1}$ cm^{-1} +3.6), 354 (−13.6), 487 (+25.5).

2.4. Δ-α-[Co(*R*,*R*-picchxn)(*R*-trp)]$(ClO_4)_2 \cdot H_2O$ (**4**)

Λ-β_1-[Co(*R*,*R*-picchxn)Cl_2]$(ClO_4) \cdot 0.5H_2O$ (1.0 g, 1.86 mmol) was dissolved in water (60 ml) at 60 °C and *R*-trpH (1.3 g, 6.4 mmol) was added. When the latter had dissolved, aqueous NaOH (2 ml, 1 M) was added dropwise and the mixture cooled to room temperature, diluted fivefold with water and chromatographed as above using aqueous 0.15 M NaCl. The main orange band that developed was collected in fractions (77×11 ml) and electronic spectra showed three isomers to be present, but pure in separate portions of the band. Fractions containing the isomer from the tail of the band were treated with solid $NaClO_4 \cdot xH_2O$ (ca. 0.15 g) and slowly evaporated over silica gel. During four weeks, orange prisms separated and these were collected at the pump, washed with ice-cold water and air-dried. Yield: 0.14 g. *Anal*. Calc. for $C_{29}H_{37}Cl_2CoN_6O_{11}$: C, 44.92; H, 4.81; N, 10.84. Found: C, 44.90; H, 4.80; N, 10.83%. Electronic spectrum: λ_{max}/nm (H_2O) 352 (ε/M^{-1} cm^{-1} 3380), 477 (1650). CD spectrum: λ_{max}/nm (H_2O) 354 ($\Delta\varepsilon/M^{-1}$ cm^{-1} +7.5), 390 (+9.2), 488 (−31.9).

2.5. Λ-β_1-[Co(*R*,*R*-picchxn)(*R*-trp)]$(CF_3SO_3)_2$ (**5**)

Fractions from the middle of the above band were combined, reduced to dryness at 40 °C and desalted with absolute ethanol. The filtrate was reduced to dryness and taken up in water (80 ml) and to the solution was added solid CF_3SO_3K (ca. 0.8 g). Evaporation over silica gel during two weeks gave deep orange prisms that were isolated as above. Yield: 0.36 g. *Anal*. Calc. for $C_{31}H_{35}CoF_6N_6O_8S_2$: C, 43.46; H, 4.12; N, 9.81. Found: C, 43.47; H, 3.86; N, 9.70%. Electronic spectrum: λ_{max}/nm (H_2O) 351 (ε/M^{-1} cm^{-1} 3080), 480 (2710). CD spectrum: λ_{max}/nm (H_2O) 327 ($\Delta\varepsilon/M^{-1}$ cm^{-1} +4.5), 383 (+5.5), 497 (+32.7).

2.6. Λ-β_2-[Co(*R*,*R*-picchxn)(*R*-trp)]$(CF_3SO_3)Cl \cdot 4H_2O$ (**6**)

Pure fractions from the front of the above band were combined and reduced to 15 ml at 40 °C. Solid CF_3SO_3K (ca. 0.1 g) was added to the pink-orange solution, which was evaporated over silica gel for two weeks. The crimson prisms that had formed were isolated as above. These slowly lose water by efflorescence when dry, but may be protected by a coating of silicone oil, or stored in contact with the mother liquor. Yield: 0.05 g. *Anal*. Calc. for $C_{30}H_{43}ClCoF_3N_6O_9S$: C, 44.20; H, 5.44; N, 10.31. Found: C, 43.99; H, 5.79; N, 10.29%. Electronic spectrum: λ_{max}/nm (H_2O) 353 (ε/M^{-1} cm^{-1} 3370), 475 (1870). CD spectrum: λ_{max}/nm (H_2O) 349 ($\Delta\varepsilon/M^{-1}$ cm^{-1} −7.6), 467 (+39.8), 551 (−1.8).

2.7. NMR spectroscopy

Concentrations of complexes were typically 10–15 mM in DMSO-d_6 and 5–10 mM in other solvents, including mixed solvents. Broadening of resonances is observed at higher concentrations, due to intermolecular interactions. Exchangeable protons for DMSO-d_6 samples were determined by addition of D_2O 5 min prior to recording the ^1H NMR spectrum. When required, sample degassing was carried out by repeated successive freeze-thaw cycles under high vacuum. Variable-temperature ^1H NMR spectra were acquired using a 15-min equilibration period at each temperature and a recycling delay of 6 s.

Two-dimensional DQF-COSY, and TOCSY experiments employing a MLEV-17 spin lock pulse sequence with 10 and 20 ms mixing times (to give predominantly $^{2-3}J_{HH}$ and strong $^4J_{HH}$ correlations) were recorded. TOCSY experiments with mixing times between 60 and 110 ms were also recorded for obtaining relayed correlations from the entire network of spin systems. 2D data sets with 2048 data points in the t_2 dimension and 256 or 512 complex points in t_1 were collected with 16–32 scans per t_1 increment. The relaxation delay was typically 2.5–3 s. All phase sensitive 2D data sets were recorded using the protocol of States et al. [24]. For the COSY, t_1 and t_2 were multiplied by a combination of sine-bell and shifted sine-bell functions prior to 2D transformation. For the TOCSY experiments, baselines were corrected with a polynomial routine in f_1 and f_2. Spectra were zero-filled and processed with a combination of exponential and Lorentzian–Gaussian window functions. ROESY [25] spectra were recorded with a relaxation delay of 2.5–5 s for mixing times of 300, 450, 600 and 1000 ms, using a pulsed spin-lock during the mixing period. Data sets consisted of 2048 complex points in the t_2 dimension and 256 or 512 in t_1 with 32–48 scans per t_1 increment. The spectra were zero-filled and processed with Gaussian weighting functions. In all cases, ridges along f_2 were reduced by multiplying the first point in the FID by 0.4–0.75 prior to the Fourier transform, then applying a polynomial baseline correction routine. HMQC [26] spectra were recorded with the delays optimized for J_{C-H} coupling constants of 125 or 140 Hz. Data sets with 2048×256 complex

Table 1
Crystal data and structure refinement for **4**, **5** and **6**

Crystal data	**4**	**5**	**6**
Empirical formula	$C_{29}H_{37}Cl_2CoN_6O_{11}$	$C_{31}H_{35}CoF_6N_6O_8S_2$	$C_{30}H_{41}ClCoF_3N_6O_8S$
Colour, habit	orange, prism	orange, prism	crimson, prism
T (K)	150(2)	150(2)	150(2)
Formula weight	775.48	856.70	797.13
Crystal size (mm)	$0.25\times0.20\times0.20$	$0.25\times0.25\times0.20$	$0.40\times0.30\times0.30$
Crystal system	orthorhombic	triclinic	monoclinic
Space group	$P2_12_12_1$	$P1$	$C2$
a (Å)	10.936(2)	8.9010(15)	24.314(11)
b (Å)	12.823(4)	9.7874(17)	9.727(5)
c (Å)	23.497(6)	10.8120(18)	18.992(9)
α (°)	90	78.303(2)	90
β (°)	90	82.258(2)	125.614(7)
γ (°)	90	69.505(2)	90
V (Å^3)	3295.2(14)	861.9(3)	3652(3)
Z	4	1	4
D_{calc} (g cm^{-3})	1.563	1.651	1.450
μ (mm^{-1})	0.752	0.712	0.671
θ Range (°)	1.73–28.25	1.93–23.28	3.52–28.01
Index ranges	$-14\leqslant h\leqslant 14$, $-17\leqslant k\leqslant 16$, $-29\leqslant l\leqslant 31$	$-9\leqslant h\leqslant 9$, $-10\leqslant k\leqslant 10$, $-12\leqslant l\leqslant 12$	$-31\leqslant h\leqslant 26$, $-12\leqslant k\leqslant 12$, $0\leqslant l\leqslant 24$
Reflections collected	31 731	5937	7876
Independent reflections (R_{int})	7868 (0.0457)	4681 (0.0153)	7876 (0.0)
Observed data [$I > 2\sigma(I)$]	6975	4517	6030
Data/restraints/parameters	7868/0/443	4681/3/488	7876/4/383
Weighting factors a, b[a]	0.0394, 2.3995	0.0320, 0	0.200, 0
Goodness-of-fit on F^2	0.835	0.943	1.536
Final R indices (observed data)	$R_1 = 0.0312$, $R_w = 0.0702$	$R_1 = 0.0254$, $R_w = 0.0613$	$R_1 = 0.1292$, $R_w = 0.3457$
R indices (all data)[b]	$R_1 = 0.0403$, $R_w = 0.0752$	$R_1 = 0.0261$, $R_w = 0.0616$	$R_1 = 0.1601$, $R_w = 0.3766$
Largest difference minimum/maximum (e Å^{-3})	−0.26/0.36	−0.36/0.37	−0.71/2.62

[a] $w = 1/[\sigma^2(F_o^2) + (aP)^2 + bP]$, where $P = [2F_c^2 + \mathrm{Max}(F_o^2, 0)]/3$.
[b] $R_1 = \sum ||F_o| - |F_c|| / \sum |F_o|$ and $R_w = \{[\sum w(F_o^2 - F_c^2)^2 / \sum w(F_o^2)^2]^{1/2}\}$.

points were then processed with a combination of Gaussian and exponential weighting functions. HMBC [27] spectra were recorded with the delays optimized for a J_{nC-H} coupling constant of 8 Hz. Data workup was similar to that employed in the HMQC experiments, with the exception that data were processed with a sine-bell weighting function in absolute-value mode. All data were processed using Varian VNMR software (version 6.1C) on a Sun workstation.

2.8. X-ray crystallography

Single-crystal, high-resolution, low-temperature data of compounds **4**, **5** and **6** were collected on a Bruker SMART 1000 CCD diffractometer using Mo Kα radiation ($\lambda = 0.71073$ Å). Data were collected at 150(2) K with ω-scan increments of 0.3°. Reflections were integrated with the program SAINT [28] and merged with the program SADABS [28]. Details concerning crystal data and refinement parameters are given in Table 1. Intensities were corrected for Lorentz and polarization effects but absorption corrections were not applied. Structures were solved by direct methods and difference Fourier techniques using the SHELX-97 system [29], and refined by full-matrix least-squares methods in which the function $\sum w(F_o^2 - F_c^2)^2$ was minimized. Refinement was terminated when the minimization factor changed by <0.1% and a final difference map showed no significant residual electron density. Weighting schemes gave uniform analyses of variance in terms of F_c^2. Non-hydrogen atoms for compounds **4** and **5** were refined anisotropically. Hydrogen atoms were positioned geometrically, riding on the atoms to which they bond, with fixed isotropic thermal parameters. Data were also collected for the Λ-β_2 complex **6**, but attempts to fully refine the structure were frustrated by the fact that the anions and molecules of water of crystallization were considerably affected by disorder. However, the structure of the complex cation was fully discernible via a combination of difference Fourier maps and careful refinement steps. This allowed the complex cation to be finally refined with anisotropic thermal parameters for the non-hydrogen atoms, enabling the Λ-β_2 topology of the cation and the nature of the intramolecular π–π interaction to be established in the solid state. Hydrogen atoms for the complex cation in **6** were positioned geometrically, riding on the atoms to which they bond, with fixed isotropic thermal parameters. Three out of four waters of crystallization (as indicated by microanalysis of the efflorescent crystals) were located in partially occupied disordered sites. Our interest in this structure has been mainly focused on the confirmation of molecular structure and the conformation of the molecular cation. Plots of the molecules were made using ORTEP [30] for Windows.

3. Results and discussion

3.1. Topological considerations

The octahedral complex cations of the species reported in this paper are Λ-β_1-[Co(*R*,*R*-picchxn)(*S*-trp)]$^{2+}$ (**3**), Δ-α-[Co(*R*,*R*-picchxn)(*R*-trp)]$^{2+}$ (**4**), Λ-β_1-[Co(*R*,*R*-picchxn)(*R*-trp)]$^{2+}$ (**5**), and Λ-β_2-[Co(*R*,*R*-picchxn)(*R*-trp)]$^{2+}$ (**6**). The various diastereoisomers examined each have a combination of π–π and/or NH–π interactions, depending on their particular topology (Fig. 3); the Λ-β_1-*R*-trp isomer possesses one conformer of tryptophan that allows an NH–π interaction between the indole ring and a secondary amine group of the tetradentate. A secondary, non-idealized [11b] NH–π interaction involving the indole ring and an amino proton from Trp is also present in this conformer. Λ-β_2-*R*-trp, Δ-α-*R*-trp and Λ-β_1-*S*-trp isomers all have an appropriate conformer of the coordinated aminoacidate that can give rise to an intramolecular π–π interaction. In the cases of the latter two species, a bifurcated NH–π interaction involving one amino proton of the tryptophan ligand being sandwiched between the π-stacking indole and pyridyl rings, accompanies this interaction. For the Δ-α-*R*-trp complex, one amino group NH–(pyridyl) interaction remains in both of the other two conformers and a different kind of NH–π(indole) interaction is possible for one of them. The latter also obtains for another conformer of Λ-β_1-[Co(*R*,*R*-picchxn)(*S*-trp)]$^{2+}$ and an NH–π(indole) interaction is possible for one rotamer of Λ-β_2-[Co(*R*,*R*-picchxn)(*R*-trp)]$^{2+}$.

3.2. Molecular structures of the complexes

The molecular structures of **3**–**6** were elucidated by NMR spectroscopy in solution, and X-ray crystallography in the solid state for compounds **4**, **5** and **6**. Through-bond ^{1}H and ^{13}C connectivities established via DQF-COSY, TOCSY, HMQC and HMBC NMR experiments enabled the complete assignment of the complexes. Through-space correlations via NOESY and ROESY measurements uniquely confirmed individual coordination topologies and dominant solution configurations of the complexes in DMSO-d_6 and D_2O solution. Full lists of ^{1}H and ^{13}C chemical shift and coupling constant data, together with observed rOe correlations (ROESY) are available as Supplementary material. A summary of the crystallographic data, experimental details and refinement results for **4**–**6** is given in Table 1. Selected bond lengths and angles in these structures are listed in Table 2.

The molecular structure of the complex cation in Δ-α-[Co(*R*,*R*-picchxn)(*R*-trp)]$(ClO_4)_2 \cdot H_2O$ (**4**), is shown in Fig. 4, together with the atom-labeling scheme applied both in the structural analysis and NMR studies. Numeric labels for hydrogen atoms correspond to those of

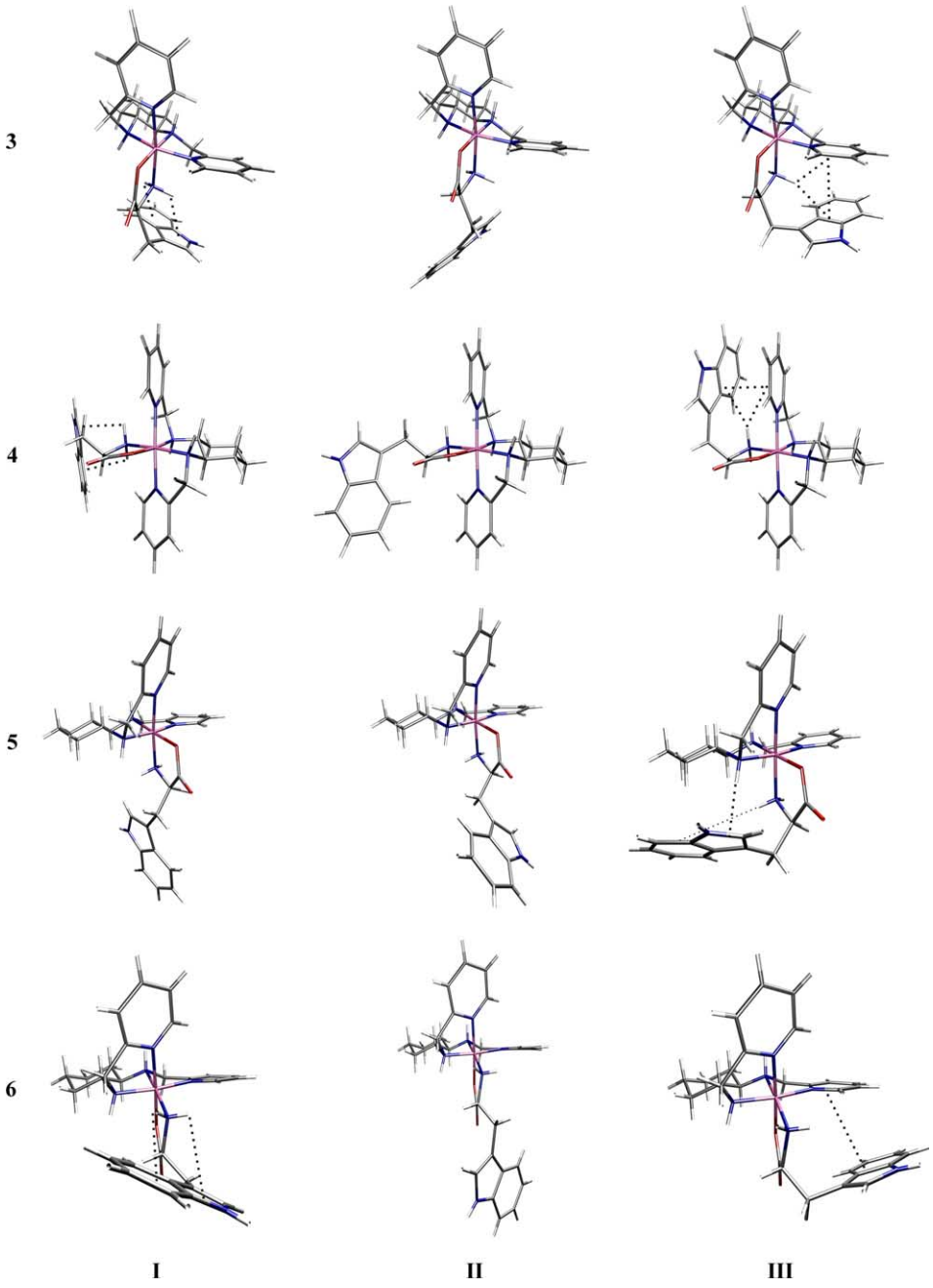

Fig. 3. Molecular conformation of the stable staggered rotamers **I**–**III** for the *R*- and *S*-aminoacidate complexes **3**–**6**. Dashed lines represent π–π and/or NH–π interactions in the individual rotamers.

the heavy atoms to which they are bonded, and where more than one hydrogen atom is bonded to a centre, it is distinguished by the suffix a, b or e. No unusual covalent bond lengths or angles were observed in the structure [13e,19–21], which clearly shows the tetradentate coordinated with α topology and the aminoacidate acting as a bidentate. In the lattice, perchlorate ions, water molecules of crystallization and the cations are linked by a hydrogen bonding network, and aromatic rings are aligned approximately parallel for adjacent cations (see Supplementary material for details of selected intermolecular contacts). Of particular note for the cation is an intramolecular π–π interaction between the indole ring of the coordinated aminoacidate and one of the pyridyl rings of the tetradentate, in a fashion akin to that observed in related structures [13e,19–21]. The conformation adopted by the molecular cation in the solid state corresponds to that of rotamer **III** in Fig. 3, as might be expected, based on a hierarchy of attractive non-covalent interactions that are possible in this species. Details of these interactions are highlighted in Fig. 5 and a summary of the intramolecular contacts is given in

Table 2
Selected bond lengths (Å) and angles (°) for **4**, **5** and **6**

	4	**5**	**6**
Bond lengths			
Co–N(1)	1.9623(17)	1.936(2)	1.963(8)
Co–O(31)	1.9245(15)	1.890(2)	1.889(6)
Co–N(21)	1.9294(18)	1.938(2)	1.927(10)
Co–N(11)	1.9496(18)	1.922(3)	1.937(7)
Co–N(2)	1.9535(18)	1.951(3)	1.961(7)
Co–N(31)[a]	1.9476(18)	1.965(2)	1.982(8)
Bond angles			
N(1)–Co(1)–O(31)	94.59(7)	178.60(11)	87.3(3)
N(1)–Co(1)–N(21)	94.42(7)	92.87(10)	94.9(4)
O(31)–Co(1)–N(21)	92.19(7)	85.73(9)	175.8(4)
N(1)–Co(1)–N(11)	81.71(8)	84.28(11)	83.4(3)
O(31)–Co(1)–N(11)	85.49(7)	95.82(10)	88.3(3)
N(21)–Co(1)–N(11)	175.30(8)	95.13(10)	95.6(4)
N(1)–Co(1)–N(2)	86.75(7)	86.68(10)	87.0(3)
O(31)–Co(1)–N(2)	175.30(7)	93.16(10)	91.7(3)
N(21)–Co(1)–N(2)	83.21(8)	82.82(10)	84.8(4)
N(11)–Co(1)–N(2)	99.16(8)	170.62(11)	170.3(4)
N(1)–Co(1)–N(31)[a]	176.34(8)	95.78(10)	171.2(4)
O(31)–Co(1)–N(31)[a]	84.53(7)	85.62(10)	84.0(3)
N(21)–Co(1)–N(31)[a]	89.17(8)	170.51(11)	93.9(4)
N(11)–Co(1)–N(31)[a]	94.68(8)	89.62(10)	95.9(3)
N(2)–Co(1)–N(31)[a]	94.41(7)	93.77(10)	93.7(3)

[a] The atom equivalent to N(31) in the Λ-β isomers **5** and **6** is labeled as N(3) in the Δ-α isomer **4**, in accordance with established nomenclature [16].

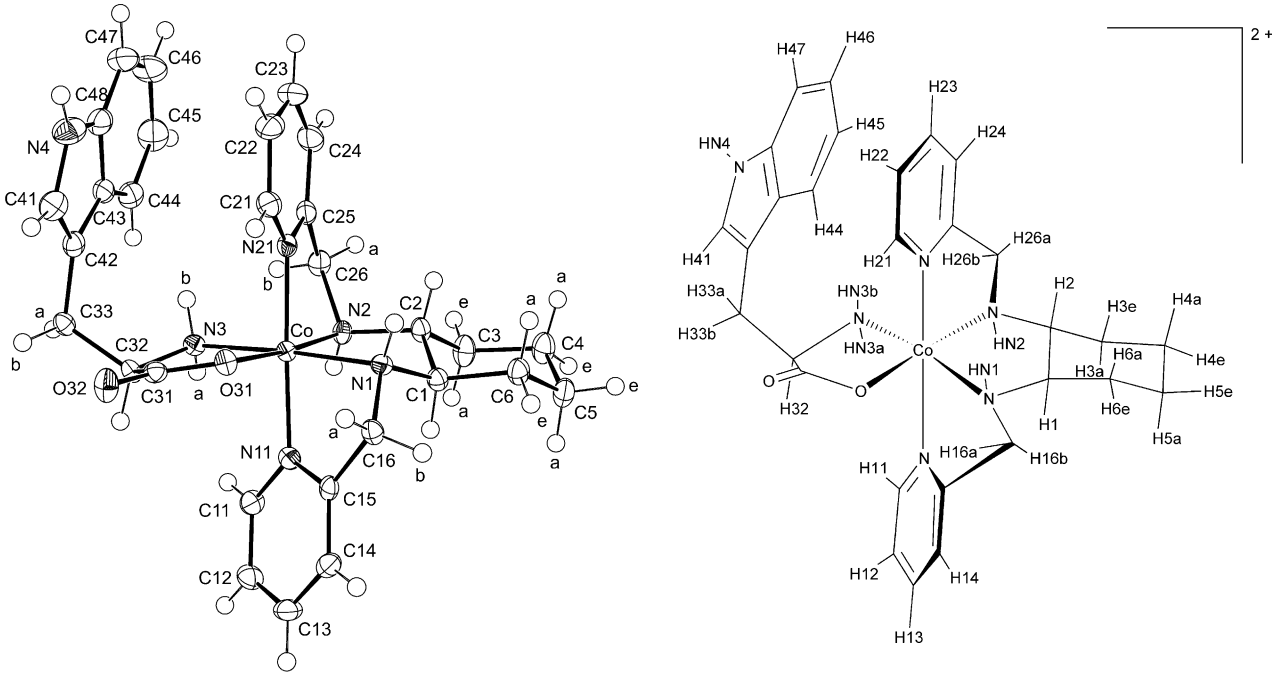

Fig. 4. Molecular structure of the Δ-α-[Co(*R*,*R*-picchxn)(*R*-trp)]$^{2+}$ cation of **4**. Thermal ellipsoids are shown at the 50% probability level. The right-hand view is a line drawing of the cation.

Table 3. The two ring planes make a dihedral angle of 7.5° and the distances between the centroid of the pyridyl ring to the centroids of the five- and six-membered rings of the adjacent indole group are 3.84 and 3.58 Å, respectively. These are characteristic of attractive π–π interactions found in a variety of systems [31], and compare well with similar contacts observed in related complexes [20]. Also shown in Fig. 5 are contacts made by the amino proton *H*N3b with the two rings, between which it is sandwiched. This proton, which participates in a bifurcated NH–π interaction, is found at the unusually high-field position of 3.49 ppm in the ^{1}H NMR

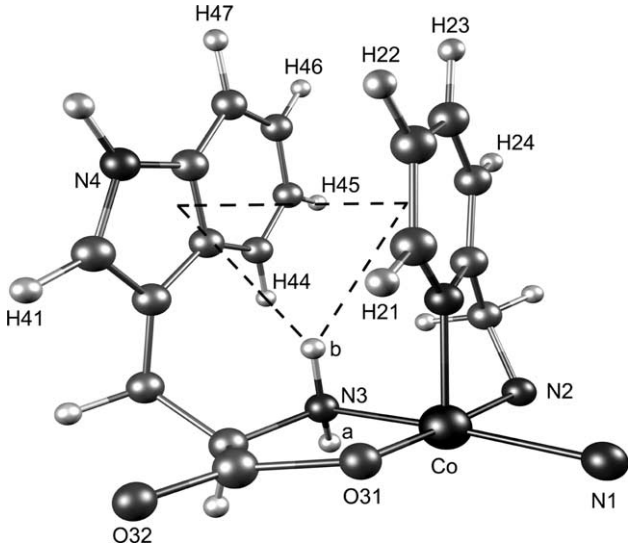

Fig. 5. Perspective view of the fragment of **4** showing the π-stacked indole and pyridyl rings. Dashed lines represent the intramolecular π–π and NH–π interactions.

spectrum recorded in DMSO-d_6 (Supplementary material). The chemical shift of *H*N3b is indicative of strong shielding effects associated with the ring current of the π-stacked aromatic rings. This non-classical hydrogen bond is not present for the geminal counterpart *H*N3a due to geometrical constraints, and accordingly this proton is observed at 6.84 ppm in DMSO-d_6. The relative chemical shifts of the two amino protons do not vary appreciably with concentration, nor under strictly anhydrous conditions (as achieved by converting the diperchlorate monohydrate **4** to the anhydrous dichloride salt via anion exchange chromatography, then dissolving this with anhydrous DMSO-d_6). This is entirely consistent with the intramolecular nature of the NH–π interaction in this complex cation.

The molecular structure of the complex cation in Λ-β_1-[Co(*R*,*R*-picchxn)(*R*-trp)]$(CF_3SO_3)_2$ (**5**), is shown in Fig. 6. Bond lengths and angles observed in the structure are quite normal [13e,19–21], and the tetradentate coordinates with β topology with the aminoacidate acting as a bidentate in β_1 fashion. In the lattice, NH groups from the indole ring, the amino group of Trp and the tetradentate are hydrogen bonded to the oxygen atoms of the triflate ions and intermolecular ring stacking interactions range from 3.6 to 3.9 Å (see Supplementary material). A different kind of intramolecular contact is evident in the complex cation of **5** (Table 3) and involves NH–π contacts between *H*N2 and the indole group of the aminoacidate (distance of 2.41 Å from *H*N2 to the centroid of the five-membered ring). This is an example of a relatively rare *facial* interaction, noted especially in certain indole and porphyrin systems [3c], and is significantly closer than a similar contact (2.72 Å) reported for another Co(III) complex containing *S*-tryptophan and *N,N*-bis(carboxymethyl)-*S*-phenylalanine [13a]. A secondary, non-ideal [11b] NH–π interaction involving the indole ring and an amino proton from Trp is also present in this conformer. It is apparent that solid-state conformation of the cation in **5** also corresponds to that of rotamer **III** in Fig. 3. This result is consistent with the solid-state conformation adopted by the closely related species Λ-β_1-[Co(*R*,*R*-picchxn)(*R*-tyr)]$(ClO_4)_2 \cdot 2H_2O$ [20a]. It is important to note, by way of contrast, that the analogous Λ-β_1-[Co(*R*,*R*-picchxn)(*R*-phe)]$(ClO_4)_2 \cdot H_2O$ complex adopts the solid-state conformation equivalent to rotamer **II** for **5** (no NH–π bond) [20a]. The results, taken together, are precisely in line with the observations of Steiner and Koellner [8], who noted that Trp and Tyr are the aromatic aminoacids most frequently involved in NH–π hydrogen bonds in proteins. The order of aromatic acceptor efficiency is Trp ≫ Tyr > Phe ≫ His [8].

The molecular structure of the complex cation in Λ-β_2-[Co(*R*,*R*-picchxn)(*R*-trp)]$(CF_3SO_3)Cl \cdot 3H_2O$, **6**, is shown in Fig. 7. A high degree of disorder of the counterions and lattice water molecules in the single-crystal structure of this compound prevented full structural refinement, but the structure of the complex cation was fully discernible. In this isomer, the indole ring of Trp participates with a pyridyl ring of the tetradentate in a π–π interaction (Table 3), but no intramolecular NH–π contacts are present. The conformation adopted by the cation of **6** in the solid state corresponds to that of rotamer **III** in Fig. 3. A quasi-parallel aromatic interaction similar to that found in compound **4** is unfavoured in this diastereoisomer due to a steric clash between H44 of the indole ring and the coordinated carboxyl group. The rings adopt a hinged π-stacking arrangement with a dihedral angle of 22.1° between the ring planes, with the principal π–π interaction occurring between the pyridyl ring and the six-membered ring of the indole group. The distance between the centroids of these two rings is 3.899 Å (Table 3).

No crystals of Λ-β_1-[Co(*R*,*R*-picchxn)(*S*-trp)]$(ClO_4)_2 \cdot NaClO_4 \cdot 2H_2O$ (**3**) suitable for X-ray analysis were obtained, but spectroscopic and analytical measurements establish the nature of the complex unambiguously. The CD spectrum indicates the Λ absolute configuration at Co [15–21] and its ^1H and ^{13}C NMR spectra are in complete agreement with the assignment. Notably, H11 is observed at δ 7.71 and 7.50 in DMSO-d_6 and D_2O, respectively, in accord with previous observations of complexes for which single-crystal structures are to hand [18,19,21]. Through-bond ^1H and ^{13}C connectivities established via DQF-COSY, TOCSY, HMQC and HMBC NMR experiments have enabled the complete assignment of this complex. Through-space correlations via NOESY and ROESY measurements in DMSO-d_6 and D_2O uniquely confirmed the

Table 3
Intramolecular contacts for compounds **4**, **5** and **6**

		Distance (Å)		Distance (Å)
4	Close contacts between π-stacked rings		Close contacts for *H*N3b	
	N4···C22	3.597	*H*N3b···C25	2.763
	C41···C21	3.849	*H*N3b···C42	2.550
	C42···C21	3.832	*H*N3b···C43	2.543
	C43···N21	3.712	*H*N3b···C44	2.512
	C44···C25	3.578	*H*N3b···pyridyl centroid	3.298
	C45···C24	3.515	*H*N3b···indole Ct(5 mem.)[a]	3.299
	C46···C24	3.521	*H*N3b···indole Ct(6 mem.)[b]	3.429
	C47···C23	3.345		
	C48···C22	3.433		
	Centroid separation between π-stacked rings			
	pyridyl···indole Ct(5 mem.)[a]	3.835		
	pyridyl···indole Ct(6 mem.)[b]	3.575		
5	Close contacts for *H*N2			
	*H*N2···N4	2.786		
	*H*N2···C41	2.496		
	*H*N2···C42	2.436		
	*H*N2···C43	2.688		
	*H*N2···C48	2.908		
	*H*N2···indole Ct(5 mem.)[a]	2.405		
	*H*N2···indole Ct(6 mem.)[b]	3.411		
6	Close contacts between π-stacked rings		Centroid separation between π-stacked rings	
	N4···C11	4.118	pyridyl···indole Ct(5 mem.)[a]	4.661
	C41···C11	4.220	pyridyl···indole Ct(6 mem.)[b]	3.899
	C42···C11	3.855		
	C43···C11	3.426		
	C44···C11	3.602		
	C45···C12	3.528		
	C46···C12	3.447		
	C47···C12	3.486		
	C48···C12	3.611		

[a] Centroid of the five-membered ring of the indole heterocycle.
[b] Centroid of the six-membered ring of the indole heterocycle.

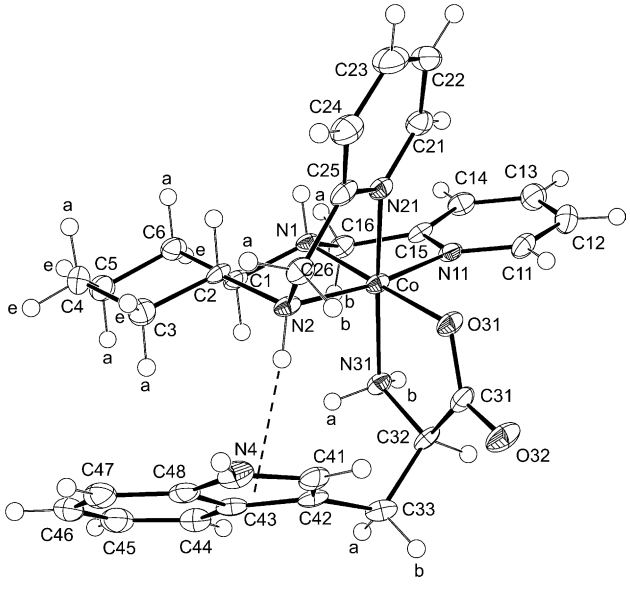

Fig. 6. Molecular structure of the Λ-β_1-[Co(*R*,*R*-picchxn)(*R*-trp)]$^{2+}$ cation of **5** with 50% probability thermal ellipsoids. A dashed line represents the intramolecular NH–π interaction.

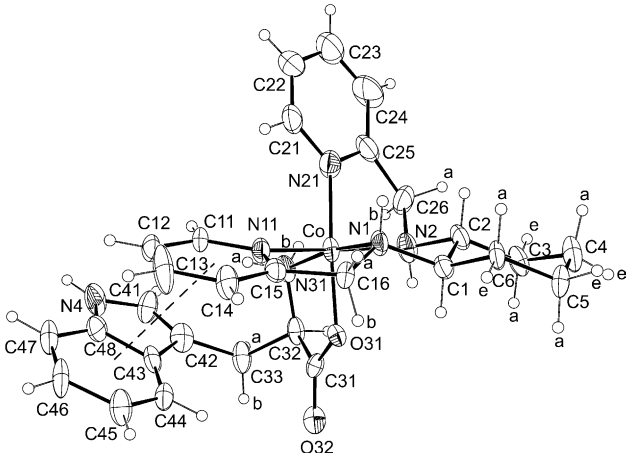

Fig. 7. Molecular structure of the Λ-β_2-[Co(*R*,*R*-picchxn)(*R*-trp)]$^{2+}$ cation of **6** with 50% probability thermal ellipsoids. A dashed line represents the intramolecular π–π interaction.

Λ-β_1 topology and molecular structure. Full lists of ^{1}H and ^{13}C chemical shift and coupling constant data, together with observed rOe correlations (ROESY) for **3** are available as Supplementary material. The molecular structure of the complex cation of **3** is shown in Fig. 8, together with the atom-labeling scheme applied in the NMR studies. The particular conformation illustrated corresponds to the dominant species in solution, as established by measurement of rotamer populations (vide infra) and through-space correlations from ROESY spectra recorded at various mixing times (vide supra). This corresponds to rotamer **III** in Fig. 3, and is consistent with the known solid-state conformation of the analogous complex with *S*-α-methyltryp [21] and other related species [20b].

3.3. Rotamer distributions and solution structures

One- and two-dimensional NMR studies confirm the structural relationships found in the solid state for the above complexes and the nature of the Λ-β_1-[Co(*R*,*R*-picchxn)(*S*-trp)]$^{2+}$ ion in solution. Rotamer populations (with respect to rotation about the C_α–C_β bond) for the coordinated *R*- or *S*-trp aminoacidate ligands in **3**–**6** were calculated from two vicinal coupling constants for the ABX systems present in their ^{1}H NMR spectra, using an established methodology (Eqs. (1)–(3)) [32]. Newman projections for the three stable staggered rotamers are shown in Fig. 9. The critical values used were $J_g = 2.60$ and $J_t = 13.56$ Hz [32e], which represent the values for the vicinal coupling constants between hydrogen atoms in the *trans*, J_t, and gauche position to each other, J_g, derived from various sources [32b–32e]:

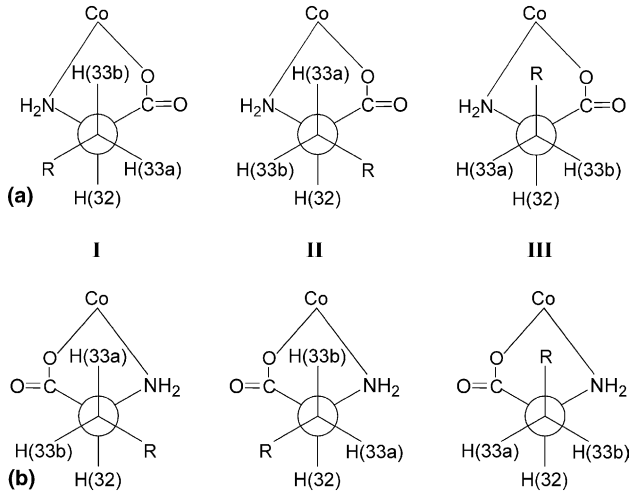

Fig. 9. Newman projections of the three staggered rotamers about the C_α–C_β bond of the coordinated aminoacidate: (a) rotamers for *R*-aa; (b) rotamers for *S*-aa.

$$p\mathbf{I} = \frac{J_{33b,32} - J_g}{J_g - J_t}, \tag{1}$$

$$p\mathbf{II} = \frac{J_{33a,32} - J_g}{J_g - J_t}, \tag{2}$$

$$p\mathbf{III} = 1 - (p\mathbf{I} + p\mathbf{II}). \tag{3}$$

It was assumed that these remained unchanged upon coordination [32a]. The relative residence times for **I** and **II** were determined from Eqs. (1) and (2), respectively, using the two measured vicinal coupling constants, $J_{33b,32}$ and $J_{33a,32}$. The residence times are normalized by

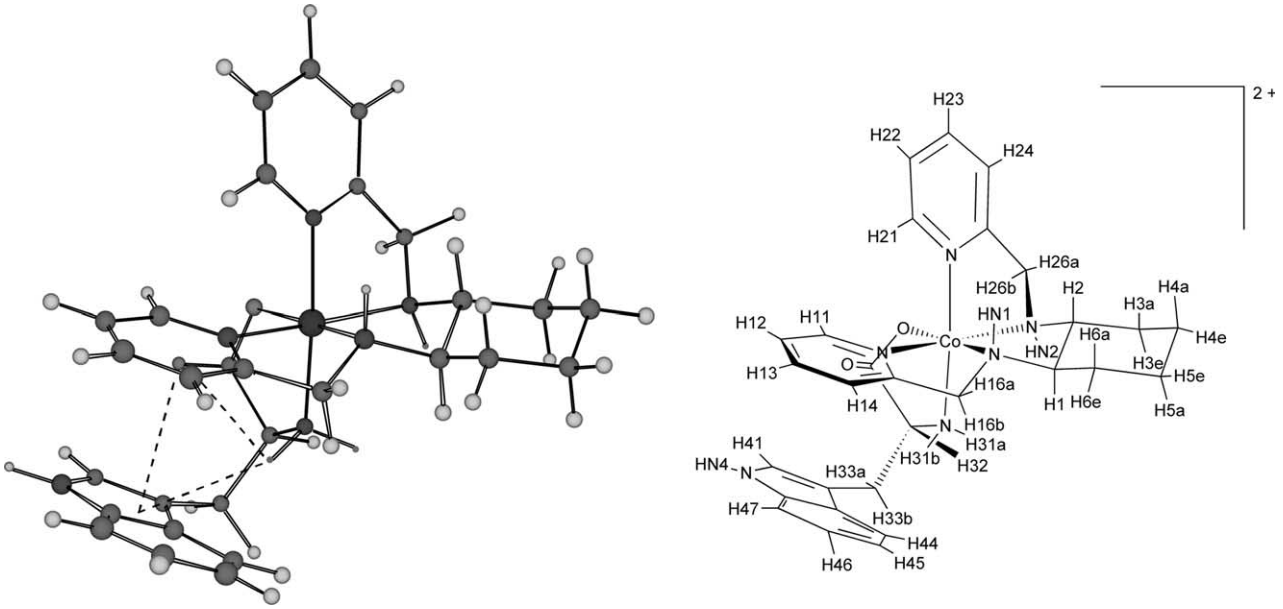

Fig. 8. Molecular structure of the Λ-β_1-[Co(*R*,*R*-picchxn)(*S*-trp)]$^{2+}$ cation of **3**. The molecular conformation was established in solution by ROESY correlations, with dashed lines representing the intramolecular π–π and NH–π interactions. The right-hand view is a line drawing of the cation.

Table 4
Vicinal coupling constants (400 MHz), rotamer populations, and selected discrimination energies for **3**–**6** in various deuterated solvents at 25 °C

	Solvent	$J_{33a,32}, J_{33b,32}$[a]	Rotamer			Discrimination (kJ mol^{-1})	
		(Hz)	**I**	**II**	**III**	ΔG_1[b]	ΔG_2[c]
3	DMSO	4.84, 4.90	0.21	0.20	0.59	−2.56 ± 0.35	−2.68 ± 0.32
	Benzene/DMSO 2:1	4.25, 4.92	0.21	0.15	0.64	−2.76 ± 0.16	−3.59 ± 0.22
	Benzene/DMSO 7:1	3.41, 5.32	0.25	0.07	0.68	−2.48 ± 0.20	−5.63 ± 0.22
	Pyridine	2.71, 5.47	0.26	0.01	0.73	−2.56 ± 0.12	−10.63 ± 0.63
	D_2O	2.73, 5.56	0.27	0.01	0.72	−2.43 ± 0.25	−10.60 ± 1.35
	D_2O/DMSO 1:2	3.59, 5.34	0.25	0.09	0.66	−2.41 ± 0.10	−4.94 ± 0.10
4	DMSO	–	–	–	–	–	–
	Benzene/DMSO 2:1	4.60, 4.73	0.19	0.18	0.63	−2.97 ± 0.17	−3.10 ± 0.13
	Benzene/DMSO 7:1	3.85, 5.10	0.23	0.11	0.66	−2.61 ± 0.20	−4.44 ± 0.34
	Pyridine	3.14, 5.31	0.25	0.05	0.70	−2.55 ± 0.13	−6.54 ± 0.34
	D_2O	2.93, 4.02	0.13	0.03	0.84	−4.62 ± 0.50	−8.26 ± 0.60
	D_2O/DMSO 1:2	2.78, 5.28	0.24	0.02	0.74	−2.79 ± 0.16	−8.95 ± 0.59
5	DMSO	5.89, 6.36	0.34	0.30	0.36	−0.14 ± 0.11	−0.45 ± 0.10
	Benzene/DMSO 2:1	5.36, 6.64	0.37	0.25	0.38	−0.07 ± 0.20	−1.04 ± 1.60
	Benzene/DMSO 7:1	5.36, 6.29	0.34	0.25	0.41	−0.46 ± 0.10	−1.23 ± 0.11
	Benzene/DMSO 10:1	5.37, 5.84	0.30	0.25	0.45	−1.00 ± 0.12	−1.46 ± 0.11
	Pyridine	4.17, 5.34	0.25	0.14	0.61	−2.21 ± 0.14	−3.65 ± 0.22
	D_2O	–	–	–	–	–	–
	D_2O/DMSO 1:2	5.93, 6.18	0.33	0.30	0.37	−0.28 ± 0.10	−0.52 ± 0.16
6	DMSO	–	–	–	–	–	–
	Benzene/DMSO 2:1	5.31, 4.80	0.20	0.25	0.55	−2.51 ± 0.15	−1.95 ± 0.12
	Benzene/DMSO 7:1	4.56, 5.19	0.24	0.18	0.58	−2.19 ± 0.12	−2.90 ± 0.16
	Pyridine	3.54, 5.80	0.29	0.09	0.62	−1.88 ± 0.10	−4.78 ± 0.29
	D_2O	2.68, 6.05	0.31	0.01	0.68	−1.95 ± 0.29	−10.45 ± 1.57
	D_2O/DMSO 1:2	3.62, 5.89	0.30	0.09	0.61	−1.76 ± 0.22	−4.74 ± 0.61

[a] Average values from at least three experiments.
[b] ΔG_1 is obtained from $K_1 = \mathbf{III}/\mathbf{I}$.
[c] ΔG_2 is obtained from $K_2 = \mathbf{III}/\mathbf{II}$. Dashes indicate rotamer populations that could not be evaluated due to deceptively simple ABX systems in the ^{1}H NMR spectra.

Eq. (3), enabling the population of **III** to be evaluated. Three-dimensional molecular models of the complexes (adopting conformations corresponding to the idealized rotamers) are illustrated in Fig. 3. Rotamer populations at 25 °C for **3**–**6** in various solvents are listed in Table 4. The dominant conformer in solution in all cases is **III**. As noted above, single-crystal structures of **4**–**6** have demonstrated that the molecular cation in each complex adopts a conformation corresponding to rotamer **III**, whereby attractive π–π and/or NH–π interactions dominate. These findings demonstrate the persistence of the weak non-covalent interactions in solution. The molecular conformation found in the solid state for **4** and **6** also dominates in solutions of Λ-β$_1$-[Co(*R*,*R*-picchxn)(*S*-trp)]$^{2+}$ (**3**). This is consistent with our recent observations [20b] for Λ-β$_1$-[Co(*R*,*R*-picchxn)(*S*-aa)]$^{2+}$ (aa = Tyr, *O*Me-tyr or Phe) complexes, for which the appropriate conformer possessing both intramolecular π–π and NH–π interactions dominates in solution in all cases.

It has been shown from an evaluation of the equilibrium rotamer distributions under a variety of conditions (Tables 4 and 5) that rotamer **III** is the dominant conformer in Δ-α-*R*-trp (**4**), Λ-β$_1$-*S*-trp (**3**), and Λ-β$_2$-*R*-trp (**6**). In each case, the dominant conformer is seen to exhibit an intramolecular π–π interaction (Fig. 3). The nature of the dominant conformers in **3**, **4** and **6** is further manifested in observations of rOe correlations between protons of the pyridyl and indole rings involved in π-stacking. Fig. 10 shows an expansion of the aromatic region of a ROESY spectrum of Δ-α-[Co(*R*,*R*-picchxn)(*R*-trp)]$^{2+}$ in D_2O, together with a perspective view of the relevant fragment of the molecule constructed using coordinates from the single-crystal X-ray structure. Cross-peaks corresponding to close proton–proton contacts between the interacting rings (depicted by dashed lines) are highlighted in the spectrum by boxes. In the solid state, all of these interproton distances are between 3.29 and 4.55 Å in distance and thus should be and are observed in the spectrum. Through-space correlations between amino proton HN3b and protons from the indole ring of Trp were only observed at shorter mixing times ($\tau_m \leqslant 300$ ms, see Supplementary material). Spectra were acquired with sufficient mixing times to allow rOe build-up, and no evidence for the effects of spin diffusion

Table 5
Vicinal coupling constants (400 MHz) and rotamer populations at various temperatures for compounds **3**, **4**, **5** and **6** in DMSO-d_6 and D_2O[a]

	Rotamer	25 °C		35 °C		45 °C		55 °C		65 °C	
		DMSO	D_2O	DMSO	D_2O	DMSO	D_2O	DMSO	D_2O	DMSO	D_2O
		(4.84, 4.90)	(2.73, 5.56)	(4.69, 4.99)	(2.75, 5.56)	(4.64, 5.05)	(2.70, 5.70)	(4.73, 5.04)	(2.81, 5.69)	(4.72, 5.13)	(2.97, 5.65)
3	**I**	0.21[b]	0.27	0.22	0.27	0.22	0.28	0.22	0.28	0.23	0.28
	II	0.20	0.01	0.19	0.01	0.19	0.01	0.19	0.02	0.19	0.03
	III	0.59	0.72	0.59	0.72	0.59	0.71	0.59	0.70	0.58	0.69
		–	(2.93, 4.02)	–	(3.26, 4.45)	–	(3.00, 4.71)	–	(2.91, 4.81)	–	(2.92, 4.98)
4	**I**	–	0.13	–	0.17	–	0.19	–	0.20	–	0.22
	II	–	0.03	–	0.06	–	0.04	–	0.03	–	0.03
	III	–	0.84	–	0.77	–	0.77	–	0.77	–	0.75
		(5.89, 6.36)	–	(5.54, 6.33)	–	(5.82, 6.31)	–	(5.64, 6.32)	–	(5.88, 6.40)	–
5	**I**	0.34	–	0.34	–	0.34	–	0.34	–	0.35	–
	II	0.30	–	0.27	–	0.29	–	0.28	–	0.30	–
	III	0.36	–	0.39	–	0.37	–	0.38	–	0.35	–
		–	(2.68, 6.05)	(4.45, 5.67)	(2.85, 6.21)	(4.91, 5.11)	(2.79, 5.98)	–	(3.07, 6.01)	–	(3.11, 6.02)
6	**I**	–	0.31	0.28	0.33	0.23	0.31	–	0.31	–	0.31
	II	–	0.01	0.17	0.02	0.21	0.02	–	0.04	–	0.05
	III	–	0.68	0.55	0.65	0.56	0.67	–	0.65	–	0.64

[a] Vicinal coupling constants in Hertz appear in the format ($J_{33a,32}$, $J_{33b,32}$) directly above populations of rotamers **I**–**III** for each given complex/solvent/temperature combination (average values from at least three separate experiments are quoted).

[b] Estimated uncertainties in the rotamer populations vary from 1% to 7% of the listed values. Dashes indicate parameters that could not be evaluated due to a deceptively-simple or obscured ABX spin system in the ^{1}H NMR spectrum at this temperature.

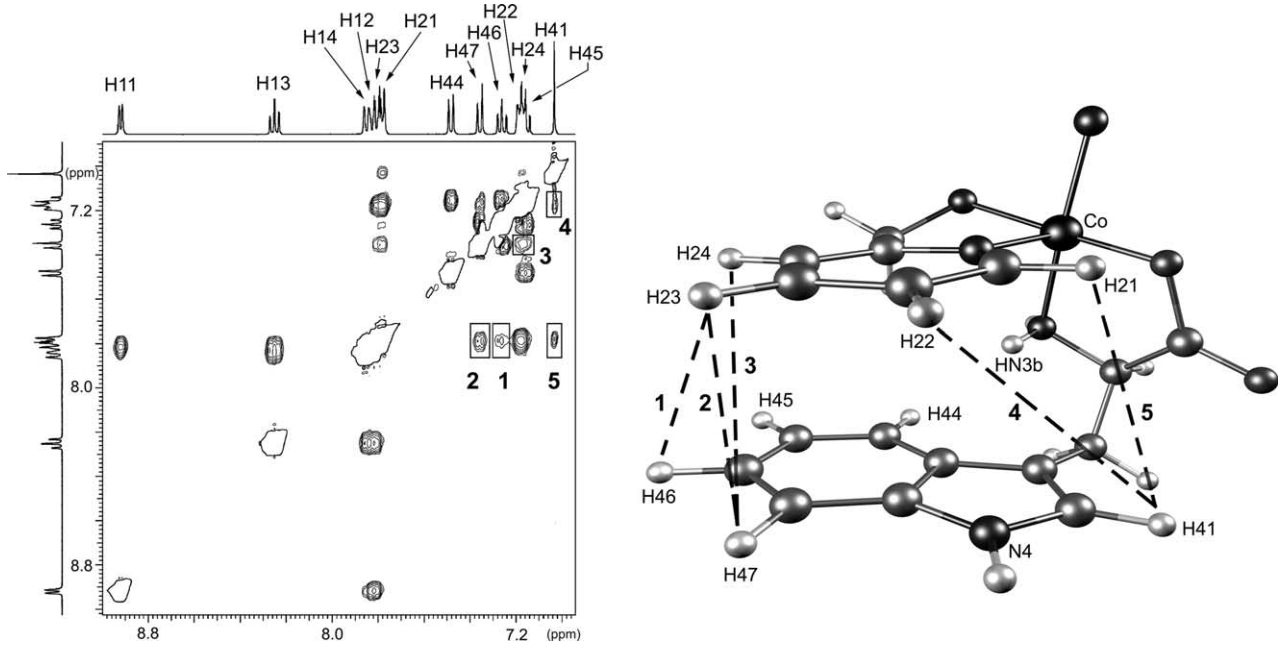

Fig. 10. ROESY spectrum of the aromatic region of Δ-α-[Co(*R*,*R*-picchxn)(*R*-trp)]$^{2+}$ in D_2O (400 MHz, 1 s mixing time, 25 °C), together with a perspective view of the relevant fragment of the complex cation as determined by single-crystal X-ray measurements. The molecular conformation observed in the solid state (at right) dominates in solution (population of π stacked rotamer **III** is 0.84).

was found for the mixing times selected. Corresponding enhancements were also observed in conventional 1D nOe difference experiments in both D_2O and DMSO-d_6. Similarly, for Λ-β_2-[Co(*R*,*R*-picchxn)(*R*-trp)]$^{2+}$ and Λ-β_1-[Co(*R*,*R*-picchxn)(*S*-trp)]$^{2+}$, definitive rOe cross-peaks are observed (Figs. 11 and 12, respectively). As far

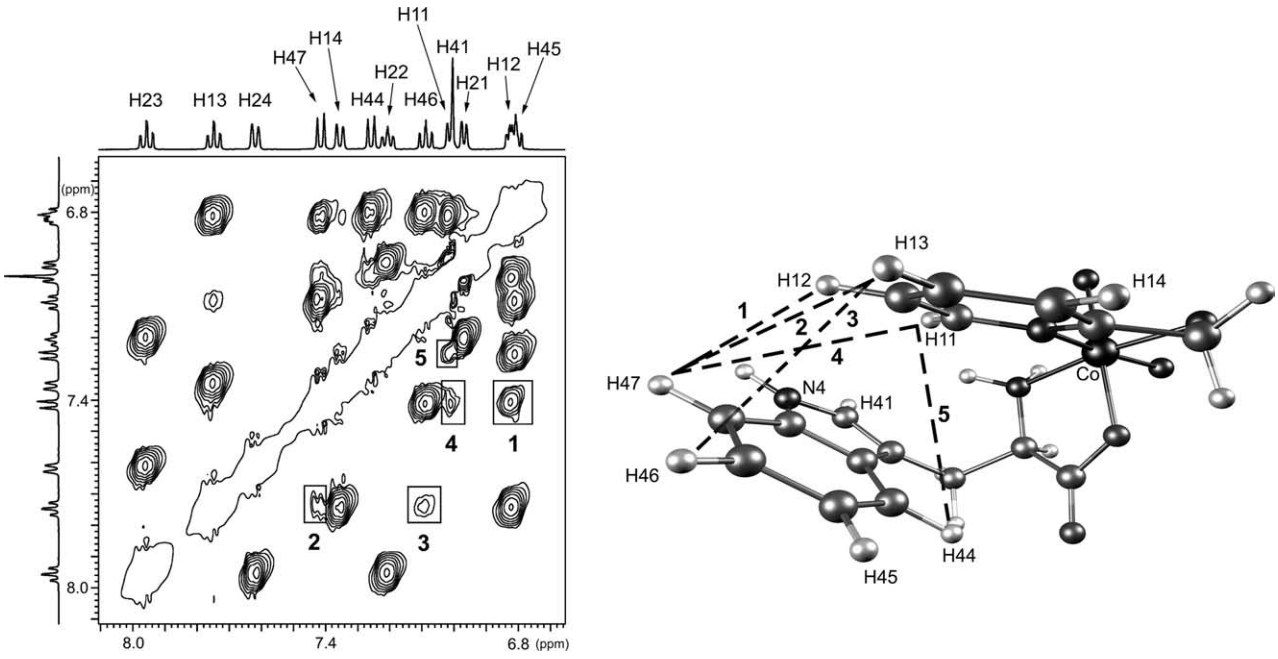

Fig. 11. ROESY spectrum of the aromatic region of the Λ-β_2-[Co(*R*,*R*-picchxn)(*R*-trp)]$^{2+}$ cation in D_2O (400 MHz, 1 s mixing time, 25 °C), together with a view of the π-stacked rings in the solid-state structure.

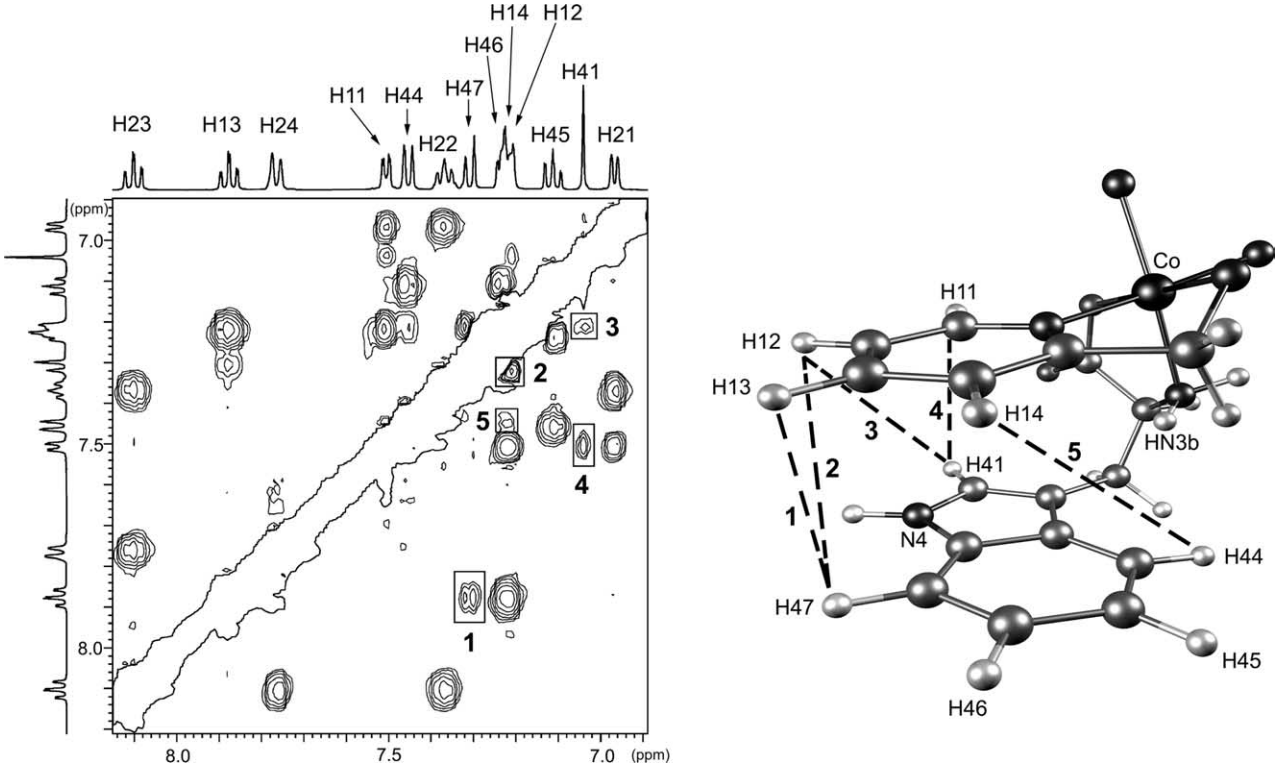

Fig. 12. ROESY spectrum of the aromatic region of the Λ-β_1-[Co(*R*,*R*-picchxn)(*S*-trp)]$^{2+}$ cation in D_2O (400 MHz, 1 s mixing time, 25 °C). A view of the dominant molecular conformation in solution (rotamer **III**) is shown, with observed intramolecular proton-to-proton contacts (<5 Å) represented by dashed lines.

as the latter is concerned, it is true that no single-crystal structure is to hand, but the NMR evidence for the interaction is supported by its observation in the solid state for the closely related analogues Λ-β_1-[Co(*R*,*R*-picchxn)(*R*-ABzH)]$^{2+}$ and, particularly, Λ-β_1-[Co(*R*,*R*-picchxn)(*S*-α-methyltryp)]$^{2+}$ [19,21].

3.4. Solvent and temperature dependence of rotamer distributions as a probe of intramolecular interactions

Few studies have been undertaken with a view to establish the effects of the solvent medium on molecules known to possess weak non-covalent interactions, particularly those possessing aromatic interactions [15]. This may be because, unlike simple dipole interactions such as classical H-bonding [1], aromatic interactions are more complicated and have proven to be more difficult to study [3d]. A majority of these studies are performed in an arbitrary solvent, or rely heavily on gas-phase calculations [12], providing limited information about the effects of the medium. We have undertaken a preliminary study of the effects of various solvents on the conformation of **3**–**6**, in an effort to probe the nature of the non-covalent interactions present in these complexes and to further demonstrate the suitability of these complexes to act as model systems for such interactions. Indeed, the primary criterion of selecting suitably simple complexes (whose molecular conformation is governed by weak intramolecular π–π and NH–π interactions) has already been realized in **3**–**6**. The other important criterion that must be demonstrated experimentally is that the molecular conformation (and hence the intramolecular π–π and NH–π interactions which govern this) of the model systems be suitably sensitive to changes in the nature of the solvent. The results of our study, which include the determination and analysis of rotamer populations of **3**–**6** in a variety of solvents, are presented in Table 4. These data show that the distributions of molecular conformations for **3**–**6** (Fig. 3) are sensitive to the nature of the medium. Indeed, consistent trends in the solvent dependencies of the rotamer populations for a given complex, as well as between different complexes, are evident on inspection of our results, confirming that gross effects due to differential solvation do not play a major role in conformational discrimination in these systems. This is in accord with the structural similarity of the complexes.

It is clear that arguments invoking a general relationship between dielectric constant and conformational stability [33,34] are inadequate for explaining our observations (Table 4). For example, in **3**, **4** and **6**, the population of the π-stacked rotamer (**III**) increases significantly when aliquots of D_2O are added to a DMSO-d_6 (or predominately DMSO-d_6) solution of the complex. This observation is consistent with the hydrophobic effect [33], where the association will increase with increasing solvent polarity. However, when increasing amounts of benzene are added to a DMSO solution of **4**, **6** or **3** in particular, the population of π-stacked rotamer **III** also increases. In addition, the population of **III** for these species dissolved in pyridine is similar to that for D_2O, for which there is a substantially different dielectric constant. At 25 °C, rotamer populations for the three stable staggered rotamers of the Λ-β_1-*R*-trp diastereoisomer **5** are approximately equal in DMSO-d_6, as might be expected due to a lack of intramolecular π–π or solvent-shielded NH–π interactions in this species. Rotamer **III** becomes more populated upon addition of benzene-d_6, and in pyridine-d_6. This is consistent with the increased magnitude of so-called *buried* hydrogen bonds found in the hydrophobic (or low polarity) regions of some proteins [4b,6b,13a]. For the Λ-β_2-*R*-trp (**6**), Δ-α-*R*-trp (**4**) and Λ-β_1-*S*-trp (**3**) diastereoisomers, that is to say those which can adopt conformations yielding an intramolecular π–π interaction, these conformers predominate in all of the selected solvents. Variable-temperature ^{1}H NMR measurements recorded for **3**–**6** in DMSO-d_6 and D_2O (25–65 °C in steps of 10°, as listed in Table 5) showed that an increase in temperature to 65 °C does not perceptibly alter the relative stability of the rotamer system. Rotamer distributions showed little variation from the values at 25 °C and an analysis of the variable-temperature data indicates that ΔH^0 and ΔS^0 contributions are small; separate energetic components that contribute to the rotamer distributions cannot be discerned. However, π–π interactions are significantly enhanced in D_2O versus DMSO-d_6 (or 2:1 DMSO-d_6/D_2O), in line with expectations associated with varying solvent polarity, dielectric constant, hydrophobic bonding, and donor-acceptor ability in charge-transfer interactions [33]. Uncertainties in the rotamer populations were estimated to be in the order of between 1 to 7% of the values listed in Table 5, and are sufficiently small to permit a comparison of these values.

Relative stabilities for individual rotamers may be simply derived from an equilibrium treatment and are listed as ΔG_1 and ΔG_2 in Table 4. For example, for Δ-α-[Co(*R*,*R*-picchxn)(*R*-trp)]$^{2+}$ (**4**) in D_2O, the equilibrium constants at 25 °C for Eqs. (4) and (5) are 6.5 and 28.0, respectively. Thus the intramolecular π–π interaction in **III** stabilizes this rotamer by some 4.6 and 8.3 kJ mol^{-1}, respectively. It is evident that cooperative effects involving NH–π interactions must also play a role and although absolute contributions are not readily evaluated, it is noted that the conformer that is least stable is that which has no NH–π interaction with the indole ring of Trp

$$\mathbf{I} \rightleftharpoons \mathbf{III} \quad K_1, \tag{4}$$

$$\mathbf{II} \rightleftharpoons \mathbf{III} \quad K_2. \tag{5}$$

The same set of intramolecular interactions are present in the preferred conformer of Λ-β_1-[Co(*R*,*R*-picchxn)(*S*-trp)]$^{2+}$, **3**, and discriminations in the equilibrium constants for Eqs. (4) and (5) in favour of **III** in this case amount to 2.4 and ca. 11 kJ mol^{-1}, respectively, in D_2O at 25 °C. Again, the least preferred rotamer is that with no possible intramolecular NH–π(indole) interaction. This is paralleled in the case of Λ-β_2-[Co(*R*,*R*-picchxn)(*R*-trp)]$^{2+}$, **6**, (Table 4), and the

least preferred rotamer is present in negligibly small amounts in D_2O at 25 °C; as expected, it is more populated at higher temperatures. Given the estimated errors for population distributions, discriminations for the equilibrium constants for Eqs. (4) and (5) in favour of **III** amount to 1.9 and ca. 10 kJ mol^{-1}, respectively, in D_2O at 25 °C.

A comparison of the rotamer distributions of **3**, **4** and **6** in DMSO (or DMSO/D_2O 2:1 for **4** and **6**) versus other selected solvents (Table 4), reveals that the general trend is for the population of the dominant rotamer (**III**) to increase, the population of **I** to remain about the same or increase slightly, and for the population of rotamer **II** to generally decrease, sometimes quite markedly. Inspection of Fig. 3 reveals that, for the aromatic complexes reported, rotamer **I** has possible intramolecular NH–π interactions involving the amino group and aromatic ring of the coordinate aminoacidate; in rotamer **II** the aminoacidate aromatic ring is extended such that the carbonyl group lies over the aromatic ring; rotamer **III** (favoured) corresponds to the solid state conformation of compounds **4** and **6** with combined intramolecular π–π and NH–π interactions possible. We note that for Λ-β_1-[Co(*R*,*R*-picchxn)(*R*-aa)]$^{2+}$ and Λ-β_2-[Co(*R*,*R*-picchxn)(*R*-aa)]$^{2+}$ complexes {aa = Trp (**5**), Phe [20b,35] or Tyr [20b,35]}, that stand-alone intramolecular NH–π interactions are observed in the solid state conformation adopted by the Λ-β_1 diastereomers, and that stand-alone intramolecular π–π interactions are similarly present in Λ-β_2 diastereomers. It may be possible to rationalise these general trends of conformational preference on the basis of a hierarchy of favourable intramolecular non-covalent interactions. This, however, is further complicated by the fact that variations in rotamer distributions of a given complex from one solvent to another (Table 4) may possibly be due to the nature of any possible solute–solvent intermolecular interactions. Intermolecular solute–solvent interactions could either enhance or compete with the forces responsible for the stabilization of a particular rotamer. Such interactions are relatively poorly understood phenomena due to their complexity, and a detailed examination of the individual contributions to subtle changes in rotamer populations from solvent to solvent is not practical. However, four trends evident in Table 4 are worthy of comment. First, the intramolecular π-stacking interaction in these complexes is not disrupted by aromatic solvents (pyridine and benzene), as might be expected to be the case given the rotational isomerism involved. This is in line with the discriminatory roles undertaken by such interactions in these complexes, and would be important for conformation analyses of aromatic residues in chelated amino acids and peptides [32b,32c]. Second, the population of rotamer **II** is substantially lower in D_2O and pyridine compared with other solvents, in particular for **3**, **4** and **6**. Kobayashi et al. [32b] have suggested the possibility of attractive interactions between the carbonyl group and the aromatic ring of aromatic amino acid derivatives, and reported that the population of the rotamer with this geometry (analogous to rotamer **II** in complexes **3**–**6**) decreased as the solvent polarity is raised. This was attributed to an attractive interaction between the carbonyl group and the polar solvent molecules (such as hydrogen bonding) disrupting the carbonyl–aromatic interaction. This may well be the case in the complexes reported here. Thirdly, intramolecular NH–π interactions that occur in solvent exposed regions (such as in rotamer **I** for **3**, **4** and **6**, and rotamer **III** for **5**) are generally weaker than, and are not favoured over π–π interactions in solution. This is manifested by the observation for **5** that in pyridine-d_6 the dominant population of conformer **III** (cf. DMSO-d_6) is achieved at the expense of *both* **I** and **II**, which lack any attractive π–π or NH–π interactions. In contrast, the dominance of rotamer **III** in all other complexes is achieved primarily at the expense of **II**. This indicates a hierarchy in terms of interaction energy to be {standalone NH–π < π–π < (NH–π + π–π)}. Finally, the estimated interaction energy of the π–π interactions in these complexes (from $|\Delta G_1|$ for **3**, **4** and **6**) varies between 1.8 ± 0.2 and 4.6 ± 0.5 kJ mol^{-1} at 25 °C. In contrast, Hunter et al. [22] recently obtained values of π–π interaction energies of between 1.0 and 4.9 kJ mol^{-1} (attractive) at 22 °C by measurement of chemical double mutant cycles in hydrogen-bonded zipper complexes. Their work involved varying combinations of *substituents* on the interacting rings in deuterochloroform, as opposed to our approach of varying the solvent medium. Given this fact, the correlation between these results is quite remarkable and serves to validate our findings based on the Co(III) model systems. The estimated interaction energy of the NH–π interactions in these complexes (from $|\Delta G_2|$ for **3**–**6**, and also $|\Delta G_1|$ for **5**) varies between 0.1 ± 0.2 and 6.0 ± 0.6 kJ mol^{-1} at 25 °C (cf. a lower limit of 4.5 ± 0.5 kJ mol^{-1} at 25 °C, also reported by Hunter et al. [4d] for a molecular zipper complex), and is highly dependent of the nature of the solvent and whether the NH proton exists in a hydrophobic or a solvent-exposed region. This is precisely in accord with the postulated sensitivity of such interactions in a variety of biopolymers [4,8], and serves to thereby highlight the suitability of these complexes to act as models for studying such interactions that occur in a variety of polar or non-polar (buried) regions within a given molecule.

3.5. Charge-transfer

Charge-transfer behaviour is observed between the π-stacked rings of complexes **3**, **4** and **6** in solution. NMR evidence for this interaction arises from the strong chemical shift dependence of these ring protons

with increased population of π-stacked rotamer **III**. The population of rotamer **III** increases with increased solvent polarity upon the addition of D_2O to a DMSO-d_6 solution of **3**, **4** and **6**, primarily due to the hydrophobic effect [33].

The Hunter and Sanders rules [31b] concerning π–π interactions dictate that polarized rings are required for charge-transfer interactions, with the interacting rings exhibiting donor-acceptor character. In complexes **3**, **4** and **6**, one coordinated pyridyl ring acts as an acceptor in such an interaction. The pyridyl ring is electron deficient due to the electron-withdrawing inductive effect of the electronegative nitrogen atom, which is involved in coordination to Co(III). The relatively electron-rich indole ring is the donor ring in the π-stacking interaction. Proton resonances of the indole donor ring shift downfield, while those of the adjacent pyridyl acceptor ring move upfield as the population of rotamer **III** increases with increasing solvent polarity. Stacked ^1H NMR spectra of the aromatic region of compound **4** in DMSO-d_6, DMSO-d_6/D_2O (5:1) and D_2O at 25 °C are shown in Fig. 13. As the solvent polarity is increased, the resonances of the pyridyl acceptor (H21–H24) progressively shift upfield, while those of the indole donor (H41–H47) generally move downfield. In contrast, the proton resonances of the *trans*-axial counterpart of the pyridyl ring involved in π-stacking (H11–H14) are relatively unchanged, consistent with the fact that this pyridyl is unable to participate in π-stacking due to geometrical constraints. This donor–acceptor behaviour is also observed for the π-stacking rings in *cis*-β complexes **3** and **6**, with resonances of the pyridyl ring *cis* to its counterpart involved in π-stacking remaining relatively unchanged. Minor changes are also possible due differential solvation, which is likely to have a bigger effect on aromatic rings that have both faces exposed to bulk solvent [31]. ^1H NMR chemical shifts and chemical shift differences for the aromatic protons of **3**, **4**, and **6** in DMSO-d_6 and D_2O at 25 °C are given in Table 6. Our observations are in accordance with the Hunter and Sanders rules [31], and may be important for the study of π–π interactions in a variety of biochemical systems.

In D_2O, of course, NH protons are readily exchanged. We note in passing that over prolonged periods, one of the protons in the methylene groups attached to the pyridyl rings of the tetradentate is also exchanged for deuterium especially for β complexes. This exchange is stereospecific; in both Λ-$β_1$-[Co(*R*,*R*-picchxn)(*R*-trp)]$^{2+}$ and Λ-$β_1$-[Co(*R*,*R*-picchxn)(*S*-trp)]$^{2+}$ H16b is completely exchanged during 3 days at room temperature. In Λ-$β_2$-[Co(*R*,*R*-picchxn)(*R*-trp)]$^{2+}$, however, both H26a and H26b exchange, the former much

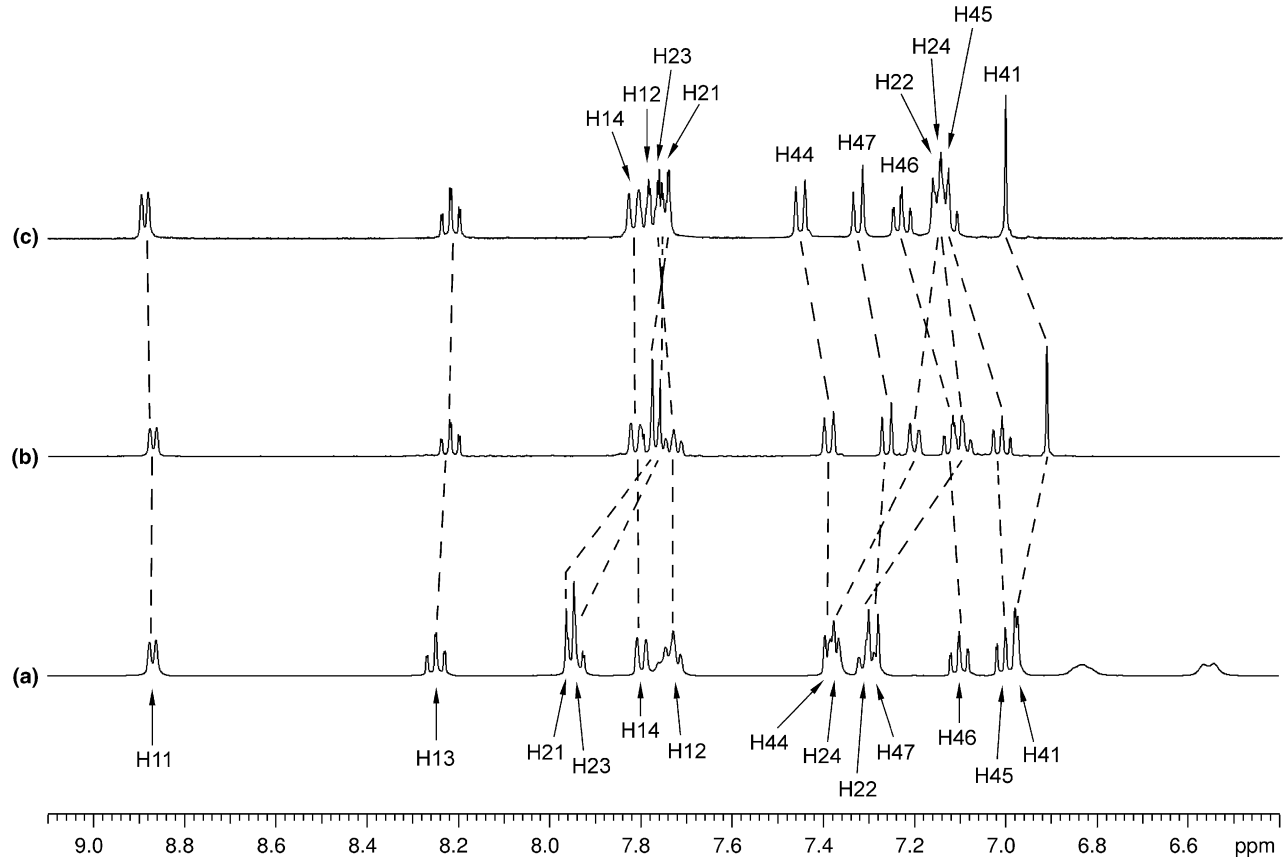

Fig. 13. Stacked ^1H NMR spectra (400 MHz) of the aromatic region of **4** at 25 °C in: (a) DMSO-d_6, (b) DMSO-d_6/D_2O (5:1), and (c) D_2O.

Table 6
^{1}H NMR chemical shift data (400 MHz) for non-exchangeable aromatic protons of **3**, **4** and **6** in DMSO-d_6 and D_2O at 25 °C

Proton	**3**			**4**			**6**		
	δ DMSO	δ D_2O	$\Delta\delta^a$	δ DMSO	δ D_2O	$\Delta\delta^a$	δ DMSO	δ D_2O	$\Delta\delta^a$
H(11)	7.705	7.501	0.204[b]	8.870	8.919	0.049	8.180	7.120	1.060[b]
H(12)	7.322	7.218	0.104[b]	7.726	7.779	0.053	7.191	6.936	0.255[b]
H(13)	8.064	7.871	0.193[b]	8.249	8.214	0.035	8.048	7.870	0.178[b]
H(14)	7.565	7.220	0.345[b]	7.798	7.814	0.016	7.680	7.481	0.199[b]
H(21)	6.940	6.962	0.022	7.951	7.746	0.205[b]	7.098	7.085	0.013
H(22)	7.481	7.363	0.118	7.302	7.142	0.160[b]	7.405	7.324	0.081
H(23)	8.141	8.096	0.045	7.944	7.752	0.192[b]	8.052	8.074	0.022
H(24)	7.744	7.760	0.016	7.373	7.138	0.235[b]	7.663	7.734	0.071
H(41)	6.960	7.035	0.075[b]	6.973	6.997	0.024[b]	7.139	7.114	0.025[b]
H(44)	7.472	7.448	0.024[b]	7.385	7.452	0.067[b]	7.438	7.376	0.062[b]
H(45)	6.943	7.107	0.164[b]	6.999	7.123	0.124[b]	6.840	6.927	0.087[b]
H(46)	7.060	7.221	0.161[b]	7.103	7.226	0.123[b]	7.040	7.207	0.167[b]
H(47)	7.240	7.304	0.064[b]	7.289	7.320	0.031[b]	7.368	7.533	0.165[b]

[a] $\Delta\delta = \delta$ DMSO $- \delta$ D_2O. Positive values indicate an upfield shift.
[b] Values correspond to protons of aromatic rings involved in π–π interactions.

more slowly (as is the case with the α isomer). The particular protons must be somewhat acidic, but the detailed reasons for this and the peculiar stereospecificities are not readily apparent.

3.6. Stereochemical change

Remarkably, these complexes can be epimerized under mild conditions with no discernible decomposition and this has enabled an assessment of chiral discrimination energies between diastereoisomers containing *R*-trp as well as the energetics involved in the NH–π versus π–π interactions. Rigorous degassing (oxygen) of aqueous (D_2O) solutions of the complexes in the presence of a mild base (TSP sodium salt present as a reference for the NMR is sufficient) serves to equilibrate diastereoisomer populations that can be measured by NMR integration. Oxygen must be strictly excluded during the reactions and any trace will halt the approach to equilibrium. Thus it is evident that the pattern of isomers produced during the syntheses of the complexes is in fact controlled by kinetic influences. It is noteworthy that the equilibrium mixtures can be produced by using any of the Δ-α-, Λ-β_1- or Λ-β_2-[Co(*R*,*R*-picchxn)(*R*-trp)]$^{2+}$ species. Approach to equilibrium is characterized by a variable induction period of minutes to hours at room temperature, indicating the possible involvement of Co(II) intermediates in an autocatalytic mechanism, details of which remain to be elucidated. Nevertheless, reaction of any starting diastereoisomer in D_2O at 25 °C results in an equilibrium mixture of isomers in the ratio Δ-α:Λ-β_1:Λ-β_2 equal to 10.2:1:2.9, estimated by a careful integration of isolated signals in the aromatic region of the ^{1}H NMR spectra with a relaxation delay long enough to ensure complete relaxation of all signals. These results give in turn values for equilibrium constants for (6) and (7) at 25 °C of 10.2 ± 0.3 and 3.5 ± 0.3, respectively. Thus the Δ-α species is more stable than the Λ-β_1 and Λ-β_2-[Co(*R*,*R*-picchxn)(*R*-trp)]$^{2+}$(aq) ions by some 5.8 ± 0.1 and 3.1 ± 0.1 kJ mol^{-1}, respectively, at this temperature

$$\Lambda\text{-}\beta_1\text{-}[\mathrm{Co}(R,R\text{-picchxn})(R\text{-trp})]^{2+}(\mathrm{aq}) \rightleftharpoons \Delta\text{-}\alpha\text{-}[\mathrm{Co}(R,R\text{-picchxn})(R\text{-trp})]^{2+}(\mathrm{aq}) \quad (6)$$

$$\Lambda\text{-}\beta_2\text{-}[\mathrm{Co}(R,R\text{-picchxn})(R\text{-trp})]^{2+}(\mathrm{aq}) \rightleftharpoons \Delta\text{-}\alpha\text{-}[\mathrm{Co}(R,R\text{-picchxn})(R\text{-trp})]^{2+}(\mathrm{aq}) \quad (7)$$

Of particular significance is the fact that no analogous Δ-α isomer could be detected in similar reactions of Λ-β_1-[Co(*R*,*R*-picchxn)(*S*-trp)]$^{2+}$ (**3**), which in the Λ-β_1 topology also possesses π–π and NH–π interactions between the indole group of the aminoacidate and the tetradentate ligand as found for Δ-α-[Co(*R*,*R*-picchxn)(*R*-trp)]$^{2+}$ and topologically related complexes [19–21]. Similarly, no Δ-α isomer was found in reactions carried out under the same conditions using Λ-$\beta_{1,2}$-[Co(*R*,*R*-picchxn)(*R*,*S*-aa)]$^{2+}$ (aa = a variety of *aliphatic* aminoacidates). Since we estimate conservatively that we could detect about 1% of any isomer in the NMR, it is therefore concluded that the Δ-α configuration of the metal-tetradentate fragment is at least 15 kJ mol^{-1} more stable than the Λ-β configuration at 25 °C, for Trp complexes of appropriate topology. This is reinforced by the observation that Δ-α-[Co(*R*,*R*-picchxn)(AbuH)]$^{2+}$ epimerizes in DMSO to the corresponding Λ-β_1 diastereoisomer with no trace of the starting material at the end of the reaction [18]. The further conclusion is thus drawn that the cooperative effects of the π–π and NH–π interactions present in Δ-α-[Co(*R*,*R*-picchxn)(*R*-trp)]$^{2+}$ must also amount to at least 15 kJ mol^{-1} at 25 °C if, as seems reasonable, contributions from solvation in the diastereoisomers are comparable. The bifurcated NH–π bond, which occurs in a hydrophobic environment,

appears to contribute the bulk of this stabilization energy (given that π–π interactions are present in both Λ-β_2 and Δ-α diastereoisomers), and is equal in magnitude to some conventional hydrogen bonds [1]. In addition, it is likely that non-covalent NH–π and π–π interactions facilitate ligand reorganization in any intermediate species involved in the Λ-β_1/Λ-β_2 to Δ-octahedral inversion. The resulting equilibrium isomer distribution of Λ-β_1 < Λ-β_2 < Δ-α is consistent with the hierarchy of favourable intramolecular non-covalent interactions possible in these diastereomers {NH–π < π–π < (NH–π + π–)}, respectively. Moreover, the ligand reorganization could occur in an analogous fashion to the role of such interactions in determining conformational preference within a given diastereoisomer.

4. Conclusions

The intramolecular π–π and NH–π interactions described above for these simple molecules have, of course, a wider context, which is all the more significant in light of the measured energetics. Some of these interactions are strong and serve to reverse expected stability trends for this class of chiral complexes containing a tetradentate ligand. It seems clear that the species described lend themselves to be excellent models for weak, non-classical bonding studies for more complicated systems including various molecular recognition phenomena, enzyme-substrate interactions, metal binding sites involving tryptophan, conformation control in the tertiary structures of peptides, proteins and the like, and for the stacking of base pairs in DNA and its congeners. All of these examples [6] display combinations of such interactions and these are sometimes overlooked [36]. We suggest that, given the measured strengths of some of them in the present system, that they may play an even more significant role than has already been suggested, depending on the microscopic environment of individual cases [8,37].

5. Supplementary material

Full lists of NMR data for complexes **3**–**6** including ^{1}H NMR spectra, tabulated ^{1}H and ^{13}C NMR assignments, selected coupling constants and ROESY correlations are available from the author (PAW) on request. Crystallographic data (excluding structure factors) for the structures reported in this paper have been deposited with the Cambridge Crystallographic Data Centre as supplementary publication numbers CCDC-200270 (**4**), CCDC-200269 (**5**), and CCDC-200268 (**6**). These data can be obtained free of charge via www.ccdc.cam.ac.uk/conts/retrieving.html (or from the CCDC, 12 Union Road, Cambridge CB2 1EZ, UK; fax: +44-1223-336033; e-mail: deposit@ccdc.cam.ac.uk).

Acknowledgements

We thank DEST for the award of an APA studentship to P.E. We gratefully acknowledge Dr. Narsimha Reddy for assistance with NMR measurements and Dr. Gary Dennis for help with inert atmosphere manipulations involving NMR sample preparation.

References

[1] (a) G.R. Desiraju, T. Steiner, The Weak Hydrogen Bond in Structural Chemistry and Biology, Oxford University Press, Oxford, 1997;
(b) J.F. Malone, C.M. Murray, M.H. Charlton, R. Docherty, A.J. Lavery, J. Chem. Soc., Faraday Trans. 93 (1997) 3429;
(c) G.A. Jeffrey, W. Saenger, Hydrogen Bonding in Biological Structures, Springer, Berlin, 1991.
[2] (a) C. Janiak, J. Chem. Soc., Dalton Trans. (2000) 3885, and references therein;
(b) C.A. Hunter, Angew. Chem. Int. Ed. 32 (1993) 1584;
(c) W.L. Jorgensen, D.L. Severance, J. Am. Chem. Soc. 112 (1990) 4768;
(d) H.-J. Schneider, R. Kramer, S. Simova, U. Schneider, J. Am. Chem. Soc. 110 (1988) 6442.
[3] (a) C.G. Claessens, J.F. Stoddart, J. Phys. Org. Chem. 10 (1997) 254, and references therein;
(b) C. Chipot, R. Jaffe, B. Maigret, D.A. Pearlman, P.A. Kollman, J. Am. Chem. Soc. 118 (1996) 11217;
(c) C.A. Hunter, Chem. Soc. Rev. (1994) 101;
(d) C.A. Hunter, J.K.M. Sanders, J. Am. Chem. Soc. 112 (1990) 5525.
[4] (a) T. Steiner, Angew. Chem. Int. Ed. 41 (2002) 48;
(b) H. Gohlke, G. Klebe, Angew. Chem. Int. Ed. 41 (2002) 2644;
(c) S. Tsuzuki, K. Honda, T. Uchimaru, M. Mikami, K. Tanabe, J. Am. Chem. Soc. 122 (2000) 11450;
(d) H. Adams, K.D.M. Harris, G.A. Hembury, C.A. Hunter, D. Livingstone, J.F. McCabe, Chem. Commun. (1996) 2531, and references therein.
[5] K. Müller-Dethlefs, P. Hobza, Chem. Rev. 100 (2000) 143, and references therein.
[6] (a) L.F. Lindoy, I.M. Atkinson, in: J.F. Stoddart (Ed.), Monographs in Supramolecular Chemistry, vol. 7, The Royal Society of Chemistry, Cambridge, 2000, pp. 7–46, and references therein;
(b) D. Philp, J.F. Stoddart, Angew. Chem. Int. Ed. 35 (1996) 1154, and references therein.
[7] (a) F. Cozzi, R. Annunzita, M. Benaglia, M. Cinquini, L. Raimondi, K.K. Baldridge, J.S. Siegel, Org. Biomol. Chem. 1 (2003) 157;
(b) K.M. Guckian, B.A. Schweitzer, R.X.–F. Ren, C.J. Sheils, D.C. Tahmassebi, E.T. Kool, J. Am. Chem. Soc. 122 (2000) 2213.
[8] T. Steiner, G. Koellner, J. Mol. Biol. 305 (2001) 535, and references therein.
[9] (a) R.E. Babine, S.L. Bender, Chem. Rev. 97 (1997) 1359;
(b) S. Liu, G.L. Gilliland, W.J. Stevens, R.N. Armstrong, J. Am. Chem. Soc. 115 (1993) 7910.
[10] (a) D.W. Christianson, W.N. Lipscomb, Acc. Chem. Res. 22 (1989) 62;
(b) A.G. Amit, R.A. Mariuzza, S.E.V. Phillips, R.J. Poljak, Science 233 (1986) 747.
[11] (a) H. Adams, F.J. Carver, C.A. Hunter, N.J. Osborne, Chem. Commun. (1996) 2529;
(b) M. Levitt, M.F. Perutz, J. Mol. Biol. 201 (1988) 751;
(c) K.M. Armstrong, R. Fairman, R.L. Baldwin, J. Mol. Biol. 230 (1993) 284.

[12] (a) M. Mons, I. Dimicoli, B. Tardivel, F. Piuzzi, V. Brenner, P. Millié, Phys. Chem. Chem. Phys. 4 (2002) 571;
(b) M. Crisma, F. Formaggio, G. Valle, C. Toniolo, M. Saviano, R. Iacovino, L. Zaccaro, E. Benedetti, Biopolymers 42 (1997) 1.
[13] (a) For recent examples pertaining to NH–π interactions: P. Emseis, P. Leverett, N. Reddy, P.A. Williams, Inorg. Chim. Acta 355 (2003) 144;
(b) H. Kumita, T. Kato, K. Jitsukawa, H. Einaga, H. Masuda, Inorg. Chem. 40 (2001) 3936, and references therein;
(c) A.I. Jiménez, C. Cativiela, J.G. Gómez-Catalán, J.J. Pérez, A. Aubry, M. Paris, M. Marraud, J. Am. Chem. Soc. 122 (2000) 5811;
(d) L.R. Hanton, C.A. Hunter, D.H. Purvis, J. Chem. Soc., Chem. Commun. (1992) 1134;
(e) For π–π interactions: P. Emseis, D.E. Hibbs, P. Leverett, N. Reddy, P.A. Williams, J. Coord. Chem. 56 (2003) 661;
(f) C.B. Martin, H.R. Mulla, P.G. Willis, A. Cammers-Goodwin, J. Org. Chem. 64 (1999) 7802;
(g) M.P. Lightfoot, F.S. Mair, R.G. Pritchard, J.W. Warren, Chem. Commun. (1999) 1945;
(h) S.P. Brown, I. Schnell, J.D. Brand, K. Müllen, H.W. Spiess, J. Am. Chem. Soc. 121 (1999) 6712;
(i) W.H. Pirkle, Y. Liu, J. Chromatogr. A 749 (1996) 19.
[14] For a review on ternary Co(III) complexes containing *picen*: J.R. Aldrich-Wright, R.S. Vagg, P.A. Williams, Coord. Chem. Rev. 166 (1997) 361.
[15] M.A. Cox, P.D. Newman, F.S. Stephens, R.S. Vagg, P.A. Williams, Inorg. Chim. Acta 221 (1994) 191, and references therein.
[16] R.R. Fenton, F.S. Stephens, R.S. Vagg, P.A. Williams, Inorg. Chim. Acta 236 (1995) 109.
[17] M.A. Anderson, E.F. Birse, M.J.E. Hewlins, J.P.G. Richards, F.S. Stephens, R.S. Vagg, P.A. Williams, Inorg. Chem. 30 (1991) 3774.
[18] E.F. Birse, M.A. Cox, P.A. Williams, F.S. Stephens, R.S. Vagg, Inorg. Chim. Acta 148 (1988) 45.
[19] M.A. Cox, T.J. Goodwin, P. Jones, P.A. Williams, F.S. Stephens, R.S. Vagg, Inorg. Chim. Acta 127 (1987) 49.
[20] (a) P. Emseis, D.E. Hibbs, P. Leverett, N. Reddy, P.A. Williams, Inorg. Chim. Acta (2004), in press;
(b) P. Emseis, D.E. Hibbs, P. Leverett, N. Reddy, P.A. Williams, Inorg. Chim. Acta (2004), in press;
(c) D. Lovejoy, P. Leverett, P.A. Williams, R.S. Vagg, J. Coord. Chem. 49 (1999) 101, and references therein.
[21] P.D. Newman, F.S. Stephens, R.S. Vagg, P.A. Williams, Inorg. Chim. Acta 204 (1993) 257.
[22] F.J. Carver, C.A. Hunter, D.J. Livingstone, J.F. McCabe, E.M. Seward, Chem. Eur. J. 8 (2002) 2848, and references therein.
[23] E.F. Birse, P.A. Williams, R.S. Vagg, Inorg. Chim. Acta 148 (1988) 57.
[24] D.J. States, R.A. Haberkorn, D.J. Ruben, J. Magn. Reson. 48 (1982) 286.
[25] H. Kessler, C. Griesinger, R. Kerssebaum, K. Wagner, R.R. Ernst, J. Am. Chem. Soc. 109 (1987) 607.
[26] A. Bax, S. Subramanian, J. Magn. Reson. 67 (1986) 565.
[27] M.F. Summers, L.G. Marzilli, A. Bax, J. Am. Chem. Soc. 108 (1986) 4285.
[28] SMART, SAINT+, SADABS and XPREP. Area detector control, data integration and reduction software, Bruker Analytical X-ray Instruments Inc. Madison, WI, 1995.
[29] G.M. Sheldrick, SHELX-97 [Includes SHELXS-97, SHELXL-97, CIFTAB]. Programs for Crystal Structure Analysis (Release 97-2), Institüt für Anorganische Chemie der Universität, Tammanstrasse 4, D-3400 Göttingen, Germany, 1998.
[30] L.J. Farrugia, J. Appl. Crystallogr. 30 (1997) 565.
[31] (a) C.A. Hunter, K.R. Lawson, J. Perkins, C.J.R. Urch, J. Chem. Soc., Perkin Trans. 2 (2001) 651, and references therein;
(b) C. Janiak, J. Chem. Soc., Dalton Trans. (2000) 3885, and references therein.
[32] (a) P. Leverett, J. Petherick, P.A. Williams, R.S. Vagg, J. Coord. Chem. 37 (1996) 195;
(b) J. Kobayashi, T. Higashijima, S. Sekido, T. Miyazawa, Int. J. Peptide Protein Res. 17 (1981) 486;
(c) P.I. Vestues, R.B. Martin, J. Am. Chem. Soc. 102 (1980) 7906;
(d) K.G.R. Pachler, Spectrochim. Acta 20 (1964) 581;
(e) K.G.R. Pachler, Spectrochim. Acta 19 (1963) 2085.
[33] M.S. Cubberley, B.L. Iverson, J. Am. Chem. Soc. 123 (2001) 7560, and references therein.
[34] T. Ren, Y. Jin, K.S. Kim, D.H. Kim, J. Mol. Biol. Struct. Dyn. 15 (1997) 401.
[35] P. Emseis, P. Leverett, N. Reddy, P.A. Williams, J. Coord. Chem. 56 (2003) 389.
[36] (a) K. Majumder, R.J. Butcher, S. Bhattacharya, Inorg. Chem. 41 (2002) 4605;
(b) J. Harrowfield, J. Chem. Soc., Dalton Trans. (1996) 3165.
[37] (a) M.J. Rashkin, M.L. Waters, J. Am. Chem. Soc. 124 (2002) 1860;
(b) H. Chen, S. Ogo, R.H. Fish, J. Am. Chem. Soc. 118 (1996) 4993.

Available online at www.sciencedirect.com
SCIENCE DIRECT®
Polyhedron 23 (2004) 1769–1775
POLYHEDRON
www.elsevier.com/locate/poly

Solution studies and structure of a dinuclear-based double-stranded helicate of $[Cu_2(p\text{-xysal})_2]$ (H_2-*p*-xysal = bis (hydroxylbenzyl)diaminoxylene)

Yufei Song [a], Iryna A. Koval [a], Patrick Gamez [a], Gerard A. van Albada [a], Ilpo Mutikainen [b], Urho Turpeinen [b], Jan Reedijk [a,*]

[a] *Leiden Institute of Chemistry, Gorlaeus Laboratories, Leiden University, P.O. Box 9502, 2300 RA Leiden, The Netherlands*
[b] *Laboratory of Inorganic Chemistry, Department of Chemistry, P.O. Box 55 (A.I. Virtasenaukio 1), University of Helsinki, FIN-00014 Helsinki, Finland*

Received 3 March 2004; accepted 8 April 2004
Available online 10 May 2004

Abstract

Reaction of a simple Schiff-base ligand bis(hydroxylbenzyl)diaminoxylene (H_2-*p*-xysal) with copper(II) perchlorate results in the formation of $Cu_2(p\text{-xysal})_2$ with a double-stranded helicate structure, constructed from two slightly different units of dinuclear Cu(II), in which all the copper(II) ions have distorted tetrahedral geometries. The two sublattices are interpenetrating where the helix axes are oriented as the monoclinic angle (116.6°). ESI-MS measurement indicates that the complex may partially dissociate in solution. The EPR spectrum in a frozen $CHCl_3$/MeOH solution shows that two different species are present. The spectrum has been satisfactory simulated with one mononuclear species and one dinuclear species. Cyclic voltammetry study shows a weakly reversible reduction wave of the Cu(II)/Cu(I) redox couple at $E_{1/2} = -0.915$ V. There are two successive oxidation waves at $E_{pa} = 0.94$ and 1.25 V. The latter one appears to be weakly reversible and it is assigned to the one electron oxidation of the phenolate group. The intra- and inter-molecular interactions are demonstrated to play important roles in the formation and the stabilization of the molecular architectures of the complex.
© 2004 Elsevier Ltd. All rights reserved.

Keywords: Self-assembly; Copper; N,O-ligands; Dinuclear; EPR

1. Introduction

It is well known that rationally designed complexes may give special functional properties, such as luminescence [1–3], redox activity [4] or magnetism [5–7]. Such materials can often be obtained by the self-assembly of well-defined architectures in a spontaneous or directed way. However, many factors may affect the self-assembly process, such as the nature of the coordination site, the structure of the bridging ligand, the geometric preferences of the metal ions and the weak intermolecular lattice interactions [7]. A considerable amount of molecular architectures have been assembled by means of metal–ligand interactions [8]. Among them, macrocyclic complexes formed by the self-assembly of transition metals with non-macrocyclic ligands give particular interesting physical properties and structural features [9].

Many systems formed by self-assembly processes have been reported to show interesting helical and non-helical structures by the complexation of designed ligands with metal ions [1,10]. The importance of the helicates is related to the development and the understanding of self-assembly processes in supramolecular chemistry [6,11].

In the present study, the synthesis, structural characterization and solution studies of a copper complex built from dinuclear units with a simple bis-bidentate Schiff-base ligand bis(2-hydroxybenzyl)-diaminoxylene (H_2-*p*-xysal) [12,13] are reported. The dinuclear coordination unit has a double-stranded helical structure,

* Corresponding author. Tel.: +715274450; fax: +715274671/31715274451.
E-mail address: reedijk@chem.leidenuniv.nl (J. Reedijk).

0277-5387/$ - see front matter © 2004 Elsevier Ltd. All rights reserved.
doi:10.1016/j.poly.2004.04.011

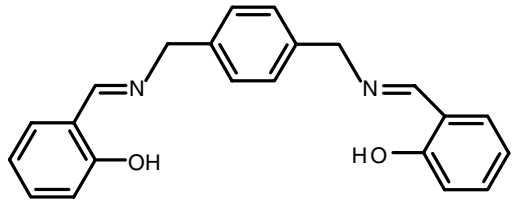

Fig. 1. The ligand bis(hydroxybenzyl)-diaminoxylene (H_2-*p*-xysal).

which is generated by coordination of two ligands twisted around two metal ions lying on the helical axis. The weak π–π and CH–π interactions between the aromatic rings of the ligands are suggested to stabilize the molecular structure and the complexation to the Cu(II) ions is the binding force which connects the two strands (see Fig. 1).

Usually Cu(II) complexes in four-coordination are found in (distorted) square-planar or tetragonal geometry. Tetrahedral geometry, on the other hand, is relatively seldom found in Cu(II) complexes, whereas it is very typical for Cu(I) complexes with four donor atoms. The present compound shows an interesting double-stranded helicate structure with a quite unusual, distorted tetrahedral coordination sphere of the copper ions. A strongly related X-ray structure has been reported recently where nitromethane molecules are present in the lattice [13]. In the present structure, no solvent molecules are included. Different methods such as ESI-MS, UV–Vis, EPR spectroscopy and cyclic voltammetry have been used to give detailed information of the solution chemistry of the complex.

2. Experimental

2.1. General remarks and physical measurements

All starting reagents and solvents were purchased from commercial sources and used as received. The ligand bis(2-hydroxybenzyl)-*p*-diaminoxylene (H_2-*p*-xylsalic) was prepared from salicylaldehyde and *p*-xylenediamine by reductive amination with $NaBH_4$ in dried methanol [12–14]. C, H, N analyses were performed on a Perkin–Elmer 2400 series II analyzer. Infrared spectra were recorded on a Perkin–Elmer Paragon 1000 spectrophotometer equipped with a Golden Gate ATR device, using the diffuse reflectance technique. X-band EPR spectra were obtained on a Jeol RE2x electron spin resonance spectrometer using DPPH ($g = 2.0036$) as a standard. The ligand-field spectra of the solid compounds were recorded in the range of 200–2000 nm on a Perkin–Elmer Lambda 900. Electrospray ionization mass spectra (ESI-MS, positive ion) in MeOH/$CHCl_3$ solutions were recorded on a Thermo Finnigan AQA apparatus. UV–Vis–NIR spectrometer in the diffuse reflectance mode with MgO as a reference. The cyclic voltammetry measurements were performed with an Autolab PGstat10 potentiostat controlled by GPES4 software. A three-electrode system was used, consisting of a glassy carbon (GC) working electrode, a platinum (Pt) auxiliary electrode and a Ag/AgCl reference electrode. All potentials are given versus Ag/AgCl. The experiments were carried out in MeOH/$CHCl_3$ solutions at room temperature under argon. Magnetic susceptibility measurements (5–300 K) were carried out using a Quantum Design MPMS-5S SQUID magnetometer, in a 1 kG applied field. Data were corrected for the experimentally determined contribution of the sample holder. Corrections for the diamagnetic responses of the complex, as estimated from Pascal's constants, were applied [15].

2.2. Synthesis

A solution of copper(II) perchlorate (0.56 g, 1.5 mmol) in methanol (15 mL) was added to the ligand (0.52 g, 1.5 mmol) and NaOH (1.20 g, 3.0 mmol) in methanol (20 mL), and a brown precipitation was produced quickly. The solution was filtered and the precipitate was washed with methanol and diethylether. It was then purified on silica gel 60 with dried chloroform (300 mL) as eluent. A clear brown solution was obtained and slow evaporation in air at room temperature led to blue rectangular-shaped needle crystals after several days. Yields 34% (0.21 g). *Anal.* Calc. $C_{44}H_{36}Cu_2N_4O_4$ (811): C, 65.1; H, 4.5; N, 6.9. Found: C, 64.7; H, 4.7; N, 7.0%. IR (solid) $\nu = 1621$, 1597, 1442, 1400, 1343, 1323, 1149, 1126, 903, 760, 751, 731, 611 cm^{-1}. UV–Vis–NIR (solid): $\lambda = 373$, 474, 635 nm. EPR (solid, room temperature): $g_z = 2.07$, $g_{x,y} = 2.01$.

2.3. X-ray crystallography

A crystal was selected and mounted on a glass fibre, using the oil-drop method and data were collected on a Nonius KappaCCD diffractometer (graphite-monochromated Mo Kα radiation, $\omega - 2\theta$ scans) at 193 K. The intensity data were corrected for Lorentz and polarization effects, for absorption (ψ-scan absorption correction) and extinction. The structures were solved by direct methods. The programmes COLLECT [16], SHELXS-97 [17], SHELXL-97 [18] were used for data reduction, structure solution and structure refinement, respectively. Refinement of F^2 was done against all reflections. The weighted *R* factor, *wR*, and goodness of fit *S* are based on F^2, the conventional *R* factor is based on *F*, with *F* set to zero for negative F^2. All non-hydrogen atoms were refined anisotropically. The H atoms were introduced in calculated positions and refined with fixed geometry with respect to their carrier atoms. Crystallographic data are collected in Table 1. Residual electron density was between −0.53 and 0.69 e $Å^{-3}$. Molecular

Table 1
Selected bond lengths (Å) and angles (°) for $[Cu_2(p\text{-xysal})_2]$ and the crystalline complex containing nitromethane molecules [13]

$Cu_2(p\text{-xysal})_2$		Cu(II) complex in [13]
Bond lengths		
Cu(1)–O(10)	1.903(2)	1.912(2)
Cu(1)–N(8)	1.964(3)	1.965(3)
Cu(1)–O(30a)	1.902(3)	1.905(2)
Cu(1)–N(38a)	1.973(3)	1.966(3)
Cu(2)–O(40)	1.891(2)	1.900(2)
Cu(2)–O50	1.917(3)	1.903(2)
Cu(2)–N(48)	1.964(3)	1.970(3)
Cu(2)–N(58)	1.957(3)	1.97293)
Bond angles		
O(10)–Cu(1)–N(18)	93.71(11)	92.47(11)
O(10)–Cu(1)–O(30a)	153.98(12)	151.34(12)
O(10)–Cu(1)–N(38a)	91.74(11)	93.43(11)
N(18)–Cu(1)–O(30a)	90.65(12)	93.77(11)
N(18)–Cu(1)–N(38a)	158.52(12)	162.47(11)
O(30a)–Cu(1)–N(38a)	93.51(11)	89.34(11)
O(40)–Cu(2)–O(50)	146.94(13)	155.18(11)
O(40)–Cu(2)–N(48)	95.34(12)	93.85(11)
O(40)–Cu(2)–N(58)	92.62(11)	92.14(11)
O(50)–Cu(2)–N(48)	95.57(12)	91.52(11)
O(50)–Cu(2)–N(58)	94.31(12)	94.12(11)
N(48)–Cu(2)–N(58)	148.20(14)	152.72(11)

illustrations and calculations were performed with the PLATON package [19].

3. Results and discussion

3.1. X-ray structure determination

It appears that the structure details of the title compound are quite similar to those in crystal structure previously reported for a nitromethane containing product [13]. Because a different crystalline composition has been obtained in the present study, we do report its molecular structure briefly and focus especially on solution chemistry studies. The dinuclear copper coordination entity of formula $[Cu_2(p\text{-xysal})_2]$ (where *p*-xysal is the dehydronated bis(2-hydroxybenzyl)-diaminoxylene) was obtained by reaction of one equivalent of H_2-*p*-xylsalic, two equivalents of NaOH and one equivalent of copper(II) perchlorate in methanol, followed by silica gel purification using chloroform as an eluent. Blue prismatic crystals suitable for single-crystal X-ray analysis were obtained after several days by slow evaporation of the solution under air. A molecular plot of two independent and slightly different units of the complex together with the used atom-labeling scheme is depicted in Fig. 2.

The unit cell of the title compound includes two independent crystallographic units, each of which consists of two symmetry-related (C_2-axis) copper(II) ions and two di-dehydronated ligands, shared by two metal centers. Each copper ion is coordinated by two oxygen donor atoms of dehydronated phenolate moieties and two imine nitrogen donor atoms, originating from two ligands. The crystal structure represents in fact a dinuclear double-stranded helicate with a C_2-axis passing through the helical axis. The tetradentate ligands adopt a bis-bidentate binding mode with two phenolate units separated by a xylene spacer. The wrapping of the strands results from a helical twist between the two coordinated bidentate binding units. Fig. 3 shows the turns of the helix of $[Cu_2(p\text{-xysal})_2]$. In the unit cell, equal amounts of right-handed and left-handed helices do occur. In Fig. 2, the helicate on the left appears to have an "arc" configuration and its assembly in Fig. 3 may be influenced by this [20]. There does appear to be an S shape aggregation pattern in Fig. 3(b), which is one of the possible aggregate patterns for an "arc" configuration.

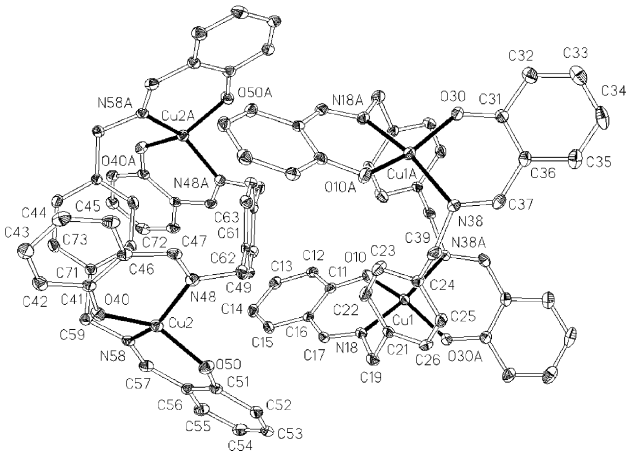

Fig. 2. Thermal ellipsoid plot (50% probability level) of two units of the dinuclear copper complex $[Cu_2(p\text{-xysal})_2]$ showing the crystallographic numbering scheme; hydrogen atom have been omitted for clarity.

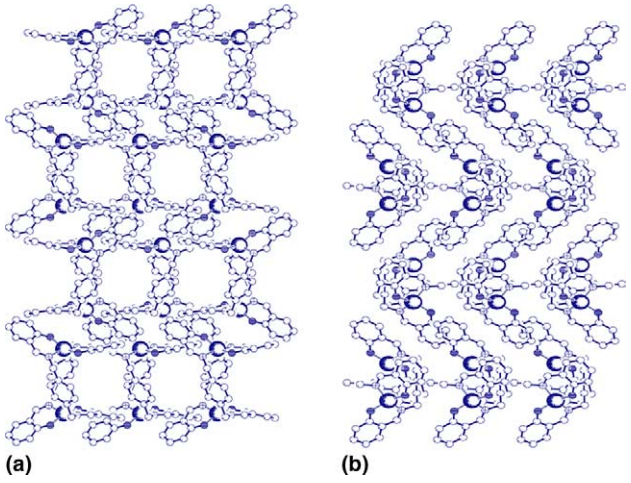

Fig. 3. Projection view along the a axis of the two independent units of the double-stranded helicates showing the turns of the helices. (a) crystal packing of the unit containing of Cu1 and Cu1a; (b) crystal packing of the other unit containing Cu2 and Cu2a.

In regard to the four-coordinated geometry of the copper ions, the discrimination between square-planar and tetrahedral geometries is partially parameterized by the angle θ, the dihedral angle between the two CuNO planes, which are 90° for a tetrahedral (D_{2d}) structure and 0° for a planar structure (D_{2h}). For the Cu1 ion, the dihedral angle between the planes O10–Cu1–N18 and O30a–Cu1–N38a is equal to 40.69(13)° [32.8(1)° for the complex in literature [13]]. For the Cu2 ions, the dihedral angle between the planes O40–Cu2–N48 and O50–Cu2–N58 is 44.52(14)° [35.9(1)° for the complex in literature [13]]. These values indicate that the coordination spheres around the copper ions can be best described as a heavily distorted tetrahedron with a CuN_2O_2 chromophore. It should be emphasized that such double-stranded helicate structures, based on four coordinated metal ions with a tetrahedral geometry, are often encountered for Cu(I) complexes [21]. However, most often the coordination geometry around the copper(II) ions in double-stranded helicates is based on a distorted octahedron [22].

The average Cu–N and Cu–O distances in the complex are 1.968(7) and 1.902(7) Å, respectively, for the Cu1 ion, and 1.960(8) and 1.904(2) Å for the Cu2 ion. The angles N/O–Cu–N/O are varying in the range of 90.65(10)°–158.52(12)°. The largest angular deviation from the regular tetrahedral geometry (109°) is 49.52° and 39.2° for the N18–Cu1–N38a (158.52°) and for N58–Cu2–N45 (148.20°). The crystal structure reveals a rather large intermetallic distance associated with the xylene spacer with 7.365 Å for the Cu1–Cu1a couple and 7.454 Å for the Cu2–Cu2a couple. Shorter intermolecular Cu–Cu contacts occur in the lattice (6.88 and 7.45 Å). Crystallographic information and selected bond lengths and angles are presented in Tables 1 and 2. (The crystal data that reported in [13] are included in Tables 1 and 2 to allow comparison).

The metal–ligand interactions lead to a ligand twisting. The flexibility of the ligand facilitated by the xylene spacer group is an important factor controlling the molecular architecture. It is worth noting that internal macrocyclic cavities are generated between the xylene groups and the coordinated phenolate units. For the cavity containing the Cu1 and Cu1a ions, the distance between ring centroids of the two benzene planes is 5.2523 Å. The dihedral angle between them is 67.63° [39.7(1)° for the complex in literature [13]]. For the cavity containing Cu2 and Cu2a, the dihedral angle between these two rings is 90°, which indicate that these two rings are strictly perpendicular to each other. These kinds of cavities may be of significance in host–guest chemistry [23].

It is interesting that the aromatic rings stack with adjacent ones from another ligand by inter-strand face to face interactions. The crystal packing of the complex is stabilized by the π–π interactions between the aromatic rings, with the shortest inter-planar ring–ring distances being 3.984 Å. These phenyl rings are stacked with each other with a dihedral angle of only 0.03°. The distances are larger than the standard distances for strong π–π stacking interactions between two aryl rings (3.35 Å for graphite [24,25]). In addition, the molecules pack together through a combination of π–π stacking and CH–π interactions [25,26]. It might be suggested that these interactions play important roles in the molecular assembly. Fig. 4 shows the crystal packing of the complex and the interactions between intermolecules. It can be seen that two independent units appear to be interpenetrating networks.

Table 2
Crystal data of $[Cu_2(p\text{-xysal})_2]$ and the crystalline complex containing nitromethane molecules [13]

$Cu_2(p\text{-xysal})_2$		Cu(II) complex in [13]
Chemical formula	$C_{44}H_{36}Cu_2N_4O_4$	$C_{45}H_{39}Cu_2N_5O_6$
Formula weight	811.85	872.89
Crystal system	monoclinic	monoclinic
Space group	C_2/c	C_2/c
a (Å)	24.619(4)	29.647(3)
b (Å)	14.366(3)	14.834(3)
c (Å)	23.064(4)	19.991(2)
β (°)	116.620(10)	115.257(5)
V (Å^3)	7293(2)	7951(2)
Z	8	8
Density (g cm^{-3})	1.479	1 458
Absorption coefficient (mm^{-1})	1.217	1.126
Crystal size (mm)	0.22×0.20×0.08	0.26×0.38×0.46
R_{int}	0.0895	0.33
Final R indices $[I > 2\sigma(I)]$	$R_1 = 0.0520$, $wR_2 = 0.0922$	$R1 = 0.0453$, $wR_2 = 0.1069$

3.2. UV–Vis and ESI-MS

The ligand-field spectrum of the complex in the solid state (diffuse reflectance) shows three absorption bands above 300 nm, centred at approximately 373 nm

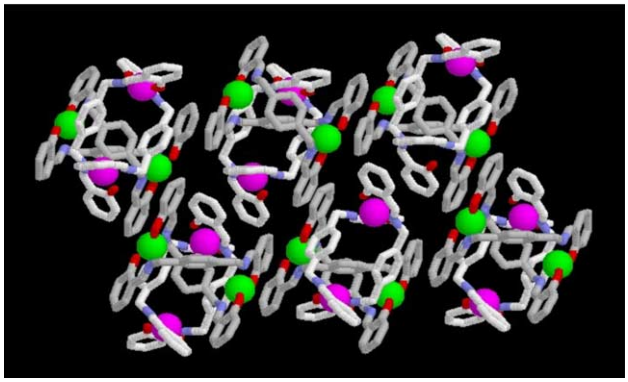

Fig. 4. Perspective view exhibiting the π–π stacking of the aromatic rings of the two units in the complex $[Cu_2(p\text{-xylsal})_2]$. Cu(II) ions are presented as large spheres.

(26.8×10^3 cm^{-1}), 474 nm (21.1×10^3 cm^{-1}) and 635 nm (15.7×10^3 cm^{-1}). The absorption at 474 nm is likely to be due to charge transfer from the nitrogen atoms to the copper ions [27]. The transition in the visible region of the electronic spectrum of this complex is a much less intense absorption at 635 nm, which is assigned to d–d transitions. The UV spectrum of the complex in a methanol:chloroform (3:7) solution shows absorptions at 271 nm ($\varepsilon = 1.6\times10^5$ M^{-1} cm^{-1}), 305 nm ($\varepsilon = 4.2\times10^4$ M^{-1} cm^{-1}), 373 nm ($\varepsilon = 5.8\times10^4$ M^{-1} cm^{-1}), and 438 nm ($\varepsilon = 680$ M^{-1} cm^{-1}) and 610 nm ($\varepsilon = 110$ M^{-1} cm^{-1}) as shoulder peaks. The difference with the solid-state spectra suggests a change in geometry upon dissolution. The intensity of the absorptions at 373 and 438 nm clearly precludes it originating from d–d transitions, hence this feature is assigned as being due to a phenolate oxygen to Cu^{II} charge-transfer (CT) transition [2,28].

The ESI-MS spectrum of the complex has been obtained in a methanol:chloroform (3:7) solution. The most intensive peak at m/z 345 corresponds to the free ligand. The peak at m/z 811.21 (relative abundance 17% to the peak at m/z 345.26) is the molecular ion peak of the targeted complex. The peak at m/z 406.12 is tentatively assigned to mononuclear species $[CuL]^+$ containing one copper ion and one ligand (the experimentally observed isotopic pattern is in a very good agreement with the theoretic result of isotope pattern calculation). However, the formation of $[Cu_2L_2]^{2+}$ can also not be excluded, since the resolution of the mass spectra is not good enough to discriminate between these two species with our experimental setup. Further studies are needed to give more detailed information. The solvent mixture of MeOH and $CHCl_3$ employed ensues from the poor solubility of the complex in pure methanol and the poor resolution of the EPR signal in pure chloroform.

3.3. EPR and magnetic susceptibility studies

The X-band EPR spectrum of the complex as a polycrystalline powder at room temperature exhibits one exchange-narrowed signal, probably caused by a dipolar interaction between the copper ions on a relatively close distance in the helical chains (Cu–Cu1a: 7.365 Å; Cu2–Cu2a: 7.45 Å; Cu1–Cu2: 8.972 Å; Cu1a–Cu2: 8.883 Å). Apparent g_z and $g_{x,y}$ values are 2.07 and 2.01, respectively. No hyperfine splitting is resolved, and no $\Delta M = \pm2$ signal, typical for dinuclear species, could be detected. The resolution does not improve upon cooling to 77 K.

The best resolved frozen-solution spectrum could be obtained in a mixture of $CHCl_3$:MeOH in 7:3 ratio (Fig. 5(b)). Now the presence of two different species in solution, as suggested by mass-spectroscopic measurements, can be clearly evidenced from the EPR spectrum. The spectrum can be best regarded as an overlap of a

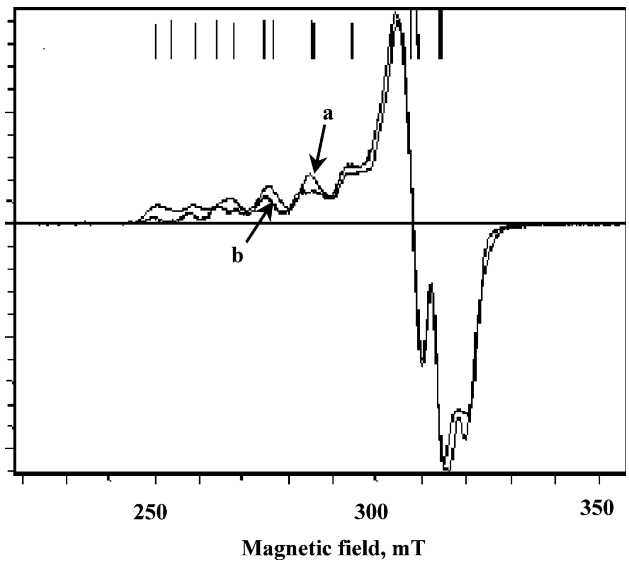

Fig. 5. X-band EPR spectrum of the complex $[Cu_2(p\text{-xysal})_2]$, recorded at 77 K in $CHCl_3$:MeOH (7:3) solution (a) and the simulated curve (b) see text for further details. Field on horizontal axis is in mT.

rhombic spectrum, derived from a mononuclear species, and a typical axial triplet spectrum ($\Delta M = \pm1$) of a dinuclear Cu(II) species. No half-field signal ($\Delta M = \pm2$), derived from a dinuclear species, could though be detected. In both cases, the ^{63,65}Cu hyperfine splitting in the g_z region is observed, although some lines are hidden due to the overlapping of two spectra with each other, or with those in the $g_{x,y}$ region. The spectrum could be satisfactory simulated [29] (Fig. 5(a)), considering two non-interacting species, one mononuclear and one dinuclear, in an approximate ratio of 1:1. The simulated parameters for the mononuclear species X are $g_x = 2.10$, $g_y = 2.11$, $g_z = 2.41$, $A_x = A_y = 0$, $A_z = 105$ Gauss). These parameters are typical for elongated rhombic octahedral CuO_6 chromophores [30] and are very close to the values observed for Cu(II) ions in a frozen methanol solution. Thus, these results suggest a partial dissociation of the complex in solution, leading to the formation of mononuclear Cu(II) species, and coordination of solvent (MeOH) molecules to the metal ions. The simulated parameters for the dinuclear species Y are $g_x \approx g_y \approx 2.07$, $g_z = 2.35$, $A_x = A_y = 0$, $A_z = 88$ Gauss, and the zero-field splitting parameter $D = 0.050$ cm^{-1}.

Magnetic susceptibility measurements have been performed on powdered crystals of the complex in the temperature range 5–300 K at 0.1 Tesla. Values for χ have been calculated for dinuclear species.

At 300 K, the χT for the complex is 0.80 cm^3 K mol^{-1}, which corresponds to an effective magnetic moment of 2.53 μB. This value is in a good agreement with the theoretically predicted one for two uncoupled Cu(II) ions ($S = 1$). This value remains almost constant upon cooling down to 5 K, as the compound exhibits a Curie–Weiss behavior over the whole temperature range. Thus,

no magnetic interaction is detected between two copper ions, which is not surprising because of the large distance between them, and thus the absence of possible exchange pathways and only dipolar exchange leading to exchange narrowing is observed. The Curie constant C is 0.42 cm^3 K mol^{-1}, resulting in a g value of 2.12. This value is fairly close to the one determined experimentally from the EPR measurements. The Curie–Weiss temperature θ is 0 K, as one would expect for such virtually uncoupled systems.

3.4. Cyclic voltammetry

The electrochemical behavior of the compound has been studied in a MeOH/$CHCl_3$ solution with tetrabutylammonium perchlorate as the supporting electrolyte in the potential range −2.0–1.8 V by cyclic voltammetry. While scanning towards the negative range of potentials, a weakly reversible reduction wave at $E_{1/2} = -0.915$ V ($\Delta E_p = 0.19$ V, $v = 0.1$ mV s^{-1}) was assigned to the Cu(II)/Cu(I) redox couple. In the anodic part of the CV curve, two successive oxidation waves at $E_{pa} = 0.94$ and 1.25 V are observed. The latter of these appears to be very weakly reversible ($\Delta E_p = 0.35$ mV, $v = 0.1$ mV s^{-1}), whereas the first one is fully irreversible. A very small reduction peak at $E_{pc} = 0.90$ V can be observed, which corresponds to $E_{pa} = 1.25$ V. These peaks are tentatively assigned to the one-electron oxidation of the phenolate group [31] (see Fig. 6).

It should be realized that coordination complexes of four-coordinated Cu(II) and Cu(I) with the same ligand, sharing the same distorted tetrahedral geometry, are rare. Due to the similar coordination spheres of Cu(I) and Cu(II) sites, the electron transfer rates between these two oxidation states are supposed to be very fast [32]. Taking into account that the two copper(II) ions in the complex have a distorted tetrahedral geometry, it is interesting to compare the redox potential of Cu(II)/Cu(I) complex couple in the complex with the values previously found in case of the Cu(I) and Cu(II) complexes sharing the same tetrahedral geometry. In the latter complexes the reduction of Cu(II) to Cu(I) oxidation state usually occurs at quite high potentials [33] (values as high as 0.92 V versus Ag/AgCl were found in some cases [34]), indicating a high stability of Cu(I) state. In our case, however, the reduction of Cu(II) to Cu(I) state takes place at much lower potential ($E_{pc} = -1.0$ V versus Ag/AgCl electrode), and is only weakly reversible. This behavior is not surprising, as the double positive charge of Cu(II) ion in the initial complex is compensated by two negatively charged ligands; thus, the reduction of Cu(II) to Cu(I) state is probably accompanied by the release of one of the two dehydronated ligands. Therefore an isolation of the respective Cu(I) complex, sharing the same coordination sphere and donor set, appears to be impossible.

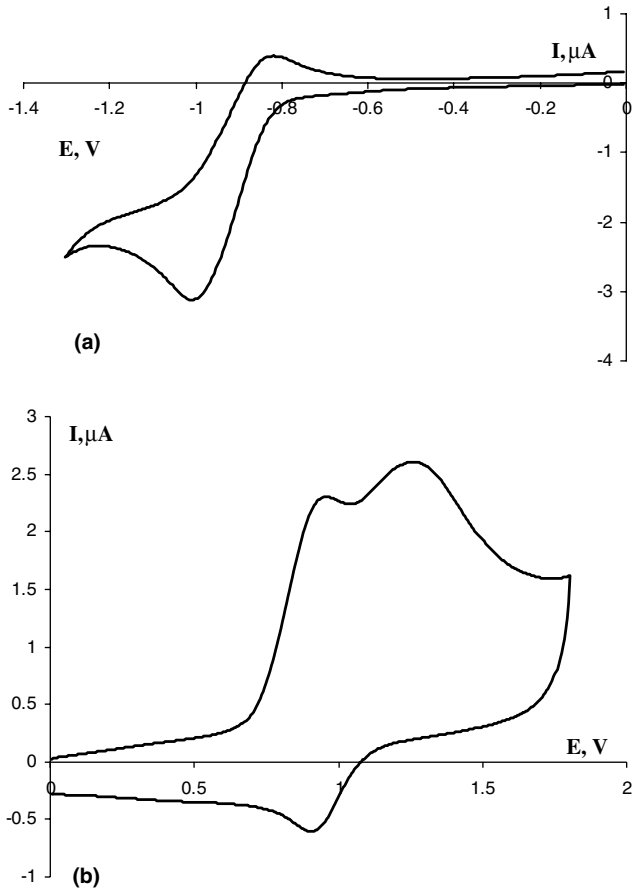

Fig. 6. Cyclic voltammograms for a solution of the complex in MeOH/$CHCl_3$ + 0.1 M TBAP, working electrode (WE): Pt (diameter 5 mm); (a) scans between −1.4 and 0 V; (b) scans between 2.0 and 0 V.

4. Conclusions

In conclusion, a dinuclear copper complex has been obtained in a tetradentate coordination mode with heavily distorted tetrahedral geometry around copper with the ligand ions. The ligands twist with each other in the molecule and allow formation of the double-stranded helical dinuclear complex by self-assembly. The cavities between the xylene spacers rings may be suitable for host–guest interactions as the nitromethane-containing copper complex found in [13]. The EPR spectrum of the frozen MeOH/$CHCl_3$ solution indicates there are two different species and the spectrum can be best simulated as one mononuclear and one dinuclear species in the solution. Cyclic voltammetry measurements indicate that the reduction of Cu(II)–Cu(I) occurs at $E_{1/2} = -0.915$ V with weakly reversible peaks. It is supposed that the intra- and inter-molecule interactions play important roles in the formation of the molecular architectures and the stabilization of the complex. Further studies by changing the bridging ligands to increase the π–π interactions are currently in progress and are likely to give better insights into the factors affecting the self-assembly process.

5. Supplementary material

Crystallographic data (excluding structure factors) for the structures have been deposited with the Cambridge Crystallographic Data Centre as publication no. CCDC-225176 for the title structure. Copies of the data can be obtained free of charge on application to CCDC, 12 Union Road, Cambridge CB2 1EZ, UK; [Fax: (internat.) +44-1223/336-033; E-mail: deposit@ccdc.cam.ac.uk, or www: http://www.ccdc.cam.ac.uk].

Acknowledgements

The work described here has been supported by the Leiden University Study group WFMO (Werkgroep Fundamenteeel-Materialen Onderzoek). Support from the NRSC Catalysis (a Research School Combination of HRSMC and NIOK) is kindly acknowledged. The project is financially supported by the Dutch Economy, Ecology, Technology (EET) program, a joint program of the Ministry of Economic Affairs, the Ministry of Education, Culture and Science, and the Ministry of Housing, Spatial Planning and the Environment.

References

[1] D. Guo, Y.T. Li, C.Y. Duan, H. Mo, Q.J. Meng, Inorg. Chem. 42 (2003) 2519.
[2] D. Guo, C.Q. Qian, C.Y. Duan, K.L. Pang, Q.J. Meng, Inorg. Chem. 42 (2003) 2024.
[3] F. Wurthner, A. Sautter, D. Schmid, P.J.A. Weber, Chem. Eur. J. 7 (2001) 894.
[4] K.D. Benkstein, J.T.S.C.L Hupp, Angew. Chem., Int. Ed. Engl. 39 (2000) 2891;
H. Hartmann, S. Berger, R. Winter, J. Fiedler, W. Kaim, Inorg. Chem. 39 (2000) 4977.
[5] C.S. Campos-Fernander, R. Clerac, K.R. Dunbar, Angew. Chem., Int. Ed. Engl. 38 (1999) 3477.
[6] J.M. Lehn, Supramolecular Chemistry, Concepts and Perspectives, VCH, Weinheim, Germany, 1995.
[7] G.F. Swiegers, T.J. Malefetse, Chem. Rev. 100 (2000) 3483.
[8] S. Leininger, B. Olenyuk, P.J. Stang, Chem. Rev. 100 (2000) 853.
[9] K. Biradha, M. Aoyagi, M. Fujita, J. Am. Chem. Soc. 122 (2000) 2397;
S.Y. Yu, T. Kusukawa, K. Biradha, M. Fujita, J. Am. Chem. Soc. 122 (2000) 2665;
M. Fujita, N. Fujita, K. Ogura, K. Yamaguchi, Nature 400 (1999) 52.
[10] E.C. Constable, R.P.G. Henney, D.A. Tocher, J. Chem. Soc., Dalton Trans. (1991) 2335;
H. Houjou, A. Iwasaki, T. Ogihara, M. Kanesato, S. Akabori, K. Hiratani, New. J. Chem. 27 (2003) 886;
T. Yano, R. Tanaka, T. Nishioka, I. Kinoshita, K. Isobe, L.J. Wright, T.J. Collins, Chem. Commun. (2002) 1396;
C. Piguet, G. Bernardinelli, G. Hopfgartner, Chem. Rev. 97 (1997) 2005;
M. Hong, G. Dong, C.Y. Duan, Y.T. Li, Q.J. Meng, J. Chem. Soc., Dalton Trans. (2002) 3422;
M.J. Hannon, C.L. Painting, A. Jackson, J. Hamblin, W. Errington, Chem. Commun. (1997) 1807;
M. Albrecht, Chem. Rev. 101 (2001) 3457;
M.J. Hannon, L.J. Childs, Supra Chem. 16 (2004) 7;
N. Yoshida, K. Ichikawa, M. Shiro, J. Chem. Soc., Perkin Trans. 2 (2000) 17;
N. Yoshida, H. Oshio, T. Ito, J. Chem. Soc., Perkin Trans. 2 (1999) 975;
N. Yoshida, H. Oshio, T. Ito, Chem. Commun. (1998) 63.
[11] M. Barboiu, G. Vaughan, R. Graff, J.M. Lehn, J. Am. Chem. Soc. 125 (2003) 10257;
M. Ruben, E. Breuning, M. Barboiu, J.P. Gisselbrecht, J.M. Lehn, Chem. Eur. J. 9 (2003) 291.
[12] W. Moneta, P. Baret, J.L. Pierre, Bull. Soc. Chim. Fr. 6 (1988) 995.
[13] B.J. McNelis, L.C. Nathan, C.J. Clark, J. Chem. Soc., Dalton Trans. (1999) 1831.
[14] Y.F. Song, P. Gamez, O. Roubeau, M. Lutz, A.L. Spek, J. Reedijk, Eur. J. Inorg. Chem. (2003) 2924.
[15] I.M. Kolthoff, P.J. Elving, Treatise on Analytical Chemistry, vol. 4, New York, 1963.
[16] Nonius, COLLECT. Nonius BV, Delft, The Netherlands, 2002.
[17] G.M. Sheldrick, SHELXL-97, Program for Crystal Structure Refinement, University of Göttingen, Germany, 1997.
[18] G.M. Sheldrick, SHELXL-97. Program for the Refinement of Crystal Structures, University of Göttingen, Germany, 1997.
[19] A.L. Spek, PLATON. A Multipurpose Crystallographic Tool, Utrecht University, The Netherlands, 2003.
[20] L.J. Childs, N.W. Alcock, M.J. Hannon, Angew. Chem., Int. Ed. Engl. 40 (2001) 1079.
[21] J.M. Lehn, R. Meric, J.P. Vigneron, I. Bkouchewaksman, C. Pascard, J. Chem, Soc., Chem. Commun. (1991) 62;
J.M. Lehn, Angew. Chem., Int. Ed. Engl. 29 (1990) 1304;
U. Koert, M.M. Harding, J.M. Lehn, Nature 346 (1990) 339.
[22] E.C. Constable, M.G.B. Drew, M.D. Ward, J. Chem. Soc., Chem. Commun. (1987) 1600;
M. Barley, E.C. Constable, S.A. Corr, R.S. McQueen, J.C. Nutkins, M.D. Ward, M.G.B. Drew, J. Chem. Soc., Dalton Trans. (1988) 2655;
C.J. Sumby, P.J. Steel, Inorg. Chem. Commun. 6 (2003) 127.
[23] A. Bilyk, M.M. Harding, J. Chem. Soc., Chem. Commun. (1995) 1697;
M. Albrecht, O. Blau, R. Frohlich, Proc. Natl. Acad. Sci. USA 99 (2002) 4867;
N. Yoshida, J. Chem. Soc., Perkin Trans. 2 (1995) 2249;
N. Yoshida, Y. Fujita, J. Phys. Chem. 99 (1995) 3671;
N. Yoshida, K. Hayashi, J. Chem. Soc., Perkin Trans. 2 (1994) 1285.
[24] D.F. Shriver, P. Arkins, C.H. Langford, Inorganic Chemistry, second ed., W.H. Freeman Co., New York, 1997.
[25] C.A. Hunter, J.K.M. Sanders, J. Am. Chem. Soc. 112 (1990) 5525.
[26] N. Yoshida, K. Ichikawa, Chem. Commun. (1997) 1091.
[27] M.H.W. Lam, Y.Y. Tang, K.M. Fung, X.Z. You, W.T. Wong, Chem. Commun. 21 (1997) 957.
[28] B.J. Hathaway, Comprehensive Coordination Chemistry, vol. 5, Pergamon Press Oxford, 1987;
D. Guo, K.L. Pang, C.Y. Duan, C. He, Q.J. Meng, Inorg. Chem. 41 (2002) 5978.
[29] F. Neese, The Program EPR, A Modeling Approach, Version 1.0, University of Konstanz, 1993.
[30] G. Wilkinson, in: G. Wilkinson (Ed.), Comprehensive Coordination Chemistry, Pergamon Press, Toronto, 1987.
[31] C. Stockheim, L. Hoster, T. Weyhermuller, K. Wieghardt, B. Nuber, J. Chem. Soc., Dalton Trans. (1996) 4409.
[32] S. Knapp, T.P. Keenan, X.M. Zhang, R. Fikar, J.A. Potenza, H.J. Shugar, J. Am. Chem. Soc. 109 (1987) 1882.
[33] P. Zanello, Stereochemistry of Organometallic and Inorganic Compounds, vol. 4, Ed: I. Bernal, Elsevier Science Publishers, Amsterdam, 1990.
[34] K. Flinzner, A.F. Stassen, A.M. Mills, A.L. Spek, J.G. Haasnoot, J. Reedijk, Eur. J. Inorg. Chem. (2003) 671.

Available online at www.sciencedirect.com
SCIENCE DIRECT®
Polyhedron 23 (2004) 1777–1784
POLYHEDRON
www.elsevier.com/locate/poly

Perhalogenated porphyrinic derivatives with indium and thallium: the X-ray structures of (β-Cl_4TPP)Tl(Cl), (β-Cl_4TPP)In(Cl) and (T*p*FTPP)Tl(Cl) ☆

Catherina Raptopoulou [a], Dimitra Daphnomili [b], Athanassios Karamalides [c], Massimo Di Vaira [c], Aris Terzis [a], Athanassios G. Coutsolelos [b,*]

[a] *NCRS, Demokritos, Agia Paraskevi, 15310 Athens, Greece*
[b] *Laboratory of Bioinorganic Coordination Chemistry, Department of Chemistry, School of Sciences, University of Crete, P.O. Box 1470, 71409 Heraklion Crete, Greece*
[c] *Universita degli Studi di Firenze, Dipartimento di Chimica, Via della Lastruccia 5, Sesto Fiorentino, Firenze, Italy*

Received 10 November 2003; accepted 24 March 2004
Available online 10 May 2004

Abstract

The synthesis and spectroscopic characterization of new substituted porphyrinate complexes are reported. The investigated compounds are represented by the formula (Porph)M(Cl) where Porph are T*p*FPP, TPyP, β-Cl_4TPP, β-Cl_8TPP or β-Cl_4TPP, and M = In or Tl.

UV–Vis and NMR spectroscopies of the title complexes confirm the proposed molecular formula and are described extracting all plausible information. The study is completed by three X-ray structures of (β-Cl_4TPP)Tl(Cl), (β-Cl_4TPP)In(Cl) and (T*p*FTPP)Tl(Cl).

Compounds (β-Cl_4TPP)Tl(Cl) and (β-Cl_4TPP)In(Cl) are isostructural and they were treated in a similar way. The chloride substituents on the porphyrin core were found to be disordered in both compounds and they were refined anisotropically with occupation factors free to vary. The porphyrin core is saddle distorted while there is no twist distortion as judged by the large values of the dihedral angles formed between the phenyl rings and the $C_{20}N_4$ mean plane. In compound (T*p*FTPP)In(Cl), the dihedral angles between the pentafluorophenyl rings and $C_{20}N_4$ are very close to the ideal value of 90°.
© 2004 Elsevier Ltd. All rights reserved.

Keywords: Metalloporphyrins; Indium; Thallium

1. Introduction

Porphyrin complexes of the main group III_B are ideal model compounds since they show considerable flexibility of the core geometries depending on the peripheral substitution and on axial ligation [1–9].

Meso-substitution as well as β-halogenation on the porphyrin core is expected to alter their spectroelectrochemical properties. Investigations have been carried out to probe the electronic structures of these systems by different approaches involving spectral and redox potential data as well as semi-empirical calculations. For β-halogenated porphyrins with more than four halogens, the electronic effects of the peripheral substituents causes a decrease of the basicity of the porphyrin ring, a red shift of the Soret band transition energy and a decrease in HOMO–LUMO energy gap [10–18].

Metal ions incorporated into perhalogenated complexes are mainly copper, zinc and nickel [10,12,14,16–18] as far as concerns the four coordinated ions, while iron complexes have also been reported due to the enhanced catalytic activity of these systems [11,18,19].

☆ Supplementary data associated with this article can be found, in the online version, at doi:10.1016/j.poly.2004.04.010.

* Corresponding author. Tel.: +30-2810-393636; fax: +30-2810-393601.
E-mail address: coutsole@chemistry.uoc.gr (A.G. Coutsolelos).

0277-5387/$ - see front matter © 2004 Elsevier Ltd. All rights reserved.
doi:10.1016/j.poly.2004.04.010

Recently the X-ray study of a lanthanide perhalogenated complex has been published [14]. It has been suggested that the metal ion and its environment influence the redox potential of these systems.

Based on a recently published procedure [14] we achieved the synthesis of halogenated In(III) and Tl(III) complexes. Their physicochemical features are compared with those of *meso*-substituted derivatives. Metallation with In or Tl offers a unique probe to study the influence of peripheral substituents and/or of the central metal on their physicochemical properties. A work correlating the ^{205}Tl NMR chemical shifts to the basicity of the ring, the axial ligation and the oxidation state has already been published by our group [20]. Monomeric thallium complexes provide ^{205}Tl signals from approximately 2850–2700 ppm following a decreasing order of basicity, while in the case of dimeric complexes (with a Rh:→Tl metal bond, typical +1 oxidation state of Tl) the signal is shifted more than 2000 ppm to the region of 180–200 ppm [21].

Finally, part of our research interest is the formation of single metal–metal bonded porphyrinic complexes. Monomeric metalloporphyrins of In or Tl are excellent precursors for the synthesis of new metal–metal bonded dimers. The nature of the monomeric complexes is expected to influence dramatically the properties of the formed dimers.

2. Experimental

2.1. Materials

All chemical were reagent grade and were used without further purification except as noted. Basic type I alumina was activated at 150 °C for at least 24 h.

2.2. Syntheses

The synthesis of free bases followed previously published procedures [14,22]. The preparation of thallium(III) complexes was based on Abraham's method [23]. The preparation of In complexes was based on the "acetate method" [24].

2.2.1. Syntheses of (Porph)Tl–Cl complexes

(T*p*FPP)TlCl (**1**): 0.1 mmol of (T*p*FPP)H_2 and 1 mmol of $Tl^{III}(CH_3COO)_3 \times 11/2H_2O$ were dissolved in 100 ml THF. The reaction mixture was refluxed for 24 h. After cooling, THF was removed and the solid residue was dissolved in CH_2Cl_2 and washed with a saturated aqueous solution of NaCl. Chromatographic separation of the crude product was performed on a SiO_2 column (4 cm × 3 cm). The metallated product was eluted with CH_2Cl_2/C_6H_{14} (4/6 v/v) as eluents (yield: 60%).

(TPyP)TlCl (**2**): The same reaction process as mentioned above was followed. The product was recovered after recrystallization from a mixture of CH_2Cl_2/C_6H_{14} (1/3 v/v), (yield: 94%).

(β-Cl_4TPP)TlCl (**3**): The reaction was performed as for compound **1**. A column of SiO_2 (4 cm × 3 cm) was used for the chromatographic separation. The desired product was eluted with CH_3OH/CH_2Cl_2 (50/50 v/v-20/80 v/v) as eluents, (yield: 65%).

(β-Br_4TPP)TlCl (**4**): The preparation of the crude product was the same as described above. The column separation was performed on SiO_2 (4 cm × 3 cm). The desired metalloporphyrin derivative was eluted with CH_2Cl_2, (yield: 67%).

(β-Cl_8TPP)TlCl (**5**): The reaction conditions mentioned before were also followed for the synthesis of the crude product **5**. The chromatographic separation was performed on SiO_2 column (6 cm × 4 cm). The product was eluted with toluene/hexane (8/2 v/v), (yield: 60%).

2.2.2. Syntheses of (Porph)In–Cl complexes

(T*p*FPP)InCl (**6**): 0.15 mmol of (T*p*FPP)H_2, 1.5 mmol of $InCl_3$ and 16 mmol of CH_3COONa were dissolved in 50 ml of glacial acetic acid. The reaction mixture was refluxed for 24 h. The solvent was removed under reduced pressure and the solid residue was dissolved in CH_2Cl_2. The solution was extracted from an aqueous solution of $NaHCO_3$ (5% w/v). The organic phase was washed two times with a saturated aqueous solution of NaCl and dried over $MgSO_4$. The solvent was removed and the solid residue was purified. A chromatographic separation was performed on SiO_2 (6 cm × 3 cm). With CH_2Cl_2/hexane (4/6 v/v) the free base was eluted. Increasing gradually the polarity of the solvents to CH_2Cl_2/hexane (8/2 v/v) the metalloporphyrin was eluted, (yield: 85%).

(TPyP)InCl (**7**): The previous synthetic route was also performed for compound **7**. Basic Al_2O_3 (5 cm × 3 cm) (Grade 1) was used in order to perform the chromatographic separation. With CH_2Cl_2/MeOH (200/5 v/v) the desired product was collected, (yield: 87%).

(β-Cl_4TPP)InCl (**8**): The preparation followed the previously described method for complex **6**. The chromatographic separation was performed on basic Al_2O_3 (5 cm × 3 cm) (Grade 1). The metalloporphyrin was eluted with a mixture of CH_2Cl_2/MeOH (7/3 v/v), (yield: 70%).

(β-Br_4TPP)InCl (**9**): The preparation was the same as described above. The crude product was chromatographed on SiO_2 (5 cm × 4 cm). The elution of the metallated porphyrin was achieved with toluene, (yield: 60%).

(β-Cl_8TPP)InCl (**10**): The reaction conditions were the same but with THF as reaction solvent due to low solubility of (β-Cl_8TPP)H_2 in the glacial acetic acid. The chromatographic separation was achieved on SiO_2 (6

cm × 4 cm) and the product was eluted with CH_2Cl_2, (yield: 70%).

3. Instrumentation and methods

^1H NMR and ^{13}C NMR spectra were recorded on a Bruker AMX-500 MHz NMR spectrometer using chloroform-D_3 as a solvent. Resonances in the ^1H NMR were referenced versus the residual proton signal of the solvent.

Absorption spectra were collected on a Perkin–Elmer Lamda 6 grating spectrophotometer.

Crystals suitable for X-ray diffraction were obtained by slow evaporation of a saturated toluene solution for compounds **3** and **8** and of a saturated solution of a mixture of 1:1 $CHCl_3$/toluene for compound **6**.

3.1. Data collection and X-ray crystal structure determination

A single crystal with approximate dimensions 0.20 × 0.20 × 0.50 mm for **3,** and 0.10 × 0.10 × 0.30 mm for **8** were mounted in air. Diffraction measurements for **3** and **8** were made on a Crystal Logic Dual Goniometer diffractometer using graphite monochromated Mo Kα radiation. Unit cell dimensions were determined and refined by using the angular settings of 25 automatically centred reflections in the range $1° < 2\theta < 23°$. Intensity data were recorded using $\theta - 2\theta$ scans. Three standard reflections were monitored every 97 reflections over the course of data collection and showed less than 3% variation and no decay. Lorentz polarization and ψ-scan absorption corrections were applied using Crystal Logic software. The structures of **3** and **8** were solved by direct methods using SHELXS-86 [25] and refined by full-matrix least-squares techniques on F^2 with SHELXL-93 [26].

A single crystal of **6**, with approximate dimensions 0.20 × 0.40 × 0.60 mm, was mounted in air on a Siemens-Bruker P4 diffractometer equipped with a rotating anode generator, graphite-monochromated Cu Kα radiation being used for all operations. Cell dimensions were determined from the angular settings of 30 reflections with $32° < \theta < 55°$. Intensity data were recorded by ω–2θ scans and three standards monitored every 90 min revealed an overall 14% intensity decay, which was accounted for at data reduction time. A ψ-scan absorption correction was applied. Structure solution and refinement were performed with SHELX [25,26].

A summary of crystallographic data for **3**, **6** and **8** is given in Table 1.

Compounds **3** and **8** are isostructural and they were treated in a similar way. The chloride substituents on the porphyrin core were found disordered in both **3** and **8** and they were refined anisotropically with occupation factors free to vary. The chlorine substitution on the

Table 1
Summary of crystal, intensity collection and refinement data for compounds (β-Cl_4TPP)TlCl (**3**), (T*p*FPP)InCl (**6**) and (β-Cl_4TPP)InCl **(8)**

Parameters	(**3**) · $C_6H_5CH_3$	(**8**) · $C_6H_5CH_3$	(**6**) · 1.5(C_6H_6)
Formula	$C_{51}H_{32}Cl_5N_4Tl$	$C_{51}H_{32}Cl_5InN_4$	$C_{53}H_{17}ClF_{20}InN_4$
Fw	1082.43	992.88	1239.98
Crystal system	triclinic	triclinic	monoclinic
Space group	$P\bar{1}$	$P\bar{1}$	$P2_1/n$
Temperature (K)	298	298	298
Unit cell dimensions			
a (Å)	13.942(6)	13.914(6)	14.775(3)
b (Å)	14.284(6)	14.198(7)	12.979(2)
c (Å)	13.368(6)	13.238(6)	26.222(6)
α (°)	105.32(1)	104.73(1)	–
β (°)	118.44(1)	118.02(1)	92.66(2)
γ (°)	90.39(1)	91.10(1)	–
V (Å^3)	2230(2)	2203(2)	5023(2)
Z	2	2	4
ρ_{calcd} (g cm^{-3})	1.612/1.60	1.497/1.48	1.640/1.63
Radiation, θ (Å)	Mo Kα 0.71073	Mo Kα 0.71073	Cu Kα 1.5418
μ (mm^{-1})	3.962	0.881	5.309
Reflections collected/unique [R_{int}]	7783/7428 [0.0156]	6412/6110 [0.0237]	9238/5827 [0.0388]
Data with $I > 2\sigma(I)$	6340	4345	5618
Parameters refined	561	562	758
$(\Delta\rho)_{max}$, $(\Delta\rho)_{min}$ (e Å^{-3})	0.696/−0.794	0.705/−0.521	1.998/−0.715
w[a]	$a = 0.0657$, $b = 1.2315$	$a = 0.0703$, $b = 9.0137$	$a = 0.0921$, $b = 9.6349$
Goodness-of-fit (on F^2)	1.179	1.014	1.134
R_1[b], wR_2[c] (all data)	0.0595, 0.1260	0.1004, 0.1984	0.0584, 0.1618
R_1[b], wR_2[c] ($I > 2\sigma(I)$)	0.0469, 0.1184	0.0680, 0.1625	0.0573, 0.1606

[a] $w = 1/[\sigma^2(F_o^2) + (aP)^2 + bP]$ and $P = (\max(F_o^2, 0) + 2F_c^2)/3$.
[b] $R_1 = \sum(|F_o| - |F_c|)/\sum(|F_o|)$.
[c] $wR_2 = \{\sum[w(F_o^2 - F_c^2)^2]/\sum[w(F_o^2)^2]\}^{1/2}$.

pyrroles of the porphyrin skeleton is unsymmetrical in both **3** and **8**. The distribution of the chloride ions is unsymmetrical because there are two pyrrole rings, which are monosubstituted, one that is doubly substituted and one unsubstituted. In compound **3,** there is 64% probability of the presence of chlorine substituents in C_2, C_7, C_{12}, C_{13} and 36% probability of the presence of the substituents in the remaining C_β atoms of the porphyrin. The corresponding probabilities in compound **8** are 60% in C_2, C_7, C_{12}, C_{13} and 40% in the remaining C_β positions. In both **3** and **8**, all the non-hydrogen atoms were refined anisotropically, except those of the toluene solvent molecule, which were refined isotropically. The toluene molecule was found disordered over two orientations and was refined with occupation factors of a total sum of one. All H atoms were introduced at calculated positions as riding on bonded atoms; no H atoms for the toluene solvent molecule were included in the refinement.

In the model for the structure of **6** all the non-hydrogen atoms were refined anisotropically and the hydrogen atoms, both of the TPP ring and of the solvent molecules, were in calculated positions, riding. Presence of solvate molecules in the structure was modelled by two benzene molecules: one was distributed over two orientations whose complementary occupancy factors were refined and the other one, lying in proximity of an inversion centre, was assigned a fixed 0.50 occupancy factor value.

4. Results and discussion

4.1. NMR

The title complexes are fully characterized by ^{1}H NMR and ^{13}C NMR, while for the case of pentafluoroporphyrins ^{19}F NMR experiments were performed.

By the performance of ^{1}H NMR we observed the characteristic differentiation of *ortho*- and *ortho′*-protons. There is only one exception for the case of octahalogenated complexes (Table 2). In the case of Tl complexes a scalar coupling of pyrrolic protons with the Tl nucleus is observed, which is measured close to 75 Hz.

Taking advantage of the 100% natural abundance of spin 1/2 ^{19}F and its high gyromagnetic ratio, ^{19}F NMR experiments were performed. Five separate signals were observed (Table 3). The porphyrin ring current and the position of the fluorine atoms related to the porphyrin ring differentiate them. The furthest downfield signals, which appeared as two doublets, are attributed to *ortho*-F and to ortho′-F ($J = 23.5$ Hz). The fluorine atom at the *para* position appeared as a triplet. Metallation mainly effects the chemical shifts of *ortho*-F, *ortho′*-F and *meta*-F compared to the free base [27].

^{13}C- NMR signals spread in a 200 ppm region (Table 4). Assignment was based on heteronuclear experiments (HMQC, HMBC). We can distinguish two major groups for carbon frequencies. The aromatic carbons resonate between 130 and 170 ppm and the methinic carbons in the region of 90–120 ppm. The chemical data does not present any unexpected information in respect to other metalloporphyrinic derivatives. However the chemical shifts for C_{ph} are sensitive to the number of the halogen atoms: 140.18 ppm for (β-Cl_4TPP)TlCl to 144.2 ppm for (β-Cl_8TPP)TlCl.

C_β are the most sensitive carbon atoms to substitution. For tetrahalogenated complexes C_β provide two signals, one which is attributed to C_β-H and one to C_β-X (X = Cl, Br). In the case of (β-Cl_4TPP)TlCl, C_β–Cl resonate at 135.34 ppm. The signal at 133.72 ppm was assigned through heteronuclear experiments to C_β-H and for the tetrabrominated analogue at 134.2 ppm. In the case of octahalogenated complexes C_β–Cl is dishielded at 137.86 ppm for (β-Cl_8TPP)TlCl.

4.2. UV–visible spectroscopy

The position (β-pyrrole or *meso*) of the substitution is the factor which affects more or less in each case the spectrochemical properties of the macrocycle (Table 5).

Table 2
^{1}H NMR chemical shifts of complexes (Porph)$In^{III}Cl$ and (Porph)$Tl^{III}Cl$ in $CDCl_3$

Complex	*para*-H (*p*-H)	*meta*-H (*m*-H)	*ortho*-H (*o*-H)	*ortho*-H′ (*o′*-H)	pyr-H
(T*p*FPP)TlCl **(1)**					9.14 ($J = 61$)[a]
(TPyP)TlCl **(2)**		9.11 (d)	8.37	8.10	9.13 ($J = 63.3$)[a]
(β-Cl_4TPP)TlCl **(3)**	7.84 (m)	7.75 (m)	8.14 (d)	8.03 (d)	8.89
(β-Br_4TPP)TlCl **(4)**	7.84 (tr)	7.73 (m)	8.14 (m)	8.04 (m)	8.97 ($J = 75$)[a]
(β-Cl_8TPP)TlCl **(5)**	7.86 (tr)	7.79 (br)	8.16 (br)	8.16 (br)	
(T*p*FPP)InCl **(6)**					9.15
(TPyP)InCl **(7)**		9.13 (d)	8.37	8.10	9.14
(β-Cl_4TPP)InCl **(8)**	7.83 (tr)	7.77 (m)	8.15 (m)	7.98 (m)	8.92
(β-Br_4TPP)InCl **(9)**	7.85 (tr)	7.77 (m)	8.15 (m)	8.01 (m)	8.95
(β-Cl_8TPP)InCl **(10)**	7.86 (tr)	7.79 (s,br)	8.15 (s,br)	8.15 (s,br)	

δ in ppm.
[a] In parenthesis ^{205}Tl–H coupling in Hz.

Table 3
^{19}F NMR data for (T*p*FPP)$M^{III}Cl$ (M = In, Tl) complexes in $CDCl_3$

	ortho-F (*o*-F)	ortho′-F (*o*′-F)	meta-F (*m*-F)	meta′-F (*m*′-F)	para-F (*p*-F)
(T*p*FPP)H_2[a]	−136.92	−136.92	−161.81	−161.81	−151.70
(T*p*FPP)$In^{III}Cl$	−135.66	−137.34	−161.03	−161.6	−150.83
(T*p*FPP)$Tl^{III}Cl$	−135.84	−137.22	−161.09	−161.56	−150.84

δ in ppm.
[a] Taken from [27].

Table 4
^{13}C NMR data of (β-X_nTPP)$In^{III}Cl$ and (β-X_nTPP)$Tl^{III}Cl$(X = Cl or Br $n = 4$ or 8) in $CDCl_3$

	C_o	$C_{o'}$	C_{meta}	$C_{meta'}$	C_{para}	C_{ph}	C_{meso}	C_a	C_β
(Cl_4TPP)TlCl	134.57	135.02	127.67	127.48	129.96	140.18	122.65	151.98	133.79 129.65
(Br_4TPP)TlCl	134.48	135.17	127.48	127.79	129.24	141.20	123.12	151.97	133.86
(Cl_8TPP)TlCl	135.80	135.44	128.64	128.41	130.15	144.20	122.8		137.86
(Cl_4TPP)InCl	134.56	134.73	127.56	127.37	129.04	140.60	121.55	150.03	133.72 135.34
(Br_4TPP)InCl	134.44	135.06	127.78	127.46	129.21	140.07	122.10	150.65	134.22
(Cl_8TPP)InCl	135.83	135.27	128.51	128.51	130.10	143.15	121.63		137.8

δ in ppm.

Table 5
UV–visible data of (Porph)$In^{III}Cl$ and (Porph)$Tl^{III}Cl$ complexes in toluene

	B bands			*Q(2,0)*	*Q(1,0)* or *β*	*Q(0,0)* or *α*	*β*/*α*
(T*p*FPP)TlCl (**1**)		412 *(4.63)*	433 *(5.70)*	523 *(3.48)*	563 *(4.38)*	596 *(3.25)*	1.35
(TPyP)TlCl (**2**)		413 *(4.53)*	434 *(5.66)*	526 *(3.41)*	565 *(4.29)*	604 *(3.77)*	1.14
(β-Cl_4TPP)TlCl (**3**)	359 *(4.33)*	422 *(4.57)*	443 *(5.47)*	535 *(3.46)*	575 *(4.14)*	614 *(3.79)*	1.09
(β-Br_4TPP)TlCl (**4**)	363 *(4.18)*	424 *(4.63)*	446 *(5.58)*	539 *(3.59)*	576 *(4.26)*	617 *(3.920)*	1.09
(β-Cl_8TPP)TlCl (**5**)	393 *(4.52)*		468 *(5.35)*	565	604 *(3.98)*	660 *(4.04)*	0.98
(T*p*FPP)InCl (**6**)		403 (4.66)	425 (5.63)	516 (3.40)	556 (4.38)	591 (3.34)	1.31
(TPyP)InCl (**7**)	330 (4.28)	405 (4.58)	426 (5.79)	520 (3.51)	559 (4.35)	597 (3,72)	1.17
(β-Cl_4TPP)InCl (**8**)	352 (4.31)	412 (4.60)	435 (5.61)	529 (3.49)	568 (4.27)	607 (3.81)	1.12
(β-Br_4TPP)InCl (**9**)	358 (4.36)	416 (4.66)	438 (5.64)	532 (3.57)	570 (4.32)	609 (3.90)	1.11
(β-Cl_8TPP)InCl (**10**)	387 (4.45)		456 (5.51)	552 (3.54)	591 (4.10)	643 (4.02)	1.02

λ_{max} (nm), $\log \varepsilon$ ($dm^{-1}\,mol^{-1}\,cm^{-1}$).

Theoretical as well as experimental work concerning the tetraphenyl porphyrin has demonstrated that the relative ordering of the a_{1u} and a_{2u} orbitals is particularly sensitive to *meso*-substitution [28]. The a_{1u} orbital localizes electron density predominantly on C_α whereas a_{2u} electron is concentrated on the *meso* position. So, an electron-withdrawing group such as a perfluorophenyl group at the *meso* position is expected to lower the energy of the a_{2u} orbital with respect to a_{1u} [15].

In the case of halogenated complexes semi-empirical AM1 and spectroscopic calculation revealed that both the electronic properties of the halogen and the distortion of the macrocycle results in a reduced HOMO–LUMO energy gap [10,12,14,18,29]. On the other hand theoretical calculations relative to the influence of metal–porphyrin interactions on the energy of the frontier orbital revealed that mainly the a_{2u} orbital sensed the metal perturbation which places considerable electron density on the pyrrole nitrogen, while a_{1u} has nodes through the nitrogen and cannot interact directly with the metal [28c,30].

The porphyrinic complexes **1**, **2**, **6** and **7** which are *meso* substituted possess spectral features of ''normal'' type porphyrins [31] (Table 5) with no significant shifts of λ_{max} relative to the corresponding tetraphenyl derivatives [2].

Metallation of tetrahalogenated porphyrin results in bathochromically shifted bands. The intensity of the α band increases relative to the tetraphenyl complexes of In and Tl. This observation is more pronounced in the case of octahalogenated complexes where the intensity ratio of the molar absorptivities (β/α) is reduced. To a first approximation the β/α value correlates with the stabilization of the central metal [32]. The porphyrin ring with a large β/α value stabilizes the central metal. This is in good agreement with the reduced electron density for the octahalogenated complexes.

The *Soret* band of the octa-halogenated complexes (**5**, **10**) is red shifted relative to the free base, in contrast to the four coordinated complexes which possess blue-shifted *Soret* bands. [10,16]. The difference in λ_{max} of the *Soret* band between octahalogenated complexes **5**, **10** and the *meso* substituted **1**, **2**, **6**, **7** reflect the reduced HOMO–LUMO energy gap expected in view of the ring distortion as well as to the inductive effect of the halogen atoms.

The differences observed concerning the λ_{max} of the *Soret* band for the two series of In and Tl complexes with the same porphyrinic ligand can be attributed to the different electronegativity values of the two metals. More electronegative metals lower the a_{2u} orbital [28c,30b]. In addition, the ionic radii of the two metals play an important role. The size of the ionic radius of Tl (1.05 Å) leads to an out of the Δ_{4N} plane displacement which is larger than that for the In complexes [33] and it is also observed in the present X-ray structures.

4.3. Description of the structures

The molecular structures of compounds **3**, **6** and **8** are shown as ORTEP plots in Figs. 1–3 respectively. Selected bond distances and angles are listed in Table 6, structural characteristics of the porphyrin core of all the three structures are given in Table 7. Compounds **3** and **8** are the corresponding thallium(III) and indium(III) complexes of tetrachloro-tetraphenylporphyrin and are isostructural, so they will be discussed together. In both compounds, the coordination geometry about the metal is square pyramidal with the four nitrogen atoms of the porphyrin defining the equatorial plane and the chloride ion occupying the apical position. The M–N bond distances range from 2.199(6) to 2.220(6) Å for **3** (average value 2.210 Å) and from 2.150(7) to 2.163(7) Å for **8**

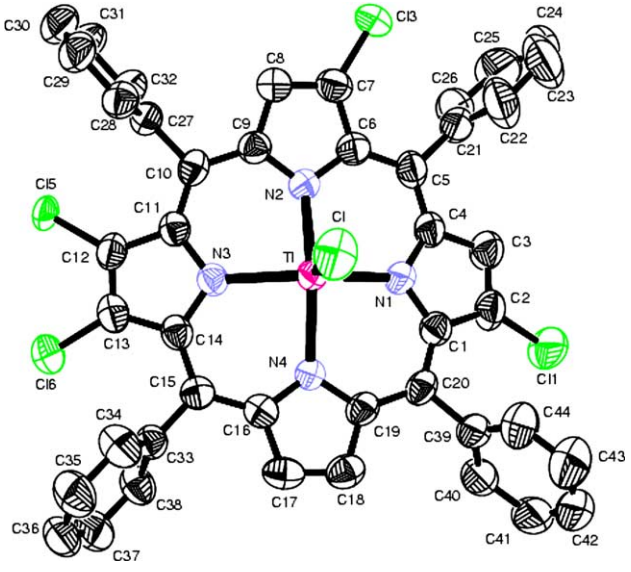

Fig. 1. ORTEP plot of (β-Cl_4TPP)TlCl (**3**).

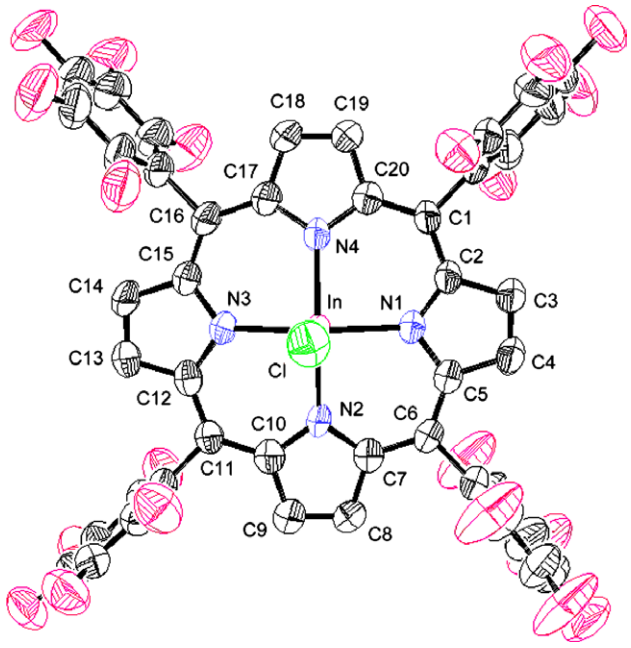

Fig. 2. ORTEP plot of (T*p*FPP)InCl (**6**).

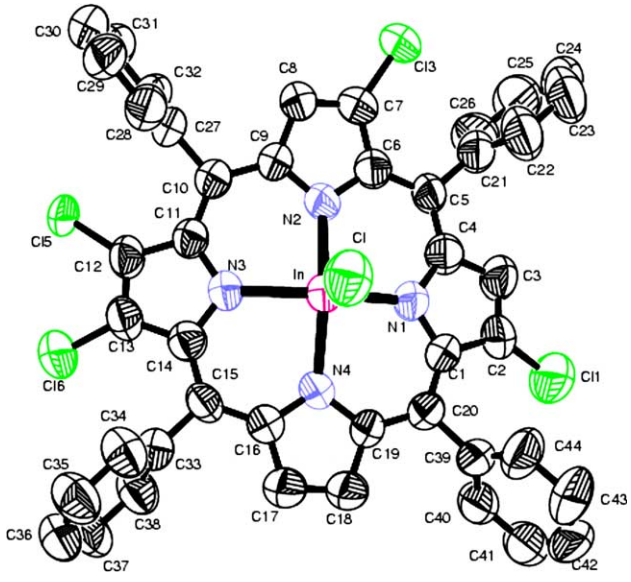

Fig. 3. ORTEP plots of (β-Cl_4TPP)InCl (**8**).

(average value 2.158 Å). The M–Cl bond lengths are 2.442(2) and 2.367(3) Å for **3** and **8** respectively. The metal ion lies 0.70 and 0.58 Å in **3** and **8** respectively, out of the equatorial plane of the square pyramid toward the axial chloride ligand. The presence of the metal ions along with the substitution on the C_β and C_m atoms of the porphyrin results in the distortion of the porphyrin core. The presence of the chlorine atoms on C_β carbon atoms of the porphyrin skeleton in both **3** and **8** results in the saddling distortion of the ligand, expressed by the mean absolute displacement of the C_β atoms from the $C_{20}N_4$ mean plane (0.39 Å for C_2, C_7, C_{12}, C_{13} in both **3** and **8**).

Table 6
Selected bond distances (Å), angles (°), and averages for (β-Cl_4TPP)TlCl · $C_6H_5CH_3$ (**3**), (β-Cl_4TPP)TlCl · $C_6H_5CH_3$ (**8**) and (T*p*FPP)InCl · 1.5(C_6H_6) (**6**)

	3 · $C_6H_5CH_3$	**8** · $C_6H_5CH_3$	**6** · 1.5(C_6H_6)
Bond distances			
M–Cl	2.442(2)	2.367(3)	2.360(2)
M–N(1)	2.212(6)	2.162(7)	2.154(5)
M–N(2)	2.207(6)	2.150(7)	2.141(5)
M–N(3)	2.199(6)	2.163(7)	2.161(5)
M–N(4)	2.220(6)	2.156(7)	2.135(5)
N–C_α	1.376	1.375	1.367
C_α–C_β	1.453	1.446	1.442
X–C_β	1.691[a]	1.674[b]	–
C_α–C_m	1.410	1.403	1.398
C_m–C_{phenyl}	1.484	1.494	1.505
Bond lengths			
$(N–M–N)_{cis}$	84.2	85.9	86.2
$(N–M–N)_{trans}$	142.9	149.0	149.9
$(Cl–M–N)_{axial}$	108.6	105.5	105.0
C_α–N–C_α	109.2	108.7	108.1
N–C_α–C_β	107.6	107.7	108.3
C_α–C_β–C_β	107.8	107.9	107.6
N–C_α–C_m	126.3	125.8	125.7

[a] For Cl(1), Cl(3), Cl(5) and Cl(6) with occupancy 64%.
[b] For Cl(1), Cl(3), Cl(5) and Cl(6) with occupancy 60% (see text for details).

Table 7
Structural characteristics of the compounds (β–Cl_4TPP)Tl–Cl · $C_6H_5CH_3$ (**3**), (β–Cl_4TPP)Tl–Cl · $C_6H_5CH_3$ (**8**) and (T*p*FPP)In–Cl · 1.5(C_6H_6) (**6**) indicating the distortion of the porphyrin core

Atom(s)	**3** · $C_6H_5CH_3$	**8** · $C_6H_5CH_3$	**6** · 1.5(C_6H_6)
N	0.017	0.031	0.074
C_m	0.081	0.094	0.061
C_β	0.387[a]	0.391[a]	0.097[b], 0.101[c]
Cl1	0.689[d]	0.689[d]	–

Dihedral angles with the $C_{20}N_4$ mean plane

Group	**3** · $C_6H_5CH_3$	**8** · $C_6H_5CH_3$	**6** · 1.5(C_6H_6)
Pyrroles	12.69, 9.97	12.33, 9.56	4.16, 5.00
	10.85, 9.21	10.85, 8.43	3.33, 7.28
Phenyls	76.71, 72.74	76.66, 72.41	74.96, 89.58
	66.70, 65.10	67.55, 64.12	87.23, 73.55

Average absolute displacement of selected atoms of the porphyrin from the $C_{20}N_4$ mean plane.
[a] Average absolute value of C(2), C(7), C(12) and C(13) displacements.
[b] Average absolute value of C(3), C(8), C(13) and C(18) displacements.
[c] Average absolute value of C(4), C(9), C(14) and C(19) displacements.
[d] Average absolute value of Cl(1), Cl(3), Cl(5) and Cl(6) displacements.

The average absolute displacement of the corresponding chlorine atoms bonded to C_β atoms is 0.69 Å (for Cl_1, Cl_3, Cl_5, Cl_6 in both **3** and **8**). On the other hand, the average absolute displacement of the C_m atoms from the porphyrin core (0.081 and 0.094 Å in **3** and **8** respectively) along with the rather large values of the dihedral angles formed between the phenyl rings and the $C_{20}N_4$ mean plane (65.10°–76.71° and 64.12°–76.66° in **3** and **8** respectively) indicate that there is no twist distortion of the porphyrin skeleton. The pyrrole rings are planar within experimental error and they are tilted alternatively up and down with respect to the porphyrin core mean plane by 9.21°–12.69° in **3** and 8.43°–12.33° in **8**.

In compound **6**, the nitrogen atoms of the tetra(pentafluorophenyl)porphyrin define the equatorial plane of the square pyramidal geometry about the indium(III) ion while the apical position is occupied by the chloride ion. The metal ion lies 0.63 Å out of the equatorial plane towards the axial ligand. The In–N bond distances range from 2.135(5) to 2.161(5) Å (average value 2.148 Å), and the In–Cl bond length is 2.360(2) Å. The lack of substitution on the C_β atoms of the porphyrin skeleton is reflected in the small average absolute displacement of these atoms from the $C_{20}N_4$ mean plane (0.097 and 0.101 Å for C_3, C_8, C_{13}, C_{18} and C_4, C_9, C_{14}, C_{19} respectively) and the small dihedral angles formed between the pyrrole rings and the $C_{20}N_4$ mean plane (3.33°–7.28°). The average absolute displacement of the C_m atoms is also very small (0.061 Å for C_1, C_6, C_{11}, C_{16}) despite the pentafluoro-phenyl substituents. The absence of C_β-substituents in the porphyrin skeleton is also reflected in the large dihedral angles formed between the pentafluoro-phenyl rings and the $C_{20}N_4$ mean plane (73.55°–89.58°) due to the minimization of the steric effects. These values are very close to the ideal value of 90°, which is expected in the non-substituted porphyrins.

5. Concluding remarks

All these complexes could be used as precursors for the synthesis of new metal–metal bonded derivates with

Rh–In or Rh–Tl bonds in order to modify the properties of the metallic bond, stability and/or reactivity. The position of substitution (β or *meso*) and the number of halogen atoms (tetra- or octahalogenated complex) impose a pronounced effect on the spectroelectrochemical features of the dimers, which will be discussed in detail in a future article [34].

6. Supplementary data

Crystallographic data for the structural analyses have been deposited with the Cambridge Crystallographic Data Center, CCDC 221431-221333. Copies of this information may be obtained free of charge from The Director, CCDC, 12 Union Road, Cambridge, CB2 1EZ, UK (fax: +44-1223-336033); e-mail: deposit@ccdc.cam.ac.uk or http://www.ccdc.cam.ac.uk.

Acknowledgements

This research was supported by the Greek General Secretariat of Research and Technology, and the ΕΠΕΑΕΚ graduate programs of "Bioinorganic Chemistry" and "Natural Products" through the Special Research Account of the University of Crete.

References

[1] W.R. Scheidt, Y. Lee, J. Struct. Bonding (Berlin) 64 (1987) 1.
[2] A.G. Coutsolelos, A. Tsapara, D. Daphnomili, D.L. Ward, J. Chem. Soc., Dalton Trans. (1991) 3413.
[3] R. Guilard, A. Zrineh, A. Tabard, A. Endo, B. Han, C. Lecomte, M. Souhassou, A. Habbou, M. Ferhat, K.M. Kadish, Inorg. Chem. 29 (1990) 4476.
[4] A. Coutsolelos, R. Guilard, A. Boukhris, C. Lecomte, J. Chem. Soc., Dalton. Trans. (1986) 1779.
[5] A. Boukhris, C. Lecomte, A. Coutsolelos, R. Guilard, J. Organomet. Chem. 29 (1990) 4476.
[6] (a) R. Guilard, S.S. Gerges, A. Tabard, P. Richard, M.A. El Borai, C. Lecomte, J. Am. Chem. Soc. 109 (1987) 7228;
(b) R. Guilard, N. Jagerovic, A. Tabard, P. Richard, L. Courthaudon, A. Louati, C. Lecomte, K.M. Kadish, Inorg. Chem. 30 (1991) 16.
[7] M.O. Senge, K. Ruhlandt-Senge, K.J. Regli, K.M. Smith, J. Chem. Soc., Dalton Trans. (1993) 3519.
[8] L.-F. Chou, Y.-H. Chen, J. Chem. Soc., Dalton Trans. (1996) 3787.
[9] C.-S. Chang, C.-H. Chen, Y.-I. Li, B.-C. Liaou, B.-T. Ko, S. Elango, J.-H. Chen, Inorg. Chem. 40 (2001) 2905.
[10] P. Bhyrappa, V. Krishnan, Inorg. Chem. 30 (2) (1991) 239.
[11] P. Tagliatesta, J. Li, M. Autret, E. Van Caemelbecke, A. Villard, F. D' Souza, K.M. Kadish, Inorg. Chem. 35 (1996) 5570.
[12] F. D' Souza, M.E. Zandler, P. Tagliatesta, Z. Ou, J. Shao, E. Van Caemelbecke, K.M. Kadish, Inorg. Chem. 37 (1998) 4567.
[13] S.G. Di Magno, A.K. Wertsching, C.R. Ros II, J. Am. Chem. Soc. 117 (1995) 8279.
[14] G.A. Spyroulias, A. Despotopoulos, C.P. Raptopoulou, A. Terzis, D. de Montauzon, R. Poilblanc, A.G. Coutsolelos, Inorg. Chem. 41 (2002) 2648, and references cited therein.
[15] P. Ochsenbein, K. Ayougou, D. Mandon, J. Fischer, R. Weiss, R.N. Austin, K. Jayaraj, A. Gold, J. Terner, J. Fajer, Angew. Chem., Int. Ed. Engl. 33 (3) (1994) 348.
[16] J.A. Hodge, M.G. Hill, H.B. Gray, Inorg. Chem. 34 (1995) 809.
[17] D. Mandon, P. Ochsenbein, J. Fischer, R. Weiss, K. Jayaraj, R.N. Austin, A. Gold, P.S. White, O. Brigaud, P. Battioni, D. Mansuy, Inorg. Chem. 31 (1992) 2044.
[18] T. Takeuchi, H.B. Gray, W.A. Goddard III, J. Am. Chem. Soc. 116 (21) (1994) 9730.
[19] P. Ochsenbein, D. Mandon, J. Fischer, R. Weiss, R. Austin, K. Jayaraj, A. Gold, J. Terner, E. Bill, M. Muther, A.X. Trautwein, Ang. Chem., Int. Ed. Engl. 32 (10) (1993) 1437.
[20] A.G. Coutsolelos, D. Daphnomili, Inorg. Chem. 34 (1997) 4614.
[21] D. Daphnomili, W.R. Scheidt, J. Zajicek, A.G. Coutsolelos, Inorg. Chem. 37 (1997) 3675.
[22] (a) J.B. Kim, J.J. Leonard, F.R. Longo, J. Am. Chem. Soc. 11 (1972) 3986;
(b) R.G. Little, J. Abraham, P.A. Loach, J.A. Ibers, J. Heterocycl. Chem. (1975) 343.
[23] R.J. Abraham, G.H. Barnett, K.M. Smith, J. Chem. Soc., Perkin I (1973) 2142.
[24] D. Dolphin, in: The Porphyrins, vol. 4, Academic press, New York, 1979, 197.
[25] G.M. Sheldrick, SHELXS-86: Structure Solving Program, University of Göttingen, Göttingen, Germany, 1986.
[26] G.M. Sheldrick, SHELXL-93: Crystal Structure Refinement, University of Göttingen, Göttingen, Germany, 1993.
[27] E.R. Birnbaum, J.A. Hodge, M.W. Grinstaff, W.P. Schaefer, L. Henling, J.A. Labinger, J.E. Bercaw, H.B. Gray, Inorg. Chem. 34 (1995) 3625.
[28] (a) J. Fajer, D.C. Borg, A. Forman, A.D. Adler, V. Varad, J. Am. Chem. Soc. 96 (1974) 1238;
(b) A.G. Skillman, J.R. Collins, G.H. Loew, J. Am. Chem. Soc. 114 (1992) 9538;
(c) J.A. Shelnutt, V.J. Ortiz, Phys. Chem. 89 (1985) 4733.
[29] (a) P. Bhyrappa, V. Krishnan, Inorg. Chem. (1991) 239;
(b) G. Hariprasad, S. Dahal, B.G. Maiya, J. Chem. Soc., Dalton Trans. (1996) 3429.
[30] (a) M.Z. Zgierski, Chem. Phys. Lett. 124 (1) (1986) 53;
(b) J.A. Shelnutt, J. Phys. Chem. 88 (1984) 4988.
[31] J.W. Buchler, W. Kokisch, P.D. Smith, Struct. Bond. 34 (1987) 79.
[32] J.E. Falk, Porphyrins and Metalloporphyrins, Elsevier, Amsterdam, 1976, p. 34.
[33] (a) R. Guilard, C. Lecomte, K.M. Kadish, Struct. Bond. (1987) 207;
(b) K. Henrick, R.W. Matthews, P.A. Tasker, Inorg. Chem. (1977) 3293;
(c) R.G. Ball, K.M. Lee, A.G. Marshall, J. Trotter, Inorg. Chem. 19 (1980) 1463.
[34] D. Daphnomili, J-H. Agondanou, S. Bénazeth, C. Raptopoulou, A. Terzis, A.G. Coutsolelos, Inorg. Chem. (2004), in press.

Available online at www.sciencedirect.com
SCIENCE DIRECT®
Polyhedron 23 (2004) 1785–1792
POLYHEDRON
www.elsevier.com/locate/poly

Synthesis, X-ray crystal structure and vibrational spectra of a polymeric copper(II) complex with 2-thiopheneacetic acid

Piotr Drożdżewski [a,*], Anna Brożyna [a], Maria Kubiak [b]

[a] *Institute of Inorganic Chemistry and Metallurgy of Rare Elements, Faculty of Chemistry, Wrocław University of Technology, Wybrzeże St., Wyspiańskiego 27, 50-370 Wrocław, Poland*
[b] *Faculty of Chemistry, University of Wrocław, F. Joliot-Curie 14, 50-383 Wrocław, Poland*

Received 17 February 2004; accepted 12 April 2004
Available online 6 May 2004

Abstract

The crystal structure of a novel polymeric copper(II) complex with 2-thiopheneacetic acid is presented and the vibrational spectra are discussed. The copper(II) atoms and coordinating carboxylate oxygen atoms form the $[Cu_2O_8]$ dinuclear units typical for other carboxylates of this metal. The units are directly linked via two, relatively short Cu–O interactions and form polymeric chains along the b axis. A structural two- and threefold disorder has been found for the thiophene rings. The IR and Raman spectra of the title complex and free ligand are interpreted with help from literature data and deuteration effects. The absorption bands that are related to Cu–Cu core vibrations have been localized by a ^{63}Cu–^{65}Cu labelling technique.
© 2004 Elsevier Ltd. All rights reserved.

Keywords: 2-Thiopheneacetic acid; Polymeric copper(II) complex; Crystal structure; Vibrational spectra; Metal isotope effect

1. Introduction

Several thiophene derivatives are known to show biological activities in point of pharmaceutical and clinical aspects. The major role of 2-thiophene carboxylates is connected with drug production. Some of these derivatives have been widely studied to focus on a family of semisynthetic cephalosporins (first-generation antibiotics), antiallergic, antimigraine and intestinal antibacterial agents as well as for influenza treatment [1]. From the clinical point of view, thiophene carboxylates have also been interesting for treatment of osteoporosis as the inhibitors of bone resorption in the tissue culture [2,3]. It has been found that the biological activities of the discussed compounds are considerably increased when they are bonded into metal complex molecules. For example, such effects have been observed for Co(II), Ni(II), Cu(II) and Zn(II) chelates with several ligands including 2-thiophenecarboxylic acid tested on some selected fungi [4]. The biological aspect concerns the wider research area of transition metal complexes with thiophene containing ligands. In recent years, the influence of Co(II), Ni(II) and Cu(II) complexes with 2-thiophenecarboxylic acid has received increasing attention as potential anticancer drugs [5]. Thus, the preparation of new naturally occurring metal complexes, which have promising biological activity, is an important aim of current chemical and medical investigations.

In the presented work, the structure of a new copper(II) complex with 2-thiopheneacetic acid is presented. This compound belongs to the large group of copper(II) carboxylates containing a very characteristic, dinuclear $[Cu_2O_8]$ unit, where each copper(II) atom is coordinated by four oxygen atoms from carboxylate groups acting in a *syn*, *syn* bridging mode Scheme 1. In most cases, the copper(II) apical position (along the Cu–Cu direction) is occupied by CH_3COOH [6] or by additional ligands, being frequently the solvent molecules of H_2O [7–11], methanol [6], DMF [6], dioxane [12,13] as well as by

* Corresponding author. Tel.: +48-71-3203909/224330; fax: +48-71-3284330.
E-mail address: drozdzewski@ichn.ch.pwr.wroc.pl (P. Drożdżewski).

0277-5387/$ - see front matter © 2004 Elsevier Ltd. All rights reserved.
doi:10.1016/j.poly.2004.04.006

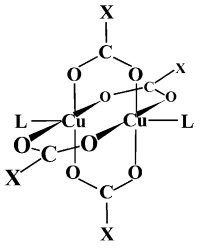

Scheme 1. The Cu(II)–Cu(II) core.

specially introduced substances e.g. pyridine [14–18], pyrazine [19], picoline [20–24], urea [16,25] and quinoline [26,27]. There are far fewer complexes where the copper atoms in the dinuclear unit are additionally coordinated by oxygen atoms of neighbouring $[Cu_2O_8]$ units, which results in a polymeric chain structure with Cu···O interactions. Such structures have been found so far for copper(II) complexes with propionic [28] and butanoic [29] acids. Here, we present another complex with a similar polymeric structure, together with its vibrational spectra, where the special metal isotope technique has been applied for detection of copper–oxygen vibrations.

2. Experimental

2.1. Preparation of the $[Cu_2(TAA)_4]_n$ complex

The ligand, 2-thiopheneacetic acid (HTAA), 98% was purchased from Sigma–Aldrich. The copper(II) chloride used was of analytical reagent grade.

The complex was prepared by neutralization of a 5 cm^3water solution containing 0.2 mmol of 2-thiopheneacetic acid with freshly precipitated $Cu(OH)_2$. The excess metal hydroxide was filtered off and the supernatant was left for crystallization at room temperature. After few days green crystals were collected, washed with water and dried in air. (Found: C, 41.44; H, 3.02; S, 18.47; $C_{12}H_{10}O_4S_2Cu$ Calc. C, 41.67; H, 2.91; S, 18.54%; melting point (m.p.) ca. 170 °C decomp.).

The complex analogues substituted with pure ^{63}Cu and ^{65}Cu isotopes were produced exactly as the compound with copper of natural abundance.

2.2. Spectral measurements

The IR spectra were collected on Perkin–Elmer FTIR 2000 and 1600 spectrometers with 0.5 and 2 cm^{-1} resolution for FIR and MIR regions, respectively. Samples were measured as Nujol mulls sandwiched between polyethylene plates and using the standard KBr pellet technique.

Raman spectra were measured on a T64000 Jobin-Yvon instrument equipped with Ar–Kr laser excitation and using the 514.5 nm line.

2.3. X-ray structure determination

For the X-ray structure determination, the data were collected on a KUMA KM4CCD diffractometer equipped with Mo Kα radiation ($\lambda = 0.71073$ Å). The structure was solved using the direct method option in

Table 1
Crystal data and structure refinement for $[Cu_2(TAA)_4]_n$

Empirical formula	$C_{12}H_{10}O_4S_2Cu$
Formula weight	345.86
Temperature (K)	100(2)
Wavelength (Å)	0.71073
Crystal system	monoclinic
Space group	$P2_1/n$
Unit cell dimensions	
a (Å)	13.244(5)
b (Å)	5.161(3)
c (Å)	19.733(6)
β (°)	103.35(3)
Volume (Å^3)	1312.3(10)
Z	2
Absorption coefficient (mm^{-1})	1.987
$F(000)$	700
D_{calc} (Mg/m^3)	1.750
Crystal size (mm)	$0.09 \times 0.08 \times 0.06$
θ Range for data collection (°)	3.38–28.46
Index ranges	$-17 \leqslant h \leqslant 17,\ -6 \leqslant k \leqslant 6,\ -26 \leqslant l \leqslant 23$
Reflections collected/unique [$R_{int} = 0.0758$]	8343/3037
Refinement method	full-matrix least-squares on F^2
Data [$I > 2\sigma(I)$]/parameters	3037/101/230
Goodness-of-fit on F^2	1.080
Final R indices [$I > 2\sigma(I)$]	$R_1 = 0.0669,\ wR_2 = 0.0634$
R indices (all data)	$R_1 = 0.1278,\ wR_2 = 0.0750$
Largest difference peak and hole (e Å^{-3})	0.40 and −0.40

the SHELXS-97 program [30] and developed using least-squares refinement and Fourier difference synthesis in the SHELXL-97 program [31]. The thiophene rings in two crystallographically different ligand forms were disordered and modelled using two or three sets of positions. For this procedure the ring distances and angles were restrained to constant values and the occupancy of two or three alternate orientations were constrained to unity. The refined occupancy was 0.851(5) and 0.149(5) for one ligand form, and 0.486(17), 0.304(5) and 0.210(17) for the second form. The hydrogen atoms were placed in geometrically calculated positions. Crystallographic parameters and structural refinement are summarized in Table 1. Selected structural parameters and best planes were calculated using the PARST97 package [32]. Diagrams were generated using ORTEP3 for Windows [33].

3. Results and discussion

3.1. Description of the structure

The core of the title compound is a dinuclear unit composed of two copper atoms and four bidentate anions forming *syn*, *syn* bridges between the metals (Fig. 1). Following the inversion symmetry, the oxygen atoms of opposite carboxylate groups form a quasi-plane together with the Cu–Cu unit. Both planes intersect along the Cu–Cu line forming a dihedral angle equal to 89.7(1)°. The copper atoms are situated in a coordination center of approximately square pyramidal shape. The four oxygen atoms of acetate anions form a base equatorial plane, and the Cu atom is 0.1717(6) Å above this plane. The apical position is occupied by a carboxylate oxygen atom from a neighbouring $[Cu_2(COO)_4]$ unit. The basal Cu–O distances are different and vary between 1.929(3) and 2.006(3) Å (Table 2). The fifth Cu–O bond, being a link between two $[Cu_2(COO)_4]$ units, is much longer and equals 2.190(3) Å.

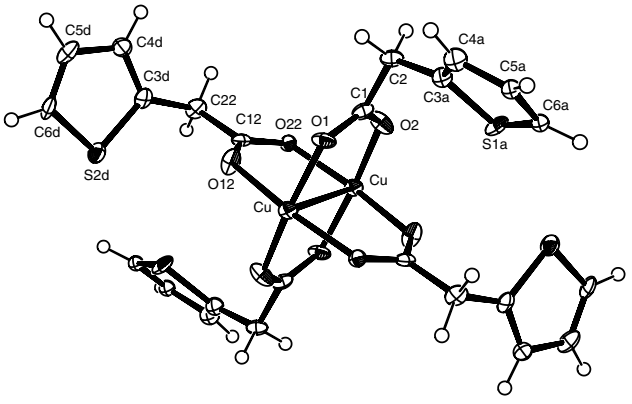

Fig. 1. View of the $[Cu_2(TAA)_4]$ unit with the atom labelling scheme and 50% probability thermal ellipsoids for non-hydrogen atoms. Atoms related by the inversion center are not labelled.

The Cu–Cu distance of 2.5867(15) Å is comparable to the respective values observed for other dinuclear copper acetates such as simple $[Cu(CH_3COO)_2(CH_3COO)]_2$ (2.581(1) Å [6]) or its analogs with water (2.6143(17) Å [7], 2.616(1) Å [8]), methanol (2.596(1) Å [6]), DMF (2.614(1) Å [6]), pyrazine (2.583(1) Å [19]) and α- or β-pyridine (2.645(3) Å [16], 2.641(1) Å [15] and 2.628(1) Å [16], 2.630(3) Å [14]) as side ligands attached along the Cu–Cu direction. Among many other dinuclear copper(II) carboxylates, similar Cu–Cu distances were found for formic (2.58(1) Å [12]), propionic (2.5634(4) Å [13], 2.578(4) Å [28] and 2.630(2) Å [18]), 2-phenylpropionic (2.589(1) Å [11]), butanoic (2.565 Å [29]), 2-thiophenecarboxylic (2.607(2) Å [9]) and 3- or 2-furancarboxylic (2.612(2) Å [9] and 2.638(1) Å [10]) acids. The symmetry of the $[Cu_2O_8]$ unit is C_i, but the distortion from the D_{4h} symmetry is rather small; the O–Cu–O angles deviate a maximum of 0.84° from a right angle, the Cu–O bond lengths differ less than 0.08 Å (~4%) and the dihedral O–Cu–Cu–O angles, measured for oxygen atoms belonging to the same carboxylate group, are a maximum of 0.3°.

As a consequence of the observed bond lengths within the Cu–O–C–O–Cu rings, the O–C–O angles are approximate 5° greater than the ideal value typical for sp^2 carbon atom hybridization. This atom is 0.038(4) Å displaced from the O1–Cu–Cu–O2 plane. The attached carbon atoms of the methylene groups are located approximately in the planes of the respective bridging rings. The C–CH_2–C angles attain values between 105(1)° and 120(3)°. These differences result from the existence of two geometrically different ligand forms and also from positional disorder of the thiophene rings. This disorder is different for two thiopheneacetic ligands as has been shown in Fig. 2, where the asymmetric unit is presented. In one case the thiophene rings are almost parallel but are rotated approximately along the C22–C3 direction forming an angle of 172(1)° between the ring best planes. In the second ligand, the disorder is more complicated. In addition to two orientations similar to those described above, a third quasi-parallel orientation has been found. The thiophene ring planes corresponding to the discussed three orientations form dihedral angles of 6(1)° (a and c indexed rings) and 173(1)° (a and b rings). Besides, the rings are shifted which causes the C1–C2–C3 angles to vary from 105.2° to 115.4°, whereas the C2–C3–S1 angles are between 119.8° and 123.3°. For the twofold disordered rings, similar angles are 113.8°, 120° and 114.6°, 121.2°, respectively. The rings are twisted with respect to the O–Cu–Cu–O planes, forming dihedral angles of approximately 80° and 62° for three- and twofold disordered

Table 2
Selected skeletal bond lengths (Å) and angles (°)

Cu–O(1)	1.929(3)	O(2)^{i}–Cu–O(22)^{ii}	96.3(1)
Cu–O(2)^{i}	1.939(3)	O(12)–Cu–O(22)^{ii}	109.8(1)
Cu–O(12)	1.960(3)	O(22)^{i}–Cu–O(22)^{ii}	80.2(1)
Cu–O(22)^{i}	2.006(3)	O(1)–Cu–Cu^{i}	83.55(9)
Cu–O(22)^{ii}	2.190(3)	O(12)–Cu–Cu^{i}	86.82(9)
Cu–Cu^{i}	2.5867(15)	O(22)^{ii}–Cu–Cu^{i}	163.21(8)
O(1)–C(1)	1.259(5)	C(1)–O(1)–Cu	124.2(3)
O(2)–C(1)	1.264(4)	C(1)–O(2)–Cu^{i}	120.4(3)
C(1)–C(2)	1.519(5)	O(1)–C(1)–O(2)	125.6(4)
C(2)–C(3A)	1.432(16)	O(1)–C(1)–C(2)	118.4(4)
C(3A)–C(4A)	1.376(8)	C(3A)–C(2)–C(1)	111.0(2)
C(3A)–S(1A)	1.729(6)	C(2)–C(3A)–S(1A)	123.3(2)
C(4A)–C(5A)	1.417(9)	C(4A)–C(3A)–S(1A)	110.4(4)
C(5A)–C(6A)	1.357(6)	C(3A)–C(4A)–C(5A)	112.8(6)
C(6A)–S(1A)	1.709(6)	C(6A)–C(5A)–C(4A)	112.5(6)
O(12)–C(12)	1.252(4)	C(5A)–C(6A)–(1A)	111.9(5)
O(22)–C(12)	1.281(4)	C(6A)–S(1A)–C(3A)	92.0(3)
C(12)–C(22)	1.519(5)	C(12)–O(12)–Cu	122.0(3)
		C(12)–O(22)–Cu^{i}	123.2(2)
O(1)–Cu–O(2)^{i}	169.8(1)	C(12)–O(22)–Cu^{iii}	136.8(3)
O(1)–Cu–O(12)	89.9(1)	Cu^{i}–O(22)–Cu^{iii}	99.8(1)
O(2)^{i}–Cu–O(12)	89.2(1)	O(12)–C(12)–O(22)	124.6(4)
O(12)–Cu–O(22)^{i}	170.1(1)	O(12)–C(12)–C(22)	119.1(4)
O(1)–Cu–O(22)^{ii}	93.5(1)	O(22)–C(12)–C(22)	116.3(4)

Symmetry transformations used to generate equivalent atoms. i: $-x, -y, -z$; ii: $x, y+1, z$; iii: $x, y-1, z$.

thiophene units. The different ring orientation is accompanied by changes in the C2–C3(a, b, c) or C22–C3(d, e) bond lengths. In the former case, the C2–C3 distances deviate up to 0.1 Å, whereas those of C22–C3 differ by 0.07 Å.

In the crystal structure, the dinuclear units are arranged in polymeric chains running parallel to the b axis. Within the chain, the units are linked by two apical Cu···O22 interactions of 2.190(3) Å to give a zigzag chain of copper atoms (Fig. 3). Copper and oxygen atoms engaged in the discussed link form a planar parallelogram with the Cu–O22···Cu angle equal to 99.83°. Similar chain structures have been found for anhydrous copper(II) propionate [28] and butyrate [29]. In these compounds, the Cu···O distances equal 2.28(1) and 2.245(no esd) Å, respectively. Thus, the complex presented here exhibits the shortest Cu···O link among those known so far. The polymeric chains are well separated, with the shortest contacts found between C5d^{i}–H5d^{i}, C6e^{i}–H6e^{i} (i: $1/2-x$, $1/2+y$, $1/2-z$) groups and O1 atoms. In these interactions the carbon–oxygen

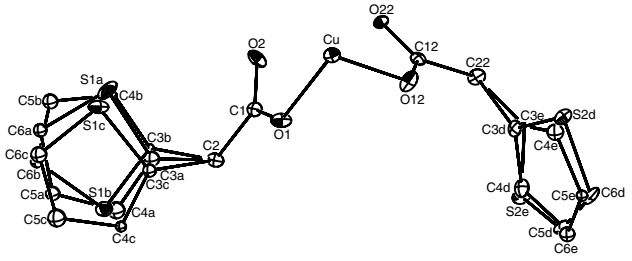

Fig. 2. A drawing of the asymmetric unit demonstrating the disordering of the thiophene rings. For better clarity the hydrogen atoms are omitted and thermal ellipsoids are reduced to 20%.

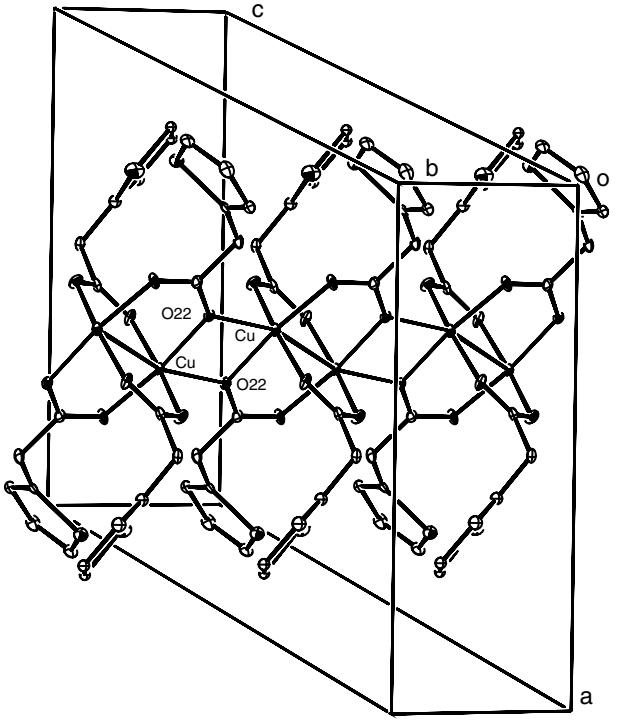

Fig. 3. Fragment of the polymer chain passing through the center of the unit cell along the *b* axis and demonstrating the Cu–O22^{i} bonds. For better clarity, the hydrogen atoms are omitted and thermal ellipsoids are reduced to 25%.

distances are 3.214(10) and 3.126(46) Å, whereas the C-H-O angles equal about 130°.

3.2. Vibrational spectra

The IR and Raman spectra of the discussed complex and free ligand have been compared in Fig. 4. The most noticeable change in IR band positions is observed for two strong ligand absorptions at 1701 and 1242 cm^{-1}. Upon coordination these bands shift to 1596 and 1285 cm^{-1}, respectively, which suggests their origin is from coordinating carboxylate group vibrations. The 105 cm^{-1} downshift of the 1701 cm^{-1} band well corresponds to the lowering of the C=O bond order caused by copper(II) coordination. Such a change is confirmed by X-ray data of the complex where all carbon–oxygen bond lengths are almost the same, within the range of 1.25 and 1.28 Å (Table 2). These distances are about 0.05 Å longer than those which are typical for the carboxylic C=O group [34]. A similar, but opposite difference is obtained when C–O bond lengths measured here are compared with those of the carboxylic C–OH group [34]. The last effect demonstrates the strengthening of the C–OH bond upon coordination and well corresponds to the positive shift of the 1242 cm^{-1} band assigned to the stretching ν(C–OH) vibration. The two recently discussed bands are frequently accompanied by another, less characteristic, absorption ranging between 1400 and 1450 cm^{-1} [35] for which the contribution of the δ(OH) mode is postulated [36]. Since this region is also occupied by thiophene ring vibration (observed for pure thiophene at 1409 cm^{-1} [36]) and $\delta(CH_2)$ mode, the coupling with the δ(OH) vibration has been utilized in the experimental detection of the third ν(COO) band. On O-deuteration of the HTAA ligand, monitored that in the discussed region, only the band at 1422 cm^{-1} is markedly shifted (to 1387 cm^{-1}) upon deuteration. Thus, this ligand absorption and corresponding 1415 cm^{-1} band in the spectrum of the complex would be the best candidates for the recently discussed transition. However, the 7 cm^{-1} difference between these band positions suggests that the contribution of the C–O vibrations is rather low in this transition where probably the modes of neighbour C–C and CH_2 groups contribute significantly. The H–D substitution also pointed the 1335 and 1293 cm^{-1} bands (not included in Table 3) as predominantly due to δ(OH) vibration. The δ(OH) counterpart has appeared as new band at 1057 cm^{-1}, which gives the H/D frequency ratio equal to 1.26 and 1.22.

As results from the location of the thiophene rings, the vibrations of these units should be much less affected by metal coordination. The comparison of the ligand and complex IR spectra shows several bands at similar positions easily comparable with normal vibrations observed for pure thiophene [37]. For nine vibrations of thiophene skeleton (listed in Table 3 as 2, 5, 11, 14, 15, 16, 21, 22 and 23) the respective wavenumbers observed for thiophene, HTAA and the complex differ by no more than 35 cm^{-1}. In the complex spectrum some

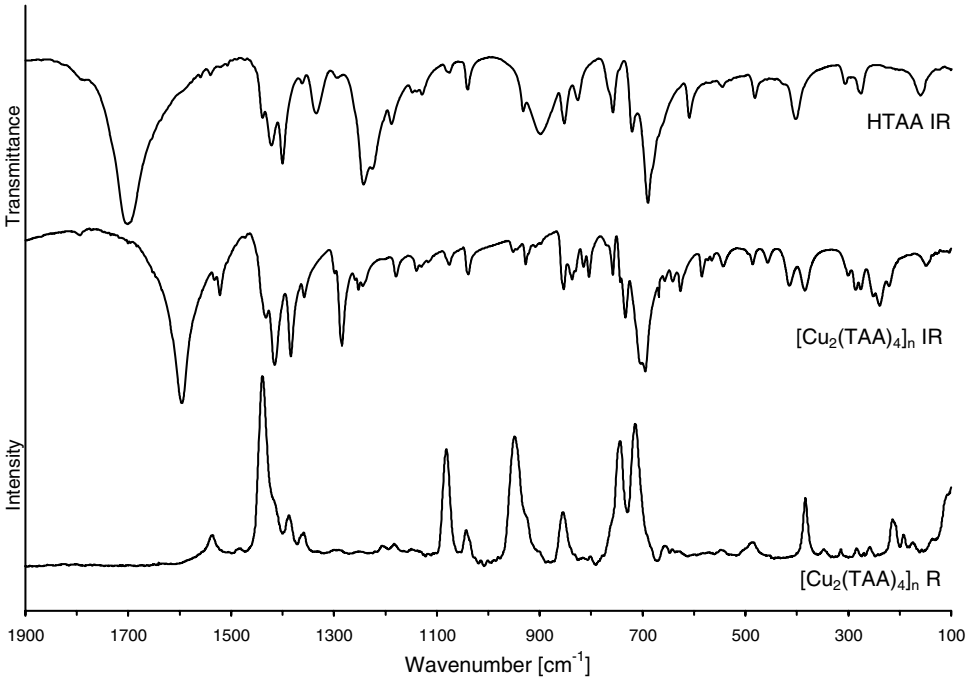

Fig. 4. IR and Raman spectra of $[Cu_2(TAA)_4]_n$ complex and pure HTAA ligand.

Table 3
Selected vibrations of the $[Cu_2(TAA)_4]_n$ complex compared with ligand (HTAA) and thiophene modes

No.	$[Cu_2(TAA)_4]_n$		HTAA	Thiophene [37]	Assignment[a]
	IR	R	IR	IR	
1	1596 vs	no[b]	1701 vs		ν_a(COO)
2	1522 m	1536 w	1540 vw	1504 vw	ν_a(C3=C4, C5=C6)
3	1433 s	1438 vs	1439 m		δ(CH_2)
4	1415 vs	1417 sh	1422 m		ν_s(COO), ν(C1–C2)
5	1383 s	1387 m	1400 s	1409 s	ν_s(C3=C4, C5=C6)
6	1358 m	1358 w	1363 w	1360 vw	δ_s(C3–H, C6–H)
7	1285 s	~1295 vw	1242 s		ν_s(COO)
8	1252 m, 1244 m	~1249 vw	1224 s	1256 s	δ_a(C4–H, C5–H)
9	1179 m	~1183 vw	1189 m,		ρ_t(CH_2)
10	1139 w, 1130 w	~1140 vw	1147 w, 1128 w		ρ_w(CH_2)
	1076 w	1081 s	1076 vw	1083 s	δ_s(C4–H, C5–H)
				1085 s	δ_a(C3–H, C6–H)
11	1039 m	1042 w	1040 w	1036 s	ν_s(C4–C5)
12	953 w	948 s	932 m		ν(C2–C3), ν(C1–C2)
13	927 w	925 sh	899 m	898	γ_s(C4–H, C5–H)
14	853 m, 837 m	854 m	853 m	867, 872 m	δ_2(R), γ_a(C4–H, C5–H)
15	815 w, 804 m	no	826 w	839 vs	ν_s(C3–S, C6–S)
16	758 m	no	757 m	751	ν_a(C3–S, C6–S)
17	743 m, 704 s	744 s, 714 vs			ρ_r(CH_2)
18	733 m	no	720 m	712	γ_a(C3–H, C6–H)
19	695 vs	no	689 vs	683	γ_s(C3–H, C6–H)
20	657 w, 642 w, 627m	657 vw			δ(C1–C2–C3–C4)
21	585 w	no	609 m	608 w	δ_1(R)
22	542 w	547 vw	546 w	565	τ_1(R)
23	486 w	485 vw	481 w	452 w	τ_2(R)
24	458 (0.5)[c]w				δ(Cu–O–C–O–Cu)
25	415 (2.0) m				ν(Cu–O)
26			402 m		ligand def.
27	385 (1.0) m	385 vs, 350 w			ν(Cu–O)
28	300 w	314 vw, 260 w	306 w, 275 w		ligand def.
29	285 (0.5) m	285 w			
30	275 (1.0) m				δ(O–Cu–O) + ν(Cu–O)
31	252 (1.0) m				
32	239 (1.0) m				
33	222 (0.5) m				
34		193 (0.5)			ligand def. + lattice
35		214 s, 174 w	159 w		ν(Cu–O[i])
36	149 (2.0) w				

Abbreviations: s – strong; m – medium; w – weak; v – very; sh – shoulder; ν – stretching; δ – in-plane bending; ρ_r – rocking; ρ_w – wagging; ρ_t – twisting; τ – out-of-plane bending; R – thiophene ring.

[a] Atom numbering is given in Fig. 1.

[b] Not observed.

[c] $\nu(^{63}Cu)$–$\nu(^{65}Cu)$ shifts are given in parentheses.

vibrations split into two or more bands (numbered in Table 3 as 8, 10, 14, 15, 17, 19 and 20). This effect is probably due to the presence of two independent ligand forms in the asymmetric unit and their structural two- or threefold disorder. Since the thiophene ring skeletons are very similar, the observed splitting may be related to bending vibrations of the CH groups or C1–C2–C3–C4 subunits, whose geometry is affected by skeletal disorder, and their vibrations may contribute in these transitions. The remaining thiophene modes are mainly due to displacements of hydrogen atoms and they preserve their positions after complexation with an accuracy similar to that of the skeletal vibrations. The stretching ν(C–H) vibrations of the thiophene units are observed in the $[Cu_2(TAA)_4]_n$ IR spectrum as broad absorptions with four distinct maxima at 3106, 3095, 3084 and 3072 cm^{-1}. Three of these maxima at 3106, 3095 and 3072 cm^{-1} well correspond to those observed for the HTAA ligand (3103, 3082 and 3070 cm^{-1}) and thiophene (3126, 3098 and 3086 cm^{-1}) [37]. The additional 3095 cm^{-1} band in the complex spectrum is probably related to an overtone or combination transition. In the Raman

spectrum of the complex, the above transitions are disturbed by luminescence, but are better seen in the corresponding spectrum of the HTAA ligand together with $\nu(CH_2)$ vibrations at 2962 and 2909 cm^{-1}. In the region below 2500 cm^{-1} this spectrum is strongly obscured by luminescence, and only the most intense transitions could be located there. These transitions mainly result from thiophene ring vibrations and appear at very similar wavenumbers as in the IR spectrum.

The most interesting transitions observed in the far-IR region are generated by stretching vibrations of copper–oxygen bonds. For copper(II) carboxylates of the structure with dimeric D_{4h} $[Cu_2O_8]$ units, two (Cu–O) ($A_{2u} + E_u$) vibrations are expected to be IR active. In the literature, those transitions were detected in the region between 300 and 400 cm^{-1} [38]. In the comparable area (420–260 cm^{-1}), the spectrum of the complex investigated here shows five mostly medium intensity bands (415, 385, 300, 285, 275 cm^{-1}) being candidates for the discussed vibrations. In the same range, the ligand shows three bands at 402, 306 and 275 cm^{-1}, which to some extent may be preserved in the spectrum of the complex. In order to distinguish the bands, which are related to the vibrations of the copper coordination sphere, the ^{63}Cu–^{65}Cu labelling technique was applied. This experiment demonstrated that bands at 415 and 385 cm^{-1} are the most sensitive (2.0 and 1.0 cm^{-1}, respectively) for isotope substitution and can be attributed to ν(Cu–O) modes, corresponding to the D_{4h} symmetry discussed before. However, as has been formerly concluded, the $[Cu_2O_8]$ unit shows small distortion from D_{4h} symmetry (the real symmetry is C_i) and more ν(Cu–O) vibrations can be IR active. Some of these modes contribute, together with bending ones, in seven other bands showing the isotope effects. As results from the X-ray data, each copper atom of the $[Cu_2O_8]$ unit forms an additional bond with one of the oxygen atoms of neighbouring unit. This bond is approximately 0.26 Å longer than those of the $[Cu_2O_8]$ unit and the energy of the corresponding vibration should be lower than in the recently presented ν(Cu–O) modes. The metal isotope substitution monitored for this vibration, the 149 cm^{-1} band, exhibited a 2.0 cm^{-1} shift.

In the discussed complex, the inversion center is located between the copper atoms, which causes in some symmetric vibrations the metal may be displaced and isotope effects can appear in the Raman spectrum. Such effects were generally not observed in the Raman scattering, except for a small shift of the 193 cm^{-1} band, but this does not exclude the contribution of copper–oxygen vibrations in particular Raman bands. Such assignment has been proposed in Table 3 for Raman bands not corresponding to 306 and 275 cm^{-1} ligand transitions. The intense band at 214 cm^{-1} could be compared with the IR, metal sensitive band at 222 cm^{-1}, but that band and those below 200 cm^{-1} may also result from lattice vibrations usually scattering strongly for molecular crystals.

4. Supplementary data

Crystallographic data for the structural analysis of the $[Cu_2(TAA)_4]_n$ complex have been deposited with the Cambridge Crystallographic Data Center, CCDC No. 229653. Copies of this information may be obtained free of charge from The Director, CCDC, 12 Union Road, Cambridge, CB2 1EZ, UK (fax: +44-1223-336033); e-mail: deposit@ccdc.cam.ac.uk or http://www.ccdc.cam.ac.uk.

References

[1] J.W. Pratt, in: Ullmann's Encyclopedia of Industrial Chemistry, vol. 36, Wiley-VCH Verlag GmbH & Co. KGaA, Weinheim, 2003, pp. 653–662, and references herein.
[2] K.O. Cameron, B.A. Lefker, R.L. Rosati, EP 911 (1999) 321.
[3] V.S. Fang, C. Minkin, P. Goldhaber, Science 172 (979) (1971) 163.
[4] R.C. Sharma, R. Nagar, Croat. Chem. Acta 61 (4) (1988) 849.
[5] P. Lumme, H. Elo, Inorg. Chim. Acta 92 (4) (1984) 241.
[6] V.M. Rao, D.N. Sathyanarayana, H. Manohar, J. Chem. Soc., Dalton Trans. (1983) 2167.
[7] G. Brown, R. Chidambaram, Acta Crystallogr., Sect. B 29 (1973) 2393.
[8] P. de Meester, S.R. Fletcher, A.C. Skapski, J. Chem. Soc., Dalton Trans. (1973) 2575.
[9] B. Paluchowska, J.K. Maurin, J. Leciejewicz, J. Coord. Chem. 51 (4) (1998) 335.
[10] F. Charbonnier, M. Petit-Ramel, R. Faure, H. Loiseleur, Rev. Chim. Miner. 21 (1984) 601.
[11] T. Fujita, S. Ohba, M. Nagamatsu, T. Tokii, C.F. Jury, O.W. Steward, Acta Crystallogr., Sect. C 49 (1993) 2095.
[12] M. Bukowska-Strzyżewska, Rocz. Chem. 40 (1966) 567.
[13] M.M. Borel, A. Leclaire, Acta Crystallogr., Sect. B 32 (1976) 1275.
[14] F. Hanic, D. Stempelova, K. Hanicova, Acta Crystallogr. 17 (1964) 633.
[15] G.A. Barclay, C.H.L. Kennard, J. Chem. Soc. (1961) 5244.
[16] H. Uekusa, S. Ohba, Y. Saito, M. Kato, T. Tokii, Y. Muto, Acta Crystallogr., Sect. C 45 (1989) 377.
[17] M.A. Bernard, M.M. Borel, F. Busnot, A. Leclaire, Rev. Chim. Miner. 16 (1979) 124.
[18] M.M. Borel, A. Leclaire, Acta Crystallogr., Sect. B 32 (1976) 3333.
[19] B. Morosin, R.C. Hughes, Acta Crystallogr., Sect. B 31 (1975) 762.
[20] M. Yamanaka, H. Uekusa, S. Ohba, Y. Saito, S. Iwata, M. Kato, T. Tokii, Y. Muto, O.W. Steward, Acta Crystallogr., Sect. B 47 (1991) 344.
[21] F. Pavelčik, F. Hanic, J. Mol. Struct. 8 (1978) 59.
[22] M.M. Borel, A. Busnot, A. Leclaire, J. Inorg. Nucl. Chem. 38 (1976) 1557.
[23] M.M. Borel, A. Leclaire, Acta Crystallogr., Sect. B 32 (1976) 1273.
[24] M.M. Borel, A. Busnot, A. Leclaire, J. Inorg. Nucl. Chem. 38 (1976) 235.
[25] D.B.W. Yawney, R.J. Doedens, Inorg. Chem. 9 (1970) 1626.
[26] Y.A. Simonov, V.I. Ivanov, A.V. Ablov, L.N. Milkova, T.I. Malinovsky, J. Struct. Chem. 17 (1976) 516 (Eng. Transl.).
[27] T.I. Tarkhova, A.V. Ablov, Kristallografiya 13 (1968) 611 (Eng. Transl.).
[28] Y.A. Simonov, T.I. Malinovsky, Kristallografiya 15 (1970) 370 (Eng. Transl.).

[29] M.J. Bird, T.R. Lomer, Acta Crystallogr., Sect. B 28 (1972) 242.
[30] G.M. Sheldrick, SHELXS97, Program for Solution of Crystal Structures, University of Göttingen, Göttingen, Germany, 1977.
[31] G.M. Sheldrick, SHELXL97, Program for Crystal Structures Refinement, University of Göttingen, Göttingen, Germany, 1977.
[32] M. Nardelli, J. Appl. Cryst. 28 (1995) 659.
[33] L.J. Farrugia, J. Appl. Cryst. 30 (1997) 565.
[34] D.R. Lide (Ed.), Handbook of Chemistry and Physics, 75th ed., CRC Press, Boca Raton, FL, 1994, Sec. 9, p. 9.
[35] M.S.C. Flett, J. Chem. Soc. (1951) 962.
[36] L.J. Bellamy, The Infrared Spectra of Complex Molecules, Chapman & Hall, London, 1975, pp. 183–200.
[37] J.S. Kwiatkowski, J. Leszczyński, I. Teca, J. Mol. Struct. 436 (1997) 451, and references herein.
[38] A.B.P. Lever, B.S. Ramaswamy, Can. J. Chem. 51 (1973) 514.

Available online at www.sciencedirect.com
SCIENCE DIRECT®
Polyhedron 23 (2004) 1793–1797
POLYHEDRON
www.elsevier.com/locate/poly

Complexation of uranium(VI) with glycerol 1-phosphate

Astrid Koban *, Gert Bernhard

Institute of Radiochemistry, Forschungszentrum Rossendorf e.V., P.O. Box 510119, D-01314 Dresden, Germany

Received 16 December 2003; accepted 13 April 2004
Available online 1 June 2004

Abstract

The complex formation of uranium(VI) with glycerol 1-phosphate was determined by potentiometric titration, and TRLFS spectroscopy. Two complexes with a metal-to-ligand stoichiometry of 1:1 and 1:2 were found by potentiometry in the pH range 3–8, and the stability constants were calculated for $I = 0.1$ M ($NaClO_4$) and $T = 25$ °C to be $\log \beta_{11} = 6.23 \pm 0.09$ for $UO_2(C_3H_7O_3PO_3)$ and $\log \beta_{12} = 10.22 \pm 0.13$ for $UO_2(C_3H_7O_3PO_3)_2^{2-}$.

The TRLFS spectra at pH = 4 show an increase of the fluorescence intensity, connected with a red shift of the emission spectra. But contrary to the potentiometric measurements only the 1:1 complex $UO_2(C_3H_7O_3PO_3)$ could be detected under the specific experimental conditions. The main fluorescence emission bands and the lifetime of this complex were determined. The complex stability constant at $I = 0.1$ M ($NaClO_4$) and $T = 25$ °C was calculated to be $\log \beta_{11} = 6.15 \pm 0.05$.
© 2004 Elsevier Ltd. All rights reserved.

Keywords: Uranium; Glycerol phosphate; Complex formation; Potentiometric titration; TRLFS

1. Introduction

Interactions of metal ions with phosphate esters play an important role in many biological processes. Glycerol 1-phosphate is widely distributed in biological systems, as constituent of phospholipids or as intermediate of metabolism or other biochemical processes like the biosynthesis of lecithin's [1]. Because of its simple and clear structure glycerol 1-phosphate can serve as model for the interaction of cations with more complex biological systems, such as phospholipids.

The understanding of the interaction of radioactive metals with biological systems on the molecular level is of great importance in view of the distribution of radioactive elements via the food chain from sources like nuclear waste disposal. There are very few data about the interactions of uranyl(VI) with bioligands in the literature. Only a couple of studies concerning the complex behavior with some amino acids [2] and nucleosides [3] are to be find. Several investigations of bio-systems like microorganisms and plants with various analytical and spectroscopic methods show that the phosphate group seems to be quite effective for uranium binding [4–7]. The complex behavior of uranium with inorganic phosphates and some organic phosphate esters was examined by different methods and some complex stability constants and spectroscopic data are well known [8–11]. However, except for the complexation of uranyl(VI) with various sugar phosphates [12,13], no investigations of the complex behavior of uranium with biorelevant organic phosphate esters have been published up to now. Therefore, we present the results of uranyl(VI) complexation with glycerol 1-phosphate ($C_3H_7O_3PO_3^{2-}$), studied by potentiometric titration, and time-resolved laser-induced fluorescence spectroscopy (TRLFS). The spectroscopic characterization of the system is the major task of our studies to get useful data sets for comparison with biological systems to understand the binding behavior of actinides in natural systems. Beside this equilibrium constants were determined to enlarge the basis for modeling the transport and binding mechanisms of actinides in bio-systems.

* Corresponding author. Tel.: +49-351-260-2076; fax: +49-351-260-3553.
E-mail address: a.koban@fz-rossendorf.de (A. Koban).

0277-5387/$ - see front matter © 2004 Elsevier Ltd. All rights reserved.
doi:10.1016/j.poly.2004.04.022

2. Experimental

2.1. Solutions and reagents

Glycerol 1-phosphate disodium salt hexahydrate was purchased from Fluka (analytical grade), the ligand stock solutions were prepared freshly for each experiment. The stock solutions of UO_2^{2+} were made from $UO_2(NO_3)_2 \cdot 6H_2O$ (Merck, p.A.). The ionic strength was kept constant by adding a $NaClO_4$ stock solution ($NaClO_4 \cdot H_2O$, Merck, p.A.). All stock solutions were prepared with deionized water. Necessary pH adjustments were made with $HClO_4$ or NaOH.

2.2. Potentiometric titration

The potentiometric titration experiments were carried out at a starting volume of 50 ml with two different uranyl concentrations (1×10^{-4} and 5×10^{-4} M) and glycerol 1-phosphate concentrations (5×10^{-4} M and 10^{-3} M) each. The corresponding glycerol 1-phosphoric acid was performed in situ by adding appropriate equimolar ratios of $HClO_4$ to the starting solution. The ionic strength was kept constant at 0.1 M ($NaClO_4$). All solutions were prepared with carbonate free deionized water under nitrogen atmosphere in a glove box. The samples were titrated in a thermostatic vessel at 25.0 ± 0.1 °C under nitrogen atmosphere in a pH range from 3 to 8 with 0.01 M NaOH (carbonate free, Merck, Titrisol) by an automatic titrator (GP Titrino 736, Metrohm, Germany) and monitored by the accompanying software (TiNet 2.2). The pH values were measured with a Schott BlueLine 11 pH combination electrode with a platinum diaphragm, the electrode was calibrated for each experimental run with NBS buffers at pH 4.01 and 6.87 (Schott). A detailed description of the titration procedure is given in [12].

Five measurements for determination of the dissociation constants of the ligand and 12 measurements for determination of the complex stability constants were accomplished. The measured titration data were analyzed with the Hyperquad least squares program, version 2.1 [14].

2.3. TRLFS measurements

The TRLFS measurements were performed at a total uranyl concentration of 10^{-5} M as a function of the ligand concentration at $pH = 4.00 \pm 0.05$. The spectra were recorded at 25 ± 2 °C using a pulsed Nd:YAG laser system (Spectron Laser Systems, SLM 400, Rugby, UK). The excitation wavelength of the uranyl fluorescence was 266 nm with a pulse energy of 0.2–0.5 mJ. The TRLFS spectra were measured from 450 to 600 nm, averaging six spectra with 100 laser pulses each and a gate time of 1 μs. The time-resolved fluorescence emission was detected using a 270 mm spectrometer (Spex 270M, Jobin–Yvon) in combination with a ICCD camera (Spectrum One, Jobin–Yvon). All functions of the laser spectrometer are computer controlled, the control software was provided from Jobin–Yvon. A detailed description of the TRLFS system is given in [15].

3. Results and discussion

3.1. Potentiometric titration

For studying the complexation behavior of glycerol 1-phosphate with uranyl(VI), it is necessary to know the acid dissociation constants of the ligand. Some data are available in the literature [10,16–21], but they differ both in values and experimental conditions. However, due to the self consistency, we determined our own pK_a values (see Table 1). Our measured value of $pK_{a1} = 2.26 \pm 0.14$ is very closed to those of André et al. [18] ($pK_{a1} = 2.28$). Other values (i.e., $pK_{a1} = 1.30$ [21]) and some values of pK_{a2} (i.e., 6.07 [16], 6.11 [17], 6.22 [18], 6.66 [20]) are more or less far away from our results ($pK_{a2} = 6.57 \pm 0.03$), but this is probably due to different definition of the constant and different experimental conditions and measuring methods.

The complexation of uranium(VI) with glycerol 1-phosphate was studied in the pH range from 3 to 8 for the general complex equilibrium

$$xUO_2^{2+} + yC_3H_7O_3PO_3^{2-} + zH^+ \rightleftharpoons (UO_2)_x(C_3H_7O_3PO_3)_yH_z^{(2x-2y+z)+} \quad (1)$$

The highest pH value we could study was limited by hydrolysis of uranium(VI); the higher the uranium concentration the lower the useable pH value. The titration measurements with the highest uranium and ligand concentration (5×10^{-4} M U(VI), 1×10^{-3} M glycerol 1-phosphate) could only be analyzed up to $pH = 4.75$.

Table 1
Summarized formation constants of the uranyl(VI) glycerol 1-phosphate system at $T = 25$ °C, $I = 0.1$ M ($NaClO_4$); $\beta_{xyz} = [(UO_2)_x(C_3H_7O_3PO_3)_yH_z]/[UO_2]^x[C_3H_7O_3PO_3]^y[H]^z$

Species	xyz	$\log \beta_{xyz}$[a]	Method
$C_3H_7O_3PO_3H^-$	011	6.57 ± 0.03[b]	Potentiometry
$C_3H_7O_3PO_3H_2$	012	8.83 ± 0.17[c]	
$UO_2(C_3H_7O_3PO_3)$	110	6.23 ± 0.09	Potentiometry
		6.15 ± 0.05	TRLFS
$UO_2(C_3H_7O_3PO_3)_2^{2-}$	120	10.22 ± 0.13	Potentiometry

[a] Errors are equal to 2σ.
[b] $\log \beta_{11} = pK_{a2}$.
[c] $\log \beta_{12} = pK_{a1} + pK_{a2}$.

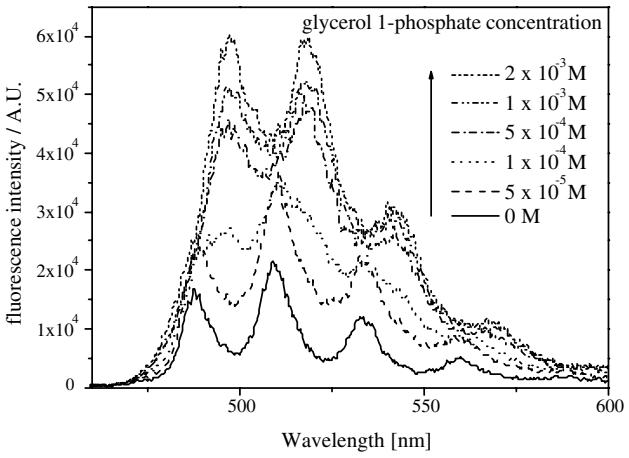

Fig. 1. TRLFS spectra of uranium(VI) (10^{-5} M) as a function of the glycerol 1-phosphate concentration at pH = 4.

Because all potentiometric titration experiments were carried out under CO_2 free and carbonate free conditions (cf. Section 2.2), the formation of uranyl carbonate complexes can be excluded. The appropriate uranyl hydroxides [10,11] were accounted for in all the refinements.

Two complexes with a metal-to-ligand ratio (M:L) of 1:1 and 1:2 could be observed. The equilibrium constants were determined to be $\log\beta_{11} = 6.23 \pm 0.09$ for $UO_2(C_3H_7O_3PO_3)$ and $\log\beta_{12} = 10.22 \pm 0.13$ for $UO_2(C_3H_7O_3PO_3)_2^{2-}$ (see Table 1). Besides at almost all titration curves any other complexes with a 1:3 or 2:3 stoichiometry or protonated species could be fitted to improve the fit parameter. Thus still more species seems to exist in this system. Further investigations are necessary to validate this presumption.

3.2. TRLFS measurements

Fig. 1 shows the fluorescence spectra of uranium(VI) as a function of the concentration of glycerol 1-phosphate at pH = 4. With increasing ligand concentration we notice a strong increase in fluorescence intensity, connected with a red shift of about 9 nm compared to the uranyl ion.

The TRLFS spectra show tri-exponential decays indicating a mixture of three species. The lifetimes are (averaged about all measurements) 155 ± 30, 800 ± 160 ns, and 7 ± 3 μs. The lifetime of 7 μs with a very low but constant intensity can be assigned to uranyl hydroxide, which is always present in small amounts under such experimental conditions. The intensity of the second lifetime (800 ± 160 ns) decreases with increasing ligand concentration, whereas the intensity of the shortest lifetime (155 ± 30 ns) increases. A lifetime of 800 ± 160 ns seems to be quite short for UO_2^{2+}(aq), but test solutions of UO_2^{2+}(aq) at pH = 4 and 1 under same conditions showed lifetimes of 761 ± 46 ns (pH = 4) and 784 ± 31 ns (pH = 1), respectively. Therefore we assign the lifetime of 800 ± 160 ns to the free uranyl ion and the lifetime of 155 ± 30 ns to the uranyl(VI) glycerol 1-phosphate complex.

To estimate the stoichiometry of this complex the series of measurements was investigated according to the complex formation reaction

$$UO_2^{2+} + nC_3H_7O_3PO_3H_2 \rightleftharpoons UO_2(C_3H_7O_3PO_3)_n^{(2-2n)+} + 2nH^+ + \log\beta_{1n}^* \quad (2)$$

A slope analysis for reaction (2) was made using the mass action law in its transformed linear form (Eq. (3))

$$\log\frac{[\text{complex}]}{[UO_2^{2+}]_{\text{free}}} = n\log[\text{ligand}]_{\text{free}} + \log\beta_{1n}^* + 2n\text{pH}. \quad (3)$$

The concentrations of the free uranyl ion were determined on the basis of the measured absorption spectra using conventional peak deconvolution. These data were used to calculate the corresponding concentrations of the complex and the non complexed ligand. This well established method for analyzing fluorescence spectra [22] is described detailed in [12]. The slope of 1.24 ± 0.04 indicates a predominant formation of the 1:1 complex $UO_2(C_3H_7O_3PO_3)$. Taking into account the dissociation of glycerol 1-phosphoric acid, the complexation reaction can be written as follows:

Table 2
Fluorescence emission bands of some uranyl compounds and uranium complexes in biosystems

	Fluorescence emission bands (nm)						References
U(VI) model compounds							
UO_2^{2+} (aq)	471.3	488.9	510.5	533.9	559.4	585.5	[15]
UO_2 (glycerol 1-phosphate)		497.2(1)	518.4(1)	542.9(3)	569.0(1)	599.1(7)	This work
UO_2 (fructose 6-phosphate)	478.9	497.1	519.0	543.3	568.9	598	[13]
Bacteria							
Thiobacillus ferrooxidans		494–495	515–517	537–540	566–568		[23]
Bacillus sphaericus		496–501	518–524	538–546	565–571		[4]
Acidithiobacillus ferrooxidans		495–496	517–518	541–542	566		[7]
Plants							
Lupines		499–504	519–526	541–549	563–573		[6]

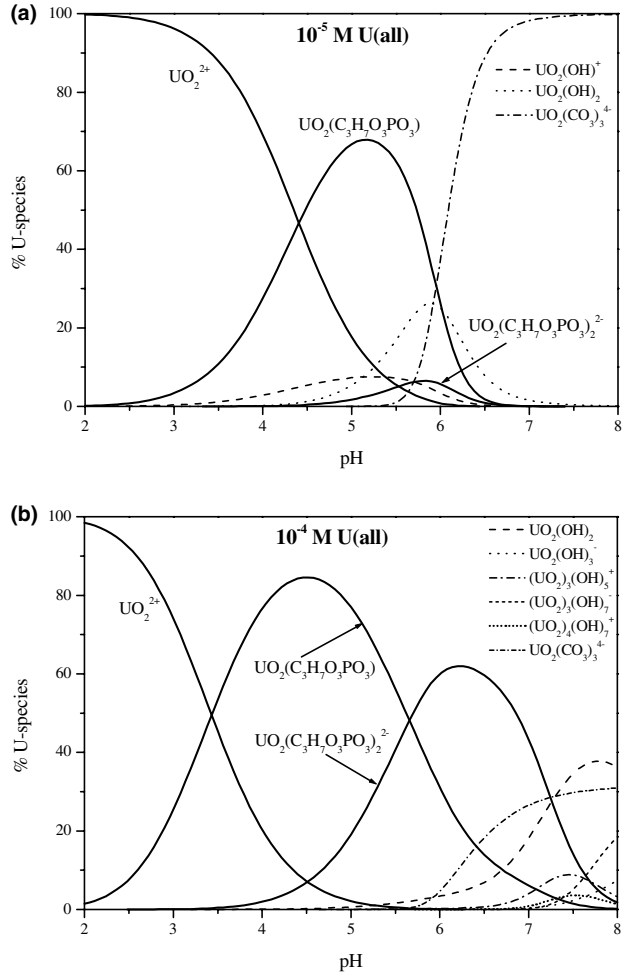

Fig. 2. Speciation of uranium(VI) in aqueous solution in dependence of the uranium and glycerol 1-phosphate concentration (10^{-4} M carbonate each): (a) 10^{-5} M U(VI), 10^{-4} M glycerol 1-phosphate; (b) 10^{-4} M U(VI), 10^{-3} M glycerol 1-phosphate. Only species $\geqslant 1\%$ were included.

$$UO_2^{2+} + C_3H_7O_3PO_3^{2-} \rightleftharpoons UO_2(C_3H_7O_3PO_3) + \log\beta_{11} \quad (4)$$

with consideration of the pH and pK_a values (from potentiometric titration, see Table 1) the complex stability constant of $UO_2(C_3H_7O_3PO_3)$ results to be $\log\beta_{11} = 6.15 \pm 0.05$.

The spectra of the uranyl glycerol 1-phosphate complex can be isolated from the composite spectra using conventional peak deconvolution. The peak maxima of the complexed uranyl species are located at 497, 518, 543, 569, and 599 nm (see Table 2). It was not possible to detect any other uranyl glycerol 1-phosphate species. Under that for TRLFS measurements optimal experimental conditions (low uranium(VI) concentrations at about 10^{-5} M and pH values up to 4), where the uranyl hydroxide species do not disturb the measurements, other complexes do not form or only in so small ratios, that they cannot be isolated from the spectra for characterization (see for example Fig. 2(a)).

4. Conclusions

The combination of potentiometric and spectroscopic methods for the investigation of the complex behavior between uranium(VI) and glycerol 1-phosphate results in a detailed characterization of this system over a wide pH and concentration range. Two different complexes, the complexes with a metal-to-ligand ratio of 1:1 and 1:2, could be detected with potentiometric titration. This method is used however with relatively high uranium concentration ratios ($1–5 \times 10^{-4}$ M). TRLFS is applied at lower uranium concentrations (10^{-5} M), which comes the biological situation more near. Under that experimental conditions only the 1:1 complex could be found and characterized. These results are in accordance with the findings made by the complexation of uranium(VI) with several sugar phosphates [12,13].

Potentiometric measurements indicate the existence of further complexes in this system. To validate this presumption UV–Vis and EXAFS measurements were done at higher uranium concentrations (10^{-3} M). But in this concentration ranges no reasonable investigations of this complex system were possible, because the solutions are only short time stable, even under cooling. Decomposition and precipitation occurs rapidly. Further investigations are necessary to identify the precipitate and to understand this complex system completely.

To estimate the relevance of the characterized complexes in bio-systems with alternating conditions concerning, for instance, the concentration of CO_2, pH value, ionic composition and ionic concentrations, Fig. 2 shows two examples of the speciation of uranium(VI) in an aqueous solution with tenfold excess of glycerol 1-phosphate and 10^{-4} M carbonate each. The speciation was done with the program Species 1.2 (Academic Software). The following uranyl species were used to obtain the speciation (additionally to the glycerol phosphates): $UO_2(OH)^+$ ($\log\beta_{11(I=0.1)} = -5.385$), $UO_2(OH)_2$ ($\log\beta_{12(I=0.1)} = -10.517$), $UO_2(OH)_3^-$ ($\log\beta_{13(I=0.1)} = -19.201$), $UO_2(OH)_4^{2-}$ ($\log\beta_{14(I=0.1)} = -32.578$), $(UO_2)_2(OH)^{3+}$ ($\log\beta_{21(I=0.1)} = -2.487$), $(UO_2)_2(OH)_2^{2+}$ ($\log\beta_{22(I=0.1)} = -5.838$), $(UO_2)_3(OH)_4^{2+}$ ($\log\beta_{34(I=0.1)} = -12.357$), $(UO_2)_3(OH)_5^+$ ($\log\beta_{35(I=0.1)} = -16.2$), $(UO_2)_3(OH)_7^-$ ($\log\beta_{37(I=0.1)} = -31.438$), $(UO_2)_4(OH)_7^{2+}$ ($\log\beta_{47(I=0.1)} = -22.767$), UO_2CO_3 ($\log\beta_{11(I=0.1)} = 7.22$), $UO_2(CO_3)_2^{2-}$ ($\log\beta_{12(I=0.1)} = 16.0$), $UO_2(CO_3)_3^{4-}$ ($\log\beta_{13(I=0.1)} = 26.5$), $(UO_2)_3(CO_3)_6^{6-}$ ($\log\beta_{36(I=0.1)} = 42.25$), $(UO_2)_2CO_3(OH)_3^-$ ($\log\beta_{213(I=0.1)} = -17.75$), $(UO_2)_3CO_3(OH)_5^-$ ($\log\beta_{315(I=0.1)} = -16.46$) [10,11]. The uranyl glycerol 1-phosphate complexes dominate over a wide uranium concentration and pH range, which

underlines the importance of this type of ligands for the complexation of heavy metals in biological systems. The formation of mixed uranyl carbonate glycerol phosphate complexes were not included in the model because there are no data available for these complexes (cf. capture 3.1).

The characteristic main emission bands received at TRLFS measurements can be used for comparison with biological samples, in order to be able to interpret the binding properties. Table 2 summarizes TRLFS data of some investigated model compounds and uranium-contaminated biosystems [4,6,7,13,15,23]. The similarity of the main emission bands with the glycerol 1-phosphate system and other organic phosphate esters substantiates the former experiences, that to organic structures bound phosphate groups dominate the uranium binding in biosystems [4–7].

References

[1] P. Nuhn, Naturstoffchemie, S. Hirzel Verlag, Stuttgart, 1997.
[2] V.V. Ramanujam, K. Rengaraj, Ind. J. Chem. A 19 (1980) 382.
[3] K. Ramalingam, C.R. Krishnamoorthy, Inorg. Chim. Acta 67 (1982) 167.
[4] P.J. Panak, J. Raff, S. Selenska-Pobell, G. Geipel, G. Bernhard, H. Nitsche, Radiochim. Acta 88 (2000) 71.
[5] C. Hennig, P.J. Panak, T. Reich, A. Roßberg, J. Raff, S. Selenska-Pobell, W. Matz, J.J. Bucher, G. Bernhard, H. Nitsche, Radiochim. Acta 89 (2001) 625.
[6] A. Günther, G. Bernhard, G. Geipel, T. Reich, A. Roßberg, H. Nitsche, Radiochim. Acta 91 (2003) 319.
[7] L.M. Merroun, G. Geipel, R. Nicolai, K.-H. Heise, S. Selenska-Pobell, BioMetals 16 (2003) 331.
[8] L.W. Kobets, E.N. Bouchikhin, R.N. Klitschewitsch, G.F. Beljatschis, Koord. Khim. 9 (1983) 103.
[9] V. Brendler, G. Geipel, G. Bernhard, H. Nitsche, Radiochim. Acta 74 (1996) 75.
[10] A.E. Martell, R.M. Smith, J.M. Ramunas, NIST Critically Selected Stability constants of Metal Complexes Database, Version 5.0, 1998.
[11] H. Wanner, J. Forest (Eds.), Chemical Thermodynamics of Uranium, North-Holland, Amsterdam, 1992.
[12] A. Koban, G. Geipel, G. Bernhard, Radiochim. Acta 91 (2003) 393.
[13] A. Koban, G. Geipel, A. Roßberg, G. Bernhard, Radiochim. Acta, (accepted).
[14] P. Gans, A. Sabatini, A. Vacca, Talanta 43 (1996) 1739.
[15] G. Geipel, A. Brachmann, V. Brendler, G. Bernhard, H. Nitsche, Radiochim. Acta 75 (1996) 199.
[16] G. Schwarzenbach, G. Anderegg, Helv. Chim. Acta 40 (1957) 1229.
[17] U. Kramer-Schnabel, P.W. Linder, J. Coord. Chem. 22 (1990) 139.
[18] J.P.R.F. André, H.D. Burrows, C.F.G.C. Geraldes, M.d.G.M. Miguel, M.H.S.F. Teixera, Polyhedron 15 (24) (1996) 4331.
[19] G. Liang, D. Chen, M. Bastian, H. Sigel, J. Am. Chem. Soc. 114 (1992) 7780.
[20] S.P. Datta, A.K. Grzybowski, Biochem. J. 69 (1958) 218.
[21] J.H. Ashby, E.M. Crook, S.P. Datta, Biochem. J. 56 (1954) 198.
[22] A. Brachmann, G. Geipel, G. Bernhard, H. Nitsche, Radiochim. Acta 90 (2002) 147.
[23] P.J. Panak, S. Selenska-Pobell, S. Kutschke, G. Geipel, G. Bernhard, H. Nitsche, Radiochim. Acta 84 (1999) 183.

Available online at www.sciencedirect.com
SCIENCE DIRECT®
Polyhedron 23 (2004) 1799–1804
POLYHEDRON
www.elsevier.com/locate/poly

Four novel sulfur-rich complexes: syntheses, crystal structures of three nickel(II) and one cobalt(II) complex with derivatives of Lawesson's Reagent ☆

Hong-Lei Liu, Hong-Yan Mao, Chen Xu, Hong-Yun Zhang *, Hong-Wei Hou, Qing-an Wu, Yu Zhu, Bao-Xian Ye, Li-Jie Yuan

Department of Chemistry, Zhengzhou University, Da Xue Road, Zhengzhou 450052, PR China

Received 8 January 2004; accepted 13 April 2004
Available online 4 May 2004

Abstract

The reaction of 2,4-bis(4-methoxyphenyl)-1,3,2,4-dithiadiphosphetane-2,4-disulfide (Lawesson's Reagent, LR) with $NiCl_2$ or $Co(CH_3COO)_2$ in methanol or ethanol gives novel sulfur-rich complexes: $C_{16}H_{20}NiO_4P_2S_4$ (**1**), $C_{18}H_{24}NiO_4P_2S_4$ (**2**) and $C_{24}H_{30}CoO_6P_3S_6$ (**4**). With the presence of ethylenediamine under the same conditions, complex $C_{24}H_{48}N_6NiO_4P_2S_4$ (**3**) is also obtained. These four novel sulfur-rich complexes were characterized by IR and X-ray crystallography, which indicate that the solvent can influence the crystal structure of complexes in the reaction between LR and metal.
© 2004 Published by Elsevier Ltd.

Keywords: Lawesson's Reagent; Thiophosphoryl compound; Sulfur-rich complex; Nickel(II) complex; Cobalt(II) complex

1. Introduction

There is much literature that reports that 2,4-bis(4-methoxyphenyl)-1,3,2,4-dithiadiphosphetane-2,4-disulfide (Lawesson's Reagent, LR, see Scheme 1) is a most effective thiation reagent for ketones, carboxamides, esters, *S*-substituted thioesters and a variety of other compounds [1–4]. LR can also participate in the preparation of many thiophosphoryl complexes [5,6]. It has been reported by Shabana and Atrees [7] and Fahmy [8] that thiophosphoryl compounds are of potential interest as fungicides, insecticide and herbicides. In order to study the influence of the thiophosphoryl metal on their biological activity, research of the syntheses and crystal structures of these thiophosphoryl metal compounds has an important role.

It has been reported that the P–S bonds in LR can easily be cleaved to offer $MeOC_6H_4PS_2$ as a ligand [9]. We found that LR can decompose into an alcohol derivative when heated in alcohol solvent (see Scheme 2).

Although a great deal of work has been reported [10–12] on thiophosphoryl compounds, these four complexes have not been reported before. We studied the syntheses and crystal structures of some metal complexes with $MeOC_6H_4P(OR)S_2$ ($R = CH_3-$ or C_2H_5-) using the direct reaction of LR with transition metal salts. In this paper, the syntheses and crystal structures of three nickel(II) and one cobalt(II) complex are reported.

2. Experimental

2.1. Materials and physical measurements

All chemicals except Lawesson's Reagent were of reagent analytical grade, purchased from Zhengzhou

☆ Supplementary data associated with this article can be found, in the online version, at doi:10.1016/j.poly.2004.04.008.

* Corresponding author. Tel.: +86-371-7763675; fax: +86-371-7761744.
E-mail address: wzhy917@zzu.edu.cn (H.-Y. Zhang).

0277-5387/$ - see front matter © 2004 Published by Elsevier Ltd.
doi:10.1016/j.poly.2004.04.008

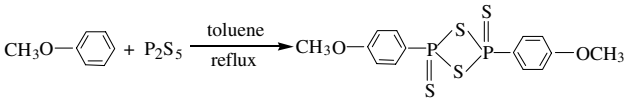

Scheme 1. Lawesson Reagent.

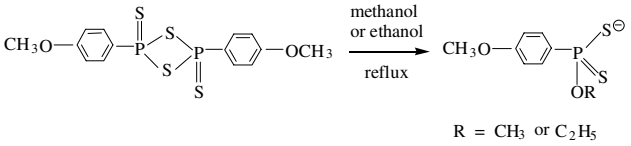

Scheme 2. The thermal decomposition reaction of Lawesson's Reagent in alcohol solvent.

Chemical Reagent Company and were used without any purification. Lawesson's Reagent ($R = p$-$MeOC_6H_4$) was prepared as described in the literature [13]. The single crystal structures were measured on a Rigaku-Raxis-IV X-ray diffractometer and IR spectra were recorded on a FTS-40 infrared spectrophotometer as KBr pellets in the range 4000–400 cm^{-1}.

2.2. Preparation of complexes *1*, *2*, *3* and *4*

Complex ***1***. 5 ml of 0.02 M solution of LR in methanol and 5 ml of 0.02 M solution of $NiCl_2$ in methanol were put into sealed vials, respectively, which were connected via a thin tube full of anhydrous ethanol. Purple crystals of complex **1** suitable for X-ray analysis were obtained in about three days.

Complex ***2***. With the same method mentioned above, purple crystals of complex **2** suitable for X-ray analysis were got using the mixed solution of ethanol and DMF (1:1, v/v).

Complex ***3***. 3.0 ml (0.04 mol) of ethylenediamine and 8.10 g (0.02 mol) of LR were refluxed in 180 ml anhydrous toluene at 110 °C with stirring for about 6 h. After cooling to room temperature, insoluble materials were filtered off. Then the reaction mixture was concentrated to about 20 ml with a vacuum rotary evaporator. This 20 ml oil liquid was diluted with 80 ml methanol, and 5 ml of the diluted solution and 5ml methanol solution of $NiCl_2$ (0.2 mmol) were mixed and run into a small vial and allowed to evaporate slowly at room temperature. Filtered, washed with anhydrous ethanol and dried naturally, pink crystals of **3** suitable for single-crystal X-ray diffraction analyses were obtained in about two weeks.

Complex ***4***. Complex **4** can be obtained by the method used in the preparation of complex **1**. 5 ml of 0.02 M solution of LR in methanol and 5 ml of 0.02 M solution of $Co(CH_3COO)_2 \cdot 4H_2O$ in methanol were put into sealed vials, respectively, which were connected via a thin tube full of anhydrous ethanol. Red crystals of **4** suitable for X-ray analysis were obtained in about three days.

2.3. X-ray crystallography

Intensity data of these complexes were measured with a Rigaku-Raxis-IV X-ray diffractometer using mono-

Table 1
Crystallographic data and structure refinement for complexes **1**, **2**, **3** and **4**

	Complex **1**	Complex **2**	Complex **3**	Complex **4**
Formula	$C_{16}H_{20}NiO_4P_2S_4$	$C_{18}H_{24}NiO_4P_2S_4$	$C_{24}H_{48}N_6NiO_4P_2S_4$	$C_{24}H_{30}CoO_6P_3S_6$
T (K)	291(2)	291(2)	291(2)	291(2)
Molecular weight	525.21	553.26	733.57	758.68
Crystal system	monoclinic	triclinic	monoclinic	monoclinic
Space group	$P2_1/c$	$P_{\bar{1}}$	$P2_1/c$	$P2_1/n$
a (Å)	11.974(2) A	6.5023(13)	15.364(3)	9.0075(18)
b (Å)	6.6343(13) A	7.6448(15)	18.929(4)	16.076(3)
c (Å)	14.750(3) A	13.109(3)	12.459(3)	23.034(5)
α (°)	90	99.37(3)	90	90
β (°)	109.69(3)	99.72(3)	94.76(3)	98.11(3)
γ (°)	90	104.09(3)	90	90
V (Å^3)	1103.3(4)	608.6(2)	3610.8(13)	3302.1(11)
D_{calc} (Mg m^{-3})	1.581	1.509	1.349	1.526
Z	2	1	4	4
Absorption coefficient (mm^{-1})	1.422	1.293	0.894	1.081
Reflections collected/unique (R_{int})	3234/1958 (0.0697)	1598/1598 (0.0000)	7464/4408 (0.0455)	8216/4758 (0.0591)
Data/restraints/parameters	1958/0/125	1598/8/134	4408/0/419	4758/0/362
R[a]	0.0417	0.0737	0.0382	0.0454
R_w[b]	0.0867	0.2060	0.0796	0.1133
Goodness-of-fit on F^2	0.970	1.122	0.897	0.987
$\Delta\rho_{max}$ and $\Delta\rho_{min}$ (e Å^{-3})	0.310 and −0.336	1.097 and −0.696	0.372 and −0.215	0.423 and −0.482

[a] $R = \sum ||F_o| - |F_c|| / \sum |F_o|$.
[b] $R_w = [\sum (||F_o| - |F_c||)^2 / \sum w|F_o|^2]^{1/2}$.

chromated Mo Kα ($\lambda = 0.71073$ Å) radiation. Raw data were corrected and the structures were solved using the SHELXL-97 program. Non-hydrogen atoms were located by direct phase determination and subjected to anisotropic refinement. The full-matrix least-squares calculation on F^2 was applied on the final refinement. Details of the crystal structure determination are summarized in Table 1. Full atomic data are available as a file in CIF format.

The IR spectra of the four complexes contain the expected bands due to the C_6H_4OMe groups. LR has two bands at 1267(s) and 1293(m) cm^{-1} due to ν_{as}(C–O–C) and a band at 2837(w) cm^{-1} of $\nu_s(CH_3)$. All these bands can be observed in complexes **1**–**4**. In the IR spectra of complex **1**, there are bands present at 1004(s), 1010(s), 1025(m) 829(w), 792(s), 666(m) and 644(m) cm^{-1} for ν_s(P–S). In that of complex **4**, the bands at 1025(m), 789(s) and 663(m) are for ν_s(P–S). All these are consistent with the literature [12]. As far as the IR spectra of the complex **3** is concerned, the bands at 3280(s) cm^{-1} for $\nu_{as}(NH_2)$, 2975(w) cm^{-1} for $\nu_{as}(CH_2)$, and 1028(vs) cm^{-1} for ν_s(CN) are also consistent with the literature [14] (s, strong; m, medium; w, weak; vs, very strong).

3. Results and discussion

3.1. The possible reaction mechanism of LR with transition metals

When Lawesson's Reagent and transition metals react in alcohol solvent the four above-mentioned complexes were obtained. The possible reaction mechanism, as shown in Scheme 3, may have one self-coordinating catalyst course. The sulfur atoms of the LR molecule have a strong coordinating tendency with the metal ion and the P–S bond of LR may easily be cleaved [9]. When Lawesson's Reagent was heated in alcohol solvent with transition metals, the fragment $CH_3OC_6H_4PS_2$, cleaved from LR, was produced and some alcohol molecules (such as methanol) were deprotonated in order to keep the phosphorus atoms with a five valence state. Finally, the fragments $CH_3OC_6H_4PS_2$ connect with a deprotonated alcohol molecule and coordinate to the metal ion. Therefore, the four title complexes (as shown in Scheme 3) are formed.

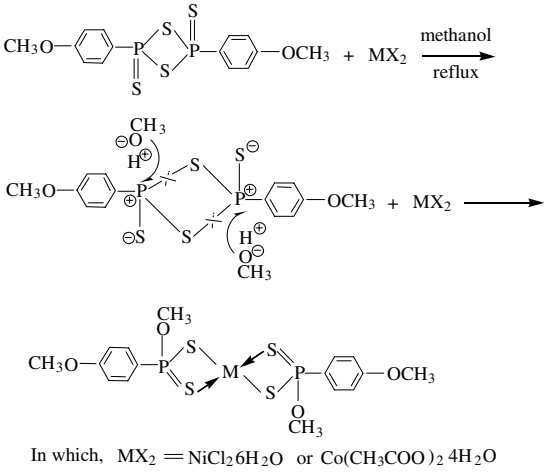

Scheme 3. The possible reaction mechanism of LR with transition metals.

3.2. The crystal structure description of complexes *1*, *2*, *3* and *4*

Crystallographic data and structure refinement for complexes **1**–**4** are given in Table 1. For complex **1**, it can be seen from Fig. 1 that the structural unit contains a crystallographic center of symmetry at the center of the four-member rings, and is therefore planar. Four sulfur atoms from two $MeOC_6H_4P(OCH_3)S_2$ ligands describe a parallelogram environment around the nickel atom, as is shown in these angles: S2AA–Ni1A–S2A = 180°, S1A–Ni1A–S1AA = 180° and S2AA–Ni1AA–S1A = 91.25°. Selected bond distances and angles for complex **1** are shown in Table 2. The two benzene rings of a certain crystal unit are parallel. The triangle P1A–S1A–S2A and another P1AA–S1AA–S2AA in the same unit lie *trans*-parallel along the central four-member ring S1A–S2A–S2AA–S1AA plane, and the dihedral angle is 19.2°.

From Figs. 1 and 2, it can be found that the molecular structure of complex **2** is similar to that of complex **1**. The only difference lies in the fact that the OCH_3 in complex **1** is replaced by OC_2H_5 in complex **2**. The nickel–sulfur bond lengths in complex **2** {2.2257(17) Å for Ni1A–S1AA and Ni1A–S1A; 2.2237(17) Å for Ni1A–S2AA and Ni1A–S2A} are a little shorter than those of complex **1** {2.2307(13) Å for Ni1A–S2AA and Ni1A–S2A; 2.2426(13) Å for Ni1A–S1AA and Ni1A–S1A}. Selected bond distances and angles for complex **2** are shown in Table 3.

As for complex **3**, it is in fact the complex $Ni(II)(en)_3^{2+}$ (en = ethylenediamine). The $MeOC_6H_4P(C_2H_5O)S_2$ can be seen as a substituted thiophosphate group which exists in the crystal structure as an electron-balancing anion. It can be seen from Fig. 3 that for every nickel(II), such as Ni1, three ethylenediamines offer four nitrogen atoms N1, N2, N4 and N5, existing in the equatorial geometry and forming a parallelogram, with the other two nitrogen atoms N3 and N6 from two ethylenediamines occupying the axial sites. So the Ni(II) ion is six-coordinated, in the center of a distorted

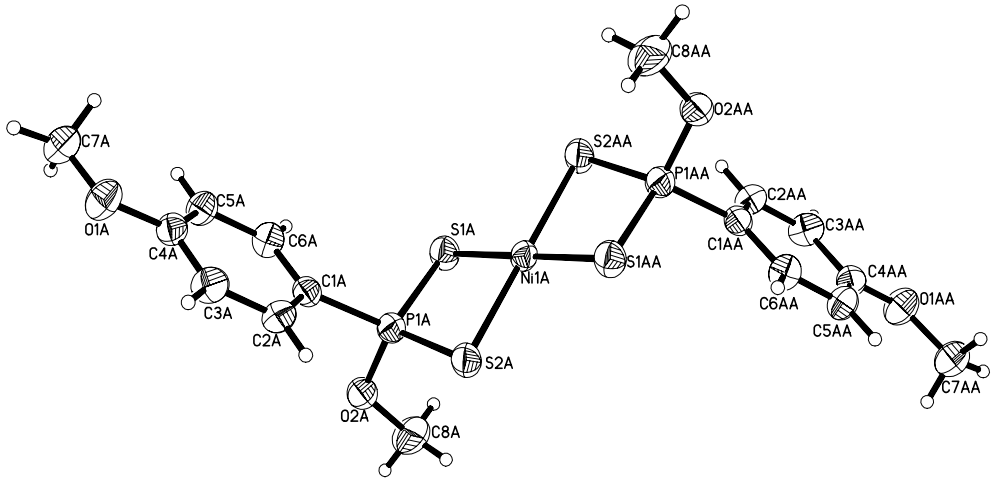

Fig. 1. The crystal structural unit of complex **1**.

Table 2
Selected bond distances (Å) and angles (°) for complex **1**

Ni1A–S2AA	2.2307(13)	S1A–Ni1A–P1AA	134.99(5)
Ni1A–S2A	2.2307(13)	S1AA–Ni1A–P1AA	45.01(5)
Ni1A–S1A	2.2426(13)	S2AA–Ni1A–P1A	135.00(4)
Ni1A–S1AA	2.2426(13)	S2A–Ni1A–P1A	45.00(4)
Ni1A–P1AA	2.8098(15)	S1A–Ni1A–P1A	45.01(5)
Ni1A–P1A	2.8098(15)	S1AA–Ni1A–P1A	134.99(5)
		P1AA–Ni1A–P1A	180.00(7)
S2AA–Ni1A–S2A	180.00(10)	S1A–Ni1A–S1AA	180.00(5)
S2AA–Ni1A–S1A	91.25(5)	S2AA–Ni1A–P1AA	45.00(4)
S2A–Ni1A–S1A	88.75(5)	S2A–Ni1A–P1AA	135.00(4)
S2AA–Ni1A–S1AA	88.75(5)		

Symmetry transformations used to generate equivalent atoms: #1, $-x, -y, -z$.

Table 3
Selected bond distances (Å) and angles (°) for complex **2**

NiA–S1AA	2.2257(17)	S1A–NiA–P1AA	135.63(6)
NiA–S1A	2.2257(17)	S2A–NiA–P1AA	135.18(6)
NiA–S2A	2.2273(17)	S2AA–NiA–P1AA	44.82(6)
NiA–S2AA	2.2273(17)	S2A–NiA(1)-P1A	180.00(5)
NiA–P1A	2.8311(19)	S1AA–NiA–S2AA	88.04(7)
NiA–P1AA	2.8311(19)	S1A–NiA–S2AA	91.96(7)
		S2A–NiA–S2AA	180.00(11)
S1AA–NiA–S1A	180.00(13)	S1AA–NiA–P1A	135.63(6)
S1AA–NiA–S2A	91.96(7)	S1A–NiA–P1A	44.37(6)
S1A–NiA–S2A	88.04(7)		

Symmetry transformations used to generate equivalent atoms: #1, $-x, -y, -z$.

octahedron. The selected bond distances and angles for complex **3** are shown in Table 4a. It is evident that in the crystal structure of complex **3** there exist numerous N–H–S hydrogen bonds which stabilize the crystal structure. The hydrogen bonds are stated in Table 4b.

For complex **4**, it can be seen from Fig. 4 that for every Co(II), such as Co1, three $MeOC_6H_4P(CH_3O)S_2$

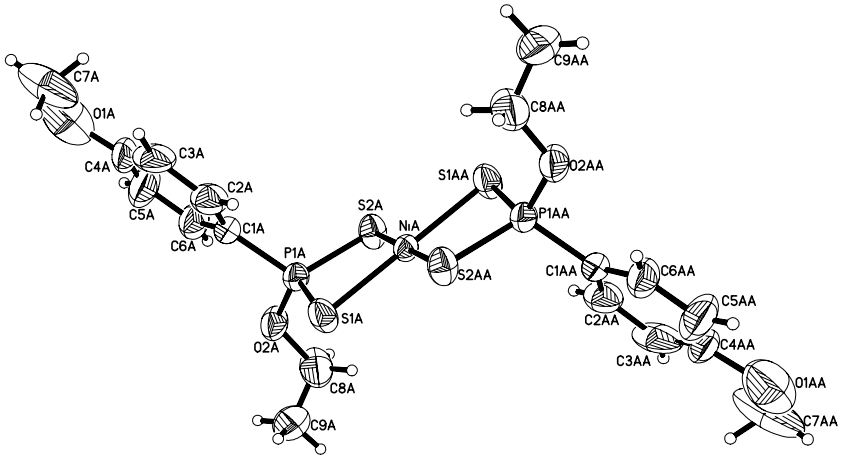

Fig. 2. The crystal structural unit of complex **2**.

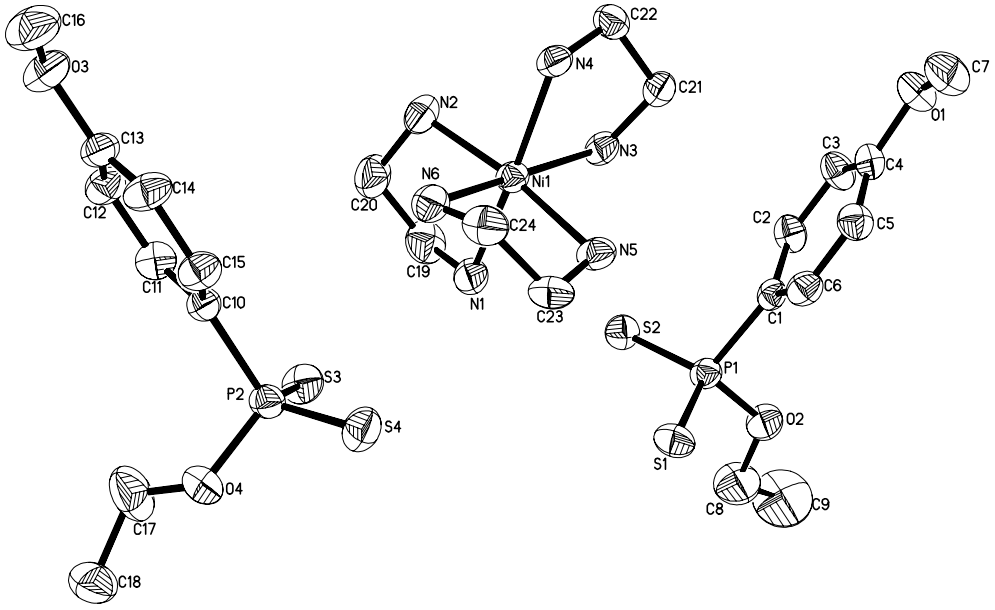

Fig. 3. The crystal structural unit of complex **3**.

Table 4a
Selected bond distances (Å) and angles (°) for complex **3**

Ni1–N3	2.113(4)	N1–Ni1–N6	94.24(19)
Ni1–N4	2.115(4)	N3–Ni1–N5	92.28(19)
Ni1–N1	2.122(4)	N4–Ni1–N5	92.7(2)
Ni1–N6	2.136(4)	N1–Ni1–N5	94.50(19)
Ni1–N5	2.145(4)	N6–Ni1–N5	80.92(19)
Ni1–N2	2.150(5)	N3–Ni1–N2	93.9(2)
		N4–Ni1–N2	91.8(2)
N3–Ni1–N4	81.51(17)	N1–Ni1–N2	81.54(19)
N3–Ni1–N1	93.04(18)	N6–Ni1–N2	93.3(2)
N4–Ni1–N1	171.1(2)	N5–Ni1–N2	172.8(2)
N3–Ni1–N6	170.4(2)		

groups offer four sulfur atoms S1, S4, S3 and S6, existing in the equatorial geometry and forming a parallelogram, with the other two sulfur atoms S2 and S5 occupying the axial sites. So the Co(II) ion is six-coordinated, in the center of a distorted octahedron. Selected bond distances and angles are shown in Table 5.

3.3. Discussion

Through the research of the syntheses and crystal structures of these four novel sulfur-rich complexes, we found that the product can be influenced by the sort of solvent used in the preparation of such complexes of LR derivatives. For example, when the solvent is methanol or ethanol, the deprotonated methanol or ethanol can attack the phosphorus atom of LR, and the product cleaved from LR containing methoxy or ethoxy was produced. It is suggested that when LR is heated in a solvent containing an active proton, solvation decomposition can easily take place.

4. Supplementary material

Crystallographic data for the structural analyses have been deposited with the Cambridge Crystallographic

Table 4b
Hydrogen-bond distances (Å) and angles (°) for complex **3**

D–H	*d*(D–H)	*d*(H···A)	∠DHA	*d*(D···A)	Assignment
N5–H5F	0.797	2.862	163.69	3.635	S1
N4–H4F	0.900	2.610	154.76	3.446	S4 $[x, -y+3/2, z+1/2]$
N1–H1F	0.954	2.581	153.18	3.459	S2
N3–H3E	0.864	2.908	140.57	3.617	S2
N1–H1E	1.020	2.586	153.08	3.525	S3
N6–H6F	0.923	2.907	171.65	3.823	S3
N2–H2E	0.953				
N6–H6E	0.936	2.523	157.24	3.405	S3 $[x, -y+3/2, z+1/2]$
N4–H4E	0.864	2.654	147.61	3.415	S1 $[x, -y+3/2, z+1/2]$
N5–H5E	0.884	2.692	148.20	3.475	S1 $[x, -y+3/2, z+1/2]$
N3–H3F	0.994	2.628	148.74	3.516	S4 $[-x+1, y+1/2, -z+3/2]$
N2–H1F	0.915	2.732	147.50	3.538	S4 $[-x+1, y+1/2, -z+3/2]$

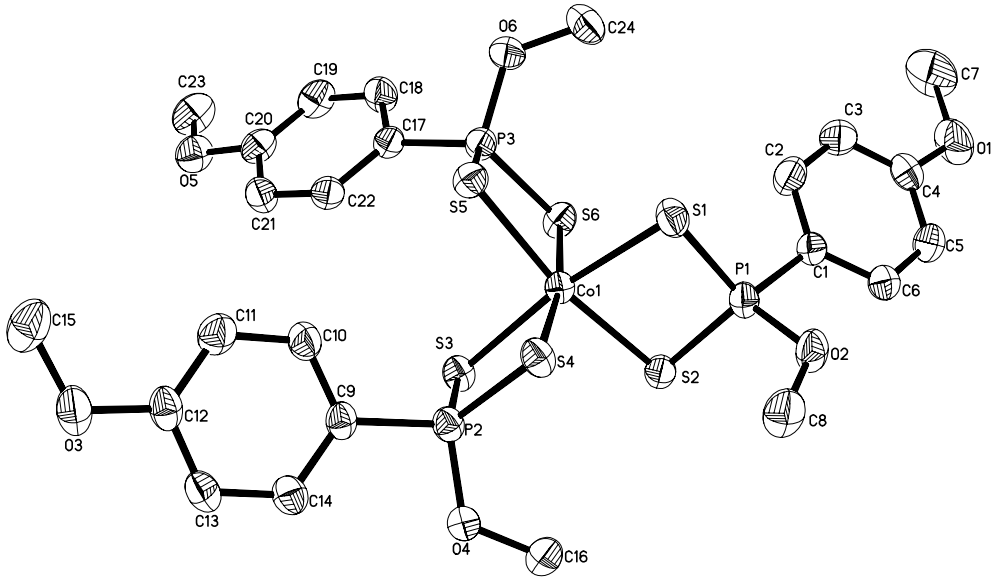

Fig. 4. The crystal structural unit of the complex **4**.

Table 5
Selected bond distances (Å) and angles (°) for complex **4**

Bond lengths					
Co1–S1	2.3029(17)	S1–Co1–S4	88.21(6)	S1–Co1–S5	89.42(6)
Co1–S4	2.3042(16)	S1–Co1–S6	97.43(6)	S4–Co1–S5	89.76(6)
Co1–S6	2.3190(16)	S4–Co1–S6	171.50(6)	S6–Co1–S5	83.97(5)
Co1–S3	2.3211(17)	S1–Co1–S3	169.98(6)	S3–Co1–S5	96.62(6)
Co1–S5	2.3292(15)	S4–Co1–S3	83.85(6)	S1–Co1–S2	84.05(6)
Co1–S2	2.3362(15)	S6–Co1–S3	91.16(6)	S4–Co1–S2	98.31(6)
Bond angles					
S3–Co1–S2	91.06(6)	S5–Co1–S2	169.42(6)	S6–Co1–S2	88.63(5)

Data Center, CCDC Nos. 222648, 222650 222647 and 228385 for complexes **1**, **2**, **3** and **4**, respectively. Copies of this information may be obtained free of charge from The Director, CCDC, 12 Union Road, Cambridge, CB2 1EZ, UK (fax: +44-1223-336033; email: deposit@ccdc.cam.ac.uk or www:http://www.ccdc.cam.ac.uk).

Acknowledgements

This work was supported by the Natural Science Foundation of China (20271046), the Natural Science Foundation of Henan Education Department (200011500027) and the Natural Foundation of Henan Province (0211020300).

References

[1] L.-N. He, R.-Y. Chen, R.-X. Zhuo, GaoDengXueXiaoHuaXueXueBao (Chinese) 18 (12) (1997) 1969.
[2] A.A. El-Barbary, S.-O. Lawesson, Tetrahedron 37 (15) (1981) 2641.
[3] B.S. Pedersen, S.-O. Lawesson, Tetrahedron 35 (1979) 2433.
[4] M. St John Foreman, R.J. Mortimen, A.M.Z. Slawin, J. Derek Woollins, J. Chem. Soc., Dalton Trans. (1999) 3419.
[5] R.A. Cherkasov, G.A. Kutyrev, A.N. Pudovik, Tetrahedron 41 (1985) 2567.
[6] Y.-G. Li, X.-F. Zhu, H.-J. Zhou, J. Org. Chem (Chinese) 15 (1995) 461.
[7] R. Shabana, S.S. Atrees, Phosphorus, Sulfur and Silicon 105 (1995) 57.
[8] A.A. Fahmy, Phosphorus, Sulfur and Silicon 68 (1992) 139.
[9] Y.-Z. Ning, B.-F. Wu, S.-T. Liu, GaoDengXueXiaoHuaXueXueBao (Chinese) 22 (8) (2001) 1286.
[10] J.R. Wasson, G.M. Waltermann, A.J. Stoklosa, Topics Current Chem. 35 (1973) 65.
[11] W. Kuchen, H. Hertel, Angew. Chem. Int. Ed. Engl. 8 (1969) 89.
[12] R.G. Cavell, W. Byers, E.D. Day, P.M. Watkins, Inorg.Chem. 11 (1972) 1598.
[13] K. Clausen, A.A. El-Barbary, S.-O. Lawesson, Tetrahedron 37 (1981) 1019.
[14] R.W. Berg, K. Rasmussen, Spectrochim. Acta A 30 (1974) 1881.

Available online at www.sciencedirect.com
SCIENCE DIRECT®
Polyhedron 23 (2004) 1805–1810
POLYHEDRON
www.elsevier.com/locate/poly

Synthesis and characterization of triphenyltin esters of heteroaromatic carboxylic acids and the crystal structure of $[Ph_3SnO_2CC_5H_4N \cdot 0.5H_2O]_\infty$

Han-Dong Yin *, Chuan-Hua Wang, Qiu-Ju Xing

Department of Chemistry, Liaocheng University, Liaocheng 252059, China

Received 3 February 2004; accepted 13 April 2004
Available online 4 May 2004

Abstract

The reaction of triphenyltin hydroxide with 2-furanyl, 2-furanvingl, 2-(5-terbutyl) furanyl, 2-(5-benzoyl) furanyl, 2-pyridinyl, 4-pyridinyl, 3-indolyl, 3-indolmethyl, 3-indolethyl and 3-indolpropyl carboxylates in 1:1 stoichiometry yields triphenyltin esters of heteroaromatic carboxylic acids Ph_3SnO_2CR. All compounds are characterized by elemental analysis, IR and ^1H NMR. The crystal structure of the triphenyltin ester of 4-pyridinyl carboxylic acid (**6**) is determined by single crystal X-ray diffraction. In compound (**6**), the tin atom is rendered five-coordinate in a trigonal bipyramidal structure by coordinating with the 4-pyridinyl carboxlate group. The resulting structure is a linear polymer containing Sn–O bond lengths of 0.2160(5)–0.2166(5) nm and Sn–N bond lengths of 0.2512(6)–0.2612(6) nm.
© 2004 Elsevier Ltd. All rights reserved.

Keywords: Heteroaromatic carboxylic acid; Triphenyltin; Synthesis; Crystal structure

1. Introduction

Organotin esters of carboxylic acid are widely used as biocides, fungicides and as homogeneous catalysts in industry [1–4]. Recently, pharmaceutical properties of organotin esters of carboxylic acid have been investigated for their antitumor activity [5,6]. In general, the biocidal activity of organotin compounds is influenced greatly by the structure of the molecule and the coordination number of the tin atom(s) [7,8]. Studies on organotin compounds containing carboxylate ligands with an additional donor atom (e.g., N, O or S) that are available for coordinating to the tin atom, have revealed that new structural types may lead to different activity [9,10]. As an extension of our studies of organotin esters of carboxylic acid with additional donor atoms residing on the carboxylate ligand [11], we have synthesized and structurally characterized a series of triorganotin compounds derived from 2-furanyl, 2-furanvingl, 2-(5-terbutyl)furanyl, 2-(5-benzoyl)furanyl, 2-pyridinyl, 4-pyridinyl, 3-indolyl, 3-indolmethyl, 3-indolethyl and 3-indolpropyl carboxylic acids and determined the crystal structure of $[Ph_3SnO_2CC_5H_4N \cdot 0.5H_2O]_\infty$. The results of these studies are reported herein.

2. Experimental

2.1. General procedures

All reactants were reagent grade. Infrared spectra were recorded on a Nicolet-460 spectrophotometer using KBr discs. ^1H NMR spectra were obtained on Mercury Plus-400 NMR spectrometer, chemical shifts are given in parts per million relative to Me_4Si in $CDCl_3$ solvent. Elemental analyses were performed with a PE-2400 II elemental apparatus. Tin was estimated as SnO_2. X-ray measurements were made on a Bruker Smart-1000 CCD diffractometer with graphite monochromated Mo Kα (0.071073 nm) radiation.

* Corresponding author. Tel./fax: +866358238121/+86-635-8239121.
E-mail address: handongyin@lctu.edu.cn (H.-D. Yin).

0277-5387/$ - see front matter © 2004 Elsevier Ltd. All rights reserved.
doi:10.1016/j.poly.2004.04.012

2.2. Synthesis of triphenyltin esters of heteroaromatic carboxylic acids

Heteroaromatic carboxylic acids (1.2 mmol) were added to a benzene solution of Ph_3SnOH (1.0 mmol). Then the mixture was refluxed for 5 h, with water formed during the reaction being removed azeotropically with a Dean and Stark apparatus. The clear solution obtained after filtration was evaporated in vacuum to give a white solid. The products were recrystallized from acetone–hexane to give colorless crystals (see Scheme 1 for compounds R).

$$Ph_3SnOH + RCOOH \rightarrow Ph_3SnOOCR$$

2.3. Crystallographic measurements of $Ph_3SnO_2CC_5H_4$-N-4 · 0.5H_2O

A colorless crystal having approximate dimensions of 0.50 mm × 0.50 mm × 0.20 mm was mounted on a glass capillary. All measurements were made on a Bruker Smart 1000 CCD diffractometer with graphite monochromated Mo Kα (0.071073 nm) radiation. The data were collected at room temperature (298 ± 2 K) using the $\omega - 2\theta$ scan technique to a maximum 2θ value of 52.9°. The crystal structure belongs to orthorhombic crystal system, with space group $P2_12_12$, $a = 1.4882(3)$, $b = 2.3802(5)$, $c = 1.2366(2)$ nm, $\alpha = \beta = \gamma = 90°$, $Z = 4$, $V = 4.3805(15)$ nm^3, $D_c = 1.459$ g/cm^3, $\mu = 1.187$ mm^{-1}, $F(000) = 1928$. The structure was solved by direct method and differential Fourier map using the SHELXL-97 program, and refined by full-matrix least-squares on F^2. All non-hydrogen atoms were refined anisotropically. The positions of hydrogen atoms were calculated and refined isotropically. The weighting scheme was $w = 1/[s^2(F_o^2) + (0.0720P)^2 + 0.0000P]$, $p = (F_o^2 + 2F_c^2)/3$. The refinement was converged to the final $R = 0.0540$, $wR = 0.1237$, $(\Delta/\sigma)_{max} = 0.001$ and $S = 0.999$. In the final difference map, the residuals are 1.074 and −1.238 e/Å^3.

3. Results and discussion

3.1. Physical properties

Physical data for compounds **1**–**10** are listed in Table 1. All compounds are colorless crystals. They are soluble in many organic solvents such as CCl_4, $CHCl_3$, C_6H_6, $(CH_3)_2CO$, but are insoluble in hexane, petroleum ether and water.

3.2. Analyses of spectroscopies

3.2.1. IR spectra

The characteristic IR spectral data of compounds **1**–**10** are shown in Table 2. The assignment of IR bands of these compounds has been determined by a comparison with the IR spectra of related organotin compounds, carboxylates and Ph_3SnOH. It is worth noting that the difference Δv between v^{as}(COO) and v^{s}(COO) is important because these frequencies can be used to determine the type of bonding between the metal and carboxylate ligand [1,12]. Generally triorganotin esters of carboxylic

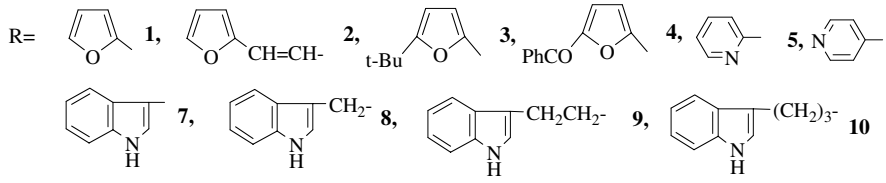

Scheme 1.

Table 1
Physical and analytical data of compounds **1**–**10**

Compound	Yield (%)	M.p. (°C)	Found (Calc.)%			
			C	H	N	Sn
1	90	102–104	59.68(59.91)	3.87(3.93)		25.79(25.74)
2	88	120–122	61.75(61.64)	4.21(4.14)		24.55(24.37)
3	76	93–95	62.91(62.70)	5.16(5.07)		22.80(22.95)
4	67	74–76	63.97(63.75)	4.05(3.92)		21.24(21.00)
5	87	151–152	61.28(61.06)	4.12(4.06)	2.90(2.97)	25.33(25.14)
6	81	210–212	59.58(59.92)	4.22(4.19)	2.87(2.91)	24.33(24.67)
7	92	134–135	63.41(63.57)	4.17(4.15)	2.70(2.75)	23.34(23.27)
8	87	123–125	64.00(64.16)	4.39(4.42)	2.73(2.67)	22.85(22.64)
9	93	110–112	62.91(62.62)	4.92(4.89)	2.47(2.52)	21.21(21.34)
10	80	84–85	65.09(65.25)	5.17(4.93)	2.62(2.54)	21.65(21.49)

Table 2
IR data (cm^{-1}) of compounds **1**–**10**

Compound	ν(C–H) (aryl)	ν^{as}(COO)	ν^{s} (COO)	ν(Sn–C)	ν(Sn–N) or (N–H)	ν(Sn–O)
1	3057w	1541s(1650)	1371s(1357)	562w		453w
2	3050w	1591s(1648)	1401s(1340)	545w		447w
3	3051w	1594s(1650)	1395s(1346)	559w		450m
4	3058m	1654(1657)	1343(1347)	547w		442w
5	3065w	1631s(1639)	1354s(1347)	557w	484w(489)	453w
6	3060w	1658s(1656)	1355s(1352)	552w	483w	460w
7	3052m	1593s(1652)	1396s(1355)	556w	3423s	443w
8	3057w	1588s(1649)	1401s(1340)	554w	3425s	438w
9	3061m	1590s(1646)	1405s(1354)	558w	3423s	435w
10	3054m	1586s(1640)	1400s(1341)	545w	3426s	443m

The parentheses give the vibration of compounds in CCl_4.

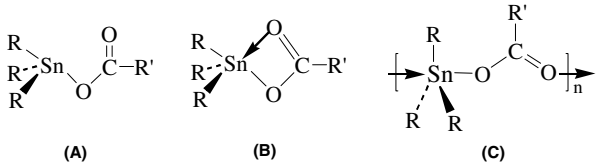

Scheme 2.

acid adopt three types of structures in the solid state (as shown in Scheme 2).

The magnitude of $\Delta\nu$ [ν^{as}(COO)–ν^{s}(COO)] of 170–199 cm^{-1} for compounds **1**–**3** and **7**–**10** is approximately equal to that for the corresponding sodium salt of the carboxylic acids. This information indicates the presence of bidentate carboxylate groups [1–4]. So it is impossible for these compounds to be structure **A**. The IR spectra of these compounds in CCl_4 are also studied in order to find out whether the ligand linkage of the C=O bond to the tin atom is intra-molecular or inter-molecular [1,13]. Because in solution the inter-molecular bond of a five-coordinated organotin polymer which belongs to structure **C** is destroyed, the polymeric structure is decomposed into mono-molecules and as a result, the $\Delta\nu$ value increases greatly [14,15]. However, the $\Delta\nu$ value for compounds with structure **B** and structure **A** do not change obviously when they are determined in solvent [14]. The results showed that the magnitude of $\Delta\nu$ 292–308 cm^{-1} in CCl_4 is much greater than that in KBr for compounds **1**–**3** and **7**–**10** (shown in Table 2). This fact reveals that the structure of these compounds might be structure **C**, not be structure **B**. The magnitude of 277–311 cm^{-1} for compounds **4**–**6** strongly indicates the unidentate bonding of the carboxylate groups, and the result in KBr is similar to that in CCl_4. But the structures of compounds **5** and **6** are different from structure **A**. One obvious feature of the IR spectra in the compounds at 484 and 483 cm^{-1} is the similarity of the stretching band arising from Sn–N [15]. Because the inter-molecular bond of Sn ← N will break in solvent, while the intra-molecular bond of Sn ← N is not influenced basically by solvent [14], whether Sn ← N of an organotin compound is inter-molecular or intra-molecular may be deduced. It is shown that the N hetero atom on the pyridine group in the carboxylate group coordinates to the tin atom [15]. In CCl_4 solution, this band is not observed in compound **6**. This indicates that the Sn ← N bond breaks up for the compound in CCl_4 solution, Thus it is proved that compound **6** contains an inter-molecular Sn ← N bond and exists as a polymer [15]. However, this difference is not observed for compound **5**. Since the intra-molecular coordination bond is not influenced by solvent [14], the Sn ← N bond existing in the compound with structure **E** can also be observed in solution. So it is possible for compound **6** to be structure **D** and compound **5** to be structure **E** [15] (see Scheme 3).

3.2.2. ^1H NMR spectra

The ^1H NMR spectra of compounds **1**–**10** are given in Table 3. It is shown that the chemical shifts of the protons on the phenyl groups of compounds **1**–**10** exhibit signals at about 7.21–7.68 ppm as multiplets.

The chemical shifts of the protons of heteroaromatic rings of compounds **1**–**10** exhibit signals in the range 6.10–8.82 ppm as multiplets (see Table 3). In compounds **1**–**4** and **7**–**10**, they are similar to that of the corresponding free heteroaromatic acid but in compounds **5** and **6** they obviously increase to be higher values than that of the corresponding free heteroaromatic acid. This finding may be consistent with previous studies that suggest that only pyridine type N atoms, present in the carboxylate R′ group, coordinate to Sn, and there is no evidence of intra- or inter-molecular coordination to Sn by the O atoms of furanyl groups

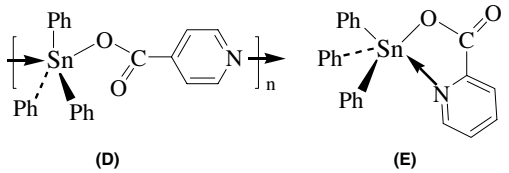

Scheme 3.

Table 3
^{1}H NMR data (ppm) for compounds **1**–**10**

Compound	^{1}H NMR
1	7.25–7.68 (16H, m, Ph-H, 5-furan-H), 7.11 (1H, d, 3-furan-H), 6.53 (1H, d, 4-furan-H)
2	7.19–7.65 (17H, m, Ph-H, 5-furan-H, C=$CHCO_2$), 6.91 (1H, d, 3-furan-H), 6.64 (1H, d, 4-furan-H), 6.38 (1H, d, C=CHAr)
3	7.21–7.67 (15H, m, Ph-H,), 6.10 (1H, d, 3-furan-H), 7.87 (1H, d, 4-furan-H), 1.33 (9H, s, CH_3)
4	7.94 (2H, br, 2,3-furan-H), 7.20–7.64 (20H, m, Ph-H)
5	8.21 (1H, br, 3-pyridine-H), 7.90 (1H, d, 6-pyridine-H), 7.51 (1H, d, 4-pyridine-H), 7.24–7.69 (16H, m, Ph-H, 5-pyridine-H)
6	8.82 (2H, d, 2,6-pyridine-H), 7.84 (2H, d, 3,5-pyridine-H), 7.35–7.75 (15H, m, Ph-H)
7	8.02 (1H, s, N–H), 7.21–7.67 (16H, m, Ph-H, 2-indole-H), 6.84–7.18 (4H, m, indole-H)
8	8.00 (1H, s, N–H), 7.22–7.62 (16H,m, Ph-H, 2-indole-H), 6.78–7.17 (4H, m, indole-H), 3.62 (2H, s, $ArCH_2CO_2$)
9	7.95 (1H, s, N–H), 7.23–7.66 (16H, m, Ph-H, 2-indole-H), 6.72–7.20 (4H, m, indole-H), 2.91 (2H, br, CH_2CO_2), 2.23 (2H, br, $ArCH_2$)
10	7.97 (1H, s, N–H), 7.21–7.69 (16H, m, Ph-H, 2-indole-H), 6.75–7.18 (4H, m, indole-H), 2.72 (2H, t, CH_2CO_2), 2.05 (2H, t, $ArCH_2$), 1.52 (2H, m, CH_2)

[10]. In addition, the presence of the N–H proton signal in the spectra of compounds **7**–**10** supports that the indolyl group N atom is not coordinated to the Sn atom.

3.2.3. X-ray crystal structure of $Ph_3SnO_2CC_5H_4N$-4·0.5H_2O (**6**)

Selected bond distances and angles are listed in Table 4. The molecular structure is shown in Fig. 1. Fig. 2 shows the packing of the molecules in the unit cell as seen in a projection onto its face.

In $[Ph_3SnO_2CC_5H_4N \cdot 0.5H_2O]_\infty$ **6**, two kinds of tin atoms with different chemical environments can be found. Each molecule of compound **6** in the unit cell possesses an unequivocally polymeric structure, but this structure differs from the tributyltin 2-(5-*tert*butyl) furanylcarboxylate [8] and tribenzyltin 2-(5-*tert*butyl)furanylcarboxylate [8]. Each tin atom is rendered five-coordinate in a trigonal bipyramidal structure by coordination of the nitrogen atom from a 4-pyridinyl carboxylate group from an adjacent molecule. The central tin atoms are surrounded axially by one oxygen atom and one nitrogen atom, and equatorially by three carbon atoms of the phenyl groups. The intra-molecular Sn(1)–O(1) and Sn(2)–O(3) bond distances are 0.2166(5) and 0.2160(5) nm, which are longer than that in $\{[^nBu_2Sn(2\text{-pic})]_2O\}_2$ [7] (0.20544 and 0.2110 nm), but are shorter than those in $Me_3SnO_2CC_5H_4N \cdot H_2O$ (0.218 and 0.221 nm) [16]. The Sn(1)–O(2) and Sn(2)–O(4) distances are 0.3237 and 0.3311 nm, which are much greater than the sum of the van der Waals radii for Sn and O of 0.280 nm. It is shown that the O(2) and O(4) atoms do not make any significant contacts with the Sn atom. The Sn(1)–N(2) and Sn(2)–N(1)#1 distances, 0.2512(6) and 0.26612(6) nm, are greater than the sum of the covalent radii of Sn and N (0.215 nm), but are considerably less than the sum of the van der

Table 4
Selected bond distances (nm) and angles (°) for compound **6**

Bond distances					
Sn(1)–O(1)	0.2166(5)	Sn(1)–N(2)	0.2512(6)	Sn(1)–C(19)	0.2129(8)
Sn(2)–N(1)#1	0.26612(6)	Sn(1)–C(7)	0.2142(9)	Sn(2)–C(37)	0.2130(7)
Sn(1)–C(13)	0.2125(8)	Sn(2)–C(31)	0.2125(8)	Sn(2)–O(3)	0.2160(5)
Sn(2)–C(43)	0.2115(8)	O(2)–C(1)	0.1208(10)	O(3)–C(25)	0.1245(9)
O(1)–C(1)	0.1276(10)	N(1)–C(4)	0.1338(11)	N(1)–C(5)	0.1300(10)
O(4)–C(25)	0.1206(9)	N(2)–C(28)	0.1336(10)	N(2)–C(29)	0.1289(9)
Bond angles					
C(13)–Sn(1)–C(7)	120.2(4)	C(13)–Sn(1)–C(19)	115.0(4)	C(7)–Sn(1)–C(19)	124.0(3)
C(13)–Sn(1)–O(1)	96.2(3)	C(7)–Sn(1)–O(1)	93.2(3)	C(19)–Sn(1)–O(1)	89.9(3)
C(13)–Sn(1)–N(2)	88.0(2)	C(19)–Sn(1)–N(2)	88.2(3)	C(7)–Sn(1)–N(2)	84.9(3)
O(1)–Sn(1)–N(2)	175.8(2)	C(37)–Sn(2)–O(3)	88.4(2)	C(43)–Sn(2)–O(3)	99.5(3)
C(31)–Sn(2)–N(1)#1	84.5(2)	C(37)–Sn(2)–N(1)#1	84.8(2)	C(43)–Sn(2)–N(1)#1	84.4(3)
O(3)–Sn(2)–N(1)#1	173.1(2)	C(31)–Sn(2)–O(3)	97.8(3)	C(28)–N(2)–Sn(1)	119.8(5)
C(1)–O(1)–Sn(1)	120.9(5)	C(29)–N(2)–Sn(1)	124.7(5)	C(12)–C(7)–Sn(1)	123.4(7)
C(8)–C(7)–Sn(1)	120.1(7)	C(14)–C(13)–Sn(1)	119.2(8)	C(18)–C(13)–Sn(1)	124.0(9)
C(24)–C(19)–Sn(1)	126.8(8)	C(20)–C(19)–Sn(1)	116.8(6)	C(36)–C(31)–Sn(2)	116.9(6)
C(32)–C(31)–Sn(2)	124.0(6)	C(25)–O(3)–Sn(2)	115.1(5)	C(42)–C(37)–Sn(2)	120.9(7)
C(44)–C(43)–Sn(2)	123.0(6)	C(38)–C(37)–Sn(2)	120.9(6)	C(4)–N(1)–C(5)	116.7(7)
C(48)–C(43)–Sn(2)	120.4(6)	O(2)–C(1)–O(1)	127.1(8)	O(1)–C(1)–C(2)	113.9(7)
N(1)–C(4)–C(3)	123.6(8)	N(1)–C(5)–C(6)	124.0(8)	O(2)–C(1)–C(2)	118.9(8)

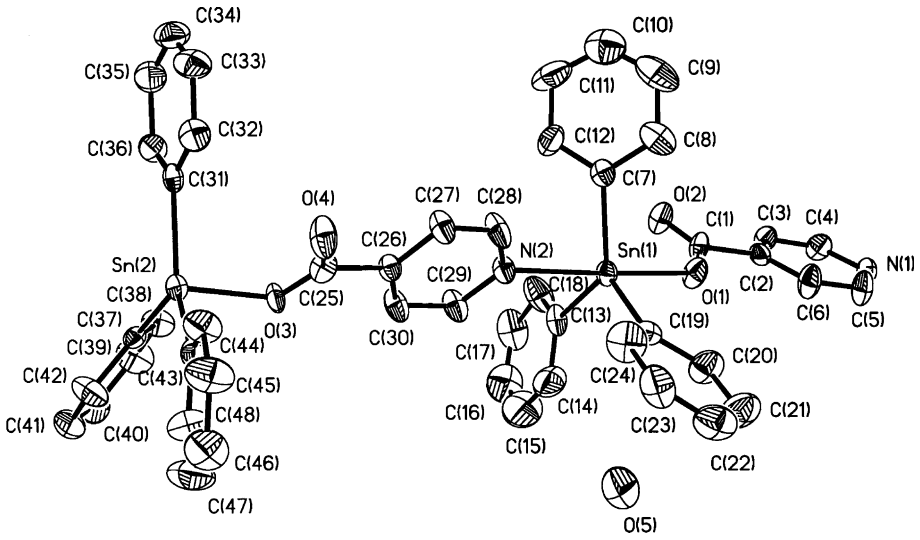

Fig. 1. The molecular structure of compound **6**.

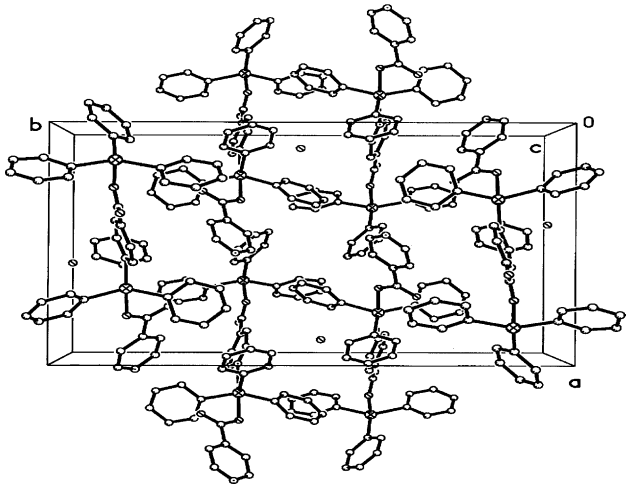

Fig. 2. Projection of compound **6**.

Waals radii (0.375 nm) [17] and should be considered as bonding interactions. In this connection it is relevant to note the Sn–N bond distances found in three other crystal structures of organotin compounds containing the pyridine carboxylate ligand. In polymeric $[Me_2SnCl(2\text{-pic})]_n$ [18] the two unique Sn–N bond distances are 0.250(3) and 0.247(2) nm, in polymeric $[Me_2Sn(2\text{-pic})_2]_n$ [9] the two Sn–N bond distances are 0.2507(4) and 0.2477(4) nm and in dicarboxylato tetraorganostannoxane $\{[^nBu_2Sn(2\text{-pic})]_2O\}_2$ [7] the two Sn–N bond distances are 0.2550(5) and 0.3150(5) nm. In compound **6**, the distortions from true trigonal bipyramidal symmetry are reflected in the interatomic angles. For instance around the Sn(1) atom of compound **6** the angles of C(7)–Sn(1)–O(1) 93.2(3)°, C(13)–Sn(1)–O(1) 96.2(3)°, C(19)–Sn(1)–O(1) 89.9(3)°, C(7)–Sn(1)–N(2) 84.9(3)°, C(13)–Sn(1)–N(2) 88.0(2)°, C(19)–Sn(1)–N(2) 88.2(3)°, all are not 90°, and only one approximates to 90°. The angle of O(1)–Sn(1)–N(2), 175.8(2)°, shows that the atoms O(1), Sn(1) and N(2) are nearly linear. The Sn(2) atom is similar to the Sn(1) atom and it has a distorted trigonal bipyramidal structure too.

4. Supplementary material

Crystallographic data for the structural analysis have been deposited with the Cambridge Crystallographic Data Center, CCDC No. 200373 for compound **6**. Copies of this information may be obtained from The Director, CCDC, 12 Union Road, Cambridge CB2 1EZ, UK (fax: +44-1233-336-033; E-mail: deposit@ccdc.cam.ac.uk, or www: http://www.ccdc.cam.ac.uk).

Acknowledgements

We acknowledge the financial support of the Shandong Province Science Foundation, and the State Key Laboratory of Crystal Materials, Shandong University, PR China.

References

[1] Q.L. Xie, S.H. Li, D.K. Zhang, Z.G. Zhang, J.M. Hu, Acta Chim. Sinica 49 (1991) 723.
[2] H.D. Yin, D.Z. Zhu, Y. Wang, C.L. Liu, F.G. Ma, Chin. J. Org. Chem. 22 (2002) 575.
[3] H.D. Yin, C.H. Wang, Y. Wang, C.L. Ma, J.X. Shao, J.H. Zhang, Acta Chim. Sinica 60 (2002) 143.
[4] H.D. Yin, C.L. Ma, Y. Wang, H.X. Fang, J.X. Sao, Acta Chim. Sinica 60 (2002) 897.
[5] H.D. Yin, C.H. Wang, Y. Wang, C.L. Ma, G.F. Liou, Chin. J. Org. Chem. 22 (2002) 590.

[6] M. Grelen, A.M. Khloufi, M. Biesmans, R. Kayser, Appl. Organomet. Chem. 7 (1993) 201.
[7] C.S. Parulekar, X.K. Jain, T.K. Das, A.R. Gupta, B.F. Hoskins, E.R.T. Tiekink, J. Organoment. Chem. 372 (1989) 193.
[8] Q.L. Xie, X.H. Xu, H.G. Wang, X.K. Yao, R.J.Z.G. Zhang, J.M. Hu, Acta Chim. Sinica 49 (1991) 1085.
[9] T.P. Lockhart, F. Davidson, Organometallics 6 (1987) 2471.
[10] C. Vatsa, V.K. Jain, T. Kesavadas, E.R.T. Tiekink, J. Organomet. Chem. 410 (1991) 135.
[11] H.D. Yin, R.F. Zhang, C.L. Ma, Chin. J .Inorg. Chem. 14 (1998) 101.
[12] S.G. Teoh, S.H. Ang, J.P.D. Declercq, Polyhedron 16 (1997) 3729.
[13] H.D. Yin, C.H. Wang, Y. Wang, C.L. Ma, D.Q. Wang, Indian J. Chem. 42B (2003) 881.
[14] Z.Q. Yang, Q.L. Xie, X.Z. Zhou, Chem. J. Chin. Univ. 16 (1995) 59.
[15] H.D. Yin, C.H. Wang, C.L. Ma, D.Q. Wang, J. Organomet. Chem. 689 (2004) 246.
[16] P.G. Harrison, R.C. Philips, J. Organomet. Chem. 182 (1979) 37.
[17] A. Bondi, J. Phys. Chem. 68 (1964) 441.
[18] I.W. Nowell, J.S. Brooks, G. Beech, R. Hill, J. Organomet. Chem. 244 (1983) 119.

Available online at www.sciencedirect.com
SCIENCE DIRECT®
Polyhedron 23 (2004) 1811–1817
POLYHEDRON
www.elsevier.com/locate/poly

Synthesis, X-ray structure and magnetic properties of the azido adducts of quadridentate Schiff base manganese(III) complexes

Sandip Saha [a], Dasarath Mal [a], Subratanath Koner [a,*], Ashis Bhattacherjee [b], Philipp Gütlich [b], Swastik Mondal [c], Monika Mukherjee [c], Ken-Ichi Okamoto [d]

[a] *Department of Chemistry, Jadavpur University, Jadavpur, Calcutta 700 032, India*
[b] *Institut für Anorganische Chemie und Analytische Chemie, Johannes Gutenberg Universität, Straudinger Weg 9, D-55099 Mainz, Germany*
[c] *Department of Solid State Physics, Indian Association for the Cultivation of Science, Jadavpur, Calcutta 700 032, India*
[d] *Department of Chemistry, University of Tsukuba, Tsukuba, Ibaraki 305-8571, Japan*

Received 10 January 2004; accepted 13 April 2004
Available online 4 May 2004

Abstract

Two new azido derivatives of quadridentate Schiff base manganese(III) complexes have been synthesized and characterized structurally and magnetically. X-ray structure analysis revealed that both complexes viz. $[Mn_2(L1)_2(N_3)_2]$ (**1**) and $[Mn_2(L2)_2(N_3)_2]$ (**2**), where $H_2L1 = N,N'$-(1,1-dimethylethylene)-bis-(salicylaldiimine) and H_2L2 = bis(*o*-hydroxyacetophenone)-ethylenediimine exist as phenoxo-bridged dimer. The magnetic susceptibility of the complexes has been measured in the 5–300 K range. At room temperature the Mn^{III} ions in complexes **1** and **2** possess an $S = 4$ ground state. The global magnetic interaction in complex **1** is found to be ferromagnetic, while for complex **2** it is anti-ferromagnetic.
© 2004 Elsevier Ltd. All rights reserved.

Keywords: Manganese(III); N,O ligands; X-ray structure; Magnetochemistry; Dimer; Azide

1. Introduction

Studies on metal assembled complexes of manganese have attracted considerable attention in recent time due to their various interesting properties like biomimetism, catalysis, molecular magnetism, etc. Manganese takes part in several essential life processes [1]. One of the most famous examples is the tetranuclear manganese cluster of the oxygen evolving complex (OEC) present in the photosystem II of green plants [2]. Dinuclear manganese clusters are present in several metalloproteins such as manganese catalase, manganese ribonucleotide reductase, etc. [3,4]. Attempts have been made to mimic the catalase activity of metalloprotein using dinuclear Mn^{III} Schiff base complexes [5]. A family of Mn^{III} Schiff base complexes also catalyzes many important reactions such as C–H bond activation, olefin epoxidation, hydroxylation, etc. [6,7]. Such complexes with chiral ligands are also employed in asymmetric catalytic reactions [7]. Exchange between two or more paramagnetic centers is the crucial criteria in manifestation of molecular magnetism. The role of bridging ligands that gives a suitable mechanism for super exchange between metal ions is important in this context. Pseudohalogens are versatile ligands for making such bridges [8–10]. Amongst them azide is the most efficient ligand with regard to super-exchange pathways between paramagnetic centers. The versatility and efficiency of azide lies on its functionality as a terminal monodentate, or bridging bi, tri and tetradentate ligand [11]. Manganese(III) Schiff bases are known to serve the required paramagnetic building block for multidimensional extended architecture. The Mn^{III} with this ligand environment could afford a ground state $S = 2$ for the monomeric entity, while $S = 4$ for dimeric forms and so on. A lot of dimeric Mn^{III} Schiff base complexes

* Corresponding author. Tel.: +91-33-2414-6666; fax: +91-33-2414-6584.
E-mail address: skoner55@hotmail.com (S. Koner).

0277-5387/$ - see front matter © 2004 Elsevier Ltd. All rights reserved.
doi:10.1016/j.poly.2004.04.007

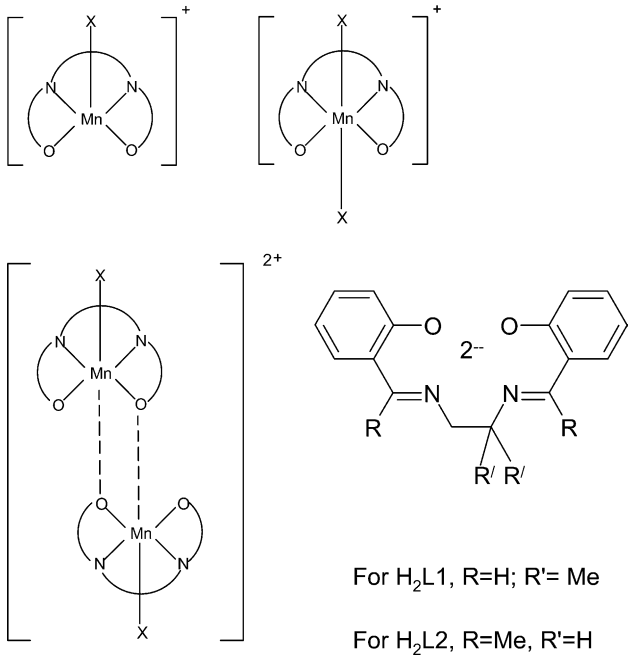

Scheme 1.

exhibiting antiferromagnetic interaction has been reported by several researchers [12–17]. But ferromagnetically coupled dimers are still scanty in the literature [18–20]. These complexes often dimerize by virtue of the formation of Mn–O–Mn* (Mn* belongs to a neighboring monomeric unit) bridge (Scheme 1) through phenoxo group present in a Schiff base [21]. In most of the cases phenoxo bridges are weak. In order to functionalize the metal centers further the azido adducts of Mn^{III} Schiff base complexes are prepared in the present study.

We report here the synthesis, structure and magnetic properties of two new azido adducts of Mn^{III} complexes containing quadridentate Schiff base ligands.

2. Experimental

2.1. Materials and synthesis

All chemicals and solvents used during the synthesis were of AR grade.

Caution!! *Azide derivatives are potentially explosive, only a small amount of materials should be prepared, and it should be handled with proper care.*

The H_2L1 was synthesized by mixing 1,1-dimethylethylenediamine with salicylaldehyde in a 1:2 molar ratio in methanol. The H_2L2 was also produced in the same method by mixing ethylenediamine with *o*-hydroxyacetophenone. The method of preparation of ligands that were followed in this study is given in [22a,22b], respectively.

2.1.1. $[Mn_2(L1^{2-})_2(N_3)_2]$ (**1**)

A methanol solution (40 ml) of H_2L1 (0.276 g, 0.932 mmol) was added to a methanol solution (20 ml) of manganese(III) acetate dihydrate (0.25 g, 0.933 mmol). After stirring the resulting brown solution for 30 min, sodium azide (0.061 g, 0.934 mmol) dissolved in minimum volume of water was added. Before filtration, the mixture was stirred for another 30 min. The filtrate was left to stand for two days at room temperature. Dark brown crystals were collected by suction filtration, washed with a minimum amount of methanol and dried in vacuo. (Yield ca. 70%.) *Anal.* Calc. for $C_{18}H_{18}MnN_5O_2$: C, 55.2; H, 4.6; N, 17.9. Found: C, 54.8; H, 4.7; N, 17.6%. IR(KBr): ν(C=N), 1635 cm^{-1}; ν(azide), 2080 cm^{-1}.

2.1.2. $[Mn_2(L2^{2-})_2(N_3)_2]$ (**2**)

The same preparation procedure as that presented for **1** was used for **2** using H_2L2 instead of H_2L1. (Yield ca. 80%.) *Anal.* Calc. for $C_{18}H_{18}MnN_5O_2$: C, 55.2; H, 4.6; N, 17.9. Found: C, 54.9; H, 4.5; N, 17.5%. IR(KBr): ν(C=N), 1601 cm^{-1}; ν(azide), 2040 cm^{-1}.

2.2. Physical measurements

The instruments used for IR and UV–Vis spectral measurement and CHN analyses were the same as reported earlier [23]. The magnetic susceptibility of complexes **1** and **2** was measured in the 5–300 K temperature range with a Quantum Design MPMS-XL SQUID susceptometer under a 1 T field. Diamagnetic corrections were estimated from Pascal constants.

2.3. X-ray crystallography

The crystal data of **1** and **2** and data collection parameters are summarized in Table 1. A black plate crystal of **1** was placed on a Rigaku AFC7S diffractometer equipped with graphite-monochromated Mo Kα radiation ($\lambda = 0.71069$ Å). The lattice parameters were obtained from a least-squares refinement of diffractometer setting angles of 12 reflections with $15.38° < 2\theta < 22.26°$. Data were collected at 300 K using the ω scan mode. The structure was solved by direct methods [24] and expanded using Fourier techniques [25]. The non-hydrogen atoms were refined anisotropically. Hydrogen atoms were included but not refined. All calculations were performed using the TEXAN [26a] crystallographic software package.

Intensity data of **2** were collected on a Bruker P4 diffractometer with graphite-monochromated Mo Kα radiation ($\lambda = 0.71073$ Å). Accurate cell parameters were obtained by least-squares refinement of diffractometer setting angles of 38 reflections with $2.07° < \theta < 14.89°$. Data were collected at 160 K using the ω scan mode. The crystal structure was solved by conventional Patterson and Fourier methods and re-

Table 1
Crystallographic data for complex **1** and **2**

Complexes	**1**	**2**
Empirical formula	$C_{18}H_{18}N_5MnO_2$	$C_{18}H_{18}N_5MnO_2$
Formula mass	391.31	391.31
Temperature (K)	300	160
Wavelength (Å)	0.71069	0.71073
Crystal system	monoclinic	monoclinic
Space group	$P2_1/a$	$P1121/n$
a (Å)	14.52(2)	7.662(9)
b (Å)	14.29(3)	11.069(7)
c (Å)	14.44(2)	19.648(9)
β (°)	144.54(5)	
γ (°)		92.81(10)
V (Å^3)	1738(5)	1664(2)
Z	4	4
ρ_{calc} (gm cm^{-3})	1.495	1.562
M (mm^{-1})	0.782	0.817
θ_{max} (°)	27.45	24.99
Crystal size (mm)	0.37×0.25×0.10	0.40×0.28×0.10
F(0 0 0)	808.00	808.00
Reflections measured	4361	2299
Unique reflections	3979	2299
R_{int}	0.078	0.000
R_1	0.087	0.0647
wR_2	0.103	0.1564

$R_1 = \sum ||F_o| - F_c|| / \sum |F_o|$.
$wR_2 = [\sum w(|F_o| - |F_c|)^2 / \sum wF_o^2]^{1/2}$.

fined by a full-matrix least-squares method with SHELXS-97 and SHELXL-97 [26b]. All non-hydrogen atoms were assigned to ideal positions and refined using a riding model.

3. Results and discussion

3.1. Description of the structures

The structure of the complexes **1** and **2** with atom numbering scheme is given in Figs. 1 and 2. The selected bond distances and angles of the complexes **1** and **2** are gathered in Table 2. These are comparable with other phenolato-bridged complexes [27]. Both complexes are the phenoxo-bridged dimers. Complexes **1** and **2** possess the same empirical formula and are ligand isomers. The quadridentate Schiff base forms the equatorial plane in these complexes. One of the axial positions of the coordination environment of Mn^{III} is occupied by a terminal azide, while the remaining axial position of the octahedron is connected to a phenoxo group of the neighboring monomeric unit which forms the bridge in the Mn_2^{III} dimer. The geometry around Mn^{III} in this molecule is best described as a tetragonally elongated octahedron. The other half of the dimer is related by a center of inversion to the first half described above (Figs. 1 and 2). The distance of Mn–O_{bridge} bonds were found to be 1.88(1) and 2.87(1) Å in complex **1**, whereas these are 1.912(4) and 2.375(5) Å in complex **2**. The [$Mn_2(\mu$-$O_2)$] diamond core in both complexes consists of

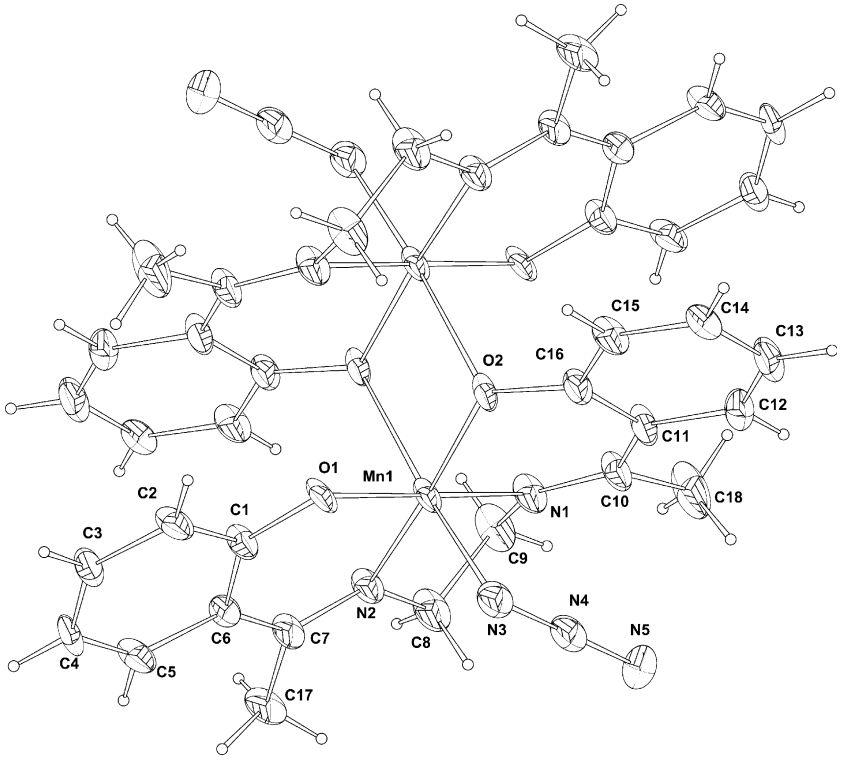

Fig. 1. ORTEP diagram of the complex **1** with the atom numbering scheme.

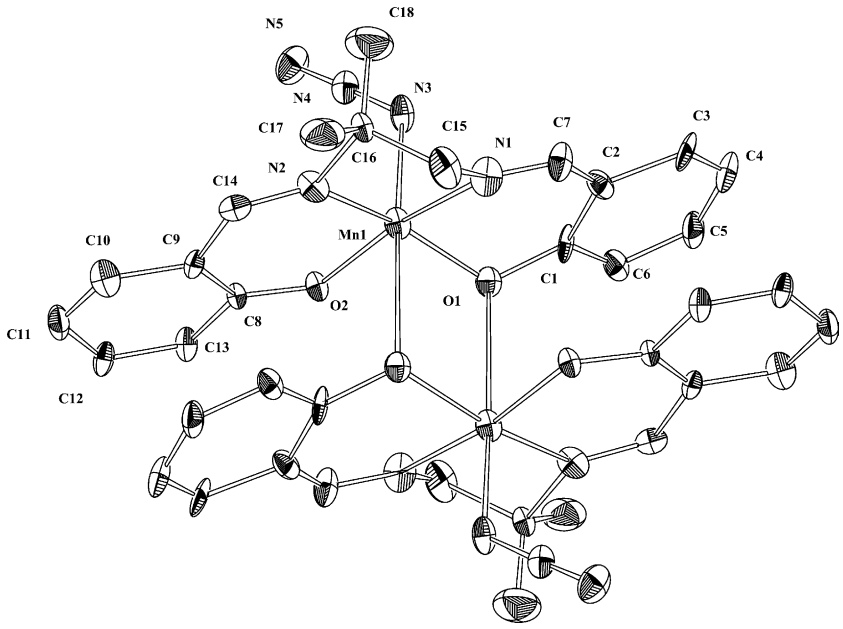

Fig. 2. ORTEP diagram of the complex **2** with the atom numbering scheme.

two significantly unequal Mn–O_{bridge} bonds. But the difference between two Mn–O_{bridge} bond distances is more prominent in complex **1** than in the complex **2**. There is also a difference between bridged and non-bridged Mn–O bond distances, obviously the Mn–O_{bridge} bond is longer than the other Mn–O bond. The Mn–Mn* distances and Mn–O–Mn* angles are 3.611(1) and 3.341(2) Å and 96.76° and 101.83°, respectively, for complexes **1** and **2**.

Table 2
Selected bond lengths (Å) and angles (°) for **1** and **2**

*Complex **1***			
Mn(1)–O(1)	1.88(1)	O(1)–Mn(1)–O(2)	92.5(5)
Mn(1)–O(2)	1.854(8)	O(1)–Mn(1)–N(1)	86.0(6)
Mn(1)–N(1)	2.033(10)	O(2)–Mn(1)–N(1)	167.5(6)
Mn(1)–N(2)	1.96(1)	O(1)–Mn(1)–N(2)	161.2(5)
Mn(1)–N(3)	2.13(2)	O(2)–Mn(1)–N(2)	92.3(5)
Mn(1)–O(2)*	2.87(1)	N(1)–Mn(1)–N(2)	85.4(6)
O(2)–Mn(1)*	2.87(1)	O(1)–Mn(1)–N(3)	96.6(6)
N(3)–N(4)	1.19(2)	O(2)–Mn(1)–N(3)	99.0(4)
N(4)–N(5)	1.15(2)	N(1)–Mn(1)–N(3)	93.5(5)
		N(2)–Mn(1)–N(3)	100.6(6)
		O(1)–Mn(1)–O(1)*	83.2(3)
*Complex **2***			
Mn(1)–O(1)	1.851(4)	O(1)–Mn(1)–O(2)	95.5(1)
Mn(1)–O(2)	1.913(1)	O(1)–Mn(1)–N(1)	172.4(2)
Mn(1)–N(1)	1.993(4)	O(2)–Mn(1)–N(1)	88.8(2)
Mn(1)–N(2)	2.016(5)	O(1)–Mn(1)–N(2)	90.5(2)
Mn(1)–N(3)	2.166(6)	O(2)–Mn(1)–N(2)	167.7(2)
Mn(1)–O(2)*	2.375(5)	N(1)–Mn(1)–N(2)	84.1(2)
O(2)–Mn(1)*	2.375(5)	O(1)–Mn(1)–N(3)	92.6(2)
N(3)–N(4)	1.199(6)	O(2)–Mn(1)–N(3)	94.8(2)
N(4)–N(5)	1.156(7)	N(1)–Mn(1)–N(3)	93.2(2)
		N(2)–Mn(1)–N(3)	95.7(2)
		O(2)–Mn(1)–O(2)*	78.2(2)

3.2. Magnetic properties

The variable temperature magnetic susceptibility of complexes **1** and **2** was measured in the range 5–300 K. A μ_{eff} (BM) versus T plot is given in Fig. 3, while the plots of χ_M versus T are given in Figs. 4 and 5 for complexes **1** and **2**, respectively. The μ_{eff} values of **1** and **2** are 6.99 and 6.89 BM, respectively, at 300 K. This suggests both the dimeric complexes possess an $S = 4$ ground state at room temperature. On lowering of temperature the μ_{eff} values of complex **1** remains almost unaltered up to ca. 100 K, then gradually increased to a value of 8.08 BM. On the other hand the μ_{eff} versus T plot for complex **2** shows a sharp downward turn at ca.

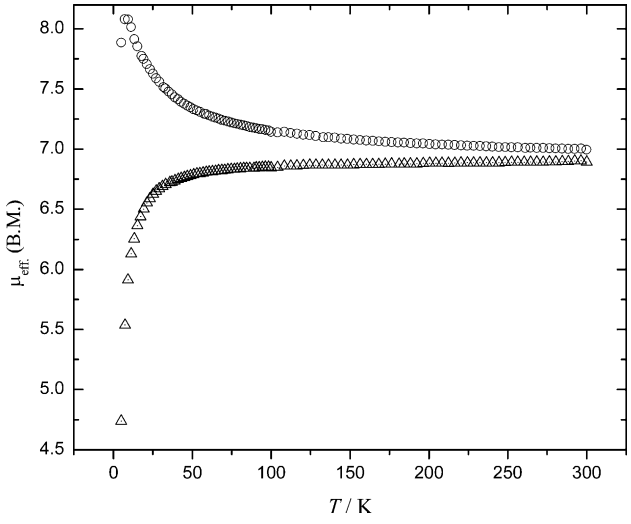

Fig. 3. A plot of μ_{eff} (BM) vs. T (K) for complex **1** (○) and **2** (△).

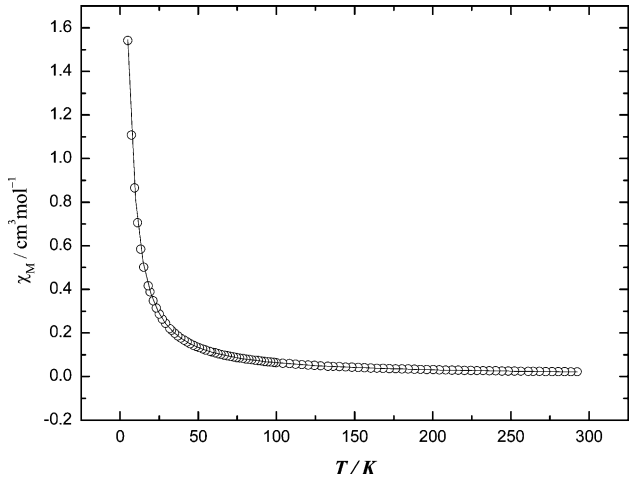

Fig. 4. A plot for complex **1** of temperature dependence of χ_M ($cm^3\ mol^{-1}$) vs. T (K). The solid lines are theoretical fits based on Eq. (I).

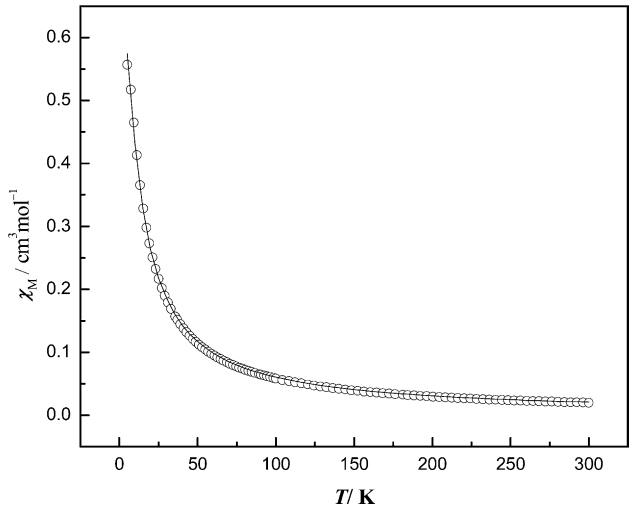

Fig. 5. A plot for complex **2** of temperature dependence of χ_M ($cm^{-3}\ mol^{-1}$) vs. T (K). The solid lines are theoretical fits based on Eq. (II).

50 K and reaches a value of 4.73 BM at 5 K. Besides, the Curie–Weiss plot (not shown) $[\chi^{-1}(T)]$ afforded the Curie (C) and Curie–Weiss (θ) constants 5.99 emu $mol^{-1}\ K^{-1}$, 4.77 K and 5.95 emu $mol^{-1}\ K^{-1}$, −2.39 K, for complex **1** and **2**, respectively. All these are indicating that the overall magnetic interaction between the Mn^{III} ions in complex **1** is ferromagnetic, whereas an antiferromagnetic coupling is operative in complex **2**.

Eqs. (I) and (II) were used for calculating the susceptibilities of complex **1** and **2**, respectively. For a ferromagnetic dimer with $S = 4$ ground state, the equation is as follows [28,29]:

$$\chi = [2Ng^2\beta^2/k(T-\alpha)][A/B],$$
$$A = 30 + 14\exp(-8J/kT) + 5\exp(-14J/kT) + \exp(-18J/kT),$$
$$B = 9 + 7\exp(-8J/kT) + 5\exp(-14J/kT) + 3\exp(-18J/kT) + \exp(-20J/kT). \quad \text{(I)}$$

For an antiferromagnetic dimeric system the equation can be written as [30]:

$$\chi = [2Ng^2\beta^2/kT][A/B],$$
$$A = \exp(J/kT) + 5\exp(3J/kT) + 14\exp(6J/kT) + 30\exp(10J/kT),$$
$$B = 1 + 3\exp(J/kT) + 5\exp(3J/kT) + 7\exp(6J/kT) + 9\exp(10J/kT). \quad \text{(II)}$$

The terms N, g, β and k have their usual meaning. The best fit of the magnetic data was obtained with the following set of parameters $J = 1.32\ cm^{-1}$, $g = 1.995$, $R = 2.52 \times 10^{-6}$ and $\alpha = -1.33$ for complex **1** (Fig. 4). The α term is introduced in the susceptibility equation (I) to account for the intradimer interaction for which the decrease of μ_{eff} in the very low temperature region was observed (Fig. 3). For complex **2** the fitting of the magnetic data afforded $J = -0.55\ cm^{-1}$, $g = 2.04$ and $R = 1 \times 10^{-5}$ (Fig. 5), where $R = \sum(\chi_{M_{obs}} - \chi_{M_{calc}})^2 / \sum(\chi_{M_{obs}})^2$.

The studies of magneto-structural correlation including theoretical calculations of phenoxo-bridged Mn^{III} complexes are sparse in the literature [31]. DFT calculations show that the phenoxo-bridged complexes of Cu^{II} and Ni^{II} are usually antiferromagnetic in nature [31]. Recently, Miyasaka et al. have studied a series of Mn^{III} Schiff base complexes structurally and magnetically [20]. Magneto-structural correlation of these complexes show that factors like Mn–O* [O* denotes the symmetry (−X,

Table 3
Important bond distances (Å) and angles (°) and magnetic parameters of some phenoxo-bridged Mn(III) complexes

Entry No.	Mn–O	Mn–O*	O–Mn–O*	Mn–O–Mn*	Mn–Mn*	F/AF	g	J/cm^{-1}	Ref.
1	1.912(4)	2.375(5)	78.17(19)	101.83	3.341(2)	AF	2.00	−0.55	This study
2	1.88(1)	2.87(1)	83.22	96.76	3.611	F	1.99	1.32	This study
a	1.872(2)	3.441(2)	83.76(8)	96.24(8)	4.0923(8)	F	1.99	0.55	[20]
b	1.877(2)	3.758(3)	83.43(10)	96.57(10)	4.3885(9)	F	2.03	0.12	[20]
c	1.912(3)	2.305(2)	76.6(1)	103.4(1)	3.318(1)	AF		−1.68	[16]
d	1.880(6)	2.750(6)	81.3(2)	98.7(2)	3.558(3)	AF			[17]

1, $[Mn_2(L1^{2-})_2(N_3)_2]$; **2**, $[Mn_2(L2^{2-})_2(N_3)_2]$; **a**, $[Mn_2(saltmen)_2(NCS)_2]$; **b**, $[Mn_2(naphtmen)_2(NCS)_2]$; **c**, $[Mn_2L_2(H_2O)_4](ClO_4)_4$; **d**, $[Mn_2(salen)_2(NCS)_2]$. saltmen, *N*,*N*′-(1,1,2,2,-tetramethylethylene)-bis-(salicylideneiminate); naphtmen, *N*,*N*′-(1,1,2,2,-tetramethylethylene)-bis-(naphthylideneiminate); AF, antiferromagnetic; F, ferromagnetic.

$-Y$, $-Z$) related phenoxo oxygen] distances, stereo-electronic character of the Schiff base, Jahn–Teller distortion have considerable influences on the characteristics of the magnetic coupling in these dimers. The Mn–O* distances are relatively longer in the case of complexes having ferromagnetic interaction, while their antiferromagnetic counterparts have shorter Mn–O* distances (Table 3). The electronic configuration of a Jahn–Teller elongated Mn^{III} ion is $t_{2g}^3e_g^1(d_z2^1)$ with a $^5B_1$ ground state [32]. The methyl group being electron releasing enhances the J–T orbital splitting. Thus the Jahn–Teller elongation increases the possibility of the orthogonality between e_g and $d\pi$ orbitals in Mn^{III} ions; as a result, a ferromagnetic interaction is favored in such cases. Both of these factors are more pronounced in complex **1** than in **2**, which might be leading the former to show a ferromagnetic coupling. It is apparent from a cursory look at Table 3 that ferromagnetic coupling predominates for a complex with smaller Mn–O–Mn* angles ($\angle$Mn–O–Mn* $\approx 96°$). Although no theoretical calculations are reported so far on the magneto-structural correlation of such Mn^{III} dimers, DFT calculation of oxo-bridged model complex $[(NH_3)_4Mn^{II}(\mu\text{-}O)_2(NH_3)_4]$ shows that J value is maximum at around $\angle$Mn–O–Mn $\approx 97°$ [31].

It is noteworthy that the azido derivatives of Mn^{III} quadridentate Schiff base complexes were synthesized in anticipation of azide being an efficient and versatile bridging ligand which would rather form a stronger bridge between metal ions and would functionalize Mn^{III} further to give a polymetallic assembly. This is indeed happened in the case of other Schiff base complexes [9,10]. Instead in the present case Mn^{III} ions prefer to form phenoxo-bridged dimers keeping the azides in the terminal positions. Although more complex and dynamic situations are encountered in metalloproteins, it is tempting to mention that the manganese catalase which consists of Mn_2^{III} moieties shows the same preference by not forming Mn^{III}–Mn^{III} bridges through azide which is often found in other metalloproteins [33,34] when azide is used as a ligand to study the interaction between small molecules and the metal centers of proteins [35].

4. Supplementary data

Supplementary data are available from The Director, CCDC, 12 Union Road, Cambridge, CB2 1EZ, UK (fax: +44-1223-336033; e-mail: deposit@ccdc.cam.ac.uk or www: http://www.ccdc.cam.ac.uk) on request, quoting the deposition number CCDC 215884 for complex **1** and 215885 for complex **2**.

Acknowledgements

The work was financially supported by the University Grants Commission by a grant (F.12-9/2002-SR-1) to S.K. P.G. and A.B. are grateful for financial help from the Deutsche Forschungsgemeinschaft (Priority program "Molecular Magnetism") and the Fonds der Chemische Industrie.

References

[1] E.J. Larson, V.L. Pecoraro, in: V.L. Pecoraro (Ed.), Manganese Redox Enzymes, VCH Publishers, New York, 1992, p. 1.
[2] R.J. Debus, Biochim. Biophys. Acta 1102 (1992) 269.
[3] G.C. Dismukes, Chem. Rev. 96 (1996) 2909.
[4] N.A. Law, M.T. Caudle, V.L. Pecoraro, Adv. Inorg. Chem. 46 (1998) 305.
[5] A. Gelasco, V.L. Pecoraro, J. Am. Chem. Soc. 115 (1993) 7928.
[6] K.A. Jørgensen, Chem. Rev. 89 (1989) 431.
[7] P. Pietikäinem, A. Haikarainen, J. Mol. Catal. A, Chem. 180 (2002) 59.
[8] L.K. Thomson, S.K. Tandon, Comments Inorg. Chem. 18 (1996) 125.
[9] S. Koner, S. Saha, K. Okamato, J.-P. Tuchagues, Inorg. Chem. 42 (2003) 4668.
[10] (a) K.R. Reddy, M.V. Rajsekharan, J.-P. Tuchagues, Inorg. Chem. 37 (1998) 5978;
(b) A. Panja, N. Shaikh, P. Vojtíšek, S. Gao, P. Banerjee, New J. Chem. 26 (2002) 1025.
[11] T.K. Maji, P.S. Mukherjee, S. Koner, G. Mostafa, J.-P. Tuchagues, N. Ray Chaudhuri, Inorg. Chim. Acta 314 (2001) 111.
[12] Y. Cringh, S.W. Gordon-Wylie, R.E. Norman, G.R. Clark, S.T. Weintraub, C.P. Horwitz, Inorg. Chem. 36 (1997) 4968.
[13] C.E. Hulme, M. Watkinson, M. Haynes, R.G. Pritchard, C.A. McAulife, N. Jaibon, B. Beagley, A. Sousa, M.R. Bermejo, M. Fondo, J. Chem. Soc., Dalton Trans. (1997) 1805.
[14] M.R. Bermejo, A. Castiñeiras, J.C. Gacia-Monteagudo, M. Rey, A. Sousa, M. Watkinson, C.A. McAulife, R.G. Pritchard, R.L. Beddoes, J. Chem. Soc., Dalton Trans. (1996) 2935.
[15] A. Garcia-Deibe, A. Sousa, M.R. Bermejo, P.P. MacRory, C.A. McAulife, R.G. Pritchard, M. Helliwell, J. Chem. Soc., Chem. Commun. (1991) 728.
[16] N. Matsumoto, Z.J. Zhong, H. Ōkawa, S. Kida, Inorg. Chim. Acta 160 (1989) 153.
[17] B.J. Kennedy, K. Murray, Inorg. Chem. 24 (1985) 1552.
[18] H. Miyasaka, N. Matsumoto, H. Ōkawa, N. Re, E. Gallo, C. Floriani, J. Am. Chem. Soc. 118 (1996) 981.
[19] H.-L. Shyu, H.-H. Wei, Y. Wang, Inorg. Chim. Acta 290 (1999) 8.
[20] H. Miyasaka, R. Clérac, T. Ishii, H.-C. Chang, S. Kitagawa, M. Yamashita, J. Chem. Soc., Dalton Trans. (2002) 1528.
[21] O. Horner, E. Anxolabéhère-Mallart, M. Charlot, L. Tchertanov, J. Guilheim, T.A. Mattioli, A. Boussac, J. Girerd, Inorg. Chem. 38 (1999) 1222.
[22] (a) H.-L. Shyu, H.-H. Wei, G.-H. Lee, Y. Wang, J. Chem. Soc., Dalton Trans. (2000) 915;
(b) H.A. Kuska, M.F. Farona, P. Pappas, S. Potterton, J. Coord. Chem. 1 (1971) 259.
[23] S. Koner, A. Ghosh, N. Ray Chaudhuri, J. Chem. Soc., Dalton Trans. (1990) 1563.
[24] A. Altmore, G. Cascarano, C. Giacovazzo, A. Gugaliradi, M.C. Burla, G. Polidori, M. Camalli, J. Appl. Cryst. 27 (1994) 435.
[25] P.T. Berskens, G. Admiraal, G. Beurskens, W.P. Bosman, R. de Gelder, R. Israel, J.M.M. Smits, DIRDIF 94, The DIRDIF 94 program system, Technical Report of the Crystallography Laboratory, University of Nijmegen, The Netherlands, 1994.
[26] (a) TEXAN, Crystal Structure Analysis Package, Molecular Structure Corporation, 1985 and 1999.

(b) G.M. Sheldrick, SHELXS-97 and SHELXL-97, University of Göttingen, Germany, 1997.
[27] S. Sailaja, K. Rajeder Reddy, M.V. Rajsekharan, C. Hureau, E. Rivèire, J. Cano, J.-J. Girerd, Inorg. Chem. 42 (2003) 180.
[28] C. Chen, D. Huang, X. Zhang, F. Chen, H. Zhu, Q. Liu, C. Zhang, D. Liao, L. Li, L. Sun, Inorg. Chem. 42 (2003) 3540.
[29] Y. Sato, H. Miyasaka, N. Matsumoto, H. Ōkawa, Inorg. Chim. Acta 247 (1996) 57.
[30] O. Kahn, Molecular Magnetism, VCH, Weinheim, Germany, 1993, p. 114.
[31] E. Ruiz, S. Alvarez, P. Alemany, Chem. Commun. (1998) 2767.
[32] M. Corbella, R. Costa, J. Ribas, P.H. Fries, J.-M. Latour, L. Öhrström, X. Solans, V. Rodríguez, Inorg. Chem. 35 (1996) 1857.
[33] E.I. Solomon, U.M. Sundaram, T.E. Machonkin, Chem. Rev. 96 (1996) 2563.
[34] F. Tuczek, E.I. Solomon, Inorg. Chem. 32 (1993) 2850.
[35] T.C. Brunold, D.R. Gamelin, T.L. Stemmler, S.K. Mandal, W.H. Armstrong, J.E. Penner-Hahn, E.I. Solomon, J. Am. Chem. Soc. 120 (1998) 8724.

Available online at www.sciencedirect.com
SCIENCE DIRECT®
Polyhedron 23 (2004) 1819–1827
POLYHEDRON
www.elsevier.com/locate/poly

X-ray and electronic structure of the $[ReCl_3(pzH)_2(PPh_3)]$ and $[ReCl_3(3,5\text{-}Me_2pzH)_2(PPh_3)]$ complexes

Barbara Machura [a,*], M. Jaworska [b], Rafal Kruszynski [c,1]

[a] Department of Inorganic and Radiation Chemistry, Institute of Chemistry, University of Silesia, 9th Szkolna St., 40-006 Katowice, Poland
[b] Department of Theoretical Chemistry, Institute of Chemistry, University of Silesia, 9th Szkolna St., 40-006 Katowice, Poland
[c] Department of X-ray Crystallography and Crystal Chemistry, Institute of General and Ecological Chemistry, Łódź University of Technology, 116 Żeromski St., 90-924 Łódź, Poland

Received 17 March 2004; accepted 13 April 2004
Available online 18 May 2004

Abstract

X-ray structures of new $[ReCl_3(pzH)_2(PPh_3)]$ and $[ReCl_3(3,5\text{-}Me_2pzH)_2(PPh_3)]$ complexes (pzH = pyrazole) have been determined, and the geometric parameters of $[ReCl_3(pzH)_2(PPh_3)]$ have been examined using density functional theory (DFT) method. The UV–Vis spectra of the complexes have been discussed on the basis of the electronic transitions of $[ReCl_3(pzH)_2(PPh_3)]$ calculated with time-dependent DFT method (TDDFT).
© 2004 Elsevier Ltd. All rights reserved.

Keywords: Rhenium complexes; Pyrazole ligand; X-ray structure; DFT calculations

1. Introduction

The noticeable growth of interest in the rhenium coordination chemistry is connected with the favourable nuclear properties of ^{186}Re and ^{188}Re nuclides, which make the radioisotopes useful for diagnostic nuclear medicine and applications in radioimmunotherapy [1,2]. Although pyrazole and its derivatives have a special place among N-donor ligands, the number of rhenium complexes containing these ligands is limited [2–6].

Previously, we investigated the reactivity of oxorhenium(V) species – $[ReO(OEt)X_2(PPh_3)_2]$, $[ReOX_3(PPh_3)_2]$ and $[ReOX_3(AsPh_3)(OAsPh_3)]$ (X = Cl or Br) – towards pyrazole (pzH) and 3,5-dimethylopyrazole (3,5-Me_2pzH) under various reaction conditions. The products of these syntheses include: (i) mononuclear $[ReOX_2\{\eta^2\text{-}N_2C_3H_3C(CH_3)_2O\}(PPh_3)]$ complexes with $C_3H_3N_2C(CH_3)_2O^-$ anion obtained in the addition reaction of pyrazole and acetone and (ii) dinuclear Re(V) compounds of types $[\{Re(O)X(PPh_3)\}_2(\mu\text{-}O)(\mu\text{-}pz)_2]$, $[\{Re(O)X_2(3,5\text{-}Me_2pzH)_2\}_2(\mu\text{-}O)]$, $[\{Re(O)Br(3,5\text{-}Me_2pzH)\}_2(\mu\text{-}O)(\mu\text{-}3,5\text{-}Me_2pz)_2]$, $[\{Re(O)X(PPh_3)\}_2(\mu\text{-}O)(\mu\text{-}3,5\text{-}Me_2pz)_2]$ and $[\{Re(O)X(PPh_3)\}(\mu\text{-}O)(\mu\text{-}3,5\text{-}Me_2pz)_2\{Re(O)X(3,5\text{-}Me_2pzH)\}]$ (X = Cl or Br) [7,8].

Here, we report the synthesis and X-ray structure of the two mononuclear Re(III) $[ReCl_3(pzH)_2(PPh_3)]$ (**1**) and $[ReCl_3(3,5\text{-}Me_2pzH)_2(PPh_3)]$ (**2**) complexes and the results of the density functional theory (DFT) calculations for **1**. The UV–Vis spectra of **1** and **2** are discussed basing on the electronic transitions of **1**, calculated using the time-dependent DFT method (TDDFT).

2. Experimental

2.1. General procedure

The reactions were carried out under argon atmosphere. All solvents were of reagent grade and were used as received. Ammonium perrhenate, Ph_3P and pyrazole (pzH) were purchased from Aldrich and used as

* Corresponding author. Tel.: +48322582441; fax: +48322599978.
E-mail addresses: basia@tc3.us.ich.edu.pl (B. Machura), mj@tc3.i-ch.us.edu.pl (M. Jaworska).
[1] A holder of the Foundation for Polish Science (FNP) scholarship.

0277-5387/$ - see front matter © 2004 Elsevier Ltd. All rights reserved.
doi:10.1016/j.poly.2004.04.017

received. $[Re(MeCN)Cl_3(PPh_3)_2]$ and $[ReOCl_3(PPh_3)_2]$ complexes and 3,5-Me_2pzH were prepared according to the literature methods [9–11].

IR spectra were recorded on a Nicolet Magna 560 spectrophotometer in the spectral range 4000–400 cm^{-1} with the samples in the form of KBr pellets. Electronic spectra were measured on a spectrophotometer Lab Alliance UV–Vis 8500 in the range 800–220 nm in deoxygenated dichloromethane solution. The magnetic susceptibility was determined with a superconducting quantum interference device (SQUID, Quantum Design) magnetometer. Elemental analyses (C, H and N) were performed on a Perkin–Elmer CHN-2400 analyser.

2.2. Preparation of $[ReCl_3(pzH)_2(PPh_3)]$ (**1**)

2.2.1. Method A (**1a**)

$[ReOCl_3(PPh_3)_2]$ (1 g, 1.20 mmol) and pzH (0.54 g, 8 mmol) in diisopropyl ketone (60 cm^3) were refluxed for 2 h. The starting material gradually dissolved and the colour of the reaction solution changed from green to dark brown. The volume of the reaction solution was condensed to 20 cm^3 and reddish-orange microcrystalline solid was formed by an addition of 100 cm^3 of diethyl ether. The product was washed with EtOH and cold ether, and dried in vacuo.

2.2.2. Method B (**1b**)

$[Re(MeCN)Cl_3(PPh_3)_2]$ (1 g, 1.20 mmol) and pzH (0.54 g, 8 mmol) in chloroform (80 cm^3) were refluxed for 4 h. The starting material gradually dissolved and the colour of the reaction solution became dark red. After 3 h, the reddish-orange microcrystalline solid started to participate. The volume was condensed to 10 cm^3, diethyl ether (100 cm^3) was added and reddish-orange microcrystalline solid was filtered. The product was washed with EtOH and cold ether, and dried in vacuo.

The crystals of **1a** and **1b** suitable for X-ray investigation were obtained by recrystallization from a mixture of acetonitrile and dichloromethane (yield 80%).

The solvents used for the reactions and recrystallization were not dried, so some water was present in the reaction systems and water molecule was found in **1b** structure.

IR(KBr, cm^{-1}) 3154 (s), 3134 (m) 3115 (w), 2939 (m), 2903 (m), 2840 (m), 2810 (w), 1610 (w) 1572 (w), 1497 (w), 1479 (m), 1458 (m), 1435 (s), 1400 (s), 1346 (w), 1317 (m), 1256 (m) 1192 (w), 1126 (s), 1093 (s), 1068 (w), 1050 (m), 1042 (s), 999 (w), 955 (w), 906 (w), 854 (w), 788 (m), 768 (m), 746 (s), 698 (s), 689 (s), 609 (w), 598 (w), 526 (s), 510 (s), 495 (m), 449 (w), 432 (w). Anal. Calc for $C_{24}H_{23}N_4Cl_3PRe$: C, 41.72; H, 3.35; N, 8.11. Found: C, 41.98; H, 3.56; N, 8.20%.

2.3. Preparation of $[ReCl_3(3,5\text{-}Me_2pzH)_2(PPh_3)]$ (**2**)

$[Re(MeCN)Cl_3(PPh_3)_2]$ (1 g, 1.20 mmol) and 3,5-Me_2pzH (0.77 g, 8 mmol) in chloroform (80 cm^3) were refluxed for 4 h. The starting material gradually dissolved and the colour of the reaction solution became dark red. After 3 h, the reddish-orange microcrystalline solid started to participate. The volume was condensed to 10 cm^3, diethyl ether (100 cm^3) was added and reddish-orange microcrystalline solid was filtered. The product was washed with EtOH and cold ether, and dried in vacuo. The crystals of **2** suitable for X-ray investigation were obtained by recrystallization from a mixture of acetonitrile and dichloromethane (yield 85%).

IR(KBr, cm^{-1}) 3384 (s), 3354 (s) 3138 (w), 3055 (m), 2922 (m), 1567 (s) 1482 (m), 1465 (w), 1432 (s), 1395 (m), 1372 (m), 1275 (s) 1177 (m), 1149 (m), 1091 (s), 1031 (s), 999 (w), 813 (w), 800 (m), 744 (s), 694 (s), 650 (m), 644 (m), 555 (w), 524 (s), 511 (s), 497 (s), 448 (m). *Anal.* Calc. for $C_{28}H_{31}N_4Cl_3PRe$: C, 45.01; H, 4.18; N, 7.50. Found: C, 45.33; H, 4.29; N, 7.60%.

2.4. Crystal structures determination and refinement

The X-ray intensity data were collected on a KM-4-CCD automatic diffractometer equipped with CCD detector with 24, 32 and 40 s exposure time (for compounds **1a**, **1b** and **2**, respectively) was used and the whole Ewald sphere (up to $2\theta = 50°$) was collected. The unit cell parameters were determined from least-squares refinement of the setting angles of 8345°, 6543° and 5421° (respectively, as above) of strongest reflections. Details concerning crystal data and refinement are given in Table 1. Lorentz, polarization and numerical absorption corrections [12] were applied. The structures was solved by the Patterson method and subsequently completed by the difference Fourier recycling. All the non-hydrogen atoms were refined anisotropically using full-matrix, least-squares technique. The hydrogen atoms of the phenyl rings were treated as ''riding'' on their parent carbon atoms [d(C–H) = 0.96 Å] and assigned isotropic temperature factors equal 1.2 times the value of equivalent temperature factor of the parent carbon atom. SHELXS 97 [13], SHELXL 97 [14] and SHELXTL [15] programs were used for all the calculations. Atomic scattering factors were those incorporated in the computer programs.

The crystals of **1a** have the diffused electron density originated from multipositional disordered solvent water molecule around special position 0, 1/2 and 1/2. This effect was repeatable for all measured crystals in the sample. In the crystals of **1b** it can be found slightly dynamically disordered water molecule that is also statically disordered in two symmetry equivalent positions.

The N2/C21 and N4/C24 atoms in structure of **1** were distinguished on the basis of anisotropic parameters. Changing the carbon atoms to nitrogen and vice versa

Table 1
Crystal data and structure refinement for **1a**, **1b** and **2**

	1a	**1b** ($1 \cdot 1/2H_2O$)	**2**
Empirical formula	$C_{24}H_{23}Cl_3N_4PRe$	$C_{24}H_{24}Cl_3N_4O_{0.5}PRe$	$C_{28}H_{31}Cl_3N_4PRe$
Formula weight	690.98	699.99	747.09
Temperature (K)	291(2)	293(2)	293(2)
Wavelength (Å)	0.71073	0.71073	0.71073
Space group	$P2_1/n$	$P2_1/n$	$P\bar{1}$
Crystal system	monoclinic	monoclinic	triclinic
Unit cell dimensions			
a (Å)	11.4910(9)	11.4101(6)	10.2682(8)
b (Å)	17.5839(15)	17.6808(9)	13.0183(15)
c (Å)	13.8284(12)	13.7198(9)	13.0572(14)
α (°)			66.249(11)
β (°)	108.030(7)	107.418(5)	76.127(8)
γ (°)			68.374(9)
Volume (Å^3)	2656.9(4)	2640.9(3)	1476.6(3)
Z	4	4	2
D_{calc} (Mg m^{-3})	1.727	1.761	1.680
Absorption coefficient (mm^{-1})	4.955	4.988	4.465
$F(000)$	1344	1364	736
Crystal size (mm)	$0.69 \times 0.26 \times 0.06$	$0.22 \times 0.11 \times 0.04$	$0.26 \times 0.12 \times 0.10$
θ range for data collection (°)	3.61–25.16	3.08–25.11	3.19–25.10
Index ranges	$-13 \leqslant h \leqslant 13$	$-13 \leqslant h \leqslant 13$	$-12 \leqslant h \leqslant 12$
	$-20 \leqslant k \leqslant 20$	$-21 \leqslant k \leqslant 21$	$-15 \leqslant k \leqslant 15$
	$-16 \leqslant l \leqslant 16$	$-16 \leqslant l \leqslant 16$	$-15 \leqslant l \leqslant 15$
Reflections collected	29 535	27 515	14 778
Independent reflections	4740 ($R_{int} = 0.0691$)	4703 ($R_{int} = 0.0566$)	5249 ($R_{int} = 0.0770$)
Completeness to 2θ (%)	96.0	96.4	99.8
Maximum and minimum transmission	0.769 and 0.130	0.887 and 0.406	0.770 and 359
Data/restraints/parameters	4740/0/298	4703/0/307	5249/0/336
Goodness-of-fit on F^2	1.156	1.096	0.991
Final R indices [$I > 2\sigma(I)$]	$R_1 = 0.0566$	$R_1 = 0.0331$	$R_1 = 0.0293$
	$WR_2 = 0.1453$	$wR_2 = 0.0727$	$wR_2 = 0.0648$
R indices (all data)	$R_1 = 0.0580$	$R_1 = 0.0482$	$R_1 = 0.0353$
	$WR_2 = 0.1465$	$wR_2 = 0.0782$	$wR_2 = 0.0667$
Largest difference peak and hole (e Å^{-3})	2.887 and −1.123	1.029 and −0.791	1.355 and −0.833

1a, data for the **1** complex obtained according to method A.
1b, data for the **1** complex obtained according to method B.

cause anisotropic displacement parameters to be senseless.

2.5. Computational details

GAUSSIAN 03 program [16] was used in the calculations. The geometry optimization was carried out using the DFT method with the use of B3LYP functional [17,18]. The electronic spectrum was calculated with the TDDFT method [19].

LANL2DZ basis set [20] was used on the rhenium atom, 6-31G(d) on the chlorine, nitrogen, phosphorus and carbon atoms and 6-31G basis on the hydrogen atoms in the calculations.

3. Results and discussion

Two different routes have been employed for the preparation of **1**. The refluxing of $[ReOCl_3(PPh_3)_2]$ with pzH in diisopropyl ketone gives the complex **1** in moderate yield. The well-known capacity of PPh_3 to interact with the Re≡O bond in the rhenium(V) oxo-complexes explains the course of the reaction between $[ReOCl_3(PPh_3)_2]$ and pyrazole:

$$2[ReOCl_3(PPh_3)_2] + 2N_2C_3H_4 \rightarrow [ReCl_3(pzH)_2(PPh_3)] + OPPh_3$$

A higher yield of **1** has been reported for the substitution reaction:

$$[ReCl_3(MeCN)(PPh_3)_2] + 2pzH \rightarrow [ReCl_3(pzH)_2(PPh_3)] + MeCN + PPh_3.$$

The complex **2** has been obtained in the reaction of $[ReCl_3(MeCN)(PPh_3)_2]$ with 3,5-Me_2pzH. The excess of pyrazole and 3,5-Me_2pzH used in the reactions ensure the maximum yield of the complexes.

3.1. X-ray structure

A perspective drawings of **1** and **2** are given in Figs. 1 and 2, respectively. The rhenium atom of the both

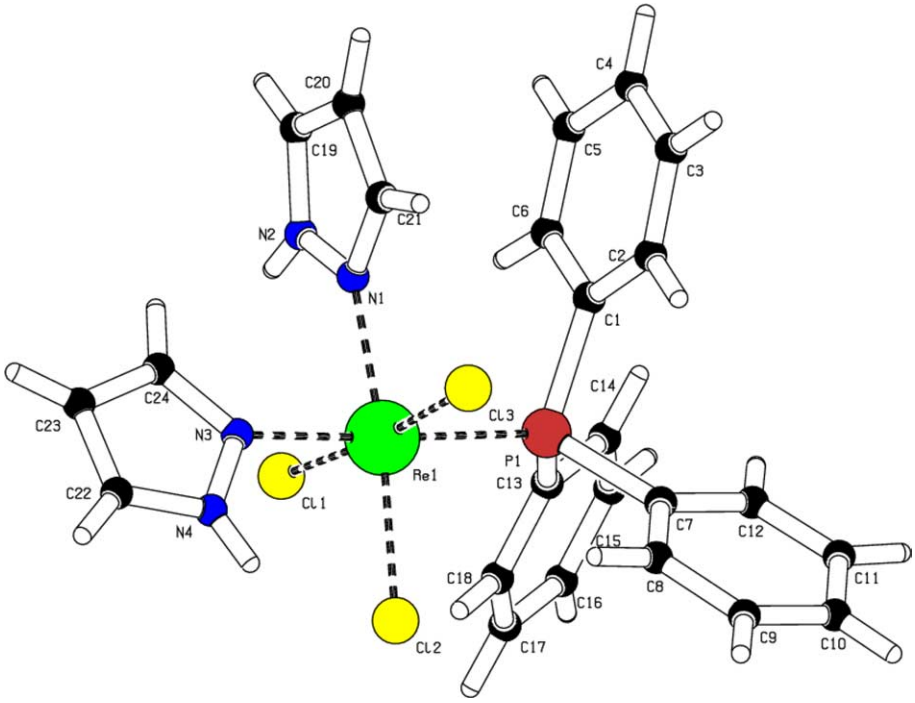

Fig. 1. The molecular structure of **1**.

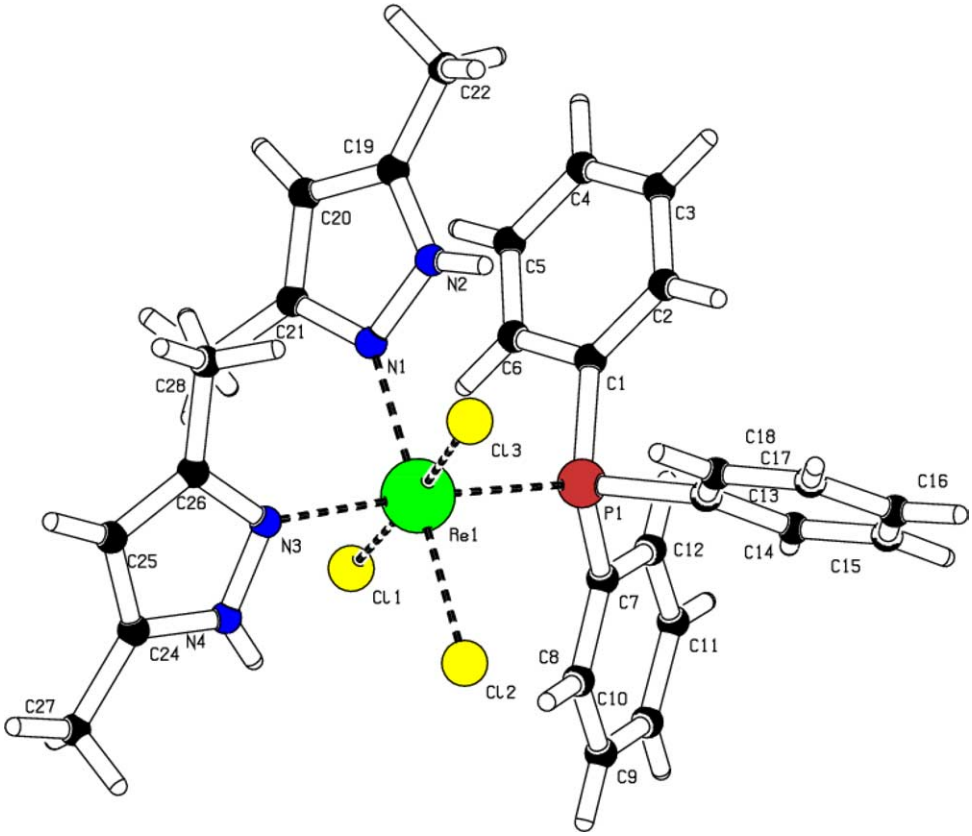

Fig. 2. The molecular structure of **2**.

complexes is in distorted octahedral environment with three chlorine ligands in *mer* geometry, two N-donor ligands (pzH or 3,5-Me_2pzH) in *cis* position to each other and one PPh_3 molecule occupying *trans* position to N(3) atom. Table 1 presents crystal data and structural refinement for **1a**, **1b** and **2**. The most important bond lengths and angles for compounds **1a**, **1b** and **2** are reported in Table 2. A notable *trans* influence of triphenylphosphine ligand is observed in both complexes; the Re–N(3) bond lengths are longer in comparison with the corresponding Re–N(1) distances. The Re–N, Re–Cl and Re–P bond lengths are unexceptional, they agree well with appropriate values found previously in similar rhenium compounds [7,8,21–23].

The weak intramolecular and intermolecular hydrogen bonds [24–26] of **1** and **2** are presented in Table 3.

3.2. Infrared data

The strong bands in the range assignable to N–H vibrations (3400–3100 cm^{-1}) in the IR spectra of **1** and **2** confirm the coordination of pyrazoles ligands in the neutral monodentate form. The characteristic bands of the C=C and C=N stretching modes, observed at 1640 and 1558 cm^{-1} in uncomplexed pyrazole and at 1663 and 1595 cm^{-1} in uncomplexed 3,5-dimethylpyrazole, are shifted to considerable lower frequencies.

3.3. Magnetochemical measurements

Magnetic susceptibilities of **1** were recorded over the temperature range 5–300 K. Temperature dependence of the molar magnetic susceptibility for **1** is presented in Fig. 3. The observed room-temperature effective magnetic moment 1.2 BM is typical of the rhenium(III) mononuclear complexes. It consistent with low-spin rhenium(III) (d^4) ions in O_h field [27] and arises because of the large spin–orbit coupling ($\xi = 2500$ cm^{-1}) [28].

3.4. The optimized geometry and molecular orbitals of *1*

The geometry of **1** was optimized in triplet and singlet states using the DFT method with the B3LYP functional. The energy of the singlet state is of 16.3 kcal higher. The optimized geometric parameters of the triplet state are gathered in Table 2. The optimized geometry of **1** is in good agreement with the experimental one and the largest differences are found for Re–Cl bond distances.

The selected HOMO and LUMO orbitals with α-spin for **1** are depicted in Fig. 4. The following orientation of the axes has been used for determination of the MO characters: the *z*-axis goes along Cl(1)–Re–Cl(3) linkage and *x* goes through the N(3)–Re–P(1) bonds. The rhenium d_π atomic orbital (d_{xz}, d_{yz} and d_{xy}) and π orbitals of chlorine ligands in anti-bonding arrangement make main contributions into the HOMO-2, HOMO-1 and

Table 2
The experimental bond lengths (Å) and angles (°) for **1a**, **1b** and **2** and the optimized bond lengths (Å) and angles (°) for **1**

	Experimental		Optimized	Experimental
	1a	**1b**	**1**	**2**
Bond lengths				
Re(1)–Cl(1)	2.345(2)	2.3452(15)	2.448	2.3713(12)
Re(1)–Cl(2)	2.400(2)	2.3993(15)	2.489	2.3956(11)
Re(1)–Cl(3)	2.357(2)	2.3614(15)	2.407	2.4009(12)
Re(1)–N(1)	2.135(7)	2.127(5)	2.166	2.135(3)
Re(1)–N(3)	2.167(8)	2.194(5)	2.164	2.185(3)
Re(1)–P(1)	2.421(2)	2.4296(14)	2.487	2.4466(11)
Bond angles				
N(1)–Re(1)–N(3)	85.8(3)	85.98(16)	87.13	89.24(12)
N(1)–Re(1)–Cl(1)	87.4(2)	86.75(13)	87.12	92.87(9)
N(3)–Re(1)–Cl(1)	87.1(2)	88.20(12)	88.59	86.70(10)
N(1)–Re(1)–Cl(2)	173.80(19)	173.97(12)	173.88	174.36(9)
N(3)–Re(1)–Cl(2)	88.2(2)	88.48(12)	87.21	87.22(9)
Cl(1)–Re(1)–Cl(2)	90.43(9)	90.71(6)	90.42	91.31(4)
N(1)–Re(1)–Cl(3)	88.7(2)	89.21(13)	87.52	85.92(9)
N(3)–Re(1)–Cl(3)	87.7(2)	87.38(12)	89.43	88.26(10)
Cl(1)–Re(1)–Cl(3)	173.77(9)	174.21(6)	174.37	174.83(4)
Cl(2)–Re(1)–Cl(3)	92.89(9)	92.90(6)	94.75	89.58(4)
N(1)–Re(1)–P(1)	92.03(19)	91.40(12)	93.40	93.47(9)
N(3)–Re(1)–P(1)	177.2(2)	175.94(12)	178.99	172.08(10)
Cl(1)–Re(1)–P(1)	94.67(8)	94.75(5)	92.30	85.73(4)
Cl(2)–Re(1)–P(1)	93.94(8)	94.26(5)	92.30	90.61(4)
Cl(3)–Re(1)–P(1)	90.36(8)	89.49(5)	89.73	99.35(4)

Table 3
Hydrogen bonds for **1a**, **1b** and **2**

D	A	H···A		D···A		D–H···A	
		1a	**1b**	**1a**	**1b**	**1a**	**1b**
N(4)	Cl(2)	2.60	2.57	3.114(8)	3.102(6)	119.8	120.6
N(4)	Cl(2#1)	2.55	2.58	3.225(8)	3.254(6)	135.7	135.5
N(2)	Cl(1)	2.65	2.63	3.148(12)	3.112(7)	117.9	116.8
C(8)	Cl(2)	2.77		3.439(11)		129.8	
C(8)	Cl(3)	2.83		3.507(11)		130.9	
C(21)	Cl(3)	2.58	2.62	3.136(10)	3.159(6)	118.7	117.4
C(14)	Cl(2)		2.74		3.425(6)		131.2
2							
N(2)	Cl(3)	2.71		3.105(4)		111.7	
N(4)	Cl(2)	2.79		3.155(4)		111.5	
C(8)	Cl(2)	2.68		3.526(6)		151.8	
C(18)	Cl(3)	2.54		3.435(6)		160.4	
C(20)	Cl(2#2)	2.81		3.629(5)		147.1	
C(28)	Cl(3)	2.68		3.511(5)		144.9	

#1: $2-x,-y,1-z$ for **1a** and $-x,-y,-z$ for **1b**.
#2: $x-1,y,z$.

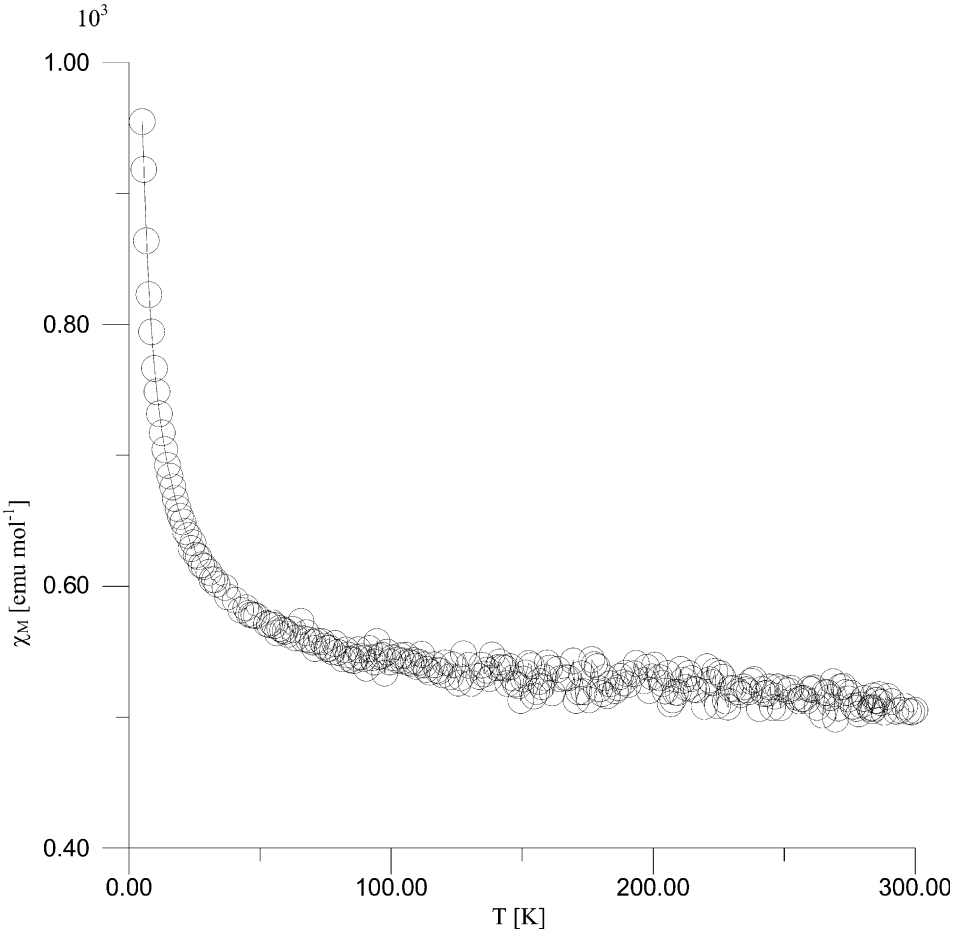

Fig. 3. Temperature dependence of the molar susceptibility for **1**.

HOMO with α-spin and HOMO, LUMO and LUMO + 1 with β-spin. The HOMO orbitals have also the antibonding contribution from the pyrazole ligands. The lower lying orbitals are π orbitals of the phenyl groups and pyrazole ligands. HOMO-11 and HOMO-5 with α-spin and HOMO-9 and HOMO-3 with β-spin

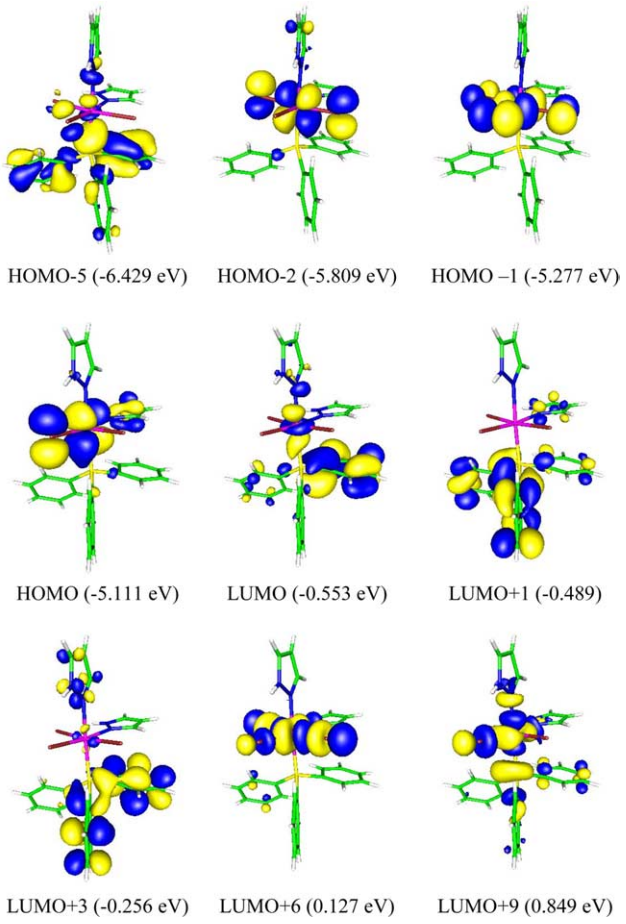

Fig. 4. The selected HOMO and LUMO orbitals with α-spin for **1**.

have a substantial contribution from the free electron pairs on the phosphorus atom. The LUMO+6 with α-spin and the LUMO+10 with β-spin are the antibonding orbital of $d_{z2} - \sigma_{Cl}$ character. The LUMO+9 with α-spin and the LUMO+11 with β-spin are the antibonding orbital of $d_{x^2-y^2} - \sigma_{Cl} - \sigma_N - \sigma_P$ character. LUMO, LUMO + 3 and LUMO + 1 with α-spin, and LUMO+2 and LUMO+3 with β-spin have large participation of p phosphorus orbitals.

3.5. UV–Vis spectra of *1* and *2* and electronic spectrum of *1* from the TDDFT calculations

The complexes under investigation are high spin systems. The calculations with TDDFT method for open-shell organic, inorganic and organometallic molecules are still limited but a few studies have already appeared and supported the TDDFT method to be applicable for such systems giving good assignment of experimental spectra [29–33]. There are also several works performed with this method for 5d-metal (including rhenium complexes) in which good correlations between experimental and calculated results have been confirmed [34–40].

The energy and molar absorption coefficients of experimental absorption bands of **1** and **2** are presented in Table 4. The spin-allowed triplet–triplet electronic transitions of **1** calculated with the TDDFT method are presented in Table 5. Except for the low energy part of the spectrum, only transitions with oscillator strengths larger than 0.01 are listed. The UV–Vis spectrum of **1** was calculated only to 260 nm. Nevertheless, on the basis of the calculated transitions for PPh_3 and [$ReCl_3(pzH)_3$] [41], it can be assumed that the experimental bands of **1** and **2** at energy below 240.0 nm correspond to intraligand $\pi \rightarrow \pi^*$ transitions in phosphine and pyrazole ligands. The solution spectra of pyrazole and PPh_3 exhibit intense absorption band at 231.6 and 217.6 nm, respectively, which can support this assignment.

The assignment of the calculated transitions to the experimental bands was based on the criterion of the energy and oscillator strength of the calculated transition. The long-wave experimental bands are of low intensity and they are compared to the calculated long-wave transitions with small oscillator strengths. The remaining absorption experimental bands are of much higher intensity and they are compared to the calculated transitions with high oscillator strengths.

The longest wave experimental bands of **1** and **2** (at 507.3 and 547.8 nm, respectively) may be attributed to the calculated transitions of $\pi_{Cl} \rightarrow d$ and $\pi_{Ph} \rightarrow d$ character (at 407.4 and 401.0 nm) and $d \rightarrow \pi^*_{Ph}$ character (at 404.5 nm) with small oscillator strengths. The transitions from π_{Ph} to metal d orbitals are mediated by phosphorus.

The next experimental bands of **1** and **2** (at 390.8 and 379.6 nm, respectively) can be assigned to the calculated transitions at 385.5 and 381.4 nm. They have MLCT ($d \rightarrow \pi^*_{pzH}$) character with small contribution of d–d

Table 4
The energy and molar absorption coefficients of experimental absorption bands for **1** and **2**

Band position (nm)	Band position (eV)	ε
1		
507.3	2.44	350
390.8	3.17	1040
331.1	3.74	1620
263.8	4.70	2200
238.0	5.21	3900
200.1	6.20	7200
2		
547.8	2.26	400
379.6	3.27	1220
338.4	3.66	3700
269.0	4.61	5470
229.0	5.41	8910
213.0	5.82	7330

ε, molar absorption coefficient ($dm^3\ mol^{-1}\ cm^{-1}$).

Table 5
The most important electronic transitions calculated with the TDDFT method for **1**

The most important orbital excitations		λ (nm)	E (eV)	f
α-spin	β-spin			
	H-5(π_{Cl}) → L(d)	407.4	3.04	0.0004
	H-2(π_{Ph}) → L(d)			
	H(d_{xy}) → L + 3(π^*_{Ph})	404.5	3.06	0.0028
	H(d_{xy}) → L + 8(π^*_{Ph})			
	H-3 (n_P + π_{Ph}) → L(d)	401.0	3.09	0.0080
	H(d_{xy}) → L + 4(π^*_{pzH})	385.5	3.22	0.0113
H(d_{xy}) → L + 6(d_{z2})	H(d_{xy}) → L + 2(π^*_{Ph})	381.4	3.25	0.0046
	H(d_{xy}) → L + 10(d_{z2})			
	H-1(π_{Ph}) → L(d_{xz})	376.1	3.30	0.0035
	H-4(π_{Ph}) → L(d_{xz})	355.3	3.49	0.0039
H(d_{xy}) → L(π^*_{Ph})		352.7	3.52	0.0033
	H-5(π_{Cl}) → L + 1(d_{yz})	351.2	3.53	0.0194
	H-2(π_{Ph}) → L + 1(d_{yz})			
H(d_{xy}) → L + 1(π^*_{Ph})		314.7	3.94	0.0266
H(d_{xy}) → L + 2(π^*_{pzH})		305.6	4.06	0.0491
	H-10(π_{Cl} + π_{pzH}) → L + 1(d_{yz})	283.7	4.37	0.0217
	H-9(π_{Cl} + π_{pzH} + π_{Ph} + n_p) → L + 1(d_{yz})			
	H-9(π_{Cl} + π_{pzH} + π_{Ph} + n_p) → L + 1(d_{yz})	280.9	4.41	0.0204
	H-6(π_{Ph}) → L + 1(d_{yz})			
H-2(d_{xz}) → L + 3(π^*_{Ph})	H-13(π_{pzH}) → L(d_{xz})	277.0	4.48	0.0253

electronic transitions. Owing to the small oscillator strengths, the three calculated transitions at 376.1, 355.3 and 352.7 nm of π_{Ph} → d and d → π^*_{Ph} character do not contribute significantly to the overall shape of the spectrum. In the experimental spectrum such small transitions are hidden under the more intense ones.

The experimental bands of **1** and **2** at 331.1 and 338.4 nm, respectively, are attributed to the calculated transitions at 351.2, 314.7 and 305.6 nm. The first one is a π_{Cl} → d(LMCT) transition, the two others have d → π^*_{pzH}(MLCT) character.

The absorption bands recorded at 263.8 and 269.0 nm for **1** and **2**, respectively, are assigned to the calculated transitions at 283.7, 280.9 and 277.0 nm with large oscillator strengths. They are of LMCT (π_{pzH} → d, π_{Cl} → d and π_{Ph} → d) character.

The LUMO + 1 and LUMO + 3 with α-spin and LUMO + 2 and LUMO + 3 orbitals with β-spin have a substantial admixture of phosphorus orbitals so the transitions from metal to π^*_{Ph} orbitals are mediated by phosphorus.

4. Supplementary data

Supplementary data are available from the CCDC, 12 Union Road, Cambridge CB2 1EZ, UK (fax: +44-1223-336033; E-mail: deposit@ccdc.cam.ac.uk or www: http://www.ccdc.cam.ac.uk) on request, quoting the deposition numbers: 233906 ($C_{24}H_{23}Cl_3N_4PRe$), 233907 ($C_{24}H_{24}Cl_3N_4O_{0.5}PRe$) and 233908 ($C_{28}H_{31}Cl_3N_4PRe$).

Acknowledgements

The GAUSSIAN 03 calculations were carried out in the WrocŁaw Centre for Networking and Supercomputing, WCSS, WrocŁaw, Poland, under calculational grant No. 51/96.

Crystallographic part was financed by funds allocated by the Ministry of Scientific Research and Information Technology to the Department of X-ray Crystallography and Crystal Chemistry, Institute of General and Ecological Chemistry, Łódź University of Technology.

The authors thank G. Jakob from University of Mainz for magnetic measurement.

References

[1] W. Volkert, W.F. Goeckeler, G.J. Ehrhardt, A.R. Ketring, J. Nucl. Med. 32 (1991) 174.
[2] E.A. Deutsch, K. Libson, J.L. Vanderheyden, Technetium and Rhenium in Chemistry and Nuclear Medicine, Raven Press, New York, 1990.
[3] S. Trofimenko, Chem. Rev. 72 (1972) 497.
[4] S. Trofimenko, Inorg. Chem. 34 (1986) 115.
[5] G. La Monica, G.A. Ardizzoia, Prog. Inorg. Chem. 46 (1997) 151.
[6] G.A. Ardizzoia, G. La Monica, A. Maspero, M. Moret, N. Masciocchi, Eur. J. Inorg. Chem. (1998) 1503.
[7] B. Machura, J.O. Dzięgielewski, S. Michalik, R. Kruszynski, T.J. Bartczak, J. Kusz, Transit. Met. Chem. 28 (2003) 939.
[8] B. Machura, J.O. Dzięgielewski, R. Kruszynski, T.J. Bartczak, J. Kusz, Inorg. Chim. Acta 357 (2004) 1011.
[9] G. Rouschias, G. Wilkinson, J. Chem. Soc. A 465 (1966).
[10] G. Rouschias, G. Wilkinson, J. Chem. Soc. A 993 (1967).
[11] A.I. Vogel, Textbook of Practical Organic Chemistry, Longman Group Limited, New York, 1978.

[12] STOE & Cie (1999), X-RED, Version 1.18, STOE & Cie GmbH, Darmstadt, Germany.
[13] G.M. Sheldrick, Acta Crystallogr., Sect. A 46 (1990) 467.
[14] G.M. Sheldrick, SHELXL 97. Program for the Solution and Refinement of Crystal Structures, University of Göttingen, Germany, 1997.
[15] G.M. Sheldrick, SHELXTL: release 4.1 for Siemens Crystallographic Research Systems, 1990.
[16] M.J. Frisch, G.W. Trucks, H.B. Schlegel, G.E. Scuseria, M.A. Robb, J.R. Cheeseman, J.A. Montgomery Jr., T. Vreven, K.N. Kudin, J.C. Burant, J.M. Millam, S.S. Iyengar, J. Tomasi, V. Barone, B. Mennucci, M. Cossi, G. Scalmani, N. Rega, G.A. Petersson, H. Nakatsuji, M. Hada, M. Ehara, K. Toyota, R. Fukuda, J. Hasegawa, M. Ishida, T. Nakajima, Y. Honda, O. Kitao, H. Nakai, M. Klene, X. Li, J.E. Knox, H.P. Hratchian, J.B. Cross, C. Adamo, J. Jaramillo, R. Gomperts, R.E. Stratmann, O. Yazyev, A.J. Austin, R. Cammi, C. Pomelli, J.W. Ochterski, P.Y. Ayala, K. Morokuma, G.A. Voth, P. Salvador, J.J. Dannenberg, V.G. Zakrzewski, S. Dapprich, A.D. Daniels, M.C. Strain, O. Farkas, D.K. Malick, A.D. Rabuck, K. Raghavachari, J.B. Foresman, J.V. Ortiz, Q. Cui, A.G. Baboul, S. Clifford, J. Cioslowski, B.B. Stefanov, G. Liu, A. Liashenko, P. Piskorz, I. Komaromi, R.L. Martin, D.J. Fox, T. Keith, M.A. Al-Laham, C.Y. Peng, A. Nanayakkara, M. Challacombe, P.M.W. Gill, B. Johnson, W. Chen, M. W. Wong, C. Gonzalez, J.A. Pople, GAUSSIAN 03, Revision B.03, Gaussian, Inc., Pittsburgh, PA, 2003.
[17] A.D. Becke, J. Chem. Phys. 98 (1993) 5648.
[18] C. Lee, W. Yang, R.G. Parr, Phys. Rev. B 37 (1988) 785.
[19] M.E. Casida, in: J.M. Seminario (Ed.), Recent Developments and Applications in Modern Density Functional Theory, Theoretical and Computational Chemistry, vol. 4, Elsevier, Amsterdam, 1996.
[20] P.J. Hay, W.R. Wadt, J. Chem. Phys. 82 (1985) 299.
[21] J.L. Lock, G. Turner, Can. J. Chem. 56 (1978) 179.
[22] G. Backes-Dahmann, J.H. Enemark, Inorg. Chem. 26 (1987) 3960.
[23] M. Cano, J.V. Heras, M. Maeso, M. Alvaro, R. Fernández, E. Pinilla, J.A. Campo, A. Monge, J. Organometal. Chem. 534 (1997) 159.
[24] G.A. Jeffrey, W. Saenger, Hydrogen Bonding in Biological Structures, Springer, New York, 1994.
[25] G.R. Desiraju, T. Steiner, The Weak Hydrogen Bond in Structural Chemistry and Biology, Oxford University Press, Oxford, 1999.
[26] R. Taylor, O. Kennard, J. Am. Chem. Soc. 104 (1982) 5063.
[27] J.E. Fergusson, Coord. Chem. Rev. 1 (1966) 459.
[28] A. Earnshaw, B.N. Figgis, J. Lewis, R.D. Peacock, J. Chem. Soc. (1961) 3132.
[29] S. Hirata, M. Head-Gordon, Chem. Phys. Lett. 302 (1999) 375.
[30] R. Andreu, J. Orduna, J. Garín, Tetrahedron 57 (2001) 1358.
[31] E. Brocławik, T. Borowski, Chem. Phys. Lett. 339 (2001) 433.
[32] M.J. Calhorda, M.G.B. Drew, V. Félix, L.P. Fonseca, C.A. Gamelas, S.S.M.C. Godinho, I.S. Gonçavles, E. Hunstock, J.P. Lopes, A.J. Parola, F. Pina, C.C. Romão, A.G. Santos, J. Organomet. Chem. 632 (2001) 94.
[33] A. Crespo, A.G. Turjanski, D.A. Estrin, Chem. Phys. Lett. 365 (2002) 15.
[34] M.C. Aragoni, M. Arca, T. Cassano, C. Denotti, F.A. Devillanova, F. Isaia, V. Lippolis, D. Natali, L. Niti, M. Sampietro, R. Tommasi, G. Verani, Inorg. Chem. Commun. 5 (2002) 869.
[35] P. Romaniello, F. Lelj, Chem. Phys. Lett. 372 (2003) 51.
[36] P. Norman, P. Cronstrand, J. Ericsson, Chem. Phys. 285 (2002) 207.
[37] J. Bossert, N.B. Amor, A. Strich, C. Daniel, Chem. Phys. Lett. 342 (2001) 617.
[38] C.E. Powell, M.P. Cifuentes, A.M. McDonagh, S.K. Hurst, N.T. Lucas, C.D. Delfs, R. Stranger, M.G. Humphrey, S. Houbrechts, I. Asselberghs, A. Persoons, D.C.R. Hockless, Inorg. Chim. Acta 352 (2003) 9.
[39] J.P. Morral, C.E. Powell, R. Stranger, M.P. Cifuentes, M.G. Humphrey, G.A. Heath, J. Organomet. Chem. 670 (2003) 248.
[40] P. Romaniello, F. Lelj, J. Mol. Struct. Theochem. 636 (2003) 23.
[41] B. Machura, M. Jaworska, R. Kruszynski, Inorg. Chem. Commun. (submitted).

Available online at www.sciencedirect.com
SCIENCE DIRECT®
Polyhedron 23 (2004) 1829–1835
POLYHEDRON
www.elsevier.com/locate/poly

Synthesis, structure and electrochemical properties of a nickel complex with the hydrotris[thioxotriazolyl-3-(2-pyridyl)]borate podand ligand ☆

Marcello Gennari, Marco Giannetto, Maurizio Lanfranchi, Luciano Marchiò *, Maria Angela Pellinghelli, Matteo Tegoni

Dipartimento di Chimica Generale ed Inorganica, Chimica Analitica, Chimica Fisica, Università degli Studi di Parma, Parco Area delle Scienze 17a, I 43100 Parma, Italy

Received 20 February 2004; accepted 14 April 2004
Available online 4 May 2004

Abstract

The complex $[Ni(Tr^{Me,o\text{-}Py})_2]$ (**2**) {$Tr^{Me,o\text{-}Py}$ = hydrotris[1,4-dihydro-4-methyl-3-(2-pyridyl)-5-thioxo-1,2,4-triazolyl]borate} was synthesized and characterized by UV–Vis spectroscopy, ESI-mass spectrometry and X-ray crystallography. Complex **2** crystallizes in the tetragonal *I*-42d space group. The metal presents a slightly distorted octahedral geometry (N_4S_2 co-ordination) bound by two ligands that behave in the S,N/N′ co-ordination mode: one of the three arms of each tripod is bound to the metal with the thioxo group, the second chelates N/N′ with the triazoline and pyridine nitrogen atoms and the third does not participate in the metal co-ordination. Ni/$Tr^{Me,o\text{-}Py}$ complexation was studied by collecting visible spectra of 16 batch samples (10 ml) containing a fixed concentration of metal (9.994×10^{-4} mol dm^{-3}) with increasing concentrations of ligand up to Ni/L = 1/3 (L = $Tr^{Me,o\text{-}Py}$). For a Ni/L ratio of 1/2, ≈38% of NiL^+ and ≈56% of NiL_2 are present with respect to the total Ni(II) concentration. Conductivity (Λ_M range 112–55 ohm^{-1} cm^2 mole^{-1} in acetonitrile and Λ_M range 15–8 ohm^{-1} cm^2 mole^{-1} in DMF) and ESI-mass spectrometry results are consistent with a partial dissociation of **2** in acetonitrile and DMF solutions according to the equilibrium $NiL_2 = NiL^+ + L^-$ in agreement with the spectrophotometric titration results. Cyclic voltammetry performed on acetonitrile solutions of **2** reveals the electrochemical activity of the $Tr^{Me,o\text{-}Py}$ ligand, which undergoes irreversible oxidation and reduction processes at potential > +0.7 and ∼0 V, respectively. The occurrence of the Ni(II)/Ni(III) and Ni(II)/Ni(I) electrochemical events could not be determined.
© 2004 Elsevier Ltd. All rights reserved.

Keywords: Nickel complex; Tripodal ligand; Cyclic voltammetry

1. Introduction

The introduction of the second generation of the hydrotris(pyrazolyl)borate ligand (Tp) was aimed at the study of the steric hindrance influence on the chemical properties of the Tp-metal complexes [1]. The steric bulk on the C^3 position of the pyrazolyl ring has a dramatic effect on the co-ordination geometry of the first row transition metal ions. In fact, tetrahedral geometry and ligand to metal ratio of 1:1 are usually found especially if the substituent on the pyrazolyl C^3 position is a *t*-Butyl group [2]. More recently, after the introduction of the softer hydrotris(methylthioxoimidazolyl)borate ligand (Tm) [3], the steric hindrance on the thioxoimidazolyl rings has been used as a 'tetrahedral enforcer' in order to obtain synthetic models of the liver alcohol dehydrogenase active site in which the zinc cation is in a tetrahedral and sulphur rich environment [4]. Another liver alcohol dehydrogenase model complex has been reported, in which the mixed hydro[pyrazolylbis(thioxoimodazolyl)]borate ligand (S,S,N donor) presents aromatic ring systems favouring the tetrahedral co-ordination at the metal [5].

☆ Supplementary data associated with this article can be found, in the online version, at doi:10.1016/j.poly.2004.04.009.

* Corresponding author. Tel.: +39-0521-905424; fax: +39-0521-905557.
E-mail address: marchio@unipr.it (L. Marchiò).

0277-5387/$ - see front matter © 2004 Elsevier Ltd. All rights reserved.
doi:10.1016/j.poly.2004.04.009

A new development of the Tp chemistry has been obtained by the synthesis of ligands bearing donor groups on the pyrazolyl C^3 position in order to expand the co-ordination capabilities of the ligand and generate new co-ordination geometries [6]. A relevant example is offered by the [CoL][PF_6] (L = hydrotris[3-(2-pyridyl)pyrazol-1-yl]borate) complex in which the metal exhibits a trigonal prismatic geometry [7]. Despite many examples of Tp N-donor podand ligands with heavy metals and lanthanide cations, relatively few mono-nuclear structures with first row transition metals have been reported. The reason for this has been ascribed to the large cavity that such ligands present, resulting in the preferred formation of poly-nuclear species when small cations are involved [7,8].

At present time no structures of Tm ligand exhibiting a podand donor group have been described, and it seemed interesting to us to investigate the co-ordination capabilities of a tripodal ligand having a thioxo group and an N,N chelating system on every arm. This could be obtained by using a thioxotriazoline-3-(2-pyridyl) precursor for the synthesis of the tripodal ligand, Scheme 1. From a previous work it was apparent how the hydrotris(thioxotriazolyl)borate ligand could behave as an S_3 or N_3 donor depending on the nature of the metal ion [9]. The introduction of a 2-pyridyl group on the thioxotriazoline moiety may render the co-ordination modes of this ligand more unpredictable as they may span from the S_3, $(N/N')_3$ to the mixed $S_x(N/N')_{3-x}$ ($x = 1, 2$).

Nickel complexes have attracted much interest in bio-inorganic chemistry [10] as nickel has been shown to be present at the catalytic core of urease [11], [NiFe] hydrogenase [12], methyl-CoM reductase [13], carbon monoxide dehydrogenase [14], acethyl CoA synthase [15] and nickel superoxide dismutase [16]. With the exception of urease, which is an hydrolytic enzyme, the catalytic activity of nickel enzymes is essentially due to the redox activity of the nickel centers and to the accessibility of the +1, +2 and +3 metal oxidation states. The redox properties of those enzymes are controlled by the presence of S (cysteinate) and N donor atoms at the nickel sites and various metal complexes have been prepared in order to mimic the redox activity of [NiFe] hydrogenase [17].

Here we wish to report the synthesis, structure, complexation studies and electrochemical properties of the [$Ni(Tr^{Me,o\text{-}Py})_2$] complex {$Tr^{Me,o\text{-}Py}$ = hydrotris[thioxotriazolyl-3-(2-pyridyl)]borate}, in which the ligand exhibits the S,N/N′ coordination mode. We can anticipate that the redox activity of $Tr^{Me,o\text{-}Py}$ narrows the potential windows at which the metal-based redox processes can be observed. In fact, irreversible oxidation and reduction peaks occur at +0.72 and ~0 V, respectively, attributable to the ligand electrochemical activity.

2. Experimental

Solvents were dried and distilled before use. The compound 1,4-dihydro-4-methyl-3-(2-pyridyl)-5-thioxo-1,2,4-triazole has been prepared according to published procedures [18]. All other reagents are commercially available (Sigma–Aldrich) and were used as received.

The ^1H and ^{13}C NMR spectra were recorded on a Bruker Avance 300 spectrometer. Chemical shifts are reported in ppm referenced to residual solvent protons (DMSO-d_6, CD_3CN).

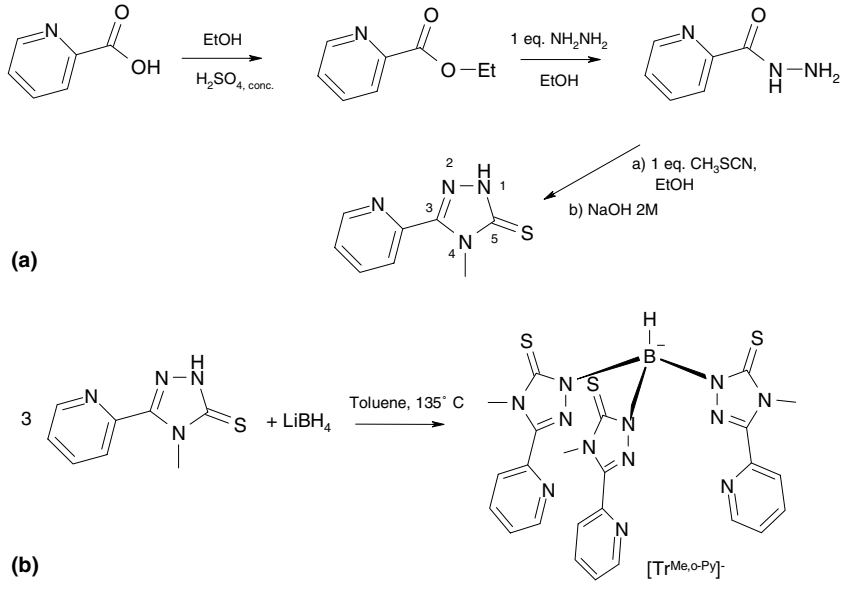

Scheme 1.

Mass spectra were obtained with a Micromass ZMD spectrometer. The mixtures were analyzed in negative and positive ionization modes by direct perfusion in ESI-MS interface; injection flow-rate = 20 μl/min; desolvation temperature = 150 °C; source block temperature = 80 °C; cone and desolvation gas flow-rates = 1.6 and 8.0 l/min, respectively; capillary = 3.0 kV; cone = 30 V; extractor = 3 V. Spectra were registered with a scansion time of 6 s.

Infrared spectra were recorded using KBr pellets from 4000 to 400 cm^{-1} on a Perkin–Elmer FT-IR Nexus spectrometer. Elemental analyses (C, H, N) were performed with a Carlo Erba EA 1108 automated analyser. Conductivity measurements were performed on a Crison microCM 2202 conductometer operating at 25 °C.

Cyclic voltammetry experiments were performed in a three-electrode cell with a Pt-disk as working electrode, a Pt-rod as counter electrode and a Ag/AgCl/KCl 0.1 M as reference electrode, by using a computerized electrochemical workstation consisting of an Autolab PGSTAT 20 potentiostat (Ecochemie, The Netherlands) controlled by the GPES 4.9 software. All measurements have been conducted in oxygen-free solutions, previously purged with N_2 for 2 min.

Magnetic susceptibility measurements were performed following Evans' method [19] using precision-made coaxial tubes (Wilmad). Cyclohexane (5% by volume) was used as internal standard in DMF-d_7. Molar susceptibilities were calculated according to

$$\chi_M = \left(\frac{3\Delta f}{2\pi f m} + \chi_0 + \frac{(d_0 - d_s)}{m}\chi_0\right)M, \quad (1)$$

where Δf is the susceptibility shift (Hz), f is the operating radio frequency (300×10^6 Hz) of the spectrometer, m is the concentration of the paramagnetic substance (grams per milliliter), χ_0 is susceptibility of the pure solvent and M is the solute molecular weight; d_0 and d_s are the densities of the pure solvent and solution, respectively. The third term in Eq. (1) has been neglected in the calculation [20]. The value of χ_0 was estimated from Pascal's constants [21]. χ_M values were corrected for the ligand diamagnetic susceptibility derived from Pascal's constants (-198×10^{-6} cgs unit).

Visible spectra were recorded on a Perkin–Elmer Lambda 25 spectrophotometer (range 200–1100 nm) using matched cells of 4 cm pathlength. Stock solutions of $Li(Tr^{Me,o\text{-}Py})$ (9.990×10^{-3} mol dm^{-3}) and of $NiCl_2 \cdot 6H_2O$ (9.994×10^{-3} mol dm^{-3}) in DMF were prepared by weight and used immediately. Complexation was studied by collecting visible spectra of 16 batch samples (10 ml) containing a fixed concentration of metal (9.994×10^{-4} mol dm^{-3}) with increasing concentrations of ligand up to Ni/L = 1/3 ($L = Tr^{Me,o\text{-}Py}$). Absorption spectra of both ligand and metal solutions were registered and used as fixed spectra. Stability constants were calculated by means of the SPECFIT program [22].

2.1. $[Li(Tr^{Me,o\text{-}Py})]$ (**1**)

Under an atmosphere of purified nitrogen, 1,4-dihydro-4-methyl-3-(2-pyridyl)-5-thioxo-1,2,4-triazole (5.00 g, 26.00 mmol) and lithium tetrahydroborate (0.189 g, 8.67 mmol) were mixed together in 80 ml of toluene in a round bottomed flask connected to a reflux condenser and to an oil bubbler. The yellow suspension was stirred at 135 °C for four days. The mixture was filtered, washed with hot toluene (3 × 20 ml), THF (2 × 20 ml) and vacuum dried yielding a pale yellow product (2.52 g, 49%). *Anal.* Calc. for $C_{24}H_{22}BN_{12}S_3Li$: C, 48.65; H, 3.74; N, 28.37. Found: C, 49.15; H, 3.42; N, 27.86%. ESI-MS (CH_3CN/MeOH, 1/1) m/z, %: 1177.4, 3, $[L_2Li]^-$; 1193.2, 7, $[L_2Na]^-$; 585.1, 100, $[L]^-$. IR data (KBr disks cm^{-1}): 3074w, 3048w, 2945w, 2531w [ν(B-H)], 1591s, 1476s, 1408s, 1337s, 1264s, 1074s, 1006m, 799s, 697m. ^1H NMR (300 MHz, DMSO-d_6) δ (ppm): 3.65 (s, 9H, CH_3), 5.18 (b, 1H, B-*H*), 7.31 (m, 3H, Py), 7.63 (t, $J = 7.8$ Hz, 3H, Py), 7.79 (d, $J = 7.8$ Hz, 3H, Py), 8.56 (d, $J = 4.5$ Hz, 3H, Py) (b = broad). ^{13}C NMR (75 MHz, DMSO-d_6) ppm: 32.35 (CH_3), 123.71 (CH, Py), 123.86 (CH, Py), 136.95 (CH, Py), 146.70 (C quat.), 147.29 (C quat.), 148.56 (CH, Py), 170.90 (C = S).

2.2. $[Ni(Tr^{Me,o\text{-}Py})_2]$ (**2**)

A mixture of $NiCl_2 \cdot 6H_2O$ (0.125 g, 0.526 mmol) and **1** (0.306 g, 0.516 mmol) in methanol (30 ml) was heated to reflux. A green precipitate formed after few minutes. After 1 h the mixture was allowed to cool to room temperature and filtered. The green solid was washed with 5 ml of hot methanol, vacuum dried and collected (0.207 g, 65%). *Anal.* Calc. for $C_{48}H_{44}B_2N_{24}S_6Ni$: C, 46.88; H, 3.61; N, 27.34. Found: C, 46.00; H, 3.89; N, 26.88%. ESI-MS (CH_3CN/MeOH, 1/1) m/z, %: positive ion mode, 1267.8, 100, $[(NiL_2)K]^+$, 1252.9, 20, $[(NiL_2)Na]^+$, 643, 70, $[NiL]^+$, 585.5, 8, $[L]^+$; negative ion mode, 585.1, 15, $[L]^-$. IR data (KBr disk, cm^{-1}): 3048w, 2947w, 2920w, 2512w [ν(B-H)], 1607m, 1590m, 1512m, 1474s, 1404s, 1342s, 1215m, 1076s, 802m, 793m. ^1H NMR (300 MHz, CD_3CN) δ (ppm): 3.58, 7.20, 7.56, 7.97, 8.33, 8.77, all signals were broad. The product was recrystallized from a dimethylsulfoxide solution from which crystals suitable for X-ray structure determination were obtained, corresponding to $[Ni(Tr^{Me,o\text{-}Py})_2] \times 1.4$ DMSO (**2a**).

2.3. X-ray crystallography

A summary of data collection and structure refinement for **2a** are reported in Table 1. Single crystal data were collected with a *Bruker AXS Smart 1000* area detector diffractometer (Mo Kα; $\lambda = 0.71073$ Å). Empirical absorption correction was applied using the program SADABS [23] (maximum and minimum absorption

Table 1
Summary of X-ray crystallographic data for **2a**

Empirical formula	$C_{50.75}H_{52.25}B_2N_{24}NiO_{1.38}S_{7.3}$
Formula weight	1337.19
Colour, habit	green, block
Crystal size (mm)	$0.45\times0.42\times0.20$
Crystal system	tetragonal
Space group	*I*-42d
a (Å)	25.224(9)
b (Å)	25.224(9)
c (Å)	23.511(7)
α (°)	90
β (°)	90
γ (°)	90
V (Å^3)	14.959(9)
Z	8
T (K)	293(2)
$\rho_{(calc)}$ (Mg/m^3)	1.187
μ (mm^{-1})	0.515
θ range (°)	1.61–26.01
Number of reflections/observed ($F > 4\sigma(F)$)	41229/3881
Goodness-of-fit	1.007
R_1	0.0490
wR_2	0.0882

$R_1 = \sum ||F_o| - |F_c||/|F_o|, wR_2 = [\sum[w(F_o^2 - F_c^2)^2]/[w(F_o^2)^2]]^{1/2}, w = 1/[\sigma^2(F_o^2) + (aP)^2 + bP]$, where $P = [\max(F_o^2, 0) + 2F_c^2]/3$.

correction coefficient: 1.000 and 0.790). The structure was solved by direct methods (SIR97) [24] and refined with full-matrix least-squares (SHELXL-97) [25], using the Wingx software package [26]. Non-hydrogen atoms were refined anisotropically; the B-*H* hydrogen atom was found and refined whereas the remaining hydrogen atoms were placed at their calculated positions. DMSO solvent molecules were severely disordered and were treated using the SQUEEZE PLATON program giving approximately 11 DMSO molecules per unit cell (469 electrons/cell) [27]. The pyridine ring of the sulfur-co-ordinated triazoline was found disordered in two positions with site occupancy factors of 0.5. The crystal was twinned (Flack parameter 0.46(2) [28]) and was refined with the Twin law 100, 010, 00–1. The programs Parst [29,30] and ORTEP for Windows [31] were also used. Full tables of bond lengths and angles, atomic positional parameters, isotropic and anisotropic displacement parameters are given in the Supplementary material.

3. Results and discussion

The synthesis of the thioxotriazoline and of the $Tr^{Me,o\text{-}Py}$ ligand is outlined in Scheme 1. This procedure allows for the synthesis of thioxotriazolines variously substituted in the third and fourth positions by using appropriate carboxylic acids and isothiocyanates as starting materials. The $[Ni(Tr^{Me,o\text{-}Py})_2]$ complex was prepared in methanol by reacting $[Li(Tr^{Me,o\text{-}Py})]$ and $NiCl_2\cdot 6H_2O$ and even if equimolar amounts of the reagents were employed, a complex of ligand/metal ratio of 2/1 was always recovered. This complex can be recrystallized from dimethylformamide, dimethylsulfoxide and acetonitrile. The X-ray structural analysis performed on crystals obtained from each one of these solvents revealed the same molecular structure together with crystallization solvent molecules.

3.1. Crystal structure of $[Ni(Tr^{Me,o\text{-}Py})_2]$

The ORTEP diagram of the complex is depicted in Fig. 1. Selected bond lengths and angles are reported in Table 2. The complex is octahedral and the metal lies on a crystallographic C_2 axis co-ordinated by four nitrogen and two sulfur atoms from two different ligands. The overall co-ordination is of the type N_4S_2 and the two

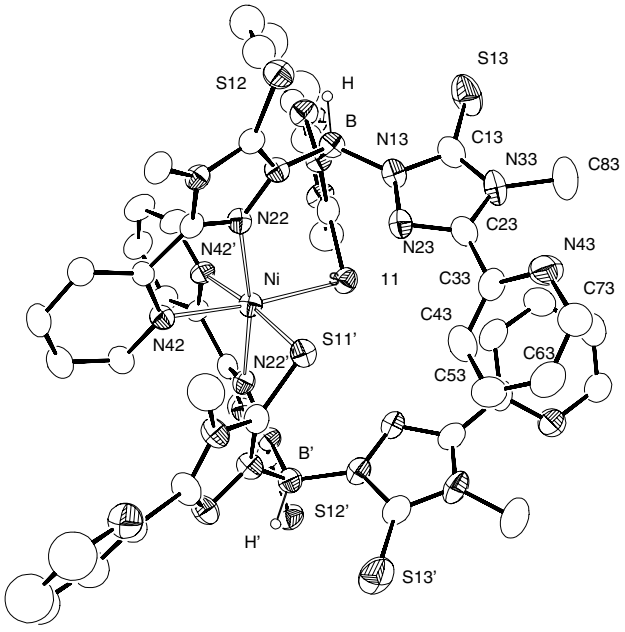

Fig. 1. ORTEP drawing of **2a** at the 30% thermal ellipsoids level.

Table 2
Selected bond lengths (Å) and angles (°) for **2a**

Bond lengths			
Ni–S(11)	2.396(1)	B–N(12)	1.548(6)
Ni–N(22)	2.118(3)	B–N(13)	1.517(6)
Ni–N(42)	2.098(3)	C(11)–S(11)	1.695(4)
B–N(11)	1.561(6)	C(12)–S(12)	1.670(4)
B–H	1.04(4)	C(13)–S(13)	1.677(5)
Bond angles			
S(11)–Ni–S(11)[a]	91.21(6)	N(42)–Ni–N(22)[a]	94.7(1)
S(11)–Ni–N(22)	97.9(1)	N(11)–B–N(12)	109.6(3)
S(11)–Ni–N(42)	174.50(9)	N(11)–B–N(13)	111.2(4)
S(11)–Ni–N(42)[a]	91.76(9)	N(12)–B–N(13)	110.4(4)
S(11)–Ni–N(22)[a]	89.51(9)	N(11)–B–H	104(2)
N(22)–Ni–N(42)	77.5(1)	N(12)–B–H	103(2)
N(42)–Ni–N(42)[a]	85.7(2)	N(13)–B–H	118(2)
N(22)–Ni–N(22)[a]	169.5(2)		

[a] $= 1 - x + 1/2, y, -z + 3/4$.

sulfur atoms are in *cis* position. The complex is chiral but both enantiomers are present in the structure. The Ni–S distance is of 2.396(1) Å and the Ni–N distances [2.118(3) (*N*-triazoline) and 2.098(3) (*N*-pyridine) Å] are nearly equivalent despite the triazoline nitrogen atom is *trans* to the thioxo group. Every arm of the ligand displays a different behaviour, as one is S co-ordinated, the second is chelating N,N′ whereas the third is not involved in the metal co-ordination. The thioxo group that is bound to the metal presents C=S bond length longer than the other two thioxo groups, Table 2. In the complex, the two ligands are arranged in a *mer* configuration with the free arms facing each other. This results in an unusual co-ordination mode if the $Tr^{Me,o\text{-}Py}$ ligand is compared to the Tp and Tm ligands, which usually act as N_3 and S_3 tripods, respectively. The reason can be ascribed to the presence of the pendant 2-pyridyl group, which introduces an additional binding site for every arm of the ligand. One of the alternative co-ordination modes of $Tr^{Me,o\text{-}Py}$ could have been the $(N/N')_3$ trigonal prismatic, where each arm of the ligand would chelate the metal through the pyridine and triazoline nitrogen atoms, as described for hydrotris[(2-pyridyl)pyrazolyl)borato [6,7]. Nevertheless, there are two major drawbacks for the trigonal prismatic geometry: (a) no sulphur atom would be involved in the metal binding and (b) this scenario is more likely for bigger metals such as the lanthanides that possess an appropriate dimension to be located into the ligand pocket, whereas for the first row transition metals, poly-nuclear complexes are preferentially formed [6,7,8b]. In the present case, the contemporary presence of the thioxo groups and the N/N′ chelating system seem to dictate the S,N/N′ ligand co-ordination giving rise to a dissymmetric ligand binding. Additional results with other metal ions are necessary to draw definitive conclusions about the co-ordination properties of $Tr^{Me,o\text{-}Py}$.

The formation constants for the complexes NiL^+ and NiL_2 were determined by collecting visible spectra of DMF solutions containing different Ni/L ratios. The obtained log β values are: $\log \beta_{[NiL]} = 3.99(6)$ and $\log \beta_{[NiL2]} = 7.47(4)$. A representative distribution diagram is reported in Fig. 2 and the calculated spectra for the complexes are reported in Fig. 3. For a Ni/L ratio of 1/2, as in the case of **2** dissolved in DMF, the concentration of the species with respect to the total Ni(II) concentration is as follow: $[NiL^+] \approx 38\%$ and $[NiL_2] \approx 54\%$.

In order to better understand the complex behaviour in solution, the molar conductivity of **2** has been measured in dry acetonitrile (concentration range $= 1.2 \times 10^{-5}$–4.9×10^{-5} M) and DMF (concentration range $= 2.4 \times 10^{-4}$–9.8×10^{-4} M) giving molar conductivity Λ_M in the range 112–55 $ohm^{-1}\,cm^2\,mole^{-1}$ (acetonitrile) and 15–8 $ohm^{-1}\,cm^2\,mole^{-1}$ (DMF), respectively. This is in accordance with the spectrophotometric titrations, which indicate a partial dissociation of **2** in DMF, according to the following equilibrium:

$$NiL_2 \leftrightarrows NiL^+ + L^-$$

The Λ_M values are in fact smaller than the lower limit of the range reported for 1:1 electrolytes in acetonitrile and DMF [32] but they are too high for a complex behaving as a non-electrolyte. This is also confirmed by ESI-MS spectrometry performed on one of the samples (conc. $= 2.4 \times 10^{-5}$ M, acetonitrile as solvent) used for the conductivity measurements, which shows the peaks corresponding to the ionic species NiL^+ and L^-, together with the un-dissociated form NiL_2 (see Section 2).

Magnetic moment (μ_{eff}) of 3.6 B.M has been observed for DMF-d_7 solutions of **2** over the 296–335 K temperature range. This unusually high value for a Ni(II) ion in an octahedral field may be explained considering the dissociation equilibrium where the NiL^+ species is in a tetrahedral geometry. This can be achieved

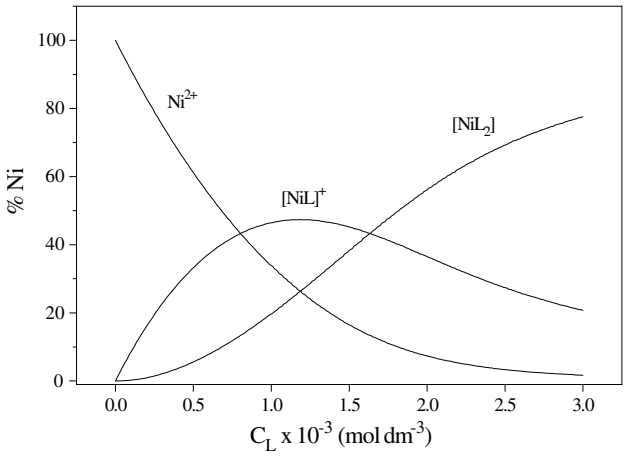

Fig. 2. Distribution diagram of the Ni/L system ($L = Tr^{Me,o\text{-}Py}$) as a function of the ligand concentration ($C_{Ni} = 1 \times 10^{-3}$ mol dm^{-3}).

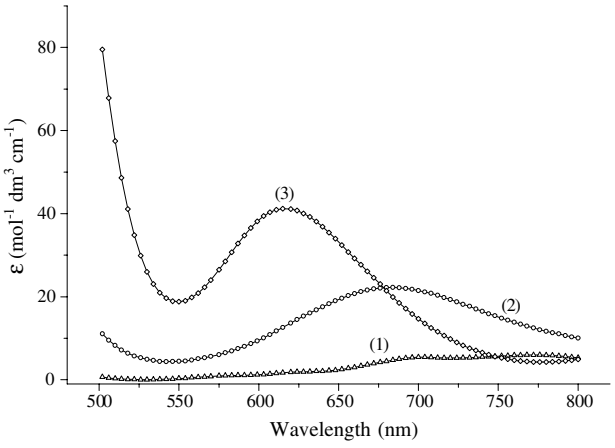

Fig. 3. Calculated spectra of the species Ni^{2+} (1), $[NiL]^+$ (2), $[NiL_2]$ (3).

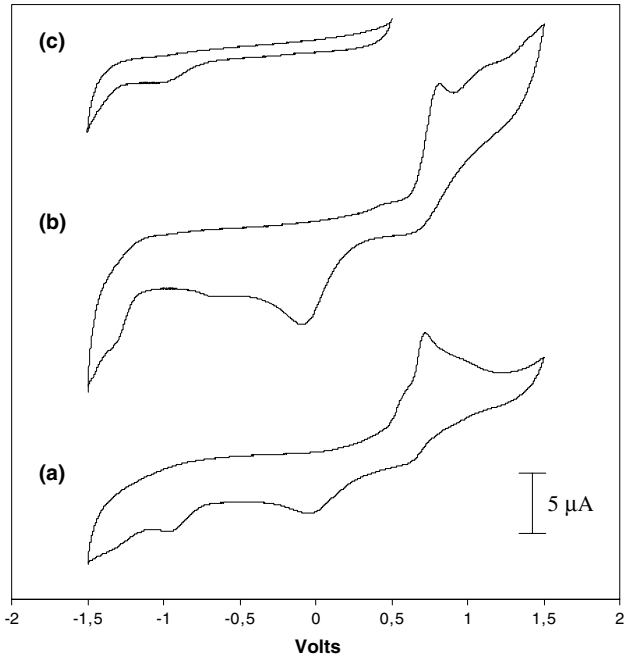

Fig. 4. Cyclic voltammograms (third scans) of saturated solutions of **1** (a) and **2** (b,c) in acetonitrile containing $TBABF_4$ as supporting electrolyte (0.1 M). Reference electrode: Ag/AgCl/KCl 0.1 M. Scan rate: 0.1 V/s.

by substitution of a ligand molecule in NiL_2 with a DMF solvent molecule. In fact, reported literature values of μ_{eff} for octahedral Ni(II) complexes fall in the range 2.8–3.3 B.M. whereas for tetrahedral Ni(II) complexes this range is usually 3.0–4.0 B.M. due to a greater spin-orbit coupling [21a,33]. According to the distribution diagram (Fig. 2), upon dissolution of **2** in DMF, the NiL^+ species occurs in ≈38% of the total metal and it may be reasonable to assume that it is a $NiL(DMF)^+$ complex exhibiting a tetrahedral geometry.

Cyclic voltammograms (acetonitrile solutions) for **1** and **2** were recorded in the −1.5 to +1.5 V potential window and starting from the Open Circuit Potential (OCP), Fig. 4. The voltammograms of **1** shows two irreversible oxidation waves at +0.72 and +1.10 V whereas for **2** these processes occur at +0.82 and +1.10 V. It seems that in the Ni(II) complex the ligand is more stabilized as it is oxidized at a slightly higher potential. The irreversible reduction process at ∼0 V is not observed when the scans are operated in the −1.5/+0.5 V potential window (Fig. 4c) and it can be concluded that it corresponds to the reduction of a species generated during the oxidation processes at potentials above +0.75 V. Furthermore, holding the potential at +0.8 V for 5 min and reversing the scan toward the cathodic direction increases only the peak at ∼0 V and confirms this assumption. From the comparison of the voltammograms of **1** and **2** it emerges that (a) the electrochemical processes are mainly due to ligand oxidation/reduction and (b) the potential window where metal-based redox processes can be observed with this ligand is limited approximately to the 0/+0.8 V range. Unfortunately, the position of the Ni(II)/Ni(III) and Ni(II)/Ni(I) couples cannot be determined. This is not surprising as in many octahedral Ni(II) complexes exhibiting mixed N/S coordination the Ni(II)/Ni(III) couple is usually found at potentials greater than +0.8 V and the Ni(II)/Ni(I) couple appears at negative potentials [17a,34], values at which the $Tr^{Me,o\text{-}Py}$ ligand is already electrochemically active.

4. Supplementary material

Listings of atomic coordinates of the non-hydrogen and hydrogen atoms, anisotropic displacement parameters and bond lengths and angles for **2a** are given in the supplementary materials. CCDC-230100 (Cambridge Crystallographic Data Centre), 12 Union Road, Cambridge CB2 1EZ, UK (Fax: +44-1223-336033, E-mail: deposit@ccdc.cam.ac.uk or www: http://www.ccdc.cam.ac.uk).

Acknowledgements

This work was supported by the Ministero dell'Istruzione, dell'Università e Ricerca (Rome, Italy).

References

[1] S. Trofimenko, J.S. Calabrese, J.S. Thompson, Inorg. Chem. 26 (1987) 1507.
[2] (a) M.H. Chisholm, N.W. Eilerts, J.C. Huffman, S.S. Iyer, M. Pacold, K. Phomphrai, J. Am. Chem. Soc. 122 (2000) 11845;
(b) J.D. Jewson, L.M. Liable-Sands, G.P.A. Yap, A.L. Rheingold, K.H. Theopold, Organometallics 18 (1999) 300;
(c) S. Thyagarajan, D.T. Shay, C.D. Incarvito, A.L. Rheingold, K.H. Theopold, J. Am. Chem. Soc. 125 (2003) 4440;
(d) H. Komatsuzaki, N. Sakamoto, M. Satoh, S. Hikichi, M. Akita, Y. Moro-oka, Inorg. Chem. 37 (1998) 6554.
[3] J. Reglinski, M. Garner, I. Cassidy, P.A. Slavin, M.D. Spicer, D. Armstrong, J. Chem. Soc. Dalton Trans. (1999) 2119.
[4] C. Kimblin, B.M. Bridgewater, D.G. Churchill, G. Parkin, Chem. Commun. (1999) 2301.
[5] J. Seebacher, M. Shu, H. Vahrenkamp, Chem. Commun. (2001) 1026.
[6] P.L. Jones, A.J. Amoroso, J.C. Jeffery, J.A. McCleverty, E. Psillakis, L.H. Rees, M.D. Ward, Inorg. Chem. 36 (1997) 10.
[7] R.L. Paul, A.J. Amoroso, P.L. Jones, S.M. Couchman, Z.R. Reeves, L.H. Rees, J.C. Jeffery, J.A. McCleverty, M.D. Ward, J. Chem. Soc., Dalton Trans. (1999) 1563.
[8] (a) E.R. Humphrey, K.L.V. Mann, Z.R. Reeves, A. Behrendt, J.C. Jeffery, J.P. Maher, J.A. McCleverty, M.D. Ward, New J. Chem. 23 (1999) 417;
(b) P.L. Jones, J.C. Jeffery, J.P. Maher, J.A. McCleverty, P.H. Rieger, M.D. Ward, Inorg. Chem. 36 (1997) 3088;
(c) A.J. Amoroso, J.C. Jeffery, P.L. Jones, J.A. McCleverty, M.D. Ward, Angew. Chem. Int. Ed. Engl. 34 (1995) 1443.

[9] P.J. Bailey, M. Lanfranchi, L. Marchiò, S. Parsons, Inorg. Chem. 19 (2001) 5030.
[10] M.A. Halcrow, G. Christou, Chem. Rev. 94 (1994) 2421.
[11] E. Jabri, M.B. Carr, R.P. Hausinger, P.A. Karplus, Science 268 (1995) 998.
[12] A. Volbeda, J.C. Fontecilla-Camps, J. Chem. Soc., Dalton Trans. (2003) 4030, and references therein.
[13] U. Empler, W. Grabarse, S. Shima, M. Goubeaud, R.K. Thauer, Science 278 (1997) 1457.
[14] C.Y. Ralston, H. Wang, S.W. Ragsdale, M. Kumar, N.J. Spangler, P.W. Ludden, W. Gu, R.M. Jones, D.S. Patil, S.P. Cramer, J. Am. Chem. Soc. 122 (2000) 10553.
[15] S.W. Ragsdale, M. Kumar, Chem. Rev. 96 (1996) 2515.
[16] S.B. Choudhury, J. Lee, G. Davidson, Y. Yim, K. Bose, M.L. Sharma, S. Kang, D.E. Cabelli, M.J. Maroney, Biochemistry 38 (1999) 3744.
[17] (a) V.V. Pavlishchuk, S.V. Kolotilov, A.W. Addison, R.J. Butcher, E. Sinn, J. Chem. Soc., Dalton Trans. (2000) 335, Electrochemistry referenced to SCE;
(b) D.C. Goodman, R.M. Buonomo, P.J. Farmer, J.H. Reibenspies, M.Y. Darensbourg, Inorg. Chem. 35 (1996) 4029;
(c) G. Musie, P.J. Farmer, T. Tuntulani, J.H. Reibenspies, M.Y. Darensbourg, Inorg. Chem. 35 (1996) 2176;
(d) H.-J. Kruger, G. Peng, R.H. Holm, Inorg. Chem. 30 (1991) 734;
(e) H.M. Alvarez, M. Krawiec, B.T. Donovan-Merkert, M. Fouzi, D. Rabinovich, Inorg. Chem. 40 (2001) 5736.
[18] (a) N.N. Gulerman, H.N. Dogan, S. Rollas, C. Johansson, C. Celik, Il Farmaco 56 (2001) 953;
(b) R. Singh, C. Fiakpui, J. Galpin, J. Stewart, M.P. Singh, R.G. Micetich, Eur. J. Med. Chem. 31 (1996) 301.
[19] D.F. Evans, J. Chem. Soc. (1959) 2003.
[20] T.H. Crawford, J. Swanson, J. Chem. Educ. 48 (1971) 382.
[21] (a) R.S. Drago, Physical Methods in Chemistry, Saunders, Philadelphia, PA, 1977, p.413;
(b) Handbook of Chemistry and Physics, 82nd ed., CRC press, LLC, Boca Raton, FL, 2002.
[22] (a) R.A. Binstead, B. Jung, A.D. Zuberbühler, Specfit/32 Ver.3.0, Spectrum Software Associates, Marlborough, MA, USA;
(b) H. Gampp, M. Maeder, C.J. Meyer, A.D. Zuberbühler, Talanta 32 (1985) 257.
[23] Area-Detector Absorption Correction; Siemens Industrial Automation, Inc., Madison, WI, 1996.
[24] A. Altomare, M.C. Burla, M. Camalli, G.L. Cascarano, C. Giacovazzo, A. Guagliardi, A.G.G. Moliterni, G. Polidori, R. Spagna, J. Appl. Cryst. 32 (1999) 115.
[25] G.M. Sheldrick, SHELX97. Programs for Crystal Structure Analysis 1997 (Release 97-2). University of Göttingen, Germany.
[26] L.J. Farrugia, J. Appl. Cryst. 32 (1999) 837.
[27] SQUEEZE - Sluis P.v.d., Spek A.L. Acta Cryst., A46 (1990) 194.
[28] H.G. Flack, G. Bernardinelli, J. Appl. Cryst. 33 (2000) 1143.
[29] M. Nardelli, Comput. Chem. 7 (1983) 95.
[30] M. Nardelli, J. Appl. Crystallogr. 28 (1995) 659.
[31] L.J. Farrugia, J. Appl. Crystallogr. 30 (1997) 565.
[32] W.J. Geary, Coord. Chem. Rev. 7 (1971) 81–122.
[33] N.N. Greenwood, A. Earnshow, in: Chemistry of the Elements, 2nd ed., Butterworth-Heinemann, London, 1998, p. 1158.
[34] (a) N. de Vries, J. Redijk, Inorg. Chem. 30 (1991) 3700, SCE as reference electrode;
(b) S.B. Choudhury, D. Ray, A. Chakravorty, Inorg. Chem. 30 (1991) 4354, SCE as reference electrode;
(c) J.G. Gilbert, A.W. Addison, R.J. Butcher, Inorg. Chim. Acta 308 (2000) 22, Ag/Ag^{+}(0.1 M) as reference electrode.

Available online at www.sciencedirect.com
SCIENCE DIRECT®
Polyhedron 23 (2004) 1837–1843
POLYHEDRON
www.elsevier.com/locate/poly

Triangulo-μ_3-sulfido-trinickel(II) cone-shaped clusters and anion traps: structural characterization

Horacio López-Sandoval [a], Arlette Richaud [a], Rosalinda Contreras [b], G. Jeffery Leigh [c], Peter B. Hitchcock [c], Angelina Flores-Parra [b], Juan Carlos Galvez-Ruíz [b], Alejandro Cruz [d], Heinrich Nöth [e], Noráh Barba-Behrens [a,*]

[a] *Departamento de Química Inorgánica y Nuclear, Facultad de Química, Universidad Nacional Autónoma de México (UNAM), CU, 04510 México DF, Mexico*
[b] *Departamento de Química, Centro de Investigación y de Estudios Avanzados del IPN, AP 14-740, CP 07000, México DF, Mexico*
[c] *Department of Chemistry, University of Sussex, Brighton BN1 9QJ, UK*
[d] *Departamento de Química, Unidad Profesional Interdisciplinaria de Biotecnología del IPN, Av. Acueducto de Guadalupe s/n Col. Barrio la Laguna, Ticomán, DF, Mexico*
[e] *Department Chemie, Ludwig-Maximiliams-Universität, Butenand-straße5-13 (Haus D), D-81377 München, Germany*

Received 17 January 2004; accepted 23 April 2004

Abstract

Trinuclear $Ni_3S_4N_3$ clusters were obtained from (1*S*,2*S*)-1-monothiasulfato-1-phenyl-2-(methylammoniumyl)propane (tpmp). Three homochiral ligand molecules together with three Ni^{II} ions give rise to a cone-shaped cluster topped by a μ_3-sulfide ion. Each Ni^{II} is in a distorted planar geometry. X-ray structural studies showed that in three cases the three phenyl groups form the rim of a cage which contains R-OSO_3 ($R = C_2H_5$, C_3H_7) or nitrate anions. The alkyl sulfates were generated during the synthesis reaction, and are hydrogen-bonded through the oxygen atoms to the amine nitrogen atoms. The corresponding compound with the methyl sulfate anion ($MeOSO_3$) reacts with Fe^{III} nitrate to form a similar compound in which the nitrate anion occupies the cavity and its crystals were analyzed by X-ray diffraction.
© 2004 Elsevier Ltd. All rights reserved.

Keywords: Pseudoephedrine; Nickel; Triangulo; Cluster; Anion exchange

1. Introduction

The chemistry and structure of nickel complexes with sulfur ligands has attracted much interest due to the biological functions of nickel–sulfur sites in enzymes [1–10]. Most of the synthetic models of such enzymes contain mono- and binuclear nickel(II) compounds with thiolate, thioester and amines [11–16]. However, some examples are known which contain trinuclear clusters and clusters of higher nuclearity [17]. We have been interested in optically active aminoalcohol and aminothiol pseudoephedrine derivatives, because of the influence of their stereochemistry on the coordination properties [18–21]. Their flexibility and the presence of different potential coordinating sites permit the formation of mono- and trinuclear coordination compounds. The *threo* stereochemistry of the pseudoephedrine derivative is important in the formation of the trinuclear complex since *erythro* isomers do not form analogous compounds [22,23]. Therefore, we investigated the coordination behaviour of 1(*S*),2(*S*)-1-monothiosulfato-1-phenyl-2-methylammoniumylpropane (tpmp) towards nickel(II), including the influence of the solvent in the synthesis reaction, and found that trinuclear nickel [17,24–29] derivatives were formed. Here, we discuss the formation and structures of new four optically active compounds $[Ni_3(pmp)_3(\mu_3\text{-}S)]$ (CH_3OSO_3) (**2**), $[Ni_3\text{-}(pmp)_3(\mu_3\text{-}S)]$ $(C_2H_5OSO_3)$ (**3**), $[Ni_3(pmp)_3(\mu_3\text{-}S)]$ $(C_3H_7OSO_3)$ (**4**) and $[Ni_3(pmp)_3(\mu_3\text{-}S)](NO_3)$ (**5**). The

* Corresponding author. Tel./fax: +52-555-6223810.
E-mail address: norah@servidor.unam.mx (N. Barba-Behrens).

0277-5387/$ - see front matter © 2004 Elsevier Ltd. All rights reserved.
doi:10.1016/j.poly.2004.04.019

parent compound, ephedrine, without sulfur was designated pmp.

2. Experimental

2.1. General remarks

All chemicals were reagent grade (Aldrich) and used without further purification. Solvents (Baker) were dried by standard procedures and freshly distilled under dinitrogen before use. IR spectra of solid samples in KBr pellets (4000–400 cm^{-1}) were obtained using a Perkin–Elmer 599B FT-IR spectrometer. UV–Vis spectra (diffuse reflectance, 40 000–4000 cm^{-1}) were recorded on a Cary-5E spectrometer. Elemental analyses were carried out with a Fisons EA 1108 analyser. Magnetic susceptibility measurements of powdered samples at room temperature were recorded on a Johnson–Matthey DG8 5HJ balance using the Gouy method. A Jeol GSX-270 spectrometer was used to obtain ^{1}H and ^{13}C NMR spectra, and a Bruker 300 for ^{15}N NMR spectra.

Details of the X-ray structural analysis, crystal data and refinement are given in Table 1. Diffraction data for compounds **3** and **5** were collected on a Nonius kappa CCD diffractometer in the hemisphere-scan mode and compound **4** on a Siemens-P4 diffractometer with CCD. The structures were solved and refined using standard methods [30,31], Crystals for compound **3** and SHELXL-97 for **4** and **5** without restrains or constraints, applying an adequate weighting scheme and an extinction correction during the least-squares cycle. Non H-atoms were refined anisotropically, while H-atoms were refined using a riding model and fixed isotropic thermal parameters. No significant residuals were observed in the final difference maps. The chiral character of the space groups were confirmed on the basis of Wilson's statistics and successful refinement. The absolute configurations were determined from refinement of the Flack parameter [32], $[Ni_3(pmp)_3(\mu_3\text{-}S)](C_2H_5OSO_3)$ (**3**) yielding $x = 0.10(3)$, $[Ni_3(pmp)_3(\mu_3\text{-}S)](C_3H_7OSO_3)$ (**4**) yielding $x = 0.04(3)$, $[Ni_3(pmp)_3(\mu_3\text{-}S)](NO_3)$ (**5**) yielding $x = 0.005(12)$, and the expected configuration for the pmp moiety.

Table 1
Crystal data and structure refinement for compounds **3**–**5**

	3	**4**	**5**
Formula	$C_{30}H_{42}N_3Ni_3S_4 \cdot C_2H_5OSO_3$	$C_{30}H_{42}N_3Ni_3S_4 \cdot C_3H_7OSO_3$	$C_{30}H_{42}N_3Ni_3S_4NO_3$
Formula weight	874.20	888.18	811.05
Temperature (K)	293	173	293
Wavelength (Å)	0.71073	0.71073	0.71073
Crystal colour	yellow	red	black
Crystal system	orthorhombic	orthorhombic	monoclinic
Space group	$P2_12_12_1$	$P2_12_12_1$	$P2_1$
Unit cell dimensions			
a (Å)	9.133(1)	9.253(1)	8.773(2)
b (Å)	17.813(2)	17.906(2)	11.827(2)
c (Å)	24.037(3)	23.781(2)	17.819(4)
α (°)	90	90	90
β (°)	90	90	103.44(3)
γ (°)	90	90	90
V (Å^3)	3910.5(8)	3940.1(5)	1798.2(7)
Z	4	4	2
D_{calc} (Mg m^{-3})	1.485	1.497	1.498
μ (mm^{-1})	1.734	1.723	1.822
$F(000)$	1824	1856	844
Crystal size (mm)	0.20 × 0.10 × 0.50	0.30 × 0.05 × 0.02	0.40 × 0.22 × 0.10
θ Range for data collection (°)	1.42–29.41	3.82–21.97	3.40–26.35
Index range	$-11 \leqslant h \leqslant 11$; $0 \leqslant k \leqslant 22$; $0 \leqslant l \leqslant 31$	$-9 \leqslant h \leqslant 9$; $-18 \leqslant k \leqslant 18$; $-22 \leqslant l \leqslant 25$	$-10 \leqslant h \leqslant 10$; $-14 \leqslant k \leqslant 14$; $-22 \leqslant l \leqslant 22$
Number reflection measured	23180	12978	16480
Number unique reflections (R_{int})[a]	6927(0.069)	4768 (0.087)	7005 (0.049)
Data/restrain/parameters	6927/0/425	4768/0/433	7005/1/398
Final R_1, $wR_2[I > 2\sigma(I)]$ (%)	6.2, 6.9	5.3, 9.8	3.65, 7.91
Final R_1, wR_2 (all data) (%)	19.7, 9.4	7.8, 10.7	4.94, 8.51
Goodness-of-fit on $F^2(S)$	0.828	1.052	1.020
Largest difference peak and hole (e Å^{-3})	1.169 and −0.444	0.927 and −0.379	0.358 and −0.307

[a] R_{int}, R_1, wR_2, and S are defined as follows: $R_{int} = \sum |F_o^2 - \langle F_o^2 \rangle| / \sum F_o^2$, $R_1 = \sum ||F_o| - |F_c|| / \sum |F_o|$, $wR_2 = \left[\sum w(F_o^2 - F_c^2)^2 / \sum (wF_o^2)^2\right]^{1/2}$, $S = \left[\sum w(F_o^2 - F_c^2)^2 / (m-n)\right]^{1/2}$.

2.2. Synthesis of (1S,2S)-1-monothiasulfato-1-phenyl-2-(methylammoniumyl)propane, (tpmp) (1) [33]

To a solution of (1*S*,2*S*)-1-chloro-1-phenyl-2-(methylamino)propane hydrochloride (4.49 g, 19.9 mmol) in dry ethanol (40 cm^3), sodium thiosulfate (3.78 g, 23.9 mmol) was added and the mixture was heated under reflux for 3 h. Then the reaction mixture was cooled to 0 °C and the sulfate derivative allowed to precipitate. It was filtered off and washed with ethanol and cold water. Yield 3.26 g, 75%, m.p. 180–182 °C. IR (ν_{max}/cm^{-1}) 1228 ($\nu_{as}RS–SO_3^-$), 1026 ($\nu_sRS–SO_3^-$), 1200 ($\nu_{as}R_2NH_2^+$). Found: C, 44.7; H, 6.0; N, 5.25; S, 24.0. $C_{10}H_{15}NO_3S_2$ requires: C, 46.0; H, 5.80; N, 5.35; S, 24.5%. $[\alpha]_D = -146.3°$ ($c = 15.0$ mg/10 cm^3, DMSO, $b = 1$ dm).

2.3. Synthesis of [Ni3(pmp)3(μ3-S)](CH3OSO3) (2)

To a solution of tpmp (2.012 g, 7.7 mmol) in methanol (50 cm^3) was added a solution which contained $Ni(CH_3COO)_2 \cdot 4H_2O$ (1.918 g, 7.7 mmol) in methanol (50 cm^3). The mixture was stirred to obtain an homogeneous solution. After 15 days, dark brown crystals were isolated. Yield 0.33 g, 15%. IR (ν_{max}/cm^{-1}) 1237 ($\nu_{as}RO–SO_3^-$), 1007 ($\nu_sRO–SO_3^-$), 1211 ($\nu_{as}R_2NH_2^+$), 579 (νM–S). Found: C, 43.60; H, 5.99; N, 4.80; S, 19.10. $C_{31}H_{45}N_3Ni_3O_4S_5$ requires: C, 43.28; H, 5.27; N, 4.88; S, 18.64%.

2.4. Synthesis of [Ni3(pmp)3(μ3-S)] (C2H5OSO3) (3)

A solution of $Ni(CH_3COO)_2 \cdot 4H_2O$ (0.266 g, 1.07 mmol) in ethanol (20 cm^3) was added to a stirred solution of tpmp (0.264 g, 1.07 mmol) in ethanol (30 cm^3). The mixture was stirred at room temperature for 30 min and filtered, and dark-brown crystals were obtained from the filtrate. Yield 0.040 g, 15%. IR (ν_{max}/cm^{-1}) 1016 ($\nu_sRO–SO_3^-$), 1236 ($\nu_{as}RO–SO_3^-$), 1206 ($\nu_{as}R_2NH_2^+$), 577 (νM–S), Found: C, 43.80; H, 5.45; N, 4.80; S, 18.60. $C_{32}H_{47}N_3Ni_3O_4S_5$ requires: C, 43.95; H, 5.42; N, 4.81; S, 18.34%.

2.5. Synthesis of [Ni3(pmp)3(μ3-S)] (C3H7OSO3) (4)

This compound was prepared analogously to **3**, using propanol as solvent. Yield 0.162 g, 30%. IR (ν_{max}/cm^{-1}) 1037 ($\nu_sRO–SO_3^-$), 1234 ($\nu_{as}RO–SO_3^-$), 1203 ($\nu_{as}R_2NH_2^+$), 577 (νM–S). Found: C, 44.50; H, 5.50; N, 4.70; S, 18.20. $C_{33}H_{49}Ni_3N_3O_4S_5$ requires: C, 44.6; H, 5.55: N, 4.75; S, 18.10%.

2.6. Synthesis of [Ni3(pmp)3(μ3-S)](NO3) (5)

A solution of $[Ni_3(pmp)_3(\mu_3\text{-}S)](CH_3OSO_3)$ (72 mg, 84 mmol) in $CHCl_3$ (4.0 cm^3) was added to a stirred solution of $Fe(NO_3)_3 \cdot 9H_2O$ (80 mg, 20 mmol) in ethanol (4.0 cm^3). The mixture was stirred at room temperature and then the excess of metal salts were filtered. Dark-brown cubic crystals were obtained from the filtrate. The yield was very low, 12.2 mg (18%), and was not enough to carry on further spectroscopic characterization. Found: C, 44.75; H, 5.25; N, 6.80; S, 15.80. $C_{30}H_{42}Ni_3N_4O_3S_4$ requires: C, 44.4; H, 5.20; N, 6.90; S, 15.8%.

3. Results and discussion

Scheme 1 shows the synthetic routes used in this work. During the synthesis of our new complexes, the alcohol solvents react with the tpmp to cleave the S–S bond and generate the anions $ROSO_3^-$ (R = Pr, Et or Me) and a cationic cluster. The positive charge should be delocalized on the Ni_3S_4 core. All four new compounds were analysed as $[Ni_3(pmp)_3(\mu_3\text{-}S)]X$ ($X^- = NO_3$ or $ROSO_3$, where R is Me, Et or Pr).

The IR spectrum of tpmp shows the ν_{as} and ν_s modes of the $RO–SO_3^-$ group at 1228 and 1026 cm^{-1}. These shifted to 1211 and 1007 cm^{-1} for **2**, 1236 and 1016 cm^{-1} for **3**, and 1234 and 1037 cm^{-1} for **4**. All three compounds (**2**–**4**) have bands assignable to ν(M–S) at ca. 578 cm^{-1}.

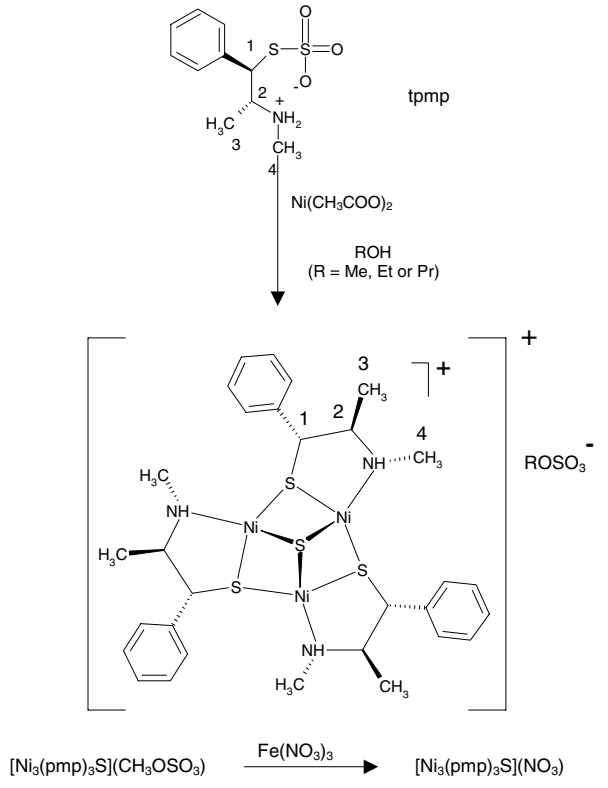

Scheme 1. General synthesis of triangular trinuclear $Ni_3S_4N_3$ clusters obtained from (1*S*,2*S*)-1-monothiasulfato-1-phenyl-2-(methylammoniumyl) propane (tpmp) and $Ni(CH_3COO)_2$.

Table 2
^{1}H NMR and ^{13}C NMR chemical shifts (δ, ppm) in $CDCl_3$ for compounds **3**–**5**

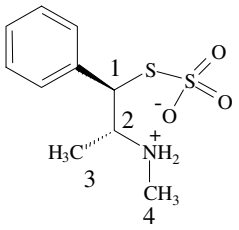

Compounds	H1	H2	H3	N–CH_3	C_6H_5
tpmp	4.42(d, $J = 8.7$ Hz)	3.81(m)	1.06(d, $J = 6.5$ Hz)	2.34	7.26–7.35
3	4.81	2.49	1.00	2.26	7.24–7.37
4	4.86 (d, $J = 11.1$ Hz)	2.46	1.00 (d, $J = 6.2$ Hz)	2.28	7.23–7.40
5	4.88	2.49	1.01	2.23	7.28–7.39
Compounds	C1	C2	C3	C4	C_6H_5
	54.7	59.0	13.9	31.1	$C_i = 138.8$, $C_o = 128.6$ $C_m = 129.2$, $C_p = 128.2$
3	54.1	72.2	15.2	41.1	$C_i = 141.0$, $C_o = 128.4$ $C_m = 128.8$, $C_p = 127.7$
4	54.1	72.2	15.6	41.0	$C_i = 141.1$, $C_o = 128.4$ $C_m = 128.7$, $C_p = 127.6$
5	54.2	72.3	15.7	41.1	$C_i = 141.1$, $C_o = 128.5$ $C_m = 128.8$, $C_p = 127.7$

Complexes **2**–**4** are diamagnetic in the solid state and in solution, and have comparable ^{1}H and ^{13}C NMR spectra (Table 2) [33]. An HETCOR experiment was carried out to correctly assign the chemical shifts for all compounds. Protons have similar shifts in the tpmp ligand and its coordination compounds. Signals for C2 and C3 are shifted to higher frequency on coordination of the amine to the nickel, by 13.2 and 10.0 ppm with respect to tpmp. There are new signals at 55.9 ppm for **2**, 64.3 and 15.3 ppm for **3** and 70.6, 23.0 and 10.6 ppm for **4** which were assigned to alkyl sulfate groups. The ^{15}N NMR spectra show only one signal characteristic of the quaternary amino group for each compound, at −364.2, −349.5 and −363.9 ppm for **2**, **3** and **4**, respectively.

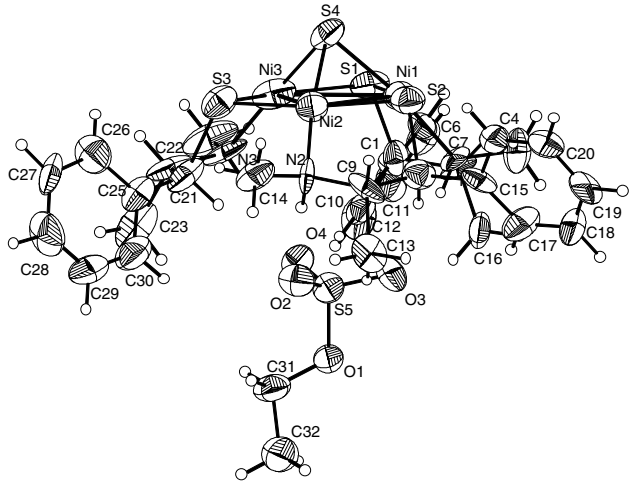

Fig. 1. ORTEP diagram for compound of $[Ni_3(pmp)_3(\mu_3\text{-}S)](C_2H_5OSO_3)$ (**3**). Displacement ellipsods are drawn at the 50% probability level and hydrogen atoms are shown as small spheres of arbitrary radii. The ethylsulfate molecule is on the rim of the cage formed by the three phenyl groups.

3.1. Crystal structures

The crystal structures of compounds **3** and **5** are presented in Figs. 1 and 2. Compound **4** has a structure very similar to that of **3**. Selected bonds distances and angles for all three structures are listed in Tables 3 and 4.

All the compounds contain the same $Ni_3S_4N_3$ cluster, Fig. 3, formed from three nickel atoms arranged in an equilateral triangle, which is capped on one face by a μ_3-sulfide ion. This core has three pendant five membered rings forming a cone shaped molecule with the capped sulfur at the apex. Each triangular edge is also bridged by a sulfur atom, which is part of the thia-pseudoephedrine, pmp. In every case, each nickel atom is also bonded to the nitrogen atom of the pmp. Since compound **5** is formed directly from compound **2**, it is likely that **2** possesses the same structure.

The phenyl groups of the three pmp molecules are so oriented as to form a cylindrical cavity which is closed at one end by the Ni_3S_4 cluster. In all three

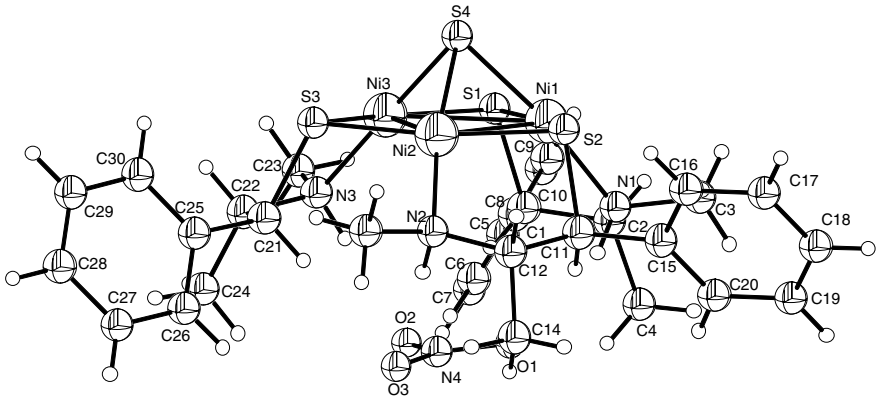

Fig. 2. ORTEP diagram for compound of $[Ni_3(pmp)_3(\mu_3\text{-}S)](NO_3)$ **5**. Displacement ellipsods are drawn at the 50% probability level and hydrogen atoms are shown as small spheres of arbitrary radii. The nitrate anion is lodged in the cavity.

Table 3
Selected bond lengths (Å) for compounds **3**–**5**

	3	4	5
Ni(1)–Ni(2)	2.758(2)	2.752(2)	2.771(9)
Ni(2)–Ni(3)	2.800(2)	2.786(2)	2.785(1)
Ni(3)–Ni(1)	2.896(3)	2.820(2)	2.742(8)
Ni(1)–S(4)	2.179(3)	2.177(3)	2.185(1)
Ni(2)–S(4)	2.179(4)	2.171(3)	2.170(1)
Ni(3)–S(4)	2.191(4)	2.176(3)	2.166(1)
Ni(1)–S(1)	2.162(4)	2.152(3)	2.150(1)
Ni(1)–S(2)	2.250(3)	2.228(2)	2.232(1)
Ni(2)–S(2)	2.172(4)	2.149(3)	2.160(1)
Ni(2)–S(3)	2.243(4)	2.223(3)	2.271(1)
Ni(3)–S(3)	2.168(4)	2.155(3)	2.158(1)
Ni(3)–S(1)	2.522(4)	2.393(3)	2.243(1)
Ni(1)–N(1)	1.976(8)	1.976(6)	1.962(4)
Ni(2)–N(2)	1.960(9)	1.951(7)	1.969(3)
Ni(3)–N(3)	1.931(1)	1.977(8)	1.953(3)

Table 4
Selected angles (°) for compounds **3**–**5**

	3	4	5
Ni(1)–S(4)–Ni(3)	83.00(1)	80.77(9)	78.13(4)
Ni(2)–S(4)–Ni(1)	78.52(1)	78.53(9)	79.02(4)
Ni(3)–S(4)–Ni(2)	79.71(1)	79.75(1)	79.93(5)
Ni(1)–S(2)–Ni(2)	77.13(1)	77.88(9)	78.22(4)
Ni(2)–S(3)–Ni(3)	78.80(1)	79.02(9)	77.89(5)
Ni(3)–S(1)–Ni(1)	75.95(1)	76.51(9)	77.22(4)
Ni(1)–Ni(2)–Ni(3)	62.79(6)	61.22(4)	59.14(3)
Ni(2)–Ni(3)–Ni(1)	57.89(6)	58.79(4)	60.16(2)
Ni(3)–Ni(1)–Ni(2)	59.32(5)	60.00(4)	60.69(3)
S(1)–Ni(1)–S(2)	166.28(1)	164.41(1)	162.35(5)
S(2)–Ni(2)–S(3)	164.13(1)	162.45(1)	160.37(5)
S(3)–Ni(3)–S(1)	156.01(1)	158.16(1)	162.66(5)
S(1)–Ni(1)–S(4)	85.87(1)	84.82(1)	82.94(5)
S(1)–Ni(3)–S(4)	77.38(1)	79.29(1)	81.24(5)
S(2)–Ni(1)–S(4)	81.49(1)	80.84(9)	80.98(5)
S(2)–Ni(2)–S(4)	83.30(1)	82.77(1)	82.97(5)
S(3)–Ni(2)–S(4)	82.30(1)	81.98(1)	81.82(5)
S(3)–Ni(3)–S(4)	83.74(1)	83.45(1)	84.55(5)
S(4)–Ni(1)–N(1)	171.6(3)	170.8(2)	170.58(5)
S(4)–Ni(2)–N(2)	173.0(3)	172.3(2)	172.86(5)
S(4)–Ni(3)–N(3)	173.4(3)	172.4(2)	172.00(5)

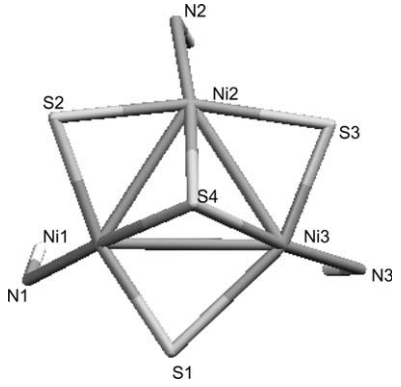

Fig. 3. Scheme showing the $Ni_3S_4N_3$ cluster in compound $[Ni_3(pmp)_3(\mu_3\text{-}S)]$ $(C_3H_7OSO_3)$ **4**.

structures the counter ion, $EtOSO_3^-$, $PrOSO_3^-$ or NO_3^-, is bound into the cavity by strong hydrogen bonds [34]. For example, in compound **4** each oxygen atom is hydrogen bonded to a N–H (N–H···O 2.089–2.149 Å) and also interacts with a benzylic C–H hydrogen (C–H···O 2.472–2.717 Å). Compound **5** (Fig. 4), contains a planar nitrate group (N–O 1.232(6)–1.248(6) Å; O–N–O 118.0(5)–121.6(5)°) with shorter N–H···O and C–H···O hydrogen bonds (2.111–2.185 and 2.370–2.413 Å, respectively).

There are at least nine compounds, including those described here, that contain the Ni_3S_4 nucleus, with the ligands (*R*,*S*)-2-[(2-mercapto-1-methylamino)ethylphenol)] [24], SMe [25], SPh [26,27], *t*-butylthiolato [28] and *o*-$(SCH_2)_2C_6H_4$) [29]. Nevertheless all nine have very similar geometries, the special characteristic of the pseudoephedrine in our compounds is its potential for hydrogen-bonding that allows the binding of the oxoanions within the cavity.

The Ni_3S_4 cluster is not significantly different in any of the compounds (**3**–**5**) or those cited in the literature. The three nickel atoms and the capping sulfur atom form a distorted tetrahedron, but perhaps the structure

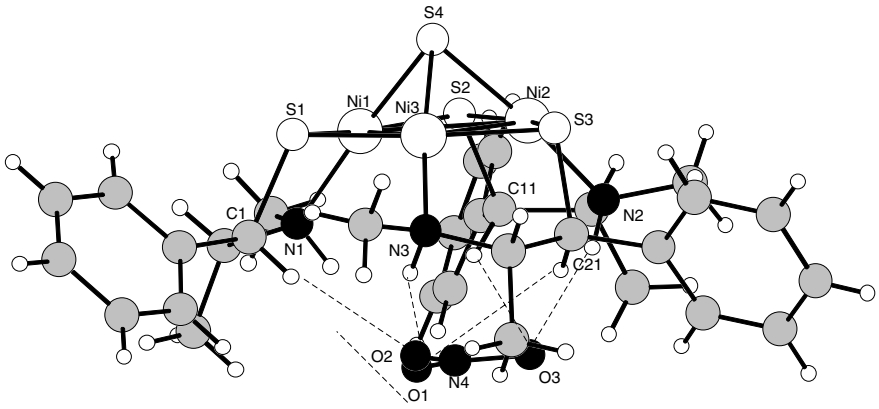

Fig. 4. Scheme of $[Ni_3(pmp)_3(\mu_3\text{-}S)](NO_3)$ **5** showing the principal hydrogen bonds between the N–H and C–H groups of pmp and oxygen atoms of the nitrate anion.

is best described as a relatively planar Ni_3S_3 array capped upon one side by a μ_3-S ion bonded directly to all three nickel ions. This has the effect of forcing other ligands attached to the nickels out of the Ni_3S_3 plane and in a direction away from the capping sulfide. This occurs with large ligands such as our own, as well as with small ligands such as SMe [25]. The three bridging sulfur atoms are little removed from the plane of the nickel atoms, so that a single plane contains not just the three nickel ions but the complete Ni_3S_3 moiety. With monodentate ligands the Ni_3S_3 unit is trigonal [25–29]. However, when bidentate ligands bridge the two positions, they introduce some distortion and two different S–Ni bond lengths, the S–Ni bonds of the five membered chelate ring being the shorter, for example 2.171(4) and 2.219(4) for the compound with (*R*,*S*)-2-[(2-mercapto-1-methylamino)ethylphenol] [24] The distances observed in our compounds are 2.158(3) and 2.513(3) Å for **3**, 2.152(3) and 2.393(3) Å for **4**, and 2.150(1) and 2.242(1) Å for **5**.

The reported Ni-μ_3S distances are all within the range 2.166(1)–2.196(3) Å, which is not a large variation, and are similar to those of our compounds. In fact, for all the recorded compounds where the μ_2-S atoms may or may not be a part of a chelating system and where the other donor atom on the nickel may be S or N or C, this range scarcely changes. The coordination about the nickel can be described as approximately square-planar. The angle S(apex)–Ni–X (X = S, C or N) in every case is of the order of 170°, which is also consistent with roughly square–planar geometry at the nickel atoms.

The Ni_3 moiety forms an equilateral triangle, the maximum variation from 60° observed in any of the examples with the Ni_3S_4 core being 2° Fig. 3. This implies some Ni–Ni bonding, which is consistent with the observed metal ion separations, none being very different from 2.75 Å. This distance is between twice the reported covalent radius of nickel(II) (1.16×2–1.21×2 Å) and twice the van der Waals radius (1.60×2 Å) [35].

4. Compound synthesis

The syntheses of all the compounds so far described, including our own, have at least one factor in common. Although all the compounds contain the capping sulfide ion, in no case was sulfide an original reactant. It must be generated in the reaction mixture. The yields of Ni_3S_4 complexes are always relatively small, less than 30% so that the reactions are not clean. In another respects, the synthesis described in the literature differ from ours. All use thiols as the source of the sulfur ligands as well as (presumably) sulfide. Our systems use a thiosulfate, tpmp, and alcohols as solvents rather than the more usual acetonitrile. It seems probable that the nickel(II) induces thiosulfate solvolysis, yielding the alkyl sulfate and the formation of a thiazolidine, where the metal ion is part of the ring system [33].

The *S*,*S* conformations at C(1) and C(2) of the initial ephedrine propane skeleton are maintained in the complexes. The cavity in our materials should be able to act as an anion trap through strong hydrogen bonding. In fact, we have already obtained compound **5** from compound **2** by treatment with $Fe(NO_3)_3$ which is essentially an anion exchange reaction. We are currently testing this kind of reaction further.

5. Supplementary material

Crystallographic data for the structural analysis have been deposited with the Cambridge Crystallographic Data Centre. The relevant CCDC references are 228424, 228425 and 22842. Copies of this information may be obtained free of charge from The Director, CCDC, 12

Union Road, Cambridge, CB2 1EZ, UK (fax: +44-1223-336033; email: deposit@ccdc.cam.ac.uk or www: http://www.ccdc.cam.ac.uk).

Acknowledgements

We thank CONACyT (Grant 41128-Q) for financial support. H.L.-S. and J.C.G.R. acknowledge scholarships from CONACyT–Mexico and G.J.L. acknowledges the support of the Royal Society and Mexican Academy. Thanks are given to Marco Antonio Leyva Ramírez for X-ray resolution of compound **3**.

References

[1] S.B. Mulrooney, R.P. Hausinger, FEMS Microbiol. Rev. 27 (2003) 239.
[2] N.-C. Ha, S.-T. Ho, J.Y. Sung, K.-A. Cha, M.H. Lee, B.-H. Ho, Nat. Struct. Biol. 8 (2001) 505.
[3] P.M. Matias, C.M. Soares, L.M. Saraiva, R. Coelho, J. Morais, J. Le Gall, M.A. Carrondo, J. Biol. Inorg. Chem. 6 (2001) 63.
[4] Y. Nicolet, C. Caravazza, J.C. Fontecilla-Camps, J. Inorg. Biochem. 91 (2002) 1.
[5] H. Dobbek, V. Svetlitchnyi, L. Gremer, R. Huber, O. Meyer, Science 293 (2001) 1281.
[6] T.I. Doukov, T.M. Iverson, J. Seravalli, S.W. Ragsdale, C.L. Drennan, Science 298 (2002) 567.
[7] W. Grabarse, F. Mahlert, E.C. Duin, M. Goubeaud, S. Shima, R.K. Thauer, V. Lamzin, U. Ermler, J. Mol. Biol. 309 (2001) 315.
[8] M.M. He, S.L. Clugston, J.F. Honek, B.W. Matthews, Biochemistry 39 (2000) 8719.
[9] T.C. Pochapsky, S.S. Pochapsky, T. Ju, H. Mo, F. Al-Mjeni, M.J. Maroney, Nat. Struct. Biol. 9 (2002) 966.
[10] S.B. Choudhury, J.W. Lee, G. Davidson, Y.I. Yim, K. Bose, M.L. Sharma, S.O. Kang, D.E. Cabelli, M.J. Maroney, Biochemistry 38 (1999) 3744.
[11] A.C. Marr, D.J.E. Spencer, M. Schröder, Coord. Chem. Rev. 219 (2001) 1055.
[12] S.A. Mirza, R.O. Day, N. Maroney, Inorg. Chem. 35 (1996) 1992.
[13] M. Cha, J. Sletten, S. Critchlow, J. Kovacs, Inorg. Chim. Acta 263 (1991) 153.
[14] J.E. Huyett, S.B. Choudhury, D.M. Eichhorn, P.A. Bryngelson, M.J. Maroney, B.M. Hoffman, Inorg. Chem. 37 (1998) 1361.
[15] C.B. Allan, G. Davidson, S.B. Choudhury, Z. Gu, K. Bose, R.O. Day, M.J. Maroney, Inorg. Chem. 37 (1998) 40166.
[16] J.A. Verhagen, D.D. Ellis, M. Lutz, A.L. Spek, E. Bowman, J. Chem. Soc., Dalton Trans. (2002) 1275.
[17] F. Cecconi, C.A. Ghilardi, S. Midollini, A. Orlandini, A. Vacca, Inorg. Chem. Commun. 3 (2000) 276.
[18] T. Mancilla, R. Contreras, J. Organomet. Chem. 321 (1987) 191.
[19] N. Farfán, T. Mancilla, P. Castillo, G. Uribe, L. Carillo, P. Joseph-Nathan, R. Contreras, J. Organomet. Chem. 381 (1990) 1.
[20] A. Cruz, A. Flores-Parra, H. Tlahuex, R. Contreras, Tetrahedron: Asymmetry 6 (1995) 1933.
[21] A. Flores-Parra, R. Contreras, Coord. Chem. Rev. 196 (2000) 85.
[22] H. López Sandoval, N. Barba-Behrens, S. Bernès, N. Farfán-García, H. Höpfl, J. Chem. Soc., Dalton Trans. (1997) 3415.
[23] H. López Sandoval, R. Contreras, A. Escuer, R. Vicente, S. Bernès, H. Nöth, G.J. Leigh, N. Barba-Behrens, J. Chem. Soc., Dalton Trans. (2002) 2648.
[24] A. Berkessel, J.W. Bats, M. Hüber, W. Haase, T. Neumann, L. Seidel, Chem. Ber. 128 (1995) 125.
[25] G. Henkel, M. Kriege, K. Matsumoto, J. Chem. Soc., Dalton Trans. (1988) 657.
[26] K. Matsumoto, I. Nakamishi, H. Nakano, S. Ooi, Polyhedron 15 (1996) 4501.
[27] K. Matsumoto, H. Nakano, S. Ooi, Chem. Lett. (1988) 823.
[28] A. Muller, G. Henkel, Chem Commun. (1996) 1005.
[29] W. Tremel, B. Krebs, G. Henkel, Inorg. Chim. Acta 80 (1983) L31.
[30] G.M. Sheldrick, SHELXTL 97. A Program for Crystal Structure Determination, University of Göttingen, Germany, 1997.
[31] D.J. Watkin, C.K. Prout, J.R. Carruthers, P.W. Betteridge, R.I. Cooper, Crystals (2001), Chemical Crystallography Laboratory, Oxford, UK, 2001.
[32] International Tables for X-Ray Crystallography, Kynoch Press, Birmingham, 1974, vol. IV, p. 99.
[33] A. Cruz, A. Vazquez-Badillo, Ramos-García, R. Contreras, Tetrahedron: Asymmetry 12 (2001) 711.
[34] G.A. Jeffrey, An Introduction to Hydrogen Bonding, Oxford University Press, New York, 1997.
[35] J.E. Huheey, E.A. Keiter, R.L. Keiter, Inorganic Chemistry, 4th ed., Harper Collins, New York, 1993, page 292.

Available online at www.sciencedirect.com
SCIENCE DIRECT®
Polyhedron 23 (2004) 1845–1849
POLYHEDRON
www.elsevier.com/locate/poly

Octakis(1-naphthylmethylthio) substituted porphyrazine derivatives

Ergün Gonca [a,b], Yüksel Köseoğlu [c], Bekir Aktaş [d], Ahmet Gül [a,*]

[a] Department of Chemistry, Technical University of Istanbul, TR34469 Maslak, Istanbul, Turkey
[b] Department of Chemistry, Fatih University, TR34500 B.Cekmece, Istanbul, Turkey
[c] Department of Physics, Fatih University, TR34500 B.Cekmece, Istanbul, Turkey
[d] Department of Physics, Gebze Institute of Technology, TR41400 Kocaeli, Turkey

Received 2 March 2004; accepted 4 May 2004
Available online 25 May 2004

Abstract

Magnesium porphyrazinate substituted with eight (1-naphthylmethylthio)groups on the peripheral positions has been synthesized by cyclotetramerization of 1,2-bis(1-naphthylmethylthio)maleonitrile in the presence of magnesium butanolate. The metal-free derivative was obtained by its treatment with trifluoroacetic acid and further reaction of this product with copper(II) acetate, zinc(II) acetate and cobalt(II) acetate led to the metal porphyrazinates (M = Cu, Zn, Co). These new compounds have been characterized by elemental analysis, together with FT- IR, ^{1}H NMR, UV–Vis and EPR spectral data.
© 2004 Elsevier Ltd. All rights reserved.

Keywords: Porphyrazine; EPR; Naphthalene; Copper; Zinc; Cobalt

1. Introduction

Porphyrins, phthalocyanines, tetrabenzoporphyrins and porphyrazines, which can be denoted as tetrapyrrole derivatives, receive extensive attention because of both theoretical studies and applications in advanced materials science [1]. Among this group, porphyrins are important not only from biological aspect but also for coordination chemistry, catalysis and material science. Phthalocyanines that are completely synthetic materials are used in electrophotography, optic data collection, gas sensor, liquid crystal, laser technology and the photodynamic therapy of tumors as well as their classical fields as pigments and dyes. Tuning of the properties of phthalocyanines has been generally achieved through changes in the nature and bonding pattern of the substituents [2–5].

In contrast to the structural similarity between phthalocyanines and porphyrazines, the latter have been relatively less studied compared to the phthalocyanines [6–8]. Starting with octakis(alkylthio) porphyrazine derivatives by Hoffman [9], in which the presence of soft S donor atoms play an important role in affecting the solid-state interactions, an extensive series of derivatives with physical and chemical properties comparable to those of phthalocyanines have been reported. Peripherally-functionalized porphyrazines have the potential to exhibit novel optical, magnetic and electronic properties. The transition metal ion in the inner core offers new ways to induce, modify and to control molecular properties. Metalloporphyrazines have been also proven to exhibit optical limiting effects comparable with phthalocyanine and naphthalocyanine derivatives [10].

During the last decade, we have been heavily engaged with the preparation of new porphyrazines in parallel with phthalocyanine analogues [11–15]. Substitution of various groups on the peripheral positions of porphyrazines has been accomplished either starting with an unsaturated dinitrile precursor with this group attached at the beginning (e.g., dimethylaminoethylthio- [16], tosylaminoethylthio- [17], etc.) or a porphyrazine with reactive functional groups has been prepared at first and then additional groups (e.g., ferrocene [18], benzo-15-crown-5 [19], pyridine [13], etc.) have been incorporated by further condensation reactions.

* Corresponding author. Tel.: +90-212-285-68-27; fax: +90-212-285-63-86.
E-mail address: ahmetg@itu.edu.tr (A. Gül).

0277-5387/$ - see front matter © 2004 Elsevier Ltd. All rights reserved.
doi:10.1016/j.poly.2004.05.001

Recently, we have reported a new group of compounds containing an aromatic phthalocyanine core at the center and four electron rich naphthoxy-substituents on the periphery with the aim of observing the consequences of the combination of these electron-rich units in the same molecule. Here in the present work, the target molecule is a further step to include a porphyrazine core with eight naphthyl units attached to the peripheral positions through methylthio bridges [20].

2. Experimental

IR spectra were recorded on a Mattson 1000 FT-IR spectrophotometer by using KBr pellets, electronic spectra on a Unicam UV–Vis spectrophotometer. Elemental analyses were performed at the Instrumental Analysis Laboratory of TUBITAK Marmara Research Center. Proton NMR spectra were recorded on a Bruker 250 MHz spectrometer using TMS as the reference. EPR spectra of (**3c**) and (**3e**) as powder form and as chloroform solution were registered by a conventional X-band ($v = 9.5$–9.8 GHz) Bruker EMX model spectrometer employing an ac magnetic modulation technique.

The disodium salt of dithiomaleonitrile (**1**) was prepared according to the previously reported procedures [21].

2.1. Synthesis of 1,2-bis(1-naphthylmethylthio)maleonitrile (2)

Disodium salt of dithiomaleonitrile (**1**) (1.12 g, 6 mmol) was mixed with 1-(chloromethyl)-naphthalene (2.65 g, 15 mmol) in methanol (50 ml) and refluxed under nitrogen for about 6 h. When MeOH was evaporated, the remaining oily product was treated with $CHCl_3$ to remove insoluble salts by filtration. The $CHCl_3$ solution was extracted several times with 15% Na_2SO_4 solution and then dried over anhydrous Na_2SO_4 overnight. After evaporation of the solvent the remaining oily product was extracted with refluxing *n*-hexane to remove any excess 1-(chloromethyl)-naphthalene. The product was very soluble in chloroform and dichloromethane. Yield: 1.90 g, 75%. FT-IR (KBr), ν_{max}/(cm^{-1}): 3055 (H–Ar), 2930–2852 (CH_2), 2212 (C≡N), 1520, 1214, 1162, 1042, 782 cm^{-1}; ^{1}H NMR (d-chloroform 250 MHz): 7.92–7.79 (m, 3H, Ar–H), 7.56–7.35 (m, 4H, Ar–H), 4.67 (s, 2H, S–CH_2). UV–Vis. ($CHCl_3$) λ_{max}/(nm): 285.

2.2. [2,3,7,8,12,13,17,18-Octakis(1-naphthylmethylthio)-porphyrazinato] Mg(II) (3a)

Mg turnings (6 mg, 0.25 mmol) and a small I_2 crystal were refluxed in *n*-BuOH (15 ml) for about 8 h to obtain $Mg(BuO)_2$. 1,2-Bis(1-naphthylmethylthio)maleonitrile (211 mg, 0.5 mmol) was added to the this solution and the mixture was refluxed for about 12 h. The blue-green product was filtered, washed with ethanol and water and dried. The crude product was dissolved in $CHCl_3$ and filtered. The $CHCl_3$ solution was dried over anhydrous Na_2SO_4. When the solvent was evaporated, dark blue-green product was obtained. Finally, pure porphyrazine was obtained by chromatography on silica gel using methanol/chloroform (1:50) mixture as eluent. The product was very soluble in chloroform, soluble in dichloromethane, acetone and toluene, but insoluble in *n*-hexane. Yield: 150 mg (70%). FT-IR (KBr), ν_{max}/(cm^{-1}): 3055 (H–Ar), 2927–2850 (CH_2), 1526, 1210, 1161, 1035, 782 cm^{-1}. ^{1}H NMR (d-chloroform 250 MHz): 8.11–7.37 (m, 7H, Ar–H), 5.40 (br s, CH_2–S).

2.3. [2,3,7,8,12,13,17,18-Octakis(1-naphthylmethylthio) H^{21}, H^{23} porphyrazine] (3b)

3a (171 mg, 0.1 mmol) was dissolved in minimum amount of trifluoroaceticacid (~3 ml) and stirred for 3 h at room temperature. When the reaction mixture was added to ice drop-by-drop and neutralized with 25% ammonia solution, precipitation occurred and it was filtered. The precipitate was extracted into the chloroform and the chloroform solution was extracted with water twice. After drying over anhydrous Na_2SO_4, the solvent was evaporated to obtain violet colored metal-free porphyrazine. The crude product was purified by chromatography on silica gel using methanol/chloroform (1:30) mixture as the eluent. Yield: 110 mg (65%). FT-IR (KBr), ν_{max}/(cm^{-1}): 3326 (N–H), 3055 (H–Ar), 2923–2855 (CH_2), 1522, 1212, 1168, 1044, 782 cm^{-1}. ^{1}H NMR (d-chloroform 250 MHz): 7.65–6.91 (m, 7H, Ar–H), 5.41 (br s, 2H, CH_2–S), −2.21 (br s, 2H, NH).

2.4. General procedure for metallo porphyrazines (3c–3e)

3b (169 mg, 0.1 mmol) in $CHCl_3$ (10 ml) was stirred with the metal salt [$Cu(OAc)_2$ (181.6 mg, 1 mmol), $Zn(OAc)_2$ (183.4 mg, 1 mmol) or $Co(OAc)_2$ (177 mg, 1 mmol)] in ethanol (15 ml) and refluxed under nitrogen for about 4 h. Then, the precipitate composed of the crude product and the excess metal salt was filtered. The precipitate was treated with $CHCl_3$ and the insoluble metal salts were removed by filtration. The filtrate was reduced to minimum volume under reduced pressure and then added into *n*-hexane (150 ml) drop by drop to realize the precipitation. Finally, pure porphyrazine derivatives were obtained by chromatography on silica gel using methanol/chloroform (1:50) mixture as the eluent.

[2,3,7,8,12,13,17,18-Octakis(1-naphthylmethylthio)-porphyrazinato] Cu(II) ***(3c)***. Yield: 58 mg (33%). FT-IR (KBr), ν_{max}/(cm^{-1}): 3055 (H–Ar), 2925–2854 (CH_2), 1522, 1213, 1162, 1039, 782 cm^{-1}.

[2,3,7,8,12,13,17,18-Octakis(1-naphthylmethylthio)-porphyrazinato] Zn(II) ***(3d)***. Yield: 67 mg (38%). FT-IR (KBr), $\nu_{max}/(cm^{-1})$: 3055 (H–Ar), 2922–2853 (CH_2), 1528, 1211, 1161, 1035, 782 cm^{-1}. ^1H NMR (d-chloroform 250 MHz): 8.29–7.35 (m, 7H, Ar–H), 4.72 (s, 2H, CH_2–S).

[2,3,7,8,12,13,17,18-Octakis(1-naphthylmethylthio)-porphyrazinato] Co(II) ***(3e)***. Yield: 75 mg (43%). FT-IR (KBr), $\nu_{max}/(cm^{-1})$: 3055 (H–Ar), 2932–2855 (CH_2), 1521, 1219, 1168, 1033, 782 cm^{-1}.

3. Results and discussion

The starting point for a novel porphyrazine structure with eight (1-naphthylmethylthio) groups bound to the periphery through flexible methylthio-chains is 1,2-bis-(1-naphthylmethylthio)maleonitrile (**2**) which was obtained from disodium salt of dithiomaleonitrile (**1**) and 1-(chloromethyl)naphthalene (Scheme1). The oily product (**2**) was obtained in relatively high yield (75%). The presence of bulky electron-donating S-groups is expected to give porphyrazines absorbing electromagnetic radiation just in the same range as phthalocyanines [10,13–16]. Conversion of bis(1-naphthylmethylthio)-maleonitrile into porphyrazine was achieved by the template effect of magnesium butanolate. Cyclotetramerization gave the blue-green octakis(1-naphthylmethylthio) porphyrazinatomagnesium (**3a**) (Fig. 1). It is very soluble in chloroform and soluble in dichloromethane, acetone and toluene, but insoluble in apolar hydrocarbon solvents such as *n*-hexane.

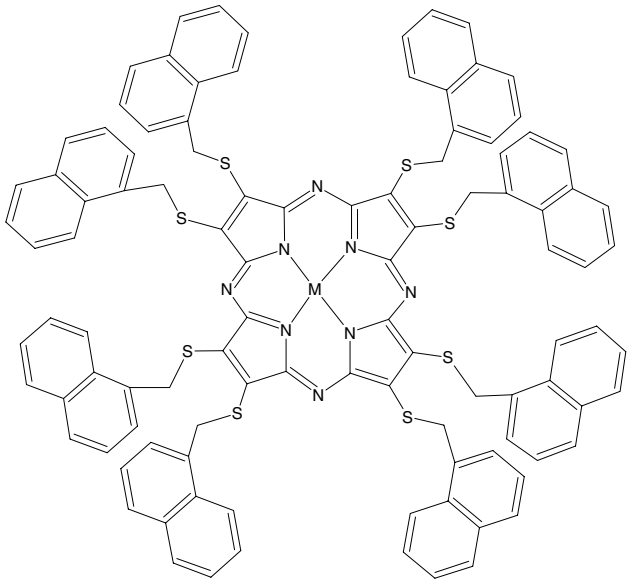

Fig. 1. Octakis (1-naphthylmethylthio) substituted porphyrazines (M = Mg (**3a**); 2H (**3b**); Cu (**3c**); Zn (**3d**); Co (**3e**)).

Elemental analyses correspond closely with the values calculated for (**2**, **3a**–**3e**) (Table 1). In the FT-IR spectrum of bis(1-naphthylmethylthio)maleonitrile (**2**) stretching vibration of C≡N is observed at 2212 cm^{-1}, the aromatic and aliphatic C–H peaks are around 2850–3055 cm^{-1} and the characteristic substituted naphthalene peak at 782 cm^{-1}. These values comply with those reported in the literature for similar compounds [20]. After conversion of dinitrile derivative (**2**) to porphyrazine (**3**), the sharp C≡N vibration around 2212 cm^{-1}

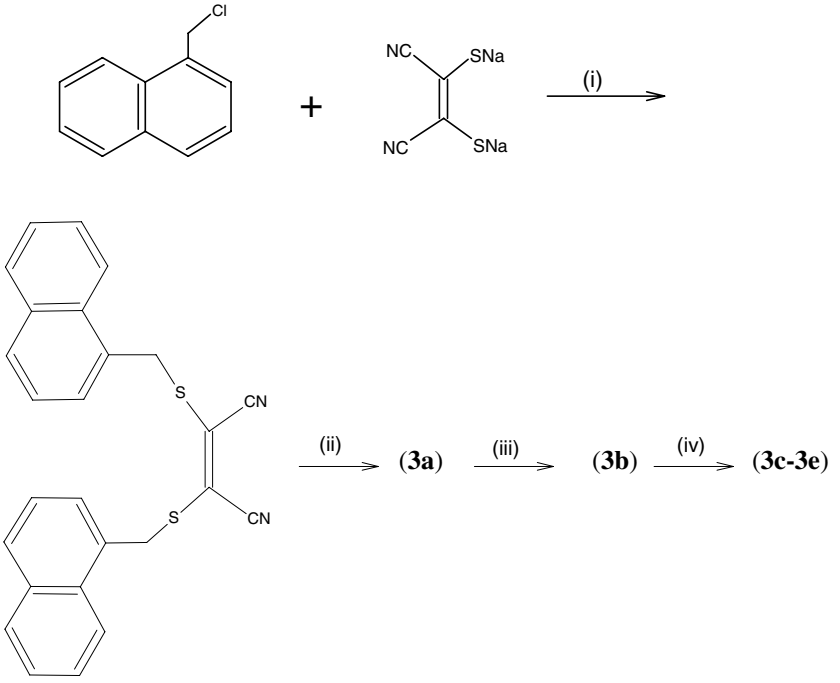

Scheme 1. (i) Methanol; (ii) Mg turnings, I_2, *n*-BuOH; (iii) CF_3CO_2H; (iv) EtOH and $Cu(OAc)_2$, $Zn(OAc)_2$, or $Co(OAc)_2$.

Table 1
Elemental analyses results of the porphyrazines[a]

Compound	C	H	N
2	73.65 (73.90)	4.45 (4.29)	6.49 (6.63)
3a	72.60 (72.86)	4.36 (4.23)	6.30 (6.54)
3b	73.68 (73.82)	4.65 (4.41)	6.78 (6.62)
3c	71.46 (71.22)	4.27 (4.14)	6.14 (6.39)
3d	70.94 (71.15)	4.28 (4.13)	6.12 (6.38)
3e	71.12 (71.41)	4.30 (4.15)	6.56 (6.41)

[a] Required values are given in parentheses.

disappeared. The N–H stretching absorption of the inner core of the metal-free porphyrazine (**3b**) was observed around 3326 cm^{-1}. FT-IR spectra of all porphyrazines derivatives (**3a**–**3e**) showed the aromatic and aliphatic C–H peaks are around 2850–3055 cm^{-1} and a characteristic substituted naphthalene peak at 782 cm^{-1} [20].

The N–H protons of the metal-free porphyrazine (**3b**) were also identified in the ^1H NMR spectrum with a broad peak at $\delta = -2.21$ ppm, presenting the typical shielding of inner core protons, which is a common feature of the ^1H NMR spectra of metal-free porphyrazines [7,12,18,19]. In the ^1H NMR spectra of diamagnetic porphyrazines **3a**, **3b**, **3d** two different types of protons are clearly seen: A multiplet around 7–8 ppm corresponding to naphthyl-protons and a singlet at 5.40 ppm (**3a**), 5.41 ppm (**3b**) or 4.72 ppm (**3d**) for methylene protons. The ratio of the integral values 7:2 also confirms the proposed structure.

Electronic spectra are especially useful to establish the structure of the porphyrazines (**3a**–**3e**). UV–Vis spectra of porphyrazine core are dominated by two intense bands, the Q band around 660 nm and the B band in the near UV region of around 355 nm, both correlated to $\pi \rightarrow \pi^*$ transitions [6,7]. The presence of an electron donating group on the periphery causes a bathochromic shift on Q bands. UV–Vis spectra of metallo-porphyrazines (**3a**, **3c**–**3e** in $CHCl_3$) prepared in the present work exhibited intense single Q band absorption of the $\pi \rightarrow \pi^*$ transitions around 643–676 nm and B bands in the UV region around 335–377 nm. For metal-free derivative (**3b**), Q band is split into two peaks at 643 and 707 nm as a consequence of the change in the symmetry of porphyrazine core from D_{4h} (in the case of metallo derivatives) to D_{2h}. Here, in the case of porphyrazines with appending (1-naphthylmethylthio) substituents in addition to these absorptions of the porphyrazine core, an intense absorption due to the $\pi \rightarrow \pi^*$ transition of naphthalene groups appeared for all these porphyrazines derivatives (**3a**–**3e**) in the UV region at about 287–289 nm [20] (Table 2).

The room temperature first-derivative EPR spectra taken from powder and solution forms of Cu(II) and Co(II) porphyrazine samples (**3c**, **3e**) are shown in Figs. 2 and 3, respectively. As seen in the figures, the first

Table 2
UV–Vis data for the porphyrazines in chloroform

Compound	λ/nm (log ε/dm^3 mol^{-1} cm^{-1})			
3a	287 (4.89)	377 (4.84)	676 (4.84)	
3b	288 (4.81)	351 (4.78)	643 (4.49)	707 (4.58)
3c	288 (4.65)	345 (4.48)	669 (4.36)	
3d	289 (4.67)	356 (4.51)	675 (4.80)	
3e	288 (4.71)	335 (4.46)	644 (4.34)	

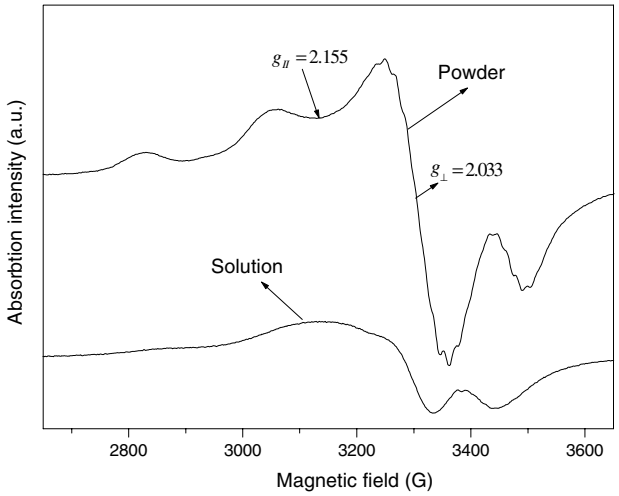

Fig. 2. X-band EPR spectra of (**3c**) as powder form and as chloroform solution at room temperature.

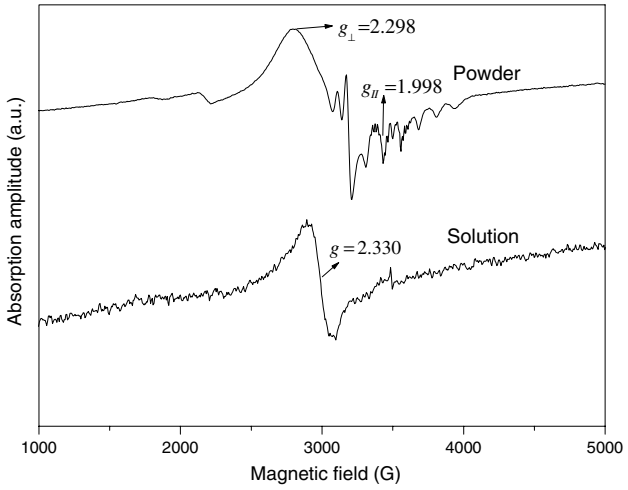

Fig. 3. X-band EPR spectra of (**3e**) as powder form and as chloroform solution at room temperature.

signals are from the powder forms and they have both parallel and perpendicular parts with hyperfine splitting. The signals have a characteristic and anisotropic main curve that satisfies an axial symmetry for the compounds. Here $g_{\|}$ and $g_{\perp}$ denote effective g-values when the applied dc field is parallel ($B_{\|}$) and perpendicular ($B_{\perp}$) to the symmetry axis of the crystalline field around the paramagnetic center, respectively. As it is well known, for statistically and randomly oriented powders,

the absorption corresponding to $g_{\perp}$ is more intensive than that corresponds to $g_{\|}$. This kind of spectrum is characteristic for a conventional powdered sample containing a paramagnetic ion with an axially symmetric g factor with $g_{\|} > g_{\perp} > g_e$ ($g_e = 2.0023$) and with hyperfine splitting [22,23]; that is, the local symmetry of the paramagnetic center giving this signal should be axial. The EPR spectrum of chloroform solution of Cu(II) porphyrazine (**3c**) (Fig. 2) is a little different from that of powder form. The hyperfine splitting can not be seen clearly. The reason for the lack of hyperfine splitting is probably due to superimposition and line broadening in the spectrum. Also, in the EPR spectrum of chloroform solution of Co(II) porphyrazine (**3e**) (Fig. 3), the signal maintains its axial symmetry character with $g_{\perp} > g_{\|}$. However, when we compare this spectrum with the previous one taken from the powder form, there are important changes at both parallel and perpendicular parts of the spectrum. The well resolved hyperfine peaks superimpose and cannot be seen at both parts of the spectrum. Also, the line width of the overall spectrum decreases. These changes observed in the EPR spectra of both samples can be attributed to the axial symmetry and highly anisotropic *g*-value. The *g*-values obtained for the copper(II) and cobalt(II) porphyrazines (**3c**) and (**3e**) closely follow those reported for other monomeric tetrapyrrole derivatives of the same paramagnetic metal centers [24–27].

In conclusion, new porphyrazines surrounded with eight bulky naphthylmethyl groups have been described; high electron density on the substituents results with a second absorption in the ultraviolet region of comparable intensity as the intense B band of porphyrazines.

Acknowledgements

This work was supported by the Research Fund of the Technical University of Istanbul.

References

[1] J.A. McCleverty, T.J. Meyer (Eds.), Comprehensive Coordination Chemistry II, vol. 9, Elsevier, Amsterdam, 2004.
[2] N. Kobayashi, Coord. Chem. Rev. 99 (2001) 219.
[3] N.B. McKeown, Adv. Mater. 11 (1999) 67.
[4] E.A. Luk'yanets, Mol. Mater. 1 (1992) 209.
[5] K.W. Poon, W. Liu, P.K. Chan, Q. Yang, T.W.D. Chan, T.C.W. Mak, D.K.P. Ng, J. Org. Chem. 66 (2001) 1553.
[6] C.F. van Nostrum, R.J.M. Nolte, Chem. Commun. (1996) 2385.
[7] A.E. Pullen, C. Faulmann, P. Cassoux, Eur. J. Inorg. Chem. (1999) 269.
[8] O.G. Khelevina, N.V. Chizhova, P.A. Stuzhin, J. Porphyr. Phthalocya. 4 (2000) 555.
[9] C.J. Schramm, B.M. Hoffman, Inorg. Chem. 19 (1980) 383.
[10] S. Vagin, M. Barthel, D. Dini, M. Hanack, Inorg. Chem. 42 (2003) 2683.
[11] M. Koçak, A.İ. Cihan, A. Okur, A. Gül, Ö. Bekaroğlu, Dyes Pigments 45 (2000) 9.
[12] B.Ş. Sesalan, A. Koca, A. Gül, Polyhedron 22 (2003) 3083.
[13] R. Öztürk, A. Gül, Tetrahedron Lett. 45 (2004) 947.
[14] B. Hasanov, A. Gül, Synth. React. Inorg. Met. Org. Chem. 31 (2001) 673.
[15] R. Öztürk, S. Güner, B. Aktaş, A. Gül, Synth. React. Inorg. Met. Org. Chem. 31 (2001) 1623.
[16] M. Polat, A. Gül, Dyes Pigments 45 (2000) 195.
[17] R.Z. Uslu, A. Gül, C.R. Acad. Sci. Paris. Ser. II C: Chim. 3 (2000) 643.
[18] H. Akkuş, A. Gül, Transition Met.Chem. 26 (2001) 689.
[19] Ö. Sağlam, A. Gül, Polyhedron 20 (2001) 269.
[20] H.Y. Yenilmez, I. Özçeşmeci, A.I. Okur, A. Gül, Polyhedron 23 (2004) 787.
[21] A. Davison, R.H. Holm, Inorg. Synth. 10 (1967) 8.
[22] J.A. Weil, J.R. Bolton, J.E. Wertz, Electron Paramagnetic Resonance, Wiley, New York, 1994.
[23] K. Golcuk, A. Altun, S. Guner, M. Kumru, B. Aktas, Spectrochim. Acta A 60 (2004) 303.
[24] C.F. van Nostrum, F.B.G. Benneker, H. Brussaard, H. Kooijman, N. Veldman, A.L. Spek, J. Schoonman, M.C. Feiters, R.J.M. Nolte, Inorg. Chem. 35 (1996) 959.
[25] B. Venkatesh, H. Hori, G. Miyazaki, S. Nagatomo, T. Kitagawa, H. Morimoto, J. Inorg. Biochem. 88 (2002) 310.
[26] K.M. Kadish, J. Shao, Z. Ou, C. Comte, C.P. Gros, R. Guilard, J. Porphyr. Phthalocya. 4 (2000) 639.
[27] F. Bonosi, G. Ricciardi, F. Lelj, G. Martini, J. Phys. Chem. 98 (1994) 10613.

Available online at www.sciencedirect.com
SCIENCE DIRECT®
Polyhedron 23 (2004) 1851–1857
POLYHEDRON
www.elsevier.com/locate/poly

Crystal structure, thermal decomposition kinetics and antimicrobial activities of $[Zn(eatz)_2(OAc)_2]$ (eatz = 5-ethyl-2-amino-1,3,4-thiadiazole) ☆

Xiao-Qing Shen [a,1], Hong-Jian Zhong [b], Hao Zheng [c], Hong-Yun Zhang [c,*], Guang-Hua Zhao [b], Qing-An Wu [c], Hong-Yan Mao [a,c], En-Bo Wang [a], Yu Zhu [c]

[a] College of Chemistry, Northeast Normal University, Changchun 130024, China
[b] Center of Experimental Research, Henan Academy of Agriculture Sciences, Zhengzhou 450008, China
[c] Department of Chemistry, Zhengzhou University, Zhengzhou 450052, China

Received 14 January 2004; accepted 18 March 2004
Available online 19 June 2004

Abstract

The synthesis and characterization of a Zn(II) complex with 5-ethyl-2-amino-1,3,4-thiadiazole (eatz) are described. The crystal structure of $[Zn(eatz)_2(OAc)_2]$ was determined by X-ray diffraction. The crystal belongs to the monoclinic system and the structural unit is a distorted tetrahedron. In this complex, eatz acts as a monodentate ligand coordinating through the thiadiazole N atom to Zn(II), and the crystal structure is mainly stabilized by both intra- and intermolecular hydrogen bonds. Thermal analysis reveals that the complex $[Zn(eatz)_2(OAc)_2]$ decomposes in three transitions to give $Zn(CN)_2$ as the end product at 650 °C in N_2 atmosphere. The thermal decomposition kinetic analysis of the title complex indicates that the first transition is a double-step reaction with the main reaction being an *n*th auto-catalysis one. A biological activity study shows that both the ligand and the complex have good antimicrobial activities against *Staphylococcus aureus*.
© 2004 Published by Elsevier Ltd.

Keywords: 1,3,4-thiadiazole; Zinc; Crystal structure; Thermal decomposition; Kinetics; Bioactivity

1. Introduction

The chemistry of thiadiazoles, their derivatives and related compounds is of great interest in chemistry owning to their bioactivity of certain plant growth regulating effects as well as antimicrobial activity [1,2]. As a series of superior ligands, thiadiazoles and their derivatives can coordinate to many metal ions with nitrogen or sulfur atoms from the five-membered ring. In particular *N*,*N*′-linkage ligands, such as 1,3,4-thiadiazoles, are very versatile ones that are able to bridge a wide range of inter-metallic separations through two close adjacent N donors [3]. These complexes have received considerable attention for the past few years due to their specific structures, characteristics and reactivities, as well as their special biological activities, exceptional pharmacological properties and potential industrial applications [4,5]. 1,3,4-thiadiazoles, which have special structures and properties, have been widely reported in the fields of synthesis and structural studies by spectroscopic analysis. But single crystal structures of 1,3,4-thiadiazole complexes with metals and their thermal analysis are rare in the literature. Up until now there have been no reports on the single-crystal structure, thermal decomposition and biological activity of the complex $[Zn(eatz)_2(OAc)_2]$, eatz = 5-ethyl-2-amino-1,3,4-thiadiazole. We have synthesized the ligand, 5-ethyl-2-amino-1,3,4-thiadiazole: 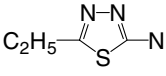 , and

☆ Supplementary data associated with this article can be found, in the online version, at doi:10.1016/j.poly.2004.03.027.

* Corresponding author. Tel.: +86-3717763675; fax: +86-37177 61744.
E-mail address: wzhy917@zzu.edu.cn (H.-Y. Zhang).
[1] Present address: College of Material Engineering, Zhengzhou University, Zhengzhou 450052, China.

0277-5387/$ - see front matter © 2004 Published by Elsevier Ltd.
doi:10.1016/j.poly.2004.03.027

the complex $[Zn(eatz)_2(OAc)_2]$. A single crystal of the complex was obtained and the crystal structure was determined by X-ray diffraction. In the present paper, we report the single crystal structure and the thermal behaviour of the complex $[Zn(eatz)_2(OAc)_2]$. The kinetic parameters for the first transition of $[Zn(eatz)_2(OAc)_2]$ decomposition have been calculated by employing both integral and differential methods and a kinetic equation has been given. In addition, bioactivity experiments of the complex and the ligand are also reported.

2. Experimental

2.1. Materials and measurement

The ligand, 5-ethyl-2-amino-1,3,4-thiadiazole, was prepared by the method described in the literature [6]. All chemicals used were of analytic reagent grade and used without further purification.

The single crystal structure was measured on a Rigaku-Raxis-IV X-ray diffractometer. The thermal behaviours were measured on NETZSCH TG209 and DSC204 instruments. The IR spectra were recorded on a Nicolet IR-470 spectrometer using KBr pellets in the range of 4000–400 cm^{-1}.

2.2. Synthesis of the complex $[Zn(eatz)_2(OAc)_2]$

0.391g (3.03 mmol) of 5-ethyl-2-amino-1,3,4-thiadiazole was added with continuous stirring to 60 ml of an acetonitrile solution containing 0.133 g (1.5 mmol) of $Zn(CH_3COO)_2 \cdot 2H_2O$. Five drops of 1 $mol1^{-1}$ HOAc solution were added to the above-mentioned solution to keep pH $\approx$ 5. The resultant solution was heated on an electro-magnetic stirring apparatus to reflux for 4 h. After a few days, 0.326 g (Yield 49.2%) poor yellow crystals of the title complex, suitable for X-ray diffraction, were obtained by being filtrated, washed with cooled water and dried under vacuum. *Anal.* Calc. for $C_{12}H_{20}N_6O_4S_2Zn$: C, 37.30; H, 5.43; N, 32.41. Found: C, 37.44; H, 5.58; N, 32.76%.

2.3. X-ray crystallography

A selected crystal of $[Zn(eatz)_2(OAc)_2]$ was mounted on a Rigaku-Raxis-IV X-ray diffractometer using graphite-monochromated Mo Kα radiation (λ = 0.71073 Å) at 293(2) K. 3534 reflections were measured over the ranges $2.56° \leqslant 2\theta \leqslant 27.52°$, $-13 \leqslant h \leqslant 10$, $-34 \leqslant k \leqslant 34$, $-10 \leqslant l \leqslant 10$, yielding 2017 unique reflections. Raw data were corrected and the structure was solved using the SHELX-97 program. Non-hydrogen atoms were located by direct phase determination and subjected to anisotropic refinement [7]. The full-matrix least-squares calculations on F^2 were applied on the final refinement. The refinement converged at $R_1 = 0.0423$ and $wR_2 = 0.0943$ values for reflections with $I > 2\sigma(I)$. Details of crystal structure determination are summarized in Table 1. Full atomic data are available as a file in CIF format.

2.4. Thermal analysis

The thermal decomposition experiments in nitrogen atmosphere with a flow rate of 20 ml min^{-1} were carried out using NETZSCH TG 209 and DSC 204 instruments. In these experiments, the complex $[Zn(eatz)_2(OAc)_2]$ was pre-triturated and pretreated in pure nitrogen atmosphere at 85 °C for 1 h to remove acetonitrile solvent completely. An Al crucible was used for DSC measurement and Al_2O_3 crucibles for TG to hold about 3–5 mg of the samples, respectively. The heating rate for thermal decomposition employed was 10 °C min^{-1}, and the rates for kinetic analysis were 5, 10, 15 and 30 °C min^{-1}, respectively.

Table 1
Crystal data and structure refinement parameters for $[Zn(eatz)_2(OAc)_2]$

Empirical formula	$C_{12}H_{20}N_6O_4S_2Zn$
Formula weight	441.83
Temperature (K)	293(2)
Wavelength (Å)	0.71073
Crystal system	monoclinic
Space group	*Cc*
Unit cell dimensions	
a (Å)	10.712(2)
b (Å)	27.651(6)
c (Å)	8.4412(17)
α (°)	90
β (°)	129.26(3)
γ (°)	90
Volume (Å^3)	1935.7(7)
Z	4
D_{calc} (Mg m^{-3})	1.516
Absorption coefficient (mm^{-1})	1.513
$F(000)$	912
Crystal color	poor yellow
Crystal size (mm)	$0.2 \times 0.18 \times 0.18$
θ Range for data collection (°)	2.56–27.52
Index ranges	$-13 \leqslant h \leqslant 10$, $-34 \leqslant k \leqslant 34$, $-10 \leqslant l \leqslant 10$
Reflections collected/unique	3534/2017 [$R_{int} = 0.0879$]
Completeness to $2\theta = 27.52$	85.7%
Refinement method	full-matrix least-squares on F^2
Data/restraints/parameters	2017/4/228
Goodness-of-fit on F^2	1.016
Final R indices [$I > 2\sigma(I)$]	$R_1 = 0.0423$, $wR_2 = 0.0943$
R indices (all data)	$R_1 = 0.0538$, $wR_2 = 0.0975$
Absolute structure parameter	0.42(4)
Extinction coefficient	0.0036(8)
Largest difference peak and hole (e Å^{-3})	0.549 and −0.407

2.5. Biological tests of the ligand and the complex $[Zn(eatz)_2(OAc)_2]$

Antimicrobial activity of the complex and the ligand eatz was qualitatively determined by a modified disc diffusion method [8] with a suspension of *Staphylococcus aureus* 1 ml in agar medium. Ethanol solutions of the complex and the ligand were prepared with concentrations of 0.0155 mmoll^{-1}.

3. Results and discussion

3.1. Crystal structure of $[Zn(eatz)_2(OAc)_2]$

Selected bond distances and angles of the complex $[Zn(eatz)_2(OAc)_2]$ are listed in Table 2. The ORTEP drawing and the packing diagram of the unit cell of $[Zn(eatz)_2(OAc)_2]$ are presented in Fig. 1(a) and (b), respectively.

In the complex $[Zn(eatz)_2(OAc)_2]$, the Zn(II) ion is linked to two thiadiazole N atoms and two acetate O atoms, and both eatz and OAc^- are coordinated to the Zn(II) ion as monodentate ligands. The lengths of Zn–O bonds (1.947(5) and 1.971(5) Å) are slightly shorter than those of Zn–N bonds (2.027(5) and 2.043(5) Å), and the maximum and minimum values of the bond angles around the Zn(II) ion are 123.0(3)° (O(3)–Zn(1)–O(1)) and 99.4(2)° (O(3)–Zn(1)–N(5)), respectively, indicating that the configuration of the structural unit of $[Zn(eatz)_2(OAc)_2]$ is very distorted from the ideal tetrahedral geometry. This severe distortion could be due to the difference in coordinate ability and steric hindrance between eatz and OAc^- ligands, as well as the stronger bonding of acetate O atoms to the Zn(II) ion than that of thiadiazole N atoms, because of the negative charge on the O atoms from OAc^-. There are complicated intra- and intermolecular hydrogen bonds in the crystal structure of $[Zn(eatz)_2(OAc)_2]$ (bonding details are given in Table 3). The tridimensional network of hydrogen bonds provides an extra stability for the crystal. Although the two thiadiazole rings of the neighboring units in different planes have a large overlap and are close to parallel to each other (the interplane angle is 1.4°), the distance between them is 4.221 Å, which is bigger than the maximum value for which π–π interactions are accepted. As a result, the structure is

Table 2
Selected bond distances (Å) and angles (°)

Bond distances	
Zn(1)–O(3)	1.947(5)
Zn(1)–O(1)	1.971(5)
Zn(1)–N(2)	2.027(5)
Zn(1)–N(5)	2.043(5)
S(1)–C(1)	1.730(6)
S(1)–C(2)	1.742(7)
S(2)–C(5)	1.732(7)
S(2)–C(6)	1.771(9)
O(1)–C(9)	1.255(8)
O(2)–C(9)	1.228(9)
O(3)–C(11)	1.272(9)
O(4)–C(11)	1.235(10)
Bond angles	
O(3)–Zn(1)–O(1)	123.0(3)
O(3)–Zn(1)–N(5)	99.4(2)
O(1)–Zn(1)–N(5)	109.1(2)
O(3)–Zn(1)–N(2)	114.0(2)
N(2)–Zn(1)–N(5)	111.0(2)
C(1)–S(1)–C(2)	87.1(3)
O(1)–Zn(1)–N(2)	100.4(2)
C(5)–S(2)–C(6)	86.8(4)
C(9)–O(1)–Zn(1)	111.1(5)

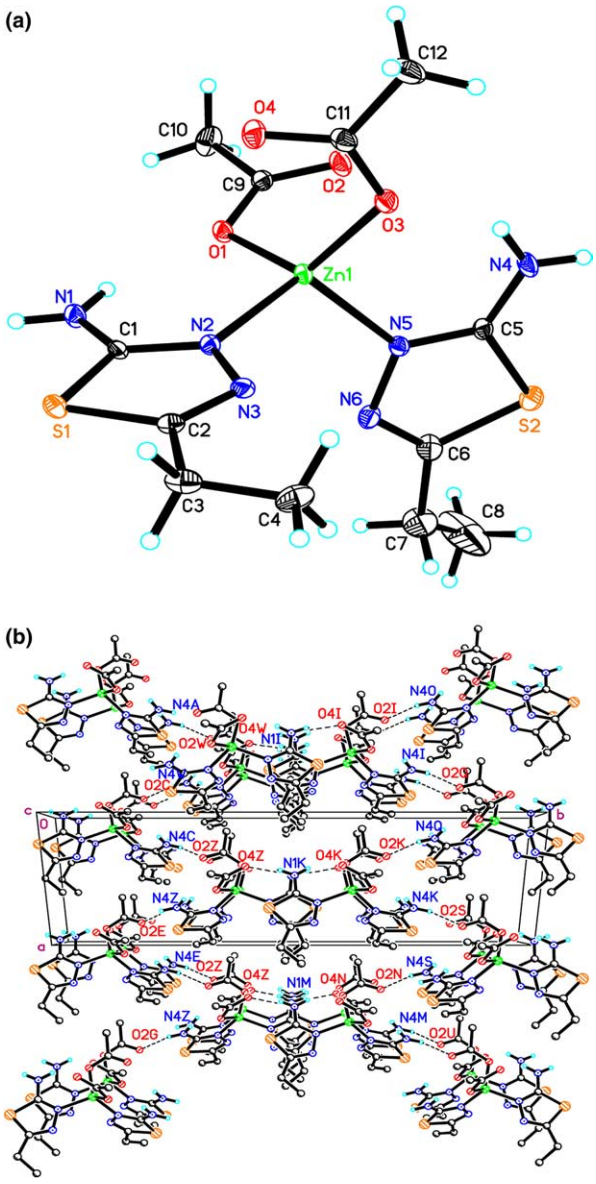

Fig. 1. (a) ORTEP drawing of $[Zn(eatz)_2(OAc)_2]$ (with 50% probability displacement ellipsoids). (b) packing diagram of the unit cell of $[Zn(eatz)_2(OAc)_2]$ looking down the *c*-axis.

Table 3
Hydrogen bonds

D–H	(D–H)	d(H···A)	∠DHA	d(D···A)	A
N1–H1A	0.860	2.062	149.81	2.838	O1
N1–H1B	0.860	1.986	165.99	2.828	O4 $[x, -y, z-1/2]$
N4–H4A	0.860	2.116	147.44	2.878	O3
N4–H4B	0.860	1.952	164.34	2.790	O2 $[x+1/2, -y+1/2, z+1/2]$

primarily stabilized by intra- and intermolecular hydrogen bonds.

3.2. Thermal decomposition

The TG and DSC curves of the title complex are shown in Fig. 2. The relatively smaller endothermic peak at 130 °C involving a ΔH value of 7.6 J g^{-1}, without mass loss associated in TG, is linked to the break of intra- and intermolecular hydrogen bonds. The endothermic peak at 150 °C without mass loss, and giving a ΔH value of 98.9 J g^{-1}, is due to the phase change of the complex. The sharp exothermic peak at 215 °C involving a ΔH value of 894.5 J g^{-1}, with a mass loss of 32.2%, may be assigned to the breaking of thiadiazole rings with the generation of NCS^- and accompanied by the formation of the $H_2[Zn(NCS)_2(OAc)_2]$ complex. The replacement of eatz by NCS^- gives rise to the more stable coordinate bond of Zn–NCS^- than that of Zn-eatz. The calculated mass loss (31.7%) for this thermal event agrees with that revealed by the TG curve (32.2%) at 217 °C. The broad shallow exothermic peak between 217 and 295 °C, giving a ΔH value of 228.3 J g^{-1} and accompanied by mass loss in TG, may mainly correspond to the breaking of Zn–OAc bonds and the decomposition of $H_2[Zn(NCS)_2(OAc)_2]$ into $Zn(NCS)_2$, with the release of CO, H_2O and H_2 [9]. The successive mass loss in TG from 300 to 650 °C may be caused by the gradual elimination of carbon as well as the decomposition of $Zn(NCS)_2$ into $Zn(CN)_2$, and the removal of sulfur. The total mass loss of 72.0% at 650 °C is quite close to the theoretical mass loss (73.4%) calculated by taking $Zn(CN)_2$ as the final product.

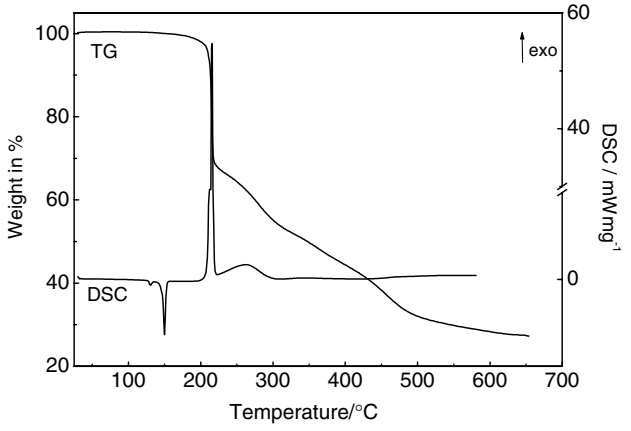

Fig. 2. TG–DSC curves of $[Zn(eatz)_2(OAc)_2]$.

The characterization frequencies of the IR spectra of the complex $[Zn(eatz)_2(OAc)_2]$ and the decomposed product at 217 °C are listed in Table 4. The peaks at 1523 and 1500 cm^{-1} in the IR spectrum of the complex, which are assigned to the characteristic vibration band of the 1,3,4-thiadiazole rings, disappear in the spectrum of the decomposed product and a new characteristic absorption peak of NCS^- appears at 2081 cm^{-1}. These results justify that the breakage of the thiadiazole ring is accompanied by the formation of NCS^-. The result of IR spectra agrees with that of the thermal analysis.

3.3. Non-isothermal kinetics of the first transition of the complex $[Zn(eatz)_2(OAc)_2]$ decomposition

3.3.1. Model-free estimation of activation energy

A series of dynamic scans with different heating rates results in a set of data which exhibits the same degree of conversion (α) at different temperatures. Based on this, two methods are developed by Friedman as well as Ozawa–Flynn–Wall to determine the kinetic parameters without having to presuppose a certain model. Fig. 3 shows the TG curves of the title complex measured in N_2 atmosphere with the heating rate of 5, 10, 15 and

Table 4
IR selected bands (cm^{-1})

Sample	$\nu(CH_3)$	$\nu(NCS^{-1})$	$\nu(COO^-)^{as}$	ν(⌬)	$\nu(COO^-)^s$
$[Zn(eatz)_2(OAc)_2]$	2979		1560–1540d	1523, 1500s	1384s
The product at 217 °C	2976	2081s	1553		1384

d, doublet; s, strong.

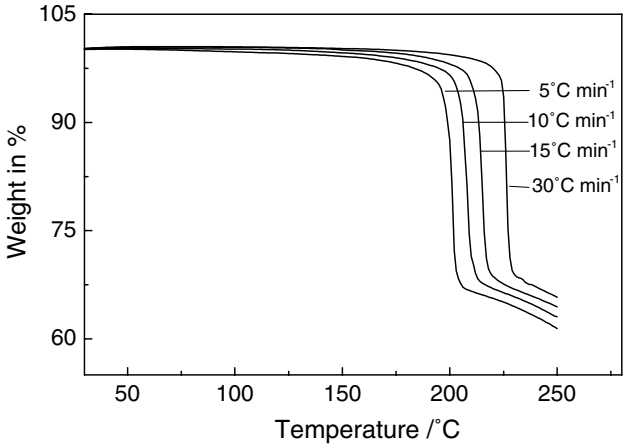

Fig. 3. TG curves of $[Zn(eatz)_2(OAc)_2]$ with different heating rates (°C min^{-1}).

30 °C min^{-1}, respectively. The basic data (β, α, T) taken from the TG curves are used in the equations below:

Ozawa–Flynn–Wall equation [10,11]:

$$\ln \beta = \ln\left(\frac{AE}{R}\right) - \ln\ g(\alpha) - 5.3305 - 1.052\frac{E}{RT}, \qquad (1)$$

where β is the heating rate, α degree of conversion, $g(\alpha)$ mechanism function, E activation energy, A pre-exponential factor and R gas constant. Friedman equation [12]:

$$\ln\left(\frac{d\alpha}{dt}\right)_{\alpha=\alpha j} = \ln[Af(\alpha)_j] - \frac{E}{RT}, \qquad (2)$$

where $d\alpha/dt$ is the rate of conversion, and $f(\alpha)$ mechanism function.

It can be seen from Eqs. (1) and (2) that the graphs ln β versus $1/T$ and ln ($d\alpha/dt$) versus $1/T$ both show straight lines with slopes $m_{(1)} = -1.052E/R$ and $m_{(2)} = -E/R$. The slopes of these straight lines are directly proportional to the reaction activation energy (E). The calculation results using the NETZSCH Thermokinetic Analysis Program [13] are shown in Table 5.

From Table 5, it can be seen that the values of E calculated by using different methods are comparable although the values obtained by the Friedman method lie on the low side. It can also be seen that the activation energy is not a constant, which indicates that the first transition of the thermal decomposition of the complex $[Zn(eatz)_2(OAc)_2]$ is a two-step reaction. The first step is a pre-reaction with $E_1 = 209.09 \pm 40.63$ kJ mol^{-1}, and the second step is the main reaction with average $\bar{E}_2 = 130.5 \pm 8.25$ kJ mol^{-1}.

3.3.2. Estimation of the kinetic model by means of multiple linear regression

From Table 5 it can be seen that the main reaction of the decomposition process comprises 96% of the total mass loss, while the pre-reaction only comprises less than 4%. For this reason, the determination of kinetic parameters and mode type for the main reaction can be turned into a problem of multiple linear regression (MLR) by an appropriate transformation. Selecting mechanism functions $f(\alpha)$ of different reaction types [14,15], given in Table 6, the calculated TG curves were obtained by plotting $\ln[(d\alpha/dt)/f(\alpha)]$ versus $1/T$ using the ACHAR equation [16]:

$$\ln\frac{d\alpha/dt}{f(\alpha)} = \ln\frac{A}{\beta} - \frac{E}{RT}. \qquad (3)$$

The calculated curves were fitted to the experimental curves by using the MLR method and corrected with least squares (LSQ). The fitting results for different reaction types are also given in Table 6.

Considering the fitting quality (characterized by the correlation coefficient), regression parameter and activation energy E from OFW analysis, it can be seen from Table 6 that the mechanism of Cn is more suitable for this reaction. That means the first thermal

Table 5
Parameters E (kJ mol^{-1}) for the first transitional thermal decomposition of $[Zn(eatz)_2(OAc)_2]$

Degree of conversion (α)	Ozawa–Flynn–Wall analysis E (kJ mol^{-1})	Friedman analysis E (kJ mol^{-1})
0.02	209.09 ± 40.63	193.09 ± 28.58
0.04	133.62 ± 26.38	133.95 ± 3.96
0.05	123.31 ± 3.26	124.22 ± 4.36
0.10	128.23 ± 3.46	126.90 ± 3.27
0.20	129.90 ± 6.73	130.94 ± 2.49
0.30	132.28 ± 11.90	132.60 ± 3.43
0.40	133.79 ± 12.19	131.15 ± 3.65
0.50	133.96 ± 11.89	127.09 ± 2.88
0.60	128.88 ± 6.44	119.81 ± 3.93
0.70	129.39 ± 2.81	120.17 ± 4.66
0.80	129.53 ± 3.88	129.47 ± 11.91
0.90	133.47 ± 2.05	129.93 ± 9.98
0.95	137.70 ± 3.13	139.45 ± 9.82
0.98	122.98 ± 13.45	139.38 ± 26.87

Table 6
Fit results for the main reaction of the thermal decomposition of $[Zn(eatz)_2(OAc)_2]$

Model	$f(\alpha)$	E (kJ mol^{-1})	lg A (s^{-1})	Correlation coefficient	Regression parameter	Order
F1	$(1-\alpha)$	185.9309	18.1583	0.9476896	0.000074	
F2	$(1-\alpha)^2$	243.5560	24.6391	0.9284248	0.001586	
Fn	$(1-\alpha)^n$	152.5736	14.3462	0.9638180	0.584508	0.003
D1	0.5α	233.5999	22.8886	0.9264153	0.000314	
D2	$[-\ln(1-\alpha)]^{-1}$	261.3192	25.7063	0.9209163	0.000033	
D3	$1.5(1-\alpha)^{2/3}[1-(1-\alpha)^{1/3}]^{-1}$	295.3493	28.8638	0.9149858	0.000160	
D4	$1.5[(1-\alpha)^{-1/3}-1]^{-1}$	272.3679	26.2917	0.9188512	0.000108	
R2	$2(1-\alpha)^{2/3}$	166.6545	15.6639	0.9563922	0.002088	
R3	$3(1-\alpha)^{2/3}$	172.3316	16.1363	0.9536346	0.000051	
B1	$(1-\alpha)\alpha$	130.2988	13.2051	0.9910313	0.000225	
Bna	$(1-\alpha)^n\alpha^n$	129.9278	13.1629	0.9923596	0.000144	1.25
C1	$(1-\alpha)(1+k\alpha)$	129.8888	9.9414	0.9924775	0.000994	
Cn	$(1-\alpha)^n(1+k\alpha)$	129.9161	9.5467	0.9984977	0.000077	1.23
A2	$(1-\alpha)[-\ln(1-\alpha)]^{1/2}$	139.4910	13.1379	0.9783842	0.000130	
A3	$3(1-\alpha)[-\ln(1-\alpha)]^{2/3}$	132.1372	12.3400	0.9874371	0.000104	
An	$n(1-\alpha)[-\ln(1-\alpha)]^{(n-1)/n}$	129.9048	12.0199	0.9920686	0.000220	0.65

$K_{CI} = 3.0967$, $K_{Cn} = 3.5354$.

decomposition transition of the complex $[Zn(eatz)_2(OAc)_2]$ preferably proceeds mainly as an nth reaction with auto-catalysis through the reactants, the order is 1.23 with $E = 129.9$ kJ mol^{-1}, lg $A = 9.55$ s^{-1} and the kinetic equation of the main reaction is:

$$d\alpha/dt = A\exp(-E/RT)(1-\alpha)^n(1+k\alpha),$$

where $n = 1.23$, $K = 3.5354$.

The result of the kinetic analysis above can also illuminate the rapid rate of decomposition of the complex during the first transition. Being an nth reaction with auto-catalysis, the main reaction is started by a pre-reaction, the reaction type of which cannot be estimated because of its smallness. It is the pre-reaction that induces the main reaction to occur so rapidly that the complex loses more than 31% of its mass within a temperature range of less than 5 °C.

3.4. Qualitative antimicrobial assay results

The results of antimicrobial activities of the complex $[Zn(eatz)_2(OAc)_2]$ and the free ligand, eatz, together with the result of the blank as a comparison, are listed in Table 7, as evaluated by the diameter of the growth inhibition zone. It can be seen that both the complex and the ligand showed a clear inhibition zone 15 mm above against *Staphylococcus aureus*, and the differences in the zone diameter between them are not obvious. These results indicate that eatz and $[Zn(eatz)_2(OAc)_2]$ are very effective against *S. aureus*.

Both the ligand and the complex have similar antimicrobial activities suggesting that the coordination of eatz with the Zn(II) ion and the formation of the complex $[Zn(eatz)_2(OAc)_2]$ do not change the biologic activity of eatz obviously. This indicates that the active group in eatz and $[Zn(eatz)_2(OAc)_2]$ is the 1,3,4-thiadiazole ring. The mechanism of antimicrobial action of these compounds still needs further investigating and the assay results above would provide basic data for the pharmacological research of thiadiazoles and their complexes.

Table 7
Results for antimicrobial assay[a] (diameter in mm)

Sample	I	II	III
Blank	8	8	8
eatz	23	24	26
$[Zn(eatz)_2(OAc)_2]$	22	22	26

[a] Diameter of 15 mm and above considered active.

4. Supplementary material

Supplementary crystallographic data have been deposited with the Cambridge Crystallographic Data Center, CCDC No. 228387. Copies of this information may be obtained free of charge from The Director, CCDC, 12 Union Road, Cambridge CB2 1EZ, UK (fax: +44-1223-336-033; e-mail: deposit@ccdc.cam.ac.uk or www: http://www.ccdc.cam.ac.uk).

Acknowledgements

This work was financially supported by the Natural Science Foundation of China (20271046), the Natural Science Foundation of Henan Province (0211020300) and the Natural Science Foundation of Henan Education Department (20011500027).

References

[1] S.N. Sawhney, A. Gupta, P.K. Sharma, Indian J. Heterocycl. Chem. 1 (1991) 8.
[2] F. Bentiss, M. Lagrene'e, J.P. Wignacourt, Polyhedron 21 (2002) 403.
[3] A. Gloria, B. Joaquý'n, E. Francisco, L.G. Malva, Inorg. Chim. Acta 343 (2003) 60.
[4] Y.J. Gao, Z.S. Wu, Z.J. Zhang, Q.J. Xue, Wear 222 (1998) 129.
[5] A.R. Katritzky, A.J. Boulton, in: Advances in Heterocyclic Chemistry, vol. 9, Academic Press, New York, 1968, pp. 166–170.
[6] C.G. Le, J.H. Ding, S.J. Yang, Chem. World 7 (2002) 366.
[7] G.M. Sheldrick, Acta Crystallogr., Sect. A 46 (1990) 467.
[8] A.W. Bauer, M.D.K. Kirny, J.C. Sherries, M. Turck, Am. J. Clin. Pathol. 45 (1966) 493.
[9] X.Y. Zhao, C.Z. Li, B.C. Zheng, H.C. Gu, L.M. Hu, J. East Chin. Uni. Sci. Tech. 23 (1997) 191.
[10] T. Ozawa, Bull. Chem. Soc. Jpn. 38 (1965) 1881.
[11] J.H. Flynn, L.H. Wall, Polym. Lett. 4 (1966) 323.
[12] H.L. Friedman, J. Macromol. Sci. (Chem.) 41 (1967) 51.
[13] NETZSCH-Gerätebau, thermo-kinetic software, Version 2000(6a).
[14] C.H. Bamford, in: C.F. Tipper (Ed.), Comprehensive Chemical Kinetics, Vol. 22, Reactions in Solid State, Elsevier, Amsterdam, 1980, p. 57.
[15] G. Pokol, S. Gal, Rr. Pungor, Anal. Chim. Acta 175 (1985) 95.
[16] B.N. Achar, G.W. Bringly, J.H. Sharp, Proc. Int. Clay Conf., Jerusalem, Vol. 1, 1966, p. 67.

Available online at www.sciencedirect.com
SCIENCE DIRECT®
Polyhedron 23 (2004) 1859–1868
POLYHEDRON
www.elsevier.com/locate/poly

Synthesis, characterization and crystal structures of molybdenum(VI) and (V) complexes with differently N-substituted β′-hydroxy-β-enaminones ☆

Marina Cindrić [a,*], Višnja Vrdoljak [a], Tanja Kajfež Novak [a], Neven Strukan [a], Ana Brbot-Šaranović [b], Predrag Novak [c,1], Boris Kamenar [a]

[a] *Laboratory of General and Inorganic Chemistry, Chemistry Department, Faculty of Science, University of Zagreb, Ulica kralja Zvonimira 8, 10000 Zagreb, Croatia*
[b] *Department of Chemistry, Veterinary Faculty, University of Zagreb, 10000 Zagreb, Croatia*
[c] *Laboratory of Analytical Chemistry, Chemistry Department, Faculty of Science, University of Zagreb, Strossmayerov trg 14, 10000 Zagreb, Croatia*

Received 26 February 2004; accepted 25 March 2004

Abstract

Mononuclear molybdenum(VI) $[MoO_2L_2]$ (**1a**, **1b**, **2a**, **2b**) and dinuclear molybdenum(V) $[Mo_2O_4(L^{1b})_2(CH_3OH)_2]$ (**3b**) complexes have been prepared by the reaction of $[MoO_2(acac)_2]$ or $[Mo_2O_3(acac)_4]$ (acac = acetylacetonate ion), respectively, with the appropriate β′-hydroxy-β-enaminones (**HL**). Also, two isomeric enaminones ($\mathbf{HL^{1a}}$ and $\mathbf{HL^{1b}}$) have been prepared by the reaction of ethyl 2-hydroxy-4-(4-hydroxy-6-methyl-2H-pyran-2-on-3-yl)-4-oxo-2-butenoate (**ehmpb**) and *o*-anisidine. All the prepared molybdenum(VI) complexes are built up of mononuclear molecules with *cis*-MoO_2^{2+} cores, while the dinuclear molybdenum(V) complex contains a $Mo_2O_4^{2+}$ core. In all complexes ligand **L** is coordinated in a didentate fashion to molybdenum through two oxygen atoms and not through the nitrogen atom. One neutral solvent molecule CH_3OH in the molybdenum(V) complex, acting as a monodentate ligand, completes the octahedral coordination of each Mo atom. All compounds have been characterized by means of chemical analyses, IR and one- and two-dimensional NMR spectroscopy. The molecular and crystal structures of the molybdenum(VI) (**1a**), molybdenum(V) (**3b**) complexes and of ligand $\mathbf{HL^{1b}}$ have been determined by a single crystal X-ray diffraction method.
© 2004 Elsevier Ltd. All rights reserved.

Keywords: Enaminones; Molybdenum(VI) complexes; Molybdenum(V) complexes; Pyrone; X-ray crystal structure; NMR spectra

1. Introduction

A series of 2-pyrone derivatives and their metal complexes have received significant attention due to their enzyme-inhibiting properties [1–4]. Similarly, the discovery of the insuline-enhancing (or insuline-mimetic) properties of oxovanadium compounds has stimulated numerous investigations concerning the syntheses, characterization and biological relevance of such complexes [5–9]. Some studies have shown that molybdenum(VI) complexes also exhibit such properties [10].

We have recently published the syntheses and structures of several isomeric enaminones containing a 4-hydroxy-2-pyrone ring, obtained by the reaction of ethyl 2-hydroxy-4-(4-hydroxy-6-methyl-2*H*-pyran-2-on-3-yl)-4-oxo-2-butenoate and the corresponding amines (*n*-butyl amine, aniline, *p*-anisidine and α-naphthyl amine) [11–13]. We have also described the preparation of several dinuclear molybdenum(V) complexes of the general formula $[Mo_2O_4L_2D_2]$ obtained by the reaction of various isomeric β′-hydroxy-β-enaminones and $[Mo_2O_3(acac)_4]$ [14–16].

☆ This paper is a part of our studies on molybdenum complexes with enaminones containing a 4-hydroxy-2-pyrone ring.

* Corresponding author. Tel.: +385-1-460-6653; fax: +385-1-461-1191.
E-mail address: marina@chem.pmf.hr (M. Cindrić).
[1] Present address: PLIVA Research Institute Ltd., Prilaz baruna Filipovića 29, 10000 Zagreb, Croatia.

0277-5387/$ - see front matter © 2004 Elsevier Ltd. All rights reserved.
doi:10.1016/j.poly.2004.03.025

In the continuation of our previous research we report here the synthesis of new ligands (HL^{1a} and HL^{1b}), and novel molybdenum(VI) $[MoO_2L_2]$ (**1a**, **1b**, **2a**, **2b**) and molybdenum(V) $[Mo_2O_4(L^{1b})_2(CH_3OH)_2]$ (**3b**) complexes with β′-hydroxy-β-enaminones (Scheme 1).

The molecular structures of a molybdenum(VI) complex (**1a**), the molybdenum(V) complex (**3b**), as well as of one ligand isomer (HL^{1b}) have been determined by a single crystal X-ray diffraction method.

The ligands and complexes have also been characterized by means of chemical analyses, high-resolution NMR spectroscopy and IR spectroscopy.

2. Experimental

All chemicals were of reagent grade and used as purchased. The starting complexes $[MoO_2(acac)_2]$ [17] and $[Mo_2O_3(acac)_4]$ [18] were prepared as described in the literature. Ethyl 2-hydroxy-4-(4-hydroxy-6-methyl-2H-pyran-2-on-3-yl)-4-oxo-2-butenoate (**ehmpb**) and the corresponding enaminones HL^{2a} and HL^{2b} (Scheme 2) were prepared according to the already described procedure [11–13]. Methanol was dried using magnesium turnings and iodine and then distilled. Dichloromethane was dried over P_2O_5.

C, H and N analyses were provided by the Analytical Services Laboratory of Rudjer Bošković Institute, Zagreb. Molybdenum was determined according to the method described in the literature [19]. Infrared spectra were recorded in KBr with an FTIR 1600, Fourier transform spectrophotometer in the 4500–450 cm^{-1} region. Elemental analyses, yields and selected IR data are given in Table 1.

2.1. Synthesis of enaminones and complexes

2.1.1. Synthesis of enaminones (HL^{1a}, HL^{1b})

A mixture of equimolar amounts (2.5 mmol) of **ehmpb** and *o*-anisidine in ethanol (20 mL) was warmed up under reflux for 1 h. The reaction mixture was cooled overnight. The formed yellow precipitate (HL^{1a}) was collected by filtration and purified by recrystallization from ethanol (m.p. = 195–196 °C). The filtrate was evaporated to half of its volume and allowed to stand at room temperature for 3–4 days. The yellow-orange crystals of HL^{1b} were collected and recrystallized from ethanol (m.p. = 146–147 °C).

2.1.2. Synthesis of the molybdenum(VI) complexes $[MoO_2L_2]$ (**1a**, **1b**, **2a**, **2b**)

$[MoO_2(acac)_2]$ (0.1 g, 0.31 mmol) was suspended in dry methanol (30 mL) and the appropriate ligand (0.31

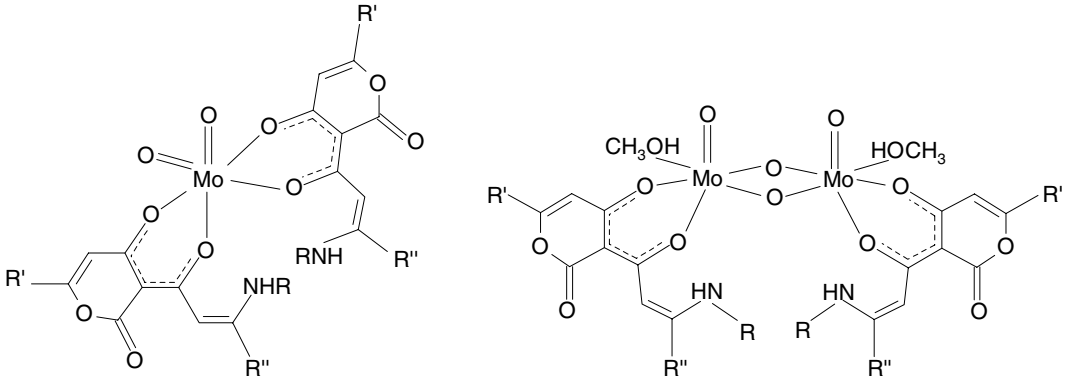

Complex	R	R'	R''
1a	*o*-$C_6H_5OCH_3$	$CO_2C_2H_5$	CH_3
1b		CH_3	$CO_2C_2H_5$
2a	α-$C_{10}H_7$	$CO_2C_2H_5$	CH_3
2b		CH_3	$CO_2C_2H_5$
3b	*o*-$C_6H_5OCH_3$	$CO_2C_2H_5$	CH_3

Scheme 1.

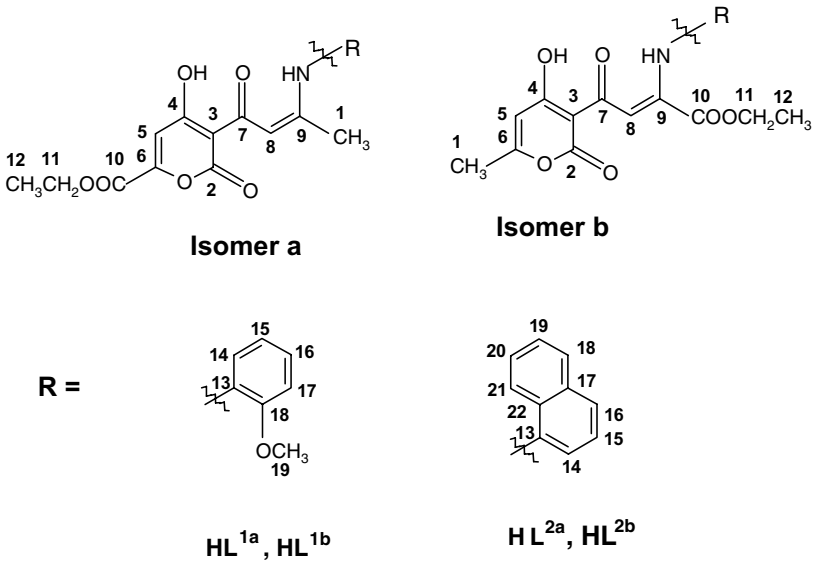

Scheme 2.

Table 1
Analytical and IR data for ligands, $[MoO_2L_2]$ and $[Mo_2O_4L_2(CH_3OH)_2]$ complexes

Formula (M_r)	Complex	Analysis found (calcd.)				Yield%	Selected IR data (cm^{-1})
		%C	%H	%N	%Mo		
$C_{19}H_{19}O_7N$ (373.356)	**HL^{1a}**	61.38 (61.12)	5.11 (5.13)	3.59 (3.75)		61	1730, 1655, 1581
	HL^{1b}	61.04 (61.12)	5.13 (5.13)	3.74 (3.75)		18	1723, 1651, 1607
$MoO_2(C_{19}H_{18}O_7N)_2$ (872.636)	**1a**	52.40 (52.30)	4.14 (4.16)	3.21 (3.21)	10.29 (10.99)	62	1723, 1649, 1577, 933, 907
	1b	52.58 (52.30)	4.75 (4.16)	3.65 (3.21)	10.45 (10.99)	50	1721, 1644, 1577, 934, 907
$MoO_2(C_{22}H_{18}O_6N)_2$ (912.701)	**2a**	57.76 (57.90)	4.08(3.98)	3.06 (3.07)	11.01 (10.51)	35	1724, 1647, 1584, 929, 906
	2b	56.63 (57.90)	3.86 (3.98)	3.35 (3.07)	10.15 (10.51)	29	1724, 1648, 1585, 929, 906
$Mo_2O_4(C_{19}H_{18}O_7N)_2(CH_3OH)_2$ (1064.658)	**3b**	45.88 (45.13)	3.86 (4.17)	2.29 (2.63)	17.84 (18.02)	42	1726, 1671, 1572, 962, 720

mmol) was added. The mixture was warmed up for 15 h. Complexes **1a** or **2a** were deposited during warming of the reaction mixture, while the complexes **1b** or **2b** were obtained when the solution was evaporated to one-third of its volume and left overnight. The obtained products were filtered off, washed with cold methanol and dried.

*2.1.3. Synthesis of the molybdenum(V) complex $[Mo_2O_4(L^{1b})_2(CH_3OH)_2]$ (**3b**)*

$[Mo_2O_3(acac)_4]$ (0.25 g, 0.39 mmol) was suspended in dry dichloromethane (25 mL) and ethyl 4-(4-hydroxy-6-methyl-2*H*-pyran-2-on-3-yl)-2-(2-methoxyanilino)-4-oxo-2-butenoate (**HL^{1b}**) (0.39 mmol) was added. The mixture was gently warmed up for 1 h, the solution was filtered off and methanol (30 mL) added to the filtrate. Upon standing at room temperature for 10 days, the obtained orange-red crystalline product was filtered off, washed with cold alcohol and dried.

2.2. X-ray crystallography

Whereas the single crystals of **HL^{1b}** and **3b** were grown by slow evaporation of solutions obtained from the above-described preparations, the single crystal of **1a** was obtained by evaporation from a mixture of methanol and dichloromethane. Intensity data for structures **HL^{1b}**, **1a** and **3b** were collected at 150 K on a Nonius Kappa CCD diffractometer with graphite-monochromated Mo Kα radiation ($\lambda = 0.71073$ Å) and reduced using the DENZO programme [20]. The structures of all

complexes were solved by Patterson and Fourier methods using the SHELXS-97 [21] programme. The refinements were performed by the full-matrix least-squares method assuming anisotropic temperature factors for all non-H atoms using SHELXL-97 [22].

Hydrogen atoms attached to carbon atoms in all structures were generated on geometrical grounds. Hydrogen atoms H1 (bonded to N1) and H4 (bonded to O4) in structure **HL^{1b}** were found in a difference Fourier map and their positions were refined, while hydrogen atoms H1 (bonded to N1) and H2 (bonded to N2) in structure **1a**, and H1 (bonded to N1) and H8 (bonded to O8) in structure **3b** were also located in a difference Fourier map but their positions were kept fixed during the refinement.

Crystal parameters, data collection details and the results of refinements are summarized in Table 2. Selected bond lengths and angles are listed in Tables 3 and 4, and hydrogen bond parameters in Table 5.

All calculations were performed on an IBM THINKPAD microcomputer (Pentium II processor, 300 MHz). The molecular structure drawings were prepared using ORTEP [23] and PLATON [24].

2.3. NMR spectroscopy

NMR experiments were carried out on a Bruker Avance DRX500 spectrometer operating at 500.13 MHz for ^{1}H, with a 5-mm diameter inverse detection probe and a *z*-axis gradient coil. The spectra of the ligands (**HL^{1a}** and **HL^{1b}**) and of all molybdenum(VI) complexes (**1a**, **1b** and **2a**) were recorded in chloroform-d_1. The spectrum of the molybdenum(V) complex (**3b**) was recorded in acetone-d_6. All experiments were performed at ambient temperature. TMS was used as the internal standard. ^{1}H NMR experiments were executed with a spectral width of 10 000 Hz, 65 K data points and 8–16 scans. The sample concentration was 20 mg mL^{-1}. The digital resolution was 0.15 Hz per point. In ^{13}C APT NMR spectra, the spectral width was 31 446 Hz, number of data points 65 K and number of scans 9000–10 000 per spectrum. The digital resolution was 0.48 Hz per point.

Two-dimensional absolute value gradient selected COSY spectra were recorded under the following conditions. The spectral width was 6660 Hz in both domains, 2K data points were applied in the time domain and 256 increments were collected for each data set with linear prediction and zero filling to 1K. The relaxation delay was 1.5 s. Spectra were processed with sine window functions. The digital resolution was 3.3 Hz per point in the f2 domain and 26.0 Hz per point in the f1 domain. The number of scans was 4.

Absolute value HMQC and HMBC spectra were recorded with a relaxation delay of 1.5 s and 8–16 scans per increment. The spectral width was 6600 Hz in acquisition domain f2 and 31000 Hz in time domain f1. Data were collected into a 1024×256 acquisition matrix and processed using a $2K \times 1K$ transformed matrix with zero filling in the f1 domain. Sine multiplication was performed prior to Fourier transformations. In HMBC spectra the delay for long range couplings was set to 60 ms.

Table 2
Crystallographic data for ligand molecule **HL^{1b}** and complexes **1a**, **3b**

	HL^{1b}	**1a**	**3b**
Chemical formula	$C_{19}H_{19}NO_7$	$MoO_2(C_{19}H_{18}O_7N)_2$	$Mo_2O_4(C_{19}H_{18}NO_7)_2(CH_3OH)_2$
Formula weight	373.35	872.63	1064.65
Crystal system	orthorhombic	triclinic	monoclinic
Crystal size (mm)	$0.25 \times 0.27 \times 0.43$	$0.29 \times 0.33 \times 0.35$	$0.28 \times 0.26 \times 0.25$
Colour	yellow	red	red
Space group	*Pbca*	$P\bar{1}$	$C2/c$
a (Å)	7.29660(10)	11.7736(4)	13.6673(2)
b (Å)	20.3517(3)	13.7891(5)	17.4014(3)
c (Å)	23.6665(4)	13.7587(6)	18.5029(3)
α (°)		69.7263(17)	
β (°)		67.9617(17)	102.745(6)
γ (°)		65.085(2)	
V (Å^3)	3514.43(9)	1830.01(12)	4292.13(16)
Z	8	2	4
D_{calc} (g cm^{-3})	1.411	1.584	1.648
μ (mm^{-1})	1.09	4.39	6.69
Data measured	12 923	13 522	7652
Unique data	3568	8027	3924
Observed data [$I > 2\sigma(I)$]	2601	6007	3554
Number of variables	254	523	299
Max/min $\Delta\rho$ (e^3/Å^3)	0.916/−0.366	0.702/−0.900	0.447/−0.609
$R(F_o)$	0.0797	0.0556	0.0239
$wR(F_o^2)$	0.2157	0.1232	0.0638

Table 3
Selected bond lengths (Å) and angles (°) for compounds HL^{1b} and **3b**

	HL^{1b}	**3b**
Bond lengths		
Mo1–Mo1^{i}		2.5491(4)
Mo1–O11		1.679(1)
Mo1–O12		1.930(1)
Mo1–O12^{i}		1.940(1)
Mo1–O3		2.097(1)
Mo1–O4		2.177(1)
Mo1–O8		2.190(1)
O1–C6	1.362(4)	1.367(3)
O1–C2	1.402(4)	1.383(2)
O2–C2	1.205(4)	1.229(2)
O3–C4	1.321(4)	1.289(2)
O4–C7	1.296(4)	1.290(2)
O4–H4	1.05(5)	
O5–C10	1.335(5)	1.330(3)
O5–C11	1.458(4)	1.458(2)
O6–C10	1.196(4)	1.202(3)
O7–C18	1.363(4)	1.364(3)
O7–C19	1.432(4)	1.429(3)
N1–C9	1.354(4)	1.345(3)
N1–C13	1.405(4)	1.421(3)
N1–H1	0.85(5)	0.923
C3–C7	1.455(5)	1.456(3)
C7–C8	1.432(5)	1.419(3)
C8–C9	1.377(5)	1.380(3)
Bond angles		
Mo1–O12–Mo1^{i}		82.39(5)
O11–Mo1–O12		105.82(7)
O11–Mo1–O12^{i}		106.36(6)
O12–Mo1–O12^{i}		94.58(6)
O11–Mo1–O3		93.58(6)
O11–Mo1–O4		162.09(6)
O12–Mo1–O3		87.50(6)
O12–Mo1–O4		88.17(6)
O3–Mo1–O4		75.56(5)
O12^{i}–Mo1–O3		158.48(6)
O12^{i}–Mo1–O4		83.09(5)
O11–Mo1–O8		87.74(7)
O12–Mo1–O8		165.71(6)
O12^{i}–Mo1–O8		85.69(6)
O3–Mo1–O8		87.12(6)
O4–Mo1–O8		77.67(6)

Symmetry code: $i = -x+1, y, -z+1/2$ for **3b**.

3. Results and discussion

3.1. Synthesis of complexes

In the course of our research on molybdenum complexes with enaminones, we have prepared novel molybdenum(VI) and molybdenum(V) complexes with polydentate β′-hydroxy-β-enaminones (Scheme 1). The complexes of the general formula $[MoO_2L_2]$ (**1a**, **1b**, **2a**, **2b**) were prepared by the reaction of $[MoO_2(acac)_2]$ with the appropriate enaminone. They were orange-red crystalline solids slightly soluble in dichloromethane and chloroform. Their solutions are quite sensitive to moisture changing colour from orange to blue.

The new molybdenum(V) complex $[Mo_2O_4(L^{1b})_2(CH_3OH)_2]$ (**3b**) was prepared in a similar way as $[Mo_2O_4L_2D_2]$, already described in the literature [13–16]. The complex was very soluble in coordinating solvents such as dmf, dmso, picoline and py, and slightly soluble in acetone, methanol and ethanol.

All complexes were characterized by IR spectroscopy and selected spectral data are given in Table 1. Two bands at 1726–1721 and 1644–1671 cm^{-1} can be attributed to the stretching vibrations of the carbonyl groups belonging to the ester $COOC_2H_5$ and 2-pyrone, respectively. The stretching frequencies at 1572–1585 cm^{-1}, attributed to the coordinated C···O, groups were observed at lower values comparing to those found in the free ligands. The intense bands in the regions 929–934 and 906–907 cm^{-1} were assigned to the ν_{asym} and ν_{sym} $Mo–O_{(terminal)}$ stretching frequencies, respectively. In the spectra of the molybdenum(V) complex, the single strong absorption maximum at about 962 cm^{-1} belongs to $Mo–O_{(terminal)}$, while the band at 720 cm^{-1} belongs to the $Mo–O_{(bridging)}$ stretching frequency. The remaining frequencies in the IR spectra are due to the vibrations within the ligands.

3.2. Crystal structure

3.2.1. Crystal structure of *HL^{1b}*

The molecular structure of compound HL^{1b} can be described as consisting of three structural fragments: a 2-pyrone ring substituted at position 6 by a methyl group, a delocalized central enaminone part and a N-substituent (phenyl ring with a methoxy group at position 2) (Fig. 1). The compound exists in the crystalline state in the enamine form (C=C–N–H) with a C8=C9 bond distance value of 1.377(5) Å and C9–N1 of 1.354(4) Å. The difference Fourier map clearly exhibits one position of a H atom (O4–H4 = 1.05(5) Å) revealing the presence of the (N–C=C–C–OH) exo–enol tautomeric form. All available O–H and N–H protons participate in hydrogen bonding. A six-membered ring formed in the β-diketone fragment is established by the resonance assisted O–H···O hydrogen bond of a very short distance, O4···O3 of 2.418(4) Å. Another six-membered heterocyclic ring containing N–H (0.85(5) Å), where H is found in the difference Fourier map, is formed by the N–H···O intramolecular hydrogen bond (N1···O4 = 2.637(4) Å).

The N-substituent shows torsion flexibility due to rotation around the single $Nsp^2–Csp^3$ bond. The value of the C9–N–C13–C14 torsion angle of 21.43(6)° in structure HL^{1b} is smaller than the values already observed in this class of compound [12,14]. Twisting around the $Nsp^2–Csp^3$ bond is reduced due to the formation of the additional intramolecular hydrogen bond, N1···O7 = 2.600(4) Å.

Table 4
Selected bond lengths and angles for compound **1a**

Bond lengths			
Mo1–O12	1.699(3)	Mo1–O103	1.999(2)
Mo1–O11	1.700(3)	Mo1–O204	2.157(2)
Mo1–O203	1.996(2)	Mo1–O104	2.159(2)
O101–C106	1.346(4)	O201–C206	1.350(4)
O101–C102	1.401(4)	O201–C202	1.405(4)
O102–C102	1.203(4)	O202–C202	1.202(4)
O103–C104	1.318(4)	O203–C204	1.312(4)
O104–C107	1.307(4)	O204–C207	1.305(4)
O105–C110	1.328(4)	O205–C210	1.331(4)
O105–C111	1.464(5)	O205–C211	1.463(4)
O106–C110	1.201(4)	O206–C210	1.201(4)
O107–C118	1.366(4)	O207–C218	1.367(4)
O107–C119	1.427(5)	O207–C219	1.433(4)
N1–C109	1.339(5)	N2–C209	1.339(4)
N1–C113	1.408(5)	N2–C213	1.412(5)
C103–C107	1.468(5)	C203–C207	1.468(5)
C107–C108	1.395(5)	C207–C208	1.389(5)
C108–C109	1.398(5)	C208–C209	1.399(5)
Bond angles			
O12–Mo1–O11	103.36(12)	O203–Mo1–O204	77.77(10)
O12–Mo1–O203	99.69(11)	O103–Mo1–O204	83.05(9)
O11–Mo1–O203	96.11(11)	O12–Mo1–O104	166.55(11)
O12–Mo1–O103	95.17(11)	O11–Mo1–O104	89.22(11)
O11–Mo1–O103	99.13(12)	O103–Mo1–O104	77.89(9)
O203–Mo1–O103	155.63(9)	O203–Mo1–O104	83.44(10)
O12–Mo1–O204	89.97(11)	O204–Mo1–O104	77.84(9)
O11–Mo1–O204	166.18(11)		

Table 5
Hydrogen bonding geometry in structures **HL^{1b}**, **1a** and **3b**

D–H···A	*d*(D–H)	*d*(H..A)	∠DHA	*d*(D···A)
O4–H4···O3	1.05(5)	1.42(5)	156(4)	2.418(4)
N1–H1···O4	0.85(5)	1.97(5)	135(4)	2.637(4)
N1–H1···O7	0.85(5)	2.23(4)	107(4)	2.600(4)
N1–H1···O104	0.923	1.927	133.3	2.647(4)
N1–H1···O107	0.923	2.139	107.0	2.565(4)
N2–H2···O204	0.902	1.934	135.0	2.650(4)
N2–H2···O207	0.902	2.086	110.9	2.552(4)
N1–H1···O4	0.923	1.888	132.4	2.602(2)
O8–H81···O2^{i}	0.990	1.676	173.2	2.662(2)
O8–H81···O1^{i}	0.990	2.470	114.6	3.019(2)

Symmetry code: i $= -x + 1/2, -y + 1/2, -z$.

The bond lengths and angles of the phenyl ring, the ethoxy-carbonyl group, as well as the pyrane ring are within expected values [25].

3.2.2. Crystal structure of *1a*

The crystal structure of compound **1a** is built up of mononuclear complex molecules $[MoO_2(C_{19}H_{18}O_7N)_2]$, with two didentate ligands **L^{1a}** coordinated to the *cis*-MoO_2^{2+} core (Fig. 2). The ligand itself is the same as described in 3.2.1. but with position 6 of the 2-pyrone ring is substituted by an ethoxycarbonyl group instead of a methyl group. The molybdenum(VI) atom is octahedrally coordinated by two terminal oxo-oxygen ligands and four oxygens from the two didentate ligands. The Mo–O distances, as already observed, indicate their dependence upon the bond order as well as their position in the molybdenum coordination sphere, i.e., *cis* or *trans* to the terminal O atoms. Consequently, the two Mo–O_{trans} bonds, amounting to 2.157(2) and 2.159(2) Å, are significantly longer than the Mo–O_{cis} bonds, amounting to 1.996(2) and 1.999(2) Å.

The characteristic bond lengths C*x*08–C*x*09 ($x = 1$ or 2) of 1.398(5) and 1.399(5) Å, and N*x*–C*x*09 of 1.339(5) Å in both cases, are indicative of the enamine

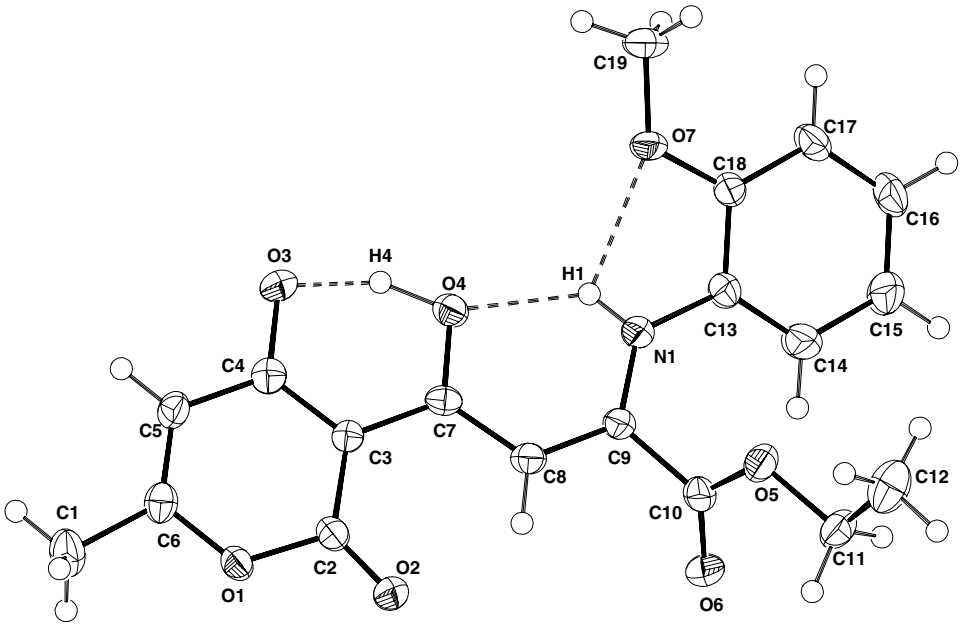

Fig. 1. Molecular structure of ligand molecule **HL[1b]**. The dashed lines indicate intramolecular hydrogen bonds. Ellipsoids are shown at the 50% probability level.

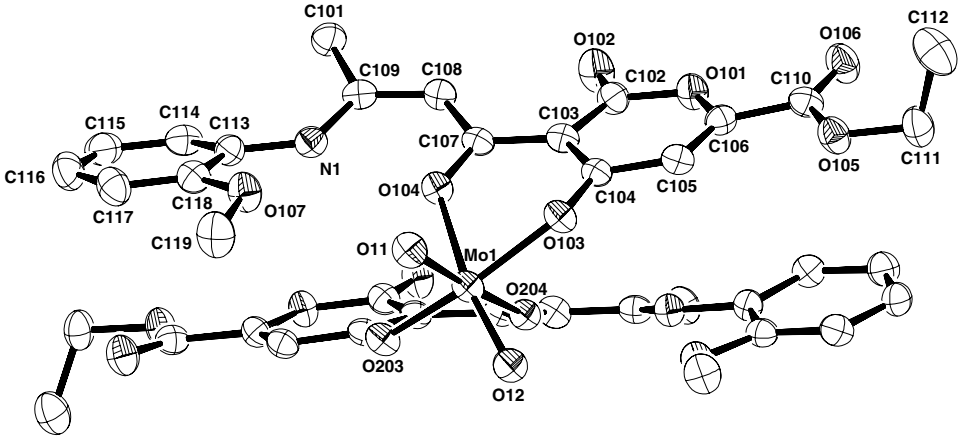

Fig. 2. Molecular structure of complex molecule **1a** showing the atom numbering scheme. Hydrogen atoms as well as the analogous labelling of lower part of the molecule are omitted for clarity. Ellipsoids are shown at the 50% probability level.

C=C–N–H form of the ligand. Due to the slight rotation around the single N–C bond, the ligands are not planar, with C*x*09–N*x*–C*x*13–C*x*14 ($x = 1$ or 2) torsion angles of 33.5(6)° and 24.5(6)°. Such a conformation is stabilized with strong intramolecular N–H···O hydrogen bonds, thus forming an additional six-membered heterocyclic ring in the enaminonic fragment of the ligand [N1···O104 = 2.647(4) Å, N2···O204 = 2.650(4) Å] and a five-membered ring with the N-substituent, [N1···O107 = 2.565(4) Å, N2···O207 = 2.552(4) Å]. Moreover, the ester groups adopt different conformations, with torsion angles C*x*05–C*x*06–C*x*10–O*x*05 ($x = 1$ or 2) of 3.6(5)° and −178.8(3)°, and C*x*10–O*x*05–C*x*11–C*x*12 of 84.4(4)° and −79.0(4)°.

3.2.3. Crystal structure of *3b*

The complex molecule $[Mo_2O_4(C_{19}H_{18}NO_7)_2(CH_3OH)_2]$, with a crystallographically imposed two-fold axis, contains a $[Mo_2O_4]^{2+}$ core, two didentate **L[1b]** ligands and two molecules of methanol (Fig. 3). Each molybdenum atom is coordinated with six oxygen atoms: one terminal oxo-O at 1.679(1) Å, two bridging oxo-O at 1.930(1) and 1.940(1) Å, two oxygen atoms from the didentate ligand at 2.097(1) and 2.177(1) Å and a oxygen atom from the methanol

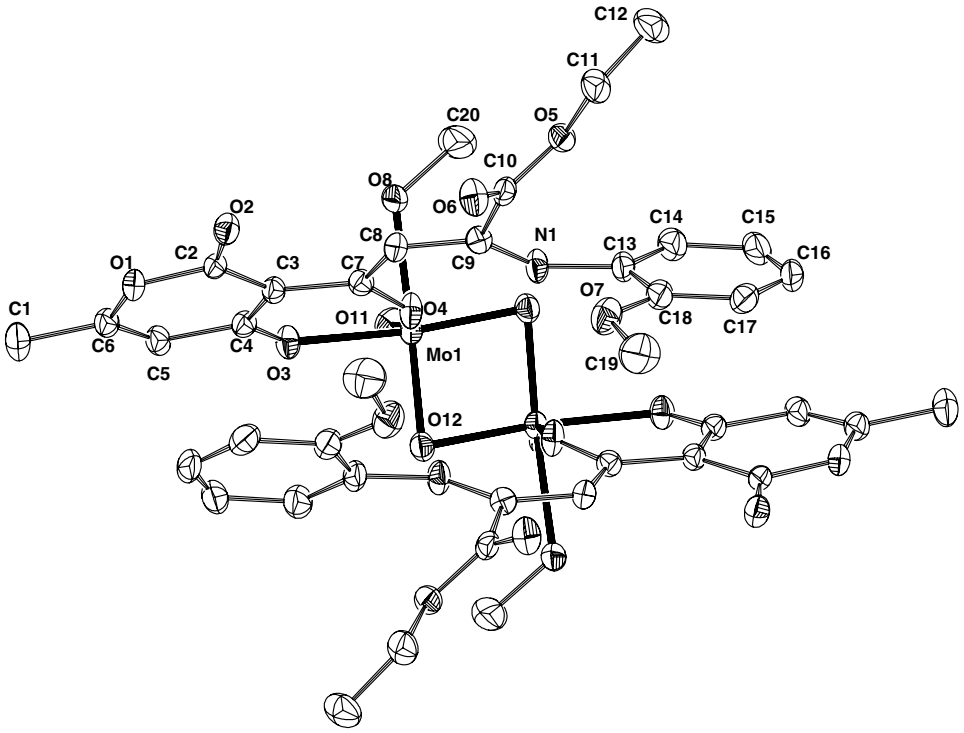

Fig. 3. Molecular structure of complex molecule **3b** showing the atom numbering scheme. Hydrogen atoms are omitted for clarity. Ellipsoids are shown at the 50% probability level.

molecule at 2.190(1) Å. The Mo–Mo distance of 2.5491(4) Å corresponds to a single bond between two molybdenum atoms [26,27]. The characteristic bond length C8═C9 of 1.380(3) Å and C9–N1 1.345(3) Å as in **1a** are indicative of the enamine C═C–N–H form of the ligand.

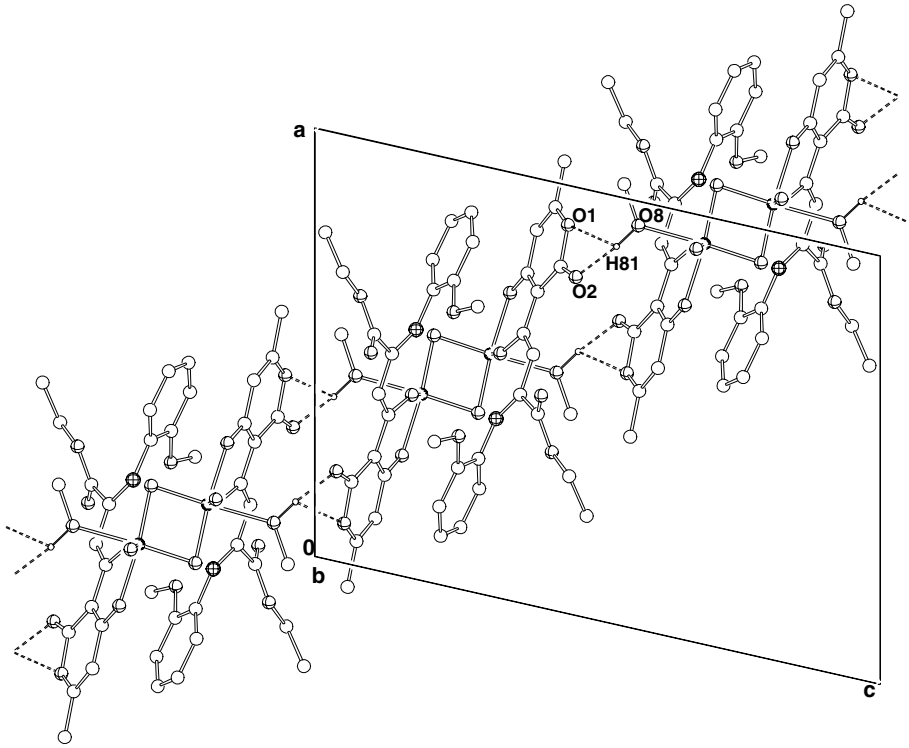

Fig. 4. Packing of **3b** complex molecules in the unit cell viewed down the *b*-axis. The hydrogen bonds are indicated by dashed lines. Chains of molecules are formed along the (1 0 1) direction.

Table 6
^{13}C chemical shifts (ppm) of carbons C-4 and C-7 for the ligands and their complexes in $CDCl_3$

Molecule	HL^{1a}	1a	Δ^*	HL^{1b}	1b	Δ^*	HL^{2a}	2a	Δ^*	HL^{2b}	$HL^{1b\#}$	$3b^{\#}$	Δ^*
Atom													
C-7	185.77	178.08	7.69	191.43	177.15	14.28	183.49	179.02	4.47	187.23	192.25	185.67	6.58
C-4	180.86	174.91	5.95	180.71	173.91	6.80	179.71	175.31	4.40	181.93	181.78	178.07	3.71

[#] In acetone-d_6.
[*] Δ (ppm) = $\delta_{Ligand} - \delta_{Complex}$.

According to the value of the C9–N1–C13–C14 torsion angle: −138.7(2)°, the N-substituent has significant flexibility around the N–C single bond.

A six-membered heterocyclic ring containing N–H is formed by the strong intramolecular hydrogen bond N–H···O [N1···O4 = 2.602(2) Å] which is reinforced with π-delocalization along the heterodienic O=C–C=C–NH moiety.

Complex molecules are interconnected through intermolecular hydrogen bonds between the coordinated methanol molecule and the 2-pyrone oxygen [O8···O1^{i} = 3.019(2) Å] and the keto-oxygen from the 2-pyrone ring [O8···O2^{i} = 2.662(2) Å; i = $-x + 1/2, -y + 1/2, -z$]. In such a way chains of molecules are formed along the (1 0 1) direction (Fig. 4). The crystal structure is additionally stabilized by C–H···O hydrogen bonds with C···O distances ranging from 2.856(2) to 3.430(3) Å.

3.3. NMR spectroscopy

The molybdenum complexes were characterized by the combined use of one- (^1H and APT) and two-dimensional (COSY, HSQC and HMBC) NMR spectra. Both proton and carbon chemical shifts resemble those previously reported for related compounds [14–16]. A complete and unambiguous atom assignment of the complex **2b** was not possible in $CDCl_3$ or acetone-d_6 owing to its very low solubility. In order to increase solubility, we added small amounts of DMSO but the complex underwent rapid decomposition.

The absence of a hydroxyl proton resonance and significant shifts of the respective carbon signals confirm the formation of complexes between molybdenum and the ligands (Scheme 2). For illustration, only chemical shifts of carbons C-4 and C-7 (being the two interacting sites) of both the ligands and the complexes are given in Table 6, together with their chemical shift differences Δ (ppm). It is clearly seen that in all complexes larger changes of chemical shift are observed for the C-7 atom (up to 14 ppm), than for C-4 (up to 7 ppm). Both effects are upfield and arise from the electron redistribution upon complexation with molybdenum. The changes in chemical shifts of the other atoms are smaller and alternate in sign. This is in accordance with the results obtained for similar compounds [14–16]. The significant downfield shifts of the amine protons in the range 10.5–12.5 ppm and the relatively broad nature of these signals are due to the formation of strong intramolecular hydrogen bonds in solution, as observed also in the solid state.

4. Supplementary material

CCDC Nos. 231337, 231338 and 231339 contain the supplementary crystallographic data for this paper. These data can be obtained free of charge via www.ccdc.cam.ac.uk/conts/retrieving.html (or from the Cambridge Crystallographic Data Centre, 12 Union Road, Cambridge CB2 1EZ, UK; fax: +44 1223 336033; or deposit@ccdc.cam.ac.uk).

Acknowledgements

This research was supported by the Ministry of Science and Technology of the Republic of Croatia Grant Nos. 0119631 and 0119641. We thank Dr. Gerald Giester from the Institute for Mineralogy and Crystallography, University of Vienna, for the data collection.

References

[1] D.T. Puerta, S.M. Cohen, Inorg. Chem. 42 (2003) 3423.
[2] G. Battaini, E. Monzani, L. Casella, L. Santagostini, R. Pagliarin, J. Biol. Inorg. Chem. 5 (2000) 262.
[3] S. Thaisrivongs, D.L. Romero, R.A. Tommasi, M.N. Janakiraman, J.W. Strohbach, S.R. Turner, C. Biles, R.R. Morge, P.D. Johnson, P.A. Aristoff, P.K. Tomich, J.C. Lynn, M.M. Horng, K.T. Chong, R.R. Hinshaw, W.J. Howe, B.C. Finzel, K.D. Watenpaugh, J. Med. Chem. 39 (1996) 4630.
[4] F.H. Vaillancourt, G. Labbe, N.M. Drouin, P.D. Fortin, L.D. Eltis, J. Biol. Chem. 277 (2002) 2019.
[5] K.H. Thompson, B.D. Liboiron, Y.S.K.D.D. Bellman, I.A. Setyawati, B.O. Patrick, V. Karunaratne, G. Rawji, J. Wheeler, K. Sutton, S. Bhanot, C. Cassidy, J.H. McNeill, V.G. Yuen, C. Orvig, J. Biol. Inorg. Chem. 8 (2003) 66.
[6] B. Song, K. Saatchi, G.H. Rawji, C. Orvig, Inorg. Chim. Acta 339 (2002) 393.
[7] M. Rangel, A. Tamura, C. Fukushima, H. Sakurai, J. Biol. Inorg. Chem. 6 (2001) 128.
[8] P. Buglyo, E. Kiss, I. Fabian, T. Kiss, D. Sanna, E. Garribba, G. Micera, Inorg. Chim. Acta 306 (2000) 174.
[9] G.R. Hanson, Y. Sun, C. Orvig, Inorg. Chem. 35 (1996) 6507.
[10] S.J-. Lord, N.A. Epstein, R.L. Paddock, C.M. Vogels, T.L. Hennigar, M.J. Zaworotko, N.J. Taylor, W.R. Driedzic, T.L. Broderick, S.A. Westcott, Can. J. Chem. 77 (1999) 1249.

[11] A. Brbot-Šaranović, B. Katušin-Ražem, I. Sušnik, Heterocycles 29 (1989) 1559.
[12] A. Brbot-Šaranović, G. Pavlović, M. Cindrić, Struct. Chem. 11 (2000) 65.
[13] A. Brbot-Šaranović, G. Pavlović, V. Vrdoljak, M. Cindrić, Croat. Chem. Acta 74 (2001) 441.
[14] M. Cindrić, V. Vrdoljak, T. Kajfež, P. Novak, A. Brbot-Šaranović, N. Strukan, B. Kamenar, Inorg. Chim. Acta 328 (2002) 23.
[15] M. Cindrić, V. Vrdoljak, N. Strukan, P. Tepeš, P. Novak, A. Brbot-Šaranović, G. Giester, B. Kamenar, Eur. J. Inorg. Chem. (2002) 2128.
[16] M. Cindrić, V. Vrdoljak, N. Strukan, A. Brbot-Šaranović, P. Novak, B. Kamenar, Inorg. Chim. Acta 375 (2004) 931.
[17] G.J. Chen, J.W. McDonald, W.E. Newton, Inorg. Chem. 15 (1976) 2612.
[18] F.W. Moore, R.E. Rice, Inorg. Chem. 7 (1968) 2510.
[19] G.A. Parker, Analytical Chemistry of Molybdenum, Springer, New York.
[20] Z. Otwinowski, in: Proceedings of the CCP4 Study Weekend: Data Collection, Warington: Daresbury Laboratory, UK, 1993.
[21] G.M. Sheldrick, SHELXS-97, Program for the Solution of Crystal Structures, University of Göttingen, Germany, 1997.
[22] G.M. Sheldrick, SHELXL-97, Program for the Refinement of Crystal Structures, University of Göttingen, Germany, 1997.
[23] C.K. Johnson, ORTEP II, Report ORNL-3794, revised, Oak Ridge National Laboratory, TN, USA, 1971.
[24] A.L. Spek, The EUCLID package, in: D. Sayre (Ed.), Computational Crystallography, Clarendon Press, Oxford, 1982, p. 528.
[25] F.A. Cotton, Inorg. Chem. 4 (1965) 334.
[26] F.A. Cotton, J. Less-Common Met. 54 (1977) 3.
[27] F.H. Allen, O. Kennard, D.G. Watson, L. Brammer, A.G. Orpen, R.J. Taylor, J. Chem. Soc., Perkin Trans. 2 (1987) S1–S19.

Available online at www.sciencedirect.com
SCIENCE DIRECT®
Polyhedron 23 (2004) 1869–1876
POLYHEDRON
www.elsevier.com/locate/poly

Electronic and magnetic properties of iron (III) dinuclear complexes with carboxylate bridges

Verónica Paredes-García [a,b,*], Ramón O. Latorre [c], Evgenia Spodine [d]

[a] Departamento de Química, Facultad de Ciencias, Universidad de Chile, Chile
[b] Departamento de Química, Universidad Tecnológica Metropolitana, José Pedro Alessandri 1242, Ñuñoa, Santiago, Chile
[c] Escuela Técnica Aeronáutica, Av. Portales 3450, Estación Central, Santiago, Chile
[d] Facultad de Ciencias Químicas y Farmacéuticas, CIMAT, Universidad de Chile, Chile

Received 5 September 2003; accepted 30 March 2004
Available online 8 June 2004

Abstract

A series of dinuclear iron (III) complexes with carboxylate bridges, of the type $[Fe_2L_2(H_20)_4](NO_3)_2(H_2O)_m$ ($m = 1$–3), where L = Schiff base derived from L-α-amino acids and salicylaldehyde have been prepared and characterised by different spectroscopic techniques, magnetic susceptibility, conductivity, and electrochemical measurements. The dimeric iron complexes contain hexa-coordinated iron (III), with the metal ion surrounded by water molecules, the salicylidenimine ligand, and the bridging carboxylate groups. The inequivalence of the iron atoms is detected by Mössbauer spectroscopy and this is reflected by the presence of two overlapping quadrupole doublets ($\delta_1 \sim 0.52$–0.67 mm s^{-1}, $\delta_2 \sim 0.64$–0.80 mm s^{-1}, $\Delta E_{Q1} \sim 0.38$–0.80 mm s^{-1}, and ΔE_{Q2} (~ 0.68–1.01 mm s^{-1}), with an approximate intensity ratio of 1:1 for all complexes. The magnetic susceptibilities of the complexes were determined over the temperature interval 5–300 K and revealed a decrease in the effective magnetic moment with decreasing temperature. The plots of the reciprocal of the molar susceptibility versus temperature indicate that the two iron (III) ions are very weakly antiferromagnetically coupled ($-J \sim 0.09$–0.21 cm^{-1}). Electrochemical studies show that the first two peaks can be assigned to two consecutive one-electron reduction process, affording $Fe^{II}Fe^{III}$ and $Fe^{II}Fe^{II}$. The comproportionation constant K_c at 298 K is in the 5.3×10^3–2.5×10^4 range. The values obtained are in agreement with an intermediate electron coupling between redox sites.
© 2004 Elsevier Ltd. All rights reserved.

Keywords: Iron (III); Dinuclear; Carboxylate; Complexes; Bridging; Mössbauer

1. Introduction

Proteins use a limited set of metal ions to mediate a variety of processes. Often the same metal centre can have a variety of roles, for example, polymetallic centres occur in numerous metalloproteins, carry out a variety of functions including electron transfer, hydroxylation of methane, the generation of amino acid radicals, hydrolysis of phosphate esters, and dioxygen transport. Furthermore, proteins that contain carboxylate-bridged diiron centres form a class of enzymes that activate molecular oxygen for diverse biological functions. These include the oxygen carrier hemerythrin, the R2 subunit of the ribonucleotide reductase, and the iron storage protein ferritin among others [1–3].

How a protein is able to fine-tune the properties of metal ions to accomplish such different functions, such as the selectivity and efficiency of these reactions, are important questions that with the development of bio-omimetics inorganic compounds have been answered in the last years [1–3]. The magnetical, electrochemical, and spectroscopical studies of these analogous synthetic systems provide important information about redox and spin states of the iron centre or centres, magnitude of exchange interaction, and the ligand environment, which have a profound influence on the functional properties [2–5].

The use of Schiff bases, derived from amino acids, as model systems has been due mainly to the participation

* Corresponding author. Tel.: +2-678-2801; fax: +2-678-2868.
E-mail address: vpg@manquehue.net (V. Paredes-García).

0277-5387/$ - see front matter © 2004 Elsevier Ltd. All rights reserved.
doi:10.1016/j.poly.2004.03.024

of similar biological compounds in key metabolic reactions. Furthermore, carboxylate-bridged diiron centres are encountered at the active sites of several proteins that bind or activate dioxygen [2,3]. The metal ions bonded to this kind of ligands promote the above-mentioned reactions by maintaining the planarity of the conjugated system [4,5].

Complexes with Schiff bases derived from salicylaldehyde and α-amino acids constitute simple models which make possible the study and the elucidation of the mechanisms of the above-mentioned reactions. These models also allow the correlation between structures and the magnetic, electronic, and optical properties of the metal sites present in biological systems [6–10].

2. Experimental

The reagents salicylaldehyde, L-glycine, L-alanine, L-valine, L-leucine, L-isoleucine, and L-phenylalanine were purchased from Merck (analytical grade) and were used without further purification.

The ligands were synthesised after introducing important modifications [11] to the method described by Heinert and Martell [12]. The amino acid was added to a solution of potassium hydroxide (1 mmol) in *i*-propanol. The amino acid was stirred with gentle warming until it had completely dissolved. The salicylaldehyde (1 mmol) was added and the reaction mixture was refluxed for 3 h. The mixture was then cooled and the product was filtered, and washed with ethanol and petroleum ether. The compounds were recrystallised from methanol and ether and dried in vacuo. (Yield 73–91%). All the ligands were prepared according to the procedure described above and were isolate as potassium salts. The Schiff bases synthesised by this method are solids of different shades of yellow and they were characterised by elementary analysis, FTIR, UV–Vis, and ^{1}H NMR spectroscopic methods [11].

The Fe(III) complexes were prepared as described by Casella et al. [13], introducing some modifications [11]. The ligand (0.001 mol) was dissolved in methanol at room temperature and 0.001 mol of potassium hydroxide was added. $Fe(NO_3)_3 9H_2O$ (0.001 mol) was added directly to the solution. The reaction mixture was left for 5–6 h at room temperature with stirring and under a nitrogen atmosphere. The KNO_3 formed was filtered off and the solution was concentrated. Finally, the product was concentrated under vacuum at room temperature to induce the precipitation, then it was filtrated and washed with *n*-hexane. A dark violet solid was obtained and was dried under vacuum. All the complexes were prepared according to the procedure described previously. The complexes synthesised by this method are dark amorphous solids of violet color with molecular formulae $[Fe_2L_2(H_2O)_4](N0_3)_2(H_2O)_{1-3}$ (Yields 70–80%).

Metal microanalyses of the complexes were performed with a Shimadzu atomic absorption spectrophotometer, model AA-6200. The infrared spectra (KBr pellets) were recorded on a Bruker, model AMX300 spectrophotometer. The Mössbauer spectra of these complexes as fine powder samples were obtained in a conventional spectrometer with constant acceleration. The source was 10 mCi ^{57}Co in a Pd matrix. The γ-ray detection was carried out with a Reutes–Stokes detector connected to an Ortec amplifying and selecting system. A 1024 channel Canberra multichannel analyser was used for the data acquisition. The reported isomer shift values are relative to sodium nitroprusside. Electrochemical studies were done with a PAR 173 potentiostat and PAR 175 programmer equipped with a Model 179 digital coulometer. Polarographic measurements were done with BAS CV27 cyclic voltammetry equipment. Molar conductance was measured at 25 °C on a Radiometer model CDM-83 conductimeter with a CDC-304 electrode. Electronic spectra were recorded on a Unicam II UV–Vis spectrophotometer. Variable temperature (5–300 K) magnetic susceptibility data were obtained with a SHE Model 906 SQUID type susceptometer–magnetometer and calibrated with $Hg[Co(NCS)_4]$. The diamagnetic corrections were calculated from Pascal's constants.

3. Results and discussion

The complexes synthesised in this work are amorphous solids of dark violet colour, with molecular formulae $[Fe_2L_2(H_2O)_4](N0_3)_2(H_2O)_m$ $(m = 1–3)$. The complexes were characterised by elementary analysis, FTIR, UV–Vis, and Mössbauer spectroscopy methods and conductivity, electrochemical, and magnetic measurements. The dimeric iron complexes contain hexacoordinated iron (III), with the metal ion surrounded by water molecules and the salicylidenimine ligand coordinated through the iminic nitrogen and the phenolic oxygen. Both metal ions are bridged by the carboxylate

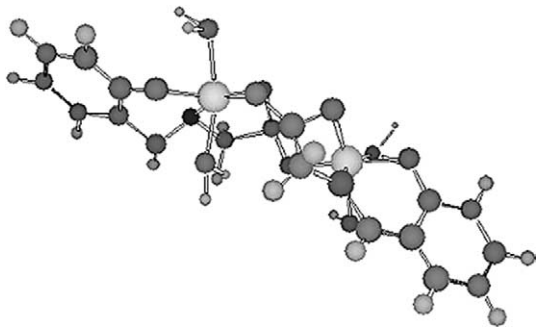

Fig. 1. Structures of dinuclear iron complexes with Schiff bases derived from salicylaldehyde and α-glicine.

Table 1
Analytical data for Fe(III) Schiff base complexes: $Fe_2L_2(H_2O)_4](N0_3)_2(H_2O)_m$

Compounds	Yield %	%Fe		%C		%H		%N		Λ^a ($Scm^2\ mol^{-1}$)
		Found	Calculated	Found	Calculated	Found	Calculated	Found	Calculated	
$[Fe_2(SA–Gly)_2(H_2O)_4](NO_3)_2 \cdot 3H_2O$(Fe–SA–Gly)	75.7	15.54	15.59	30.27	30.19	3.93	3.94	7.84	7.82	175.96
$[Fe_2(SA–Ala)_2(H_2O)_4](NO_3)_2.H_2O$(Fe–SA–Ala)	60.4	15.71	15.77	34.01	33.92	3.98	3.98	7.94	7.91	162.51
$[Fe_2(SA–Val)_2(H_2O)_4](NO_3)_2 \cdot 3H_2O$(Fe–SA–Val)	77.3	13.90	13.95	35.91	36.02	5.05	5.04	6.98	7.00	176.01
$[Fe_2(SA–Leu)_2(H_2O)_4](NO_3)_2 \cdot 3H_2O$(Fe–SA–Leu)	82.5	13.44	13.48	37.79	37.70	5.35	5.35	6.79	6.76	154.33
$[Fe_2(SA–Ile)_2(H_2O)_4](NO_3)_2 \cdot 3H_2O$(Fe–SA–Ile)	80.1	13.44	13.48	37.82	37.70	5.33	5.35	6.78	6.79	190.31
$[Fe_2(SA–Phe)_2(H_2O)_4](NO_3)_2 \cdot 3H_2O$(Fe–SA–Phe)	75.4	12.42	12.46	42.96	42.88	4.52	4.50	6.28	6.25	187.67

[a] Conductivity data for the dimeric iron complexes in DMF at 25 °C.

groups of the amino acids residue, Fig. 1. The physical characteristics of the complexes are summarised in Table 1. In general, the complexes are highly insoluble in most organic solvents of low polarity, and although they are soluble in water, they decompose releasing the free ligand.

3.1. Magnetic susceptibilities

The magnetic susceptibilities of the $[Fe_2(L_2(H_2O)_4](NO_3)_2(H_2O)_m$ set were determined over the temperature range 5–300 K. The plot of the reciprocal of the molar susceptibility versus temperature for Fe–SA–Ala complex is shown in Fig. 2 and is similar for the rest of the complexes. The alanine complex, for example, has an effective magnetic moment per molecule (μ_{eff}), which slightly decreases from $7.10\mu_B$ at 300 K to $7.03\mu_B$ at 60 K, after which there is a major decrease to $5.85\mu_B$ at 5 K. The trend is similar for the rest of the complexes. The μ_{eff} values at 300 K for complexes are lower than the theoretical value of $8.37\mu_B$ for effective moment of two independent high spin iron (III) ions ($S = 5/2$). The decrease of μ_{eff} at lower temperatures indicates that two high-spin iron (III) centres are weakly antiferromagnetically coupled [14].

The magnetic susceptibility of the binuclear iron (III) complexes was analysed using the van Vleck equation [14] with a spin exchange Hamiltonian, $H = -JS_1S_2$, where $S_1 = S_2 = 5/2$. All the calculations were performed using a least-squares minimisation routine,

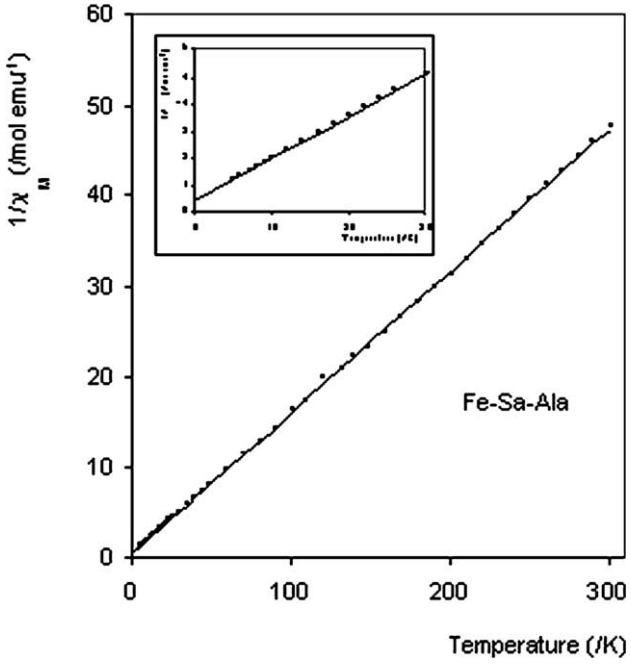

Fig. 2. Temperature dependence of the reciprocal molar susceptibility of Fe–SA–Ala.

Table 2
Magnetic parameters for dinuclear iron (III) complexes

Complexes	μ_{eff} (300 K) dimeric complex (μ_B)	g	$-J$ (cm^{-1})	R	θ (K)
Fe–SA–Gly	7.05	2.37	0.12	4.2×10^{-6}	−1.46
Fe–SA–Ala	7.10	2.37	0.21	2.1×10^{-5}	−2.68
Fe–SA–Val	6.86	2.18	0.16	3.1×10^{-4}	−4.27
Fe–SA–Leu	6.71	2.20	0.15	6.1×10^{-5}	−2.36
Fe–SA–Ile	7.00	2.19	0.12	4.8×10^{-4}	−5.14
Fe–SA–Fen	7.24	2.39	0.09	5.6×10^{-5}	−1.66

where $SSQ = \sum_i [(\chi_i^{obs} - \chi_i^{calc})/\chi_i^{obs}]^2$. We report the parameter $R = SSQ/(n-p)$, where n is the number of experimental data points and p is the number of parameters allowed to vary in the minimisation routine. The final magnetic parameters for the different complexes are summarised in Table 2. For all complexes, a very small negative value was obtained for J (−0.09 to −0.21 cm^{-1}), indicating that the two iron (III) ions are very weakly antiferromagnetically coupled [14]. The g values were somewhat greater than expected for ferric ions. We attribute this to the difficulty of fitting them when the J values are so small. These values are comparable with those reported for other tris-carboxylate-bridged complexes $[Fe_2(O_2CH)_4(BIPhMe)_2]$ [15], in which the J value is −0.16 cm^{-1}. Other complexes derived from $[Fe_2(salen)_2L_2]$, where L = oxalate and squarate as bridging ligands have J values of −7.1 and −0.39 cm^{-1}, respectively [16]. For bis-carboxylate complexes such as $[Fe_2(O_2CCH_3)_2L_2](ClO_4)_2$, where L = *N*,*N*′-dimethyl-*N*,*N*′-bis-(2-pyridylmethylethane)-1,2-diamine, the value of the antiferromagnetic exchange coupling constant is also very small, J value, i.e., −1.5 cm^{-1} [15].

The magnetic properties of carboxylate-bridged di-iron (III) complexes depend significantly on the nature of the bridging ligands. For example, the values for J vary between −13 and −26 cm^{-1} for hydroxo and alkoxo carboxylate-bridged complexes [17–20].

3.2. Mössbauer spectroscopy

Mössbauer spectra for all complexes were recorded at 4, 298 and 300 K. Fig. 3 shows a representative spectrum and theoretical least-squares fit of the data. The parameters obtained for the series of carboxylate-bridged iron (III) complexes, derived from salicylaldehyde and the different α-amino acids, are summarised in Table 3. The values of the chemical shifts are referred to sodium nitroprusside.

The spectra of all the complexes show two overlapping doublets that are revealed by shoulders in each spectrum, and by the width and asymmetry of the obtained signals [11]. The integrated absorption intensities of the two spectral subcomponents show a 1:1 ratio, and consequently, the relative proportion of iron in both sites is the same. The above indicates the presence of two inequivalent iron (III) centres in the dinuclear complexes.

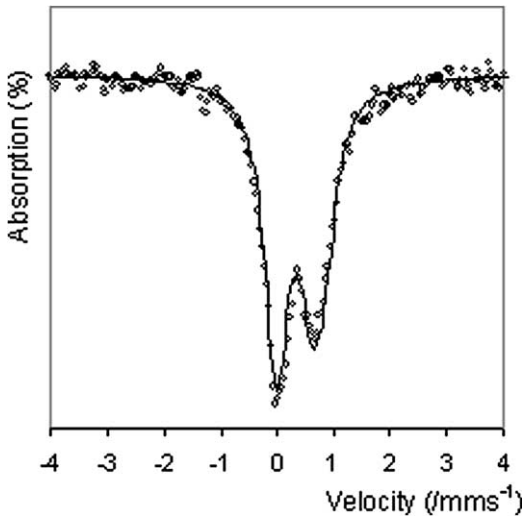

Fig. 3. Mössbauer spectrum for Fe–SA–Ala at 300 K.

The isomer shifts are similar for both doublets ($\delta_1 \sim 0.60$ mm s^{-1}, $\delta_2 \sim 0.70$ mm s^{-1}), as expected for very similar ligand environment for the iron centres, and the values correspond to high spin Fe(III) [21–23]. In all the complexes, the second site shows a higher quadrupolar splitting value ($\Delta E_Q = 0.68$–1.01 mm s^{-1}), that is indicative of a variation in the electric field gradient, probably caused by greater distortions of the octahedral geometry at this site [23,24]. The Mössbauer spectra at room temperature show an asymmetric doublet. At lower temperature this asymmetry is partially lost, but a slight asymmetry is retained even at 4 K. The asymmetry of the lines is probably due to Gol'danskii–Karyagin and spin–spin relaxation combined effects, since it disappears partially with decreasing temperature [21,24]. The isomer shift values of 0.50 mm s^{-1} and quadrupolar splitting in order to 0.9 mm s^{-1} are in accord with pseudo-octahedral system, with a N,O coordination sphere and carboxylate bridges, like in $[Fe_2O(O_2CH_3)_2(Me_3TACN)](ClO_4)_2$ (Me_3TACN = 1,4,7-trimethyl-1,4,7-triazacyclo-nonane) [25]. These parameters are similar for those derived from iron ions in hemerythrin forms,

Table 3
Mössbauer parameters for dinuclear iron complexes at 77 and 300 K

Complexes	Temperature (K)	I.S.[a] ($mm\,s^{-1}$)		ΔE_Q[b] ($mm\,s^{-1}$)		A_1/A_2[c]
		Site 1	Site 2	Site 1	Site 2	
Fe–SA–Gly	298	0.60	0.70	0.60	0.85	1.01
	77	0.61	0.71	0.59	0.89	1.15
Fe–SA–Ala	298	0.61	0.68	0.58	0.72	1.13
	77	0.63	0.69	0.55	0.70	1.08
Fe–SA–Val	298	0.52	0.64	0.64	0.88	1.07
	77	0.55	0.65	0.60	0.85	1.08
Fe–SA–Leu	298	0.64	0.66	0.64	0.82	1.23
	77	0.65	0.68	0.62	0.80	1.14
Fe–SA–Ile	298	0.66	0.76	0.82	1.01	1.15
	77	0.66	0.75	0.80	0.98	1.09
Fe–SA–Fen	298	0.66	0.80	0.39	0.68	1.09
	77	0.67	0.80	0.38	0.68	1.07

[a] Isomer shift.
[b] Quadrupolar splitting.
[c] Area ratio.

in which a coordination sphere also formed by nitrogen and oxygen atoms and carboxylate bridges is present [26]. On the other hand, the difference in ΔE_Q values for sites 1 and 2 is indicative of different local symmetries for the two ferric sites, producing the splitting of the T_{2g} orbital triplet by crystal field distortion. The values indicate a lower symmetry for site 2 compared to site 1 [18a]. Since the quadrupolar splitting values are not significantly different, the ferric ions at both sites must have a pseudo-octahedral arrangement [23,24]. It is also possible to consider that the dinuclear iron (III) complexes synthesised in this work have a more symmetric conformation at 77 K than at 298 K.

Although big fluctuations do not exist in the value of the isomer shift, this value increases as the amino acid side chain increases. A higher electronic density on the metal atom could also explain these fluctuations. The fact that these differences are small may be due to retrodonation effects of ligand to metal donation, thus leaving a constant electron density on each iron atom [11,27,28].

3.3. Cyclic voltammetry

The electrochemistry of the dinuclear complexes was studied by cyclic voltammetry. Cyclic voltammetry of the complexes was recorded in DMF with [TBA][PF_6] as supporting electrolyte, in the potential range +1.3 to −1.8 V versus SCE. The redox parameters are summarised in Table 4. In all cases, three redox processes

Table 4
Electrochemical data for dinuclear iron (III) complexes[a]

Complexes	Redox wave	E_{pa}	E_{pc}	ΔE	$E_{1/2}$	i_{pa}/i_{pc}	K_c
Fe–SA–Gly	I	−0.27	−0.33	0.06	−0.30	1.66	8.02×10^3
	II	−0.56	−0.62	0.06	−0.59	2.20	
	III	−1.02	−1.17	0.15	−1.10	1.33	
Fe–SA–Ala	I	−0.29	−0.36	0.07	−0.33	0.66	2.49×10^4
	II	−0.56	−0.62	0.06	−0.59	2.40	
	III	−1.10	−1.22	0.12	−1.16	1.65	
Fe–SA–Val	I	−0.28	−0.33	0.05	−0.29	1.70	1.14×10^4
	II	−0.52	−0.59	0.07	−0.53	1.98	
	III	−1.10	−1.22	0.11	−1.16	1.23	
Fe–SA–Leu	I	−0.29	−0.35	0.06	−0.31	2.40	5.25×10^3
	II	−0.55	−0.62	0.07	−0.53	1.33	
	III	−1.07	−1.25	0.18	−1.16	1.14	
Fe–SA–Ile	I	−0.30	−0.36	0.06	−0.32	0.75	5.25×10^3
	II	−0.52	−0.59	0.07	−0.54	1.34	
	III	−1.09	−1.20	0.11	−1.18	1.34	
Fe–SA–Fen	I	−0.31	−0.38	0.07	−0.30	1.32	1.69×10^4
	II	−0.50	−0.57	0.07	−0.55	2.05	
	III	−1.05	−1.17	0.12	−1.12	1.16	

[a] Potential values are in volts and referred to SCE. $\Delta E = E_{pa} - E_{pc}$; $E_{1/2} = (E_{pa} + E_{pc})$. E_{pa} and E_{pc} are the anodic and cathodic peak potentials, respectively.

were observed at essentially identical potentials. This result is indicative of a similar electronic environment for the iron in all complexes. The first and second processes can be ascribed to successive redox reactions with approximately $E^1_{1/2} = -0.3$ V and $E^2_{1/2} = -0.6$ V versus SCE,

$$[Fe_2L_2(H_2O)_4]^{2+} \overset{E^1_{1/2}}{\underset{-e^-}{\overset{+e^-}{\rightleftharpoons}}} [Fe_2L_2(H_2O)_4]^{+} \overset{E^1_{1/2}}{\underset{-e^-}{\overset{+e^-}{\rightleftharpoons}}} [Fe_2L_2(H_2O)_4] \quad (1)$$

where L = Schiff base ligand.

Both couples were quasireversible, and with potential separations (ΔE^1, ΔE^2) between 60 and 70 mV, indicating a one-electron transfer per dimer. The ratio $i_p/v^{1/2}$ was constant in accord with a diffusion-controlled process.

The first two peaks can be assigned to two consecutive one-electron reduction process, affording $Fe^{II}Fe^{III}$ and $Fe^{II}Fe^{II}$ species, similar to those observed for other binuclear carboxylate-bridged iron (III) complexes [29–31].

The separation between redox potentials $E^1_{1/2}$ and $E^2_{1/2}$ ($\Delta E_{1,2} = E^1_{1/2} - E^2_{1/2}$) is between 0.22 and 0.29 V. The comproportionation constant K_c at 298 K for Eq. (2) were calculated using Eq. (3) and are in the 5.3×10^3–2.5×10^4 range (Table 3),

$$Fe^{III}Fe^{III} + Fe^{II}Fe^{II} \overset{K_c}{\rightleftharpoons} 2Fe^{II}Fe^{III} \quad (2)$$

$$K_c = \exp\left(\frac{\Delta E_{1,2} nF}{RT}\right). \quad (3)$$

The K_c values obtained are in agreement with an intermediate electron coupling between redox sites, which is indicative of a moderate charge delocalisation between metal centres, class II, Robin–Day classification [32–34].

The third redox process with $E^3 1/2 = -1.10$ V (versus SCE) involves more than one electron and may be attributed to the reduction of the Fe^{II}–Fe^{II} species [35,36]. The analysis of the polarographic waves indicates that the electron ratio between the first two reduction processes and the third reduction process is 1:1:2.

3.4. Spectroscopy data

Infrared data were recorded in KBr pellets at room temperature. The vibrational data for all dinuclear iron complexes and the free ligand are summarised in Table 5. For all complexes it can be seen that the vibration of the –C=N bond in the complexes is displaced toward lower energy, in comparison to the free ligand; the opposite is observed for the –C–O (phenolic) group [37]. On the other hand, the symmetric and asymmetric stretching absorption bands associated with the carboxylate group show a decrease in energy for both bands. Furthermore, since the difference between these bands is about 170 cm^{-1}, it may be assumed that the carboxylate group is bridging the two metal atoms [38]. At lower energy, an absorption is present around 800–810 cm^{-1}, and this can be assigned to chelate ring vibrations, since it is not present in the free ligand [39]. Around 645–680 cm^{-1}, the band corresponding to out-of-plane vibrations, δO–C–O of the carboxylate bridge can be identified [40]. The absorptions at approximately 560 and 450 cm^{-1} were assigned to the metal–ligand vibrations Fe–N and Fe–O, respectively, in agreement with Nakamoto [39]. These bands are of low intensity and are not present in the free ligand spectrum. The spectra of all the complexes showed a broad band at 3400 cm^{-1} due to lattice water. The single absorption at 1445 cm^{-1} is indicative of an ionic nitrate group [41].

In agreement with infrared data and reported assignments for similar Schiff bases, it is possible to infer that these dimeric complexes have six-coordinated structures in which the metal ion is coordinated to water oxygen, phenol oxygen, imine nitrogen, and carboxylate oxygen, the latter group bridging both iron atoms (Fig. 1).

The low solubility of the complexes in a great variety of solvents allowed the electronic spectra to be recorded

Table 5
Characteristic infrared absorptions for the ligands and complexes[a]

Compounds	$\nu_{C=N}$	ν_{O-Ph}	ν_{COOs}	ν_{COOas}	$\nu_{quelate\ ring}$	ν_{Fe-N}	ν_{Fe-O}	ν_{H_2O}
Fe–SA–Gly	1630 s	1300 m	1366 m	1541 m	804 m	549 m	451 m	3432 b
Fe–SA–Ala	1626 s	1306 m	1369 m	1543 m	806 m	552 m	452 m	3431 b
Fe–SA–Val	1624 s	1312 m	1377 m	1542 m	804 m	555 m	457 m	3438 b
Fe–SA–Leu	1626 s	1310 m	1367 m	1541 m	800 m	555 m	459 m	3438 b
Fe–SA–Ile	1624 s	1311 m	1368 m	1541 m	800 m	559 m	459 m	3439 b
Fe–SA–Fen	1624 s	1308 m	1356 m	1541 m	800 m	550 m	455 m	3435 b
SA–Gly	1636 s	1297 w	1404 m	1590 s				
SA–Val	1638 s	1278 w	1376 m	1605 s				
SA–Leu	1637 s	1279 w	1377 m m	1609 s				
SA–Ile	1639 s	1275 w	1377 m	1608 s				
SA–Phe	1634 s	1277 w	1376 m	1616 s				

[a] b, broad; s, strong; m, medium; w, weak.

only in methanol. The electronic spectra of the complexes are strongly dominated by the electronic transitions due to the iron-salicylaldiminate chromophores. The charge transfer bands from phenolate to the metal (causing the red-purple color of the complexes) are of intermediate intensity and appear near 450 nm. These bands correspond to a charge transfer from the pπ orbital of phenolic oxygen to the dπ orbital of the iron [42]. The absorption bands between 230 and 260 nm are assigned to π–π^* transitions of benzenoid type [30,38]. The absorption bands near 295 and 420 nm have been assigned to the π–π^* and n–π^* transitions, originating mainly in the azomethine chromophore [32,38]. The other bands near 320 and 480 nm should correspond to ligand–metal charge transfer bands [37].

4. Conclusions

By Mössbauer spectroscopy, it is possible to identify two different sites for iron. For the whole series of complexes derived from salicylaldehyde and different α-amino acids, the isomer shift and quadrupolar splitting for both sites correspond to high spin Fe(III). The quadrupolar splitting for these two sites is different, due to different distortions at each iron centre with a pseudo octahedral arrangement. The values of chemical shift and quadrupolar splitting are similar to those shown by iron nuclei in biological compounds with N and O coordination spheres and with carboxylate bridges. The observed weak antiferromagnetic interactions are in agreement with other iron polynuclear complexes with carboxylate bridges.

From the cyclic voltammetry measurements, it was possible to determine two redox couples which identified the process of reduction of Fe(III) to Fe(II) and one redox couple for the reduction of iron II. Polarographic measurements indicate that for the reductions of iron (III), there is one electron involved and the reduction of Fe(II) is related to a two-electron transfer.

From the results obtained by infrared, electronic, and Mössbauer spectroscopy, besides the electrochemical, conductimetric, and magnetic measurements, the structures of dimeric complexes with Schiff bases derived from α-amino acids and salicylaldehyde (Fig. 1) are confirmed.

Acknowledgements

Financial support for this work provided by FONDECYT (Grant 2960043) is gratefully acknowledged. We thank Dr. A.B.P. Lever (York University), for his support and important discussion, and Dr. Octavio Peña for recording the susceptibility data (Université de Rennes 1, France) and FONDAP 11980002 and PICS 922 project for financial support.

References

[1] A.L. Feig, S.J. Lippard, Chem. Rev. 94 (1994) 759.
[2] E.I. Solomon, T.C. Brunold, M.I. Davis, J.N. Kemsley, S.K. Lee, N. Lehnert, F. Neese, A.J. Skulan, Y.S. Yang, J. Zhou, Chem. Rev. 100 (2000) 235.
[3] Y. Mathews, P. Joy, H. Manohar, Polyhedron 30 (1991) 2163.
[4] F. Dianzhong, W. Bo, Trans. Met. Chem. 18 (1993) 101.
[5] R.E. Norman, S. Yan, G. Backes, J. Ling, S. O'Connor, J.H. Zhang, L. Que, J. Am. Chem. Soc. 112 (1990) 1554.
[6] W. Kwik, A.W.N. Tay, Tetrahedron 9 (1990) 1293.
[7] L. Canali, D.C. Sherrington, Chem. Soc. Rev. 28 (1999) 85.
[8] Y.Z. Voloshin, O.A. Varzatskii, E.Yu. Tkachenko, Y.A. Maletin, S.P. Degtyarov, D.I. Kochubey, Inorg. Chim. Acta 255 (1997) 255.
[9] (a) G. Blondin, J. Girerd, Chem. Rev. 90 (1990) 1359;
(b) D.M. Kurtz, Chem. Rev. 90 (1990) 585;
(c) J. Vincent, G. Olivier, B. Averill, Chem. Rev. 90 (1990) 1447;
(d) S. Lippard, Angew. Chem., Int. Ed. Engl. 27 (1988) 344.
[10] A. Nivorozhkin, P. Mialane, R. Davydov, J. Guilhem, J.J. Girerd, S. Styring, Inorg. Chem. 36 (1997) 846.
[11] V. Paredes-García, Ph.D. Thesis, Universidad de Chile, 2000.
[12] D.H. Heinert, A.T. Martell, J. Am. Chem. Soc. 84 (1962) 3257.
[13] L. Casella, M. Gullotti, A. Pintar, L. Messori, M. Gyór, Inorg. Chem. 26 (1987) 1031.
[14] (a) Y. Maeda, K. Kawano, T. Oniki, J. Chem. Soc., Dalton Trans. (1995) 3533;
(b) A. Earnshaw, Introduction to Magnetochemistry, Academic Press, London, 1968;
(c) B. Snyder, G. Patterson, A. Abrahamson, R.H. Holm, J. Am. Chem. Soc. 111 (1989) 5214.
[15] V. Grillo, R. Hanson, W.H. Trevor, L. Gaham, K. Murray, B. Molubaraki, J. Chem. Soc., Dalton Trans. (1997) 305.
[16] S. Herold, S.J. Lippard, J. Am. Chem. Soc. 119 (1997) 145.
[17] (a) D.P. Goldberg, J. Telser, C.M. Bastos, S.J. Lippard, Inorg. Chem. 34 (1995) 3011;
(b) S. Dutta, R. Werner, S. Mohonta, K. Nag, Inorg. Chem. 35 (1996) 2292.
[18] (a) A. Boudalis, N. Lalioti, G.A. Spyroulias, C.P. Raptopoulou, A. Terzis, V. Tangoulis, J.P. Tuchagues, S. Perlepes, Inorg. Chem. 41 (2002) 6474;
(b) B.T. Weldon, D.E. Wheeler, J.P. Kirby, J.K. McCusker, Inorg. Chem. 40 (2001) 6802.
[19] P. Kopel, M. Biler, Z. Trávnicek, M. Nádvorník, Acta Univ. Palackianae Olomucenesis. Chem. 37 (1998) 17.
[20] C. Wu, S.A. Hunt, P.K. Gantzel, G. Gütlich, D.N. Hendrickson, Inorg. Chem. 36 (1997) 4717.
[21] S. Herold, S.J. Lippard, Inorg. Chem. 36 (1997) 50.
[22] G. Long, Mössbauer Spectroscopy Applied to Inorganic Chemistry, Plenum Press, New York, 1984, p. 43.
[23] L. May, An Introduction to Mössbauer Spectroscopy, Plenum Press, New York, 1971.
[24] V.I. Gol'danskii, R.H. Herber, Chemical Applications of Mössbauer Spectroscopy, Academic Press, New York, 1968.
[25] (a) R. Wu, M. Poyzarz, F. Sowry, Inorg. Chem. 37 (1998) 1913;
(b) P. Poganiuch, S. Liu, G. Papaly, S.J. Lippard, J. Am. Chem. Soc. 113 (1991) 4645.
[26] (a) M. Matsumoto, J. Chem. Soc., Dalton Trans. (1985) 2575;
(b) J.C. Daran, J.C. Daran, Y. Yeami, L.M. Martin, Inorg. Chem. 19 (1980) 2395.
[27] W. Quayle, G. Peeters, G. Deroy, E. Vanssant, J. Lunsford, Inorg. Chem. 21 (1982) 2226.

[28] (a) L.K.F Joop, J. De Vries, E. De Boer, J. Chem. Soc., Dalton Trans. (1974) 1771;
(b) M. Blume, Phys. Rev. Lett. 18 (1967) 305.
[29] C. He, S.J. Lippard, Inorg. Chem 40 (2001) 1414.
[30] A. Neves, M. Brito, I. Vencato, V. Drago, K. Griesar, W. Haase, Inorg. Chem. 35 (1996) 2360.
[31] M. Kodera, H. Shimakoshi, M. Nishimura, H. Okawa, S. Iijima, K. Kano, Inorg. Chem. 35 (1996) 4967.
[32] M.B. Robin, P. Day, Adv. Inorg. Chem. Radiochem. 10 (1967) 247.
[33] B. Carré, J.P. Costes, J.B. Tommasino, D. De Montauzon, F. Soulet, P.L. Fabre, Polyhedron 12 (1993) 641.
[34] K. Kadish, M. Autret, P. Tagliatesta, T. Boschi, V. Fares, Inorg. Chem. 36 (1997) 204.
[35] (a) L. Casella, M. Gullotti, J. Am. Chem. Soc. 103 (1981) 6338;
(b) P. Teyssie, J.J. Charette, Spectrochim. Acta 19 (1963) 1407;
(c) J.E. Kovacic, Spectrochim. Acta 23A (1967) 183.
[36] D. Lee, S.J. Lippard, Inorg. Chem. 41 (2002) 2704.
[37] D. Sattari, E. Alipour, S.J. Shirani, Inorg. Biochem. 45 (1992) 115.
[38] R.C. Burrows, J.C. Bailar, J. Am. Chem. Soc. 88 (1966) 4150.
[39] K. Nakamoto, Infrared and Raman Spectra of Inorganic Coordination Compounds, Wiley, New York, 1986, p. 232.
[40] K. Ramesh, R. Murherjee, J. Chem. Soc., Dalton Trans. (1992) 83.
[41] D. Cook, D. Cummins, E.D. McKenzie, J. Chem. Soc., Dalton Trans. (1976) 1369.
[42] R. Santhi, K.S. Nangajara, R. Udupa, Inorg. Chim. Acta 133 (1987) 211.

Available online at www.sciencedirect.com
SCIENCE DIRECT®
Polyhedron 23 (2004) 1877–1888
POLYHEDRON
www.elsevier.com/locate/poly

Syntheses, structures and fluorescence of three novel 3D coordination polymers $[Cd_3(TMA)_2(H\text{-}PRZ)(H_2O)_3(OH)]\cdot H_2O$, $Cd_2Na_2(TMA)_2(H_2O)_4$ and $[Cd_2Co(TMA)_2(H_2O)_4]\cdot 2H_2O$ (TMA = trimesic acid, PRZ = piperazine) ☆

Jian-Xin Chen [a,b], Shi-Xiong Liu [a,*], En-Qing Gao [c]

[a] Central Laboratory, Fuzhou University, Fuzhou 350002, PR China
[b] College of Chemistry and Materials Science, Fujian Normal University, Fuzhou 350007, PR China
[c] Shanghai Key Laboratory of Green Chemistry and Chemical Processes, East China Normal University, Shanghai 200062, P.R. China

Received 21 March 2004; accepted 31 March 2004
Available online 25 May 2004

Abstract

The hydrothermal reactions of H_3TMA (or Na_3TMA) with metal acetate yield three novel coordination polymers $[Cd_3(TMA)_2(H\text{-}PRZ)(H_2O)_3(OH)]\cdot H_2O$ (**1**), $Cd_2Na_2(TMA)_2(H_2O)_4$ (**2**) and $[Cd_2Co(TMA)_2(H_2O)_4]\cdot 2H_2O$ (**3**) (TMA = trimesic acid, PRZ = piperazine). The three Cd(II) centers in **1** are bridged by TMA ligands and a μ_3-O atom of coordinated hydroxide to generate a sandwich-liked tri-layer motif. These motifs with a Cd_3O core are further interlinked by hydrogen bond interactions to stack in a 3D coordination framework with a porous dimension of ca. 7.5×5.5 Å. Complex **2** is a three-dimensional polymer based on tetranuclear heterometallic clusters. The centrosymmetric tetranuclear heterometallic cluster contains a Cd_2Na_2 parallelogram cluster core. These clusters are connected through the coordination of carboxylate oxygen atoms of TMA ligands to form a 3D coordination framework. Complex **3** represents the first structural characterization of a trimesate complex containing two different transitional metals. Each TMA^{3-} ligand in the $Cd_2Co(C_9H_3O_6)_2(H_2O)_4$ structure unit of **3** binds to other three structure units, resulting in a 3D coordination polymer. The three complexes exhibit strong fluorescent emission bands at 420 nm (λ_{ex} = 314 nm) for complex **1**, 424 nm (λ_{ex} = 314 nm) for complex **2**, and 419 nm (λ_{ex} = 308 nm) for complex **3** in the solid state at room temperature. The preliminary magnetic property of complex **3** has been investigated.
© 2004 Elsevier Ltd. All rights reserved.

Keywords: Supramolecular chemistry; Self-assembly; Polymers; Transition metal; Crystal engineering

1. Introduction

The construction of inorganic coordination polymers with unusual electrical, magnetic, optical and catalytic properties is currently considered as one of the most important issues [1–3]. Hydrogen bonding and coordinative metal–ligand interactions are two principal methods for the construction of extended structural coordination polymer solids. The assembly of a wide variety of 1D, 2D and 3D extended porous metal–organic supramolecular polymers exhibiting unusual ion exchange, neutral guest exchange and selective adsorptive behavior from hydrogen bonding interactions has still to reach a new level as a hot subject [4], and yet the construction of extended metal–organic architectures from metal–ligand interactions has been widely studied. For example, some very interesting functional coordination solids with cyclic or porous structures based on metal ions and bridging ligands containing N-donors have been prepared [5–7]. Another approach to novel porous networks involves the reaction

☆ Supplementary data associated with this article can be found, in the online version, at doi:10.1016/j.poly.2004.04.018.

* Corresponding author. Tel./fax: +86-591-3729860.
E-mail address: shixiongliu@yahoo.com (S.-X. Liu).

0277-5387/$ - see front matter © 2004 Elsevier Ltd. All rights reserved.
doi:10.1016/j.poly.2004.04.018

of organic ligands containing O-donors such as multicarboxylates with alkaline earths or transition metal ions under hydrothermal conditions [8]. As a building block to construct some porous or cyclic coordination polymer, the trimesic acid (H_3TMA) ligand exhibits a variety of coordination fashions and holds the capability of generating coordination architectures of diverse sizes and shapes. Although there have been a lot of reports [9–14] on infinite 1D, 2D and 3D coordination polymers assembled by trimesate, however, so far as we know, most of them contain a single metal atom, whereas those constructed by two different metal atoms and TMA ligands are very rare, with the reported compound [NaCu-$TMA(H_2O)_4]\cdot 2H_2O$ [10b]. In this paper, we report three novel compounds of metal-trimesate $[Cd_3(TMA)_2(H\text{-}PRZ)(H_2O)_3(OH)]\cdot H_2O$ (**1**), $Cd_2Na_2(TMA)_2(H_2O)_4$ (**2**)

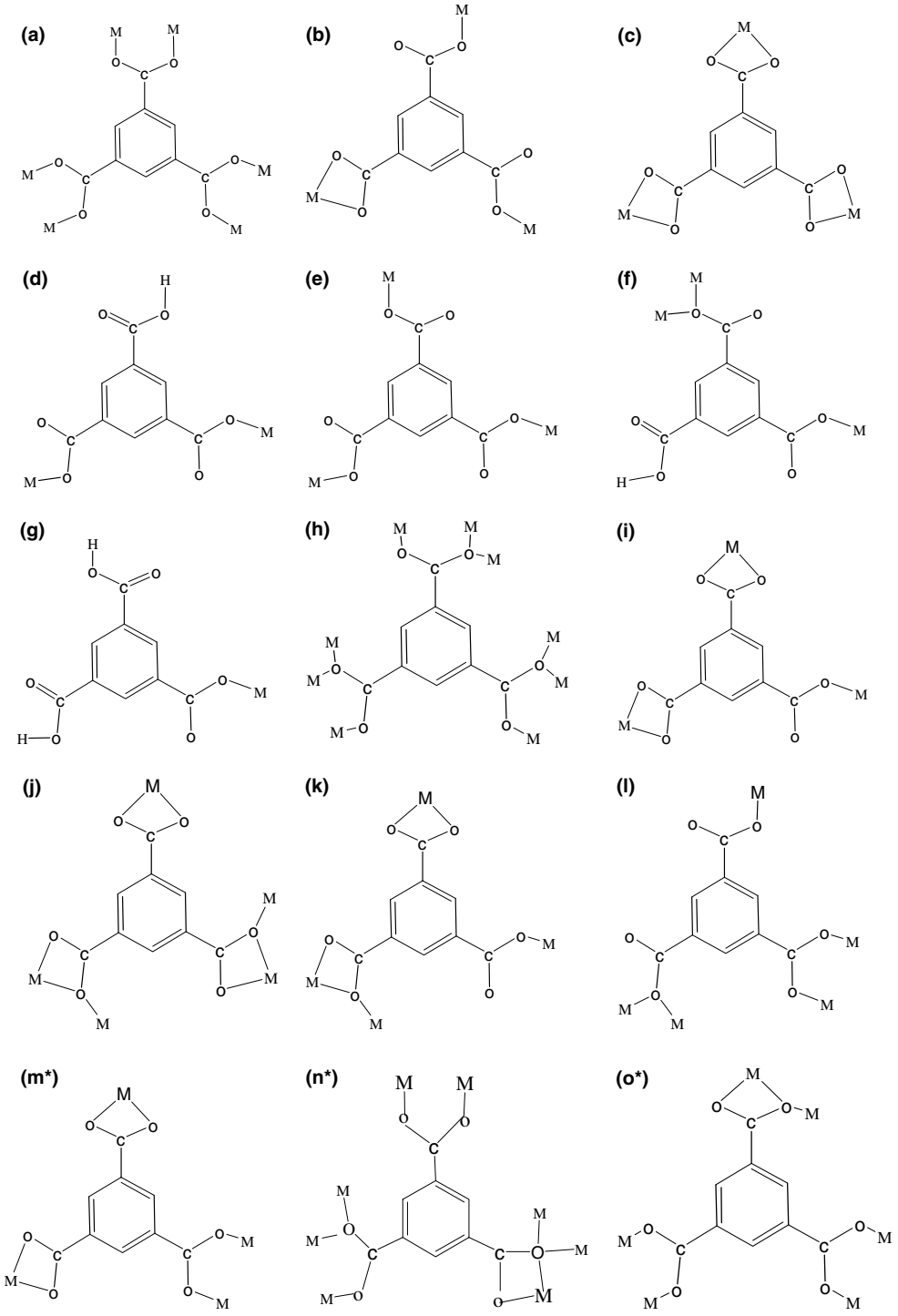

Fig. 1. Coordination fashions of TMA (*discovered first in this work).

Table 1
Summary of crystallographic data for $[Cd_3(TMA)_2(H\text{-}PRZ)(H_2O)_3(OH)]\cdot H_2O$ (**1**), $Cd_2Na_2(TMA)_2(H_2O)_4$ (**2**) and $[Cd_2Co(TMA)_2(H_2O)_4]\cdot 2H_2O$ (**3**)

	1	**2**	**3**
Formula	$C_{22}H_{26}N_2O_{17}Cd_3$	$C_{18}H_{14}O_{16}Cd_2Na_2$	$C_{18}H_{18}O_{18}Cd_2Co$
Formula weight	927.65	757.07	806.05
Crystal system	orthorhombic	triclinic	monoclinic
Space group	*Pbca*	$P\bar{1}$	$C2/c$
a (Å)	16.6518(4)	7.8484(4)	19.4353(12)
b (Å)	14.0862(5)	8.7280(3)	7.1029(3)
c (Å)	22.7124(4)	8.9316(4)	18.0458(10)
α (°)	90	68.485(3)	90
β (°)	90	73.048(2)	118.030(2)
γ (°)	90	70.509(2)	90
V (Å^3)	5327.4(2)	526.49(4)	2199.0(2)
Z	8	1	4
D_{calc} (Mg m^{-3})	2.313	2.388	2.435
Crystal size (mm)	0.15×0.15×0.08	0.35×0.20×0.14	0.25×0.15×0.04
μ (mm^{-1})	2.463	2.152	2.760
$F(000)$	3616	368	1572
θ_{max}, θ_{min} (°)	27.48, 1.79	27.48, 2.5	27.48, 2.37
Index range			
h	$0\rightarrow 21$	$-10\rightarrow 9$	$-25\rightarrow 0$
k	$0\rightarrow 18$	$-11\rightarrow 0$	$-9\rightarrow 0$
l	$-29\rightarrow 0$	$-11\rightarrow 10$	$-20\rightarrow 23$
R_{int}	0.0381	0.0177	0.0342
Number of independent reflections	6019	2383	2528
Number of observed reflections	4281	2333	2186
Number of variables	409	177	183
R_1[a]	0.0209	0.0170	0.0221
wR^2[b]	0.0419	0.0438	0.0525
Goodness-of-fit	0.918	1.145	0.995
Largest difference peak and hole[c] (e Å^{-3})	0.520 and −0.554	0.558 and −0.704	0.828 and −0.703
Δ/σ	0.002/0.000	0.001/0.000	0.001/0.000

[a] $R_1 = \sum ||F_o| - |F_c|| / \sum |F_o|$.
[b] $wR = \{\sum[w(F_o^2 - F_c^2)^2]/[\sum w(F_o^2)^2]\}^{1/2}$, $w = [\sigma^2(F_o^2) + (Ap)^2 + BP]^{-1}$, $P = (F_o^2 + 2F_c^2)/3$.
[c] Largest peak (hole) in difference Fourier map.

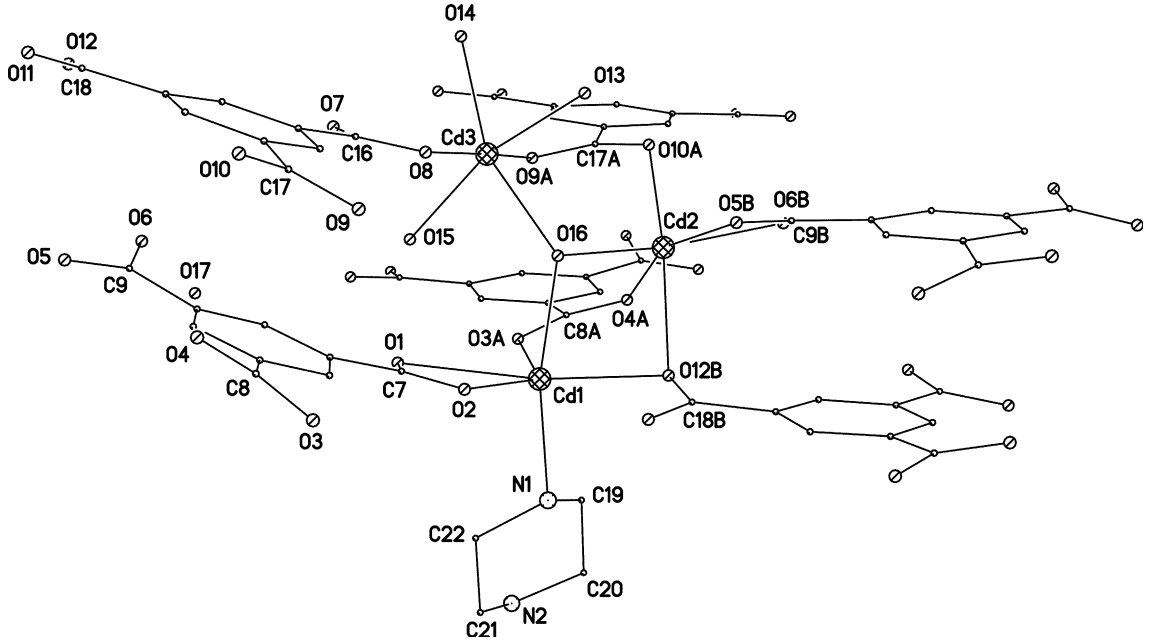

Fig. 2. The coordination environments of the cadmium atoms in **1**. Symmetry codes: A, $x-1/2, y, 1/2-z$; B, $x, 3/2-y, z-1/2$.

Table 2
Selected bond lengths (Å) and angles (°) for **1**

Bond lengths			
Cd(1)–O(16)	2.263(3)	Cd(1)–N(1)	2.330(4)
Cd(1)–O(2)	2.332(3)	Cd(1)–O(12B)	2.346(3)
Cd(1)–O(3A)	2.410(3)	Cd(1)–O(1)	2.566(3)
Cd(2)–O(16)	2.203(3)	Cd(2)–O(6B)	2.232(3)
Cd(2)–O(10A)	2.270(3)	Cd(2)–O(4A)	2.279(3)
Cd(2)–O(12B)	2.383(3)	Cd(2)–O(5B)	2.536(3)
Cd(3)–O(8)	2.204(3)	Cd(3)–O(9A)	2.244(3)
Cd(3)–O(16)	2.303(3)	Cd(3)–O(14)	2.310(3)
Cd(3)–O(13)	2.387(4)	Cd(3)–O(15)	2.393(3)
Cd(1)···Cd(2)	3.3629(4)	Cd(2)···Cd(3)	3.6612(4)
Cd(1)··· Cd(3)	4.1762(5)		
Bond angles			
O(16)–Cd(1)–N(1)	165.6(1)	O(16)–Cd(1)–O(2)	90.9 (1)
N(1)–Cd(1)–O(2)	102.5(1)	O(16)–Cd(1)–O(12B)	81.1(1)
N(1)–Cd(1)–O(12B)	86.4(1)	O(2)–Cd(1)–O(12B)	129.0(1)
O(16)–Cd(1)–O(3A)	82.8(1)	N(1)–Cd(1)–O(3A)	91.2(1)
O(2)–Cd(1)–O(3A)	134.5(1)	O(12B)–Cd(1)–O(3A)	94.6(1)
O(16)–Cd(1)–O(1)	91.2(1)	N(1)–Cd(1)–O(1)	101.0(1)
O(2)–Cd(1)–O(1)	53.1(1)	O(12B)–Cd(1)–O(1)	171.9(1)
O(3A)–Cd(1)–O(1)	82.0(1)	O(16)–Cd(2)–O(6B)	145.5(1)
O(16)–Cd(2)–O(10A)	102.6(1)	O(6B)–Cd(2)–O(10A)	88.9(1)
O(16)–Cd(2)–O(4A)	98.2(1)	O(6B)–Cd(2)–O(4A)	115.6(1)
O(10A)–Cd(2)–O(4A)	83.7(1)	O(16)–Cd(2)–O(12B)	81.6(1)
O(6B)–Cd(2)–O(12B)	98.1(1)	O(10A)–Cd(2)–O(12B)	161.2(1)
O(4A)–Cd(2)–O(12B)	77.6(1)	O(16)–Cd(2)–O(5B)	90.9(1)
O(6B)–Cd(2)–O(5B)	54.7(1)	O(10A)–Cd(2)–O(5B)	110.9(1)
O(4A)–Cd(2)–O(5B)	160.9(1)	O(12B)–Cd(2)–O(5B)	87.2(1)
O(8)–Cd(3)–O(9A)	173.3(1)	O(9A)–Cd(3)–O(16)	91.3(1)
O(8)–Cd(3)–O(16)	91.8(1)	O(9A)–Cd(3)–O(14)	79.4(1)
O(8)–Cd(3)–O(14)	99.3(1)	O(8)–Cd(3)–O(13)	83.3(1)
O(16)–Cd(3)–O(14)	158.5(1)	O(16)–Cd(3)–O(13)	79.0(1)
O(9A)–Cd(3)–O(13)	103.3(1)	O(8)–Cd(3)–O(15)	97.4(1)
O(14)–Cd(3)–O(13)	84.0(2)	O(16)–Cd(3)–O(15)	86.5(1)
O(9A)–Cd(3)–O(15)	76.7(1)	O(13)–Cd(3)–O(15)	165.5(1)
O(14)–Cd(3)–O(15)	109.9(1)	Cd(3)–O(16)–Cd(2)	108.7(1)
Cd(1)–O(16)–Cd(3)	132.3(1)	Cd(3)···Cd(1)···Cd(2)	56.9(0)
Cd(2)–O(16)–Cd(1)	97.7(1)	Cd(1)···Cd(2)···Cd(3)	72.8(0)

Symmetry codes: A, $x-1/2, y, -z+1/2$; B, $x, -y+3/2, z-1/2$.

and $[Cd_2Co(TMA)_2(H_2O)_4]\cdot 2H_2O$ (**3**), measuring their strong fluorescence emissions in the solid state at room temperature, based on diverse coordination architectures.

2. Experimental

2.1. Materials

All analytical grade chemicals and solvents were purchased commercially and used without further purification.

2.2. Preparations

2.2.1. Na_3TMA

Na_3TMA was synthesized according to the chemical reaction equation: $H_3TMA + 3NaOH \rightarrow Na_3TMA + 3H_2O$.

2.2.2. $[Cd_3(TMA)_2(H\text{-}PRZ)(H_2O)_3(OH)]\cdot H_2O$ (**1**)

0.134 g (0.502 mmol) cadmium(II) acetate dihydrate, 0.106 g H_3TMA (0.504 mmol), 0.0493 g (0.254 mmol) piperazine hexahydrate ($C_4H_{10}N_2\cdot 6H_2O$) and 12 ml water were loaded into a 23 cm^3 Teflon-lined stainless-steel vessel, which was then sealed and placed in a programmable furnace. The resulting mixture was heated at 100 °C h^{-1} to 160 °C and held at that temperature for 10 h, then cooled to 140 °C at 4 °C h^{-1} and held for 5 h, followed by further cooling at the same rate to room temperature to give a 44.67% yield of **1** (0.207 g) based on Cd, as primrose yellow crystals which were collected by mechanical isolation and washed with water (3 × 10 ml) and absolute alcohol (3 × 10 ml), then dried at 40 °C. *Anal.* Calc. for $Cd_3C_{22}H_{26}N_2O_{17}$, $[Cd_3(TMA)_2(H\text{-}PRZ)(H_2O)_3(OH)]\cdot H_2O$: C, 28.47; H, 2.80; N, 3.02; O, 29.34. Found: C, 28.21; H, 2.85; N, 3.12; O, 29.45%. FT-IR (KBr pellet, 4000–400 cm^{-1}): 3380(vs, br), 3244(vs, sh), 2364(m), 1612(vs, sh), 1561(vs, sh),

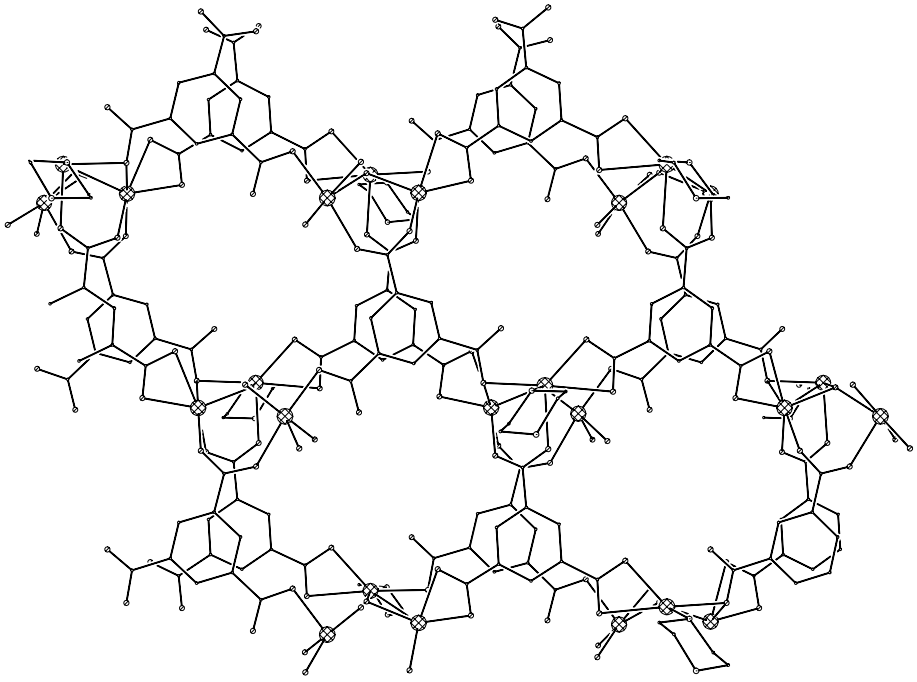

Fig. 3. The 3D porous structure of **1** along the *b*-axis. All hydrogen atoms are omitted for clarity.

1438(vs, sh), 1366(vs), 1204(w), 1103(w), 1094(m), 1027(vw), 997(w), 936(vw), 874(w), 813(vw),762(s), 725(vs), 626(m), 526(m), 459(m), 414(m), 409(m), 403(m).

2.2.3. $[Cd_2Na_2(TMA)_2(H_2O)_4]$ (**2**)

0.134 g (0.502 mmol) cadmium(II) acetate dihydrate, 0.139 g Na_3TMA (0.504 mmol) and 12 ml water were loaded into a 23 cm^3 Teflon-lined stainless-steel vessel, which was then sealed and placed in a programmable furnace. The resulting mixture was heated at a rate of ca. 100 °C h^{-1} to 160 °C and held at that temperature for 8 h, then cooled to 140 °C at 3 °C h^{-1} and held for four days, followed by further cooling at the same rate to room temperature to give a 34.84% yield of **2** based on Cd, as colorless crystals which were collected by mechanical isolation and washed with water (3×10 ml) and absolute alcohol (3×10 ml), then dried at 40 °C. *Anal.* Calc. for $Cd_2Na_2C_{18}H_{14}O_{16}$, $[Cd_2Na_2(TMA)_2(H_2O)_4]$: C, 28.53; H, 1.86; O, 33.81. Found: C, 28.69; H, 1.92; O, 33.55%. FT-IR (KBr pellet, 4000–400 cm^{-1}): 3442(s,br), 3080(s), 2355(m), 1872(w), 1611(vs, sh), 1556(vs, br), 1438(vs), 1368(vs, br), 1205(m), 1104(m), 934(m), 768(m), 726(vs, sh), 671(m), 560(m), 518(m), 469(m), 448(m), 407(m).

2.2.4. $[Cd_2Co(TMA)_2(H_2O)_4]\cdot 2H_2O$ (**3**)

0.134 g (0.502 mmol) cadmium(II) acetate dihydrate, 0.063 g (0.250 mmol) cobalt(II) acetate tetrahydrate, 0.106 g H_3TMA (0.504 mmol), 1 ml pyridine and 12 ml water were loaded into a 23 cm^3 Teflon-lined stainless-steel vessel, which was then sealed and placed in a programmable furnace. The resulting mixture was heated at a rate of ca. 100 °C h^{-1} to 140 °C and held at that temperature for three days, then cooled to room temperature at a rate of ca. 3 °C h^{-1} to give a 24.14% yield of **3** based on Cd, as pink crystals which were mechanically separated from the reaction mixture of a white solid, and washed with water (3×10 ml) and absolute alcohol (3×10 ml), then dried at 40 °C. *Anal.* Calc. for $Cd_2CoC_{18}H_{18}O_{18}$, $[Cd_2Co(TMA)_2(H_2O)_4]\cdot 2H_2O$: C, 26.58; H, 2.22; O, 35.45. Found: C, 26.20; H, 2.54; O, 35.50%. FT-IR (KBr pellet, 4000–400 cm^{-1}): 3614(s), 3414(vs, br), 3103(s), 2926(m), 2380(w), 1885(vw), 1619(vs, sh), 1541(vs, br), 1435(vs, sh),

Table 3
Hydrogen-bonding geometry (Å, °) in complex **1**

D–H···A	D–H	D···A	D–H···A
O13–H13B···O2#1	0.843	2.753(5)	163.26
O13–H13C···O11#2	0.968	2.791(5)	136.67
O14–H14B···O1#7	0.889	2.836(5)	139.90
O14–H14C···O3#1	0.953	2.795(5)	148.98
O15–H15B···O1	0.970	2.738(4)	152.91
O15–H15C···O3#3	0.903	2.858(4)	151.94
O17–H17B···O6#4	0.993	2.770(5)	152.43
O17–H17C···O10#5	0.850	2.824(6)	172.32
N1–HN1···O5#6	0.888	3.255(6)	154.85
N2–HN3···O17	0.983	2.708(5)	156.52
N2–HN2···O7#4	0.851	2.939(5)	170.95
N2–HN2···O15#4	0.851	2.950(5)	110.63

Symmetry codes: #1, $-x+1/2, y+1/2, z$; #2, $-x+1/2, -y+2, z-1/2$; #3, $x-1/2, y, -z+1/2$; #4, $-x, y-1/2, -z+1/2$; #5, $x-1/2, y-1, -z+1/2$; #6, $-x+1/2, -y+1, z-1/2$; #7, $-x, y+1/2, -z+1/2$.

Table 4
Selected bond lengths (Å) and angles (°) for **2**

Bond lengths			
Cd(1)–O(2)	2.227(2)	Cd(1)–O(6I)	2.263(1)
Cd(1)–O(4H)	2.296(2)	Cd(1)–O(5E)	2.400(2)
Cd(1)–O(3C)	2.418(2)	Cd(1)–O(3H)	2.581(2)
Na(1)–O(1)	2.372(2)	Na(1)–O(3C)	2.377(2)
Na(1)–O(7)	2.422(2)	Na(1)–O(6G)	2.439(2)
Na(1)–O(7F)	2.490(2)	Na(1)–O(8)	2.545(2)
O(2)–C(7)	1.271(3)	O(1)–C(7)	1.245(3)
O(3)–C(8)	1.276(2)	O(4)–C(8)	1.246(3)
O(5)–C(9)	1.258(2)	O(6)–C(9)	1.264(3)
Cd(1)···Na(1)	3.826(1)	Cd(1)···Na(1A)	3.642(1)
Bond angles			
O(2)–Cd(1)–O(6I)	123.83(6)	O(2)–Cd(1)–O(4H)	111.01(6)
O(2)–Cd(1)–O(5E)	87.23(5)	O(2)–Cd(1)–O(3C)	90.43(6)
O(2)–Cd(1)–O(3H)	151.97(6)	O(6I)–Cd(1)–O(4H)	124.93(6)
O(6I)–Cd(1)–O(5E)	92.18(5)	O(6I)–Cd(1)–O(3C)	83.22(5)
O(6I)–Cd(1)–O(3H)	77.57(5)	O(4H)–Cd(1)–O(5E)	85.28(5)
O(4H)–Cd(1)–O(3C)	102.20(5)	O(4H)–Cd(1)–O(3H)	53.39(5)
O(5E)–Cd(1)–O(3C)	172.51(5)	O(5E)–Cd(1)–O(3H)	111.72(5)
O(3C)–Cd(1)–O(3H)	73.13(5)	O(1)–Na(1)–O(3C)	85.95(6)
O(1)–Na(1)–O(7)	173.57(7)	O(1)–Na(1)–O(6G)	100.34(6)
O(1)–Na(1)–O(7F)	91.96(6)	O(1)–Na(1)–O(8)	73.12(7)
O(3C)–Na(1)–O(7)	89.35(6)	O(3C)–Na(1)–O(6G)	78.41(5)
O(3C)–Na(1)–O(7F)	99.76(6)	O(3C)–Na(1)–O(8)	155.66(7)
O(7)–Na(1)–O(6G)	82.96(6)	O(7)–Na(1)–O(7F)	84.52(6)
O(7)–Na(1)–O(8)	110.43(7)	O(6G)–Na(1)–O(7F)	167.36(7)
O(6G)–Na(1)–O(8)	116.88(7)	O(7F)–Na(1)–O(8)	69.41(7)
Na(1A)···Cd(1)···Na(1)	114.99(2)	Cd(1A)···Na(1)···Cd(1)	65.01(2)

Symmetry codes: A, $-x, -y+2, -z$; C, $-x+1, -y+1, -z$; E, $-x+1, -y+1, -z+1$; F, $-x, -y+1, -z$; G, $-x, -y+1, -z+1$; H, $x-1, y+1, z$; I, $x, y+1, z-1$.

1365(vs, sh), 1206(w), 1108(w), 942(vw), 829(w, sh), 809(w, sh), 772(m), 736(s, sh), 725(s, sh), 587(m, br), 537(m), 452(m), 426(w), 406(w).

2.3. Physical measurements

Infrared spectra were measured on a Perkin–Elmer FT-IR 2000 spectrometer using KBr pellets in the 4000–400 cm^{-1} region. Elemental analyses were carried out by an EA1112 CHNS elemental analyzer. Fluorescent data were collected on an Edinburgh FL-FS920 TCSPC system, thermal gravimetric analysis (TGA) was tested under nitrogen with a heating rate of 10 °C min^{-1} using a Perkin–Elmer TGA-7 Thermal Analysis system. The magnetic susceptibility was measured on a SQUID magnetometer.

2.4. Crystal structure determination

Crystals of a suitable size for the three title compounds were mounted on glass fibers. Intensity data were collected with graphite-monochromated Mo Kα radiation ($\lambda = 0.71073$ Å) and the ω scan mode, using a Rigaku R-AXIS RAPID Weissengberg IP diffractometer. The structures were solved by direct methods using SHELXS-97 [15] and refined by full-matrix least-squares calculations with SHELXL-97 [16]. All non-hydrogen atoms in the three title complexes were refined with anisotropic thermal parameters. Most of the hydrogen atoms in the three complexes were located in calculated positions or found from difference Fourier maps.

3. Results and discussion

3.1. A summary of coordination fashions for the TMA ligand

As mentioned above, TMA has a great ability to construct different coordination frameworks with metal ions using various coordination fashions. We now summarized fifteen coordination models in Fig. 1, three (Fig. 1, M–O) of which are discovered first in this work. It is noticeable that one carboxylic group of TMA contains a bridging μ_3-O atom in coordination pattern N.

3.2. Structures

The crystallographic data of complexes **1**, **2** and **3** are given in Table 1.

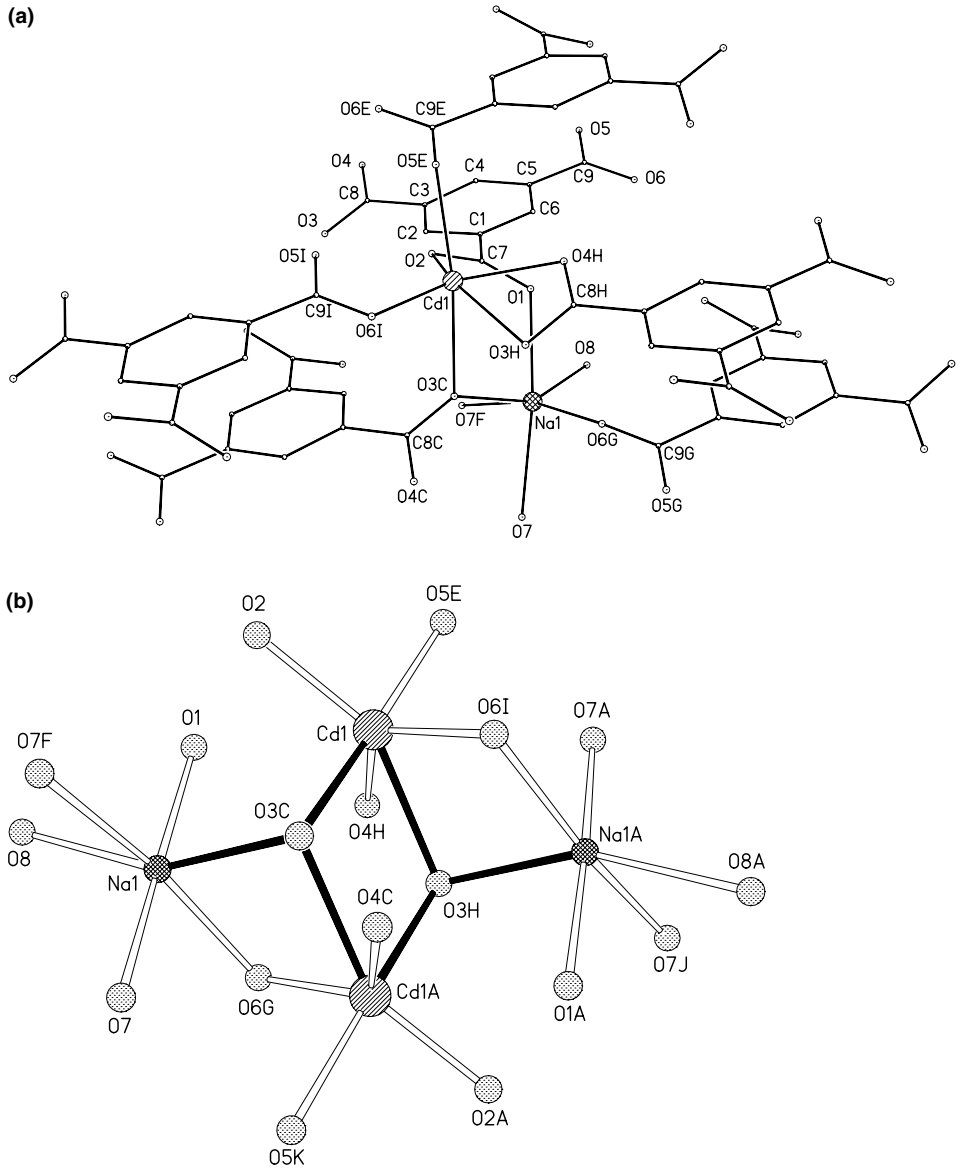

Fig. 4. (a) The local coordination environments of Cd1 and Na1 in **2**. Symmetry codes: C, $-x+1,-y+1,-z$; E, $-x+1,-y+1,-z+1$; F, $-x,-y+1,-z$; G, $-x,-y+1,-z+1$; H, $x-1,y+1,z$; I, $x,y+1,z-1$. (b) The Cd_2Na_2 core in the tetranuclear cluster unit. Symmetry codes: A, $-x,-y+2,-z$; C, $-x+1,-y+1,-z$; E, $-x+1,-y+1,-z+1$; F, $-x,-y+1,-z$; G, $-x,-y+1,-z+1$; H, $x-1,y+1,z$; I, $x,y+1,z-1$; J, $x,y+1,z$; K, $x-1,y-1,z-1$.

3.2.1. $[Cd_3(TMA)_2(H\text{-}PRZ)(H_2O)_3(OH)]\cdot H_2O$ (1)

As shown in Fig. 1, L and M, the TMA ligand has two coordination fashions in complex **1**. In one fashion (Fig. 1, L), the three carboxylate groups of the TMA ligand bind to metal ions adopting unidentate, bidentate and bridging unidentate patterns. In the other fashion (Fig. 1, M), the three carboxylate groups of the TMA ligand link to metal ions using bidentate and chelating bis-bidentate forms. The local coordination environment of the three Cd(II) centers is described in Fig. 2. The trinuclear Cd_3O core, which is constructed by three Cd(II) centers and a capped μ_3-O atom (O16 from a coordinated hydroxide ion), fabricates the principal architecture of complex **1**. Selected bond lengths and bond angles are listed in Table 2. Bond lengths of Cd1–O16, Cd2–O16 and Cd3–O16 are 2.263(3), 2.203(3) and 2.303(3) Å, respectively; and distances of Cd···Cd separation are 3.3629(4) Å (Cd1···Cd2), 3.6612(4) Å (Cd2···Cd3) and 4.1762(5) Å (Cd1···Cd3). The bond angles of Cd1–O16–Cd3, Cd3–O16–Cd2, Cd2–O16–Cd1 and the interatomic angles of Cd3···Cd1···Cd2 and Cd1···Cd2···Cd3 are 132.3(1)°, 108.7(1)°, 97.7(1)°, 56.9(0)° and 72.8(0)°, respectively.

The Cd1 atom is coordinated by four oxygen atoms (O1, O2, O3A, O12B), a capped μ_3-O atom (O16) and a nitrogen atom (N1) from a PRZ molecule, forming a distorted octahedral geometry. The O1 and O2 atoms come from a chelating bidentate carboxylate group

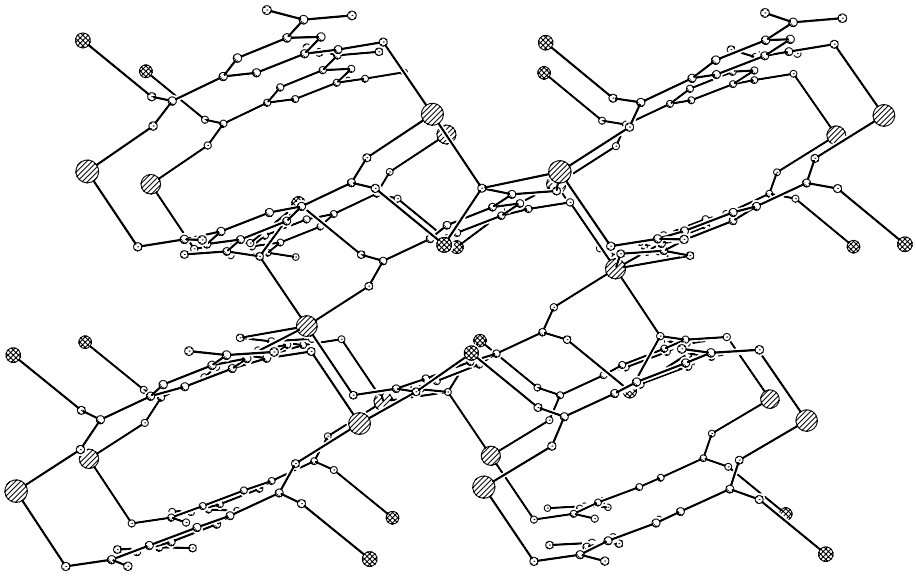

Fig. 5. The 3D structure of compound **2**. All the hydrogen atoms and coordinated water molecules on the Na atoms are omitted for clarity.

(Fig. 1, M) of the first TMA ligand; O3A atom comes from a bidentate carboxylate group (Fig. 1, M) of the second TMA ligand; whereas the atom O12B comes from the bridging unidentate carboxylate group (Fig. 1, L) of the third TMA ligand. Similar to Cd1, besides being coordinated by the capped unitary μ_3-O atom (O16), the six-coordinated Cd2 atom is coordinated by three oxygen atoms [O4A and (O5B, O6B)], which come from two different bidentate and chelating bidentate carboxylate groups (Fig. 1, M) of two separate TMA ligands; meanwhile, it is bound to two oxygen atoms (O10A and O12B) from two diverse bidentate and bridging unidentate carboxylate groups (Fig. 1, L) of two separate TMA ligands. The Cd3 atom is also six-coordinated by the capped unitary μ_3-O atom (O16), three terminal coordinated water molecules (O13, O14 and O15), as well as two oxygen atoms (O8 and O9A) from two different unidentate and bidentate carboxylate groups (Fig. 1, L) of two

Table 5
Hydrogen-bonding geometry (Å, °) in **2**

D–H···A	D–H	D···A	D–H···A
O(7)–H(7A)···O(8)#1	0.869	2.867(5)	124.0
O(7)–H(7A)···O(5)#2	0.869	2.979(6)	118.0
O(7)–H(7B)···O(2)#3	0.868	2.857(6)	167.9
O(8)–H(8A)···O(1)#4	0.755	2.939(5)	118.1
O(8)–H(8B)···O(1)	0.819	2.932(6)	128.9

Symmetry codes: #1, $-x,-y+1,-z$; #2, $x-1,y+1,z-1$; #3, $x-1,y,z$; #4, $-x,-y+1,-z+1$.

Table 6
Selected bond lengths (Å) and angles (°) for **3**

Bond lengths			
Cd(1)–O(4B)	2.223(2)	Cd(1)–O(5C)	2.232 (2)
Cd(1)–O(2)	2.328(2)	Cd(1)–O(3A)	2.338(2)
Cd(1)–O(6D)	2.338(2)	Cd(1)–O(1)	2.618(2)
Co(1)–O(8)	2.049(2)	Co(1)–O(1)	2.133(2)
Co(1)–O(7)	2.134(2)		
Bond angles			
O(4B)–Cd(1)–O(5C)	138.59(6)	O(4B)–Cd(1)–O(2)	82.06(6)
O(4B)–Cd(1)–O(3A)	104.79(7)	O(4B)–Cd(1)–O(6D)	85.98(7)
O(4B)–Cd(1)–O(1)	132.14(6)	O(5C)–Cd(1)–O(2)	139.20(6)
O(5C)–Cd(1)–O(3A)	82.85(6)	O(5C)–Cd(1)–O(6D)	92.01(6)
O(5C)–Cd(1)–O(1)	88.76(6)	O(2)–Cd(1)–O(3A)	82.20(6)
O(2)–Cd(1)–O(6D)	95.23(6)	O(2)–Cd(1)–O(1)	52.00(5)
O(3A)–Cd(1)–O(6D)	168.43(6)	O(3A)–Cd(1)–O(1)	83.78(6)
O(6D)–Cd(1)–O(1)	85.77(5)	O(8)–Co(1)–O(1)	92.17(7)
O(8)–Co(1)–O(7)	88.06(8)	O(8)–Co(1)–O(1A)	93.19(7)
O(8)–Co(1)–O(7A)	86.75(8)	O(8)–Co(1)–O(8A)	172.3(1)
O(1)–Co(1)–O(7)	86.46(7)	O(1)–Co(1)–O(1A)	91.90(9)
O(1)–Co(1)–O(7A)	177.97(8)	O(7)–Co(1)–O(7A)	95.2(1)

Symmetry codes: A, $-x+1,y,-z+1/2$; B, $x-1/2,-y+1/2,z-1/2$; C, $x-1/2,y+1/2,z$; D, $-x+1,-y+1,-z$.

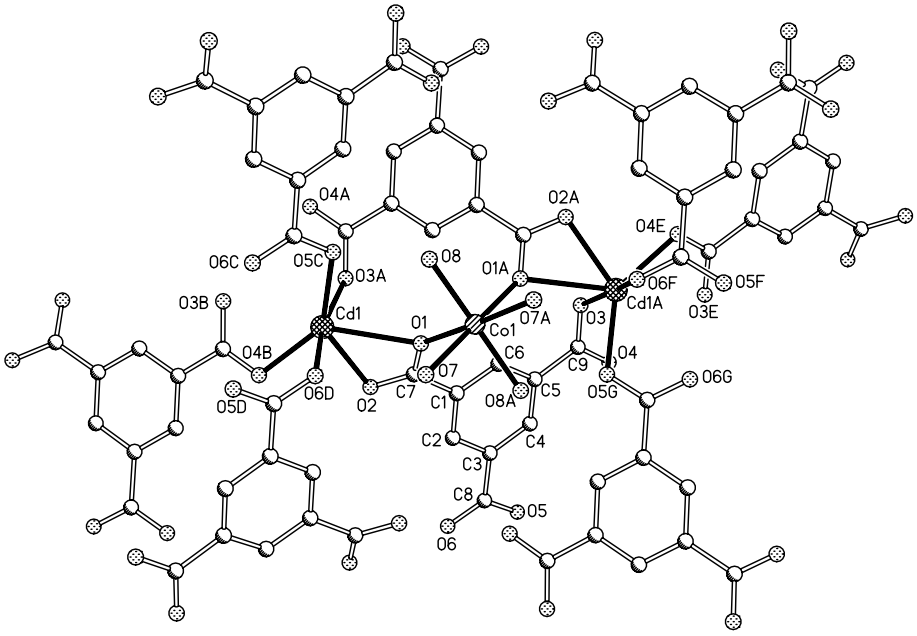

Fig. 6. The local coordination environments of Cd1 and Co1 in **3**. Symmetry codes: A, $-x+1, y, -z+1/2$; B, $x-1/2, -y+1/2, z-1/2$; C, $x-1/2, y+1/2, z$; D, $-x+1, -y+1, -z$; E, $3/2-x, 1/2-y, 1-z$; F, $x, -y, 1/2+z$; G, $3/2-x, y-1/2, 1/2-z$.

separate TMA ligands. The non-coordinated nitrogen atom (N2) of piperazine is protonated. The rudimental building block of compound **1** is constructed by two TMA ligands with two diverse coordination fashions, three Cd(II) centers, a protonated PRZ molecule as well as a capped unitary μ_3-O atom (from an hydroxide ion). As shown in Fig. 3, the rudimental building blocks are interlinked along the *ac*-plane to yield a sandwich-like tri-layer molecular motif subunit with a porous dimension of ca. 7.5×5.5 Å (based on nuclei separation). These independent 2D sandwich-like sheet subunits are further interconnected by hydrogen bond interactions (Table 3) between layers to stack in a 3D coordination framework.

3.2.2. $Cd_2Na_2(TMA)_2(H_2O)_4$ (**2**)

Complex **2** is a three-dimensional polymer based on tetranuclear heterometallic clusters. Selected bond lengths and angles in **2** are listed in Table 4.

The coordination fashion of the TMA ligand in **2** is depicted in Fig. 1, N, where the TMA ligand possesses three different carboxylate groups of bidentate, bridging bidentate and chelating/bridging bidentate bonding modes. Different from complex **1**, complex **2** contains two diverse metal ions [Cd(II) and Na(I)], which is rare in all coordination polymers of TMA [10b]. Fig. 4(a) reveals the local coordination environment around the Na(I) and Cd(II) centers. The metal atoms (Cd1 and Na1) are in distorted octahedral geometry. The Na1 atom is coordinated by six oxygen atoms (O1, O3C, O6G, O7, O7F and O8), three of which (O1, O3C and O6G) come from a bidentate carboxylate group, a chelating/bridging bidentate carboxylate group and a bridging bidentate carboxylate group (Fig. 1, N) of three separate TMA ligands, respectively; the remaining oxygen atoms (O7, O7F and O8) come from three terminal water molecules. The Cd1 atom is coordinated by six oxygen atoms (O2, O3C, O3H, O4H, O5E and O6I), of which atom O2 comes from a bidentate carboxylate group of TMA; O3C, O3H and O4H come from two chelating/bridging bidentate carboxylate groups of two separate TMA ligands; whereas the O5E and O6I atoms come from two bridging bidentate carboxylate groups of two separate TMA ligands.

The tetranuclear heterometallic cluster in complex **2** and its parallelogram Cd_2Na_2 cluster core are shown in Fig. 4(b). The centrosymmetric tetranuclear cluster is constructed from two Cd atoms (Cd1 and Cd1A, symmetry code A: $-x, -y+2, -z$), two Na atoms (Na1 and Na1A), eight TMA ligands and four-coordinated water molecules. Two longer Cd–Na edges of 3.826(1) Å (Cd1–Na1 and Cd1A–Na1A) and two shorter Cd–Na edges of 3.642(1) Å (Cd1–Na1A and Cd1A–Na1) construct a parallelogram Cd_2Na_2 cluster core, angles of Na1A–Cd1–Na1 and Cd1–Na1–Cd1A being 114.99(2)° and 65.01(2)°, respectively. The symmetrical center $(0, 1, 0)$ is between the two Cd atoms and between the two Na atoms in the tetranuclear cluster Cd_2Na_2 core. There are two μ_3-O atoms from carboxylate groups (O3C and O3H) in the cluster core. These tetranuclear heterometallic clusters are connected through the coordination of carboxylate oxygen atoms of TMA ligands, forming a 3D polymer (Fig. 5). A 3D polymer based on tetranuclear heterometallic clusters is rarely found in all known coordination polymers of TMA complexes [10b].

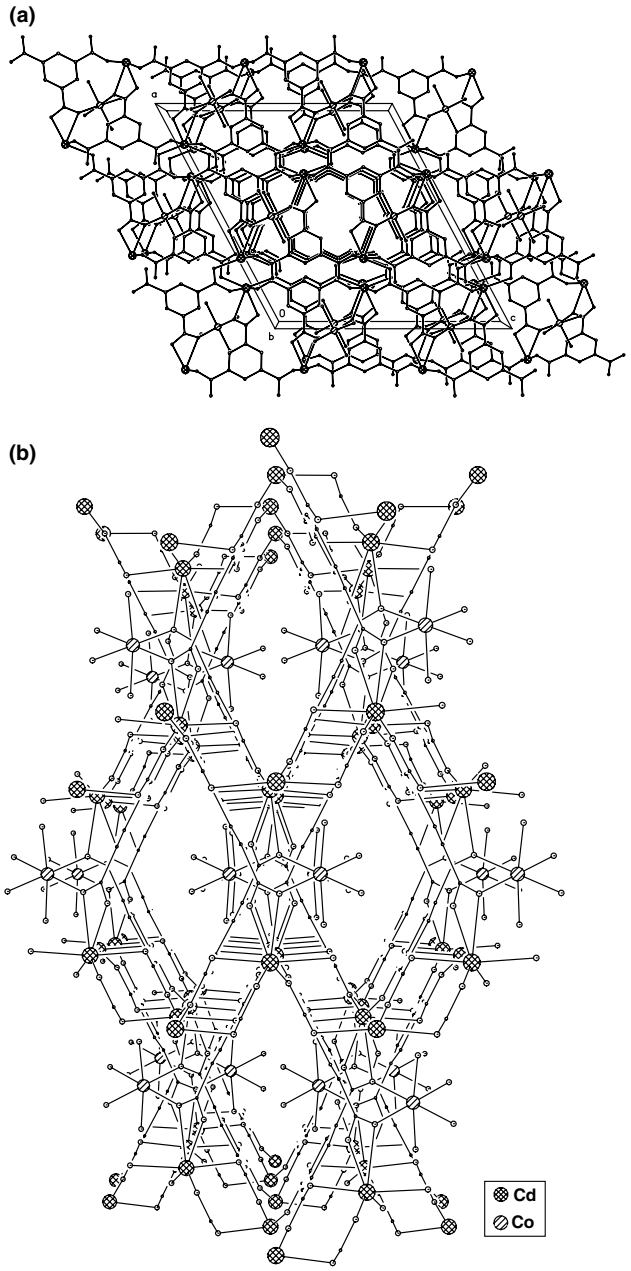

Fig. 7. (a) The 3D structure of **3** along the *b*-axis. (b) The 3D structure of **3** viewed down the *c*-axis showing the channel. All the hydrogen atoms are omitted for clarity.

As given in Table 5, there are several intermolecular hydrogen bonds between the TMA ligands and the coordinated water molecules.

3.2.3. $[Cd_2Co(TMA)_2(H_2O)_4]\cdot 2H_2O$ (3)

The selected bond lengths and bond angles of complex **3** are shown in Table 6. To our knowledge, complex **3** is the first trimesate containing two different transitional metals. As illustrated in Fig. 6, the coordination sphere in **3**, $Cd_2Co(C_9H_3O_6)_2(H_2O)_4$, has a crystallographic symmetry C_2, in which Co1 atom is on the twofold rotation axis 2[0 1 0], and two $Cd(C_9H_3O_6)$ groups and four-coordinated water molecules (O7, O8, O7A, and O8A, symmetry code A: $1-x, y, 1/2-z$) are on the two sides of the axis 2[0 1 0].

Each TMA^{3-} ligand in the coordination sphere $Cd_2Co(C_9H_3O_6)_2(H_2O)_4$ bridges to three other coordination spheres, resulting in a 3D coordination polymer (see Fig. 7(a) and (b)). There is a channel with dimensions of ca. 6.5×6 Å (based on nuclei separation) in the 3D framework, and the Co(II) coordination spheres are located in the 1D channels (see Fig. 7(b)).

The coordination fashion of the TMA ligand in **3** is illustrated in Fig. 1, O. The six-coordinated Cd1 and Co1 centers have a distorted octahedral geometry. The Cd1 atom is coordinated by six oxygen atoms from a chelating/bridging bidentate carboxylate group (O1, O2) and four different bidentate carboxylate groups (O3A, O4B, O5C, O6D) of five separate TMA ligands. The Co1 atom is coordinated by six oxygen atoms (O1, O1A, O7, O7A, O8, O8A), two of which (O1 and O1A) come from two different chelating/bridging bidentate carboxylate groups of two separate TMA ligands, the remaining four (O7, O7A O8 and O8A) come from four terminal coordinated water molecules.

As shown in Table 7, there are several intermolecular hydrogen bonds between the O–H group of coordinated water molecules and the carboxylate oxygen atoms.

3.3. Elemental analysis and TGA measurement

The elemental analysis data for the three complexes are consistent with the formulas of $[Cd_3(TMA)_2(HPRZ)(H_2O)_3(OH)]\cdot H_2O$ (**1**), $Cd_2Na_2(TMA)_2(H_2O)_4$ (**2**), and $[Cd_2Co(TMA)_2(H_2O)_4]\cdot 2H_2O$ (**3**). The TGA data of complex **1** indicates two obvious weight losses. The first weight loss starts at ca. 103–151 °C to give a total weight loss of ca. 11.2%, corresponding to loss of one guest H_2O molecule and one PRZ molecule per formula unit. The second weight loss starts at ca. 314–462 °C to give a total weight loss of ca. 52.4%, corresponding to loss of $4H_2O$ molecules and two TMA molecules per formula unit, which indicates that the framework of complex **1** is stable. The TGA data of complex **2** shows an obvious weight loss starting at ca. 100–150 °C to give a total loss of ca. 9.5%, corresponding to loss of $4H_2O$ molecules per formula unit. TMA removal starts at ca. 355–492 °C, which sug-

Table 7
Hydrogen-bonding geometry (Å, °) in **3**

D–H···A	D–H	D···A	D–H···A
O(7)–H(4w)···O(3)#1	0.724	2.927(3)	136.6
O(7)–H(4w)···O(6)#2	0.724	2.975(3)	115.2
O(7)–H(3w)···O(1w)#2	0.730	2.916(3)	152.6
O(8)–H(5w)···O(5)#3	0.878	2.739(3)	159.4
O(8)–H(6w)···O(1w)#4	0.934	2.701(3)	164.9
O(1w)–H(1w)···O(2)	1.003	2.710(3)	161.7

Symmetry codes: #1, $-x, 1+y, 1/2-z$; #2, $1-x, 1-y, -z$; #3, $-1/2x, y+1/2, z$; #4, $x, 1-y, z+1/2$.

gests that TMA ligands are strongly coordinated with the metal centers to form a stable architecture. Similar to complex **2**, the TGA of compound **3** exhibits an obvious weight loss starting at ca. 80–200 °C, to give a total loss of ca. 13.3% which corresponds to loss of $6H_2O$ molecules per formula unit. TMA removal starts at ca. 350–512 °C, which accounts for the framework of **3** being rather stable, too.

3.4. Spectroscopy and fluorescent properties

The IR spectra of these complexes show the characteristic bands of the TMA ligand at 1622–1551 cm^{-1} for the asymmetric vibration $\nu_{as}(COO^-)$ and at 1441–1367 cm^{-1} for the symmetric vibration $\nu_s(COO^-)$, and the broad bands of water at 3215–3442 cm^{-1}. In the three complexes, the absence of the expected characteristic bands at 1730–1690 cm^{-1} attributed to the protonated carboxylate groups accounts for the complete deprotonation of H_3TMA ligands in the course of the hydrothermal reactions [17]. For complex **1**, the presence of characteristic bands at 1027–997 cm^{-1} are assigned to absorption vibrations of the PRZ ligand.

The emission spectra of complexes **1**–**3** in the solid state at room temperature are depicted in Fig. 8. It can be observed that intense emissions occurring at 420 nm (Fig. 8(a), $\lambda_{ex} = 314$ nm) for **1**, 424 nm (Fig. 8(b), $\lambda_{ex} = 314$ nm) for complex **2**, and 419 nm (Fig. 8(c), $\lambda_{ex} = 308$ nm) for complex **3** are attributed to the ligand-to-metal charge-transfer (LMCT) bands. It is worthy of statement that complex **1** exhibits a quenching of the fluorescence with $\tau = 3.47$ ns, which suggests that complex **1** may be an excellent candidate for potentially photoactive material.

3.5. Magnetic investigation of complex 3

The magnetic susceptibility of complex **3** was measured in the 5–300 K temperature range and is shown as

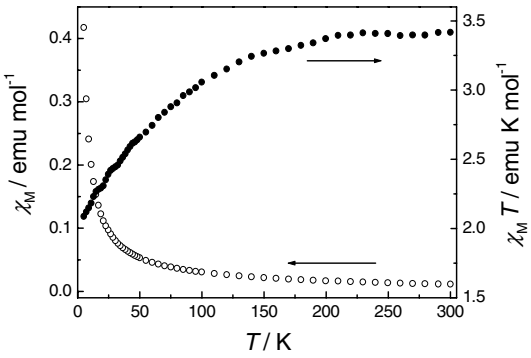

Fig. 9. The χ_M and $\chi_M T$ vs. T plots for complex **3**.

χ_M and $\chi_M T$ versus T plots in Fig. 9. The experimental $\chi_M T$ value of the complex at room temperature is ca. 3.41 emu mol^{-1} K per Cd_2Co unit, indicating significant contributions from the orbital momentum, typical of the Co(II) ion ($^4T_{1g}$) in an octahedral field. Upon cooling, the χT value decreases monotonously and reaches 2.09 emu mol^{-1} K at 5 K. Since the Co(II) ions are well isolated from one another by the TMA ligand and the Cd(II) ions, the magnetic interaction between Co(II) ions should be negligible. The temperature-dependent behavior should be mainly due to the combination of spin-orbit coupling and low-symmetry ligand field effects that cause splitting of the $^4T_{1g}$ levels [18,19].

3.6. Reaction condition dependence of structures

As illustrated in Fig. 1, the TMA ligand has a considerable variety of coordination fashions when it reacts with metal ions, and the resulting coordination polymer solids usually possess 1D, 2D or 3D structural characteristics. Yaghi et al. [9c] described that the dimensionality of the resulting coordination framework topology constructed by metal ions and TMA is extremely dependent on the deprotonation level of H_3TMA. Another noticeable experimental phenomenon

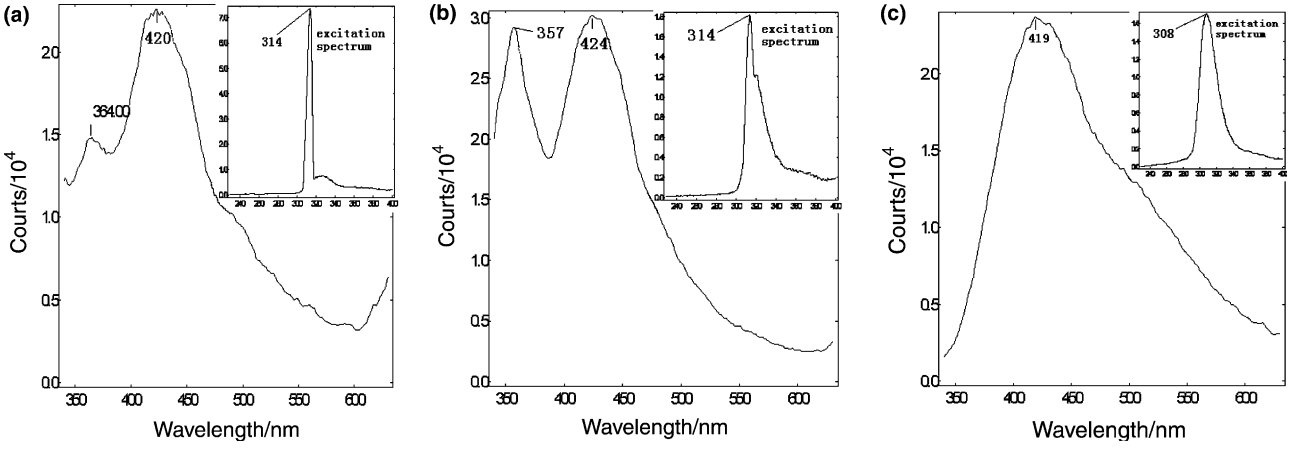

Fig. 8. Solid-state emission spectra for complexes **1**–**3**: (a) complex **1**; (b) complex **2**; (c) complex **3**.

is that different polymer solids constructed by TMA and metal ions are often obtained synchronously in the same reaction vessel under hydrothermal condition, which indicates the mechanisms of those reactions are very complex. Of course, the temperature, crystallisation time, pH value and cooling rate are also important influential factors on the structures of the resulting coordination solids. Revelation of the microscopic reaction mechanisms of H_3TMA may lead to new strategies for inorganic synthetic chemistry and design of supramolecular hosts.

It has now been demonstrated that the three novel title polymer solids with 3D porous frameworks have been synthesized through hydrothermal reactions of TMA with transition metal ions. The title complexes **2** and **3** contain two different metal centers in the coordination architectures. Similar to zeolitic properties, the TGA data of the three title compounds indicate the backbones of the polymers are very stable. The intense fluorescent emissions show that the title complexes could have roles as potential photoactive materials. The experimental $\chi_M T$ value of complex **3** at room temperature is ca. 3.41 emu mol^{-1} K per Cd_2Co unit. Upon cooling, the χT value decreases steadily and reaches 2.09 emu mol^{-1} K at 5 K.

4. Supplementary material

Crystallographic data for the structural analysis have been deposited with the Cambridge Crystallographic Data Centre, CCDC Nos. 214205 for compound **1**, 214204 for compound **2** and 214203 for compound **3**. Copies of this information may be obtained free of charge from The Director, CCDC, 12 Union Road, Cambridge CB2 1EZ, UK (fax: +44-1223-336033; email: deposit@ccdc.cam.ac.uk or www:http://www.ccdc.cam.ac.uk).

Acknowledgements

The authors are grateful for financial support from the National Natural Science Foundation of China (No. 20171012) and the Natural Science Foundation of Fujian Province, China (No. E0110010).

References

[1] (a) O.M. Yaghi, M. O'Keeffe, J. Solid State Chem. 152 (2000) 1;
(b) Z. Xu, Y.H. Kiang, S. Lee, E.B. Lobkovsky, N. Emmott, J. Am. Chem. Soc. 122 (2000) 8376;
(c) C.J. Kepet, M.J. Rosseinsky, Chem. Commun. (1999) 375.

[2] (a) R.-G. Xiong, S.R. Wilson, W.B. Lin, J. Chem. Soc., Dalton Trans. (1998) 4089;
(b) C. Kaes, M.W. Hosseini, C.E.F. Rickard, B.W. Skelton, A.H. White, Angew. Chem. Int. Ed. 37 (1998) 920.

[3] (a) N. Takeda, K. Umemto, K. Yamaguchi, M. Fujita, Nature 398 (1999) 794;
(b) B.F. Abrahams, S.J. Egan, R. Robson, J. Am. Chem. Soc. 121 (1999) 3535.

[4] (a) C.B. Aakeröy, A.M. Beatty, B.A. Helfrich, Angew. Chem. Int. Ed. 40 (2001) 3240;
(b) T.J. Prior, M.J. Rosseinsky, Chem. Commun. (2001) 1222.

[5] M. Fujita, K. Ogura, Bull. Chem. Soc. Jpn. 69 (1996) 1471.

[6] L. Carlucci, G. Cani, D.M. Proserpio, A. Sironi, J. Chem. Soc., Chem. Commun. (1994) 2755.

[7] M.-L. Tong, H.-J. Chen, X.-M. Chen, Inorg. Chem. 39 (2000) 2235.

[8] (a) S.O.H. Gutschke, M. Molinier, A.K. Powell, P.T. Wood, Angew. Chem. Int. Ed. 36 (1997) 991;
(b) R.H. Groeneman, L.R. MacGillivray, J.L. Atwod, Chem. Commun. (1998) 273;
(c) H.J. Choi, T.S. Lee, M.P. Suh, Angew. Chem. Int. Ed. 38 (1999) 1405;
(d) F.A. Cotton, L.M. Daniels, C. Lin, C.A. Murillo, Chem. Commun. (1999) 841.

[9] (a) O.M. Yaghi, G. Li, H. Li, Nature 3788 (1995) 703;
(b) O.M. Yaghi, H. Li, T.L. Groy, J. Am. Chem. Soc. 118 (1996) 9096;
(c) O.M. Yaghi, C.E. Davis, G. Li, H. Li, J. Am. Chem. Soc. 119 (1997) 2861;
(d) M. Eddaoudi, D.B. Moler, H.L. Li, B.L. Chen, T.M. Reineke, M. O'Keeffe, O.M. Yaghi, Acc. Chem. Res. 34 (2001) 319.

[10] (a) S.S.-Y. Chui, S.M.F. Lo, J.P.H. Charmant, A.G. Orpen, I.D. Williams, Science 283 (1999) 1148;
(b) S.S.-Y. Chui, A. Siu, I.D. Williams, Acta Crystallogr., Sect. C 55 (1999) 194.

[11] M.J. Plater, M.R.S.J. Foreman, R.A. Howie, J.M.S. Skakle, E. Coronado, C.J. Gómez-García, T. Gelbrich, M.B. Hursthouse, Inorg. Chim. Acta 319 (2001) 159.

[12] T.J. Prior, M.J. Rosseinsky, Chem. Commun. (2001) 1222.

[13] (a) D.-F. Sun, R. Cao, J.-B. Weng, M.-C. Hong, Y.-C. Liang, J. Chem. Soc., Dalton Trans. (2002) 291;
(b) J.-C. Dai, X.-T. Wu, Z.-Y. Fu, C.-P. Cui, S.-M. Hu, W.-X. Du, L.-M. Wu, H.-H. Zhang, R.-Q. Sun, Inorg. Chem. 41 (2002) 1391.

[14] (a) G. Wu, X. Shi, Q.-R. Fang, G. Tian, L.-F. Wang, G.-S. Zhu, A.W. Addison, Y. Wei, S.L. Qiu, Inorg. Chem. Commun. 6 (2003) 402;
(b) H.-F. Zhu, W.-Y. Sun, T. Okamura, N. Ueyama, Inorg. Chem. Commun. 6 (2003) 168;
(c) Z.L. Lü, W. Chen, J.-Q. Xu, L.-J. Zhang, C.-L. Pan, T.-G. Wang, Inorg. Chem. Commun. 6 (2003) 244.

[15] G.M. Sheldrick, SHELXS-97: Program for X-ray Crystal Structure Solution, University of Göttingen, Göttingen, Germany, 1997.

[16] G.M. Sheldrick, SHELXL-97: Program for X-ray Crystal Structure Refinement, University of Göttingen, Göttingen, Germany, 1997.

[17] L.J. Bellamy, The Infrared Spectra of Complex Molecules, Wiley, New York, 1958.

[18] O. Kahn, Molecular Magnetism, VCH, New York, 1993.

[19] P. Jensen, S.R. Batten, B. Moubaraki, K.S. Murray, R. Robson, J. Solid State Chem. 159 (2001) 352.

Available online at www.sciencedirect.com
SCIENCE DIRECT®
Polyhedron 23 (2004) 1889–1896
POLYHEDRON
www.elsevier.com/locate/poly

Polyynes: a new class of carbon allotropes. About the formation of dicyanopolyynes from an electric arc between graphite electrodes in liquid nitrogen

Franco Cataldo *

Soc. Lupi Chemical Research Institute, Via Casilina 1626/A, 00133 Rome, Italy

Received 2 January 2004; accepted 6 April 2004
Available online 19 June 2004

Abstract

A mixture of dicyanopolyynes having the general formula N≡C–(C≡C)$_n$–C≡N with $n = 2$, 3 and 4 is formed and collected in a simple apparatus when graphite electrodes are arced in liquid nitrogen. As secondary products regular polyynes, i.e. hydrogen-terminated polyynes with the general formula H–(C≡C)$_n$–H with $n = 4$, 5 and 6 are formed together with the cyanopolyynes. It is shown that the hydrogen for carbon chain end-capping is supplied by the plasmalysis of traces of water present in the liquid nitrogen while nitrogen end groups of cyanopolyynes derive from the plasmalysis of molecular nitrogen. This study has confirmed the key role played by the graphite electrodes as the source of elemental carbon under the form of sp-hybridized carbon chains which are then terminated by atoms derived from the medium where the electric arc is struck. The analysis of the reaction products was made by electronic absorption spectroscopy and the separation and identification of the molecular species produced was made with a liquid chromatographic analysis (HPLC) coupled with a diode-array (DAD) detector. The importance of the polyynes and their role as a class of carbon allotropes has been discussed.
© 2004 Elsevier Ltd. All rights reserved.

Keywords: Carbon allotropes; Polyynes; Carbyne; Dicyanopolyynes; Cyanopolyynes; Electric arc; Graphite; Liquid nitrogen

1. Introduction

The concept of allotropy sometimes appears too limited when applied to the richness of chemical structures that have been observed or theorized for elemental carbon [1]. In fact, elemental carbon occurs in a plethora of forms and mixed structures. For this reason it is convenient to classify carbon allotropes and other forms of carbon based on the degree of hybridization as proposed by Heimann et al. [2]. According to the proposed classification (see Fig. 1), there are three fundamental carbon allotropes: diamond, graphite and polyynes. In each of these elemental forms the carbon atoms are sp^3, sp^2 and sp hybridized, respectively.

Fullerenes, carbon nanotubes and related structures (see Fig. 1) are considered intermediate forms of carbon in this classification, because of the deviation from planarity imposed by the curved surfaces observed in these molecules; the carbon hybridization is no longer pure sp^2 but an intermediate value between sp^2 and sp^3 [3].

Acetylenic chains like H–(C≡C)$_n$–H are constituted by a sequence of sp hybridized carbon atoms. If the chain is relatively short and terminated with hydrogen atoms or with other groups, it is called a polyyne chain. In such a case it is an almost linear carbon chain although deviations from linearity have been observed experimentally in some cases [4]. However, when a polyyne chain is closed into a ring, we obtain a cyclopolyyne which again is no longer bonded by purely sp hybridized carbon. The distortion from linearity introduces a higher degree of hybridization and hence the carbon atoms are at an intermediate level of hybridization between sp and sp^2. Carbyne is instead an ideal form of solid elemental carbon made by sp-hybridized

* Tel./fax: +39062050800.
E-mail address: cdcata@flashnet.it (F. Cataldo).

0277-5387/$ - see front matter © 2004 Elsevier Ltd. All rights reserved.
doi:10.1016/j.poly.2004.04.024

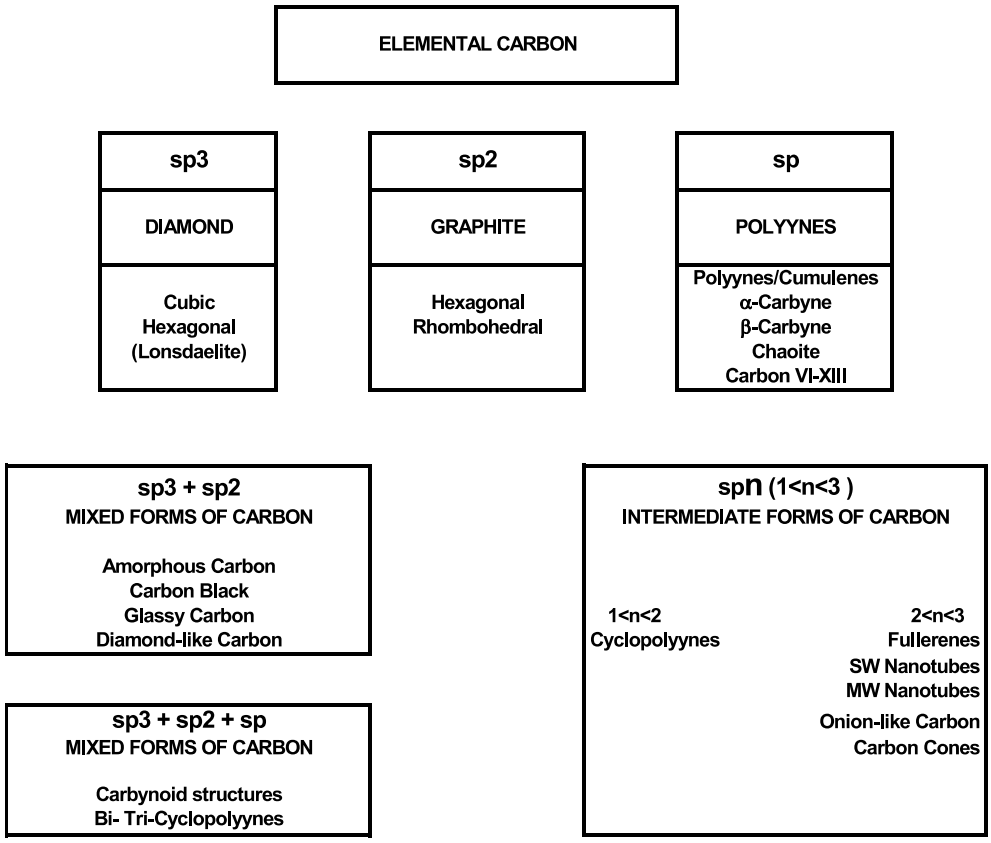

Fig. 1. Carbon allotropes and other forms of carbon. Elaborated and updated by the author; after Heimann et al. [2].

carbon chains whose length is so high that they can be considered infinite. By using the language of polymer chemistry, it is possible to state that polyynes are oligomeric forms of sp-hybridized carbon atoms which have been synthesized and observed experimentally essentially in solution and in vapour phase, while carbyne is a high polymer made again by sp-hybridized carbon atoms but it has never been produced in pure form experimentally. Instead of carbyne, several times carbynoid structures have been obtained as results of attempted synthesis of carbyne. The distinction between carbyne and carbynoid structures was proposed by Heimann [5] and is useful to distinguish between ideal and real sp-carbon solid. In fact, the literature is confusing since often the synthesis of carbyne has been reported while actually the synthesis was of carbynoid structures [5]. Carbynoid structures are essentially made by carbyne chains or, better, by polyyne chains or domains embedded in a carbonaceous matrix of mixed forms of carbon or stabilized by certain metal ions.

It is possible to talk about mixed forms of carbon when carbon atoms with different types of hybridization occur simultaneously in the same solid. Examples of mixed forms of carbon are the already mentioned carbynoid structures where it is possible to detect the coexistence of hybridized sp, sp^2 and sp^3 carbon atoms [6]. Other examples of mixed forms of carbon are represented by diamond-like carbon and glassy carbon.

Probably the carbonaceous solids closest to carbyne were synthesized under special conditions for instance by Kavan and co-workers [7], by Ravagnan et al. [8] and by Tanuma and Palnichenko [9].

Based on the preceding discussion, polyynes are a class of molecules which simultaneously can be viewed as a class of carbon allotropes, exactly as fullerenes are: a special class of molecules made exclusively by elemental carbon.

The bulk synthesis of polyynes belonged to the realm of organic chemistry and was achieved in 1972 [10] by a complex, impressive and elegant synthetic procedure. Recently, we have shown that a polyynes mixture can be easily synthesized in one shot and in relatively bulk quantities when an electric arc is struck between two graphite electrodes submerged in a solvent like methanol, acetonitrile or *n*-hexane [11–14]. The graphite electrodes play a key role in the polyynes synthesis as will be discussed elsewhere [15]. Moreover the temperature and the nature of the solvent also seem to be important in the arc synthesis. For instance, when acetonitrile was used as solvent, polyynes chains having up to 18 carbon atoms were obtained, provided that the arc between the graphite electrodes was struck in the solvent cooled at

−40 °C [12,13]. In acetonitrile the polyynes series was accompanied by a monocyanopolyynes series described by the general formula H–(C≡C)$_n$–C≡N [12,13]. Instead, when *n*-hexane was used as solvent at room temperature, although the polyynes series with chains having the maximum length of 16 carbon atoms were the dominant products, significant traces of polycyclic aromatic hydrocarbons (PAH) and other by-products were found in the solution [15].

To maximize the beneficial effects of the low temperatures, which permit the synthesis of the longest polyynes chains and to reduce the solvent interference, which tends also to produce by-products, we have studied the products formed in the electric arc between graphite electrodes submerged in liquid nitrogen. The present work is a complete account of our investigation on this specific subject.

2. Experimental

Graphite rods 6 mm diam. × 150 mm length (99.999% purity) used as electrodes were obtained from Aldrich. All solvents used were analytical or high performance liquid chromatographic (HPLC) grades from Fluka or Riedel de Haen. Liquid nitrogen was supplied by SIAD gas tecnici (Italy).

The electric arc was conducted using DC current. The DC power supply was from KERT (Italy) model Cosmo 3000 (0–30 V and 0–10 A). The electronic absorption spectra were recorded on a Shimadzu UV160A spectrophotometer on filtered solutions in *n*-octane. The solution containing the crude mixture of polyynes in *n*-octane was filtered through a PVDF Acrodisc® membrane having a pore size of 0.45 μm, to remove carbon particles suspended in the solvent, before recording electronic spectra or before running HPLC analysis.

The HPLC analysis of the solutions was conducted on an Agilent Technologies System Model 1100 equipped with a diode-array detector (DAD) and a C-8 column Zorbax Eclipse XDB-C8. A mixture of CH_3CN/water 80/20 v/v was used as the mobile phase and pumped at a rate of 1.5 ml/min into the HPLC column. Further details on the analysis can be found in previous works [12–14].

2.1. The electric arc in liquid nitrogen between graphite electrodes

A three-necked round bottomed Duran flask of 100 ml equipped with two graphite electrodes arranged in a "V" geometry was filled with liquid nitrogen and immersed in liquid nitrogen in a Dewar flask. The third neck of the flask was fitted with a valve connected with a Drechsel tube (a gas washing bottle) of 250 ml filled with 100 ml of *n*-octane.

The electric arc was ignited and sustained at 9.5 A and 15–30 V (DC current) by putting in contact and by moving slightly up and down the two graphite electrodes submerged in liquid nitrogen in the three-necked flask. The bright light of the arc can be easily observed and the heat generated by the arc caused the partial vaporization of the liquid nitrogen, which was forced to bubble into the gas washing bottle attached to the reaction flask. The products formed in the electric arc were forced to pass into the octane solvent outside the reactor and hence were trapped in the solvent. Periodically samples of the *n*-octane solution were collected and analyzed by electronic absorption spectroscopy and by HPLC–DAD analysis. The following polyynes were identified based on the retention time and the electronic spectra: C_6N_2, C_8H_2, C_8N_2, $C_{10}H_2$, $C_{10}N_2$.

2.2. Electric arc between graphite electrodes submerged in n-octane

To create a "blank" or a reference to the products formed by the carbon arc in liquid nitrogen, we have arced also graphite electrodes directly in *n*-octane at 10 A under the same conditions described elsewhere [12,14] for *n*-hexane. Indeed the products were practically the same as detected and reported previously for *n*-hexane [12–14], namely, a polyynes mixture with polyyne C_8H_2 as the most abundant component (see the spectrum in Fig. 2(a)).

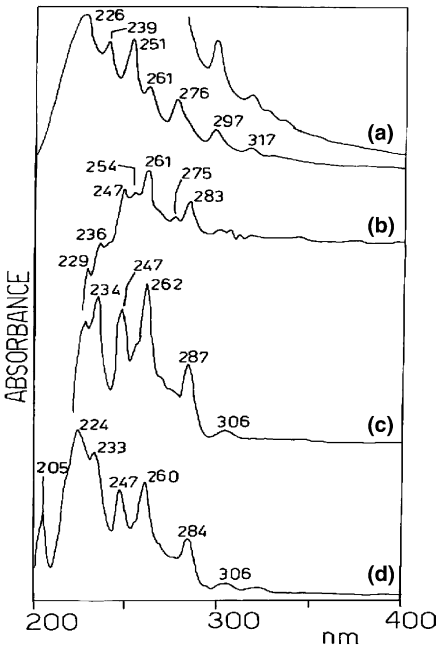

Fig. 2. Electronic absorption spectra of polyynes mixtures. (a) Polyynes obtained by arcing graphite directly into *n*-octane. (b) Initial spectrum of the polyynes mixtures produced from the graphite arc in liquid nitrogen and trapped in *n*-octane at the beginning of the experiment. (c) Same as (b) but after prolonged arcing in liquid nitrogen. (d) Same as (c) at the end of the experiment; a final total concentration of polyynes estimated at about 8×10^{-6} M was achieved.

2.3. The electric arc between graphite electrodes submerged in water

The arc was conducted between graphite electrodes submerged in distilled water at 10 A. The electronic absorption spectrum of the crude aqueous solution of polyynes and other products showed the following absorption bands: 200, 215 and 226 nm as the most intense. Other weaker bands were observed at 238, 246, 250, 259, 274, 284, 300 and 323 nm.

The HPLC–DAD analysis revealed the presence of the following polyynes: C_4H_2, C_6H_2, C_8H_2 and $C_{10}H_2$. Polyyne C_8H_2 was by far the most abundant product.

3. Results and discussion

3.1. General remarks

At atmospheric pressure, carbon sublimes above 3500 °C. The complex nature of carbon vapour has been known since the end of the fifties of the last century [16,17]. The mass analysis of the carbon vapour formed in an electrical discharge between graphite electrodes has revealed all ions from C_1 up to C_{33}^+ and C_{35}^- [17,18]. Alternatively, the laser ablation of graphite by a ruby laser produced a series of species ranging from C_1 to C_{10}, the most abundant being C_2 and C_3 [16,19]. The properties of the carbon vapour have been studied theoretically by using molecular orbital theory computations. The results indicate the growth of linear polyatomic molecules essentially of the polyyne type. Extrapolation of the calculations to liquid carbon shows that this should consist of essential long chains of carbon atoms [16]. The laser vaporization of graphite [20] confirmed the earlier results, namely odd and even clusters were obtained up to C_{38}, but only even clusters above that value. It was shown later [21] that the carbon clusters larger than C_{38}, having only even numbers of carbon atoms, are made by fullerenes with a neat predominance of C_{60} and C_{70}. Conversely, the clusters having less than 38 carbon atoms have been assigned to polyynes and/or cyclopolyynes which are considered the precursors of fullerenes which, in fact, by a crosslinking reaction yield fullerenes [22,23] as it has been postulated and also demonstrated by using appropriate precursors [21]. High intensity laser ablation of graphite and other carbonaceous substrates produces also higher homologues of C_{60} and C_{70} fullerenes [24,25].

3.2. Formation of polyynes from an electric arc in liquid nitrogen between graphite electrodes

Recently we have shown that an electric arc between two graphite electrodes in a solvent produces polyyne solutions in the given solvent. The basic mechanism proposed involves carbon vaporization from the graphite electrodes under the high temperature produced by the electric arc, estimated to be above 4000 °C [11–14] and thus above the vaporization point of elemental carbon. Carbon is vaporized from the electrodes in the form of polyyne chains and then is quenched into the solvent surrounding the plasma ball of the arc. Thus, polyyne solutions are obtained.

When the graphite electrodes are arced in liquid nitrogen the polyynes formed in the arc are quenched into the very cold reservoir of the liquid nitrogen surrounding the plasma ball. During arcing, part of the liquid nitrogen vaporizes to dissipate the heat generated by the electric arc. When the liquid nitrogen vaporizes, a continuous stream of gaseous nitrogen drags the polyynes, which presumably are insoluble but are embedded in liquid nitrogen, outside the reactor (see Section 2) into the gas washing bottle connected to the reactor and filled with a solvent (*n*-octane). When nitrogen bubbles into the bottle, it releases the polyynes into the *n*-octane solvent, which acts as a trap. In fact in Fig. 2 it is possible to observe the typical polyyne spectrum from the octane solution used as a trap for these molecules. As reported and discussed in our earlier works [11–14], the polyynes are characterized by very peculiar electronic absorption spectra which permit their easy identification. When the polyynes are in a mixture they show spectra composed of several bands as reported in Fig. 2(a) obtained by arcing graphite electrodes directly into *n*-octane [11–14].

Fig. 2(b) shows the initial spectrum of the polyyne mixtures produced from the graphite arc in liquid nitrogen at the beginning of the experiment. Under these conditions, the initial concentration of polyynes was estimated from their optical density in the spectrum to be around 10^{-7} M in the *n*-octane trap. Furthermore, the spectrum in Fig. 2(b) of the polyynes produced from the arc in liquid nitrogen shows a different band pattern than the mixture of polyynes produced by arcing graphite electrodes directly into *n*-octane (compare Fig. 2(b) with Fig. 2(a)). In particular in Fig. 2(b) we can observe two main bands at 261 and 283 nm while the most intense bands in Fig. 2(a) are located at 226, 239 and 251 nm. Since the end groups of polyyne chains are affected by the nature of the solvent where the graphite arc is struck, and since we know that usually the polyynes are hydrogen-terminated when the arc is made in hydrocarbon solvents like *n*-hexane or *n*-octane and they are also cyano-terminated when the arc is made in acetonitrile, these spectral differences can be taken as a first hint that the polyynes formed in liquid nitrogen are nitrogen and hence cyano-terminated.

From our previous works on polyynes, we know the electronic absorption spectra of a series of monocyanopolyynes and from literature [26,27] we know the spectrum of the dicyanopolyyne C_8N_2 whose maximum

wavelength absorption band lies just at 261 nm. In principle, it is quite obvious to expect to produce nitrogen-terminated polyynes by arcing graphite in liquid nitrogen since the high temperatures of the electric arc may cause the plasmalysis of molecular nitrogen into atomic nitrogen which in its turn can easily form cyano-groups with carbon vapour and hence can terminate the polyyne chains into dicyanopolyynes:

$$N{\equiv}C{-}(C{\equiv}C)_n{-}C{\equiv}N$$

It is fascinating to think that similar synthetic processes leading to these or similar molecules are known to occur in the outflow of certain carbon-rich giant stars in the space [28].

By continuing arcing in liquid nitrogen with graphite electrodes, it is possible to accumulate the reaction products into the octane trap. This is illustrated in Fig. 2(c) where the bands become more intense and better defined as a function of the arcing time. In particular in Fig. 2(c) the concentration of the polyynes can be estimated at about 2.5×10^{-6} M. Arcing was stopped when all the liquid nitrogen in the reaction flask was consumed, i.e. disappeared by vaporization. The final spectrum of the products collected is shown in Fig. 2(d), with a final total concentration of polyynes estimated at about 8×10^{-6} M.

The crude *n*-octane solution, after filtration, was chromatographed in the HPLC apparatus (see Section 2). The complex polyynes mixture formed by arcing graphite directly into liquid nitrogen was resolved into six main components whose electronic absorption spectra are shown all together in Fig. 3. The three main components are easily and definitively identified from their electronic absorption spectra and are, respectively, C_6N_2, C_8N_2 and $C_{10}N_2$ (see below for further details), the former being the most abundant followed by the other two in lower concentrations. Other minor components detected were hydrogen-terminated polyynes C_8H_2, $C_{10}H_2$ and $C_{12}H_2$ in decreasing concentration and in general at much lower concentration than the corresponding dicyanopolyynes ($C_{12}H_2$ is not shown in Fig. 3).

The individual spectra of the molecular species separated by the liquid chromatographic analysis are shown in Fig. 4, following their retention time (R_t) from the bottom to top of Fig. 4. The first molecular species eluted with a $R_t = 1.55$ min was identified as C_6N_2 from its absorption spectrum ($\lambda_m = \mathbf{235}$, 222, 213 and 205 nm) in comparison to the well known [11–14] spectrum of C_8H_2 which eluted immediately after the species with a $R_t = 1.64$ min ($\lambda_m = \mathbf{227}$, 218 and 208 nm). It can be observed that both C_6N_2 and C_8H_2 have similar molecular weight (about 100 versus 98 Da, respectively), but from our previous study on polyynes and cyanopolyynes [12–14] we know that at more or less equal molecular weight the nitrogen-capped polyynes have a shorter retention time than the hydrogen-capped polyynes. Thus, the assignment appears correct. The

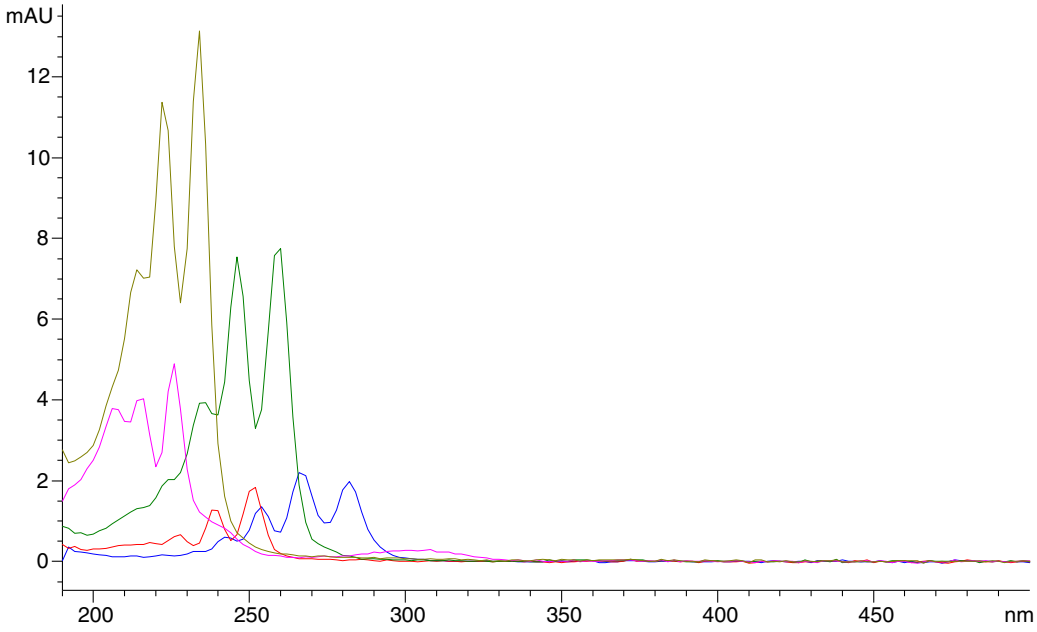

Fig. 3. Electronic absorption spectra of the polyynes formed from graphite arcing in liquid nitrogen. The liquid chromatographic analysis (HPLC) was able to separate the mixture into its components. The electronic spectrum of each component eluted was recorded by the diode-array detector (DAD). The three main components are easily and definitively identified from their electronic absorption spectra and are, respectively, C_6N_2, C_8N_2 and $C_{10}N_2$. The spectra of these three dicyanopolyynes in the figure are easily identifiable from the longest wavelength absorption band lying at 233, 260 and 283 nm, respectively. There are also two other minor components in the figure: the hydrogen-terminated polyynes C_8H_2 and $C_{10}H_2$. Furthermore, $C_{12}H_2$ has also been identified although at very low concentration (not shown in the figure).

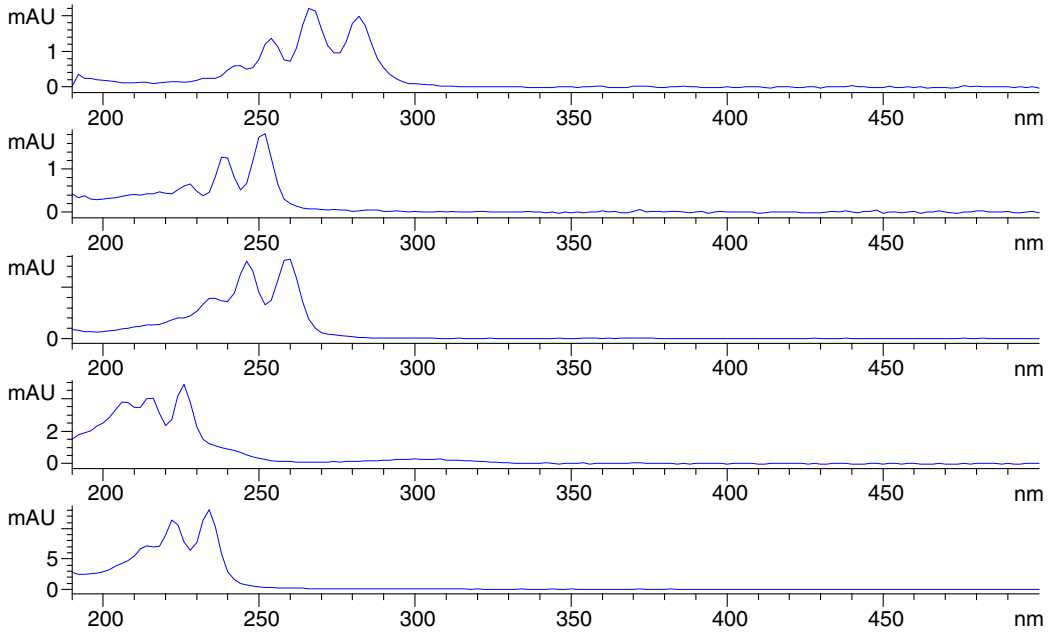

Fig. 4. Individual spectra of each molecular species separated by the liquid chromatographic analysis. From bottom to top of the figure it is possible to distinguish the spectrum of C_6N_2 with $R_t = 1.55$, then C_8H_2 with $R_t = 1.64$ followed by C_8N_2 ($R_t = 1.87$), $C_{10}H_2$ ($R_t = 2.11$) and $C_{10}N_2$ ($R_t = 2.39$).

next compound eluted with a $R_t = 1.87$ min is C_8N_2, which has been recognized from the band pattern of its spectrum which matches that reported in literature for this compound [26,27] (λ_m (found) = **260**, 247, 233, 223 and 214 nm; λ_m (literature [26]) = 261, 248, 236, 225 and 215 nm). After C_8N_2 with a molecular weight of about 124 Da, the hydrogen-capped polyyne $C_{10}H_2$ is eluted, having a molecular weight of 122 Da and a $R_t = 2.11$ min. Its spectrum matches completely the known [12–14] band pattern of this compound (λ_m = **251**, 239, 227 and 218 nm). Finally, the detection of $C_{10}N_2$ occurs at a $R_t = 2.39$ min and the spectrum is characterized by λ_m = 303, 283, **268**, 253, 243 and 232 nm. In all the spectral wavelengths reported, the most intense band is written in bold. It is also important to underline that in the assignments reported here we have been guided also by the typical retention times we have measured in earlier works for hydrogen-capped polyynes of monocyanopolyynes as reported in Table 1.

The formation of polyynes in the electric arc in liquid nitrogen represents a clear indication that the elemental carbon for the polyynes chains is supplied essentially from the graphite electrodes and not from the solvent. This result is quite expected since we know that the electric arc in vacuum conditions between graphite electrodes produces polyynes ions. Furthermore, Hirsch and colleagues [26,27] have shown that the electric arc between graphite electrodes under Kratschmer–Huffman conditions [29] in a reduced pressure of cyanogen (C_2N_2) produces a mixture of dicyanopolyynes whose main components are C_8N_2 and $C_{10}N_2$ (respectively, 55% and 35%). Also $C_{12}N_2$, $C_{14}N_2$ and $C_{16}N_2$ were detected [26,27].

Table 1
HPLC retention times of the dicyanopolyynes versus other polyynes

$R_t = 1.55$ for C_6N_2 in comparison to $R_t = 1.547$ for HC_7N [12–14]
$R_t = 1.64$ for C_8H_2 as already found in [12–14]
$R_t = 1.87$ for C_8N_2 in comparison to $R_t = 1.89$ for HC_9N [12–14]
$R_t = 2.11$ for $C_{10}H_2$ as already found in [12–14]
$R_t = 2.39$ for $C_{10}N_2$ in comparison to $R_t = 2.41$ for $HC_{11}N$ [12–14]

In the products of the electric arc in liquid nitrogen (Fig. 3), we can estimate from the chromatographic analysis that C_6N_2 represents approximately 50% (by mol.) of the mixture followed by C_8N_2 with about 25% and $C_{10}N_2$ with about 5%. The remaining products are essentially C_8H_2, $C_{10}H_2$ and $C_{12}H_2$.

The hydrogen-terminated polyynes formed in minor quantities in our synthesis derive their hydrogen end-groups from the plasmalysis of the humidity present in the reactor and in the liquid nitrogen. Therefore, they must be regarded merely as secondary products. In the next section, we demonstrate experimentally that the hydrogen-terminated polyynes are formed from the water plasmalysis. In fact, in our electric arc in liquid nitrogen we have excluded the presence of any organic solvent but not the presence of humidity. Therefore, the arc between graphite electrodes in liquid nitrogen involves necessarily also the plasmalysis of small amounts of water which supplies the hydrogen necessary for end-capping the polyynes chain.

3.3. Polyynes from the electric arc from graphite electrodes in water

As reported in our previous works [11–14] when arcing between graphite electrodes is conducted in organic solvents usually hydrogen-capped polyynes are obtained. In general, it is believed at present that the hydrogen end capping is derived from the solvent plasmalysis. Under special conditions e.g. in acetonitrile, monocyanopolyynes are produced together with normal hydrogen-terminated polyynes. The solvent plasmalysis caused by the electric arc generates atomic hydrogen, which then reacts with the diradicalic carbon chains produced by carbon vaporization from the electrodes.

In Section 3.2, the electric arc in liquid nitrogen produces cyanopolyynes as expected but also hydrogen-terminated polyynes, which are rather unexpected unless we should admit that traces of water play the role of the supplier of hydrogen atoms during the plasmalysis caused by the electric arc. In Section 2.3, we have clearly demonstrated that when the submerged electric arc between graphite electrodes is struck under distilled water, it is possible to observe the typical electronic spectrum of a mixture of polyynes in water. Furthermore, the liquid chromatographic analysis permits to separate and identify all the hydrogen-terminated polyynes series normally observed in organic solvents like methanol and *n*-hexane (see Fig. 5). Thus, it is demonstrated that the hydrogen atoms in a system of graphite electrodes and water are supplied by the plasmalysis of the water molecules. Consequently, it is now clear that the hydrogen-terminated polyynes observed as secondary products in the arcing experiment in liquid nitrogen derive from the humidity and traces of water present in the liquid nitrogen itself and in the reactor.

4. Conclusions

Polyynes represent the oligomers of carbyne, which is thought as a carbon chain of very high molecular weight: a high polymer. Although carbyne has not yet been produced in pure form and remains a limiting structure, polyynes can be produced in bulk quantity by certain multistep synthetic routes or by the electric arc between graphite electrodes submerged in organic solvents or in liquids. Polyynes are thus a class of molecules made exclusively by a chain of sp-hybridized carbon atoms and represent a class of molecules which can be regarded as a class of carbon allotropes. Of course, carbon chains of any length must be terminated by end groups to ensure stability, otherwise we are dealing with diradical chains. The simplest end groups are hydrogen atoms:

$$H–(C{\equiv}C)_n–H$$

When arcing is made between graphite electrodes submerged in organic solvents, the elemental carbon is supplied from the vaporization of the graphite electrodes under the high plasma temperature produced by the high speed electron impacts on the surface of the electrodes. The nature of the solvent does not seem to play any role in the elemental carbon supply. This has been demonstrated in the present work, where the polyynes have been formed in an "inorganic" liquid: liquid nitrogen

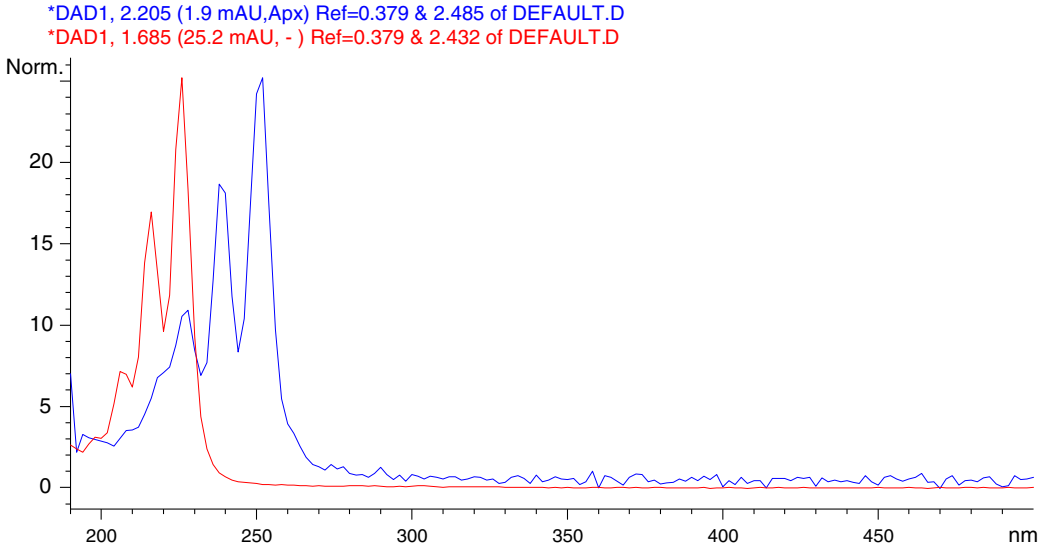

Fig. 5. Hydrogen-terminated polyynes C_8H_2 and $C_{10}H_2$ produced by arcing graphite electrodes in pure distilled water as identified by HPLC–DAD analysis of the mixture. The former polyyne was the dominant product.

instead of the organic solvents used previously, provided that graphite electrodes were used. Obviously, by arcing electrodes of other elements than carbon in liquid nitrogen no polyynes must be expected [15].

Concerning the end-groups of the polyynes, the medium where the graphite electrodes are arced seems instead to be of great importance. We have shown that in liquid nitrogen the polyynes are nitrogen terminated:

$$N{\equiv}C{-}(C{\equiv}C)_n{-}C{\equiv}N$$

The nitrogen end groups derive necessarily from the plasmalysis in the electric arc of molecular N_2 into atomic nitrogen. The nitrogen atoms react with the polyynes carbon chains produced from the graphite electrodes yielding the cyanopolyynes. However, even in liquid nitrogen the formation of cyanopolyynes is accompanied by the formation of hydrogen-terminated or regular polyynes. We have demonstrated that these secondary products are formed from the plasmalysis of traces of water present in liquid nitrogen and in the reactor. The resulting hydrogen atoms then terminate the carbon chains. In fact, if the graphite electrodes are arced submerged in distilled water regular polyynes are formed easily in detectable quantities, exactly as it happens by arcing graphite electrodes in organic solvents like methanol or *n*-hexane [11–14]. In these last two cases the hydrogen atoms are supplied from the plasmalysis of these solvents and regular polyynes are obtained [11–14].

This study has shown the easy access to cyanopolyynes in solution with a simple apparatus. The availability of cyanopolyynes will permit us to study their chemistry and physical properties, which until now have been explored mainly on a theoretical basis. It is expected that the end-capping of polyynes chains with cyano groups must give a significant stability to these molecules. Cyanopolyynes are present in the interstellar and circumstellar shells of carbon rich stars [28,29] as well as in the interstellar medium, and are thought to contribute to certain spectral features of the interstellar medium [30]. Furthermore, cyanopolyynes are known to be present in the atmospheres of the giant plants of the solar system and also on Titan, the giant moon of Saturn [31]. The results of the present work may be used to explain the easy formation of these complex molecules in space and can be also used in laboratory simulations and studies of the interstellar conditions with a very easy access to these species.

References

[1] F. Diederich, Y. Rubin, Angew. Chem., Int. Ed. Engl. 31 (1992) 1101.
[2] R.B. Heimann, S.E. Evsyukov, Y. Koga, Carbon 35 (1997) 1654.
[3] F. Cataldo, Carbon 38 (2000) 623.
[4] S. Szafert, J.A. Gladysz, Chem. Rev. 103 (2003) 4175.
[5] R.B. Heimann, S.E. Evsyukov, L. Kavan, Carbyne and Carbynoid Structures, Kluwer Academic Publishers, Dordrecht, The Netherlands, 1999.
[6] F. Cataldo, D. Capitani, Mater. Chem. Phys. 59 (1999) 225.
[7] J. Kastner, H. Kuzmany, L. Kavan, F.P. Dousek, J. Kurti, Macromolecules 28 (1995) 344.
[8] L. Ravagnan, F. Siviero, C. Lenardi, P. Piseri, E. Barborini, P. Milani, C.S. Casari, A. Li Bassi, C.E. Bottani, Phys. Rev. Lett. 89 (2002) 2855061.
[9] S. Tanuma, A. Palnichenko, J. Mater. Res. 10 (1995) 1120.
[10] R. Eastmond, T.R. Johnson, D.R.M. Walton, Tetrahedron 28 (1972) 4601.
[11] F. Cataldo, Carbon 41 (2003) 2671.
[12] F. Cataldo, Tetrahedron Lett. 45 (2004) 141.
[13] F. Cataldo, Carbon 42 (2004) 129.
[14] F. Cataldo, Fullerenes, Nanotubes Carbon Nanostruct. 12(3) (2004) (in press).
[15] F. Cataldo, Tetrahedron 60 (2004) 4265.
[16] A.K. Holliday, G. Hughes, S.M. Walkers, in: J.C. Bailar, H.J. Emeleus, R. Nyholm, A.F. Trotman-Dickenson (Eds.), Comprehensive Inorganic Chemistry, Pergamon Press, London, 1973.
[17] H. Hintenberger, J. Franzen, K.D. Schuy, Z. Naturforsch. A 18 (1963) 1236.
[18] J.R. Heath, Q. Zhang, S.C. O'Brien, R.F. Curl, H.W. Kroto, R.E. Smalley, J. Am. Chem. Soc. 109 (1987) 359.
[19] F. Cataldo, Y. Keheyan, Fullerene Sci. Technol. 9 (2001) 553.
[20] E.A. Rohlfing, D.M. Cox, A. Kaldor, J. Chem. Phys. 81 (1984) 3322.
[21] H.W. Kroto, D.R.M. Walton, Phil. Trans. R. Soc. Lond. A 343 (1993) 103.
[22] J.R. Heath, in: G.S. Hammond, V.J. Kuck (Eds.), Fullerenes: synthesis, properties and chemistry of large carbon clusters. ACS Symposium Series 481, Atlanta, GA, 1992 (Chapter 1).
[23] N.I. Alekseev, G.A. Dyuzhev, Tech. Phys. 47 (2002) 634, and 643.
[24] F. Cataldo, Y. Keheyan, Fullerenes Nanotubes Carbon Nanostruct. 10 (2002) 99.
[25] F. Cataldo, Y. Keheyan, Fullerenes Nanotubes Carbon Nanostruct. 10 (2002) 313;
F. Cataldo, Y. Keheyan, Fullerenes Nanotubes Carbon Nanostruct. 10 (2002) 333.
[26] T. Grosser, A. Hirsch, Angew. Chem., Int. Ed. Engl. 32 (1993) 1340.
[27] G. Schermann, T. Grosser, F. Hampel, A. Hirsch, Chem. Eur. J. 3 (1997) 1105.
[28] H.W. Kroto, Angew. Chem., Int. Ed. Engl. 31 (1992) 111.
[29] W. Kratschmer, L. Lamb, K. Fostiropoulos, D.R. Huffman, Nature 347 (1990) 354.
[30] P. Thaddeus, M.C. McCarthy, M.J. Travers, C.A. Gottlieb, W. Chien, Faraday Discuss. 109 (1998) 121.
[31] A. Coustenis, F. Taylor, Titan. The Earth-like Moon, World Scientific, Singapore, 1999.

Available online at www.sciencedirect.com
SCIENCE DIRECT®
Polyhedron 23 (2004) 1897–1901
POLYHEDRON
www.elsevier.com/locate/poly

Effect of pH and temperature on the formation of hydroxyapatite at low temperatures by decomposition of a Ca–EDTA complex

Heilen Arce [a], Mavis L. Montero [a,b,*], Alejandro Sáenz [b,c], Victor M. Castaño [d]

[a] Escuela de Química, Universidad de Costa Rica, San José, Costa Rica
[b] Centro de Investigación en Ciencia e Ingeniería de Materiales, Universidad de Costa Rica, Costa Rica, San José, Costa Rica
[c] Escuela de Física, Universidad de Costa Rica, San José, Costa Rica
[d] Centro de Física Aplicada y Tecnología Avanzada, UNAM, Querétaro, Qro., Mexico

Received 22 December 2003; accepted 8 April 2004
Available online 15 June 2004

Abstract

Hydroxyapatite (HAp) was synthesized through the decomposition of a Ca(EDTA) complex in presence of phosphate ions. Ion concentrations are much higher than previously reported. This route allows the formation of HAp at temperatures below 140 °C and at different pH values. Phase identification, crystallinity and morphology of the obtained products were studied via FTIR, SEM, XRD and EDS.
© 2004 Elsevier Ltd. All rights reserved.

Keywords: Hydroxyapatite; Complex; EDTA; Hydrothermal; Low temperature; Calcium phosphates

1. Introduction

Hydroxyapatite (HAp) is the main inorganic constituent of bone tissue. Synthetic HAp has been successfully used for synthetic bone, metal coatings and other materials of biomedical interest [1–4]. A number of different methodologies for producing synthetic calcium phosphates are available in the literature, ranging from updates of long-known techniques, to reports on novel synthetic routes, including solution processes, hydrothermal systems, bio-mimetic systems and sol–gel methods, among others [5–18]. The preparation of homogeneous HAp precipitates via decomposition of chemical complexes through chelating agents are simple processes, particularly associated with hydrothermal reactions. These kind of processes have been used to produce HAp whiskers and coatings on metals and ceramic materials. Chelates including EDTA, citric acid and lactic acid have been tested [19–24]. Our group has recently succeeded in synthesizing SiO_2–HAp composites by decomposing the Ca(EDTA) complex under reflux conditions. In addition, HAp coatings on metals with orthopedic interest have been produced at temperatures below 150 °C [25–28].

The production of Hap through homogeneous solutions of complexed calcium yields a versatile synthetic route, which allows to experiment with different temperatures, pH conditions and concentrations of both calcium and phosphate ions. The present work shows the results of synthesizing HAp through the decomposition of the Ca(EDTA) complex in presence of phosphate ions, at concentrations five times larger than previously reported [19–24]. HAp has been produced at temperatures of 140 °C or lower. Besides, the formation and morphology of the precipitates is studied as a function of pH.

2. Experimental

2.1. Calcium/EDTA/phosphate solution

Complexed solutions were prepared with $CaCl_2 \cdot 2H_2O$ (Riedel-de Haën, analytical grade), Na_2

* Corresponding author. Fax: +506-253-5020.
E-mail addresses: heilenarce@costarricense.cr (H. Arce), mmontero@equi.ucr.ac.cr (M.L. Montero), asaenz@cariari.ucr.ac.cr (A. Sáenz), castano@fata.unam.mx (V.M. Castaño).

0277-5387/$ - see front matter © 2004 Elsevier Ltd. All rights reserved.
doi:10.1016/j.poly.2004.04.021

EDTA · $2H_2O$ (Aldrich Chemical Co., analytical grade), and K_2HPO_4 (Riedel-de Haën, analytical grade). One liter of the solutions were prepared as to obtain $CaCl_2$ 0.25 M, Na_2 EDTA 0.25 M and K_2HPO_4 0.15 M at pH values of 5.0, 7.0 and 9.0. Two hundred millilitres of the calcium/EDTA/phosphate solution at the mentioned pH values were refluxed until the production of a precipitate was observed. Solutions were also heated in a Mini-reactor Parr up to 120 and 140 °C during 4 h.

2.2. Characterization

Sample morphology and constituent elements were determined through a Low Vacuum Scanning Electron Microscope, JEOL-5900LV (LV-SEM), equipped with an energy dispersive X-ray analysis probe, Oxford (EDS) and a Hitachi S-570 with an Aspe model Sirius 10/7.5 EDS. Samples were fixed to the aluminum holder via adhesive carbon foil and secondary electrons were employed. FTIR was performed in a Perkin–Elmer Spectrum 1000. XRD was carried out in a Siemens D5000 and a Rigaku Mini Flex.

3. Results and discussion

The calcium/EDTA/phosphate solution at pH 5.0 was refluxed until a precipitate was observed after at least 20 h. Figs. 1–3 show a series of SEM micrographs showing the different morphologies obtained for pH 5.0 under the three different conditions, i.e.: reflux, 120 and 140 °C. In the solid obtained under reflux, Fig. 1, bars are present with sizes of the order of 10 μm long and 1 μm in diameter and platelets of various sizes, ranging between 1/2 and 2 μm. When the solution is heated to 120 °C, the solid obtained, Fig. 2, consists mostly of platelets with sizes ranging from 1.5 to 3 μm, in addition several needles about 1 μm long are present. The solid obtained when the solution is heated to 140 °C, Fig. 3, presents different morphology to those previously described. Crystallites resemble clustered thin blades between 2 and 3 μm long. Fig. 5 shows the corresponding X-ray diffractograms, which clearly show that the nature of the solid precipitated obtained depends on temperature. The one corresponding to the refluxed solution (the lowest in Fig. 5) shows the presence of monetite and HAp as a minority phase. The one for the solid obtained at 120 °C clearly indicates that HAp is now more abundant and, for that obtained with the reactor at 140 °C, HAp is the main phase. It is important to point out that no report on the production of HAp at temperatures below 150 °C and pH 5.0 in so short period of time is available in the literature. Thus, the presence of much higher concentrations of calcium and phosphate ions achieved in this work allow the formation of HAp under these conditions. It is also important to emphasize that

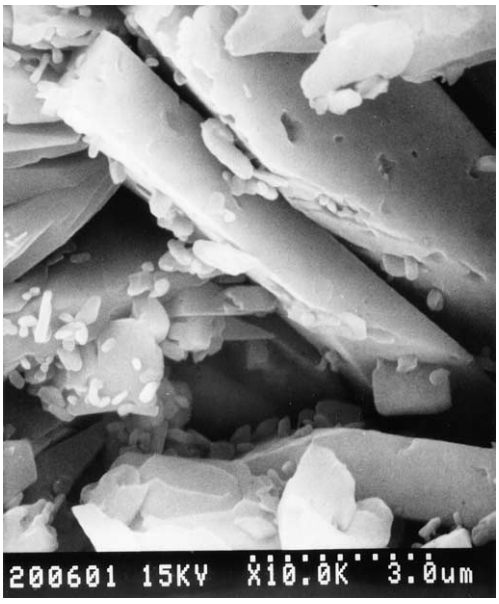

Fig. 1. Morphology and size for the solid obtained as precipitates at pH 5.0 and at reflux temperature.

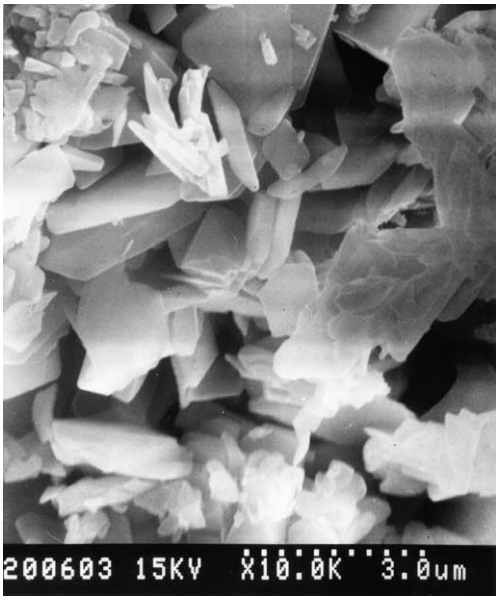

Fig. 2. Morphology and size for the solid obtained as precipitates at pH 5.0 and 120 °C.

the solubility diagram for calcium phosphates shows that at pH values smaller or equal to 5.0, HAp becomes less stable than dicalcium phosphate. Therefore, the HAp phase exposed to more acidic conditions may coexist with this compound [29,30].

Table 1 summarizes the Ca/P ratio for the solids obtained at different pH values and temperatures. For pH 5.0, the increase in this ratio with increasing temperature confirms that the solid obtained is richer in HAp as temperature is raised. However, the Ca/P ratio

Fig. 3. Morphology and size for the solid obtained as precipitates at pH 5.0 and 140 °C.

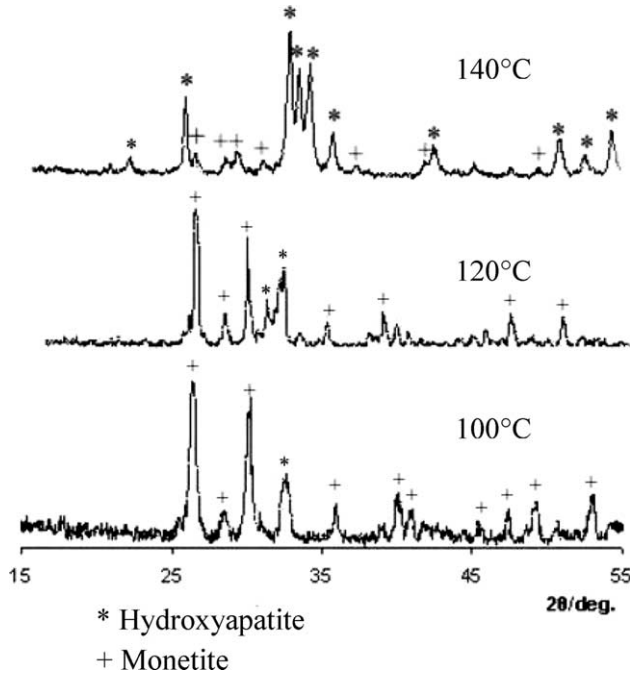

Fig. 5. X-ray diffractograms for samples prepared at pH 5.0. Temperatures are indicated above each spectra.

Table 1
Ca/P ratio for solids obtained at different pH values and temperatures by decomposition of a Ca–EDTA complex in presence of phosphate

Temperature (°C)	Ca/P (pH 5)	Ca/P (pH 7)	Ca/P (pH 9)
100	1.01	1.57	1.59
120	1.14	1.57	1.60
140	1.41	1.59	1.61

for the solid produced at 140 °C (1.41) is well below the stoichiometric ratio for HAp (1.67); this is a consequence of monetite still being present.

The solids precipitated at pH 7.0 after 96 h under reflux and for the solution heated up to 120 and 140 °C in the reactor were analyzed with scanning microscopy. Under these three conditions elongated crystallites between 5 and 10 μm are found. The image for the 140 °C case is shown in Fig. 4. X-ray diffractograms for these

Fig. 4. Morphology and size for solids obtained as precipitates at pH 7.0 and 140 °C.

Fig. 6. Morphology and size for solids obtained as precipitates at pH 9.0 and reflux temperature.

powders prove HAp to be the only phase present. XRD spectra are very similar for these samples and for those prepared at pH 9.0, the solid obtained at pH 9.0 and 140 °C is shown in Fig. 7. In Table 1, the Ca/P ratio for pH 7.0 varies between 1.57 and 1.60 showing a calcium-deficient HAp; this is typical for HAp obtained from decomposition of complexes.

It was necessary to reflux the calcium/EDTA/phosphate solution at pH 9.0 for 120 h in order to obtain a precipitate. The solid from the refluxed solution presents elongated crystallites 0.1 m in diameter and about 1.5 μm long, Fig. 6. It is important to mention that the use of complexing agents for the production of HAp via hydrothermal methods has traditionally being associated to the production of whiskers (about 15 μm in length) [29]. In this case, however, with much larger concentrations of calcium and phosphate, at reflux temperature, the size of the crystallites is significantly smaller. After heating for 4 h at 120 and 140 °C, the crystals consist of needles about 12 μm long, resembling those synthesized at pH 7.0 but some groups grow up from a common origin, see Fig. 7. Powder X-ray diffractograms show, for all samples obtained at pH 9.0, that the only phase is Hap, Fig. 8 shows the one corresponding to reflux at 140 °C.

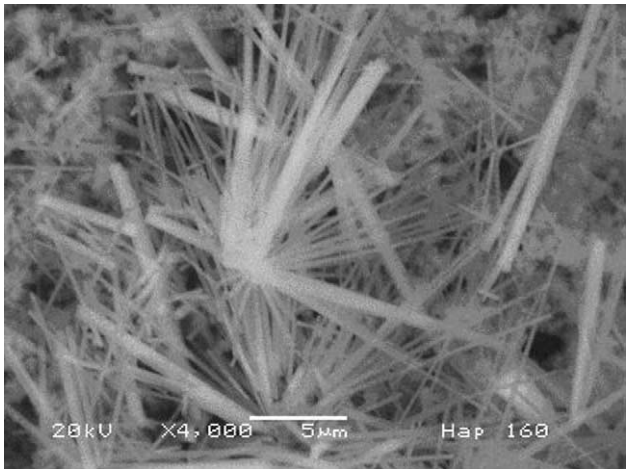

Fig. 7. Morphology and size for solids obtained as precipitates at pH 9.0 and 140 °C.

IR spectra for samples prepared at pH 7.0 and 9.0 show all bands corresponding to the PO_4^{3-} and to OH^-. A weaker band from 1400 to 1500 cm^{-1} shows the presence of traces of CO_3^{2-}. A signal at around 859 cm^{-1} shows the HPO_4^{2-} functional group.

From Table 1 it is evident that those solids with HAp as the only present phase (pH 7.0 and 9.0), are not stoichiometric but calcium-deficient. Several theories have being develop to explain this phenomenon. They consider: (a) the presence of other phases like amorphous calcium phosphate or octacalcium phosphate, (b) the absorption of phosphate species by the surface, (c) lattice defects combinations, (d) Ca^{2+} and OH^- vacancies and (e) the substitution of some phosphate groups by HPO_4^{2-} [31,32]. The presence of IR bands corresponding to CO_3^{2-} and HPO_4^{2-} in these samples could support the last model.

4. Conclusions

HAp has been prepared by a hydrothermal method under reflux and at 120 and 140 °C during 4 h at pH values of 7.0 and 9.0; by decomposition of a Ca–EDTA complex. At pH 5.0 there is a direct influence of temperature on the solid obtained; at reflux the main component of the solid is monetite. When temperature is raised, HAp phase becomes predominant. The

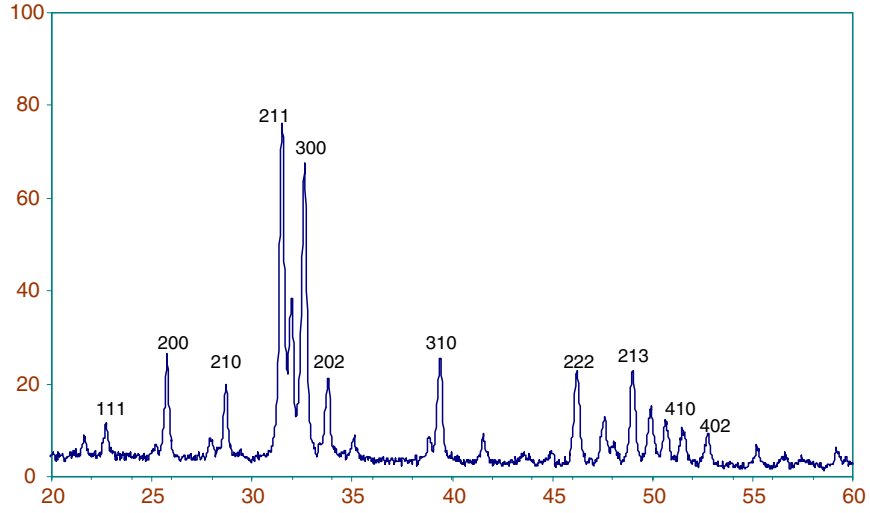

Fig. 8. X-ray diffractograms for sample prepared at pH 9.0 and 140 °C. It is totally alike to those obtained for all samples prepared at pH 7.0 and 9.0.

morphology of the solid synthesized at pH 5.0 changes with temperature, from plate like monetite to thin blades of HAp mixed with monetite. For crystals produced at pH 7.0 the morphology is elongated, with sizes between 5 and 10 μm which do not change significantly with temperature,. The crystals corresponding to pH 9.0 are all elongated with sizes varying from 1.5 μm in length and 0.1 μm in diameter for reflux temperature to about 12 μm for temperatures of 120 and 140 °C. It is important to remark that in order to obtain a solid at reflux temperatures, rather long reaction times were needed, which became even longer with increasing pH. An increase of 20 °C has the effect of reducing to 4 h the time needed to obtain a solid for the different pH values studied.

The Ca/P ratio increases with temperature for pH 5.0, this fact is explained by the formation of HAp in larger quantities. It reaches up to 1.41, due to the presence of monetite in the solid. This ratio varies from 1.57 to 1.61 for pH 7.0 and 9.0. The crystallites obtained are calcium-deficient for all pH values and temperatures investigated, this could be related to the presence of HPO_4^{2-} for all samples, as shown by its bands in the IR spectra.

Acknowledgements

This work was partially supported by Consejo Nacional de Investigaciones (CONICIT), Programa Mesoamericano de Intercambio Académico ANUIES-CSUCA and CLAFM. We acknowledge the use of XRD facilities at ININ, México and at Recursos Geotérmicos, ICE, Costa Rica.

References

[1] J.C. Elliott, Recent studies of apatites and other calcium orthophosphates, in: E. Bres, P. Hadouin (Eds.), Calcium Phosphates Materials, Fundamentals, Sauramps Medical, Monpellier, 1998, p. 25.
[2] S. Dorozhkin, M. Epple, Angew. Chem. Int. Ed. 41 (2002) 3130.
[3] K. Mattox, in: D. Muster (Ed.), Biomaterials – Hard Tissue Repair and Replacement, vol. 3, Elsevier, Amsterdam, 1992.
[4] W. Suchanek, M. Yoshimura, J. Mater. Res. 13 (1998) 94.
[5] L.M. Rodríguez-Lorenzo, M. Vallet-Regí, Chem. Mater. 12 (2000) 2460.
[6] M. Vallet-Regí, J. Chem. Soc. Dalton Trans. (2001) 97.
[7] P.A.A.P. Maques, A.P. Serro, V.J. Saramago, A.C. Fernades, M.C.F. Magalhaes, R. Correira, J. Mater. Chem. 13 (2003) 1484.
[8] E.A.P. De Maeyer, R.M.H. Verbeeck, D.E. Naessens, J. Cryst. Growth 135 (1994) 539.
[9] S.W. Russell, K.A. Luptak, Suchicital, T.L. Alford, V.B. Pizziconi, J. Am. Ceram. Soc. 79 (1996) 837.
[10] D. Walsh, J.L. Kingston, B.R. Heywood, S. Mann, J. Cryst. Growth 133 (1993) 1.
[11] M. Yoshimura, H. Suda, in: P.W. Brown, B. Constantz (Eds.), Hydroxyapatite and Related Materials, CRC Press, Boca Raton, FL, 1994, p. 45.
[12] R.Z. LeGeros, in: P.W. Brown, B. Constantz (Eds.), Hydroxyapatite and Related Materials, CRC Press, Boca Raton, FL, 1994, p. 3.
[13] F. Peters, M. Epple, J. Chem. Soc. Dalton Trans. (2001) 3577.
[14] A. López-Macipe, J. Gómez-Morales, R. Rodríguez-Clemente, Adv. Mater. 10 (1998) 49.
[15] A. Jillavenkatesa, D.T. Hoelzer, R.A. Condrate, J. Mater. Sci. 34 (1999) 4821.
[16] S.W. Ruseel, K.A. Luptak, C. Suchicital, T.L. Alford, V.B. Pizziconi, J. Am. Ceram. Soc. 79 (1996) 837.
[17] K. Schwarz, M. Epple, Chem. Eur. J. 10 (1998) 1898.
[18] E. Rivera, M. Araiza, W. Brostow, V. Castaño, J.R. Díaz-Estrada, R. Hernández, J.R. Rodríguez, Mater. Lett. 41 (1999) 128.
[19] W. Suchanek, H. Suda, M. Yashima, M. Kakihana, M. Yoshimura, J. Mater. Res. 10 (1995) 521.
[20] Y. Fujishiro, S. Uchida, T. Sato, Bioceramics 12 (1999) 141.
[21] N. Cristiansen, R.E. Riman, Bioceramics: A future through Microstructural and Chemical Design, in: Proceedings of the Fifth Scandinavian Symposium on Material Science, New Materials and Processes, 22–23 May 1989, p. 209.
[22] Y. Fujishiro, A. Fujimoto, T. Sato, A. Okuwaki, J. Coll. Interf. Sci. 173 (1995) 119.
[23] M. Toriyama, Y. Kawamoto, T. Suzuki, Y. Yokogawa, K. Nishizawa, F. Nagata, M.R. Mucalo, J. Mater. Sci. Lett. 15 (1996) 179.
[24] M. Yoshimura, H. Suda, K. Okamoto, K. Ioku, J. Mater. Sci. 29 (1994) 3399.
[25] A. Saenz, M.L. Montero, V.M. Castaño, Phys. Stat. Solidi 230 (2002) 347.
[26] A. Sáenz, M.L. Montero, V.M. Castaño, Surf. Rev. Lett. 9 (2002) 1795.
[27] A. Sáenz, M.L. Montero, V.M. Castaño, Surf. Rev. Lett. 9 (2002) 1799.
[28] A. Sáenz, M.L. Montero, G. Mondragón-Galicia, V. Rodríguez-Lugo, V.M. Castaño, Mat. Res. Innovat. 7 (2003) 68.
[29] P.W. Browen, J. Am. Ceram. Soc. 75 (1992) 17.
[30] G. Vereecke, Lamaitre, J. Cryst. Growth 104 (1990) 521.
[31] J.L. Meyer, B.O. Fowler, Inorg. Chem. 21 (1982) 3029.
[32] R.Z. LeGeros, Monographs in Oral Science, in: Calcium Phosphates in Oral Biology and Medicine, vol. 15, Karger AG, Basel, 1991.

Available online at www.sciencedirect.com
SCIENCE DIRECT®
Polyhedron 23 (2004) 1903–1907
POLYHEDRON
www.elsevier.com/locate/poly

Syntheses and crystal structures of two mononuclear Zn(II) complexes with the 2,5-bis(2-pyridyl)-1,3,4-thiadiazole ligand ☆

Fouad Bentiss [a], Michel Lagrenée [a,*], Hervé Vezin [b], Jean-Pierre Wignacourt [a], Elizabeth M. Holt [c]

[a] *Laboratoire de Cristallochimie et Physicochimie du Solide, CNRS UMR 8012, ENSCL, BP 108, F-59652 Villeneuve d'Ascq Cedex, France*
[b] *Laboratoire de Chimie Organique et Macromoleculaire, CNRS UMR 8009, USTL Bat C3, F-59655 Villeneuve d'Ascq Cedex, France*
[c] *Formerly: Department of Chemistry, Oklahoma State University, Stillwater, OK 74078, USA*

Received 9 February 2004; accepted 13 April 2004
Available online 8 June 2004

Abstract

Crystal structure and minimum energy calculations show that 2,5-bis(2-pyridyl)-1,3,4-thiadiazole exists in the solid state in one of two minimum energy forms. Uncomplexed, both nitrogen atoms of the pyridyl rings facing in the direction of the sulfur atom of the five-membered hetero ring in the planar molecule. Two different single crystal structures of zinc complexed to this ligand with a Zn/ligand ratio of 1/2 show a rotation of one of the pyridyl rings of each ligand molecule to allow complexation of the metal to the pyridyl nitrogen atom of this ring and the near diazole nitrogen atom. Axial coordination to water molecules completes the octahedral geometry at zinc.
© 2004 Elsevier Ltd. All rights reserved.

Keywords: 2,5-Bis(2-pyridyl)-1,3,4-thiadiazole; Zinc; Energy minimization; Crystal structures; Monomeric complexes

1. Introduction

There is interest in dimeric metal complexes with close metal–metal contacts and appropriate bridging atoms for their magnetic properties [1–7]. These properties may be modified by the character of the bridging species and by the geometry of the metal atoms and bridging species. 1,2,4-Triazoles (1A, 1B), 1,3,4-oxadiazoles (1C) and 1,3,4-thiadiazoles (1D) with *o*-pyridine substitution at the carbon positions of the hetero ring (Scheme 1) have been used as bridging ligands capable of enforcing suitable geometry and proximity of metal atoms, while providing a σ overlap superexchange pathway. Structural parameters such as magnitude of the M–N=N angles, coplanarity of the extended π network of the ligand with the metal, and conformation of N7 and N13 nitrogen atoms play a role in determination of the magnitude and type of magnetic interaction.

When the pyridyl nitrogen atoms face in the same direction as the N1 and N2 positions and the four nitrogen atoms bond to two metal atoms (Scheme 1D), metal–metal distances of about 4 Å are seen [8]. However, one pyridine ring may rotate 180° to bond to a metal atom along with the nitrogen atom in the 4 position. A second metal is found on the opposite side of the ligand, bound to the nitrogen atom of the remaining pyridine ring and to the near nitrogen of the oxadiazole ring [9]. In this conformation, metal–metal interactions are absent.

We have recently reported the structures of monomeric complexes of Co(II), Ni(II) and Cu(II) with the neutral 2,5-bis(2-pyridyl)-1,3,4-thiadiazole derivative

☆ Supplementary data associated with this article can be found, in the online version, at doi:10.1016/j.poly.2004.04.025.

* Corresponding author. Tel.: +33-320-337-746; fax: +33-320-436-814.
E-mail address: michel.lagrenee@ensc-lille.fr (M. Lagrenée).

0277-5387/$ - see front matter © 2004 Elsevier Ltd. All rights reserved.
doi:10.1016/j.poly.2004.04.025

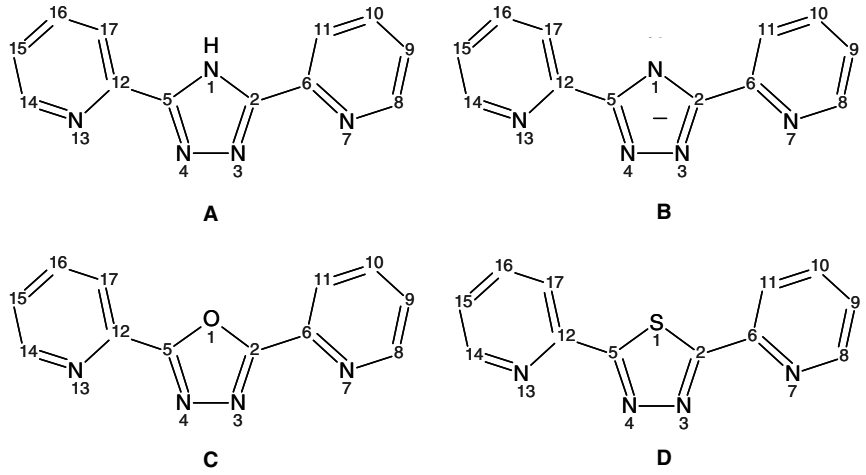

Scheme 1.

[10]. We report here the structures of the uncomplexed ligand 1D (structure I) along with the monomeric zinc (diaquo-2,5-bis(2-pyridyl)-1,3,4-thiadiazole) cationic complexes with zinc tetrachloride (**II**) and perchlorate (**III**) as counter ions. Comparison of the energy-minimized structure [11] of the solid-state uncoordinated ligand and of the two monomeric zinc(2,5-bis(2-pyridyl)-1,3,4-thiadiazole)$_2$ complexes permits an evaluation of the relative importance of conformation and planarity in complex formation. From this information, the potential of the ligand as a bridging unit may be evaluated.

2. Experimental

2.1. Synthesis

2.1.1. Ligand (*I*)

2,5-Bis(2-pyridyl)-1,3,4-thiadiazole (**I**) was synthesized as described previously [12,13]. M.p., 218 °C. ^{1}H NMR (200 MHz, dmso): δ (ppm) 7.60 (t, 2H, $J = 7.5$ Hz), 8.05 (t, 2H, $J = 7.7$ Hz), 8.31 (d, 2H, $J = 7.9$ Hz), 8.71 (d, 2H, $J = 5.1$ Hz). ^{13}C NMR (200 MHz, $CDCl_3$): δ (ppm) 157.32, 150.30, 144.72, 137.7, 124.04, 118.76. *Anal.* Calc. for $C_{12}H_8N_4S$: C, 60.00; H, 3.33; N, 23.33; S, 32.00. Found: C, 60.11; H, 3.21; N, 23.36; S, 32.06%.

2.1.2. $[ZnL_2(H_2O)_2](ZnCl_4)(H_2O)_2$ (*II*)

$ZnCl_2$ (1.5 mmol, 0.2 g) in 8 ml of water was added to (0.42 mmol, 0.1 g) of ligand (**I**) dissolved in 8 ml of ethanol. The solution was filtered and after 24 h, the colorless compound (**II**) crystallized at room temperature. Crystals (**II**) were washed with water and dried under vacuum. *Anal.* Calc. for $C_{24}H_{24}N_8O_4S_2Cl_4Zn_2$: C, 34.93; H, 2.91; N, 13.58; S, 7.76; Cl, 17.20. Found: C, 34.99; H, 2.99; N, 13.51; S, 7.72; Cl, 17.39%.

2.1.3. $[ZnL_2(H_2O)_2](ClO_4)_2$ (*II*)

$Zn(ClO_4)_2$, $6H_2O$ (1.5 mmol, 0.56 g) in 8 ml of water was added to (0.42 mmol, 0.1 g) of ligand (**I**) dissolved in 8 ml of ethanol. The solution was filtered and after 24 h, the colorless compound (**III**) crystallized at room temperature. Crystals were washed with water and dried under vacuum. *Anal.* Calc. for $C_{24}H_{20}N_8O_{10}S_2Cl_2Zn$: C, 36.91; H, 2.56; N, 14.35; S, 8.20; Cl, 9.09. Found: C, 36.87; H, 2.59; N, 14.43; S, 8.26; Cl, 9.21%.

2.2. Crystal structure determinations

Single crystals of **I**, **II** and **III** were mounted on a Brucker AXS SMART three-circle diffractometer using graphite monochromated Mo Kα radiation ($\lambda = 0.71073$ Å), equipped with a CCD two-dimensional detector [14]. Data (Table 1) were corrected for Lorentz, polarization, background and decomposition effects. Atomic positions were determined using SHELXS [15] and refined using full-matrix least-squares [16]. Hydrogen positions were calculated and included in the final cycles of refinement in constrained positions and with fixed isotropic thermal parameters. Absorption corrections were not made due to the small value of the absorption coefficients (Table 1). Extinction was refined for all three structures but was minimal. Tables 2–4 present the bond angles and distances for **I**, **II** and **III**, respectively.

2.3. Theoretical calculations

All quantum theoretical calculations were performed with SPARTAN PRO V. 1.05 software package for PC (Irvine Inc.) using ab initio Hartree–Fock 6-21G** basis set at RHF (Restricted Hartree–Fock) level. Prior full ab initio optimization, the three conformers were optimized with semi-empirical PM3 method.

Table 1
Crystal data for compounds **I**, **II** and **III**

	I	**II**	**III**
Formula	$C_{12}H_8N_4S$	$C_{24}H_{24}N_8O_4S_2Cl_4Zn_2$	$C_{24}H_{20}N_8O_{10}S_2Cl_2Zn$
Formula weight	240.28	825.17	780.86
Crystal system	monoclinic	monoclinic	monoclinic
Space group	$P2_1/n$	$C2/c$	$P2_1/n$
a (Å)	4.8279(8)	17.137(3)	10.910(3)
b (Å)	20.811(3)	13.226(3)	11.126(3)
c (Å)	11.2751(8)	14.125(3)	13.173(3)
β (°)	99.304(3)	91.805(5)	100.541(5)
V (Å^3)	1118.0(3)	3199.8(11)	1571.9(6)
Z	4	4	2
D_{calc} (Mg/m^3)	1.428	1.713	1.650
T (K)	293(2)	293(2)	293(2)
$F(0\,0\,0)$	496	1664	792
Crystal size (mm)	$0.1 \times 0.1 \times 0.1$	$0.1 \times 0.1 \times 0.1$	$0.1 \times 0.1 \times 0.1$
Lattice determination	48 reflections ($11.6 < 2\theta < 25.8$)	48 reflections ($9.6 < 2\theta < 25.8$)	68 reflections ($8.4 < 2\theta < 20.8$)
μ (mm^{-1})	0.270	2.009	1.151
Data collection range (°)	($3.92 < 2\theta < 46.5$)	($3.90 < 2\theta < 57.4$)	($4.46 < 2\theta < 61$)
Range of indices	h, −5 to 5; k, −21 to 22; l, −12 to 12	h, −23 to 23; k, −17 to 17; l, −19 to 19	h, −15 to 15, k; −15 to 15; l, −18 to 18
Reflections measured	4797	16 183	17 314
Unique reflections	1102	4134	4699
R_{int}	2.65	8.1	8.05
Observed reflections ($F > 2.0\sigma(F)$)	1102	1881	1565
R	2.77	5.48	5.98
wR	8.45	8.44	14.38
Goodness-of-fit on F^2	0.89	0.924	0.919
Number of parameters	154	217	251
Maximum peak in final ΔF map (e/Å^3)	0.040	0.089	0.047
Minimum peak in final ΔF map (e/Å^3)	−0.025	−0.058	−0.029

Table 2
Bond angles (°) and distances (Å) for 2,5-bis(2-pyridyl)-1,3,4-thiadiazole (**I**)

Bond distances			
S1–C5	1.712(2)	C8–C9	1.364(4)
S1–C2	1.714(2)	C9–C10	1.363(4)
C2–N3	1.306(3)	C10–C11	1.374(4)
C2–C6	1.470(3)	C12–N13	1.332(3)
N3–N4	1.369(3)	C12–C17	1.386(3)
N4–C5	1.307(3)	N13–C14	1.333(3)
C5–C12	1.466(3)	C14–C15	1.374(3)
C6–N7	1.327(3)	C15–C16	1.371(3)
C6–C11	1.374(3)	C16–C17	1.374(3)
N7–C8	1.332(3)		
Bond angles			
C5–S1–C2	86.90(11)	N7–C8–C9	124.9(3)
N3–C2–C6	123.5(2)	C10–C9–C8	118.0(3)
N3–C2–S1	114.3(2)	C9–C10–C11	119.0(3)
C6–C2–S1	122.2(2)	C6–C11–C10	118.5(2)
C2–N3–N4	112.2(2)	N13–C12–C17	123.4(2)
C5–N4–N3	112.2(2)	N13–C12–C5	115.4(2)
N4–C5–C12	123.7(2)	C17–C12–C5	121.1(2)
N4–C5–S1	114.4(2)	C14–N13–C12	117.0(2)
C12–C5–S1	121.9(2)	N13–C14–C15	123.3(2)
N7–C6–C11	123.7(2)	C16–C15–C14	119.1(3)
N7–C6–C2	115.6(2)	C17–C16–C15	118.7(2)
C11–C6–C2	120.7(2)	C16–C17–C12	118.5(2)
C6–N7–C8	115.8(2)		

Table 3
Bond angles (°) and distances (Å) for $ZnL_2(H_2O)_2](ZnCl_4)(H_2O)_2$ (**II**)

Bond distances			
Zn1–N3	2.078(4)	C6–N7	1.356(6)
Zn1–N7	2.129(5)	C6–C11	1.375(7)
Zn1–O1	2.129(5)	N7–C8	1.333(7)
Zn2–Cl2	2.2532(19)	C8–C9	1.377(8)
Zn2–Cl1	2.2946(18)	C9–C10	1.371(8)
S1–C2	1.700(5)	C10–C11	1.385(8)
S1–C5	1.737(6)	C12–N13	1.327(7)
C2–N3	1.305(7)	C12–C17	1.368(8)
C2–C6	1.475(7)	N13–C14	1.334(8)
N3–N4	1.376(6)	C14–C15	1.372(10)
N4–C5	1.294(7)	C15–C16	1.352(9)
C5–C12	1.459(8)	C16–C17	1.388(9)
Bond angles			
N3^{i}–Zn1–N3	180.0	N4–N3–Zn1	130.7(3)
N3^{i}–Zn1–N7	102.33(17)	N7–Zn1–O1^{i}	92.04(19)
N3–Zn1–N7	77.67(17)	O1–Zn1–O1^{i}	180.0(3)
N7–Zn1–N7^{i}	180.0	Cl2–Zn2–Cl2	112.11(10)
N3^{i}–Zn1–O1	89.8(2)	Cl2–Zn2–Cl1^{ii}	108.23(8)
N3–Zn1–O1	90.2(2)	Cl2–Zn2–Cl1	111.03(8)
N7–Zn1–O1	87.96(19)	Cl1^{ii}–Zn2–Cl1	106.05(10)

$^{i} = -x + 1/2,\ -y + 1/2,\ -z$; $^{ii} = -x,\ y,\ -z + 1/2$.

Table 4
Bond angles (°) and distances (Å) for $[ZnL_2(H_2O)_2](ClO_4)_2$ (**III**)

Bond distances			
Zn1–N3	2.080(4)	N3–N4	1.368(6)
Zn1–N7	2.155(4)	N4–C5	1.296(6)
Zn1–O99	2.163(4)	C5–C12	1.475(7)
Cl1–O33′	1.28(2)	C6–N7	1.339(6)
Cl1–O22′	1.279(18)	C6–C11	1.374(7)
Cl1–O11′	1.297(16)	N7–C8	1.325(7)
Cl1–O44′	1.374(16)	C8–C9	1.371(7)
Cl1–O33	1.395(12)	C9–C10	1.357(8)
Cl1–O22	1.401(16)	C10–C11	1.378(8)
Cl1–O44	1.454(13)	C12–N13	1.326(7)
Cl1–O11	1.498(15)	C12–C17	1.350(8)
S1–C2	1.702(5)	N13–C14	1.339(8)
S1–C5	1.721(6)	C14–C15	1.333(10)
C2–N3	1.308(6)	C15–C16	1.359(10)
C2–C6	1.467(7)	C16–C17	1.392(9)
Bond angles			
$N3^i$–Zn1–N3	180.0(3)	C2–N3–N4	113.6(4)
$N3^i$–Zn1–N7	101.98(17)	C2–N3–Zn1	114.4(3)
N3–Zn1–N7	78.02(17)	N4–N3–Zn1	131.9(3)
N7–Zn1–$N7^i$	180.0(3)	C5–N4–N3	110.9(4)
N3–Zn1–$O99^i$	89.31(16)	N4–C5–C12	123.8(5)
N7–Zn1–$O99^i$	91.94(16)	N4–C5–S1	115.0(4)
N3–Zn1–O99	90.69(16)	C12–C5–S1	121.2(4)
N7–Zn1–O99	88.06(16)	C8–N7–Zn1	128.8(4)
$O99^i$–Zn1–O99	180.00(14)	C6–N7–Zn1	113.6(3)
O33–Cl1–O22	141.5(13)	O33′–Cl1–O22′	102.5(18)
O33–Cl1–O44	106.8(10)	O33′–Cl1–O11′	119.6(18)
O22–Cl1–O44	93.1(10)	O22′–Cl1–O11′	110.9(12)
O33–Cl1–O11	103.9(9)	O33′–Cl1–O44′	122.2(18)
O22–Cl1–O11	97.8(9)	O22′–Cl1–O44′	125.0(19)
O44–Cl1–O11	112.8(9)	O11′–Cl1–O44′	75.1(13)

Symmetry_equiv_pos_as_xyz.
$^i = -x, -y, -z'$.

3. Discussion

2,5-Bis(2-pyridyl)-1,3,4-thiadiazole (**I**) (L = ligand) exists with the 2-pyridyl rings relatively coplanar with the central 1,3,4-thiadiazole ring, rotation angles 4.9° and 2.8°. Both pyridyl nitrogen atoms are found on the sulfur side of the 1,3,4-thiadiazole ring (Fig. 1) [17].

Minimum energy calculations at the Hartree–Fock level using the 6-31G** basis set (Spartan [11]) show a difference of 11.7 kcal/mol between this and the local minima form with both pyridyl nitrogen atoms rotated to the 'azide side' of the five-membered ring. The conformation with a single pyridyl ring rotated to the 'azide side' is at an intermedial level in energy (5.4 kcal/mol greater than the local minimum form). All three energy-minimized conformations show total coplanarity of all atoms with a calculated dihedral angle of 0.02°.

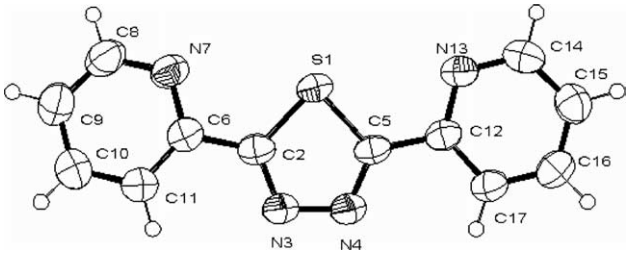

Fig. 1. Projection view of 2,5-bis(2-pyridyl)-1,3,4–thiadiazole (**I**) (thermal ellipsoids are shown at the 50% probability level).

Complexes **II** and **III** show zinc(+2) in octahedral coordination. Each zinc(+2) atom exists on a center of symmetry and is coordinated to two molecules of ligand L and to two molecules of water. Coordination to the ligands (**I**) is achieved by interaction with the nitrogen atom of a single pyridyl ring and with the near nitrogen of the azide group. Zn–N, 2.078(4) and 2.129(5) Å (**II**), 2.080(4) and 2,155(4) Å (**III**) (Figs. 2 and 3). The nitrogen atom of the remaining pyridyl ring is rotated to the sulfur side of the thiadiazole ring. In **II**, both pyridyl rings, complexed and uncomplexed, display near coplanarity with the central thiadiazole ring (0.9° and 3.2°, respectively). However in **III** the complexed pyridyl ring displays an interplanar angle of 4.3° with the thiadiazole ring, whereas the noncomplexed ring subtends an angle of 20.9°, a significant rotation from coplanarity. Thus the ligand, L, is seen in a conformation close to that of the form of intermediate energy. In that conformation,

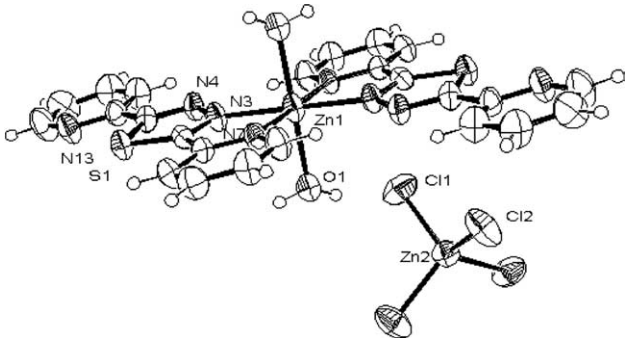

Fig. 2. Projection view of $[ZnL_2(H_2O)_2](ZnCl_4)(H_2O)_2$ (**II**) (thermal ellipsoids are shown at the 50% probability level).

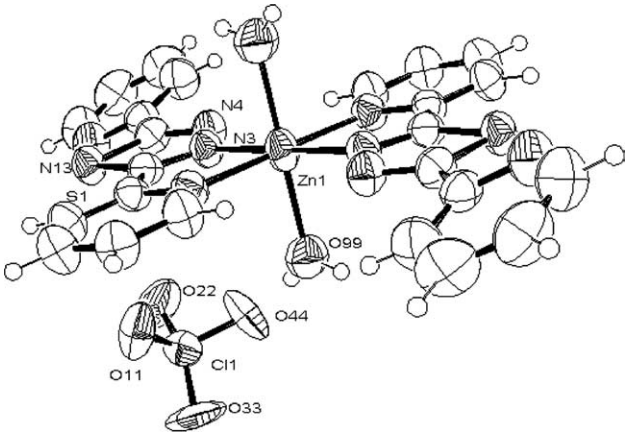

Fig. 3. Projection view of $[ZnL_2(H_2O)_2](ClO_4)_2$ (**III**). Only one of the two disordered sets of oxygens of ClO_4 are represented for clarity (thermal ellipsoids are shown at the 50% probability level).

it is not capable of complexing to two metal atoms in close proximity.

Important to potential overlap mechanisms of dimeric complexes of these ligands are the N3–Zn1–N7 and N3–Zn1–N7′ angles which should be close to the 90° angle between $d_{x^2-y^2}$ orbitals which are normally found in the equatorial plane. These angles are 77.67(17)° and 102.33(17)° in **II** and 78.02(17)° and 101.98(17)° in **III**, far from the ideal 90° value. Similarly M–N=N angles may be used to evaluate an overlap of greater efficiency. Values approaching 120° seen in dimers with effective orbital overlap between metal atoms. In **II** and **III**, these angles are 130.7(3)° (**II**) and 131.9(3)° (**III**), larger than ideal.

The water molecules are found in axial positions and at distances which substantiate the lack of axial distortion, Zn–O, 2.129(5) Å (**II**) and Zn–O 2.163(4) Å (**III**).

The counter ion, $ZnCl_4$ in **II** is well ordered. Hydrogen bonding links bound and unbound water molecules and also the unbound water molecule and N13. In **III**, the ClO_4 moiety shows disorder over more than two sets of positions. Refinement was unstable when attempts were made to introduce more than two sets of disordered oxygen positions. Hydrogen bonding links the two hydrogen atoms of the bound water molecule to oxygen atoms of each of the disordered ClO_4 groups.

Consideration of the solid-state structures seen for coordinated and uncoordinated 2,5-bis(2-pyridyl)-1,3,4-thiadiazole shows that the ligand is likely to maintain a coplanar or near coplanar conformation when coordinated. The rotation of a single pyridyl ring nitrogen atom to the 'azide side' of the five-membered hetero ring to bind one metal atom is accomplished without energy penalty. The rotation of the second pyridyl ring to provide bidentate binding to a second metal atom involves a relatively small energy cost. However, potentially effective orbital overlap between two bound metal atoms and thus significant magnetic interaction when 2,5-bis(2-pyridyl)-1,3,4-thiadiazole serves as a bridging ligand seem impeded by unfavorable M–N–N and N–M–N angles.

4. Supplementary material

The supplementary material has been sent to the Cambridge Crystallographic Data Center, 12 Union Road, Cambridge CB2 1EZ, UK (fax: +44-1223-336033; E-mail: deposit@ccdc.cam.ac.uk or www: http://www.ccdc.cam.ac.uk) as supplementary material No. SUP 200909–200911 and can be obtained by contacting the CCDC (quoting the article details and the corresponding SUP number).

References

[1] J.K. Tang, H.M. Wang, P. Cheng, X. Liu, D.Z. Liao, Z.H. Jiang, S.P. Yan, Polyhedron 20 (2001) 675.
[2] J.K. Tang, H.M. Wang, P. Cheng, X. Liu, D.Z. Liao, Z.H. Jiang, S.P. Yan, Pol. J. Chem. 74 (2000) 1651.
[3] M.I. Gabryszewski, B. Wieczorek, Spectrosc. Lett. 33 (2000) 23.
[4] S. Ferrer, P.J. vanKoningsbruggen, J.G. Haasnoot, J. Reedjijk, H. Kooijman, A.L. Spek, L. Lezama, A. Arif, J.S. Miller, J. Chem. Soc., Dalton Trans. (1999) 4269.
[5] J.C. Liu, D.G. Fu, J.Z. Zhuang, C.Y. Duan, X.Z. You, J. Chem. Soc., Dalton, Trans. 14 (1999) 2337.
[6] V.K. Singh, R. Sinha, R. Kant, B.K. Sinha, Asian J. Chem. 10 (1998) 532.
[7] P.J. Van Koningsbuggen, J.G. Haasnoot, W. Vreugdenhil, J. Reedijk, O. Kahn, Inorg. Chim. Acta 239 (1995) 5.
[8] A. Escuer, R. Vicente, B. Mernari, A. El Gueddi, M. Pierrot, Inorg. Chem. 36 (1997) 2511.
[9] J.P. Wignacourt, S. Sueur, M. Lagrenée, Acta Crystallogr., Sect. C 46 (1990) 394.
[10] F. Bentiss, M. Lagrenée, J.P. Wignacourt, E.M. Holt, Polyhedron 21 (2002) 403.
[11] SPARTAN PRO, V 1.0.1, Wavefunction Inc., Irvine, CA 92612.
[12] A.R. Katritzky, A.J. Boulton, in: Advances in Heterocyclic Chemistry, vol. 9, Academic Press, New York, 1968, p. 166.
[13] G. Mazzone, G. Puglisi, F. Bonina, A. Corsaro, J. Heterocyclic Chem. 20 (1983) 1399.
[14] Bruker AXS, SMART, Madison, WI, USA, 1998.
[15] G.M. Sheldrick, Acta Crystallogr., Sect. A 24 (1985) 4128.
[16] G.M. Sheldrick, SHELXL97, Program for the Refinement of Crystal Structures, University of Göttingen, Germany, 1997.
[17] L.F. Farrugia, J. Appl. Crystallogr. 30 (1997) 565.

Available online at www.sciencedirect.com
SCIENCE DIRECT®
Polyhedron 23 (2004) 1909–1914
POLYHEDRON
www.elsevier.com/locate/poly

New β-aminovinylketonates with annealated 1,2-benzothiazine-1,1-dioxide fragment

A.D. Garnovskii [a], Boris I. Kharisov [b,*], E.L. Anpilova [a], A.V. Bicherov [a,d], O.Yu. Korshunov [a], A.S. Burlov [a], Miguel A. Méndez-Rojas [e], L.M. Blanco [b], G.S. Borodkin [a], I.E. Uflyand [a], U. Ortiz Méndez [c]

[a] *Institute of Physical and Organic Chemistry, Rostov State University, Rostov-on-Don 344006, Russia*
[b] *Facultad de Ciencias Químicas, Universidad Autónoma de Nuevo León, San Nicolás de los Garza, N.L., A.P.18-F, C.P. 66450, Mexico*
[c] *Facultad de Ingeniería Mecánica y Eléctrica, Universidad Autónoma de Nuevo León, San Nicolás de los Garza, N.L., A.P.18-F, C.P. 66450, Mexico*
[d] *Southern Scientific Center of Russian Academy of Sciences, Rostov-on-Don 344006, Russia*
[e] *Universidad de las Américas, Puebla, Mexico*

Received 15 March 2004; accepted 13 April 2004
Available online 24 June 2004

Abstract

New β-aminovinylketones with heterocyclic 1,2-benzothiazine-1,1-dioxide and antipyrine moieties (LH) and their 3d-metal (Co^{II}, Ni^{II}, Cu^{II}, Zn^{II}) chelates have been synthesized. Two types of chelates can be obtained based on the coordination of the LH ligand, depending when an available carbonyl (C=O) group of the antipyrine fragment is coordinated (M = Co, Ni) or not (M = Cu) to the metal center. The molecular structure of compound **5b** was obtained by X-ray diffraction, indicating that the ligand **2b** forces the complex to adopt a highly distorted tetracoordinate square planar structure. Details on the synthesis and characterization of these complexes are discussed.
© 2004 Elsevier Ltd. All rights reserved.

1. Introduction

Although β-aminovinylketones have been subject of permanent interest in coordination chemistry [1–4], a relatively small number of their metal-chelate complexes, specially those containing heterocyclic fragments attached to the amino functionality, have been reported to the date [4–12]. Among them, the complexes based on azomethine derivatives of 1,2-benzothiazine-1,1-dioxide β-diketones are of especial interest due to their chances to act as anti-inflammatory drugs [13] as well as their potential as interesting ambidentate ligands [6–8]. According to previous studies by several other research groups, which includes X-ray diffraction analysis, molecules such as piroxicam, **1** [4-hydroxy-2-methyl-*N*-(2-pyridyl)-2H-1,2-benzothiazine-3-carboxamide-1,1-dioxide] a non-steroidal anti-inflammatory drug widely used for arthritis treatment can act as mono- [7] or bidentate [6,8] ligands.

As a contribution to the development of this research area, we have synthesized a series of ligands derived from the β-aminovinylketone, **2a**–**2c**, which can be considered as being potentially a mono (O)-, bi (N,O)- or tri (N,O,O)-dentate ligand, depending on the number of donor atoms bound to the metal center [14,15].

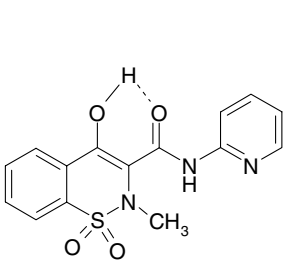

1

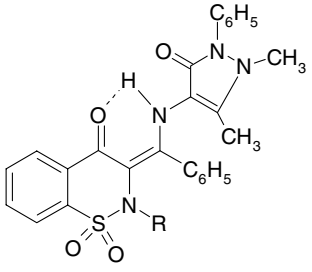

2a (R=H)
2b (R=CH_3)
2c (R=CH_2CH_3)

* Corresponding author. Tel.: 52-81-83727031/375-3068; fax: 52-81-83727031/3753851.
E-mail address: bkhariss@ccr.dsi.uanl.mx (B.I. Kharisov).

0277-5387/$ - see front matter © 2004 Elsevier Ltd. All rights reserved.
doi:10.1016/j.poly.2004.04.020

2. Experimental

2.1. Materials

β-Diketones **3a**–**3c** were synthesized from a known procedure [16]. 4-Aminoantipyrine, **4** was purchased from Aldrich and used as supplied. Metal acetates and pure metals in the form of foils or wire were purchased from Aldrich.

2.2. Instrumentation

^{1}H NMR spectra were recorded in a UNITY (Varian) 300 MHz instrument at room temperature and using DMSO-d_6 as solvent (TMS as internal reference). Melting points were determined in a MeltTemp apparatus. Infrared spectra were registered in vaseline oil using a Specord IR-75 spectrophotometer. Magnetochemical studies were carried out on a Quantum Design MPMS-5S SQUID apparatus using the Faraday's method at 21 °C. TESWARE (Sigma–Aldrich, model PS500-1) power supply was used for the electrolysis experiments.

2.3. Synthesis of the ligands

The β-aminovinylketones, **2a**–**2c**, were obtained by Schiff-base condensation of the corresponding *N*-*R*-1,2-benzothiazine-1,1-dioxide, **3** (a β-diketone, where R = H, Me, Et), with a small excess of 4-amino-2,3-dimethyl-1-phenylpyrazolone-5 (4-aminoantipyrine), **4**. The general procedure is illustrated as follow: In a round bottom flask, a mixture of 0.01 mol of (III) and 0.015 mol of (IV) was heated up to 180 °C and kept at this temperature before total elimination of water (30–40 min). After cooling the reaction mixture, 10 mL of acetonitrile were added and the mixture was refluxed; a precipitate formed and was filtered after cooling. The recovered solid was recrystalized from *i*-propanol, and dried at vacuum at 150 °C. Analytical data. Compound **2a**: R = H ($C_{26}H_{22}N_4O_4S$). NMR (DMSO-d_6, ppm): 1.95 (CH_3, s, 3H); 2.8 (CH_3N, s, 3H); 7.20–8.20 (Ar, m, 14H); 8.85 (NH, s, 1H); 12.2 (NH, s, 1H). Calculated: C, 64.18; H, 4.56; N, 11.51. Found: C, 63.90; H. 5.10; N, 11.65%. Compound **2b**: R = CH_3 ($C_{27}H_{24}N_4O_4S$). NMR (DMSO-d_6, ppm): 1.95 (CH_3, s, 3H); 2.8–3.0 (CH_3N, s, 3H); 2.8 (CH_3, s, 3H); 7.20–8.20 (Ar, m, 14H); 12.2 (NH, s, 1H). Calculated: C, 64.78; H, 4.83; N, 11.90. Found: C, 64.10; H, 5.00; N, 11.69%. Compound **2c**: R = CH_2CH_3 ($C_{28}H_{26}N_4O_4S$). NMR (DMSO-d_6, ppm): 0.5 (CH_3CH_2, t, 3H); 1.95 (CH_3, s, 3H); 2.8–3.0 (CH_3N, s, 3H); 2.8–3.0 (CH_2CH_3, q, 2H); 7.20–8.20 (Ar, m, 14H); 12.2 (NH, s, 1H). Calculated: C, 65.35; H, 5.09; N, 10.90. Found: C, 64.80; H, 5.39; N, 10.75%.

2.4. Synthesis of metal-chelates

2.4.1. Chemical synthesis (A)

The complexes were synthesized by refluxing for a short time (10–20 min) 0.001 mol of the ligand **2a**–**2c** and 0.0005 mol of the corresponding hydrated metal acetate ($Co(OAc)_2 \cdot 4H_2O$, $Ni(OAc)_2 \cdot 4H_2O$, $[Cu(OAc)_2 \cdot H_2O]_2$ or $Zn(OAc)_2 \cdot 2H_2O$) in methanol (15 mL). The solids obtained, usually crystalline, were filtered, washed with hot methanol, and dried at 150 °C. Analytical and physical-chemical data for compounds **5a**–**5c** **6a**–**6c** **7b, 7c** and **8c** are presented in Table 1.

2.4.2. Direct electrochemical synthesis (B)

The electrochemical cell consisted on a Zn cathode (counter electrode) and a sacrificial anode (M = Cu, Zn, working electrode). To avoid the formation of a mixture of products, sometimes obtained during conventional electrochemical synthesis [17], the experiment was carried out without using any of the common supporting electrolytes. According to [9] in order to provide an electron carrier in the electrochemical cell, the sodium salt of the corresponding ligand was generated in situ and used as supporting electrolyte. It was obtained by the reaction of 2 mg of metallic sodium and 0.001 mol of the ligands **2a**–**2c** in 25 mL of a methanol. The electrolysis was carried out at fixed voltages during 2.5 h (M = Zn) or 1.5 h (M = Cu). The applied voltage varied with the time, as the in situ generated supporting electrolyte was consumed, and it was optimal at 30 V. The applied current ranged from 10 to 20 mA. After electrolysis, the solid products were filtered and washed with hot methanol. Analytical and physical–chemical data for compounds **6a′**, **6c′** and **8c′** are presented in Table 1.

3. Results and discussion

β-Aminivinylketones **2a**–**2c**, containing an antipyrine fragment, were synthesized following a classic technique of interaction of β-diketones with primary amines [3,18]. However, in contrast with previously reported similar syntheses in low-boiling solvents [3], harder conditions (fusion of reagents occurred at 180 °C) are needed to carry out the reaction when the β-diketones **3a**–**3c** and aminoantipyrine **4**, are used (Scheme 1).

This transformation can take place in two different routes depending on the reaction site, so it can generate any of two tautomers **2a**–**2c** or **2a′**–**2c′**, or both.

Table 1
Elemental analysis and related data for β-aminovinylketone ligands and their chelates

	R	M	Synthetic route	Yield, %	Color, m.p., C	Gross formula	Contents, % (found/calculated)		ν(C=O), cm^{-1}	$\nu(SO_2)$, cm^{-1}	$\mu_{\ni\phi\phi}$,B M., 293 K
							N	M			
2a	H	–		62	Light-orange, >250	$C_{26}H_{22}N_4O_4S$	11.65/11.51	–	1663	1327 1180	
5a		Ni	(A)	16	Yellow-brown, >250	$C_{52}H_{42}NiN_8O_8S_2$	10.68/10.88	5.90/5.71	1613	1327 1180	3.18
6a		Cu	(A)	71	Light-brown, 207–209	$C_{52}CuH_{42}N_8O_8S_2$	11.40/10.83	6.01/6.15	1663 1663	1327 1180	2.05
6a′		Cu	(B)	51	Light-brown, 207–209	$C_{52}CuH_{42}N_8O_8S_2$	10.25/10.83	5.98/6.15	1663 1633	1327 1180	2.19
2b	Me	–		63	Yellow, >250	$C_{27}H_{24}N_4O_4S$	11.69/11.90	–	1667	1327 1180	
5b		Ni	(A)	57	Red-brown, >250	$C_{54}H_{46}NiN_8O_8S_2$	10.27/10.59	5.40/5.56	1607	1327 1180	3.21
6b		Cu	(A)	71	Dark brown, >250	$C_{54}CuH_{46}N_8O_8S_2$	10.34/10.54	5.85/5.99	1667 1663	1327 1180	2.08
7b		Co	(A)	47	Brown, >250	$C_{54}CoH_{46}N_8O_8S_2$	10.36/10.59	5.35/5.58	1607	1327 1180	5.62
2c	Et	–		77	Yellow, 204–206	$C_{28}H_{26}N_4O_4S$	10.75/10.90	–	1673	1327 1180	
5c		Ni	(A)	88	Yellow-brown, >250	$C_{56}H_{50}NiN_8O_8S_2$	10.03/10.32	5.38/5.40	1633	1327 1180	3.14
6c		Cu	(A)	85	Dark-brown, >250	$C_{56}CuH_{50}N_8O_8S_2$	10.20/10.28	6.36/5.83	1673 1647	1327	1.81
6c′		Cu	(B)	28	Dark-brown, >250	$C_{56}CuH_{50}N_8O_8S_2$	10.20/10.28	6.02/5.83	1673 1647	1327 1180	2.05
7c		Co	(A)	48	Red-brown, 223–224	$C_{56}CoH_{50}N_8O_8S_2$	10.05/10.32	5.90/5.42	1633	1327 1180	5.76
8c		Zn	(A)	71	Orange, >250	$C_{56}H_{50}N_8O_8S_2Zn$	10.38/10.26	4.30/5.08	1653 1633	1327 1180	
8c′		Zn	(B)	52	Orange, >250	$C_{56}H_{50}N_8O_8S_2Zn$	10.12/10.26	4.35/5.08	1653 1327	1327 1180	

A, traditional synthetic methods; B, direct electrosynthesis.

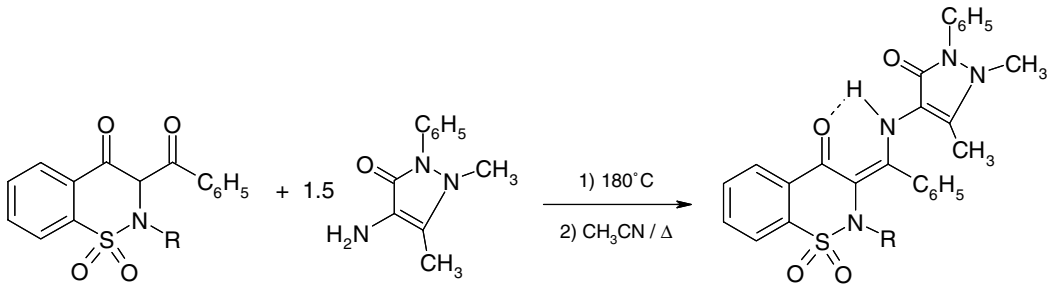

3a (R=H)
3b (R=CH_3)
3c (R=CH_2CH_3)

4

2a (R=H)
2b (R=CH_3)
2c (R=CH_2CH_3)

Scheme 1.

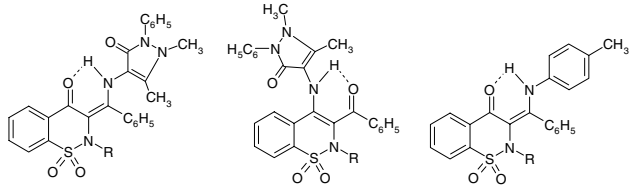

(a) **2a-c** (b) **9**

It can be guessed than the structure of compounds **2a**–**2c** can be represented by tautomer (a) on analogy with other β-aminovinylketones for which the aminoketone tautomer with similar structure are mostly obtained [19], as well by comparison with compound **9** whose structure has been proved by X-ray diffraction analysis to be almost exclusively as tautomer (a) [20].

In accordance, IR and NMR data for compounds **2a**–**2c** agree with that supposition. The IR spectra (see Table 1) show several absorption bands corresponding to different vibrational modes for C═O (antipyrine, 1663–1673 cm^{-1}) [21], SO_2 (1180, 1327 cm^{-1}), and N–H (~3200–3450 cm^{-1}) groups [22]. The presence of a wide low-intense band at 3000–3500 cm^{-1} (max. at ~3400 cm^{-1}), as well as signals corresponding to a NH fragment at 12.2 ppm in the ^1H NMR spectra, suggest the existence of an intra-molecular hydrogen bond of the type N─H···O═C─ as occurs in tautomer (a).

According to elemental analysis data (see Table 1), the synthesized compounds have the general composition ML_2 (where LH is the pro-ligand **2a**–**2c** and L is the corresponding deprotonated ligand), which is typical for describing other previously synthesized metal-chelates of aliphatic and aromatic β-aminovinylketonates [1–4], β-diketonates of 1,2-benzothiazine-1,1-dioxide [10,23], and 3-carboxamido-4-hydroxy-1,2-benzothiazine-1,1-dioxide [6]. The chelate structure of the described complexes is confirmed by disappearance of the typical vibrational bands for secondary amino group in the IR spectra of the complexes (for the pure ligand, LH, **2a**–**2c**, the NH group vibrational band appears at 3300–3450 cm^{-1}) and also is supported by the ^1H NMR data of the zinc complex.

The tautomeric form of ligands **2a**–**2c** (a) should be considered as an ambidentate ligand [4,14,24,25], which can act as bi- or tridentate ligands with or without participation of the C═O group of the antipyrine fragment in binding with the metal. In this sense, the structures of the novel coordination compounds can be represented as shown in Scheme 2.

Complexes **5a**, **5b**, **5c**, **7b** and **7c** should adopt an octahedral geometry according with IR and magnetochemical data (see Table 1). A shift of the C═O vibrational band of the antipyrine fragment [21,24–30] of around 20–60 cm^{-1}, in comparison with the free ligands was observed. The magnetochemical information for these coordination compounds (where $M = Co^{2+}$, Ni^{2+}) indicate that they are high-spin complexes, as should be expected for octahedral complexes [31].

In contrast, complexes **6a**, **6a′**, **6b**, **6c**, **6c′**, **8c** and **8c′** present two absorption bands corresponding to vibrational stretching modes of the non-coordinated and coordinated C═O group of the antipyrine fragment. Small prismatic green crystals of 6c, suitable for X-ray diffraction analysis, were grown by slow evaporation from a methanolic solution (monoclinic system; $a = 15.565(4)$ Å, $b = 25.911(4)$ Å, $c = 13.821(3)$ Å; $\beta = 99.25(2)°$; $V = 5501(2)$ $Å^3$; $\mu = 1090.7$; $F(000) = 2268$; $\rho_{calc} = 1.317$ g/cm^3; $\mu_{Mo} = 0.53$ mm^{-1}; $Z = 4$; space group = $P2_1/c$). X-ray data indicates that the oxygen atom of one antipyrine fragment is oriented toward the metal center (Cu). However, the interatomic distance

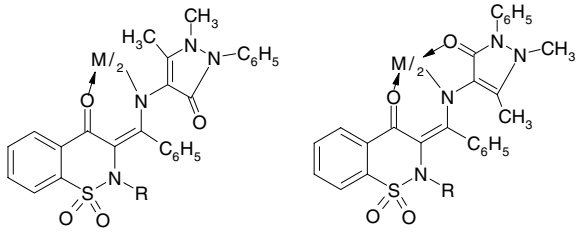

6a, 6a', 6b, 6c, 6c'
8c, 8c'

5a, 5b, 5c
7b, 7c

Scheme 2.

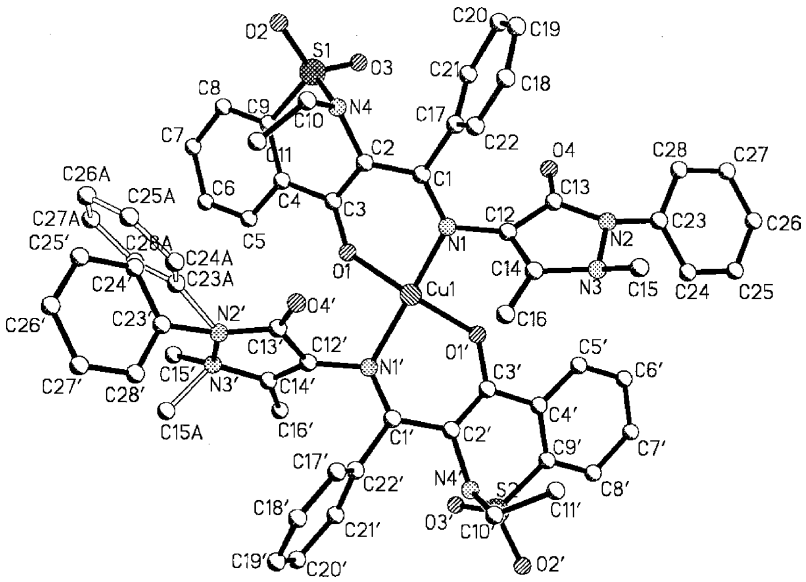

Fig. 1. Thermal ellipsoid plot of compound **6c**. Thermal ellipsoids are drawn at the 30% probability level. H atoms are represented by spheres of arbitrary size.

C=O···Cu of 3.41 Å [32], is too large to be considered a coordination bond (Fig. 1). Furthermore, the tetrahedral geometry is highly distorted, as evidenced by the 47° dihedral angle between the planes formed by the Cu(1)O(1)N(1) and Cu(1)O(1′)N(1′) planes, being more precisely an intermediate structure between a tetrahedral and a square planar arrangements. Table 2 contains selected bond distances and angles for compound **6c**. The magnetochemical data (Table 1) is in agreement with a tetracoordinated system and is supports the idea of a mononuclear structure for compound **6c**.

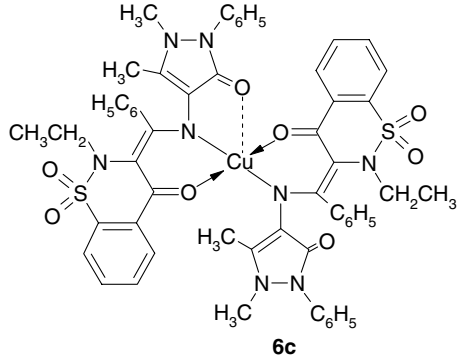

6c

Table 2
Selected bond distances (Å) and angles(°) for compound **6c** (for detailed data see [32])

Cu(1)–O(1)	1.875(9)
Cu(1)···O(4′)	3.41(2)
Cu(1)–N(1′)	1.93(1)
Cu(1)–O(1′)	1.928(9)
Cu(1)–N(1)	1.93(1)
O(1) Cu(1)N(1′)	93.0(4)
O(1′)Cu(1)N(1)	91.4(5)

4. Conclusions

The synthesis, by conventional chemical as well as by direct electrochemical methods, of 12 new coordination complexes of three early unknown-aminovinylketonates with 1,2-benzothiazine-1,1-dioxide fragments and a coordinatively active antipyrine substituent has been reported. It was shown that, depending on the metal nature, the studied ligand system may behave as an ambidentate ligand, forming metal-chelates with both distorted tetrahedral (Cu^{2+} and Zn^{2+}) or octahedral (Co^{2+} and Ni^{+}) geometries around the metal center. Spectrophotometrical and magnetochemical studies, as well as X-ray diffraction for one compound, support our findings. Further studies on other systems is currently undergoing.

Acknowledgements

The authors are very grateful to the Ministry of Education of Russian Federation (Grant E 02-50-334), MINPROMNAUKI (Grant HIII-945.2003.3), CONACYT-México (Grant 39558), and the *Universidad Autónoma de Nuevo León* (Monterrey, Mexico, project PAICyT) for financial support.

References

[1] R.H. Holm, M.J. O'Connor, Progr. Inorg. Chem. 14 (1971) 214.
[2] A.D. Garnovskii, A.L. Nivorozhkin, V.I. Minkin, Coord. Chem. Rev. 126 (1993) 1.
[3] Y.-L. Tung, W.-C. Tseng, C.-Y. Lee, P.-F. Hsu, Y. Chi, S.-M. Peng, G.H. Lee, Organometallics 18 (1999) 864.
[4] A.D. Garnovskii, I.S. Vasilchenko, Usp. Khim+ 71 (2002) 1064.
[5] A. Bury, A.E. Underhill, D.R. Kemp, N.Y. O'Shea, Y.P. Smith, P.S. Gomm, Inorg. Chim. Acta 138 (1987) 85.

[6] R. Cini, G. Giorgi, A. Guantini, C. Rossi, M. Sabat, Inorg. Chem. 29 (1990) 5197.
[7] D. Dileo, F. Berrettini, R. Cini, J. Chem. Soc., Dalton Trans. (1998) 1993.
[8] S.K. Hadjikakou, M.A. Demertzis, J.R. Miler, D. Kovala-Demertzi, J. Chem. Soc. Dalton Trans. (1999) 663.
[9] M.A. Mendez-Rojas, F. Cordova-Lozano, G. Gójon-Zorrilla, E. González-Vergara, M.A. Quiroz, Polyhedron 18 (1999) 2651.
[10] A.V. Bicherov, B.I. Kharisov, L.M. Blanco, O.Yu. Korshunov, E.L. Koroleva, I.E. Uflyand, A.D. Garnovskii, J. Coord. Chem. 54 (2001) 337.
[11] E.Y. Fursova, V.I. Ovcharenko, G.V. Romanenko, V.N. Ikorskii, Y.G. Shvedenkov, I.P. Asanov, L.N. Masalov, Zhurn. Strukt. Khim. 42 (2001) 302.
[12] E.Y. Fursova, V.N. Ikorskii, G.V. Romanenko, V.A. Reznikov, Yu.G. Shedenkov, V.I. Ovcharenko, Zhurn. Strukt. Khim. 43 (2002) 706.
[13] G.E. Jackson, M.J. Kelly, J. Chem. Soc., Dalton Trans. (1989) 2429.
[14] A.D. Garnovskii, D.A. Garnovskii, I.S. Vasilchenko, A.S. Burlov, A.P. Sadimenko, I.D. Sadekov, Russ. Chem. Rev. 66 (1997) 389.
[15] A.D. Garnovskii, B.I. Kharisov, I.S. Vasilchenko, L.M. Blanco, D.A. Garnovskii, M.A. Méndez-Rojas, in: A.D. Garnovskii, B.I. Kharisov (Eds.), Synthetic Coordination and Organometallic Chemistry, Marcel Dekker, New York, 2003.
[16] K. Abe, S. Yamamoto, K. Matsui, J. Pharm. Soc. Jpn. 76 (1956) 1058.
[17] A.D. Garnovskii, B.I. Kharisov, V.I. Skopenko, L.M. Blanco-Jerez, V.N. Kokozay, A.S. Kuzharov, D.A. Garnovskii, A.S. Burlov, V.A. Pavlenko, in: A.D. Garnovskii, B.I. Kharisov (Eds.), Direct Synthesis of Coordination and Organometallic Compounds, Elsevier, Amsterdam, 1999, p. 244.
[18] J.V.J. Greenhill, Chem. Soc. Rev. 6 (1977) 277.
[19] V.A. Bren, V.I. Minkin, Izv. Vissh. Uchebn. Zaved. Khim. I Khim. Tehn. 25 (1982) 663.
[20] A.S. Antsyshkina, G.G. Sadikov, O.Yu. Korshunov, E.L. Anpilova, A.V. Bicherov, V.S. Sergienko, I.E. Uflyand, A.D. Garnovskii, Koord. Khim. 29 (2003) 782.
[21] E.N. Naprienko, N.A. Skorik, N.N. Shaforostova, Zhurn. Neorg. Khim. 45 (2000) 1344.
[22] L. Bellamy, Advances in Infrared Group Frequencies, Methuen & Co LTD., Bungay, Suffolk, 1968.
[23] O.Yu. Korshunov, A.S. Bicherov, A.D. Garnovskii, Koord. Khim. 26 (2000) 949.
[24] A.D. Garnovskii, A.S. Burlov, T.A. Yusman, V.G. Zaletov, Koord. Khim. 21 (1995) 62.
[25] A.D. Garnovskii, A.S. Burlov, T.A. Yusman, V.V. Litvinov, S.G. Kochin, Koord. Khim. 21 (1995) 471.
[26] B. Kuncheria, P. Indrasenan, Polyhedron 7 (1988) 143.
[27] A.M. Dania, F.A. El-Saied, Polyhedron 7 (1988) 2149.
[28] M. Gaber, H.E. Mobrouk, A. Ba-Issa Aebada, M. Ayad Mochamed, Monatsh. Chem. 123 (1992) 1089.
[29] Yu.N. Medvedev, B.E. Zaitzev, M.L. Kuznetzov, B.V. Lokshin, F.M. Spiridonov, Zhurn. Neorg. Khim. 38 (1993) 1832.
[30] N.T. Madhu, P.K. Padhakrishnan, Synt. React. Inorg. Metal Org. Chem. 30 (2000) 1561.
[31] J. Lavis, R.G. Wilkins, Modern Coordination Chemistry. Principles and Methods, Interscience Publishers, New York, 1960.
[32] A.D. Garnovskii, A.S. Antsyshkina, E.L. Anpilova, O.Yu. Korshunov, A.V. Bicherov, A.S. Burlov, G.G. Sadikov, V.S. Sergienko, I.E. Uflyand, Zhurn. Neorg. Khim. 48 (2003) 1992.

Available online at www.sciencedirect.com
SCIENCE DIRECT®
Polyhedron 23 (2004) 1915–1921
POLYHEDRON
www.elsevier.com/locate/poly

Synthesis and spectroscopic properties of Mo(VI) complexes with phosphine oxide ligands and the crystal structures of $[MoO_2X_2(OPMe_3)_2]$ (X = Cl or Br) and $[MoO_2Br_2\{o\text{-}C_6H_4(P(O)Ph_2)_2\}]\cdot 2CH_2Cl_2$

Michael B. Hursthouse [a], William Levason [a], Raju Ratnani [b,*], Gillian Reid [a]

[a] Department of Chemistry, University of Southampton, Highfield, Southampton SO17 1BJ, UK
[b] Department of Pure and Applied Chemistry, M.D.S. University, Ajmer-305009, India

Received 10 February 2004; accepted 19 April 2004
Available online 15 June 2004

Abstract

The colourless neutral Mo(VI) complexes $[MoO_2Cl_2(OPMe_3)_2]$, $[MoO_2Cl_2(L\text{–}L)]$ (L–L = $Ph_2P(O)CH_2P(O)Ph_2$, $Ph_2P(O)CH_2CH_2P(O)Ph_2$ and $o\text{-}C_6H_4(P(O)Ph_2)_2$) have been obtained in good yield by reaction of MoO_2Cl_2 with the ligand in anhydrous CH_2Cl_2 solution. The corresponding light yellow bromo species were obtained from reaction of a CH_2Cl_2 solution of the phosphine oxide ligand with MoO_3 and HBr. The complexes have been characterised by IR, ^1H, $^{31}P\{^1H\}$ and where possible by ^{95}Mo NMR spectroscopy and trends in the spectroscopic data are discussed. Crystal structures of $[MoO_2X_2(OPMe_3)_2]$ (X = Cl or Br) and $[MoO_2Br_2\{o\text{-}C_6H_4(P(O)Ph_2)_2\}]\cdot 2CH_2Cl_2$ are also described. Each of the compounds adopts a distorted octahedral geometry at Mo(VI) with *trans* halo ligands, a *cis* dioxo unit and with the O-bound phosphine oxide ligands completing the coordination environment.
© 2004 Elsevier Ltd. All rights reserved.

Keywords: Molybdenum; ^{95}Mo NMR; X-ray structures; Phosphine oxide

1. Introduction

Molybdenum coordination chemistry continues to be the subject of much research effort. This is in part due to the occurrence of Mo in the active sites of biologically important species, the molybdoenzymes [1]. Further interest derives from the ability to vary the Mo oxidation state from Mo(VI) to Mo(0) (and even Mo(–II)) under ligand control. Molybdenum(VI) oxo complexes are also of interest as oxo transfer agents [2] and as catalyst precursors, e.g., in the selective epoxidation of olefins [3].

We have been interested for some time in the synthesis and properties of coordination complexes involving hard, high oxidation state acceptors with soft ligands, such as chalcogenoethers and phosphines and arsines. Recent examples include the preparations, spectroscopic and structural properties of complexes involving six-, seven- and eight-coordinate Ti(IV), Zr(IV) and Hf(IV) with these types of ligand, for example the eight-coordinate $[TiX_4\{o\text{-}C_6H_4(EMe_2)_2\}_2]$ (X = Cl or Br; E = P or As) and $[MCl_4\{MeE'(CH_2)_2\text{-}E'Me\}_2]$ (M = Zr or Hf; E′ = S or Se), the seven-coordinate $[MCl_4([9]aneS_3)]$ and the octahedral dinuclear $[(ZrCl_4)_2\{\mu_2\text{-}MeS(CH_2)_3SMe\}_2]$ [4–7]. In an extension of this work, we are now attempting to investigate the properties of rare examples of complexes of Mo(VI) based upon the MoO_2X_2 (X = Cl or Br) core, with neutral Group 15 and 16 ligands. We are not aware of any molybdenum(VI) dioxo complexes with phosphine and arsine ligands. The only reported thioether complexes involving the MoO_2X_2 unit are those of the macrocyclic [14]aneS$_4$ (1,4,8,11-tetrathiacyclotetradecane)

* Corresponding author. Tel.: +91-141-787412; fax: +91-141-787049.
E-mail address: ratnaniraju@rediffmail.com (R. Ratnani).

0277-5387/$ - see front matter © 2004 Elsevier Ltd. All rights reserved.
doi:10.1016/j.poly.2004.04.023

and [18]aneS$_6$ (1,4,7,10,13,16-hexathiacyclooctane) [8], and there are no selenoether or telluroether derivatives.

Under some conditions reaction of the quite strongly oxidising [MoO_2Cl_2(solvent)$_2$] (solvent = dmso or dmf) with phosphines results in oxidation and oxygen atom transfer to afford the corresponding phosphine oxide and reduction to Mo(IV) [9]. A number of phosphine oxide complexes of Mo(VI) have also been reported, however in many cases the data are quite old and rather fragmented and spectroscopic data are limited. Structurally characterised examples include [MoO_2X_2-(OPPh$_3$)$_2$] (X = Cl or Br), [MoO_2Cl_2(OPMePh$_2$)$_2$], [MoO_2Br_2{$Ph_2P(O)CH_2P(O)Ph_2$}], [MoO_2Cl_2{$Ph_2P(O)$-$(CH_2)_3P(O)Ph_2$}] and [MoO_2Cl_2{$(CH_2P(O)(CH_2CH_2O$-Me)$_2$)$_2$}] [10–16]. Therefore, in our preliminary work we have investigated a series of Mo(VI) complexes with phosphine oxide ligands, including ^{95}Mo NMR spectroscopic data where possible. We report here the synthesis and spectroscopic properties of [MoO_2X_2(OPMe$_3$)$_2$], [MoO_2X_2{$Ph_2P(O)CH_2P(O)Ph_2$}], [MoO_2X_2{o-C_6H_4(P(O)Ph$_2$)$_2$}] and [MoO_2Cl_2-{$Ph_2P(O)(CH_2)_2P(O)Ph_2$}]. The crystal structures of [MoO_2X_2(OPMe$_3$)$_2$] (X = Cl or Br) and [MoO_2Br_2{o-C_6H_4(P(O)Ph$_2$)$_2$}]$\cdot$ 2CH_2Cl_2 are also described and compared with the related literature compounds.

2. Results and discussion

Reaction of MoO_2Cl_2 with two molar equivalents of L (L = OPMe$_3$ or OPPh$_3$) or one molar equivalent of L–L (L–L = $Ph_2P(O)CH_2P(O)Ph_2$, $Ph_2P(O)CH_2CH_2P(O)$-Ph_2 or o-C_6H_4(P(O)Ph$_2$)$_2$) in anhydrous CH_2Cl_2, followed by concentration of the solvent in vacuo, affords the six-coordinate [$MoO_2Cl_2L_2$] or [MoO_2Cl_2(L–L)], respectively, as white solids in good yield. The corresponding bromo derivatives [MoO_2-Br_2L_2] and [MoO_2Br_2(L–L)] (L–L = $Ph_2P(O)CH_2P(O)$-Ph_2 and o-C_6H_4(P(O)Ph$_2$)$_2$) were obtained as light yellow solids from reaction of MoO_3, L or L–L and concentrated HBr in CH_2Cl_2/EtOH. The products were characterised by IR, ^{1}H, ^{31}P{^{1}H} and (where possible) ^{95}Mo NMR spectroscopy and analysis.

IR spectra (Table 1) show two peaks in the range 900–960 cm^{-1}, indicative of the *cis*-dioxo unit and either one or two P=O stretching vibrations significantly to low frequency of the uncoordinated phosphine oxide, consistent with coordination to the metal centre. The spectra for the chloro and bromo complexes are very similar, although the spectra of the chloro complexes exhibit a reasonably strong peak at ca. 320 cm^{-1} which is not evident in the bromo species and is therefore attributed to ν($MoCl_2$) of a *trans*-$MoCl_2$ unit. A peak at ca. 235 cm^{-1} in the bromo complexes is tentatively assigned to ν($MoBr_2$) of a *trans*-$MoBr_2$ unit.

The products are air stable solids, most of which show modest solubility in CH_2Cl_2, $CHCl_3$ and acetone without degradation. They are rather more soluble in O-donor solvents such as dmf, however ^{31}P{^{1}H} NMR studies show that the monodentate phosphine oxide ligands are readily displaced by the dmf, while the diphosphine dioxide ligands are displaced more slowly (1–2 h).

The ^{1}H NMR spectra of the compounds are generally not very informative, but confirm the presence of the coordinated L or L–L. Although the OPPh$_3$ complexes have been reported previously, ^{31}P{^{1}H} and ^{95}Mo NMR spectroscopic data on these are not known. The ^{31}P{^{1}H} NMR spectra for each of the compounds in this study reveal a single resonance ca. 10 ppm to high frequency of the uncoordinated phosphine oxide, indicating the presence of a single isomer for each, and that there is no significant chelate ring effect in the bidentate ligand species between the six-membered ring present in [MoO_2X{$Ph_2P(O)CH_2P(O)Ph_2$}] and the seven-membered rings in the other L–L complexes (Table 1). The coordination shifts in these compounds are similar to those observed in other hard, early transition metal

Table 1
Selected spectroscopic data

Compound	δ(^{31}P{^{1}H})/ppm[a]	δ(^{95}Mo)/ppm ($w_{1/2}$/Hz)[a,b]	ν(Mo=O)[c]	ν(P=O)[c]	ν(Mo–X)[c]
[MoO_2Cl_2(OPPh$_3$)$_2$]	40.6	137 (370)	945, 905	1148	320
[MoO_2Cl_2(OPMe$_3$)$_2$]	59.1	149 (400)	957, 936, 903, 895[d]	1120, 1099	318
[MoO_2Cl_2{$Ph_2P(O)CH_2P(O)Ph_2$}]	39.1	n.o.	951, 905	1154	315
[MoO_2Cl_2{$Ph_2P(O)CH_2CH_2P(O)Ph_2$}]	45.3	n.o.	944, 900	1172, 1149	324
[MoO_2Cl_2{o-C_6H_4(P(O)Ph$_2$)$_2$}]	43.5	n.o.	944, 909	1175, 1152	323
[MoO_2Br_2(OPPh$_3$)$_2$]	42.0	171 (380)	946, 905	1169, 1152	244
[MoO_2Br_2(OPMe$_3$)$_2$]	60.6	179 (350)	955, 927, 890[d]	1108, 1091	236
[MoO_2Br_2{$Ph_2P(O)CH_2P(O)Ph_2$}]	40.0	n.o.	947, 902	1165, 1147	235
[MoO_2Br_2{o-C_6H_4(P(O)Ph$_2$)$_2$}]	44.7	n.o.	943, 905	1170, 1149	234

n.o. = not observed, see text.
[a] Spectra recorded in CH_2Cl_2.
[b] δ(^{95}Mo) = 162 (X = Cl) and 224 (X = Br), respectively, for solutions of [MoO_2X_2(dmf)$_2$] in CH_2Cl_2.
[c] Nujol mull.
[d] ρ(PMe) in uncoordinated OPMe$_3$ occur at 955, 937 and 867 cm^{-1}, [24] therefore assignment of ν(MoO_2) is uncertain.

complexes with phosphine oxide ligands, for example yttrium(III) halide complexes [17]. The $^{31}P\{^{1}H\}$ NMR shifts of the Mo-chloro complexes are consistently to high frequency of the bromo analogues by ca. 1 ppm. This very small difference suggests that the electronic environment at Mo(VI) is little influenced by X and L (or L–L), but is probably dominated by the Mo-dioxo unit as expected.

The ^{95}Mo isotope (15.7%, $D_c = 0.489$), although quadrupolar ($I = 5/2$), has proved to be a useful and informative spectroscopic probe in diamagnetic Mo-containing complexes, with the chemical shift showing significant dependence on the Mo oxidation state, the ligand set around the metal and the coordination geometry [18,19]. ^{95}Mo NMR spectroscopy has been widely used to study zero-valent molybdenum carbonyl complexes, however, despite offering a direct probe of the electronic environment at the metal centre, there have been fewer studies on Mo(VI) coordination complexes.

^{95}Mo NMR spectra were obtained for the $OPPh_3$ and $OPMe_3$ ligand complexes in this work from solutions in CH_2Cl_2, as well as for $[MoO_2X_2(dmf)_2]$ for comparison and are in the range observed for other Mo(VI) complexes (Table 1) [18]. The $[MoO_2Cl_2L_2]$ species each show a single broad resonance (137 ppm for $L = OPPh_3$ and 149 ppm for $L = OPMe_3$). The corresponding resonances for the bromo analogues are observed at 171 ppm for $L = OPPh_3$ and 179 ppm for $L = OPMe_3$. The linewidths are approximately 350–400 Hz for these compounds. The ^{95}Mo NMR nucleus appears to be much more sensitive than ^{31}P to both the halide and the phosphine oxide ligand in these complexes, although the chemical shift range for ^{95}Mo is substantially larger than for ^{31}P. These shifts compare with $\delta(^{95}Mo) = 157$ and 216 for $[MoO_2Cl_2(H_2O)_2]$ and $[MoO_2Br_2(H_2O)_2]$, respectively [20]. This inverse dependence of $\delta(^{95}Mo)$ upon the halide is also consistent with that seen in other molybdenum-dioxo complexes with halide co-ligands [18]. The resonances for the phosphine oxide species are also to low frequency of $[MoO_2X_2(dmf)_2]$ for a given X.

The diphosphine dioxide ligand complexes were not sufficiently soluble in non-coordinating CH_2Cl_2 solution to observe the ^{95}Mo NMR resonance, and attempts to obtain the spectra from freshly prepared solutions of these compounds in dmf resulted in partial dissociation of the diphosphine dioxide ligand and resonances associated with $[MoO_2X_2(dmf)_2]$. This was confirmed from $^{31}P\{^{1}H\}$ NMR spectra recorded after the ^{95}Mo NMR spectra which revealed resonances associated with free L–L.

Attempts to obtain electrospray, APCI or FAB mass spectra for these compounds gave peaks consistent L or L–L, but no Mo-containing species were evident.

In order to confirm the structures of the new complexes and to establish bond length and angle distributions, X-ray crystallographic studies were undertaken on four examples. Crystals were obtained as described in Section 3. The structures of $[MoO_2X_2(OPMe_3)_2]$ (X = Cl or Br), although not isostructural, each show (Figs. 1 and 2, Table 2) distorted octahedral coordination to Mo(VI) through two *cis* oxo groups, two *trans* X ligands and two *cis* $OPMe_3$ ligands. Other than *d*(Mo–X), which increase as a consequence of the larger size of Br over Cl, there are no significant differences in the bond lengths and angles around the Mo centre in these compounds. The O–Mo–O angles in the *cis*-dioxo unit are 102.21(14)° and 102.72(13)°, whereas the O–Mo–O angle involving the $OPMe_3$ ligands are much more acute (78.77(10)° and 78.31(9)°).

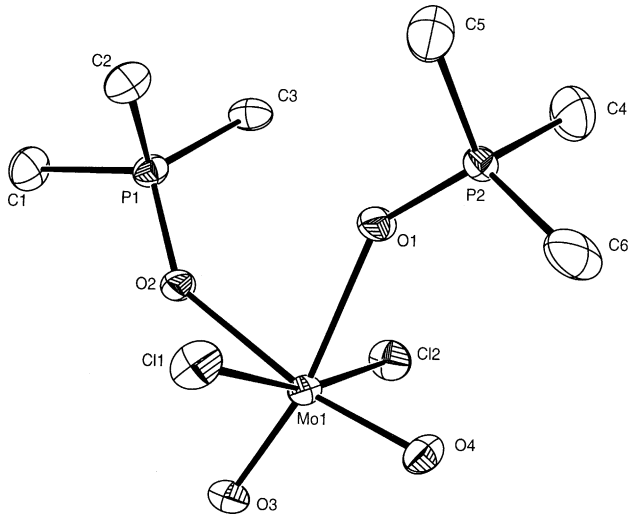

Fig. 1. View of the structure of $[MoO_2Cl_2(OPMe_3)_2]$ with numbering scheme adopted. Ellipsoids are shown at the 40% probability level and H atoms are omitted for clarity.

The X-ray structure of $[MoO_2Br_2\{o\text{-}C_6H_4(P(O)Ph_2)_2\}]\cdot 2CH_2Cl_2$ shows (Fig. 3 and Table 3) a similar distorted octahedral arrangement to the $OPMe_3$ complexes above, with similar bond lengths and angles around the molybdenum ion. In this species, the diphosphine dioxide ligand forms a seven-membered chelate ring, with the O–Mo–O angle involved in this chelate ring = 76.22(14)°, almost identical to the corresponding angle in the $OPMe_3$ complexes above. This suggests that the $o\text{-}C_6H_4(P(O)Ph_2)_2$ ligand can adjust its bite angle to accommodate the preference of the central metal fragment. These structures are very similar to those of other reported phosphine oxide complexes involving the MoO_2X_2 unit [12–16].

Very small, weakly diffracting crystals of $[MoO_2Cl_2\text{-}\{Ph_2P(O)CH_2P(O)Ph_2\}]\cdot 1/2Me_2CO$ [1] were also

[1] Crystal data for $[MoO_2Cl_2\{Ph_2P(O)CH_2P(O)Ph_2\}]\cdot 1/2Me_2CO$: MW = 644.25; monoclinic, space group $P2_1/c$, $Z = 4$, $a = 9.2075(4)$, $b = 20.4599(13)$, $c = 15.7724(10)$ Å, $\beta = 104.217(3)°$, $V = 2880.3(2)$ Å^3, $Z = 4$; 6492 unique data, giving $R_1 = 0.0853$, $wR_2 = 0.1990 (I > 2\sigma(I))$ based upon 327 independent parameters and $S = 1.005$.

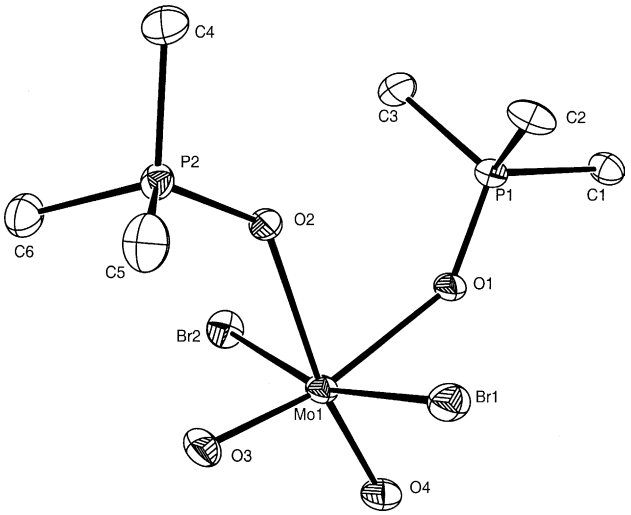

Fig. 2. View of the structure of $[MoO_2Br_2(OPMe_3)_2]$ with numbering scheme adopted. Ellipsoids are shown at the 40% probability level and H atoms are omitted for clarity.

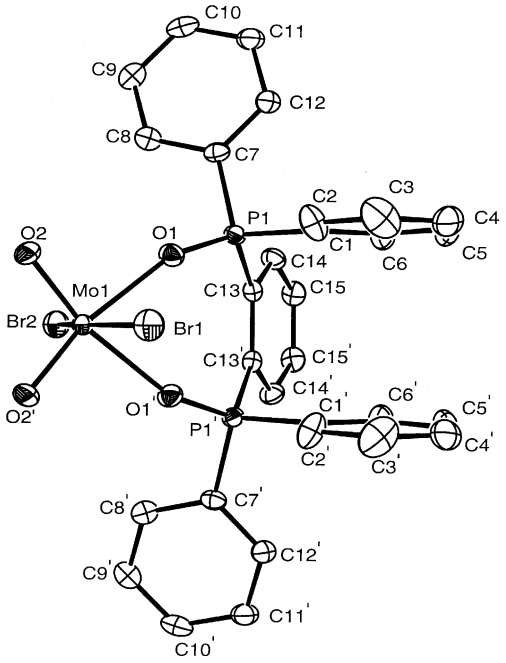

Fig. 3. View of the structure of $[MoO_2Br_2\{o\text{-}C_6H_4(P(O)Ph_2)_2\}]$ with numbering scheme adopted (symmetry operation: $' = x, 1\frac{1}{2} - y, z$). Ellipsoids are shown at the 40% probability level and H atoms are omitted for clarity.

Table 2
Selected bond lengths (Å) and angles (°) for $[MoO_2X_2(OPMe_3)_2]$

	X = Cl	X = Br
Bond lengths		
Mo1–O1	2.145(3)	2.127(2)
Mo1–O2	2.192(3)	2.194(2)
Mo1–O3	1.685(3)	1.691(3)
Mo1–O4	1.685(3)	1.691(3)
Mo1–X1	2.3840(10)	2.5560(5)
Mo1–X2	2.4078(11)	2.5551(5)
P1–O1	1.513(3)	1.514(3)
P2–O2	1.502(3)	1.518(2)
Bond angles		
O1–Mo1–O2	78.77(10)	78.31(9)
O3–Mo1–O1	168.96(12)	166.75(11)
O3–Mo1–O2	90.20(12)	88.47(11)
O4–Mo1–O1	88.82(12)	90.53(11)
O4–Mo1–O2	167.54(12)	168.62(11)
O4–Mo1–O3	102.21(14)	102.72(13)
O1–Mo1–X1	83.99(8)	85.00(6)
O2–Mo1–X1	83.34(8)	84.89(6)
O1–Mo1–X2	84.66(8)	84.87(6)
O2–Mo1–X2	83.08(8)	82.58(6)
O3–Mo1–X1	94.74(10)	92.94(9)
O3–Mo1–X2	94.17(10)	94.47(9)
O4–Mo1–X1	96.57(10)	96.42(9)
O4–Mo1–X2	94.77(10)	94.36(9)
X1–Mo1–X2	163.76(4)	165.254(18)

Table 3
Selected bond lengths (Å) and angles (°) for $[MoO_2Br_2\{o\text{-}C_6H_4(POPh_2)_2\}] \cdot 2CH_2Cl_2$

Bond lengths	
Mo1–O2	1.694(3)
Mo1–O1	2.173(3)
Mo1–Br1	2.5541(7)
Mo1–Br2	2.5585(7)
Bond angles	
O2–Mo1–O2′	102.79(18)
O2–Mo1–O1	90.49(12)
O2–Mo1–O1′	166.71(11)
O2′–Mo1–O1	166.71(11)
O1–Mo1–O1′	76.22(14)
O2–Mo1–Br1	94.88(10)
O1–Mo1–Br1	84.09(7)
O2–Mo1–Br2	94.63(10)
O1–Mo1–Br2	83.91(7)
Br1–Mo1–Br2	164.74(3)

Symmetry operation: $' = x, 1\frac{1}{2} - y, z$.

examined. The structure determination confirms that the coordination environment at Mo is very similar (Fig. 4) to that reported previously for $[MoO_2Br_2\{Ph_2P(O)CH_2P(O)Ph_2\}]$. However, the quality of the structure determination was poorer than for the other structures described, with higher *R*-factors and esds, precluding detailed comparisons of the geometric parameters.

Studies on the preparation and properties of MoO_2X_2 complexes incorporating soft phosphine, arsine, thioether and selenoether ligands are now underway in our laboratories. The results described here provide useful comparative data since as we have already noted, oxo-transfer from Mo(VI) to P(III) is a possible decomposition pathway in this chemistry.

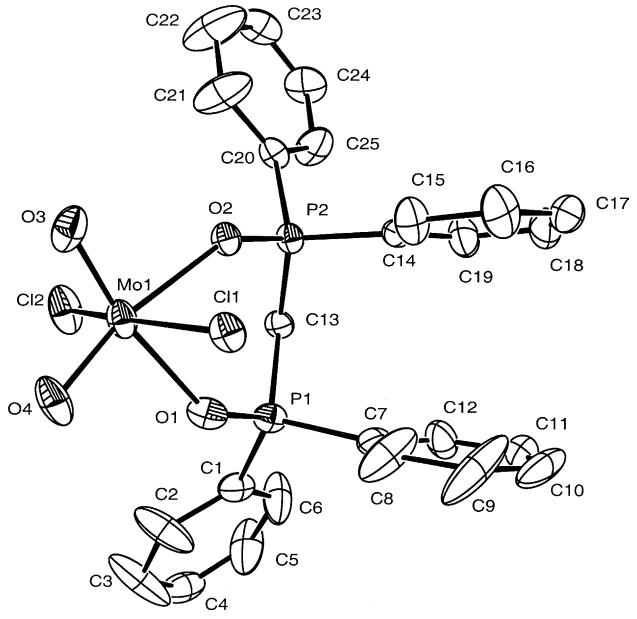

Fig. 4. View of the structure of $[MoO_2Cl_2\{Ph_2P(O)CH_2P(O)Ph_2\}]$ with numbering scheme adopted. Ellipsoids are drawn at 40% probability and H atoms are omitted for clarity. Selected bond lengths (Å): Mo1–O1 = 2.213(6), Mo1–O2 = 2.198(6), Mo1–O3 = 1.696(7), Mo1–O4 = 1.695(6), Mo1–Cl1 = 2.402(2), Mo2–Cl2 = 2.383(2).

3. Experimental

Infrared spectra were recorded as Nujol mulls between CsI plates using a Perkin–Elmer 983G spectrometer over the range 4000–200 cm^{-1}. ^1H NMR spectra were recorded using a Bruker AM300 spectrometer. $^{31}P\{^1H\}$ and ^{95}Mo NMR spectra were recorded using a Bruker DPX400 spectrometer operating at 162.00 or 26.08 MHz, respectively, and are referenced to external 85% H_3PO_4 and 1 mol dm^{-3} aqueous $Na_2[MoO_4]$, respectively. Microanalyses were undertaken by the University of Strathclyde microanalytical service.

Solvents were dried prior to use and all preparations were undertaken using standard Schlenk techniques under a N_2 atmosphere. MoO_2Cl_2, $OPMe_3$ and $OPPh_3$ were obtained commercially (Aldrich), while the other phosphine oxides were obtained by oxidation of the parent phosphine by the literature method [21]. MoO_3 was obtained by heating $[NH_4]_6[Mo_7O_{24}]\cdot 4H_2O$ in a furnace at ca. 250 °C to constant weight. $[MoO_2X_2(OPPh_3)_2]$ (X = Cl or Br) were obtained by the literature method [10].

3.1. Preparation of $[MoO_2Cl_2(OPMe_3)_2]$

MoO_2Cl_2 (0.17 g, 0.85 mmol) with $OPMe_3$ (0.16 g, 1.74 mmol) were stirred in CH_2Cl_2 (5 cm^3) under N_2 for ca. 2 h. The resulting white precipitate was filtered, washed with hexane and dried in vacuo. Yield 0.32 g, 97%. *Anal.* Calc. for $C_6H_{18}Cl_2MoO_4P_2$: C, 18.8; H, 4.7. Found: C, 18.7; H, 5.0%. ^1H NMR ($CDCl_3$): δ 1.83 (d, $J = 13.2$ Hz, Me) ppm.

3.2. Preparation of $[MoO_2Cl_2\{Ph_2P(O)CH_2P(O)Ph_2\}]$

Method as above to give a white solid. Yield 76%. *Anal.* Calc. for $C_{25}H_{22}Cl_2MoO_4P_2$: C, 48.8; H, 3.6. Found: C, 48.3; H, 3.4%. ^1H NMR ($CDCl_3$): δ 7.35–7.85 (m, 10H, Ph), 3.75 (t, 2H, CH_2) ppm.

3.3. Preparation of $[MoO_2Cl_2\{Ph_2P(O)CH_2CH_2P(O)Ph_2\}]$

Method as above to give a white solid. Yield 88%. *Anal.* Calc. for $C_{26}H_{24}Cl_2MoO_4P_2\cdot 0.25CH_2Cl_2$: C, 48.5; H, 3.8. Found: C, 48.4; H, 3.8%.

3.4. Preparation of $[MoO_2Cl_2\{o\text{-}C_6H_4(P(O)Ph_2)_2\}]$

Method as above to give a white solid. Yield 78%. *Anal.* Calc. for $C_{30}H_{24}Cl_2MoO_4P_2\cdot 0.25CH_2Cl_2$: C, 52.0; H, 3.5. Found: C, 51.9; H, 3.5%. ^1H NMR ($CDCl_3$): δ 7.20–7.60 (m, aromatic CH) ppm.

3.5. Preparation of $[MoO_2Br_2(OPMe_3)_2]$

To a flask containing MoO_3 (0.12 g, 0.83 mmol) in concentrated HBr (0.5 cm^3) was added $OPMe_3$ (0.16 g, 1.73 mmol) in ethanol. The resulting mixture was stirred under N_2 overnight. The resulting precipitate was filtered, washed with hexane and dried in vacuo to give a light yellow solid. Yield 0.20 g, 71%. *Anal.* Calc. for $C_6H_{18}Br_2MoO_4P_2$: C, 15.5; H, 4.1. Found: C, 15.3; H, 3.8%. ^1H NMR ($CDCl_3$): δ 1.88 (d, $J = 12.5$ Hz, Me) ppm.

3.6. Preparation of $[MoO_2Br_2\{Ph_2P(O)CH_2P(O)Ph_2\}]$

Method as above to give a light yellow solid. Yield 73%. *Anal.* Calc. for $C_{25}H_{22}Br_2MoO_4P_2$: C, 42.6; H, 3.2. Found: C, 42.6; H, 3.3%. ^1H NMR (CD_2Cl_2): δ 7.30–7.90 (m, 10H, Ph), 3.80 (t, H, CH_2) ppm.

3.7. Preparation of $[MoO_2Br_2\{o\text{-}C_6H_4(P(O)Ph_2)_2\}]$

Method as above to give a yellow solid. Yield 65%. *Anal.* Calc. for $C_{30}H_{24}Br_2MoO_4P_2$: C, 47.0; H, 3.2. Found: C, 46.5; H, 3.6%. ^1H NMR ($CDCl_3$): δ 7.20–7.65 (m, aromatic CH) ppm.

3.8. X-ray crystallography

Details of the crystallographic data collection and refinement parameters are given in Table 4. Colourless crystals of $[MoO_2Cl_2(OPMe_3)_2]$ and light yellow

Table 4
Crystallographic parameters

Complex	$[MoO_2Cl_2(OPMe_3)_2]$	$[MoO_2Br_2(OPMe_3)_2]$	$[MoO_2Br_2\{o\text{-}C_6H_4(POPh_2)_2\}]\cdot 2CH_2Cl_2$
Formula	$C_6H_{18}Cl_2MoO_4P_2$	$C_6H_{18}Br_2MoO_4P_2$	$C_{32}H_{28}Br_2Cl_4MoO_4P_2$
M	382.98	471.90	936.04
Crystal system	orthorhombic	monoclinic	monoclinic
Space group	*Pbca*	$P2_1/n$	$P2_1/m$
a (Å)	12.1802(3)	10.6760(3)	9.1777(3)
b (Å)	14.6037(6)	11.7465(4)	20.4793(8)
c (Å)	16.6626(7)	12.3415(4)	9.4379(4)
β (°)	90	92.241(2)	98.923(2)
U (Å^3)	2963.88(19)	1546.51(8)	1752.41(12)
Z	8	4	2
μ(Mo Kα) (cm^{-1})	14.54	62.15	30.87
Number of reflections measured	23731	15309	13399
Unique reflections	3381	3525	4116
Unique reflections with $I_0 > 2\sigma(I_0)$	2426	2862	3539
R_{int}	0.0798	0.0570	0.0583
Numbers of parameters	136	136	208
R_1, $wR_2[I_0 > 2\sigma(I_0)]$	0.0403, 0.0913	0.0356, 0.0741	0.0446, 0.0961
R_1, wR_2 [all data]	0.0700, 0.1019	0.0506, 0.0791	0.0552, 0.1007

$R_1 = \sum ||F_o| - |F_c||_i / \sum |F_o|$ and $wR_2 = [\sum w(F_o^2 - F_c^2)^2 / \sum wF_{oi}^4]^{1/2}$.

crystals of $[MoO_2Br_2(OPMe_3)_2]$ and $[MoO_2Br_2\{o\text{-}C_6H_4\text{-}(POPh_2)\}]\cdot 2CH_2Cl_2$ were obtained by cooling a solution of the appropriate complex in CH_2Cl_2. Extremely small and weakly diffracting crystals of $[MoO_2Cl_2\text{-}\{Ph_2P(O)CH_2P(O)Ph_2\}]\cdot 1/2Me_2CO$ were obtained by cooling a solution of this complex in Me_2CO. Data collection used a Nonius Kappa CCD diffractometer ($T = 120$ K) with graphite monochromated Mo Kα X-radiation ($\lambda = 0.71073$ Å). Structure solution and refinement were routine [22–24], except for the $[MoO_2Cl_2\{Ph_2P(O)CH_2P(O)Ph_2\}]$ where the difference map indicated the presence of two partially occupied and disordered Me_2CO solvent molecules in asymmetric unit. This was modelled reasonably successfully to give two 25% occupied molecules disordered over one site. Selected bond lengths and angles are given in Tables 2 and 3.

4. Supplementary material

Crystallographic data for the structural analyses have been deposited with the Cambridge Crystallographic Data Centre, CCDC nos. 230190 ($[MoO_2Br_2\{o\text{-}C_6H_4(P(O)Ph_2)_2\}]\cdot 2CH_2Cl_2$), 230191 ($[MoO_2Cl_2\text{-}(OPMe_3)_2]$) and 230192 ($[MoO_2Br_2(OPMe_3)_2]$). Copies of this information may be obtained free of charge from The Director, CCDC, 12 Union Road, Cambridge CD2 1EZ, UK (Fax: +44-1223-336033; email: deposit@ccdc.cam.ac.uk or www: http://www.ccdc.cam.ac.uk).

Acknowledgements

R.R. would like to thank the Commonwealth Scholarship Commission, UK (INCF-2003-85) and M. D. S. University, Ajmer (India) for granting a leave of absence.

References

[1] J.M. Tunney, J. McMaster, C.D. Garner, in: J.A. McCleverty, T.J. Meyer (Eds.), Comprehensive Coordination Chemistry II, vol. 8, Elsevier, Amsterdam, 2003, p. 459.
[2] R.H. Holm, Chem. Rev. 87 (1987) 1401.
[3] F.E. Kuhn, M. Groarke, E. Bencze, E. Herdtweck, A. Prazeres, A.M. Santos, M.J. Calhorda, C.C. Romao, I.S. Goncalves, A.D. Lopes, M. Pillinger, Chem. Eur. J. 8 (2002) 2370.
[4] R. Hart, W. Levason, B. Patel, G. Reid, Eur. J. Inorg. Chem. (2001) 2927.
[5] W. Levason, B. Patel, G. Reid, V.-A. Tolhurst, M. Webster, J. Chem. Soc., Dalton Trans. (2000) 3001.
[6] R. Hart, W. Levason, B. Patel, G. Reid, J. Chem. Soc., Dalton Trans. (2002) 3153.
[7] W. Levason, B. Patel, G. Reid, M. Webster, unpublished work.
[8] D. Sevdic, L. Fekete, Inorg. Chim. Acta 57 (1982) 111.
[9] F.J. Arnaiz, R. Aguado, J.M. Martinez de Ilarduya, Polyhedron 23 (1994) 3257.
[10] S.M. Horner, S.Y. Tyree Jr., Inorg. Chem. 1 (1962) 122.
[11] F.J. Kohl, J. Lewis, R. Whyman, J. Chem. Soc. A (1965) 630.
[12] S.-O. Oh, S.-J. Mo, J. Korean Chem. Soc. 39 (1995) 318.
[13] R.J. Butcher, B.R. Penfold, E. Sinn, J. Chem. Soc., Dalton Trans. (1979) 668.
[14] F.R. Fronczek, R.L. Luck, G. Wang, Inorg. Chim. Acta 342 (2003) 247.
[15] A. Herbowski, T. Lis, E.A. Deutsch, J. Organomet. Chem. 460 (1993) 25.
[16] F.J. Arnaiz, R. Aguado, M.R. Pedrosa, J. Mahia, M.A. Maestro, Polyhedron 21 (2002) 1635.
[17] W. Levason, M.C. Popham, G. Reid, M. Webster, Polyhedron 21 (2002) 445.
[18] M. Minelli, J.H. Enemark, R.T.C. Brownlee, M.J. O'Connor, A.G. Wedd, Coord. Chem. Rev. 68 (1985) 169.

[19] P.S. Pregosin, in: P.S. Pregosin (Ed.), Transition Metal Nuclear Magnetic Resonance, Elsevier, Amsterdam, 1991.
[20] J.M. Coddington, M.J. Taylor, J. Chem. Soc., Dalton Trans. (1990) 41.
[21] A.R.J. Genge, W. Levason, G. Reid, Inorg. Chim. Acta 288 (1999) 142.
[22] G.M. Sheldrick, SHELXS-97, Program for Crystal Structure Solution, University of Göttingen, 1997.
[23] G.M. Sheldrick, SHELXL-97, Program for Crystal Refinement, University of Göttingen, 1997.
[24] R. Pantzer, W. Schmidt, J. Goubeau, Z. Anorg. Allgem. Chem. 395 (1973) 262.

Available online at www.sciencedirect.com
SCIENCE DIRECT®
Polyhedron 23 (2004) 1923–1929
POLYHEDRON
www.elsevier.com/locate/poly

Synthesis and characterization of chalcogenoic aminophosphines: X-ray structures of $Bu^t_2P(E)NHPr^n$ (E = Se, Te), $Ph_2P(Se)NHPr^n$ and $\{Et_2P(Se)\}_2NPr^n$

Martin D. Rudd [a,*], Matt A. Creighton [b], Jason A. Kautz [c]

[a] Department of Chemistry, University of Wisconsin – Fox Valley, Menasha, WI 54952, USA
[b] Department of Chemistry and Physics, Northwestern State University, Natchitoches, LA 71497, USA
[c] Department of Chemistry and Biochemistry, Baylor University, Waco, TX 76798, USA

Received 3 February 2004; accepted 20 April 2004
Available online 19 June 2004

Abstract

The four title compounds have been synthesized and characterized by ^1H, ^{13}C and ^{31}P NMR spectroscopy and their identities confirmed by elemental analysis and X-ray crystallography. $Bu^t_2P(E)NHPr^n$ [E = Se (**1**); E = Te (**2**)] and $Ph_2P(E)NHPr^n$ [E = Se (**3**)] were prepared by the metathesis reaction of $LiNHPr^n$ with the appropriate chlorophosphine in diethylether at −78 °C, followed by reaction with elemental selenium or tellurium at reflux temperatures. (**1**) and (**2**) are isostructural with P═Se 2.1163(14) Å and P═Te 2.3642(13) Å. In (**3**) a P═Se bond length of 2.1159(10) Å is observed. (**4**) was prepared by the additional of two equivalents of diethylchlorophosphine to the dilithium salt of *n*-propylamine.
© 2004 Elsevier Ltd. All rights reserved.

Keywords: Phosphine chalcogenides; X-ray structure; ^{31}P NMR; Tellurium; Selenium

1. Introduction

Over the past several years, there has been a great deal of interest in the design and synthesis of precursors suitable for the chemical vapor deposition of metal chalcogenides [1]. These have included several investigations into the properties of ligands that can coordinate to suitable metal fragments to produce volatile materials that deposit thin films in a clean manner [2,3].

One such class of ligands that have been investigated is the aminophosphine chalcogenides of the general formula $R_2P(E)–NHR'$ (R and R′ = alkyl/aryl groups). By altering the R/R′ groups it was found that the volatility of any subsequently formed metallo-complexes could be changed. Bochmann et al. [4] have synthesized and characterized a series of seleno- and telluro-aminophosphines and some associated Ti, Zn and Cd complexes. In a later paper, they investigated the chemical vapor deposition potential of these materials [5] and determined that at temperatures generally above 150 °C (sublimation temperatures) and under reduced pressures (10^{-6} mbar), films of cadmium telluride, zinc telluride or cadmium selenide could be deposited and readily identified by X-ray diffraction. Compared to arene chalcogenato compounds [6], the zinc and cadmium complexes of phosphinochalcogenic amines showed better volatility and stability as suitable single-source precursors for metal selenides and tellurides.

In this paper, we present the synthesis and characterization of some seleno- and telluro-aminophosphines, whose reactions with main group elements and transition metals are part of an ongoing investigation.

2. Results and discussion

The chalogenophosphinic amides presented in this paper were prepared through a metathesis reaction of

* Corresponding author. Tel.: +1-920-832-2694.
E-mail address: mrudd@uwc.edu (M.D. Rudd).

0277-5387/$ - see front matter © 2004 Elsevier Ltd. All rights reserved.
doi:10.1016/j.poly.2004.04.028

the corresponding lithium amide and di(alkyl/aryl)chlorophosphine. Further reaction with the elemental chalcogen (selenium or tellurium) at refluxing solvent temperatures resulted in the formation of the title compounds as depicted in Scheme 1.

The isolated compounds were obtained in moderate to high yields (60–80%) as white microcrystalline powders (selenium derivatives) or pale yellow powders (tellurium derivatives). The spectroscopic and analytical data for (**1**–**4**) are presented in Section 3. These compounds are generally air stable although the tellurium analogs have a tendency to decompose, depositing elemental tellurium, upon exposure to warm, humid air. The selenium compounds are stable in solution indefinitely at −20 °C, but the tellurium compounds should be handled only in oxygen free solvents. We also prepared $Ph_2P(Te)NHPr^n$ but the compound was too unstable for us to grow crystals.

The molecular structures of **1**–**3** show the expected geometries for molecules of this type. The central phosphorus atom lies in a distorted tetrahedral environment coordinated to a chalcogen atom, an amino nitrogen atom and two carbon atoms of the alkyl/aryl substituents. We were also able to prepare compound **4** through a double substitution by two equivalents of diethylchlorophosphine on dilithium *n*-propylamide followed by oxidation with selenium. To our knowledge, this is the first time such a doubly substituted amide has been structurally characterized.

2.1. $Bu^t_2P(Se)NHPr^n$

The structure of this compound is shown in Fig. 1 together with the atom notation used. The central phosphorus atom lies in a distorted tetrahedral environment surrounded by two carbon atoms of the *tert*-butyl groups, an amine nitrogen group and a selenium atom with bond distances P=Se [2.1163(14) Å], P–N

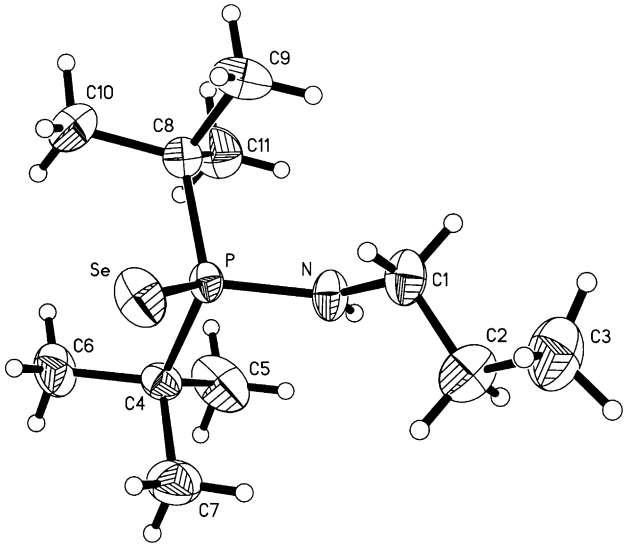

Fig. 1. Molecular structure of $Bu^t_2P(Se)NHPr^n$ showing atomic numbering.

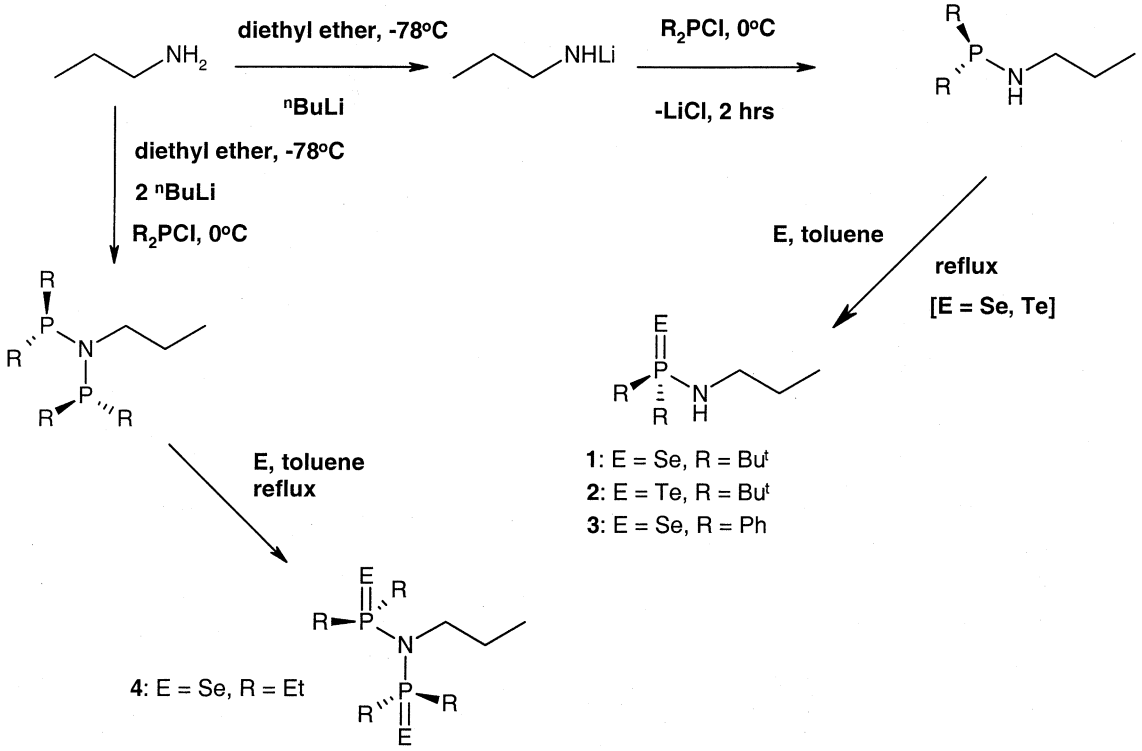

Scheme 1. Synthesis of chalcogenoic aminophosphines.

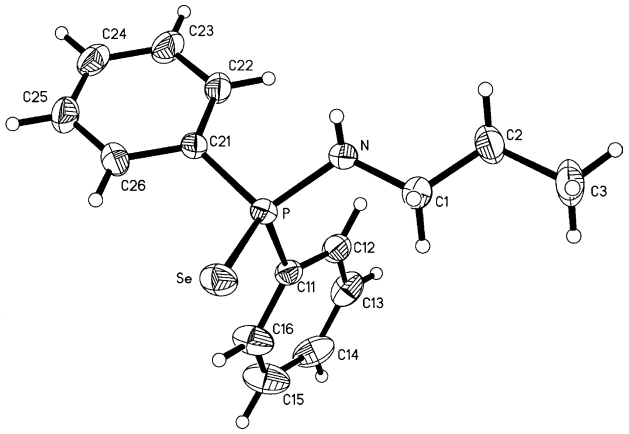

Fig. 2. Molecular structure of $Bu^t_2P(Te)NHPr^n$ showing atomic numbering.

[1.649(4) Å], and P–C_{ave} [1.857 Å]. These molecular dimensions are very similar to those described by Bochmann in the related $Bu_2P(Se)NHPr^i$ structure [4].

2.2. $Bu_2P(Te)NHPr^n$

The structure of this compound is shown in Fig. 2. As with compound **1** above, the aminophosphine has been chalcogenated, this time with tellurium. There are only a few known P=Te compounds that have been crystallographically characterized. These include a related structure reported by Bochmann et al. [4], Bu_2P-(Te)NHCy in which a P=Te distance of 2.371(1) Å is found. In a related, but disordered structure of $Ph_3PTe{\cdot}PPh_3$ [7] the phosphorus–tellurium bond distances are 2.27–2.42 Å. For comparison purposes, it is interesting to note that the P=Te distance in the tungsten carbonyl complex, $[W(CO)_5(Bu^t_3PTe)]$ is 2.439(2) Å [8]. Interestingly enough, in his discussion of phosphine telluride bond lengths in known crystal structures, Gilheany [9] indicates that the bond length of 2.368 Å in Bu^t_3PTe is probably not typical of tertiary phosphine tellurides and that this corresponds to a bond order of 1.5 according to the covalent radii of Schomaker and Stevenson.

2.3. $Ph_2P(Se)NHPr^n$

Fig. 3 shows the atomic labeling and molecular structure of compound **3**. This compound was prepared by the metathesis reaction of Ph_2PCl with lithium *n*-propylamine in diethylether followed by addition of selenium at reflux temperatures. Some considerable deviations away from the tetrahedral bonds angles are found, most probably due to the steric requirements of the two phenyl groups. A review of the bond lengths and angles found in triaminophosphine selenides and tellurides, in particular their deviation away from the ideal structure, has recently been published [10].

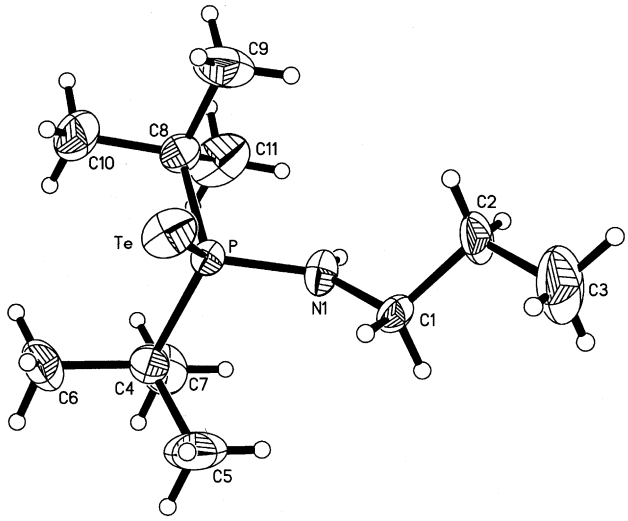

Fig. 3. Molecular structure of $Ph_2P(Se)NHPr^n$ showing atomic numbering.

2.4. $\{Et_2P(Se)\}_2NPr^n$

The structure of this doubly substituted primary amine is shown in Fig. 4. The addition of two molar equivalents of *n*-butyl lithium to *n*-propylamine followed by treatment with two equivalents of diethylchlorophosphine and oxidation with selenium yielded the title compounds which was readily obtained as

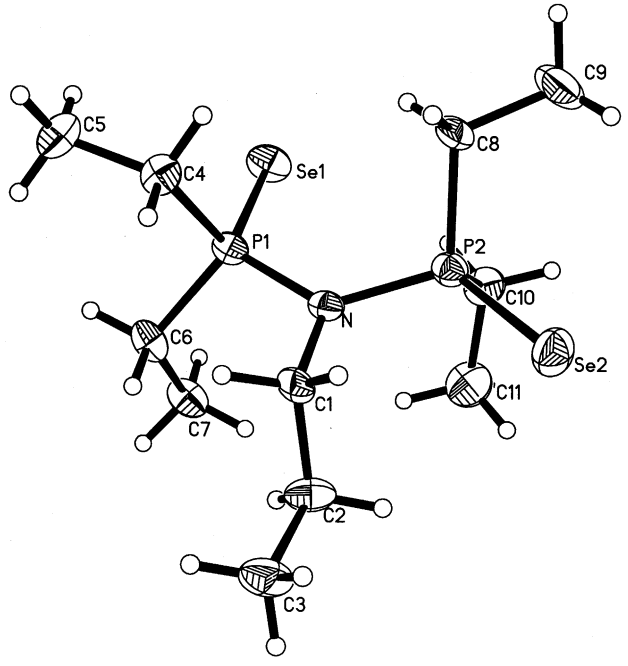

Fig. 4. Molecular structure of $\{Et_2P(Se)\}_2NPr^n$ showing atomic numbering.

colorless crystals. The two selenium atoms lie in an anti-arrangement. Both P=Se bonds distances are typical of the range observed in phosphine selenides (2.09–2.11 Å) [9]; the less bulky nature of the alkyl groups in this study, compared with the Ph and Bu^t substituents in **1** and **3**, give rise to a less strained tetrahedral environment around the two phosphorus atoms.

3. Experimental

3.1. General and instrumental

NMR spectra were obtained on a Bruker AMX-360 spectrometer and recorded in $CDCl_3$ except where noted. ^1H NMR were recorded at 360 MHz, ^{13}C at 90.6 MHz and ^{31}P at 161.9 MHz (using an external H_3PO_4 reference). Et_2PCl (Strem), Ph_2PCl (Strem) and Bu^t_2PCl (Aldrich), *n*-butyllithium (1.6 M in hexanes, Aldrich) and *n*-propylamine were used as received. All solvents (toluene, diethylether and hexanes) were dried and purified using standard reagents and distilled from a dry nitrogen atmosphere prior to use. All reactions were carried out using Schlenk techniques under an atmosphere of argon. Elemental analyzes were performed at Atlantic Microlab. Inc. (Norcross, GA).

3.2. Synthesis of $Bu^t_2P(Se)NHPr^n$ (**1**)

To a cooled solution (−78 °C) of *n*-propylamine (0.46 mL, 5.6 mmol) in diethylether (10 mL) was added *n*-butyllithium (1.6 M in hexane; 3.52 mL, 5.6 mmol). After allowing the reaction to slowly warm to room temperature, a thick white precipitate of $LiNHPr^n$ formed which was stirred for 1 h. The precipitate was cooled back to 0 °C and di-*t*-butylchlorophosphine (1.09 mL, 5.6 mmol) was added via syringe. The reaction immediately became clear and colorless and was stirred at room temperature for 2 h during which time a small amount of precipitate formed. The precipitate was allowed to settle and the solution filtered onto elemental selenium (0.44 g, 5.7 mmol) through a Whatman 1μm on-line filter. Toluene (10 mL) was added and the mixture was refluxed for 2 h until all the selenium had been consumed. Whilst hot, the solution was again filtered through a Whatman filter and allowed to cool. Large colorless block crystals formed directly at −10 °C suitable for X-ray structure determination. Yield: 1.55 g, 81%. M.p.: 150–2 °C. *Elem. Anal.* Calc. for $C_{11}H_{26}NPSe$ ($M_w = 282.26$) C: 46.80; H 9.30. Found: C 46.78; H 9.24%. ^1H NMR: 0.88 (t, 3H, $CH_3CH_2CH_2$); 1.29 (d, 18H, $J(PH) = 15.6$ Hz, $C(CH_3)_3$); 1.48 (d of q, 2H, $CH_3CH_2CH_2$); 1.77 (s, br, 1H, NH); 3.03 (q, 2H, $CH_3CH_2CH_2$); ^{13}C NMR 11.2 (s, $CH_3CH_2CH_2$); 25.6 (d, $J(PC) = 5$ Hz $CH_3CH_2CH_2$); 27.7 (s, ^{t}Bu); 40.8 (d, $J(PC) = 46.3$ Hz, CMe_3); 45.9 (s, $CH_3CH_2CH_2$) $^{31}P\{^1H\}$ NMR: 98.74 ppm (s, $J(PSe) = 731$ Hz).

3.3. Synthesis of $Bu^t_2P(Te)NHPr^n$ (**2**)

An analogous procedure to that described above was used. Amounts used: *n*-propylamine (0.42 mL, 5.1 mmol); *n*-butyllithium (1.6 M in hexane; 3.2 mL, 5.2 mmol); di-*t*-butylchlorophosphine (0.97 mL, 5.1 mmol); Te powder (0.65 g, 5.1 mmol). The reaction was refluxed for 3 h and then filtered. Recrystallization from diethylether gave small colorless block crystals. Yield: 1.66 g, 67%. M.p.: 150 °C (dec). *Elem. Anal.* Calc. for $C_{11}H_{26}PNTe$ ($M_w = 330.91$) C: 39.93; H 7.92. Found: C 39.82; H 7.95%. ^1H NMR: 0.93 (t, 3H, $CH_3CH_2CH_2$); 1.33 (d, 18H, $J(PH) = 19.0$ Hz, $C(CH_3)_3$); 1.53 (d of q, 2H, $CH_3CH_2CH_2$); 1.71 (s, br, 1H, NH); 3.05 (q, 2H, $CH_3CH_2CH_2$); ^{13}C NMR 11.6 (s, $CH_3CH_2CH_2$); 25.6 (d, $J(PC) = 7$ Hz $CH_3CH_2CH_2$); 28.6 (s, ^{t}Bu); 40.2 (d, $J(PC) = 34.0$ Hz, CMe_3); 50.1 (s, $CH_3CH_2CH_2$); $^{31}P\{^1H\}$ NMR: 85.02 (s, J (PTe) = 1784 Hz).

3.4. Synthesis of $Ph_2P(Se)NHPr^n$ (**3**)

An analogous procedure to that described above was used. Amounts used: *n*-propylamine (0.50 mL, 6.0 mmol); *n*-butyllithium (1.6 M in hexane; 3.8 mL, 6.0 mmol); diphenylchlorophosphine (1.11 mL, 6.0 mmol); Se powder (0.46 g, 6.0 mmol). The reaction was refluxed for 2 h and then filtered. Small colorless block crystals were obtained from the reaction liquors. Yield: 2.03 g, 67%. M.p.: 126–131 °C. *Elem. Anal.* Calc. for $C_{15}H_{18}NPSe$ C: 55.90; H 5.64. Found: C 55.90; H 5.56%. ^1H NMR: 0.94 (t, 3H, $CH_3CH_2CH_2$); 1.61 (d of q, 2H, $CH_3CH_2CH_2$); 2.27 (s, br, 1H, NH); 2.87 (q, 2H, $CH_3CH_2CH_2$); 7.19–7.52 (m, Ph, 10H); ^{13}C NMR: 11.9 (s, $CH_3CH_2CH_2$); 24.8 (d, $J(PC) = 12$ Hz $CH_3CH_2CH_2$); 44.6 (s, $CH_3CH_2CH_2$); 128.4–134.5 (m, Ph); $^{31}P\{^1H\}$ NMR: 58.10 (s, $J(PSe) = 739$ Hz).

3.5. Synthesis of $\{Et_2P(Se)\}_2NPr^n$ (**4**)

To a cooled solution of *n*-propylamine (0.2 mL, 2.4 mmol) in diethylether (10mL) was added two equivalents of *n*-butyllithium (1.6 M in hexane; 3.0 mL, 4.8 mmol) forming a white precipitate. This was stirred for 2 h at room temperature and then cooled to ca. −20 °C. Diethylchlorophosphine (0.58 mL, 4.8 mmol) was introduced via a syringe and a vigorous exothermic reaction occurred. The reaction was allowed to warm to room temperature, stirred for 1 h and then filtered onto selenium powder (0.37 g, 4.8 mmol) suspended in dry toluene (10 mL). The reaction was refluxed for 1 h until the selenium had been consumed and then filtered while still hot. Cooling to −20 °C for 3 weeks yielded large colorless block crystals. Yield: 0.68 g, (67%). M.p.:

67–70 °C. *Elem. Anal.* Calc. for $C_{11}H_{27}NP_2Se_2$ ($M_w = 393.20$) C: 33.60; H 6.92. Found: C 33.86; H 6.90%. ^{1}H NMR: 0.79 (t, 3H, $CH_3CH_2CH_2$); 1.17 (d of t, 12H, CH_3CH_2P); 1.63 (d of q, 2H, $CH_3CH_2CH_2$); 2.87 (d of d of q, 8H, CH_3CH_2P); 3.41 (q, 2H, $CH_3CH_2CH_2$); ^{13}C NMR: 7.7 (s, PCH_2CH_3); 10.3 (s, N–$CH_2CH_2CH_3$); 26.0 (s, N–$CH_2CH_2CH_3$); 29.7 (d, $J(PC) = 54.9$ Hz P–CH_2CH_3); 51.3 (s, N–$CH_2CH_2CH_3$); ^{31}P{^{1}H} NMR: 83.92 (s, $J(PSe) = 745$ Hz).

3.6. Structure determinations

Crystal data are given in Table 1, together with some data collection and refinement parameters.

The following general method was used: Diffracted intensities were collected on an Enraf–Nonius CAD-4 operating in the ω–2θ scan mode, using graphite-monochromated Mo Kα radiation. Final unit cell dimensions were determined from the setting angles of 25 accurately centered reflections. Crystal stability during the data collection was monitored by measuring the intensities of three standard reflections every 2 h. Data were collected at a constant rate, 5.17° min^{-1} in ω, with a scan range of $1.30 + 0.34 \tan\theta$. The data were corrected for Lorentz, polarization and X-ray absorption effects, the latter by a numerical method based on the measurements of six crystal faces.

The structure was solved by direct methods and successive difference Fourier syntheses were used to locate all non-hydrogen atoms using SHELXTL Version 5.03 [11]. Refinements were made by full-matrix least-squares on all F^2 data using SHELX-97 [12]. Anisotropic thermal parameters were included for all non-hydrogen atoms. All hydrogen atoms were included in calculated positions and allowed to ride on their parent nitrogen or carbon atoms with fixed isotropic thermal parameters ($U_{iso} = 1.2U_{iso}$ of the parent atom, or $U_{iso} = 1.5U_{iso}$ of the parent for CH_3 hydrogens).

Some differences in the individual methods for solving the crystal structures **1**–**4** are given below.

For **1**: The *n*-propyl group was disordered with the methylene carbons (C1, C2 and C1a, C2a) occupying two distinct sites in a 70:30 ratio. Insignificant residual electron density in the difference Fourier synthesis was found near the Se atom.

For **2**: The C1 and C2 atoms of the *n*-propyl group were found to be disordered over two distinct sites in a 60:40 ratio. The C–C distances were restrained in the minor component. Insignificant residual electron density in the difference Fourier syntheses was found near the Te atom.

For **3**: Diffracted intensities were collected on an Enraf–Nonius CAD-4 operating in the ω–$5/3\theta$ scan mode. Data were collected at a constant rate, 5.17° min^{-1} in ω, with a scan range of $1.10 + 0.34 \tan\theta$. The data were corrected for Lorentz, polarization and X-ray absorption effects, the latter by a numerical method based on the measurements of seven crystal faces. Insignificant residual

Table 1
Crystal structure data and refinement details for compounds **1**–**4**

Compound	**1**	**2**	**3**	**4**
Empirical formula	$C_{11}H_{26}NPSe$	$C_{11}H_{26}NPTe$	$C_{15}H_{18}NPSe$	$C_{11}H_{27}NP_2Se_2$
Formula weight	282.26	330.90	322.23	393.20
Crystal color, habit	colorless, acicular	yellow blocks	clear colorless prisms	clear colorless prisms
Crystal size (mm)	$0.41 \times 0.23 \times 0.19$	$0.56 \times 0.37 \times 0.20$	$0.51 \times 0.33 \times 0.23$	$0.38 \times 0.361 \times 0.361$
Crystal system	monoclinic	monoclinic	monoclinic	monoclinic
Space group	$P2(1)/c$	$P2(1)/c$	$P2(1)/n$	$P2(1)/n$
Unit cell dimensions				
a (Å)	8.7123(9)	8.8262(5)	12.539(2)	11.6069(10)
b (Å)	11.1470(8)	11.710(2)	9.4529(13)	11.883(2)
c (Å)	15.583(2)	15.4929(12)	12.844(2)	12.701(2)
α (°)	90	90	90	90
β (°)	104.922(10)	105.889(7)	95.372(13)	104.591(10)
γ (°)	90	90	90	90
V (Å^3)	1462.3(3)	1540.1(2)	1515.6(4)	1695.2(4)
Z	4	4	4	4
λ	0.71073	0.71073	0.71073	0.71073
Reflections collected	2057	2156	2781	1994
Independent reflections	1911	2004	2653	1880
Data/parameters	1911/134	2004/153	2653/166	1880/146
Final R	0.0448	0.0379	0.0371	0.0518
wR_2	0.0857	0.0923	0.0671	0.1214
R indices (all data)	0.0813	0.0451	0.0737	0.0785
WR_2	0.0985	0.0981	0.0764	0.1375
Largest difference peak	0.306/−0.469	0.657/−0.837	0.303/−0.310	0.737/−0.953

Table 2
Selected bond distances (Å) and angles (°) for compounds **1**–**4**

	1 (E = Se)	**2** (E = Te)	**3** (E = Se)	**4** (E = Se)
Bond lengths				
P═E	2.1163(14)	2.3642(13)	2.1159(10)	2.106(2); 2.102(2)
P–N	1.649(4)	1.647(4)	1.647(3)	1.714(6); 1.697(6)
P–C	1.865(5)	1.865(5)	1.807(3)	1.796(8); 1.801(8)
	1.848(6)	1.877(5)	1.810(3)	1.814(8); 1.819(8)
Bond angles				
N–P–E	111.7(2)	111.7(2)	117.66(11)	116.4(2); 113.0(2)
C–P–C	112.8(4)	112.9(3)	104.3(2)	106.2(2); 106.6(4)
N–P–C	105.5(2)	103.9(3)	103.8(2)	107.1(4); 105.6(3)
	104.7(2)	106.3(3)	104.0(2)	108.0(4); 107.2(3)
P–N–P				125.9(4)

electron density in the difference Fourier syntheses was found near the Se atom.

For **4**: Diffracted intensities were collected on an Enraf–Nonius CAD-4 operating in the ω–4/3θ scan mode. Data were collected at a constant rate, 5.17° min^{-1} in ω, with a scan range of $1.15 + 0.34 \tan\theta$. The data were corrected for Lorentz, polarization and X-ray absorption effects, the latter by a semi-empirical method based on azimuthal scans of ψ-data. Insignificant residual electron density in the difference Fourier syntheses was found near the Se atoms.

Some of the significant bond distances and angles are given in Table 2.

3.7. Spectroscopy

All of the new ligands were fully characterized using multi-nuclear NMR spectroscopy. The ^{1}H and ^{13}C NMR spectra are as expected for this type of organophosphorus compound. As is typical of P(V)═E compounds, ^{31}P chemical shifts occurred in the δ 20–100 ppm range, depending on the exact nature of the R and amino groups [13]. Bochmann reported a value [4] of δ 97.6 ppm for $Bu^{t}_{2}P(Se)NHPr^{i}$. As indicated in the literature, coupling constants of $^{1}J_{PSe}$ 700–800 Hz are often seen for E = Se [14], and closer to 1500–2000 Hz for E = Te [15,16].

4. Conclusions

In this work, we have shown that the synthesis of chalcogenoic aminophosphines can be readily achieved through a facile synthetic route giving moderate to high yields of the desired products. We have established that a variety of alkyl and aryl groups can be used to prepare these compounds and that ^{31}P NMR spectroscopy is a useful technique for their characterization. We are currently probing the reactions of these ligands (neutral and deprotonated) with a variety of transition metal and main group halides.

5. Supplementary data

CCDC Nos. 236222–236225 [236222 (**4**); 236223 (**3**); 236224 (**2**) and 236225 (**1**)] contains the supplementary crystallographic data for this paper. These data can be obtained free of charge via www.ccdc.cam.ac.uk/data_request/cif, by emailing data_request@ccdc.cam.ac.uk, or by contacting The Cambridge Crystallographic Data Centre, 12, Union Road, Cambridge CB2 1EZ, UK; fax: +44 1223 336033.

Acknowledgements

M.D.R. thanks the NSU CURIA for generous financial support of this project and UW – Fox Valley for travel monies. M.A.C expresses his thanks to Dr. Gary White (Society of Physics Students) for his support in this undergraduate research. We are grateful to Dr. Paul Jelliss (Baylor University) for assistance in obtaining the NMR spectra and to Professor Bob Angelici (Iowa State University) for computing facilities.

References

[1] See, for example: P. O'Brien, J.R. Walsh, I.M. Watson, M. Motevalli, L. Henriksen, J. Chem. Soc., Dalton Trans. (1996) 2491;
J.R. Walsh, A.C. Jones, J. Cryst. Growth 10 (1997) 170;
P. O'Brien, T. Trinade, Adv. Mater. 8 (1998) 161.
[2] A.P. Coleman, R.S. Dickson, G.B. Deacon, G.D. Fallon, M. Ke, K. McGregor, B.O. West, Polyhedron 13 (1994) 1277.
[3] M.L. Stiegerwald, C.E. Rice, J. Am. Chem. Soc. 110 (1988) 4228.
[4] M. Bochmann, X. Song, J. Chem. Soc., Dalton Trans. (1997) 2689;
M. Bochmann, G.C. Bwembya, M.B. Hursthouse, S.J. Coles, J. Chem. Soc., Dalton Trans. (1995) 1887;
M. Bochmann, G.C. Bwembya, M.B. Hursthouse, S.J. Coles, J. Chem. Soc., Dalton Trans. (1995) 2815.

[5] M. Bochmann, Chem. Vap. Depos. 2 (1996) 95;
G.C. Bwembya, X. Song, M. Bochmann, Chem. Vap. Depos. 1 (1995) 78.
[6] J. Arnold, J.M. Walker, K.M. Yu, P.J. Bonaria, A.L. Seligson, E.D. Bourret, J. Cryst. Growth 124 (1992) 647.
[7] T. Austad, T. Rød, K. Åse, J. Songstad, A.H. Norbury, Acta. Chem. Scand. 27 (1973) 1939.
[8] H. Schumann, N. Kuhn, G. Wolmershäuser, J. Chem. Soc., Chem. Commun. (1985) 1595.
[9] D.G. Gilheany, in: F.R. Hartley (Ed.), The Chemistry of Organophosphorus Compounds, vol. 2, Wiley, New York, 1992 (Chapter 1).
[10] M.D. Rudd, S.V. Lindeman, S. Husebye, Acta Chem. Scand. 50 (1996) 759.
[11] SHELXTL Version 5.03, Bruker AXS, Madison, WI, 1995.
[12] G.M. Sheldrick, University of Göttingen, Germany, 1997.
[13] G. Davidson, in: F.R. Hartley (Ed.), The Chemistry of Organophosphorus Compounds, vol. 2, Wiley, New York, 1992 (Chapter 5).
[14] W. McFarlane, D.S. Rycroft, J. Chem. Soc., Dalton Trans. (1973) 2162.
[15] I.A. Nuretdinov, E.I. Loginova, Bull. Acad. Sci. USSR, Chem. Sci. (1973) 2765.
[16] W.W. DuMont, H.J. Kroth, Z. Naturforsch., Teil B 36 (1981) 332.

Available online at www.sciencedirect.com
SCIENCE DIRECT®
Polyhedron 23 (2004) 1931–1937
POLYHEDRON
www.elsevier.com/locate/poly

Synthesis and liquid-crystalline behaviour of Ni(II) and Zn(II) phthalocyanines with peripheral monoazacrown ethers

Fatma Yılmaz [a], Devrim Atilla [a], Vefa Ahsen [a,b,*]

[a] *Department of Chemistry, Gebze Institute of Technology, P.O. Box 141, Gebze 41400, Turkey*
[b] *TUBITAK-Marmara Research Center, Materials and Chemical Technologies Research Institute, P.O. Box 21, Gebze 41440, Turkey*

Received 4 March 2004; accepted 21 April 2004

Abstract

The synthesis of metallo derivatives (Ni, Zn) of phthalocyanines obtained from a 4,5-dicyanobenzomonoazacrown ether substituted with a long alkoxyphenyl chain (**5a, 5b**) are described. The new compounds have been characterized by elemental analysis, IR, NMR and electronic spectroscopy, and mass spectra. The thermal stabilities of the pc compounds were determined by thermogravimetric analysis. The mesogenic properties of these new materials were studied by differential scanning calorimetry (DSC), optical microscopy and X-ray diffraction patterns of the mesophases.
© 2004 Elsevier Ltd. All rights reserved.

Keywords: Phthalocyanine; Metallo phthalocyanine; Liquid crystal; Metallo mesogen; Crown ether; Aza ether

1. Introduction

Phthalocyanines (Pcs) have been under systematic study more than 70 years; however, researchers are still interested in this class of compounds [1]. There is great interest in designing and using phthalocyanine (pc) compounds and their metal derivatives as materials in chemical sensors, liquid crystals, catalysis, nonlinear optics, optical data storage and nanotechnology. Substituted pc derivatives can also be used for photodynamic cancer therapy and other processes driven by visible light. Phthalocyanine derivatives offer a very wide choice of molecular physicochemical properties by changing the type of metal complex and/or the nature of substituent [1–4].

Phthalocyanines are well-known as a disc-like molecule and form a one-dimensional columnar structure in condensed phases. The first thermotropic discotic liquid crystalline pc was reported in 1982 [5] and since then numerous liquid crystalline pc derivatives have been synthesized with the aim of producing more easily controllable macroscopic structures [6]. It has recently been found that numerous phthalocyanine derivatives exhibit thermotropic or lyotropic mesomorphism [7–17]. The liquid crystalline properties of these compounds depend on the number, position and character of peripheral substituents and the nature of the central complex-forming ion. For example pcs, when peripherally substituted with alkyl [7], alkoxy [8], alkoxymethyl [5], oligo(ethyleneoxy) [10–12], alkylthia [13], oligo (ethyleneoxy)thia [14] or even ''crowned'' [15,16] groups form thermotropic discotic liquid crystals. Most of the liquid crystals based on pc or porphyrins contain alkyl side chains [17]. Although a number of benzo-15-crown-5 substituted pcs have been shown to form discotic mesophases [15,16] and there are no pcs showing mesogenic properties, which contain monoazacrown ether moieties.

Aza-crown ether-substituted pcs have been previously described in the literature [18–22]. Different substituents have been introduced on the nitrogen atom of the aza-crown moiety to improve the solubility, liquid crystal properties and the intrinsic amphiphilic character of these pcs.

* Corresponding author. Tel.: +90-262-754-2360/2611; fax: +90-262-754-2385.
E-mail address: ahsen@gyte.edu.tr (V. Ahsen).

0277-5387/$ - see front matter © 2004 Elsevier Ltd. All rights reserved.
doi:10.1016/j.poly.2004.04.031

Recently we have essentially focused on the synthesis of new pcs exhibiting gas sensor [23–25] and liquid crystal properties [13,14,27,28]. Pc films have been proven to be used as photoconductors and gas sensors in molecular electronic devices and ordered pc films are more sensitive than disordered pc films [25,26]. In this study, pcs with monoazacrown ether moieties on the periphery containing a long alkyloxyphenyl N-pivotal group were synthesized for investigation of their liquid crystalline behaviour. These compounds contain a central pc core, four monoaza 15-crown-5 rings and a total of four 3,4,5-tri(decyloxy) phenyl N-pivotal groups.

2. Experimental

2.1. Materials

4,5-Dibromomonoazabenzo-15-crown-5 (**1**) [18] and 3,4,5-tri(decyloxy)-1-benzenecarbonyl chloride (**2**) [29] were prepared according to the literature procedures. All other reagents and solvents were reagent-grade quality, were obtained from commercial suppliers, and were dried as described in Perrin and Armarego [30] before use.

2.2. Measurements

Elemental analyses were obtained from a Carlo Erba 1106 Instrument. Infrared spectra in KBr pellets were recorded on a Bio-Rad FTS 175C FT-IR spectrophotometer. Optical spectra in the UV–Vis region were recorded with a Shimadzu 2001 UV Pc spectrophotometer using 1 cm pathlength cuvettes at room temperature. The mass spectra were acquired on an LCQ-ion trap (Thermofinnigan, San Jose, CA, USA), equipped with an electrospray source and were recorded on a VG Zab Spec GC–MS spectrometer using the liquid secondary ion mass spectrometer (LSIMS). Electrospray full scan spectra, in the range of m/z 50–2000 amu or m/z 2000–3000 amu, were obtained by infusion through fused silica tubing at 2–10 μl min^{-1}. The solutions were analyzed in the positive mode. The LCQ calibration (m/z 50–2000) was achieved according to the standard calibration procedure from the manufacturer (mixture of caffeine, MRFA and Ultramark 1621). An ES-Tuning Mix solution (Agilent) was used to calibrate the spectrometer between 2000 and 3000 amu. The temperature of the heated capillary of the LCQ was set to the range of 180–200 °C, the ion spray voltage was in the range of 1–7 kV with an injection time of 5–200 ms. ^1H and ^{13}C NMR spectra were recorded in $CDCl_3$ solutions on a Bruker 500 MHz spectrometer using TMS as an internal reference. Thermogravimetric analyses were carried out on a Mettler Toledo Star^e Thermal Analysis System at a rate of 10 °C min^{-1} in a nitrogen flow (50 ml min^{-1}). Transition temperatures were determined with scan rates of 10 °C min^{-1} using a Mettler Toledo Star^e Thermal Analysis System/DSC 822^e System differential scanning calorimeter calibrated with indium from 3 to 4 mg samples under a nitrogen atmosphere. Optical textures were observed with the polarizing microscope Leitz Wetzler Orthoplan-pol equipped with the hot stage Linkam TMS 93 and temperature-controller Linkam LNP. X-ray measurements were performed with Cu Kα-radiation using a Rigaku Kristalloflex diffractometer (D_{max} 2200) at 30 °C.

2.3. Synthesis

2.3.1. 4,5-Dibromo-1,2-[7-(3,4,5-tri-decyloxyphenyl-1-carbonyl)-7-aza-1,4,10,13-tetraoxatridecamethylene]-benzene (3)

3,4,5-Tri(decyloxy)-1-benzenecarbonyl chloride (**2**) (0.93 g, 1.54 mmol) was added to a mixture of 4′,5′-dibromomonoazabenzo-15-crown-5 (**1**) (0.60 g, 1.41 mmol) and Et_3N (0.29 g, 2.82 mmol) in CH_2Cl_2 (10 ml) and stirred at room temperature. After 18 h, the crude mixture was washed with water (3 × 10 ml) and the organic solution was dried with anhydrous Na_2SO_4. The solvent was removed and the crude mixture was further purified by column chromatography (Silica gel, CH_2Cl_2) to afford of **3** as a white solid. Yield: 1.31 g (93%); mp. 53 °C. *Anal.* Calc. for $C_{51}H_{83}Br_2NO_8$: C, 61.41; H, 8.36; N, 1.41. Found: C, 61.38; H, 8.38; N, 1.40%. IR (KBr): ν_{max} (cm^{-1}) 3047, 2927–2857 (CH_2, CH_3), 1634 (C=O), 1583, 1487, 1455, 1354, 1252, 1175 (C–O–C), 1135 (C–N), 1056 ($C_{ar}O$–CH_2), 1013, 927, 843, 803, 765. MS (LSIMS): m/z (%) 998 (70) [M^+], 573 (100) [$M^+-3(C_{10}H_{21})$], 433 (76), 153 (27). ^1H NMR ($CDCl_3$): δ 0.87 (t, 9H, CH_3), 1.40 (m, 42H, CH_2), 1.76 (m, 6H, CH_2), 3.54–4.06 (m, 22H, CH_2O), 6.57 (s, 2H, CH_{ar}), 7.05 (s, 2H, CH_{ar}). ^{13}C NMR ($CDCl_3$, APT): δ 14.04 (CH_3), 22.83–31.87 (CH_2), 69.15–73.40 (CH_2O), 105.31 ($C_{ar}H$), 115.33 (C_{ar}–Br), 118.06 ($C_{ar}H$), 131.35 (C_{ar}–C=O), 139.12 (C_{ar}–$OC_{10}H_{21}$), 148.89 (C_{ar}–OCH_2CH_2O), 153.103 (C_{ar}–$OC_{10}H_{21}$), 172.11 (C=O).

2.3.2. 4,5-Dicyano-1,2-[7-(3,4,5-tri-decyloxyphenyl-1-carbonyl)-7-aza-1,4,10,13-tetraoxatridecamethylene]-benzene (4)

A mixture of **3** (0.73 g, 0.73 mmol), CuCN (0.20 g, 2.17 mmol) and dry DMF (4.50 ml) were heated to reflux for 18 h under argon. After cooling to room temperature, the solvent was removed and the reaction mixture was diluted with ammonium hydroxide solution (25%) and air bubbled through the mixture for 18 h. Then the mixture was filtered and the precipitate was washed with water until it became neutral. The precipitate crude product was further purified by column chromatography (Silica gel, CH_2Cl_2) to afford of **4** as a white solid. Yield: 0.32 g (50%); mp. 84 °C. *Anal.* Calc.

for $C_{53}H_{83}N_3O_8$: C, 71.46; H, 9.32; N, 4.73. Found: C, 71.50; H, 9.40; N, 4.72%. IR (KBr): ν_{max} (cm^{-1}) 3063, 2927–2856 (CH_2, CH_3), 2229 (C≡N), 1635 (C=O), 1518, 1352 (C–N), 1290 (C–O–C), 1246, 1232, 1174 (C–N), 1133, 936, 835, 765. MS (LSIMS): *m/z* (%) 912 (100) [M^+ + Na], 889 (23) [M^+], 573 (83) [$M^+-2(C_{10}H_{21})$], 433 (95) [$M^+-3(C_{10}H_{21})$]. ^{1}H NMR ($CDCl_3$,): δ 0.85 (t, 9H, CH_3), 1.38 (m, 42H, CH_2), 1.80 (m, 6H, CH_2), 3.48 – 4.10 (m, 22H, CH_2O), 6.50 (s, 2H, CH_{ar}), 7.05 (s, 2H, CH_{ar}). ^{13}C NMR ($CDCl_3$, APT): δ15.06 (CH_3), 21.60–32.05 (CH_2), 66.10–71.15 (CH_2O), 103.40 ($C_{ar}H$), 109.40 (C≡N), 116.80 (C_{ar}–C≡N), 116.95 ($C_{ar}H$), 130.00 (C_{ar}–C=O), 139.80 (C_{ar}–$OC_{10}H_{21}$), 151.30 (C_{ar}–OCH_2CH_2O), 151.60 (C_{ar}–$OC_{10}H_{21}$), 172.20 (C=O).

2.3.3. Synthesis of phthalocyanine derivatives

*2.3.3.1. 2,3;9,10;16,17;23,24-Tetrakis-[1,4,10,13-tetraoxatridecamethylene-7-aza-(3,4,5-tri-decyloxyphenyl-1-carbonyl) phthalocyaninato] nickel (II) (**5a**).* A mixture of **4** (1.07 g, 1.21 mmol), anhydrous $NiCl_2$ (0.32 g, 2.47 mmol), 0.27 ml (1.80 mmol) DBU and dried 1-hexanol (10 ml) were heated to reflux for 18 h under argon. The solvent was removed, the crude product diluted with CH_2Cl_2 and filtered to remove any participates. The solvent was removed and the crude green product was purified by column chromatography over silica gel with CH_2Cl_2. This compound was soluble in $CHCl_2$ and $CHCl_3$, slightly soluble in ethyl acetate, *n*-hexane and *n*-heptane, and insoluble in ethanol, methanol, acetone and DMF. Yield: 0.25 g (23%). *Anal.* Calc. for $C_{212}H_{332}N_{12}NiO_{32}$: C, 70.33; H, 9.18; N, 4.61. Found: C, 70.35; H, 9.24; N, 4.64%. IR (KBr): ν_{max} (cm^{-1}) 3055, 2927–2856 (CH_2, CH_3), 1635 (C=O), 1609 (C_{ar}=N), 1359 (C–N), 1284 (C–O–C), 1248, 1208, 1172 (C–N), 1128, 936, 839,749. MS (ES-MS), *m/z* (%): 3618 (90) $[M+H]^+$, 3046 (35) [$M^+-OCC_6H_23(C_{10}H_{21})$] and 1807 (100). ^{1}H NMR ($CDCl_3$): δ 0.71 (t, 36H, CH_3), 0.78–1.31 (m, 168H, CH_2), 1.61 (t, 24H, CH_2), 3.66–4.71 (m, 64H, CH_2O), 6.65 (s, 8H, CH_{ar}), 7.20 (s, 8H, CH_{ar}). ^{13}C NMR ($CDCl_3$, Decoupled): δ 12.04 (CH_3), 23.40–32.78 (CH_2), 68.03–78.30 (CH_2O), 102.20 (C–C=N), 104.30 ($C_{ar}H$), 123.40 ($C_{ar}H$), 126.47 (C_{ar}–C=O), 130.70 (C=N), 138.14 (C_{ar}–$OC_{10}H_{21}$), 150.45 (C_{ar}–OCH_2CH_2O), 152.74 (C_{ar}–$OC_{10}H_{21}$), 162.25 (C=O).

*2.3.3.2. 2,3;9,10;16,17;23,24-Tetrakis-[1,4,10,13-tetraoxatridecamethylene-7-aza-(3,4,5-tri-decyloxyphenyl-1-carbonyl) phthalocyaninato] zinc (II) (**5b**).* A mixture of **4** (1.07 g, 1.21 mmol), anhydrous Zn $(O_2CMe)_2$ (0.319 g, 2.47 mmol), 0.27 ml (1.8 mmol) DBU and dried 1-hexanol (10 ml) were heated to reflux for 18 h under argon. After that, **5b** was isolated and purified following the same procedure as for **5a**. This compound was soluble in CH_2Cl_2 and $CHCl_3$, slightly soluble in ethyl acetate, *n*-hexane and *n*-heptane, and insoluble in ethanol, methanol, acetone and DMF. Yield: 0.27 g (26%). *Anal.* Calc. for $C_{212}H_{332}N_{12}O_{32}Zn$: C, 70.19; H, 9.16; N, 4.65. Found: C, 70.22; H, 9.23; N, 4.63%. IR (KBr): ν_{max} (cm^{-1}) 3055, 2926–2854 (CH_2, CH_3), 1635 (C=O), 1582 (C_{ar}=N), 1359 (C–N), 1281 (C–O–C), 1248, 1208, 1172 (C–N), 1109, 1069, 936, 839,749. MS (ES-MS), *m/z* (%): 3624 (45) $[M+H]^+$, 2721 (100) [$M^+-6(C_{10}H_{21})$]. ^{1}H NMR ($CDCl_3$): δ 0.75 (t, 36H, CH_3), 0.80–1.37 (m, 168H, CH_2), 1.65 (t, 24H, CH_2), 3.68–4.73 (m, 64H, CH_2O), 6.59 (s, 8H, CH_{ar}), 7.19 (s, 8H, CH_{ar}). ^{13}C NMR ($CDCl_3$, Decoupled): δ 14.09 (CH_3), 22.64–31.94 (CH_2), 69.02–77.28 (CH_2O), 105.12 (C–CN), 106.40 ($C_{ar}H$), 125.40 ($C_{ar}H$), 127.60 (C_{ar}–C=O), 131.55 (C=N), 139.18 (C_{ar}–$OC_{10}H_{21}$), 150.45 (C_{ar}–OCH_2CH_2O), 153.24 (C_{ar}–$OC_{10}H_{21}$), 173.30 (C=O).

3. Results and discussion

The starting compound 4,5-dibromomonoazabenzo-15-crown-5 (**1**), 3,4,5-tri(decyloxy)-1-benzenecarbonyl chloride (**2**) were obtained as described in the literature [18,29], respectively. 4,5-Dibromomonoazabenzo-15-crown-5 (**1**) was treated with **2** to prepare the dibromo monoazacrown ether substituted with a long alkyloxyphenyl chain (**3**). This reaction was carried out in the presence of triethylamine as the base in dichloromethane at room temperature and the yield was relatively high (93–97%). Dibromo compound (**3**) was treated with CuCN in dimethylformamide (DMF) to prepare the corresponding dinitrile derivative (**4**). The synthetic pathways are shown in Fig. 1.

The preparation of pc derivatives from aromatic dinitriles might be carried out under different reaction conditions [1]. For various substituted dinitriles, the reactions in the presence of strong nitrogen bases such as 1,8-diazabicyclo [5.4.0] undec-7-ene (DBU), or 15-diazabicyclo [4.3.0] non-5-ene (DBN) in 1-hexanol are the most efficient ones in comparison to other methods [31–33]. In addition, these reactions are easily to perform and the conditions are relatively mild, together with a relatively high yield of pure pcs. Therefore, the pc derivatives (**5a** and **5b**) were obtained from the reaction of the dicyano compound (**4**) in the presence of the corresponding metal salt and DBU in 1-hexanol at reflux temperature.

Spectral investigations on the newly synthesized intermediates and pcs are in accordance with the proposed structures. Comparison of the IR spectra of each step gave some hints as to the nature of the product. In the IR spectrum of **3**, CH_2, CH_3 groups gave absorptions at 2927, 2856 cm^{-1} and the amidic C=O group stretched around 1635 cm^{-1}. The IR spectrum of **4** was easily verified with the sharp C≡N vibrations around 2229 cm^{-1}. The IR spectra of **5a** and **5b** are very similar.

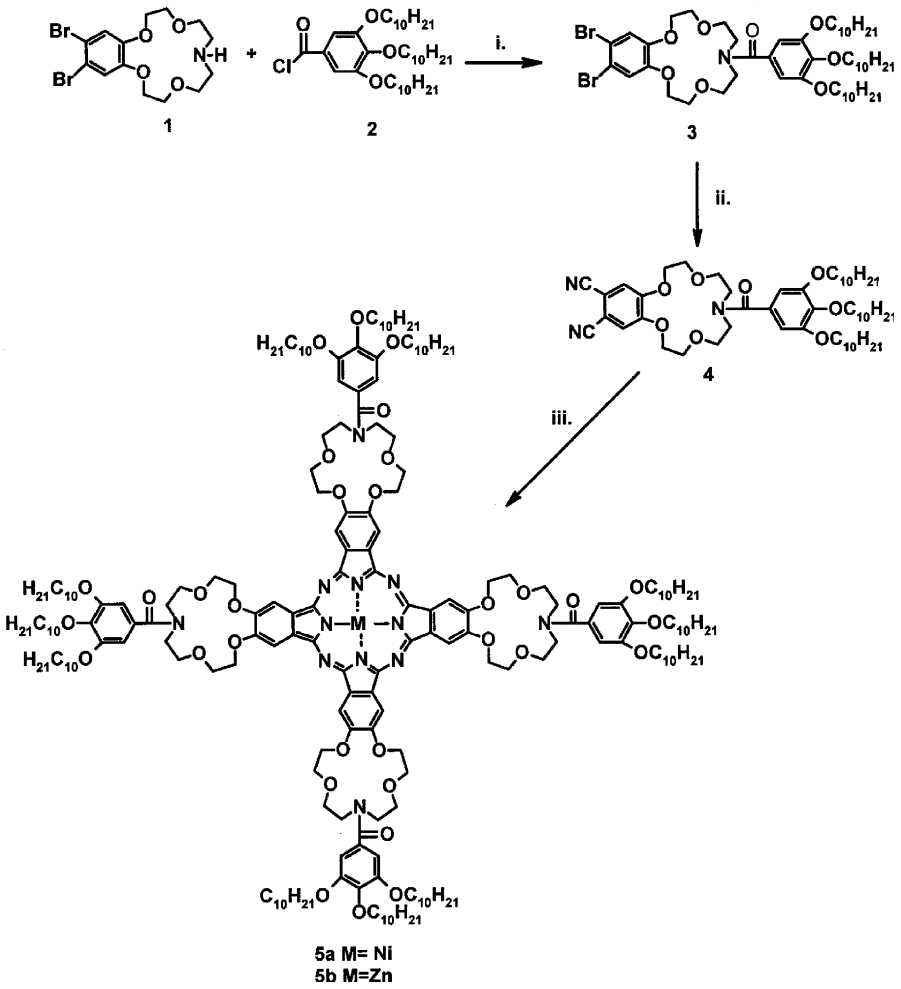

Fig. 1. Synthetic pathway for the preparation of **3**, **4**, **5a** and **5b**. (i) Triethylamine, dichloromethane. (ii) CuCN, DMF, reflux. (iii) DBU, 1-hexanol and metal salt.

In the ^{1}H NMR spectrum of **3**, the aromatic protons of the benzo group of the monoaza crown ether and the benzo group of the substituted alkyl chain give singlets at 6.57 and 7.05 ppm, respectively. The ^{1}H NMR spectrum of **4** indicates the aromatic protons of the benzo group of the monoaza crown ether at 6.5 ppm, shifting 0.7 ppm because of the CN substitution. A common feature of the ^{1}H NMR spectra of the pcs (**5a** and **5b**) is the broad absorptions when compared with that of the cyano derivatives.

In the ^{13}C APT (Attached Proton Test) NMR spectrum of **4**, the nitrile carbons appeared at 107.80 ppm. The ^{13}C NMR spectra of **5a** and **5b** indicate C=N carbons at 130.70 and 131.55 ppm, respectively.

A close investigation of the mass spectra of the dibromo (**3**) and dinitrile (**4**) derivatives and pcs (**5a, 5b**) confirmed the proposed structures. The mass spectra of **5a** and **5b** were obtained by the Electron Spray technique and the molecular ion peaks at m/z: 3618 for **5a** and m/z: 3624 for **5b** were observed. The mass spectra of **3** and **4**, obtained by the LSIMS technique show molecular ion peaks for these molecules. In the mass spectra of **3** and **4** the region of the molecular ion and of the bigger fragment ions are shown together with the corresponding leaving groups. In the mass spectra of **3** and **4**, in addition to the [M^{+}] peaks at 998 and 889, respectively, fragment ions corresponding to the loss of 3($C_{10}H_{21}$) [M^{+}−425] for **3** and [M^{+}−(425+Na)] for **4** were easily identified.

In the electronic spectra of the pcs (**5a** and **5b**) intense Q absorption bands were observed at 667 and 674 nm, respectively, with weaker absorptions at 601 and 609 nm, respectively. Weaker absorptions on the higher energy side of the Q bands are generally observed in the case of metallophthalocyanines, indicating the presence of aggregated species together with the monomeric ones which are essentially responsible for the intense absorption occurring in the main Q bands [34]. B band absorptions of the pcs (**5a** and **5b**) were observed at 312 and 355 nm, respectively (Fig. 2). Although the NiPc (**5a**) and ZnPc (**5b**) have a typical spectral pattern in the UV–Vis region for pcs, only the NiPc (**5a**) showed a new

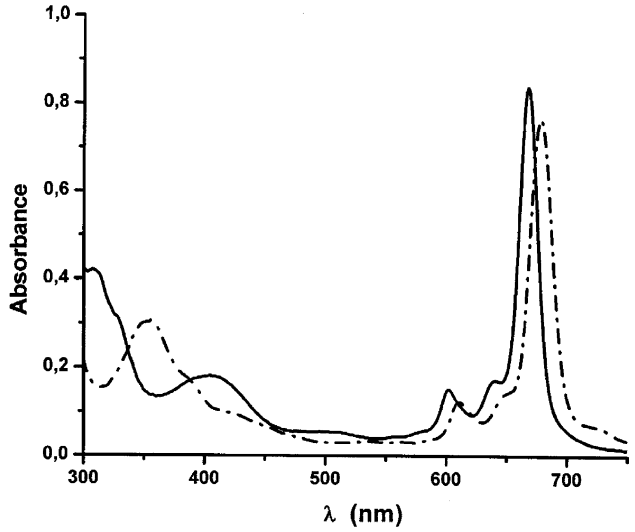

Fig. 2. Absorption spectra of **5a** (—) and **5b** (- - -) in chloroform at 3.76×10^{-6} M concentration.

absorption band at 405 nm in addition to a B band. This new absorption band due to the effect of the metal can be characteristically observed for a number of Ni Pcs [19,22,28]. For pcs complexed with metals having partially filled d orbitals, further bands are sometimes observed which can be ascribed to metal-to-ligand charge transfer (MLCT) or ligand-to-metal charge transfer (LMCT) transitions. So the spectrum of NiPc shows three transitions in the region of the B and N bands which are not present in the zinc analogue [35].

Although the thermal stability of pcs is well known, the pc compounds are not stable above 320 °C. The initial and main decomposition temperatures of **5a** and **5b** are 320 and 396 °C, respectively.

3.1. Characterization of the mesophases

3.1.1. Thermotropic phase-behaviour

The phase transition behaviours of pcs **5a** and **5b** were determined by differential scanning calorimetry (DSC) and polarizing microscopic observations. The DSC-measurement of **5a** shows an endothermic peak at about 109 °C in the vicinity which relates to the phase transition ($\Delta H = 78.1$ kJ/mol). The cooling cycle shows no peak representing a phase transition compared with the heating cycle. A phase transition is not observed at the second heating and cooling cycles nor the third cycle. However, compound **5b** shows a broad peak at about 117 °C for the first heating cycle ($\Delta H = 16.2$ kJ/mol). The cooling cycle shows a broad peak at about 111 °C ($\Delta H = 16.9$ kJ/mol). The heating cycles were interrupted before reaching any clearing point to avoid decomposition. In all cases, decomposition of the pcs are around 320–396 °C (determined by Thermal Gravimetric Analysis, TGA). We assume that the peaks of **5a** and **5b** in the heating cycles are related to the transition from the crystal phase to the mesophase and the peak of **5b** in the cooling cycle is related to the transition from the mesophase to the crystal phase. These investigations indicate that compound **5a** exhibits a thermotropic liquid crystalline behaviour over a wide temperature range, including room temperature, and compound **5b** exhibits no liquid crystalline behaviour at room temperature.

Fig. 3. Optical texture of **5a** observed at 110 °C (magnification × 25).

Fig. 4. Optical texture of **5b** observed at 118 °C (magnification × 16).

3.1.2. Optical microscopy of the thermotropic mesophase

The textures observed by polarizing optical microscopy for the compounds **5a** and **5b** are very similar to those described in the literature [12,36–38]. Good textures of the samples of the mesophases were obtained by slowly cooling (5 °C min^{-1}) from the isotropic melt, and mosaic textures appear (notice the decomposition). A phase transition from the mesophase to isotropic liquid is for **5a** and **5b** >320 °C. The textures of compound **5a** and **5b** under polarizing optical microscopy at 110 and 118 °C, respectively, are presented in Figs. 3 and 4.

Table 1
X-Ray diffraction data of compound **5a** at room temperature

Compound	Spacing (Å)		Ratio	Miller indices	Lattice constant
	$d_{calculated}$	$d_{observed}$			
5a	34.86	34.86	1	1 0 0	$a = 40.26$ Å
	20.05	20.13	$\sqrt{3}$	1 1 0	
	17.01	17.43	$\sqrt{4}$	2 0 0	
	13.19	13.17	$\sqrt{7}$	2 1 0	
	11.12	11.62	$\sqrt{9}$	3 0 0	
	10.11	10.06	$\sqrt{12}$	2 2 0	
	7.35				
	4.46				

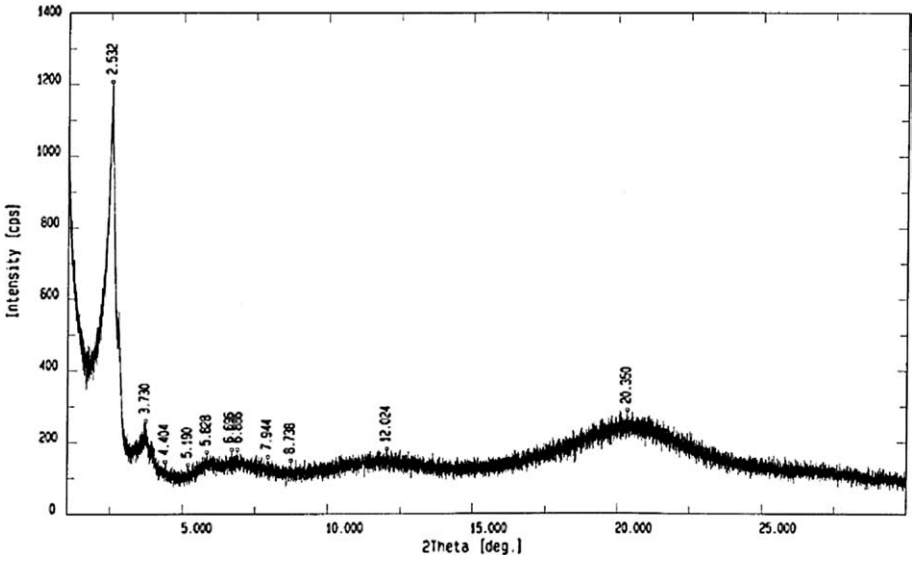

Fig. 5. X-ray diffraction pattern of complex **5a** at 30 °C.

3.1.3. X-ray diffraction

The mesophase of **5a** was identified by microscopic observation and X-ray diffraction measurements at 30 °C. The X-ray data is summarized in Table 1. Powder diffraction patterns of **5a** contain the typical reflections of a columnar mesophase of substituted pcs [17]. The low angle of the X-ray diffraction diagram of compound **5a** (Fig. 5) shows up to seven sharp Bragg reflections with a d-spacing ratio $1{:}1/\sqrt{3}{:}1/\sqrt{4}{:}1/\sqrt{7}{:}1/\sqrt{9}{:}1/\sqrt{12}{:}1/\sqrt{13}$ [5,7,10,13,14,17,39]. The lattice constant (**a**) is 40.26 Å for compound **5a**. This results suggests a two-dimensional hexagonal lattice with disk-like molecules stacked in columns in the hexagonal arrangement. In the wide angle regions the compound shows a diffuse band around 4.46 Å ($2\theta = 20.36°$) which corresponds to the melting of alkyl chains, and a band at about 3.5 Å ($2\theta \cong 25°$) which would correspond to fluctuation of the inter-disk distance in the one-dimensional molecular stack was not observed. Hence, this mesophase could be identified as a Col_h mesophase. The X-ray diffraction measurement of **5b** could not be measured at room temperature because this compound does not exhibit a mesophase at this temperature.

The diameter of the pc molecules (**5a** and **5b**) were calculated as ≈57 Å by means of semi-empirical method AM1 with full geometry optimization (GAUSSIAN 03W program package) in the gas phase. If the alkyl chains break then the diameter of the molecule is calculated as 35.8 Å. The experimental result from X-ray analysis data does not fit the corresponding theoretical result. It may be concluded that, according to the X-ray analysis data, the alkyl chains do not prefer a straight form but a frizzed form.

Acknowledgements

This work was supported by the Research Fund of Gebze Institute of Technology. We thank Professor Anatoly Dimoglo and Dr. Ayşe Gül Gürek at Gebze Institute of Technology, Department of Chemistry for fruitful discussions.

References

[1] C.C. Leznoff, A.B.P. Lever (Eds.), Phthalocyanines: Properties and Applications, vol. 1–4, VCH, New York, 1989, 1993, 1996.
[2] S. Huang, L. Dai, A.W.H. Mau, J. Phys. Chem. B 103 (1999) 4223.
[3] M. Hanack, M. Lang, Adv. Mater. 6 (1994) 819.
[4] P. Matlaba, T. Nyokong, Polyhedron (2002) 2463.
[5] C. Piechocki, J. Simon, A. Skoulios, D. Guillon, P. Weber, J. Am. Chem. Soc. 104 (1982) 5245.
[6] J.L. Serrano (Ed.), Metallomesogens, VCH, Weinheim, 1996, p. 160 (Chapter 4).
[7] K. Ohta, L. Jacquemin, C. Sirlin, L. Bosio, J. Simon, New J. Chem. 12 (1988) 751.
[8] D. Masurel, C. Sirlin, J. Simon, New J. Chem. 11 (1987) 455.
[9] P. Humberstone, G.J. Clarkson, N.B. McKeown, K.E. Treacher, J. Mater. Chem. 6 (1996) 315.
[10] D. Guillon, A. Skoulios, C. Piechocki, J. Simon, P. Weber, Mol. Cryst. Liq. Cryst. 100 (1983) 275.
[11] G.J. Clarkson, N.B. McKeown, K.E. Treacher, J. Chem. Soc., Perkin Trans. 1 (1995) 1817.
[12] J.M. Kroon, R.B.M. Koehorst, M. van Dijk, G.M. Sanders, E.J.R. Sudhölter, J. Mater. Chem. 7 (1997) 615.
[13] A.G. Gürek, V. Ahsen, F. Heinemann, P. Zugenmaier, Mol. Cryst. Liq. Cryst. 338 (2000) 75.
[14] S. Dabak, V. Ahsen, F. Heinemann, P. Zugenmaier, Mol. Cryst. Liq. Cryst. 348 (2000) 111.
[15] C.F. Van Nostrum, S.J. Picken, R.J.M. Nolte, Angew. Chem. Int. Ed. Engl. 33 (1994) 2173.
[16] C.F. Van Nostrum, S.J. Picken, A.J. Schouten, R.J.M. Nolte, J. Am. Chem. Soc. 117 (1995) 9965.
[17] J. Simon, P. Bassoul, in: C.C. Leznoff, A.B.P Lever (Eds.), Phthalocyanines: Properties and Applications, vol. 2, VCH, New York, 1993 (Chapter 5).
[18] V. Ahsen, A.G. Gürek, E. Musluoğlu, A. Gül, Ö. Bekaroğlu, Chem. Ber. 122 (1989) 1073.
[19] V. Ahsen, A.G. Gürek, E. Musluoğlu, A. Gül, Ö. Bekaroğlu, Chem. Ber. 124 (1991) 2531.
[20] M. Kandaz, Ö. Bekaroğlu, J. Porphyr. Phthalocya. 3 (1999) 339.
[21] B. Cabezon, E. Quesada, S. Esperanza, T. Torres, Eur. J. Org. Chem. (2000) 2767.
[22] D. Atilla, V. Ahsen, J. Porphyr. Phthalocya. 6 (2002) 593.
[23] V. Ahsen, M. Özdemir, Z.Z. Öztürk, A. Gül, Ö. Bekaroğlu, J. Chem. Res. (S) 2 (1995) 348.
[24] T.V. Basova, B.A. Kolesov, A.G. Gürek, V. Ahsen, Thin Solid Films 385 (2001) 246.
[25] T.V. Basova, A.G. Gürek, V. Ahsen, Mater. Sci. Eng. C 22 (2002) 99.
[26] T.V. Basova, C. Taşaltn, A.G. Gürek, M.A. Ebeoğlu, Z.Z. Öztürk, V. Ahsen, Sensor Actuator B 96 (2003) 70.
[27] A.G. Gürek, M. Durmuş, V. Ahsen, New J. Chem. 28 (2004) 693.
[28] M. Durmuş, C. Lebrun, V. Ahsen, J. Porphyr. Phthalocya., in press.
[29] C. Mertesdorf, H. Ringsdorf, Liq. Cryst. 5 (1989) 1757.
[30] D.D. Perrin, W.L.F. Armarego, Purification of Laboratory Chemicals, 2nd ed., Pergamon, Oxford, 1989.
[31] D. Wöhrle, G. Schnurpfeil, G. Knothe, Dyes Pigments 18 (1992) 91.
[32] H. Tomoda, S. Saito, S. Ogawa, S. Shiraishi, Chem. Lett. (1980) 1277.
[33] H. Tomoda, S. Saito, S. Shiraishi, Chem. Lett. (1983) 313.
[34] M.J. Stilmann, T. Nyokong, in: C.C. Leznoff, A.B.P. Lever (Eds.), Phthalocyanines: Properties and Applications, vol. 1, VCH, New York, 1993 (Chapter 3).
[35] M.J. Cook, in: R.J.H. Clark, R.E. Hester (Eds.), Spectroscopy of New Materials, Wiley, New York, 1989 (Chapter 3).
[36] J.A. Duro, G. de la Torre, J. Barbera, J.L. Serrano, T. Torres, Chem. Mater. 8 (1996) 1061.
[37] T. Hegmann, B. Neumann, J. Kains, S. Diele, C. Tschierske, J. Mater. Chem. 10 (2000) 2244.
[38] J. Sleven, C. Görller-Walrand, K. Binnemans, Mater. Sci. Eng. C 18 (2001) 229.
[39] A.S. Cherodian, A.N. Davies, R.M. Richardson, M.J. Cook, N.B. McKeown, A.J. Thomson, J. Feijoo, G. Ungar, K.J. Harrison, Mol. Cryst. Liq. Cryst. 196 (1991) 103.

Available online at www.sciencedirect.com
SCIENCE DIRECT®
Polyhedron 23 (2004) 1939–1946
POLYHEDRON
www.elsevier.com/locate/poly

Copper(II) complexes of several monophosphono dipeptides: the role of phosphonic oxygen and thioether sulfur in complex stabilization

Barbara Kurzak [a,*], Agnieszka Woźna [a], Julia Jezierska [b], Małgorzata Jeżowska-Bojczuk [b], Wojciech Szczepanik [b], Paweł Kafarski [c]

[a] *Institute of Chemistry, University of Podlasie, 3-Maja 54, 08-110 Siedlce, Poland*
[b] *Faculty of Chemistry, University of Wrocław, F. Joliot-Curie 14, 50-383 Wrocław, Poland*
[c] *Institute of Organic Chemistry, Biochemistry and Biotechnology, Wrocław University of Technology, Wybrzeże Wyspiańskiego 27, 50-370 Wrocław, Poland*

Received 6 January 2004; accepted 23 April 2004
Available online 24 June 2004

Abstract

Potentiometric, UV–Vis, CD and EPR studies were performed on the copper(II) complexes of oxygen and nitrogen donor ligands (monophosphono dipeptides: 1-(*N*-L-leucylamino)methylphosphonic acid – Leu–Gly(P), 1-(*N*-L-leucylamino)valylphosphonic acid – Leu–Val(P)) and a thioether sulfur donor ligands (monophosphono dipeptides: 1-*N*-(glycyloamino)-2-(*S*-benzylthio)ethanephosphonic acid – Gly–(Bz)Cys(P), D(+) and Gly–(Bz)Cys(P), D(−)). Complex formation reaction between copper(II) and dipeptides were very similar to each other, $[MLH_{-1}]^-$ being the major species in wide pH region. CD spectroscopy, however, was a very sensitive tool for the elucidation of small structural differences among peptide complexes, including the weak interaction in an axial and equatorial position of thioether residues. The complexes of the thioether donors have higher thermodynamic stability constants than the other ones.
© 2004 Elsevier Ltd. All rights reserved.

Keywords: Copper(II) complexes; Thioether ligands; Stability constants; Monophosphono dipeptides; Potentiometry; Vis, CD, EPR spectroscopy

1. Introduction

In contrast to the aminoalkylphosphonic acids complexes (see review [1] and references therein), which were intensively investigated in solution, studies on the chemistry of complex equilibria of the phosphonodipeptides containing N-terminal aminoalkylphosphonic acids with different metal ions in solution are rather poor [2–5]. Phosphonodipeptides containing terminal aminoalkylphosphonic acids have exhibited bacteriostatic ([6] and references therein) and herbicidal [7] activity. Their synthesis and properties have been reported by Kafarski et al. [8].

Besides, a good implementation of organophosphonates requires reliable data on the stability constants of the corresponding complexes. These permit modeling and prediction of the technological, environmental and pharmaco-kinetic equilibrium. So, chemical speciations based on numerical chemical equilibrium data are of extreme importance for different applications.

In earlier publications we have characterized the complex forming abilities of some aminodiphosphonic acids as iminodimethylenediphosphonic acids [1], and aminomethane-1,1-diphosphonic acids [9] with different metal ions in aqueous solutions. In the present work, our studies have been extended to various monophosphono dipeptides: 1-(*N*-L-leucylamino)methylphosphonic acid – Leu–Gly(P), 1-(*N*-L-leucylamino)valylphosphonic acid – Leu–Val(P) and 1-*N*-(glycyloamino)-2-(*S*-benzylthio) ethanephosphonic acid – Gly–(Bz)Cys(P). The aim of

* Corresponding author. Tel.: +48-25-643-1097; fax: +48-25-644-2045.
E-mail address: bkurzak@ap.siedlce.pl (B. Kurzak).

0277-5387/$ - see front matter © 2004 Elsevier Ltd. All rights reserved.
doi:10.1016/j.poly.2004.04.027

the present paper was to study the influence of a thioether sulfur in the side chain on the complexing properties of Gly–(Bz)Cys(P), D(+) and Gly–(Bz)Cys(P), D(−) towards Cu^{2+} metal ion. We have chosen copper(II) (the coordination sphere of this metal ion is characterized by the phenomena of its plasticity) because of question, which still exists in the literature: does a thioether sulfur interact with Cu^{2+} or not?

Coordination properties of the ligands are important factors to understand the coordination ability of the hard–soft metals towards biological materials. Combination of different spectroscopic method was applied to identify the complexes in solution. Tentative structures for the complexes are discussed.

2. Experimental

2.1. Materials

Monophosphono dipeptides used in this study (Table 1) were obtained according to previously described procedures [10,11]. The purity and the exact concentrations of the solutions of the ligands used for potentiometric measurements were determined by the Gran method [12]. The concentration of copper(II) chloride stock solution was standardized by complexometric ethylenedinitrilotetraacetate (EDTA) titration. Carbonate-free sodium hydroxide (the titrant) was prepared and standardized against a standard potassium hydrogenphthalate solution.

2.2. Potentiometric measurements

The stability constants of the proton and copper(II) complexes were determined by pH-metric titration of 5 cm^3 samples in water solutions. The ligand concentration was 4×10^{-3} or 2×10^{-3} mol dm^{-3} and the metal ion:ligand ratios were 0:1; 1:1; 1:1.5; 1:2 or 1:4. The ionic strength was adjusted to 0.2 mol dm^{-3} with KCl in each case. The titrations were performed over the range pH 2–11 with a carbonate-free KOH solution of known concentration (ca. 0.15 mol dm^{-3}). All titration solutions were thermostated at 25 ± 0.1 °C using a constant-temperature water-bath.

The data for the Cu^{2+}–Leu–Gly [13] and for the Cu^{2+}–Leu–Gly(P) [4] systems can be found in the literature but the stability constants were reinvestigated by us under the condition identical to those applied for other systems. In the case of Leu–Val(P), Gly–(Bz)Cys(P), D(−) and Gly–(Bz)Cys(P), D(+) our data are the first reported.

The pH was measured with a Radelkis OP-208/1 instrument with a combination pH electrode (SINGLE PORE, Hamilton) using a microburette ABU-80 (Radiometer). The electrode system was calibrated by periodic titrations of HCl solution (7.5×10^{-3} mol dm^{-3} in KCl) against standard KOH solution. The resulting titration data were used to calculate the standard

Table 1
The formulae of the studied ligands

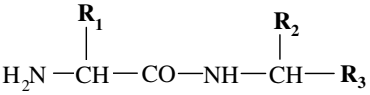

R_1	R_2	R_3	Abbreviation
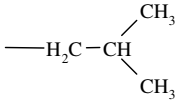	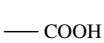		Leu – Gly
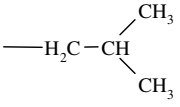			Leu – Gly(P)
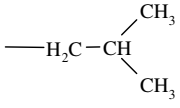		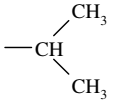	Leu – Val(P)
		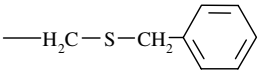	Gly-(Bz)Cys(P), D(-) Gly-(Bz)Cys(P), D(+)

electrode potentials, E^0, and the dissociation constant for water ($pK_w = 13.73$). These values were then used to calculate the hydrogen-ion concentration [H^+] from e.m.f. readings [14]; number of titration, 3; calculations, SUPERQUAD computer program [15]. The reported standard deviations were calculated by assuming random errors.

The charges of the complexes have been omitted in the text and tables. However, for clarity, it should be mentioned that the fully deprotonated forms have negative charges L^{2-} and L^- for the monophosphono dipeptides and simple dipeptide, Leu–Gly, respectively.

2.3. UV/Vis spectroscopy

The absorption spectra were obtained on a SPECORD M40 spectrophotometer using 5-cm quartz cells at room temperature. The spectra were recorded digitally (1.5 nm) over the range 400–900 nm. The metal ion concentration was 3×10^{-3} mol dm^{-3} and concentration ratio of copper(II):ligand were 1:1 and 1:2. The individual spectra of the copper(II) complexes were calculated by means of method described in [16].

2.4. CD spectroscopy

The spectra were recorded at 25 °C on a Jasco J-715 spectropolarimeter (JASCO, Japan Spectroscopic Co.), over the range of 200–800 nm, using 1 cm and 0.1 cm cells. Samples contained 5.0×10^{-3} mol dm^{-3} ligand concentrations and 1:1.5 Cu^{2+}-to-ligands molar ratios. Such molar complex ratio exactly reflects the species distribution at the ratio 1:2, however, at the ligand concentration applied (2.5×10^{-3} mol dm^{-3} of Cu^{2+} ions) were too low to obtain readable spectra. The spectra are expressed in terms of $\Delta\varepsilon = \varepsilon_l - \varepsilon_r$, where ε_l and ε_r are molar absorption coefficients for left and right circularly polarized light, respectively.

2.5. EPR spectroscopy

Electron paramagnetic resonance (EPR) spectra were performed on a Bruker ESP 300E spectrometer at the X-band frequency (9.45 GHz) at 77 K in ethylene glycol–water (1:1 v/v) solutions. The ligand concentration was 4.0×10^{-3} mol dm^{-3} and the molar ratios of metal–ligand were 1:1 and 1:2. The spectra were analyzed by computer simulation program [17] based on resonance fields calculated according to method of Sakaguchi et al. [18].

3. Results and discussion

The acid dissociation constants of the studied monophosphono dipeptides together with those of simple dipeptide, Leu–Gly, are given in Table 2. The fully protonated form (H_3L^+) of Leu–Gly–PO_3H_2, Leu–Val–PO_3H_2 or Gly–(Bz)Cys–PO_3H_2, D(−) and Gly–(Bz)

Table 2
Logarithmic protonation constants ($\log\beta_n^H$) and stability constants ($\log\beta_n$) for their complexes with Cu^{2+} at 25 °C and $I = 0.2$ mol dm^{-3} (KCl)

Assignments	Compound						
	Leu–Gly		Leu–Gly(P)		Leu–Val(P)	Gly–(Bz) Cys(P)	Gly–(Bz) Cys(P)
	This work	Ref. [13]	This work	Ref. [4]		D(−)	D(+)
[HL]	8.02(1)	8.24	8.26(1)	8.07	8.32(1)	8.35(1)	8.33(1)
[H_2L]	11.11(2)	11.44	14.71(1)	14.17	14.92(3)	14.50(1)	14.46(1)
[H_3L]			15.95(8)		16.15(15)		
[Cu(HL)]			11.76(2)	11.29(3)	12.06(2)	12.04(1)	12.00(2)
[CuL]	5.33(3)	5.11	6.70(2)	6.21(1)	6.87(2)	7.07(1)	7.02(2)
[CuLH_{-1}]	1.36(1)	1.28	1.66(1)	1.46(6)	1.37(2)	1.57(1)	1.51(2)
[CuLH_{-2}]	−7.91(1)	−8.50	−8.24(2)	−7.46(3)	−8.20(2)	−7.88(2)	−7.93(3)
[CuL_2]			12.19(4)		12.25(4)	11.80(13)	11.87(13)
[CuL_2H_{-1}]	3.89(3)	3.59	3.55(13)	4.37(7)	3.64(9)	4.62(3)	4.59(4)
[CuL_2H_{-3}]		−5.24					
$\log K_{[CuL_2]}$			5.49		5.38	4.73	4.85
$pK_{[Cu(HL)]}$			5.06	5.08	5.19	4.97	4.98
$pK_{[CuL]}$	3.97	3.83	5.04	4.75	5.50	5.50	5.51
$pK_{[CuLH_{-1}]}$	9.27	9.78	9.90	8.92	9.57	9.45	9.44
$pK_{[CuL_2]}$			8.64		8.61	7.18	7.28
$\log\beta_{[Cu(HL)]} - pK_{PO_3H^-}$			5.31		5.46	5.89	5.87
$\log\beta_{[CuLH_{-1}]} - \sum pK$	−9.75		−13.05		−13.55	−12.93	−12.95

Cys–PO_3H_2, D(+) can release three protons. The first proton of the –PO_3H_2 group is very acidic (p$K \approx 1.0$–2.0), and thus this function is fully deprotonated in the pH range studied in potentiometric titrations (2–10.5) and does not take part in metal coordination equilibria. In this connection the acidic dissociation constants of these protons are not given in Table 2. The second proton comes from the phosphonic function –PO_3H^- and the last one from the amino group –NH_3^+.

Comparison of the corresponding pK values with each other: the pK(NH_3^+) values with that of Leu–Gly, and of the pK(–PO_3H^-) values with that of Leu–Gly–PO_3H^-, shows that the pK(NH_3^+) values of the peptide-phosphonic acids are in good agreement with one another and slightly differ from that of Leu–Gly. It is seen (Table 2) that in case of the phosphonodipeptides, the –NH_3^+ group shows a higher basicity (ca. 0.3 log units) than Leu–Gly, probably because of a weak interaction with negatively charged phosphonic group (the fully deprotonated phosphonate group has a charge of 2–).

The electron donating by the R_3 substituent, which is present in the Leu–Val–PO_3H^-, results from the more basic character of the –PO_3H^- group in this molecule, if compare with Leu–Gly–PO_3H^-. The more acidic character of the –PO_3H^- group of Gly–(Bz)Cys–PO_3H^-, D(–) and Gly–(Bz)Cys–PO_3H^-, D(+) than of Leu–Gly–PO_3H^- ($\log \Delta K = 0.30$), can be explained by the electron-withdrawing effects of the R_3 substituent in the former case. The differences between the pK values of the corresponding amino groups are not as big as the differences between the pK's of the – PO_3H^- groups.

The titration curves for the systems containing copper(II) and studied ligand were evaluated by assuming the same type of complexes as were determined for the simple aliphatic dipeptides [19]. Due to the higher basicity of PO_3^{2-}, as compared to that for CO_2^-, the formation of protonated LH was also taken into account. The best fits between the measured and calculated titration curves were obtained by assuming the species given in Table 2. Formation of the [CuL_2] complex, which is not found by Herman and Lukes [4] for Cu^{2+}–Leu–Gly(P) system, is observed by us for all the phosphonodipeptides. As an illustration, the concentration distribution curves for the complexes formed in the Cu^{2+}–Leu–Gly and Cu^{2+}–Leu–Gly(P) systems are depicted in Figs. 1 and 2, and for the Cu^{2+}–Gly–(Bz)Cys(P), D(–) system in Fig. 3.

To clarify the binding modes of the complexes formed – visible, CD and EPR spectral measurements were performed (Tables 3 and 4). The analysis of the EPR spectra measured for all the systems as a function of pH and molar relation Cu:L, allows to find a specific EPR parameters which differentiate the species predicted by the potentiometric studies. In general, the EPR parameters are in some extent modified due to substitution of –CO_2^- by –PO_3H^- (or –PO_3^{2-}) group. The

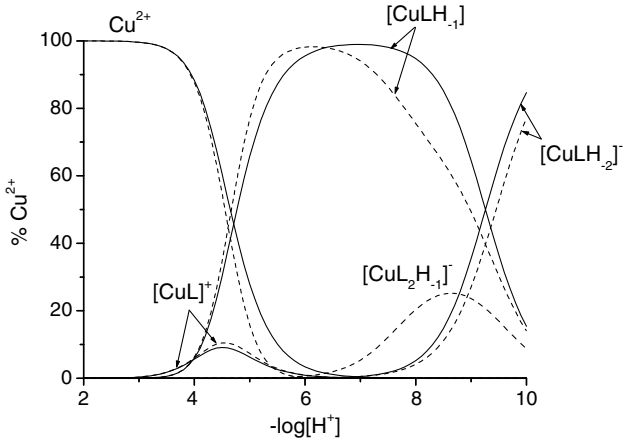

Fig. 1. Distribution diagrams of the complexes formed in the Cu^{2+}–Leu–Gly system as a function of $-\log[H^+]$, $c_L = 0.004$ mol dm^{-3}; (–) $c_{Cu^{2+}} = 0.004$ mol dm^{-3}, (···) $c_{Cu^{2+}} = 0.002$ mol dm^{-3}.

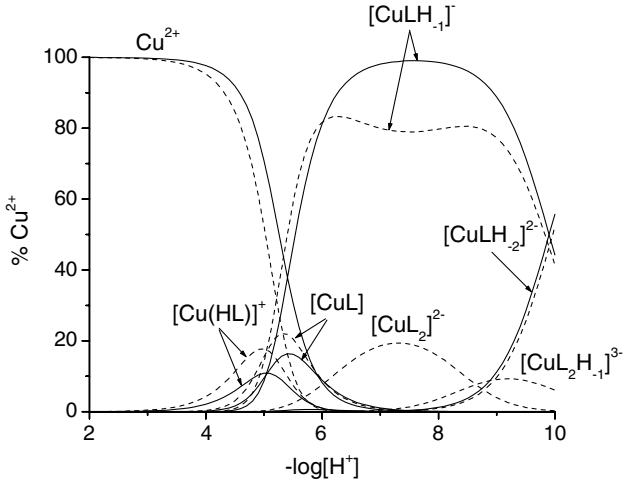

Fig. 2. Distribution diagrams of the complexes formed in the Cu^{2+}–Leu–Gly(P) system as a function of $-\log[H^+]$, $c_L = 0.002$ mol dm^{-3}; (–) $c_{Cu^{2+}} = 0.002$ mol dm^{-3}, (···) $c_{Cu^{2+}} = 0.001$ mol dm^{-3}.

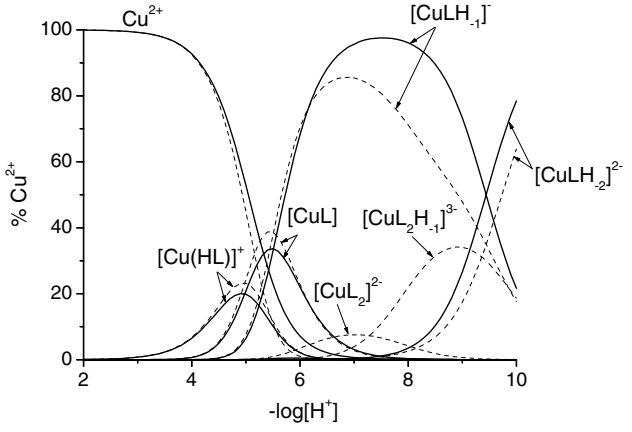

Fig. 3. Distribution diagrams of the complexes formed in the Cu^{2+}–Gly–(Bz)Cys(P), [D(+)] system as a function of $-\log[H^+]$, $c_L = 0.002$ mol dm^{-3}; (–) $c_{Cu^{2+}} = 0.002$ mol dm^{-3}, (···) $c_{Cu^{2+}} = 0.001$ mol dm^{-3}.

Table 3
Spectroscopic parameters for the copper(II) complexes with dipeptide (Leu–Gly) and phosphonodipeptides

Species	Vis		CD	
	λ (nm)[a]	ε (dm^3 mol^{-1} cm^{-1})[a]	λ (nm)	$\Delta\varepsilon$ (dm^3 mol^{-1} cm^{-1})
Leu–Gly				
[CuL]	653	78		
[CuLH$_{-1}$]	634	88		
[CuLH$_{-2}$]	628	82		
[CuL$_2$H$_{-1}$]	620	105		
Leu–Gly(P)				
[CuLH$_{-1}$]	623	66		
[CuLH$_{-2}$]	620	68		
[CuL$_2$]	620	104		
[CuL$_2$H$_{-1}$]	611	121		
Leu–Val(P)				
[CuLH$_{-1}$]	620	73		
[CuLH$_{-2}$]	614	74		
Gly–(Bz)Cys(P), D(−)				
[CuLH$_{-1}$]	631	69	676	−0.50
			327	+0.68
			273	−2.10
[CuLH$_{-2}$]	630	64	679	−0.53
			572	+0.03
			518	−0.04
			322	+0.75
			264	−2.70
Gly–(Bz)Cys(P), D(+)				
[CuLH$_{-1}$]	631	67	674	+0.42
			326	−0.57
			272	+1.87
[CuLH$_{-2}$]	630	62	676	+0.45
			573	−0.03
			518	+0.03
			321	−0.63
			263	+2.27

[a] The Vis absorption bands presented in the table arise from distribution-corrected absorption spectra.

Table 4
EPR parameters for the Cu^{2+} complexes with dipeptide (Leu–Gly) and phosphonodipeptides

	g_{iso}	A_{iso}[a]	$g_{\parallel}$	$g_{\perp}$	$A_{\parallel}$[b]
Leu–Gly					
[Cu(HL)]/[CuL]	2.119	65	2.331	2.065	158
[CuLH$_{-1}$]	2.117	67	2.249	2.055	180
[CuLH$_{-2}$]	2.118	68	2.251	2.055	165
[CuL$_2$H$_{-1}$]	2.120	66	2.232	2.055	160
Leu–Gly(P)					
[Cu(HL)]/[CuL]	2.119	75	2.330	2.065	157
[CuLH$_{-1}$]	2.114	74	2.248	2.050	185
[CuLH$_{-2}$]	2.115	74	2.246	2.055	184
Leu–Val(P)					
[Cu(HL)]/[CuL]	2.118	76	2.330	2.065	157
[CuLH$_{-1}$]	2.115	78	2.248	2.050	185
[CuLH$_{-2}$]	2.114	77	2.243	2.055	177
Gly–(Bz)Cys(P), D(+) and D(−)					
[Cu(HL)]/[CuL]	2.119	73	2.330	2.065	157
[CuLH$_{-1}$]	2.118	73	2.255	2.055	180
[CuLH$_{-2}$]	2.117	74	2.240	2.055	165
[CuL$_2$H$_{-1}$]	2.119	73	2.250	2.058	183

A parameters are given in 10^{-4} cm^{-1}. For all liquid solution spectra a fourth line of copper hyperfine structure exhibits hyperfine splitting of 13 G due to interaction with two nitrogen nuclei.
[a] A_{iso} is close to 15×10^{-4} cm^{-1}.
[b] $A_{\parallel}$ is close to 15×10^{-4} cm^{-1}.

complexes with phosphonodipeptides exhibit in general higher values of copper hyperfine coupling parameter A, due to a greater negative charge provided by deprotonated phosphono groups.

In the copper(II)–dipeptide–PO_3H_2 systems, the first complex formed at pH ca. 4 is [Cu(HL)]. This species is not formed with amino acid dipeptides because of the lower basicity of the carboxylate group. Taking into account a fact that the values of $\log K_{[Cu(HL)]} = \log \beta_{[Cu(HL)]} - pK_{PO_3H^-}$ of the phosphonodipeptides and of $\log \beta_{[CuL]}$ of the simple dipeptides [20,21] are about of the same order of magnitude, we can conclude that in the [Cu(HL)] species the phosphonodipeptides are coordinated to the metal ion in the same way as in the simple dipeptides, i.e. in a bidentate way, via the terminal amino and the peptide carbonyl group. This leads to the formation of the thermodynamically stable five-membered chelate ring, while the phosphonate group is still protonated, similarly to Kiss's [5] and Herman's [4] systems. The formation of this complex is evident from frozen solution EPR spectra at pH range 4.5–5.5. The signals of the species in the EPR spectra (in equilibrium with Cu^{2+}–aqua and with the signals from the next complex) correspond to the parameters $A_{\parallel} = 158 \times 10^{-4}$ cm^{-1} and $g_{\parallel} = 2.330$, which are associated with {3O, N} donor set around Cu^{2+} plane in [Cu(HL)] complex. On the other hand, the EPR spectrum of liquid solution at pH 5.3 is separated from the next spectrum and corresponds to the different parameters, than those observed at higher pH. The spectrum exhibits a hyperfine structure from two nitrogen atoms at the fourth line at high magnetic field suggesting, that in the second complex [CuL] metal ion is surrounded by two nitrogen atoms (Scheme 1).

Deprotonation of [Cu(HL)] and formation of the minor [CuL] species begins at pH below 5. The next step in the ligand dissociation and formation of the dominant species [CuLH$_{-1}$] occurs at the same pH. The loss of these two protons can presumably be ascribed to the terminal PO_3H^- and the peptide amide groups. These two processes overlap with each other (see $pK_{[Cu(HL)]}$ and $pK_{[CuL]}$ values in Table 2 and Scheme 1). If the next two consecutive deprotonations are separated by less than ca. 0.6 log units [22] a correct assignment of their pK values cannot be achieved.

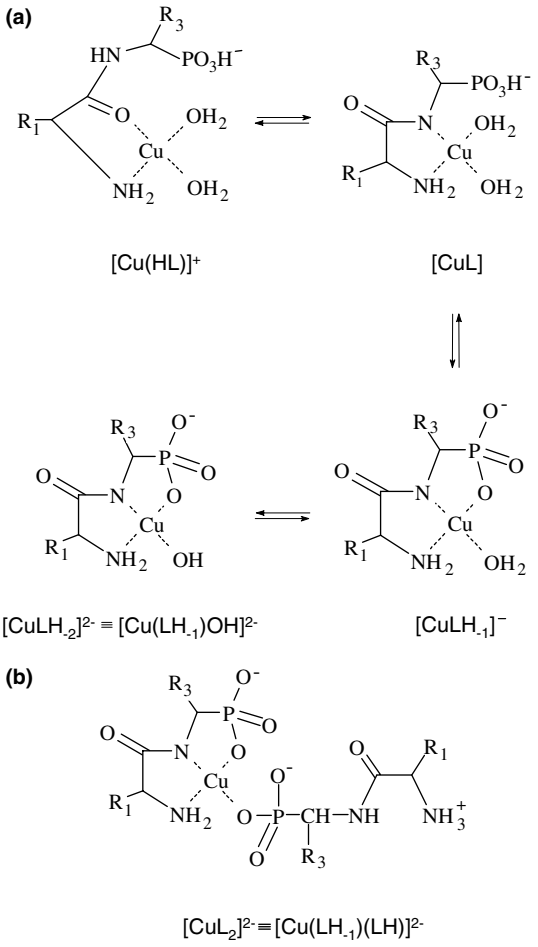

Scheme 1. Tentative structures of the species formed in the Cu^{2+}–phosphonodipeptides systems at 1:1 molar ratio (a) and additional structure formed at 1:2 molar ratio (b).

Nevertheless, the $pK_{[CuL]}$ values are the same for Leu–Val(P), Gly–(Bz)Cys(P), D(−) and Gly–(Bz)Cys(P), D(+) and higher than for Leu–Gly(P) (Table 2) suggesting that substitution of C-terminal part of the phosphonodipeptide by R_3 has effect on the metal ion-binding ability of the ligands. On the other hand, all these values are distinctly higher for the complexes with Leu–Gly (Table 2), indicating that PO_3^{2-}/CO_2^- substitution makes the copper(II) ion-induced deprotonation and simultaneous coordination of the peptide amide somewhat disfavored [5].

In the first major complex $[CuLH_{-1}]$ phosphonodipeptides coordinate in a tridentate manner with {2N, O} binding mode. Besides the considerable increase in energy of the d–d transition, the change of EPR parameters is seen. An increase of $A_{\|}$ to about 180×10^{-4} cm^{-1} and decrease of $g_{\|}$ to about 2.25 may be unambiguously assigned to coordination of two nitrogen atoms in Cu^{2+} plane. This coordination mode is supported additionally by ^{14}N hyperfine splitting, which comes from two nitrogens, observed in liquid solution EPR spectra.

The CD spectra, obtained for both Cu^{2+}–Gly–(Bz)Cys(P) complexes confirm nitrogen coordination with the distinct $N\rightarrow Cu^{2+}$ CT band at around 260–270 nm. The intensity of this band increases drastically upon pH increase in comparison with that observed at pH 4.5, where only one nitrogen donor is coordinated in [Cu(HL)] species. The most probable arrangement of the donor atoms around the Cu^{2+} ion in $[CuLH_{-1}]$ can be seen in Scheme 1. The deprotonation and simultaneous coordination of the peptide–amide group are accompanied by an appreciable spectral change. Fig. 4 shows the changes in energy of the d–d transition as a function of pH for several of the Cu^{2+}–ligand systems studied. It can be seen that until pH ca. 4.5 there are small spectral changes in the copper(II)–phosphonodipeptide systems. Due to the very close overlap of the two deprotonation processes (Figs. 1–3), a correct assignment of the two pK values cannot be achieved. It is most probable that parallel deprotonation of the terminal $-PO_3H^-$ and the peptide amide take place. In the [CuL] species, ligands coordinate in a bidentate manner with $\{NH_2, N^-\}$ binding modes and in $[CuLH_{-1}]$ – in a tridentate manner with $\{NH_2, N^-, O\}$ binding modes. Besides the considerable increase in energy of the d–d transition ($\lambda_{max}\approx 625$ nm) the EPR parameters also indicate 2N coordination in these two species.

A further deprotonation process of $[CuLH_{-1}]$, leading to the formation of $[CuLH_{-2}]$ is detected potentiometrically in all studied systems. This complex is regarded as a mixed hydroxo-complex $[Cu(LH_{-1})(OH)]$, in which the water molecule in the horizontal plane is replaced by $[OH]^-$. This process is accompanied by almost no change in the d–d transition on visible spectra for all the systems studied, but the CD spectra for Gly–(Bz)Cys(P), D(−) and Gly–(Bz)Cys(P), D(+) show that the sum of d–d bands which occurs at around 670 nm splits up into three individual bands following deprotonation and formation of $[CuLH_{-2}]$. The formation of

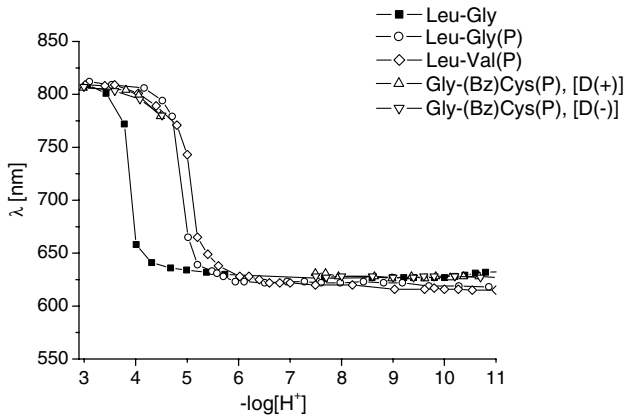

Fig. 4. Changes of the d–d absorption in the 1:1 Cu^{2+}/ligand systems as a function of $-\log[H^+]$.

the transitions at ca. 570 and 520 nm for the complexes of both ligands indicates the distortion of the tetragonal symmetry towards more tetrahedral environment, due to increasing repulsion between negatively charged ligands around copper(II) ion (Table 3).

For the systems with L = Leu–Val(P) and Gly–(Bz)Cys(P) at pH 10.5, a new EPR spectrum is observed for Cu^{2+}:L molar ratios equal to 1:1 and 1:2 indicating that the spectrum is most likely associated with formation of $[CuLH_{-2}]$ complex. A significant decrease of $A_{\|}$ values for the spectra at pH higher than 10 additionally supports a lowering of the complex symmetry upon including of OH^- into Cu^{2+} coordination sphere. The effect appears to be smaller in the case of the ligand with $R_3 = H$.

Ligands Gly–(Bz)Cys(P), D(−) and Gly–(Bz)Cys(P), D(+) are more effective chelating agents than other ones. This is reflected in the pH value of complexation of 50% of Cu^{2+}, which is about 30% for other ligands (Fig. 3) and also in the higher basicity-adjusted stability constants, $\log \beta_{[CuLH-1]} - \sum pK$ (Table 2). Taking these into account, comparison of the $[Cu(Leu–Val(P)H_{-1})]$ species and $[Cu(Gly–(Bz)Cys(P)H_{-1})]$ complexes still reveals a difference in stabilities of about 0.98 log units. The presence of an aromatic ring (e.g. Bz) in the C-terminal residue gives generally a more stable $[MLH_{-1}]$ species [23]. This stabilizing effect is often attributed to an interaction between the metal ion and the aromatic ring [24–27]. In the case of both Gly–(Bz)Cys(P) ligands, this effect may also arise from the interaction of thioether sulfur in an axial position with the copper(II) center. As an evidence for this, the formed complexes exhibit a distinct band in CD spectra in the region 320–330 nm. A similar band was previously observed in the absorption spectra for a set of thioether ligands and was assigned to $S \rightarrow d_{x^2-y^2}$ charge transfer transition [28]. Also, a wide range of studies focused on copper(II) binding to a variety of oligopeptides containing methionyl residue revealed the possibility of S–Cu^{2+} interactions [29–33]. Methionine itself was reported to act as tridentate ligand for copper(II) ions but only at low temperatures and at low pH values [29]. This type of chelation was verified in comparison to norleucine, which possesses a similar hydrophobic side chain [30]. Moreover, dipeptides and tripeptides containing methionine gave with Cu^{2+} ions similar CT bands in UV–Vis and CD spectra, assigned to the $S \rightarrow Cu^{2+}$ transition, regardless the position of thioether group [31,32]. The CT band in CD spectra was relatively weak [31] and the analogous band in UV–Vis existed only at acidic and neutral pH [32]. In our experiments, the intensity of the band between 320 and 330 nm in CD spectra for both Gly–(Bz)Cys(P) ligands arises with the change of the complex stoichiometry from $[CuLH_{-1}]$ to $[CuLH_{-2}]$.

However, the benzyl ring may also participate in complex stabilization through an interaction in an axial position with Cu^{2+} center. Such phenomenon may compete with thioether sulfur coordination. It was proved for both methionyl sulfur and phenyl aromatic ring in Met–Phe and Phe–Met ligands to exhibit similar potency towards their copper complexes stabilization [33]. This occurred through the distortion of the carboxylic oxygen–copper(II) bond, which is energetically weak, by sulfur donor or phenyl residue. In the case of Gly–(Bz)Cys(P), both benzyl ring and thioether group can stabilize the complex by competition with the phosphonic oxygen towards copper ion coordination in an axial position. A distinct CT transition band observed at around 320 nm suggests that this is rather S–Cu^{2+} interaction. The inspection of (Table 4) (X-EPR) reveals that liquid- and frozen-state EPR spectra of all the complexes formed by both Cu^{2+}–Gly–(Bz)Cys(P) ligands are in small extent but consequently different as compared to those observed for the remaining Cu^{2+}–phosphonodipeptides. The change in the EPR parameters [slightly decreased $A_{\|}$ (and A_{iso}) and increased $g_{\|}$ (and g_{iso})] at pH range of dominant contribution of $[CuLH_{-1}]$ is opposite the change observed [32] due to coordination of methionine sulphur in the *xy*-plane of copper. This tendency supports the binding of thioether sulfur at an axial position and the weakness of the equatorial ligand bonds.

In the presence of excess of the ligand a species with $[CuL_2]$ composition is also formed in all studied systems in the pH range 6–8. Our results concerning the system with Leu–Gly(P) are not consistent with those reported by Herman and Lukes [4]. The formation of 1:2 complex was not observed by them. For other systems, contrary to [5] and [4], the $[CuL_2]$ species is regarded as a $[Cu(LH_{-1})(HL)]$ complex. Because deprotonation of the amide function takes place around pH 5, tridentate and monodentate binding of the ligands is possible. So, binding mode of this species can be interpreted as $\{NH_2, N^-, PO_3^{2-}, PO_3^{2-}\}$, see Scheme 1.

The calculations performed with use of the complex stabilities, $\log K_{[CuL]}/K_{[CuL_2]}$, show the decreasing ability to form the bis-complexes as the size of R_3 increases (Table 2).

Deprotonation of the $[CuL_2]$ species starting at pH 5.5 and giving $[CuL_2H_{-1}]$ is overlapped by deprotonation process of dominant $[CuLH_{-1}]$ species, accompanied by formation $[CuLH_{-2}]$, which concentration reaches about 80% at pH ca. 10.5. It is noteworthy that similarly to the complex with Leu–Gly, the greatest content of $[CuL_2H_{-1}]$ is predicted potentiometrically at pH about 9 for both L = Gly–(Bz)Cys(P), in contrast to other phosphono dipeptides. In this case the species $[CuL_2H_{-1}]$ are separated from $[CuL_2]$. The signals of the corresponding EPR spectra are shifted into slightly lower values of $g_{\|}$ and higher values of $A_{\|}$ suggesting a stronger donor character of the ligands; this effect may be diminished by a simultaneous distortion of the complex geometry.

4. Conclusion

Because of the more basic character of the phosphonic group, PO_3^{2-}/CO_2^- substitution leads to the formation of various protonated 1:1 and 1:2 complexes in copper(II)–monophosphono dipeptides systems in compare to system with Leu–Gly (see Table 2).

From the comparative analysis of the stability and the spectroscopic (UV–Vis, CD and EPR) data, it has been established that the coordination in $[CuLH_{-1}]$, the major species in the studied systems, is realized by the $\{PO_3^{2-}, NH_2, N^-\}$ donor set. Both ligands Gly–(Bz)Cys(P) are more effective chelating agents than other ones. In this case both benzyl ring and thioether group can stabilize this complex by competition with the phosphonic oxygen towards copper ion coordination in an axial position. A distinct CT transition band observed at around 320 nm suggests that this is rather S–Cu^{2+} interaction. In addition the inspection of X-EPR reveals that liquid- and frozen-state EPR spectra of all the complexes formed by both Cu^{2+}–Gly–(Bz)Cys(P) ligands are in small extent but consequently different as compared to those observed for the remaining Cu^{2+}–monophosphono dipeptides.

References

[1] B. Kurzak, A. Kamecka, Pol. J. Chem. 77 (2003) 1059.
[2] L. Blaha, I. Lukes, J. Rohovec, P. Herman, J. Chem. Soc., Dalton Trans. (1997) 2621.
[3] I. Lukes, L. Blaha, F. Kesner, J. Rohovec, P. Herman, J. Chem. Soc., Dalton Trans. (1997) 2629.
[4] P. Herman, I. Lukes, J. Chem. Soc., Dalton Trans. (1995) 2605.
[5] T. Kiss, E. Farkas, H. Kozlowski, Z. Siatecki, P. Kafarski,, B. Lejczak, J. Chem. Soc., Dalton Trans. (1989) 1053.
[6] F.R. Atherton, C.H. Hasal, R.W. Lambert, J. Med. Chem. 29 (1986) 29.
[7] P. Wieczorek, B. Lejczak, M. Kaczanowska, P. Kafarski, Pestic. Sci. 30 (1990) 43.
[8] P. Kafarski, B. Lejczak, P. Mastalerz, Beitr. Wirkstofforschung 25 (1985) 1.
[9] E. Matczak-Jon, B. Kurzak, A. Kamecka, P. Kafarski, Polyhedron 21 (2002) 321.
[10] M. Soroka, P. Mastalerz, Pol. J. Chem. 50 (1976) 661.
[11] J. Oleksyszyn, E. Gruszecka, P. Kafarski, P. Mastalerz, Monatsh. Chem. 113 (1982) 1138.
[12] G. Gran, Acta Chem. Scand. 4 (1950) 599.
[13] The IUPAC Stability Constants Database, Academic Software, 1999.
[14] M. Molina, C. Melios, J.O. Tognalli, L.C. Luchiari, M. Jafelicci Jr., J. Electroanal. Chem. 105 (1979) 237.
[15] P. Gans, A. Sabatini, A. Vacca, J. Chem. Soc., Dalton Trans. (1985) 1195.
[16] T. Murakami, K. Murata, Y. Ishikawa, Inorg. Chim. Acta 244 (1996) 51.
[17] A. Ożarowski, unpublished program.
[18] U. Sakaguchi, Y. Arata, S. Fujiwara, J. Magn. Res. 9 (1973) 118.
[19] A. Gergely, I. Nagypal, J. Chem. Soc., Dalton Trans. (1977) 1104.
[20] A.E. Martell, R.M. Smith, Critical Stability Constants, Plenum Press, New York, 1974–1989, pp. 1–6.
[21] V. Cucionatta, R. Purello, E. Rizazarelli, Comment Inorg. Chem. 11 (1990) 85.
[22] B. Noszal, in: K. Burger (Ed.), Biocoordination Chemistry – Coordination Equilibria in Biologically Active Systems, Ellis Horwood, Chichester, 1990, pp. 18–55.
[23] L.D. Pettit, J.E. Gregor, H. Kozłowski, Perspect. Bioinorg. Chem. 1 (1991) 1.
[24] O. Yamauchi, K. Tsujide, A. Odani, J. Am. Chem. Soc. 107 (1985) 659.
[25] W.L. Kwik, K.P. Ang, G.I. Chen, J. Inorg. Nucl. Chem. 42 (1980) 303.
[26] P.I. Vestues, R.B. Martin, J. Am. Chem. Soc. 102 (1980) 7906.
[27] S.H. Kim, R.B. Martin, J. Am. Chem. Soc. 106 (1984) 1707.
[28] A.R. Amundsen, J. Whelan, B. Bosnich, J. Am. Chem. Soc. 99 (1977) 6730.
[29] H. Kozłowski, T. Kowalik, Inorg. Nucl. Chem. Lett. 14 (1978) 201.
[30] C.A. McAuliffe, J.V. Quagliano, L.M. Vallarino, Inorg. Chem. 5 (1966) 1996.
[31] T. Kowalik-Jankowska, A. Kiss, I. Sovago, H. Kozłowski, Pol. J. Chem. 68 (1994) 1093.
[32] K. Varnagy, B. Boka, I. Sovago, D. Sanna, P. Marras, G. Micera, Inorg. Chim. Acta 275–276 (1998) 440.
[33] L. Xiao, M. Jouini, B.T. Fan, G. Lapluye, J. Huet, J. Chem. Soc., Dalton Trans. (1990) 1137.

Available online at www.sciencedirect.com
SCIENCE DIRECT®
Polyhedron 23 (2004) 1947–1952
POLYHEDRON
www.elsevier.com/locate/poly

Synthesis and structural characterization of two new chiral coordination polymers of Cu(nicotinate)$_2$(H_2O) and Co(nicotinate)$_2$

Chun-Wei Yeh [a], Maw-Cherng Suen [b], Hui-Ling Hu [c], Jhy-Der Chen [a,*], Ju-Chun Wang [d]

[a] *Department of Chemistry, Chung-Yuan Christian University, No. 22 Pu Ren, Chung-Li 320, Taiwan, ROC*
[b] *Department of Textile Science, Nanya Institute of Technology, Chung-Li, Taiwan, ROC*
[c] *Department of Chemical Engineering, Nanya Institute of Technology, Chung-Li, Taiwan, ROC*
[d] *Department of Chemistry, Soochow University, Taipei, Taiwan, ROC*

Received 18 March 2004; accepted 26 April 2004
Available online 24 June 2004

Abstract

The syntheses and structural characterization of two new chiral coordination polymers, Cu(nic)$_2$(H_2O)·CH_3OH (nic = nicotinate) (**1**), and Co(nic)$_2$·H_2O (**2**), which were prepared by reactions of nicotinic acid with $CuCl_2 \cdot 2H_2O$ and $Co(NO_3)_2 \cdot 6H_2O$, respectively, are reported. Single-crystal X-ray crystallography structure determinations show that complexes **1** and **2** crystallize in the chiral space groups $P3_221$ and $C2$, respectively. The Cu(II) centers in **1** adopt a slightly distorted square pyramidal geometry, while the Co(II) centers in **2** exhibit a distorted octahedral coordination geometry. The metal centers in **1** and **2** coordinate to both the pyridyl and carboxylate groups to form 3-D and 2-D framework structures, respectively. Complex **1** exhibits open channels that are occupied by removable CH_3OH molecules, while complex **2** shows planar molecular grids.
© 2004 Elsevier Ltd. All rights reserved.

Keywords: Chiral; Coordination polymers; Nicotinate; Open channel; Grid

1. Introduction

Recently, great effort has been devoted to the self-assembly of organic and inorganic molecules in the solid state because it extends the range of new solids with desirable physical and chemical properties [1]. The range and variety of self-assembled inorganic structures that can be constructed relies on suitable metal–ligand interactions and hydrogen bondings, and the various types of polymeric structures include 1-D, 2-D and 3-D network structures [2]. Chiral coordination polymers containing nicotinate ligands [3], which display optical properties [3a], were the subject of several studies during recent years. Despite some recent progress for the synthesis of chiral coordination polymers, the ability to predict and control the supramolecular assembly of these molecules remains an elusive goal, and much more work is required to understand the effects of the metal center and ligand on the patterns of the molecular structure in the solid state. During our investigation on the reactions of transition metal (II) complexes with nicotinic acid, we have obtained two chiral polymeric complexes which show 3-D and 2-D framework structures. The syntheses and crystal structures of Cu(nic)$_2$(H_2O)·CH_3OH (nic = nicotinate) (**1**), and Co(nic)$_2$·H_2O (**2**), form the subject of this report.

2. Experimental

2.1. General procedures

All manipulations were carried out under dry, oxygen-free nitrogen by using Schlenk techniques, unless otherwise noted. Solvents were dried and deoxygenated

* Corresponding author. Tel.: +88632653351; fax: +88632653399.
E-mail address: jdchen@cycu.edu.tw (J.-D. Chen).

0277-5387/$ - see front matter © 2004 Elsevier Ltd. All rights reserved.
doi:10.1016/j.poly.2004.04.026

by refluxing over the appropriate reagents before use. The visible absorption spectra were recorded on a Hitachi U-2000 spectrophotometer. IR spectra were obtained from a Jasco FT/IR-460 plus spectrometer. Elemental analyses were obtained from a PE 2400 series II CHNS/O analyzer.

2.2. Materials

The reagents $CuCl_2 \cdot 2H_2O$, $Co(NO_3)_2 \cdot 6H_2O$ and nicotinic acid were purchased from Aldrich Chemical Co. and used as received.

2.3. Preparation of the $Cu(nic)_2(H_2O)$ (1)

$CuCl_2 \cdot 2H_2O$ (0.43 g, 2.52 mmol) was added to a methanolic solution (25 ml) containing nicotinic acid (0.75 g, 6.09 mmol). The mixture was then heated to reflux for 6 h until some blue solid began to precipitate. The solid was filtered out, washed with diethylether (2×10 ml) and dried under vacuum to give a blue powder. Yield: 0.75 g (91%). UV–Vis (DMF): 438 nm ($\varepsilon = 1406.2\ M^{-1}\,cm^{-1}$). *Anal.* Calc. for $C_{13}H_{14}CuN_2O_6$ ($M_w = 357.80$), C, 44.24; H, 3.09; N, 8.60. Found: C, 43.75; H, 3.01; N, 9.08%. IR (KBr disk): 1636(m), 1560(s), 1543(s), 1508(w), 1457(m), 1384(s), 1307(w), 1191(m), 762(m), 683(m), 669(w), 651(m), 472(w). Dark blue crystals suitable for X-ray crystallography were obtained by slow diffusion of CH_3OH into a DMF solution of **1**.

2.4. Preparation of $Co(nic)_2$ (2)

$Co(NO_3)_2 \cdot 6H_2O$ (0.29 g, 1.0 mmol) was added to a CH_2Cl_2 solution (20 ml) containing nicotinic acid (0.25 g, 2.0 mmol). The mixture was then refluxed for 48 h to afford a red solution and a red solid. The precipitate was filtered and washed with ether (3×10 ml) and then dried under reduced pressure to give a dark red solid. Yield: 0.28 g (92%). UV–Vis (DMF): 382 nm ($\varepsilon = 1045.8\ M^{-1}\,cm^{-1}$). *Anal.* Calc. for $C_{12}H_8CoN_2O_4$ ($M_w = 303.14$), C, 47.55; H, 2.66; N, 9.24. Found: C, 47.54; H, 3.03; N, 9.67%. IR (KBr disk): 1385(s), 1192(s), 1048(s), 828(m), 756(s), 698(m), 451(w). Red crystals suitable for X-ray crystallography were obtained by slow diffusion of ether into a $MeOH/H_2O$ solution of **2**.

3. X-ray crystallography

The diffraction data for complexes **1** and **2** were collected at 25 °C on Bruker AXS P4 and Siemens CCD diffractometers, respectively, which were equipped with graphite-monochromated Mo K_α ($\lambda_\alpha = 0.71073$ Å) radiation. Data reduction was carried out by standard methods with the use of well-established computational procedures [4]. The structure factors were obtained after Lorentz and polarization correction. The positions of some of the heavier atoms, including the copper atom, were located by the direct method. The remaining atoms were found in a series of alternating difference Fourier maps and least-square refinements [5]. The CH_3OH molecule was found to be disordered, and the occupancies for the carbon and the oxygen atoms were set to be 0.5. The final residuals of the final refinement were $R_1 = 0.0552$, $wR_2 = 0.1490$. The crystallographic procedures for **2** were similar to those for **1**. Basic information pertaining to crystal parameters and structure refinement is summarized in Table 1.

4. Results and discussion

4.1. Syntheses

The complex $Cu(nic)_2(H_2O)$ (nic = nicotinate) (**1**), was prepared by reaction of $CuCl_2 \cdot 2H_2O$ with nicotinic acid in refluxing methanol while the complex $Co(nic)_2$ (**2**), was prepared by reaction of $Co(NO_3)_2 \cdot 6H_2O$ with nicotinic acid in refluxing CH_2Cl_2. Their structures have been determined by spectroscopic methods and by X-ray crystallography.

4.2. Structure of 1

A single crystal X-ray structural analysis of **1** reveals the formation of a complex of stoichiometry $Cu(nic)_2(H_2O) \cdot CH_3OH$. Complex **1** conforms to the chiral space group $P3_221$. Fig. 1 shows the coordination geometry about the Cu metal center, which adopts a slightly distorted square pyramidal coordination geometry with the bond angles only slightly deviated from 90° or 180°. The Cu atom is bonded to two *trans* pyridyl nitrogen atoms (Cu–N = 2.032 (6) Å) and two *trans* oxygen atoms of the monodentate carboxylate groups (Cu–O = 1.964 (4) Å) in the equatorial plane. The dihedral angles of the two *trans* pyridyl rings that coordinated to the Cu atom through the nitrogen atoms is 83.0°, while that of the other set is 18.1°. The Cu atom is also bonded to one H_2O ligand (Cu–O = 2.332 (1) Å) in the axial position to complete the distorted-square-pyramidal coordination geometry. Noticeably, each bidentate nicotinate ligand links two Cu(II) metal centers, and all the ligands extend approximately along the *c*-axis to form an infinite helical chain (Fig. 2, top). The most striking feature of this complex is that the infinite helices form a two-dimensionally extended hexagonal array with open pores (9.1×11.3 Å) that accommodate the water molecules that are coordinated to the Cu(II) atoms and the non-coordinating methanol molecules. The open channels are further linked through the nico-

Table 1
Crystal data for complexes **1** and **2**

Compound	**1**	**2**
Formula	$CuC_{13}H_{14}O_6N_2$	$CoC_{12}H_{10}O_5N_2$
Formula weight	357.80	321.15
Crystal system	trigonal	monoclinic
Space group	$P3_221$	$C2$
a (Å)	9.0718(14)	11.225(3)
b (Å)	9.0718(14)	10.786(3)
c (Å)	16.891(2)	6.8130(16)
α (°)	90	90
β (°)	90	107.690(5)
γ (°)	120	90
V (Å^3)	1203.9(3)	785.9(3)
Z	4	2
D_{calc} (g/cm^3)	1.947	1.357
$F(0\,0\,0)$	732	326
Crystal size (mm)	$0.1 \times 0.1 \times 0.4$	$0.02 \times 0.1 \times 0.2$
μ (Mo K$_\alpha$) (mm^{-1})	1.852	1.109
Data collection instrument	Bruker AXS P4	Siemens CCD
Radiation monochromated in incident beam (λ(Mo K$_\alpha$)) (Å)	0.71073	0.71073
Range (2θ) for data collection (°)	$5.18 \leqslant 2\theta \leqslant 49.16$	$5.36 \leqslant 2\theta \leqslant 50.06$
Temperature (°C)	22	22
Limiting indices	$-1 \leqslant h \leqslant 10$, $-10 \leqslant k \leqslant 1$, $-20 \leqslant l \leqslant 1$	$-13 \leqslant h \leqslant 9$, $-12 \leqslant k \leqslant 3$, $-7 \leqslant l \leqslant 6$
Reflections collected	2033	785
Independent reflections [R_{int}]	1408 [0.0479]	671 [0.0259]
Refinement method	full-matrix least-squares on F^2	full-matrix least-squares on F^2
Data/restraints/parameters	1408/0/110	671/1/96
Quality-of-fit indicator[c]	1.106	1.310
Final R indices [$I > 2\sigma(I)$][a,b]	$R_1 = 0.0552$, $wR_2 = 0.1490$	$R_1 = 0.0423$, $wR_2 = 0.1342$
R indices (all data)	$R_1 = 0.0625$, $wR_2 = 0.1550$	$R_1 = 0.0440$, $wR_2 = 0.1354$
Largest differential peak and hole (e/Å^3)	0.809 and −0.642	0.786 and −0.418

[a] $R_1 = \sum ||F_o| - |F_c|| / \Sigma |F_o|$.
[b] $wR_2 = \left[\sum w(F_o^2 - F_c^2)^2 / \sum w(F_o^2)^2\right]^{1/2}$, $w = 1/[\sigma^2(F_o^2) + (ap)^2 + (bp)]$, $p = [\max(F_o^2 \text{ or } 0) + 2(F_c^2)]/3$, $a = 0.0995$, $b = 0.7189$, for **1**; $a = 0.0765$, $b = 1.7429$, for **2**.
[c] Quality-of-fit $= \left[\sum w(|F_o^2| - |F_c^2|)^2 / N_{observed} - N_{parameters}\right]^{1/2}$.

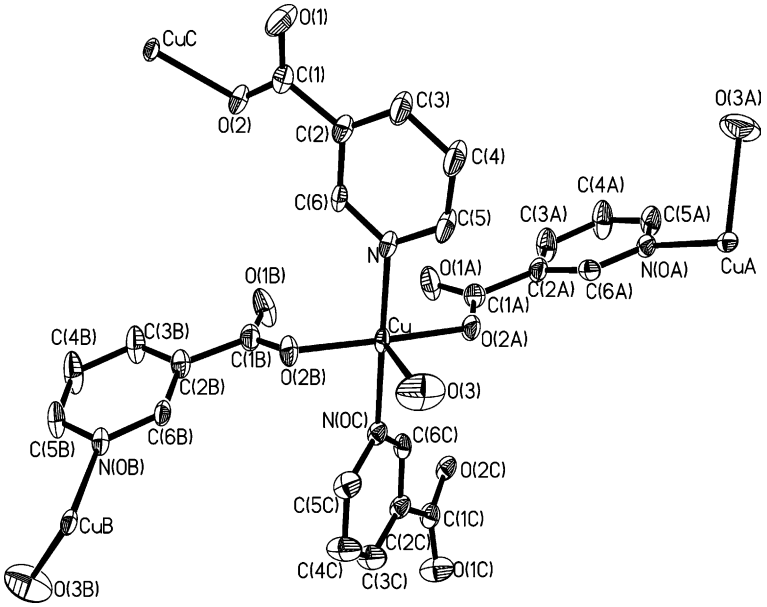

Fig. 1. An ORTEP drawing showing the coordination geometry of the copper metal center. Ellipsoids are scaled to enclose 20% of the electron density.

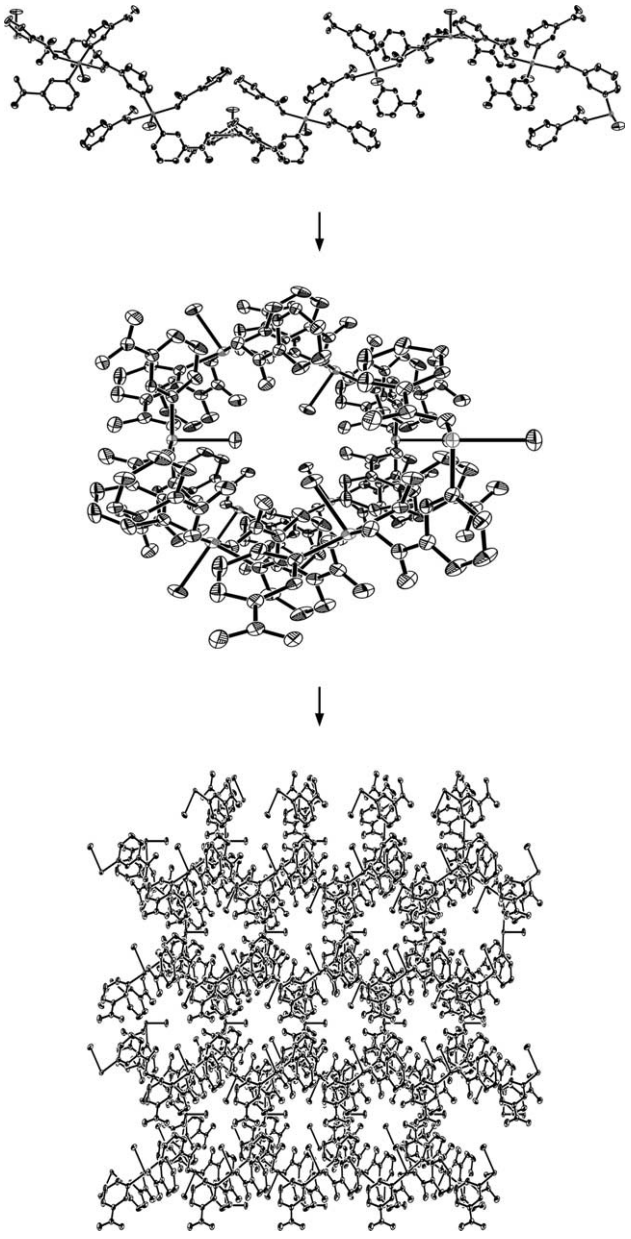

Fig. 2. A helical chain with *P* configuration formed by the bidentate nicotinate groups and Cu centers running along the *a* axis (top), Chiral channel formed by the helical chain running along the *c* axis (middle) and the polymeric structure of **1** (bottom).

tinate groups to form a 3-D framework structure (Fig. 2, bottom). It is also seen from Fig. 2 that the water molecules are all pointing to the centers of the pores. This helical structure is in marked contrast to the one found in the complex $[Cu(pzca)(Me_2CO)_{0.5}](BF_4)$ (pzca = 2-pyrazinecarboxamide) where the cavities are occupied by the BF_4^- anions [6]. It is also noted that helical coordination polymers with large chiral cavities have been prepared by dissolving $[Ni(acetate)_2]$ and benzoic acid in MeOH and layering with a solution of 4,4′-bipyridine in MeOH [7].

4.3. Structure of **2**

A single X-ray structural analysis of crystals of **2**, obtained by slow diffusion of ether into a MeOH solution of **2**, reveals the formation of a complex of stoichiometry $Co(nic)_2 \cdot H_2O$. Complex **2** was solved in the chiral space group *C*2. Fig. 3 shows the coordination geometry about the Co metal center. The cobalt metal center, which resides on a crystallographic 2-fold axis, adopts a distorted octahedral coordination geometry with the bond angles significantly deviated from 90° or 180° (Table 2), presumably due the chelation of the bidentate carboxylate groups to the Co metal center. The Co atom is bonded to two *cis* pyridyl nitrogen atoms (Co–N = 2.075 (6) Å) and two *cis* bidentate carboxylate groups (Co–O = 2.059 (6) and 2.291 (7) Å). The carboxylate groups are coordinated to the metal centers in unsymmetrical fashions. All the Co metal centers in complex **2** are chiral and have the same handedness Δ. Adjacent Co atoms are linked to each other through the pyridyl nitrogen atoms and the oxygen atoms of the bidentate carboxylate groups to form the two-dimensional square grid, Fig. 4(a). The complex shows void space with a Co–Co separation of 7.748 Å. The cavities are occupied by the solvent molecules and the squares are further linked through extensive C–H- - -O hydrogen bondings (H- - -O = 2.523 Å; ∠C–H–O = 130.5°), Fig. 4(b). The square grids in complex **2** are in contrast to those found in the chiral complex Zn(nicotinate)$_2$ where the pyridine rings of the nicotinate groups intrude into the square cavities to result in interdigitation of the 2-D square networks [3].

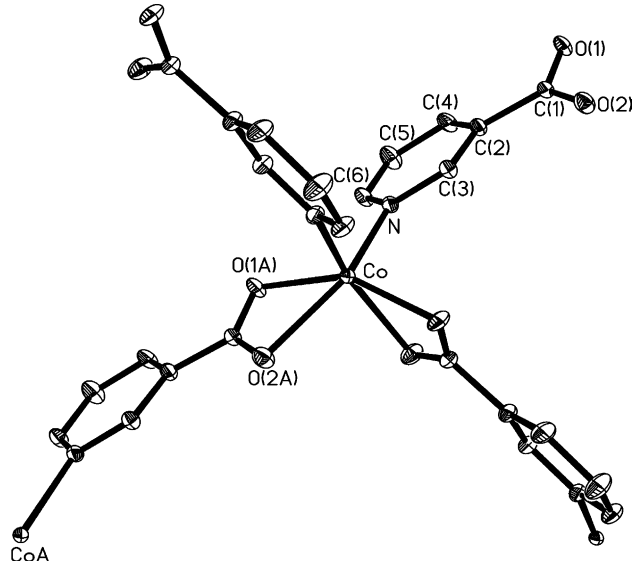

Fig. 3. An ORTEP drawing showing the coordination geometry of the cobalt metal center. Ellipsoids are scaled to enclose 20% of the electron density.

Table 2
Selected bond distances (Å) and angles (°) complexes **1** and **2**

Complex **1**			
Distances			
Cu–O(2A)	1.964(4)	Cu–N	2.032(6)
Cu–O(3)	2.332(10)		
Angles			
O(2A)–Cu–O(2B)	176.9(3)	O(2A)–Cu–N	92.01(19)
O(2B)–Cu–N	88.0(2)	N(C)–Cu–N	178.1(3)
O(2A)–Cu–O(3)	91.55(15)	N–Cu–O(3)	89.03(15)
Complex **2**			
Distances			
Co–O(1A)	2.059(6)	Co–O(2A)	2.291(7)
Co–N	2.075(6)		
Angles			
O(1A)–Co–O(1B)	148.6(3)	O(1A)–Co–N	104.8(3)
O(1B)–Co–N	95.3(3)	N–Co–N(C)	100.0(4)
O(1A)–Co–O(2B)	96.6(2)	O(1A)–Co–O(2A)	60.0(2)
N–Co–O(2B)	155.1(3)	N–Co–O(2A)	90.5(2)
O(2B)–Co–O(2A)	89.2(3)	O(1A)–Co–C(1B)	122.7(3)

Symmetry transformations used to generate equivalent atoms: (A) $x-y, -y+1, -z+1/3$; (B) $-y+1, x-y, z-1/3$ for **1**. (A) $x+1/2, y+1/2$, z; (B) $-x-1/2, y+1/2, -z$ for **2**.

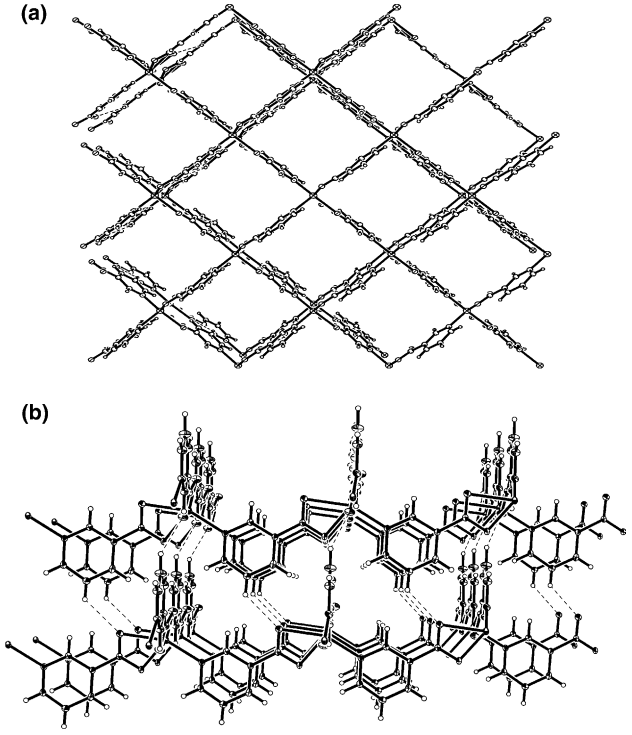

Fig. 4. (a) The polymeric structure of **2**. The solvent molecules which occupy the cavities are removed for clarity. (b) A diagram showing the interactions among the square grids of **2**.

Complexes **1** and **2** make interesting comparisons with the mononuclear complexes $Cu(nic)_2(H_2O)_4$ and $Co(nic)_2(H_2O)_4$ [8] and the three-dimensional Cu(II) coordination polymer $Cu(nic)_2$ [9,10]. The complexes $Cu(nic)_2(H_2O)_4$ and $Co(nic)_2(H_2O)_4$ were prepared by the reactions of $CuCl_2 \cdot 2H_2O$ and $CoCl_2 \cdot 6H_2O$, respectively, with nicotinic acid in NaOH solution (pH = 6) at 60 °C. The coordination spheres of these two mononuclear complexes are octahedral, with two pyridyl nitrogen atoms and two aqua oxygen atoms in the equatorial positions and two aqua oxygen atoms in the axial positions. The complex $Cu(nic)_2$ was synthesized by treating copper nitrate with nicotinic acid under hydro(solvo)thermal conditions, and the Cu(II) centers adopt a coordination geometry intermediate between square pyramidal and trigonal bipyramidal. The tridentate nicotinate groups (with bridging carboxylate) link doubly carboxylate bridged Cu(II) dimers into a pleated-sheet structure through the coordination of their pyridyl nitrogen atoms, while the bidentate nicotinate groups link adjacent Cu centers to form zigzag chains along the *a*-axis and thus cross-link the pleated sheets formed by the Cu centers and tridentate nicotinate groups to result in a complex 3-D framework structure [9]. A complex of the same formula of $Cu(nic)_2$ has also been prepared by reacting $Cu(NO_3)_2 \cdot 2.5H_2O$ with nicotinic acid in the mole ratio of 2:1 for three days at 170 °C under hydrothermal conditions [10].

The two main factors that govern the structures of **1** and **2** and all the complexes mentioned above are the coordination of the H_2O molecules and the role of the metal centers in influencing the coordination geometry. It is clearly seen that changing the metal center and introducing the water molecule can drastically modify the structures of the coordination polymers.

4.4. Thermal properties

Complex **1** is very stable in air at ambient temperature and almost insoluble in common solvents such as water, alcohol, acetonitrile, chloroform, methanol and acetone. Complex **2** is also stable in air at room temperature but soluble in methanol. Thermal gravimetric analyses (TGA) were carried out to examine the thermal stability of **1** and **2**. The samples were heated up in air at 1 atm pressure with the heating rate of 20 °C min^{-1}. The TGA curve shows that **1** is stable up to 120 °C. A total weight loss of 16.3% occurred in the temperature range 120–230 °C, presumably due to the removal of the guest methanol molecules and the bonded H_2O molecules per formula unit (Calc. 16.4%), and a sharp weight loss occurred in the temperature range 230–320 °C, consistent with the removal of nicotinate ligands and decomposition of the framework. The TGA curve shows that **2** is stable up to 100 °C. A total weight loss of 5.6% occurred in the temperature range 100–150 °C, corresponding to the removal of the guest H_2O molecules per formula unit (Calc. 5.9%), and a sharp weight loss occurred in the temperature range 380–420 °C, consistent with the removal of nicotinate ligands and

decomposition of the framework. Their T_m values have been measured by using differential scanning calorimetry (DSC), and these are 107.2° and 134.9° for complexes **1** and **2**, respectively.

5. Supplementary material

Crystallographic data (CIF files) for the structures **1** and **2** have been deposited with the Cambridge Crystallographic Data Centre, CCDC no. 226294 and 228646, respectively. Copies of this information may be obtained free of charge from The Director, CCDC, 12 Union Road, Cambridge, CB2 1EZ, UK (Fax: +44-1223-336-033; e-mail: deposit@ccdc.cam.ac.uk or www: http://www.ccdc.cam.ac.uk).

Acknowledgements

We are grateful to the National Science Council of the Republic of China for support.

References

[1] (a) G.R. Desiraju, Angew. Chem., Int. Ed. Engl. 34 (1995) 2311;
(b) G.R. Desiraju, Chem. Commun. (1997) 1475;
(c) J.M. Lehn, Supramolecular Chemistry, VCH, Weinheim, 1995.
[2] (a) A.J. Blake, N.R. Champness, P. Hubberstey, W.-S. Li, M.A. Withersby, M. Schröder, Coord. Chem. Rev. 183 (1999) 117;
(b) S. Muthu, J.H.K. Yip, J.J. Vittal, J. Chem. Soc., Dalton Trans. (2002) 4561, and references therein.
[3] (a) W. Lin, O.R. Evans, R.-G. Xiong, Z. Wang, J. Am. Chem. Soc. 120 (1998) 13272;
(b) J.Y. Lu, E.E. Kohler, Inorg. Chem. Commun. 5 (2002) 600.
[4] (a) XSCANS, Release, 2.1, Siemens Energy and Automation, Inc, Madison, WI, 1995;
(b) SMART/SAINT/ASTRO, Release, 4.03, Siemens Energy and Automation, Inc, Madison, WI, 1995.
[5] SHELXTL 5.10. Bruker Analytical X–ray Instruments Inc., Karlsruche, Germany, 1997.
[6] M. Munakata, L.P. Wu, T. Kuroda-Sowa, M. Maekawa, K. Moriwaki, S. Kitagawa, Inorg. Chem. 36 (1997) 5416.
[7] K. Biradha, C. Seward, M.J. Zaworotko, Angew. Chem. Int. Ed. 38 (1999) 492.
[8] K. Waizumi, M. Takuno, N. Fukushima, H. Masuda, J. Coord. Chem. 44 (1998) 269.
[9] M.E. Chapman, P. Ayyappan, B.M. Foxman, G.T. Yee, W. Lin, Crystal Growth Design 1 (2001) 159.
[10] J.Y. Lu, A.M. Babb, Inorg. Chem. Commun. 4 (2001) 716.

Available online at www.sciencedirect.com
SCIENCE DIRECT®
Polyhedron 23 (2004) 1953–1960
POLYHEDRON
www.elsevier.com/locate/poly

Synthesis, characterization and electropolymerization of a new polypyrrole iron(II) Schiff-base complex

Glaico Chiericato Júnior [a,*], Ana Paula Saldanha Silva [a], Luciana Simionatto Guinesi [b]

[a] *Departamento de Química, Faculdade de Filosofia Ciências e Letras de Ribeirão Preto, Universidade de São Paulo, 14040-901 Ribeirão Preto, SP, Brazil*
[b] *Instituto de Química, Universidade Estadual Paulista P.O. Box. 355, Araraquara, SP, Brazil*

Received 12 January 2004; accepted 28 April 2004

Abstract

This work presents the synthesis of the complex $[Fe(\mathbf{L})_2](PF_6)_2 \cdot H_2O$ ($\mathbf{L}$ = 2,6-bis[1-(3-pyrrol-1-yl-propylimino)ethyl]pyridine (Fig. 1) and its characterization through elemental and thermal analysis, X-ray diffraction and UV–Vis, IR and ^{1}H NMR spectra. The use of this compound in the preparation of modified electrodes is also described. The best electrochemical parameters to achieve optimum film formation have been established and the effects of both the upper-limit of the applied scanning potential (E_{aul}) and the number of scans on the efficiency of film formation have been investigated. Film surface morphology has been characterized by atomic force microscopy.
© 2004 Elsevier Ltd. All rights reserved.

Keywords: Schiff-base; Polypyrrole; Electropolymerization; Iron complex; AFM; Polymer

1. Introduction

Chemically modified electrodes have been the subject of considerable attention since their inception about 27 years ago [1]. This is due to their potential application in electrochromic devices, electrocatalysis, electroanalysis and in the design of molecular electronic devices [2]. With the deliberate immobilization of a modifier agent onto an electrode surface, it is hoped that the physicochemical properties of the modifier will be transferred to the electrode surface. This modification seeks to dictate and control the behavior of the electrode/solution interface [2]. The electrochemical polymerization and precipitation of films directly onto an electrode surface offer some advantages when compared with the deposition of chemically preformed polymers. Electropolymerization allows the deposition of insoluble polymers, uniform coating on irregular surfaces and easy electrochemical control of the film thickness. The electrochemical polymerization of the pyrrole group is convenient for carrying out the coating of electrode surfaces by non-passivating polymer films containing active centers, especially transition metal complexes [3].

This work presents the synthesis of the complex $[Fe(\mathbf{L})_2](PF_6)_2 \cdot H_2O$ ($\mathbf{L}$ = 2,6-bis[1-(3-pyrrol-1-yl-propylimino)ethyl]pyridine (Fig. 1) and its characterization through elemental and thermal analysis, X-ray diffraction and UV–Vis, IR and ^{1}H NMR spectra. The use of this compound in the preparation of modified electrodes is also described. The best electrochemical parameters to achieve optimum film formation have been established and the effects of both the upper limit of the applied scanning potential (E_{aul}) and the number of scans on the efficiency of film formation have been investigated. Film surface morphology has been characterized by atomic force microscopy.

* Corresponding author. Tel.:+55-16-6023755; fax: +55-16-6338151.
E-mail address: gchieric@usp.br (G.C. Júnior).

0277-5387/$ - see front matter © 2004 Elsevier Ltd. All rights reserved.
doi:10.1016/j.poly.2004.04.029

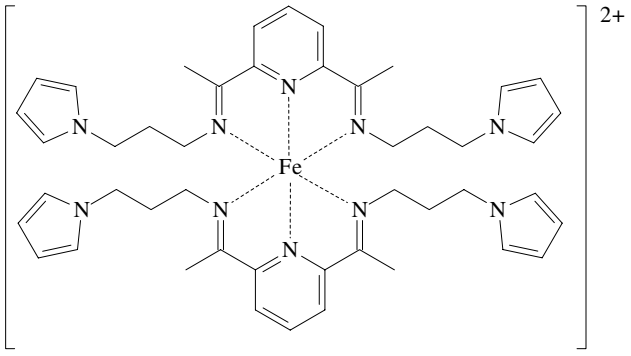

Fig. 1. Structural representation of $[Fe(\mathbf{L})_2]^{2+}$ ion complex.

2. Experimental

2.1. Materials

2,6-Diacetylpyridine, *N*-(2-cyanoethyl)pyrrole, lithium aluminium hydride and dichloromethane (DCM) were obtained from Aldrich Chemical Co., Ltd. Tetrabutylammonium perchlorate (TBAP) was purchased from Fluka. All other reagents and solvents were of the highest purity grade available from Merck, Mallinckrodt and Sigma Chemical Co., Ltd. and were used without prior purification.

2.2. Synthesis of the ligand

N-(2-cyanoethyl)pyrrole was reduced to *N*-(3-aminopropyl)pyrrole with $LiAlH_4$ in dry diethyl ether through a procedure described in the literature [4]. The product was purified by distillation under reduced pressure. Yield 62%.

^{1}H NMR in $CDCl_3$: δ 1.12 (s, 2H, NH_2); δ 1.87 (q, 2H,); δ 2.67 (t, 2H); δ 3.94 (t, 2H); δ 6.12 (t, 2H); δ 6.64 (t, 2H).

IR: $\nu(NH_2)$ 3365, 3293 cm^{-1}.

2.3. Synthesis of the complex $[Fe(L)_2](PF_6)_2 \cdot H_2O$

The complex was synthesized through Schiff-base condensation between 2,6-diacetylpyridine (143.4 mg, 0.88 mM) and *N*-(3-aminopropyl)pyrrole (219.4 mg, 1.77 mM), in the presence of ferrous ammonium sulfate (172.4 mg, 0.44 mM) and dry ethanol (10 mL), under nitrogen atmosphere. The mixture was stirred at 70 °C for 3 h and filtered through a fine filter. The desired complex was precipitated from the filtrate by adding 2 mL of saturated aqueous NH_4PF_6 to it. The precipitate was collected, washed with cold water and dried under vacuum. Yield 68%. Results from CHN elemental analysis were in good agreement with the expected theoretical composition for $[Fe(C_{46}H_{58}N_{10})](PF_6)_2 \cdot 1H_2O$ (M quelate) = 1114.81 g mol^{-1}. Calc.: C, 49.56; H, 5.42; N, 12.56. Found: C, 49.17; H, 5.03; N, 12.18%.

2.4. Characterization

Elemental analysis was performed on a Carlo Erba Elemental Analyzer model EA1110. ^{1}H NMR spectra were obtained in $CDCl_3$ solutions in a Bruker 300 MHz spectrometer model DPX 300. UV–Vis spectra were obtained in quartz cells by using a 8452A Hewlett–Packard spectrophotometer. Thermogravimetry (TG) and differential thermal analysis (DTA) experiments were performed by using a module of thermal analysis, SDT 2960, from TA Instruments under dynamic atmosphere of oxygen and nitrogen with a heating rate of 20 °C min^{-1} from 40 to 1200 °C. The residual oxide was characterized through DXR using a Siemens D 5000 diffractometer with Cu Kα radiation, submitted to 40 KV, 30 mA and 0.05° s^{-1} step. The oxide was placed on a proper support and exposed to radiation from 4° to 70° (2θ). Differential scanning calorimetry (DSC) curves were obtained by using a DSC 2910 from TA Instruments under nitrogen dynamic atmosphere, at a heating rate of 20 °C min^{-1} from 40 to 600 °C. IR spectra were recorded on a 1600 FT Perkin–Elmer spectrophotometer as KBr discs. Electrochemical experiments were conducted on a PAR model 273 Potentiostat/Galvanostat. Cyclic voltammetric experiments were carried out in conventional three-compartment glass cells under argon atmosphere using a glassy-carbon disc working electrode (0.08 cm^2 area), a platinum wire auxiliary electrode and a saturated calomel reference electrode (SCE). The glassy-carbon electrode was polished to a mirror finish with different grades of alumina as low as 0.05 μm and ultrasonically cleaned before the experiments. All experiments were done in dichloromethane 0.1 M in TBAP.

Apparent surface coverages (Γ_T^{APP}, mol cm^{-2}) were calculated using the equation $\Gamma_T^{APP} = Q/nFA$ (where n is the number of transferred electrons, F is Faraday's constant, A is the electrode area in cm^2 and Q is the charge (area) under the cyclic voltammetric oxidation $Fe^{II/III}$ wave at 50 mV s^{-1}.

The surface morphology of the electrodeposits was analyzed by AFM in a Nanoscope IIIa electronics (Digital Instruments, Inc.). Polymer films of different thickness were grown on indium/tin oxide electrodes (1 cm^2) by cycling (20 and 50 times) the potential (0–1.25 V). One modified electrode was cycled between 0 and −2.0 V to deactivate the polymer. The electrodes were removed from the electrochemical cell after electrodeposition, washed with anhydrous dichloromethane and dried under vacuum. During AFM measurements, considerable search was done to find images on various parts of the surface. The images that were found in several parts of the film will be shown herein.

3. Results and discussion

The free ligand (L) was prepared by heating a solution of 2,6-diacetylpyridine and *N*-(3-aminopropyl)pyrrole (1:2 equivalents) at reflux in dry benzene for 2 h. Upon removal of the solvent by roto-evaporation, the ligand was collected as a yellow oil. However, a carbonyl containing material, probably due to the unreacted 2,6-diacetylpyridine, remained in the reaction product, as detected by ^{1}H NMR spectrum. Sub products of this condensation were not observed when it was performed in the presence of ferrous ammonium sulfate, yielding the complex straightforwardly.

The IR spectrum of the complex showed one band at ca. 1648 cm^{-1}, assigned to the ν(C=N) imine bond stretch. No ν(C=O) or $\nu(NH_2)$ signals were observed, indicating that no unreacted reagents remained in the sample. The sharp bands at 840 and 558 cm^{-1} were assigned to the hexafluorophosphate ion.

The electronic spectrum of $[Fe(\mathbf{L})_2]^{2+}$ in dichloromethane solution shows two absorption bands in the visible region (494 and 597 nm) characteristic of metal-to-ligand charge-transfer transitions (MLCT) in iron(II)–diimine complexes [5]. The electronic spectra of this complex is very similar to that reported by Wieghardt and coworkers [6]. for iron(II) complexes containing the ligand 2,6-bis[1-(4-methoxyphenylimino) ethyl]pyridine. The intense bands observed in the region from 219 to 292 nm are assigned to internal ligand transitions of the type $\pi \rightarrow \pi^*$ [7] and $n \rightarrow \pi^*$ [8] type.

The TG curves for $[Fe(\mathbf{L})_2]^{2+}$ under oxygen and nitrogen (Fig. 2(a)) shows the first mass loss step to be between 40 and 165.5 °C, which is related to the dehydration of 1 H_2O per mol of the compound. This thermal event displays the endothermic peaks at 133.0 and 91.8 °C in DTA (Fig. 2(b)) and DSC (Fig. 2(c)) curves, respectively.

The complex shows distinct thermal behavior depending on the employed atmosphere. Under oxygen, the thermal decomposition of the ligand occurs in two consecutive steps: between 187.5–461.4 °C and 462.3–833.7 °C (Fig. 2(a)), corresponding to the exothermic peaks at 297.4 and 573.7 °C (Fig. 2(b)). These events result in the formation of 14.25% of a Fe(III) oxide residue above 834.0 °C. Such oxide corresponds to $FePO_4$ in the hexagonal phase and it is generated because of the oxidizing atmosphere (calculated 13.53%), as revealed by the X-ray diffraction pattern.

Under nitrogen, the compound shows a mass loss of 46.81% between 230.5 and 440.4 °C (Fig. 2(a)), with a wide endothermic peak around 255.2 °C and another one defined at 363.9 °C in the corresponding DSC curve (Fig. 2(c)). This thermal event may be due to the decomposition of propylpyrrole and ethyl groups that were not coordinated to the metal (calculated 46.74%). The remaining complex shows subsequent continuous

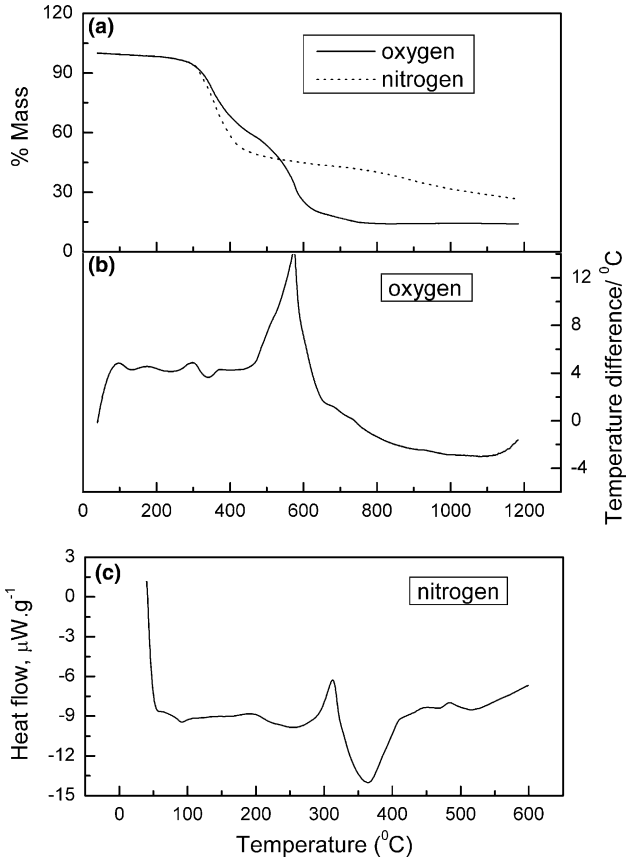

Fig. 2. Thermal analysis of the $[Fe(\mathbf{L})_2](PF_6)_2 \cdot 1H_2O$ under oxidant and inert atmospheres at 20 °C min^{-1}: (a) TG curves; (b) DTA curve; (c) DSC curve.

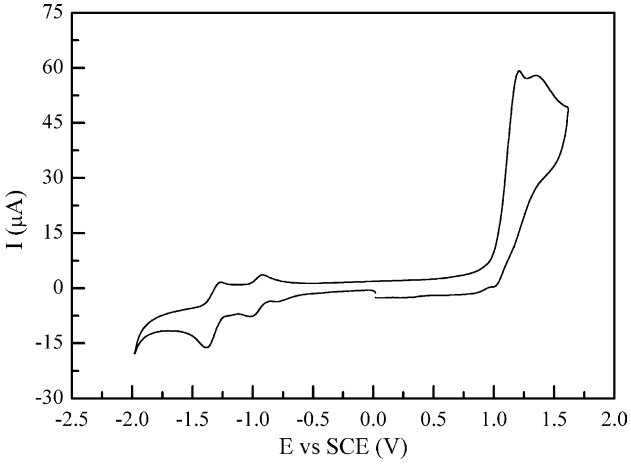

Fig. 3. Cyclic voltammogram of $[Fe(\mathbf{L})_2]^{2+}$ (1×10^{-3} M) in dichloromethane 0.1 M in TBAP; glassy-carbon electrode, scan rate = 100 mV s^{-1}.

$$[Fe^{II}L_2{}^0]^{2+} \underset{+e}{\overset{-e}{\rightleftharpoons}} [Fe^{II}L_0L_1]^{+} \underset{+e}{\overset{-e}{\rightleftharpoons}} [Fe^{II}L_2{}^1]^{0}$$

Scheme 1.

mass loss up to 1200 °C, forming a carbonaceous compound as residue. The acquisition of the DSC curve was necessary because the DTA one does not show adequate resolution due to the low reaction enthalpies observed under nitrogen atmosphere.

The electrochemical behavior of 1.0 mM $[Fe(\mathbf{L})_2]^{2+}$ in dichloromethane 0.1 M in TBAP was investigated by cyclic voltammetry on a glassy-carbon electrode (Fig. 3). The voltammogram shows two redox pairs corresponding to two quasi- reversible one-electron reductions ($E^1_{1/2} = -0.98$ V; $E^2_{1/2} = -1.34$ V) that must be ligand-centered as depicted in Scheme 1 [6].

Upon oxidation, the cyclic voltammogram shows two overlapped waves with peak potential values of 1.21 and 1.35 V, which can be ascribed to the reversible $Fe^{II/III}$ oxidation and irreversible pyrrole oxidation, respectively. This was also earlier observed for a similar iron complex [9]. The plot of i_p versus $v^{1/2}$ (square root of the scan rate), was linear for both peaks in the 20–500 mV s^{-1} range, indicating that both charge-transfer reactions are diffusion controlled in this interval. For higher scan rates, there is total overlap so only one peak is observed, and the peak potential shifts anodically as the scan rate increases.

The oxidative electrodeposition of $[Fe(\mathbf{L})_2]^{2+}$ in anhydrous dichloromethane is shown in Fig. 4. The continuous current increase in the cyclic voltammetric peaks during repeated potential scans from 0.0 to 1.25 V indicates film growth on the electrode surface. As described by Deronzier and Moutet [10], the poor reversibility of the $Fe^{II/III}$ couple suggests that pyrrole groups are catalytically oxidized by electrogenerated Fe(III) species. The parent cobalt complex $[Co(\mathbf{L})_2]^{2+}$ has the Co(II)/Co(III) couple potential at 0.38 V, far from the pyrrole function oxidation potential. Attempts to electropolymerize this complex were unsuccessful, supporting the suggestion above. Visual inspection of the electrode also shows the deposition of a purple film. The film is not dissolved upon subsequent anodic or cathodic potential sweeps; i.e., it is not simply the result of the precipitation of an insoluble monomeric $Fe(\mathbf{L})_2$-based complex. In agreement with the work of Vilas-Boas et al. [11] and references therein, one can conclude that the product of $[Fe(\mathbf{L})_2]^{2+}$ oxidation is a polymeric material.

The modified electrode transferred to clean electrolyte solution exhibits only one redox couple with diffusional shape at $E_{1/2} = 1.26$ V (which is an average value between $Fe^{II/III}$ and pyrrole oxidations). Broad waves, normally associated with conducting polypyrrole, are not observed in the voltammogram. These results demonstrate that only the electroactivity of the iron complex is maintained (Fig. 5). In the case of a chemically stable redox species and an electrochemically reversible system, the voltammetric behavior of an electrode coated with a monolayer of a redox couple is characterized by symmetrical anodic and cathodic waves with a difference in the peak potential values (ΔE_p) close to zero. Surface-confined redox couples with slow charge-transfer kinetics, on the other hand, exhibit higher ΔE_p values which increase with the scan rate. For relatively thicker films, further deviations from the monolayer behavior normally occur, indicating the appearance of some mass transport limitations in the film. Note that for $[Fe(\mathbf{L})_2^{2+}]_n$ films, even in the case of low coverage and low scan rates, the cyclic voltammetry waves exhibited peak potential separations greater than 200 mV and diffusional shape, thus indicating a relatively slow charge transfer rate from the interface between the electrode substrate and the $Fe^{II/III}$ redox centers through the film.

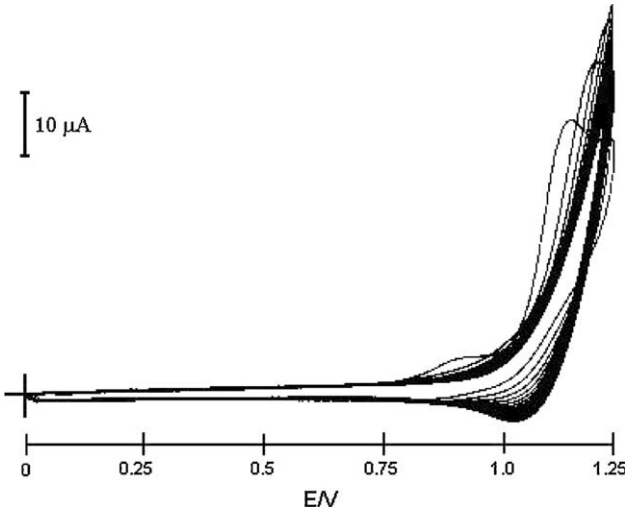

Fig. 4. Cyclic voltammogram showing deposition of poly-$[[Fe(\mathbf{L})_2]^{2+}]_n$ onto a glassy-carbon electrode in dichloromethane 0.1 M in TBAP, scan rate = 100 mV s^{-1}.

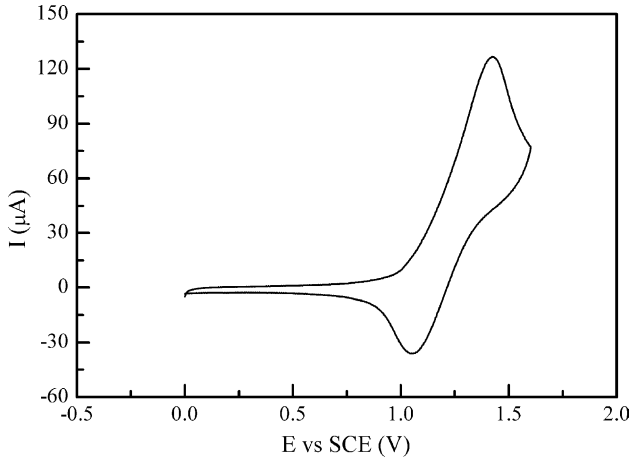

Fig. 5. Cyclic voltammogram of a poly-$[[Fe(\mathbf{L})_2]^{2+}]_n$-coated glassy-carbon electrode in dichloromethane 0.1 M in TBAP, scan rate = 100 mV s^{-1}.

The successful growth of polypyrrole films from substituted pyrroles requires carefully controlled experimental conditions. No electropolymerization is observed at monomer concentrations below 0.5 mM. A determining factor for successful electropolymerization is solvent choice. Electropolymerization does not occur in acetonitrile, *N*,*N*-dimethylformamide and propylene carbonate, for example. The choice of an appropriate scan upper-limit potential also determines the electropolymerization success. In order to establish the optimum parameters for efficient polymer film electrodeposition, E_{aul} was systematically changed from 0.70 to 1.6 V versus SCE (five cycles), with scans always beginning at 0.0 V. The $Fe^{II/III}$ couple peak intensities were monitored in clean electrolyte solutions. Fig. 6 shows the modified electrode apparent surface coverage (Γ_T^{APP} mol cm^{-2}) in a clean electrolyte solution (no monomers) as a function of E_{aul}. Electrochemical polymerization does not occur for potentials below 0.95 V. Above this potential, a nearly linear continuous increase in the apparent surface coverage is observed, reaching a maximum at 1.25 V. The value of Γ_T^{APP} increases with successive scans, indicating continued polymer deposition on the electrode. The value of Γ_T^{APP} abruptly decreases at upper-limits (beyond 1.25 V), so this potential has been established as the optimum upper-limit potential for growing polymeric films on glassy-carbon electrode surfaces.

It was observed that the number of cycles affects Γ_T^{APP} values. In order to improve electrodeposition efficiency, experiments were conducted to investigate the relationship between film formation and the number of voltammetric scans for an E_{aul} of 1.25 V. A plot of Γ_T^{APP} versus the number of cycles (Fig. 7) reveals an increase in the apparent surface coverage for up to 20 cycles,

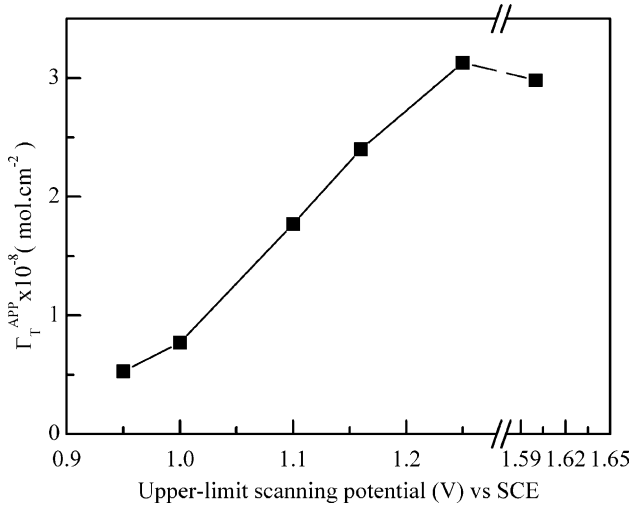

Fig. 6. Plot of Γ_T^{APP} vs. upper-limit scanning potential for poly-$[[Fe(\mathbf{L})_2]^{2+}]_n$ in dichloromethane 0.1 M in TBAP; glassy-carbon electrode, scan rate = 50 mV s^{-1}.

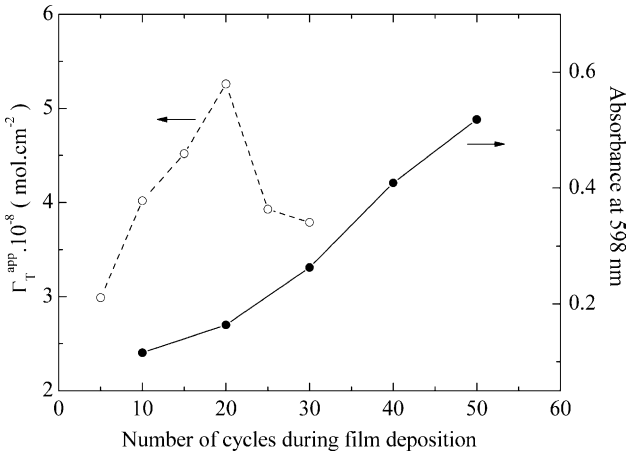

Fig. 7. Plot of Γ_T^{APP} vs. number of potential sweep voltammetric cycles of poly-$[[Fe(\mathbf{L})_2]^{2+}]_n$ (—) for an upper-limiting potential of 1.25 V; glassy-carbon electrode, dichloromethane 0.1 M in TBAP, scan rate = 50 mV s^{-1}. Absorbance at 598 nm vs. number of potential sweep voltammetric cycles of poly-$[[Fe(\mathbf{L})_2]^{2+}]_n$ (– – –) in dichloromethane. Films were deposited on ITO electrode in the same conditions as for glassy-carbon electrode.

followed by a decrease in the coverage. Each point was obtained from a modified electrode grown from freshly prepared monomer solution which was then transferred to a clean electrolytic solution (no monomers). Franco et al. [12] observed the same behavior for polypyrrole films functionalized with ruthenium and they attributed it to film formation with relatively poor charge transfer kinetics. The above experiment was repeated using an ITO working electrode for the electrodeposition. Each freshly modified electrode was copiously washed with dichloromethane and the electronic spectrum was acquired in the same solvent. The spectrum shows the same absorption bands obtained for the monomer in solution, suggesting that intact $[Fe(\mathbf{L})_2^{2+}]$ complex is incorporated into the deposited film. The absorbance at 598 nm almost linearly increases with the number of cycles (up to 50 cycles), indicating that an increasing number of layers is being deposited (Fig. 7). These results are clearly in contrast with those obtained before, where maximum surface coverage was obtained with 20 cycles, as discussed above. An explanation for that can be given as follows. An electrode coated with a redox polymer film exhibiting diffusive charge transport may do so at a fast, slow or intermediate rate with respect to the experimental time scale. If the charge transport rate is significantly faster than the experimental time scale, the oxidized/reduced site concentration ratio Γ_o/Γ_r will be uniform throughout the film and will be in thermodynamic equilibrium with the applied electrode potential. Cyclic voltammetric current–potential peaks will thus have a symmetrical shape in this case. If on the other hand, the diffusive charge transport is small, the cyclic voltammetric response will quantitatively be

the same as when reactants freely diffuse to the electrode from an infinite volume of solution. In other words, the depletion layer of the diffusion profile never reaches the cell wall. In the case of a coated electrode, the "cell" dimension is the thickness of the polymerized film itself, which is quite small. For films that present diffusional shape, as the one observed in Fig. 5, the electrochemical charge diffusion rate through the polymer must be very slow in comparison with diffusion rates common to electrolyte solutions. So it is obvious, that a good deal of electroactive Fe^{II} sites remains unoxidized as the potential is swept through the peak. This happens even more frequently at fast sweep rates and on thicker films, misleading the measured charge under the voltammetric wave. In our case, it is believed that estimated surface coverage values higher than $\sim 5 \times 10^{-8}$ mol cm^{-2} are significantly smaller than the real ones due to charge transport limitations imposed by film thickness. This is supported by AFM studies (see below).

The stability of the films has been checked by repetitive potential cycling in both anodic and cathodic sides. $[[Fe(\mathbf{L})_2]^{2+}]_n$ films exhibit low stability toward electrochemical cycling between the Fe(II) and Fe(III) states. For example, 42% of the integrated anodic peak current is lost after cycling a film 10 times between 0 and 1.6 V at 100 mV s^{-1}. After only one cathodic cycle in the 0–2.0 V range, all electroactivity is lost and no electrochemical response is observed at all.

Electrodes coated with $[[Fe(\mathbf{L})_2]^{2+}]_n$ films have been examined by cyclic voltammetry in the presence of ferrocene, which undergoes one-electron oxidation at less positive potentials than the Fe(II)/Fe(III) couple inside the film ($E_{sol} = 0.62$ V and $E_{pol} = 1.330$ V, respectively). These experiments were done with five electrodes (5, 10, 15, 20, 25 cycles) prepared by cycling the potential (0–1.25 V, 50 mV s^{-1}) in a 10^{-3} M solution of $[Fe(\mathbf{L})_2]^{2+}$ in dichloromethane 0.1 M in TBAP. They were washed with dichloromethane and transferred to a solution of ferrocene 4×10^{-3} M in clean supporting electrolyte. It is know that ferrocene may be oxidized at the electrode/polymer interface after diffusion through a continuous polymer film. Alternatively, it may be oxidized at a polymer film/solution interface, a process that requires either redox conduction through the film or an electronically conducting film. In the case of redox-conductivity-mediated electron transfer, irreversible oxidation of the solution species will occur at or near E_{pol}. For electron transfer mediated by an electronically conducting film, reversible oxidation will occur at or near E_{sol} [9].

A cyclic voltammogram for a solution of 4×10^{-3} M ferrocene at an electrode freshly coated with 3.95×10^{-8} mol cm^{-2} (10 cycles) of $[Fe(\mathbf{L})_2]^{2+}$ is shown in Fig. 8.

Ferrocene seems unable to penetrate the film, even the thinnest one (5 cycles), once the normally reversible wave at E_{sol} is completely suppressed. Similar behavior has been reported for cobaltocene and ferrocene at polypyrrole films [2]. On the other hand, the wave at E_{pol} is enhanced in the presence of ferrocene, while the cathodic wave in the reverse scan is reduced. This effect is qualitatively indicative of concurrent electrocatalytic oxidation of ferrocene by Fe^{3+} species inside the film [3]. For thicker films, there is no increase in the oxidation current in the presence of ferrocene, but the cathodic wave is again reduced. In summary, for an electrode modified with $[[Fe(\mathbf{L})_2]^{2+}]_n$, the most likely pathway for ferrocene oxidation in solution is via redox conduction through the film, which can in turn be classified as a redox polymer.

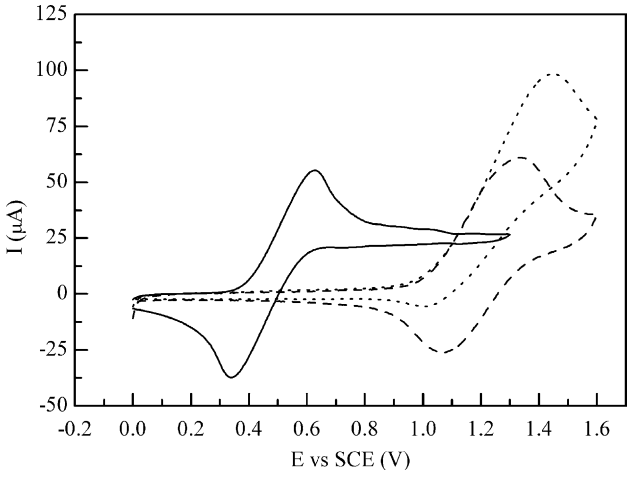

Fig. 8. Cyclic voltammogram of 4×10^{-3} M ferrocene in dichloromethane 0.1 M in TBAP (scan rate = 100 mV s^{-1}): (—) bare glassy-carbon electrode; (– – –) glassy-carbon coated with 3.95×10^{-8} mol cm^{-2} (10 cycles) of $[[Fe(\mathbf{L})_2]^{2+}]_n$; (. . .) glassy-carbon/poly-$[[Fe(\mathbf{L})_2]^{2+}]_n$ without ferrocene.

Atomic force microscopy was used to provide information concerning polymer morphology. Values of roughness and film thickness are listed in Table 1. It can be observed that there is an increase in roughness and film thickness values with the number of voltammetric scans. Films without electrochemical activity present smaller values than electroactive ones.

A typical 3-D AFM image of an electrochemically active film is shown in Fig. 9. The image reveals that the surface morphology is granular, indicating that the nuclei growth rates are essentially equal or comparable in directions parallel or perpendicular to the electrode surface [13]. From the observation of the AFM image, it is clear that nuclei are formed in large number and different sizes. No channels or holes are observed and the film surface is substantially rough with small and large nuclei in conical form. The 3-D image of a film without electrochemical activity is shown in Fig. 10.

Such images were obtained to verify if any alteration in film morphology would be responsible for the loss of electrochemical response. From Fig. 10, it can be ob-

Table 1
Roughness and thickness of poly-$[Fe(\mathbf{L})_2]_n$ with deposition time

	20 cycles		50 cycles	
	Active	Without activity	Active	Without activity
Thickness (nm)	211	166	493	277
Roughness (nm)	152	74	309	238

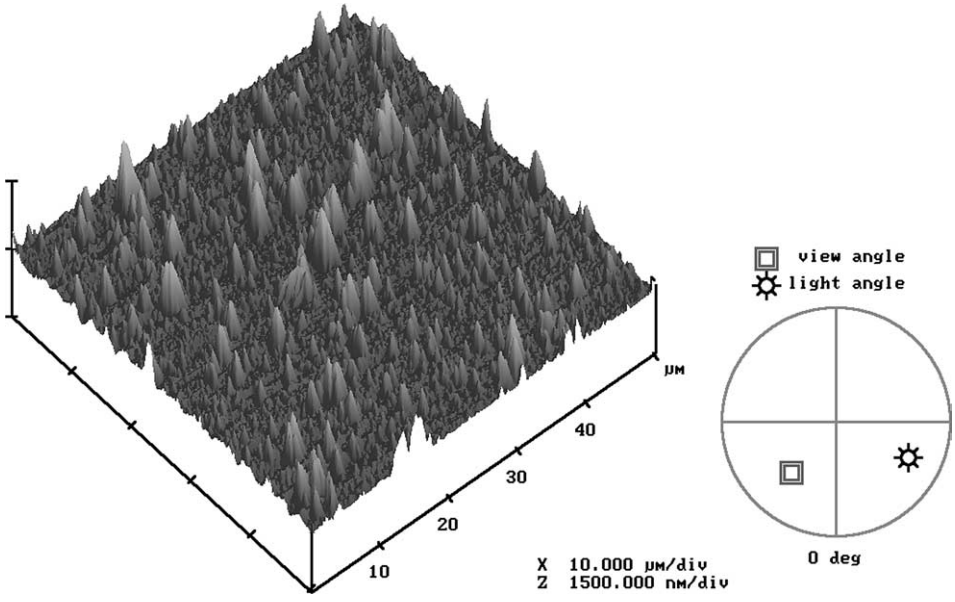

Fig. 9. AFM image of the surface morphology of a poly-$[[Fe(\mathbf{L})_2]^{2+}]_n$ film deposited on ITO, prepared by 20 voltammetric scans (0–1.25 V). 3-D view, scan scale: 10 μm.

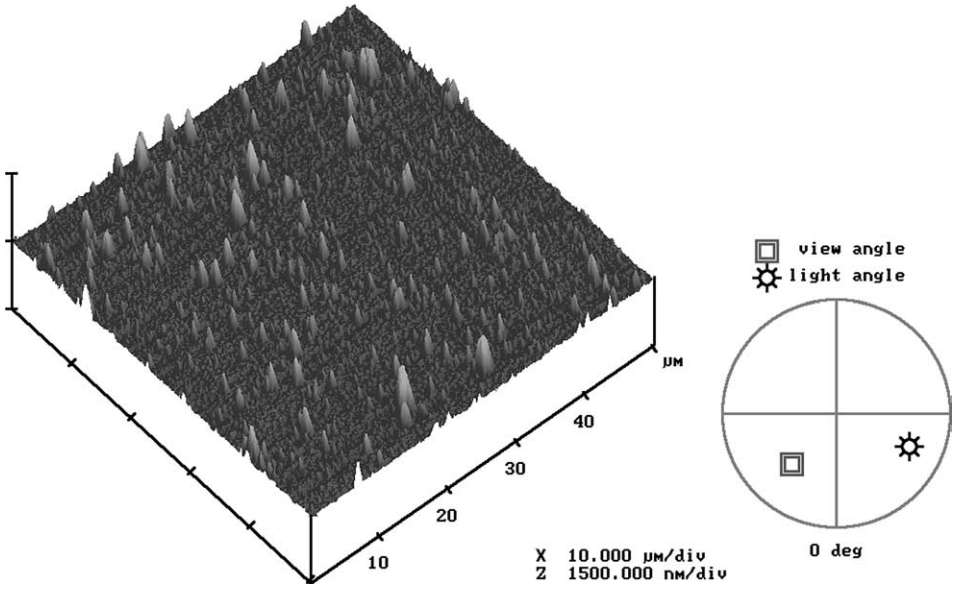

Fig. 10. AFM image of the surface morphology of a poly-$[[Fe(\mathbf{L})_2]^{2+}]_n$ film deposited on ITO, prepared by 20 voltammetric scans (0–1.25 V) followed by one scan in the cathodic direction (0 to −2.0 V). 3-D view, scan scale: 10 μm.

served that film morphology for the non-active film is about the same as for the active one. Although some film has been lost, it is clear that it still is on the electrode surface and the complete absence of electrochemical activity cannot be attributed to morphology modification or film destruction. Therefore, we suppose

that Fe(II) and/or ligand reduction modifies the complex coordination environment in an irreversible way, although there is no evidence to support such suggestion.

4. Conclusions

In the complex synthesis, the condensation between 2,6-diacetylpyridine and *N*-(3-aminopropyl)pyrrole in the presence of ferrous ions in a template reaction mode gives better results than the reaction between the free ligand and the metal ions.

Through TG, DTA and DSC curves, the composition of the complex could be established as being $[Fe(\mathbf{L})_2]^{2+}$ monomers that show distinct thermal behaviors under oxygen and nitrogen atmospheres. There is no formation of $FePO_4$ as residual oxide in the former case. Elemental analysis supports this composition.

Results reported herein demonstrate the successful preparation of modified electrodes by electropolymerization of the pyrrole-substituted Schiff-base iron complex using the potentiometric technique and an adequate solvent. The established optimum conditions are: tetrabutylammonium perchlorate 0.1 M in dichloromethane as solvent, 1.25 V as upper-limit potential and 20 as maximum number of electropolymerization cycles. From the results of our electrochemical studies carried out in the presence of ferrocene, the film can be classified as a redox polymer.

AFM analysis showed neighboring globular deposits under the experimental conditions. Surface morphology is maintained for films with or without electrochemical activity.

This work is an initial study in the coordination chemistry of iron(II) Schiff-base complexes bearing a pyrrole unit and a study on the nucleation and growth mechanism of $[Fe(\mathbf{L})_2]^{2+}$ is currently under investigation in our laboratory.

Acknowledgements

We gratefully acknowledge the financial support from FAPESP and CAPES.

References

[1] P.R. Moses, P. Wier, R.W. Murray, Anal. Chem. 47 (1975) 1882.
[2] H.D. Abruña, Coord. Chem. Rev. 86 (1988) 135.
[3] A. Deronzier, J.-C. Moutet, Coord. Chem. Rev. 147 (1996) 339.
[4] N.C. Foulds, C.R. Lowe, Anal. Chem. 60 (1988) 2473.
[5] H.E. Toma, T. Chavez-Gil, Inorg. Chim. Acta 257 (1997) 197.
[6] B. Bruin, E. Bill, E. Bothe, T. Weyhermuller, K. Wieghardt, Inorg. Chem. 39 (2000) 2936.
[7] P. Krumholz, O.A. Serra, M.A. De Paoli, Inorg. Chim. Acta 15 (1975) 25.
[8] G.J. Brealey, M. Kasha, J. Am. Chem. Soc. 77 (1955) 4462.
[9] J.G. Eaves, H.S. Munro, D. Parker, Inorg. Chem. 26 (1987) 644.
[10] A. Deronzier, J.-C. Moutet, Curr. Top. Electrochem. 3 (1994) 159.
[11] M. Vilas-Boas, C. Freire, B. Castro, P.A. Christensen, A.R. Hillman, Inorg. Chem. 36 (1997) 4919.
[12] C.V. Franco, P.B. Prates, V.N. Moraes, M.M.S. Paula, Synth. Met. 90 (1997) 81.
[13] B.J. Hwang, R. Santhanam, Y.L. Lin, Electrochim. Acta 46 (2001) 2843.

Available online at www.sciencedirect.com
SCIENCE DIRECT®
Polyhedron 23 (2004) 1961–1967
POLYHEDRON
www.elsevier.com/locate/poly

Novel hydrogen-bonded and π–π interaction networks generated from the reaction of copper(II) chloride hydrates with heterocyclic diimines (2,2′-bipyridine, 1,10-phenanthroline) and bidentate diamine (ethylenediamine)

Hong-Yan Mao [a,b], Xiao-Qing Shen [a,b], Gang Li [b], Hong-Yun Zhang [b,*], Chen Xu [b], Hong-Lei Liu [b], En-Bo Wang [a], Qing-An Wu [b], Hong-Wei Hou [b], Yu Zhu [b]

[a] *Department of Chemistry, Northeast Normal University, Changchun 130024, PR China*
[b] *Department of Chemistry, Zhengzhou University, Zhengzhou 450052, PR China*

Received 14 April 2004; accepted 28 April 2004

Abstract

The reaction of copper dichloride dihydrate, heterocyclic diimine (bipy, phen) and bidentate diamine (en) ligands under mild conditions affords two novel supramolecular complexes containing $Cu^{II}N_4Cl$ chromophores, $[Cu(en)(bipy)Cl][OH]\cdot(H_2O)_3$ (**1**) (en = ethylenediamine, bipy = 2,2′-bipyridine) and $[Cu(phen)_2Cl][OH]\cdot(CH_3OH)_2\cdot(H_2O)_6$ (**2**) (phen = 1,10-phenanthroline). Complex **1** involves a $Cu^{II}N_4Cl$ chromophore with a regular square based pyramidal stereochemistry, while complex **2** involves a regular trigonal bipyramidal one. To our knowledge, **1** is the first example of a $Cu^{II}N_4X$ complex generated from mixed ligands. Both of the two compounds were constituted through hydrogen bonding and π–π interactions between the heterocyclic rings. The magnetic properties of **2** were studied in the temperature range 5–300 K. The results reveal the occurrence of a weak antiferromagnetic coupling with $J = -1.9\ cm^{-1}$.
© 2004 Elsevier Ltd. All rights reserved.

Keywords: $Cu^{II}N_4Cl$ chromophores; Bidentate diimine; Bidentate diamine; π–π Interactions; Hydrogen bonding; Magnetic property

1. Introduction

The penta-coordinated copper(II) complexes comprising of both molecules of bidentate diimine, 2,2′-bipyridine (bipy) and 1,10-phenanthroline (phen), and one monodentate co-ligand have been attracting great interest for their diverse stereo and physicochemical properties [1–8]. The molecular structures of five-coordinate copper(II) complexes show an extensive variability, ranging from regular trigonal bipyramidal (RTBP) to regular square based pyramidal (RSBP) with most complexes displaying a structure that is intermediate between the two extremes. In such materials, interesting properties and potentials in spectroscopy, electrochemistry, biological activity and magnetism, etc. can be introduced from either the inorganic species or the organic linker molecules [9–15]. Therefore, the evaluations for correlations of stereochemistry with the corresponding properties are of fundamental importance for these copper(II) complexes. Although many five-coordinated copper(II) complexes are well documented, the presence of a mixed ligand compound has been rarely observed [8]. Here we describe the synthesis and crystal structures of two novel supramolecular complexes containing $Cu^{II}N_4Cl$ chromophores, $[Cu(en)(bipy)Cl][OH]\cdot(H_2O)_3$ (**1**) (en = ethylenediamine, bipy = 2,2′-bipyridine) and $[Cu(phen)_2Cl][OH]\cdot(CH_3OH)_2\cdot(H_2O)_6$ (**2**) (phen = 1,10-phenanthroline). To the best of our knowledge, compound **1** is the first example of a $Cu^{II}N_4X$ ($X = Cl^-$, Br^-, I^-) complex generated from mixed ligands and **2**

* Corresponding author. Tel.: +86-371-7763675; fax: +86-371-7761744.
E-mail address: wzhy917@zzu.edu.cn (H.-Y. Zhang).

0277-5387/$ - see front matter © 2004 Elsevier Ltd. All rights reserved.
doi:10.1016/j.poly.2004.04.034

provides a novel case of a dimeric unit formed through weak hydrogen bonding C–H···Cl and π–π interactions between phen rings. The magnetic properties of compound **2** are also investigated. The results indicate that the magnetic behavior of the compound obeys the Curie–Weiss law over the whole temperature range and weak antiferromagnetic coupling can be observed between the copper(II) ions.

2. Experimental

2.1. Materials and physical techniques

All chemicals were of analytical reagent grade quality, obtained from commercial sources and used without further purification. IR spectra were recorded on a FTS-40 spectrophotometer with pressed KBr pellets in the 400–4000 cm^{-1} region. Elemental analyses (C, H and N) were carried out on a Carlo-Erba 1106 elemental analyzer. The thermogravimetric analyses were performed on a NETZSCH TG 209 system at a rate of 10 °C min^{-1} in nitrogen atmosphere over the range 30–700 °C. DSC traces were obtained with the aid of a NETZSCH DSC 204 calorimeter at 10 °C min^{-1} in N_2 over the range 20–400 °C. Variable-temperature magnetic susceptibility data were obtained on a Quantum Design MPMS-5 SQUID magnetometer in the temperature range 5–300 K with an applied field of 500 G. Diamagnetic corrections were calculated from Pascal's constants [16].

2.2. Synthesis of the complexes

2.2.1. Synthesis of $[Cu(en)(bipy)Cl][OH]\cdot(H_2O)_3$ (**1**)

Copper dichloride dihydrate (0.0850 g, 0.5 mmol) dissolved in 20 cm^3 of water was allowed to react with 20 cm^3 of a methanolic solution of 2,2′-bipyridine (0.1562 g, 1.0 mmol), and stirred for 10 min. Into the resulting solution was poured slowly 10 cm^3 of a methanolic solution of ethylenediamine (0.030 g, 0.5 mmol), the entire mixture was stirred for 30 min and then allowed to evaporate slowly in an open atmosphere. After a few weeks, clear blue purple blocks of **1** suitable for X-ray structural study were obtained. These crystals were separated, washed with ethanol, and dried (yield: 82%, based on $CuCl_2\cdot H_2O$). *Anal.* Calc. for $C_{12}H_{23}ClCuN_4O_4$: C, 37.31; H, 6.00; N, 14.50. Found: C, 37.45; H, 5.98; N, 14.54%. IR (ν, cm^{-1}): 3384 (s, br), 3222 (s), 3135 (s), 2948 (m), 2889 (m), 1632 (m), 1610 (m), 1601 (s), 1567 (m), 1481 (m), 1441(m), 1327 (w), 1132 (m), 1056 (s), 1031 (m), 775 (s), 732 (s), 662 (m), 524 (m), 419 (m).

2.2.2. Synthesis of $[Cu(phen)_2Cl][OH]\cdot(CH_3OH)_2\cdot(H_2O)_6$ (**2**)

Into an aqueous solution (5 cm^3) of $CuCl_2\cdot 2H_2O$ (0.0425 g, 0.25 mmol) was poured slowly 20 cm^3 of a methanolic mixture of 1,10-phenanthroline monohydrate (0.0991 g, 0.5 mmol) and pyrazine (0.020 g, 0.25 mmol). The entire mixture was stirred for 30 min at 70 °C and allowed to evaporate slowly in an open atmosphere. After a few weeks, clear blue prismatic crystals of **2** suitable for X-ray structural study were obtained. These crystals were separated, washed with methanol, and dried (yield: 76%, based on $CuCl_2\cdot H_2O$). *Anal.* Calc. for $C_{26}H_{37}ClCuN_4O_7$: C, 50.65; H, 6.05; N, 9.09. Found: C, 50.58; H, 6.02; N, 9.12%. IR (ν, cm^{-1}): 3529 (m), 3382 (m), 3327 (m), 1627 (m), 1605 (w), 1585 (m), 1518 (s), 1495 (m), 1428 (s), 1426 (m), 1342 (w), 1228 (w), 1151 (w), 1103 (w), 869 (m), 853 (s), 778 (w), 722 (s), 648 (w), 629 (w), 430 (m).

2.3. X-ray crystallography

Crystal data and experimental details for compounds **1** and **2** are contained in Table 1. All measurements were made on a Rigaku RAXIS-IV imaging plate area detector with graphite-monochromated Mo Kα radiation ($\lambda = 0.71073$ Å). Prismatic single crystals were selected and mounted on a glass fiber. All data were collected using the ω–2θ scan technique and corrected for Lorenz-polarization effects. A correction for secondary extinction was applied. The two structures were solved by direct methods and expanded using Fourier techniques. All non-hydrogen atoms were described anisotropically; hydrogen atoms were included but not refined. The final cycle of full-matrix least-squares refinement was based on 3156 observed reflections and 200 variable parameters for **1**, 3561 observed reflections and 308 variable

Table 1
Crystallographic data and structure refinement

Structural parameter	**1**	**2**
Formula	$C_{12}H_{23}ClCuN_4O_4$	$C_{26}H_{37}ClCuN_4O_7$
Formula weight	386.34	616.59
T (K)	293(2)	291(2)
Crystal system	triclinic	monoclinic
Crystal size (mm)	0.30×0.30×0.30	0.20×0.18×0.18
Space group	$P\bar{1}$	$C2/c$
a (Å)	6.8731(14)	23.367(5)
b (Å)	11.532(2)	30.316(6)
c (Å)	12.595(3)	7.5084(15)
α (°)	65.73(3)	90
β (°)	77.19(3)	97.75(3)
γ (°)	77.42(3)	90
V (Å^3)	878.3(3)	5270.4(18)
D_{calc} (g cm^{-3})	1.465	1.554
Z	2	8
μ (mm^{-1})	1.416	0.985
Reflns collected/ unique (R_{int})	3156/3156 (0.0000)	5864/3561 (0.0711)
R_1, wR_2 [$I > 2\sigma(I)$]	0.0695[a], 0.2028[b]	0.0772[a], 0.2083[b]
$\Delta\rho_{min}$ and $\Delta\rho_{max}$ (e Å^{-3})	1.287 and −0.580	0.705 and −0.536

[a] $R = \sum||F_o| - |F_c||/\sum|F_o|$.
[b] $R_w = [\sum(||F_o| - |F_c||)^2/\sum w|F_o|^2]^{1/2}$.

Table 2
Selected bond distances (Å) and angles (°) for **1** and **2**

1		**2**	
Bond distances			
Cu(1)–N(3)	1.998(5)	Cu(1)–N(4)	1.981(7)
Cu(1)–N(1)	2.009(5)	Cu(1)–N(1)	1.982(7)
Cu(1)–N(4)	2.024(5)	Cu(1)–N(2)	2.097(6)
Cu(1)–N(2)	2.028(5)	Cu(1)–N(3)	2.110(7)
Cu(1)–Cl(1)	2.733(2)	Cu(1)–Cl(1)	2.336(2)
Bond angles			
N(3)–Cu(1)–N(1)	177.4(2)	N(4)–Cu(1)–N(1)	176.1(3)
N(3)–Cu(1)–N(4)	84.7(2)	N(4)–Cu(1)–N(2)	95.4(3)
N(1)–Cu(1)–N(4)	96.7(2)	N(1)–Cu(1)–N(2)	81.0(3)
N(3)–Cu(1)–N(2)	97.1(2)	N(4)–Cu(1)–N(3)	81.3(3)
N(1)–Cu(1)–N(2)	81.1(2)	N(1)–Cu(1)–N(3)	99.2(3)
N(4)–Cu(1)–N(2)	167.6(2)	N(2)–Cu(1)–N(3)	123.5(2)
N(3)–Cu(1)–Cl(1)	93.4(2)	N(4)–Cu(1)–Cl(1)	91.1(2)
N(1)–Cu(1)–Cl(1)	88.70(14)	N(1)–Cu(1)–Cl(1)	92.2(2)
N(4)–Cu(1)–Cl(1)	97.4(2)	N(2)–Cu(1)–Cl(1)	121.26(18)
N(2)–Cu(1)–Cl(1)	94.77(14)	N(3)–Cu(1)–Cl(1)	115.20(18)

parameters for **2**. All calculations were performed using the SHELXL-97 crystallographic software package [17]. Selected bond lengths and bond angles are listed in Table 2.

3. Results and discussion

3.1. Preparation of complexes

The self-assembly reaction of $CuCl_2 \cdot H_2O$ and the chelating bidentate ligands (bipy, en, phen) in H_2O–MeOH is an effective route for preparation of novel penta-coordinated copper(II) complexes containing $[Cu^{II}N_4X]^+$ and OH^-. Although it has the same cation as $\{[Cu(phen)_2Cl][OH] \cdot 6H_2O\}_2$ (**3**) [13], complex **2** obtained the hydroxide counter-ions in a quite different way. The structure of **3** was gained by treating $CuCl_2 \cdot 2H_2O$ with phen (1:2 metal-to-ligand ratio) in H_2O–EtOH and using NaOH to adjust the pH. In our synthesis (but not in compound **3**s) it appears that the (unincorporated) pyrazine molecules and non-coordinating methanol solvent used are critical in influencing the product. When the experiment was performed in the absence of pyrazine, extremely unstable crystals which turned opaque immediately under ambient atmosphere were obtained, a property distinctly different from the air-stable **2**. Similar results were obtained for complex **1**, all attempts to obtain a $Cu^{II}N_4Cl$ complex failed in a water solution instead of H_2O–MeOH.

3.2. Infrared spectra

The infrared spectrum of compound **1** exhibits characteristic bands for both 2,2′-bipyridine and ethylenediamine ligands. The presence of the bipy ligand is confirmed by bands due to the skeletal vibrations of the pyridine ring at 1610, 1567, 1481 and 1441 cm^{-1}. In addition, the band at 775 cm^{-1} can be assigned to the CH out-of-plane bend of the pyridine ring (four adjacent H). Moreover, the peaks at 3384, 3222, 3135 and 1601 cm^{-1} are the characteristic bands of N–H(en), and the bands in the region 3300–3500 cm^{-1} are assigned to the stretching vibrations, ν(O–H), of the hydroxyl groups. The slight variation of O–H(H_2O) and N–H(en) vibrations for these complexes is probably mainly due to the hydrogen bonds. The Cu–N stretching is tentatively assigned at 419 cm^{-1}.

In the IR spectrum of complex **2**, the aromatic C=C and C=N stretching vibration absorptions of the phen ring appear at 1627, 1585, 1518 and 1428 cm^{-1}. The band at 853 and 722 cm^{-1} is assigned to the CH out-of-plane bend (two adjacent H), ring breathing and deformation absorptions of coordinated 1,10-phenanthroline. Meanwhile the peaks at 3529 (ν_{O-H}) and 1426 (ν_{bend}) cm^{-1} are the characteristic bands of H_2O, which indicates the existence of molecular lattice water. In addition, the new band at ca. 430 cm^{-1} was recorded which shows the stretch vibrating frequency of the Cu–N coordinated bond [18].

3.3. Thermal behavior

The thermogravimetric analyses of compounds **1** and **2** show the occurrence of three consecutive processes, namely dehydration, ligand pyrolysis and inorganic residue formation. The DSC and TGA analysis for **1** shows that the lattice water molecule is lost at ~89 °C as indicated by a weight loss of 12.10% (Calc. 13.99%) corresponding to three moles of water per formula unit. As the temperature increases simultaneous en and 2,2′-bipy ligand pyrolyses occurs between 146 and 271 °C with a total weight loss of 57.70% (Calc. 55.99%), by the occurrence of endothermic and exothermic peaks overlapping with each other. Thermogravimetric analysis of **2** indicates that the thermal decomposition of **2** is initiated between 99 and 112 °C by a weight loss of 27.10%, corresponding to the loss of six water and two methanol molecules (Calc. 27.93%). The six water molecules are released before the temperature of 112 °C which suggests that these water molecules are the crystallized ones instead of the coordinated ones. There is a further 58.0% weight loss in two continuous steps in the 278–384 °C range, which compares with the calculated loss (58.45%) for the two phen molecules.

3.4. Crystal structures

3.4.1. $[Cu(en)(bipy)Cl][OH] \cdot (H_2O)_3$ (**1**)

Compound **1** consists of discrete monovalent complex cations, hydrogen bonded separate hydroxide ions and solvent H_2O molecules. An ORTEP drawing of the unit with the atomic numbering scheme is depicted in

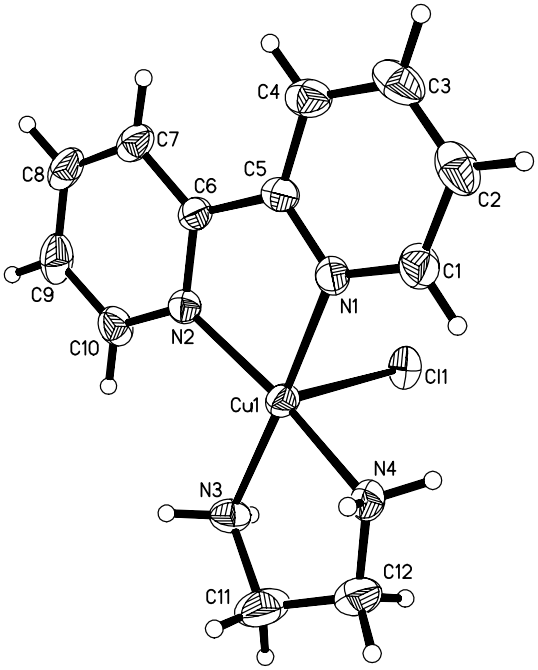

Fig. 1. Structural unit of $[Cu(en)(bipy)Cl]^+$ with atom numberings, showing 30% thermal ellipsoids.

Fig. 1. The complex cations possess five-coordinated environments with $Cu^{II}N_4Cl$ chromophores, namely, each of the Cu atoms is coordinated by four nitrogen atoms from one bidentate diimine (2,2′-bipy) and one bidentate diamine (en) ligand with one chloride anion forming weak Cu–Cl apex bonds. Although the hydroxide ion is geometrically oriented for potential axial Cu–O bonding, the distance (Cu–O = 2.762 Å) is greater than 2.7 Å, and the axial bonding is considered to be absent. The Cu–N bond lengths and the N–Cu–N bite angles are comparable to those found in en and bipy copper(II) structures (see Table 2) [8–10]. However, the Cu–Cl distance (2.733(2) Å) is significantly longer than that in the common $Cu^{II}N_4Cl$ complexes [9–13]. Furthermore, the largest angle around the Cu(II) center (β: N3–Cu1–N1 = 177.4(2)°) is slightly larger than the second-largest one (α: N4–Cu1–N2 = 167.6(2)°). The value of the differences between the longest and shortest Cu–N bond distances ΔCu–N is 0.030 Å. These imply that the geometries around the Cu(II) centers in **1** are of distorted square-pyramidal or trigonal-bipyramidal one. Since the angular structural index parameter, $\tau = (\beta - \alpha)/60$, is evaluated by the two largest angles ($\alpha < \beta$) in the five-coordinated geometry [19], the value of $\tau = 0.16$ seems to indicate a RSBP. The two pyridine rings in the heterocyclic diimine ligands are not coplanar. Each dihedral angle is twisted by 3.8°, similar to that of closely related compound [8–10]. The hydroxide ions appear to be loosely held in lattice holes by Coulombic forces and by weak hydrogen bonds to the chloride and bipyridine C–H groups as shown in Fig. 2.

The most interesting feature of **1** is that the inter-ionic hydrogen bonds play an important role in the crystal packing and the stability of the inclusion complex (Fig. 2). Adjacent units are cross-linked by four types of intermolecular hydrogen bonds, which stabilize the conformation with the distances of 2.369 Å for $(OH^-)O\cdots H$–C(bipy), 3.115 Å for $Cl\cdots H$–$O(OH^-)$, 2.816 Å for $Cl\cdots H$–C(bipy), 2.478 and 2.697 Å for $Cl\cdots H$–N(en). Through the interionic hydrogen bonds, the cations are linked into two-dimensional layers parallel to the crystallographic *ab*-plane with interdigitation of neighboring parallel pyridyl ligands. The bipy ligands engage in face-to-face C–H$\cdots\pi$ aromatic stacking in-

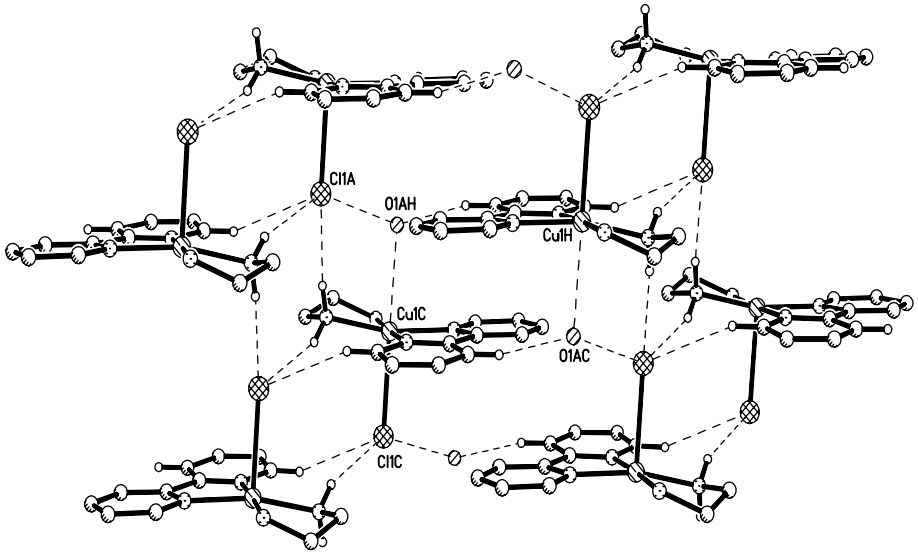

Fig. 2. The layer structure of **1** formed by hydrogen bondings. The non-hydrogen bonding H atoms have been omitted for clarity.

teractions (d(C···C) = 3.035–3.148 Å). In the crystal, the infinite considerably puckered sheets are parallel on each other along the c-axis and stack with an interpenetrating mode to give an extended three-dimensional network with spacious and straight channels, in which the hydrogen bonded H_2O molecules are sandwiched.

3.4.2. $[Cu(phen)_2Cl][OH]\cdot(CH_3OH)_2\cdot(H_2O)_6$ (2)

The X-ray structural analyses reveals that **2** consists of discrete monovalent complex cations, hydrogen bonded free hydroxide ions and solvent H_2O molecules, and that **2** additionally involves hydrogen bonded dimers of methanol. As shown in Fig. 3, the complex cations possess five-coordinated environments with $Cu^{II}N_4Cl$ cores similar to that in complex **3** [13]. Namely, each of the Cu atoms is coordinated by four N atoms from two phen frameworks and one Cl atom. The Cu–N distances of ~2.02 Å and the bite angles of ~81° of the phen ligands are close to the average values for phen copper(II) complexes (Table 2) [11]. The Cu–Cl distance (2.336(2) Å) is slightly longer, while the value of ΔCu–N (0.129 Å) is slightly shorter than that for **3**. The largest angle β(N4–Cu1–N1 = 176.1(3)°) is considerably different from the second-largest one α(N2–Cu1–N3 = 123.5(2)°). The value of the angular structural index parameter τ(0.88) shows a much more limited range of distortion from the RTBP stereochemistry (regular trigonal bipyramidal).

In crystals of **2**, no hydroxide ions are close enough to interact with the Cu(II) centers in the complex cations. However, one phen framework in the complex cation in **2** is in close proximity to that in the other complex cation accompanied by the formation of a dimeric unit. Namely, the interplane distance and angle between the neighboring two phen frameworks are ca. 3.425 Å and 0.0°, respectively, indicating the interaction between the two π-electronic systems of the phen frameworks. In addition, the Cl atoms form double hydrogen bonds with the C atoms in the phen ring of the dimer and the O atom of adjacent lattice water. The crystal lattice water molecules and hydroxyl groups are involved in the hydrogen bonding network, making the system stable. Thus, the dimers are propagated into a 2D architecture through the C–H···Cl, O–H···Cl and O–H···O hydrogen bonds (Fig. 4). A statistical analysis based on CSD suggests that C–H··· Cl contacts are within the range 2.7–3.0 Å. In this case, the C–H···Cl distance is 2.759 Å, which is in accordance with the statistical analysis. Furthermore, the C–H···Cl bond angles of **2** exhibit a directionality of 159.0°, which further suggests that the C–H···Cl hydrogen bonds are available in the structure of **2**. The remaining one of the phen rings in the $[Cu(phen)_2Cl]^+$ cation also produces π–π interactions between dimers as shown in Fig. 5. The center-to-center and interplanar distances are 3.687 and 3.426 Å, respectively. Thus, the binuclear $[Cu(phen)_2Cl]_2^{2+}$ units are linked to each other to give an extended three-dimensional network with void space, in which the hydrogen bonded hydroxide ions, solvent H_2O molecules and tetramers of methanol are sandwiched.

It is interesting that the phen components play double roles in the structure of **2**. One is acting as a ligand covalently linked to the copper centers. The adjacent phen rings are parallel to each other and cause signifi-

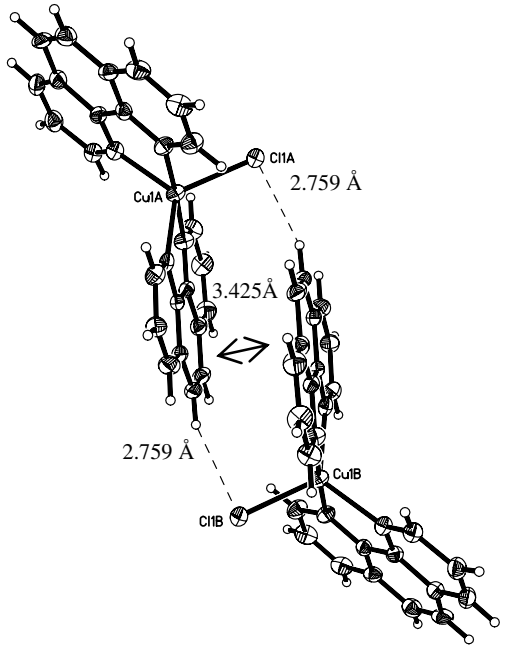

Fig. 3. Dimer structure of $[Cu(phen)_2Cl]_2^{2+}$ formed by C–H···Cl hydrogen bondings and π–π interactions.

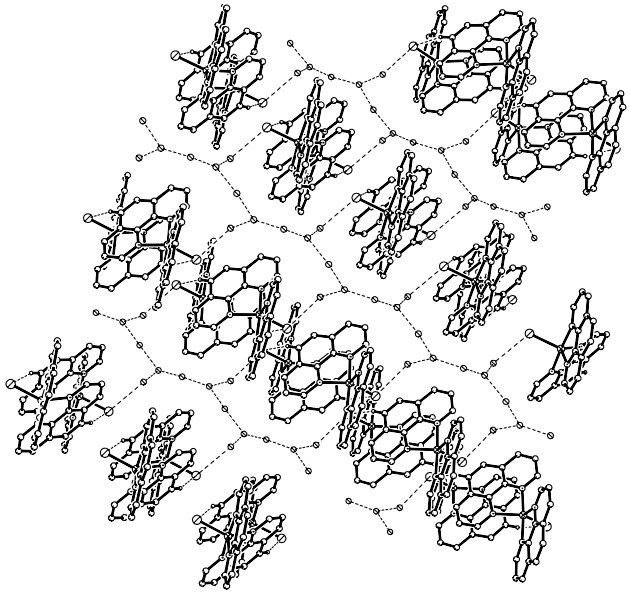

Fig. 4. The layer structure of complex **2** formed by hydrogen bonds. Hydrogen atoms have been omitted for clarity.

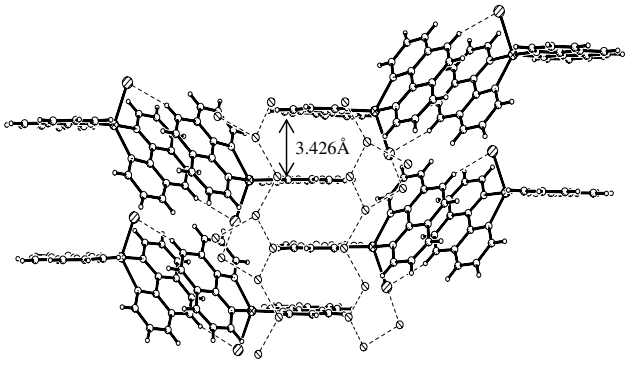

Fig. 5. The π–π interactions between the adjacent phen rings of the dimers in **2**.

cant π–π stacking interactions in and between dimers. Therefore, the dimer unit is highly strengthened by the strong π–π interactions. The other role is acting as the donors of hydrogen bonding which leads to the generation of the 3D supermolecular architecture. It is worth noting that a dimer structure constructed through C–H···Cl hydrogen bonding and π–π interactions is rare, and **2** is a new case of the RTBP stereochemistry for the $[Cu(phen)_2Cl]^+$ series of compounds.

3.5. Magnetic properties of 2

Variable-temperature magnetic susceptibility measurements were performed in the range of 5–300 K. The thermal variation of the molar susceptibility χ_M together with a plot of χ_M^{-1} versus T of complex **2** is shown in Fig. 6. The magnetic moment at 300 K ($\mu_{eff} = 2.04\ \mu_B$) per copper(II) center is higher than that expected for an isolated paramagnetic system with $S = 1/2$ ($\mu_{eff} = 1.73\ \mu_B$). By the value of magnetic moment measured at 300 K, the 2+ oxidation state of copper in **2** could be confirmed with a calculation of the spin-only magnetic moment. The increase in χ_M with decreasing temperature at very low temperatures is due to the presence of traces of monomeric paramagnetic impurity. The thermal evolution of χ_M^{-1} obeys the Curie–Weiss law, $\chi_M = C_M/(T-\theta)$, over the whole temperature range with $C_M = 0.5190$ cm^3 K mol^{-1} and $\theta = -0.302$ K. In general, the negative Weiss constant indicates an antiferromagnetic interaction between the copper ions. In addition, the variation of magnetic susceptibility with temperature for **2** can be fitted to the Bleaney–Bowers model (see Eq. (1)); J is the exchange coupling constant; N, g, β, K have their usual meanings; χ_M is expressed per mole of copper atoms, ρ is the fraction of monomeric impurity [20]

$$\chi_M = \frac{Ng^2\beta^2}{3KT}[1 + 1/3\exp(-2J/KT)]^{-1}(1-\rho) + \frac{Ng^2\beta^2}{4KT}\rho + N_a. \quad (1)$$

However, the magnetism of the dimer could not be simulated in the region between 5 and 60 K. In this temperature range the observed and calculated data diverge slightly, therefore we have concentrated our efforts in the range 60–300 K. Magnetic parameters thus determined are $g = 2.36$, $J = -1.9$ cm^{-1}, $N_a = 2.23 \times 10^{-3}$ cm^3 mol^{-1}, $\rho = 0.02$. The discrepancy factor $\sigma = [\sum(\chi_{obs} - \chi_{calc})^2 / \sum \chi_{obs}]^{1/2}$ in the least-squares fits was 1.03×10^{-4}. Obviously, the negative and small J value suggests the antiferromagnetic interaction between the copper(II) ions in the complex is very weak and C–H···Cl hydrogen bonding in the dimers does not apparently facilitate exchange between the paramagnetic atoms. Moreover, from 300 to 5 K, the slightly decreased $\chi_M T$ value is also consistent with the above conclusion.

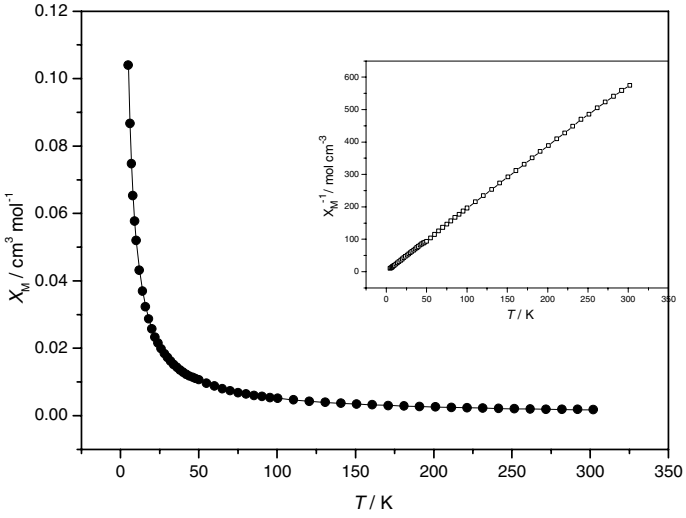

Fig. 6. Thermal variation of χ_M and χ_M^{-1} for **2**. The solid line corresponds to the best theoretical fit.

4. Supplementary material

Crystallographic data for the structural analyses have been deposited with the Cambridge Crystallographic Data Center, CCDC Nos. 197217 and 227506 for **1** and **2**, respectively. Copies of this information may be obtained free of charge from The Director, CCDC, 12 Union Road, Cambridge CB2 1EZ, UK (fax: +44-1223-336033; e-mail: deposit@ccdc.cam.ac.uk or www: http://www.ccdc.cam.ac.uk).

Acknowledgements

We gratefully acknowledge financial support from the National Natural Science Foundation of China (20271046), the Natural Science Foundation of Henan Education Department (200011500027) and the Natural Science Foundation of Henan Province (0211020300).

References

[1] S. Tyagi, B. Hathaway, S. Kremer, H. Stratemeier, D. Reinen, J. Chem. Soc., Dalton Trans. (1984) 2087.
[2] W.D. Harrison, D.M. Kennedy, M. Power, R. Sheahan, B.J. Hathaway, J. Chem. Soc., Dalton Trans. (1981) 1556.
[3] O. Carugo, C.B. Castellani, J. Chem. Soc., Dalton Trans. (1990) 2895.
[4] P.M. Bush, J.P. Whitehead, C.C. Pink, E.C. Gramm, J.L. Eglin, S.P. Watton, L.E. Pence, Inorg. Chem. 40 (2001) 1871, and references therein.
[5] S.M. Morehouse, H. Suliman, J. Haff, D. Nguyen, Inorg. Chim. Acta 297 (2000) 411.
[6] D. Tran, B.W. Skelton, A.H. White, L.E. Laverman, P.C. Ford, Inorg. Chem. 37 (1998) 2505.
[7] P. Nagle, E. O'Sullivan, B.J. Hathaway, E. Muller, J. Chem. Soc., Dalton Trans. (1990) 3399.
[8] C.-C. Su, Y.-L. Lin, S.-J. Liu, T.-H. Chang, S.-L. Wang, F.-L. Liao, Polyhedron 12 (1993) 2687.
[9] C. O'Sullivan, G. Murphy, B. Murphy, B. Hathaway, J. Chem. Soc., Dalton Trans. (1999) 1835.
[10] M. Brophy, G. Murphy, C. O'Sullivan, B. Hathaway, B. Murphy, Polyhedron 18 (1999) 611.
[11] G. Murphy, P. Nagle, B. Murphy, B. Hathaway, J. Chem. Soc., Dalton Trans. (1997) 2645, and references therein.
[12] E.C. O'Brien, E. Farkas, M.J. Gil, D. Fitzgerald, A. Castineras, K.B. Nolan, J. Inorg. Biochem. 79 (2000) 47.
[13] B.-Q. Ma, S. Gao, T. Yi, C.-H. Yan, G.-X. Xu, Inorg. Chem. Commun. 3 (2000) 93.
[14] O.J. Parker, G.T. Greiner, G.L. Breneman, R.D. Willett, Polyhedron 13 (1994) 267.
[15] G. Murphy, C. O'Sullivan, B. Murphy, B. Hathaway, Inorg. Chem. 37 (1998) 240.
[16] R.L. Carlin, Magnetochemistry, Springer, New York, 1986, pp. 125–200.
[17] G.M. Sheldrick, SHELXL-97: Program for Crystal Structure Refinement, University of Göttingen, Göttingen, Germany, 1997.
[18] P.G. Slade, M. Raupach, E.W. Radoslovich, Acta Crystallogr., Sect. B 29 (1973) 279.
[19] A.W. Addison, T.N. Rao, J. Reedijk, J. Rijn, G.C. Verschoor, J. Chem. Soc., Dalton Trans. (1984) 1349.
[20] K.E. Hyde, G. Gordon, G.F. Kokoszka, J. Inorg. Nucl. Chem. 30 (1968) 2155.

Available online at www.sciencedirect.com
SCIENCE DIRECT®
Polyhedron 23 (2004) 1969–1973
POLYHEDRON
www.elsevier.com/locate/poly

Crystal structures, spectroscopy and EPR of two distortion isomers of Cu(II) perchlorate with 2,2′-bi-imidazoline

Aminou Mohamadou [a,1], Gerard A. van Albada [a], Willem L. Driessen [a], René de Gelder [b], Jan Reedijk [a,*]

[a] Gorlaeus Laboratories, Leiden Institute of Chemistry, Leiden University, P.O. Box 9502, NL-2300 RA Leiden, The Netherlands
[b] Departement of Inorganic Chemistry, University of Nijmegen, Toernooiveld 1, 6525 ED Nijmegen, The Netherlands

Received 21 January 2004; accepted 29 April 2004
Available online 24 June 2004

Abstract

The synthesis, crystal structures, as well as the electronic and spectroscopic properties, of two new mononuclear Cu(II) isomeric compounds containing the ligand 2,2′-bi-imidazoline (biz) are reported. Both Cu(II) compounds, the blue $[Cu(biz)_2(ClO_4)_2]$ (**1**) and the violet $[Cu(biz)_2](ClO_4)_2$ (**2**), have the same stoichiometry and but differ in the location of the perchlorate anions. The basal plane of both compounds is formed by four nitrogen atoms of two dichelating biz ligands. In compound **1**, the apical position is occupied by two oxygen atoms of two perchlorate anions, resulting in an elongated octahedral geometry around the Cu ion. In compound **2**, the perchlorate anions are not coordinating to the Cu ion, resulting in a square planar geometry around the Cu atom. Both isomers show different and interesting H-bonding properties. The electronic, EPR and IR spectroscopy results are in agreement with the structural geometry. In frozen solution (at 77 K) the EPR spectrum is identical for both compounds, so in that case they have both the same geometry.
© 2004 Elsevier Ltd. All rights reserved.

Keywords: Copper; Structure; Infrared; Hydrogen bonds; Distortion isomers

1. Introduction

The organic ligand 2,2′-bi-imidazoline (biz) (see Fig. 1) is an interesting and flexible bifunctional ligand. This heterocyclic didentate ring ligand is of special interest as it deviates from the more "flat" molecules, like bisimidazole, bipyridine or bipyrimidine, due to the fact that the steric effects at the rear side of the molecule are influenced by two acidic hydrogen atoms. These two N–H donor groups can form polymeric aggregates by hydrogen bonding [1,2].

So far X-ray structures with biz and transition metals have only been reported for a few Fe(II), Fe(III) and Co(II), Co(III) compounds [1,2], in which neutral and mono-deprotonated biz are present. With Cu(II), Ni(II) and Co(II) as transition metal ions recently X-ray structures with this ligand and the anion dicyanamide and a copper(II) azide compound have been reported by some of us [3,4]. Especially, the chemistry of the Cu(II) compounds appears to be rich.

In this study, we present the molecular and X-ray structure of two new mononuclear compounds with the same stoichiometry, a blue $[Cu(biz)_2(ClO_4)_2]$ (**1**) and a violet $[Cu(biz)_2](ClO_4)_2$ (**2**) compound. The compounds can be described as examples of the rare case of distortion isomers; in the literature only a few of such cases are reported [5–8]. The two studied compounds could be reproducible synthesized by using a different Cu–ligand ratio of Cu–L 1:2 and Cu–L 1:1 for compounds **1** and **2**, respectively.

* Corresponding author. Tel.: +31-71-527-4459; fax: +31-71-527-4451.
E-mail address: reedijk@chem.leidenuniv.nl (J. Reedijk).
[1] On leave from GRECI, Faculté des Sciences, Université de Reims Champagne-Ardenne, Reims, France.

0277-5387/$ - see front matter © 2004 Elsevier Ltd. All rights reserved.
doi:10.1016/j.poly.2004.04.030

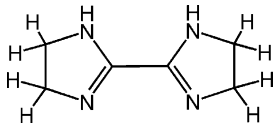

Fig. 1. Chemical structure of 2,2′-bi-imidazoline (biz).

2. Experimental

2.1. Syntheses

The ligand, 2,2′-bi-imidazoline (biz), was prepared by the method reported in the literature [9].

The compounds **1** and **2** were prepared by using a different Cu(II) ligand ratio, according to the following procedure: 1.2 mmol of the metal perchlorate salt and 2.4 mmol ligand (for the synthesis of compound **1**) or 1.2 mmol ligand (for the synthesis of compound **2**) were each dissolved in 10 ml of ethanol and 1 ml water. The ligand solution was then added slowly to the metal perchlorate solution and filtered to remove any undissolved material. Usually, after a few days to at most one week, the product separates as crystalline products. Violet crystals of compound **2** separates as a pure compound within a few days. The blue compound **1** also separates within a week, but contains always a small amount (5% at most) of the violet crystals of compound **2**. These violet crystals were easily removed by hand under the microscope obtaining in this way the pure compound **1**, which could be used for XRD, spectroscopic measurements and EPR. The crystalline products were isolated by filtration and dried in air, and characterized by elemental analysis and spectroscopic methods. Yield varies from 40% to 60%. *Anal*. Calc. for $C_{12}H_{20}Cl_2CuN_8O_8$: (Compound **1**): C, 26.3; H, 4.2; N, 20.2. Found: C, 26.7; H, 3.7; N, 20.8%. *Anal*. Calc. for $C_{12}H_{20}Cl_2CuN_8O_8$: (Compound **2**): C, 26.2; H, 3.9; N, 20.5. Found: C, 26.7; H, 3.7; N, 20.8%.

2.2. Physical measurements

C, H, N determinations were performed on a Perkin–Elmer 2400 Series II analyser. Ligand-field spectra were obtained on a Perkin–Elmer Lambda 900 spectrophotometer using the diffuse-reflectance technique, with MgO as a reference. X-band powder EPR spectra were obtained on a Jeol RE2× electron spin resonance spectrometer, using DPPH ($g = 2.0036$) as a standard.

FT-IR spectra were obtained on a Perkin–Elmer Paragon 1000 FT-IR spectrophotometer equipped with a Golden Gate ATR device, using the reflectance technique (4000–300 cm^{-1}, resolution 4 cm^{-1}).

2.3. Crystal structure determination and refinement of the structures

The reflection intensities were measured on a four-circle Enraf-Nonius CAD-4 diffractometer using graphite-monochromated Cu Kα radiation ($\lambda = 1.54184$ Å).

Table 1
Crystal data and details of the structure determination

	1	**2**
Crystal data		
Compound	$C_{12}H_{20}Cl_2CuN_8O_8$	$C_{12}H_{20}Cl_2CuN_8O_8$
Molecular weight	538.81	538.81
Crystal system	monoclinic	monoclinic
Space group	$P2_1/n$	$P2_1/c$
a (Å)	7.7199(5)	7.1261(6)
b (Å)	9.8205(7)	14.2991(11)
c (Å)	13.3434(7)	9.5305(4)
α (°)	90	90
β (°)	92.807(5)	92.998(5)
γ (°)	90	90
V (Å^3)	1010.39(11)	969.80(12)
Z	2	2
D_{calc} (g cm^{-3})	1.771	1.845
$F(000)$	550	550
μ (mm^{-1})	4.500	4.700
Crystal size (mm)	0.09×0.21×0.25	0.12×0.33×0.46
Data collection and refinement		
T (K)	293	293
θ_{min}; θ_{max}	5.6; 69.9	5.6; 69.8
Total data collected	1990	1984
Independent reflections (R_{int})	1990 (0.000)	1984 (0.000)
Observed reflections ($I > 2\sigma(I)$)	1561	1814
Number of refined reflections and parameters	1555 and 122	1798 and 142
Final R_1, wR_2 ($I > 2\sigma(I)$)	0.1020, 0.1630	0.070, 0.1090
Goodness-of-fit on F^2	0.82	0.77
Minimum and maximum residual density (e Å^{-3})	−1.32 and 1.28	−1.18 and 0.97

The cell dimensions were determined using 25 independent reflections. Intensity data were corrected for Lorentz and polarization effects. Absorption correction was not applied. The positions of heavy atoms were determined from a Patterson map (DIRDIF) [10]. The atomic scattering factors were taken from the International Tables for X-ray Crystallography [11]. The remainder of the non-H atoms were located in subsequent difference Fourier syntheses. Hydrogen atoms were placed at calculated positions (at 0.95 Å) from their parent atoms. Full-matrix least-squares refinement on F using the XTAL 3.4 set of programs [12] with the function minimized being $\sum w(|F_o| - |F_c|)^2$ with $w = 1/\sigma^2(F)$. Positional refinement of all non-H atoms, anisotropic for the non-hydrogen atoms, fixed isotropic thermal parameters for the hydrogens. Geometric calculations and molecular graphics were performed with the PLATON package [13]. (Details are given in Table 1.)

3. Results and discussion

3.1. Description of the crystal structures of $[Cu(biz)_2(ClO_4)_2]$ (1) and $[Cu(biz)_2](ClO_4)_2$ (2)

Both structures **1** and **2** are quite similar, and are discussed together. The only important difference is the location of the perchlorate anion and the hydrogen bonding system. The structure of the complete units is depicted in Figs. 2 and 3, for structures **1** and **2**, respectively. Relevant bond length and bond angle information is given in Table 2. A centre of symmetry is located on the Cu atom.

The basal plane in both compounds is occupied by four nitrogen atoms of two dichelating biz ligands with distances of 1.977(7) and 2.021(6) Å for compound **1** and 1.965(4) and 1.982(4) Å for compound **2**. In compound **1**, the apical positions are occupied by two oxygen atoms of two perchlorate anions with a semi-coordination distance of 2.594(8) Å, resulting in a elongated octahedral geometry around the Cu ion. In compound **2**, the perchlorate anions are not coordinating to the Cu ion (shortest Cu···O contact = 3.183(4) Å), resulting in a square planar geometry around the Cu ion. This also agrees with the somewhat shorter Cu–N distances in compound **2** (averaged Cu–N distance 1.973 Å), compared to compound **1** (averaged Cu–N distance 1.999 Å). The difference in coordination of the perchlorate anion for the two compounds results mainly in a quite different lattice structure. The hydrogen bonds in compound **1** occur between the uncoordinated nitrogen atoms of the biz ligand at the rear side of the molecule and the oxygen atoms of the perchlorate anions of a neighbouring unit as bifurcated bonds with distances that vary from 2.946(12) to 3.201(14) Å. The hydrogen bonds in compound **2** exist between the uncoordinated nitrogen atoms of the biz ligand and the O3 of the uncoordinating perchlorate anion with distances of 2.941(6) and 2.938(6) Å. Details of the hydrogen bonds are given in Table 2 and in Figs. 4 and 5. The lattice is further stabilised by ring–ring contacts of imidazoline units of 4.094 and 3.784 Å, for compounds **1** and **2**, respectively.

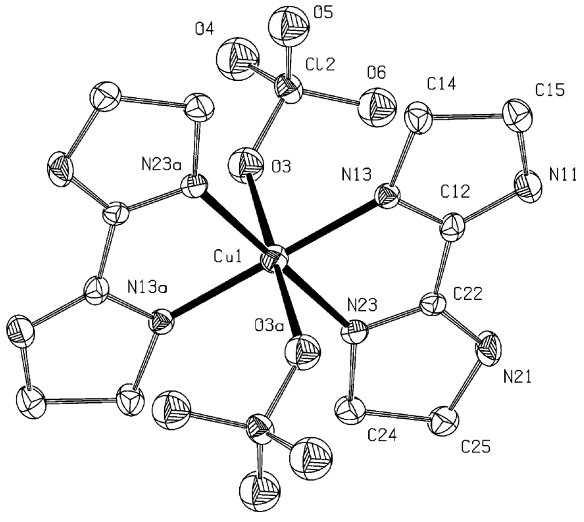

Fig. 2. Thermal ellipsoid plot at 50% probability of $[Cu(biz)_2(ClO_4)_2]$ (**1**) with atom-labelling scheme. Hydrogen atoms are omitted for clarity. Atoms marked with an "a" are generated by an inversion centre.

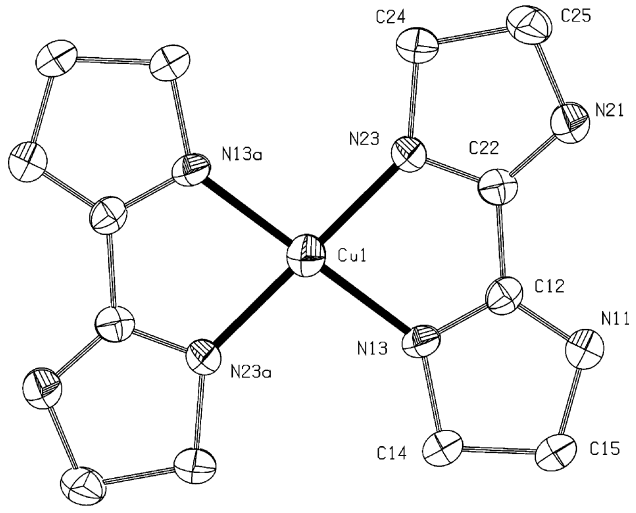

Fig. 3. Thermal ellipsoid plot at 50% probability of the cation in $[Cu(biz)_2](ClO_4)_2$ (**2**) with atom-labelling scheme. Hydrogen atoms and the uncoordinating perchlorate anions are omitted for clarity. Atoms marked with an "a" are generated by an inversion centre.

3.2. Electronic and infrared spectra

The diffuse reflectance spectra of the powdered solids are observed as broad bands at 16.3 and 17.5×10^3 cm^{-1}, for compound **1** and **2**, respectively. These band positions are to be considered as normal for a square-planar based CuN4 or $CuN_4(O_2)$ chromophore [14,15].

Table 2
Selected bond distances (Å), angles (°) and H-bond information for structures $[Cu(biz)_2(ClO_4)_2]$ (**1**) and $[Cu(biz)_2](ClO_4)_2$ (**2**)

	1	**2**		
Bond distances				
Cu1–N13	2.021(6)	1.982(4)		
Cu1–N23	1.977(7)	1.965(4)		
Cu1–O3	2.594(8)			
Bond angles				
N13–Cu1–N23	81.2(3)	81.56(16)		
N13–Cu1–N23a	98.8(3)	98.44(16)		
O3–Cu1–N13	92.6(3)			
O3–Cu1–N23	88.4(2)			
O3–Cu1–N13a	87.4(3)			
O3–Cu1–N23a	91.6(2)			
Hydrogen bond properties for structure **1**				
		D···A	Observed ν_{NH} (cm^{-1})	Calculated (Å) [18]
N(11)–H(11)···O(3) $[1+x,y,z]$[a]		2.982(11)		
N(11)–H(11)···O(4) $[1+x,y,z]$[a]		3.201(14)	3385	3.10
N(21)–H(21)···O(5) $[3/2-x,-1/2+y,1/2-z]$[a]		2.946(12)		
N(21)–H(21)···O(6) $[3/2-x,-1/2+y,1/2-z]$[a]		3.117(12)	3291	2.95
Hydrogen bond properties for structure **2**				
		D···A		
N(11)–H(11)···O(3)		2.938(6)		
N(21)–H(21)···O(3)		2.941(6)	3306	2.96

a: $1-x,1-y,1-z$ for **1** and $-x,-y,-z$ for **2**.
[a] Bifurcated hydrogen bonds.

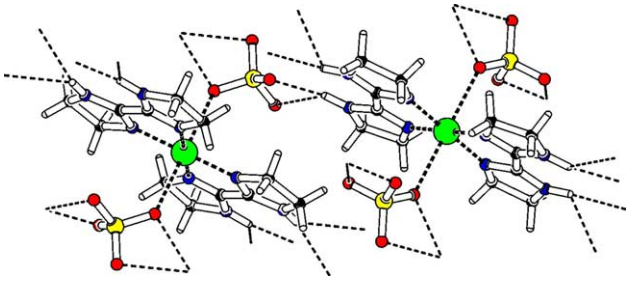

Fig. 4. Hydrogen bonds of compound **1**.

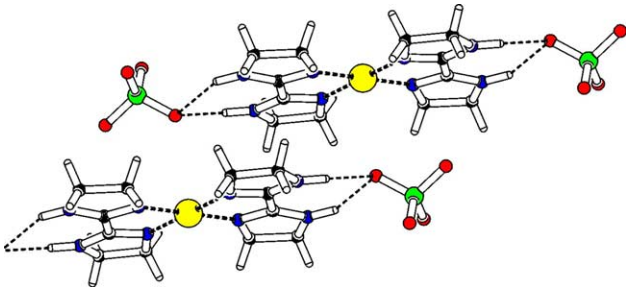

Fig. 5. Hydrogen bonds of compound **2**.

The IR spectra of compounds **1** and **2** are almost identical, except the area between 1000 and 1100 cm^{-1}, in which the strong anionic vibrations occur. These perchlorate vibrations are found around 1030 and 1066 cm^{-1} for compound **1** and around 1028 and 1091 cm^{-1} for compound **2**. Also a remarkable difference is seen in the region of the NH and OH vibrations, around 3300 cm^{-1}. Compound **1** has medium to strong peaks at 3385 and 3291 cm^{-1}, while compound **2** has only one strong broad vibration at 3306 cm^{-1}. This difference is due to the difference in the H-bonding properties (see Table 2). The two bands in compound **1** nicely agree with two different N···O contacts and calculations according to Bellamy and Owens [18] would have predicted N···O distances of 2.95 and 3.10 Å (assuming the free ligand having a NH vibration of 3450 cm^{-1} [18]). The one band at 3306 cm^{-1} for compound **2** agrees with the almost identical N···O contacts (calculated to be 2.96 Å). This is in close agreement with the observations made.

Another small difference is present in the region around 950 cm^{-1}, where medium strong CH_2 out-of-plane vibrations of the ligand occur [16]. Compound **1** has a medium strong doublet at 938 and 924 cm^{-1}, while compound **2** has a medium strong doublet shifted to 934 and 925 cm^{-1}.

3.3. EPR

X-band EPR spectra of polycrystalline powders were recorded at room temperature (RT) and in liquid nitrogen (77 K). Firstly, the difference in coordination geometry in the two Cu(II) compounds, **1** and **2**, is clearly demonstrated here. Compound **1** exhibits at RT a strong broad signal at $g_\perp$ at 2.07 with an unresolved $g_\parallel = 2.27$. At 77 K, $g_\parallel$ is more resolved and two hyperfine peaks are resolved with $A_\parallel = 18.2$ mT. Com-

pound **2**, however, gives only one strong isotropic signal at RT with $g = 2.07$, which sharpens up at 77 K, but no hyperfine is resolved. These values are in agreement with a $d_{x^2-y^2}$ ground state [14,15] and in good agreement with the square planar/octahedral topology of the CuN_4 or $CuN_4(O)_2$ chromophore [17].

In frozen solution (DMF/methanol 1:1) at 77 K, however, identical signals are obtained for both compounds. A resolved signal with $g_\perp = 2.04$, $g_\parallel = 2.24$ and $A_\parallel = 18.5$ mT. Even the superhyperfine splitting is observed with $A_{N\parallel} = 1.55$ mT. Also nine lines, though not clearly by overlap of the fourth band of the $A_\parallel$ signal, is in agreement with four nitrogen donors. So in solution both isomers must have the same geometry.

4. Concluding remarks

The research described in this paper has shown that the proper choice of the ligands, 2,2′-bi-imidazoline, can give interesting structural compounds, due to its steric properties. With Cu(II) perchlorate a blue and a violet compound could be synthesized using a different Cu:ligand ratio. These two compounds which are so-called distortion isomers, and differ in geometry by the (non) coordination of the perchlorate anion. These differences have also been observed in the IR and in the solid-state EPR. In frozen solution EPR (DMF/MeOH) the same signal is obtained and it has been concluded that in solution both isomers have the same geometry.

5. Supplementary material

Crystallographic data (excluding structure factors) for the structures in this paper have been deposited with the Cambridge Crystallographic Data Centre as Supplementary Publication Nos. CCDC-228514 and 228515, for compounds **1** and **2**, respectively.

Copies of the data can be obtained free of charge on application to CCDC, 12 Union Road, Cambridge CB2 1EZ, UK [Fax: (internat.) +44-1223-336-033, e-mail: deposit@ccdc.cam.ac.uk or www: http://www.ccdc.cam.ac.uk].

Acknowledgements

The work described in the present paper has been supported by the Leiden University Study group WFMO (Werkgroep Fundamenteel Materialen Onderzoek).

References

[1] J.P. Roth, S. Lovell, J.M. Mayer, J. Am. Chem. Soc. 122 (2000) 5486.
[2] J.C. Yoder, J.P. Roth, E.M. Gussenhoven, A.S. Larsen, J.M. Mayer, J. Am. Chem. Soc. 125 (2003) 2629.
[3] A. Mohamadou, G.A. van Albada, H. Kooijman, B. Wieczorek, A.L. Spek, J. Reedijk, New J. Chem. 27 (2003) 983.
[4] A. Mohamadou, G.A. van Albada, A. Mills, A.L. Spek, J. Reedijk, J. Chem. Cryst. 34 (2004) 233.
[5] G.A. van Albada, I. Mutikainen, U. Turpeinen, J. Reedijk, Polyhedron 23 (2003) 993.
[6] S. Youngme, N. Chaichit, N. Koonsang, Inorg. Chim. Acta 335 (2002) 36.
[7] R. Uggla, M. Melník, J. Valo, A. Pajunen, M.R. Sundberg, Acta Chem. Scand. 49 (1995) 585.
[8] M. Brophy, G. Murphy, C. O'Sullivan, B. Hathaway, B. Murphy, Polyhedron 18 (1999) 611.
[9] J.C. Wang, J.E. Bauman Jr., Inorg. Chem. 4 (1965) 1613.
[10] P.T. Beurskens, G. Admiraal, G. Beurskens, W.P. Bosman, S. Garcica-Granda, R.O. Gould, J.M.M. Smits, C. Smykalla, The DIRDIF Program System: Techmical Report of the Crystallography Laboratory, University of Nijmegen, Nijmegen, The Netherlands, 1992.
[11] C.J. Wilson, in: International Tables for X-ray Crystallography, vol. C, Kluwer Academic Publishers, Dordrecht, 1992.
[12] S.R. Hall, G.S.D. King, J.M. Steward, XTAL 3.4: Users Manual, University of Western Australia and Maryland, 1995.
[13] A.L. Spek, J . Appl. Crystallogr. 36 (2003) 7.
[14] B.J. Hathaway, in: G. Wilkinson, R.D. Gillard, J.A. McCleverty (Eds.), Comprehensive Coordination Chemistry, vol. 5, Pergamon Press, Oxford, 1987.
[15] A.B.P. Lever, Inorganic Electronic Spectroscopy, second ed., Elsevier, Amsterdam, 1984.
[16] J.B. Lambert, H.F. Shurvell, D. Lightner, R.G. Cooks, Organic Structural Spectroscopy, Prentice-Hall, Pavia, 1998.
[17] J.A. Weil, J.R. Bolton, E. Wertz, Electron Spin Resonance: Elementary Theory and Practical Applications, 2nd ed., Wiley, New York, 1994.
[18] L.J. Bellamy, A.J. Owens, Spectr. Chim. Acta A 25 (1969) 329.

Available online at www.sciencedirect.com
SCIENCE DIRECT®
Polyhedron 23 (2004) 1975–1980
POLYHEDRON
www.elsevier.com/locate/poly

Synthesis and characterization of vanadium(IV)–M (M = Mn, Zn) and vanadium(IV)–Ln (Ln = La, Nd) complexes with nitrilotriacetate ligands: $\{(NH_4)_2[(V^{IV}O)_2(\mu_2\text{-}O)(nta)_2M(H_2O)_4]\cdot 2H_2O\}_n$ and $NH_4[Ln(H_2O)_9][(V^{IV}O)_2(\mu_2\text{-}O)(nta)_2]$ ☆

Quanzheng Zhang, Canzhong Lu *, Wenbin Yang, Shumei Chen, Yaqin Yu, Xiang He, Ying Yan, Jiuhui Liu, Xinjiang Xu, Changkun Xia, Lijuan Chen, Xiaoyuan Wu

The State Key Laboratory of Structural Chemistry, Fujian Institute of Research on the Structure of Matter, Chinese Academy of Sciences, Fuzhou 350002, China

Received 10 March 2004; accepted 3 May 2004

Abstract

Four heterometal complexes, namely $\{(NH_4)_2[(V^{IV}O)_2(\mu_2\text{-}O)(nta)_2Mn(H_2O)_4]\cdot 2H_2O\}_n$ (**1**), $\{(NH_4)_2[(V^{IV}O)_2(\mu_2\text{–}O)(nta)_2Zn(H_2O)_4]\cdot 2H_2O\}_n$ (**2**), $NH_4[La(H_2O)_9][(V^{IV}O)_2(\mu_2\text{–}O)(nta)_2]$ (**3**) and $NH_4[Nd(H_2O)_9][(V^{IV}O)_2(\mu_2\text{–}O)(nta)_2]$ (**4**), where nta = nitrilotriacetate, have been prepared and characterized by single-crystal X-ray diffraction analyses. Complexes **1** and **2** exhibit heterometallic one-dimensional chain structures formed by polymeric $[(V^{IV}O)_2(\mu_2\text{-}O)(nta)_2M(H_2O)_4]^{2-}$ anions (M = Mn, Zn). Moreover, the one-dimensional chains are further linked together through hydrogen bonding into a three-dimensional framework. Compounds **3** and **4** display discrete units, however, these molecules are built up into three-dimensional structures through hydrogen bonding.
© 2004 Published by Elsevier Ltd.

Keywords: Vanadium complexes; Nitrilotriacetate; X-ray crystal structure; Hydrogen bonding

1. Introduction

Contemporary interest in the coordination chemistry of oxovanadium (IV), oxovanadium (V) and dioxovanadium (V) derives from their important biological and medicinal applications [1]. Recently, inorganic–organic hybrid materials based on vanadium oxides have attracted much attention. Therefore, the discovery of new vanadium oxide complexes especially possessing one-, two- or three-dimensional structures and the rational design of such solid materials remain an important and very active subject. In view of this point, some novel vanadium oxide complexes with polymeric structures have been prepared through the use of organically templated metal coordination subunits [2] or bridging organic ligands [3] as structural directors.

As one of the important derivatives of glycine, nitrilotriacetate (nta) can act as a potential bifunctional ligand with variable multi-dentate coordination modes. For instance, a series of nta complexes of transition metals have been isolated and structurally characterized [4]. Among these numerous studies on nta complexes, vanadium nitrilotriacetate (nta) complexes have been reported over the past decades, and some crystal structures have been described: $(NH_4)_3[V_2O_3(nta)_2]\cdot 3H_2O$ [5], $Na_3[VO(O_2)(nta)]\cdot 5H_2O$ [6], $[V(nta)(H_2O)_3]\cdot 4H_2O$ [7], $Na_3[V_2O_3(nta)_2]\cdot 5H_2O$ [8], $Ba[VO(O_2)(nta)]\cdot 3H_2O$ [9], $K_2[VO(O_2)(nta)]\cdot 2H_2O$ [10], $K_2[VO(O_2)(nta)]$ [11], $K_2[VO(O_2)(nta)]\cdot 2H_2O$ [12], $(NH_4)_2[VO_2(nta)]$ [13], $K_3[V_2O_3(nta)_2]\cdot 3H_2O$ [14]. In these vanadium nta complexes, each exhibits a discrete structure. Therefore, how to design and synthesize a polymeric structure of this type of vanadium nta complex will be an interesting

☆ Supplementary data associated with this article can be found, in the online version, at doi:10.1016/j.poly.2004.05.008.

* Corresponding author. Fax: +86-591-3714946.
E-mail address: czlu@ms.fjirsm.ac.cn (C. Lu).

0277-5387/$ - see front matter © 2004 Published by Elsevier Ltd.
doi:10.1016/j.poly.2004.05.008

work. In this paper, we present four heterometal complexes with nta ligands, $\{(NH_4)_2[(V^{IV}O)_2(\mu_2\text{-}O)(nta)_2\text{-}Mn(H_2O)_4]\cdot 2H_2O\}_n$ (**1**), $\{(NH_4)_2[(V^{IV}O)_2(\mu_2\text{-}O)(nta)_2\text{-}Zn(H_2O)_4]\cdot 2H_2O\}_n$ (**2**), $NH_4[La(H_2O)_9][(V^{IV}O)_2(\mu_2\text{-}O)\text{-}(nta)_2]$ (**3**) and $NH_4[Nd(H_2O)_9][(V^{IV}O)_2(\mu_2\text{-}O)(nta)_2]$ (**4**) (nta = nitrilotriacetate). In **1** and **2**, the binuclear vanadium $[(V^{IV}O)_2(\mu_2\text{-}O)(nta)_2]^{4-}$ anions are linked up by $[M(H_2O)_4]^{2+}$ (M = Mn, Zn) cations into heterometallic one-dimensional chain structures. The one-dimensional chains are further linked together through hydrogen bonds into a three-dimensional structure. Although compounds **3** and **4** exhibit discrete structures, the molecules are built up into three-dimensional structures through complex hydrogen bonding.

2. Experimental

2.1. Reagents and apparatus

All chemical used during the course of this work were of reagent grade and were used as received from a commercial source without further purification. Elemental analysis (C, H, N) was performed with a Vario EL *III* CHNOS Elemental Analyzer and the inductively coupled plasma (ICP) analysis was performed on a Perkin–Elmer optima 3300 DV ICP spectrometer. The IR spectra were recorded from KBr pellets in the range of 4000–400 cm^{-1} on a FTS-40 spectrophotometer. ESR spectra were recorded on a FD-ESR-I spectrometer in an aqueous solution.

2.2. Synthesis

2.2.1. $\{(NH_4)_2[(V^{IV}O)_2(\mu_2\text{-}O)(nta)_2Mn(H_2O)_4]\cdot 2H_2O\}_n$ (*1*)

A mixture of NH_4VO_3 (0.31 g, 2.65 mmol), H_3nta (1.20 g, 6.28 mmol), $Mn(CH_3COO)_2\cdot 4H_2O$ (0.33 g, 1.35 mmol) and H_2O (25 ml) was heated to boiling until NH_4VO_3 dissolved completely. The deep blue solution was allowed to stand at room temperature without any further disturbance for about three days to give deep blue crystals. *Anal.* Calc. for **1**: C, 19.86; H, 4.41; N, 7.72; Mn, 7.58; V, 14.05 (%). Found: C, 19.78; H, 4.36; N, 7.75; Mn, 7.39; V, 14.12 (%). IR (KBr pellet, cm^{-1}): 3498 (s), 3190 (s), 1614 (s), 1454 (m), 1398 (s), 1283 (w), 1124 (m), 1001 (m), 953 (s), 910 (s), 733 (s), 625 (s). Yield: ≈67%.

2.2.2. $\{(NH_4)_2[(V^{IV}O)_2(\mu_2\text{-}O)(nta)_2Zn(H_2O)_4]\cdot 2H_2O\}_n$ (*2*)

A mixture of NH_4VO_3 (0.28 g, 2.39 mmol), H_3nta (1.20 g, 6.28 mmol), $Zn(CH_3COO)_2\cdot 2H_2O$ (0.46 g, 2.09 mmol) and H_2O (25 ml) was heated to boiling until NH_4VO_3 dissolved completely. The deep blue solution was allowed to stand at room temperature without any further disturbance for about five days to give deep blue crystals. *Anal.* Calc. for **2**: C, 19.57; H, 4.35; N, 7.61; Zn, 8.89; V, 13.85 (%). Found: C, 19.51; H, 4.36; N, 7.52; Zn, 8.71; V, 13.23 (%). IR (KBr pellet, cm^{-1}): 3537 (s), 3383 (s), 1603 (s), 1460 (m), 1412 (m), 1385 (s), 1281 (w), 1126 (w), 958 (s), 912 (s), 746 (s), 629 (w). Yield: ≈73%.

Table 1
Crystal data and structure refinement parameters for the compounds

	1	**2**	**3**	**4**
Empirical formula	$C_{12}H_{32}MnN_4O_{21}V_2$	$C_{12}H_{32}ZnN_4O_{21}V_2$	$C_{12}H_{34}LaN_3O_{24}V_2$	$C_{12}H_{34}NdN_3O_{24}V_2$
Molecular weight	725.24	735.67	845.21	850.54
Crystal system	monoclinic	monoclinic	monoclinic	monoclinic
Space group	$P2_1/n$	$P2_1/n$	$C2/c$	$C2/c$
a (Å)	10.8755(9)	10.738(6)	23.6566(9)	23.494(3)
b (Å)	10.2993(8)	10.217(5)	11.0073(4)	10.9874(12)
c (Å)	11.2187(10)	11.070(6)	10.8987(3)	10.8731(12)
β (°)	99.190(2)	99.480(7)	92.975(2)	92.982(2)
V (Å^3)	1240.48(2)	1198.0(1)	2834.15(17)	2803.0(5)
Z	2	2	4	4
T (K)	293(2)	293(2)	293(2)	293(2)
D_C (g cm^{-3})	1.942	2.039	1.981	2.016
$F(000)$	742	752	1688	1700
μ (mm^{-1})	1.344	1.866	2.230	2.583
λ (Å)	0.71073	0.71073	0.71073	0.71073
Goodness-of-fit on F^2	1.133	1.065	1.097	1.108
Largest differential peak and hole (e Å^{-3})	0.567 and −0.583	0.706 and −0.791	1.269 and −1.307	1.640 and −1.822
Final R indices $[I > 2\sigma(I)]$[a]	$R_1 = 0.0732$, $wR_2 = 0.1626$	$R_1 = 0.0529$, $wR_2 = 0.1193$	$R_1 = 0.0429$, $wR_2 = 0.1070$	$R_1 = 0.0763$, $wR_2 = 0.1554$
R indices (all data)	$R_1 = 0.0988$, $wR_2 = 0.1827$	$R_1 = 0.0633$, $wR_2 = 0.1255$	$R_1 = 0.0475$, $wR_2 = 0.1121$	$R_1 = 0.1049$, $wR_2 = 0.1748$

[a] $R_1 = \sum(|F_o| - |F_c|)/\sum|F_o|$. $wR_2 = \left[\sum w(F_o^2 - F_c^2)^2 \Big/ \sum w(F_o^2)^2\right]^{0.5}$.

*2.2.3. $NH_4[La(H_2O)_9][(V^{IV}O)_2(\mu_2\text{-}O)(nta)_2]$ (**3**)*

A mixture of NH_4VO_3 (0.15 g, 1.28 mmol), H_3nta (1.36 g, 7.12 mmol), $LaCl_3$ (0.32 g, 1.30 mmol) and H_2O (25 ml) was heated to boiling until NH_4VO_3 dissolved completely. The deep blue solution was allowed to stand at room temperature without any further disturbance for about five days to give deep blue crystals. *Anal.* Calc. for **3**: C, 17.03; H, 4.02; N, 4.97 (%). Found: C, 16.89; H, 3.96; N, 4.78 (%). IR (KBr pellet, cm^{-1}): 3379 (s), 1614 (s), 1406 (s), 1375 (s), 1275 (m), 1219 (m), 1126 (m), 1007 (w), 957 (s), 916 (s), 737 (s), 627 (w). Yield: ≈62%.

*2.2.4. $NH_4[Nd(H_2O)_9][(V^{IV}O)_2(\mu_2\text{-}O)(nta)_2]$ (**4**)*

A mixture of NH_4VO_3 (0.18 g, 1.53 mmol), H_3nta (1.25 g, 6.54 mmol), $NdCl_3$ (0.36 g, 1.44 mmol) and H_2O (25 ml) was heated to boiling until NH_4VO_3 dissolved

Table 2
Selected bond lengths (Å) and angles (°) for the compounds

1					
Bond lengths					
Mn(1)–O(9)	2.128(5)	V(1)–O(7)	1.601(5)	V(1)–O(5)	1.984(6)
Mn(1)–O(6)	2.166(5)	V(1)–O(8)	1.8164(1)	V(1)–O(1)	2.052(5)
Mn(1)–O(10)	2.183(5)	V(1)–O(3)	1.977(5)	V(1)–N(1)	2.294(5)
Bond angles					
O(9)–Mn(1)–O(6)	90.6(3)	O(7)–V(1)–O(5)	104.4(3)	O(5)–V(1)–O(1)	84.7(2)
O(9)–Mn(1)–O(10)	89.5(2)	O(8)–V(1)–O(5)	91.21(2)	O(7)–V(1)–N(1)	168.9(2)
O(6)–Mn(1)–O(10)	91.7(2)	O(3)–V(1)–O(5)	153.0(2)	O(8)–V(1)–N(1)	87.18(1)
O(7)–V(1)–O(8)	103.8(2)	O(7)–V(1)–O(1)	92.5(2)	O(3)–V(1)–N(1)	76.5(2)
O(7)–V(1)–O(3)	101.8(3)	O(8)–V(1)–O(1)	163.65(2)	O(5)–V(1)–N(1)	76.5(2)
O(8)–V(1)–O(3)	88.58(2)	O(3)–V(1)–O(1)	88.0(2)	O(1)–V(1)–N(1)	76.47(2)
2					
Bond lengths					
Zn(1)–O(9)	2.034(4)	V(1)–O(7)	1.613(4)	V(1)–O(3)	1.984(4)
Zn(1)–O(10)	2.087(3)	V(1)–O(8)	1.8220(11)	V(1)–O(1)	2.047(4)
Zn(1)–O(6)	2.109(4)	V(1)–O(5)	1.978(4)	V(1)–N(1)	2.280(4)
Bond angles					
O(9)–Zn(1)–O(10)	91.10(15)	O(7)–V(1)–O(3)	101.3(2)	O(3)–V(1)–O(1)	87.60(15)
O(9)–Zn(1)–O(6)	90.2(2)	O(8)–V(1)–O(3)	88.23(12)	O(7)–V(1)–N(1)	169.83(17)
O(6)–Zn(1)–O(10)	90.53(15)	O(5)–V(1)–O(3)	154.16(16)	O(8)–V(1)–N(1)	86.26(11)
O(7)–V(1)–O(8)	103.79(14)	O(7)–V(1)–O(1)	93.33(17)	O(5)–V(1)–N(1)	77.11(15)
O(7)–V(1)–O(5)	103.9(2)	O(8)–V(1)–O(1)	162.86(10)	O(3)–V(1)–N(1)	77.08(15)
O(8)–V(1)–O(5)	91.19(11)	O(5)–V(1)–O(1)	85.40(15)	O(1)–V(1)–N(1)	76. 61(14)
3					
Bond lengths					
V(1)–O(7)	1.607(4)	V(1)–O(3)	2.061(4)	La(1)–O(13)	2.535(4)
V(1)–O(8)	1.8045(9)	V(1)–N(1)	2.297(5)	La(1)–O(12)	2.598(4)
V(1)–O(1)	1.992(4)	La(1)–O(10)	2.526(4)	La(1)–O(9)	2.602(4)
V(1)–O(5)	2.015(4)	La(1)–O(11)	2.532(6)		
Bond angles					
O(7)–V(1)–O(8)	103.67(14)	O(1)–V(1)–O(5)	151.87(2)	O(7)–V(1)–N(1)	167.75(2)
O(7)–V(1)–O(1)	103.88(19)	O(7)–V(1)–O(3)	91.75(2)	O(8)–V(1)–N(1)	88.57(1)
O(8)–V(1)–O(1)	89.74(12)	O(8)–V(1)–O(3)	164.29(1)	O(1)–V(1)–N(1)	75.40(2)
O(7)–V(1)–O(5)	103.41(19)	O(1)–V(1)–O(3)	89.43(2)	O(5)–V(1)–N(1)	76.48(2)
O(8)–V(1)–O(5)	90.36(12)	O(5)–V(1)–O(3)	83.05(2)	O(3)–V(1)–N(1)	76.04(2)
4					
Bond lengths					
V(1)–O(7)	1.606(9)	V(1)–O(3)	2.071(8)	Nd(1)–O(13)	2.488(8)
V(1)–O(8)	1.8017(19)	V(1)–N(1)	2.298(10)	Nd(1)–O(12)	2.548(9)
V(1)–O(1)	1.991(9)	Nd(1)–O(10)	2.475(8)	Nd(1)–O(9)	2.556(9)
V(1)–O(5)	2.006(8)	Nd(1)–O(11)	2.485(11)		
Bond angles					
O(7)–V(1)–O(8)	104.1(3)	O(1)–V(1)–O(5)	152.2(4)	O(7)–V(1)–N(1)	167.5(4)
O(7)–V(1)–O(1)	103.9(4)	O(7)–V(1)–O(3)	91.3(4)	O(8)–V(1)–N(1)	88.4(3)
O(8)–V(1)–O(1)	89.8(3)	O(8)–V(1)–O(3)	164.5(3)	O(1)–V(1)–N(1)	75.2(4)
O(7)–V(1)–O(5)	102.9(4)	O(1)–V(1)–O(3)	88.9(4)	O(5)–V(1)–N(1)	77.1(3)
O(8)–V(1)–O(5)	91.0(3)	O(5)–V(1)–O(3)	83.0(4)	O(3)–V(1)–N(1)	76.3(3)

completely. The deep blue solution was allowed to stand at room temperature without any further disturbance for about six days to give deep blue crystals. *Anal.* Calc. for **4**: C, 16.93; H, 3.99; N, 4.93 (%). Found: C, 16.86; H, 3.58; N, 4.71 (%). IR (KBr pellet, cm^{-1}): 3381 (s), 1612 (s), 1406 (s), 1375 (s), 1275 (m), 1219 (m), 1128 (m), 1007 (w), 957 (s), 916 (s), 739 (s), 629 (w). Yield: ≈68%.

2.3. Crystallography

Crystals with dimensions $0.08 \times 0.12 \times 0.21$ mm for **1**, $0.06 \times 0.10 \times 0.16$ mm for **2**, $0.11 \times 0.25 \times 0.31$ mm for **3** and $0.11 \times 0.19 \times 0.27$ mm for **4** were selected for indexing and intensity data collections at 293 K on a Siemens SMART CCD diffractometer with graphite monochromated Mo Kα radiation ($\lambda = 0.71073$ Å) at room temperature. The structures were solved by direct methods, successive Fourier difference synthesis and refined by full matrix least-squares based on F^2 using the SHELXTL-97 program package. In all cases, all non-hydrogen atoms were refined anistropically. All the hydrogen atoms based on C atoms were generated theoretically, while other hydrogen atoms were not located. The crystallographic data for **1**, **2**, **3** and **4** are listed in Table 1. Selected bond lengths and angles are given in Table 2.

3. Results and discussion

Complexes **1** and **2** are isostructural compounds. Each consists of one heterometal $[(V^{IV}O)_2(\mu_2\text{-}O)(nta)_2M(H_2O)_4]^{2-}$ anion, two ammonium cations and two free water molecules. A locally expanded unit for complex **1** is shown in Fig. 1. The heterometal $[(V^{IV}O)_2\text{-}(\mu_2\text{-}O)(nta)_2M(H_2O)_4]^{2-}$ anion is formed by the connection of a binuclear vanadium $[(V^{IV}O)_2(\mu_2\text{-}O)(nta)_2]^{4-}$ anion and a metal $[M(H_2O)_4]^{2+}$ (M = Mn, Zn) cation. As described before [5,8,14], the binuclear $[(V^{IV}O)_2(\mu_2\text{-}O)(nta)_2]^{4-}$ anion can be considered as two similar mononuclear $[(V^{IV}O)(nta)]^{-}$ anions connected together by one μ_2-O atom (O8). The two $[(V^{IV}O)(nta)]$ units are centrosymmetric via the O8 atom which is located on the special position (1/2, 0, 1/2). Each vanadium atom in the mononuclear unit is in an octahedral coordination environment. The distorted octahedron is defined by one vanadyl oxygen atom (O7), one bridging oxygen atom (O8), three carboxyl oxygen atoms (O1, O3 and O5) and one nitrogen atom. The V–O distances of **1** can be divided into three groups: (a) The V=O bond length is 1.601(5) Å, which is in the normal range of 1.56–1.63 Å for the V^{IV}=O bond length [15]; (b) The V–O μ_2 bond length is 1.8164(1) Å, showing partial multiple bond character; (c) The V–O_{nta} bond distances are 1.977(5), 1.984(6) and 2.052(5) Å. The V–N distance is 2.294(5) Å, which is slight longer than that in other analogous nta complexes, but is shorter than that in vanadium EDTA complexes [16].

In compound **1**, the tetradentate nta ligand forms three glycinate rings with the V atom. The N–V–O bond angles are 76.46(2)°, 76.5(2)° and 76.5(2)°. The N–C and C–C distances are as expected. It is worthwhile to point out that there exists one carboxyl oxygen atom (O6) coordinated to the Mn atom. Thus, the C–O bond lengths can be divided into three groups: (a) C–O_V 1.283(8), 1.279(11) and 1.261(10) Å; (b) C–O_{Mn} 1.250(9) Å; (c) C–O_{unco} 1.235(8) and 1.231(10) Å. As a bridging metal, the Mn atom is coordinated by four water molecules and two bridging O atoms. A regular octahedral MnO_6 is formed with the corresponding Mn–O6, Mn–O9 and Mn–O10 distances of 2.166(5), 2.128(5) and 2.183(5) Å, respectively.

As shown in Fig. 2, the most interesting feature of **1** is its novel one-dimensional chain structure, which is formed by the binuclear $[(V^{IV}O)_2(\mu_2\text{-}O)(nta)_2]^{4-}$ ions and the bridging metal $[Mn(H_2O)_4]^{2+}$ ions. The free ammonium ions and water molecules are hydrogen bonded to the carboxylate O atoms of the neighboring nta ligands with corresponding N···O contacts of 2.795 Å and O···O contacts in the range of 2.750–3.198 Å. Thus, the one-dimensional chains are further bound together through the hydrogen bonding into a three-dimensional network (Fig. 3).

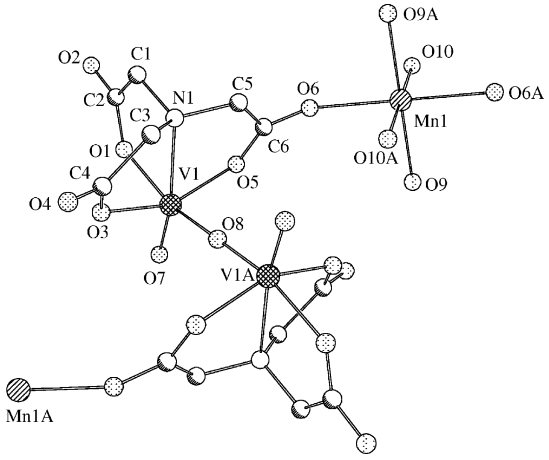

Fig. 1. The locally expanded unit of **1**, showing the structure of the heterometal $[(V^{IV}O)_2(\mu_2\text{-}O)(nta)_2M(H_2O)_4]^{2-}$ anion.

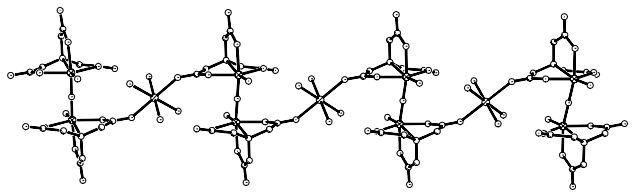

Fig. 2. The one-dimensional chain of **1** formed by the polymeric $[(V^{IV}O)_2(\mu_2\text{-}O)(nta)_2M(H_2O)_4]^{2-}$ anion (viewed along the *a*-axis).

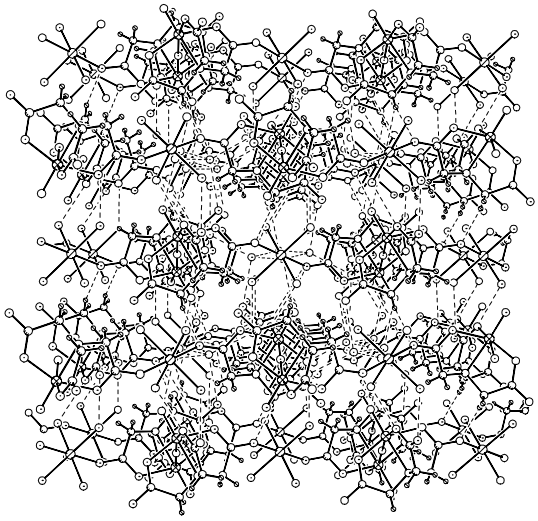

Fig. 3. Packing framework of **1** viewed along the *c*-axis. All hydrogen atoms are omitted for clarity.

As shown in Fig. 4, compound **3** contains one binuclear $[(V^{IV}O)_2(\mu_2\text{-}O)(nta)_2]^{4-}$ anion unit, one $[La(H_2O)_9]^{3+}$ cation and one ammonium ion. The binuclear $[(V^{IV}O)_2(\mu_2\text{-}O)(nta)_2]^{4-}$ anion unit of **3** displays a similar structure to that of **1**, which is formed by the means of the connection of one bridging oxygen atom (μ_2-O) and two mononuclear $[(V^{IV}O)(nta)]^-$ anions. In the binuclear vanadium anion of **3**, the V=O, V–Oμ_2, and V–O_{nta} (average) bond lengths are 1.607(4), 1.8045(9) and 2.0226 (4) Å, respectively. The V–N distance is 2.297(5) Å, which is comparable to that of compound **1** (2.294(5) Å). The La ion is coordinated by nine water molecules with La–O distances in the range of 2.526(4)–2.602(4) Å.

A remarkable feature of compound **3** is that there exists hydrogen bonding between the coordinated water molecules and the binuclear vanadium units. The coordinated water molecules not only link up the adjacent binuclear vanadium clusters into a two-dimensional layer, but they also connect the two-dimensional layers

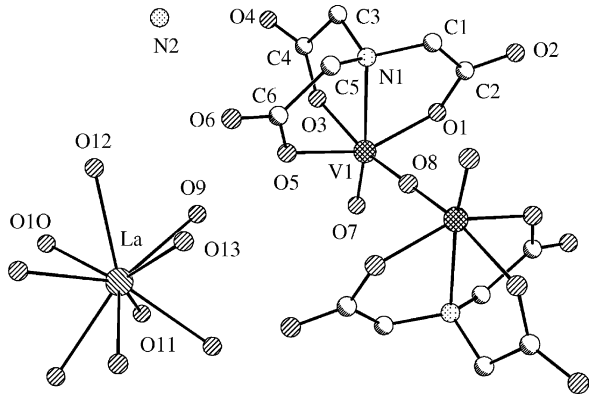

Fig. 4. The molecule structure of **3**.

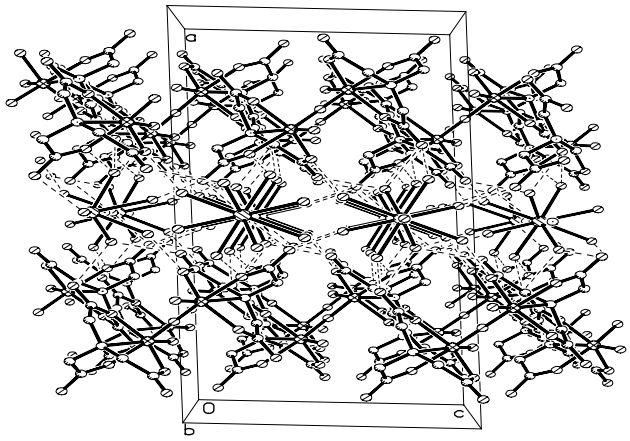

Fig. 5. Packing framework of **3**. All hydrogen atoms are omitted for clarity.

into a three-dimensional framework through hydrogen bonding (Fig. 5). The distances between the coordinated water molecules and the oxygen atoms of binuclear vanadium units are in the 2.701–3.159 Å range. However, no hydrogen bonding is involved between the ammonium cations and the binuclear vanadium units.

The structure of the Nd derivative $NH_4[Nd(H_2O)_9][(V^{IV}O)_2(\mu_2\text{-}O)(nta)_2]$ (**4**) is isomorphous with **3**. As shown in Table 2, among the metrical parameters for structures the Nd–O distances are in the range of 2.475(8)–2.556(9) Å, showing the predicted changing trend compared with the La–O counterparts. In addition, the distances involving the hydrogen bonding between the coordination water molecules and the oxygen atoms of the binuclear vanadium units are in the 2.697–3.139 Å range.

The IR spectra show that the ν(C–N) of the compounds are in the 1124–1128 cm^{-1} range (free H_3nta is at 1200 cm^{-1}), indicating the N atoms of nta ligands coordinate to V atoms. The ν_{as}(COOH) at 1725 cm^{-1} of H_3nta now red-shifts to the 1603–1614 cm^{-1} range, and the ν_s(COO) at 1340 cm^{-1} of H_3nta blue-shifts to the 1375–1398 cm^{-1} range, which confirm that the O atoms of the COO^- groups coordinate to the V atoms. Moreover, in **1** and **2**, the relative positions of the ν_{as}(COO) and ν_s(COO), $\Delta = \nu_{as}(COO) - \nu_s(COO)$, are 216 and 218 cm^{-1}, while in **3** and **4**, the relative positions (Δ) are 239 and 237 cm^{-1}, respectively. This fact indicates that there exist different coordination modes of the carboxylate groups in **1**, **2** (containing bidentate bridging) and **3**, **4** (monodentate). The bands in the 958–625 cm^{-1} range for all the compounds are attributed to the ν(V=O) and ν(V–O–V) vibrations. The EPR spectrum of **3** has been performed at room temperature, providing eight hyperfine peaks with g_o and A_o values of 1.985 and 112.62 G, respectively. The observed g tensor value is expected for oxo-vanadium (IV) ions, and eight $(2nI + 1)$ peaks are should be attributed to the coupling

of the unpaired electron ($n = 1$) with the nuclear spin ($I = 7/2$). In view of this point, we can deduce that the oxidation state of each vanadium atom in the other three compounds is in a reduced oxidation state (V^{IV}). This is also in agreement with the charge balance. Actually, all the complexes are synthesized in low pH solutions (pH < 1). When the pH values of the reaction solution are raised to above 1, the complexes cannot be obtained. Therefore it is easy to understand that the VO^{2+} ion is from the redox of the VO_3^- ion and nitrilotriacetic acid in the low pH value solution.

To date, some vanadium nitrilotriacetate complexes have been reported [5–14], however, each exhibits a discrete structure. In the reported vanadium nta complexes with alkali or alkaline-earth metal ions [6,8–12,14], the alkali or alkaline-earth metal ions only act as counter ions to balance the negative charges of the molecules. In compound **1**, the transition metal ion takes part in coordination as a bridge, playing an important role in the formation of this kind of polymeric structure. Compound **3** is synthesized in a similar aqueous solution to that of **1**, but displays a different structure feature. This might be attributed to the different influence of electronic structures of the lanthanide and transition metal on the formation of this type of complex.

4. Supplementary material

Crystallographic data for the structure reported in this paper have been deposited with the Cambridge Crystallographic Data Center as Supplementary Publication No. CCDC-233302 for **1**, CCDC-233303 for **2**, CCDC-233304 for **3** and CCDC-233305 for **4**. Copies of the data can be obtained free of charge on application to CCDC, 12 Union Road, Cambridge CB2 1EZ, UK (fax; (+44) 1223-336-033; e-mail: deposit@ccdc.cam.ac.uk or www: http://www.ccdc.cam.ac.uk).

Acknowledgements

This work was supported by the 973 program of the MOST (001CB108906), the National Natural Science Foundation of China (90206040, 20333070 and 20303021), the Natural Science Foundation of Fujian Province (20002F015 and 2002J006) and the Chinese Academy of Sciences.

References

[1] (a) K.H. Thompson, J.H. McNeill, C. Orvig, Chem. Rev. 99 (1999) 2561;
(b) D. Rehder, J. Costa Pessoa, C.F.G.C. Geraldes, M.M.C.A.M. Rangel, A. Salifoglou, I. Turel, Dongren Wang, J. Biol. Inorg. Chem. 7 (2002) 384;
(c) D. Rehder, Inorg. Chem. Commun. 6 (2003) 604.
[2] (a) X.B. Cui, Z.E. Lin, G.Y. Yang, Solid State Sci. 5 (2003) 311;
(b) Z.M. Dai, X.B. Chen, Z. Shi, D. Zhang, G.H. Li, S.H. Feng, Inorg. Chem. 42 (2003) 908;
(c) G.H. Li, Z. Shi, Y.H. Xu, S.H. Feng, Inorg. Chem. 42 (2003) 1170.
[3] (a) R.G. Xiong, Y.R. Xie, X.Z. You, C.M. Che, J. Chem. Soc., Dalton Trans. (2001) 777;
(b) X.M. Zhang, M.L. Tong, H.K. Zee, X.M. Chen, J. Solid State Chem. 160 (2001) 118;
(c) K. Barthelet, D. Riou, M. Nogues, G. Ferey, Inorg. Chem. 42 (2003) 1739;
(d) M. Yuan, E.B. Wang, Y. Lu, S.T. Wang, Y.G. Li, L. Wang, C.W. Hu, Inorg. Chim. Acta 344 (2003) 257.
[4] (a) S.L. Heath, A.K. Powell, H.L. Utting, M. Helliwell, J. Chem. Soc., Dalton Trans. (1992) 305;
(b) I. Malfant, I. Morgenstern-Badarau, M. Philoche-Levisalles, F. Lioret, J. Chem. Soc., Chem. Commun. (1990) 1338;
(c) H.G. Visser, W. Purcell, S.S. Basson, Q. Claassen, Polyhedron 16 (1997) 2851;
(d) H.G. Visser, W. Purcell, S.S. Basson, Polyhedron 20 (2001) 185;
(e) Yugen Zhang, Jianmin Li, M. Nishiura, T. Imamoto, Chem. Lett. (1999) 543;
(f) Q.D. Liu, J.R. Li, S. Gao, B.Q. Ma, Q.Z. Zhou, K.B. Yu, H. Liu, Chem. Commun. (2000) 1685;
(g) I.N. Polyakova, A.L. Poznyak, V.S. Sergienko, Z. Neorg. Khim. 45 (2000) 1649;
(h) H.G. Visser, W. Purcell, S.S. Basson, Polyhedron 18 (1999) 2795.
[5] M. Nishizawa, K. Hirotsu, S. Ooi, K. Saito, J. Chem. Soc., Chem. Commun. (1979) 707.
[6] D.X. Wu, X.J. Lei, R. Cao, M.C. Hong, Chin. J. Struct. Chem. 11 (1992) 65.
[7] K. Okamoto, J. Hidaka, M. Fukagawa, K. Kanamori, Acta Crystallogr. C 48 (1992) 1025.
[8] D.X. Wu, X.J. Lei, R. Rong, M.C. Hong, Chin. J. Struct. Chem. 12 (1993) 79.
[9] L. Kuchta, M. Sivák, F. Pavelčík, J. Chem. Res. 393 (1993) 2801.
[10] A.E. Lapshin, Y.I. Smolin, Y.F. Shepelev, M. Sivák, D. Gyepesová, Acta Crystallogr. C 49 (1993) 867.
[11] Y.G. Wei, S.W. Zhang, G.Q. Huang, M.C. Shao, Polyhedron 13 (1994) 1587.
[12] C. Djordjevic, P.L. Wilkins, E. Sinn, R.J. Butcher, Inorg. Chim. Acta 230 (1995) 241.
[13] Man-Ho Lee, Nam Ho Heo, Bull. Korean Chem. Soc. 18 (1997) 544.
[14] J.M. Shi, J.Q. Xu, W.T. Yu, L.D. Liu, C.J. Wu, Pol. J. Chem. 75 (2001) 1695.
[15] A. Kahn, J. Livage, R. Collongues, Phys. Status Solidi (A) 26 (1974) 175.
[16] W.R. Scheidt, R. Countryman, J.L. Hoard, J. Am. Chem. Soc. 93 (1971) 3878.

Available online at www.sciencedirect.com
SCIENCE DIRECT®
Polyhedron 23 (2004) 1981–1986
POLYHEDRON
www.elsevier.com/locate/poly

Syntheses, characterizations and crystal structures of new triorgano-tin or -germanium complexes with 1H-5-mercapto-1,2,3-triazolato

Chunlin Ma [a,b,*], Junhong Zhang [a], Rufen Zhang [a]

[a] Department of Chemistry, Liaocheng University, 34 Wenhua Road, Liaocheng 252059, China
[b] Department of Chemistry, Taishan University, Taian 271021, China

Received 15 March 2004; accepted 4 May 2004

Abstract

A series of triorganotin and triorganogermanium(IV) complexes with 1H-5-mercapto-1,2,3-triazolato, of the type $R_3MSC_2H_2N_3$ (M = Sn, R = CH_3, (**1**); C_2H_5, (**2**); *n*-C_4H_9, (**3**); C_6H_5, (**4**); M = Ge, R = CH_3, (**5**); C_2H_5, (**6**); *n*-C_4H_9, (**7**); C_6H_5, (**8**)), have been synthesized. All the complexes **1**–**8** have been characterized by elemental, IR and ^{1}H NMR analyses. Among them complexes **4** and **8** have also been characterized by X-ray crystallography diffraction analyses, which revealed that the Sn and Ge atom environments are distorted tetrahedral coordination polyhedrons, coordinated to three phenyl groups and to one sulfur atom of the ligand. The packing of complexes **4** and **8** is stabilized into a one-dimensional infinite chain by intermolecular N–H···N hydrogen bonds.
© 2004 Elsevier Ltd. All rights reserved.

Keywords: 1H-5-mercapto-1,2,3-triazolato; Organotin; Organogermanium(IV); Crystal structure; X-ray crystallography

1. Introduction

Metal thiolato complexes have been extensively studied because of their ability to adopt various nuclearities and their relevance in biology, since they form the inorganic part of the biologically active centers of some metalloproteins and enzymes [1–3]. Recently, attention has been paid to the coordination chemistry of heterocyclic thiol/thione donors, which can give potential access to new compounds with unusual structures and reactivities [4]. For example, triazyl- and tetrazole-thiol organometallic derivatives have been reported. A related class of such compounds is thiosemicarbazones in which the structure unit HS–C–N–N or S=C–N–N can bond to metal ions through S or N or both atoms [5–8].

As a result of our continuing interest in the coordination of main group metals with polydentate S, N ligands [9–11], here we report the studies on the syntheses of a series of organotin and organogermanium complexes $R_3MSC_2H_2N_3$ (M = Sn, R = CH_3, (**1**); C_2H_5, (**2**); *n*-C_4H_9, (**3**); C_6H_5, 4; M = Ge, R = CH_3, (**5**); C_2H_5, (**6**); C_4H_9, (**7**); C_6H_5, (**8**)) and their characterization by elemental, IR and ^{1}H NMR analyses. X-ray crystallography analyses of the complexes **4** and **8** have also been given in the present paper.

2. Experimental

2.1. Materials and measurements

All reagents and the sodium salt of the ligand (1H-5-mercapto-1,2,3-triazole) were purchased commercially and used without further purification unless otherwise noted. The melting points were obtained with a Kofler micro-melting point apparatus and were uncorrected. Infrared-spectra were recorded on a Nicolet-460 spectrophotometer using KBr discs and sodium chloride optics. ^{1}H NMR spectra were recorded on a JEOL-FX-90Q spectrometer using TMS as internal standard and

* Corresponding author. Tel.: +86-635-8238121; fax: +86-635-8238274/86-538-671-5521.
E-mail address: macl@lctu.edu.cn (C. Ma).

0277-5387/$ - see front matter © 2004 Elsevier Ltd. All rights reserved.
doi:10.1016/j.poly.2004.05.005

$CDCl_3$ as solvent. The chemical shifts are reported in ppm. Elemental analyses were performed with a PE-2400II apparatus.

2.2. Syntheses of the complexes **1–8**

2.2.1. $(CH_3)_3Sn(SC_2H_2N_3)$ (**1**)

The reaction was carried out under nitrogen atmosphere. The sodium salt of 1H-5-mercapto-1,2,3-triazole (0.123 g, 1 mmol) and trimethyltin chloride (0.199 g, 1 mmol) were added to a solution of absolute benzene (20 ml) in a Schlenk flask, stirred for 12 h at 40 °C and then filtered. The filtered solution was gradually reduced by evaporation under vacuum until a solid product was obtained. The solid was then recrystallized from ether. The white crystal complex **1** was formed. Yield, 89%. M.p.: 121–123 °C. *Anal*. Calc. for $C_5H_{11}N_3SSn$: C, 22.76; H, 4.20; N, 15.93. Found: C, 22.72; H, 4.18; N, 15.96%. IR (KBr, cm^{-1}): 3251 (br, N–H), 3052 (w, C–H), 1605 (m, C=C), 1596 (C–N), 1442 (m, N=N), 1156, 1078 (m, C–S), 560, 535 (m, Sn–C), 319 (m, Sn–S). ^1H NMR ($CDCl_3$): δ 10.9 (br, 1H, N-H), 1.53 (m, 9H, CH_3), 7.30 (s, 1H, =CH).

2.2.2. $(C_2H_5)_3Sn(SC_2H_2N_3)$ (**2**)

The synthesis procedure was the same as in Section 2.2.1, using the sodium salt of 1H-5-mercapto-1,2,3-triazole (0.123 g, 1 mmol), triethyltin chloride (0.241 g, 1 mmol) and benzene (20 ml). The colorless crystal complex **2** was obtained from *n*-hexane. Yield: 82%. M.p.: 124–126 °C. *Anal*. Calc. for $C_8H_{17}N_3SSn$: C, 31.41; H, 5.60; N, 13.74. Found: C, 31.38; H, 5.46; N, 13.79%. IR (KBr, cm^{-1}): 3250 (br, N–H), 3050 (w, C–H), 1605 (m, C=C), 1595 (C–N), 1443 (m, N=N), 1152, 1076 (m, C–S), 561, 524 (m, Sn–C), 317 (m, Sn–S). ^1H NMR ($CDCl_3$): δ 10.5 (br, 1H, N–H), 1.76 (q, 6H, $-CH_2$), 0.88 (t, 9H, CH_3), 7.28 (s, 1H, =CH).

2.2.3. $(n\text{-}C_4H_9)_3Sn(SC_2H_2N_3)$ (**3**)

The synthesis procedure was the same as in Section 2.2.1, using the sodium salt of 1H-5-mercapto-1,2,3-triazole (0.123 g, 1 mmol), tributyltin chloride (0.325 g, 1 mmol) and benzene (20 ml). The colourless crystal complex **3** was obtained from benzene. Yield: 80%. M.p.: 58–60 °C. *Anal*. Calc. for $C_{14}H_{29}N_3SSn$: C, 43.11; H, 7.50; N, 10.78. Found: C, 43.14; H, 7.53; N, 10.76%. IR (KBr, cm^{-1}): 3249 (br, N–H), 3050 (w, C–H), 1605 (m, C=C), 1595 (C–N), 1443 (m, N=N), 1152, 1076 (m, C–S), 565, 540 (m, Sn–C), 316 (m, Sn–S). ^1H NMR ($CDCl_3$): δ 10.6 (br, 1H, N–H), 1.79 (t, 6H, $-CH_2$), 1.13–1.50 (m, 12H, CH_2), 0.86 (t, 9H, CH_3), 7.28 (s, 1H, =CH).

2.2.4. $Ph_3Sn(SC_2H_2N_3)$ (**4**)

The synthesis procedure was the same as in Section 2.2.1, using the sodium salt of 1H-5-mercapto-1,2,3-triazole (0.123 g, 1 mmol), triphenyltin chloride (0.385 g, 1 mmol) and benzene (30 ml). The yellow crystal complex **4** was obtained from hexane–dichloromethane. Yield, 89%. M.p.: 128–130 °C. *Anal*. Calc. for $C_{20}H_{17}N_3SSn$: C, 53.37; H, 3.81; N, 9.33; S, 7.12. Found: C, 53.24; H, 3.76; N, 9.28; S, 6.97%. IR (KBr, cm^{-1}): 3250 (br, N–H), 3050 (w, C–H), 1605 (m, C=C), 1595 (C–N), 1443 (m, N=N), 1152, 1076 (m, C–S), 561, 533 (m, Sn–C), 317 (m, Sn–S). ^1H NMR ($CDCl_3$): δ 11.0 (br, 1H, N–H), 7.31–7.96 (m, 15H, Ph–H), 7.28 (s, 1H, =CH).

2.2.5. $(CH_3)_3Ge(SC_2H_2N_3)$ (**5**)

The synthesis procedure was the same as in Section 2.2.1, using the sodium salt of 1H-5-mercapto-1,2,3-triazole (0.123 g, 1 mmol), trimethylgermanium chloride (0.153 g, 1 mmol) and benzene (20 ml). The yellow crystal complex **5** was obtained from hexane–dichloromethane. Yield, 78%. M.p.: 120–122 °C. *Anal*. Calc. for $C_5H_{11}N_3SGe$: C, 27.57; H, 5.02; N, 19.29. Found: C, 27.40; H, 5.06; N, 19.05%. IR (KBr, cm^{-1}): 3251 (br, N–H), 3120 (w, C–H), 1608 (m, C=C), 1595 (C–N), 1445 (m, N=N), 1160, 1073 (m, C–S), 587, 505 (m, Ge–C), 455 (m, Ge–S). ^1H NMR ($CDCl_3$): δ 10.8 (br, 1H, N–H), 1.71 (s, 9H, Ge–CH_3), 7.29 (s, 1H, =CH).

2.2.6. $(C_2H_5)_3Ge(SC_2H_2N_3)$ (**6**)

The synthesis procedure was the same as in Section 2.2.1, using the sodium salt of 1H-5-mercapto-1,2,3-triazole (0.123 g, 1 mmol), triethylgermanium chloride (0.195 g, 1 mmol) and benzene (20 ml). The yellow crystal complex **6** was obtained from hexane–dichloromethane. Yield, 79%. M.p.: 119–121 °C. *Anal*. Calc. for $C_8H_{17}N_3SGe$: C, 36.97; H, 6.60; N, 16.17. Found: C, 36.94; H, 6.57; N, 16.19%. IR (KBr, cm^{-1}): 3252 (br, N–H), 3121 (w, C–H), 1608 (m, C=C), 1596 (C–N), 1443 (m, N=N), 1161, 1073 (m, C–S), 579, 516 (s, Ge–C), 457 (m, Ge–S). ^1H NMR (90 MHz, $CDCl_3$): δ 10.8 (br, 1H, N–H), 1.76 (q, 6H, Ge–CH_2), 0.88 (t, 9H, CH_3), 7.30 (s, 1H, =CH).

2.2.7. $(n\text{-}C_4H_9)_3Ge(SC_2H_2N_3)$ (**7**)

The synthesis procedure was the same as in Section 2.2.1, using the sodium salt of 1H-5-mercapto-1,2,3-triazole (0.123 g, 1 mmol), triphenylgermanium chloride (0.279 g, 1 mmol) and benzene (20 ml). The yellow crystal complex **7** was obtained from hexane–dichloromethane. Yield, 71%. M.p.: 49–51 °C. *Anal*. Calc. for $C_{14}H_{29}N_3SGe$: C, 48.89; H, 8.50; N, 12.21. Found: C, 48.87; H, 8.53; N, 12.19%. IR (KBr, cm^{-1}): 3250 (br, N–H), 3120 (w, C–H), 1605 (m, C=C), 1592(C–N), 1442 (m, N=N), 1162, 1073 (m, C–S), 585, 531 (m, Ge–C), 461 (m, Ge–S). ^1H NMR ($CDCl_3$): δ 10.7 (br, 1H, N–H), 1.79 (t, 6H, Ge–CH_2), 1.13–1.50 (m, 12H, CH_2), 0.86 (t, 9H, CH_3), 7.30 (s, 1H, =CH).

*2.2.8. $Ph_3Ge(SC_2H_2N_3)$ (**8**)*

The synthesis procedure was the same as in Section 2.2.1, using the sodium salt of 1H-5-mercapto-1,2,3-triazole (0.123 g, 1 mmol), triphenylgermanium chloride (0.339 g, 1 mmol) and benzene (25 ml). The yellow crystal complex **8** was obtained from hexane–dichloromethane. Yield, 73%. M.p.: 130–132 °C. *Anal*. Calc. for $C_{20}H_{17}N_3SGe$: C, 59.46; H, 4.24; N, 10.40. Found: C, 59.40; H, 4.19; N, 10.36%. IR (KBr, cm^{-1}): 3250 (br, N–H), 3120 (w, C–H), 1608 (m, C=C), 1595 (C–N), 1445 (m, N=N), 1160, 1073 (m, C–S), 591, 535 (m, Ge–C), 453 (m, Ge–S). ^1H NMR ($CDCl_3$): δ 11.2 (br, 1H, N–H), 7.33–7.74 (m, 15H, Ph–H), 7.30 (s, 1H, =CH).

*2.3. X-ray crystallographic studies of complexes **4** and **8***

All X-ray crystallographic data were collected on a Bruker SMART CCD 1000 diffractometer. The φ/ω, scan technique was employed. Corrections were applied for Lorentz and polarization effects but not for absorption, satisfying $I \geqslant \sigma(I)$. Criterion of observability was used for the solution and refinement. The structure was solved by direct methods and refined by a full-matrix least-squares procedure based on F^2 using the SHELXL-97 program system. All data were collected at 298(2) K using graphite-monochromated Mo Kα radiation ($\lambda = 0.71073$ Å) and corrected for Lorentz and polarization effects but not for absorption. All non-H atoms were included in the model at their calculated positions. The positions of hydrogen atoms were calculated, and their contributions in structural factor calculations were included.

3. Results and discussion

*3.1. Syntheses of the complexes **1**–**8***

The synthesis procedure was as in the following Scheme 1:

*3.2. IR spectroscopic studies of the complexes **1**–**8***

The assignment of the IR bands of all the complexes **1**–**8** have been made by a comparison with the IR spectra of related organotin(IV) and organogermanium(IV) compounds. A new absorption band that appears at about 309–316 cm^{-1} for complexes **1**–**4** can be attributed to the vibration of the Sn–S bond, which is consistent with that detected for a number of organotin(IV)–sulfur derivatives [12], and the absorption band that appears at 453–461 cm^{-1} for complexes **5**–**8** can be attributed to the vibrations of the Ge–S bond according to the literature [13].

In complexes **1**–**4**, two strong or medium absorptions are observed at 560–565 and 524–540 cm^{-1}. They are due to ν_{asym} and ν_{sym} Sn–C stretching vibrations, respectively. In complexes **5**–**8**, ν_{asym} and ν_{sym} Ge–C stretching vibrations are at 579–591 and 505–535 cm^{-1}, respectively. This suggests that there are no-planar SnC_3 fragments for all the complexes **1**–**8**.

The middle intensity bands observed at 1592–1596 cm^{-1} in the spectra of all the complexes **1**–**8** have been assigned to ν(C–N), according to the literature [14], together with the absorption region ranging from 1442 to 1445 cm^{-1} attributed to the vibration of ν(N=N), which are all consistent with the free ligand. In the 2800–2600 cm^{-1} region the ligands exhibit a broad band typical of N–H stretching. In the organotin(IV) and organogermanium(IV) adducts this shifts to 3250 cm^{-1}. The position and character of the broadened N–H stretching band are consistent with the presence of a NH···N intermolecular hydrogen bond, as reported in the literature [15].

All the above data indicate the coordination of the ligand to tin or germanium only by the sulfur atom in all the complexes **1**–**8**. So it can be concluded that complexes **1**–**8** are four-coordinate, with a sulfur atom and three alkyl (or phenyl) groups bonded to the central metal atom. The conclusion well coincides with the following X-ray crystallographic analysis of complexes **4** and **8**.

*3.3. ^1H NMR data of the complexes **1**–**8***

The ^{1}HNMR spectra show that the chemical shifts of the proton on the phenyl group (Sn–C_6H_6) 7.31–7.96 ppm for **4** and (Ge–C_6H_6) 7.30–7.74 ppm for **8** and those of the methylene connected directly with tin in complexes **1**–**3** and with germanium in complexes **5**–**7**,

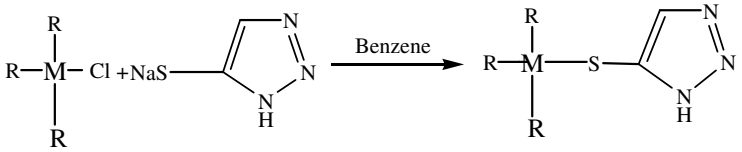

M=Sn, R=CH_3, **1**; C_2H_5, **2**; n-C_4H_9, **3**; C_6H_5, **4**; M=Ge, R=CH_3, **5**; C_2H_5, **6**; C_4H_9, **7**; C_6H_5, **8**

Scheme 1.

1.53–1.79 ppm, upfield shift when compared with those of their corresponding precursors. All these data are similar to those cases that appear in the literature [16], indicating there may exist coordination of the ligand to the metal atom for all the complexes. In addition, the broad resonance of the (N–H) proton appears at 10.5–11.2 ppm for all the complexes **1**–**8**.

3.4. Crystal structures of complexes *4* and *8*

The structure details of complexes **4** and **8** are shown in Figs. 1 and 2, respectively. The intermolecular hydrogen-bond packing of complexes **4** and **8** are similar, one of which is displayed in Fig. 3. Single crystal X-ray diffraction study details are shown in Table 1, and selected bond lengths and angles are listed in Table 2. The complexes **4** and **8** exhibit the tin(IV) and the germanium(IV) in a distorted tetrahedral geometry defined by three phenyl groups and one sulfur atom, which exists as a bridge between the tin or the germanium atom and the triazole ring.

For complex **4**, Sn–C bond lengths (2.121(5) to 2.135(5) Å) are comparable with the complex: triphenyl(5-mercapto-1-phen-1,2,3,4-tetralato)tin (2.120–2.127 Å) [17]. The Sn–S distance is 2.4354(15) Å, which is consistent with the sum of the covalent radii (2.42 Å) [18] and the complex $[Cy_2NeophylSnS_2P(OC_6H_4{}^tBu\text{-}4)_2]$ (2.477(3) Å) [19], and this distance is much shorter than the sum of the van der Waals' radii (4.0 Å) [18]. The S–Sn–C bond angles are more acute and the C–Sn–C bond angles are larger than the theoretical tetrahedral angle, the largest deviations occurring in S(1)–Sn(1)–C(15) [101.32(14)°] and C(15)–Sn(1)–C(9) [116.12(17)°].

For complex **8**, the germanium atom environment is similar to that of the tin atom in complex **4**. The Ge–C bond lengths (1.925(2)–1.929(3) Å) are in the normal range (1.93 Å for Ge–Cp) [20]. The Ge–S bond length (2.2406(11) Å) is a little longer than that reported in dichloro-(ferrocene-1,1′-dithiolato)-germanium (2.19 Å) [20], and is consistent with that in complex 4-$CH_3C_6H_5CS_2GePh_3$ (2.2526(8) Å) [21]. The angles around the center Ge element range from 103.00° to 113.40°, which all depart from the theoretical tetrahedral angle.

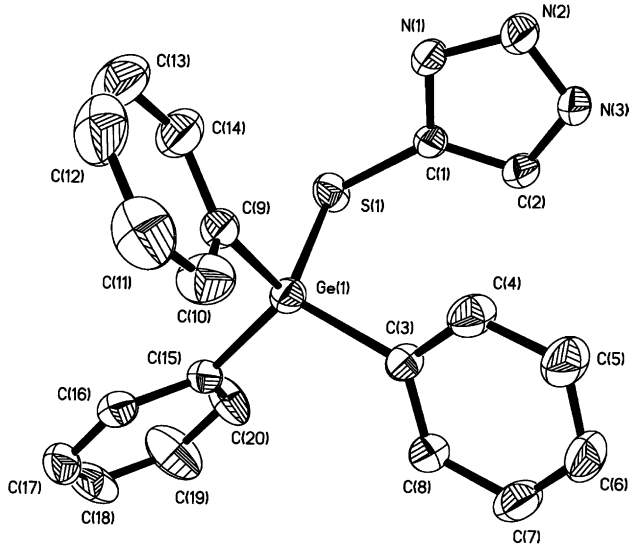

Fig. 2. SHELX view of complex **8** (30% probability thermal ellipsoids).

Furthermore, the salient feature of the superamolecular structure of complexes **4** and **8** is that of a one-dimensional hydrogen-bonded polymer, as shown in Fig. 3, in which N(3) of the triazole bonds to N(1) of a neighboring triazole through a hydrogen bond [$H(1)\cdots N(1)^i$ 1.966 Å, N(3)–$H(1)\cdots N(1)^i$ 173.93° for **4**); $H(1)\cdots N(1)^i$ 1.880 Å, N(3)–$H(1)\cdots N(1)^i$ 165.56° for **8**, (i) $X+1/2, -Y+1/2, -Z$], the parameters of which are consistent with that reported, $H(1)\cdots N(1)$ 1.92(3) Å, for the complex $[(C_6H_5)_3SnSCNH_2{=}N{-}N{=}C(CH_3)(C_6H_4\text{-}2\text{–}OH)]$ [22].

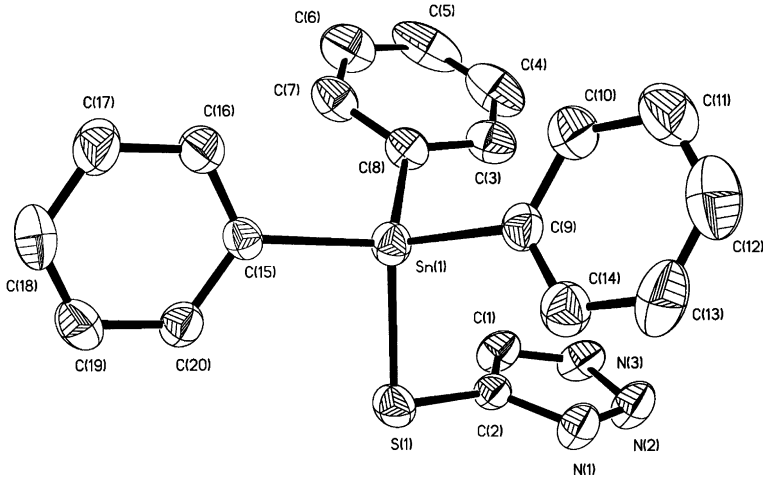

Fig. 1. SHELX view of complex **4** (30% probability thermal ellipsoids).

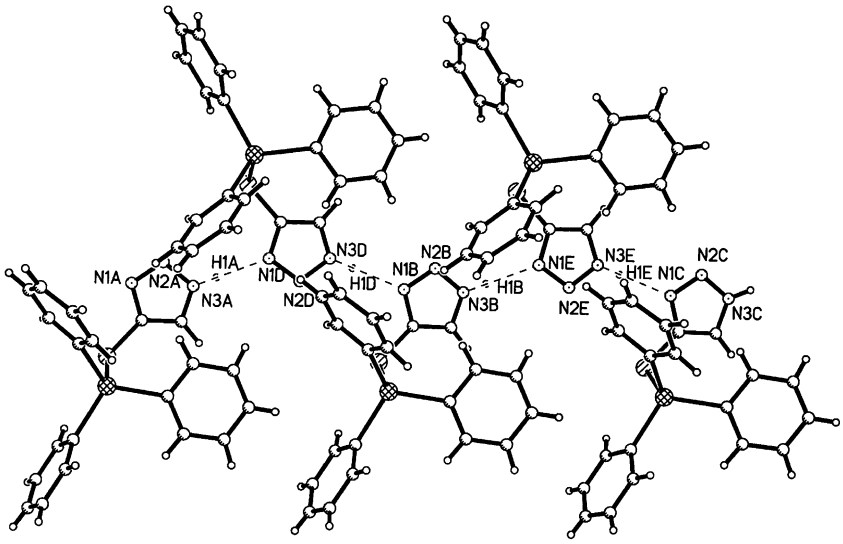

Fig. 3. A drawing showing the intermolecular hydrogen-bonds in complex **8** (the intermolecular hydrogen-bonds in complex **4** are similar to complex **8**).

Table 1
Crystal data and refinement details for complexes **4** and **8**

Data and details	**4**	**8**
Empirical formula	$C_{20}H_{17}N_3SSn$	$C_{20}H_{17}N_3SGe$
Formula weight	450.12	404.02
Temperature (K)	298(2)	298(2)
Wavelength (nm)	0.71073	0.71073
Crystal system	monoclinic	orthorhombic
Space group	$P2_1/c$	$P2(1)2(1)2(1)$
Unit cell dimensions		
a (Å)	9.539(2)	9.184(4)
b (Å)	21.892 (5)	9.657(4)
c (Å)	9.441(2)	21.283(8)
β (°)	93.846 (4)	90
V (Å^3)	1967.1(8)	1887.7(12)
Z	4	4
D_{calc} (Mg/m^3)	1.520	1.422
Absorption coefficient (mm^{-1})	1.412	1.740
Maximum and minimum transmission factors	0.8162 and 0.6768	0.7803 and 0.6059
$F(000)$	896	824
Crystal size (mm)	$0.30 \times 0.20 \times 0.15$	$0.32 \times 0.18 \times 0.15$
θ Data collection (°)	1.86–26.44	1.91–26.37
Index ranges	$-11 \leqslant h \leqslant 11$, $-15 \leqslant k \leqslant 27$, $-11 \leqslant l \leqslant 11$	$-10 \leqslant h \leqslant 11$, $-12 \leqslant k \leqslant 11$, $-21 \leqslant l \leqslant 26$
Reflections collected	11458	10994
Independent reflections	4034	3842
R_{int}	0.0543	0.0382
Completeness to $\theta = 26.37$	99.7%	99.5%
Refinement method	full-matrix least-squares on F^2	full-matrix least-squares on F^2
Absorption correction	semi-empirical from equivalents	semi-empirical from equivalents
Number of parameters	294	294
Goodness-of-fit on F^2	0.903	0.857
Final R indices [$I > 2.0\sigma(I)$]	$R_1 = 0.0409$, $wR_2 = 0.0726$	$R_1 = 0.0293$, $wR_2 = 0.0467$
R indices (all data)	$R_1 = 0.0881$, $wR_2 = 0.0859$	$R_1 = 0.0455$, $wR_2 = 0.0495$
Largest difference peak and hole (e Å^{-3})	0.584 and −0.724	0.289 and −0.223

4. Supplementary material

Crystallographic data (excluding structure factors) for the structures reported in this paper have been deposited with the Cambridge Crystallographic Data Center as supplementary publication Nos. CCDC-192514 and CCDC-207060. Copies of the data can be obtained free of charge on application to the Director,

Table 2
Selected bond lengths (Å) and angles (°) for complexes **4** and **8**

4		**8**	
Bond lengths			
Sn(1)–S(1)	2.4354(15)	Ge(1)–S(1)	2.2406(11)
Sn(1)–C(8)	2.121(5)	Ge(1)–C(3)	1.926(2)
Sn(1)–C(9)	2.135(5)	Ge(1)–C(9)	1.925(3)
Sn(1)–C(15)	2.133(4)	Ge(1)–C(15)	1.929(3)
S(1)–C(2)	1.746(4)	S(1)–C(2)	1.743(3)
N(1)–N(2)	1.316(5)	N(1)–N(2)	1.314(3)
N(2)–N(3)	1.329(5)	N(2)–N(3)	1.321(3)
N(1)–C(2)	1.348(5)	N(1)–C(2)	1.347(3)
N(3)–C(1)	1.317(6)	N(3)–C(1)	1.316(4)
N(3)–H(1)	0.858	N(3)–H(1)	0.985
$N(1)^{i}\cdots H$	1.966	$N(1)^{i}\cdots H$	1.880
Bond angles			
C(8)–Sn(1)–S(1)	110.20(13)	C(3)–Ge(1)–S(1)	109.00(8)
C(9)–Sn(1)–S(1)	107.11(15)	C(9)–Ge(1)–S(1)	110.08(11)
C(15)–Sn(1)–S(1)	101.32(14)	C(15)–Ge(1)–S(1)	103.00(10)
C(8)–Sn(1)–C(15)	113.45(19)	C(3)–Ge(1)–C(9)	108.70(13)
C(8)–Sn(1)–C(9)	108.2(2)	C(15)–Ge(1)–C(9)	112.49(14)
C(9)–Sn(1)–C(15)	116.12(17)	C(3)–Ge(1)–C(15)	113.40(11)
$N(3)–H(1)\cdots N(1)^{I}$	173.93	$N(3)–H(1)\cdots N(1)^{i}$	165.56
C(1)–S(1)–Sn(1)	98.83(16)	C(1)–S(1)–Sn(1)	99.79(10)
N(2)–N(1)–C(2)	109.7(4)	N(2)–N(1)–C(1)	108.8(2)
N(1)–N(2)–N(3)	105.7(4)	N(1)–N(2)–N(3)	106.4(2)
C(1)–N(3)–N(2)	112.0(4)	C(2)–N(3)–N(2)	111.4(3)
N(1)–C(1)–S(1)	122.2(3)	N(1)–C(1)–S(1)	122.3(2)
C(1)–C(2)–S(1)	130.6(4)	C(2)–C(1)–S(1)	129.8(2)
N(3)–C(1)–C(2)	105.4(5)	N(3)–C(2)–C(1)	105.8(3)
N(1)–C(2)–C(1)	107.2(4)	N(1)–C(1)–C(2)	107.6(3)

CCDC, 12 Union Road, Cambridge, CB2 1EZ, UK (fax: +44-1223-336033; e-mail: deposit@ccdc.cam.ac.uk or www: http://www.ccdc.cam.ac.ck).

Acknowledgements

This work was supported by the Natural Science Foundation of Shandong Province, and the Key Teachers Foundation from the State Education Ministry of China (2050).

References

[1] E.I. Stiefel, K. Matsumoto, in: Transtion Metal Sulfur Chemistry, ASC Symposium Series, 653, American Chemistry Society, Washington, DC, 1995, p. 2.
[2] E.S. Rasper, Coord. Chem. Rev. 165 (1997) 475.
[3] B. Krebs, G. Henkel, Angew. Chem., Int. Ed. Engl. 30 (1991) 769.
[4] C.J. Jones, Chem. Soc. Rev. 27 (1998) 289.
[5] I. Awad, A.A. Abdel-Rahman, E. Bakite, J. Chem. Technol. Biotechnol. 51 (1991) 483.
[6] R. Cea-Olivares, O. Jimenez-Sandoval, G. Espinosa-Perez, C. Silvestru, J. Organomet. Chem. 484 (1994) 33.
[7] R. Cea-Olivares, O. Jimenez-Sandoval, G. Espinosa-Perez, C. Silvestru, Polyhedron 13 (1994) 2809.
[8] S. Bhandari, M.F. Mahon, J.G. McGinley, K.C. Molly, C.E. Roper, J. Chem. Soc., Dalton Trans. (1998) 3425.
[9] C.L. Ma, F. Li, D.Q. Wang, H.D. Yin, J. Organomet. Chem. 667 (2003) 5.
[10] C.L. Ma, F. Li, Chin. J. Chem. 21 (2003) 146.
[11] H.D. Yin, R.F. Zhang, L.Y. Zhang, C.L. Ma, ACH-Models Chem. 137 (2000) 103.
[12] C.V.R Moura, A.P.G. de Sousa, R.M. Silva, A.R. Abras, M. Horner, A.J. Bortoluzzi, C.A.L. Filgueiras, J.L. Wardell, Polyhedron 18 (1999) 2961.
[13] R.A. Chadha, J.E. Drake, A.B. Sarkar, Inorg. Chem. 25 (1986) 2201.
[14] A. Růžička, A. Lyčka, R. Jambor, P. Novák, L. Čísařová, M. Holčapek, M. Erben, J. Holeček, Appl. Organomet. Chem. 17 (2003) 168.
[15] A. Tarassoli, T. Sedaghat, Inorg. Chim. Commun. 2 (1999) 595.
[16] Y. Ye, Q. Zeng, L.Z. Liu, Synth. Commun. 31 (2001) 2373.
[17] J. Bravo, M.B. Cordero, J.S. Casas, A. Sanchez, S. Sordo, E.E. Castellano, J. Zukerman-Schpector, J. Organomet. Chem. 482 (1994) 147.
[18] J.E. Huheey, Inorganic Chemistry, third ed., Harper Int, Cambridge, 1983.
[19] F. Yuan, Y.Q. Huang, Q.L. Xie, Appl. Organomet. Chem. 16 (2002) 660.
[20] S. Zurcher, V. Gramlich, A. Togni, Inorg. Chim. Acta 291 (1999) 355.
[21] S. Kato, K. Tani, N. Kitaoka, K. Yanada, H. Mifune, J. Organomet. Chem. 611 (2000) 190.
[22] S.W. Ng, V.G. Kumar Das, J. Organomet. Chem. 377 (1989) 211.

Available online at www.sciencedirect.com
SCIENCE DIRECT®
Polyhedron 23 (2004) 1987–1996
POLYHEDRON
www.elsevier.com/locate/poly

A new redox-active multisite ligand: synthesis, spectroscopy and electrochemistry of its mono and dinuclear complexes, and the interaction of (*E*,*E*)M (M = Ni) complex with Pd^{II} and Ag^{I}

Mehmet Kandaz [a,*], Atıf Koca [b], Ali Rıza Özkaya [c]

[a] *Department of Chemistry, Sakarya University, 54100 Mithatpaşa, Sakarya, Turkey*
[b] *Chemical Engineering Department, Engineering Faculty, Marmara University, 81040 Kadıköy, Istanbul, Turkey*
[c] *Department of Chemistry, Marmara University, 81040 Kadıköy, Istanbul, Turkey*

Received 9 January 2004; accepted 5 May 2004

Abstract

A novel redox active (*E*,*E*)-dioxime ligand, *S*,*S*′-bis-[2(2′-ferrocenemethylaminobenzyl)]-dithioglyoxime (LH_2), containing ferrocene and flexible aminobenzenesulfanyl-moieties on the periphery has been synthesized from 2-(2′-ferrocenemethylamino)benzenethiol, which was obtained by the reduction of 2,2′-pyridylbenzothiazolidine with a large excess of $NaBH_4$. Mononuclear $(LH)_2M$ ($M = Ni^{II}$, Cu^{II}, Co^{II}, Fe^{II} and Mn^{II}), homodinuclear $(LH)_2(UO_2)_2(OH)_2$ and heterotrinuclear $(LH)_2MM'_2X_n$ ($M = Ni^{II}$ and $M' = Pd^{II}$, $X = Cl^-$, $n = 4$ and $M' = Ag^{I}$, $X = NO_3^-$, $n = 2$) complexes have been obtained with the metal:ligand ratios of 1:2, 2:2 and 3:2, respectively. Flexible ferrocenemethylaminobenzenesulfanyl moieties bearing two different heteroatoms, –S and –N, on the periphery of the *vic*-dioxime serve as weak binding sites for Pd^{II} and Ag^{I} ions. The detection of H-bonding in all complexes except the uranyl complex by IR revealed square-planar MN_4 coordination of the mono- and trinuclear complexes. The MN_4 coordination of the Ni^{II} complex was also determined by the ^1H NMR spectroscopy. The structures of the complexes were characterized by elemental analysis, ^1H NMR, IR, MS, UV–Vis spectral and cyclic voltammetry. The voltammetric analyses of the complexes showed metal, ligand, and ferrocene based signals. The redox chemistry of the complexes exhibited both M^{I} and M^{III} oxidation states of the central metals of the complexes.
© 2004 Published by Elsevier Ltd.

Keywords: *Vic*-dioximes; Thiazolidine; Ferrocene; Transition metal complexes; Electrochemistry

1. Introduction

The importance of polytopic *vic*-dioximes containing functional sites for binding different guest species is increasing rapidly [1–6]. Their metal complexes are of current concern for their rich physcochemical, optical, catalytic, redox and medical properties [7–14]. The desired properties of the complexes can be altered by peripheral and central substitutions [5–21]. Polytopic *vic*-dioximes form polynuclear metal complexes, which exhibit novel allosteric, catalytic and sensor properties [22–24]. The oxidation states of the central metals, type and number of donor atoms, and core structures of the complexes are major factors in determining structure–function relationships of the transition metal complexes [15–21,25,26].

Although a large number of *vic*-dioxime complexes possessing core structural types, such as MN_2, MS_2, MN_4, MN_2S_2, MS_4, MN_2S_2, $MN_2S_2O_2$ and MO_4S_2, have been synthesized and characterized [15–21,27–29], the studies on complexes containing peripheral redox-active substituents are rather scarce [30]. Therefore, we are currently interested in fabricating new reactive *vic*-dioxime ligands containing multiple redox-active peripheral groups and/or external transition metal recognition sites as precursors for further applications.

* Corresponding author. Tel.: +90-264-2760237; fax: +90-264-3460371.
E-mail address: mkandaz@sakarya.edu.tr (M. Kandaz).

0277-5387/$ - see front matter © 2004 Published by Elsevier Ltd.
doi:10.1016/j.poly.2004.05.009

In this study, as a continuity of our previous studies on *vic*-dioximes with multifunctional substituents [18–20], we reported for the first time the preparation and characterization of a novel mixed-donor *vic*-dioxime ligand, *S*,*S*′-bis-[2(2′-ferrocenemethylaminobenzyl)]-dithioglyoxime (LH_2) (**3**), containing N_2S_2 external chelating donor sites. It was synthesized from (*E*,*E*)-dichloroglyoxime and 2-(2′-ferrocenemethylamino)-benzenethiol (**2**). Compound **2** was prepared by the reduction of the condensation product, 2,2′-pyridylbenzothiazolidine (**1**), of 2-ferrocenecarboxyaldehyde and 2-aminothiophenol with a large excess of $NaBH_4$ [31,32]. Compound **3** gave *N*,*N*-coordinated planar mononuclear complexes with Ni^{II}, Cu^{II}, Fe^{II}, Co^{II} and Mn^{II} in the rigid core of the *vic*-dioxime groups as MN_4 type complexes. But, compound **3** gave *N*,*O*-coordinated dinuclear complexes with $UO_2{}^{II}$ as MN_2O_2 type complex. We also isolated heterotrinuclear complexes of $(LH)_2MM'_2X_n$ with Pd^{II} ($n = 4$) and Ag^{I} ($n = 2$), having one metal ion for each dithioamino-substituted benzenoid group.

The stability of the oxidation states of the metal center in these complexes depends on the metal coordination environment [33,34]. The ability of donor atoms to stabilize reduced and/or oxidized forms of metal has sparked interest in their role in bioinorganic systems. Hence, for a better understanding of their properties, the investigation of redox behavior has a vital importance. Although various oximes and their metal and non-metal compounds have been studied extensively, electrochemistry of *vic*-dioximes is scarce [18–20]. Therefore, the redox properties of the complexes synthesized in this study were investigated by cyclic voltammetry.

2. Experimental

All reagents and solvents were of reagent-grade quality and obtained from commercial suppliers. (*E*,*E*)-Dicholoroglyoxime was prepared by a reported procedure [31,32]. ^{1}H NMR spectra were recorded on Bruker 200 and 250 MHz spectrometers. FT-IR spectra were recorded on a Mattison 1000 FT-IR spectrometer using KCl pellets, and electronic spectra on a Unicam UV2 spectrophotometer. The elemental analyses were performed using a Carlo Erba 1106 Instrument. Mass spectra were recorded on a VG Zabspec GSMS Spectrometer by the EI and LSIMS methods (MNBA matrix: *meta*-nitrobenzylalcohol). The metal contents of the complexes were determined with a Hitachi 180-80 Atomic Absorption Spectrophotometer in solution prepared by decomposition of the compounds in aqua regia followed by dilution with water. The homogeneity of 2-(2′-ferrocenemethylamino)benzenethiol (**2**) and **3** were tested by TLC (SiO_2, $CHCl_3$:MeOH).

Cyclic voltammetric (CV) and controlled potential coulometric (CPC) measurements were carried out at 25 ± 1 °C with a Princeton Applied Research Model 273 potentiostat controlled by an external PC, using the computer program, HEADSTRT. The Origin 6.0 graph program was used to evaluate HEADSTRT data, to draw voltammograms and to analyze them. The working electrode was a Pt plate with an area of 1.0 cm^2 and a Pt-spiral wire served as the counter electrode in the voltammetric measurements. A saturated calomel electrode (SCE) was employed as the reference electrode. Ferrocene was used as an internal reference and the potentials are also reported with respect to the Fc/Fc^+ couple. Dimethylsulfoxide (DMSO) over molecular sieves was employed as the solvent. Electrochemical grade tetraethylammonium perchlorate (TEAP) (0.1 mol dm^{-3}) was employed as the supporting electrolyte. High-purity nitrogen was used for deaeration and to maintain a nitrogen blanket for at least 15 min prior to each run. For CPC studies, a platinum gauze working electrode (10.5 cm^2 surface area), a Pt wire counter electrode separated by a glass bridge, a SCE as reference, and a model 377/12 Synchronous stirrer were used.

2.1. Synthesis

2.1.1. S,S-Bis-[2(2′-ferrocenemethylaminophenyl)]-dithioglyoxime(LH_2) (3)

[2-(2′-Ferrocenemethylamino)]benzenethiol (**2**) (0.50 g, 1.87 mmol) was dissolved in 30 cm^3 absolute ethanol under nitrogen. Then anhydrous $NaHCO_3$ (0.157 g, 1.87 mmol) was added and the mixture was stirred for about half an hour at room temperature. To this solution, (*E*,*E*)-dicholoroglyoxime (0.046 g, 0.291 mmol) in 15 cm^3 ethanol was added dropwise. The reaction mixture was stirred for 1 h at this temperature and then 4 h at reflux temperature. During the reaction, the mixture was monitored by TLC (chloroform/MeOH; 98:2 v/v). After the mixture had been filtered to separate the NaCl formed, the solvent was removed under reduced pressure until a volume of about 10–15 cm^3 remained. The yellowish mixture was taken up in $CHCl_3$, washed successively with H_2O, 5% $NaHCO_3$ and then H_2O to remove any thiol or inorganic reagents, dried with Na_2SO_4, and finally evaporated under reduced pressure to give a yellow oily residue. The crude product was purified by chromatography on silica gel (MeOH:$CHCl_3$ 2/98 v/v) and dried in vacuo to give the pure compound. This compound is soluble in THF, DMSO, DMF and hot ethanol, and slightly soluble in diethyl ether. Yield: 0.55 g (40.29%); m.p.: 196 °C. IR (Thin film, cm^{-1}): 3380 (s, NH), 3240 (N–OH), 3068, 3019 (Ar-H), 2963, 2924, 2854 (Aliph-H), 1729 (O–H···O), 1606 (C=C), 1587 (C=N), 1566, 1497, 1476, 1448, 1409 (Fc), 1383 (Ar-skel-vib), 1314–1279, 1251, 1174, 1159, 1105, 1032, 1005 (br, st, N–O and Fc), 924, 817 (Fc), 742 (st), 668. ^{1}H NMR (250 MHz, DMSO-d_6) δ: 9.97 (s, 2H, =N–OH, D-exchangeable), 7.62 (dd, $^3J = 7.5$ Hz, 2H, C_6H_4

ortho to SCH_2), 7.44 (dt, $^3J = 7.0$ Hz, 2H, C_6H_4 *meta* to SCH_2), 7.25 (d, $^3J = 7.0$ Hz, 2H, C_6H_4 *para* to NH), 6.62–6.48 (dd, $^3J = 7.8$ Hz, 2H, C_6H_4 *ortho* to NH), 5.84 (s, br, 2H, –NH, D-exchangeable), 4.82 (2H, t, $^3J = 5.0$, C_5H_4), 4.68 (2H, t, $^3J = 5.2$, C_5H_4), 4.27 (s, 2H, NH–CH_2), 4.11 (2H, s, $^3J = 5.2$, C_5H_5), UV–Vis (in DMSO) λ_{max}/nm ($\log \varepsilon$): 375(sh) (2.2), 338(sh), (2.8), 262 (11.34). MS (LSIMS,*m*-NBA): m/z (%) = 731.2 $[M + 1]^+$ (5), 711.4 $[(M–H_2O)]^+$ (5), 673.2 $[(M–Cp)]^+$ or $[(M–Fe)]^+$ (10), 543.4$[(M–Fc)]^+$ (3), 536.2 $[(M–FcCH_2)]^+$, 394.7 $[(M–FcCH_2C_7H_5NS)]^+$ (4), 358.4 $[(M–2Fc)]^+$ (7), 213.3 $[(M–FcCH_2C_7H_5NS–Fc)]^+$ (13), 234.3 (50), 157. 0 $[(DCGO)]^+$ (45).

2.2. Mononuclear complexes: $(LH)_2M$ ($M = Ni^{II}$ (**4**), Cu^{II} (**5**), Co^{II} (**6**), Fe^{II} (**7**) and Mn^{II} (**8**))

2.2.1. $(LH)_2Ni$ (**4**)

To a solution of LH_2 (**3**) (0.050 g, 0.068 mmol) in 20 cm^3 THF, a solution of $Ni(NO_3)_2 \cdot 6H_2O$ (0.010 g, 0.034 mmol) in 10 cm^3 THF was added by dropwise. The complex started to precipitate after a distinct change in color and a decrease in pH had been observed. The mixture was stirred for 2 h at 40 °C to complete the reaction. An equivalent amount of $(C_2H_5)_3N$ was then added dropwise to adjust the pH of the mixture to about 6–7 and complete the precipitation of the complex. After the mixture had been cooled to room temperature and stored in a deep-freeze for 1–2 h, a red-brown precipitate was isolated by successive centrifugation. The product was filtered off, washed with H_2O, MeOH and Et_2O, and finally dried in vacuo. It is soluble in DMSO, DMF and pyridine, and insoluble in methanol, THF and diethylether. Yield: 0.017 g (32.95%); m.p.: >200 °C. IR (Thin film, cm^{-1}): 3376 (–NH), 3073, 3028 (Ar-H), 2974, 2924 (Aliph-H), 1728 (O–H···O bridge), 1632 (C=C), 1586 (C=N), 1504, 1458, 1412, 1291, 1212, 1161, 1065 (N–O), 838, 750, 653, 519. ^{1}H NMR (200 MHz, DMSO-d_6) $\delta = 15.34$ (s, 2H, O–H···O), 7.47(dd, $^3J = 7.5$Hz, 4H, Ar-H, H3), 7.22(dt, $^3J = 6.5$ Hz, 4H, C_6H_4, H5), 6.76 (dt, $^3J = 6.8$ Hz, 4H, C_6H_4, H6), 6.48 (dd, $^3J = 6.4$ Hz, 4H, C_6H_4, H4), 5.84 (s, br, 2H, –NH, D-exchangeable), 4.81(2H, t, $^3J = 5.0$, C_5H_4), 4.68 (2H, t, $^3J = 5.2$, C_5H_4), 4.23 (s, 2H, NH–CH_2), 4.01 (2H, s, $^3J = 5.2$, C_5H_5). UV–Vis (in DMSO) λ_{max}/nm ($\log \varepsilon$): 426(sh) (1.8), 365(sh) (3.8), 264 (10.14). MS (LSIMS, *m*-NBA): $m/z = 1517.3$ $[M + 1]^+$ (3), 1572.3 $[(M + Fe)]^+$ (5), 1499.2 $[M + H_2O]^+$, 1458.2 $[M–Ni]^+$, 1331.7 $[M–Fc]^+$ (3), 1145.3 $[M–2xFc]^+$ (3), 1089.9 $[M–2Fc\text{-}Ni]^+$ (5), 825.7 $[M–2FcCH_2\text{-}C_7H_5NS]^+$ (6), 715.3 (5), 692.3 (10), 676.4 (100), 663.3 (20), 621.4 (10), 583.4 (15), 509.2 (5), 453.2 (8), 337.2 (5), 227.2 (15), 175.1 (20), 157. 0 $[(DCGO)]^+$ (15).

2.2.2. $(LH)_2Cu$ (**5**)

This brown complex was prepared by following the same procedure as described for the preparation of **4**, starting from **3** (0.050 g, 0.068 mmol) and $Cu(NO_3)_2 \cdot 6H_2O$ (0.010 g, 0.034 mmol). This compound is soluble in DMF, DMSO and pyridine, and insoluble in THF, alcohol, hexane and diethyl ether. Yield: 0.20 g (38.66%); m.p.: >200 °C. IR (Thin film, cm^{-1}): 3373 (–NH), 3060, (Ar-H), 2963, 2926 (Aliph-H), 1757 (O–H...O bridge), 1630 (C=C), 1580 (C=N), 1501, [1462–1380] (alip-skel-vib and Fc), 1284, 1106 (Fc), 1032, (N–O), 827 (Fc), 745, 672, 618, 497(Fc), 482 (Fc). UV–Vis (in DMSO) λ_{max}/nm ($\log \varepsilon$): 387(sh) (1.86), 340(sh) (2.4), 261 (12.26). MS (LSIMS, *m*-NBA): m/z (%) = 1523.3 (15) $[M + 3]^+$, 1485.3 $[M–2H_2O]^+$, 1335.8 $[M–Fc]^+$ (5), 1187.9 $[M–FcCH_2C_7H_5NS]^+$ (7), 1153.3 $[M–2Fc]^+$ (3), 829.4 (10), 682.3 (30), 563.3 (12), 457.2 (15), 311.2 (10), 147.4 (5), 228.0 (20), 157.3 $[(DCGO)]^+$ (35), 136.0 (25).

2.2.3. $(LH)_2Co$ (**6**)

The preparation method as described for **4** gave the brown complex, **6**, as powder, starting from **3** (0.050 g, 0.068 mmol) and $Co(NO_3)_2 \cdot 6H_2O$ (0.010 g, 0.034 mmol). This compound is soluble in DMF, DMSO and pyridine, and insoluble in THF, alcohol, hexane and diethyl ether. Yield: 0.025 g (48.47%); m.p.: >200 °C. IR (Thin film, cm^{-1}): 3376 (–NH), 3063 (Ar-H), 2968, 2928 (Aliph-H), 1771 (O–H···O bridge), 1626 (br, C=C), 1589 (C=N), 1508, [1458, 1406 (Fc), 1317] (alip-skel-vib), 1261, 1161, 1063, 1033 (N–O), 1001 (Fc), 942, 823 (Fc), 752, 598, 517 (S–CH_2). UV–Vis (in DMSO) λ_{max}/nm ($\log \varepsilon$): 378(sh) (2.0), 309(sh) (4.65), 264 (12.12).

2.2.4. $(LH)_2Fe$ (**7**)

This red-brown complex **7** was prepared by following the same procedure as described for the preparation of **4**, starting from **3** (0.050 g, 0.068 mmol) and $Fe(NO_3)_2 \cdot 6H_2O$ (0.010 g, 0.034 mmol). This compound is soluble in DMF, DMSO, pyridine and quinoline, and insoluble in THF, alcohol and diethyl ether. Yield: 0.025 g (48.56%); m.p.: >200 °C. IR (Thin film, cm^{-1}): 3343 (–NH), 3035 (Ar-H), 2967, 2923 (Aliph-H), 1774 (O–H···O bridge), 1638 (br, C=C), 1568 (C=N), 1500, [1460, 1441, 1405 (Fc), 1384] (alip-skel-vib), 1275, 1174, 1106, 1015 (N–O), 1003 (Fc), 926, 828 (Fc), 753, 668, 582, 500, 482 (S–CH_2 and Fc). UV–Vis (in DMSO) λ_{max}/nm ($\log \varepsilon$): 384(sh) (8.2), 308(sh) (3.13), 264 (10.80).

2.2.5. $(LH)_2Mn$ (**8**)

A preparation method similar to that used for compound **4** gave the brown complex, **8** as powder, starting from **3** (0.050 g, 0.068 mmol) and $MnCl_2 \cdot 4H_2O$ (0.007 g, 0.034 mmol). This compound is soluble in DMF, DMSO, pyridine, quinoline and insoluble in THF, alcohol and diethyl ether. Yield: 0.014 g (27.22%); m.p.: >200 °C. IR (Thin film, cm^{-1}): 3347 (–NH), 3055 (Ar-H), 2965, 2926 (Aliph-H), 1819 (O–H···O bridge), 1630 (C=C), 1589 (C=N), [1501, 1460, 1400 (Fc) 1384] (alip-

skel-vib), 1316, 1281, 1161, 1105 (Fc), 1033 (N–O), 1005 (Fc), 820 (Fc), 748, 669, 617, 561 (S–CH_2). UV–Vis (in DMSO) λ_{max}/nm ($\log \varepsilon$): 412(sh) (2.18), 359 (sh) (5.14), 262 (9.08).

2.3. Dinuclear uranyl complex $[(LH)_2(UO_2)_2(OH)_2]$ (9)

A solution of $UO_2(NO_3)_2 \cdot 6H_2O$ (0.068 g, 0.166 mmol) in 15.0 cm^3 THF was slowly added with stirring to a solution of **3** (0.100 g, 0.136 mmol) in 15.0 cm^3 THF at room temperature. The color of the solution immediately turned into orange. The pH of the mixture was about 4–5. $(C_2H_5)_3N$ was added to the mixture to adjust the pH of the mixture and to complete the precipitation after the mixture had been heated on water-bath for 1 h. Finally, the mixture was centrifuged several times with THF and Et_2O and the product dried in vacuo to afford an orange powder. This compound is soluble in DMF, DMSO, pyridine and quinoline, and insoluble in THF, alcohol and diethyl ether. Yield: 0.023 g (16.64%); m.p: >200 °C. IR (Thin film, cm^{-1}): 3256 (N–OH), 3067, (Ar-H), 2971, 2925 (Aliph-H), 1642 (C=C), 1576 (C=N), 1515, 1453, 1407 (st, Fc), 1370, 1253, 1068, 1025 (N–O), 1003 (st, Fc), 908 (st, O=U=O), 816 (Fc), 738, 666, 535, 523, 440. UV–Vis (in DMSO) λ_{max}/nm ($\log \varepsilon$): 412(sh), 378(sh), 283 (sh), 264 (10.12). ^{1}H NMR (250 MHz, DMSO-d_6) $\delta = 10.45$ (s, 1H, N–OH, D-exchangeable), 10.22 (s, 1H, N–OH, D-exchangeable), 7.38 (dd, $^3J = 6.5$ Hz, 4H, Ar-H, H3), 7.08 (dt, $^3J = 6.5$ Hz, 4H, C_6H_4, H5), 6.66 (dt, $^3J = 6.0$ Hz, 4H, C_6H_4, H6), 6.51 (dd, $^3J = 6.0$ Hz, 4H, C_6H_4, H4), 5.92, 5.84 (s,s br, 2H, –NH, D-exchangeable), 4.82 (2H, t, $^3J = 6.0$ Hz, C_5H_4), 4.64 (2H, t, $^3J = 6.2$ Hz, C_5H_4), 4.22 (s, 2H, NH–CH_2), 4.12 (2H, s, $^3J = 6.0$ Hz, C_5H_5).

2.4. Heterotrinuclear complexes $[(LH)_2MM'_2X_n$ ($M = Ni^{II}$ and $M' = Pd^{II}$, $X = Cl^-$, $n = 4$ and $M' = Ag^I$, $X = NO_3^-$, $n = 2$) (10, 11)

The mononuclear nickel complex, **4**, (0.05 g, 0.033 mmol) was dissolved in DMF–water (5.0:0.3 cm^3). An excess $Na_2[PdCl_4] \cdot 3H_2O$ or $AgNO_3$ in the same solvent was added. The color became brown-black while stirring for 2 h at 60–70 °C and some precipitation occurred. After adding ethanol to the mixture, the precipitates were separated by filtration and washed successively with hot water, ethanol and diethylether to yield brown-black products $[Ni(LH)_2 (PdCl_2)_2]$ and $[Ni(LH)_2 (AgNO_3)_2]$.

Complex **10**: Yield: 0.025 g (40.49%); ν_{max} 3343 (–NH), 3055, 3019 (Ar-H), 2988, 2945 (Aliph-H), 1713 (O–H···O bridge), 1612 (C=C), 1577 (C=N), 1498, 1443, 1409, 1280, 1156, 1051 (N–O), 886, 714, 648, 512. UV–Vis (in DMSO) λ_{max}/nm ($\log \varepsilon$): 403 (1.92), 363(sh) (3.2), 264 (11.08). MS (FAB): 1871 $[M]^+$ (5), 1873 $[M]^+$ (3), 1836.3 $[M–PdCl_2]^+$ (4), 1517 $[(LH)_2M]$ (5), 1431 $[(LH)_2M–2Fc]$, 1154 (10), 833.5 (10), 231.0 (20), 157.0 $[DCGO]^+$ (55).

Complex **11**: Yield: 0.034 g (55.48%), ν_{max} 3340 (–NH), 3082, 3013 (Ar-H), 2975, 2933 (Aliph-H), 1702 (O–H···O bridge), 1604 (C=C), 1595 (C=N), 1498, 1443, 1385, 1280, 1132, 1103 (N–O), 1078, 976, 879, 828, 710, 658, 534. UV–Vis (in DMSO) λ_{max}/nm ($\log \varepsilon$): 398(sh) (1.7), 352(sh) (4.04), 264 (9.40). MS (FAB): 1857 $[M]^+$ (3), 1685.3 $[M–AgNO_3]^+$ (4), 1517 $[(LH)_2M]$, 1483.1 (5) 1325.1 (8), 1150.7 (15), 835.5 (17), 675.3 (25), 322.0 (30), 224.4 (45),157.0 $[DCGO]^+$ (75).

3. Results and discussion

2-(2′-Ferrocenemethylamino)benzenethiol (**2**) was prepared by a two-step reaction sequence according to the previously reported procedure [31,32]. Compound **3** was prepared by the reaction of the mixture of **2** and (*E*,*E*)-dichlorodioxime [35,36] in THF at reflux temperature in the presence of $NaHCO_3$ (Scheme 1). It was isolated in a moderate yield after chromatography with silica gel. Mononuclear $(LH)_2M$ ($M = Ni^{II}$ (**4**), Cu^{II} (**5**), Co^{II} (**6**), Fe^{II} (**7**) and Mn^{II} (**8**)) (Scheme 1), and dinuclear uranyl complexes $(LH)_2(UO_2)_2(OH)_2$ (**9**) (Fig. 1) of the *vic*-dioxime were prepared with a metal/ligand molar ratio of 1:2 and 2:2, respectively, in moderate yield by treating the metal(II)nitratehexahydrate, except **8** where manganese(II)chloridetetrahydrate was used, with the ligand in THF in the presence of basic Et_3N [13–21]. These products were isolated as pure species via spontaneous precipitation. Further precipitation was achieved by adding Et_3N to the crude product after the first precipitation. The formation of mono-, di- and trinuclear complexes with **3** depends on the tendency of the metal ion to coordinate to the "hard" and/or "soft" sites of the ligand. In trinuclear complexes, two metal ions are coordinated by the two nitrogen and two sulfur atoms of each peripheral site whereas the third metal ion is coordinated by the *N*,*N*′ atoms of each oxime group in the two ligand molecules (Scheme 1). The acidity of peripheral –NH donors in **3** coming from the condensation between ferrocenecarboxyaldehyde and 2-aminothiophenol is rather low when compared with that of amides because of their position far away from oxime groups [37]. Therefore, the trinuclear complex was obtained without deprotonation of these –NH groups under the basic conditions in DMF.

The routes for the synthesis of **3** are given in Scheme 1. The structural formula of **3** and its complexes (**4**, **5**, **6**, **7**, **8** and **9**) were deduced by elemental analysis, IR, ^{1}H NMR, UV–Vis spectroscopic and mass spectral data. The colors, yields and elemental analyses of **3** and its complexes are listed in Table 1. In the IR spectrum of **3**, the –[NOH] stretching absorption was observed at 3240

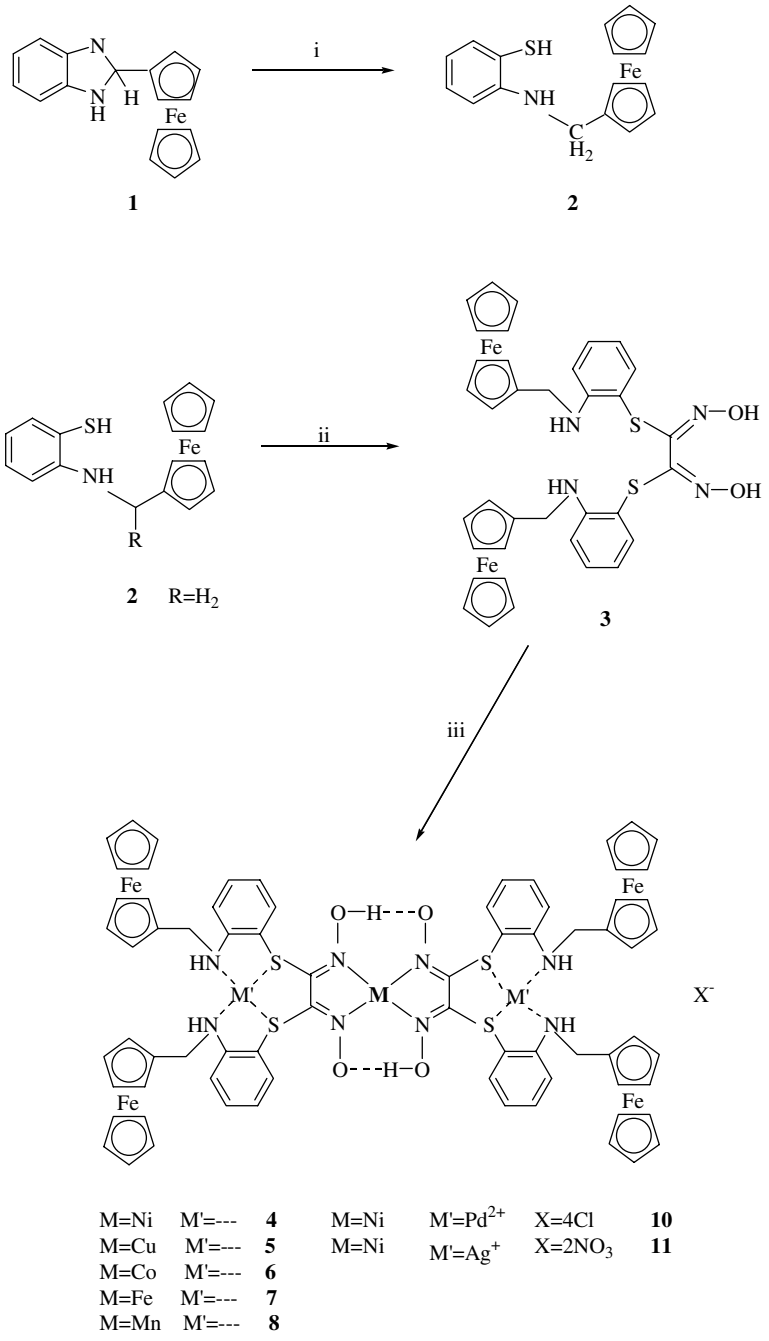

Scheme 1. (i) MeOH, $NaBH_4$, HCl; (ii) MeOH, $NaHCO_3$, DCGO, reflux; (iii) $MX_2 \cdot 6H_2O$ ($M = Ni^{II}$, Cu^{II}, Co^{II}, Fe^{II}; $X = NO_3$; $M = Mn^{II}$, $X = Cl$), Et_3N, THF.

cm^{-1} while the [ν(SH)] band for **1** at 2519 cm^{-1} is not observed. The missing of N–OH stretching band at ca 3200 cm^{-1} in the IR spectrum of **3** together with the existence of a H-bridge (O–H···O) at near 1700–1850 cm^{-1} and the shifting of –C=N and –N–O stretches in the IR spectra of the complexes provide support for MN_4-type coordination in the complexes. While the ν(N–O) stretching vibrations for the ligand shifted to slightly higher frequencies, ν(C–N) stretching vibrations shifted to slightly lower frequencies upon complexation. On the other hand, in the IR spectrum of the uranyl complex **9** [ν(O=U=O)], [ν(N–O)] and [ν(N–OH)] frequencies were observed at 908, 1025 and 3256 cm^{-1}, respectively, as strong bands which are consistent with the dimeric structure. Characteristic ferrocene frequencies were also detected at 816, 1003 and 1407 cm^{-1}. These values are also in harmony with the previously reported dithioglyoxime derivatives [14–20,27–29].

The ^1H NMR data gave reasonable information about the proposed structures of the *vic*-dioxime ligand

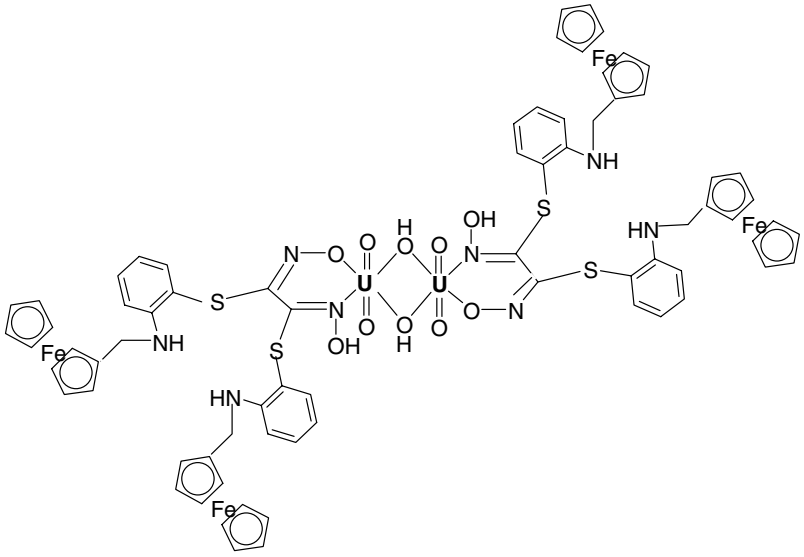

Fig. 1. Binuclear uranyl complex (**9**).

Table 1
Analytical and physical data for LH_4 and its complexes

Compounds	Color	Calc. (Found) %				
		C	H	N	Fe	M
(LH_2) (**3**)	Cream	59.18 (58.79)	4.66 (4.52)	7.67 (7.40)	15.34 (15.55)	
$Ni(LH)_2$ (**4**)	Reddish brown	56.95 (56.37)	4.35 (3.98)	7.38 (6.99)	14.77 (14.40)	3.89 (3.77)
$Cu(LH)_2$ (**5**)	Brown	56.79 (56.72)	4.33 (4.20)	7.36 (7.06)	14.72 (14.77)	4.17 (4.10)
$Co(LH)_2$ (**6**)	Dark brown	56.95 (56.41)	4.35 (4.02)	7.38 (7.08)	14.77 (14.39)	3.89 (8.63)
$Fe(LH)_2$ (**7**)	Red-brown	57.07 (57.04)	4.36 (4.30)	7.40 (7.28)	18.49 (18.27)	
$Mn(LH)_2$ (**8**)	Light-brown	57.11 (57.08)	4.36 (4.05)	7.40 (15.13)	14.79 (14.09)	3.63 (3.52)
$(UO_2)_2(LH)_2(OH)_2$ (**9**)	Orange	23.52 (38.88)	3.34 (2.95)	5.51 (9.99)	11.02 (10.99)	
$Ni(LH)_2 \cdot 2PdCl_2$ (**10**)	Brown-black	46.18 (46.77)	3.39 (3.90)	5.97 (5.73)	11.97 (12.04)	3.15 (3.17)
$Ni(LH)_2 \cdot 2AgNO_3$ (**11**)	Brown-black	56.95 (56.37)	4.35 (3.98)	7.38 (6.99)	10.23 (10.15)	2.69 (2.71)

and its metal complexes. The resonances due to the –N–OH, –NH, ferrocene and S-donor of the benzene moiety were the most dominant signals indicating the formation of **3**. The ^1H NMR spectrum of **3** in DMSO exhibited D_2O-exchangeable signals for the N–OH and NH protons at 9.97 and 5.84 ppm, respectively. These signals are indicative of the *anti*-isomer form of the *vic*-dioxime. The singlets, which belong to NH and N–OH, disappeared after addition of D_2O. In addition, the signals resulting from the moieties in **3** were observed as a double-doublet at 7.44, a double-triplet at 7.25, a doublet at around 6.62–6.48, and a double-doublet at around 4.82–4.68 for benzene, at 4.11 for ferrocene and at 4.24 ppm for N–CH_2. The ^1H NMR spectrum of complex **4** confirms the hydrogen-bridged structure. The existence of an intra-molecular H-bridge was observed by a new signal at lower field, $\delta = 15.34$ ppm, in addition to the second deuterium-exchangeable-NH protons. The signal from the deuterium-exchangeable O–H$\cdots$O group disappeared upon addition of D_2O. The shifts and changes in the intensity of certain peaks in the NMR spectra of **4** and **9** as compared to **3** are consistent with the coordination of **3**. The signals for the ferrocene, methylene and benzene in **4** and **9** are similar with those of **3** with small shifts. The NMR spectrum of **9** contained two peaks for the oxime N–OH group at low field ($\delta = 10.45$, 10.22 ppm, s, 1H, N–OH, D-exchangeable), which can be attributed to the magnetic anisotropy of the uranyl ion, as discussed in previous works [18–20]. It is known that the uranyl ion enhances the chemical shift differences between non-equivalent protons.

The UV–Vis spectra of the ligand and its complexes (**4**, **5**, **6**, **7**, **8** and **9**) in DMF showed two or three absorption bands between 260 and 550 nm. These bands are assigned to both a charge transfer transition from the metal to π^* anti-bonding orbital of the ligand and a spin-allowed π–π^* transition of the ligand. The general character of these spectra are very similar to that of the corresponding complexes of symmmetrically disubstituted dioximate ligands. This is probably due to the fact that metal to ligand charge transfer and ligand to metal charge transfer transitions have similar energy differ-

ences. The d^8 metal ion, Pd^{II} exhibits a preference for square planar geometry with dithioether complexes [37]. The decrease in the intensities of π–π^* and n–π^* transitions indicates the coordination to the peripheral sulfur and nitrogen atoms [17–21,38]. Consequently, the two PdS_2N_2 planes are directed out of the plane of the *vic*-dioxime complex as expected, which causes decomposition of aggregates of the planar *vic*-dioxime molecule in solution. The metal contents of the trinuclear complexes were determined quantitatively by atomic absorption spectrophotometry.

The mass spectra of **3**, **4**, **5**, **10** and **11** were obtained by the LSIMS technique using *m*-NBA (*meta*-nitrobenzylalcohol) as the matrix and they showed molecular ion peaks at $m/z = 731.2$ $[L + 1]^+$ for **3**, $m/z = 1517.3$ $[2L + M + H]^+$ for **4**, $m/z = 1523.3$ $[2L + M + 3H]^+$ for **5**, 1871 $[M]^+$ for **10** and 1857 $[M]^+$ for **11**. These data confirm the proposed structures and obey the rules of dithiosubstituted *vic*-dioxime and its complexes in addition to major fragments.

The electrochemical properties of **4**–**9** were investigated using voltammetric techniques. The results are summarized in Table 2. With the controlled potential coulometry studies, complete electrolysis of the solution at the working electrode at constant potential ($E_{p,c}$ of the redox couple) was achieved, and the time integration of the electrolysis current was recorded and the charge, Q, at the end of the electrolysis was calculated using the current-time response of the solution. Faraday's law was used to estimate the number of electrons transferred. The number of electrons was found to be two for the U(VI)/U(V) couple of **9** and one for all other redox processes.

Figs. 2 and 3 show the cyclic voltammograms of **4** and **7**, respectively. The first reduction and first oxidation processes for these complexes (Ic/Ia and IIIa/IIIc in Figs. 2 and 3) take place on the metal center of the complexes, whose voltammetric data are given in Table 2. For both **4** and **7**, the second reduction process corresponds to the oxime moieties and the second oxidation process to Fc/Fc^+. Addition of ferrocene compound into the solution of **4** gives an oxidation signal almost at the same potential with the couple at $E_{1/2} = 0.466$ V indicating that the second one of these oxidations corresponds to the ferrocene substituents attached to the oxime moieties. ΔE_p and $\partial E_p/\partial \log v$ values indicated that for both complexes the metal-based processes have quasi-reversible character while the ferrocene oxidation processes have reversible behavior. The redox chemistry of the Ni^{II} (**4**) and Fe^{II} (**7**) complexes exhibit both M(III)/M(II) and M(II)/M(I) redox couples. It is clearly stated in the literature that oxime containing metal

Table 2
Voltammetric data for the complexes in DMSO–TBAP

Complexes	Redox couple	Peak ratio[a]	$E_{1/2}$[b] (V)	$\partial E_p/\partial \log v$ (V)	ΔE_p[c] (V)
$[Ni(LH)_2]$ (**4**)	Fc/Fc^+	0.96	0.466 (−0.009)	0.030	0.066
	Ni(II)/Ni(III)	3.20	0.205 (−0.270)	0.050	0.095
	Ni(II)/Ni(I)	1.08	−0.430 (−0.905)	−0.055	0.200
	L/L^-		−1.225 (−1.700)	−0.090	
$[Cu(LH)_2]$ (**5**)	Cu(II)/Cu(III)	0.256	0.128 (−0.352)	0.140	0.203
	Cu(II)/Cu(I)		−0.730 (−1.210)	[d]	
	Cu(I)/Cu(0)		−1.130 (−1.610)	[d]	
	L/L^-	0.48	−1.330 (−1.810)	−0.016	0.080
$[Co(LH)_2]$ (**6**)	Fc/Fc^+	1.00	0.466 (0.006)	0.050	0.157
	Co(II)/Co(I)	1.00	−0.290 (−0.750)	−0.020	0.470
	L/L^-		−1.070 (−1.530)	−0.070	
$[Fe(LH_3)_2]$ (**7**)	Fc/Fc^+	1.00	0.455 (−0.010)	0.035	0.050
	Fe(II)/Fe(III)	1.00	0.215 (−0.250)	0.025	0.070
	Fe(II)/Fe(I)	0.98	−0.465 (−0.930)	−0.010	0.635
	L/L^-	0.10	−0.825 (−1.290)	−0.060	0.450
$[Mn(LH_3)_2]$ (**8**)	Fc/Fc^+	0.70	0.473 (0.003)	0.060	0.055
	Mn(II)/Mn(I)	1.00	−0.853 (−1.323)	−0.015	0.565
$(UO_2)_2(LH)_2(OH)_2$ (**9**)	L/L^+	1.00	0.730 (0.250)	0.035	0.060
	Fc/Fc^+	0.90	0.460 (−0.020)	0.010	0.060
	$U(VI)O_2/U(V)O_2$	1.00	−0.508 (−0.988)	−0.015	0.058
	L/L^-		−1.140 (−1.620)	−0.095	

[a] $i_{p,a}/i_{p,c}$ for reduction, $i_{p,c}/i_{p,a}$ for oxidation at 0.100 V s^{-1} scan rate.
[b] Cathodic peak potential for reduction, anodic peak potential for oxidation for irreversible processes. The values in parenthesis indicate the half-peak potentials vs. Fc/Fc^+.
[c] $\Delta E_p = E_{p,a} - E_{p,c}$ at 0.100 V s^{-1} scan rate.
[d] These data could not be determined due to weak signals.

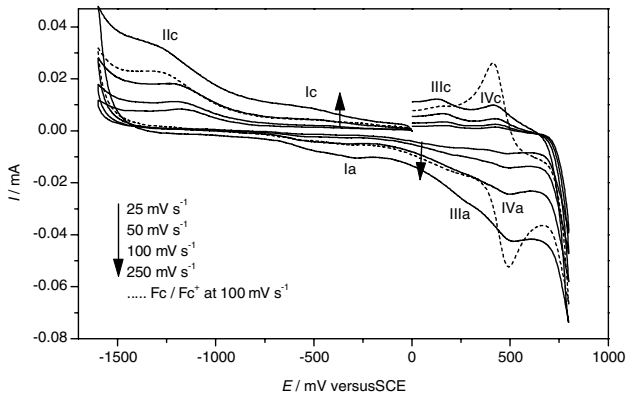

Fig. 2. Cyclic voltammograms of $[Ni(LH)_2]$ (**4**) in DMSO–TBAP at various scan rates.

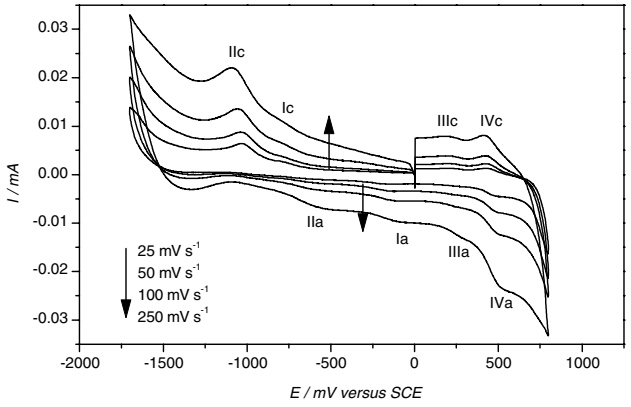

Fig. 3. Cyclic voltammograms of $[Fe(LH)_2]$ (**7**) in DMSO–TBAP at various scan rates.

complexes give redox signals involving both higher and lower oxidation states of the metal depending on the coordination environment of metal center [39,40].

In the CV measurements upon scanning cathodically at the negative potential side, with the exception of **5**, all complexes display first a one-electron peak assigned to the reduction of the metal center of the complexes and then an irreversible oxime-based reduction peak without the corresponding anodic wave. As shown in Fig. 4(b), **5** has a different redox behavior compared to the others. It displays two one-electron totally irreversible reduction peaks at −0.730 and −1.130 V without the corresponding anodic waves during the reverse scan. Since the first reduction wave is irreversible, the first electron transfer step is probably being rapidly followed by a chemical reaction which gives a daughter product which is responsible for the second irreversible process. It also displays a third reduction peak with the corresponding anodic wave at $E_{1/2} = -1.330$ V which can be attributed to the oxime moieties. The oxidation process of **5** (IVa in Fig. 4(a)) had an adsorption behavior. Direct proportionality of the anodic peak current with scan rate provided evidence for the adsorption character of this process. This adsorption behavior was also observed previously in our works involving voltammetric behaviors of various copper-oxime complexes [18–20]. Although the ferrocene substituents are redox active within the accessible potential range of the DMSO/TBAP solvent system, their voltammetric signal was not observed. This signal probably coincides with the adsorption peak having a high-current, and cannot be observed.

Figs. 5 and 6 indicate the CVs of **6** and **8**, respectively. These complexes give a one-electron M^{II}/M^{I} couple (Ic/Ia) with a high peak separation probably due to a slow charge transfer process. The peak separation value of the Ic/Ia couple of **6** is considerably high ($\Delta E_p = 0.470$ V at 0.100 V s^{-1}). However, the $\partial E_p/\partial \log v$ value for this couple (−0.020 V) is indicative of a quasi-reversible character of the process. ΔE_p of the Ic/Ia couple of **8** is also very high (0.565 V at 0.100 V s^{-1}) while the $\partial E_p/\partial \log v$ value (−0.015 V) is within the range for a quasi-reversible peak character. In the case of **6**, the Co^{II}/Co^{I} couple is followed with an irreversible oxime reduction peak (IIc) at −1.070 V, while this peak was not observed with **8**. The redox peak of the oxime reduction

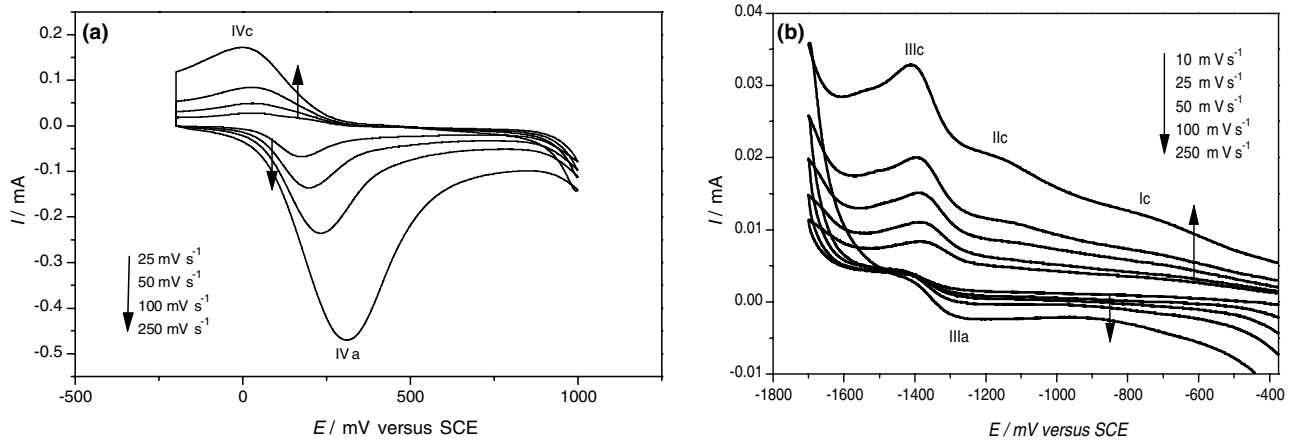

Fig. 4. Cyclic voltammograms of $[Cu(LH)_2]$ (**5**) in DMSO–TBAP at various scan rates.

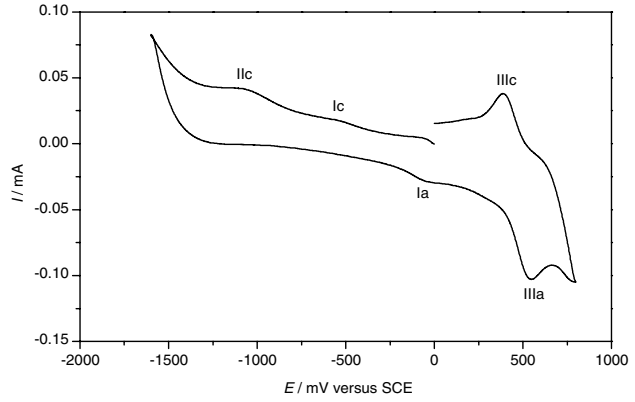

Fig. 5. Cyclic voltammograms of $[Co(LH)_2]$ (**6**) in DMSO–TBAP at 100 mV s^{-1}.

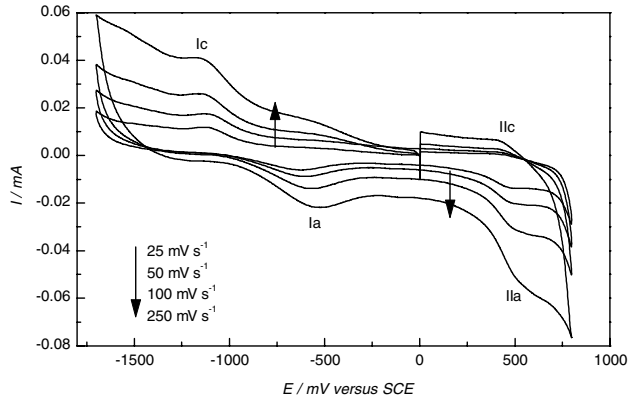

Fig. 6. Cyclic voltammograms of $[Mn(LH)_2]$ (**8**) in DMSO–TBAP at various scan rates.

for **8** is probably weak and it is difficult to resolve it from the background current of the CV. Both **6** and **8** also show a reversible oxidation couple corresponding to Fc/Fc^+. The ferrocene signal of **6** is considerably higher than those of the other complexes. This is probably due to the coincidence of the Co(II)/Co(III) and Fc/Fc^+ redox processes.

Fig. 7 represents the cyclic voltammograms of **9** at different scan rates. Complex **9** displays a reversible reduction couple assigning to $U^{VI}O_2/U^{V}O_2$ at $E_{1/2} = -0.508$ V followed by an irreversible reduction of the oxime moieties at −1.140 V and two oxidation couples at 0.460 V (IIIa/IIIc) and at 0.730 V (IVa/IVc). Addition of ferrocene compound into the solution of **9** give an oxidation signal almost at the same potential with the couple at $E_{1/2} = 0.460$ V indicating that first one of these oxidations corresponds to the ferrocene substituents attached to the oxime moieties. Moreover, addition of ferrocene does not change remarkably the position of other voltammetric signals indicating the absence of any considerable substituent effect on the potentials of the oxime and metal based redox processes. The second oxidation signal is attributed to the oxime

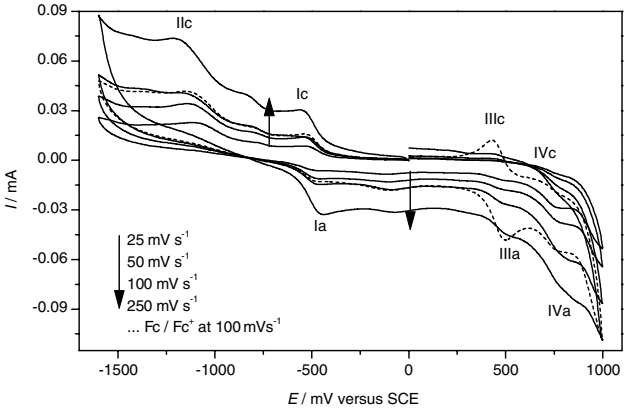

Fig. 7. Cyclic voltammograms of $[(UO_2)_2(LH)_2(OH)_2]$ (**9**) in DMSO–TBAP at various scan rates.

moieties, and observed only for the uranyl complex. For the other complexes, this signal is probably out of the accessible potential window of the DMSO/TBAP solvent system, and thus cannot be monitored.

4. Conclusion

The present work introduces the preparation, characterization and electrochemical properties of a novel *vic*-dioxime ligand and its mono and dinuclear metal complexes which were substituted peripherally with redox active ferrocenyl and ionophore aminothiophenyl moieties. The external aminobenzylthio moieties provided the complexes with the capability of binding various metal ions. Electron donating nitrogen or sulfur atoms render the chelating centers very electron rich. This makes this family of molecules ideally suited for the development of new charge-transfer complexes and as precursors to magnetic or conductive materials. Voltammetric results showed that the metal-oxime complexes indicated metal, ligand and ferrocene based signals. The electrochemistry of the oxime containing metal complexes clearly showed that the reduction of the oxime moiety in non-aqueous media is very difficult due to the polarization of the hydroxyl groups, so the redox signals involving the oxime moiety were observed after central metal-based redox processes and at considerably negative potentials. Addition of ferrocene into the complex solutions did not change remarkably the position of other voltammetric signals indicating the absence of any considerable substituent effect on the potentials of the oxime and metal-based redox processes.

Acknowledgements

We thank the Research Fund of Sakarya University (Project Nos. 2000-013 and 2002-45), TÜBİTAK (Pro-

ject No. TBAG-2241 (102T167)) and The Research Fund of Marmara University (Project No. SCIENCE-107/020603).

References

[1] G.A. Melson, Coordination Chemistry of Macrocyclic Compounds, Plenum Press, New York, 1979.
[2] B. Meunier (Ed.), DNA Cleavers and Chemotherapy of Cancer and Viral Diseases, Kluwer Academic Publishers, Dordrecht, 1996.
[3] G. Pratviel, J. Bernadou, B. Meunier, Adv. Inorg. Chem. (1998) 251.
[4] M. Kandaz, S.L.J. Michel, B.M. Hoffman, J. Porphyr. Phthalocya. 7 (2004) 700.
[5] R. Kramer, Coord. Chem. Rev. 182 (1999) 243.
[6] J.P. Leonard, D.P. Novotnik, R.D. Neirinckx, J. Nucl. Med. 27 (1986) 1819.
[7] P.L. Boulas, M. Gomez-Kaifer, L. Echegoyen, Angew. Chem. Int. Ed. 37 (1998) 216.
[8] D. Bhuniya, S. Mohan, S. Narayanan, Synthesis-Stuttgart 7 (2003) 1018.
[9] E. Lukevics, R. Abele, M. Fleisher, J. Popelis, E. Abele, J. Mol. Catal. 198 (2003) 89.
[10] M.J. Baena, J. Barbera, P. Espinet, A. Ezcurra, M.B. Ros, J.L. Serrano, J. Am. Chem. Soc. 116 (1994) 1899.
[11] K. Ohta, H. Hasebe, M. Moriya, T. Fujimoto, I. Yamamoto, Mol. Cryst. Liq. Cryst. 208 (1991) 43.
[12] K. Ohta, R. Higashi, M. Ikejima, I. Yamamoto, N. Kobayashi, J. Mater. Chem. 8 (1998) 1979.
[13] A. Gül, Ö. Bekaroğlu, J. Chem. Soc., Dalton Trans. (1983) 2537.
[14] I. Gürol, V. Ahsen, Ö. Bekaroğlu, J. Chem. Soc., Dalton Trans. (1992) 2283.
[15] G. Gümüş, V. Ahsen, Mol. Cryst. Liq. Cryst. 348 (2000) 167.
[16] Y. Gök, Polyhedron 15 (1996) 1355.
[17] H. Kantekin, U. Ocak, Y. Gök, J. Incl. Phenom. Macro. 43 (2002) 175.
[18] M. Kandaz, İ. Yılmaz, S. Keskin, A. Koca, Polyhedron 21 (2002) 825.
[19] İ. Yılmaz, M. Kandaz, A.R. Özkaya, A. Koca, Monatsh. Chem. 133 (2002) 609.
[20] M. Kandaz, S.Z. Çoruhlu, İ. Yılmaz, A.R. Özkaya, Transition Metal Chem. 27 (2002) 877.
[21] H. Temel, H. Hoşgören, Transition Metal Chem. 27 (2002) 609.
[22] P.D. Beer, O.R. Kocian, J. Mortinos, R. Spencer, J. Chem. Soc., Chem. Commun. (1992) 602.
[23] J.D. Carr, S.J. Coles, W.W. Hassan, M.B. Hursthouse, K.M. Abdul Malik, J.H.R. Tucker, J. Chem. Soc., Dalton Trans. (1999) 57.
[24] Z.N. Chen, H.X. Zhang, K.B. Yu, C.Y. Su, B.S. Kang, Polyhedron 17 (1998) 1535.
[25] D. Sellmann, J. Utz, F.W. Heinemann, Inorg. Chem. 38 (1999) 459.
[26] D. Christodoulou, M.G. Kanatzidis, D. Coucouvanis, Inorg. Chem. 29 (1990) 191.
[27] E. Musluoğlu, Ö. Bekaroğlu, J. Coord. Chem. 39 (1996) 253.
[28] M. Ertaş, A.R. Koray, V. Ahsen, Ö. Bekaroğlu, J. Organomet. Chem. 319 (1987) 197.
[29] V. Ahsen, A. Gürek, A. Gül, Ö. Bekaroğlu, J. Chem. Soc., Dalton Trans. (1990) 5.
[30] E. Sharon, A. Davis, C. Cameron, S. Ashley, H.L. Scott, S. Throckmorton, L. Studer-Martinez, C.F. Beam, J. Organomet. Chem. 533 (1997) 125.
[31] U. Brand, H. Vahrenkamp, Chem. Ber. 129 (1996) 435.
[32] Z. Zhang, A.E. Martell, R.T. Motekaitis, L. Fu, Tetrahedron Lett. 40 (1999) 4615.
[33] V.V. Pavlishchuk, S.V. Kolotilov, A.W. Addison, M.J. Prushan, R.J. Butcher, L.K. Thompson, Inorg. Chem. 38 (1999) 1759.
[34] V.V. Pavlishchuk, S.V. Kolotilov, E. Sinn, M.J. Prushan, A.W. Addison, Inorg. Chim. Acta 278 (1998) 217.
[35] P. Panzio, F. Baldrocca, Gazz. Chim. Ital. 60 (1930) 415.
[36] H. Brinizinger, R. Titman, Chem. Ber. 85 (1952) 344.
[37] E. Hamuryudan, Ö. Bekaroğlu, Chem. Ber. 127 (1994) 2483.
[38] S.J. Loeb, K.D.L. Smith, Inorg. Chem. 32 (1993) 1297.
[39] M.J. Prushan, A.W. Addison, R.J. Butcher, Inorg. Chim. Acta 300–302 (2000) 992.
[40] N. Sengottuvelan, J. Manonmani, M. Kandaswamy, Polyhedron 21 (2002) 2767.

Available online at www.sciencedirect.com
SCIENCE DIRECT®
Polyhedron 23 (2004) 1997–2004
POLYHEDRON
www.elsevier.com/locate/poly

Complexes of nickel with tetradentate ligands formed by ring opening of 1-benzoyl-3,5-dimethyl-5-(1′-benzoylhydrazido)pyrazoline

Abhik Mukhopadhyay, Samudranil Pal *

School of Chemistry, University of Hyderabad, Hyderabad 500 046, India

Received 25 March 2004; accepted 7 May 2004
Available online 15 June 2004

Abstract

The condensation of acetylacetone with benzoylhydrazine in a 1:2 mol ratio in methanol to prepare acetylacetone bis(benzoylhydrazone) (H_3bbhac) resulted in the formation of the cyclized product 1-benzoyl-3,5-dimethyl-5-(1′-benzoylhydrazido)-pyrazoline (bzpyzn). The pyrazoline structure has been confirmed by X-ray crystallography. In methanol, treatment of bzpyzn with $Ni(O_2CCH_3)\cdot 4H_2O$ in a 1:1 mol ratio under aerobic conditions results in the pyrazoline ring opening and formation of a complex with the deprotonated acetylacetone bis(benzoylhydrazone) ($bbhac^{3-}$). The room temperature magnetic moment (1.71 μ_B) of [Ni(bbhac)] is consistent with an $S = 1/2$ spin state. However, the EPR spectral features indicate that [Ni(bbhac)] is on the borderline between an authentic nickel(III) complex and a nickel(II) stabilized ligand radical. In our attempts to grow single crystals of [Ni(bbhac)], the transformation of the central –CH= moiety of the acetylacetone residue in $bbhac^{3-}$ to a keto group has been realized. The molecular structure of the resulting nickel(II) complex of the formula [Ni(bbhacO)] has been determined by X-ray crystallography.
© 2004 Elsevier Ltd. All rights reserved.

Keywords: Nickel complexes; Pyrazoline; Ring opening; Ligand oxidation; Structures

1. Introduction

The chemistry of trivalent nickel complexes has been the subject of considerable interest due to the important roles played by nickel(III) in catalytic and biological processes [1–4]. Ligands containing N-coordinating deprotonated amide functionality are well known to stabilize higher-valent (>+2) late first transition series metal ions [5]. Schiff bases derived from semicarbazides and acyl- or aroylhydrazines contain this high oxidation state promoting amide functionality that can coordinate a metal ion through the O atom. Thus these ligands provide the scope to study the effect of the amide protonation state on the structural and physical properties of the complexes, which is rather intricate for amide-N coordinated species. We have been working on these aspects of transition metal complexes with tridentate acyl- or aroylhydrazones [6–11]. In the present work, we have reported the results obtained in our attempt to prepare a similar tetradentate Schiff base acetylacetone bis(benzoylhydrazone) (H_3bbhac) and to explore the nickel coordination chemistry with it. Deprotonation of the two amide functionalities and the active methylene group of H_3bbhac will produce the trianionic planar N_2O_2 donor ligand $bbhac^{3-}$ which in principle can stabilize nickel(III). To synthesize H_3bbhac we have reacted benzoylhydrazine and acetylacetone in a 2:1 mol ratio. However, a new cyclized product 1-benzoyl-3,5-dimethyl-5-(1′-benzoyl-hydrazido)pyrazoline (bzpyzn) has been isolated instead of H_3bbhac. Formation of substituted pyrazolines from semicarbazide or thiosemicarbazide and 1,3-diketones (in a 2:1 mol ratio) has been reported before [12–14]. It has been shown that in the presence of transition metal ions (Cu^{2+}, Zn^{2+}) under anaerobic conditions, the pyrazoline derived from thiosemicarbazide and acetylacetone undergoes ring

* Corresponding author. Tel.: +91-40-2313-4756; fax: +91-40-2301-2460.
E-mail address: spsc@uohyd.ernet.in (S. Pal).

0277-5387/$ - see front matter © 2004 Elsevier Ltd. All rights reserved.
doi:10.1016/j.poly.2004.05.002

opening and neutral complexes of the general formula [ML] are formed where H_2L is the acetylacetone bis(thiosemicarbazone) [14]. It is also observed that under aerobic conditions, the central methylene group of the acetylacetone residue of the ligand in [ML] (Ni, Cu, Zn) is oxidized to a keto group [14,15]. The reaction of bzpyzn with $Ni(O_2CCH_3)\cdot 4H_2O$ under aerobic condition causes a similar pyrazoline ring opening in bzpyzn. However, this ring opening leads to the formation of a formal nickel(III) complex [Ni(bbhac)], of the intended ligand instead of the nickel(II) complex of the oxidized ligand, as observed for acetylacetone bis(thiosemicarbazone). Interestingly in solution under wet conditions, the methine fragment in [Ni(bbhac)] gets oxidized to a keto group leading to the formation of a new nickel(II) complex of the formula [Ni(bbhacO)]. Herein, we describe the synthesis and physical properties of bzpyzn, [Ni(bbhac)] and [Ni(bbhacO)]. Solid state molecular structures of bzpyzn and [Ni(bbhacO)] have been determined by X-ray crystallography.

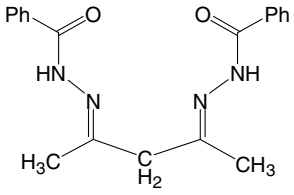

(H_3bbhac)

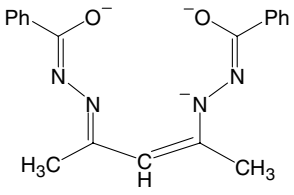

($bbhac^{3-}$)

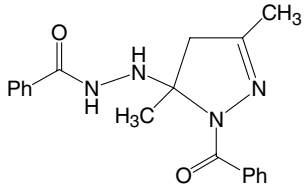

(bzpyzn)

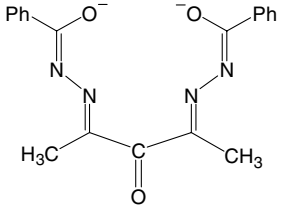

($bbhacO^{2-}$)

2. Experimental

2.1. Materials

The chemicals and the solvents used in this work were of analytical grade, available commercially and were used without further purification.

2.2. Physical measurements

Microanalytical (C, H, N) data were obtained with a Perkin–Elmer Model 240C elemental analyzer. Infrared spectra were collected by using KBr pellets on a Jasco-5300 FT-IR spectrophotometer. Solution electrical conductivities were measured with a Digisun DI-909 conductivity meter. Room temperature (300 K) solid state magnetic susceptibility was measured by using a Sherwood Scientific magnetic susceptibility balance. $Hg[Co(NCS)_4]$ was used as the standard. A diamagnetic correction (-186×10^{-6} emu mol^{-1} for [Ni(bbhac)]), calculated from Pascal's constants [16], was used to obtain the molar paramagnetic susceptibility. EPR spectra were recorded on a Jeol JES-FA200 spectrometer. A Shimadzu 3101-PC UV/vis/NIR spectrophotometer was used to record the electronic spectra. Proton NMR spectra of bzpyzn (in $CDCl_3$) and [Ni(bbhacO)] (in $(CD_3)_2SO$) were recorded on a Bruker 200 MHz spectrometer using $Si(CH_3)_4$ as an internal standard.

2.3. Synthesis of 1-benzoyl-3,5-dimethyl-5-(1′-benzoylhydrazido)pyrazoline (bzpyzn)

To a methanol solution (25 ml) of benzoylhydrazine (545 mg, 4 mmol) 0.21 ml of acetylacetone (205 mg, 2.05 mmol) was added. The mixture was refluxed for 6 h followed by evaporation to about 1/5th of the original volume on a rotary evaporator. It was then cooled to room temperature. The white solid thus obtained was collected by filtration and recrystallized from methanol. Yield, 430 mg (64%). A single crystal suitable for X-ray structure determination was selected from this material. *Anal*. Calc. for $C_{19}H_{20}N_4O_2$: C, 67.84; H, 5.99; N, 16.65. Found: C, 67.55; H, 5.82; N, 16.53%. Selected IR bands (cm^{-1}): 3277(s), 1659(s), 1605(s), 1572(m), 1537(m), 1489(w), 1456(s), 1427(s), 1375(s), 1329(s), 1306(m), 1134(m), 1105(m), 1061(w), 1026(m), 993(m), 934(w), 910(s), 862(s), 789(s), 708(s), 638(w), 488(m). ^{1}H NMR (200 MHz) data in CD_3OD (δ): 1.88 (s, 3H, 5-CH_3); 1.98 (s, 3H, 3-CH_3); 2.90 and 3.22 (2H, CH_AH_B, $J_{AB}=18$ Hz); 5.30 (s, 1H, 5-NH); 7.38–7.50 (m, 6H, aromatic protons); 7.73–7.84 (m, 4H, aromatic protons); 8.27 (s, 1H, NHN*H*). Electronic spectral data in CH_3OH (λ (nm) (ε ($M^{-1}\,cm^{-1}$))): 322 (1760), 264sh (9700), 225 (24 600).

2.4. Synthesis of [Ni(bbhac)]

To a methanol solution (20 ml) of bzpyzn (572 mg, 1.7 mmol) a methanol solution (20 ml) of $Ni(O_2CCH_3)\cdot 4H_2O$ (425 mg, 1.7 mmol) was added dropwise over a period of 5 min. with stirring in air. The mixture was stirred for another 5 h. The green solid that precipitated was collected by filtration, washed thoroughly with methanol and dried in vacuum over anhydrous $CaCl_2$. Yield, 500 mg (75%). *Anal*. Calc. for $C_{19}H_{17}N_4O_2Ni$: C, 58.21; H, 4.37; N, 14.29. Found: C, 57.85; H, 4.25; N, 14.07%. ESI mass spectrum: highest m/z at 392 ($[M]^+$). Selected IR bands (cm^{-1}): 1632(m), 1597(m), 1539(w), 1472(s), 1412(s), 1379(s), 1279(m), 1215(w), 1171(m), 1117(w), 1086(s), 1009(s), 920(s),

880(s), 787(m), 731(m), 698(s), 534(w). Electronic spectral data in CH_2Cl_2 (λ (nm) (ε ($M^{-1}\,cm^{-1}$))): 772 (130), 644 (640), 595sh (330), 439 (4 600), 372sh (4 580), 346 (5 860), 267 (9 440). μ_{eff} (μ_B) at 300 K: 1.71.

2.5. Synthesis of [Ni(bbhacO)]

[Ni(bbhac)] (100 mg, 0.25 mmol) was dissolved in 25 ml of dichloromethane–acetonitrile (1:1) mixture and left in air at room temperature for slow evaporation. The initial green colour of the solution slowly became brown and in about 4–5 days a brown crystalline solid separated. The complex was collected by filtration and dried in air. Yield, 30 mg (29%). A single crystal suitable for X-ray structure determination was selected from this material. *Anal*. Calc. for $NiC_{19}H_{16}N_4O_3$: C, 56.06; H, 3.96; N, 13.76. Found: C, 55.84; H, 3.73; N, 13.51%. Selected IR bands (cm^{-1}): 1649(m), 1591(m), 1541(s), 1491(m), 1443(w), 1368(s), 1242(w), 1208(w), 1169(m), 1138(w), 1067(w), 1026(m), 955(w), 924(w), 870(w), 787(w), 700(s), 599(m), 474(w). ^1H NMR (200 MHz) data in $(CD_3)_2SO$ (δ): 2.35 (s, 3H, CH_3); 7.46 (m, 3H, phenyl); 7.93 (m, 2H, phenyl). Electronic spectral data in CH_3CN (λ (nm) (ε ($M^{-1}\,cm^{-1}$))): 577sh (95), 398sh (3 670), 364 (6 830), 269 (7 330), 223 (8 100).

2.6. X-ray crystallography

For each of the two compounds, bzpyzn and [Ni(bbhacO)], the crystal was mounted at the end of a glass fibre and covered with a thin layer of epoxy. The data were collected on an Enraf-Nonius Mach-3 single crystal diffractometer using graphite monochromated Mo Kα radiation ($\lambda = 0.71073$ Å) by the ω-scan method. Unit cell parameters of bzpyzn and [Ni(bbhacO)] were determined by the least-squares fit of 25 reflections having 2θ values in the range 18°–22° and 19°–29°, respectively. In each case, the stability of the crystal was monitored by measuring the intensities of three check reflections after every 1.5 h during the data collection. No decay was observed in either case. An empirical absorption correction was applied to the data of [Ni(bbhacO)] based on the ψ-scans of three reflections. The compounds bzpyzn and [Ni(bbhacO)] crystallize in *Pbca* and $P\bar{1}$ space groups, respectively. The structures were solved by using direct methods and refined by full-matrix least-squares procedures on F^2. In each case, the asymmetric unit contains a single molecule of the compound. For both structures all the non-hydrogen atoms were refined using anisotropic thermal parameters. The hydrogen atoms were included at calculated positions by using a riding model and were used for the structure factor calculation, but were not refined. Calculations were done using the programs of WINGX [17] for data reduction and absorption correction, and SHELX-97 programs [18] for structure solution and refinement. The ORTEX6a [19] and PLATON [20] packages were used for molecular graphics. Significant crystal data are summarized in Table 1.

Table 1
Crystallographic data for bzpyzn and [Ni(bbhacO)]

Compound	bzpyzn	[Ni(bbhacO)]
Chemical formula	$C_{19}H_{20}N_4O_2$	$C_{19}H_{16}N_4O_3Ni$
Formula weight	336.39	407.07
Crystal system	orthorhombic	triclinic
Space group	*Pbca*	$P\bar{1}$
Unit cell dimensions		
a (Å)	10.287(2)	7.5030(11)
b (Å)	12.667(3)	11.1159(12)
c (Å)	27.550(6)	11.605(2)
α (°)	90	106.857(13)
β (°)	90	99.946(9)
γ (°)	90	102.851(13)
V (Å^3)	3590.2(15)	873.4(2)
Z	8	2
μ (mm^{-1})	0.083	1.139
Total reflections	4645	3453
Independent reflections	4124	3186
R_1, wR_2 [$I \geqslant 2\sigma(I)$]	0.0489, 0.0963	0.0387, 0.0959
R_1, wR_2 (all data)	0.1448, 0.1258	0.0556, 0.1031
Goodness-of-fit on F^2	1.003	1.072
Largest peak and hole (e Å^{-3})	0.166 and −0.189	0.784 and −0.405

3. Results and discussion

3.1. Synthesis and characterization of bzpyzn

Reaction of 1 mol equivalent of acetylacetone with 2 mol equivalents of benzoylhydrazine in methanol produced a white product in good yield. The elemental analysis data for this compound are consistent with the formula $C_{19}H_{20}N_4O_2$ for the desired acetylacetone bis(benzoylhydrazone) (H_3bbhac). However, as it is known that this type of reaction leads to cyclized 3,5-substituted pyrazolines [12–14], we have determined the molecular structure of bzpyzn by single crystal X-ray crystallography. The structure obtained confirms the cyclization reaction and formation of the pyrazoline derivative (Fig. 1). Selected bond parameters are listed in Table 2. The intramolecular bond distances are comparable to other similar structurally characterized compounds [13,14,21,22]. In the solid state, a one-dimensional assembly of the bzpyzn molecules is formed via intermolecular hydrogen bonding (Fig. 2). The oxygen atom (O2) of the benzoyl group attached to N3 and one of the hydrazide protons of the benzoylhydrazide group attached to C3 (Fig. 1) are involved in the hydrogen bonding. The N1···O2 distance and N1–H···O2 angle are 2.871(2) Å and 160.0(2)°, respectively.

The infrared spectrum of bzpyzn shows a strong peak at 3277 cm^{-1}, possibly due to the N–H groups [23]. Two

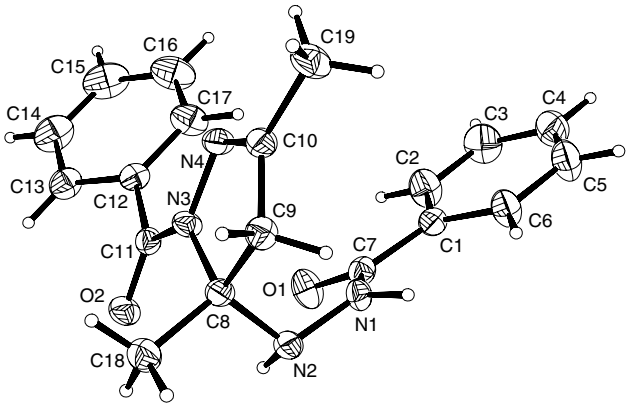

Fig. 1. Molecular structure of bzpyzn with the atom labelling scheme. All non-hydrogen atoms are represented by their 30% probability thermal ellipsoids.

Table 2
Selected bond lengths (Å) and bond angles (°) for bzpyzn

Bond lengths			
O(1)–C(7)	1.231(2)	N(3)–N(4)	1.406(2)
O(2)–C(11)	1.233(2)	N(4)–C(10)	1.276(3)
N(1)–C(7)	1.344(3)	C(9)–C(10)	1.487(3)
N(1)–N(2)	1.414(2)	C(8)–C(9)	1.526(3)
N(2)–C(8)	1.459(3)	N(3)–C(8)	1.502(3)
N(3)–C(11)	1.355(3)	C(8)–C(18)	1.515(3)
Bond angles			
N(4)–N(3)–C(8)	112.36(15)	N(2)–C(8)–C(18)	108.02(17)
C(10)–N(4)–N(3)	107.56(17)	N(3)–C(8)–C(18)	113.46(17)
N(4)–C(10)–C(9)	114.54(18)	C(11)–N(3)–N(4)	122.19(17)
C(10)–C(9)–C(8)	103.94(17)	C(11)–N(3)–C(8)	124.50(17)
N(3)–C(8)–C(9)	99.96(16)	C(19)–C(10)–C(9)	123.54(19)
N(2)–C(8)–C(9)	110.91(16)	N(4)–C(10)–C(19)	121.9(2)

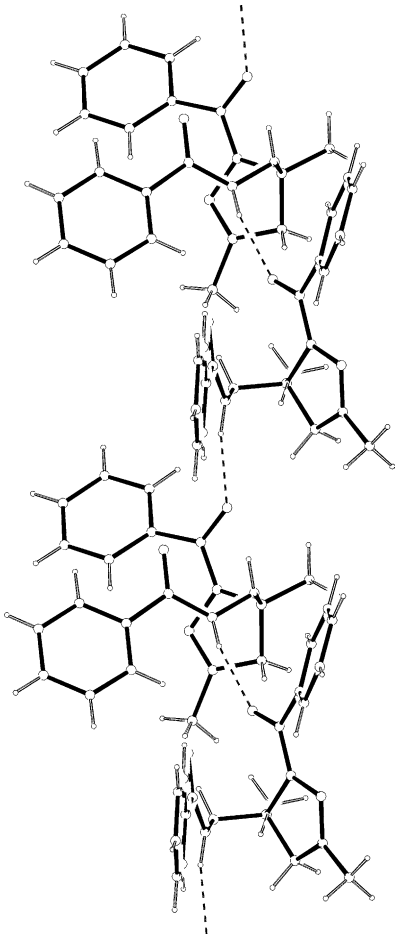

Fig. 2. One-dimensional ordering of the bzpyzn molecules via N–H···O interactions.

strong peaks observed at 1659 and 1605 cm^{-1} are assigned to the C=O and C=N stretches, respectively [22,23]. The electronic spectrum of bzpyzn in methanol solution displays three strong absorptions in the range 322–225 nm. The proton NMR spectrum of bzpyzn in $CDCl_3$ solution is consistent with the pyrazoline structure. The 5-methyl and 3-methyl protons appear as singlets at 1.88 and 1.98 δ, respectively. As observed in other similar compounds [12–14,22], the methylene group protons of bzpyzn are diastereotopic and observed as an AB type quartet centred at 3.06 δ. Each of the two N–H group protons appear as a singlet. They are observed at 5.30 and 8.27 δ. The aromatic protons appear as two multiplets centred at 7.44 and 7.78 δ.

3.2. Formation of [Ni(bbhac)] by ring opening of bzpyzn

Under aerobic conditions, reaction of 1 mol equivalent of bzpyzn with 1 mol equivalent of $Ni(O_2CCH_3)\cdot 4H_2O$ in methanol results in the formation of a green solid. In the infrared spectrum of this green solid there is no peak near 3300 cm^{-1} attributable to an N–H group. The strong peak at 1659 cm^{-1} displayed by free bzpyzn, due to the C=O stretch, is also absent. The non-appearance of the N–H and C=O stretches is consistent with the ring opening of bzpyzn and complexation of the metal ion by the tetradentate N_2O_2 donor $Hbbhac^{2-}$ (H represents the active methylene proton) or $bbhac^{3-}$. Two medium intensity peaks observed at 1632 and 1597 cm^{-1} are most likely due to the deprotonated O-coordinating amide functionalities and the C=N moieties of the tetradentate ligand [6–11,24]. The complex is electrically non-conducting in CH_2Cl_2 solution. The elemental analysis data are consistent with the formula [Ni(bbhac)]. It has been reported that in the presence of oxygen or iodine, oxidative C–C coupling involving the central C-atom of the acetylacetone residue in complexes with similar tetradentate Schiff bases leads to dinuclear species [25–27]. Although [Ni(bbhac)] has been isolated in the presence of air, the ESI mass spectral data indicates that the complex is mononuclear. Furthermore, oxidation of the –CH= moiety of the acetylacetone residue to a keto group and the formation of [Ni(bbhacO)] (vide infra) also supports the mononuclear nature of [Ni(bbhac)]. The electronic spectrum

of the complex in CH_2Cl_2 solution displays several absorptions in the range 772–267 nm. The three weak absorptions at 772, 644 and 595 nm are most likely due to d–d transitions [28]. The remaining intense bands are likely to be due to ligand-to-metal charge transfer and intra-ligand transitions.

The solid state magnetic moment (1.71 μ_B) of [Ni(bbhac)] at 300 K indicates an $S = 1/2$ spin state. A non-innocent nature of the ligands in complexes with tetradentate Schiff bases derived from acetylacetone has been noted before [25–27]. Thus, to resolve the ambiguity between an authentic nickel(III) complex and a nickel(II) stabilized ligand radical system we have examined the EPR spectral features of [Ni(bbhac)] (Fig. 3). At room temperature (300 K) in the powdered phase the complex displays an isotropic signal centred at $g = 2.01$. The peak-to-peak width for this signal is 70 G. At low temperature (115 K) this signal becomes rhombic and the corresponding g values are 2.02, 2.01 and 1.98. Like the solid sample, a dichloromethane solution of the complex at room temperature also displays a similar isotropic signal at $g = 2.01$. However, the peak-to-peak width (17 G) for this signal is significantly smaller compared to that in the solid state spectrum (Fig. 3). The spectrum of the complex in frozen (115 K) dichloromethane solution is again rhombic in character (g values are 2.02, 2.01 and 1.98). However, in this spectrum the lowest field signal is well resolved and the highest field signal is significantly broadened compared to the corresponding signals observed in the spectrum obtained from the solid sample of the complex at the same temperature (Fig. 3). The observed g values are very close to those for a nickel(II) stabilized ligand radical species [29–31]. However, the peak-to-peak width for the isotropic signal observed at room temperature in the solid state spectrum is rather large for a ligand radical system [31]. Although the room temperature isotropic signal displayed by the dichloromethane solution of [Ni(bbhac)] is sufficiently narrow, it is devoid of any nitrogen hyperfine structure to suggest a ligand radical system. In addition, at low temperature both solid state and frozen solution spectra are rhombic in character. Such rhombic spectra are not unusual for square-planar nickel(III) complexes, due to distortion from the square-planar geometry or weak coordination at the apical site [32,33]. Considering all the EPR features it is difficult to describe [Ni(bbhac)] as a genuine nickel(III) species or a nickel(II) stabilized ligand radical system. Thus the best description for [Ni(bbhac)] may perhaps be that it is border-line between the two possible situations. However, the typical rhombic nature of both low temperature solid state and frozen solution spectra suggests that [Ni(bbhac)] may be slightly biased towards the nickel(III) side.

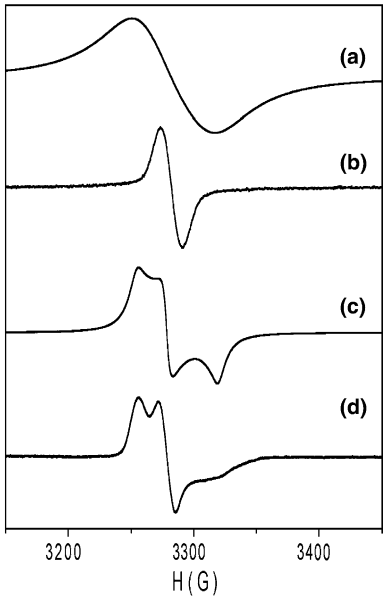

Fig. 3. EPR spectra of [Ni(bbhac)]: (a) in powder phase at 300 K; (b) in dichloromethane solution at 300 K; (c) in powder phase at 115 K; (d) in frozen (115 K) dichloromethane solution.

3.3. Isolation and characterization of [Ni(bbhacO)]

Slow evaporation of a green dichloromethane–acetonitrile (1:1) solution of [Ni(bbhac)] in air produces a brown crystalline substance. However, if the same procedure is performed using dry solvents under moisture free atmosphere in the presence or absence of oxygen, the unchanged [Ni(bbhac)] is recovered as a green amorphous material. Interestingly [Ni(bbhac)] also remains unchanged in wet solvent under dinitrogen atmosphere. Thus, the brown complex is formed in the presence of both water and oxygen. Solid state magnetic susceptibility measurements with this brown crystalline substance indicate the diamagnetic character of this material. In acetonitrile solution, this new species is electrically non-conducting. Thus the brown complex is most likely a neutral square-planar nickel(II) complex. In the electronic spectrum, the complex displays a weak absorption at ~577 nm. This absorption has been assigned to the spin-allowed d–d transition ($^1A_{1g} \rightarrow {}^1A_{2g}$). Four more absorptions observed in the range 398–223 nm are possibly due to ligand-to-metal charge transfer and intra-ligand transitions. The proton NMR spectrum of the complex displays only three signals. The singlet observed at 2.35 δ, corresponding to three protons, has been assigned to the methyl group. The multiplets centred at 7.46 and 7.93 δ correspond to three and two protons, respectively. These signals are assigned to the phenyl ring protons. Observation of only one methyl group and one phenyl ring in the NMR spectrum suggests that both halves of the tetradentate ligand in the complex are magnetically equivalent, at least on an NMR time-scale. There is no signal assignable to

methylene or N–H groups. The infrared spectrum of the solid also does not display any peak that could be associated with the N–H group. The absence of an N–H group indicates deprotonation of the amide functionalities in the ligand. However, one medium intensity peak observed at 1649 cm^{-1} is very likely to be due to a C=O group. The origin of another medium intensity peak at 1591 cm^{-1} is most likely the C=N moieties of the ligand. As mentioned before, under aerobic conditions square-planar bivalent 3d metal ion complexes of the formula [ML] (H_2L = acetylacetone bis(thiosemicarbazone)), the central methylene of the acetylacetone residue of L^{2-} gets oxidized and a keto group is formed [14,15]. The infrared spectrum and other physical properties indicate that the brown material obtained from [Ni(bbhac)] is possibly a similar square-planar nickel(II) complex with the oxidized ligand $bbhacO^{2-}$.

We have determined the X-ray structure of the brown complex to confirm the above conjecture. The structure reveals that indeed the middle C-atom of the acetylacetone residue has been oxidized with the formation of a keto group (Fig. 4). The molecule is a square-planar nickel(II) species having a tetradentate dianionic ligand ($bbhacO^{2-}$). Selected bond parameters are listed in Table 3. Intra-ligand bond distances and angles are unexceptional and consistent with the deprotonation of both amide functionalities and C9–O3 being a keto group [6–11,22,34,35]. The ligand binds the metal ion via two amide-O atoms and two imine-N atoms providing an N_2O_2 square-plane around the metal ion. In this process, it forms two five- and one six-membered chelate ring. The chelate bite angles for the five membered rings are essentially identical (84.77(9)° and 84.69(9)°), and are smaller than that (97.40(10)°) of the six-membered ring. There is no displacement of the nickel(II) centre from the N_2O_2 square plane. The maximum deviation from the mean plane formed by NiN_2O_2 is 0.0055(11) Å for O1 (Fig. 4). However, the molecule as a whole is not perfectly planar. The two phenyl ring planes are slightly tilted from the mean plane constituted by the rest of the molecule. The dihedral angles thus formed are very similar (7.43(15)° and 7.17(14)°). The angle between the two phenyl ring planes is 10.96(18)°. The Ni–N(imine) distances (1.836(2) and 1.841(2) Å) are very similar. The same is true for the Ni–O(amide) distances (1.8418(19) and 1.8479(19) Å). These distances are comparable with the distances observed for square-planar nickel(II) complexes having imine-N or deprotonated amide-O coordinating atoms [22,26,27,34,35].

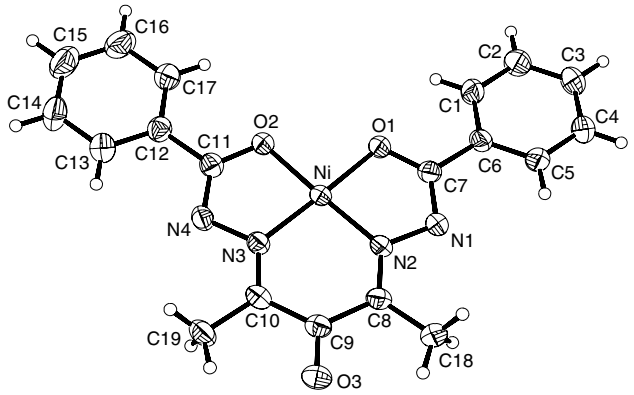

Fig. 4. Molecular structure of [Ni(bbhacO)] with the atom labelling scheme. All non-hydrogen atoms are represented by their 40% probability thermal ellipsoids.

Table 3
Selected bond lengths (Å) and bond angles (°) for [Ni(bbhacO)]

Bond lengths			
Ni–O(1)	1.8418(19)	N(1)–N(2)	1.392(3)
Ni–O(2)	1.8479(19)	N(3)–N(4)	1.396(3)
Ni–N(2)	1.841(2)	N(1)–C(7)	1.325(4)
Ni–N(3)	1.836(2)	N(4)–C(11)	1.317(4)
O(1)–C(7)	1.293(3)	N(2)–C(8)	1.301(3)
O(2)–C(11)	1.294(3)	N(3)–C(10)	1.294(4)
O(3)–C(9)	1.215(3)		
Bond angles			
O(1)–Ni–O(2)	93.15(8)	O(2)–Ni–N(2)	177.90(9)
O(1)–Ni–N(2)	84.77(9)	O(2)–Ni–N(3)	84.69(9)
O(1)–Ni–N(3)	177.79(9)	N(2)–Ni–N(3)	97.40(10)

[Ni(bbhacO)] does not have any good conventional hydrogen bond donor. However, intermolecular C–H···π interactions [11,36–38] lead to the self-assembly of [Ni(bbhacO)] molecules into a one-dimensional array in

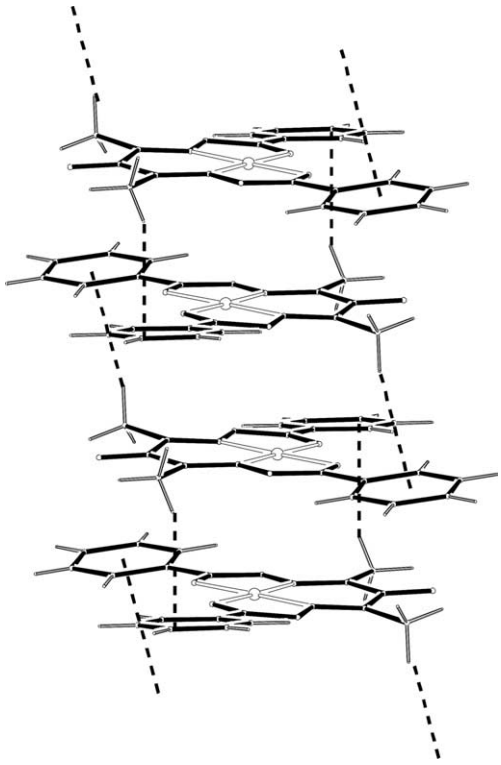

Fig. 5. One-dimensional ordering of the [Ni(bbhacO)] molecules via C–H···π interactions.

the crystal lattice. In this one-dimensional arrangement, two methyl group C–Hs of each molecule are interacting with the phenyl rings of the two adjacent molecules in a reciprocal manner (Fig. 5). Thus, both methyl groups and both phenyl rings of every molecule are involved in these interactions. The H···centroid (cg) distances are 2.801 and 2.952 Å for C18–H···cg (of C12–C17 ring) and C19–H···cg (of C1–C6 ring) interactions, respectively. The corresponding C–H···cg angles are 137.2° and 125.4°, respectively. The Ni···Ni distance for the pair of molecules involved in C18–H···cg interactions is 4.142 Å and that for the pair of molecules involved in C19–H···cg interactions is 3.586 Å . The differences in the structural parameters associated with the two C–H···π interactions and the tilted nature of the two phenyl rings compared to the rest of the molecule (vide supra) are possibly responsible for the alternating short and long Ni···Ni distances in the chain-like arrangement of the metal ions.

4. Conclusion

Our objective was to study the nickel coordination chemistry with the Schiff base acetylacetone bis(benzoylhydrazone) (H_3bbhac) containing two higher oxidation state promoting amide functionalities. In our attempt to prepare this Schiff base from acetylacetone and benzoylhydrazine, we have isolated a new substituted pyrazoline. Treatment of this pyrazoline with nickel acetate tetrahydrate leads to metal ion assisted pyrazoline ring opening and the formation of a neutral complex of the formula [Ni(bbhac)], having the intended ligand. The molecular formula and the magnetic moment of [Ni(bbhac)] are consistent with the +3 formal oxidation state of the metal ion in this complex. However, the EPR spectral characteristics of this complex indicate a border-line situation between a nickel(III) species and a nickel(II) stabilized ligand radical species. In wet dichloromethane–acetonitrile solution, the –CH═ moiety of the ligand in [Ni(bbhac)] gets oxidized to –C(═O)– and a square-planar nickel(II) complex of the formula [Ni(bbhacO)] is formed. Considering the border-line nature of [Ni(bbhac)] and the need of moisture for this transformation to take place, a possible mechanism for this oxidation could be as follows: shift of the unpaired electron from the nitrogen atom to the methine carbon of the ligand, followed by homolytic cleavage of the C–H bond and addition of water to form –CH(OH)–, and finally a $2e^-$, $2H^+$ oxidation to the keto group by oxygen. Similar mechanisms have been suggested for platinum(IV) and Ru(III) assisted conversion of a methine group to a keto group in guanine [39,40].

Although the oxidation of the methylene group to a keto group for the complexes [ML] of the deprotonated acetylacetone bis(thiosemicarbazone) (H_2L) in the presence of oxygen has been observed before [14,15], nothing has been reported about the nature of the intermediate involved during the formation of [MLO] from [ML]. In this work, we have been able to isolate and establish the nature of this intermediate which provides us with some clues about the possible pathways for the transformation to the final complex of the oxidized ligand. We are currently investigating the chemistry of other transition metal ions with the same ligand and those prepared from 3-substituted 2,4-pentanediones for a better understanding of the intricacies involved in this ligand oxidation process.

5. Supplementary material

Crystallographic data have been deposited with the Cambridge Crystallographic Data centre (deposition numbers are CCDC-233762 and CCDC-233763 for bzpyzn and [Ni(bbhacO)], respectively). Copies of this information may be obtained from The Director, CCDC, 12 Union Road, Cambridge CB2 1EZ, UK (fax: +44-1233-336033; email: deposit@ccdc.cam.ac.uk or www: http://www.ccdc.cam.ac.uk).

Acknowledgements

X-ray crystallographic data were obtained from the National Single Crystal Diffractometer Facilities (established by the Department of Science and Technology, New Delhi) at the School of Chemistry, University of Hyderabad and at the Department of Chemistry, Indian Institute of Technology, Bombay. We thank the University Grants Commission, New Delhi for the facilities provided under the UPE program. Mr. A. Mukhopadhyay thanks the Council of Scientific and Industrial Research, New Delhi for a research fellowship.

References

[1] J.R. Lancaster (Ed.), The Bioinorganic Chemistry of Nickel, VCH, New York, 1988.
[2] A.E. Przybyla, J. Robbins, N. Menon, H.D. Peck Jr., FEMS Microbiol. Rev. 88 (1992) 109.
[3] H. Yoon, T.R. Wagler, K.J. O'Connor, C.J. Burrows, J. Am. Chem. Soc. 112 (1990) 4568.
[4] P.J. Chmielewski, L. Latos-Grażyński, Inorg. Chem. 36 (1997) 840.
[5] D.W. Margerum, Pure Appl. Chem. 32 (1983) 297.
[6] N.R. Sangeetha, C.K. Pal, P. Ghosh, S. Pal, J. Chem. Soc., Dalton Trans. (1996) 3293.
[7] A.V. Lakshmi, N.R. Sangeetha, S. Pal, Indian J. Chem. Sect. A 36 (1997) 844.
[8] G.V. Karunakar, N.R. Sangeetha, V. Susila, S. Pal, J. Coord. Chem. 50 (2000) 51.
[9] S.N. Pal, S. Pal, J. Chem. Soc., Dalton Trans. (2002) 2102.
[10] S. Pal, Proc. Indian Acad. Sci. (Chem. Sci.) 114 (2002) 417.
[11] S.N. Pal, S. Pal, Eur. J. Inorg. Chem. (2003) 4244.
[12] H. Buttkus, R.J. Bose, J. Org. Chem. 36 (1971) 3895.

[13] D.H. Hunter, C. McRoberts, J.J. Vittal, Can. J. Chem. 76 (1998) 522.
[14] S.C. Davies, M.C. Durrant, D.L. Hughes, A. Pezeshk, R.L. Richards, J. Chem. Res. (S) (2001) 100.
[15] V.B. Arion, N.V. Gerbeleu, K.M. Indrichan, Russ. J. Inorg. Chem. 30 (1985) 70.
[16] W.E. Hatfield, in: E.A. Boudreaux, L.N. Mulay (Eds.), Theory and Applications of Molecular Paramagnetism, Wiley, New York, 1976, p. 491.
[17] L.J. Farrugia, J. Appl. Crystallogr. 32 (1999) 837.
[18] G.M. Sheldrick, SHELX-97, Structure Determination Software, University of Göttingen, Göttingen, Germany, 1997.
[19] P. McArdle, J. Appl. Crystallogr. 28 (1995) 65.
[20] A.L. Spek, PLATON – A Multipurpose Crystallographic Tool, Utrecht University, Utrecht, The Netherlands, 2002.
[21] E.C. Constable, M.J. Doyle, S.M. Elder, P.R. Raithby, J. Chem. Soc., Chem. Commun. (1989) 1376.
[22] K.C. Joshi, R. Bohra, B.S. Joshi, Inorg. Chem. 31 (1992) 598.
[23] W. Kemp, Organic Spectroscopy, Macmillan, Hampshire, 1987, p. 65.
[24] K. Nakamoto, Infrared and Raman Spectra of Inorganic and Coordination Compounds, Wiley, New York, 1986, pp. 241–244.
[25] U. Knof, T. Weyhermüller, T. Wolter, K. Weighardt, E. Bill, C. Butzlaff, A.X. Trauwein, Angew. Chem., Int. Ed. Engl. 32 (1993) 1635.
[26] V.B. Arion, N.V. Gerbeleu, V.G. Levitsky, Y.A. Simonov, A.A. Dvorkin, P.N. Bourosh, J. Chem. Soc., Dalton Trans. (1994) 1913.
[27] V.B. Arion, K. Weighardt, T. Weyhermüller, E. Bill, V. Leovac, A. Rufinska, Inorg. Chem. 36 (1997) 661.
[28] C. Daul, C.W. Schläpfer, A. von Zelewsky, Struct. Bonding (Berlin) 36 (1979) 129.
[29] J.A. McCleverty, Prog. Inorg. Chem. 10 (1968) 49.
[30] R.S. Drago, I. Baucom, Inorg. Chem. 11 (1972) 2064.
[31] R.R. Gagné, D.M. Ingle, Inorg. Chem. 20 (1981) 420.
[32] T.J. Collins, T.R. Nichols, E.S. Uffelman, J. Am. Chem. Soc. 113 (1991) 4708.
[33] Y. Shimazaki, F. Tani, K. Fukui, Y. Naruta, O. Yamauchi, J. Am. Chem. Soc. 125 (2003) 10512.
[34] A. Mukhopadhyay, G. Padmaja, S.N. Pal, S. Pal, Inorg. Chem. Commun. 6 (2003) 381.
[35] H. Yin, S.-X. Liu, Chinese J. Inorg. Chem. 18 (2002) 269.
[36] M. Nishio, Y. Umezawa, M. Hirota, Y. Takeuchi, Tetrahedron 51 (1995) 8665.
[37] K.S.B. Hancock, J.W. Steed, Chem. Commun. (1998) 1409.
[38] K. Biradha, M.J. Zaworotko, J. Am. Chem. Soc. 120 (1998) 6431.
[39] S. Choi, S. Delaney, L. Orbai, E.J. Padgett, A.S. Hakemian, Inorg. Chem. 40 (2001) 5481.
[40] K.C. Cariepy, M.A. Curtin, M.J. Clarke, J. Am. Chem. Soc., 111 (1989) 4947.

Available online at www.sciencedirect.com
SCIENCE DIRECT®
Polyhedron 23 (2004) 2005–2011
POLYHEDRON
www.elsevier.com/locate/poly

DFT calculation and X-ray structure of the $[ReCl_3(pzH)_3]$ complex

Barbara Machura [a,*], M. Jaworska [b], Rafal Kruszynski [c,1]

[a] Department of Inorganic and Radiation Chemistry, Institute of Chemistry, University of Silesia, 9th Szkolna St., 40-006 Katowice, Poland
[b] Department of Theoretical Chemistry, Institute of Chemistry, University of Silesia, 9th Szkolna St., 40-006 Katowice, Poland
[c] X-Ray Crystallography Laboratory, Institute of General and Ecological Chemistry, Technical University of Łódź, 116 Żeromski St., 90-924 Łódź, Poland

Received 24 March 2004; accepted 11 May 2004
Available online 24 June 2004

Abstract

The X-ray structure of a new paramagnetic $[ReCl_3(pzH)_3]$ complex (pzH = pyrazole) has been determined and its geometric parameters have been examined using the density functional theory (DFT) method. The UV–Vis spectrum of the complex has been discussed on the basis of the electronic transitions of $[ReCl_3(pzH)_3]$ calculated with the time-dependent DFT method (TDDFT).
© 2004 Elsevier Ltd. All rights reserved.

Keywords: Rhenium complexes; Pyrazole ligand; X-ray structure; DFT calculations

1. Introduction

Pyrazole and its derivatives possess two adjacent nucleophilic sites and their steric and electronic properties can be modified by the substituents of the heterocyclic ring. They (i) can act as monodentate, *exo*- or even *endo*-bidentate anionic ligands, (ii) can afford oligomers of different nuclearities depending on the used synthesis methods and (iii) have been shown to possess a rather wide conformational variability [1–4].

Previously, we investigated the reactivity of oxorhenium(V) species – $[ReO(OEt)X_2(PPh_3)_2]$, $[ReOX_3(PPh_3)_2]$ and $[ReOX_3(AsPh_3)(OAsPh_3)]$ (X = Cl or Br) – towards pyrazole (pzH) and 3,5-dimethylpyrazole (3,5-Me_2pzH) under different reaction conditions. The products of these syntheses include (i) mononuclear $[ReOX_2\{\eta^2\text{-}N_2C_3H_3C(CH_3)_2O\}(PPh_3)]$ complexes with the $C_3H_3N_2C(CH_3)_2O^-$ anion obtained in the addition reaction of pyrazole and acetone, and (ii) dinuclear Re(V) compounds of the types $[\{Re(O)X(PPh_3)\}_2(\mu\text{-}O)(\mu\text{-}pz)_2]$, $[\{Re(O)X_2(3,5\text{-}Me_2pzH)_2\}_2(\mu\text{-}O)]$, $[\{Re(O)Br(3,5\text{-}Me_2pzH)\}_2(\mu\text{-}O)(\mu\text{-}3,5\text{-}Me_2pz)_2]$, $[\{Re(O)X(PPh_3)\}_2(\mu\text{-}O)(\mu\text{-}3,5\text{-}Me_2pz)_2]$ and $[\{Re(O)X(PPh_3)\}(\mu\text{-}O)(\mu\text{-}3,5\text{-}Me_2pz)_2\{Re(O)X(3,5\text{-}Me_2pzH)\}]$(X = Cl or Br) [5,6].

Here, we report the synthesis and X-ray structure of $[ReCl_3(pzH)_3]$ complex (**1**) and the results of DFT calculations for **1**, based on B3LYP theory, carried out by using the GAUSSIAN 03 program package. The UV–Vis spectrum of the title complex is discussed based on the electronic transitions of **1**, calculated using the time-dependent DFT method (TDDFT).

Reports of $[ReX_3L_3]$ rhenium complexes with monodentate N-donor ligands (L) are restricted, and the only structurally characterized complexes of this type appear to be *mer*-$[ReFI_2(py)_3]$ [7], *mer*-$[ReCl_3(py)_3]$, *mer*-$[ReBr_3(py)_3]$ [8] and *mer*-$[ReCl_3(3,5\text{-lut})_3]$ [9].

2. Experimental

2.1. General procedure

The reaction was carried out under argon atmosphere. All solvents were of reagent grade and were used as received. Ammonium perrhenate, Ph_3P and pyrazole (pzH) were purchased from Aldrich and used as

* Corresponding author. Tel.: +48322582441; fax: +48322599978.
E-mail addresses: basia@tc3.ich.us.edu.pl (B. Machura), mj@tc3.ich.us.edu.pl (M. Jaworska).
[1] A holder of the Foundation for Polish Science (FNP) scholarship.

0277-5387/$ - see front matter © 2004 Elsevier Ltd. All rights reserved.
doi:10.1016/j.poly.2004.05.003

received. The $[ReOCl_3(PPh_3)_2]$ complex was prepared according to the literature method [10].

IR spectra were recorded on a Nicolet Magna 560 spectrophotometer in the spectral range 4000–400 cm^{-1} with the samples in the form of KBr pellets. Electronic spectra were measured on a spectrophotometer Lab Alliance UV–Vis 8500 in the range 800–220 nm in deoxygenated dichloromethane solution. Magnetic susceptibilities were measured at 296 K by the Faraday method. Elemental analyses (C, H, N) were performed on a Perkin–Elmer CHN-2400 analyzer.

2.2. Preparation of $[ReCl_3(pzH)_3]\cdot H_2O\cdot HCl$ ($\mathbf{1}\cdot H_2O\cdot HCl$)

$[ReOCl_3(PPh_3)_2]$ (1 g, 1.20 mmol) and pzH (0.54 g, 8 mmol) in benzene (100 cm^3) were refluxed overnight. The color of the reaction mixture changed quickly from yellow-green to dark brown. The volume was condensed to 10 cm^3 and a reddish-brown microcrystalline solid was formed on addition of 100 cm^3 of diethyl ether. The product was washed with EtOH and cold ether, and dried in vacuo. Crystals of $\mathbf{1}\cdot H_2O\cdot HCl$ suitable for X-ray investigation were obtained by recrystallization from $CHCl_3$–EtOH. Yield: 55%.

IR (KBr, cm^{-1}) 3406 (m), 3341 (m), 3142 (s), 1618 (w, br), 1513 (w), 1490 (m), 1470 (m), 1405 (m), 1348 (m), 1327 (m), 1265 (m), 1241 (w), 1125 (s), 1106 (s), 1086 (m), 1052 (vs), 910 (m), 783 (s), 702 (w), 603 (m). Calc. for $C_9H_{15}N_6Cl_4ORe$: C, 19.61; H, 2.74; N, 15.24. Found: C, 19.73; H, 2.6; N, 15.30%.

2.3. Crystal structure determination and refinement

The X-ray intensity data of $\mathbf{1}\cdot H_2O\cdot HCl$ were collected on a KM-4-CCD automatic diffractometer equipped with a CCD detector with 21 s exposure time, and a half of the Ewald sphere was collected. The unit cell parameters were determined from least-squares refinement of the setting angles of the 5023 strongest reflections. Details concerning crystal data and refinement are given in Table 1. Lorentz, polarization and numerical absorption corrections [11] were applied. The structure was solved by means of the Patterson method and subsequently completed by difference Fourier recycling. All the non-hydrogen atoms were refined anisotropically using a full-matrix, least-squares technique. The hydrogen atoms of the phenyl rings were treated as "riding" on their parent carbon atoms [d(C–H) = 0.96 Å] and assigned isotropic temperature factors equal to 1.2 times the value of the equivalent temperature factor of the parent carbon atom. SHELXS-97 [12], SHELXL-97 [13] and SHELXTL [14] programs were used for all the calculations. Atomic scattering factors were those incorporated in the computer programs.

Table 1
Crystal data and structure refinement for $\mathbf{1}\cdot H_2O\cdot HCl$

Empirical formula	$C_9H_{15}Cl_4N_6ORe$
Formula weight	551.27
Temperature (K)	291(2)
Wavelength (Å)	0.71073
Crystal system	triclinic
Space group	$P\bar{1}$
Unit cell dimensions	
a (Å)	7.7451(7)
b (Å)	8.1581(9)
c (Å)	14.1257(10)
α (°)	75.507(10)
β (°)	84.050(8)
γ (°)	81.453(9)
Volume (Å^3)	852.48(14)
Z	2
D_{calc} (Mg/m^3)	2.148
Absorption coefficient (mm^{-1})	7.760
$F(000)$	524
Crystal size (mm)	$0.42\times0.21\times0.20$
θ Range for data collection (°)	3.46–25.14
Index ranges	$-9\leqslant h\leqslant 9$, $-9\leqslant k\leqslant 9$, $-15\leqslant l\leqslant 16$
Reflections collected	8672
Independent reflections (R_{int})	3037 (0.0362)
Completeness to 2θ (%)	99.1
Maximum and minimum transmission	0.3046 and 0.1398
Data/restraints/parameters	3037/0/191
Goodness-of-fit on F^2	1.174
Final R indices [$I > 2\sigma(I)$]	$R_1 = 0.0300$, $wR_2 = 0.0723$,
R indices (all data)	$R_1 = 0.0331$, $wR_2 = 0.0732$
Largest difference peak and hole (e Å^{-3})	1.508 and −1.387

2.4. Computational details

The GAUSSIAN 03 program [15] was used in the calculations. The geometry optimization was carried out using the DFT method with the use of the B3LYP functional [16,17]. The electronic spectrum was calculated with the TDDFT method [18]. The LANL2DZ basis set [19] was used on the rhenium atom, 6-31G(d) on the chlorine, nitrogen and carbon atoms and 6-31G basis on the hydrogen atoms in the calculations.

3. Results and discussion

Refluxing the $[ReOCl_3(PPh_3)_2]$ complex with an excess of pzH in wet benzene under argon atmosphere leads to the isolation of the mononuclear $\mathbf{1}\cdot H_2O\cdot HCl$ complex. The well-known capacity of PPh_3 to interact with the Re≡O bond in rhenium(V) oxo-complexes explains the course of the reaction between $[ReOCl_3(PPh_3)_2]$ and pyrazole:

$$[ReOCl_3(PPh_3)_2] + 3N_2C_3H_4 \rightarrow [ReCl_3(pzH)_3] + PPh_3 + OPPh_3$$

3.1. Geometry and charge distribution

Complex **1** crystallizes as the solvate $\mathbf{1}\cdot H_2O\cdot HCl$. A perspective drawing of $\mathbf{1}\cdot H_2O\cdot HCl$ is shown in Fig. 1. The two groups of ligands of **1** (halide ions and pyrazole molecules) are arranged in a *meridional* fashion and the departure from the ideal octahedron is very limited. Table 1 presents crystal data and structural refinement for **1**. The most important experimental bond lengths and angles for compound **1** are reported in Table 2. The Re–N bond lengths of **1** are similar to those of [{$ReOCl_2py_2$}$_2$(μ-O)] and [{$ReOCl_2$(3,5-Me_2pzH)$_2$}$_2$(μ-O)] [20,21], and the bond distances and angles in the pyrazole rings are in good agreement with expected values [22,23].

The structure of $\mathbf{1}\cdot H_2O\cdot HCl$ is assembled via strong N–H···Cl, N–H···O, Cl–H···O, O–H···N, O–H···Cl and weak C–H···Cl [24–26] intermolecular hydrogen bonds (Table 3) into a three-dimensional network. Three pairs of intermolecular hydrogen bonds: Cl(99)–H99···O(99# $-x,-y,-z+1$), O(99)–H99B···Cl(99# $-x,-y,-z+1$); N(4)–H(4N)···O(99), O(99)–H(99A)···N(4) and Cl(99)–H(99)···O(99# $x-1,y+1,z$), O(99)–H99A···Cl(99# $x+1,y-1,z$) can be considered as double hydrogen bonds [25]. This causes the existence of three relatively short intermolecular contacts H(99)···H(99A) – 2.07 Å, H(4N)···H(99A) – 1.54 Å and H99···H99B – 1.36 Å. In the title compound strong N–H···Cl and weak C–H···Cl intramolecular hydrogen bonds can be also found (Table 3), which provides additional stabilization to the molecule conformation. In this way five-membered rings in spiro arrangement are created.

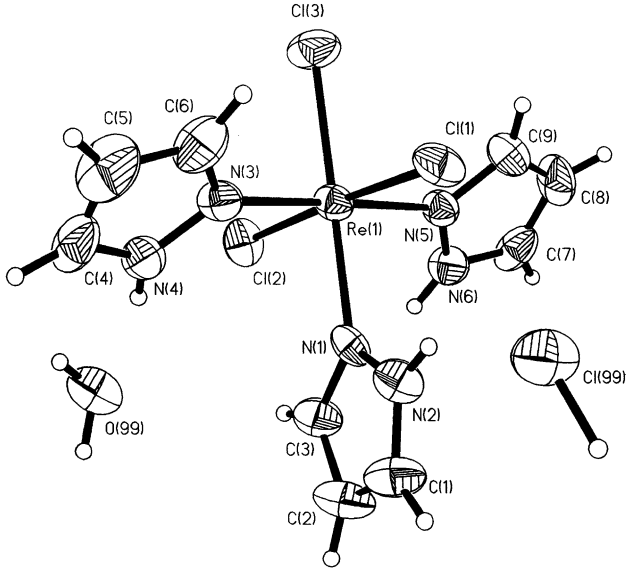

Fig. 1. The molecular structure of $\mathbf{1}\cdot H_2O\cdot HCl$.

Table 2
The experimental and optimized bond lengths (Å) and angles (°) for $\mathbf{1}\cdot H_2O\cdot HCl$

	Experimental	Optimized
Bond lengths		
Re(1)–Cl(1)	2.3220(18)	2.505
Re(1)–Cl(2)	2.3101(18)	2.525
Re(1)–Cl(3)	2.3120(18)	2.390
Re(1)–N(1)	2.133(5)	2.159
Re(1)–N(3)	2.095(5)	2.118
Re(1)–N(5)	2.093(5)	2.118
N(1)–N(2)	1.353(8)	1.352
N(1)–C(3)	1.329(9)	1.344
N(2)–C(1)	1.331(9)	1.345
C(1)–C(2)	1.345(12)	1.388
C(2)–C(3)	1.384(11)	1.401
Bond angles		
N(1)–Re(1)–Cl(2)	89.04(15)	88.04
N(3)–Re(1)–Cl(3)	91.01(16)	89.29
N(5)–Re(1)–Cl(3)	90.87(16)	89.28
N(1)–Re(1)–Cl(3)	177.76(14)	179.56
N(3)–Re(1)–Cl(2)	91.36(17)	89.63
N(5)–Re(1)–Cl(2)	89.43(16)	89.63
N(1)–Re(1)–Cl(1)	88.43(15)	86.41
N(3)–Re(1)–Cl(1)	89.32(17)	90.44
N(5)–Re(1)–Cl(1)	89.81(16)	90.44
N(3)–Re(1)–N(1)	87.1(2)	90.71
N(5)–Re(1)–N(1)	91.0(2)	90.71
N(5)–Re(1)–N(3)	177.9(2)	178.37
Cl(2)–Re(1)–Cl(1)	177.35(7)	174.46
Cl(3)–Re(1)–Cl(1)	90.29(7)	94.03
Cl(2)–Re(1)–Cl(3)	92.26(8)	91.52

Table 3
Hydrogen bonds for $\mathbf{1}\cdot H_2O\cdot HCl$

		H···A	D···A	D–H···A
N(2)	Cl(99)	2.36	3.087(6)	142.8
N(2)	Cl(1)	2.52	3.054(6)	120.8
N(4)	O(99)	1.90	2.726(9)	161.4
N(4)	Cl(2)	2.86	3.261(6)	110.7
N(6)	Cl(99)#1	2.37	3.133(6)	147.4
Cl(99)	O(99)#2	2.16	3.143(7)	125.0
Cl(99)	O(99)#3	2.30	3.145(7)	116.5
O(99)	Cl(99)#5	2.82	3.145(7)	100.9
O(99)	N(4)	2.21	2.726(9)	113.0
O(99)	Cl(99)#2	2.25	3.143(7)	163.8
C(3)	Cl(2)	2.78	3.246(8)	111.8
C(8)	Cl(1)#4	2.78	3.509(8)	136.0

#1 $x+1,y,z$; #2 $-x,-y,-z+1$; #3 $x-1,y+1,z$; #4 $-x,-y+1,-z$; #5 $x+1,y-1,z$.

3.2. Infrared data

The presence of strong bands in the range assignable to N–H vibrations in the spectrum of **1** confirms the coordination of pyrazoles in the neutral monodentate form. The characteristic bands of the C=C and C=N stretching modes, observed at 1640 and 1558 cm^{-1} in uncomplexed pyrazole, are shifted to considerable lower frequencies, which is consistent with the somewhat

longer C=C and C=N bonds in these complexes compared with the same distances in the uncomplexed ligand [27].

3.3. Magnetochemical measurements

Complex **1** shows a room temperature magnetic moment of 1.8 BM. This value is characteristic of mononuclear complexes with low-spin rhenium(III) (d^4) ions in an O_h field [28], and arises because of the large spin–orbit coupling ($\xi = 2500\ cm^{-1}$) [29]. A similar deviation from the expected value (2.8 BM) has been found for $[ReX_2(pymS)(PPh_3)]$ (X = Cl, Br, I) [30,31], $[ReCl_3(NCR)(PPh_3)_2]$ (R = Me, Et, Ph), $[ReCl_3(NCR)(P(p\text{-tol})_3)]$ (R = Me, Et) [32] and $[ReCl_3(\eta^3\text{-}N,N,P\text{–}N\{CH_2CH_2PPh_2\}_2\{CH_2CH_2P(O)Ph_2\})]$ [33].

Table 4
The Mulliken atomic charges for **1**

Atom	
Re(1)	0.571
Cl(1)	−0.413
Cl(2)	−0.399
Cl(3)	−0.296
N(1)	−0.312
N(2)	0.034
N(3)	−0.389
N(4)	0.013
N(5)	−0.318
N(6)	0.003

3.4. The optimized geometry and molecular orbitals of *1*

The geometry of **1** was optimized in triplet and singlet states using the DFT method with the B3LYP functional, but the singlet state could not be converged. Because of that only the triplet state has been calculated, but other calculations show that the B3LYP method gives the proper ordering of spin states of rhenium complexes [34]. The optimized bond lengths and angles for **1** are presented in Table 2. In general, the predicted bond lengths and angles are in agreement with the values based upon the X-ray crystal structure data. The largest differences between the experimental and optimized values may be noticed for Re–Cl distances in *trans* positions to each other (~0.2 Å). The elongation of the rhenium–chlorine bond lengths (up to 0.25 Å) in the B3LYP with different basis sets has been found in other rhenium–chlorine complexes [35]. The optimized length of the Re–Cl *trans* to pyrazole is in good agreement with the experimental data. The differences in the calculated and experimental Re–Cl(1,2) bonds lengths can be explained by strong hydrogen bonding involving Cl(1) and Cl(2) atoms. In the experimental structure the transfer of electron density between the hydrogen bond acceptor and donor causes its local deficiency on the chlorine atoms and thus these atoms are closer to the rhenium atom. The atomic charges calculated with the DFT method presented in Table 4 also confirm the stronger delocalizaton of the electron density of Cl(3) in comparison with Cl(2) and Cl(1) ligands.

Table 5
The energy and character of the selected molecular orbitals with α and β spins for **1**

	α MO		β MO	
	E (eV)	Character	*E* (eV)	Character
HOMO − 11	−8.120	π(pzH), π(Cl)	−8.441	σ(Cl), π(pzH)
HOMO − 10	−7.921	π(pzH), π(Cl)	−8.228	σ(Cl)
HOMO − 9	−7.811	π(pzH), π(Cl)	−8.011	π(pzH), π(Cl)
HOMO − 8	−7.751	π(Cl), π(pzH)	−7.870	π(pzH), π(Cl)
HOMO − 7	−7.570	π(Cl), π(pzH), σ(Cl)	−7.755	π(pzH), (Cl)
HOMO − 6	−7.475	π(pzH), σ(Cl)	−7.642	π(Cl), π(pzH)
HOMO − 5	−7.434	π(pzH), π(Cl)	−7.460	π(pzH), π(Cl)
HOMO − 4	−6.812	π(pzH), π(Re−Cl)	−7.377	π(Cl)
HOMO − 3	−6.576	π(Re-Cl), π(Cl)	−7.361	π(pzH), π(Cl)
HOMO − 2	−5.119	d_{xz}(Re), π(Cl)	−6.700	π(Re-Cl), π(pzH)
HOMO − 1	−4.956	d_{yz}(Re), π(Cl)	−6.304	π(Cl)
HOMO	−4.620	d_{xy}(Re), π(Cl)	−4.085	d_{xy}(Re), π(Cl)
LUMO	−0.530	π*(pzH), d_{xy}(Re)	−2.252	d_{xz}(Re), π(Cl)
LUMO + 1	−0.433	π*(pzH)	−1.820	d_{yz}(Re), π(Cl)
LUMO + 2	0.031	π*(pzH), d_{xy}(Re)	−0.507	π*(pzH), d_{xy}(Re)
LUMO + 3	0.612	d_{z2}(Re)–σ(Cl)	−0.356	π*(pzH)
LUMO + 4	1.111	π*(pzH)	0.391	π*(pzH), d_{xy}(Re)
LUMO + 5	1.299	σ*(N–H)	1.041	d_{z2}(Re)–σ(Cl)
LUMO + 6	1.299	d_{x2-y2}–σ_{pzH}–σ(Cl)	1.117	π*(pzH)
LUMO + 7	1.4106	π*(pzH)	1.319	σ*(N–H)
LUMO + 8	1.566	d_{x2-y2}–σ_{pzH}–σ_{Cl}	1.470	π*(pzH)
LUMO + 9	1.698	π*(pzH)	1.497	π*(pzH)

3.5. Molecular orbitals

The energies and characters of the selected MOs for **1** are presented in Table 5. The following orientation of the axes has been used for determination of the MO characters: the *z* axis goes along the Cl(1)–Re–Cl(2) linkage and *x* goes through the N(3)–Re–N(5) bonds. Several HOMOs and LUMOs of **1** with α and β spins are depicted in Fig. 2. The rhenium d_π atomic orbital (d_{xz}, d_{yz} and d_{xy}) and π orbitals of the chlorine ligands, in anti-bonding arrangement, make the main contributions into the HOMO-2, HOMO-1 and HOMO with α-spin and HOMO, LUMO and LUMO + 1 with β-spin. The α LUMO orbital has predominantly π^*(pzH) character. The LUMO + 3 with α-spin and the LUMO + 5 with β-spin are antibonding orbitals of d_{z2}–σ_{Cl} character. The LUMO + 6 with α-spin is the antibonding orbital of $d_{x^2-y^2}$–σ_{Cl}–σ_{pzH} character.

3.6. Electronic spectrum from the TDDFT calculations

The electronic absorption spectrum of **1** is typical of mononuclear rhenium(III) complexes [30,31]. The solution spectrum of **1** exhibits two intense absorption bands at 269 and 226 nm and some weaker absorptions in the low energy range 520–380 nm.

Considering the significant elongation of the Re–Cl distances in *trans* positions to each other, the spin-allowed triplet–triplet electronic transitions of **1** were calculated with the TDDFT method using the experimental data. The assignment of the calculated transitions to the experimental absorption bands was based on the criterion of the energy and oscillator strength of the calculated transition. Due to the complex character of the MOs of **1**, only the main contributions were taken into consideration for the discussion of the electronic transitions. The assignments of the calculated transitions to the experimental absorption bands are presented in Table 6.

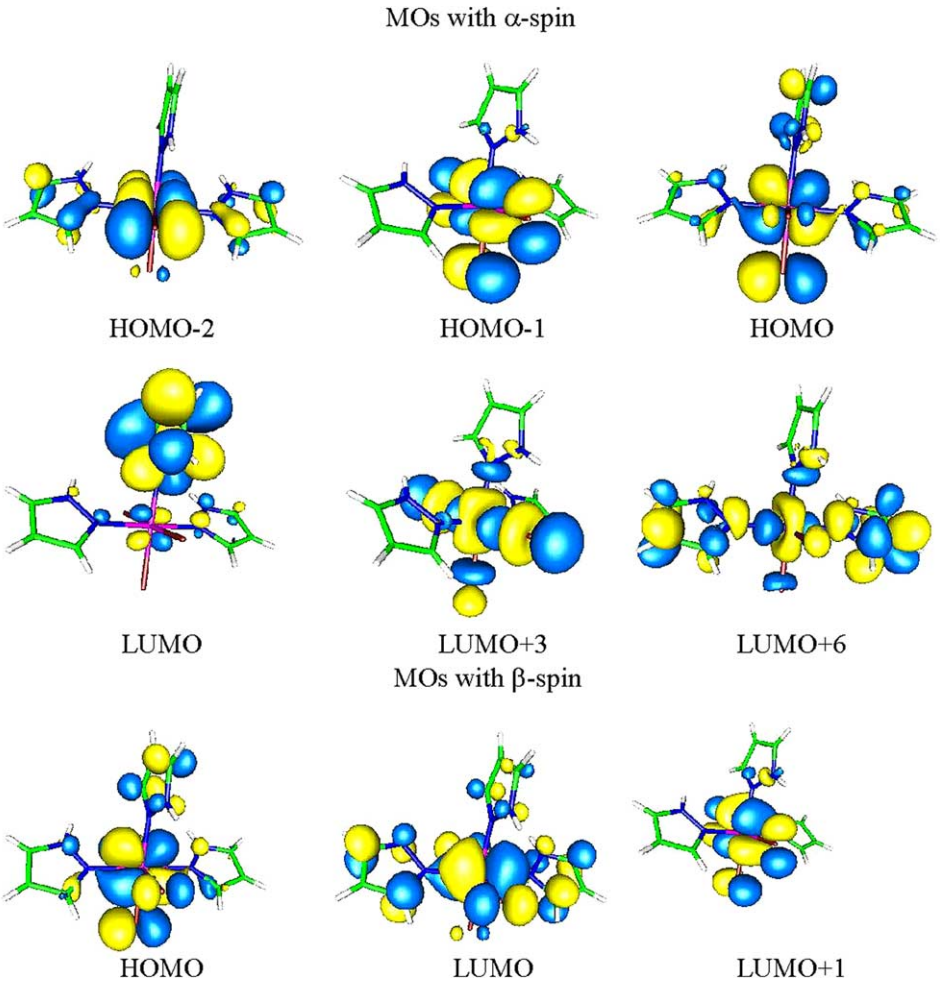

Fig. 2. The selected HOMO and LUMO orbitals with α and β spins for **1**. Positive values of the orbital contour are represented in blue (0.03 a.u.) and negative values in yellow (−0.03 a.u.). (For interpretation of the references to color in this figure legend, the reader is referred to web version of this article.)

Table 6
The energy and molar absorption coefficients of absorption bands and the electronic transitions calculated with the TDDFT method for **1**

The most important orbital excitations		λ (nm)	E (eV)	f	Experimental ΔE/nm(E/eV)ε
α-spin	β-spin				
$H(d_{xy}) \rightarrow L(\pi^*_{pzH})$	$H(d_{xy}) \rightarrow L+2(\pi^*_{pzH})$	475.1	2.61	*0.0142*	518.0(2.39)280
	$H(d_{xy}) \rightarrow L+3(\pi^*_{pzH})$	439.2	2.82	*0.0088*	465.9(2.66)400
$H(d_{xy}) \rightarrow L+3(d_{z2})$	$H(d_{xy}) \rightarrow L+3(\pi^*_{pzH})$	394.2	3.15	*0.0009*	412.9(3.00)580
$H(d_{xy}) \rightarrow L(\pi^*_{pzH})$	$H(d_{xy}) \rightarrow L+4(\pi^*_{pzH})$	377.0	3.29	*0.0360*	
$H(d_{xy}) \rightarrow L+1(\pi^*_{pzH})$		375.8	3.30	*0.0358*	
$H(d_{xy}) \rightarrow L(\pi^*_{pzH})$	$H(d_{xy}) \rightarrow L+4(\pi^*_{pzH})$	366.3	3.39	*0.0121*	391.0(3.17)820
	$H-1(\pi_{Cl}) \rightarrow L+1(d_{yz})$				
$H(d_{xy}) \rightarrow L(\pi^*_{pzH})$	$H-2(\pi_{Cl}) \rightarrow L(d_{xz})$	364.95	3.40	*0.0286*	
	$H-1(\pi_{Cl}) \rightarrow L+1(d_{yz})$	354.1	3.50	*0.0352*	
$H-2(d_{xz}) \rightarrow L+1(\pi^*_{pzH})$		332.7	3.73	*0.0309*	
$H(d_{xy}) \rightarrow L+2(\pi^*_{pzH})$	$H-1(d_{xy}) \rightarrow L+4(\pi^*_{pzH})$	328.7	3.77	*0.0217*	
	$H-5(\pi_{pzH}) \rightarrow L(d_{xz})$	288.8	4.29	*0.1833*	268.8(4.61)2250
	$H-6(\pi_{Cl}) \rightarrow L(d_{xz})$	278.7	4.45	*0.0326*	
	$H-4(\pi_{Cl}) \rightarrow L+1(d_{yz})$				
	$H-9(\pi_{pzH}) \rightarrow L(d_{xz})$	268.2	4.62	*0.0116*	
	$H-8(\pi_{pzH}) \rightarrow L(d_{xz})$				
$H-6(\pi_{pzH}) \rightarrow L+2(\pi^*_{pzH})$	$H-5(\pi_{pzH}) \rightarrow L+1(d_{yz})$	260.6	4.76	*0.0086*	
	$H(d_{xy}) \rightarrow L+9(\pi^*_{pzH})$	253.8	4.88	*0.0082*	
	$H-1(\pi_{Cl}) \rightarrow L+2(\pi^*_{pzH})$	240.5	5.16	*0.0090*	
$H(d_{xy}) \rightarrow L+7(\pi^*_{pzH})$	$H-14(\pi_{pzH}) \rightarrow L+1(d_{yz})$	228.8	5.42	*0.0098*	224.8(5.52)2990
$H-11(\pi_{pzH}) \rightarrow L+1(\pi^*_{pzH})$	$H-9(\pi_{pzH}) \rightarrow L+2(\pi^*_{pzH})$				
$H-10(\pi_{pzH}) \rightarrow L+1(\pi^*_{pzH})$	$H-8(\pi_{pzH}) \rightarrow L+2(\pi^*_{pzH})$				
$H-9(\pi_{pzH}) \rightarrow L+2(\pi^*_{pzH})$	$H-7(\pi_{pzH}) \rightarrow L+3(\pi^*_{pzH})$				
$H-8(\pi_{pzH}) \rightarrow L+1(\pi^*_{pzH})$	$H-5(\pi_{pzH}) \rightarrow L+3(\pi^*_{pzH})$				
$H-5(\pi_{pzH}) \rightarrow L+2(\pi^*_{pzH})$	$H-3(\pi_{pzH}) \rightarrow L+2(\pi^*_{pzH})$				

The experimental bands at 518 and 465 nm are attributed to the calculated transitions at 475.1 and 439.2 nm, respectively. The experimental band at 412.9 nm is assigned to the calculated transitions at 394.2, 377.0 and 375.8 nm. All these transitions have MLCT ($d \rightarrow \pi^*_{pzH}$) character with a small contribution of d–d electronic transitions.

The absorption band at 391.0 nm can be assigned to the calculated transitions in the range 365–328 nm. They have MLCT ($d \rightarrow \pi^*_{pzH}$) and LMCT ($\pi_{Cl} \rightarrow d$) character.

The experimental band at 268.8 nm with $\varepsilon = 2250$ is ascribed to the calculated transitions with large oscillator strengths at 288 and 278 nm of LMCT ($\pi_{pzH} \rightarrow d$ and $\pi_{Cl} \rightarrow d$) character.

The absorption band at 224 nm is attributed to the calculated transition at 228.8 nm. This transition consists mainly of the $\pi \rightarrow \pi^*$ excitations in the pyrazole ligands (intra-ligand LL). We expect additional $\pi \rightarrow \pi^*$ transitions to be found in the calculation at higher energies, but it is outside the range of our calculated spectrum, and it is not of significant interest to the present work. The solution spectrum of pyrazole exhibits an intense absorption band at 231.6 nm, which supports this assignment.

4. Supplementary data

Supplementary data for $C_9H_{15}Cl_4N_6ORe$ are available from the CCDC, 12 Union Road, Cambridge CB2 1EZ, UK (fax: +44-1223-336033; E-mail: deposit@ccdc.cam.ac.uk or www: http://www.ccdc.cam.ac.uk) on request, quoting the deposition number 224809.

Acknowledgements

The Gaussian 03 calculations were carried out in the Wrocł'aw Centre for Networking and Supercomputing, WCSS, Wrocł'aw, Poland under Calculational Grant No. 51/96.

References

[1] S. Trofimenko, Chem. Rev. 72 (1972) 497.
[2] S. Trofimenko, Inorg. Chem. 34 (1986) 115.
[3] G. La Monica, G.A. Ardizzoia, Prog. Inorg. Chem. 46 (1997) 151.
[4] G.A. Ardizzoia, G. La Monica, A. Maspero, M. Moret, N. Masciocchi, Eur. J. Inorg. Chem. (1998) 1503.
[5] B. Machura, J.O. Dziegielewski, S. Michalik, R. Kruszynski, T.J. Bartczak, J. Kusz, Transition Met. Chem. 28 (2003) 939.
[6] B. Machura, J.O. Dziegielewski, S. Michalik, R. Kruszynski, T.J. Bartczak, J. Kusz, Inorg. Chim. Acta 357 (2004) 1011.
[7] J. Holzbock, W. Sawodny, U. Thewalt, Z. Anorg. Allg. Chem. 626 (2000) 321.
[8] O. Arp, W. Preetz, Z. Anorg. Allg. Chem. 622 (1996) 219.
[9] F. Tisato, F. Refosco, A. Dolmella, G. Bandoli, Polyhedron 17 (1998) 3947.
[10] G. Rouschias, G. Wilkinson, J. Chem. Soc. A (1966) 465.
[11] STOE & Cie, X-RED, Version 1.18, STOE & Cie GmbH, Darmstadt, Germany, 1999.

[12] G.M. Sheldrick, Acta Crystallogr., Sect. A 46 (1990) 467.
[13] G.M. Sheldrick, SHELXL97. Program for the Solution and Refinement of Crystal Structures, University of Göttingen, Germany, 1997.
[14] G.M. Sheldrick, SHELXTL: release 4.1 for Siemens Crystallographic Research Systems (1990).
[15] M.J. Frisch, G.W. Trucks, H.B. Schlegel, G.E. Scuseria, M.A. Robb, J.R. Cheeseman, J.A. Montgomery Jr., T. Vreven, K.N. Kudin, J.C. Burant, J.M. Millam, S.S. Iyengar, J. Tomasi, V. Barone, B. Mennucci, M. Cossi, G. Scalmani, N. Rega, G.A. Petersson, H. Nakatsuji, M. Hada, M. Ehara, K. Toyota, R. Fukuda, J. Hasegawa, M. Ishida, T. Nakajima, Y. Honda, O. Kitao, H. Nakai, M. Klene, X. Li, J.E. Knox, H.P. Hratchian, J.B. Cross, C. Adamo, J. Jaramillo, R. Gomperts, R.E. Stratmann, O. Yazyev, A.J. Austin, R. Cammi, C. Pomelli, J.W. Ochterski, P.Y. Ayala, K. Morokuma, G.A. Voth, P. Salvador, J.J. Dannenberg, V.G. Zakrzewski, S. Dapprich, A.D. Daniels, M.C. Strain, O. Farkas, D.K. Malick, A.D. Rabuck, K. Raghavachari, J.B. Foresman, J.V. Ortiz, Q. Cui, A.G. Baboul, S. Clifford, J. Cioslowski, B.B. Stefanov, G. Liu, A. Liashenko, P. Piskorz, I. Komaromi, R.L. Martin, D.J. Fox, T. Keith, M.A. Al-Laham, C.Y. Peng, A. Nanayakkara, M. Challacombe, P.M.W. Gill, B. Johnson, W. Chen, M.W. Wong, C. Gonzalez, J.A. Pople, GAUSSIAN 03, Revision B.03, Gaussian, Inc., Pittsburgh, PA, 2003.
[16] A.D. Becke, J. Chem. Phys. 98 (1993) 5648.
[17] C. Lee, W. Yang, R.G. Parr, Phys. Rev. B 37 (1988) 785.
[18] M.E. Casida, in: J.M. Seminario (Ed.), Recent Developments and Applications in Modern Density Functional Theory, Theoretical and Computational Chemistry, vol. 4, Elsevier, Amsterdam, 1996.
[19] P.J. Hay, W.R. Wadt, J. Chem. Phys. 82 (1985) 299.
[20] J.L. Lock, G. Turner, Can. J. Chem. 56 (1978) 179.
[21] G. Backes-Dahmann, J.H. Enemark, Inorg. Chem. 26 (1987) 3960.
[22] M. Cano, J.V. Heras, M. Maeso, M. Alvaro, R. Fernández, E. Pinilla, J.A. Campo, A. Monge, J. Organomet. Chem. 534 (1997) 159.
[23] G. Esquius, J. Pons, R. Yáñez, J. Ros, X. Solans, M. Font-Bardía, J. Organomet. Chem. 605 (2000) 226.
[24] G.A. Jeffrey, W. Saenger, Hydrogen Bonding in Biological Structures, Springer, Berlin, 1994.
[25] G.R. Desiraju, T. Steiner, The Weak Hydrogen Bond in Structural Chemistry and Biology, Oxford University Press, Oxford, 1999.
[26] R. Taylor, O. Kennard, J. Am. Chem. Soc. 104 (1982) 5063.
[27] A. Baldy, J. Elguero, R. Faure, M. Pierrot, E.J. Vincent, J. Am. Chem. Soc. 107 (1985) 5290.
[28] J.E. Fergusson, Coord. Chem. Rev. 1 (1966) 459.
[29] A. Earnshaw, B.N. Figgis, J. Lewis, R.D. Peacock, J. Chem. Soc. (1961) 3132.
[30] G. Battistuzzi, M. Cannio, R. Battistuzzi, Polyhedron 19 (2000) 2163.
[31] G. Battistuzzi, M. Borsari, R. Battistuzzi, Polyhedron 16 (1997) 2093.
[32] C. Pearson, A.L. Beauchamp, Inorg. Chim. Acta 237 (1995) 13.
[33] V. Bertolasi, A. Marchi, L. Marvelli, R. Rossi, C. Bianchini, I. De los Rios, M. Peruzzini, Inorg. Chim. Acta 327 (2002) 140.
[34] B. Machura, M. Jaworska, R. Kruszynski, Polyhedron 23 (2004) 1819.
[35] N. Psaroudakis, K. Mertis, D.G. Liakos, E.D. Simandiras, Chem. Phys. Lett. 369 (2003) 490.

Available online at www.sciencedirect.com
SCIENCE DIRECT®
Polyhedron 23 (2004) 2013–2020
POLYHEDRON
www.elsevier.com/locate/poly

Heterobimetallic complexes of palladium(II) and platinum(II) bridged by the ligand 5-phenyl-1,3,4-oxadiazole-2-thione

Othman H. Amin [a], Lamaan J. Al-Hayaly [b], Subhi A. Al-Jibori [c], Talal A.K. Al-Allaf [d,*]

[a] Department of Chemistry, College of Science, University of Salahaddin, Erbil, Iraq
[b] Department of Chemistry, College of Education, University of Tikrit, Tikrit, Iraq
[c] Department of Chemistry, College of Science for Women, University of Tikrit, Tikrit, Iraq
[d] Department of Chemistry, College of Basic Sciences, Applied Science University, Shafa Badran, Amman 11931, Jordan

Received 12 May 2004; accepted 18 May 2004

Abstract

The complexes $[ML_2A_2]$ or $[ML_2B]$ where M = Pd or Pt, L = 5-phenyl-1,3,4-oxadiazole-2-thione ion, A = tertiary monophosphines and B = tertiary diphosphines have been used effectively to prepare bimetallic complexes of the type $[A_2M(\mu\text{-}L)_2M'Cl_2]$ or $[BM(\mu\text{-}L)_2M'Cl_2]$, where M′ = Co, Pd or $SnCl_2$. The prepared complexes were characterized by elemental analysis, magnetic susceptibility, IR and UV–Vis spectral data. $^{31}P\text{–}\{^1H\}$ NMR data have been applied to characterize the produced linkage isomers.
© 2004 Elsevier Ltd. All rights reserved.

Keywords: Palladium; Platinum; Heterobimetallic; Phosphine; Oxadiazole ligand complexes

1. Introduction

The metal complexes of some heterocyclic thiones attract much attention. The interactions of heavy metals such as platinum and gold with N,S-donor atoms have been recognized for their anticancer properties with the potential to develop metal based drugs [1–6]. Recently, some research works involving platinum(II) and palladium(II) ions with 8-thiotheophylline and dppm to give homo- and heterobimetallic complexes have been published [7,8]. Other related works on platinum(II) or (IV) complexes with tertiary phosphines and ligands containing sulfur have been also published recently [9,10]. However, metal complexes containing bis-tertiary phosphines and heterocyclic-2-thiones are rare [11].

In our recent work [12,13], we reported the preparation of some palladium(II) and platinum(II) complexes containing mixed ligands; tertiary monophosphines or diphosphines and 5-phenyl-1,3,4-oxadiazole-2-thione (LH). We found that the tertiary monophosphines or diphosphines reacted with the chelated complexes of the above ligand (L) to give complexes in which L behaves as a monodentate ligand coordinated to the metal centre through either S, N or mixture of both (Fig. 1).

In the present work, we used the uncoordinated end of the ligand (L) in the complexes $[ML_2A_2]$ and $[ML_2B]$ to build up some new types of heterobimetallic complexes bridged by L, i.e., $[A_2M(\mu\text{-}L)_2M'Cl_2]$ and $[BM(\mu\text{-}L)_2M'Cl_2]$, where M = Pt or Pd; M′ = Co, Pd or $SnCl_2$; A = $PMePh_2$; B = $Ph_2P(CH_2)_nPPh_2$ {$n = 1$, dppm; $n = 2$, dppe; $n = 3$, dppp; $n = 4$, dppb} and L = 5-phenyl-1,3,4-oxadiazole-2-thione (–H) (Fig. 1). To the best of our knowledge, this work is novel.

2. Experimental

2.1. General

$^{31}P\text{–}\{^1H\}$ NMR spectra were performed in the laboratories of Prof. Dr. Wilhelm Keim, Insitute for Techische Chemie der RWTH Achen, Worringer Weg 1, D-52074 Achen, Germany. IR spectra were recorded on a PYE-Unicam SP3-300s spectrophotometer in the 200–4000 cm^{-1} range using CsI discs. Electronic spectra were

* Corresponding author. Tel.: +962-6-5609999; fax: +962-6-5232899.
E-mail address: talal_al_allaf@hotmail.com (T.A.K. Al-Allaf).

0277-5387/$ - see front matter © 2004 Elsevier Ltd. All rights reserved.
doi:10.1016/j.poly.2004.05.006

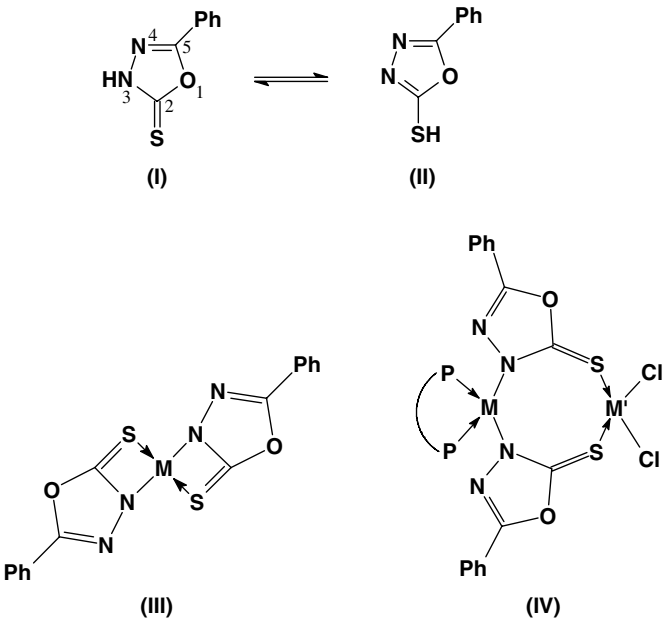

Fig. 1. The ligand 5-phenyl-1,3,4-oxidiazole-2-thione (LH), its tautomeric forms (I) and (II) and the suggested structure of its bis(chelated) complexes (III) and the bridging bimetallic complexes (IV), M = Pd or Pt, M′ = Co, Pd or $SnCl_2$, P···P = 2PMePh$_2$, dppm, dppe, dppp or dppb.

obtained using a Perkin–Elmer lambda 9 spectrophotometer. Elemental analyses were carried out on a CHN Analyzer, type 1106 (Carlo Erba). Magnetic measurements were recorded on a Bruker BH6 instrument at room temperature following the Faraday method. Conductivity measurements were made on a conductivity meter type CDM 83 70. Melting points were measured on an Electrothermal 9300 melting point apparatus.

2.2. Starting materials

The compounds K_2PtCl_4, $Na_2PdCl_4 \cdot 3H_2O$, $PdCl_2$, $CoCl_2$, $SnCl_4 \cdot 5H_2O$, $PMePh_2$, dppm, dppe, dppp and dppb were commercial products and used as supplied. The ligand 5-phenyl-1,3,4-oxadiazole-2-thione (LH) its potassium salt (LK) [14], *trans*-[$PdCl_2$ $(DMSO)_2$], *cis*-[$PtCl_2(DMSO)_2$] [15], [PdL_2]$\cdot H_2O$, [PtL_2], [PdL_2 (dppm)]$\cdot H_2O$, [PtL_2(dppm)], [PdL_2(dppe)], [PtL_2(dppe)] [12], [$PdL_2(PMePh_2)_2$] and [$PtL_2(PMePh_2)_2$] [13] were prepared according to the literature.

2.3. [PdL_2(dppp)] (**4**) and [PdL_2(dppb)] (**5**)

These complexes were prepared by a method similar to that reported for the preparation of [PdL_2-(dppm)]$\cdot H_2O$ [12].

2.4. [PtL_2(dppp)] (**9**) and [PtL_2(dppb)] (**10**)

These complexes were prepared by a method similar to that reported for the preparation of [PtL_2(dppm)] [12].

2.5. [$(PMePh_2)_2Pd(\mu$- L)$_2CoCl_2$]$\cdot 2H_2O$ (**11**)

Solid $CoCl_2$ (0.05 g, 0.38 mmol) was added to a solution of [$PdL_2(PMePh_2)_2$] (0.15 g, 0.17 mmol) in chloroform (15 ml). The yellow solution turned green. The mixture was stirred at room temperature for ca. 10 h. The unreacted $CoCl_2$ was removed by filtration and the green filtrate was evaporated to dryness. Diethylether was added and the green solid was filtered off and dried under vacuum (yield, 0.13 g, 75%).

The following complexes were prepared and isolated by a similar method: **13**, **17**, **20**, **23**, **25**, **28** and **31**.

2.6. [$(PMePh_2)_2Pd(\mu$-L)$_2PdCl_2$] (**12**)

Solid *trans*-[$PdCl_2(DMSO)_2$] (0.13 g, 0.38 mmol) was added with stirring to a solution of [$PdL_2(PMePh_2)_2$] (0.2 g, 0.23 mmol) in chloroform (15 ml). The mixture was stirred at room temperature for ca. 8 h, then filtered. The filtrate was evaporated to dryness and diethylether was added. The orange–brown solid thus formed was filtered off and dried in vacuum (yield, 0.23 g, 95%).

The following complexes were prepared and isolated by a similar method: **15**, **18**, **21**, **24**, **26**, **29** and **32**.

2.7. [$(PMePh_2)_2Pd(\mu$-L)$_2SnCl_4$] (**13**)

Solid $SnCl_4 \cdot 5H_2O$ (0.07 g, 0.22 mmol) was added with stirring to a clear yellow solution of [$PdL_2(PMePh_2)_2$] (0.14 g, 0.16 mmol) in chloroform (12 ml). The mixture was stirred at room temperature for ca. 10 h, then filtered. The filtrate was evaporated to dryness

and diethylether was added. The resulting yellow solid was filtered off and dried in vacuum (yield, 0.13 g, 71%).

The following complexes were prepared and isolated by a similar method: **16**, **19**, **22**, **27**, **30** and **33**.

3. Results and discussion

3.1. Synthesis of the complexes

We reported previously that the reaction of *cis*-$[PtCl_2(B)]$ {B = $Ph_2P(CH_2)PPh_2$ (dppm) and $Ph_2P(CH_2)_2PPh_2$ (dppe)} with the potassium salt of the ligand 5-phenyl-1,3,4-oxadiazole-2-thione (LK) or the reaction of *trans*-$[PtL_2]$ with dppm or dppe gave complexes of the type $[PtL_2(B)]$ which was a single linkage isomer when B = dppm [12]. From the *J*(Pt–P) value (2714 Hz), we believed that this was the S-bonded isomer. When B = dppe, two linkage isomers in the ratio 1:1 were obtained, the S-bonded isomer with a low *J*(Pt–P) value (2346 Hz) and the N-bonded isomer with high *J*(Pt–P) value (3088 Hz). Now, we have extended this series to include the ligands $Ph_2P(CH_2)_3PPh_2$ (dppp) and $Ph_2P(CH_2)_4PPh_2$ (dppb). From the $^{31}P–\{^1H\}$ NMR data, we found that for the complex $[PtL_2(dppp)]$, a single isomer is obtained and from its *J*(Pt–P) value (3023 Hz), we believed that it is the N-bonded isomer.

Treatment of a solution of $[ML_2(PMePh_2)_2]$ or $[ML_2(B)]$ (B = dppm, dppe, dppp or dppb) with solid $CoCl_2$, *trans*-$[PdCl_2(DMSO)_2]$ or $SnCl_4 \cdot 5H_2O$ in chloroform yielded heterobimetallic complexes of the type $[(PMePh_2)_2M(\mu\text{-}L)_2M'Cl_2]$ or $[(B)M(\mu\text{-}L)_2M'Cl_2]$.

3.2. Characterization of complexes

The complexes were identified by elemental analysis, $^{31}P–\{^1H\}$ NMR, IR, UV–Vis spectra, magnetic susceptibility and conductivity measurements and their data are listed in Tables 1–4.

The synthesised heterobimetallic complexes are stable in the solid state as well as in solution except for the cobalt complexes which showed some instability in aqueous or alcoholic solvents. For this reason, these solvents were avoided in the preparation and characterization of the cobalt complexes Although the molar conductivities of the complexes in acetonitrile are greater than those in chloroform (Table 3), due to the higher dielectric constant of acetonitrile, nevertheless the values in both solvents are too low to suggest that they are non-electrolytes [16].

3.2.1. IR spectra and magnetic moments

The IR spectra of the prepared complexes (Table 2) showed weak to strong bands at ca. 1550, 1435, 960 and 775 cm^{-1}, which may be assigned to the thioamide vibrational bands I, II, III and IV, respectively [17]. The IR spectra of the Pd–Co or Pt–Co complexes showed two medium to strong bands at around 310–330 cm^{-1}, assigned to *ν*(Co–Cl) in an octahedral environment (complexes **11**, **17**, **20**, **25**, **28** and **31**), or a single strong band at around 310 or 315 cm^{-1} for square planar and tetrahedral cobalt complexes (complexes **14** and **23**) [18]. The far IR spectra of the Pd–Sn complexes showed a strong single band at around 310–330 cm^{-1} assigned to (Sn–Cl) [19], while the IR spectra of the Pd–Pd complexes (**12**, **15**, **18**, **21** and **24**) showed in each case two medium intensity bands at 350, 290 or 310, 290 cm^{-1}, respectively, which are assigned to (Pd–Cl) in a *cis*-arrangement [20]. Other IR data are given in Table 2.

The magnetic susceptibility measurements for the prepared complexes indicated that all of them are diamagnetic except for some of the cobalt complexes (**11**, **17**, **20**, **23**, **25**, **28** and **31**). The magnetic susceptibility value of complex **23** is 4.5 BM, which on the basis of this value and the spectral data was assigned to have a tetrahedral geometry [21]. The values 4.9–5.2 BM for the remaining cobalt complexes suggest an octahedral arrangement around cobalt(II), which compare very well with reported values for octahedral complexes of cobalt(II) (4.7–5.2 BM) [22–24].

3.2.2. $^{31}P–\{^1H\}$ NMR spectra

The $^{31}P–\{^1H\}$ NMR data of some of the prepared complexes are given in Table 4.

The spectrum of $[PtL_2(dppm)]$ showed a singlet at $\delta P - 49.2$ ppm with associated platinum satellites, *J*(Pt–P) = 2714 Hz. The negative value of the δP indicates that dppm behaves as a chelating ligand [25]. The low *J*(Pt–P) value suggests that the *trans*-atom is a sulfur rather than a nitrogen atom [8]. The sulfur atom has the ability to compete with the phosphorus atom on back donation from the platinum. Therefore, it lowers the *J*(Pt–P) value. The small volume occupied by dppm permits the ligand (L) to bond through the preferable sulfur atom. This makes the ligands occupy a bigger volume [26]. The $^{31}P–\{^1H\}$ NMR spectrum of $[(dppm)Pt(\mu\text{-}L)_2PdCl_2]$ showed a singlet at $\delta P - 63.0$ ppm associated with platinum satellites, *J*(Pt–P) = 3106 Hz; i.e., 392 Hz higher than that of the starting complex $[PtL_2(dppm)]$, indicating a single isomer and that the bridging ligand (L) is bonded to platinum via the sulfur end, while it is bonded to palladium via the nitrogen end.

We reported in our recent work that the $^{31}P–\{^1H\}$ NMR spectrum of $[PtL_2(dppe)]$ showed two singlets at δP 48.1 and 48.8 ppm in the ratio of 1:1, each associated with platinum satellites, *J*(Pt–P) = 3088 and 2346 Hz, respectively, assigned to the linkage N-bonded and the S-bonded isomers, respectively [12]. Reaction of the isomeric mixture with *trans*-$[PdCl_2(DMSO)_2]$ gave a single heterobimetallic isomer at δP 42.4 ppm with *J*(Pt–P) = 3727 Hz, i.e., 639 Hz higher than that of the starting complex $[PtL_2(dppe)]$. The *J*(Pt–P) value

Table 1
Physical properties of complexes **1**–**33**

Sequence	Complex	Colour	Yield	Melting point (°C)[a]	Found (calc) (%)		
					C	H	N
1	$[PdL_2(PMePh_2)_2]$	yellow	95	229–231	58.7 (58.9)	4.2 (4.2)	6.5 (6.7)
2	$[PdL_2(dppm)]$	orange	76	140–142	58.3 (57.8)	3.8 (3.7)	6.6 (6.7)
3	$[PdL_2(dppe)]$	yellow	93	233–234	58.7 (59.1)	3.9 (3.9)	6.5 (6.8)
4	$[PdL_2(dppp)]$	yellow	94	136–138	59.1 (60.0)	4.1 (3.7)	6.4 (6.2)
5	$[PdL_2(dppb)]$	yellow–orange	94	232–235	59.6 (59.8)	4.3 (4.2)	6.3 (6.3)
6	$[PtL_2(PMePh_2)_2]$	pale yellow	56	261–263	53.1 (52.7)	3.8 (3.8)	5.9 (6.1)
7	$[PtL_2(dppm)]$	off white	77	146–148	52.8 (53.1)	3.4 (3.3)	6.0 (5.8)
8	$[PtL_2(dppe)]$	off white	83	264–268	53.2 (53.0)	3.6 (3.4)	5.9 (6.0)
9	$[PtL_2(dppp)]$	off white	76	176–178	53.7 (53.9)	3.7 (3.7)	5.8 (5.9)
10	$[PtL_2(dppb)]$	pale yellow	82	168–169	54.2 (54.4)	3.9 (3.8)	5.7 (5.9)
11	$[(PMePh_2)_2Pd(\mu\text{-}L)_2CoCl_2]\cdot 2H_2O$	green	75	251–252	49.1 (48.7)	3.5 (3.4)	5.5 (5.4)
12	$[(PMePh_2)_2Pd(\mu\text{-}L)_2PdCl_2]$	orange–brown	95	203–210	48.8 49.2	3.5 (3.3)	5.4 (5.6)
13	$[(PMePh_2)_2Pd(\mu\text{-}L)_2SnCl_4]$	yellow	71	148–150	44.9 (44.6)	3.2 (3.4)	5.0 (4.9)
14	$[(dppm)Pd(\mu\text{-}L)_2CoCl_2]$	green	73	186–187	50.5 (50.4)	3.3 (3.4)	5.7 (5.6)
15	$[(dppm)Pd(\mu\text{-}L)_2PdCl_2]$	orange	97	279–281	49.2 (49.1)	3.1 (3.0)	5.5 (5.6)
16	$[(dppm)Pd(\mu\text{-}L)_2SnCl_4]$	yellow	89	189–191	44.5 (44.3)	2.9 (3.0)	5.1 (4.9)
17	$[(dppe)Pd(\mu L)_2CoCl_2]\cdot 2HO$	green	75	265–258	49.6 (49.7)	3.3 (3.3)	5.5 (5.5)
18	$[(dppe)Pd(\mu\text{-}L)_2PdCl_2]$	orange	60	314–316	47.8 (47.9)	3.5 (3.4)	5.4 (5.5)
19	$[(dppe)Pd(\mu\text{-}L)_2SnCl_4]$	yellow	61	154–156	45.0 (44.8)	3.0 (3.0)	5.0 (5.1)
20	$[(dppp)Pd(\mu\text{-}L)_2CoCl_2]\cdot H_2O$	green	79	196–198	48.7 (48.9)	3.5 (3.4)	5.4 (5.3)
21	$[(dppp)Pd(\mu\text{-}L)_2PdCl_2]$	orange–brown	72	208–210	49.1 (49.3)	3.4 (3.3)	5.3 (5.4)
22	$[(dppp)Pd(\mu\text{-}L)_2SnCl_4]$	yellow	83	152–154	45.5 (45.8)	3.2 (3.2)	4.9 (4.9)
23	$[(PMePh_2)_2Pt(\mu\text{-}L)_2CoCl_2]$	blue–green	87	187–189	46.7 (46.4)	3.3 (3.3)	5.2 (5.1)
24	$[(PMePh_2)_2Pt(\mu\text{-}L)_2PdCl_2]$	pale orange	95	245–247	44.8 (45.1)	3.2 (3.4)	5.0 (5.3)
25	$[(dppm)Pt(\mu\text{-}L)_2CoCl_2]\cdot 2H_2O$	blue–green	95	118–120	44.7 (44.7)	2.9 (2.9)	5.1 (5.2)
26	$[(dppm)Pt(\mu\text{-}L)_2PdCl_2]$	orange	97	326–328	46.3 (46.0)	2.9 (2.9)	5.0 (5.2)
27	$[(dppm)Pd(\mu\text{-}L)_2SnCl_4]$	pale yellow	48	198–199	41.2 (41.5)	2.7 (2.7)	5.7 (5.6)
28	$[(dppe)Pt(\mu\text{-}L)_2CoCl_2]\cdot 2H_2O$	green	91	218–220	46.1 (46.0)	3.3 (3.2)	5.0 (5.0)
29	$[(dppe)Pt(\mu\text{-}L)_2PdCl_2]$	orange–brown	94	294–296	44.9 (44.8)	3.0 (3.1)	5.0 (5.1)
30	$[(dppe)Pt(\mu\text{-}L)_2SnCl_4]$	pale brown	94	178–180	42.0 (42.1)	2.8 (2.8)	4.6 (4.5)
31	$[(dppp)Pt(\mu\text{-}L)_2CoCl_2]\cdot 2H_2O$	blue–green	88	228–230	46.8 (47.0)	3.2 (3.2)	5.0 (4.9)
32	$[(dppp)Pt(\mu\text{-}L)_2PdCl_2]$	orange–brown	89	318–320	44.9 (44.8)	3.2 (3.1)	4.9 (5.1)
33	$[(dppp)Pt(\mu\text{-}L)_2SnCl_4]$	off white	90	197–199	42.5 (42.7)	2.9 (3.1)	4.6 (4.5)

[a] Complexes melt with decomposition.

indicated that it is the N-bonded isomer *cis–cis*-$[(dppe)Pt\{\mu\text{-}L(NS)\}_2PdCl_2]$. However, the difference in J(Pt–P) values, i.e., 392 Hz in the case of the dppm complex and 639 Hz in the case of dppe may be explained on the basis of the strain presented by the dppm chelate ring which is not present in the dppe and dppp chelate rings.

The $^{31}P\text{–}\{^1H\}$ NMR spectrum of $[PtL_2(dppp)]$ showed a singlet at $\delta P - 1.92$ ppm with $J(Pt\text{–}P) = 3023$ Hz, indicating the presence of a single isomer. The J(Pt–P) value indicates that it is the N-bonded isomer. Reaction of this complex with *trans*-$[PtCl_2(DMSO)_2]$ gave the heterobimetallic complex *cis–cis*-$[(dppp)Pt\{\mu\text{-}L(NS)\}_2PdCl_2]$ as indicated from the δP which is −4.37 ppm and J(Pt–P) which is 3375 Hz.

The above trend of changing the point of attachment of the ligand 5-phenyl-1,3,4-oxadiazole-2-thione from an S-bonded, in the presence of the dppm ligand, to a 1:1 mixture of the S- and N-bonded with dppe, to an N-bonded in the presence of dppp reflects the steric effect exerted by the diphosphine ligands on the type of linkage isomer produced. This trend is in consistent with that reported for the complexes $[Pd(SCN)_2\{Ph_2P(CH_2)_nPPh_2\}]$ $n = 1$, 2 or 3 [26].

On the other hand, the $^{31}P\text{–}\{^1H\}$ NMR spectrum of *trans*-$[PdL_2(PMePh_2)_2]$ showed two singlets at δP 13.5 and 12.4 ppm in the ratio of 80% and 20%, respectively. No coupling between the two signals was observed which indicates the presence of two compounds. We believe that these are, probably, due to the two linkage isomers, the S-bonded and the N-bonded 5-phenyl-1,3,4-oxadiazole-2-thione. The possibility of having an S,N-bonded isomer is ruled out since the complex we obtained has a *trans*-configuration and not the *cis*-one. The *cis*-isomer should give an AX spin system (doublet of doublets) in the ^{31}P NMR spectrum and in our case we found only two singlets in the spectrum. Several attempts carried out to grow a crystal of the complex for X-ray analysis were unsuccessful. On treatment of this isomeric mixture with *trans*-$[PdCl_2(DMSO)_2]$, a mixture of linkage heterobimetallic isomers of the type *trans*-$[(PMePh_2)_2Pd(\mu\text{-}L)_2PdCl_2]$ were observed, as shown

Table 2
IR spectral data[a] of complexes **1**–**33**

Complex	Thioamide bands				Others							
	I	II	III	IV	*v*(OH)	*v*(CH)	*v*(M–N)	*v*(M–S)	*v*(M–Cl)	*v*(P–Me)	*v*(COC)	*v*(N–N)
1	1550w	1435s	995m	777m, 760s		3055w, 2920w	510s, 459m	445m		890s	1160m	1480m
2	1545w	1430s	960m	772s, 745s	3415w	3045m, 2890w	500s, 480m	450w			1154s	1475m
3	1545m	1435s	960w	780m, 752m		3045m, 2960m	530a, 483m	437m			1150s	1480m
4	1545w	1430s	960w	775m, 745s	3400s	3050m, 2920w	515s, 490m	435w			1163s	1480s
5	1570w	1430s	970	470s	3400s	3050m, 2920w	520s, 500s				1175s	1477m
6	1550w	1430s	960w	775m		3050m, 2920w	510s, 490m	420m		895s	1155s	1478m
7	1555w	1430s	960m	772s, 740s	3420s	3055m, 2960w	510s, 486m	428w			1160s	1480s
8	1543w	1425s	960m	772m, 738s	3380s	3040m, 2940w	530s, 480m	438w			1170m	1480s
9	1545w	1430s	970w	775m, 745s		3040m, 2905w	520s	440w			1152s	1475m
10	1550w	1430s	965w	775m, 745s		3045w, 2910w	515s, 485m	430w			1165m	1480m
11	1555w	1425s	960m	775m, 745s	3400m	3050w, 2910w	510s, 490m		340s, 315m	890s	1160m	1480m
12	1558w	1430s	960m	775m, 740s	3450w	3050w, 2910w	512s, 490m	450m	350s, 314m	900s	1165m	1480m
13	1550w	1430s	960m	772m, 740s	3240w	3050w, 2910w	510s, 485m	450m	325s	890s	1170m	1477m
14	1555w	1430s	955w	775s, 740s	3400s	3040w, 2900w	500s, 475m	430w	315s		1177s	1475m
15	1555w	1435s	950w	773m, 740s	3450m	3040w, 2900w	520s, 480m	435	350m, 290s		1165m	1480w
16	1568w	1432s	970s	772s, 740s		3040m, 2950w	505m	425m	303m		1180m	1478sw
17	1557w	1435s	960w	775m, 753m	3400s	3050w, 2915w	530s, 485m	440w	340m, 315s		1170s	1480m
18	1565w	1430s	1000m	760s, 720s		3050w, 2980w	530s, 485m	440w	315s, 290m		1163m	1477m
19	1565w	1430s	970m	775m, 750m	3400s	3050, 2950w	350s, 490m	445w	330s		1163s	1480s
20	1555s	1430s	950m	773m, 750s	3440s	3046m, 2980w	500s	430w	330s, 316s		1160s	1480s
21	1555s	1430s	950m	775m, 750s	3450s	3042m, 2980w	510s	430	312s, 290s		1155m	1477m
22	1548w	1435s	945m	772m, 750s		3140w, 2950w	510s	430w	330s		1172s	1478s
23	1524m	1425s	995m	775m, 740s		3040s, 2960w	510s, 490s	430w	310s	895s	1170s	1475m
24	1556m	1430s	965m	775m, 740s		3060m, 2920w	510s, 490s	420w	350s, 320m	900s	1160s	1480m
25	1552m	1430s	955m	775m, 742s	3400s	3050m, 2940w	510s, 485m	450w	330m, 310m		1170s	1477m
26	1555m	1430s	955m	775m, 742s	3400b	3040m, 2910w	520s, 485m	430w	310m, 295m		1175m	1480m
27	1555m	1440s	965m	775m, 735s		3040w, 2900w	490s	460w	315m		1175m	1480m
28	1550w	1430s	960m	778m, 732s		3050w, 2950w	535s, 485m	430w	340m, 320m		1170m	1480m
29	1555m	1435s	955w	775m, 755s	3480b	3050, 2910w	530s, 490m	438w	318s, 293s		1160m	1480m
30	1560w	1435s	955w	775m, 755s		3060w, 2940w	530s, 490m	438w	330s		1175m	1480m
31	1552m	1425s	975w	775m, 745s		3040w, 2920w	510s	430w	335m, 320m		1155m	1475m
32	1557m	1430s	950m	775m, 750s		3050w, 2912w	518s	440w	310s, 290m		1158m	1480m
33	1552m	1432s	970w	770w, 750s		305w, 2920w	518s	435w	325s		1165m	1480s

[a]For IR data (cm^{-1}); b: broad, m: medium, s: strong, w: weak bands.

Table 3
Electronic spectra, magnetic moments and molar conductivity of complexes **1**–**33**

Complex	λ_{max} (nm)	Assignments	μ_{eff} (BM)[a]	Λ_M (Ω^{-1} cm^2 mol^{-1})	
				$CHCl_3$	CH_3CN
1	375	$^1A_1g \rightarrow {}^1B_1g$	0.2 Pd sq.pl.	0.2	3.2
	336	$^1E_1g \rightarrow {}^1A_1g$			
	266	c.t.			
2	440	$^1A_1g \rightarrow {}^1B_1g$	0.2 Pd sq.pl.	0.16	3.2
	337	$^1E_1g \rightarrow {}^1A_1g$			
	300	c.t.			
3	416	$^1A_1g \rightarrow {}^1A_2g$	0.2 Pd sq.pl.	0.18	3.0
	350	$^1Eg \rightarrow {}^1B_1g$			
	272	c.t.			
4	330	$^1Eg \rightarrow {}^1B_1g$	0.2 Pd sq.pl.	0.2	3.4
	265	c.t			
5	414	$^1A^1g \rightarrow A_2g$	0.1 Pd sq.pl.	0.2	3.0
	355	$E_1g \rightarrow {}^1Bg$			
	265	c.t.			
6	375	$^1A_1g \rightarrow {}^1B_1g$	0.1 Pt sq.pl.	0.16	2.6
	324	c.t			
7	660	$B_2g \rightarrow B_1g$	0.2 Pt sq.pl.	0.2	2.1
	370	$A_1g \rightarrow {}^1B_1g$			
	262	c.t			
8	262	c.t.	0.2 Pt sq.pl.	0.2	3.7
	250	c.t.			
9	262	c.t.	0.2 Pt sq.pl.	0.18	5.0
10	342	$A_1g \rightarrow {}^1B_1g$	0.1 Pt sq.pl.	0.19	4.5
	260	c.t.			
11	633	$^4A_2F \rightarrow {}^4T_{1F}$	4.9 Pd sq.pl., Co o.h.	0.24	14.6
	390	$^1A_1g \rightarrow {}^1B_1g$			
	340	$E_1g \rightarrow {}^1A_1g$			
	300	c.t.			
12	420	$^1A_1g \rightarrow {}^1B_1g$	0.1 Pd sq.pl.	0.24	5.8
	330	$^1E_1g \rightarrow A_1g$			
	260	c.t			
13	440	$^1A_1g \rightarrow {}^1B_1g$	0.2 Pd sq.pl.	0.25	5.7
	332	$^1E_1g \rightarrow {}^1A_1g$			
	265	c.t.			
14	420	$^2A_1g \rightarrow {}^2Eg$	0.1 Pd	0.20	3.7
	334	c.t.	sq. pl., Co sq.pl.		
	263	c.t.			
15	345	$^1E_1g \rightarrow {}^1B_1g$	0.1 Pd sq.pl.		
	260	c.t.			
16	480	$^1A_1g \rightarrow {}^1A_2g$	0.1 Pd sq.pl.	0.22	11.2
	350	$^1E_1g \rightarrow {}^1B_1g$			
	264	c.t.			
17	631	$^4T_1gF \rightarrow {}^4A_2g(F)$	5.1 Pd sq.pl., Co o.h.	0.20	15.9
	442	$^4T_1gF \rightarrow {}^4T_1g(P)$			
	325	c.t.			
	262	c.t.			
18	450	$^1A_1g \rightarrow {}^1B_1g$	0.2 Pd sq.pl.	0.21	2.5
	332	$^1Eg \rightarrow {}^1B_1g$			
	264	c.t.			
19	355	$E_1g \rightarrow {}^1B_1g$	0.2 Pd sq.pl.	0.23	20.7
	262	c.t.			
20	620	$^4T_1gF \rightarrow {}^4A_2g(F)$	4.9 Pd sq.pl., Co o.h.	0.21	14.0
	454	$^4T_1gF \rightarrow {}^4T_1g(P)$			
	264	c.t.			
21	461	$A_1g \rightarrow A_2g$	0.1 Pd sq.pl.	0.21	23.0
	339	$E_1g \rightarrow {}^1B_1g$			
	265	c.t.			
22	420	$A_1g \rightarrow A_2g$	0.1 Pd sq.pl.	0.23	18.3
	335	$E_1g \rightarrow {}^1B_1g$			
	266	c.t			

Table 3 (*continued*)

Complex	λ_{max} (nm)	Assignments	μ_{eff} (BM)[a]	Λ_M (Ω^{-1} cm^2 mol^{-1})	
				$CHCl_3$	CH_3CN
23	622	$^4A_2F \rightarrow {}^4T_1g(P)$	4.5 Pt sq.pl., Co t.h.	0.20	3.6
	370	$A_1g \rightarrow B_1g$			
	348	$E_1g \rightarrow B_1g$			
	264	c.t			
24	318	$E_1g \rightarrow {}^1B_1g$	0.1 Pt sq.pl.	0.20	20.9
	266	c.t.			
25	621	$^4T_1gF \rightarrow {}^4A_2g(F)$	5.2 Pt sq.pl., Co o.h.	0.20	8.5
	389	$^1A_1g \rightarrow {}^3B_1(g)$			
	330	$E_1g \rightarrow B_1g$			
	259	c.t.			
26	262	c.t.	0.1 Pt sq.pl.	0.20	2.7
27	335	$^1A_1g \rightarrow {}^3B_1g$	0.2 Pt sq.pl.	0.23	8.0
	263	c.t.			
28	621	$^4A_2gF \rightarrow {}^4T_1g(F)$	0.1 Pt sq.pl., Co o.h.	0.20	2.1
	416	$^4T_1gF \rightarrow {}^4T_1g(P)$			
	272	c.t.			
29	450	$A_1g \rightarrow B_1g$	0.1 Pt sq.pl.	0.20	3.1
	332	$E_1g \rightarrow B_1g$			
	264	c.t.			
30	335	$^1A_1g \rightarrow {}^3B_1g$	0.2 Pt sq.pl.	0.20	7.6
	263	c.t.			
31	634	$^4A_2gF \rightarrow {}^4T_1g(F)$	5.0 Pt sq.pl., Co o.h.	0.20	13.8
	480	$^4T_1gF \rightarrow {}^4T_1g(P)$			
	303	c.t.			
32	490	$^1A_1g \rightarrow {}^1A_2g$	0.1 Pt sq.pl., Pd sq.pl.	0.20	12.0
	370	$A_1g \rightarrow B_1g$			
	272	c.t			
33	336	$A_1g \rightarrow {}^1B_1g$	0.1 Pt sq.pl.	0.20	14.0
	264	c.t.			

[a] Abbreviations, sq.pl., o.h. and t.h. are for square planar, octahedral and tetrahedral environment, respectively.

Table 4
$^{31}P-\{^1H\}$ NMR data (δ ppm and J Hz)[a] of some of the prepared complexes

Complex	Sequence	δp	J(Pt–P)	Comments
cis-$[PdCl_2(PMePh_2)_2]$[c]		−19.1		
trans-$[PdCl_2(PMePh_2)_2]$[c]		−7.8		
trans-$[PdL_2(PMePh_2)_2]$	**1**	13.5		80% S-bonded
		12.4		20% N-bonded
trans-$[(PMePh_2)_2Pd(\mu\text{-}L)_2PdCl_2]$	**12**	23.0		65% S-bonded
		23.6		35% N-bonded
$[PdL_2(dppm)]$	**2**	−39.2		
$[(dppm)Pd(\mu\text{-}L)_2PdCl_2]$	**15**	−53.2		
$[PdL_2(dppe)]$	**3**	63.0		
$[(dppe)Pd(\mu\text{-}L)_2PdCl_2]$	**18**	65.2		
$[(dppe)Pd(\mu\text{-}L)_2SnCl_4]$	**19**	72.0		
cis-$[PtCl_2(PMePh_2)_2]$[c]		−1.2	3616	
trans-$[PtCl_2(PMePh_2)_2]$		41.3	2028	
cis-$[PtL_2(PMePh_2)_2]$	**6**	9.6	2567	
$[PtCl_2(dppm)]$[c]		−64.3	3078	
$[PtL_2(dppm)]$	**7**	−49.2	2714	
$[(dppm)Pt(\mu\text{-}L)_2PdCl_2]$	**26**	−63.0	3106	
$[PtCl_2(dppe)]$[c]		45.3	3618	
$[PtL_2(dppe)]$	**8**	48.1	3088[b]	50% N-bonded
		48.8	2346[b]	50% S-bonded
$[(dppe)Pt(\mu\text{-}L)_2PdCl_2]$	**29**	42.4	3727	
$[PtCl_2(dppp)]$[c]		−5.6	3420	
$[PtL_2(dppp)]$	**9**	−1.9	3023	
$[(dppp)Pt(\mu\text{-}L)_2PdCl_2]$	**32**	−4.4	3375	

[a] Measured in $CDCl_3$ downfield from 85% H_3PO_4.
[b] Published previously [12] in a reverse order.
[c] These are listed here for comparison.

from the $^{31}P–\{^1H\}$ NMR spectrum. The spectrum of this heterobimetallic mixture showed two singlets at δP 23.0 and 23.6 ppm in the ratio of 65% and 35%, respectively. We believe that these correspond to the S-bonded and N-bonded heterobimetallic isomers, i.e., *cis–cis*-$[(PMePh_2)_2Pd\{\mu\text{-}L(SN)\}_2PdCl_2]$ and *cis–cis*-$[(PMePh_2)_2Pd\{\mu\text{-}L(NS)\}_2PdCl_2]$, respectively.

The $^{31}P–\{^1H\}$ NMR spectrum of $[PdL_2(dppm)]$ showed a singlet at $\delta P - 39.2$ ppm while that of the bimetallic complex $[(dppm)Pd(\mu\text{-}L)_2PdCl_2]$ showed it to be at $\delta P - 53.3$ ppm. The negative sign of the chemical shifts indicate again that dppm behaves as a chelating ligand in both the mononuclear and the binuclear complexes [25]. Other $^{31}P–\{^1H\}$ NMR data of the other palladium complexes are given in Table 4.

Acknowledgements

We thank Prof. Dr. Wilhelm Keim, Institute for Technische Chemie der RWTH Aachen, Worringer Weg1, D-52074 Aachen, Germany, for his help in obtaining the $^{31}P–\{^1H\}$ NMR data.

References

[1] T.A.K. Al-Allaf, L.J. Rashan, Boll. Chim. Farm (Italy) 22 (2001) 205.
[2] A.S. Abu-Surrah, T.A.K. Al-Allaf, M. Klinga, M. Ahlgren, Polyhedron 22 (2003) 1529.
[3] T.A.K. Al-Allaf, L.J. Rashan, A. Stelzner, D.R. Powell, Appl. Organomet. Chem. 17 (2003) 891.
[4] E.S. Raper, Coord. Chem. Rev. 165 (1997) 475.
[5] J. Reedijk, Inorg. Chim. Acta 198–200 (1992) 873.
[6] L.T. McCaffrey, W. Henderson, B.K. Nicholson, J.E. Mackay, M.B. Dinger, J. Chem. Soc., Dalton Trans. (1997) 2577.
[7] L.T. McCaffrey, W. Henderson, B.K. Nicholson, Polyhedron 17 (1998) 221.
[8] E. Colacio, R. Cuesta, M. Ghazi, M. Angeles Huertas, J.M. Moreno, A. Navarrete, Inorg. Chem. 36 (1997) 1652.
[9] J.M. Teuben, S.S.G.E. van Boom, J. Reedijk, J. Chem. Soc., Dalton Trans. (1997) 3979.
[10] E.G. Talman, W. Bruning, J. Reedijk, A.L. Spek, N. Veldman, Inorg. Chem. 36 (1997) 854.
[11] T.S. Lobana, R. Verma, G. Hundal, A. Castineiras, Polyhedron 19 (2000) 899.
[12] S.A. Al-Jibori, I.N. Al-Nassiri, L.J. Al-Hayaly, Transit. Met. Chem. 27 (2002) 191.
[13] A.M. Qadir, A.I. Abdulla, S.A. Al-Jibori, T.A.K. Al-Allaf, Asian J. Chem. 16 (2004) 1180.
[14] R.W. Young, K.H. Wood, J. Am. Chem. Soc. 77 (1955) 400.
[15] J.H. Price, A.N. Williamson, R.F. Schram, B.B. Wayland, Inorg. Chem. 11 (1972) 1280.
[16] W.J. Geary, Coord. Chem. Rev. 7 (1971) 81.
[17] A.H. Jassim, Ph.D. Thesis, Saddam University of Engineering and Science, Baghdad, Iraq, 1993.
[18] A.K. El-Sawaf, D.X. West, Transit. Met. Chem. 23 (1998) 227.
[19] T.A.K. Al-Allaf, J. Organomet. Chem. 590 (1999) 25.
[20] N.H. Buttrus, A.K. Hussain, T.A.K. Al-Allaf, Asian J. Chem. 15 (2003) 1617.
[21] A. Cukurovali, I. Yilmas, H. Ozmen, M. Almedzade, Transit. Met. Chem. 27 (2002) 171.
[22] C. Pelizzi, G. Pelizzi, Inorg. Nucl. Lett. 16 (1980) 451.
[23] T.S. Lobana, H.S. Cheema, S.S. Sandhu, Polyhedron 4 (1985) 717.
[24] S.A. Al-Jibori, O.H. Amin, T.A.K. Al-Allaf, R. Davis, Transit. Met. Chem. 26 (2001) 186.
[25] P.G. Pringle, D.Phil. Thesis, Leeds University, 1983.
[26] G.J. Palenik, M. Mathew, W.L. Steffen, G. Beran, J. Am. Chem. Soc. 97 (1975) 1059.

Available online at www.sciencedirect.com
SCIENCE DIRECT®
Polyhedron 23 (2004) 2021–2030
POLYHEDRON
www.elsevier.com/locate/poly

Organotin adducts of indomethacin: synthesis, crystal structures and spectral characterization of the first organotin complexes of indomethacin

Angeliki Galani [a], Dimitra Kovala-Demertzi [a,*], Nikolaos Kourkoumelis [a], Aglaia Koutsodimou [a], Vaso Dokorou [a], Zbigniew Ciunik [b], Umberto Russo [c], Mavroudis A. Demertzis [a,*]

[a] *Inorganic Chemistry, Department of Chemistry, University of Ioannina, 45110 Ioannina, Greece*
[b] *Faculty of Chemistry, University of Wrocław, 14 F. Joliot-Curie Street, 50-383 Wrocław, Poland*
[c] *Dipartimento di Chimica Inorganica, Metallorganica e Analitica, Università di Padova, Via Loredan 4, I-35131 Padova, Italy*

Received 19 April 2004; accepted 18 May 2004
Available online 19 June 2004

Abstract

The complexes $[Me_2(Indo)SnOSn(Indo)Me_2]_2$, (**1**) $[Bu_2(Indo)SnOSn(Indo)Bu_2]_2$, (**2**), where Hindo is indomethacin, have been prepared and structurally characterized by means of ^{119}Sn Mössbauer, vibrational, and NMR (^1H and ^{13}C) spectroscopy. The crystal structures of the complexes $[Me_2(Indo)SnOSn(Indo)Me_2]_2 \cdot 2C_4H_8O_2$, **3** and **2** have been determined by X-ray crystallography. Each structure is centro-symmetric and features a central rhombus Sn_2O_2 unit with two additional tin atoms linked at the O atoms. Pairs of tin atoms are bridged by bidentate carboxylate ligands and by a monoatomic bridging oxygen. C–H→ π, π → π, stacking interactions, inter and intramolecular hydrogen bonds stabilize the structures **2** and **3**. Complexes **2** and **3** are self-assembled via π → π, C–H-π and stacking interactions.
© 2004 Elsevier Ltd. All rights reserved.

Keywords: Indomethacin; Diorganotin; Crystal structures; Spectroscopic studies

1. Introduction

Indomethacin (1-(4-chlorobenzoyl)-5-methoxy-2-methyl-1Hindole-3-acetic acid), Hindo, scheme 1, is one of the most potent of the clinically used non-steroidal anti-inflammatory drugs, NSAIDs, and interferes with prostaglandin synthesis by direct inhibition of the two cyclooxygenase enzyme systems, Cox-I and Cox-II. Inhibition of the Cox-II system results in anti-inflammatory action, while inhibition of the Cox-I enzyme system results in anti-inflammatory action as well as gastric irritation [1,2]. It was proposed that Hindo binds to Arg 120 of both the COX-I and COX-II enzymes by a carboxylate bridge and by slow and time-dependent reaction, competing with arachidonic acid for the COX site, and blocking the COX action of the enzyme [3,4]. A Cu(II) dimer of indomethacin with low toxicity is commercially available in Australasia, South East Asia and South Africa in a variety of oral pharmaceutical dosage forms for veterinary use [4–6]. Additional interest in NSAIDs lies in their possible therapeutic benefits in the prevention of various cancers including colorectal and lung cancers [7] and even in the treatment of Alzheimer's disease [8]. It was found that, indomethacin and mefenamic, at non-toxic levels, significantly increased the cytotoxicity of the anthracyclines, doxorubicin, daunorubicin and epirubicin, as well as teniposide, VP-16 and vincristine [9]. The crystal structure of Copper(II) dimers of Indomethacin have been reported [10,11].

* Corresponding authors. Tel.: +30-265098425/30-2651098422; fax: +30-265044825/30-2651044831.
E-mail addresses: dkovala@cc.uoi.gr (D. Kovala-Demertzi), mdemert@cc.uoi.gr (M.A. Demertzis).

0277-5387/$ - see front matter © 2004 Elsevier Ltd. All rights reserved.
doi:10.1016/j.poly.2004.05.004

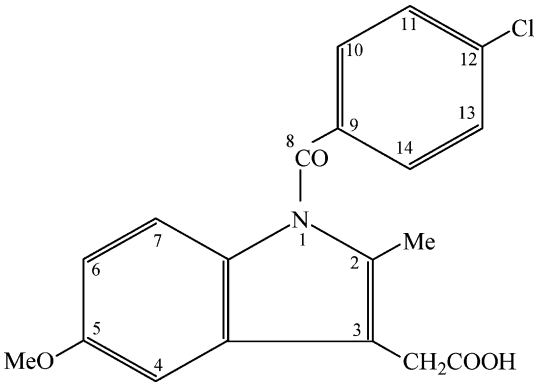

Scheme 1.

Organotin(IV) carboxylates form an important class of compound and have received increasing attention in recent years, not only because of their intrinsic interest but owing to their varied applications [12,13]. Investigations have been carried out to test their anti-tumour activity and it has been observed that indeed several diorganotin and triorganotin species show potentiality as anti-neoplastic and anti-tuberculosis agents [14–16].

Given the pharmacological importance of indomethacin acid and the potential biological activity of organotin carboxylates, it was thought of interest to explore the chemistry of organotin/indomethacin compounds. As a continuation of our studies of biological organotin chemistry and on the coordination chemistry and anti-inflammatory properties of NSAIDs such as diclofenac, tolfenamic acids and lornoxicam [17–21], we report here the synthesis and spectral characterization of $[R_2(Indo)SnOSn(Indo)R_2]_2$ (where $R = CH_3$, **1**, Bu, **2**, Indo is the deprotonated indomethacin. The complexes have been structurally characterized in the solid state by means of ^{119}Sn Mössbauer and vibrational spectroscopy and in solution by ^{1}H and ^{13}C NMR spectroscopic studies and electrochemical measurements. The crystal and molecular structures of **2** and $[Me_2(Indo)SnOSn(Indo)Me_2]_2 \cdot 2C_4H_8O_2$, **3** are also described, these being the first structures of organometallic indomethacin acid derivatives to be reported.

2. Experimental

2.1. Physical measurements

The reagents (Aldrich, Merck) were used as supplied while the solvents were purified according to standard procedures. Indomethacin was a gift from "Genepharm S.A". C, H, and N analyses were carried out by the microanalytical service of the University of Ioannina. Melting points were determined in open capillaries and are uncorrected. Infrared and far-infrared spectra were recorded on a Nicolet 55XC Fourier transform spectrophotometer using KBr pellets (4000–400 cm^{-1}) and nujol mulls dispersed between polyethylene disks (400–40 cm^{-1}). The ^{1}H (250.13 MHz), and ^{13}C (62.90 MHz) NMR spectra were recorded on a Bruker AC-250 spectrometer. Samples were dissolved in $CDCl_3$ or DMSO-d6 and spectra were obtained at room temperature with the signal of the free DMSO or $CHCl_3$ (at 2.49 and 7.24 ppm, respectively) as a reference. 2D ^{1}H–^{1}H shift correlated spectra (COSY), 2D ^{13}C–^{1}H shift correlated spectra (HETCOR) and 2D long-range ^{13}C–^{1}H shift correlated spectra (COLOC) of indomethacin were performed. Mössbauer spectra were recorded on finely ground materials at 80.0 K using an Air Liquid cryostat. The $Ca^{119}SnO_3$ source (15mCi New England Nuclear) at room temperature was moved in a constant acceleration mode with a triangular wave form. Suitable computer programs were employed in the fitting procedure of the experimental spectra to Lorentzian line shapes. The estimated errors on the Mössbauer parameters are ±0.01 mm/s. Electrochemical measurements were made using an AUTOLAB PGSTAT30 potentiostat with a platinum microsphere as working electrode, a platinum wire auxiliary electrode and an Ag/AgCl reference electrode in a three electrode configuration. Ferrocene was added at the end of each experiment and

Table 1
Crystal data and structure refinement parameters for **3** and **2**

	3	**2**
Empirical formula	$C_{96}H_{108}Cl_4N_4O_{24}Sn_4$	$C_{108}H_{132}Cl_4N_4O_{18}Sn_4$
Formula weight	2318.42	2390.74
Temperature (K)	100(2)	100(2)
Wavelength (A)	0.71073	0.71073
Crystal system	triclinic	triclinic
Space group	$P\bar{1}$	$P\bar{1}$
a (Å)	12.4429(7)	13.423(2)
b (Å)	14.5161(12)	15.4278(18)
c (Å)	15.9753(11)	15.996(2)
α (°)	71.259(7)	109.864(11)
β (°)	67.833(6)	99.629(12)
γ (°)	71.136(6)	114.199(13)
Volume (Å^3)	2462.4(3)	2654.1(6)
Z	1	1
D_x (g cm^{-3})	1.563	1.496
μ (mm^{-1})	1.185	1.098
$F(0\,0\,0)$	1172	1220
Crystal size (mm)	$0.20 \times 0.15 \times 0.15$	$0.12 \times 0.12 \times 0.05$
θ Range (°)	3.60–28.37	3.27–28.49
Ranges of h,k,l	−15–16, −12–19, −21–20	−17–17, −20–14, −20–21
Reflections		
collected	17,171	18,475
unique (R_{int})	10,836 (0.0457)	11,670 (0.0691)
Data/parameters	10,836/604	11,670/630
Goodness-of-fit (F^2)	0.958	0.927
Final R_1/wR_2 indices ($I > 2sI$)	0.0446/0.0664	0.0623/0.0868
Max/min $\Delta\rho$ (e Å^{-3})	1.174/−0.856	1.138/−1.020

used as an internal standard. All potentials are reported relative to a Ag/AgCl reference electrode and ferrocenium/ferrocene (Fe^{+}/Fc, $E_{1/2} = 0.173$ V in DMF); under the experimental conditions used (scan rate 100 mV s^{-1}). Et_4NClO_4 (0.1 M) was used as supporting electrolyte, the solutions were 1×10^{-3}M in complex, and carried out under a dinitrogen atmosphere.

2.2. Preparation of the complexes

2.2.1. Synthesis of [Me_2(Indo)SnOSn(Indo)Me_2]$_2$ 1,2:3,4-di-μ_2-1-(4chlorobenzoyl)-5-methoxy-2-methyl-1H-Indole-3-acetato-O,O-1,3-bis-1-(4-chlorobenzoyl)-5-methoxy-2-methyl-1H-Indole-3-acetato-μ_3-oxo-tetrakis[di-methyltin(IV)] (**1**)

Me_2SnO, (0.164 g, 1 mmol) was added to a solution of Hindo (0.357 g, 1 mmol) in benzene (50 cm^3) and the reaction mixture was refluxed overnight with azeotropic removal of water via a Dean–Stark trap. The resultant clear solution was rotary evaporated under vacuum to a small volume, chilled and triturated with diethyl ether to give a yellow solid. The powder was redissolved (suspended) in dry diethyl ether and the same procedure was repeated twice. The yellow powder was filtered and dried in vacuum over silica gel. M.p. 192–194 °C; Yield 92%. IR: 1614 ν_{as}(COO), 1362 ν_{sym}(COO), 1560 ν_{as}(COO), 1402 ν_{sym}(COO), 588, 575, 547 ν(Sn–C), 645br v(SnOSn), 314, 279 νSn–O(COO);). *Anal.* Calc. for $C_{84}H_{84}Cl_4N_4O_{18}Sn_4$: C, 49.1; H, 4.1; N, 2.7. Found: C, 48.7; H, 4.4; N, 2.6%. Crystals of [Me_2(Indo)SnOSn(Indo)Me_2]$_2 \cdot 2C_4H_8O_2$ (**3**) suitable for X-ray analysis were obtained by slow evaporation of a fresh *n*-C_6H_{12}/$CHCl_3$/$C_4H_8O_2$ solution of **1**.

2.2.2. Synthesis of [Bu_2(Indo)SnOSn(Indo)Bu_2]$_2$, 1,2:3,4-di-μ_2-1-(4-chlorobenzoyl)-5-methoxy-2-methyl-1H-Indole-3-acetato-O,O-1,3-bis-1-(4-chlorobenzoyl)-5-methoxy-2-methyl-1H-Indole-3-acetato-μ_3-oxo-tetrakis[di-n-butyltin(IV)] (**2**)

Di-*n*-butyl oxide (0.250 g, 1 mmol), Hindo (0.3578 g, 1 mmol) and 40 ml of benzene were refluxed overnight with azeotropic removal of water via a Dean–Stark trap. The resulting clear solution was rotary evaporated under vacuum to a small volume, chilled and triturated

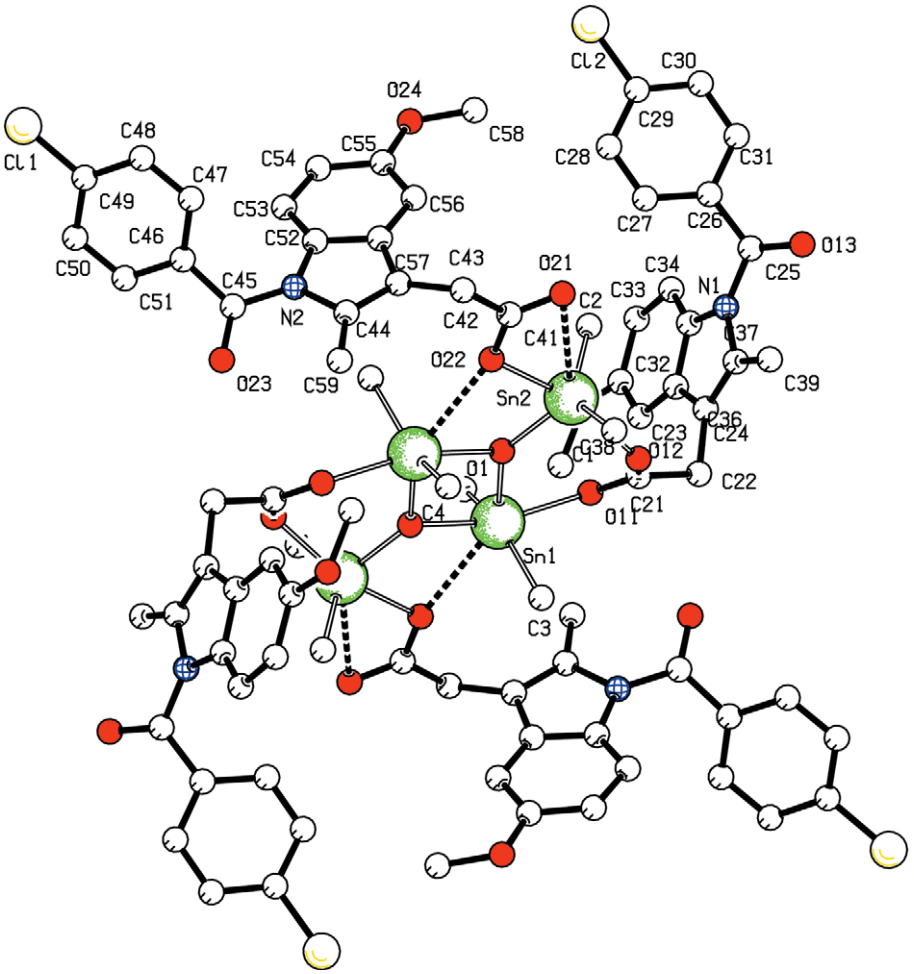

Fig. 1. Perspective view of [$Me_2SnLOLSnMe_2$]$_2$ (**1**) showing the atomic numbering scheme.

with diethyl ether to give a yellow solid. The powder was redissolved (suspended) in dry diethyl ether and the same procedure was repeated twice. The light yellow powder was dried in vacuo over silica gel. 180–183 °C; Yield, 85%. IR: 1622 v_{as}(COO), 1369 v_{sym}(COO), 1566 v_{as}(COO), 1402 v_{sym}(COO), 564, 545 v(Sn–C), 640, 635br v(SnOSn), 295, 277 vSn–O(COO); *Anal*. Calc. for $C_{108}H_{132}Cl_4N_4O_{18}Sn_4$: C, 54.2; H, 5.5; N, 2.3. Found: C, 54.4; H, 6.1; N, 2.1%. Crystals of (**2**) suitable for X-ray analysis were obtained by slow evaporation of a fresh *n*-C_6H_{12}/$CHCl_3$ solution of **2**.

2.3. X-ray crystallography

Crystal data for **2** and **3** are given in Table 1, together with refinement details. All measurements of crystals were performed in low temperature using an Oxford Cryosystem device on a Kuma KM4CCD κ-axis diffractometer with graphite-monochromated Mo Kα radiation. The crystal was positioned at 65 mm from the CCD camera. Six hundred and twelve frames were measured at 0.75° intervals with a counting time of 20 s. Accurate cell parameters were determined and refined by least-squares fit of 2100 the strongest reflections. The data were corrected for Lorentz and polarization effects. No absorption correction was applied. Data reduction and analysis were carried out with the Oxford Diffraction (Poland) Sp. z o.o (formerly Kuma Diffraction Wroclaw, Poland) programs. The structure was solved by direct methods (program SHELXS-97 [11]) and refined by the full-matrix least-squares method on all F^2 data using the using the WinGX version of SHELXL-97 programs [22,23]. Non-hydrogen atoms were refined with anisotropic displacement parameters; hydrogen atoms were included from geometry of molecules and $\Delta\rho$ maps but were not refined. Molecular graphics were performed from PLATON2001 [24,25].

3. Results and discussion

3.1. Crystal structures of 3 and 2

Compounds **1** and **2** are obtained by azeotropic removal of water produced by the reaction between the diorganotin oxide and indomethacin in the molar ratio 1:1. Recrystallization of **1** from a fresh *n*-C_6H_{12}/$CHCl_3$ solution gives the adduct $C_4H_8O_2$, **3**. The molecular structures of **3** and **2** are shown in Figs. 1 and 2 and selected interatomic parameters are collected in Table 2. Compounds **3** and **2** are centrosymmetric dimers built up around the planar cyclic Sn_2O_2 unit. The two oxygen

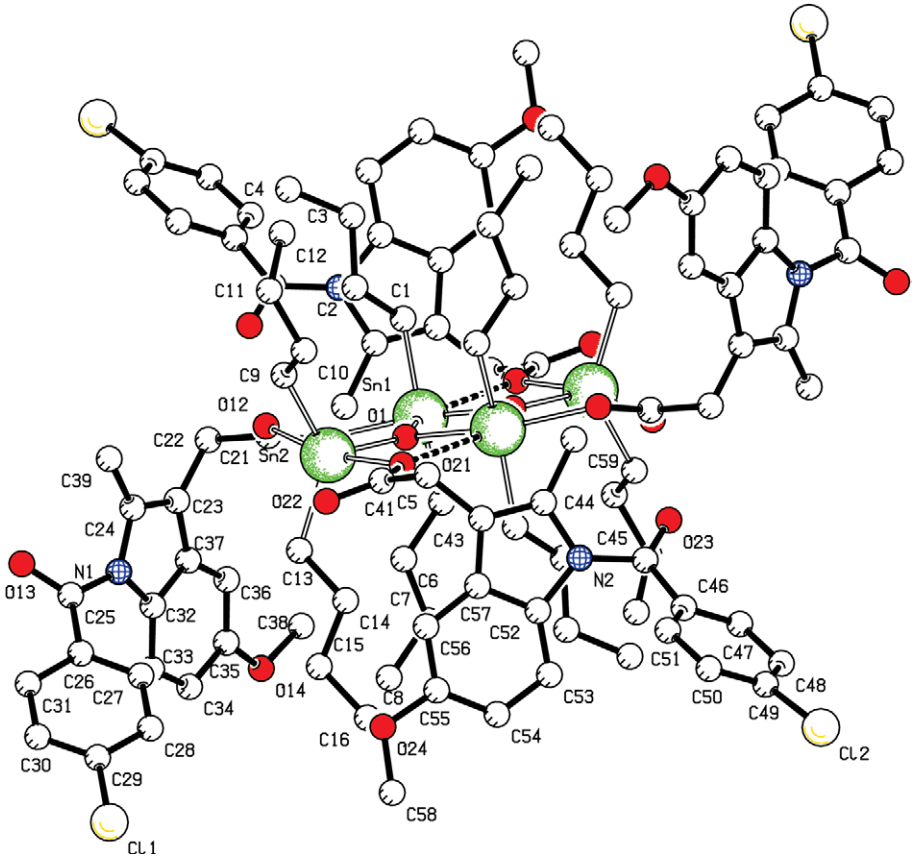

Fig. 2. Perspective view of $[Bu_2SnLOLSnBu_2]_2$ (**2**) showing the atomic numbering scheme.

atoms O(1) and O(1a) are triply bridging, each linking one exo-cyclic (Sn(2) or Sn(2a)) and two endo-cyclic (Sn(1) and Sn(1a)) atoms (see Fig. 3). The additional links between the endo- and exo-cyclic Sn atoms are provided by two bidentate bridging carboxylate ligands that form symmetrical bridges (Sn(1)–O(11) 2.262(3) Å and Sn(2)–O(12) 2.2361(3) Å for **3** and Sn(1)–O(11) 2.242(4) Å and Sn(2)–O(12) 2.243(4) Å) for **2**. Each exocyclic Sn atom is also coordinated by an anisobidentate chelating carboxylate ligand (Sn(2)–O(22) 2.176(3) Å and Sn(2)–O(21) 2.874(3) Å for **3** and Sn(2)–O(22) 2.178(4) Å and Sn(2)–O(21) 2.970(6) Å for **2**. The distance of O(22) atoms from endocyclic Sn are 2.741(3) and 2.752(5) for **3** and **2** respectively. The Sn–O distance of 2.741(3)–2.970(6) Å is considered long to indicate significant bonding interactions, however, the range of distances Sn–O of 2.61–3.02 Å, has been confidently reported for intramolecular bonds [26,27]. It is considered that the close approach of 2.970(6) Å is long for primary Sn–O bonding, but represent a type of secondary interaction. The coordination number around each tin is six for **3** and five and six around Sn(1) and Sn(2) respectively for **2**. Analysis of the shape determining angles for **2**, using the approach of Reedijk and coworkers [28], yields τ ($(\alpha - \beta)/60$) value of 0.54 for Sn(2) ($\tau = 0.0$ and 1.0 for *SP* and *TBP* geometries respectively). The metal co-ordination geometry is therefore described as very distorted trigonal bipyramidal with the O(21) and O(12) atoms occupying the axial positions and O(1), C(13) and C(9) the equatorial

Table 2
Selected bond distances and angles

3		**2**	
Bond distances			
Sn(1)–O(1)	2.050(3)	Sn(1)–O(1)	2.041(4)
Sn(1)–C(3)	2.101(4)	Sn(1)–C(1)	2.118(7)
Sn(1)–C(4)	2.110(4)	Sn(1)–C(5)	2.118(7)
Sn(1)–O(1)[a]	2.156(3)	Sn(1)–O(1)[b]	2.168(4)
Sn(1)–O(11)	2.262(3)	Sn(1)–O(11)	2.242(4)
Sn(2)–O(1)	2.025(3)	Sn(2)–O(1)	2.029(4)
Sn(2)–C(2)	2.106(4)	Sn(2)–C(9)	2.128(8)
Sn(2)–C(1)	2.115(4)	Sn(2)–C(13)	2.132(7)
Sn(2)–O(22)	2.176(3)	Sn(2)–O(21)	2.178(4)
Sn(2)–O(12)	2.236(3)	Sn(2)–O(12)	2.243(4)
Cl(1)–C(49)	1.739(4)	Cl(1)–C(29)	1.743(8)
Cl(2)–C(29)	1.745(4)	Cl(2)–C(49)	1.735(8)
O(1)–Sn(1)[a]	2.156(3)	O(21)–C(41)	1.300(7)
O(21)–C(41)	1.234(5)	O(22)–C(41)	1.261(8)
O(22)–C(41)	1.307(4)	O(23)–C(45)	1.212(8)
O(23)–C(45)	1.221(5)	O(24)–C(55)	1.395(8)
O(24)–C(55)	1.375(5)	O(24)–C(58)	1.418(9)
O(24)–C(58)	1.425(5)		
Bond angles			
O(1)–Sn(1)–C(3)	106.17(14)	O(1)–Sn(1)–C(1)	106.3(3)
O(1)–Sn(1)–C(4)	110.28(13)	O(1)–Sn(1)–C(5)	107.4(2)
C(3)–Sn(1)–C(4)	142.66(16)	C(1)–Sn(1)–C(5)	146.2(3)
O(1)–Sn(1)–O(1)[a]	75.19(11)	O(1)–Sn(1)–O(1)[b]	75.70(18)
C(3)–Sn(1)–O(1)[a]	99.79(13)	C(1)–Sn(1)–O(1)[b]	97.0(3)
C(4)–Sn(1)–O(1)[a]	97.02(13)	C(5)–Sn(1)–O(1)[b]	94.2(2)
O(1)–Sn(1)–O(11)	89.82(10)	O(1)–Sn(1)–O(11)	91.18(16)
C(3)–Sn(1)–O(11)	88.69(13)	C(1)–Sn(1)–O(11)	91.2(3)
C(4)–Sn(1)–O(11)	83.66(14)	C(5)–Sn(1)–O(11)	85.1(2)
O(1)[a]–Sn(1)–O(11)	164.31(10)	O(1)[b]–Sn(1)–O(11)	166.04(16)
O(1)–Sn(2)–C(2)	109.23(14)	O(1)–Sn(2)–C(9)	115.7(2)
O(1)–Sn(2)–C(1)	115.52(14)	O(1)–Sn(2)–C(13)	109.1(2)
C(2)–Sn(2)–C(1)	134.88(17)	C(9)–Sn(2)–C(13)	134.0(3)
O(1)–Sn(2)–O(22)	78.29(10)	O(1)–Sn(2)–O(21)	78.82(17)
C(2)–Sn(2)–O(22)	99.53(14)	C(9)–Sn(2)–O(21)	96.2(2)
C(1)–Sn(2)–O(22)	94.90(13)	C(13)–Sn(2)–O(21)	102.5(2)
O(1)–Sn(2)–O(12)	88.81(10)	O(1)–Sn(2)–O(12)	90.14(16)
C(2)–Sn(2)–O(12)	90.73(14)	C(9)–Sn(2)–O(12)	80.8(2)
C(1)–Sn(2)–O(12)	84.78(13)	C(13)–Sn(2)–O(12)	89.0(2)
O(22)–Sn(2)–O(12)	165.58(10)	O(21)–Sn(2)–O(12)	166.08(17)

[a] $-x+1, -y+2, -z$.
[b] $1-x, 1-y, 1-z$.

positions. For **3** and **2** the bond distances involving the bridging carboxylate ligand differ by only 0.024 and 0.002 Å respectively indicating a nearly symmetrical bridge, while the variations in the C–O bond distances, 0.002 and 0.025 Å suggest charge delocalization over the carboxylato group. The two rings of indole, the five and six-membered rings, are nearly planar, the dihedral angle is 3.6(3)° and 2.7(4)° for **3** and **2** respectively. The dihedral angles between the planes of the two phenyl rings are 62.2(2)° and 64.1(2)° for **3** and 63.2(4)° and 63.5(4)° for **2** and for the bidentate bridging and the anisobidentae chelating ligands respectively. The conformation of the co-ordinated indomethacin is similar to the two adducts and is similar to the structure of indomethacin. The dihedral angle of indomethacin between the planes of the two phenyl rings and the two rings of indole is 67.3(9)° and 2.0(8)° respectively [29]. The crystal structure of **3** shows ring stacking interactions. The monomers are stacked by double strong $\pi \rightarrow \pi$ interactions (C(2)–C(4)N(1) → C(4A)–C(9A), C(4A)–C(9A) → C(2)–C(4)N(1); the two rings of indole, the six and five-membered C(4A)–C(9A) and C(2)–C(4)N(1) 'face' the rings C(2)–C(4)N(1) and C(4A)–C(9A) respectively at a distance of 3.915(4) Å. These $\pi \rightarrow \pi$ interactions play an important role in the stabilization of the stacked molecular units. Weaker $\pi \rightarrow \pi$ and C–H→ π interactions play a role in the stabilization of the units. The crystal structure of **2** exhibits weak $\pi \rightarrow \pi$ and C–H→ π interactions, Table 3, in this case complex **2** is self-assembled via C–H→ π and $\pi \rightarrow \pi$ stacking interactions [30]. The overall geometry found in **2** and **3** allowing for differences in chemistry, is similar to compounds with the general formula $[R_2(R'CO_2)SnOSn(O_2CR')R_2]_2$ [31]. View of the crystal packing for **2** is shown in Fig. 4.

3.2. Spectroscopy

3.2.1. Infrared spectroscopy

Hindo displays a very broad, intense O–H stretching absorption in the region of 3300–2500 cm^{-1} with weaker and much sharper C–H stretches superimposed. The absence of the O–H absorption bands of the carboxylic acid in the IR spectra of **1** and **2** are indicative of carboxylato group binding. All the complexes exhibit characteristic IR spectra due to the ligand vibration modes. The major characteristic of the IR spectra is the frequency of the υ_{asym}(COO) and υ_{sym}(COO) stretching

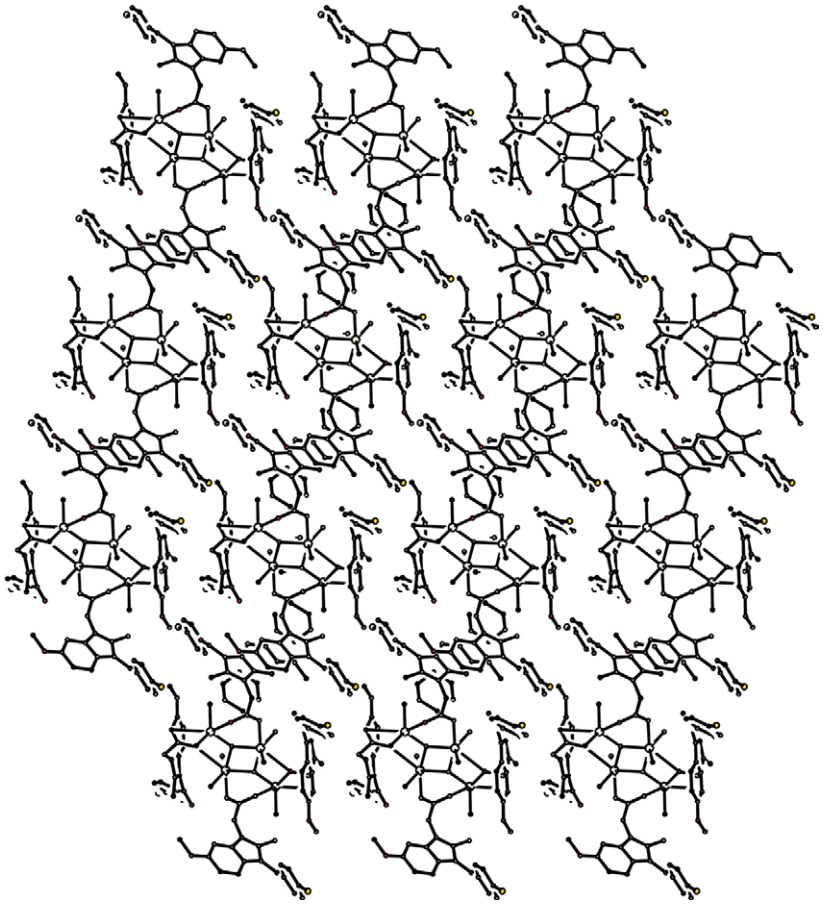

Fig. 3. Packing diagram of the complex of $[Me_2SnLOLSnMe_2]_2$ (**1**) viewed along the α axis.

Table 3
Proton and ^{13}C NMR data

		CH_3	CH_2	H4	OCH_3	H6	H7	H10,14	H11,13									
Hindo		2.36s	3.67s	6.92d	3.81s	6.65dd	6.83d	7.45d	7.64d									
1	Me_2Sn: 0.52s, 0.47s	2.33s	3.45s	6.98d	3.78s	6.62dd	6.79d	7.43d	7.61d									
2	Bu_2Sn Hδ: 0.71t/0.79t; Hγ: 1.45m; Hα, β: 1.18m	2.36s	3.49s	6.90d	3.75s	6.58dd	6.74d	7.41d	7.59d									
		COOH	C2	C3	C3α	C4	C5	C6	C7	C7α	CO	C9	C10,14	C11,13	C12	OCH_3	CH_2	CH_3
Hindo		176.9	136.2	130.4	111.8	101.2	156.0	111.7	115.0	130.7	168.3	133.7	129.1	131.1	139.3	55.7	30.0	13.3
1	Bu_2Sn, Cδ: 13.6/13.5; Cγ: 177.0 26.8/26.7; Cβ: 27.6/27.2; Cα: 28.6/27.6		135.3	–	114.3	101.8	156.0	111.0	114.9	130.8	168.1	134.0	129.0	131.0	139.1	55.5	32.3	13.3

vibrations. The frequency of these bands depends upon the co-ordination mode of the carboxylato ligand. The ν_{as}(COO) and ν_{sym}(COO) bands appear at ~1630–1560 cm^{-1} and ~1400–1370 cm^{-1} respectively. The ν_{as}(COO) and ν_{sym}(COO) bands appear at 1614, 1560 cm^{-1} and at 1394, 1402 cm^{-1}, respectively, for **1**. The difference, Δ [ν_{as}(COO)−ν_{sym}(COO)] between these frequencies for **1** is close to that found for aniso-bidentate (252 cm^{-1}) and bridging bidentate carboxylato groups (158 cm^{-1}). The ν_{as}(COO) and ν_{sym}(COO) bands appear at 1622, 1566 cm^{-1} and at 1369, 1401 cm^{-1}, respectively, for **2**. The difference, Δ [ν_{as}(COO)−ν_{sym}(COO)] between these frequencies for **2** is close to that found for aniso-bidentate (253 cm^{-1}) and bridging bidentate carboxylato groups (163 cm^{-1}). Two bands at 600–620 for **1** and **2**, are assigned to $\nu_{as,sym}(SnO)_2$, indicating non-linear O–Sn–O moieties, while the bands at 320–280 cm^{-1} are assigned to the tin-oxygen (COO) stretching modes. The absorption bands at 580–540 cm^{-1} are attributed to ν(Sn–C) stretching modes [18–20,32].

3.2.2. Mössbauer spectra

The Mössbauer spectra of **1** and **2** consist of a clearly asymmetric doublet that can be fitted only by assuming it derives from the overlap of two doublets due to two different tin sites present in a 1:1 atomic ratio. For both complexes, the two doublets present very similar values for the isomer shift, while the quadrupole splitting values are rather different indicating different contributions to the electric field gradient due to the lattice. The fitting of the experimental data points by two overlapping Lorentzian doublets for **1** and **2**, shows the occurrence of two distinct crystallographic environments around tin atoms, present in a 1:1 ratio. The hyperfine values for **1** are: $\delta = 1.51$, 1.46 $mm\,s^{-1}$; $\Delta E_Q = 3.76$, 2.88 $mm\,s^{-1}$; and for **2** are: $\delta = 1.50$, 1.44 $mm\,s^{-1}$; $\Delta E_Q = 3.63$, 2.86 $mm\,s^{-1}$. The very similar values for the isomer shift are indicative of the comparable electronic density at the two tin sites for both complexes.

From the quadrupole splitting values (ΔE_Q) and the point-charge model formalism, the relation $\Delta E_Q = 4[R](1 - 3\sin^2\theta\cos^2\theta)^{1/2}$ gives an estimate of θ, where 180°–2θ is the R–Sn–R bond angle [33]. In **1**, the bond angles calculated for the two tin sites are 151.8° for the high ΔE_Q value and 132.1° for the low ΔE_Q value. The X-ray crystal structure for this compound indicates C–Sn–C bond angles of 142.4(2)° and 135.1(2)°. For **2** similar results are confirmed by the X-ray diffraction analysis where the experimental values, 146.2(3)° and 134.0(3)°, are very close to the theoretical ones, 146.9° and 131.4°.

3.2.3. NMR spectra

The ^1H and ^{13}C NMR data for indomethacin (scheme 1) and the complexes **1** and **2** are summarized in Table 4. Complete assignment of the indomethacin

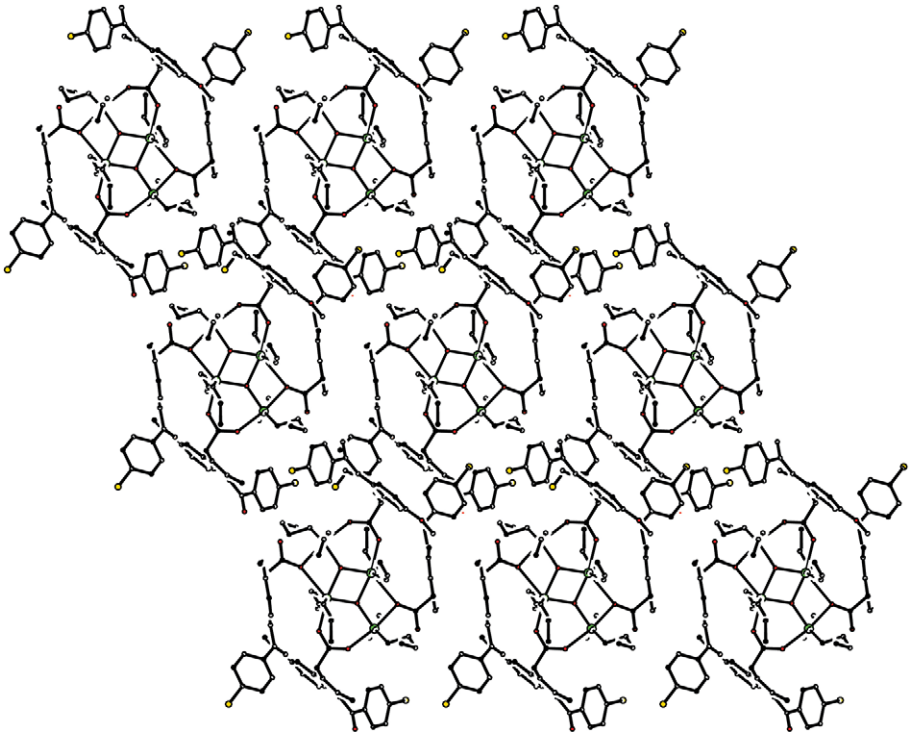

Fig. 4. Packing diagram of the complex of $[Bu_2SnLOLSnBu_2]_2$ (**2**) viewed along the α axis.

resonances in $CDCl_3$ has been based on ^1H (250.13 MHz), ^{13}C (62.90 MHz), 2D ^1H–^1H shift correlated spectra (COSY), 2D ^{13}C–^1H shift correlated spectra (HETCOR) and 2D long range ^{13}C–^1H shift correlated spectra (COLOC) and on previously reported data [34]. In **1** and **2**, most of the proton atoms of indomethacin show upfield shifts upon interaction of the ligand with organotin. These shifts mainly lie close to 0.1 ppm. When looking only at the proton resonances, no clear conclusion can be drawn concerning the possible coordination site of the metal. The ^{13}C NMR spectra of the complexes synthesized reveal major changes in the exocyclic carboxylic group, indicative of metal interaction through the carboxylic group. The latter exhibits either a major downfield shift (4.2 ppm in **1**) or a considerably broadened signal accompanied by a significant downfield shift for the methylene carbon attached to the carboxylato group, as observed in complex **2**. The ^1H NMR resonances of **2** are broadened in comparison to the free ligand and exhibit small upfield shifts, with the greatest shift (0.18 ppm) demonstrated by the CH_2 peak. In the ^{13}C NMR spectrum of **2**, the greatest shifts are observed for the C(3a) (2.5 ppm, downfield) and CH_2 (+2.3 ppm, downfield) atoms. Negligible shifts ranging between 0.0 and 0.9 ppm are found for the other carbon atoms. It is worth mentioning that the peak corresponding to the carboxyl group remains unshifted. However, upon interaction with the metal, it exhibits considerable loss in intensity and broadening. Keeping this in mind and taking also into consideration the shifts exhibited by the neighboring atoms (C(3a) and CH_2), interaction of the metal with the carboxyl group is infered. In both the ^1H and ^{13}C NMR spectra of complex **2**, two peaks of equal height appear for the methyl group of dibutyltin (IV). It is presumed that two types of tin centres are present. This is confirmed by the crystal structure of **2**. The greatest shift at **1** is exhibited by the CH_2 peak implicating coordination through the carboxyl group of the ligand. Two peaks of equal height appear for the methyl group of dimethylltin(IV), reflecting the presence of two types of tin centres. This is confirmed by the crystal structure of **3**. No J ($^{119/117}Sn$–^1H) fine couplings could be observed for **1** and **2**.

3.3. Electrochemical measurements

The ability of the complexes to gain or to lose electrons was studied in anhydrous DMF solution by cyclic voltammetry. The ligand exhibits irreversible reduction peaks at −0.618 and −1.130 V. Complex **1** shows irreversible reductions at −0.610 and −1.123 V, while complex **2** at −0.613 and −1.189 V. The electrochemical data suggest that the reduction of **Hindo**, **1** and **2** might be regarded as being more or less centered on the ligand system [20]. The electron transfers from the platinum cathode and is directed to the π^* LUMO orbital. The first reduction potential of **1** is less negative than **2** and decreased in the order **1** < **2** < **Hindo**.

Table 4
Distances (Å) and angles (°) of C–H-π, π–π interactions and interamolecular hydrogen bonds for **3** and **2**

C–H(I)-Cg(J)		H–Cg	C–Cg	∠C–H–Cg
C–H–π, π–π interactions and interamolecular hydrogen bonds for **3**				
C(42)–H → Cg(3)[A]		2.6319	3.431(5)	84.70
C(3)–H → Cg(3)[B]		2.6577	3.445(6)	137.57
C(22)–H → Cg(7)[C]		3.3283	3.734(6)	106.62
Cg(I) → Cg(J)[a]	Cg–Cg[b]	β[c]	CgI-Perp[d]	CgJ-Perp[e]
Cg(2) → Cg(7)[C]	3.915(4)	28.07	3.521	3.456
Cg(7) → Cg(2)[C]	3.917(3)	26.15	3.456	3.516
C–H(I) → Cg(J)		H–Cg	C–Cg	∠C–H-Cg
C–H–π, π–π interactions and intramolecular hydrogen bonds for **2**				
C(1)–H → Cg(3)[D]		2.565	3.596(10)	176.21
C(42)–H → Cg(8)[C]		2.567	3.385(9)	138.47
C(56)–H → Cg(3)[C]		3.3867	3.610(9)	95.88
Cg(I) → Cg(J)[a]		β[c]	CgI-Perp [d]	CgJ-Perp[e]
Cg(5) → Cg(5)[E]	4.083(5)	26.25	3.661	3.662
Cg(5) → Cg(7)[F]	4.086(6)	20.55	3.826	3.935
Cg(7) → Cg(5)[F]	4.087(6)	15.66	3.935	3.826

[A] 1−x, 1−y, −z.
[B] 1−x, 2−y, −z.
[C] 1−*x*, 2−*y*, 1−*z*.
[D] 1−*x*, 1−*y*, 1−*z*.
[E] −*x*, 1−*y*, −*z*.
[F] −1 + *x*, −1 + *y*, −1 + *z*.
[a] Where Cg(2), Cg(3) and Cg(7) are referred to the centroids N(2)–C(23)–C(24)–C(32)–C(37), N(2)–C(43)–C(44)–C(52)–C(57) and C(32)C(24)–C(37), for **3**, Cg(3), Cg(5) and Cg(7), Cg(8), are referred to the centroids N(2)–C(43)–C(44)–C(52)–C(57), C(26)–C(31) and C(46)–C(51), C(52)–C(57) for 3.
[b] Cg–Cg is the distance between ring centroids; symmetry transformations.
[c] Where β is the angle Cg(I)-→Cg(J) or Cg(i)-→Me vector and normal to plane I (°).
[d] CgI-Perp is the perpendicular distance of Cg(I) on ring J.
[e] CgJ-Perp is the perpendicular distance of Cg(J) on ring I.

4. Supplementary material

Crystallographic data for the structures reported in this paper have been deposited with the Cambridge Crystallographic Data Centre, CCDC, 233948 and 233949 for compounds **3** and **2**. Copies of this information may be obtained free of charge from The Director, CCDC, 12, Union Road, Cambridge CB2 1EZ [FAX +44(1223)336-033] or e-mail deposit@ccdc.cam.ac.uk or http://www.ccdc.cam.ac.uk.

Acknowledgements

We thank the European Community and the Greek Ministry of Education and Religion for the funding support from the research program EPEAEK HERAKLEITOS and V.D. and A.G. thank the same project for a scholarship. We also thank the NMR service of the University of Ioannina.

References

[1] M.N.G. Dukes, Meyler's Side Effects of Drugs, An Encyclopedia of Adverse Reactions and Interactions, 13th ed., Elsevier, Amsterdam, 1996.
[2] J.R. Vane, R.M. Botting, Semin. Arthritis Rheum. 26 (1997) 2.
[3] R.G. Kurumbail, A.M. Stevens, J.K. Gierse, J.J. McDonald, R.A. Stegeman, J.Y. Pak, D. Gildehaus, J.M. Miyashiro, T.D. Penning, K. Seibert, P.C. Isakson, W.C. Stalling, Nature (London) 384 (1996) 644.
[4] J.E. Weder, C.T. Dillon, T.W. Hambley, B.J. Kennedy, P.A. Lay, J.R. Biffin, H.L. Regtop, N.M. Davies, Coord. Chem. Rev. 232 (2002) 95.
[5] IVS Annual; MIMS Publishing, Crows Nest, NSW, Sydney, 1997, p. 145, 276.
[6] J.R. Biffin, Safe Administration of Copper Indomethacin to Dogs, personal communication, 2000.
[7] T. Hida, J. Leyton, A.N. Makheja, P. Benav, T. Hla, A. Martinez, J. Mulshine, S. Malkani, P. Chung, T.W. Moody, Anticancer Res. 18 (1998) 775.
[8] E.E. Netland, J.L. Newton, R.E. Majocha, B.A. Tate, Neurobiol. Aging 19 (1998) 201.
[9] C.P. Duffy, C.J. Elliott, R.A. O'Connor, M.M. Heenan, S. Coyle, I.M. Cleary, K. Kavanagh, S. Verhaegen, C.M. O'Loughlin, R. NicAmhlaoibh, M. Clynes, Eur. J. Cancer 34 (8) (1998) 1250.
[10] Y.R. Morgan, P. Turner, B.J. Kennedy, T.W. Hambley, P.A. Lay, J.R. Biffin, H.L. Regtop, B. Warwick, Inorg. Chim. Acta 324 (2001) 150.
[11] J.E. Weder, T.W. Hambley, B.J. Kennedy, P.A. Lay, G.J. Foran, A.M. Rich, Inorg. Chem. 40 (2001) 1295.
[12] V. Chandrasekhar, S. Nagendram, V. Baskar, Coord. Chem. Rev. 235 (2002) 1.
[13] M. Gielen, Appl. Organomet. Chem. 16 (2002) 481.
[14] D. Kovala-Demertzi, V. Dokorou, Z. Ciunik, N. Kourkoumelis, M.A. Demertzis, Appl. Organomet. Chem. 16 (2002) 360.

[15] D. Kovala-Demertzi, P. Tauridou, U. Russo, M. Gielen, Inorg. Chim. Acta 239 (1995) 177.
[16] S.K. Hadjikakou, M.A. Demertzis, J.R. Miller, D. Kovala-Demertzi, J. Chem. Soc. Dalton Trans. (1999) 663.
[17] M.A. Demertzis, S.K. Hadjikakou, D. Kovala-Demertzi, A. Koutsodimou, M. Kubicki, Helvet. Chim. Acta 83 (2000) 2787.
[18] V. Dokorou, Z. Ciunik, U. Russo, D. Kovala-Demertzi, J. Organomet. Chem. 630 (2001) 205.
[19] D. Kovala-Demertzi, N. Kourkoumelis, A. Koutsodimou, A. Moukarika, E. Horn, E.R.T. Tiekink, J. Organomet. Chem. 620 (2001) 194.
[20] A. Galani, M.A. Demertzis, M. Kubicki, D. Kovala-Demertzi, Eur. J. Inorg. Chem. (2003) 1761.
[21] D. Kovala-Demertzi, J. Inorg. Biochem. 79 (1–4) (2000) 153.
[22] G.M. Sheldrick, Acta Crystallogr. Sect. A 46 (1990) 467.
[23] G.M. Sheldrick, SHELXL 97 and SHELXS 97, University of Gottingen, Germany.
[24] L.J. Farrugia, J. Appl. Cryst. 32 (1999) 837.
[25] A.L. Spek, PLATON, A Program for the automated generation of a variety of geometrical entities, University of Utrecht, The Netherlands, 2001.
[26] K.C. Molloy, T.G. Purcell, K. Quill, I.W. Nowell, J. Organomet. Chem. (1984) 267.
[27] A.R. Forrester, S.J. Garden, R.A. Howie, J.L. Wardell, J. Chem. Soc. Dalton Trans. (1992) 2615.
[28] A. Addison, R.T. Nageswara, J. Reedijk, J. Van Rijn, G.C. Verschoor, J. Chem. Soc. Dalton Trans. (1984) 1349.
[29] T.J. Kistenmacher, R.E. Marsh, J. Am. Chem. Soc. 94 (1972) 1340.
[30] Th. Steiner, Cryst. Rev. 6 (1996) 57.
[31] E.R.T. Tiekink, Trends Organomet. Chem. 1 (1994) 71.
[32] K. Nakamoto, Infrared and Raman Spectra of Inorganic and Coordination Compounds, 4th ed., Wiley, New York, 1986.
[33] G. Fronza, A. Mele, E. Redenti, P. Ventura, J. Org. Chem. 61 (1996) 909.
[34] G.M. Banroft, T.K. Sham, Inorg. Chem. 14 (1975) 2281.

Available online at www.sciencedirect.com
SCIENCE DIRECT®
Polyhedron 23 (2004) 2031–2036
POLYHEDRON
www.elsevier.com/locate/poly

Synthetic, spectroscopic and X-ray crystallographic structural study of the monomeric [Cu(pysme)(sac)(MeOH)] and dimeric $[Cu(6mptsc)(sac)]_2$ complexes [pysme = anion of the pyridine-2-carboxaldehyde Schiff base of *S*-methyldithiocarbazate, 6mptsc = the anion of the 6-methyl-2-pyridinecarbaldehydethiosemicarbazone and sac = the saccharinate anion]

Mohammad Akbar Ali [a,*], A.H. Mirza [a], Thahira B.S.A. Ravoof [a], Paul V. Bernhardt [b]

[a] *Department of Chemistry, University of Brunei Darussalam, Jalan Tungku Link, Gadong BE 1410, Brunei*
[b] *Department of Chemistry, The University of Queensland, Brisbane 4072, Australia*

Received 30 March 2004; accepted 24 May 2004

Abstract

New mixed-ligand copper(II) complexes of empirical formulas [Cu(pysme)(sac) (CH_3OH)] and $[Cu(6mptsc)(sac)]_2$ have been synthesized and characterized by conductance, magnetic, IR and electronic spectroscopic techniques. X-ray crystallographic structure analyses of these complexes indicate that in both complexes the copper(II) ions adopt a five-coordinate distorted square-pyramidal geometry with an N_3SO donor environment. The Schiff bases are coordinated to the copper(II) ions as tridentate NNS chelates via the pyridine nitrogen atom, the azomethine nitrogen atom and the thiolate sulfur atom. In the monomeric [Cu(pysme)(sac)(MeOH)] complex, the saccharinate anion acts as a monodentate ligand coordinating the copper(II) ion via the imino nitrogen atom whereas in the dimeric $[Cu(6mptsc)(sac)]_2$ complex, the sac anion behaves as a bridging bidentate ligand providing the imino nitrogen donor atom to one of the copper(II) ions and the carbonyl oxygen as a weakly coordinated axial ligand atom to the other Cu(II) ion. In both complexes, the copper(II) ions have distorted square-pyramidal environments. The distortion from an ideal square-pyramidal geometry is attributed to the restricted bite angles of the planar tridentate ligand.
© 2004 Elsevier Ltd. All rights reserved.

Keywords: Copper(II) complexes; Dithiocarbazates; Saccharin complexes

1. Introduction

Saccharin (*o*-sulfobenzoimide) is a commercially important artificial sweetener and is widely used as a food additive [1]. The saccharinate anion (sac^-) is also an interesting polyfunctional ligand since it has several potential donor atoms and consequently, its coordination chemistry with several metal ions has been studied in some detail [1–5].

In view of the interesting coordination chemistry of both the saccharinate anion and tridentate Schiff bases derived from *S*-alkyl- and *S*-aryldithiocarbazates and thiosemicarbazide [6–10], which are also analogues of the well-known experimental anticancer drug, pyridine-2-aldehydethiosemicarbazone [11], we report here the synthesis, characterization and X-ray crystal structures of two new mixed-ligand copper(II) complexes [Cu(pysme)(sac)(MeOH)] and $[Cu(6mptsc)(sac)]_2$ which contain both coordinated saccharinate anion and tridentate NNS ligands.

* Corresponding author. Tel.: +673-2-463001x1341; fax: +673-2-461502.
E-mail address: akbar@fos.ubd.edu.bn (M. Akbar Ali).

0277-5387/$ - see front matter © 2004 Elsevier Ltd. All rights reserved.
doi:10.1016/j.poly.2004.05.007

2. Experimental

2.1. Materials and instrumentation

The electronic spectra were recorded both in the solid state (as Nujol mulls) and in solution on a Shimadzu UV-3100 spectrophotometer. The IR spectra were recorded as KBr discs on either a Perkin–Elmer 1600 FT IR spectrometer or a Perkin–Elmer 2000 spectrometer. Conductance measurements were made by means of a CMD 400 conductivity meter. Magnetic susceptibilities were measured with a Sherwood Scientific magnetic susceptibility balance calibrated with $HgCo(NCS)_4$. Diamagnetic corrections were applied using Pascal's constants.

2.2. Preparation of the Schiff bases

These bases were prepared by literature methods [12,13].

2.3. Preparation of the complexes

The complexes were prepared by the following general method: $[Cu(sac)_2(H_2O)_4]\cdot 2H_2O$ [4] (0.6 mmol) dissolved in boiling methanol (25 ml) was mixed with a solution of the appropriate Schiff base (0.6 mmol) in the same solvent (25 ml) and the resulting mixture was heated on a water bath for 40 min. On standing overnight in a refrigerator, the mixture yielded crystalline complexes suitable for X-ray work (yield: 40–60%). *Anal.* Calcd. for [Cu(pysme)(sac)(CH_3OH)] ($C_{16}H_{16}N_4O_4S_3$Cu): C, 37.84; H, 3.39; N, 11.77. Found: C, 38.01; H, 2.97; N, 11.74%. *Anal.* Calcd. for $[Cu(6mptsc)(sac)]_2$ ($C_{30}H_{26}N_{10}O_6S_4Cu_2$): C, 37.64; H, 3.20; N, 15.20. Found: C, 37.64; H, 3.18; N, 15.03%.

2.4. X-ray crystallography

A crystal of the appropriate complex was mounted on a glass fibre. Cell constants were determined by a least-squares fit to the setting parameters of 25 independent reflections, measured on an Enraf–Nonius CAD 4 four-circle diffractometer using graphite monochromated Mo Kα radiation (0.71073 Å) and operating in the ω–2θ mode within the range $2° < 2\theta < 50°$. An empirical absorption correction (ψ scans) and data reduction were performed with the WINGX [14] suite programmes. The structures were solved by direct methods with SHELX86 [15] of programmes and refined by full-matrix least-squares analysis with SHELXL97 [16]. Non-hydrogen atoms were refined with anisotropic thermal parameters whereas H-atoms were restrained at calculated positions using a riding model. Drawings of the molecules were produced with ORTEP3 [17]. A summary of the crystal data, structure solution and refinement parameters are given in Table 1.

3. Results and discussion

The Schiff bases (Fig. 1(a); R = H, CH_3; X = SCH_3 or NH_2) although, in principle, could exhibit thione (**1a**)

Table 1
Crystallographic data for [Cu(pysme)(sac)(MeOH)] and $[Cu(6mptsc)(sac)]_2$

Formula	$C_{16}H_{16}CuN_4O_4S_3$	$C_{30}H_{26}Cu_2N_{10}O_6S_4$
Formula weight	488.08	877.92
Temperature (K)	296(2)	296(2)
Crystal size (mm)	$0.5 \times 0.40 \times 0.20$	$0.27 \times 0.20 \times 0.20$
Crystal system	monoclinic	triclinic
Space group	$P2_1/n$	$P\bar{1}$
a (Å)	12.897(4)	9.309(5)
b (Å)	11.589(1)	9.351(4)
c (Å)	14.247(2)	10.816(5)
α (°)		101.06(4)
β (°)	114.03(1)	96.96(4)
γ (°)		103.11(4)
Volume (Å^3)	1944.9(7)	886.5(7)
Z	4	1
D_{calc} (g cm^{-3})	1.667	1.645
Absorption coefficient (mm^{-1})	1.476	1.494
$F(000)$	996	446
Reflections collected	3578	3308
Independent reflections (R_{int})	3418 (0.0270)	3098 (0.0263)
Observed reflections [$I > 2\sigma(I)$]	2930	2346
Parameters	255	236
Goodness-of-fit	1.094	1.101
R_1 [$I > 2\sigma(I)$]	0.0284	0.0634
wR_2 (all data)	0.0841	0.1674

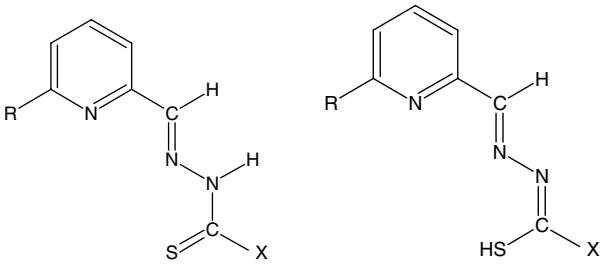

(**1a**; thione form; R =H, CH_3 X = SCH_3 or NH_2) (**1b**;thiol form)

Fig. 1. The thione (**1a**) and thiol (**1b**) forms of the Schiff bases (**1a**: thione form; R = H, CH_3, X = SCH_3 or NH_2) (**1b**: thiol form).

and thiol (**1b**) tautomerism, our previous studies have shown that, in the solid state, they remain in the thione forms (**1a**) [12,13]. However, in boiling methanol, they readily react with $[Cu(H_2O)_4(sac)_2]\cdot 2H_2O$ yielding mixed-ligand complexes of empirical formula $[Cu(NNS)(sac)(MeOH)_x]$ (NNS = anionic form of the Schiff base; sac^- = the saccharinate anion; $x = 1, 0$). These complexes are quite stable in the atmosphere and could be kept in a desiccator for a long period of time without any sign of decomposition. Their molar conductance values in MeCN fall in the range 18–19 $\Omega^{-1}\,cm^2\,mol^{-1}$. These values, although significant, are much lower than that shown by 1:1 electrolytes in this solvent [18]. The conductivity data indicate that the sac^- ligands remain predominantly coordinated to the copper(II) ions as uninegatively charged ligands in MeCN. The IR spectra of the complexes do not exhibit the *v*NH bands of the free ligands supporting deprotonation of the ligands during coordination with the copper(II) ion. An examination of the IR data in Table 2 also shows that the Schiff bases are coordinated to the copper(II) ions via the azomethine nitrogen atoms (shift of *v*C=N and *v*N–N bands of the free ligands at ca. 1584–1559 and 1046–1076 cm^{-1}, respectively), the thiolate sulfur atom (splitting of the $vCSS_a$ bands of the free ligands in the spectrum of the [Cu(pysme)(sac)(MeOH)] complex) and the pyridine nitrogen atoms (shift of the pyridine ring vibration from ca. 634 to ~647 cm^{-1}).

The room temperature magnetic moments of 1.88 B.M. for [Cu(pysme)(sac)(CH_3OH)] and 1.85 B.M. for $[Cu(6mptsc)(sac)]_2$ indicate that they are magnetically dilute in nature. The electronic spectra of the copper(II) complexes, in addition to showing the intra-ligand $n \Rightarrow \pi^*$ bands in the range 369–358 nm and $\pi \Rightarrow \pi^*$ in the 293–254 nm range, display a $S \Rightarrow Cu^{II}$ charge-transfer band in the 406–430 nm range and a weaker d–d band in the range 600–620 nm. The presence of a $S \Rightarrow Cu$ LMCT band at ca. 406–430 nm in the electronic spectra of the present copper(II) complexes is strong evidence that the Schiff bases are coordinated to the copper(II) ions via the thiolate sulfur atom. Such LMCT bands are quite common in the electronic spectra of copper(II) complexes of tridentate NNS thiosemicarbzone ligands [19,20]. The appearance of a d–d band at ca. 600–620 nm in their electronic spectra is consistent with a five-ccordinate geometry and is similar to that observed for $[\{Cu(pytsc)(CH_3COO)\}_2]$ (λ_{max} = 640 nm) which also contains five-coordinate copper(II) ions [21].

3.1. The crystal structure of the [Cu(pysme)(sac)(MeOH)] complex

A thermal ellipsoid drawing of the structure indicating atom numbering scheme is shown in Fig. 2. Bond lengths and bond angles are given in Table 3. The complex crystallizes as a five-coordinate monomeric species. As indicated from the physicochemical results, the copper(II) ion adopts a distorted square-pyramidal geometry with the equatorial donor atoms being the pyridine nitrogen atom (N3), the azomethine nitrogen atom (N2) and the sulfur atom (S1) from the

Table 2
Selected IR bands and electronic spectral data for the ligands and their copper(II)–saccharinate complexes

Compound	IR bands							Electronic spectra bands[a]	
	*v*NH	*v*CN	*v*NN	$vCSS_a$	v_sSO_2	$v_{as}SO_2$	*v*CO	State	λ_{max} (nm)
Hpysme	3093m, 2913m 2799br	1584s	1046s	956m				Nujol	358, 254
								MeCN	339(5.1), 219(4.6)
H6mptsc·H_2O	2973w,br	1580s	1117s					Nujol	352, ca. 250
								MeCN	324(4.6), 233(4.3)
[Cu(pysme)(sac)(MeOH)]		1559s	1077m	965s	1154s	1301vs	1653s	Nujol	625, 359, 228
								MeCN	ca. 625, 421(4.1), 332(4.5)
$[Cu(6mptsc)(sac)]_2$	3585m 3456m	1591s	1056s		1144s	1281s	1651s 1621s	Nujol	ca. 680, 360, 351
	3341m							MeCN	ca. 600, 406(3.2), 285(3.6), 230

[a] $\log \varepsilon$ ($l\,mol^{-1}\,cm^{-1}$) are given in parentheses.

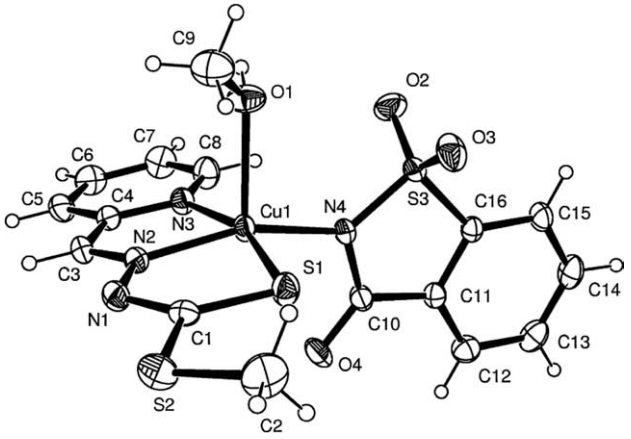

Fig. 2. The structure of [Cu(pysme)(sac)(MeOH)].

Table 3
Selected bond lengths (Å) and bond angles (°) for the copper(II) complexes

Bond lengths		Bond angles	
(a) [Cu(pysme)(sac)(CH$_3$OH)]			
Cu1–O1	2.228(2)	O1–Cu1–S1	99.61(6)
Cu(1)–N(3)	2.062(2)	N3–Cu1–S1	161.87(6)
Cu(1)–N(2)	1.958(2)	N4–Cu1–S1	97.05(7)
Cu(1)–S(1)	2.2951(9)	N2–Cu1–S1	83.51(7)
Cu(1)–N(4)	1.967(2)	N3–Cu1–O1	90.39(9)
N(1)–N(2)	1.381(3)	N4–Cu1–O1	97.99(8)
C(1)–S(1)	1.710(3)	N2–Cu1–O1	101.12(8)
C(1)–N(1)	1.312(4)	N4–Cu1–N3	96.48(9)
C3–N2	1.273(3)	N2–Cu1–N3	79.71(9)
C3–C4	1.461(4)	N2–Cu–N4	160.54(9)
C1–S2	1.752(3)		
(b) [Cu(6mptsc)(sac)]$_2$			
Cu(1)–S(1)	2.2741(19)	N(5)–Cu(1)–N(4)	102.50(16)
Cu(1)–N(5)	1.992(4)	N(2)–Cu(1)–S(1)	83.29(13)
Cu (1)–N(4)	2.123(4)	N(2)–Cu(1)–O(1)′	102.04(16)
Cu(1)–N(2)	1.961(4)	N(4)–Cu(1)–O(1)′	85.55(15)
Cu(1)–O(1)′	2.276(4)	N(4)–Cu(1)–S(1)	163.30(12)
C(1)–S(1)	1.715(5)	N(2)–Cu(1)–N(4)	80.12(16)
C(1)–N(1)	1.333(7)	N(2)–Cu(1)–N(5)	157.43(18)
N(1)–N(2)	1.340(7)	N(5)–Cu(1)–O(1)′	100.52(16)
C(2)–N(2)	1.286(6)	S(1)–Cu(1)–O(1)′	99.77(12)
C(2)–C(3)	1.454(7)		
C(3)–N(4)	1.356(6)		

O(1)′ symmetry operation $2-x, 1-y, 2-z$.

tridentate dithiocarbazate Schiff base plus the nitrogen N(4) from the saccharinate ion. The methanol ligand coordinates weakly in the apical site through O(1), which is typical of similar five-coordinate complexes [21]. The Schiff base is coordinated to the copper(II) ion in its iminothiolate form. While coordinating in this form, the negative charge generated upon deprotonation of the NH proton is delocalized across the S1–C1–N1 group as indicated by the intermediate C1–N1 {1.312(4) Å} and C1–S1 bond distances {1.710(3) Å}. These bonds may be compared with the true double bond seen in C3=N2 {1.273(3) Å} and C=S bonds are found in the (metal free) methylpyruvate Schiff base of *S*-methyldithiocarbazate {1.652(6) Å} [22], methylpyruvatethiosemicarbazone hemihydrate {1.684(4) Å} [23] and pyridine-2-carboxaldehydethiosemicarbazone {1.698(3) Å} [24].

The Cu–S {2.2951(9) Å}, Cu–$N_{azomethine}$ {1.958(2) Å} and Cu–N_{py} {2.062(2) Å} bond distances compare well with those of the analogous five-coordinate square-pyramidal copper(II) complex, [Cu(pytsc)(sac)(H_2O)] (pytsc = anionic form of the pyridine-2-carboxaldehydethiosemicarbazone), whose structure has been confirmed by X-ray diffraction [25]. The saccharinate ion is coordinated to the copper(II) ion via the deprotonated imino nitrogen atom. The Cu–N_{sac} distance {1.967(2) Å} also compares well that found in the above mixed-ligand copper(II)-thiosemicarbazone–saccharinate complex. The geometry of the complex is distorted square-pyramidal as a consequence of the restricted bite of the tridentate Schiff base ligand.

3.2. The crystal structure of the [Cu(6mptsc)(sac)]$_2$ complex

The structure shows that, in contrast with [Cu(pysme)(sac)(MeOH)] which is a monomer, the complex [Cu(6mptsc)(sac)]$_2$ is a centrosymmetric dimer. The symmetry related copper(II) ions adopt a five-coordinate geometry with the unique thiosemicarbazone ligand coordinating in its deprotonated thiolate form via the pyridine nitrogen atom, the azomethine nitrogen atom and the thiolate sulfur atom, while the saccharinate anion behaves as a bridging bidentate ligand providing an imino nitrogen donor atom to one copper(II) ion and the carbonyl oxygen donor to the second copper(II) ion. The structure of the dimer, [Cu(6mptsc)(sac)]$_2$ with atom numbering scheme adopted is shown in Fig. 3. The important bond lengths and angles are listed in Table 3. The resulting coordination spheres, (CuN_3SO) are similar to that found in the monomeric [Cu(pysme)(sac)(MeOH)] complex. The delocalization of electrons in the thiosemicarbazide chain is again reflected in the intermediate C1–N1 {1.333(7) Å} and C1–S1 bond lengths {1.715(5) Å}. The Cu–S {2.2741(19) Å}, Cu–$N_{azomethine}$ {1.961(4) Å}, Cu–N_{py} {2.123(4) Å} and Cu–N_{sac} {1.992(4) Å} bond distances compare well with those of other five-coordinate mixed-ligand copper(II)–saccharinate complexes containing tridentate thiosemicarbazones as co-ligands. However, the apical Cu–O_{sac} bond length {2.276(4) Å} is longer than that found in other O-bonded saccharinate complexes such as in [Cu(sac)(NH_3)$_4$] [3], indicating weaker copper(II)–carbonyl oxygen interaction in the present dimer. Of course these variations in the strength of axial coordination are relatively minor perturbations on the

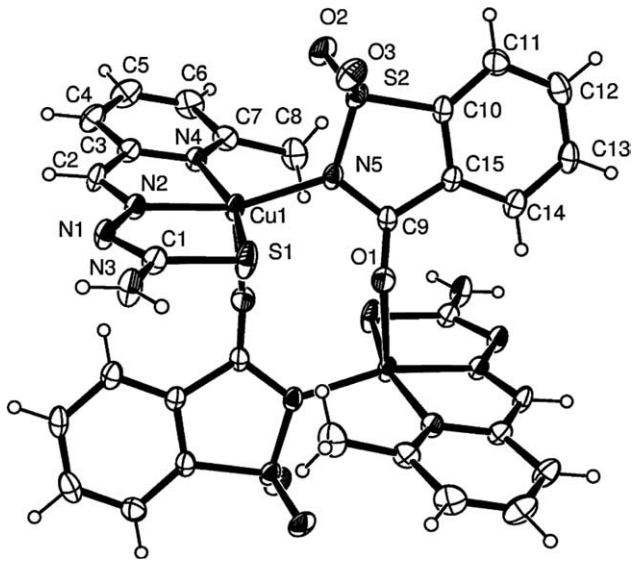

Fig. 3. The structure of $[Cu(6mptsc)(sac)]_2$.

over-riding axial elongation that ensues from the electronic (Jahn–Teller) effect inherent to five- and six-coordinate Cu(II) complexes, and they are correlated with changes in the equatorial ligands as well. The stereochemistry adopted by each copper(II) ion in the dimer is a distorted square-pyramid as a result of the restricted bite size of the ligand.

Given the very similar solution electronic spectra of $[Cu(6mptsc)(sac)_2]$ and [Cu(pysme)(sac)(MeOH)] and the lability of the metal ions, we wished to investigate whether the solid state structural differences identified crystallographically persisted in solution. EPR spectroscopy is a particularly powerful technique for the discrimination of monomeric and dimeric copper(II) complexes. Dipole–dipole coupling between neighbouring Cu(II) ($S = 1/2$) centres in a dimeric configuration leads to completely different EPR spectra to those found in isolated mononuclear analogues. The 77K EPR spectrum of 1 mM solution of $[Cu(6mptsc)(sac)]_2$ in DMF is characteristic of a monomeric Cu(II) complex with the spin Hamiltonian parameters $g_z = 2.205$ ($A_z = 168$ G), $g_x = g_y = 2.057$ ($A_x = A_y = 20$ G) obtained by spectral simulation. The spectrum of [Cu(pysme)(sac)(MeOH)] measured under identical conditions was the same. The A_z value (hyperfine coupling constant ^{65,67}Cu $I = 3/2$) is consistent with a distorted square-pyramidal coordination environment and a $d_{x^2} - d_{y^2}$ ground state [26]. Furthermore, the spectra are unlike those seen for genuine dinuclear five-coordinate copper(II) complexes [27,28], so the dimeric solid-state structure of $[Cu(6mptsc)(sac)]_2$ clearly does not persist in DMF solution. Presumably the competitive O-donor DMF occupies the axial coordination site in place of the O-bound sac^- ligand seen in the crystal structure.

4. Conclusions

The reaction of $[Cu(sac)_2(H_2O)_4]$ with tridentate sulfur–nitrogen chelating agents such the pyridine-2-carboxaldehyde Schiff base of *S*-methyldithiocarbazate or the 6-methyl-2-pyiridinecarboxaldehydethiosemicarbazone in methanol proceeds smoothly yielding crystalline mixed-ligand copper(II) complexes containing both coordinated saccharinate ion and deprotonated NNS donor ligands. The formation of a monomeric five-coordinate [Cu(pysme)(sac)(MeOH)] complex with an N-bonded saccharinate ligand and a dimeric $[Cu(6mptsc)(sac)]_2$ complex in which each of the saccharinate ions behaves as a bidentate chelating agent providing a nitrogen donor atom to one copper and the carbonyl oxygen donor atom to the other, demonstrates the versatility of the saccharinate anion as a polyfunctional ligand. In both the monomeric and dimeric complexes the $Cu–N_{sac}$ and $Cu–N_{imine}$ bonds are shorter than the $Cu–N_{py}$ bond.

5. Supplementary data

Crystallographic data for the structure analyses have been deposited with the Cambridge Crystallographic Data Centre, CCDC No. 204485 for [Cu(pysme)(sac)(MeOH)] and 204491 for $[Cu(6mptsc)(sac)]_2$. Copies of these information may be obtained free of charge from the Director, CCDC, 12 Union Road, Cambridge, CB2 1EZ, UK (fax: +44-123-333-6033; e-mail: deposit@ccdc.cam.ac.uk or http://www.ccdc.cam.ac.uk).

Acknowledgements

We thank the Department of Chemistry, Universiti Brunei Darussalam for support.

References

[1] L.O. Nabors, C.G. Robert, Alternative Sweeteners, 2nd ed., Marcel-Dekker, New York, 1991.
[2] C.A. Johns, G.M.G. Hossain, K.M.A. Malik, S.Z. Haidur, U.K.R. Romman, Polyhedron 56 (2000) 142, and references therein.
[3] L.R. Falvello, J. Gomez, I. Pascual, M. Thomas, E.P. Urriolabeitia, A.J. Schultz, Inorg. Chim. Acta 40 (2001) 4455;
F.A. Cotton, L.R. Falvello, W. Schwotzer, C.A. Murillo, G. Valle-Bourrouet, Inorg. Chim. Acta 190 (1991) 89, and references therein.
[4] S.Z. Haider, K.M.A. Malik, K.J. Ahmad, H. Hess, H. Riffel, M.B. Hursthouse, Inorg. Chim. Acta 72 (1983) 21.
[5] V.T. Yilmaz, A. Karadag, C. Thoene, J. Coord. Chem. 55 (2002) 609.
[6] M. Akbar Ali, A.H. Mirza, C.W. Voo, Ai Ling Tan, P.V. Bernhardt, Polyhedron 22 (2003) 1471, and references cited therein.

[7] M. Akbar Ali, A.H. Mirza, R.J. Butcher, M.T.H. Tarafdar, T.B. Keat, A.M. Ali, J. Inorg. Biochem. 92 (2002) 141.
[8] D.X. West, S.B. Padhye, P.B. Sonawane, Struct. Bonding (Berlin) 76 (1991) 1.
[9] D.X. West, A.E. Liberta, S.B. Padhye, R.C. Chikate, P.B. Sonawane, A.S. Kumbhar, R.G. Yerande, Coord. Chem. Rev. 123 (1993) 49.
[10] V. Philip, V. Suni, M.R.P. Kurup, M. Nethaji, Polyhedron 23 (2004) 1225, and references therein.
[11] H.A. Saryan, E. Ankel, C. Krishnamurti, D.H. Petoring, J. Med. Chem. 22 (1979) 1218.
[12] M. Akbar Ali, S.E. Livingstone, D.J. Phillips, Inorg. Chim. Acta 5 (1971) 493.
[13] M. Akbar Ali, K.K. Dey, M. Nazimuddin, F.E. Smith, R.J. Butcher, J.P. Jasinski, J.M. Jasisnski, Polyhedron 15 (1996) 3331.
[14] L. Farrugia, J. Appl. Cryst. 31 (1999) 837.
[15] SHELX 97 – G.M. Sheldrick programme for crystal structure solution, Institut fur Anorganische Chemie der Universitat Gottingen, Germany.
[16] SHELX 97 – G.M. Shildrick programme for crystal structure solution, Institut fur Anorganische Chemie der Universitat Gottingen, Germany.
[17] ORTEP 3 for Windows: L.J. Farrugia, J. Appl. Cryst. 30 (1997) 565.
[18] W.J. Geary, Coord. Chem. Rev. 7 (1971–72) 81.
[19] A.G. Bingham, H. Bogge, A. Muller, E.W. Ainscough, A.M. Brodie, J. Chem. Soc., Dalton Trans. (1987) 493.
[20] E.W. Ainscough, A.M. Brodie, N.G. Larson, Inorg. Chim. Acta 60 (1982) 25;
E.W. Ainscough, A.M. Brodie, N.G. Larson, J. Chem. Soc., Dalton Trans. (1982) 815.
[21] A.G. Bingham, H. Bogge, A. Muller, E.W. Ainscough, A.M. Brodie, J. Chem. Soc., Dalton Trans. (1987) 493.
[22] M. Akbar Ali, A.H. Mirza, R.J. Butcher, Polyhedron 20 (2001) 1037.
[23] M.B. Ferrai, G.G.C. Pelizzi, P. Tarasconi, J. Chem. Soc., Dalton Trans. (1989) 119.
[24] V.N. Biyushk, Chumakov, N.M. Samus, J. Struct. Chem. (Eng. Transl.) 28 (1987) 119.
[25] E.W. Ainscough, E.N. Baker, A.M. Brodie, R.J. Cresswell, J.D. Ranford, J.M. Waters, Inorg. Chim. Acta 172 (1990) 185.
[26] P.V. Bernhardt, J.M. Harrowfield, D.C.R. Hockless, A.M. Sargeson, Inorg. Chem. 33 (1994) 5659.
[27] P.V. Bernhardt, E.J. Hayes, J. Chem. Soc., Dalton Trans. (1998) 1037.
[28] D.G. Lennon, D.C. Craig, S.B. Colbran, P.V. Bernhardt, J. Chem. Soc. Dalton Trans. (2004) 778.

Available online at www.sciencedirect.com
SCIENCE DIRECT®
Polyhedron 23 (2004) 2037–2043
POLYHEDRON
www.elsevier.com/locate/poly

The preparation and characterization of seven-coordinate tin(IV) complexes of the 2,6-diacetylpyridine Schiff bases of *S*-alkyl/aryl-dithiocarbazates and the X-ray crystal structure of the [Sn(dapsme)I_2] complex (dapsme = doubly deprotonated form of the 2,6-diacetylpyridine Schiff base of *S*-methyldithiocarbazate)

Mohammad Akbar Ali [a,*], Aminul Huq Mirza [a], Ai Ling Tan [a], Lim Kok Wei [a], Paul V. Bernhardt [b]

[a] *Department of Chemistry, Universiti Brunei Darussalam, Jalan Tungku Link, BE 1410, Negara Brunei Darussalam*
[b] *Department of Chemistry, The University of Queensland, QLD 4072, Australia*

Received 13 May 2004; accepted 28 May 2004

Abstract

New tin(IV) complexes of empirical formula, Sn(SNNNS)I_2 (SNNNS = anionic form of the 2,6-diacetylpyridine Schiff bases of *S*-methyl- or *S*-benzyldithiocarbazate) have been prepared and characterized by a variety of physico-chemical techniques. The structure of Sn(dapsme)I_2 has been determined by single crystal X-ray crystallographic structural analysis. The complex has a seven-coordinate distorted pentagonal-bipyramidal geometry with the Schiff base coordinated to the tin(IV) ion as a dinegatively charged pentadentate chelating agent via the pyridine nitrogen atom, the two azomethine nitrogen atoms and the two thiolate sulfur atoms. The ligand occupies the equatorial plane and the iodo ligands are coordinated to the tin(IV) ion at axial positions. The distortion from an ideal pentagonal bipyramidal geometry is attributed to the restricted bite size of the pentadentate ligands.
© 2004 Elsevier Ltd. All rights reserved.

Keywords: Tin(IV) complexes; Dithiocarbazates; 2,6-diacetylpyridine Schiff bases of *S*-alkyldithiocarbazates; Seven-coordinate tin(IV) complexes

1. Introduction

Schiff bases formed from *S*-alkyl- and *S*-aryldithiocarbazates and heterocyclic aldehydes and ketones contain both hard 'nitrogen' and soft 'sulfur' donor atoms and consequently, they are capable of forming stable complexes with a wide variety of metal ions some of which have been shown to exhibit interesting physico-chemical properties and potentially useful chemotherapeutic properties [1–10]. Although a large number of studies involving complexes of these ligands with transition metal ions have been reported, there have been fewer studies on complexes of these ligands with main group elements such as tin. We have previously reported some transition metal complexes of the 2,6-diacetylpyridine Schiff bases of *S*-methyl- [11] and *S*-benzyldithiocarbazates [12,13]. The 2,6-diacetylpyridine Schiff base of *S*-benzyldithiocarbazate has been shown to act as an interesting chelating agent yielding a novel dinuclear pyridine-nitrogen-bridged nickel(II) complex whose structure has been determined by X-ray diffraction [12]. Recently we have also reported a novel binuclear zinc(II) complex in which the mode of coordination of the ligand is entirely different from that found in the dimeric nickel(II) complex [2]. The related 2,6-diacetylpyridinebis(thiosemicarbazone) has also been found to act as a versatile chelating agent producing zinc(II) complexes with different geometry

* Corresponding author. Tel.: +673-2-463001x1341; fax: +673-2-461502.
E-mail address: akbar@fos.ubd.edu.bn (M.A. Ali).

0277-5387/$ - see front matter © 2004 Elsevier Ltd. All rights reserved.
doi:10.1016/j.poly.2004.05.010

depending on the nature of the zinc(II) salts and reaction conditions used in the preparation of the complexes [13]. In view of very little work done on tin complexes of Schiff bases derived from *S*-alkyl/aryl esters of dithiocarbazic acid and as part of our ongoing work on metal-dithiocarbazates, we report here the first examples of two seven-coordinate tin(IV) complexes of the 2,6-diacetylpyridine Schiff bases of *S*-methyl- and *S*-benzyl esters of dithiocarbazic acid together with the X-ray crystal structure of the Sn(dapsme)I_2 complex.

2. Experimental

2.1. Reagents

All chemicals were of analytical reagent grades and used without any further purification. Tin(IV) iodide was prepared according to the published procedure [14]. The ligands were prepared as described in our previous papers [11,12]. All physical measurements and analytical procedures used in the present work were similar to those described previously [1].

2.2. Preparation of the complexes

Tin(IV) iodide (0.18 g; 0.3 mmol) dissolved in boiling absolute ethanol (20 ml) was mixed with a boiling solution of the appropriate Schiff base (0.3 mmol) in a mixture of ethanol (20 ml) and dichloromethane (250 ml). The mixture was refluxed for 5 h and then left to stand overnight. The crystals of the tin complexes which had formed were then filtered off, washed with cold ethanol and dried in a desiccator over silica gel. Yield: 50–60%. Crystals of Sn(dapsme)I_2 suitable for X-ray analysis were obtained during preparation of the complex. *Anal.* Calc. for $C_{13}H_{15}N_5S_4SnI_2$: C, 21.04; H, 2.02; N, 9.40%. Found: C, 21.25; H, 1.95; N, 9.09%. *Anal.* Calc. for $C_{23}H_{25}N_5OS_4SnI_2$: C, 32.92; H, 2.75; N, 7.68%. Found: C, 32.46; H, 2.32; N, 6.60%.

2.3. Crystallography

For the compound Sn(dapsme)I_2 cell constants were determined by a least-squares fit to the setting parameters of 25 independent reflections, measured on an Enraf-Nonius CAD 4 four-circle diffractometer using graphite monochromated Mo Kα radiation (0.71073 Å) and operating in the ω–2θ mode within the range $2° < 2\theta < 50°$. Empirical absorption correction (ψ scans) and data reduction were performed with the WINGX [15] suite of programmes. The structures were solved by direct methods with SHELX-86 and refined by full-matrix least-squares analysis with SHELXL-97 [16]. Non-hydrogen atoms were refined with anisotropic thermal parameters whereas H-atoms were included at estimated positions.

Table 1
Crystallographic data and structure refinement details for Sn(dapsme)I_2

Formula	$C_{13}H_{15}I_2N_5S_4Sn$
Formula weight	742.03
Temperature (K)	293
Wavelength (Å)	0.71073
Crystal system	Monoclinic
Space group	$C2/c$
Unit cell dimensions	
a (Å)	8.071(1)
b (Å)	15.5217(9)
c (Å)	17.691(1)
β (°)	103.076(7)
Volume (Å^3)	2158.8(3)
Z	4
D_{calc} (g cm^{-3})	2.283
Absorption coefficient (mm^{-1})	4.439
$F(0\,0\,0)$	1392
Reflections collected	2053
Independent reflections [R_{int}]	1908 [0.0209]
Observed reflections [$I > 2\sigma(I)$]	1373
Parameters	118
Goodness-of-fit on F^2	1.003
R_1 [$I > 2\sigma(I)$]	0.0276
wR_2 (all data)	0.0697

The drawing of the molecule (Fig. 2) was produced with ORTEP3 [17]. A summary of the crystal data, structure solution and refinement parameters are given in Table 1 and selected bond lengths appear in Table 4.

3. Results and discussion

Schiff bases derived from *S*-alkyl/aryl esters of dithiocarbazic acid possess the thioamide –NH– C(S)– functional group and consequently, they are capable of exhibiting thione-thiol tautomerism. In the solid state, the 2,6-diacetylpyridine Schiff bases of *S*-methyl- and *S*-benzyldithiocarbazate (Fig. 1(a); R = –SCH_3, SCH_2-C_6H_5), have previously been found to remain soley as the thione tautomer. In solution, they however, can exist as an equilibrium mixture of both the thione (**1a**) and thiol (**1b**) tautomers. Their ^{1}H NMR spectra in DMSO-d_6 show a broad signal at ≈12.60 ppm attributable to the resonance of the sec. NH proton. The appearance of the –NH– signal at ≈13 ppm and the absence of any signal at ≈4.00 ppm which can be attributed to the –SH proton, indicate that in DMSO, both the Schiff bases also remain in their thione forms. The presence of the N(H) signal at ≈12.60 ppm in the ^{1}H NMR spectra also indicates that the sec. NH protons are probably intermolecularly hydrogen bonded with a thione sulfur of another molecule or the NH protons participate in hydrogen bonding with the solvent DMSO. Although the Schiff bases remain in thione forms both in the solid state and in solution, in an ethanolic solution and in the presence of tin(IV) iodide, they quickly convert to the thiol forms with the con-

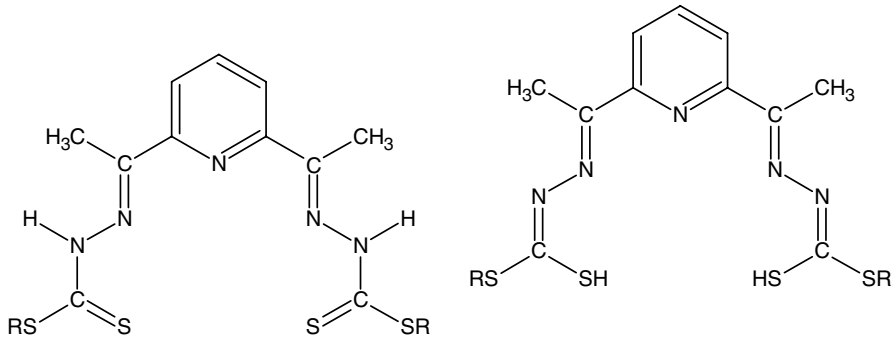

(**1a; R=CH_3, $CH_2C_6H_5$**) **(1b)**

Fig. 1. The thione (**1a**) and thiol (**1b**) forms of the Schiff bases.

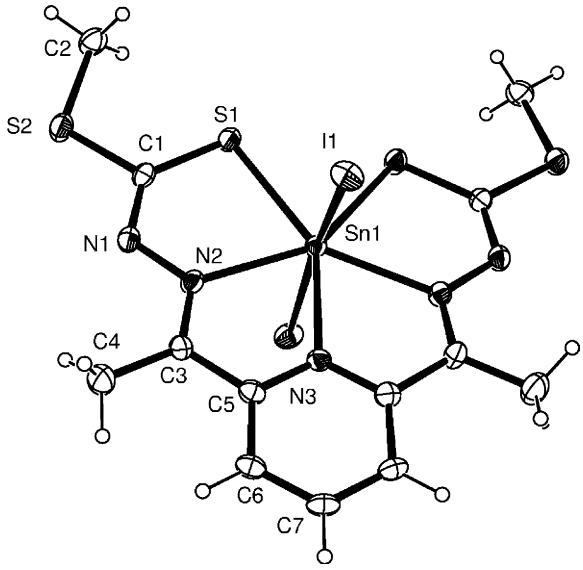

Fig. 2. ORTEP drawing of [Sn(dapsme)I_2] (30% ellipsoids shown).

comitant formation of tin(IV) complexes of their deprotonated mercaptide forms. This behaviour has been found to be common with almost all Schiff bases derived from *S*-alkyldithiocarbazates [1–10]. Thiosemicarbazones, which are structurally similar to Schiff bases derived from *S*-alkyl/aryl esters of dithiocarbazic acid, do not always deprotonate in neutral media and consequently, their complexes of in both protonated [18–21] and deprotonated [22,23] forms have been prepared. There are also interesting examples of complexes in which both protonated and deprotonated forms of a thiosemicarbazone ligand have been found to be present in the same complex [24]. In contrast with thiosemicarbazones, Schiff bases derived from *S*-alkyl/aryl esters of dithiocarbazic acid, almost invariably coordinate in their deprotonated forms even in the presence of mineral acids.

Reaction of tin(IV) iodide with the Schiff bases in a mixture of absolute ethanol and dichloromethane afforded beautiful bright orange coloured crystalline tin(IV) complexes of empirical formula, Sn(SNNNS)I_2 (SNNNS = anionic form of the Schiff bases) which are quite stable in the atmosphere and could be stored in a desiccator over anhydrous silica gel for a long period of time without any sign of decomposition. These complexes are sparingly soluble in methyl cyanide, chloroform and dichloromethane but dissolve readily in DMSO. Their molar conductances in DMSO are in the range 34.8–36.8 $ohm^{-1}\,cm^2\,mol^{-1}$, indicating that there is substantial dissociation of the complexes in this solvent but the conductivity values are much lower than those shown by 1:1 electrolytes in this solvent. The conductivity data, therefore, support coordination of the ligands to the tin(IV) ion in their deprotonated anionic forms and that the two iodide ions are also coordinated to the tin(IV) ion.

Table 3 lists the main IR bands of the ligand and their tin complexes. The IR spectra of the ligands when compared with those of the tin complexes indicate that the νNH bands of the free ligands disappear in the spectra of the complexes supporting deprotonation of the ligand during coordination with the tin ion. Coordination of the azomethine nitrogen to the tin atom is indicated by the shift the the νC=N bands of the free H_2dapsme ligand from 1617 to 1596 cm^{-1} in the spectrum of Sn(dapsme)I_2. However, in the IR spectrum of Sn(dapsbz)I_2 the νC=N band of the free H_2dapsbz ligand at 1600 cm^{-1} does not exhibit any shift after coordination. This is not surprising since the C=N band is expected to couple with other bands and therefore, its shifting will be dependent on how much it is in combination with other bands. However, support in favour of coordination of H_2dapsbz to the tin(IV) ion via the azomethine nitrogen atoms comes from the shift of the νN–N bands of the free ligand to higher wave numbers in the spectra of the tin complex [25]. The splitting of the ν_aCSS band of the ligand at $\approx$959 cm^{-1} in the IR spectra of the complexes indicates coordination of the ligands to the tin ion via one of the sulfur atoms [26]. Coordination via the pyridine nitrogen atom is also indicated by the shift of the pyridine ring breathing vibration of the ligands at 697–700 cm^{-1}.

Table 2
^{1}H and ^{13}C NMR spectral data for the Schiff bases and their tin(IV) complexes in DMSO-d_6

	H_2dapsme	H_2dapsbz	Sn(dapsme)I_2	Sn(dapsbz)I_2
^{1}H NMR assignments				
–NH	12.45(s,br,1H)	12.70(s,br, 1H)		
py–H	7.90–7.93(m)	8.05(d, 2H)	8.47–8.48(m,3H)	8.58(t, 1H)
	7.74–7.79(m)	7.90(t, 1H)		8.74(d, 2H)
	7.60(t, 2H)			
Ar–H		[7.22–7.30, 7.33–7.39](m, 5H)		7.28–7.47(m, 5H)
–N=C–CH_3	2.30(s, 6H)	2.50(s, 6H)	2.30(s, 6H)	Obscured by DMSO
–SCH_2/SCH_3	3.12(s, 6H)	4.48(s, 4H)	2.75(s, 6H)	4.58(d, 4H)
^{13}C NMR assignments				
CS	201.6	199.8	183.0	184.1
–C=N	154.5	154.3	155.0	154.4
C_{py}	152.2	152.2	146.3	140.3
	138.3	138.4	142.9	133.3
	121.7	121.8	130.4	129.1
C_{Ar}		137.6		129.5
		130.1		123.7
		129.4		112.7
		129.4		105.5
SCH_2/SCH_3	18.0	39.0	17.5	36.8
–CH_3	13.7	13.8	14.3	17.6

The electronic spectra of the Schiff bases and their tin(IV) complexes are shown in Table 3. The spectra of the ligands exhibit bands in the range 389–345 and 264–256 nm assignable to the $n \rightarrow \pi^*$ and $\pi \rightarrow \pi^*$ transitions, respectively. In addition to the intra-ligand bands, a shoulder appears at 410–420 nm in the spectra of the complexes which could be attributed to the $S \rightarrow Sn^{IV}$ charge-transfer band. Such CT bands are quite common in the electronic spectra of metal complexes of thiosemicarbazones [27,28].

The ^{1}H and ^{13}C NMR spectral data for the ligands and their tin complexes in DMSO-d_6 are compiled in Table 2. The changes in the spectra of the ligands upon complexation with the tin(IV) ion are closely related to those observed for other Schiff bases derived from *S*-alkyl/aryl esters of dithiocarbazic acid, when they are coordinated to metal ions via the thiolate sulfur, the azomethine nitrogen and pyridine nitrogen atoms. In the ^{1}H NMR spectra of the complexes the following changes are observed: (i) The N(H) signal at ≈12.65 ppm of the free ligand disappears as a result of their deprotonation during coordination and (ii) the protons attached to the pyridine ring are deshielded as a result of coordination via the pyridine nitrogen atom but the –N=C(CH_3) protons are not affected even though coordination via the azomethine nitrogen atom occurs. In the ^{13}C NMR spectra, the carbon atom of the thiocarbonyl group undergoes a significant shielding effect on coordination to the tin(IV) ion. This is in contrast with the ^{13}C NMR spectra of the seven-cordinate tin(IV) complex of the related 2,6-diacetylpyridine thiosemicarbazone where a very little shift of this signal was observed [29]. The carbon atoms of the methyl groups (attached to the carbon atom of the azomethine group) are deshielded on coordination with the tin atom similar to that found in related tin complexes [30].

3.1. The structure of Sn(dapsme)I_2

Fig. 2 shows the ORTEP drawing of the [Sn(dapsme)I_2] complex together with the numbering scheme adopted. The molecule has crystallographic twofold

Table 3
IR and electronic spectral data

	IR				UV spectra in Nujol
Compound	*ν*NH	*ν*C=N	*ν*N–N	*ν*CSS	λ_{max} (nm)
H_2dapsme	3176s,br	1617m	1065s	959s	345(4.2)[a], 256(4.5)[a]
H_2dapsbz	3157br,w	1600m	1102m	993w	358[b] , 263[b]
Sn(dapme)I_2		1596w		972s	≈425br, ≈363, 275, 230
				968sh	
Sn(dapsbz)I_2		1600m	1114w	961br	≈425br, ≈337, 281

[a] In CH_2Cl_2, data taken from [6].
[b] Data taken from [12].

Table 4
Selected bond lengths (Å) and angles (°) for [Sn(dapsme)I_2]

Bond lengths	
C(1)–N(1)	1.309(7)
C(1)–S(1)	1.719(6)
C(1)–S(2)	1.750(6)
C(2)–S(2)	1.804(6)
C(3)–N(2)	1.278(7)
N(1)–N(2)	1.374(6)
N(2)–Sn(1)	2.354(5)
N(3)–Sn(1)	2.280(6)
I(1)–Sn(1)	2.8128(5)
S(1)–Sn(1)	2.563(2)
Bond angles	
N(3)–Sn(1)–N(2)	68.82(11)
N(2)–Sn(1)–N(2)#1	137.6(2)
N(2)–Sn(1)–S(1)#1	148.35(11)
N(3)–Sn(1)–S(1)	142.27(3)
N(2)–Sn(1)–S(1)	73.76(11)
S(1)#1–Sn(1)–S(1)	75.46(7)
N(3)–Sn(1)–I(1)	84.118(13)
N(2)–Sn(1)–I(1)	90.19(12)
N(2)#1–Sn(1)–I(1)	85.56(11)
S(1)#1–Sn(1)–I(1)	97.80(4)
S(1)–Sn(1)–I(1)	91.51(4)
I(1)–Sn(1)–I(1)#1	168.24(3)

Symmetry transformation $-x, y, -z + 1/2$.

symmetry, with the rotation axis passing through the Sn atom and the pyridyl N3 atom. Selected bond lengths and angles are given in Table 4. The structure shows that the complex is monomeric and the tin(IV) ion is in a seven-coordinate pentagonal bipyramidal environment being ligated by the two iodide ions at apical positions and the planar pentadentate SNNNS coordinated Schiff base in its deprotonated thiolate form through the thiolate sulfur atoms, the two azomethine nitrogen atoms and the pyridine nitrogen atom. The two Sn–N distances [Sn(1)–N(2) = 2.354(5) and Sn(1)–N(3) = 2.280(6)] are slightly higher than the sum of the non-polar covalent radii 2.15 Å indicating strong tin(IV)-nitrogen interaction. However, as found in other tin(IV) complexes of related pentadentate thiosemicarbazone ligands [29,30], the Sn–N_{py} bond distance [2.280(6) Å] in the present complex is shorter than the Sn–$N_{azomethine}$ distance [2.354(5) Å]. The higher basicity of the azomethine nitrogen atoms relative to that of the pyridine nitrogen atom should lead to shorter M–$N_{azomethine}$ distances than the M–N_{py} distances. This has in fact been observed in most four-, five- and six-coordinate metal complexes of thiosemicarbazones [31–33] and dithiocarbazates [1]. The shorter Sn–N_{py} distance compared with the the Sn–$N_{azomethine}$ distance in the present complex as well as in other related seven-coordinate tin(IV) complexes may be due to the geometric requirement of the structure in which the tin(IV) ion bonds with the pyridine nitrogen atom in such a way that it prevents the closer approach of the two imine nitrogen atoms. The Sn–S distance [2.563(2) Å] is longer than the sum of the covalent radii (2.42 Å) but it is considerably shorter than the van der Waals radii (4.0 Å) [34] suggesting a fairly strong bond. For the purpose of comparison, the Sn-donor atom distances of Sn(dapsme)I_2 together with those of other seven-coordinate complexes of related pentadentate chelating agents are shown in Table 5. The

Table 5
Comparison of bond tin-donor atom distances (Å) in some seven-coordinate tin complexes

Compound	Sn–S/O	Sn–$N_{azom.}$	Sn–N_{py}	Sn–C	Sn–X	Reference
[Sn(Hadaptsc)Ph_2]Cl	2.592(1) 2.703(1)	2.353(4) 2.491(4)	2.348(4)	2.163(4) 2.170(4)		[30]
[Sn(daptsc)Ph_2] · 2DMF	2.593(1) 2.603(1)	2.427(4) 2.421(4)	2.368(3)	2.178(4) 2.179(4)		[29]
[Sn(H_2dapsc)Cl_2] · $2H_2O$	2.123(6) 2.127(5)	2.259(6)	2.272(7)			[37]
[Sn(CH_3)(Cl)Hdaptsc]Cl · CH_3OH	2.527(2) 2.633()	2.288(6) 2.430(6)	2.238(6)	2.166(8)	2.476(2)	[38]
[CH_3Sn(H_2dapsc)Cl]Cl_2 · $2H_2O$	2.177(6) 2.180(6)	2.284(7) 2.252(7)	2.262(2)	2.122(9)	2.386(2)	[38]
[Sn(dapsme)I_2]	2.5629(15)	2.354(5)	2.280(6)		2.28128(5)	This work
[Sn(H_2daptsz-Me)(CH_3OH)$_2$]· CH_3OH	2.554(5) 2.567(6)	2.349(17) 2.317(15)	2.24(2)		1.971(14) 1.979(5)	[39]
[Sn(dapcheximtsc)Bu_2]	2.6924(6) 2.6924(6)	2.437(5) 2.437(5)	2.415(6)	2.148(10) 2.170(8)		[40]

Hadaptsc, monodeprotonated form of the 2,6-diacetylpyridinebis(thiosemicarbazone); H_2dapsc, neutral form of the 2,6-diacetylpyridinebis(semicarbazone); dapsme, doubly deprotonated form of the 2,6-diacetylpyridine Schiff base of *S*-methyldithiocarbazate; H_2daptsz-Me, Bis(4-*N*-methylthiosemicarzone)-2,6-diacetylpyridine; dapcheximtsc, doubly deprotonated form of 2,6-diacetylpyridine bis(3-hexamethyleneiminylthiosemicarbazone).

data indicate that all these complexes have comparable tin-donor atom distances irrespective of the oxidation state of the tin atom. An examination of bond distances in the dithiocarbazate chain shows that the C(1)–S(1) bond {1.719(6) Å} is longer than than that observed in free *S*-benzyldithiocarbazate [35] and other Schiff bases derived from related dithiocarbazates [36], being intermediate between 1.82 Å for a single and 1.56 Å for a double bond. While coordinating in its iminothiolate form, the negative charge generated upon deprotonation of the thiol group is delocalized across the coordinated N(1)–C(1)–S(1) group as supported by the intermediate (single/double bond) N(1)–C(1) distance [1.309(7) Å].

The coordinated dapsme^{2-} ligand presents an almost ideal pentagonal array of donor atoms. The five-membered chelate rings each have bite angles (Table 4) within 3° of their ideal value (72°). The N_3S_2 coordination core is approximately planar with deviations of 0.139 Å for S(1) and −0.099 Å for N(2) from the SnN_3S_2 least squares plane (where Sn(1) and N(3) lie on the plane). The symmetry related iodo ligands are distorted somewhat away from linear *trans*-conformation (168.24(3)°).

4. Conclusions

The 2,6-diacetylpyridine Schiff bases of *S*-methyl- and *S*-benzyldithiocarbazates, like most Schiff bases derived from *S*-alkyl esters of dithiocarbazic acid, remain as the thione tautomer in both the solid state as well as in solution but, in the presence of tin(IV) iodide they convert to the iminothiol form, deprotonate and coordinate with the tin(IV) ion as a dinegatively charged pentadentate SNNNS chelating agent. The tendency of the ligands to deprotonate even in a neutral solution may be attributed to the extra stability gained by them through π-electron delocalization along the –C–N–N–C–S–chains in the two arms of these ligands. The ready formation of stable 1:1 metal-ligand complexes with tin(IV) iodide with the elimination of HI indicates that these ligands are capable of coordinating with non-transition metals like tin even though they have both soft sulfur donor atoms in their backbones. The adoption of a distorted pentagonal-bipyramidal geometry by the Sn(SNNNS)I_2 complexes is due to the restricted bite sizes of the ligands.

5. Supplementary materials

Full crystallographic data (CCDC No. 237458) for Sn(dapsme)I_2 have been deposited at the Cambridge Crystallographic Data Centre and are available on request from the Director, CCDC, 12 Union Road, Cambridge, CB2 1EZ, UK (fax: +44-1223-336033; e-mail: deposit@ccdc.cam.ac.uk or http://www.ccdc.cam.ac.uk).

Acknowledgements

M. Akbar Ali, A.H. Mirza and L.K. Wei gratefully acknowledge the Department of Chemistry, Universiti Brunei Darussalam for supporting this work.

References

[1] M. Akbar Ali, A.H. Mirza, M. Nazimuddin, R. Ahmed, L.H. Gahan, P.V. Bernhardt, Polyhedron 22 (2003) 1471.
[2] M. Akbar Ali, A.H. Mirza, C.W. Voo, A.L. Tan, P.V. Bernhardt, Polyhedron, and references cited therein.
[3] M.T.H. Tarafder, T.-J. Khoo, K.A. Crouse, A.M. Ali, Polyhedron 25 (2002) 27.
[4] P. Bera, R.J. Butcher, S. Chowdhury, Polyhedron 21 (2002) 1.
[5] T. Yu-Peng, D. Chung-Ying, Y. Xia-Xeng, T.C.W. Mak, L. Qing, Z. Jian-Ying, Trans. Met. Chem. 23 (1998) 17.
[6] M. Akbar Ali, A.H. Mirza, S.T.W. Keng, R.J. Butcher, Trans. Met. Chem. 28 (2003) 241.
[7] M. Akbar Ali, S.E. Livingstone, Coord. Chem. Rev. 13 (1974) 101, and references therein.
[8] M. Das, S.E. Livingstone, Br. J. Cancer 37 (1978) 101.
[9] D.X. West, S.B. Padhye, P.B. Sonawane, Struct. Bond. (Berlin) 76 (1991) 1.
[10] M. Akbar Ali, A.H. Mirza, R.J. Butcher, M.T.H. Tarafder, Tan B. Keat, A.M. Ali, J. Inorg. Biochem. 92 (2002) 141.
[11] S.M.M.H. Majumder, M. Akbar Ali, F.E. Smith, M.A.U. Mridha, Polyhedron 7 (1988) 2183.
[12] M. Akbar Ali, A.H. Mirza, R.J. Butcher, M.T.H. Tarafder, M.A. Ali, Inorg. Chim. Acta 320 (2001) 1.
[13] A. Bino, N. Cohen, Inorg. Chim. Acta 210 (1993) 11.
[14] T. Moeller, D.C. Edwards, R.L. Brandt, J. Kleinberg, in: Inorganic Synthesis, vol. 4, Robert K. Krieger Publishing, Huntington, NY, 1978, p. 119.
[15] L.J. Farrugia, J. Appl. Cryst. 32 (1999) 837.
[16] G.M. Sheldrick, SHELX. Programs for Crystal Structure Analysis, University of Göttingen, Germany, 1997.
[17] L.J. Farrugia, J. Appl. Cryst. 30 (1997) 565.
[18] R. Gronbaek-Hazell, Acta Chem. Scand. 26 (1972) 1365.
[19] A. Mohan, P. Sharma, N.K. Jha, Inorg. Chim. Acta 106 (1985) 117.
[20] A. Castneiras, R. Carballo, T. Perez, Polyhedron 20 (2001) 441.
[21] D.X. West, T.J. Tomack, A.E. Liberta, Trans. Met. Chem. 17 (1992) 256.
[22] L. Carvalica, M. Nardelli, G. Fava, Acta Crystallogr. 15 (1962) 1139.
[23] J. Valdez-Martinez, A. Sierra-Ramoco, C. Alvarez-Toledano, R.A. Toscano, H. Garcia-Topia, J. Organomet. Chem. 352 (1983) 321.
[24] P. Souza, A.I. Matesanz, V. Fernandez, J. Chem. Soc., Dalton Trans. (1996) 3011.
[25] R. Ugo, J. Organomet. Chem. 9 (1967) 395.
[26] P. Pelagatti, A. Venturini, A. Leporati, M. Carcelli, M. Costa, A Bacchi, G. Pelizzi, C. Pelizzi, J. Chem. Soc., Dalton Trans. (1998) 2715.
[27] E.W. Ainscough, E.N. Baker, A.M. Brodie, R.J. Cresswell, J.D. Ranford, J.M. Waters, Inorg. Chim. Acta 170 (1990) 185.
[28] E.W. Ainscough, A.M. Brodie, J.D. Ranford, J.M. Waters, K.S. Murray, Inorg. Chim. Acta 197 (1992) 107.

[29] J.S. Casas, A. Castineiras, A. Sanchez, J. Sordo, A. Vazquez-Lopez, M.C. Rodriguez-Arguelles, M.C. Rodriguez-Arguelles, U. Russo, Inorg. Chim. Acta 221 (1994) 61.
[30] P.C. Moreno, R.H.P. Francisco, M.T. do, P. Gambardella, G.F. deSousa, A. Abras, Acta Crystallogr. Sect. C. 53 (1997) 1411.
[31] D.K. Sau, R.J. Butcher, S. Chaudhuri, Polyhedron 23 (2004) 5.
[32] N.C. Kasuga, K. Sekino, C. Koumo, N. Shimada, M. Ishikawa, K. Nomiya, J. Inorg. Biochem. 84 (2001) 55.
[33] E.W. Ainscough, A.M. Brodie, J.A. Ramnford, J.M. Waters, J. Chem. Soc., Dalton Trans. (1997) 1251.
[34] A. Bondi, J. Phys. Chem. 68 (1964) 441.
[35] S. Shanmuga, S. Raj, B.M. Yamin, Y.A. Yusof, M.T.H. Tarafder, H.-K. Fun, K.A. Crouse, Acta Crystallogr. C 56 (2000) 1236.
[36] K.A. Crouse, K.-B. Chew, M.T.H. Tarafder, K.A. Kasbollah, A.M. Ali, B.M. Yamin, H.-K. Fun, Polyhedron 23 (2004) 161.
[37] S.O. Sommerer, G.J. Palenik, Inorg. Chim. Acta 183 (1991) 217.
[38] G.F. de Sousa, C.A.L. Filgueiras, A. Abras, S.S. Al-Juaid, P.B. Hitchcock, J.F. Nixon, Inorg. Chim. Acta 218 (1994) 139.
[39] M.R. Berjemo, R. Pedrido, M.I. Fernandez, A.M. Gonzalez-Noya, M. Maneiro, M.J. Rodriguez, M.J. Romero, M. Vazquez, Inorg. Chem. Commun. 7 (2004) 4.
[40] G.F. de Sousa, D.X. West, C.A. Brown, J.K. Swearingen, J. Valdes-Martinez, R.A. Toscano, S. Hernandez-Ortega, M. Horner, A.J. Bortulluzzi, Polyhedron 19 (2000) 841.

Available online at www.sciencedirect.com
SCIENCE DIRECT®
Polyhedron 23 (2004) 2045–2053
POLYHEDRON
www.elsevier.com/locate/poly

Polymeric end-to-end bibridged cadmium(II)thiocyanates containing monodentate and bidentate N-donor organic blockers: supramolecular synthons based on π–π and/or C–H···π interactions

Doyel Bose [a], Jaya Banerjee [a], Sk Hafijur Rahaman [a], Golam Mostafa [b], Hoong-Kun Fun [c], Rosa D. Bailey Walsh [d], Michael J. Zaworotko [d], Barindra Kumar Ghosh [a,*]

[a] Department of Chemistry, The University of Burdwan, Burdwan 713104, India
[b] Department of Physics, Jadavpur University, Kolkata 700 032, India
[c] School of Physics, University Sains Malaysia, 11800 USM Penang, Malaysia
[d] Department of Chemistry, The University of South Florida, 4202 East Fowler Avenue, Tampa, FL 33620-5250, USA

Received 2 February 2004; accepted 29 April 2004

Abstract

Treatment of $Cd(NO_3)_2 \cdot 4H_2O$ with two equivalents of NH_4NCS in combination with two equivalents of imH [imH = imidazole] or one equivalent of pfan [pfan = ((pyridin-2-yl)formylidene)aniline] results neutral 1D polymers of the type $[Cd(imH)_2(NCS)(SCN)]_n$ (**1**) or $[Cd(pfan)(NCS)(SCN)]_n$ (**2**). X-ray structure determinations show that in both polynuclear **1** and **2**, octahedral Cd^{II} ions occupy centre of symmetry with a CdN_4S_2 chromophore. The metal ions are linked through N and S atoms of NCS^- alternately in doubly bridged end-to-end fashion; two mutually *trans* N atoms of monodentate imH units complete hexacoordination of each metal centre in **1**. Similar NCS-bibridging chain is present in **2** with one bidentate (N,N) Schiff base chelator (pfan) in *cis* orientation. The 1D chains in **1** are further engaged in intermolecular hydrogen bonding (N–H···S) between N of imH and coordinated S of NCS^- along with aromatic π–π stacking of imH moieties that constrain the 1D chains to lie in *bc*-plane, which are further linked via C–H···π interactions. In **2**, 1D chains participate in two kinds of π–π interactions. Supramers **1** and **2** display intraligand $^1(\pi–\pi^*)$ fluorescence and intraligand $^3(\pi–\pi^*)$ phosphorescence in glassy solutions (MeOH at 77 K).
© 2004 Elsevier Ltd. All rights reserved.

Keywords: Cadmium(II)thiocyanate; Polymer; Schiff base; Imidazole; Supramolecular synthon

1. Introduction

The construction [1] of sophisticated inorganic–organic hybrid [2] supramolecular networks [3] based on organised strong covalent interactions [4] and extensive lateral weak non-covalent forces like hydrogen bonding [5], π–π stacking [6] and C–H···π interactions [7] is an area of great activity due to fabrication of functional materials [8–13] utilizing the wide variety in properties associated with each suitably tailored component. Among the weak forces, hydrogen bonding is a general protocol for structure directing master key interaction, and has been widely used towards crystal design [5,14,15]. On the contrary, less attention [6,7,16,17] has been paid to cooperative weaker π···π and C–H···π interactions, which may tune topology [18] effectively and untangle the intrigue interactions in peptide and protein structures and associated properties [19]. Recently, we have established the composition tailored superstructures [20] on luminous zinc(II)azides containing a tailored diimine, 2,2′-dipyridylamine (dpa) with active amine (–NH–) hydrogen and aromatic π rings. In continuation of our research on congeneric cadmium, we have investigated its binding with

* Corresponding author. Tel.: +91-342-255-8545; fax: +91-342-253-0452.
E-mail address: barin_1@yahoo.co.uk (B.K. Ghosh).

0277-5387/$ - see front matter © 2004 Elsevier Ltd. All rights reserved.
doi:10.1016/j.poly.2004.04.035

thiocyanate in combination with a monodentate blocker, imidazole (imH), and bidentate Schiff base chelator, ((pyridin-2-yl)formylidene)aniline (pfan), with or without active hydrogen on ligand network coping with possible H-bonding, face-to-face $\pi\cdots\pi$ and/or edge-to-face C–H$\cdots\pi$ interactions due to the presence of aromatic π-rings towards preparation of metallosupramolecules of different aggregates. Polynuclear cadmium complexes in which the metal centres are in close proximity has received much attention due to study of electronic and optoelectronic properties [21] towards designing of new inorganic materials [22]. Thiocyanate is a putative ambidentate ligand, which results in different molecular architectures through its versatile ligation modes [23]. Imidazole [24] with its active –NH– hydrogen and aromatic π-ring, is a versatile blocker and the interest in its chemistry arises from the use as ionic liquids [25] and in different compounds from a biological and pharmacological applications [26]. Schiff bases [27,28] have recently been focussed by the coordination chemists due to their preparational accessibilities, structural varieties and varied denticities. The present work stems from our interest to build new crystalline aggregates in cadmium bound states with such bridging units. Successfully we have prepared and X-ray crystallographically characterized two one-dimensional (1D) coordination polymers of the type $[Cd(imH)_2(NCS)(SCN)]_n$ (**1**) and $[Cd(pfan)(NCS)(SCN)]_n$ (**2**). **1** and **2** exhibit fascinating self-assembled structural topologies via cooperative H-bonds and aromatic face-to-face $\pi\cdots\pi$ and edge-to-face C–H$\cdots\pi$ interactions (in **1**) or via $\pi\cdots\pi$ interactions (in **2**). In this paper an emphasis has been made to show how use of such intermolecular cooperative forces may be harnessed to engineer novel crystalline architectures.

2. Experimental

2.1. Materials

High purity imidazole (SRL, India), aniline (E. Merck, India), pyridine-2-carboxaldehyde (Lancester, UK), cadmium nitrate tetrahydrate (E. Merck, India) and ammonium thiocyanate (E. Merck, India) were purchased from respective concerns and used as received. The Schiff base (pfan) was prepared [28b] by condensing pyridine-2-carboxaldehyde with aniline in dehydrated alcohol in the 1:1 molar ratio. After 8 h reflux the reaction solution was evaporated under reduced pressure to a gummy mass, which was dried and stored in vacuo over $CaCl_2$ for subsequent use. Yield: 0.137 g (70%). *Anal.* Calc. for $C_{12}H_{10}N_2$: C, 79.10; H, 5.53; N, 15.37. Found: C, 78.98; H, 5.46; N, 15.65%. IR (KBr, cm^{-1}): ν(C=N), 1590 cm^{-1}. UV–Vis (λ, nm): 254, 390. All other chemicals and solvents were AR grade and were used as received.

2.2. Physical measurements

Elemental analyses (carbon, hydrogen and nitrogen) were performed on a Perkin–Elmer 2400 CHNS/O elemental analyzer. IR spectra (KBr discs, 4000–300 cm^{-1}) were recorded using a JASCO FTIR model 420 spectrometer. Molar conductances were measured using a Systronics conductivity meter where the cell constant was calibrated with 0.01 M KCl solution and dry MeOH was used as solvent. Ground state absorption and steady-state fluorescence measurements were made with a JASCO model V-530 UV–Vis spectrophotometer and Hitachi model F-4010 spectrofluorimeter, respectively. Time-resolved fluorescence measurements were carried out using a time-correlated single photon counting (TCSPC) spectrometer Edinburgh Instruments, model 199; a hydrogen filled coaxial flash lamp with a pulse width of 1.2 ns at FWHM and a Philips XP-2020Q Photomultiplier tube were, respectively, used as the excitation source and the fluorescence detector.

2.3. Preparation of the complexes

The complexes were prepared using 1:2:2 and 1:1:2 mole ratio of the metal, ligand and thiocyanate for **1** and **2**, respectively. The typical syntheses are described below.

2.3.1. $[Cd(imH)_2(NCS)(SCN)]_n$ (**1**)

Solid imH (0.136 g, 2 mmol) was added slowly to $Cd(NO_3)_2\cdot 4H_2O$ (0.308 g, 1 mmol) dissolved in methanol (10 cm^3). To this, a methanol solution (5 cm^3) of NH_4NCS (0.152 g, 2 mmol) was added (5 cm^3). The resulting colourless solution was filtered and was kept for slow evaporation. After seven days colourless crystals that were separated, was collected by filtration, washed with toluene and dried in vacuo over silica gel indicator. Yield: 0.095 g (80%). *Anal.* Calc. for $C_8H_8N_6S_2Cd$ (**1**): C, 26.34; H, 2.21; N, 23.04. Found: C, 26.52; H, 2.31; N, 22.31%. IR (KBr, cm^{-1}): ν(N–H) 3310; ν(CN), 2120, 2106. Λ_M (MeOH, Ω^{-1} cm^2 mol^{-1}): 5; UV–Vis (λ, nm): 311.

2.3.2. $[Cd(pfan)(NCS)(SCN)]_n$ (**2**)

Pfan (0.182 g, 1 mmol) in MeOH (10 cm^3) was added dropwise to a solution of $Cd(NO_3)_2\cdot 4H_2O$ (0.308 g, 1 mmol) in the same solvent (10 cm^3). To the resulting yellowish brown mixture, aqueous solution (5 cm^3) of NH_4NCS (0.152 g, 2 mmol) was added slowly. The final mixture was filtered and the supernatant liquid was kept in air for slow evaporation. After about a week compound **2** was separated which was collected by filtration, washed with toluene and dried in vacuo over silica gel

indicator. Yield: 0.093 g (70%). *Anal.* Calc. for $C_{14}H_{10}N_4S_2Cd$ (**2**): C, 40.94; H, 2.45; N, 13.64. Found: C, 40.68; H, 2.57; N, 13.52%. IR (KBr, cm^{-1}): ν(CN), 2120, 2104. Λ_M (MeOH, Ω^{-1} cm^2 mol^{-1}): 5; UV–Vis (λ, nm): 328.

2.4. X-ray crystallographic analyses

Single crystals of the title complexes were obtained by slow evaporation of methanol (**1**) and 4:1 methanol–water (**2**) solutions of the reaction mixtures at room temperature (298 K). Suitable colourless crystals were mounted on a Siemens SMART CCD (**1**) and Bruker-AXS SMART APEX/CCD (**2**) diffractometers equipped with a graphite-monochromator and Mo Kα ($\lambda = 0.71073$ Å) radiation. Diffraction data for both **1** and **2** were measured using the ω-scan method. Crystal data, data collection parameters and the results of analyses can be found in Table 1. The intensity data were corrected for Lorentz and polarization effects and an empirical absorption correction was employed using the SAINT [29] and SADABS [30] program for crystal **1**, and no absorption correction was made for **2**. The structures were solved by direct methods and the structure solution and refinement were based on $|F|^2$. All non-hydrogen atoms were refined with anisotropic displacement parameters whereas hydrogen atoms were placed in calculated positions when possible and given isotropic U values 1.2 times that of the atom to which they are bonded. The final difference Fourier map showed the highest residual electron density of 1.091 e $Å^{-3}$ at a distance of 0.62 Å from Cd(II) atom for **2**, having no chemical significance. All crystallographic calculations were conducted with SHELXL-97 [31], ORTEP-32 [32], PLATON programs [33] for **1** and the SHELXTL v.6.1 program package [34] for **2**.

3. Results and discussion

3.1. Synthesis and formulation

The coordination polymer $[Cd(imH)_2(NCS)(SCN)]_n$ (**1**) was prepared as a colourless powder through one-pot reactions of a 1:2:2 molar ratio of the metal nitrate, organic blocker and the pseudohalide from methanolic solutions. The other polymer $[Cd(pfan)(NCS)(SCN)]_n$ (**2**) was obtained with a 1:1:2 molar ratio of cadmium nitrate tetrahydrate, pfan and ammonium thiocyanate, respectively, in aqueous alcohol. The compounds have been characterized by microanalytical (C, H and N) results, IR, UV–Vis spectral data and other physicochemical properties. The air-stable moisture-insensitive complexes $[Cd(imH)_2(NCS)(SCN)]_n$ (**1**) and $[Cd(pfan)(NCS)(SCN)]_n$ (**2**) are soluble in common organic solvents like, methanol, ethanol, dichloromethane, dimethylformamide and dimethylsulfoxide. In methanol both behave as non-electrolytes as is evident [35] from their low conductivity values (ca. 5 Ω^{-1} cm^2 mol^{-1}). The IR spectra show two strong peaks at 2120, 2106 cm^{-1} in

Table 1
Crystallographic data and details of data collection for $[Cd(imH)_2(NCS)(SCN)]_n$ (**1**) and $[Cd(pfan)(NCS)(SCN)]_n$ (**2**)

	1	**2**
Chemical formula	$C_8H_8N_6S_2Cd$	$C_{14}H_{10}N_4S_2Cd$
Formula weight	364.72	410.78
Crystal size (mm)	0.44×0.14×0.14	0.20×0.20×0.05
Crystal system	monoclinic	triclinic
Space group	$P2_1/c$	$P\bar{1}$
a (Å)	7.8105(5)	8.9730(12)
b (Å)	5.7689(4)	9.2498(13)
c (Å)	14.6495(9)	10.0061(14)
α (°)	90.00	99.915(2)
β (°)	108.999(3)	99.601(2)
γ (°)	90.00	103.337(2)
V ($Å^3$)	624.12	777.33(19)
Z	2	2
T (K)	293(2)	293(2)
λ (Mo Kα) (Å)	0.71073	0.71073
ρ_{calc} (Mg m^{-3})	1.941	1.755
μ (Mo Kα) (mm^{-1})	2.070	1.670
Reflections collected	3753	4787
θ Range (°)	2.76–28.29	2.12–28.22
Unique data/restraints/parameters	1518/0/95	3440/0/190
Goodness-of-fit on F^2	1.163	1.008
Final R indices [$I > 2\sigma(I)$]	$R_1 = 0.0208$, $wR_2 = 0.0481$	$R_1 = 0.0384$, $wR_2 = 0.0860$
Largest difference peak and hole (e $Å^{-3}$)	0.290 and −0.626	1.091 and −0.717

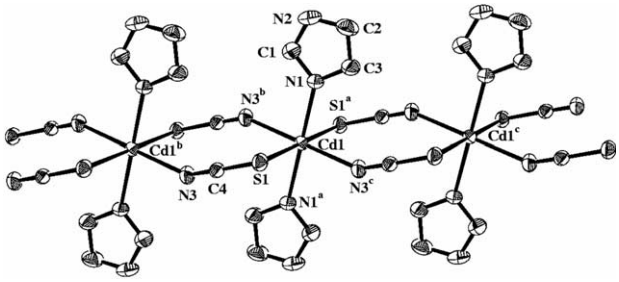

Fig. 1. ORTEP diagram of $[Cd(imH)_2(NCS)(SCN)]_n$ (**1**) with atom numbering scheme and 40% probability ellipsoids for all non-hydrogen atoms.

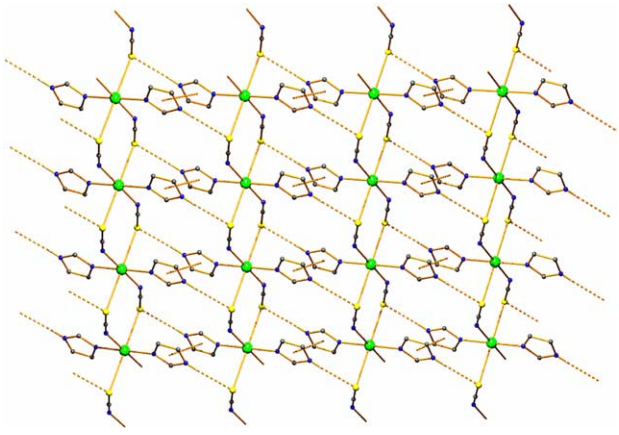

Fig. 2. Packing view of 2D supramolecular sheet formed by N–H···S H-bonding and π···π interaction in **1**.

1 and 2120, 2104 cm^{-1} in **2**, which are assigned to ν_{as}(CN) stretching vibrations [36]. The position (>2100 cm^{-1}) and number of signals strongly suggest mutual *cis* alignment as well as N- and S-coordinated bridging nature of the bound thiocyanates. The X-ray diffraction study confirms this hypothesis. The solution of **1** in MeOH is colourless and exhibits absorption at 311 nm while the faint yellow solution of complex **2** displays bands at 328 nm. Reflectance spectra [**1**: λ, 310 nm; **2**: λ, 325 nm] in nujol and electronic spectra in MeOH solutions are akin in both complexes reflecting similar gross structure and electronic structure in solid state and in solution in each case.

3.2. Structure

The structural analyses show that **1** and **2** consist of strong 1D covalent chains cooperated by weak N–H···S hydrogen bonding, π···π stacking and C–H···π interactions in **1** and two kinds of π···π interactions in **2**. The ORTEP diagrams of part of the chains with atom labeling scheme, perspective view of the 2D sheets and arrangement of these sheets are shown in Figs. 1–3 (for **1**) and Figs. 4–6 (for **2**), respectively. Selected interatomic bond distances and bond angles of **1** and **2** are set in Tables 2 and 3, respectively. The significant hydrogen bonding, π···π interaction and C–H··· interaction parameters can be found in Table 4 following the criteria of Janiak [37].

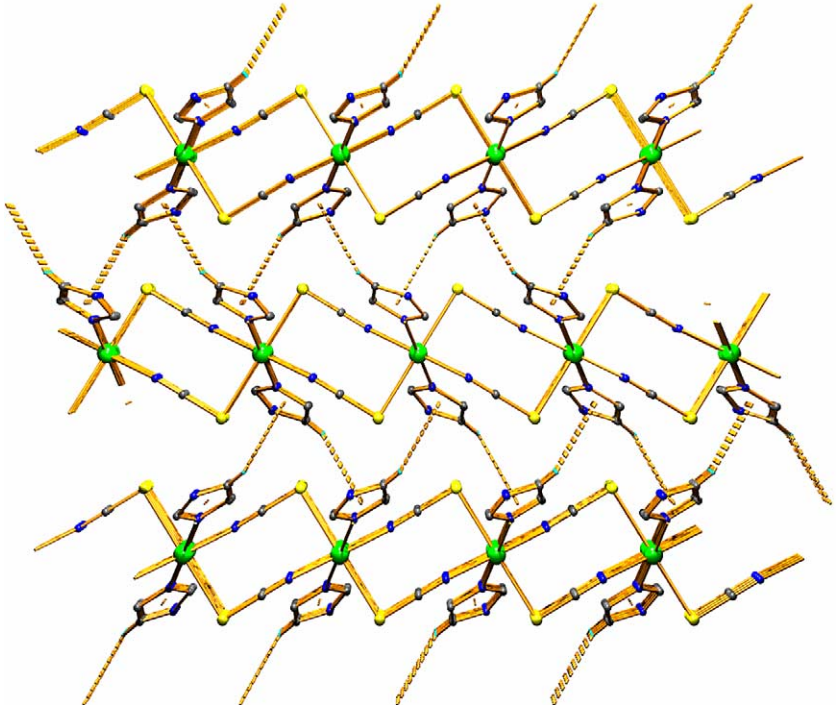

Fig. 3. C–H···π in **1** interactions among the supramolecular sheets.

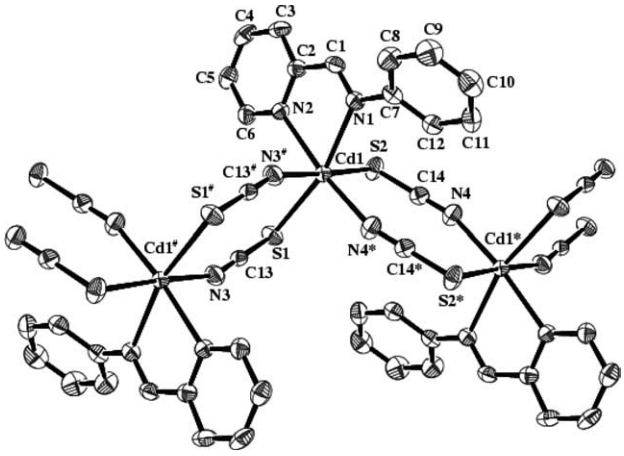

Fig. 4. ORTEP plot of $[Cd(pfan)(NCS)(SCN)]_n$ (**2**) with atom numbering scheme and 40% probability ellipsoids for all non-hydrogen atoms.

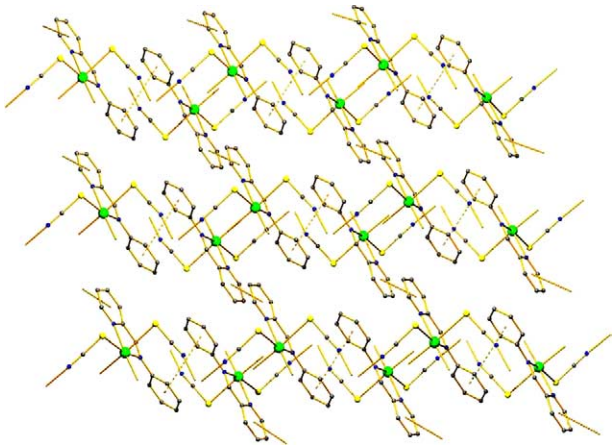

Fig. 6. $\pi\cdots\pi$ interactions in **2** among the supramolecular sheets.

Complex **1** is made up of 1D chains along *c*-axis. The coordination environment around each cadmium(II) is best described as distorted octahedron with CdN_4S_2 chromophore (Fig. 1) in a *trans*,*trans*,*trans* geometry of imH nitrogens and nitrogen and sulphur atoms of coordinated NCS^-. Each cadmium(II) is attached to four NCS^- bridges and two pendant imH ligands. The metal ion occupies centre of inversion. Two N atoms (N1, $N1^a$) of pendant imH ligands and two N atoms ($N3^c$, $N3^b$) of bridging NCS^- form the equatorial plane. The *trans* axial positions are occupied by the two symmetry related S atoms. The distortion of each cadmium(II) is reflected from the *cisoid* angles [87.80(5)°–92.20(5)°] (Table 2). The eight-membered Cd–$(SCN)_2$–Cd rings adopt chair conformation. The intrachain Cd···Cd separation is 5.769 Å.

The polymeric chains of $[Cd(imH)_2(NCS)(SCN)]_n$ (**1**) pack alongside each other to give a 2D sheet-like structure in *bc*-plane. Closest 1D chains are arranged side by side to facilitate a weak N–H···S hydrogen bond (Table 4). The 2D sheets are further stabilised by a

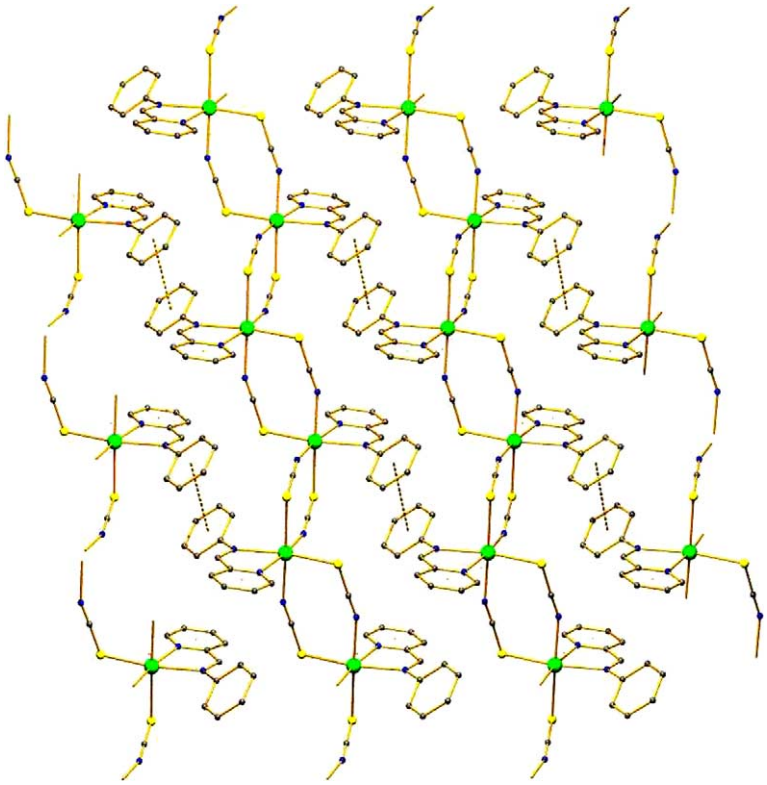

Fig. 5. Packing diagram of 2D supramolecular sheet formed only by $\pi\cdots\pi$ interaction in **2**.

Table 2
Selected bond distances (Å) and angles (°) for **1**

Bond distances			
Cd(1)–N(1)[a]	2.2749(16)	Cd(1)–N(3)[b]	2.3262(18)
Cd(1)–N(1)	2.2749(16)	Cd(1)–S(1)	2.8538(6)
Cd(1)–N(3)[c]	2.3262(18)	Cd(1)–S(1)[a]	2.8538(6)
Cd(1)···Cd(1)[c]	5.769(1)		
Bond angles			
N(3)[c]–Cd(1)–S(1)[a]	92.20(5)	N(3)[c]–Cd(1)–N(3)[b]	180.00(11)
N(3)[b]–Cd(1)–S(1)[a]	87.80(5)	N(1)[a]–Cd(1)–S(1)	90.06(5)
S(1)–Cd(1)–S(1)[a]	180.00(2)	N(1)–Cd(1)–S(1)	89.94(5)
N(1)–Cd(1)–N(1)[a]	180.00(9)	N(3)[c]–Cd(1)–S(1)	87.80(5)
N(1)[a]–Cd(1)–N(3)[c]	88.84(7)	N(3)[b]–Cd(1)–S(1)	92.20(5)
N(1)–Cd(1)–N(3)[c]	91.16(7)	N(1)[a]–Cd(1)–S(1)[a]	89.94(5)
N(1)[a]–Cd(1)–N(3)[b]	91.16(7)	N(1)–Cd(1)–S(1)[a]	90.06(5)
N(1)–Cd(1)–N(3)[b]	88.84(7)	Cd(1)[c]···Cd(1)···Cd(1)[d]	180.0

Symmetry code: [a] $-x,-y,-z$; [b] $-x,1-y,-z$; [c] $x,-1+y,z$; [d] $x,1+y,z$.

Table 3
Selected bond distances (Å) and angles (°) for **2**

Bond distances			
Cd(1)–N(4)*	2.247(3)	Cd(1)–S(2)	2.7263(11)
Cd(1)–N(3)[#]	2.337(3)	N(3)–Cd(1)[#]	2.337(3)
Cd(1)–N(2)	2.370(3)	N(4)–Cd(1)*	2.247(3)
Cd(1)–N(1)	2.398(3)	S(1)-C(13)	1.650(4)
Cd(1)–S(1)	2.6899(10)	S(2)-C(14)	1.646(4)
Cd(1)···Cd(1)[#]	5.908(1)	Cd(1)···Cd(1)*	5.795(10)
Bond angles			
N(4)*–Cd(1)–N(3)[#]	89.40(12)	N(3)[#]–Cd(1)–N(1)	87.01(11)
N(4)*–Cd(1)–N(2)	171.92(11)	N(2)–Cd(1)–N(1)	70.89(10)
N(3)[#]–Cd(1)–N(2)	90.26(12)	N(4)*–Cd(1)–S(1)	96.06(9)
N(4)*–Cd(1)–N(1)	101.03(12)	N(3)[#]–Cd(1)–S(1)	93.73(8)
S(1)–Cd(1)–S(2)	86.21(3)	C(14)–S(2)–Cd(1)	96.97(13)
N(2)–Cd(1)–S(1)	92.01(8)	N(1)–Cd(1)–S(1)	162.90(8)
N(4)*–Cd(1)–S(2)	94.09(9)	N(3)[#]–Cd(1)–S(2)	176.49(9)
N(2)–Cd(1)–S(2)	86.23(8)	N(1)–Cd(1)–S(2)	92.02(8)
C(1)–N(1)–Cd(1)	113.9(2)	C(13)–S(1)–Cd(1)	100.53(13)
Cd(1)[#]···Cd(1)···Cd(1)*	117.5(1)		

Symmetry code: *$2-x,-y,-z$; [#]$2-x,-y,1-z$.

Table 4
Hydrogen bond distances (Å) and angles (°) for **1**

Complex	D–H···A	D–H	H···A	D···A	D–H···A
1	N(2)–H(1N2)···S(1)[i]	0.78(4)	2.70(4)	3.471(2)	167(4)
1	C(2)–H(2)···π[ii]	0.96	3.15(3)	3.636(3)	113(2)

*π–π interaction for **1** and **2***

	Ring(*i*) → Ring(*j*)	Dihedral angle(*i*,*j*) (°)	Centroid separation Cg–Cg (Å)	Vertical displacement of Cg's (Å)	Ring slippage (°)
1	**Ring1 → Ring1[iii]	0.0	4.324	3.090	44.0
2	Ring2 → Ring2[iv]	0.0	4.196	3.735	27.1
2	Ring3 → Ring3[v]	0.0	5.416	2.815	58.7

Symmetry code: [i]$1+x,y,z$; [ii]$1-x,-1/2+y,1/2-z$; [iii]$1-x,-y,-z$; [iv]$1-x,1-y,1-z$; [v]$2-x,1-y,-z$. **Ring1, N1–C1–N2–C2–C3; Ring2, N1–C2–C3–C4–C5–C6; Ring3, C7–C8–C9–C10–C11–C12.

face-to-face π···π interactions from two terminal imH rings of two closest chains (Fig. 2). Every such sheet is further locked by a C–H···π interaction (Table 4) to generate an aesthetically pleasant solid state continuum (Fig. 3).

In **2** cadmium(II) centres are linked by bibridged end-to-end thiocyanato ligands resulting a 1D polymeric infinite chain (Fig. 4) which is composed of [Cd(pfan)-(NCS)(SCN)] monomer where the metal centres are coordinated by both N and S in *cis* position. Each cadmium(II) ion is linked with two of its neighbouring symmetry related counterparts (Cd1*), by two end-to-end thiocyanate ligands, and effectively each metal centre is ligated with four bridging pseudohalides producing two eight-membered loops. Similar to **1**, the eight-membered Cd–$(SCN)_2$–Cd loops adopt chair conformation. Octahedral coordination around each metal centre is completed through binding to one bidentate pfan chelator forming a five-membered loop. This feature makes the polymeric structure unique. One nitrogen atom (N1) from bidentate Schiff base chelator, one nitrogen atom ($N3^{\#}$) and two sulphur atom (S1, S2) of the three NCS^- define the equatorial plane around cadmium. The *trans* axial sites are occupied by nitrogen atom (N2) from bidentate organic blocker and fourth nitrogen (N4*) of the bridging thiocyanate. Deviation of cadmium(II) from the mean plane formed by four equatorial atoms (N1, $N3^{\#}$, S1, S2) is about 0.1713 Å. The Cd–N bond lengths are shorter than the bridging Cd–S distances (Table 3) and are consistent with the corresponding values of cadmium(II)thiocyanato bridging system [23]. Cd1-N1 [imine] distance is slightly greater than Cd1–N2 [pyridine] bond length. Angles in the equatorial plane are close to the ideal 90.00° and lie within a close range [86.21(3)°–93.73(8)°]. *Trans* axial angle N2–Cd1–N4* shows slight deviation from ideal 180.00°. The dihedral angle between the planar pyridine and benzene moieties of pfan ligand is 47.3(2)°. The nearest neighbouring Cd···Cd distances within the chain are 5.908 and 5.795 Å.

The chains of $[Cd(pfan)(NCS)(SCN)]_n$ (**2**) pack alongside each other to give a sheet-like structure (Fig. 5) in *bc*-plane containing only π···π interactions. Here, two pyridyl rings from two closest chains are linked through face-to-face π-interactions (Table 4). The 2D sheets are further locked by another weaker face-to-face π···π interactions from two terminal benzene rings (Fig. 6), where the π-interactions (Table 4) are mainly responsible for the formation of solid state.

Recent literature on π···π interactions in metal complexes containing pyridyl-type ligands [38,39] shows that such non-covalent interaction plays an important role on crystal packing, and aromatic N-heterocycles are well suited for fabricating congregated π···π motifs because of their low π-electron density. Likewise, the presence of two N atoms in imH blocker in **1** facilitates such relatively stronger non-covalent interactions as compared to that in **2**.

3.3. Luminescence spectra

The spectroscopic data in methanol solutions and glasses are listed in Table 5. **1** shows emission spectrum at 348 nm while compound **2** has a band at 395 nm at 298 K (Fig. 7). These are assignable to intraligand $^1(\pi–\pi^*)$ fluorescence. **2** has very weak fluorescence; the lifetimes are 2.04 ns (**1**) and 2.42 ns (**2**), respectively. Though complex **1** shows overall stronger weak interaction, this higher lifetime in **2** may be due to the presence of a stronger π···π interactions (pyridyl–pyridyl), which is mainly responsible for fluorescence. In

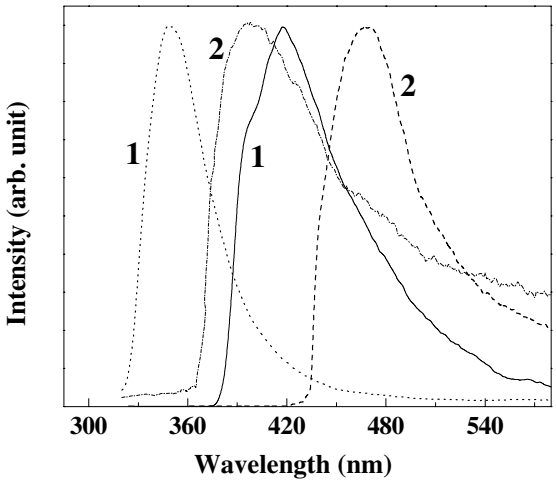

Fig. 7. Fluorescence of **1** in MeOH solution at 298 K (·····), phosphorescence in MeOH glassy solution (——); fluorescence of **2** in MeOH solution at 298 K (–·–·–), phosphorescence in MeOH glassy solution (- - - - -).

Table 5
Photophysical data for **1** and **2**

Sample	Absorption (λ (nm))	Emission (λ (nm))		Lifetime (ns)
		Fluorescence[a]	Phosphorescence[b]	
1	311	348	417	2.04
2	328	395	470	2.42

[a] In MeOH at room temperature (298 K).
[b] In MeOH at 77 K.

glassy solutions (77 K) a red shift is observable (417 nm for **1** and 470 nm for **2**) which is presumably due to $^3(\pi$–$\pi^*)$ phosphorescence.

4. Conclusion

Two new inorganic organic composite luminous polymers are synthesised through single-pot reactions of the building components with preassigned ratios. The C–H(imH)$\cdots\pi$ interaction in **1** indicates acidity of C–H proton of imH ring. No such hydrogen bonding in **2** indicates less acidity of the C–H proton in pfan Schiff base. The presence of more than one hetero N in imH compared to single N in pyridine ring of pfan facilitates such weak force, and topology is engineered accordingly. Structures **1** and **2** represent the reliability of combinations of strong/weak interactions in crystal engineering because of the concomitant predictability of the crystal design. This work reflects that a combination of a moderate to strong interaction and a weaker interaction seems to result synthon robustness giving variable architectures. In the future, we will expand the types of networks through change of organic blocker, metal template and bridging unit.

5. Supplementary data

Crystallographic data (excluding structure factors) for the structures reported in this paper have been deposited with the Cambridge Crystallographic Data Centre as supplementary publication nos. CCDC-217234 (**1**) and 211535 (**2**). Copies of this information can be obtained, free of charge from The Director, CCDC, 12 Union Road, Cambridge CB2 1EZ, UK (fax: +44-1223-336033; e-mail: deposit@ccdc.cam.ac.uk or www:http://www.ccdc.cam.ac.uk).

Acknowledgements

Financial support from the Department of Science and Technology (DST) and Council of Scientific and Industrial Research (CSIR), New Delhi, India is gratefully acknowledged. D.B. and H.R. are, respectively, thankful to the CSIR and UGC for their fellowships.

References

[1] P. Comba, T.W. Hambley, Molecular Modeling of Inorganic and Coordination Compounds, 2nd ed., VCH, Weinheim, 2001.
[2] (a) D.B. Mitzi, Prog. Inorg. Chem. 48 (1999) 1;
(b) B. Moulton, M.J. Zaworotko, Chem. Rev. 101 (2001) 1629.
[3] (a) J.-M. Lehn, Supramolecular Chemistry: Concepts and Perspectives, VCH, Weinheim, 1995;
(b) J.W. Steed, J.L. Atwood, Supramolecular Chemistry, Wiley, New York, 2000.
[4] S. Leininger, B. Olenyuk, P.J. Stang, Chem. Rev. 100 (2000) 853.
[5] (a) T. Steiner, Angew. Chem. Int. Ed. 41 (2002) 48;
(b) G.R. Desiraju, Acc. Chem. Res. 35 (2002) 565.
[6] (a) M.J. Zaworotko, Chem. Commun. (2002) 199;
(b) L. Pan, N.W. Zheng, N.W. Wu, X.Y. Huang, J. Coord. Chem. 41 (1999) 551;
(c) C.A. Hunter, Chem. Soc. Rev. 23 (1994) 101.
[7] (a) S.V. Lindeman, D. Kosynkin, J.K. Kochi, J. Am. Chem. Soc. 120 (1998) 6431;
(b) C.D. Abernethy, C.L.B. Macdonald, J.A.C. Clyburne, A.H. Cowley, Chem. Commun. (2001) 61;
(c) L. Rong-Guang, T. Zhu, X. Sai-Feng, Z. Quin-Jiang, W.G. Jackson, W. Zhan-Bing, L. La-Sheng, Polyhedron 22 (2003) 3467.
[8] B. Cornils, W.A. Herrmann, R. Schlogl (Eds.), Catalysis from A to Z: A Concise Encyclopedia, Wiley, New York, 2000.
[9] (a) S.R. Marder, J.E. Sohn, G.D. Stucky (Eds.), Materials for Nonlinear Optics: Chemical Perspectives, ACS Symposium Series, Washington, DC, 1991;
(b) O.R. Evans, W. Lin, Acc. Chem. Res. 35 (2002) 511.
[10] J.S. Miller, M. Drillon (Eds.), Magnetism: Molecules to Materials IV, Wiley–VCH, Weinheim, 2003.
[11] D. Demus, J.W. Goodby, G.W. Gray, H.-W. Spiess, V. Vill (Eds.), Handbbok of Liquid Crystals, Wiley–VCH, Weinheim, 1998.
[12] (a) J.R. Farraro, J.M. Williams, Introduction to Synthetic Electrical Conductors, Academic Press, New York, 1987;
(b) Special issue on Chemical Sensors, Chem. Rev. 100 (2000) Number 7.
[13] (a) C. Janiak, J. Chem. Soc., Dalton Trans. (2003) 2781;
(b) S.L. James, Chem. Soc. Rev. 32 (2003) 276.
[14] G.R. Desiraju (Ed.), Crystal Design: Structure and Function. Perspectives in Supramolecular Chemistry, vol. 7, Wiley, Chichester, 2003.
[15] D. Braga, F. Grepioni, A.G. Orpen (Eds.), Crystal Engineering: From Molecules and Crystals to Materials, Kluwer, Dordrecht, 1999.
[16] (a) G.W. Rabe, H. Heise, G.P.A. Yap, L.M. Liable-Sands, I.A. Guzei, A.L. Rheingold, Inorg. Chem. 37 (1998) 4235;
(b) M.-L. Tong, H.-J. Chen, X.-M. Chen, Inorg. Chem. 39 (2000) 2235;
(c) D.L. Long, A.J. Blake, N.R. Champness, C. Wilson, M. Schroder, Chem. Eur. J. 8 (2002) 2026.
[17] (a) W. Clegg, K.W. Henderson, L. Horsburgh, F.M. Mackenzie, R.E. Mulvey, Chem. Eur. J. 4 (1998) 53;
(b) L. Carlucci, G. Ciani, D.M. Proserpio, Chem. Commun. (1999) 449.
[18] (a) K.N. Power, T.L. Hennigar, M.J. Zaworotko, Chem. Commun. (1998) 595;
(b) K.L.V. Mann, E. Psillakis, J.C. Jeffery, L.H. Rees, N.M. Harden, J.A. McCleverty, M.D. Ward, D. Gatteschi, F. Totti, F.E. Mabbs, E.J.L. McInnes, P.C. Riedi, J.M. Smith, J. Chem. Soc., Dalton Trans. (1999) 339.
[19] (a) N. Motohiro, M. Hirota, Y. Umezawa, The CH/π Interaction. Evidence Nature and Consequences, Wiley–VCH, New York, 1998;
(b) G.R. Desiraju, T. Steiner, The Weak Hydrogen Bond in Structural Chemistry and Biology, Oxford University Press, Oxford, 1999.
[20] D. Bose, Sk.H. Rahaman, G. Mostafa, R.D. Bailey Walsh, M.J. Zaworotko, B.K. Ghosh, Polyhedron 23 (2004) 545.
[21] (a) S. Subramanian, M.J. Zaworotko, Angew. Chem., Int. Ed. Engl. 34 (1995) 2127;
(b) K. Biradha, Y. Hongo, M. Fujita, Angew. Chem. Int. Ed. 39 (2000) 3843.

[22] D.W. Bruce, D. O'Hare (Eds.), Inorganic Materials, second ed., Wiley, New York, 1996.
[23] (a) H. Zhang, X. Wang, K. Zhang, B.K. Teo, Coord. Chem. Rev. 183 (1999) 157;
(b) A. Mondal, G. Mostafa, A. Ghosh, I.R. Laskar, N. Ray Chaudhuri, J. Chem. Soc., Dalton Trans. (1999) 9;
(c) N. Mondal, M.K. Saha, S. Mitra, V. Gramlich, J. Chem. Soc., Dalton Trans. (2000) 3218;
(d) J.M. Clemente-Juan, B. Chansou, B. Donnadieu, J.-P. Tuchagues, Inorg. Chem. 39 (2000) 5515.
[24] (a) F.F. Jian, P.S. Zhao, S.Y. Wang, S.S. Zhang, J. Chem. Crystallogr. 32 (2002) 395;
(b) A.M. Galibert, O. Cortedellas, B. Soula, B. Donnadieu, P.B. Fabre, J. Chem. Soc., Dalton Trans. (2002) 3743;
(c) G.W. Gokel, L.B. Barbour, R. Ferdani, J.X. Hu, Acc. Chem. Res. 35 (2002) 878.
[25] T. Welton, Chem. Rev. 99 (1999) 1071.
[26] W. Plass, Coord. Chem. Rev. 237 (2003) 205.
[27] (a) A.D. Garnovskii, A.L. Nivorozhkin, V.I. Minkin, Coord. Chem. Rev. 126 (1993) 1;
(b) V. Alexander, Chem. Rev. 95 (1995) 273.
[28] (a) T.K. Karmakar, S.K. Chandra, J. Ribas, G. Mostafa, T.-H. Lu, B.K. Ghosh, Chem. Commun. (2002) 2364;
(b) E.-Q. Gao, S.-Q. Bai, Y.-F. Yue, Z.-M. Wang, C.-H. Yan, Inorg. Chem. 42 (2003) 3642;
(c) R. Paschke, S. Liebsch, C. Tschierske, M.A. Oakley, E. Sinn, Inorg. Chem. 42 (2003) 8230.
[29] G.M. Sheldrick, SAINT: Ver. 5, Siemens Analytical X-ray Instrument Inc., Madison, WI, 1995.
[30] SADABS v2.02: Area-Detector Absorption Correction, Siemens Industrial Automation, Inc., Madison, WI, 1996.
[31] G.M. Sheldrick, SHELXL-97: Program for Refinement of Crystal Structures, University of Gottingen, Gottingen, Germany, 1997.
[32] L.J. Farrugia, J. Appl. Crystallogr. 30 (1997) 565.
[33] A.L. Spek, PLATON-99: Molecular Geometry Program, University of Utrecht, The Netherlands, 1999.
[34] SHELXTL-6.1, Bruker AXS Inc., Madison, WI, 2001.
[35] W.J. Geary, Coord. Chem. Rev. 7 (1971) 81.
[36] K. Nakamoto, Infrared and Raman Spectra of Inorganic and Coordination Compounds: Part B, 5th ed., Wiley, New York, 1997, p. 116.
[37] C. Janiak, J. Chem. Soc., Dalton Trans. (2000) 3885.
[38] (a) V. Lozan, P.-G. Lassahn, C. Zhang, B. Wu, C. Janiak, G. Rheinwald, H. Lang, Z. Naturforsch. 58b (2003) 1152;
(b) E. Craven, C. Zhang, C. Janiak, G. Rheinwald, H. Lang, Z. Anorg. Allg. Chem. 629 (2003) 2282;
(c) C. Zhang, C. Janiak, Z. Anorg. Allg. Chem. 627 (2001) 1972;
(d) C. Zhang, C. Janiak, J. Chem. Crystallogr. 31 (2001) 29.
[39] (a) H.-P. Wu, C. Janiak, G. Rheinwald, H. Lang, J. Chem. Soc., Dalton Trans. (1999) 183;
(b) C. Janiak, L. Uehlin, H.-P. Wu, P. Klufers, H. Piotiowski, T.G. Scharmann, J. Chem. Soc., Dalton Trans. (1999) 3121;
(c) C. Zhang, C. Janiak, H. Brombacher, Z. Naturforsch. 56b (2001) 1205.

Available online at www.sciencedirect.com
SCIENCE DIRECT®
Polyhedron 23 (2004) 2055–2061
POLYHEDRON
www.elsevier.com/locate/poly

Anionic capsules of *p*-sulfonatothiacalix[4]arene with trivalent lanthanide ions and diaza-crown ether

Qian-Ling Guo, Wen-Xiang Zhu *, Ying-Chun Liu, Da-Qiang Yuan, Jing Zhang, Shu-Lan Ma

Department of Chemistry, Beijing Normal University, Xinjiekou Waidajie Street 19, Beijing 100875, People's Republic of China

Received 16 March 2004; accepted 3 May 2004
Available online 3 July 2004

Abstract

4,13-Diaza-18-crown-6 is shrouded by two *p*-sulfonatothiacalix[4]arenes in the presence of trivalent lanthanide ions in two different types of arrangements: (4,13-diaza-18-crown-6){(4,13-diprotodiaza-18-crown-6) ⊂ {[La(H_2O)$_8$(*p*-sulfonatothiacalix[4]arene)$^{4-}$]$^-$}$_2$} · 17H_2O **(1)** and (4,13-diprotodiaza-18-crown-6){[Eu(NO_3)(H_2O)$_7$]$^{2+}$}$_2$}{(4,13-diprotodiaza-18-crown-6) ⊂ [(*p*-sulfonatothiacalix[4]arene)$^{4-}$]$_2$} · 17H_2O **(2)**. In complex **1**, one sulfonato group of thiacalixarene ligates to the La^{3+} ion, but in complex **2,** the *p*-sulfonatothiacalixarene does not directly coordinate to the Eu^{3+} ion which exists as [Eu(NO_3)(H_2O)$_7$]$^{2+}$ but acts as a second-sphere ligand through hydrogen bonding. In both complexes, thiacalixarenes form irregular bi-layer structures in which the exo-capsule diaza-18-crown-6 traverses the hydrophobic layers.
© 2004 Elsevier Ltd. All rights reserved.

Keywords: Sulfonatothiacalixarene; Capsules; Diaza-18-crown-6; Lanthanide ions

1. Introduction

Water-soluble calix[*n*]arenes have been widely investigated and are becoming increasingly important in the field of supramolecular chemistry and crystal engineering, showing interesting inclusion properties and a wide range of metal coordination complexes both in solution and in the solid state [1]. *p*-Sulfonatocalix[4]arene is a highly versatile tecton, generating various structural motifs which include 'molecular capsules' [2–7], 'ferris wheels' [8], hydrogen bonded polymers [9], 2-D coordination polymers [9–11], as well as nanometer scale spheres and tubules [12].

Similar to *p*-sulfonatocalix[4]arene, Na_4[thiacalix[4]arene tetrasulfonate] · ethanol · 8H_2O also shows a bi-layer structure in the solid state [13] and the thiacalixarene unit adopts the cone configuration. It is also shown to form large molecular assemblies with highly complex supramolecular architectures in the presence of suitable guest molecules. In our recent studies, we focused on the supramolecular chemistry of water-soluble *p*-sulfonatothiacalix[4]arene [14–17]. In this paper, we report the formation of ionic capsules where the di-protonated 4,13-diaza-18-crown-6 is shrouded by two *p*-sulfonatothiacalix[4]arenes in the presence of lanthanide ions.

2. Experimental

2.1. Materials and methods

4,13-Diaza-18-crown-6 [18] and tetrasodium *p*-sulfonatothiacalix[4]arene [13] were synthesized by literature methods. All other reagents were commercially available and used without further purification.

C, H and N were determined using an Elementar Vario EL analyzer. The UV spectra in aqueous solution were measured using a GBC Cintra 10e UV–Vis spectrophotometer. The IR spectra were recorded on a

* Corresponding author. Tel.: +861062207838; fax: +861062200567.
E-mail address: wx-zhu@263.net (W.-X. Zhu).

0277-5387/$ - see front matter © 2004 Elsevier Ltd. All rights reserved.
doi:10.1016/j.poly.2004.05.011

Nicolet Avatar 360 FT-IR spectrometer using the KBr pellet technique in the 400–4000 cm^{-1} regions.

2.2. Preparation of (4,13-diaza-18-crown-6){(4,13-diprotodiaza-18-crown-6) ⊂ {[La(H_2O)$_8$(p- sulfonatothiacalix[4]arene)$^{4-}$]$^-$}$_2$}·17H_2O (1) and (4,13-diprotodiaza-18-crown-6){[Eu(NO_3)(H_2O)$_7$]$^{2+}$}$_2${(4,13-diprotodiaza-18-crown-6) ⊂ [(p-sulfonatothiacalix[4]arene)$^{4-}$]$_2$}·17H_2O (2)

4,13-Diaza-18-crown-6 (26 mg, 0.1 mmol) and tetrasodium *p*-sulfonatothiacalix[4]arene (45 mg, 0.05 mmol) were dissolved in deionized water (5 mL), and the solution was acidified up to pH ≈ 2 with perchloric acid, to which 0.2 mmol $Ln(NO_3)_3$ ($Ln^{3+} = La^{3+}$, Eu^{3+}) was added. After several days, large crystals suitable for X-ray diffraction analysis were formed. The crystals quickly cracked when removed from the mother liquor. UV (in water): $\lambda_{max}/nm(\varepsilon_{max}/dm_3\,mol^{-1}\,cm^{-1}) = 208$ (9.07×10^4), 305 (1.45×10^4) (for complex **1**), λ_{max}/nm ($\varepsilon_{max}/dm_3\,mol^{-1}\,cm^{-1}) = 208$ (1.04×10^5), 305 (1.60×10^4) (for comp1ex **2**). IR: sulfonate absorptions: $\nu = 1221$, 1146, 1037 cm^{-1} (for comp1ex **1**), $\nu = 1221$, 1145, 1037 cm^{-1} (for comp1ex **2**). Elem. *Anal*. Calc. for $C_{36}H_{62}LaN_2O_{31.5}S_8$: C, 30.40; H, 4.40; N, 1.97. Found: C, 30.11; H, 4.26; N, 2.11% (the analytical data is only for the samples having lost five water molecules during transport), *Anal*. Calc. for $C_{36}H_{54}EuN_3O_{30}S_8$: C, 30.51; H, 3.85; N, 2.97. Found: C, 30.15; H, 3.99; N, 2.59% (the analytical data is only for the samples having lost 8.5 water molecules during transport).

2.3. X-ray data collections and structure determinations

X-ray data were collected at 293(2) K on a Bruker SMART 1000 CCD diffractometer using Mo Kα radiation ($\lambda = 0.71073$ Å). The crystals were sealed in a glass capillary with a few drops of mother liquor in order to prevent cracking owing to solvent loss. The structures were solved by direct methods and refined by full-matrix least-square techniques on F^2 using the SHELXL-97 program. All non-hydrogen atoms were refined anisotropically. The hydrogen atoms on the crown ether and the thiacalixarene were placed at their calculated positions and assigned with isotropic displacement parameters. The hydrogen atoms on the water molecules could not be located. A number of lattice water molecules were disordered and were given partial occupancies. The experimental details for X-ray data collection of the complexes are presented in Table 1. Selected bond lengths and angles are listed in Table 2.

3. Results and discussion

The complexes were prepared by mixing the corresponding lanthanide ion (III) nitrates, 4,13-diaza-18-crown-6 and tetrasodium *p*-sulfonatothiacalix[4]arene in an aqueous solution, with the pH adjusted to 2 (see Scheme 1).

The structure of complex **1** is shown in Fig. 1. It consists of several structural components: the anionic capsule {(4,13-diprotodiaza-18-crown-6) ⊂ {[La(H_2O)$_8$

Table 1
Crystal data for the complexes

	1	**2**
Empirical formula	$C_{36}H_{72}La\ N_2O_{36.5}S_8$	$C_{36}H_{71}EuN_3O_{38.5}S_8$
Formula weight	1512.35	1570.40
Temperature (K)	293(2)	293(2)
Wavelength (Å)	0.71073	0.71073
Crystal system	monoclinic	triclinic
Space group	$P2_1/n$	$P\bar{1}$
Unit cell dimensions		
a (Å)	18.261(8)	14.814(8)
b (Å)	14.613(6)	16.432(9)
c (Å)	25.92(1)	16.61(1)
α (°)	90	115.41(1)
β (°)	90.881(9)	98.369(9)
γ (°)	90	110.139(9)
Volume (Å^3)	6916(5)	3218(3)
Z, D_{Calc} (g cm^{-3})	4, 1.453	2, 1.621
Absorption coefficient (mm^{-1})	0.945	1.332
F(000)	3116	1614
Crystal size (mm)	0.52 × 0.50 × 0.44	0.20 × 0.16 × 0.14
Range for data collection (°)	1.94–26.55	1.45–26.57
Limiting indices	$-22 \leqslant h \leqslant 21$, $-18 \leqslant k \leqslant 12$, $-29 \leqslant l \leqslant 32$	$-18 \leqslant h \leqslant 18$,$-20 \leqslant k \leqslant 14$, $-15 \leqslant l \leqslant 20$
Reflections collected/unique [R_{int}]	38 690/14 020 [0.1199]	18 630/13 082 [0.0403]
Completeness to θ_{max} (%)	97.2	97.3
Goodness-of-fit on F^2	0.945	1.042
Final *R* indices [$I > 2\sigma(I)$]	$R_1 = 0.0873$, $wR_2 = 0.1973$	$R_1 = 0.0557$, $wR_2 = 0.1141$

Table 2
Selected bond lengths (Å) and bond angles (°) for complexes **1** and **2**

1		**2**	
Bond lengths			
La(1)–O(18)	2.474(7)	Eu(1)–O(24)	2.396(5)
La(1)–O(5)	2.503(7)	Eu(1)–O(20)	2.414(5)
La(1)–O(17)	2.52(1)	Eu(1)–O(25)	2.424(5)
La(1)–O(23)	2.52(1)	Eu(1)–O(23)	2.446(5)
La(1)–O(19)	2.55(1)	Eu(1)–O(22)	2.449(5)
La(1)–O(20)	2.555(9)	Eu(1)–O(26)	2.477(5)
La(1)–O(21)	2.560(9)	Eu(1)–O(21)	2.495(5)
La(1)–O(24)	2.579(9)	Eu(1)–O(18)	2.508(5)
La(1)–O(22)	2.59(1)	Eu(1)–O(17)	2.528(5)
Bond angles			
O(18)–La(1)–O(5)	70.8(2)	O(24)–Eu(1)–O(20)	81.3(2)
O(18)–La(1)–O(17)	135.6(4)	O(24)–Eu(1)–O(25)	75.9(2)
O(5)–La(1)–O(17)	70.5(4)	O(20)–Eu(1)–O(25)	136.8(2)
O(18)–La(1)–O(23)	140.0(5)	O(24)–Eu(1)–O(23)	82.9(2)
O(5)–La(1)–O(23)	100.3(5)	O(20)–Eu(1)–O(23)	139.5(2)
O(17)–La(1)–O(23)	68.3(6)	O(25)–Eu(1)–O(23)	73.1(2)
O(18)–La(1)–O(19)	77.4(4)	O(24)–Eu(1)–O(22)	75.5(2)
O(5)–La(1)–O(19)	75.1(4)	O(20)–Eu(1)–O(22)	72.6(2)
O(17)–La(1)–O(19)	72.5(5)	O(25)–Eu(1)–O(22)	133.4(2)
O(23)–La(1)–O(19)	139.6(6)	O(23)–Eu(1)–O(22)	67.5(2)
O(18)–La(1)–O(20)	71.9(3)	O(24)–Eu(1)–O(26)	140.4(2)
O(5)–La(1)–O(20)	133.8(3)	O(20)–Eu(1)–O(26)	137.5(2)
O(17)–La(1)–O(20)	125.0(4)	O(25)–Eu(1)–O(26)	68.9(2)
O(23)–La(1)–O(20)	125.9(5)	O(23)–Eu(1)–O(26)	70.3(2)
O(19)–La(1)–O(20)	71.0(4)	O(22)–Eu(1)–O(26)	117.2(2)
O(18)–La(1)–O(21)	138.4(3)	O(24)–Eu(1)–O(21)	145.6(2)
O(5)–La(1)–O(21)	143.3(3)	O(20)–Eu(1)–O(21)	73.2(2)
O(17)–La(1)–O(21)	73.2(4)	O(25)–Eu(1)–O(21)	138.4(2)
O(23)–La(1)–O(21)	70.7(5)	O(23)–Eu(1)–O(21)	101.7(2)
O(19)–La(1)–O(21)	89.1(4)	O(22)–Eu(1)–O(21)	75.0(2)
O(20)–La(1)–O(21)	66.6(3)	O(26)–Eu(1)–O(21)	70.5(2)
O(18)–La(1)–O(24)	72.8(3)	O(24)–Eu(1)–O(18)	122.9(2)
O(5)–La(1)–O(24)	64.6(3)	O(20)–Eu(1)–O(18)	79.9(2)
O(17)–La(1)–O(24)	108.3(4)	O(25)–Eu(1)–O(18)	82.5(2)
O(23)–La(1)–O(24)	68.4(5)	O(23)–Eu(1)–O(18)	138.9(2)
O(19)–La(1)–O(24)	135.8(4)	O(22)–Eu(1)–O(18)	144.1(2)
O(20)–La(1)–O(24)	126.6(3)	O(26)–Eu(1)–O(18)	70.2(2)
O(21)–La(1)–O(24)	134.5(3)	O(21)–Eu(1)–O(18)	75.3(2)
O(18)–La(1)–O(22)	80.8(3)	O(24)–Eu(1)–O(17)	72.5(2)
O(5)–La(1)–O(22)	129.7(3)	O(20)–Eu(1)–O(17)	68.1(2)
O(17)–La(1)–O(22)	142.2(5)	O(25)–Eu(1)–O(17)	70.2(2)
O(23)–La(1)–O(22)	75.9(5)	O(23)–Eu(1)–O(17)	139.7(2)
O(19)–La(1)–O(22)	137.9(4)	O(22)–Eu(1)–O(17)	132.1(2)
O(20)–La(1)–O(22)	68.1(4)	O(26)–Eu(1)–O(17)	110.2(2)
O(21)–La(1)–O(22)	83.8(4)	O(21)–Eu(1)–O(17)	116.7(2)
O(24)–La(1)–O(22)	67.7(3)	O(18)–Eu(1)–O(17)	50.4(2)

(*p*-sulfonatothiacalix[4]arene)$^{4-}$]$^{-}$}$_2$}, one disordered exo-capsule diaza-crown ether, and two water molecules hydrogen bonded to the crown ether, along with several disordered lattice water molecules. An oxygen atom of a sulfonato group coordinates to a lanthanum ion at a La–O bond distance of 2.503 Å. The metal ion is also ligated to eight aqua ligands at an average La–O bond distance of 2.544 Å. The cation is ligated in a distorted mono-capped tetragonal *anti*-prismatic geometry.

A di-protonated diaza-crown ether is sandwiched by two thiacalixarenes, each of which has two sulfonato groups disordered in an 'up–down' fashion forming a capsule. There is a water molecule on either side of the di-protonated diaza-crown ether guest molecule. This is reminiscent of the capsule created by the di-protonated diaza-crown ether and *p*-sulfonatocalix[4]arene [7], but in the present structure, the water molecules hydrogen are bonded to two *trans* oxygen atoms of the crown ether with O···O distances of 2.874 and 3.093 Å, not to the di-protonated nitrogen atoms.

In the present structure, the splaying effect of the thiacalixarene is observed, which is the decisive factor in

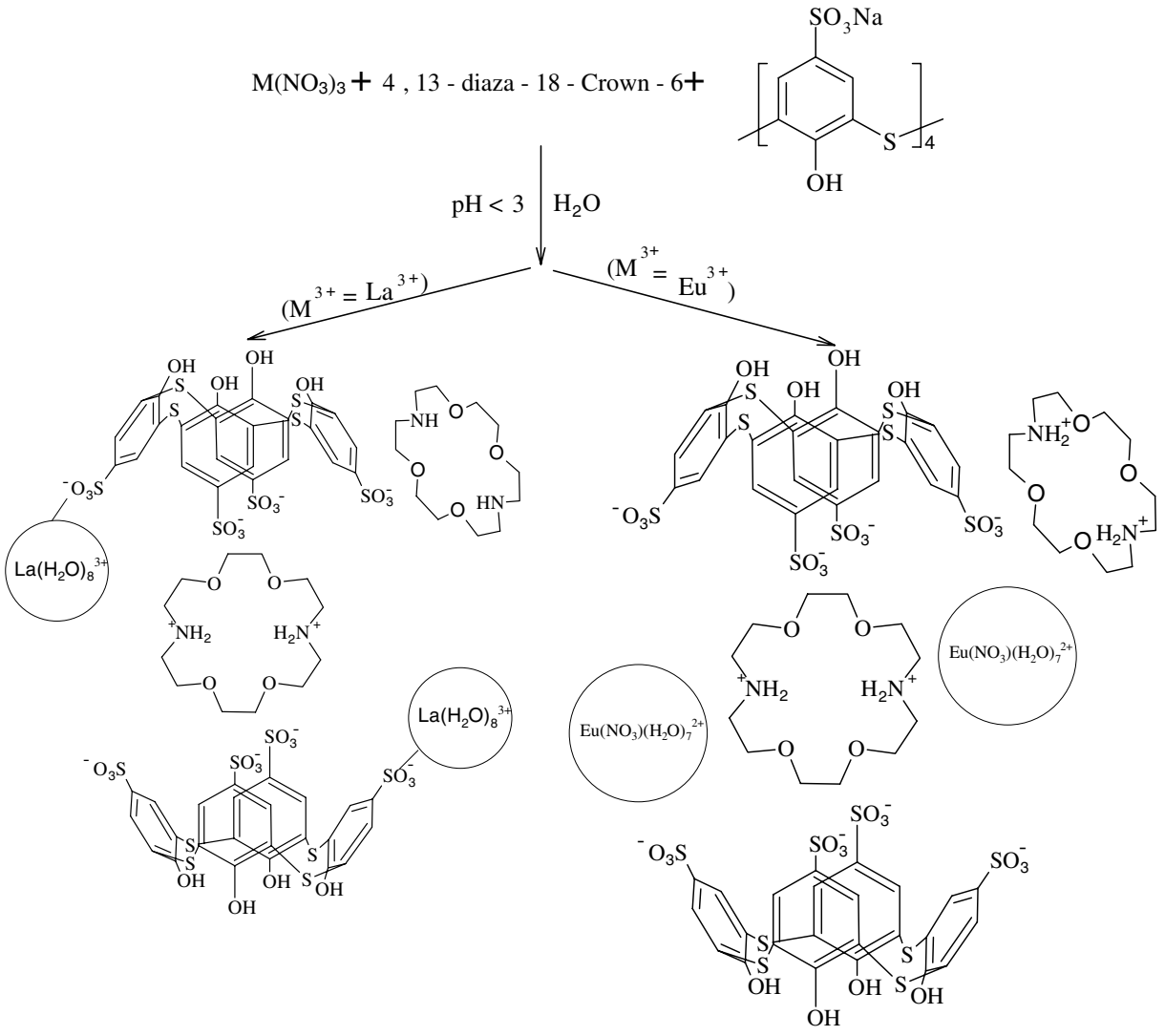

Scheme 1.

the formation of an 'ion capsule'. The dihedral angles between the two splaying aromatic rings and the plane of the four phenolic oxygens are 146.8° and 138.3°. The other two are 118° and 105.4°. There are also hydrogen bonds from the lattice water molecules to the sulfonato groups of the two thiacalixarenes with O···O distances from 2.742 to 2.921 Å.

There is an exo-capsule crown ether which is interspersed between columns of 'up–down' thiacalixarenes, so an irregular bi-layer assembly is formed (see Fig. 2). The interactions between the adjacent thiacalixarenes are not π–π stacking, but are hydrogen bonds between the sulfonato groups and the phenolic groups or hydrogen bonds mediated by lattice water molecules. The interaction between the thiacalixarene and the exo-capsule crown ether are hydrogen bonds bridged by lattice water molecules.

The structure of complex **2** is shown in Fig. 3. It consists of several structural components: the anionic capsule {(4,13-diprotodiaza-18-crown-6) ⊂ [(*p*-sulfonato-thiacalix[4]arene)$^{4-}$]$_2$}, one exo-capsule di-protonated diaza-crown ether and two $[Eu(NO_3)(H_2O)_7]^{2+}$ ions, along with several disordered lattice water molecules. The Eu^{3+} ion is not bound directly to any sulfonato groups, but exists as the $[Eu(NO_3)(H_2O)_7]^{2+}$ ion, forming part of the secondary coordination sphere through hydrogen bonding. This is different from that of complex **1**. A NO_3^- anion coordinates to Eu^{3+} as a bidentate ligand, at an average Eu–O bond distance of 2.518 Å. The metal ion is also ligated to seven aqua ligands at an average Eu–O bond distance of 2.443 Å. There is extensive hydrogen bonding from the ligated water molecules of the europium ion to sulfonato groups of the two thiacalixarenes in the nearest 'ionic capsule' with hydrogen bonding MO···OS distances of 2.968 and 2.975 Å.

In this structure, a disordered di-protonated diaza-18-crown-6 is at the core of the 'ionic capsule'. In

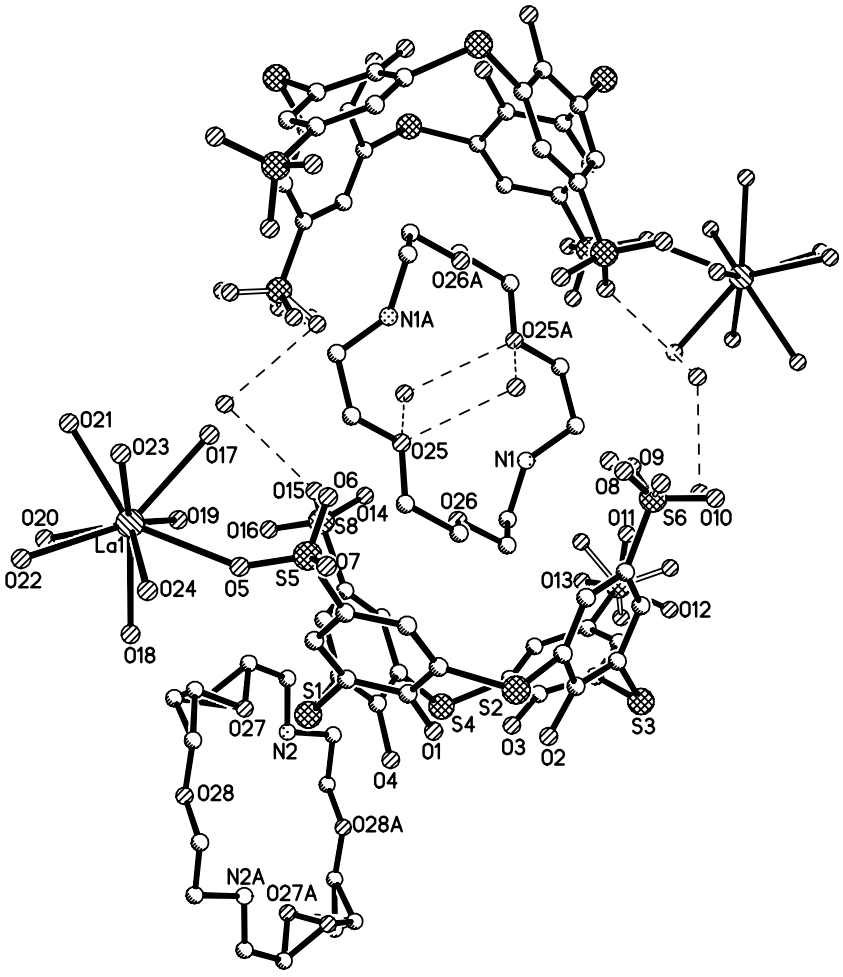

Fig. 1. An 'ionic capsule' in **1**; dashed lines indicate hydrogen bonds (hydrogen atoms and lattice water molecules have been omitted for clarity).

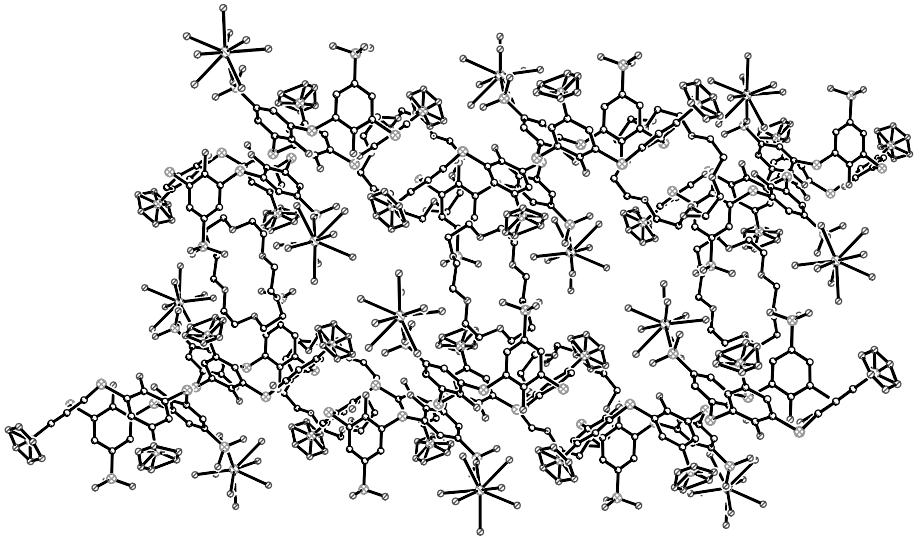

Fig. 2. Projection of **1,** showing the bi-layer packing.

addition to the splaying effect (the dihedral angles between the two splaying aromatic rings and the plane of the four phenolic oxygens are 141.4° and 134°, the other two are 113.9° and 109.8°), the hydrogen bonds between the di-protonated nitrogen atoms of the crown ether and the disordered sulfonato groups of the two

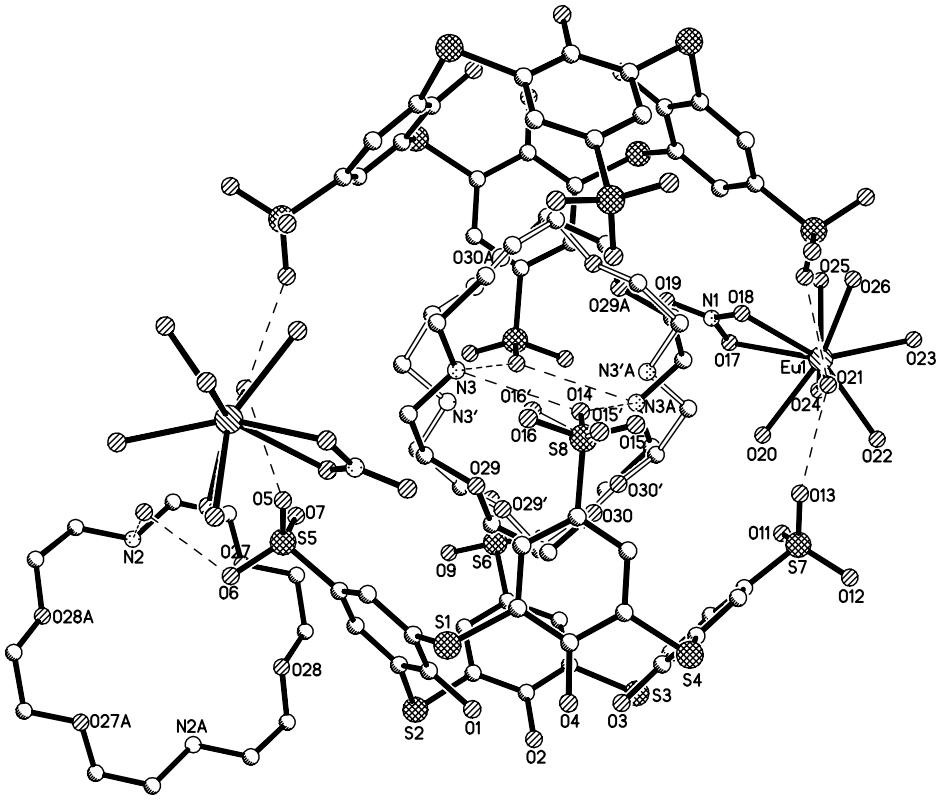

Fig. 3. An 'ionic capsule' in **2**; dashed lines indicate hydrogen bonds (hydrogen atoms and lattice water molecules have been omitted for clarity).

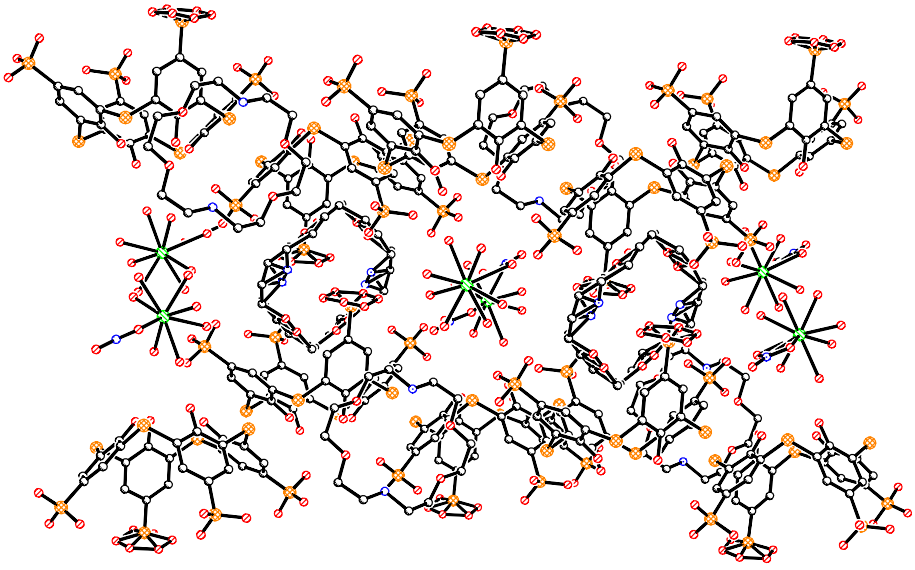

Fig. 4. Projection of **2**, showing the bi-layer packing.

thiacalixarenes which form the shell of the capsule stabilize the ionic capsule assembly. The distances of N···O range from 2.673 to 3.067 Å.

Similar to complex **1**, as an exo-capsule di-protonated diaza crown ether intersperses into the hydrophobic layer, a particular bi-layer structure is formed (see Fig. 4).

4. Conclusion

In both complexes, the 4,13-diaza-18-crown-6 is shrouded by two thiacalixarenes in the presence of trivalent lanthanide ions to form an ionic capsule. In addition to forming 'ionic capsules', the diaza-crown ethers can also insert into the hydrophobic layers via a

variety of supramolecular interactions. These are similar to the related complexes of transition metal ions ($M^{2+} = Co^{2+}$, Ni^{2+}, Cu^{2+}) with 4,13-diaza-18-crown-6 and *p*-sulfonatothiacalix[4]arene [17]. But the coordination modes of the cations with the *p*-sulfonatothiacalix[4]arenes in the lanthanide ionic complexes are different from that in the related transition metal ionic complexes in which the thiacalixarenes coordinate to transition metal ions through phenolic groups and a bridging sulfur atom at the base due to the fact that the bridging sulfur atom tends to bind the transition metal ions.

5. Supplementary data

CCDC-230797 (complex **1**) and CCDC-230796 (complex **2**) contain the supplementary crystallographic data for this paper. These data can be obtained free of charge at www.ccdc.cam.ac.uk/conts/retrieving.html or from the Cambridge Crystallographic Data Centre, 12, Union Road, Cambridge, CB2 1EZ, UK [fax: (internat.) +44-1223/336-033; E-mail: deposit@ccdc.cam.ac.uk].

Acknowledgements

We are grateful to the Municipal Natural Science Foundation of Beijing (No. 2022011).

References

[1] J.L. Atwood, L.J. Barbour, M.J. Hardie, C.L. Raston, Coord. Chem. Rev. 222 (2001) 3.
[2] A. Drljaca, M.J. Hardie, C.L. Raston, J. Chem. Soc., Dalton Trans. (1999) 3639.
[3] A. Drljaca, M.J. Hardie, C.L. Raston, L. Spiccia, Chem. Eur. J. 5 (1999) 2295.
[4] S. Airey, A. Drljaca, M.J. Hardie, C.L. Raston, Chem. Commun. (1999) 1137.
[5] A. Drljaca, M.J. Hardie, T.J. Ness, C.L. Raston, Eur. J. Inorg. Chem. (2000) 2221.
[6] M.J. Hardie, J.A. Johnson, C.L. Raston, H.R. Webb, Chem. Commun. (2000) 849.
[7] S.J. Dalgarno, C.L. Raston, J. Chem. Soc., Dalton Trans. (2003) 287.
[8] A. Drljaca, M.J. Hardie, J.A. Johnson, C.L. Raston, H.R. Webb, Chem. Commun. (1999) 1135.
[9] J.L. Atwood, L.J. Barbour, S. Dalgarno, C.L. Raston, H.R. Webb, J. Chem. Soc., Dalton Trans. (2002) 4351.
[10] H.R. Webb, M.J. Hardie, C.L. Raston, Chem. Eur. J. 7 (2001) 3616.
[11] S.J. Dalgarno, C.L. Raston, Chem. Commun. (2002) 2216.
[12] G.W. Orr, L.J. Barbour, J.L. Atwood, Science 285 (1999) 1049.
[13] D. Yuan, W.-X. Zhu, S. Ma, X. Yan, J. Mol. Struct. 616 (2002) 241.
[14] Q. Guo, W.-X. Zhu, S. Dong, X. Yan, J. Mol. Struct. 650 (2003) 159.
[15] Q.-L. Guo, W.-X. Zhu, S.-L. Ma, D.-Q. Yuan, S.-J. Dong, M.-Q. Xu, J. Mol. Struct. 690 (2004) 63.
[16] Q.-L Guo, W.-X. Zhu, S. Gao, S.-L. Ma, S.-J. Dong, M.-Q. Xu, Inorg. Chem. Commun. 7 (2004) 467.
[17] Q.-L. Guo, W.-X. Zhu, S.-L. Ma, S.-J. Dong, M.-Q. Xu, Polyhedron 23 (2004) 1461.
[18] S. Kulstad, L.A. Malmaston, Acta Chem. Scand. B33 (1979) 469.

Available online at www.sciencedirect.com
SCIENCE DIRECT®
Polyhedron 23 (2004) 2063–2067
POLYHEDRON
www.elsevier.com/locate/poly

Synthesis and characterization of a chiral Zn(II) complex based on a *trans*-1,2-diaminocyclohexane derivative and catalytic reduction of acetophenone

Soo Gyun Roh, Jong Uk Yoon, Jong Hwa Jeong *

Department of Chemistry, Kyungpook National University, 1370 Sankyuk-dong, Taegu 702-701, Republic of Korea

Received 28 February 2004; accepted 28 April 2004
Available online 7 July 2004

Abstract

Reaction of $ZnCl_2$ with *R*,*R*-bmbcd (= *N*,*N*′-bis(4-methoxy-benzyl)-cyclohexane-1,2-diamine) **1** in ethanol yields the chiral [$ZnCl_2$(*R*,*R*-bmbcd)] **2**, which crystallizes in the monoclinic space group $P2_1$. The Zn atom has a distorted tetrahedral geometry involving two nitrogen atoms of *R*,*R*-bmbcd and two chloro ligands with the range of bond lengths, 2.066(2)–2.2289(9) Å. The result of the catalytic enantioselective reduction of acetophenone promoted by *R*,*R*-bmbcd:$Zn(OTf)_2$ = 1:1 mole ratio in the presence of catecholborane for 48 h at 0 °C give (*S*)-(−)-1-phenylethanol in 48% ee with 77% yield.
© 2004 Elsevier Ltd. All rights reserved.

Keywords: *trans*-1,2-Diaminocyclohexane; Crystal structure; Zinc complex; Catalytic enantioselective reduction

1. Introduction

Catalytic asymmetric synthesis is a key technique for preparing optically active substances in biologically medical science and fine chemicals [1]. Enantioselective syntheses such as the alkylation of aldehydes [2], the epoxidation of olefines [3] and the asymmetric reduction of ketones [4] have been extensively studied. In particular, asymmetric alkylation of aldehydes with dialkylzinc in the presence of chiral bidentate ligands such as diol [5], aminoalcohol [6], diamine [7], ditriflamide [2,8], diaminocyclohexane [9] have been well-established as contrasted with the asymmetric reduction of ketones. The Kobayashi and co-workers [2a] has obtained highly optically pure alcohols by using a (*R*,*R*)-*trans*-1,2-diaminocyclohexane derivative containing an electron withdrawing group in the presence of $Ti(O^iPr)_4$. Recently, the Walsh and co-worker [10] has worked to optimize the enantioselectivity of the catalyst by varying the achiral ligands, described as chiral environment amplifications, which is a modular approach to asymmetric catalysis. Enantioselective reduction of α-alkoxy ketones in the presence of $Zn(OTf)_2$ and bis-oxazolines afforded the chiral alochols in good yields and high ee's [11], but the extended studies for enantioselective reduction of α-alkoxy ketones are limited.

The enantiomeric purity of a chiral auxiliary in asymmetric catalysis is a major factor for alkylation of benzaldehyde. The reaction rate is also considerably influenced by the enantiomeric purity, and is significantly faster with pure chiral auxiliaries than with the racemic ones [12]. The structure of the catalyst in the asymmetric reduction of ketones can be a key parameter for the development of a better catalyst, providing the coordination environments at the centre atom, the reaction mechanism and the steric effect. Diaminocyclohexane derivatives involving functional groups such as hydrogen, isopropyl, isobutyl, etc., are not satisfied with the enantioselective reduction of ketones by comparing with the enantioselective reduction of aldehydes. However, the enantioselective reduction of acetophenone to secondary alcohols with polymethylhydrosiloxane (PMHS) was carried out with high yields and ee's in the

* Corresponding author. Tel.: +82-539-506-343; fax: +82-539-506-330.

0277-5387/$ - see front matter © 2004 Elsevier Ltd. All rights reserved.
doi:10.1016/j.poly.2004.04.033

presence of chiral zinc catalysts [13] or chiral titanocene [14]. More recently, we have reported our results for the catalytic reduction of acetophenone using the $Zn(OTf)_2$ and N,N'-bis(3,5-dimethylpyrazolylmethyl)-L-alanine-methylester system, in which (*S*)-(−)-1-phenylethanol was obtained in low yield and ee [15].

Optically pure 1,2-diaminocyclohexane derivatives have been extensively utilized as chiral reagents, auxiliary catalysts and chiral ligands in various asymmetric synthetic routes [16]. However, these ligands are rare in the asymmetric reduction of ketones. The studies of the enantiomeric reduction of acetophenone activated by diaminocyclohexane derivatives bearing secondary and tertiary diamine bidentate ligands under mild conditions have not been reported. Herein, we have synthesized optically pure *R*,*R*-bmbcd and its complex of $ZnCl_2$, and describe its catalytic reduction of acetophenone by considering its structural property and the steric effect through the function of the methoxy-benzyl group.

2. Experimental

2.1. General remark

All reagents were of reagent grade and solvents were freshly distilled prior to use. ^{1}H NMR spectra were recorded on a Varian 300-NMR Spectrometer at ambient temperature and chemical shifts were referenced to internal tetramethylsilane. HPLC with a chiralcel OD-H (0.46 cm $\Phi \times 25$ cm) column was used for measurement of ee. Elemental analyses were performed at the Chemical Analysis Laboratory of the Center for Scientific Instruments of Kyungpook National University.

2.2. Syntheses of the compounds

2.2.1. *N,N'-bis(4-methoxy-benzyl)-cyclohexane-1,2-diamine (R,R-bmbcd),* **1**

Absolute ethanol was added to *trans*-*R*,*R*-1,2-diaminocyclohexane (19.81 g, 0.17 mol) until it was completely dissolved. *p*-Anisaldehyde (43.077 ml, 0.347 mol) was added and the yellow solution was stirred at room temperature for two days. The solvent was then removed under reduced pressure to obtain a thin yellow solid. This solid was recrystallized in diethyl ether to give colorless crystals (55.00 g, 90%). To a solution of the colorless crystals an ice bath (16.81 g, 0.0478 mol) in dry THF, in an ice bath, was slowly added $LiAlH_4$ (1 M solution in THF, 143.904 ml, 3 equiv.) by syringe. This solution was refluxed for 24 h, cooled to room temperature and then distilled water (12 ml) and 2 M NaOH (30 ml) were added. After filtering, the solvent was removed under reduced pressure, the remaining solid was extracted with CH_2Cl_2, dried with $MgSO_4$, filtered, and then the solvent was evaporated to give a thin yellow solid. This solid was recrystallized in diethyl ether to give colorless crystals (13.60 g, 80%). *Anal.* Calc. for $C_{22}H_{30}N_2O_2$: C, 74.54; H, 8.53; N, 7.90. Found: C, 74.57; H, 8.49; N, 7.87%. ^{1}H NMR ($CDCl_3$); δ 7.2 (d, 4H, Ph, $J = 8.7$ Hz), 6.8 (d, 4H, Ph, $J = 8.4$ Hz), 3.77 (s, 6H, OCH_3), 3.84–3.56 (dd, 4H, CH_2, $J = 13.2$ Hz), 2.22 (m, 2H, CHA), 2.12 (m, 2H, CHA), 1.74 (m, 2H, CHA), 1.69 (m, 2H, CHA), 1.20 (m, 1H, CHA), 1.01 (m, 1H, CHA).

2.2.2. *$ZnCl_2$(R,R-bmbcd),* **2**

To a solution of $ZnCl_2$ (0.7900 g, 5.79 mmol) in ethanol (10 ml) was added dropwise a solution of **1** (2.0548 g, 5.796 mmol) in ethanol (25 ml). The mixture was stirred overnight at ambient temperature. The white precipitate that formed was filtered off and washed several times with *n*-hexane and diethyl ether. The white solid was recrystallized from methanol to obtain colorless crystals (2.625 g, 92%). *Anal.* Calc. for $C_{22}H_{30}Cl_2N_2O_2Zn$: C, 53.84; H, 6.16; N, 5.71. Found: C, 53.82; H, 6.16; N, 6.18%. ^{1}H NMR ($CDCl_3$); δ 7.4 (d, 4H, Ph, $J = 8.7$ Hz), 6.8 (d, 4H, Ph, $J = 8.4$ Hz), 3.73 (s, 6H, OCH_3), 3.99–3.82 (dd, 4H, CH_2, $J = 13.2$ Hz), 2.46 (m, 4H, CHA), 2.08 (m, 2H, CHA), 1.85 (m, 2H, CHA), 1.26 (m, 1H, CHA), 1.13 (m, 1H, CHA).

2.3. Crystal structure determination of **2**

A colorless single crystal of **2** suitable for X-ray analysis was sealed in a thin walled glass capillary and mounted on an Enraf-Nonius CAD-4 diffractometer with Mo Kα radiation ($\lambda = 0.71073$ Å). Unit cell dimensions with estimated standard deviations were determined by least-squares using 25 well-centered reflections in the range of 10°–13°. A total of 2469 unique reflections were collected using the ω–2θ scan mode. The intensities of the reflections were corrected for Lorentz and polarization effects. Crystal data, data collection, and refinement for the complex are listed in Table 1. Data reduction was carried out using a MOLEN program package; a decay correction based on the intensities of three standard reflections measured every hour was performed; empirical absorption corrections were applied based on Ψ scans [17]. The structure in $P2_1$ for the complex was determined by direct methods and refined by full-matrix least-squares using SHELXS-97 and SHELXL-97 program packages [18,19] using reflections with $I > 2\sigma(I)$. All non-hydrogen atoms were refined anisotropically. Hydrogen atoms were constrained by using riding models. The final cycle of the refinement yielded $R = 0.021$ and $wR = 0.057$. Selected bond distances and bond angles are given in Table 2.

2.4. Catalytic enantioselective reduction of acetophenone

The flame-dried Schlenk flask was charged with the chiral ligand **1** (0.078 mmol), $Zn(OTf)_2$ (0.078 mmol) and

Table 1
Crystallographic data and structure refinement of **2**

Empirical formula	$C_{22}H_{30}Cl_2N_2O_2Zn$
Formula weight	490.75
Temperature (K)	293(2)
Wavelength, λ (Mo Kα) (Å)	0.71073
Crystal system	monoclinic
Space group	$P2_1$
Unit cell dimensions	
a (Å)	8.0309(5)
b (Å)	13.0098(7)
c (Å)	11.2650(6)
β (°)	99.092(5)
Volume V (Å^3)	1162.2(1)
Formula units per cell Z	2
D_{calc} (Mg/m^3)	1.402
Absorption coefficient (mm^{-1})	1.306
$F(000)$	512
θ Range for data collection (°)	1.83–25.47
Index ranges	$-9 \leqslant h \leqslant 9, 0 \leqslant k \leqslant 15, 0 \leqslant l \leqslant 13$
Reflections collected/unique	2469/2259 [$R_{int} = 0.0117$]
Refinement method	full-matrix least-squares on F^2
Data/restraints/parameters	2259/1/263
Goodness-of fit on F^2	1.060
Final R indices [$I > 2\sigma(I)$]	$R_1 = 0.021, wR_2 = 0.057$
Largest differential peak and hole (e/Å^3)	0.19 and 0.15

Table 2
Selected bond lengths (Å) and angles (°) for **2**

Bond lengths			
Zn–N(1)	2.066(2)	Zn–N(2)	2.092(2)
Zn–Cl(1)	2.2289(2)	Zn–Cl(2)	2.2036(8)
N(1)–C(8)	1.489(4)	N(1)–C(9)	1.486(3)
N(2)–C(14)	1.492(4)	N(2)–C(15)	1.499(4)
C(9)–C(14)	1.533(4)		
Bond angles			
N(1)–Zn–N(2)	85.66(9)	N(1)–Zn–Cl(1)	111.55(7)
N(1)–Zn–Cl(2)	113.32(7)	N(2)–Zn–Cl(1)	108.43(7)
N(2)–Zn–Cl(2)	110.60(7)	Cl(1)–Zn–Cl(2)	121.42(3)
N(1)–C(8)–C(5)	112.1(3)	N(2)–C(15)–C(16)	111.0(2)
C(8)–N(1)–C(9)	114.1(2)	C(14)–N(2)–C(15)	112.0(2)
C(8)–N(1)–Zn	115.3(2)	C(9)–N(1)–Zn	104.5(2)
C(14)–N(2)–Zn	106.2(2)	C(15)–N(2)–Zn	114.14(9)

dry CH_2Cl_2 (2 ml) under nitrogen atmosphere via syringe. The mixture was stirred for 30 min, cooled to 0 °C and then acetophenone (0.078 mmol) was added. The mixture was then stirred for 5 min and catecholborane (100 μl, 0.94 mmol) was added. The procedures were same as the methods used in the previous paper [15]. The enantiomeric excess was measured by HPLC (a chiral OD column), affording (*S*)-(−)-1-phenylethanol in 48% ee with 77% yield.

3. Results and discussion

3.1. Synthesis and chemical properties

The pure optical material, diaminocyclohexane derivative **1**, which was afforded from the cyclohexyldiimine derivative by reduction with $LiAlH_4$, gives in quantitative yield a colorless solid. It is soluble in polar solvents and insoluble in non-polar solvents such as hydrocarbons.

The reaction of $ZnCl_2$ with **1** afforded **2** in a high yield as white crystals after the usual workups. The chiral Zn(II) complex is readily soluble in polar solvents such as alcohols, yet poorly soluble in most polar solvents such as chloroform and THF.

3.2. Crystal structure of complex 2

The crystal structure of the chiral Zn(II) complex **2**, for getting binding information of the catalytic species, is confirmed by X-ray analysis as shown in Fig. 1. The central Zn atom is coordinated by two nitrogen atoms from a bidentate *R*,*R*-bmbcd and two chloro atoms in a distorted tetrahedral arrangement. The bond distances Zn–N(1) and Zn–N(2) are 2.066(2) and 2.092(2) Å, respectively, which are comparable to those in related compounds of the type $ZnCl_2$(L), i.e., 2.029(3) and 2.157(3) Å in $ZnCl_2$(Clemizole) where Clemizole is 1-(*p*-chloro-phenylmethyl)-2-(1-pyrrolidinylmethyl)benzimidazole [20], 2.006(3) and 2.008(3) Å in $ZnCl_2$(1,2-dimethylimidazole)$_2$ [21], and 2.050(3) and 2.074(3) Å in $ZnCl_2$(quinoline) [22]. The bond distances Zn–Cl(1) and Zn–Cl(2) [2.2289(9) and 2.2036 (8) Å] are close to those of similar complexes which are in the range of 2.196(2)–2.2509(8) Å [20–22]. The long bond distances of Zn–Cl are comparable with the bond distances of Zn–N, giving rise to those reported for the $ZnCl_2N_2$ core. The bond angles of N–Zn–Cl are in the range of 108.43(7)°–113.32(7)°, which are distorted from ideal tetrahedral geometry as a consequence of the opening of the two chloro ligands. The bond angle N(1)–Zn–N(4) [85.66(9)°] is smaller than that [89.5(1)°] found in $ZnCl_2$(2,2′-bis(pyrazolyl-1-ylpropane) and that [109.3(1)°]

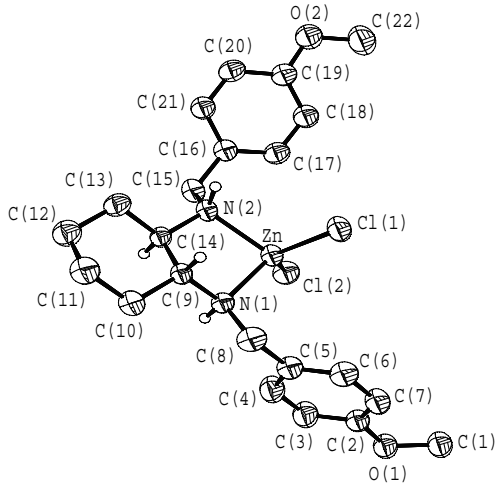

Fig. 1. Crystal structure with the labelling scheme for compound **2**.

in $ZnCl_2$(quinoline)$_2$ [21], but larger than that [81.7(1)°] in $ZnCl_2$(Clemizole) [20]. The bond angle of 121.42(3)° for Cl(1)–Zn–Cl(2) is quite similar to that [120.18(6)°] found in $ZnCl_2$(Clemizole) [20] and is larger than that [114.54(7)°] in $ZnCl_2$(bdmpame) (bdmpame = *N*,*N*-bis(3,5-dimethylpyrazolylmethyl)-L-alaninemethyl ester) [15], that [114.59(8)°] in $ZnCl_2(MeImOH)_2$ (MeImOH = 2-hydroxymethyl-1-methylimidazole) [23], and that [115.47(5)°] in $ZnCl_2$(quinoline)$_2$ [21].

3.3. Catalytic enantioselective reduction of acetophonone

Recently, the enantioselective reduction of ketones prompted by chiral zinc complexes has been well-established, and very high enantioselectivity has been accomplished by using various chiral diimine ligands [11,13]. We have investigated the catalytic enantioselective reduction of acetophenone (Eq. (1)) using in situ $Zn(OTf)_2$/*R*,*R*-bmbcd as the catalyst.

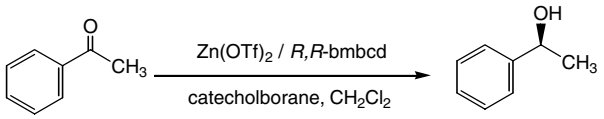

(1)

The reaction was carried out under the standard set of conditions described in Section 2. The enantiomeric excess of the catalytic reduction was moderate to give 48% ee with 77% yield. The enantioselective reduction of acetophenone using lithiated α-stannylbenzyl sulfide or α-lithio benzyl 2-pyridyl sulfide with *N*,*N*,*N*′,*N*′-tetramethyl-cyclohexane-1,2-diamine as the chiral ligand show 1% ee in 8% yield and 21% ee in 70% yield, respectively [24]. The low enantiomeric excess may be explained by the lack of stereoselective control of the functional groups at the reaction center, coupled with the fact that the blocking from the steric hinderance of the methyl or dimethyl groups the near chiral center washes out any chiral discrimination formed in the catalyst.

4. Conclusions

We have attempted to establish the synthesis and characterization of *R*,*R*-bmbcd and its Zn complex **2**. In particular, the catalytic enantioselective reduction of acetophenone promoted by $Zn(OTf)_2$ with *R*,*R*-bmbcd in the presence of catecholborane as reductant has shown that a chiral cyclohexane-1,2-diamine derivative **1** is an exploratory precursor. The zinc catalyst of the new chiral 1,2-diaminocyclohexane derivative ligand, through the steric effect of functional groups and the enhancement of the absolute stereoselective control, could give significant enantiometric excess. We are currently investigating in this area.

5. Supplementary data

Supplementary data are available from the Cambridge Crystallographic Data Centre, 12 Union Road, Cambridge CB2 1EZ, UK (fax: +44-1223-336033; E-mail: deposit@ccdc.cam.ac.uk or www: http://www.ccdc.cam.ac.uk) on request, quoting the deposit number CCDC 231764.

Acknowledgements

We gratefully acknowledge financial support by grant No. R05-2001-000-00202-0 from the Korean Science & Engineering Foundation.

References

[1] (a) I. Ojima (Ed.), Catalytic Asymmetric Synthesis, VCH Publishers, Cambridge, 1993;
(b) R. Noyori, Asymmetric Catalysis in Organic Synthesis, Wiley, New York, 1994;
(c) R.E. Gawley, J. Aube, in: J.E. Baldwin, P.D. Magnus (Eds.), Principles of Asymmetric Synthesis, Pergamon Press, Oxford, 1996;
(d) V.D. Singh, Synthesis (1992) 606.
[2] (a) H. Takahashi, T. Kawakita, M. Ohno, M. Yoshioka, S. Kobayashi, Tetrahedron 48 (1992) 5691;
(b) H. Takahashi, T. Kawakita, M. Ohno, Tetrahedron Lett. 30 (1989) 1657.
[3] W. Zhang, J.L. Loebach, S.R. Wilson, E.N. Jacobsen, J. Am. Chem. Soc. 112 (1990) 2801.
[4] P. Gamez, F. Fache, M. Lemaire, Tetrahedron: Asymmetr. 6 (1995) 705.
[5] B. Schmidt, D. Seebach, Angew. Chem., Int. Ed. Engl. 30 (1991) 99.
[6] R. Noyori, M. Kitamura, Angew. Chem., Int. Ed. Engl. 30 (1991) 49.
[7] K. Soai, S. Niwa, Chem. Rev. 92 (1992) 833.
[8] M. Yoshioka, T. Kawakita, M. Ohno, Tetrahedron Lett. 30 (1989) 1657.
[9] (a) P. Knochel, R.D. Singer, Chem. Rev. 93 (1993) 2117;
(b) C. Lutz, P. Knochel, J. Org. Chem. 62 (1997) 7895;
(c) Š. Vyskoil, S. Jaracz, M. Smrčina, M. Štícha, V. Hanuš, M. Polášek, P. Kočovský, J. Org. Chem. 63 (1998) 7727;
(d) S.E. Denmark, S.P. O'Connor, S.R. Wilson, Angew. Chem. Int. Ed. 37 (1998) 1149;
(e) M. Shi, W.-S. Sui, Tetrahedron: Asymmetr. 10 (1999) 3319;
(f) F. Fache, E. Schulz, M.L. Tommasino, M. Lemaire, Chem. Rev. 100 (2000) 2159.
[10] J. Balsells, P.J. Walsh, J. Am. Chem. Soc. 122 (2000) 1801.
[11] M. Bandini, P.G. Cozzi, M. de Angelis, A. Umani-Ronchi, Tetrahedron Lett. 41 (2000) 1601.
[12] M. Kitamura, H. Oka, R. Noyori, Tetrahedron 55 (1999) 3605.
[13] H. Mimoun, J.Y.S. Laumer, L. Giannini, R. Scopelliti, C. Floriani, J. Am. Chem. Soc. 121 (1999) 6158.
[14] M.B. Carter, B. Schiott, A. Guttierrez, S.L. Buchwald, J. Am. Chem. Soc. 116 (1994) 11667.
[15] S.-G. Roh, Y.-C. Park, D.-K. Park, T.-J. Kim, J.H. Jeong, Polyhedron 20 (2001) 1961.

[16] (a) J. Seyden-Penne, Chiral Auxiliaries and Ligands in Asymmetric Synthesis, Wiley-Interscience, New York, 1995, pp. 57–67; (b) H. Brunner, W. Zettlmeier, in: Handbook of Enantioselective Catalysis, vol. 2, VCH, Weinheim, 1993.
[17] C.K. Fair, MOLEN, An Interactive Intelligent System for Crystal Structure Analysis, Enraf-Nonius, Deft, The Netherlands, 1990.
[18] G.M. Sheldrick, SHELXS-97, Program for the Solution of Crystal Structure, University of Göttingen, Göttingen, Germany, 1990.
[19] G.M. Sheldrick, SHELXL-97, Program for Crystal Structure Refinement, University of Göttingen, Göttingen, Germany, 1997.
[20] M. Parvez, A.P. Sabir, Acta Crystallogr., Sect. C52 (1996) 1651.
[21] P.K. Bharadwaj, H.J. Schugar, J.A. Potenza, Acta Crystallogr., Sect. C47 (1991) 754.
[22] Y. Cui, D. Long, W.D. Chen, J.S. Huang, Acta Crystallogr., Sect. C54 (1998) 1605.
[23] S.-P. Yang, L.-S. Long, X.-M. Chen, L.-N. Ji, Acta Crystallogr., Sect. C55 (1999) 869.
[24] S. Nakamura, R. Nakagawa, Y. Watanabe, T. Toru, J. Am. Chem. Soc. 122 (2000) 11340.

Available online at www.sciencedirect.com
SCIENCE DIRECT®
Polyhedron 23 (2004) 2069–2074
POLYHEDRON
www.elsevier.com/locate/poly

An unusual vanadium(II) promoted hydrogenation of a magnesium tetraiminediphenolate compound yielding an asymmetric oxovanadium(IV) macrocyclic complex

Angela C. Raimondi [a], Vagner R. de Souza [b], Henrique E. Toma [b], Antonio S. Mangrich [a], Tai Hasegawa [c], Fábio S. Nunes [a,*]

[a] *Departamento de Química, Universidade Federal do Paraná, Centro Politécnico, C.P. 19081, 81531-990 Curitiba, PR, Brazil*
[b] *Instituto de Química, Universidade de São Paulo, C.P. 26077, 05599-970 São Paulo, SP, Brazil*
[c] *Henry Taube Institute, P.O. Box 19585, Stanford, CA 94309, USA*

Received 17 December 2003; accepted 13 April 2004
Available online 15 July 2004

Abstract

The complex $[VO(didadf)(H_2O)](BF_4)_2$ (didadf = diiminediaminediphenolate ligand) has been prepared from a vanadium(II) salt under strict inert atmosphere conditions and characterized by analytical, magnetic and spectroscopic methods (EPR, FTIR, UV–Vis), cyclic voltammetry as well as by spectroelectrochemistry. These techniques along with the mass spectrum (FAB^+) were important to understand the nature and the redox properties of the metal ion complex.
© 2004 Elsevier Ltd. All rights reserved.

Keywords: Vanadium; Diiminediaminediphenolate macrocycle; Magnetochemistry; EPR; FTIR; Spectroelectrochemistry

1. Introduction

Selectivity, inertia, high thermodynamic stability and structural flexibility of their metal complexes have proved macrocycles to be suitable ligands to produce specific metal–ion environments [1,2]. The macrocyclic ligand tetraiminediphenolate (tidf) was first prepared by Pilkington and Robson [3] by a template reaction involving 4-methyl-2,6-diformylphenol, 1,3-diaminepropane, lead acetate and lead nitrate (magnesium and other transition metal salts can also be employed) [1b].

Tidf binds metal ions such as copper(II), nickel(II), cobalt(II), iron(II), manganese(II), lead(II) and zinc(II) giving either mono- or di-nuclear complexes [4]. All metal(II) mononuclear complexes have both uncoordinated diimine nitrogen atoms protonated, so the complexes have a total charge of 2+. Transmetallation reactions from Mg^{II} or Pb^{II} compounds allow the preparation of new mononuclear complexes that are good starting materials for binuclear macrocycle compounds, as recently reported by our group [5].

In contrast to other first row transition elements [6], the chemistry of vanadium-macrocyclic complexes has not been extensively investigated, up to the present time. In this work, we report the synthesis of the $[VO(didadf)(H_2O)](BF_4)_2$(didadf = diiminediaminediphenolate ligand) complex and its characterization by means of elemental analysis, mass spectrometry, magnetochemistry, EPR, FTIR and UV–Vis spectroscopy, cyclic voltammetry and spectroelectrochemistry. This compound was obtained from the reaction between $[V(H_2O)_6]^{2+}$ and tidf under severe inert atmosphere conditions through an unusual hydrogenation reaction. The didadf ligand can form two complexes, by coordinating to the central phenolate groups and either two amine or two imine groups in the lateral positions, as shown in Scheme 1. A detailed assignment of the spectra and the electrochemical behavior is provided, and the reaction steps for the formation of the complex are discussed.

* Corresponding author. Tel.: +55-41-361-3180; fax: +55-41-361-3186.
E-mail address: fsnunes@quimica.ufpr.br (F.S. Nunes).

0277-5387/$ - see front matter © 2004 Elsevier Ltd. All rights reserved.
doi:10.1016/j.poly.2004.04.032

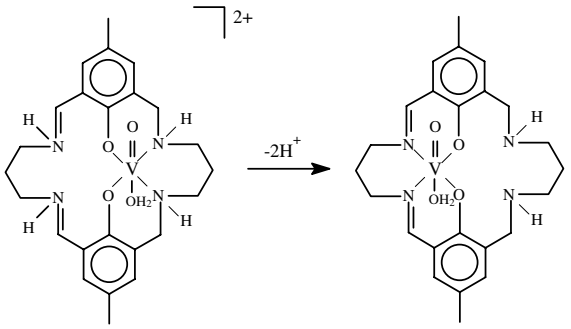

Scheme 1. The oxovanadium complexes.

The relative stability of the two possible complexes was evaluated theoretically, based on molecular mechanics (MM^+) and semiempirical methods (ZINDO/S).

2. Experimental

2.1. Physical measurements and instrumentation

X-band electron paramagnetic resonance (epr) spectra were recorded on a Bruker ESP300-E instrument from acetonitrile solutions of the complex (1×10^{-2} mol L^{-1}) at room-temperature.

The mass spectrum (FAB^+ technique) was recorded on a VG Autospec spectrometer (Fisons Instruments) equipped with a CsI gun at 25 kV in 3-nitrobenzyl alcohol as the matrix.

Magnetic susceptibility measurements were carried out in the solid state at room-temperature using a MKII magnetic susceptibility balance from Johnson–Matthey. Corrections for the diamagnetism of the ligands were applied by the use of Pascal constants [10].

Infrared spectra were obtained with a Bomen Hartmann and Braun MB series spectrophotometer in the region 4000–400 cm^{-1} as nujol mulls spread on KBr windows.

Electronic spectra in the UV–Vis range (190–820 nm) were obtained on a Hewlett–Packard Model 8452A diode-array spectrophotometer in acetonitrile solutions.

Cyclic voltammetry was carried out with a Princeton Applied Research Potentiostat (PARC) model 273A. A platinum disc electrode was employed for the measurements at $I = 0.1$ mol L^{-1}, kept constant with $TEAClO_4$ (tetraethylammonium perchlorate). $Ag/AgNO_3$ ($[Ag^+] = 0.01$ mol L^{-1} in an MeCN solution of $TEAClO_4$ 0.1 mol L^{-1}) and a platinum wire were used as reference and auxiliary electrodes, respectively. Typical experiments were conducted with a 3.0×10^{-3} mol L^{-1} complex concentration in acetonitrile solutions at ambient temperature.

Spectroelectrochemical measurements were performed with the PARC potentiostat attached to a diode-array spectrophotometer, from ≈1 mmol L^{-1} complex and 0.1 mol L^{-1} $TEAClO_4$ acetonitrile solutions. A three-electrode system was designed for a thin layer cell of 0.025 cm internal optical path length. A gold minigrid was used as transparent working electrode in the presence of a small Ag/AgCl (1 mol L^{-1}) reference electrode and a platinum auxiliary electrode.

Microanalyses were done under dinitrogen by MEDAC Ltd. laboratories in Egham, Surrey, UK.

Molecular modelling calculations were carried out for the two possible forms of the $[VO(didadf)(H_2O)](BF_4)_2$complex, using the HYPERCHEM 7.1 package, from Hypercube Inc., Gainesville, FL, USA. Geometry optimization was carried out using the MM^+ method, with a gradient of 1×10^{-5} kcal as a convergence criterion, in combination with SCF calculations performed at the RHF level using the ZINDO/S method. In this case, default parameters were employed for single CI excitations in an active space involving 20 frontier molecular orbitals (10 highest occupied and 10 lowest unoccupied MOs).

2.2. Materials

Magnesium acetate tetrahydrate, magnesium nitrate (Mallinckrodt), 4-methyl-2,6-diformylphenol (Aldrich) and 1,3-diaminopropane (Merck) were used as supplied. Methanol (Merck) was degassed exhaustively before use. $[V(H_2O)_6](BF_4)_2$ was prepared as described previously [7]. The complex $[VO(acac)_2]$ (acac = acetylacetonate) was prepared according to Fernelius [8].

2.3. Synthesis

2.3.1. $[Mg_2(tidf)](NO_3)_2 \cdot 4H_2O$

This compound was prepared by an adaptation of the synthesis described by Mohanta et al. [9] for a less symmetric macrocyclic ligand. To a boiling solution containing magnesium acetate tetrahydrate (1.63 g, 7.5 mmol), magnesium nitrate (1.95 g, 7.5 mmol) and 4-methyl-2,6-diformylphenol (2.50 g, 15 mmol) in methanol (80 mL) was added a solution (50 mL) of 1,3-diaminopropane (1.13 g, 15 mmol) in methanol, over a period of 4 h. The mixture was refluxed for 2 h. After cooling to room-temperature, diethyl ether was added to the bright yellow solution and a colorless solid was removed by filtration and discarded. The solution was concentrated under vacuum and an orange-yellowish solid was obtained, filtered-off, washed with diethyl ether/methanol (1:1) and vacuum-dried. Yield 95% (4.69 g). *Anal.* Calc. for $C_{24}H_{34}N_6O_{12}Mg_2$: C, 44.54; H, 5.30; N, 12.99. Found: C, 43.50; H, 5.77; N, 12.32%.

2.3.2. $[VO(didadf)(H_2O)](BF_4)_2$

This product was prepared in a nitrogen-saturated glove-box. $[V(H_2O)_6](BF_4)_2$ (1.36 g, 4.0 mmol) was dissolved in 30 mL of methanol. The resulting purple

solution was added to a yellow suspension of $[Mg_2(tidf)](NO_3)_2 \cdot 4H_2O$ (1.22 g, 2.0 mmol) in 80 mL of methanol. The system was stirred for 1 h and a reddish solid was filtered-off, washed with methanol and dried under vacuum. Yield was 58% (0.84 g). *Anal*. Calc. for $C_{24}H_{30}N_4O_4B_2F_8V$: C, 43.49; H, 4.53; N, 8.45. Found: C, 43.55; H, 4.94; N, 8.50%.

3. Results and discussion

3.1. Electron paramagnetic resonance and magneto chemistry

The eight-line epr spectrum of $[VO(didadf)(H_2O)](BF_4)_2$ at room-temperature (Fig. 1) is typical of a single species in which the unpaired electron in a d_{xy} orbital is coupled to the nuclear spin of the vanadium nucleus with $I = 7/2$, ruling out the occurrence of any mixture of species. The values of $g = 2.014$ and $A = 100$ G are very similar to those observed for other $V^{IV}ON_2O_2$ systems [11].

The room-temperature magnetic moment of $[VO(didadf)(H_2O)](BF_4)_2$ is 1.78, consistent with the spin only value predicted for a VO^{2+} ($S = 1/2$) species [12].

3.2. Mass spectrum

FAB^+ mass spectrum of the vanadyl complex shows a base peak (intensity of 100%) at $m/z = 470$ assigned to the molecular ion $\{[VO(didadf\text{-}H)]\}^+$ (didadf-H = the macrocyclic ligand with the loss of a hydrogen ion), produced by the dissociation of a water molecule and a proton.

3.3. Infrared spectrum

IR spectrum of $[VO(didadf)(H_2O)](BF_4)_2$ exhibits very intense bands at 1644 and 1555 cm^{-1} assigned to ν(C=N) and ν(C–O) and, respectively. A band at 870 cm^{-1} with strong intensity was attributed to ν(V=O). This ν(V=O) band was reported at 844 cm^{-1} for the tetraaminediphenolate complex $[VO(tadf)] \cdot H_2O$ (tadf = tetraaminodiphenolate) [13], in which case intermolecular V=O···V=O interactions were observed. The bands at 3480 and 3558 cm^{-1} assigned to ν(O–H) are in agreement with the microanalysis as these results support the presence of a water molecule in the composition of the complex. Other important bands occurs at 1050(s) cm^{-1} (ν_s(B–F)), 770(m) and 544(m) cm^{-1} (δ(B–F)) in accordance with the positive charge of the ion complex.

3.4. Spectroelectrochemistry

UV–Vis spectra of $[VO(didadf)(H_2O)](BF_4)_2$ show bands at 212 and 265 nm (Fig. 2) assigned to π–π^* transitions, also seen in the magnesium complex $[Mg_2(tidf)](NO_3)_2 \cdot 4H_2O$. The strong absorption band at 395 nm was tentatively assigned to a ligand-to-metal

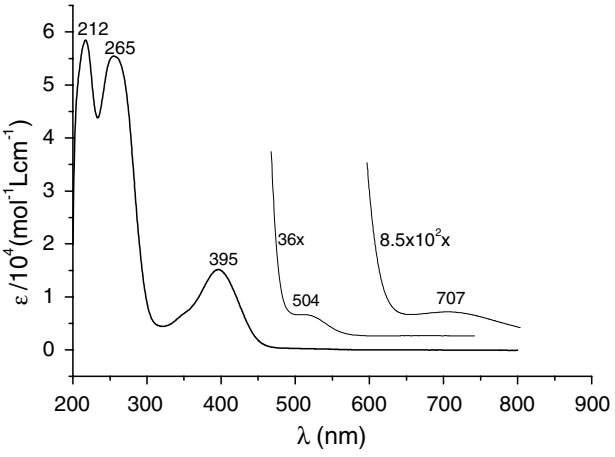

Fig. 2. UV–Vis spectra of $[VO(didadf)(H_2O)]^{2+}$ in CH_3CN.

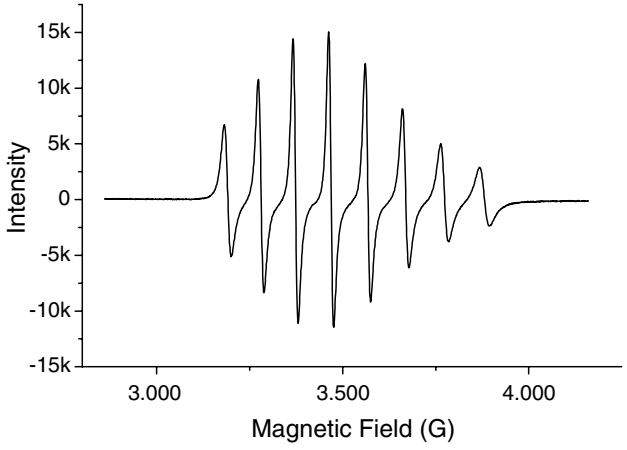

Fig. 1. The epr spectrum of $[VO(didadf)(H_2O)](BF_4)_2$ in CH_3CN at room-temperature.

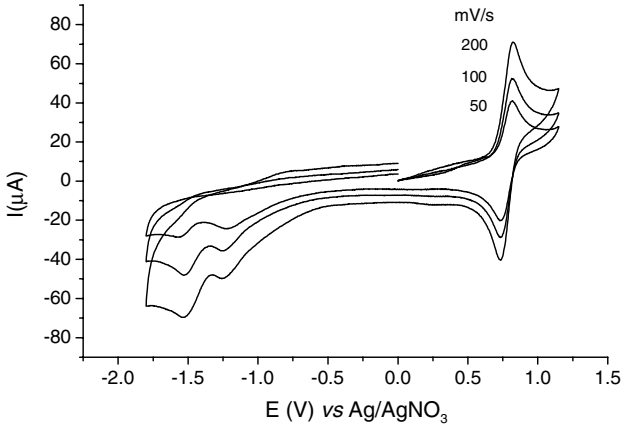

Fig. 3. Cyclic voltammograms of $[VO(didadf)(H_2O)]^{2+}$ (3 mmol L^{-1}), 0.10 mol L^{-1} $TEAClO_4$ in CH_3CN.

charge transfer transition, since it is not observed in the magnesium complex. The bands at 504 nm and 707 nm have intensities ($\varepsilon = 433$ and 18 $L\,mol^{-1}\,cm^{-1}$) compatible with d–d transitions (d_{xy} to $d_{x^2-y^2}$ and to (d_{yz}, d_{xz}), respectively), similar to the ones seen at 584 and 707 nm in the $[VO(acac)_2]$ complex and at 520 and 820 nm in $[VO(tadf)]\cdot H_2O$ [13]. Cyclic voltammograms of $[VO(didadf)(H_2O)](BF_4)_2$ show typical reversible behavior between −0.75 and 1.25 V with a formal reduction potential $E^f = 0.80$ V versus Ag/Ag^+ (1.30 versus SHE) and assigned to the $V^{IV/V}$ process (Fig. 3), and two irreversible waves below −1 V, ascribed to the successive reduction of the macrocyclic ligand.

Spectroelectrochemical measurements between 0.68 and 0.90 V (Fig. 4(a)) shows a decrease in the intensity of the band at 395 nm, accompanying the reversible oxidation of the vanadium(IV) center. An interesting observation is that this process is followed by a second electrochemical reaction in the 0.90–0.98 V range (Fig. 4(b)), not apparent in the cyclic voltammograms. This process can be ascribed to the oxidation of the didadf ligand, since a similar behavior was also observed in the electrochemistry of the magnesium complex $[Mg_2(tidf)](NO_3)_2\cdot 4H_2O$ at 1.1 V. These two processes exhibit rather close E^fs, giving rise to a single reversible wave in the cyclic voltammograms. The two-step process can also be observed by reversing the potentials in the spectroelectrochemical experiments, as shown in Fig. 4(c). The band at 395 nm is regenerated in the catodic scan between +0.90 and +0.1 V consistent with a

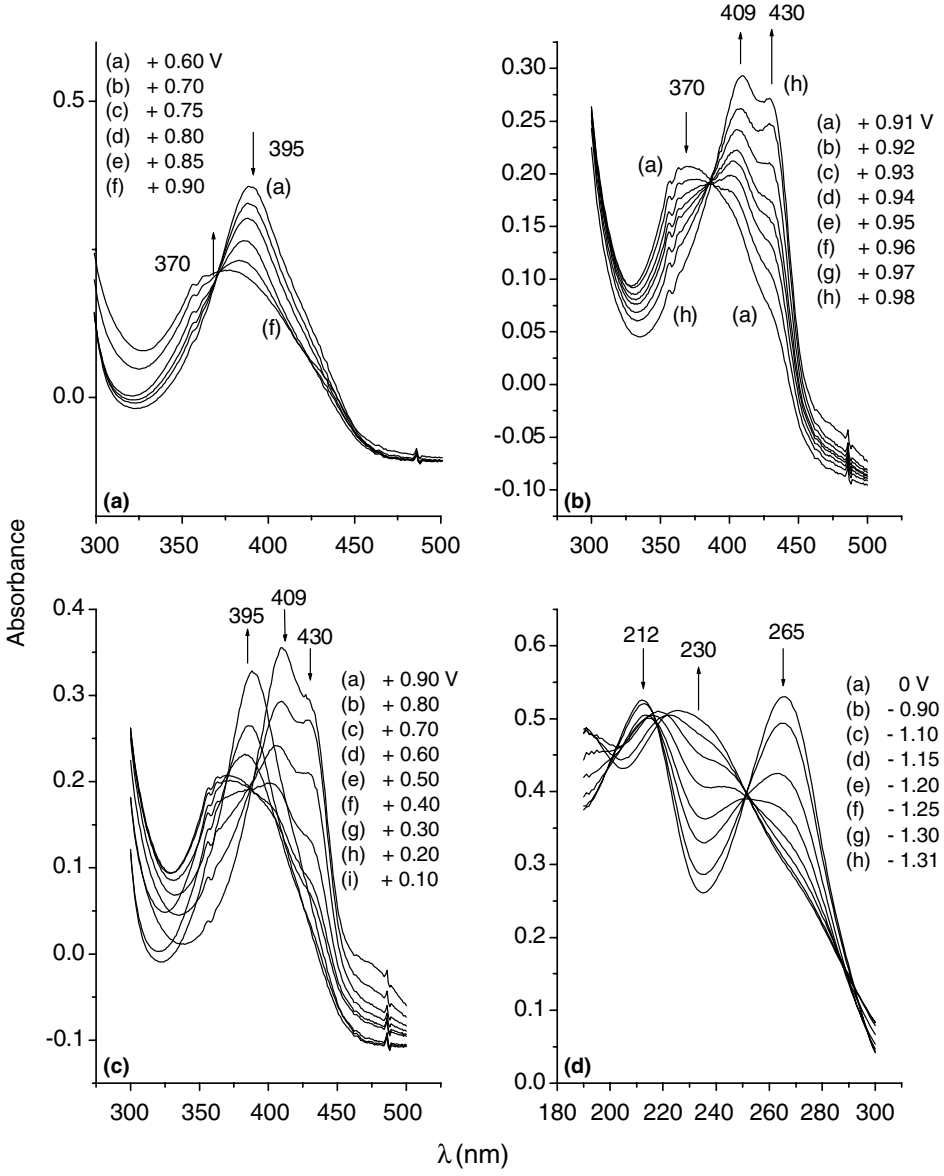

Fig. 4. Spectroelectrochemistry of $[VO(didadf)(H_2O)]^{2+}$ (≈1 mmol L^{-1}), 0.10 mol L^{-1} $TEAClO_4$ in CH_3CN. Oxidation process starting from +0.60 V (a) and +0.91 V vs Ag/Ag^+ (b), and the reduction of the VO^{IV} complex starting from +0.90 V (c) and 0 V (d).

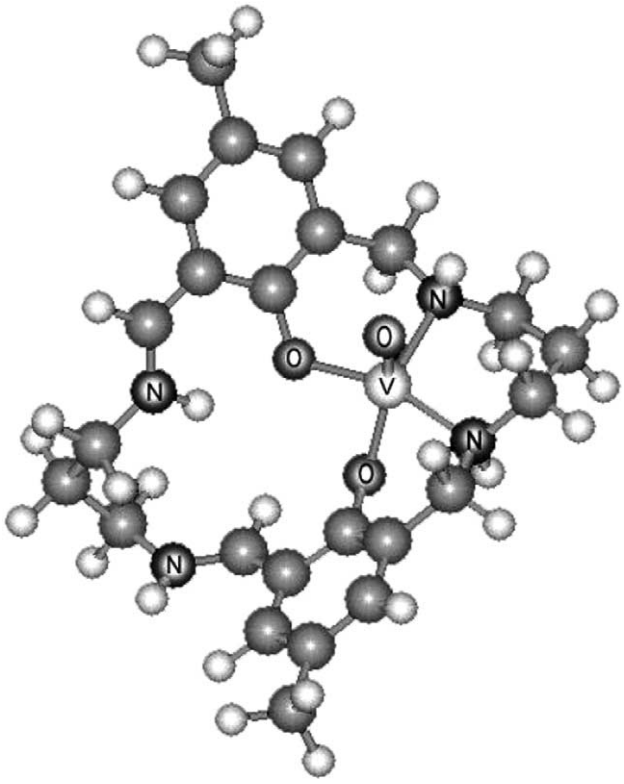

Fig. 5. Molecular simulation (MM^{+}) for the most stable complex.

thermodynamic reversibility of the two processes involved.

The π–π^{*} bands at 212 and 265 nm tend to vanish at very negative potentials, 0 to −1.31 V (Fig. 4(d)) as a new band, with the same assignment, appears at 230 nm. This behavior occurs in a range of potentials where an irreversible reduction of the ligand didadf with Ep_c at −1.3 V (Fig. 3) is observed.

3.5. Molecular mechanics MM^{+}

The corresponding structures generated by (MM^{+}/ZINDO) molecular simulation exhibit strong distortions from the planar configuration, with the vanadyl center in an intermediate geometry between square pyramidal and trigonal bipyramid, as shown in Fig. 5. However, according to ZINDO/S calculations, the complex where the vanadyl ion is bound to the two-amine groups is thermodynamically favored with respect to the diimine species. This is also in agreement with the hard acid behavior of the V^{IV} ion, in relation to the strong donor amine group and the predominantly acceptor diimine group. The protonation of the imines is not unusual in the chemistry of the tidf macrocycle, and was reported in the crystal structure investigation of the $[Fe(tidf)(CH_3OH)_2](NO_3)_2$ complex [5b].

4. Conclusions

Our attempts to prepare the vanadium(II) complex always ended up with oxovanadium(IV) complex in a high yield, even using strict inert atmosphere conditions (glove-box with $[O_2] < 0.1$ ppm and solvents thoroughly degassed. Apparently there was no oxidation of the starting solution of vanadium(II) as it maintained its original purple color until the reaction with $[Mg_2(tidf)](NO_3)_2 \cdot 4H_2O$. A possible explanation is summarized in Scheme 2, where it is believed that vanadium(II) reduces the macrocyclic ligand. This would be supported by the presence of the weak band at 3090 cm^{-1} assigned to ν(N–H) in the infrared spectrum of the product. The expected band at ca. 1600 cm^{-1} due to the δ(N–H) mode is masked by the strong and broad band at 1644 cm^{-1} attributed to ν(C=N).

Acknowledgements

This work was supported by Brazilian PRONEX Program (Contract Number 41.96.0884.00), whose help we gratefully acknowledge. We thank Prof. G.J. Leigh and A. Abdul Sada (CPES, University of Sussex, UK) for the mass spectrum and elemental analysis. A.C.R.

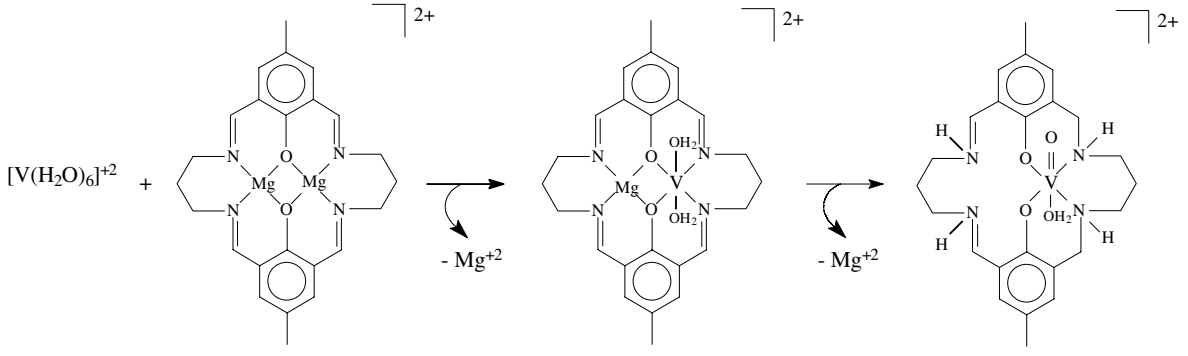

Scheme 2. Proposed reaction steps toward the formation of $[VO(didadf)(H_2O)]^{2+}$.

thanks Brazilian Research Council (CNPq) for a research fellowship.

References

[1] (a) L. Latos-Grazynski, K. Rachlewicz, J. Wojaczynski, Coord. Chem. Rev. 109 (1999) 192;
(b) H. Okawa, H. Furutachi, D.E. Fenton, Coord. Chem. Rev. 174 (1998) 51;
(c) R. Panicucci, T.C. Bruice, J. Am. Chem. Soc. 112 (1990) 6023;
(d) C.A. Koval, R.D. Noble, J.D. Way, B. Louie, E. Reyes, R. Bateman, G.M. Horn, D.L. Reed, Inorg. Chem. 24 (1985) 1148;
(e) R.D. Jones, D.A. Summerville, F. Basolo, Chem. Rev. 79 (1979) 139.

[2] (a) F.S. Nunes, P. De, M.L. Murta, C.J. da Cunha, J. Coord. Chem. 47 (1999) 251;
(b) F.S. Nunes, P. De, M.L. Murta, I. Vencato, C.J. da Cunha, J. Chem. Crystallogr. 27 (1997) 721;
(c) H.E. Toma, F.S. Nunes, J. Coord. Chem. 36 (1995) 33;
(d) H.E. Toma, F.S. Nunes, Int. J. Chem. Kinet. 25 (1993) 205;
(e) H.E. Toma, F.S. Nunes, Spectrosc. Lett. 25 (1992) 757.

[3] R. Robson, N.H. Pilkington, Aust. J. Chem. 23 (1970) 2225.

[4] (a) L.K. Thompson, S.K. Mandal, S.S. Tandon, J.N. Bridson, M.K. Park, Inorg. Chem. 35 (1996) 3117;
(b) R.R. Gagné, C.L. Spiro, T.J. Smith, C.A. Hamann, W.R. Thies, A.K. Shiemke, J. Am. Chem. Soc. 103 (1981) 4073;
(c) C.L. Spiro, L.L. Lambert, T.J. Smith, E.N. Duesler, R.R. Gagné, D.N. Hendrickson, Inorg. Chem. 20 (1981) 1229;
(d) R.R. Gagné, L.M. Henling, T.J. Kistenmacher, Inorg. Chem. 19 (1980) 1226;
(e) S.L. Lambert, D.N. Hendrickson, Inorg. Chem. 18 (1979) 2683;
(f) H. Okawa, S. Kida, Bull. Chem. Soc. Jpn. 45 (1972) 1759.

[5] (a) A.C. Raimondi, P.B. Hitchcock, G.J. Leigh, F.S. Nunes, J. Chem. Crystallogr. 34 (2004) 83;
(b) A.C. Raimondi, P.B. Hitchcock, G.J. Leigh, F.S. Nunes, J. Chem. Crystallogr. 32 (2002) 363.

[6] (a) M.R. Maurya, Coord. Chem. Rev. 237 (2003) 163;
(b) D.R. Wang, W.J. Zhang, K. Gruning, D. Rehder, J. Mol. Struct. 656 (2003) 79;
(c) S.K. Sengupta, O.P. Pandey, J.K. Pandey, G.K. Pandey, J. Coord. Chem. 55 (2002) 1455;
(d) R.J. Baker, P.C. Davies, P.G. Edwards, R.D. Farley, S.S. Liyanage, D.M. Murphy, B. Yong, Eur. J. Inorg. Chem. (2002) 1975;
(e) T. Weyhermuller, H. Schucht, K. Mochizuki, K. Wieghardt, J. Inorg. Biochem. 86 (2001) 478;
(f) Z.L. Wang, N.H. Hu, K. Sakata, M. Hashimoto, J. Chem. Soc., Dalton Trans. (1999) 1695;
(g) S.C. Davies, M.C. Durrant, D.L. Hughes, C. Le Floc'h, S.J.A. Pope, G. Reid, R.L. Richards, J.R. Sanders, J. Chem. Soc., Dalton Trans. (1998) 2191;
(h) S.K. Sengupta, O.P. Pandey, G.K. Pandey, Ind. J. Chem. Sec. A 37 (1998) 644;
(i) S. Mohanta, K.K. Nanda, L.K. Thompson, U. Florke, K. Nag, Inorg. Chem. 37 (1998) 1465;
(j) K.K. Nanda, S. Mohanta, S. Ghosh, Inorg. Chem. 34 (1995) 2861.

[7] D.G.L. Holt, L.F. Larkworthy, D.C. Povey, G.W. Smith, G.J. Leigh, Inorg. Chim. Acta 169 (1990) 201.

[8] W.C. Fernelius, Inorg. Synth. 5 (1957) 105.

[9] S. Mohanta, S. Baitalik, S.K. Dutta, K. Adhikary, Polyhedron 17 (1998) 2669.

[10] A. Earnshaw, Introduction to Magnetochemistry, Academic Press, London, 1961, p. 115.

[11] S.A. Amer, M. Gaber, R.M. Issa, Polyhedron 7 (1988) 2635.

[12] J.E. Huheey, E.A. Keitter, R.L. Keitter, Principles of Structure and Reactivity, 4th ed., Harper Collins, New York, 1993, p. 465.

[13] R. Das, K.K. Nanda, A.K. Mukherjee, M. Mukherjee, M. Helliwell, K. Nag, J. Chem. Soc., Dalton Trans. (1993) 2241.

Available online at www.sciencedirect.com
SCIENCE DIRECT®
Polyhedron 23 (2004) 2075–2079
POLYHEDRON
www.elsevier.com/locate/poly

Facile synthesis and structures of infinite one-dimensional silver(I) coordination polymers

Alexandra L. Pickering, Geoffrey J.T. Cooper, De-Liang Long, Leroy Cronin *

Department of Chemistry, Joseph Black Building, University of Glasgow, University Avenue, Glasgow G12 8QQ, UK

Received 17 March 2004; accepted 7 June 2004

Abstract

The synthesis and characterization of the isolated, infinite tubular coordination polymers $\{[Ag(cis\text{-tach})]ClO_4\}_\infty$ (**1**), $\{[Ag(trans\text{-tach})]ClO_4\}_\infty$ (**2**) and $\{[Ag(cis\text{-tach})]BF_4\}_\infty$ (**3**) has been achieved with the isomers *cis,cis*-1,3,5-triaminocyclohexane and *cis,trans*-1,3,5-triaminocyclohexane. Each new material has been fully characterized by single crystal X-ray diffraction, NMR, IR and elemental analysis. Compounds **1**–**3** form definite channels by the trigonal planar coordination of silver(I) metal centres to rigid, aliphatic triamino ligands, forming $4^2 \cdot 6$ topological networks.
© 2004 Elsevier Ltd. All rights reserved.

Keywords: One-dimensional; Silver(I); Aliphatic amino ligands; Coordination polymers; Tubes; Topology; Supramolecular chemistry; Self assembly; Nanotubes

1. Introduction

Since their discovery in 1991 [1], carbon nanotubes have become of increasing interest due to their uniqueness in size, shape and extraordinary physical properties. Experiments are emerging that investigate the properties of carbon nanotubes, whose structural properties are determined by such features as length, diameter and chirality. Such studies have shown carbon nanotubes to be extremely robust materials, and research into the construction of fibre-composite materials using carbon nanotubes is underway [2]. However, production of single (SWNT) [3–6] and multiple (MWNT) [7] walled carbon nanotubes is both expensive and challenging. Coordination polymers are attractive alternatives as the self-assembly of polynuclear, functional materials provides a flexible and facile route to systems more traditionally formed using a covalent approach [8,9]. This methodology uses coordinative or weaker forces to build-up networks of specific topologies, and has been successful in creating a great number of functional materials that contain channels within a higher dimensionality array [10–13], and a much smaller number that exist as isolated one-dimensional polymers [14–16]. We have recently published the first synthesis of infinite, isolated silver(I) coordination tubes by incorporating a pre-organized, tridentate ligand system that is flexible enough to 'wrap' its number of arms to form a tubular network [17].

We herein report the extended synthesis of a variety of silver(I) nanotubes using the isomerically related ligands *cis,cis*-1,3,5-triaminocyclohexane (*cis*-tach) and *cis,trans*-1,3,5-triaminocyclohexane (*trans*-tach) (Fig. 1). The ligand system in each case has combined rigidity due to the cyclohexane backbone and flexibility due to the primary aliphatic amino groups. The formation of the tubular networks appears to be a function of the nitrogen donor geometry combined with anion effects, and as such comprise a novel synthetic route to the construction of the isolated nanotubes $\{[Ag(cis\text{-tach})]ClO_4\}_\infty$ (**1**), $\{[Ag(trans\text{-tach})]ClO_4\}_\infty$ (**2**) and $\{[Ag(cis\text{-tach})]BF_4\}_\infty$ (**3**).

* Corresponding author. Tel.: +44-141-330-6650; fax: +44-141-330-4888.
E-mail address: L.Cronin@chem.gla.ac.uk (L. Cronin).

0277-5387/$ - see front matter © 2004 Elsevier Ltd. All rights reserved.
doi:10.1016/j.poly.2004.06.002

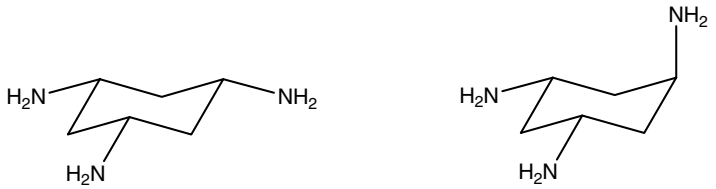

cis,cis-1,3,5-triaminocyclohexane *cis,trans*-1,3,5-triaminocyclohexane

Fig. 1. Ligand geometry facilitating network formation.

2. Experimental

2.1. Materials and physical measurements

Ligands *cis,cis*- and *cis,trans*-1,3,5-triaminocyclohexane were synthesized according to literature methods [18]. All other solvents and reagents were used as purchased without further purification. NMR spectra were measured in D_2O on a Bruker DPX-400 (400 MHz ^1H, 100 MHz ^{13}C). Infrared spectra were obtained from samples prepared as KBr discs in the 650–4000 cm^{-1} range using a Jasco FTIR-410 spectrometer. Elemental analyses were performed on a CE-440 Elemental Analyser.

2.2. Synthesis of compounds **1–3**

2.2.1. Synthesis of [Ag(cis-tach)]ClO_4 (**1**)

Silver perchlorate (40 mg, 0.19 mmol) in methanol (3 ml) was added dropwise to a methanolic solution of *cis,cis*-1,3,5-triaminocyclohexane (50 mg, 0.39 mmol) and stirred at room temperature for 1 h, during which white precipitate occurred. Water (5 ml) was added and the mixture stirred for a further 30 min. The resulting cloudy solution was filtered and the clear colourless filtrate yielded colourless needle-like crystals suitable for diffraction by diffusion with ethanol. Yield: 20 mg (0.06 mmol, 32%) $[Ag(C_6H_{15}N_3)]ClO_4$ (334.98); Found (Calc.)%: C 20.99 (21.49), H 4.32 (4.49), N 11.98 (12.48); ^1H NMR (ppm) 0.96 (q, 3H, *J* 11.62 Hz), 2.19 (dt, 3H, *J* 3.83, 11.42 Hz), 3.12 (m, 3H); ^{13}C NMR (ppm) 40.154 (CH_2), 47.124 (CH); FTIR (wavenumbers in cm^{-1}) 3332 (m), 3284 (m), 2919 (w), 2850 (w), 1581 (m), 1457 (w), 1378 (m), 1199 (m), 1074 (s), 1047 (s), 948 (m), 921 (m), 856 (w).

2.2.2. Synthesis of [Ag(trans-tach)]ClO_4 (**2**)

Silver perchlorate (53 mg, 0.25 mmol) in methanol (3 ml) was added dropwise to a methanolic solution of *cis,trans*-1,3,5-triaminocyclohexane (65 mg, 0.51 mmol) and stirred at room temperature for 1 h, during which a small amount of white precipitate occurred. The cloudy solution was filtered through a cotton wool plug until clear. The clear colourless filtrate yielded pale brown, block-like crystals suitable for diffraction by slow evaporation over two months. Yield: 41 mg (0.12 mmol, 48%). $[Ag(C_6H_{15}N_3)]ClO_4$; Found (Calc.)%: C 21.38 (21.49), H 4.69 (4.55), N 11.65 (11.72); ^1H NMR (ppm) 1.15 (q, 1H, *J* 11.60 Hz), 1.42 (tt, 2H, *J* 3.93, 12.81 Hz), 1.88 (d, 2H, *J* 13.61 Hz), 2.17 (dt, 1H, *J* 1.80, 11.86 Hz), 3.23 (tt, 2H, *J* 3.83, 11.68 Hz), 3.47 (quin, 1H, *J* 3.41 Hz); ^{13}C NMR (ppm) 37.96 (CH_2), 44.53 (CH_2), 45.19 (CH), 45.73 (CH); FTIR (wavenumbers in cm^{-1}) 3332 (m), 3282 (m), 2904 (w), 2389 (w), 1716 (m), 1579 (m), 1454 (w), 1365 (m), 1351 (m), 1211 (w), 1187 (w), 1068 (s), 993 (s), 970 (s), 875 (m), 844 (m), 806 (m).

2.2.3. Synthesis of [Ag(cis-tach)]BF_4 (**3**)

Silver(I) tetrafluoroborate (75 mg, 0.39 mmol) in water (3 ml) was added dropwise to a solution of *cis,cis*-1,3,5-triaminocyclohexane (100 mg, 0.78 mmol) in methanol (2 ml) and the solution stirred for 1 h. The resulting clear, colourless solution was filtered and single crystals suitable for X-ray diffraction were grown by diffusion of ether. Yield: 116 mg (0.358 mmol, 46%). $[Ag(C_6H_{15}N_3)]BF_4$; Found (Calc.)%: C 22.32 (22.25), H 4.65 (4.66), N 12.74 (12.97); ^1H NMR (ppm) 1.03 (q, 3H, *J* 11.60 Hz), 2.17 (dt, 3H, *J* 3.53, 11.34 Hz), 3.15 (tt, 3H, *J* 3.73, 11.05 Hz); ^{13}C NMR (ppm) 39.195 (CH_2), 47.096 (CH); FTIR (wavenumbers in cm^{-1}) 3372 (w), 3347 (m), 3301 (w), 2923 (m), 2852 (m), 2237 (w), 1587 (s), 1459 (s), 1382 (m), 1359 (m), 1290 (w), 1261 (w), 1201 (s), 1074 (s), 948 (m), 923 (m), 856 (w), 806 (m).

2.3. X-ray crystallography

Suitable single crystals of **1**–**3** were prepared and the crystals were mounted on a thin glass fibre using Fomblin oil. X-ray intensity data were measured at 150 K on a Nonius Kappa-CCD diffractometer [λ(Mo Kα) = 0.7107 Å]. Structure solution and refinement for **1**–**3** was carried out with SHELXS-97 [19] and SHELXL-97 [20] via WinGX [21]. Corrections for incident and diffracted beam absorption effects were applied using empirical [22] and numerical methods [23]. None of the crystals showed evidence of crystal decay during data collection. Compounds **1**–**3** crystallized in the space group $P2_1/c$, as determined by systematic absences in the intensity data, intensity statistics and the successful solution and refinement of the structures. All structures were solved

Table 1
Crystallographic data for compounds **1**–**3**[a]

	1	**2**	**3**
Empirical formula	$C_6H_{15}AgClN_3O_4$	$C_6H_{15}AgClN_3O_4$	$C_6H_{15}AgBF_4N_3$
Formula weight	336.53	336.53	323.89
Crystal system	monoclinic	monoclinic	monoclinic
a (Å)	8.4778(5)	7.3136(8)	8.4228(4)
b (Å)	7.6947(3)	8.0334(13)	7.6234(4)
c (Å)	16.6640(12)	8.9245(12)	16.4719(8)
α (°)	90	90	90
β (°)	96.803(2)	101.289(8)	97.792(3)
γ (°)	90	90	90
Space group	$P2_1/c$	$P2_1/c$	$P2_1/c$
V (Å^3)	1079.41(11)	514.20(12)	1047.90(9)
Z value	4	2	4
ρ_{calc} (g/cm^3)	2.071	2.174	2.053
μ (cm^{-1})	2.114	2.219	1.950
T (K)	150(2)	150(2)	150(2)
Number of observations	2121	1559	2061
Residuals: R; R_w	0.0295; 0.0578	0.0590; 0.1041	0.0308; 0.0500

[a] $R_1 = \sum \|F_o| - |F_c\| / \sum |F_o|$.
$wR_2 = \left\{ \sum [w(F_o^2 - F_c^2)^2] \Big/ \sum [w(F_o^2)^2] \right\}^{1/2}$.

Table 2
Bond lengths and angles for compounds **1**–**3**

Compound	Bond lengths (Å)		Bond angles (°)	
1	Ag–N(1)	2.403(3)	N(1)–Ag–N(2)	98.15(10)
	Ag–N(2)	2.222(3)	N(1)–Ag–N(3)	111.44(11)
	Ag–N(3)	2.224(3)	N(2)–Ag–N(3)	150.28(11)
2	Ag–N(1)	2.273(11)	N(1)–Ag–N(2)	133.5(4)
	Ag–N(2)	2.276(10)	N(1)–Ag–N(3)	108.4(4)
	Ag–N(3)	2.345(11)	N(2)–Ag–N(3)	118.1(4)
3	Ag–N(1)	2.227(3)	N(1)–Ag–N(2)	150.33(11)
	Ag–N(2)	2.227(3)	N(1)–Ag–N(3)	111.71(11)
	Ag–N(3)	2.391(3)	N(2)–Ag–N(3)	97.89(10)

by a combination of direct methods and difference Fourier syntheses and refined against F^2 by the full-matrix least-squares technique. Crystal data, data collection parameters and refinement statistics for **1**–**3** are listed in Table 1. Relevant interatomic bond distances and bond angles for **1**–**3** are given in Table 2.

3. Results and discussion

3.1. Structural analysis of compounds *1*–*3*

Crystallization of a methanolic mixture of *cis,cis*-1,3,5-triaminocyclohexane with $AgClO_4$ and $AgBF_4$ and *cis,trans*-1,3,5-triaminocyclohexane with $AgClO_4$ results in the formation of infinite one-dimensional coordination polymers. Each structure contains a metal to ligand ratio of 1:1 and the asymmetric unit in each case consists of one ligand, one silver(I) ion and one counter ion. None of the structures presented here contain solvent molecules (see Fig. 2).

Both the trigonal planar silver(I) ions and the tridentate amino ligands can be seen as three-coordinate units, which self-assemble to form $4^2 \cdot 6$ topological networks. The macrocycles formed upon coordination facilitate a tubular structure with a definite channel. The channels found in compounds **1**, **2** and **3** are not large enough to encapsulate a further molecule, having dimensions of 5.4, 5.3 and 5.6 Å, respectively. The isolated one-dimensional polymers together form an extensive three-dimensional hydrogen-bonded network linked via interactions between the coordinating amino groups and the counter ions (Fig. 3).

The manner in which these rigid ligands facilitate the formation of tubular networks is dependent upon their coordination geometry. The molecule *cis*-tach is a tripodal ligand, where the three equatorial amino residues can wrap around the walls of the channel (Fig. 4(a)). *trans*-Tach, on the other hand, has the ability to coordinate in a linear polymer via the two equatorial groups along a chain (Fig. 4(b)), and further coordination via the axial amino group connects to a silver(I) centre of a second chain and forms the tubular structure (Fig. 4(c)). The macrocyles formed in each case by two silver(I) ions and two ligands consist of 12 atoms and have an inversion centre.

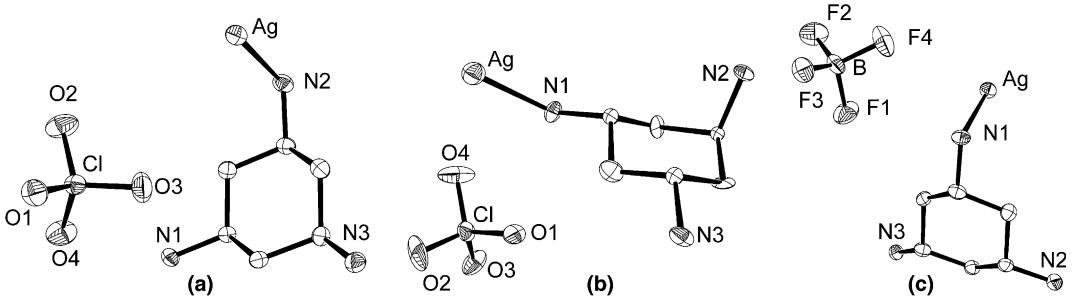

Fig. 2. Asymmetric unit of **1 (a)**, **2 (b)** and **3 (c)**. Note the coordination environment of the silver ion lies between T-shaped planar and trigonal planar, with the Ag ion being ligated to three amino groups of different tach ligands.

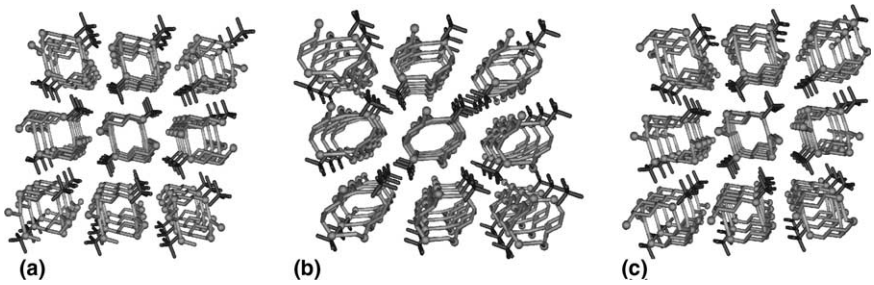

Fig. 3. Three-dimensional hydrogen bonded networks of (a) compound **1**, (b) compound **2** and (c) compound **3** showing isolated coordination polymers. The anions are shown by the black tetrahedra and the nitrogen atoms of the tach-based ligands are shown as spheres.

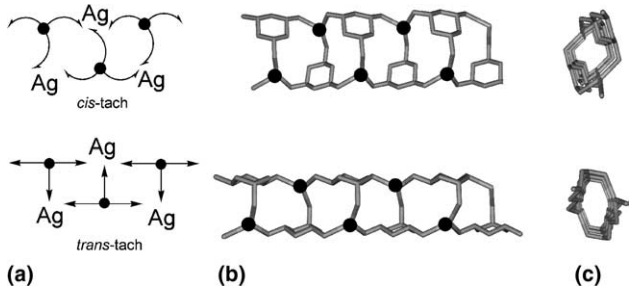

Fig. 4. (a) Ligand motifs of *cis*- and *trans*-tach shown as black dots with arrows. (b) Macrocycle formation utilizing the different ligand geometries with the silver ions show as black dots. (c) End-on view of tubes showing channels.

3.2. Conclusions

We have investigated the synthesis of a number of infinite one-dimensional coordination polymers of aliphatic triamino ligands with a variety of silver(I) salts in order to determine whether such ligand systems can be used as building blocks in the rational design of new functional materials. The isomeric ligands *cis,cis*-1,3,5-triaminocyclohexane and *cis,trans*-1,3,5-triaminocyclohexane have aliphatic amino groups, the direction of which have been proven to provide valuable freedom in the self-assembly process. The construction of these infinite tubular polymers from metal–ligand systems that posses a degree of pre-organization and a number of arms that can 'wrap' can be seen as a noteworthy development in the self-assembly of nanotubular compounds. We are currently extending this work by investigation into the coordination of our rigid amines with other metals and also via derivatization of the amino residues in order to enlarge the channel dimensions and increase the functionality of the materials.

4. Supplementary material

Crystallographic data (X-ray data in *.cif files) for structures **1**–**3** have been deposited with the Cambridge Crystallographic Data Centre, CCDC No. 233831 for compound **1**, CCDC No. 233832 for compound **2** and CCDC No. 233833 for compound **3**. Copies of this information may be obtained from the Director, CCDC, 12 Union Road, Cambridge, CB21EZ, UK (fax: +44-1223-336033; e-mail: deposit@ccdc.cam.ac.uk or http://www.ccdc.cam.ac.uk).

Acknowledgements

The authors are grateful to the EPSRC and the University of Glasgow for financial support.

References

[1] S. Iijima, Nature 56 (1991) 354.
[2] A.A. Mamedov, N.A. Kotov, M. Prato, D.M. Guldi, J.P. Wicksted, A. Hirsch, Nature Mater. 1 (2002) 190.
[3] S. Iijima, T. Ichihashi, Nature 363 (1993) 603.
[4] D.S. Bethune, C.H. Kiang, M.S. de Vries, G. Gorman, R. Savoy, J. Vazquez, R. Beyers, Nature 363 (1993) 605.
[5] P.M. Ajayan, J.M. Lambert, P. Bernier, L. Barbedette, C. Colliex, J.M. Planeix, Chem. Phys. Lett. 215 (1993) 509.
[6] T. Guo, P. Nikolaev, A. Thess, D.T. Colbert, R.E. Smalley, Chem. Phys. Lett. 243 (1995) 49.
[7] T.W. Ebbesen, P.M. Ajayan, Nature 358 (1992) 220.
[8] H. Liu, S. Xiao, H. Gan, T. Jiu, H. Li, L. Jiang, D. Zhu, D. Yu, B. Xiang, Y. Chen, J. Am. Chem. Soc. 125 (2003) 10794.
[9] J. Liu, M. Shao, X. Chen, W. Yu, X. Liu, Y. Qian, J. Am. Chem. Soc. 125 (2003) 8088.
[10] M.J. Zaworotko, Angew. Chem. Int. Ed. 39 (2000) 3052.
[11] Y. Cui, J. Lee, W. Lin, J. Am. Chem. Soc. 125 (2003) 6014.
[12] P. Jenson, S.R. Batten, B. Moubaraki, K.S. Murray, J. Chem. Soc., Dalton Trans. (2002) 3712.
[13] M. Hong, Y. Zhao, W. Su, R. Cao, M. Fujita, Z. Zhou, A.S.C. Chan, Angew. Chem. Int. Ed. 39 (2000) 2468.
[14] M. Aoyagi, S. Tashiro, M. Tominaga, K. Biradha, M. Fujita, Chem. Commun. (2002) 2036.
[15] J. Fan, H.-F. Zhu, T.-A. Okamura, W.-Y. Sun, W.-X. Tang, N. Ueyama, Inorg. Chem. 42 (2003) 158.
[16] Y. Kang, S.S. Lee, K.-M. Park, S.H. Lee, S.O. Kang, J. Ko, Inorg. Chem. 40 (2001) 7027.
[17] A.L. Pickering, G. Seeber, D.-L. Long, L. Cronin, Chem. Commun. (2004) 136.
[18] F. Lions, K.V. Martin, J. Am. Chem. Soc. 79 (1957) 15721.
[19] G.M. Sheldrick, Acta Crystallogr., Section A A46 (1998) 467.

[20] G.M. Sheldrick, SHELXL-97. Program for Crystal Structure Analysis, University of Göttingen, Germany, 1997.
[21] L.J. Farrugia, J. Appl. Crystallogr. 32 (1999) 837.
[22] R.H. Blessing, Acta Crystallogr., Section A 51 (1995) 33.
[23] P. Coppens, L. Leiserowitz, D. Rabinovich, Acta Crystallogr. 18 (1965) 1035.

Available online at www.sciencedirect.com
SCIENCE DIRECT®
Polyhedron 23 (2004) 2081–2083
POLYHEDRON
www.elsevier.com/locate/poly

Is bipyridine planar in metal complexes?

Alan Hazell *

Department of Chemistry, Aarhus University, Langelandsgade 140, DK-8000 Århus C, Denmark

Received 22 April 2004; accepted 8 June 2004
Available online 3 July 2004

Abstract

Deviations from planarity of the bipyridine ligand are discussed in terms of bow and twist angles and an S-shaped deformation. The angle φ between the best-planes through the pyridine moieties is related to the bow and twist angles by $\varphi \sim \sqrt{(\theta_B^2 + \theta_T^2)}$. The values are compared with the results of crystal structure determinations. A further deviation from ideality is the in-plane distortion of the ligand that is seen to decrease with increasing metal–nitrogen distances.
© 2004 Elsevier Ltd. All rights reserved.

Keywords: Bipyridine; Distortions

1. Introduction

Bipyridine, $C_{10}H_8N_2$, is a very popular complexing agent. In the uncoordinated molecule the nitrogen atoms are *trans* [1], whereas in the vast majority of metal complexes studied by X-ray diffraction they are *cis* (the Cambridge Structural Data Base [2] contains 2506 *N*,*N*′ complexes, three *N*,*C* complexes and one *N*,*C*,*N*′,*C*′ complex). The ligand is often regarded as either being planar or that the two pyridine moieties are twisted about the central C–C single bond. In the latter case crystallographers are then often asked for the angle between the planes, φ, this angle is then claimed to be the twist angle, θ_T. In practice the distortion from planarity is more complex [3,4] with a bow distortion, θ_B, and an S-shaped distortion. There is also an in-plane distortion, θ_P. These distortions are shown in Fig. 1 for real structures.

In most cases, the deformation is a combination of these effects and the purpose of this paper is to describe a simple method of decomposing the deformation into the individual components.

2. Calculation of the distortion angles

Atomic positions are usually given by a set of fractional coordinates obtained by X-ray diffraction, these are then converted to orthogonal coordinates, in Å, relative to the centre of gravity of the ligand. These are then transposed to the inertial axial system, with *x* parallel to the long dimension of the bipyridine and *z* perpendicular to the best plane through the ligand. The various deformation angles are then obtained by examining the projections down the inertial axes. The pyridine moieties are considered to be planar.

2.1. The in-plane distortion, θ_P

The angle, θ_P, is the angle between the two lines through the pyridine rings in the *xy* projection, Fig. 1(a), these are calculated as the mean of vectors 1–2, 3–4, and 5–6 for the left hand pyridine and similarly for the right hand pyridine. The required angle is then the angle between these two lines. Since the atoms of the pyridine ring lie almost on a circle a 'best straight line' cannot be calculated.

2.2. The bow distortion, θ_B, and S-shaped distortions

The best straight lines, $ax + c = z$, through each of the two pyridine rings in projection have gradients θ_1

* Tel.: +45-8942-3891; fax: +45-8619-6199.
E-mail address: ach@chem.au.dk (A. Hazell).

0277-5387/$ - see front matter © 2004 Elsevier Ltd. All rights reserved.
doi:10.1016/j.poly.2004.06.001

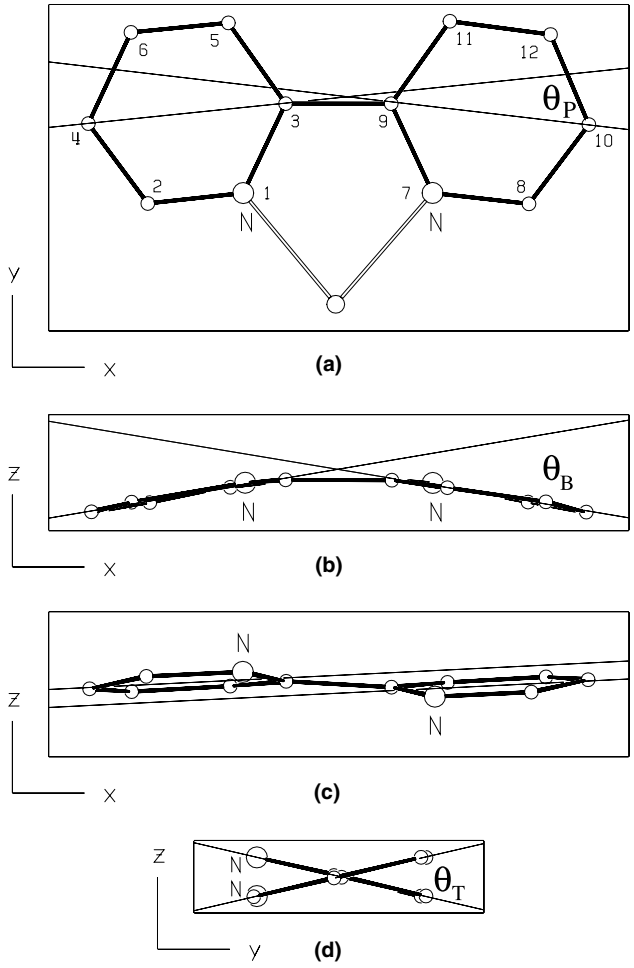

Fig. 1. Distortions in bipyridyl ligands, (a) in-plane, θ_P, Refcode HAJZOH01, (b) bow form, θ_B, Refcode JOYWAV (c) S-shaped, Refcode FUPQUEM, (d) twist, θ_T, Refcode JEVWAI. The Refcodes refer to the Cambridge Structural Data Base [2].

and θ_r and make intercepts c_l and c_r with the z-axis. For a pure bow distortion, Fig. 1(b), $\theta_l = -\theta_r$ and $c_l = c_r$ whilst for a pure S-shaped distortion, Fig. 1c, $\theta_l = \theta_r$ and $c_l = -c_r$. For a combination of the two effects $\theta_B = \theta_l - \theta_r$ and $d_z = c_l - c_r$, d_z is the separation of the two parallel lines along the z-axis. The perpendicular distance between the lines is $d_s = d_z \cos((\theta_l + \theta_r)/2)$.

The S distortion is generally small and in Fig. 1(c) the z-axis has been drawn on double the scale of the x-axis. For structures with a 2-fold axis through the bipyridine ring, $\theta_B = 0$.

2.3. The twist distortion, θ_T

This is the angle between the two best lines through the pyridine rings in the yz projection, Fig. 1(d). For structures with a mirror plane perpendicular to the bipyridine ring, $\theta_T = 0$.

3. Comparison with observed values

The Cambridge Structural Data Base [2] contains 2506 N,N' coordinated bipyridyl ligands, many of these are poorly determined, so only those in which the average σ(C–C) was smaller than 0.005 Å were considered, this reduced the number to 563 this number was further reduced to 551 by rejecting three structures which clearly contained errors, e.g., bond lengths differing by more than 0.2Å from expected values. The pyridine rings are usually not coplanar, Fig. 2.

The values of θ_T range from 0.0° to 26.1° and for θ_B from 0.0° to 19.8°, a plot, Fig. 3, of θ_T versus θ_B shows that in many cases both distortions occur.

There is a high concentration of points on the axes, those where the distortions are constrained to be zero by the crystallographic symmetry are shown with filled circles. The angle φ between the pyridine rings is seen to be $\sqrt{(\theta_B^2 + \theta_T^2)}$. The parameter d_s is in the range 0–0.127 Å, 90% of the values being less than 0.053 Å. This is a small distortion, $d_s = 0.05$ Å corresponds to the central C–C bond making an angle of 1.9° with the plane through a pyridine ring. For all of these distortions the absolute value is given since the sign has no meaning.

The in-plane angle, θ_P, differs from the other distortions in that here the sign has been retained, all the angles are positive, i.e., the nitrogen atoms are displaced towards the metal atom. Fig. 4, shows that θ_P lies in the range 2.9°–12.5° with a mean value of 7.8° and decreases with increasing metal–nitrogen distance.

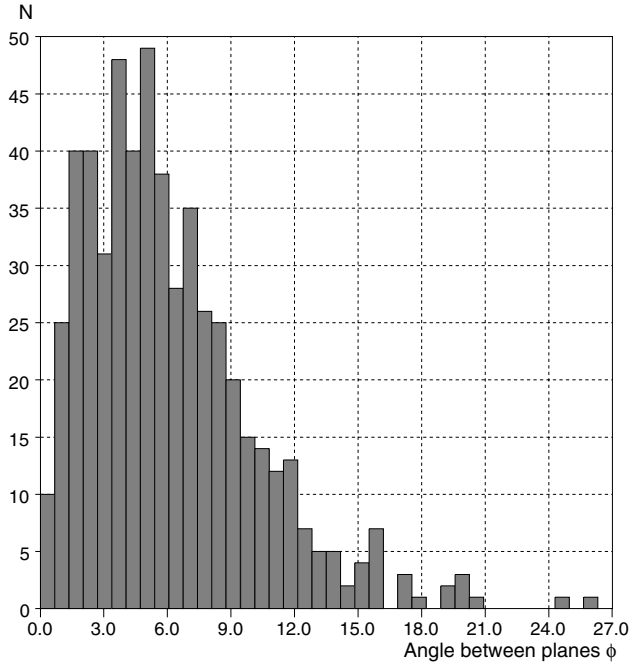

Fig. 2. The angle, φ, between the best planes through the pyridine moieties.

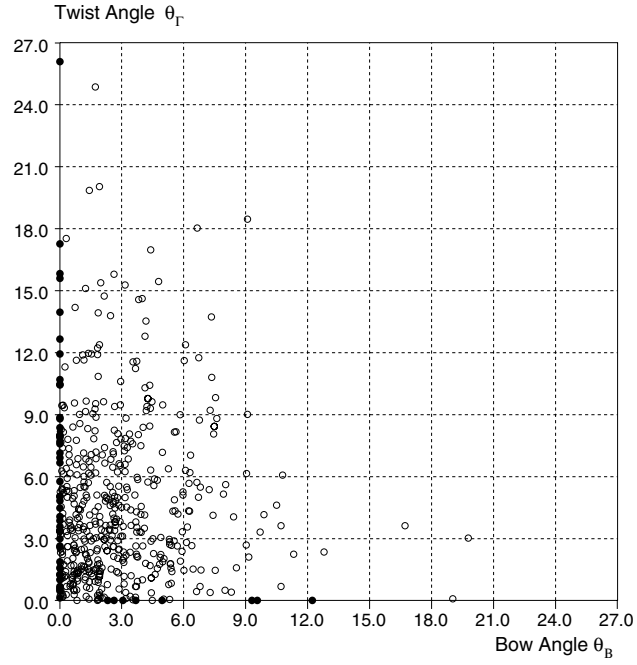

Fig. 3. The bow angle, θ_B, vs. the twist angle, θ_T. Points representing structures where one of the angles is exactly zero from symmetry considerations are shown as filled circles.

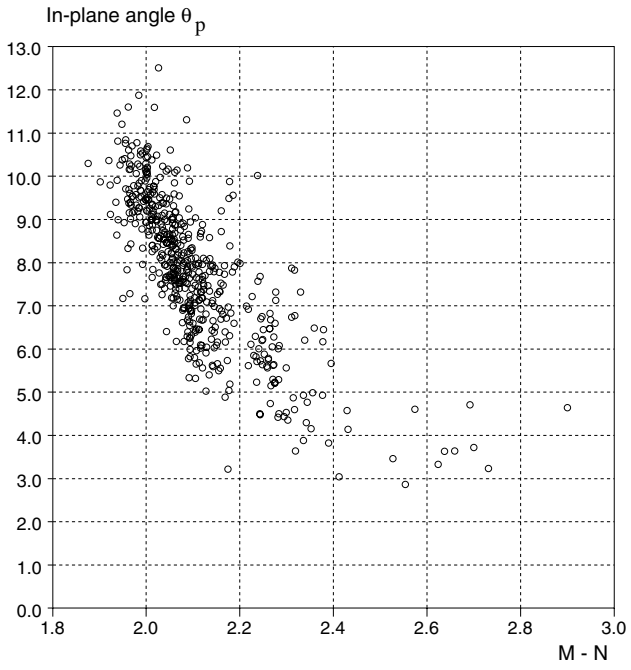

Fig. 4. The in-plane distortion, θ_P, plotted against the mean M–N distance.

There is however a large scatter and the correlation coefficient is only 0.77. In the free bipyridine [1], the CCN angle involving the central bond is 118.26° that would give an in-plane distortion of 3.5°. The in-plane distortion of the Mbipy group is a combination of distortions of the CCN and of the MNC angle, and the sum of these distortions $(240° - \theta_{CCN} - \theta_{MNC})$ correlates inversely with M–N, the correlation coefficient is 0.96. The M–N distance for which there would be no in-plane distortion is 2.72 Å.

4. Conclusions

The answer to the question in the title is that bipyridine is seldom planar in metal complexes and that the deviation from planarity can be described in terms of bow and twist deformations and to a lesser extent in terms of an S-shaped distortion. There is also an in-plane deformation, which is far from negligible.

References

[1] F.E. Kühn, M. Groarke, E. Bencze, E. Herdtweck, A. Prazares, A.M. Santos, M.J. Calhorda, C.C. Romão, I.S. Gonçalves, A.D. Lopes, M. Pillinger, Chem. Eur. J. 8 (2002) 2370.
[2] F.H. Allen, Acta Crystallogr. Sect. B 58 (2002) 380.
[3] A. Hazell, A. Mukhopadhyay, Acta Crystallogr. Sect. B 36 (1980) 1647.
[4] A. Hazell, O. Simonsen, O. Wernberg, Acta Crystallogr. Sect. C 42 (1986) 1707.

Available online at www.sciencedirect.com
SCIENCE DIRECT®
Polyhedron 23 (2004) 2085–2093
POLYHEDRON
www.elsevier.com/locate/poly

Hydrothermal synthesis and characterization of the first examples of lanthanide(III) isoorotates with a 3D supramolecular network

Chang-Yan Sun, Lin-Pei Jin *

Department of Chemistry, Beijing Normal University, Xinjiekou Road, Beijing 100875, PR China

Received 10 February 2004; accepted 25 May 2004
Available online 3 July 2004

Abstract

The first examples of lanthanide(III) isoorotates were synthesized by hydrothermal reactions and characterized by single crystal X-ray diffraction. Isoorotate ions (H_2iso^- and $Hiso^{2-}$) act as bidentate ligands and coordinate to the Ln(III) ions through the carboxylate oxygen and the adjacent carbonyl oxygen, forming a stable six-membered ring. But in the Pr(III) complex, $Hiso^{2-}$ acts as a tetradentate ligand, and in addition to the formation of the six-membered ring, another carbonyl oxygen atom and a deprotonated amido nitrogen atom are involved in coordination. There are O–H···O, N–H···O and/or N–H···N hydrogen bonds, and/or π–π stacking interactions in these complexes, resulting in the formation of 3D supramolecular networks.
© 2004 Elsevier Ltd. All rights reserved.

Keywords: Lanthanide(III) complexes; Hydrothermal syntheses; Isoorotic acid; Hydrogen bonds; Supramolecule

1. Introduction

It is well known that orotic acid (6-carboxyuracil, H_3oro) plays a significant role in many biological processes, since this compound is the only effective precursor of pyrimidine bases of nucleic acids in living systems [1]. Also, it has been extensively used in medicine for the treatment of some pathologies [2]. The coordination chemistry of this compound has been intensively investigated. Isoorotic acid (5-carboxyuracil, H_3iso), the isomer of orotic acid, has not received so much attention yet, although it exhibits anticancer, antibacterial and antihypertensive properties and is an interesting species from a medical and pharmacological point of view [3]. Apart from that, isoorotic acid possesses fascinating coordination characteristics: first, it is an interesting multidentate ligand capable of coordinating to metal ions through the nitrogen atoms, the two carbonyl oxygen atoms and the carboxylate oxygen atoms; second, the carboxylic and amido hydrogens may be completely or partially removed, so that metal complexes of H_2iso^-, $Hiso^{2-}$ and/or iso^{3-} are formed; and third, it can act not only as a hydrogen-bond acceptor, but also a hydrogen-bond donor, depending on the deprotonated groups. Because of the different position of the carboxylate group in orotic acid and isoorotic acid, we expect that there are many differences in their coordination behavior. Previous studies on the coordination chemistry of isoorotic acid mainly focused on transition metals [4–10] and those on lanthanide ones were by and large neglected. With the above consideration in mind, we report the synthesis and characterization of the first examples of lanthanide complexes with isoorotic acid.

2. Experimental

2.1. Materials and apparatus

All reagents were used as received without further purification. The C, H, N microanalyses were carried out with a Vario EL elemental analyzer. The IR spectra were recorded with a Nicolet Avatar 360 FT-IR spectrometer using the KBr pellet technique. Thermogravimetric

* Corresponding author. Tel.: +8601062205522; fax: +8601062202075.
E-mail address: lpjin@bnu.edu.cn (L.-P. Jin).

0277-5387/$ - see front matter © 2004 Elsevier Ltd. All rights reserved.
doi:10.1016/j.poly.2004.05.013

analyses were conducted on a ZRY-2P Thermal Analyzer using a heating rate of 10 °C/min from room temperature to 900 °C.

2.2. Synthesis

Tb(Hiso)(H2iso)(H2O)4·3H2O (1). A mixture of H_3iso (0.017 g, 0.1 mmol), $TbCl_3 \cdot 6H_2O$ (0.038 g, 0.1 mmol), an aqueous solution of NaOH (0.2 ml, 0.65 mol l^{-1}) and deionized water (5 ml) was sealed in a Teflon-lined stainless vessel (25 ml) and heated at 140 °C for 72 h. The vessel was then cooled at 10 °C/3 h to 100 °C, followed by slow cooling to room temperature. Colourless crystals were obtained by filtration, and washed with water and ethanol. Yield: 0.019 g (64%). *Anal.* Calc. for $C_{10}H_{19}N_4O_{15}Tb$: C, 20.20; H, 3.20; N, 9.43. Found: C, 20.05; H, 3.03; N, 9.23%. IR (KBr, cm^{-1}): 3378s, 1625s, 1552m, 1469m, 1426m, 1370s, 1304m, 1192m, 1142m, 1011m, 919m, 812m, 653m, 584m.

Yb(Hiso)(H2iso)(H2O)4·3H2O (2). The synthesis of complex **2** followed the same procedure as for **1**, but using $YbCl_3 \cdot 6H_2O$. Yield: 0.012 g (39.5%). *Anal.* Calc. for $C_{10}H_{19}N_4O_{15}Yb$: C, 19.73; H, 3.12; N, 9.21. Found: C, 19.61; H, 2.92; N, 9.06%. IR (KBr, cm^{-1}): 3418s, 1626s, 1548m, 1470m, 1427m, 1384s, 1304m, 1196m, 1142m, 1010m, 919m, 812m, 653m, 584m.

Pr2(Hiso)(H2iso)4(phen)2(H2O)2·5H2O (3). A mixture of H_3iso (0.017 g, 0.1 mmol), $PrCl_3 \cdot 6H_2O$ (0.036 g, 0.1 mmol), phen·H_2O (0.02 g, 0.1 mmol), an aqueous solution of NaOH (0.2 ml, 0.65 mol l^{-1}) and deionized water (5 ml) was sealed in a Teflon-lined stainless vessel (25 ml) and heated at 140 °C for 72 h. The vessel was then cooled at 10 °C/3 h to 100 °C, followed by slow cooling to room temperature. Colourless crystals were obtained by filtration, and washed with water and ethanol. Yield: 0.023 g (74.5%). *Anal.* Calc. for $C_{49}H_{44}N_{14}O_{27}Pr_2$: C, 38.11; H, 2.85; N, 12.70. Found: C, 38.35; H, 2.56; N, 12.34%. IR (KBr, cm^{-1}): 3428s, 3073m, 2969m, 2798m, 1716m, 1643s, 1559m, 1422s, 1384s, 1300m, 1198m, 1142m, 1101m, 1046m, 846m, 812m, 648m, 567m.

Eu(Hiso)(H2iso)(phen)2·2H2O (4). The synthesis of complex **4** followed the same procedure as for **3**, but using $EuCl_3 \cdot 6H_2O$. Yield: 0.031 g (72.3%). *Anal.* Calc. for $C_{34}H_{25}N_8O_{10}Eu$: C, 47.60; H, 2.92; N, 13.07. Found: C, 47.47; H, 2.60; N, 13.07%. IR (KBr, cm^{-1}): 3459s, 3059m, 2972m, 1638s, 1547m, 1514m, 1468m, 1415s, 1341m, 1301m, 1256m, 1102m, 1050m, 848m, 731m, 637m.

Tb(Hiso)(H2iso)(phen)2·2H2O (5). A mixture of H_3iso (0.017 g, 0.1 mmol), $TbCl_3 \cdot 6H_2O$ (0.038 g, 0.1 mmol), phen·H_2O (0.02 g, 0.1 mmol), an aqueous solution of NaOH (0.3 ml, 0.65 mol l^{-1}) and deionized water (5 ml) was sealed in a Teflon-lined stainless vessel (25 ml), and heated at 120 °C for 72 h. The vessel was then cooled slowly to room temperature. Colourless crystals were obtained by filtration, and washed with water and ethanol. Yield: 0.023 g (74.5%). *Anal.* Calc. for $C_{34}H_{25}N_8O_{10}Tb$: C, 47.22; H, 2.89; N, 12.96. Found: C, 46.63; H, 2.66; N, 12.85%. IR (KBr, cm^{-1}): 3451s, 3061m, 2927m, 1637s, 1545m, 1515m, 1496m, 1418s, 1342m, 1301m, 1257m, 1103m, 1049m, 847m, 731m, 638m.

Yb(Hiso)(H2iso)(phen)2·2H2O (6). The synthesis of complex **6** followed the same procedure as for **5**, but using $YbCl_3 \cdot 6H_2O$. Yield: 0.016 g (36.4%). *Anal.* Calc. for $C_{34}H_{25}N_8O_{10}Yb$: C, 46.43; H, 2.85; N, 12.75. Found: C, 45.68; H, 2.64; N, 12.42%. IR (KBr, cm^{-1}): 3464s, 3062m, 2926m, 1636s, 1544m, 1513m, 1473m, 1420s, 1379m, 1302m, 1256m, 1103m, 996m, 848m, 730m, 638m.

Yb(Horo)(OH)(H2O) (7). A mixture of H_3oro (0.017 g, 0.1 mmol), $YbCl_3 \cdot 6H_2O$ (0.039 g, 0.1 mmol), an aqueous solution of NaOH (0.2 ml, 0.65 mol l^{-1}) and deionized water (5 ml) was sealed in a Teflon-lined stainless vessel (25 ml), and heated at 160 °C for 72 h. The vessel was then cooled slowly to room temperature. Colourless crystals were obtained by filtration, and washed with water and ethanol. Yield: 0.011 g (30.4%). *Anal.* Calc. for $C_5H_5N_2O_6Yb$: C, 16.57; H, 1.38; N, 7.73. Found: C, 16.84; H, 1.26; N, 7.65%. IR (KBr, cm^{-1}): 3373m, 3113m, 1631s, 1486m, 1425s, 1374m, 1346m, 1320m, 1162m, 1018m, 848s, 798m, 723m, 620m.

2.3. X-ray diffraction determination

Diffraction intensities for the complexes were collected at 293 K on a Bruker SMART 1000 CCD area detector diffractometer employing graphite monochromatized Mo Kα radiation ($\lambda = 0.71073$ Å) in ϕ and ω scan modes. Semi-empirical absorption correction was applied on the complexes using the SADABS program [11]. The structures were solved by direct methods [12] and refined by full-matrix least squares method on F^2 using SHELXS-97 and SHELXL-97 programs, respectively [12,13]. Non-hydrogen atoms were refined anisotropically. Hydrogen atoms were placed in geometrically calculated positions. The crystallographic data for complexes **1**–**7** are listed in Table 1, and selected bond lengths (Å) and bond angles (°) in Tables 2–5.

3. Results and discussion

3.1. Description of the structures

Compounds **1** and **2** are isomorphous, while **4**, **5** and **6** are isomorphous, too. Only the structures of **2, 3, 6** and **7** will be described in detail. It is noted that the site occupancy of hydrogen atoms on N(2) and N(2A) for **1** and **2**, and on N(4) and N(4A) for **4**–**6**, is 0.5.

Table 1
Crystal data and structure refinement parameters for **1**–**7**

	1	**2**	**3**	**4**	**5**	**6**	**7**
Chemical formula	$C_{10}H_{19}N_4O_{15}Tb$	$C_{10}H_{19}N_4O_{15}Yb$	$C_{49}H_{44}N_{14}O_{27}Pr_2$	$C_{34}H_{25}N_8O_{10}Eu$	$C_{34}H_{25}N_8O_{10}Tb$	$C_{34}H_{25}N_8O_{10}Yb$	$C_5H_5N_2O_6Yb$
Crystal system	monoclinic	monoclinic	triclinic	monoclinic	monoclinic	monoclinic	orthorhombic
Space group	$P2(1)/m$	$P2(1)/m$	$P\bar{1}$	$C2/c$	$C2/c$	$C2/c$	$Pna2(1)$
θ Range (°)	1.98–26.40	1.97–26.40	1.77–26.49	1.85–26.40	2.28–26.42	2.28–26.40	3.25–25.03
a (Å)	5.3645(2)	5.384(3)	10.239(4)	17.111(6)	17.156(4)	17.142(8)	9.927(4)
b (Å)	20.558(6)	20.684(1)	12.902(5)	14.495(5)	14.486(4)	14.341(8)	16.194(6)
c (Å)	8.200(3)	8.230(4)	13.342(5)	13.137(4)	13.218(3)	13.267(7)	4.5801(2)
α (°)	90	90	61.364(5)	90	90	90	90
β (°)	93.954(5)	93.454(8)	89.874(7)	99.570(5)	100.216(4)	101.633(1)	90
γ (°)	90	90	71.341(6)	90	90	90	90
V (Å^3)	902.2(5)	914.8(8)	1441.2(1)	3213.1(1)	3232.7(1)	3194(3)	736.3(5)
Z	2	2	1	4	4	4	4
D_{calc} (Mg/m^3)	2.187	2.208	1.778	1.773	1.776	1.827	3.267
μ (mm^{-1})	4.011	5.202	1.772	2.028	2.263	3.004	12.709
F (0 0 0)	584	594	770	1712	1720	1740	668
Formula weight	594.21	608.33	1542.80	857.58	864.54	878.66	362.15
R_{int}	0.0293	0.0342	0.0314	0.0646	0.0691	0.0382	0.0396
R indices	$R_1 = 0.0339$,	$R_1 = 0.0339$,	$R_1 = 0.0483$,	$R_1 = 0.0495$,	$R_1 = 0.0431$,	$R_1 = 0.0254$,	$R_1 = 0.0280$,
$[I > 2\sigma(I)]$	$wR_2 = 0.0995$	$wR_2 = 0.0856$	$wR_2 = 0.1173$	$wR_2 = 0.1027$	$wR_2 = 0.0540$	$wR_2 = 0.0512$	$wR_2 = 0.0649$
R indices	$R_1 = 0.0369$,	$R_1 = 0.0367$,	$R_1 = 0.0725$,	$R_1 = 0.0787$,	$R_1 = 0.0737$,	$R_1 = 0.0343$,	$R_1 = 0.0342$,
(all data)	$wR_2 = 0.1153$	$wR_2 = 0.0866$	$wR_2 = 0.1331$	$wR_2 = 0.1106$	$wR_2 = 0.0599$	$wR_2 = 0.0538$	$wR_2 = 0.0693$

Table 2
Selected bond lengths (Å) and angles (°) for **1** and **2**

*Compound **1***			
Bond lengths			
Tb(1)–O(1)	2.328(5)	Tb(1)–O(6)	2.373(5)
Tb(1)–O(3)	2.375(5)	Tb(1)–O(7)	2.408(8)
Tb(1)–O(5)	2.404(7)		
Bond angles			
O(1)–Tb(1)–O(1)#1	73.9(3)	O(3)–Tb(1)–O(7)	73.10(1)
O(1)–Tb(1)–O(3)	72.09(2)	O(3)#1–Tb(1)–O(3)	127.4(3)
O(1)–Tb(1)–O(3)#1	140.4(2)	O(5)–Tb(1)–O(7)	94.0(3)
O(1)–Tb(1)–O(5)	86.7(2)	O(6)–Tb(1)–O(3)	74.47(2)
O(1)–Tb(1)–O(6)	79.1(2)	O(6)–Tb(1)–O(3)#1	135.6(2)
O(1)–Tb(1)–O(6)#1	118.0(2)	O(6)–Tb(1)–O(5)	145.95(2)
O(1)–Tb(1)–O(7)	143.03(1)	O(6)–Tb(1)–O(7)	80.0(2)
O(3)–Tb(1)–O(5)	71.73(2)	O(6)#1–Tb(1)–O(6)	66.4(3)
*Compound **2***			
Bond lengths			
Yb(1)–O(1)	2.285(5)	Yb(1)–O(6)	2.337(5)
Yb(1)–O(3)	2.360(4)	Yb(1)–O(7)	2.349(7)
Yb(1)–O(5)	2.353(6)		
Bond angles			
O(1)–Yb(1)–O(1)#1	72.6(2)	O(5)–Yb(1)–O(3)	72.02(1)
O(1)–Yb(1)–O(3)	73.51(2)	O(6)–Yb(1)–O(3)	74.60(2)
O(1)–Yb(1)–O(3)#1	140.73(2)	O(6)–Yb(1)–O(3)#1	135.16(2)
O(1)–Yb(1)–O(5)	86.8(2)	O(6)–Yb(1)–O(5)	146.23(1)
O(1)–Yb(1)–O(6)	79.0(2)	O(6)–Yb(1)–O(7)	80.5(2)
O(1)–Yb(1)–O(6)#1	117.08(2)	O(7)–Yb(1)–O(3)	72.30(1)
O(1)–Yb(1)–O(7)	143.70(1)	O(7)–Yb(1)–O(3)#1	72.30(1)
O(3)#1–Yb(1)–O(3)	126.6(2)	O(7)–Yb(1)–O(5)	94.0(2)

Symmetry transformations used to generate equivalent atoms: #1 $x, -y + 3/2, z$.

*Yb(Hiso)(H$_2$iso)(H$_2$O)$_4\cdot$3H$_2$O (**2**).* The asymmetric unit of **2** consists of one Yb(III) ion, two isoorotate groups, four coordinated water and three lattice water molecules (Fig. 1). The Yb(III) ion is eight-coordinated by oxygen atoms, four of which come from water molecules and the others belong to two isoorotate groups.

Table 3
Selected bond lengths (Å) and angles (°) for **3**

*Compound **3***			
Bond lengths			
Pr(1)–O(1)	2.367(5)	Pr(1)#1–O(1)#1	2.367(5)
Pr(1)–O(4)	2.543(4)	Pr(1)#1–O(4)#1	2.543(4)
Pr(1)–O(5)	2.412(5)	Pr(1)#1–O(5)#1	2.412(5)
Pr(1)–O(8)	2.589(5)	Pr(1)#1–O(8)#1	2.589(5)
Pr(1)–O(9)	2.514(5)	Pr(1)#1–O(9)#1	2.514(5)
P r(1)–O(13)	2.63(2)	Pr(1)#1–O(10)	2.508(1)
Pr(1)–N(1)	2.669(5)	Pr(1)#1–O(11)	2.47(3)
Pr(1)–N(2)	2.741(5)	Pr(1)#1–N(1)#1	2.669(5)
Pr(1)–N(7)	2.527(6)	Pr(1)#1–N(2)#1	2.741(5)
Bond angles			
O(1)–Pr(1)–O(4)	71.39(1)	O(9)–Pr(1)–O(13)	139.4(1)
O(1)–Pr(1)–O(5)	139.81(2)	O(9)–Pr(1)–N(1)	75.64(2)
O(1)–Pr(1)–O(8)	73.02(2)	O(9)–Pr(1)–N(2)	72.71(2)
O(1)–Pr(1)–O(9)	95.54(2)	O(9)–Pr(1)–N(7)	147.56(2)
O(1)–Pr(1)–O(10)#1	69.0(3)	O(10)#1–Pr(1)–O(4)	76.1(3)
O(1)–Pr(1)–O(11)#1	129.6(1)	O(10)#1–Pr(1)–O(8)	134.1(3)
O(1)–Pr(1)–O(13)	124.6(9)	O(10)#1–Pr(1)–O(9)	138.2(3)
O(1)–Pr(1)–N(1)	133.44(2)	O(10)#1–Pr(1)–O(13)	64.0(8)
O(1)–Pr(1)–N(2)	72.98(2)	O(10)#1–Pr(1)–N(1)	87.4(3)
O(1)–Pr(1)–N(7)	80.27(2)	O(10)#1–Pr(1)–N(2)	65.7(3)
O(4)–Pr(1)–O(8)	68.04(2)	O(10)#1–Pr(1)–N(7)	13.5(2)
O(4)–Pr(1)–O(13)	70.3(1)	O(11)#1–Pr(1)–O(4)	73.3(1)
O(4)–Pr(1)–N(1)	142.34(2)	O(11)#1–Pr(1)–O(8)	123.5(1)
O(4)–Pr(1)–N(2)	134.80(2)	O(11)#1–Pr(1)–O(9)	134.5(1)
O(5)–Pr(1)–O(4)	86.26(2)	O(11)#1–Pr(1)–O(10)#1	68.5(8)
O(5)–Pr(1)–O(8)	67.67(2)	O(11)#1–Pr(1)–O(13)	5.0(2)
O(5)–Pr(1)–O(9)	78.44(2)	O(11)#1–Pr(1)–N(1)	69.2(1)
O(5)–Pr(1)–O(10)#1	138.2(2)	O(11)#1–Pr(1)–N(2)	111.3(1)
O(5)–Pr(1)–O(11)#1	70.3(8)	O(11)#1–Pr(1)–N(7)	55.1(8)
O(5)–Pr(1)–O(13)	74.4(7)	O(13)–Pr(1)–N(1)	72.0(1)
O(5)–Pr(1)–N(1)	84.04(2)	O(13)–Pr(1)–N(2)	110.3(1)
O(5)–Pr(1)–N(2)	138.63(2)	N(1)–Pr(1)–N(2)	60.67(2)
O(5)–Pr(1)–N(7)	124.72(2)	N(7)–Pr(1)–O(4)	72.04(2)
O(8)–Pr(1)–O(13)	124.3(1)	N(7)–Pr(1)–O(8)	137.18(2)
O(8)–Pr(1)–N(1)	138.27(2)	N(7)–Pr(1)–O(13)	50.6(7)
O(8)–Pr(1)–N(2)	125.17(2)	N(7)–Pr(1)–N(1)	84.0(2)
O(9)–Pr(1)–O(4)	137.30(2)	N(7)–Pr(1)–N(2)	75.34(2)
O(9)–Pr(1)–O(8)	69.27(2)		

Symmetry transformations used to generate equivalent atoms: #1 $-x+1, -y+1, -z$.

In the complex, the isoorotate group (H_2iso^- or $Hiso^{2-}$) acts as a bidentate ligand through the carboxylate group and the adjacent carbonyl oxygen, forming a stable six-membered ring. This is the same as in the Mn(II) [5], Zn(II) [7], Fe(II) [8] and Mg(II) [10] complexes with H_2iso^-. The Yb–O distances range from 2.285 to 2.360 Å and the average value is 2.333 Å (2.371 Å for **1**).

There are several kinds of hydrogen bonds in **2**: (1) the O_w–H$\cdots O_{cc}$ hydrogen bond between the coordinating water molecule (O_w) and the coordinating carboxyl oxygen (O_{cc}); (2) the O_w–H$\cdots O_c$ hydrogen bond between the coordinating water molecule and the uncoordinating carbonyl oxygen (O_c); (3) the O_w–H$\cdots O_w$ hydrogen bond among the coordinating water molecules; (4) the N–H$\cdots O_c$ hydrogen bond between the amido group and the uncoordinating carbonyl oxygen. All these hydrogen bonds link the moieties into a 2D layer structure along the ab plane, as shown in Fig. 2. The lattice water molecules in **2** can form hydrogen bonds with the aqua ligands, uncoordinating carbonyl oxygen and coordinating carboxyl oxygen, which connect the 2D layer into a 3D supramolecular architecture [14]. The details of the hydrogen bonds are listed in Table 6.

*$Pr_2(Hiso)(H_2iso)_4(phen)_2(H_2O)_2\cdot 5H_2O$ (**3**).* The coordination environments of the Pr(III) ions in **3** are shown in Fig. 3. Both Pr(III) ions are coordinated by four oxygen atoms (O(1), O(4), O(5), O(8) or O(1A), O(4A), O(5A), O(8A)) from two H_2iso^- anions, one oxygen atom (O(9) or O(9A)) from one coordinated water molecule and two nitrogen atoms (N(1), N(2) or N(1A), N(2A)) from one chelating phen molecule. For Pr(1), one oxygen atom (O(13)) and one nitrogen atom (N(7)) from one $Hiso^{2-}$ anion occupy the last two sites to complete the nine-coordination. On the other hand, for Pr(1A) they are O(10) and O(11) from the $Hiso^{2-}$

Table 4
Selected bond lengths (Å) and angles (°) for **4** and **5**

*Compound **4***			
Bond lengths			
Eu(1)–O(1)	2.284(4)	Eu(1)–N(1)	2.593(6)
Eu(1)–O(3)	2.355(4)	Eu(1)–N(2)	2.616(5)
Bond angles			
O(1)–Eu(1)–O(1)#1	88.1(2)	O(3)–Eu(1)–N(1)#1	134.87(2)
O(1)–Eu(1)–O(3)	73.27(1)	O(3)–Eu(1)–N(2)	122.17(2)
O(1)–Eu(1)–O(3)#1	82.93(2)	O(3)–Eu(1)–N(2)#1	75.19(2)
O(1)–Eu(1)–N(1)	105.19(2)	O(3)#1–Eu(1)–O(3)	146.8(2)
O(1)–Eu(1)–N(1)#1	149.32(1)	N(1)–Eu(1)–N(1)#1	77.4(2)
O(1)–Eu(1)–N(2)	81.42(2)	N(1)–Eu(1)–N(2)	62.79(2)
O(1)–Eu(1)–N(2)#1	147.73(1)	N(1)–Eu(1)–N(2)#1	72.62(2)
O(3)–Eu(1)–N(1)	74.97(2)	N(2)–Eu(1)–N(2)#1	122.1(3)
*Compound **5***			
Bond lengths			
Tb(1)–O(1)	2.275(3)	Tb(1)–N(1)	2.575(4)
Tb(1)–O(3)	2.333(3)	Tb(1)–N(2)	2.593(3)
Bond angles			
O(1)–Tb(1)–O(1) #1	88.64(2)	O(3)–Tb(1)–N(1)#1	74.84(1)
O(1)–Tb(1)–O(3)	73.97(1)	O(3)–Tb(1)–N(2)	74.53(1)
O(1)–Tb(1)–O(3)#1	82.42(1)	O(3)–Tb(1)–N(2)#1	122.39(1)
O(1)–Tb(1)–N(1)	148.68(1)	O(3)#1–Tb(1)–O(3)	146.87(1)
O(1)–Tb(1)–N(1)#1	105.07(1)	N(1)–Tb(1)–N(2)	63.53(1)
O(1)–Tb(1)–N(2)	147.67(1)	N(1)–Tb(1)–N(2)#1	73.21(1)
O(1)–Tb(1)–N(2)#1	80.21(1)	N(1)#1–Tb(1)–N(1)	77.73(2)
O(3)–Tb(1)–N(1)	134.87(1)	N(2)–Tb(1)–N(2)#1	123.71(2)

Symmetry transformations used to generate equivalent atoms: #1 $-x+1, y, -z+1/2$.

anion. The $Hiso^{2-}$ anion is disordered and its occupancy is 0.5. The average distance of Pr–O is 2.498 Å, while that of Pr–N is 2.676 Å. In the complex, the coordination modes of H_2iso^- and $Hiso^{2-}$ anions are different. The H_2iso^- anion acts as an O,O-chelating bidentate ligand, the same as in complexes **1** and **2**, while the $Hiso^{2-}$ anion acts as a tetradentate ligand. In addition to the formation of a six-membered ring, another carbonyl oxygen and one deprotonated amido nitrogen are involved in the coordination. So one $Hiso^{2-}$ anion bridges two Pr(III) ions. This coordination mode has not been reported before. The separation between Pr(1) and Pr(1A) is 8.717 Å.

The dinuclear $Pr_2(Hiso)(H_2iso)_4(phen)_2(H_2O)_2$ is the building block of **3**. Every two such building blocks are linked by O_w–H···O_c hydrogen bonds, forming a grid of 10.239×8.717 Å (Fig. 4a). There are N–H···O_c, O_w–H···O_{uc}, O_w–H···O_{uc} and O_w–H···O_w hydrogen bonds between the grids, resulting in the formation of a 3D supramolecular structure, as shown in Fig. 4b. The details of the hydrogen bonds are depicted in Table 6. All phen molecules are perfectly parallel to each other and the average distance between two adjacent phen planes is 3.58 Å, indicating the existence of π-aromatic interactions.

*$Yb(Hiso)(H_2iso)(phen)_2 \cdot 2H_2O$ (**6**)*. There is only one metal environment in **6** as shown in Fig. 5. The Yb(III) ion is eight-coordinated and is surrounded by four nitrogen atoms belonging to two chelating phen molecules and four oxygen atoms from two isoorotate groups. The distances of Yb–O are 2.222 and 2.272 Å, and those of Yb–N are 2.513 and 2.544 Å. The average distance of Yb–O is 2.247 Å, which is much shorter than that of Yb–N (2.529 Å). The dihedral angle between two phen molecules is 35.8°. In the complex, the isoorotate groups (H_2iso^- or $Hiso^{2-}$) also act as bidentate ligands as in **1** and **2**, but leading to a different architecture.

A 3D supramolecular network (see Fig. 6) results from the hydrogen bonds among the amido groups (N–H···N), and the hydrogen bonds between the amido group and the uncoordinating carbonyl oxygen (N–H···O_c), the lattice water and the uncoordinating carbonyl oxygen (O–H···O_c), the lattice water and the uncoordinating carboxyl oxygen (O–H···O_{uc}).The details of the hydrogen bonds are shown in Table 6.

*$Yb(Horo)(OH)(H_2O)$ (**7**)*. The structure of **7** is similar to that of $Gd(Horo)(OH)(H_2O)$ [15], which is a coordination polymer with a 3D network. Each Yb(III) ion is coordinated to one nitrogen and seven oxygen atoms, of which three oxygen atoms come from OH^- groups, three from different orotate ligands and one from a coordinating water molecule. In the complex, the orotate group acts as a tetradentate ligand, coordinating

Table 5
Selected bond lengths (Å) and angles (°) for **6** and **7**

Compound ***6***[a]			
Bond lengths			
Yb(1)–O(1)	2.222(2)	Yb(1)–N(1)	2.513(3)
Yb(1)–O(3)	2.272(2)	Yb(1)–N(2)	2.544(3)
Bond angles			
O(1)–Yb(1)–O(1)#1	89.86(1)	O(3)–Yb(1)–N(1)#1	74.31(9)
O(1)–Yb(1)–O(3)	75.22(8)	O(3)–Yb(1)–N(2)	74.34(9)
O(1)–Yb(1)–O(3)#1	81.42(9)	O(3)–Yb(1)–N(2)#1	122.13(1)
O(1)–Yb(1)–N(1)	146.68(8)	O(3)#1–Yb(1)–O(3)	146.83(1)
O(1)–Yb(1)–N(1)#1	105.28(1)	N(1)–Yb(1)–N(2)	64.64(9)
O(1)–Yb(1)–N(2)	148.61(8)	N(1)–Yb(1)–N(2)#1	73.50(9)
O(1)–Yb(1)–N(2)#1	78.23(9)	N(1)#1–Yb(1)–N(1)	78.16(1)
O(3)–Yb(1)–N(1)	135.52(8)	N(2)–Yb(1)–N(2)#1	125.38(1)
Compound ***7***[b]			
Bond lengths			
Yb(1)–O(2)	2.243(1)	Yb(1)–O(6)	2.294(9)
Yb(1)–O(5)	2.267(1)	Yb(1)–O(6)#2	2.469(2)
Yb(1)–O(3)#1	2.295(1)	Yb(1)–O(6)#3	2.36(2)
Yb(1)–O(4)#2	2.333(8)	Yb(1)–N(2)	2.511(1)
Bond angles			
O(2)–Yb(1)–O(3)#1	83.3(4)	O(5)–Yb(1)–O(3)#1	70.8(4)
O(2)–Yb(1)–O(4)#2	148.4(4)	O(5)–Yb(1)–O(4)#2	117.7(4)
O(2)–Yb(1)–O(5)	74.7(5)	O(5)–Yb(1)–O(6)	143.4(6)
O(2)–Yb(1)–O(6)	112.1(5)	O(5)–Yb(1)–O(6)#2	138.6(5)
O(2)–Yb(1)–O(6)#2	74.8(4)	O(5)–Yb(1)–O(6)#3	76.2(5)
O(2)–Yb(1)–O(6)#3	139.0(4)	O(5)–Yb(1)–N(2)	77.0(4)
O(2)–Yb(1)–N(2)	66.1(4)	O(6)–Yb(1)–O(3)#1	143.9(4)
O(3)#1–Yb(1)–O(4)#2	75.0(4)	O(6)–Yb(1)–O(4)#2	76.2(3)
O(3)#1–Yb(1)–O(6)#2	78.4(4)	O(6)–Yb(1)–O(6)#2	75.0(4)
O(3)#1–Yb(1)–O(6)#3	113.2(3)	O(6)–Yb(1)–O(6)#3	77.2(5)
O(3)#1–Yb(1)–N(2)	140.4(4)	O(6)–Yb(1)–N(2)	73.9(4)
O(4)#2-Yb(1)–O(6)#2	78.5(4)	O(6)#2–Yb(1)–N(2)	114.4(3)
O(4)#2-Yb(1)–O(6)#3	71.8(4)	O(6)#3–Yb(1)–O(6)#2	143.2(4)
O(4)#2-Yb(1)–N(2)	142.5(4)	O(6)#3–Yb(1)–N(2)	79.8(3)

[a] Symmetry transformations used to generate equivalent atoms: #1 $-x+1, y, -z+1/2$.
[b] Symmetry transformations used to generate equivalent atoms: #1 $-x+3/2, y+1/2, z-1/2$ #2 $-x+2, -y+1, z-1/2$ #3 $-x+2, -y+1, z+1/2$.

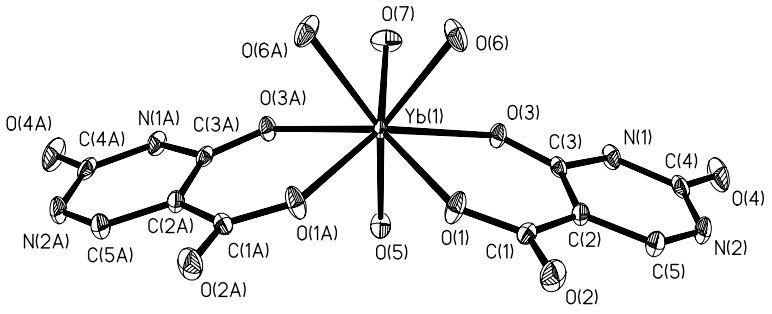

Fig. 1. Asymmetric unit of complex **2** with 30% thermal ellipsoids, lattice water molecules and hydrogen atoms are omitted for clarity.

through two carbonyl oxygen, one carboxylate oxygen and one deprotonated amido nitrogen.

Comparing the structures of **2** and **7**, we can see some differences: (1) **2** is mononuclear while **7** is a 3D coordination polymer. This is the result of the different coordination modes of isoorotate and orotate anions. The former coordinates to metal atoms through the carboxylate group and the adjacent carbonyl oxygen, forming a stable six membered ring, while the latter acts as a bridging ligand to link the metals. (2) The position

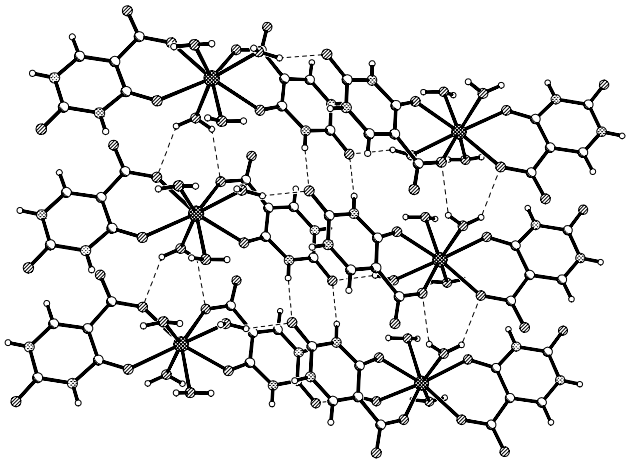

Fig. 2. The 2D layer structure of complex **2** viewed along the *c*-axis.

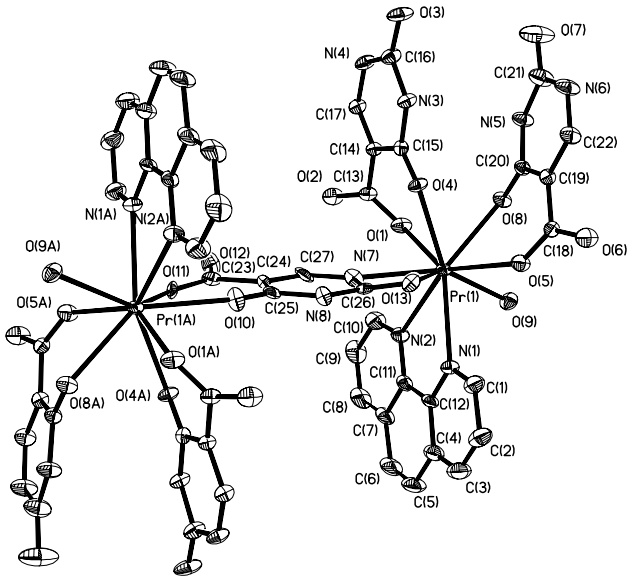

Fig. 3. The coordination environments of Pr(III) ions in **3** with 30% thermal ellipsoids, all hydrogen atoms and lattice water molecules are omitted for clarity.

of carboxylate is important for the deprotonation of the amido group. In **2**, H_3iso only loses one hydrogen atom of the carboxylate group; while in **7**, H_3oro loses two hydrogen atoms, including one hydrogen of the carboxylate group and one hydrogen of the adjacent amido group, so that $Horo^{2-}$ coordinates to the metal ion through the carboxylate oxygen and the adjacent deprotonated amido nitrogen, forming a five membered ring.

Phen is a versatile ligand to construct supramolecular structures, as it is often involved with π–π stacking interactions and C–H···O hydrogen bonds. When phen was introduced to the mixture of H_3iso and lanthanide

Table 6
Hydrogen bonding geometry (Å) and (°) for **2**, **3** and **6**

D–H	*d*(D–H)	*d*(H..A)	<DHA	*d*(D..A)	A
Compound ***2***					
N1–H1	0.860	2.008	170.74	2.860	O4 $[-x+2,-y+1,-z+1]$
O5–H5A	0.855	2.161	136.47	2.842	O1 $[x+1,-y+3/2,z]$
O6–H6A	0.855	1.940	152.59	2.727	O4 $[-x+1,-y+1,-z+1]$
O6–H6B	0.852	2.195	154.23	2.986	O7 $[x-1,y,z]$
O7–H7A	0.853	1.942	172.38	2.790	O8 $[-x+1,y+1/2,-z+1]$
O8–H8A	0.856	1.891	166.54	2.731	O2 $[-x,-y+1,-z]$
O8–H8B	0.866	2.255	119.87	2.790	O7 $[-x+1,-y+1,-z+1]$
O9–H9A	0.851	2.347	134.40	3.005	O1 $[x,-y+3/2,z+1]$
O9–H9A	0.851	2.347	134.40	3.005	O1 $[x,y,z+1]$
O9–H9B	0.857	2.347	129.14	2.964	O6
O9–H9B	0.857	2.347	129.14	2.964	O6 $[x,-y+3/2,z]$
Compound ***3***					
O9–H9A	0.930	2.149	130.09	2.839	O16 $[-x+2,-y+1,-z+1]$
O9–H9A	0.930	2.186	132.64	2.898	O3 $[x+1,y,z]$
O9–H9B	0.930	2.293	115.78	2.824	O6 $[-x+2,-y,-z+1]$
N3–H3	0.860	1.868	167.96	2.715	O6 $[-x+1,-y,-z+1]$
N4–H4	0.860	1.954	163.50	2.790	O3 $[-x,-y+1,-z+1]$
N5–H5	0.860	1.894	176.12	2.753	O2 $[-x+1,-y+1,-z+1]$
N6–H6	0.860	2.121	152.33	2.910	O11 $[x,y-1,z+1]$
N6–H6	0.860	2.123	151.10	2.905	O13 $[-x+1,-y,-z+1]$
N6–H6	0.860	2.177	136.97	2.867	O12 $[x,y-1,z+1]$
Compound ***6***					
N3–H3A	0.860	1.973	176.40	2.832	O2 $[x,-y+1,z-1/2]$
N4–H4	0.860	1.798	173.37	2.654	N4 $[-x+1/2,-y+3/2,-z]$
O5–H5A	0.842	2.255	146.05	2.990	O2 $[-x+1/2,y-1/2,-z+1/2]$
O5–H5B	0.843	2.117	179.18	2.961	O4 $[x,-y+1,z+1/2]$

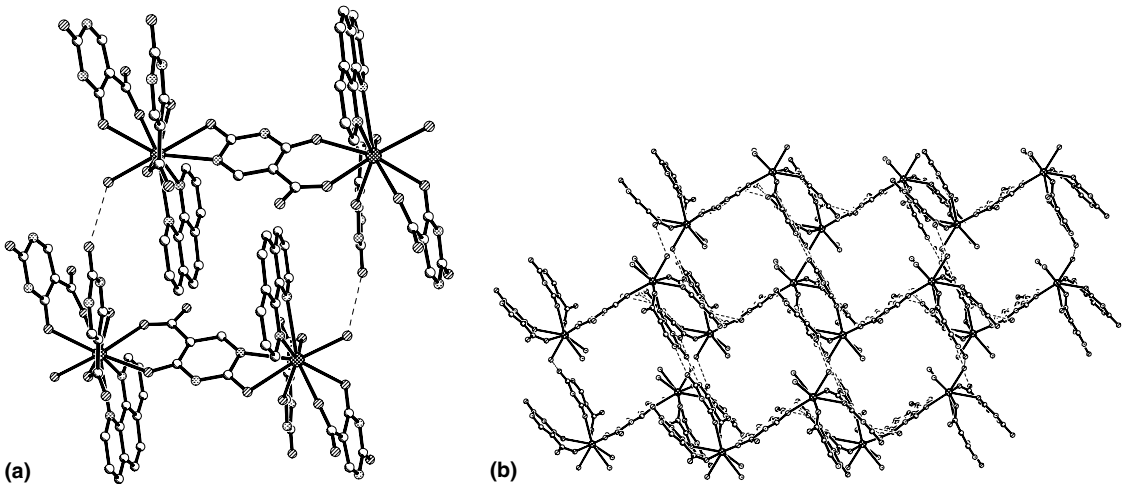

Fig. 4. (a) The grid formed by the O_w–H$\cdots$$O_c$ hydrogen bonds; (b) The 3D supramolecular network of **3** viewed along the *b*-axis, carbon atoms of phen molecules and all the hydrogen atoms are omitted for clarity.

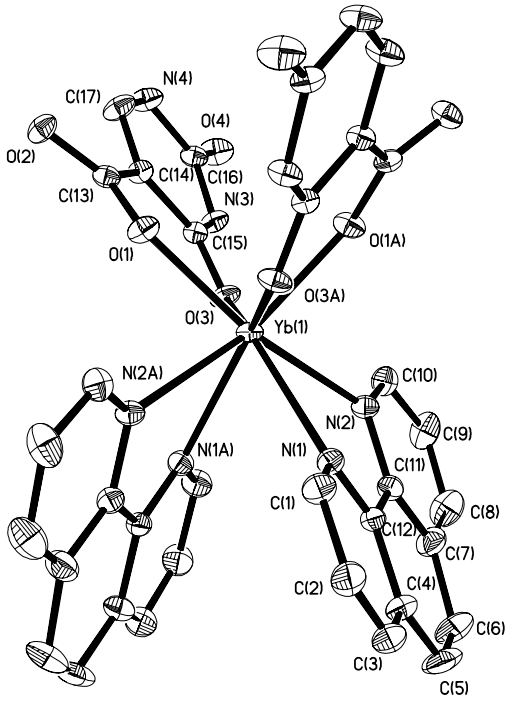

Fig. 5. Asymmetric unit of the complex **6** with 30% thermal ellipsoids; two lattice water molecules and all hydrogen atoms are omitted for clarity.

ions, different results were obtained. In **3**, there are weak π–π stacking interactions between phen molecules as expected. But in complexes **4**–**6**, two phen molecules coordinate to one lanthanide ion. In order to decrease the steric hindrance, the phen molecules are separated with a large distance and there are no π–π stacking interactions.

From **3** to **6**, with increasing atomic number, the mean distance of Ln–O bonds are in the following order:

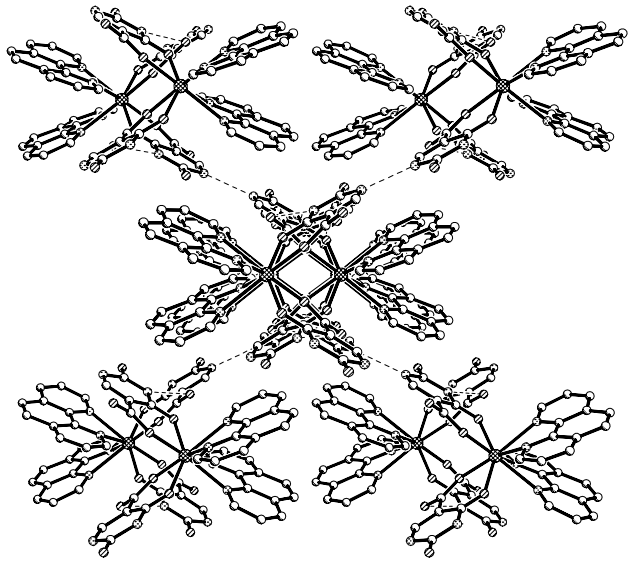

Fig. 6. The 3D supramolecular network of **6** viewed along the *c*-axis.

Pr–O (2.498 Å) > Eu–O (2.320 Å) > Tb–O (2.304 Å) > Yb–O (2.247 Å); the mean Ln–N bond distances are 2.676, 2.605, 2.584 and 2.529 Å for Pr, Eu, Tb and Yb, respectively. This is consistent with the lanthanide contraction.

3.2. Thermal analyses

Thermogravimetric analyses of the seven complexes were carried out to examine their thermal stabilities. The data of the thermogravimetric analyses for **1**–**7** are listed in Table 7. The complexes **1**–**6** lost their coordinated or/and lattice water molecules at the first weight loss, while complex **7** began to decompose above 250 °C.

Table 7
Thermogravimetric analyses data of **1**–**7**

	Dehydration temperature (°C)	Loss of water: Cacl. (Found) (%)	Further decomposition temperature (°C)
1	84–168	21.2 (20.8)	258
2	75–177	20.7 (20.4)	260
3	48–199	5.8 (5.5)	232
4	69–141	4.2 (3.8)	291
5	63–160	4.2 (3.6)	310
6	64–151	4.1 (3.8)	320
7			250

From Table 7 we can see that the dehydration temperature for **1–6** ranges from 48 to 199 °C. They further decompose beyond 230 °C. Taking **2** as an example, the TGA curve shows that the first weight loss of 20.4%, which occurs between 75 and 177 °C, corresponds to the loss of four coordinated and three crystal water molecules (calculated: 20.7%). Further decomposition of **2** occurs above 260 °C, whereas for **3** the first weight loss of 5.5%, from 48 to 199 °C, corresponds to the loss of five crystal water molecules (calculated: 5.8%) and further decomposition occurs above 232 °C.

4. Supplementary data

Crystallographic data for the structural analysis have been deposited with the Cambridge Crystallographic Data Centre, CCDC Nos. 227488 to 227494 for **1**–**7**, respectively. Copies of this information may be obtained free of charge from the CCDC, 12 Union Road, Cambridge, CB2 1EZ, UK (fax: +44-1223-336-033; e-mail:deposit@ccdc.cam.ac.uk or www:http://www.ccdc.cam.ac.uk).

Acknowledgements

This project is supported by National Nature Science Foundation of China (20071004, 20331010).

References

[1] I. Lieberman, A. Kornberg, E.S. Simms, J. Biol. Chem. 215 (1955) 403.
[2] N.K. Davidenko, N.N. Zinich, Russ. J. Chem. 24 (1979) 891.
[3] H. Tobiki, H. Yamada, Y. Nakatsuka, K. Shimago, I. Eda, N. Noguchi, T. Komatsu, T. Nakagome, Yakugaku Zasshi 100 (1980) 38.
[4] F. Hueso-Ureña, M.N. Moreno-Carretero, J.M. Salas-Peregrin, G.A. de Cienfuegos-López, J. Inorg. Biochem. 43 (1991) 17.
[5] G. Maistralis, N. Katsaros, D. Mentzafos, A. Terzis, Acta Cryst. Sect. C 47 (1991) 740.
[6] G. Maistralis, N. Katsaros, S.P. Perlepes, D. Kovala-Demertzi, J. Inorg. Biochem. 45 (1992) 1.
[7] F. Hueso-Ureña, M.N. Moreno-Carretero, M.A. Romero-Molina, J.M. Salas-Peregrin, M.P. Sanchez-Sanchez, G.A. de Cienfuegos-López, R. Faure, J. Inorg. Biochem. 51 (1993) 613.
[8] E.J. Baran, R.C. Mercader, F. Hueso-Ureña, M.N. Moreno-Carretero, M. Quiros-Olozabal, J.M. Salas-Peregin, Polyhedron 15 (1996) 1717.
[9] F. Hueso-Ureña, M.N. Moreno-Carretero, M. Quiros-Olozabal, J.M. Salas-Peregin, R. Faure, G.A. de Cienfuegos-López, Inorg. Chim. Acta 241 (1996) 61.
[10] C.C. Wagner, E.J. Baran, O.E. Piro, J. Inorg. Biochem. 73 (1999) 259.
[11] G.M. Sheldrick, SADABS, Program for Empirical Absorption Correction of Area detector Data, University of Göttingen, Germany, 1997.
[12] G.M. Sheldrick, SHELXS-97, Program for Crystal Structure Solution, University of Göttingen, Germany, 1997.
[13] G.M. Sheldrick, SHELXL-97, Program for Crystal Structure Refinement, University of Göttingen, Germany, 1997.
[14] J. Lehn, Angew. Chem. Int. Ed. Engl. 29 (1990) 1304.
[15] X. Li, R. Cao, D. Sun, Q. Shi, M. Hong, Y. Liang, Inorg. Chem. Commun. 5 (2002) 589.

Available online at www.sciencedirect.com
SCIENCE DIRECT®
Polyhedron 23 (2004) 2095–2101
POLYHEDRON
www.elsevier.com/locate/poly

Synthesis, characterization, thermodynamic and thermal studies of Zn(II) complexes with di-2-pyridyl ketone salicyloylhydrazone

Ivanise Gaubeur [a,b], Márcia Guekezian [b], Lúcia H.S. Ávila Terra [c], Maria Carolina B. Moraes [d], Claudimir L. Lago [e], Jivaldo R. Matos [e], Maria Encarnación V. Suárez-Iha [e,*]

[a] *E. Engenharia, Universidade Presbiteriana Mackenzie*
[b] *FCBE e Experimentais, Universidade Presbiteriana Mackenzie*
[c] *EFO de Alfenas, Centro Universitário Federal*
[d] *Embrapa Cenargen Pq EB*
[e] *Instituto de Química, Universidade de São Paulo, Caixa Postal 26077, CEP 05513-970, São Paulo, Brasil*

Received 19 March 2004; accepted 3 June 2004

Abstract

This paper shows the characteristics of a coordinated compound formed by zinc(II) and di-2-pyridyl ketone salicyloylhydrazone (DPKSH). The synthesized complex shows the formula: $Zn(DPKSH)_2$. Elemental analysis, electron ionization and electrospray mass spectra indicated the 1:2 metal/ligand molar ratio. The IR spectra show that DPKSH is coordinated to zinc(II) through the oxygen from the enolic or the phenolic group as the *v*CO frequency was suppressed and the *v*CO (phenolic) band was shifted to higher frequency in the IR spectrum of the complex. Two other interactions can be attributed to the nitrogens from the azo and the pyridine groups. Thermal decomposition and differential scanning calorimetry (DSC) are different for the ligand and the complex. The overall formation constants were obtained in ethanolic solution 50% (V/V), at pH 4.5 and 25 °C, resulting in $\beta_1 = 1.07\times10^5$ and $\beta_2 = 1.05\times10^{10}$. The molar absorptivies of the 1:1 (ε_1) and 1:2 (ε_2) complexes (Zn(II):DPKSH) were found to be 1.1×10^4 and 4.5×10^4 ($M^{-1}cm^{-1}$), respectively.
© 2004 Elsevier Ltd. All rights reserved.

Keywords: Di-2-pyridyl ketone salicyloylhydrazone; Zinc(II) complexes; Stability constants; Spectroscopy; Thermal analysis

1. Introduction

Hydrazones are azomethines characterized by the triatomic grouping C═N–N and they are interesting substances because some of them may play an important role in the treatment of several diseases, such as tuberculosis. Such an activity is directly attributed to the formation of stable chelates with transition metals that catalyze the corresponding physiological processes [1–3]. Such compounds are often synthesized and are widely used in analytical chemistry, chiefly as colorimetric or fluorimetric reagents or in liquid–liquid extraction methods combined with atomic absorption, colorimetric or fluorimetric methods for the determination of metallic ions [4–17]. In these chelates the aroylhydrazones ($R^1R^2CN_2(H)C(O)R^3$) may behave as a bidentate, tridentate or tetradentate ligand when R^1, R^2 and/or R^3 have a donor atom in an appropriate position [1,2,17–19]. When R^1 and R^2 are pyridine groups and R^3 is an

* Corresponding author. Tel.: +55-11-30-210-473; fax: +55-11-38-155-579.
E-mail address: maevsiha@iq.usp.br (Maria Encarnación V. Suárez-Iha).

0277-5387/$ - see front matter © 2004 Elsevier Ltd. All rights reserved.
doi:10.1016/j.poly.2004.06.004

o-hydroxy-phenolic group, the result is di-2-pyridyl ketone salicyloylhydrazone (DPKSH).

Di-2-pyridyl ketone salicyloylhydrazone is a reagent soluble in different organic solvents but only slightly soluble in water. In aqueous/ethanolic solutions, DPKSH shows tautomeric structures (I and II) [20] and it may be coordinated to the metallic ion through the nitrogen atoms either alone or in combination with an oxygen atom, of the enolic or phenolic group. Neutral metallic complexes are formed in many cases.

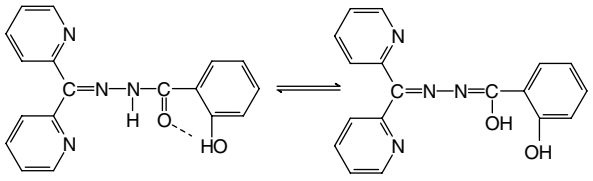

(I) ketonic form (II) enolic form

Recently, complexes of zinc(II) with DPKSH were used to develop a highly sensitive spectrophotometric method [16]. The highest sensitivity was achieved in 50% (V/V) ethanol–water solvent and pH 4.5, maintained with acetic acid/acetate buffer. The main advantages of this method consist of low detection limit (8.1 $\mu g\,L^{-1}$), high sensitivity (4.8×10^{4} $L\,mol^{-1}\,cm^{-1}$ at 376 nm) and the use of simple instrumentation with the possible application in field analysis.

For a better understanding of the bonds, structure and stoichiometry of DPKSH/Zn(II) complexes, as well as the knowledge of some spectroscopic, thermal and thermodynamic properties, a thorough report on the experiments and the results obtained from DPKSH and the DPKBH/Zn(II) complex is provided.

2. Experimental

2.1. Reagents and solutions

All reagents and solvents were of analytical grade from Merck. A standard solution of Zn(II) was prepared by dissolving reagent-grade $ZnSO_4\cdot7H_2O$ in de-ionized water and sulfuric acid. The final pH was adjusted to ≈2.5 in order to avoid the hydrolysis of the metallic ion and the zinc(II) concentration was determined by titration with a standard EDTA solution [21].

The synthesis of DPKSH was performed in accordance with the procedure outlined by Garcia-Vargas et al. [20]. After synthesis, the melting point of the product was verified to be 179 °C and its absorption spectrum was checked and compared with previously reported values [20]. The DPKSH stock solution was prepared by dissolving the reagent in ethanol and may be stored for 30 days.

The complex was obtained by reacting the zinc hydrated salt and the ligand (molar ratio 1:2) in ethanol. This molar ratio was achieved by mixing 50 mL of each solution: 2×10^{-2} $mol\,L^{-1}$ Zn(II) and 4×10^{-2} $mol\,L^{-1}$ DPKSH. After a slow evaporation of this solvent, the complex was dried under vacuum over anhydrous calcium chloride leading to a yellow solid.

The electrospray ionization spectra were recorded from a solution of the complex in ethanol/methanol 40/60% (v/v). Another electrolyte was not added because the synthesis was carried out in presence of buffer solution (acetic acid/potassium acetate).

The necessary experimental data for the application of the continuous variations [22,23] or Job's method are made up of the absorbances related to solutions with different ligand molar fractions, varying the concentrations of both Zn(II) and DPKSH, but keeping the sum of the ligand and the metal ion concentrations constant at 1.0×10^{-4} $mol\,L^{-1}$. Such solutions are obtained from complementary volumes of equimolar solutions where the total volume is constant. The stoichiometry of the Zn(II)/DPKSH complexes was determined by using a series of solutions having a constant sum of the DPKSH and Zn(II) concentrations, in 50% ethanol–water and at pH 4.5. The molar ratio was varied from 0 to 1 and the absorbance values were measured at $\lambda = 376$ nm.

The necessary absorbance measurements to determine the overall formation constants [24] of the complexes were obtained at 376 nm. Three series of solutions with 1.10×10^{-5}, 1.52×10^{-5} and 2.01×10^{-5} $mol\,L^{-1}$ Zn(II) were prepared with different ligand concentrations ranging from 0.01×10^{-5} to 5.0×10^{-5} $mol\,L^{-1}$, in 50% EtOH/water, at pH 4.5.

2.2. Apparatus

All spectrophotometric measurements were carried out on a Hitachi model U-3000 spectrophotometer using 1.00 cm quartz cells. The pH measurements were performed with a Metrohm 654 pH meter equipped with a Metrohm glass electrode of which the Ag/AgCl reference was filled with 3 $mol\,L^{-1}$ NaCl. FTIR spectra (4000—500 cm^{-1}; KBr pellets) were recorded on a Perkin–Elmer 1750 series FTIR spectrophotometer. The electron ionization spectra were obtained from a Hewlett Packard HP 5988A. The electrospray mass spectra were obtained from Platform II Micromass in high capillary and cone tension (2.90 kV and 53 V, respectively). A CHN Elemental Analyser instrument from Perkin–Elmer, model 2400 was used to determine the C, H and N percentages both in DPKSH and the Zn(II)/DPKSH complex. The percentage of oxygen in the ligand was calculated by difference and the Zn(II) percentage present in the complex was obtained from TG experiments. Thermogravimetry (TG) and derivative thermogravimetry (DTG) curves were obtained on a model TGA-50

Thermogravimetric Analyzer in the temperature range 25–900 °C with a heating rate of 10 °C min^{-1} under dynamic air atmosphere (ca. 50 mL min^{-1}) and with a sample weighing 3.1–3.2 mg in a Pt crucible. Differential scanning calorimetry (DSC) curves were obtained on a DSC50 cell (Shimadzu) in the temperature range 25–600 °C with a heating rate of 10 °C min^{-1}, under dynamic nitrogen atmosphere (ca. 50 mL min^{-1}) with a sample weighing in the range of 0.9–1.3 mg in an Al crucible. The DSC system was calibrated with indium (m.p. = 156.6 °C; $\Delta H_{fus.}$ = 28.54 J g^{-1}) and zinc (m.p. = 419.6 °C).

3. Results and discussion

DPKSH is a crystalline and very light yellow solid and the Zn(II)/DPKSH complexes obtained as previously described have a darker yellow color. The main IR frequencies for DPKSH and Zn(II)/DPKSH are summarized in Table 1. IR spectrum of the complex differs significantly from that of the free ligand. The ν(N–H) at 3059 cm^{-1}, δ(C═O) at 1636 cm^{-1} (amide I) and δ(C–O) phenolic group at 1133 cm^{-1}, observed for the ligand, are suppressed in the spectrum [25–27] of the complex. The shift of the carbonyl stretching mode to lower frequencies is in accordance with coordination through the oxygen. The band at 1583 cm^{-1} (amide II) is shifted to a higher frequency and intensity in the complex (1593 cm^{-1}). The band due to the phenolic group from the ligand at 1133 cm^{-1} [25] is shifted to a higher frequency (1151 cm^{-1}) in the complex. These observations suggest that DPKSH is coordinated to Zn(II) through the oxygen from the enolic (amide I) or phenolic group (C–O 1133 cm^{-1}) and through nitrogens of one of the pyridines and from the principal chain (amide II).

Electron ionization spectra of the ligand and the Zn(II)/DPKSH complex were registered in a range of m/z from 0 to 400. Main fragments found for DPKSH are indicated in Table 2. The base peak was found at m/z = 169 for both the ligand and the complex. The molecular ion peak at m/z = 318 corresponds to the formula weight of the ligand. The peak m/z = 121 was found for the ligand but it was not observed for the Zn(II) complex. In the spectrum of the complex the molecular ion peak formed at m/z = 350 probably corresponds to its formula weight when z = 2 ($Zn(C_{18}H_{13}N_4O_2)_2$, 700 g mol^{-1}).

The mass spectrum with electrospray ionization [28–30] was obtained. The cluster registered at m/z = 701, corresponds to the protonated complex $[Zn(C_{18}H_{13}N_4O_2)_2H]^+$ and confirms the composition of the Zn(II)/DPKSH complex with a 1:2 ratio of Zn(II)/ligand. A peak at m/z = 723 may be related to the species $[Zn(DPKSH)_2Na]^+$ and the presence of Na is probably due to a very common electrode contamination. A cluster at m/z = 739 was also observed and it can be correlated to the $[Zn(DPKSH)_2K]^+$ species. The presence of K is probably explained by the use of buffer solution (acetic acid/potassium acetate) in the synthesis of the complex.

Table 3 shows the elemental analysis results for DPKSH and its complexes with Zn(II). These data are in excellent compliance with the calculated C, H and N percentages for the ligand and the respective complex of Zn(II) considering the 1:2 stoichiometry $[Zn(DPKSH)_2]$. The calculation was made considering

Table 1
Main IR frequencies (cm^{-1}) of DPKSH and the Zn(II)/DPKSH complex and their assignments[a]

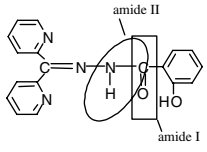

DPKSH	Zn(II)/DPKSH	Characteristic groups
3059 s		νN–H (free); νC–H (aromatic)
1636 s		C═O (amide I)
1583 m	1593 s	δN–H (amide II); νC–C e νC–N (pyridine)
1506 w	1513 s	νC–C; νC–N (pyridine)
	1399 s	νC–C; νC–N (pyridine)
1329 w	1323 s	δO–H (phenolic); νC–C e νC–N (pyridine)
1155 w	1151 s	νC–O (phenolic)
1133 s		νC–O (phenolic)
1086 w	1095 m	νC–O (phenolic)
905 s		δC–H (out of plane)
805 s	797 m	δC–H (out of plane)
757 m	751 s	δC–H (out of plane)
742 s		δC–H (out of plane)

[a] s, strong; m, medium; w, weak.

Table 2
Main DPKSH fragments related to the main peaks registered in the mass spectrum

m/z	Fragment	%
318	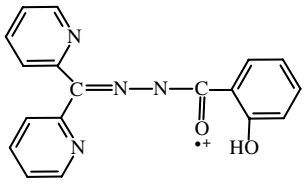	**5**
197	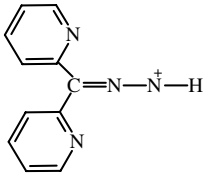	**76**
169	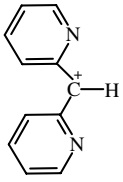	**100**
121	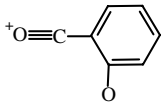	**11**

the formula weight of the DPKSH being equal to 318.3 and 317.3 g mol^{-1} for the ligand coordinated to Zn(II) ions as an anion ($[C_{18}N_4H_{13}O_2]^-$).

The concordance between the experimental and theoretical percentages of C, N and H found for the ligand shows the absence of water molecules. Considering the elemental analysis data (Table 3) for the complex it is possible to confirm the presence of a water molecule in the composition, namely $Zn(DPKSH)_2 \cdot H_2O$.

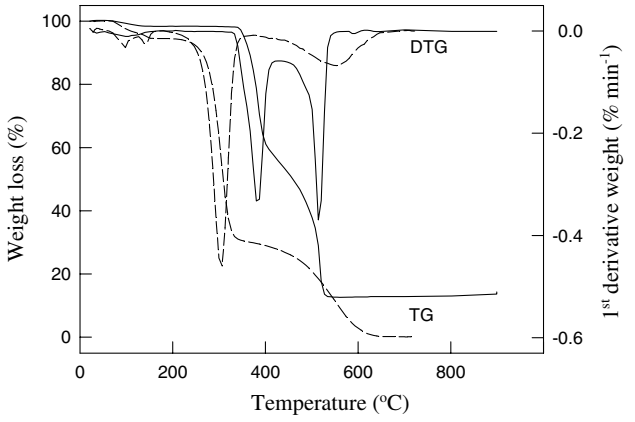

Fig. 1. TG/DTG curves: for (– – –) DPKSH ($m = 3.134$ mg) and (—) $Zn(DPKSH)_2$ ($m = 3.271$ mg). Both of the curves were obtained in air atmosphere (ca. 50.0 mL min^{-1}) and a heating rate of 10 °C min^{-1}.

Fig. 1 shows TG/DTG curves for the ligand and the Zn(II) complex. Thermal decomposition of DPKSH occurs in three main steps, with DTG peaks at 91 and 146 (related to dehydration), 295 and 493 °C. The weight loss observed between 50 and 160 °C may be attributed to an intramolecular reaction that involves the loss of a water molecule as the TG curve shows a mass variation of 5.41%. Considering this probable reaction, the mass loss calculated corresponds to 5.67%, which is quite similar to the experimental value.

TG/DTG curves of the complex show a mass loss of 2.6% over temperatures ranging from 30 to 200 °C that corresponds to the complex dehydration, indicating the presence of one coordinated water molecule. The anhydrous species is stable thermally up to ≈350 °C. In a temperature range from 350 to 730 °C, the thermal decomposition occurs at two distinctive stages. The mass loss between 350 and 430 °C with a DTG peak at 383 °C and $\Delta m = 43.9\%$ corresponds to the elimination of one molecule of DPKSH (calculated value, 45.5%). The mass loss observed in a range from 430 to 730 °C with a DTG peak at 515 °C was found to have a $\Delta m = 42.8\%$ and it corresponds to the final decomposition resulting in ZnO (Table 3).

Table 3
Elementary analysis of DPKSH and the Zn(II)/DPKSH complex

DPKSH				$Zn(DPKSH)_2 \cdot H_2O$		
%	Calculated	Experimental	Error %	Calculated	Experimental	Error %
C	67.9	67.7	−0.3	60.22	60.3	+0.1
H	4.43	4.54	2.4	3.93	3.99	+1.5
N	17.6	17.6		15.61	15.6	−0.1
H_2O				2.51	2.61	+3.8
ZnO				11.3	11.1[a]	−1.8

[a] Calculated from TG/DTG curves.

Considering the total decomposition of the [Zn(DPKSH)$_2$] complex and the formation of ZnO as a residue at 730 °C, the experimental value (11.1%) conforms to the calculated value (11.3%). This good agreement is another evidence of the coordination of two molecules of DPKBH to the Zn(II) cation and confirms the proposed stoichiometry for this complex.

Comparison between TG/DTG curves of the ligand and the complexes shows a higher thermal stability for the complex, as the mass losses after its dehydration begin at 350 for the complex and at 200 °C for the ligand. The higher stability of the ligand – when coordinated to Zn(II) – may be attributed to ligand–metal interactions.

DSC curves of DPKSH and [Zn(DPKSH)$_2$H$_2$O] are shown in Fig. 2. As it can be seen, the DSC curve profiles of the ligand and complex are quite different. Some endothermic events observed for DPKSH at the lower temperature range (<160 °C) may also be associated to the intramolecular reaction (water molecule loss) proposed on the TG curve basis. The anhydrous DPKSH shows an intense sharp endothermic peak between 169 and 189 °C and, $\Delta H = 36$ kJ mol^{-1} which corresponds to the melting of DPKSH. The onset temperature, 179 °C, is in agreement with the melting temperature range indicated in the literature (172–174 °C) [20]. Above 297 °C, several exothermic events can be seen and they are related to thermal decomposition processes. The DSC curve of the complex shows a sharp endothermic peak which characterizes the melting process at 336 °C with $\Delta H = 60$ kJ mol^{-1}. After the complex melts, some exothermic events are observed and the thermal decomposition is associated with a gradual mass loss process.

The molar ratio relative to the maximum of the Job's curve corresponds to the more favorable species present in the equilibrium [22,23]. That molar ratio is obtained from the intersection between the tangents of the curve.

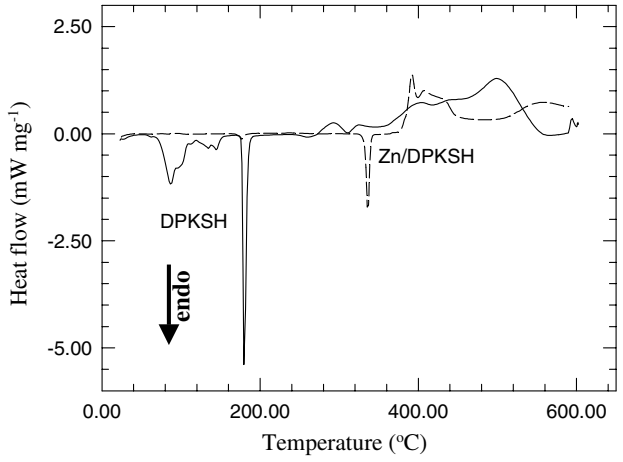

Fig. 2. DSC curves of the ligand DPKSH and Zn(DPKSH)$_2$ obtained in dynamic nitrogen atmosphere (ca. 50.0 mL min^{-1}) and heating rate of 10 °C min^{-1}, with mass 1.365 and 0.9220 mg, respectively.

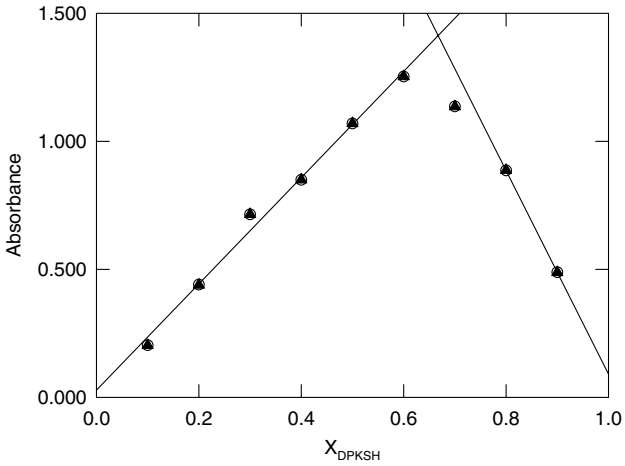

Fig. 3. Values of absorbance vs. molar fraction of the ligand, $C_{DPKSH}/(C_{Zn(II)} + C_{DPKSH})$. Pathlength = 1 cm, $\lambda = 376$ nm, pH 4.5. $C_{DPKSH} + C_{Zn(II)} = 1.00 \times 10^{-4}$ mol L^{-1} in ethanol/water 50% (v/v).

Fig. 3 shows the absorbances at $\lambda = 376$ nm for several solutions with different molar ratios. The maximum absorbance was found at a molar ratio equal to 0.67 and this value corresponds to a 1:2 metal/ligand ratio or the coordination of two molecules of DPKSH to Zn(II).

In order to obtain the stability constants of the complexes [24] formed by Zn(II) and DPKSH, absorbances were measured at 376 nm for three different total metal concentrations with variable ligand-to-metal ratios. Median molar absorptivities ($\bar{\varepsilon}$) were obtained as follows:

$$\bar{\varepsilon} = \frac{A}{C_{Zn} \cdot b} \quad (1)$$

where A is the measured absorbance, C_{Zn} is the analytical molar concentration of Zn(II) and b is the pathlength (cm) of the spectrophotometric cell.

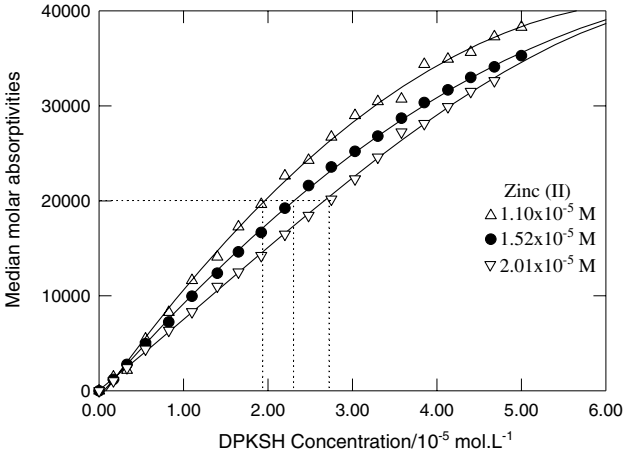

Fig. 4. Experimental data of median molar absorptivities vs. analytical concentrations of DPKSH for Zn(II) at three different concentrations. Calculated curves from stability constants and individual molar absorptivities. An example of three corresponding solutions is showed by the dashed lines.

Fig. 4 shows the data obtained for three representative Zn(II) concentrations: 1.10×10^{-5}, 1.52×10^{-5} and 2.01×10^{-5} mol L^{-1}. Considering the favorable changes in the absorbance with variable metal and ligand concentrations, the spectrophotometric method of corresponding solutions [11,12] was employed to determine the overall formation constants.

With the available experimental data ($\bar{\varepsilon}$, C_{Zn} and C_L), the average ligand number, $\bar{n}$, and the free ligand concentrations, [DPKSH]=[L], were determined according to Eq. (2) in which a plot of C_{DPKSH} versus C_{Zn} should yield a straight line with an intercept that corresponds to the free ligand concentration and a slope that corresponds to the $\bar{n}$ value.

$$C_{DPKSH} = [DPKSH] + \bar{n}C_{Zn} \quad (2)$$

Considering the region (Fig. 4) where the variation of the median molar absorptivities is the maximum, Eq. (2) can be used to obtain a set of $\bar{n}$ and [DPKSH] values. The average ligand number – $\bar{n}$ – according to Eq. (3) is related to [DPKSH].

$$\bar{n} = \frac{C_L - [L]}{C_M} = \frac{\beta_1[L] + 2\beta_2[L]^2}{1 + \beta_1[L] + \beta_2[L]^2} \quad (3)$$

A nonlinear variation of $1/\bar{n}$ versus [DPKSH] shows the existence of more than one species at equilibrium. A weighted least-square analysis of the data Eq. (3) yields *overall stability constants* for the 1:1 (β_1) and 1:2 (β_2) complexes, being $\beta_1=(1.07\pm0.02)\times10^5$ and $\beta_2=(1.05\pm0.01)\times10^{10}$. The individual formation constants are $K_1=1.07\times10^5$ and $K_2=9.81\times10^4$.

Calculation of the individual molar absorptivities (ε_1 and ε_2) for the respective complexes was simplified due to the low number of species present at equilibrium. Eq. (1) can be rewritten as:

$$\bar{\varepsilon} = \frac{\varepsilon_0 + \varepsilon_1\beta_1[L] + \varepsilon_2\beta_2[L]^2}{1 + \beta_1[L] + \beta_2[L]^2} \quad (4)$$

Here ε_0 was experimentally determined and corresponds to the Zn(II) molar absorptivity in the absence of DPKSH. A weighted least-square analysis of the data ($\bar{\varepsilon}$, [L], $\varepsilon_0=0$) yields Eq. (4) the molar absorptivities ($M^{-1}cm^{-1}$) of the Zn(II)/DPKSH 1:1 and 1:2 complexes of $\varepsilon_1=(1.1\pm0.3)\times10^4$ and $\varepsilon_2=(4.5\pm0.1)\times10^4$ L $mol^{-1}cm^{-1}$, respectively. The last molar absorptivity (ε_2) is in excellent agreement with the slope of the analytical curve by Gaubeur et al. 4.83×10^4 L $mol^{-1}cm^{-1}$ [16]. This means that the use of excess of ligand in the spectrophotometric method [16] leads to the predominance of the 1:2 species.

The distribution diagram of the species is presented in Fig. 5. It shows that in the range of concentrations employed to determine the stability constants, the Zn(II)DPKSH 1:1 species predominates. Even though the [$Zn(DPKSH)_2$] concentration is low, the determination of the respective stability constants is possible due to the fact that the K_1/K_2 ratio is favorable.

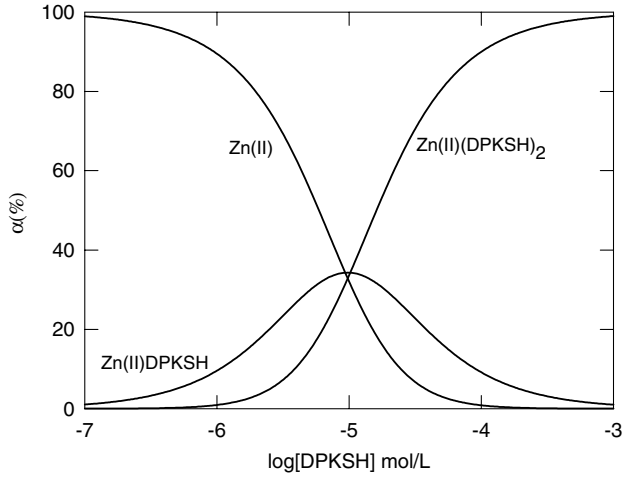

Fig. 5. Distribution diagram for the species present in the system Zn(II)-DPKSH. $T=25.0\pm0.1$ °C, pH 4.5 and 50% ethanol.

Acknowledgments

The authors gratefully acknowledge the financial support granted by FAPESP (Fundação de Amparo à Pesquisa do Estado de São Paulo) and CNPq (Conselho Nacional de Desenvolvimento Científico e Tecnológico).

References

[1] M. Katyal, Y. Dutt, Talanta 22 (1975) 151.
[2] R.B. Singh, P. Jain, Talanta 29 (1982) 77.
[3] M. Moham, M.P. Gupta, L. Chandra, N.K. Jha, Inorg. Chim. Acta 151 (1988) 61.
[4] T. Nakanishi, M. Otomo, Microchem. J. 33 (1986) 172.
[5] N.A. Zatar, A.Z. Abu-Zuhri, M.A. Al-Nuri, F.M. Mahmoud, A.A. Abu-Obaid, Spectrosc. Lett. 22 (1989) 1203.
[6] S.O. Pehkonen, Y. Erel, M.R. Hoffmann, Environ. Sci. Technol. 26 (1992) 1731.
[7] Y. Erel, S.O. Pehkomem, M.R. Hoffmann, J. Geophys. Res. 98 (1993) 18423.
[8] A. Zatar, Mohmmed, A. Al-Nuri, M. Abu-Eid, M. Hannoun, A.Z. Abu-Zuhri, S. Khalaf, M. Kramis, Spectrosc. Lett. 24 (1991) 1145.
[9] M.A. Al-Nuri, M. Abu-Eid, N.A. Zatar, S. Khalaf, M. Hannoun, Anal. Chim. Acta 259 (1992) 175.
[10] T. Nakanishi, M. Otomo, Anal. Sci. 1 (1985) 161.
[11] M.E.V. Suárez-Iha, S.O. Pehkonen, M.R. Hoffmann, Environ. Sci. Technol. 28 (1994) 2080.
[12] M.V. Rossi, M.E.V. Suárez-Iha, M.R. Hoffmann, Spectrosc. Lett. 28 (1995) 1153.
[13] L.H.S. Ávila Terra, M.E.V. Suárez-Iha, Spectrosc. Lett. 30 (1997) 625.
[14] L.H.S. Ávila Terra, M.C.C. Areias, I. Gaubeur, M.E.V. Suárez-Iha, Spectrosc. Lett. 32 (1999) 257.
[15] M.C.C. Areias, L.H.S. Ávila Terra, I. Gaubeur, M.E.V. Suárez-Iha, Spectrosc. Lett. 34 (2001) 289.

[16] I. Gaubeur, M.C.C. Areias, L.H.S. Ávila Terra, M.E.V. Suárez-Iha, Spectrosc. Lett. 35 (2002) 455.
[17] M.M. Kamal, A.Z. Abu Zuhri, M.M. Hannoun, Fresen. J. Anal. Chem. 344 (1992) 275.
[18] W.C. Vosburgh, G.R. Cooper, J. Am. Chem. Soc. 63 (1941) 437.
[19] L.H.S. Ávila Terra, M. Guekezian, I. Gaubeur, J.R. Matos, M.E.V. Suárez-Iha, Polyhedron 21 (2002) 2375.
[20] M. Garcia-Vargas, M. Belizón, M.P. Hernández-Artiga, C. Martinez, J.A. Pérez-Bustamante, Appl. Spectrosc. 40 (1986) 1058.
[21] F.J. Welcher, The analytical uses of ethylenediamine tetracetic acid, first ed., Van Nostrand, New York, 1965.
[22] P. Job, Anal. Chem. 9 (1928) 113.
[23] F. Woldbye, Acta Chem. Scand. 9 (1955) 299.
[24] L. Sommer, M. Langová, CRC Crit. Rev. Anal. Chem. 19 (1988) 225.
[25] R.M. Silverstein, G.C. Bassler, T.C. Morril, Spectrometric Identification of Organic Compounds, fifth ed., Wiley, New York, 1991.
[26] R.T. Conley, Infrared Spectroscopy, second ed., Allyn & Bacon, Boston, 1972.
[27] L.J. Bellammy, The Infrared Spectra of Complex Molecules, first ed., Wiley, New York, 1954.
[28] N.S. Biradar, B.R. Havinale, Inorg. Chim. Acta 17 (1976) 157.
[29] B. Paschold, T. Seshadri, A. Kettrup, Fresen. Z. Anal. Chem. 311 (1982) 98.
[30] S.J. Gaskell, J. Mass Spectrom. 32 (1997) 677.

Available online at www.sciencedirect.com
SCIENCE DIRECT®
Polyhedron 23 (2004) 2103–2109
POLYHEDRON
www.elsevier.com/locate/poly

Synthesis, characterisation and thermal decomposition of tin(IV) dithiocarbamate derivatives – single source precursors for tin sulfide powders

D.C. Menezes [a], G.M. de Lima [a,*], A.O. Porto [a,*], C.L. Donnici [a], J.D. Ardisson [b], A.C. Doriguetto [c], J. Ellena [c]

[a] *Laboratório de Química de Coordenação e Organometálica do Estanho, Departamento de Química, Universidade Federal de Minas Gerais (UFMG), Avenida Antonio Carlos 6627, Belo Horizonte – MG, CEP 31270-901, Brazil*
[b] *Laboratório de Física Aplicada –CDTN/CNEN, Belo Horizonte – MG, Brazil*
[c] *Grupo de Cristalografia, FFI, IFSC, USP, CP 369, São Carlos – SP, CEP 13560-970, Brazil*

Received 21 April 2004; accepted 4 June 2004

Abstract

The reaction of ammonium pyrrolidinedithiocarbamate with $SnPh_2Cl_2$ and $SnPh_3Cl$ produced in good yield the compounds $[Sn\{S_2CN(CH_2)_4\}_2\{C_6H_5\}_2]\cdot$toluene (**1**) and $Sn\{S_2CN(CH_2)_4\}\{C_6H_5\}_3$ (**2**). They were fully characterised by multinuclear NMR [^1H,$^{13}C\{^1H\}$ and $^{119}Sn\{^1H\}$] and ^{119}Sn Mössbauer spectroscopies. In addition the structure of **1** was determined, and **2** was revised by X-ray crystallographic studies. Finally, thermal decomposition experiments were carried out for both compounds in nitrogen and the residues were characterised by X-ray powder diffraction (XRD), X-ray electron probe microanalysis (EPMA), scanning electron microscopy (SEM) and ^{119}Sn Mössbauer spectroscopy. The results clearly indicate the formation of a mixture of γ-Sn_2S_3 and SnS, both orthorhombic phases.
© 2004 Elsevier Ltd. All rights reserved.

Keywords: Pyrolysis; Organotin derivatives; Tin sulfide

1. Introduction

Tin sulfides are narrow-bandgap semiconductors with special optical and electronic properties [1]. Tin sulfides have three main phases: (i) SnS_2, (ii) SnS that exhibit layer structures and (iii) Sn_2S_3 which is a mixed valence Sn(II)/Sn(IV) compound with the same local order as the former sulfide, but with a ribbon-like structure [2]. Tin(II) sulfide displays a distorted rock-salt arrangement which is isostructural to GeS (orthorhombic, *Pbnm* group). Six sulfur atoms surround each tin centre with three short Sn–S bonds within the layer and three long bonds to the sulfur of the next layer [3,4].

Tin sulfides might encounter applications as low-cost green materials for photovoltaic devices either replacing cadmium chalcogenides, which have been banned in many countries because of their toxicity, or else as substitute to the expensive silicon-based sensors. Their preparation methods require high temperature reactions (more than 300 °C) or special reactors [5,6]. Atmospheric pressure chemical vapour deposition (APCVD) and pyrolysis using unsymmetrical organotin dithiocarbamates complexes, like $[(CH_3)_3Sn(S_2CN(C_4H_9)CH_3)]$ and $[(CH_3CH_2CH_2CH_2)Sn(S_2CN(C_4H_9)CH_3)]_3$, or heteroleptic thiolate/dithiocarbamate derivatives, $(Et_2NCS_2)(RS)_2$-Sn (R = Cy, CH_2CF_3), have already been reported [7–9].

* Corresponding authors. Tel.: +553134997544; fax: +553134995720.
E-mail addresses: gmlima@ufmg.br (G.M. de Lima), aporto@dedalus.lcc.ufmg.br (A.O. Porto).

0277-5387/$ - see front matter © 2004 Elsevier Ltd. All rights reserved.
doi:10.1016/j.poly.2004.06.007

However, either the decomposition temperatures are still too high or the process goes on in complicated many step mechanisms. Therefore the search for more appropriate single source precursors for Sn–S based materials is still justified.

The work reported here is part of a more general study performed by our research team concerning precursors for tin sulfide and oxide powders, which is still under investigation [10,11]. So far we have employed organotin derivatives such as $Sn_4S_4R_6$ and $Sn_4O_4R_6$ {R = methyl (Me), *n*-butyl or phenyl}. We found those economically attractive not only because of the facile preparation method but also due to their air stability, however, the decomposition temperatures are still high. In order to explore other promising starting materials and check the viability as a good precursor, we have also an interest in tin-containing dithiocarbamates complexes, and herein we describe the first outcomes of our investigations.

2. Experimental

2.1. Instrumentation and techniques:

IR spectra were obtained as KBr plates on a Mattson Galaxy Model ST 3000 spectrometer in the 4000–400 cm^{-1} range. NMR spectra were record in $CDCl_3$ at 25 °C on a Brucker Avance DRX 400. The values were referenced to internal $SiMe_4$ and $SnMe_4$. C, H, N analyses were performed using a Perkin–Elmer Model PE 2400 CHN.

Thermal decomposition of **1** and **2** were carried out in a tube furnace in N_2 atmospheres up to 500 °C for **1** and 750 °C for **2** using a heating rate of 5 °C/min and a gas flux of 100 ml/min.

XRD patterns were collected with Rigaku Geigerflex equipment by using Ni-filtered Cu Kα radiation ($\lambda = 1.5418$ Å) and a graphite monochromator in the diffracted beam. A scan rate of 4 °/min was applied to record a pattern in the 2θ range of 4–80°.

^{119}Sn Mössbauer measurements were performed on conventional apparatus with the samples at liquid N_2 temperature and a $CaSnO_3$ source kept at room temperature, for compounds **1** and **2** and both the residues in order to identify the Sn oxidation state and number of different sites.

The scanning electron microscopies (SEM) were taken in JEOL JSM-840A equipment and the samples were previously covered with a thin gold layer. The X-ray electron probe microanalyses (EPMA) were carried out in a JXA 89000 RL wavelength /energy dispersive combined microanalyser with samples covered with a thin film of carbon deposited by sputtering.

The intensity data for the X-ray crystallographic determination of **1** were collected at 293(2) K on an Enraf-Nonius Kappa CCD diffractometer with Mo Kα, $\lambda = 0.71073$ Å, radiation. Programs used: COLLECT, HKL Denzo-Scalepack, WINGX, SHELXS-97 [12], SHELXL-97 and ORTEP-3 [13] and the refinements were carried out on F^2 using SHELXL-97 software [14]. Further details are given in Table 1. All non-H atoms were refined anisotropic. The carbons' H atoms were positioned stereochemically and were refined with fixed individual displacement parameters [U_{iso} (H) = 1.2U_{eq} (C)] using the SHELXL riding model.

2.2. Synthesis of $[Sn\{S_2CN(CH_2)_4\}_2\{C_6H_5\}_2]\cdot$toluene (1)

$[NH_4][(CH_2)_4NCS_2]$ (1.32 g, 8 mmol) was dissolved in 20 cm^3 of ethanol and added dropwise to a solution of $(C_6H_5)_2SnCl_2$ (1.38 g, 4 mmol) in the same solvent. The mixture was stirred for two hours and then the solvent was removed by filtration and a white solid, $(C_6H_5)_2Sn[S_2CN(CH_2)_4]_2$, was obtained. The ammonium salt was removed by washing the product with hot water (80 °C). X-ray quality colourless crystals were obtained by cooling a dichloromethane/toluene solution of the compound. Yield: 85%. M.p. 222.5–223.1 °C. IR (cm^{-1}, KBr): 990 and 1050 (s, ν_{C-S}), 1560 (s, ν_{C-N}). ^1H NMR (δ, $CDCl_3$): 1.95–2.01; 3.60–3.66 (t); 7.23–7.90

Table 1
Crystal data for $[(C_6H_5)_2Sn\{S_2CN(CH_2)_4\}_2]\cdot$toluene

Empirical formula	$C_{22}H_{26}SnN_2S_4$
Molecular weight	581.38
T (K)	100(2)
λ (Å)	0.71073
Crystal system	triclinic
Space group	$P\bar{1}$
Unit cell dimensions	
a (Å)	8.7355(11)
b (Å)	9.1326(7)
c (Å)	16.72.88(17)
α (°)	83.704(4)
β (°)	84.318(6)
γ (°)	88.979(5)
V (Å^3)	1320.0(2)
Z	2
ρ_{calc} (Mg/m^3)	1.463
Absorption coefficient (mm^{-1})	1.300
$F(000)$	588
Crystal size (mm^3)	0.18×0.08×0.04
θ Range for data collection (°)	3.23–25.00
Reflections collected	28 756
Independent reflections (R_{int})	4634 (0.0392)
Completeness to $\theta = 25.00°$ (%)	99.7
Maximum and minimum transmission	0.9498 and 0.7997
Refinement method	full-matrix least-squares on F^2
Data/restraints/parameters	4634/0/282
Goodness-of-fit on F^2	0.999
Final R indices [$I > 2\sigma(I)$]	$R_1 = 0.0503$, $wR_2 = 0.1168$
R indices (all data)	$R_1 = 0.0555$, $wR_2 = 0.1209$
Largest difference peak and hole (e Å^{-3})	2.859 and −1.520
CCDC reference	236258

(m, 2 C_6H_5). ^{13}C NMR (δ, $CDCl_3$): 26.7; 54.9; 128.1; 128.3 [$^1J(^{119}Sn–^{13}C) = 811$ Hz]; 134.3 [$^2J(^{119}Sn–^{13}C) = 621$ Hz]; 151.6; 194.5. ^{119}Sn NMR (δ, $CHCl_3$): −500 [$^1J(^{119}Sn–^{13}C) = 811$ Hz, $^2J(^{119}Sn–^{13}C) = 621$ Hz]. *Anal.* Calc. for $C_{22}H_{26}SnN_2S_4$: C, 46.75; H, 4.60; N, 4.95. Found: C, 46.62; H, 4.54; N, 4.84%.

2.3. Synthesis of $Sn\{S_2CN(CH_2)_4\}\{C_6H_5\}_3$ (2)

Prepared accordingly using $[NH_4][(CH_2)_4NCS_2]$ (0.56 g, 4 mmol) and $SnCl_2(C_6H_5)_2$ (1.54 g, 4 mmol) dissolved in 20 cm^3 of ethanol. Yield: 89%. M.p. 171–171.4 °C. IR (cm^{-1}, KBr): 990 and 1060 ($\nu_{C–S}$), 1460 and 1570($\nu_{C–N}$). ^1H NMR (δ, $CDCl_3$): 1.85–1.97 (m); 3.59–3.70 (t); 7.28–7.90 (m, 2 C_6H_5). ^{13}C NMR (δ, $CDCl_3$): 26.64; 55.05; 128.45 [$^2J(^{119}Sn–^{13}C) = 62$ Hz]; 129.06; 136.71 [$^3J(^{119}Sn–^{13}C) = 51$ Hz]; 142.07 [$^1J(^{119}Sn–^{13}C) = 606$ Hz]; 191.57. ^{119}Sn NMR (δ, $CHCl_3$): −174 [$^1J(^{119}Sn–^{13}C) = 606$ Hz, $^2J(^{119}Sn–^{13}C) = 62$ Hz, $^3J(^{119}Sn–^{13}C) = 51$ Hz]. *Anal.* Calc. for $C_{23}H_{23}SnNS_2$: C, 55.67; H, 4.64; N, 2.82. Found: C, 55.47; H, 4.73; N, 2.81%.

3. Results and discussion

Compounds **1** and **2** were isolated as mixture-free derivatives and after re-crystallisation they showed acceptable melting points, as well as satisfactory elemental analyses. They were obtained as air- and moisture-stable white crystalline solids, readily soluble in polar organic solvents.

Compound **1** was studied by X-ray crystallography and the results are displayed in Table 1. It is shown that the crystalline compound possesses a very disordered molecule of toluene in its structure (Fig. 1).

Table 2 comprises selected bond lengths and angles. A similar derivative, $[Sn\{S_2CN(CH_2)_4\}_2Me_2]$, previously published, crystallises as orthorhombic in the *Pmmn* space group [15]. In this compound, the Sn atom lies at the centre of an almost perfect octahedron with a plane of symmetry, containing the R group and the metal centre, and dividing equally the two ligands. Compound **1** has kept the hexacoordination and the pseudo-octahedral geometry, but the crystals have grown in the triclinic system with the space group $P\bar{1}$. Unlike the published derivative, which displays two sets of Sn–S bonds, 2.518(1) and 2.9938(1) Å, all four Sn–S distances in **1** are different. There are three slightly different short bonds, S(22)–Sn 2.5727(13), S(12)–Sn 2.5864(14) and S(11)–Sn 2.6850(17) Å, and a long one S(21)–Sn 2.9495(16) Å, which seems not to remain in solution as will be discussed later. Apart from the longer bond, the former bonds correlate very well with those observed for the methyl derivative. Because of the lack

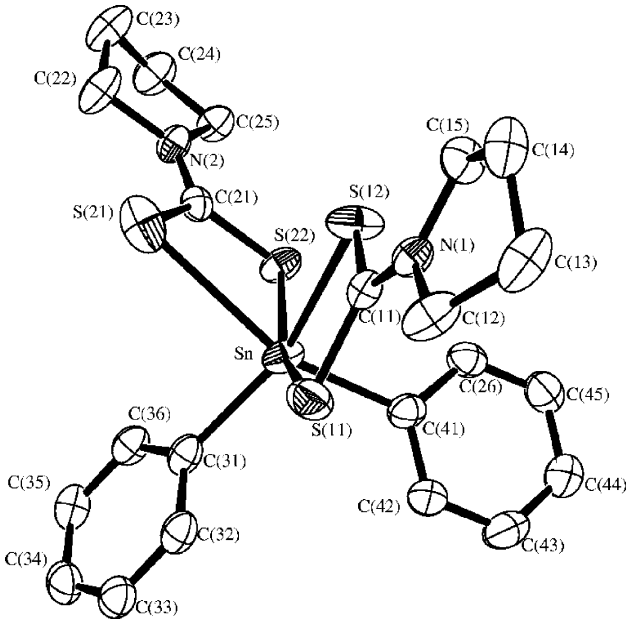

Fig. 1. The Molecular structure of **1** and the atom numbering scheme.

of symmetry, two Sn–C bond lengths are observed, Sn–C(41) 2.166(5) Å and Sn–C(41) 2.156(6) Å, for the Sn–phenyl interactions. The S–Sn–S angles, S(22)–Sn–S(12) 89.77(5)°, S(22)–Sn–S(11) 157.20(5)°, S(12)–Sn–S(11) 67.55(5)° are close to those found in the literature. We have also reviewed the X-ray crystallographic structure of **2** and the data does not differ from the reported structure [16]. The Sn(IV) displays a geometric arrangement between tetrahedral and bipyramidal trigonal.

The ^1H NMR of **1** and **2** revealed signals for the organic groups. Besides the expected resonances for the R groups the ^{13}C spectra revealed first and second-order $^{119}Sn–^{13}C$ couplings. Unlike other reported examples found in the literature, which normally describe more than one isomer in solution, detected by ^{119}Sn NMR experiments, in our case only one signal was observed, δ −500 $^1J(^{13}C–^{19}Sn) = 811$Hz for **1** and −174 $^1J(^{119}Sn–^{13}C) = 606$ Hz for **2**. The latter signal appeared upfield compared to the former because of the higher coordination number of the Sn(IV) centre in compound **2**.

Table 2
Selected bond lengths (Å) and angles (°) for **1**

C(31)–Sn	2.156(6)	S(12)–Sn	2.5864(14)
C(41)–Sn	2.166(5)	S(21)–Sn	2.9495(16)
S(11)–Sn	2.6850(17)	S(22)–Sn	2.5737(13)
C(31)–Sn–C(41)	107.58(19)	C(41)–Sn–S(11)	92.66(14)
C(31)–Sn–S(12)	152.82(14)	C(41)–Sn–S(22)	91.18(14)
C(31)–Sn–S(22)	105.35(14)	C(41)–Sn–S(12)	94.29(14)
C(31)–Sn–S(11)	94.87(14)	S(12)–Sn–S(11)	67.55(5)
S(22)–Sn–S(12)	89.77(5)	S(22)–Sn–S(11)	157.20(5)

Table 3
^{119}Sn Mössbauer parameters[a] (isomer shift (IS), quadrupole splitting (QS), area and width) obtained at liquid nitrogen temperature for the compounds **1** and **2** and their respective residues obtained in N_2

Material	Sn site	IS (mm s^{-1})	QS (mm s^{-1})	Area (%)	Width (mm s^{-1})
1	Sn(IV)	1.09	1.72	100	0.90
2	Sn(IV)	1.26	1.65	100	0.90
Residue of **1**	Sn(II)	3.31	1.03	88	0.90
	Sn(IV)	0.17	0.59	12	0.90
Residue of **2**	Sn(II)	3.08	1.07	77	0.90
	Sn(IV)	0.14	0.56	21	0.90

[a] The errors associated to IS, QS and width are ±0.05 mm s^{-1} and 1% for the area.

It is possible to estimate the C–Sn–C bond angle employing methods encountered in the literature, which correlates the angle with the first-order coupling constant between ^{119}Sn and ^{13}C, in solution [17]. The methods have provided a C–Sn–C angle for compound **1** ranging from 154.57° to 157.34°, in disagreement with the experimental data, 107.58(19)°. Either because the structure of **1** in solution differs drastically from that in the solid state, or the reported methods do not apply to this system. The latter could be justified by the dissociation of the long Sn–S bond, discussed in the X-ray results, effecting a change in the coordination of the metal.

The ^{119}Sn Mössbauer parameters, isomer shift (IS) and quadrupolar splitting (QS) obtained for compounds **1** and **2** indicate a strong dependence upon the coordination number, hybridisation and symmetry around the Sn(IV) nucleus. The IS for **1**, 1.09 mm s^{-1} is smaller than that for **2**, 1.65 mm s^{-1}, Table 3, suggesting higher coordination, as attested by the X-ray and ^{119}Sn-NMR spectroscopic results. It is consistent with a smaller contribution of *s* electrons to the hybridisation scheme at the tin atom in **1** as compared to **2**. The quadrupole splitting parameters 1.30 and 1.80 mm s^{-1} points to a lower symmetry for complex **1**. These data match perfectly with other known values for penta and hexacoordinated Sn(IV) derivatives [18].

*3.1. Thermal decomposition of **1** and **2** and characterisation of the residues*

The thermogravimetric curves of **1** and **2**, Fig. 2, shows that the decomposition processes begin at 207 and 233 °C (±2 °C), respectively, and at about 350 °C both materials have been consumed. The presence of one more phenyl group in the structure of **2** increases its T_d (temperature of decomposition) by approximately 26 °C. In both cases, the decomposition take place in a pseudo-single step and the decomposition temperatures are lower than those found for organotin sulfides, reported by us, which have been considered a promising single source precursor [10a].

The residue obtained after the pyrolysis of **1** and **2** carried out in a tube furnace in N_2 were chemically and structurally characterised. The EPMA results, Fig. 3, clearly indicate the presence of Sn and S as major elements in the residues. However, a tiny amount of oxygen has also been revealed, which might be due to the formation of SnO_2 as a much lesser product. It has possibly originated from the N_2, which was not completely free from moisture or oxygen, however, it is much smaller than the quantity of carbon, employed to cover the sample.

The diffraction patterns of the residues, Fig. 4, suggested the formation of γ-Sn_2S_3 and SnS, both orthorhombic phases, in view of the diffraction lines. The lines of SnO_2, which is quite sensitive to this technique, were not detected. A poor crystallinity of the sample has rendered low quality XRD patterns for residue **1**. Nevertheless, lines at 2θ/° 27.19, 31.80, 31.46 and 38,99 assigned to γ-Sn_2S_3 and SnS were identified. A better diffractogram was obtained for **2** and it was possible to connect the lines at 2θ/° 31.61 (201), 31.86 (131), 25.94 (101), 27.22 (140) and 38.94 (301) to γ-Sn_2S_3 (JCPDS-ICCD 1996 card no. 39-0354). Likewise, those diffractions at 2θ/° 31.50 (111), 31.73 (040), 25.94 (110), 27.36 (021), 30.46 (101) and 39.24 (131) were attributed to SnS (JCPDS-ICCD 1996 card no.

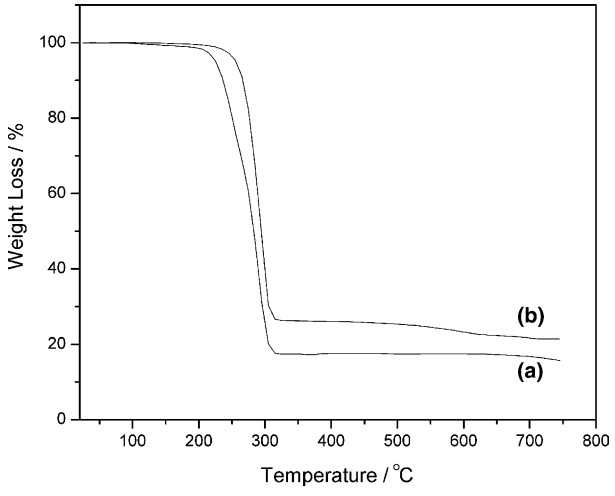

Fig. 2. The thermogravimetric curves of **1** (a) and **2** (b) in nitrogen.

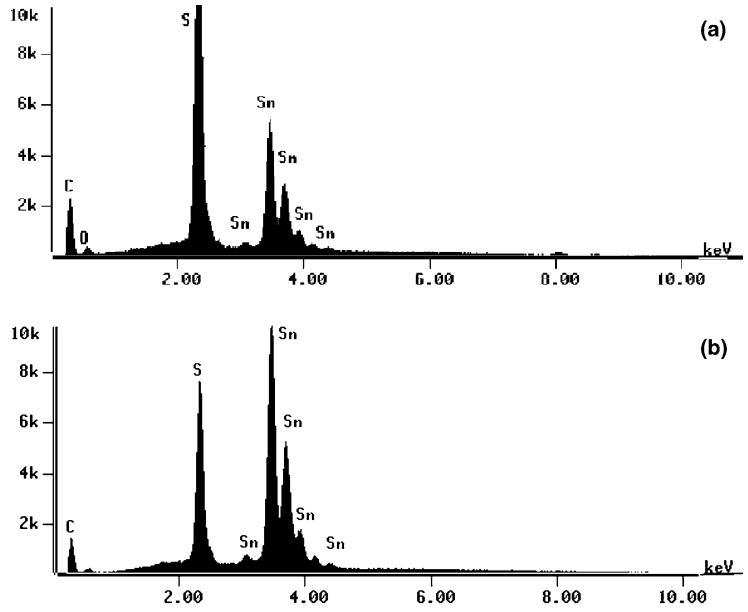

Fig. 3. The X-ray electron probe microanalysis (EPMA) of the residue of **1** (a) and **2** (b).

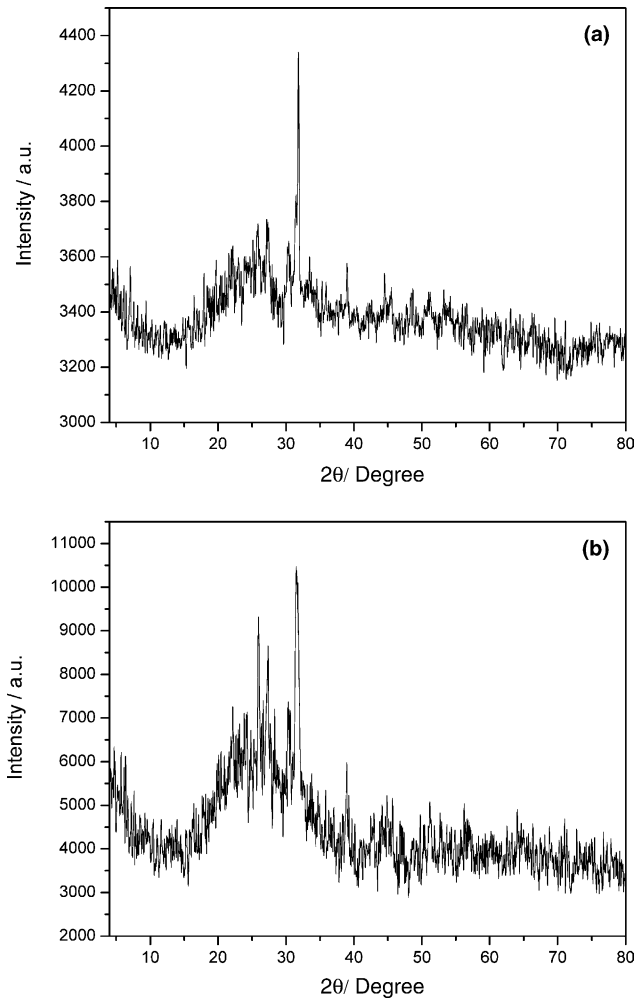

Fig. 4. The X-ray powder diffraction patterns of the residue **1** (a) and **2** (b).

30-13790). The respective Miller indexes are indicated in parenthesis.

The ^{119}Sn Mössbauer spectra were important to confirm the results of XRD and EPMA, Fig. 5. The experiments have clearly shown the presence of two Sn sites corresponding to Sn(II) and Sn(IV) in the residues, in the form of SnS and Sn_2S_3. Since the amount of SnO_2 is not detectable, it is not absurd to assume that all the Sn nuclei exist as tin-sulfides. For the residue of **1** there are two sets of signals, IS 3.31 mm s^{-1}, QS 1.03 mm s^{-1} and IS 0.17 mm s^{-1}, QS 0.59 mm s^{-1}. Similarly, for **2** IS 3.08 mm s^{-1}, QS 1.07 mm s^{-1} and IS 0.14 mm s^{-1}, QS 0.56 mm s^{-1} are observed. The Mössbauer parameters for both residues are in good agreement with similar data reported in one of our previous works [10a]. It is important to observe that a smaller amount of Sn(II) was produced in the decomposition of **2** (area = 77%) compared to the residue of **1** (area = 88%). In either case there is more SnS than the required amount to match the Sn_2S_3 stoichiometry. It is possible that a mixture of the two sulfides is present, which the ^{119}Sn Mössbauer experiments cannot reveal. We have also performed the same study on a standard of Sn_2S_3 and the same pattern of two set of signals with IS = 3.35 mm s^{-1}, QS = 0.97 mm s^{-1} for Sn(II) and IS = 0.46 mm s^{-1}, QS = 0.88 mm s^{-1} for Sn(IV) was encountered.

The scanning electron micrographs showed that layered and ribbon-like crystals basically compose the residues, Fig. 6. It is a very common characteristic of SnS and Sn_2S_3 systems. The SEM images have revealed the particle size of microns and also confirmed the low crystallinity of the samples, as pointed out by the XRD diffractograms.

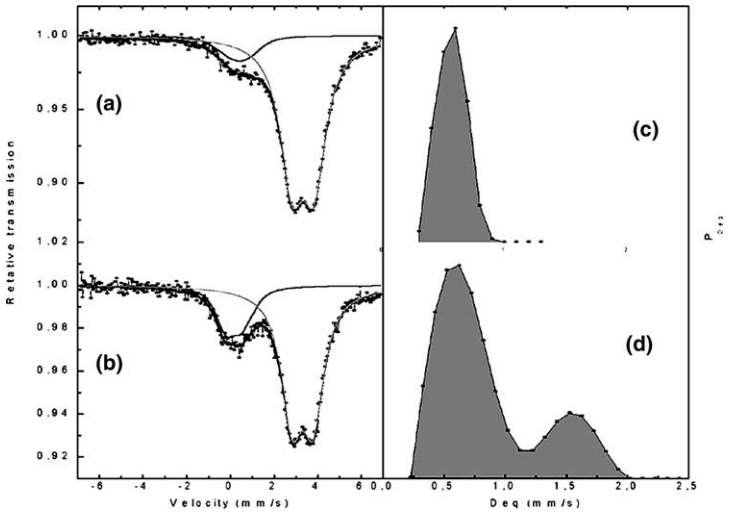

Fig. 5. The ^{119}Sn Mössbauer spectra and the respective quadrupole distribution of the residue of **1** (a) and **2** (b).

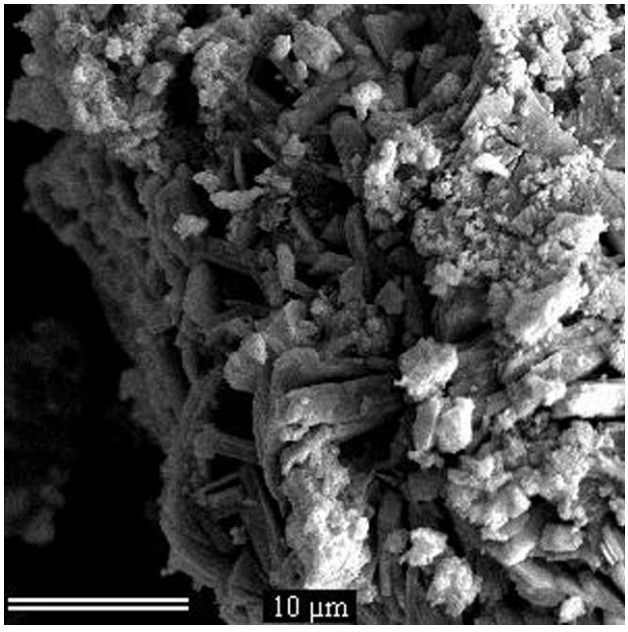

Fig. 6. The scanning electron microscopy (SEM) image of the residue of **1**.

4. Conclusions

We have described in this paper the synthesis, characterisation and thermal decomposition of two dithiocarbamate tin-based derivatives. The versatility of compounds **1** and **2** has been proved as single source precursor for SnS and Sn_2S_3. They were obtained by a pyrolysis experiment in N_2 in sharp steps at a much lower temperature compared to other compounds. Only a negligible amount of SnO_2 was revealed by EPMA, and was not detected in the XRD or in ^{119}Sn Mössbauer experiments.

5. Supplementary data

Crystallographic data for the structural analysis for complex **1** have been deposited at the Cambridge Crystallographic Data Centre, 12 Union Road, Cambridge CB2 1EZ, UK, and are available on request quoting the deposition number CCDC-236258.

Acknowledgements

We thank CNPq-Brazil for granting a scholarship to D.C. Menezes. We are in debit to the Laboratório de Microscopia Eletrônica e Microanálise (LMA) for performing part of the analysis – financed by FAPEMIG (Project CEX 1074/95).

References

[1] J. Morales, V.C. Perez, J. Santos, L.J. Tiraldo, J. Electrochem. Soc. 143 (1996) 2847.
[2] T. Jiang, G.A. Ozin, J. Mater. Chem. 8 (1998) 1099.
[3] R. Hertzenberg, Ver. Minerals 4 (1932) 33.
[4] R. Kneip, D. Mootz, U. Severin, H. Wunderlich, Acta Crystallogr., Sect. B 38 (1982) 2022.
[5] R.W. ParryInorganic Synthesis, vol. 12, McGraw-Hill, New York, 1995.
[6] I.P. Parkin, A.T. Rowley, Polyhedron 12 (1993) 2961.
[7] A.T. Kana, T.G. Hibbert, M.F. Mahon, K.C. Molloy, I.P. Parkin, L.S. Price, Polyhedron 20 (2001) 2989.
[8] G. Barone, T. Chaplin, T.G. Hibbert, A.T. Kana, M.F. Mahon, K.C. Molloy, I.D. Worsley, I.P. Parkin, L.S. Price, J. Chem. Soc., Dalton Trans. (2002) 1085.
[9] A.C. Fabretti, A. Giusti, C. Preti, G. Tosi, P. Zannini, Polyhedron 5 (1986) 871.
[10] (a) A.O. Porto, G.M. de Lima, A.G. Pereira, L.A.R. Batalha, J.D. Ardisson, Appl. Organometal. Chem. 18 (2004) 39;
(b) A.G. Pereira, A.O. Porto, G.M. de Lima, H.G.L. Siebald, J.D. Ardisson, Solid State Commun. 127 (2003) 223;

(c) A.G. Pereira, L.A.R. Batalha, A.O. Porto, G.M. de Lima, G.G. Silva, J.D. Ardisson, H.G.L. Siebald, Mater. Res. Bull. 38 (2003) 1805.
[11] A.G. Pereira, A.O. Porto, G.G. Silva, G.M. de Lima, H.G.L. Siebald, J.L. Neto, Phys. Chem. Chem. Phys. 4 (2002) 4528.
[12] G.M. Sheldrick, SHELXS-97: Program for Crystal Structure Resolution, University of Göttingen, Göttingen, Germany, 1997.
[13] G.M. Sheldrick, SHELXL-97: Program for Crystal Structures Analysis, University of Göttingen, Göttingen, Germany, 1997.
[14] L.J. Farrugia, ORTEP-3 for Windows, J. Appl. Crystallogr. 30 (1997) 565.
[15] P.F. Lindley, P.J. Carr, Cryst. Mol. Struct. 4 (1974) 173.
[16] (a) V. Vrabel, J. Lokaj, E. Kello, J. Kozlsek, V. Rettay, Proc. Conf. Coord. Chem. 12 (1989) 441;
(b) E.M. Holl, F.A.K. Nasser, A. Wilson Jr., J.J. Zuckerman, Organometallics 4 (2073) 1985.
[17] (a) T.P. Lockhart, W.F. Manders, J.J. Zuckerman, J. Am. Chem. Soc. 107 (1985) 4546;
(b) J. Holeçek, M. Nádvornik, K. Handlič, A. Lyčka, J. Organomet. Chem. 315 (1986) 299;
(c) J. Holeček, M. Nádvornik, K. Handlič, S.M. Teleb, A. Lyčka, J. Organomet. Chem. 339 (1988) 61.
[18] P.J. Smith, Organomet. Chem. Rev. A 5 (1970) 373.

Available online at www.sciencedirect.com
SCIENCE DIRECT®
Polyhedron 23 (2004) 2111–2115
POLYHEDRON
www.elsevier.com/locate/poly

Synthesis and physicochemical properties of charge transfer compounds derived from the reaction of tetrathiafulvalene with copper(II)

Sung-Nak Choi, Woo-Sung Jung, Min-Joo Lee, Yong-Min Lee, Young-Inn Kim *

Chemistry Institute for Functional Materials, Department of Chemistry and Chemistry Education, Pusan National University, Jangjeon-Dong, Kumjeong-Gu, Pusan 609-735, Korea

Received 2 March 2004; accepted 9 June 2004

Abstract

Charge transfer compounds with the general formula $(TTF)_4CuX_2$ (TTF=tetrathiafulvalene; X = NCS, NO_3, Cl, Br, NCO and NO_2) were prepared by the reaction of excess TTF with the precursor $Cu(Sp)X_2$[Sp = (–)-sparteine] complexes in dichloromethane. The TTF radical patterns were observed in EPR spectra and a signal attributable to Cu(II) was not detected in the solid state for the prepared compounds, indicating that there is charge transfer from the TTF donors to the copper metal(II) ions and that the copper center in $(TTF)_4CuX_2$ is in a diamagnetic Cu(I) state. The powdered electrical conductivities of some $(TTF)_4CuX_2$ (X = NCS, NO_3, Cl and Br) compounds are in the semiconductor region ($\sigma_{r.t} = 10^0$–10^1 S cm^{-1}), whereas the other compounds (X = NCO and NO_2) are in the insulator range ($\sigma_{r.t} < 10^{-4}$ S cm^{-1}) at room temperature. The electrical conductivities of the prepared six compounds are closely related to the charge transfer rate from TTF to $Cu(Sp)X_2$ in the formation of $(TTF)_4CuX_2$ and the reduction potential of the precursor $Cu(Sp)X_2$ complexes.
© 2004 Elsevier Ltd. All rights reserved.

Keywords: Tetrathiafulvalene; Copper(II); Charge transfer compounds; Electrical conductivity

1. Introduction

Tetrathiafulvalene (TTF) is an excellent electron donor for the purpose of forming a wide class of electrical conductive materials ranging from insulators to superconductors [1,2]. Its electrical properties depend on the degree of charge transfer (stoichiometry) as well as the stacking mode of TTFs in the resulting charge transfer compounds [3]. For example, in TTF compounds with copper(II) halides, the partially ionized $(TTF)n^{+1}Cu(I)X_2$ ($n = 4/3$–$7/3$, X = Cl, Br) exhibits $\sigma_{rt} = 10^{-1}$–10^{+1} S cm^{-1} [4], whereas the completely ionized $(TTF)^{+1}Cu(I)Cl_2$ has been reported to be an insulator, $\sigma_{rt} = 10^{-4}$–10^{-5} S cm^{-1} [5]. In those compounds, the composition of TTF is dependent on the reaction conditions such as the solvent used, the ratio of the reactants, and other conditions.

Previously we proposed a convenient method for the preparation of $(TTF)_nCuX_2$ charge transfer compounds of varying ratios of TTF to copper using copper halides complexes [6]. $(TTF)_4CuX_2$ (X = Cl, Br) and $(TTF)_2CuX_2$ compounds were obtained using $Cu(Sp)X_2$ [Sp = (–)-sparteine, $C_{15}H_{26}N_2$] and $Cu(nic)X_2$ [nic = (–)-nicotine, $C_{10}H_{14}N_2$] respectively with excess TTF in dichloromethane. In this work, we expand this method of preparing TTF complexes with variable

* Corresponding author. Tel.: +82-51-510-2695; fax: +82-51-581-2348.
E-mail address: yikim@pusan.ac.kr (Y.-I. Kim).

0277-5387/$ - see front matter © 2004 Elsevier Ltd. All rights reserved.
doi:10.1016/j.poly.2004.06.008

counter ions of the copper metal; $(TTF)_4CuX_2$ (X = NCS, NO_3, Cl, Br, NCO and NO_2) were prepared using $Cu(Sp)X_2$ complexes as the precursors. The composition of TTF was constant, independent of the counter ions of the copper metal in the prepared compounds; therefore, we examined the conductivity of the prepared $(TTF)_4CuX_2$ in terms of the nature of the counter anions and the difference of the reduction potential of $Cu(Sp)X_2$ compounds, since the reduction potential of the electron acceptor also plays an important role in the strength of the ionicity of the charge transfer compounds [7]. The rates of electron transfer from TTF to the copper(II) metal center in the reaction of TTF with $Cu(Sp)X_2$ complexes are also investigated here, and the correlation of the charge transfer rate with the conductivity is an interesting further step since both the electrochemical and kinetic properties of $Cu(Sp)X_2$ complexes are known to be related to the copper coordination geometry [8–15].

2. Experimental section

2.1. Synthesis

All reagents and solvents were obtained commercially from either Aldrich or Sigma Chemicals and the precursor copper(II)-sparteine $Cu(Sp)X_2$ complexes were synthesized by a method reported previously [8]. The $(TTF)_4Cu(NO_3)_2$ complex was prepared from the direct reaction of TTF with $Cu(Sp)(NO_3)_2$. A solution of $Cu(Sp)(NO_3)_2$ (0.3 mmol) in 40 ml of dichloromethane was added dropwise to 20 ml of TTF (1 mmol) dichloromethane solution. The solution changed to a dark purple color immediately. The resulting mixture was stirred for approximately 2 h and then refrigerated overnight. The deep purple precipitates were isolated by filtration and washed several times with dichloromethane. The microcrystalline precipitates were dried in a vacuum at room temperature. Other $(TTF)_4CuX_2$ (X = NCS, Cl, Br, NCO and NO_2) type complexes were obtained by an analogous method using the corresponding $Cu(Sp)X_2$ complexes. All of the prepared compounds are stable in air. Elemental analyses were performed by the Korean Basic Science Center (Busan Branch). *Anal.* Calc. for $(TTF)_4Cu(NCS)_2$: C, 31.32; H, 1.62; N, 2.81. Found: C, 31.06; H, 1.56; N, 3.03%. Calc. for $(TTF)_4Cu(NO_3)_2$: C, 28.68; H, 1.60; N, 2.79. Found: C, 28.44; H, 1.53; N, 2.85%. Calc. for $(TTF)_4CuBr_2$: C, 27.69; H, 1.55. Found: C, 27.27; H, 1.63%. Calc. for $(TTF)_4CuCl_2$: C, 30.28; H, 1.69. Found: C, 30.29; H, 1.56%. Calc. for $(TTF)_4Cu(NCO)_2$: C, 32.36; H, 1.67; N, 2.90. Found: C, 32.50; H, 1.72; N, 2.99%. Calc. for $(TTF)_4Cu(NO_2)_2$: C, 29.63; H, 1.66; N, 2.88. Found: C, 30.07; H, 1.69; N, 2.84%.

2.2. Physical measurements

The electrical conductivities for the prepared compounds were determined with compressed pellets using a two-electrode system connected to a potentiostat at room temperature. The EPR spectral measurements were carried out for powered samples both at room temperature and at 77 K using an ESP-300S EPR spectrometer at the X-band frequency. The field modulation frequency was 100 kHz and DPPH was used as a reference. Cyclic voltammograms were recorded on an EG& PAR Inc. model 273 Potentiostat and a Galvanostat with a model BD X–Y recorder (Kipp & Zonen). The charge transfer rates from TTF to $Cu(Sp)X_2$ complexes was followed by the use of a Union Giken RA-401 stopped-flow spectrophotometer. All of the kinetic runs were carried out at 25 °C and 0.1 M ionic strength. The rate of formation of the charge transfer complexes was determined spectrophotometerically at 580 nm. The total concentration of [TTF] was 100-fold in excess over that of $[Cu(Sp)X_2]$ and the pseudo-first order condition was maintained. Pseudo-first order rate constants were evaluated using the conventional $\ln(A_t - A_\infty)$ vs. time plot and were linear for about 90% of the reaction times for most of the experiments. All of the test solutions were purged with dried nitrogen gas before each run.

3. Results and discussion

$(TTF)_4CuX_2$ (X = NCS, NO_3, Cl, Br, NCO and NO_2) complexes were prepared from the reaction of TTF with the copper(II)-sparteine $Cu(Sp)X_2$ complexes. The reaction of TTF with $Cu(Sp)X_2$ is interesting in that sparteine is replaced by TTF molecules. Fraenkel et al. [16] reported on the kinetics of the complexation of magnesium complexes with the sparteine ligand, in which one of the two nitrogen atoms in sparteine bound to the metal ion can be replaced by a solvent molecule in solution. The complex with sparteine bound by two nitrogen atoms is in equilibrium with a complex with a monodentate sparteine and a coordinated solvent molecule. It is likely that sparteine in $Cu(Sp)X_2$ could dissociate in the reaction with a strong reductant such as TTF, through this equilibrium. In all of the prepared compounds, the composition of TTF was always four per copper atom, provided that excess TTF in dichloromethane was used.

The powdered electrical conductivities of the compounds at room temperature are summarized in Table 1. On the basis of the electrical conductivity, the prepared compounds can be divided into two groups. One is the compounds, $(TTF)_4CuX_2$ (X = NCS, NO_3, Br and Cl), the electrical conductivities of which are in the semiconductor region ($\sigma_{r.t} = 10^0$–10^1 $S\,cm^{-1}$), and

Table 1
Electrical conductivities and EPR parameters of $(TTF)_4CuX_2$ charge transfer compounds

Compound	Electrical conductivity ($S\,cm^{-1}$)	EPR parameters[a]	
		$g_{\parallel}$	$g_{\perp}$
$(TTF)_4Cu(NCS)_2$	6.0×10^{1}	2.002	2.008
$(TTF)_4Cu(NO_3)_2$	7.5×10^{0}	2.002	2.008
$(TTF)_4CuBr_2$	4.8×10^{0}	2.0002[b]	2.0074[b]
$(TTF)_4CuCl_2$	2.9×10^{0}	1.9989[b]	2.0049[b]
$(TTF)_4Cu(NCO)_2$	1.8×10^{-4}	2.007 (isotropic)	
$(TTF)_4Cu(NO_2)_2$	~0	2.006	2.009

[a] EPR parameters were obtained at 77 K.
[b] Ref. [6].

the other group (X = NCO and NO_2) are insulators ($\sigma_{r.t} < 10^{-4}\ S\,cm^{-1}$) at room temperature.

The powdered EPR spectra for each compound exhibit a sharp singlet at around $\langle g\rangle \sim 2.006$ at room temperature. The EPR line shapes for each compounds exhibit good resolution for parallel ($g_{\parallel}$) and perpendicular ($g_{\perp}$) components at 77 K, except for $(TTF)_4Cu(NCO)_2$, and the results are summarized in Table 1. It is well known that the g values of sulfur radicals in which unpaired electrons are localized on the sulfur atoms are ~2.03, which is somewhat larger than the value of 2.003 of carbon radicals because of the larger spin–orbital coupling constants of sulfur atoms [17]. The observed g values for $(TTF)_4CuX_2$ are nearly equal to that of TTF^{+} radicals in solution ($\langle g\rangle = 2.00838$), indicating that the EPR signals arose from the unpaired electrons distributed on TTF stacks in $(TTF)_4CuX_2$ and that they have the same spin density as a TTF moiety. No EPR signals attributed to the Cu(II) metal ions were detected in any case, indicating that the copper center in $(TTF)_4CuX_2$ is in the diamagnetic Cu(I) state in the solid state; therefore the compounds are formulated as $(TTF)_4{}^{+1}Cu(I)X_2$. The partially ionized $(TTF)_4{}^{+1}$ oxidation state was confirmed by IR spectral investigations. The CS stretch band in the TTF ring (ν_{16}) of the prepared compounds was observed in the range of 821–828 cm^{-1}, which are higher than the value of 781 cm^{-1} for the TTF molecule and lower than the value of 836 cm^{-1} for TTF^{+1} free radicals [18].

We examined the correlation between the electrical conductivity and both the stability of $(TTF)_4CuX_2$ and the rate of charge transfer from TTF to the copper(II) metal in the reaction in order to examine how the nature of the counter anion in $(TTF)_4CuX_2$ affects the electrical conductivity.

Fig. 1 shows the electronic absorption spectra of TTF, $Cu(Sp)(NCS)_2$ and $(TTF)_4Cu(NCS)_2$, respectively. A new intense band appears at 580 nm in $(TTF)_4Cu(NCS)_2$, which is considered to arise from the charge transfer from the sulfur atom in TTF to the copper metal ion ($b_{2g} \rightarrow b_{1u}$) [19]. These charge transfer bands of all of the prepared compounds with an initial concentration of $[TTF]_0 = 5.0\times10^{-3}$ M and $[Cu(Sp)X_2]_0 = 2.5\times10^{-4}$ M centered at 580 nm at 298 K are also shown in a box in Fig. 1. The absorption intensities depend on the type of precursor copper complex used. The absorption intensities are parallel to the electrical conductivities of the charge transfer compounds produced. This result shows that the electrical conductivity increases as the quantity of charge transfer compound produced increases, suggesting that the more stable charge transfer compound exhibits the higher electrical conductivity.

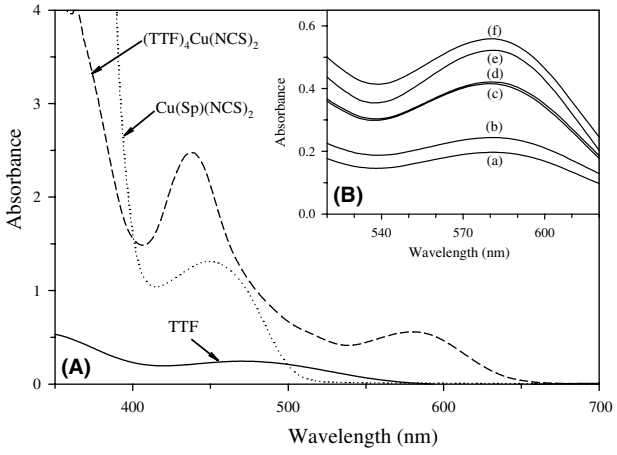

Fig. 1. (A) Electronic absorption spectra of the charge transfer complex, TTF and precursor complex $Cu(Sp)(NCS)_2$, A new intense band appears when TTF reacts with $(TTF)_4Cu(NCS)_2$. (B) The charge transfer bands centered at 580 nm are shown in a box. (The initial concentrations of $[TTF]_0 = 5.0\times10^{-4}$ M and $[Cu(Sp)X_2]_0 = 2.5\times10^{-4}$ M at 298 K, The absorption intensities are different depending on the type of precursor complexes used.) (a) $(TTF)_4Cu(NCO)_2$, (b) $(TTF)_4Cu(NO_2)_2$, (c) $(TTF)_4CuBr_2$, (d) $(TTF)_4CuCl_2$, (e) $(TTF)_4Cu(NO_3)_2$ and (f) $(TTF)_4Cu(NCS)_2$.

We measured the charge transfer rate from TTF to the copper metal ion for the following reaction.

$$4TTF + Cu(Sp)X_2 \rightarrow (TTF)_4CuX_2 + Sp$$

when $Cu(Sp)X_2$ and TTF are mixed in acetonitrile in a stopped-flow system, a very rapid increase in the absorption of 580 nm was observed. The pseudo-first order k_{obs}

Table 2
The second order rate constants (k_2)[a] in the reaction with TTF and the redox potential[b] for the precursor $Cu(Sp)X_2$ complexes

Complexes	k_2 ($M^{-1}s^{-1}$)	Redox potential				References
		E_{pc} (V)	$E_{1/2}$(V)	E_{pa}(V)	ΔE_p[c] (V)	
$Cu(Sp)(NCS)_2$	334.0 ± 0.1	+0.175	+0.228	+0.280	0.105	This work
$Cu(Sp)(NO_3)_2$	235.7 ± 0.1	−0.105	−0.056	−0.006	0.099	[8]
$Cu(Sp)Br_2$	102.0 ± 0.1	−0.050	+0.025	+0.100	0.150	[8]
$Cu(Sp)Cl_2$	1.07 ± 0.09	−0.220	−0.150	−0.080	0.140	This work
$Cu(Sp)(NCO)_2$	52.6 ± 0.1	−0.286	−0.235	−0.183	0.103	[8]
$Cu(Sp)(NO_2)_2$	0.42 ± 0.04	−0.400	−0.325	−0.250	0.150	[8]

[a] The k_2 values were evaluated from the equation $k_{obs} = k_2$[TTF] at 25 °C and 0.1 M ionic strength.
[b] Working electrode: Pt disk (ϕ = 1.6 mm). Reference electrode: Ag/Ag^+ electrode. Concentration: 0.5 mM. Supporting electrolyte: 0.1 M TBAP in CH_3CN. Scan rate: 100 mV/s. $E_{1/2}$ for the ferrocium/ferrocene couple is at +0.47 V vs. Ag/AgCl under the experimental conditions.
[c] ΔE_p is defined as E_{pa}–E_{pc}.

values for the above reaction were determined from the $\ln(A_t - A_\infty)$ vs. time plot which yields a good straight line. The second order rate constants k_2, for $k_{obs} = k_2$ [TTF], were evaluated from the plot of the k_{obs} values vs. [TTF] concentrations. The slope gives the second order rate constant k_2 value and the evaluated k_2 values are also summarized in Table 2. The k_2 values vary appreciably depending on the nature of anions in the precursor copper complexes. The highest value was observed for $(TTF)_4Cu(NCS)_2$. The $(TTF)_4Cu(NO_3)_2$ and $(TTF)_4CuBr_2$ complexes show relatively higher values than those of $(TTF)_4CuCl_2$, and $(TTF)_4Cu(NO_2)_2$. The softer sulfur and bromide donor atoms can stabilize the +1 state of the copper metal ion more efficiently than the oxygen atom.

We reported the reduction potentials of some $Cu(Sp)X_2$ complexes for the process $Cu^{II}(Sp)X_2 + e \rightarrow Cu^{I}(Sp)X_2$ [8], and newly examined the reduction potentials of $Cu(Sp)(NCS)_2$ and $Cu(Sp)Cl_2$ to compare the stability of the precursor copper complexes. In the potential range of −1.00 to +0.50 V vs. Ag/AgCl in acetonitrile, a single peak was observed which was described as $Cu(II) + e \rightarrow Cu(I)$ [20]. The half-wave $E_{1/2}$ values for $Cu(II) \rightarrow Cu(I)$ were estimated by averaging the anionic and cathodic peak potentials, and these values are listed in Table 2. Two $E_{1/2}$ values at +0.42 V and +0.66 V were observed in the TTF molecule, and were assigned to the TTF^{+1}/TTF and TTF^{+2}/TTF^{+1} couples respectively by comparing them with the reported reduction potential of TTF [21]. It is well known that conducting material of a mixed valence state can be obtained by the reaction of donors and acceptors with moderate redox potentials, and it is proposed that the value of the difference (ΔE_{redox}) between the first oxidation potential of the donors and the first reduction potential of the acceptors must be below ≈+0.25 V in order to form a partially ionized charge transfer compound [22]. The ΔE_{redox} of $(TTF)_4Cu(NCS)_2$ is +0.19 V and those of the other prepared compounds are above +0.25 V. For example, the ΔE_{redox} of $(TTF)_4Cu(NO_2)_2$ is as large as +0.76 V. In spite of these relatively high ΔE_{redox} values, partially ionized $(TTF)_4^{1-n}$ species are formed in these compounds; however, the ΔE_{redox} value plays an important role in forming the electrical conductive materials. The compounds that have ΔE_{redox} larger than +0.66 V exhibit poor electrical conductivities, acting as insulators, in this study.

It was found that the faster the charge transfer rate from TTF to the precursor copper(II) complex in the formation of $(TTF)_4CuX_2$ as well as the higher the reduction potential of the precursor copper complexes, the higher the electrical conductivity of $(TTF)_4CuX_2$ that was produced. A quasi-linear relationship between $E_{1/2}$ and k_2 values was discovered for $(TTF)_4CuX_2$ (X = NCS, NO_3, NCO and NO_2), as seen in Table 2.

But the compounds with the anions Cl and Br deviated from this linearity, showing the relatively low k_2 values even though the electrical conductivities are in the semiconductor region. The relatively high electrical conductivities of $(TTF)_4CuCl_2$ and $(TTF)_4CuBr_2$ are attributable to the thermodynamic stability of the corresponding precursor compounds rather than the charge transfer rate in the formation of $(TTF)_4CuX_2$.

4. Conclusions

We prepared the charge transfer compounds $(TTF)_4CuX_2$ (X = NCS, NO_3, Cl, Br, NCO and NO_2) from the direct reaction of TTF with the precursor $Cu(Sp)X_2$ complexes in dichloromethane. The TTFs were partially ionized and the copper metals were reduced $Cu(II) \rightarrow Cu(I)$ in the formation of $(TTF)_4CuX_2$. The electrical conductivity increases by increasing the reduction potential of the precursor compound $Cu(Sp)X_2$ and the charge transfer rate from TTF to $Cu(Sp)X_2$. This observed result may provide useful information in the design of molecular-based conductive material with prescribed thermodynamic and kinetic

properties, even though more data is needed in order to confirm this conclusion.

Acknowledgement

This work was supported by the Korean Science and Engineering Foundation (KOSEF project No. R01-2001-000055-0).

References

[1] J.P. Farges, Organic Conductors, Marcel Dekker, New York, 1994.
[2] J.M. Williams, J.R. Ferraro, R.J. Thorn, K.D. Carlson, U. Geiser, H.H. Wang, A.M. Kini, M.-H. Whangbo, Organic Superconductors (including Fullerenes), Prentice-Hall, Englewood Cliffs, NJ, 1992.
[3] L. Ouahab, Chem. Mater. 9 (1997) 1909.
[4] M.B. Inoue, M. Inoue, Q. Fernando, K.W. Nebesny, Inorg. Chem. 25 (1986) 3976.
[5] A.R. Siedle, G.A. Candela, T.F. Finnegan, R.P. Van Duyne, T. Cape, G.F. Kokoszka, P.M. Woyciejes, J.A. Hashmall, Inorg. Chem. 20 (1981) 2635.
[6] Y.I. Kim, W.E. Hatfield, Inorg. Chim. Acta 189 (1991) 237.
[7] J.B. Torrance, Acc. Chem. Res. 12 (1979) 79.
[8] Y.M. Lee, Y.K. Kim, H.C. Jung, Y.I. Kim, S.N. Choi, Bull. Kor. Chem. Soc. 23 (2002) 404.
[9] S.-N. Choi, M.-A. Kwon, Y. Kim, R.D. Bereman, P. Singh, B. Knight, K. Seff, J. Coord. Chem. 34 (1995) 241.
[10] Y.-M. Lee, S.-N. Choi, I.-H. Suh, R.D. Bereman, Acta Cryst. C 54 (1998) 1582.
[11] S. Lopez, I. Muravyov, S.R. Pulley, S.W. Keller, Acta Cryst. C 54 (1998) 355.
[12] L.S. Childers, K. Folting, L.L. Merritt Jr., W. Streib, Acta Cryst. B 31 (1975) 924.
[13] A. Togni, G. Rihs, P.S. Pregosin, C. Ammann, Helv. Chim. Acta 73 (1990) 723.
[14] S.-N. Choi, R.D. Bereman, J.R. Wasson, J. Inorg. Nucl. Chem. 37 (1975) 2087.
[15] Y.-M. Lee, M.-A. Kwon, S.K. Kang, J.H. Jeong, S.-N. Choi, Inorg. Chem. Commun. 6 (2003) 197.
[16] G. Fraenkel, B. Appleman, J.G. Ray, J. Am. Chem. Soc. 96 (1974) 5113.
[17] A. R Siedle, G.A. Candela, T.F. Finnegan, R.P. Van Duyne, T. Cape, G.F. Kokoszka, P.M. Woyciejes, J.A. Hashmall, Inorg. Chem. 20 (1981) 2635.
[18] R. Bozio, I. Zanon, A. Girlando, C. Pecile, J. Chem. Phys. 71 (1979) 2282.
[19] T. Sugano, H. Kuroda, K. Yakushi, Bull. Chem. Soc. Jpn. 51 (1978) 1041.
[20] A.J. Burd, R. Pasons, J. Jordans, Standard Potential in Aqueous Solution, Marcel Dekker, New York, 1985.
[21] D.L. Coffer, J.Q. Chambers, D.R. Williams, P.E. Garret N.D. Canfield, J. Am. Chem. Soc. 93 (1971) 2258.
[22] R.C. Wheland, J. Am. Chem. Soc. 98 (1976) 3936.

Available online at www.sciencedirect.com
SCIENCE DIRECT®
Polyhedron 23 (2004) 2117–2123
POLYHEDRON
www.elsevier.com/locate/poly

Dinuclear silver(I) complexes of N,N'-dibenzyl-4,13-diaza-18-crown-6-ether and dibenzo-24-crown-8-ether

Ming Wen [a,d,*], Megumu Munakata [b], Yusaku Suenaga [b], Takayoshi Kuroda-Sowa [b], Masahiko Maekawa [c], Iwade Kodai [b]

[a] Department of Chemistry, Tongji University, 1239# Siping Road, Shanghai 200092, China
[b] Department of Chemistry, Kinki University, Kowakae, Higashi-Osaka, Osaka 577-8502, Japan
[c] Research Institute for Science and Technology, Kinki University, Kowakae, Higashi-Osaka, Osaka 577-8502, Japan
[d] State Key Laboratory of Coordination Chemistry, Nanjing University, 210093, China

Received 5 February 2004; accepted 23 March 2004
Available online 28 July 2004

Abstract

Three silver(I) coordination complexes of diaza- and dibenzo-crown ethers, $[Ag(DDAC)](CF_3SO_3)$ (**1**), $[Ag_2(DDAC)(CF_3SO_3)_2]$ (**2**) and $[Ag_2(DB24C8)(CF_3SO_3)_2]$ (**3**) have been synthesized by using different molar ratios of ligand to silver triflate salt, and characterized structurally. A large excess of DDAC ligand leads to mononuclear complex **1**, and a large excess of silver triflate gives rise to dinuclear complex **2**, based on metal–heteroatom and metal–oxygen interactions. Ligand DB24C8 coordinates two silver(I) ions to afford dinuclear complex **3**.
© 2004 Elsevier Ltd. All rights reserved.

Keywords: Silver(I) complexes; Dinuclear complex; Mononuclear complex

1. Introduction

Macrocyclic ligands have long been employed for studies involving transition metal ion recognition [1,2]. There has been tremendous development with respect to cyclic type ligands like crown ethers [3] which are able to perform specific functions. When the macrocyclic ligands are bound to polymeric supporting materials, the resulting materials can serve as ion sensors, exchange resins, metal ion extractors, phase transfer catalysts, mimics of enzyme systems and photoresponsive chromophores [4–6].

Cryptand type ligands, crown ether systems are suitable to be used in the design of complexation agents for metal ions [7–13]. We have been continuously studying dibenzo-crown ether complexes with silver(I) ions [14,15], because these silver(I) complexes used usually involve the oxygen base cavities and π-donor phenyl groups. Same as the reported example [16], two different coordination complexes can be constructed by using different molar ratios of crown ether ligand to silver(I) ion in this work. The macrocyclic crown ether and cryptand ligands were incorporated into the dimers.

In this work, two cryptand type ligands of crown ethers, N,N'-dibenzyl-4,13-diaza-18-crown-6-ether (DDAC) and dibenzo-24-crown-8-ether (DB24C8), as a continuation of our previous work [15], have been selected as ligands to synthesize three silver(I) coordination complexes, $[Ag(DDAC)](CF_3SO_3)$ (**1**), $[Ag_2(DDAC)(CF_3SO_3)_2]$ (**2**) and $[Ag_2(DB24C8)(CF_3SO_3)_2]$ (**3**). The cryptand crown ether hosts, diaza-crown ether and dibenzo-crown ether, using different coordination modes bind the guest silver(I) ions and build up distinctive molecular architectures.

* Corresponding author. Fax: +86-21-6598-2287.
E-mail address: m_wen@mail.tongji.edu.cn (M. Wen).

0277-5387/$ - see front matter © 2004 Elsevier Ltd. All rights reserved.
doi:10.1016/j.poly.2004.03.026

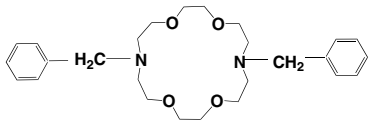

N,N'-Dibenzyl-4,3-diaza-18-crown-6-ether
(DDAC)

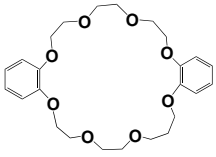

Dibenzo-24-crown-8-ether
(DB[24]C8)

2. Experimental

2.1. General procedures

All reactions and manipulations were performed under an argon atmosphere by using Schlenk techniques. All chemicals were reagent grade and used as supplied without further purification. Solvents were dried and distilled by using standards methods before use. Reagent grade DDAC was purchased from Tokyo Chemical Industry Co. Ltd., whereas silver perchlorate and all other chemicals were purchased from Wako Pure Chemical, Inc. and used as received. The IR spectra were measured as KBr disks on a JASCO FT/IR-8000 spectrometer at room temperature. All crystallizations of the silver complexes were performed in the dark.

2.2. Syntheses

2.2.1. [Ag(DDAC)](CF$_3$SO$_3$) (**1**)

To a toluene solution (8 ml) containing Ag(CF$_3$SO$_3$) (12.6 mg, 0.048 mmol), DDAC (106.2 mg, 0.24 mmol) was added. The mixture was stirred at room temperature for 20 min and filtered. A portion of the filtrate (2 ml) was introduced into a 7 mm glass tube and layered with *n*-hexane as a diffusion solvent. After the glass tube was sealed under argon and left standing at room temperature for one week, colorless block crystals of **1** suitable for X-ray determination were isolated. The theoretical value of elemental analysis and the isolated yield (21.4 mg, 18%) are based on the formula without THF molecules. *Anal.* Calc. for $AgSF_3O_7N_2C_{27}H_{38}$: C, 46.36; H, 5.48; N, 4.00. Found: C, 46.35; H, 5.06; N, 3.96%. Main IR bands (KBr, ν/cm^{-1}): 2858(m), 1494(w), 1452(m), 1266(s), 1145(s), 1106(s), 1030(s), 749(m), 709(m), 638(s).

2.2.2. [Ag$_2$(DDAC)(CF$_3$SO$_3$)$_2$] (**2**)

A solution of DDAC (12.8 mg, 0.03 mmol) in toluene (10 ml) was treated with Ag(CF$_3$SO$_3$) (38.8 mg, 0.30 mmol). The above procedure was repeated to yield colorless platelet single crystals of **2** (13.4 mg, yields 26%). *Anal.* Calc. for $Ag_2S_2F_6O_{10}N_2C_{28}H_{38}$: C, 34.42; H, 4.09; N, 2.81. Found: C, 35.16; H, 4.00; N, 2.93%. Main IR bands (KBr, ν/cm^{-1}): 2887(m), 2370(w), 1458(w), 1285(s), 1267(s), 1148(s), 1106(s), 1036(s), 736(m), 708(m), 638(m).

2.2.3. [Ag$_2$(DB24C8)(CF$_3$SO$_3$)$_2$] (**3**)

Similar to the previous complexes, DB[24]C8 (44.8 mg, 0.10 mmol) was added to a solution of AgCF$_3$SO$_3$ (51.4 mg, 0.20 mmol) in toluene, and yielded colorless platelet single crystals of **3** (26.9 mg, yield 28%). *Anal.* Calc. for $Ag_2S_2F_6O_{14}C_{26}H_{32}$: C, 32.42; H, 6.88. Found: C, 32.05; H, 6.56%. Main IR bands (KBr, ν/cm^{-1}): 3547(m), 2910(s), 1597(s), 1504(s), 1456(s), 1352(s), 1278(s), 1224(s), 1160(s), 1116(s), 1083(s), 1047(s), 1033(s), 951(s), 938(s), 905(m), 746(m), 634(s).

2.3. Crystallography

Single crystal X-ray data for all complexes were measured on a Rigaku/MSC Mercury CCD diffractometer with graphite monochromated Mo Kα radiation ($\lambda = 0.71073$ Å) at -123 ± 1 °C for **1** and **2**, and 26.0 ± 1 °C for **3**. Details are summarized in Table 1. Selected bond lengths and angles for the three complexes are given in Table 2.

3. Results

3.1. Syntheses and infrared spectroscopy

3.1.1. Syntheses

It is noted that in the preparations described above different metal:ligand ratios were used. Generally, coordination of an aromatic ligand to silver ions can be achieved via a stoichiometric reaction [17,18], but sometimes an excess of ligand or metal ion has to be used to obtain coordinated complexes [19–23]. In this work, the complexes presented here are prepared via reactions of excess ligand or metal ion. In the experiments, when the molar ratios of M:L were 5:1, 1:10 and 1:2 for **1**, **2** and **3**, respectively, crystallized solids were isolated at room temperature, and the different molar ratios led to different crystal structures. Reasons for the use of silver salt excesses in **3** are as follows: (i) The solvent toluene may form metal complexes in solution with silver ions [24] which partially consumes the metal salt. Thus, the preparation of silver(I) complexes in toluene sometimes requires an excess of the silver salt

Table 1
Crystallographic data for complexes **1**–**3**

Complex	**1**	**2**	**3**
Formula	$AgSF_3O_7N_2C_{27}H_{38}$	$Ag_2S_2F_6O_{10}N_2C_{28}H_{38}$	$AgSF_3O_7C_{13}H_{16}$
Formula weight	699.53	1912.92	481.19
Crystal system	monoclinic	triclinic	monoclinic
Space group	$P2_1/n$ (#14)	$P\bar{1}$ (#2)	$P2_1/c$ (#14)
a (Å)	11.261(3)	12.603(6)	10.0449(3)
b (Å)	13.523(4)	15.094(7)	21.051(3)
c (Å)	20.222(6)	10.252(6)	8.6860(5)
α (°)		98.76(2)	
β (°)	109.870(3)	100.34(2)	110.4894(6)
γ (°)		109.46(1)	
V (Å^3)	2896(1)	1760(1)	1720.5(2)
Z	4	2	4
$F(0\,0\,0)$	1440.00	960.00	960.00
T (°C)	−123.0	−123.0	26.0
ρ (g/cm^3)	1.604	1.804	1.858
λ, Å (Mo Kα)	0.71069	0.71069	0.71069
μ (cm)	8.33	13.15	13.53
Number of reflections measured	9062 (total) 6594 (unique)	19 999 (total) 7949 (unique)	20 973 (total) 2018 (unique)
Number of observed reflections [$I > 2\sigma(I)$]	6049	5651	3912
Number of variable parameters	370	452	274
Residuals: R; R_w	0.026; 0.053	0.066; 0.128	0.055; 0.108
Goodness-of-fit	1.07	1.07	1.44

$R = \sum ||F_o| - |F_c|| / \sum |F_o|$. $R_w = [\sum w(F_o^2 - F_c^2)^2 / \sum w(F_o^2)^2]^{1/2}$.

[25]. (ii) When a compound (complex) in solution is "incongruently saturating", its crystal cannot be obtained via a stoichiometric reaction [26]. We examined the effect of a different molar ratio on the nature of the final product. The reactivity of $AgCF_3SO_3$ with DB24C8 was systematically studied in toluene with

Table 2
Selected bond lengths (Å) and bond angles (°) for complexes **1**–**3**

Complex **1**					
Bond lengths					
Ag(1)–O(3)	2.598(1)	Ag(1)–O(4)	2.686(2)	Ag(1)–N(1)	2.305(2)
Ag(1)–N(2)	2.316(2)				
Bond angles					
O(3)–Ag(1)–O(4)	63.6(4)	O(3)–Ag(1)–N(1)	71.7(4)	O(3)–Ag(1)–N(2)	121.9(4)
O45)–Ag(1)–N(1)	113.8(4)	O(4)–Ag(1)–N(2)	73.6(4)	N(1)–Ag(1)–N(2)	166.1(4)
Ag(1)–O(3)–C(21)	110.7(8)	Ag(1)–O(3)–C(23)	117.5(1)	Ag(1)–O(4)–C(17)	102.5(9)
Ag(1)–O(4)–C(24)	103.9(1)	Ag(1)–N(1)–C(19)	113.9(1)	Ag(1)–N(1)–C(22)	108.4(1)
Ag(1)–N(1)–C(25)	108.4(1)	Ag(1)–N(2)–C(16)	111.5(1)	Ag(1)–N(2)–C(18)	111.8(9)
Ag(1)–N(2)–C(26)	107.0(1)				
Complex **2**					
Bond lengths					
Ag(1)–O(1)	2.511(4)	Ag(1)–O(2)	2.589(4)	Ag(1)–O(3)	2.203(4)
Ag(1)–N(1)	2.287(4)	Ag(2)–O(6)	2.592(4)	Ag(2)–O(7)	2.506(5)
Ag(2)–O(8)	2.252(3)	Ag(2)–N(2)	2.325(4)		
Bond angles					
O(1)–Ag(1)–O(2)	115.5(1)	O(1)–Ag(1)–O(3)	121.4(2)	O(1)–Ag(1)–N(1)	78.8(2)
O(2)–Ag(1)–O(3)	105.2(1)	O(2)–Ag(1)–N(1)	73.7(1)	O(3)–Ag(1)–N(1)	161.5(2)
O(6)–Ag(2)–O(7)	121.5(1)	O(6)–Ag(2)–O(8)	113.0(1)	O(6)–Ag(2)–N(2)	71.0(1)
O(7)–Ag(2)–O(8)	113.4(1)	O(7)–Ag(2)–N(2)	74.5(1)	O(8)–Ag(2)–N(2)	163.5(2)
Complex **3**					
Bond lengths					
Ag(1)–O(1)	2.450(4)	Ag(1)–O(5)	2.538(5)	Ag(1)–O(6)	2.634(6)
Bond angles					
Ag(1)–O(1)–C(1)	112.3(3)	Ag(1)–O(1)–C(2)	113.6(4)		

different M:L ratios. Reactions similar to that described in the experimental section but performed with M:L ratios of 1:1 led to no evidence for formation of an isolable complex. In order to obtain polymeric complexes by connecting silver(I) ions and the phenyl group of DDAC besides silver(I) locating in the cavities, a large excess of silver triflate was used with L:M = 1:10 which led to dinuclear complex **2**. The effect of a different molar ratio was studied by employing a large ligand excess with L:M = 5:1. The result was the mononuclear complex **1**.

3.1.2. Infrared spectroscopy

In the IR spectra of **1**–**3**, a broad strong absorption occurs in the region 638–1254 cm^{-1}, and their peaks are shifted to slightly different frequencies compared with the normal absorption of $AgCF_3SO_3$ at 1256, 1179, 1037, and 629 cm^{-1}. This suggests that the triflate groups in these complexes are present not as ionic species, but as coordinated ones [27]. The coordination of silver(I) ions to oxygen or nitrogen atoms of diaza-crown ether and dibenzo-crown ether can also be seen by comparing the spectra of **1**–**3** with those of the two free ligands (DDAC at 1453, 1123, 1056, 749, 701 cm^{-1}, DB24C8 at 1594, 1507, 1357, 1225, 960, 740 cm^{-1}).

3.2. Description of the structures

3.2.1. Mononuclear complex [Ag(DDAC)](CF$_3$SO$_3$) (1)

Molecules of triflate anion exist independently of the complex in lattice interstices. The molecular structure of complex **1** together with the numbering scheme is shown in Fig. 1. The silver(I) ion is in a distorted tetrahedral environment, being coordinated by two nitrogen atoms and two oxygen atoms on the same side of the N–Ag–N system, in which Ag–O bond lengths are 2.598(1) and 2.686(2) Å and Ag–N bond lengths are 2.305(2) and 2.315(2) Å. The O–Ag–O and N–Ag–N angles are 63.6(4)° and 166.13(4)°, respectively. The remaining two ligand oxygen atoms are not involved in coordination, and the triflate ion only plays a charge-balance and space-filling role.

3.2.2. Dinuclear complex [Ag$_2$(DDAC)(CF$_3$SO$_3$)$_2$] (2)

An ORTEP drawing of complex **2** with the atom numbering scheme is shown in Fig. 2. The symmetric unit contains two independent dinuclear molecules each located at an inversion center. The coordination environment of each metal atom is almost tetrahedral, comprising of three oxygen atoms of which two are from DDAC and one from a triflate group, plus a nitrogen atom. The DDAC ligand thus contains two silver(I) centers in its heterocyclic hard donor cavity with Ag–O bond lengths ranging from 2.203(4) to 2.592(4) Å and Ag–N bond lengths of 2.287(4) and 2.325(4) Å. The present Ag–O bond lengths are well within the normal range 2.17–2.61 Å observed in silver(I)–crown ether complexes [15] and the Ag–N bond lengths are normal

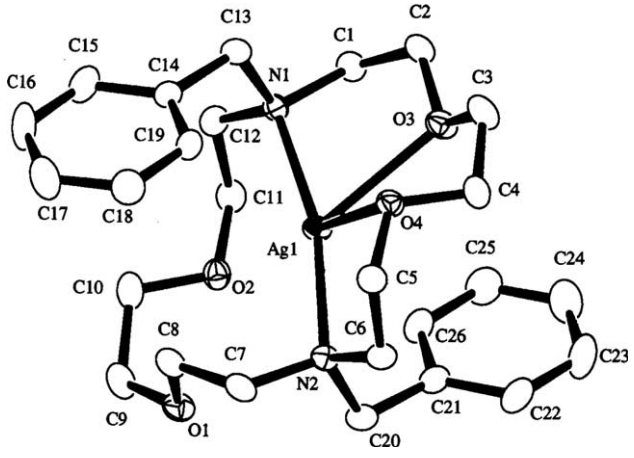

Fig. 1. ORTEP view of the molecular structure of **1**.

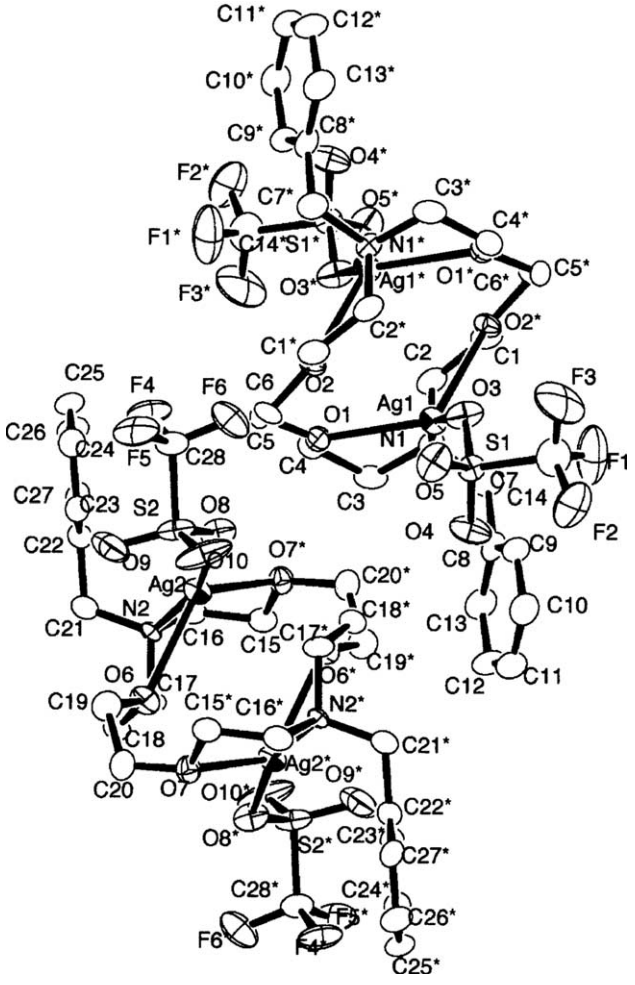

Fig. 2. Molecular structure of the dinuclear unit of **2**.

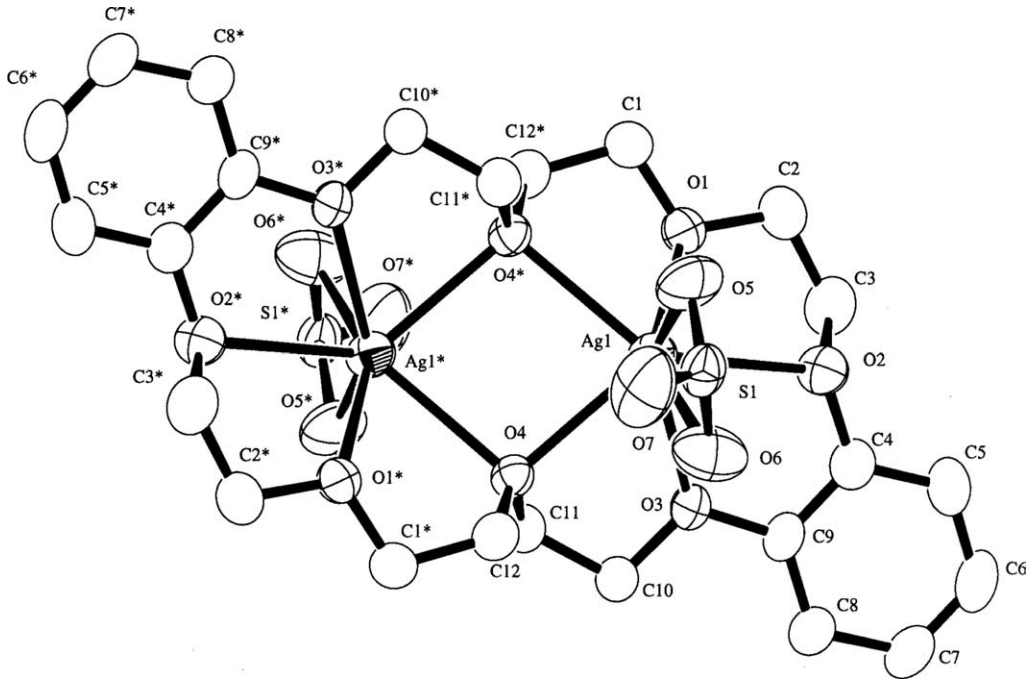

Fig. 3. Molecular structure of the dinuclear unit of **3**.

compared with those in previously reported crystate–silver(I) complexes [10].

3.2.3. Dinuclear complex $[Ag_2(DB24C8)(CF_3SO_3)_2]$ (**3**)

Fig. 3 depicts a perspective view with the atom numbering of centrosymmetric complex **3**, in which each silver(I) ion is octahedrally coordinated by two triflate oxygens with an average Ag–O length of 2.586 Å and five oxygens of the ligand with an average Ag–O bond length of 2.450 Å. Each DB24C8 host molecule contains two silver(I) ions as guests with a Ag···Ag distance of 3.95 Å. Unlike dinuclear silver(I) coordination complexes of the dibenzo-crown ether family in our previous works, [Ag(DB[18]C6)(ClO_4)](THF) [15a], the silver(I) ions are not coordinated to phenyl groups.

4. Discussion

In this work, the diaza- and dibenzo-crown ether hosts accommodate silver(I) ions as guests in their cyclic hard donor base cavities. The structures of these three silver(I) complexes display different characteristics with the cation being encapsulated in a macrocyclic environment with different L:M stoichiometries. A large excess of DDAC ligand leads to mononuclear complex **1**, and a large excess of silver triflate gives rise to dinuclear complex **2** based on metal–heteroatom and metal–oxygen interactions. DB24C8 coordinates to two silver(I) ions to afford dinuclear complex **3**.

The average Ag–O bond lengths of 2.642, 2.442 and 2.540 Å observed for **1**, **2** and **3**, respectively, are within the normal range observed in silver(I)–crown ether complexes [10]. The average Ag–N bond lengths of 2.310 Å in **1** and 2.306 Å in **2** are virtually the same and a little longer than that in the silver(I) complex of 1,4,10,13-tetraoxa-7,16-diazacyclooctadecane, but slight shorter than that in the silver(I) complex of N-methylated (L^2) and N-benzylated 1,4,10,13-tetraoxa-7,16-diazacyclooctadecane (L^3) [10]. In the present complexes, each silver(I) ion is not coordinated to all oxygen and nitrogen atoms as in [Ag(L^3)]PF_6 [10]. In addition, triflate oxygen atoms are not coordinated to silver(I) ions in **1**, but are coordinated to silver(I) ions in **2**, and the Ag–O bond length of silver(I) with triflate is shorter than that of silver(I) with the ligand oxygen atoms.

Furthermore, the crown ether hosts in this work are not involved in coordination of the phenyl group to silver(I) via a π interaction, as our previous work in DB18C6–Ag(I) complexes [15a] (Fig. 4). Two symmetry-related silver(I) ions can be located in the oxygen base cavity of DB24C8 without silver(I)–π interaction and π–π interaction (Fig. 4(c)). On the other hand, even though DDAC has the same size, six-membered hard donor cavity as that of DB18C6, the silver(I) guest number and coordination fashion differ distinctly. The coordination unit of DB18C6-Ag(I) complexes can involve both σ bonding at an oxygen group and silver–π as well as π–π interaction between two parallel phenyl groups (Fig. 4(a)). DDAC only contains two symmetry-related silver(I) ions in its

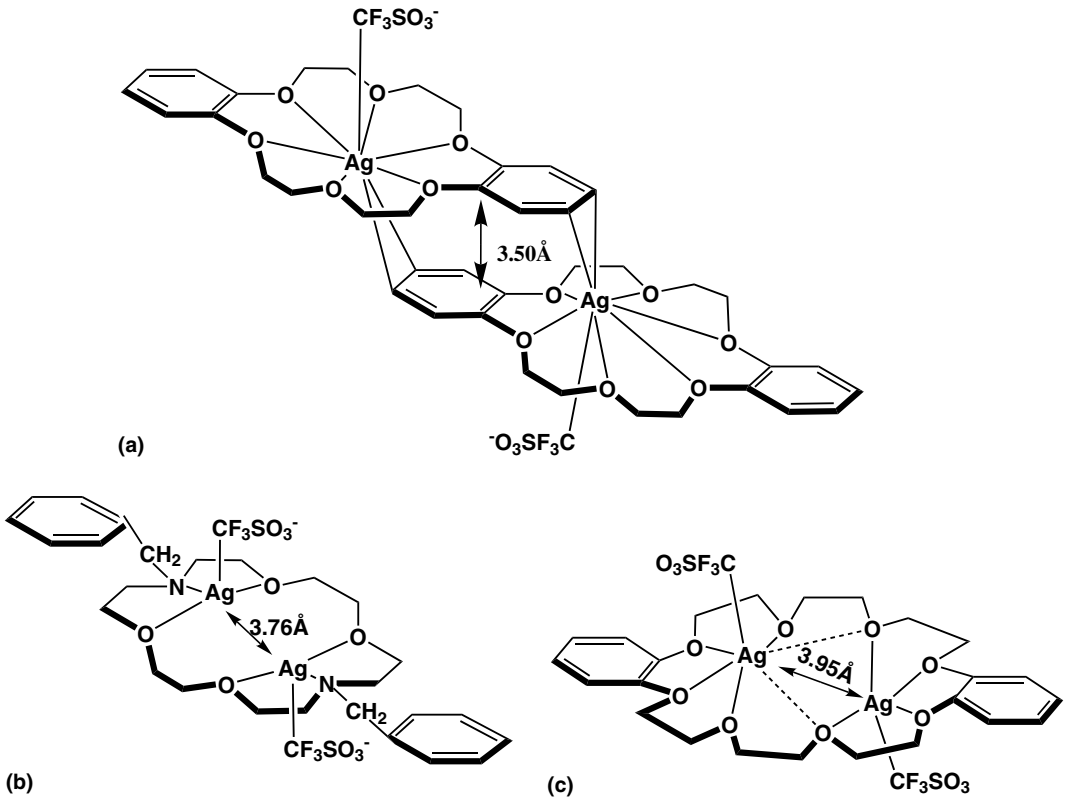

Fig. 4. Schematic view of dinuclear Ag(I) complexes with dibenzo- and diaza-crown ethers. $[Ag(DB18C6)(CF_3SO_3)]_2(acetone)_2$ (a), $[Ag_2(DDAC)(CF_3SO_3)_2]$ (b), $[Ag_2(DB24C8)(CF_3SO_3)_2]$ (c).

six-membered heterocyclic hard donor cavity without silver–π and π–π interaction (Fig. 4(b)). This case is the same as the formation of the Ag(I)–DB24C8 complex with a eight-membered hard donor cavity. This indicates that the structure construction process in the crown ether–silver(I) complex system is strongly dependent on the ligand: cavity size and the existence of heteroatoms as well as flexibility of the phenyl group.

In conclusion, with the cryptand type ligands, two distinct coordination complexes **1** and **2**, have been synthesized with different L:M stoichiometry. With regard to silver(I) complexes with diaza- and dibenzo-crown ethers (Fig. 4), there are two kinds of substantial dinuclear complexes. The ligand DB18C6 is based on the silver(I)–π interaction, in which the coordination unit involves both σ bonding at oxygen donor sites and π–π interaction between two phenyl groups. The other kind comprise dinuclear complex **2** and **3** in this work, in which two silver(I) ions occupy the cyclic or heterocyclic base cavity to coordinate to oxygen atoms without Ag(I)–π interaction or π–π interaction. It is believed that self-assembly of macrocyclic cryptand or dibenzo-crown ether compounds with transition metal ions can be constructed using stereospecific diaza- and dibenzo-crown ethers ligands (cavity size, the existence of heteroatoms as well as the flexibility of phenyl groups) and the molar ratio effect [10].

5. Supplementary material

Crystallographic data for the structures reported here have been deposited with the Cambridge Crystallographic Data Center as Supplementary Publication Nos. CCDC-220695, 220694 and 220693 for complex **1**, **2** and **3**, respectively. Copies of this information may be obtained free of charge from: The Director, CCDC, 12 Union Road, Cambridge, CB2 1EZ, UK (fax: +44-1223-336-033; e-mail: deposit@ccdc.cam.ac.uk or www:http//www.ccdc.cam.ac.uk).

Acknowledgements

This work was partially supported by Grants-in-Aid for Science Research [Nos. 10440201, 11874092, 12440189, 10016743 (priority area: metal-assembled complexes)] from the Ministry of Education, Science, Culture, Sports of Japan, and the Project-sponsored by SRF for ROCS from the SEM [No. 1380241005], the

Science Fund [No. 1380219042] from Tongji University of China.

References

[1] L.F. Lindoy, The Chemistry of Macrocyclic Ligand Complexes, Cambridge University Press, Cambridge, 1989.
[2] C.J. Pedersen, H.K. Frensdorff, Angew. Chem. Int. Ed. Eng. 11 (1972) 16.
[3] J.M. Lehn, Pure Appl. Chem. 50 (1978) 871.
[4] H. Dürr, Photochromism of Dihydroindolizines and Related Systems, in: J.C. Cranno, R.J. Guglielmetti (Eds.), Organic Photochromic and Thermochromic Compounds, vol. 1, Plenum Press, New York, 1999, p. 223.
[5] Y.A. Zolotov (Ed.), Macrocyclic Compounds in Analytical Chemistry, Wiley, New York, 1997, Chapter 4.
[6] J. Smid, R. Sinta, in: F. Vögtle, W. Weber (Eds.), Topic in Current Chemistry, vol. 121, Springer-Verlag, Berlin, 1984, p. 105.
[7] (a) P.D. Prince, P.J. Cragg, J.W. Steed, Chem. Commun. (1999) 1179;
(b) J.W. Steed, P.C. Junk, B.J. McCool, J. Chem. Soc., Dalton Trans. (1998) 3417.
[8] K. Kubo, T. Sakurai, N. Kato, A. Mori, Heterocycles 51 (1999) 1229.
[9] S.H. Chan, L.S.M. Lam, W.T. Wong, W.K. Chan, Macromol. Rapid Commun. 21 (2000) 1075.
[10] T.W. Hambley, L.F. Lindoy, J.R. Reimers, P. Turner, G. Wei, A.N. Widmer-Cooper, J. Chem. Soc., Dalton Trans. (2001) 614.
[11] H. Plenio, J. Hermann, Acta Crystallogr. C55 (1999) 62.
[12] K. Kubo, N. Kato, T. Sakurai, Acta Crystallogr. C53 (1997) 132.
[13] N. Heidari, A. Thaler, H. Schneider, B.G. Cox, Inorg. Chim. Acta 279 (1998) 186.
[14] T.B. Lu, X.M. Gan, M.Y. Tan, K.B. Yu, Polyhedron 12 (1993) 621.
[15] (a) M. Wen, M. Munakata, Y. Suenaga, T. Kuroda-Sowa, M. Maekawa, Inorg. Chim. Acta 322 (2002) 18;
(b) M. Wen, M. Munakata, Y. Suenaga, T. Kuroda-Sowa, M. Maekawa, Inorg. Chim. Acta 338 (2002) 111.
[16] A.J. Blake, G. Reid, M. Schröder, J. Chem. Soc. Chem. Commun. 15 (1992) 1074.
[17] M. Munakata, L.P. Wu, T. Kuroda-Sowa, M. Meakawa, S. Suenaga, K. Sugimoto, Inorg. Chem. 36 (1997) 4903.
[18] M. Munakata, L.P. Wu, T. Kuroda-Sowa, M. Maekawa, Y. Suenaga, G.L. Ning, T. Kojima, J. Am. Chem. Soc. 120 (1998) 8610.
[19] P. Paul, B. Tyagi, A.K. Bilakhiya, P. Dastidar, E. Suresh, Inorg. Chem. 39 (2000) 14.
[20] S.R. Batten, B.F. Hoskins, B. Moubaraki, K.S. Murray, R. Robson, Chem. Commun. (2000) 1095.
[21] B.F. Abrahams, S.R. Batten, M.J. Grannas, H. Hamit, B.F. Hoskins, R. Robson, Angew. Chem. Int. Ed. Eng. 38 (1999) 1475.
[22] D. Venkataraman, S. Lee, J.S. Moore, P. Zhang, K.A. Hirsch, G.B. Gardner, A.C. Covey, C.L. Prentice, Chem. Mater. 8 (1996) 2030.
[23] A.J. Blake, N.R. Brooks, N.R. Champness, L.R. Hanton, P. Hubberstey, M. Schröder, Pure Appl. Chem. 70 (1998) 2351.
[24] H.K. Hofstee, J. Organomet. Chem. 168 (1979) 241.
[25] (a) M. Munakata, L.P. Wu, T. Kuroda-Sowa;, M. Maekawa, Y. Suenaga, G.L. Ning, T. Kojima, J. Am. Chem. Soc. 120 (1998) 8610;
(b) M. Munakata, L.P. Wu, G.L. Ning, T. Kuroda-Sowa;, M. Maekawa, Y. Suenaga, N. Maeno, J. Am. Chem. Soc. 121 (1999) 4968.
[26] A.N. Cambell, N.O. Smith, Phase Rule, Dover Publications Inc., Mineola, NY, 1951, p. 348.
[27] B.J. Hathaway, A.E. Underhill, J. Chem. Soc., Dalton Trans. (1961) 3091.

Available online at www.sciencedirect.com
SCIENCE DIRECT®
Polyhedron 23 (2004) 2125–2134
POLYHEDRON
www.elsevier.com/locate/poly

Self-assembly, structure and magnetic properties of carboxylate-bridged Cu(II)–M(II) (M = Mg, Ca, Sr, Ba) complexes with a new metalloligand as a building block

Wen-Long Liu [a], Yang Zou [a], Chang-Sheng Lu [a], Dong-Bin Dang [a], Yi-Zhi Li [a], Yuan-Gen Yao [b], Qing-Jin Meng [a,*]

[a] *Coordination Chemistry Institute, State Key Laboratory of Coordination Chemistry, Nanjing University, Nanjing 210093, PR China*
[b] *State Key Laboratory of Structural Chemistry, Fujian Institute of Research on the Structure of Matter, Fuzhou 350002, PR China*

Received 3 May 2004; accepted 1 June 2004
Available online 3 August 2004

Abstract

Schiff base complex $[CuL]^-$ anions, used as metalloligands, are assembled by alkaline earth metal cations M^{2+} (M = Mg, Ca, Sr, Ba) leading to mononuclear $[Mg(H_2O)_6][CuL]_2\cdot 4H_2O$ (**1**), tri- and tetranuclear $[Ca_4(CuL)_8(H_2O)_{16}]\cdot 22H_2O$ (**2**), a 1D ladder-like polymer $\{[Sr(CuL)_2(H_2O)_3]\cdot 2H_2O\}_n$ (**3**) and a 2D layer polymer $\{[Ba(CuL)_2(H_2O)_4]\}_n$, (**4**), ($H_3L$ = *N*-2-hydroxyacetophenoneglycylglycine), depending on the radius of the alkaline earth metal cations. Single crystal X-ray diffraction analyses show that the deprotonated Schiff base ligand (L) in **1**–**4** is a triple negatively charged quadridentate ONNO chelant, coordinating to the Cu(II) atom in a square-planar geometry. Compound **1** is stacked to form a three-dimensional network consisting of $[CuL]^-$ and $Mg(H_2O)_6^{2+}$ via hydrogen bonding. In **2**, three moieties, mononuclear($[CuL]^-$), trinuclear($[Ca(CuL)_2(H_2O)_4]$) and tetranuclear($[Ca_2(CuL)_2(H_2O)_8]^{2+}$), are co-existent and are linked together by a network of hydrogen-bonding to form a three-dimensional network. In **3**, The ligand $[CuL]^-$ is assembled by the cation Sr^{2+} to form a 1D ladder-like coordination polymeric chain via Sr–O bonds. In **4**, $[CuL]^-$ coordinates to Ba(II) via the carboxylate and carbonyl oxygen atoms to form a 2D polymeric plane. Variable-temperature magnetic susceptibility measurements indicate that all complexes exhibit weak antiferromagnetic interactions between the Cu(II) paramagnetic centers.
© 2004 Elsevier Ltd. All rights reserved.

Keywords: Self-assemble; Carboxylate bridges; Copper complexes; Dipeptides; Alkaline earth metals; Magnetic properties

1. Introduction

The design of metal-containing building blocks to spontaneously assembly into higher order architectures is of considerable interest in relation to their resemblance to biopolymers as well as their potential applications in catalysis and advanced materials such as magnetic, optic and electronic materials [1–8]. Recently, some stable coordination compounds containing potential bridging blocks have been used as metalloligands to bind other metal ions to form one-, two- and three-dimensional (1D, 2D, 3D) systems [9–16]. Some transition metal complexes of Schiff bases derived from amino acids and peptides comprising two types of ligating atoms (such as N and O) have interesting coordination capability (especially as carboxylate-bridged ligands) to metal ions [17–22]. These precursors are good candidates to be used as metalloligands and are particularly suitable for designing carboxylate-bridged heterometallic polynuclear complexes and constructing

* Corresponding author. Tel: +86-25-83597266; fax: +86-25-83314502.
E-mail address: mengqj@netra.nju.edu.cn (Q.-J. Meng).

0277-5387/$ - see front matter © 2004 Elsevier Ltd. All rights reserved.
doi:10.1016/j.poly.2004.06.003

extended 1D or 2D heterometallic supramolecular coordination polymers. Although carboxylate-bridged heteronuclear transition metal complexes containing multidentate ligands have been investigated with respect to their role in biological systems [23,24] and some of other areas [25–27] in recent years, the understanding of the chemistry of carboxylate-bridged heterometallic polynuclear compounds, especially for the heteronuclear complexes and polymers containing transition metals and main group metals, is very limited [28–30].

Here we report the synthesis of the novel Cu(II) Schiff base complex $K[CuL]\cdot 2.5H_2O$ (H_3L = *N*-2-hydroxyacetophenoneglycylglycine), and then use the metalloligand $[CuL]^-$ as a building block, reacting it with alkaline earth metal cations leading to a series of carboxylate-bridged heteronuclear Cu(II)–M(II) compounds $[M(CuL)_2(H_2O)_{x1}]_{x2}\cdot xH_2O$ (M = Mg, Ca, Sr, Ba) (**1**–**4**). Compound **4** has been briefly reported in a preliminary communication [31]. The present paper is devoted to the structural studies and magnetic properties of these compounds.

2. Experimental

2.1. Reagents and physical measurements

Reagent grade 2-hydroxyacetophenone (Fluka) and glycylglycine (Sigma) were used without further purification. All other reagents and solvents were analytical grade.

The IR spectra using KBr discs were recorded on a Bruker Vector 22 spectrophotometer in the 400–4000 cm^{-1} region. The UV–Vis spectra were recorded with a Shimadzu UV-3100 spectrophotometer. Elemental analyses (H, C, N) were determined using a Perkin–Elmer model 240C automatic instrument. Electrospray mass spectra were recorded on a LCQ system (Finnigan MAT, USA) using methanol/water as the mobile phase. All ESR spectra were obtained using a Bruker JES-FEIXG spectrometer with the X-band. Variable-temperature magnetic susceptibility measurements for complexes **1** and **2** were performed on a CAHN-2000 Faraday balance from 300 to 75 K, and for coordination polymers **3** and **4** were carried out with a Quantum Design MPMS SQUID magnetometer down to 2 K. Diamagnetic correction for the constituent atoms was made using Pascal's constants.

2.2. Preparation of Cu(II) Schiff base complex $K[CuL]\cdot 2.5H_2O$ (H_3L = *N*-2-hydroxyacetophenoneglycylglycine)

Glycylglycine (1.32 g, 10 mmol) was dissolved in 30 mL of aqueous ethanol (1:2 by volume mixture) containing KOH (0.56 g, 10 mmol). After cooling to room temperature, a solution of 2-hydroxyacetophenone (1.36 g, 10 mmol) in 10 mL absolute ethanol was added slowly with stirring for half an hour. An aqueous solution of copper(II) acetate (2.00 g, 10 mmol) in 10 mL was added dropwise and the resulting solution was adjusted to pH 9–10 by addition of concentrated KOH solution. After stirring at about 50 °C for 8 h and then filtering, the volume of the filtrate was reduced to ca. 5 mL in vacuo using a rotary evaporator. A large quantity of acetone was added to precipitate the violet product, which was recrystallized from water/acetone, dried in vacuo at 35 °C over P_2O_5. Yield 89%. *Anal.* Calc. for $K[Cu(C_{12}H_{11}N_2O_4)]\cdot 2.5H_2O$: C, 36.5; H, 4.1; N, 7.1. Found: C, 36.4; H, 4.1; N, 7.1%. FTIR (KBr; cm^{-1}): 3421s, 1651s, 1618s, 1343m, 1530m, 1297m. UV–Vis (in CH_3OH, λ_{max}, nm): 345, 568. ESI-MS (*m*/*z*): 310.1 $[CuL]^-$.

2.3. Synthesis of Cu(II)–M(II) (M = Mg, Ca, Sr, Ba) Schiff bases complexes

2.3.1. Synthesis of $[Mg(H_2O)_6][CuL]_2\cdot 4H_2O$ (**1**)

$K[CuL]\cdot 2.5H_2O$ (2 mmol) was dissolved in 20 mL H_2O. $MgCl_2\cdot 6H_2O$ (1 mmol) was then added to the filtrate with stirring at 25 °C for half an hour. A violet precipitate was obtained, which could be recrystallized from hot water (90 °C). The filtrate was allowed to evaporate slowly at room temperature. After several days violet red crystals, which were suitable for X-ray diffraction, were obtained. Yield 72%. *Anal.* Calc. for $C_{24}H_{42}N_4O_{18}MgCu_2$: C, 34.9; H, 5.1; N, 6.8. Found: C, 34.6; H, 5.2; N, 6.6%. FTIR (KBr; cm^{-1}): 3242s, 1640s, 1601s, 1351m, 1538m, 1292m. UV–Vis (in CH_3OH, λ_{max}, nm): 346, 567.

2.3.2. Synthesis of $[Ca_4(CuL)_8(H_2O)_{16}]\cdot 22H_2O$ (**2**), $[Sr(CuL)_2(H_2O)_3]\cdot 2H_2O$ (**3**) and $[Ba(CuL)_2(H_2O)_4]$ (**4**)

Complexes **2**–**4** were obtained using a similar method but by replacing $MgCl_2\cdot 6H_2O$ with $CaCl_2$, $SrCl_2\cdot 6H_2O$ and $BaCl_2\cdot 2H_2O$. Yield 68% for **2**; 76% for **3** and 52 % for **4**. *Anal.* Calc. for $C_{96}H_{164}N_{24}O_{70}Ca_4Cu_8$ (**2**): C, 33.5; H, 4.8; N, 9.8. Found: C, 33.4; H, 4.8; N, 9.7%. FTIR (KBr; cm^{-1}): 3453s, 1649s, 1609s, 1341m, 1538m, 1292m. UV–Vis (in CH_3OH, λ_{max}, nm): 346, 567. *Anal.* Calc. for $C_{24}H_{32}N_4O_{13}SrCu_2$ (**3**): C, 36.1; H, 4.0; N, 7.0. Found: C, 35.8; H, 4.1; N, 6.9%. FTIR (KBr; cm^{-1}): 3396s, 1658s, 1604s, 1340m, 1537m, 1290m. UV–Vis (in CH_3OH, λ_{max}, nm): 345, 566. *Anal.* Calc. for $C_{24}H_{30}N_4O_{12}BaCu_2$ (**4**): C, 34.7; H, 3.6; N, 6.7. Found C, 34.6; H, 3.6; N, 6.7%. FTIR (KBr; cm^{-1}): 3442s, 1655s, 1609s, 1340m, 1537m, 1297m. UV–Vis (in CH_3OH, λ_{max}, nm): 344, 563.

Table 1
Crystal data and structure refinement for **1**–**4**

	1	**2**	**3**	**4**
Empirical formula	$C_{24}H_{42}N_4O_{18}MgCu_2$	$C_{96}H_{164}N_{24}O_{70}Ca_4Cu_8$	$C_{24}H_{33}N_4O_{13}SrCu_2$	$C_{24}H_{30}N_4O_{12}BaCu_2$
Formula weight	826.03	3331.15	799.26	830.95
Crystal system	triclinic	triclinic	triclinic	monoclinic
Space group	$P\bar{1}$	$P\bar{1}$	$P\bar{1}$	$P2(1)/c$
a (Å)	7.551(1)	14.667(8)	8.020(1)	21.532(4)
b (Å)	11.223(2)	14.996(8)	9.537(1)	7.266(1)
c (Å)	11.590(2)	18.998(11)	20.004(3)	18.353(3)
α (°)	115.28(1)	68.08(1)	80.07(1)	
β (°)	106.46(1)	75.04(1)	81.15(1)	91.57(1)
γ (°)	95.58(1)	71.78(1)	79.44(1)	
V (Å^3)	824.3(3)	3634(3)	1469.7(3)	2870.3(8)
Z	1	1	2	4
D_{calc} (Mg m^{-3})	1.664	1.522	1.806	1.923
μ(Mo Kα) (cm^{-1})	1.394	1.387	3.315	2.895
T (K)	293(2)	293(2)	293(2)	293(2)
F(000)	428	1724	808	1848
Crystal size (mm^3)	0.15×0.20×0.15	0.3×0.20×0.20	0.30×0.20×0.20	0.15×0.15×0.20
θ range for data collection	2.1–25.0	1.7–25.0	2.1–25.0	1.9–25.0
Index ranges	$-8\leqslant h\leqslant 8$	$-16\leqslant h\leqslant 17$	$-9\leqslant h\leqslant 9$	$-25\leqslant h\leqslant 25$
	$-13\leqslant k\leqslant 1$	$-16\leqslant k\leqslant 17$	$-9\leqslant k\leqslant 11$	$0\leqslant k\leqslant 8$
	$-13\leqslant l\leqslant 13$	$0\leqslant l\leqslant 22$	$-23\leqslant l\leqslant 23$	$0\leqslant l\leqslant 21$
Reflections collected	4120	18015	7357	13627
Independent reflections	2861	12489	5089	5018
Data/restraints/parameters	2861/0/224	12489/0/923	5089/0/381	5018/0/390
R_{int}	0.0733	0.0391	0.0390	0.0587
Final R_1, $wR_2[I>2\sigma(I)]$	0.0460, 0.1189	0.0541, 0.1345	0.0433, 0.0624	0.0321, 0.0618
Goodness-of-fit on F^2	1.013	1.001	0.836	0.993
Largest difference: peak and hole (e Å^{-3})	0.55 and −0.73	0.85 and −0.98	0.65 and −0.51	0.98 and −0.77

2.4. X-ray crystallography

The diffraction experiments were carried out on a Bruker AXS SMART APEX CCD diffractometer. Data were collected with graphite-monochromated Mo Kα radiation ($\lambda = 0.71073$ Å) using SMART and SAINT programs [32]. Absorption corrections were calculated and applied for each structure by using SADABS [33]. The structures were solved by direct methods and non-hydrogen atoms were anisotropically refined by full-matrix least-squares based on F^2 using SHELXTL [34]. All hydrogen atoms were included in the refinement in calculated positions, riding on their carrier atoms. The hydrogen thermal displacement parameters were fixed at 1.2 and 1.5 times the equivalent isotropic thermal displacement parameters of their internal and terminal carrier atoms, respectively. A summary of the data collection and structure refinement is listed in Table 1.

3. Results and discussion

3.1. Syntheses

Heteronuclear compounds and inorganic polymers containing main group metals are very important and present synthetic challenges [35–37]. Supramolecular self-assembly processes allow these materials to be prepared with high yield. As mentioned in the experimental (Scheme 1), the synthetic approach to prepare heteronuclear complexes is based on two major step reactions. The first step is to synthesize the complex K[CuL] in which L is a Schiff base ligand derived from 2-hydroxyacetophenone and dipeptides. The second step is using $[CuL]^-$ as a metalloligand to prepare heteronuclear complexes. The $[CuL]^-$ core with a terminal carboxylic group is easy to coordinate to the other hard (lewis acid) metal ions. As long as M^{2+} (M = Mg, Ca, Sr or Ba) were added to the solution of $[CuL]^-$, the final heteronuclear compounds were precipitated immediately. The simple general method provides a facile way to include more than one type of metal center into the system.

3.2. Crystal structure of $[Mg(H_2O)_6][CuL]_2\cdot 4H_2O$ (1)

An ORTEP plot with non-hydrogen atomic labelling is shown in Fig. 1. Selected bond distances and angles are listed in Table 2. The compound crystallizes in the centrosymmetric space group $P\bar{1}$. The unit cell of **1** consists of two $[CuL]^-$ cores, one $Mg(H_2O)_6^{2+}$ core and four water molecules. $[CuL]^-$ has approximately square-planar structure. The deprotonated Schiff base ligand is a triple negatively charged quadridentate ONNO chelant, coordinating to the Cu(II) atom via

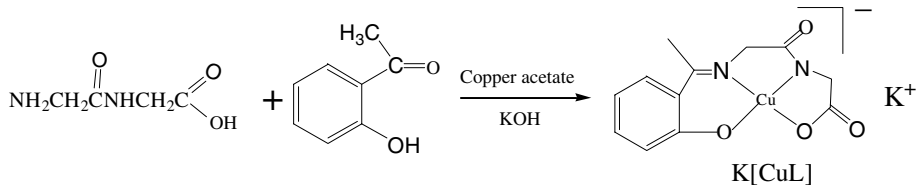

$MCl_2 \cdot nH_2O$

M=Mg, Sr, n=6
M=Ca, n=0
M=Ba, n=2

$[M(CuL)_2(H_2O)_{x1}]_{x2} \cdot xH_2O$

1 M=Mg; X1=6; X2=1; X=4
2 M= Ca; X1=4; X2=4; X=22
3 M= Sr; X1=3; X2=1; X=2
4 M= Ba; X1=4; X2=1; X=0

Scheme 1.

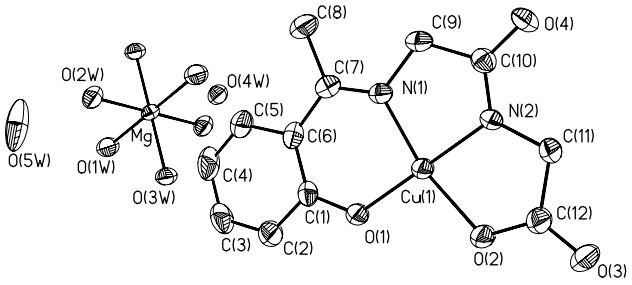

Fig. 1. ORTEP view of **1,** with hydrogen atoms omitted for clarity. Thermal ellipsoids are drawn at the 35% probability level.

one phenolic oxygen (O(1)), one deprotonated amide nitrogen atom (N(2)), one imino nitrogen atom (N(1)) and one carboxylate oxygen (O(3)). The phenyl ring [C(1)–C(6)] and the chelate ring C(6), C(1), C(7), N(1), O(1), Cu(1) are almost coplanar with a small dihedral angle of 3.7°, suggesting a large π-electron delocalization. Mg(II) lies on an inversion center and is almost octahedrally coordinated by six aqua ligands.

The anions and cations form well-separated columns along the *a*-axis in the stacking structure of **1**. Hydrogen bonds play a very important role (see supplementary material, Table S1). In the presence of water molecules, intermolecular and intramolecular hydrogen bonds result in the compound forming a 3D network.

Table 2
Selected bond lengths (Å) and angles (°) for **1**

Bond lengths			
Cu1–O1	1.867(2)	Cu1–N1	1.948(4)
Cu1–O2	1.996(3)	Cu1–N2	1.883(3)
Mg1–O2W	2.043(3)	Mg1–O1W	2.078(3)
Mg1–O3W	2.050(2)		
Bond angles			
O1–Cu1–O2	97.97(10)	O2–Cu1–N1	166.80(11)
O1–Cu–N1	95.13(12)	O2–Cu1–N2	82.39(13)
O1–Cu1–N2	179.32(14)	N1–Cu1–N2	84.49(14)
O2Wa–Mg–O3W	88.20(10)	O1W–Mg–O2W	91.85(12)
O1W–Mg–O3W	89.93(11)	O1Wa–Mg–O2W	88.15(12)
O2W–Mg–O3W	91.80(10)	O1W–Mg–O3Wa	90.07(11)

Symmetry transformations used to generate equivalent atoms: $(-x+1, -y+1, -z+1)$.

3.3. Crystal structure of $[Ca_4(CuL)_8(H_2O)_{16}] \cdot 22H_2O$ (**2**)

Compound **2** has an interesting structure, its ORTEP view is shown in Fig. 2 with water molecules omitted for clarity. In the solid state, the compound crystallizes in the centrosymmetric space group $P\bar{1}$ and three Cu(II) containing moieties co-exist simultaneously: mononuclear ($[CuL]^-$), trinuclear ($[Ca(CuL)_2(H_2O)_4]$) and tetranuclear ($[Ca_2(CuL)_2(H_2O)_8]^{2+}$). Selected bond distances and angles are listed in Table 3. The coordination environment of the Cu(II) centers of all $[CuL]^-$ groups in the three moieties are similar to that of complex **1**.

For the trinuclear moieties, two $[CuL]^-$ are connected by Ca(2). Each calcium atom is coordinated by four carboxylate oxygen atoms (O(7), O(8), O(11), O(12)) and four water molecule oxygen atoms. The carboxylates in two $[CuL]^-$ groups chelate the calcium atom in a bidentate manner (Fig. 3(a)). The chelate rings C(25), C(30), C(31), N(5), O(9), Cu(3) and C(13), C(18), C(19), N(3), O(5), Cu(2) are almost perpendicular, with a dihedral angle of 94.1°. The chelate rings C(25), C(30), C(31), N(5), O(9), Cu(3) and C(37), C(42), C(43), N(7), O(13), Cu(4) in the mononuclear moieties are almost parallel, with a small dihedral angle of 11.7°.

In the tetranuclear moieties, two $[CuL]^-$ groups are connected by two Ca cations (Ca(1), Ca(1A)) to form a $[Ca_2(CuL)_2(H_2O)_8]^{2+}$ structure. The Ca cation has 7 coordination atoms: three carboxylate oxygen atoms (O(3), O(4), O(4A)) and four water molecule oxygens. The carboxylate group shows two different coordination modes: to one calcium in a bidentate chelating manner, to the other one in a monodentate manner (Fig. 3(b)). Ca(1) and Cu(1) are bridged by carboxylate oxygen O(3) with a Ca···Cu distance of 4.30 Å, and Ca(1)

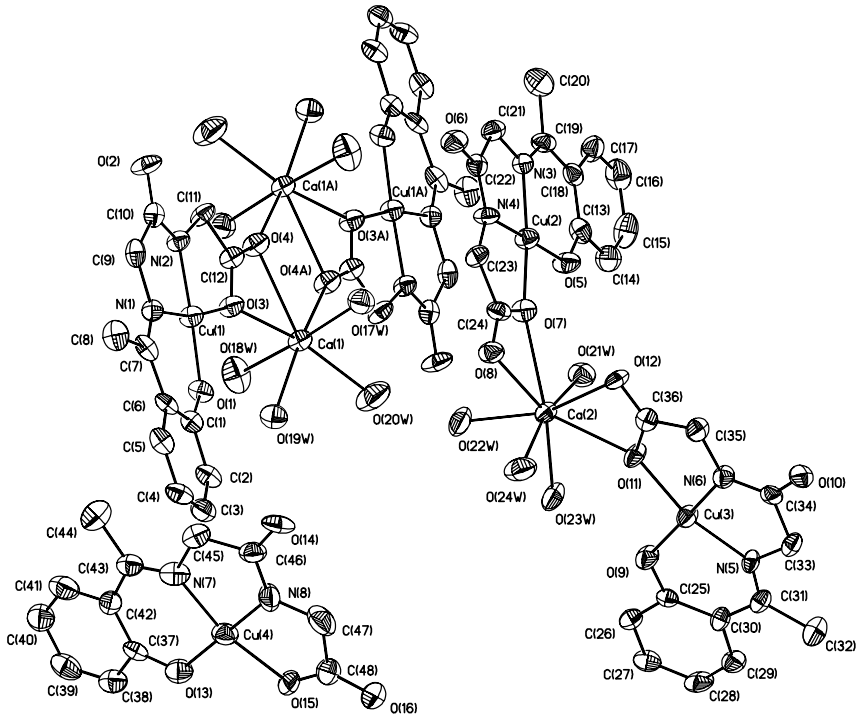

Fig. 2. ORTEP view of **2,** with lattice water molecules and hydrogen atoms omitted for clarity. Thermal ellipsoids are drawn at the 35% probability level.

and Ca(1A) are bridged by the carboxylate oxygen O(4) and O(4A). The Ca–Ca distance is longer (4.14 Å) than those of usual dimeric complexes [38]. The chelate rings C(6), C(1), C(7), N(1), O(1), Cu(1) and C(13), C(18), C(19), N(3), O(5), Cu(2) are almost parallel with a small dihedral angle of 4.7°.

The molecule packs along the *b*-axis to form a main chain that is stabilized by H-bond interactions between water molecules and their symmetric atoms (see supplementary material, Table S2). Adjacent main chains are associated by extensive H-bonds form the three-dimensional network.

3.4. Crystal structure of coordination polymer $\{[Sr(CuL)_2(H_2O)_3]\cdot 2H_2O\}_n$ (3)

The crystal structure of **3** consists of 1D coordination polymer chains and water molecules. An ORTEP view of the polymer is shown in Fig. 4(a). Selected bond distances and angles are listed in Table 4. Compound **3** crystallizes in the triclinic centrosymmetric space group $P\bar{1}$. The coordination environment of Cu(II) is similar to complex **1**. $[Cu(1)L]^-$ and $[Cu(2)L]^-$ groups are attached to Sr(II) ions by two different modes: $[Cu(1)L]^-$ through one carbonyl oxygen atom (O(2)) (Fig. 3(c)), and $[Cu(2)L]^-$ through two carboxylate oxygen atoms(O(8), O(7)) and one carbonyl oxygen atom(O(6)) (Fig. 3(d)). The carboxylate group in $[Cu(2)L]^-$ is similar to that of the tetranuclear moiety ($[Ca_2(CuL)_2(H_2O)_8]^{2+}$) in **2** and shows two different coordination

Table 3
Selected bond lengths (Å) and angles (°) for **2**

Bond lengths			
Cu1–O1	1.843(3)	Cu1–N1	1.932(5)
Cu1–O3	1.995(4)	Cu1–N2	1.884(4)
Cu2–N3	1.911(4)	Cu2–O5	1.855(4)
Cu2–N4	1.866(4)	Cu2–O7	1.977(3)
Cu3–N5	1.910(4)	Cu3–O9	1.849(4)
Cu3–N6	1.858(4)	Cu3–O11	1.972(3)
Cu4–N7	1.942(5)	Cu4–O13	1.858(4)
Cu4–N8	1.863(6)	Cu4–O15	1.981(4)
Ca1–O3	2.469(4)	Ca2–O7	2.550(4)
Ca1–O4	2.587(4)	Ca2–O8	2.638(4)
Ca1–O4a	2.388(4)	Ca2–O11	2.472(4)
		Ca2–O12	2.494(4)
Bond angles			
O1–Cu1–O3	94.69(14)	O11–Cu3–N6	82.37(15)
O1–Cu1–N1	96.80(15)	O13–Cu4–O15	96.92(17)
O1–Cu1–N2	175.39(17)	O13–Cu4–N7	94.69(19)
O3–Cu1–N1	168.38(15)	O13–Cu4–N8	177.8(2)
O3–Cu1–N2	83.19(17)	O15–Cu4–N7	167.00(19)
N1–Cu1–N2	85.49(18)	O15–Cu4–N8	83.8(2)
O7–Cu2–N3	168.18(16)	N7–Cu4–N8	84.8(2)
O7–Cu2–N4	83.52(16)	O4–Ca1–O4a	67.48(12)
N3–Cu2–N4	84.72(18)	O3–Ca1–O4a	118.59(12)
O5–Cu2–O7	95.24(14)	O3–Ca1–O4	51.24(11)
O5–Cu2–N3	96.53(17)	O7–Ca2–O11	126.95(13)
O9–Cu3–O11	96.57(15)	O7–Ca2–O12	80.53(12)
O9–Cu3–N5	95.30(17)	O8–Ca2–O11	123.53(12)
O9–Cu3–N6	175.4(2)	O8–Ca2–O12	75.65(12)
N5–Cu3–N6	86.39(17)	O11–Ca2–O12	52.60(10)
O11–Cu3–N5	165.90(15)	O7–Ca2–O8	49.62(11)

Symmetry transformations used to generate equivalent atoms: (a: $-x+1, -y+1, -z+2$.)

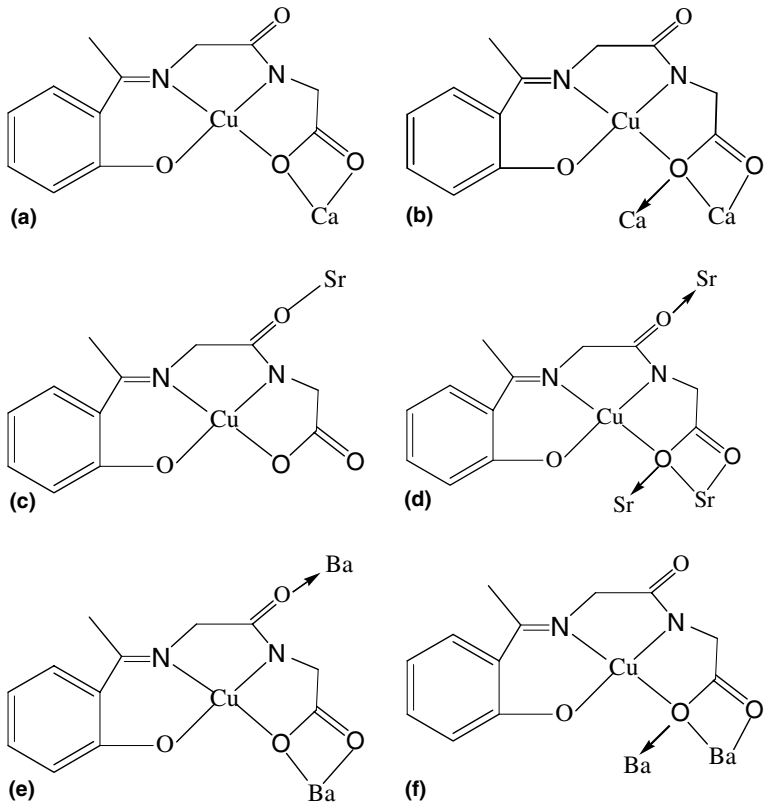

Fig. 3. Schematic diagram of the coordination behavior of the metalloligand $[CuL]^-$ in **2**–**4**

modes: to one strontium in a bidentate chelating manner, to the other one in a monodentate manner. The chelate ring planes of the two metalloligands ($[Cu(1)L]^-$ and $[Cu(2)L]^-$) are almost parallel with a small dihedral angle of 5.6°. In each unit, Sr and SrA are bridged by carboxylate oxygen atoms (O(8), O(8A)). The Sr···SrA distance is 4.34 Å.

The strontium cations in **3** are eight-coordinated as in the case of the calcium cations in the trinuclear moieties ($[Ca(CuL)_2(H_2O)_4]$) of **2**. However, the coordination environment around the strontium varies significantly to that found in **2**. Each strontium cation is coordinated by three carboxylate oxygen atoms (O(7), O(8), O(8A)), two carbonyl oxygen atoms (O(2) from the $[Cu(1)L]^-$ group and O(6B) from another $[Cu(2B)L]^-$ group, related by a symmetry operation) and three aqua ligands (O(1w), O(2w), O(3w)).

Two strontium cations link the four $[CuL]^-$ groups together via Sr–O bonds to form a new building block {[Cu(1)L][Cu(2)L]SrSr(A)[Cu(1A)L][Cu(2A)L]}. The two carbonyl oxygen atoms (O(6B) and O(6D)) from the adjacent building blocks are connected to Sr and SrA in the new building block respectively. The coordination of the symmetry-related strontium cations link the adjacent building blocks together to generate a 1D ladder-like polymeric chain along the *a*-axis (Fig. 4(b)). The intermolecular and intramolecular hydrogen bonds play an important role in the stabilization of the whole structure (Table S3, Supplementary material). Adjacent 1D chains are associated by hydrogen bonds to form 2D planes. The entire structure is held together to form a two-dimensional layer structure by van der Waals contacts.

3.5. Crystal structure of polymer $\{[Ba(CuL)_2(H_2O)_4]\}_n$ (**4**)

The crystal structure of **4** has been briefly reported in our previous communication [31]. Compound **4** crystallizes in the monoclinic centrosymmetric space group $P2_1/c$. The coordination environment of all Cu(II) ions is similar to **1**. In each unit, the metalloligand $[Cu(1)L]^-$ coordinates to Ba(II) ions through two carboxylate oxygen atoms(O(7), O(8)) in a bidentate chelating manner and one carbonyl oxygen atom (O(6)) (Fig. 3(e)), and $[Cu(2)L]^-$ has the same coordination mode as the tetranuclear moiety ($[Ca_2(CuL)_2(H_2O)_8]^{2+}$) in **2** (Fig. 3(f)). The Ba(II) ion is 10-coordinated to five carboxylate oxygen, one carbonyl oxygen (from another $[Cu(2A)L]^-$ ligand related by a symmetry operation) and four aqua ligands.

Two barium cations link the four $[CuL]^-$ metalloligands together via Ba–O bonds to form a hexanuclear building block {[Cu(1)L][Cu(2)L]Ba(1)Ba(1A)[Cu(1A)L]-

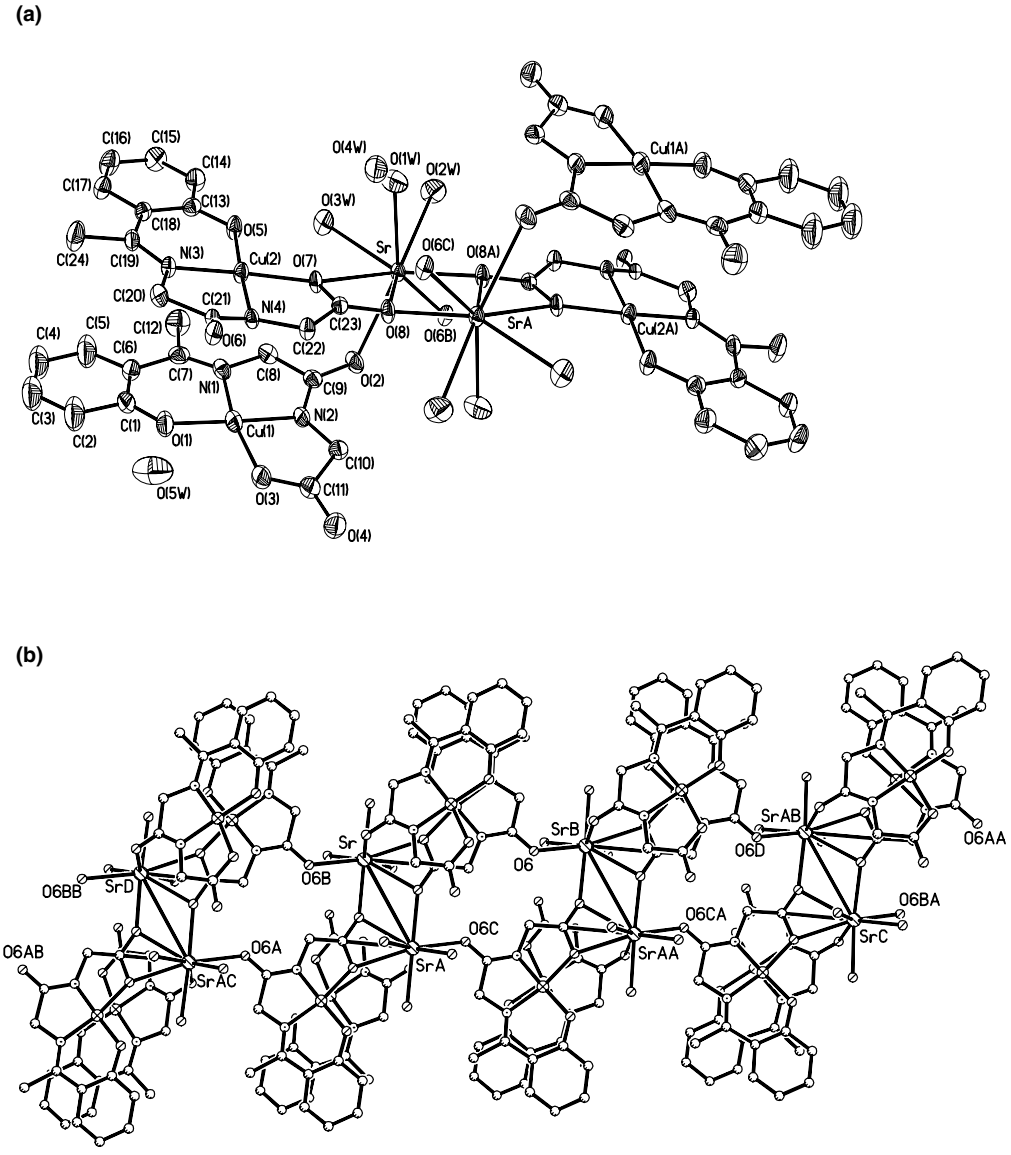

Fig. 4. (a) ORTEP view of **3**, with hydrogen atoms omitted for clarity. Thermal ellipsoids are drawn at the 35% probability level. (b) A view of the packing of the 1D ladder-like polymeric chain in **3** along the *a*-axis.

[Cu(2A)L]}. The symmetry-related Ba–O(6) bonds further join adjacent building blocks together to give an extended 2D network structure along the *bc*-plane (see Fig. 5). The intermolecular and intramolecular hydrogen bonds (Table S4, Supplementary material) and π–π interactions also potentially contribute to the stability of the whole structure. The entire structure is held together to form a 2D layer structure by van der Waals contacts.

3.6. Infrared, electronic and ESR spectra

The IR spectra of all the complexes show broad bands in the 3000–3500 cm^{-1} region, which may be ascribed to hydrogen-bonded *v*(O–H) and/or *v*(N–H), and may also include *v*(C–H). The broad bands at 1640–1658 and 1601–1618 cm^{-1} correspond to *v*(C═N) and v_{as}(COO). The symmetric carboxylate stretch, v_s(COO), probably corresponds to the medium/strong bands in the range 1340–1351 cm^{-1}. A medium band at 1530–1538 cm^{-1}, always present in the four compounds, may originate from the vibration of the *v*(Ph–)C–C(═N) bond [39] and typifies complexes derived from salicylaldehyde or 2-hydroxyacetophenone [39,40]. Medium bands in the range 1290–1297 cm^{-1} can be assigned to *v*(C–O) of the phenolic group in the complexes [41].

The UV absorption band observed at 344–346 nm in the complexes are assigned to the imino n–π^* transitions. The d–d transition spectra of the complexes show broad bands centered at 562–568 nm, being suggestive of approximate square-planar geometry at the Cu(II) ion.

Table 4
Selected bond lengths (Å) and angles (°) for **3**

Bond lengths			
Cu1–O1	1.861(4)	Cu1–N1	1.935(4)
Cu1–O3	1.949(3)	Cu1–N2	1.877(4)
Sr–O7	2.707(3)	Cu2–O5	1.858(3)
Sr–O8	2.714(3)	Cu2–O7	1.963(3)
Sr–O8a	2.525(3)	Cu2–N3	1.917(4)
Sr–O6b	2.562(3)	Cu2–N4	1.874(4)
Bond angles			
O2–Sr–O7	74.14(11)	O3–Cu1–N1	168.21(16)
O2–Sr–O8	86.13(11)	O3–Cu1–N2	83.40(15)
O2–Sr–O8a	120.20(11)	N1–Cu1–N2	84.87(18)
O7–Sr–O8	47.69(9)	O5–Cu2–O7	93.93(13)
O7–Sr–O8a	114.10(9)	O5–Cu2–N3	95.87(15)
O8–Sr–O8a	68.25(9)	O5–Cu2–N4	176.86(15)
O1–Cu1–O3	96.49(15)	O7–Cu2–N3	169.46(14)
O1–Cu1–N1	95.27(18)	O7–Cu2–N4	83.69(15)
O1–Cu1–N2	178.11(17)	N3–Cu2–N4	86.38(16)

Symmetry transformations used to generate equivalent atoms: (a: x, $y-1$, z; b: $-x+1$, $-y+2$, $-z+1$).

ESR spectra of complex **2** at room temperature in DMSO are shown in Fig. 6. Simulated spectra obtained by using the WINEPR SimFonia program gave good agreement. ESR spectra of complexes **1**, **3** and **4** are similar to that of complex **2**. The spectra exhibited a lineshape with five nitrogen superhyperfine (shf) structure peaks indicating ligation of two nitrogen atoms to the metal ion.

The four compounds all have similar IR, electronic and ESR spectra, which shows they have the same coordination environment around the Cu(II) ions.

3.7. Magnetic properties

The magnetic behaviours of compounds **1** and **2** showed that in the studied temperature range (75–300 K) the $\chi_M T$ (where χ_M is the molar magnetic susceptibility) values decrease regularly with cooling (see supplementary material, Fig. S1). The data can be nicely fitted to the Curie–Weiss expression $\chi_M = C/(T-\theta)$, affording $C = 0.677$ cm^3 mol^{-1}, $\theta = -12.18$ K for **1** and $C = 1.05$ cm^3 mol^{-1}, $\theta = -7.39$ K for **2**. The negative Weiss constant θ could suggest a weak antiferromagnetic interaction between the copper(II) ions in both compounds.

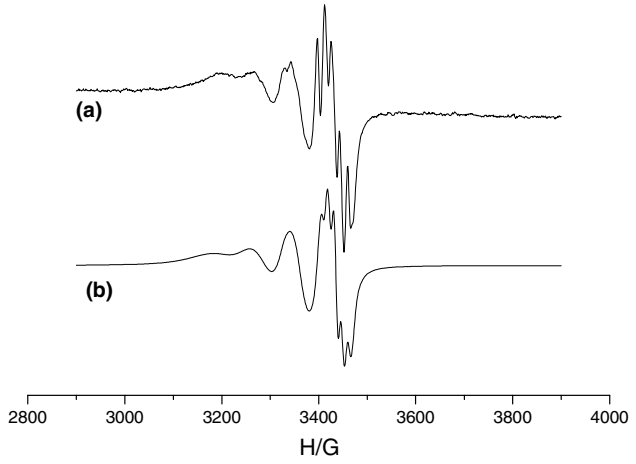

Fig. 6. Experimental ESR spectrum of **2** taken in DMSO at room temperature (a), together with the calculated curve (b).

The magnetic susceptibility of the two coordination polymers **3** and **4** was measured in the temperature range of 2–300 K on a SQUID magnetometer in an applied magnetic field of 1000 G (Fig. 7). The μ_{eff} values are equal to 2.74 (**3**) and 2.88 μ_B (**4**) at room temperature. These values are a little larger than those expected for two isolated copper(II) ions (for **3**, 2.45 μ_B, $g = 2.00$; for **4**, 2.58 μ_B, $g = 2.11$). For **3** (**4**), the $\chi_M T$ values decline gradually between 300 and ca. 11 (15) K, where the value is 0.720 (0.771) cm^3 mol^{-1} K; below 11 (15) K, it falls

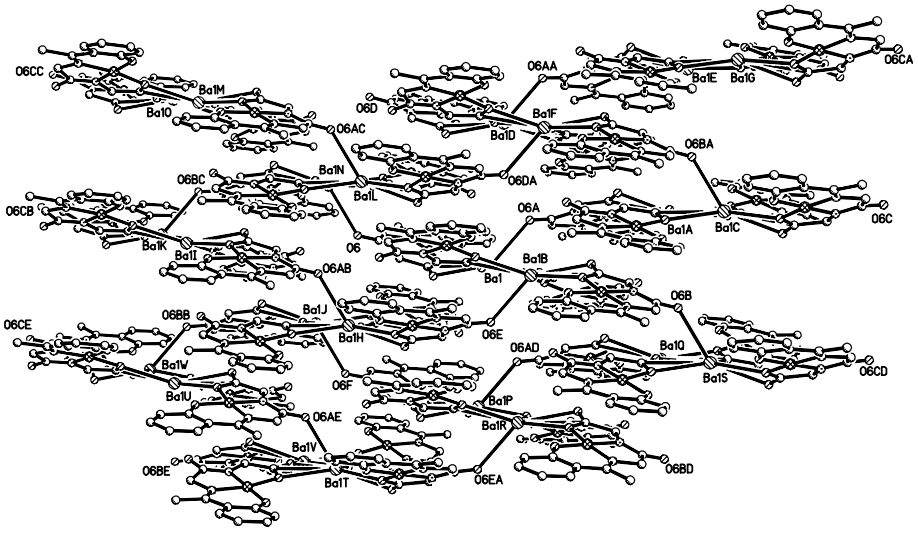

Fig. 5. A view of the packing of the 2D polymeric plane in **4** along the *a*-axis.

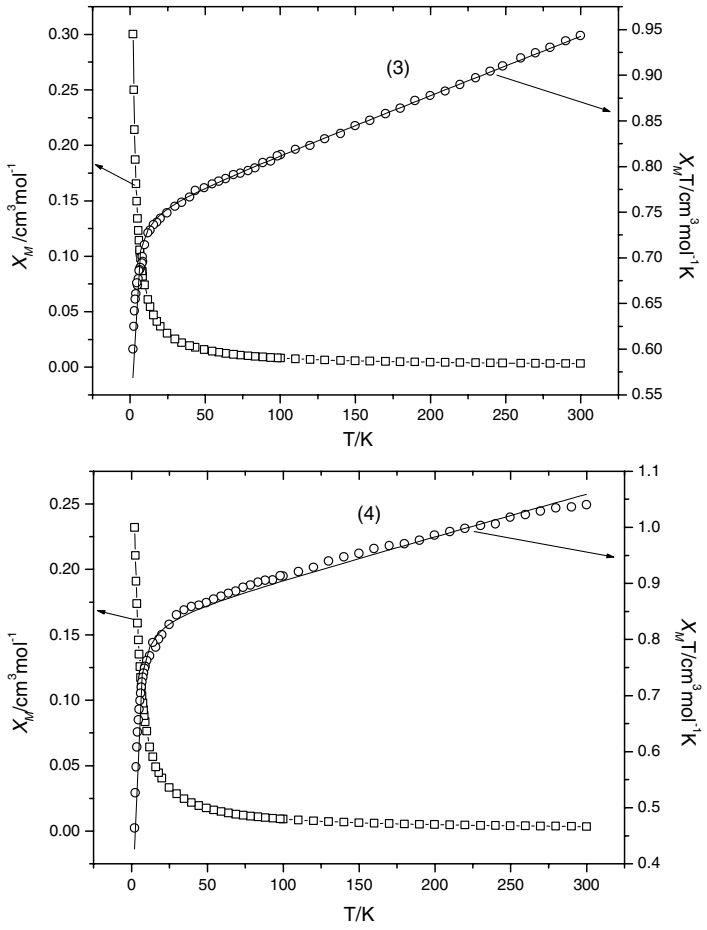

Fig. 7. χ_M (□) versus T and $\chi_M T$ (○) versus T plots for the coordination polymers **3** and **4**. The solid lines represent the best-fit curves to Eq. (1).

sharply to 0.600 (0.464) cm^3 mol^{-1} K at 2 K. These magnetic behaviors provide evidence of the presence of a weak antiferromagnetic spin-exchange interaction between two Cu(II) centres through the oxygen bridges. The experimental magnetic susceptibility data were fitted to the modified Bleaney–Bowers equation [42] for exchange-coupled dinuclear copper(II) complexes

$$\chi_M = \frac{2Ng^2\beta^2}{3kT}\left[1+\frac{1}{3}\exp(-2J/kT)\right]^{-1} + \text{Tip}. \qquad (1)$$

Here, Tip is the corrected value of temperature-independent paramagnetism and the remaining symbols have their usual meanings. A least-squares fitting procedure led to $J/k = -0.83$ K, $g = 2.00$ and Tip $= 6.5\times10^{-4}$, with an agreement factor of $R = 8.00\times10^{-5}$ (R is defined as $\sum[(\chi_M)_{obs}-(\chi_M)_{calc}]^2/\sum[(\chi_M)_{obs}]^2$) for **3** and $J/k = -1.58$ K, $g = 2.11$ and Tip $= 7.5\times10^{-4}$, with R value of 1.30×10^{-4} for **4**.

4. Conclusion

A series of heterometallic supramolecules have been constructed by a Cu(II) Schiff base complex K[CuL] (H_3L = *N*-2-hydroxyacetophenoneglycylglycine) with alkaline earth metal cations M^{2+} (M = Mg, Ca, Sr or Ba). The supramolecules are assembled by carboxylate bridges of the metalloligand $[CuL]^-$. With the ionic radii increase from Mg^{2+} to Ba^{2+}, they formed a mononuclear entity, trinuclear and tetranuclear clusters, a 1D ladder-like chain polymer and a 2D extended layer polymer. For a given M/[CuL] ratio (1:2), the coordinating behavior of the $[CuL]^-$ ligand to M can be fine tuned depending on the nature and size of the M^{2+} ions in the study. The $[CuL]^-$ ligand does not coordinate to the metal ion Mg^{2+} in **1** wherein the Mg^{2+} ion preferentially binds to water molecules, in the form of $[Mg(OH_2)_6]^{2+}$. While the $[CuL]^-$ ligands in **2** make only three and four bonds to the central calcium through the carboxylate oxygen atoms, the number of contacts with M ions are increased to five and six in **3** and **4**, respectively. The carbonyl oxygen atom of the $[CuL]^-$ ligand in **2** does not coordinate to the metal, presumably because the calcium dication has a smaller coordination sphere. Thus, five different modes of coordination of the metalloligand $[CuL]^-$ have been realized for complexes **2**–**4** (Fig. 3). The magnetic behaviours indicate that all complexes exhibit weak

antiferromagnetic interactions between the Cu(II) paramagnetic centers.

Acknowledgement

This work was supported financially by the National Natural Science Foundation of China (No. 20171022), The Center of Materials Analysis of Nanjing University.

Appendix A. Supplementary material

Crystallographic data for the structural analysis have been deposited with the Cambridge Crystallographic Data Centre, CCDC Nos. 202242–202245 for compounds **1**–**4**, respectively. Copies of this information may be obtained free of charge from The Director, CCDC, 12 Union Road, Cambridge, CB2 1EZ, UK (fax: +44-1223-336033; email: deposit@ccdc.cam.ac.uk or www: http://www.ccdc.cam.ac.uk). Supplementary data associated with this article can be found, in the online version at doi:10.1016/j.poly.2004.06.003.

References

[1] J.-M. Lehn, Supramolecular Chemistry, VCH, Weiheim, 1995.
[2] A.F. Williams, Chem. Eur. J. 3 (1997) 15.
[3] K. Wieghardt, Angew. Chem., Int. Ed. Engl. 28 (1989) 1153.
[4] M. Kondo, T. Yoshitomi, K. Seki, H. Matsuzaka, S. Kitagawa, Angew. Chem., Int. Ed. Engl. 36 (1997) 1725.
[5] H. Li, M. Eddaoudi, M. O'Keeffe, O.M. Yaghi, Nature 402 (1999) 276.
[6] B.Q. Ma, H.L. Sun, S. Gao, G.X. Xu, Inorg. Chem. 40 (2001) 6247.
[7] P.D. Beer, P.A. Gale, Angew. Chem., Int. Ed. 40 (2001) 486.
[8] S. Wang, Z. Pang, D.L. Smith, Inorg. Chem. 32 (1993) 4992.
[9] S.-Q. Zang, R.-J. Tao, Q.-L. Wang, N.-H. Hu, Y.-X. Cheng, J.-Y. Niu, D.-Z. Liao, Inorg. Chem. 42 (2003) 761.
[10] Y.-Y. Yang, Y.-L. Wu, L.-S. Long, X.-M. Chen, J. Chem. Soc., Dalton Trans. (1999) 2005.
[11] H.O. Stumpf, L. Ouahab, Yu Pei, P. Bergerat, O. Kahn, J. Am. Chem. Soc. 116 (1994) 3866.
[12] M. Ohba, N. Mamono, H. Okawa, T. Enoki, J.-M. Latour, J. Am. Chem. Soc. 116 (1994) 11566.
[13] H. Miyasaka, N. Matsumoto, H. Okawa, N. Re, E. Gallo, C. Floriani, J. Am. Chem. Soc. 118 (1996) 981.
[14] O. Kahn, J. Larionova, J.V. Yakhmi, Chem. Eur. J. 5 (1999) 3443.
[15] H.-Z. Kou, W.-M. Bu, S. Gao, D.-Z. Liao, Z.-H. Jiang, S.-P. Yan, Y.-G. Fan, G.-L. Wang, J. Chem. Soc., Dalton Trans. (2000) 2996.
[16] H.-Z. Kou, S. Gao, B.-Q. Ma, D.-Z. Liao, Chem. Commun. (2000) 713.
[17] C.T. Yang, B. Moubaraki, K.S. Murray, J.D. Ranford, J.J. Vittal, Inorg. Chem. 40 (2001) 5934.
[18] J.D. Ranford, J.J. Vittal, D. Wu, X. Yang, Angew. Chem., Int. Ed. 38 (1999) 3498.
[19] C.T. Yang, B. Moubaraki, K.S. Murray, J.J. Vittal, J. Chem. Soc., Dalton Trans. (2003) 880.
[20] A. Erxleben, D. Schumacher, Eur. J. Inorg. Chem. (2001) 3039.
[21] E. Colacio, J.M. Domínguea-Vera, M. Ghazi, R. Kivekäs, M. Klinga, J.M. Moreno, Eur. J. Inorg. Chem. (1999) 441.
[22] E. Colacio, M. Ghazi, R. Kivekäs, J.M. Moreno, Inorg. Chem. 39 (2000) 2882.
[23] R. Holtzelmann, K. Wieghardt, J. Ensling, H. Romstedt, P. Gütlich, E. Bill, U. Flörke, H.-J. Haupt, J. Am. Chem. Soc. 114 (1992) 9470.
[24] T. Tanase, S.P. Watton, S.J. Lippard, J. Am. Chem. Soc. 116 (1994) 9401.
[25] O. Kahn, Molecular Magnetism, VCH, Weinheim, 1993.
[26] L. Chen, S.R. Breeze, R. Rousseau, S. Wang, L.K. Thompson, Inorg. Chem. 34 (1995) 454.
[27] S.R. Breeze, S. Wang, J.E. Greedan, N.P. Raju, J. Chem. Soc., Dalton Trans. (1998) 2327.
[28] A. Ouchi, Y. Suzuki, Y. Ohki, Y. Koizumi, Coord. Chem. Rev. 92 (1988) 29.
[29] R.D. Cannon, R.P. White, Prog. Inorg. Chem. 36 (1988) 195.
[30] X.-M. Chen, T.C.W. Mak, Inorg. Chem. 33 (1994) 2444.
[31] W.-L. Liu, Y. Zou, C.-S. Lu, C.-L. Ni, D.-B. Dang, Y.-Z. Li, Q.-J. Meng, Inorg. Chem. Commun. 7 (2004) 434.
[32] SMART and SAINT Software Reference manuals, Version 6.22; Bruker AXS Inc., Madison, WI, 2000.
[33] G.M. Sheldrick, SADABS software for empirical absorption correction, University of Gottingen, Germany, 1996.
[34] SHELXTL Reference manuals, Version 6.10; Bruker AXS Inc., Madison, WI, 2000.
[35] I. Manners, Science 294 (2001) 1664.
[36] I. Manners, J. Polym. Sci. Part A: Polym. Chem. 40 (2002) 182.
[37] I. Manners, Macromol. Symp. 196 (2003) 57.
[38] S. Ivanov, N. Snezko, A. Hyukhin, V. Sergienko, Polyhedron 16 (1997) 2527.
[39] J.W. Leadbetter Jr., J. Phys. Chem. 81 (1977) 54.
[40] L. Casella, M. Gullotti, J. Am. Chem. Soc. 103 (1981) 6338.
[41] K. Nakamoto, Infrared and Raman Spectra of Inorganic and Coordination Compounds, fourth ed., John Wiley & Sons, New York, 1986.
[42] B. Bleaney, K.D. Bowers, Proc. R. Soc. Lodon A 214 (1952) 451.

Available online at www.sciencedirect.com
SCIENCE DIRECT®
Polyhedron 23 (2004) 2135–2139
POLYHEDRON
www.elsevier.com/locate/poly

Reactions of *closo*-$[B_{12}H_{12}]^{2-}$ anion with aromatic acylchlorides: synthesis of novel 1,2-disubstituted dodecaborates $[1\text{-HO-2-ArCOB}_{12}H_{10}]^{2-}$

A. Semioshkin [a,*], B. Brellochs [b], V. Bregadze [a]

[a] *Laboratory of Organoaluminium and Organoboron Compounds, A.N. Nesmeyanov Institute of Organoelement Compounds, Russian Academy of Sciences, Vavilov Street, 28, 119991, Moscow, Russia*
[b] *Department Chemie, Ludwig-Maximilians-Universität München, Butenandt Street, 5-13, Haus, D-81377 München, Germany*

Received 29 March 2004; accepted 17 June 2004
Available online 29 July 2004

Abstract

Synthesis of disubstituted derivatives of the dodecahydro-*closo*-dodecaborate anion is described and the reaction mechanism is discussed. Derivatives of the $[B_{12}H_{12}]^{2-}$ anion containing hydroxyl and arylated carbonyl functions ($[1\text{-HO-2-ArCOB}_{12}H_{10}]^{2-}$) were prepared from different acylchlorides. The major advantage of these compounds is their possibility to provide two different binding sites in one molecule. These compounds are suitable for the development of new precursors for boron neutron capture therapy (BNCT).
© 2004 Elsevier Ltd. All rights reserved.

Keywords: *closo*-Dodecaborate; Hydroxy and acyl derivatives; Disubstituted functional derivatives; Boron neutron capture therapy

1. Introduction

Our continuing interest in the chemistry of the dodecahydro-*closo*-dodecaborate anion $[B_{12}H_{12}]^{2-}$ aims towards facile, reliable and rational introduction of a broad variety of substituents [1–4]. Especially water-soluble functionalized derivatives of the dodecahydro-*closo*-dodecaborate anion are promising candidates for boron neutron capture therapy (BNCT) [5,6]. In our previous work [1], we described the reaction of $Na_2[B_{12}H_{12}]$ with various acylchlorides in acetone at room temperature, leading to a mixture of the acylated product $[B_{12}H_{11}COR]^{2-}$ and the monohydroxy derivative $[B_{12}H_{11}OH]^{2-}$.

The ratio of the products depends on the nature of the R used. The mechanism of the reaction was studied and intermediate (**A**) was characterized [1] (cf. (Scheme 1)). In this paper, we present the results of the study of the same reaction in boiling acetone.

2. Results and discussion

We found, that aromatic acylchlorides react with $Na_2[B_{12}H_{12}]$ (**1**) in boiling acetone resulting after work up with water in 1-hydroxy-2-acyl-*closo*-dodecaborates $[1\text{-HO-2-ArCOB}_{12}H_{10}]^{2-}$ (**2a**–**c**) with ca. 70% yield. In contrast the reaction with aliphatic acylchlorides in boiling acetone leads to a mixture of the acylated product and the monohydroxy derivative as at ambient temperature [1].

The structure of **2a**–**c** was determined using methods of NMR and IR spectroscopy. The $^{11}B\{^1H\}$ NMR

* Corresponding author. Tel.: +7-951-359-242; fax: +7-951-355-085.
E-mail addresses: semi@ineos.ac.ru (A. Semioshkin), b.brellochs@gmx.net (B. Brellochs).

0277-5387/$ - see front matter © 2004 Elsevier Ltd. All rights reserved.
doi:10.1016/j.poly.2004.06.005

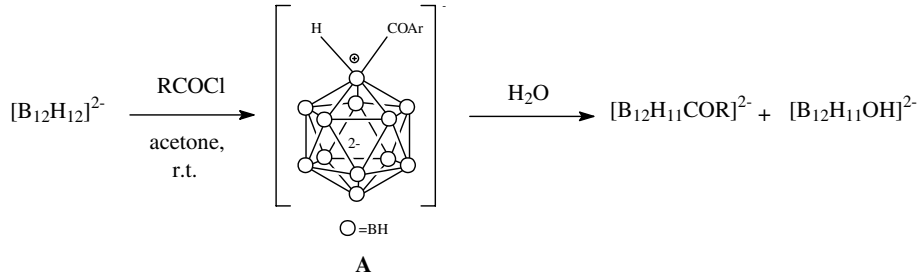

A

Scheme 1.

spectra of **2a**–**c** (Table 1) show 6 signals with the intensity ratio of 1:1:6:2:1:1. This pattern is not inconsistent with the expected 1:1:2:2:2:2:1:1 pattern for a $[B_{12}H_{10}XY]^{2-}$-system with 2 different substituents. The coinciding ^{11}B resonances B(3,6), B(4,5) and B(7,11) show separated ^{1}H resonances in the corresponding $^{1}H\{^{11}B\}$ NMR spectra. The two lowfield singlets at ~4.5 and ~2.7 ppm are assigned to B(1)–OH and B(2)–COAr. The assignment of B(1) and B(2) is based on the data found for the monosubstituted derivatives $[B_{12}H_{11}OH]^{2-}$ (B(1) 5.4 ppm [2]) and $[B_{12}H_{11}COR]^{2-}$ (B(1) ~3 ppm [1]). The 1,2-substitution in **2a**–**c** and assignment of the B–H-bonded (non-substituted) boron atoms is based on the ^{11}B-^{11}B-COSY NMR spectra (Scheme 2).

In the ^{1}H NMR spectra of **2a**–**c** the signals of the cation and the COAr protons were observed. The shifts of the B–H protons were determined by ^{1}H-^{11}B-2D NMR spectra (Table 1). The 5 signals in the $^{1}H\{^{11}B\}$ NMR spectra (intensity ratio of 2:2:2:2:2) correspond to disubstitution of the *closo*-dodecaborate anion. The B–H protons of B(9)–H and B(12)–H (antipodal to B(2)–COAr and B(1)–OH) show coincidence for all synthesized dodecaborates $[1\text{-HO-2-ArCOB}_{12}H_{10}]^{2-}$ (**2a**–**c**).

The ^{13}C NMR spectra of **2a**–**c** contain signals of the CO-group at ~170 ppm. These signals are shifted by approximately 5 ppm to the lower field in the comparison with signals of the corresponding monoacylated derivatives $[B_{12}H_{11}COR]^{2-}$ [1].

The IR spectra of **2a**–**c** contain the characteristic bands of CO (~1650 cm^{-1}), BH (~2500 cm^{-1}) and OH (~3425 cm^{-1}) groups. The signals of carbonyl and hydroxyl groups are shifted in the comparison with signals of monosubstituted acylderivatives $[B_{12}H_{11}COR]^{2-}$ (1675–1690 cm^{-1}) [1] and hydroxyl derivative $[B_{12}H_{11}OH]^{2-}$ (3565cm^{-1}) [2]. Such trends, as well as the corresponding shift of the carbonyl ^{13}C NMR signals, can be explained by the formation of a intramolecular hydrogen bond between the hydroxy and carbonyl groups (Scheme 3).

Earlier we studied the mechanism of the room temperature reaction of **1** with acylchlorides [1]. To understand the reason of the selective 1,2-disubstitution in the present work we studied the reaction of **1** with 4-chlorobenzoylchloride in acetone-d_6 in a NMR tube at 52 °C. We monitored the reaction by measuring ^{1}H and ^{11}B NMR spectra every 5 min and ^{13}C NMR spectra every 30 min. After heating the tube for 2.5 h the same intermediate as in the reaction at room temperature (**A**) was formed (cf. Scheme 1). The NMR data of **A** match perfectly with those obtained earlier [1].

Through further heating of the tube for additional 3 h hydrogen is evolved and **A** is nearly quantitatively transformed to the new intermediate **B**. Intermediate **B**

Table 1
^{11}B and $^{1}H\{^{11}B\}$ NMR data of $[1\text{-OH-2-COArB}_{12}H_{10}]^{2-}$ **2a**–**c**

Compound	**2a**		**2b**		**2c**	
	δ (ppm)	J_{BH} (Hz)	δ (ppm)	J_{BH} (Hz)	δ (ppm)	J_{BH} (Hz)
B (1)	4.8		4.5		4.4	
B (2)	2.1		1.7		2.2	
B (3,4,5, 6,7,11)	−15.0	not resolved	−15.4	122.6	−15.4	122.5
B (8,10)	−16.9	not resolved	−17.2	128.5	−17.3	127.5
B (9)	−19.6	not resolved	−20.6	not resolved	−20.2	130.1
B (12)	−20.8	not resolved	−21.5	124.3	−21.6	125.5
H (3,6)	1.72		1.70		1.70	
H (4,5)	1.59		1.58		1.54	
H (7,11)	1.41		1.38		1.37	
H (8,10)	1.16		1.16		1.16	
H (9), H (12)	1.02		1.02		1.00	

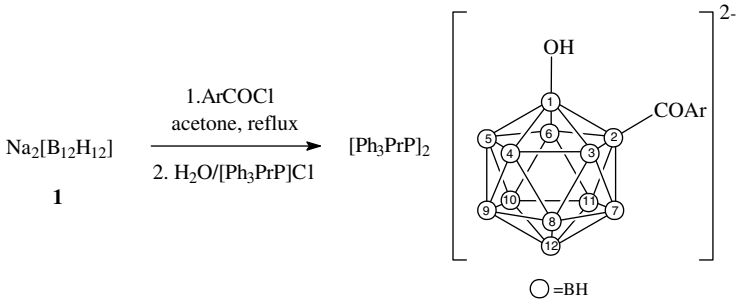

2a-c

Ar = Ph (**2a**), 4-ClC_6H_4 (**2b**), 4-BrC_6H_4 (**2c**)

Scheme 2.

is stable at room temperature for several hours. It reacts to **2b** after the addition of water. In the ^1H NMR spectrum of **B** the signals of the aromatic ring protons are shifted to lower field (8.21 and 7.72 ppm for this AX-system) compared to **A** [1]. The ^{13}C NMR spectrum shows that all signals of the aromatic ring carbons are shifted to lower field compared to **A**. The signal of C_i (C–CO–) is shifted by ca. 5 ppm (143.4 and 137.9 ppm for **A** [1]). ^{13}C NMR shift for the former carbonyl C-atom is found at 185.3 ppm (167.0 for **A** [1]). The ^{11}B NMR spectrum of **B** shows the expected 1:1:2:2:2:2:1:1 pattern for a disubstituted dodecaborate with two different substituents (5.00 and 2.9 ppm for B(1)–O– and B(2)–C^+(Ar)–). The shifts of the substituted boron atoms are close to the product **2b** (4.5 and 1.7 ppm), but both shifted to the lowfield side. The 2:2:2:2:1:1 pattern of the $^1H\{^{11}B\}$ NMR spectrum provides another convincing proof for the proposed structure of **B**. According to the data it is possible to propose a mechanism for the formation of **2** (Scheme 4).

After the elimination of hydrogen from **A** the formation of **B** through transient intermediate **I** is reasonable. All NMR data match with the proposed structure **B**. The work up of **B** with water or dry methanol only results in **2b**. This strongly supports structure **B**. If the reaction mixture contained substantial amounts of **I**, after work up with MeOH the methoxylated derivative [1-MeO-2-(4-ClC_6H_4CO)-$B_{12}H_{10}$]$^{2-}$ should be formed as well.

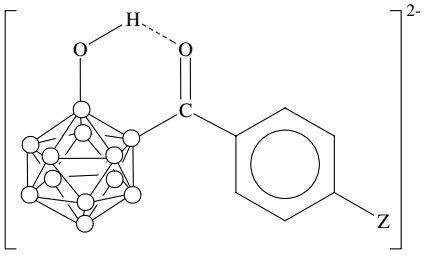

Scheme 3.

3. Experimental

3.1. Materials and equipments

Chemicals were reagent grade and used as received from standard commercial vendors, acetone and acetone-d_6 was distilled from dry K_2CO_3, methanol was distilled from magnesium. IR spectra were recorded on NICOLET 520 FR/FT spectrometer. The ^1H, ^{13}C, and ^{11}B NMR spectra were recorded at 200.13. 50.32 and 64.21 MHz on a BRUKER-ACP-200 spectrometer in acetone-d_6/D_2O (10:1,v/v). Melting points were measured in open capillary and are not corrected.

3.2. Preparation of compounds

3.2.1. Bis-(triphenyl-n-propylphosphonium)-1-hydroxy-2-benzoyl-decahydrodo-closo-decaborate, *2a*

To a solution of 0.95 g (5.0 mmol) $Na_2[B_{12}H_{12}]$ in 50 ml absolute acetone 1.4 ml (5.2 mmol) benzoylchloride was added and the solution was refluxed for 48 h. The precipitated NaCl was filtered. To the filtrate 1.52 g (10.0 mmol) CsF in 50 ml dry MeOH was added. The precipitate formed was recovered by filtration and dissolved in 50 ml H_2O. After addition of 3.85 g (10.0 mmol) Ph_3PrPBr in 50 ml water the Ph_3PrP-salt precipitated. The solid was filtered, washed with 2×30 ml H_2O, dried in vacuum giving 3.13 g (71.7%, yield) of **2a,** m.p. = 84–85 °C. *Anal*. Calc. for $C_{49}H_{60}B_{12}O_2P_2$; C, 67.44; H, 6.93; B, 14.86. Found: C, 66.98; H, 6.94; B, 14.47%. IR (Nujol, cm^{-1}): 3401 (OH), 2499 (B–H), 1648 (C═O). ^1H NMR (ppm): 8.1–7.7 (30H, m, Ph–P), 7.6–7.3 (5H, m, Ph–CO), 3.56 (4H, m, P–CH_2), 1.81 (4H, m, P–CH_2-CH_2), 1.20 (6H, t, P–CH_2–CH_2–

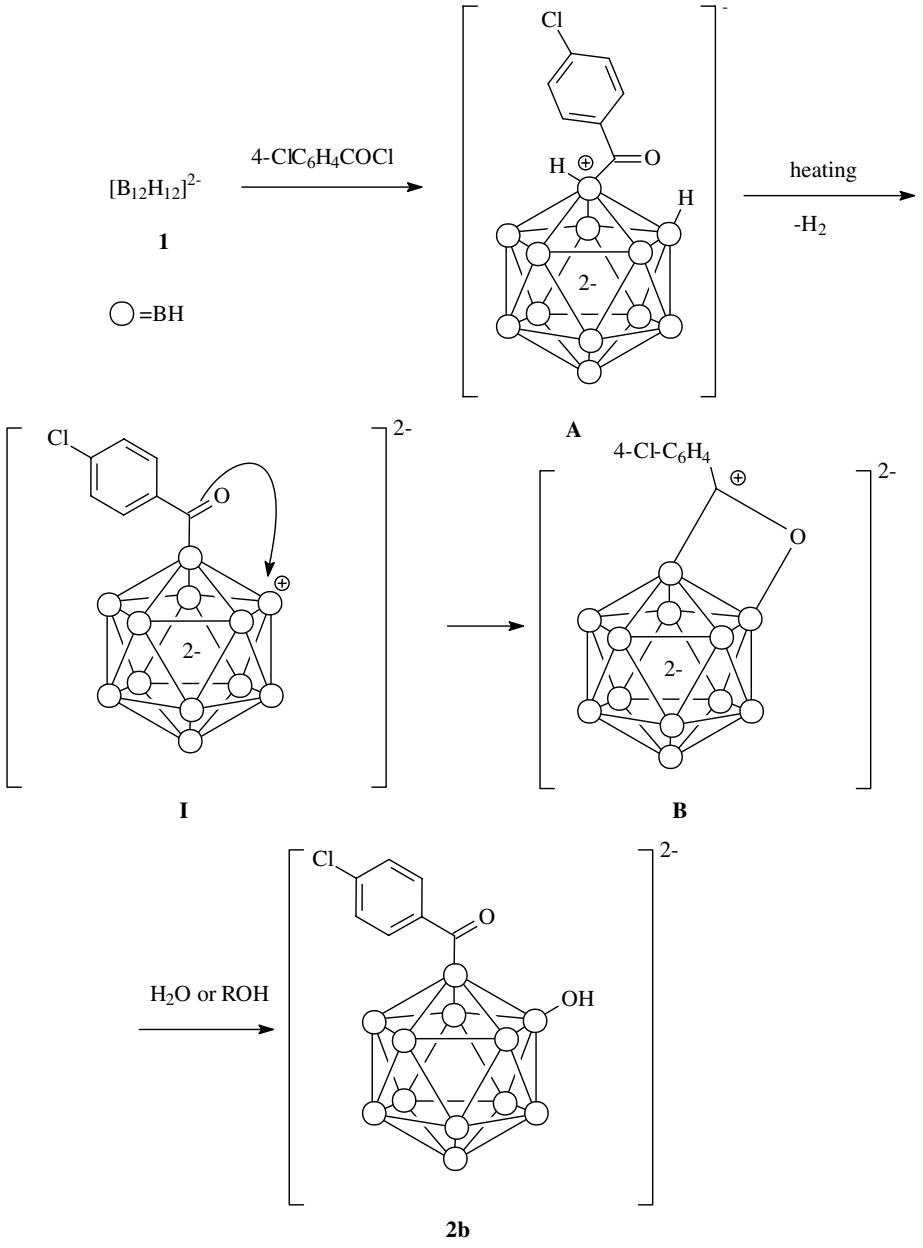

Scheme 4.

CH_3). ^{13}C NMR (ppm): 171.6 (C═O), 133.6, 131.6, 130.5, 129.9 (Ph–CO), 135.8 (d), 134.2 (d), 131.0 (d), 119.5 (d, –Ph–P), 23.6 (d), 16.8 (d), 15.2 (d, –Pr–P).

3.2.2. Bis-(triphenyl-n-propyl-phosphonium)-1-hydroxy-2-(4-chlorobenzoyl)-decahydro-closo-dodecaborate ***2b***

$Na_2[B_{12}H_{12}]$ (0.95 g, 5.0 mmol) was dissolved in 50 ml absolute acetone and 0.7 ml (5.2 mmol) *p*-chlorobenzoylchlorid was added. The reaction mixture was refluxed for 24 h. The solvent was evaporated to dryness, 100 ml H_2O were added and insoluble material was filtered off. One gram NMe_4Br in 10 ml H_2O was added to precipitate by – products. After filtering, the pure product was precipitated after the addition of 3.85 g (10.0 mmol) Ph_3PPrBr in 100 ml H_2O. The precipitate was recovered by filtration, washed 2×30 ml H_2O, dried in vacuo, yielding −3.1 g (68.5%) of **2b,** m.p. = 72 °C. *Anal*. Calc. for $C_{49}H_{59}B_{12}ClO_2P_2$; C, 64.88; H, 6.56; B, 14.30. Found: C, 64.27; H, 6.59; B, 14.14%. IR (Nujol, cm^{-1}): 3447 (OH), 2495 (B–H), 1650 (C═O). ^1H NMR (ppm): 7.7 (30H, m, Ph–P), 7.43 (2H,d,1/2Ar–CO), 3.56 (4H, m, P–CH_2): 1.81 (4H, m, P–CH_2–CH_2), 1.20 (6H, t, P–CH_2–CH_2–CH_3). ^{13}C NMR (ppm): 169.5 (C═O), 138.6; 135.9, 132.3; 129.0 (4-C_6H_4–CO), 135.8 (d), 134.4 (d), 131.1 (d), 119.0 (d, –Ph–P), 23.5 (d), 17.0 (d), 15.0 (d, –Pr–P).

3.2.3. Bis-(triphenyl-n-propylphosphonuim)-1-hydroxy-2-(4-bromobenzoyl)-decahydro-closo-dodecaborate, ***2c***

2c was synthesized by the same way as **2b** from 0.95 g (5.0 mmol) $Na_2[B_{12}H_{12}]$ in 50 ml absolute acetone and 1.2 ml (5.0 mmol) 4-bromobenzoylchloride. Yield 3.22 g (67.4%) **2c**, m.p. = 83 °C. *Anal.* Calc. for $C_{49}H_{59}B_{12}BrO_2P_2$; C, 61.85; H, 6.25; B, 13.63. Found: C, 61.17; H, 6.22; B, 13.34%. IR (Nujol, cm^{-1}): 3429 (OH), 2495 (B–H), 1651 (C═O). ^1H NMR (ppm): 8.1–7.7 (30H, m, Ph–P), 7.87, 7.60 (4H, dd, 4-BrC_6H4CO), 3.57 (4H, m, P–CH_2), 1.82 (4H, m, P–CH_2CH_2), 1.18 (6H, t, P–CH_2–CH_2–CH_3), ^{13}C NMR (ppm): 169.1 (C═O), 135.8, 134.6, 131.7, 129.2 (4-BrC_6H_4–CO–), 135.5 (d); 134.1 (d), 130.9 (d), 118.5 (d, –P–Ph), 23.5 (d), 17.0 (d), 15.3 (d, –P–Pr).

3.2.4. Studies of mechanism

To a solution of $Na_2[B_{12}H_{12}]$ (71 mg, 0.37 mmol) in 0.5 ml absolute acetone-d_6 in the NMR-tube 50 μl (0.39 mmol) *p*-chlorobenzoylchloride was added. The tube was heated to 52°C for 2.5 h (formation of **A**) and than for additional 3 h. The resulting solution contained nearly quantitatively **B**. The tube was cooled to room temperature and the NMR data were taken.

^{11}B NMR (ppm): 5.0 (1B, s, B–O–), 2.9 (1B, s, B–$C(Ar)^+$–), −14.5 (2B), −15.6 (2B), −16.2 (2B), −17.0 (2B), −20.5 (1B, B(9)), −22.4 (1B, B(12)); ^1H NMR (ppm): 8.21, 7.72 (4H,dd,Ar), 3.0–0.5 (10H, broad, BH); $^1H\{^{11}B\}$NMR (ppm): 1.67 (2H), 1.51 (2H), 1.30 (2H), 1.14 (2H), 1.05 (1H), 0.96 (1H); ^{13}C NMR (ppm): 185.3 (C^+), 143.4 (C(Ar)–C^+), 137.6 (C(Ar)–Cl), 134.2, 131.5(CH)Ar)).

Acknowledgement

The authors thank Russian foundation for basic research for the support.

References

[1] A.A. Semioshkin, P.V. Petrovskii, D. Gabel, B. Brellochs, V.I. Bregadze, Russ. Chem. Bull. 47 (1998) 950.
[2] A.A. Semioshkin, P.V. Petrovskii, I.B. Sivaev, E.G. Balandina, V.I. Bregadze, Russ. Chem. Bull. 45 (1996) 683.
[3] I.B. Sivaev, A.B. Bruskin, V.V. Nesterov, M. Yu. Antipin, V.I. Bregadze, S. Sjöberg, Inorg. Chem. 38 (1999) 5887.
[4] I.B. Sivaev, A.A. Semioshkin, B. Brellochs, S. Sjöberg, V.I. Bregadze, Polyhedron 19 (2000) 627.
[5] M.F. Hawthorne, Angew. Chem., Int. Ed. Engl. 32 (1993) 950.
[6] I.B. Sivaev, V.I. Bregadze, N.T. Kuznetsov, Russ. Chem. Bull. 51 (2002) 1362.

Available online at www.sciencedirect.com
SCIENCE DIRECT®
Polyhedron 23 (2004) 2141–2151
POLYHEDRON
www.elsevier.com/locate/poly

Iron complexes of 3-(pyrazinyl)-1,2,4-triazole ligands

Faye E. Bradford, Lee P. Connor, Colin A. Kilner, Malcolm A. Halcrow *

Department of Chemistry, University of Leeds, Woodhouse Lane, Leeds LS2 9JT, UK

Received 25 May 2004; accepted 11 June 2004
Available online 30 July 2004

Abstract

The iron complex chemistry of the ligands 3-(pyrazinyl)-1,2,4-triazole (L^2H) and 1-methyl-3-(pyrazinyl)-1,2,4-triazole (L^2Me) has been investigated. The complexes $[Fe(L^2H)_3](ClO_4)_2$, $[Fe(L^2Me)_3]X_2$ ($X^- = BF_4^-$ or PF_6^-), $[Fe(L^2Me)_3](ClO_4)_2 \cdot xH_2O$ ($x = 0$ or 1) and $[Fe(L^2Me)_3]SO_4 \cdot 2H_2O$ have been isolated by complexation of the appropriate hydrated iron(II) salt by 3 equiv. of an L^2R ligand. Attempts to prepare other salts of these complexes gave intractable oil products; the autooxidation product $[\{FeCl(L^2Me)_2\}_2(\mu\text{-}O)](PF_6)_2$ slowly crystallised from one such reaction mixture, and was identified by crystallography. The single crystal structure of $[Fe(L^2Me)_3](ClO_4)_2 \cdot H_2O$ contains *mer*-six-coordinate Fe(II) centres, that are essentially fully low-spin at 150 and 296 K. The anhydrous powders $[Fe(L^2H)_3](ClO_4)_2$ and $[Fe(L^2Me)_3]Y_2$ ($Y^- = BF_4^-$, ClO_4^- or PF_6^-) undergo gradual spin-state transitions with $182 \leqslant T_{1/2} \leqslant$ ca. 400 K, that range from 61% to 100% completeness at 50 K. $[Fe(L^2Me)_3]SO_4 \cdot 2H_2O$ is high-spin above 200 K, but shows a decline in $\chi_M T$ at lower temperatures whose origin is uncertain. The single crystal X-ray structure of 1,4-dihydro-3,6-dipyrazinyl-1,2,4,5-tetrazine, a byproduct from an attempted synthesis of 5-methyl-3-(pyrazinyl)-1,2,4-triazole, is also reported.
© 2004 Elsevier Ltd. All rights reserved.

Keywords: Iron; Spin-crossover; Crystal structure; Magnetic measurements

1. Introduction

There is continuing interest in the chemistry and physics of compounds that exhibit spin-state transitions upon cooling, irradiation and/or the application of pressure [1–3]. Since these transitions are usually accompanied by a colour change in the sample, such compounds in the solid state have potential for application in information storage and display devices [4]. In order to be useful, a thermal spin-crossover compound must exhibit an abrupt transition with a pronounced hysteresis loop, which should ideally occur close to room temperature [5,6]. Abrupt spin-state transitions are a consequence of strong, cooperative interactions between the spin centres in the solid [1–3]. Hence, it can be generalised that coordination polymers, or solids containing discrete complex molecules linked by hydrogen-bonding or strong π–π interactions, are the most likely to exhibit this property. Otherwise, the synthesis of new abrupt spin-crossover materials still involves a significant degree of trial-and-error.

During our own studies of spin-crossover Fe(II) compounds [7–11] we reported Fe(II) complexes of 3-(pyrazinyl)pyrazole (L^1), which contains both hydrogen bond-donor and -acceptor sites when coordinated to a metal ion [11]. We thought that this might result in networks of Fe complex centres linked by hydrogen bonding, which could undergo cooperative spin-state transitions. In fact, while crystals of $[Fe(L^1)_3]X \cdot n_2O$ ($X^- = BF_4^-$, $n = 2$; $X^- = ClO_4^-$, $n = 1$) do show the desired intermolecular N–H···N hydrogen bonding, they are also fully low-spin at or below room-temperature [11]. We reasoned that, in order to obtain spin-crossover

* Corresponding author. Tel.: +44-113-343-6506; fax: +44-113-343-6565.
E-mail address: m.a.halcrow@chem.leeds.ac.uk (M.A. Halcrow).

0277-5387/$ - see front matter © 2004 Elsevier Ltd. All rights reserved.
doi:10.1016/j.poly.2004.06.018

compounds from this type of system, we would need to make one or other of the heterocycles in the L^1 framework less basic. We now report an investigation of the iron(II) complex chemistry of two 3-(pyrazinyl)-1,2,4-triazole derivatives, L^2R (R = H or Me). The synthesis of these ligands, and of L^3H, has been reported by others, although only their ruthenium complex chemistry has been investigated to date [12–14]. However, several iron(II) complexes of closely related 35-(pyrid-2-yl)-1,2,4-triazoles L^4R are known, all of which undergo spin-state transitions below room temperature [15–18].

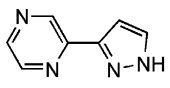

L^1

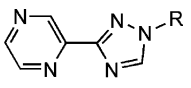

R = H, L^2H
R = CH_3, L^2Me

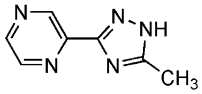

L^3

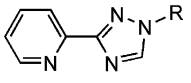

R = H, L^4H
R = CH_3, L^4Me

2. Experimental

All manipulations were carried out in air, using distilled water or reagent-grade solvents, and all organic and inorganic reagents were used as supplied. The syntheses of **I**, **II**, L^2H and L^2Me are modifications of the literature procedures [12]. *Caution*. While we have experienced no difficulty in handling the ClO_4^- salts in this study, metal–organic perchlorates are potentially explosive and should be handled with due care in small quantities.

2.1. Synthesis of pyrazinylamidrazone (*I*)

An ethanol (40 cm^3) solution of cyanopyrazine (10.0 g, 9.5×10^{-2} mol) and hydrazine monohydrate (4.8 g, 9.5×10^{-2} mol) was stirred at room temperature for 1 h, yielding a yellow precipitate. The reaction mixture was stored at −30 °C overnight. The solid product was then collected by filtration, washed with the minimum amount of cold ethanol and dried over P_2O_5. Yield 12.1 g (93%). Calc. for $C_5H_7N_5$: C, 43.8; H, 5.1; N, 51.1. Found: C, 44.0; H, 5.2; N, 51.1%. M.p. 127–129 °C. EI mass spectrum: *m/z* 137 (M^+), 106 (M^+–N_2H_3), 79 (M^+–$CNHN_2H_3$). ^{1}H NMR spectrum ({CD_3}$_2$SO, 293 K): δ, ppm 5.64 (br s, 2H, N*H*), 5.81 (br s, 2H, N*H*), 8.56 (m, 2H, pz H^5 + H^6), 9.18 (s, 1H, pz H^3).^{13}C NMR spectrum ({CD_3}$_2$SO, 293 K): δ, ppm 141.6 (*C*═NH), 142.1, 142.6, 143.1 (pz C^3 + C^5 + C^6), 147.5 (pz C^2).

2.2. Synthesis of pyrazinyl-N′-methylamidrazone (*II*)

A solution of cyanopyrazine (10.0 g, 9.5×10^{-2} mol) and methylhydrazine (23.8 g, 0.48 mol) in ethanol (100 cm^3) was stirred at room temperature for 1 h, yielding a yellow solution. The reaction mixture was quenched with water, and the aqueous phase extracted with Et_2O (3×50 cm^3). The organic washing were dried over $MgSO_4$, then concentrated in vacuo until the product began to precipitate. Overnight storage of the solution at −30 °C yielded fine yellow needles, which were collected by filtration and dried over P_2O_5. Yield 12.6 g (88%). Calc. for $C_6H_9N_5$: C, 47.7; H, 6.0; N, 46.3. Found: C, 47.8; H, 6.0; N, 46.3%. M.p. 106–108 °C. EI mass spectrum: *m/z* 151 (M^+), 122 (M^+–$NHCH_2$), 79 (M^+–$CNHN_2H_2$ CH_3). ^{1}H NMR spectrum ({CD_3}$_2$SO, 293 K): δ, ppm 2.88 (s, 3H, CH_3), 5.29 (br s, 1H, N*H*), 5.79 (br s, 2H, N*H*), 8.53 (d, 2.7 Hz, 1H, pz H^6), 8.54 (dd, 1.4 and 2.7 Hz, 1H, pz H^5), 9.13 (d, 1.4 Hz, 1H, pz H^3). 13C NMR spectrum ({CD_3}$_2$SO, 293 K): δ, ppm 38.3 (C_3), 140.6 (*C*═NH), 142.1, 142.8, 143.2 (pz C^3 + C^5 + C^6), 147.0 (pz C^2).

2.3. Synthesis of pyrazinyl-N′-phenylamidrazone (*III*)

Method as for **I**, using phenylhydrazine (10.3 g, 9.5×10^{-2} mol). Evaporation of the reaction mixture to dryness yielded an orange oil, which partially crystallised on standing at room temperature. Yield 18.1 g (89%). Calc. for $C_{11}H_{11}N_5$: C, 62.0; H, 5.2; N, 32.8. Found: C, 61.8; H, 5.3; N, 32.8%. EI mass spectrum: ***m/z*** 214 (M+H^+), 77 (Ph^+). ^{1}H NMR spectrum ({CD_3}$_2$SO, 293 K): δ, ppm 3.63 (br s, 3H, N*H*), 6.73 (m, 2H, Ph $H^{2/6}$), 7.16 (m, 3H, Ph H^{3-5}), 8.65 (dd, 1.2 and 2.6 Hz, 1H, pz H^5), 8.83 (d, 2.6 Hz, 1H, pz H^6), 9.39 (d, 1.2 Hz, 1H, pz H^3).13C NMR spectrum ({CD_3}$_2$SO, 293 K): δ, ppm 112.5 (Ph $C^{2/6}$), 119.8 (Ph C^4), 129.6 (Ph $C^{3/5}$), 131.5 (Ph C^1), 145.9, 147.8, 148.7 (pz C^3 + C^5 + C^6), 151.7 (pz C^2), 162.2 (*C*═NH).

2.4. Synthesis of 3-(pyrazinyl)-1,2,4-triazole (L^2H)

Pyrazinylamidrazone (2.7 g, 0.020 mol) was added in small portions, with stirring, to formic acid (9.0 g, 0.20 mol) at 0 °C. The mixture was allowed to warm to room temperature, then refluxed for 2 h. The excess formic acid was removed by evaporation under reduced pressure, and the solid residue neutralised with aqueous Na_2CO_3. Silica column chromatography using a 1:3 MeOH:CH_2Cl_2 eluent yielded the pure product as yellow-brown platelets. Yield 0.95 g (32%). Calc. for $C_6H_5N_5$: C, 49.0; H, 3.4; N, 47.7. Found: C, 49.1; H, 3.7; N, 47.7%. M.p. 210–212 °C. EI mass spectrum: *m/z*

147 (M^+), 119 (M^+–N_2). ^{1}H NMR spectrum ({CD_3}$_2$SO, 293 K): δ, ppm 8.50 (s, 1H, tz H^5), 8.70 (d, 2.5 Hz, 1H, pz H^6), 8.73 (dd, 1.5 and 2.5 Hz, 1H, pz H^5), 9.25 (d, 1.4 Hz, 1H, pz H^3).^{13}C NMR spectrum ({CD_3}$_2$SO, 293 K): δ, ppm 142.9, 144.9, 145.5 (pz C^3 + C^5 + C^6), 148.3 (pz C^2), tz C^3 and C^5 not observed [19].

2.5. Synthesis of 1-methyl-3-(pyrazinyl)-1,2,4-triazole (L^2Me)

Method as for L^2H, except pyrazinyl-*N*′-methylamidrazone (3.0 g, 0.020 mol) was used. The product was a cream powder. Yield 1.3 g (40%). Calc. for $C_7H_7N_5$: C, 52.2; H, 4.4; N, 43.5. Found: C, 52.0; H, 4.2; N, 43.3%. M.p. 174–176 °C. EI mass spectrum: *m/z* 161 (M^+), 133 (M^+–N_2), 118 (M^+–N_2CH_3). ^{1}H NMR spectrum ({CD_3}$_2$SO, 293 K): δ, ppm 3.98 (s, 3H, CH_3), 8.63 (s, 1H, tz H^5), 8.67 (d, 2.6 Hz, 1H, pz H^6), 8.72 (dd, 1.5 and 2.6 Hz, 1H, pz H^5), 9.21 (d, 1.5 Hz, 1H, pz H^3).^{13}C NMR spectrum ({CD_3}$_2$SO, 293 K): δ, ppm 36.6 (C_3), 142.9, 144.9, 145.1, 146.6 (pz C^3 + C^5 + C^6 + tz C^5), 145.5 (tz C^3), 159.3 (pz C^2).

2.6. Attempted synthesis of 5-methyl-3-(pyrazinyl)-1,2,4-triazole (L^3H)

Pyrazinylamidrazone (2.7 g, 0.020 mol) was added in small portions, with stirring, to acetic acid (12.0 g, 0.20 mol) at 0 °C. The mixture was allowed to warm to room temperature, then stirred for 2 h. The excess acetic acid was removed by evaporation under reduced pressure, and the solid residue neutralised with aqueous Na_2CO_3. Silica column chromatography using a 1:3 MeOH:CH_2Cl_2 eluent demonstrated the presence of several coloured products, with dark orange 1,4-dihydro-3,6-dipyrazinyl-1,2,4,5-tetrazine (**IV**) [20] being the only component to elute cleanly.^{1}H NMR spectroscopy implied that **IV** was the most abundant species in the crude product mixture (ca. 30%).

2.7. Synthesis of[Fe(L^2H)$_3$](ClO_4)$_2$ [**1(ClO_4)$_2$**]

A mixture of $Fe(ClO_4)_2 \cdot 6H_2O$ (0.38 g, 1.0×10^{-3} mol) and L^2H (0.46 g, 3.1×10^{-3} mol) in MeOH (50 cm^3) was stirred at room temperature until all the solid had dissolved. The deep red solution was filtered to remove a black impurity, and concentrated to ca. 5 cm^3. Diffusion of Et_2O vapour into this solution yielded a dark red-brown powder which was filtered, washed with Et_2O and dried in vacuo. Yield 0.29 g, 42%. Calc. for $C_{18}H_{15}Cl_2FeN_{15}O_8$: C, 31.1; H, 2.2; N, 30.1. Found: C, 31.0; H, 2.2; N, 29.7%. ESMS: *m/z* 627 [Na_5(L^2H)$_3$(OH)(OH$_2$)$_3$]$^+$, 591 [Na_5(L^2H)$_3$(OH)(OH$_2$)]$^+$, 427 [Na_2(L^2H)$_2$(OH)$_3$(OH$_2$)$_2$]$^+$, 390 [Na(L^2H)$_2$(OH$_2$)$_4$+H]$^+$, 358 [Na_2(L^2H)$_2$(OH$_2$)]$^+$, 285 [Na_3(L^2H)(OH)$_3$(OH$_2$)]$^+$, 263 [Na_2(L^2H)(OH)$_2$(OH$_2$)$_2$]$^+$, 245 [Na_2(L^2H)(OH)$_2$(OH$_2$)]$^+$, 212 [Na_2(L^2H)(OH$_2$)+H]$^+$, 148 [L^2H+H]$^+$. IR (nujol): 3460br w, 3130br w, 1606m, 1561w, 1405m, 1344m, 1297m, 1274m, 1165s, 1105br vs, 1000m, 972m, 930w, 856m, 767m, 736m, 722m, 622s, 511m cm^{-1}. ^{1}H NMR spectrum (CD_3 CN, 293 K): δ, ppm 45.5, 55.2 (both 1H, pz H^3+H^5), 108.1 (1H, tz H^5).

2.8. Synthesis of [Fe(L^2Me)$_3$](BF_4)$_2$ [**2(BF_4)$_2$**]

A mixture of $Fe(BF_4)_2 \cdot 6H_2O$ (0.34 g, 1.0×10^{-3} mol) and L^2Me (0.50 g, 3.1×10^{-3} mol) in MeCN (50 cm^3) was stirred at room temperature for 1 h. The deep red solution was filtered, and concentrated to ca. 5 cm^3. Diffusion of Et_2O vapour into this solution yielded dark red microcrystals which were filtered, washed with Et_2O and dried in vacuo. Yield 0.46 g, 63%. Calc. for $C_{21}H_{21}B_2F_8FeN_{15}$: C, 35.4; H, 3.0; N, 29.5. Found: C, 35.6; H, 3.1; N, 29.7%. IR (nujol): 3146w, 1603m, 1558s, 1512m, 1351m, 1285m, 1223s, 1151s, 1020br vs, 939m, 873w, 855s, 849s, 832m, 771s, 733m, 699s, 664s, 642m, 636m, 540m, 523m cm^{-1}.

2.9. Synthesis of [Fe(L^2Me)$_3$](ClO_4)$_2$ [**2(ClO_4)$_2$**]

A solution of $Fe(ClO_4)_2 \cdot 6H_2O$ (0.37 g, 1.0×10^{-3} mol) and L^2Me (0.50 g, 3.1×10^{-3} mol) in acetone (50 cm^3) was stirred at room temperature for 1 h. The resultant red solution was filtered, and concentrated to ca. 5 cm^3. Diffusion of Et_2O vapour into this solution gave a red microcrystalline solid which was filtered, washed with Et_2O and dried in vacuo. Yield 0.52 g, 68%. Calc. for $C_{21}H_{21}Cl_2FeN_{15}O_8$: C, 34.2; H, 2.9; N, 28.5. Found: C, 34.0; H, 3.0; N, 28.4%. ESMS: *m/z* 569 [Na_3(L^2Me)$_3$(OH)]$^+$, 423 [Na_2(L^2Me)$_2$(OH$_2$)$_3$+H]$^+$, 385 [Na_2(L^2Me)$_2$(OH)]$^+$, 303 [Na_3(L^2Me)$_3$(OH$_2$)$_3$]$^{2+}$, 259 [Na_2(L^2Me)(OH)$_2$(OH$_2$)]$^+$, 225 [Na_2(L^2Me)(OH$_2$)]$^+$, 162 [L^2Me+H]$^+$. IR (nujol): 3124w, 1597m, 1549m, 1513s, 1346m, 1296m, 1222s, 1166s, 1100br vs, 1034s, 932m, 879m, 864m, 767s, 734m, 695m, 636m, 625s, 514m cm^{-1}. ^{1}H NMR spectrum (CD_3 CN, 293 K): δ, ppm 9.6 (3H, CH_3), 41.7, 45.9 (both 1H, pz H^3 + H^5), 97.2 (1H, tz H^5).

2.10. Synthesis of [Fe(L^2Me)$_3$](PF_6)$_2$ [**2(PF_6)$_2$**]

A mixture of $FeCl_2 \cdot 4H_2O$ (0.21 g, 1.0×10^{-3} mol), L^2Me (0.50 g, 3.1×10^{-3} mol) and NH_4PF_6 (0.34 g, 2.1×10^{-3} mol) in H_2O (50 cm^3) was stirred with mild heating until all the solid had dissolved. Allowing the red solution to stand at room temperature overnight afforded a red polycrystalline solid contaminated with a small amount of white powder. Recrystallisation of this material from MeCN/Et_2O afforded dark red microcrystals which were filtered, washed with Et_2O and dried in vacuo. Yield 0.32 g, 37%. Calc. for $C_{21}H_{21}F_{12}FeN_{15}P_2$:

C, 30.4; H, 2.6; N, 25.3. Found: C, 30.7; H, 2.8; N, 25.5%. IR (nujol): 3143w, 1607m, 1559s, 1511m, 1349m, 1287m, 1220s, 1165s, 1149m, 1066m, 1046m, 1018m, 1008m, 923m, 860br vs, 770s, 735m, 701m, 645m, 634m, 558m, 522m cm^{-1}.

2.11. Synthesis of $[Fe(L^2Me)_3]SO_4 \cdot 2H_2O$ [$2SO_4 \cdot 2H_2O$]

An aqueous (50 cm^3) mixture of $FeSO_4 \cdot 6H_2O$ (0.34 g, 1.0×10^{-3} mol) and L^2Me (0.50 g, 3.1×10^{-3} mol) was stirred with mild heating until all the solid had dissolved. Slow evaporation of the resultant red solution afforded a red polycrystalline solid which was dried in vacuo and analysed without further purification. Yield 0.46 g, 66%. Calc. for $C_{21}H_{25}FeN_{15}O_6S$: C, 37.6; H, 3.7; N, 31.3. Found: C, 37.7; H, 3.7; N, 31.6%. IR (nujol): 3098w, 1634br m, 1603m, 1552w, 1536m, 1511m, 1496m, 1345m, 1294m, 1278m, 1224s, 1193s, 1146s, 1020br vs, 943m, 914m, 858s, 766m, 760m, 739s, 722m, 698m, 690m, 642m, 608m, 597m, 512m cm^{-1}.

2.12. Single crystal X-ray structure determinations

Red needles of **IV** were grown from CH_2Cl_2/MeOH. For **2(ClO$_4$)$_2$ · H$_2$O**, a mixture of $Fe(ClO_4)_2 \cdot 6H_2O$ (0.38 g, 1.0×10^{-3} mol) and L^2Me (0.50 g, 3.1×10^{-3} mol) in H_2O (50 cm^3) was stirred with mild heating until all the solid had dissolved. The resultant dark red solution was filtered, and then allowed to evaporate slowly to yield clusters of small, dark red plates. Different crystals, cleaved from these clusters, were used for the two datasets of this compound. For **3 · 1.5CH$_3$CN**, a mixture of $FeCl_2 \cdot 4H_2O$ (0.21 g, 1.0×10^{-3} mol), L^2Me (0.50 g, 3.1×10^{-3} mol) and NH_4PF_6 (0.34 g, 2.1×10^{-3} mol) in MeCN (50 cm^3) was stirred at room temperature for 1 h, yielding a red solution with a small amount of white precipitate. The solution was filtered and concentrated to ca. 5 cm^3. Diffusion of Et_2O vapour into this solution initially afforded an orange oil, which slowly crystallised over several days to yield red single crystals of the product, mixed with **2(PF$_6$)$_2$** as a red powder.

Experimental details from the structure determinations are given in Table 1. Data for **IV**, **3 · 1.5CH$_3$CN** and **2(ClO$_4$)$_2$ · H$_2$O** at 150 K were collected on a Nonius KappaCCD area-detector diffractometer, using graphite-monochromated Mo Kα radiation. The data for **2(ClO$_4$)$_2$ · H$_2$O** at 296 K were obtained from a Bruker X8 Apex diffractometer, using graphite-monochromated Mo-K_α radiation generated by a rotating anode. All the structures were solved by direct methods (SHELXS-97 [21]) and refined by full-matrix least-squares on F^2 (SHELXL-97 [22]).

2.13. Single crystal X-ray structure of IV

No disorder was detected during refinement, and no restraints were applied. All non-H atoms were refined anisotropically, while all C-bound H atoms were placed in calculated positions and refined using a riding model. The two N-bound H atoms were located in the difference map and allowed to refine freely with a common isotropic thermal parameter. A Flack parameter of 4(4) was calculated from 940 Friedel pairs, meaning that the absolute configuration of the crystal could not be determined. Hence, all Friedel opposites in the data were merged for the final least-squares refinement cycles.

2.14. Single crystal X-ray structures of 2(ClO$_4$)$_2$ · H$_2$O

The asymmetric unit contains one complex dication, two ClO_4^- anions and one water molecule, all lying on a general position. At 150 K, one ClO_4^- ion was found to be disordered over three equally occupied orientations. At 296 K both ClO_4^- anions were disordered: one over two orientations with a 0.60:0.40 occupancy ratio; and the other over three orientations with occupancies of 0.50, 0.30 and 0.20. The three disorder orientations of the latter anion contained a common, wholly occupied Cl atom. At both temperatures, this disorder was modelled using the restraints Cl–O = 1.42(2) Å and O···O = 2.32(2) Å. At 150 K, the water molecule was crystallographically ordered and wholly occupied. In the 296 K crystal, however, two partial water environments were refined with occupancies of 0.50 and 0.20. At both temperatures, all wholly occupied non-H atoms were refined anisotropically, while all C-bound H atoms were placed in calculated positions and refined using a riding model. The H atoms attached to the water molecule(s) could not be located in the difference map and so were not included in the final model although they were included in the final density calculation.

2.15. Single crystal X-ray structure of 3 · 1.5CH$_3$CN

The asymmetric unit contains one complex dication, two PF_6^- anions and one MeCN molecule lying on general positions, and a second, half occupied MeCN site that is disordered across the crystallographic inversion centre $1-x, -y, 1-z$. One of the two PF_6^- anions is disordered over three equally occupied orientations. All disordered P–F bonds were restrained to 1.59(2) Å, *cis*-F···F distances to 2.25(2) Å and *trans*-F···F distances to 3.18(2) Å. The solvent molecule on a general position is also disordered over two equally occupied sites. All the solvent C–C bonds were restrained to 1.46(2) Å, C≡N bonds to 1.13(2) Å and 1,3-C···N distances to 2.59(2) Å. All wholly occupied non-H

Table 1
Experimental details for the single crystal structure determinations in this study

	IV	**$2(ClO_4)_2 \cdot H_2O$**		**$5 \cdot 1.5CH_3CN$**
Formula	$C_{10}H_8N_8$	$C_{21}H_{23}Cl_2FeN_{15}O_9$	$C_{21}H_{22.4}Cl_2FeN_{15}O_{8.7}$	$C_{31}H_{32.5}Cl_2F_{12}Fe_2N_{21.5}OP_2$
M_r	240.24	756.29	750.89	1194.82
Crystal size (mm)	$0.34 \times 0.09 \times 0.09$	$0.12 \times 0.07 \times 0.04$	$0.21 \times 0.16 \times 0.01$	$0.20 \times 0.13 \times 0.09$
Crystal class	orthorhombic	orthorhombic	orthorhombic	triclinic
Space group	$Pca2_1$	$Pbca$	$Pbca$	$P\bar{1}$
a (Å)	10.7073(4)	10.9543(2)	11.0809(11)	12.7800(2)
b (Å)	3.6015(1)	21.0815(3)	21.117(2)	13.4066(2)
c (Å)	26.0523(12)	26.9525(4)	27.030(2)	14.4853(2)
α (°)				92.6129(7)
β (°)				103.7550(7)
γ (°)				100.5058(9)
V (Å^3)	1004.64(7)	6223.8(2)	6324.9(10)	2359.97(6)
Z	4	8	8	2
μ (Mo Kα) (mm^{-1})	0.110	0.731	0.719	0.899
T (K)	150(2)	150(2)	296(2)	150(2)
Radiation λ (Å)	0.71073	0.71073	0.71073	0.71073
Absorption correction	multi-scan	multi-scan	multi-scan	multi-scan
Minimum and maximum transmission	0.96/0.99	0.92/0.97	0.86/0.99	0.84/0.92
Measured reflections	5890	45013	72710	53167
Independent reflections	1169	7128	3446	10774
R_{int}	0.073	0.106	0.070	0.098
Observed reflections [$I > 2\sigma(I)$]	893	4269	2777	7903
Range in 2θ (°)	$6.2 \leqslant 2\theta \leqslant 55.0$	$4.8 \leqslant 2\theta \leqslant 55.0$	$3.0 \leqslant 2\theta \leqslant 42.2$	$5.0 \leqslant 2\theta \leqslant 55.0$
Parameters/restraints	170/1	453/30	444/50	669/72
$R(F)$[a], $wR(F^2)$[b]	0.042, 0.110	0.059, 0.174	0.064, 0.183	0.059, 0.175
Goodness-of-fit	1.024	1.025	1.030	1.025
Weighting scheme[c]	$w = 1/[\sigma^2(F_0^2) + (0.0619P)^2 + (0.1269P)]$	$w = 1/[\sigma^2(F_0^2) + (0.0817P)^2 + (6.9711P)]$	$w = 1/[\sigma^2(F_0^2) + (0.0903P)^2 + (33.7120P)]$	$w = 1/[\sigma^2(F_0^2) + (0.0937P)^2 + (2.1496P)]$
$\Delta\rho$ (maximum/minimum) (e Å^{-3})	0.24/−0.24	0.89/−0.67	1.02/−0.69	0.78/−0.95

[a] $R = \sum[|F_o| - |F_c|]/\sum|F_o|$.
[b] $wR = [\sum wF_o^2 - F_c^2)/\sum wF_o^4]^{1/2}$.
[c] $P = (F_0^2 + 2F_c^2)/3$.

atoms were refined anisotropically, and all H atoms were placed in calculated positions and refined using a riding model, with the methyl group torsions allowed to refine freely.

2.16. Other measurements

Infra-red spectra were obtained as Nujol mulls pressed between KBr windows, between 400 and 4000 cm^{-1} using a Nicolet Avatar 360 spectrophotometer. UV/visible spectra were obtained with a Perkin–Elmer Lambda 900 spectrophotometer, operating between 1100 and 200 nm, in 1 cm quartz cells. EI mass spectra were performed on a VG AutoSpec spectrometer while electrospray mass spectra were obtained on a Micromass LCT TOF spectrometer, employing a MeOH matrix. CHN microanalyses were performed by the University of Leeds Department of Chemistry microanalytical service. NMR spectra were run on a Bruker ARX250 spectrometer, operating at 250.1 MHz (^1H) or (^{13}C). Magnetic susceptibility measurements were obtained using a Quantum Design SQUID magnetometer in an applied field of 1000 G. Diamagnetic corrections were estimated from Pascal's constants [23].

3. Results and discussion

The ligands L^2H and L^2Me have been synthesised previously by Nieuwenhuis et al. [12], by the method shown in Scheme 1. We obtained a higher yield of the amidrazone derivative **II**, compared to these workers, by using an excess of methylhydrazine reagent and a modified work-up procedure. However the method of Nieuwenhuis et al. using a stoichiometric amount of hydrazine was followed for **I** and **III**, since separation of these crude products from an excess of hydrazine reagent proved difficult. We also obtained higher yields for the second step of the synthesis [(ii) in Scheme 1] compared to the literature method, by carrying out the reactions at reflux and through a modified work-up. Our attempts to extend this methodology to the preparation of L^2Ph were unsuccessful, with **III** being recovered largely unchanged following step (ii). Nieuwenhuis et al. [12] have also reported the synthesis of L^3H, by treatment of **I** with acetic acid. Our own attempts to replicate that reaction at reflux or at room temperature yielded 1,4-dihydro-3,6-dipyrazinyl-1,2,4,5-tetrazine (**IV**) [20] as a major product, together with several other unidentified byproducts. The identity of **IV**was unambiguously confirmed from an X-ray crystal structure (Fig.1). However, the bulk sample of **IV** also showed the correct highest molecular ion by EI mass spectrometry ($m/z = 240$) and an identical ^1H NMR spectrum to that reported previously for this compound [20], thus confirming its identity. The formation of **IV** implies that acetic acid is a weaker electrophile than **I** under the reaction conditions, so that **I** prefers to nucleophilically attack another molecule of itself [24]. In the light of this result, the synthesis of L^3H and other L^3R ligands was not pursued further. Although they are not isostructural, the molecular structure of **IV** in the crystal closely resembles that of 1,4-dihydro-3,6-dipyridyl-1,2,4,5-tetrazine [25].

The red complexes $[Fe(L^2Me)_3](BF_4)_2$ [**2(BF$_4$)$_2$**] and $[Fe(L^2Me)_3](ClO_4)_2$ [**2(ClO$_4$)$_2$**] were readily obtained by direct complexation of the appropriate ligand and hydrated Fe(II) salt in MeCN or acetone, respectively. In addition, slow evaporation of a mixture of $Fe(ClO_4) \cdot 6H_2O$ or $FeSO_4 \cdot 6H_2O$ and 3 equiv. of L^2Me in water afforded the red polycrystalline hydrates $[Fe(L^2Me)_3](ClO_4)_2 \cdot H_2O$ [**2(ClO$_4$)$_2$ · H$_2$O**] and $[Fe(L^2Me)_3]SO_4 \cdot 2H_2O$ [**2(SO$_4$) · 2H$_2$O**]. The presence of water in these materials was confirmed from a characteristic H–O–H bending vibration near 1635 cm^{-1} in their IR spectra [26]. While **2(SO$_4$) · 2H$_2$O** retains its water content in vacuo, drying **2(ClO$_4$)$_2$ · H$_2$O** in vacuo over P_2O_5 afforded analytically pure anhydrous **2(ClO$_4$)$_2$**. Finally, $[Fe(L^2Me)_3](PF_6)_2$ [**2(PF$_6$)$_2$**] was synthesised by reaction of $FeCl_2 \cdot 4H_2O$, L^2Me and NH_4PF_6 in a 1:3:2 molar ratio in water. The resultant red polycrystalline precipitate

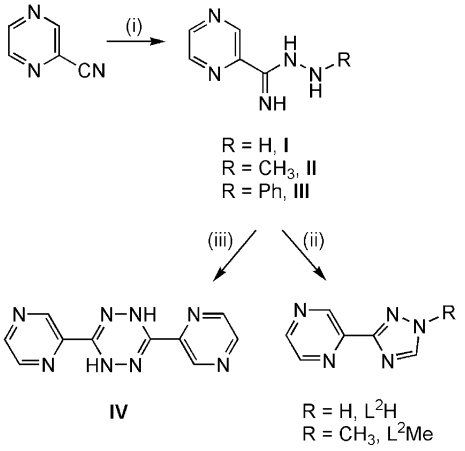

Scheme 1. Syntheses of the ligands used in this study. (i) 1 eq. (R = H) or 5 eq. (R = Me) H_2NNHR, EtOH, RT, 2 h. (ii) **I** or **II**, HCO_2H, 0 °C → reflux, 2 h. (iii) **I**, CH_3CO_2H, 0 °C → reflux, 2 h.

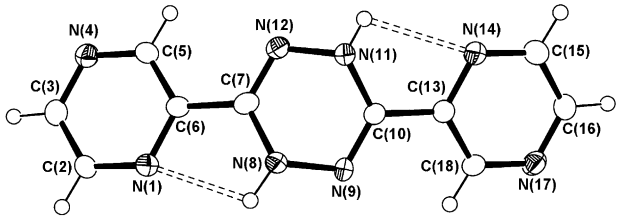

Fig. 1. View of the asymmetric unit in the single crystal structure of 1,4-dihydro-3,6-dipyrazinyl-1,2,4,5-tetrazine (**IV**). Thermal ellipsoids are at the 50% probability level and H atoms have arbitrary radii.

was recrystallised from MeCN/Et_2O to remove a white impurity, yielding an anhydrous product that contained no chloride by microanalysis (see below). Preparing salts of $[Fe(L^2H)_3]^{2+}$ proved more difficult. Solvent-free $[Fe(L^2H)_3](ClO_4)_2$ [**1(ClO$_4$)$_2$**] was obtained as a dark red-brown powder, upon reaction of $Fe(ClO_4) \cdot 6H_2O$ and 3 equiv. of L^2H in MeOH. Attempts to prepare this complex, or the BF_4^-, PF^{6-} and SO^{42-} salts of the same dication, in water or any other of the common organic solvents led only to intractable oils. Similarly, impure compounds were obtained following attempts to prepare the salts of $[Fe(L^2Me)_3]^{2+}$ by procedures different from those described above. This is discussed further below.

Complex **2(ClO$_4$)$_2$ · H$_2$O** crystallises from water as clusters of plates, from which small fragments could be cleaved for X-ray analysis. A full dataset to $2\theta = 55°$ from one such fragment was achieved at 150 K. Unfortunately, the crystals diffracted very weakly at higher temperatures. We were able to collect a complete dataset of **2(ClO$_4$)$_2$ · H$_2$O** to $2\theta = 42°$ at 296 K, using a different diffractometer fitted with a more intense, rotating anode X-ray source. Although the observed data:parameter ratio was low, this determination did show that the bond lengths and angles at Fe(1) are equal to within four standard uncertainties at the two temperatures (Table 2). Hence, only the 150 K crystal structure will be described in detail.

The $[Fe(L^2Me)_3]^{2+}$ dication in **2(ClO$_4$)$_2$.H$_2$O** has an octahedral geometry, that is slightly distorted by the bite angle of the chelating ligands (Table 2, Fig. 2). The triazole ring of the L^2Me ligand is coordinated through *N*4,

Table 2
Selected bond lengths (Å) and angles (°) in the single crystal X-ray structure of $[Fe(L^2Me)_3](ClO_4)_2 \cdot H_2O$[**2(ClO$_4$)$_2$ · H$_2$O**]

	150 K	296 K
Fe(1)–N(2)	1.971(3)	1.991(5)
Fe(1)–N(9)	1.968(3)	1.976(5)
Fe(1)–N(14)	1.977(3)	1.992(5)
Fe(1)–N(21)	1.963(3)	1.969(5)
Fe(1)–N(26)	1.987(3)	2.004(5)
Fe(1)–N(33)	1.972(3)	1.975(5)
N(2)–Fe(1)–N(9)	81.62(13)	81.2(2)
N(2)–Fe(1)–N(14)	95.04(13)	95.4(2)
N(2)–Fe(1)–N(21)	92.26(13)	92.5(2)
N(2)–Fe(1)–N(26)	172.24(13)	172.1(2)
N(2)–Fe(1)–N(33)	91.16(13)	91.3(2)
N(9)–Fe(1)–N(14)	171.68(13)	172.0(2)
N(9)–Fe(1)–N(21)	91.37(13)	92.1(2)
N(9)–Fe(1)–N(26)	97.06(13)	97.3(2)
N(9)–Fe(1)–N(33)	91.73(13)	91.3(2)
N(14)–Fe(1)–N(21)	81.12(13)	80.7(2)
N(14)–Fe(1)–N(26)	87.26(13)	87.0(2)
N(14)–Fe(1)–N(33)	95.96(13)	96.0(2)
N(21)–Fe(1)–N(26)	95.42(13)	95.3(2)
N(21)–Fe(1)–N(33)	175.69(13)	175.2(2)
N(26)–Fe(1)–N(33)	81.22(13)	81.0(2)

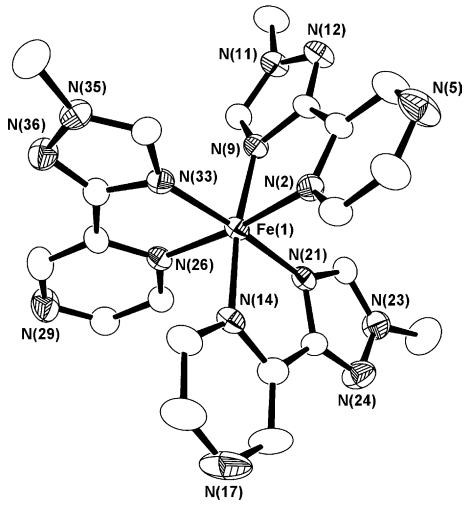

Fig. 2. View of the complex dication in the single crystal structure of $[Fe(L^2Me)_3](ClO_4)_2 \cdot H_2O$ [**2(ClO$_4$)$_2$ · H$_2$O**] at 150 K. All H atoms have been omitted for clarity. Thermal ellipsoids are at the 50% probability level. The structure of this compound at 296 K is visually indistinguishable from that shown here, and uses the same atom numbering scheme.

as is usual in iron complexes of triazole-containing chelates [17,18,27]. The complex crystallises as its *mer* isomer, which is the more commonly observed isomer for Fe(II) complexes of asymmetric heterocyclic chelates [11,17,18,28], including $[Fe(L^4H)_3](BF_4)_2 \cdot 2H_2O$ [17]. The Fe–N bond lengths clearly demonstrate that the complex is fully low spin at both 150 and 296 K (Table 2). While the H atoms of the lattice water molecule O(48) could not be located in the difference map, it is clear that the molecule is positioned to hydrogen bond to the disordered ClO_4^- anion Cl(43)–O(47) (not shown in Fig. 2), and to its symmetry equivalent Cl(43^i)–O(47^i) related by $0.5 + x$, y, $-0.5 + z$. This is evidenced by a range of O(48)···O distances between the water molecule and partial O atoms from these disordered anions, of 2.79–3.19 Å. The water molecule also accepts a C–H···O hydrogen bond from the pyrazine C–H group C(4)–H(4), with C(4)···O(48) = 3.375(5) Å, H(4)···O(48) = 2.44 Å and C(4)–H(4)···O(48) = 167.0°. Importantly, there is no hydrogen bonding to any of the non-coordinated pyrazine or triazole N atoms in the $[Fe(L^2Me)_3]^{2+}$ dication.

Variable temperature susceptibility measurements between 5 and 340 K were run on all of the complex salts prepared in this study. The sample of **2(ClO$_4$)$_2$** employed for these measurements was obtained from dried polycrystalline **2(ClO$_4$)$_2$ · H$_2$O**. All of the compounds except one (see below) undergo spin-state transitions, although these differ substantially in form (Fig. 3). Three different types of behaviour can be distinguished, which will be discussed in turn. The compounds **1(ClO$_4$)$_2$** and **2(ClO$_4$)$_2$** exhibit a very gradual and incomplete spin-state transition upon cooling, with a substantial residual

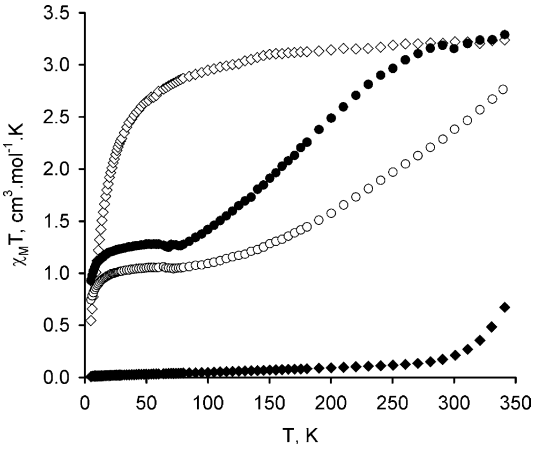

Fig. 3. Variable temperature susceptibility data from powdered **1(ClO$_4$)$_2$** (○), **2(ClO$_4$)$_2$** (●), **2(PF$_6$)$_2$** (♦) and **2(SO$_4$)·2H$_2$O** (◇). The behaviour of **2(BF$_4$)$_2$**, not shown in the figure, is very similar to that of **2(PF$_6$)$_2$**.

high-spin fraction below the transition temperature range (Table 3). A small additional decrease in $\chi_M T$ below 50 K for these compounds reflects zero-field splitting of the residual high-spin $S = 2$ manifold (Fig. 3). $\chi_M T$ for **2(ClO$_4$)$_2$** at 340 K is 3.29 cm^3 mol^{-1} K, showing that it is fully high-spin at this temperature [23]. However, **1(ClO$_4$)$_2$** shows $\chi_M T \approx 2.76$ cm^3 mol^{-1} K at 340 K, implying that this compound is in a mixture of spin-states. If $\chi_M T$ for fully high-spin **1(ClO$_4$)$_2$** is also 3.3 cm^3 mol^{-1} K, then $T_{1/2} \approx 277$ K and ca. 68% of the iron sites in this material undergo spin-crossover.

In contrast to these data, **2(BF$_4$)$_2$** (not shown in Fig. 3) is essentially diamagnetic at low temperatures, but exhibits an increase in $\chi_M T$ upon warming above ca. 200 K to reach 0.85 cm^3 mol^{-1} K at 340 K. The behaviour of **2(PF$_6$)$_2$** is similar, with $\chi_M T$ increasing from 0.09 cm^3 mol^{-1} K at 200 K to 0.68 at 340 K (Fig. 3). These data indicate that both compounds undergo a complete, high-temperature spin-state transition. The midpoint $T_{1/2}$ for both compounds is near 400 K if the $\chi_M T$ versus T curves below 340 K are extrapolated, and if $\chi_M T$ for their fully high-spin states is 3.3 cm^3 mol^{-1} K.

Finally, $\chi_M T$ for **2(SO$_4$)·2H$_2$O** is near-constant at 3.20 ± 0.05 cm^3 mol^{-1} K upon cooling to ca. 200 K, before decreasing in a smooth curve to 0.54 cm^3 mol^{-1} K at 5 K without reaching a plateau (Fig. 3). This curve can be modelled reasonably using the Curie–Weiss law for a $S = 2$ paramagnet with $g = 2.14$ and $\theta = -16.8$ K. The low-temperature decrease in $\chi_M T$ is unlikely to arise from zero-field splitting of the high-spin iron(II) spins, because the zero-field splitting constant $|D|$ obtained by fitting these data [23] is 41.7 cm^{-1}. That is an extremely high value for high-spin Fe(II) with six N-donor ligands; by comparison, $|D|$ calculated for the high-spin fractions of **1(ClO$_4$)$_2$** and **2(ClO$_4$)$_2$** below 80 K ranges from 7.8 to 8.7 cm^{-1}. Rather, the low-temperature decrease in $\chi_M T$ may be caused by a spin-state transition with $T_{1/2} = 15$ K and 83% completeness at 5 K. Or, it could reflect weak ($|J| = 1$–2 cm^{-1}) antiferromagnetic coupling between high-spin iron(II) centres in the solid. In the absence of any structural or Mössbauer spectroscopic data on **2(SO$_4$)·2H$_2$O**, it is impossible to distinguish between these two possibilities.

The ^{1}H NMR spectra of **1(ClO$_4$)$_2$** and **2(ClO$_4$)$_2$** in CD_3CN or $\{CD_3\}_2CO$ at 293 K are strongly contact-shifted, demonstrating that they are predominantly high-spin in these solvents. The spectra of **1(ClO$_4$)$_2$** both show three contact-shifted peaks, while those of **2(ClO$_4$)$_2$** show four peaks. In both cases, this is one fewer than the number of unique C-bound H environments in the relevant L^{2}R (R = H or Me) ligands. It is most likely the pyrazine *H* 6 environment that is not detected in these spectra owing to dipolar broadening, since this H atom will be the closest in space to the high-spin Fe(II) centre [29]. Importantly, the spectra of **1(ClO$_4$)$_2$** and **2(ClO$_4$)$_2$** in both solvents show the same number of peaks with chemical shifts that vary by up to 7 ppm between solvents. This suggests that there are only small differences between the chemical and/or magnetic structures of these compounds in different solvents. Importantly, however, electrospray mass spectra of all the complexes in this study showed substantial exchange of Na for the Fe content of the samples, to the extent that no Fe-containing molecular ions were detected under the conditions used. This shows that these complexes are in fact labile in solution, as we have previously noted for [Fe(L^1)$_3$]$^{2+}$ [11].

Some insight into our difficulties preparing other salts of [Fe(L^{2}H)$_3$]$^{2+}$ (see above) was provided by the crystallisation of [{FeCl(L^{2}Me)$_2$}$_2$(μ-O)](PF$_6$)$_2$·1.5CH$_3$CN

Table 3
Summary of the magnetic data for the spin-state transitions shown by the compounds in this study

	$\chi_M T$ (340 K) (cm^3 mol^{-1} K)	$\chi_M T$ (70 K) (cm^3 mol^{-1} K)	$T_{1/2}$ (K)	Completeness (%)
1(ClO$_4$)$_2$	2.76	1.05	≈277	≈68
2(BF$_4$)$_2$	0.85	0.03	≈385	≈100
2(ClO$_4$)$_2$	3.29	1.27	182	61
2(PF$_6$)$_2$	0.68	0.04	≈400	≈100
2(SO$_4$)·2H$_2$O[a]	3.25	2.81	15	83 [at 5 K]

$T_{1/2}$ corresponds to the temperature at which $\chi_M T = [3.3 + \chi_M T(70\text{ K})]/2$.
[a] It is uncertain whether this compound actually undergoes a spin-state transition. See text for more details.

Table 4
Selected bond lengths (Å) and angles (°) in the single crystal X-ray structure of $[\{FeCl(L^2Me)_2\}_2(\mu\text{-}O)](PF_6)_2 \cdot 1.5CH_3CN$ [**5 · 1.5CH$_3$CN**]

Fe(1)–O(3)	1.773(2)	Fe(2)–O(3)	1.772(2)
Fe(1)–Cl(4)	2.2664(10)	Fe(2)–Cl(29)	2.2848(9)
Fe(1)–N(5)	2.322(3)	Fe(2)–N(30)	2.326(3)
Fe(1)–N(12)	2.118(3)	Fe(2)–N(37)	2.109(3)
Fe(1)–N(17)	2.308(3)	Fe(2)–N(42)	2.317(3)
Fe(1)–N(24)	2.135(3)	Fe(2)–N(49)	2.116(3)
O(3)–Fe(1)–Cl(4)	101.78(8)	O(3)–Fe(2)–Cl(29)	102.38(8)
O(3)–Fe(1)–N(17)	87.78(10)	O(3)–Fe(2)–N(30)	170.34(10)
O(3)–Fe(1)–N(12)	97.66(11)	O(3)–Fe(2)–N(37)	98.19(10)
O(3)–Fe(1)–N(17)	87.78(10)	O(3)–Fe(2)–N(42)	88.18(10)
O(3)–Fe(1)–N(24)	99.20(11)	O(3)–Fe(2)–N(49)	98.48(11)
Cl(4)–Fe(1)–N(5)	86.40(7)	Cl(29)–Fe(2)–N(30)	85.08(7)
Cl(4)–Fe(1)–N(12)	100.18(9)	Cl(29)–Fe(2)–N(37)	102.51(8)
Cl(4)–Fe(1)–N(17)	166.06(8)	Cl(29)–Fe(2)–N(42)	164.74(7)
Cl(4)–Fe(1)–N(24)	94.58(9)	Cl(29)–Fe(2)–N(49)	93.23(8)
N(5)–Fe(1)– N(12)	73.60(11)	N(30)–Fe(2)–N(37)	73.97(10)
N(5)–Fe(1)– N(17)	85.52(10)	N(30)–Fe(2)– N(42)	85.75(9)
N(5)–Fe(1)– N(24)	87.15(11)	N(30)–Fe(2)–N(49)	87.09(10)
N(12)–Fe(1)–N(17)	88.40(11)	N(37)–Fe(2)–N(42)	86.60(10)
N(12)–Fe(1)–N(24)	154.78(11)	N(37)–Fe(2)–N(49)	153.99(11)
N(17)–Fe(1)–N(24)	73.70(11)	N(42)–Fe(2)–N(49)	74.13(10)
		Fe(1)–O(3)–Fe(2)	177.20(15)

(**3 · 1.5CH$_3$CN**) from a reaction of $FeCl_2 \cdot 4H_2O$, 3 equiv. L^2Me and 2 equiv. NH_4PF_6 in MeCN. The theoretical C, H and N microanalyses of **3** and **2(PF$_6$)$_2$** are indistinguishable within experimental error. However, from the Cl analysis of the bulk material of $1.6 \pm 0.2\%$, the products of this reaction appeared to be a mixture of these two compounds in approximately a 1:3 **3**:**2(PF$_6$)$_2$** ratio. Compound **3** is a product of the aerobic autooxidation of the Fe(II) content of the reaction mixture to Fe(III), a common feature of the iron chemistry of N-donor ligands. The molecular structure of **3** resembles those of $[\{FeCl(L)_2\}_2(\mu\text{-}O)]^{2+}$ (L = bipy, 4,4′-Me$_2$ bipy or phen) [30], bearing two *cis*-$[FeCl(L^2Me)_2]^{2+}$ moieties linked by a near-linear oxo bridge (Table 4, Fig. 4). The two octahedral Fe centres adopt a near-staggered conformation, with the torsion Cl(4)–Fe(1)···Fe(2)–Cl(29) being 87.38(5)°. This facilitates an intramolecular π–π interaction between the ligands N(17)–C(28) and N(42)–C(53) which lie 3.617(16) Å apart, with a dihedral angle of 8.60(11)° between their least squares planes. There are two apparent intramolecular C–H···Cl hydrogen bonds between the triazole C–H groups C(13)–H(13) and C(38)–H(38), and the Cl ligands bound to the opposite Fe atom (Fig. 4). This is suggested by the distances H(13)···Cl(29) = 2.86 Å and H(38)···Cl(4) = 2.81 Å, which are substantially shorter than the 3.0 Å sum of the van der Waals radii of a H and a Cl atom [31], and the angles C(13)–H(13)···Cl(29) = 152.5 and C(38)–H(38)···Cl(4) = 152.7°. These C–H···Cl contacts are also most likely to be responsible for the displacement of Fe(1) and Fe(2) out of their equatorial planes of ClN_3 ligand donors towards O(3), by 0.2688(13) [Fe(1)] and 0.2795(12) Å [Fe(2)]. The other bond lengths and angles in **3** are unexceptional.

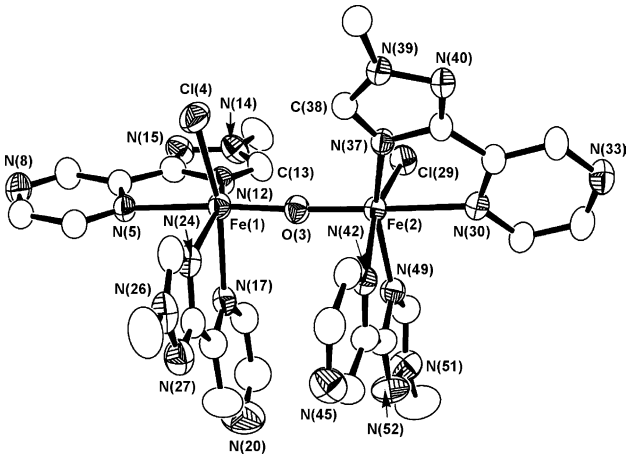

Fig. 4. View of the complex dication in the single crystal structure of $[\{FeCl(L^2Me)_2\}_2(\mu\text{-}O)](PF_6)_2 \cdot 1.5CH_3CN$ [**5 · 1.5CH$_3$CN**]. All H atoms have been omitted for clarity. Thermal ellipsoids are at the 50% probability level.

4. Concluding remarks

The only structural information we were able to gain from a $[Fe(L^2R)_3]^{2+}$ complex was from **2(ClO$_4$)$_2$ · H$_2$O**. The low-spin nature of this hydrate at 296 K is inconsistent with the spin-state transition shown by anhydrous **2(ClO$_4$)$_2$** upon cooling, but does resemble **2(BF$_4$)$_2$** and **2(PF$_6$)$_2$** which are predominantly low-spin at room temperature. With that in mind, it is a little surprising that **2(ClO$_4$)$_2$** does not show the same type of complete high-temperature spin-state transition as these other two compounds, given that the ClO_4^- counterion has the same near-spherical shape as BF_4^- and PF_6^-, and lies between them in size [32]. Notwithstanding this anomaly, the very different spin-state regimes shown by several of the complexes in this study demonstrate that spin-crossover in this system is dependent on the local environment of the $[Fe(L^2R)_3]^{2+}$ centres in their solids. While the presence (or absence) of lattice water is clearly important, in **2(ClO$_4$)$_2$ · H$_2$O** at least this influence does not arise from hydrogen bonding to the complex dications. Rather, the dominant factor controlling the different spin-state regimes in this system is probably the local steric environment about the complex dications in each material. Unfortunately more detailed explanations for the anomalous spin-state transition of **2(ClO$_4$)$_2$**, and whether or not **2(SO$_4$) · 2H$_2$O** actually undergoes spin-crossover at very low temperatures, are unclear in the absence of structural and/or Mössbauer spectroscopic data on these compounds.

The magnetochemistry of **1(ClO$_4$)$_2$** and **2(ClO$_4$)$_2$** strongly resembles that of many hydrated or anhydrous salts of $[Fe(L^4R)_3]^{2+}$ (R = H, Me) in showing a gradual, incomplete spin-state transition upon cooling with a large residual high-spin fraction [15–18]. In the one case where this transition been fully characterised, namely $[Fe(L^4H)_3](BF_4)_2 \cdot 2H_2O$, the incompleteness of the spin-state transition was attributed to anion/water site disorder in the crystal, which results in different molecules in the sample having different local environments [17,18]. Since we do not have structural data on **1(ClO$_4$)$_2$** and anhydrous **2(ClO$_4$)$_2$**, it is unclear whether anion disorder is also the origin of their incomplete spin-crossover. There are two other potential explanations for the incomplete spin-state transitions in this study, however. First, it might be that a fraction of the $[Fe(L^2R)_3]^{2+}$ sites in **1(ClO$_4$)$_2$** and **2(ClO$_4$)$_2$** contain triazole centres coordinated through *N*2 rather than *N*4. This coordination mode is unusual for mononuclear complexes of 3-pyridyl-1,2,4-triazole-type chelates, and is apparently unknown for compounds of this type containing first row transition ions [17,18,29] (the only crystallographically characterised examples have the formula $[Ru(bipy)_2(L)]^{2+}$ {L = L^4H or a 5-substituted derivative of it} [14,33]). However, linkage isomerism of the triazole donors in bulk samples of $[Fe(L^2R)_3]^{2+}$ and $[Fe(L^4R)_3]^{2+}$ cannot be ruled out. Alternatively, is that the six-coordinate Fe(II) centres in **1(ClO$_4$)$_2$** and **2(ClO$_4$)$_2$** exist as a mixture of *fac*- and *mer*-stereoisomers. That is certainly possible; for example, both *fac*- and *mer*-isomers of $[Fe(L^1)_3]^{2+}$ have been crystallised using different counterions [11]. This explanation would require that the *mer*-complex centres give rise to the residual high-spin iron fraction at low temperatures, as precedent suggests that *fac*-isomers of $[FeL_3]^{2+}$ (L = a bis-N-donor chelate) tend to favour low-spin configurations more than their corresponding *mer*-isomers [34].

5. Supplementary data

Full crystallographic data for the structure analyses in this study are available on request from the Cambridge Crystallographic Data Centre, 12 Union Road, Cambridge CB2 1EZ, UK. The CCDC deposition numbers are 236851 [**3 · 1.5CH$_3$CN**], 236852 [**IV**], 236853 [**2(ClO$_4$)$_2$ · H$_2$O** at 150 K] and 236854 [**2(ClO$_4$)$_2$ · H$_2$O** at 296 K].

Acknowledgements

The authors thank Dr. H.J. Blythe (University of Sheffield, UK) for the susceptibility data, and the EPSRC and the University of Leeds for funding.

References

[1] P. Gütlich, A. Hauser, H. Spiering, Angew. Chem. Int. Ed. 33 (1994) 2024.
[2] P. Gütlich, Y. Garcia, H.A. Goodwin, Chem. Soc. Rev. 29 (2000) 419.
[3] J.A. Real, A.B. Gaspar, V. Niel, M.C. Muñoz, Coord. Chem. Rev. 236 (2003) 121.
[4] O. Kahn, C.J. Martinez, Science 279 (1998) 44.
[5] (a) J. Kröber, E. Codjovi, O. Kahn, F. Grolière, C. Jay, J. Am. Chem. Soc. 115 (1993) 9810;
(b) J. Kröber, J.-P. Audière, E. Codjovi, O. Kahn, J.G. Haasnoot, F. Grolière, C. Jay, A. Bousseksou, J. Linarès, F. Varret, A. Gonthier-Vassal, Chem. Mater. 6 (1994) 1404;
(c) Y. Garcia, P.J. van Koningsbruggen, R. Lapouyade, L. Fournès, L. Rabardel, O. Kahn, V. Ksenofontov, G. Levchenko, P. Gütlich, Chem. Mater. 10 (1998) 2426;
(d) O. Roubeau, J.M. Alcazar Gomez, E. Balskus, J.J.A. Kolnaar, J.G. Haasnoot, J. Reedijk, New J. Chem. 25 (2001) 144.
[6] (a) W. Fujita, K. Agawa, Science 286 (1999) 261;
(b) G.D. McManus, J.M. Rawson, N. Feeder, J. van Duijn, E.J.L. McInnes, J.J. Novoa, R. Burriel, F. Palacio, P. Oliete, J. Mater. Chem. 11 (2001) 1992.
[7] (a) J.M. Holland, J.A. McAllister, Z. Lu, C.A. Kilner, M. Thornton-Pett, M.A. Halcrow, Chem. Commun. (2001) 577;
(b) J.M. Holland, J.A. McAllister, C.A. Kilner, M. Thornton-Pett, A.J. Bridgeman, M.A. Halcrow, J. Chem. Soc., Dalton Trans. (2002) 548;
(c) V.A. Money, I. Radosavljevic Evans, M.A. Halcrow, A.E. Goeta, J.A.K. Howard, Chem. Commun. (2003) 158;
(d) V.A. Money, J. Sánchez Costa, S. Marcén, G. Chastanet, J. Elhaúk, M.A. Halcrow, J.A.K. Howard, J.-F. Létard, Chem. Phys. Lett. 391 (2004) 273.
[8] J.M. Holland, C.A. Kilner, M.A. Halcrow, Inorg. Chem. Commun. 5 (2002) 328.
[9] V.A. Money, J. Elhaúk, M.A. Halcrow, J.A.K. Howard, Dalton Trans. (2004) 1516.
[10] (a) J. Elhaïk, V.A. Money, S.A. Barrett, C.A. Kilner, I. Radosavljevic Evans, M.A. Halcrow, Dalton Trans. (2003) 2053;
(b) V.A. Money, J. Elhaïk, I. Radosavljevic Evans, M.A. Halcrow, J.A.K. Howard, Dalton Trans. (2004) 65;
(c) V.A. Money, I. Radosavljevic Evans, J. Elhaïk, M.A. Halcrow, J.A.K. Howard, Acta Crystallogr., Sect. B 60 (2004) 41.
[11] R.J. Smithson, C.A. Kilner, A.R. Brough, M.A. Halcrow, Polyhedron 22 (2003) 725.
[12] H.A. Nieuwenhuis, J.G. Hasnoot, R. Hage, J. Reedijk, T.L. Snoeck, D.J. Stufkens, J.G. Vos, Inorg. Chem. 30 (1991) 48.
[13] (a) T.E. Keyes, C.M. O'Connor, U. O'Dwyer, C.G. Coates, P. Callaghan, J.J. McGarvey, J.G. Vos, J. Phys. Chem. A 103 (1999) 8915;
(b) S. Fanni, C. Di Pietro, S. Serroni, S. Campagna, J.G. Vos, Inorg. Chem. Commun. 3 (2000) 42;
(c) C. Di Pietro, S. Serroni, S. Campagna, M.T. Gandolfi, R. Ballardini, S. Fanni, W.R. Browne, J.G. Vos, Inorg. Chem. 41 (2002) 2871.
[14] W.R. Browne, D. Hesek, J.F. Gallagher, C.M. O'Connor, J.S. Killeen, F. Aoki, H. Ishida, Y. Inoue, C. Villani, J.G. Vos, Dalton Trans. (2003) 2597.
[15] (a) P. Stupik, J.H. Zhang, M. Kwiecen, W.M. Reiff, J.G. Haasnoot, R. Hage, J. Reedijk, Hyperfine Interact. 28 (1986) 725;
(b) P. Stupik, W.M. Reiff, R. Hage, J. Jacobs, J.G. Haasnoot, J. Reedijk, Hyperfine Interact. 40 (1988) 343.
[16] K.H. Sugiyarto, D.C. Craig, A.D. Rae, H.A. Goodwin, Aust. J. Chem. 48 (1995) 35.
[17] A.F. Stassen, M. de Vos, P.J. van Koningsbruggen, F. Renz, J. Ensling, H. Kooijman, A.L. Spek, J.G. Haasnoot, P. Gütlich, J. Reedijk, Eur. J. Inorg. Chem. (2000) 2231.

[18] O. Roubeau, M. de Vos, A.F. Stassen, R. Burriel, J.G. Haasnoot, J. Reedijk, J. Phys. Chem. Solids 64 (2003) 1003.
[19] V.I. Minkin, A.D. Garnovskii, J. Elguero, A.R. Katritzky, O.V. Denisko, Adv. Heterocycl. Chem. 76 (2000) 157.
[20] B. Sarkar, W. Kaim, T. Schleid, I. Hartenbach, J. Fiedler, Z. Anorg. Allg. Chem. 629 (2003) 1353.
[21] G.M. Sheldrick, Acta Crystallogr., Sect. A 46 (1990) 467.
[22] G.M. Sheldrick, SHELXL-97, Program for the refinement of crystal structures, University of Göttingen, 1997.
[23] C.J. O'Connor, Prog. Inorg. Chem. 29 (1982) 203.
[24] J.F. Geldard, F. Lions, J. Org. Chem. 30 (1965) 318.
[25] (a) M.R. Caira, R.G.F. Giles, L.R. Nassimbeni, G.M. Sheldrick, R.G. Hazell, Acta Crystallogr., Sect. B 32 (1976) 1467;
(b) L.-S. Liou, P.-S. Chen, C.-H. Sun, J.-C. Wang, Acta Crystallogr., Sect. C 52 (1996) 1841.
[26] K. Nakamoto, Infrared and Raman Spectra of Inorganic and Coordination Compounds, Part B, fifth ed., Wiley–Interscience, New York, 1997 p. 54.
[27] (a) See e.g . R. Hage, R. Prins, R.A.G. de Graaff, J.G. Haasnoot, J. Reedijk, J.G. Vos, Acta Crystallogr., Sect. C 44 (1988) 56;
(b) R.J. Forster, A. Boyle, J.G. Vos, R. Hage, A.H.J. Dijkhuis, R.A.G. de Graaff, J.G. Haasnoot, R. Prins, J. Reedijk, J. Chem. Soc., Dalton Trans. (1990) 121;
(c) J.H. van Diemen, J.G. Haasnoot, R. Hage, J. Reedijk, J.G. Vos, R. Wang, Inorg. Chem. 30 (1991) 4038;
(d) K.H. Sugiyarto, D.C. Craig, A.D. Raue, H.A. Goodwin, Aust. J. Chem. 46 (1993) 1269;
(e) K.H. Sugiyarto, D.C. Craig, H.A. Goodwin, Aust. J. Chem. 49 (1996) 497;
(f) B.J. Childs, D.C. Craig, M.L. Scudder, H.A. Goodwin, Aust. J. Chem. 51 (1998) 895;
(g) E. Szłyk, I. Łakomska, J. Kobe, A. Surdykowski, T. Głowiak, J. Sitkowski, Polyhedron 21 (2002) 2001.
[28] (a) See e.g. A. Katz, C.E. Strouse, J. Am. Chem. Soc. 101 (1979) 6214;
(b) L. Wiehl, G. Kiel, C.P. Köhler, H. Spiering, P. Gütlich, Inorg. Chem. 25 (1986) 1565;
(c) M.J. Blandamer, J. Burgess, D.L. Elvidge, P. Guardado, A.W. Hakin, L.J.S. Prouse, S. Radulovic, J.R. Russell, Transition Met. Chem. 16 (1991) 82;
(d) L.S. Harimanow, K.H. Sugiyarto, D.C. Craig, M.L. Scudder, H.A. Goodwin, Aust. J. Chem. 52 (1999) 109;
(e) D. Onggo, M.L. Scudder, D.C. Craig, H.A. Goodwin, Aust. J. Chem. 53 (2000) 153.
[29] I. Bertini, C. Luchinat, Coord. Chem. Rev. 150 (1996) 77.
[30] (a) P.C. Healy, B.W. Skelton, A.H. White, Aust. J. Chem. 36 (1983) 2057;
(b) S.R. Choudhury, J.A. Traquair, J.J. Vittal, Z. Kristallogr. 212 (1997) 44;
(c) D.F. Xiang, X.S. Tan, S.W. Zhang, Y. Han, K.B. Yu, W.X. Tang, Polyhedron 17 (1998) 2095;
(d) M.-N. Collomb, A. Deronzier, K. Gorgy, J.-C. Leprêtre, J. Pecaut, New J. Chem. 23 (1999) 785.
[31] L. Pauling, The Nature of the Chemical Bond, third ed., Cornell University Press, Ithaca, NY, 1960 pp. 257–264.
[32] D.M.P. Mingos, A.L. Rohl, J. Chem. Soc., Dalton Trans. (1991) 3419.
[33] (a) See e.g. R. Hage, J.P. Turkenburg, R.A.G. de Graaff, J.G. Haasnoot, J. Reedijk, J.G. Vos, Acta Crystallogr., Sect. C 45 (1989) 381;
(b) B.E. Buchanan, J.G. Vos, M. Kaneko, W.J.M. van der Putten, J.M. Kelly, R. Hage, R.A.G. de Graaff, R. Prins J.G. Haasnoot, J. Reedijk, J. Chem. Soc., Dalton Trans. (1990) 2425;
(c) P. Passaniti, W.R. Browne, F.C. Lynch, D. Hughes, M. Nieuwenhuyzen, P. James, M. Maestri, J.G. Vos, J. Chem. Soc., Dalton Trans. (2002) 1740;
(d) W.R. Browne, C.M. O'Connor, H.P. Hughes, R. Hage, O. Walter, M. Doering, J.F. Gallagher, J.G. Vos, J. Chem. Soc., Dalton Trans. (2002) 4048;
(e) B. Mehmetaj, J.G. Haasnoot, L. De Cola, G.A. van Albada, I. Mutikainen, U. Turpeinen, J. Reedijk, Eur. J. Inorg. Chem. (2002) 1765;
(f) W.R. Browne, D. Hesek, J.F. Gallagher, C.M. O'Connor, J.S. Killeen, F. Aoki, H. Ishida, Y. Inoue, C. Villani, J.G. Vos, Dalton Trans. (2003) 2597.
[34] (a) A.M. Greenaway, E. Sinn, J. Am. Chem. Soc. 100 (1978) 8080;
(b) B.A. Katz, C.E. Strouse, Inorg. Chem. 19 (1980) 658.

Available online at www.sciencedirect.com
SCIENCE DIRECT®
Polyhedron 23 (2004) 2153–2159
POLYHEDRON
www.elsevier.com/locate/poly

Hydrothermal synthesis and structure of a molybdenum(VI) phosphate cluster and a three dimensional cobalt molybdenum(V) phosphate

Xin He [a], Ping Zhang [a,*], Tian-You Song [a], Zhong-Cheng Mu [b], Jie-Hui Yu [a], Yue Wang [b], Jia-Ning Xu [a,*]

[a] *Department of Chemistry, Jilin University, Changchun 130012, PR China*
[b] *Key Laboratory for Supramolecular Structure and Materials of the Ministry of Education, Jilin University, Changchun 130012, PR China*

Received 12 March 2004; accepted 1 June 2004
Available online 30 July 2004

Abstract

Two new molybdenum phosphates, $[Co(en)_3][C_4H_{12}N_2]_{0.5}[(Mo_5O_{15})(HOPO_3)_2]\cdot 3H_2O$ (**1**) (en = ethylenediamine) and $(C_4N_2H_{10})_5[Co_3Mo_{12}O_{18}(HOPO_3)_6(PO_4)_2(OH)_{12}(H_2O)_4]\cdot 9H_2O$ (**2**), have been synthesized hydrothermally. **1** is constructed from $[Mo_5P_2O_{21}(OH)_2]^{4-}$ clusters, $Co(en)_3^{3+}$ and piperazine, which are linked together through hydrogen-bonding interactions. The enantiomers of $Co(en)_3^{3+}$ in **1** are separated as Δ and Λ configurations. **2** is composed of centrosymmetric $Co[Mo_6O_9(OH)_6(HOPO_3)_3(PO_4)]_2$ clusters linked by dinuclear cobalt cations forming a three dimensional structure. The interconnected voids and channels in **2** are filled with piperazine and water molecules. The three dimensional **2** was obtained from the zero dimensional **1** under hydrothermal reaction conditions. This experiment demonstrates that molybdenum phosphates of low dimensional structure could be employed as starting materials to prepare molybdenum phosphates of high dimensional structure.
© 2004 Elsevier Ltd. All rights reserved.

Keywords: Transformation; Molybdenum phosphate; Hydrothermal synthesis; Crystal structure

1. Introduction

The cooperative assembly of organic and inorganic components has given rise to a wide variety of new materials [1]. Among the organic–inorganic hybrid materials reported, molybdenum phosphates have become good candidates owing to their attractive characters ranging from potential applications such as catalysis and medicine [2,3] to the diversity of their structures [4–10]. The investigation of incorporating d-block elements into molybdenum phosphates [4,8–25] as stoichiometric framework constituents has resulted in metal molybdenum phosphates with remarkable structural diversities [8–10] when compared with the well-characterized building units $[P_4Mo_6O_{25}(OH)_3]^{9-}$ [11–21] and $[P_2Mo_5O_{23}]^{6-}$ [22–25]. Recently, chiral transitional metal complexes have been often used as template agents in the synthesis of phosphates since the first example was reported by Morgan et al. [26]. Some studies have demonstrated that the chirality of these complexes could be transferred to the inorganic networks through the formation of "chiral pockets" [27–30]. In 2001, Rao et al. showed that low dimensional zinc phosphates could transform into complex open-framework structures under appropriate reaction conditions [31–33]. In our experiments, $Co(en)_3Cl_3$, MoO_3, piperazine and H_3PO_4 were selected as starting materials to prepare a molybdenum phosphate $[Co(en)_3(C_4H_{12}N_2)_{0.5}(Mo_5O_{15})(HOPO_3)_2]\cdot 3H_2O$ (en = ethylenediamine) (**1**), which has a

* Corresponding authors.
E-mail address: zhangping@mail.jlu.edu.cn (P. Zhang).

0277-5387/$ - see front matter © 2004 Elsevier Ltd. All rights reserved.
doi:10.1016/j.poly.2004.06.010

zero dimensional structure constructed from monomers of $[Mo_5P_2O_{21}(OH)_2]^{4-}$ clusters, $Co(en)_3^{3+}$ and piperazine. Then **1** was disposed in the mother liquor and heated at a higher temperature. Another product, $(C_4N_2H_{10})_5[Co_3Mo_{12}O_{18}(HOPO_3)_6(PO_4)_2(OH)_{12}(H_2O)_4]\cdot 9H_2O$ (**2**), with a three dimensional framework was obtained.

2. Experimental

2.1. Synthesis

1 was synthesized through the hydrothermal reaction of $Co(en)_3Cl_3$, MoO_3, H_3PO_4, $C_4N_2H_{10}$ and H_2O in a molar ratio of 1.0:2.4:6.0:3.0:288.0. Typically, 0.8 g $Co(en)_3Cl_3$, 0.8 g MoO_3 and 0.6 g piperazine were dissolved in 12 ml of water, 1 ml H_3PO_4 (85 wt%) was added dropwise with stirring. After stirring for 1h, the mixture was transferred into a Teflon-lined stainless steel autoclave and heated at 413 K for 4 days under autogenous pressure. Orange rod-like crystals as a single phase (90% based on Mo) were then filtered, washed with distilled water and dried at room temperature. *Anal*. Calc. for $C_8H_{38}CoMo_5N_7O_{26}P_2$: C, 7.69; H, 3.04; N, 7.85. Found: C, 7.83; H, 2.97; N, 7.94%. The simulation of single-crystal X-ray diffraction data accords with the experimental X-ray powder diffraction data well.

2 was prepared by heating **1** (0.5 g), which was dried at room temperature for 2 days, in 10 ml of the mother liquor of **1** at 443K for 2 days. Dark red crystals were obtained as a single phase in good yield (80% based on Mo). *Anal*. Calc. for $C_{20}H_{94}Co_3Mo_{12}N_{10}O_{75}P_8$: C, 7.38; H, 2.89; N, 4.31. Found: C, 7.47; H, 2.78; N, 4.44%.

2.2. Measurements and materials

X-ray powder diffraction (XRD) data were collected on a Shimadazu XRD-6000 diffractometer with Cu Kα radiation ($\lambda = 1.5418$ Å).

Elemental analyses (C, H and N) were performed on a Perkin–Elmer 2400 CHN Elemental Analyzer.

A Perkin–Elmer TGA 7 unit was used to carry out the thermogravimetric analysis (TGA) in air with a heating rate of 20 °C/min.

IR spectra were recorded in the range 400–4000 cm^{-1} on a Nicolet 5PC FT-IR spectrophotometer using KBr pellets.

2.3. X-ray crystallography

The X-ray single-crystal structure analyses of **1** and **2** were performed on a Rigaku R-AXIS RAPID diffractometer (Mo Kα radiation, $\lambda = 0.71073$ Å, graphite monochromator) in the Ψ rotation scan mode. The structure determinations were done with direct methods by using SHELXL 5.01v and refinements with full-matrix least squares on F^2. The structures were solved by direct methods and refined on F^2 by full-matrix least squares using SHELXTL-97 [34]. No adsorption correction was applied. H atoms were placed geometrically and refined using a riding model. All non-hydrogen atoms were refined anisotropically. Experimental details for the structure determinations are presented in Table 1.

Table 1
Crystal data and structure refinement for **1** and **2**

Compound	**1**	**2**
Empirical formula	$C_8H_{38}CoMo_5N_7O_{26}P_2$	$C_{20}H_{94}Co_3Mo_{12}N_{10}O_{75}P_8$
Formula weight	1249.02	3251.08
Temperature (K)	193(2)	293(2)
Wavelength (Å)	0.71073	0.71073
Crystal system	monoclinic	triclinic
Space group	$P2_1/n$ (No. 11)	$P\bar{1}$ (No. 2)
a (Å)	13.0081(4)	12.7846(11)
b (Å)	19.9798(4)	12.8311(11)
c (Å)	13.3511(6)	15.9937(17)
α (°)	90	67.358(4)
β (°)	110.336(2)	67.224(5)
γ (°)	90	63.053(2)
Volume (Å^3)	3253.66(19)	2085.1(3)
Z	4	1
μ (mm^{-1})	2.573	2.599
Reflections collected/unique [R_{int}]	21642/7134 [0.0269]	8468/6423 [0.0392]
Reflections with $I > 2\sigma(I)$	5688	6423
Final R indices [$I > 2\sigma(I)$]	$R_1 = 0.0202$, $wR_2 = 0.0518$	$R_1 = 0.0351$, $wR_2 = 0.0746$
R indices (all data)	$R_1 = 0.0312$, $wR_2 = 0.0751$	$R_1 = 0.0505$, $wR_2 = 0.0775$

3. Results and discussions

3.1. Structure of $[Co(en)_3][C_4H_{12}N_2]_{0.5}[(Mo_5O_{15})(HOPO_3)_2]\cdot 3H_2O$ (1)

In **1**, the inorganic cluster, $[(Mo_5O_{15})(HOPO_3)_2]^{4-}$ (Fig. 1), is quite similar to that reported by Burkholder and Zubieta [22] and Hedman [35]. Selected bond distances of **1** are summarized in Table 2. The structure of **1** consists of $[Co(en)_3]^{3+}$, $[(Mo_5O_{15})(HOPO_3)_2]^{4-}$ clusters, piperazine and water molecules, which construct the framework though hydrogen-bonding (Fig. 2). The structure of $[(Mo_5O_{15})(HOPO_3)_2]^{4-}$ can be considered as a ring formed by five distorted edge- and corner-sharing MoO_6 octahedra capped on both poles by a phosphate tetrahedron sharing three vertices with the ring molybdenum centers. Based on the bond parameter results from bond valence sum calculations [36], all the Mo atoms have a +6 oxidation state, which agrees with the expected value of 6.00 for Mo atoms in the $[(Mo_5O_{15})(HOPO_3)_2]^{4-}$ building block. Bond lengths of MoO_6 and PO_4 are all within the expected range.

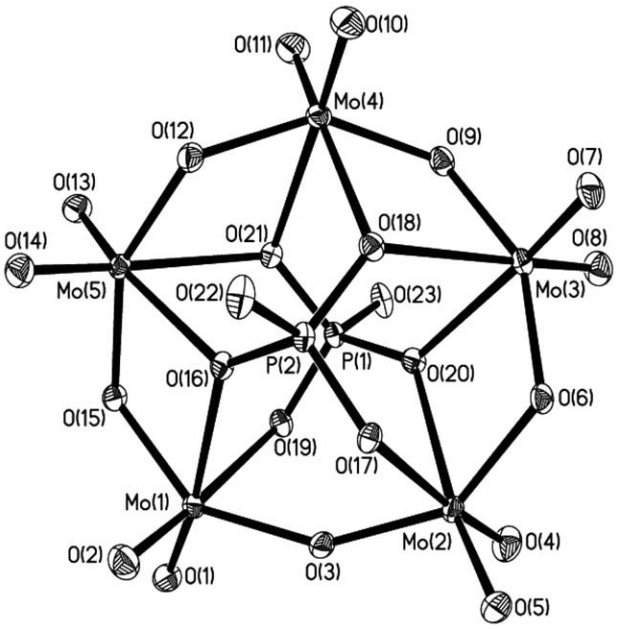

Fig. 1. The structure of $[(Mo_5O_{15})(HOPO_3)_2]^{4-}$ anionic cluster showing the atom-labelling scheme and the 50% probability displacement ellipsoids. H atoms have been omitted for clarity.

Table 2
Selected bond lengths (Å) for **1**

Mo(1)–O(2)	1.708(3)	Mo(1)–O(1)	1.713(2)
Mo(1)–O(3)	1.905(2)	Mo(1)–O(15)	1.925(2)
Mo(1)–O(16)	2.344(2)	Mo(1)–O(19)	2.358(2)
Mo(2)–O(3)	1.898(2)	Mo(2)–O(6)	1.921(2)
Mo(2)–O(4)	1.704(3)	Mo(2)–O(5)	1.717(3)
Mo(2)–O(17)	2.318(2)	Mo(2)–O(20)	2.363(2)
Mo(3)–O(8)	1.701(3)	Mo(3)–O(7)	1.722(2)
Mo(3)–O(9)	1.898(2)	Mo(3)–O(6)	1.940(2)
Mo(3)–O(20)	2.206(2)	Mo(3)–O(18)	2.403(3)
Mo(4)–O(10)	1.696(3)	Mo(4)–O(11)	1.712(3)
Mo(4)–O(12)	1.902(3)	Mo(4)–O(9)	1.927(3)
Mo(4)–O(18)	2.289(2)	Mo(4)–O(21)	2.384(2)
Mo(5)–O(14)	1.706(3)	Mo(5)–O(13)	1.712(2)
Mo(5)–O(12)	1.918(2)	Mo(5)–O(15)	1.929(2)
Mo(5)–O(16)	2.231(2)	Mo(5)–O(21)	2.371(2)
P(1)–O(19)	1.521(3)	P(1)–O(21)	1.526(3)
P(1)–O(20)	1.544(2)	P(1)–O(23)	1.568(3)
P(2)–O(17)	1.521(2)	P(2)–O(18)	1.533(3)
P(2)–O(16)	1.536(2)	P(2)–O(22)	1.563(3)

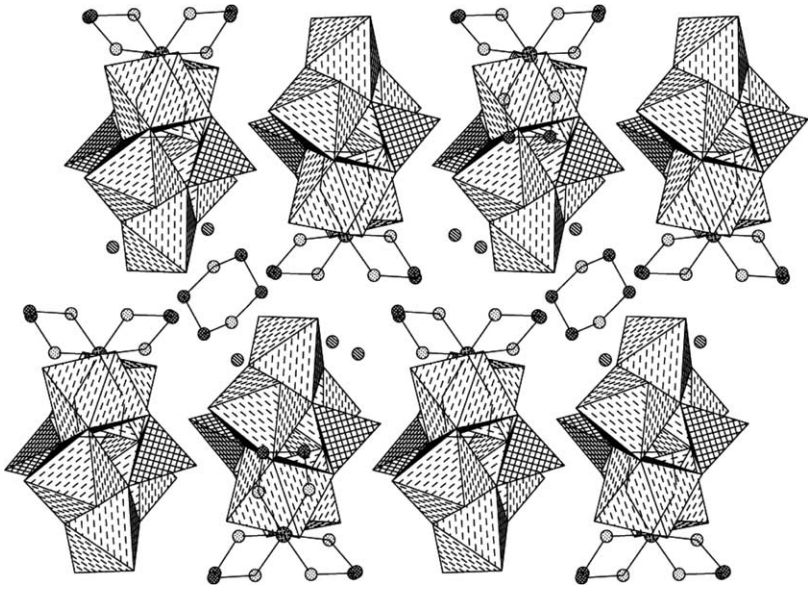

Fig. 2. Polyhedral representation of $[(Mo_5O_{15})(HOPO_3)_2]^{4-}$ anion and ball-and-stick representation of the $[Co(en)_3]^{3+}$ cations and piperazines along the *a*-axis. Water molecules and H atoms have been omitted for clarity.

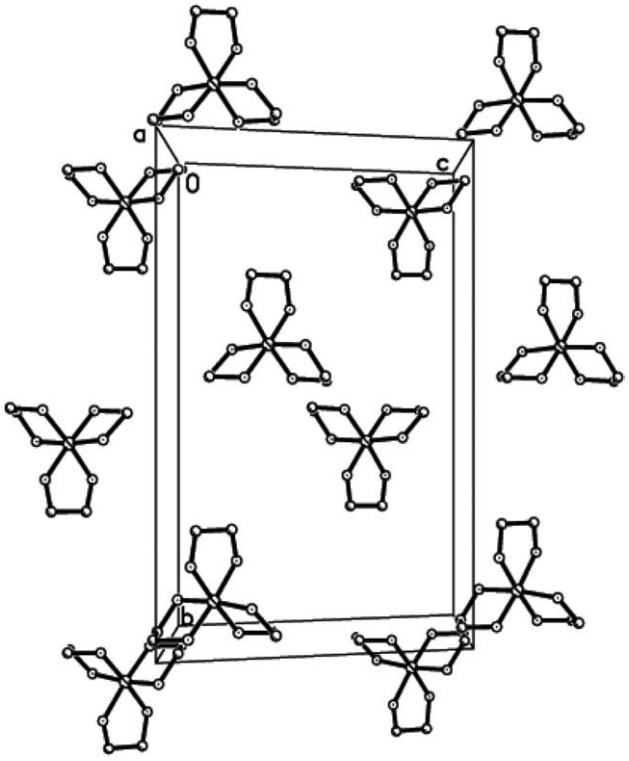

Fig. 3. Δ and Λ configurations of $[Co(en)_3]^{3+}$ pairs in alternative regions in the structure of **1**.

The metal complexes $[Co(en)_3]^{3+}$ in **1** separate the inorganic clusters of $[(Mo_5O_{15})(HOPO_3)_2]^{4-}$. Interestingly, the enantiomers of the cobalt complexes are separated as Δ and Λ configurations and appear as pairs of enantiomers (Fig. 3). Similar results have been reported by other authors when $[Co(en)_3]^{3+}$ is used as a template in the synthesis of phosphates [26,27].

The framework of **1** is stabilized by extensive intermolecular multi-point hydrogen bonding involving inorganic clusters, $Co(en)_3^{3+}$, piperazine and water molecules. Hydrogen-bonding occurs between the P–OH groups with μ_2-O(17) and μ_2-O(19) in adjacent $[(Mo_5O_{15})(HOPO_3)_2]^{4-}$ clusters. As a result, the inorganic clusters form a chain-like structure (Fig. 4). Each amino group in $[Co(en)_3]^{3+}$ and the piperazine form extensive hydrogen bonds with oxygen atoms in the $[(Mo_5O_{15})(HOPO_3)_2]^{4-}$ luster and water molecules with N···O separation distances ranging from 2.726 to 3.320 Å. Water molecules also form hydrogen bonds with three terminal oxygen atoms O(2), O(4) and O(7) in the inorganic clusters.

3.2. Structure of $(C_4N_2H_{10})_5[Co_3Mo_{12}O_{18}(HOPO_3)_6(PO_4)_2(OH)_{12}(H_2O)_4]\cdot 9H_2O$ (**2**)

In **2,** the building block (Fig. 5) of the crystal consists of two $Co(1)_{0.5}[Mo_6O_9(OH)_6(HOPO_3)_3(PO_4)]$ (Co-$[Mo_6P_4]$) units and dinuclear Co cations in an octahedral environment. The geometry of the Co(1)-$[Mo_6O_9(OH)_6(HOPO_3)_3(PO_4)]_2$(Co$[Mo_6P_4]_2$) unit (Fig. 6) is very similar to that observed in several sodium, iron or zinc molybdenum phosphates [14–21]. Six MoO_6 in Co$[Mo_6P_4]$ units form a hexagonal ring by sharing edges, and the four phosphate tetrahedra are corner-sharing with the corresponding molybdenum octahedron. Among the four phosphate groups, three around the periphery of the ring bridge the three non-bonded Mo···Mo dimers and the one in the center bridges the three non-bonded Mo atoms from the ''inside'' of the Mo_6 ring. Bond valence sum calculations [36] indicate that all the molybdenum atoms are pentavalent, the cobalt atoms are bivalent, the phosphate atoms are pentavalent, O(1), O(3), O(4), O(13), O(23), O(26), O(28), O(29) and O(30) are oxygen atoms of OH groups, and O(8) and O(24) are oxygen atoms of water molecules. The oxidation state of all other oxygen atoms is −2. In **2,** there are three Mo–Mo bonding contacts and the Mo–Mo bond distances are 2.5898(6), 2.5914(6) and 2.5943(6) Å for Mo(1)–Mo(5), Mo(2)–Mo(3) and Mo(4)–Mo(6), respectively (Table 3).

In the structure of **2**, each Co$[Mo_6P_4]_2$ unit is coordinated to six dinuclear Co cation via six oxygen atoms of six peripheral phosphate groups, and each dinuclear Co cations in turn contacts six phosphate groups from six different Co$[Mo_6P_4]_2$ units (Figs. 6 and 7). The resulting three dimensional anionic framework delimits channels running along the [1 0 0] axes. The structure is similar to two molybdenum phosphates $(TMA)_2(NH_4)_2[Fe_2$-

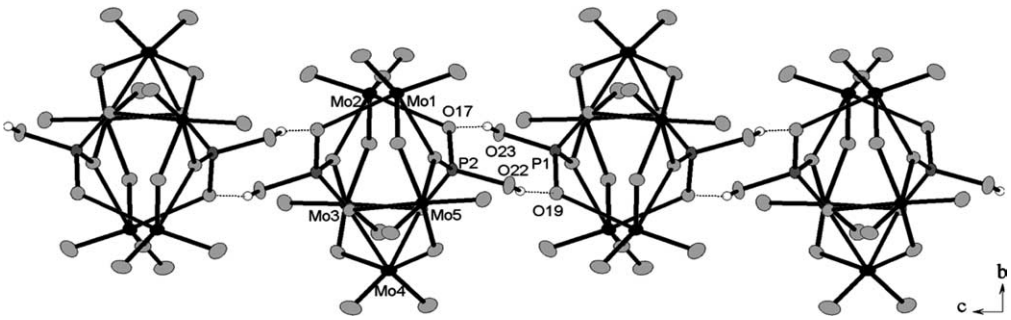

Fig. 4. View of connection of $[(Mo_5O_{15})(HOPO_3)_2]^{4-}$ clusters forming a chain-like structure by hydrogen bonds interactions shown by dotted lines.

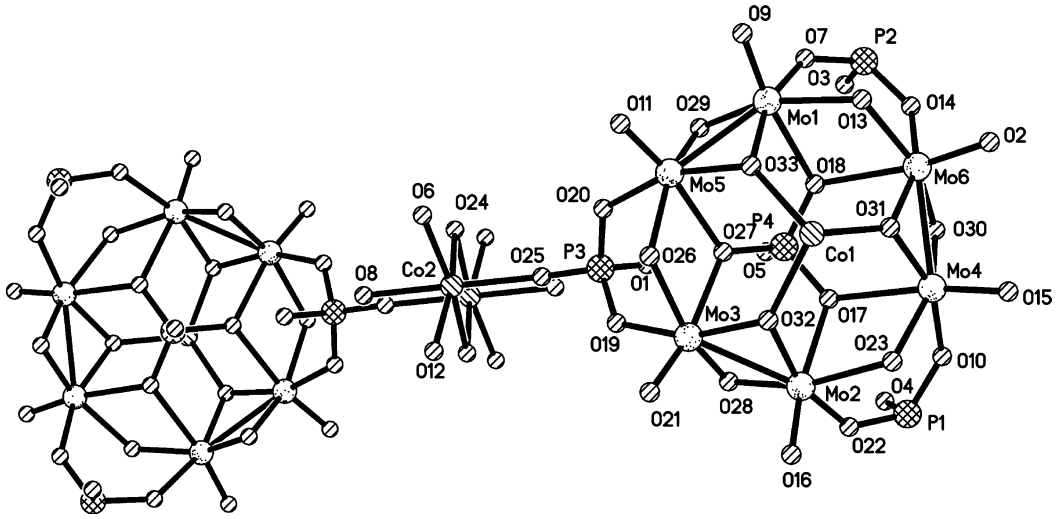

Fig. 5. Perspective view of a representative fragment of **2** showing the atom numbering scheme and the 50% probability displacement ellipsoids. H atoms have been omitted for clarity.

$Mo_{12}O_{30}(H_2PO_4)_6(HPO_4)_2]\cdot nH_2O$ [14] and $Na_{12}Co_3$-$[(PO_4)_4Mo_6O_{12}(OH)_3]_2\cdot 44H_2O$ [11]. A noteworthy feature in the structure of **2** is the presence of the dinuclear Co cations, while in other molybdenum phosphates [11–15,17,19–21] containing $[Mo_6P_4]$ building units, the three dimensional frameworks are formed through coordination of the inorganic groups with transition metal cations in the mononuclear form. The structure of **2** is stabilized by multipoint hydrogen bonds among $[(Mo_5O_{15})(HOPO_3)_2]^{4-}$ clusters, piperazine and lattice water molecules.

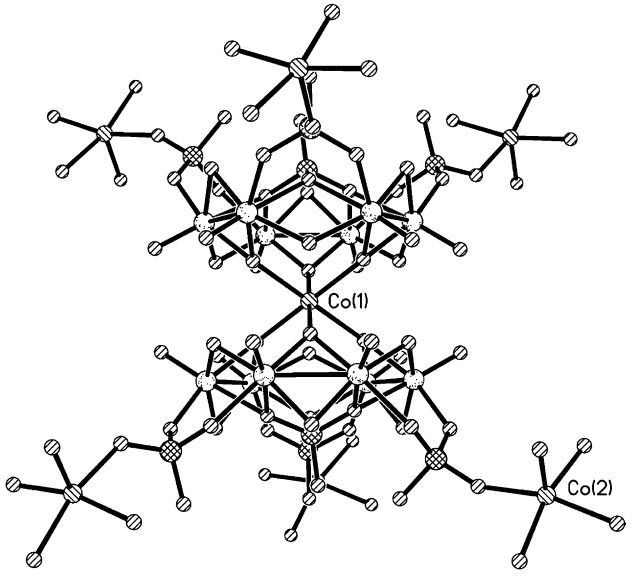

Fig. 6. Perspective view of the $Co[Mo_6P_4]_2$ building unit.

Table 3
Select bond lengths (Å) for **2**

Mo(1)–O(9)	1.673(3)	Mo(1)–O(29)	1.942(3)
Mo(1)–O(33)	1.986(3)	Mo(1)–O(7)	2.047(3)
Mo(1)–O(13)	2.081(3)	Mo(1)–O(18)	2.293(3)
Mo(1)–Mo(5)	2.5898(6)	Mo(2)–O(16)	1.678(3)
Mo(2)–O(28)	1.951(3)	Mo(2)–O(32)	1.984(3)
Mo(2)–O(22)	2.052(3)	Mo(2)–O(23)	2.072(3)
Mo(2)–O(17)	2.314(3)	Mo(2)–Mo(3)	2.5914(6)
Mo(3)–O(21)	1.672(3)	Mo(3)–O(28)	1.939(3)
Mo(3)–O(32)	1.976(3)	Mo(3)–O(19)	2.081(3)
Mo(3)–O(26)	2.108(3)	Mo(3)–O(27)	2.239(3)
Mo(4)–O(15)	1.676(3)	Mo(4)–O(30)	1.945(3)
Mo(4)–O(31)	1.982(3)	Mo(4)–O(10)	2.047(3)
Mo(4)–O(23)	2.097(3)	Mo(4)–O(17)	2.308(3)
Mo(4)–Mo(6)	2.5943(6)	Mo(5)–O(11)	1.668(3)
Mo(5)–O(29)	1.950(3)	Mo(5)–O(33)	1.983(3)
Mo(5)–O(20)	2.077(3)	Mo(5)–O(26)	2.117(3)
Mo(5)–O(27)	2.235(3)	Mo(6)–O(2)	1.671(3)
Mo(6)–O(30)	1.950(3)	Mo(6)–O(31)	1.983(3)
Mo(6)–O(14)	2.040(3)	Mo(6)–O(13)	2.095(3)
Mo(6)–O(18)	2.295(3)	Co(1)–O(31)	2.121(3)
Co(1)–O(31)#1	2.121(3)	Co(1)–O(33)#1	2.147(3)
Co(1)–O(33)	2.147(3)	Co(1)–O(32)	2.168(3)
Co(1)–O(32)#1	2.168(3)	Co(2)–O(6)	2.034(3)
Co(2)–O(25)	2.044(4)	Co(2)–O(12)	2.052(3)
Co(2)–O(8)	2.151(4)	Co(2)–O(24)#2	2.198(3)
Co(2)–O(24)	2.206(3)	P(1)–O(6)#3	1.509(3)
P(1)–O(4)	1.531(4)	P(1)–O(10)	1.546(3)
P(1)–O(22)	1.551(4)	P(2)–O(12)#4	1.519(3)
P(2)–O(3)	1.520(4)	P(2)–O(14)	1.551(3)
P(2)–O(7)	1.558(4)	P(3)–O(25)	1.490(4)
P(3)–O(20)	1.534(3)	P(3)–O(19)	1.536(3)
P(3)–O(1)	1.579(4)	P(4)–O(5)	1.495(3)
P(4)–O(18)	1.547(3)	P(4)–O(17)	1.554(3)
P(4)–O(27)	1.563(3)	O(6)–P(1)#5	1.509(3)
O(12)–P(2)#6	1.519(3)	O(24)–Co(2)#2	2.198(3)

Symmetry transformations used to generate equivalent atoms: #1 $-x+1,-y+2,-z$; #2 $-x,-y+1,-z+1$; #3 $x,y+1,z$; #4 $x+1,y,z$; #5 $x,y-1,z$; #6 $x-1,y,z$.

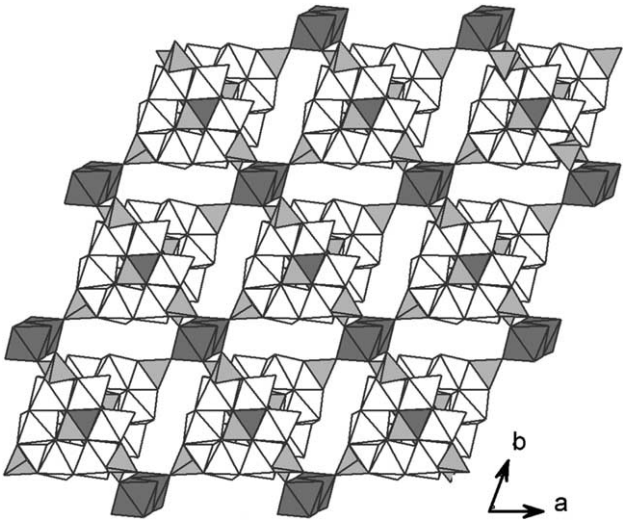

Fig. 7. Polyhedral view of the 3D network parallel to the *c*-axis in **2** showing that each $Co[Mo_6P_4]_2$ unit is coordinated to six dinuclear Co cations via six oxygen atoms of six peripheral phosphate groups, and each dinuclear Co cation in turn contacts six phosphate groups from six different $Co[Mo_6P_4]_2$ units. All C, H, N atoms and water guests are omitted for clarity.

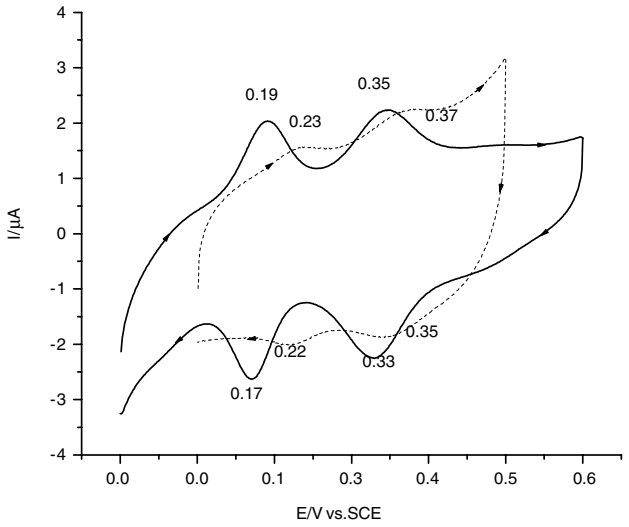

Fig. 8. Cyclic voltammograms (100 mV/s) in hydrochloric acid solution of **1** (solid line) and **2** (dashed line). Peak potentials vs. SCE are indicated.

3.3. TGA-DSC thermal analysis and IR spectra

TG analysis of **1** shows that a weight loss of about 4.0 wt% occurs below 200°C, which is attributed to the loss of water molecules in **1** (calc. 4.3 wt%). A weight loss of 20.5 wt% occurring in the temperature range 250–650 °C is attributed to the decomposition of the metal complexes and organic amines (calc. 19.4 wt%). X-ray powder diffraction analysis indicates that the crystal structure collapses upon decomposition of the metal complexes and organic amines.

TG analysis of **2** shows a weight loss of about 5.0 wt% occurring below 250 °C, which is attributed to the loss of water molecules in **2** (calc. 4.98 wt%). A weight loss of 14.0 wt% occurring in the temperature range 250–650 °C is attributed to the decomposition of the organic amines (calc. 13.35 wt%).

The IR spectrum of **1** contains characteristic bands at 927 cm^{-1} attributed to the Mo═O group, in the region of 688–407 cm^{-1} attributed to the bridging Mo–O–Mo group, in the region of 1000–1200 cm^{-1} associated to the P–O bond and in the region 1530–1340 cm^{-1} assigned to the C–C and C–N stretching vibrations of the organic amines.

The IR spectrum of **2** exhibits an absorption at 952 cm^{-1}, characteristic of ν(Mo═O), and bands at 738 and 1010 cm^{-1} which are attributed to ν(Mo–O–M) and ν(P–O), respectively. A series of bands in the 1455–1314 cm^{-1} region are assigned to the C–C and C–N stretching vibrations of the organic amines.

3.4. Electrochemistry

Complexes **1** and **2** were sampled from hydrochloric acid solution. As shown in Fig. 7, in the potential range from 0 to 700 mV, **1** exhibits two couples of reversible redox peaks at 180 and 340 mV, while **2** has two couples of quasi-reversible redox peaks at 230 and 360 mV. The peak current of **1** is thus much larger than that of **2**; this indicates that the redox ability of **1** is stronger than that of **2**. The potential separations of two couples of peaks of **1** are 20 mV, so according to the formula $\Delta ep = Ep_a - Ep_c = 57–63/n$, the two couples of peaks correspond to three-electron redox processes (see Fig. 8).

4. Conclusion

We have reported the synthesis, crystal structures, TGA-DSC thermal analysis and IR spectra of two new molybdenum phosphates **1** and **2**. It was demonstrated that the three dimensional **2** was synthesized from the zero dimensional **1** by a hydrothermal reaction. Though the mechanism of the transformation is not yet clear, the reaction temperature plays a key role for the product. Our experimental results show that novel architectures can be achieved by using a simple molybdenum phosphate cluster as a starting material.

Acknowledgement

This work was financially supported by the National Natural Science Foundation of China (50225313, 50073008).

Appendix A. Supplementary materials

Crystallographic data for **1** and **2** have been deposited with the Cambridge Crystallographic Data Centre, CCDC Nos. 211838, 220649, respectively. Copies of this data can be obtained free of charge on application to CCDC, 12 Union Road, Cambridge CB2 1EZ, UK (fax: (44) 1223-336-033; e-mail: deposit@ccdc.cam.ac.uk or www: http://www.ccdc.cam.ac.uk). Supplementary data associated with this article can be found, in the online version at doi:10.1016/j.poly.2004.06.010.

References

[1] P.J. Hagrman, D. Hagrman, J. Zubieta, Angew. Chem. Int. Ed. 38 (1999) 2638.
[2] N. Mizuno, M. Misono, Chem. Rev. 98 (1998) 199.
[3] J.T. Rhule, C.L. Hill, D.A. Judd, R.F. Schinazi, Chem. Rev. 98 (1998) 327.
[4] R.C. Haushalter, L.A. Mundi, Chem. Mater. 4 (1992) 31.
[5] N. Guillou, G. Ferey, M.S. Whittingham, J. Mater. Chem. 8 (10) (1998) 2277.
[6] D. Hagrman, P.J. Zapf, J. Zubieta, Chem. Commun. (1998) 1283.
[7] C.D. Wu, C.Z. Lu, H.H. Zhuang, J.S. Huang, J. Am. Chem. Soc. 124 (2002) 3836.
[8] C.D. Peloux, A. Dolbecq, P. Mialane, J. Marrot, E. Riviere, F. Secheresse, Angew. Chem. Int. Ed. 40 (2001) 2455.
[9] J.J. Lu, Y. Xu, N.K. Goh, L.S. Chia, Chem. Commun. (1998) 1709.
[10] C.M. Liu, D.Q. Zhang, M. Xiong, D.B. Zhu, Chem. Commun. (2002) 1416.
[11] C.D. Peloux, P. Mialane, A. Dolbecq, J. Marrot, E. Riviere, F. Secheresse, J. Mater. Chem. 11 (2001) 3392.
[12] Y.S. Zhou, L.J. Zhang, H.R. Fun, J.L. Zuo, I.A. Razak, S. Chantrapromma, X.Z. You, New J. Chem. 25 (2001) 1342.
[13] Y.S. Zhou, L.J. Zhang, X.Z. You, S. Natarajan, J. Solid State Chem. 159 (2001) 209.
[14] L.A. Mundi, R.C. Haushalter, Inorg. Chem. 32 (1993) 1579.
[15] L.A. Mundi, R.C. Haushalter, Inorg. Chem. 31 (1992) 3050.
[16] Y. Xu, B. Zhang, N.K. Goh, L.S. Chia, Inorg. Chim. Acta. 282 (1998) 10.
[17] A. Guesdon, M.M. Borel, A. Leclaire, B. Raveau, Chem. Eur. J. 3 (1997) 1797.
[18] A. Leclaire, C. Biot, H. Rebbah, M.M. Borel, B. Raveau, J. Mater. Chem. 8 (2) (1998) 439.
[19] L. Xu, Y.Q. Sun, E.B. Wang, E.H. Shen, Z.G. Liu, C.W. Hu, Y. Xing, Y.H. Lin, H.Q. Jia, New J. Chem. 23 (1999) 1041.
[20] M. Yuan, E.B. Wang, Y. Lu, Y.G. Li, C.W. Hu, N.H. Hu, H.Q. Jia, J. Solid. State. Chem. 170 (2003) 192.
[21] M. Yuan, E.B. Wang, Y. Lu, Y.G. Li, C.W. Hu, N.H. Hu, H.Q. Jia, Inorg. Chem. Commun. 5 (2002) 505.
[22] E. Burkholder, J. Zubieta, Chem. Commun. (2001) 2056.
[23] R.C. Finn, E. Burkholder, J. Zubieta, Chem. Commun. (2001) 1852.
[24] J.J. Lu, Y. Xu, N.K. Goh, L.S. Chia, Chem. Commun. (1998) 2733.
[25] J.B. Weng, M.C. Hong, Y.C. Liang, Q. Shi, R. Cao, J. Chem. Soc., Dalton. Trans. 3 (2002) 289.
[26] K. Morgan, G. Gainsford, N. Milestone, J. Chem. Soc., Chem. Commun. (1995) 425.
[27] J.H. Yu, Y. Wang, Z. Shi, R.R. Xu, Chem. Mater. 13 (2001) 2972.
[28] M.J. Gray, J.D. Jasper, A.P. Wilkinson, J.C. Hanson, Chem. Mater. 9 (1997) 976.
[29] S.M. Stalder, A.P. Wilkinson, Chem. Mater. 9 (1997) 2168.
[30] D.A. Bruce, A.P. Wilkinson, M.G. White, J.A. Bertrand, J. Solid. State. Chem. 125 (1996) 228.
[31] C.N.R. Rao, S. Natarajan, A. Choudhury, S. Neeraj, A.A. Ayi, Acc. Chem. Res. 34 (2001) 80.
[32] A.A. Ayi, A. Choudhury, S. Natarajan, S. Neeraj, C.N.R. Rao, J. Mater. Chem. 11 (2001) 1181.
[33] A. Choudhury, S. Neeraj, S. Natarajan, C.N.R. Rao, J. Mater. Chem. 11 (2001) 1537.
[34] G.M. Sheldrick, SHELXL-97: A Program for Crystal Structure Determination, University of Gottingen, Germany, 1997.
[35] B. Hedman, Acta Chem. Scand. 27 (1973) 3335.
[36] I.D. Brown, Acta Cryst. B 41 (1985) 244.

Available online at www.sciencedirect.com
SCIENCE DIRECT®
Polyhedron 23 (2004) 2161–2167
POLYHEDRON
www.elsevier.com/locate/poly

Hydrothermal synthesis of two new lead-containing coordination polymers: $^{2}_{\infty}[PbCl_2(4,4'\text{-bipy})]$ and $^{2}_{\infty}[Pb_2(NO_3)_4(H_2O)_2(4,4'\text{-bipy})_2](4,4'\text{-bipy})_2$

Karen J. Nordell [a,*], Kristin N. Schultz [a], Khadine A. Higgins [a], Mark D. Smith [b]

[a] Department of Chemistry, Lawrence University, Appleton, WI 54912, USA
[b] Department of Chemistry and Biochemistry, University of South Carolina, Columbia, SC 29208, USA

Received 18 March 2004; accepted 9 June 2004
Available online 29 July 2004

Abstract

Hydrothermal reaction of $Pb(II)X_2$ ($X = Cl^-$, NO_3^-) and 4,4′-bipyridine in a molar ratio of 1:1 resulted in the formation of two new Pb(II) coordination polymers, $^{2}_{\infty}[PbCl_2(4,4'\text{-bipy})]$, (**1**), and $^{2}_{\infty}[Pb_2(NO_3)_4(H_2O)_2(4,4'\text{-bipy})_2](4,4'\text{-bipy})_2$, (**2**). Compound **1** crystallizes in the triclinic crystal system ($P\bar{1}$), and the stereochemically active lone pair generates a distorted structure different from the similar bromide analogue reported previously, where the Pb^{2+} lone pair is apparently not "active". Compound **2** crystallizes in the monoclinic crystal system ($P2_1/c$), with an unusual layered structure consisting of flat slabs of $\{Pb(NO_3)_{4/2}Pb(H_2O)_2(NO_3)_2\}$ bilayers linked into a 3D network via hydrogen bonds involving undulating layers of two independent uncoordinated 4,4′-bipyridine molecules.
© 2004 Elsevier Ltd. All rights reserved.

Keywords: Lead; Coordination polymer; Hydrothermal synthesis; X-ray structure determination

1. Introduction

Crystal engineering, the domain of organic chemists for more than 30 years, has been refined and extended in recent years by inorganic and materials chemists to synthesize a new class of organic–inorganic hybrid materials called coordination polymers [1]. These materials represent a new and expanding research area that weds the fields of coordination chemistry, polymer synthesis and solid state chemistry by the linking of metal ions, complexes or clusters via organic ligands to create polymeric structures. The field began (ca. 1992) with studies employing 4,4′-bipyridine (4,4′-bipy), and this simple rigid bidentate ligand has been responsible for a bewildering number of compounds, primarily with first row transition elements. Despite the thousands of structures already reported with 4,4′-bipy, new M-4,4′-bipy structural motifs continue to be discovered. Indeed, the variety of structures obtained from M-4,4′-bipy systems (M = Fe, Co, Ni, Cu, Zn, Cd) is surprisingly vast [2] and hints at the yet undiscovered structural variety of other less-well characterized ligand systems. Recent coordination polymer discoveries have impacted catalysis, molecular recognition, ion exchange, luminescence, nonlinear optics and magnetism [3].

Hydrothermal synthesis as a preparative route to new coordination polymer materials is well established and can produce compounds not achievable by other routes. This technique is well-suited to solubilizing materials which are only slightly soluble at room temperature or at temperatures accessible by reflux. It also often yields crystals of high quality for single crystal X-ray diffraction analysis.

* Corresponding author. Tel.: +1-9208327262; fax: +1-9208326962.
E-mail address: nordellk@lawrence.edu (K.J. Nordell).

0277-5387/$ - see front matter © 2004 Elsevier Ltd. All rights reserved.
doi:10.1016/j.poly.2004.06.012

Here we report the hydrothermal synthesis and structural characterization of two new coordination polymers based on 4,4′-bipyridine and Pb(II)X_2 salts ($X = Cl^-$, NO_3^-), two novel additions to the sparse field of Pb(II)-containing coordination polymers [4].

2. Experimental

All reagents were commercially available and used without further purification. Elemental analyses were carried out by Desert Analytics Inc.

2.1. Synthesis of [$PbCl_2$(4,4′-bipy)] (1)

$PbCl_2$ (27.1 mg, 0.10 mmol), 4,4′-bipyridine (4,4′-bipy) (15.7 mg, 0.10 mmol) and 0.80 ml of distilled water were sealed in an evacuated Pyrex tube (7 mm ID, 11 cm long). The reaction was heated to 130 °C at 1 °C/min, soaked at 130 °C for 10 h, and cooled to 30 °C at 0.2 °C/min. Colorless crystals formed in the tube. *Anal.* Calc. for $C_{10}H_8N_2PbCl_2$: C, 27.66; H, 1.86; N, 6.45. Found: C, 27.34; H, 1.69; N, 6.28%.

2.2. Synthesis of [$Pb(NO_3)_2(H_2O)$(4,4′-bipy)$_2$] (2)

$Pb(NO_3)_2$ (33.0 mg, 0.10 mmol), 4,4′-bipyridine (4,4′-bipy) (15.8 mg, 0.10 mmol), and 0.80 ml of distilled water were sealed in an evacuated Pyrex tube (7 mm ID, 11 cm long). The reaction was heated to 130 °C at 1 °C/min, soaked at 130 °C for 10 h and cooled to 30 °C at 0.2 °C/min. Over the course of 24–48 h, plentiful colorless bar shaped crystals and a variety of very thin, small colorless crystals grew throughout the ampoule. The analysis of the crystalline products in multiple ampoules demonstrated that while compound **2** was the major product, small amounts of other crystalline products formed. Due to the fragility and poor crystal quality of these other products, it was not possible to fully characterize these products. Several samples were sent for elemental analysis, but the results were inconclusive due to the difficulties of getting enough pure product for analysis. The IR (cm^{-1}) results: 1590 (s), 1406 (s), 1323 (s), 1216 (m), 805 (s), clearly indicate the presence of nitrate groups coordinated to the metal.

2.3. X-ray crystallography

Crystals of each compound formed as colorless blocks (**1**) or bars (**2**). X-ray intensity data for both were measured at room temperature on a Bruker SMART APEX CCD-based diffractometer (Mo Kα radiation, $\lambda = 0.71073$ Å). [5] Raw data frame integration and Lp corrections were performed with SAINT+ [5]. Final unit cell parameters were determined by least-squares refinement of all reflections from each data set with $I > 5(\sigma)I$ (4102 for **1** and 5219 for **2**). Analysis of the data sets showed negligible crystal decay during collection. Both data sets were corrected for absorption with SADABS [5]. Patterson methods structure solution, difference Fourier calculations and full-matrix least-squares refinement against F^2 were performed with SHELXTL [6].

2.3.1. [$PbCl_2$(4,4′-bipy)] (1)

1 crystallizes in the triclinic crystal system. The space group $P\bar{1}$ was assumed and confirmed by the successful solution and refinement of the structure. The asymmetric unit consists of one Pb atom, two Cl atoms and one 4,4′-bipy ligand. All species reside on positions of general crystallographic symmetry. Non-hydrogen atoms were refined with anisotropic displacement parameters; hydrogen atoms were placed in geometrically idealized positions and included as riding atoms. The largest peak/hole remaining in the final difference map are +1.80/−0.72 $e^-/Å^3$ respectively, both located near Pb1.

2.3.2. [$Pb_2(NO_3)_4(H_2O)_2$(4,4′-bipy)$_2$](4,4′-bipy)$_2$ (2)

The space group $P2_1/c$ was uniquely determined by the pattern of systematic absences in the intensity data. The asymmetric unit consists of two crystallographically independent Pb centers, four nitrate anions, two 4,4′-bipy ligands coordinated to the Pb atoms, two uncoordinated 4,4′-bipy ligands and two coordinated H_2O ligands. All species are located on positions of general crystallographic symmetry. Non-hydrogen atoms were refined with anisotropic displacement parameters. Hydrogen atoms bound to carbon were placed in geometrically idealized positions and included as riding atoms; water hydrogens were located in difference maps and refined subject to O–H = 0.9 Å and H···H = 1.5 Å distance restraints, and $U_{eq}(H) = 1.5U_{eq}(O)$. The largest peak/hole remaining in the final difference map are +2.55/−1.68 $e^-/Å^3$ respectively, both located near Pb1.

3. Results and discussion

3.1. Crystal structure of $^2{}_\infty$[$PbCl_2$(4,4′-bipy)] (1)

Hydrothermal reaction (130 °C, 24 h) between equimolar amounts of $PbCl_2$ and 4,4-bipy yields plentiful colorless block-like crystals. Details of the X-ray data and structural refinement are in Table 1. Table 2 contains selected bond distances and angles. The details of the structure were established by single crystal X-ray diffraction, which revealed infinite two-dimensional layers parallel to the crystallographic *ab* plane (Fig. 1). The layers themselves are comprised of linear one-dimensional ribbons of composition $PbCl_{4/2}$ running along the crystallographic *a*-axis (Fig. 2). These constituent ribbons are linked into sheets by 4,4′-bipy spacers.

Table 1
Crystal data and structure refinement for $[PbCl_2(4,4'\text{-bipy})]$ (**1**) and $[Pb_2(NO_3)_4(H_2O)_2(4,4'\text{-bipy})_2]\ (4,4'\text{-bipy})_2$ (**2**)

Empirical formula	$C_{10}H_8C_{12}N_2Pb$	$C_{40}H_{36}N_{12}O_{14}Pb_2$
Formula weight	434.27	1323.19
Temperature (K)	294(2)	294(2)
λ (Å)	0.71073	0.71073
Crystal system	triclinic	monoclinic
Space group	$P\bar{1}$	$P2_1/c$
a (Å)	3.9813(3)	19.0473(13)
b (Å)	11.9563(10)	8.1540(6)
c (Å)	12.3748(10)	29.083(2)
α (°)	93.535(2)	90
β (°)	92.737(2)	91.183(2)
γ (°)	94.481(2)	90
V (Å^3)	585.32(8)	4515.9(6)
Z	2	4
D_{calc} (Mg m^{-3})	2.464	1.946
μ (mm^{-1})	14.835	7.527
$F(000)$	396	2544
Crystal size (mm)	$0.07 \times 0.04 \times 0.02$	$0.22 \times 0.10 \times 0.04$
θ Range (°)	1.65–27.07	1.40–26.41
h, k, l ranges	−5 to 5, −15 to 15, −15 to 15	−23 to 23, −10 to 10, −36 to 36
Reflections collected	5635	40,283
Independent reflections (R_{int})	2560 (0.0287)	9265 (0.0735)
Data/parameters	2560/136	9265/625
Goodness-of-fit (F^2)	1.054	1.042
Final R_1/wR_2 indices ($I > 2\sigma_i$)	0.0328/0.0677	0.0539/0.1131
Largest difference peak/hole (e Å^{-3})	1.797/−0.725	2.551/−1.685

There is one crystallographically independent lead (II) atom, which is situated in a severely distorted octahedral coordination environment consisting of four Cl atoms (Pb–Cl1 = 2.741(2), 3.052(2) Å; Pb–Cl2 = 2.736(2), 3.005(2) Å) and two nitrogen atoms from two symmetry-equivalent 4,4′-bipy ligands (Pb–N1 = 2.557(6) Å, Pb−N2 = 2.834(6) Å). The distorted Pb environment is caused by the Pb(II) lone pair, which is clearly stereochemically active (Fig. 3). Its impact is plainly evident in the *trans* N1–Pb–N2 bond angle of 151.3(2)° and in the slight lifting of Pb out of the plane formed by the four equatorial Cl atoms ($Pb–Cl_4$ plane distance = 0.387 Å). With the exception of the stereochemical distortion at the metal center, the structural motif observed in **1** is the same as that observed in $[PbI_2(4,4'\text{-bipy})]_n$ [4a], $[PbBr_2(4,4'\text{-bipy})]_n$ [4b], $[HgBr_2(4,4'\text{-bipy})]_n$ [7] and $[MCl_2(4,4'\text{-bipy})]_n$ (M = Fe, Co) [8]. The Cl2–Pb–Cl2 angle is 87.65(5)° and the Cl1–Pb–Cl1 angle is 86.65(5)° in **1**. In the related lead-containing compounds the X1–Pb–X1 angles are 87.94(2)° for X = I and 89.22(4)° for X = Br. The distorted Pb environment caused by the stereochemically active lone pair in **1** is the reason **1** is not isostructural with $[PbX_2(4,4'\text{-bipy})]_n$ (X = Br, I). The lone pair distortion is also responsible for the non-planarity of the 4,4-bipy ligand observed in **1**. The dihedral angle between the symmetry-inequivalent pyridyl ring planes of the 4,4′-bipy ligand in **1** is 28.5°, compared to 0.0° (exactly planar) for the symmetry-equivalent pyridyl rings in the Br and I compounds. Within the layers, the 4,4′-bipy ligands stack on top of each other at a perpendicular distance of 3.69 Å, and like the related Br and I compounds, the $PbCl_2(4,4'$-bipy) layers themselves stack along the c-axis at a

Table 2
Selected bond lengths (Å) and angles (°) for $[PbCl_2(4,4'\text{-bipy})]$ (**1**)

Pb(1)–N(1)	2.557(6)
Pb(1)–Cl(2)	2.7375(18)
Pb(1)–Cl(1)	2.7409(18)
Pb(1)–N(2)#1	2.834(6)
Pb(1)–Cl(2)#2	3.0051(18)
Pb(1)–Cl(1)#2	3.0524(18)
Cl(1)–Pb(1)#3	3.0524(18)
Cl(2)–Pb(1)#3	3.0051(18)
N(1)–Pb(1)–Cl(2)	82.62(15)
N(1)–Pb(1)–Cl(1)	83.58(14)
Cl(2)–Pb(1)–Cl(1)	96.58(6)
N(1)–Pb(1)–N(2)#1	151.3(2)
Cl(2)–Pb(1)–N(2)#1	78.52(14)
Cl(1)–Pb(1)–N(2)#1	77.39(14)
N(1)–Pb(1)–Cl(2)#2	80.81(14)
Cl(2)–Pb(1)–Cl(2)#2	87.65(5)
Cl(1)–Pb(1)–Cl(2)#2	163.16(6)
N(2)#1–Pb(1)–Cl(2)#2	119.45(14)
N(1)–Pb(1)–Cl(1)#2	81.81(15)
Cl(2)–Pb(1)–Cl(1)#2	163.64(6)
Cl(1)–Pb(1)–Cl(1)#2	86.65(5)
N(2)#1–Pb(1)–Cl(1)#2	117.81(14)
Cl(2)#2–Pb(1)–Cl(1)#2	84.93(5)
Pb(1)–Cl(1)–Pb(1)#3	86.65(5)
Pb(1)–Cl(2)–Pb(1)#3	87.65(5)

Symmetry transformations used to generate equivalent atoms: #1 $x-1,y-1,z$; #2 $x+1,y,z$; #3 $x-1,y,z$.

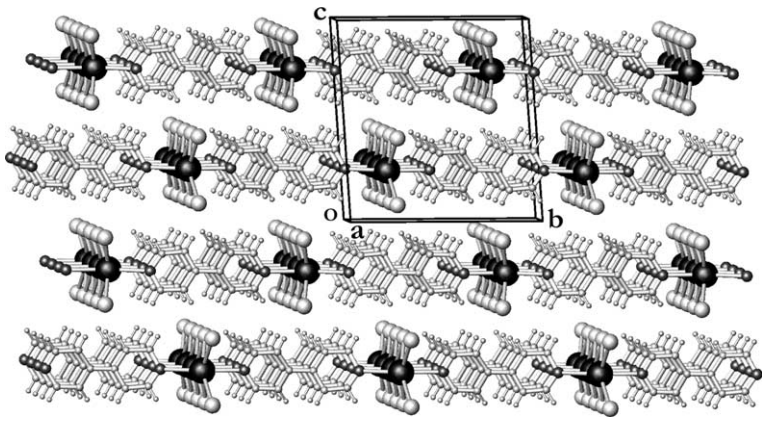

Fig. 1. View of **1** along the *a*-axis, showing the layers parallel to the *ab* plane.

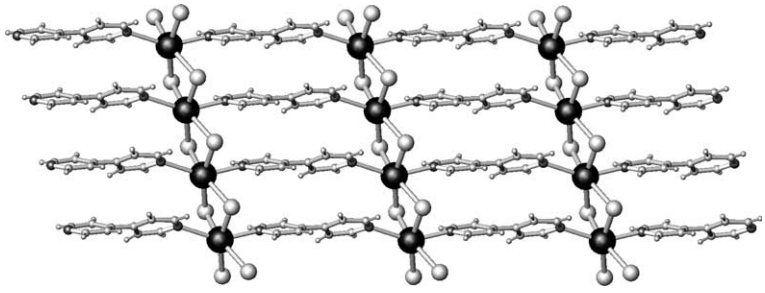

Fig. 2. View perpendicular to one individual layer in **1**.

distance of *c*/2 or 6.1874 Å. Our attempts to prepare either $[PbBr_2(4,4'\text{-bipy})]_n$ or $[PbI_2(4,4'\text{-bipy})]_n$ via hydrothermal synthesis have been to date unsuccessful.

3.2. Crystal structure of $^2{}_\infty[Pb_2(NO_3)_4(H_2O)_2(4,4'\text{-bipy})_2]\cdot(4,4'\text{-bipy})_2$ (**2**)

Plentiful colorless plate crystals of **2** were obtained from the hydrothermal reaction of equimolar amounts of $Pb(NO_3)_2$ and 4,4′-bipy in a sealed pyrex tube (130 °C). The structure of **2** was established by single crystal X-ray diffraction. Details of the X-ray data and structural refinement are in Table 1. Table 3 contains selected bond distances and angles. Compound **2** adopts a layered structure quite different from the rather common structural motif adopted by **1**. Two crystallographically and chemically different Pb(II) centers are present in **2**. Pb1 sits in an irregular eight-coordinate $\{PbN_2O_6\}$ environment (Fig. 4) composed of two nitrogen donors from two crystallographically inequivalent 4,4′-bipy ligands (Pb1–N1 = 2.643(7), Pb1–N11 = 2.721(7) Å); two oxygen atoms from two independent water molecules (Pb1–O1W = 2.471(7); Pb1–O2W = 2.515(7) Å) and four oxygen atoms from two independent bidentate nitrate anions (Pb1–O range = 2.742(7)–2.817(8) Å). Pb2 sits in an irregular 10-coordinate environment (Fig. 4) formed by two inequivalent 4,4′-bipy nitrogen donors (Pb2–N2 = 2.785(7); Pb2–N12 = 2.841(7) Å), and eight oxygen atoms from four chelating nitrate anions. These Pb–O distances (2.563(8)–3.068(8) Å) are in the range commonly observed in Pb–NO_3 complexes [9].

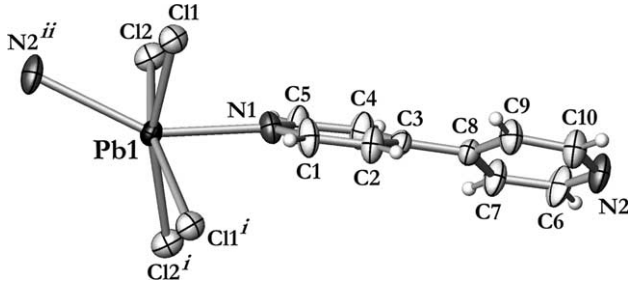

Fig. 3. Pb1 coordination environment. Displacement ellipsoids drawn at the 50% probability level.

The two inequivalent Pb centers are linked into one-dimensional chains by the two inequivalent bridging 4,4′-bipy ligands (Fig. 4). These chains run along the crystallographic [1,−2,0] direction and lie side-by-side

Table 3
Selected bond lengths (Å) and angles (°) for $[Pb_2(NO_3)_4(H_2O)_2(4,4'\text{-bipy})_2]$ $(4,4'\text{-bipy})_2$ (**2**)

Pb(1)–O(2W)	2.471(7)
Pb(1)–O(1W)	2.515(7)
Pb(1)–N(1)	2.643(7)
Pb(1)–N(11)	2.721(7)
Pb(1)–O(4)	2.742(7)
Pb(1)–O(2)	2.778(8)
Pb(1)–O(1)	2.784(7)
Pb(1)–O(5)	2.817(8)
Pb(2)–O(10)	2.563(8)
Pb(2)–O(8)	2.599(8)
Pb(2)–O(7)	2.640(8)
Pb(2)–O(11)	2.680(8)
Pb(2)–N(2)#1	2.785(7)
Pb(2)–O(6)	2.837(7)
Pb(2)–N(12)#2	2.841(7)
Pb(2)–O(3)#3	2.883(8)
Pb(2)–O(5)	3.051(8)
Pb(2)–O(2)#3	3.068(8)
O(2W)–Pb(1)–O(1W)	83.4(2)
O(2W)–Pb(1)–N(1)	87.9(3)
O(1W)–Pb(1)–N(1)	75.9(2)
O(2W)–Pb(1)–N(11)	80.3(2)
O(1W)–Pb(1)–N(11)	93.3(3)
N(1)–Pb(1)–N(11)	164.9(3)
O(2W)–Pb(1)–O(4)	74.3(2)
O(1W)–Pb(1)–O(4)	142.5(2)
N(1)–Pb(1)–O(4)	73.6(2)
N(11)–Pb(1)–O(4)	111.7(2)
O(2W)–Pb(1)–O(2)	162.5(3)
O(1W)–Pb(1)–O(2)	92.0(3)
N(1)–Pb(1)–O(2)	74.6(2)
N(11)–Pb(1)–O(2)	116.9(2)
O(4)–Pb(1)–O(2)	100.3(3)
O(2W)–Pb(1)–O(1)	149.6(2)
O(1W)–Pb(1)–O(1)	82.4(2)
N(1)–Pb(1)–O(1)	114.3(2)
N(11)–Pb(1)–O(1)	73.8(2)
O(4)–Pb(1)–O(1)	130.2(2)
O(2)–Pb(1)–O(1)	44.8(2)
O(2W)–Pb(1)–O(5)	89.9(3)
O(1W)–Pb(1)–O(5)	165.6(3)
N(1)–Pb(1)–O(5)	116.7(2)
N(11)–Pb(1)–O(5)	73.0(3)
O(4)–Pb(1)–O(5)	45.4(2)
O(2)–Pb(1)–O(5)	98.0(3)
O(1)–Pb(1)–O(5)	97.4(3)
O(10)–Pb(2)–O(8)	74.1(3)
O(10)–Pb(2)–O(7)	74.0(3)
O(8)–Pb(2)–O(7)	47.4(3)
O(10)–Pb(2)–O(11)	47.0(3)
O(8)–Pb(2)–O(11)	79.5(3)
O(7)–Pb(2)–O(11)	110.4(3)
O(10)–Pb(2)–N(2)#1	71.4(3)
O(8)–Pb(2)–N(2)#1	116.1(2)
O(7)–Pb(2)–N(2)#1	72.0(3)
O(11)–Pb(2)–N(2)#1	110.2(3)
O(10)–Pb(2)–O(6)	135.7(2)
O(8)–Pb(2)–O(6)	95.6(3)
O(7)–Pb(2)–O(6)	68.2(2)
O(11)–Pb(2)–O(6)	173.6(3)
N(2)#1–Pb(2)–O(6)	75.6(2)
O(10)–Pb(2)–N(12)#2	114.8(2)
O(8)–Pb(2)–N(12)#2	71.8(3)
O(7)–Pb(2)–N(12)#2	114.6(3)
O(11)–Pb(2)–N(12)#2	73.1(3)
N(2)#1–Pb(2)–N(12)#2	171.6(3)
O(6)–Pb(2)–N(12)#2	101.6(2)
O(10)–Pb(2)–O(3)#3	97.4(3)
O(8)–Pb(2)–O(3)#3	137.4(2)
O(7)–Pb(2)–O(3)#3	169.3(3)
O(11)–Pb(2)–O(3)#3	66.0(3)
N(2)#1–Pb(2)–O(3)#3	99.3(2)
O(6)–Pb(2)–O(3)#3	116.5(2)
N(12)#2–Pb(2)–O(3)#3	74.7(2)
O(10)–Pb(2)–O(5)	173.3(3)
O(8)–Pb(2)–O(5)	99.5(3)
O(7)–Pb(2)–O(5)	100.3(3)
O(11)–Pb(2)–O(5)	134.7(2)
N(2)#1–Pb(2)–O(5)	110.6(3)
O(6)–Pb(2)–O(5)	41.72(19)
N(12)#2–Pb(2)–O(5)	64.0(2)
O(3)#3–Pb(2)–O(5)	88.6(3)
O(10)–Pb(2)–O(2)#3	104.2(3)
O(8)–Pb(2)–O(2)#3	178.0(3)
O(7)–Pb(2)–O(2)#3	133.5(3)
O(11)–Pb(2)–O(2)#3	98.5(3)
N(2)#1–Pb(2)–O(2)#3	64.0(3)
O(6)–Pb(2)–O(2)#3	86.4(3)
N(12)#2–Pb(2)–O(2)#3	108.1(3)
O(3)#3–Pb(2)–O(2)#3	41.3(2)
O(5)–Pb(2)–O(2)#3	82.2(3)

Symmetry transformations used to generate equivalent atoms: #1 $-x,y+3/2,-z+3/2$; #2 $-x+1,y-1/2,-z+3/2$; #3 $x,y+1,z$; #4 $-x,y-3/2,-z+3/2$; #5 $x,-y+1/2,z+1/2$; #6 $x,-y+3/2,z+1/2$; #7 $-x,y+1/2,-z+3/2$.

forming sheets in the *ab* plane. There is no direct linkage between individual unidirectional chains in these sheets; however two such sheets of chains are connected via bridging nitrates to form a bilayer of composition $[Pb_2(NO_3)_4(H_2O)_2(4,4'\text{-bipy})_2]$. The operation of the 2_1 axis causes the constituent chains of each sheet of the bilayer to crisscross at an angle of (ca. ~90°) relative to the chains in the other sheet (Fig. 5). An alternative view of the bilayers is of infinite undulating $\{Pb(NO_3)_2\}$ ribbons running parallel to the *b*-axis (Fig. 5) which are linked in a crisscross fashion by 4,4′-bipy ligands. This view highlights the inorganic–organic hybrid nature of **2**, grossly similar to that in **1**.

The two water molecules bound to Pb1 protrude to the outside surfaces of the bilayers and play a critical role in assembling the full three-dimensional hydrogen-bonded structure. The bilayer sheets lie parallel the crystallographic *ab* plane, and are interleaved by layers of 'free' (uncoordinated to Pb1 or Pb2) 4,4′-bipy molecules. These interstitial 4,4′-bipy molecules adopt a sinusoidally undulating pattern, with the extrema of the troughs and crests coinciding with the water molecules bound to Pb1, forming hydrogen bonds (Fig. 6). All four water hydrogens on the two waters on Pb1

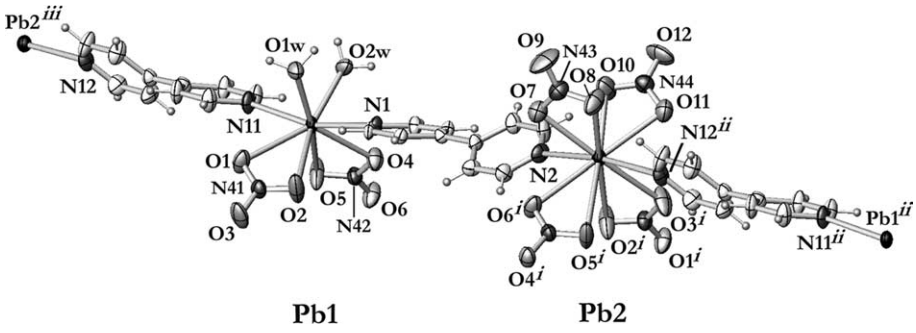

Fig. 4. Coordination environments of Pb1 and Pb2. Displacement ellipsoids drawn at the 40% probability level.

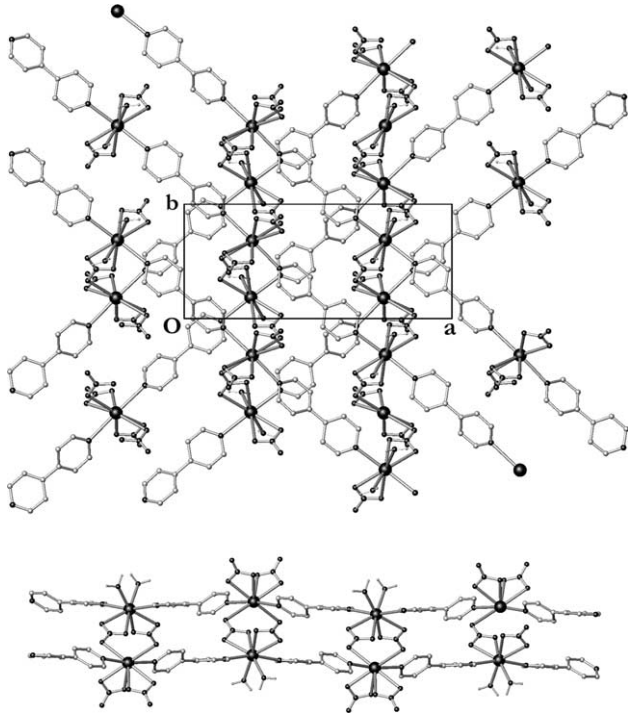

Fig. 5. View perpendicular (top) and parallel (bottom) to the double layers of chains created by the bridging nitrates in **2**.

participate in the hydrogen bonding network (Table 4). The relative positions of the two waters along the undulation direction created a slight ''phase lag'' in the sine wave chains of uncoordinated 4,4′-bipys, illustrated schematically in Fig. 6.

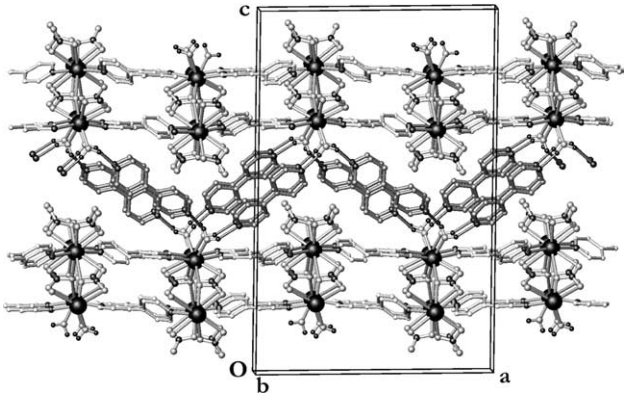

Fig. 6. View of the Pb bilayer – 4,4′-bipyridine hydrogen bonding in **2**.

4. Conclusions

Whereas the slow addition of a methanol solution of 4,4′bipy to a dimethylformamide solution of PbX_2 (X = Br, I) resulted in the formation of isostructural Pb-containing coordination polymers $[PbX_2(4,4'\text{-bipy})]_n$ (X = Br, I) [4], our hydrothermal synthesis resulted in the formation of two new lead-containing coordination polymers. Compound **1** is nearly isomorphous with the two previously reported (Br and I) compounds except for the profound distorting impact of the stereochemically active lone pair on the Pb(II) coordination environment. In an excellent discussion, Shimoni–Livny et al. list factors favoring an active lone pair in Pb(II) compounds [10]. They point out that based on a search of the Cambridge Structural Database, it is unusual for a Pb(II)

Table 4
Hydrogen bonds for $[Pb_2(NO_3)_4(H_2O)_2(4,4'\text{-bipy})_2]$ $(4,4'\text{-bipy})_2$ (**2**) (Å and °)

D–H...A	*d*(D–H)	*d*(H...A)	*d*(D...A)	<(DHA)
O(1W)–H(1WA)...N(21)#5	0.901(10)	1.91(3)	2.793(11)	167(10)
O(1W)–H(1WB)...N(31)#2	0.900(10)	2.00(4)	2.842(12)	155(8)
O(2W)–H(2WA)...N(32)#6	0.902(10)	2.14(9)	2.807(13)	131(10)
O(2W)–H(2WB)...N(22)#7	0.903(10)	2.00(5)	2.800(11)	147(8)

Symmetry transformations used to generate equivalent atoms: #1 $-x,y+3/2,-z+3/2$; #2 $-x+1,y-1/2,-z+3/2$; #3 $x,y+1,z$; #4 $-x,y-3/2,-z+3/2$; #5 $x,-y+1/2,z+1/2$; #6 $x,-y+3/2,z+1/2$; #7 $-x,y+1/2,-z+3/2$.

compound with several soft Cl^- ligands to show the effects of an active lone pair. However, this may be mitigated by the presence of harder ligating atoms such as nitrogen in the presence of Pb, and by attractive interactions between ligands. The π–π interactions between pyridyl rings present in compound **1** may thus also contribute to the geometry at the Pb center. Finally, the authors say inter-ligand repulsions show a tendency to favor more symmetrical Pb coordination geometries. Therefore the smaller size of Cl relative to Br and I provides a more roomy coordination environment around the Pb(II) thereby allowing the lone pair to exert a stronger stereochemical influence in **1**. Compound **2** is an interesting layered structure stuffed with free 4,4′-bipy molecules, arranged to maximize their hydrogen-bonding capability. Both structures display inorganic $\{Pb(anion)_2\}$ ribbons linked together by organic 4,4′-bipy ligands.

5. Supplementary material

Crystallographic data (excluding structure factors) for the structures in this paper have been deposited with the Cambridge Crystallographic Data Centre as supplementary publication nos. CCDC 234033 and 234034. Copies of the data can be obtained, free of charge, on application to CCDC, 12 Union Road, Cambridge CB2 1EZ, UK (fax: +44-1223-336033 or e-mail: deposit@ccdc.cam.ac.uk or www.ccdc.cam.ac.uk).

References

[1] (a) For reviews on the crystal engineering of coordination polymers M.J. Zaworotko, Chem. Commun. (2001) 1;
(b) S.R. Batten, Curr. Opin. Sol. State Mater. Sci. 5 (2001) 107;
(c) B. Moulton, M.J. Zaworotko, Chem. Rev. 101 (2001) 1629;
(d) M. Eddaoudi, D.B. Moler, H. Li, B. Chen, T.M. Reineke, M. O'Keeffe, O.M. Yaghi, Acc. Chem. Res. 34 (2001) 319;
(e) D. Braga, J. Chem. Soc., Dalton Trans. (2000) 3705;
(f) O.M. Yaghi, M. O'Keeffe (Eds.), J. Solid State Chem.(2000) 152 (special issue);
(g) A.J. Blake, N.R. Champness, P. Hubberstey, W.-S. Li, M.A. Withersby, M. Schroder, Coord. Chem. Rev. 183 (1999) 117;
(h) M. Munakata, L.P. Wu, T. Kuroda-Sowa, Adv. Inorg. Chem. 46 (1999) 173.

[2] The Cambridge Structural Database: a quarter of a million structures and rising F.H. Allen, Acta Crystallogr. B 58 (2002) 380.

[3] (a) For utilization of coordination polymers see: O.R. Evans, W. Lin, Chem. Mater. 13 (2001) 3009;
(b) K. Matsuda, K. Takayama, M. Irie, Chem. Commun. (2001) 363;
(c) Z. Xu, S. White, L.K. Thompson, D.O. Miller, M. Ohba, H. Okawa, C. Wilson, J.A.K. Howard, J. Chem. Soc., Dalton, Trans. (2000) 1751;
(d) L. Pan, E.B. Woodlock, X. Wang, Inorg. Chem. 39 (2000) 4174;
(e) O. Kahn, Acc. Chem. Res. 33 (2000) 647;
(f) G.B. Gardner, D. Venkataraman, J.S. Moore, S. Lee, Nature 374 (1995) 792;
(g) B.F. Abrahams, D.M. Hoskins, R. Robson, Nature 369 (1994) 727.

[4] (a) Y.-J. Shi, Y. Xu, Y. Zhang, B. Huang, D.-R. Zhu, C.-M. Jin, H.-G. Zhu, Z. Yu, X.-T. Chen, X.-Z. You, Chem. Lett. (2001) 678;
(b) Y. Cui, J. Ren, G. Chen, W. Yu, Y. Qian, Acta Cryst. C 56 (2000) e552;
(c) Y.-J. Shi, X.-T. Chen, C.-X. Cai, Y. Zhang, Z. Xue, X.-Z. You, S.-M. Peng, G.-H. Lee, Inorg. Chem. Commun. 5 (2002) 621.

[5] SMART Version 5.624 and SAINT+ Version 6.02a. Bruker Analytical X-ray Systems, Inc., Madison, Wisconsin, USA, 1998.

[6] G.M. Sheldrick, SHELXTL Version 5.1; Bruker Analytical X-ray Systems, Inc., Madison, Wisconsin, USA, 1997.

[7] L. Pan, N. Zheng, Y. Wu, S. Wu, X. Huang, Acta Cryst. C 55 (1999) 343.

[8] M.A. Lawandy, X. Huang, R.-J. Wang, J. Li, J.Y. Lu, T. Yeun, C.L. Lin, Inorg. Chem. 38 (1999) 5410.

[9] (a) J.M. Grevy, F. Tellez, S. Bernes, H. Noth, R. Contreras, N. Barba-Behrens, Inorg. Chim. Acta 339 (2002) 532;
(b) X. Meng, Y. Song, H. Hou, Y. Fan, G. Li, Y. Zhu, Inorg. Chem. 42 (2003) 1306.

[10] L. Shimoni-Livny, J.P. Glusker, C.W. Bock, Inorg. Chem. 37 (1998) 1853.

Available online at www.sciencedirect.com
SCIENCE DIRECT®
Polyhedron 23 (2004) 2169–2176
POLYHEDRON
www.elsevier.com/locate/poly

Synthesis, characterization, and cytotoxicities of palladium(II) and platinum(II) complexes containing fluorinated pyridinecarboxaldimines

Stephen J. Scales [a], Haiwen Zhang [a], Paul A. Chapman [a], Ciara P. McRory [a], Eric J. Derrah [a], Christopher M. Vogels [a], Mazen T. Saleh [b], Andreas Decken [c], Stephen A. Westcott [a,*]

[a] Department of Chemistry, Mount Allison University, 63C York Street, Sackville, NB, Canada E4L 1G8
[b] Department of Biology and Biochemistry, Mount Allison University, Sackville, NB, Canada E4L 1G7
[c] Department of Chemistry, University of New Brunswick, Fredericton, NB, Canada E3B 5A3

Received 9 May 2004; accepted 9 June 2004
Available online 29 July 2004

Abstract

Condensation of 2-pyridinecarboxaldehyde with several primary amines containing fluorine groups gave the corresponding pyridinecarboxaldimines (N-N′). Addition of these ligands to $[MCl_2(coe)]_2$ (M = Pd, Pt; coe = *cis*-cyclooctene) gave complexes of the type *cis*-MCl_2(N-N′) [Pd (**3**), Pt (**4**)] in moderate to high yields. All palladium and platinum complexes were examined for their potential cytotoxicities against OV2008 (human ovarian carcinoma) and the analogous cisplatin-resistant C13.
© 2004 Elsevier Ltd. All rights reserved.

Keywords: Pyridinecarboxaldimine; Cytotoxicity; Platinum; Palladium; Fluorine

1. Introduction

Cisplatin, *cis*-$[PtCl_2(NH_3)_2]$ and a few related platinum-based complexes are currently used as anticancer agents against testicular and ovarian malignancies [1–7]. There are several limitations to platinum therapy, however, such as neural and kidney toxicity as well as intrinsic and acquired resistance of tumor cells to the drugs [1]. These complications have provided an incentive for further research into the development of platinum-based complexes with increased solubility and enhanced specificity towards cancer cells. Recent studies have shown that *cis*-amminedichloro(2-methylpyridine)platinum(II) (AMD473 or ZD0473, Fig. 1) shows considerable cytotoxicity in cisplatin-resistant cell lines [8,9]. Steric crowding from the methyl group is believed to decrease the rates of hydrolysis and substitution reactions of AMD473 by effectively shielding the platinum atom and thereby permitting high selectivity in binding to DNA [10]. The primary mechanism of action in these platinum drugs is believed to arise from the metal's interaction with DNA.

We have begun to develop AMD473 analogues by replacing the NH_3 group with a pendant imine group. Previous studies have shown that the platinum complex derived from aniline, **2** (Fig. 1), has shown considerable activity against the hormone independent human mammary carcinoma cell line MDA-MB 231 [11]. Varying the aniline functionality allows us to design compounds with a wide range of physical and chemical properties

* Corresponding author. Tel.: +1-506-364-2351/2372; fax: +1-506-364-2313.
E-mail address: swestcott@mta.ca (S.A. Westcott).

0277-5387/$ - see front matter © 2004 Elsevier Ltd. All rights reserved.
doi:10.1016/j.poly.2004.06.013

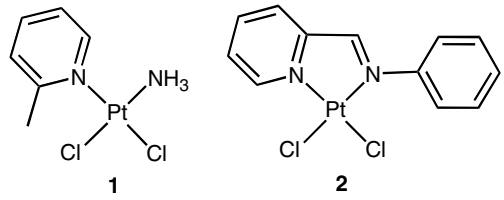

Fig. 1. Structure of AMD473 (**1**) and complex **2**.

that may provide steric congestion around the platinum atom. As well, the use of bidentate ligands prevents trans labilization and undesired displacement of the ligands by sulfur and nitrogen donors in biomolecules, interactions believed responsible for some of the adverse side effects associated with cisplatin [1–3]. We report herein our results on the synthesis and initial cytotoxicity testing of *cis*-dichloro(pyridin-2-ylcarboxaldimine)-palladium(II) and -platinum(II) compounds containing bulky fluorinated aryl groups (Fig. 2).

2. Experimental

2.1. General procedures and methods

Reagents and solvents used were obtained from Aldrich Chemicals. $PdCl_2$ and K_2PtCl_4 were purchased from Precious Metals Online Ltd. and $[PdCl_2(coe)]_2$ and $[PtCl_2(coe)]_2$ were made by established procedures [12]. Pyridinecarboxaldimine ligands were prepared as previously reported [13]. NMR spectra were recorded on a JEOL JNM-GSX270 FT NMR or Varian Mercury Plus 200 NMR spectrometer. ^1H NMR chemical shifts are reported in ppm and are referenced to residual protons in deuterated solvent at 270 and 200 MHz. ^{13}C NMR chemical shifts are referenced to solvent carbon resonances as internal standards at 68 and 50 MHz. ^{19}F NMR chemical shifts are referenced to CF_3CO_2H. Multiplicities are reported as singlet (s), doublet (d), triplet (t), quartet (q), multiplet (m), broad (br) and overlapping (ov). Infrared spectra were obtained using a Mattson Genesis II FT-IR spectrometer and are reported in cm^{-1}. Melting points were measured uncorrected with a Mel-Temp apparatus. Microanalyses for C, H and N were carried out at Guelph Chemical Laboratories Ltd. (Guelph, Ont.).

2.2. General procedure for the preparation of metal complexes

A CH_2Cl_2 (5 ml) solution of ligand (0.55 mmol) was added to the appropriate $[MCl_2(coe)]_2$ (where M = Pd or Pt) (0.25 mmol) in CH_2Cl_2 (5 ml). The reaction mixture was stirred for 5 h at room temperature and the precipitate was collected by suction filtration and washed with CH_2Cl_2 (3×5 ml) to afford the metal complex.

2.2.1. Compound ***3a***

Yield: 80% as an orange solid; m.p. 280–281 °C (decomposition). Spectroscopic NMR data (in DMSO-d_6): ^1H δ: 9.05 (d, $J = 6$ Hz, 1H, Ar), 8.89 (s, 1H, C(*H*)═N), 8.43 (t of d, $J = 8$, 1 Hz, 1H, Ar), 8.23 (d, $J = 8$ Hz, 1H, Ar), 7.97 (t of d, $J = 6$, 1 Hz, 1H, Ar), 7.48–7.27 (ov m, 4H, Ar); $^{13}C\{^1H\}$ δ: 175.7, 155.9, 154.5 (d, $J_{C-F} = 274$ Hz, *C*F), 150.9, 142.0, 135.6 (d, $J_{C-F} = 12$ Hz), 130.7 (d, $J_{C-F} = 8$ Hz), 130.5, 130.2, 125.7, 124.9 (d, $J_{C-F} = 4$ Hz), 116.4 (d, $J_{C-F} = 20$ Hz); $^{19}F\{^1H\}$ δ: −118.4. IR (nujol): 2949, 2904, 2860, 1581, 1460, 1377, 1250, 1228, 1159, 1101, 955, 798, 771, 739. *Anal*. Calc. for $C_{12}H_9N_2Cl_2FPd$: C, 38.16; H, 2.41; N, 7.42. Found: C, 38.20; H, 2.29; N, 7.13%.

2.2.2. Compound ***3b***

Yield: 76% as an orange solid; m.p. 278–280 °C (decomposition). Spectroscopic NMR data (in DMSO-d_6): ^1H δ: 9.05 (d, $J = 6$ Hz, 1H, Ar), 8.80 (s, 1H, C(*H*)═N), 8.42 (t, $J = 8$ Hz, 1H, Ar), 8.21 (d, $J = 8$ Hz, 1H, Ar), 7.96 (t, $J = 6$ Hz, 1H, Ar), 7.55–7.47 (m,

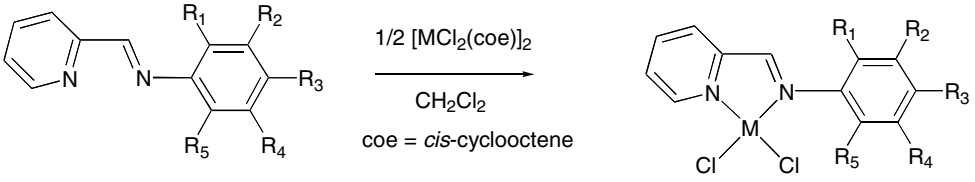

a: $R_1 = F$, $R_2 = R_3 = R_4 = R_5 = H$
b: $R_2 = F$, $R_1 = R_3 = R_4 = R_5 = H$
c: $R_3 = F$, $R_1 = R_2 = R_4 = R_5 = H$
d: $R_1 = CF_3$, $R_2 = R_3 = R_4 = R_5 = H$
e: $R_2 = CF_3$, $R_1 = R_3 = R_4 = R_5 = H$
f: $R_3 = CF_3$, $R_1 = R_2 = R_4 = R_5 = H$
g: $R_2 = R_4 = CF_3$, $R_1 = R_3 = R_5 = H$
h: $R_1 = R_2 = R_3 = R_4 = R_5 = F$

3: M = Pd
4: M = Pt

Fig. 2. Synthesis of palladium and platinum complexes **3**–**4**.

1H, Ar), 7.34–7.24 (ov m, 3H, Ar); $^{13}C\{^1H\}$ δ: 174.0, 161.7 (d, J_{C-F} = 245 Hz, *C*F), 156.2, 150.7, 148.8 (d, J_{C-F} = 10 Hz), 141.9, 130.6 (d, J_{C-F} = 9 Hz), 130.3, 129.9, 120.7, 115.9, (d, J_{C-F} = 21 Hz), 112.4 (d, J_{C-F} = 25 Hz); $^{19}F\{^1H\}$ δ: −112.8. IR (nujol): 2951, 2927, 2854, 1591, 1460, 1377, 1360, 1300, 1269, 1252, 1228, 1167, 1138, 980, 897, 856, 796, 771, 723, 692. *Anal*. Calc. for $C_{12}H_9N_2Cl_2FPd$: C, 38.16; H, 2.41; N, 7.42. Found: C, 38.22; H, 2.13; N, 7.25%.

2.2.3. Compound **3c**

Yield: 60% as an orange solid; m.p. 328 °C (decomposition). Spectroscopic NMR data (in DMSO-d_6): ^1H δ: 9.05 (d, J = 6 Hz, 1H, Ar), 8.75 (s, 1H, C(*H*)═N), 8.40 (t, J = 8 Hz, 1H, Ar), 8.20 (d, J = 8 Hz, 1H, Ar), 7.94 (t, J = 6 Hz, 1H, Ar), 7.51–7.46 (m, 2H, Ar), 7.34–7.28 (m, 2H, Ar); $^{13}C\{^1H\}$ δ: 173.4, 162.2 (d, J_{C-F} = 246 Hz, *C*F), 156.4, 150.6, 143.9 (d, J_{C-F} = 2 Hz), 141.9, 130.1, 129.7, 126.8 (d, J_{C-F} = 9 Hz), 115.6 (d, J_{C-F} = 22 Hz); $^{19}F\{^1H\}$ δ: −113.0. IR (nujol): 3109, 3041, 3016, 2920, 1597, 1579, 1498, 1479, 1308, 1296, 1242, 1228, 1196, 1157, 1103, 960, 850, 806, 795, 768, 579. *Anal*. Calc. for $C_{12}H_9N_2Cl_2FPd$: C, 38.16; H, 2.41; N, 7.42. Found: C, 37.98; H, 2.10; N, 7.10%.

2.2.4. Compound **3d**

Yield: 70% as an orange solid; m.p. 324–326 °C (decomposition). Spectroscopic NMR data (in DMSO-d_6): ^1H δ: 9.04 (d, J = 6 Hz, 1H, Ar), 8.97 (s, 1H, C(*H*)═N), 8.44 (t of d, J = 8, 1 Hz, 1H, Ar), 8.25 (d, J = 8 Hz, 1H, Ar), 8.01 (t of d, J = 6, 1 Hz, 1H, Ar), 7.82–7.76 (ov m, 2H, Ar), 7.61 (t, J = 8 Hz, 1H, Ar), 7.51 (d, J = 8 Hz, 1H, Ar); $^{13}C\{^1H\}$ δ: 175.2, 155.6, 151.2, 145.3, 142.1, 133.5, 130.6 (2C), 129.0, 126.8 (q, J_{C-F} = 5 Hz), 126.2, 124.5 (q, J_{C-F} = 274 Hz, *C*F_3), 122.2 (q, J_{C-F} = 30 Hz); $^{19}F\{^1H\}$ δ: −55.9. IR (nujol): 3074, 3014, 2952, 2925, 2854, 1593, 1471, 1456, 1319, 1296, 1269, 1203, 1155, 1124, 1055, 1034, 984, 768, 571. *Anal*. Calc. for $C_{13}H_9N_2Cl_2F_3Pd$: C, 36.51; H, 2.13; N, 6.55. Found: C, 36.57; H, 1.98; N, 6.54%.

2.2.5. Compound **3e**

Yield: 65% as an orange solid; m.p. 346–348 °C (decomposition). Spectroscopic NMR data (in DMSO-d_6): ^1H δ: 9.06 (d, J = 6 Hz, 1H, Ar), 8.85 (s, 1H, C(*H*)═N), 8.42 (t, J = 8 Hz, 1H, Ar), 8.23 (d, J = 8 Hz, 1H, Ar), 7.97 (t, J = 6 Hz, 1H, Ar), 7.85 (s, 1H, Ar), 7.80 (m, 1H, Ar), 7.77–7.68 (ov m, 2H, Ar); $^{13}C\{^1H\}$ δ: 175.0, 156.8, 151.3, 148.2, 142.5, 130.8, 130.5 (2C), 129.9 (q, J_{C-F} = 32 Hz), 129.4, 128.7 (q, J_{C-F} = 274 Hz, *C*F_3), 126.1 (q, J_{C-F} = 4 Hz), 122.0 (q, J_{C-F} = 4 Hz); $^{19}F\{^1H\}$ δ: −61.0. IR (nujol): 3074, 3014, 2953, 2854, 1593, 1450, 1362, 1329, 1238, 1184, 1159, 1117, 1068, 808, 773, 700, 658. *Anal*. Calc. for $C_{13}H_9N_2Cl_2F_3Pd$: C, 36.51; H, 2.13; N, 6.55. Found: C, 36.23; H, 2.11; N, 6.33%.

2.2.6. Compound **3f**

Yield: 65% as an orange solid; m.p. 301–302 °C (decomposition). Spectroscopic NMR data (in DMSO-d_6): ^1H δ: 9.06 (d, J = 6 Hz, 1H, Ar), 8.83 (s, 1H, C(*H*)═N), 8.42 (t of d, J = 8, 1 Hz, 1H, Ar), 8.22 (d, J = 8 Hz, 1H, Ar), 7.97 (t of d, J = 6, 1 Hz, 1H, Ar), 7.87 (d, J = 8 Hz, 2H, Ar), 7.63 (d, J = 8 Hz, 2H, Ar); $^{13}C\{^1H\}$ δ: 174.4, 156.3, 150.7, 150.4, 142.0, 130.4, 130.0, 129.1 (q, J_{C-F} = 35 Hz), 126.0 (q, J_{C-F} = 4 Hz), 125.6, 124.5 (q, J_{C-F} = 274 Hz, *C*F_3); $^{19}F\{^1H\}$ δ: −60.8. IR (nujol): 3074, 2870, 1460, 1377, 1186, 1169, 1107, 966, 854, 766, 721, 607. *Anal*. Calc. for $C_{13}H_9N_2Cl_2F_3Pd$: C, 36.51; H, 2.13; N, 6.55. Found: C, 36.66; H, 1.97; N, 6.45%.

2.2.7. Compound **3g**

Yield: 60% as an orange solid; m.p. 358–360 °C (decomposition). Spectroscopic NMR data (in DMSO-d_6): ^1H δ: 9.07 (d, J = 6 Hz, 1H, Ar), 8.98 (s, 1H, C(*H*)═N), 8.45 (t of d, J = 8, 1 Hz, 1H, Ar), 8.27 (d, J = 8 Hz, 1H, Ar), 8.24 (s, 1H, Ar), 8.19 (s, 2H, Ar), 8.00 (t of d, J = 6, 1 Hz, 1H, Ar); $^{13}C\{^1H\}$ δ: 175.7, 156.1, 150.9, 148.2, 142.1, 130.8, 130.6 (q, J_{C-F} = 34 Hz), 130.3, 126.1, 123.5 (q, J_{C-F} = 274 Hz, *C*F_3), 122.6 (q, J_{C-F} = 4 Hz); $^{19}F\{^1H\}$ δ: −61.2. IR (nujol): 3107, 3020, 2951, 2922, 2854, 1371, 1358, 1292, 1279, 1242, 1184, 1174, 1126, 970, 901, 881, 777, 702, 683. *Anal*. Calc. for $C_{14}H_8N_2Cl_2F_6Pd$: C, 33.92; H, 1.63; N, 5.65. Found: C, 33.50; H, 1.39; N, 5.43%.

2.2.8. Compound **3h**

Yield: 65% as an orange solid; m.p. 288 °C (decomposition). Spectroscopic NMR data (in DMSO-d_6): ^1H δ: 9.21 (s, 1H, C(*H*)═N), 9.04 (d, J = 6 Hz, 1H, Ar), 8.46 (t, J = 8 Hz, 1H, Ar), 8.34 (d, J = 8 Hz, 1H, Ar), 8.06 (t, J = 6 Hz, 1H, Ar); $^{19}F\{^1H\}$ δ: −145.4 (d, J_{F-F} = 19 Hz), −154.2 (t, J_{F-F} = 19 Hz), −162.8 (t, J_{F-F} = 9 Hz). IR (nujol): 3095, 3016, 2951, 2924, 2856, 1591, 1512, 1470, 1433, 1352, 1294, 1221, 1103, 1009, 995, 960, 885, 793, 781. *Anal*. Calc. for $C_{12}H_5N_2Cl_2F_5Pd$: C, 32.06; H, 1.12; N, 6.23. Found: C, 31.91; H, 0.83; N, 5.99%.

2.2.9. Compound **4a**

Yield: 65% as an orange solid; m.p. 282 °C (decomposition). Spectroscopic NMR data (in DMSO-d_6): ^1H δ: 9.51 (s, J_{H-Pt} = 92 Hz, 1H, C(*H*)═N), 9.47 (d, J_{H-H} = 6 Hz, J_{H-Pt} = 40 Hz, 1H, Ar), 8.47 (t, J_{H-H} = 8 Hz, 1H, Ar), 8.25 (d, J_{H-H} = 8 Hz, 1H, Ar), 8.04 (t, J_{H-H} = 6 Hz, 1H, Ar), 7.50–7.31 (ov m, 4H, Ar); $^{13}C\{^1H\}$ δ: 175.4, 157.1, 154.9 (d, J_{C-F} = 250 Hz, *C*F), 149.8, 141.4, 135.4 (d, J_{C-F} = 12 Hz), 131.1 (d, J_{C-F} = 8 Hz), 130.8 (2C), 126.5, 124.9 (d, J_{C-F} = 4 Hz), 116.5 (d, J_{C-F} = 20 Hz); $^{19}F\{^1H\}$ δ: −120.0. IR (nujol): 2941, 2902, 2860, 1589, 1558, 1493, 1456, 1377, 1348, 1300, 1250, 1228, 1159, 1101, 937, 856, 800, 766, 739,

667, 596. *Anal.* Calc. for $C_{12}H_9N_2Cl_2FPt$: C, 30.91; H, 1.95; N, 6.01. Found: C, 30.44; H, 1.73; N, 5.68%.

2.2.10. Compound **4b**

Yield: 81% as an orange solid; m.p. 286 °C (decomposition). Spectroscopic NMR data (in DMSO-d_6): ^{1}H δ: 9.48 (d, J_{H-H} = 6 Hz, J_{H-Pt} = 47 Hz, 1H, Ar), 9.40 (s, J_{H-Pt} = 91 Hz, 1H, C(*H*)═N), 8.45 (t, J_{H-H} = 8 Hz, 1H, Ar), 8.24 (d, J_{H-H} = 8 Hz, 1H, Ar), 8.01 (t, J_{H-H} = 6 Hz, 1H, Ar), 7.60–7.52 (m, 1H, Ar), 7.40–7.29 (ov m, 3H, Ar); ^{13}C{^{1}H} δ: 174.0, 161.8 (d, J_{C-F} = 247 Hz, *C*F), 157.5, 149.7, 148.7 (d, J_{C-F} = 10 Hz), 141.3, 130.7, 130.5, 130.4, 121.2 (d, J_{C-F} = 3 Hz), 116.2 (d, J_{C-F} = 21 Hz), 112.7 (d, J_{C-F} = 25 Hz); ^{19}F{^{1}H} δ: −112.7. IR (nujol): 2931, 2912, 2856, 1593, 1460, 1377, 1358, 1300, 1269, 1252, 1230, 1138, 984, 897, 858, 796, 769, 694. *Anal.* Calc. for $C_{12}H_9N_2Cl_2FPt$: C, 30.91; H, 1.95; N, 6.01. Found: C, 31.27; H, 1.65; N 6.00%.

2.2.11. Compound **4c**

Yield: 85% as an orange solid; m.p. 327 °C (decomposition). Spectroscopic NMR data (in DMSO-d_6): ^{1}H δ: 9.47 (d, J_{H-H} = 6 Hz, J_{H-Pt} = 40 Hz, 1H, Ar), 9.34 (s, J_{H-Pt} = 93 Hz, 1H, C(*H*)═N), 8.45 (t of d, J_{H-H} = 8, 1 Hz, 1H, Ar), 8.23 (d, J_{H-H} = 8 Hz, 1H, Ar), 8.00 (t of d, J_{H-H} = 6, 1 Hz, 1H, Ar), 7.56–7.51 (ov m, 2H, Ar), 7.39–7.33 (ov m, 2H, Ar); ^{13}C{^{1}H} δ: 172.8, 161.8 (d, J_{C-F} = 250 Hz, *C*F), 157.1, 149.1, 143.3 (d, J_{C-F} = 2 Hz), 140.7, 129.8, 129.7, 126.6 (d, J_{C-F} = 9 Hz), 115.0 (d, J_{C-F} = 23 Hz); ^{19}F{^{1}H} δ: −112.7. IR (nujol): 2951, 2939, 2914, 2852, 1462, 1377, 1298, 1244, 1228, 1157, 1101, 1059, 1039, 972, 947, 932, 920, 850, 806, 766, 752, 586. *Anal.* Calc. for $C_{12}H_9N_2Cl_2FPt$: C, 30.91; H, 1.95; N, 6.01. Found: C, 30.75; H, 1.69; N, 5.72%.

2.2.12. Compound **4d**

Yield: 75% as an orange solid; m.p. 315 °C (decomposition). Spectroscopic NMR data (in DMSO-d_6): ^{1}H δ: 9.59 (s, J_{H-Pt} = 90 Hz, 1H, C(*H*)═N), 9.48 (d, J_{H-H} = 6 Hz, J_{H-Pt} = 40 Hz, 1H, Ar), 8.48 (t, J_{H-H} = 8 Hz, 1H, Ar), 8.30 (d, J_{H-H} = 8 Hz, 1H, Ar), 8.06 (t, J_{H-H} = 6 Hz, 1H, Ar), 7.88–7.79 (ov m, 2H, Ar), 7.67 (t, J_{H-H} = 8 Hz, 1H, Ar), 7.54 (d, J_{H-H} = 8 Hz, 1H, Ar); ^{13}C{^{1}H} δ: 174.9, 163.2, 156.9, 150.1, 141.5, 133.4, 131.1, 130.9, 129.4, 127.1, 126.9 (q, J_{C-F} = 5 Hz), 125.0 (q, J_{C-F} = 274 Hz, *C*F$_3$), 122.9 (q, J_{C-F} = 30 Hz); ^{19}F{^{1}H} δ: −56.2. IR (nujol): 2945, 2902, 2868, 1560, 1460, 1377, 1317, 1306, 1271, 1234, 1201, 1163, 1124, 1055, 1032, 968, 781, 762, 723, 596. *Anal.* Calc. for $C_{13}H_9N_2Cl_2F_3Pt$: C, 30.24; H, 1.76; N, 5.43. Found: C, 29.81; H, 1.69; N, 5.25%.

2.2.13. Compound **4e**

Yield: 65% as an orange solid; m.p. 336 °C (decomposition). Spectroscopic NMR data (in DMSO-d_6): ^{1}H δ: 9.48 (d, J_{H-H} = 6 Hz, J_{H-Pt} = 40 Hz, 1H, Ar), 9.45 (s, J_{H-Pt} = 88 Hz, 1H, C(*H*)═N), 8.47 (t of d, J_{H-H} = 8, 1 Hz, 1H, Ar), 8.26 (d, J_{H-H} = 8 Hz, 1H, Ar), 8.02 (t of d, J_{H-H} = 6, 1 Hz, 1H, Ar), 7.90 (s, 1H, Ar), 7.85–7.75 (ov m, 3H, Ar); ^{13}C{^{1}H} δ: 174.5, 157.6, 149.7, 147.6, 141.4, 130.6, 130.5, 130.2 (q, J_{C-F} = 31 Hz), 130.0, 129.2, 128.3 (q, J_{C-F} = 274 Hz, *C*F$_3$), 126.0 (q, J_{C-F} = 4 Hz), 121.9 (q, J_{C-F} = 4 Hz); ^{19}F{^{1}H} δ: −61.0. IR (nujol): 2943, 2910, 2860, 1460, 1377, 1327, 1240, 1182, 1161, 1117, 1066, 941, 808, 771, 700, 660, 596. *Anal.* Calc. for $C_{13}H_9N_2Cl_2F_3Pt$: C, 30.24; H, 1.76; N, 5.43. Found: C, 30.20; H, 1.50; N, 5.43%.

2.2.14. Compound **4f**

Yield: 85% as an orange solid; m.p. 300 °C (decomposition). Spectroscopic NMR data (in DMSO-d_6): ^{1}H δ: 9.48 (d, J_{H-H} = 6 Hz, J_{H-Pt} = 40 Hz, 1H, Ar), 9.43 (s, J_{H-Pt} = 97 Hz, 1H, C(*H*)═N), 8.47 (t of d, J_{H-H} = 8, 1 Hz, 1H, Ar), 8.26 (d, J_{H-H} = 8 Hz, 1H, Ar), 8.03 (t of d, J_{H-H} = 6, 1 Hz, 1H, Ar), 7.92 (d, J_{H-H} = 8 Hz, 2H, Ar), 7.68 (d, J_{H-H} = 8 Hz, 2H, Ar); ^{13}C{^{1}H} δ: 174.4, 157.5, 149.7, 149.5, 141.3, 130.6, 130.5, 130.2 (q, J_{C-F} = 31 Hz), 126.5 (q, J_{C-F} = 274 Hz, *C*F$_3$), 126.0 (2C); ^{19}F{^{1}H} δ: −60.8. IR (nujol): 2958, 2939, 2883, 1416, 1325, 1201, 1111, 1066, 856, 825, 808, 760, 731, 700, 685, 669, 606, 596, 515. *Anal.* Calc. for $C_{13}H_9N_2Cl_2F_3Pt$: C, 30.24; H, 1.76; N, 5.43. Found: C, 29.98; H, 1.42; N, 5.22%.

2.2.15. Compound **4g**

Yield: 60% as an orange solid; m.p. 338 °C (decomposition). Spectroscopic NMR data (in DMSO-d_6): ^{1}H δ: 9.59 (s, J_{H-Pt} = 85 Hz, 1H, C(*H*)═N), 9.49 (d, J_{H-H} = 6 Hz, J_{H-Pt} = 40 Hz, 1H, Ar), 8.49 (t, J_{H-H} = 8 Hz, 1H, Ar), 8.31 (d, J_{H-H} = 8 Hz, 1H, Ar), 8.27 (s, 1H, Ar), 8.25 (s, 2H, Ar), 8.05 (t, J_{H-H} = 6 Hz, 1H, Ar); ^{13}C{^{1}H} δ: 175.6, 157.4, 149.9, 148.1, 141.5, 130.9, 130.6 (q, J_{C-F} = 34 Hz), 130.4, 126.5, 123.5 (q, J = 274 Hz, *C*F$_3$), 123.1 (q, J_{C-F} = 4 Hz); ^{19}F{^{1}H} δ: −61.2. IR (nujol): 2935, 2904, 2870, 1460, 1377, 1290, 1173, 1126, 974, 900, 847, 773. *Anal.* Calc. for $C_{14}H_8N_2Cl_2F_6Pt$: C, 28.77; H, 1.38; N, 4.80. Found: C, 28.57; H, 1.16; N, 4.57%.

2.2.16. Compound **4h**

Yield: 60% as an orange solid; m.p. 302 °C (decomposition). Spectroscopic NMR data (in DMSO-d_6): ^{1}H δ: 9.85 (s, J_{H-Pt} = 82 Hz, 1H, C(*H*)═N), 9.47 (d, J_{H-H} = 6 Hz, J_{H-Pt} = 38 Hz, 1H, Ar), 8.50 (t, J_{H-H} = 8 Hz, 1H, Ar), 8.40 (d, J_{H-H} = 8 Hz, 1H, Ar), 8.14 (t, J_{H-H} = 6 Hz, 1H, Ar); ^{19}F{^{1}H} δ: −145.9 (d, J = 19 Hz), −153.6 (t, J = 19 Hz), −162.6 (t, J = 19 Hz). IR (nujol): 3041, 3016, 2960, 2939, 2864, 1512, 1471, 1433, 1350, 1292, 1223, 1105, 1026, 1011, 993, 939, 887, 779, 667. *Anal.* Calc. for $C_{12}H_5N_2Cl_2F_5Pt$: C, 26.77; H, 0.94; N, 5.21. Found: C, 26.53; H, 0.75; N, 5.15%.

2.3. X-ray crystallography

Crystals of **3d**·**DMF** were grown from a saturated DMF solution at 20 °C. Single crystals were coated with Paratone-N oil, mounted using a glass fibre and frozen in the cold stream of the goniometer. A hemisphere of data was collected on a Bruker AXS P4/SMART 1000 diffractometer using ω and θ scans with a scan width of 0.3° and 10 s exposure time. The detector distance was 4 cm. The data were reduced [14] and corrected for absorption [15]. The structure was solved by direct methods and refined by full-matrix least-squares on F^2 [16]. All non-hydrogen atoms were refined anisotropically. Hydrogen atoms were located in Fourier difference maps and refined isotropically.

2.4. Cell culture

OV2008 (human ovarian carcinoma) and the analogous cisplatin-resistant cell line C13 were a generous gift from Dr. Barbara C. Vanderhyden of the Centre for Cancer Therapeutics, Ottawa Regional Cancer Centre, Ont., Canada. Both cell lines were cultured in complete RPMI-1640 medium with L-glutamine, supplemented with 5% fetal bovine serum, penicillin (50 units/ml) and streptomycin (50 mg/ml). Cells were incubated in a humidified atmosphere of 5% CO_2 at 37 °C and were subcultured twice weekly using trypsin–EDTA.

2.5. Cell growth inhibition assay

Cells were seeded in 96-well plates at a concentration of $0.1–1.0 \times 10^4$ cells/well in 200 μl of complete media and incubated for 24 h at 37 °C in a 5% CO_2 atmosphere to allow for cell adhesion. Stock solutions (15 mM) of the compounds made in DMSO were filter sterilized, then diluted to 10 mM in phosphate-buffered saline (PBS, 0.02 M phosphate, 0.11 M NaCl, pH 7.0, sterile). The 10 mM solutions were diluted to 50 μM and 1.4 mM in complete media for treatment against OV2008 and C13 cell lines, respectively, where 20 μl of compound solutions were added to 180 μl of fresh medium in wells to give final concentrations of 5 μM against OV2008 and 140 μM for C13. All assays were performed in two independent sets of quadruplicate tests. Control groups containing no drug were run in each assay, along with standards of cisplatin and a previously studied *cis*-dichloro(pyridin-2-ylcarboxaldimine)platinum(II) complex (**2**) [11].

Following 48 h of exposure, each well was carefully rinsed with 200 μl PBS buffer. MTT solution (50 μl, 1 mg/ml ddH_2O) along with 200 μl of fresh, complete media were added to each well, and plates were incubated for 45 min. Following incubation, the medium was removed and the purple formazan precipitate in each well was solubilized in 200 μl DMSO. Absorbances were measured using a VersaMax tunable microplate reader (Molecular Devices) at 570 nm. Reduction of cell proliferation was determined as a fraction of the absorbance values for each drug treatment (T) to the mean absorbance of the no-drug control (C), and calculated using the expression $1 - T/C \times 100\%$. Data from the separate trials were combined using a t test ($P < 0.05$).

3. Results and discussion

3.1. Synthesis and structure

The addition of a primary amine to commercially available 2-pyridinecarboxaldehyde to afford the corresponding pyridinecarboxaldimine ligand is a well-known route to a versatile class of bidentate ligands [17–27]. Variation of the amine therefore allows for the facile design of ligands and subsequent metal complexes with different physical and chemical properties. In this study, the metal complexes **3**–**4** (Fig. 2) were prepared by addition of the pyridin-2-ylcarboxaldimine ligands to CH_2Cl_2 solutions of $[MCl_2(coe)]_2$ (M = Pd, Pt; coe = *cis*-cyclooctene) [12,13]. Palladium complexes were also prepared because of recent interest for their anticancer potential. Compounds of the type $[Pd(en)Cl_2]$ and [Pd(en)L] (en = ethylenediamine; L = malonato, methylmalonato, dimethylmalonato and 1,1-cyclobutanedicarboxylato) were recently shown to bind to DNA in a manner similar to that proposed for cisplatin [28].

Complexes containing fluorine groups are of particular interest as substitution of hydrocarbon fragments with C–F moieties can dramatically alter the properties of biologically active compounds and can influence the metabolism and distribution of drug molecules in the body [29–31]. For instance, substitution of fluorine on the aromatic ring of the neurotransmitter norepinephrine produces large differences in its adrenergic activities [32].

In this study, complexes **3**–**4** have been characterized by a number of physical methods, including multinuclear NMR spectroscopy. A significant downfield shift in the ^1H NMR is observed for the imine sp^2 proton upon coordination of the ligand to the metal center. For instance, the singlet at δ 8.59 ppm for the free ligand derived from 2-pyridinecarboxaldehyde and 4-fluoroaniline shifts to 9.34 ppm in complex **4c**. Platinum satellites are also observed for this resonance (J_{H-Pt} = 93 Hz) upon complexation of the ligand to the metal. Similar trends are observed for the pyridine hydrogen α to the nitrogen atom as the chemical shift changes from δ 8.71 to 9.47 ppm (J_{H-Pt} = 40 Hz). The ^{19}F NMR spectra for compounds **3**–**4** are similar to analogous palladium and platinum complexes containing fluorinated imines [33–36]. For instance, three distinct resonances appear

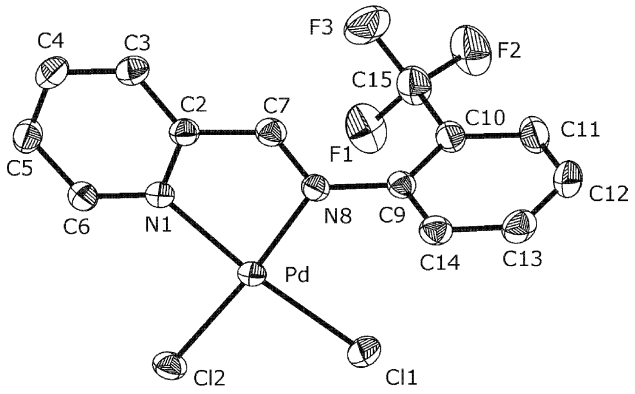

Fig. 3. A view of molecule **3d·DMF**, with displacement ellipsoids drawn at the 30% probability level. H atoms and the molecule of DMF have been omitted for clarity.

in the aromatic region for complexes **3**, **4h**, derived from pentafluoroaniline, and coupling constants are in the expected range for analogous compounds [37]. It is interesting to note, however, that metal complexes **3**, **4h** were unstable in DMSO and decomposed after ca. 12 h to give a number of unidentified products, precluding the acquisition of ^{13}C NMR data. As late metals are known to activate the C–F bond in related pentafluoropyridine [38], it is plausible that compounds **3**, **4h** are also decomposing via a similar mechanism [39,40].

Complex **3d·DMF** has also been characterized by an X-ray diffraction study (Fig. 3). Crystallographic data are given in Table 1 and selected bond lengths and angles provided in Table 2. The nitrogen–palladium bonds of 2.0296(15) Å (pyridine) and 2.0181(16) Å (imine) are similar to those reported in other imine palladium systems [41–43]. The imine C(7)–N(8) distance of 1.286(2) Å is in the range of accepted carbon–nitrogen double bonds [44]. Interesting, the aromatic ring on the imine nitrogen is almost perpendicular to the N(1)–Pd–N(8) plane (83.4°), a trend that is observed in related diimine platinum systems [45]. Indeed, this structural feature has been used to create active and selective catalyst precursors for the polymerization of α-olefins, where *ortho* substitution of the aniline group with bulky groups is believed to shield and stabilize the metal center. The structure of the related $[PtCl_2(R\text{-pea})]$ (pea = 1,(2-pyridyl)ethylamine) has been reported recently [46], where the methyl group of the backbone lies in an equatorial plane and results in a close contact between it and the pyridine, which would otherwise not be present if the methyl group were in the axial position. In the case of **3d·DMF**, a closest contact of Pd with F is 3.387 Å, where the trifluoromethyl group is canted over the plane of the metal center. This observation suggests that complexes with CF_3 groups in the *ortho* position of the imine aryl ring may shield the metal atom in a similar way to AMD473.

Table 1
Crystallographic data collection parameters for **3d·DMF**

Complex	**3d·DMF**
Formula	$C_{16}H_{16}Cl_2F_3N_3OPd$
Formula weight	500.62
Crystal system	triclinic
Space group	$P\bar{1}$
a (Å)	7.9624(5)
b (Å)	9.4425(5)
c (Å)	12.8704(7)
α (°)	77.022(1)
β (°)	76.213(1)
γ (°)	89.263(1)
V (Å^3)	914.93(9)
Z	2
D_{calc} (Mg m^{-3})	1.817
Crystal size (mm^3)	$0.375 \times 0.30 \times 0.15$
T (K)	173(1)
Radiation	Mo Kα ($\lambda = 0.71073$)
μ (mm^{-1})	1.346
Total reflections	7377
Total unique reflections	4769
Number of variables	299
R_{int}	0.0244
θ Range (°)	2.22–30.00
Largest difference peak/hole (e Å^{-3})	0.918/−0.2828
S (Goodness-of-fit) on F^2	1.063
R_1[a] ($I > 2\sigma(I)$)	0.0272
wR_2[b] (all data)	0.0703

[a] $R_1 = \sum||F_o| - |F_c||/\sum|F_o|$.

[b] $wR_2 = (\sum[w(F_o^2 - F_c^2)^2/\sum[F_o^4]])^{1/2}$, where $w = 1/[\sigma^2(F_o^2) + (0.0354 \times P)^2 + (0.2668 * P)]$, where $P = (\max(F_o^2, 0) + 2 \times F_c^2)/3$.

Table 2
Selected bond lengths (Å) and angles (°) for **3d·DMF**

Pd–N(8)	2.0181(16)
Pd–N(1)	2.0296(15)
Pd–Cl(1)	2.2663(5)
Pd–Cl(2)	2.2841(5)
N(1)–C(6)	1.327(2)
N(1)–C(2)	1.357(2)
C(7)–N(8)	1.286(2)
N(8)–C(9)	1.424(2)
C(15)–F(2)	1.325(2)
C(15)–F(1)	1.334(3)
C(15)–F(3)	1.341(3)
N(8)–Pd–N(1)	80.39(6)
N(8)–Pd–Cl(1)	93.28(5)
N(1)–Pd–Cl(1)	173.64(4)
N(8)–Pd–Cl(2)	174.97(4)
N(1)–Pd–Cl(2)	94.66(5)
Cl(1)–Pd–Cl(2)	91.673(19)
C(6)–N(1)–C(2)	118.60(17)
C(6)–N(1)–Pd	128.69(14)
C(2)–N(1)–Pd	112.68(12)
F(2)–C(15)–F(1)	106.7(2)
F(2)–C(15)–F(3)	106.8(2)
F(1)–C(15)–F(3)	105.64(19)
F(2)–C(15)–C(10)	112.02(18)
F(1)–C(15)–C(10)	112.97(19)
F(3)–C(15)–C(10)	112.2(2)

3.2. Cytotoxic activity

We have tested the cytotoxic activity of all the new palladium and platinum complexes against both cisplatin-sensitive and cisplatin-resistant human ovarian cells (Table 3), OV2008 and C13, respectively, at concentrations corresponding to cisplatin's IC_{50} value against either cell line [47–49]. While marginal activity was observed for palladium complexes against cisplatin-sensitive cells OV2008, most of the analogous platinum complexes showed significantly less activity. Indeed, the platinum complexes **4a** and **4h**, which contain a F group in the α position showed no activity against the cisplatin-sensitive cell line. In contrast, however, is the observation that **4d**, with a bulky CF_3 group in the α position, showed considerable activity against OV2008 while **4e** showed no activity with the CF_3 group in the *meta* position. More remarkable is that almost all palladium and platinum complexes displayed substantial activity against cisplatin-resistant cell lines C13. Only compound **4a** does not show any significant activity. Compound **3d**, with the CF_3 group in the *ortho* position of the aryl group, was significantly more active than its platinum analogue **4d**. The platinum compounds **4e** and 4**g** contain a CF_3 moiety in the *meta* position and show enhanced activities towards C13 as compared to OV2008. Interestingly, increased activities were observed for both metal complexes when the CF_3 group was bound in the *para* position (complexes **3f** and **4f** show the greatest activity against C13). While these initial studies have shown that some compounds show promise against the cisplatin-resistant cell line, further in vitro studies are needed to address the structure activity relationships in these complexes in order to design a potent drug candidate.

Table 3
Percent reduction of cell proliferation of cisplatin-sensitive (OV2008) and cisplatin-resistant (C13) cancer cells to compounds at 5 and 140 μM, respectively ($n = 8$; ±SD)

Compound	OV2008	C13
cisplatin	44 ± 11	41 ± 8
2	21 ± 3	37 ± 8
3a	25 ± 11	78 ± 8
3b	21 ± 7	31 ± 9
3c	28 ± 12	31 ± 7
3d	28 ± 10	79 ± 11
3e	20 ± 11	29 ± 16
3f	24 ± 12	83 ± 15
3g	23 ± 10	39 ± 15
3h	25 ± 8	56 ± 13
4a	0	4 ± 4
4b	10 ± 16	83 ± 4
4c	26 ± 5	78 ± 7
4d	70 ± 14	28 ± 13
4e	0	81 ± 6
4f	45 ± 12	96 ± 2
4g	12 ± 9	87 ± 9
4h	0	35 ± 12

4. Conclusion

Pyridinecarboxaldimines derived from the condensation of 2-pyridinecarboxaldehyde and fluorine-containing amines have been prepared in high yields and used as ligands for palladium and platinum salts. The resulting metal complexes have shown considerable cytotoxicity against the OV2008 (human ovarian carcinoma) cisplatin-resistant C13 cell line. Future work in this area will continue to develop bulkier metal complexes containing highly fluorinated groups.

Acknowledgements

Thanks are gratefully extended to the Research Corporation (Cottrell College Science Award), NSERC, Canada Research Chair/Canadian Foundation for Innovation/Atlantic Innovation Fund programs and Mount Allison University for financial support. We also thank Roger Smith, Dan Durant and Barbie Sears (MAU) for expert technical assistance, Dr. Barbara C. Vanderhyden of the Centre for Cancer Therapeutics (Ottawa Regional Cancer Centre, Ont., Canada) for providing us with the OV2008 and C13 cell lines, and anonymous reviewers for helpful comments.

Appendix A. Supplementary material

Full crystallographic data in CIF format have been deposited with The Director, CCDC, 12 Union Road, Cambridge, CB2 1EZ, UK (fax: +44-1223-366033; e-mail: deposit@ccdc.cam.ac.uk or www: http//www.ccdc.cam.ac.uk) and are available on request, quoting deposition number 237107 for compound **3d·DMF**. Supplementary data associated with this article can be found, in the online version at doi:10.1016/j.poly.2004.06.013.

References

[1] E.R. Jamieson, S.J. Lippard, Chem. Rev. 99 (1999) 2467.
[2] J. Reedijk, Chem. Rev. 99 (1999) 2499.
[3] E. Wong, C.M. Giandomenico, Chem. Rev. 99 (1999) 2451.
[4] H. Rauter, R.D. Domencio, E. Menta, A. Oliva, Y. Qu, N. Farrell, Inorg. Chem. 36 (1997) 3919.
[5] Y.-P. Ho, S.C.F. Au-Yeung, K.K.W. To, Med. Res. Rev. 23 (2003) 633.
[6] N. Poklar, D.S. Pilch, S.J. Lippard, E.A. Redding, S.U. Dunham, K.J. Breslauer, Proc. Natl. Acad. Sci. USA 93 (1996) 7606.

[7] E.T. Martins, H. Baruah, J. Kramarczyk, G. Saluta, C.S. Day, G.L. Kucera, U. Bierbach, J. Med. Chem. 44 (2001) 4492.
[8] J.L. Butour, J.-P. Macquet, Eur. J. Biochem. 78 (1977) 455.
[9] K. Neplechová, J. Kašpárková, O. Vrána, O. Nováková, A. Habtemariam, B. Watchman, P.J. Sadler, V. Brabec, Mol. Pharmacol. 56 (1999) 20.
[10] A.C.G. Hotze, Y. Chen, T.W. Hambley, S. Parsons, N.A. Kratochwil, J.A. Parkinson, V.P. Munk, P.J. Sadler, Eur. J. Inorg. Chem. (2002) 1035.
[11] H. Brunner, M. Schmidt, H. Schönenberger, Inorg. Chim. Acta 123 (1986) 201.
[12] S. Otto, A. Roodt, L.I. Elding, J. Chem. Soc., Dalton Trans. (2003) 2519.
[13] L.G. Nikolcheva, C.M. Vogels, R.A. Stefan, H.A. Darwish, S.J. Duffy, R.J. Ireland, A. Decken, R.H.E. Hudson, S.A. Westcott, Can. J. Chem. 81 (2003) 269.
[14] SAINT 6.02, Bruker AXS, Inc., Madison, Wisconsin, USA (1997–1999).
[15] G.M. Sheldrick, SADABS, Bruker AXS, Inc., Madison, WI, USA, 1999.
[16] G.M. Sheldrick, SHELXTL-5.1, Bruker AXS, Inc., Madison, WI, USA, 1997.
[17] P. Krumholz, Inorg. Chem. 4 (1965) 609.
[18] J. Burgess, J. Chem. Soc. (A) (1968) 497.
[19] H. Brunner, B. Reiter, G. Riepl, Chem. Ber. 177 (1984) 1330.
[20] P. Pointeau, H. Patin, A. Mousser, J.-Y. Le Marouille, J. Organomet. Chem. 312 (1986) 263.
[21] G.J.P. Britovsek, G.Y.Y. Woo, N. Assavathorn, J. Organomet. Chem. 679 (2003) 110.
[22] M. Crespo, Polyhedron 15 (1996) 1981.
[23] J.H. Groen, M.J.M. Vlaar, P.W.N.M. van Leeuwen, K. Vrieze, H. Kooijman, A.L. Spek, J. Organomet. Chem. 551 (1998) 67.
[24] M.L. Ferrara, I. Orabona, F. Ruffo, M. Funicello, A. Panunzi, Organometallics 17 (1998) 3832.
[25] S.-J. Kim, N. Yang, D.-H. Kim, S.O. Kang, J. Ko, Organometallics 19 (2000) 4036.
[26] A. Kundu, B.P. Buffin, Organometallics 20 (2001) 3635.
[27] X.–F. He, C.M. Vogels, A. Decken, S.A. Westcott, Polyhedron 23 (2004) 155.
[28] J.M. Tercero, A. Matilla, M.A. Sanjuán, C.F. Moreno, J.D. Martín, J.A. Walmsley, Inorg. Chim. Acta 342 (2003) 77.
[29] B.K. Park, N.R. Kitteringham, P.M. O'Neill, Annu. Rev. Pharmacol. Toxicol. 41 (2001) 443.
[30] Z.-M. Qiu, D.J. Burton, J. Org. Chem. 60 (1995) 5570.
[31] H.L. Bardlow, C.A. VanderWerf, J. Am. Chem. Soc. 70 (1948) 654.
[32] A. Adejare, J.-Y. Nie, D. Hebel, L.E. Brackett, O. Choi, F. Gusovsky, W.L. Padgett, J.W. Daly, C.R. Creveling, K.L. Kirk, J. Med. Chem. 34 (1991) 1063.
[33] M. Crespo, X. Solans, M. Font-Bardía, Organometallics 14 (1995) 355.
[34] J. Albert, J. Granell, R. Moragas, J. Sales, M. Font-Bardía, X. Solans, J. Organomet. Chem. 494 (1995) 95.
[35] O. López, M. Crespo, M. Font-Bardía, X. Solans, Organometallics 16 (1997) 1233.
[36] M. Crespo, M. Font-Bardía, X. Solans, Polyhedron 21 (2002) 105.
[37] C. Crocker, R.J. Goodfellow, J. Gimeno, R. Usón, J. Chem. Soc., Dalton Trans. (1977) 1448.
[38] T. Braun, S. Rothfeld, V. Schorlemer, A. Stammler, H.-G. Stammler, Inorg. Chem. Commun. 6 (2003) 752.
[39] E.F. Murphy, R. Murugavel, H.W. Roesky, Chem. Rev. 97 (1997) 3425.
[40] J.L. Kiplinger, T.G. Richmond, C.E. Osterberg, Chem. Rev. 94 (1994) 373.
[41] A. Bacchi, M. Carcelli, L. Gabba, S. Ianelli, P. Pelagatti, G. Pelizzi, D. Rogolino, Inorg. Chim. Acta 342 (2003) 229.
[42] R. Ares, M. López-Torres, A. Fernández, M.T. Pereira, G. Alberdi, D. Vázquez-García, J.J. Fernández, J.M. Vila, J. Organomet. Chem. 665 (2003) 76.
[43] C. Navarro-Ranninger, I. López-Solera, V.M. González, J.M. Pérez, A. Alvarez-Valdés, A. Martín, P.R. Raithby, J.R. Masaguer, C. Alonso, Inorg. Chem. 35 (1996) 5181.
[44] A.I. Kltaigorodskii, Organic Chemical Crystallography, Consultants Bureau, New York, NY, 1961.
[45] S.D. Ittel, L.K. Johnson, M. Brookhart, Chem. Rev. 100 (2000) 1169.
[46] V.P. Munk, C.I. Diakos, L.T. Ellis, R.R. Fenton, B.A. Messerle, T.W. Hambley, Inorg. Chem. 42 (2003) 3582.
[47] M.S. Robillard, M. Bacac, H. van den Elst, A. Flamigni, G.A. van der Marel, J.H. van Boom, J. Reedijk, J. Comb. Chem. 5 (2003) 821.
[48] A. Trevisan, C. Marzano, P. Cristofori, M.B. Venturini, L. Giovagini, D. Fregona, Arch. Toxicol. 76 (2002) 262.
[49] M.D. Todd, X. Lin, L.F. Stankowski Jr., M. Desai, G.H. Wolfgang, J. Biomol. Screen. 5 (1999) 259.

Available online at www.sciencedirect.com
SCIENCE DIRECT®
Polyhedron 23 (2004) 2177–2182
POLYHEDRON
www.elsevier.com/locate/poly

Dicopper(II) Schiff base aminobenzoates with discrete molecular and 1D-chain polymeric structures

Arindam Mukherjee, Manas K. Saha, Munirathinam Nethaji, Akhil R. Chakravarty *

Department of Inorganic and Physical Chemistry, Indian Institute of Science, Sir C. V. Raman Avenue, Bangalore 560012, India

Received 2 June 2004; accepted 23 June 2004
Available online 29 July 2004

Abstract

Dicopper(II) complexes $[Cu_2L(O_2CC_6H_4\text{-}o\text{-}NH_2)]$ (**1**) and $[Cu_2L(O_2CC_6H_4\text{-}p\text{-}NH_2)]$ (**2**) are prepared from a reaction of $[Cu_2L(O_2CMe)]$ with the corresponding aminobenzoic acid and a base in MeOH, where L is a trianionic pentadentate Schiff base ligand *N*,*N*′-(2-hydroxypropane-1,3-diyl)bis(salicylaldimine). The complexes are structurally characterized by X-ray crystallography. The crystal structures show the presence of an asymmetrically dibridged $\{Cu_2^{II}(\mu\text{-}OR)(\mu\text{-}O_2CR)\}$ core where the endogenous monoatomic bridging alkoxo group is derived from the Schiff base and the aminobenzoate ligand displays *syn–syn* bridging mode. The Cu···Cu separation and Cu–OR–Cu bond angle in **1** and **2** are 3.472(1) Å, 131.02(18)° and 3.511(1) Å, 132.20(17)°, respectively. The *o*-aminobenzoate complex is discrete dimeric nature. The pendant *o*-amino group is involved in an intramolecular hydrogen bonding interaction with one carboxylate oxygen atom. The crystal structure of the *p*-aminobenzoate species **2** shows the formation of a one-dimensional polymeric chain resulting from the axial binding of the pendant *p*-amino group to one copper center belonging to another dimeric unit. Magnetic studies show that both the complexes are antiferromagnetic in nature giving a singlet–triplet energy separation of −130 and −150 cm^{-1} for **1** and **2**, respectively. The 1D chain complex **2** magnetically behaves like the discrete dimeric complex **1**.
© 2004 Elsevier Ltd. All rights reserved.

Keywords: Dicopper(II) complex; 1D Coordination polymer; Crystal structure; Magnetic properties; Schiff base

1. Introduction

Binuclear copper(II) complexes are of interest as models for investigating intramolecular magnetic-exchange interactions between two metal centers in different structural motifs, viz. the ''paddle-wheel'' dicopper(II) tetracarboxylates, symmetrically dibridged hydroxo or alkoxo species, and asymmetrically dibridged complexes with a (μ-hydroxo/alkoxo)(μ-carboxylato)dicopper(II) core [1–10]. Dicopper(II) complexes are also of importance as precursors in the chemistry of supramolecular and discrete molecular high-nuclearity copper(II) complexes [11–20]. In our recent publications, we have shown that dicopper(II) complexes containing pentadentate Schiff base ligands *N*,*N*′-(2-hydroxypropane-1,3-diyl)bis(salicylaldimine) (H_3L) or *N*,*N*′-(2-hydroxypropane-1,3-diyl)bis(acetylacetoneimine) (H_3L^1) are useful for the synthesis of high nuclearity copper(II) complexes showing interesting magneto-structural properties [16–20].

We have observed that the dicopper(II) Schiff base complexes having bridging carboxylate like *p*-hydroxycinnamate with a pendant hydroxyl group form helical supramoleclar structure due to hydrogen bonding interactions involving one phenoxo oxygen atom of the Schiff base and the hydroxyl group of the carboxylate [21]. In contrast, the *p*-hydroxybenzoate complex is a discrete tetranuclear species resulting from the self-assembly of

* Corresponding author. Tel.: +918022932533; fax: +918023600683.
E-mail address: arc@ipc.iisc.ernet.in (A.R. Chakravarty).

0277-5387/$ - see front matter © 2004 Elsevier Ltd. All rights reserved.
doi:10.1016/j.poly.2004.06.014

two dicopper(II) units [22]. The present work stems from our interest to prepare analogous dicopper(II) Schiff base (H_3L) complexes containing *o*- and *p*-aminobenzoate ligands with an aim to explore the effect of the pendant amino group on the structure and magnetic properties of the complexes. Herein we report the synthesis, crystal structure and magnetic properties of two new dicopper(II) complexes $[Cu_2L(O_2CC_6H_4\text{-}o\text{-}NH_2)]$ (**1**) and $[Cu_2L(O_2CC_6H_4\text{-}p\text{-}NH_2)]$ (**2**) having a (μ-alkoxo)(μ-carboxylato)dicopper(II) core. While **1** is discrete dimeric, **2** is a one-dimensional coordination polymer.

2. Experimental

2.1. Materials and measurements

Chemicals and reagents were procured from commercial sources and were used as received. The Schiff base *N*,*N*′-(2-hydroxypropane-1,3-diyl)bis(salicylaldimine) (H_3L) and the precursor complex $[Cu_2L(O_2CMe)]$ were prepared following literature procedures [7]. The elemental analyses were done using Thermo Finnigan FLASH EA 1112 CHN analyser instrument. The infrared and electronic spectra were obtained from Bruker Equinox 55 and Perkin–Elmer Lamda 35 spectrometers, respectively. Variable temperature magnetic susceptibility data for the polycrystalline samples of the complexes in the temperature range 18–300 K were obtained using a Model 300 Lewis Coil Force magnetometer (George Associates Inc., Berkeley, CA), equipped with a closed cycle cryostat (Air Products) and a Cahn balance. $Hg[Co(NCS)_4]$ was used as a standard. The experimental susceptibility data were corrected for diamagnetic contributions and temperature independent paramagnetism [23]. The magnetic susceptibility data were fitted to the modified Bleaney–Bowers expression by means of a least-squares computer program [23,24]. The Hamiltonian and susceptibility equation used were: $\hat{H} = -2J\hat{S}_1\hat{S}_2$ ($S_1 = S_2 = 1/2$ for a d^9–d^9 dicopper(II)core) and $\chi_{Cu} = [Ng^2\beta^2/k(T-\theta)][3+\exp(-2J/k(T-\theta))]^{-1}(1-\rho) + (Ng_1^2\beta^2/4kT)\rho + N_\alpha$, where ρ is the fraction of paramagnetic impurity and $2J$ is the singlet–triplet energy separation. The expression used to calculate *R* value is: $R = \sum_i[\{\chi_{obs}(T_i) - \chi_{calc}(T_i)\}^2/\chi_{obs}(T_i)^2]$. The best theoretical fit gave $2J = -130$ cm^{-1}, $g = 2.06$, $\rho = 0.011$, $g1 = 2.2$, $\theta = 0$ K, $R = 6.5\times10^{-3}$ for **1** and $2J = -150$ cm^{-1}, $g = 2.19$, $\rho = 0.02$, $g1 = 2.2$, $\theta = 6$ K, $R = 7.9\times10^{-3}$ for **2**. The magnetic moments were calculated in μ_B unit ($\mu_B \approx 9.274\times10^{-24}$ JT^{-1}).

2.2. Synthesis

The complexes were prepared by a common synthetic procedure in which the *ortho*- or *para*-aminobenzoic acid (0.24 g, 1.7 mmol) taken in methanol (10 ml) was initially treated with piperidine (0.15 ml, 1.5 mmol), followed by reaction with a methanol solution of $[Cu_2L(O_2CMe)]$ (0.71 g, 1.5 mmol). The solution was refluxed for 30 min, cooled to an ambient temperature and the product, isolated as a green solid, was washed with ethanol and finally dried in vacuum over P_4O_{10} (~65% yield). *Anal.* Calc. for $C_{24}H_{21}Cu_2N_3O_5$ (**1**): C, 51.6; H, 3.8; N, 7.5. Found: C, 51.3; H, 4.0; N, 7.7%. FT-IR (KBr phase), cm^{-1}: 3478m, 3351m, 3051w, 2908w, 1635s, 1601m, 1570m, 1538s, 1467m, 1449s, 1397s, 1343m, 1317s, 1261m, 1196m, 1151m, 1110m, 1107w, 1055w, 1030w, 967w, 895w, 862w, 760s, 706m, 671w, 593w, 573w, 469w (s, strong; m, medium; w, weak). Electronic spectral data in MeOH [λ_{max}, nm (ε, M^{-1}cm^{-1})]: 635 (370), 354 (8600), 269 (22600), 242 (42000), 222 (54000). Magnetic susceptibility data [χ_M^{corr} (per copper), cm^{3}M^{-1}]: 1.17×10^{-3} at 300 K; 0.35×10^{-3} at 18 K. Magnetic moment (μ_{eff} per copper): 1.67 μ_B at 300 K and 0.22 μ_B at 18 K. *Anal.* Calc. for $C_{24}H_{21}Cu_2N_3O_5$ (**2**): C, 51.6; H, 3.8; N, 7.5. Found: C, 51.4; H, 4.0; N, 7.6%. FT-IR (KBr phase), cm^{-1}: 3419m, 3341m, 3052w, 2925w, 2899w, 1632s, 1600s, 1587s, 1548s, 1449s, 1390s, 1349m, 1319m, 1281m, 1186m, 1167m, 1148m, 1132m, 1055w, 1027w, 966w, 858w, 792m, 758m, 698m, 625w, 587w, 513w, 475w, 437w. Electronic spectral data in MeOH [λ_{max}, nm (ε, M^{-1}cm^{-1})]: 640 (370), 364 (10100), 273 (41600), 242 (43600), 223 (50000). Magnetic susceptibility data [χ_M^{corr} (per copper), cm^{3}M^{-1}]: 1.29×10^{-3}at 300 K; 0.73×10^{-3} at 18 K. Magnetic moment (μ_{eff} per copper): 1.76 μ_B at 300 K and 0.33 μ_B at 18 K.

2.3. X-ray crystallography

Single crystals of the complexes were obtained on slow concentration of the mother liquor at room temperature. The crystals were mounted on glass fibers using epoxy cement. All geometric and intensity data for **1** were collected using an automated Enraf-Nonius CAD4 diffractometer equipped with graphite monochromated Mo Kα radiation. Intensity data were collected using a ω–2θ scan mode and the data were corrected for Lorentz-polarization effects and for absorption [25a]. Intensity data for **2** were measured in frames with increasing ω (width of 0.3°/frame) at a scan speed of 12 s/frame using a Bruker SMART APEX CCD diffractometer, equipped with a fine-focus sealed tube X-ray source. The SMART software was used for data acquisition and the SAINT software for data extraction. Empirical absorption correction was made on the data [25b]. The structures were solved by heavy atom method and refined on F^2 by full-matrix least-squares using SHELX programs [26]. All the non-hydrogen atoms were refined anisotropically. Hydrogen atoms were generated in their calculated positions, assigned fixed ther-

Table 1
Selected crystallographic data for discrete dimeric [$Cu_2L(O_2CC_6H_4$-*o*-$NH_2)$] (**1**) and 1D-chain polymeric [$Cu_2L(O_2CC_6H_4$-*p*-$NH_2)$] (**2**)

	1	**2**
Empirical formula	$C_{24}H_{21}Cu_2N_3O_5$	$C_{24}H_{21}Cu_2N_3O_5$
Formula weight	558.52	558.52
Temperature (K)	293(2)	293(2)
λ(Mo Kα) (Å)	0.71073	0.71073
Crystal system	orthorhombic	orthorhombic
Space group (no.)	*Pcab* (no. 61)	*Pbca* (no. 61)
Unit cell dimensions		
a (Å)	16.920(2)	9.3620(11)
b (Å)	11.017(5)	18.642(2)
c (Å)	24.199(4)	25.440(3)
V (Å^3)	4511(2)	4440.1(9)
Z	8	8
D_{calc} (Mg m^{-3})	1.645	1.671
Absorption coefficient (mm^{-1})	1.928	1.959
F(000)	2272	2272
Crystal size (mm)	0.32×0.32×0.2	0.27×0.11×0.03
θ Range for data collection (°)	1.68–25.0	1.60–23.25
Index ranges	$0 \leqslant h \leqslant 20$, $0 \leqslant k \leqslant 13$, $0 \leqslant l \leqslant 28$	$-10 \leqslant h \leqslant 10$, $-20 \leqslant k \leqslant 20$, $-28 \leqslant l \leqslant 25$
Reflections collected [R_{int}]	3965 [0.0000]	25870 [0.0806]
Reflections observed [$I > 2\sigma(I)$]	3965 [2738]	3173 [2157]
Number of parameters refined	315	315
Maximum and minimum transmission	0.6798, 0.5347	0.7572, 0.6114
Goodness-of-fit on F^2	1.109	0.834
R (observed data) [*R* (all data)]	0.0590 [0.0988]	0.0384 [0.0686]
R_w (observed data) [R_w (all data)]	0.1097 [0.1240]	0.0760 [0.0845]
Largest difference peak and hole (eÅ^{-3})	0.486 and −0.332	0.352 and −0.407
Weight factor: $w = 1/[\sigma^2(F_o^2) + (AP)^2 + BP]$	$A = 0.0562$, $B = 2.4706$	$A = 0.0441$, $B = 1.8437$

mal parameters and refined using a riding model. They were used for structure factor calculation only. Selected crystallographic data are given in Table 1. Perspective views of the complexes were obtained by ORTEP [27].

3. Results and discussion

3.1. Synthesis and general properties

Complexes **1** and **2** are prepared in high yield by reacting [$Cu_2L(O_2CMe)$] with the respective *ortho*- and *para*-aminobenzoate ligand in methanol. The complexes show a visible spectral band near 640 nm in MeOH, assignable to the d–d transition. The infrared spectra display characteristic bands for the amino group near 3450 and 3350 cm^{-1}. The IR spectral band for the imine group [ν(C=N)] is observed near 1640 cm^{-1}.

3.2. Crystal structures

The molecular structures of **1** and **2** are obtained from single crystal X-ray crystallographic studies. Selected bond distances and angles are listed in Table 2 and the ORTEP views are given in Figs. 1 and 2. Complex **1** is a discrete dimeric species in which the metal atoms are bonded to a pentadentate Schiff base and a carboxylate ligand. The Schiff base provides the endogenic alkoxo bridge, while the carboxylate displays three-atom bridging mode in the {Cu_2(μ-OR)(μ-O_2CR)} core. Each copper has $CuNO_3$ square-planar coordination geometry. The Cu···Cu distance and Cu–O–Cu angle are 3.472(1) Å and 131.02(18)°, respectively. The copper atoms are deviated by ∼0.01 Å from the basal plane. The alkoxo oxygen atom O(2) has a planar geometry as the sum of three angles is ∼359°. The pendant *o*-amino group is involved in moderately strong intramolecular hydrogen bonding interaction with the oxygen atom O(4) of the carboxylate [N(3)···O(4), 2.65(1) Å].

Complex **2** with *p*-aminobenzoate ligand forms a one-dimensional coordination polymer in which the [$Cu_2L(O_2CC_6H_4$-*p*-$NH_2)$] units are linked via axial coordination of the amino group of one unit to the copper center of another dimeric unit. The Cu(1) atom has a square pyramidal (4 + 1) coordination geometry, while the Cu(2) atom is square planar. The Cu···Cu distance and Cu–O–Cu angle are 3.511(1) Å and 132.20(17)°, respectively. The Cu(1) atom is deviated by ∼0.1 Å from the basal plane due to the formation of the axial bond. The polymeric structure of **2** displays an isotactic arrangement of the Cu(2) atom protruding to one side of the polymeric chain that contains the Cu(1) atom. The polymeric structure of **2** is significantly different from its isonicotinate analogue $Cu_2L(O_2CC_5H_4N)$] in which the Cu_2L^+ units are covalently linked by the

Table 2
Selected bond distances (Å) and angles (°) for discrete dimeric $[Cu_2L(O_2CC_6H_4\text{-}o\text{-}NH_2)]$ (**1**) and 1D-chain polymeric $[Cu_2L(O_2CC_6H_4\text{-}p\text{-}NH_2)]$ (**2**)

	1	2
Cu(1)···Cu(2)	3.472(1)	3.511(1)
Cu(1)–O(1)	1.905(3)	1.891(3)
Cu(1)–O(2)	1.914(3)	1.927(3)
Cu(1)–O(5)	1.932(3)	1.974(3)
Cu(1)–N(1)	1.941(4)	1.943(4)
Cu(1)–N(3)#1[a]		2.552(5)
Cu(2)–O(2)	1.901(3)	1.913(3)
Cu(2)–O(3)	1.886(4)	1.892(3)
Cu(2)–O(4)	1.925(4)	1.927(3)
Cu(2)–N(2)	1.927(5)	1.926(4)
Cu(1)–O(2)–Cu(2)	131.02(18)	132.20(17)
O(1)–Cu(1)–O(2)	176.47(15)	177.23(14)
O(1)–Cu(1)–O(5)	87.35(15)	89.25(14)
O(1)–Cu(1)–N(1)	92.44(16)	93.14(15)
O(2)–Cu(1)–O(5)	96.17(14)	93.45(13)
O(2)–Cu(1)–N(1)	84.04(16)	84.09(15)
O(5)–Cu(1)–N(1)	179.39(17)	166.22(15)
O(2)–Cu(2)–O(3)	178.55(16)	175.24(14)
O(2)–Cu(2)–O(4)	94.83(14)	94.61(13)
O(2)–Cu(2)–N(2)	84.16(16)	84.47(15)
O(3)–Cu(2)–O(4)	86.32(16)	88.38(14)
O(3)–Cu(2)–N(2)	94.65(18)	93.09(15)
O(4)–Cu(2)–N(2)	177.44(17)	171.87(15)

[a] Symmetry operation (#1): $x-1, y, z$.

pyridine nitrogen atom of the isonicotinate ligand to give a syndiotactic arrangement of the copper ions protruding outside the chain [28].

3.3. Magnetic properties

The variable temperature magnetic susceptibility data for the complexes in the temperature range 300–18 K show an antiferromagnetic (AF) behavior of the complexes (Fig. 3). The magnetic moment values (per copper) of ~1.7 μ_B at 300 K and ~0.3 μ_B at 18 K indicate significant AF spin–spin coupling in the asymmetrically dibridged dicopper(II) core. A theoretical fitting of the magnetic susceptibility data for **1** gave the singlet–triplet energy separation ($-2J$) of 130 cm^{-1} with the singlet as the ground state. Complex **1** is a discrete dimeric species and the observed magnitude of the exchange coupling constant compares well with that of the precursor complex (-170 cm^{-1}) [7]. The nature and magnitude of the magnetic exchange interaction in the {Cu_2(μ-OR)(μ-

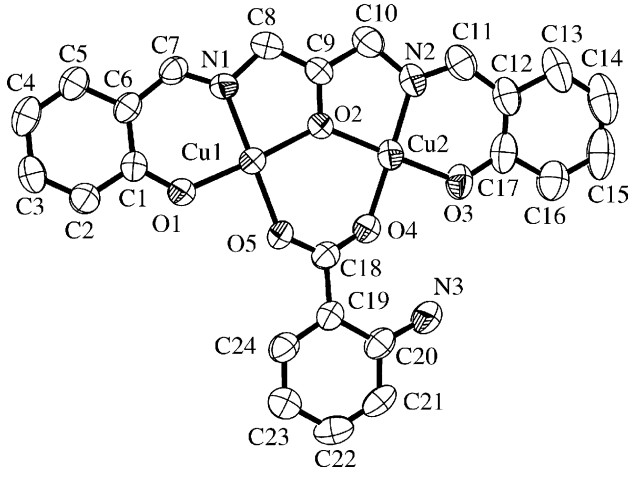

Fig. 1. An ORTEP view of $[Cu_2L(O_2CC_6H_4\text{-}o\text{-}NH_2)]$ (**1**) showing 50% probability thermal ellipsoids and the atom labeling scheme.

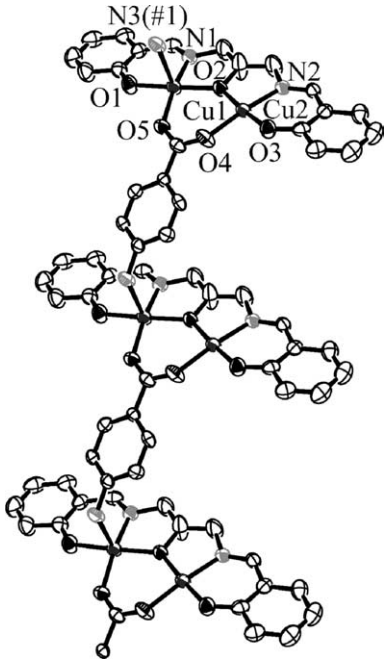

Fig. 2. An ORTEP view of the one-dimensional chain polymeric complex $[Cu_2L(O_2CC_6H_4\text{-}p\text{-}NH_2)]$ (**2**) showing 50% probability thermal ellipsoids and the atom numbering scheme.

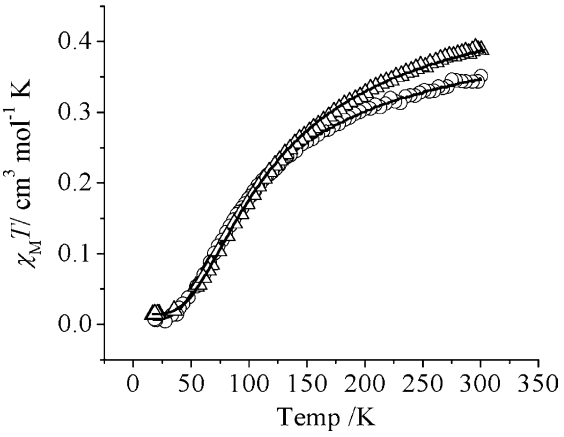

Fig. 3. Plots of $\chi_M T$ vs. T for the polycrystalline samples of $[Cu_2L(O_2CC_6H_4\text{-}o\text{-}NH_2)]$ (**1**, ○) and 1D-chain polymeric $[Cu_2L(O_2CC_6H_4\text{-}p\text{-}NH_2)]$ (**2**, △). The solid lines are the theoretical fits to the experimental data.

$O_2CR)\}$ core primarily depends on the Cu–O–Cu angle. The magnitude of $-2J$ in such a core is generally small due to counter-complimentary nature of overlap of the magnetic orbitals [4,5,7].

The magnetic behavior of the 1D chain coordination polymer **2** is similar to those observed for the discrete dicopper(II) complexes with a $\{Cu_2(\mu\text{-}OR)(\mu\text{-}O_2CR)\}$ core. Complex **2** has been modeled as an isolated dimeric species and good theoretical fitting of the magnetic susceptibility data is obtained using modified Bleaney–Bowers expression [23,24]. The $2J$ value is -150 cm^{-1} with a θ value of 6 K. While an antiferromagnetic coupling is predominant in the dicopper(II) unit having a large Cu–O–Cu angle of 132°, a positive value of θ suggests the presence of minor ferromagnetic interaction involving the dimeric units through the axial bond. The involvement of the $d_{x^2-y^2}$ orbital of the Cu(1) atom and the d_{z^2} orbital of the adjacent copper atom along the chain could promote weak ferromagnetic interaction. The magnetic behavior of **2** is significantly different from that of the isonicotinate complex $[Cu_2L(O_2CC_5H_4N)]_x$ for which the magnetic data do not show any good fit with the Bleaney–Bowers expression. The magnetic model assumes the isonicotinate complex as an equimolar mixture of copper atoms belonging to an antiferromagnetically coupled one-dimensional Heisenberg chain with the other copper atoms outside the chain behaving like paramagnetic centers [28]. The 1D chain of **2** magnetically behaves like the discrete dimeric complex **1**.

In summary, two new Schiff base copper(II) complexes having asymmetrically dibridged dicopper(II) cores are prepared and structurally characterized. The *o*-aminobenzoate complex is discrete dimeric in nature. The *p*-aminobenzoate species shows the formation of a one-dimensional coordination polymer. The dicopper(II) cores in the complexes show antiferromagnetic magnetic exchange. The magnetic interaction between two copper centers along the 1D chain in **2** is weakly ferromagnetic in nature.

Acknowledgments

We thank the Department of Science and Technology, Government of India, for the financial support and for the CCD diffractometer facility. We also thank the Convener of the Bioinformatics Center of our Institute for database search.

Appendix A. Supplementary data

Crystallographic data for **1** and **2** in the CIF format have been deposited with the Cambridge Crystallographic Data Center, CCDC Nos. 240088 and 240089. Copies of this information may be obtained free of charge from The Director, CCDC, 12 Union Road, Cambridge, CB2 1EZ, UK (fax: +44-1223-366-033; e-mail: deposit@ccdc.ac.uk or http://www.ccdc.cam.ac.uk). Supplementary data associated with this article can be found, in the online version at doi:10.1016/j.poly.2004.06.014.

References

[1] (a) M. Kato, Y. Muto, Coord. Chem. Rev. 92 (1988) 45;
(b) M. Melnik, Coord. Chem. Rev. 42 (1982) 1981;
(c) R.J. Doedens, Prog. Inorg. Chem. 21 (1976) 209.
[2] (a) W.E. Hatfield, Comments Inorg. Chem. 1 (1981) 105;
(b) D.J. Hodgson, Prog. Inorg. Chem 19 (1975) 173;
(c) V.H. Crawford, H.W. Richardson, J.R. Wasson, D.J. Hodgson, W.E. Hatfield, Inorg. Chem. 15 (1976) 2107.
[3] (a) O. Kahn, Angew. Chem., Int. Ed. Engl. 24 (1985) 834;
(b) O. Kahn, Comments Inorg. Chem. 3 (1984) 105.
[4] P.J. Hey, J.C. Thibeault, R. Hoffmann, J. Am. Chem. Soc. 97 (1975) 4884.
[5] W. Mazurek, B.J. Kennedy, K.S. Murray, M.J. O'Connor, J.R. Rodgers, M.R. Snow, A.G. Wedd, P.R. Zwack, Inorg. Chem. 24 (1985) 3258.
[6] (a) Y. Nishida, M. Takeuchi, K. Takahashi, S. Kida, Chem. Lett. (1982) 1815;
(b) Y. Nishida, M. Takeuchi, K. Takahashi, S. Kida, Chem. Lett. (1985) 631.
[7] Y. Nishida, S. Kida, J. Chem. Soc., Dalton Trans. (1986) 2633.
[8] M. Handa, N. Koga, S. Kida, Bull. Chem. Soc. Jpn. 61 (1988) 6853.
[9] (a) K. Geetha, M. Nethaji, N.Y. Vasanthacharya, A.R. Chakravarty, J. Coord. Chem. 47 (1999) 77;
(b) S. Meenakumari, S.K. Tiwari, A.R. Chakravarty, J. Chem. Soc., Dalton Trans. (1993) 2175;
(c) K. Geetha, M. Nethaji, A.R. Chakravarty, N.Y. Vasanthacharya, Inorg. Chem. 35 (1996) 7666.
[10] (a) T.N. Sorrell, C.J. O'Connor, D.P. Anderson, J.H. Reibenspies, J. Am. Chem. Soc. 107 (1985) 4199;
(b) V. McKee, M. Zvagulis, J.V. Dagdigian, M.G. Patch, C.A. Reed, J. Am. Chem. Soc. 106 (1984) 4765.
[11] R.E.P. Winpenny, Adv. Inorg. Chem. 52 (2001) 1.
[12] S.P. Perlepes, E. Libby, W.E. Streib, K. Folting, G. Christou, Polyhedron 8 (1992) 923.
[13] (a) S.R. Batten, B.F. Hoskins, B. Moubaraki, K.S. Murray, R. Robson, Chem. Commun. (2000) 1095;
(b) B. Graham, M.T.W. Hearn, P.C. Junk, C.M. Kepert, F.E. Mabbs, B. Moubaraki, K.S. Murray, L. Spiccia, Inorg. Chem. 40 (2001) 1536.
[14] M.-L. Tong, K.H. Lee, Y.-X. Tong, X.-M. Chen, T.C.W. Mak, Inorg. Chem. 39 (2000) 4666.
[15] (a) V. Tangoulis, C.P. Raptopoulou, S. Paschalidou, E.G. Bakalbassis, S.P. Perlepes, A. Terzis, Angew. Chem., Int. Ed. Engl. 36 (1997) 1083;
(b) V. Tangoulis, C.P. Raptopoulou, A. Terzis, S. Paschalidou, S.P. Perlepes, E.G. Bakalbassis, Inorg. Chem. 36 (1997) 3996;
(c) H. Annetha, K. Panneerselvam, T.-F. Liao, T.-H. Lu, C.-S. Chung, J. Chem. Soc., Dalton Trans. (1999) 2869.
[16] A. Mukherjee, I. Rudra, M. Nethaji, S. Ramasesha, A.R. Chakravarty, Inorg. Chem. 42 (2003) 463.
[17] K. Geetha, M. Nethaji, A.R. Chakravarty, Inorg. Chem. 36 (1997) 6134.
[18] A. Mukherjee, M. Nethaji, A.R. Chakravarty, Angew. Chem. Int. Ed. 43 (2004) 87.

[19] A. Mukherjee, M. Nethaji, A.R. Chakravarty, Chem. Commun. (2003) 2978.
[20] A. Mukherjee, I. Rudra, S.G. Naik, S. Ramasesha, M. Nethaji, A.R. Chakravarty, Inorg. Chem. 42 (2003) 5660.
[21] A. Mukherjee, M.K. Saha, M. Nethaji, A.R. Chakravarty, Chem. Commun. (2004) 716.
[22] A. Mukherjee, M.K. Saha, I. Rudra, S. Ramasesha, M. Nethaji, A.R. Chakravarty, Inorg. Chim. Acta 357 (2004) 1077.
[23] O. Kahn, Molecular Magnetism, VCH, Weinheim, Germany, 1993.
[24] B. Bleaney, K.D. Bowers, Proc. R. Soc. Lond. A 214 (1952) 451.
[25] (a) A.C.T. North, D.C. Phillips, F.S. Mathews, Acta. Crystallogr., Sect. A 24 (1968) 351;
(b) G.M. Sheldrick, SADABS, Version 2, Multi-Scan Absorption Correction Program, University of Göttingen, Germany, 2001.
[26] G.M. Sheldrick, SHELX 97, Programs for Crystal Structure Solution and Refinement, University of Göttingen, Göttingen, Germany, 1997.
[27] M.N. Burnett, C.K. Johnson, ORTEP-III, Report ORNL-6895, Oak Ridge National Laboratory, Oak Ridge, TN, 1996.
[28] K. Geetha, S.K. Tiwary, A.R. Chakravarty, G. Ananthakrishna, J. Chem. Soc., Dalton Trans. (1999) 4463.

Available online at www.sciencedirect.com
SCIENCE DIRECT®
Polyhedron 23 (2004) 2183–2192
POLYHEDRON
www.elsevier.com/locate/poly

Alkaline earth metal complexes of the edta-type with a six-membered diamine chelate ring: crystal structures of $[Mg(H_2O)_6]$ $[Mg(1,3\text{-pdta})] \cdot 2H_2O$ and $[Ca(H_2O)_3Ca(1,3\text{-pdta})(H_2O)] \cdot 2H_2O$: comparative stereochemistry of edta-type complexes

Dušanka D. Radanović [a,*], Urszula Rychlewska [b,**], Miloš I. Djuran [c], Beata Warżajtis [b], Nenad S. Drašković [c], Dejan M. Gurešić [c]

[a] *Institute of Chemistry, Technology and Metallurgy, University of Belgrade, Njegoševa 12, P.O. Box 815, 11001 Belgrade, Serbia and Montenegro*
[b] *Faculty of Chemistry, Adam Mickiewicz University, 60-780 Poznan, Poland*
[c] *Department of Chemistry, Faculty of Science, University of Kragujevac, R. Domanovića 12, P.O. Box 60, 34000 Kragujevac, Serbia and Montenegro*

Received 29 March 2004; accepted 28 May 2004
Available online 28 August 2004

Abstract

Starting from $Ba[Ba(1,3\text{-pdta})] \cdot 2H_2O$ (where 1,3-pdta is the 1,3-propanediaminetetraacetate ion) two new hexadentate complexes: $[Mg(H_2O)_6][Mg(1,3\text{-pdta})] \cdot 2H_2O$ (**1**) and $[Ca(H_2O)_3Ca(1,3\text{-pdta})(H_2O)] \cdot 2H_2O$ (**2**) have been prepared and characterized. The complexes differ in coordination numbers and geometry, and in coordinative bond distances. They also display dramatically different packing patterns: while the structural units of (**1**) consist of discrete $[Mg(1,3\text{-pdta})]^{2-}$ and $[Mg(H_2O)_6]^{2+}$ octahedra arranged in the solid-state in a close packed fashion, the crystals of (**2**) are composed of one-dimensional chains of ligand-bridged coordination complexes, such that no discrete complex units exist. The calcium(II) ion (Ca1), coordinated with the 1,3-pdta ligand and two symmetry-related water molecules, forms an irregular square-antiprismatic structure, which is not common for the M-1,3-pdta system. The coordination polyhedron formed around the counter ion (Ca2) can best be described as a dodecahedron. Six-membered diamine chelate rings in complexes (**1**) and (**2**) are found to be in *twist-boat* and distorted *chair* conformations, respectively. Infrared and solid-state ^{13}C NMR spectra of Ba-, Mg- and Ca-1,3-pdta complexes have also been presented.
© 2004 Elsevier Ltd. All rights reserved.

Keywords: Alkaline earth metal complexes; Crystal structures

1. Introduction

The metal ion (M) complexes with edta-type ligands (edta is the ethylenediaminetetraacetate ion) exhibit a variety of coordination numbers (C.N.) and geometries [1]. Factors that govern the stereochemistry of this type of complex have been considered by different authors [2–4]. According to Yamamoto et al. [2], the elements that dictate the structural types of M-edta complexes include d-electron configuration and the size of the central metal ion (M). When the ionic radius of the metal ion, [5] with other than spherically symmetric electron configurations, exceeds the size of a "critical" ionic radius, [2,4] a C.N. of six is preferred by ligand field stabilization. In some cases, edta cannot easily span the large

* Corresponding authors. Fax: +381 11 636 061
** Fax: +48 61 865 8008.
E-mail addresses: radanovic@helix.chem.bg.ac.yu (D.D. Radanović), urszular@amu.edu.pl (U. Rychlewska).

0277-5387/$ - see front matter © 2004 Elsevier Ltd. All rights reserved.
doi:10.1016/j.poly.2004.05.019

ion as a hexadentate ligand and the complex is expected to contain pentadentate edta having one carboxylate arm dechelated and a monodentate ligand occupying the sixth position. However, for M-edta complexes, where the ionic radius of M, [5] with d^0, d^5 (high-spin) or d^{10} configurations, exceeds the size of the "critical" ionic radius, [2,4] the C.N. can be expected to increase to 7. Seven-coordinate metal complexes, which adopt in most cases either a pentagonal-bipyramidal (PB) or mono-capped trigonal-prismatic (CTP) structure, have attracted an increasing interest of coordination chemists, [4] because they are relatively rare and play key roles in associative substitution reactions of the by-far more common six-coordinate, octahedral metal complexes.

The theory that treats the role of chelate ring size to be a very important factor in determining the coordination number and geometry, and the complex stability, has been reported by Hancock [3]. He has established that the ligand edta which is capable of forming only five-membered chelate rings, favours coordination with larger metal ions with an ionic radii of about 1.0 Å. The M-edta system is of minimum strain when the M–N bond length is 2.5 Å and the N–M–N bond angle is 69°. This is consistent with a coordination number higher than six and indeed there are several examples of complexes of the $[M(edta)(H_2O)]^{n-}$ type (M = Mg(II), [6,7] Mn(II), [8] Fe(II), [4] Co(II), [9] Fe(III), [10] V(III) [11] and Ca(II) [12]). In contrast to this, a six-membered diamine ring of 1,3-pdta (1,3-pdta is the 1,3-propanediaminetetraacetate) was found to have minimum strain when the metal ion (M) is small with a M–N bond distance of 1.6 Å and a N–M–N bond angle of 109.5° [3].

All hexadentate $[M(1,3\text{-pdta})]^{n-}$ (M = Co(III), [13] Cr(III), [14] Rh(III), [14] Fe(III), [2,15] V(III), [16] Cu(II), [17,18] Ni(II) [19] and Co(II) [20]) complexes known so far, adopt more or less distorted octahedral geometry. Comparing the X-ray data [1,19,20] of edta and 1,3-pdta complexes it has been found that the hexadentate 1,3-pdta ligand containing a lengthened diamine chain, with respect to edta, is able to form less strained octahedral systems with metal ions of different size.

The aim of the present work was to investigate the stereochemical properties of 1,3-pdta complexes with spherically symmetric metal ions of different size. For this purpose two hexadentate complexes, $[Mg(H_2O)_6][Mg(1,3\text{-pdta})]\cdot 2H_2O$ (**1**) (C.N. = 6) and $[Ca(H_2O)_3Ca(1,3\text{-pdta})(H_2O)]\cdot 2H_2O$ (**2**) (C.N. = 8) were prepared, and characterized. The structural characteristics of **1** and **2** were studied by single-crystal X-ray crystallography, and spectral infrared and solid-state ^{13}C NMR characterizations for these and the $[Ba(1,3\text{-pdta})]^{2-}$ complex have also been given.

2. Experimental

All commercially obtained reagent-grade chemicals were used without further purification. The preparation of barium (1,3-propanediaminetetraacetato)barium(II) dihydrate, $Ba[Ba(1,3\text{-pdta})]\cdot 2H_2O$, has been reported elsewhere [17,21].

2.1. Preparation of hexaaquamagnesium(II) (1,3-propanediaminetetraacetato)magnesium(II) dihydrate, $[Mg(H_2O)_6][Mg(1,3\text{-pdta})]\cdot 2H_2O$ (1)

$MgSO_4\cdot 6H_2O$ (4.56 g, 20.0 mmol) was dissolved in 160 cm^3 of water. To this solution, solid $Ba[Ba(1,3\text{-pdta})]\cdot 2H_2O$ (6.13 g, 10.0 mmol) was added and the reaction mixture was stirred with heating for 9 h at 90 °C. During this time the volume of the reaction mixture was kept at about 160 cm^3 by adding distilled water. The precipitated $BaSO_4$ was removed by filtration, and the volume of filtrate was reduced to 25 cm^3. After cooling at room temperature, the solution was left to stand in a refrigerator overnight. The colorless crystals of $[Mg(H_2O)_6][Mg(1,3\text{-pdta})]\cdot 2H_2O$ (**1**) were filtered, washed with ethanol, then ether, and air-dried. Yield: 4.36 g, 88%. Recrystallization of the compound was easily achieved from hot water and cooling the solution at room temperature. *Anal.* Calc. for $[Mg(H_2O)_6][Mg(1,3\text{-pdta})]\cdot 2H_2O$ (**1**), $Mg_2C_{11}H_{30}N_2O_{16}$ (FW = 494.99): C, 26.69; H, 6.11; N, 5.66. Found: C, 26.84; H, 5.91; N, 5.70%.

2.2. Preparation of (aqua)(1,3-propanediaminetetraacetato)calcium(II)-triaquacalcium(II) dihydrate, $[Ca(H_2O)_3Ca(1,3\text{-pdta})(H_2O)]\cdot 2H_2O$ (2)

$CaSO_4\cdot 1/2H_2O$ (2.90 g, 20.0 mmol) was dissolved in 1200 cm^3 of water. Into this solution solid $Ba[Ba(1,3\text{-pdta})]\cdot 2H_2O$ (6.13 g, 10.0 mmol) was added, and the reaction mixture was stirred with heating for 18 h at 90 °C. During this time, the volume of the reaction mixture was reduced to 400 cm^3 and the precipitated $BaSO_4$ was removed by filtration. The volume of the filtrate was reduced to 200 cm^3 and then cooled at room temperature. The white compound $[Ca(H_2O)_3Ca(1,3\text{-pdta})(H_2O)]\cdot 2H_2O$ (**2**) (2.23 g) was collected by filtration and air-dried. The volume of mother liquor was reduced to 80 cm^3. After cooling at room temperature, 10 cm^3 of ethanol was added and the solution was left to stand at room temperature for several days. From this solution an additional amount of $[Ca(H_2O)_3Ca(1,3\text{-pdta})(H_2O)]\cdot 2H_2O$ (**2**) (1.12 g) was precipitated, then filtered and air-dried. Yield: 3.35 g, 68%. The complex was recrystallized from a water solution left to stand in a desiccator over methanol for several weeks. The recrystallized

product was checked by elemental microanalyses and IR spectroscopy, and the obtained results were equal to those for the precipitates obtained before recrystallization. *Anal.* Calc. for $[Ca(H_2O)_3Ca(1,3\text{-}pdta)(H_2O)] \cdot 2H_2O$ (**2**), $Ca_2C_{11}H_{26}N_2O_{14}$ (FW = 490.50): C, 26.94; H, 5.34; N, 5.71. Found: C, 27.10; H, 5.24; N, 5.71%.

2.3. Physical measurements

The IR spectra in the solid-state were recorded on a JASCO FT/IR-5300 spectrophotometer using KBr pellets. Solid-state ^{13}C NMR spectra were recored on a Varian Infinityplus-400 spectrometer at 100.4 MHz, using CP/MAS. Spinning speeds of 8 kHz and a contact time of 1 ms were used. Elemental microanalyses for carbon, hydrogen and nitrogen were done by the Department of Chemistry, University of Belgrade, Serbia.

2.3.1. Crystallographic data collection and refinement of the structures

The crystal data for (**1**) and (**2**) and the parameters of data collection are summarized in Table 1. The intensity data were measured with a KM4CCD kappa-geometry diffractometer [22] using graphite monochromated Mo Kα radiation (λ = 0.71073 Å) at 293(2) and 150(2) K for (**1**) and (**2**), respectively. The structures were solved by direct methods using SHELXS97 [23] and refined by least-squares techniques with SHELXL97 [24]. The intensity data were corrected for Lp effects as well as for absorption. Anisotropic thermal parameters were employed for the non-hydrogen atoms. All of the water hydrogen atoms were located in the Fourier map, while the remaining H atoms were placed at calculated positions. The H-atom positions were refined in a so called "riding model" with the atomic displacement parameters 30% higher than the displacement parameters for the atom to which the H atoms were bonded. A Siemens Stereochemical Workstation was used to prepare drawings [25].

Table 1
Crystallographic data collection and structure refinement information

	1	**2**
Formula	$Mg_2C_{11}H_{30}N_2O_{16}$	$Ca_2C_{11}H_{26}N_2O_{14}$
Formula weight	494.99	490.50
Temperature (K)	293	150
Wavelength Mo Kα (Å)	0.71073	
Crystal system	orthorhombic	triclinic
Space group	*Pnna*	$P\bar{1}$
Unit cell dimensions		
a (Å)	13.258(3)	8.574(2)
b (Å)	11.661(2)	10.594(2)
c (Å)	13.941(3)	12.329(2)
α (°)	90.0	102.35(3)
β (°)	90.0	108.20(3)
γ (°)	90.0	101.13(3)
V (Å^3)	2155.3(8)	997.7(3)
Z	4	2
D_{calc} (g cm^{-3})	1.525	1.633
μ (mm^{-1})	0.192	0.645
F (000)	1048	516
Crystal size (mm)	$0.50 \times 0.25 \times 0.25$	$0.20 \times 0.04 \times 0.03$
θ Range (°)	3.49 25.05	3.41 24.11
Index ranges	$-15 \leqslant h \leqslant 15$, $-13 \leqslant k \leqslant 10$, $-16 \leqslant l \leqslant 16$	$-6 \leqslant h \leqslant 9$, $-12 \leqslant k \leqslant 12$, $-14 \leqslant l \leqslant 14$
T_{min}, T_{max}	0.901, 1.000	0.864, 1.000
N_{total}	10761	9521
N_{ind}	1910	3153
N_{obs}	1637 [$I > 2\sigma(I)$]	1691 [$I > 2\sigma(I)$]
Refinement method	full-matrix least squares (F^2)	
$S(F^2)$	1.314	0.834
R	0.0334 [$I > 2\sigma(I)$]	0.0469 [$I > 2\ \sigma(I)$]
wR	0.0952	0.0881
Weighting scheme	$w = 1/[\sigma^2(F_o)^2 + (0.0459\ P)^2 + 0.1782P]$, where $P = (F_o^2 + 2F_c^2)/3$	$w = 1/[\sigma^2(F_o)^2 + (0.0184\ P)^2]$, where $P = (F_o^2 + 2F_c^2)/3$
Extinction correction	SHELXL	
Extinction coefficient	0.052(10)	
ρ_{max}, ρ_{min} (e Å^{-3})	0.634, −0.298	0.390, −0.328

3. Results and discussion

The influence of metal ion radius and d-electron configuration on the geometry of the complex is precisely defined for the M-edta system [2,4]. However, this effect on the geometry of complexes with ligands containing lengthened chains with respect to edta has not been explored yet. The reason for this may lie in the fact that crystallographic data for such systems are limited. The crystal structures of these hexadentate $[M(1,3\text{-pdta})]^{n-}$ complexes, for which coordinates are available through the Cambridge Crystallographic Database, [1] can roughly be divided into two series, depending on the valence of the central metal atom. All so far reported $[M(1,3\text{-pdta})]^{2-}$ complexes crystallize in the space group, Pnna, forming an isomorphic series, [17–20] while the majority of $[M(1,3\text{-pdta})]^{-}$ complexes crystallize in either $P2_12_12_1$[14,15a,16] or $C222_1$ [13] space groups, again displaying an identical packing pattern within the series. The packing pattern in the $[M(1,3\text{-pdta})]^{2-}$ series can be characterized as constituting of discrete complexed cations and anions of octahedral geometry arranged in the crystal in a close packed fashion and connected via numerous hydrogen bonds. On the other hand, in the $[M(1,3\text{-pdta})]^{-}$ series, the cations and anions are connected via carboxylate bridges. The complex anions are situated in layers perpendicular to the 16 Å direction, while the cations and water molecules are arranged in between these layers. The crystal structure containing the $[Fe(1,3\text{-pdta})]^{-}$ unit, [2,15b] that crystallizes in space group $P2_1/n$ and therefore seems to be an exception to this generalization, possesses similar unit cell parameters and displays a very similar packing pattern as the remaining $[M(1,3\text{-pdta})]^{-}$ crystals.

Our main interest in this work was to investigate the influence of metal ion radius on the geometry of the M-1,3-pdta system. To prepare the model complexes, metal ions of varying size (Mg(II) (0.86 Å) [5] and Ca(II) (1.14 Å) [5]) were chosen for which a C.N. 6 is not preferred by ligand field stabilization. Comparison of the coordinative behavior, of calcium and magnesium from data deposited in the CSD [26] has revealed that although both cations display some similarities in their coordinative behavior, such as formation of highly ionic coordinative bonds and a marked preference for oxygen donor atoms, they do differ in their coordination numbers which in the case of Mg(II) is fairly strictly confined to 6, while for Ca(II) the coordination numbers 6 and 8 are readily accessible. In the synthetic reactions of the dibarium complex of 1,3-pdta with magnesium or calcium sulfates two new hexadentate complexes were obtained ($[Mg(H_2O)_6][Mg(1,3\text{-pdta})]\cdot 2H_2O$ (**1**) and $[Ca(H_2O)_3Ca(1,3\text{-pdta})(H_2O)]\cdot 2H_2O$ (**2**)). The X-ray analyses of these revealed that 1,3-pdta-chelated Mg(II) and Ca(II) metal ions are significantly different in coordination number and geometry.

3.1. Crystal structure of $[Mg(H_2O)_6][Mg(1,3\text{-pdta})]\cdot 2H_2O$ (1)

The crystal of the studied complex (**1**) appears to be isomorphic with the other (1,3-propanediaminetetraacetato)metal(II) complexes: $[M(H_2O)_6][Cu(1,3\text{-pdta})]\cdot 2H_2O$ (M = Mg(II) [17] or Mn(II) [18]), $[Mg(H_2O)_6][Ni(1,3\text{-pdta})]\cdot 2H_2O$ [19] and $[M(H_2O)_6][Co(1,3\text{-pdta})]\cdot 2H_2O$ (M = Mg(II) or Co(II)) [20]. The ORTEP diagram of $[Mg(H_2O)_6][Mg(1,3\text{-pdta})]\cdot 2H_2O$ (**1**) is depicted in Fig. 1 where the numbering scheme adopted for the respective atoms is also given. Selected bond distances and bond angles for complex (**1**) are listed in Table 2. The structural unit in the crystal structure of (**1**) consists of $[Mg(1,3\text{-pdta})]^{2-}$ and $[Mg(H_2O)_6]^{2+}$ octahedra, and two water solvent molecules, all of which lie on a special position in the unit cell. The highest symmetry (C_2) axis of the complex anion passes through the Mg1and C2 atoms and bisects the N1–Mg1–N1^{i} bond angle (where the symmetry code i = x, $0.5-y$, $-0.5-z$) making the two out-of-plane glycinate rings (R rings), as well as the two in-plane (G rings), identical. In this structure, the six-membered 1,3-propanediamine ring (T ring) adopts a flexible *twist-boat* conformation with the average torsion angle moduli of 44.0°. The R rings are almost flat, while the G-rings are much more puckered and are halfway between *envelope* and *twist* conformations. The mean deviation from octahedral angles (average

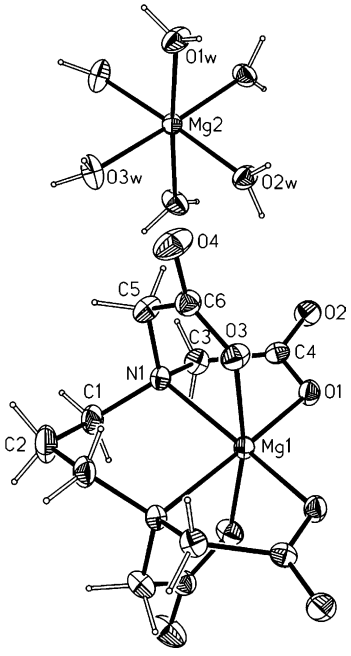

Fig. 1. The ORTEP drawing of the $[Mg(1,3\text{-pdta})]^{2-}$ and $[Mg(H_2O)_6]^{2+}$ octahedra. As the molecules are situated on a two-fold symmetry axis, generation of the second half of the complex anion and cation requires the symmetry operations x, $0.5-y$, $-0.5-z$ and x, $0.5-y$, $0.5-z$, respectively.

Table 2
Selected bond distances (Å) and bond angles (°) for complexes **1** and **2**

Bond distances			
Mg1–O1	2.0151(12)	Mg2–O1W	2.0493(13)
Mg1–O3	2.0870(13)	Mg2–O2W	2.0678(13)
Mg1–N1	2.1993(15)	Mg2–O3W	2.0745(14)
Bond angles			
O1–Mg1–O1^{i}	106.32(7)	O1W–Mg2–O1W^{ii}	176.00(9)
O1–Mg1–O3	95.05(5)	O1W–Mg2–O2W^{ii}	88.33(6)
O1–Mg1–O3^{i}	91.79(5)	O1W–Mg2–O2W	88.94(5)
O3–Mg1–O3^{i}	168.59(8)	O2W–Mg2–O2W^{ii}	93.98(8)
O1–Mg1–N1	81.42(5)	O1W–Mg2–O3W^{ii}	91.84(5)
O1–Mg1–N1^{i}	168.67(5)	O1W–Mg2–O3W	91.01(6)
O3–Mg1–N1^{i}	92.93(5)	O2W–Mg2–O3W^{ii}	177.50(6)
O3–Mg1–N1	79.12(5)	O2W–Mg2–O3W	88.42(5)
N1–Mg1–N1^{i}	92.22(8)	O3W–Mg2–O3W^{ii}	89.19(8)
Bond distances			
Ca1–O3	2.381(3)	Ca2–O1	2.492(3)
Ca1–O1	2.397(4)	Ca2–O2	2.414(4)
Ca1–O5	2.414(4)	Ca2–O3^{iii}	2.572(3)
Ca1–O7	2.467(3)	Ca2–O4^{iv}	2.370(4)
Ca1–O1W^{iii}	2.504(3)	Ca2–O3W	2.422(3)
Ca1–O1W	2.603(4)	Ca2–O4^{iii}	2.431(4)
Ca1–N2	2.654(4)	Ca2–O2W	2.450(3)
Ca1–N1	2.708(4)	Ca2–O4W	2.491(4)
Bond angles			
O3–Ca1–O1	158.83(12)	O4^{iv}–Ca2–O2	101.62(13)
O3–Ca1–O5	103.80(13)	O4^{iv}–Ca2–O3W	142.42(12)
O1–Ca1–O5	86.99(13)	O2–Ca2–O3W	87.06(12)
O3–Ca1–O7	75.93(11)	O4^{iv}–Ca2–O4^{iii}	74.86(13)
O1–Ca1–O7	108.32(12)	O2–Ca2–O4^{iii}	166.59(12)
O5–Ca1–O7	137.86(12)	O3W–Ca2–O4^{iii}	88.27(11)
O3–Ca1–O1W^{iii}	82.95(11)	O4^{iv}–Ca2–O2W	72.14(11)
O1–Ca1–O1W^{iii}	80.46(11)	O2–Ca2–O2W	102.67(12)
O5–Ca1–O1W^{iii}	82.50(12)	O3W–Ca2–O2W	141.99(12)
O7–Ca1–O1W^{iii}	137.66(12)	O4^{iii}–Ca2–O2W	88.69(12)
O3–Ca1–O1W	79.37(12)	O4^{iv}–Ca2–O4W	73.00(11)
O1–Ca1–O1W	81.82(12)	O2–Ca2–O4W	83.94(12)
O5–Ca1–O1W	147.28(11)	O3W–Ca2–O4W	71.68(12)
O7–Ca1–O1W	74.80(11)	O4^{iii}–Ca2–O4W	82.65(12)
O1W–Ca1–O1W^{iii}	65.40(12)	O2W–Ca2–O4W	145.13(11)
O3–Ca1–N2	65.13(13)	O4^{iv}–Ca2–O1	133.34(12)
O1–Ca1–N2	135.86(13)	O2–Ca2–O1	53.78(12)
O5–Ca1–N2	65.63(13)	O3W–Ca2–O1	81.02(12)
O7–Ca1–N2	77.12(12)	O4^{iii}–Ca2–O1	137.57(13)
O1W^{iii}–Ca1–N2	125.68(12)	O2W–Ca2–O1	76.00(11)
O1W–Ca1–N2	138.99(12)	O4W–Ca2–O1	130.68(12)
O3–Ca1–N1	132.36(13)	O4^{iv}–Ca2–O3^{iii}	117.55(12)
O1–Ca1–N1	65.23(12)	O2–Ca2–O3^{iii}	136.97(12)
O5–Ca1–N1	87.47(13)	O3W–Ca2–O3^{iii}	73.02(11)
O7–Ca1–N1	65.97(12)	O4^{iii}–Ca2–O3^{iii}	52.59(11)
O1W^{iii}–Ca1–N1	144.70(12)	O2W–Ca2–O3^{iii}	75.19(11)
O1W–Ca1–N1	114.82(12)	O4W–Ca2–O3^{iii}	122.65(13)
N2–Ca1–N1	78.98(13)	O1–Ca2–O3^{iii}	85.09(12)

^{i} x, $0.5-y$, $-0.5-z$.
^{ii} x, $0.5-y$, $0.5-z$.
^{iii} $1-x$, $1-y$, $2-z$.
^{iv} x, $1+y$, z.

(ΔO_h)) for $[Mg(1,3\text{-pdta})]^{2-}$ equals 7.4°, which indicates the nearly regular octahedral geometry of the complex anion.

Table 3 lists bond lengths to the metal(II) atoms observed in a series of isomorphic crystals for complexes of the $[M^{II}(H_2O)_6][M^{II}(1,3\text{-pdta})]\cdot 2H_2O$ type and the mean deviation from octahedral angles (average (ΔO_h) parameter). The closest to the ideal regular octahedral geometry is displayed by the $[Ni(1,3pdta)]^{2-}$ complex anion in which the Ni–N and Ni–O_R bonds are equal in length. On the contrary, in the Mg(II) complex, the Mg–N bond lengths are significantly longer than the corresponding Mg–O bonds, in line with the observation that for edta-like complexes of predominantly electrostatic binding metal ions the interactions of such metals with amine nitrogens are relatively weak.

Similar to other crystal structures of divalent metal ions with the 1,3-pdta ligand, [17–20] the discrete $[Mg(1,3\text{-pdta})]^{2-}$ and $[Mg(H_2O)_6]^{2+}$ octahedra alternate in the crystal in such a way that each complex anion is surrounded by six complex cations situated at the corners of a distorted octahedron and vice versa. As a result, not only the first but also the second metal coordination sphere displays nearly octahedral geometry. Such an alternating arrangement of the cationic and anionic species might indicate nearly spherical charge distribution on each of the complex units, which is consistent with their first coordination sphere being close to a regular octahedron.

The packing in the structure is determined by an extended network of relatively strong hydrogen bonds predominantly involving water molecules (coordinated to Mg2 or two water solvent molecules) and carboxylate oxygens. The two coordination polyhedra are connected via hydrogen bonds in three dimensions.

3.2. Crystal structure of $[Ca(H_2O)_3Ca(1,3\text{-pdta})(H_2O)]\cdot 2H_2O$ (2)

The crystal structure of (**2**) consists of infinite one-dimensional chains of ligand-bridged coordination complexes connected by hydrogen bonds, such that no discrete complexes exist. The ORTEP diagram of the $[Ca(H_2O)_3Ca(1,3\text{-pdta})(H_2O)]$ unit is presented in Fig. 2, where the numbering scheme adopted for the respective atoms is also given. Selected bond distances and bond angles for complex (**2**) are listed in Table 2.

The Ca1 has eightfold coordination with the hexadentate 1,3-pdta ligand and two symmetry-related water molecules O1W and O1W^{iii} (where the symmetry code iii = $1-x$, $1-y$, $2-z$). Distribution of the values of the valence angles around the Ca1 metal center resembles a set of values expected for the ideal square antiprism (70.5°, 109.5°, 82.1° and 160.5°), thus the coordination polyhedron formed around Ca1 may be described as distorted square antiprism. Conformations of the chelate rings are found to be *twist* or *envelope* for the glycinates and a distorted *chair* for the six-membered diamine ring. Two symmetry related calcium ions Ca1 and Ca1^{iii} are

Table 3
Geometry around divalent cations in a series of isomorphic crystals of the $[M^{II}(H_2O)_6][M^{II}(1,3\text{-pdta})]\cdot 2H_2O$ type

Metal ion octahedrally coordinated by the 1,3-pdta ligand	M–N (Å)	M–O_G(Å)[a]	M–O_R(Å)[a]	av. ΔO_h	Ref.
Mg(II)	2.199	2.015	2.087	7.4	this work
Co(II)[b,c]	2.142	2.055	2.111	6.7	[20]
Ni(II)	2.073	2.027	2.078	5.2	[19]
Cu(II)[c]	2.048	1.974	2.279	5.8	[17,18]

[a] M–O_G is the mean in plane bond length; M–O_R is the mean out-of-plane bond length.
[b] Measured at 120 K.
[c] Average of two independent measurements.

bridged by water molecules (O1W and O1W^{iii}) around the center of symmetry at (1/2 1/2 0), and in this way two complex units are joined into a dimer. The distance between two metal centers in the dimer is 4.281(1) Å . By sharing both oxygen atoms of the C(5) and C(7) carboxylate groups, the two Ca1 and Ca1^{iii} ions join in a bidentate fashion to the same two Ca2 ions (at distances of 4.632 and 4.704 Å) forming a tetramer structure. Further, Ca2 and Ca2^{v} (where the symmetry code v = $1-x$, $2-y$, $2-z$) are bridged by carbonyl oxygen atoms O4^{iii} and O4^{iv} (where the symmetry code iv = x, $1+y$, z) around the center of symmetry at (1/2 0 0). The two Ca2 metal centers approach each other at a distance of only 3.829(1)Å . In this way the tetramers are joined together by coordination bonds into one-dimensional chains parallel to the *b*-axis (Fig. 3). Within the chains the C(5) and C(7) carboxylate groups act as a bridge between metal centers: the C(5) carboxylate bridging two metal centers and C(7) carboxylate bridging three metal centers. Interactions between the neighboring polymeric chains include not only numerous hydrogen bonds but also dipolar interactions between antiparallel C(10)=O(8) groups around the symmetry center at 0 1/2 0 (Table 4). The two crystal water molecules (O5W and O6W) serving as hydrogen bond donors and acceptors connect the polymeric chains in three dimensions. Distances and angles for all hydrogen bonds that participate in the structure and geometrical parameters describing dipolar carbonyl interactions are listed in Table 4.

The coordination number of Ca2 is eight and the coordination polyhedron is very irregular in shape and may best be described as a dodecahedron. The Ca2 ion is surrounded by five oxygen atoms (O1, O2, O3^{iii}, O4^{iii} and O4^{iv}) which belong to three different but symmetry-related 1,3-pdta ligands, and by three water molecules (O2W, O3W and O4W). Two carboxylate groups of 1,3-pdta are coordinated in a bidentate fashion (over O1, O2, O3^{iii} and O4^{iii} oxygen atoms) to Ca2, and two carbonyl oxygens (O4^{iii} and O4^{iv}) are shared between two Ca2 ions.

A complex of a metal ion that is fairly large in size, such as Ca(II), with the 1,3-pdta ligand is much less favored with respect to that of edta [3,27]. Despite this, complex **2** is similar in structure to the three known crystal structures containing $[Ca(edta)]^{2-}$, units [12a–c]. For each edta-chelated Ca(II), the coordination number is also eight and the coordination polyhedron is approximately square-antiprismatic [12a–c]. In Ca(II)-edta, the two sites that supplement the C.N. 8 (in addition to the six sites occupied by the hexadentate edta ligand) are filled by a water molecule and a symmetry-related edta oxygen atom [12a,b] or by two water molecules [12c]. A noticeable difference in the stereochemistry of the three $[Ca(edta)]^{2-}$ anions is observed in the conformation of the ethylenediamine ring, which for the same configuration of the complex isomer adopts in two cases the λ conformation [12a,c] and in one case the δ conformation [12b].

3.3. Comparative stereochemistry and strain analysis of edta-type complexes

The critical radii between C.N. = 6 and 7 are successfully used to predict the coordination numbers of edta complexes in cases where the central metal ions have one of the spherically symmetric configurations (d^0, high-spin d^5 and d^{10}) [2,4]. For trivalent metal ions, the C.N. changes from 6 to 7 around Fe(III) (0.785 Å), [5] and for divalent metal ions around Zn (II) (0.88 Å) [5] or Mg(II) (0.86 Å) [5]. However, judging from an electronic point of view the metal ions with d^1, d^2, low-spin d^3, low-spin d^4, high-spin d^6 or high-spin d^7 configurations are also able to form seven-coordinate edta complexes [4]. Structural parameters reflecting the geometry of complexes with edta and 1,3-pdta ligands, containing metal ions that are common for both type of ligands, are presented in Table 5. The restriction was also imposed on metal ions that may form edta complexes of C.N. higher than six. The $[M(edta)(H_2O)]^{n-}$ (M = V(III) (**3**), Fe(III) (**4**), Mg(II) (**5** and **6**) and Co(II) (**7**)) complexes listed are of C.N. = 7 and adopt either PB or CTP structure, while complexes of Mg(II) (**1**), V(III) (**9**), Fe(III) (**10**) and Co(II) (**11**) with the 1,3-pdta ligand (which differs from edta in the length of the diamine chain) are all of C.N. = 6 and adopt an octahedral structure. This indicates that the critical ionic radii for the M-1,3-pdta system should be greater than that for edta. This well

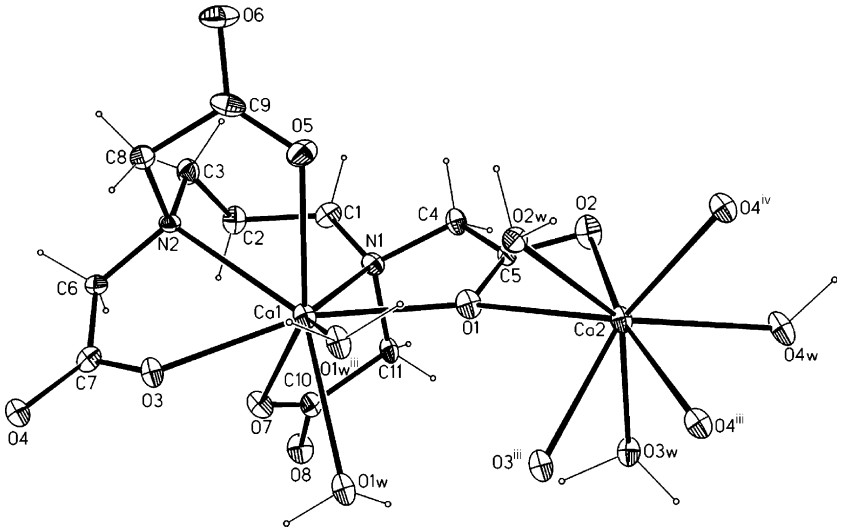

Fig. 2. Coordination sphere around two independent calcium ions (Ca1 and Ca2). The 1,3-pdta ligand is bound to other symmetry-related metal ions by five O atoms: O1, O2, O3 and O4 (the latter is bound to two different Ca^{II} ions). Symmetry codes: iii = $1-x$, $1-y$, $2-z$ and iv = x, $y+1$, z.

pronounced tendency within the two series is perturbed by the complex of Ca(II) which is of C.N. = 8 and has square-antiprismatic geometry with both the edta (complex (**8**)) and 1,3-pdta ligands (complex (**2**)) (Table 5).

The edta complexes listed in Table 5 exhibit nearly an ideal coordination geometry of the ethylenediamine rings as evidenced by N–M–N bond angles close to the value of 69° which is obtained for the energy minimized coordination [3]. With respect to the value of 69°, the N–M–N bond angle in the $[Co(edta)(H_2O)]^{2-}$ (**7**) complex shows the maximum deviation of +9.7° among the edta complexes listed. The minimum deviation of the N–M–N bond angle was registered for $[Ca(edta)(H_2O)]^{2-}$ (**8**) complexes of C.N. = 8 and equals, on average, −0.5°. A six-membered chelate ring involving 1,3-propanediamine as a ligand was found to be of minimum strain when the N–M–N bond angle equals 109.5° [3]. For the $[M(1,3\text{-pdta})]^{n-}$ [M = Co(III), Cr(III), V(III), Fe(III), Rh(III), Ni(II), Cu(II), Co(II) and Mg(II)] complexes, which adopt a nearly octahedral structure, the N–M–N bite angle was found to be in the range 92.2°–99.0° [19,20]. These values are closer to the value of an ideal octahedral bond angle rather than that of a tetrahedral one. For both series of complexes (edta and 1,3-pdta), with the exception for complex (**7**), the mean M–O distances are shorter than the mean M–N distances. In addition, the mean M–O distances for the 1,3-pdta series increase systematically with an increasing size of the ionic radii. It might also be interesting to note that Ca(II) complexes with edta and 1,3-pdta ligands contain almost identical metal–ligand bond lengths.

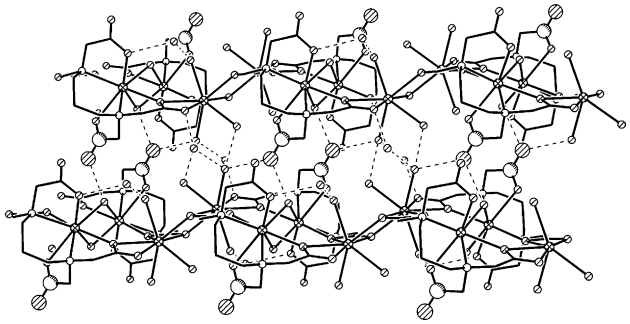

Fig. 3. Infinite one-dimensional chains parallel to the *b*-axis joined together by hydrogen bonds and carbonyl dipolar interactions in the crystal structure of complex (**2**). View along *x*-axis. Atoms constituting carbonyl groups involved in dipolar iteractions are drawn as bigger circles.

The effect of chelation on the distortion of the tetrahedral bonding geometry of the nitrogen atoms is much greater for $[M(edta)]^{n-}$ than for $[M(1,3\text{-pdta})]^{n-}$ octahedral systems [19]. However, an increase of the C.N. from 6 to 7 releases this strain and, accordingly, in the $[M(edta)(H_2O)]^{n-}$ systems of CTP or PB geometry and in the octaheral $[M(1,3\text{-pdta})]^{n-}$ complexes the strain formed around chelating N atoms seems comparable. As can be seen in Table 5, the total deviation from the tetrahedral values of the six bond angles around the N atoms measured for seven-coordinate edta complexes ((**3**)–(**7**)) varies from 8° to 17°, while for 1,3-pdta complexes ((**1**), (**9**)–(**11**)) it is somewhat greater and covers the range from 11° to 21°. For the two square-antiprismatic structures it was observed that the strain formed around chelating N atoms in $[Ca(edta)(H_2O)]^{2-}$ (**8**) is much less than that in $[Ca(1,3\text{-pdta})(H_2O)]^{2-}$ (**2**) (12° *vs.* 28°). Of all complexes considered in Table 4, $[Ca(1,3\text{-pdta})(H_2O)]^{2-}$ (**2**) contains the most strained bonds around chelating nitrogen atoms indicating possible C–N bond rupture in substitution reactions.

Table 4
Parameters describing hydrogen bonding and dipolar C=O interactions in $[Ca(H_2O)_3Ca(1,3\text{-pdta})(H_2O)]\cdot 2H_2O$ (**2**)

	D–H (Å)	H···A (Å)	D–H···A (°)	D···A (Å)	Symmetry operations on A
O1W–H1W···O8	0.965	1.73	174	2.70	$-x+2, -y+1, -z+2$
O1W–H2W···O2W	1.002	1.75	169	2.74	$-x+1, -y+1, -z+2$
O2W–H3W···O5W	1.058	1.53	175	2.58	
O2W–H4W···O4W	0.939	2.05	137	2.81	$-x+1, -y+2, -z+2$
O3W–H5W···O6W	1.076	1.68	157	2.70	
O3W–H6W···O8	1.075	1.79	144	2.73	$-x+2, -y+1, -z+2$
O4W–H7W···O7	1.038	1.77	168	2.79	x, y + 1, z
O4W–H8WA···O3W	0.854	1.96	167	2.80	$-x+2, -y+2, -z+2$
O5W–H9W···O5	1.022	1.78	153	2.73	
O5W–H10W···O6	0.948	1.79	160	2.71	$-x, -y+1, -z+1$
O6W–H11W···O6	0.989	1.94	169	2.91	x + 1, y + 1, z + 1
O6W–H12W···O2	0.984	1.84	163	2.79	$-x+2, -y+2, -z+2$
C10···O8[i]			3.556 Å		
C10 = O8···C10[i]			77.8°		
O8 = C10···O8[i]			102.2°		
C10 = O8···C10[i] = O8[i]			0.0°		

[i] $-x+2, -y+1, -z+2$.

Table 5
The mean M–L bond distances and N–M–N bond angles in edta and 1,3-pdta complexes with common metal ions[a]

Complexes	r(M)[b] (Å)	C.N.	Geometry	N–M–N (°)	M–N (Å)	M–O (Å)	$\sum\Delta$(N)[c] (°)	No.m.av[d]	Ref.
EDTA:									
$[V^{III}(edta)(H_2O)]^-$ (**3**)	0.780	7	CTP	75.6(6)	2.23(3)	2.05(2)	11	5	[11a–c]
$[Fe^{III}(edta)(H_2O)]^-$ (**4**)	0.785	7	PB	73.9(4)	2.32(4)	2.03(7)	17	10	[10a–g]
$[Mg^{II}(edta)(H_2O)]^{2-}$ (**5**)	0.860	7	CTP	75.3(1)	2.378(2)	2.17(11)	9	1	[7]
$[Mg^{II}(edta)(H_2O)]^{2-}$ (**6**)	–	7	PB	74.1(2)	2.39(5)	2.18(17)	10	2	[6a–b]
$[Co^{II}(edta)(H_2O)]^{2-}$ (**7**)	0.885	7	CTP	78.7(6)	2.24(2)	2.23(14)	8	4	[8e,9]
$[Ca^{II}(edta)(H_2O)]^{2-}$ (**8**)	1.140	8	square antiprismatic	68.5(1.3)	2.63(5)	2.42(5)	12	3	[12a–c]
1,3-PDTA:									
$[V^{III}(1,3\text{-pdta})]^-$ (**9**)	0.780	6	octahedral	96.7(1)	2.143(2)	1.98(2)	14	1	[16]
$[Fe^{III}(1,3\text{-pdta})]^-$ (**10**)	0.785	6	octahedral	93.6(7)	2.18(1)	1.98(1)	21	2	[2,15]
$[Mg^{II}(1,3\text{-pdta})]^{2-}$ (**1**)	0.860	6	octahedral	92.2(1)	2.199(2)	2.05(4)	13	1	this work
$[Co^{II}(1,3\text{-pdta})]^{2-}$ (**11**)	0.885	6	octahedral	95.7(1)	2.142(2)	2.08(3)	11	2	[20][e]
$[Ca^{II}(1,3\text{-pdta})(H_2O)]^{2-}$ (**2**)	1.140	8	square antiprismatic	79.0(1)	2.68(3)	2.41(3)	28	1	this work[e]

[a] The values in parentheses are the standard deviations of the sample.
[b] Ionic radius for C.N. = 6 [5].
[c] $\sum\Delta$(N) is the sum of the absolute values of the deviations from 109.5° of the six bond angles made by the chelate nitrogen atoms. A mean value for the two nitrogens is reported.
[d] Number of molecules averaged.
[e] Low temperature data.

3.4. Spectral characteristics of the complexes

In this paper the $[Ba(1,3\text{-pdta})]^{2-}$ complex has been used in the simple method for preparation of the corresponding magnesium and calcium complexes. To compare these complexes with structurally investigated complexes of known X-ray structure, their infrared (IR) and solid-state ^{13}C NMR spectra have been recorded. No signal in the solid-state ^{13}C NMR spectrum of the 1,3-pdta-Ca complex was observed. The IR spectrum of $[Mg(1,3\text{-pdta})]^{2-}$ in the carboxylate region for coordinated glycinates showed only one very strong band at 1596 cm^{-1} indicating that all glycinate rings in this complex are equivalent. However, in accordance with its lower symmetry $[Ca(1,3\text{-pdta})(H_2O)]^{2-}$ showed two bands, a very weak one at 1638 cm^{-1} and a strong one at 1587 cm^{-1}, both assigned to the asymmetric carbonyl stretching vibrations of non-equivalent glycinate rings. In this region two bands have also been observed for $[Ba(1,3\text{-pdta})]^{2-}$ (a shoulder at 1600 cm^{-1} and a very strong band at 1568 cm^{-1}) indicating that glycinate rings in this system should also be non-equivalent. The solid-state ^{13}C CP/MAS NMR spectra of $[Mg(1,3\text{-pdta})]^{2-}$ and $[Ba(1,3\text{-pdta})]^{2-}$ are presented in Fig. 4. On the basis of their chemical shifts, the lowest-field peaks (C1) at ~180 ppm can be assigned to the carboxy-

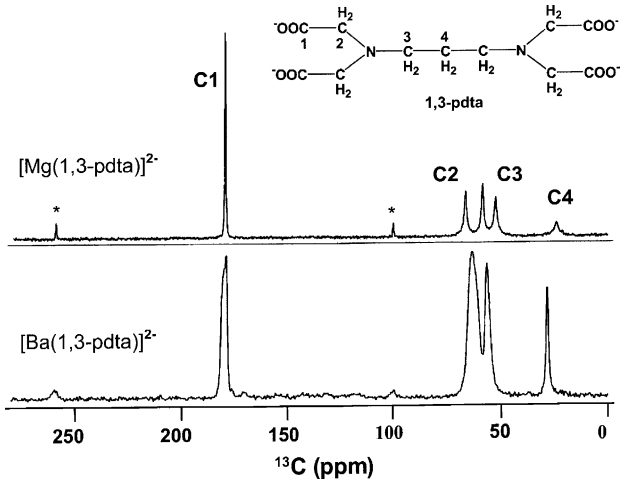

Fig. 4. Solid-state CP/MAS ^{13}C NMR spectra of $[Mg(1,3\text{-pdta})]^{2-}$ and $[Ba(1,3\text{-pdta})]^{2-}$. The assignments together with the structure of 1,3-pdta are also shown. The peaks marked with "*" are spinning side-bands.

lates and the peaks (C2) at 66.6 and 58.6 ppm for $[Mg(1,3\text{-pdta})]^{2-}$ and the very broad peak at 63.0 ppm for $[Ba(1,3\text{-pdta})]^{2-}$ can be assigned to the methylene carbons of the two pairs of non-equivalent glycinate rings in each complex. The highest field methylene resonances (C4) at 24.3 ppm for $[Mg(1,3\text{-pdta})]^{2-}$ and 27.9 ppm for $[Ba(1,3\text{-pdta})]^{2-}$ are due to the middle carbon of the propylenediamine backbone since this carbon is in the greatest shielded environment. The rest of the peaks, (C3) at 52.5 ppm for $[Mg(1,3\text{-pdta})]^{2-}$ and at 56.2 ppm for $[Ba(1,3\text{-pdta})]^{2-}$, are due to the two terminal carbons of the propylenediamine backbone. Additionally, in the carboxylate region for $[Ba(1,3\text{-pdta})]^{2-}$ two well resolved peaks (179.9 and 178.9 ppm) for the two pairs of non-equivalent rings were obtained. This is in accordance with the ^{13}C NMR spectra of 1,3-pdta complexes containing Co(III) [28] and Rh(III) [29] ions. Better resolution of these resonances for $[Ba(1,3\text{-pdta})]^{2-}$ in relation to the corresponding magnesium complex (signal at 180.2 ppm) can be explained in terms of the size differences between these two ions and the greater system strain in $[Ba(1,3\text{-pdta})]^{2-}$.

4. General conclusions

The hexadentate $[M(1,3\text{-pdta})]^{n-}$ complexes are much less distorted from a regular octahedral structure than $[M(edta)]^{n-}$ complexes, as has been evidenced by comparison of the X-ray data of the series of complexes [19]. This is due to the presence of the flexible M-1,3-propanediamine ring system, which releases the strain of the complex as a whole. Thus, it is not unexpected that all but one of the known crystal structures of M-1,3-pdta complexes are so far octahedral. The only exception is the $[Ca(1,3\text{-pdta})(H_2O)]^{2-}$ (**2**) complex, presented in this paper, which has the coordination number eight. On the other hand, M-edta complexes show varieties in stereochemistry, and the critical ionic radii between coordination number six and seven have been successfully used to predict the coordination numbers of edta complexes [2,4]. By comparing the systems of the two ligands, we came to the conclusion that the critical ionic radii for the M-1,3-pdta system should be greater than that for the M-edta system. However, the precise definition would require further X-ray studies of several new and closely related compounds.

As it follows from this study and from previous observations, six of the seven investigated crystals of transition metal(II) complexes with the 1,3-pdta ligand and divalent counter cations: $[Mg(H_2O)_6][Mg(1,3\text{-pdta})]\cdot 2H_2O$ (**1**), $[M(H_2O)_6][Cu(1,3\text{-pdta})]\cdot 2H_2O$ (M = Mg(II) [17] or Mn(II) [18]), $[Mg(H_2O)_6][Ni(1,3\text{-pdta})]\cdot 2H_2O$ [19] and $[M(H_2O)_6][Co(1,3\text{-pdta})]\cdot 2H_2O$ (M = Mg(II) or Co(II)), [20] are isomorphic. The crystal packing of these compounds is characterized by the alternating arrangement of complex cations and anions leading to an approximately octahedral surrounding in the second coordination sphere of the metal. This can be achieved because the first coordination sphere of both metals shows nearly ideal octahedral geometry and thus nearly spherical charge distribution, and the complex ions form discrete units not connected by carboxylate bridges. As a result, the packing is mostly governed by electrostatic forces. However, this way of molecular organization in the solid-state is not favoured by the homometallic complex of Ca(II) with the hexadentate 1,3-pdta ligand (**2**), which in the crystal builds one-dimensional polymeric chains such that no discrete complexes exist.

The observation that the homometallic complex of Ca(II) with the hexadentate 1,3-pdta ligand displays a different geometry and a different packing mode than all other $[M(1,3\text{-pdta})]^{2-}$ complexes may be attributed to the specific properties of the calcium ion, which is known as a "soft" cation, rather than to the properties of the ligands surrounding the metal center. This conclusion is supported by the fact that calcium(II) forms not only six- but seven-, eight- and nine-coordinated aqua ions [1].

5. Supplementary data

Supplementary data are available from the CCDC, 12 Union Road, Cambridge CB2 1EZ, UK (fax: + 44-1223-336-033; e-mail: deposit@ccdc.cam.uk or www: http://www.ccdc.cam.ac.uk) on request, quoting the Deposition No. CCDC 217531 and 217530 for complexes **1** and **2**, respectively.

Acknowledgements

The authors D.D.R. and M.I.D. are grateful to the Ministry of Science, Technologies and Development of the Republic of Serbia for the financial support (Projects No. 1569 and No. 1254) and Drs. F. Deng (Wuhan, China) and H. Sun (Hong Kong) for the solid-state ^{13}C NMR.

This work was partially financed during the years 2003–2006 by the Polish State Committee for Scientific Research as a Scientific Project No. 4 T09A 185 25.

References

[1] F.H. Allen, O. Kennard, Chem. Des. Autom. News 8 (1993) 1 31.
[2] T. Yamamoto, K. Mikata, K. Miyoshi, H. Yoneda, Inorg. Chim. Acta 150 (1988) 237.
[3] R.D. Hancock, Perspectives in Coordination Chemistry, Verlag Helvetica Chimica Acta, Basel, Switzerland, 1992 p. 129.
[4] T. Mizuta, J. Wang, K. Miyoshi, Bull. Chem. Soc. Jpn. 66 (1993) 2547 and references therein.
[5] R.D. Shannon, Acta Crystallogr. Sect. A 32 (1976) 751.
[6] (a) E. Passer, J.G. White, K.L. Cheng, Inorg. Chim. Acta 24 (1977) 13;
(b) A.I. Pozhidaev, T.N. Polynova, M.A. Porai-Koshits, V.A. Logvinenko, Zh. Strukt. Khim. 14 (1973) 746.
[7] J.J. Stezowski, R. Countryman, J.L. Hoard, Inorg. Chem. 12 (1973) 1749.
[8] (a) X. Solans, S. Gali, M. Font-Altaba, J. Oliva, J. Herrera, Afinidad 45 (1988) 243;
(b) N.N. Anan'eva, T.N. Polynova, M.A. Porai-Koshits, Zh. Strukt. Khim. 15 (1974) 261;
(c) I.N. Polyakova, A.L. Poznyak, V.S. Sergienko, L.V. Stopolyanskaya, Kristallografiya 46 (2001) 47;
(d) S. Richards, B. Pedersen, J.V. Silverton, J.L. Hoard, Inorg. Chem. 3 (1964) 27;
(e) T. Yi, S. Gao, B. Li, Polyhedron 17 (1998) 2243;
(f) I.N. Polyakova, V.S. Sergienko, A.L. Poznyak, Kristallografiya 47 (2002) 280.
[9] S. Gao, O. Bai, B.-Q. Ma, T. Yi, C.-H. Yan, G.-X. Xu, J. Chem. Cryst. 30 (2000) 163.
[10] (a) X. Solans, M. Font-Altaba, J. Garcia-Oricain, Acta Crystallogr. Sect. C 40 (1984) 635;
(b) X. Solans, M. Font-Altaba, J. Garcia-Oricain, Acta Crystallogr. Sect. C 41 (1985) 525;
(c) X. Solans, M. Font-Altaba, J. Garcia-Oricain, Afinidad 41 (1984) 572;
(d) Ya.M. Nesterova, T.N. Polynova, M.A. Porai- Koshits, Koord. Khim. 1 (1975) 966;
(e) M.J. Hamor, T.A. Hamor, J.L. Hoard, Inorg. Chem. 3 (1964) 34;
(f) M.D. Lind, J.L. Hoard, Inorg. Chem. 3 (1964) 34;
(g) J.M. Lopez-Alcala, M.C. Puerta-Vizcaino, F. Gonzalez-Vilchez, E.N. Duesler, R.E. Tapscott, Acta Crystallogr. Sect. C 40 (1984) 939.
[11] (a) M. Shimoi, Y. Saito, H. Ogino, Bull. Chem. Soc. Jpn. 64 (1991) 2629;
(b) R.E. Marsh, Acta Crystallogr. Sect. B 53 (1997) 317;
(c) M. Shimoi, Y. Saito, H. Ogino, Chem. Lett. (1989) 1675.
[12] (a) B.L. Barnett, V.A. Uchtman, Inorg. Chem. 18 (1979) 2674;
(b) M.I. Arriortua, M. Insausti, M.K. Urtiaga, J. Via, T. Rojo, Acta Crystallogr. Sect. C 48 (1992) 779;
(c) A.S. Antsyshkina, G.G. Sadikov, A.L. Poznyak, V.S. Sergienko, Zh. Neorg. Khim. 47 (2002) 43.
[13] R. Nagao, F. Marumo, Y. Saito, Acta Crystallogr. Sect. B 28 (1972) 1852.
[14] R. Herak, G. Srdanov, M.I. Djuran, D.J. Radanovic, M. Bruvo, Inorg. Chim. Acta 83 (1984) 55.
[15] (a) K. Okamoto, K. Kanamori, J. Hidaka, Acta Crystallogr. Sect. C 46 (1990) 1640;
(b) H.P. Bommeli, G. Anderegg, W. Petter, Z. Kristallogr. 174 (1986) 23.
[16] J.C. Robles, Y. Matsuzaka, S. Inomata, M. Shimoi, W. Mori, H. Ogino, Inorg. Chem. 32 (1993) 13.
[17] U. Rychlewska, D.D. Radanović, V.S. Jevtović, D.J. Radanović, Polyhedron 19 (2000) 1.
[18] M. Hernandez-Padilla, E. Chinea, S. Dominguez, A. Mederos, M.C. Munoz, F. Lloret, Polyhedron 19 (2000) 1175.
[19] D.J. Radanović, T. Ama, H. Kawaguchi, N.S. Drašković, D.M. Ristanović, S. Janićijević, Bull. Chem. Soc. Jpn. 74 (2001) 701.
[20] D.D. Radanović, U. Rychlewska, M.I. Djuran, N.S. Drašković, M.M. Vasojević, I.M. Hodžić, D.J. Radanović, Polyhedron 22 (2003) 2745.
[21] J.A. Weyh, R.E. Hamm, Inorg. Chem. 7 (1968) 2431.
[22] Kuma Diffraction KM4CCD Software. Version 1.168. Kuma Diffraction Instruments GmbH, Wrocław, Poland, 1999.
[23] G.M. Sheldrick, Acta Crystallogr. Sect. A 46 (1990) 467.
[24] G.M. Sheldrick, SHELXL97, Program for the Refinement of Crystal Structures, University of Göttingen, Germany, 1997.
[25] Stereochemical Workstation Operation Manual, Release 3.4. Siemens Analytical X-ray Instruments, Inc., Madison, WI, 1989.
[26] O. Carugo, K. Djinovic, M. Rizzi, J. Chem. Soc., Dalton Trans. (1993) 2127.
[27] R.D. Hancock, Pure Appl. Chem. 58 (1986) 1445.
[28] C.A. Chang, B.E. Douglas, J. Coord. Chem. 9 (1979) 93.
[29] K.D. Gailey, D. J Radanović, M.I. Djuran, B.E. Douglas, J. Coord. Chem. 8 (1978) 161.

Available online at www.sciencedirect.com
SCIENCE DIRECT®
Polyhedron 23 (2004) 2193–2202
POLYHEDRON
www.elsevier.com/locate/poly

Synthesis, X-ray and Mössbauer study of iron(II) complexes with trithiocyanuric acid ($ttcH_3$). The X-ray structures of $[Fe(bpy)_3](ttcH) \cdot 2bpy \cdot 7H_2O$ and $[Fe(phen)_3](ttcH_2)(ClO_4) \cdot 2CH_3OH \cdot 2H_2O$

Pavel Kopel [a,*], Zdeněk Trávníček [a], Radek Zbořil [b], Jaromír Marek [c]

[a] Department of Inorganic Chemistry, Palacký University, Křížkovského 10, CZ-771 47 Olomouc, Czech Republic
[b] Department of Physical Chemistry, Palacký University, Tř. Svobody 8, CZ-771 46 Olomouc, Czech Republic
[c] Laboratory of Functional Genomics and Proteomics, Faculty of Sciences, Masaryk University, Kotlářská 2, CZ-611 37 Brno, Czech Republic

Received 26 April 2004; accepted 17 June 2004
Available online 25 August 2004

Abstract

Iron(II) complexes with a combination of nitrogen-donor ligands and trithiocyanuric acid ($ttcH_3$) of the composition $[Fe(bpy)_2(ttcH)] \cdot 2H_2O$ (**1**), $[Fe(bpy)_3](ttcH) \cdot 2bpy \cdot 7H_2O$ (**2**), $[Fe(terpyCl)_2](ttcH_2)_2 \cdot H_2O$ (**3**), $[Fe(phen)_2(ttcH)] \cdot 2H_2O$ (**4**), $[Fe(nphen)_2(ttcH)] \cdot 4H_2O$ (**5**) and $[Fe(phen)_3](ttcH_2)(ClO_4) \cdot 2CH_3OH \cdot 2H_2O$ (**6**), where bpy = 2,2′-bipyridine, terpyCl = 4′-chloro-2,2′:6′,2′-terpyridine, phen = 1,10-phenanthroline, nphen = 5-nitro-1,10-phenanthroline, have been prepared. The compounds, except for **6**, have been characterized by elemental analysis, ^{57}Fe Mössbauer, IR and UV–Vis spectroscopies. It has been found that the trithiocyanurate ion is either coordinated to the metal centre (**1**, **4** and **5**) or situated outside the inner coordination sphere of the iron(II) ion (**2**, **3** and **6**). The X-ray crystal structures of complexes **2** and **6** demonstrate that the ligands enforce a distorted octahedral geometry on the Fe^{II} ions with monoanionic **2** and dianionic **6** forms of uncoordinated trithiocyanuric acid. Density-functional theory (DFT) calculations (B3LYP/6-31 + G*) were used for the geometry optimisation and infrared frequencies calculations of differently protonated forms of the acid ($ttcH_3$, $ttcH_2^-$ and $ttcH^{2-}$).
© 2004 Elsevier Ltd. All rights reserved.

Keywords: Iron(II) complexes; Trithiocyanuric acid; Mössbauer spectra; Crystal structures; Spectroscopic properties; DFT calculations

1. Introduction

Trithiocyanuric acid (2,4,6-trimercapto-1,3,5-triazine, $ttcH_3$) and its trisodium salt ($ttcNa_3 \cdot 9H_2O$) are widely applied in industry, analytical chemistry and biochemistry. For example, $ttcNa_3 \cdot 9H_2O$ is used as a precipitating agent for many heavy metals from contaminated water [1], as a component of the zinc electroplating bath, in PVC floor coverings and it may be also used instead of thiourea in the bleaching of wool [2–4]. Moreover, it was found that the acid inhibits the *Toxoplasma gondii uracil phosphoribosyltransferase* enzyme in vitro better than 5-fluorouracil and emimycin, i.e. compounds showing an antitoxoplasmal activity [5,6].

At first, Beezer et al. [7] studied complexes of trithiocyanuric acid. The authors found that the formation of mononuclear, binuclear as well as trinuclear complexes depends on the molar stoichiometry of reactants (i.e. on the molar ratio between metal ions and ligands) and the pH of the water solution. Bailey et al. [8] studied

* Corresponding author. Tel.: +420 58 563 4354; fax: +420 58 522 5737.
E-mail address: kopel@risc.upol.cz (P. Kopel).

0277-5387/$ - see front matter © 2004 Elsevier Ltd. All rights reserved.
doi:10.1016/j.poly.2004.06.024

the influence of pH and different stoichiometry on the formation of Co^{II}, Cu^{II} and Cd^{II} complexes in detail. Moreover, they have found that the complexes can be used as precursors for the preparation of transition metal sulfide nanomaterials. To date, X-ray crystal structures of some complexes involving trithiocyanurate anions have been determined, e.g. $[\{Os_3H(CO)_{10}\}_3(ttc)]$ [9], $[\{Co(en)_2\}_2(ttc)](ClO_4)_3 \cdot 2H_2O$ (en = ethylenediamine) [10], $[\{Cu(PPh_3)\}_6(ttc)_2]$ (PPh_3 = triphenylphosphine) [11], $[\{Au(ttc)\}\{Au(PPhMe_2)_2\}]_2$, $[(AuPPh_3)_3(ttc)] \cdot 2DMF$ [12], $[(AuPPh_3)_3(ttc)] \cdot 2Et_2O$, $[Au_6(L)_4(ttc)_2] \cdot C_6H_5NO_2$, (L = *t*-butylcyanate) [13], $[(SnPh_3)_3(ttc)]$, $[(SnMe_3)_3(ttc)]$ [14], $Ca(ttcH_2)_2 \cdot 11H_2O$, $Sr(ttcH_2)_2 \cdot 11H_2O$, $Ba(ttcH_2)_2 \cdot 4.5H_2O$ [15], $Mg(ttcH_2)_2 \cdot 6H_2O$, $Ba(ttcH_2)_2 \cdot 7H_2O$, $Ba(ttcH) \cdot 3H_2O$ [16], $Li(ttcH_2) \cdot 2HMPA$, (HMPA = hexamethylphosphoramide) and $Li_3(ttc) \cdot 4THF$ [17,18].

Recently, we have prepared and structurally characterized a series of nickel(II) complexes containing the trithiocyanurate dianion and nitrogen-donor ligands [19]. It has been found that the nickel atom is both five- and six-coordinated in these complexes and $ttcH^{2-}$ is monodentately bonded only through a N atom or chelated via N and S atoms. All the prepared complexes are mononuclear only. Moreover, it has been found that $ttcH^{2-}$ can be also situated outside the coordination sphere of the nickel. The latter mode is preferred in the case when the coordination sphere of the central atom is completely occupied by N-donor ligands such as 1,10-phenanthroline (phen) or 2,2′-bipyridine (bpy).

The complexes of iron(II) with 2,2′-bipyridine and 1,10-phenantholine and their derivatives are of general interest to coordination chemists [20]. In these compounds, the iron(II) ions with octahedral surroundings can be either in a low-spin ($S = 0$) or in a high-spin ($S = 2$) ground state. It is well known that the $[Fe(bpy)_3]^{2+}$ and $[Fe(phen)_3]^{2+}$ complex cations are mostly low-spin, but their magnetochemical behaviour also depends on the counter-ion used, e.g. the $[Fe(bpy)_3](BF_4)_2 \cdot 2H_2O$ complex exhibits a thermally induced low-spin to high-spin crossover [21]. The substitution of one bpy or phen ligand by a monodentate N-donor ligand in similar complexes can also lead to the formation of compounds where transition from a low-spin to a high-spin state can be observed. The spin-crossover behaviour, which can be either thermally or light induced, was intensively studied on the $[Fe(bpy)_2X_2]$ and $[Fe(phen)_2X_2]$ complexes, where $X = NCS^-$ or $NCSe^-$ [21].

The aim of this work was to prove the coordination abilities of the trithiocyanurate ion to iron(II). In this study, we used the combination of $ttcH_3$ and N-donor organic molecules as ligands. Here, we report X-ray structures of two iron(II) complexes: $[Fe(bpy)_3](ttcH) \cdot 2bpy \cdot 7H_2O$ (**2**) and $[Fe(phen)_3](ttcH_2)(ClO_4) \cdot 2CH_3OH \cdot 2H_2O$ (**6**). It was also our interest to find if the presence of the trithiocyanurate ion in the iron(II) complexes can cause their spin-crossover behaviour.

2. Experimental

2.1. General procedures

The chemicals and solvents were purchased from Aldrich co. and Lachema co. and were used as received. The C, H, N, S analyses were carried out on an EA 1108 instrument (FISONS). IR spectra (400–4000 cm^{-1}) were recorded on a Nexus 670 FTIR spectrometer (ThermoNicolet) using KBr pellets. The diffuse-reflectance spectra (11000–35000 cm^{-1}) were obtained on a Specord M40 (Carl Zeiss, Jena) using the nujol technique. The transmission Mössbauer spectra were recorded using a Mössbauer spectrometer in constant acceleration mode with a $^{57}Co(Rh)$ source. A cryostat with closed He-cycle (Janis Research Company, USA) was used as the basis of a refrigerating system that allowed measurements in the 15–300 K temperature range. Isomer shift parameters are related to metallic iron (with a calibration temperature of 300 K).

2.2. Preparation of the complexes **1**–**6**

2.2.1. Preparation of $[Fe(bpy)_2(ttcH)] \cdot 2H_2O$ (**1**)

2,2′-Bipyridine (bpy) (320 mg, 2 mmol) in 15 ml of EtOH was added to an aqueous solution (10 ml) of $(NH_4)_2Fe(SO_4)_2 \cdot 6H_2O$ (390 mg, 1 mmol). The mixture was stirred at room temperature for 3 h. The white solid that formed was filtered off. Consecutively, a solution of $ttcNa_3 \cdot 9H_2O$ (400 mg, 1 mmol) in water (5 ml) was added dropwise to the red filtrate. Then, the mixture was stirred for 2 h, and a red microcrystalline product was separated by filtration, washed with EtOH and dried under an infra lamp at 40 °C. Yield: 498 mg, 86%. *Anal.* Calc.: C, 47.7; H, 3.7; N, 16.9; S, 16.6. Found: C, 47.6; H, 3.5; N, 16.6; S, 17.0%. IR (cm^{-1}): 401w, 423m, 456m, 488w, 616w, 658w, 720w, 734m, 772s, 874m, 966w, 1021w, 1134s, 1188w, 1227s, 1323w, 1343w, 1443s, 1468vs, 1529s, 1603m, 1632m, 1723w, 1738w, 2855w, 2925m, 3072w, 3103w, 3452vs. UV–Vis (cm^{-1}): 18700, 20200, 28600. Mössbauer spectrum (300 K): doublet with isomer shift (i.s.) = 0.29 ± 0.01 mm s^{-1}, quadrupole splitting (q.s.) = 0.33 ± 0.01 mm s^{-1}, half-width of the spectral line (Γ) = 0.26 ± 0.01 mm s^{-1} and relative spectrum area (A) = 100%.

2.2.2. Preparation of $[Fe(bpy)_3](ttcH) \cdot 2bpy \cdot 7H_2O$ (**2**)

A suspension of iron(II) oxalate dihydrate (180 mg, 1 mmol) and bpy (320 mg, 2 mmol) in water (50 ml) was stirred with heating until all the yellow iron(II) oxa-

late salt disappeared. After cooling, an aqueous solution (5 ml) of $ttcNa_3 \cdot 9H_2O$ (400 mg, 1 mmol) was added dropwise with stirring to the reaction mixture. The mixture was filtered off to remove a small amount of red precipitate, which was discarded, and the filtrate was left for crystallization. Dark red needle like crystals suitable for X-ray analysis were obtained after one week. They were filtered off, washed with a small amount of EtOH and dried in air. Yield: 270 mg, 58%. *Anal.* Calc.: C, 55.9; H, 4.9; N, 16.0; S, 8.5. Found: C, 55.7; H, 4.6; N, 16.0; S, 8.2%. IR (cm^{-1}): 423m, 457w, 473m, 551w, 571w, 620m, 639w, 657w, 668w, 734m, 766vs, 772vs, 852s, 898w, 991w, 1020w, 1040w, 1067w, 1122m, 1187vs, 1250m, 1269w, 1314m, 1427s, 1454vs, 1559m, 1581m, 1602s, 1622m, 1636m, 1698w, 2041w, 2907m, 3021w, 3048m, 3065m, 3409s. UV–Vis (cm^{-1}): 18300, 19850, 28800. Mössbauer spectrum (300 K): doublet with i.s. = 0.29 ± 0.01 mm s^{-1}, q.s. = 0.34 ± 0.01 mm s^{-1}, Γ = 0.25 ± 0.01 mm s^{-1}, A = 100%.

2.2.3. Preparation of $[Fe(terpyCl)_2](ttcH_2)_2 \cdot H_2O$ (3)

$Fe(ClO_4)_2 \cdot 6H_2O$ (125 mg, 0.34 mmol) was dissolved in EtOH (50 ml) and 1 ml of 0.1 M $HClO_4$ and iron chips were added. Then, 4′-chloro-2,2′:6′,2′-terpyridine (terpyCl) (140 mg, 0.5 mmol), dissolved in 20 ml of EtOH, was added to the solution with stirring at room temperature. The color of the reaction mixture turned to violet immediately and a violet precipitate was formed. Consecutively, $MeNO_2$ (10 ml) was added until all the precipitate disappeared. After that a solution of $ttcNa_3 \cdot 9H_2O$ (200 mg, 0.5 mmol) in 10 ml of EtOH:water (1:1) mixture was added. A small amount of the precipitate was removed and a dark violet crystalline product, obtained from solution after two days, was filtered off, washed with EtOH and dried in air. Yield: 82 mg, 34%. *Anal.* Calc.: C, 45.0; H, 2.7; N, 17.5; S, 20.0. Found: C, 44.8; H, 2.8; N, 17.4; S, 20.2%. IR (cm^{-1}): 420w, 458s, 483m, 541s, 567m, 619w, 652w, 670w, 690w, 719s, 728m, 751s, 787s, 828m, 874vs, 965w, 1019w, 1034w, 1057w, 1132vs, 1232vs, 1283m, 1346s, 1394vs, 1424vs, 1460vs, 1529vs, 1600vs, 1631s, 1737m, 1776w, 1849w, 2015w, 2112w, 2344w, 2361m, 2849vs, 2911vs, 3063s, 3410s. UV–Vis (cm^{-1}): 17200, 19400, 28000. Mössbauer spectrum (300 K): doublet with i.s. = 0.20 ± 0.01 mm s^{-1}, q.s. = 0.96 ± 0.01 mm s^{-1}, Γ = 0.28 ± 0.01 mm s^{-1}, A = 100%.

2.2.4. Preparation of $[Fe(phen)_2(ttcH)] \cdot 2H_2O$ (4)

The procedure similar to that used for the preparation of **1** was applied, only 1,10-phenanthroline monohydrate (400 mg, 2 mmol) was used instead of 2,2′-bipyridine. Yield: 364 mg, 58%. *Anal.* Calc.: C, 51.7; H, 3.4; N, 15.6; S, 15.3. Found: C, 51.6; H, 3.5; N, 15.2; S, 16.1%. IR (cm^{-1}): 435w, 409w, 420w, 458m, 483w, 530m, 558w, 620m, 671w, 722s, 775m, 845vs, 876s, 967w, 998m, 1040w, 1057w, 1133vs, 1188s, 1233vs, 1344s, 1425vs, 1485vs, 1527vs, 1578m, 1631s, 1985w, 2059w, 2247w, 2291w, 2362w, 2922m, 3070s, 3431vs. UV–Vis (cm^{-1}): 19100, 20400, 28800. Mössbauer spectrum (300 K): doublet *I* with i.s. = 0.29 ± 0.01 mm s^{-1}, q.s. = 0.24 ± 0.01 mm s^{-1}, Γ = 0.28 ± 0.01 mm s^{-1}, A = 71.1%; doublet *II* with i.s. = 0.25 ± 0.01 mm s^{-1}, q.s. = 0.83 ± 0.01 mm s^{-1}, Γ = 0.29 ± 0.01 mm s^{-1}, A = 28.9%.

2.2.5. Preparation of $[Fe(nphen)_2(ttcH)] \cdot 4H_2O$ (5)

5-Nitro-1,10-phenanthroline (440 mg, 2 mmol) in EtOH (100 ml) was added with stirring to an aqueous solution (10 ml) of $(NH_4)_2Fe(SO_4)_2 \cdot 6H_2O$ (390 mg, 1 mmol). Then, $ttcNa_3 \cdot 9H_2O$ (400 mg, 1 mmol) with 1 ml of 1 M HCl in water:EtOH (1:1) mixture was added dropwise to the solution. A dark violet product, which appeared during the addition of the solution of $ttcNa_3$, was filtered off, washed with EtOH and dried under an infra lamp at 40 °C. Yield: 482 mg, 64%. *Anal.* Calc.: C, 43.0; H, 3.1; N, 16.7; S, 12.8. Found: C, 43.1; H, 2.8; N, 16.2; S, 12.5%. IR (cm^{-1}): 409w, 420w, 428w, 458m, 482w, 505w, 538w, 618m, 657w, 669w, 721s, 734m, 755w, 810m, 843m, 859m, 907w, 1002w, 1039w, 1064w, 1130s, 1189m, 1232m, 1350s, 1420s, 1458vs, 1514s, 1534vs, 1579w, 1630m, 1684w, 2925w, 3090s, 3456vs. UV–Vis (cm^{-1}): 17900, 21600, 29000. Mössbauer spectrum (300 K): doublet *I* with i.s. = 0.29 ± 0.01 mm s^{-1}, q.s. = 0.27 ± 0.01 mm s^{-1}, Γ = 0.27 ± 0.01 mm s^{-1}, A = 20.0%, doublet *II* with i.s. = 0.35 ± 0.01 mm s^{-1}, q.s. = 0.64 ± 0.01 mm s^{-1}, Γ = 0.29 ± 0.01 mm s^{-1}, A = 80.0%.

2.2.6. Preparation of $[Fe(phen)_3](ttcH_2)(ClO_4) \cdot 2CH_3OH \cdot 2H_2O$ (6)

$Fe(ClO_4)_2 \cdot 6H_2O$ (250 mg, 0.68 mmol) was dissolved in 50 ml of MeOH and 1 ml of 0.1 M $HClO_4$ and iron chips were added. A solution of 1,10-phenanthroline monohydrate (400 mg, 2 mmol) dissolved in 10 ml of MeOH was added to this mixture, with stirring at room temperature. The color of the reaction mixture turned into red immediately. Finally, a solution of $ttcNa_3 \cdot 9H_2O$ (400 mg, 1 mmol) in water (5 ml) was added. A red precipitate (its composition was identical to $[Fe(phen)_2(ttcH)] \cdot 2H_2O$ (**4**), as was proven by elemental analysis) was filtered off and the filtrate was left to stand at room temperature for crystallization. A small amount of red crystals was obtained after two weeks. The crystals were characterized only by a single crystal X-ray analysis. Yield: 77 mg, 12%.

2.3. X-ray crystallography

Diffraction experiments for complexes $[Fe(bpy)_3](ttcH) \cdot 2bpy \cdot 7H_2O$ (**2**) and $[Fe(phen)_3](ttcH_2)(ClO_4) \cdot 2CH_3OH \cdot 2H_2O$ (**6**), were carried out on a

four circle κ-axis KUMA KM-4 diffractometer using graphite-monochromated MoK_α radiation (λ = 0.71073 Å) at 120(2) K. Data collections for both complexes were performed using a CCD detector (KUMA Diffraction, Wroclaw). KUMA KM4RED software was used for data reduction. Both structures were solved by direct methods [22]. All non-hydrogen atoms of **2** and **6** were refined anisotropically by the full-matrix least-squares procedure [SHELXL-97] [23] with weight: $w = 1/[\sigma^2(F_o^2) + (0.050P)^2 + 10.000P]$ for **2** and $w = 1/[\sigma^2(F_o^2) + (0.075P)^2 + 3.000P]$ for **6**, where $P = (F_o^2 + 2(F_c^2)/3$. The O(1), O(5) and O(7) atoms in **2** are disordered. All H-atom positions, except for one hydrogen atom of O(7) in **2**, were located from Fourier difference maps. In **6**, two methanol molecules are disordered over two positions and their hydrogen atoms were not found in the Fourier difference maps. All remaining hydrogen atoms were localized and their parameters were refined. The largest peak and hole on the final difference map for **2** and **6** were 0.711 [0.11 Å from H(7W)] and −0.425 [0.46 Å from O(7)] e Å^{-3}, and 0.550 [0.79 Å from N(5)] and −0.606 [0.61 Å from C(41)] e Å^{-3}, respectively. Important crystallographic parameters are given in Table 1.

2.4. Computational details

The geometry optimisations and infrared frequency calculations of differently protonated *thion*-forms of the trithiocyanuric acid ($ttcH_3$, $ttcH_2^-$ and $ttcH^{2-}$) were performed employing hybrid density functional B3LYP as implemented in the Gaussian98W [24] and Spartan'02 [25] programs. All calculations were performed with the 6-31 + G* basis set and the theoretical infrared frequencies were not scaled.

3. Results and discussion

3.1. Infrared and electronic spectra

The experimental vibrational frequencies with their relative intensities are given in Section 2.2. In general, the IR spectra of the iron(II) complexes **1**–**5** are quite similar. It is typical that the IR spectra of iron complexes having aromatic heterocycles such as bpy or phen as ligands contain several bands in the regions 1400–1600 and 700–900 cm^{-1}, which are connected with the ring modes [ν(C–C) and ν(C–N)] and the ring deformation vibrations, respectively [20]. For instance, the bands

Table 1
Data collection and refinement parameters for $[Fe(bpy)_3](ttcH) \cdot 2bpy \cdot 7H_2O$ (**2**) and $[Fe(phen)_3](ttcH_2)(ClO_4) \cdot 2CH_3OH \cdot 2H_2O$ (**6**)

	Complex **2**	Complex **6**
Empirical formula	$C_{43}H_{44}FeN_{11}O_{5.5}S_3$	$C_{41}H_{36}ClCFeN_9O_8S_3$
Formula weight	954.92	970.27
Temperature (K)	120(2)	120(2)
Wavelength (Å)	0.71073	0.71073
Crystal system	monoclinic	triclinic
Space group	*C2/c*	$P\bar{1}$
Unit cell dimensions		
a (Å)	28.943(2)	10.4767(7)
b (Å)	13.3723(7)	12.5987(9)
c (Å)	25.485(10)	17.0441(12)
α (°)	–	97.342(6)
β (°)	116.039(4)	103.604(6)
γ (°)	–	103.041(6)
Volume (Å^3)	8862(4)	2091.0(3)
Z	8	2
Density (calc.) (g/cm^3)	1.431	1.541
Absorption coefficient (mm^{-1})	0.542	0.640
F(0 0 0)	3976	1000
Crystal size (mm)	0.40 × 0.15 × 0.15	0.70 × 0.50 × 0.30
Index ranges	$-34 \leqslant h \leqslant 34$, $-8 \leqslant k \leqslant 15$, $-30 \leqslant l \leqslant 30$	$-12 \leqslant h \leqslant 12$, $-14 \leqslant k \leqslant 14$, $-13 \leqslant l \leqslant 20$
Reflections collected	23516	11388
Independent reflections	7657 [$R_{(int)}$ = 0.0321]	7076 [$R_{(int)}$ = 0.0318]
Refinement method	full-matrix least-squares on F^2	full-matrix least-squares on F^2
Data/restraints/parameters	7657/4/744	7076/4/703
Goodness-of fit on F^2	0.943	1.002
Final *R* indices [$I > 2\sigma(I)$]	R_1 = 0.0320, wR_2 = 0.0784	R_1 = 0.0454, wR_2 = 0.1230
R indices (all data)	R_1 = 0.0406, wR_2 = 0.0830	R_1 = 0.0509, wR_2 = 0.1269
Largest differential peak and hole (e Å^{-3})	0.711 and −0.425	0.550 and −0.606

observed in the IR spectrum of the free bpy ligand at 1414, 1452, 1456 and 1578 cm^{-1} are shifted to higher frequencies upon coordination and are observed at 1427, 1454, 1559 and 1581 cm^{-1} in the spectrum of **2**. The peaks connected with the ring deformation of the aromatic N-donor heterocycles are observed in the IR spectra of all the complexes at ca. 620, 720, 775, 845 and 870 cm^{-1} [26]. The bands observed near 3060 and 3450 cm^{-1} can be connected with $\nu(C_{ar}–H)$ and $\nu(N_{ttc}–H)$ vibrations, respectively. At this point, it is necessary to mention that the interpretation of IR spectra is somewhat difficult in connection with the fact that many vibrations can be overlapped. However, based on the DFT/6-31 + G* calculated infrared frequencies (see Section 3.4), we can conclude that the bands connected with the ν(C–N) and ν(C–S) vibrations of the 2,4,6-trimercapto-1,3,5-triazine ring are observed in IR spectra of the complexes **1**–**5** at 1514–1559 and 1172–1227 cm^{-1}, and 845–874 and 420–435 cm^{-1}, respectively.

The diffuse-reflectance spectra of **1**–**5** are also very similar. The bands observed in the 17200–19100 cm^{-1} range may be associated with d–d transitions or identically, and more probably, like the bands with the maxima recorded in the regions of 19850–21600 and 27500–30000 cm^{-1}, with metal-to-ligand charge transfer (MLCT) transitions [27].

3.2. Mössbauer spectroscopy

The hyperfine parameters of the room temperature ^{57}Fe Mössbauer spectra of the iron(II) complexes **1**–**5** are given in Section 2. The experimental data were fitted by a least squares procedure with Lorentzian profiles used to determine the line positions, widths and relative spectra areas. The continuous lines represent the computer's fitted data. Fig. 1 demonstrates the room temperature Mössbauer spectra of complexes **1** and **2**. The spectra are almost identical with a distinct doublet with an isomer shift i.s. = 0.29 mm s^{-1} and quadrupole splitting parameter q.s. = 0.33 and 0.34 mm s^{-1}, respectively. The value of the isomer shift is typical for octahedral complexes of iron(II) in the low-spin state. For example, the isomer shifts measured for $[Fe(bpy)_3]Cl_2$ and $[Fe(bpy)_3](ClO_4)_2$ are 0.33 and 0.30 mm s^{-1}, respectively [28,29]. The octahedral coordination of iron(II) in the complex **2** was unambiguously confirmed by X-ray analysis.

The room temperature Mössbauer spectrum of complex **3** (Fig. 2) consists of a doublet with a relatively low value of isomer shift (0.20 mm s^{-1}) corresponding to low-spin iron(II). In the structure of this complex, two 4′-chloro-2,2′:6′,2′-terpyridines are probably coordinated to the central atom in a meridional fashion, as in complex $[Fe(terpy)_2](ClO_4)_2$ [30]. This type of coordi-

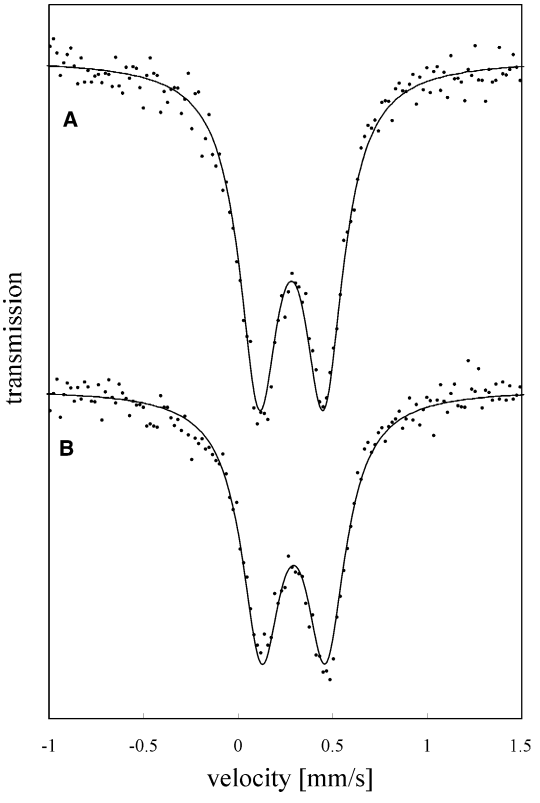

Fig. 1. Room temperature Mössbauer spectra of the complexes **1** (A) and **2** (B). I.s. are related to metallic iron. The solid line results from least-squares fitting of the data to the theoretical equation.

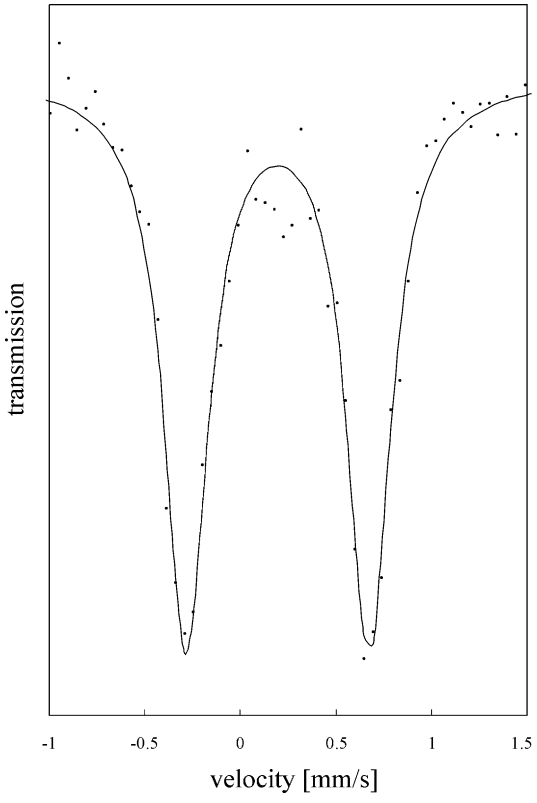

Fig. 2. The room temperature Mössbauer spectrum of complex **3**.

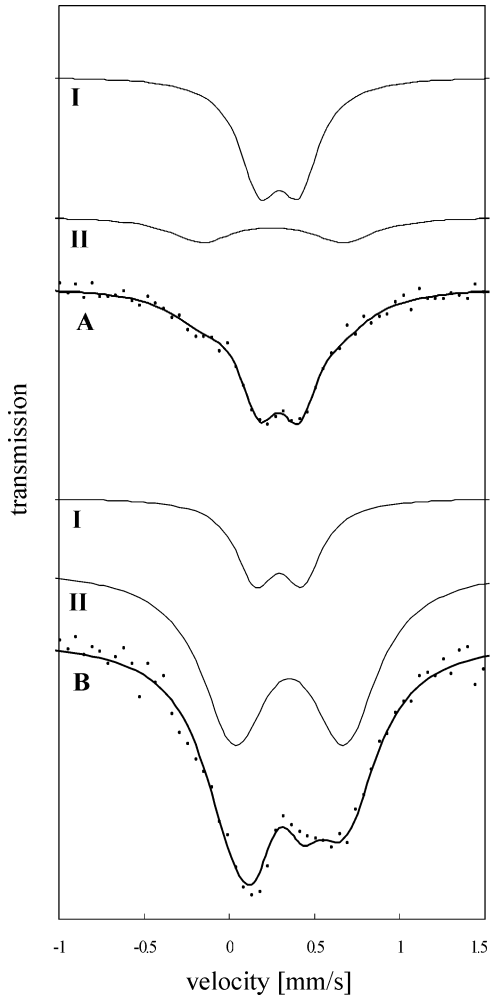

Fig. 3. The room temperature Mössbauer spectra of the complexes **4** (A) and **5** (B) with the results of their mathematical deconvolution (curves I, II).

nation leads to a lowering of the symmetry in the iron environment resulting in the relatively high value of the quadrupole splitting (0.96 mm s^{-1}).

The room temperature Mössbauer spectra of the complexes **4** and **5** are composed of two doublets corresponding to two non-equivalent coordination modes of iron (see Fig. 3). In the spectrum of **4** (Fig. 3A), the doublet *I* with relative spectrum area $A = 71.1\%$ shows hyperfine parameters well comparable to those found for complexes **1** and **2**. Therefore, we can suggest that this doublet also corresponds to octahedrally coordinated low-spin iron(II), where iron is coordinated by four N-atoms of two phen ligands and S and N atoms of trithiocyanurate(2-). The doublet *II* ($A = 28.9\%$) has a significantly higher q.s. value (0.83 mm s^{-1}) indicating distortion from the octahedral coordination geometry. We assume that the trithiocyanurate anion is coordinated to iron(II) only via a N atom as in the case of [Ni (taa)(ttcH)] {taa = tris-(2-aminoethyl)amine} [31] or in $[Cu(PPh_3)_2(ttcH_2)]$ [32]. Two doublets in the room temperature Mössbauer spectrum of complex **5** (Fig. 3B) can be interpreted as well as in the former case. However, the relative spectral areas proved the higher content of iron atoms with a distorted octahedral environment ($A_{II} = 80\%$) in comparison with complex **4**. The higher tendency towards the distorsion of the octahedral Fe environment in the case of complex **5** can be assigned to the effect of NO_2 groups although the influence of water of crystallization cannot be excluded. The low temperature Mössbauer spectra (25 K) of the complexes **4** and **5** are very similar (the spectrum of complex **4** is depicted in Fig. 4) and show only one component with a high value of i.s. = 0.40 mm s^{-1} due to the temperature shift and q.s. = 0.17 mm s^{-1}. It is evident that the distortion is eliminated by temperature lowering as can be deduced on the basis of the absence of second doublet in the spectrum. The subsequent heating to room temperature caused the repeated appearance of two doublets in the spectrum that indicates a thermally induced reversible character of the structural ordering.

In general, the obtained results are in good accordance with the literature data for iron(II) low-spin complexes [21]. The found values of q.s. parameters indicate the differences in the symmetry of central atom environment and reflect the non-equivalent coordination modes of individual complexes.

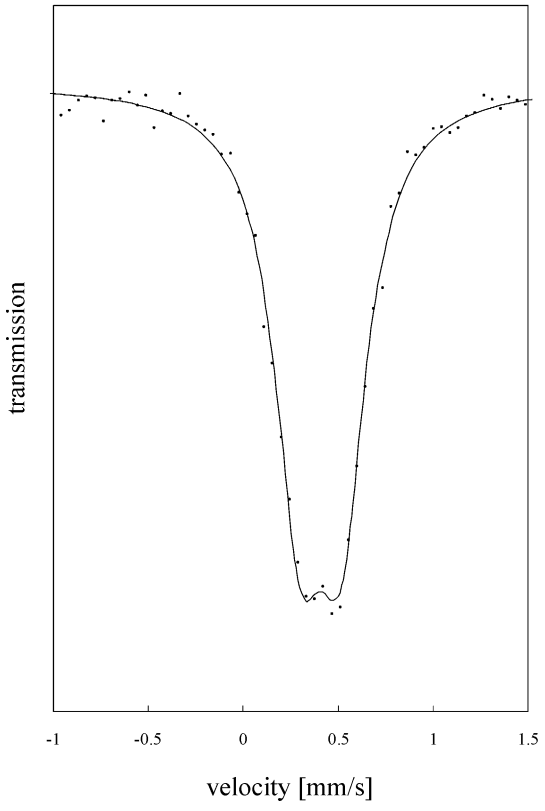

Fig. 4. The Mössbauer spectrum of complex **4** measured at 25 K.

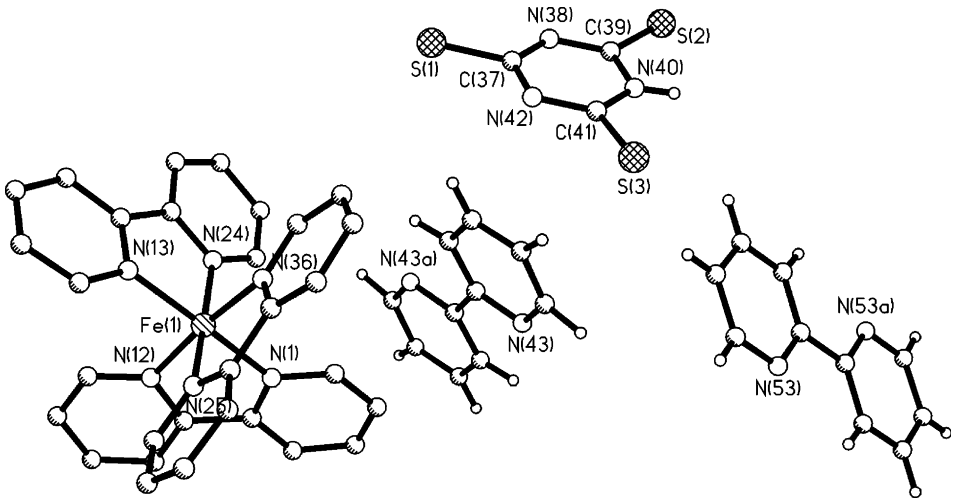

Fig. 5. Molecular structure of $[Fe(bpy)_3](ttcH) \cdot 2bpy \cdot 7H_2O$ (**2**). Solvent water molecules and the hydrogen atoms of coordinated bpy ligands are omitted for clarity.

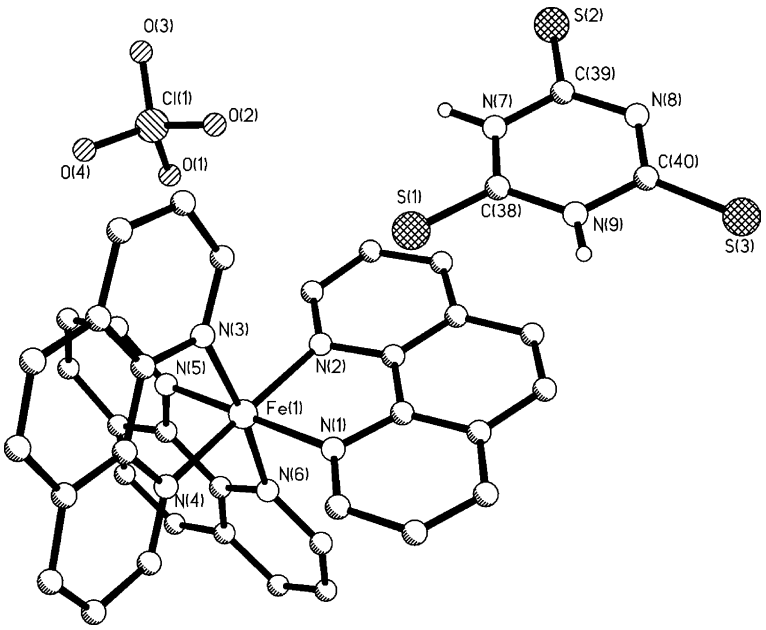

Fig. 6. Molecular structure of $[Fe(phen)_3](ttcH_2)(ClO_4) \cdot 2CH_3OH \cdot 2H_2O$ (**6**). Molecules of solvents as well as hydrogen atoms of phen ligands are omitted for clarity.

3.3. X-ray structures

The molecular structures of **2** and **6** are shown in Figs. 5 and 6. Selected bond lengths and angles for the complexes are listed in Table 2. Both structures consist of hexacoordinated $[Fe(N–N)_3]^{2+}$ cations (N–N = bpy or phen) and uncoordinated trithiocyanurate anions. There are also seven water molecules and two bpy (in **2**) and one perchlorate anion, two water and two methanol molecules (in **6**) in the crystal lattices. Both iron(II) ions in **2** and **6** are coordinated in distorted octahedral arrangements. The Fe–N bond lengths are quite comparable and vary from 1.9715(17) to 1.9834(16) Å (in **2**) and from 1.973(2) to 1.985(2) Å (in **6**). In both structures, the trithiocyanurate anions are situated outside the coordination sphere of the central atom. However, the extent of deprotonation of the anion is different. Only one hydrogen atom at the N(40) position of the triazine ring was located in **2** (see Fig. 5), while two protons were found in **6** (see Fig. 6). It is evident that a different manner of deprotonation causes the changes in bond lengths and angles of the trithiocyanurate anion. The C–S bond distances in **2** {1.7213(19), 1.708(2), 1.7091(19) Å} are intermediate between single and double bonds (a typical value for the single C–S bond length equals 1.81 Å), whilst the C–S bond

Table 2
Selected bond lengths [Å] and angles [°] in the vicinity of the central atom for $[Fe(bpy)_3](ttcH) \cdot 2bpy \cdot 7H_2O$ (**2**) and $[Fe(phen)_3](ttcH_2)(ClO_4) \cdot 2\text{-}CH_3OH \cdot 2H_2O$ (**6**)

Complex **2**		Complex **6**	
Bond lengths			
Fe(1)–N(25)	1.9715(17)	Fe(1)–N(2)	1.973(2)
Fe(1)–N(1)	1.9721(16)	Fe(1)–N(3)	1.974(2)
Fe(1)–N(13)	1.9741(16)	Fe(1)–N(5)	1.978(2)
Fe(1)–N(24)	1.9775(17)	Fe(1)–N(4)	1.979(2)
Fe(1)–N(12)	1.9816(16)	Fe(1)–N(6)	1.980(2)
Fe(1)–N(36)	1.9834(16)	Fe(1)–N(1)	1.985(2)
Bond angles			
N(25)–Fe(1)–N(1)	91.01(7)	N(2)–Fe(1)–N(3)	94.21(9)
N(25)–Fe(1)–N(13)	94.40(7)	N(2)–Fe(1)–N(5)	93.63(9)
N(1)–Fe(1)–N(13)	172.46(7)	N(3)–Fe(1)–N(5)	92.70(9)
N(25)–Fe(1)–N(24)	173.46(7)	N(2)–Fe(1)–N(4)	174.07(9)
N(1)–Fe(1)–N(24)	93.34(7)	N(3)–Fe(1)–N(4)	82.49(9)
N(13)–Fe(1)–N(24)	81.74(7)	N(5)–Fe(1)–N(4)	91.45(9)
N(25)–Fe(1)–N(12)	94.15(6)	N(2)–Fe(1)–N(6)	91.12(9)
N(1)–Fe(1)–N(12)	81.64(7)	N(3)–Fe(1)–N(6)	173.06(8)
N(13)–Fe(1)–N(12)	92.71(7)	N(5)–Fe(1)–N(6)	82.52(9)
N(24)–Fe(1)–N(12)	91.31(6)	N(4)–Fe(1)–N(6)	92.57(9)
N(25)–Fe(1)–N(36)	81.41(6)	N(2)–Fe(1)–N(1)	82.86(9)
N(1)–Fe(1)–N(36)	94.25(6)	N(3)–Fe(1)–N(1)	93.14(9)
N(13)–Fe(1)–N(36)	91.75(6)	N(5)–Fe(1)–N(1)	173.40(9)
N(24)–Fe(1)–N(36)	93.39(6)	N(4)–Fe(1)–N(1)	92.37(9)
N(12)–Fe(1)–N(36)	173.93(6)	N(6)–Fe(1)–N(1)	91.93(9)

distances in **6** (1.678(3), 1.665(3), 1.682(3) Å) are more characteristic for C=S double bonds (a typical value for the double C=S bond ranges from 1.61 to 1.68 Å [18]). The bond angles of the triazine rings lie in the ranges of 116.15(16)°–125.80(17)° (for **2**) and 115.7(2)°–123.2(3)° (for **6**). The actual value of the angles inside the triazine ring strongly depends on the extent of deprotonation as well as on the protonation site.

3.4. DFT calculations

The DFT/6-31 + G* optimised structures of differently protonated *thion*-forms of the trithiocyanuric acid ($ttcH_3$, $ttcH_2^-$ and $ttcH^{2-}$) are shown in Fig. 7. The comparison of the calculated interatomic parameters with the experimental data (X-ray) [33] is presented in Table 3. Overall, the calculations gave a good agreement with the experimental data. The differences between experimental and theoretical bond lengths and angles for $ttcH_3$, $ttcH_2^-$ and $ttcH^{2-}$, expressed as an average absolute deviation, were the following (Spartan'02/Gaussian98W): 0.012/0.011 Å and 1.38°/1.38° for $ttcH_3$, 0.014/0.013 Å and 1.89°/1.73° for $ttcH_2^-$, and 0.016/0.014 Å and 1.42°/1.41° for $ttcH^{2-}$, respectively. As for theoretical infrared vibrational frequencies, we have focused our attention on interpretation of the bands belonging to ν(C–N),ν(C–S), δ(CNH) and δ(CNC) vibrations. The B3LYP calculations predicted two C–N stretching bands at 1573.8 and 1279.4 cm^{-1} (for $ttcH_3$), 1539.3 and 1209.3 cm^{-1} (for $ttcH_2^-$), and 1514.5 and 1175.1 cm^{-1} (for $ttcH^{2-}$). The experiment is consistent in finding one strong and one medium strong band at 1577 and 1260 cm^{-1}, as measured for $ttcH_3$ using the KBr technique. On the other hand, the calculated bands at 922.1 and 444.7 cm^{-1} (for $ttcH_3$), 886.4 and 431.5 cm^{-1} (for $ttcH_2^-$), and 842.3 and 411.3 cm^{-1} (for $ttcH^{2-}$) can be assigned to ν(C–S). The bands observed in the IR spectrum of $ttcH_3$ at 892 and 458 cm^{-1} can be connected with the same vibration. The theoretical bands at 1385.0 cm^{-1} (for $ttcH_3$), 1294.0 cm^{-1} (for $ttcH_2^-$) and 1236.7 cm^{-1} (for $ttcH^{2-}$) are attributable to δ(CNH), while the bands at 988.7 cm^{-1} (for $ttcH_3$), 975.4 cm^{-1} (for $ttcH_2^-$) and 961.3 cm^{-1} (for $ttcH^{2-}$) can be assigned to δ(CNC). In conclusion, we can state that although the values of calculated infrared frequencies are non-scaled, a good agreement between theoretical and experimental data has been found.

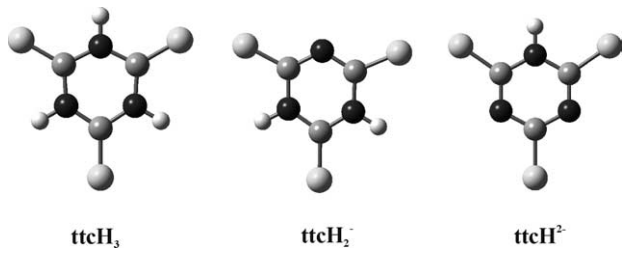

Fig. 7. The optimised geometries of differently protonated *thion*-forms of trithiocyanuric acid.

Table 3
Comparison of X-ray and DFT-calculated (B3LYP/6-31 + G*) bond lengths [Å] and angles [°] for differently protonated *thion*-forms of trithiocyanuric acid ($ttcH_3$, $ttcH_2^{(1-)}$ and $ttcH^{(2-)}$)

$ttcH_3$[a]	X-ray	Sp02	G98W	$ttcH_2^{(1-)}$	X-ray[b]	Sp02	G98W	$ttcH^{(2-)}$	X-ray[c]	Sp02	G98W
S(2)–C(2)	1.650	1.650	1.651	S(1)–C(38)	1.678(3)	1.684	1.689	S(1)–C(37)	1.7213(19)	1.728	1.727
S(4)–C(4)	1.641	1.650	1.651	S(2)–C(39)	1.665(3)	1.689	1.689	S(2)–C(39)	1.708(2)	1.736	1.730
S(6)–C(6)	1.657	1.650	1.651	S(3)–C(40)	1.682(3)	1.689	1.689	S(3)–C(41)	1.7091(19)	1.736	1.730
N(1)–C(2)	1.363	1.381	1.380	N(7)–C(38)	1.344(4)	1.360	1.360	C(37)–N(42)	1.360(3)	1.376	1.370
N(1)–C(6)	1.371	1.381	1.380	N(7)–C(39)	1.389(4)	1.414	1.410	C(37)–N(38)	1.361(3)	1.376	1.370
N(3)–C(2)	1.365	1.381	1.380	N(8)–C(40)	1.341(4)	1.341	1.340	N(38)–C(39)	1.330(2)	1.327	1.320
N(3)–C(4)	1.361	1.381	1.380	N(8)–C(39)	1.353(4)	1.341	1.340	C(39)–N(40)	1.370(2)	1.386	1.380
N(5)–C(4)	1.380	1.381	1.380	N(9)–C(38)	1.357(4)	1.360	1.360	N(40)–C(41)	1.365(3)	1.386	1.380
N(5)–C(6)	1.354	1.381	1.380	N(9)–C(40)	1.385(4)	1.414	1.410	C(41)–N(42)	1.339(2)	1.327	1.320
C(2)–N(3)–C(4)	125.5	126.79	126.81	C(38)–N(7)–C(39)	123.0(2)	125.10	124.94	C(39)–N(38)–C(37)	116.15(16)	118.39	118.24
C(4)–N(5)–C(6)	124.8	126.80	126.77	C(40)–N(8)–C(39)	120.2(3)	120.19	120.50	C(41)–N(40)–C(39)	122.63(17)	122.82	122.79
C(6)–N(1)–C(2)	124.2	126.77	126.75	C(38)–N(9)–C(40)	123.2(3)	124.93	124.86	C(41)–N(42)–C(37)	117.07(16)	118.39	118.52
N(1)–C(2)–N(3)	115.1	113.26	113.24	N(7)–C(38)–N(9)	115.7(2)	112.84	112.71	N(42)–C(37)–N(38)	125.80(17)	123.60	123.55
N(3)–C(4)–N(5)	114.2	113.19	113.19	N(8)–C(39)–N(7)	118.8(3)	118.40	118.49	N(38)–C(39)–N(40)	119.71(17)	118.40	118.69
N(5)–C(6)–N(1)	115.7	113.21	113.23	N(8)–C(40)–N(9)	118.8(3)	118.40	118.43	N(42)–C(41)–N(40)	118.57(17)	118.40	118.16
N(1)–C(2)–S(2)	122.4	123.36	123.38	N(7)–C(38)–S(1)	123.1(2)	123.56	123.69	N(42)–C(37)–S(1)	116.84(15)	118.20	118.23
N(3)–C(2)–S(2)	122.4	123.37	123.37	N(9)–C(38)–S(1)	121.3(2)	125.56	123.59	N(38)–C(37)–S(1)	117.36(14)	118.20	118.23
N(3)–C(4)–S(4)	123.2	123.41	123.39	N(8)–C(39)–S(2)	121.4(2)	125.05	124.89	N(38)–C(39)–S(2)	122.06(14)	124.82	124.62
N(5)–C(4)–S(4)	122.6	123.39	123.41	N(7)–C(39)–S(2)	119.7(2)	116.57	116.58	N(40)–C(39)–S(2)	118.22(15)	116.78	116.65
N(5)–C(6)–S(6)	122.4	123.37	123.38	N(8)–C(40)–S(3)	123.0(2)	125.05	124.99	N(42)–C(41)–S(3)	123.13(15)	124.82	124.88
N(1)–C(6)–S(6)	121.9	123.41	123.38	N(9)–C(40)–S(3)	118.2(2)	116.57	116.53	N(40)–C(41)–S(3)	118.29(14)	116.78	116.92

Sp02 = Spartan'02 (Windows Version 1.0.2); G98W = Gaussian98W (Rev. A.11).

[a] The atoms are numbered following the nomenclature used in [33] for $ttcH_3 \cdot THF$.

[b] X-ray data for $[Fe(bpy)_3](ttcH) \cdot 2bpy \cdot 7H_2O$ (**2**).

[c] X-ray data for $[Fe(phen)_3](ttcH_2)(ClO_4) \cdot 2CH_3OH \cdot 2H_2O$ (**6**).

4. Supplementary material

Crystallographic data for the structures **2** and **6** have been deposited with the Cambridge Crystallographic Data Centre, CCDC nos. 197713 and 197712. The copies of this information may be obtained free of charge from the Director, CCDC, 12 Union Road, Cambridge, CB2 1EZ, UK (fax: +44-1223-336033; e-mail: deposit@ccdc.cam.ac.uk or http://www.ccdc.cam.ac.uk).

Acknowledgement

The crystallographic part of this work was supported by the GAČR (a grant no. 203/02/0436).

References

[1] K.R. Henke, D. Robertson, M.K. Krepps, D.A. Atwood, Water Res. 34 (2000) 3005.
[2] Y. Nakamura, M. Saito, K. Mori, K. Tamura, Nippon Gomu Kyokaishi 53 (5) (1980) 294.
[3] E.S. Raper, Coord. Chem. Rev. 61 (1985) 115.
[4] W.N. Marmer, J.M. Cardamone, B. Guoping, F. Casado, Textile Research J. 27 (9) (1995) 75.
[5] M. Iltzsch, K.O. Tankersley, Biochem. Pharmacol. 46 (1993) 1849.
[6] M. Iltzsch, K.O. Tankersley, Biochem. Pharmacol. 48 (1994) 781.
[7] A.E. Beezer, J.C. Chudy, Thermochim. Acta 6 (1973) 231.
[8] J.R. Bailey, M.J. Hatfield, K.R. Henke, M.K. Krepps, J.L. Morris, T. Otieno, K.D. Simonetti, E.A. Wall, D.A. Atwood, J. Organomet. Chem. 623 (2001) 185.
[9] E.W. Ainscough, A.M. Brodie, R.K. Coll, A.J.A. Mair, J.M. Waters, Inorg. Chim. Acta 214 (1993) 21.
[10] K. Yamanari, Y. Kushi, M. Yamamoto, A. Fuyuhiro, S. Kaizaki, T. Kawamoto, Y. Kushi, J. Chem. Soc., Dalton. Trans. (1993) 3715.
[11] C.K. Chan, K.K. Cheung, C.M. Che, Chem. Commun. (1996) 227.
[12] B.C. Tzeng, C.M. Che, S.M. Peng, Chem. Commun. (1997) 1771.
[13] W.J. Hunks, M.C. Jennings, R.J. Puddephatt, Inorg. Chem. 38 (1999) 5930.
[14] I. Haiduc, M.F. Mahon, K.C. Molloy, M.M. Venter, J. Organomet. Chem. 627 (2001) 6.
[15] K. Henke, D.A. Atwood, Inorg. Chem. 37 (1998) 224.
[16] K.R. Henke, A.R. Hutchison, M.K. Krepps, S. Parkin, D.A. Atwood, Inorg. Chem. 40 (2001) 4443.
[17] W. Clegg, J.E. Davies, M.R.J. Elsegood, E. Lamb, J.J. Longridge, J.M. Rawson, R. Snaith, E.H. Wheatley, Inorg. Chem. Commun. 1 (1998) 58.
[18] D.A. Armstrong, J.E. Davies, N. Feeder, E. Lamb, J.J. Longridge, J.M. Rawson, R. Snaith, A.E.H. Wheatley, J. Mol. Model. 6 (2000) 234.
[19] P. Kopel, Z. Trávníček, L. Kvítek, M. Biler, M. Pavlíček, Z. Šindelář, J. Marek, Transition Met. Chem. 26 (2001) 282, and references therein.
[20] P. Gütlich, A. Hauser, H. Spiering, Angew. Chem., Int. Ed. Engl. 33 (1994) 2024, and references therein.
[21] H.A. Goodwin, Coord. Chem. Reviews 18 (1976) 293, and references therein.
[22] G.M. Sheldrick, SHELXS-97: enhanced version of SHELX-S, Acta Crystallogr. A 46 (1990) 467.
[23] G.M. Sheldrick, SHELXL-97: Program for Crystal Structure Refinement, University of Göttingen, 1997.
[24] GaussianW98, Revision A.11, M.J. Frisch, G.W. Trucks, H.B. Schlegel, G.E. Scuseria, M.A. Robb, J.R. Cheeseman, V.G. Zakrzewski, J.A. Montgomery, Jr., R.E. Stratmann, J.C. Burant, S. Dapprich, J.M. Millam, A.D. Daniels, K.N. Kudin, M.C. Strain, O. Farkas, J. Tomasi, V. Barone, M. Cossi, R. Cammi, B. Mennucci, C. Pomelli, C. Adamo, S. Clifford, J. Ochterski, G.A. Petersson, P.Y. Ayala, Q. Cui, K. Morokuma, P. Salvador, J.J. Dannenberg, D.K. Malick, A.D. Rabuck, K. Raghavachari, J.B. Foresman, J. Cioslowski, J.V. Ortiz, A.G. Baboul, B.B. Stefanov, G. Liu, A. Liashenko, P. Piskorz, I. Komaromi, R. Gomperts, R.L. Martin, D.J. Fox, T. Keith, M.A. Al-Laham, C.Y. Peng, A. Nanayakkara, M. Challacombe, P.M.W. Gill, B. Johnson, W. Chen, M.W. Wong, J.L. Andres, C. Gonzalez, M. Head-Gordon, E.S. Replogle, J.A. Pople, Gaussian, Inc., Pittsburgh, PA, 2001.
[25] Spartan'02 (Version for Windows 1.0.2), Wavefunction Inc., 18401 Von Karman Avenue, Suite 370, Irvine, CA 92612, USA.
[26] C.J. Pouchert, The Aldrich Library of Infrared Spectra, third ed., Aldrich Chemical Company, Milwaukee, WI, 1981.
[27] A.B.P. Lever, Inorganic Electronic Spectroscopy, Elsevier, Amsterdam, 1984.
[28] L.Y. Johansson, R. Larsson, Chem. Phys. Lett. 24 (1974) 508.
[29] H. Sato, T. Tominaga, Bull. Chem. Soc. Jpn. 49 (1976) 697.
[30] A.T. Baker, H.A. Goodwin, Aust. J. Chem. 38 (1985) 207.
[31] P. Kopel, Z. Trávníček, R. Panchártková, M. Biler, J. Marek, Transition Met. Chem. 24 (1999) 239.
[32] M.F. Mahon, K.C. Molloy, M.M. Venter, I. Haiduc, Inorg. Chim. Acta 348 (2003) 75.
[33] F. Belaj, R. Tripolt, E. Nachbaur, Monatsh. Chem. 121 (1990) 99.

Available online at www.sciencedirect.com
SCIENCE DIRECT®
Polyhedron 23 (2004) 2203–2208
POLYHEDRON
www.elsevier.com/locate/poly

A novel 3D malonato-bridged compound Cu(mal)(pz)$_2$: synthesis, spectroscopy, crystal structure and magnetism

Mao Liang [a], Qing-Lun Wang [a], Li-Hua Yu [a], Dai-Zheng Liao [a,b,*], Zong-Hui Jiang [a], Shi-Ping Yan [a,c], Peng Cheng [a]

[a] *Department of Chemistry, Nankai University, Weinjin Road 91, Tianjin 300071, China*
[b] *State Key Laboratory of Structural Chemistry, Fujian Institute of Research on the Structure of Matter, Chinese Academy of Sciences, Fuzhou 350002, China*
[c] *State Key Laboratory of Earth Material Chemistry and Applications, Peking University, Peking 100871, China*

Received 11 March 2004; accepted 18 June 2004
Available online 12 August 2004

Abstract

A novel 3D malonato-bridged copper(II) complex of formula Cu(mal)(pz)$_2$ (**1**) (mal = malonate dianion; pz = pyrazole) has been prepared and characterized by elemental analyses, IR, electronic and EPR spectroscopies, TG analysis, single crystal X-ray diffraction and magnetic susceptibility. **1** crystallizes in the tetragonal space group *I4(1)*, a = 9.4951(16) Å, b = 9.4951(16) Å, c = 12.620(4) Å, V = 1137.8(5) Å^3, Z = 4. The 3D framework of the title compound is formed by the connection of malonate bridges. Magnetic characterization of **1** suggests that the complex exhibits overall a weak ferromagnetic coupling with an antiferromagnetic interaction in the very low temperature range.
© 2004 Elsevier Ltd. All rights reserved.

Keywords: Copper(II) complex; Crystal structure; Magnetic properties; Coordination polymers

1. Introduction

Pronounced attention has currently been paid to the crystal engineering of 2D and 3D metal–ligand coordination polymers due to their fascinating network topologies and potential applications as functional materials [1,2]. Dicarboxylic acids are capable of binding metals to form new types of polymers and oligomers, which can considerably influence the magnetic, optical or catalytic properties of the ultimate product [3]. Among the dicarboxylates, the major studies have been done on oxalate and terephthalate and a few examples with malonate, fumarate, maleate, adipate, etc. [4–15]. The malonate exhibits a rather flexible stereochemistry and variable mode of binding with metal ions in the crystalline state. Research works using malonate as a bridging ligand in copper(II) complexes have shown the versatility of this ligand [6,7,16–23]. Its versatility as a ligand is illustrated by the variety of its coordination modes when acting as a bridge, the most common being the so-called *syn–syn*, *syn–anti* and *anti–anti* modes (Scheme 1). In addition, the adoption of bidentate and/or bridging coordination modes makes this ligand very appropriate in designing mono- and polynuclear species. In order to design high-dimensional (2D or 3D) copper(II) malonate complexes and to gain a better understanding of the correlation between structure and magnetism, we selected the malonate dianion as a linker and pyrazole as the auxiliary ligand, and succeeded in obtaining the novel 3D malonato-bridged copper(II) complex Cu(mal)(pz)$_2$ (**1**). In this paper, we report the synthesis, structure, properties and characterization of **1**.

* Corresponding author. Tel.: +86 23509957; fax: +86 23502779.
E-mail address: coord@nankai.edu.cn (D.-Z. Liao).

0277-5387/$ - see front matter © 2004 Elsevier Ltd. All rights reserved.
doi:10.1016/j.poly.2004.06.027

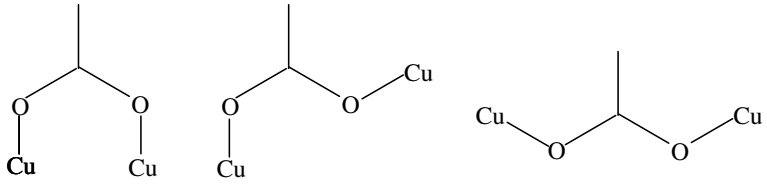

Scheme 1.

2. Experimental

2.1. Physical measurements

All the starting reagents are of A.R. grade and used as purchased. Elemental analyses (C, H, N) were performed on a Perkin–Elmer 240 analyzer. Infrared spectra on KBr pellets were recorded on a Shimadzu IR-408 spectrophotometer in the range 4000–600 cm^{-1} and the TG runs were taken on a Rigaku TG-DTA standard type thermal analysis system. The compound was heated up to 600 °C in the atmosphere of nitrogen, at a heating rate of 10 °C per min. The variable temperature susceptibility measurements were carried out with a MagLab System 2000 magnetometer in the temperature range 2–300 K at a magnetic field of 10,000 G. The electronic spectrum was measured with a Jasco-570 spectrophotometer and X-band EPR spectrum on a Bruker ER 200 D-SRC EPR spectrometer.

2.2. Synthesis

An aqueous solution of pyrazole (27 mg 0.4 mmol) was added to an aqueous solution of $Cu(NO_3)_2 \cdot 2H_2O$ (44 mg, 0.20 mmol). To this mixture an aqueous solution of Na_2(mal) (29 mg, 0.2 mmol) was added after a few minutes. This solution was stirred at room temperature for half an hour. Slow evaporation of the resulting mixture led to blue crystals of **1**. *Anal.* Calc. for $C_9H_{10}CuN_4O_4$: C, 35.82; H, 3.31; N, 18.56. Found: C 35.72; H, 3.44; N, 18.63%.

Table 1
Crystallographic data and structure refinement for **1**

Formula	$C_9H_{10}CuN_4O_4$
Formula weight	301.75
Crystal system	tetragonal
Space group	*I*4(1)
Unit cell dimensions	
a (Å)	9.4951(16)
b (Å)	9.4951(16)
c (Å)	12.620(4)
V (Å^3)	1137.8(5)
Z	4
D_{calc} (g cm^{-1})	1.762
Crystal size (mm^3)	$0.24 \times 0.18 \times 0.14$
F(000)	612
θ Range for data collection	2.68–26.31
Reflections measured	3254
Unique reflections	969
R_{int}	0.0270
Goodness-of-fit	1.041
R_1, wR_2 [$I > 2\sigma(I)$]	0.0247, 0.0510
R_1, wR_2 (all data)	0.0334, 0.0533

2.3. X-ray crystal structure determination

The crystal data were collected with a Bruker Smart 1000 CCD diffractometer equipped with graphite monochromated Mo Kα radiation ($\lambda = 0.71073$ Å) by the $\omega - 2\theta$ scan technique at 293(2) K. A total of 3254 reflections were measured to give 969 independent reflections ($R_{int} = 0.0391$). The structure was solved by direct methods using the SHELXS-97 [24] program. Data were corrected for Lorentz and polarization effects. The final refinement was performed using SHELXL-97 [25] by full-matrix least-squares methods with anisotropic thermal parameters for non-hydrogen atoms on F^2. The crystal data and structure refinement details for **1** are given in Table 1.

3. Results and discussion

3.1. Crystal structure

The coordination environment of the copper(II) ion, with the atom numbering scheme, is shown in Fig. 1. The selected bond lengths and angles are listed in Table 2. The copper(II) ion displays a slightly distorted octahedral coordination environment with the two chelated oxygen atoms (O(1), O(1a)) of one malonate ligand and two nitrogen atoms (N(1), N(1a)) from two pyrazole ligands in the equatorial plane, while two bridging oxygen atoms (O(1w), O(2w)) from two different malonate ligands occupy the axial positions. Both the distances Cu(1)–O(1w) and Cu(1)–O(2w) are the same (2.516 Å), which can be considered as weakly coordinated bonds. The value of the equatorial Cu–O bond distances is 1.948 Å. These structural parameters are within the range observed in previous malonate-contain-

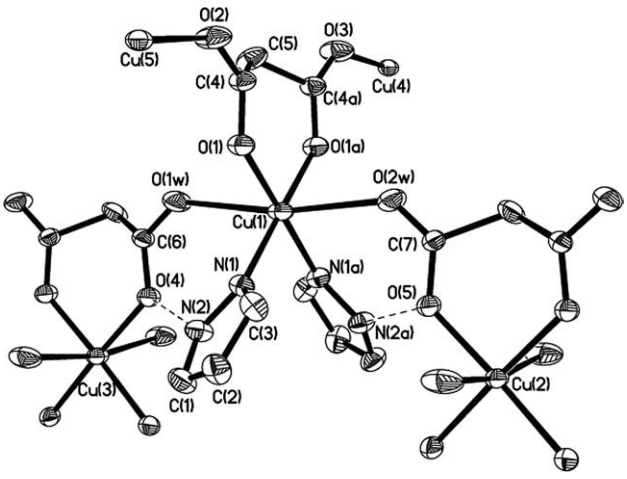

Fig. 1. Perspective diagram of the complex **1** with thermal ellipsoids at 30% probability (Symmetry codes: a = $-x + 1$, $-y + 0$, $z + 0$).

Table 2
Selected bond lengths (Å) and angles (°) for the title compound

Cu(1)–O(1)	1.948(2)	Cu(1)–O(1a)	1.948(2)
Cu(1)–N(1)	2.003(2)	Cu(1)–N(1a)	2.003(2)
Cu(1)–O(1w)	2.516	Cu(1)–O(2w)	2.516
N(1)–C(3)	1.318(4)	N(1)–N(2)	1.339(3)
O(1)–Cu(1)–O(1a)	93.76(12)	O(1)–Cu(1)–N(1)	177.50(11)
O(1a)–Cu(1)–N(1)	88.49(8)	O(1)–Cu(1)–N(1a)	88.49(8)
N(1)–Cu(1)–N(1a)	89.28(14)	O(2)–C(4)–C(5)	115.3(3)
C(4)–O(1)–Cu(1)	128.12(17)	O(2)–C(4)–O(1)	125.1(2)
O(1)–C(4)–C(5)	114.2(4)	N(2)–N(1)–Cu(1)	123.71(18)

a = $-x + 1$, $-y + 0$, $z + 0$.

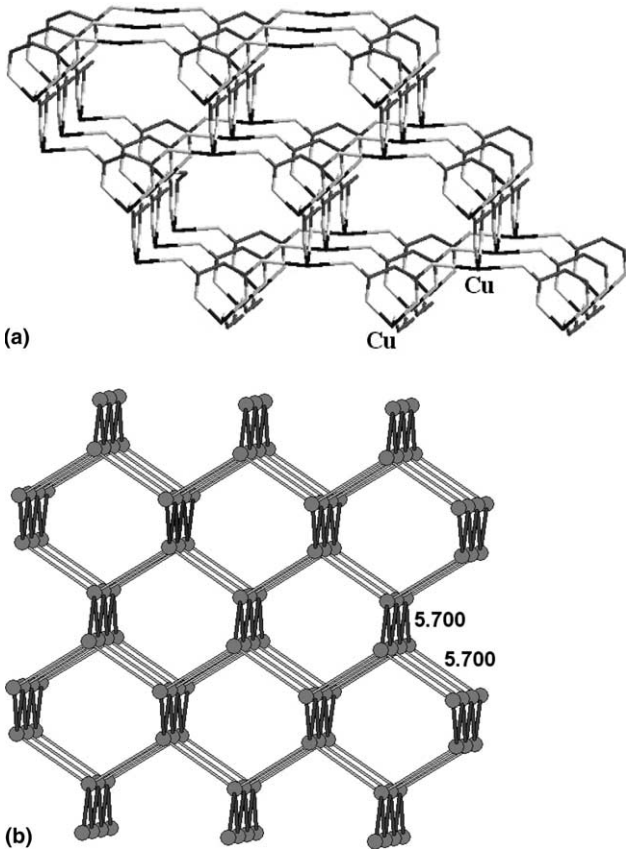

Fig. 2. (a) A perspective view of the 3D framework of **1** (the pyrazole ligands are omitted for clarity). (b) Projection of **1** showing the honeycomb-like structure based on the topology of Cu–Cu connections viewed along the a axis (C, H, O and N atoms are omitted for clarity).

ing copper(II) complexes [18]. Each malonate group adopts simultaneously bidentate (O(1), O(1a) toward Cu(1)) and bis-monodentate coordination modes (through O(3) toward Cu(4) and O(2) toward Cu(5)), and it exhibit an envelope conformation. In addition, the carboxylate-bridges exhibit a *syn–anti* conformation (Cu(1)–O(2w)–C(7)–O(5)–Cu(2)), which connect an equatorial site of one copper atom with an apical site of the adjacent copper atom.

The dihedral angle between the basal plane defined by O(1), O(1a), (N(1), N(1a) and the plane defined by O(1w), O(2w), O(4), O(5) is nearly a right angle (92.2°). The angle (O(1)–Cu(1)–O(1a)) subtended at the copper atom by the chelating malonate group is 80.3°, which is smaller than that previously reported [b]. The value of the O(1w)–Cu(1)–O(2w) bond angle (170.05°) reflects the slightly distorted octahedral surrounding at Cu(1). The average C–O bond distance is 1.241 Å and the O–C–O bond angles are the same (125.11°). Nevertheless, its unique 3D topological architecture, shown in Fig. 2(b), is worth mentioning. Each copper atom is six-connected with four malonate bridged copper atoms and two pyrazole bridged Cu atoms. If the pyrazole bridges are omitted, the four-connected network can be viewed as a metal-apex 3D honeycomb-like structure from the *a* axis, based on the topology of Cu–Cu connections. Each copper atom is connected with one copper in a *syn–anti* conformation with Cu···Cu separations of 5.700 Å. The nitrogen atoms of the pyrazole ligand link the oxygen atoms of malonate via hydrogen bonds (N(2)···O(4) = N(2a)···O(5) = 2.790 Å), which contribute to the stabilization of the crystal structure. Thus, the 3D framework of the title compound is formed by the connection of malonate in orthogonal directions as shown in Fig. 2(a).

3.2. Spectrospic properties

The IR spectrum of **1** shows the main bands as followed: 3275m, 1590s, 1405m, 1350m, 1150w, 1135w, 1050m, 1040m, 930w, 860w, 750m, 720m cm^{-1}, of which the 1590 cm^{-1} band belongs to the C═O stretching vibration of the malonate group, appearing as a strong

band. The medium bands at 1405 and 1350 cm^{-1} are assigned to the absorption of the C=C and C=N groups of the pyrazole ligand, which are shifted to considerable lower frequencies compared with the uncoordinated ligand [26,27].

The electronic spectrum of complex **1** shows a strong absorption at 43 500 cm^{-1} ($\varepsilon = 4.5 \times 10^3$ L mol^{-1} cm^{-1}) and a weak absorption at 14 000 cm^{-1} ($\varepsilon = 344$ L mol^{-1} cm^{-1}). The former may be assigned to an intra-ligand and/or change-transfer transition in the copper(II) chromophore and the latter is the d–d transitions of copper(II) ions in a distorted octahedral environment.

The EPR spectrum of complex **1** measured on a polycrystalline power at 110 K shows an isotropic signal centered at $g = 2.15$, line width 198 G. Two g values ($g_{\|}$, $g_{\perp}$) correspond to a tetragonally ligand field formed by an elongated octahedron. The computer simulation gave the ESR parameters ($g_{\|} = 2.19$, $g_{\perp} = 2.08$ as shown in Fig. 3.

3.3. TG analysis

The TG curve of compound **1** is shown in Fig. 4. The TG curve of **1** exhibits three steps of weight losses. The first weight loss is 45.6% from 230 to 240 °C, which is assigned to the loss of pyrazole groups. The whole weight loss of the second and the third stage is 26.1% from 260 to 500 °C. The second loss of weight is due to the start of decarboxylation of the malonate ligand and finally the metal oxide is formed as expected, which is in agreement with the calculated weight loss value (71.7%).

3.4. Magnetic properties

Fig. 5 describes the temperature variation of the effective magnetic moment μ_{eff}. The μ_{eff} value of the title complex is 1.79 BM at room temperature, which is a slightly higher than the spin-only value of one copper(II) ion (1.73 BM), due to mixing of angular momentum from excited states via spin–orbit coupling. The μ_{eff} value increases smoothly upon cooling, to 1.83 BM at 8 K, then decreases to 1.72 BM at 3 K. This curve is typical of overall weak ferromagnetic coupling with antiferromagnetic coupling between chains in the very low temperature range. The magnetic behavior within the chain may be described by the series expansion for the Heisenberg model ($H = -2J\sum_i \hat{S}_i\hat{S}_{i+1}$) for ferromagnetically coupled $S = 1/2$ ions, which was derived by Baker et al. [28] (Eq. (1)). Taking into account the interaction between chains, the magnetic susceptibility expansion involving a mean field correction is given by Eq. (2) [29].

$$\chi_{\text{Chain}} = \frac{Ng^2\beta^2}{4KT}\left\{\frac{1.0 + 5.7979916x + 16.902653x^2 + 29.376885x^3 + 29.832959x^4 + 14.036918x^5}{1.0 + 2.7979916x + 7.0086780x^2 + 8.6538644x^3 + 4.5743114x^4}\right\}^{2/3}, \quad (1)$$

$$\chi = \frac{\chi_{\text{Chain}}}{1 - (ZJ'/Ng^2\beta^2)\chi_{\text{Chain}}}, \quad (2)$$

where $x = 2J/KT$, J is the interaction parameter between two copper(II) centers. ZJ' is the exchange parameter between the chains and the rest of the symbols have their usual meanings. Magnetic data were well fitted to Eqs. (1) and (2) with $g = 2.07$, $J = +0.32$ cm^{-1}, $ZJ' = -0.02$ cm^{-1} and $R = 5.76 \times 10^{-3}$, where R is the agreement factor: $R = \sum(\chi_{obsd} - \chi_{calcd})^2/\sum\chi_{obsd}^2$. The small value of J indicates a weak ferromagnetic exchange interaction between copper(II) ions within the chain. The decrease of

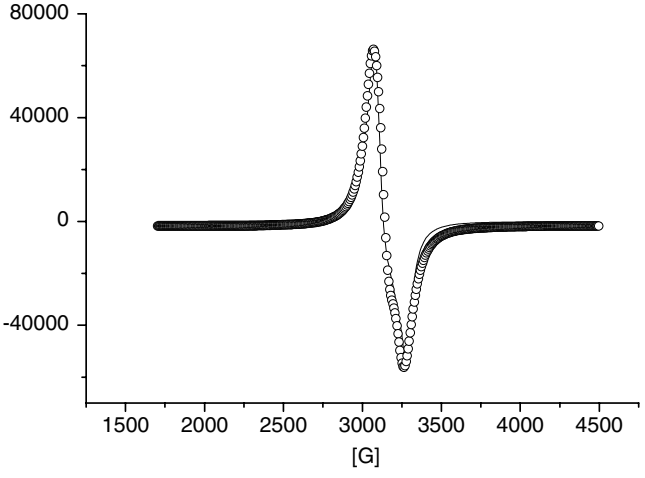

Fig. 3. Experimental (solid line) and simulated (O) X-band EPR spectra of **1**.

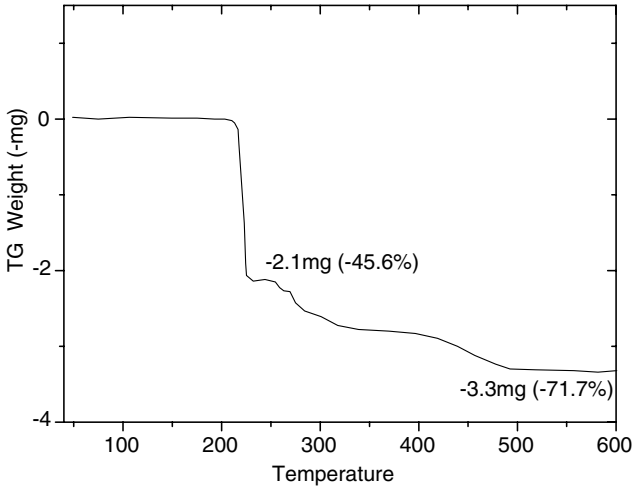

Fig. 4. The TG curve of compound **1**.

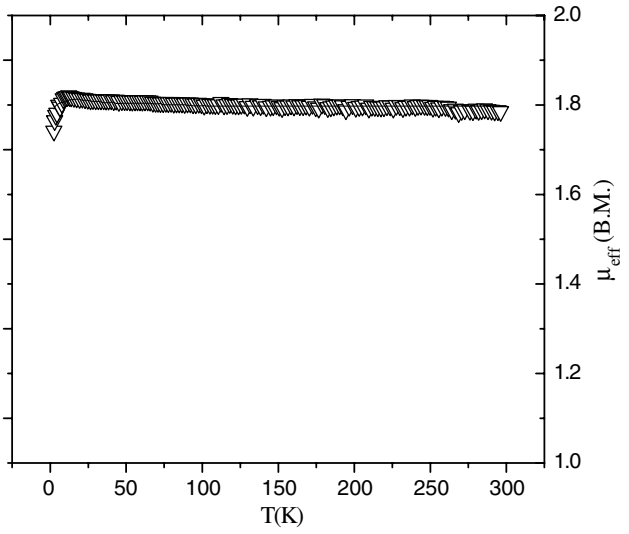

Fig. 5. Plot of μ_{eff} (△) vs. T. The solid lines represent the theoretical values based on the equations.

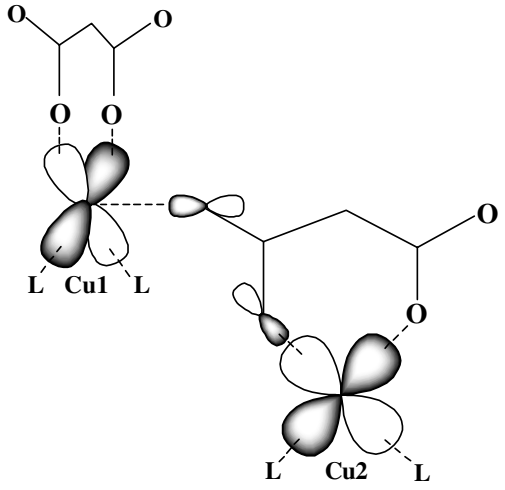

Scheme 2.

the values of the effective magnetic moment below 8 K is due to the antiferromagnetic interaction between the chains.

Details of the magneto-structural correlation of carboxylato-bridged copper(II) complexes have been well explored [18e,22], and it is found that the magnetic interaction between metal centers is dependant on the relative position of the carboxylato bridge of the malonate with respect to the copper(II) ions: equatorial–equatorial (strong antiferromagnetic interaction), equatorial–apical (weak ferromagnetic interaction) and apical–apical (negligible interaction). The crystal structure shows that the copper(II) ion is in an elongated octahedral coordination environment. One of the bridging oxygen atoms (O(2w)) is in an axial position to Cu(1), the other bridging oxygen (O(5)) is in an equatorial position of Cu(2). Scheme 2 shows the relative orientation (equatorial–apical) of the malonato-bridge with respect to the copper(II) ions in the title complex. Since the exchange pathway involves an equatorial position on one copper ($d_{x^2-y^2}$ orbital) and an axial position on the other copper atom (d_{z^2}), this would lead to a ferromagnetic interaction between the copper(II) ions within the chain.

Acknowledgements

The work was supported by the National Natural Science Foundation of China (Nos. 20071019, 50172021, 90101028).

Appendix A. Supplementary data

Crystallographic data for the structure reported in this paper have been deposited with the Cambridge Crystallographic Data Centre as supplementary publication no. CCDC-226527. Copies of the data can be obtained free of charge from CCDC, 12 Union Road, Cambridge CB2 1EZ, UK (fax (44) 1223-336-033; e-mail: deposit@ccdc.cam.ac.uk). Supplementary data associated with this article can be found, in the online version at doi:10.1016/j.poly.2004.06.027.

References

[1] (a) R. Robson, B.F. Abrahams, S.R. Batten, R.W. Gable, B.F. Hoskins, J. Liu, Supramolecular Architecture, ACS, Washington, DC, 1992;
(b) S.R. Batten, R. Robson, Angew. Chem., Int. Ed. 37 (1998) 1460;
(c) M.J. Zaworotko, Chem. Commun. 1 (2001) 9;
(d) P.J. Hagrman, J. Zubieta, Angew. Chem., Int. Ed. 38 (1999) 2638;
(e) O.M. Yaghi, H. Li, C. Davis, D. Richardson, T.L. Groy, Acc. Chem. Res. 31 (1998) 474;
(f) M. Munakata, L. Wu, T.K. Sowa, Adv. Inorg. Chem. 46 (1999) 173;
(g) A.J. Blake, N.R. Champness, P. Hubberstey, W.S. Li, M.A. Withersby, M. Schröder, Coord. Chem. Rev. 183 (1999) 117;
(h) J.M. Lehn, Angew. Chem., Int. Ed. 27 (1988) 89.
[2] (a) O. Kahn, C. Martinez, Science 279 (1998) 44;
(b) O.M. Yaghi, G.M. Li, H.L. Li, Nature 378 (1995) 703;
(c) M. Fujita, Y.J. Kwon, S. Washizu, K. Ogura, J. Am. Chem. Soc. 116 (1994) 1151;
(d) S. Subramanian, M.J. Zaworotko, Angew. Chem., Int. Ed. Engl. 34 (1995) 2127;
(e) J.S. Miller, A.J. Spstein, Chem. Commun. 13 (1998) 1319;
(f) M.S.E. Fallah, E. Rentschler, A. Caneschi, R. Sessoli, D. Gatteschi, Angew. Chem., Int. Ed. Engl. 35 (1996) 1947;
(g) C.B. Ma, C.N. Chen, Q.T. Liu, D.Z. Liao, L.C. Li, L.C. Sun, New J. Chem. 27 (2003) 890.

[3] S.G. Baca, Y.A. Simonov, N.V. Gerbeleu, M. Gdaniec, P.N. Bourosh, G.A. Timco, Polyhedron 20 (2001) 831.
[4] J. Li, H. Zeng, J. Chen, Q. Wang, X. Wu, Chem. Commun. 13 (1997) 1213.
[5] T.K. Maji, S. Sain, G. Mostafa, T.H. Lu, J. Ribas, M. Monfort, N.R. Chaudhuri, Inorg. Chem. 42 (2003) 709.
[6] C. Ruiz-Pérez, M. Hernández-Molina, P. Lorenzo-Luis, F. Lloret, J. Cano, M. Julve, Inorg. Chem. 39 (2000) 3845.
[7] C. Ruiz-Pérez, J. Sanchiz, M. Hernández-Molina, F. Lloret, M. Julve, Inorg. Chem. 39 (2000) 1363.
[8] (a) P. Lightfoot, A. Snedden, J. Chem. Soc., Dalton Trans. 20 (1999) 3549;
(b) T. Lis, J. Matuszewski, Acta Crystallogr. 35B (1979) 2212.
[9] G.D. Muro, F.A. Mautner, M. Insausti, L. Lezema, M.I. Arriortua, T. Rojo, Inorg. Chem. 37 (1998) 3243.
[10] (a) P.S. Mukherjee, S. Dalai, G. Mostafa, E. Zangrando, T.H. Lu, G. Rogez, T. Mallah, N. Ray Chaudhuri, Chem. Commun. 15 (2001) 1346;
(b) S. Dalai, P.S. Mukherjee, E. Zangrando, F.N. Lloret, Ray Chaudhuri, J. Chem. Soc., Dalton Trans. 6 (2002) 822.
[11] P.S. Mukherjee, T.K. Maji, G. Mostafa, J. Ribas, M. Salah El Fallah, N. Ray Chaudhuri, Inorg. Chem. 40 (2001) 928.
[12] S. Konar, P.S. Mukherjee, E. Zangrando, F. Lloret, N. Ray Chaudhuri, Angew. Chem. Int. Ed. 41 (2002) 1561.
[13] Z. Shi, L. Zhang, S. Gao, G. Yang, H. Jia, L. Gao, S. Feng, Inorg. Chem. 39 (2000) 1990.
[14] E.C. Alyea, S.A. Dias, G. Ferguson, M.A. Khan, P.J. Roberts, Inorg. Chem. 18 (1979) 2433.
[15] Y. Kim, D.K. Jung, Inorg. Chem. 39 (2000) 1470.
[16] D. Chattopadhyay, S.K. Chattopadhyay, P.R. Lowe, C.H. Schwalke, S.K. Mazumber, A. Rana, S. Ghosh, J. Chem. Soc., Dalton Trans. (1993) 913.
[17] I. Gil de Muro, F.A. Mautner, M. Insausti, L. Lezama, M.I. Arriortua, T. Rojo, Inorg. Chem. 37 (1998) 3243.
[18] (a) C. Ruiz-Pérez, J. Sanchiz, M. Hernández-Molina, F. Lloret, M. Julve, Inorg. Chim. Acta 298 (2000) 202;
(b) J. Sanchiz, Y. Rodríguez-Martín, C. Ruiz-Pérez, A. Mederos, F. Lloret, M. Julvec, New J. Chem. 26 (2002) 1624;
(c) Y. Rodríguez-Martín, J. Sanchiz, C. Ruiz-Pérez, F. Lloretc, M. Julve, Cryst. Eng. Commun. 107 (2002) 631;
(d) Y. Rodríguez-Martín, C. Ruiz-Pérez, J. Sanchiz, F. Lloret, M. Julve, Inorg. Chim. Acta 318 (2001) 159;
(e) F.S. Delgado, J. Sanchiz, C. Ruiz-Pérez, F. Lloret, M. Julve, Inorg. Chem. 42 (2003) 5938.
[19] J.M. Li, Y.G. Zhang, J.H. Chen, L. Rui, Q.M. Wang, X.T. Wu, Polyhedron 19 (2000) 1117.
[20] N. Lah, I.K. Cigi, I. Leban, Inorg. Chem. Commun. 6 (2003) 1441.
[21] T.F. Liu, H.L. Sun, S. Gao, S.W. Zhang, T.C. Lau, Inorg. Chem. 42 (2003) 4792.
[22] J. Pasán, F.S. Delgado, Y. Rodríguez-Martín, M. Hernández-Molina, C. Ruiz-Pérez, J. Sanchiz, F. Lloret, M. Julve, Polyhedron 22 (2003) 2143.
[23] X.T. Zhang, C.Z. Lu, Q.Z. Zhang, S.F. Lu, W.B. Yang, J.C. Liu, H.H. Zhuang, Eur. J. Inorg. Chem. 6 (2003) 1181.
[24] G.M. Sheldrick, Acta Crystallogr., Sect. A 46 (1990) 467.
[25] G.M. Sheldrick, SHELXL-97, University of Göttingen, Göttingen, Germany, 1997.
[26] B. Machura, J.O. Dziezgielewski, R. Kruszynski, T.J. Bartczak, J. Kusz, Inorg. Chem. Commun. 12 (2003) 1436.
[27] H.W.W. Ehrlich, Acta Crystallogr., Sect. C 13 (1960) 946.
[28] G.A. Baker, G.S. Rushbrooke, H.E. Gilbert, Phys. Rev. A 135 (1964) 1272.
[29] C.J. Óconnor, Prog. Inorg. Chem. 29 (1982) 203.

Available online at www.sciencedirect.com
SCIENCE DIRECT®
Polyhedron 23 (2004) 2209–2215
POLYHEDRON
www.elsevier.com/locate/poly

Syntheses, structures and photoluminescent properties of 1D, 2D, 3D silver (I) coordination polymers with flexible long-chain dinitriles and tetranitriles

Jian-Kai Cheng, Jian Zhang, Yao Kang, Ye-Yan Qin, Zhao-Ji Li, Yuan-Gen Yao *

State Key Laboratory of Structural Chemistry, Fujian Institute of Research on the Structure of Matter, The Chinese Academy of Sciences, Fuzhou, Fujian 350002, PR China

Received 27 May 2004; accepted 23 June 2004
Available online 25 August 2004

Abstract

Three Ag(I) coordination polymers with flexible long-chain multi-nitrile ligands, $[Ag(TDPN)(NO_3)]_n$ (**1**), $[Ag(TDPN)(ClO_4)]_n$ (**2**) (TDPN = β,β′- thiodipropionitrile), $[Ag_2(TCEB)(NO_3)_2]_n$ (**3**) (TCEB = 1, 2, 3, 4-tetrakis (2-cyanoethoxy)butane) have been synthesized and structurally characterized by IR spectra and X-ray crystallography. In particular, TCEB is a meso compound. Single-crystal X-ray analysis shows that it contains two chiral carbon atoms with *R*- and *S*-configurations. The structures of **1**, **2** and **3** consist of a 1-D ladder-like chain, a 2-D boxlike network and a 3-D framework of $CdSO_4$ topology, respectively. IR spectra of the free and coordinated CN groups, the correlation between the counter anions and the topological structures, and the photoluminescent properties of complexes **1–3** are also discussed.
© 2004 Elsevier Ltd. All rights reserved.

Keywords: Silver coordination complex polymers; 1D, 2D, 3D topological structure; Multi-nitriles

1. Introduction

Self-assembly of metal-based supramolecules has attracted considerable interest in current coordination chemistry owing to their potential as functional materials [1]. Much effort has been devoted to the investigation of multi-dimensional networks based primarily on linking metal centers with rigid bridging components, such as 4,4′-bipyridine [2]. Far less common is the use of flexible bridging ligands in the construction of extended networks. However, the use of flexible ligands is attractive because the flexibility and conformation freedom of such ligands offer the possibility for the construction of novel frameworks with tailored properties and functions. On the other hand, Ag(I) as a soft acid, being inclined to coordinate to soft base such as *S*- and unsaturated *N*-containing ligands, is a favorable and fashionable building block and connecting node for coordination polymers [3]. For example, Carlucci et al. reported a series of silver coordination architectures with flexible long-chain dinitrile ligands. However, the architectures of coordination polymers constructed by silver ions and flexible long-chain multi-nitrile ligands with ether or thioether groups, have not been reported to our knowledge.

A major challenge in crystal engineering using flexible building blocks is the predictability of the polymeric network topology, which may depend on several factors such as the coordination geometry and the oxidation state of the metal centers [5], the metal-to-ligand ratio [6], the nature of the ligands used [7] and the presence of solvents [8] and/or counter anions [4,9]. In particular,

* Corresponding author. Tel.: +86 591 371 1523; fax: +86 591 371 4946.
E-mail address: yyg@ms.fjirsm.ac.cn (Y.-G. Yao).

0277-5387/$ - see front matter © 2004 Elsevier Ltd. All rights reserved.
doi:10.1016/j.poly.2004.06.035

counter anions exert an important influence on the self-assembly of silver salts and flexible ligands. Herein, we report our recent successful results in the construction of three Ag(I) coordination polymers with flexible multi-nitriles TDPN and TCEB, and the effects of counter anions on the coordination modes of the ligands and the geometries of the Ag(I) ions are also discussed in detail.

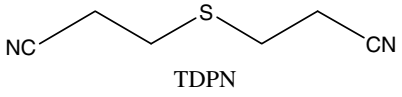

TDPN

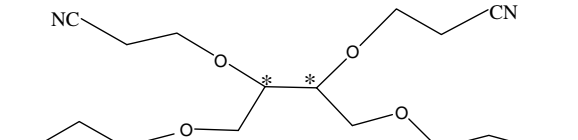

TCEB

2. Experimental

2.1. Materials and physical measures

All reagents were commercial grade and were used as received. Elemental analyses for C, H, N were determined on an Elementar Vario EL-III analyzer. IR spectra were measured as KBr pellets on a Nicolet Magna 750 FT IR spectrometer in the range of 400–4000 cm^{-1}. Fluorescence measurements were made on an Edinburgh Analytical Instrument FLS920.

2.2. Syntheses of the complexes

2.2.1. Synthesis of $[Ag(TDPN)(NO_3)]_n$ (1)

TDPN (1 mmol) was dissolved in CH_3CN (20 ml), then $AgNO_3$ (1 mmol) was added. The resulting mixture was stirred at 50 °C for 30 min and then filtered. Colorless block crystals were obtained after slow evaporation at room temperature for two days. Yield: 68% (on the basis of silver). *Anal.* Calc. for $C_6H_8N_3O_3SAg$: C, 23.24; H, 2.60; N, 13.55; S, 10.34. Found: C, 23.13; H, 2.46; N, 13.59; S, 10.61%. IR (cm^{-1}): 2933w, 2426w, 2395w, 2251m, 1763m, 1626w, 1385vs, 1284w, 1238w, 904w, 825m.

2.2.2. Synthesis of $[Ag(TDPN)(ClO_4)]_n$ (2)

TDPN (1 mmol) was dissolved in CH_3CN (20 ml), then $AgClO_4$ (1 mmol) was added. The resulting mixture was stirred at 50 °C for 30 min and then filtered. Colorless block crystals were obtained after slow evaporation at room temperature for five days. Yield: 63% (on the basis of silver). *Anal.* Calc. for $C_6H_8N_2O_4SClAg$: C, 20.74; H, 2.32; N, 8.06; S, 9.23. Found: C, 20.75; H, 2.60; N, 7.87; S, 9.12%. IR (cm^{-1}): 2933m, 2251s, 1626w, 1421s, 1284m, 1088vs, 627vs.

Table 1
Crystallographic graphic data for the title three complexes and TCEB

Compound	1	2	3	TCEB
Empirical formula	$C_6H_8N_3O_3SAg$	$C_6H_8N_2O_4SClAg$	$C_{16}H_{22}N_6O_{10}Ag_2$	$C_{16}H_{22}N_4O_4$
Crystal size (mm)	$0.36\times0.30\times0.20$	$0.38\times0.20\times0.16$	$0.82\times0.62\times0.40$	$0.62\times0.37\times0.45$
Formula weight	310.08	347.52	674.14	334.38
T (K)	293(2)	293(2)	293(2)	293(2)
Crystal system	monoclinic	monoclinic	monoclinic	monoclinic
Space group	$P2(1)/n$	$P2(1)/c$	$P2(1)/c$	$P2(1)/c$
a (Å)	6.7852(9)	8.259(1)	7.7378(2)	9.228(1)
b (Å)	10.806(1)	7.624(1)	9.8032(1)	12.244(1)
c (Å)	13.586(2)	16.677(3)	15.2834(5)	8.209(1)
α (°)	90	90	90.015(2)	90
β (°)	99.417(2)	93.224(2)	90.099(2)	98.398(2)
γ (°)	90	90	95.032(2)	90
V (Å^3)	982.7(2)	1048.4(3)	1154.86(5)	917.6(2)
Z	4	4	2	2
D_{calc} (g cm^{-3})	2.096	2.202	1.939	1.210
μ (mm^{-1})	2.248	2.371	1.760	0.089
$F(000)$	608	680	340	356
θ Range (°)	2.42–25.05	2.45–25.07	1.33–25.04	2.23–25.02
Independent reflections	1714	1827	3184	1599
Observed reflections	1510 ($I > 2\sigma(I)$)	1468($I > 2\sigma(I)$)	2945 ($I > 2\sigma(I)$)	1112($I > 2\sigma(I)$)
Parameter	128	137	307	110
S on F^2	1.044	0.938	1.076	1.024
$R(F_o)$	0.0402	0.0420	0.0382	0.0699
$R_w(F_o)$	0.1219	0.1174	0.1118	0.2260

*2.2.3. Synthesis of $[Ag_2(TCEB)(NO_3)_2]_n$ (**3**)*

TCEB (1 mmol) was dissolved in CH_3CN (30 ml), then $AgNO_3$ (1 mmol) was added. The resulting mixture was stirred at 50 °C for 30 min and then filtered. Colorless block crystals were obtained after slow evaporation at room temperature for two days. Yield: 63% (on the basis of silver). *Anal*. Calc. for $C_6H_8N_2O_4SClAg$: C, 20.74; H, 2.32; N, 8.06; S, 9.23. Found: C, 20.75; H, 2.60; N, 7.87; S, 9.12%. IR (cm^{-1}): 2970s, 2941m, 2924m, 2906s, 2885s, 2800m, 2737w, 2426m, 2395w, 2247s, 1763m, 1385vs, 1252m, 1225m, 1128s, 1107 vs, 1068m, 1043m, 598w, 823m, 490m.

2.3. Crystal structure determination

Measurements were made on a Siemens SMART platform diffractometer with graphite monochromatized Mo Kα ($\lambda = 0.71073$ Å) radiation. Data reductions and cell refinements were performed with SMART CCD software [10]. The structures were solved by direct methods with the SHELXTL-97 program [11]. Absorption corrections were carried out using SADABS [12]. Crystallographic data for complexes **1**–**3** and TCEB are listed in Table 1. Selected bond lengths and bond angles for complexes **1**–**3** are summarized in Table 2.

Table 2
Selected bond length (Å) and angles (°) for complexes **1**–**3** and TCEB

*Complex **1***			
Bond distances			
Ag(1)–N(2)	2.221(5)	Ag(1)–O(1)	2.447(5)
Ag(1)–N(1)	2.398(6)	Ag(1)–S(2)	2.497(1)
Bond angles			
N(2)–Ag(1)–N(1)	106.4(2)	N(2)–Ag(1)–S(2)	146.6(1)
N(2)–Ag(1)–O(1)	98.44(17)	N(1)–Ag(1)–S(2)	100.5(2)
N(1)–Ag(1)–O(1)	87.62(18)	O(1)–Ag(1)–S(2)	102.06(12)
*Complex **2***			
Bond distances			
Ag(1)–N(1)#1	2.283(6)	Ag(1)–S(1)	2.544(2)
Ag(1)–N(2)#2	2.303(6)	Ag(1)–S(1)#3	2.635(2)
Bond angles			
N(1)#1–Ag(1)–N(2)#2	115.7(2)	C(6)–N(2)–Ag(1)#4	172.2(5)
N(1)#1–Ag(1)–S(1)	103.6(2)	S(1)–Ag(1)–S(1)#3	140.43(3)
N(2)#2–Ag(1)–S(1)	108.2(2)	N(2)#2–Ag(1)–S(1)#3	92.3(2)
N(1)#1–Ag(1)–S(1)#3	96.8(2)		
*Complex **3***			
Bond distances			
Ag(1)–N(2)	2.209(4)	Ag(1)–O(3)	2.395(4)
Ag(1)–N(1)	2.239(4)	Ag(1)– O(2)#1	2.660(4)
N(2)–C(5)	1.124(6)	N(1)–C(4)	1.126(6)
Bond angles			
N(2)–Ag(1)–N(1)	127.0(2)	N(1)–Ag(1)–O(3)	102.4(2)
N(2)–Ag(1)–O(3)	120.9(2)	N(2)–Ag(1)–O(2)#1	99.1(2)
N(1)–Ag(1)–O(2)#1	103.4(1)	O(3)–Ag(1)–O(2)#1	98.4(2)
TCEB			
Bond distances			
C(2)–N(1)	1.132(6)	C(6)–N(2)	1.136(5)

Symmetry modes: #1 $-x+2, -y, -z+1$; #2 $-x+2, y+1/2, -z+3/2$; #3 $-x+2, y-1/2, -z+3/2$ for complex **2**. #1 $-x+1, -y, -z+2$ for complex **3**.

3. Results and discussion

3.1. IR spectra

The main absorption peaks in the IR spectra of complexes **1**–**3**, TDPN and TCEB are listed in Table 3. The presence of characteristic bands around 2250 cm^{-1} indicates that the complexes all contain CN groups. As shown in Table 3, we found that the ν_{CN} values of coordinated CN groups of complexes **1**–**3** are the same as those of the corresponding ligands. Therefore, the silver ions exert no influence on the ν_{CN} values. In addition, complexes **1** and **3** show the same absorption at 1385 cm^{-1}, which should be assigned to $\nu_{NO_3^-}$. According to the result of $[Ag(EDTPN)(ClO_4)]_n$ reported by Min et al., the strong absorption peak at 1088 cm^{-1} corresponds to $\nu_{ClO_4^-}$ [4].

3.2. Fluorescence spectra

The fluorescence emission spectra for complexes **1** and **2**, and complex **3** in the solid-state are shown in Figs. 1 and 2, respectively. It can be observed that the intense emission for complex **1** occurs at 426 nm ($\lambda_{max} = 363$ nm) and complex **2** at 436 nm ($\lambda_{max} = 371$ nm), while the intense emission for complex **3** occurs at 440 nm ($\lambda_{max} = 368$ nm). These emissions may be assigned to the CN groups in the TDPN and TCEB ligands to Ag ion charge-transfer bands (LMCT). It is notable that a blue shift (10 nm) occurs in complex **1**, although complexes **1** and **2** are constructed by the same metal ion and ligands. We assume that the different topological structures and metal coordination environments are mostly responsible for the blue shift.

Table 3
IR spectra data for complexes **1**–**3** T(DPN) and TCEB

Compound	ν_{CN} (cm^{-1})	ν_{anion} (cm^{-1})
1	2251	1385
2	2251	1088
3	2247	1385
TDPN	2251	
TCEB	2247	

*3.2.1. Crystal structures of complexes **1** and **2***

Fig. 3 shows an ORTEP view of the coordination sphere of the Ag(I) ion and atom labelling in $[Ag(TDPN)(NO_3)]_n$ **(1)**. TDPN as a flexible multi-functional ligand contains rich structural information in which both nitrile nitrogen and sulfur atoms can act as donors to coordinate to Ag ions. As shown in Fig. 3, two TDPN ligands exhibit a "W" and an inverse "W" motif. Two nitrogen atoms and one sulfur atom occupy the summit of the "W" motif, and then coordinate to the three different Ag ions. The two motifs are linked with two Ag ions, thus a 20-membered ring is formed in which the S···S distance is 3.541(2) Å and the Ag···Ag distance is 10.224(6) Å. Each silver ion exhibits tetrahedral coordination geometry and is surrounded by two N atoms (Ag(1)–N(1) 2.398(6), Ag(1)–N(2) 2.221(5) Å) and one S atom (Ag(1)–S(2) 2.497(1) Å) from two different TDPN ligands, as well as one O atom from the nitrate anion (Ag(1)–O(1) 2.447(5) Å). In the whole structure, each Ag ion is linked with three TDPN ligands, and each TDPN binds three Ag ions. Therefore, **1** is a 1-D ladder-like coordination polymer, which propagates along *c*-axis (Fig. 4).

An ORTEP drawing of **2** is represented in Fig. 5. Similar to complex **1**, the silver ion also displays tetrahedral coordination geometry. In contrast to complex **1**, the coordination sites are defined by two N atoms (Ag(1)–N(1)#1 2.283(6), Ag(1)–N(2)#2 2.303(6) Å) and two S atoms (Ag(1)–S(1) 2.5437(15), Ag(1)–S(1)#3 2.635(2) Å) from four different TDPN ligands (Fig. 5). As a result, S atoms in complex **2** act as μ_2-bridges to complete the tetrahedral coordination geometry. Similar to complex **1**, a 20-membered ring is also observed in complex **2** (Fig. 5), although the motif is distinct from that of **1**. As each TDPN ligand binds four different Ag(I) ions and each Ag(I) is linked with four TDPN ligands, whole structure becomes a box-like 2-D layer, as shown in Fig. 6. The uncoordinated perchlorate ions are located between the layers to balance the electric charge (Fig. 7).

*3.2.2. Crystal structures of complex **3** and TCEB*

Figs. 8 and 9 show ORTEP diagrams of complex **3** and TCEB, respectively. It is notable that TCEB is a *meso* compound as it possesses two chiral carbon atoms, *R*-C8 and *S*-C8# 1(Fig. 8). Space groups *P*2(1)/*c* of TCEB and complex **3** also confirm that they are achiral. TCEB, acting as a symmetrical tetra-dentate ligand, has a volute motif. It seems a good ligand to coordinate to metal ions, but, to our surprise, a search of the Cambridge Crystallographic Database revealed that metal TCEB complexes do not exist. The X-ray crystallography of complex **3** shows that the silver ion in **3** also displays a tetrahedral coordination geometry, being coordinated by two cyano groups from two different TCEB ligands and two O atoms from two different ni-

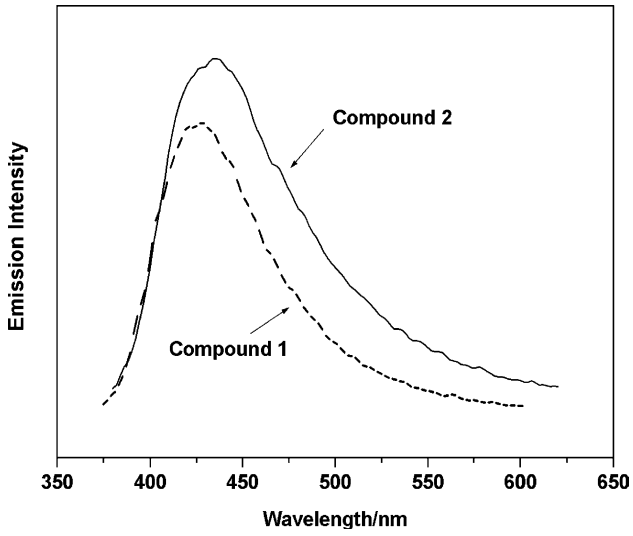

Fig. 1. The solid-state emission spectra of complexes **1** and **2** at room temperature.

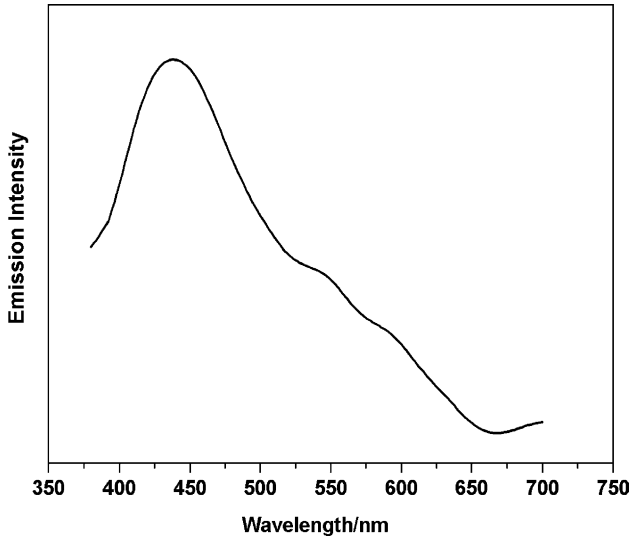

Fig. 2. The solid-state emission spectrum of complex **3** at room temperature.

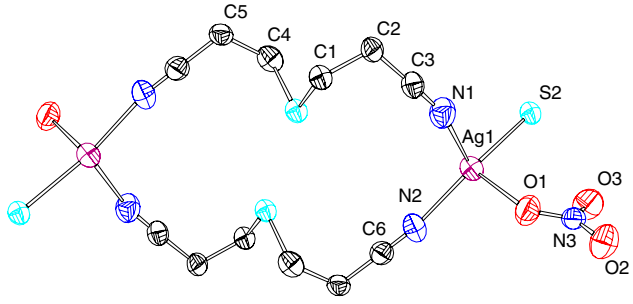

Fig. 3. An ORTEP drawing of $[Ag(TDPN)(NO_3)]_n$ **1** with atomic numbering scheme.

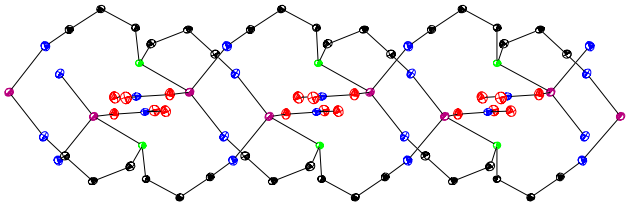

Fig. 4. The one-dimensional ladder-like chain structure in **1** (down the *c*-axis).

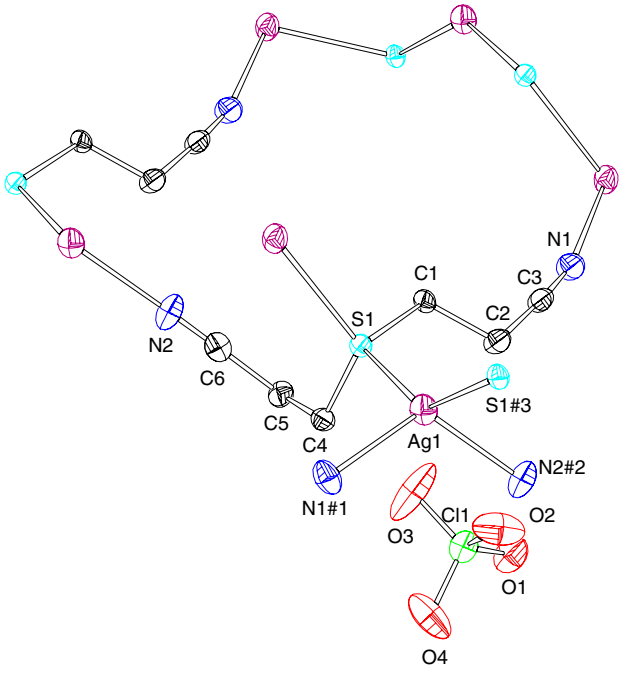

Fig. 5. An ORTEP drawing of $[Ag(TDPN)(ClO_4)]_n$ **2** with atomic numbering scheme.

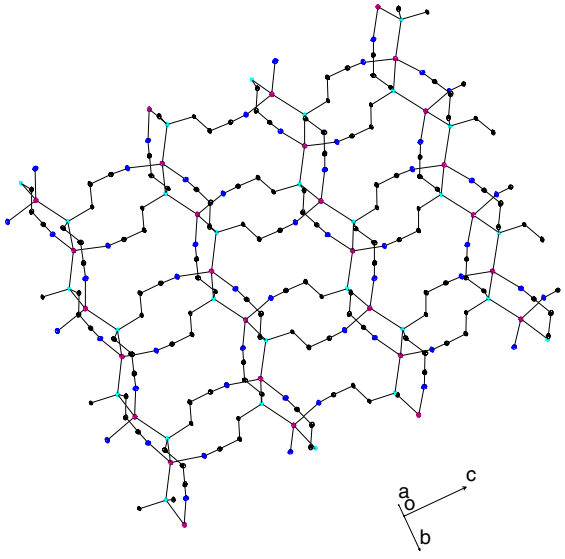

Fig. 6. The 2-D box-like structure in **2** (ClO_4^- anions are omitted for clarity).

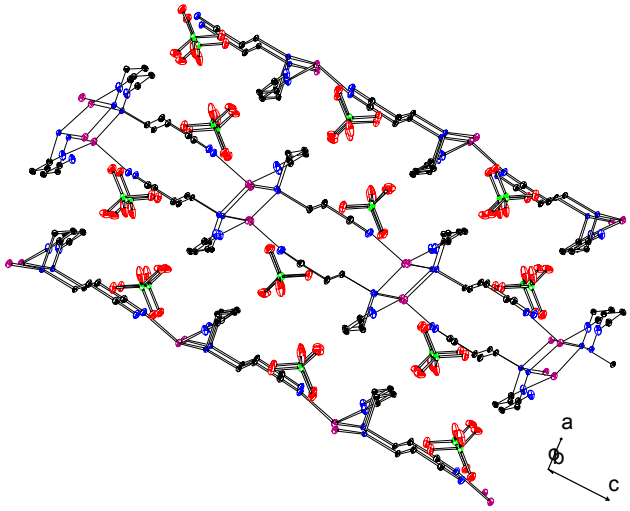

Fig. 7. The side view of the packed structure of **2**, showing the position of ClO_4^- anions.

trate ions. The Ag–N bond distances are 2.209(4) and 2.239(4) Å. For the coordinated nitrate anions, the two Ag–O bond distances are 2.395(4) and 2.660(4) Å. Each TCEB acts as a μ_4-bridge to link four silver ions, and each nitrate ion acts as a μ_2-bridge to link two Ag(I) ions, which gives rise to a 3-D network as shown in Fig. 10. Evidently, complex **3** exhibits a 3-D inorganic–organic hybrid coordination architecture, in which inorganic layers are constructed by rare

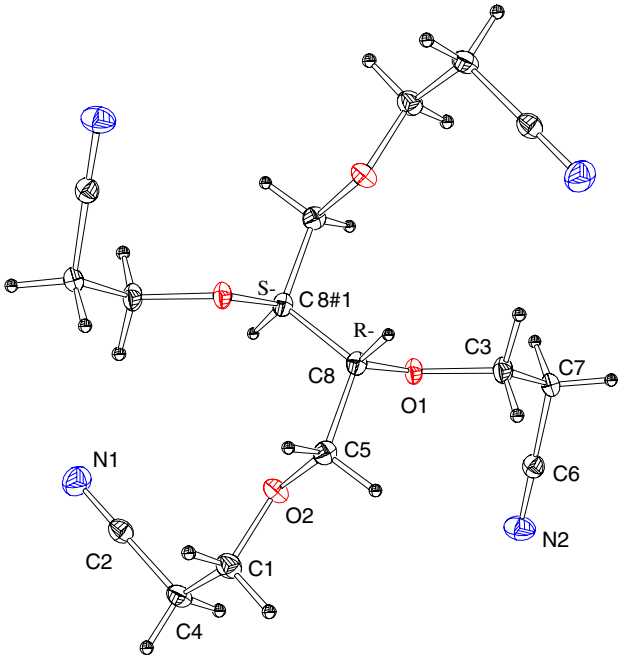

Fig. 8. An ORTEP drawing of TCEB with atomic numbering scheme. Symmetry mode: (# 1) $1-x, 1-y, -z$.

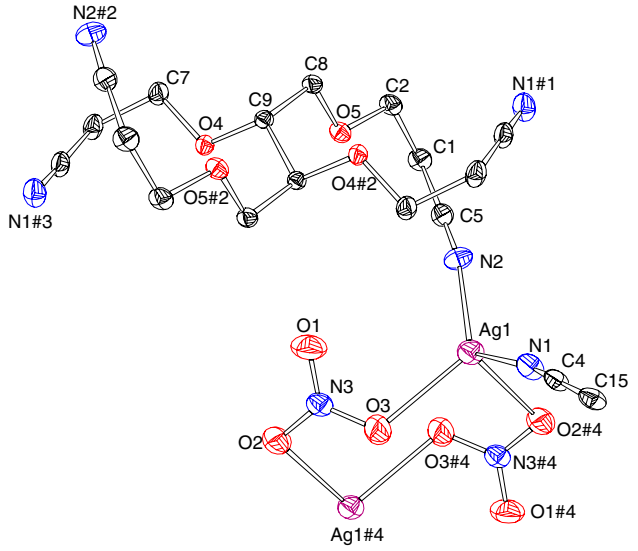

Fig. 9. An ORTEP drawing of $[Ag_2(TCEB)(NO_3)_2]_n$**3** with atomic numbering scheme. Symmetry modes: (#1)x, $-1/2-y$, $-1/2+z$; (#2) $2-x$, $-y$, $1-z$; (#3) $2-x$, $1/2+y$, $3/2-z$; (#4) $1-x$, $1-y$, $2-z$.

eight-membered silver nitrate rings with an Ag···Ag distance of 4.463(1) Å, while organic layers are formed by TCEB ligands. In addition, the 3D network of **3** could be simplified to a 4-connected network if the $Ag_2(NO_3)_2$ dimer is simplified to the baricenter and the ligand becomes another four-connected center. The overall topology could be described as a simple single (not interpenetrated) uninodal four-connected net of $CdSO_4$ topology. Compared to the S atoms of TDPN in complex **1** and **2**, the O atoms of TCEB in **3** do not participate in coordination to the Ag^+ ions. This indicates that the order of affinity to Ag ions can be ranked as S > O, which is in accord with conventional wisdom that a soft acid, such as Ag^+ ions, is inclined to coordinate to a soft base such as a *S*-ligand [4].

4. Conclusion

It is interesting that although complexes **1** and **2** are both synthesized by the self-assembly of silver salts with the same ligand TDPN, X-ray analysis reveals that they display completely different topological structures, which are an infinite one-dimensional array with a ladder-like chain structure (Fig. 4) and a box-like layer structure (Fig. 6), respectively. Different anions thus exert an important influence on the assembly of metal–organic frameworks, including their topologies and dimensionality. Such a phenomenon was observed in the self-assembly of other silver coordination architectures [4]. We have used a *meso* ligand to construct a novel complex **3** with a four-connected net of $CdSO_4$ topology. The IR spectra for the three title complexes and their ligands TDPN and TCEB show that free and coordinated CN groups have virtually the same ν_{CN} value. In addition, the fluorescence spectra for complexes **1**–**3** indicate that they may be good blue-light emitting materials since they are insoluble in common polar and non-polar solvents.

In summary, three silver coordination polymers have been synthesized and characterized. The present study shows that the counter anion plays an important role in the construction of coordination architectures from silver salts and flexible multi-nitriles.

5. Supplementary data

CCDC Nos. 236187 and 236190 contain the supplementary crystallographic data for this paper. These data can be obtained free of charge via http://www.ccdc.cam.ac.uk/data_request/cif, by emailing data_request@ccdc.cam.ac.uk, or by contacting The Cambridge Crystallographic Data Centre, 12, Union Road, Cambridge CB2 1EZ, UK; fax: +44-1223-336033.

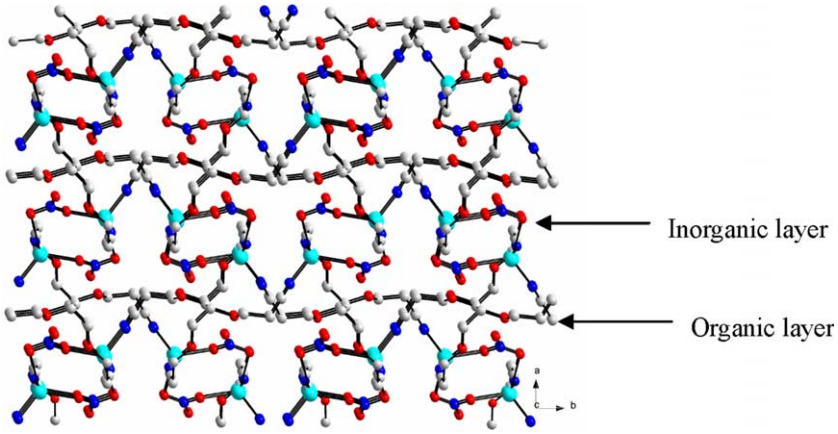

Fig. 10. The 3D structure in **3**, showing inorganic layers ($AgNO_3$) with eight-membered rings and organic layers (TCEB).

Acknowledgements

This work is supported by the National Natural Science Foundation of China under project No. 20173063, the State Key Basic Research and Developement Plan of China (001CB108906), and the NSF of Fujian Province (E0020001).

References

[1] (a) D. Braga, F. Grepioni, G.R. Desiraju, Chem. Rev. 98 (1998) 1375;
(b) H.O. Stumpt, L. Ouahab, Y. Pei, D. Grandjean, O. Kahn, Science 261 (1993) 447;
(c) O.M. Yaghi, G. Li, H. Li, Nature 378 (1995) 703;
(d) D.B. Amabilino, J.F. Stoddart, Chem. Rev. 95 (1995) 2725;
(e) D.S. Lawrence, T. Jiang, M. Levett, Chem. Rev. 95 (1995) 2229.

[2] (a) M. Fujita, D. Oguro, M. Miyazawa, H. Oka, K. Yamaguchi, K. Ogura, Nature 378 (1995) 469;
(b) M. Fujita, M. Aoyagi, K. Ogura, Bull. Chem. Soc. Jpn. 71 (1998) 1799;
(c) A.J. Blake, M. Schroder, Coord. Chem. Rev. 183 (1999) 117;
(d) C.V.K. Sharma, G.A. Broker, J.G.. Huddleston, J.W. Baldwin, R.M. Metzger, R.D. Rogers, J. Am. Chem. Soc. 121 (1999) 1137;
(e) K. Biradha, C. Seward, M.J. Zaworotko, Angew. Chem. Int. Ed. 38 (1999) 492;
(f) S. Leininger, B. Olenyuk, P.J. Stang, Chem. Rev. 100 (2000) 853.

[3] (a) Z.N. Chen, W.J. Li, B.S. Kang, M.C. Hong, Z.Y. Zhou, T.C.W. Mak, Z. Lin, X.M. Chen, H.Q. Liu, Inorg. Chem. 36 (1997) 208;
(b) X.H. Bu, W. Chen, W.F. Hou, M. Du, R.H. Zhang, F. Brisse, Inorg. Chem. 41 (2002) 3477;
(c) M. Munakata, L.P. Wu, T. Kuroda-Sowa, Bull. Chem. Soc. Jpn. 70 (1997) 1727.

[4] (a) L. Carlucci, G. Ciani, D.M. Proserpio, S. Rizzato, Chem. Eur. J. 8 (2002) 1519;
(b) L. Carlucci, G. Ciani, P. Macchi, D.M. Proserpio, S. Rizzato, Chem. Eur. J. 8 (1999) 237;
(c) L. Carlucci, G. Ciani, D.M. Proserpio, S. Rizzato, Cryst. Eng. Commun. 4 (2002) 413;
(d) K.S. Min, M.P. Suh, J. Am. Chem. Soc. 122 (2000) 6834.

[5] (a) M.C. Hong, Y.J. Zhao, W.P. Su, R. Cao, M. Fujita, Z.Y. Zhou, A.S.C. Chan, Angew. Chem. Int. Ed. 39 (2000) 2468;
(b) H.P. Wu, C. Janiak, G. Rheinwald, H. Lang, J. Chem. Soc., Dalton Trans. (1999) 183.

[6] A.J. Blake, N.R. Champness, P.A. Cooke, A.M. Deveson, D. Fenske, P. Hubberstey, W.S. Li, M. Schroder, J. Chem. Soc., Dalton Trans. (1999) 2103.

[7] S. Lopez, M. Kaharaman, M. Harmata, S.W. Keller, Inorg. Chem. 36 (1997) 961.

[8] T.L. Hennigar, D.C. MacQuarri, P. Losier, R.D. Rogers, M.J. Zaworotko, Angew. Chem. Int. Ed. 36 (1997) 972.

[9] M.A. Withersby, A.J. Blake, N.R. Champness, P. Hubberstey, W.S. Li, M. Schroder, Angew. Chem. Int. Ed. 36 (1997) 2327.

[10] Siemens, Smart Version 4.0. User manual, Siemens Analytical X-ray Instruments Inc., Madison, WI, 1994.

[11] G.M. Sheldrick, SHELX-97, Program for structure refinement, University of Gottingen, Germany, 1997.

[12] G.M. Sheldrick, SADABS, Program for Siemens area detector absorption correction, University of Gottingen, 1996.

Available online at www.sciencedirect.com
SCIENCE DIRECT®
Polyhedron 23 (2004) 2217–2226
POLYHEDRON
www.elsevier.com/locate/poly

Synthesis and characterization of cobalt(III) complexes with sinambic amplector ligands

Clint A. Sharrad, Lawrence R. Gahan *

Chemistry Department, The University of Queensland, Brisbane, Qld 4072, Australia

Received 25 May 2004; accepted 24 June 2004
Available online 28 August 2004

Abstract

The synthesis of the hexadentate ligand 5,6-dimethyl-2,2,9,9-tetra(methyleneamine)-4,7-dithiadecane (1,2-$Me_2EtN_4S_2$amp) is reported. The diastereiosomers were separated as cobalt(III) complexes using cation exchange chromatography. The *rac* and *meso* isomers were characterized by NMR (^{13}C, ^{1}H, ^{59}Co), ESI-MS, UV–Vis spectroscopy and cyclic voltammetry. Single crystals of [Co(*rac*-1,2-$Me_2EtN_4S_2$amp)] $Cl_2(ClO_4) \cdot 2H_2O$ were characterized by X-ray diffraction. The low-temperature (11 K) absorption spectra of the complexes have been measured in Nafion films and from the observed positions of both spin-allowed $^{1}A_{1g} \rightarrow {}^{1}T_{1g}$ and $^{1}A_{1g} \rightarrow {}^{1}T_{2g}$ and spin forbidden $^{1}A_{1g} \rightarrow {}^{3}T_{2g}$ bands, octahedral ligand-field parameters (10Dq, *B* and *C*) were determined. These results, in conjunction with the ^{59}Co NMR data, are used to further explore the relationship between the ^{59}Co magnetogyric ratio (γ_{Co}) and the product of the nephelauxetic ratio and the wavelength of the $^{1}A_{1g} \rightarrow {}^{1}T_{1g}$ transition ($\beta(\Delta E)^{-1}$) for complexes of mixed donor nitrogen–thioether ligands.
© 2004 Elsevier Ltd. All rights reserved.

Keywords: Multidentate ligand; Cobalt(III); Sinambic; ^{59}Co NMR

1. Introduction

A new class of mixed donor nitrogen–thioether ligands, known as *amplectors* (amp), with a tetrapodal branched topology has been developed [1–3]. A series of cobalt(III) complexes, $[Co(RN_4S_2amp)]^{3+}$, have been synthesized and characterized where the hinge moieties (R) include straight chain (R = Et, Pr, Bu) and aromatic entities (R = Xy) [1,2] (Chart 1). Our interest in these and other mixed donor nitrogen–thioether complexes has focussed on structural, electronic, ^{59}Co NMR and electrochemical properties [1–8]. The amplector complexes can be used also as templates for the synthesis of encapsulated structures with larger cavities [1].

The use of 2,3-butanethiol in the readily adaptable amplector synthetic methodology allows for the possible introduction of chirality into the ligand structure by forming 5,6-dimethyl-2,2,9,9-tetra(methyleneamine)-4,7-dithiadecane (1,2-$Me_2EtN_4S_2$amp; Chart 1). This expansion of the class of hexadentate amplectors results in the formation of a sinambic (Latin: *without rotation*) ligand, the term sinambic ligands used to describe bidentates with rotationally non-equivalent donor atoms [9–11]. The terminology is applicable to these amplector ligands as the chiral carbons are located within the dithio-hinge moiety. This paper reports the preparation and characterization of the sinambic ligand and the cobalt(III) complexes which were separated into their diastereoisomeric forms and characterized.

* Corresponding author. Tel.: +61 7 3365 3844; fax: +61 7 3365 4299.
E-mail address: gahan@mailbox.uq.edu.au (L.R. Gahan).

0277-5387/$ - see front matter © 2004 Elsevier Ltd. All rights reserved.
doi:10.1016/j.poly.2004.06.033

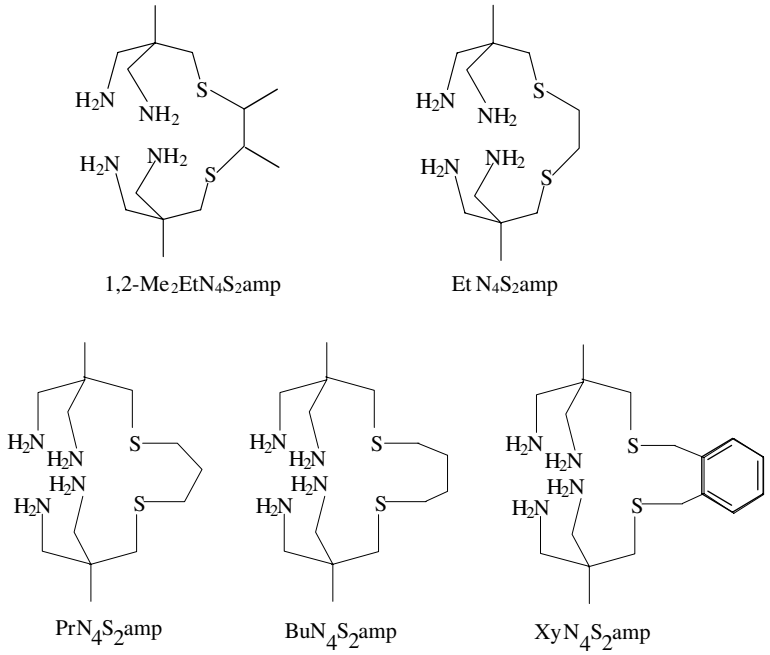

Chart 1.

2. Experimental

2.1. Physical measurements

NMR (^{13}C, ^{1}H and ^{59}Co) spectroscopy, cyclic voltammetry, mass spectrometry, solution and Nafion film UV-Vis spectroscopy were performed as described previously [1–4]. The chemical shifts of ^{13}C NMR spectra (D_2O) for the metal complexes are reported in parts per million (δ_C) as positive downfield and negative upfield of the internal reference 1,4-dioxane, as described previously [1–3]. Where necessary, peak positions in UV–Vis spectra were determined using Peakfit [12] obtaining a correlation coefficient (R^2) greater than 0.997.

Analytical HPLC was performed with a Shimadzu HPLC system comprised of a Shimadzu LC-10ATvp liquid chromatograph, Shimadzu FCV-10ALvp low-pressure gradient flow control valve, Shimadzu DGU-14A degasser, Shimadzu SCL-10Avp system controller and a Shimadzu SPD-10Avp UV–Vis detector. A Waters Protein-Pak SP 5PW (7.5 mm × 7.5 cm) analytical column was used. All eluent solutions were prepared using Milli-Q water and were degassed and filtered through an all-glass filter unit fitted with a 0.45 μm membrane (Millipore MF type membrane). All metal complex solutions (Milli-Q H_2O) were passed through syringe filters (pore size 0.2 μm) prior to injection. The column was prepared by an initial washing with water (30 min, 0.5 cm^3/min) followed by the eluent (60 min, 0.5 cm^3/min). Metal complex solutions (5–50 μL; Hamilton 250 μL syringe) were injected into the injector assembly unit. Chromatograms were recorded from 0 to 90 min at two detection wavelengths. Concentrations of metal complex solutions were adjusted so that all absorbance readings were below 2.0.

2.2. Ligand synthesis

2,3-Butanedithiol was purchased from Aldrich Chemical Company and used without further purification.

2.2.1. 5,6-dimethyl-2,2,9,9-tetra(methyleneamine)-4,7-dithiadecane (1,2-$Me_2EtN_4S_2$amp)

The synthetic methodology for 1,2-$Me_2EtN_4S_2$amp was essentially identical to that described for the analogous ligand 2,2,9,9-tetra(methyleneamine)-4,7-dithiadecane (EtN_4S_2amp) but replacing 1,2-ethanedithiol in the latter synthesis with 2,3-butanedithiol in the former [1–3]. In all steps of the synthesis of 1,2-$Me_2EtN_4S_2$amp, the same reagents, solvents and methodologies were employed as described for EtN_4S_2amp, and on the same scale.

2.3. Preparation of cobalt(III) complexes

Caution: Although the perchlorate salts described in this work do not appear to be sensitive to shock or heat these materials, like all perchlorates, should be treated with caution.

2.3.1. [Co(rac-1,2-$Me_2EtN_4S_2$amp)] $Cl_2(ClO_4)\cdot 2H_2O$

Cobaltous nitrate hexahydrate (13.1 g) in methanol (200 cm^3) was added dropwise to a stirred solution of

1,2-$Me_2EtN_4S_2$amp (13.1 g) in methanol (300 cm^3). A stream of air was bubbled through the ligand solution for the duration of the metal addition and the aeration continued for a further four hours. The solvent was removed under reduced pressure, the residue dissolved in water and the solution filtered. The filtrate was diluted to 2 l and loaded on Dowex cation exchange resin (50W × 2 (200–400 mesh) H^+ form). The column was washed with water and 1 M HCl to elute minor products. The major red band was eluted with 3 M HCl. The solvent was removed under reduced pressure to give a red residue, which was dissolved in water (500 cm^3) and loaded onto Sephadex C-25 cation exchange resin (Na^+ form). The column was washed with water then 0.2 M NaCl to elute a series of minor pink and purple products followed by a red-brown band. A major orange band was eluted with 0.3 M NaCl. The orange eluent was loaded onto Dowex cation exchange resin and washed with 1 M HCl. The orange band was eluted with 3 M HCl and the solvent removed to give an orange solid. HPLC of a small sample of the orange compound resolved two compounds when eluted with 0.1 M Na_2SO_4 adjusted to pH 4 with H_2SO_4 (see Fig. 1). The orange solid was dissolved in water (500 cm^3) and loaded onto Sephadex cation exchange resin. The orange band was eluted with 0.1 M Na_2SO_4, adjusted to pH 4 with H_2SO_4. The orange band was collected in three approximately even fractions as band separation was not clearly evident. Fraction 3 was loaded onto Dowex cation exchange resin, washed with 1 M HCl and eluted with 3 M HCl. The solvent was removed from the eluent under reduced pressure to give an orange solid. Analytical HPLC showed the fraction consisted of predominantly one compound. A small amount of the compound predominant in Fraction 1, subsequently identified as [Co(*meso*-1,2-$Me_2EtN_4S_2$amp)]$^{3+}$, was eluted immediately before the major product. The orange solid was dissolved in a minimum volume of aqueous $NaClO_4$, and the solution left to stand overnight to give orange crystals (0.3 g). (Found: C, 27.87; H, 6.28, N, 9.30%. $[C_{14}H_{34}N_4S_2Co]Cl_2(ClO_4)\cdot 2H_2O$ requires: C, 28.60; H, 6.52; N, 9.53%.) UV–Vis spectrum [λ_{max}, nm (ε_{max}, L mol^{-1} cm^{-1}) in H_2O]: 475 (390), 284 (16000), 232 (15000). ^{13}C NMR (D_2O): δ_C −49.9 (–CH_3*(hinge)*); −43.0 (—CH_3); −29.0 (–CH_2–S); −26.5 (C_q); −21.9, −20.0 (–CH_2–N); −11.3 (—CH—S). ^1H NMR (D_2O): δ_H 1.07 (–CH_3, s); 1.67 (–CH_3*(hinge)*, d); 2.3–3.3 (–CH_2–, m) ; 3.52 (—CH—S, m). ^{59}Co NMR (H_2O): δ_{Co} 5579 ($\nu_{1/2}$ = 630 Hz). ESI-MS: Calc. for [Co(*rac*-1,2-$Me_2EtN_4S_2$amp)]$^{3+}$ − $2H^+$, *m/z* 379; found, *m/z* 379 (65%). Calc. for [Co(*rac*-1,2-$Me_2EtN_4S_2$amp)]$^{3+}$ − H^+, *m/z* 190; found, *m/z* 190 (100%).

2.3.2. [Co(meso-1,2-$Me_2EtN_4S_2$amp)]Cl $(ClO_4)_2\cdot 3H_2O$

Fraction 1 of the initial Sephadex purification from the synthesis of [Co(*rac*-1,2-$Me_2EtN_4S_2$amp)]$^{3+}$ was loaded onto Dowex cation exchange resin and washed with 1 M HCl. The orange band was eluted with 3 M HCl and the solvent was removed under reduced pressure. Analytical HPLC showed the fraction consisted of predominantly one compound. A small amount of

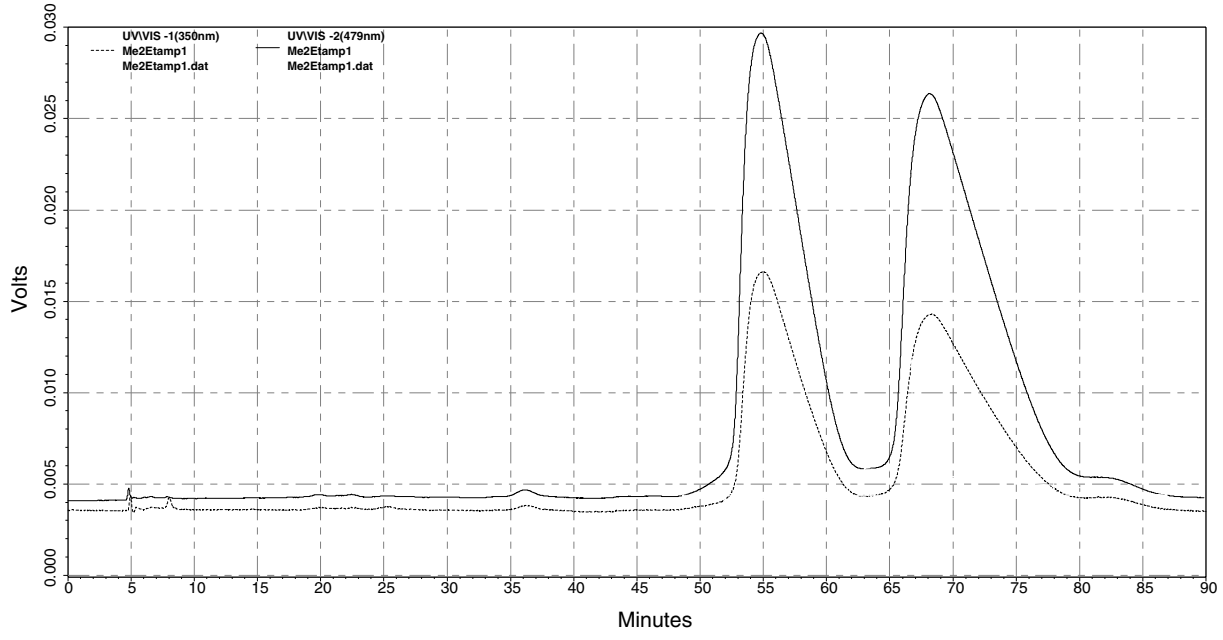

Fig. 1. HPLC trace of the crude orange product from the synthesis of [Co(1,2-$Me_2EtN_4S_2$amp)]$^{3+}$ (eluent: 0.1 M Na_2SO_4, pH 4; detection wavelengths: 479 and 350 nm; flow rate = 0.5 cm^3/min; column: Waters Protein-Pak SP 50PW).

the compound predominant in Fraction 3, subsequently identified as [Co(*rac*-1,2-$Me_2EtN_4S_2$amp)]$^{3+}$, was eluted immediately after the major product. The orange solid was dissolved in a minimum volume of aqueous $NaClO_4$ and the solution allowed to stand for several days to give orange crystals (0.2 g). ($[C_{14}H_{34}N_4S_2Co]Cl(ClO_4)_2 \cdot 3H_2O$ requires: C, 25.10; H, 6.02; N, 8.37. Found: C, 24.89; H, 5.68; N, 8.20%.) UV–Vis spectrum [λ_{max}, nm (ε_{max}, L mol^{-1} cm^{-1}) in H_2O]: 481 (350), 289 (11 000), 234 (10 000). ^{13}C NMR (D_2O): δ_C −55.8, −52.0 (–CH_3*(hinge)*); −43.0, −42.9 (–CH_3); −32.4, −31.6 (–CH_2–S); −25.7, −25.5 (C_q); −21.9, −20.8, −20.7, −20.4 (–CH_2–N); −18.4, −11.7 (–CH–). ^{1}H NMR (D_2O): δ_H 1.08, 1.08 (–CH_3, s); 1.50, 1.76 (–CH_3*(hinge)*, d); 2.3–3.3 (–CH_2–, m); 3.68, 3.72 (–CH–, m). ^{59}Co NMR: δ_{Co} 5661 ($\nu_{1/2}$ = 370 Hz). ESI-MS: Calc. for $[Co(meso-1,2-Me_2EtN_4S_2amp)]^{3+} - H^+ + {}^{35}ClO_4^-$, *m*/*z* 479; found, *m*/*z* 479 (100%). Calc. for [Co(*meso*-1,2-$Me_2EtN_4S_2$amp)]$^{3+}$ − 2H$^+$, *m*/*z* 379; found, *m*/*z* 379 (89%).

2.4. X-ray crystallography

For diffractometry a crystal of the metal complex was mounted onto glass fibres with Supa Glue. Lattice parameters were determined by least squares fits to the setting parameters of 25 independent reflections, measured and refined on an Enraf-Nonius CAD4 diffractometer using graphite-monochromated Mo Kα radiation.

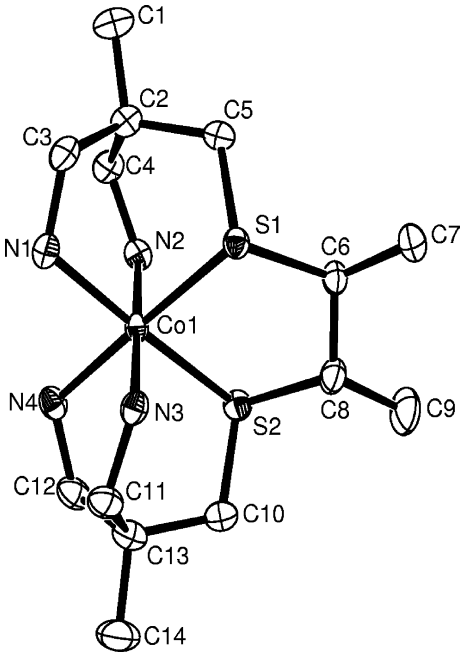

Fig. 2. ORTEP plot of the complex cation of [Co(*rac*-1,2-$Me_2EtN_4S_2$amp)]$Cl_2(ClO_4) \cdot 2H_2O$, giving the crystallographic atom numbering scheme.

Table 1
Crystal data for [Co(*rac*-1,2-$Me_2EtN_4S_2$amp)]$Cl_2(ClO_4) \cdot 2H_2O$

Empirical formula	$C_{14}H_{38}Cl_3CoN_4O_6S_2$
Formula weight	587.88
Crystal system	monoclinic
Space group	$P2_1/c$
a (Å)	11.549(1)
b (Å)	14.563(2)
c (Å)	15.365(1)
β (°)	91.278(7)
V (Å)^3	2583.6(5)
D_{calc} (g cm^{-3})	1.511
Z	4
Crystal dimensions (mm)	0.40 × 0.40 × 0.10
Colour	orange
Habit	prism
Temperature (K)	293(2)
λ (Å)	0.71073
Absorption coefficient (cm^{-1})	11.71
F(000)	1232
θ Range (°)	1.76–24.97
Range of *h k l*	$0 \leqslant h \leqslant 13$, $0 \leqslant k \leqslant 17$, $-18 \leqslant l \leqslant 18$
Reflections collected	4784
Independent reflections	4543
Restraints/parameters	4/287
R_{int}	0.0181
Goodness-of-fit on F^2	1.037
Largest difference peak and hole (e Å^3)	0.567 and −0.523
$R(F_o)$, R_w	0.0353, 0.0556

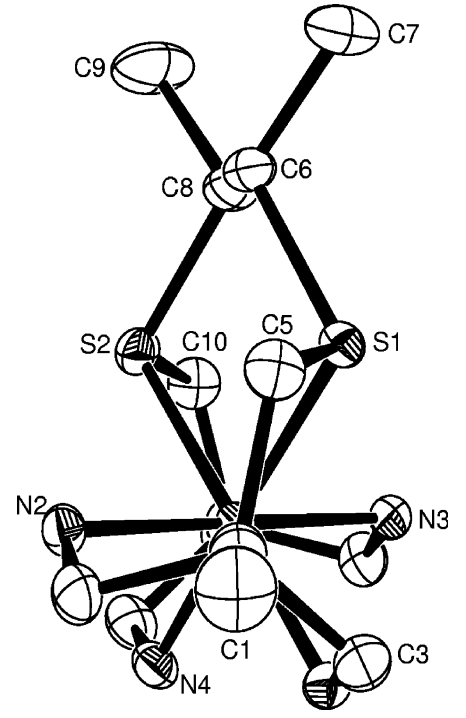

Fig. 3. ORTEP plot of the complex cation of [Co(*rac*-1,2-$Me_2EtN_4S_2$amp)]$Cl_2(ClO_4) \cdot 2H_2O$, view along the *pseudo*-C_3 axis. Probability ellipsoids of 30% are shown.

Table 2
Selected interatomic distances (Å) and angles (°) for [Co(*rac*-1,2-$Me_2EtN_4S_2$amp)]$Cl_2(ClO_4) \cdot 2H_2O$

Bond lengths			
Co(1)–N(1)	1.980(3)	Co(1)–N(2)	1.981(3)
Co(1)–N(3)	1.976(3)	Co(1)–N(4)	1.976(3)
Co(1)–S(1)	2.2248(9)	Co(1)–S(2)	2.2232(9)
Bond angles			
N(1)–Co(1)–N(2)	88.07(11)	N(3)–Co(1)–S(2)	90.18(8)
N(1)–Co(1)–S(1)	90.23(8)	N(4)–Co(1)–N(1)	90.36(11)
N(1)–Co(1)–S(2)	177.35(8)	N(4)–Co(1)–N(2)	91.71(11)
N(2)–Co(1)–S(1)	90.61(8)	N(4)–Co(1)–N(3)	87.53(11)
N(2)–Co(1)–S(2)	89.74(8)	N(4)–Co(1)–S(1)	177.62(8)
N(3)–Co(1)–N(1)	92.03(11)	N(4)–Co(1)–S(2)	91.20(9)
N(3)–Co(1)–N(2)	179.24(11)	S(2)–Co(1)–S(1)	88.29(3)
N(3)–Co(1)–S(1)	90.15(8)		

The structure was solved by heavy-atom methods (direct methods) and refined using full-matrix least-squares on F^2. Programs used were SIR-92 [13] for solution, SHELXL-97 [14] for refinement and *ORTEP-3 for Windows* [15] for plotting. Crystal data are given in Table 1. The geometry of the complex cation [Co(*rac*-1,2-$Me_2EtN_4S_2$amp)]$^{3+}$ is displayed in Figs. 2 and 3 with crystallographic atom numbering schemes. Selected bond lengths and bond angles are given in Table 2.

3. Results and discussion

3.1. Nomenclature

The nomenclature employed for amplector ligands synthesized from straight chain dithiols will be used [1,2]. The abbreviated nomenclature for the amplector (amp) ligand can be considered in terms of the donor set and a hinge moiety connecting them. Thus, for 1,2-$Me_2EtN_4S_2$amp (*5,6-dimethyl-2,2,9,9-tetra(methyleneamine)-4,7-dithiadecane*) the hinge derived from 2,3-butanedithiol is abbreviated to 1,2-Me_2Et, where Et refers to the ethyl link between thio donors. The 1,2-Me_2 prefix refers to the methyl groups bonded to each of the methine carbons of the ethyl hinge. The two diastereoisomeric forms of the ligand, upon complexation, are referred to as *rac*-1,2-$Me_2EtN_4S_2$amp and *meso*-1,2-$Me_2EtN_4S_2$amp.

3.2. Synthesis

The synthetic methodology reported previously for this type of ligand [1–3] employing straight chain and substituted dithiols has been utilized in this work. Thus, the reaction sequence employed is essentially that described for the EtN_4S_2amp analogue [1]; however, a diastereomeric mixture of 2,3-butanedithiol was employed instead of 1,2-ethanedithiol. The desired ligand 1,2-$Me_2EtN_4S_2$amp was reacted with a cobalt(II) salt and air in methanol and, after initial purification with Dowex resin, cation exchange chromatography of the crude mixture of the Co(III) complex using Sephadex resin resulted in the isolation of an orange band in a similar manner to the purification of [Co(EtN_4S_2amp)]$^{3+}$ [1].

The NMR spectrum of this material indicated that it consisted of a mixture of isomers. High performance liquid chromatography of this material using a Waters Protein-Pak SP 5PW (cation exchange) column, eluting with Na_2SO_4 (adjusted to pH 4), indicated that two complexes were present (Fig. 1). Assuming that the extinction coefficients for both complexes are similar at the detection wavelengths used, the peak areas obtained for the HPLC trace suggested the complexes are present in approximately equivalent amounts. Preparative scale chromatography of this orange band with a Sephadex cation column (0.1 M Na_2SO_4, pH 4; H_2SO_4) gave two bands. The complexes were separately crystallized as mixed chloride/perchlorate salts by the addition of $NaClO_4$ to an aqueous solution. The first eluted complex was found to be [Co(*meso*-1,2-$Me_2EtN_4S_2$amp)]$^{3+}$ by microanalysis and NMR spectroscopy while the [Co(*rac*-1,2-$Me_2EtN_4S_2$amp)]$^{3+}$ isomer was eluted second. No evidence from either the HPLC or preparative scale chromatography separations indicated the resolution of *lel* and *ob* isomers [16] for [Co(1,2-$Me_2EtN_4S_2$amp)]$^{3+}$ for both *rac* and *meso* ligands. Attempts to resolve the racemic complex into stereoisomers using sodium $(+)_{589}$-tartrate as eluent on a column of Sephadex SP C25 cation exchange resin (Na^+ form) were unsuccessful.

The chemistry of Co(III) complexes with chiral carbons in disubstituted ethyl dithio-chelate rings is limited, but the chemistry of analogous diamine chelate rings is more extensive. Examples include numerous complexes with the bidentate 2,3-butanediamine ligand [8,17–20], straight chain tetradentate ligands like 5,6-dimethytriethylenetetraamine (5,6-dmtrien) and 5,6-dimethyl-3,7-diaza-2,9-diaminodecane (tmtrien) [21], and branched ligands like 2,3-butanediamine-*N*,*N*,*N*′,*N*′-tetraacetic acid (H_4bdta) [22].

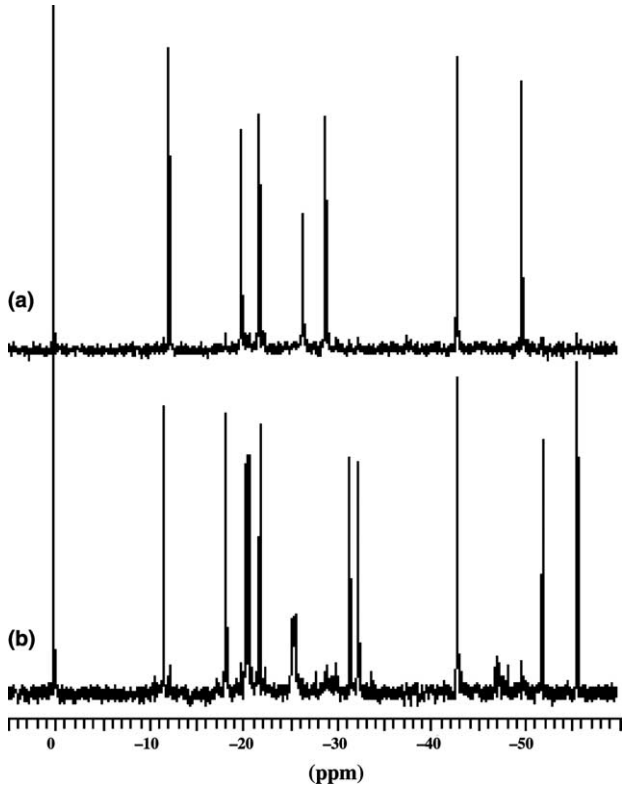

Fig. 4. ^{13}C NMR spectra of $[Co(1,2\text{-}Me_2EtN_4S_2amp)]^{3+}$ in D_2O: (a) *rac* isomer, (b) *meso* isomer (δ_C 0 ppm – 1,4-dioxane).

3.3. NMR spectroscopy

The ^{13}C NMR spectrum of $[Co(rac\text{-}1,2\text{-}Me_2EtN_4S_2amp)]^{3+}$ (Fig. 4(a)) exhibits seven resonances for this symmetric molecule which has a C_2 rotation axis bisecting the dithio-hinge and the cobalt centre. The methyl carbon resonance in the dithio-hinge (δ_C −49.9 ppm) is shifted upfield relative to the apical methyl carbon resonance (δ_C −43.0 ppm). The methine carbons on the dithio-hinge display a resonance (δ_C −12.3 ppm) which is shifted significantly downfield compared to resonances of methylene carbons adjacent to thioethers for both this complex (δ_C −29.0 ppm) and $[Co(EtN_4S_2amp)]^{3+}$ (δ_C −28.4, −27.5 ppm) [1]. The remaining ^{13}C resonances of $[Co(rac\text{-}1,2\text{-}Me_2EtN_4S_2amp)]^{3+}$ are found to have similar shifts to those for the analogous resonances of $[Co(EtN_4S_2amp)]^{3+}$ [1].

The ^{13}C NMR spectrum of $[Co(meso\text{-}Me_2EtN_4S_2amp)]^{3+}$ (Fig. 4(b)) displays 14 resonances and is characteristic of an asymmetric molecule. In comparison to the *rac* isomer, the ^{13}C NMR signals for the *meso* isomer can be considered as ''pairs'' of resonances for each type of carbon atom present. The greatest difference in chemical shift within a single ''pair'' of signals is seen for the chiral methine carbons (δ_C −11.7, −18.4 ppm). The difference between shifts within a ''pair'' of resonances decreases with decreasing proximity to the chiral carbons.

3.4. X-ray crystal structure

The structure of $[Co(rac\text{-}1,2\text{-}Me_2EtN_4S_2amp)]Cl_2(ClO_4)\cdot 2H_2O$ (Fig. 2) consists of the molecular cation, two chloride anions, a perchlorate anion and two water molecules. The structure of the molecular cation is similar to that of $[Co(EtN_4S_2amp)]^{3+}$ [1]. The cation adopts the *lel* conformation [16] for the dithio-chelate ring (Fig. 3) as for the Co(III) complexes of amplectors with straight chain dithio-hinges. The chiral carbons of the dithio-hinge both adopt the *S* (or *R*) configuration while the coordinated thioethers are *R* (or *S*). Thus, the methyl groups of the dithio-chelate ring are equatorial with the average plane of this chelate ring. When both thioethers are *R*, the dithio-chelate ring has the δ conformation for the *lel* form. Conversely, for its mirror image, the dithio-chelate ring has the λ conformation and both thioether donors are *S* for the *lel* form. The *ob* conformation would require one thioether donor to adopt the *R* configuration while the other thioether donor would have the *S* configuration. The remaining six-membered chelate rings all adopt the unsymmetrical skew-boat conformation [23].

Selected bond lengths and bond angles for $[Co(rac\text{-}Me_2EtN_4S_2amp)]Cl_2(ClO_4)\cdot 2H_2O$ are shown in Table 2. The coordination bond lengths are typical for both Co(III)-amine and Co(III)-thioether bonds [24–27]. In comparison to $[Co(EtN_4S_2amp)]^{3+}$ [1], the Co–N and Co–S bonds of $[Co(rac\text{-}1,2\text{-}Me_2EtN_4S_2amp)]^{3+}$ are slightly shorter. The S–Co–S bite angle for $[Co(rac\text{-}1,2\text{-}Me_2EtN_4S_2amp)]^{3+}$ (88.29(3)°) is slightly smaller than that of $[Co(EtN_4S_2amp)]^{3+}$ (88.72(7)°) [1]. The structural parameters of $[Co(rac\text{-}1,2\text{-}Me_2EtN_4S_2amp)]^{3+}$ and $[Co(EtN_4S_2amp)]^{3+}$ show only minor differences suggesting there is little steric hindrance from the methyl groups of the 1,2-dimethylethyl dithio-hinge.

3.5. Electrochemistry

The cyclic voltammograms of the cobalt(III) complexes of the diastereoisomers of $1,2\text{-}Me_2EtN_4S_2amp$ (Fig. 5) exhibit irreversible $Co^{3+/2+}$ redox couples as is the case for all the other cobalt(III) amplector complexes studied to date [1,2]. The cathodic peak attributed to the $Co^{3+/2+}$ couple for $[Co(rac\text{-}1,2\text{-}Me_2EtN_4S_2amp)]^{3+}$ (−412 mV, versus Ag/AgCl) is clearly shifted to a more negative value in comparison to that for $[Co(EtN_4S_2amp)]^{3+}$ (−330 mV, versus Ag/AgCl)) [1]. The difference in potential and the differences in the structural properties between $[Co(rac\text{-}1,2\text{-}Me_2EtN_4S_2amp)]^{3+}$ and $[Co(EtN_4S_2amp)]^{3+}$ suggest a preference for the smaller Co(III) ion in the former complex.

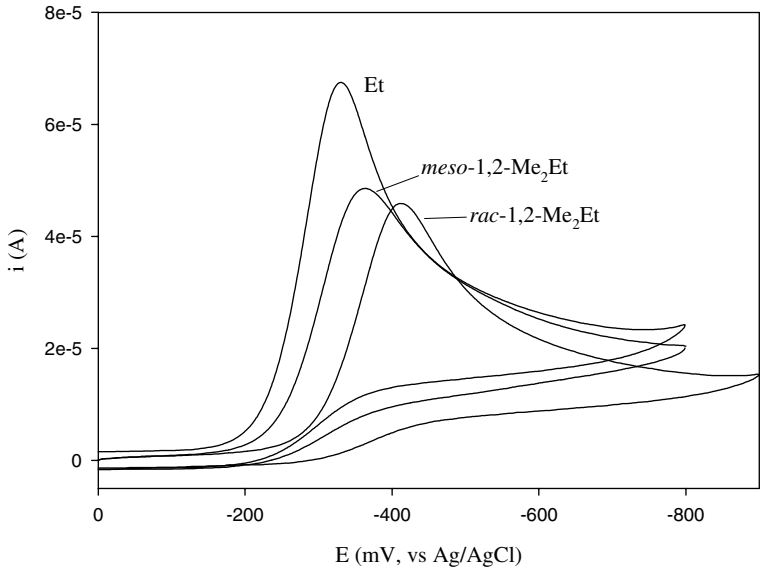

Fig. 5. Cyclic voltammograms of $[Co(RN_4S_2amp)]^{3+}$ (R = Et, *meso*-1,2-Me_2Et, *rac*-1,2-Me_2Et, pH < 2.5; Glassy C working electrode, 100 mV/s).

The cathodic peak for the $Co^{3+/2+}$ couple of [Co(*meso*-1,2-$Me_2EtN_4S_2amp$)]$^{3+}$ (−364 mV, versus Ag/AgCl) falls between those for [Co(*rac*-1,2-$Me_2EtN_4S_2amp$)]$^{3+}$ and $[Co(EtN_4S_2amp)]^{3+}$. The difference in redox potentials for the diastereoisomers of [Co(1,2-Me_2Et-N_4S_2amp)]$^{3+}$ is of similar magnitude to the $Co^{3+/2+}$ couples observed for other diastereoisomeric complexes such as [Co(salbn)] (salbn = *N*,*N*′-butane-2,3-diylbis(salicylideneiminato)) [28].

3.6. UV–Vis spectroscopy

The room temperature aqueous solution UV–Vis spectra of [Co(*rac*-1,2-$Me_2EtN_4S_2amp$)]$Cl_2(ClO_4)$ and [Co(*meso*-1,2-$Me_2EtN_4S_2amp$)]$Cl(ClO_4)_2$ were recorded. The spectra are typical of low spin Co(III) systems, with no spin forbidden transitions observed. For each spectrum, the peak attributed to the $^1A_{1g} \rightarrow {}^1T_{1g}$ transition is clearly seen. The higher energy $^1A_{1g} \rightarrow {}^1T_{2g}$ transition is observed as a shoulder upon an intense charge transfer band for both complexes.

Spectra recorded in Nafion film at low temperature (11 K) for [Co(*rac*-1,2-$Me_2EtN_4S_2amp$)]$^{3+}$ and [Co(*meso*-1,2-$Me_2EtN_4S_2amp$)]$^{3+}$ are similar to those of $[Co(EtN_4S_2amp)]^{3+}$ although the $^1A_{1g} \rightarrow {}^1T_{2g}$ transition is less obscured by the charge transfer band for the complexes with the dimethyl substituted hinge [1].

The observation of one spin forbidden band ($^1A_{1g} \rightarrow {}^3T_{2g}$) for both [Co(*rac*-1,2-$Me_2EtN_4S_2amp$)]$^{3+}$ and [Co(*meso*-1,2-$Me_2EtN_4S_2amp$)]$^{3+}$ complexes allows for the unique determination of spectrophotometric parameters 10Dq, *B* and *C* using perturbation equations described previously [7]. The equations assume O_h symmetry and are corrected for configuration interaction. The complexes $[Co(EtN_4S_2amp)]^{3+}$, [Co(*rac*-1,2-$Me_2EtN_4S_2amp$)]$^{3+}$ and [Co(*meso*-1,2-$Me_2EtN_4S_2amp$)]$^{3+}$ are found to have similar B values (551, 535 and 549 cm^{-1}, respectively; Table 3) as expected. It is clearly evident that the Racah parameter $C \approx 6B$ as previously reported [1,2,4,7,8,25]. 10 Dq for these complexes is essentially constant, as expected, and supports previous observations that this parameter is relatively insensitive for mixed nitrogen–thioether cobalt(III) complexes [4,7,8].

3.7. ^{59}Co NMR resonances and line-widths

^{59}Co resonances for the ethyl hinged amplector complexes are found within the relatively narrow chemical shift range of 5570–5670 ppm ($[Co(EtN_4S_2amp)]^{3+}$, δ_{Co} 5638 ppm; [Co(*rac*-1,2-$Me_2EtN_4S_2amp$)]$^{3+}$, δ_{Co} 5579 ppm; [Co(*meso*-1,2-$Me_2EtN_4S_2amp$)]$^{3+}$, 5661 ppm) and have similar ^{59}Co NMR chemical shifts to other Co(III) complexes with N_4S_2 donor sets (5000–6500 ppm) [2]. The linewidths of the ^{59}Co NMR resonances are known to be dependent upon electric field gradients at the cobalt nucleus and departures from strict octahedral symmetry about the cobalt atom cause line broadening [29]. The ^{59}Co linewidth of [Co(*rac*-1,2-$Me_2EtN_4S_2amp$)]$^{3+}$ ($\nu_{1/2}$ = 630 Hz) is similar to that of $[Co(EtN_4S_2amp)]^{3+}$ ($\nu_{1/2}$ = 740 Hz), whilst that of [Co(*meso*-1,2-$Me_2EtN_4S_2amp$)]$^{3+}$ ($\nu_{1/2}$ = 370 Hz) is decidedly less than that of the *rac* isomer. This is a somewhat surprising result as the *meso* isomer is asymmetric by ^{1}H and ^{13}C NMR spectroscopy while [Co(*rac*-1,2-$Me_2EtN_4S_2amp$)]$^{3+}$ and $[Co(EtN_4S_2amp)]^{3+}$ both exhibit a C_2 rotation axis. The ^{59}Co NMR linewidth is not only seen to be dependent on the symmetry of the donor set but also the rigidity of the ligand structure, as the

Table 3
Spectroscopic parameters for Co(III) complexes of nitrogen–thioether ligands[a] [2]

Ligand[b]	Donor set	$^1A_{1g} \rightarrow {}^1T_{1g}$ (cm^{-1})	$^1A_{1g} \rightarrow {}^1T_{2g}$ (cm^{-1})	$^1A_{1g} \rightarrow {}^3T_{1g}$ (cm^{-1})	$^1A_{1g} \rightarrow {}^3T_{2g}$ (cm^{-1})	10Dq (cm^{-1})	B (cm^{-1})	C[c] (cm^{-1})	$\beta(\Delta E)^{-1}$[d] (nm)	γ_{Co}[e] (MHz T^{-1})	Compound no.[f]	Ref.
N_3S_3	3N 3S	20860	27280	14535	17625	23360	452	3040	203.46	10.1507	1	[4] [g]
$AMN_3S_3sarH^+$	3N 3S	20460	26960	14145	17240	21920	459	3030	210.65	10.1506	2	[4] [g]
N_4S_2	4N 2S	20800	27950			22140	516		232.94	10.1602	3	[6] [h]
$AMN_4S_2sarH^+$	4N 2S	20450	27700			21750	526		241.51	10.1604	4	[6] [h]
EtN_4S_2amp	4N 2S	21140	28800	13800	17400	22570	551	3500	244.74	10.1627	5	[3] [g]
rac-1,2-$Me_2EtN_4S_2amp$	4N 2S	21240	28620		17800	22600	535	3350	243.58	10.1686	6	[g]
meso-1,2-$Me_2EtN_4S_2amp$	4N 2S	20970	28500		17400	22310	549	3430	245.82	10.1629	7	[g]
$Me_6docosadieneN_4S_2$	4N 2S	19380	26450			20580	516		250.00	10.1714	8	[g]
N_5S	5N S	20900	28700			22200	572		256.98	10.1686	9	[8] [h]
$AZAN_5Ssar$	5N S	20700	28200			22000	547		248.12	10.1686	10	[h]
$(NH_3)_6$	6N	21200	29550	13000	17200	22400	626	3790	277.26	10.1881	11	[24]
$(en)_3$	6N	21500	29600	13700	17500	23000	583	3730	254.61	10.178	12	[24]
Sen	6N	21400	29400			22710	587		257.56	10.1756	13	[24] [h]
Sep	6N	21200	29400			22400	607		268.85	10.1758	14	[24] [h]
$diAMN_6sarH_2^{2+}$	6N	21100	29030			22400	583		259.44	10.1752	15	[24] [h]

[a] All energies determined by Peakfit [12] using the residuals method with Gaussian + Lorentzian amplitude curves with no base line.
[b] Ligand nomenclature described elsewhere [2].
[c] For values of C not given, $C = 6B$ is assumed in order to determine 10Dq and B.
[d] $\beta = B/B_0$ ($B_0 = 1065$ cm^{-1}) [36].
[e] $\gamma_{Co} = \gamma_s(1+\delta_{Co})$ where $\gamma_s = 10.1057$ MHz T^{-1} (the magnetogyric ratio of $[Co(CN)_6]^{3-}$); δ_{Co} [2].
[f] See Fig. 6.
[g] Spectra obtained from Nafion films at 11 K.
[h] Solution spectra.

encapsulated complexes have a markedly larger ^{59}Co linewidth than the branched precursor complexes.

3.8. Correlation between the ^{59}Co chemical shift and $E(^1A_{1g} \rightarrow {}^1T_{1g})$

Griffith and Orgel [30] showed that for low spin d^6 systems the $^1T_{1g}$ state can mix with the ground state ($^1A_{1g}$) on exposure to a magnetic field. They predicted that the paramagnetic screening constant σ_p was inversely proportional to $\Delta E_{(^1A1g \rightarrow {}^1T1g)}$, the energy separation of the $^1T_{1g}$ and $^1A_{1g}$ states [30]

$$\sigma_p = -32\beta_M^2 \langle r^{-3} \rangle \Delta E^{-1}_{(^1A_{1g} \rightarrow {}^1T_{1g})}, \quad (1)$$

where r is the distance of a given 3d electron from the cobalt nucleus and β_M is the Bohr magneton. The theoretical expression for the magnetogyric ratio, γ, as a function of screening constants is given by [31]

$$\gamma = \gamma_o(1 - \sigma_d - \sigma_p), \quad (2)$$

where σ_d and σ_p are diamagnetic and paramagnetic screening constants, respectively. Experimentally, $\gamma = \gamma_S(1 + \delta_{Co})$ where γ_S, the magnetogyric ratio of $[Co(CN)_6]^{3-}$, is 10.1057 MHz T^{-1} and δ_{Co} is the ^{59}Co chemical shift. Assuming $\langle r^{-3} \rangle$ to be constant, it was expected that γ would be inversely proportional to $\Delta E_{(^1A_{1g} \rightarrow {}^1T_{1g})}$. Freeman et al. [32], the first to investigate whether such a correlation existed using homoleptic and mixed donor cobalt(III) complexes, concluded that a linear correlation between ^{59}Co chemical shifts and the wavelength of the $^1A_{1g} \rightarrow {}^1T_{1g}$ transition existed for symmetrical complexes. Deviations from the best fit line for symmetrical structures were observed for asymmetric complexes and those with 3rd and 4th period ligators [32]. The difference was attributed to increases in the covalency of the coordination sphere delocalizing the cobalt d-electron shell, thus decreasing $\langle r^{-3} \rangle$. Introduction of the nephelauxetic ratio, β_{Racah} ($= B_{complex}/B_{free\ ion}$)

$$\sigma_p \alpha \beta_{Racah} \Delta E^{-1}_{(^1A_{1g} \rightarrow {}^1T_{1g})}$$

was proposed to rationalize the observed deviations from linearity [33].

The series of non-orthoaxial complexes $[Co(EtN_4S_2amp)]^{3+}$, $[Co(meso\text{-}1,2\text{-}Me_2EtN_4S_2amp)]^{3+}$, $[Co(rac\text{-}1,2\text{-}Me_2EtN_4S_2amp)]^{3+}$ and the $N_{6-x}S_x$ ($x = 1, 2, 3$) complexes [5–8] for which both spin-allowed and spin-forbidden transitions are observed permits unique determination of β and therefore an examination of the relationship between γ_{Co} and $\beta\Delta E^{-1}$ [2]. The plot of $\gamma(^{59}Co)$ and $\beta_{Racah}(\Delta E)^{-1}$ for these complexes (Table 3, Fig. 6) results in a linear relationship ($r^2 = 0.93$) with an intercept of 10.047 MHz T^{-1}, giving $\gamma_0(^{59}Co)$ as 10.049 ± 0.013 MHz T^{-1} ($\sigma_d = 0.0021$) [32]. Independently determined values of γ_0 (the magnetogyric ratio of the bare cobalt nucleus) include 10.054 ± 0.002 MHz T^{-1} [34,35].

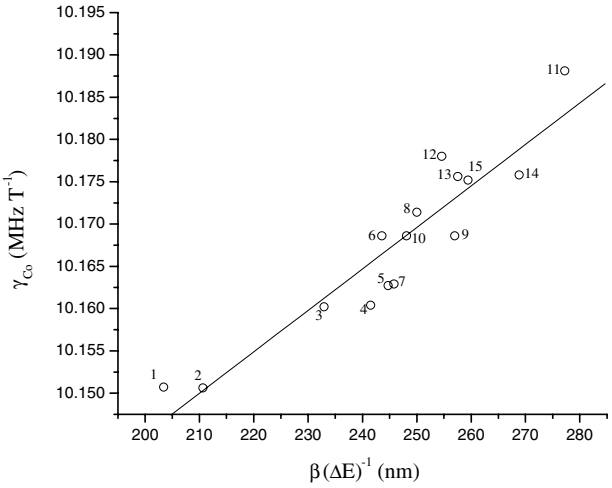

Fig. 6. Plot of ^{59}Co magnetogyric ratio vs $\beta(\Delta E)^{-1}$ for the series of complexes with N_6, N_5S, N_4S_2 and N_3S_3 donors (see Table 3 for data; the solid line represents the line of best fit).

4. Conclusions

The amplector synthetic methodology has been shown to be readily adapted to allow the formation of ligands possessing substituents on the dithio-chelate ring – in this case resulting in an example of a sinambic ligand. The complexes characterized in this work have permitted the further investigation of the spectroscopic characteristics of mixed donor (sulfur–nitrogen) multidentate ligands. Future work will investigate the inclusion of more elaborate functional groups (e.g primary amine) on the dithio-hinge presenting the possibility for further synthetic elaboration.

5. Supplementary material

Crystallographic data for $[Co(rac\text{-}1,2\text{-}Me_2Et\text{-}N_4S_2amp)]Cl_2(ClO)_4 \cdot 2H_2O$ (CCDC 239514) have been deposited with the Cambridge Crystallographic Data Centre. A copy of this information may be obtained free of charge from: The Director, CCDC, 12 Union Road, Cambridge, CB2 1EZ, UK (fax: +44-1223-3360333; e-mail: deposit@ccdc.cam.ac.uk; www: http://www.ccdc.cam.ac.uk).

References

[1] C.A. Sharrad, S.R. Lüthi, L.R. Gahan, J. Chem. Soc., Dalton Trans. (2003) 3693.
[2] C.A. Sharrad, G.E. Cavigliasso, R. Stranger, L.R. Gahan, J. Chem. Soc., Dalton Trans. (2004) 767.

[3] C.A. Sharrad, G.E. Cavigliasso, R. Stranger, L.R. Gahan, J. Chem. Soc., Dalton Trans. (2004) 1166.
[4] T.M. Donlevy, L.R. Gahan, T.W. Hambley, K.L. McMahon, R. Stranger, Aust. J. Chem. 46 (1993) 1799.
[5] L.R. Gahan, T.W. Hambley, A.M. Sargeson, M.R. Snow, Inorg. Chem. 21 (1982) 2699.
[6] L.R. Gahan, T.M. Donlevy, T.W. Hambley, Inorg. Chem. 29 (1990) 1451.
[7] T.M. Donlevy, L.R. Gahan, T.W. Hambley, R. Stranger, Inorg. Chem. 31 (1992) 4376.
[8] J.I. Bruce, L.R. Gahan, T.W. Hambley, R. Stranger, Inorg. Chem. 52 (1993) 5997.
[9] M.F. Gargallo, J.D. Mather, E.N. Duesler, R.E. Tapscott, Inorg. Chem. 22 (1983) 2888.
[10] J.D. Mather, R.E. Tapscott, C.F. Campana, Inorg. Chim. Acta 73 (1983) 235.
[11] J.D. Mather, R.E. Tapscott, J. Coord. Chem. 11 (1981) 5.
[12] PeakFit, Version 4, AISN Software Inc., 1991–1995.
[13] A. Altomare, G. Cascorano, C. Giacovazzo, A. Gualardi, J. Appl. Cryst. 26 (1993) 343.
[14] G.M. Sheldrick, SHELXL-97, A Program for Crystal Structure Refinement, University of Göttingen, Germany, 1997, Release 97-2.
[15] L.J. Farrugia, J. Appl. Cryst. 30 (1997) 565.
[16] *lel*, and *ob* refer to limiting conformations of five-membered chelate rings in which the C–C axis is respectively parallel and oblique to the (pseudo) C_3 axis of the complex cation. See Inorg. Chem. 9 (1970) 1.
[17] E.N. Duesler, M.F. Gargallo, R.E. Tapscott, Acta Crystallogr., Sect. B 38 (1982) 1300.
[18] M. Kojima, H. Funaki, Y. Yoshikawa, K. Yamasaki, Bull. Chem. Soc. Jpn. 48 (1975) 2801.
[19] S.R. Niketić, K. Rasmussen, Acta Chem. Scand. A 32 (1978) 391.
[20] C.J. Hilleary, T.F. Them, R.E. Tapscott, Inorg. Chem. 19 (1980) 102.
[21] M. Goto, H. Matsushita, M. Saburi, S. Yoshikawa, Inorg. Chem. 12 (1973) 1498.
[22] M. Kalina, V. Kettmann, F. Pavelčik, J. Majer, Coll. Czech. Chem. Commun. 50 (1985) 171.
[23] C.J. Hawkins, Absolute Configuration of Metal Complexes, Wiley–Interscience, New York, 1971.
[24] P. Hendry, A. Ludi, Adv. Inorganic Chem. 35 (1990) 117.
[25] P. Osvath, A.M. Sargeson, A. McAuley, R.E. Mendelez, S. Subramanian, M.J. Zaworotko, L. Broge, Inorg. Chem. 38 (1999) 3634.
[26] G.J. Grant, S.S. Shoup, C.E. Hadden, D.G. VanDerveer, Inorg. Chim. Acta 274 (1998) 192.
[27] G. Wei, C.C. Allen, T.W. Hambley, G.A. Lawrance, M. Maeder, Inorg. Chim. Acta 261 (1997) 197.
[28] J. Hanzlik, A. Puxeddu, G. Costa, J. Chem. Soc., Dalton Trans. (1977) 543.
[29] R.G. Kidd, R.J. Goodfellow, in: R.K. Harris, B.E. Mann (Eds.), NMR and the Periodic Table, Academic Press, New York, 1978.
[30] J.S. Griffith, L.E. Orgel, Trans. Faraday Soc. 53 (1957) 601.
[31] R. Bramley, M. Brorson, A.M. Sargeson, C.E. Schäffer, J. Am. Chem. Soc. 107 (1985) 2780.
[32] R. Freeman, G.R. Murray, R.E. Richards, Proc. R. Soc. Lond. A 242 (1957) 455.
[33] N. Juranić, J. Chem. Phys. 74 (1981) 3690.
[34] R.E. Walstedt, J.H. Wernick, V. Jaccarino, Phys. Rev. 162 (1967) 30.
[35] H.W. Spiess, H. Haas, H. Hartmann, J. Chem. Phys. 50 (1969) 3057.
[36] C.R. Hare, in: K. Nakamoto, P.J. McCarthy (Eds.), Spectroscopy and Structure of Metal Chelate Compounds, Wiley, New York, 1968.

Available online at www.sciencedirect.com
SCIENCE DIRECT®
Polyhedron 23 (2004) 2227–2233
POLYHEDRON
www.elsevier.com/locate/poly

Three-dimensional porous frameworks constructed by transition metal ions and isoorotic acid

Chang-Yan Sun, Lin-Pei Jin *

Department of Chemistry, Beijing Normal University, Xinjiekou Road, Beijing 100875, PR China

Received 31 May 2004; accepted 25 June 2004
Available online 25 August 2004

Abstract

Four new coordination polymers, $[M(Hiso)(H_2O)_3]_n$ (M = Co (**1**); M = Ni (**2**)) and $\{[M_2(Hiso)_2(bipy)_2(H_2O)_4]\cdot 2(bipy)\}_n$ (M = Co (**3**); M = Ni (**4**)) (H_2iso = isoorotic acid, bipy = 4,4′-bipyridine), were synthesized by hydrothermal reactions and characterized by single-crystal X-ray diffraction. The four complexes all comprise 1D chains that are further interlinked via hydrogen bonds, resulting in the formation of 3D frameworks. There are small channels in **1** and **2** and two kinds of larger channels in **3** and **4**, in which free bipy molecules residue. In **1** and **2**, the $Hiso^{2-}$ anions act as tridentate ligands to link metal ions; in **3** and **4**, the $Hiso^{2-}$ anions act as bidentate ligands and the metal ions are bridged by bipy.
© 2004 Elsevier Ltd. All rights reserved.

Keywords: Isoorotic acid; Co(II) and Ni(II) complexes; Hydrothermal synthesis; Hydrogen bonds; Supramolecular frameworks

1. Introduction

The rational self-assembly of supramolecular frameworks using noncovalent forces such as hydrogen bonds and π–π stacking interactions is a rapidly expanding field due to their fascinating crystal structures, electronic, optical and magnetic properties, and potential applications [1–5]. Hydrogen bonding, as the strongest and most directional intermolecular force, has been intensively investigated in organic crystalline solids [6–9]. Attempts have been made to combine both metal–ligand coordination bonds and hydrogen bonds in the crystal engineering of porous metal–organic hybrid materials. For example, the construction of a porous solid from hydrogen bonded metal complexes of 1,3,5-benzenetricarboxylic acid with interesting properties has been achieved by Yaghi, and Munakata has described the design of 3D supramolecular channel-like copper compounds that host a variety of anions by changing the hydrogen-bonding modes and distances [10,11]. This approach provides a means to control the rigidity of a supramolecular framework joined by metal–ligand interactions by selectively incorporating more flexible hydrogen bonds between molecules. This should promote crystalization since hydrogen-bonded structures form reversibly and exhibit slower kinetics for nucleation and growth of crystals than coordination polymers.

In this work, we used transition metal ions, 4,4′-bipyridine (bipy) and a multifunctional ligand, namely, isoorotic acid (5-carboxyuracil acid, H_3iso) to construct coordination complexes. Bipy is an efficient ligand to link transition metal ions. The choice of H_3iso was driven by following factors. First, H_3iso possesses multiple coordination sites and can bond to metal ions with versatile coordination modes. Moreover, it can act as a hydrogen bond donor or acceptor. Finally, there are only a few reports on the coordination chemistry of H_3iso [12–16].

* Corresponding author. Tel.: +01062205522; fax: +8601062 202075.
E-mail address: lpjin@bnu.edu.cn (L.-P. Jin).

0277-5387/$ - see front matter © 2004 Elsevier Ltd. All rights reserved.
doi:10.1016/j.poly.2004.06.032

Hydrothermal synthesis has been employed extensively to obtain single crystals because the properties and the interactions of the reactants are quite different from those under conventional conditions [17–20]. Herein, we report the hydrothermal syntheses and structures of four new complexes $[M(Hiso)(H_2O)_3]_n$ (M = Co (**1**), Ni (**2**)) and $\{[M_2(Hiso)_2(bipy)_2(H_2O)_4]\cdot 2(bipy)\}_n$ (M = Co (**3**), Ni (**4**)).

2. Experimental

2.1. Materials and apparatus

All reagents were used as received without further purification. The C, H, N microanalyses were carried out with a Vario EL elemental analyzer. The IR spectra were recorded with a Nicolet Avatar 360 FT-IR spectrometer using the KBr pellet technique. Thermogravimetric analyses were conducted on a ZRY-2P Thermal Analyzer using a heating rate of 10 °C/min from room temperature to 900 °C.

2.2. Synthesis

2.2.1. $[Co(Hiso)(H_2O)_3]_n$ (*1*)

A mixture of H_3iso (0.017 g, 0.1 mmol), $CoCl_2\cdot 6H_2O$ (0.048 g, 0.2 mmol), NaOH aqueous solution (0.35 ml, 0.65 mol l^{-1}) and deionized water (5 ml) was sealed in a Teflon-lined stainless vessel (25 ml), heated to 120 °C for 72 h, and then cooled at 5 °C/3 h to 100 °C, followed by slow cooling to room temperature. Red crystals were obtained, washed with water and ethanol, and dried in air. Yield: 0.02 g (74.9%). *Anal*. Calc. for $C_5H_8N_2O_7Co$: C, 22.47; H, 3.00; N, 10.49. Found: C, 22.35; H, 2.74; N, 10.31%. IR data (KBr pellet, cm^{-1}): 3480m, 1646s, 1571m, 1526m, 1404s, 1386m, 1325m, 1297m, 1028m, 887w, 670m.

2.2.2. $[Ni(Hiso)(H_2O)_3]_n$ (*2*)

The synthesis of complex **2** followed the same procedure as for complex **1**. Yield: 0.022 g (82.4%). *Anal*. Calc. for $C_5H_8N_2O_7Ni$: C, 22.49; H, 3.00; N, 10.49. Found: C, 22.33; H, 2.75; N, 10.35%. IR data (KBr pellet, cm^{-1}): 3483m, 1646s, 1571m, 1528m, 1404s, 1386s, 1325m, 1295m, 1209m, 883w, 675m.

2.2.3. $\{[Co_2(Hiso)_2(bipy)_2(H_2O)_4]\cdot 2(bipy)\}_n$ (*3*)

A mixture of H_3iso (0.017 g, 0.1 mmol), $CoCl_2\cdot 6H_2O$ (0.024 g, 0.1 mmol), bipy (0.016 g, 0.1 mmol), NaOH aqueous solution (0.18 ml, 0.65 mol l^{-1}) and deionized water (5 ml) was sealed in a Teflon-lined stainless vessel (25 ml), heated to 120 °C for 72 h, and then cooled at 5 °C/3 h to 100 °C, followed by slow cooling to room temperature. Red crystals were obtained, washed with water and ethanol, and dried in air. Yield: 0.02 g (35.6%). *Anal*. Calc. for $C_{50}H_{44}N_{12}O_{12}Co_2$: C, 53.44; H, 3.92; N, 14.97. Found: C, 53.48; H, 3.52; N, 14.90%. IR data (KBr pellet, cm^{-1}): 3414m, 2920m, 1611s, 1564m, 1536m, 1477m, 1402s, 1376m, 1310m, 1294m, 816m, 660m, 609w.

Table 1
Crystal data and structure refinement parameters for **1**–**4**

	1	**2**	**3**	**4**
Chemical formula	$C_5H_8N_2O_7Co$	$C_5H_8N_2O_7Ni$	$C_{50}H_{44}N_{12}O_{12}Co_2$	$C_{50}H_{44}N_{12}O_{12}Ni_2$
Formula weight	267.06	266.84	1122.84	1122.39
Crystal system	monoclinic	monoclinic	triclinic	triclinic
Space group	*P*2(1)/*n*	*P*2(1)/*n*	$P\bar{1}$	$P\bar{1}$
Unit cell dimensions				
a (Å)	5.2084(14)	5.1645(16)	11.241(3)	11.232(4)
b (Å)	12.185(3)	12.172(4)	11.553(3)	11.570(4)
c (Å)	13.617(4)	13.459(4)	11.736(3)	11.728(4)
α (°)	90	90	72.094(4)	71.251(6)
β (°)	91.103(4)	91.169(5)	67.041(5)	67.067(6)
γ (°)	90	90	65.249(5)	65.244(5)
V (Å^3)	864.0(4)	845.9(5)	1255.4(6)	1251.6(8)
Z	4	4	1	1
F(000)	540	544	578	580
D_c (Mg m^{-3})	2.053	2.095	1.485	1.489
T (°C)	293(2)	293(2)	293(2)	293(2)
θ Range (°)	2.24–26.38	2.26–26.38	1.91–26.43	1.92–26.41
Absorption coefficient (mm^{-1})	2.009	2.317	0.737	0.828
Goodness-of-fit on F^2	1.035	1.020	1.011	0.954
$R(wR)$ $[I > 2\sigma(I)]$	0.0229 (0.0589)	0.0338 (0.0659)	0.0595 (0.1109)	0.0465 (0.0953)
$R(wR)$ (all data)	0.0283 (0.0610)	0.0570 (0.0734)	0.1198 (0.1364)	0.1023 (0.1146)
Largest difference peak and hole (e Å^{-3})	0.368 and −0.275	0.362 and −0.365	0.514 and −0.561	0.536 and −0.589

Table 2
Selected bond lengths (Å) and angles (°) for **1** and **2**

1			
Bond lengths			
Co(1)–O(1)	2.047(2)	Co(1)–O(6)	2.107(1)
Co(1)–O(3)	2.081(1)	Co(1)–O(7)	2.113(2)
Co(1)–O(5)	2.132(2)	Co(1)–N(2)#1	2.157(2)
Bond angles			
O(1)–Co(1)-O(3)	86.89(6)	O(3)–Co(1)–N(2)#1	179.21(6)
O(1)–Co(1)–O(5)	91.86(6)	O(5)–Co(1)–N(2)#1	96.06(6)
O(1)–Co(1)–O(6)	174.86(5)	O(6)–Co(1)–O(5)	87.57(6)
O(1)–Co(1)–O(7)	91.52(6)	O(6)–Co(1)–O(7)	88.36(6)
O(1)–Co(1)–N(2)#1	93.89(6)	O(6)–Co(1)–N(2)#1	91.25(6)
O(3)–Co(1)–O(5)	83.84(6)	O(7)–Co(1)–O(5)	171.50(6)
O(3)–Co(1)–O(6)	87.96(6)	O(7)–Co(1)–N(2)#1	91.49(6)
O(3)–Co(1)–O(7)	88.56(6)		
2			
Bond lengths			
Ni(1)–O(1)	2.020(2)	Ni(1)–O(6)	2.069(2)
Ni(1)–O(3)	2.032(2)	Ni(1)–O(7)	2.072(2)
Ni(1)–O(5)	2.089(2)	Ni(1)–N(2)#1	2.118(3)
Bond angles			
O(1)–Ni(1)–O(3)	88.49(9)	O(3)–Ni(1)–N(2)#1	178.6(1)
O(1)–Ni(1)–O(5)	91.46(9)	O(5)–Ni(1)–N(2)#1	95.48(9)
O(1)–Ni(1)–O(6)	175.67(9)	O(6)–Ni(1)–O(5)	88.02(9)
O(1)–Ni(1)–O(7)	91.8(1)	O(6)–Ni(1)–O(7)	88.22(9)
O(1)–Ni(1)–N(2)#1	92.8(1)	O(6)–Ni(1)–N(2)#1	91.6(1)
O(3)–Ni(1)–O(5)	83.86(9)	O(7)–Ni(1)–O(5)	172.08(9)
O(3)–Ni(1)–O(6)	87.18(9)	O(7)–Ni(1)–N(2)#1	91.60(9)
O(3)–Ni(1)–O(7)	88.99(9)		

Symmetry transformations used to generate equivalent atoms: #1 $x + 1/2$, $-y + 3/2$, $z - 1/2$.

Table 3
Selected bond lengths (Å) and angles (°) for **3** and **4**

3			
Bond lengths			
Co(1)–O(1)	2.058(3)	Co(2)–O(5)	2.022(3)
Co(1)–O(3)	2.056(3)	Co(2)–O(6)	2.206(3)
Co(1)–N(3)	2.133(4)	Co(2)–N(4)	2.134(4)
Bond angles			
O(1)–Co(1)–N(3)	88.67(1)	O(5)–Co(2)–O(6)	88.94(1)
O(3)–Co(1)–O(1)	90.36(1)	O(5)–Co(2)–N(4)	88.92(1)
O(3)–Co(1)–N(3)	89.36(1)	N(4)–Co(2)–O(6)	87.58(1)
4			
Bond lengths			
Ni(1)–O(1)	2.049(2)	Ni(2)–O(5)	2.020(2)
Ni(1)–O(3)	2.041(2)	Ni(2)–O(6)	2.164(2)
Ni(1)–N(3)	2.094(3)	Ni(2)–N(4)	2.090(3)
Bond angles			
O(1)–Ni(1)–N(3)	88.85(1)	O(5)–Ni(2)–O(6)	89.55(1)
O(3)–Ni(1)–O(1)	91.19(9)	O(5)–Ni(2)–N(4)	88.40(1)
O(3)–Ni(1)–N(3)	89.43(1)	N(4)–Ni(2)–O(6)	88.34(1)

2.2.4. $\{[Ni_2(Hiso)_2(bipy)_2(H_2O)_4]\cdot 2(bipy)\}_n$ (**4**)

The synthesis of complex **4** followed the same procedure as for complex **3**, except that the temperature was 140 °C and the mixture cooled at 10 °C/3 h to 100 °C, followed by slow cooling to room temperature. Yield: 0.016 g (28.5%). *Anal.* Calc. for $C_{50}H_{44}N_{12}O_{12}Ni_2$: C, 53.46; H, 3.92; N, 14.97. Found: C, 53.31; H, 3.59; N, 14.96%. IR data (KBr pellet, cm^{-1}): 3432s, 2919m,

1613s, 1565m, 1537m, 1478w, 1402m, 1378m, 1310m, 1295m, 816w, 661w, 608w.

2.3. X-ray diffraction determination

Diffraction intensities for the four complexes were collected at 293 K on a Bruker SMART 1000 CCD diffractometer employing graphite monochromatized Mo Kα radiation ($\lambda = 0.71073$ Å). A semi-empirical absorption correction was applied using the SADABS program [21]. The structures were solved by direct methods [22] and refined by full-matrix least squares on F^2 using SHELXS-97 and SHELXL-97 programs, respectively [22,23]. Non-hydrogen atoms were refined anisotropically. All hydrogen atoms were initially located in a difference Fourier map. The O–H distances were then fixed at 0.85 Å and Uiso(H) of the hydrogen atoms of H_2O was 1.5 times of Ueq(O) in the next refinement. The crystallographic data for complexes **1**–**4** are listed in Table 1, and selected bond lengths (Å) and bond angles (°) in Tables 2 and 3.

3. Results and discussion

3.1. Description of the structures

Complexes **1** and **2**, **3** and **4** are two isomorphous pairs. Because of the different radii of the Co(II) and Ni(II) ions, there are corresponding differences in the distances of M–O and M–N (M = Co or Ni), but only the structures of **1** and **3** will be described in detail.

3.1.1. $[Co(Hiso)(H_2O)_3]_n$ (*1*)

As shown in Fig. 1, the Co(II) ion is six-coordinated and surrounded by two oxygen atoms from one $Hiso^{2-}$ anion, one nitrogen atom from another $Hiso^{2-}$ anion and three aqua ligands. In this complex the $Hiso^{2-}$ anion acts as a tridentate ligand through O(1), O(3) and N(2). This kind of coordination mode has not been reported before. The bridging $Hiso^{2-}$ anions link the Co(II) ions into infinite polymeric zigzag chains parallel to the *c*-axis. The Co···Co distance in the chain is 7.574 Å (7.488 Å for Ni) and the Co–Co–Co angle is 151.2° (151.5° for Ni).

In **1**, the amido groups, the carbonyl oxygen atoms, the carboxylate groups and the aqua ligands are all involved in hydrogen bonds. The amido groups and the aqua ligands act as hydrogen bonding donors, while the carboxylate and the carbonyl oxygen atoms act as hydrogen bonding acceptors. There are O_w–H···O_w (a), O_w–H···O_{cc} (b), O_w–H···O_{uc} (c), O_w–H···O_c (d) and N–H···O_c (e) hydrogen bonds between the chains (O_w, water molecule oxygen atom; O_{cc}, coordinating carboxyl oxygen atom; O_{uc}, uncoordinating carboxyl oxygen atom; O_c, uncoordinating carbonyl oxygen atom), resulting in the formation of a 3D-supramoleclar structure (see Fig. 2). There are two kinds of channels (A and B) in the structure, but they are too small for any host molecules to reside. The geometry of the hydrogen bonds is shown in Table 4. There is a weak π–π stacking interaction between the pyramidine rings at a distance of 3.76 Å, which stabilizes the complex.

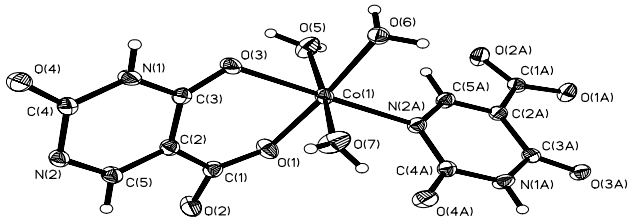

Fig. 1. The coordination environment of the Co(II) ion in complex **1** with 50% thermal ellipsoids.

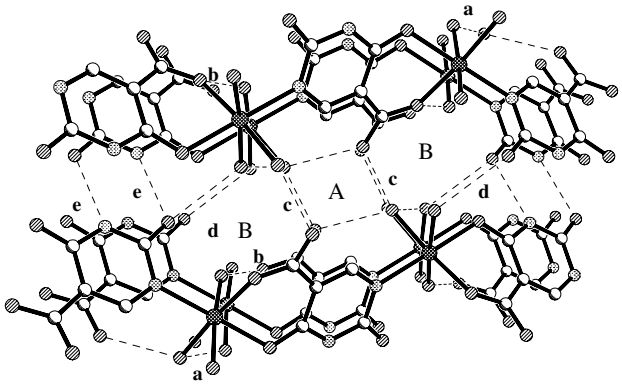

Fig. 2. 3D network constructed by hydrogen bonds of complex **1** viewed along the a axis, all hydrogen atoms are omitted for clarity.

3.1.2. $\{[Co_2(Hiso)_2(bipy)_2(H_2O)_4]\cdot 2(bipy)\}_n$ (*3*)

There are two kinds of metal coordination environments in **3**, as shown in Fig. 3. Although Co(1) and Co(2) are both six-coordinate and their coordination geometries can be described as distorted octahedrons, the coordination environments around them are different. Co(1) is coordinated by four oxygen atoms belonging to two $Hiso^{2-}$ anions and two nitrogen atoms from two bipy molecules, while Co(2) is coordinated by two nitrogen atoms of bipy and four aqua ligands. Co(1) and Co(2) are in the center of symmetry and are connected by bipy at a separation of 11.365 Å (11.288 Å for Ni). In complex **3**, the $Hiso^{2-}$ anion acts as a bidentate ligand through O(1) and O(3). It is worth noting that although N(2) in the $Hiso^{2-}$ anion is deprotonated, it is not coordinated as in **1** and **2** owing to the strong coordination ability of bipy to Co(II) ions. There are two kinds of bipy that have different roles in the structure (see Fig. 3). One kind of bipy bridges Co(II) ions and the dihedral angle of the two pyridine rings of this bipy is 6.1°; while the other

Table 4
Hydrogen bonding geometry (Å and °) for **1**–**4**

D–H	*d*(D–H)	*d*(H···A)	∠(DHA)	*d*(D···A)	A
1					
N1–H1	0.860	1.990	160.51	2.815	O4 [$-x$, $-y+1$, $-z+1$]
O5–H5A	0.850	2.080	164.24	2.907	O4 [$-x+1$, $-y+1$, $-z+1$]
O5–H5B	0.850	1.989	172.95	2.835	O6 [$x+1$, y, z]
O6–H6A	0.850	1.847	165.87	2.680	O2 [$x-1/2$, $-y+3/2$, $z-1/2$]
O6–H6B	0.850	1.869	155.03	2.664	O2 [$-x+3/2$, $y-1/2$, $-z+1/2$]
O7–H7A	0.850	1.831	153.03	2.617	O4 [$x+1/2$, $-y+3/2$, $z-1/2$]
O7–H7B	0.850	1.920	169.04	2.759	O1 [$x-1$, y, z]
2					
N1–H1	0.860	1.992	161.40	2.821	O4 [$-x$, $-y+1$, $-z+1$]
O5–H5A	0.857	2.080	165.05	2.916	O4 [$-x+1$, $-y+1$, $-z+1$]
O5–H5B	0.857	1.993	172.69	2.846	O6 [$x+1$, y, z]
O6–H6A	0.859	1.842	167.72	2.687	O2 [$x-1/2$, $-y+3/2$, $z-1/2$]
O6–H6B	0.853	1.873	154.10	2.666	O2 [$-x+3/2$, $y-1/2$, $-z+1/2$]
O7–H7A	0.853	1.851	152.62	2.638	O4 [$x+1/2$, $-y+3/2$, $z-1/2$]
O7–H7B	0.858	1.928	169.08	2.775	O1 [$x-1$, y, z]
3					
O5–H5B	0.850	1.777	157.33	2.582	O2 [$x+1$, $y-1$, z]
O5–H5C	0.845	2.124	119.46	2.644	N2 [$-x+2$, $-y$, $-z+2$]
O6–H6B	0.858	2.369	115.57	2.847	O4 [x, $y-1$, z]
N1–H1A	0.919	1.865	176.10	2.783	O4 [$-x+2$, $-y+1$, $-z+1$]
4					
O5–H5B	0.850	1.780	157.13	2.584	O2 [$x+1$, $y-1$, z]
O5–H5C	0.850	2.146	118.01	2.653	N2 [$-x+2$, $-y$, $-z+2$]
O6–H6B	0.850	2.372	116.60	2.856	O4 [x, $y-1$, z]
N1–H1A	0.919	1.868	175.52	2.785	O4 [$-x+2$, $-y+1$, $-z+1$]

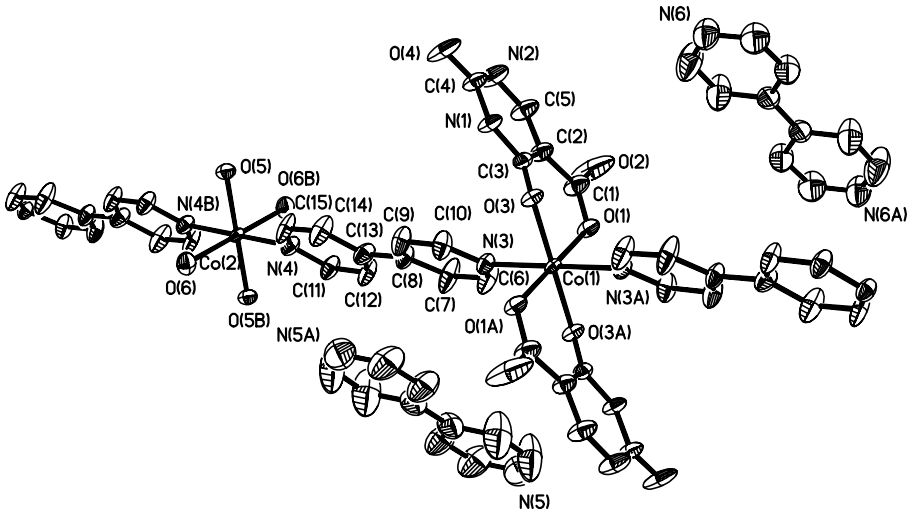

Fig. 3. The coordination environments of Co(II) ions in complex **3** with 50% thermal ellipsoids, all hydrogen atoms are omitted.

kind, with the two pyridine rings being coplanar, is free and does not take part in coordination.

As shown in Fig. 4, the octahedral Co(II) ions are bridged into 1D infinite chains by bipy, and the $Hiso^{2-}$ ligands stay up and down the chains. The uncoordinating carbonyl oxygen atoms and amido groups of $Hiso^{2-}$ ligands form hydrogen bonds with the aqua water molecules of the adjacent chain (O_w–H···O_c and O_w–H···N hydrogen bond), building a rhomboid-type 2D network. The rhomboid-grid dimensions are about 11.365 × 9.579 Å (see Fig. 4, 11.288 × 9.570 Å for Ni). Furthermore, the uncoordinating carboxylate oxygen atoms of $Hiso^{2-}$ ligands also form hydrogen bonds with the aqua water molecules of the adjacent chain (O_w–H···O_{uc}

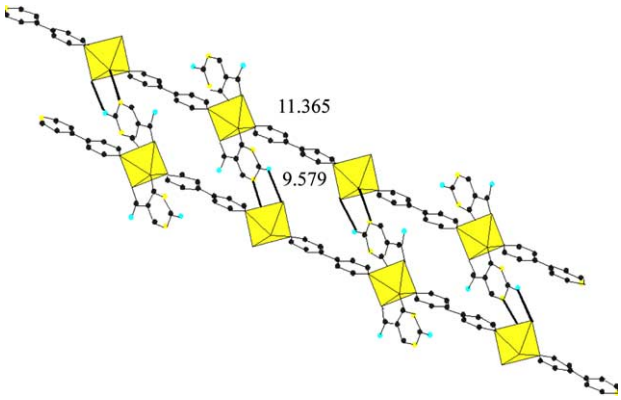

Fig. 4. Rhomboid-type 2D network of complex **3** viewed along the [1 1 0] direction. The thick line represents hydrogen bonds, and all hydrogen atoms are omitted for clarity.

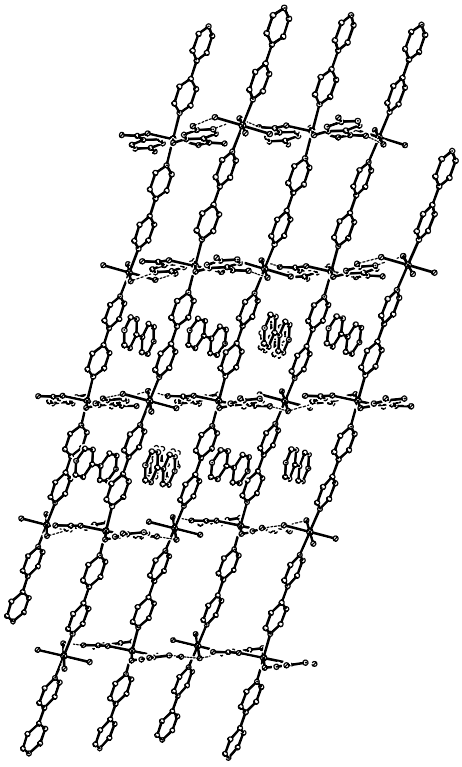

Fig. 5. 3D network of complex **3** viewed along the *a* axis, all hydrogen atoms are omitted for clarity.

hydrogen bonds), building a similar rhomboid-grid of 11.365 × 6.348 Å (11.288 × 6.345 Å for Ni). The 3D supramolecular structure of complex **3** is shown in Fig. 5. Free bipy molecules residue in the channels. The details of the hydrogen bonds are listed in Table 4.

Comparing the structures of **1** and **3**, several differences are noted: (1) In complex **1**, there is only one kind of metal environment, while in complex **3** there are two. The different coordination environments of Co(II) ions help to form the ordered packing. (2) In complex **1**, $Hiso^{2-}$ acts as a tridentate ligand, coordinating through the carboxylate group, carbonyl oxygen and deprotonated amido group; while in complex **3**, $Hiso^{2-}$ acts as a bidentate ligand, coordinating through the carboxylate group and carbonyl oxygen, but the amido group is left to form hydrogen bonds. (3) The channels in complex **3** are much larger than those in complex **1**. This must be attributed to the introduction of bipy, which acts as a bridging ligand to link the metal ions, leaving $Hiso^{2-}$ anions to form hydrogen bonds and resulting in the formation of large channels.

3.2. Thermal analyses

Thermogravimetric analyses of the four complexes were carried out to examine their thermal stabilities. The data for **1**–**4** are listed in Table 5. The complexes **1** and **2** lost their aqua ligands at the first weight loss, while **3** and **4** lost their free bipy molecules. Taking **1** and **3** as examples, the TGA curves show that the first weight loss of 18.7% from 206 to 258 °C corresponds to the loss of three aqua water molecules in complex **1** (calcd 18.8%) and the first weight loss of 28.1% from 131 to 219 °C corresponds to the loss of two free bipy molecules in complex **3** (calcd 27.8%). Increasing temperature led to further decomposition of **1** and **3** at 276 and 342 °C. The final pyrolysis was completed at 615 and 537 °C, respectively, giving CoO powder.

4. Supplementary data

Crystallographic data for the structural analyses have been deposited with the Cambridge Crystallographic Data Centre, CCDC Nos. 218806, 218807, 234940 and 234939 for **1**–**4**, respectively. Copies of this information may be obtained free of charge from the CCDC, 12 Union Road, Cambridge, CB2 1EZ, UK (fax: +44-1223-

Table 5
Thermogravimetric analyses data of **1**–**4**

	1	**2**	**3**	**4**
The first weight loss temperature (°C)	206–258	223–274	131–219	142–229
Loss of weight: Calc. (Found) (%)	18.8 (18.7)	20.6 (20.2)	28.1 (27.8)	28.0 (27.8)
Further decomposition temperature (°C)	276–615	318–440	342–537	350–520
The residue	CoO	NiO	CoO	NiO

336-033; e-mail: deposit@ccdc.cam.ac.uk or www: http://www.ccdc.cam.ac.uk).

Acknowledgement

This project is supported by the National Nature Science Foundation of China (20071004, 20331010).

References

[1] J.S. Miller, A.J. Epstein, Angew. Chem. Int. Ed. Engl. 33 (1994) 385.
[2] P.L. Fagan, M.D. Ward, Sci. Am. (1992) 28.
[3] M.S. Wong, C. Bosshard, P. Günter, Adv. Mater. 9 (1997) 837.
[4] K. Miyamura, A. Mihara, T. Fujii, Y. Gohshi, Y. Ishii, J. Am. Chem. Soc. 117 (1995) 2377.
[5] M. Munakata, L.P. Wu, T. Kuroda-Sowa, M. Maekawa, Y. Suenaga, K. Furuichi, J. Am. Chem. Soc. 118 (1996) 3305.
[6] P. Brunet, M. Simard, J.D. Wuest, J. Am. Chem. Soc. 119 (1997) 2737.
[7] J.A. Swift, A.M. Pivovar, A.M. Reynolds, M.D. Ward, J. Am. Chem. Soc. 120 (1998) 5887.
[8] T. Sawaki, T. Dewa, Y. Aiyama, J. Am. Chem. Soc. 120 (1998) 8539.
[9] A. Ranganathan, V.R. Pedireddi, C.N.R. Rao, J. Am. Chem. Soc. 121 (1999) 1752.
[10] O.M. Yaghi, H.L. Li, T.L. Groy, J. Am. Chem. Soc. 118 (1996) 9096.
[11] M. Munakata, L.P. Wu, M. Yamamoto, T. Kuroda-Sowa, M. Mackawa, J. Am. Chem. Soc. 118 (1996) 3117.
[12] F. Hueso-Ureña, M.N. Moreno-Carretero, M.A. Romero-Molina, J.M. Salas-Peregrin, M.P. Sanchez-Sanchez, G.A. de Cienfuegos-López, R. Faure, J. Inorg. Biochem. 51 (1993) 613.
[13] G. Maistralis, N. Katsaros, S.P. Perlepes, D. Kovala-Demertzi, Acta Crystallogr., Sect. C 47 (1991) 740.
[14] E.J. Baran, R.C. Mercader, F. Hueso-Ureña, M.N. Moreno-Carretero, M. Quiros-Olozabal, J.M. Salas-Peregin, Polyhedron 15 (1996) 1717.
[15] C.C. Wagner, E.J. Baran, O.E. Piro, J. Inorg. Biochem. 73 (1999) 259.
[16] F. Hueso-Ureña, M.N. Moreno-Carretero, M. Quiros-Olozabal, J.M. Salas-Peregin, R. Faure, G.A. de Cienfuegos-López, Inorg. Chim. Acta 241 (1996) 61.
[17] L. Pan, X. Huang, J. Li, Y. Wu, N. Zheng, Angew. Chem. Int. Ed. 39 (2000) 527.
[18] Y.C. Liang, R. Cao, W.P. Su, M.C. Hong, W.J. Zhang, Angew. Chem. Int. Ed. 39 (2000) 3304.
[19] R. Cao, D. Sun, Y. Liang, M. Hong, K. Tatsumi, Q. Shi, Inorg. Chem. 41 (2002) 2087.
[20] O.M. Yaghi, H. Li, T.L. Groy, J. Am. Chem. Soc. 118 (1996) 9096.
[21] G.M. Sheldrick, SADABS Program for Empirical Absorption Correction of Area Detector Data, University of Göttingen, Germany, 1997.
[22] G.M. Sheldrick, SHELXS-97, Program for Crystal Structure Solution, University of Göttingen, Germany, 1997.
[23] G.M. Sheldrick, SHELXL-97, Program for Crystal Structure Refinement, University of Göttingen, Germany, 1997.

Available online at www.sciencedirect.com
SCIENCE DIRECT®
Polyhedron 23 (2004) 2235–2242
POLYHEDRON
www.elsevier.com/locate/poly

MP2 studies of the bis(methoxycarbimido)amine ligand and its anion

Kateřina Brudíková [a], Martin Breza [b,*]

[a] Department of Physical and Applied Chemistry, Brno University of Technology, CZ-612 00 Brno, Czech Republic
[b] Department of Physical Chemistry, Slovak Technical University, Radlinskeho 9, SK-81237 Bratislava, Slovakia

Received 4 May 2004; accepted 29 June 2004
Available online 28 August 2004

Abstract

Various conformations of bis(methoxycarbimido)amine, $[HN{=}C(OCH_3)]_2NH$ (Hmici), and of it anion, $[HN{=}C(OCH_3)]_2N^-$ ($mici^-$), have been optimized at MP2 level of theory. Their electronic structures have been investigated in terms of Mulliken population analysis and topological analysis of electron density. The experimentally observed conformations are not the most stable ones and the determining role of the central atom for the geometry and electronic structure of Hmici and $mici^-$ complexes may be concluded. The preferential methoxy group positions may be explained by energy arguments of the free ligands. Shielding (especially by methoxy groups) should increase the electron density at the central H atom in Hmici.
© 2004 Elsevier Ltd. All rights reserved.

Keywords: MP2 geometry optimization; Bis(methoxycarbimido)amine; Topological analysis of electron density

1. Introduction

Transition metal compounds with dicyanamide (or dicyanimide) bridges exhibit interesting magnetic properties [1]. Dicyanamide anions, $[N(CN)_2]^-$, form both mono- and multinuclear complexes with various metals [2] but no compound of this type with its neutral form has been found in the Cambridge Structural Database (CSD) [3]. Neutral dicyanamide molecules exist in solutions only [2]. Depending on the reaction conditions, the hydrolysis of dicyanamide salts may result in various products. If not accounting for polymerisation products, it proceeds in several steps.

In the first hydration step, a cyanourea H_2N–CO–NH–CN is obtained. Only a single tetranuclear Ag complex of its anionic form [4] has been found in the CSD.

In the second step, a biuret H_2N–CO–NH–CO–NH_2 is formed. Only mononuclear complexes of its neutral form are known (such as $[Cu(biuret)_2]^{2+}$ [5], $[Co(biuret)_3]^{3+}$ [6] and $[Ni(biuret)_2]^{2+}$ [7]).

In methanolic solutions, the third solvation step may be observed [1]. It results in the formation of neutral bis(methoxycarbimido)amine, HN–$C(OCH_3)$–NH–$C(OCH_3)$–NH, (Hmici) or its anion, [HN–$C(OCH_3)$–N–$C(OCH_3)$–$NH]^-$, ($mici^-$). On the contrary to the previous compounds, mononuclear complexes of both forms are known.

$[Cu(mici)_2]$ has a square-planar structure (Fig. 1) [8,9]. An attempt to replace the central atom by its reaction with CoS in dimethylsulfoxide led to the formation of $[Co(mici)_3]$ [10] whereas FeS caused the formation of $[Fe(Hmici)_2(H_2O)(SO_4)] \cdot 2H_2O$ [11]. The same neutral ligand is bonded in bis(bis(methoxycarbimido)amine)-copper(II) tetrakis(biuret)dibromide methanol acetonitrile solvate [12] (Fig. 2). It is interesting that the methoxy groups in the planar anionic $mici^-$ (in the complexes with Cu(II) [8,9] and Co(III) [10]) and in the neutral Hmici ligand (in the complexes with Cu(II) [12] and

* Corresponding author. Tel.: +42 125 932 5482; fax: +42 125 249 3198.
E-mail addresses: k.brudikova@email.cz (K. Brudiková), breza@cvtstu.cvt.stuba.sk (M. Breza).

0277-5387/$ - see front matter © 2004 Elsevier Ltd. All rights reserved.
doi:10.1016/j.poly.2004.06.034

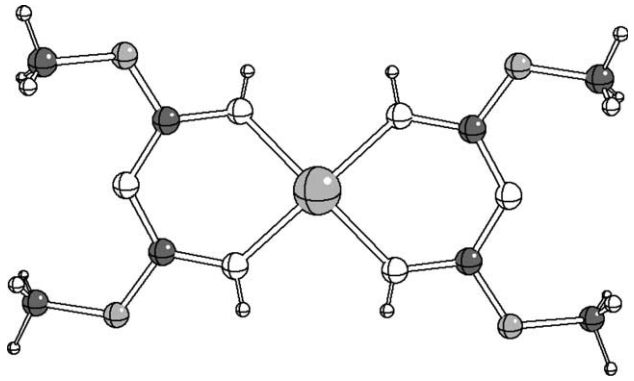

Fig. 1. Structure of $[Cu(mici)_2]$ [8,9].

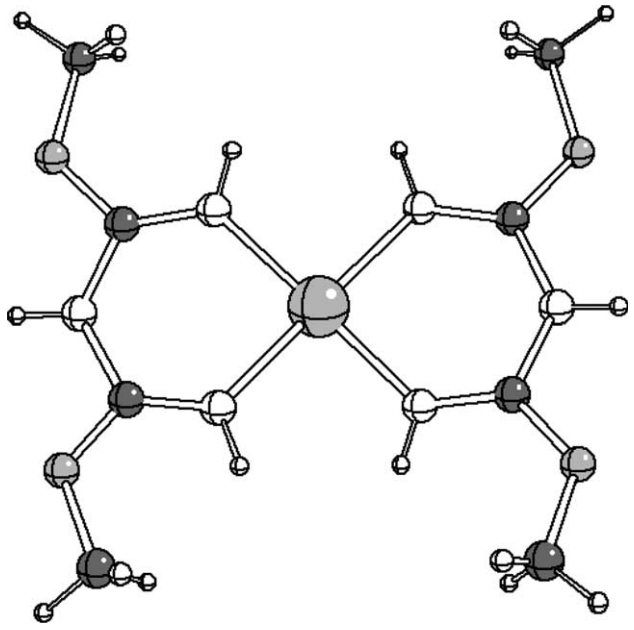

Fig. 2. Structure of $[Cu(Hmici)_2]^{2+}$ in bis(bis(methoxycarbimido)amine)copper(II) tetrakis(biuret)dibromide methanol acetonitrile solvate [12].

Fe(II) [11]) are in opposite positions (compare Figs. 1 and 2).

It is evident that the relative stability of transition metal complexes with Hmici and $mici^-$ ligands should depend on a delicate balance between intrinsic properties of the complex (such as electronic structure) and environmental influences of the solvent (such as pH). Experimental data on Hmici powder (confirmed by NMR measurements) obtained from a DMSO solution at various conditions indicate its existence in (at least) two forms, one of them sublimating at room temperature [13]. Unfortunately, no quantum-chemical studies on this type of molecule have been found in the literature. Very recently, a HF/6-31G* study [14] of substituted 1,3-diazabuta-1,3-dienes (such as HN=CR–N=CH–NH_2, R = H or NH_2) in various conformations has been published. Geometry optimizations confirmed the earlier observation that there is a delicate balance between π conjugative effects (forcing the molecule to planarity) and 1,4-steric repulsions, and this balance determines the conformational preferences in these systems. Under solvent conditions the electron delocalisations in these systems get reduced and the torsional angles in non-planar structures are larger than in the gas phase. π Donating substituents (at both carbons) increase the conjugation in the π frame of the diazadienes.

The aim of our study is to investigate mutual relations between geometry and electronic structure of $mici^-$ and Hmici ligands (the shielding by methoxy and imine groups, π-bond signification, etc.) within a suitable series of conformations. This might help to explain the reasons of preferential methoxy group positions as well as the role of transition metals in the solvation.

2. Method

Ab initio molecular MP2 orbital calculations were performed using the standard GAUSSIAN94 program package [15] with Dunning's correlation consistent cc-pVDZ basis sets [16]. The geometries of all the systems under study (Table 1) were optimized using the Berny algorithm [17] with standard accuracy. The electronic structure was evaluated in terms of Mulliken population analysis (gross atomic charges for atoms and overlap populations for bonds).

Using the AUG-cc-pVDZ basis set [16,18], a topological analysis of electron density [19] has been elaborated (AIM2000 program package [20]) and the results have been evaluated in terms of electron density ρ, density Laplacian L and bond ellipticity ε at bond critical points (BCP) as well as in terms of atomic volumes and atomic charges evaluated using the electron density integrated over atomic basins (up to the 0.001 e/$bohr^3$ level).

3. Results and discussion

Studied conformations of $mici^-$ (A1–A6 models, see Fig. 3) and Hmici (B1–B6 models, see Fig. 4) systems (for the atoms notation see Scheme 1) differ in N(2) (and H(2)) atom shielding by methoxy and imine groups. For the sake of simplicity, the equivalent atoms (with the same numbers – see Scheme 1) are symmetry related (by a mirror plane or C_2 symmetry axis) in the starting conformations and full geometry optimizations started from planar structures. The optimized geometries are presented in Figs. 3 and 4 and Tables 1 and 2. According to our results all systems are planar except A4 and B4 ones. Non-planar A4 and B4 systems contain two planar subsystems with torsion angles of ca. 70° about the central N(2)–C(1) bond. This indicates significant π character of C–N and C–O bonds. The C(1)–N(2), C(1)–O and N(1)–H(1) bonds are longer than their

Table 1
Bond lengths (10^{-10} m) in the systems under study

System	A1	A2	A3	A4	A5	A6	B1	B2	B3	B4	B5	B6
N(1)–C(1)	1.305	1.301	1.310/1.309	1.296/1.314	1.311	1.311	1.278	1.275	1.287/1.281	1.281/1.280	1.287	1.287
C(1)–N(2)	1.349	1.354	1.350/1.346	1.372/1.337	1.344	1.354	1.389	1.398	1.392/1.387	1.423/1.407	1.391	1.404
C(1)–O	1.434	1.423	1.413/1.435	1.405/1.413	1.426	1.392	1.380	1.383	1.352/1.378	1.349/1.365	1.357	1.341
O–C(Met)	1.400	1.411	1.400/1.402	1.414/1.421	1.402	1.413	1.422	1.420	1.422/1.424	1.431/1.434	1.424	1.434
N(1)–H(1)	1.026	1.033	1.025/1.024	1.030/1.033	1.023	1.028	1.024	1.029	1.024/1.023	1.028/1.029	1.022	1.025
N(2)–H(2)	–	–	–	–	–	–	1.013	1.007	1.015	1.021	1.016	1.014

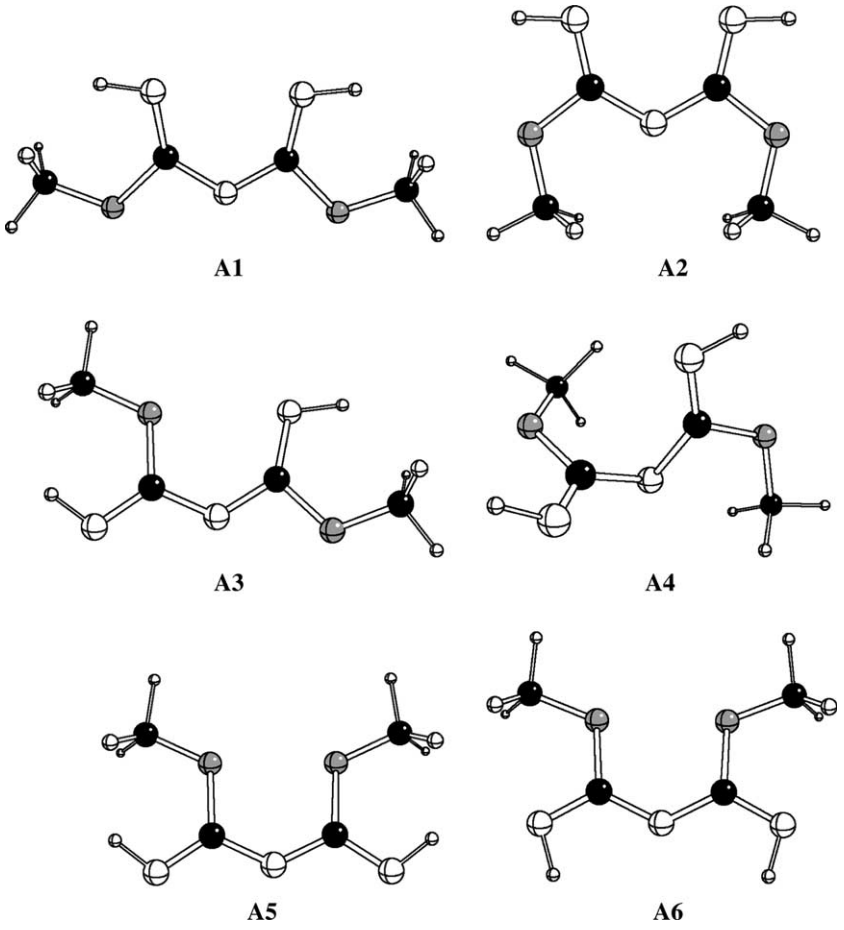

Fig. 3. Investigated conformations of the anionic form of bis(methoxycarbimido)amine, HN=C(OCH$_3$)–N–C(OCH$_3$)=NH$^-$ (mici$^-$).

C(1)–N(1), C(Met)–O and N(2)–H(2) counterparts, respectively. The longer C–N and C–O bonds are shortened and the shorter ones lengthened (i.e., the bonds length alternation is lower) in mici$^-$ in comparison with Hmici. The geometries of our systems are significantly influenced by mechanical strain due to non-bonding interatomic interactions. The flexibility of C(1) atoms is higher than of N(2) ones, as may be deduced from N(1)–C(1)–N(2) and C(1)–N(2)–C(1′) bond angles (their deviations from 120°), respectively. The same data indicate that the interatomic repulsion decreases in the order O–O′ > O–N(1′) > N(1)–N(1′) for the planar structures. C(1)–O–C(Met) bond angles in mici$^-$ are nearly constant whereas in Hmici they are influenced by the interaction of the methyl group with H(1) or H(2) atoms.

Energy data (Table 3) exhibit the lowest values for A6 and B6 systems. The differences in zero-point energy (ZPE) corrections are one order lower than in MP2 energies and cannot cause any changes in the relative stability of the systems under study. Nevertheless, only planar A1/B1 and non-planar A4/B4 geometries have not any imaginary frequencies and may be ascribed to energy minima. The remaining ones should decrease in energy on account of their planarity.

According to our results, the geometries A1 and B2 observed in experimental structures are not the most

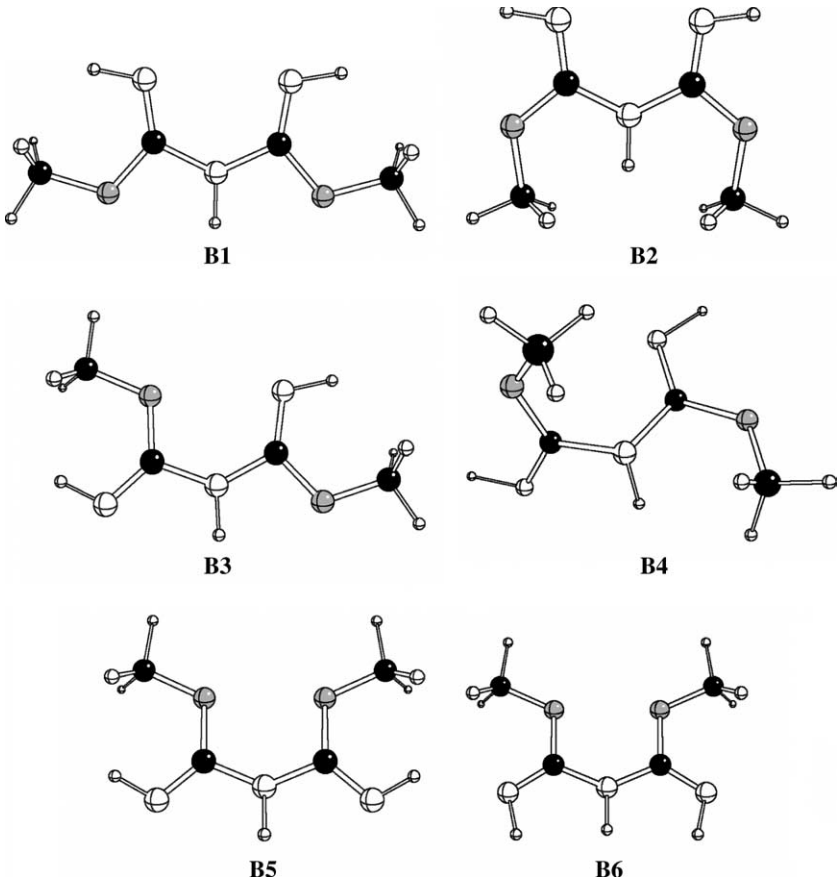

Fig. 4. Investigated conformations of the neutral bis(methoxycarbimido)amine, HN=C(OCH$_3$)–NH–C(OCH$_3$)=NH (Hmici).

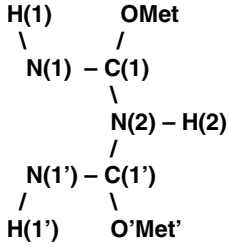

Scheme 1. Schematic description of neutral bis(methoxycarbimido)-amine.

stable ones. It implies a determining role of the central atom for the geometry and electronic structure of our ligands.

Electronic structural characteristics are usually described in terms of Mulliken population analysis (MPA). However, MPA results for our systems using the aug-cc-pVDZ basis are evidently incorrect (negative bond orders, negative H charges) and so cc-pVDZ data are presented. Nevertheless, the trends in MPA data (gross atomic charges and overlap populations) and in

Table 2
Selected bond and dihedral angles (°) in the systems under study

System	A1	A2	A3	A4	A5	A6	B1	B2	B3	B4	B5	B6
N(1)–C(1)–N(2)	131.9	132.3	121.4/133.1	124.2/130.1	121.2	124.9	124.8	124.3	117.6/125.4	117.9/122.3	117.5	125.2
C(1)–N(2)–C(1′)	120.1	120.7	123.8	118.1	128.7	127.2	128.9	127.0	131.5	119.2	134.6	133.8
N(2)–C(1)–O	105.5	112.0	116.0/105.1	118.9/113.7	117.0	118.9	105.4	114.1	112.0/105.3	118.1/114.8	112.7	112.8
C(1)–O–C(Met)	116.0	116.6	116.4/116.3	116.5/115.4	116.3	114.0	115.2	120.7	115.1/115.4	118.8/118.7	114.9	113.8
C(1)–N(1)–H(1)	108.5	104.0	108.4/108.6	105.3/104.8	108.8	103.1	109.4	106.1	110.4/109.3	107.5/107.4	110.5	109.9
C(1)–N(2)–H(1)	–	–	–	–	–	–	115.5	116.5	113.0/115.6	106.7/112.0	112.7	113.1
N(1)–C(1)–N(2)–C(1′)	0.0	0.0	0.0/180.0	2.2/114.5	180.0	180.0	0.0	0.0	0.0/180.0	12.1/116.1	180.0	180.0
O–C(1)–N(2)–C(1′)	180.0	180.0	0.0/180.0	72.8/177.8	0.0	0.0	180.0	180.0	0.0/180.0	67.9/168.9	0.1	0.0
C(Met)–O–C(1)–N(2)	180.0	0.0	180.0	175.4/3.5	180.0	180.0	180.0	0.0	180.0	16.9/15.4	180.0	180.0
H(1)–N(1)–C(1)–N(2)	180.0	180.0	180.0	173.3/177.6	180.0/0.0	0.0	180.0	180.0	180.0	172.3 174.9	180.0	0.0
O–C(1)–N(2)–H(2)	–	–	–	–	–	–	0.0	0.0	180.0/0.0	164.1/43.3	180.0	180.0

Table 3
MP2 energies related to the B6 ones (ΔE), zero-point energy corrections (ZPE) and numbers of imaginary frequencies (N_{imag}) of the systems under study

	ΔE (hartree)	ZPE (hartree)	N_{imag}	ΔE (hartree)
Basis	cc-pVDZ	cc-pVDZ	cc-pVDZ	aug-cc-pVDZ
A1	0.59834	0.13248	0	0.57463
A2	0.58266	0.13291	1	0.56095
A3	0.60022	0.13265	1	0.57599
A4	0.58049	0.13355	0	0.55756
A5	0.60455	0.13265	1	0.58015
A6	0.57527	0.13408	1	0.55398
B1	0.00252	0.14724	0	0.00322
B2	0.02310	0.14598	2	0.02273
B3	0.00068	0.14766	1	0.00123
B4	0.00589	0.14803	0	0.00708
B5	0.00131	0.14780	2	0.00192
B6	0.00000	0.14762	2	0.00000

Table 4
Mulliken population analysis of the systems under study

System	A1	A2	A3	A4	A5	A6	B1	B2	B3	B4	B5	B6
Atomic charges												
N(1)	−0.29	−0.30	−0.32/−0.32	−0.36/−0.31	−0.32	−0.37	−0.21	−0.201	−0.23/−0.27	−0.24	−0.27	−0.28
N(2)	−0.39	−0.49	−0.38	−0.44	−0.36	−0.44	−0.24	−0.275	−0.23	−0.27	−0.22	−0.26
C(1)	0.18	0.25	0.20/0.18	0.25/0.23	0.19	0.23	0.27	0.295	0.27	0.27	0.27	0.30
C(Met)	0.10	0.14	0.10	0.13/0.11	0.10	0.13	0.07	0.062	0.07	0.07/0.08	0.07	0.10
O	−0.33	−0.38	−0.33/−0.30	−0.37/−0.36	−0.33	−0.32	−0.33	−0.332	−0.32/−0.26	−0.32/−0.30	−0.28	−0.28
H(1)	0.03	0.04	0.03	0.04/0.05	0.03	0.04	0.09	0.100	0.09	0.10	0.09	0.08
H(2)	–	–	–	–	–	–	0.13	0.100	0.13	0.14	0.14	0.11
Overlap populations												
N(1)–C(1)	0.61	0.66	0.64/0.60	0.68/0.62	0.63	0.61	0.66	0.700	0.67/0.65	0.70/0.67	0.67	0.65
C(1)–N(2)	0.50	0.44	0.49/0.50	0.40/0.47	0.49	0.49	0.35	0.318	0.35	0.29/0.32	0.35	0.35
C(1)–O	0.34	0.31	0.34	0.33/0.33	0.32	0.31	0.38	0.348	0.39	0.37	0.38	0.37
O–C(Met)	0.32	0.32	0.32/0.33	0.32/0.30	0.33	0.32	0.30	0.303	0.30	0.29	0.30	0.30
N(1)–H(1)	0.34	0.32	0.36/0.35	0.33/0.33	0.36	0.34	0.35	0.337	0.37/0.36	0.35/0.34	0.37	0.35
N(2)–H(2)	–	–	–	–	–	–	0.35	0.370	0.35	0.33	0.35	0.35

Table 5
Atomic charges and volumes in terms of topological analysis of electron density in the systems under study

System	A1	A2	A3	A4	A5	A6	B1	B2	B3	B4	B5	B6
Charges												
N(1)	−1.13	−1.10	−1.14	−1.17/−1.13	−1.13	−1.17	−1.10	−1.06	−1.11/−1.12	−1.13/−1.12	−1.12	−1.12
N(2)	−1.15	−1.22	−1.16	−1.21	−1.18	−1.21	−1.26	−1.26	−1.25	−1.19	−1.25	−1.22
C(1)	1.55	1.57	1.59/1.55	1.61/1.57	1.58	1.60	1.71	1.70	1.74/1.71	1.72/1.69	1.73	1.74
C(Met)	0.64	0.65	0.65/0.64	0.62/0.57	0.64	0.63	0.57	0.58	0.58/0.57	0.56/0.54	0.57	0.55
O	−1.03	−1.06	−1.02/−1.03	−1.06/−1.05	−1.02	−1.05	−1.06	−1.05	−1.06/−1.06	−1.06/−1.07	−1.06	−1.07
H(1)	0.35	0.36	0.37/0.36	0.36/0.37	0.34	0.38	0.40	0.42	0.40/0.41	0.43	0.42	0.40
H(2)	–	–	–	–	–	–	0.50	0.46	0.50	0.47	0.51	0.46
Volumes (bohr^3)												
N(1)	147.	148.	146./154.	148./152.	153.	148.	138.	136.	137./144.	134./144.	144.	139.
N(2)	125.	110.	126.	115.	127.	130.	98.	97.	98.	92.	99.	100.
C(1)	40.	39.	39.	37.	39.	38.	36.	37.	35./36.	35./36.	35.	35.
C(Met)	54.	55.	54./55.	56./58.	54.	56.	57.	56.	57.	57./58.	57.	58.
O	105.	106.	105./99.	106./105.	98.	99.	102.	102.	101./97.	103./101.	96.	96.
H(1)	30.	35.	30.	35./34.	30.	34.	29.	31.	29./29.	31.	29.	32.
H(2)	–	–	–	–	–	–	26.	20.	26.	27.	26.	28.

Table 6
Electron density ρ_{BCP}, its Laplacian L_{BCP} and bond ellipticity ε_{BCP} at bond critical points in the systems under study

System	A1	A2	A3	A4	A5	A6	B1	B2	B3	B4	B5	B6
ρ_{BCP} (*e/bohr*^{3})												
N(1)–C(1)	0.367	0.374	0.365/0.364	0.377/0.364	0.365	0.368	0.388	0.394	0.383/0.387	0.389/0.390	0.383	0.384
C(1)–N(2)	0.338	0.332	0.335/0.338	0.322/0.339	0.335	0.329	0.302	0.293	0.300/0.303	0.286/0.296	0.300	0.290
C(1)–O	0.241	0.247	0.252/0.241	0.258/0.253	0.245	0.266	0.277	0.272	0.295/0.278	0.294/0.283	0.291	0.304
O–C(Met)	0.263	0.252	0.263/0.260	0.250/0.244	0.260	0.251	0.240	0.243	0.240/0.239	0.235/0.230	0.239	0.231
N(1)–H(1)	0.322	0.316	0.324/0.322	0.317	0.324	0.321	0.322	0.319	0.323/0.322	0.320/0.319	0.323	0.321
N(2)–H(2)	–	–	–	–	–	–	0.332	0.338	0.331	0.327	0.330	0.333
L_{BCP} (*e/bohr*^{5})												
N(1)–C(1)	−1.312	−1.357	−1.321/−1.291	−1.395/−1.269	−1.312	−1.326	−1.418	−1.473	−1.409/−1.421	−1.414/−1.442	−1.411	−1.414
C(1)–N(2)	−1.118	−1.095	−1.118/−1.122	−1.011/−1.143	−1.130	−1.064	−0.986	−0.916	−0.976/−0.986	−0.857/−0.907	−0.971	−0.888
C(1)–O	−0.454	−0.475	−0.496/−0.457	−0.516/−0.495	−0.470	−0.522	−0.575	−0.545	−0.554/−0.580	−0.516/−0.536	−1.406	−0.559
O–C(Met)	−0.532	−0.468	−0.534/−0.510	−0.451/−0.404	−0.517	−0.452	−0.346	−0.388	−0.345/−0.344	−0/345/−0.296	−0.348	−0.293
N(1)–H(1)	−1.373	−1.353	−1.384/−1.375	−1.364/−1.352	−1.385	−1.388	−1.409	−1.399	−1.418/−1.409	−1.413/−1.408	−1.419	−1.403
N(2)–H(2)	–	–	–	–	–	–	−1.542	−1.550	−1.545	−1.429	−1.547	−1.521
ε_{BCP}												
N(1)–C(1)	0.257	0.281	0.269/0.250	0.299/0.256	0.274	0.258	0.312	0.344	0.295/0.305	0.341/0.328	0.298	0.290
C(1)–N(2)	0.160	0.144	0.159/0.163	0.056/0.206	0.166	0.150	0.174	0.169	0.163/0.177	0.102/0.142	0.173	0.142
C(1)–O	0.019	0.016	0.005/0.021	0.035/0.141	0.011	0.015	0.051	0.063	0.056/0.048	0.073/0.060	0.054	0.086
O–C(Met)	0.014	0.022	0.013/0.010	0.028/0.044	0.013	0.027	0.001	0.016	0.003	0.011/0.025	0.000	0.110
N(1)–H(1)	0.001	0.001	0.005/0.004	0.002/0.010	0.006	0.002	0.007	0.010	0.001/0.005	0.007/0.006	0.001	0.004
N(2)–H(2)	–	–	–	–	–	–	0.048	0.048	0.046	0.038	0.045	0.051

the corresponding characteristics of topological analysis of electron density (atomic charges and BCP electron density, ρ_{BCP}) within the aug-cc-pVDZ basis may be different (Tables 4–6).

Our results (Tables 4 and 5) indicate that N(2) are more negative than N(1) atoms whereas H(2) and C(1) are more positive than H(1) and C(Met) atoms (in agreement with the observed H(2) dissociation), respectively. In anionic systems, the electron density at N(1), N(2), O and C(1) atoms increases but decreases at C(Met) atoms in comparison with neutral molecules. Shielding (especially by methoxy groups) should increase H(2) electron density. As expected, volumes of atomic basins exhibit reverse trends (higher electron densities correspond to lower atomic volumes). Significant changes in atomic volumes of N(2) in mici$^-$ and H(2) in Hmici are not caused by mechanical strain but by space restrictions of the shielding methoxy groups (compare N(2) in mici$^-$ – see Table 5). The changes in H(1) volumes may be explained analogously. On the other hand, mechanical strain explains the (smaller) changes in C(1) volumes.

As indicated by overlap populations as well as by ρ_{BCP} values (Tables 4 and 6), N(1)–C(1) bonds are stronger than C(1)–N(2) ones in all systems. C(1)–O bonds are stronger than O–C(Met) ones in neutral Hmici molecules. In anionic mici$^-$, C(1)–N(2) and O–C(Met) bonds are stronger whereas N(1)–C(1) and C(1)–O ones are weaker than in neutral Hmici. These trends are in agreement with the bond lengths (Table 1) and Laplacian BCP electron densities (Table 6, longer bond lengths correspond to weaker bonds and a less negative Laplacian). Nevertheless, analogous C–O and N–H bond length trends have been confirmed by the above electronic characteristics in neutral Hmici molecules only.

Ellipticity ε data (Table 6) confirm the π character of all C–N bonds whereas the remaining ones correspond to typical σ bonds. Ellipticity of N(1)–C(1) bonds is significantly higher than of C(1)–N(2) ones. In neutral Hmici molecules, a non-vanishing π contribution to C(1)–O bonds may be observed. Ellipticities in mici$^-$ are lower (especially in N(1)–C(1) bonds) than in neutral Hmici molecules (except non-planar structures) in agreement with lower bond length alternations in mici$^-$.

4. Conclusions

Finally it may be concluded that mici$^-$ and Hmici are typical examples of the failure of traditional MPA treatment to electronic structure investigations using basis sets with polarization and diffusion functions. Higher flexibility of C(1) atoms than of the central N(2) ones reflects the unusual electron structure of our ligands (especially mici$^-$). Shielding the central H(2) atom in Hmici causes its protection against splitting not only sterically, but also by increasing its electron density (less positive H(2) charge). Comparison of our results with experimental structural data on transition metal complexes shows that preferential methoxy group positions may be explained by energy arguments of the free ligands, but their formation should be conditioned by complexation with transition metals (in agreement with [1]). In further studies, solvent influences are to be considered. Quantum-chemical studies on individual solvation stages as well as on transition metal complexes of these ligands are in progress.

Acknowledgements

The work reported in this paper has been funded by the Slovak Grant Agency (Project No. 1/0052/03). IBM Slovakia Ltd. is acknowledged for computing facilities. We thank Professor I. Mayer (Hungarian Academy of Science, Budapest, Hungary) and Professor J. Kožíšek (STU Bratislava, Slovakia) for valuable comments and discussions.

References

[1] J. Kohout, L. Jäger, M. Hvastijová, J. Kožíšek, J. Coord. Chem. 51 (2000) 169.
[2] D. Koschel (Ed.), Gmelins Handbuch der anorganischen Chemie. 8. Auflage. 14. Kohlenstoff. Teil D1. Kohlenstoff-Stickstoff-Verbindungen, Verlag Chemie GmbH, Weinheim, Germany, 1971, p. 295.
[3] F.H. Allen, Acta Crystallogr. B 58 (2002) 380.
[4] D. Britton, Acta Crystallogr. C 43 (1987) 2442.
[5] A. Pajunen, S. Pajunen, Acta Crystallogr. B 38 (1982) 1586.
[6] P.J.M.W.L. Birker, J.M.M. Smits, J.J. Bour, P.T. Beurskens, Rec. Trav. Chim. Pays.-Bas. (Rec. J. R. Neth. Chem. Soc.) 92 (1973) 1240.
[7] A. Pajunen, S. Pajunen, Acta Crystallogr. C 50 (1994) 1884.
[8] J. Kožíšek, M. Hvastijová, J. Kohout, Inorg. Chim. Acta (L) 168 (1990) 157.
[9] R. Boča, M. Hvastijová, J. Kožíšek, M. Valko, Inorg. Chem. 35 (1996) 4794.
[10] R. Boča, M. Hvastijová, J. Kožíšek, J. Chem. Soc., Dalton Trans. (1995) 1921.
[11] M. Fronc, J. Kožíšek, M. Breza, M. Hvastijová, I. Svoboda, M.T. Duarte, in: K. Stadnicka, W. Nitek (Eds.), Crystallography in Natural Sciences and Technology, EJB Publishers, Krakow, Poland, 2001, p. 167.
[12] M.M. Bishop, L.F. Lindoy, S. Mahadev, P. Turner, J. Chem. Soc., Dalton Trans. (2000) 233.
[13] J. Kožíšek, unpublished results.
[14] R.S. Kumar, A. Marwaha, P.V. Bharatam, M.P. Mahajan, J. Mol. Struct. (Theochem.) 640 (2003) 1.
[15] M.J. Frisch, G.W. Trucks, H.B. Schlegel, P.M.W. Gill, B.G. Johnson, M.A. Robb, J.R. Cheeseman, T.A. Keith, G.A. Petersson, J.A. Montgomery, K. Raghavachari, M.A. Al-Laham, V.G. Zakrzewski, J.V. Ortiz, J.B. Foresman, J. Cioslowski, B.B. Stefanov, A. Nanayakkara, M. Challacombe, C.Y. Peng, P.Y. Ayala, W. Chen, M.W. Wong, J.L. Andres, E.S. Replogle, R. Gomperts, R.L. Martin, D.J. Fox, J.S. Binkley, D.J. Defrees, J. Baker, J.P. Stewart, M. Head-Gordon, C. Gonzales, J.A. Pople, GAUSSIAN94 (Revision D.1), Gaussian Inc., Pittsburgh, PA, 1995.

[16] T.H. Dunning Jr., J. Chem. Phys. 90 (1989) 1007.
[17] C. Peng, P.Y. Ayala, H.B. Schlegel, M.J. Frisch, J. Comp. Chem. 17 (1996) 49.
[18] R.A. Kendall, T.H. Dunning Jr., J. Harrison, J. Chem. Phys. 96 (1992) 6796.
[19] R.F.W. Bader, Atoms in Molecules: A Quantum Theory, Clarendon Press, Oxford, 1990.
[20] (a) F. Biegler-König, J. Schönbohm, D. Bayles, J. Comp. Chem. 22 (2001) 545;
(b) http://www.aim2000.de/ .

Available online at www.sciencedirect.com
SCIENCE DIRECT®
Polyhedron 23 (2004) 2243–2252
POLYHEDRON
www.elsevier.com/locate/poly

Synthesis and crystal structure of complexes of bipodal thiophosphorylated thioureas with divalent transition metals

Nail G. Zabirov [a,*], Vasiliy V. Brusko [a], Alexander Y. Verat [a,1], Dmitry B. Krivolapov [b], Igor A. Litvinov [b], Rafael A. Cherkasov [a]

[a] Department of Chemistry, Kazan State University, Kremlevskaya Street 18, 420008, Kazan, Russia
[b] Arbusov Institute of Organic and Physical Chemistry, Arbuzov St. 8, 420088, Kazan, Russia

Received 7 November 2003; accepted 1 July 2004
Available online 28 August 2004

Abstract

New complexes of bipodal thiophosphorylated thioureas $\{[(i\mathrm{PrO})_2\mathrm{P(S)NC(S)NH}]_2\mathrm{Z}\}\mathrm{M}$, where Z = *m*-$C_6H_4$, *p*-$C_6H_4$, M = Co, Ni, Zn, Cd have been prepared and characterized. The crystal and molecular structures of Cd(II), Z = CH_2CH_2 and Pd(II), Z = $(CH_2CH_2)_2O$ complexes have been determined by single crystal X-ray diffraction analyses. Both complexes are binuclear in the solid state with a M_2L_2 stoichiometry. The cadmium and palladium atoms are four-coordinated and have the configuration of a slightly distorted tetrahedron for cadmium and a distorted square plane for palladium. Metal-containing macrocycles are formed as well as two spirocycles.
© 2004 Elsevier Ltd. All rights reserved.

Keywords: *P*,*S*-metallocycles; Supramolecular chemistry; Bipodal ligands; Crystal structures; Macrocycles; Phosphorylated urea complexes

1. Introduction

We have recently reported the syntheses and complexing properties of bipodal thiophosphorylated thioureas $[(i\mathrm{PrO})_2\mathrm{P(S)NHC(S)NH}]_2\mathrm{Z}$, where Z = $(CH_2)_2$, $(CH_2)_7$, $(CH_2)_2O(CH_2)_2$, $(CH_2)_2O(CH_2)_2O(CH_2)_2$, and some properties of the chelate complexes formed by these ligands with a series of metal ions [1,2].

In this paper, we report on the synthesis of the bis-urea $[(i\mathrm{PrO})_2\mathrm{P(S)NHC(S)NH}]_2\mathrm{Z}$ complexes with Co(II), Ni(II), Zn(II) and Cd(II) (Z = *m*-C_6H_4, *p*-C_6H_4), together with the X-ray study of the bis-urea $[(i\mathrm{PrO})_2\mathrm{P(S)NHC(S)NHCH_2}]_2$ and the complexes with the cadmium(II) ion (**1**) (Z = CH_2CH_2) and the palladium(II) ion (**2**) (Z = $(CH_2CH_2)_2O$).

* Corresponding author. Tel./fax: +7 8432 543734.
E-mail addresses: zabirov@mi.ru (N.G. Zabirov), averat@mail.ru (A.Y. Verat).
[1] Tel.: +7 8432 607654; fax: +7 8432 543734.

0277-5387/$ - see front matter © 2004 Elsevier Ltd. All rights reserved.
doi:10.1016/j.poly.2004.07.005

2. Experimental

2.1. Synthesis of $[(iPrO)_2P(S)NHC(S)NH]_2$-*m*-C_6H_4 (**3**)

A solution of *m*-phenylenediamine (2.163 g, 0.02 mol) in anhydrous benzene (50 ml) was added dropwise under stirring to a benzene solution (25 ml) of diisopropylthiophosphoryl isothiocyanate (9.572 g, 0.04 mol). The mixture was heated to 60 °C and stirred for 2 h. The solvent was removed in vacuum. A colourless precipitate was crystallized from benzene. Yield: 8.33 g (~71%), m.p. 122 °C. *Anal.* Calc. for $C_{20}H_{36}N_4O_4P_2S_4$: C, 40.95; H, 6.14; P, 10.58. Found: C, 41.58; H, 6.25; P, 10.30%. ^{1}H NMR (C_6D_6) 1.33 (d, 24H, CH_3, $^3J_{HH}$ 6.1 Hz), 4.78 (d, sept, 4H, OCH, $^3J_{HH}$ 6.3 Hz, $^3J_{POCH}$ 10.7 Hz), 6.86 (d, 2H, NHP(S), $^2J_{PH}$ 9.8 Hz), 7.24 (t, 1H, *m*-C_6H_4, $^3J_{HH}$ 8.2 Hz), 7.46 (d. d, 2H, *m*-C_6H_4, $^3J_{HH}$ 7.8 Hz, $^4J_{HH}$ 1.9 Hz), 8.14 (m, 1H, *m*-C_6H_4), 9.68 (s, 2H, C_6H_4NH). $^{31}P\{^1H\}$ NMR (ppm), 53.5. IR (cm^{-1}):

3430(s) (NH), 3190(br, s) (NH), 1550(s) (S═C─N), 1315(m) (C═S), 1000(vs) (POC), 980(vs) (POC), 655(m) (P═S).

2.2. Synthesis of [(iPrO)$_2$P(S)NHC(S)NH]$_2$-p-C$_6$H$_4$ (4)

A solution of diisopropylthiophosphoryl isothiocyanate (9.572 g, 0.04 mol) in anhydrous benzene (25 ml) was added dropwise under stirring to a solution of *p*-phenylenediamine (2.163 g, 0.02 mol) in 50 ml of benzene heated to 60 °C. The mixture was refluxed with stirring for 3 h. *n*-Hexane (30 ml) was added, the mixture cooled down to 0 °C and then a white solid precipitated. The precipitate was crystallized twice from benzene. Yield: 8.8 g (~75%), m.p. 139 °C. *Anal*. Calc. for $C_{20}H_{36}N_4O_4P_2S_4$: C, 40.95; H, 6.14; P, 10.58. Found: C, 41.09; H, 6.25; P, 10.18%. ^{1}H NMR (C_6D_6) 1.22 (d, 12H, CH_3, $^3J_{HH}$ 6.0 Hz), 1.25 (d, 12H, CH_3, $^3J_{HH}$ 6.4 Hz), 4.90 (d, sept, 4H, OCH, $^3J_{HH}$ 6.2 Hz, $^3J_{POCH}$ 10.6 Hz), 6.50 (d, 2H, NHP(S), $^2J_{PH}$ 8.4 Hz), 7.83 (s, 4H, C_6H_4), 10.19 (s, 2H, C_6H_4*NH*). ^{31}P{^{1}H} NMR (ppm), 53.28. IR (cm^{-1}): 3360(s) (NH), 3110(s) (NH), 1565(s) (S═C─N), 1335(m) (C═S), 980(vs) (POC), 655(m) (P═S).

2.3. Synthesis of [(iPrO)$_2$P(S)NHC(S)NHCH$_2$]$_2$ (5)

The compound was prepared as described above for **3** from ethylenediamine (1.202 g, 0.02 mol, as an acetonitrile solution, 15 ml) and diisopropylthiophosphoryl isothiocyanate (9.572 g, 0.04 mol) in benzene (25 ml) to give 7.54 g (~70%, after crystallization from benzene) of **5** as colourless crystals. M.p. 111 °C. *Anal*. Calc. for $C_{16}H_{36}N_4O_4P_2S_4$: C, 35.67; H, 6.74; P, 11.50. Found: C, 35.64; H, 6.67; P, 11.09%. ^{1}H NMR (C_6D_6) 1.404 (d, 12H, CH_3, $^3J_{HH}$ 6.2 Hz), 1.409 (d, 12H, CH_3, $^3J_{HH}$ 6.3 Hz), 3.97 (m, 4H, CH_2CH_2), 4.88 (d. sept, 4H, OCH, $^3J_{HH}$ 6.3 Hz, $^3J_{POCH}$ 10.4 Hz), 7.53 (d, 2H, NHP(S), $^2J_{PH}$ 8.3 Hz), 8.35 (br. s, 2H, CH_2*NH*). ^{31}P{^{1}H} NMR (ppm), 51.46. IR (cm^{-1}): 3440(s) (NH), 1560(s) (S═C─N), 1315(m) (C═S), 1010(vs) (POC), 640(m) (P═S).

2.4. Synthesis of {[(iPrO)$_2$P(S)NC(S)NH]$_2$-m-C$_6$H$_4$Co} (6)

A suspension of **3** (1.173 g, 2 mmol) in anhydrous ethanol (20 ml) was mixed with an ethanol solution of potassium hydroxide (0.224 g, 4 mmol). To the resulting potassium salt, a water (20 ml) solution of $Co(NO_3)_2 \cdot 6H_2O$ (0.579 g, 2.2 mmol) was added dropwise with vigorous stirring. The mixture was stirred at room temperature for a further 3 h and left overnight. The resulting complex was extracted with methylene chloride, washed with water and dried over $MgSO_4$. Then the solvent was removed in vacuum. A green precipitate was precipitated from methylene chloride by *n*-hexane. Yield: ~41%, m.p. 156 °C. *Anal*. Calc. for $C_{20}H_{34}CoN_4O_4P_2S_4$: C, 37.29; H, 5.28; P, 9.63; Co, 9.15. Found: C, 37.67; H, 5.72; P, 9.32; Co, 8.86%. ^{31}P{^{1}H} NMR (acetone; ppm; width at half height, Hz; integral intensity, %), 56.46 (58 Hz, 64.6%), 58.632 (79 Hz, 35.4%). IR (cm^{-1}): 3350(s) (NH), 1550(s) (SCN), 970(br, vs) (POC), 560, 580 (m) (P═S).

2.5. Synthesis of {[(iPrO)$_2$P(S)NC(S)NH]$_2$-m-C$_6$H$_4$Ni} (7)

This was prepared similarly to compound **6** by using $Ni(NO_3)_2 \cdot 6H_2O$. Yield: ~45%, m.p. 140 °C. *Anal*. Calc. for $C_{20}H_{34}N_4NiO_4P_2S_4$: C, 37.30; H, 5.28; P, 9.63; Ni, 9.12. Found: C, 37.22; H, 5.68; P, 9.98; Ni, 9.95%. ^{31}P{^{1}H} NMR (CH_2Cl_2; ppm; width at half height, Hz; integral intensity, %), 51.20 (187 Hz, 51.3%), 53.05 (58 Hz, 36.6%), 54.40 (90 Hz, 12.1%). IR (cm^{-1}): 3345(s) (NH), 1545(s) (SCN), 975(br, vs) (POC), 573, 589(m) (P═S).

2.6. Synthesis of {[(iPrO)$_2$P(S)NC(S)NH]$_2$-m-C$_6$H$_4$Zn} (8)

This was prepared similarly to compound **6** by using $ZnCl_2$. Yield: ~84%, m.p. 150 °C. *Anal*. Calc. for $C_{20}H_{34}N_4O_4P_2S_4Zn$: C, 36.94; H, 5.23; P, 9.53; Zn, 10.06. Found: C, 37.16; H, 5.17; P, 9.24; Zn, 9.76%. ^{31}P{^{1}H} NMR ($(CD_3)_2CO$; ppm), 56.24. ^{1}H NMR ($(CD_3)_2CO$; ppm): 1.478 (d, 12H, $^3J_{HH}$ 5.5 Hz); 1.482 (d, 12H, $^3J_{HH}$ 6.0 Hz), 4.92 (d. sept, 4H, $^3J_{POCH}$ 9.9 Hz; $^3J_{HH}$ 6.1 Hz), 7.44 (m, 3H, Ph); 8.15 (m, 1H), 9.59 (br. d, 2H, $^4J_{PNCNH}$ 7.8 Hz). IR (cm^{-1}): 3340(br, s) (NH), 1520(s) (SCN), 1000(b, vs) (POC), 569, 595(m) (P═S).

2.7. Synthesis of {[(iPrO)$_2$P(S)NC(S)NH]$_2$-m-C$_6$H$_4$Cd} (9)

This was prepared similarly to compound **6** by using $Cd(CH_3COO)_2 \cdot H_2O$. Yield: ~69%, m.p. 146–147 °C. *Anal*. Calc. for $C_{20}H_{34}CdN_4O_4P_2S_4$: H, 4.88; P, 8.88. Found: H, 5.59; P, 8.20%. ^{31}P{^{1}H} NMR ($(CD_3)_2CO$; ppm), 55.54. ^{1}H NMR ($(CD_3)_2CO$; ppm): 1.496 (d. 12H, $^3J_{HH}$ 6.5 Hz); 1.471 (d, 12H, $^3J_{HH}$ 6.5 Hz), 4.92 (d. sept, 4H, $^3J_{POCH}$ 10.2 Hz; $^3J_{HH}$ 6.1 Hz), 7.39 (m, 3H, Ph), 8.30 (m, 1H, Ph), 9.64 (br. d, 2H, NH, $^4J_{PNCNH}$ 8.2 Hz). IR (cm^{-1}): 3200(br, s) (NH), 1490(s) (SCN), 1005(br, vs) (POC), 573, 594(m) (P═S).

2.8. Synthesis of {[(iPrO)$_2$P(S)NC(S)NH]$_2$-p-C$_6$H$_4$Co} (10)

A suspension of 1.173 g (2 mmol) of [(*i*PrO)$_2$P(S)NHC(S)NH]$_2$-*p*-C$_6$H$_4$ in anhydrous ethanol (20 ml) was mixed with an ethanol solution of potassium

hydroxide (0.224 g, 4 mmol). To the resulting potassium salt, a water (20 ml) solution of $Co(NO_3)_2 \cdot 6H_2O$ (0.579 g, 2.2 mmol) was added dropwise with vigorous stirring. The resulting complex was extracted with methylene chloride as a suspension and then the organic phase was washed with water (20 ml). The solvent was removed in vacuum. The residue was dried over $MgSO_4$ as an acetone solution and the solvent was removed in vacuum. A green solid was precipitated from acetone by *n*-hexane and dried in vacuum at 50 °C. Yield: 66%, m.p. 190–200 °C, decomposes. *Anal*. Calc. for $C_{20}H_{34}CoN_4O_4P_2S_4$: C, 37.29; H, 5.28; P, 9.63; Co, 9.15. Found: C, 36.60; H, 5.38; P, 11.94; Co, 11.37%. $^{31}P\{^1H\}$ NMR (CH_2Cl_2; ppm; width at half height, Hz); 169.54 (341 Hz). IR (cm^{-1}): 3360(br, s) (NH), 1504(s) (SCN), 1000(br, vs) (POC), 568(m) (P═S).

2.9. Synthesis of {[(iPrO)$_2$P(S)NC(S)NH]$_2$-p-C$_6$H$_4$Zn} (11)

This was prepared similarly to compound **10** by using $ZnCl_2$. Yield: ~65%, m.p. 305 °C, decomposes. *Anal*. Calc. for $C_{20}H_{34}N_4O_4P_2S_4Zn$: C, 36.94; H, 5.23; P, 9.53; Zn, 10.06. Found: C, 36.60; H, 5.22; P, 9.89; Zn, 10.04%. $^{31}P\{^1H\}$ NMR ($(CD_3)_2CO$; ppm), 56.39. ^1H NMR ($(CD_3)_2CO$; ppm): 1.475 (d, 24H, $^3J_{HH}$ 6.2 Hz), 4.90 (d. sept, 4H, $^3J_{POCH}$ 10.2 Hz; $^3J_{HH}$ 6.1 Hz), 7.79 (s, 4H, Ph), 9.577 (d, 2H, NH, $^4J_{PNCNH}$ 8.2 Hz). IR (cm^{-1}): 3280(br, s) (NH), 1500(s) (SCN), 980(br, vs) (POC), 575(m) (P═S).

2.10. Synthesis of {[(iPrO)$_2$P(S)NC(S)NH]$_2$-p-C$_6$H$_4$Cd} (12)

This was prepared similarly to compound **10** by using $Cd(CH_3COO)_2 \cdot H_2O$. Yield: ~20%, m.p. 175 °C. *Anal*. Calc. for $C_{20}H_{34}CdN_4O_4P_2S_4$: C, 34.46; H, 4.88; P, 8.88; Cd, 16.12. Found: C, 34.71; H, 4.56; P, 9.06; Cd, 16.71%. $^{31}P\{^1H\}$ NMR ($(CH_3)_2CO$; ppm), 55.29. IR (cm^{-1}): 3220(br, s) (NH), 1510(s) (SCN), 980–1000 (POC), 568(m) (P═S).

2.11. Physical measurements

Infrared spectra (Nujol) were recorded on a Specord M-80 spectrometer in the range 400–3600 cm^{-1}. NMR spectra were obtained on a Varian Unity-300 NMR spectrometer at 25 °C. ^1H and ^{31}P spectra were recorded

Table 1
Crystal data, data collection and refinement parameters for **1**, **2** and **5**

	1	**2**	**5**
Empirical formula	$C_{32}H_{68}N_8O_8P_4S_8Cd_2$	$C_{36}H_{76}N_8O_{10}P_4S_8Pd_2 \cdot 2CH_2Cl_2$	$C_{16}H_{36}N_4O_4P_2S_4$
Formula weight	1298.1	772.03	538.69
Space group	$P2_1/n$	$P\bar{1}$	$P2_1/n$
Unit cell dimensions			
a (Å)	15.297(2)	9.883(4)	10.556(2)
b (Å)	12.938(5)	12.368(2)	12.521(1)
c (Å)	30.089(5)	14.481(4)	10.723(2)
α (°)	90	73.75(2)	90
β (°)	103.55(1)	82.74(3)	103.41(1)
γ (°)	90	72.12(2)	90
V (Å^3)	5787(2)	1616(1)	1378.5(4)
Z	4	1	2
D_{calc} (g cm^{-3})	1.49	1.59	1.30
$F(000)$	664	792	572
Crystal colour	colourless	orange	colourless
Crystal form	prismatic	prismatic	prismatic
Crystal size (mm)	0.4 × 0.3 × 0.2	0.4 × 0.3 × 0.4	0.4 × 0.3 × 0.4
Radiation (Å)	0.71073	0.71073	0.71073
Temperature (K)	294	143	294
Scan mode	$\omega/2\theta$	$\omega/2\theta$	ω
Recording range θ_{max} (°)	33.76	26.28	32.28
Absorption correction	ψ-scans	none	none
μ (cm^{-1})	11.81	11.3	4.9
Scan speed (° min^{-1})	Variable, 1-16.4	Variable, 1-16.4	Variable, 1-16.4
Index ranges	$0 \leqslant h \leqslant 16$, $-16 \leqslant k \leqslant 0$, $-36 \leqslant l \leqslant 37$	$-11 \leqslant h \leqslant 0$, $-15 \leqslant k \leqslant 13$, $-16 \leqslant l \leqslant 16$	$0 \leqslant h \leqslant 12$, $0 \leqslant k \leqslant 12$, $-13 \leqslant l \leqslant 13$
No. of recorded reflections	11091	5944	1895
Observed reflections $F^2 \geqslant 4\sigma(F^o)$	6704	3693	784
R (%)	0.038	0.058	0.057
R_w (%)	0.087	0.138	0.149
S	1.000	0.997	0.991

at 299.948 and 121.420 MHz, respectively. Chemical shifts are reported with reference to $SiMe_4$ (^1H) and H_3PO_4 (^{31}P).

2.12. Crystal structure determination and refinement

The crystals of **1** were obtained from the mixture of dichloromethane and *n*-hexane (1:13) and the crystals of **2** via the slow evaporation of solvent from a dichloromethane solution. At room temperature the crystals of **2**, taken from the saturated solution, lose solvents molecules and destroy themselves.

The X-Ray diffraction data for the crystals of **1** and **2** were collected on a CAD4 Enraf-Nonius automatic diffractometer using graphite monochromated Mo Kα (0.71073 Å) radiation. Molecules of **2** and **5** in the crystals are in special positions. The details of crystal data, data collection and the refinement are given in Table 1. The stability of the crystals and the experimental conditions were checked every 2 h using three control reflections, while the orientation was monitored every 200 reflections by centreing two standards. No significant decay was observed. An empirical absorption correction based on ψ-scans was applied. The structures were solved by direct methods using the SIR 92 [3] program and refined using the SHELXL-97 program [4]. For the crystals (**1**, **2**, **5**) all non-hydrogen atoms were refined anisotropically. The positions of the hydrogen atoms were idealised. All figures were made using the program PLATON [5].

3. Results and discussion

3.1. Synthesis

Ligands were prepared by the addition reaction of bis-amines $H_2N–Z–NH_2$ to diisopropoxythiophosphoryisothiocyanate $(iPrO)_2P(S)NCS$.

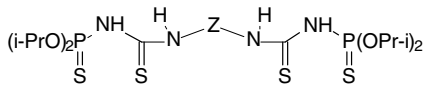

3–5

Complexes of $[(iPrO)_2P(S)NHC(S)NH]_2(m\text{-}C_6H_4)$ and $[(iPrO)_2P(S)NHC(S)NH]_2(p\text{-}C_6H_4)$ with Co(II), Ni(II), Zn(II) and Cd(II) **6–12** were prepared by the following procedure: the ligands were converted to their potassium salts, followed by interaction with inorganic salts of the corresponding metals. The obtained compounds are crystalline solids, soluble in most polar solvents. According to elemental analyses, they have a ratio M/L = 1:1. Complexes of bis-urea $[(iPrO)_2P(S)NHC(S)NH]_2(p\text{-}C_6H_4)$ are unstable in solution, in the presence of moisture, alcohols and air oxygen.

3.2. IR and NMR spectroscopy

The IR spectra of **1**, **2**, **6–12** exhibit absorptions at 450–300 cm^{-1}, which correspond to the stretching vibration of M–S bonds. The absorption band of the P=S group is shifted from 630–655 cm^{-1} in the parent ligands to 560–595 cm^{-1} in the complexes. The strong infrared absorption observed for all complexes in the region 1490–1570 cm^{-1} was assigned to the group vibrations of the SCN fragment. The signal of the C(S)NHP(S) group proton is absent in NMR ^1H spectra. The signal of the ZNH proton is shifted upfield with respect to the same signal of free ligands. High $^4J_{PNCNH}$ coupling constants, about 8 Hz, were noted previously for the complexes of *N*-diisopropoxyphosphoryl-*N*′-phenyl thiourea [6]. Such a high constant can be explained by the almost planar bond arrangement in the PNCNH backbone and by the accordance of this fragment configuration to the so-called *W*-criterion [7]. ^{31}P NMR spectra of complexes **1**, **2**, **6–9**, **11** and **12** each show a resonance in the region 51–59 ppm. As a rule the signals are shifted downfield with respect to the parent ligands. Obtained IR and NMR spectral data are evidence of the chelate knot formation with participation of C=S and P=S groups and the metal cation. Due to the presence of the paramagnetic centres, the signals for the ^1H NMR spectrum of cobalt and nickel complexes **6**, **7** and **10** are broadened and their number increased, this makes assignment of the signals much more complicated.

Divalent metals can form complexes of 1:1 ML **A** and 2:2 M_2L_2 **B** compositions with such a kind of bipodal ligands. Formation of oligomeric or polymeric compositions M_nL_n (**C**) is also possible.

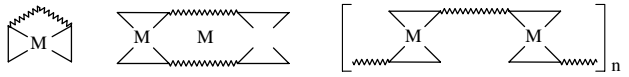

A **B** **C**

Thus, there is the possibility of an equilibrium in solution between all described types of complexes. We suppose that the equilibrium state depends first of all on the bridging chain Z length and secondly on the nature of the metal.

The ^{31}P NMR spectra of cobalt and nickel complexes **6**, **7** and **10** show several (up to three) signals of different intensities and widths at half height, which correspond to the different metal cation environments in the complexes. Such behaviour is common of the other complexes of bipodal thiophosphorylated thiourea [1]. The nickel cation has a *cis*-square-planar coordination environment in a dimer **B** and a *trans*-square-planar in an oligomer **C**. Nickel can also stay tetrahedral. Moreover, Ni(II) cations can be coordinated by lone pair donors,

such as nitrogen or oxygen, which are present in the ligand molecules. Different signals in the phosphorus spectrum of **7** can be due to any of proposed forms. Cobalt(II) cations are usually tetrahedral, but they can also form adducts with donor molecules.

^{31}P NMR spectra of complexes **1**, **8**, **9**, **11** and **12** exhibit only one signal. Cd(II) and Zn(II) cations are diamagnetic and their signals in ^{31}P NMR spectra are less sensitive to the environment of the metal cation. That is why both forms can have the same chemical shift.

In contrast to nickel, palladium(II) does not give a tetrahedral form or adducts and *cis*- and *trans*-isomers have different signals in spectra, as shown for the complex of *N*-diisopropoxythiophosphoryl-*N*′-phenylthiourea with Pd(II) [6]. Nonetheless, the ^{31}P spectrum of compound **2** shows a single resonance, which could correspond to the binuclear complex as the only form present in solution.

3.3. Crystal structure of *5*

Ligand **5** has been studied by X-ray analysis in order to compare its structure with the structures of **1** and **2**. The crystal structure of **5** is shown in Fig. 1, selected values of bond lengths, bond and torsion angles are given in Table 2. The NC(S)N fragment is almost planar, which is evidence of the resonance between the nitrogen lone pair and the double C=S bond. The conformation of the P–N–C–N fragment is almost shielded, torsion ∠P(1)–N(1)–C(1)–N(2) = 8.5(1)°. The NH group protons stay in an anti-disposition. The molecule has an inversion centre (see Table 3).

In the crystals of bisthiourea intra- and inter-molecular H-bonds of the NH···S type were found. Their parameters are presented in Table 3. Intermolecular H-bonds form endless chains. In the crystal these chains are oriented parallel to each other, along the *OY* axis.

3.4. Crystal structures of *1* and *2*

Figs. 2 and 3 show the structures of **1** and **2**, respectively, selected values of bond lengths, bond and torsion angles are given in Tables 4 and 5. For compound **1** only the data concerning one chelate knot are presented. The second one has a very similar geometry. According to the X-ray data these complexes are of M_2L_2 structure.

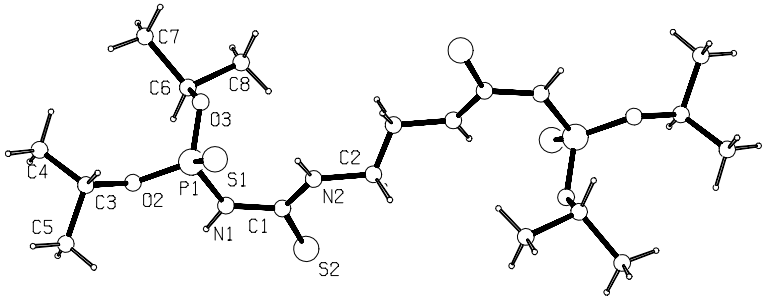

Fig. 1. Molecular structure of **5**.

Table 2
Selected bond distances (Å), bond and torsion angles (°) for the ligand **5**

Bond distances			
P(1)–S(1)	1.921(4)	P(1)–N(1)	1.684(5)
S(2)–C(1)	1.683(6)	N(1)–C(1)	1.382(7)
P(1)–O(2)	1.546(5)	N(2)–C(1)	1.306(8)
P(1)–O(3)	1.522(6)	N(2)–H(2)	0.8597
N(1)–H(1)	0.8597		
Bond angles			
S(1)–P(1)–N(1)	117.0(2)	N(1)–C(1)–N(2)	117.5(5)
P(1)–N(1)–C(1)	127.5(4)	S(2)–C(1)–N(2)	124.0(5)
S(2)–C(1)–N(1)	118.5(5)	C(1)–N(2)–C(2)	125.3(5)
P(1)–N(1)–H(1)	116.22	C(1)–N(1)–H(1)	116.23
Torsion angles			
P(1)–N(1)–C(1)–N(2)	8.5(1)	S(1)–P(1)–N(1)–C(1)	–52.7(7)
P(1)–N(1)–C(1)–S(2)	–170.9(4)		

Table 3
Parameters of H-bonds in the bisthiourea **5**

Bond	Symmetry operation	d(D–H)	d(H···A)	d(D···A)	∠(DHA)
N1–H1···S2	$-x, 1-y, 1-z$	0.86	2.62	3.467(4)	170.0
N2–H2···S1	intramolecular	0.86	2.59	3.332(6)	145.0

Bond lengths in Å and bond angles in degrees.

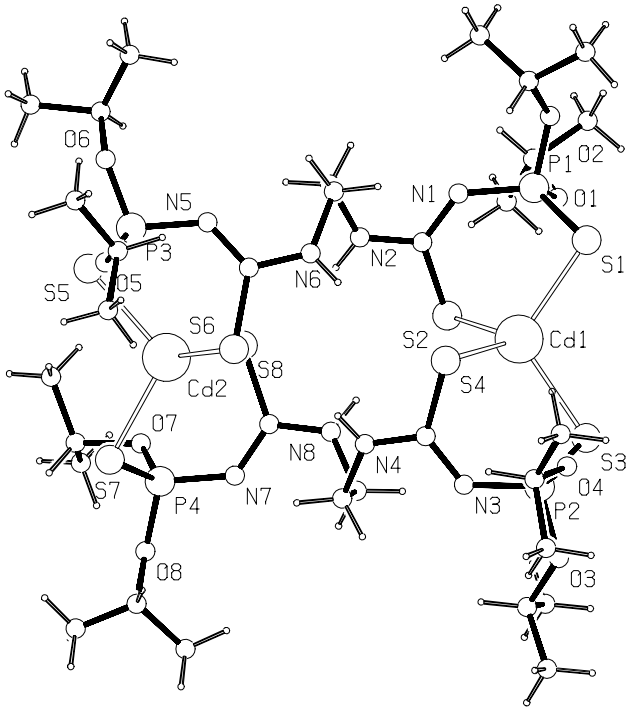

Fig. 2. Molecular structure of complex **1**.

Each ligand "tail" covers only its own metal atom. The coordination sphere of the metal includes a second ligand molecule. The structures of the described complexes are similar to the structures of the complexes of *para*-phenylene bis(imines) and *para*-phenylene methylpyridines [8,9]. In the crystal of compound **1** there is only the independent molecule in the asymmetric part of the lattice. In compound **2** the molecule is in a special position respective to the centre of symmetry. The cadmium and palladium atoms are four-coordinated and have the configuration of a slightly distorted tetrahedron for cadmium and a distorted square plane for palladium. The tetrahedral configuration of the cadmium atoms in compound **1** resembles those previously found in imidobis-seleno-$[Ph_2P(Se)NP(Se)Ph_2]_2Cd$ [10] and -thiophosphinyl $[iPr_2P(S)NP(S)iPr_2]_2Cd$ [11] cadmium complexes. They have a bis-chelate structure with a tetrahedral configuration of the central atom.

In compound **1** the Cd–S(C) bond lengths range from 2.527(1) to 2.536(1) Å, and Cd–S(P) bond lengths range from 2.503(2) to 2.523(1) Å. This reveals the equalization of the metal bond lengths with either the thiophosphoryl or the thiocarbonyl sulfur atoms. The values of the P–S (1.990 Å mean) and C–S (1.760 Å mean) bond

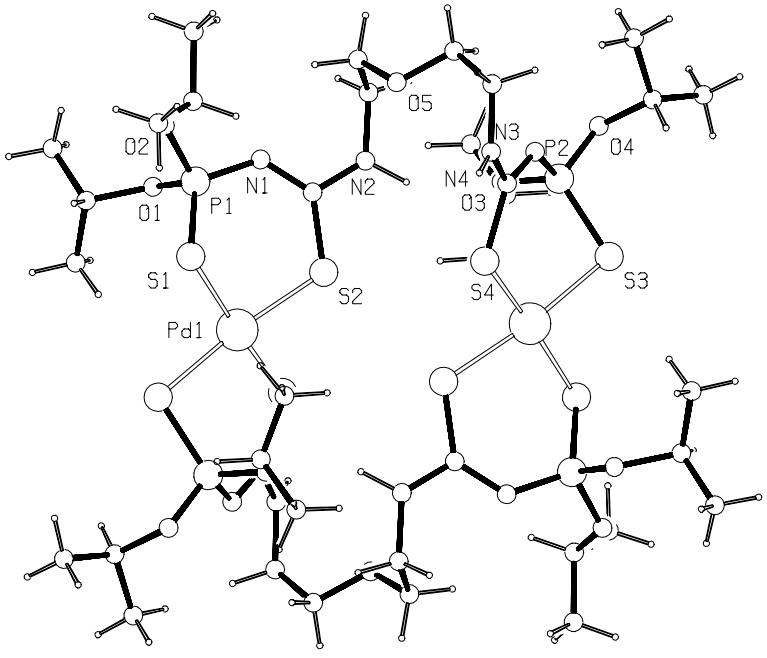

Fig. 3. Molecular structure of complex **2**.

Table 4
Selected bond distances (Å), bond and torsion angles (°) for complex **1**

Bond distances			
Cd(1)–S(1)	2.522(1)	Cd(1)–S(2)	2.536(1)
Cd(1)–S(3)	2.522(1)	Cd(1)–S(4)	2.532(1)
S(1)–P(1)	1.989(2)	S(3)–P(2)	1.986(2)
S(2)–C(1)	1.764(4)	S(4)–C(2)	1.758(4)
P(1)–N(1)	1.603(4)	P(2)–N(3)	1.595(4)
N(1)–C(1)	1.310(5)	N(3)–C(2)	1.317(6)
Bond angles			
S(1)–Cd(1)–S(2)	100.62(4)	S(2)–Cd(1)–S(4)	105.68(4)
S(3)–Cd(1)–S(4)	103.49(4)	S(1)–Cd(1)–S(4)	118.96(4)
S(1)–Cd(1)–S(3)	111.47(5)	S(2)–Cd(1)–S(3)	117.22(4)
Cd(1)–S(1)–P(1)	97.84(5)	Cd(1)–S(2)–(1)	92.9(1)
Cd(1)–S(3)–P(2)	96.49(7)	Cd(1)–S(4)–(2)	92.2(1)
P(1)–N(1)–C(1)	127.9(3)	P(2)–N(3)–C(2)	128.7(3)
S(1)–P(1)–N(1)	116.4(1)	S(3)–P(2)–N(3)	115.7(1)
S(2)–C(1)–N(1)	126.4(3)	S(4)–C(2)–N(3)	127.0(3)
Torsion angles			
P(1)–N(1)–C(1)–S(2)	−1.1(5)	P(2)–N(3)–C(2)–S(4)	−8.5(6)
S(1)–P(1)–N(1)–C(1)	−68.9(4)	S(3)–P(2)–N(3)–C(2)	−67.3(4)

Table 5
Selected bond distances (Å), bond and torsion angles (°) for complex **2**

Bond distances			
Pd(1)–S(1)	2.342(2)	Pd(1)–S(3)	2.354(2)
Pd(1)–S(2)	2.289(2)	Pd(1)–S(4)	2.296(2)
S(1)–P(1)	2.004(3)	S(3)–P(2)	1.993(3)
S(2)–(1)	1.733(8)	S(4)–(2)	1.739(8)
P(1)–N(1)	1.580(6)	P(2)–N(3)	1.579(6)
N(1)–C(1)	1.333(9)	N(3)–C(2)	1.319(9)
Bond angles			
S(1)–Pd(1)–S(2)	96.05(7)	S(2)–Pd(1)–S(4)	80.31(7)
S(1)–Pd(1)–S(3)	85.26(7)	S(3)–Pd(1)–S(4)	99.32(7)
Pd(1)–S(1)–P(1)	99.48(9)	Pd(1)–S(3)–P(2)	97.57(9)
Pd(1)–S(2)–C(1)	115.0(2)	Pd(1)–S(4)–C(2)	115.4(3)
P(1)–N(1)–C(1)	128.9(5)	P(2)–N(3)–C(2)	126.5(5)
S(1)–P(1)–N(1)	119.0(2)	S(3)–P(2)–N(3)	117.1(2)
S(2)–C(1)–N(1)	129.9(6)	S(4)–C(2)–N(3)	129.7(6)
Torsion angles			
P(1)–N(1)–C(1)–S(2)	15(1)	P(2)–N(3)–C(2)–S(4)	−2(1)
S(1)–P(1)–N(1)–C(1)	23.2(8)	S(3)–P(2)–N(3)–C(2)	−48.4(7)

lengths also correspond to the values intermediate between double (P═S 1.91–1.92 Å, C═S 1.68 Å in the thioureas) and the single (P–S 2.05–2.11 Å, C–S 1.751 Å) bonds [12]. The P═S bonds order stays in agreement with IR spectroscopy observations. Meanwhile, the C–N and P–N bonds are shorter on comparison with those in the free ligand **5** (C–N 1.382(7), P–N 1.684(5) Å). This picture is characteristic for the complexes discussed.

The metal-containing heterocycles CdSPNCS have the conformation of a non-symmetric boat, with the most deviation of P and S(C) atoms from the mean square planes of these fragments (Table 6).

In complex **2** the palladium atom has a distorted square-planar configuration. The deviations of the S(1) and S(4a) atoms from the plane S(1)S(2)S(3a)S(4a) are −0.147(2) and −0.154(2) Å, respectively, S(2) and S(3a) atoms are 0.158(2) and 0.154(2) Å, respectively. The palladium atom deviates from the plane S(1)S(2)S(3a)S(4a) by 0.0305(6) Å. The Pd–S(C) and Pd–S(P) bond lengths are within the usual limits for bonds of these kinds. For example, in the complex $[PhC(S)NP(S)(O\textit{i}Pr)_2]_2Pd$ (**13**) Pd–S(C) is 2.310 Å and Pd–S(P) is 2.341 Å [13]. The Pd–S(P) bond lengths in the compounds $Pd[(EtO)_2P(S)NP(S)Ph_2]_2$ (**14**) [14], $Pd[\{(PhO)_2P(S)\}_2N]_2$ [15], $Pd[\{\textit{i}Pr_2P(S)\}_2N]_2$ [16] are in the range 2.325–2.351 Å. The Pd–S(C) bond lengths in the complex $Pd[Et_2NC(S)NC(O)Ph]_2$ (**15**) are 2.310–2.315 Å [17]. The values of the bond lengths also show the equalization of the bond lengths, but in contrast to complex **1**, there is an evident difference between the bonds M–S(P) and M–S(C) in complex **2**.

The metal-containing six-membered heterocycle Pd(1)S(1)P(1)N(1)C(1)S(2) is in a ''sofa'' conformation. The conformation of the second metal-containing heterocycle Pd(1)($-x$, $-y$, $1-z$)S(3)P(2)N(3)C(2)S(4) is a non-symmetric boat, see Table 7. The conformation of the SCNPS backbone in **1** and **2** is similar: the NC(S)NP fragment is almost planar and the phosphoryl sulfur is deviated from its least-square plane. Torsion S–P–N–C angles range from 67.3(4)° to 72.3(5)° for **1** and 23.2(8)° to 48.4(7)° for **2**. The values of torsion angles in compounds **1** and **2** show that these deviations are higher in the cadmium complex **1**.

Table 6
Deviations (Å) from the mean-square planes CdSPNCS in **1**

Atoms in plane	Deviation	Atoms in plane	Deviation	Atoms in plane	Deviation	Atoms in plane	Deviation
Cd(1)	−0.4825	Cd(1)	−0.3911	Cd(2)	−0.4419	Cd(2)	−0.3636
S(1)	0.0958	S(3)	−0.1801	S(5)	−0.1369	S(7)	−0.2061
P(1)	0.4879	P(2)	0.5063	P(3)	0.5083	P(4)	0.5205
N(1)	−0.3018	N(3)	−0.2614	N(5)	−0.3009	N(7)	−0.2652
C(1)	−0.2765	C(2)	−0.3098	C(3)	−0.2779	C(4)	−0.3045
S(2)	0.6687	S(4)	0.6360	S(6)	0.6493	S(8)	0.6189

Table 7
Deviations (Å) from the mean-square planes PdSPNCS in **2**

Atoms in plane	Deviation	Atoms in plane	Deviation
Pd(1)	−0.4537	Pd(1)	0.2818
S(1)	0.5521	S(3) (−*x*, −*y*, 1 − *z*)	0.5275
P(1)	−0.2806	P(2) (−*x*, −*y*, 1 − *z*)	−0.4083
N(1)	−0.0894	N(3) (−*x*, −*y*, 1 − *z*)	0.0435
C(1)	0.1879	C(2) (−*x*, −*y*, 1 − *z*)	0.2021
S(2)	0.0837	S(4) (−*x*, −*y*, 1 − *z*)	−0.0829

Table 8
Parameters of intramolecular H-bonds of the complex **1**

Bond	d(D–H)	d(H···A)	d(D···A)	∠(DHA)
N2–H2···S8	0.86	2.66	3.504(3)	168.0
N4–H4···S6	0.86	2.69	3.529(4)	167.0
N6–H6···S4	0.86	2.82	3.662(4)	167.0
N8–H8···S2	0.86	2.63	3.477(3)	170.0

Bond lengths in Å and bond angles in degrees.

In the crystal of complex **1** intramolecular H-bonds of the NH···S type were found (Fig. 4). In contrast to complex **1**, in the crystal of complex **2** both inter- and intramolecular H-bonds take place (Fig. 5). The H-bonds parameters of complexes **1** and **2** are presented in Tables 8 and 9. As a result of hydrogen bonding in **2** centrosymmetric dimers are formed. Since the first molecule of the dimer lies in the local symmetry centre, the second molecule is linked to another dimer's molecule. Finally, due to this interaction the dimers are linked into endless chains.

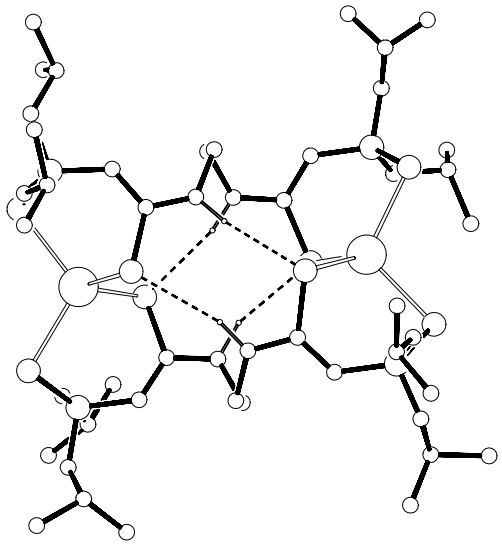

Fig. 4. H-bonds in complex **1**.

The nature of the close chemical environment of the central atom imposes a major impact on the chelate knot structure. If these atoms are the same then the square-planar complexes of "soft" metals with anionic ligands of the [A(X)NB(Y)] type have, as a rule, a *trans*-structure: **13** [13], **14** [14], [PhNHC(S)NP(S)(O*i*Pr)$_2$]$_2$Ni [18], [Pr$_2$NC(S)NP(S)(OPh)$_2$]$_2$Ni [19], [MeNHC(S)NP(S)Ph$_2$]$_2$Ni [20], [(EtO)$_2$P(S)NP(S)Ph$_2$]$_2$Pt [14], [Me$_2$P(S)NP(S)Ph$_2$]$_2$Ni [21], [Et$_2$NC(S)NC(S)Ph]$_2$Ni [22]. The only exception is the complex {[H$_2$NC(S)NP(S)Ph$_2$]$_2$Pt}(Et$_2$O) [23]. If $X \neq Y$ the *cis*-structure is preferable due to the *trans*-influence: **15** [17], [Et$_2$NC(S)NC(O)Ph]$_2$Cu [24], [Ph$_2$P(Se)NP(O)Ph$_2$]$_2$Pd [25], [(*i*PrO)$_2$P(O)NC(S)Ph]$_2$Cu [26], [(*i*PrO)$_2$P(O)NC(S)NEt$_2$]$_2$Cu [27]. The central atom's surroundings affects in turn the structure of the macrocyclic complexes with bipodal ligands. For example the dimer

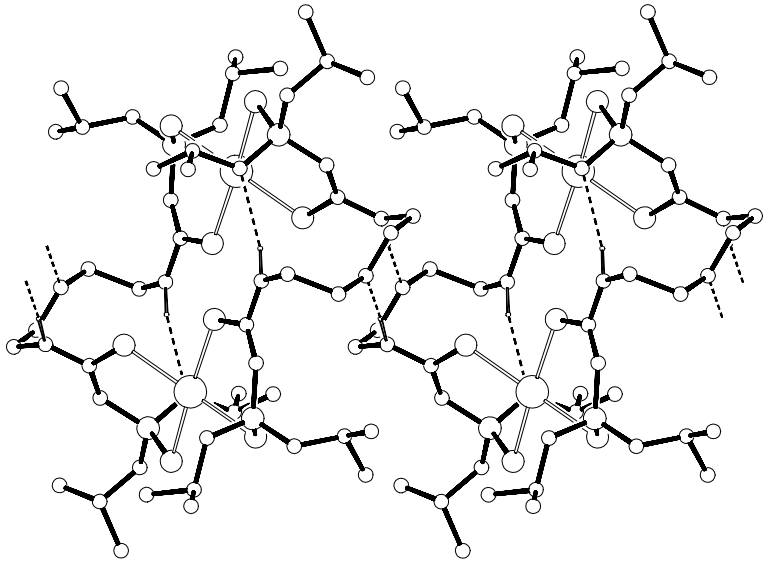

Fig. 5. H-bonds in complex **2**.

Table 9
Parameters of H-bonds of the complex **2**

Bond	Symmetry operation	d(D–H)	d(H···A)	d(D···A)	∠(DHA)
N2–H2···O3	Intramolecular	1.00	2.34	3.177(7)	141.0
N4–H4···O5	$-x$, $1-y$, $-z$	0.86	1.99	2.823(8)	164.0

Bond lengths in Å and bond angles in degrees.

and trimer complexes with bipodal *O*,*S*-acylthioureas have the *cis*-structure only [28,29].

Ligands having coordinating atoms with similar donor abilities can form both *cis*- and *trans*-isomers depending on slight peculiarities like the entropy of an isomer, steric preferences, polarity of media. Hence, it is evident, why the complexes with *S*,*S*-bipodal ligands form both polymers [1,2] and dimers as in this case. When there is a tendency to form chelate molecules with a *trans*-structure, the minimal accepted size for the cyclic molecule $(ML)_n$ should be $n = 4$.

The results of the presented work are in a good agreement with the data published by Kluiber and Lewis [30], Kobuke and Satoh [31], – both the dimeric complexes **1** and **2** are formed with ligands that contain less than 7 atoms in the bridging chain Z.

Acknowledgements

Financial support from the Russian Foundation for Basic Research (Grants #00-03-32742 and 03-03-32372-a) and joint program of CRDF and Russian Ministry of Education "Basic Research & High Education" (Grant REC-007) is gratefully acknowledged.

Appendix A. Supplementary material

Crystallographic data for the structural analysis have been deposited with the Cambridge Crystallographic Data Centre CCDC Nos. 189278, 189279 and 218902. Copies of the data can be obtained free of charge from The Director, CCDC, 12 Union Road, Cambridge, CB2 1EZ, UK (fax: +44-(1223)-336033; e-mail: deposit@ccdc.cam.ac.uk or www: http://www.ccdc.cam.ac.uk). Supplementary data associated with this article can be found, in the online version, at doi:10.1016/j.poly.2004.07.005.

References

[1] N.G. Zabirov, V.V. Brus'ko, S.V. Kashevarov, F.D. Sokolov, V.A. Sherbakova, A.Yu. Verat, R.A. Cherkasov, Russ. J. Gen. Chem. 70 (2000) 1214.
[2] V.V. Brus'ko, F.D. Sokolov, N.G. Zabirov, R.A. Cherkasov, A.I. Rakhmatullin, A.Yu. Verat, Russ. J. Gen. Chem. 69 (1999) 664.
[3] A. Altomare, G. Cascarano, C. Giacovazzo, D. Viterbo, Acta Crystallogr. A 47 (1991) 744.
[4] G.M. Sheldrick, SHELX-97 Program for Crystal Structure Analysis (Release 97-2), University of Göttingen, Göttingen, Germany.
[5] A.L. Spek, Acta Crystallogr. A 46 (1990) 3440.
[6] V.V. Brus'ko, A.I. Rakhmatullin, N.G. Zabirov, Russ. J. Gen. Chem. 70 (2000) 1603.
[7] H. Günter, NMR Spectroscopy: An Introduction, Wiley, 1980.
[8] B.J. McNelis, L.C. Nathan, C.J. Clark, J. Chem. Soc., Dalton Trans. (1999) 1831.
[9] B. Kirson, H. Sechter, Bull. Soc. Chim. France (1965) 2743.
[10] V. Garcia-Montalvo, J. Novosad, P. Kilian, J.D. Woollins, A.M.Z. Slawin, P. Garcia y Garcia, M. Lopez-Cardozo, G. Espinosa-Perez, R. Cea-Olivares, J. Chem. Soc., Dalton Trans. (1997) 1025.
[11] D. Cupertino, R. Keyte, A.M.Z. Slawin, D.J. Williams, J.D. Woollins, Inorg. Chem. 35 (1996) 2695.
[12] F.H. Allen, O. Kennard, D.G. Watson, L. Brammer, A.G. Orpen, R. Taylor, J. Chem. Soc., Perkin Trans. II (1987) S1.
[13] N.G. Zabirov, I.A. Litvinov, O.N. Kataeva, S.V. Kashevarov, F.D. Sokolov, R.A. Cherkasov, Russ. J. Gen. Chem. 68 (1998) 1408.
[14] D.C. Cupertino, R.W. Keyte, A.M.Z. Slawin, J.D. Woollins, Polyhedron 18 (1998) 311.
[15] M. Nouaman, Z. Zak, E. Herrmann, O. Navratil, Z. Anorg. Allg. Chem. 619 (1993) 1147.
[16] D. Cupertino, R. Keyte, A.M.Z. Slawin, J.D. Woollins, Polyhedron 15 (1996) 4441.
[17] V.G. Fitzl, L. Beyer, J. Sieler, R. Richter, J. Kaiser, E. Hoyer, Z. Anorg. Allg. Chem. 433 (1977) 237.
[18] V.V. Brus'ko, A.I. Rakhmatullin, V.G. Shtyrlin, D.B. Krivolapov, I.A. Litvinov, N.G. Zabirov, in: 34th International Conference on Coordination Chemistry (ICCC34), Edinburgh, UK. 2000 (Abstracts. P. 0782).
[19] Z. Zak, T. Glowiak, N.T.T. Chau, E. Herrmann, Z. Anorg. Allg. Chem. 586 (1990) 136.
[20] T. Iwamoto, F. Ebina, H. Nakazawa, C. Nakatsuka, Bull. Chem. Soc. Jpn. 52 (1979) 1857.
[21] R. Rosler, C. Silvestru, G. Espinosa-Perez, I. Haiduc, R. Cea-Olivares, Inorg. Chim. Acta 241 (1996) 47.
[22] S. Seiler, R. Richter, U. Braun, L. Beyer, O. Lindqvist, L. Andersen, Z. Anorg. Allg. Chem. 528 (1985) 107.
[23] D.J. Birdsall, J. Green, T.Q. Ly, J. Novosad, M. Necas, A.M.Z. Slawin, J.D. Woollins, Z. Zak, Eur. J. Inorg. Chem. (1999) 1445.
[24] R. Richter, L. Beyer, J. Kaiser, Z. Anorg. Allg. Chem. 461 (1980) 67.
[25] A.M.Z. Slawin, M.B. Smith, J.D. Woollins, J. Chem. Soc., Dalton Trans. (1996) 3659.
[26] A.L. Kon'kin, V.G. Shtyrlin, N.G. Zabirov, I.A. Litvinov, A.T. Gubaidullin, R.R. Garipov, A.V. Aganov, A.V. Zakharov, Phosphorus Sulfur Silicon 147 (1999) 449.
[27] V.G. Shtyrlin, A.L. Kon'kin, V.V. Brusko, F.D. Sokolov, R.R. Garipov, N.G. Zabirov, I.A. Litvinov, D.B. Krivolapov, A.V. Zakharov, A.V. Aganov, in: 34th International Conference on

Coordination Chemistry (ICCC34), Edinburgh, UK, 2000 (Abstracts. P. 0784).
[28] R. Kohler, R. Kirmse, R. Richter, J. Sieler, E. Hoyer, L. Beyer, Z. Anorg. Allg. Chem. 537 (1986) 133.
[29] K.R. Koch, S.A. Bourne, A. Coetzee, J. Miller, J. Chem. Soc., Dalton Trans. (1999) 3157.
[30] R.W. Kluiber, J.W. Lewis, J. Am. Chem. Soc. 82 (1960) 5777.
[31] Y. Kobuke, Y. Satoh, J. Amer. Chem. Soc. 114 (1992) 789.

Available online at www.sciencedirect.com
SCIENCE DIRECT®
Polyhedron 23 (2004) 2253–2258
POLYHEDRON
www.elsevier.com/locate/poly

Synthesis, structure and magnetic properties of carboxylate-bridged polynuclear copper(II)–lanthanide(III) rings: $[Ln(H_2O)_5(CuL)_2][CuL]\cdot 8H_2O$ (Ln = La, Ce)

Yang Zou [a], Wen-Long Liu [a], Song Gao [b], Chang-Shen Lu [a], Dong-Bin Dang [a], Qing-Jin Meng[a,*]

[a] State Key Laboratory of Coordination Chemistry, Coordination Chemistry Institute, Nanjing University, Nanjing 210093, PR China
[b] Earth Materials Chemistry and Applications, Peking University, Beijing 10871, PR China

Received 9 March 2004; accepted 2 July 2004
Available online 28 August 2004

Abstract

Reaction of Na[CuL] (H_3L = the Schiff base derived from 5-bromosalicylaldehyde and glycylglycine) with $Ln(NO_3)_3$ leads to the formation of the title complexes $[Ln(H_2O)_5(CuL)_2][CuL]\cdot 8H_2O$ (Ln = La (**1**) and Ce (**2**)), which contain ring-like hexanuclear $[Ln_2(H_2O)_{10}(CuL)_4]^{2+}$ cations. The Ln(III) cations in **1** and **2** are coordinated by five water molecules, one carbonyl oxygen and three carboxylic oxygen atoms, and the copper(II) cations are coordinated by one phenolic oxygen, one carboxylate oxygen atom, one deprotonated amide nitrogen atom and one imino nitrogen atom. Complex **1** exhibits a ferromagnetic interaction and **2** exhibits an antiferromagnetic interaction in the solid state.
© 2004 Elsevier Ltd. All rights reserved.

Keywords: Cu(II)–Ln(III) complexes; Dipeptides; Carboxylate bridge; Hexanuclear cations; Crystal structures; Magnetic properties

1. Introduction

Study on the synthetic methods, structures and properties of heterometallic compounds consolidated by carboxylate groups is currently of interest because of the magnetic interaction between transition and rare-earth ions in bridged systems, and their possible application in production of high temperature superconductors [1–4]. Heterometallic compounds ligated by carboxylate groups have not been well documented [5–7]; some examples of heteronuclear Cu–Ln (Ln = lanthanide) compounds have recently been uncovered [8–15]. This may be attributed to the fact that Cu and Ln have different coordination capabilities. Therefore heteronuclear Cu–Ln compounds have commonly been synthesized with hetero-donor ligands, comprising two types of ligating atoms (such as N and O) coordinated each to Cu and Ln atoms, respectively.

Some transition metal complexes of Schiff bases derived from amino acids and peptides comprising two types of ligating atoms (such as N and O) have interesting coordination capabilities (especially as carboxylate-bridged ligands) to metal ions [16–21]. We have recently found that the stable $[CuL]^-$ (H_3L = 5-bromosalicylideneglycylglycine) core can be used as a ''metallo-ligand'' to bind other hard metal ions such as Ba^{II} to form a heterometallic complex [22,23], thus providing a new synthetic route for heterometallic complexes in metal carboxylate chemistry. Since the lanthanide^{III} ions are very similar to hard barium ions in coordination chemistry, the above-mentioned interesting strategy can also

* Corresponding author. Tel.: +862583597266; fax: +86258331-4502.
E-mail addresses: njuzyang@163.com (Y. Zou), mengqj@netra.nju.edu.cn (Q.-J. Meng).

0277-5387/$ - see front matter © 2004 Elsevier Ltd. All rights reserved.
doi:10.1016/j.poly.2004.07.006

be applied to the preparation of carboxylate-bridged heterometallic hexanuclear $Cu_4^{II}Ln_2^{III}$ compounds. Herein we described their preparation and magnetic properties, and the crystal structure of $[Ln(H_2O)_5(CuL)_2][CuL]\cdot 8H_2O$.

2. Experimental

2.1. Materials and methods

All reagents were commercially available and used as received. Elemental analyses (H, C, N) were performed on a Perkin–Elmer 240 analytical instrument. FT-IR spectra were recorded on a Bruker vector22 spectrophotometer as KBr pellets in the 4000–400 cm^{-1} region. Magnetic measurements were performed on a Quantum Design MPMS-7 SQUID magnetometer and an Oxford MagLab2000 System in the temperature range 2–300 K and under an applied external magnetic field of 2–3 T. Diamagnetic corrections were estimated on the basis of Pascal's constants.

2.2. Preparation of compounds

2.2.1. $Ln(H_2O)_5(CuL)_2][CuL]\cdot 8H_2O$ (1–2)

These complexes were all prepared using the same method as described in detail for complex **1** as an example (Scheme 1): glycylglycine (10 mmol), 5-bromosalicylaldehyde (10 mmol) and LiOH (20 mmol) were dissolved and refluxed in MeOH/H_2O (v:v = 1:1). $CuCl_2\cdot 2H_2O$ (10 mmol) was then added to the solution and the resulting solution was adjusted to pH 9–11. Last excess $LaCl_3$ (15 mmol) was added. A violet precipitate was obtained, which can be recrystallized from hot water (90 °C). The filtrate was allowed to evaporate slowly at room temperature. After several days violet red crystals, which were suitable for X-ray diffraction were obtained. Yield: 78%. *Anal.* Calc. for $C_{33}H_{48}O_{24}N_6Br_3Cu_3La$: C, 26.7; H, 3.3; N, 5.7. Found: C, 26.6; H, 3.3; N, 5.6%. IR (KBr, cm^{-1}): ν_{sh}(COO) 1686, ν(C=N) 1646s, ν_{as}(COO) 1600 and ν_s(COO) 1403. MS ($[C_{11}H_8N_2O_4BrCu]^-$, *m/z*): 375.7.

2: violet red crystals. Yield: 80%. *Anal.* Calc. for $C_{33}H_{50}N_6O_{25}Br_3CeCu_3$: C, 26.4; H, 3.4; N, 5.6. Found: C, 26.7; H, 3.4; N, 5.7%. IR (KBr, cm^{-1}): ν_{sh}(COO) 1688, ν(C=N) 1645s, ν_{as}(COO) 1599 and ν_s(COO) 1400 (see Table 1).

2.3. X-ray crystallography

A summary of the data collection and structure refinement is listed in Table 2. Data were collected on a Bruker SMART 1000 diffractometer equipped with a CCD detector and graphite-monochromated Mo Kα (λ = 0.71073 Å) radiation. The structure solution by direct methods revealed the metal atom coordinates and subsequent difference Fourier methods yielded the positions of all remaining non-H atoms and all of the hydrogen atoms. All other non-H atoms were refined anisotropically by full-matrix least-squares calculations using SHELXTL version 5.1 [24]. For the two complexes all the hydrogen atoms were found in difference Fourier maps, assigned fixed isotropic displacement parameters 1.2 times the equivalent isotropic *U* value of the attached atoms and allow to ride on their respective parent atoms.

3. Results and discussion

3.1. Crystal structures

3.1.1. $La(H_2O)_5(CuL)_2][CuL]\cdot 8H_2O$ (1)

The crystal structure of **1** consists of a centrosymmetric hexanuclear $[La_2(H_2O)_{10}(CuL)_4]^{2+}$ ring-like cation,

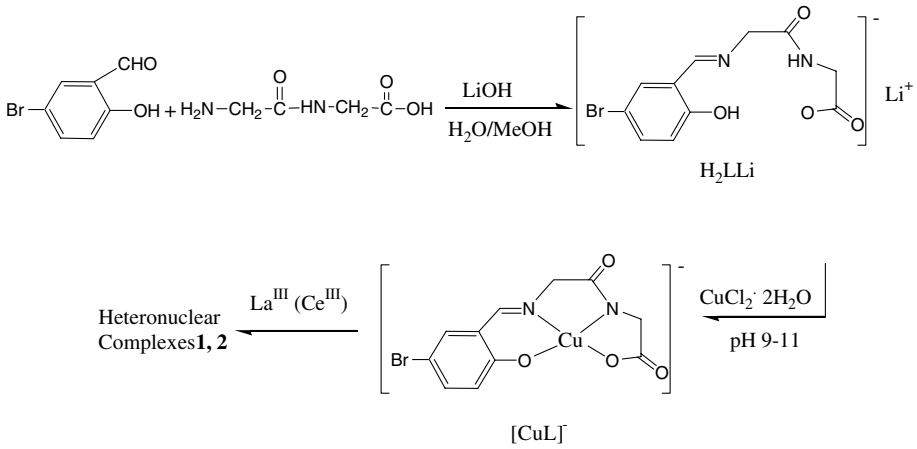

Scheme 1. Synthetic route to the Cu–Ln heteronuclear complexes **1** and **2**.

Table 1
Crystal data for complexes **1** and **2**

	1	**2**
Empirical formula	C66H96O48 N12Br6Cu6La2	C33H50O25N6Br3Cu3Ce
Molecular weight	2964.07	1501.26
Crystal system	triclinic	triclinic
Space group	$P\bar{1}$	$P\bar{1}$
a (Å)	11.390(2)	11.432(5)
b (Å)	12.618(2)	12.616(5)
c (Å)	19.237(3)	19.262(8)
γ (°)	83.95(1)	84.05(1)
β (°)	77.03(1)	76.91(1)
γ (°)	66.03(1)	66.03(1)
U (Å^3)	2461.5(7)	2472.3(18)
Z	1	2
μ(Mo Kα) (mm^{-1})	4.651	4.690
Reflections collected	13320	12392
Independent reflections	9448 (R_{int} = 0.017)	8545 (R_{int} = 0.029)
Goodness-of-fit on F^2	1.03	1.08
Final R_1, wR_2 ($I > 2\sigma$)	0.0544, 0.1420	0.0544, 0.1095

Table 2
Selected bond lengths (Å) and angles (°) for **1** and **2**

1		**2**	
Bond lengths			
Cu(1)–O(1)	1.869(5)	Cu(1)–O(1)	1.869(4)
Cu(1)–O(4)	1.944(5)	Cu(1)–O(4)	1.993(4)
Cu(1)–N(1)	1.925(6)	Cu(1)–N(1)	1.922(5)
Cu(1)–N(2)	1.868(6)	Cu(1)–N(2)	1.895(6)
La(1)–O(2)^{i}	2.385(5)	Ce(1)–O(7)^{ii}	2.421(5)
La(1)–O(3)	2.433(5)	Ce(1)–O(6)	2.382(4)
La(1)–O(7)	2.630(5)	Ce(1)–O(3)	2.608(5)
La(1)–O(8)	2.633(5)	Ce(1)–O(4)	2.625(4)
La(1)–O(13)	2.566(5)	Ce(1)–O(13)	2.539(5)
La(1)–O(14)	2.539(5)	Ce(1)–O(14)	2.540(5)
La(1)–O(15)	2.587(5)	Ce(1)–O(15)	2.564(5)
La(1)–O(16)	2.583(5)	Ce(1)–O(16)	2.556(5)
La(1)–O(17)	2.525(5)	Ce(1)–O(17)	2.561(5)
N(1)–C(7)	1.298(9)	N(1)–C(7)	1.266(8)
N(1)–C(8)	1.444(9)	N(1)–C(8)	1.483(8)
N(2)–C(9)	1.342(10)	N(2)–C(9)	1.338(8)
N(2)–C(10)	1.444(9)	N(2)–C(10)	1.436(8)
Bond angles			
N(2)–Cu(1)–O(1)	177.6(3)	N(2)–Cu(1)–O(1)	178.1(2)
N(2)–Cu(1)–N(1)	84.7(3)	N(2)–Cu(1)–N(1)	85.2(2)
O(1)–Cu(1)–N(1)	95.5(2)	O(1)–Cu(1)–N(1)	96.6(2)
N(2)–Cu(1)–O(4)	82.9(2)	N(2)–Cu(1)–O(4)	83.4(2)
O(1)–Cu(1)–O(4)	96.9(2)	O(1)–Cu(1)–O(4)	94.73(19)
N(1)–Cu(1)–O(4)	167.6(3)	N(1)–Cu(1)–O(4)	166.3(2)
O(2)^{i}–La(1)–O(3)	105.08(17)	O(7)^{ii}–Ce(1)–O(6)	104.46(16)
O(2)^{i}–La(1)–O(7)	141.00(18)	O(7)^{ii}–Ce(1)–O(3)	80.15(16)
O(2)^{i}–La(1)–O(8)	133.02(17)	O(7)^{ii}–Ce(1)–O(4)	120.70(16)
O(3)–La(1)–O(7)	81.07(17)	O(6)–Ce(1)–O(3)	140.40(17)
O(3)–La(1)–O(8)	121.04(17)	O(6)–Ce(1)–O(4)	133.75(15)
O(7)–La(1)–O(8)	49.28(16)	O(3)–Ce(1)–O(4)	49.69(14)

Symmetry code: (i) $1-x,-y,-z$; (ii) $-x,2-y,-$z.

two [CuL]$^-$ anions and lattice water molecules. An ORTEP view of the hexanuclear cation in **1** is shown in Fig. 1. The coordination environment of the copper(II) centers is approximately square-planar. The Schiff base ligand is deprotonated and acts as a triple negatively charged quadridentate ONNO chelate, coordinated to

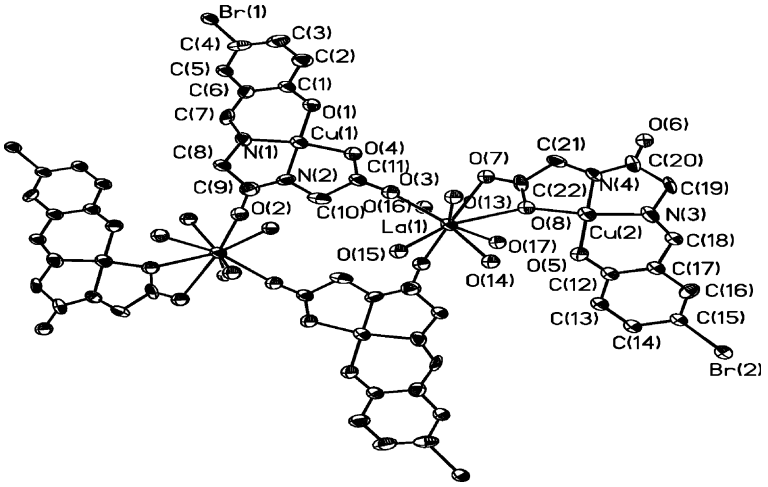

Fig. 1. An ORTEP view of the crystal structure of $[La_2(H_2O)_{10}(CuL)_4]^{2+}$ showing the 50% probability thermal ellipsoid.

the copper(II) atom via one phenolic oxygen (O(1)), one deprotonated amide nitrogen atom (N(2)), one imino nitrogen atom (N(1)) and one carboxylate oxygen atom (O(4)). The value of 1.444(9) Å for the C(8)–N(1) bond, shorter than the usual C–N single bond, and the double bond C(7)–N(1) length of 1.298(9) Å agree well with the values of Schiff base type I [25]. The C(9)–N(2) bond length is 1.342(10) Å and the C(10)–N(2) bond length is 1.444(9) Å. The best-fit least-squares plane through the four basal and Cu atoms shows these atoms to be nearly coplanar. The O(1)–Cu(1)–N(2) angle of 177.6(3)° is nearly linear. The N(1)–Cu(1)–O(4) bond angle is 167.6(3)°. The phenyl ring [C(1)–C(6)] and the C(1), C(6), C(7), N(1), O(1), Cu(1) chelate ring are almost coplanar with a small dihedral angle of 0.3°. There are three types of $[CuL]^-$ subunits in the crystal. $[Cu(3)L]^-$ act as a counter ion; $[Cu(1)L]^-$ coordinate to La(III) through one carboxylate oxygen (O(3)) and one carbonyl oxygen (O(2)), and $[Cu(2)L]^-$ coordinates to La(III) though two carboxylate oxygens (O(7), O(8)).

La(III) is 9-coordinated by five water molecules (O(13), O(14), O(15), O(16), O(17)), three carboxylic oxygen atoms (O(3), O(7), O(8)) and one carbonyl oxygen $(O(2)^i$; symmetry code (i): $1-x,-y,-z$). The La–O(water) distances, ranging from 2.525(5) to 2.587(5) Å, are similar to reported values [26]. The La–O(carboxylic oxygen) distances range from 2.433(5) to 2.633(5)Å. The La–O(carbonyl oxygen) distances is 2.385(5) Å. The $[CuL]^-$ and the lanthanum ions join together to form a ring structure. The nearest La–La distance is 8.093 Å.

In the packing scheme of the compound, intermolecular and intramolecular hydrogen bonds plays a very important role. The hydrogen atoms of water are involved in both intra- and intermolecular hydrogen bonds, bonding with the carbonylic, carboxylic and phenolic oxygen of the Schiff base ligand. The intermolecular bonds have $\cdots$O distances ranging from 1.87 to 2.87 Å. The molecules are linked by the extensive hydrogen bonding to form a three-dimensional network in the solid state.

$[Ce(H_2O)_5(CuL)_2][CuL]\cdot 8H_2O$ (**2**). The crystal structure of complex **2** is isomorphic to that of **1**, only small metric differences being observed for the two complexes. Owing to the slightly smaller radius of Ce^{III} than that of La^{III} [27], all the metal–ligand bonds in **2** are slightly shorter than the corresponding bonds in **1**, as compared in Table 2, however the bond angles in both are almost the same.

3.2. Magnetic properties of $[La(H_2O)_5(CuL)_2][CuL]\cdot 8H_2O$ (*1*)

The temperature dependency of magnetic susceptibilities $\chi_m T$ for **1** measured at 10 kOe field using a SQUID magnetometer are shown in Fig. 2. The $\chi_m T$ value at room temperature (2.252 emu K mol^{-1}) is very close to the expected value of 2.25 emu K mol^{-1} for six non-interacting spin-only Cu^{II} ions (La^{III} is a diamagnetic ion). As the temperature is decreased from 300 to 14.1 K, the values of $\chi_m T$ show a gradual increase, indicating a ferromagnetic coupling. After passing though a maximum of 5.13 emu K mol^{-1} at 14.1 K, $\chi_m T$ shows an abrupt decrease, suggesting a weak antiferromagnetic coupling between the ferromagnetic units. Ferromagnetic ordering is demonstrated further by the field dependence of isothermal magnetization performed at 1.9 K (inset of Fig. 2). The magnetization at 1.9 K increases very rapidly in low fields, and reaches the saturation value of ca. 25846 emu G mol^{-1} at 60 kOe.

For complex **2**, The $\chi_m T$ value at room temperature (3.36 emu K mol^{-1}) is slightly smaller than the calculated value (3.86 emu K mol^{-1}) for two Ce^{III} and six spin-only Cu^{II}. As the temperature decreases, the $\chi_m T$ value first decreases slowly between 300 and 21 K (3.09 emu K mol^{-1}) and then drops very rapidly to

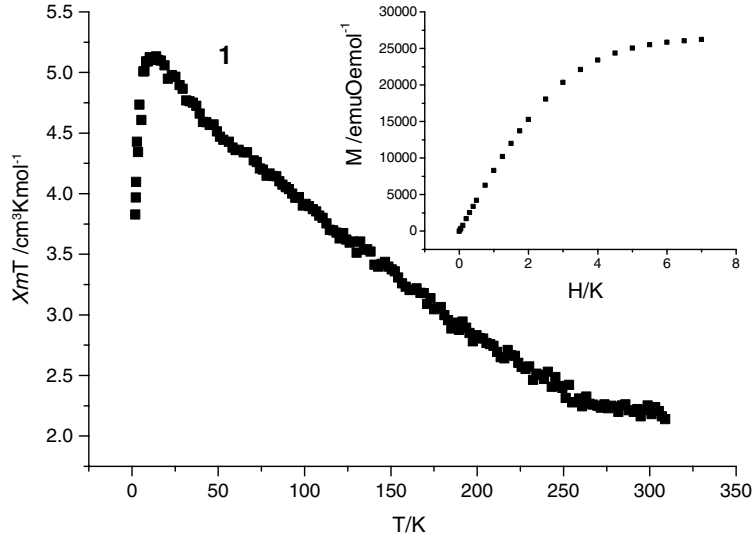

Fig. 2. Temperature dependence of $\chi_m T$ for a powder sample of $[La(H_2O)_5(CuL)_2]_2[CuL]_2\cdot 16H_2O$ (**1**). The field dependence of magnetization M for $[La(H_2O)_5(CuL)_2]_2[CuL]_2\cdot 16H_2O$ at 1.9 K is given in the inset.

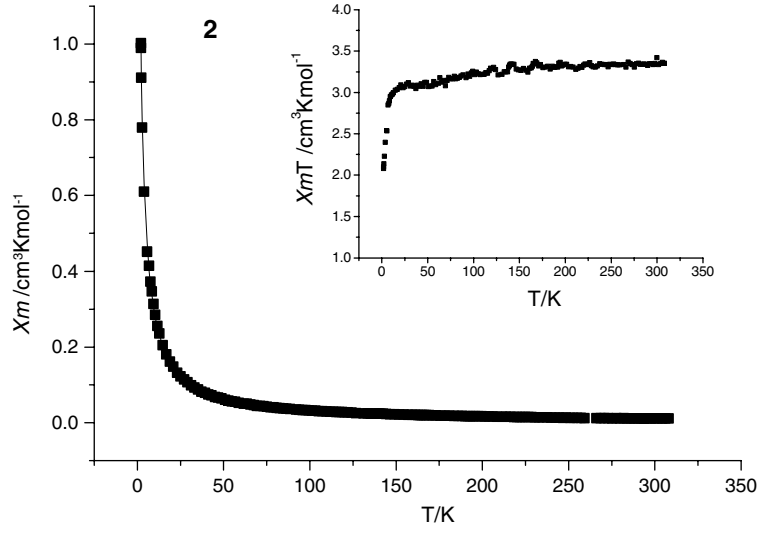

Fig. 3. Temperature dependence of χ_m for a powder sample of $[Ce(H_2O)_5(CuL)_2]_2[CuL]_2\cdot 16H_2O$ (**2**). The $\chi_m T$ vs T plot is given in the inset.

2.08 emu K mol^{-1} at 2 K (see Fig. 3). Fitting the data to the Curie–Weiss law gives $C = 3.22$ emu K mol^{-1}, $\theta = -1.17$ K with a final agreement factor $R = 2.0 \times 10^{-5}$ $[R = \sum(\chi_m^{obs} - \chi_m^{calc})^2 / \sum(\chi_m^{obs})^2]$, showing antiferromagnetic interactions.

4. Conclusion

In summary, we have prepared two novel hexanuclear complexes $[Ln(H_2O)_5(CuL)_2][CuL]\cdot 8H_2O$ constructed from the "metallo ligand" $[CuL]^-$ and the rare-earth ions La or Ce, and have reported their magnetic properties. Many fascinating structures will be assembled by the versatile building block $[CuL]^-$.

5. Supplementary data

CCDC 225171 and 225172 contain the supplementary crystallographic data for this paper. These data can be obtained free of charge at www.ccdc.cam.ac.uk/conts/retrieving.html [or from the Cambridge Crystallographic Data Centre, 12, Union Road, Cambridge CB2 1EZ, UK; fax: +44-1223/336-033; E-mail: deposit@ccdc.cam.ac.uk].

Acknowledgement

We thank the National Nature Science Foundation of China (No. 20171022); Jiangsu Science & Technology

Department and the Center of Analysis and Determining of Nanjing University for financial support.

References

[1] M. Andruh, I. Ramade, E. Codjovi, O. Guillou, O. Kahn, J.C. Trombe, J. Am. Chem. Soc. 115 (1993) 1822.
[2] R. Georges, O. Kahn, O. Guillou, Phys. Rev. B 49 (1994) 3235.
[3] S. Wang, Z. Pang, D.L. Smith, Inorg. Chem. 32 (1993) 4992.
[4] E.K. Brechin, S.G. Harris, S. Parson, R.E. Winpenny, J. Chem. Soc., Dalton Trans. (1997) 1665, and refs. therein.
[5] Y.Y. Yang, Y.L. Wu, L.S. Long, X.M. Chen, J. Chem. Soc., Dalton Trans. (1999) 2005.
[6] A. Ouchi, Y. Suzuki, Y. Ohki, Y. Koizumi, Coord. Chem. Rev. 92 (1988) 29.
[7] C. Benelli, D. Gatteschi, Chem. Rev. 102 (2002) 2369.
[8] (a) J.J. Bodwin, A.D. Cutland, R.G. Malkani, V.L. Pecoraro, Coord. Chem. Rev. 216 (2001) 489;
(b) A.J. Stemmler, J.W. Kampf, M.L. Kirk, B.H. Atasi, V.L. Pecoraro, Inorg. Chem. 38 (1999) 2807.
[9] (a) X.M. Chen, S.M.J. Aubin, Y.L. Wu, Y.S. Yang, T.C.W. Mak, D.N. Hendrickson, J. Am. Chem. Soc. 117 (1995) 9600;
(b) Y.C. Liang, R. Cao, W.P. Su, M.C. Hong, W.J. Zhang, Angew. Chem., Int. Ed. Engl. 39 (2000) 3304;
(c) Y. Cui, G. Chen, J. Ren, Y.T. Qian, J.S. Huang, Inorg. Chem. 39 (2000) 4165;
(d) J.J. Zhang, S.M. Hu, L.M. Zheng, X.T. Wu, Z.Y. Fu, J.C. Dai, W.X. Du, H.H. Zhang, R.Q. Sun, Chem.-Eur. J. 8 (2002) 5742.
[10] A.C. Rizzi, R. Calvo, R. Baggio, M.T. Garland, O. Pena, M. Perec, Inorg. Chem. 41 (2002) 5609.
[11] J.P. Costes, F. Dahan, C. R. Acad. Sci. II C 4 (2001) 97.
[12] R. Baggio, M.T. Garland, Y. Moreno, O. Pena, M. Perec, E. Spodine, J. Chem. Soc., Dalton Trans. (2002) 2061.
[13] (a) T. Kido, Y. Ikuta, Y. Sunatsuki, Y. Ogawa, N. Matsumoto, Inorg. Chem. 42 (2003) 398;
(b) T. Kido, S. Nagasato, Y. Sunatsuki, N. Matsumoto, Chem. Commun. (2000) 2113.
[14] (a) Q.D. Liu, S. Gao, J.R. Li, Q.Z. Zhou, K.B. Yu, B.Q. Ma, S.W. Zhang, X.X. Zhang, T.Z. Jin, Inorg. Chem. 39 (2000) 2488;
(b) Y. Zou, W.L. Liu, C.L. Ni, Z.P. Ni, Y.G. Yao, Q.J. Meng, Inorg. Chem. Commun. 7 (2004) 101.
[15] M.L. Kahn, C. Mathoniere, O. Kahn, Inorg. Chem. 38 (1999) 3692.
[16] C.T. Yang, B. Moubaraki, K.S. Murray, J.D. Ranford, J.J. Vittal, Inorg. Chem. 40 (2001) 5934.
[17] J.D. Ranford, J.J. Vittal, D. Wu, X. Yang, Angew. Chem., Int. Ed. 38 (1999) 3498.
[18] C.T. Yang, B. Moubaraki, K.S. Murray, J.J. Vittal, J. Chem. Soc., Dalton Trans. (2003) 880.
[19] A. Erxleben, D. Schumacher, Eur. J. Inorg. Chem. (2001) 3039.
[20] E. Colacio, J.M. Domínguea-Vera, M. Ghazi, R. Kivekäs, M. Klinga, J.M. Moreno, Eur. J. Inorg. Chem. (1999) 441.
[21] E. Colacio, M. Ghazi, R. Kivekäs, J.M. Moreno, Inorg. Chem. 39 (2000) 2882.
[22] Y. Zou, W.L. Liu, C.S. Lu, J.L. Xie, C.L. Ni, Q.J. Meng, Inorg. Chem. Commun. 6 (2003) 1217.
[23] Y. Zou, W.L. Liu, S. Gao, J.L. Xie, Q.J. Meng, Chem. Commun. (2003) 2946.
[24] G.M. Sheldrick, SHELXTL. Structure Determination Software Programs. Version 5.10, Bruker Analytical X-ray Systems Inc., Madison, WI, USA, 1997.
[25] T. Ueki, T. Ashida, V. Sasada, K. Kakudo, Acta Crystallogr. B25 (1969) 328.
[26] Q.D. Liu, J.R. Li, S. Gao, B.Q. Ma, Q.Z. Zhou, K.B. Yu, H. Liu, Chem. Commun. (2000) 1685.
[27] R.D. Shannon, Acta Crystallogr., Sect. A 32 (1976) 751.

Available online at www.sciencedirect.com
SCIENCE DIRECT®
Polyhedron 23 (2004) 2259–2264
POLYHEDRON
www.elsevier.com/locate/poly

π ··· π Interaction assembled silver(I) complexes with the ligand 4′,5′-diaza-9′-(4,5-disubstituted-1,3-dithiol-2-ylidene)fluorene

Qin-Yu Zhu [a,b], Jie Dai [a,b,*], Ding-Xian Jia [a], Li-Hui Cao [a], Hai-Hong Lin [a]

[a] Department of Chemistry and Chemical Engineering, Suzhou University, Suzhou 215006, PR China
[b] Key Laboratory of Organic Synthesis of Jiangsu Province, Suzhou University 215006, PR China

Received 23 May 2004; accepted 5 July 2004
Available online 27 August 2004

Abstract

Six silver(I) complexes with a new type of ligand, 4′,5′-diaza-9′-(4,5-disubstituted-1,3-dithiol-2-ylidene)fluorene (L^n, n = 1, Me; 2, Et; 3, Bu substituted) have been obtained. Two of the complexes $[Ag(L^1)_2]ClO_4$ (**1**) and $[Ag(L^1)_2]SO_3CF_3$ (**4**) have been structurally characterized by single-crystal X-ray diffraction. All of the Ag(I) ions are coordinated linearly by two ligands and the cations take planar structures. These planes are further assembled into one dimensional columns by Ag–Ag weak bonds, π–π stacking and Ag···N interactions. The UV–Vis and fluorescence spectra of the complexes were studied and the ligand-centered energy levels are not changed dramatically when the complexes are formed.
© 2004 Elsevier Ltd. All rights reserved.

Keywords: Diaza-fluorene; Silver complexes; Crystal structures; Intermolecular interactions; Electronic spectra

1. Introduction

The research on metal complexes with bipyridine and 1,10–phenanthroline ligands has attracted great interest due to their long-standing application in electronic and luminescent photochemistry [1,2]. Several efforts were reported to tune the physical and chemical properties of the π system through chemical modification of the phenanthroline [3–6]. 1,10-Phenanthroline behaves as a σ chelator donor/π acceptor ligand, which implies that the low-lying π^* orbits are an attractive target for modifying the electrochemical or excited state properties of the corresponding complexes. Furthermore, great efforts on crystal engineering have been reported to design and prepare supramolecules or complexes having π···π stacking [7–9]. Recently much more attention has been paid to silver(I) compounds [10–13]. In view of these facts, we became interested in the ligands 4′,5′-diaza-9′-(4,5-disubstituted-1,3-dithiol-2-ylidene)fluorene, which are a derivative of bipyridine and has a similar structure to 1,10-phenanthroline (Scheme 1) [14,15]. Besides, these ligands have a conjugated dithiole moiety that changes the relative levels of the π orbitals, compared with those of phenanthroline and bipyridine. In this paper, we present the synthesis, spectroscopic properties and crystal structures of a series of Ag(I) complexes with this type of diaza fluorene. These complexes are expected to be a new molecular system.

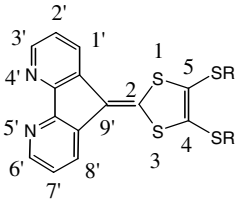

L^1: R= Me
L^2: R= Et
L^3: R= Bu

Scheme 1.

* Corresponding author. Tel.: +86 512 65224783; fax: +86 512 65224783.
E-mail address: daijie@suda.edu.cn (J. Dai).

0277-5387/$ - see front matter © 2004 Elsevier Ltd. All rights reserved.
doi:10.1016/j.poly.2004.07.007

2. Experimental

2.1. Materials and methods

The reagents L^1, 4′,5′-diaza-9 ′-(4,5-bis(methylthio)-1,3-dithiol-2-ylidene) fluorene; L^2, 4′,5′-diaza-9′-(4,5-bis-(ethylthio)-1,3-dithiol-2-ylidene)fluorene; L^3, 4′,5′-diaza-9′-(4,5-bis(butylthio)-1,3-dithiol-2-ylidene)fluorene were prepared according to the literature [16–19]. Acetonitrile was dried and distilled by a standard method before use. Elemental analyses of C, H and N were performed using an EA1110 elemental analyzer. The IR spectra were recorded as KBr discs on a Nicolet Magma 550 FT-IR spectrometer. ^{1}H NMR spectra were measured by an UNITYNOVA-400 spectrophotometer. UV–Vis spectra were recorded using a Shimadzu UV-240 spectrometer. The fluorescence spectra were recorded on a RF-540 fluorescent photometer.

2.2. Synthesis of the complexes

2.2.1. $[Ag(L^1)_2]ClO_4 \cdot 2CH_2Cl_2$ (1)

To an acetonitrile solution (1 ml) of $AgClO_4 \cdot H_2O$ (0.1 mmol, 20.76 mg) was slowly dropped a dichloromethane solution (15ml) of the ligand L^1 (0.1 mmol, 36 mg). The mixture was stirred for 30 min at room temperature. After that, an orange precipitate formed which was filtrated, washed with the solvents, and finally dried in vacuum over silica gel (Yield 61%). *Anal.* Calc. for $C_{34}H_{28}AgCl_5N_4O_4S_8$: C, 37.30; H, 2.58; N, 5.12. Found: C, 37.12; H, 2.38; N, 5.49%.

2.2.2. $[Ag(L^2)_2]ClO_4 \cdot CH_2Cl_2$ (2)

Complex **2** was synthesized by a similar procedure as for complex **1** (Yield 69%). Anal. Calc. for $C_{37}H_{34}AgCl_3N_4O_4S_8$: C, 41.55; H, 3.20; N, 5.24. Found: C, 41.50; H, 3.23; N, 5.41%.

2.2.3. $[Ag(L^3)_2]ClO_4 \cdot CH_2Cl_2$ (3)

Complex **3** was also synthesized by a similar procedure as for complex **1** (Yield 60%). Anal. *Calc.* for $C_{45}H_{50}AgCl_3N_4O_4S_8$: C, 45.74; H, 4.27; N, 4.74. Found: C, 45.40; H, 4.19; N, 4.62%.

2.2.4. $[Ag(L^1)_2]SO_3CF_3 \cdot 1/2\,CH_2Cl_2$ (4)

To an acetonitrile solution (1 ml) of $AgSO_3CF_3$ (0.05 mmol, 13.7 mg) was slowly dropped a dichloromethane solution (8 ml) of the ligand L^1 (0.05 mmol, 18 mg). The mixture was stirred for 30 min at room temperature. After that, an orange precipitate formed which was filtrated, washed with the solvents, and finally dried in vacuum over silica gel (Yield 65%). *Anal.* Calc. for $C_{33.5}H_{25}AgCl_1F_3N_4O_3S_9$: C, 39.43; H, 2.47; N, 5.49. Found: C, 39.93; H, 2.39; N, 5.54%.

2.2.5. $[Ag(L^2)_2]SO_3CF_3 \cdot 1/2\,CH_2Cl_2$ (5)

Complex **5** was synthesized by a similar procedure as for complex **4** (Yield 62%). *Anal.* Calc. for $C_{37.5}H_{33}AgCl_1F_3N_4O_3S_9$: C, 41.84; H, 3.07; N, 5.21. Found: C, 41.99; H, 3.14; N, 5.20%.

2.2.6. $[Ag(L^2)_2]SO_3CF_3 \cdot CH_2Cl_2$ (6)

Complex **6** was also synthesized by a similar procedure as for complex **4** (Yield 68%). *Anal.* Calc. for $C_{46}H_{50}AgCl_2F_3N_4O_3S_9$: C, 44.84; H, 4.06; N, 4.55. Found: C, 44.75; H, 4.09; N, 4.57%.

2.3. X-ray crystallography

X-ray crystallographic data for complexes **1** and **4** were obtained using a Rigaku Mercury CCD area detector with graphite monochromated Mo Kα (λ = 0.71070 Å) radiation. The data of **1** have been reported as a letter [15]. The data of **4** were collected at a temperature of 193.15 K to a maximum 2θ value of 55.0° using ω scans. An empirical absorption correction was applied and the structure was solved by the SHELXS-97 software package. The non-hydrogen atoms were refined anisotropically and hydrogen atoms were added theoretically. The final cycle of full-matrix least-squares refinement on F^2 was based on all unique reflections of **4**. The weighted *R*-factor and goodness-of-fit *S* are based on F^2 and conventional *R*-factors are based on *F*. Calculations were performed using the SHELXL-97 software package. Table 1 lists relevant crystallographic data for complex **4** and details of data collection. Table 2 lists the selected bond lengths and angles and the important

Table 1
Crystallographic data for complex **4**

Empirical formula	$C_{102}H_{76}Ag_3Cl_4F_{12}N_{12}O_{12}S_{28}$
Formula weight	3252.84
Crystal size (mm)	$0.25 \times 0.65 \times 0.07$
Crystal system	triclinic
Space group	$P\bar{1}$
Unit cell dimensions	
a (Å)	11.008(2)
b (Å)	12.759(3)
c (Å)	22.870(4)
α (°)	98.038(4)
β (°)	94.900(3)
γ (°)	105.203(4)
V (Å^3)	3043.9(10)
Z	1
$D_{calc.}$ (Mg m^{-3})	1.775
Absorption coefficient (mm^{-1})	1.129
F(000)	1633
Temperature (K)	193.15
$2\theta_{max}$ (°)	55.0
Number of unique reflections	13605
Number of reflections (gt) [$I > 2.0\sigma(I)$]	11209
Goodness-of-fit	1.089
R (gt)	0.0709
wR (gt)	0.1644

Table 2
Selected bond lengths (Å), angles (°) and important interaction distances (Å) for complex **4**

Bond lengths		Bond angles	
Ag(1)–N(1)	2.200(5)	N(1)–Ag(1)–N(1′)	180
Ag(2)–N(3)	2.193(4)	N(3)–Ag(2)–N(5)	177.60(15)
Ag(2)–N(5)	2.200(4)		
Intra- or inter-molecular contacts			
Ag(2)···Ag(2′)	3.564	Ag(2)···C(5)	3.401
Ag(1)···N(6)	3.267	C(1)···C(41)	3.352
C(8)···C(18)	3.339	C(21)···C(11)	3.382

interaction distances for **4** (shorter than the sum of Van der Waals radii). Disorder was found for one Cl atom of the solvent, one F and one O atom of the anion. For the same reason, the H atoms of dichloromethane could not be located.

3. Results and discussion

3.1. Synthesis of the compounds

The ligands were prepared according to the literature [16–19] and were characterized before being used. These molecules, L^n ($n = 1$–3), have part of a TTF (tetrathiafulvalene) moiety and showed quasi-reversible one-electron redox behavior [19]. Due to the ligands having good solubility only in dichloromethane, the complexes of $[Ag(L^n)_2]ClO_4 \cdot mCH_2Cl_2$ (**1**–**3**) and $[Ag(L^n)_2]SO_3CF_3 \cdot mCH_2Cl_2$ (**4**–**6**) was synthesized by reaction of the ligands L^n with $AgClO_4$ or $AgSO_3CF_3$ in mixed solvents of acetonitrile and dichloromethane. Although complex **1** has been reported previously as a communication for discussion of the conversion of molecular configuration in the solid state and in solution [15], it is still mentioned here for the integrity of the silver complexes. The red single crystals suitable for X-ray diffraction were obtained from the filtrate of a diluted reaction solution at room temperature under ambient conditions. X-ray crystal structure determination showed that solvent molecules CH_2Cl_2 are included in the crystals, but they are lost quickly when the crystals are separated from the mother liquid for a period. Thus the elemental analysis was carried out immediately after the micro-crystal powders were separated.

3.2. Structural descriptions

The crystal structure of $[Ag(L^1)_2]ClO_4 \cdot 2CH_2Cl_2$ (**1**) and $[Ag(L^1)_2]SO_3CF_3 \cdot 1/2\,CH_2Cl_2$ (**4**) are shown in Fig. 1. In **1**, the silver ion is coordinated linearly by two nitrogen atoms from two ligands. It is noteworthy that although the linear coordinated planar structure of $[Ag(L^1)_2]^+$ in **4** is similar to that of **1**, the crystal structure of **4** is quite different from **1**. Two types of silver

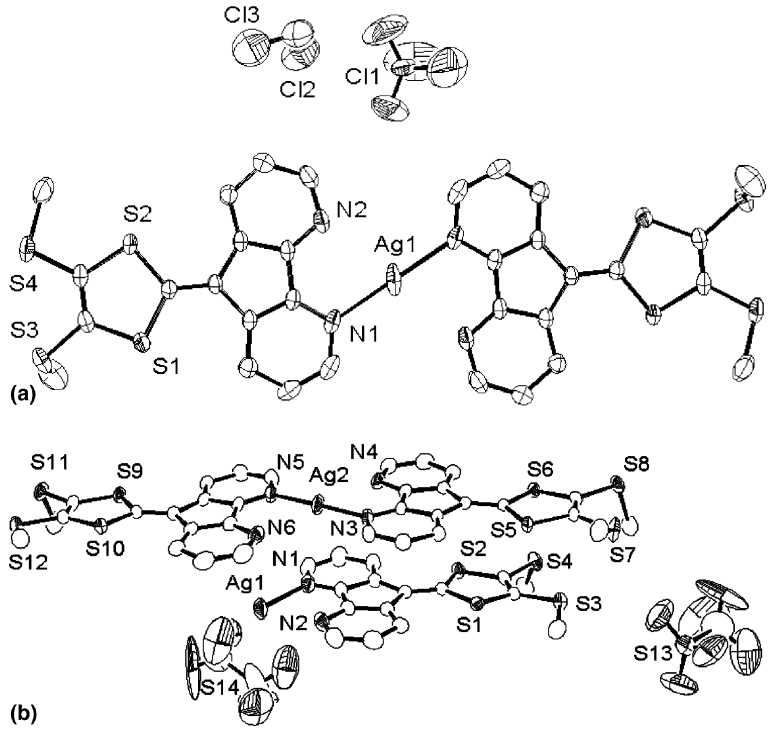

Fig. 1. ORTEP view of $[Ag(L^1)_2]ClO_4 \cdot 2CH_2Cl_2$ (**1**) (a) and $[Ag(L^1)_2]SO_3CF_3 \cdot 1/2\,CH_2Cl_2$ (**4**) (b), showing the selected atom labels. Non-H atoms are shown as 50% probability displacement ellipsoids. The solvent is omitted for clarity for **4**.

centers were found within the compound. Ag(1) is coordinated linearly by two ligands via N(1) and N(1′) atoms with an inversion center. The two Ag(1)–N(1) distances of **4** are equivalent (2.200 Å) and the two other Ag–N distances are 2.727 Å, longer than the coordination bonds. Ag(2) is also linearly coordinated by two N atoms from two ligands, but they are not equivalent in the operation of crystallographic symmetry, due to the methylthio groups of the two ligands being orientated on the same side of the ion's plane (Fig. 1(b)). The distances of Ag(2)–N(3) and Ag(2)–N(5), 2.193 and 2.200 Å, respectively, are approximately equivalent to the Ag(1)–N(1) distance. The other Ag–N distances are 2.714 Å for Ag(2)–N(6) and 2.732 Å for Ag(2)–N(4). Although linear coordination is very common for Ag(I) complexes, it is not for 2,2′-bipyridine and phenanthroline complexes. In contrast, a number of four coordinated Ag(I) complexes are reported [11,12]. Burke has indicated that complexes of the type $[M(bpy)_2]^{n+}$ and $[M(phen)_2]^{n+}$ are unable to adopt a square-planar configuration because of steric interaction between α-H atoms [13]. For the same reason most octahedral $[M(bpy)_2X_2]^{n+}$ and $[M(phen)_2X_2]^{n+}$ ions take on a *cis*-structure rather than a *trans*-one. Thus the planar structure of $[Ag(L)_2]^+$ is unusual and it is benefited by the linear coordination of the Ag(I) ion and the intermolecular interactions of the extended molecular planes. The linear coordination keeps away from the steric hindrance of the α-H atoms of the two ligands and the planar structure can be further stabilized by the layered close-packing with strong interactions.

In complex **4**, three $[Ag(L^1)_2]^+$ cations form a unit in which two form a pair which is interconnected by a weak Ag(2)···Ag(2′) bond (3.56 Å) and the other is independent (Fig. 2) with a Ag(1) to Ag(2) separation of 4.307 Å. All the molecules are found in columns propagated in the direction of the *a* axis and displaying three distinct forms of intermolecular interaction of Ag···C (3.40 Å), Ag···N (3.28 Å) and C···C (3.34–3.38 Å). It is interesting that unlike the structure of **1**, in which the Ag···S and C···C interactions act continuously along the column, the interactions in **4** only exist within the planes of Ag(1) and Ag(2) and there is no interaction within the Ag(2) planes except the weak

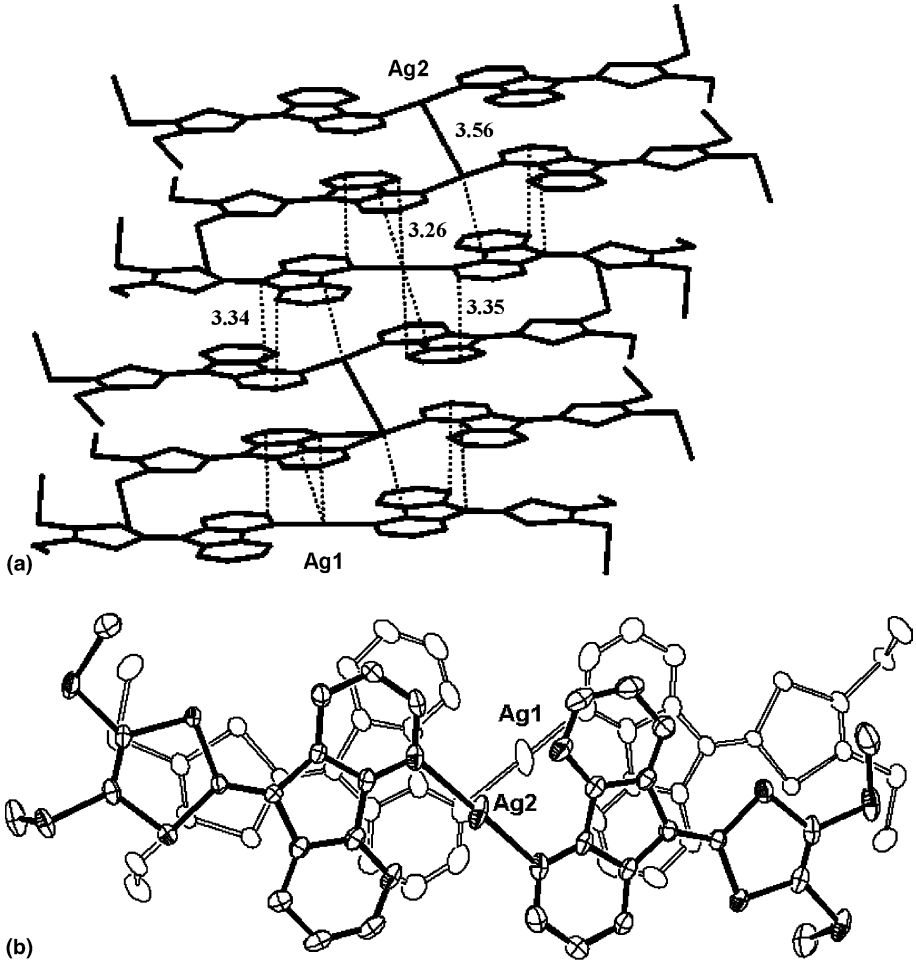

Fig. 2. (a) Molecular packing of **4** within a column, the dashed lines are used to represent inter-planar π–π stacking and Ag···N interactions. (b) Top view of the two units of $[Ag(L^1)_2]^+$ showing the overlap areas.

Table 3
^{1}H NMR chemical shifts of the ligands and their complexes

Compound	H'_1, H'_8	H'_2, H'_7	H'_3, H'_6	
L^1	8.68	7.39	8.06	2.58 ($-CH_3$)
1 $[Ag(L^1)_2]ClO_4$	8.78	7.55	8.24	2.63 ($-CH_3$)
4 $[Ag(L^1)_2]SO_3CF_3$	8.81	7.60	8.28	2.62 ($-CH_3$)
L^2	8.68	7.39	8.07	1.41, 3.02 ($-CH_2CH_3$)
2 $[Ag(L^2)_2]ClO_4$	8.82	7.62	8.29	1.43, 3.05 ($-CH_2CH_3$)
5 $[Ag(L^2)_2]SO_3CF_3$	8.93	7.79	8.49	1.44, 3.07 ($-CH_2CH_3$)
L^3	8.68	7.41	8.08	0.96, 1.50, 1.70, 2.98 ($-CH_2CH_2CH_2CH_3$)
3 $[Ag(L^3)_2]ClO_4$	8.81	7.70	8.35	0.97, 1.52, 1.74, 3.05 ($-CH_2CH_2CH_2CH_3$)
6 $[Ag(L^3)_2]SO_3CF_3$	8.82	7.76	8.41	0.96, 1.51, 1.73, 3.03 ($-CH_2CH_2CH_2CH_3$)

Ag···Ag bond. Fig. 2 shows the alternant interaction structure and a top view of the planes of Ag(1) and Ag(2) showing the overlap areas.

3.3. Spectral properties

The ^{1}H NMR spectra and signal assignments of ligands L^1–L^3 and the complexes **1**–**6** in $CDCl_3$ are summarized in Table 3. As an example, for complex **4** two doublet signals at 8.81 and 8.28 ppm are assigned to ^{1}H at 1′, 8′ and 3′, 6′ ring sites of the fluorene, respectively (Scheme 1). The signal at 7.60 with a quartet-split is assigned to the ^{1}H at 2′ and 7′ ring sites. The signals below 3.10 ppm are attributed to the alkyl groups. The general downfield shifts can be attributed to the coordination of the ligands with the positive silver ion. All the chemical shifts of the aromatic protons of **4**–**6** are somewhat larger than those of **1**–**3**, which might have arisen from the polarized anion.

The important IR vibration bands and their assignments are given in Table 4. The ν(C=N) band at 1540 cm^{-1} for the free ligand L^n is somewhat shifted to lower energy in the case of the complexes $[Ag(L^n)_2]ClO_4$ and $[Ag(L^n)_2]SO_3CF_3$, due to the coordination of the imino group in the pyridyl ring. The same results were also found for the C=C vibration bands at about 1480 cm^{-1}. In contrast to the C=N and C=C bands, the S–C–S vibrations at about 856 cm^{-1} are enhanced on the formation of the complexes. The ClO_4^- vibrations of **1**–**3** were observed at around 1090 cm^{-1}, and the $SO_3CF_3^-$ vibrations of the complexes **4**–**6** were observed at around 1265 cm^{-1}, which confirms the presence of the counterions.

The UV–Vis spectral data of phenanthroline, the ligands and their complexes in dichloromethane have been measured. In contrast to the spectrum of phenanthroline (no absorption bands above 300 nm) a strong absorption band at about 410–415 nm appeared when the ligand was modified with the extended and conjugated dithiole structure. An intramolecular charge transfer, from dithiole to the bipyridine moieties, is attributed to the new absorption. The representative spectra of L^3 (R = Bu) and complex **3** are given in Fig. 3. This new absorption band red shifts to 420–435 nm on the formation of the complex, which is due to the influence of the electron withdrawing property of the Ag(I) ion. Since the tail of this band develops over 500 nm, these complexes are red in color in contrast to the yellow ligands.

Fluorescence spectra show that the ligand emits a strong fluorescence at 365 nm (λ_{ex} 300 nm, $CHCl_3$). This fluorescence band is still observed and does not change

Table 4
Characteristic IR bands of the ligands and their complexes (cm^{-1})

Compound	ν(C=N)	ν(C=C)	ν(S–C–S)	ν(C–N)	$\nu(ClO_4)$	$\nu(SO_3CF_3)$
L^1	1540vs	1488vs	857m	738vs		
1 $[Ag(L^1)_2]ClO_4$	1539s	1483s	862m	740m	1094vs	
4 $[Ag(L^1)_2]SO_3CF_3$	1539s	1480s	861m	740m		1268vs
L^2	1540vs	1480vs	856m	745s		
2 $[Ag(L^2)_2]ClO_4$	1536vs	1474vs	859m	739s	1093vs	
5 $[Ag(L^2)_2]SO_3CF_3$	1534s	1472s	860m	740vs		1261vs
L^3	1542vs	1487m	855m	741s		
3 $[Ag(L^3)_2]ClO_4$	1537s	1478s	859m	739s	1081vs	
6 $[Ag(L^3)_2]SO_3CF_3$	1537s	1481m	860m	740m		1266vs

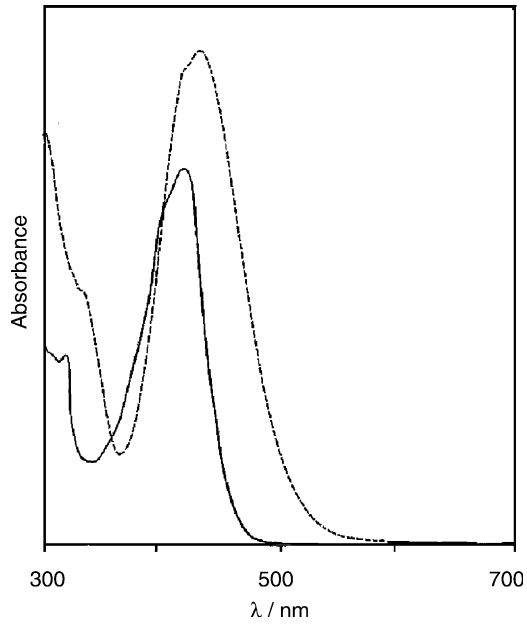

Fig. 3. UV–Vis spectra of the ligand L^3 (solid line) and complex **3** (dash-line) in dichloromethane.

when the complex is formed (ligand centered π–π emission). This result has been explained by the tetrahedral configuration of the complex in solution [15]. On the other hand, the emission spectra in the visible range are dramatically different (Fig. 4). Although self-absorption should also be considered at about 400–480 nm for both the ligands and the complexes, the weak emission above 550 nm is clearly a new band which can be assigned to the fluorescence of the Ag(I) ion of the d^{10} metal. However the energy level of the complexes and the assignment of the emission bands need to be studied further.

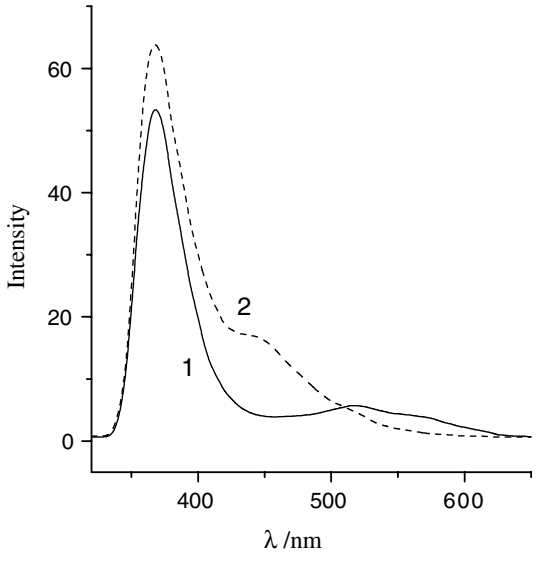

Fig. 4. Fluorescence spectra of ligand L^3 (line 2) and complex **3** (line 1) in trichloromethane (λ_{ex} 300 nm).

4. Supplementary data

Crystallographic data for the structural analyses have been deposited with the Cambridge Crystallographic Data Centre, CCDC Nos. 209123 and 228492 for compounds **1** and **4**, respectively. These data can be obtained free of charge via www: http://www.ccdc.cam.ac.uk or from the Cambridge Crystallographic Data Centre, 12 Union Road, Cambridge CB2 1EZ, UK; fax: +44 1223 336 033, or e-mail: deposit@ccdc.cam.ac.uk.

Acknowledgements

This work was supported by the National Natural Science Foundation (20071024, 20371033), PR China. The authors are also grateful to the Laboratory of Organic Solids, Institute of Chemistry, Chinese Academy of Sciences, Beijing 100080, PR China for financial support.

References

[1] N.P. Ayala, C.M. Flynn Jr., L. Sacksteder, J.N. Demas, B.A. DeGraff, J. Am. Chem. Soc. 112 (1990) 3837.
[2] L. Kenneth Kam-Wing, H. Wai-Ki, N. Dominic Chun-Ming, C. Kung-Kai, Inorg. Chem. 41 (2002) 40.
[3] P.G. Sammes, G. Yahioglu, Chem. Soc. Rev. (1994) 327.
[4] E. Peña-Cabrera, P.O. Norrby, M. Sjögren, A. Vitagliano, V. De Felice, J. Oslob, S. Ishii, D. O'Neill, B. Akermark, P. Helquist, J. Am. Chem. Soc. 118 (1996) 4299.
[5] A. Klein, W. Kaim, E. Waldhör, H.D. Hausen, J. Chem. Soc., Perkin Trans. 2 (1995) 2121.
[6] S. Ernst, C. Vogler, A. Klein, W. Kaim, S. Zalis, Inorg. Chem. 35 (1996) 1295.
[7] M. Kato, K. Sasano, C. Kosuge, M. Yamazaki, S. Yano, M. Kimura, Inorg. Chem. 35 (1996) 116.
[8] M. Munakata, T. Kuroda-Sowa, M. Maekawa, M. Nakamura, S. Akiyama, S. Kitagawa, Inorg. Chem. 33 (1994) 1284.
[9] M. Munakata, J. Dai, M. Maekawa, T. Kuroda-Sowa, J. Fukui, J. Chem. Soc., Chem. Commun. (1994) 2331.
[10] J.P. Alexander, M.M. Thomas, M.B. David, Polyhedron 16 (1997) 2711.
[11] T. Christoph, K. Wolfgang, Z. Stanislav, Inorg. Chem. 36 (1997) 2505.
[12] M.C. Samantha, C.J. John, D.W. Michael, Polyhedron 18 (1999) 2633.
[13] P.J. BurKe, D.R. McMillin, W.R. Rosinson, Inorg. Chem. 19 (1980) 1211.
[14] Q.Y. Zhu, G.Q. Bian, J. Dai, D.X. Jia, J.S. Zhang, L. Guo, Inorg. Chim. Acta 351:1 (2003) 177.
[15] Q.Y. Zhu, Y. Zhang, J. Dai, G.Q. Bian, D.X. Jia, J.S. Zhang, L. Guo, Chem. Lett. 32 (2003) 762.
[16] L.J. Henderson, J. Frank, R. Fronczek, R. William, J. Am. Chem. Soc. 106 (1984) 5876.
[17] N. Svenstrup, K.M. Rasmussen, T.K. Hansen, J. Becher, Synthesis (1994) 809.
[18] N. Svenstrup, J. Becher, Synthesis (1995) 215.
[19] K. Sako, M. Kusakabe, H. Tatemitsu, Mol. Cryst. Liq. Cryst. 285 (1996) 101.

Available online at www.sciencedirect.com
SCIENCE DIRECT®
Polyhedron 23 (2004) 2265–2272
POLYHEDRON
www.elsevier.com/locate/poly

Syntheses and characterizations of a series of heptanuclear octahedral polyhedra {$LnNi_6$} with different amino acids as ligands in aqueous media

Jian-Jun Zhang, Sheng-Chang Xiang, Sheng-Min Hu, Sheng-Qing Xia, Rui-Biao Fu, Xin-Tao Wu *, Ya-Min Li, Hui-Shuang Zhang

Department of Chemistry, State Key Laboratory of Structural Chemistry, Fujian Institute of Research on the Structure of Matter, Chinese Academy of Sciences, Fuzhou, Fujian 350002, PR China

Received 20 May 2004; accepted 6 July 2004
Available online 28 August 2004

Abstract

$Ln(ClO_4)_3$ and $Ni(ClO_4)_2$ self-assemble in the presence of amino acids (glycine, L-alanine or L-threonine) to form seven novel heptanuclear octahedral clusters {$LnNi_6$} (Ln = La, Pr). X-ray structures are reported for $Na[LaNi_6(Gly)_{12}](ClO_4)_4(H_2O)_{11}$ (**1**), $Na_5[LaNi_6(Gly)_{12}](ClO_4)_8(H_2O)_{10}$ (**2**), $Na[PrNi_6(Gly)_{12}](ClO_4)_4(H_2O)_{11}$ (**3**), $[LaNi_6(Gly)_{12}][Ni(im)(H_2O)_5]\cdot(ClO_4)_5(H_2O)_5$ (**4**) and $[LaNi_6(Gly)_{12}][Ni(NCS)_3(H_2O)_3][Ni(NCS)_2(H_2O)_4]\cdot(ClO_4)_2(H_2O)_6$ (**5**). L-Alanine and L-threonine were used as ligands to synthesize $[LaNi_6(Ala)_{12}](ClO_4)_3\cdot(H_2O)_{15}$ (**6**) and $[LaNi_6(Thr)_{12}](ClO_4)_3\cdot(H_2O)_{15}$ (**7**). In the $[LnNi_6(Gly)_{12}]^{3+}$ ions, the Ln^{3+} ion is in the center of the octahedral cage formed by six nickel atoms and coordinates to 12 carboxylate oxygen atoms. Its coordination polyhedron may be best described as an icosahedron. Complexes **1, 3** and **4** exhibit ferromagnetic interactions.
© 2004 Elsevier Ltd. All rights reserved.

Keywords: Nickel(II); Lanthanides(III); Amino acid; Heptanuclear; Cluster compound

1. Introduction

Sparked by the structural diversity and interesting luminescence and magnetic properties found and proposed for 3d–4f clusters [1], interest in their rational synthesis has been increasing rapidly since the pioneering work of Gatteschi [2]. Up until now many heterometallic compounds of transition metals and rare earth metals have been synthesized with pyridones [3], Schiff-base [4], oxalato [5], oximates [6] or oxamides [7], cyano groups [8] and carboxylic acids [9] as ligands. However, despite extensive research on low-nuclearity 3d–4f complexes, only a few studies have focused on the design and synthesis of high-nuclearity compounds of 3d–4f clusters [9a,10].

Amino acid is one of the most important biological ligands. Research on the coordination of metal–amino acid complexes has contributed to our understanding of the function of metal ions in organisms. Up until now many Ln–amino acid complexes [11] and 1:1 or 1:2 transition metal–amino acid complexes [12] with a mononuclear or chain structure motif have been synthesized, though only recently a series of poly-nuclear lanthanide clusters with amino acid as the ligand were reported [13]. Recently we also showed that amino acid is a useful ligand for the construction of poly-nuclear copper clusters [14]. But until now, only three reports have focused on the 3d–4f-amino acid system, which are the $LnNi_6$ octahedral complex [15], the series of

* Corresponding author. Tel.: +865913792837; fax: +865913714946.
E-mail address: wxt@ms.fjirsm.ac.cn (X.-T. Wu).

0277-5387/$ - see front matter © 2004 Elsevier Ltd. All rights reserved.
doi:10.1016/j.poly.2004.07.012

$LnNi_6$ trigonal prismatic complexes [16] and the 32-nuclearity complex $\{La_6Cu_{26}\}$ reported by our group [10c]. The difficulty in obtaining this kind of complex may be attributed to the fact that 3d and 4f ions have distinctly different chemical behavior and the difficulty of seeking a suitable pH window so that the ligand can use both amino and carboxylate groups to coordinate to 3d and 4f metal ions. As amino acid ligands have a variety of coordinated modes, their use for the synthesis of 3d–4f heteronuclear compounds can lead to structures much more complex and intriguing than those of simple carboxylic acids [10c,16].

Up until now there are five kinds of heptanuclear 3d–4f clusters with the general formula of LnM_6 (M = transition metal) with the wheel ($LnCu_6$) [17], trigonal prismatic ($LnCu_6$ or $LnNi_6$) [16,18] and octahedral ($LnNi_6$) [15] structure motifs. Yukawa et al. [15] have synthesized an octahedral $SmNi_6$ cluster by the reaction of Sm^{3+} and bis(L-prolinato)nickel(II) in a non-aqueous medium, but the crystal is unstable. In this paper we report a series of octahedral $LnNi_6$ clusters obtained by the reaction of Ln^{3+}, Ni^{2+} and amino acid (glycine, L-alanine or L-threonine) in aqueous solution. The crystals obtained are very stable in air. The effect of solvent, the ionic radii of the lanthanide ions and other small molecular ligands, such as imidazole and SCN^-, on the synthesis are discussed. The magnetic behaviours were also studied.

2. Experimental

2.1. Materials and instrumentation

$Ln(ClO_4)_3 \cdot 6H_2O$ was synthesized by dissolving lanthanide oxide in an excess amount of perchloric acid. Other starting materials were of reagent grade and used without further purification. Elemental analyses were carried out by the Elemental Analysis Laboratory of our Institute. Magnetic measurements were carried out with a Quantum Design PPMS model 6000 magnetometer.

2.2. Synthesis of the complexes

2.2.1. $Na[LaNi_6(Gly)_{12}](ClO_4)_4(H_2O)_{11}$ (1)

To an aqueous solution (10 ml) of $La(ClO_4)_3 \cdot 6H_2O$ (0.545 g, 1 mmol), $Ni(ClO_4)_2 \cdot 6H_2O$ (2.184 g, 6 mmol) and glycine (0.90 g, 12 mmol) were added. Then the pH value of the reaction mixture was carefully adjusted to about 6.6 by slow addition of 0.1 M NaOH solution. After 2 h of stirring, the solution was filtered to remove a small amount of precipitate formed due to hydrolyzation of metal ions, and placed in a desiccator filled with phosphorus pentaoxide. Blue crystals were obtained about one month later. Yield: 0.76 g, 38%. *Anal*. Calc. for $C_{24}H_{70}Cl_4LaN_{12}NaNi_6O_{51}$: C, 14.42; H, 3.53; N, 8.41. Found: C, 14.32; H, 3.63; N, 8.58%.

2.2.2. $Na_5[LaNi_6(Gly)_{12}](ClO_4)_8 \cdot (H_2O)_{10}$ (2)

The above procedure was repeated except that the proportion of the reactants was controlled to be La^{3+}:Ni^{2+}:Gly = 1:9:9. Yield: 1.26 g, 51%. *Anal*. Calc. for $C_{24}H_{68}Cl_8LaN_{12}Na_5Ni_6O_{66}$: C, 11.67; H, 2.77; N, 6.80. Found: C, 11.46; H, 2.83; N, 6.51%.

2.2.3. $Na[PrNi_6(Gly)_{12}](ClO_4)_4 \cdot (H_2O)_{11}$ (3)

The above procedure was repeated except that $Pr(ClO_4)_3 \cdot 6H_2O$ was used and the proportion of the reactants was controlled to be Pr^{3+}:Ni^{2+}:Gly = 1:6:12. Yield: 0.71 g, 36%. *Anal*. Calc. for $C_{24}H_{70}Cl_4N_{12}NaNi_6O_{51}Pr$: C, 14.41; H, 3.53; N, 8.40. Found: C, 14.12; H, 3.43; N, 8.14%.

2.2.4. $[LaNi_6(Gly)_{12}][Ni(im)(H_2O)_5](ClO_4)_5(H_2O)_5$ (4)

The above procedure was repeated except imidazole was added and the proportion of the reactants was controlled to be La^{3+}:Ni^{2+}:Gly:im = 1:6:12:3. Yield: 0.66 g, 30%. *Anal*. Calc. for $C_{27}H_{72}Cl_5LaN_{14}Ni_7O_{54}$: C, 14.85; H, 3.32; N, 8.98. Found: C, 14.80; H, 2.95; N, 8.74%.

2.2.5. $[LaNi_6(Gly)_{12}][Ni(NCS)_3(H_2O)_3][Ni(NCS)_2(H_2O)_4] \cdot (ClO_4)_2 \cdot (H_2O)_6$ (5)

The above procedure was repeated except NaSCN was added and the proportion of the reactants was controlled to be La^{3+}:Ni^{2+}:Gly:SCN = 1:6:6:3. Yield: 0.56 g, 25%. *Anal*. Calc. for $C_{29}H_{74}Cl_2LaN_{17}Ni_8O_{45}S_5$: C, 15.69; H, 3.36; N, 10.72. Found: C, 15.43; H, 3.17; N, 10.32%.

2.2.6. $[LaNi_6(Ala)_{12}](ClO_4)_3 \cdot (H_2O)_{15}$ (6)

The above procedure was repeated except L-alanine was used and the proportion of the reactants was controlled to be La^{3+}:Ni^{2+}:Ala = 1:6:12. Yield: 0.87 g, 41%. *Anal*. Calc. for $C_{36}H_{102}Cl_3LaN_{12}Ni_6O_{51}$: C, 20.43; H, 4.86; N, 7.94. Found: C, 20.67; H, 5.16; N, 8.02%.

2.2.7. $[LaNi_6(Thr)_{12}](ClO_4)_3 \cdot (H_2O)_{15}$ (7)

The above procedure was repeated except L-threonine was used and the proportion of the reactants was controlled to be La^{3+}:Ni^{2+}:Thr = 1:6:12. Yield: 0.87 g, 35%. *Anal*. Calc. for $C_{48}H_{126}Cl_3LaN_{12}Ni_6O_{63}$: C, 23.28; H, 5.13; N, 6.79. Found: C, 23.18; H, 5.02; N, 6.94%.

2.3. X-ray crystallography

Intensity data for the five complexes **1**–**5** were collected at 293(2) K on a Siemens Smart/CCD area-detector diffractometer with Mo Kα radiation ($\lambda = 0.71073$

Table 1
Crystallographic and data collection parameters for **1**–**5**

	1	**2**	**3**	**4**	**5**
Formula	$C_{24}H_{70}Cl_4LaN_{12}NaNi_6O_{51}$	$C_{24}H_{68}Cl_8LaN_{12}Na_5Ni_6O_{66}$	$C_{24}H_{70}Cl_4N_{12}NaNi_6O_{51}Pr$	$C_{27}H_{72}Cl_5\ LaN_{14}Ni_7O_{54}$	$C_{29}H_{74}Cl_2LaN_{17}Ni_8O_{45}S_5$
M_r	1998.88	2470.62	2000.88	2184.12	2220.84
Crystal system	orthorhombic	monoclinic	orthorhombic	triclinic	monoclinic
Space group	*Pbca*	*P*2(1)/*n*	*Pbca*	$P\bar{1}$	*P*2(1)/*n*
Unit cell dimensions					
a (Å)	13.8190(3)	12.0188(1)	13.9159(2)	12.1754(1)	11.8213(2)
b (Å)	21.8328(5)	23.5126(2)	21.9051(2)	12.2494(2)	22.6328(4)
c (Å)	22.7222(5)	13.7395(2)	22.7883(3)	24.2394(4)	14.0375(1)
α (°)	90	90	90	84.549(1)	90
β (°)	90	97.627(1)	90	77.970(1)	107.780(1)
γ (°)	90	90	90	80.336(0)	90
Volume (Å^3)	6855.5(3)	3848.34(7)	6946.54(15)	3478.78(9)	3576.33(9)
Z	4	2	4	2	2
D_{calc} (g/cm^3)	1.937	2.132	1.913	2.085	2.062
F(0 0 0)	4040	2480	4048	2204	2244
Measured reflections	20191	11 768	22 136	18 172	11 529
Independent reflections	6070	6676	6037	12174	6300
$R_{(int)}$	0.0411	0.0296	0.0403	0.0225	0.0336
Goodness-of-fit on F^2	1.086	1.070	1.102	1.153	1.265
R[a]	0.0546	0.0483	0.0541	0.0428	0.0773
R_w[b]	0.1474	0.1059	0.1417	0.0932	0.1617

(**1**) $a = 0.0809$, $b = 41.4523$; (**2**) $a = 0.0452$, $b = 19.5793$; (**3**) $a = 0.0749$, $b = 39.6582$; (**4**) $a = 0.0215$, $b = 19.6060$; (**5**) $a = 0.0000$, $b = 56.5282$.

[a] $R = \sum \| F_o| - |F_c \| / \sum |F_o|$.

[b] $R_w = \left\{ \sum w[(F_o^2 - F_c^2)^2] / \sum w[(F_o^2)^2] \right\}^{1/2}$, $w = 1/[\sigma^2(F_o^2) + (aP)^2 + bP]$, $P = (F_o^2 + F_c^2)/3$.

Å). Data reduction and unit cell refinement were performed with Smart-CCD software [19a]. An absorption correction using SADABS software was applied [19b]. The structures were solved by direct methods using SHELXS-97 [20] and refined by full-matrix least squares using SHELXL-97 [20]. Anisotropic displacement parameters were refined for all non-hydrogen atoms. Hydrogen atoms of the methylene and amine groups of the amino acid have been placed in calculated positions (AFIX 23) and refined with a riding model. No attempt was made to locate the hydrogen atoms of water. The crystallographic data are summarized in Table 1.

3. Results and discussion

3.1. Synthesis of the complexes

Until now many Ln–amino acid complexes [11] and 1:1 or 1:2 transition metal–amino acid complexes [12] with a mononuclear or chain structure motif have been synthesized below pH 1–4. We have now developed a high pH synthesis procedure and have successfully prepared a series of 3d–4f heptanuclear clusters. During the synthesis process, we observed an interesting phenomenon controlled mainly by the ionic radii of the lanthanide ions. We have tried many times and various molar ratios of reagents to synthesize a $\{LaNi_6\}$ trigonal prismatic cluster, but failed [16]. In our attempted synthesis of $\{LnNi_6\}$ octahedral clusters in aqueous solution, only $\{LaNi_6\}$ and $\{PrNi_6\}$ octahedral clusters could be obtained though we have tried La^{3+}, Pr^{3+}, Nd^{3+}, Sm^{3+}, Eu^{3+}, Gd^{3+} and Er^{3+}. The ionic radii of the lanthanide ions were presumed to play an important role in the synthesis. Of the lanthanide ions, La^{3+} has the largest ionic radius (1.50 Å, 12-coordinated) [21]. In this system it prefers a stable 12-coordinated icosahedral configuration regardless of the molar ratios of reagents employed. For those lanthanide ions following Pr^{3+}, their ionic radii are not large enough to satisfy a 12-coordinate icosahedral configuration, so only $\{LnNi_6\}$ trigonal prismatic clusters have been obtained. Previously a heptanuclear octahedral cluster was synthesized with Sm^{3+} as the central ion and bis(L-prolinato)nickel(II) as the "ligand" in acetonitrile [15]. Thus the solvent can also affect the synthesis of the octahedral cluster, as the coordination ability of water to Ln^{3+} is superior to a non-aqueous solvent molecule. The competition of solvent effect and ionic radii effect account for the fact that $\{LnNi_6\}$ (Ln = Nd–Lu) octahedral clusters cannot be synthesized in aqueous solution.

In order to build new clusters, we tried to introduce some small molecular ligand, such as imidazole or SCN^- into the system, but failed. The $\{LnNi_6\}$ octahedral cluster is so stable that it does not take up any additional ligand.

3.2. IR spectra

Using **1** as an example, the complex has two ν_s(N–H) peaks at about 3350 and 3298 cm^{-1}, compared with 3130 and 3105 cm^{-1} of the free glycinato ligand. The spectrum of **1** also shows two strong peaks at ca. 1414 and 1578 cm^{-1} which may be assigned to stretching vibrations ν_{sym}(COO) and ν_{asym}(COO) of the carboxylate group of glycine. The strong bands at 1090 and 625 cm^{-1} may be assigned to the vibrations of ClO_4^-. The presence of water molecules was proven by the strong and broad OH resonance at 3300–3500 cm^{-1}. The spectra of other complexes were found to be similar to that of **1**, except that **4** has several peaks at about 1621 and 1537 cm^{-1} which may be attributed to the presence of imidazole and **5** has strong peak at about 2083 cm^{-1} (ν(SCN)).

3.3. Description of structures

X-ray diffraction analyses indicate that complexes **1**–**5** all have the same heptanuclear octahedral $\{LnNi_6\}$ cation. In the cations, all the lanthanide atoms sit on crystallographic centres of symmetry and thus the entire clusters are centrosymmetric. The structure of the cation of **1** is shown in Fig. 1 as an example. Selected bond distances and bond angles of **1** are shown in Table 2. The La^{3+} ion is situated in the center of a large octahedral cage formed by six Ni^{2+} ions with La···Ni distances and Ni···Ni distances of about 3.6950(0.0009)–3.7019(0.0009) and 5.2309(0.0013)–5.2424(0.0013) Å, respectively, compared with those observed in the $\{SmNi_6\}$ cluster (3.7 and 5.23 Å, respectively) [15] and the $\{LaNi_6\}$ cluster with imino-carboxylate as the ligand [18a] (3.63 and 5.12–5.15 Å, respectively).

The coordination polyhedron of the O_{12} coordinated centered La^{3+} ion, as shown in Fig. 2, may be best described as an icosahedron. The 12 carboxyl oxygen atoms from 12 glycinato ligands coordinate to the central lanthanide ion with distances of about 2.692–2.761 Å. The average nearest neighboring O···O distance is about 2.745–2.980 Å and the angles between two adjacent metal–ligand bonds are in the range of 61.49–65.80° (see Table 3).

Each Ni atom has an N_2O_4 donor set which consists of two amino nitrogen atoms and four carboxyl oxygen atoms from four glycinato ligands. The Ni–O and Ni–N distances are about 2.04–2.07 Å. For Ni(1), small deviations of bond angles from 180° of the idealized octahedral geometry are found for angles O(1)–Ni(1)–N(2) [174.8(2)°], O(3)–Ni(1)–N(1) [174.5(2)°] and O(6A)–Ni(1)–O(8) [176.5(2)°], implying it has a slightly distorted octahedral configuration. Other Ni ions show similar behavior.

In the cation, each glycinato ligand adopts a η^4-coordination mode, being bound to two Ni^{2+} and one La^{3+}

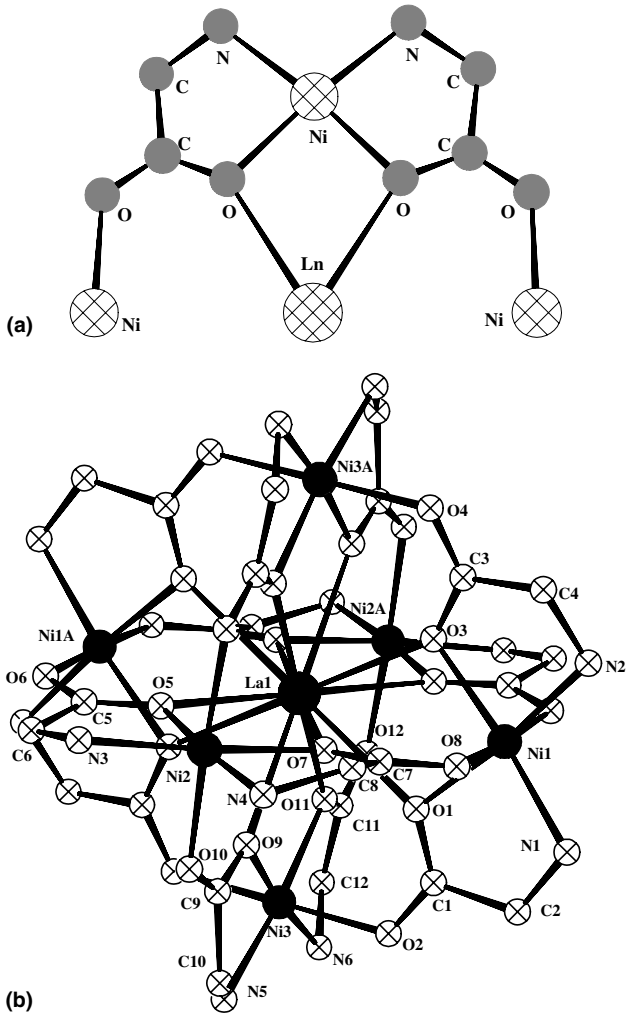

Fig. 1. (a) The structure of the $Ni(Gly)_2$ unit. (b) A perspective view of the $\{LaNi_6\}$ cation of **1** with the atom numbering scheme. Symmetry code: A = $-x + 2$, $-y$, $-z + 1$.

ion (as shown in Scheme 1). The N–Ni–O angles in the five-membered chelate rings formed in the η^4-coordination mode are about 82°.

The structure of the $\{LaNi_6\}$ cation of **2** is same as that of **1**, though **2** crystallizes in a different space group. Another structural difference between **1** and **2** is that **2** has more Na^+ and ClO_4^- ions. Compounds **3** and **1** are isomorphous. Complex **4** has two kinds of cations, and one is the $\{LaNi_6\}$ cluster, the other is $[Ni(im)(H_2O)_5]^{2+}$ (Fig. 3(a)). In the latter, the Ni^{2+} ion is six-coordinated, with an octahedral NO_5 donor set which consists of one nitrogen atom from imidazole and five aqua ligands. The Ni–O and Ni–N distances are in the range of 2.03–2.14 Å. Compound **5** contains the complex anion $[Ni(NCS)_3 \cdot (H_2O)_3]^{-1}$ and the neutral complex $[Ni(NCS)_2 \cdot (H_2O)_4]$ as well as $[LaNi_6(Gly)_{12}]^{3+}$. In $[Ni(NCS)_3 \cdot (H_2O)_3]^{-1}$ and $[Ni(NCS)_2 \cdot (H_2O)_4]$, the Ni^{2+} ions adopt a distorted octahedral configuration and coordinate to nitrogen and oxygen atoms.

Table 2
Selected bond lengths (Å) and bond angles (°) for **1**

Bond lengths			
La(1)–O(1)	2.708(4)	Ni(2)–O(5)	2.045(5)
La(1)–O(3)	2.722(4)	Ni(2)–O(7)	2.052(4)
La(1)–O(5)	2.710(4)	Ni(2)–O(2)	2.056(5)
La(1)–O(7)	2.716(4)	Ni(2)–N(4)	2.060(6)
La(1)–O(9)	2.708(4)	Ni(2)–N(3)	2.064(6)
La(1)–O(11)	2.712(4)	Ni(2)–O(4)#1	2.071(5)
Ni(1)–O(1)	2.048(4)	Ni(3)–O(11)	2.040(4)
Ni(1)–O(3)	2.051(4)	Ni(3)–O(9)	2.043(4)
Ni(1)–O(12)#1	2.056(5)	Ni(3)–N(6)	2.058(6)
Ni(1)–N(1)	2.055(6)	Ni(3)–N(5)	2.064(6)
Ni(1)–N(2)	2.056(6)	Ni(3)–O(8)	2.065(5)
Ni(1)–O(10)	2.064(5)	Ni(3)–O(6)#1	2.065(5)
Bond angles			
O(9)–La(1)–O(1)	61.7(1)	O(3)–Ni(1)–N(1)	174.8(2)
O(9)–La(1)–O(5)#1	63.7(1)	O(1)–Ni(1)–N(2)	174.4(2)
O(1)–La(1)–O(5)	63.9(1)	O(12)#1–Ni(1)–O(10)	178.2(2)
O(9)–La(1)–O(11)	65.7(1)	O(5)–Ni(2)–N(4)	173.6(2)
O(1)–La(1)–O(11)	117.8(1)	O(7)–Ni(2)–N(3)	174.3(2)
O(5)–La(1)–O(11)#1	61.5(1)	O(2)–Ni(2)–O(4)#1	177.9(2)
O(9)–La(1)–O(7)	62.0(1)	O(9)–Ni(3)–N(6)	173.0(2)
O(1)–La(1)–O(7)	63.3(1)	O(11)–Ni(3)–N(5)	173.4(2)
O(5)–La(1)–O(7)	65.8(1)	O(8)–Ni(3)–O(6)#1	178.9(2)
O(11)–La(1)–O(7)	64.2(1)	Ni(1)–O(1)–La(1)	101.3(2)
O(9)–La(1)–O(3)	64.6(1)	Ni(1)–O(3)–La(1)	100.8(2)
O(1)–La(1)–O(3)	65.8(1)	Ni(2)–O(5)–La(1)	101.3(2)
O(5)–La(1)–O(3)	117.3(1)	Ni(2)–O(7)–La(1)	100.9(2)
O(11)–La(1)–O(3)	116.7(1)	Ni(3)–O(9)–La(1)	101.2(2)
O(7)–La(1)–O(3)	118.4(1)	Ni(3)–O(11)–La(1)	101.1(2)

Symmetry transformations used to generate equivalent atoms: #1 $-x + 2$, $-y$, $-z + 1$.

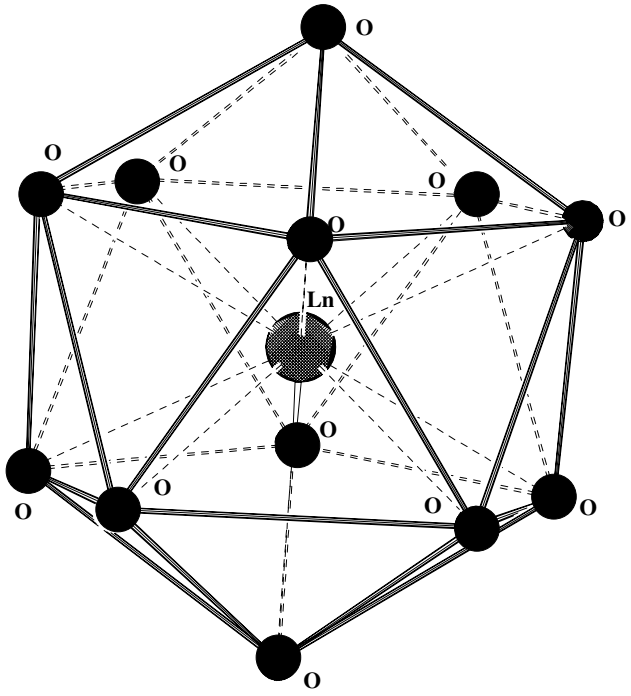

Fig. 2. Coordination polyhedron of the Ln^{3+} ion in the clusters.

Table 3
Bond length (Å) and angle (°) ranges in the coordination of Ln ions in compounds **1** to **5**

	1	2	3	4		5
				Mol. 1	Mol. 2	
Bond lengths						
Ln–O (min)	2.710(5)	2.689(4)	2.711(5)	2.699(4)	2.678(4)	2.703(7)
Ln–O (max)	2.721(5)	2.759(4)	2.727(4)	2.745(4)	2.745(4)	2.741(7)
Bond angles						
Angle A (min)	61.47(15)	60.78(11)	61.41(14)	61.56(11)	61.52(11)	62.0(2)
Angle A (max)	65.79(14)	66.73(11)	66.02(14)	66.33(11)	66.51(11)	65.4(2)
Angle B (min)	114.21(14)	113.27(11)	114.04(13)	113.67(11)	113.49(11)	114.6(2)
Angle B (max)	118.53(15)	119.22(11)	118.53(13)	118.44(11)	118.48(11)	118.0(2)
Angle C	180	180	180	180	180	180

Note: Angle A is O–Ln–O, where O are adjacent vertices of a triangular icosahedron face, e.g. O(9)–La(1)–O(1) in Table 2. Angle B is O–Ln–O, where O are the unshared vertices of a pair of edge sharing icosahedron faces, e.g. O(1)–La(1)–O(11) in Table 2. Angle C is O–Ln–O, where O are vertices with the longest distance between themselves.

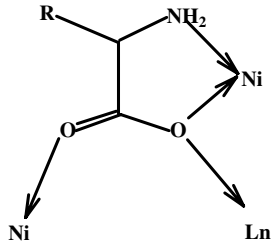

Scheme 1. The η^4-coordination mode of amino acid.

We also obtained well-shaped blue crystals of **6** and **7**. Complex **6** crystallizes in the tetragonal system ($a = b = 27.5708(3)$, $c = 40.3522(7)$ Å) and **7** belongs to the cubic system with $a = b = c = 33.696(8)$ Å. Because of the weak intensities, we only obtained incomplete structures, which indicated both to have an analogous $\{LaNi_6\}$ heptanuclear octahedral metal skeleton.

3.4. Magnetic properties

Temperature dependent magnetic susceptibilities of complexes **1**, **3** and **4** were measured in the range 2–300 K at 10 kOe. Fig. 4 shows the $\chi_M T$ versus T curves for **1** and **3**. At 300 K, the $\chi_M T$ values for **1**, **3** and **4** are 8.35($LaNi_6$), 9.79 ($PrNi_6$), 9.68 $cm^3\,mol^{-1}\,K$ ($LaNi_7$), respectively, larger than the expected values (7.46 $cm^3\,mol^{-1}\,K$ for **1**, 9.06 $cm^3\,mol^{-1}\,K$ for **3**, 8.70 $cm^3\,mol^{-1}\,K$ for **4**) for one Ln^{III} ion with a free-ion state and six or seven spin only Ni^{II} ions ($S = 1$, $g = 2.23$).

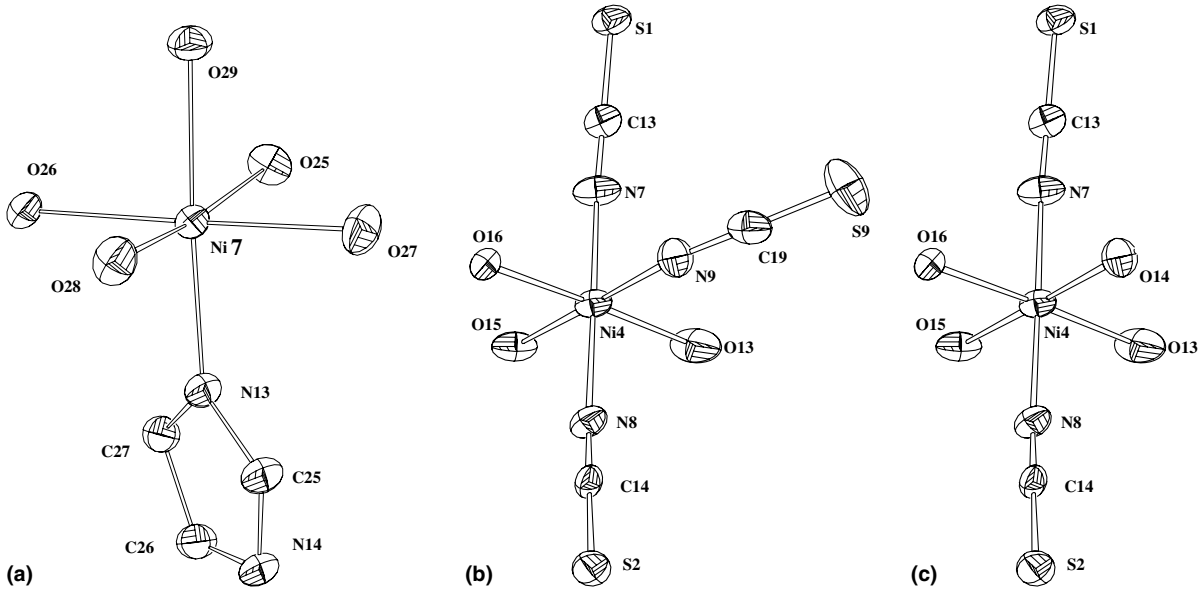

Fig. 3. ORTEP drawing of the complex species in **4** and **5** with the atom numbering scheme (ellipsoids at 25% probability). (a) $[Ni(im)(H_2O)_5]^{2+}$; (b) $[Ni(NCS)_3(H_2O)_3]^-$; (c) $[Ni(NCS)_2 \cdot (H_2O)_4]$.

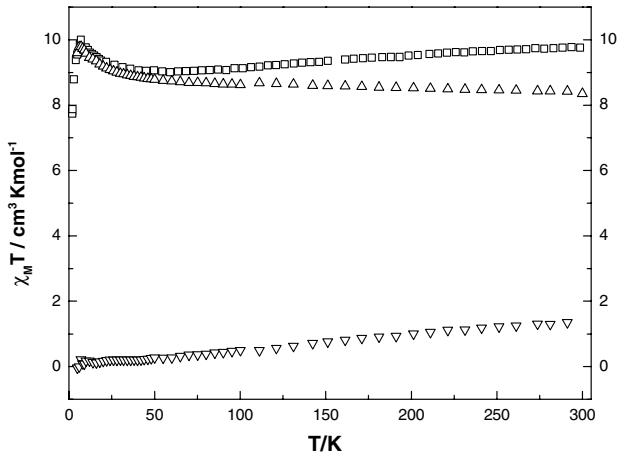

Fig. 4. Plots of $\chi_M T$ vs T for **1** (△) and **3** (□), and for the difference $\Delta\chi_M T = \chi_M T$ (**3**) $- \chi_M T$ (**1**) (▽).

Upon cooling, the $\chi_M T$ value for **1** increase slightly when the temperature is cooled to about 60 K and more rapidly up to about 7 K, where it reaches a maximum of 9.79 cm^3 mol^{-1} K. This phenomenon corresponds to a ferromagnetic interaction. Further decreasing of $\chi_M T$ below 7 K may be due to anisotropic effects, like zero field splitting or spin orbit coupling. This Ni–Ni ferromagnetic interaction in the $LaNi_6$ cluster is also confirmed by the positive Weiss constants ($\theta = 2.35$ K), determined by data in the temperature range 10–300 K. Ferromagnetic coupling was also observed in a similar heptanuclear $NaCu_6$ compound [22]. With the decreasing temperature, $\chi_M T$ for **3** first decreases slowly, reaches 9.35 cm^3 mol^{-1} K at 150 K, and then remains almost constant down to ca. 60 K, where it begins to increase smoothly until reaching a maximum of 10.00 cm^3 mol^{-1} K at ca. 6 K. It shows an overall ferromagnetic interaction, compared with the antiferromagnetic interaction in the $\{PrNi_6\}$ trigonal prismatic cluster [16].

As **1** and **3** are isomorphous, we can deduct the Ni···Ni interaction by subtracting the $\chi_M T$ (**1**) from $\chi_M T$ (**3**), similarly to that done by Kahn and Costes [23]. The $\Delta\chi_M T$ is the sum of the Pr···Ni interaction and the crystal field effect of the Pr^{3+} ion (as shown in Fig. 4). Pr^{3+} ion has a $^3H_4$ ground state and is not a Kramers ion. The crystal field alone can resolve degeneracy to give a non-magnetic ground state [24]. $\Delta\chi_M T$ decreases slowly with decreasing temperature and tends to zero as the temperature approaches absolute zero, suggesting that the Pr···Ni interaction may be small or negligible. As the crystal field effect will also decrease the $\chi_M T$ value upon cooling and we cannot obtain an isostructural $\{PrZn_6\}$ cluster, we cannot tell the nature of the Pr···Ni interaction based on the experiments. The $\chi_M T$ versus T curve of **4** is similar to that of **3** and also shows an overall ferromagnetic interaction with positive Weiss constants ($\theta = 1.53$ K).

4. Conclusion

In summary, a family of seven novel heptanuclear octahedral clusters $\{LnNi_6\}$ have been synthesized, among which five have been characterized by X-ray structure analysis. Previous studies [10c,14,16] and this work together show that under high pH conditions, amino acids have the unique ability in adopting different coordination modes to co-existing different transition metal ions and lanthanide ions to form high-nuclearity 3d–4f-amino acid clusters. Future work will be aimed at the synthesis of high-nuclearity Ln–V, Ln–Cr clusters with novel structures using amino acid ligands.

5. Supplementary data

CCDC 225803-225807 contain the supplementary crystallographic data for this paper. These data can be obtained free of charge via www.ccdc.cam.ac.uk/conts/retrieving.html (or from the Cambridge Crystallographic Data Centre, 12 Union Road, Cambridge CB2 1EZ, UK; fax: (+44) 1223-336-033; or e-mail: deposit@ccdc.cam.ac.uk).

Acknowledgements

This research was supported by Grants from the State Key Laboratory of Structural Chemistry, Fujian Institute of Research on the Structure of Matter, Chinese Academy of Sciences (CAS), The Ministry of Science and Technology of China (001CB1089), the National Science Foundation (20333070, 20273073, 90206040) of China and Fujian Province (2002F014, 2003J042) for research funding support.

References

[1] (a) C. Benelli, D. Gatteschi, Chem. Rev. 102 (2002) 2369;
(b) M. Sakamoto, K. Manseki, H. Okawa, Coord. Chem. Rev. 379 (2001) 219.
[2] A. Bencini, C. Benelli, A. Caneschi, R.L. Carlin, A. Dei, D. Gatteschi, J. Am. Chem. Soc. 107 (1985) 8128.
[3] R.E.P. Winpenny, Chem. Soc. Rev. 27 (1998) 447, and references therein.
[4] (a) J.-P. Costes, F. Dahan, A. Dupuis, Inorg. Chem. 39 (2000) 5994;
(b) Q.-Y Chen, Q.-H. Luo, Z.-L. Wang, J.-T. Chen, Chem. Commun. (2000) 1033;
(c) M. Sassaki, K. Manseki, H. Horiuchi, M. Kumagai, M. Sakamoto, H. Sakiyama, Y. Nishida, Y. Sadaoka, M. Ohba, H. Okawa, J. Chem. Soc., Dalton Trans. (2000) 259.
[5] (a) N. Sakagami, K. Okamoto, Chem. Lett. (1998) 201;
(b) S. Decurtins, M. Gross, H.W. Schmalle, S. Ferlay, Inorg. Chem. 37 (1998) 2443.
[6] (a) A.D. Cutland, R.G. Malkani, J.W. Kampf, V.L. Pecoraro, Angew. Chem., Int. Ed. Engl. 39 (2000) 2689;

(b) M.L. Kahn, C. Mathoniere, O. Kahn, Inorg. Chem. 38 (1999) 3692;
(c) M.L. Kahn, M. Verelst, M. Lecantes, C. Mathoniere, O. Kahn, Eur. J. Inorg. Chem. (1999) 527.
[7] T. Sanada, T. Suzuki, S. Kaizaki, J. Chem. Soc., Dalton Trans. (1998) 959.
[8] B.-Q. Ma, S. Gao, G. Su, G.-X. Xu, Angew. Chem., Int. Ed. Engl. 40 (2001) 434.
[9] (a) X.-M. Chen, S.M.J. Aubin, Y.-L. Wu, Y.-S. Yang, T.C.W. Mak, D.N. Hendrickson, J. Am. Chem. Soc. 117 (1995) 9600;
(b) Y. Cui, G. Cheng, J. Ren, Y.-T. Qian, J.-S. Huang, Inorg. Chem. 39 (2000) 4165;
(c) R.A. Reynolds, D. Coucouvanis, J. Am. Chem. Soc. 120 (1998) 209.
[10] (a) S.N. Wang, Z. Pang, M.J. Wagner, Inorg. Chem. 31 (1992) 5381;
(b) A.J. Blake, R.O. Gould, C.M. Grant, P.E.Y. Milne, S. Parsons, R.E.P. Winpenny, J. Chem. Soc., Dalton Trans. (1997) 485;
(c) S.-M. Hu, J.-C. Dai, X.-T. Wu, L.-M. Wu, C.-P. Cui, Z.-Y. Fu, M.-C. Hong, Y.-C. Liang, J. Cluster Sci. 13 (2002) 33 (included in the special memorial issue in honor of Professor Jia-Xi Lu, the founder of the Fujian Institute of Research on the Structure of Matter).
[11] R.Y. Wang, F. Gao, T.-Z. Jin, Huaxuetongbao (Chemistry, in China) 10 (1996) 14.
[12] (a) M.A.A.F. de C.T. Carrondo, M.T.L.S. Duarte, M.L.S.S. Goncalves, P. O'Brien, M.B. Hursthouse, J. Chem. Soc., Dalton Trans. (1990) 213;
(b) N. Ohata, H. Masuda, O. Yamauchi, Angew. Chem., Int. Ed. Engl. 35 (1996) 531;
(c) H. Masuda, A. Odani, T. Yamazaki, T. Yajima, O. Yamauchi, Inorg. Chem. 32 (1993) 1111.
[13] Z.-P. Zheng, Chem. Commun. (2001) 2521.
[14] S.-M. Hu, W.-X. Du, J.-C. Dai, L.-M. Wu, C.-P. Cui, Z.-Y. Fu, X.-T. Wu, J. Chem. Soc., Dalton Trans. (2001) 2963.
[15] (a) Y. Yukawa, S. Igarashi, A. Yamano, S. Sato, Chem. Commun. (1997) 711;
(b) S. Igarashi, Y. Hoshino, Y. Masuda, Y. Yukawa, Inorg. Chem. 39 (2000) 2509.
[16] J.-J. Zhang, S.-M. Hu, L.-M. Zheng, X.-T. Wu, Z.-Y. Fu, J.-C. Dai, W.-X. Du, H.-H. Zhang, R.-Q. Sun, Chem. Eur. J. 8 (2002) 5742.
[17] Y.-J. Zhang, B.-Q. Ma, S. Gao, J.-R. Li, Q.-D. Liu, J. Chem. Soc., Dalton Trans. (2000) 2249.
[18] (a) D.M.J. Doble, C.H. Benison, A.J. Blake, D. Fenska, M.S. Jackson, R.D. Kay, W.-S. Li, M. Schroder, Angew. Chem., Int. Ed. Engl. 38 (1999) 1915;
(b) Q.-D. Liu, S. Gao, J.-R. Li, Q.-Z. Zhou, K.-B. Yu, B.-Q. Ma, S.-W. Zhang, X.-X. Zhang, T.-Z. Jin, Inorg. Chem. 39 (2000) 2488.
[19] (a) XSCANS (Version 2.1), Siemens Analytical X-Ray Instruments Inc., Madison, WI, 1994;
(b) G.M. Sheldrick, Program for Empirical Absorption Correction of Area Detector Data, University of Göttingen, Germany, Göttingen, Germany, 1996.
[20] G.M. Sheldrick, SHELXS-97, Program for X-ray Crystal Structure Solution, University of Göttingen, Göttingen, Germany, 1997.
[21] J.E. Huheey, E.A. Keiter, R.L. Keiter, Inorganic Chemistry: Principles of Structure and Reactively, 4th ed., HarperCollins College Publishers, New York, 1993, pp. 114–115.
[22] L.-Y. Wang, S. Igarashi, Y. Yukawa, Y. Hoshino, O. Roubeau, G. Aromi, R.E.P. Winpenny, Dalton Trans. (2003) 2318.
[23] (a) M.L. Kahn, P. Lecante, M. Verelst, C. Mathonière, O. Kahn, Chem. Mater. 12 (2000) 3073;
(b) J.-P. Costes, F. Dahan, A. Dupuis, J.-P. Laurent, Chem. Eur. J. 4 (1998) 1616.
[24] R.L. Carlin, Magnetochemistry, Springer, Berlin, 1986.

Available online at www.sciencedirect.com
SCIENCE DIRECT®
Polyhedron 23 (2004) 2273–2280
POLYHEDRON
www.elsevier.com/locate/poly

Synthesis of phosphine stabilised group 11 1-azaallyl complexes; molecular structure of $bu^i_3PAuCH(R)C(bu^t) = NR$ (R = $SiMe_3$)

Richard J. Bowen [a,b], Judy Caddy [a,b], Manuel A. Fernandes [a], Marcus Layh[a,*], Messai A. Mamo [a]

[a] *Molecular Sciences Institute, School of Chemistry, University of the Witwatersrand, Private Bag 3, Wits 2050, Johannesburg, South Africa*
[b] *Project AuTEK, Mintek, Private Bag X 3015, Randburg 2125, South Africa*

Received 14 June 2004; accepted 12 July 2004

Abstract

The phosphine complexes bu^i_3PMX (**2a**: M = Cu, X = Cl, **2b**: M = Cu, X = I, **2c**: M = Ag, X = Cl, **2d**: M = Au, X = Cl) were synthesised in high yields from bu^i_3P and MX. Their reaction with $[Li\{\mu\text{-}N(R)C(bu^t)C(H)R\}]_2$ (R = $SiMe_3$) gave the monomeric complexes $bu^i_3PCuN(R)C(bu^t) = C(H)R$ (**3a**) and $bu^i_3PMC(H)RC(bu^t) = NR$ (**3b**: M = Ag, **3c**: M = Au) in moderate to high yields. All compounds were fully characterised by multinuclear NMR spectroscopy, microanalysis [not $bu^i_3PCuN(R)C(bu^t) = C(H)R$ (**3a**) and $bu^i_3PAgC(H)RC(bu^t) = NR$ (**3b**)] and for **2c**, **2d** and **3c** by single crystal X-ray diffraction. The bonding mode in the 1-azaallyl complexes **3a**–**c** was found to depend strongly on the metal ion, with **3a** being an enamide complex and **3b** and **3c** iminoalkyl complexes.
© 2004 Elsevier Ltd. All rights reserved.

Keywords: Group 11 phosphine complexes; 1-azaallyls; X-ray crystallography; Iminoalkyl bonding mode

1. Introduction

Metal η^3-allyl complexes have been studied extensively and found numerous applications in organic chemistry [1]. 1-Azaallyl complexes in contrast had initially attracted much less interest and have only become popular in the last decade with a recent review [2] summarising the field. The ligands steric and electronic properties have given access to complexes with the metal in an unusual oxidation state or coordination number. Another feature of interest is the ligands flexibility in adopting different bonding modes as shown in **I**–**IV** depending on the substituents on the ligand, the nature of the metal and the presence or absence of a neutral co-ligand(s) [2].

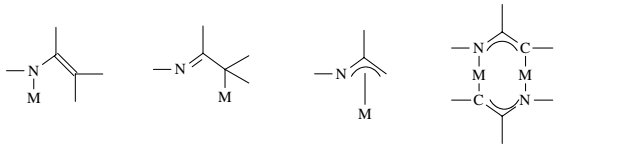

I η^1-enamide complex; II η^1-iminoalkyl complex; III η^3-azaallyl complex; IV μ^2-bridging complex

As part of our continuing investigations into the chemistry of the 1-azaallyl ligand in the context of Group 11 metals we have previously reported the bridged (**IV**), dimeric complexes $[CuLL']_2$ [L′ = $RNC(bu^t)CHR$] [3], $[MLL'']_2$ [4] [M = Cu, Au, LL″ = RNC(Ph)CR_2], the monomeric phosphine adduct Ph_3PCuLL' [3] and a lithium cuprate $(dme)_3LiCu(LL')_2$ (dme = 1,2 dimethoxyethane; R = $SiMe_3$) [3]. It was shown that Ag and Au analogues of $[CuLL']_2$ were

* Corresponding author. Tel.: +27 11 7176744; fax: +27 11 7176749.
E-mail address: marcus@aurum.wits.ac.za (M. Layh).

0277-5387/$ - see front matter © 2004 Elsevier Ltd. All rights reserved.
doi:10.1016/j.poly.2004.07.008

not stable and attempts to their synthesis led to the reduction of the Group 11 metal precursor by the ligand transfer reagent $[LiLL']_2$ [5]. The sterically more demanding ligand LL″ [6] provided access to $[AuLL'']_2$ [4] but a silver analogue remained elusive. In this paper we report the synthesis, solid and solution structures of a series of phosphine stabilised Group 11 metal 1-azaallyl complexes bu^i_3PMLL' and their metal halide precursors.

2. Experimental

2.1. Reagents and general procedures

All manipulations were carried out under argon, using standard Schlenk techniques. Solvents were distilled from drying agents and degassed. The NMR spectra were recorded in C_6D_6 at ambient probe temperature using the following Bruker instruments: DRX 400 (^{1}H, 400.13 MHz, ^{31}P, 162.0 MHz), DXP 300 (^{1}H, 300.13; ^{13}C 75.5 MHz) or AC200 (^{1}H, 200.13 MHz) and referenced internally to residual solvent resonances (chemical shift data in δ). ^{13}C NMR spectra were all proton-decoupled. Elemental analyses were determined by the Institute for Soil, Climate and Water, Pretoria, South Africa. The following abbreviations are used throughout this section: bs = broad singlet, d = doublet, dd = doublet of doublet, m = multiplet, s = singlet. Coupling constants (J) are given in Hz. Me_2SAuCl [7] was synthesised according to the literature [8].

2.2. Synthesis of phosphine complexes

2.2.1. Synthesis of bu^i_3PCuCl (**2a**)

(a) bu^i_3P (0.64 cm^3, 2.53 mmol) was added to a suspension of CuCl (0.25 g, 2.53 mmol) in thf (20 cm^3). The initially yellow, later colourless solution was stirred for 3 h at room temperature. The solvent was removed in vacuo and the residue extracted into hexane. The solution was filtered of some dust and the solvent was then removed from the filtrate to give a colourless, viscous oil, that was sufficiently pure for further reactions.

(b) bu^i_3P (0.80 cm^3, 3.16 mmol) was added to acetonitrile (25 cm^3) followed by the addition of CuCl (0.38 g, 3.84 mmol). The resulting mixture was stirred overnight to give a colourless solution. After keeping the reaction mixture for two days at −20 °C colourless crystals of bu^i_3PCuCl (**2a**) (0.35 g, 30%) were isolated. ^{1}H NMR (C_6D_6): δ = 1.02 [d, CHMe_2, 18H, $^3J_{H-H}$ = 6.6 Hz], 1.22 [dd, CH_2, 6H, $^2J_{P-H}$ = 10.5 Hz; $^3J_{H-H}$ = 6.6 Hz], 2.03 (m, CHMe$_2$, 3H); ^{13}C NMR (C_6D_6): δ = 24.0 (s, CHMe_2), 26.3 (br s, CHMe$_2$), 37.5 (br s, CH$_2$); ^{31}P NMR (C_6D_6): δ = −25.1.

2.2.2. Synthesis of bu^i_3PCuI (**2b**)

CuI (0.38 g, 2.00 mmol) was dissolved in 25 cm^3 acetonitrile. The solution was cooled to 0 °C and 0.50 cm^3 (2.00 mmol) bu^i_3P were added. Immediately a colourless precipitate formed that was isolated by removing all volatiles in vacuo to give 0.82 g of crude material. Recrystallisation from diethyl ether (25 cm^3) at −60 °C gave colourless crystals of bu^i_3PCuI (**2b**) (0.53 g, 67%). (Found: C, 36.48; H, 6.97. $C_{12}H_{27}CuI$ requires C, 36.70; H, 6.93%); ^{1}H NMR (C_6D_6): δ = 1.05 [d, CHMe_2, 18H, $^3J_{H-H}$ = 8.8 Hz], 1.39 [dd, CH_2, 6H, $^2J_{P-H}$ = 9.6 Hz; $^3J_{H-H}$ = 9.4 Hz], 2.05 (m, CHMe$_2$, 3H); ^{13}C NMR (C_6D_6): δ = 25.3 [d, CHMe_2, $^3J_{C-P}$ = 7.8 Hz], 26.0 [d, CHMe$_2$, $^2J_{C-P}$ = 3.8 Hz], 36.7 [d, CH$_2$, $^1J_{C-P}$ = 36.7 Hz]; ^{31}P NMR (C_6D_6): δ = −29.6.

2.2.3. Synthesis of bu^i_3PAgCl (**2c**)

A mixture of AgCl (0.29 g, 2.00 mmol) and bu^i_3P (0.50 cm^3, 2.00 mmol) was stirred in 25 cm^3 acetonitrile overnight. After filtration and cooling the filtrate to −20 °C colourless crystals of bu^i_3PAgCl (**2c**) (0.61 g, 87%) were obtained. (Found: C, 42.14; H, 8.10. $C_{12}H_{27}AgCl$ requires C, 41.70; H, 7.87%); ^{1}H NMR (C_6D_6): δ = 1.08 [d, CHMe_2, 18H, $^3J_{H-H}$ = 8.4 Hz], 1.30 [dd, CH_2, 6H, $^2J_{P-H}$ = 9.7 Hz; $^3J_{H-H}$ = 9.6 Hz], 2.02 (m, CHMe$_2$, 3H); ^{13}C NMR (C_6D_6): δ = 25.0 (m, CHMe_2), 26.9 (br s, CHMe$_2$), 37.8 (m, CH$_2$); ^{31}P NMR (C_6D_6): δ = −15.6 [d, ^1J = 599.4 Hz]; ^{31}P NMR (C_7D_8) (−15 °C): δ = −16.1 [dd, $^1J(^{31}P-^{107}Ag)$ 592.2 Hz; $^1J(^{31}P-^{109}Ag)$ 683.3 Hz].

2.2.4. Synthesis of bu^i_3PAuCl (**2d**)

Me_2SAuCl (1.00 g, 3.4 mmol) was dissolved in thf (approx. 25 cm^3) at room temperature and 0.87 g (4.3 mmol) bu^i_3P was added. The resulting mixture was stirred for 2 h. The solution was concentrated to 2/3 of its volume and stored at −20 °C to give colourless crystals of bu^i_3PAuCl (**2d**) (1.31 g, 89%). (Found: C, 33.34; H, 6.29. $C_{12}H_{27}AuCl$ requires C, 33.15; H, 6.26%); ^{1}H NMR (C_6D_6): δ = 0.86 [d, CHMe_2, 18H, $^3J_{H-H}$ = 6.7 Hz], 1.09 [dd, CH_2, 6H, $^2J_{P-H}$ = 10.4 Hz;$^3J_{H-H}$ = 6.7 Hz], 1.56 (m, CHMe$_2$, 3H); ^{13}C NMR (C_6D_6): δ = 24.6 [d, CHMe_2 $^3J_{C-P}$ = 19.0 Hz], 26.3 (s, CHMe$_2$), 36.7 [d, CH$_2$, $^1J_{C-P}$ = 74.5 Hz]; ^{31}P NMR (C_6D_6): δ = 11.9.

2.2.5. Synthesis of $bu^i_3PCuN(R)C(bu^t)=C(H)R$ (**3a**)

(a) bu^i_3P (0.29 cm^3, 1.18 mmol) was dissolved in hexane (12 cm^3) and added dropwise at −40 °C to a solution of $[CuN(R)C(bu^t)=CHR]_2$ (0.36 g, 0.58 mmol). The reaction mixture was allowed to warm up to room temperature and stirred for 1.5 h to give a yellow reaction mixture that was filtered. The filtrate was concentrated and cooled to −60 °C to give colourless crystals of $bu^i_3PCuN(R)C(bu^t)=CHR$ (**3a**) (0.29 g, 48%).

(b) A solution of $LiC(H)RC(bu^t)NR$ (0.40 g, 1.60 mmol) in hexane (10 cm^3) was added to a solution of

bu^i_3PCuCl (**2a**) (0.48 g, 1.60 mmol) in hexane (20 cm^3) at −20 °C. The reaction mixture was allowed to warm up to room temperature and stirred for 6 h to give a pale yellow, slightly turbid solution. Filtration of the reaction mixture and concentration of the filtrate gave after cooling to −60 °C colourless crystals of **3a** (0.51 g, 63%). Isolation of the crystals by removal of the mother liquor led to a slow decomposition of the sample as evident by the crystals turning brown and becoming sticky. ^{1}H NMR (C_6D_6): δ = 0.45 (s, Si*Me*$_3$, 9H), 0.49 (s, Si*Me*$_3$, 9H), 0.94 [d, CH*Me*$_2$, 18H, $^3J_{H-H}$ = 6.6 Hz], 1.38 [dd, C*H*$_2$, 6H, $^2J_{P-H}$ = 16.8 Hz; $^3J_{H-H}$ = 3.4 Hz], 1.41 (s, C*Me*$_3$, 9H), 1.66 (m, C*H*Me$_2$, 3H), 4.95 (s, C*H*, 1H); ^{13}C NMR (C_6D_6) δ = 2.3 (s, NSi*Me*$_3$), 5.1 (s, CSi*Me*$_3$), 25.0 [d, CH*Me*$_2$, $^3J_{C-P}$ = 8.3 Hz], 26.2 [d, *C*HMe$_2$, $^2J_{C-P}$ = 3.0 Hz], 32.0 (s, C*Me*$_3$), 37.0 [d, *C*H$_2$, $^1J_{C-P}$ = 24.5 Hz], 40.0 (s, *C*Me$_3$), 103.1 (s, *C*H), 177.8 (s, *C*N); ^{31}P NMR (C_6D_6) δ = −19.2.

2.2.6. Synthesis bu^i_3PAgC(H)RC(bu^t)=NR (**3b**)

A solution of LiC(H)RC(bu^t)NR (0.38 g, 1.52 mmol) in hexane (10 cm^3) was added dropwise to a solution of (bu^i)$_3$PAgCl (**2c**) (0.45 g, 1.3 mmol) in hexane (10 cm^3) at −60 °C. The reaction mixture was kept at that temperature for 20 min and then slowly warmed to room temperature. The reaction mixture was stirred for 6 h at room temperature to give a yellow solution with a fine black precipitate. The solvent was removed in vacuo to give a blackish/white solid that was found to be light and temperature sensitive. The solid was extracted with hexane (30 cm^3), it was filtered and the pale brown filtrate was concentrated (to approx. 4 cm^3) and cooled to −60 °C to give after several days slightly brownish, highly sensitive crystals of **3b** (0.42 g, 58%). ^{1}H NMR (C_6D_6): δ = 0.51 (s, Si*Me*$_3$, 9H), 0.54 (s, Si*Me*$_3$, 9H), 0.92 [d, CH*Me*$_2$, 18H, $^3J_{H-H}$ = 6.5 Hz], 1.05 (bs, C*H*$_2$, 6H), 1.43 (s, C*Me*$_3$, 9H), 1.63 (bs, C*H*Me$_2$, 3H), 3.50 (s, C*H*, 1H); ^{13}C NMR (C_6D_6): δ = 2.8 (s, CSi*Me*$_3$), 4.6 (bs, NSi*Me*$_3$), 24.6 [d, CH*Me*$_2$, $^3J_{C-P}$ = 9.0 Hz], 26.7 [d, *C*HMe$_2$, $^2J_{C-P}$ = 5.9 Hz], 31.5 (s, *C*Me$_3$), 37.5 [d, *C*H$_2$, $^1J_{C-P}$ = 15.1 Hz], 41.7 (s, *C*Me$_3$), 60.1 (s, *C*H), 189.8 (s, *C*N); ^{31}P NMR (C_6D_6): δ = −17.4 (bs).

2.2.7. Synthesis bu^i_3PAuC(H)RC(bu^t)=NR (**3c**)

To a solution of (bu^i)$_3$PAuCl (**2d**) (0.68 g, 1.56 mmol) in diethyl ether (40 cm^3) was added dropwise a solution of LiC(H)RC(bu^t)NR (0.39 g, 1.56 mmol) in diethyl ether (20 cm^3) at −60 °C. Initially a white precipitate was formed that redissolved at −40 °C to give a colourless solution once the reaction mixture had reached room temperature. After stirring for 1 h at room temperature a fine colourless precipitate started to form. The reaction mixture was stirred overnight and the solvent removed in vacuo to give a colourless solid. Extraction with hexane (30 cm^3) and filtration gave a colourless solution that was concentrated and cooled to −20 °C. A first crop of crystals (0.18 g, 0.4 mmol, 26%) was identified as starting material **2d**. Concentration of the mother liquor and cooling to −60 °C gave colourless crystals of **3c** (0.68 g, 68%). (Found: C, 44.03; H, 7.61; N 2.05. $C_{24}H_{55}AuNPSi_2$ requires C, 44.91; H, 8.64; N 2.18%); ^{1}H NMR (C_6D_6): δ = 0.45 (s, Si*Me*$_3$, 9H), 0.49 (s, Si*Me*$_3$, 9H), 0.98 [d, CH*Me*$_2$, 18H, $^3J_{H-H}$ = 8.0 Hz], 1.15 [dd, C*H*$_2$, 6H, $^2J_{P-H}$ = 9.6 Hz; $^3J_{H-H}$ = 6.8 Hz], 1.39 (s, C*Me*$_3$, 9H), 1.88 (m, C*H*Me$_2$, 3H), 3.01 [d, C*H*, 1H, $^3J_{P-H}$ = 10.9 Hz]; ^{13}C NMR (C_6D_6): δ = 2.1 (s, CSi*Me*$_3$), 3.0 (bs, NSi*Me*$_3$), 24.9 [d, CH*Me*$_2$, $^3J_{C-P}$ = 8.05 Hz], 26.4 (s, *C*HMe$_2$), 30.7 (s, C*Me*$_3$), 38.3 [d, *C*H$_2$, $^1J_{C-P}$ = 47.2 Hz], 42.3 (s, *C*Me$_3$), 50.3 [d, *C*H, $^2J_{C-P}$ = 56.3 Hz], 193.7(s, *C*N); ^{31}P NMR (C_6D_6): δ = 21.4.

2.3. Crystal structure determination

Intensity data were collected on a Bruker SMART 1K CCD area detector diffractometer with graphite monochromated Mo Kα radiation (50 kV, 30 mA). The collection method involved ω-scans of width 0.3°. Data reduction was carried out using the program SAINT+ [9] and face indexed absorption corrections were made using the program XPREP [9].

The crystal structures were solved by direct methods using SHELXTL [10]. Non-hydrogen atoms were first refined isotropically followed by anisotropic refinement by full matrix least-squares calculation based on F^2 using SHELXTL. Hydrogen atoms were located from the difference map and then positioned geometrically and allowed to ride on their respective parent atoms. The isobutyl groups of compound **2c** exhibited very large thermal vibration as indicated by the large thermal ellipsoids. Attempts to apply a disorder model proved to be unsuccessful. Several low temperature collections were attempted on crystals grown from various solvents without success due to a phase transition at around −70 °C. A data collection at −50 °C was found to be of lower quality than the presented room temperature data. Bond lengths and angles from **2d** were used as restraints in the final structure solution of **2c**. Compound **3c** was found to be disordered in a ratio of 0.9379(8):0.0621(8) although only a partial refinement on the minor component was possible. Only the equivalent atoms of Au, P, C2, C13, C17 and C21 were refined as a rigid body on the disordered component, with the occupancies of the two components being summed to unity. This was necessary as a refinement of the major component only would lead to a residual peak of about 9 e $Å^{-3}$ corresponding to the Au atom from the minor component.

Further crystallographic data are summarised in Table 1. Diagrams and publication material were generated using SHELXTL [10], PLATON [11] and ORTEP3 [12].

Table 1
Crystal data and refinement for compounds **2c**, **2d**, **3c**

Compound	**2c**	**2d**	**3c**
Empirical formula	$C_{48}H_{108}Ag_4Cl_4P_4$	$C_{12}H_{27}AuClP$	$C_{24}H_{55}AuNPSi_2$
M	1382.50	434.72	641.81
T (K)	293 (2)	293 (2)	173 (2)
Wavelength (Å)	0.71073	0.71073	0.71073
Crystal system	rhombohedral	monoclinic	monoclinic
Space group	$R\bar{3}$	$P2(1)/n$	$P2(1)/n$
Unit cell dimensions			
a (Å)	22.654 (4)	9.296 (2)	8.9678 (11)
b (Å)	22.654 (4)	9.2668 (19)	17.093 (2)
c (Å)	11.656 (2)	19.291 (4)	20.747 (3)
α (°)	90	90	90
β (°)	90	101.299 (4)	94.337 (2)
γ (°)	120	90	90
U (Å^3)	5180.8 (15)	1629.6 (6)	3171.1 (7)
Z	3	4	4
D_{calc} (Mg/m^3)	1.329	1.772	1.344
μ (mm^{-1})	1.390	9.264	4.776
$F(000)$	2136	840	1312
Crystal size (mm)	$0.38 \times 0.29 \times 0.13$	$0.29 \times 0.20 \times 0.09$	$0.22 \times 0.22 \times 0.12$
θ Range for data collection (°)	1.80–25.97.	2.15–28.35	1.55–26.00
Index ranges	$-27 \leqslant h \leqslant 27$	$-11 \leqslant h \leqslant 12$	$-10 \leqslant h \leqslant 11$
	$-23 \leqslant k \leqslant 27$	$-12 \leqslant k \leqslant 11$	$-21 \leqslant k \leqslant 11$
	$-13 \leqslant l \leqslant 14$	$-25 \leqslant l \leqslant 17$	$-25 \leqslant l \leqslant 25$
Reflections collected	10 302	11 009	18 588
Independent reflections	4379 [R_{int} = 0.0597]	4019 [R_{int} = 0.0380]	6226 [R_{int} = 0.0330]
Completeness to theta	100	98.3	100.0
Absorption correction	semi-empirical from equivalents	integration	integration
Maximum and minimum transmission	0.8399 and 0.6201	0.4894 and 0.1742	0.5405 and 0.3648
Refinement method	full-matrix least-squares on F^2	full-matrix least-squares on F^2	full-matrix least-squares on F^2
Data/restraints/parameters	4379/33/181	4019/0/143	6226/12/288
Goodness-of-fit on F^2	0.958	1.042	1.085
Final R indices [$I > 2\sigma(I)$]	R_1 = 0.0512, wR_2 = 0.1326	R_1 = 0.0236, wR_2 = 0.0510	R_1 = 0.0334, wR_2 = 0.0658
R indices (all data)	R_1 = 0.0931, wR_2 = 0.1571	R_1 = 0.0348, wR_2 = 0.0538	R_1 = 0.0471, wR_2 = 0.0695
Extinction coefficient	−0.04(6)	0.00106(9)	
Largest difference peak and hole (e Å^{-3})	0.321 and −0.322	0.739 and −0.567	0.837 and −0.595

3. Results and discussion

3.1. Synthesis

Ph_3PCuLL' had previously been synthesised by the addition of stoichiometric amounts of triphenylphosphine to the dimeric complex $[CuLL']_2$ [LL′ = RNC(bu^t)CHR, R = $SiMe_3$] [3] [cf. (i) in Scheme 1]. The same synthetic route gave the copper complex bu^i_3PCuLL' (**3a**) in moderate yield [(i) in Scheme 1] but was not applicable for the Ag and Au analogues as the respective parent compounds [MLL′] were not accessible. It was, therefore, decided to first synthesise the easily accessible and stable phosphine adducts bu^i_3PM-X (**2a**–**d**) from the metal halides and free phosphine [(ii) in Scheme 1], which were then reacted with $[LiLL']_2$ [5] to give the 1-azaallyl complexes bu^i_3PMLL' (**3a**–**c**) [(iii) in Scheme 1]. Pbu^i_3 was selected as the phosphine of choice as its sterically demanding alkyl groups were expected to convey stability to the metal complexes as well as solubility in non-polar solvents. Preliminary experiments involving the treatment of $(Me_2S)AuCl$ with PPh_3 and subsequent reaction with $[LiLL']_2$ [5] led to the NMR-spectroscopically characterised complex Ph_3PAuLL' but attempts to purify the product by recrystallisation were unsuccessful. The bu^i_3P-derivatives (**3a**–**c**) were in contrast obtained after recrystallisation from hexane as colourless, air- and moisture sensitive crystals in moderate to high yields. While **3c** was indefinitely stable at room temperature in an inert gas atmosphere, the copper (**3a**) and especially the silver analogue (**3b**) were found to be sensitive to light and heat, depositing metal from dissolved and solid samples of the complex even at low temperatures. An attempt to synthesise the aurate complex $(dme)_3LiAu(LL')_2$ from **3c** and a second equivalent of $[LiLL']_2$ [5] in the presence of dme was not successful and led to the recovery of the starting materials.

3.2. NMR-spectroscopic studies and solution behaviour

It had been shown previously that ^1H and ^{13}C NMR spectroscopy is a powerful tool to distinguish different

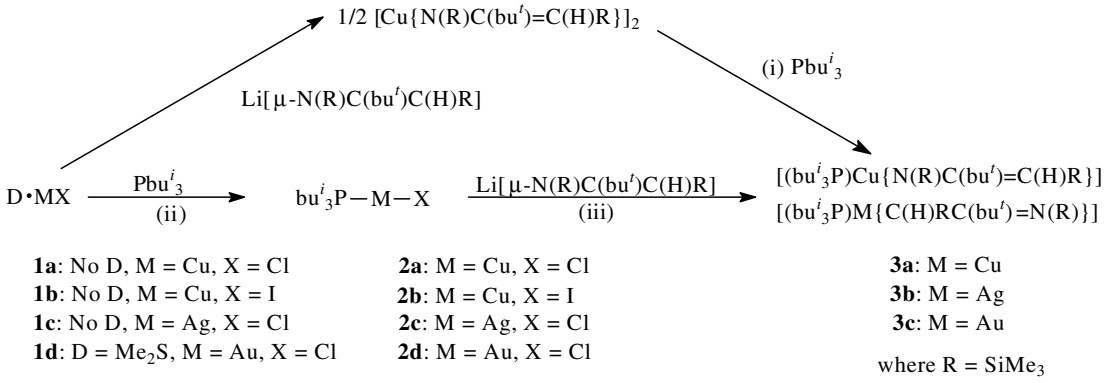

Scheme 1. Synthesis of Group 11 metal 1-azaallyl complexes.

Table 2
Selected NMR-spectroscopic data of 1-azaallyl metal complexes

Compound	CH (^{1}H)	CH (^{13}C)	CN (^{13}C)	^{31}P	Bonding mode	Ref.
$(dme)_3LiCuLL'_2$	5.05	101.9	177.5		**(I)**	[3]
Ph_3PCuLL'	4.83	101.9	182.3	12.7	**(I)**	[3]
$[LiLL']_2$	4.54	93.7	170.8		**(I,III)**	[5]
bu^i_3PCuLL' (**3a**)	4.95	103.1	177.8	−19.1	**(I)**	this work
$[CuLL']_2$	3.11	48.1	220.8		**(IV)**	[3]
bu^i_3PAgLL' (**3b**)	3.50	60.1	189.8	−17.4	**(II)**	this work
Ph_3PAuLL'	3.10 (d)			42.2	**(II)**	this work
bu^i_3PAuLL' (**3c**)	3.01 (d)	50.3 (d)	193.7	21.4	**(II)**	this work
$Ph_3PNi(LL')I$	2.50 (d)	56.1 (d)	172.1	31.0	**(III)**	[22]

LL′ = C(H)RC(bu^t)NR.

bonding modes in 1-azaallyl complexes [3,13]. Table 2 summarises NMR-spectroscopic data of **3a**–**c** and some related metal complexes featuring the LL′ ligand. Previously a signal at low frequency in the ^{1}H ($\delta \approx 3$) and ^{13}C ($\delta \approx 50$) NMR spectrum for CH and a signal at high frequency for CN ($\delta \approx 190$) was found to be indicative for an iminoalkyl metal complex (**II**) while the reverse situation with signals for CH at high frequency [$\delta \approx 5$ (^{1}H), 100 (^{13}C)] and CN at low frequency [$\delta \approx 180$ (^{13}C)] were observed for enamide metal complexes (**I**). In line with this interpretation the copper phosphine complexes Ph_3PCuLL' and bu^i_3PCuLL' (**3a**) may be classified as enamide complexes (**I**) with a direct bond between Cu and N and no direct contact to CH while the heavier analogues bu^i_3PAgLL' (**3b**), Ph_3PAuLL' and bu^i_3PAuLL' (**3c**) are better described as iminoalkyl complexes (**II**).

Further support for this classification comes from the ^{1}H and ^{13}C NMR spectra of **3c** that show doublets for the CH group of the 1-azaallyl ligand with coupling constants ^3J(P,H) and ^2J(P,C) of 10.9 (10.5 for Ph_3PAuLL') and 56.3 Hz, respectively, as a consequence of coupling to P. Coupling constants for ^3J(P,H) in the region of 4–16 Hz and ^2J(P,C) around 100 Hz have been reported for other phosphine alkyl complexes [14–18].

The silver complex **3b** in contrast showed singlets in the ^{13}C NMR ($\delta = 24.6$) and the ^{1}H NMR spectrum ($\delta = 3.50$). The latter was broad and probably not resolved due to additional J(Ag,C) coupling and the occurrence of exchange between **3b** and free bu^i_3P formed from the decomposition of the silver complex. Similar observations have previously been described for phosphine gold complexes $RAuPR'_3$ (R = alkyl, R′ = alkyl, aryl) where the doublet of the HCAu-fragment either broadens significantly [18] or else collapses to a sharp singlet [17] as a consequence of the addition of small quantities of free phosphine to the metal complexes.

A noteworthy observation is the appearance of two overlapping doublets [attributable to unequal $^1J(^{31}P–^{109}Ag)$ and $^1J(^{31}P–^{107}Ag)$ coupling constants] in the $^{31}P\{^1H\}$ NMR spectrum at near ambient temperature (298 K). This is unusual for monodentate phosphine silver complexes, since rapid ligand exchange usually precludes the observation of P–Ag spin–spin coupling. For example, for a series of $XAg\{P(p\text{-tol})_3\}_n$ complexes (where $n = 2$–4 and X = a range of counter-anions), the ligands were labile in all the complexes studied so that P–Ag spin–spin coupling was not resolved above −70 °C [19]. Where ligands are too sterically encumbered to

participate in the association process believed to be involved in the exchange, most notably, $XAg(PMe_3)_2$ and $XAg(Pbu^t_3)_2$, well resolved P–Ag spin–spin coupling is exhibited at ambient temperature [20,21].

Consistent with the copper complexes being enamide complexes (**I**) no coupling was observed in their ^1H or ^{13}C NMR spectrum. The solid state structures of Ph_3PCuLL' [3], $(dme)_3LiCuLL'_2$ [3] and bu^i_3PAuLL' (see below) lend the above arguments further support.

The distinction between an η^3-1-azaallyl (**III**) and an iminoalkyl metal complex (**II**) on the basis of NMR spectroscopy is, however, more ambiguous as may be deduced from the close similarity of the NMR-spectrum (cf. Table 2) of $Ph_3PNi(I)LL'$ [22] as an example for an η^3-1-azaallyl complex (**III**) and the discussed iminoalkyl metal complexes (**II**).

The observed difference in bonding modes between Cu- and Ag/Au-azaallyl complexes, respectively, may be explained on the basis of HSAB theory [23] with the softer, larger metal ion [Ag(I), Au(I)] having a preference for the softer atom (C^-) of the bidentate 1-azaallyl ligand and the harder cation [Cu(I)] binding preferentially to the harder atom (N^-).

3.3. Solid state structures of complexes *2c*, *2d* and *3c*

Copper- and silver phosphine halides of monodentate phosphines are frequently found to aggregate in the solid state into dimers or higher molecular species by increasing the coordination number of the metal via additional metal halogen bonds [24,25]. Gold analogues in contrast are known to show linear two coordinate metal atoms that may dimerise via relativistic Au···Au interactions [25,26]. In order to minimise steric repulsion between the phosphine substituents while at the same time maximising aurophilic interactions the dimers are arranged in a paddle-like fashion with P–Au–Au–P torsion angles close to 90° [25–27]. Mononuclear complexes in contrast are found in case of sterically demanding phosphines with cone angles [28] larger than 130°.

In line with these general trends the crystal structures of **2c** and **2d** show no surprises. $[bu^i_3PAgCl]_4$ (**2c**) crystallises as a tetramer with a cubic AgCl core that has threefold rotation symmetry (Fig. 1). The Cl–Ag–Cl and Ag–Cl–Ag angles (see Table 3) are close to 90° with the former being slightly larger [92.67(8)–94.00(6)°] than the latter [86.03(8)–87.50(6)°]. A considerable larger distortion of the cube was observed in $[(2\text{-}Py_2Ph)PAgCl]_4$ [29] and $[Ph_3PAgCl]_4$ [30]. The Ag–P and Ag–Cl distances of 2.371(2), 2.383(4) and 2.645(3), 2.648(2), 2.690(2), 2.676(3) Å, respectively, in **2c** compare well to those found in related complexes such as $[(H_{11}C_6)_3PAgCl]_4$ [31] or $[Et_3PAgCl]_4$ [32] (see also [26,27]).

bu^i_3PAuCl (**2d**) (cone angle for Pbu^i_3 143°) [28] is a monomer (shortest Au···Au contact 4.450 Å; Fig. 2(a), Table 4) in the solid state with a linear two coordinate gold atom [(P–Au–Cl 178.41(3)°]. The Au–P and Au–Cl bond distances of 2.239(1) and 2.292(1) Å are comparable to related complexes such as $(c\text{-}H_{11}C_6)_3PAuCl$ [33], $(H_7C_{10})_3PAuCl$ [8], (TPA)-AuCl (TPA = 1,3,5-triaza-7-phosphaadamantane) [27], Et_3PAuCl [34], $(NCCH_2CH_2)_3PAuCl$ [35], $2\text{-}Py_3PAuCl$ [36], Ph_3PAuCl [37] or Pr^i_3PAuCl [38] but slightly shorter than those in related silver complexes. This is thought to be a consequence of the relativistic contraction of gold [25,39]. Two monomeric units of **2d** are linked via weak CH···Cl contacts (C1–H1···C1′ 2.82 Å, Fig. 2(b)) between the Cl atom and a CH_2 group of the neighbouring phosphine (Fig. 2(b)). $(c\text{-}H_{11}C_6)_3PAuCl$ was found to associate in a similar fashion to polymeric chains (Cl···HC 2.91–3.27 Å) [33a].

Compound **3c** crystallises in the monoclinic space group $P2(1)/n$ with one molecule in the asymmetric unit (Fig. 3, Table 5). It is a monomer with a linear P–Au–C unit [P–Au–C2 178.3 (1)°] and represents to the best of

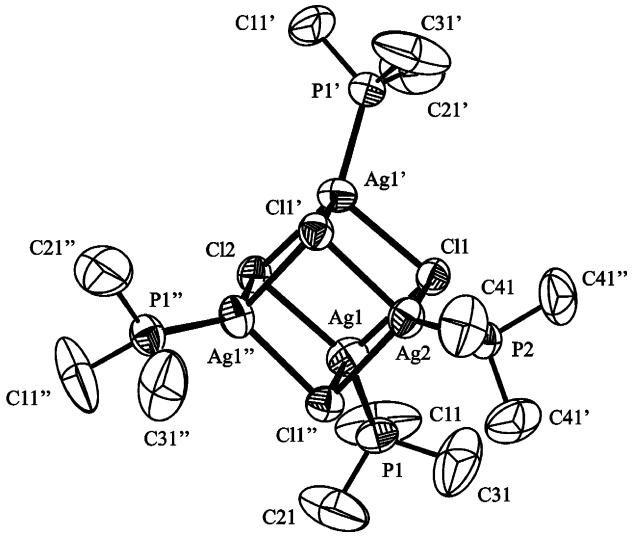

Fig. 1. Molecular structure of $[bu^i_3PAgCl]_4$ (**2c**). Thermal ellipsoids are drawn on the 30% probability level. H atoms and isobutyl groups except C atoms directly bound to P have been omitted for clarity.

Table 3
Selected bond distances (Å) and angles (°) for compound **2c**

Bond distances			
Ag1–P1	2.371(2)	Ag2–P2	2.383(4)
Ag1–C11	2.645(3)	Ag1–C12	2.648(2)
Ag1–C11*	2.690(2)	Ag2–C11	2.676(3)
Bond angles			
C11–Ag1–C12	94.00(6)	C11–Ag1–C11*	93.04(11)
C12–Ag1–C11*	92.99(6)	C11–Ag2–C11*	92.67(8)
Ag1–C11–Ag2	87.50(6)	Ag1–C11–Ag1**	86.03(8)
Ag2–C11–Ag1**	86.60(6)	Ag1*–C12–Ag1	86.81(8)

Symmetry transformations used to generate equivalent atoms: *, $-x+y+1, -x+2, z$; **, $-y+2, x-y+1, z$.

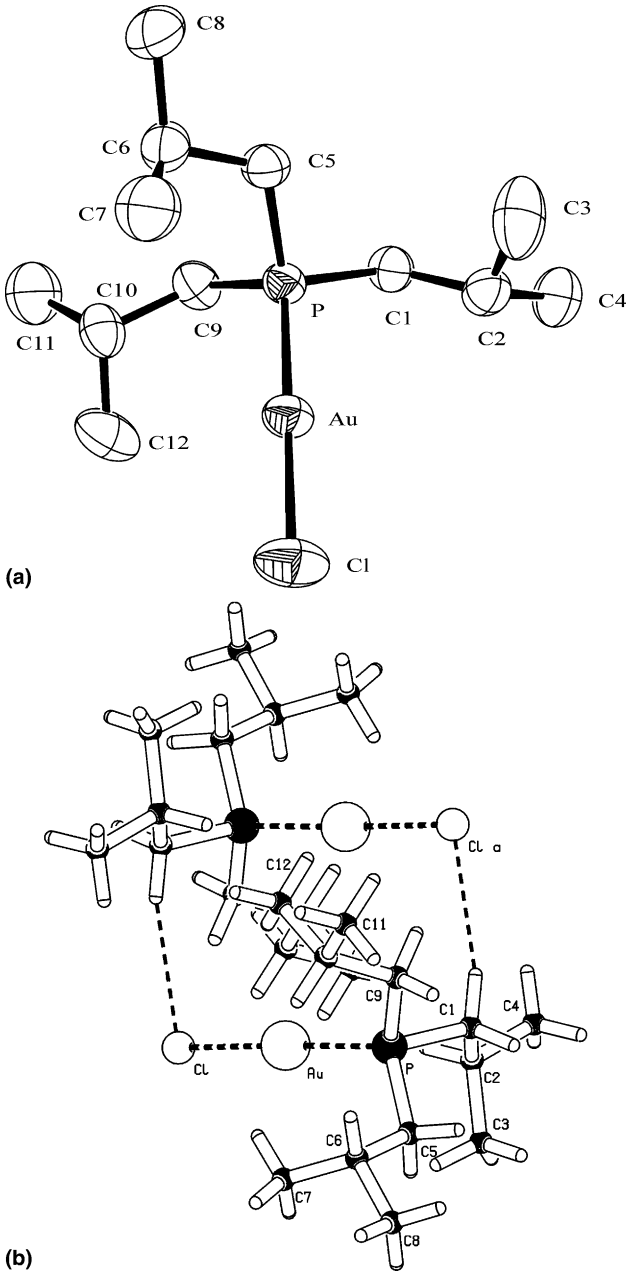

Fig. 2. (a) Molecular structure of $bu^{i}_{3}PAuCl$ (**2d**). Thermal ellipsoids are drawn on the 50% probability level. H atoms have been omitted for clarity. (b) Molecular structure of $bu^{i}_{3}PAuCl$ showing CH···Cl contacts.

Table 4
Selected bond distances (Å) and angles (°) for compound **2d**

Bond distances			
Au–P	2.239(1)	Au–C1	2.292(1)
P–C1	1.830(3)	P–C5	1.833(3)
P–C3	1.827(4)		
Bond angles			
C1–H1···C1′	2.82	C1···C1	3.76
P–Au–C1	178.41(3)	C1–H1–C1′	164.96

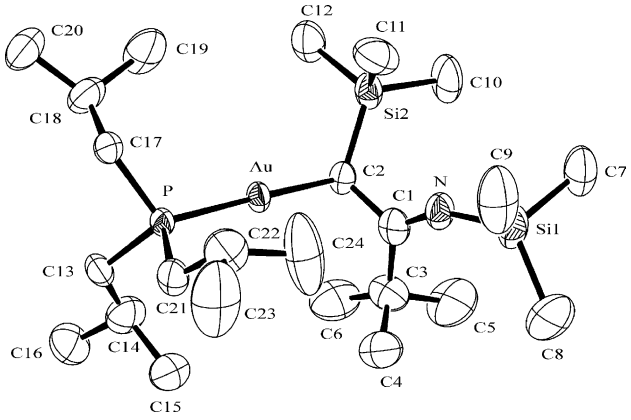

Fig. 3. Molecular structure of $bu^{i}_{3}PAuLL'$ (**3c**). Thermal ellipsoids are drawn on the 50% probability level. H atoms have been omitted for clarity.

Table 5
Selected bond distances (Å) and angles (°) for compound **3c**

Bond distances			
Au–P	2.284(1)	Au–C2	2.100(5)
N–C1	1.266(6)	C1–C2	1.493(7)
P–C13	1.842(5)	P–C17	1.830(5)
P–C21	1.825(5)		
Bond angles			
C2–Au–P	178.3(1)		

our knowledge the first example of a crystallographically characterised 1-azaallyl complex that adopts an iminoalkyl configuration (**II**) and may be best compared to the enolate complex $Ph_3PAuCH_2C(O)Ph$ [40]. The Au–P distance of 2.284(1) Å is unexceptional as is the Au–C2 distance of 2.100(5) Å that is within the range expected for a Au–C σ bond to an sp^3-hybridised C-atom [$Ph_3PAuCH_2C(O)Ph$ [40], $Ph_3PAuCH_2CH_2C(O)Ph$ [40], $Ph_3PAuC_5HPh_4$ [18], Ph_3PAuMe [41], Ph_3PAuCH_2Cl [15], Ph_3PAuCH_2SPh [15], $Ph_3PAuCH(SiMe_3)_2$ [14], ($Ph_3PAuC_{13}H_9$ [16]) but slightly longer than those found in aryl gold complexes as for example $Ph_3PAuC_6H_3(OMe)_2$-2,6 [42], $bu^{t}_{3}PAuPh$ [43], $Ph_3PAuC_4H_4O$ [44] or $Ph_3PAuC_6H_3Mes_2$-2,6 [45] (2.04–2.08 Å). The coordination geometry around C2 is a distorted tetrahedron with the angle C1–C2–Si1 (114.2°) between the two sterically most demanding groups showing the largest deviation from 109.5°. The iminoalkyl configuration is further confirmed by the C1–C2 and C2–N bond distances of 1.493(7) and 1.2666(6) Å that correspond to C–C single and CN double bonds, respectively. The sum of angles of 360° around the N atom are in line with an sp^2-hybridisation at the N.

4. Supplementary data

Full crystallographic data (CCDC No. 232066 for compound **2c**, 232067 for compound **3c** and 232068 for

compound **2d**) have been deposited at the Cambridge Crystallographic Database Centre and are available on request from the Director, CCDC, 12 Union Road, Cambridge, CB2 1EZ, UK (Fax: +44-1223-336-033; Email: deposit@ccdc.cam.ac.uk or http://www.ccdc.cam.ac.uk).

Acknowledgements

The authors thank Mintek (project AuTEK), CANSA, THRIP and the University of the Witwatersrand for financial support.

References

[1] (a) A.J. Pearson, Syn. lett. (1990) 10;
(b) S.L. Blystone, Chem. Rev. 89 (1989) 1663;
(c) J.W. Faller, K.-H. Chao, J. Am. Chem. Soc. 105 (1983) 3893;
(d) K. Yamamoto, J. Tsuji, Tetrahedron Lett. 23 (1982) 3089;
(e) B.M. Trost, Tetrahedron 33 (1977) 2615;
(f) B.M. Trost, T.R. Verhoeven, Compr. Organomet. Chem. 8 (1982) 799 (and references therein).
[2] C.F. Caro, M.F. Lappert, P.G. Merle, Coord. Chem. Rev. 219-221 (2001) 605.
[3] P.B. Hitchcock, M.F. Lappert, M. Layh, J. Chem. Soc., Dalton Trans. (1998) 1619.
[4] P.B. Hitchcock, M.F. Lappert, M. Layh, A. Klein, J. Chem. Soc., Dalton Trans. (1999) 1455.
[5] P.B. Hitchcock, M.F. Lappert, D.-S. Liu, J. Chem. Soc., Chem. Commun. (1994) 1699.
[6] M.F. Lappert, M. Layh, Tetrahedron Lett. 39 (1998) 4745.
[7] K.C. Dash, H. Schmidbaur, Chem. Ber. 106 (1973) 1221.
[8] T.E. Müller, J.C. Green, D.M.P. Mingos, C.M. McPartlin, C. Wittingham, D.J. Williams, T.M. Woodroffe, J. Organomet. Chem. 551 (1998) 313.
[9] (a) Bruker, SAINT+. Version 6.02 (includes XPREP and SADABS), Bruker AXS INC., Madison, WI, USA, 1999;
(b) G.M. Sheldrick, SADABS, University of Göttingen, Germany, 1996.
[10] Bruker, SHELXTL, Version 5.1 (includes XS, XL, XP, XSHELL), Bruker AXS INC., Madison, WI, USA, 1999.
[11] A.L. Spek, J. Appl. Cryst. 36 (2003) 7.
[12] L.J. Farrugia, J. Appl. Cryst. 30 (1997) 565.
[13] P.B. Hitchcock, J. Hu, M.F. Lappert, M. Layh, J. Severn, J. Chem. Soc., Chem. Commun. (1997) 1189.
[14] S. Bommers, H. Beruda, N. Dufour, M. Paul, A. Schier, H. Schmidbaur, Chem. Ber. 128 (1995) 137.
[15] D. Steinborn, S. Becke, R. Herzog, M. Günther, R. Kircheisen, H. Stoeckli-Evans, C. Bruhn, Z. Anorg. Allg. Chem. 624 (1988) 1303.
[16] Y.T. Struchkov, Y.L. Slovokhotov, D.N. Kravtsov, T.V. Baukova, J. Organomet. Chem. 338 (1988) 269.
[17] H. Schmidbaur, A. Shiotani, Chem. Ber. 104 (1971) 2821.
[18] T.V. Baukova, Y.L. Slovokhotov, Y.T. Struchkov, J. Organomet. Chem. 220 (1981) 125.
[19] E.L. Muetterties, C.W. Alegranti, J. Am. Chem. Soc. 94 (1972) 6386.
[20] R.C. Gael, P. Pilon, Inorg. Chem. 17 (1978) 2876.
[21] E.C. Alyea, S.A. Dias, S. Stevens, Inorg. Chim. Acta 44 (1980) L203.
[22] P.B. Hitchcock, M.F. Lappert, M. Layh, Z. Anorg. Allg. Chem. 626 (2000) 1081.
[23] (a) R.G. Pearson, J. Am. Chem. Soc. 85 (1963) 3533;
(b) R.G. Pearson, Inorg. Chem. 27 (1988) 734;
(c) R.G. Pearson, Inorg. Chim. Acta 240 (1995) 93.
[24] P.D. Akrivos, H.J. Katsikis, A. Koumoutsi, Coord. Chem. Rev. 167 (1997) 95.
[25] P. Schwerdtfeger, H.L. Hermann, H. Schmidbaur, Inorg. Chem. 42 (2003) 1334.
[26] P. Pyykkö, Chem. Rev. 97 (1997) 597.
[27] Z. Assefa, B.G. McBurnett, R.J. Staples, J.P. Fackler Jr., B. Assmann, K. Angermaier, H. Schmidbaur, Inorg. Chem. 34 (1995) 75.
[28] C.A. Tolman, Chem. Rev. (1977) 315.
[29] Y. Inoguchi, B. Milewski-Mahrla, D. Neugebauer, P.G. Jones, H. Schmidbaur, Chem. Ber. 116 (1983) 1487.
[30] B.-K. Teo, J. Calabrese, Inorg. Chem. 15 (1976) 2467.
[31] G.A. Bowmaker, Effendy, P.J. Harvey, P.C. Healy, B.W. Skelton, A.H. White, J. Chem. Soc., Dalton Trans. (1996) 2459.
[32] M.R. Churchill, J. Donahue, F. Rotella, Inorg. Chem. 15 (1976) 2752.
[33] (a) R.C. Bott, G.A. Bowmaker, R.W. Buckley, P.C. Healy, M.C.S. Perera, Aust. J. Chem. 52 (1999) 271;
(b) J.A. Muir, M.M. Muir, L.B. Pulgar, Acta Crystallogr., Sect. C 41 (1985) 1174.
[34] E.R.T. Tiekink, Acta Crystallogr., Sect. C 45 (1989) 1233.
[35] J.P. Fackler Jr., R.J. Staples, M.N.L. Khan, R.E.P. Winpenny, Acta Crystallogr., Sect. C 50 (1994) 1020.
[36] C.J.L. Lock, M.A. Turner, Acta Crystallogr., Sect. C 43 (1987) 2096.
[37] N.C. Baenzinger, W.E. Bennet, D.M. Soboroff, Acta Crystallogr., Sect. B 32 (1976) 962.
[38] K. Angermaier, E. Zeller, H. Schmidbaur, J. Organomet. Chem. 472 (1994) 371.
[39] A. Bayler, A. Schier, G.A. Bowmaker, H. Schmidbaur, J. Am. Chem. Soc. 118 (1996) 7006.
[40] Y. Ito, M. Inouye, M. Suginome, M. Murakami, J. Organomet. Chem. 342 (1988) C41.
[41] P.G. Gavens, J.J. Guy, M.J. Mays, G.M. Sheldrick, Acta Crystallogr., Sect. B 33 (1977) 137.
[42] P.E. Riley, R.E. Davis, J. Organomet. Chem. 192 (1980) 283.
[43] A. Sladek, S. Hofreiter, M. Paul, H. Schmidbaur, J. Organomet. Chem. 501 (1995) 47.
[44] K.A. Porter, A. Schier, H. Schmidbaur, Organometallics 22 (2003) 4922.
[45] G.W. Rabe, N.W. Mitzel, Inorg. Chim. Acta 316 (2001) 132.

Available online at www.sciencedirect.com
SCIENCE DIRECT®
Polyhedron 23 (2004) 2281–2284
POLYHEDRON
www.elsevier.com/locate/poly

Zwitterionic ferrocenyldithiophosphonates: the molecular structure of [FcP(S)S($OCH_2CH_2NH_2Me$)] [Fc = Fe(η^5-C_5H_4)(η^5-C_5H_5)]

Mehmet Karakus [a,*], Peter Lönnecke [b], Evamarie Hey-Hawkins [b,*]

[a] Department of Chemistry, Faculty of Arts and Science, Pamukkale University, Kinikli, 20017 Denizli, Turkey
[b] Institut für Anorganische Chemie der Universität Leipzig, Johannisallee 29, D-04103 Leipzig, Germany

Received 22 June 2004; accepted 14 July 2004
Available online 28 August 2004

Abstract

Ferrocenyldithiodiphosphetane [FcPS(μ-S)]$_2$ [Fc = Fe(η^5-C_5H_4)(η^5-C_5H_5)] reacts with the aminoethanol derivatives $HOCH_2CH_2NHMe$ and $HOCH_2CH_2NEt_2$ to give the first structurally characterised examples of zwitterionic (*O*-ethylammonium)ferrocenyldithiophosphonates, [FcP(S)S($OCH_2CH_2NHR^1R^2$)] (R^1 = H, R^2 = Me (**1**); R^1 = R^2 = Et (**2**)). **1** and **2** were characterised by elemental analyses, IR, NMR spectroscopy (^{1}H, ^{13}C (for **2**) and ^{31}P) and mass spectrometry. A crystal structure determination was carried out on **1**.
© 2004 Elsevier Ltd. All rights reserved.

Keywords: Zwitterionic ferrocenyldithiophosphonates; Molecular structures

1. Introduction

Organophosphorus-containing dithiolato-type compounds are of interest due to their agricultural and industrial applications, such as insecticides, pesticides, antioxidants, additives for lubricants, solvent-extraction reagents for metals and flotation agents for mineral ores [1,2]. Reactions of [FcPS(μ-S)]$_2$ [Fc = Fe(η^5-C_5H_4)(η^5-C_5H_5)] [3] with alcohols [4–7] or sodium alkoxides [8], silanols [6,9], dienes [10,11], alkenes [11] and cyanamides [12,13] were already described.

We now report the reaction of [FcPS(μ-S)]$_2$ with methylaminoethanol and diethylaminoethanol to give the zwitterionic complexes [FcP(S)S($OCH_2CH_2NHR^1R^2$)] (R^1 = H, R^2 = Me (**1**); R^1 = R^2 = Et (**2**)), in which the H atom of the initially formed P–SH group was transferred to the amino group (Scheme 1). We also report the molecular structure of **1**, which to the best of our knowledge is the first example of this type of compounds to be structurally characterised.

2. Results and discussion

We previously observed that [FcPS(μ-S)]$_2$ [3] reacts with alcohols ROH (R = Me, Et, Pr^i, Bu^s, Bu^i) to give the corresponding ferrocenyldithiophosphonic acids [FcPS(OR)(SH)], which could, however, not be isolated in pure form, but were sufficiently pure for further reaction with nickel(II) acetate to yield the square-planar heterobimetallic trinuclear complexes [{FcP(OR)S$_2$}Ni] [7]. We have therefore now employed aminoalcohols as bifunctional reagents in an attempt to prepare the corresponding ferrocenyldithiophosphonic acids [FcPS($OCH_2CH_2NR^1R^2$)(SH)], which could act as *S*,*S*′ chelating ligands towards soft transition metals and simultaneously as amino ligands towards hard transition metals, thus enabling the synthesis of multinuclear complexes.

* Corresponding authors. Tel.: +49 341 973 6151; fax: +49 341 973 9319.
E-mail address: hey@rz.uni-leipzig.de (M. Karakus).

0277-5387/$ - see front matter © 2004 Elsevier Ltd. All rights reserved.
doi:10.1016/j.poly.2004.07.003

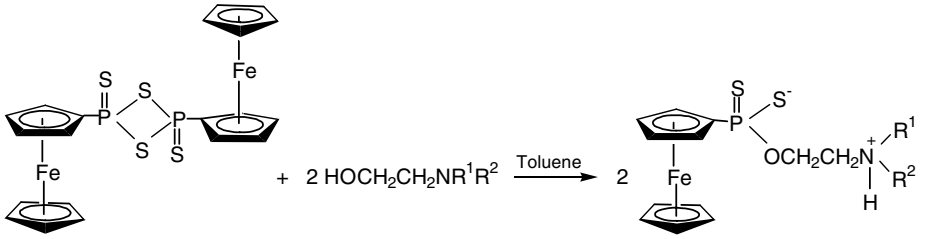

$R^1 = H$, $R^2 = Me$ (**1**)
$R^1 = R^2 = Et$ (**2**)

Scheme 1.

However, reaction of 2,4-diferrocenyl-1,3-dithiadiphosphetane 2,4-disulfide $[FcPS(\mu\text{-}S)]_2$ with the aminoethanol derivatives $HOCH_2CH_2NHMe$ and $HOCH_2CH_2NEt_2$ in a 1:2 ratio gave the zwitterionic complexes $[FcP(S)S(OCH_2CH_2NHR^1R^2)]$ ($R^1 = H$, $R^2 = Me$ (**1**); $R^1 = R^2 = Et$ (**2**)) as yellow solids in good yield (Scheme 1).

Compounds **1** and **2** were characterised by elemental analyses (C, H, N, S), ^1H and ^{31}P NMR and IR spectroscopy and by MS. The solubility of **1** is very low, even in $CHCl_3$ and CH_3CN, in which **2** is slightly soluble. Both compounds are soluble in DMSO, but decomposition occurs with the yellow solution turning darker. Therefore, ^{13}C NMR spectra could only be obtained for **2**, but the signal of the *ipso*-C atom of the cyclopentadienyl ring could not be observed due to low solubility in $CDCl_3$. The ^1H NMR spectra of **1** and **2** are consistent with the formation of zwitterionic dithiodiphosphonates, as indicated by a broad singlet at δ 9.85 (for **1**) and 11.50 ppm (for **2**), which can be assigned to the NH proton of the ammonium group [14]. In the ^{31}P NMR spectra of **1** and **2** triplets are observed at 114.1 and 115.4 ppm ($^2J_{PH} = 14.8$ and 16.5 Hz) due to coupling to the OCH_2 protons. Due to low solubility, no NMR data are available for the starting material $[FcPS(\mu\text{-}S)]_2$ [3], but similar chemical shifts and coupling constants were observed in [FcP(S)(SH)(OR)] and $[\{FcP(OR)S_2\}_2Ni]$ [7].

In the IR spectra of **1** and **2** characteristic bands are observed for νPO (1025 or 1028 cm^{-1}), and two strong bands about at 654 or 656 cm^{-1} and 582 or 584 cm^{-1} are attributed to $\nu_{asym}(PS_2)$ and $\nu_{sym}(PS_2)$, respectively. A medium band at 2745 (for **1**) or 2697 cm^{-1} (for **2**) can be attributed to the N-H vibration in the ammonium salt [14].

In the ESI mass spectra of **1** and **2** molecular ion peaks are observed at *m/z* 355 and 397, respectively, while only fragment ions (*m/z* 121 (CpFe), 186 (Fc) and 217 (FcP)) occur in the EI mass spectrum. In the ESI mass spectrum, signals for a dimer (for **1** and **2**) and trimer (for **1**) are also observed.

Compounds **1** and **2** do not dissolve in water but dissolve in aqueous NaOH, probably with formation of the sodium salts $Na[FcP(S)S(OCH_2CH_2NR^1R^2)]$ ($R^1 = H$, $R^2 = Me$; $R^1 = R^2 = Et$). Attempts to isolate these salts by evaporating the solvent at room temperature produced only **1** or **2** and NaOH. This reaction is presently under further investigation.

Attempts to prepare transition metal complexes of **1** and **2** by reaction with nickel acetate in acetic acid/chloroform, $ZnSO_4$ in aqueous NaOH or cadmium acetate in chloroform/ethanol were unsuccessful; no reaction was observed under these conditions.

3. Molecular structure of 1

Single crystals of **1** were obtained from $CHCl_3$/CH_3CN. Compound **1** crystallises in the orthorhombic space group *Pbca* with $Z = 8$. The crystallographic data indicate that **1** is a zwitterion (Fig. 1). The P–S(1) and P–S(2) bond lengths are similar (1.975(1) and 1.993(1) Å) and longer than observed for a P–S double bond (1.94 Å) [15] as would be expected for a delocalised PS_2 fragment. The phosphorus atom has a tetrahedral coordination environment with a small O(1)–P–C(1) bond angle (97.5(1)°) and three bond angles (O(1)–P–S(1), O(1)–P–S(2) and C(1)–P–S(2)) close to the ideal value of 109.5°

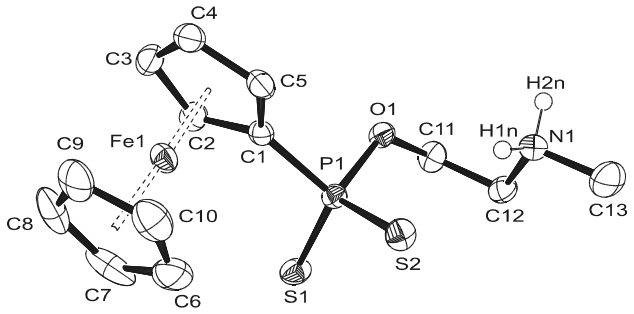

Fig. 1. Molecular structure of **1** (ORTEP, 50% probability, SHELXTL PLUS; XP) [18].

(110.03(9), 108.36(8) and 109.8(1)°). However, larger bond angles (112.5(1) and 116.91(5)°) are observed for C(1)–P–S(1) and S(1)–P–S(2), respectively, probably due to steric reasons (see Table 2).

4. Experimental

Solvents were dried and distilled prior to use by standard methods. Compounds were handled with exclusion of air and moisture. $[FcPS(\mu\text{-}S)]_2$ was prepared according to the literature procedure [16]. Elemental analyses were determined with a VARIO EL (Heraeus). The mass spectra were recorded on a MAT-8230 (EI-MS, 70 eV) or on an FT-ICR-MS Bruker-Daltonics ESI mass spectrometer (APEX II, 7 Tesla). IR spectra were recorded as KBr disks with a Perkin–Elmer 2000 FT-IR spectrometer in the range 400-4000 cm^{-1}. Melting points (Gallenkamp) are uncorrected. Methylaminoethanol and diethylaminoethanol were purchased from ACROS.

5. Syntheses

5.1. [FcP(S)S(OCH$_2$CH$_2$NH$_2$Me)] (1)

$[FcPS(\mu\text{-}S)]_2$ (0.6 g, 1 mmol) was treated with methylaminoethanol (0.18 mL, 2 mmol) in hot toluene (10 mL). The mixture was refluxed for 30 min and a yellow solid was obtained. The yellow solid was isolated by filtration and washed with toluene and diethyl ether. The product was recrystallised from chloroform/acetonitrile (2/1) and obtained as a yellow solid (0.35 g, 58%), m.p. 193–194 °C (decomp); $C_{13}H_{18}FeNOPS_2$: requires C, 43.95; H, 5.10; N, 3.90; S, 18.05. Found: C, 41.5; H, 5.15; N, 3.77; S, 21.0%. MS (ESI): *m/z* 354.99 $[M]^+$, 710.99 $[2M]^+$, 1065.99 $[3M]^+$; MS (EI): *m/z* 337 $[M - CH_3 - 2H, 100\%]^+$, 280 $[FcPS_2, 93\%]^+$, 217 $[FcP, 66\%]^+$, 184 $[Fc, 88\%]^+$, 121 $[CpFe, 88\%]^+$. δ_H ($CDCl_3$): 9.85 (br, 2H, NH_2), 4.76 (br s, 2H, C_5H_4), 4.64 (d of m, 2H, $^3J_{PH} = 14.8$ Hz, C_5H_4), 4.43 (br s, 2H, OCH_2), 4.36 (s, 5H, C_5H_5), 3.32 (br, 2H, CH_2N), 2.94 (s, 3H, CH_3). δ_P($CDCl_3$): 114.1 (t, $^3J_{PH} = 14.8$ Hz). Due to low solubility, ^{13}C NMR spectra could not be obtained. Selected IR bands (cm^{-1}): 2745 s (νNH), 1025 versus (νPO), 654 versus ($\nu_{asym}(PS_2)$), 582 s ($\nu_{sym}(PS_2)$).

5.2. [FcP(S)S(OCH$_2$CH$_2$NHEt$_2$)] (2)

$[FcPS(\mu\text{-}S)]_2$ (0.52 g, 0.9 mmol) was treated with diethylaminoethanol (0.25 mL, 1.8 mmol) in hot toluene (10 mL). The mixture was refluxed for 30 min and a yellow solid was obtained, which was isolated by filtration and washed with toluene and diethyl ether. The product was recrystallised from chloroform/acetonitrile (2/1) to give a yellow solid (0.41 g, 68%), m.p. 182–183 °C (decomp); $C_{16}H_{24}FeNOPS_2$: requires C, 48.32; H, 6.08; N, 3.52; S, 16.14. Found: C, 47.80; H, 5.83; N, 3.58; S, 16.90%. MS (ESI): *m/z* 397.5 $[M]^+$, 398.05 $[M + H]^+$, 795.09 $[2M]^+$; MS (EI): *m/z* 340 $[M - 2C_2H_5, 41\%]^+$, 248 $[FcPS, 33\%]^+$, 217 $[FcP, 35\%]^+$, 186 $[Fc, 100\%]^+$, 121 [CpFe,

Table 1
Crystal data and structure refinement for **1**

Empirical formula	$C_{13}H_{18}FeNOPS_2$
Formula weight	355.22
Temperature	208(2) K
Wavelength	71.073 pm
Crystal system	orthorhombic
Space group	*Pbca*
Unit cell dimensions	
a	919.4(1) pm
b	1221.2(2) pm
c	2758.8(4) pm
α	90°
β	90°
γ	90°
V	3.0974(7) nm^3
Z	8
$D_{calc.}$	1.524 Mg/m^3
Absorption coefficient	1.337 mm^{-1}
F(000)	1472
Crystal size	0.40 × 0.30 × 0.20 mm
θ Range for data collection	1.48–29.20
Index ranges	$-12 \leqslant h \leqslant 11$, $-11 \leqslant k \leqslant 16$, $-35 \leqslant l \leqslant 36$
Reflections collected	15660
Independent reflections	3884 [$R_{int} = 0.0374$]
Completeness to $\theta = 29.11°$	92.5%
Maximum and minimum transmission	0.7758 and 0.6168
Refinement method	full-matrix least-squares on F^2
Data/restraints/parameters	3884/0/244
Goodness-of-fit on F^2	1.362
Final *R* indices [$I > 2\sigma(I)$]	$R_1 = 0.0609$, $wR_2 = 0.0966$
R indices (all data)	$R_1 = 0.0721$, $wR_2 = 0.0993$
Largest difference peak and hole	0.389 and −0.371 e $Å^{-3}$

Table 2
Selected bond lengths (Å) and angles (°) for **1**

P–S(1)	1.975(1)
P–S(2)	1.993(1)
P–O(1)	1.636(2)
P–C(1)	1.785(3)
N–C(12)	1.475(3)
N–C(13)	1.481(5)
O(1)–P–S(1)	110.03(9)
O(1)–P–S(2)	108.36(8)
S(1)–P–S(2)	116.91(5)
P(1)–C(1)–Fe(1)	127.6(2)
O(1)–P–C(1)	97.5(1)
C(1)–P–S(1)	112.5(1)
C(1)–P–S(2)	109.8(1)
C(11)–O(1)–P(1)	122.2(2)

69%]$^+$. $\delta_H(CDCl_3)$: 11.50 (br, 1H, NH), 4.72 (br m, 2H, C_5H_4), 4.49 (d of m, 2H, $^3J_{PH}$ 16.5 Hz, C_5H_4), 4.36 (s, 5H, C_5H_5), 4.35 (m, 2H, OCH_2), 3.32 (br m, 4H, CH_2 in Et), 3.22 (br t, 2H, NCH_2), 1.44 (t, 6H, $^3J_{HH}$ 6.8 Hz, CH_3 in Et). δ_C ($CDCl_3$): 8.44 (CH_2CH_3), 47.08 (CH_2CH_3), 54.04 (CH_2CH_2N), 57.73 (OCH_2), 70.60 (C_5H_5), 70.74 (C_5H_4), 72.02 (C_5H_4), *ipso*-C in C_5H_4 not observed. $\delta_P(CDCl_3)$: 115.4 (t, $^3J_{PH}$ = 16.5 Hz). Selected IR bands (cm^{-1}): 2697 s (νNH), 1028 versus (νPO), 656 versus $\nu_{asym}(PS_2)$, 584 s $\nu_{sym}(PS_2)$.

5.3. X-ray crystallography

Crystallographic data for **1** are given in Table 1. Data [λ (Mo Kα) = 0.71073 Å] were collected with a Siemens CCD (SMART) diffractometer. 900 reflections were used for determination of the unit cell parameters. Empirical absorption correction with SADABS [17]. The structure was solved by direct methods (SHELXTL PLUS) [18]. H atoms were located by difference maps and refined isotropically.

6. Supplementary material

CCDC-242555 (**1**) contains the supplementary crystallographic data for this paper. These data can be obtained free of charge via www.ccdc.cam.ac.uk/conts/retrieving.html (or from the Cambridge Crystallographic Data Centre, 12 Union Road, Cambridge CB2 1EZ, UK; fax: +44 1223 336 033; or deposit@ccdc.cam.uk).

Acknowledgement

M. Karakus is grateful to DAAD for a postdoctoral fellowship (A/03/21316).

References

[1] M.C. Aragoni, M. Arca, F. Demartin, F.A. Devillanova, C. Graiff, F. Isaia, V. Lippolis, A. Tiripicchio, G. Verani, Eur. J. Inorg. Chem. (2000) 2239.
[2] M.C. Aragoni, M. Arca, F. Demartin, F.A. Devillanova, C. Graiff, F. Isaia, V. Lippolis, A. Tiripicchio, G. Verani, J. Chem. Soc., Dalton Trans. (2001) 2671.
[3] M.R.St.J. Foreman, A.M.Z. Slawin, J.D. Woollins, J. Chem. Soc., Dalton Trans. (1996) 3653.
[4] W.E. van Zyl, J.P. Fackler Jr., Phosphorus Sulfur Silicon 167 (2000) 117.
[5] C.M. Thomas, A. Neels, H. Stœckli-Evans, G. Süss-Fink, J. Organomet. Chem. 633 (2001) 85.
[6] W.E. van Zyl, J.M. López-de-Luzuriaga, A.A. Mohamed, R.J. Staples, J.P. Fackler Jr., Inorg. Chem. 21 (2002) 4579.
[7] M. Karakus, P. Lönnecke, D. Yakhvarov, E. Hey-Hawkins, Z. Anorg. Allg. Chem. 630 (2004) 1249.
[8] I.P. Gray, H.L. Milton, A.M.Z. Slawin, J.D. Woollins, Dalton Trans. (2003) 3450.
[9] W.E. van Zyl, R.J. Staples, J.P. Fackler Jr., Inorg. Chem. Commun. 1 (1998) 51.
[10] M.R.St.J. Foreman, A.M.Z. Slawin, J.D. Woollins, Chem. Commun. (1997) 855.
[11] M.R.St.J. Foreman, A.M.Z. Slawin, J.D. Woollins, J. Chem. Soc., Dalton Trans. (1999) 1175.
[12] M.R.St.J. Foreman, A.M.Z. Slawin, J.D. Woollins, Chem. Commun. (1997) 1269.
[13] M.R.St.J. Foreman, R.J. Mortimer, A.M.Z. Slawin, J.D. Woollins, J. Chem. Soc., Dalton Trans. (1999) 3419.
[14] M. Hesse, H. Meier, B. Zeeh, Spektroskopische Methoden in der organischen Chemie, 5. Aufl., G. Thieme Verlag, Stuttgart, New York, 1995.
[15] V.K. Jain, B. Varghese, J. Organomet. Chem. 584 (1999) 159.
[16] M.D. Santana, G. García, C.M. Navarro, A.A. Lozano, J. Pérez, L. García, G. López, Polyhedron 21 (2002) 1935.
[17] G.M. Sheldrick, SADABS – A Program for Empirical Absorption Correction, Göttingen, 1998.
[18] SHELXTL PLUS, Siemens Analyt. X-ray Inst. Inc., XS: Program for Crystal Structure Solution, XL: Program for Crystal Structure Determination, XP: Interactiv Molecular Graphics, 1990.

Available online at www.sciencedirect.com
SCIENCE DIRECT®
Polyhedron 23 (2004) 2285–2291
POLYHEDRON
www.elsevier.com/locate/poly

Separation of actinides and lanthanides: crystal and molecular structures of *N,N′*-bis(3,5-di-*t*-butylsalicylidene)-4,5-dimethyl-1, 2-phenylenediamine and its uranium complex

Ramu Kannappan [a], Stefania Tanase [a], Duncan M. Tooke [b], Anthony L. Spek [b], Iipo Mutikainen[c], Urho Turpeinen [c], Jan Reedijk [a,*]

[a] *Gorlaeus Laboratories, Leiden Institute of Chemistry, Leiden University, P.O. Box 9502, 2300 RA Leiden, The Netherlands*
[b] *Department of Crystal and Structural Chemistry, Bijvoet Center for Biomolecular Research, Utrecht University, Padualaan 8, 3584 CH Utrecht, The Netherlands*
[c] *Laboratory of Inorganic Chemistry, Department of Chemistry, P.O. Box 55 (A.I.Virtasen aukio 1), 00014 University of Helsinki, Finland*

Received 9 June 2004; accepted 16 July 2004
Available online 28 August 2004

Abstract

The preparation of the tetradentate dianionic ligand *N,N′*-bis(3,5-di-*t*-butylsalicylidene)-4,5-dimethyl-1,2-phenylenediamine [H_2L] is described, together with the corresponding uranium complex [$UO_2(L)CH_3OH$]. H_2L has been found to selectively bind to a representative actinide (UO_2^{2+}) rather than to lanthanum (La^{3+}) due to its cavity size. Both the free ligand and uranyl complex were characterized by elemental analysis, spectroscopic methods and single-crystal X-ray diffraction. The crystal structure of [$UO_2(L)CH_3OH$] complex show that uranyl cation adopts a distorted pentagonal bipyramidal conformation, with two imine nitrogen atoms, two phenolic oxygen atoms and a methanol oxygen in the coordination sphere, together with two *trans* oxo groups. The oxo groups have a (O–U–O, 176.85(15)°) angle consistent with linear coordination and U–O bond lengths of 1.786(4) and 1.805(4) Å. The difference in the bond distances can be ascribed to the existence of a hydrogen bond between one uranyl oxygen and the O–H of a methanol of neighboring molecule. This complex has one of the highest solubilities in organic solvents of all uranium compounds, making it a potential candidate for applications in solvent extraction.
© 2004 Elsevier Ltd. All rights reserved.

Keywords: Uranium; Crystal structure; N, O donor ligands

1. Introduction

One of the critical tasks in the restoration and nuclear waste is the separation of radioactive waste for disposal and for long term storage. There has been great interest in the separation of actinides (Ac) and lanthanides (Ln) in solution to aid the safe management of nuclear waste [1–3]. Many Schiff-base ligands have been designed and prepared with the aim of discriminating between Ln and Ac [4–7]. Tetradentate Schiff-base ligands are suitable for coordination to d-block transition metals due to their cavity size and planarity, but very few ligands have been found that chelate to f-block metals. One noticeable limitation in using these kinds of ligands lies in the fact that they are generally insoluble after binding to form a neutral complex [8]. The title complex is highly soluble in a range of solvents, which is likely due to the incorporation of *t*-butyl groups into the ligand.

* Corresponding author. Tel.: +31 715 274 450; fax: +31 715 274 671.
E-mail address: reedijk@chem.leidenuniv.nl (J. Reedijk).

0277-5387/$ - see front matter © 2004 Elsevier Ltd. All rights reserved.
doi:10.1016/j.poly.2004.07.004

Our research is currently focused on the synthesis of related ligands and the formation of analogous Ln^{3+} and (UO_2^{2+}) coordination complexes.

In this paper, we explore the synthesis, spectroscopic characterization, crystal structures and hydrogen bonding interactions of the first of our ligands, *N,N′*-bis(3,5-di-*t*-butylsalicylidene)-4,5-dimethyl-1,2-phenylenediamine, and its corresponding uranyl complex. This ligand has a cavity for which preliminary modelling had shown that a Ln^{3+} ion would probably not bind in the chelating mode, whereas the uranyl groups would bind.

2. Experimental

2.1. Synthesis of *N,N′*-bis(3,5-di-*t*-butylsalicylidene)-4,5-dimethyl-1,2-phenylenediamine [H_2L]

3,5-di-*t*-Butylsalicylaldehyde (4.68 g, 0.02 mol, 2 equiv.) and 4,5-dimethyl-1,2-phenylenediamine (1.32 g, 0.01 mol, 1 equiv.) were refluxed overnight in methanol (50 ml). The solution was allowed to cool to room temperature, yielding a yellow precipitate, which was filtered off and washed with diethyl ether. This solid was dissolved in a $CH_3OH/CHCl_3$ mixture and a small quantity of activated charcoal was added. The solution was heated to reflux and filtered, and the yellow crystalline compound obtained by solvent evaporation. Yield: 2.84 g (47.8%); m.p. 135 °C. *Anal.* Calc. for $C_{38}H_{52}N_2O_2$: C, 80.19; H, 9.21; N, 4.46. Found: C, 77.47; H, 8.89; N, 4.22%. FT-IR (ν_{max}/cm^{-1}): 1615 ν(C=N) and 1590 ν(C=C). MS (*m/z*): 569. ^1H NMR ($CDCl_3$): δ 8.33 (s, 2H), 7.36 (m, 2H), 7.25 (m, 2H), 7.07 (m, 2H), 2.20 (s, 6H), 1.53 (s, 6H), 1.45 (s, 15H) and 1.31 (s, 15H).

2.2. Synthesis of [$UO_2(L)CH_3OH$]

Uranyl nitrate (0.25 g, 0.0005 mol) was dissolved in the minimum amount of methanol and added to an equimolar solution of H_2L (0.284 g, 0.0005 mol) in methanol (50 ml). A red precipitate was formed, which was filtered and dried in vacuo. The crude product was recrystallized from chloroform to obtain the pure compound. Red single crystals for X-ray diffraction were grown in a $CH_3OH/CHCl_3$ mixture by solvent evaporation at room temperature over three days. Yield: 0.346 g (79%). *Anal.* Calc. for $C_{39}H_{54}N_2O_5U$: C, 53.91; H, 6.26; N, 3.22. Found: C, 53.11; H, 7.18; N, 4.04%. IR (ν_{max}/cm^{-1}): 1609 (C=N); 1533 (C=C) and 888 (O=U=O). UV/Vis (λ_{max}/nm): 398, 295.

2.3. Physical measurements

All the chemicals and solvents were of analytical grade and were used as received (Caution! *Uranyl nitrate is a weak radioactive salt and care should be taken in handling the compound*). C, H and N analyses were performed with a Perkin–Elmer 2400 series II analyzer. Infrared spectra (4000–300 cm^{-1}, resp. 4 cm^{-1}) were recorded on a Perkin–Elmer Paragon 1000 FTIR spectrometer equipped with a Golden Gate ATR device, using the reflectance technique. ^1H NMR spectra were recorded on a Bruker 300 DPX MHz spectrometer in $CDCl_3$ solution, using TMS as the internal standard. Diffuse reflectance spectra were obtained on a Perkin–

Table 1
Selected crystallographic data

	[H_2L] · acetone	[$UO_2(L)CH_3OH$]
Empirical formula	$C_{38}H_{52}N_2O_2 \cdot C_3H_6O$	$C_{39}H_{54}N_2O_5U$
Formula weight	626.89	868.87
Temperature (K)	150(2)	173(2)
Crystal system	monoclinic	monoclinic
Space group	$P2_1/c$	$P2_1/c$
a (Å)	9.9077 (8)	13.637(3)
b (Å)	35.083(3)	29.118(6)
c (Å)	11.9115(1)	10.476(2)
β (°)	113.93(1)	112.26(3)
Volume ($Å^3$)	3784.5(5)	3849.8(14)
Z	4	4
D_{calc} (Mg/m^3)	1.100	1.499
Absorption coefficient (mm^{-1})	0.07	4.26
Measured reflections	48 657	34 578
Independent reflections	6647	8864
R_{int}	0.0635	0.0788
Reflections with $I > 2\sigma(I)$	4739	6008
Final R indices [$I > 2\sigma(I)$]	$R_1 = 0.063$; $wR_2 = 0.174$	$R_1 = 0.044$; $wR_2 = 0.076$
R indices (all data)	$R_1 = 0.088$; $wR_2 = 0.191$	$R_1 = 0.088$; $wR_2 = 0.084$
Goodness-of-fit on F^2	1.06	1.02
Largest difference peak and hole (e $Å^{-3}$)	−0.30 and 0.47	−0.764 and 1.316

Elmer Lambda 900 spectrophotometer using MgO as a reference. Electrospray mass spectra (ESI-MS) in methanol were recorded on Thermo finnigan AQA apparatus.

2.4. Single crystal X-ray structures

2.4.1. $(H_2L)\cdot(acetone)$ and $[UO_2(L)CH_3OH]$

The X-ray data were collected with a Nonius Kappa CCD diffractometer using graphite-monochromatized Mo Kα radiation. An initial unit cell determination was performed using the NONIUS COLLECT software suite [9] and the DIRAX [10] indexing program. A complete dataset for each compound was collected, and integrated by the HKL2000 [11] and SORTAV [12] programs. No absorption correction was applied. The ligand structure was solved using the SHELXS-86 program [13], and refined with SHELXL-97 [14]. The program PLATON [15] was used for space group determination, validation and the preparation of diagrams. An empirical absorption correction was applied using the SADABS program [16] for the Uranyl complex. The structure was solved and refined using SHELXS-97 [17], SHELXL-97 [14] for structure solution and structure refinement, respectively. All non-hydrogen atoms were refined anisotropically. Hydrogen atoms were placed at idealized positions and allowed to ride on the connecting atom. Selected crystal data are given in Table 1.

3. Results and discussion

3.1. Ligand and metal coordination

The new tetradentate ligand *N,N′*-bis(3,5-di-*t*-butylsalicylidene)-4,5-dimethyl-1,2-phenylenediamine was synthesized from a reaction of 4,5-dimethyl-1,2-phenylenediamine with 3,5-di-*t*-butylsalicylaldehyde, using the synthetic procedure described above. Schiff-base uranyl complexes are generally soluble only in donor solvents such as DMSO and DMF, whereas the title compound is highly soluble in ethanol, methanol, chloroform, dichloromethane and acetone. This good solubility may be due to the presence of tertiary butyl groups, which will improve the solubility of the complex in less strong donor or organic solvents [18]. The IR spectrum of the ligand shows the formation of a ν(C=N) peak [19] at 1615 cm^{-1}, which, together with the disappearance of the ν(C=O) peak is indicative of a Schiff-base condensation.

The uranyl complex $[UO_2(L)CH_3OH]$ was prepared using the method described above. The IR spectrum shows subtle differences in comparison to the free ligand, with peaks at 1609 cm^{-1} ν(C=N) and 1533 cm^{-1} ν(C=C). A new peak was observed at 888 cm^{-1} due to ν(O=U=O), which indicates the presence of a linear, symmetric dioxouranium(VI) group [20]. The ligand field spectrum of the complex in the solid state

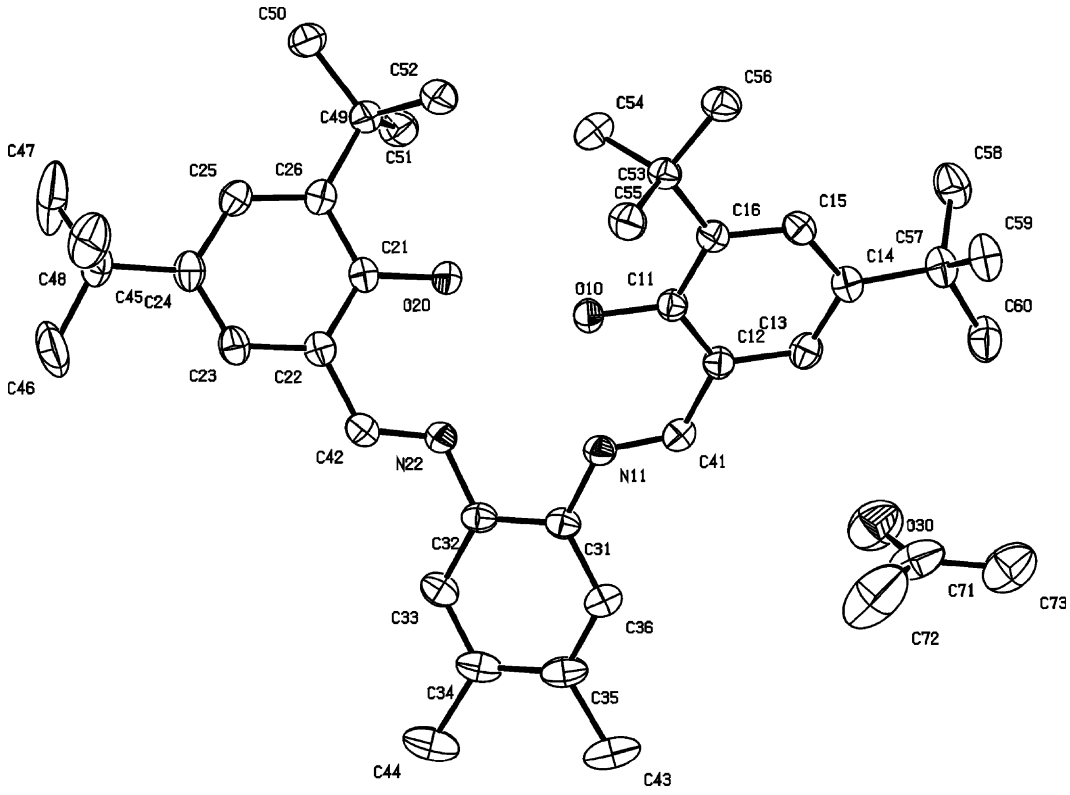

Fig. 1. Crystal structure of ligand (H_2L) and acetone, with hydrogen atoms omitted for clarity and displacement ellipsoids drawn at the 50% probability level.

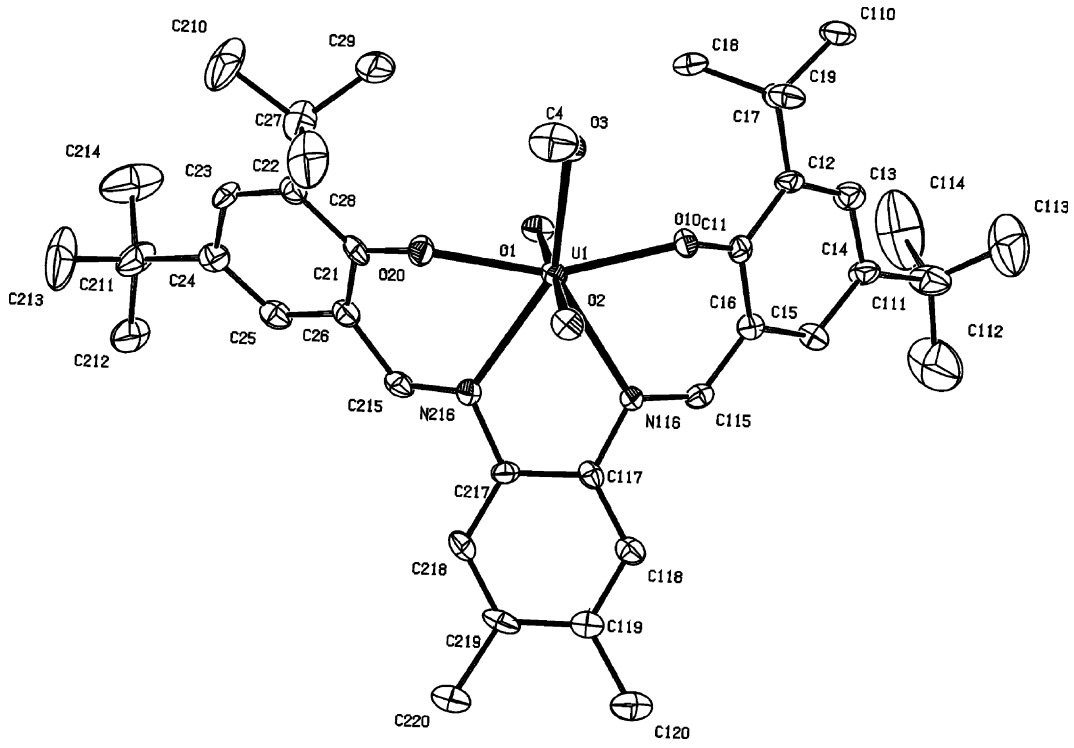

Fig. 2. Crystal structure of $[UO_2(L)CH_3OH]$ with hydrogen atoms omitted for clarity and displacement ellipsoids drawn at the 50% probability level.

shows absorptions around 398 nm with a shoulder of 295 nm, assigned to the charge transfer (phenolato-O–U) and $\pi-\pi^*$ of ligand. As expected, the proton NMR spectrum of the complex shows the imine proton shifted downfield from 8.33 to 8.86 ppm. The aromatic as well as methyl protons were found to be unaltered.

We tried to prepare lanthanide complexes by using the above method with a 1:1 mole ratio of the ligand and metal salt in methanol solvent. At the final stage after evaporation, we observed the formation of crystals of the ligand and metal salt separately. The ligand crystal was obtained with one acetone molecule. We also change the reaction conditions with different temperatures and times, and periods of 3, 6 h and overnight reflux were used. These repeated attempts to prepare lanthanide complexes starting from $LnCl_3$, $La(NO_3)_3$, $Pr(NO_3)_3$, $GdCl_3$ and $Gd(NO_3)_3$ with the same ligand were also unsuccessful, which may be due to a mismatch of its ionic size (radii, La^{3+}: 1.02 Å for 8 coordination; U^{6+}: 0.80 Å for 6–8 coordination) with the cavity of the ligand.

3.2. Crystal structures

The crystal structures of (H_2L) and $[UO_2(L)CH_3OH]$ are depicted in Figs. 1 and 2, with selected crystal data in

Table 2
Selected bond lengths (Å) and angles (°) for complex $[UO_2(L)CH_3OH]$

Bond lengths	
U(1)–O(1)	1.786(4)
U(1)–O(2)	1.805(4)
U(1)–O(10)	2.228(3)
U(1)–O(20)	2.240(3)
U(1)–N(216)	2.521(4)
U(1)–O(3)	2.530(4)
U(1)–N(116)	2.590(4)
Bond angles	
O(1)–U(1)–O(2)	176.85(15)
O(1)–U(1)–O(10)	86.33(14)
O(2)–U(2)–O(10)	95.65(14)
O(1)–U(1)–O(20)	86.89(14)
O(2)–U(1)–O(20)	92.18(14)
O(10)–U(1)–O(20)	157.14(13)
O(1)–U(1)–N(216)	86.51(15)
O(2)–U(1)–N(216)	90.34(15)
O(10)–U(1)–N(216)	131.56(13)
O(20)–U(1)–N(216)	69.65(13)
O(1)–U(1)–O(3)	99.98(14)
O(2)–U(1)–O(3)	82.86(14)
O(10)–U(1)–O(3)	77.89(12)
O(20)–U(1)–O(3)	81.83(12)
N(216)–U(1)–O(3)	150.42(12)
O(1)–U(1)–N(116)	93.16(14)
O(2)–U(1)–N(116)	85.25(15)
O(10)–U(1)–N(116)	69.79(13)
O(20)–U(1)–N(116)	132.43(13)
N(216)–U(1)–N(116)	62.88(13)
O(3)–U(1)–N(116)	144.16(12)

Table 1 and selected bond distances and angles given in Table 2.

The molecular structure of the H_2L ligand crystallized with one acetone molecule is shown in Fig. 1, which shows that in the uncoordinated ligand, the molecule is distinctly non-planar. In order to accommodate the two central O–H groups the 3,5-di-*t*-butylsalicylidene groups are displaced to opposite sides of the 4,5-dimethyl-1,2-phenylenediamine ring plane, with dihedral angles of 34.97(11)° between the C(31)–C(36) plane and C(11)–(C16) plane, and −37.39(11)° between the C(31)–C(36) plane and C(21)–(C26) plane (Fig. 1, Supplementary material).

The tetradentate dianionic ligand binds equatorially to the dioxouranium(VI) group leading to a seven-coordinated center with a distorted pentagonal bipyramidal coordination geometry. The uranium oxide coordination sphere contains two imine nitrogen atoms, two phenol oxygen atoms and a third oxygen atom from the methanol molecule. The oxo groups of the uranyl moiety lie *trans* to one another with a nearly linear O–U–O angle of 176.85(15)° and U–O bond length of 1.786(4) Å for U–O(1) and 1.805(4) Å for U–O(2). The lengthening of the U–O(2) bond length can be ascribed to the existence of a hydrogen bond, D–H···A length of 2.831(6) Å, between O(2) and the O–H group of the methanol molecule.

The uranium atom, N(116), N(216), and O(20) all lie approximately in a plane, with a maximum deviation from the mean squares plane of 0.0383(3) Å for U(1). O(10) is displaced significantly out of the plane by 0.390(4) Å. The U–N(116), U–N(216), U(1)–O(10) and

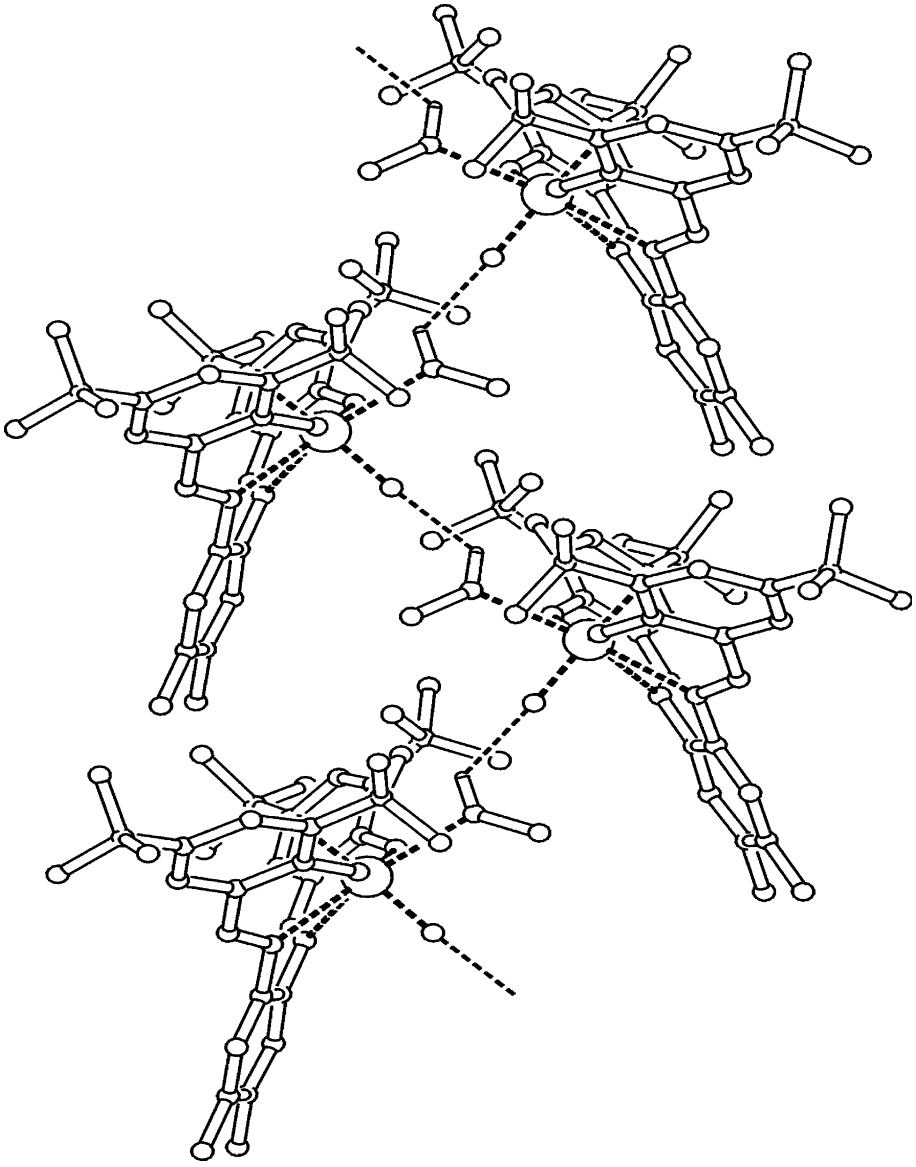

Fig. 3. Molecular packing of $[UO_2(L)CH_3OH]$ complex showing hydrogen bonded zigzag infinite chain.

U(1)–O(20) bond distances, of 2.590(4), 2.521(4), 2.228(3) and 2.240(3) Å, respectively, are in good agreement with those reported previously [8,21–23]. U–N distances are typically found to be longer than U–O distances, a behavior which can be explained by Pearson's hard and soft acid–base concept [24,25]. This concept agrees well with what is observed in the title compound, as nitrogen would be expected to be bonded less strongly to a hard acid such as (UO_2^{2+}), while oxygen has relatively higher base strength towards uranium. The methanol oxygen atom, O(3), also lies outside the main U–N–N–O plane, though on the other side to O(10), with a deviation of −0.334(4) Å. The U–O(3) bond length is 2.530(4) Å, which is comparable with related complexes in the literature [25].

The ligand is not planar, but, in contrast to the uncoordinated structure, the two 3,5-di-*t*-butylsalicylidene groups are now on the same side of the 4,5-dimethyl-1,2-phenylenediamine ring, which gives the complex a distinctive "book" appearance when viewed from the side (Fig. 2, Supplementary material). Evidently, in the five-membered ring (C117, C217, N116, N216 and U1), the small bite angle (62.88°), may enhance the planarity of chelating mode to non-binding with lanthanides.

Due to the hydrogen-bonding between the methanol molecule and O(2) the structure forms an infinite polymer with a distinctive 'zigzag' motif (Fig. 3). No π–π stacking is present, due to the unfavorable orientations of the aromatic rings in the structure.

4. Conclusions

In this paper, we have described the successful synthesis of a ligand that is suitable for coordination to the actinide (UO_2^{2+}), but not to lanthanides (La, Pr, Eu and Gd). Uranium exists as the uranyl cation (UO_2^{2+}) in aqueous solution, where the oxo groups of the uranyl moiety lie *trans* to one another with an angle that is close to linear with the uranium as the center. This linear arrangement appears to help the uranyl cation enter into the cavity of the ligand frame like a "pen" into the "cap". The uranium center is seven coordinate with a distorted pentagonal bipyramidal geometry. The lengthening of one U=O distance can be ascribed to the presence of a hydrogen bond between the oxygen and the O–H of a neighboring methanol molecule. Hydrogen bonding will lead to the sequestration of the uranium to achieve the high selectivity over competing cations in solution.

Apparently the spherical shape and the large size of the Ln(III) ions do not match with the ligand cavity, whereas the smaller size of U(VI) and the ellipsoid of the (UO_2^{2+}) fit better. This principle is now further developed for a potential use in the separation of uranium and lanthanum.

Acknowledgements

This research has been financially supported by the Netherlands Technology Research Foundation (STW) applied science division of The Netherlands Organisation for Scientific Research. We thank Dr. Lies Bouwman for fruitful discussion. We thank Dr. W. Verboom (Twente university) for valuable discussion. Thanks are due to Meenal Godbole and Nilesh Mehendale for rendering their assistance.

Appendix A. Supplementary material

Complementary data for the ligand and complex are available upon request from the Cambridge Crystallographic Data center, 12 Union Road, Cambridge CB2 1EZ, UK, Fax: +44-1223-336-033; www: http://www.ccdc.cam.ac.uk or by e-mail from deposit@ccdc.cam.ac.uk. Please quote the deposition number in all correspondence (CCDC 243295, CCDC 243296). Supplementary data associated with this article can be found, in the online version, at doi:10.1016/j.poly. 2004.07.004.

References

[1] L.F. Rao, A.Y. Garnov, J. Jiang, P. Di Bernardo, P. Zanonato, A. Bismondo, Inorg. Chem. 42 (2003) 3685.
[2] C. Den Auwer, R. Drot, E. Simoni, S.D. Conradson, M. Gailhanou, J.M. de Leon, New J. Chem. 27 (2003) 648.
[3] O. Terra, N. Clavier, N. Dacheux, R. Podor, New J. Chem. 27 (2003) 957.
[4] L. Salmon, P. Thuery, M. Ephritikhine, Polyhedron 23 (2004) 623.
[5] D.J. Evans, P.C. Junk, M.K. Smith, Polyhedron 21 (2002) 2421.
[6] M. Vidali, P.A. Vigato, U. Casellato, E. Tondello, O. Traverso, J. Inorg. Nucl. Chem. 37 (1975) 1715.
[7] U. Casellato, P. Guerriero, S. Tamburini, P.A. Vigato, R. Graziani, J. Chem. Soc., Dalton Trans. (1990) 1533.
[8] M.S. Hill, P.R. Wei, D.A. Atwood, Polyhedron 17 (1998) 811.
[9] B.V. Nonius, Software Suite, Delft University, Delft, 2004.
[10] A.J.M. Duisenberg, J. Appl. Crystallogr. 25 (1992) 92.
[11] Z. Otwinowski, W. MinorMacromolecular Crystalography, vol. 276, Academic Press, London, 1992.
[12] R.H. Blessing, Acta Crystallogr. A 51 (1995) 33.
[13] G.M. Sheldrick, Program for Crystal Structure refinement, University of Gottingen, Germany, 1986.
[14] G.M. Sheldrick, Program for Crystal Structure refinement, University of Gottingen, Germany, 1997.
[15] A.L. Spek, J. Appl. Crystallogr. 36 (2003) 7.
[16] G.M. Sheldrick, SADABS Program for Empirical Absorption Correction, Bruker AXS.
[17] G.M. Sheldrick, SHELXS-97, Program for Crystal Structure Determination, University of Gottingen, Germany, 1997.
[18] S. Sitran, D. Fregona, U. Casellato, P.A. Vigato, R. Graziani, G. Faraglia, Inorg. Chim. Acta 132 (1987) 279.
[19] G. Das, R. Shukla, S. Mandal, R. Singh, P.K. Bharadwaj, J. van Hall, K.H. Whitmire, Inorg. Chem. 36 (1997) 323.
[20] D.E. Fenton, P.A. Vigato, U. Casellato, R. Graziani, M. Vidali, Inorg. Chim. Acta 51 (1981) 195.
[21] G. Bandoli, D.A. Clemente, U. Croatto, M. Vidali, P.A. Vigato, J. Chem. Soc., Chem. Commun. (1971) 1330.

[22] G. Bandoli, D.A. Clemente, M. Vidali, P.A. Vigato, J. Chem. Soc., Chem. Commun. (1972) 344.
[23] M.N. Akhtar, E.D. McKenzie, R.E. Paine, A.J. Smith, J. Inorg. Nucl. Chem. 5 (1969) 673.
[24] E.O. Schlempe, Inorg. Chem. 6 (1967) 2012.
[25] G. Bandoli, D.A. Clemente, U. Croatto, M. Vidali, P.A. Vigato, J. Chem. Soc., Dalton Trans. (1973) 2331.

Available online at www.sciencedirect.com
SCIENCE DIRECT®
Polyhedron 23 (2004) 2293–2301
POLYHEDRON
www.elsevier.com/locate/poly

Syntheses of lanthanide bromide complexes from oxides and the crystal structures of $[LnBr_3(DME)_2]$ (Ln = Pr, Nd, Sm, Eu), $[LnBr_3(THF)_4]$ (Ln = Pr, Sm) and $[EuBr_2(THF)_5][EuBr_4(THF)_2]$

S. Petriček *

Faculty of Chemistry and Chemical Technology, University of Ljubljana, Aškerčeva 5, 1001 Ljubljana, Slovenia

Received 14 June 2004; accepted 16 July 2004

Abstract

Lanthanide bromide complexes were prepared in excellent yields by reactions of lanthanide oxides and hydrogen bromide, which was formed *in situ* from bromotrimethylsilane and water, in DME (DME = dimethoxyethane). The crystals for X-ray structural analyses were grown from DME and from THF (THF = tetrahydrofuran) solutions. Three bromine and four oxygen atoms from DME are coordinated to a central lanthanide atom in the crystal structures of lanthanide complexes $[LnBr_3(DME)_2]$ (Ln = Pr (**1**), Nd (**2**), Sm (**3**), Eu (**4**)). Crystallization from THF resulted in two types of complexes, molecular $[LnBr_3(THF)_4]$ (Ln = Pr (**5**), Sm (**6**)) and ionic $[EuBr_2(THF)_5][EuBr_4(THF)_2]$ (**7**). Complexes **1**, **4**, **5** and **7** are the first crystallographically characterized water-free complexes of praseodymium or europium tribromides.
© 2004 Elsevier Ltd. All rights reserved.

Keywords: Lanthanide oxides; Bromotrimethylsilane; O-donor ligands; Complexes of lanthanide bromides; Crystal structure; Coordination number

1. Introduction

Lanthanide(III) halides and their complexes with simple donors such as THF [1–16] and DME [6,9,10,15,17–20] are useful starting compounds in syntheses of lanthanide complexes, organolanthanide compounds and in organic synthesis [21]. Base-free lanthanide trihalides with an extended structure (CN = 9 for Ln = La–Gd) are in many cases less appropriate starting substances than mononuclear complexes of lanthanide halides with simple donors due to their low solubility and reactivity. For example, carbamato complexes of the lighter lanthanides $[Ln(O_2CNR_2)_3]$ were successfully synthesized only by using $[LnCl_3L_n]$, while experiments using anhydrous lanthanide chlorides failed due to lower reactivity of $LnCl_3$ (Ln = La–Gd) [22]. A choice of an appropriate lanthanide halide in metathesis reactions also plays an important role. A softer iodide could be displaced by some ligands [11], but a similar reaction does not take place, if a harder chloride is used.

Crystal structures of lanthanide chloride and some iodide complexes with THF and DME have been well investigated in the past due to their broad application (references in Table 1). In the crystal structures of lanthanide chlorides with DME only two types of molecules were found, binuclear $[LnCl_3(DME)_2]_2$ and mononuclear $[LnCl_3(DME)_2]$. In the case of iodide complexes with DME are reported only crystal structures of lanthanide(II) compounds [23–27]. A higher structural diversity is characteristic for lanthanide trichloride complexes with THF where are coordination numbers from

* Tel.: +38612419120; fax: +38612419220.
E-mail address: sasa.petricek@uni-lj.si (S. Petriček).

0277-5387/$ - see front matter © 2004 Elsevier Ltd. All rights reserved.
doi:10.1016/j.poly.2004.07.009

Table 1
References for crystallographically characterized complexes of lanthanide trihalides with DME or THF

CN	**8** in $[LnX_3(DME)_2]_2$	**8** in $[LnX_3(DME)_2]_2$	**7** in $[LnX_3(DME)_2]$	**7** in $[LnX_3(DME)_2]$
Ln/X	Cl	Br	Cl	Br
DME complexes				
La	19	15		
Ce	19			
Pr	19			[a]
Nd	10,19		17	[a]
Sm			20	[a]
Eu			19	[a]
Gd			18	
Tb			19	
Dy			9	
Ho			19	
Er			6, 15	
Tm			19	
Yb			15	15
Lu			19	

CN	8	**7**				**7/6**			**6**		**6**
	$[LnX_3(THF)_2]_n$	$[LnX_3(THF)_2]_n$	$[LnX_3(THF)_4]$			$[LnX_2(THF)_5][LnX_4(THF)_2]$			$[LnX_3(THF)_3]$		$[LnX_3(THF)_2]_2$
Ln/X	Cl	Cl	Cl	Br	I	Cl	Br	I	Cl	Br	Cl
THF complexes											
La	1			15	14						
Ce		1, 3									
Pr		1, 2		[a]	11						
Nd		3	5	16				11			
Sm			6	[a]				12			
Eu			7				[a]				
Gd			2			1		11			
Tb						3					
Dy						2,9					
Er						1,6					
Yb						10		13	1	15	4
Lu									8		

six to eight. Several lanthanides form two (Nd, Gd) [1–3,5] or three (Yb) [1,4,10] different types of chloride complexes with THF, simultaneously revealing transitions to lower coordination numbers (Gd, Yb) [1,2,4,10]. Structural diversity diminishes along with the coordination numbers range in the THF complexes of larger halides, bromides and iodides, as seen in Table 1.

In contrast to lanthanide chloride and iodide complexes only a few bromide complexes have been described in the literature by now [15,16]. The known complexes of lanthanide bromides were prepared from $LnBr_3 \cdot 6H_2O$ (Ln = Nd, Sm) [16,28] or from metals (Ln = La, Yb) [15]. A dehydration of $LnBr_3 \cdot 6H_2O$ was done by trimethylorthoformate. The metals reacted with dibromomethane or dibromoethane in THF and DME under ultrasound conditions. We chose lanthanide oxides as starting compounds to prepare lanthanide bromide complexes with DME similar as in syntheses of lanthanide chloride complexes [29]. The new syntheses from lanthanide oxides are effective and simple by using trimethylbromosilane as bromide donor at room temperature. New THF complexes of lanthanide bromides were prepared to check the structural diversity of bromides and compare it to the well known variety of crystal structures reported for analogous chlorides. We provide additional structural data to establish at which elements occur transitions to lower coordination numbers in the series of lanthanide bromide complexes with THF and DME.

2. Experimental

2.1. General

All the manipulations were carried out under an atmosphere of purified argon using Schlenk tubes or in a dry box. Lanthanide oxides (Aldrich), bromotrimethylsilane (Aldrich) and DME (Fluka) were used as received, THF and pentane were dried over Na/K and distilled before use. When a bottle of bromotrimethylsilane (Aldrich) was opened, the substance was used within a few days. A later use is not recommended due to a partial decomposition of the reagent to bromine, which resulted in a contamination of the products and lower yields.

The samples were ground in nujol mull and IR spectra were recorded on a Perkin–Elmer 1720X instrument between 400 and 4000 cm^{-1}.

The bromine content was determined by a potentiometric titration of bromide ions with silver nitrate and lanthanide content by a gravimetric analysis. Elemental analyses were carried out on a Perkin–Elmer 2400 CHN analyzer at the University of Ljubljana (Department of Organic Chemistry).

2.2. Synthesis of $[PrBr_3(DME)_2]$ (1) and $[PrBr_3(THF)_4]$ (5)

To 0.420 g (0.622 mmol) of Pr_4O_7 were added 10.53 g (117 mmol) of DME, 7.81 g (51 mmol) of $(CH_3)_3SiBr$ and water (0.01 g, 0.56 mmol). The suspension was stirred for eight days at room temperature and after drying in vacuum 1.40 g (100% yield) of the complex **1** was gained. *Anal.* Calc. for **1**: H, 3.95; C, 17.13. Found: H, 3.97; C, 17.69%. IR (Nujol): 1311 w, 1280 w, 1260 m, 1239 w, 1187 m, 1081 vs, 1030 vs, 993 m, 914 m, 911 m, 898 m, 859 s, 822 m, 800 m, 674 w, 598 w, 551 w, 464 w cm^{-1}. Dried product was dissolved in DME and THF. Complex **1** crystallized from DME solution and **5** from THF solution during slow diffusion of pentane vapor to the solution. IR of **5** (Nujol): 1169 w, 1074 w, 1019 vs, 917 w, 863 s, 669 w cm^{-1}.

2.3. Synthesis of $[NdBr_3(DME)_2]$ (2)

To 0.460 g (1.37 mmol) of Nd_2O_3 were added 29.39 g (327 mmol) of DME, 6.80 g (44.4 mmol) of $(CH_3)_3SiBr$ and water (0.01 g, 0.56 mmol). The suspension was stirred for eight days at room temperature and after drying in vacuum 1.54 g (99.6% yield) of the complex **2** was gained. *Anal.* Calc. for **2**: H, 3.57; C, 17.03; Br, 42.5; Nd, 25.7. Found: H, 3.67; C, 16.89; Br, 42.1; Nd, 25.2%. IR (Nujol): 1259 w, 1189 w, 1086 s, 1028 vs, 998 m, 899 m, 856 m, 826 w cm^{-1}. Dried product was dissolved in DME and complex **2** crystallized during slow diffusion of pentane vapor to the solution.

2.4. Synthesis of $[SmBr_3(DME)_2]$ (3) and $[SmBr_3(THF)_4]$ (6)

To 0.540 g (1.55 mmol) of Sm_2O_3 were added g 12.79 g (142 mmol) of DME, 6.71 g (43.8 mmol) of $(CH_3)_3SiBr$ and water (0.01 g, 0.56 mmol). The suspension was stirred for nine days at room temperature and after drying in vacuum 1.68 g (95.0% yield) of the product was gained. *Anal.* Calc. for **3**: Br, 42.0; Sm, 26.3. Found: Br, 42.3; Sm, 26.9%. IR (Nujol): 1305 w, 1285 w, 1260 w, 1240 w, 1188 w, 1072 vs, 1028 s, 1017 s, 1002 m, 992 s, 974 m, 896 m, 856 s, 825 w, 550 w cm^{-1}. Dried product was dissolved in DME and in THF. Complex **3** crystallized from DME solution and **6** from THF solution during slow evaporation of the solvent. IR of **6** (Nujol): 1260 m, 1177 w, 1074 w, 1019 vs, 919 w, 862 s, 669 w cm^{-1}.

2.5. Synthesis of $[EuBr_3(DME)_2]$ (4) and $[EuBr_2(THF)_5][EuBr_4(THF)_2]$ (7)

To 0.440 g (1.25 mmol) of Eu_2O_3 were added 15.36 g (171 mmol) of DME, 7.26 g (47.4 mmol) of

$(CH_3)_3SiBr$ and water (0.01 g, 0.56 mmol). The suspension was stirred for nine days at room temperature and after drying in vacuum 1.24 g of the yellow product was gained. The traces of Eu_2O_3were observed in IR spectra of this crude product. The crude product was dissolved in DME or THF and filtered. Yellow crystals of **4** grew out of DME solution during evaporation of the solvent. *Anal.* Calc. for **4**: H, 3.52; C, 16.80. Found: H, 3.56; C, 16.85%. IR of **4** (Nujol): 1306 w, 1260 m, 1188 w, 1111m, 1084s, 1073 s, 1026 vs, 973 m, 859 s, 850 s, 826 w, 801 w, 556 w, 459 w cm^{-1}. Complex **7** crystallized from THF solution during slow evaporation of the solvent. IR of **7** (Nujol): 1170 w, 1074 w, 1040m, 1011 s, 919 m, 855 vs, 670 m cm^{-1}.

2.6. Crystal structure determination

The details of crystal data collection and refinement parameters are listed in Table 2 (**1**–**4**) and Table 3 (**5**–**7**). All studied compounds were hygroscopic. The crystals were greased on a glass thread. Diffraction data were collected on a Nonius Kappa CCD diffractometer with CCD area detector at 150(2) K. A Cryostream Cooler (Oxford Cryosystems) was used for cooling of the samples. A graphite monochromatic Mo Kα radiation ($\lambda = 0.71073$ Å) was employed in all measurements. The structures were solved by direct methods implemented in SHELXS-97 [30] and refined by a full-matrix least-squares procedure based on F^2 (SHELXL-97) [31]. Combined general twinning by pseudo-merohedry and racemic twinning (Flack parameter 0.44(3)) [32] was considered in the refinement of the complex **4**. The twin law in SHELXL-97 for monoclinic unit cell ($\beta \sim 90°$), which emulate orthorhombic one, was employed in the refinement. All non-hydrogen atoms except one carbon atom in methyl group in complexes **4** were refined anisotropically. The calculated fraction of orthorhombic structure in **4** was 11.2(1)%. All non-hydrogen atoms in complexes **1**, **2**, **3**, **5**, **6** and **7** were refined anisotropically. The hydrogen atoms were included in the model at geometrically calculated positions and refined using a riding model except in the crystal structure of **2**, where were all hydrogen atoms located from difference Fourier syntheses.

Table 2
Crystallographic data for $[LnBr_3(DME)_2]$ complexes **1**–**4**

	1	**2**	**3**	**4**
Chemical formula	$[PrBr_3(O_2C_4H_{10})_2]$	$[NdBr_3(O_2C_4H_{10})_2]$	$[SmBr_3(O_2C_4H_{10})_2]$	$[EuBr_3(O_2C_4H_{10})_2]$
Formula mass (g/mol)	560.86	564.21	570.32	571.93
Crystal system	orthorhombic	orthorhombic	monoclinic	monoclinic
Space group	*Pcab* (no. 61)	*Pcab* (no. 61)	$P2_1/n$ (no. 14)	*Cc* (no. 9)
Unit cell dimensions				
a (Å)	9.5455(1)	9.5341(1)	10.0561(1)	9.6296(2)
b (Å)	14.3946(2)	14.3679(1)	13.2333(2)	12.0428(3)
c (Å)	24.4039(3)	24.3443(2)	12.5219(2)	13.9186(3)
α (°)	90	90	90	90
β (°)	90	90	96.950(1)	91.000(1)
γ (°)	90	90	90	90
V (Å^3)	3353.19(7)	3334.80(5)	1654.11(4)	1613.86(6)
Z (asym. unit)	8	8	4	4
$D_{cal.}$ (g/cm^3)	2.222	2.248	2.290	2.354
μ (mm^{-1})	10.05	10.30	10.79	11.31
Crystal color	light brown	light blue	colorless	Yellow
Crystal size (mm)	0.08 × 0.08 × 0.08	0.07 × 0.06 × 0.05	0.1 × 0.1 × 0.08	0.08 × 0.08 × 0.05
θ Range (°)	3.29–27.50	3.29–27.48	3.28–30.48	1.46–27.46
Total number of collected reflections	7225	7183	9573	3619
Number of unique reflections	3849	3820	5025	1842 + 1680 (Friedel related refl.)
R_{int}	0.0295	0.0142	0.0233	0.0118
Number of reflections used	2870	3303	4318	3356
Threshold	$[I > 2.0\sigma(I)]$	$[I > 2.0\sigma(I)]$	$[I > 2.0\sigma(I)]$	$[I > 2.0\sigma(I)]$
Number of parameters	149	225	149	146
Number of restraints	0	0	0	2
R[a] (observed)	0.027	0.0177	0.0252	0.0482
wR_2[b]	0.051	0.036	0.0544	0.134
S	1.066	1.069	1.051	1.033
Maximum/minimum residual electron density (e/Å^3)	0.575, −1.265	0.468, −0.845	1.018, −1.175	2.15*,−1.91

[a] $R = \sum(|F_o| - |F_c|)/\sum|F_o|$.

[b] $wR_2 = \left(\sum\left[w(F_o^2 - F_c^2)^2\right]/\sum(wF_o^2)^2\right)^{1/2}$.

* 0.97 Å from Eu1.

Table 3
Crystallographic data for compounds $[LnBr_3(THF)_x]$

	5	6	7
Chemical formula	$[PrBr_3(OC_4H_8)_4]$	$[SmBr_3(OC_4H_8)_4]$	$[EuBr_2(OC_4H_8)_5][EuBr_4(OC_4H_8)_2]$
Formula mass (g/mol)	669.06	678.50	1288.10
Crystal system	triclinic	triclinic	monoclinic
Space group	$P\bar{1}$ (no.2)	$P\bar{1}$ (no.2)	$C2/c$ (no. 15)
Unit cell dimensions			
a (Å)	8.2146(1)	8.2640(2)	12.5673(1)
b (Å)	9.3914(2)	9.3033 (2)	11.5253(1)
c (Å)	15.4795(3)	15.4107(4)	28.1373(4)
α (°)	78.781(1)	79.316(1)	90
β (°)	86.997(1)	86.882(1)	90.474(1)
γ (°)	74.886(1)	75.051(1)	90
V (Å^3)	1130.85(4)	1124.84 (5)	4075.32(8)
Z (formula)	2	2	4
$D_{cal.}$ (g/cm^3)	1.965	2.003	2.099
μ (mm^{-1})	7.469	7.954	8.97
Crystal color	light green	colorless	Yellow
Crystal size (mm)	$0.1 \times 0.1 \times 0.08$	$0.1 \times 0.1 \times 0.08$	$0.08 \times 0.04 \times 0.04$
θ Range (°)	2.97–27.42	3.44–27.39	1.45–27.48
Total number of collection reflections	9318	9241	8600
Number of unique reflections	5121	5066	4630
R_{int}	0.021	0.030	0.027
Number of reflections used	4510	4277	4014
Threshold	$[I > 2.0\ \sigma\ (I)]$	$[I > 2.0\ \sigma\ (I)]$	$[I > 2.0\ \sigma\ (I)]$
Number of parameters	217	218	197
R[a] (observed)	0.0249	0.0306	0.0309
wR_2[b]	0.0536	0.0767	0.0756
S	1.043	1.01	1.05
Maximum/minimum residual electron density (e/Å^3)	1.123,−1.058	1.027, −0.819	1.62, −1.294

[a] $R = \sum(|F|-|F_c|)/\Sigma|F_o|$.

[b] $wR_2 = \left(\sum\left[w(F_o^2 - F_c^2)^2\right]\Big/\sum(wF_o^2)^2\right)^{1/2}$.

3. Results and discussion

3.1. Syntheses

The syntheses of the lanthanide bromide complexes were achieved according to the reactions:

$$2(CH_3)_3SiBr + H_2O \rightarrow (CH_3)_3SiOSi(CH_3)_3 + 2HBr$$

$$6HBr + Ln_2O_3 + 4DME \rightarrow 2[LnBr_3(DME)_2] + 3H_2O$$

Bromotrimethylsilane reacts with water generating hydrogen bromide in situ, which reacts with lanthanide oxides in dimethoxyethane giving the lanthanide bromide complexes. The water, formed in the second reaction reacts with $(CH_3)_3SiBr$ and therefore, only a small amount of water is added (n(Ln):n(H_2O) ~ 5:1). The excess of $(CH_3)_3SiBr$ guarantees the total consumption of water. High yields were achieved by this simple method, which is carried out at room temperature. The side products, HBr and $(CH_3)_3SiOSi(CH_3)_3$, are volatile and easily removable. Crystallization of the products from DME resulted in mononuclear compounds $[LnBr_3(DME)_2]$ (**1**–**4**) and from THF in the neutral $[LnBr_3(THF)_4]$ (**5**, **6**) or ionic complex of $[LnBr_2(THF)_5][LnBr_4(THF)_2]$ (**7**). To the best of our knowledge are compounds **1**, **4**, **5** and **7** the first crystallographically characterized water-free lanthanide tribromide complexes containing Pr–Br and Eu–Br bonds.

3.2. Crystal structures of DME complexes *1*–*4*

The structures of the complexes **1**–**4** (see Fig. 1 for **1**, Table 4) consist of three bromine and four oxygen atoms from DME coordinated to the central lanthanide atom in a distorted pentagonal bipyramidal geometry. Two bromine atoms, Br1 and Br3, occupy the axial sites with Br1–Ln–Br3 angle from 166.72(1)° in **1** to 171.15(1)° in **3**. Molecules **1**–**4** have similar structures to $[LnCl_3(DME)_2]$ [6,9,15,17–20] and $[YbBr_3(DME)_2]$ [15]. On the contrary to chlorides $[LnCl_3(DME)_2]$, where all mononuclear complexes (Ln = Nd–Lu) crystallize in the same monoclinic space group with similar unit cells, different packing of molecules in the bromides resulted either in orthorhombic or monoclinic crystal system. Only the complex **3** crystallize in the same monoclinic space group as analogous chlorides, **1** and **2** are isostructural orthorhombic complexes, while monoclinic emulate

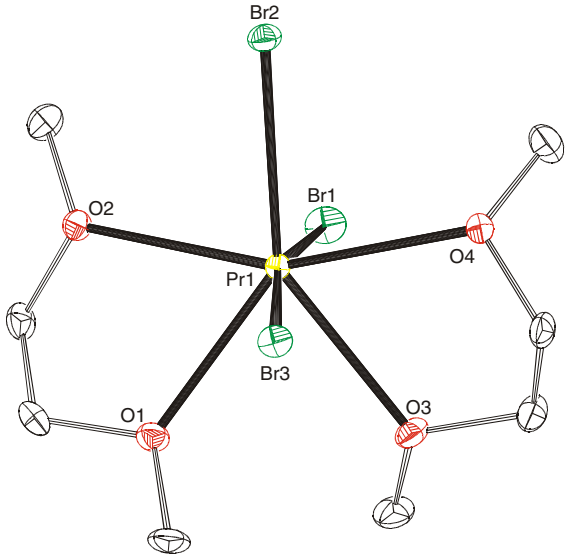

Fig. 1. The crystal structure of **1** with the numbering scheme adopted also in **2**–**4**. Hydrogen atoms are omitted for clarity.

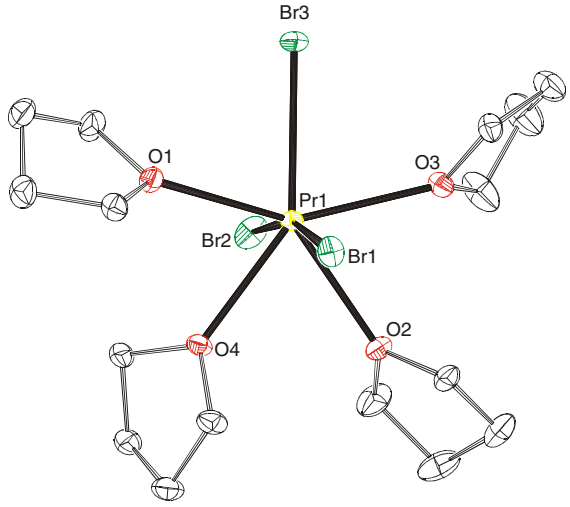

Fig. 2. The crystal structure of **5** with the numbering scheme adopted also in **6**. Hydrogen atoms are omitted for clarity.

Table 4
Selected bond lengths and their average values (Å) in **1**–**4**

	Pr	Nd	Sm	Eu
Br1	2.8591(4)	2.8559(3)	2.8313(3)	2.807(2)
Br2	2.8449(4)	2.8307(2)	2.8182(3)	2.799(2)
Br3	2.8672(4)	2.8474(2)	2.8272(3)	2.826(2)
O1	2.506(2)	2.4900(14)	2.462(2)	2.45(1)
O2	2.539(2)	2.5276(15)	2.467(2)	2.44(1)
O3	2.579(2)	2.5603(14)	2.482(2)	2.52(1)
O4	2.476(2)	2.4596(15)	2.460(2)	2.43(1)
$Br_{av.}$	2.857(1)	2.845(1)	2.826(1)	2.811(6)
$O_{av.}$	2.525(8)	2.509(6)	2.468(8)	2.46(4)

orthorhombic compound in **4** (Table 2). Unit cell volumes in **1** and **2** are approximately two times larger than in **3** and **4** because of doubled *c* axes in **1** and **2**.

Average Ln–Br and Ln–O bond lengths in the series of complexes decrease as expected due to lanthanide contraction [33]. The average Ln–Br bond distances in **2** and **3** (Table 4) are similar to the Ln–Br distances in the published $[NdBr_3(THF)_4]$ (2.86(2) Å) [16] and $[SmBr_3(Pr^iOH)_4]$ (2.834(3) Å) [28]. A Sm–$Br_{terminal}$ bond distance in $[SmBr_2(DME)_2]_2$ (2.994(2) Å) [23] is longer due to larger Sm^{2+} ion. Ln–O bond lengths within each lanthanide compound differ significantly for **1**, **2** and **4** similar as in $[LnCl_3(DME)_2]$ [19]. One DME molecule is coordinated to lanthanide with two similar Ln–O bonds and the other with one short and one long Ln–O bond. The average Ln–O bond lengths are similar in the prepared complexes **2**–**4** (Table 4) as reported for $[LnCl_3(DME)_2]$ (Ln = Nd (2.52(1) Å), Sm (2.50(1) Å), Eu (2.48(1) Å)) [17,19]. Pr–O bonds in mononuclear complex **1** are shorter than in $[PrCl_3(DME)_2]_2$ (from 2.586(3) to 2.654(3) Å) [19] as expected for a lower coordination number of praseodymium in **1** than in the binuclear chloride.

3.3. Crystal structure of THF complexes 5–7

Crystallization of lanthanide bromide complexes from THF resulted in the compounds **5**–**7**. The com-

Table 5
The praseodymium environment in **5**

Atom	*r* (Å)	Br2	Br3	O1	O2	O3	O4
Br1	2.8577(3)	166.08(1)	104.89(1)	86.63(5)	85.42(5)	85.42(5)	86.36(5)
Br2	2.8826(4)		89.03(1)	96.90(5)	83.40(5)	98.13(5)	82.31(5)
Br3	2.8977(3)			77.15(5)	141.57(5)	75.37(5)	144.22(5)
O1	2.491(2)				141.10(7)	148.29(7)	69.62(7)
O2	2.544(2)					68.58(7)	71.91(7)
O3	2.489(2)						140.13(7)
O4	2.508(2)						
$Br_{av.}$	2.879(1)						
$O_{av.}$	2.51(1)						

r is praseodymium–ligand atom distance or the average distance. Other entries in the matrix are the angles (°) subtended by the relevant atoms at the head of the row and column.

Table 6
The samarium environment in **6**

Atom	*r* (Å)	Br2	Br3	O1	O2	O3	O4
Br1	2.8083(4)	168.49(2)	101.55(2)	88.35(7)	85.54(6)	86.36(7)	87.77(6)
Br2	2.8314(4)		89.88(2)	95.75(7)	84.42(6)	95.27(7)	83.59(7)
Br3	2.8582(4)			76.76(7)	143.07(7)	75.30(7)	144.94(6)
O1	2.430(3)				140.07(9)	149.85(10)	69.74(9)
O2	2.497(3)					68.99(9)	70.62(9)
O3	2.451(3)						139.50(9)
O4	2.474(3)						
$Br_{av.}$	2.833(1)						
$O_{av.}$	2.46(1)						

r is samarium–ligand atom distance or the average distance. Other entries in the matrix are the angles (°) subtended by the relevant atoms at the head of the row and column.

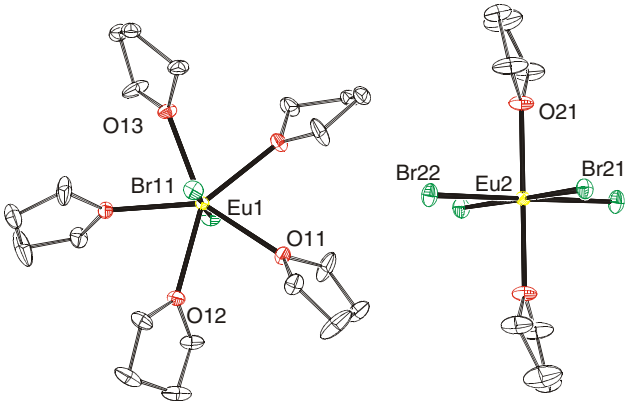

Fig. 3. The crystal structure of **7** with the numbering scheme adopted. Hydrogen atoms are omitted for clarity.

Table 7
Selected bond lengths and their average values (Å) and bond angles (°) in **7**

Cation–CN = 7		Anion–CN = 6	
Bond lengths			
Eu1–O11	2.418(3)	Eu2–O21	2.364(3)
Eu1–O13	2.429(3)	Eu2–Br22	2.7927(4)
Eu1–O12	2.443(4)	Eu2–Br21	2.8262(5)
Eu1–Br11	2.7883(4)	Eu1–$Br_{av.}$	2.809(1)
Eu1–$O_{av.}$	2.43(1)		
Bond angles			
Br11–Eu1–Br11a	179.75(2)	O21–Eu2–O21	180.000(18)
O11–Eu1–Br11	94.38(8)	Br22–Eu2–Br21	87.674(15)
O12–Eu1–Br11	89.875(11)	O21–Eu2–Br21	88.71(9)
O13–Eu1–Br11	85.04(8)	O21–Eu2–Br22	89.04(8)
O11–Eu1–O12	71.60(8)		
O11–Eu1–O13a	73.13(11)		
O13–Eu1–O13a	72.33(16)		

plexes **5** and **6** are isostructural to the previously described $[LnBr_3(THF)_4]$ (Ln = La [15], Nd [16]), while **7** is the first known ionic complex of lanthanides containing only bromo and THF ligands.

Three bromine atoms and four molecules of THF are coordinated to each praseodymium in **5** (Fig. 2) or samarium in **6** resembling a distorted pentagonal bipyramid. Two bromine atoms are in the apical *trans* and one

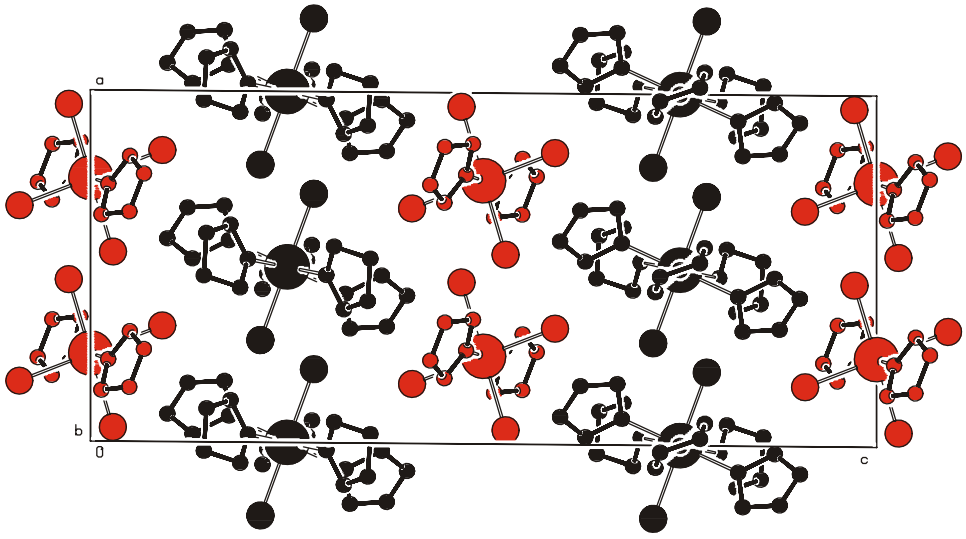

Fig. 4. Alternating layers of cations and anions in **7** along *c* axis. Hydrogen atoms are omitted for clarity.

bromine atom plus four oxygens of THF in equatorial positions. A comparison to the crystal structures of the known $[LnBr_3(THF)_4]$ (Ln = La [15], Nd [16]) shows an expected shortening of Ln–Br and Ln–O bonds and a reduction of unit cell volume in **5** and **6** [33]. The average Ln–Br bond lengths in **5** and **6** are similar as in **1**, **3** (Tables 4–6) and Ln–O as in $[PrCl_3(THF)_2]_n$ [1,2], $[PrI_3(THF)_4]$ [11] or $[SmCl_3(THF)_4]$ [6].

The ionic structure of **7** is presented in Fig. 3 and alternating layers of cations and anions lie along *c* axis in Fig. 4. The complex **7** is isostructural to analogous ionic lanthanide chloride (Gd–Yb) [3,6,9,10] and iodide (Nd–Yb) [6,11–13] complexes with THF. The two bromine atoms in the cation are in the *trans* positions and five oxygen atoms from THF in the equatorial plane of a rather undistorted pentagonal bipyramid. Only six ligands are octahedrally coordinated to europium in the centrosymmetric anion with two oxygens in *trans* positions. Despite lower coordination number in anion than in cation of **7**, the average Eu–Br bond lengths are similar in cation, anion (Table 7) and neutral complex **4** (Table 4). A higher negative partial charge on the europium centrum in the anion compensate a lower coordination number of the anion leading to elongation of Eu–Br bonds in the six-coordinated anion. The neutral ligands are expectedly less sensitive to ion charge and the average Eu–O distance in anion **7** is shorter than in the cation **7** (Table 7), complex **4** (Table 4) or $[EuCl_3(THF)_4]$ [7], which all poses the higher coordination number.

4. Conclusion

$[LnBr_3(DME)_2]$ (Ln = Pr, Nd, Sm, Eu), $[LnBr_3(THF)_4]$ (Ln = Pr, Sm) and $[EuBr_2(THF)_5]$ $[EuBr_4(THF)_2]$ were prepared following a new convenient synthetic route. Ln_2O_3 reacts with Me_3SiBr in the presence of DME and small amounts of water (n(Ln):n(H_2O) $\sim$ 5:1) at room temperature. The soluble products were crystallized from DME and THF in high yields.

A structural variety of different lanthanide halide complexes depends upon size and coordination mode of halide and neutral ligands. A transition from one to another type of crystal structure could be associated to a change of coordination number because of lanthanide contraction and/or coordination mode of halide, which is either a terminal or bridging one. A decrease of coordination number and associated transition to another structural type appears at lighter lanthanides, if larger halides are present in both, THF and DME complexes.

The complexes of lanthanide trichlorides or tribromides with DME crystallize as binuclear $[LnX_3(DME)_2]_2$ (CN = 8) or mononuclear $[LnX_3(DME)_2]$ (CN = 7). A polymeric structure was only proposed for $[LnCl_3(DME)]_n$ (Ln = La, Pr) [15,34]. A border between binuclear and mononuclear chlorides is set by neodymium complexes, which are known in both forms [10,17,19]. The X-ray crystal structures of **1** confirmed that the same change of coordination appears in bromide complexes of DME already for praseodymium, an earlier lanthanide than neodymium in chloride complexes. A crystal structure of analogous cerium complex should be determined to get undoubtedly the first lanthanide in the row, which forms mononuclear DME complexes of bromides.

Our results make possible to compare a transition between the mononuclear and ionic structures of different halide complexes with THF in the lanthanide row. The coordination number seven extends in $[LnBr_3(THF)_4]$ from lanthanum [15] to praseodymium in **5**, samarium in **6** and changes to the mixed, seven/six at europium in **7**. The same transition in crystal structures occurs in the analogous chloride at an later lanthanide, gadolinium, and in the analogous iodide complexes at an earlier lanthanide, neodymium. It would be interesting to determine the coordination numbers in THF complexes for lanthanide bromides from gadolinium to thulium to find the first complex with six-coordinated lanthanide. A mononuclear $[LnBr_3(THF)_3]$ could be expected for a lighter lanthanide than for the published ytterbium [15] according to the known crystal structures of lanthanide chloride and iodide complexes with THF.

5. Supplementary material

The CCDC Nos. 240791 (**1**), 240792 (**2**), 240793 (**3**), 240794 (**4**), 240788 (**5**), 240789 (**6**) and 240790 (**7**) contain the supplementary crystallographic data for this paper. These data can be obtained free of charge via www.ccdc.cam.ac.uk/data_request/cif, by emailing data_request@ccdc.cam.ac.uk, or by contacting The Cambridge Crystallographic Data Centre, 12, Union Road, Cambridge CB2 1EZ, UK; fax: +44 1223 336033.

Acknowledgements

The Ministry of Education, Science and Sport, Republic of Slovenia supported this work, through Grants MŠZŠP1-0175 and X-2000. Special thanks are given to Prof. Alojz Demšar for helpful discussions.

References

[1] G.B. Deacon, T. Feng, P.C. Junk, B.W. Skelton, A.N. Sobolev, A.H. White, Aust. J. Chem. 51 (1998) 75.
[2] G.R. Willey, T.J. Woodman, M.G.B. Drew, Polyhedron 16 (1997) 3385.
[3] W.J. Evans, J.L. Shreeve, J.W. Ziller, R.J. Doedens, Inorg. Chem. 34 (1995) 576.

[4] G.B. Deacon, T. Feng, S. Nickel, B.W. Skelton, A.H. White, J. Chem. Soc., Chem. Commun. (1993) 1328.
[5] W. Chen, Z. Jin, Y. Xing, Y. Fan, G. Yang, Inorg. Chim. Acta 130 (1987) 125.
[6] S. Anfang, M. Karl, N. Faza, W. Massa, J. Magull, K. Dehnicke, Z. Anorg. Allg. Chem. 623 (1997) 1425.
[7] S.H. Lin, Z.C. Dong, J.S. Huang, Q.E. Zhang, J.X. Lu, Acta Cryst. C47 (1991) 426.
[8] G.K.I. Magomedov, A.Z. Voskoboinikov, N.I. Kirillova, A.I. Gusev, I.N. Parshina, I.P. Beletskaya, Metalloorg. Khim. 5 (1992) 679.
[9] S. Anfang, K. Dehnicke, J. Magull, Z. Naturforsch. 51b (1996) 531.
[10] G.B. Deacon, D.J. Evans, P.C. Junk, Z. Anorg. Allg. Chem. 628 (2002) 2033.
[11] K. Izod, S.T. Linddle, W. Clegg, Inorg. Chem. 43 (2004) 214.
[12] Z. Xie, K. Chiu, B. Wu, T.C.W. Mak, Inorg. Chem. 35 (1996) 5957.
[13] M. Niemayer, Acta Crystallogr. E57 (2001) 363.
[14] A.A. Trifonov, P.V. de Weghe, J. Collin, A. Domingos, I. Santos, J. Organomet. Chem. 527 (1997) 225.
[15] G.B. Deacon, T. Feng, P.C. Junk, G. Meyer, N.M. Scott, B.W. Skelton, A.H. White, Aust. J. Chem. 53 (2000) 853.
[16] M.C. Gallazzi, F. Bianchi, L. Depero, M. Zocchi, Polymer 29 (1988) 1516.
[17] G. Zi, H.W. Li, Z. Xie, Organometallics 21 (2002) 1136.
[18] Crystallographic data obtained through the Cambridge Crystallographic Data Centre, [$GdCl_3(DME)_2$], refcode: VAKMID G. Wei, H. Gao, Z. Jin, Q. Shen, J. Struct. Chem. 8 (1989) 61.
[19] U. Baisch, D.B. Dell'Amico, F. Calderazzo, R. Conti, L. Labella, F. Marchetti, E.A. Quadrelli, Inorg. Chim. Acta 357 (2004) 1538.
[20] U. Baisch, W. Schnick, Z. Anorg. Allg. Chem. 629 (2003) 2073.
[21] P.G. Steel, J. Chem. Soc. Perkin Trans. 1 (2001) 2727, and references therein.
[22] U. Baisch, D.B. Dell'Amico, F. Calderazzo, L. Labella, F. Marchetti, A. Merigo, Eur. J. Inorg. Chem. (2004) 1219.
[23] A. Mandel, J. Magull, Z. Anorg. Allg. Chem. 623 (1997) 1542.
[24] T. Gröb, G. Seybert, W. Massa, K. Harms, K. Dehnicke, Z. Anorg. Allg. Chem 626 (2000) 1361.
[25] W.J. Evans, N.T. Allen, J.W. Ziller, J. Am. Chem. Soc. 122 (2000) 11749.
[26] M.N. Bocharev, I.L. Fedushkin, A.A. Fagin, T.V. Petrovskaya, J.W. Ziller, R.N.R. Broomhall-Dilard, W.J. Evans, Angew. Chem., Int. Ed. Engl. 36 (1997) 133.
[27] D.E. Hibbs, C. Jones, A.F. Richards, J. Chem. Cryst. 29 (1999) 1107.
[28] L. Depero, M.T. Arienti, M. Zocchi, M.C. Gallazzi, Struct. Chem. 2 (1991) 595.
[29] S. Petriček, A. Demšar, L. Golič, Polyhedron 18 (1998) 529.
[30] G.M. Sheldrick, SHELXS-97, A Program for Automatic Solution of Crystal Structures, University of Göttingen, Göttingen, Germany, 1997.
[31] G.M. Sheldrick, SHELXL-97, A Program for Crystal Structure Refinement, University of Göttingen, Göttingen, Germany, 1997.
[32] R. Herbst-Irmer, G.M. Sheldrick, Acta Cryst. B54 (1998) 443.
[33] R.D. Shannon, Acta Cryst. A32 (1976) 751.
[34] S. Petriček, A. Demšar, L. Golič, J. Košmrlj, Polyhedron 19 (2000) 199.

Available online at www.sciencedirect.com
SCIENCE DIRECT®
Polyhedron 23 (2004) 2303–2313
POLYHEDRON
www.elsevier.com/locate/poly

Spectral and structural studies of Zn and Cd complexes of 2-pyridineformamide N(4)-ethylthiosemicarbazone

Elena Bermejo [a], Alfonso Castiñeiras [a,*], Larissa M. Fostiak [b], Isabel García Santos [a], John K. Swearingen [b], Douglas X. West [c]

[a] Departamento de Química Inorgánica, Universidad de Santiago de Compostela, E-15706 Santiago de Compostela, Spain
[b] Department of Chemistry, Illinois State University, Normal, IL 61790-4160, USA
[c] Department of Chemistry, 351700, University of Washington, Seattle, WA 98195-1700, USA

Received 18 May 2004; accepted 19 July 2004
Available online 28 August 2004

Abstract

Reduction of 2-cyanopyridine in the presence of N(4)-ethylthiosemicarbazide produces 2-pyridineformamide N(4)-ethylthiosemicarbazone, HAm4E. Complexes with various zinc(II) and cadmium(II) salts have been prepared and characterized using physical and spectral methods. In addition, the crystal and molecular structure of $[Zn(Am4E)(OAc)]_2$ (**1**), $[Zn(HAm4E)I_2]$ (**4a**), $[Cd(Am4E)_2]$ (**5a**), $[Cd(HAm4E)Br_2] \cdot DMSO$ (**7a**) and $[Cd(HAm4E)I_2] \cdot DMSO$ (**8a**) have been obtained. Coordination is via the pyridyl nitrogen, imine nitrogen and thione or thiolato sulfur when coordinating as the neutral and anionic ligand, respectively. $[Zn(Am4E)(OAc)]_2$ is the first example of a binuclear complex with a 2-pyridineformamide thiosemicarbazonato ligand in which the two acetate bridging groups are equivalent resulting in a center of symmetry.
© 2004 Elsevier Ltd. All rights reserved.

Keywords: Thiosemicarbazone; 2-pyridineformamide; Crystal structure; Zinc; Cadmium

1. Introduction

Thiosemicarbazones and their metal complexes have been subject of interest in numerous studies because of their chemical and biological activities [1,2], in as much as possess a wide range of beneficial medicinal properties [3,4] that are often attributed to their chelating ability with metals ions [5]. Really, an important number of thiosemicarbazones being NNS tridentate donors possess carcinostatic efficacy [6] and substantial in vivo activity against various human tumor lines [7,8] but structural variations on some thiosemicarbazones with regard to the chelating ability may be destroy or reduce its medicinal values [9].

Complexes of Group 12 metals, zinc and cadmium, can provide an interesting range of stoichiometries depending on the preparative salt. Although complexes with 2-formyl- and 2-acetylpyridine N(4)-substituted thiosemicarbazones [10–13] have been studied previously, thiosemicarbazones in which the thiosemicarbazone moiety is attached to an amide carbon rather than an aldehyde or ketone carbon have been less studied.

Previously, we have reported our studies of metal complexes of 2-pyridineformamide thiosemicarbazone [14,15], 2-pyridineformamide N(4)-methylthiosemicarbazone [16–18], 2-pyridineformamide N(4)-dimethylthiosemicarbazone [19–21] and 2-pyridine-formamide 3-piperidylthiosemicarbazone [22–24] and 3-hexamethyleneiminylthiosemicarbazone [25]. We

* Corresponding author. Tel.: +34 981 594 636; fax: +34 981 547 163.
E-mail address: qiac01@usc.es (A. Castiñeiras).

0277-5387/$ - see front matter © 2004 Elsevier Ltd. All rights reserved.
doi:10.1016/j.poly.2004.07.010

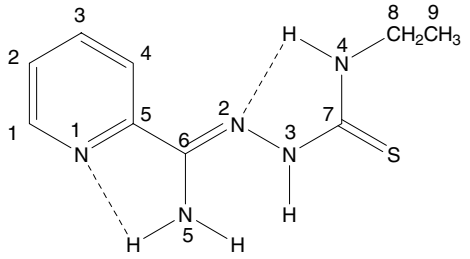

Fig. 1. Depiction of HAm4E showing the weak intramolecular N–H...N interactions.

report here our studies of the zinc(II) and cadmium(II) complexes of 2-pyridineformamide N(4)-ethylthiosemicarbazone, HAm4E (Fig. 1).

2. Experimental

HAm4E was prepared by reduction of 2-cyanopyridine [26] with sodium in the presence of N(4)-ethylthiosemicarbazide and is described elsewhere [27].

*Synthesis of [Zn(Am4E)(OAc)]$_2$ (**1**):* A solution of $Zn(OOCH_3)_2 \cdot 2H_2O$ (0.25 g, 1.12 mmol) in EtOH (30 ml) was mixed with a solution of HAm4E (0.25 g, 1.12 mmol) in EtOH (30 ml). The resultant solution is stirred at room temperature for 7 days and a yellow precipitate was filtered off. Recrystallization from DMSO gave yellow crystals of $[Zn(Am4E)(OAc)]_2$.

Yield: 0.29 g (74.5%). *Anal.* Calc. for $C_{22}H_{30}N_{10}O_4S_2Zn$: C, 38.4; H, 4.4; N, 20.2, S, 9.2. Found: C, 38.1; H, 4.4; N, 20.2; S, 9.3 %. IR (KBr, ν/cm^{-1}): 3360, 3320 (NH); 1570, 1516 (CN + CC), 1011 (NN), 862 (CS), 427 (ZnN), 327 (ZnS). ^{1}H NMR (DMSO-d$_6$, δ/ppm): 8.47 (d, 1H, H1); 8.08 (s, br, 2H, H3 + H4); 7.87 (s, br, 1H, H2); 6.87 (s, br, 2H, N5); 6.31 (s, br, 1H, N4H); 3.37 (q, 2H, CH_2); 1.14 (t, 3H, CH_3). ^{13}C NMR (DMSO-d$_6$, δ/ppm): 170.43 (C7), 147.78 (C1), 146.12 (C5), 144.54 (C6), 139.53 (C3), 125.21 (C2), 119.73 (C4), 36.93 (C8), 14.75 (C9). FAB$^+$ MS *m*/*z* (assignment): 286 ([Zn(Am4E)]$^+$).

*Synthesis of [Zn(HAm4E)Cl$_2$] (**2**):* A solution of $ZnCl_2$ (0.15 g, 1.12 mmol) in EtOH (30 ml) was mixed with a solution of HAm4E (0.25 g, 1.12 mmol) in EtOH (30 ml). The resultant yellow solution is stirred at room temperature for 7 days and the yellow precipitate was filtered off.

Yield: 0.36 g (88.3%). *Anal.* Calc. for $C_9H_{13}Cl_2N_5SZn$: C, 30.2; H, 3.6; N, 20.2, S, 8.0. Found: C, 30.1; H, 3.6; N, 19.5; S, 8.9%. IR (KBr, ν/cm^{-1}): 3365–3052 (NH); 1595, 1563 (CN + CC), 1012 (NN), 861 (CS), 456 (ZnN), 324 (ZnS), 282, 263 (ZnCl). ^{1}H NMR (DMSO-d$_6$, δ/ppm): 9.96 (s, 1H, N3H); 8.55 (d, 1H, H1); 8.29 (d, 2H, H4 + N4H); 7.86 (s, br, 1H, H3); 7.44 (dd, 1H, H2); 6.93 (s, br, 2H, N5); 3.58 (q, 2H, CH_2); 1.14 (t, 3H, CH_3). ^{13}C NMR (DMSO-d$_6$, δ/ppm): 171.45 (C7), 149.41 (C1), 148.67 (C5), 147.98 (C6), 139.71 (C3), 124.18 (C2), 121.09 (C4), 38.13 (C8), 14.88 (C9). FAB$^+$ MS *m*/*z* (assignment): 289 ([Zn(HAm4E + 2H)]$^+$).

*Synthesis of [Zn(HAm4E)Br$_2$] (**3**):* A solution of $ZnBr_2$ (0.25 g, 1.12 mmol) in EtOH (30 ml) was mixed with a solution of HAm4E (0.25 g, 1.12 mmol) in EtOH (30 ml). The resultant solution is stirred at room temperature for 7 days. The white product was filtered off.

Yield: 0.5 g (89.2%). *Anal.* Calc. for $C_9H_{13}Br_2N_5SZn$: C, 24.3; H, 2.9; N, 15.6, S, 6.7. Found: C, 24.1; H, 2.9; N, 15.6; S, 7.2 %. IR (KBr, ν/cm^{-1}): 3371–3052 (NH); 1632–1538 (CN + CC), 1016 (NN), 863 (CS), 457 (ZnN), 324 (ZnS), 218, 195 (ZnCl). ^{1}H NMR (DMSO-d$_6$, δ/ppm): 9.96 (s, 1H, N3H); 8.56 (s, 1H, H1); 8.42 (d, 1H, H4); 8.31 (s, br, 1H, N4H); 7.86 (s, br, 1H, H3); 7.45 (s, br, 1H, H2); 6.97 (s, br, 2H, N5H); 3.57 (q, 2H, CH_2); 1.14 (t, 3H, CH_3). ^{13}C NMR (DMSO-d$_6$, δ/ppm): 175.94 (C7), 149.40 (C1), 148.66 (C5), 145.82 (C6), 137.90 (C3), 127.23 (C2), 121.12 (C4), 38.66 (C8), 14.11 (C9).

*Synthesis of [Zn(HAm4E)$_2$I$_2$] · 3H$_2$O (**4**):* A solution of ZnI_2 (0.36 g, 1.12 mmol) in EtOH (30 ml) was mixed with a solution of HAm4E (0.25 g, 1.12 mmol) in EtOH (30 ml). The resultant solution is stirred at room temperature for 7 days and the yellow product was separated by filtration.

Yield: 0.05 g (11.1%). *Anal.* Calc. for $C_{18}H_{32}I_2N_{10}O_3S_2Zn$: C, 26.8; H, 3.2; N, 16.9, S, 6.7. Found: C, 27.0; H, 3.8; N, 17.3; S, 7.2 %. IR (KBr, ν/cm^{-1}): 3388–3041 (OH, NH); 1634, 1563 (CN + CC), 1015 (NN), 856 (CS), 340 (ZnS), 202, 177 (ZnI). ^{1}H NMR (DMSO-d$_6$, δ/ppm): 9.90 (s, br, 1H, N3H); 8.44 (d, 1H, H1); 8.09 (s, br, 2H, H3 + H4); 7.06 (s, br, 3H, H2 + N5H); 6.53 (s, br, 1H, N4H); 3.27 (s, br, 2H, CH_2); 1.02 (s, br, 3H, CH_3). FAB$^+$ MS *m*/*z* (assignment): 509.2 ([Zn(HAm4E)-(Am4E)]$^+$).

Upon slow evaporation of the solvent a large yield of crystals of $[Zn(HAm4E)I_2]$ (**4a**) were isolated.

*Synthesis of [Cd(Am4E)(OAc)]$_2$ (**5**):* A solution of $Cd(OAc)_2 \cdot 2H_2O$ (0.30 g, 0.90 mmol) in EtOH (30 ml) was mixed with a solution of HAm4E (0.25 g, 0.90 mmol) in EtOH (30 ml). The resultant solution is stirred at room temperature for 7 days and after that the yellow precipitate was filtered off.

Yield: 0.41 g (93.9%). *Anal.* Calc. for $C_{22}H_{30}N_{10}O_4S_2Cd$: C, 33.5; H, 3.7; N, 16.2, S, 6.2. Found: C, 33.6; H, 3.8; N, 17.8; S, 8.1 %. IR (KBr, ν/cm^{-1}): 3427–3134 (NH); 1562, 1539 (CN + CC), 1011 (NN), 859 (CS), 423 (CdN), 319 (CdS). ^{1}H NMR (DMSO-d$_6$, δ/ppm): 8.44 (d, 1H, H1); 8.06 (s, 2H, H3 + H4); 7.56 (s, br, 1H, H2); 6.86 (s, 2H,

N5H); 6.30 (s, br, 1H, N4H); 3.36 (m, 2H, CH_2); 1.10 (t, 3H, CH_3). FAB^+ MS *m/z* (assignment): 223.1 ($[HAm4E]^+$), 335.9 ($[Cd(Am4E)]^+$), 558.0 $(Cd(Am4E)_2]^+$).

Recrystallization from DMSO gave crystals of $[Cd(Am4E)_2]$ (**5a**).

*Synthesis of [Cd(HAm4E)Cl$_2$] (**6**):* A solution of $CdCl_2$ (0.21 g, 1.12 mmol) in EtOH (30 ml) was mixed with a solution of HAm4E (0.25 g, 1.12 mmol) in EtOH (30 ml). The resultant solution is stirred at room temperature for 7 days and the white solid was separated by filtration.

Yield: 0.35 g (76.7%). *Anal.* Calc. for $C_9H_{13}Cl_2N_5SCd$: C, 26.5; H, 3.0; N, 17.0, S, 7.8. Found: C, 26.6; H, 3.2; N, 17.2; S, 7.9 %. IR (KBr, ν/cm^{-1}): 3383–3055 (NH); 1629–1563 (CN + CC), 1013 (NN), 855 (CS), 401 (CdN), 323 (CdS), 262, 243 (CdCl). ^{1}H NMR (DMSO-d$_6$, δ/ppm): 9.97 (s, 1H, N3H); 8.55 (s, br, 1H, H1); 8.31 (s, br, 2H, H4 + N4H); 7.85 (t, 1H, H3); 7.44 (dd, 1H, H2); 6.92 (s, br, 2H, N5H); 3.57 (q, 2H, CH_2); 1.14 (t, 3H, CH_3). ^{13}C NMR (DMSO-d$_6$, δ/ppm): 167.55 (C7), 149.35 (C1), 148.68 (C5), 145.76 (C6), 137.86 (C3), 125.24 (C2), 123.11 (C4), 37.97 (C8), 14.23 (C9). FAB^+ MS *m/z* (assignment): 371.0 ($[Cd(Am4E)Cl]^+$).

Upon slow evaporation of the solvent crystals of $[Cd(Am4E)_2]$ (**5a**) were isolated.

*Synthesis of [Cd(HAm4E)Br$_2$] (**7**):* A solution of $CdBr_2$ (0.21 g, 1.12 mmol) in EtOH (30 ml) was mixed with a solution of HAm4E (0.25 g, 1.12 mmol) in EtOH (30 ml). The resultant solution is stirred at room temperature for 7 days and the yellow formed solid was filtered off.

Yield: 0.51 g (92.3%). *Anal.* Calc. for $C_9H_{13}Br_2N_5SCd$: C, 22.2; H, 2.4; N, 14.1, S, 6.4. Found: C, 21.8; H, 2.6; N, 14.1; S, 6.5%. IR (KBr, ν/cm^{-1}): 3334–3014 (NH); 1622–1526 (CN + CC), 1014 (NN), 848 (CS), 402 (CdN), 330 (CdS), 183, 163 (CdBr). ^{1}H NMR (DMSO-d$_6$, δ/ppm): 9.97 (s, 1H, N3H); 8.56 (s, br, 1H, H1); 8.42 (d, 1H, H4); 7.83 (s, br, 1H, H3); 7.82 (s, br, 1H, N4H); 7.45 (dd, 1H, H2); 6.92 (s, br, 2H, N5H); 3.57 (q, 2H, CH_2); 1.15 (t, 3H, CH_3). ^{13}C NMR (DMSO-d$_6$, δ/ppm): 167.66 (C7), 149.42 (C1), 148.68 (C5), 145.83 (C6), 137.99 (C3), 125.32 (C2), 123.18 (C4), 38.67 (C8), 14.29 (C9).

Recrystallization from DMSO gave colourless crystals of $[Cd(HAm4E)Br_2] \cdot DMSO$ (**7a**).

*Synthesis of [Cd(HAm4E)I$_2$] (**8**):* A solution of CdI_2 (0.41 g, 1.12 mmol) in EtOH (30 ml) was mixed with a solution of HAm4E (0.25 g, 1.12 mmol) in EtOH (30 ml). The resultant solution is stirred at room temperature for 7 days and the yellow precipitate was filtered off.

Yield: 0.6 g (90.2%). *Anal.* Calc. for $C_9H_{13}I_2N_5SCd$: C, 18.8; H, 2.2; N, 11.8, S, 5.8. Found: C, 18.3; H, 2.6; N, 11.9; S, 5.4%. IR (KBr, ν/cm^{-1}): 3381–3033 (NH); 1615–1548 (CN + CC), 1012 (NN), 849 (CS), 406 (CdN), 326 (CdS), 163, 140 (CdI). ^{1}H NMR (DMSO-d$_6$, δ/ppm): 9.96 (s, 1H, N3H); 8.55 (s, br, 1H, H1); 8.42 (d, 1H, H4); 7.85 (s, br, 2H, H3 + N4H); 7.51 (s, br, 1H, H2); 6.95 (s, br, 2H, N5H); 3.55 (m, 2H, CH_2); 1.15 (d, 3H, CH_3). ^{13}C NMR (DMSO-d$_6$, δ/ppm): 167.55 (C7), 149.35 (C1), 148.64 (C5), 147.76 (C6), 137.85 (C3), 125.24 (C2), 123.11 (C4), 37.97 (C8), 14.23 (C9). FAB^+ MS *m/z* (assignment): 224.1 ($[H_2Am4E^+]$), 336.0 ($[Cd(Am4E)]^+$), 463.9 ($[Cd(HAm4E)I]^+$).

Recrystallization from DMSO gave colourless crystals of $[Cd(HAm4E)I_2] \cdot DMSO$ (**8a**).

Elemental analyses were performed with a Carlo Erba 1108 and Perkin–Elmer 240B microanalyser. NMR spectra were obtained as dmso solutions with a Brucker AMX300 spectrometer and chemical shifts are reported in parts per million downfield from Me_4Si. IR spectra were recorded as KBr disks (4000–400 cm^{-1}) or polyethylene-sandwiched Nujol mulls (500–100 cm^{-1}) with a Bruker IFS-66V spectrophotometer. Mass spectra were obtained in a Hewlett Packard HP598A. Yellow prismatic crystals of $[Zn(Am4E)(OAc)]_2$, $[Cd(Am4E)_2]$, $[Cd(HAm4E)Br_2] \cdot DMSO$, $[Cd(HAm4E)I_2] \cdot DMSO$ as well as a yellow plate crystal of $[Zn(HAm4E)I_2]$ were mounted on a glass fiber and used for data collection. Cell constants and an orientation matrix for data collection were obtained by least-squares refinement of the diffraction data from 25 reflections in the range $5.81° < \theta < 10.21°$ for $[Zn(Am4E)(OAc)]_2$, $9.980° < \theta < 20.899°$ for $[Zn(HAm4E)I_2]$, $15.694° < \theta < 46.261°$ for $[Cd(HAm4E)Br_2] \cdot DMSO$, $18.631° < \theta < 45.792°$ for $[Cd(HAm4E)I_2] \cdot DMSO$ and $12.994° < \theta < 23.762°$ for $[Cd(Am4E)_2]$ with an Enraf-Nonius CAD4 or MACH3 automatic diffractometer. The structures were solved by direct methods [28], which revealed the position of all non-hydrogen atoms, and refined on F^2 by a full matrix least-squares procedure using anisotropic displacement parameters [29]. The H atoms were included in geometrically idealized positions employing appropriate riding models with isotropic displacement parameters constrained to $1.2U_{eq}$ of their carrier atoms. For $[Cd(HAm4E)Br_2] \cdot DMSO$ and $[Cd(HAm4E)I_2] \cdot DMSO$ the Flack x parameter (absolute structure parameter) was calculated to be 0.00(3) and 0.03(3) for the present structure and 1.04(3) and 0.97(3) for the inverted structure, respectively, thus providing strong evidence that the absolute structure has been assigned correctly [30]. Atomic scattering factors are from *International Tables for Crystallography* [31] and molecular graphics from PLATON [32]. A summary of the crystal data, experimental details and refinement results are listed in Table 1.

Table 1
Crystal data and structure refinement for $[Zn(Am4E)(OAc)]_2$ (**1**), $[Zn(HAm4E)I_2]$ (**4a**), $[Cd(Am4E)_2]$ (**5a**) $[Cd(HAm4E)Br_2]\cdot DMSO$ (**7a**) and $[Cd(HAm4E)I_2]\cdot DMSO$ (**8a**)

Empirical formula	$C_{22}H_{30}N_{10}O_4S_2Zn_2$	$C_9H_{13}I_2N_5SZn$
Color; habit	yellow, prism	yellow, plate
Formula weight	693.42	542.47
Temperature (K)	293(2)	293(2)
Crystal size (mm)	$0.24\times0.16\times0.12$	$0.45\times0.15\times0.10$
Crystal system	monoclinic	triclinic
Space group:	$P2_1/c$ (No. 14)	$P\bar{1}$ (No. 2)
Unit cell dimensions		
a (Å)	10.305(2)	8.322(1)
b (Å)	8.404(5)	8.491(3)
c (Å)	19.266(3)	11.546(2)
α (°)	90(–)	88.07(3)
β (°)	120.81(1)	82.72(2)
γ (°)	90(–)	87.58(2)
Volume (Å^3)	1433.0(9)	808.1(2)
Z	2	2
Density (Mg/m^3)	1.607	2.229
Diffractometer	nonius MACH3	nonius MACH3
Radiation (λ, AA)	Mo Kα (0.71073)	Mo Kα (0.71073)
Absorption coefficient (mm^{-1})	1.868	5.460
Absorption correction	Ψ-scan	Ψ-scan
θ Range for data collection (°)	3.13–23.36	2.47–27.97
Index ranges	$-11\leqslant h\leqslant 11$, $-9\leqslant k\leqslant 0$, $-11\leqslant l\leqslant 21$	$-10\leqslant h\leqslant 0$, $-11\leqslant k\leqslant 11$, $-15\leqslant l\leqslant 15$
Maximum and minimum transmission	0.857, 0.679	0.975, 0.829
Reflections collected	2164	4397
Independent reflections	2084 (R_{int} = 0.0506)	3880 (R_{int} = 0.0532)
Data/restraints/parameters	2084/0/182	3880/0/164
Final R indices [$I > 2\sigma(I)$]	R_1 = 0.0733 wR_2 = 0.0935	R_1 = 0.0490 wR_2 = 0.1072
R indices (all data)	R_1 = 0.1169 wR_2 = 0.1539	R_1 = 0.1484 wR_2 = 0.1366
Goodness-of-fit	0.878	0.955
Extinction coefficient		
Largest differential peak/hole (e Å^{-3})	0.569/−0.957	1.797/−0.784

	$C_{18}H_{24}CdN_{10}S_2$	$C_{11}H_{19}Br_2CdN_5OS_2$	$C_{11}H_{19}CdI_2N_5OS_2$
Color; habit	yellow, prism	yellow, prism	yellow, prism
Formula weight	556.99	573.65	667.63
Temperature (K)	293(2)	293(2)	293(2)
Crystal size (mm)	$0.40\times0.25\times0.15$	$0.35\times0.30\times0.30$	$0.40\times0.25\times0.25$
Crystal system	monoclinic	monoclinic	monoclinic
Space group	$P2_1/c$ (No.14)	Cc (No. 9)	Cc (No. 9)
Unit cell dimensions			
a (Å)	9.284(3)	13.5493(10)	13.5557(13)
b (Å)	15.096(3)	12.9870(6)	13.2459(10)
c (Å)	16.933(5)	11.1062(6)	11.5450(14)
β (°)	95.042(7)	94.076(6)	94.107(9)
Volume (Å^3)	2364.0(1)	1437.0(5)	2067.7(4)

Z	4	4	4
Density (Mg/m^3)	1.565	1.956	2.145
Diffractometer	nonius CAD4	nonius CAD4	nonius CAD4
Radiation (λ, Å)	Mo Kα (0.71073)	Cu Kα (1.54184)	Cu Kα (1.54184)
Absorption coefficient (mm^{-1})	1.127	15.854	33.857
Absorption correction	Ψ-scan	Ψ-scan	Ψ-scan
θ Range for data collection (°)	1.81–26.47	4.72–75.82	4.67–75.95
Index ranges	$-10 \leqslant h \leqslant 11$, $-18 \leqslant k \leqslant 18$, $-17 \leqslant l \leqslant 21$	$-17 \leqslant h \leqslant 16$, $-16 \leqslant k \leqslant 16$, $0 \leqslant l \leqslant 13$	$-16 \leqslant h \leqslant 17$, $-16 \leqslant k \leqslant 1$, $-14 \leqslant l \leqslant 0$
Maximum/minimum transmission	0.849/0.661	0.964/0.662	0.969/0.533
Reflections collected	19820	4165	2518
Independent reflections	4825 (R_{int} = 0.0545)	2132 (R_{int} = 0.0834)	2266 (R_{int} = 0.1337)
Data/restraints/parameters	4825/0/280	2132/2/203	2266/2/203
Final R indices [$I > 2\sigma(I)$]	R_1 = 0.0618, wR_2 = 0.0833	R_1 = 0.056, wR_2 = 0.169	R_1 = 0.054, wR_2 = 0.144
R indices (all data)	R_1 = 0.1610, wR_2 = 0.1745	R_1 = 0.063, wR_2 = 0.179	R_1 = 0.057, wR_2 = 0.146
Goodness-of-fit	1.036	1.047	1.076
Extinction coefficient		0.00068(13)	0.00058(8)
Largest differential peak/hole (e Å^{-3})	0.984/−1.339	2.150/−1.039	1.111/−1.390

3. Results and discussion

The bond distances for the zinc(II) and cadmium(II) complexes are shown in Table 2 and their bond angles in Table 3. Table 4 lists the hydrogen bonding interactions and Table 5 the mean plane data and angles between planes.

3.1. Structural properties of [Zn(Am4E)(OAc)]$_2$ (1)

Previously, the crystal structures of acetate bridged zinc(II) complexes of 2-pyridineformamide N(4)-substituted thiosemicarbazones, as well as other heterocyclic thiosemicarbazones, have been reported. [Zn(Am4DH)(OAc)]$_2$, where Am4DH is the anion of 2-pyridineformamide thiosemicarbazone [33], [Zn(Ampip)OAc]$_2$, where Ampip is the anion of 2-pyridineformamide 3-piperidylthiosemicarbazone [16], and [Zn(Amhexim)(OAc)]$_2$, where Amhexim is the anion of 2-pyridineformamide 3-hexamethyleneiminylthiosemicarbazone [25] are all unsymmetrical with one acetate bridging with two oxygen atoms and the other with one oxygen; the second oxygen is weakly coordinated, at best, to one of the zinc centers. In addition, [Zn(Ac4E)(OAc)]$_2$, where Ac4E is the anion of 2-acetylpyridine N(4)-ethylthiosemicarbazone [34], is also bridged in an unsymmetrical manner by the two acetate ligands. However, [Zn(Am4M)(OAc)], where Am4M is the anion of 2-pyridineformamide N(4)-methylthiosemicarbazone [18], was found to be symmetrically bridged with a *syn–syn* arrangement of the two acetate ligands like the present [Zn(Am4E)(OAc)]$_2$ with a center symmetry (Fig. 2) in which the Zn–Zn distance is of 3.707(5) Å. The Am4E anion (i.e., loss of the hydrogen from N13) coordinates as a NNS tridentate ligand to give 5-coordinate zinc(II) centers. The bond distances for the coordinating atoms is Zn–N(im) < Zn–N(py) < Zn–S and the Zn–O distances which are different have the shortest bond distances to Zn(II). The anionic ligand has a longer C17–S1 bond (which formally becomes a single bond in [Zn(Am4E)(OAc)]$_2$), 1.759(19) Å, compared to an average of 1.696(3) Å for HAm4E [27], a shorter C16–N12 bond, 1.24(2) Å compared to an average of 1.292(3) Å and a shorter N13–C17 bond (which formally becomes a double bond), 1.31(2) Å compared to an average of 1.354(6) Å. The difference in the C–O bond distances, 1.270(19) and 1.18(2) Å, is caused by the difference in their coordination distances to Zn. Compared to [Zn(Am4M)(OAc)]$_2$ there are some differences in bond distances: Zn–S is longer in [Zn(Am4E)(OAc)]$_2$, 2.431(6) Å compared to 2.3697(9) Å and the C–O bond distances are closer to being the same in [Zn(Am4M)(OAc)]$_2$.

The identical ZnN_2O_2S chromophores in [Zn(Am4E)(OAc)]$_2$ have a N11–Zn1–S1 angle of 151.2(5)° compared to 156.58(6)° for [Zn(Am4M)(OAc)]$_2$. With

Table 2
Selected bond distances (Å) for $[Zn(Am4E)(OAc)]_2$ (**1**), $[Zn(HAm4E)I_2]$ (**4a**), $[Cd(Am4E)_2]$ (**5a**), $[Cd(HAm4E)Br_2]\cdot DMSO$ (**7a**), and $[Cd(HAm4E)I_2]\cdot DMSO$ (**8a**)

Bond	1	4a	5a[a]	7a	8a
M–S1	2.431(6)	2.502(3)	2.590(3)/2.558(2)	2.607(5)	2.580(4)
M–N11	2.204(18)	2.170(7)	2.445(8)/2.447(5)	2.307(10)	2.363(10)
M–N12	2.033(18)	2.120(7)	2.338(6)/2.317(5)	2.368(12)	2.362(10)
M–X11	2.014(12)	2.6184(13)		2.5957(18)	2.7932(13)
M–X12	1.961(13)	2.6370(14)		2.587(2)	2.7544(15)
S1–C17	1.759(19)	1.701(9)	1.751(15)/1.734(8)	1.699(16)	1.700(14)
C16–N12	1.24(2)	1.284(10)	1.304(16)/1.282(7)	1.314(18)	1.308(15)
N12–N13	1.40(2)	1.371(10)	1.416(15)/1.394(7)	1.364(15)	1.354(14)
N13–C17	1.31(2)	1.353(11)	1.22(2)/1.325(8)	1.350(17)	1.363(16)
C17–N14	1.35(2)	1.311(11)	1.413(7)/1.373(8)	1.317(19)	1.335(16)
N14–C18	1.40(2)	1.466(12)	1.46(2)/1.439(14)	1.48(2)	1.471(14)
C16–N15	1.34 (2)	1.336(10)	1.367(13)/1.360/8)	1.312(19)	1.345(17)

[a] Second number refers to S2 ligand.

Table 3
Selected bond angles (°) for for $[Zn(Am4E)(OAc)]_2$ (**1**), $[Zn(HAm4E)I_2]$ (**4a**), $[Cd(Am4E)_2]$ (**5a**), $[Cd(HAm4E)Br_2]\cdot DMSO$ (**7a**), and $[Cd(HAm4E)I_2]\cdot DMSO$ (**8a**)

Angle	1	4a	7a	8a	Angle	5a[a]
S1–M–X1	100.1(4)	97.28((7)	103.62(12)	103.23(13)	S1–Cd–N22	113.20(15)
S1–M–N1	151.2(5)	148.5(2)	142.1(3)	142.3(3)	S1–Cd–N11	141.7(2)
S1–M–N2	81.1(6)	78.4(2)	74.3(3)	73.7(3)	S1–Cd–N12	73.6(3)
S1–M–X2	109.4(5)	105.16(8)	103.80(13)	103.48(15)	S1–Cd–N21	100.27(17)
N1–M–N2	73.5(8)	73.8(3)	68.0(3)	69.0(4)	S1–Cd–S2	107.25(8)
N1–M–X2	92.4(6)	96.9(2)	97.2(3)	97.1(3)	N11–Cd–N12	68.8(3)
N1–M–X1	84.2(5)	96.0(2)	95.8(3)	96.0(3)	N11–Cd–N21	85.2(2)
N2–M–X2	110.4(5)	106.9(2)	117.4(2)	115.8(3)	N11–Cd–N22	104.1(2)
N2–M–X1	125.6(6)	142.7(2)	127.3(2)	128.4(3)	N12–Cd–N22	156.4(2)
X2–M–X1	119.8(5)	109.94(4)	114.21(5)	114.93(10)		
M–S1–C7	93.6(8)	97.6((3)	101.4(4)	101.8(5)		96.7(6)
M–N2–C6	122.1(17)	119.8(6)	121.0(8)	119.8(9)		118.1(8)
M–N2–N3	122.5(13)	120.6(5)	120.7(7)	120.4(8)		122.1(8)
N5–C6–N2	124(2)	124.7(8)	127.0(12)	125.7(13)		119.7(17)/124.1(6)
C5–C6–N2	116(2)	115.4(7)	115.0(11)	114.6(13)		118.6(9)/118.1(5)
C6–N2–N3	115(2)	119.6(7)	118.3(10)	119.8(12)		117.2(10)/116.2(5)
N2–N3–C7	114.4(17)	119.9(7)	120.3(10)	121.6(12)		114.0(10)/114.4(5)
N3–C7–N4	116.8(19)	116.1(8)	116.0(12)	116.3(14)		116.0(14)/114.1(7)
N3–C7–S1	125.5(16)	121.4(7)	123.2(10)	122.4(11)		131.3(13)/128.7(5)
N4–C7–S1	117.7(18)	122.6(7)	120.8(10)	121.2(11)		112.6(14)/117.2(6)
C7–N4–C8	124.7(19)	126.3(8)	123.6(13)	124.7(16)		121.3(17)/126.7(9)

[a] Second number refers to S2 ligand.

N11–Zn–S1 assigned as β and N12–Zn1–O11 as α, $\tau = 0.43$ [35], compared to 0.56 for $[Zn(Am4M)(OAc)]_2$, indicates that the arrangement about Zn is not as close to a trigonal bipyramid (i.e., N11 and S11 apical and N12, O1a and O2 basal) than $[Zn(Am4M)(OAc)]_2$.

Intermolecular hydrogen bonding, Table 4, by N14H and $N15H_2$ is common to the 2-pyridineformamide thiosemicarbazone [14,15,32] and N-alkylthiosemicarbazones [16,17]. The distances and angles for the interactions with the coordinated thiol sulfur atoms are comparable to the N–H···S intermolecular interactions of N-2-pyridyl-N′-arylthioureas [36]. For $[Zn(Am4M)(OAc)]_2$ the N14–H14···S1 interaction was stronger based on H14···S1 and N14···S1 distances of 2.67 and 3.466(3) Å and the N15–H15···O11 interaction was also stronger, H15···O11 and N15···O11 distances of 2.20 and 2.973 Å. However, a N15–H15···S1 interaction, which is the stronger of the interactions with sulfur for $[Zn(Am4E)(OAc)]_2$, was not detected in $[Zn(Am4M)(OAc)]_2$.

As might be expected due to the greater bulkiness of the ethyl group compared to a methyl group, the thiosemicarbazone moiety has a mean plane deviation in $[Zn(Am4E)(OAc)]_2$, 0.0717, compared to $[Zn(Am4M)(OAc)]_2$, 0.0316. Also, the angle between the mean planes of the thiosemicarbazone moiety and the pyridine ring is considerably larger, 15.9(9)° compared to 3.8(2)°. However, because the stereochemistry about the Zn center in $[Zn(Am4M)(OAc)]_2$ is closer to a regular trigonal bipyramid, the thiosemicarbazone moiety makes an angle with the bridging acetate group's O11–C2–O12 of 87.3(1)° compared to 75.5(6)° for $[Zn(Am4E)(OAc)]_2$.

Table 4
Hydrogen bonding interactions for [Zn(Am4E)(OAc)]$_2$ (**1**), [Zn(HAm4E)I$_2$] (**4a**), Cd(Am4E)$_2$] (**5a**), [Cd(HAm4E)Br$_2$] · DMSO (**7a**) and [[Cd(HAm4E)I$_2$] · DMSO (**8a**)

Compound	D–H···A	*d*(D–H)	*d*(H···A)	*d*(D···A)	∠(DHA)
[Zn(Am4E)(OAc)]$_2$[a]	N14–H14···S1#2	0.86	2.87	3.61(2)	145.5
	N15–H15A···O11#3	0.86	2.71	3.15(2)	113.8
	N15–H15B···S1#3	0.86	2.71	3.51(2)	155.2
[Zn(HAm4E)I$_2$][b]	N3–H3··· I2#1	0.86	2.80	3.619(7)	158.9
	N4–H4···I2#1	0.86	2.94	3.759(8)	158.7
	N5–H5A···I2#1	0.86	3.22	4.038(8)	158.7
	N5–H5A···I1#2	0.86	3.25	3.789(9)	123.2
	N5–H5B···S1#3	0.86	2.88	3.663(8)	152.6
[Cd(HAm4E)I$_2$][c]	N3–H3···O20#1	0.86	1.92	2.73(2)	175.0
	N5–H5A···O20#1	0.86	2.02	2.87(2)	168.7
	N4–H4···I1#2	0.86	3.17	3.86(1)	139.0
[Cd(HAm4E)Br$_2$][d]	N3–H3···O20#1	0.86	1.87	2.72(2)	170.3
	N4–H4···Br1#2	0.86	2.98	3.67 (1)	138.6
	N5–H5B···Br2#1	0.86	3.04	3.82(1)	151.7
	N5–H5A···O20#1	0.86	2.04	2.89(2)	170.4
[Cd(Am4E)$_2$]	N15–H15A···N13	0.86	2.36	2.66(1)	101.4
	N24–H24A···S1#1	0.86	2.61	3.46(1)	169.2

Symmetry transformations used to generate equivalent atoms: (a) #1: $-x+1$, $-y+1$, $-z+1$; #2 $-x+2$, $-y+1$, $-z+1$; #3 $-x+1$, $y-1/2$, $-z+1/2$. (b) #1: $-x-1$, $-y+2$, $-z+1$; #2: $-x$, $-y+2$, $-z+1$; #3: x, $y+1$, z. (c) #1: x, $-y$, $z+1/2$; #2: x, $-y$, $z-1/2$. (d) #1: x, $-y$, $z+1/2$; #2: x, $-y$, $z-1/2$. (e) #1: $-x+1$, $y+1/2$, $-z+1/2$.

Table 5
Rms planes for [Zn(Am4E)(OAc)]$_2$ (**1**), [Zn(HAm4E)I$_2$] (**4a**), [Cd(Am4E)$_2$] (**5a**), [Cd(HAm4E)Br$_2$] · DMSO (**7a**), and [Cd(HAm4E)I$_2$] · DMSO (**8a**)

Compound	Plane	Rms deviation	Largest deviation	Angle with previous plane
[Zn(Am4E)(OAc)]$_2$	N11–C11–C12–C13–C14–C15	0.0086	N11, 0.010 (14)	
	C16–N12–N13–C17–N14–S1	0.0717	N12, 0.138(15)	15.9(9)
	O11–C2–O12	0.0000		75.5(6)
[Zn(HAm4E)I$_2$]	C6–N2–N3–C7–N4–S1	0.0650	C6, 0.113 (7)	
	N1–C1–C2–C3–C4–C5	0.0035	C4, 0.006(8)	8.9(4)
[Cd(Am4E)$_2$]	N11–C11–C12–C13–C14–C15	0.0176	C15, 0.028(9)	
	C16–N12–N13–C17–N14–S1	0.0268	N12, 0.044(6)	12.4(4)
	C25–C26–N22–N23–C27–N24–S2	0.0497	C26, 0.076(4)	85.3(2)
	N21–C21–C22–C23–C24–C25	0.0041	C22, 0.007(7)	5.6(4)
[Cd(HAm4E)Br$_2$]	C6–N2–N3–C7–N4–S1	0.0115	C7, 0.022 (12)	
	N1–C1–C2–C3–C4–C5	0.0125	C2, 0.018 (12)	3.7(6)
[Cd(HAm4E)I$_2$]	C6–N2–N3–C7–N4–S1	0.0041	N2, 0.008(8)	
	N1–C1–C2–C3–C4–C5	0.0047	N1, 0.006 (10)	3.9(6)
	S1–N2–N1–I1	0.3198	N2, 0.430 (6)	26.3(5)

*3.2. Structural properties of [Zn(HAm4E)I$_2$] (**4a**)*

The molecular structure of the complex is represented in Fig. 3. The only other crystal structure reported for a 2-pyridineformamide thiosemicarbazone complex prepared with zinc(II) iodide, [Zn(HAm4DH)I$_2$] [13], crystallized in the monoclinic space group $P2_1/n$ while [Zn(HAm4E)I$_2$] is triclinic and $P\bar{1}$. The bond distances to Zn are in the expected order Zn–N(im) < Zn–N(py) < Zn–S with Zn–S and Zn–N(py) longer than for [Zn(Am4E)(OAc)]$_2$, with Zn–N(im) marginally shorter (Table 2). Compared to [Zn(HAm4DH)I$_2$] [13], Zn–S is longer, 2.502(3) Å compared to 2.436(3) Å, Zn–N(py) marginally longer and Zn(im) essentially the same. The Zn–I bond distances are all above 2.6 Å in the two complexes, but there is a difference of >0.06 Å between the Zn–I bonds of [Zn(HAm4DH)I$_2$]. Because the anionic form of the ligand is present in [Zn(Am4E)(OAc)]$_2$

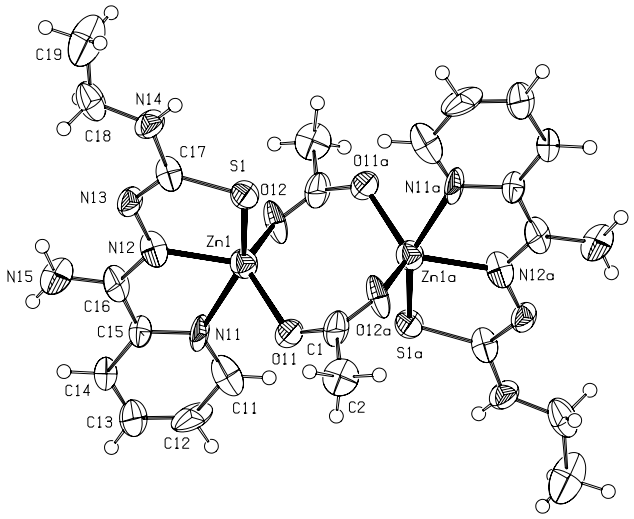

Fig. 2. A view of the molecular structure of $[Zn(Am4E)(OAc)]_2$ (**1**), showing the atom labeling scheme. The thermal motion ellipsoids are drawn at the 50% probability; (a: $-x+1, -y+1, -z+1$).

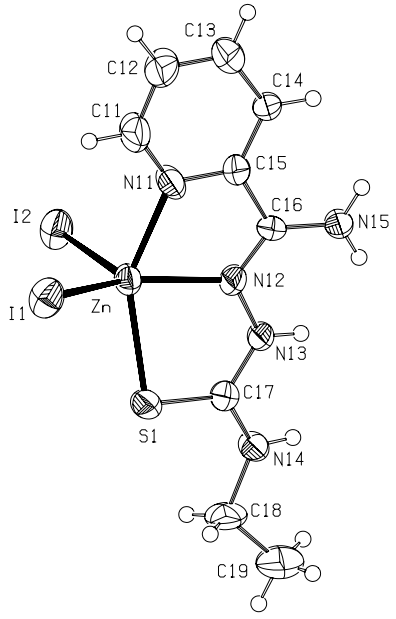

Fig. 3. Molecular structure of $[Zn(HAm4E)I_2]$ (**4a**).

and the neutral ligand in $[Zn(HAm4E)I_2]$, there are difference in the bond distances of the thiosemicarbazone moiety in the two complexes; the biggest difference in S1–C17, which has considerably more double bond character in $[Zn(HAm4E)I_2]$ and essentially the same as the average distance in HAm4E [27]. The bond distances throughout the thiosemicarbazone moiety in $[Zn(HAm4E)I_2]$ are comparable to those of $[Zn(HAm4DH)I_2]$ [14]. The bond angles involving the Zn center, as well as the thiosemicarbazone moiety, of the two complexes are also essentially the same. The parameter $\tau = 0.10$ for $[Zn(HAm4E)I_2]$ and indicates that it is closer to square planar than $[Zn(HAm4DH)I_2]$ ($\tau = 0.23$) [14]. The basal plane could involve either I1 or I2 with the thiosemicarbazone moiety, but because Zn–I1 is marginally shorter it can be designated as the apical donor.

There are a number of weak intermolecular interactions involving all of the hydrogens attached nitrogens in $[Zn(HAm4E)I_2]$, the distances and angles of these interactions are similar to those of $[Zn(HAm4DH)I_2]$ [14]. The angle between the best planes of the pyridine ring and the thiosemicarbazone moiety is smaller than 11.4(6)° found for $[Zn(HAm4DH)I_2]$; Zn is 0.489(8) Å from the mean plane of the thiosemicarbazone moiety.

3.3. Structural properties of $[Cd(Am4E)_2]$ (*5a*)

Fig. 4 shows the molecular structure of the compound along with the atom numbering scheme. $[Cd(Am4E)_2]$, like $[Cd(Ampip)_2]$ and $[Cd(Amhexim)_2]$, is 6-coordinate environment in which both ligands are coordinated in their deprotonated thiolate forms via the pyridine nitrogen, azomethine nitrogen and thiolate sulphur atoms. The two HAm4E are in a meridional position due to the planarity imposed by the conjugated system causing a distortion from octahedral symmetry due to the restricted bite angles for their chelation. One of the ligands HAm4E (S1) is disorder, so that we will consider only the ligand without disorder (S2).

The distances to the cadmium atom differ slightly from that found in $[Cd(HAm4E)Br_2] \cdot DMSO$ and $[Cd(HAm4E)I_2] \cdot DMSO$ and there are significant modifications in bond distances in the thiocarbamide group, C-S is longer than in the free ligand suggesting a degree

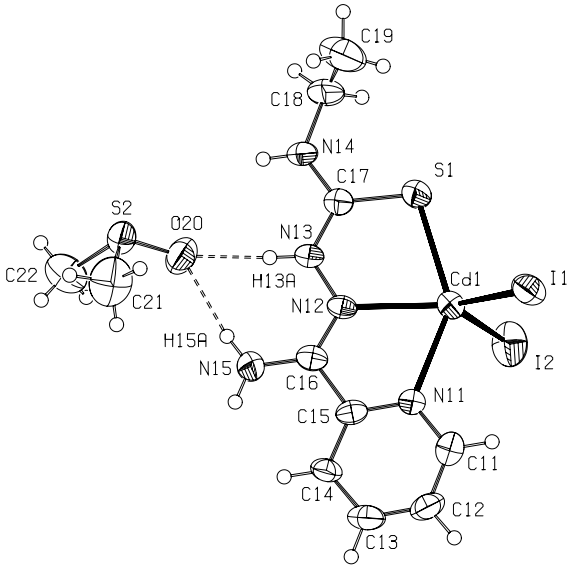

Fig. 4. Atomic displacement plot (50% probability level) of the molecular structure of $[Cd(Am4E)_2]$ (**5a**).

of thione to thiol change which also increase to bond order and shortens the bond length of C7–N3. The C6–N4 distance is longer in $[Cd(Am4E)_2]$ than in HAm4E probably because deprotonation of N(3) reduce the resonance contribution of the thiosemicarbazone chain. These changes in bond distances also differentiate from $[Cd(HAm4E)Br_2]\cdot\cdot$DMSO and $[Cd(HAm4E)I_2]\cdot$DMSO keeping with seems to be a general difference between complexes with neutral and deprotonated ligand.

The mean planes of the thiosemicarbazone moieties are at an angle of 85.3(2)°, similar to 86.5(2)° for $[Cd(Amhexim)_2]$ and 87.2(1)° for $[Cd(Ampip)_2]$, consistent with a nearly 90° octahedral angle.

3.4. Structural properties of $[Cd(HAm4E)Br_2]\cdot DMSO$ (*7a*)

$[Cd(HAm4E)Br_2]\cdot$DMSO (Fig. 5) is (configurationally) isotypic with $[Cd(HAm4E)I_2]\cdot$DMSO, both crystallizing as monoclinic in the space group *Cc* which allows a meaningful comparison of the differences caused by a change in the electronic and steric factor. Beside the difference in the Cd–X bond distances, the Cd–N11 bond is much shorter in $[Cd(HAm4E)Br_2]$ and also significantly shorter than the Cd–N12 bond, which is unusual for thiosemicarbazone complexes. However, a shorter Cd–N11 than Cd–N12 bond distance has also been found for $[Cd(HAc4M)Br_2]\cdot 2$DMSO [37], the only other example to our knowledge. There are no significant differences in the bond distances and angles of the thiosemicarbazone moieties of $[Cd(HAm4E)Br_2]$ and $[Cd(HAm4E)I_2]$. The bond angles involving Cd are also essentially the same for the two complexes and the value of τ, 0.25, for $[Cd(HAm4E)Br_2]$ is similar to the value for $[Cd(HAm4E)I_2]$.

The hydrogen bonding interactions with the oxygen of DMSO are essentially the same as for $[Cd(HAm4E)I_2]$, but the smaller and more electronegative Br allows for another weak interaction with a bromo ligand of a neighboring molecule, N15H15B...Br2. The planarity of the HAm4E ligand in the two cadmium complexes is essentially the same.

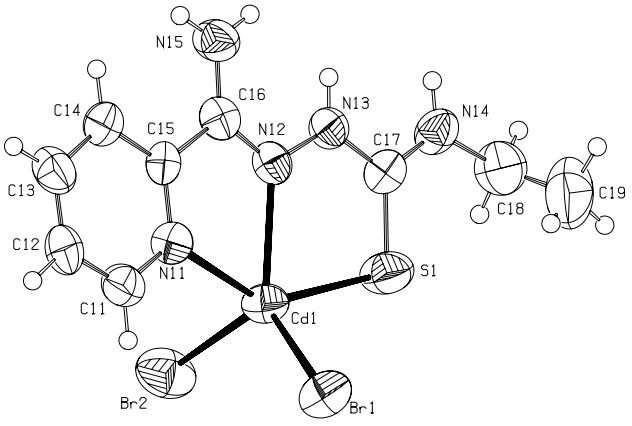

Fig. 5. Molecular structure of $[Cd(HAm4E)Br_2]\cdot$DMSO (**7a**). Solvent DMSO molecule is omitted for clarity.

3.5. Structural properties of $[Cd(HAm4E)I_2]\cdot DMSO$ (*8a*)

The structure of (**8a**) is shown in Fig. 6. The crystal structures of $[Cd(HAc4E)I_2]\cdot 2$DMSO (i.e, HAc4E represents 2-acetylpyridine N(4)-ethylthiosemicarbazone) [37], $[Cd(HAm4DH)I_2]$ [15], $[Cd(HAm4DM)I_2]$ (i.e., HAm4DM represents 2-pyridineformamide N(4)-dimethylthiosemicarbazone) [21], $[Cd(HAmpip)I_2]\cdot$DMSO (i.e., HAmpip represents 2-pyridineformamide 3-piperidylthiosemicarbazone) [23] and $[Cd(HAmhexim)I_2]\cdot$EtOH (i.e., HAmhexim represents 2-pyridineformamide 3-hexamethyleneiminyl thiosemicarbazone) [25] have been reported recently. This allows comparison of identical thiosemicarbazones of 2-acetylpyridine and 2-pyridineformamide, the electronic and steric effects of the N(4)-substituent of the thiosemicarbazone moiety, and the previously discussed $[Zn(HAm4E)I_2]$. As expected all bonds to Cd in $[Cd(HAm4E)I_2]$ are longer than in $Zn(HAm4E)I_2]$, but there are not significant differences between the bond distances of thiosemicarbazone moieties (Table 2). Similarly, there are not significant differences in the bond distances to cadmium in any of the complexes involving 2-pyridineformamide thiosemicarbazones except that in the previously reported structures

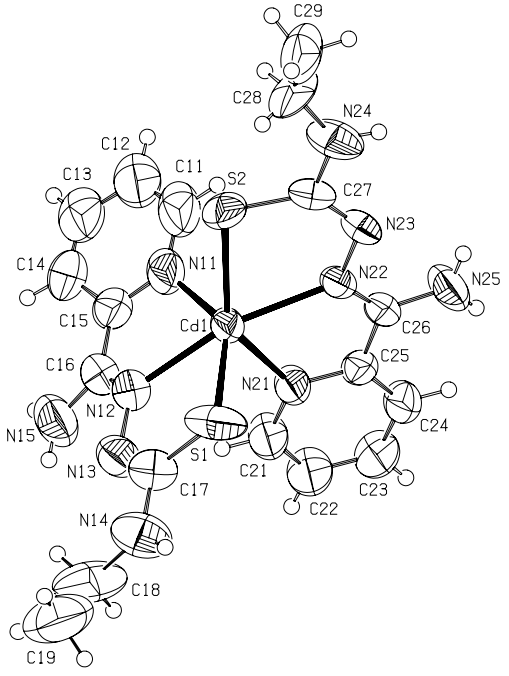

Fig. 6. Perspective view of the structure of $[Cd(HAm4E)I_2]\cdot$DMSO (**8a**). Hydrogen bonding interactions involving the solvent DMSO are also shown.

the Cd–N11 distance is longer than the Cd–N12 distance [15,19,23,25]. In contrast, in [Cd(HAc4E)I_2] the Cd–N12 is marginally longer, 2.398(9) Å compared to 2.362(10) Å, demonstrating the weaker inductive effect of a CH_3 group compared to NH_2 group and Cd–N12 is significantly longer than Cd–N11 in [Cd(HAc4E)I_2] [36], whereas they are the same in [Cd(HAm4E)I_2].

One measure of a steric effect among these complexes prepared with CdI_2 appears to be the τ parameter [35] which has a value of 0.23 for [Cd(HAm4E)I_2]. Other values of τ for related iodo complexes with tridentate neutral thiosemicarbazone ligands are [Cd(HAm4DH)I_2], 0.14 [15]; [Cd(HAm4DM)I_2], 0.21 [21]; [Cd(HAmpip)I_2], 0.10 [27]; [Cd(HAmhexim)I_2], 0.04 [25]; [Cd(HAc4M)I_2], 0.08 [38], [Cd(HAc4E)I_2], 0.05 [37] and [Cd(HAc4DM)I_2], 0.23 [39]. It appears that there is a steric effect which reaches a maximum with the N(4)-ethylthiosemicarbazone of the 2-pyridineformamide series; structures have not been solved for complexes with larger alkyl substituents in the 2-acetylpyridine series. Thus, more members of each series (i.e., Ac, Am), as well as more series (i.e., 2-formyl-, 2-benzoylpyridine etc.), are needed to establish where the actual maximum occurs. It should be noted that the N11–Cd–S1 angle ranges from 131.6(2)° for [Cd(HAm4DM)I_2] [19] to 142.3(3)° for [Cd(HAm4E)I_2], the two complexes with the largest values of τ and greatest distortion toward a trigonal bipyramid structure; the N12–Cd–X1 angle is larger than N11–Cd–S1 in [Cd(HAm4DM)I_2], which shows that these two complexes have very different structural details, despite similar values of τ. [Zn(HAm4E)I_2], $\tau = 0.10$, is closer to square planar than [Cd(HAm4E)I_2], as is [Cd(Ac4E)I_2] [37].

Stronger hydrogen bonding interactions occur for [Cd(HAm4E)I_2] · DMSO than for [Zn(HAm4E)I_2] due to interactions with the DMSO oxygen, Table 4. However, only one of the amide hydrogens, N15H15A, has a intermolecular interaction in contrast to [Zn(HAm4E)I_2] and [Cd(HAm4E)Br_2] · DMSO (vide infra). The larger cadmium atom in [Cd(HAm4E)I_2] places less of a demand on the ligand resulting in an angle between the best planes of the pyridine ring and thiosemicarbazone moiety of 3.9(6)°, substantially less than 8.9(4)° for [Zn(HAm4E)I_2].

3.6. Spectral and physical properties of [Zn(Am4E)(OAc)]$_2$, [Zn(HAm4E)Cl_2], [Zn(HAm4E)Br_2] and [Zn(HAm4E)$_2I_2$]

These zinc complexes have varying shades of yellow due to a $S \rightarrow Zn$ charge transfer band. Although [Zn(HAm4E)$_2I_2$] was isolated, crystals of [Zn(HAm4E)I_2] were obtained from solution. The mass spectra of these zinc complexes show an ion fragment centered at $m/z = 289$ assignable to {Zn(Am4E)$^+$} and the spectrum of [Zn(HAm4E)$_2I_2$] has an ion fragment at $m/z = 509$ which is likely {Zn(HAm4E)(Am4E)$^+$}. Compared to the IR spectrum of HAm4E, the spectra of [Zn(Am4E)(OAc)]$_2$, [Zn(HAm4E)Cl_2] and [Zn(HAm4E)Br_2] show a decrease in the energy of ν(CN), increase in ν(NN) and decrease in ν(CS) (i.e., the thioamide IV band which contains a significant contribution from ν(CS)), which along with bands assignable to ν(ZnN) and ν(ZnS), indicate coordination of the imine nitrogen and thione/thiolato sulfur. The ratio of ν_a(ZnBr)/ν_a(ZnCl) = 0.77 is consistent with [Zn(HAm4E)Cl_2] and [Zn(HAm4E)Br_2] having the same structure. Coordination of the anionic ligand in [Zn(Am4E)(OAc)]$_2$ causes a much larger decrease in the energy of the ν(CS) and bands at 1589 and 1406 cm^{-1} assignable to $\nu_a(CO_2)$ and $\nu_s(CO_2)$, respectively, are consistent with bridging acetate ligands in agreement with crystal structure. Based on IR, it appears that [Zn(HAm4E)$_2I_2$] is tetrahedral with coordination of the two iodo ligands and two thione sulfur atoms. The ^{1}H NMR spectra of these zinc complexes are not significantly different from spectrum of HAm4E except in the spectrum of [Zn(Am4E)(OAc)]$_2$ where the anionic ligand and coordination of the thiolato sulfur causes an upfield shift of N14H. This upfield was observed in [Zn(HAm4E)$_2I_2$] indicating the different structure of this complex respecting to the other halo zinc complexes. The CH_3 resonance of the bridging acetate ligands is at 1.76 ppm. In the ^{13}C spectra in the zinc halo complexes the C7 is the signal more deshield except in the [Zn(Am4E)(OAc)]$_2$ where the C(OAc) appears at 173.40 and the Me(OAc) appears at 23.02 ppm.

3.7. Spectral and physical properties of [Cd(Am4E)(OAc)]$_2$, [Cd(HAm4E)Cl_2], [Cd(HAm4E)Br_2] and [Cd(HAm4E)I_2]

The mass spectra of the cadmium complexes is less regular than the zinc complexes with only [Cd(Am4E)(OAc)]$_2$ and [Cd(HAm4E)I_2] having the ion fragment at $m/z = 336$ assignable to {Cd(HAm4E)$^+$}. Like the zinc complexes, however, the spectrum of [Cd(Am4E)(OAc)]$_2$ has a ion fragment at $m/z = 558$ consistent with {Cd(HAm4E)(Am4E)$^+$} and the spectrum of [Cd(HAm4E)I_2] and [Cd(HAm4E)Cl_2] at $m/z = 464$ and 371 consistent with {Cd(HAm4E)I$^+$} and {Cd(HAm4E)Cl$^+$}, respectively. In contrast to the zinc complexes ν(CS) in the cadmium complexes with neutral HAm4E is not shifted to lower energy due to back donation of electron density from the cadmium centers, which is consistetnt with ν(CdS) and ν(ZnS) being essentially the same. The ratios of ν_a(CdBr)/ν_a(CdCl) = 0.70 and ν_a(CdI)/ν_a(CdBr) = 0.89 are consistent with [Cd(HAm4E)Cl_2], [Cd(HAm4E)Br_2] and [Cd(HAm4E)I_2] being isostructural. Like [Zn(Am4E)(OAc)]$_2$ only the upfield shift of N14H in the spectrum of [Cd(A-

m4E)(OAc)]$_2$ compared to HAm4E is a significant difference on coordination and besides the disappearance of the proton N3 indicatives the deprotonation of the ligand. The ^{13}C NMR resonance assigned to the thione/thiolato carbon, C17, does shift upfield more for the cadmium complexes than the zinc complexes again indicating greater back donation of electron density from he cadmium centers. The resonances in ^{113}Cd NMR spectra for [Cd(Am4E)(OAc)]$_2$ are 254.8 and 415.1 ppm, which is compatible with a dinuclear complex and for [Cd(HAm4E)Cl$_2$], [Cd(HAm4E)Br$_2$] and [Cd(HAm4E)I$_2$] are 388.9, 294.6 and 366.6 ppm, respectively, where the progressive increase in shielding upon replacement of Cl by Br and Br by I is consistent with the decreasing electronegativity of the halide. The observed chemical shifts are in the range expected for 5-coordinate cadmium(II) complexes.

4. Supplementary data

Crystallographic data for the structures have been deposited with the Cambridge Crystallographic Data Centre, CCDC Nos. 236646–236650 for [Zn(Am4E)(OAc)]$_2$, [Zn(HAm4E)I$_2$], [Cd(Am4E)$_2$], [Cd(HAm4E)Br$_2$] · DMSO and [Cd(HAm4E)I$_2$] · DMSO, respectively. Copies of this information may be obtained free of charge from The Director, CCDC, 12 Union Road, Cambridge, CB2 1EZ, UK (Fax: +44 1223/336 033; e-mail for inquiry: fileserv@ccdc.cam.uk; e-mail for deposition: deposit@ccdc.cam.ac.uk

References

[1] D.X. West, S.B. Padye, P.B. Sonawane, Struct. Bonding 76 (1991) 1.
[2] S. Padye, G.B. Kauffmann, Coord. Chem. Rev. 63 (1985) 127.
[3] M.J.M. Campbell, Coord. Chem. Rev. 15 (1975) 279.
[4] A. Mohsen, M.E. Omar, I.M. Labouta, M.G. Kasem, J. Boudais, J. Pharm. Sci. 72 (1983) 1226.
[5] D.L. Klayman, J.F. Bartosecich, T.S. Griffin, C.J. Mason, J.P. Scoveill, J. Med. Chem. 22 (1979) 885.
[6] E.J. Blanz, F.A. French, Cancer Res. 28 (1968) 2419.
[7] M.C. Miller, C.N. Stineman, J.R. Vance, D.X. West, I.M. Hall, Anticancer Res. 18 (1998) 4131.
[8] M.C. Miller, C.N. Stineman, J.R. Vance, D.X. West, I.M. Hall, Appl. Organomet. Chem. 13 (1999) 9.
[9] J.P. Scovill, D.L. Klayman, C. Lambros, G.E. Childs, W. Antholing, D.H. Petering, J. Chem. Med. 27 (1984) 87.
[10] L. Bresolin, R.A. Burrow, M. Hörner, E. Bermejo, A. Castiñeiras, Polyhedron 16 (1997) 3947.
[11] E. Bermejo, R. Carballo, A. Castiñeiras, R. Domínguez, A.E. Liberta, C. Maichle-Mössmer, M.M. Salberg, D.X. West, Eur. J. Inorg. Chem. (1999) 965.
[12] E. Bermejo, A. Castiñeiras, R. Domínguez, R. Carballo, C. Maichle-Mössmer, D.X. West, Z. Anorg. Allg. Chem. 625 (1999) 961.
[13] E. Bermejo, R. Carballo, A. Castiñeiras, R. Domínguez, C. Maichle-Mössmer, A.E. Liberta, D.X. West, Z. Naturforsch. B 54 (1999) 777.
[14] A. Castiñeiras, I. García, E. Bermejo, D.X. West, Z. Naturforsch. 55 (2000) 511.
[15] A. Castiñeiras, I. García, E. Bermejo, D.X. West, Polyhedron 19 (2000) 1873.
[16] D.X. West, J.K. Swearingen, J. Valdés-Martínez, S. Hernández-Ortega, A.K. El-Sawaf, F. van Meurs, A. Castiñeiras, I. García, E. Bermejo, Polyhedron 18 (1999) 2919.
[17] D.X. West, J.K. Swearingen, A.K. El-Sawaf, Transition Met. Chem. 25 (2000) 80.
[18] I. García, E. Bermejo, A.K. El-Sawaf, A. Castiñeiras, D.X. West, Polyhedron 21 (2002) 729.
[19] L.M. Fostiak, I. García, J.K. Swearingen, E. Bermejo, A. Castiñeiras, D.X. West, Polyhedron 22 (2003) 83.
[20] E. Bermejo, A. Castiñeiras, I. García, D.X. West, Polyhedron 22 (2003) 1147.
[21] E. Bermejo, A. Castiñeiras, L.M. Fostiak, Isabel García, A.L. Llamas-Saiz, J.K. Swearingen, D.X. West, Z. Naturforsch. 56b (2001) 1297.
[22] K.A. Ketcham, J.K. Swearingen, A. Castiñeiras, I. García, E. Bermejo, D.X. West, Polyhedron 20 (2001) 3265.
[23] A. Castiñeiras, I. García, E. Bermejo, K.A. Ketcham, D.X. West, A.K. El-Sawaf, Z. Anorg. Allg. Chem. 628 (2002) 492.
[24] K.A. Ketcham, I. García, J.K. Swearingen, E. Bermejo, A.K. El-Sawaf, A. Castiñeiras, D.X. West, Polyhedron 21 (2002) 859.
[25] I. García Santos, E. Bermejo, A. Castiñeiras, D.X. West, Z. Anorg. Allg. Chem. 630 (2004) 1086.
[26] J. van Koningsbruggen, J.G. Haasnoot, R.A.G. De Graaff, J. Reedijk, Inorg. Chim. Acta 234 (1995) 87.
[27] I. García, L M. Fostiak, E. Bermejo, A. Castiñeiras, J.K. Swearingen, D.X. West, Anorg. Allg. Chem., submitted for publication.
[28] G.M. Sheldrick, Acta Crystallogr. A 46 (1990) 467.
[29] G.M. Sheldrick, SHELXL97. Progam for the Refinement of Crystal Structures, University of Göttingen, Germany, 1997.
[30] H.D. Flack, Acta Crystallogr. A 39 (1983) 876.
[31] International Tables for Crystallography (1995), vol. C, Kluwer Academic Publishers, Dordrecht, The Netherlands.
[32] A.L. Spek, PLATON. A Multipurpose Crystallographic Tool (1999) Utrecht University, Utrecht, The Netherlands.
[33] I. García, E. Bermejo, A. Castiñeiras, D.X. West, Z. Naturforsch., submitted for publication.
[34] L. Bresolin, R.A. Burrow, M. Hörner, E. Bermejo, A. Castiñeiras, Polyhedron 16 (1997) 3947.
[35] A.W. Addison, T.N. Rao, J. Reedijk, J. van Rijn, G.C. Verschoor, J. Chem. Soc. Dalton Trans. (1984) 1349.
[36] D.X. West, J.K. Swearingen, A.K. Hermetet, L.J. Ackerman, C. Presto, J. Mol. Struct. 522 (2000) 27.
[37] E. Bermejo, R. Carballo, A. Castiñeiras, R. Domínguez, C. Maichle-Mössmer, J. Strähle, D.X. West, Polyhedron 18 (1999) 3695.
[38] E. Bermejo, R. Carballo, A. Castiñeiras, R. Domínguez, C. Maichle-Mössmer, A.E. Liberta, D.X. West, Z. Naturforsch. 54 (1999) 777.
[39] E. Bermejo, R. Carballo, A. Castiñeiras, R. Domínguez, A.E. Liberta, C. Maichle-Mössmer, M.M. Salberg, D.X. West, Eur. J. Inorg. Chem. (1999) 965.

Available online at www.sciencedirect.com
SCIENCE DIRECT®
Polyhedron 23 (2004) 2315–2321
POLYHEDRON
www.elsevier.com/locate/poly

Syntheses and spectroscopy of diamine complexes of Zn(II) and Cd(II) ethylxanthates and the molecular structures of $[M(S_2COEt)_2TMEDA]$: formation of CdS nanoparticles from $[Cd(S_2COEt)_2]$ and $[Cd(S_2COEt)_2TMEDA]$

Jacqui Cusack [a,*], Michael G.B. Drew [b], Trevor R. Spalding [a]

[a] *Department of Chemistry, University College Cork, College Road, Cork, Ireland*
[b] *School of Chemistry, University of Reading, Reading RG6 6AD, UK*

Received 27 May 2004; accepted 26 July 2004
Available online 28 August 2004

Abstract

The zinc and cadmium ethylxanthate complexes of *N*,*N*,*N*′,*N*′-tetramethylethylenediamine (TMEDA), $[M(S_2COEt)_2TMEDA]$, were synthesized and characterized with infrared, ^1H and ^{13}C NMR spectroscopy, mass spectrometry and X-ray crystallography. Whereas the cadmium complex has a six-coordinate $\{CdS_4N_2\}$ centre with bidentate xanthate ligands, the zinc complex contains four coordinate $\{ZnS_2N_2\}$ zinc with two monodentate xanthate groups. The cadmium species $[Cd(S_2COEt)_2(diamine)]$ (where diamine = *N*,*N*-dimethylethylenediamine or *N*,*N*′-diisopropylethylenediamine) were also synthesized. The surfactant-assisted formation of nanoparticles from $[Cd(S_2COEt)_2]$ and $[Cd(S_2COEt)_2TMEDA]$ was studied with TEM, XRD and XRF techniques. From $[Cd(S_2COEt)_2]$, spherical nanoparticle aggregates 140–200 nm in diameter were obtained but from $[Cd(S_2COEt)_2TMEDA]$, single nanoparticles were produced with estimated diameters in the range of 4–7 nm and almost no aggregation.
© 2004 Elsevier Ltd. All rights reserved.

Keywords: Xanthate; Diamine; Zinc; Cadmium; CdS; Nanoparticles

1. Introduction

Much attention has been given recently to the relatively new field of "quantum dot" nanoparticles [1,2] and their applications as optoelectronic materials [1,3]. The burgeoning interest in nanoparticles in general is due to their unique chemical and electronic properties, which have potential applications in non-linear optics, luminescence, electronics, catalysis and solar energy conversion [4–10] as well as optoelectronics. In order to make functioning devices, it will be necessary to synthesize nanomaterials which will have uniform size and properties. A major interest at the moment is in the development of single-source precursors of metal chalcogenides [11–15]. In the case of MX (M = Zn, Cd; X = S, Se) particular attention has been paid to dithiocarbamates and diselenocarbamates [16–19].

Suitable single-source precursors for MS (M = Zn or Cd) would contain direct metal–sulfur bonds. We have already shown the suitability of $[Zn(S_2COEt)_2]$ for the production of thin films of zinc sulphide [20]. However, relatively little use has been made of xanthates in the formation of nanoparticles [21]. We decided to investigate the synthesis of novel molecular precursors based on xanthates and to study their potential for the production of CdS nanoparticles.

* Corresponding author. Tel.: +353 21 4902911; fax: +353 21 4274097.
E-mail address: jacqui_cusack@hotmail.com (J. Cusack).

0277-5387/$ - see front matter © 2004 Elsevier Ltd. All rights reserved.
doi:10.1016/j.poly.2004.07.014

Many methods have been devised for the preparation of nanoparticles and nanowires of metal sulphides. The most common methods for the synthesis of nanoparticles and nanowires involve reverse micelles [22,23], organic templates [24], inorganic templates, including mesoporous silica [25,26] and the thermal decomposition of precursors in the presence of capping ligands [27–29]. This last method has been especially successful with tri-*n*-octylphosphine oxide (TOPO) as the capping ligand [12–14,16]. With the exception of the thermal decomposition "TOPO method", only a small number of methods have employed single-source precursors. With this in mind it was decided to investigate the possibility of using a surfactant to enable the production of CdS nanoparticles from $[Cd(S_2COEt)_2]$ and $[Cd(S_2COEt)_2TMEDA]$ precursors. The method used was broadly based on that reported by Zhao et al. [30].

2. Experimental

All chemicals $[ZnCl_2 \cdot 4H_2O]$, $[CdCl_2 \cdot 2\frac{1}{2}H_2O]$, [K($S_2$COEt)], *N*,*N*,*N*′,*N*′-tetramethylethylenediamine (TMEDA), *N*,*N*-dimethylethylenediamine (DMEDA), *N*,*N*′-diisopropylethylenediamine (DiPEDA), Brij 52 and solvents were supplied by Aldrich Chemical Co. and used as received. Microanalyses were recorded on an Exeter Analytical Inc. CE 444 CHN elemental analyzer at UCC. FT-IR spectra were recorded on a Perkin–Elmer Paragon 1000 spectrometer as KBr discs. NMR spectra (^{1}H and ^{13}C) were obtained in $CDCl_3$ solution at ambient temperature using a Bruker-Avance 300 spectrometer with TMS as an internal standard. Mass spectra were obtained on a KRATOS HV5 profile machine. XRD data was collected on a Philips PW3710 X'Pert diffractometer, equipped with a Cu Kα radiation source and accelerator detector at 40 kV/40 mA. X-ray fluorescence data were recorded on a Phillips Minipal PW4025, at 30 kV, 50 μA using an Al filter and a Kapton ray source. TEM was carried out on a JEOL 2000 microscope operating at 200 kV.

2.1. Synthesis and characterization of $[M(S_2COEt)_2]$ where M = Zn and Cd

2.1.1. General procedure

All reactions and workup procedures were carried out in air. The compounds $[Zn(S_2COEt)_2]$ [31] and $[Cd(S_2COEt)_2]$ [32] are well known and were prepared by methods based on the literature reports. Typically, an aqueous solution of K[S_2COEt] (13 mmol in 10 ml water) was added drop-wise to an aqueous solution of the metal chloride (6.5 mmol in 20 ml water) with continuous stirring. There was immediate formation of a cream coloured precipitate of $[M(S_2COEt)_2]$. The mixture was stirred for 20 min, the solid product filtered, washed with water and dried for 16 h at 60 °C.

2.1.1.1. $Cd(S_2COEt)_2$.

Elemental *Anal.* Calc. for $Cd(S_2COEt)_2$: C, 20.3; H, 2.8. Found: C, 20.3; H, 2.7%. IR (KBr): ν_{max} (cm^{-1}); 1198, 1122, 1031. ^{1}H NMR (300 MHz, $CDCl_3$, 298 K) ordered as δ (ppm), multiplicity, relative ratio, assignment: 4.53 (q, 2H, $S_2COCH_2CH_3$), 1.48 (t, 3H, $S_2COCH_2CH_3$). ^{13}C NMR (300 MHz, $CDCl_3$, 298 K) ordered as δ (ppm), assignment: 231.64 ($S_2COCH_2CH_3$), 72.07 ($S_2COCH_2CH_3$), 14.12 ($S_2COCH_2CH_3$). Yield: 94.5%. M.p. (°C): 158–159 (dec.).

2.1.1.2. $Zn(S_2COEt)_2$.

Elemental *Anal.* Calc. for $Zn(S_2COEt)_2$: C, 23.4; H, 3.3. Found: C, 23.2; H, 3.2%. IR (KBr): ν_{max} (cm^{-1}); 1210, 1125, 1047, 1028. ^{1}H NMR (300 MHz, $CDCl_3$, 298 K) ordered as δ (ppm), multiplicity, relative ratio, assignment: 4.58 (q, 2H, $S_2COCH_2CH_3$), 1.49 (t, 3H, $S_2COCH_2CH_3$). ^{13}C NMR (300 MHz, $CDCl_3$, 298 K) ordered as δ (ppm), assignment: 226.64 ($S_2COCH_2CH_3$), 70.70 ($S_2COCH_2CH_3$), 14.08 ($S_2COCH_2CH_3$). Yield: 85.5%. M.p. (°C): 139–140 (dec.).

2.2. Synthesis and characterization of $[M(S_2COEt)_2TMEDA]$ where M = Zn and Cd

TMEDA, equimolar to the $[M(S_2COEt)_2]$ used, was added drop-wise with stirring to a solution of $[M(S_2COEt)_2]$ in a minimum amount of methanol. The reaction mixture was stirred for 20 min, solid product filtered, washed with water and dried for 16 h at 60 °C.

2.2.1. $[Cd(S_2COEt)_2TMEDA]$

Elemental *Anal.* Calc. for $[Cd(S_2COEt)_2TMEDA]$: C, 30.6; H, 5.6; N, 5.95. Found: C, 30.4; H, 5.5; N, 5.6%. IR (KBr): ν_{max} (cm^{-1}); 1292, 1185, 1116, 1035, 1028. ^{1}H NMR (300 MHz, $CDCl_3$, 298 K) ordered as δ (ppm), multiplicity, relative ratio, assignment: 4.45 (q, 2H, $S_2COCH_2CH_3$), 2.64 (s, 2H, $(CH_3)_2N(CH_2)_2N(CH_3)_2$), 2.55 (s, 6H, $(CH_3)_2N(CH_2)_2N(CH_3)_2$) 1.42 (t, 3H, $S_2COCH_2CH_3$). ^{13}C NMR (300 MHz, $CDCl_3$, 298 K) ordered as δ (ppm), assignment: 231.55 ($S_2COCH_2CH_3$), 73.46 ($S_2COCH_2CH_3$), 56.54 ($(CH_3)_2N(CH_2)_2N(CH_3)_2$), 46.00 ($(CH_3)_2N(CH_2)_2N(CH_3)_2$), 14.24 ($S_2COCH_2CH_3$). EI-MS: *m*/*z* 474 pmi ($[Cd(S_2COEt)_2TMEDA]$), 473 $[pmi - 1]^+$ ($[Cd(S_2COEt)_2TMEDA–H]^+$) for ^{116}Cd. Yield: 83.5%. M.p. (°C): 169 (dec.).

2.2.2. $[Zn(S_2COEt)_2TMEDA]$

Elemental *Anal.* Calc. for $[Zn(S_2COEt)_2TMEDA]$: C, 34.0; H, 6.2; N, 6.6. Found: C, 33.8; H, 6.2; N, 6.45%. IR (KBr): ν_{max} (cm^{-1}); 1290, 1176, 1122, 1047, 1026. ^{1}H NMR (300 MHz, $CDCl_3$, 298 K) ordered as δ (ppm), multiplicity, relative ratio, assignment: 4.47 (q, 2H, $S_2COCH_2CH_3$), 2.61 (s, 2H, $(CH_3)_2N(CH_2)_2N(CH_3)_2$),

2.53 (s, 6H, $(CH_3)_2N$–$(CH_2)_2N(CH_3)_2$) 1.40 (t, 3H, $S_2COCH_2CH_3$). ^{13}C NMR (300 MHz, $CDCl_3$, 298 K) ordered as δ (ppm), assignment: 225.64 ($S_2COCH_2CH_3$), 71.00 ($S_2COCH_2CH_3$), 56.98 ($(CH_3)_2N(CH_2)_2N(CH_3)_2$), 46.85 ($(CH_3)_2N(CH_2)_2N(CH_3)_2$), 14.17 ($S_2COCH_2CH_3$). EI-MS: *m/z* 305 $[Zn(S_2COEt)_2–H]^+$. Yield: 85.5%. M.p. (°C): 129–130 (dec.).

2.3. Synthesis and characterization of $[Cd(S_2COEt)_2$ (diamine)] where diamine = N,N-dimethylethylenediamine (DMEDA) and N,N′-diisopropylethylenediamine (DiPEDA) in a 'one-pot' reaction

To an aqueous solution of $[CdCl_2 \cdot 2\frac{1}{2}H_2O]$ (4.5 mmol in 20 ml water) the diamine ligand was added drop-wise, with stirring. After 5 min, an aqueous solution of $K[S_2COEt]$ (9 mmol in 10 ml water) was added. The reaction mixture was stirred for 20 min, solid product filtered, washed with water and dried for 16 h at 40 °C.

2.3.1. $[Cd(S_2COEt)_2DMEDA]$

Elemental *Anal.* Calc. for $[Cd(S_2COEt)_2DMEDA]$: C, 27.1; H, 5.0; N, 6.1. Found: C, 27.15; H, 5.0; N, 6.1%. IR (KBr): ν_{max} (cm^{-1}); 1188, 1114, 1036, 1003. ^1H NMR (300 MHz, $CDCl_3$, 298 K) ordered as δ (ppm), multiplicity, relative ratio, assignment: 4.47 (q, 2H, $S_2COCH_2CH_3$), 3.06 (broad singlet, H, $(CH_3)_2NCH_2CH_2NH_2$), 2.64 (t, H, $(CH_3)_2NCH_2CH_2NH_2$), 2.54 (s, 3H $(CH_3)_2NCH_2CH_2NH_2$), 1.42 (t, 3H, $S_2COCH_2CH_3$). ^{13}C NMR (300 MHz, $CDCl_3$, 298 K) ordered as δ (ppm), assignment: 231.24 ($S_2COCH_2CH_3$), 73.38 ($S_2COCH_2CH_3$), 59.65 ($(CH_3)_2NCH_2CH_2NH_2$), 45.85 ($(CH_3)_2NCH_2CH_2NH_2$), 37.34 ($(CH_3)_2NCH_2CH_2NH_2$), 14.24 ($S_2COCH_2CH_3$). Yield: 90%. M.p. (°C): 96–97.

2.3.2. $[Cd(S_2COEt)_2DiPEDA]$

Elemental *Anal.* Calc. for $[Cd(S_2COEt)_2DiPEDA]$: C, 33.7; H, 6.1; N, 5.6. Found: C, 33.5; H, 6.0; N, 5.5%. IR (KBr): ν_{max} (cm^{-1}); 1178, 1110, 1042. ^1H NMR (300 MHz, $CDCl_3$, 298 K) ordered as δ (ppm), multiplicity, relative ratio of H atoms, assignment: 4.46 (q, 2H, $S_2COCH_2CH_3$), 3.17 (septet, H, $(CH_3)_2CHN(CH_2)_2NCH(CH_3)_2$), 3.00 (s, 2H, $(CH_3)_2CHN(CH_2)_2NCH(CH_3)_2$), 1.42 (t, 3H, $S_2COCH_2CH_3$) 1.29 (d, 6H $(CH_3)_2CHN(CH_2)_2$ $NCH(CH_3)_2$). ^{13}C NMR (300 MHz, $CDCl_3$, 298 K) ordered as δ (ppm), assignment: 229.65 ($S_2COCH_2CH_3$), 72.84 ($S_2COCH_2CH_3$), 50.02 ($(CH_3)_2CHN(CH_2)_2NCH(CH_3)_2$), 45.29 ($(CH_3)_2CHN(CH_2)_2NCH(CH_3)_2$), 22.44 ($(CH_3)_2CHN(CH_2)_2N$–$CH(CH_3)_2$), 14.21 ($S_2COCH_2CH_3$). Yield: 89%. M.p. (°C): 128.9–129.1 (dec.).

2.4. Preparation of CdS nanoparticles by a surfactant-assisted method using a single-source precursor

Brij 52 (5 g) in 10 ml water was stirred at 40 °C for 15 min. Five mmol of the precursor (0.18 g $[Cd(S_2COEt)_2]$, or 0.24 g of $[Cd(S_2COEt)_2TMEDA]$) was added. The mixture was heated at the reflux temperature for 8 h. The yellow precipitate was separated from the mixture by means of centrifugation. The precipitate was repeatedly washed with ethanol and ultrasonically dispersed in ethanol. A drop of the mixture was deposited on a copper grid and dried in air overnight for TEM analysis. The precipitate was also characterized by XRF and XRD.

2.5. X-ray crystallographic analyses of $[M(S_2COEt)_2TMEDA]$ where M = Zn (**1**) and Cd (**2**)

Crystals of crystallographic quality were obtained when $[Zn(S_2COEt)_2TMEDA]$ (**1**) and $[Cd(S_2COEt)_2$-TMEDA] (**2**) were synthesized in THF. Details of the crystals of complexes **1** and **2** are shown in Table 1. Data for **1** and **2** were measured with Mo Kα radiation using the MAR research Image Plate System. The crystals were positioned at 70 mm from the Image Plate. 100 frames were measured at 2° intervals with a counting time of 2 min. Data analysis was carried out with the XDS program [33]. The structure was solved using direct methods with the SHELX-86 program [34]. Non-hydrogen atoms were refined with anisotropic thermal parameters. The hydrogen atoms bonded to carbon were included in geometric positions and given thermal parameters equivalent to 1.2 times those of the atom to which they were attached. Empirical absorption corrections were applied using the DIFABS program [35]. The structures were refined on F^2 using the SHELXL program [36].

Table 1
Comparison of structure characteristics of complexes $[M(S_2COEt)_2$-TMEDA]

M	**1** · Zn	**2** · Cd
Empirical formula	$C_{12}H_{26}ZnN_2O_2S_4$	$C_{12}H_{26}CdN_2O_2S_4$
Formula weight	423.96	470.99
Colour, habit	colourless	yellow
Crystal size (mm)	$0.25 \times 0.25 \times 0.20$	$0.20 \times 0.15 \times 0.10$
Crystal system	orthorhombic	monoclinic
Space group	*Pnca* (No. 60)	$P2_1/c$
Z	4	
Unit cell dimensions		
a (Å)	20.41(2)	11.780(14)
b (Å)	12.260(15)	12.090(14)
c (Å)	8.043(11)	15.293(16)
β (°)	(90)	109.90(1)
V (Å^3)	2013(4)	2048(4)
D_{calc} (g cm^{-3})	1.386	1.515
μ (mm^{-1})	1.634	1.473
R_1, wR_2 [$I > 2\sigma(I)$]	0.078, 0.184	0.077, 0.196
R_1, wR_2 (all data)	0.095, 0.193	0.092, 0.207
Maximum, minimum residual density (e Å^{-3})	1.005, −1.110	1.609, −1.677

3. Results and discussion

3.1. Syntheses

The success of the synthetic procedure was dependent on the choice of solvent and reagents. Thus, although a 'two-pot' method could be used with either methanol or THF as solvent to prepare the $[M(S_2COEt)_2TMEDA]$ complexes where M = Zn and Cd, it was not possible to obtain analytically pure samples of $[Cd(S_2COEt)_2$-(diamine)] with diamine = DMEDA or DiPEDA in these solvents. With water as solvent in a 'one-pot' reaction it was possible to obtain all three $[Cd(S_2COEt)_2$-(diamine)] complexes.

3.2. X-ray structural studies of $[M(S_2COEt)_2TMEDA]$ where M = Zn (1) and Cd (2)

The molecular structure of **1** which has a crystallographic twofold axis is shown in Fig. 1. The zinc atom is four-co-ordinate being bonded to two nitrogen atoms of the TMEDA ligand and to two xanthate ligands each via a single sulfur atom. The geometry of the coordination sphere is distorted tetrahedral. The chelating TMEDA ligand subtends an angle of 85.5(4)° at the metal while the S–Zn–S angle is 130.8(2)°, the remaining angles ranging from 105.9(2)° to 109.8(2)°. The Zn–N and Zn–S(2) bond lengths at 2.147(7) and 2.304(3) Å, respectively, are within the expected range of values for such bonds. The non-bonded sulfur atom, S(3), is 3.33 Å from the zinc atom and hence the molecules of **1** are essentially monomeric. In the $\{S_2C\}$ section of the xanthate ligands, the carbon to sulfur, S(2), distance is 1.729(9) Å which is typical of a single bond whereas the carbon to sulfur S(3) distance of 1.646(9) Å is typical of a carbon to sulfur double bond [37]. Indeed, the carbon to sulfur S(3) distance is shorter than the reported mean of C=S distances in $(X)_2$–C=S compounds (X = C, N, O or S) 1.671 Å and thioureas, 1.681 Å. The monomeric nature of **1** is in contrast to $[Zn(S_2COEt)_2]$ which has polymeric structure of xanthate-bridged zinc atoms [31].

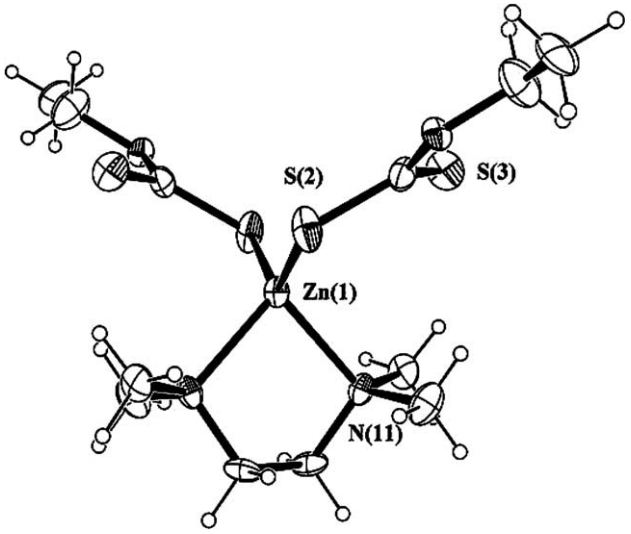

Fig. 1. The structure of $[Zn(Xan)_2TMEDA]$ which contains a crystallographic twofold axis, with ellipsoids at 30% probability. Unique bond lengths in the coordination sphere are Zn(1)–S(2) 2.304(3), Zn(1)–N(11) 2.147(6) Å. The Zn(1)–S(3) distance is 3.33 Å. The S–Zn–S angle is 130.8(2)°, N–Zn–N angle is 85.5(4)° and the remaining S–Zn–N angles are 105.88(18)° and 109.76(18)°. The C(4)–S(2) distance is 1.729(9) Å and the C(4)–S(3) distance is 1.649(9) Å.

In **2** the metal atom is bonded to two nitrogen atoms at 2.421(8), 2.420(9) Å and four sulfur atoms at distances in the range 2.680(5)–2.706(3) Å, values that are usual for cadmium. The distortions from octahedral geometry are primarily caused by the small S···S bite in the xanthate ligand that gives rise to S–Cd–S angles of 66.9(2)° and 67.2(11)° in the two ligands (see Fig. 2).

3.3. Spectroscopy

The ^1H NMR spectra of the zinc and cadmium TMEDA complexes are almost indistinguishable. However, the ^{13}C spectra show a significant difference between the compounds in the S_2COEt carbon signal region. The chemical shift moves 5.9 ppm downfield in the zinc complex with respect to the cadmium compound. This may be related to the coordination of the xanthate ligands in the structures of **1** and **2**. In general, the xanthate ligand is either a bidentate ligand on a single metal, as in **2**, or it bridges two metals [38]. The zinc complex **1** in the solid state has one sulfur atom from each xanthate bonded to the zinc and the other participating in what is essentially a C=S bond. The cadmium structure **2** is six-coordinate with bidentate xanthate ligands and partial C to S double bond character in both carbon–sulfur bonds. The difference is reflected in the downfield shift of the S_2COEt signal in the NMR spectra of complex **1** compared to **2** and also slightly affects the methylene carbon in the xanthate ligand.

The FT-IR spectra of all the complexes show three very strong bands in the region 1190–1035 cm^{-1} which are characteristic of xanthate compounds [39].

3.4. Preparation of CdS nanoparticles by the surfactant-assisted method using a single-source precursor

Both precursors, $[Cd(S_2COEt)_2]$ and $[Cd(S_2COEt)_2TMEDA]$ produced orange-yellow powders, after their ethanol solutions were allowed to evaporate in air. Initial characterization was by XRD and XRF analysis. The XRD analysis showed four major peaks at $2\theta = 26.5°$, 44, 52°, and 64°, corresponding to the (111), (220), (311) and (400) planes of cubic CdS (JCPRD card 10-0454), respectively. The XRD peaks are quite broad, for example, the peak corresponding

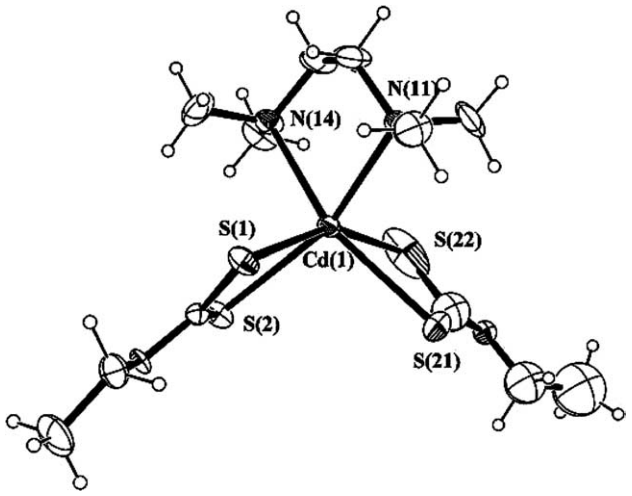

Fig. 2. The structure of $[Cd(Xan)_2TMEDA]$ with ellipsoids at 30% probability. Bond lengths (Å) in the metal coordination sphere are Cd(1)–S(1) 2.706(3), Cd(1)–S(2) 2.697(3), Cd(1)–S(21) 2.680(5), Cd(1)–S(22) 2.700(4), Cd(1)–N(11) 2.421(8), Cd(1)–N(14) 2.420(9). Bond angles (°) of note are: S(1)–Cd(1)–S(2) 67.2(1), S(1)–Cd(1)–S(21) 157.71(1), S(1)–Cd(1)–S(22) 97.83(16), S(2)–Cd(1)–S(21) 98.53(2), S(2)–Cd(1)–S(22) 100.38(13), S(22)–Cd(1)–S(21) 66.9(3), N(11)–Cd(1)–N(14) 76.0(3), N(11)–Cd(1)–S(1) 97.4(2), N(11)–Cd(1)–S(2) 159.4(2), N(11)–Cd(1)–S(22) 95.0(2), N(11)–Cd(1)–S(21) 100.0(3), N(14)–Cd(1)–S(1) 101.9(3), N(14)–Cd(1)–S(2) 93.4(2), N(14)–Cd(1)–S(22) 159.1(3), N(14)–Cd(1)–S(21) 95.7(3).

to the (3 1 1) reflection at 44° had a FWHM of 0.23. The XRF spectrum shows strong peaks for cadmium and sulfur.

Further characterization was by TEM. Fig. 3, shows pseudo-spherical nanoparticle aggregates produced from $[Cd(S_2COEt)_2]$. These aggregates are 140–200 nm in diameter. A small number of nanorods about 1.5 μm long and 100 nm wide in size was also observed. Heating the nanoparticle reaction mixture for 24 h instead of 8 h did not increase the relative number of nanorods or the size of either the nanoparticle aggregates or the nanorods.

In the work of Zhao et al. [30], who used Brij 58 surfactant and a mixture of $[Cd(NO_3)_2]$, thiourea and excess ethylenediamine, 8–15 nm nanorods of hexagonal CdS were reported and there was no mention of aggregated nanoparticles like those shown in Fig. 3. Spherical nanoparticles with a mean diameter of 4.2 ± 0.4 nm of hexagonal CdS were produced by Nair et al. [40] who used $[Cd(S_2COEt)_2]$ in the TOPO capping method. Although TEM analysis showed the particles grouping together in the work by Nair et al., there were no clearly defined aggregates. The difference between the nanoparticles produced by Nair et al. and the aggregates obtained in the present work is due presumably to the presence of the TOPO capping ligand which prevents aggregation of the CdS/TOPO nanoparticles.

It is noteworthy that, if the reaction leading to the nanoparticle aggregates was stopped after 6 h rather than 8 h, the aggregated nanoparticles had not fully formed, as can be seen in Fig. 4. Instead, a mixture of nanoparticles with an estimated diameter of between 4 and 7 nm and aggregates with diameters of ~20 nm were present.

Nanoparticle formation using the Brij surfactant and $[Cd(S_2COEt)_2TMEDA]$ as a single CdS source produced, after 8 h, nanoparticles with estimated diameters in the range of 4–7 nm. There was almost no aggregation. Clearly, the diamine in the cadmium reactant affects the final size of the CdS particles most probably by acting as an effective capping ligand.

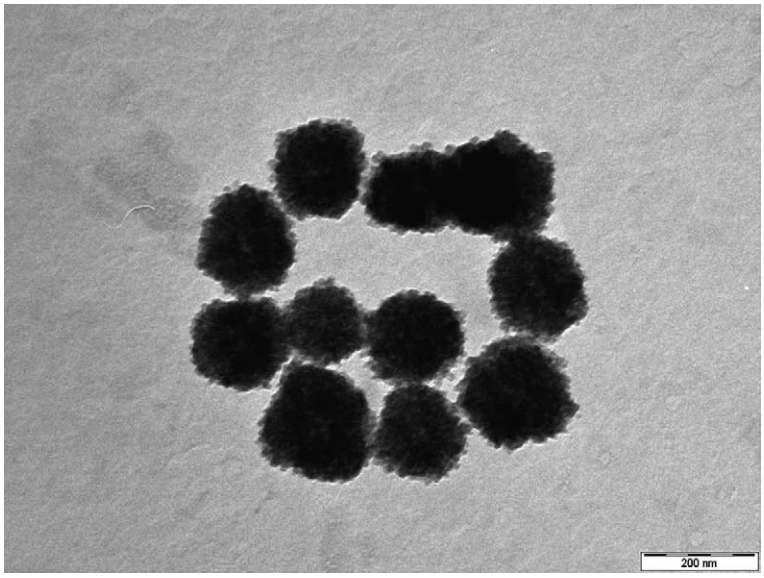

Fig. 3. CdS pseudo-spherical nanoparticle aggregates of 140–200 nm in diameter produced from $[Cd(S_2COEt)_2]$ single-source precursor via the Brij method after refluxing for 8 h.

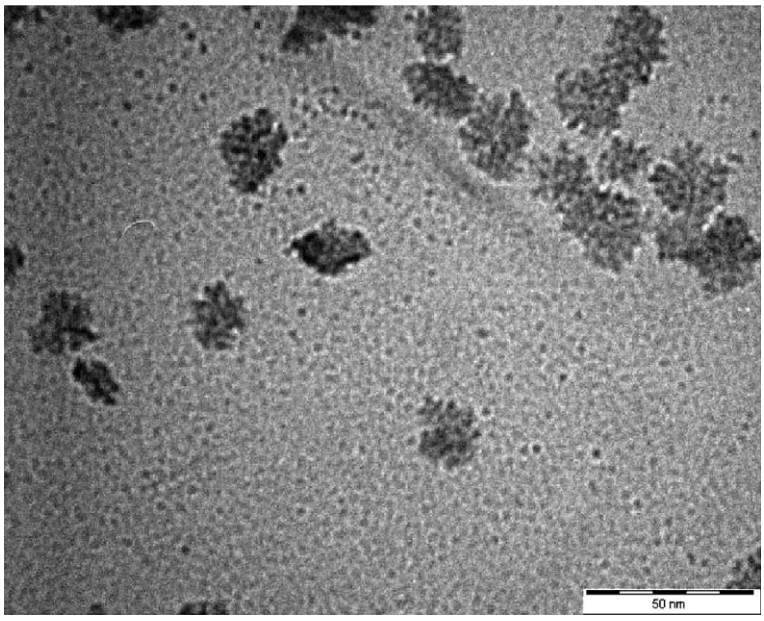

Fig. 4. TEM of nanoparticles produced via the Brij method from $[Cd(S_2COEt)_2]$ after refluxing for 6 h.

4. Supplementary material

Details in the CIF format of the two structures, $[Zn(S_2COEt)_2TMEDA]$ **1** and $[Cd(S_2COEt)_2TMEDA]$ **2**, have been deposited at the Cambridge Crystallographic Data Centre, 12 Union Road, Cambridge CB2 1EZ, UK; fax: (+44) 1223-336-033; or e-mail: deposit@ccdc.cam.ac.uk (Reference Nos. 239456 and 239457, respectively).

Acknowledgements

We thank the EPSRC and the University of Reading for funding of the image-plate system, Higher Education Authority (Ireland) PRTLI – III grant to J.C. and colleagues K.B., J.L., F.D., A.O'D. M.C. and E.B. for discussions.

References

[1] T. Trindade, P. O'Brien, N.L. Pickett, Chem. Mater. 13 (2001) 3843.
[2] M. Green, P. O'Brien, Chem. Commun. (1999) 2235.
[3] N.P. Gaponik, D.V. Talapin, A.L. Rogach, A. Eychmuller, J. Mater. Chem. 10 (2000) 2163.
[4] L. Francois, M. Mostafavi, J. Belloni, J.A. Delaire, Phys. Chem. Chem. Phys. 3 (2001) 4965.
[5] M. Nirmal, B.O. Dabbousi, M.G. Bawendi, J.J. Macklin, J.K. Trautman, T.D. Harris, L.E. Brus, Nature 383 (1996) 802.
[6] Y.-C. Zhu, Y. Bo, Chem. Phys. Lett. 377 (2003) 367.
[7] S. Wageh, L. Shu-Man, F.T. You, X. Xu-Rong, J. Lumin. 102–103 (2003) 768.
[8] V.I. Roldughin, Russ. Chem. Rev. 69 (2000) 821.
[9] L. Guo, Q. Huang, X.-Y. Li, S. Yang, Phys. Chem. Chem. Phys. 3 (2001) 1661.
[10] Z.-H. Yuan, L.-D. Zhang, J. Mater. Chem. 11 (2001) 1265.
[11] Y.-W. Jun, C.-S. Choi, J. Cheon, Chem. Commun. (2001) 101.
[12] M.A. Malik, P. O'Brien, N. Revaprasadu, J. Mater. Chem. 12 (2002) 92.
[13] T. Trindade, P. O'Brien, X.-M. Zhang, M. Motevalli, J. Mater. Chem. 7 (1997) 1011.
[14] P.S. Nair, T. Radhakrishnan, N. Revaprasadu, G.A. Kolawole, P. O'Brien, Polyhedron 22 (2003) 3129.
[15] S.L. Cumberland, K.M. Hanif, A. Javier, G.A. Khitrov, G.F. Strouse, S.M. Woessner, C.S. Yun, Chem. Mater. 14 (2002) 1576.
[16] N. Revaprasadu, M.A. Malik, P. O'Brien, G. Wakefield, J. Mater. Res. 14 (1999) 3237.
[17] C.J. Barrelet, Y. Wu, D.C. Bell, C.M. Lieber, J. Am. Chem. Soc. 125 (2003) 11498.
[18] B. Ludolph, M.A. Malik, P. O'Brien, N. Revaprasadu, Chem. Commun. (1998) 1849.
[19] M. Lazell, S.J. Nøranger, P. O'Brien, N. Revaprasadu, Mater. Sci. Eng. C 16 (2001) 129.
[20] D. Barreca, E. Tondello, D. Lydon, T.R. Spalding, M. Fabrizo, Chem. Vapor Depos. 9 (2003) 93.
[21] J. Cheon, H.-K. Kang, J.I. Zink, Coord. Chem. Rev. 200–202 (2000) 1009.
[22] J. Zhang, B. Han, J. Liu, X. Zhang, Z. Liu, J. He, Chem. Commun. (2001) 2724.
[23] J. Xu, Y. Li, J. Colloid Interface Sci. 259 (2002) 275.
[24] Z.-L. Zhang, Q.-S. Wu, Y.-P. Ding, Inorg. Chem. Commun. 6 (2003) 1393.
[25] W.-H. Zhang, J.-l. Shi, H.-R. Shen, Z.-L. Hua, D.-S. Yan, Chem. Mater. 13 (2000) 648.
[26] F.J. Brieler, M. Fröba, L. Chen, P.J. Klar, W. Heimbrodt, H.-A.K.V. Nidda, Chem. Eur. J. 8 (2002) 187.
[27] Y. Zhang, M. Ma, X. Wang, D. Fu, H. Zhang, N. Gu, J. Liu, Z. Lu, L. Xu, K. Chen, J. Phys. Chem. Solids 64 (2003) 927.
[28] J.-X. Yao, G.-L. Zhao, G.-R. Han, Microelectron. Eng. 66 (2003) 115.
[29] S.K. Kulkarni, U. Winkler, N. Deshmukh, P.H. Borse, R. Fink, E. Umbach, Appl. Surf. Sci. 169–170 (1999) 438.

[30] Q. Zhao, L. Hou, R. Huang, S. Li, Inorg. Chem. Commun. 6 (2003) 1459.
[31] T. Ikeda, H. Hagihara, Acta Crystallogr. 21 (1966) 919.
[32] Y. Iimura, T. Ito, H. Hitoshi, Acta Crystallogr., Sect. B 28 (1972) 2271.
[33] W. Kabsch, J. Appl. Crystallogr. 21 (1988) 916.
[34] G.M. Sheldrick, SHELX-86, Acta Crystallogr., Sect. A 46 (1990) 4670.
[35] N. Walker, D. Stuart, DIFABS program, Acta Crystallogr., Sect. A 39 (1983) 158.
[36] G.M. Sheldrick, SHELXL: Program for Crystal Refinement, University of Göttingen, Göttingen, Germany, 1993.
[37] F.H. Allen, O. Kennard, D.G. Watson, L. Brammer, A.G. Orpen, R. Taylor, J. Chem. Soc., Perkin Trans. II (1987) S1.
[38] S.S. Garje, V.K. Jain, Coord. Chem. Rev. 236 (2003) 35.
[39] K. Nakamoto, Infrared Raman Spectroscopy of Inorganic Coordination Compounds, Wiley–Interscience, New York, 1997.
[40] P.S. Nair, T. Radhakirshnan, N. Revaprasadu, G. Kolawole, P. O'Brien, J. Chem. Soc., Mater. Chem. 12 (2002) 2722.

Available online at www.sciencedirect.com
SCIENCE DIRECT®
Polyhedron 23 (2004) 2323–2329
POLYHEDRON
www.elsevier.com/locate/poly

Synthesis, X-ray crystal structures and multinuclear NMR characterization of Hg(II) complexes of 2-[(*E*)-2-(aryl)-1-diazenyl]pyridine

Tushar S. Basu Baul [a,*], Antonin Lycka [b], Ray Butcher [c], Frank E. Smith [d,**]

[a] *Department of Chemistry, North-Eastern Hill University, NEHU Permanent Campus, Umshing, Shillong 793 022, India*
[b] *Research Institute for Organic Syntheses, CZ-532 18 Pardubice-Rybitvi, Czech Republic*
[c] *Department of Chemistry, Howard University, Washington, DC 20059, USA*
[d] *Weill Cornell Medical College in Qatar, P.O. Box 24144, Doha, Qatar*

Received 2 April 2004; accepted 2 August 2004
Available online 28 August 2004

Abstract

Syntheses and structural studies for the two complexes dichloro-{2-[(*E*)-2-(4-methylphenyl)-1-diazenyl]pyridine}Hg(II) (**1**) and dichloro-{2-[(*E*)-2-(3-methylphenyl)-1-diazenyl]pyridine}Hg(II) (**2**) are reported. The solid-state structures of the complexes were determined by X-ray diffraction methods and in addition, the complexes were characterized in solution using ^{1}H, ^{13}C and ^{199}Hg NMR spectroscopy. The X-ray structures reveal that the complexes adopt surprisingly different structures. Complex **2** has an extended polymeric structure with 2-[(*E*)-2-(3-methylphenyl)-1-diazenyl]pyridine behaving as a monodentate ligand via the pyridyl nitrogen, and all the chlorine atoms serving to bridge mercury atoms, whereas complex **1** has a dimeric structure with 2-[(*E*)-2-(4-methylphenyl)-1-diazenyl]pyridine behaving as a bidentate ligand via the pyridyl nitrogen and one of the azo nitrogens, with a terminal chlorine on each Hg and a μ,μ′-dichloro bridge between the mercury atoms. But the coordination geometry around the mercury atom is similar in both complexes, each showing a distorted trigonal bipyramidal arrangement of the donor atoms. These complexes were characterized in solution by ^{1}H, ^{13}C, ^{199}Hg NMR spectroscopy.
© 2004 Elsevier Ltd. All rights reserved.

Keywords: 2-[(*E*)-2-(aryl)-1-diazenyl]pyridine; Hg(II) complexes; NMR; Crystal structures

1. Introduction

The metal complexes of heterocyclic α-diimine ligands such as 2,2′-bipyridine and 1,10-phenanthroline have proven to be useful for studying such phenomena as luminescence and photo reduction/oxidation. It is for this reason that extensive studies with the 2-(arylazo)pyridine (hereafter named as 2-[(*E*)-2-(aryl)-1-diazenyl]pyridine, Fig. 1) system have been undertaken and a number of studies of metal complexes containing this type of ligand have been reported. These include investigations of complexes of Fe(II) [1,2], Ni(II) [2], Hg(II) [3,4], Os(II) [5,6], Ru(II) [7–19], Cr(0), Mo(0), W(0) [20,21], Cr(II) [22], Cu(I) [23], Rh(III) [24,25], Rh(I) [26], Ag(I) [27], Re(III) [28], Co(II) [29], Mo(IV) [15], Ru(III) [30], Sn(IV) [31] and organometallic complexes of Re(I) [32] and Sn(IV) [33–37]. In spite of such a wide-ranging series of studies on a variety of metal complexes involving these ligands, the structures of the mer-

* Corresponding authors. Tel.: +91 364 2722627; fax: +91 364 2721000.
** Tel.: 974 492 8206.
E-mail addresses: basubaul@nehu.ac.in (T.S. Basu Baul), frs2003@med.cornell.edu (F.E. Smith).

0277-5387/$ - see front matter © 2004 Elsevier Ltd. All rights reserved.
doi:10.1016/j.poly.2004.08.003

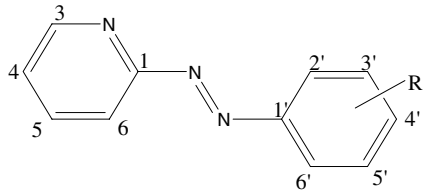

(L^1: R = 4-CH_3 and L^2: R = 3-CH_3)

Fig. 1. Generic structure of the ligand.

cury complexes have remained uncertain [3,4]. A mercuration reaction was attempted with 2-[(*E*)-2-(phenyl)-1-diazenyl]pyridine but gave no detectable mercuration products, instead an addition product was isolated [3]. The same product (which was characterized by m.p. and microanalytical data) was again prepared by reacting mercuric chloride and 2-[(*E*)-2-(phenyl)-1-diazenyl]pyridine. Structures for the Hg(II) complexes of analogous ligands have been proposed on the basis of electronic, infrared and ^{1}H NMR spectra. However these studies cannot provide definitive conclusions concerning the co-ordination geometry of the complexes [4]. In this paper, X-ray diffraction results are reported for two mercury complexes in combination with their detailed ^{1}H, ^{13}C, ^{199}Hg NMR spectroscopic data. Consequently, we are able to be quite confident of our descriptions of the structures of these complexes at least in the solid state.

2. Experimental

2.1. Materials

$HgCl_2$ (Merck) was used without further purification. All the solvents used in the reactions were of AR grade and dried using standard literature procedures. The ligands, viz., 2-[(*E*)-2-(4-methylphenyl)-1-diazenyl]pyridine and 2-[(*E*)-2-(3-methylphenyl)-1-diazenyl]pyridine (abbreviated as L^1 and L^2, respectively) were prepared according to the literature methods [38,39]. The complexes, dichloro-{2-[(*E*)-2-(4-methylphenyl)-1-diazenyl]pyridine}Hg(II); L^1HgCl_2 (**1**) and dichloro-{2-[(*E*)-2-(3-methylphenyl)-1-diazenyl]pyridine}Hg(II); L^2HgCl_2 (**2**) were prepared by a method similar to that reported earlier with slight modifications [4]. A typical procedure is described below (see Section 2.3).

2.2. Physical measurements

Carbon, hydrogen and nitrogen analyses were performed with a Perkin–Elmer 2400 series II instrument. IR spectra in the range 4000–400 cm^{-1} were obtained on a Perkin Elmer 983 spectrophotometer with samples as KBr discs. For the ^{1}H (500.13 MHz) and ^{13}C (125.76 MHz) NMR spectra and two-dimensional experiments, the instrument used was a Bruker Avance 500 NMR spectrometer equipped with a triple (^{1}H/^{13}C/broadband) 5 mm inverse probe. The ^{1}H and ^{13}C chemical shifts were referred to internal TMS ($\delta = 0.00$). Samples were dissolved either in acetone-d_6 or DMSO-d_6. Two-dimensional experiments (gradient-selected (gs)-COSY, gs-HSQC and gs-HMBC) were performed using the manufacturer's software (XWINNMR version 3.1). The ^{199}Hg (64.50 MHz) NMR spectra were recorded on a Bruker AMX 360 NMR spectrometer equipped with a 5 mm tunable broadband probe. The ^{199}Hg chemical shifts were referred to $Hg(CH_3)_2$ ($\delta = 0.0$) by a calculation procedure using $\Xi(^{199}\text{Hg}) = 17\,910\,841$ Hz and $\Xi(^1\text{H}) = 100\,000\,000$ Hz for proton resonance in tetramethylsilane [40]. Positive values of chemical shifts denote shifts to higher frequencies.

2.3. Preparation of dichloro-{2-[(E)-2-(4-methylphenyl)-1-diazenyl]pyridine}Hg(II) (1)

$HgCl_2$ (0.345 g, 1.27 mmol) in 25 ml of acetone was added drop-wise to a stirred acetone solution (15 ml) containing L^1 (0.25 g, 1.26 mmol). The reaction mixture was stirred for 6 h at ambient temperature, and the solvent was removed using a rotary evaporator. The resulting dry mass was washed thoroughly with petroleum ether to remove any unreacted ligand, extracted into acetone (20 ml) and filtered. The red solution was allowed to evaporate slowly at ambient temperature until crystallization occurred. This yielded red crystals of **1** in 90 % yield; m.p.: 192–194 °C (180–181 °C) [4]. *Anal.* Calc. for $C_{12}H_{11}N_3HgCl_2$: C, 30.73; H, 2.35; N, 8.96. Found: C, 30.71; H, 2.38; N, 8.92%. IR (cm^{-1}): $\nu(C{=}N)_{py}$: 1599 vs. ^{1}H NMR (acetone-d_6) δ: 8.83 (dd, 1H, 3-H), 8.20 (ddd, 1H, 5-H), 8.00 (a part of AA′MM′ system, 2H, 2′ and 6′-H), 7.96 (dd, 1H, 6-H), 7.70 (ddd, 1H, 4-H), 7.47 (a part of AA′MM′ system, 2H, 3′ and 5′-H), 2.47 (s, 3H, CH_3), ppm. (DMSO-d_6) δ: 8.80 (dd, 1H, 3-H), 7.96 (a part of AA′MM′ system, 2H, 2′ and 6′-H), 7.90 (dd, 1H, 6-H), 7.70 (ddd, 1H, 4-H), 7.49 (a part of AA′MM′ system, 2H, 3′ and 5′-H), 7.17 (ddd, 1H, 5-H), 2.46 (s, 3H, CH_3), ppm. ^{13}C NMR (acetone-d_6) δ: (C-1; not observed due to very low solubility), 151.09 (C-1′), 150.31 (C-3), 144.87 (C-4′), 140.69 (C-5), 131.12 (C-3′ and 5′), 127.24 (C-4), 124.56 (C-2′ and 6′), 117.85 (C-6), 21.34 (CH_3), ppm. (DMSO-d_6) δ: 161.40 (C-1), 149.93 (C-1′), 149.65 (C-3), 144.08 (C-4′), 140.37 (C-5), 130.58 (C-3′ and 5′), 126.73 (C-4), 123.68 (C-2′ and 6′), 116.11 (C-6), 21.51 (CH_3), ppm. ^{199}Hg NMR (DMSO-d_6) δ: = −1460.2 ppm.

2.4. Preparation of dichloro-{2-[(E)-2-(3-methylphenyl)-1-diazenyl]pyridine}Hg(II) (2)

An identical method to that used to prepare **1** was employed. This led to the formation of red crystals of

2 which were dried in vacuo. Yield, 82%; m.p.: 178–179 °C (158 °C) [4]. *Anal*. Calc. for $C_{12}H_{11}N_3HgCl_2$: C, 30.73; H, 2.35; N, 8.96. Found: C, 30.70; H, 2.36; N, 8.95%. IR (cm^{-1}): $\nu(C{=}N)_{py}$: 1593 vs. ^1H NMR (acetone-d_6) δ: 8.88 (dd,1H, 3-H), 8.26 (ddd, 1H, 5-H), 8.07 (dd, 1H, 6-H), 7.93 (m, 1H, 2′-H), 7.92 (m, 1H, 6′-H), 7.76 (ddd, 1H, 4-H), 7.55 (m, 1H, 5′-H), 7.50 (m, 1H, 4′-H), 2.48 (s, 3H, CH_3), ppm. (DMSO-d_6) δ: 8.83 (dd, 1H, 3-H), 8.22 (ddd, 1H, 5-H), 7.93 (dd, 1H, 6-H), 7.66 (m, 2H, 2′ and 6′-H), 7.74 (ddd, 1H, 4-H), 7.56 (m, 2H, 5′-H), 7.51 (m, 1H, 4′-H), 2.46 (s, 3H, CH_3), ppm. ^{13}C NMR (acetone-d_6) δ: 161.68 (C-1), 152.79 (C-1′), 150.33 (C-3), 141.35 (C-5), 140.66 (C-3′), 134.80 (C-4′), 130.41 (C-5′), 127.94 (C-4), 124.60 (C-2′), 122.38 (C-6′), 119.77 (C-6), 21.33 (CH_3), ppm. (DMSO-d_6) δ: 160.89 (C-1), 151.72 (C-1′), 149.61 (C-3), 140.56 (C-5), 139.57 (C-3′), 133.99 (C-4′), 129.76 (C-5′), 126.89 (C-4), 123.42 (C-2′), 121.34 (C-6′), 116.44 (C-6), 20.08 (CH_3) ppm. ^{199}Hg NMR (acetone-d_6) δ: = −1349.8 and (DMSO-d_6) δ: = −1433.2 ppm.

2.5. X-ray crystallography

The intensity data for dark red block-shaped crystals of complexes **1** and **2** were measured on a Bruker P4S using Cu Kα radiation (λ = 1.54178 Å) and on a Bruker SMART 1K using Mo Kα radiation (λ = 0.71073 Å), respectively. Empirical corrections were made from psi-scan curves [41]. The structures were solved by direct methods. All hydrogen atoms were given calculated positions. Neutral atom scattering factors were taken from the literature [42]. All computations were performed using the SHELXTL programmes [43]. All refinements were performed by full-matrix least-squares on F^2. The data were corrected for Lorentz and polarization effects.

3. Results and discussion

3.1. Syntheses

The complexes dichloro-{2-[(*E*)-2-(4-methylphenyl)-1-diazenyl]pyridine}Hg(II) (**1**) and dichloro-{2-[(*E*)-2-(3-methylphenyl)-1-diazenyl]pyridine}Hg(II) (**2**) were prepared in good yield by stirring stoichiometric amounts of $HgCl_2$ and L^1 or L^2 in acetone. The complexes are stable and can be stored in the solid state at room temperature for months. Selected characterization data for the complexes are presented in the experimental section. The microanalytical data are in agreement with the calculated values and thus confirm the composition. They are highly soluble in acetone and DMSO but poorly soluble in common organic solvents.

3.2. NMR data

The ^1H and ^{13}C NMR spectra of the complexes display distinct signals for the ligand skeletons. The numbering scheme employed for the assignments of individual ^1H and ^{13}C signals are shown in Fig. 1. The efforts to use the NMR data in the elucidation of the coordination mode of the ligand and the geometries of the complexes were not successful since the solvents used for the spectra (DMSO-d_6 and acetone-d_6) could influence the nature of the coordination sphere.

3.3. X-ray diffraction analysis for complexes *1* and *2*

Pertinent crystallographic parameters are summarised in Table 1. The atomic numbering scheme and the coordination around the mercury atom for the complexes **1** and **2** are illustrated in Figs. 2 and 3, respectively. Selected bond lengths and bond angles are listed in Table 2 (for **1**) and 3 (for **2**). Considering the similarity of the ligands, the two complexes adopt surprisingly different structures. Complex **2** has an extended polymeric structure with 2-[(*E*)-2-(3-methylphenyl)-1-diazenyl]pyridine behaving as a monodentate ligand via the pyridyl nitrogen, and all the chlorine atoms serving to bridge mercury atoms, whereas complex **1** has a dimeric structure with 2-[(*E*)-2-(4-methylphenyl)-1-diazenyl]pyridine behaving as a bidentate ligand via the pyridyl nitrogen and one of the azo nitrogens, with a terminal chlorine on each Hg and a μ,μ′-dichloro bridge between the mercury atoms. But the coordination geometry around the mercury atom is similar in both complexes, each showing a distorted trigonal bipyramidal arrangement of the donor atoms.

3.3.1. Dichloro-{2-[(E)-2-(4-methylphenyl)-1- diazenyl]pyridine}Hg(II) (1)

This complex occurs as centro-symmetric dimers in the solid state with the ligand 2-[(*E*)-2-(4-methylphenyl)-1-diazenyl]pyridine behaving as a bidentate via the pyridyl nitrogen and one of the azo nitrogens, with one bridging and one terminal chlorine atom. The geometry around each mercury atom is probably best described as being that of a distorted trigonal bipyramid, with the terminal chlorine, one bridging chlorine and the pyridyl nitrogen forming the trigonal plane and the other bridging chlorine and one of the azo-nitrogen atoms taking the axial positions. The structure is very similar in many regards to that recently reported for dichloro-mercury(II)-2-(phenylazo)-pyrimidine [44]. The bond angles making up the trigonal plane in **1** are N(1)–Hg–Cl(2), 105.3(2)°; Cl(1)–Hg–Cl(2), 137.5(9)° and N(1)–Hg–Cl(1), 117.0(2)°, giving a total of 359.8°. The corresponding bond angles found for dichloro-mercury(II)-2-(phenylazo)-pyrimidine are 105.3(2)°, 137.53(9)° and 117.0(2)°, giving a total of 359.8°. The

Table 1
Crystallographic data and structure refinement for L^1HgCl_2 (**1**) and L^2HgCl_2 (**2**)

Parameters	L^1HgCl_2 (**1**)	L^2HgCl_2 (**2**)
Empirical formula	$C_{24}H_{22}Cl_4Hg_2N_6$	$C_{24}H_{22}Cl_4Hg_2N_6$
Formula weight	937.46	937.46
Temperature (K)	293 (2)	103 (2)
Crystal size (mm)	$0.06 \times 0.25 \times 0.04$	$0.12 \times 0.40 \times 0.48$
Crystal system	triclinic	triclinic
Space group	$P\bar{1}$	$P\bar{1}$
Radiation (λ, Å)	Cu Kα (1.54178)	Mo Kα (0.71073)
a (Å)	7.4967 (13)	7.5149 (6)
b (Å)	9.416 (2)	9.2126 (6)
c (Å)	10.224 (3)	10.6784 (8)
α (°)	87.363 (16)	111.1840 (10)
β (°)	78.346 (15)	97.7140 (10)
γ (°)	80.456 (15)	91.3030 (10)
V (Å^3)	696.9 (3)	681.06 (9)
Z	1	1
D_{calc} (Mg/m^3)	2.234	2.286
μ (mm^{-1}), F (000)	23.211, 436	11.676, 436
θ Range (°)	4.42–68.05	2.38–28.28
Reflections collected	2657	5226
Independent reflections (R_{int})	2447 (0.0540)	3194 (0.0399)
Absorption correction	empirical	semi-empirical from equivalents
Maximum and minimum transmission	0.94 and 0.11	0.89 and 0.62
Refinement method	full-matrix least-squares on F^2	full-matrix least-squares on F^2
Data/restraints/parameters	2447/0/165	3194/0/165
Goodness-of-fit on F^2	1.040	1.080
Final R indices [$I > 2\sigma(I)$]	$R_1 = 0.0540$, $wR_2 = 0.1448$	$R_1 = 0.0433$, $wR_2 = 0.1177$
R indices (all data)	$R_1 = 0.0588$, $wR_2 = 0.1514$	$R_1 = 0.0433$, $wR_2 = 0.1186$
Extinction coefficient	0.0008 (3)	0.0018 (11)
Largest differential peak and hole (e/Å^3)	1.566 and −2.092	4.345 and −4.800

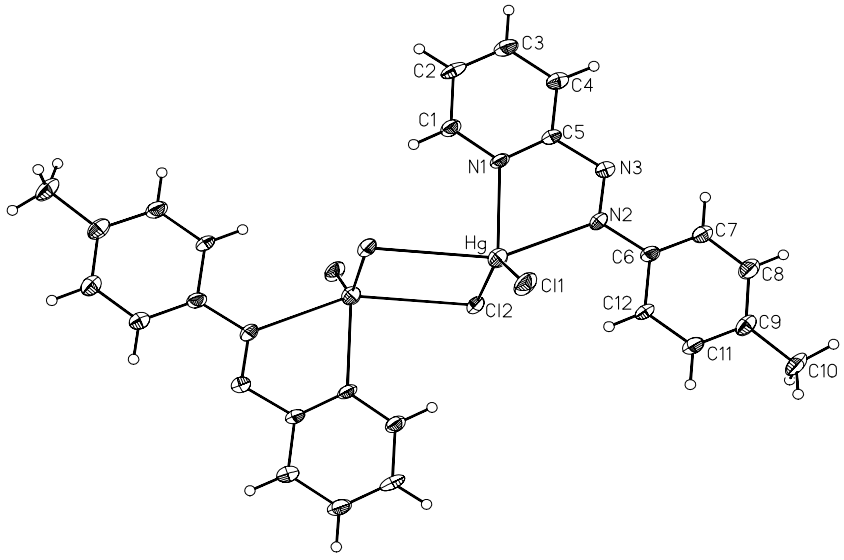

Fig. 2. Molecular structure and crystallographic numbering scheme for **1**.

angle between the two ''axial'' bonds in **1**, [N(2)–Hg–Cl(2)] is 153.5(2)° whereas the corresponding angle for dichloro-mercury(II)-2-(phenylazo)-pyrimidine is 161.3°, indicating considerable distortions from linearity in both complexes. Both of these complexes exhibit both bridging and terminal Hg–Cl bonds, with bridging Hg–Cl bond lengths of 2.428(2) and 2.909(2) Å for **1** compared to 2.42 and 2.92 Å, for dichloro-mercury(II)-2-(phenylazo)-pyrimidine. The equivalent terminal Hg–Cl distances are found to be 2.368(3) and 2.369(2) Å, respectively, in **1** and **2**, which is similar to terminal Hg–Cl distances reported elsewhere [45]. A fea-

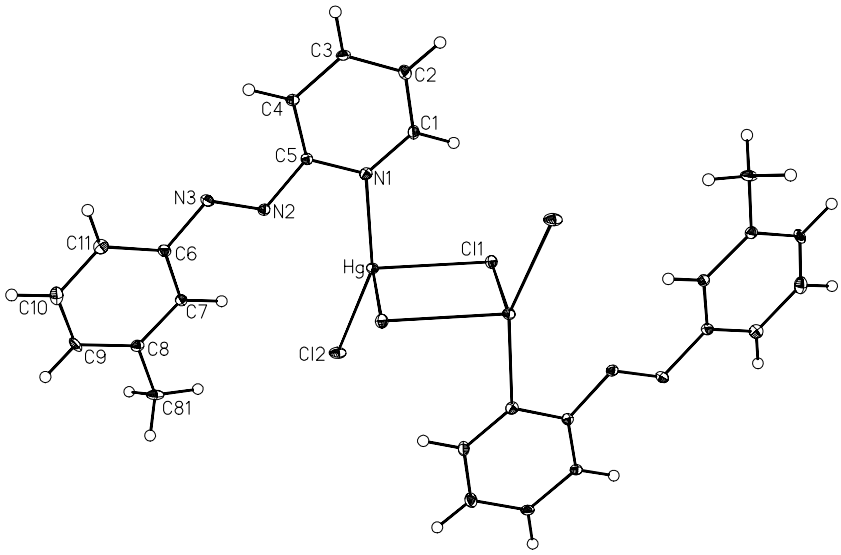

Fig. 3. Molecular structure and crystallographic numbering scheme for **2**.

Table 2
Selected bond lengths (Å) and angles (°) for L^1HgCl_2 (**1**)

Bond length		Bond angle	
Hg–N(1)	2.368 (7)	N(1)–Hg–Cl(2)	105.26 (19)
Hg–Cl(1)	2.368 (3)	N(1)–Hg–Cl(1)	117.03 (19)
Hg–Cl(2)	2.428 (2)	N(1)–Hg–N(2)	65.1 (3)
Hg–N(2)	2.541 (8)	Cl(1)–Hg–Cl(2)	137.53 (9)
Hg–Cl(2)#1	2.909 (2)	Cl(2)–Hg–N(2)	95.71 (17)
Cl(2)–Hg#1	2.909 (2)	Cl(1)–Hg–N(2)	98.38 (17)
N(2)–N(3)	1.265 (11)	Cl(1)–Hg–Cl(2)#1	96.67 (9)
N(2)–C(6)	1.413 (12)	N(1)–Hg–Cl(2)#1	88.6 (2)
N(3)–C(5)	1.444 (13)	N(2)–Hg–Cl(2)#1	153.47 (17)
		Cl(2)–Hg–Cl(2)#1	87.68 (8)
		C(1)–N(1)–Hg	123.1 (6)
		Hg–Cl(2)–Hg#1	92.32 (8)
		N(3)–N(2)–Hg	119.8 (6)
		C(5)–N(1)–Hg	119.2 (6)
		N(2)–N(3)–C(5)	113.5 (8)
		N(3)–N(2)–C(6)	114.4 (8)
		N(1)–C(5)–N(3)	121.6 (7)
		C(6)–N(2)–Hg	125.8 (5)
		C(12)–C(6)–N(2)	114.7 (8)
		C(4)–C(5)–N(3)	114.8 (9)
		C(7)–C(6)–N(2)	125.4 (8)

Symmetry transformations used to generate equivalent atoms: #1 $-x$, $-y+1$, $-z$.

Table 3
Selected bond lengths (Å) and angles (°) for L^2HgCl_2 (**2**)

Bond length		Bond angle	
Hg–N(1)	2.223 (6)	N(1)–Hg–Cl(1)	92.51 (16)
Hg–Cl(1)	2.6071(16)	N(1)–Hg–Cl(2)	156.27 (16)
Hg–Cl(2)	2.3691 (17)	N(1)–Hg–Cl(1)#1	88.08 (15)
Hg–Cl(1)#1	2.7857 (15)	Cl(2)–Hg–Cl(1)	109.49 (6)
Cl(1)–Hg#1	2.7857(15)	Cl(1)–Hg–Cl(1)#1	91.30 (4)
N(2)–N(3)	1.249 (8)	Cl(2)–Hg–Cl(1)#1	99.82 (5)
N(2)–C(5)	1.423 (9)	C(5)–N(1)–Hg	113.4 (4)
N(3)–C(6)	1.417 (9)	Hg–Cl(1)–Hg#1	88.70 (4)
		N(2)–N(3)–C(6)	114.4 (6)
		C(1)–N(1)–Hg	126.7 (5)
		N(3)–N(2)–C(5)	113.7 (6)
		C(11)–C(6)–N(3)	114.5 (6)

Symmetry transformations used to generate equivalent atoms: #1 $-x$, $-y+4$, $-z+1$.

ture of the structures of these two complexes is the occurrence of a dinuclear μ,μ-chloro bridged Hg_2Cl_2 fragment, of almost identical dimensions in both. The Hg–N distances in the two complexes are also comparable, being 2.541(8) Å (Hg–N(azo)) and 2.368(7) Å (Hg–N(pyridyl)) in **1** and 2.55 Å (Hg–N(azo)) and 2.41 Å (Hg–N(pyrimidyl)) in dichloro-mercury(II)-2-(phenylazo)-pyrimidine. The N–N distance for the azo groups of the respective coordinated ligand molecules are 1.26 Å in both instances. Despite the great difference in the overall structures of **1** and **2**, the two complexes still share several common structural features. The geometry around the Hg atoms in both is essentially that of a distorted trigonal bipyramid, but in **2**, the axial atoms are the pyridyl nitrogen and one of the bridging chlorines whilst the trigonal plane comprises the remaining three bridging chlorine atoms. Another similar compound, dichloro-mercury(II)-1-ethyl-2-(phenylazo)-imidazole [44] has the same dimeric structure reported here for **1** and dichloro-mercury(II)-2-(phenylazo)-pyrimidine. However, the presence of the five-membered imidazole ring in the ligand of this complex rather than the six-membered pyridine or pyrimidine rings in the other ligands results in some differences in individual bond distances. But the overall structural features are the same in all three complexes.

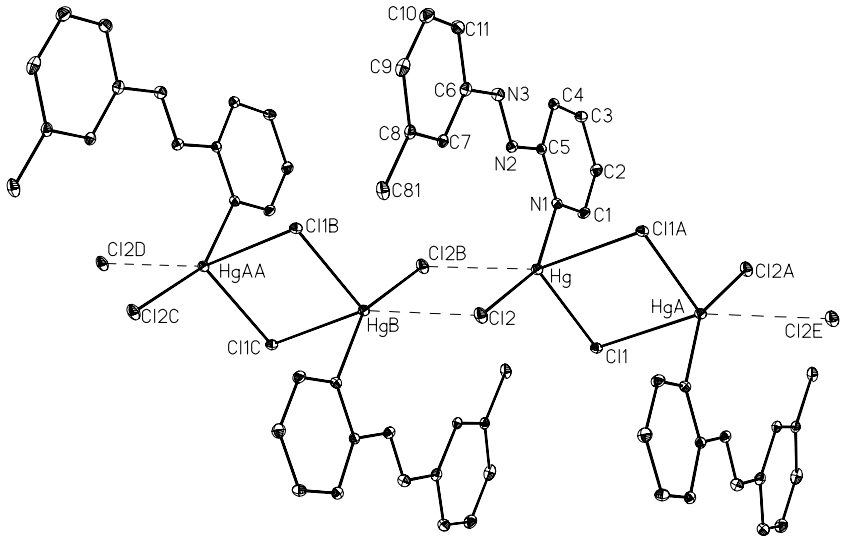

Fig. 4. Illustration of chlorine-bridging and polymeric structure of **2**.

*3.3.2. Dichloro-{2-[(E)-2-(3-methylphenyl)-1- diazenyl]pyridine}Hg(II) (**2**)*

Modifying the structure of the ligand by shifting the methyl group on the phenyl ring from the *para-* (in **1**) to the *meta-* (in **2**) position has a profound effect on the structure of the resulting complex. In contradistinction to **1** (as described above), compound **2** has an extended polymeric structure with 2-[(*E*)-2-(3-methylphenyl)-1-diazenyl]pyridine behaving as a monodentate ligand via the pyridyl nitrogen, and all the chlorine atoms serving to bridge mercury atoms. In this case, neither of the azo nitrogens is coordinated to mercury. A skewed repeating chain of Hg_2Cl_2 rhombohedra links the molecular units together, as shown in Fig. 4. Adjacent Hg_2Cl_2 units are staggered, whereas alternate ones lie in planes aligned parallel to one another. The coordinated ligand molecules are all aligned along planes parallel to each other, but in a third direction, roughly at right angles to the planes of each of the Hg_2Cl_2 rhombohedra. In addition to the chlorine bridges, which hold the units together in the polymeric structure, there are hydrogen-bonding interactions which provide some end-to-end cohesion between the monomeric units. These hydrogen bonds link the hydrogen atom on the carbon *para-* to the nitrogen in the pyridyl ring of each ligand with one of the bridging chlorines on an adjacent unit. The relevant bond distances are C(3)–H(3A) = 0.95 Å, H(3A)...Cl(1) = 2.80 Å and C(3)–Cl(1) = 3.49 Å and the angle C(3)–H(3A)...Cl(1) is 130.3°. These hydrogen-bonding interactions as well as the packing arrangements in the crystal and the chlorine bridges are shown in Fig. 5. The bond angles making up the trigonal plane in **2** are N(1)–Hg–Cl(1), 92.5(2)°; N(1)–Hg–Cl(2), 156.3(2)°; and Cl(1)–Hg–Cl(1A), 109.5(6)° giving a total of 358.3°. The angle between the two axial bonds in **2**, [Cl(1A)–Hg–Cl(2B)] is 161.3°. These values are comparable to those in **1**.

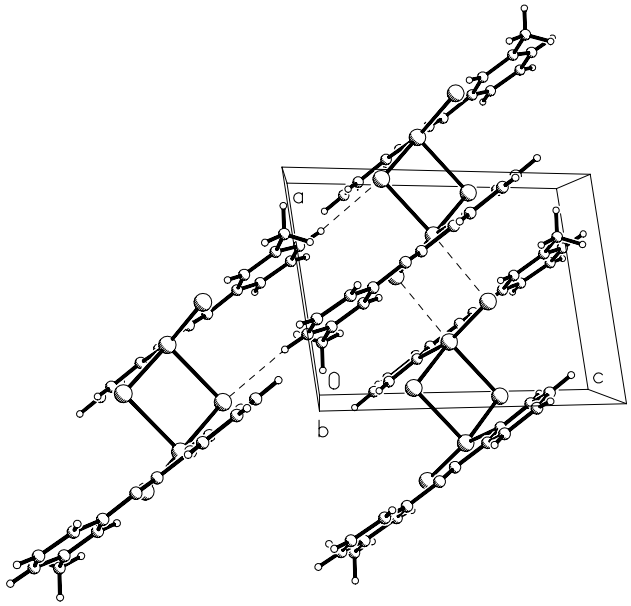

Fig. 5. Unit cell, chlorine bridging, and hydrogen bonding for **2**.

4. Supplementary material

Full tables of bond lengths and angles, tables of non-hydrogen and hydrogen atomic coordinates, anisotropic thermal parameters for non-hydrogen atoms have been deposited with Cambridge Crystallographic data center, CCDC No. 230005 and 230006 for L^1HgCl_2 (**1**) and L^2HgCl_2 (**2**), respectively. Copies of this information may be obtained free of charge from the Director, CCDC, 12 Union Road, Cambridge, CB2 1EZ, UK

(Fax: +44-1223-336-033; e-mail: deposit@ccdc.cam.ac.uk or http://www.ccdc.cam.ac.uk).

Acknowledgements

The financial support of the Department of Science & Technology, New Delhi, India (Grant No. SP/S1/F26/99, TSBB) and the support of the Grant Agency of the Czech Republic (Grant No. 104/03/0393, AL) are gratefully acknowledged.

References

[1] S. Gupta, A. Chakravorty, Inorg. Nucl. Chem. Lett. 9 (1973) 109.
[2] B.S. Raghavendra, A. Chakravorty, Indian J. Chem. Sect. A 14 (1976) 166.
[3] P.V. Roling, D.D. Kirt, J.L. Dill, S. Hall, C.J. Hollstrom, J. Organomet. Chem. 116 (1976) 39.
[4] T.S. Basu Baul, D. Dey, Synth. React. Inorg. Met. Org. Chem. 20 (1990) 541.
[5] H.K. Ghosh, S. Goswami, A. Chakravorty, Inorg. Chem. 22 (1983) 3358.
[6] B.K. Ghosh, A. Mukhopadhyay, S. Goswami, S. Ray, A. Chakravorty, Inorg. Chem. 23 (1984) 4633.
[7] R.A. Krause, K. Krause, Inorg. Chem. 21 (1982) 1714.
[8] R.A. Krause, K. Krause, Inorg. Chem. 19 (1980) 2600.
[9] S. Goswami, A.R. Chakravarty, A. Chakravorty, Inorg. Chem. 20 (1981) 2246.
[10] S. Goswami, A.R. Chakravarty, A. Chakravorty, Inorg. Chem. 21 (1982) 2737.
[11] S. Goswami, A.R. Chakravarty, A. Chakravorty, Inorg. Chem. 22 (1983) 602.
[12] S. Goswami, R. Mukherjee, A. Chakravorty, Inorg. Chem. 22 (1983) 2825.
[13] D. Datta, J. Chem. Soc., Dalton Trans. (1986) 1907.
[14] P. Munshi, R. Samanta, G.K. Lahiri, Polyhedron 17 (1998) 1913.
[15] R. Samanta, P. Munshi, B. Santra, G.K. Lahiri, Polyhedron 18 (1999) 995.
[16] N. Bag, A. Pramanik, G.K. Lahiri, A. Chakravorty, Inorg. Chem. 31 (1992) 40.
[17] R.A. Krause, K. Krause, Inorg. Chem. 23 (1984) 2195.
[18] A.K. Deb, M. Kakoti, S. Goswami, J. Chem. Soc., Dalton Trans. (1991) 3249.
[19] N. Chanda, R.H. Laye, S. Chakraborty, R.L. Paul, J.C. Jeffery, M.D. Ward, G.K. Lahiri, J. Chem. Soc., Dalton Trans. (2002) 3496.
[20] M.N. Ackermann, C.R. Barton, E.M. Specht, W.E. Schreiber, Abstracts of papers, in: 187th National Meeting of the American Chemical Society, St. Louis, MO, American Chemical Society, Washington, DC, 1984, INOR 133.
[21] M.N. Ackermann, C.R. Barton, C.J. Deodene, E.M. Specht, S.C. Keill, W.E. Schreiber, H. Kim, Inorg. Chem. 28 (1989) 397.
[22] V. Ferreira, R.A. Krause, S. Larsen, Inorg. Chim. Acta 145 (1988) 29.
[23] D. Datta, A. Chakravorty, Inorg. Chem. 22 (1983) 1085.
[24] B. Divisia-Blohorn, G. Kyriakakou, J. Ulrich, Org. Mass Spectrom. 20 (1985) 463.
[25] A.K. Deb, S. Goswami, J. Chem. Soc., Dalton Trans. (1989) 1635.
[26] J.J. Robertson, A. Kadziola, R.A. Krause, S. Larsen, Inorg. Chem. 28 (1989) 2097.
[27] A.K. Deb, S. Choudhury, S. Goswami, Polyhedron 9 (1990) 2251.
[28] P. Ghosh, A. Pramanik, N. Bag, A. Chakravorty, J. Chem. Soc., Dalton Trans. (1992) 1883.
[29] A. Bharath, B.K. Santra, G.K. Lahiri, J. Chem. Soc., Dalton Trans. (1998) 2643.
[30] G.K. Lahiri, S. Bhattacharya, S. Goswami, A. Chakravorty, J. Chem. Soc., Dalton Trans. (1990) 561.
[31] T.S. Basu Baul, W.L. Basaiawmoit, J. Indian Chem. Soc. 70 (1993) 151.
[32] R. Samanta, P. Munshi, B.K. Santra, N.K. Lokanath, M.A. Sridhar, J.S. Prasad, G.K. Lahiri, J. Organomet. Chem. 579 (1999) 311.
[33] A.K. Kumar, T.K. Chattopadhyay, E. Rivarola, Indian J. Chem. Sect. A 27 (1988) 912.
[34] T.S. Basu Baul, A. Lycka, Polyhedron 11 (1992) 2423.
[35] T.S. Basu Baul, D. Dey, D.D. Mishra, Synth. React. Inorg. Met. Org. Chem. 23 (1993) 53.
[36] D. Dey, T.S. Basu Baul, E. Rivarola, Bull. Chem. Soc. Jpn. 66 (1993) 1556.
[37] D. Dey, T.S. Basu Baul, E. Rivarola, Indian J. Chem. Sect. A 34 (1995) 239.
[38] N. Campbell, A.W. Henderson, D. Taylor, J. Chem. Soc. (1953) 1281.
[39] R.W. Faessinger, E.V. Brown, J. Am. Chem. Soc. 73 (1951) 4608.
[40] R. Garth Kidd, R.J. Goddfellow, in: R.K. Harris, B.E. Mann (Eds.), NMR and the Periodic Table, Academic Press, London, 1978, p. 266.
[41] D.C. Phillips, A.C.T. North, F.S. Mathews, Acta Crystallogr. 24 (1968) 351.
[42] D.T. Cromer, J.T. Waber, International Tables for X-ray Crystallography, vol. 4, Kynoch Press, Birmingham, 1974 (Table 2.2A).
[43] G.M. Sheldrick, SHELXTL Software Package, Version 5.10, Bruker AXS Inc., Madison, WI, USA, 1997.
[44] B. Chand, U. Ray, P.K. Santra, G. Mostafa, T.H. Lu, C. Sinha, Polyhedron 22 (2003) 1205.
[45] I. del Hierro, I. Sierra, D. Pérez-Quintanilla, F. Carrillo-Hermosilla, I. Lopez-Solera, M. Fajardo, Inorg. Chim. Acta 355 (2003) 347.

Available online at www.sciencedirect.com
SCIENCE DIRECT®
Polyhedron 23 (2004) 2331–2336
POLYHEDRON
www.elsevier.com/locate/poly

Further study of tris(cyclohexyl)stannane compounds, Cy_3SnX. Syntheses of the compounds with X = Br, I, N_3 and NCS and redetermination of the crystal structures of Cy_3SnX (X = Br and I)

R. Alan Howie [a,*], Marcelo V.H. Moura [b], James L. Wardell [b], Solange M.S.V. Wardell [c]

[a] Department of Chemistry, University of Aberdeen, Old Aberdeen, AB24 3UE, Scotland, UK
[b] Departamento de Química Inorgânica, Instituto de Química, Universidade Federal do Rio de Janeiro, CP 68563, 21945-970 Rio de Janeiro, RJ, Brazil
[c] Far-Manguinhos, Fiocruz, Rua Sizenando Nabuco 100, Manguinhos, CEP 21041-250, Rio de Janeiro, RJ, Brazil

Received 21 July 2004; accepted 3 August 2004
Available online 28 August 2004

Abstract

Methods of preparation and far IR data are presented for various Cy_3SnX compounds. The synthesis of tris(cyclohexyl)tin hydroxide, Cy_3SnOH, is also described. Redeterminations of the crystal structures of tris(cyclohexyl)tin bromide and iodide, Cy_3SnBr and Cy_3SnI, confirm their molecular nature and improve considerably upon the results reported earlier [S. Calogero, P. Ganis, V. Peruzzo, G. Tagliavini, G. Valle, J. Organomet. Chem. 220 (1981) 11] providing, in both cases, lower R-factors and, in particular, a revised estimate of the Sn–I bond length, now 2.7463(6) Å.
© 2004 Elsevier Ltd. All rights reserved.

Keywords: Tris(cyclohexyl)tin; Halostannanes; Crystal structure

1. Introduction

Halo- and pseudo-halostannanes of the general form $R_{4-n}SnX_n$, (R = an organic group, X = halide or pseudo halide and n =1–13), have received much attention. Of interest in compounds of this type, particularly for those with $n = 2$ and more especially those with $n = 1$, has been the investigation of the occurrence and nature of secondary Sn–X contacts to establish whether they contribute to the coordination of tin and change its nominal tetrahedral nature to one with a higher coordination number. Typical examples of this are the detailed report of the temperature dependent order–disorder transition in tris(cyclohexyl)tin chloride, **1** (X = Cl), [1, and references therein], and reports on the structures of **1** (X = F, Br and I) [2] and of various tris(2-methyl-2-phenyl-propyl)stannane derivatives $(Neo)_3SnX$, **2** (X = Cl, Br, I, N_3 and NCS) [3]. We now report the synthesis of **1** (X = Br, I, N_3 and NCS) and of tris(cyclohexyl)tin hydroxide, along with redeterminations of the structures of **1** (X = Br) and **1** (X = I). Far IR data are also presented for various Cy_3SnX compounds.

2. Experimental

Melting points were measured on Melt-Temp-II equipment. Far IR spectra were obtained using a Nicolet

* Corresponding author. Tel.: +44 1224 272907; fax: +44 1224 272921.
E-mail address: r.a.howie@abdn.ac.uk (R.A. Howie).

0277-5387/$ - see front matter © 2004 Elsevier Ltd. All rights reserved.
doi:10.1016/j.poly.2004.08.001

Magna 760 FTIR instrument with samples suspended in Nujol between polythene plates. Cy_3SnCl was a recrystallised commercial sample, m.p. 127–129 °C.

Far IR: *v* 492, 439, 420, 327, 271, 252, 199 cm^{-1}.

2.1. Preparation of tris(cyclohexyl)tin iodide, **I** (X = I)

Solutions of Cy_3SnCl (2 mmol) in Me_2CO (15 ml) and NaI (5 mmol) in Me_2CO (15 ml) were mixed. After stirring at RT for 4 h the reaction mixture was filtered and the filtrate evaporated to leave a residue which was extracted into $CHCl_3$. The chloroform extract was evaporated and the solid residue was recrystallised from EtOH, m.p. 64–66 °C.

Far IR: *v*: 492, 439, 420, 324, 250(sh), 239, 212, 161 cm^{-1}.

2.2. Preparation of tris(cyclohexyl)tin hydroxide, **I** (X = OH)

A solution of Cy_3SnCl (2 mmol) in Et_2O (15 ml) was added to a solution of NaOH (5%) in H_2O (15 ml) and the mixture was stirred for 1 h, and then filtered. The ether layer in the filtrate was collected, dried and evaporated. The residue from the ether layer was added to the original solid collected by filtration and the combined solids were recrystallised from aqueous EtOH, m.p.174–179 °C. The wide m.p. range is attributed to the presence in trace amounts, and in situ formation, of bis[tris(cyclohexyl)tin] oxide, $(Cy_3Sn)_2O$, in accord with the previous report [4] that only with great difficulty can pure samples of either the oxide or the hydroxide be obtained, *v*(OH) 3623 cm^{-1}.

2.3. Preparation of tris(cyclohexyl)tin bromide, **I** (X = Br)

Concentrated HBr (2 ml) was added to a solution of Cy_3SnOH (0.5 mmol) in EtOH (20 ml). The mixture was stirred at room temperature for 2 h, the volatiles removed under vacuum and the solid product recrystallised from $CHCl_3$; m.p. 77–79 °C.

Far IR: *v*: 491, 438, 419, 322, 250(sh), 228(br), 203(sh) cm^{-1}.

2.4. Preparation of tris(cyclohexyl)tin azide, **I** ($X = N_3$)

A solution of Cy_3SnCl (2 mmol) in Me_2CO (15 ml) and a suspension of NaN_3 (5 mmol) in Me_2CO (15 ml) were mixed. After stirring at RT overnight, the reaction mixture was filtered. The filtrate was shaken with a further suspension of NaN_3 (5 mmol) in Me_2CO (15 ml) for 4 h, all volatiles removed by rotary evaporation and the residue extracted into $CHCl_3$. The chloroform extract was dried and rotary evaporated to leave a solid residue. $\nu(N_3)$ 2071 cm^{-1}: no *v*(OH)

2.5. Preparation of tris(cyclohexyl)tin isothiocyanate, **I** (X = NCS)

A solution of Cy_3SnCl (2 mmol) in Me_2CO (15 ml) and a suspension of NaNCS (5 mmol) in Me_2CO (15 ml) were mixed. After stirring at RT overnight, the reaction mixture was filtered and the filtrate collected. The filtrate was shaken with a further suspension of NaNCS (5 mmol) in Me_2CO (15 ml) for 4 h, all volatiles removed by rotary evaporation and the residue extracted into $CHCl_3$. The chloroform extract was dried and rotary evaporated to leave a solid residue which was recrystallised from CH_2Cl_2/hexane, m.p. 120–122 °C.

IR: *v*: 2071 cm^{-1}. Far IR: *v*: 570(br), 491, 439, 420, 326, 252, 220, 200 cm^{-1}

2.6. X-ray crystallography

2.6.1. Data collection

Intensity data for **1** (X = Br and I) were obtained with Mo Kα radiation, $\lambda = 0.71073$ Å, by means of the Enraf Nonius KappaCCD area diffractometer of the EPSRC's crystallography service at Southampton. For **1** (X = Br), for which the crystal shattered on cooling, the data were obtained at 298 K and at 120 K for **1** (X = I). The entire process of data collection, cell refinement and data reduction was accomplished by means of the programs DENZO [5] and COLLECT [6]. Correction for absorption by a semi-empirical method based upon the variation in intensity of equivalent reflections was achieved with the program SORTAV [7,8]. The transmission factors for each compound (Table 1) are not then on an absolute scale. Unfortunately both data sets have proved to be less than fully complete (see Table 1). This is especially true in the case of **1** (X = Br), where the available crystals were of particularly dubious quality, but is perceived to have no more deleterious effect than to limit the precision with which derived quantities such as bond lengths and bond angles are estimated.

2.6.2. Structure solution and refinement

In both cases initial solution of the structure was obtained by the heavy atom technique with the program SHELXS-86 [9] and completed and refined by full matrix least squares on F^2 with SHELXL-97 [10]. In the case of **1** (X = Br) the structure was finally re-refined with the atomic coordinates from the refinement of **1** (X = I) as starting parameters but with bromine substituted for iodine thus ensuring total equivalence between the labelling schemes of these two refinements. One reflection showing particularly poor agreement due to extinction was omitted from the refinement of **1** (X = Br). Despite a degree of disorder affecting the atoms of the cyclohexyl groups of **1** (X = Br), which was not modelled in detail, anisotropic thermal vibration parameters were refined for all non-H atoms. In all cases the residual electron

Table 1
Crystal data and structure refinement

Compound	**1** (X = Br)	**1** (X = I)
Empirical formula	$C_{18}H_{33}BrSn$	$C_{18}H_{33}ISn$
Formula weight	448.04	495.03
Temperature (K)	298(2)	120(2)
Crystal system	orthorhombic	orthorhombic
Space group	*Pnma*	*Pnma*
Unit cell dimensions		
a (Å)	11.2576(10)	12.2446(8)
b (Å)	16.6583(17)	17.1651(14)
c (Å)	10.2199(9)	9.0044(6)
Volume (Å^3)	1916.6(3)	1892.5(2)
Z	4	4
Calculated density (Mg/m^3)	1.553	1.737
Absorption coefficient (mm^{-1})	3.410	2.973
F(000)	904	976
Crystal[a] size (mm)	0.22 × 0.16 × 0.07	0.30 × 0.20 × 0.20
θ range for data collection (°)	2.69–20.97	3.05–27.50
Index ranges	$-10 \leqslant h \leqslant 10$, $-15 \leqslant k \leqslant 12$, $-7 \leqslant l \leqslant 10$	$-15 \leqslant h \leqslant 13$, $-19 \leqslant k \leqslant 22$, $-11 \leqslant l \leqslant 10$
Reflections collected/unique	1346/741 [R_{int} = 0.0955]	10576/2179 [R_{int} = 0.0737]
Completeness to max. θ (%)	69.4	97.1
Absorption correction *T*min/max	0.2059/0.3222	0.7415/0.8258
Data/restraints/parameters	741/0/97	2179/0/97
Goodness-of-fit on F^2	1.026	1.018
Final *R* indices [$I > 2\sigma(I)$]	R_1 = 0.0690, wR_2 = 0.1826	R_1 = 0.0402, wR_2 = 0.0763
R indices (all data)	R_1 = 0.0930, wR_2 = 0.2085	R_1 = 0.0674, wR_2 = 0.0855
Largest peak and hole (e/Å^3)	0.405 and −0.460	1.218 and −1.307

[a] Colourless crystals in every case.

density features noted in Table 1 are in the vicinity (within 0.90 Å) of heavy atoms. In the final stages of refinement H atoms were introduced in calculated positions and refined with a riding model. The program ORTEP-3 for Windows [11] was used in the preparation of the Figures and SHELXL-97 and PLATON [12] for bond length and angle and other molecular geometry calculations. PLATON was used, in particular, for calculations based upon crystallographic data extracted from the Cambridge Structural Database [13]. It is noted here that in Table 4 for those compounds with more than one molecule in the asymmetric unit, e.g. all 2, the bond distances and bond angles and the associated estimated errors are average values. Further details of the data collection and structure refinement processes are available in Table 1.

3. Results and discussion

3.1. General features of the structures

All of the cyclohexyl rings are found to be in the chair conformation with C–C distances and internal C–C–C angles more or less as expected provided that due allowance is made for the disorder in **1** (X = Br) noted above. Apart from this the real significance of the structures presented here lies in the nature of the tin coordination which they reveal which is discussed below.

3.2. Crystal structures of *1* (*X = Br and I*)

The compounds **1** (X = Br) and **1** (X = I) are isomorphous and it is for this reason that both the drawing of the molecule (Fig. 1) and the layer of molecules shown in Fig. 2, although based on data for **1** (X = I), are applicable to both compounds. In these structures the tin and halogen atoms lie on a crystallographic mirror plane which also bisects one of the cyclohexyl groups and re-

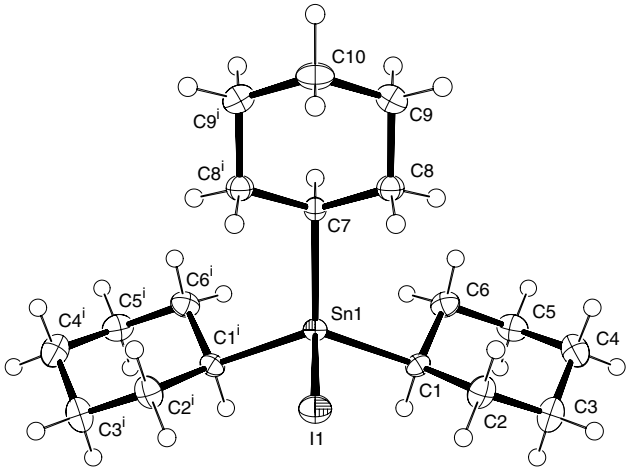

Fig. 1. The molecule of **1** (X = I) showing the labelling scheme. Non-H atoms are shown as 50% probability displacement ellipsoids and H atoms as small circles of arbitrary radius. Symmetry code (i) $x, 3/2 - y, z$.

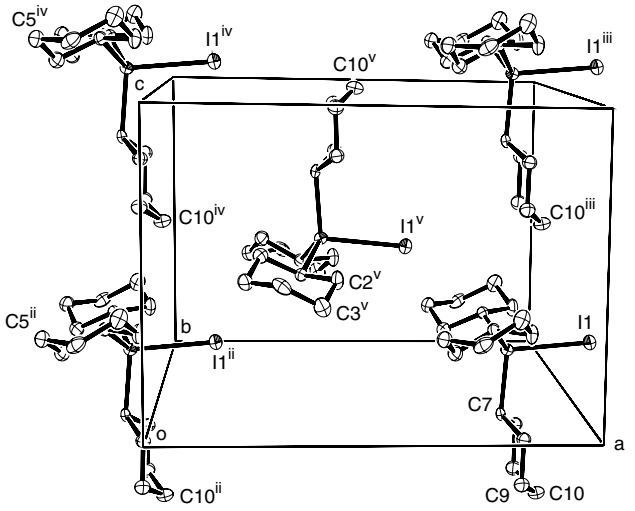

Fig. 2. A layer of molecules of **1** (X = I). Non-H atoms are shown as 50% probability displacement ellipsoids and H atoms have been omitted for clarity. Only selected atoms are labelled. Symmetry codes (ii) $x-1, y, z$; (iii) $x, y, 1+z$; (iv) $x-1, y, 1+z$; (v) $x-1/2, y, 1/2-z$.

lates the two remaining cyclohexyl groups by symmetry. Thus the asymmetric unit consists of one complete cyclohexyl group [C(1–6)], four atoms of another cyclohexyl group [C(7–10)] and the tin and halogen atoms (see Fig. 1). In both cases the bond length and bond angle data in Table 2 are consistent with tin in a tetrahedral environment distorted primarily in order to accommodate the steric requirements of the cyclohexyl groups. Particularly notable in this table is the Sn(1)–I(1) bond length of 2.7463(6) Å which is much more reasonable than the previous published value [2] of 2.54(1) Å. The molecules are found in layers on the crystallographic mirror planes as shown in Fig. 2 within which the next nearest neighbour Sn–X distances are 5.375(5) and 4.8013(7) Å for X = Br and X = I, respectively. The surprisingly shorter next nearest neighbour distance for X = I is attributed primarily to the different temperatures at which the intensity data were collected (see Table 1).

Table 2
Selected bond lengths and angles (Å, °) for isomorphous **1** (X = Br and I)

	X = Br	X = I
Bond lengths		
Sn(1)–C(1)	2.09(2) × 2	2.167(4) × 2
Sn(1)–C(7)	2.09(2)	2.166(6)
Sn(1)–X(1)	2.501(4)	2.7463(6)
Bond angles		
C(1)–Sn(1)–C(1^{i})	119.6(16)	115.9(2)
C(1)–Sn(1)–C(7)	112.6(7) × 2	114.45(12) × 2
C(1)–Sn(1)–X(1)	102.5(9) × 2	104.90(10) × 2
C(7)–Sn(1)–X(1)	104.5(6)	99.71(14)

Symmetry code: (*i*) $x, 3/2-y, z$.

3.3. Structural trends in R_3SnX compounds with X = F, Cl, Br and I

The nature, polymeric or molecular, of the solid state structure of **1** (X = Cl) has been a matter of conjecture for many years. Initial X-ray structural results [14] were taken to be indicative of a molecular structure with four coordinate tin in contrast to earlier results from Mössbauer spectoscopy suggestive of a polymeric structure with five coordinate tin. Means were then found [2] to resolve this disparity in favour of the molecular structural model. Further support for this model was obtained, by comparison of ^{119}Sn chemical shifts in the solid state (CP/MAS) with those found for the compounds in solution, by Harris et al. [15]. The results of this study were considered to be compatible with **1** (X = Cl) existing as a molecular species in the solid state in the same manner as **1** (X = Br) and **3** (X = Cl). Most recently Asadi et al. [1] have investigated the X-ray crystal structure of **1** (X = Cl) over the temperature range 120–298 K. This study reveals, in addition to an order–disorder transition at about 248 K, an inverse and temperature dependent relationship between the nearest, Sn–Cl, and next nearest, Sn···Cl′, distances. These distances tend to equality with reducing temperature. Also present are essentially linear Cl–Sn···Cl′ and Sn–Cl···Sn′ groups (see Table 3). The findings of Asadi et al. support the earlier suggestion [4], based on NMR (solution) and Mössbauer spectroscopy, that **1** (X = Cl) is weakly polymeric in the solid state but

Table 3
Comparison table of selected geometric parameters (Å, °) in **1** (X = F, Cl, Br and I)

X	Temperature[a] (K)	Sn–X[b]	Sn···X′	Sn–X···Sn′	X–Sn···X′	Reference
F		2.052(10)	2.302(10)	180	180	[16]
Cl	298	2.415(3)	3.298(3)	178.95(17)	178.95(12)	[1]
Cl	108	2.4657(7)	3.0077(7)	171.95(3)	178.58(3)	[1]
Br	298	2.501(4)	5.375(5)	135.39(15)	116.67(9)	[c]
I	120	2.7463(6)	4.8013(7)	140.03(2)	129.70(2)	[c]

[a] Room temperature unless otherwise stated.
[b] Primed and unprimed labels indicate next nearest and nearest neighbour atoms, respectively.
[c] Isomorphs, this work.

Table 4
Comparison of selected interatomic distances (Å) in $(Neo)_3$ SnX, **2**, and Ph_3 SnX, **3**

	Ph_3Sn–X				$(Neo)_3Sn$–X			
X	Sn–X[a]	Sn···X′	Temperature[b] (K)	Reference	Sn–X	Sn···X′	Temperature (K)	Reference
Cl[c]	2.3548(17)	>5.84		[17]	2.382(3)	>7.31	150	[21]
Cl[c]	2.3605(12)	>5.63	110	[17]				
Br[c]	2.495(2)	>5.79		[18]	2.5444(14)	>5.64	150	[3][d]
I	2.6988(9)[e]	>6.30		[19]	2.7424(6)	>5.67	150	[3][d]
I	2.7080(7)[f]	>6.30		[20]				

[a] Primed and unprimed labels indicate next nearest and nearest neighbour atoms, respectively.
[b] Room temperature unless otherwise stated.
[c] Isomorphous pairs of compounds.
[d] Isomorphous pairs of compounds.
[e] Triclinic polymorph with $Z = 4$.
[f] Triclinic polymorph with $Z = 2$.

monomeric in solution. Thus in the context of compounds of the form R_3 SnCl (R = alkyl or aryl) **1** (X = Cl) is perceived as being polymeric but intermediate in this respect between, on the one hand, such as polymeric Me_3 SnCl and on the other, for example, molecular Ph_3 SnCl, **3** (X = Cl).

With the information now available the status of various **1** can be considered further in terms of the nature of X as well as R. Thus from the data in Table 3 **1** (X = F and Cl), with Sn···X′ distances much shorter than the sums of the contact radii of the relevant atoms (PLATON contact radii 2.26, 1.47, 1.75, 1.85 and 1.98 Å for Sn, F, Cl, Br and I, respectively) and essentially linear X–Sn···X′ groups, are clearly polymeric. The remainder, **1** (X = Br and I) with Sn···X′ distances greater than the relevant contact radii sums and non-linear X–Sn···X′ groups, are equally clearly molecular species. Table 4 shows Sn–X and Sn···X′ distances for compounds of the form R_3 SnX, R = Neo, **2**, and R = Ph, **3**, with, in both cases, X = Cl, Br and I. All of these compounds are molecular species as shown by the Sn···X′ distances, all much greater than the sums of the contact radii. For **2** this is largely because of the bulk of the non-halogen substituents. For **3** it comes about because the molecules occur in stacks in such a way as to permit large numbers of C–H–π intermolecular contacts. The Sn–X bonds of successive molecules in the stack are then directed in opposite directions away from the mid-line of the stack. In other words, in the case of **3** (X = Cl, Br and I), the stacking of the molecules favours interactions between the phenyl groups rather than Sn···X′ intermolecular contacts.

Three notable features arise from comparison of Tables 3 and 4. First, whereas in **3** (X = Cl), the only case for which the necessary data are available in Table 4, reduced temperature has virtually no effect on the Sn–Cl distance but shortens the Sn···Cl′ contact dramatically, in **1** (X = Cl) both types of distance are temperature dependent but in opposite senses. Second, the Sn–Cl distance is longer in polymeric **1** (X = Cl) than in either of the corresponding, but molecular, **2** and **3** in which last two this distance is very similar. Third, for all molecular **1**, **2** and **3** (X = Br and I) the Sn–X distances are much the same for any particular X. The implication of the above is that, at least for X = halogen, a polymeric compound of the form R_3Sn–X will display temperature dependency of the type noted above for **1** (X = Cl), more or less linear X–Sn···X′ groups and an Sn–X distance longer than that found in a molecular compound with the same X but, obviously, a different R. In general terms it appears that the formation of polymeric species with bridging X in R_3SnX (X = halogen) in the solid state is favoured for more electronegative and smaller X and disfavoured by large R. On the other hand, as in the case of **3** (X = Cl, Br and I), polymerisation with bridging X may be supplanted by other intermolecular interactions.

The structures for **1** (X = Br and I) presented here improve upon those previously reported [2] not only because they are better determined but also, in the case of **1** (X = I), because the data derived from the original structure determination are very similar to those obtained both here and previously for **1** (X = Br). Likewise the previously reported [2] structure of **1** (X = F) has been ignored in favour of that of Tudela et al. [16] because the data derived from the original determination closely resembled that of **1** (X = Cl). There is, therefore, doubt as to the authenticity of the samples used in the original structure determinations [2] of **1** (X = F and I).

4. Supplementary material

Supplementary data, including atomic coordinates, anisotropic thermal parameters and bond lengths and angles are available from the Cambridge Crystallographic Data Centre with reference codes CCDC 231208 and 231209 for **1** (X = I) and **1** (X = Br), respectively. Copies of this information may be obtained, free of charge, from the Director, CCDC, 12 Union Road,

Cambridge CB2 1EZ, UK (fax: +44 1223 336033; e-mail: deposit@ccdc.cam.ac.uk) or via http://www.ccdc.cam.ac.uk/conts/retrieving.html.

Acknowledgements

We are indebted to the EPSRC for the use of both the Chemical Database Service at Daresbury, primarily for access to the Cambridge Structural Database, and the X-ray service at the University of Southampton for data collection. We thank CNPq and FUJB, Brazil, for financial support.

References

[1] A. Asadi, C. Eaborn, P.B. Hitchcock, M.M. Meehan, J.D. Smith, Inorg. Chem. 42 (2003) 4141.
[2] S. Calogero, P. Ganis, V. Peruzzo, G. Tagliavini, G. Valle, J. Organomet. Chem. 220 (1981) 11.
[3] J.A.S. Bomfim, C.A.L. Filgueiras, R.A. Howie, J.N. Low, J.M.S. Skakle, J.L. Wardell, S.M.S.V. Wardell, Polyhedron 21 (2002) 1667.
[4] S.J. Blunden, R. Hill, Inorg. Chim. Acta 98 (1985) L7.
[5] Z. Otwinowski, W. Minor, Macromolecular Crystallography, Part A, in: C.W. CarterJr., R.M. Sweet (Eds.), Methods in Enzymology, vol. 276, Academic Press, New York, 1997, pp. 307–326.
[6] R. Hooft, COLLECT, Nonius BV, Delft, The Netherlands, 1998.
[7] R.H. Blessing, Acta Crystallogr., Sect. A 51 (1995) 33.
[8] R.H. Blessing, J. Appl. Crystallogr. 30 (1997) 421.
[9] G.M. Sheldrick, Acta Crystallogr., Sect. A 46 (1990) 467.
[10] G.M. Sheldrick, SHELXL-97, Program for Crystal Structure Refinement, University of Göttingen, Germany, 1997.
[11] L.J. Farrugia, J. Appl. Crystallogr. 30 (1997) 565.
[12] A.L. Spek, J. Appl. Crystallogr. 36 (2003) 7.
[13] F.H. Allen, Acta Crystallogr., Sect. B 58 (2002) 380.
[14] S. Calogero, P. Ganis, V. Peruzzo, G. Tagliavini, J. Organomet. Chem. 179 (1979) 145.
[15] R.K. Harris, A. Sebald, D. Furlani, G. Tagliavini, Organometallics 7 (1988) 388.
[16] D. Tudela, R. Fernandez, V.K. Belsky, V.E. Zavodnic, J. Chem. Soc., Dalton Trans. (1996) 2123.
[17] J.S. Tse, F.L. Lee, E.J. Gabe, Acta Crystallogr., Sect. C 42 (1986) 1876.
[18] H. Preut, F. Huber, Acta Crystallogr., Sect. B 35 (1979) 744.
[19] M.G. Simard, I. Wharf, Acta Crystallogr., Sect. C 50 (1994) 397.
[20] S.W. Ng, Acta Crystallogr., Sect. C 51 (1995) 2292.
[21] J.N. Low, J. Wardell, J.A.S. Bomfim, S.M.S.V. Wardell, Acta Crystallogr., Sect. C 56 (2000) e554.

Available online at www.sciencedirect.com
SCIENCE DIRECT®
Polyhedron 23 (2004) 2337–2348
POLYHEDRON
www.elsevier.com/locate/poly

Versatile coordination mode of dicyanamide in nickel(II) complexes containing polyamines as blocking ligands

Roman Boča [a,*], Miroslav Boča [b,c], Milan Gembický [a], Lothar Jäger [d], Christoph Wagner [d], Hartmut Fuess [c]

[a] Department of Inorganic Chemistry, Slovak Technical University, SK-812 37 Bratislava, Slovakia
[b] Institute of Inorganic Chemistry, Slovak Academy of Sciences, SK-845 36 Bratislava, Slovakia
[c] Materials Science, Darmstadt University of Technology, D-64287 Darmstadt, Germany
[d] Department of Chemistry, Martin-Luther-University, D-06099 Halle/Saale, Germany

Received 9 January 2004; accepted 14 June 2004
Available online 21 September 2004

Abstract

Triethylenetetramine (L^4) and dipropylenetriamine (L^3) were used as blocking ligands (tetradentate and tridentate, respectively) that, after complexation with Ni(II), leave two or three sites ready for ligation with $N(CN)_2^-$ (dicyanamide, abbr. *dca*). The formed complexes are mononuclear, binuclear or polymeric. This was proven by the X-ray structure analysis for $[NiL^4(dca)_2]$ (mononuclear, **1**), $[(dca)L^3Ni(dca)_2NiL^3(dca)]$ (binuclear, **2**) and $[NiL^4(dca)](ClO_4)$ (polymeric, **3**). The magnetic susceptibility measurements for **1** confirm that the Curie law is obeyed at higher temperatures whereas the zero-field splitting is effective below 10 K ($D/hc = -4\ cm^{-1}$); **2** shows a weak antiferromagnetic coupling ($J/hc = -0.6\ cm^{-1}$); **3** exhibits a negligible exchange coupling ($J/hc \approx 0$).
© 2004 Elsevier Ltd. All rights reserved.

Keywords: Crystal structure; Nickel(II) complexes; Magnetism, Pseudohalides

1. Introduction

Halides and pseudohalides (both linear, CN^-, N_3^-, NCO^-, NCS^-, $NCSe^-$, CNO^-, and non-linear, $N(CN)_2^-$, $C(CN)_3^-$, $ONC(CN)_2^-$, etc.) represent versatile ligands which can form mononuclear, dinuclear, polynuclear and polymeric complexes. For instance, $[Ni(en)_2(NCS)_2]$ is a mononuclear complex [1], whereas $[(en)_2Ni(NCS)_2Ni(en)_2]I_2$ represents a typical dimer in which the thiocyanate bears a bridging functionality [2]; *en* = 1,2-diaminoethane (ethylenediamine), boldfaces visualise the donor atoms hereafter. Such dinuclear units are formed also in the $[(en)_2Ni(NCS)_2Ni(en)_2](ClO_4)_2$ complex [3] and an analogous coordination mode has been found in $[(en)_2NiCl_2Ni(en)_2]Cl_2$ [4] and $[(en)_2NiBr_2Ni(en)_2]Br_2$ [5]. A similar coordination mode is maintained when the tetradentate ligand *tren* is used for the complexation (*tren* = 2,2′,2″-triaminotriethylamine), as found in $[(tren)Ni(NCO)_2Ni(tren)](BPh_4)_2$ [6], and assumed also when NCO^- is substituted for NCS^- and $NCSe^-$ [7]. The dinuclear character has been assumed and later confirmed in $[(tren)Ni(N_3)_2Ni(tren)](BPh_4)_2$ [8,9]. The ligand–isomer of the latter complex, $[(teta)Ni(N_3)_2Ni(teta)](BPh_4)_2$, *teta* = triethylenetetramine, adopts a dinuclear structure, too [10]. Notice, the $[Ni(tren)(NCS)_2]$ complex again is mononuclear. A different dinuclear structure held only by a single $(N)_3^-$ bridge has been found in $[(N_3)(macro)Ni(N_3)Ni(macro)(N_3)]I$, *macro* = *N*-tetramethylcyclam where two $(N)_3^-$ ligands adopt a terminal functionality [11].

On changing the stoichiometry and nature of the *N*-donor neutral ligand, different structural types

* Corresponding author. Tel.: +421 2 59325 610; fax: +421 2 524 931 98.
E-mail address: roman.boca@stuba.sk (R. Boča).

0277-5387/$ - see front matter © 2004 Elsevier Ltd. All rights reserved.
doi:10.1016/j.poly.2004.06.022

occur. For example, $[Ni(L^2)_2(NO_2)]X$ complexes (L^2 = the bidentate ligand *en* or 1,3-diaminopropane; $X = (ClO)_4^-$ or $(I)_3^-$) adopt the single-chain structure with a $(NO)_2^-$ bridge; the modified complexes with tetradentate ligands L^4, i.e. $[NiL^4(NO_2)](ClO_4)$, behave analogously [12]. Chain structures are present, for instance, in $Ni(en)_2Ni(CN)_4$ and $Ni(dien)(mea)Ni(CN)_4$, *dien* = diethylenetriamine, *mea* = 2-aminoethanole [13,14]; here the diamagnetic square planar $[Ni(CN)_4]^{2-}$ ion bears the role of the bridging and charge-balancing agent.

The complex $[Ni(im)_2(NCS)_2]$, where *im* = imidazole, is a coordination polymer with the basal plane formed of $Ni(NCS)_4$-units showing a two-arm chain, and completed in the axial positions by two unidentate *im* ligands [15]; interesting is the ferromagnetic ordering below 5 K and the cobalt-analogue exhibits a ferromagnetic ordering with hysteresis too. A similar structural motif has been found in the $[Cu(ampym)_2(dca)_2]$ complex (*ampym* = 2-aminopyrimidine; *dca* = dicyanamide, $NCNCN^-$) [16]. Two reports on $(Ph_4P)_2$ $[Co(dca)_4]$ confirm a 1D two-arm chain held by the bidentate *dca* ligands, with the axial positions terminated by additional unidentate *dca* ligands [17,18]; at $T_c = 1.75$ K a ferromagnetic ordering starts to apply [17]. The complex $(Ph_4P)[Co(dca)_3]$ adopts a layered (2D) network structure where each *dca* ligand is bidentate [18]. Such a cation-templation into the $Mn(dca)_3^-$ polymer resulted in an analogous network [19]. The binary α-$M(dca)_2$ complexes possess a rutile-like structure and show either ferromagnetism (M = Co and Ni) or antiferromagnetism (M = Cr, Mn and Fe); the Cu-complex is a paramagnet. Just the interesting magnetic properties of these materials represent the driving force of the contemporary interest and a renaissance in research of the pseudohalide complexes [20]. Let us exemplify some recent investigations of magnetic properties of *dca* -containing complexes [21–28] and complexes of $C(CN)_3^-$ (tricyanomethanide, abbr. *tcm*) [29–33]. The coordination chemistry of *dca* and *tcm* ligands has been intensively studied in a systematic way for a longer period [34,35]. The magnetism of such a complexes has been reviewed elsewhere [36].

In the present communication we are focusing on the coordination mode of the *dca* ligand in Ni(II) complexes along with their associated magnetic properties. There exists a structural report on the mononuclear complex $[Ni(tren)(dca)_2]$ and its ligand–isomer $[Ni(teta)(dca)_2]$ at $T = 150$ K [37]; the synthesis and characterization of the complexes $[Ni(tren)(dca)](ClO_4)$ and $[Ni(teta)(dca)](ClO_4)$ are also reported but the structures of these complexes have not been determined by X-ray structure analysis. An analogous complex with the *tcm* ligand has been confirmed as binuclear, i.e. $[(teta)Ni(tcm)_2Ni(teta)](ClO_4)_2$, with a ferromagnetic ordering below 16 K [38,39].

We are reporting the synthesis, structure and magnetic properties of $[Ni(teta)(dca)_2]$, $[(dca)(dpt)Ni(dca)_2Ni(dpt)(dca)]$ and $[Ni(teta)(dca)](ClO_4)$ complexes, where *teta* is a tetradentate ligand and *dpt* = dipropylenetriamine is tridentate one.

2. Experimental

Caution: Perchlorate salts of metal complexes with organic ligands are potentially explosive. Only a small amount of material should be prepared, and handled with caution.

The chemicals used were commercial products and were used without further purification. $NiSiF_6 \cdot 6H_2O$ was prepared with quantitative yield by combining a solution of hexafluorosilicic acid in water and an equimolar amount of basic nickel carbonate. For magnetic measurements pure macro crystalline materials were grounded into Agate mortar.

$[Ni(teta)(N(CN)_2)_2]$, **1.** $KN(CN)_2$ (10 mmol) in 10 cm^{-3} of water was added to a solution ($V = 20$ cm^3) obtained by mixing $Ni(NO_3)_2 \cdot 6H_2O$ (5 mmol), triethylenetetramine (5 mmol) and water. From the resulting blue solution a small quantity of nickel hydroxide was removed by filtration, and **1** was obtained by a slow evaporation of the filtrate (in one week) as blue-violet well-formed crystals suitable for the X-ray crystal structure analysis. Yield 26%. Complex **1** can also be prepared by the same procedure with $NiSiF_6 \cdot 6H_2O$. Found: C, 35.7; H, 5.55; N, 41.4; Ni, 16.9. Calc. for $C_{10}H_{18}N_{10}Ni$: C, 35.6; H, 5.38; N, 41.6; Ni, 17.4%. IR (cm^{-1}, KBr) 2282vs ($\nu_s + \nu_{as}$ C–N), 2224vs (ν_{as} NCN), 2159 vs, br (ν_s NCN), 1360s (ν_{as} C–N), 944m (ν_s C–N). UV–Vis (nm, MgO) 934, 559, 362.

$[Ni_2(dpt)_2(N(CN)_2)_4]$, **2.** A solution of $Ni(ClO_4)_2 \cdot 6H_2O$ (2.5 mmol) containing dipropylenetriamine (2.5 mmol) in 15 cm^3 of water was combined with $KN(CN)_2$ (2.5 mmol) in 15 cm^3 of water. Nickel hydroxide was removed by filtration, and from the filtrate violet crystals of **2** were collected the next day. Yield 28%. Found: C, 37.2; H, 5.23; N, 38.9, Ni, 18.0. Calc. for $C_{10}H_{17}N_9Ni$: C, 37.3; H, 5.29; N, 39.2; Ni, 18.2%. IR (cm^{-1}, KBr) 2243m, 2211vs, 2185vs (ν CN). UV–Vis (nm, MgO) 894, 554, 358.

$[Ni(teta)(N(CN)_2)](ClO_4)$, **3.** The complex was synthesized from a dilute aqueous solution containing $KN(CN)_2$ (5 mmol), $Ni(ClO_4)_2 \cdot 6H_2O$ (5 mmol) and triethylenetetramine (5 mmol) in 50 cm^3 of water. Nickel hydroxide was removed by filtration and **3** was separated as violet crystals by slow evaporation of the filtrate. Yield 10%. Found: C, 25.9; H, 4.91; N, 25.7; Cl, 9.3; Ni, 14.9. Calc. for $C_8H_{18}N_7ClNiO_4$: C, 26.0; H, 4.86; N, 26.5; Cl, 9.57; Ni, 15.8%. IR (cm^{-1}, KBr) 2308s ($\nu_s + \nu_{as}$ C–N), 2230m (ν_{as} NCN), 2159vs (ν_s

NCN), 1267s (ν_{as} C–N), 990m (ν_s C–N). UV–Vis (nm, MgO) 972, 568, 362.

2.1. Spectra and magnetic measurements

Infrared spectra were recorded on a FTIR spectrometer MATTSON 5000 in the range of 400–4000 cm^{-1} as KBr pellets. Electronic spectra were monitored on an UV–Vis spectrometer Lambda 19 (Perkin–Elmer) between 200–2000 nm at room temperature.

Magnetic susceptibility data were taken with an alternating current susceptometer (LakeShore, model 7221); field parameters were $f = 222$ Hz, $H_{AC} = H_{DC} = 800$ A m^{-1}. Corrections to the underlying diamagnetism were estimated on the basis of Pascal constants. The magnetic susceptibility was converted to the effective magnetic moment $\mu_{eff}/\mu_B = 798(\chi'_{mol}T)^{1/2}$ (SI units are employed). The magnetisation measurements were done on a similar apparatus (LakeShore, model 7225) and a SQUID magnetometer (Quantum Design) until $B = 6$ T.

2.2. Structure analysis and refinement

Suitable single crystals of **1** and **2** were mounted on a STOE-STADI-IV diffractometer equipped with graphite monochromated Mo Kα radiation. Single crystals of 3 were mounted on a STOE-IPDS diffractometer. In all cases corrections to Lorentz and polarisation effects have been applied, and also for **1** an absorption correction.

Direct methods (SHELXS-97) and full least-squares refinement (SHELXL-97) with all non-H-atoms refined anisotropically have been applied [40,41]. Crystal data and refinement parameters are collected in Table 1. For the plots of the molecular structures, the program DIAMOND [42] was used.

3. Results and discussion

3.1. Crystal and molecular structure

The X-ray crystal structure analysis showed that complex **1**, [Ni(*teta*)(**N**CNCN)$_2$], is mononuclear (Fig. 1) with *cis* positioned $NCNCN^-$ ligands and with the terminal N atoms of the neutral ligand L^4 in *trans* positions. The $\{NiN_4N'_2\}$ chromophore is nearly octahedral. In fact this represents a room-temperature reinvestigation of the crystal structure already published elsewhere [37]. The former, low-temperature data (hereafter **1b**) show a compression of the unit cell on cooling to 150 K except the *a*-parameter; $a = 9.948$ (9.974), $b = 11.201$ (11.067), $c = 14.102$ (14.058), $V = 1481$ (1463) for $T = 293$ (150) K.

The bond lengths Ni−N in **1** vary scarcely and values were found between Ni−N(1) = 2.090(3) Å and Ni−N(9) = 2.118(3) Å (Table 2). For the angles N−Ni−N maximum deviations from 90° were found for N(7)−Ni−N(9) = 99.5(1)° and N(9)−Ni−N(10) = 81.3(1)°. A comparison with **1b** shows that on cooling not all Ni−N distances contract, and some of them expand. A new feature is the identification of close contacts typical for hydrogen bonds: 3.045, 3.101 and a longer pair of 3.314, 3.409 Å. These contacts form a complex network that can transmit an exchange interaction. These contacts contract on cooling to 150 K to 3.031, 3.096, 3.306, 3.380 Å.

Table 1
Crystallographic data and data collection parameters of **1–3**

	1	**2**	**3**
Formula	$C_{10}H_{18}N_{10}Ni$	$C_{20}H_{34}N_{18}Ni_2$	$C_8H_{18}ClN_7NiO_4$
M (g mol^{-1})	337.05	644.07	370.45
Crystal system	monoclinic	triclinic	orthorhombic
Space group	*Cc*	$P\bar{1}$	*Pcam*
Unit cell dimensions			
a (Å)	9.948(2)	8.415(6)	8.591(2)
b (Å)	11.201(2)	9.332(6)	11.113(3)
c (Å)	14.102(2)	10.595(7)	15.056(3)
α (°)	90	84.37(5)	90
β (°)	109.48(2)	70.85(6)	90
γ (°)	90	66.47(5)	90
V (Å^3)	1481.4(5)	720.1(8)	1437.5(5)
Z	4	1	4
μ (mm^{-1})	1.321	1.353	1.563
Reflections collected/unique	2553/2547 [$R_{int} = 0.0170$]	4003/2544 [$R_{int} = 0.0664$]	10118/1303 [$R_{int} = 0.0665$]
Final $R1/wR2[I > 2\sigma(I)]$	0.0255/0.0654	0.0362/0.0836	0.0517/0.1455
Final $R1/wR2$ (all data)	0.0267/0.0668	0.0497/0.0932	0.0557/0.1499
CCDC deposit number	168452	220110	168453
T (K)	293(2)	293(2)	220(2)

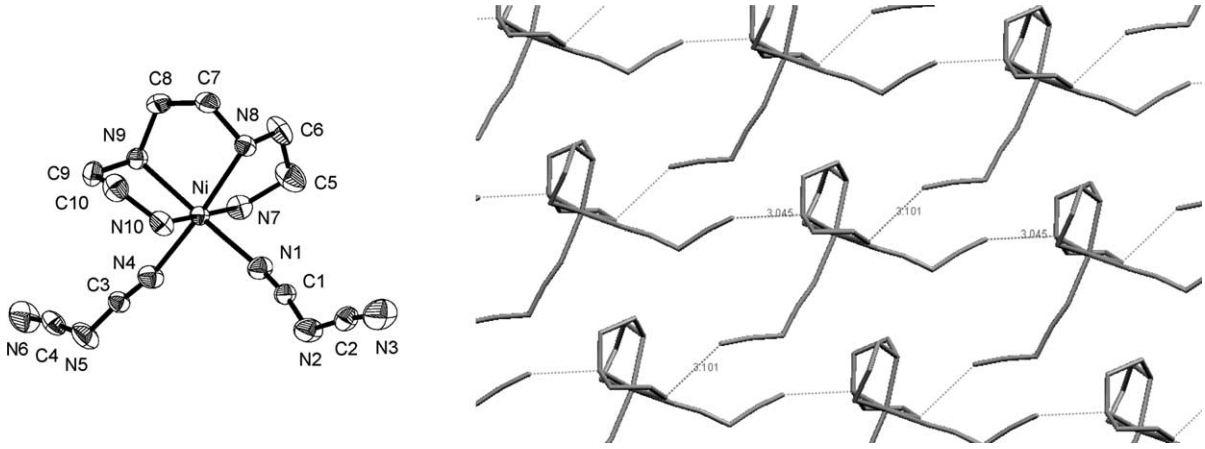

Fig. 1. Molecular structure of **1** (hydrogen atoms are omitted for clarity).

Table 2
Selected bond lengths (Å) within the chromophore of complexes **1**–**3**[a]

1, T = 293 K	**1b**, T = 150 K [37]	**2**	**2b** [44]	**3**
NCNCN group				
Ni–N(1) = 2.090	Ni–N(1) = 2.087	Ni–N(1) = 2.087	Ni–N(7) = 2.146	Ni–N(1) = 2.121
Ni–N(4) = 2.095	Ni–N(4) = 2.099	Ni–N(3) = 2.135	Ni–N(9) = 2.217	
		Ni–N(4) = 2.108	Ni–N(4) = 2.130	
Polyamine group				
Ni–N(7) = 2.093	Ni–N(7) = 2.109	Ni–N(7) = 2.078	Ni–N(1) = 2.087	Ni–N(3) = 2.144
Ni–N(8) = 2.124	Ni–N(8) = 2.127	Ni–N(8) = 2.127	Ni–N(2) = 2.208	Ni–N(4) = 2.118
Ni–N(9) = 2.118	Ni–N(9) = 2.127	Ni–N(9) = 2.098	Ni–N(3) = 2.082	
Ni–N(10) = 2.100	Ni–N(10) = 2.094			
Close contacts				
N3···N9 = 3.045	N3···N8 = 3.031			
N3···N7 = 3.409	N3···N10 = 3.380			
N6···N10 = 3.101	N6···N7 = 3.096			
N6···N8 = 3.314	N6···N9 = 3.306			

[a] Standard deviations 0.003–0.005 Å.

Complex **2**, [(NCNCN)(*dpt*)Ni(NCNCN)$_2$Ni(*dpt*)-(NCNCN)], possesses isolated binuclear units (Fig. 2). The hexacoordinated nickel(II) atoms are capped by the tridentate polyamine with the terminal NH_2 groups in *trans* positions. Two *cis*-positioned vertices are occupied by *dca* anions that bear bridging-ligand functionality. The sixth site is occupied by a non-bridging, terminal ligand $NCNCN^-$. The interatomic distances Ni−N in the chromophore $\{NiN_3N'_2N''\}$ are almost equal and amount on average to 2.105(5) Å which cor-

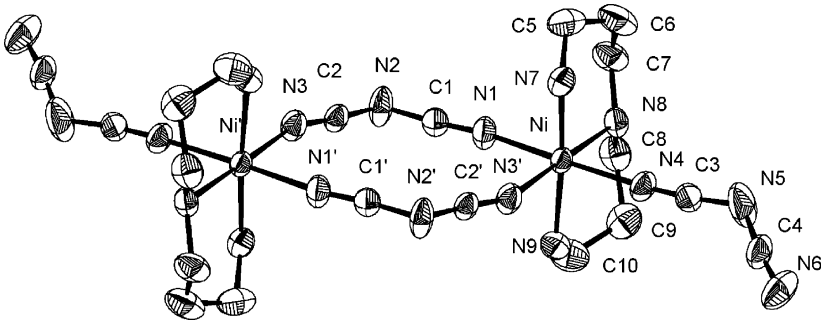

Fig. 2. Molecular structure of the complex **2** (hydrogen atoms are omitted for clarity); 50% probability thermal ellipsoids; [a] Symmetry code:^{i} $1-x$, $1-y$, $1-z$.

responds with the upper range for Ni–N (primary, secondary amines) bonds in octahedral complexes [43]. The almost planar *dca* utilizes two of three possible N-donors to coordinate which results in the formation of a twelve-membered, slightly puckered ring. The bond angle inside the ring, N(1)–Ni–N(3)^{i}, is 90.4(1)°. The intramolecular Ni–Ni separation is 7.328 Å. These molecules, formed in the *a*-direction, stack with parallel lying rings and a Ni···Ni distance of 8.415 Å. There are two other kinds of intermolecular Ni···Ni contacts: a very short one of 5.525 Å, and a long one of 9.332 Å.

Recently a structural report on **2** (hereafter **2b**) appeared [44]. Surprisingly, there are some different features for **2** (**2b**), of which the cell parameters $b = 70.8$ (79.8) and $V = 720$ (753) are the most significant. Thus, it is problematic to claim that our results on **2** represent a reinvestigation of **2b**. Different cell parameters reflect into significantly different Ni–N distances as seen from Table 2. Also the Ni···Ni separation differs for **2** and **2b**: 7.328 and 7.270 Å, respectively.

Complex **3**, [Ni(**NCNCN**)(*teta*)](ClO$_4$), adopts a polymeric (chain) structure along the *c*-axis where one *dca* ligand links two adjacent centres (Fig. 3). The coordination polyhedron of nickel is an octahedron with nitrogen atoms of the *dca* in *cis* positions and with terminal N atoms of the amine in *trans* positions. Within the 3σ criterion all Ni–N distances are equal [on average 2.13(1) Å] and the angles N–Ni–N vary between 82.1(1)° and 95.7(2)°. The intrachain Ni···Ni separation is 7.528 Å but interchain distances are 5.551 and 8.591 Å.

The structural data on *dca*-containing Ni(II) complexes, available from the CCDB, are collected in Table 3. The geometric parameters of *dca*-complexes **1–3** correspond well with those in a variety of other *dca*-complexes [55]. The comparison of the uni- (**1**) and bidentately (**2**, **3**) coordinated ligand shows scarcely significantly different parameters. The NCN arms are almost linear and the angles C–N–C lie between 121.2(5)° (**3**) and 123.4(3)° (**1**). The *dca* anions (**1–3**) are almost planar with maximum deviations from the plane formed by all five atoms of 0.009 Å for C(1) in complex **1**.

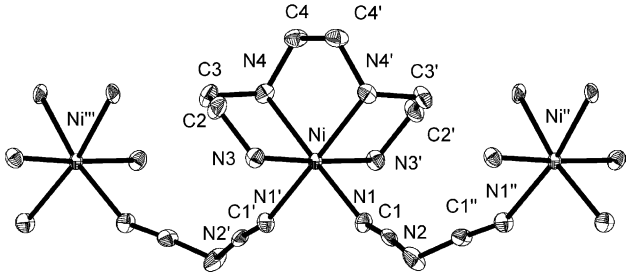

Fig. 3. Structural motif of the complex cation **3** (hydrogen atoms are omitted for clarity); 50% probability thermal ellipsoids; symmetry codes: [i] 0.5 −*x*; *y*; −z; x;[ii] y; −0.5 − z; [iii] x; y; 0.5 − z.

3.2. Magnetic data

The mononuclear Ni(II) complex **1** obeys the Curie law at temperature above 10 K because the effective magnetic moment stays almost temperature-independent (Fig. 4). Its value, $\mu_{\mathrm{eff}} = 2.76\ \mu_{\mathrm{B}}$ is a bit lower than the spin-only value of 2.83 μ_{B} for the $S = 1$ system. With temperature lowering the effective magnetic moment drops down as a consequence of the zero-field splitting. As the effective magnetic moment turns towards a constant value (not to zero), a negative zero-field splitting parameter D is expected with the Kramers doublet $|S,M_S\rangle = |1,\pm1\rangle$referring to the ground state [56].

The magnetic susceptibility data were fitted by assuming the usual form of the spin Hamiltonian

$$\hat{H} = D[S_z^2 - S(S+1)/3]\hbar^{-2} + g_a\mu_{\mathrm{B}}B\hat{S}_a\hbar^{-1} \qquad (1)$$

that accounts for an axial zero-field splitting parameter D and the anisotropic Zeeman term ($a = z$ or x). Within the spin Hamiltonian formalism the set of magnetic parameters is constrained through the relationship $D = (g_z - g_x)\lambda/2$, where $\lambda = \pm\xi^{\mathrm{so}}/2S$ and stands for the spin-orbit splitting parameter ($\lambda/hc = -315\ \mathrm{cm}^{-1}$ for Ni(II) complexes). The fitting procedure gave $g_z = 1.971$ and $g_x = 1.945$ whereas the constrained D-value was $D/hc = -4.00\ \mathrm{cm}^{-1}$. The quality of the fit is excellent: $R(\chi) = 0.0036$. The subnormal values of the *g*-parameters are assigned to a complex network (Fig. 1) that can transmit some exchange interaction.

The magnetisation data show some deviation from the Brillouin function at fields of about $B = 6$ T, which is a consequence of the zero-field splitting. The magnetisation data recovered by the above-mentioned set of magnetic parameters are also displayed in Fig. 4.

The magnetic properties of **2** are dominated by the exchange interaction between $S_{\mathrm{A}} = S_{\mathrm{B}} = 1$ local spins. The effective magnetic moment is temperature-independent down to 20 K and then drops down more abruptly (Fig. 5).

The magnetic susceptibility can be fitted using an isotropic exchange Hamiltonian of the type

$$\hat{H} = -J_{\mathrm{Ni-Ni}}\hbar^{-2}(\vec{S}_{\mathrm{A}}\cdot\vec{S}_{\mathrm{B}}) + \mu_{\mathrm{B}}\hbar^{-1}Bg_{\mathrm{Ni}}(\hat{S}_{\mathrm{A},z} + \hat{S}_{\mathrm{B},z}) - (zJ')\hbar^{-1}\langle S_z\rangle\hat{S}_z. \qquad (2)$$

For $S_{\mathrm{A}} = S_{\mathrm{B}} = 1$ one can handle an explicit formula for the magnetic susceptibility [57]. A fitting procedure gave the magnetic parameters $J_{\mathrm{Ni-Ni}}/hc = -1.00\ \mathrm{cm}^{-1}$ and $g_{\mathrm{Ni}} = 2.073$ (the discrepancy factor of the fit $R = 0.016$). A rather small value of the exchange-coupling constant of antiferromagnetic nature is consistent with an increasing magnetic susceptibility on cooling; its maximum will appear at a temperature T_{max} far below 4 K as the following equation holds true for the $S_{\mathrm{A}} = S_{\mathrm{B}} = 1$ system: $|J|/k = 0.976\ T_{\mathrm{max}}$ [57].

Table 3
Metal–ligand distances in *dca* containing Ni(II) complexes

CCDC-code/deposit No	Formula[a]	Ni–N(*dca*)	Ni–N(other)	References
Mononuclear				
168452	cis-[Ni(*teta*)(*dca*)$_2$], T = 293 K	2.090, 2.095	2.093, 2.124 2.118, 2.100	this work
BARHUX	*cis*-[Ni(*teta*)(*dca*)$_2$], T = 150 K	2.087, 2.098	2.094, 2.128 2.109, 2.127	[37]
BARHEH	*cis*-[Ni(*tren*)(*dca*)$_2$]	2.064, 2.108	2.100, 2.090 2.104, 2.148	[37]
MOFXIO	*trans*-[Ni(*macro*1)(*dca*)$_2$]·H$_2$O	2.163	2.053, 2.078	[45]
MOFXOU	*trans*-[Ni(*macro*2)(*dca*)$_2$] · H$_2$O	2.122	2.081, 2.098	[45]
TICBIQ	*trans*-[Ni(*Meiz*)$_4$(*dca*)$_2$]	2.114	2.090, 2.114	[46]
IHIDOS	*trans*-[Ni(*biim*)$_2$(*dca*)$_2$]	2.095	2.062, 2.106	[47]
Oligomeric				
220110	[Ni$_2$(*dpt*)$_2$(*dca*)$_4$]	2.087, 2.135, 2.108	2.078, 2.127, 2.098	this work
200891	[Ni$_2$(*dpt*)$_2$(*dca*)$_4$]	2.146, 2.217, 2.130	2.087, 2.208, 2.082	[44]
200892	[Ni$_2$(*medpt*)$_2$(*dca*)$_4$]	2.158, 2.117, 2.092	2.082, 2.176, 2.071	[44]
200894	[Ni$_2$(*dca*)$_2$(*dpt*)$_2$(H$_2$O)$_2$ (*ter*)]	2.062		[44]
KAFJOR	[Ni$_3$(*dpa*)$_4$(*dca*)$_2$] · 2.5CH$_2$Cl$_2$	2.003, 2.055		[48]
Polymeric				
168453	*catena*-[Ni(*teta*)(*dca*)]ClO$_4$	2.121	2.144, 2.118	this work
BALKUV	*catena*-[Ni(*pn*)$_2$(*dca*)]$_n$ · n(ClO$_4$)	2.095, 2.116	2.006 2.107	[49]
MEKMAQ	*catena*-[Ni(*apy*)(*dca*)$_2$]$_n$	2.049, 2.074 2.200 (N$_{am}$)		[50]
NEHYII	*catena*-n(AsPh$_4$)$_2$ · [Ni$_2$(*dca*)$_6$]$_n$	2.075, 2.076, 2.101, 2.072, 2.080, 2.098		[51]
NEHYUU	*catena*-n(AsPh$_4$)$_2$ · [Ni$_2$(*dca*)$_6$]H$_2$O]$_n$ · nH$_2$O · 1/2n MeOH	2.055, 2.057, 2.076,2.077, 2.069, 2.085		[51]
OFABEC	*catena*-[Ni$_2$(*dca*)$_4$(H$_2$O)$_2$]$_n$ · n(*phena*)	2.032, 2.040, 2.198, 2.073, 2.125	2.038 (OH$_2$)	[52]
XAPBAR	*catena*-[Ni(*apyNO*)(*dca*)$_2$]	2.043, 2.058, 2.077, 2.096	2.082, 2.106	[53]
ECAVIN	*catena*-[C$_{16}$H$_6$N$_{16}$Ni$_2$]$_n$ · n(H$_2$O)	not available		[54]

[a] Ligand abbreviations: *ter* = terephthalato, *apy* = 2-amino-pyrimidine, *pn* = propane-1,3-diamine, *tren* = tris(2-aminoethyl)amine, *phena* = phenazine, *apyNO* = aminopyridine N-oxide, *biim* = 2,2′-biimidazoline, *dpa* = di(2-pyridyl)amido, *macro* 1 = 3,10-bis(2-hydroxyethyl)-1,3,5,8,10,12-hexaazacyclotetradecane, *macro* 2 = 3,14-dimethyl-2,6,13,17-tetraazatricyclo[14,4,$0^{1.18}$,$0^{7.12}$]-docosane.

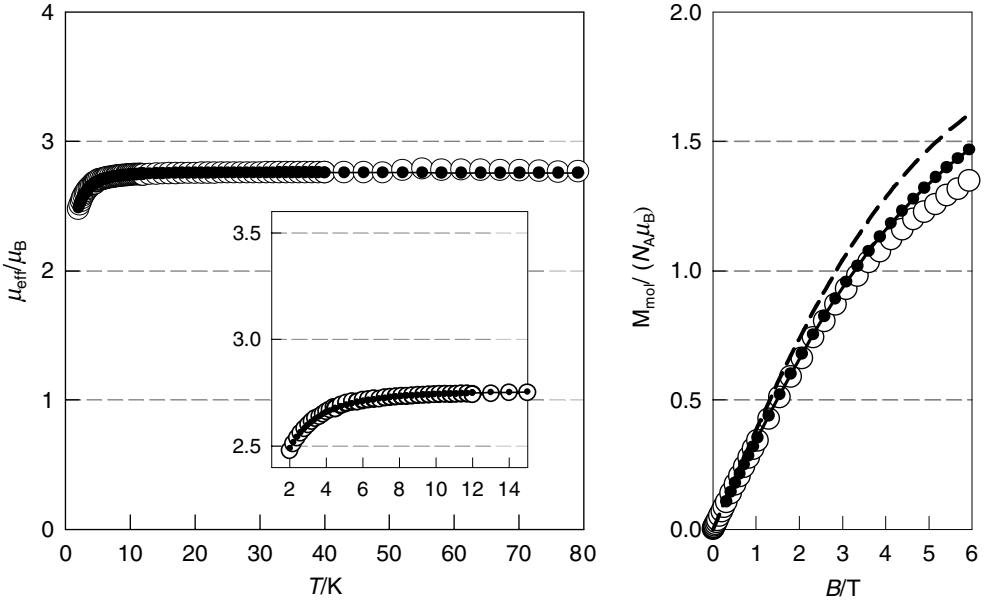

Fig. 4. Magnetic functions for **1**: temperature dependence of the effective magnetic moment (left) and field dependence of the magnetisation at $T = 4.60$ K (right); inset – enlarged low-temperature window; open circles – experimental data; full points and solid lines – the fitted data; dashed – the Brillouin function.

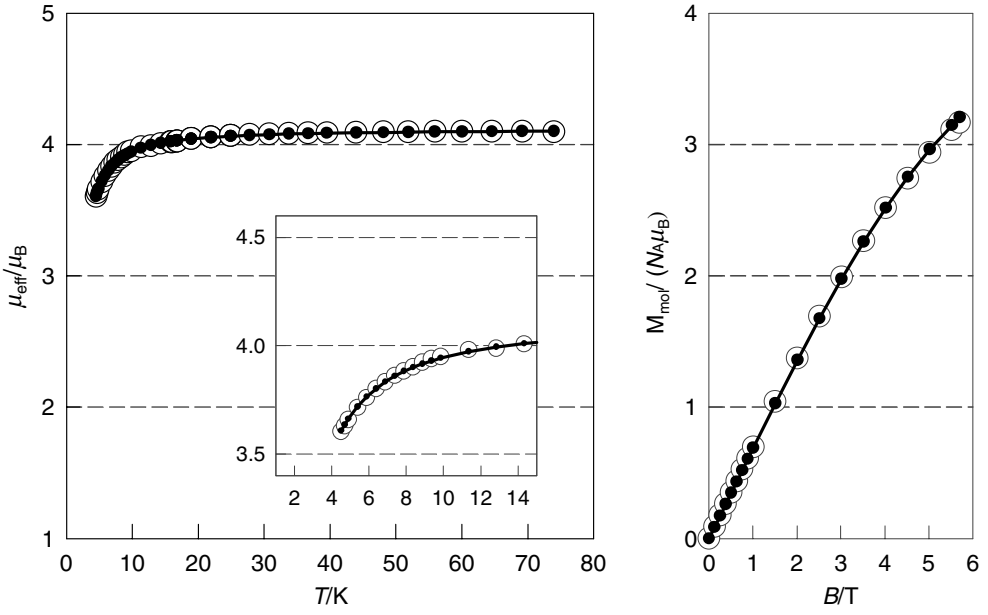

Fig. 5. Magnetic functions for **2** per dimer: temperature dependence of the effective magnetic moment (left) and field dependence of the magnetisation at $T = 4.40$ K (right); inset – enlarged low-temperature window; open circles – experimental data; full points and solid lines – the fitted data.

A slight antiferromagnetic nature of the exchange coupling constant in **2** results from a partial cancellation of the ferromagnetic and antiferromagnetic contributions. In the present case of an odd number of spacers (atoms) separating the metal centres the ferromagnetic portion becomes substantial and the spin-polarisation mechanism applies [58]. The counter parting antiferromagnetic portion, on the contrary, could be suppressed owing to a large intramolecular Ni···Ni separation (7.3 Å). Therefore the resulting value of the exchange coupling constant could be either slightly positive or slightly negative depending upon delicate balance between its ferromagnetic and antiferromagnetic portions.

Attempts to improve the fit of the experimental data by adding the molecular field correction with the molecular field parameter zJ' did not lead to the desired effect.

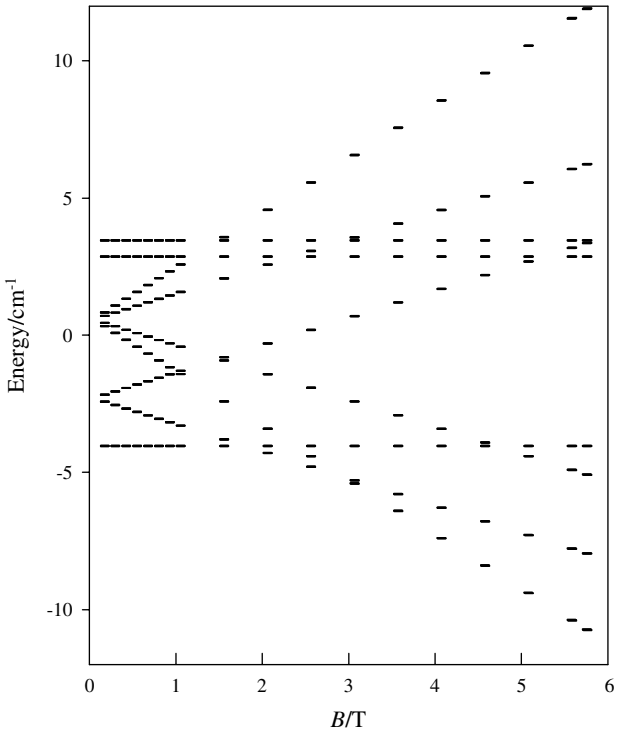

Fig. 6. Field dependence of the calculated energy levels for **2**.

Another extension is to consider the asymmetric exchange by considering an additional term to the Hamiltonian

$$\hat{H}_S^{(2)} = \hbar^{-2}(\vec{S}_A \cdot \bar{\bar{D}}_{AB} \cdot \vec{S}_B + \vec{S}_A \cdot \bar{\bar{D}}_A \cdot \vec{S}_A + \vec{S}_B \cdot \bar{\bar{D}}_B \cdot \vec{S}_B) = \hbar^{-2}(\vec{S} \cdot \bar{\bar{D}}_S \cdot \vec{S}). \quad (3)$$

The molecular-state D-tensor results from the combination of the local D_A- and D_B-tensors, and the pair-interaction D_{AB}-tensor. When the isotropic exchange coupling constant is large (positive, or negative, $|J| \gg |D|$), a contribution of D_S to the off-diagonal blocks of the exchange Hamiltonian would be ineffective: the energy levels are then dominated by the diagonal matrix elements only. In such a strong-exchange limit the asymmetric exchange results in the zero–field splitting: the situation would be analogous to the mononuclear case as the sublevels are separated by D_1 for $S = 1$, by D_2 and $3D_2$ for $S = 2$.

The strong-exchange limit is surely not a proper assumption in the present case so we are left with a need to construct and then to diagonalise the entire exchange Hamiltonian numerically. The easiest way is to skip the coupling process (as the coupling is only a unitary transformation that leaves the eigenvalues invariant) and to work in the basis set of uncoupled spin functions; the formulae for the matrix elements can be found elsewhere [57]. The fitting procedure enriched with the asymmetric exchange led to the following set of magnetic parameters for **2**: $J_{Ni-Ni}/hc = -0.577$ cm^{-1}, $g_{Ni} = 2.122$, $D_{Ni}/hc = +2.58$ cm^{-1} and $D_{Ni-Ni}/hc = -2.58$ cm^{-1}; the goodness of the fit is excellent ($R = 0.002$, both high-temperature and low-temperature data agree within ± 0.005 μ_B). As seen from Fig. 6, the energy levels no longer follow the usual strong-exchange picture.

The magnetisation measurements for **2** up to $B = 5.7$ T bring no evidence for a saturation at low temperature. The limiting value of magnetisation per particle, $M_{mol}/N_A = 4.0$ μ_B, will evidence the $S = 2$ ground state of

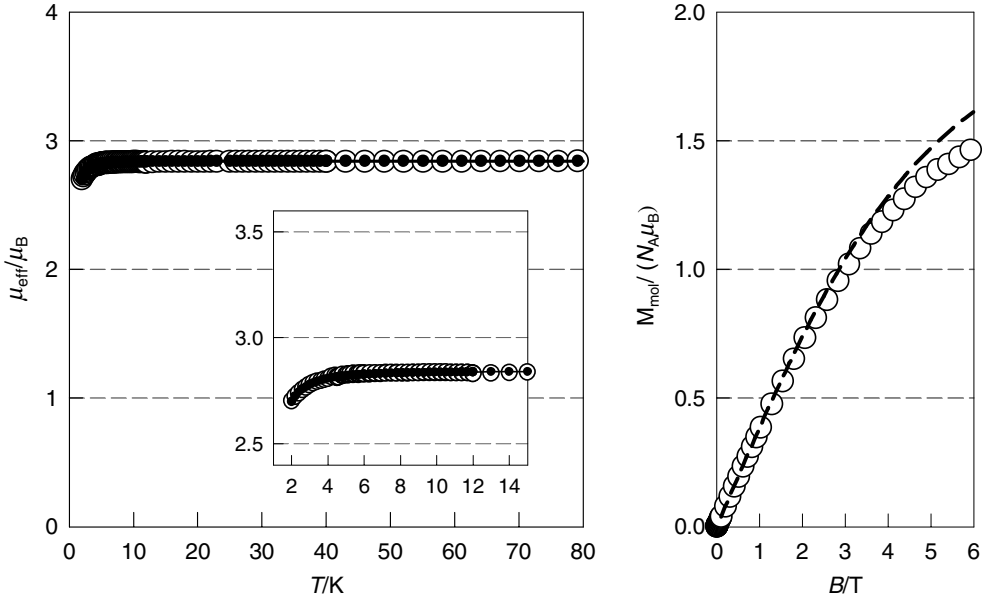

Fig. 7. Magnetic functions for **3**: temperature dependence of the effective magnetic moment (left) and field dependence of the magnetisation at $T = 4.60$ K (right); inset – enlarged low-temperature window; open circles – experimental data; full points and solid lines – the fitted data; dashed – the Brillouin function.

Table 4
Magnetic parameters (in cm^{-1}) for related mononuclear, binuclear and polymeric Ni(II) complexes

Complex[b]	Experimental	D/hc	g	zj/hc	J/hc[a]	Structure; magnetism
Mononuclear $[Ni(L^2)_2X_2]$ or $[NiL^4\ X_2]$						
trans-$[Ni(en)_2(NCS)_2]$	T = 0.3–20 K	+6.24;		E, 1.13		[1]; [60]
	(calorimetry)	− 4.81		E, 2.55		
$[Ni(tren)(NCS)_2]$	T = 4.2–289 K	−0.76	2.181	−1.52		–; [7]
cis-$[Ni(tren)(dca)_2]$	R.T.		2.24			[37];–
cis-$[Ni(teta)(dca)_2]$	R.T.		2.06			[37];–
	T = 2.0–90 K	−4.00	g_z, 1.97			this work
	B = 0.1 T		g_x, 1.94			
Binuclear $[(L^2)_2NiX_2Ni(L^2)_2]Y_2$, $[L^4NiX_2NiL^4]Y_2$, or $[XL^3NiX_2NiL^3X]Y_2$						
$[Ni(en)_2\mu\text{-}Cl]_2Cl_2$	T = 1.5–300 K	+6.5	2.14	−0.33	+19.7	[4]; [61]
	Set-2:	−11	2.12	−0.04	+20.8	
$[Ni(en)_2\mu\text{-}Br]_2Br_2$	T = 1.5–300 K	+6.6	2.12	−0.56	+17.2	[2]; [61]
	Set-2:	−7.6	2.12	−0.32	+15.1	
$[Ni(en)_2\mu\text{-}(SCN)]_2I_2$	T = 1.5–300 K	+4.7	2.14	−0.36	+9.7	[3]; [61]
	Set-2:	−3.3	2.14	−0.31	+9.0	
$[Ni(mepn)_2\mu\text{-}(SCN)]_2(PF_6)_2$	T = 4.2–300 K	−2.0	2.14	−0.14	+12.7	[62]; [62]
	B = 1.5 T					
$[\mu-(NCS)_2(Ni^{II}_2(mepn))_3(NCS)_2]_2[Ni^{II}(mepn)_2(NCS)_2]\cdot H_2O$	T = 4–300 K	−20.0	2.13	+0.20	+8.6	[62]; [62]
	B = 1.5 T					
$[Ni(teta)\mu\text{-}(N_3)]_2(BPh_4)_2$	T = 4.2–300 K		2.43		−83.6	[10]; [10]
$[Ni(tren)\mu\text{-}(N_3)]_2(BPh_4)_2$	T = 4.2– 300 K	+6.8	2.325	+0.50	−70.2	[9]; [8,9]
	B = 1.48 T					
$[\mu\text{-}(N_3)(Ni(macro)(N_3))_2]I$	T = 4.2– 300 K	4.9	2.233	−2.4	−24.6	[11]; [9]
	B = 1.48 T					
$[Ni(tren)\mu\text{-}(NCO)]_2(BPh_4)_2$	T = 4.2–289 K	10.1	2.282	+1.42	−8.8	[6]; [7]
$[Ni(tren)\mu\text{-}(NCS)]_2(BPh_4)_2$	T = 4.2–289 K	0.45	2.255	−0.32	+4.8	–; [7]
$[Ni(tren)\mu\text{-}(NCSe)]_2(BPh_4)_2$	T = 4.2–289	K–0.49	2.247	−0.14	+3.2	–; [7]
$[Ni(CH_2(dmpz)_2)\mu\text{-}Cl_2]_2$	T = 4.2–90 K	2.17	2.310	−0.78	+5.16	[63]; [63]
	B = 0.38 T					
$[Ni(terpy)(H_2O)(NCO)]_2(PF_6)_2$	T = 2– 300 K	−12.2	2.21	+0.40	+9.2	[64]
	B = 0.2 T					
$[Ni(terpy)(N_3)_2]_2\cdot 2H_2O$	T = 2– 100 K	−12.5	2.26	+0.76	+40.2	[65]
$[\mu\text{-}(NCSe)_2(Ni(medpt)_2(NCSe))_2]$	T = 4–300 K	1.5	2.15	+0.22	+17.6	[66]
	B = 1.5 T					
$[\mu\text{-}(NCS)_2(Ni(terpy)(NCS))_2]$	T = 2–300 K	−4.3	2.10	+0.02	+9.8	[67]
	B=0.2T					
$[\mu\text{-}(NCS)_2(Ni(terpy)(NCSe))_2]$	T = 2–300 K	−10.0	2.15	+0.01	+20.2	[67]
	B = 0.2 T					
$[\mu\text{-}BiIm(Ni(tren))_2](BPh_4)_2$	T = 4.2–286 K	53 (problematic)	2.082	+2.50	−5.8	[68]
$[Ni(teta)\mu\text{-}(tcm)]_2(ClO_4)_2$	T = 25 −80 K		2.126	+0.071	+0.15	[39]
	$B_{AC} \approx 0$					

(*continued on next page*)

Table 4 (*continued*)

Complex[b]	Experimental	D/hc	g	zj/hc	J/hc[a]	Structure; magnetism
[(*dca*)Ni(*dpt*)μ-(*dca*)]$_2$	T = 4.2–80 K $B_{AC} \approx 0$		2.073		−1.0	this work
	Set-2 (best):	+2.58	2.122	D_{Ni-Ni}, −2.58	−0.58	this work
	T = 2–300 K B = 0.5 T		2.29		−1.2	[44]; [44]
	Set-2:	−10.9	2.16		–	[44]; [44]
[(*dca*)Ni(*medpt*)μ-(*dca*)]$_2$	T = 5–300 K B = 0.5 T		2.17		+0.7	[44]; [44]
[μ-(*ter*){Ni(*dpt*)(*dca*)(H_2O)}$_2$]	T = 4–300 K B = 1.5 T		2.13		−0.3	[44]; [44]
Polymeric chains [(L^2)$_2$NiX^2], [(L^3 L^1)NiX^2], or [(L^4)NiX]Y						
[Ni(*en*)$_2${μ-Ni(CN)$_4$}]	T = 0.05–20 K $M(B \rightarrow 6$ T), T = 4.27 K	6.6	2.24		−0.06	[13]
[Ni(*dien*)(*mea*){μ-Ni(CN)$_4$}]	T = 4.2–140 K $B_{AC} \approx 0$,	−6.98	2.145	2.101	–	[14]; [14]
[Ni(*im*$_2$$\mu$-NCS)$_2$]	T = 2–290 K, B=1 T	0.2	2.18		8	[15]; [15]
[Ni(*am1*)(μ-NO_2)](ClO_4)	T = 4.2–140K		2.36		−27.4	[12]
[Ni(*am2*)(μ-NO_2)](ClO_4)	B = 1.5 T		2.33		−32.3	[12]
[Ni(*am3*)(μ-NO_2)](ClO_4)			2.30	J_2/J_1, 0.88	−31.8	[12]
[Ni(*teta*)(μ-*dca*)](ClO_4)	T = 2.0–90 K, B = 0.1 T		2.016		− 0.07	this work
		Set-2:	1.81 g_x, 2.013	g_z, 2.002	–	this work
	R.T.		1.91			[37]
[Ni(*tren*)(μ*dca*)](ClO_4)	R.T.		2.19			[37]

[a] The published exchange coupling constants have been re-adjusted to the definition of the exchange coupling Hamiltonian according to Eq. (2).

[b] Abbreviation for ligands: *BiIm* = biimidazolate; *dca* = $N(CN)_2^-$, dicyanamide; *dien* = diethylenetriamine; *dmpz* = 3,5-dimethypyrazolyl; *en* = $NH_2CH_2CH_2NH_2$, 1,2-diaminopropane (ethylenediamine); *im* = imidazole; *macro* = 1,4,8,11-tetramethyl-1,4,8,11-tetraazacyclotetradecane; *mea* = 2-aminoethanole; *medpt* = *N*,*N*-bis(3-aminopropyl)methylamine; *mepn* = 1,2-diamino-2-methylpropane; *tcm* = $C(CN)_3^-$, tricyanomethanide; *terpy* = 2,2′:6′,2″-terpyridine; *teta* = $NH_2CH_2CH_2NHCH_2CH_2NHCH_2CH_2NH_2$, triethylenetetramine (abbr. also *tta*); *tren* = $N(CH_2CH_2NH_2)_3$, 2,2′,2″-triaminotriethylamine (abbr. also *taa*); *ter* = terephthalato; *am1* = *N*,*N*′ -bis(2-aminoethyl)propane-1,3-diamine; *am2* = *N*,*N*′ -bis(3-aminopropyl)ethane-1,2-diamine; *am3* = *N*,*N*′ -bis(3-aminopropyl)propane-1,3-diamine.

the complex (Fig. 5). The experimental data on magnetisation were perfectly reconstructed by using the thermodynamic partition function based upon the above mentioned magnetic parameters.

The magnetic properties of **3** show an almost constant effective magnetic moment of $\mu_{\mathrm{eff}} \approx 2.84\ \mu_{\mathrm{B}}$ (Fig. 7); this is a very typical feature of Ni(II) chains [59]. A fit to the equation suitable for an antiferromagnetic chain [59]

$$\bar{\chi}_{\mathrm{mol}} = \left(\frac{N_{\mathrm{A}}\mu_0\mu_{\mathrm{B}}^2}{k}\right)\frac{g_{\mathrm{Ni}}^2}{T}\,\frac{2 + 0.0194x + 0.777x^2}{3 + 4.346x + 3.232x^2 + 5.834x^3} \tag{4}$$

with $x = |J|/kT$ gave a negligible exchange coupling constant $J/hc = -0.07\ \mathrm{cm}^{-1}$ and $g_{\mathrm{Ni}} = 2.016$. This means that effectively a Curie-Weiss law holds true for isolated $S = 1$ centres. A fit with the simple Hamiltonian according to Eq. (1) gave $g_z = 2.002$, $g_x = 2.013$ and $D/hc = 1.81\ \mathrm{cm}^{-1}$.

The available magnetic data for related mononuclear, binuclear and polymeric Ni(II) complexes are collected in Table 4. (A more extensive tabulation can be found elsewhere [56]. Original literature sources can differ in definition of J and also D.) It can be seen that the local magnetogyric ratio falls into the interval $g_{\mathrm{Ni}} = 2.1$–2.4. The values of the local magnetic anisotropy ranges between moderate negative and positive values: $D_{\mathrm{Ni}}/hc = -12$ to $+7\ \mathrm{cm}^{-1}$ (with two exceptions). With small D-values the g-factor anisotropy is negligible and needs not to be accounted for. The only report that brings a value of the pair-wise magnetic anisotropy, $D_{\mathrm{Ni–Ni}}$ is the present communication. The isotropic exchange coupling constant in binuclear compounds varies between $J_{\mathrm{Ni–Ni}}/hc = -80$ to $+20\ \mathrm{cm}^{-1}$.

4. Supplementary material

Crystallographic data for the structural analyses have been deposited with the Cambridge Crystallographic Data Centre, CCDC Nos. 168452 (**1**), 220110 (**2**), 168453 (**3**). Copies of the data can be obtained free of charge from The Director, CCDC, 12 Union Road, Cambridge, CB2 1EZ, UK (fax: +44-(1223)-336033; email: deposit@ccdc.cam.ac.uk or www: http://www.ccdc.cam.ac.uk).

Acknowledgements

The authors are thankful to the Grant agencies (VEGA, 1/9252/02; APVT, 20-009902, Slovakia), as well as the Fonds der Chemischen Industrie (Germany) for generous financial support. M.B. is thankful to Humboldt Stiftung (TU Darmstadt, Germany).

References

[1] B.W. Brown, E.C. Lingafelter, Acta Crystallogr. 16 (1963) 753.
[2] A.E. Shvelashvili, M.A. Porai-Koshits, A.S. Antsyshkina, J. Struct. Chem. (USSR) 10 (1969) 552.
[3] J.M. Shi, C.Y. Shu, W.T. Yu, L.J. Sun, C.J. Wu, J.J. Lu, Pol. J. Chem. 75 (2001) 1067.
[4] K.O. Joung, C.J. O'Connor, E. Sinn, R.L. Carlin, Inorg. Chem. 18 (1979) 804.
[5] A.S. Antsyshkina, M.A. Porai-Koshits, Dokl. Akad. Nauk SSSR 143 (1962) 105.
[6] D.M. Duggan, D.N. Hendrickson, Inorg. Chem. 13 (1974) 2056.
[7] D.M. Duggan, D.N. Hendrickson, Inorg. Chem. 13 (1974) 2929.
[8] D.M. Duggan, D.N. Hendrickson, Inorg. Chem. 12 (1973) 2422.
[9] C.G. Pierpont, D.N. Hendrickson, D.M. Duggan, F. Wagner, E.K. Barefield, Inorg. Chem. 14 (1975) 604.
[10] A. Escuer, I. Castro, F. Mautner, M. Salah El Fallah, R. Vicente, Inorg. Chem. 36 (1997) 4633.
[11] F. Wagner, M.T. Mocella, M.J. D'Aniello Jr., A.H.-J. Wang, E. Kent Barefield, J. Am. Chem. Soc. 96 (1974) 2625.
[12] A. Escuer, R. Vicente, X. Solans, J. Chem. Soc., Dalton Trans. (1997) 531.
[13] M. Orendáč, A. Orendáčová, J. Černák, A. Feher, P.J.C. Signore, M.W. Meisel, S. Merah, M. Verdaguer, Phys. Rev. B52 (1995) 3535.
[14] J. Paharová, J. Černák, R. Boča, Z. Žák, Inorg. Chim. Acta 346 (2003) 25.
[15] B. Żurowska, J. Mrozinski, M. Julve, F. Lloret, A. Mašlejová, W. Sawka-Dobrowolska, Inorg. Chem. 41 (2002) 1771.
[16] C.A. van Albada, M.E. Quiroz-Castro, I. Mutikainen, U. Turpeinen, J. Reedijk, Inorg. Chim. Acta 298 (2000) 221.
[17] L. Jäger, Ch. Wagner, M. Korabik, A. Zygmunt, J. Mrozinski, J. Mol. Struct. 570 (2001) 159.
[18] J.W. Raebiger, J.L. Manson, R.D. Sommer, U. Geiser, A.L. Rheingold, J.S. Miller, Inorg. Chem. 40 (2001) 2578.
[19] P.M. van der Werff, S.R. Batten, P. Jensen, B. Mourbaraki, K.S. Murray, Inorg. Chem. 40 (2001) 1718.
[20] H. Miyasaka, R. Clerac, C.S. Campos-Fernandez, K.R. Dunbar, Inorg. Chem. 40 (2001) 1663.
[21] J. Mroziński, M. Hvastijová, J. Kohout, Polyhedron 11 (1992) 2867.
[22] M. Hvastijová, J. Kohout, M. Okruhlica, J. Mroziński, L. Jäger, Transit. Metal Chem. 18 (1993) 579.
[23] P. Jensen, S.R. Batten, G.D. Fallon, D.C.R. Hockless, B. Moubaraki, K.S. Murray, R. Robson, J. Solid State Chem. 145 (1999) 387.
[24] I. Dasna, S. Golhen, L. Ouahab, P. Pena, J. Guillevic, M. Fettouhi, J. Chem. Soc., Dalton Trans. (2000) 129.
[25] P. Jensen, S.R. Batten, G.D. Fallon, B. Moubaraki, K.S. Murray, D.J. Price, Chem. Commun. (1999) 177.
[26] J.L. Manson, C.R. Kmety, A.J. Epstein, J.S. Miller, Inorg. Chem. 38 (1999) 2552.
[27] S.R. Batten, P. Jensen, B. Moubaraki, K.S. Murray, R. Robson, Chem. Commun. (1998) 439.
[28] J.L. Manson, A.M. Arif, J.S. Miller, J. Mater. Chem. 9 (1999) 979.
[29] J.L. Manson, C. Campana, J.S. Miller, Chem. Commun. (1998) 251.
[30] S.R. Batten, B.F. Hoskins, R. Robson, J. Chem. Soc., Chem. Commun. (1991) 445.
[31] H. Hoshino, K. Iida, T. Kawamoto, T. Mori, Inorg. Chem. 38 (1999) 4229.
[32] J. Kožíšek, M. Hvastijová, J. Kohout, J. Mroziński, H. Köhler, J. Chem. Soc., Dalton Trans. (1991) 1773.
[33] J. Mroziński, J. Kohout, M. Hvastijová, Pol. J. Chem. 71 (1997) 883.

[34] M. Hvastijová, J. Kohout, J. Kožíšek, R. Boča, J. Buchler, L. Jäger, Coord. Chem. Rev. 175 (1998) 17.
[35] J. Kohout, L. Jäger, M. Hvastijová, J. Kožíšek, J. Coord. Chem. 51 (2000) 169.
[36] S.R. Batten, K.S. Murray, Coord. Chem. Rev. 246 (2003) 103.
[37] F. Březina, Z. Trávníček, Z. Šindelář, R. Pastorek, J. Marek, Transit. Metal Chem. 24 (1999) 459.
[38] M. Gembický, R. Boča, L. Jäger, C. Wagner, Inorg. Chem. Commun. 3 (2000) 566.
[39] R. Boča, M. Gembický, R. Herchel, W. Haase, L. Jäger, C. Wagner, H. Ehrenberg, H. Fuess, Inorg. Chem. 22 (2003) 6965.
[40] G.M. Sheldrick, SHELXS-97, Program for Crystal Structure DeterminationActa Crystallogr., 46 A, University of Göttingen, 1990, 467.
[41] G.M. Sheldrick, SHELXL-97, Program for the Refinement of Crystal Structures, University of Göttingen, 1997.
[42] K. Brandenburg, DIAMOND, Crystal Impact GbR, Visual Information System for Crystal Structures, V2.01d, 1996–2000.
[43] A.G. Orpen, L. Brammer, F.H. Allen, O. Kennard, D.G. Watson, R. Taylor, J. Chem. Soc., Dalton Trans. (1989) S1.
[44] D. Ghoshal, H. Bialas, A. Escuer, M. Font-Bardia, T. Kumar Maji, J. Ribas, X. Solans, R. Vicente, E. Zangrando, N.R. Chaudhuri, Eur. J. Inorg. Chem. (2003) 3929.
[45] J. Cho, U. Lee, J.C. Kim, Transit. Metal Chem. 27 (2002) 429.
[46] J. Kozisek, H. Paulus, M. Dankova, M. Hvastijova, Acta Crystallogr., Sect. C: Cryst. Struct. Commun. 52 (1996) 3019.
[47] A. Mohamadou, G.A. van Albada, H. Kooijman, B. Wieczorek, A.L. Spek, J. Reedijk, Nouv. J. Chim. 27 (2003) 983.
[48] J.F. Berry, F.A. Cotton, C.A. Murillo, J. Chem. Soc., Dalton Trans. (2003) 3015.
[49] B. Li, J. Ding, J. Lang, Z. Xu, J. Chen, J. Mol. Struct. 616 (2002) 175.
[50] P. Jensen, S.R. Batten, B. Moubaraki, K.S. Murray, Chem. Commun. (2000) 793.
[51] P.M. van der Werff, S.R. Batten, P. Jensen, B. Moubaraki, K.S. Murray, E.H.-K. Tan, Polyhedron 20 (2001) 1129.
[52] A.M. Kutasi, S.R. Batten, B. Moubaraki, K.S. Murray, J. Chem. Soc., Dalton Trans. (2002) 819.
[53] B.-W. Sun, S. Gao, B.-Q. Ma, D.-Z. Niu, Z.-M. Wang, J. Chem. Soc., Dalton Trans. (2000) 4187.
[54] S. Martin, M.G. Barandika, R. Cortes, J.I. Ruiz de Larramendi, M.K. Urtiaga, L. Lezama, M.I. Arriortua, T. Rojo, Eur. J. Inorg. Chem. (2001) 2107.
[55] J. Kohout, L. Jäger, M. Hvastijová, J. Kožíšek, J. Coord. Chem. 51 (2000) 169.
[56] R. Boča, Coord. Chem. Rev. 248 (2004) 757.
[57] R. Boča, Theoretical Foundations of Molecular Magnetism, Elsevier, Amsterdam, 1999.
[58] J. Cano, E. Ruiz, S. Alvarez, M. Verdaguer, Comments Inorg. Chem. 20 (1998) 27.
[59] O. Kahn, Molecular Magnetism, VCH, New York, 1993.
[60] S. Murakawa, T. Wakamatsu, M. Nakano, M. Sorai, H. Suga, J. Chem. Thermodyn. 19 (1987) 1275.
[61] A.P. Ginsberg, R.L. Martin, R.W. Brookes, R.C. Sherwood, Inorg. Chem. 11 (1972) 2884.
[62] M. Monfort, J. Ribas, X. Solans, Inorg. Chem. 33 (1994) 4271.
[63] J.C. Jansen, H. van Koningsveld, J.A.C. Van Ooijen, J. Reedijk, Inorg. Chem. 19 (1980) 170.
[64] M.I. Arriortua, R. Cortes, J.L. Mesa, L. Lezama, T. Rojo, G. Villeneuve, Transit. Metal Chem. 13 (1988) 371.
[65] M.I. Arriortua, R. Cortes, J.L. Mesa, L. Lezama, T. Rojo, X. Solans, M. Font-Bardia, Inorg. Chim. Acta 174 (1990) 263.
[66] R. Vicente, A. Escuer, J. Ribas, X. Solans, M. Font-Bardia, Inorg. Chem. 32 (1993) 6117.
[67] T. Rojo, R. Cortes, L. Lezama, M.I. Arriortua, K. Urtiaga, G. Willeneuve, J. Chem. Soc., Dalton Trans. (1991) 1779.
[68] M.S. Haddad, D.N. Hendrickson, Inorg. Chem. 17 (1978) 2622.

Available online at www.sciencedirect.com
SCIENCE DIRECT®
Polyhedron 23 (2004) 2349–2356
POLYHEDRON
www.elsevier.com/locate/poly

New metal(II) complexes containing monodentate and bridging 3-aminopyridine and azido ligands

Mohamed A.S. Goher [a,*], Afaf K. Hafez [a], Morsy A.M. Abu-Youssef [a], Ahmed M.A. Badr [a], Christian Gspan [b], Franz A. Mautner [b,*]

[a] Department of Chemistry, Faculty of Science, Alexandria University, P.O. Box 426, Ibrahimia, Alexandria 21321, Egypt
[b] Institut für Physikalische und Theoretische Chemie, Technische Universität Graz, A-8010 Graz, Austria

Received 17 March 2004; accepted 16 June 2004
Available online 11 September 2004

Abstract

Three new metal (II) complexes namely $[Mn(3\text{-ampy})_4(N_3)_2]$ (**1**), $[Cd(3\text{-ampy})(H_2O)_4]_n(SO_4)_n\cdot(H_2O)_n$ (**2**) and $[Cd(3\text{-ampy})(N_3)_2]_n$ (**3**) (3-ampy = 3-aminopyridine), have been synthesized and characterized by spectroscopic and crystallographic methods. The structure of **1** contains distorted octahedral Mn (II) atoms, monodentate 3-ampy and azide ligands. The structure of **2** consists of a packing of $[Cd(3\text{-ampy})(H_2O)_4]^{2+}$ cations and SO_4^{2-} anions and lattice water molecules. The Cd(1) center in the cation is coordinated by four O atoms from aqua molecules [Cd–O from 2.261(3) to 2.409(2) Å] and two N atoms; the hetero nitrogen atoms of 3-ampy [Cd–N 2.262(3) Å], whereas Cd(2) atom is surrounded by four aqua molecules and two nitrogen atoms of two amino groups of 3-ampy molecules [Cd–N 2.378(3) Å]. 3-Aminopyridine, therefore, acts as bidentate bridging ligands generating a 1D chain along $[0,1,-1]$. Different hydrogen bonds are formed extending the structure to a 3D network. Complex **3** contains dimeric units Cd_2N_2 through double μ-1,1 azide bridges, *N*,*N*′-3-ampy ligand and μ-1,3 azides generating a 3D network structure. There are hydrogen bonds of the type N–H···N between the NH_2 and azido groups consolidating the structure. The thermal properties of the three complexes have been recorded and discussed.
© 2004 Elsevier Ltd. All rights reserved.

Keywords: Mn(II) and Cd(II) complexes; Azides, 3-Aminopyridine; Synthesis; Spectra; X-ray structures; Thermal properties

1. Introduction

The chemistry of coordination polymers has evolved rapidly in recent years and a variety of topologies has been constructed through ligand design and the use of different transition metal geometries. These polymers may have interesting properties and applications, e.g. adsorption, ion exchange, non-linear optical and magnetic materials [1–6]. On the other hand, thermal properties of metal azido complexes have received very little attention [7], due to their sensitivity to friction and heat. This explosive nature, however, is dependent on the mode of bonding of bridged azides [8]. Thermal properties of azido complexes are important for determination of the temperature at which the complex explodes, as well as its stability above room temperature, particularly when phase transitions are expected.

We have recently reported a number of cadmium(II) azido and thiocyanato coordination polymers with some pyridine derivative ligands containing different bridging modes and topologies of the $[Cd(N_3)_2]_n$ and $[Cd(NCS)_2]_n$ chains [9–13]. We now extend our work to include the reaction of cadmium(II) and manganese(II) ions with 3-aminopyridine (3-ampy) in presence of azide or thiocyanate ions. In case of the azide ion, manganese(II) forms a 1:4, $Mn(N_3)_2$: 3-ampy complex, whereas a 1:1

* Corresponding authors.
E-mail addresses: masidahmed@hotmail.com (M.A.S. Goher), mautner@ptc.tu-graz.ac.at (F.A. Mautner).

0277-5387/$ - see front matter © 2004 Elsevier Ltd. All rights reserved.
doi:10.1016/j.poly.2004.06.011

complex is obtained between $Cd(N_3)_2$ and 3-ampy. In case of the thiocyanate ion, however, our trials afforded a mixture of few good quality crystals of a polymeric ionic complex containing sulfate anion rather than the desired thiocyanate complex. In this paper we report the synthesis and structural characterization of the three complexes for which we isolated suitable crystals for X-ray measurements.

2. Experimental

2.1. Materials and instrumentation

Elemental analyses were carried out using a perkin-Elmer analysis. Infrared spectra were recorded on a Bruker IFS-125 model FT-IR spectrophotometer as KBr pellets. Other physical measurements have been done as described previously [10]. 3-Aminopyridine was purchased from Aldrich company and other chemicals were of analytical grade quality and used as received.

Caution! Metal azide complexes are potential explosives. Only a small amount of material should be prepared and handled with caution.

2.2. Synthesis

2.2.1. $[Mn(3\text{-ampy})_4(N_3)_2]$ (**1**)

The complex was prepared by combining 15 ml of an aqueous solution of NaN_3 (0.98 g, 15 mmol) saturated with hydrazoic azid [9] with an aqueous solution (20 ml) of $Mn(NO_3)_2\cdot 4H_2O$ (1.88 g, 7.5 mmol) and 3-aminopyridine (5.10 g, 54 mmol). After 1 day transparent brown crystals were separated from the clear solution at room temperature. Yield: 55%. *Anal.* Calc.: C, 46.6; H, 4.7; Mn, 10.7; N, 38.0. Found: C, 46.3; H, 4.9; Mn, 10.9; N, 37.9%. IR, KBr (cm^{-1}) (v, very; s, strong; m, medium; w, weak; br, broad): 3449 m, 3378 m, 3324 s, 3214 m (H-bonded NH_2), 2063 vs (ν_{as}-N_3), 1341 wm (ν_s-N_3), 1628 m (NH_2 sessors), 1589 m, 1579 s, 1485 m, 1443 ms, 1301 ms, 1263 m, 1192 wm, 1098 wm, 1019 w, 806 m, 706 ms, 640 m, 546 w, 5 (pyridine vibrations).

2.2.2. $[Cd(3\text{-ampy})(H_2O)_4]_n(SO_4)_n(H_2O)_n$ (**2**)

This complex was prepared by mixing $3CdSO_4\cdot 8H_2O$ (0.55 g, 1.99 mmol) in water (30 cm^3) with 3-aminopyridine hydrochloride (0.370 g, 4.0 mmol) in methanol (5 cm^3). An aqueous solution (5 cm^3) of NaNCS (0.32 g, 4 mmol) was added dropwise with continuous stirring. The final solution mixture was filtered off and then allowed to stand for several days in a refrigerator to yield colorless crystals of the complex, suitable for X-ray diffraction (20% yield) and a pale yellow microcrystalline powder of the thiocyanato complex. Analytical data for the colorless crystals of $C_5H_{16}N_2O_9CdS$: Calc.: C, 15.3; H, 4.1; N, 7.1; Cd, 28.6. Found: C, 15.5; H, 4.4; N, 7.0; Cd, 28.9%. IR, KBr (cm^{-1}): 3229 s, 3261 s, 1587 ms, 1488 s, 1266 m, 1251 ms, 1203 ms, 1119 vs, br (ν3-SO_4^{2-}), 1053 w, 967 m, 933 m, 809 ms, 699 s, 645 wm, 620 vs (ν4-SO_4^{2-}), 595 ms, 533 wm. Analytical data of the yellow thiocyanato complex: $C_{12}H_{12}N_6CdS_2$: Calc.: C, 34.6; H, 2.9; N, 20.2; Cd, 27.0. Found: C, 34.8; H, 3.0; N, 20.0; Cd, 26.9%.

2.2.3. $[Cd(3\text{-ampy})(N_3)_2]_n$ (**3**)

This complex was prepared by addition of a methanol solution(5 cm) of 3-aminopyridine hydrochloride (0.5 g, 3.8 mmol) to 30 cm^3 aqueous solution of $3CdSO_4\cdot 8H_2O$ (0.5 g, 2 mmol) followed by drop wise addition of (0.5 g, 7.6 mmol) NaN_3 in water (10 cm). Colorless crystals suitable for X-ray diffraction were obtained by allowing the final mixture to stand over several days in a refrigerator. Yield for $C_5H_6N_8Cd$: 62%. *Anal.* Calc.: C, 20.7; H, 2.1; N, 38.5; Cd, 38.7. Found: C, 20.9; H, 2.2; N, 38.1; Cd, 38.8%. IR, KBr (cm^{-1}): 3450 m, 3323 s, 3267 s, 3157 m (H-bonded NH_2), 2116 vs (ν_{as}-N_3), 2040 vs (ν_{as}-N_3), 1585 s, 1491 m, 1448 s, 1327 s (ν_s-N_3), 1286 m, 1263 s, 1201 wm, 1101 wm, 1055 vm, 954 m, 926 vm, 799 m, 703 s, 645 m, 558 m.

2.3. X-ray crystallography

Single crystal X-ray data were measured at 90(2) K on a modified STOE four circle diffractometer using graphite crystal-monochromatized Mo Kα radiation (λ = 0.71069 Å). The intensities were corrected for Lorentz-polarisation effects, intensity decay and for absorption. Crystallographic data and processing parameters are given in Table 1. The structures were solved by direct methods and subsequent Fourier analyses. The program DIFABS [14] and the SHELXTL/PC program package [15] were used for computations. Analytical expressions of neutral-atom scattering factors were employed, and anomalous dispersion corrections were incorporated. Anisotropic displacement parameters were applied to non-hydrogen atoms in full-matrix least-squares refinements based on F^2. All hydrogen atoms were located from difference Fourier maps assigned with isotropic displacement factors and included in the final refinement cycles by use of geometrical restraints. Selected bond distances and bond angles are given in Tables 2–4, for complexes **1**, **2** and **3**, respectively.

3. Results and discussion

The reaction between manganese (II) ions and 3-ampy in presence of azide ion afforded a 1:4 complex (**1**), but in case of cadmium (II) ions a 1:2 complex (**3**) is obtained. In presence of the thiocyanate ions, however, cadmium (II) afforded few colorless crystals

Table 1
Crystallographic data and processing parameters

Compound	1	2	3
Empirical formula	$C_{20}H_{24}MnN_{14}$	$C_5H_{16}CdN_2O_9S$	$C_5H_6CdN_8$
Formula mass	515.47 392.68	290.59	
System	triclinic	triclinic	triclinic
Space group	$P\bar{1}$	$P\bar{1}$	$P\bar{1}$
a (Å)	7.609(2)	7.833(4)	6.625(3)
b (Å)	8.795(2)	8.339(3)	7.799(4)
c (Å)	9.640(2)	10.922(3)	8.923(5)
α (°)	91.60(2)	90.12(3)	71.14(3)
β (°)	101.26(2)	103.17(3)	88.34(3)
γ (°)	107.93(2)	111.73(3)	89.06(3)
V (Å^3)	599.3(2)	642.3(4)	436.1(4)
Z		1	2
μ(Mo Kα) (mm^{-1})	0.591	1.903	2.476
D_{calc} (Mg/m^3)	1.428	2.030	2.213
Approximate crystal size (mm)	$0.50 \times 0.25 \times 0.16$	$0.32 \times 0.18 \times 0.11$	$0.25 \times 0.10 \times 0.06$
θ range (°)	2.88–25.00	2.89–26.79	2.76–26.50
Reflections collected	2515	3188	2169
Independent reflections/R_{int}	2107/0.0263	2725/0.0213	1805/0.0210
Parameters	173	204	138
Goodness-of-fit on F^2	1.075	1.073	1.095
R_1 (observed/all data)	0.0348/0.0401	0.0297/0.0338	0.0261/0.0272
wR_2 (observed/all data)	0.0869/0.0958	0.0732/0.0767	0.0674/0.0683
Largest peak/hole (e/Å^3)	0.299/−0.291	0.702/−1.338	0.811/−0.993

Table 2
Selected bond lengths (Å) and angles (°) for (**1**)

Bond lengths			
Mn(1)–N(11)	2.209(2)	Mn(1)–N(11A)	2.209(2)
Mn(1)–N(3)	2.281(2)	Mn(1)–N(3A)	2.281(2)
Mn(1)–N(1)	2.312(2)	Mn(1)–N(1A)	2.312(2)
N(11)–N(12)	1.190(3)	N(12)–N(13)	1.165(3)
Bond angles			
N(11)–Mn(1)–N(11A)	180.0	N(11)–Mn(1)–N(3)	91.28(7)
N(3)–Mn(1)–N(3A)	180.0	N(11A)–Mn(1)–N(1)	91.31(7)
N(3)–Mn(1)–N(1A)	93.17(6)	N(1)–Mn(1)–N(1A)	180.0
N(12)–N(11)–Mn(1)	131.6(2)	N(13)–N(12)–N(11)	178.5(2)
Hydrogen bonds			
N(2)···N(11B)	3.132(3)	N(2)···N(13C)	3.099(3)
N(4)···N(13D)	3.075(3)	H(22)···N(11B)	2.27(2)
H(21)···N(13C)	2.21(2)	H(24)···N(13D)	2.19(2)
N(11B)···N(2)···N(13C)	109.48(8)	N(2)–H(22)···N(11B)	158(3)
N(2)–H(21)···N(13C)	168(3)	N(4)–H(24)···N(13D)	165(3)

Symmetry codes: (A) $-x+1,-y,-z+1$; (B) $-x,-y,-z+1$; (C) $x,y+1,z$; (D) $x+1,y,z$.

of a sulfate ionic complex (**2**) and a pale yellow 1:2 thiocyanato complex. The stoichiometry of complex **1** is quite different from that of a polymeric complex of the same components: $[\{Mn_2(3\text{-ampy})_4(N_3)_4(H_2O)\cdot 4H_2O\}_n]$ [16]. This later complex was synthesized by different route. Complexes **1** and **2** are soluble in solvents like DMSO and DMF giving non-conducting solutions for **1** and 1:1 electrolytes for **2**. Although **3** is less soluble in these solvents it gives non-conducting solutions.

3.1. Structures

3.1.1. *[Mn(3-ampy)$_4$(N$_3$)$_2$] (**1**)*

Fig. 1 illustrates the principle structural features of complex **1**. The structure consists of isolated *trans* coordinated manganese(II) polyhedra, in which the manganese center is located at an inversion center (Fig. 2). Each metal atom is linked by a pair of *trans* azido ligands and the hetero nitrogen atom from the four 3-ampy ligands. The terminal azido ligands are linear

Table 3
Selected bond lengths (Å) and angles (°) for (**2**)

Bond lengths			
Cd(1)–N(1A)	2.262(3)	Cd(1)–O(6A)	2.280(3)
Cd(1)–O(5A)	2.409(2)	Cd(2)–O(8B)	2.261(3)
Cd(2)–O(7B)	2.287(3)	Cd(2)–N(2B)	2.378(3)
N(2)–C(2)	1.425(4)	N(2)–H	0.91
O–H	0.85		
Bond angles			
N(1)–Cd(1)–O(6)	93.44(10)	N(1)–Cd(1)–O(5A)	91.07(9)
O(6)–Cd(1)–O(5A)	95.07(9)	O(8B)–Cd(2)–O(7B)	92.12(10)
O(7)–Cd(2)–N(2B)	93.53(10)	O(8B)–Cd(2)–N(2)	92.79(10)
C(2)–N(2)–Cd(2)	113.6(2)		
Hydrogen bonds			
O(5)···O(9) [$x-1,y,z$]	2.759(4)	O(5)···O(4)	2.771(4)
O(6)···O(2) [$1-x,-1-y,2-z$]	2.686(3)	O(6)···O(2) [$x-1,y,z$]	2.702(4)
O(7)···O(4) [$1-x,-1-y,1-z$]	2.746(3)	O(7)···O(4)	2.723(4)
O(8)···O(1) [$1-x,-y,1-z$]	2.687(4)	O(8)···O(9) [$1-x,-1-y,1-z$]	2.751(4)
O(9)···O(3)	2.786(4)	O(9)···O(3) [$2-x,-1-y,1-z$]	2.750(3)
N(2)···O(3) [$x-1,y,z$]	3.118(4)	N(2)···O(5) [$x,1+y,z$]	3.250(4)

Symmetry codes: (A) $-x+1,-y-1,-z+2$; (B) $-x+1,-y,-z+1$.

Table 4
Selected bond lengths (Å) and angles (°) for (**3**)

Bond lengths			
Cd(1)···Cd(1A)	3.655(2)	Cd(1)···Cd(1B)	6.282(4)
Cd(1)···Cd(1C)	6.475(4)	Cd(1)···Cd(1D)	6.661(4)
Cd(1)–N(31)	2.273(3)	Cd(1)–N(1)	2.319(3)
Cd(1)–N(11)	2.324(3)	Cd(1)–N(21)	2.370(3)
Cd(1)–N(2)	2.455(3)	N(11)–N(12)	1.204(4)
N(12)–N(13)	1.146(4)	N(21)–N(22)	1.176(3)
N(22)–N(21B)	1.176(3)	N(31)–N(32)	1.171(3)
N(32)–N(31C)	1.171(3)	C(2)–N(2D)	1.410(4)
Bond angles			
N(31)–Cd(1)–N(1)	87.88(11)	N(31)–Cd(1)–N(11)	170.41(10)
N(1)–Cd(1)–N(11)	101.71(11)	N(31)–Cd(1)–N(11A)	94.07(11)
N(1)–Cd(1)–N(11A)	177.41(9)	N(11)–Cd(1)–N(11A)	76.35(12)
N(31)–Cd(1)–N(21)	90.69(11)	N(1)–Cd(1)–N(21)	87.81(11)
N(11)–Cd(1)–N(21)	89.68(11)	N(11A)–Cd(1)–N(21)	93.87(11)
N(31)–Cd(1)–N(2)	92.27(10)	N(1)–Cd(1)–N(2)	86.02(10)
N(11)–Cd(1)–N(2)	88.44(11)	N(11a)–Cd(1)–N(2)	92.19(10)
N(21)–Cd(1)–N(2)	173.05(10)	N(12)–N(11)–Cd(1)	130.4(2)
N(12)–N(11)–Cd(1A)	125.6(2)	Cd(1)–N(11)–Cd(1A)	103.65(12)
N(13)–N(12)–N(11)	179.5(3)	N(22)–N(21)–Cd(1)	121.0(2)
N(21B)–N(22)–N(21)	180.0	N(32)–N(31)–Cd(1)	137.8(2)
N(31)–N(32)–N(31C)	180.0		
N(2)···N(21E)	3.125(4)	N(2)···N(13F)	3.090(5)
N(2)–H(6)···N(21E)	168(3)	N(2)–H(7)···N(13F)	173(3)

Symmetry codes: (A) $-x+1,-y+1,-z+2$; (B) $-x,-y+1,-z+2$; (C) $-x+1,-y+1,-z+1$; (D) $-x+1,-y+2,-z+1$; (E) $x+1,y,z$; (F) $-x+1,-y+2,-z+2$.

and asymmetric [N(11)–N(12) = 1.190(3), N(12)–N(13) = 1.165(3) Å, N(11)–N(12)–N(13) = 178.5(2)°]; as for other metal complexes with terminal azides, the shorter N–N bonds are more remote from the metal atom. The Mn–N(3-ampy) bond lengths are comparable with corresponding values found in the structure of [Mn(picolinate) $(N_3)(H_2O)]_n$ [2.278(3) Å] [17] and [Mn(4-acetylpyridine)$_2(N_3)_2]_n$ [2.291(3) Å] [18], but little longer than those reported in the structure of *trans*-[Mn(3-picoline)$(N_3)_2(H_2O)_2$] [2.252(27) Å] [19] and polymeric [Mn(pyridine)$_2(N_3)_2]_n$ [2.259(3) Å] [20]. The structure of **1** is consolidated by hydrogen bonds of the type N–H···N between the NH_2 group of 3-ampy and the uncoordinated nitrogen atom of terminal azides (Fig. 1).

The structure of **1** closely related to that of [Mn(pyrazole)$_4(N_3)_2$] [21] (**4**) with subtle differences. Although the pyrazole complex contains isolated coordinated

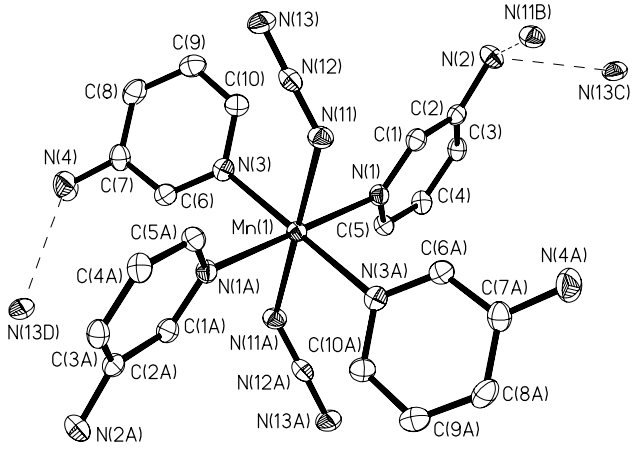

Fig. 1. Perspective view and atom labeling scheme of [Mn(3-ampy)$_4$(N$_3$)$_2$] (**1**). Broken lines indicate hydrogen bonds.

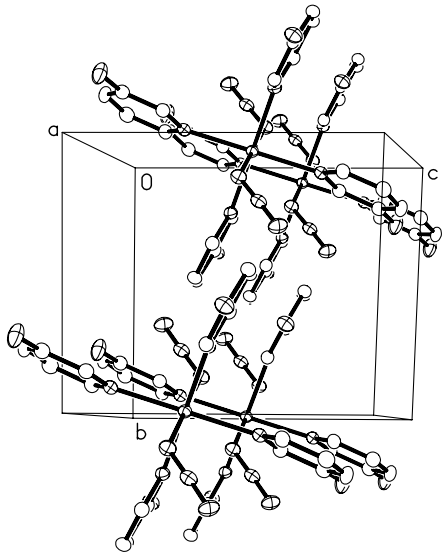

Fig. 2. Packing plot of [Mn(3-ampy)$_4$(N$_3$)$_2$] (**1**) along *a*-axis of unit cell.

manganese and contains N–H···N bonds between the NH of pyrazole and the uncoordinated nitrogen atom of terminal azides, its crystals are monoclinic with *C*2/*c* space group. The structural parameters for **4**, are : Mn(1)–N(11) = 2.182(4) Å, Mn–N(pyrazole) from 2.249(4) to 2.265(4) Å, N(12)–N(11)–Mn(1) = 38.0(4)°, N(11)–N(12) = 1.187(6) and N(12)–N(13) = 1.145(4) Å.

3.1.2. [Cd(3-ampy)(H$_2$O)$_4$]$_n$(SO$_4$)$_n$(H$_2$O)$_n$ (**2**)

The atom labeling scheme for complex **2** is shown in Fig. 3. The structure of **2** consists of a packing of [Cd(3-ampy)(H$_2$O)$_4$]$^{2+}$ cation, SO_4^{2-} anion and lattice water molecule. The cation contains two crystallographically different Cd centers. Cd(1) atom is *trans* coordinated by two hetero N atoms of 3-ampy ligands [Cd(1)–N(1) = 2.262(3) Å] whereas Cd(2) is *trans* coordinated by two amino N atoms of two 3-ampy molecules [Cd(2)–N(2) = 2.378(3) Å], in addition to four aqua molecules for each Cd center [Cd–O from 2.261(3) to 2.409(2) Å]. Thus 3-aminopyridine behaves as a *N*,*N*′-bidentate bridging ligand giving a 1D chain along [0, 1, −1] direction. Both Cd(II) centers are located at inversion centers. The intrachain Cd···Cd distance is 6.878(4) Å and the Cd(2)–N(2)–C(2) angle is 113.6(2)°. The interchain Cd···Cd distances are 6.864(4), 7.833(4) and 8.049(4) Å. Complex **2** contains different types of hydrogen bonds consolidating the structure: (a) O–H···O hydrogen bond between oxygen atoms of the SO_4^{2-} anion and oxygen atoms of aqua molecules and/or lattice water molecules, (b) O–H···O bond between oxygen atoms of aqua molecules and lattice water. These hydrogen bonds connect the 1D chains generating a supramolecular 3D network structure (Fig. 4).

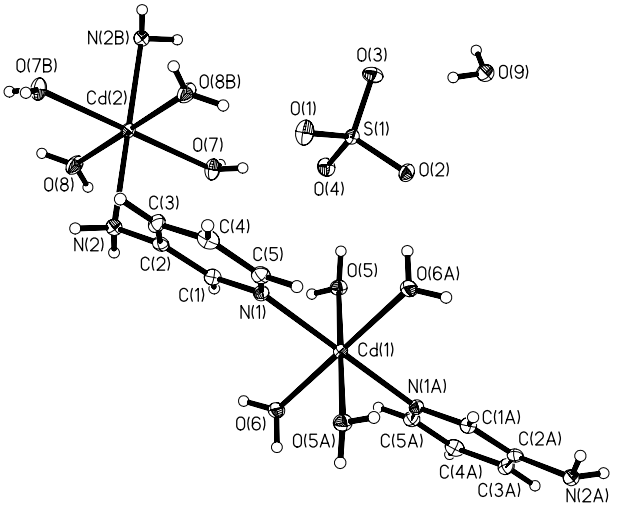

Fig. 3. [Cd(3-ampy)(H$_2$O)$_4$]$_n$(SO$_4$)$_n$(H$_2$O)$_n$ (**2**): perspective view with atom labeling scheme.

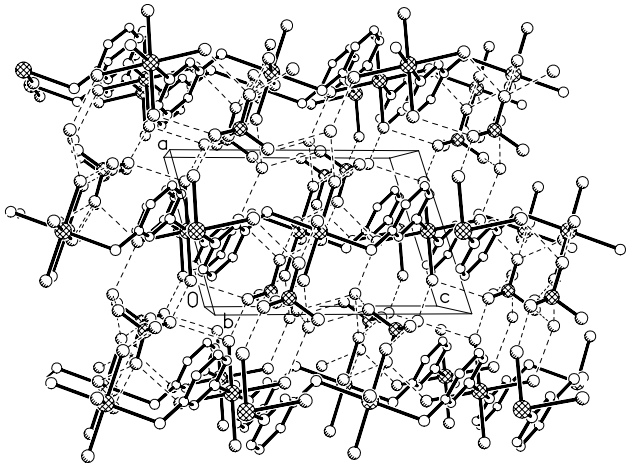

Fig. 4. [Cd(3-ampy)(H$_2$O)$_4$]$_n$(SO$_4$)$_n$(H$_2$O)$_n$ (**2**): packing view along the *b*-axis of the unit cell. Broken lines indicate hydrogen bonds.

3.1.3. $[Cd(3\text{-ampy})(N_3)_2]_n$ (3)

The principle structural features of complex **3** are illustrated in Fig. 5. In this structure each Cd(II) center is six-coordinated by four azido groups [Cd–N distances from 2.273(3) to 2.370(3) Å], a hetero N atom of 3-ampy [Cd–N = 2.319(3) Å] and the amino N atom of another 3-ampy ligand [Cd–N = 2.455(3) Å]. Two of the four azido groups act as μ(1,1) bridges [N(11)–N(12)–N(13)] linking two Cd(II) centers forming four-member Cd_2N_2 rings. The *N*,*N*′-bridging 3-ampy connect the Cd_2N_2 rings forming 1D subunits. These 1D subunits are connected via the other two μ(1,3) azide bridges (with their central nitrogen atoms N(22) and N(32) located at inversion centers) giving rise to a 3D network structure for **3** (Fig. 6). While the μ(1,1) azides are asymmetric the μ(1,3) bridges are symmetrical (Table 4), both types, however are linear [N–N–N angles 179.5(3)° and 180°]. The Cd···Cd distances are 3.655(2) Å in the four-member rings and 6.282(4)–6.661(4) Å in the other rings. The Cd–N_3 sublattice with *cis*-arrangement of 3-ampy ligands is similar to that of Mn(II) complex $[Mn(L)(N_3)_2]_n$ (L=4,4′-dimethyl-2,2′-bipyridine) [22]. The structure of **3** is further consolidated by two hydrogen bonds between the amino group and N atoms of a μ(1,1) and a μ(1,3) azide bridges [N···N distances are 3.125(4) and 3.090(4) Å] (Fig. 5).

At this point it is noteworthy to mention that although the metal center is octahedrally coordinated in the three complexes, 3-aminopyridine acts as a monodentate ligand in **1**, whereas it behaves as a *N*,*N*′-bidentate bridge in **2** and **3**. For complex **1** this is expected from ist chemical composition of 1:4 metal:3-ampy ratio, and is similar to that found in the structure of $[\{Mn_2(3\text{-ampy})_4(N_3)_4(H_2O)\}]_n$ [16] and $[\{Cu_2(3\text{-ampy})_4(N_3)_2(NO_3)_2\}(C_2H_5OH)]_n$ [23]. In case of **2**, this complex, which contains the sulfate counter ion, crystallizes with four aqua molecules, and as it contains only one 3-ampy, two of such molecules are expected to behave as *N*,*N*′-bidentate bridges to occupy the last two positions of each Cd center. In **3**, the $[Cd(N_3)_2]_n$ sublattice is similar to that of $[Mn(N_3)_2]_n$ found in the structures of many $[MnL_2(N_3)_2]_n$ complexes [24–26], in which the azides occupy four sites of the six positions around each metal center, and therefore the existing single 3-ampy per Cd is expected to act as *N*,*N*′-bridge, as in **2**, in order to complete the octahedral geometry. The *N*,*N*′-bridging mode of the 3-ampy ligand was observed in the dinuclear complex $[Ni(NCS)_2(3\text{-ampy})_2(H_2O)]_2\cdot 2H_2O$ [27]. To the best of our knowledge, in all other structurally characterized metal-(3-ampy) or related metal-(5,5′-diamino-2,2′-bipyridine) complexes, the aminopyridine ligand binds the metal center through the heterocyclic N atom and the amino group only functions as a hydrogen bond donor [28–35].

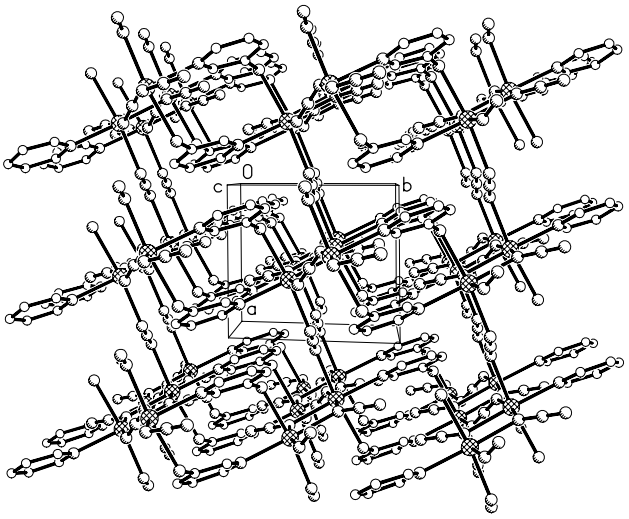

Fig. 6. Packing plot of $[Cd(3\text{-ampy})(N_3)_2]_n$ (**3**) viewed along the *c*-axis of the unit cell.

3.2. Spectra

The IR spectrum of **1** shows the vibrations of the hydrogen bonded NH_2 group as sharp bands at 3448

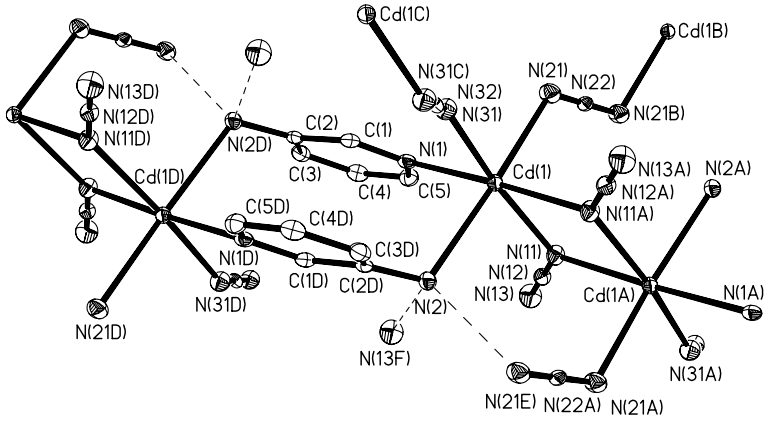

Fig. 5. Perspective view of $[Cd(3\text{-ampy})(N_3)_2]_n$ (**3**) with atom labeling scheme. Symmetry codes according to Table 4. Broken lines indicate hydrogen bonds.

ms, 3376 s, 3324 ms, 3214 ms, but the 1629 cm^{-1} (NH_2-sessors) band remains at the same position as in the spectrum of free 3-ampy, suggesting that the amino group is not involved in complexation. The position of the 2063 cm^{-1} (ν_{as}-N_3) falls within the absorption range of terminal azides in Mn(II) complexes [19,20], and the appearance of the ν_s-N_3 band at 1341 cm^{-1} indicates the asymmetric nature of the azide groups in **1**. The medium intensity broad band in the range 3500–3000 cm^{-1} with two strong peaks at 3329 and 3261 cm^{-1} in the IR spectrum of **2** is due to hydrogen bonded aqua and lattice molecules as well as NH_2 group. The disappearance of the 1629 cm^{-1} band from the IR spectrum of **2** suggests the participation of the NH_2 group in complex formation. The systematic blue shifts of the vibration bands due to pyridine moiety indicate that 3-ampy behaves as *N*,*N*′ bidentate bridging ligand in complex **2**. The ionic nature of the SO_4^{2-} group is indicated by the appearance of a very strong broad band centered around 1120 cm^{-1} (ν_3) and a sharp band at 620 cm^{-1} (ν_4) [36]. The IR spectrum of **3** is very similar to that of **2** for the NH_2 and pyridine ring vibrations, indicating that 3-ampy acts as a *N*,*N*′ bidentate bridging ligand and that NH_2 is H-bonded. Additionally, the spectrum exhibits two very strong bands at 2116 and 2040 cm^{-1} due to $\nu_{as}(N_3)$. The 2040 cm^{-1} band falls well within the range for μ(1,3) azide bridges [37], whereas the 2116 cm^{-1} is due to the μ(1,1) bridges [38].

The room temperature X-band ESR spectrum of polycrystalline samples of the manganese complex (**2**) have been recorded. The spectrum shows a broad intense isotropic signal centered at $g = 2.0$. In DMSO the spectrum of **1** shows a hyperfine structure due to Mn(II) ($I = 5/2$) with (A) of 92 G. These spectra of the solid as well as DMSO solution are very similar to those of hexa-coordinate manganese(II) complexes [39].

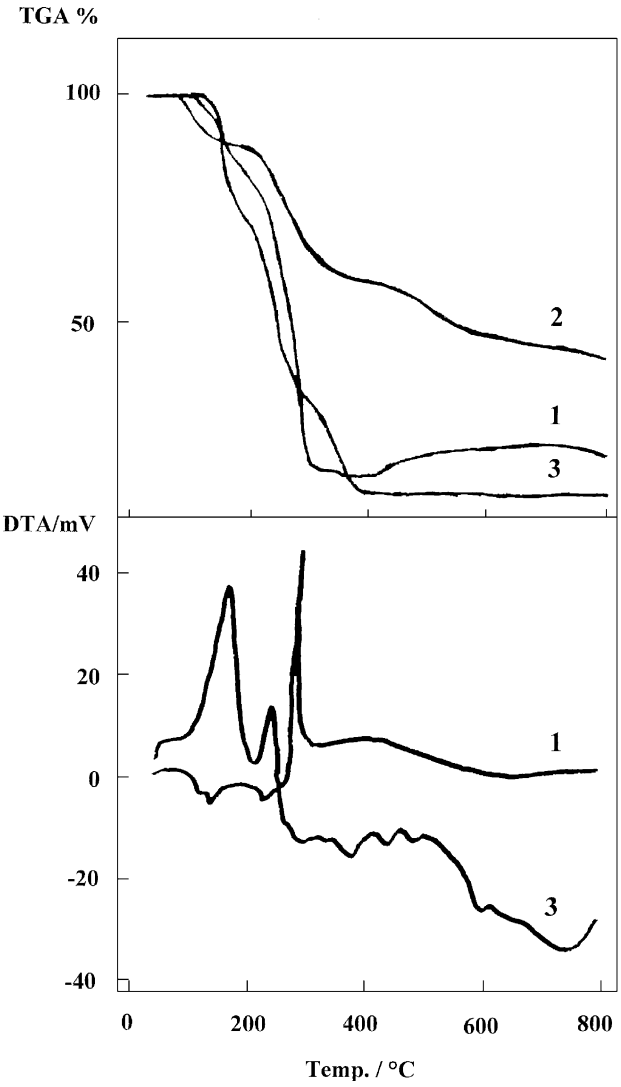

Fig. 7. Thermal behaviour of complexes **1**–**3**.

3.3. Thermal properties

The results of the thermal decomposition of complexes **1**, **2** and **3** are represented in Fig. 7. The first step of the thermal decomposition of **1** consists of a loss of one azide group and two amino groups from two 3-ampy ligands (loss of weight; exper. 13.9% and theor. 14.2%). The DTA shows two successive endothermic peaks with maxima at 125 and 150 °C. The residual polymeric complex is not stable and decomposes immediately with a weight loss of 33.2% which corresponds a loss of one py moiety and one 3-ampy. The theoretical loss in this step (160–254 °C) is 33.4%. In the third step the loss of 35.5%, is suggestive of the loss of 3-ampy, py and one nitrogen atom from the azide group (theor. loss 36.1%) with a residue of 17.4%. These two steps, however, are not well separated, suggesting that they are two stages of one step rather than two steps as seen from the TG curve. The DTA curve shows a weak endothermic peak at 260 °C followed by an exothermic peak at 335 °C. The weight of the final residue is a little higher than that corresponding to MnN_2 (16.1%). As the decomposition takes place under air, it is possible to suggest that the residue is MnO_2 (16.9%). The TG curve shows that the residual weight is about 15.5% just below 400 °C, increases again above 410 °C and reaches about 17%. The thermal decomposition of **1** differs from that of the corresponding $Mn(pyrazole)_4(N_3)_2$ [21].

The first step of decomposition of **2** starts at 80 °C with a weight loss of 9.6% which corresponds to the loss of two H_2O molecules (theor. loss 9.2%). In the second step (140–327 °C) the weight loss of 29.7% corresponds to the loss of 3-ampy and 1.25 water molecules (29.7%) leaving $CdSO_4 \cdot 1.75H_2O$, as a residue. In the third step which ends around 800 °C, the weight loss is 20%, which is less than that required for complete decomposition of the $CdSO_4 \cdot 1.75H_2O$, additionally the final residue weight is about 41%, which is much higher than that

assuming the final product to be CdO (32%). According to a previous study [40] the initial decomposition temperature of $CdSO_4$ is around 780 °C depending on the heating rate and the complete decomposition occurs around 950 °C. As a consequence the weight loss of 20% in this step is due to the loss of the water molecules and the decomposition of some $CdSO_4$.

Complex **3** loses an azide and N atom of the amino group of 3-ampy ligand with a weight loss of 18.8% (Theor. 19.3%). This step appears in the DTA curve as a strong exotherm at 168.6 °C. In the second step the weight loss of 30.1% is a little higher than the loss of 3-ampy ligand residue (27.6%) suggesting that the release of the second azide group starts before the third step, and this appears in the DTA curve as a weak exotherm at 241.9 °C. The DTA curve shows the last step as several weak endotherms, the first peak at 374 °C. The final residue of 34.5% is less than that calculated assuming only Cd (38.6%), suggesting that some explosion takes place.

4. Supplementary material

Supplementary data are available from the CCDC, 12 Union Road, Cambridge CB2 1EZ, UK (Fax: +44-1223-336-033 or e-mail: deposit@ccdc.cam.ac.uk or www: http://www.ccdc.cam.ac.uk), on request, quoting the deposition numbers: CCDC-233523–CCDC-233525 for **1**–**3**.

Acknowledgements

F.A.M. thanks Prof. Kratky and Prof. Belaj (Univ. Graz) for the use of the STOE 4-circle diffractometer.

References

[1] R.F. Hoskins, R. Robson, J. Am. Chem. Soc. 112 (1990) 1564.
[2] M. Fujita, Y.J. Kwan, S. Washizu, K. Ogura, J. Am. Chem. Soc. 116 (1994) 1151.
[3] O.M. Yaghi, J. Li, J. Am. Chem. Soc. 117 (1995) 10401.
[4] P.J. Hagrman, D. Hagrman, J. Zubieta, Angew. Chem., Int. Ed. Engl. 38 (1999) 2638.
[5] C. Janiak, J. Chem. Soc., Dalton Trans. (2003) 2781.
[6] S.L. James, Chem. Soc. Rev. 32 (2003) 267.
[7] M.A.S. Goher, Thermochim. Acta 336 (1999) 61, and refs. therein.
[8] I. Agrell, Acta Chem. Scand. 24 (1970) 3575, and refs. therein.
[9] M.A.S. Goher, F.A. Mautner, M.A.M. Abu-Youssef, A.K. Hafez, A.M.A. Badr, J. Chem. Soc., Dalton Trans. (2002) 3309.
[10] M.A.S. Goher, F.A. Mautner, A.K. Hafez, M.A.M. Abu-Youssef, C. Gspan, A.M.A. Badr, Polyhedron 22 (2003) 975.
[11] F.A. Mautner, C. Gspan, M.A.S. Goher, M.A.M. Abu-Youssef, Monatsh. Chem. 134 (2003) 1311.
[12] M.A.S. Goher, F.A. Mautner, M.A.M. Abu-Youssef, A.K. Hafez, A.M.A. Badr, C. Gspan, Polyhedron 22 (2003) 3137.
[13] F.A. Mautner, C. Gspan, K. Gatterer, M.A.S. Goher, M.A.M. Abu-Youssef, E. Bucher, W. Sitte, Polyhedron 23 (2004) 1217.
[14] H. Walker, D. Stuart, Acta Crystallogr. A 39 (1983) 158.
[15] SHELXTL/PC 5.03, Siemens Analytical Automation, Inc., Madison, W1, 1995.
[16] M.A.M. Abu-Youssef, A. Escuer, M.A.S. Goher, F.A. Mautner, R. Vicente, J. Chem. Soc., Dalton Trans. (2000) 413.
[17] M.A.S. Goher, M.A.M. Abu-Youssef, F.A. Mautner, A. Popitsch, Polyhedron 11 (1992) 2137.
[18] A. Escuer, R. Vicente, M.A.S. Goher, F.A. Mautner, Inorg. Chem. 34 (1995) 5707.
[19] M.A.S. Goher, F.A. Mautner, Cryst. Res. Technol. 25 (1990) 1271.
[20] M.A.S. Goher, F.A. Mautner, Croat. Chim. Acta 63 (1990) 559.
[21] M.A.S. Goher, F.A. Mautner, M.A.M. Abu-Youssef, Trans. Met. Chem. 24 (1999) 29.
[22] Z. Shen, J.-L. Zuo, Z. Yu, Y. Zhang, J.-F. Bai, C.-M. Che, H.-K. Fun, J.J. Vittal, X.-Z. You, J. Chem. Soc., Dalton Trans. (1999) 3393.
[23] A. Escuer, M.A.S. Goher, F.A. Mautner, R. Vicente, Inorg. Chem. 39 (2000) 2107.
[24] M.A.S. Goher, F.A. Mautner, N.A. Al-Salem, J. Coord. Chem. 44 (1998) 119.
[25] A. Escuer, R. Vicente, M.A.S. Goher, F.A. Mautner, Inorg. Chem. 35 (1996) 6386.
[26] A. Escuer, R. Vicente, M.A.S. Goher, F.A. Mautner, Inorg. Chem. 36 (1997) 3440.
[27] M.H. Moore, L.R. Nassimbeni, M.L. Niven, Inorg. Chim. Acta 132 (1987) 61.
[28] F. Vallach, M. Dunaj-Jurco, Acta Crystallogr. B 38 (1982) 2145.
[29] A. Sekine, Y. Ohashi, Bull. Chem. Soc. Jpn. 64 (1991) 2183.
[30] O. Castillo, A. Luque, P. Roman, F. Lloret, M. Julve, Inorg. Chem. 40 (2001) 5526.
[31] L.-G. Zhu, S. Kitagawa, Z. Kristallgr.–New Cryst. Struct. 217 (2002) 579.
[32] X.-J. Yang, B. Wu, W.-H. Sun, C. Janiak, Inorg. Chim. Acta 343 (2003) 366.
[33] I. Csoregh, G. Kennessey, T. Wadsten, G. Liptay, B.R. Carson, Z. Kristallogr. 215 (2000) 547.
[34] X.-Y. Huang, R.-G. Xiong, X.-Z. You, Acta Crystaollgr. C 51 (1995) 2261.
[35] C. Janiak, S. Deblon, H.-P. Wu, M.J. Kolm, P. Klüfers, H. Piotrowski, P. Mayer, Eur. J. Inorg. Chem. (1999) 1507.
[36] K. Nakamoto, Infrared Spectra of Inorganic and Coordination Compounds, 2nd ed., Wiley, New York, 1978.
[37] (a) M.A.S. Goher, Acta Chim. Hung. 117 (1984) 215;
(b) Z. Dori, R.F. Ziolo, Chem. Rev. 31 (1973) 247.
[38] (a) J.L. Manson, A.M. Arif, J.S. Miller, J. Chem. Soc., Chem. Commun. (1999) 1479;
(b) J. Ribas, M. Monfort, B.K. Ghosh, X. Solans, Angew. Chem., Int. Ed. Engl. (1994) 2087;
(c) X. Hao, Y. Wei, S.-W. Zhung, J. Chem. Soc., Chem. Commun. (2000) 2271.
[39] (a) B.R. Srinivasan, S. Sakar, Inorg. Chem. 29 (1990) 3898;
(b) T.S. Lobana, N. Bala, Trans. Met. Chem. 19 (1994) 115;
(c) G. Batra, P. Mathur, Trans. Met. Chem. 19 (1004) 160.
[40] H. Tagawa, Thermochim. Acta 80 (1984) 23.

Available online at www.sciencedirect.com
SCIENCE DIRECT®
Polyhedron 23 (2004) 2357–2362
POLYHEDRON
www.elsevier.com/locate/poly

Hydrothermal synthesis and characterization of a new 3D iron phosphatooxalate templated by organo-amine

He Meng, Guang-Hua Li, Yan Xing, Yu-Lin Yang, Yan-Jie Cui, Li Liu, Hong Ding, Wen-Qin Pang *

State Key Laboratory of Inorganic Synthesis and Preparative Chemistry, College of Chemistry, Jilin University, Changchun 130012, P.R. China

Received 16 March 2004; accepted 7 July 2004
Available online 11 September 2004

Abstract

A new organically templated iron(II) phosphatooxalate, $(N_2C_4H_{12})[Fe_4(C_2O_4)_3(HPO_4)_2(H_2O)_2]$ **I**, has been synthesized under hydrothermal conditions and characterized by single-crystal X-ray diffraction. The structure possesses infinite chains made from Fe_2O_{10} dimers and PO_4 tetrahedra bridged by bidentate oxalate units and strong interlayer P–O–H-oxalate hydrogen bonds. The diprotonated piperazinium cations are located in the intersecting tunnels parallel to the [1 0 0] and [0 1 0] directions.
© 2004 Elsevier Ltd. All rights reserved.

Keywords: Hydrothermal synthesis; Crystal structure; Iron phosphatooxalate; Template; Oxalate acid; Piperazine

1. Introduction

The study of framework materials continues to be of interest not only because of the wide variety of structures but also due to their potential applications in the areas of catalysis, sorption and separation processes [1]. Recent developments in the area of hybrid structures have placed special emphasis on metal phosphate chains or layers that are connected by oxalate moieties. Up to now, a few metal phosphatooxalates such as Al [2], V [3], Co [4], Mn [5], Zn [6] and Ga [7] have been reported in the literature. Most of the framework inorganic materials are normally synthesized under mild hydro/solvothermal conditions in the presence of a structure-directing agent. It has been shown recently that the oxalate units generally cross-link the inorganic parts and act as a bridge in the phosphatooxalates. In recent years, several iron phosphatooxalates [8] have also been expatiated, which exhibit interesting magnetic properties originating from the super-exchange interactions that are predominantly antiferromagnetic, involving the iron phosphates and the oxalate moieties. Here we report the synthesis, crystal structure, Mössbauer and magnetic behavior of a new iron phosphatooxalate $(N_2C_4H_{12})[Fe_4(C_2O_4)_3(HPO_4)_2(H_2O)_2]$ **I**, which was synthesized hydrothermally using piperazine as the template.

2. Experimental

Compound **I** was synthesized under hydrothermal conditions in a 15 ml Teflon-lined autoclave under autogenous pressure. The reagents used were deoxidized ferric powder (Beijing Chemical Plant, A.R.), phosphoric acid (Beijing Chemical Plant, 85%), oxalic acid dihydrate (Beijing Chemical Plant, A.R.), piperazine (PIP, Acros, 99%) and deionized water.

* Corresponding author. Tel.: +86 431 5168546; fax: +86 431 5168624.
E-mail address: wqpang@mail.jlu.edu.cn (W.-Q. Pang).

0277-5387/$ - see front matter © 2004 Elsevier Ltd. All rights reserved.
doi:10.1016/j.poly.2004.07.016

2.1. Synthesis and characterization

In a typical synthesis, a mixture of Fe:$2H_3PO_4$:1.6-PIP:$1.1H_2C_2O_4$:$155.6H_2O$ was stirred to form a homogeneous solution. The reaction was carried out in a Teflon-lined stainless-steel autoclave (70% filling rate) at 393 K for ca. 48 h. The product was cleaned by ultrasonication and filtration, washed with distilled water several times, and dried at room temperature. The final product consisted of pale green plates with a small amount of black solid.

The powder X-ray diffraction (XRD) pattern was recorded on a Siemens D5005 diffractometer with Cu Kα radiation ($\lambda = 1.5418$ Å). Element analyses were performed on a Perkin–Elmer 2400 element analyzer and the inductively coupled plasma (ICP) analysis on a Perkin–Elmer Optima 3300 DV ICP instrument. Thermogravimetric analysis (TGA) was conducted on a Netzsch STA 449C thermogravimetric analyzer with a heating rate of 10 °C min^{-1} in air. Magnetic susceptibility data were obtained on polycrystalline samples from 2 to ca. 300 K in a magnetic field of 5k Oe after zero-field cooling using a Quantum Design MPMS-7 SQUID magnetometer. The ^{57}Fe Mössbauer measurements were made on a XOFORD-500 instrument at room temperature. Isomer shifts are reported with respect to an iron foil standard at 300 K.

2.2. Determination of crystal structure

The intensity data were collected on a Siemens Smart CCD diffractometer equipped with a normal-focus, 2.4 kW sealed-tube X-ray source (graphite-monochromated Mo Kα radiation, λ(Mo Kα) = 0.71073 Å) operating at 50 kV and 40 mA. The structure was solved by direct methods and refined by full-matrix least-squares on F^2 using SHELXTL [10]. Version 5.1 [9]. It is noteworthy that the atoms (C5, C6, N1, N2) of piperazine are disordered over two positions with occupancy factors 0.5 in the crystal structure, and H atoms on the coordinated water molecules of Fe(2) in **I** were not located because of the large thermal parameter of $O(9)_w$. Further details of the X-ray structural analysis are given in Table 1.

Table 1
Crystal data and structure refinement for compound **I**

Empirical formula	$C_{10}H_{18}Fe_4N_2O_{22}P_2$
Formula weight	803.60
Temperature (K)	293(2)
Wavelength (Å)	0.71073
Crystal system	triclinic
Space group	$P\bar{1}$
Unit cell dimensions	
a (Å)	7.6329(2)
b (Å)	7.9591(3)
c (Å)	9.7361(3)
α (°)	75.74(1)
β (°)	79.87(2)
γ (°)	85.83(2)
Volume (Å^3)	564.05(3)
Z	1
D_{calc} (mg/m^3)	2.366
Absorption coefficient (mm^{-1})	2.776
F (000)	402
Crystal size (mm)	$0.11 \times 0.11 \times 0.09$
θ Range for data collection (°)	2.19–30.01
Limiting indices	$-8 \leqslant h \leqslant 10$, $-11 \leqslant k \leqslant 11$, $-13 \leqslant l \leqslant 10$
Reflections collected/unique	4630/3237 [R_{int} = 0.0320]
Completeness to θ = 30.01 (%)	98.2
Absorption correction	empirical
Maximum and minimum transmission	0.3494 and 0.2673
Refinement method	full-matrix least-squares on F^2
Data/restraints/parameters	3237/0/203
Goodness-of-fit on F^2	0.987
Final R indices [$I>2\sigma(I)$]	[a]R_1 = 0.0342, [b]wR_2 = 0.0866
R indices (all data)	[a]R_1 = 0.0486, [b]wR_2 = 0.0919
Largest different peak and hole (e Å^{-3})	0.798 and −0.560

[a] $R_1 = \sum || F_o | - | F_c || / \sum | F_o |$.
[b] $wR_2 = [\sum[w(F_o^2 - F_c^2)^2] / \sum[w(F_o^2)^2]]^{1/2}$.

3. Results and discussion

3.1. Characterization

The experimental and simulated powder X-ray diffraction patterns are in excellent agreement with each other, proving the phase purity of the sample.

The ICP analysis shows that compound **I** contains 28.85 wt% Fe and 7.69 wt% P, suggesting a molar ratio of Fe:P of 2:1, which is in good agreement with the value (28.87 wt% Fe and 7.71 wt% P) based on the single-crystal structure analysis. Elemental analysis indicates that the C, H and N contents are 14.89, 2.29 and 3.44 wt%, respectively, corresponding well to the values 14.93, 2.24 and 3.48 wt% on the basis of the structural formula.

The TGA studies for the title compound **I** carried out from 33–600 °C in air showed a sharp weight loss with a broad tail that begins at ca. 200 °C and is complete ca. 500 °C (the observed total weight loss is 43.6%). The DTA curve shows only one strong exothermic peak at ca. 323 °C. The weight loss is attributed to dehydration of hydrogen phosphate groups, decomposition of oxalate anions and release of organic components, giving $Fe_4(P_2O_7)_3$ and Fe_2O_3 as the final products. The observed total weight loss is close to the calculated value of 44.7% based on the empirical formula.

3.2. Description of the structure

The coordination geometry in compound **I** is shown in Fig. 1. Both distinct Fe^{II} atoms are in distorted octahedral environments (the Fe(1)–O bond lengths are in

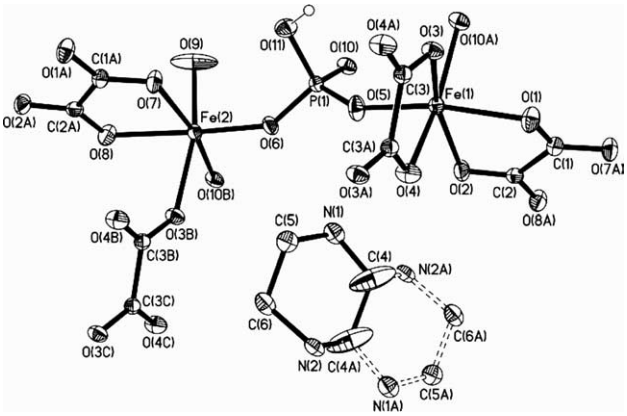

Fig. 1. ORTEP view of the structure of **I** showing the atom labelling scheme (50% thermal ellipsoids).

the range 1.980–2.244 Å, Fe(2)–O 1.985–2.202 Å. O–Fe(1)–O bond angles 75.53°–164.93°, O–Fe(2)–O 75.72°–168.20°). Fe(1) is coordinated by two bidentate oxalates and two phosphate units, while Fe(2) is coordinated by one bidentate oxalate, one monodentate oxalate, two phosphate units and one aqua ligand. The selected bond lengths and bond angles are listed in Table 2.

The $Fe(1)O_6$ and $Fe(2)O_6$ octahedra share corners to form a dimer $[Fe_2O_{10}]$ (Fig. 2(a)). The dimers and the phosphate groups are connected alternatively to form an infinite chain with four-membered rings (Fig. 2(b)). Such chains are further connected with each other via the oxalate bridges along [1 0 0] and [0 0 1], completing a three dimensional architecture (Fig. 2(c)). The connectivity between the chains and the oxalates creates an eight-membered (four $[Fe_2O_{10}]$ dimers, two phosphates and two oxalate units) one-dimensional (1-D) channel. The protonated piperazinium cation resides in the middle of the channel along the [0 1 0] direction. Along the [1 0 0] direction, the connectivity between these units also creates eight-membered one-dimensional channels, and also gives rise to a narrow elliptical 1-D channel formed by four $[Fe_2O_{10}]$ dimers and four oxalates (Fig. 3).

The structure-directing amine molecules are located within the channels of **I**, interacting with the framework via multipoint hydrogen bonding. Such multipoint hydrogen bonding is known to be associated with the formation as well as structural stability of various open-framework materials [10]. The hydrogen bond interactions in **I** between the framework and the protonated piperazinium cation are quite strong. The terminal –OH group of the HPO_4 unit and terminal H_2O of a $Fe(2)O_6$ unit participate in intra- as well as inter-framework hydrogen bonding. A complete list of hydrogen bond interactions is listed in Table 3.

Table 2
Selected bond lengths (Å) and angles (°) for compound **I**

Bond lengths			
Fe(1)–O(5)	1.980(2)	Fe(2)–O(9)	2.159(3)
Fe(1)–O(3)	2.138(2)	Fe(2)–O(7)	2.177(2)
Fe(1)–O(1)	2.143(2)	Fe(2)–O(8)	2.197(2)
Fe(1)–O(10)#1	2.153(2)	Fe(2)–O(3)#3	2.202(2)
Fe(1)–O(2)	2.194(2)	P(1)–O(6)	1.512(2)
Fe(1)–O(4)	2.244(2)	P(1)–O(5)	1.515(2)
Fe(2)–O(6)	1.985(2)	P(1)–O(10)	1.536(2)
Fe(2)–O(10)#2	2.113(2)	P(1)–O(11)	1.589(2)
Bond angles			
O(5)–Fe(1)–O(3)	106.60(8)	O(6)–Fe(2)–O(7)	93.22(8)
O(5)–Fe(1)–O(1)	164.93(9)	O(10)#2–Fe(2)–O(7)	168.18(7)
O(3)–Fe(1)–O(1)	88.35(7)	O(9)–Fe(2)–O(7)	88.80(9)
O(5)–Fe(1)–O(10)#1	96.12(9)	O(6)–Fe(2)–O(8)	168.20(8)
O(3)–Fe(1)–O(10)#1	80.16(7)	O(10)#2–Fe(2)–O(8)	92.47(7)
O(1)–Fe(1)–O(10)#1	88.07(8)	O(9)–Fe(2)–O(8)	84.16(1)
O(5)–Fe(1)–O(2)	89.24(8)	O(7)–Fe(2)–O(8)	75.72(7)
O(3)–Fe(1)–O(2)	161.62(8)	O(6)–Fe(2)–O(3)#3	97.06(8)
O(1)–Fe(1)–O(2)	75.71(8)	O(10)#2–Fe(2)–O(3)#3	79.61(7)
O(10)#1–Fe(1)–O(2)	107.90(8)	O(9)–Fe(2)–O(3)#3	161.36(1)
O(5)–Fe(1)–O(4)	89.70(8)	O(7)–Fe(2)–O(3)#3	97.83(8)
O(3)–Fe(1)–O(4)	75.53(7)	O(8)–Fe(2)–O(3)#3	80.67(8)
O(1)–Fe(1)–O(4)	92.40(8)	O(6)–P(1)–O(5)	110.07(12)
O(10)#1–Fe(1)–O(4)	155.67(7)	O(6)–P(1)–O(10)	112.02(1)
O(2)–Fe(1)–O(4)	95.75(8)	O(5)–P(1)–O(10)	112.41(1)
O(6)–Fe(2)–O(10)#2	98.53(8)	O(6)–P(1)–O(11)	106.64(1)
O(6)–Fe(2)–O(9)	99.96(1)	O(5)–P(1)–O(11)	108.39(1)
O(10)#2–Fe(2)–O(9)	90.34(9)	O(10)–P(1)–O(11)	107.03(12)

Symmetry transformations used to generate equivalent atoms: # $1-x, -y+1, -z+2$; # $2-x, -y+2, -z+2$; # $3x, y+1, z$.

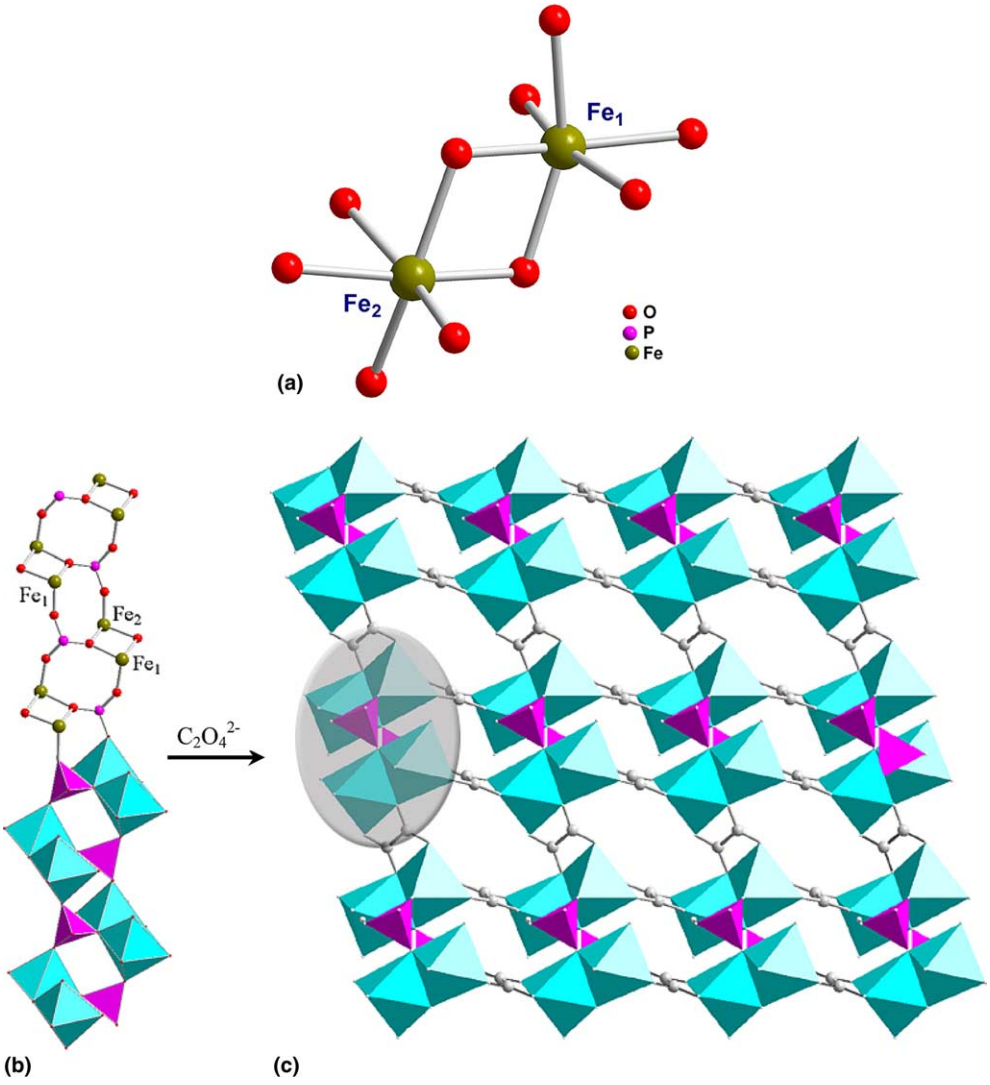

Fig. 2. The description of the structural fashion of compound **I**. (a) Fe(1)O_6 and Fe(2)O_6 octahedrons are corner shared in the dimer [Fe_2O_{10}]. (b) The infinite chain-like structure is formed by the dimers connecting with PO_4 tetrahedra alternatively. (c) The structure of compound **I** viewed along the [0 1 0] direction.

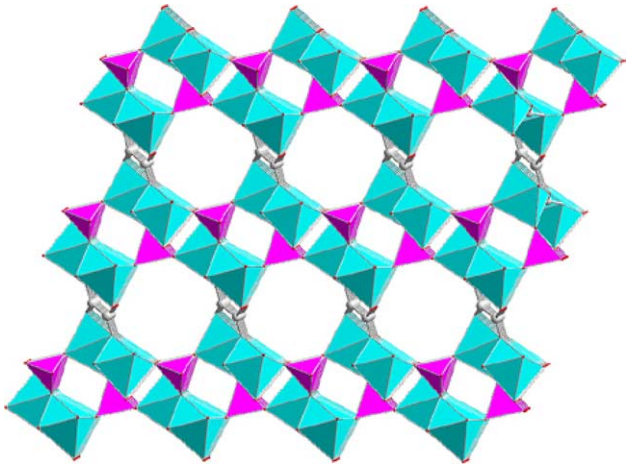

Fig. 3. The structure of compound **I** viewed along the [1 0 0] direction.

The magnetic behavior of a powdered sample of compound **I** was measured in the temperature range 2–300 K. The temperature dependence of χ_m and χ_m^{-1} curves, where χ_m is the molar magnetic susceptibility, are shown in Fig. 4. The maximum around 23 K suggests the presence of an antiferromagnetic coupling, the thermal variation of the molar susceptibility follows a Curie–Weiss law ($1/\chi_m = (T-\theta)/C_m$) with values of the Curie–Weiss constants of $C_m = 13.74\ \mathrm{cm^3\,K\,mol^{-1}}$ and $\theta = -17.97$ K. Although the computed curve does not match the χ_m^{-1} curve very well, the values of the magnetic interactions obtained are correct in sign and the magnitude is physically reasonable. The mismatch between the calculated curve and the experimental data may be due to the orbital contribution of the distorted octahedral high spin iron(II) ion, because of the Jahn–Teller compres-

Table 3
Hydrogen bonds for compound **I** (Å and °)

D–H ⋯ A	*d*(D–H)	*d*(H ⋯ A)	*d*(D ⋯ A)	∠(D–H ⋯ A)
O(11)–H(11) ⋯ O(8)#1	0.88(4)	1.84(4)	2.716(3)	172(4)
N(1)–H(1A) ⋯ O(1)#2	0.90	2.09	2.903(5)	150.1
N(1)–H(1A) ⋯ O(9)#3	0.90	2.28	2.790(6)	115.9
N(1)–H(1B) ⋯ O(5)	0.90	2.11	2.952(6)	155.6
N(2)–H(2A) ⋯ O(7)#4	0.90	1.99	2.893(5)	179.7
N(2)–H(2B) ⋯ O(2)#5	0.90	1.93	2.786(5)	157.7
N(2)–H(2B) ⋯ O(9)#6	0.90	2.41	2.852(6)	110.5

Symmetry transformations used to generate equivalent atoms: #1 $x, y-1, z$; #2 $x, y+1, z$; #3 $-x, -y+2, -z+2$; #4 $-x, -y+2, -z+1$; #5 $-x+1, -y+2, -z+1$; #6 $x+1, y, z-1$.

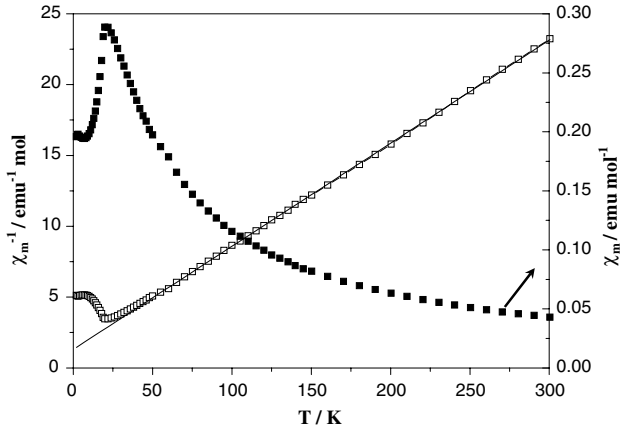

Fig. 4. Temperature variation of the magnetic susceptibility of compound **I**.

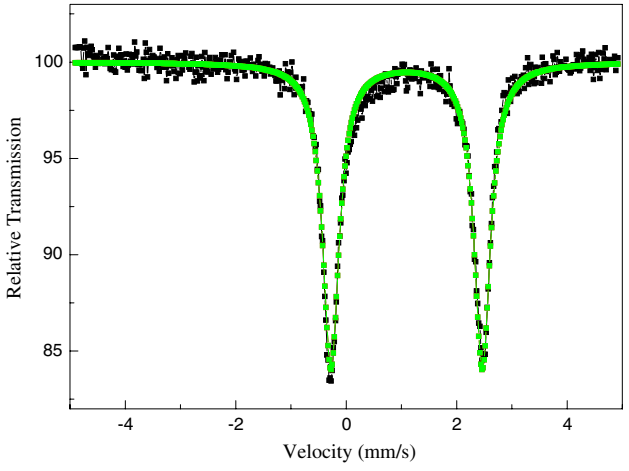

Fig. 5. Mössbauer spectroscopy of compound **I** at 300 K.

sion. Furthermore, the magnetic interaction could be due to super-exchange coupling between Fe(1) and Fe(2) via O(3) and O(10) within the dimeric units. Similar interactions have been reported in some iron phosphates [11] and oxalates [12].

The room temperature ^{57}Fe Mössbauer spectrum of **I** was least-squares fitted by one doublet (Fig. 5). The obtained parameters are δ (isomer shift) = 1.21 mm s^{-1}, ΔE_Q (quadrupole splitting) = 2.74 mm s^{-1}, and Γ (full-width at half-height) = 0.18 mm s^{-1}. The large quadrupole splitting corresponds to a large octahedral distortion. According to Menil, the isomer shift is characterisitic of high-spin Fe^{II} [13]. Therefore, the valence of the iron atoms in **I** is confirmed by Mössbauer spectroscopy.

It is instructive to compare the structural features of **I** with those of others metal phosphate-oxalates. Since we completed the present study, we also noticed two papers on Fe(II) oxalate-phophates by K.H. Lii [10a] and C.N.R. Rao [10b] which have an analogous structural formula to **I** and have comparable structural features. In the reported structures, FeO_6 and FeO_5 share their edges forming a dimeric unit [Fe_2O_9], the dimers are linked to each other via the phosphate, with the oxalate units forming the framework structures. In most of the oxalate-phosphates based open-framework structures iron is present in either five or six coordination, forming trigonal bipyramidal FeO_5 or octahedral FeO_6 as the building units. Here in the reported compound **I**, both Fe(II) centres have six coordination. According Choudhury and Natarajan [8e], this is because the average charge per oxygen on the oxalate (0.5) is less than that on the phosphate (0.75), such that more oxalate oxygens are needed to satisfy the valence of iron.

4. Conclusion

In conclusion, a new open-framework iron phosphatooxlate has been synthesized hydrothermally in the presence of a structure-directing amine. The 3-D architecture of the title compound **I** contains Fe_2O_{10} dimers and PO_4 moieties connected with each other to form infinite chains, which are linked via oxalate units to form a 3-D structure. Such a dual role of the oxalate unit is noteworthy. The magnetic behavior indicates the presence of antiferromagnetic interactions. It would be worthwhile to explore the possibility of introducing other magnetic components into the iron phosphatooxalate framework, in order to obtain materials with novel magnetic properties.

Acknowledgements

We are grateful to the National Natural Science Foundation of China (20233030) and the State Basic Research Project (G200077507) for financial support.

Appendix A. Supplementary material

Crystallographic data for $(N_2C_4H_{12})[Fe_4(C_2O_4)_3(HPO_4)_2(H_2O)]$ has been deposited with the Cambridge Crystallographic Center, CCDC No. 233538. Copies of this information may be obtained free of charge from The Director, CCDC, 12 Union Road, Cambridge, CB2, IEZ, UK (fax: +44-1233-336-033, email: deposit@ccdc.cam.ac.uk or www:http//www.ccdc.cam.ac.uk). Supplementary data associated with this article can be found, in the online version, at doi:10.1016/j.poly.2004.07.016.

References

[1] (a) R.C. Haushalter, L.A. Mundi, Chem. Mater. 4 (1992) 31;
(b) X. Bu, P. Feng, G.D. Strucky, Science 278 (1997) 2080;
(c) R.M. Barrer, Hydrothermal Chemistry of Zeolites, Academic Press, New York, 1982;
(d) G. Ozin, Adv. Mater. 4 (1992) 612;
(e) J.M. Thomas, Angew. Chem., Int. Ed. Engl. 33 (1994) 913.
[2] (a) P. Lightfoot, Z.A.D. Lethbridge, R.E. Morris, D.S. Wragg, P.A. Wright, J. Solid State Chem. 143 (1999) 74;
(b) K. Kedarnath, A. Choudhury, S. Natarajan, J. Solid State Chem. 150 (2000) 324;
(c) N. Rajic, N.Z. Logar, G. Mali, V. Kaucic, Chem. Mater. 15 (2003) 1734.
[3] J. Do, R.P. Bontchev, A.J. Jacobson, Inorg. Chem. 39 (2000) 3230.
[4] A. Choudhury, S. Natarajan, Solid State Sci. 2 (2000) 365.
[5] (a) Z.A.D. Lethbridge, A.D. Hillier, R. Cywinski, P. Lightfoot, J. Chem. Soc. Dalton Trans. 1595 (2000);
(b) Z.A.D. Lethbridge, M.J. Smith, S.K. Tiwary, A. Harrison, P. Lightfoot, Inorg. Chem. 43 (2004) 11.
[6] S.N. Srinivasan, C.N.R. Rao, J. Chem. Soc., Dalton Trans. 289 (2001).
[7] (a) C.T.S. Choi, E.V. Anokhina, C.S. Day, Y. Zhao, F. Taulelle, C. Huguenard, Z. Gan, A. Lachgar, Chem. Mater. 14 (2002) 4096;
(b) M. Mrak, U. Kolitsh, C. Lengauer, V. Kaucic, E. Tillmanns, Inorg. Chem. 42 (2003) 598.
[8] (a) A. Choudhury, S. Natarajan, J. Mater. Chem. 9 (1999) 3113;
(b) A. Choudhury, S. Natarajan, C.N.R. Rao, Chem. Eur. J. 7 (2000) 6;
(c) A. Choudhury, S. Natarajan, C.N.R. Rao, Chem. Mater. 11 (1999) 2316;
(d) A. Choudhury, S. Natarajan, C.N.R. Rao, Chem. Commun. 1305 (1999);
(e) A. Choudhury, S. Natarajan, J. Mater. Chem. 9 (1999) 3113;
(f) W.J. Chang, H.M. Lin, K.H. Lii, J. Solid State Chem. 157 (2001) 233.
[9] G.M. Sheldrick, SHELXL-97, Program for Refinement of Crystal Structures, University of Göttingen, Germany, 1997.
[10] (a) H.M. Lin, K.H. Lii, Chem. Mater. 11 (1999) 519;
(b) A.C. Choudhury, S. Natarajan, C.N.R. Rao, J. Solid State Chem. 146 (1999) 538;
(c) L.Y. Na, Y.L. Liu, W.Q. Pang, R.R. Xu, Chin. J. Inorg. Chem. 16 (2000) 287.
[11] (a) M. Cavellec, G. Ferey, Micro. Mater. 8 (1997) 103;
(b) M.B. Korzenski, J.W. Kolis, J. Solid State Chem. 139 (1998) 152;
(c) A. Choudhury, S. Natarajan, J. Solid State Chem. 154 (2000) 507;
(d) L.K. Elbouaanani, R. Gerardin, J. Solid State Chem. 163 (2002) 412;
(e) H.H. Song, L.M. Zheng, J. Solid State Chem. 164 (2002) 367;
(f) P. Yin, S. Gao, L.M. Zheng, Chem. Mater. 15 (2003) 3233.
[12] (a) L.M. Zheng, K.H. Lii, J. Chem. Soc., Dalton Trans. 2311 (1999);
(b) D.J. Price, A. K Powell, P.T. Wood, J. Chem. Soc., Dalton Trans. 2478 (2003);
(c) D. Armentano, G. Munno, New J. Chem. 27 (2003) 161.
[13] F. Menil, J. Phys. Chem. Solids 46 (1985) 763.

Available online at www.sciencedirect.com
SCIENCE DIRECT®
Polyhedron 23 (2004) 2363–2371
POLYHEDRON
www.elsevier.com/locate/poly

Electronic structure and UV–Vis spectroscopy of $[Re(NO)Br_3(PPh_3)_2]$ and $[Re(NO)Br_3(OPPh_3)_2]$ complexes

Barbara Machura *

Department of Inorganic and Radiation Chemistry, Institute of Chemistry, University of Silesia, 9th Szkolna Street, 40-006 Katowice, Poland

Received 31 May 2004; accepted 12 July 2004
Available online 12 September 2004

Abstract

Density functional calculations for the $[ReBr_3(NO)(PPh_3)_2]$ (**1**) and $[ReBr_3(NO)(OPPh_3)_2]$ (**2**) complexes have been carried out using the DFT method with the B3LYP functional. The experimentally characterised molecular structures of **1** and **2** have been properly reproduced by the B3LYP method. The UV–Vis spectra of both complexes have been interpreted on the basis of the electronic transitions calculated with the time-dependent DFT method (TDDFT) for **1** and **2**.
© 2004 Elsevier Ltd. All rights reserved.

Keywords: Rhenium; Nitrosyls; Phosphine complexes; DFT calculations

1. Introduction

For many years nitrosyl compounds of transition metals have been the centre of interest for scientists both engaged in basic research and trying to employ these complexes as catalysts of polymerisation, oligomerisation, metathesis, epoxidation, oxidation and reduction [1–7].

One of the most important aspects of metal nitrosyl complexes is the bonding nature of the nitric oxide to the metal centre. Historically, the bonding of the M–NO unit has been described by assigning formal oxidation states to the metal centre and the nitrosyl ligand. In such an assignment, the linear M–NO unit is deemed to possess a bound NO^+ ligand, and conversely, a bent M–NO core is deemed to possess a bound NO^- ligand. However, the bonding in the $M(NO)_x$ moieties of metal nitrosyl complexes is largely of a covalent nature, and the electron distribution in the M–NO unit is more or less evenly distributed in this group. Enemark and Feltham have proposed the $\{M(NO)_x\}^n$ formalism for metal nitrosyls in which n is taken as the total number of electrons associated with the metal d and π*(NO) [5].

Studies of the electronic structure and electronic spectroscopy of nitrosyl complexes of transition metals are dominated by investigations of the nitroprusside ion $[Fe(CN)_5(NO)]^{2-}$ [8,9] and ruthenium nitrosyls [10–13]. To our knowledge, only the model $[Re(NO)_2(PH_3)_2L]$ nitrosyl complexes (L = H^-, CO, $CNCH_3$, PH_3, CN^-, $NCCH_3$, Cl^-) have been the subject of quantum chemical calculations based on density functional theory (DFT) [14].

The papers [15–19] present the preparation, structural and some spectroscopic characterisation of rhenium nitrosyl complexes of the general formula $[ReX_3(NO)L_2]$, where X = Cl or Br and L = PPh_3, $AsPh_3$, $OPPh_3$ or $OAsPh_3$.

This study presents a comparison of the electronic structure and bonding nature of $[ReBr_3(NO)(PPh_3)_2]$ (**1**) and $[ReBr_3(NO)(OPPh_3)_2]$ (**2**), based on the results of DFT calculations. The paper also includes calculations of electronic transitions with the time-dependent

* Tel.: +48322582441; fax: +48322599978.
E-mail address: bmachura@poczta.onet.pl.

0277-5387/$ - see front matter © 2004 Elsevier Ltd. All rights reserved.
doi:10.1016/j.poly.2004.07.021

DFT method (TDDFT) for **1** and **2**, and discussion of their UV–Vis spectra on the basis of the TDDFT calculations.

Calculations with the TDDFT method for open-shell organic, inorganic and organometallic molecules are still limited, but a few studies have already appeared and support the TDDFT method to be applicable for such systems giving good assignment of experimental spectra [20–23]. There are also several works performed with this method for 5d-metals (including rhenium complexes) in which good correlations between experimental and calculated results have been confirmed [24–30].

2. Experimental

$[ReBr_3(NO)(PPh_3)_2]$ (**1**) and $[ReBr_3(NO)(OPPh_3)_2]$ (**2**) complexes were prepared according to the literature methods [16,17].

Electronic spectra of **1** and **2** were measured on a spectrophotometer Lab Alliance UV–VIS 8500 in the range 800–220 nm in deoxygenated dichloromethane solution.

3. Computational details

The GAUSSIAN 03 program [31] was used in the calculations. The geometry optimisation was carried out with the DFT method with the use of the B3LYP functional [32,33]. The LANL2DZ basis set [34] was used on the rhenium and bromine atoms, 6-31G(d) on the nitrogen and carbon atoms and 6-31G basis on the hydrogen atoms in the calculations.

4. Results and discussion

4.1. Molecular geometries

The geometries of **1** and **2** were optimised in the doublet state by the DFT method with the B3LYP functional. Table 1 shows the possible electronic configurations and spin multiplicities of the $[ReBr_3(NO)L_2]$ (L = PPh_3 or $OPPh_3$) complexes. The doublet state agrees well with the experimental values of the effective magnetic moment for **1** and **2**, they are both equal, ~1.8 BM, and correspond to one unpaired electron.

The structures and atomic numbering schemes of the examined complexes are shown in Figs. 1 and 2. Complex **1** has pseudooctahedral geometry with *trans* phosphine molecules, *meridional* bromo ligands and a linear nitrosyl group. The rhenium atom of **2** is also in a distorted octahedral environment with three bromine ligands in *meridional* geometry, but the linear N–O group is *trans* to one of $OPPh_3$ ligands, and the two $OPPh_3$ molecules are mutually *cis*. The geometric parameters of **1** and **2** optimised by the DFT method are gathered in Table 2. For comparison, the experimental bonds and bond angles are also included. Two polymorphs, orthorhombic with all atoms in general positions and monoclinic with the rhenium atom on the special position *e* of the space group *C*2/*c* with multiplicity 4 and site symmetry 2, were isolated for complex **2** [17,19]. Table 1 shows only the X-ray crystal structure data for orthorhombic polymorph [19]. The optimised geometries are in good agreement with the experimental ones, the largest differences are found for the Re–Br bond distances. A similar elongation of the rhenium–halogen bond lengths in the B3LYP with different basis sets has been found in other rhenium complexes [35]. In the X-ray structure of **1**, the

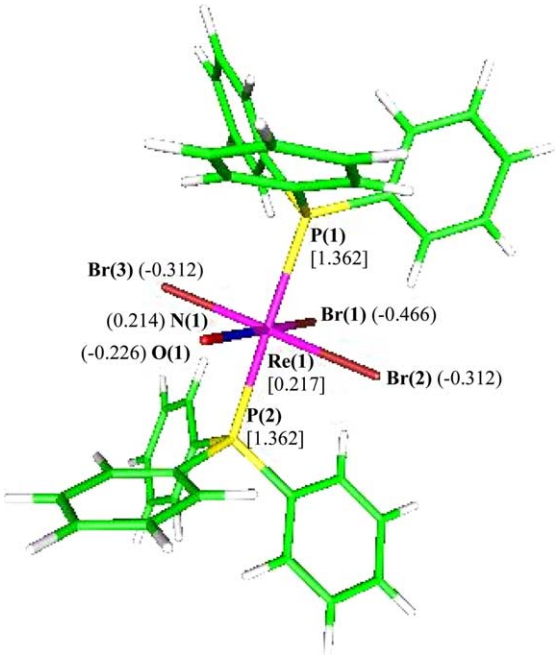

Fig. 1. Structure of **1** and atomic charges from the Natural Population (NP) analysis.

Table 1
Possible oxidation numbers and spin multiplicities of Re and NO in $[ReBr_3(NO)L_2]$ complexes (L = PPh_3 or $OPPh_3$)

Re	Spin of Re	NO	Spin of NO	Total spin	Spin multiplicity
Re(II)	5/2, 3/2, 1/2	$NO^+(\pi_1^*)^0(\pi_2^*)^0$	0	5/2, 3/2, 1/2	6, 4, 2
Re(III)	2, 1, 0	$NO(\pi_1^*)^1(\pi_2^*)^0$	1/2	5/2, 3/2, 1/2	6, 4, 2
Re(IV)	3/2, 1/2	$NO^-(\pi_1^*)^1(\pi_2^*)^1$	1	5/2, 3/2, 1/2	6, 4, 2

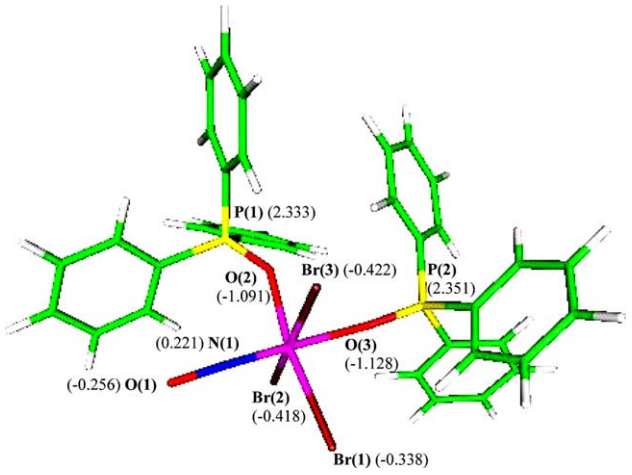

Fig. 2. Structure of **2** and atomic charges from the Natural Population (NP) analysis.

rhenium, NO and bromine species are sited on a crystallographic twofold axis, so the N–O–Re–Br unit is perfectly linear. In the optimised structure, the N–Re–Br and N–O angles are almost linear. There is no significant difference in the calculated Re–N and N–O bond lengths for **1** and **2**. The shortening of the experimental N–O bond length in **2** may be a consequence of crystal packing. In monoclinic polymorph of *mer-cis*-[$ReBr_3(NO)(OPPh_3)_2$] the N–O distance is equal 1.26(1) Å [19], in *mer-cis*-[$ReCl_3(NO)(OPPh_3)_2$] – 1.21(3) Å [15] and in *mer-cis*-[$ReBr_3(NO)(OAsPh_3)_2$] – 1.156(6) Å [18]. A similar shortening of the N–O bond as a result of steric requirements or some disorders is observed in [NEt_4][$ReBr_4(NO)(MeCN)$] – 0.99(2) Å [36] and *mer*-[$RuCl_3(NO)\{PPh_2(CH_2)_3PPh_2$] – 0.907(7) Å [37]. The general trends observed in the experimental data are well reproduced in the calculations, e.g., the significant shortening of the Re–Br bond length in the *trans* position to the $OPPh_3$ molecule in **2**, the notable differences in O–P–Re angle values and O–P bond lengths in **2**, and the lengthening of the Re–Br bond length in the *trans* position to NO in **1**.

4.2. Charge distribution and spin densities

Figs. 1 and 2 present the atomic charges from the Natural Population (NP) analysis [38] for **1** and **2**, respectively. For both complexes **1** and **2**, the charges on the nitrogen atoms of the nitrosyl groups are positive, whereas the oxygen atoms are negatively charged. The total charges on the NO groups of these complexes are close to zero, −0.012 and −0.035 for **1** and 2, respectively. The more negative total charge of the NO ligand in **2** indicates the stronger electron acceptor ability of the NO group in this complex. The calculated charge on the rhenium atom of **1** is far from the formal charge +2. It results from charge donation from the bromine

Table 2
The experimental and optimised bond lengths (Å) and angles (°) for **1** and **2**

1						**2**					
Bond lengths	Experimental	Optimised	Bond angles	Experimental	Optimised	Bond lengths	Experimental	Optimised	Bond angles	Experimental	Optimised
Re(1)–N(1)	1.769(12)	1.759	N(1)–Re(1)–Br(2)	90.57(4)	89.25	Re(1)–N(1)	1.87(2)	1.744	N(1)–Re(1)–O(2)	99.2(4)	98.43
Re(1)–P(1)	2.540(2)	2.604	N(1)–Re(1)–Br(2a)	90.57(4)	89.25	Re(1)–O(2)	2.071(9)	2.118	N(1)–Re(1)–O(3)	179.2(5)	178.63
Re(1)–P(1a)	2.540(2)	2.604	N(1)–Re(1)–Br(1)	180.000(1)	179.49	Re(1)–O(3)	2.076(7)	2.126	N(1)–Re(1)–Br(1)	92.0(3)	91.00
Re(1)–Br(1)	2.496(3)	2.681	Br(2)–Re(1)–Br(2a)	178.86(7)	178.49	Re(1)–Br(1)	2.473(2)	2.596	N(1)–Re(1)–Br(2)	93.6(5)	93.01
Re(1)–Br(2)	2.4811(14)	2.618	Br(2)–Re(1)–Br(1)	89.43(4)	90.77	Re(1)–Br(2)	2.511(2)	2.653	N(1)–Re(1)–Br(3)	92.4(5)	93.76
Re(1)–Br(2a)	2.4811(14)	2.618	Br(2a)–Re(1)–Br(1)	89.43(4)	90.74	Re(1)–Br(3)	2.534(2)	2.658	O(2)–Re(1)–Br(1)	168.8(3)	170.56
N(1)–O(1)	1.12(2)	1.172	N(1)–Re(1)–P(1a)	90.75(6)	91.87	O(2)–P(1)	1.533(9)	1.530	O(2)–Re(1)–Br(3)	88.4(3)	85.68
			Br(2)–Re(1)–P(1a)	87.59(6)	89.88	O(3)–P(2)	1.497(8)	1.514	O(2)–Re(1)–O(3)	80.5(3)	87.47
			Br(2a)–Re(1)–P(1a)	92.39(6)	90.18	N(1)–O(1)	0.94(1)	1.175	O(2)–Re(1)–Br(2)	86.2(3)	82.94
			Br(1)–Re(1)–P(1a)	89.25(6)	88.12				Br(2)–Re(1)–Br(3)	172.51(6)	171.00
			N(1)–Re(1)–P(1)	90.75(6)	91.84				Br(2)–Re(1)–Br(1)	92.92(6)	93.54
			Br(2)–Re(1)–P(1)	92.39(6)	90.18				Br(3)–Re(1)–Br(1)	91.36(6)	92.26
			Br(2a)–Re(1)–P(1)	87.59(6)	89.86				O(3)–Re(1)–Br(1)	88.3(2)	87.63
			Br(1)–Re(1)–P(1)	89.25(6)	88.17				O(3)–Re(1)–Br(2)	87.2(2)	87.07
			P(1a)–Re(1)–P(1)	178.50(12)	176.29				O(3)–Re(1)–Br(3)	86.8(2)	86.29
			O(1)–N(1)–Re(1)	180.000(2)	177.99				O(1)–N(1)–Re(1)	175(1)	177.36
									O(2)–P(1)–Re(1)	140.4(6)	142.78
									O(3)–P(2)–Re(1)	174.1(6)	165.30

ions and triphenylphosphine ligands, which act as σ-donors. There are large positive charges on the phosphorus atoms, and the charges on the bromine ligands are significantly smaller than −1. There is a noticeable difference between the calculated charge on the bromine ion in the *trans* position to the NO group and the charges on two mutually *trans* bromine ligands. The second ones are less negative. The positive charge on the rhenium atom of **2** is higher in comparison with 1, but it is also considerable smaller than the formal +2 charge. It results mainly from strong charge donation from bromine ions, the charges on the bromine ligands are significantly smaller than −1. A visible difference between the calculated charge on the bromine ion in the *trans* position to the $OPPh_3$ molecule and charges on two mutually *trans* bromine ligands is also noticed for complex **2**. A smaller negative charge is observed on the bromine ion in the *trans* position to the $OPPh_3$ molecule. The oxygen atoms of $OPPh_3$ ligands are negatively charged, whereas the phosphorous atoms are positively charged.

For both complexes, there are positive spin densities on the rhenium atoms of about **1** (0.988 for **1** and 1.072 for **2**) and small negative spin densities of about −0.1 on the nitrogen and oxygen atoms of the nitrosyl ligands. The spin densities on the bromine ligands and phosphorous atoms of PPh_3 ligands for complex **1** are as follows: Br(1), −0.003; Br(2/3), −0.131; P(1/2), −0.034. The spin densities on the phosphorous and oxygen atoms of $OPPh_3$ ligands and the bromine ligands for complex **2** are also close to zero and they are: Br(1), −0.068; Br(2/3), −0.029; P(1), −0.002, P(2)/O(2), 0.000 and O(1), 0.014.

4.3. Electronic structure

The energies and characters of several highest occupied and lowest unoccupied molecular orbitals of **1** and **2** are presented in Table 3. The selected HOMO and LUMO of **1** and **2** with α spin are depicted in Figs. 3 and 4, respectively. Most of the MOs of **1** and **2** have complicated characters. The percent participation of atomic orbitals in the selected HOMO and LUMOs of **1** and **2** is given in Table 3.

4.3.1. $[ReBr_3(NO)(PPh_3)_2]$ (**1**)

Among the MOs of **1** there are no orbitals of pure π_{Re-NO} character. The π_{ReNO} bonding interaction makes the largest contribution into HOMO − 22 and HOMO − 19 with α-spin, and HOMO − 21 and HOMO − 19 with β-spin. A substantial contribution of π_{Re-NO} orbitals is also shown in HOMO − 2 with α spin and HOMO − 1 with β spin, but the π bromine orbitals are the main components of these MOs (see Table 3). The bonding π_{Re-NO} orbitals with and β spin are localised mainly on the rhenium d orbitals and they are mixed with π_{Br} and π_{Ph} orbitals. LUMO + 1 and LUMO + 2 with α-spin and β-spin are of π^*_{Re-NO} antibonding character. They have prevalent NO character. On the basis of the molecular orbital composition and the small charge on the NO group, the NO^+ character of the nitrosyl in this complex can be confirmed.

The HOMO with α-spin and HOMO with β-spin are mainly localised on the bromine ligands, but they have a substantial contribution from the free electron pairs on the phosphorus atom. They present an interaction between the free phosphorus electron pairs and rhenium d_{yz} orbitals, which explains the strong donation of electron density from the phosphorous atoms to the rhenium atom. HOMO − 23 is of σ_{Re-P} character.

The d_{xy} rhenium orbital and π orbitals of bromine ligands in an anti-bonding arrangement make the main contributions into HOMO − 1 with α-spin and the LUMO with β-spin. The LUMO with α-spin and LUMO + 3 with β-spin are of $d_{x^2-y^2} - \sigma_{Br}$ character. LUMO + 3 with α-spin and LUMO + 7 with β-spin are mainly localised on the rhenium d_{x^2} orbital. LUMO + 4, LUMO + 5 with α-spin and LUMO + 5, LUMO + 6 with β-spin present a π interaction of the phosphorous orbitals with the π* orbitals of the phenyl groups.

4.3.2. $[ReBr_3(NO)(OPPh_3)_2]$ (**2**)

The largest participation of the bonding π_{Re-NO} orbitals are shown in HOMO − 12, HOMO − 7, HOMO − 2 and HOMO − 1 with α-spin and HOMO − 6, HOMO − 2, HOMO − 1 and HOMO with β spin. Similar to **1**, they are mixed with π_{Br} and π_{Ph} orbitals. However, the contribution of π_{Br} and π_{Ph} orbitals is significantly larger in comparison with the corresponding orbitals of **1**. The percent participation of the rhenium d orbitals and π^*_{NO} orbitals in the bonding π_{Re-NO} orbitals are very similar. LUMO + 6, LUMO + 7, LOMO + 8 and LUMO + 9 with α-spin and LUMO + 7, LUMO + 9, LUMO + 11 and LUMO + 11 with β-spin present a π-antibonding interaction between d_{yz} and d_{xz} metal orbitals and π^*_{NO} orbitals. For complex **2**, the number of unoccupied MOs with significant contribution of π^*_{Re-NO} orbitals is larger in comparison with compound **1**. It is a consequence of the *trans* position of the nitrosyl group to $OPPh_3$ ligand. All the π^*_{Re-NO} orbitals are mixed with π^*_{Ph} orbitals. Moreover, the percent participation of the rhenium d orbitals and π^*_{NO} orbitals in the antibonding π^*_{Re-NO} orbitals are very similar. Nevertheless, the character of the nitrosyl ligand in **2** may be described as NO^+.

The LUMO, LUMO + 2 and LUMO + 3 with α-spin and LUMO + 1, LUMO + 2 and LUMO + 3 with β-spin present the π interaction of phosphorous orbitals with π* orbitals of the phenyl groups. The HOMO with α-spin and LUMO with β-spin consist of the rhenium d_{xy} orbital and π orbitals of bromine ligands in an anti-bonding phase.

Table 3
The energy and character of the selected molecular orbitals with α and β spin for **1** and **2**

	1				**2**			
	α MO		β MO		α MO		β MO	
	E (eV)	Character	*E* (eV)	Character	*E* (eV)	Character	*E* (eV)	Character
HOMO − 12	−7.048	π(Ph)	−7.051	π(Ph)	−7.196	d_{yz}(14.1) + π*(NO) (10.0), π(Ph) (45.1), π(Br) (15.1), π(O) (11.1)	−7.274	π(Ph)
HOMO − 11	−6.980	π(Ph) (57.7), π(Br) (28.4)	−7.032	π(Ph) (78.9), π(Br) (11.4)	−7.091	π(Ph)	−7.197	π(Ph)
HOMO − 10	−6.962	π(Ph) (71.3), π(Br) (12.3)	−6.956	π(Ph) (63.1), π(Br) (24.6)	−7.022	π(Ph)	−7.095	π(Ph)
HOMO − 9	−6.858	π(Ph) (76.0), π(Br) (12.7)	−6.911	π(Ph) (71.6), π(Br) (11.9)	−6.950	π(Ph)	−7.054	d_{yz}(11.9) + π*(NO) (7.0), π(Ph) (38.3), π(Br) (29.2), π(O) (12.1)
HOMO − 8	−6.821	π(Ph)	−6.804	π(Ph)	−6.923	π(Ph)	−7.018	π(Ph)
HOMO − 7	−6.781	π(Ph) (65.6), π(Br) (29.1)	−6.793	π(Ph)	−6.862	d_{xz}(23.3) + π*(NO) (14.9), π(Ph) (23.3), π(Br) (18.8), π(O) (17.7)	−6.920	π(Ph)
HOMO − 6	−6.688	π(Ph) (74.6), π(Br) (15.7)	−6.756	π(Br) (49.1), π(Ph) (42.1)	−6.422	σ(Br) (43.2), π(O) (17.8), d(Re) (9.8)	−6.830	d_{xz} + π*(NO) (43.1), π(Br) (26.6), π(O) (16.5)
HOMO − 5	−6.673	π(Ph)	−6.653	π(Ph) (79.7), π(Br) (10.0)	−6.386	π(Br)	−6.718	σ(Br) (63.7), π(O) (15.3), d(Re) (7.6)
HOMO − 4	−6.563	π(Ph) (44.4), π(Br) (31.6), *n*(P) (9.3), d_{yz}(4.4) + π*(NO) (6.0)	−6.592	π(Ph) (78.3), π(Br) (14.7)	−5.962	π(Br)	−6.392	π(Br)
HOMO − 3	−6.309	π(Br)	−6.396	π(Br) (53.7), π(Ph) (24.5)	−5.962	π(Br)	−6.264	π(Br)
HOMO − 2	−6.154	π(Br)(51.4), d_{xz}(23.2) + π*(NO) (16.7)	−6.287	π(Br)	−5.840	π(Br) (57.3), d_{xz}(19.4) + π*(NO) (14.0)	−5.789	d_{xz}(7.9) + π*(NO) (9.9), π(Br) (76.3)
HOMO − 1	−6.064	d_{xy}(39.7), π(Br) (50.0)	−6.076	π(Br) (47.9), d_{xz}(16.7) + π*(NO) (20.3),	−5.764	d_{yz}(21.5) + π*(NO) (14.5), π(Br) (30.1)	−5.753	d_{xz}(10.8) + π*(NO) (13.9), π(Br) (70.1)
HOMO	−6.052	π(Br) (50.0), d_{yz}(5.6), *n*(P) (16.6)	−6.022	π(Br) (47.7), d_{yz}(7.5) + π*(NO) (9.3), *n*(P) (16.1)	−5.418	d_{xy}(51.8), π(Br) (42.0)	−5.694	d_{yz}(19.0) + π*(NO) (22.0), π(Br) (53.5)
LUMO	−1.619	$d_{x^2-y^2}$(34.1) − σ(Br) (14.2) − σ(P)(29.7)	−3.659	d_{xy}(64.7), π(Br) (28.2)	−1.468	π(P)(13.2) + π*(Ph)(57.4), $d_{x^2-y^2}$(12.5)	−2.593	d_{xy}(73.2), π(Br) (17.9)
LUMO + 1	−1.519	π*(NO) (53.2) − d_{yz}(20.7)	−1.523	π*(NO) (48.0) − d_{yz}(23.5)	−1.277	π*(Ph)	−1.423	π(P)(14.4) + π*(Ph)(68.8), $d_{x^2-y^2}$(5.8)
LUMO + 2	−1.474	π*(NO) (57.4) − d_{xz}(25.9)	−1.450	π*(NO) (51.6) − d_{xz}(34.9)	−1.180	π(P)(5.8) + π*(Ph)(47.8), $d_{x^2-y^2}$(24.7)	−1.274	π(P) (11.4) + π*(Ph) (81.0)
LUMO + 3	−0.966	d_{z^2}(Re)(25.9) − σ(Br)(23.7) −σ(NO)(7.3)	−1.447	$d_{x^2-y^2}$(32.3) − σ(Br)(11.5) −σ(P)(14.4)	−1.102	π(P)(7.9) + π*(Ph)(64.1), $d_{x^2-y^2}$(13.4)	−1.130	π(P) (11.2) + π*(Ph) (88.3)
LUMO + 4	−0.875	π(P) (15.6) + π*(Ph) (68.6)	−0.891	π(P) (15.8) + π*(Ph) (78.9)	−0.997	π*(Ph)	−1.018	π*(Ph)(74.9), $d_{x^2-y^2}$(7.8)
LUMO + 5	−0.832	π(P) (9.9) + π*(Ph) (83.6)	−0.827	π(P) (8.9) + π*(Ph) (84.1)	−0.934	π*(Ph)	−0.974	π*(Ph)(81.4), $d_{x^2-y^2}$(5.6)
LUMO + 6	−0.703	π*(Ph)	−0.696	π*(Ph)	−0.828	π*(NO) (33.6) − d_{yz}(15.6), π*(Ph) (38.1)	−0.838	$d_{x^2-y^2}$(31.7) − σ(Br) −σ(P), π*(Ph)(30.6)
LUMO + 7	−0.654	π*(Ph)	−0.679	d_{z^2}(Re)(24.2), π*(Ph)(31.1)	−0.715	π*(NO) (10.1) − d_{xz}(5.7), π*(Ph) (76.3)	−0.808	π*(NO) (20.1) − d_{yz}(21.2), π*(Ph) (40.8)
LUMO + 8	−0.455	π*(Ph)	−0.613	d_{z^2}(Re)(11.9), π*(Ph)(55.2)	−0.666	π*(NO) (21.2) − d_{yz}(16.1), π*(Ph) (42.4)	−0.706	π*(Ph)
LUMO + 9	−0.412	π*(Ph)	−0.444	π*(Ph)	−0.615	π*(NO) (32.2) − d_{xz}(14.2), π*(Ph) (53.3)	−0.635	π*(NO) (21.6) − d_{yz}(30.3), π*(Ph) (39.3)
LUMO + 10	−0.288	π*(Ph)	−0.398	π*(Ph)	−0.565	π*(Ph)	−0.585	π*(NO) (11.8) − d_{xz}(14.1), π*(Ph) (62.3)
LUMO + 11	−0.200	π*(Ph)	−0.289	π*(Ph)	−0.547	π*(Ph)	−0.551	π*(NO) (17.3) − d_{xz}(11.2), π*(Ph) (66.9)
LUMO + 12	−0.054	π*(Ph)	−0.165	π*(Ph)	−0.315	π*(Ph)	−0.544	π*(Ph)

The percent participation of the atomic orbitals is given in round brackets.

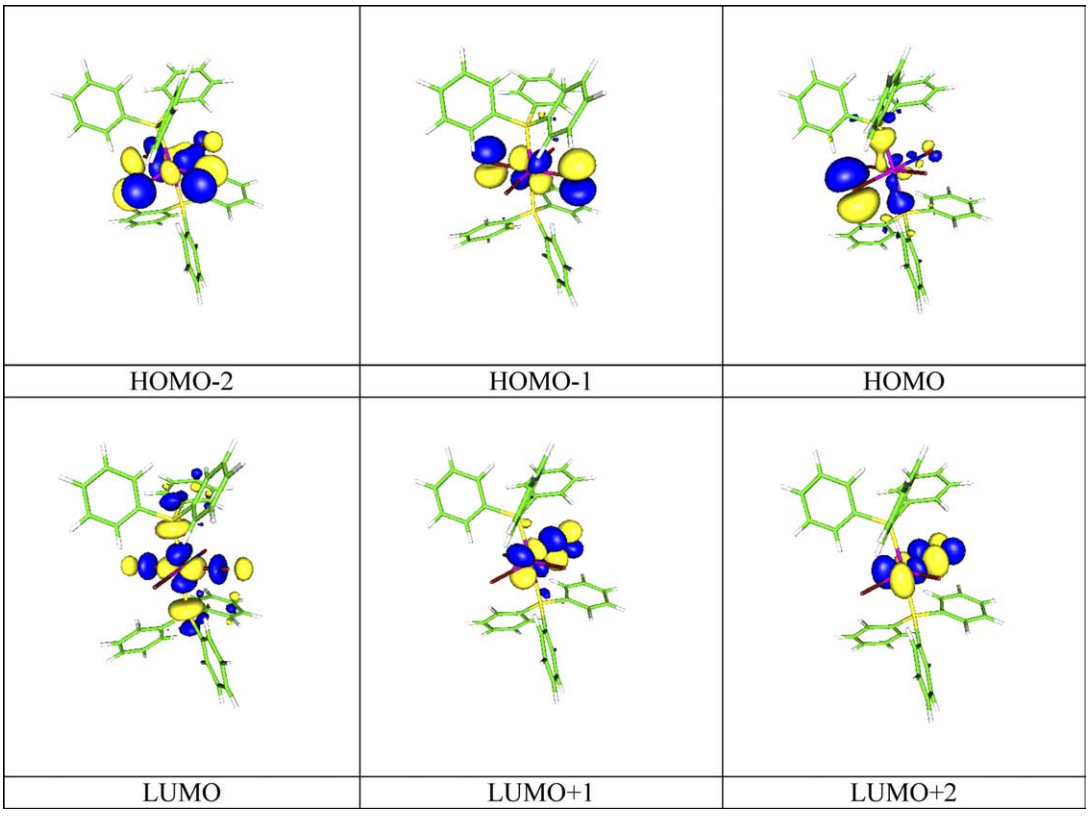

Fig. 3. Selected HOMO and LUMO orbitals with α spin for **1**. Positive values of the orbital contour are represented in blue (0.04 au) and negative values in yellow (−0.04 au). (For interpretation of the references to colour in this figure legend, the reader is referred to the web version of this article.)

4.4. Electronic spectra

The investigated molecules are of large size, the numbers of basis functions are equal to 674 and 702 for **1** and **2**, respectively. For both complexes, 80 electron transitions were calculated by the TDDFT method. However, the calculated transitions do not comprise all the experimental absorption bands, and some of the experimental bands (of the highest energy) are not assigned to the calculated transitions.

It is known that commonly used functionals, including B3LYP have incorrect asymptotic properties. However, the transitions of energies smaller than the energy of the HOMO orbital are well reproduced by this method [39–41]. In the present calculations the highest calculated transitions are of energy 4.44 and 4.23 eV for **1** and **2**, respectively. This is much smaller than the energy of the HOMO orbitals for **1** and **2** (Table 3).

Table 4 presents the energy and molar absorption coefficients of experimental absorption bands and the spin-allowed doublet–doublet electronic transitions calculated with the TDDFT method for **1** and **2**. The calculations result in many transitions with very small oscillator strengths. Except for the electronic transition of $d \rightarrow \pi^*_{NO}$ character and the low energy part of the spectrum, only transitions with oscillator strengths larger than 0.0050 and 0.0020 are listed for **1** and **2**, respectively. The assignment of the calculated transitions to the experimental bands is based on the criterion of the energy and oscillator strength of the calculated transitions. In the description of the electronic transitions the main components of the molecular orbital are used. The bonding π_{Re-NO} orbitals are described as d orbitals, and the antibonding π^*_{Re-NO} as π^*_{NO}.

*4.4.1. [$ReBr_3(NO)(PPh_3)_2$] (**1**)*

The longest wavelength experimental band at 645 nm is low in intensity and it may be attributed to the transition of $\pi_{Br}/n(P) \rightarrow d$ character with a small oscillator strength calculated at 885.4 nm.

The next experimental band at 571.0 nm is much more intense and it is assigned to the calculated transition at 648.5 nm. The transition is of $\pi_{Br} \rightarrow d$ origin and its oscillator strength is large.

The absorption band at 456.0 nm is ascribed to the calculated transitions in the range 545–475 nm. These transitions have $\pi_{Ph} \rightarrow d$ (LMCT) character and they are mediated by phosphorus orbitals.

The experimental band at 420 nm can be attributed to two calculated transitions at 419.4 and 409.6 nm. The first one is a $d \rightarrow d$ transition, and the second has $\pi_{Br} \rightarrow d$ character.

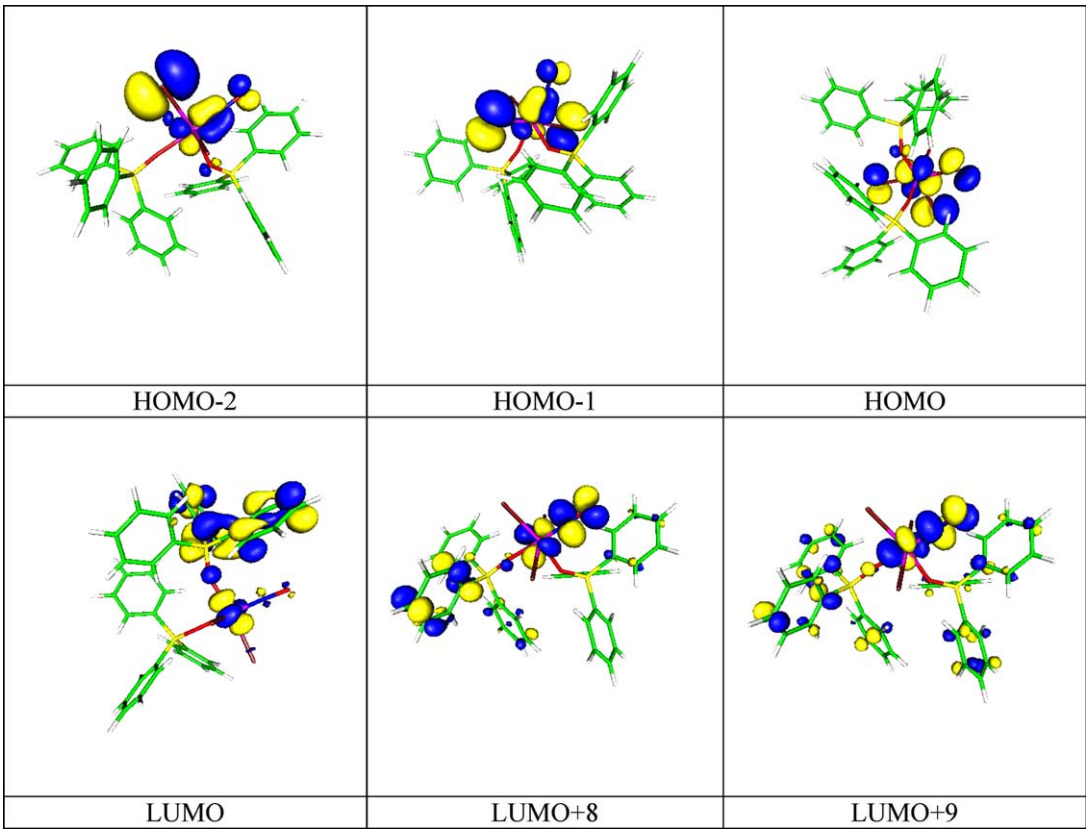

Fig. 4. Selected HOMO and LUMO orbitals with α spin for **2**. Positive values of the orbital contour are represented in blue (0.04 au) and negative values in yellow (−0.04 au). (For interpretation of the references to colour in this figure legend, the reader is referred to the web version of this article.)

The intense absorption band at 307 nm is assigned to two electronic transitions with large oscillator strengths calculated at 329.3 and 297.1 nm, respectively. Both the transitions are of LMCT ($\pi_{Br}/n(P) \rightarrow d$) character.

The shortest wavelength experimental band at 241.8 nm is attributed to the calculated transitions of LLCT character, but this assignment is not completed. The UV–Vis spectrum of **1** was calculated only to 277 nm and additional intraligand and interligand transitions are expected to be found in the calculation at higher energies. The solution spectra of PPh_3 exhibit an intense absorption band at 263.2 nm, which can support this assignment.

The electronic transition from the rhenium d orbitals to the π* orbitals of the nitrosyl group are calculated at 529.4, 366.0 and 363.0 nm. Considering the large contribution of π bromine orbitals in HOMO − 2 with α spin and HOMO − 1 with β spin, the transition at 529.4 nm is of mixed character $d_{xz}/\pi(Br) \rightarrow \pi^*(NO)$. The transitions at 366.0 and 363.0 nm are of $d_{xy} \rightarrow \pi^*(NO)$ origin. Owing to the small oscillator strengths, none of the transitions contribute significantly to the overall shape of the spectrum. In the experimental spectrum they are hidden under the more intense transitions of LMCT ($\pi_{Br} \rightarrow d$ and $\pi_{Ph} \rightarrow d$) character. Such small values of the oscillator strengths seem to be typical of the $d \rightarrow \pi^*_{NO}$ transitions, and they have been supported by the calculations for other metal nitrosyls [10,11].

4.4.2. *[$ReBr_3(NO)(OPPh_3)_2$] (**2**)*

The TDDFT calculations for complex **2** resulted in many transitions with oscillator strengths close to zero. Similarly as for complex **1**, the spectrum of **2** was calculated only to 290 nm, and the experimental absorption bands recorded below 290 nm were not assigned to the calculated transitions. Considering our previous calculations [42], it can be assumed that the transitions in the high energy part of the spectrum correspond mainly to intraligand $\pi \rightarrow \pi^*$ transitions in the phosphine ligands and interligand transitions. However, the calculations in the range 700–290 nm enable the comparison of the $d \rightarrow \pi^*_{NO}$ transition energy for complexes **1** and **2**.

The longest wavelength experimental bands at 689.2 and 647.4 nm are of low intensity and they are attributed to the transitions of $\pi_{Br}/d_{yz} \rightarrow d$ character with small oscillator strengths calculated at 697.7 and 677.8 nm, respectively.

Table 4
The energy and molar absorption coefficients of experimental absorption bands and the electronic transitions calculated with the TDDFT method for **1** and **2**

The most important orbital excitations	Character	λ [nm]	E [eV]	f	Experimental Λ [nm] (E [eV]) ε
1					
H(β) → L(β)	π(Br), *n*(P) → d	885.4	1.40	*0.0012*	645.0 (1.92) 292
H − 3(β) → L(β)	π(Br) → d	648.5	1.91	*0.0232*	571.0 (2.17) 1766
H − 5(β) → L(β)	π(Ph) → d	545.1	2.27	*0.0115*	456.0 (2.72) 906
H − 2(α) → L + 2(α)	d_{xz}, π(Br) → π*(NO)	529.4	2.34	*0.0002*	
H − 1(β) → L + 2(β)					
H − 5(β) → L(β)	π(Ph) → d	505.2	2.45	*0.0035*	
H − 9(β) → L(β)					
H − 8(β) → L(β)	π(Ph) → d	478.2	2.59	*0.0029*	
H − 18(β) → L(β)	d → d	419.4	2.96	*0.0063*	420.0 (2.95) 908
H − 19(β) → L(β)	π(Br) → d	409.6	3.03	*0.0050*	
H − 1(α) → L + 1(α)	d_{xy} → π*(NO)	366.0	3.39	*0.0011*	
H − 1(α) → L + 2(α)	d_{xy} → π*(NO)	363.0	3.42	*0.0026*	
H(β) → L + 3(β)	π(Br), *n*(P) → d	329.3	3.77	*0.0887*	307.0 (4.04) 2216
H − 1(β) → L + 3(β)					
H − 3(β) → L + 3(β)	π(Br), *n*(P) → d	297.1	4.17	*0.1373*	
H − 4(α) → L(α)					
H(β) → L + 7(β)	π(Br), *n*(P) → d	280.5	4.42	*0.0204*	241.8 (5.13) 12510
H(β) → L + 8(β)	π(Br), *n*(P) → π*(Ph)				
H(β) → L + 4(β)	π(Br), *n*(P) → π*(Ph)	279.2	4.44	*0.0239*	
2					
H(β) → L(β)	π(Br), d_{yz} → d	696.7	1.78	*0.0001*	689.2 (1.80) 39
H − 1(β) → L(β)	π(Br), d_{yz} → d	677.8	1.83	*0.0001*	647.4 (1.92) 66
H − 2(β) → L(β)					
H − 2(β) → L(β)	π(Br), d_{yz} → d	539.3	2.30	*0.0192*	429.9 (2.88) 1686
H − 1(β) → L(β)					
H − 3(β) → L(β)	π(Br) → d	454.4	2.73	*0.0140*	
H − 4(β) → L(β)	π(Br) → d	449.1	2.76	*0.0066*	
H − 5(β) → L(β)	π(Br), π(O) → d	413.8	3.00	*0.0067*	368.3 (3.37) 4 656
H − 9(β) → L(β)	π(Br), π(NO), π(O), *n*(P) → d	387.0	3.20	*0.0104*	
H − 16(β) → L(β)	π(Br), π(O), *n*(P) → d	347.0	3.57	*0.0027*	
H − 14(β) → L(β)					
H − 2(β) → L + 1(β)	π(Br), d_{yz} → π*(Ph)	328.5	3.77	*0.0020*	321.0 (3.86) 1913
H − 2(α) → L + 6(α)	d_{xz}, π(Br) → π*(NO), π*(Ph)	327.7	3.78	*0.0014*	
H − 1(α) → L + 6(α)	d_{xz}, π(Br) → π*(NO), π*(Ph)	326.5	3.80	*0.0009*	
H(α) → L + 6(α)	d_{xy} → π*(NO), π*(Ph)	317.4	3.91	*0.0004*	
H(α) → L + 6(α)	d_{xy} → π*(NO), π*(Ph)	295.6	4.19	*0.0002*	
H − 3(β) → L + 1(β)	π(Br) → π*(Ph)	294.4	4.21	*0.0033*	
H(α) → L + 7(α)	d_{xy} → π*(NO), π*(Ph)	293.6	4.22	*0.0010*	
H − 1(β) → L + 4(β)	π(Br), d_{yz} → π*(Ph)	293.2	4.23	*0.0022*	
					274.0 (4.52) 6859
					268.0 (4.63) 7624
					261.9 (4.73) 7029
					236.8 (5.54) 11841

The next experimental band at 429.9 nm is much more intense and it is assigned to the calculated transitions of $\pi_{Br}/d_{yz} \rightarrow d$ (at 539.3 nm) and $\pi_{Br} \rightarrow d$ (at 454.4 and 449.1 nm) character with large oscillator strengths.

The absorption band at 368.3 nm is attributed to the transitions of $\pi_{Br}/\pi_O \rightarrow d_{yz}$ character calculated at 413.8, 387.0 and 347.0 nm.

The experimental band at 321.0 nm is assigned to the calculated transitions of $\pi(Br)/d_{yz} \rightarrow \pi^*$(Ph) character (at 328.5 and 293.2 nm) and π(Br → π*(Ph) origin (at 294.4 nm).

The electronic transition from the rhenium d orbitals to the π* orbitals of the nitrosyl ligand are calculated at 327.7, 326.5, 317.4, 295.6 and 293.6 nm. The larger number of $d \rightarrow \pi^*_{NO}$ transitions for complex **2** compared to complex **1** results from the larger number of molecular orbitals with substantial contribution of the bonding and antibonding π_{Re-NO} orbitals. In the case of **2**, the π-bonding π_{Re-NO} orbitals are mixed with π bromine orbitals, and the π-antibonding π_{Re-NO} orbitals with π* orbitals of the phenyl groups. Consequently, the transitions at 327.7 and 326.6 nm are of d_{xz}/π(Br → π*(NO)/π*(Ph) origin, and the other ones have

$d_{xy} \rightarrow \pi^*(NO)/\pi^*(Ph)$ character. All the $d \rightarrow \pi^*(NO)$ transitions of complex **2** are shifted towards higher energy in comparison with **1**. The replacement of the triphenylphosphine (strong σ-donor and π-acceptor) by the triphenylphosphine oxide (weak σ-donor and strong π-donor) [43] causes an increase in the energy of the π^*_{Re-NO} orbitals of **2**, whereas the energies of the molecular orbitals of d(Re) character are similar for both **1** and **2**. Similar to complex **1**, the oscillator strengths of the $d_{xy} \rightarrow \pi^*(NO)$ transitions are very small and all the transitions are hidden under the more intense transitions of LMCT ($\pi_{Br} \rightarrow d$, $n(P) \rightarrow d$ and $\pi_O \rightarrow d$) character.

References

[1] N.G. Connelly, Inorg. Chim. Acta Rev. 6 (1972) 47.
[2] K.G. Caulton, Coord. Chem. Rev. 14 (1975) 317.
[3] W.L. Gladfelter, Adv. Organomet. Chem. 24 (1985) 41.
[4] G.B. Richter-Addo, P. Legzdins, Metal Nitrosyls, Oxford University Press, Oxford, 1992.
[5] G.B. Richter-Addo, P. Legzdins, J. Burstyn, Chem. Rev. 102 (2002) 857.
[6] T.W. Hayton, P. Legzdins, W.B. Sharp, Chem. Rev. 102 (2002) 935.
[7] J.A. McCleverty, Chem. Rev. 104 (2004) 403.
[8] E. Hollauer, J.A. Olabe, J. Braz, Chem. Soc. 8 (1997) 495.
[9] B.L. Westcott, J.H. Enemark, in: E.I. Solomon, A.B.P. Lever (Eds.), Inorganic Electronic Structure and Spectroscopy, vol. 2, Wiley, New York, 1999, p. 403.
[10] S.C. da Silva, D.W. Franco, Spectrochim. Acta 55A (1999) 1515.
[11] S.I. Gorelsky, S.C. da Silva, A.B.P. Lever, D.W. Franco, Inorg. Chim. Acta 300–302 (2000) 698.
[12] J.A. Gómez, D. Guenzburger, Chem. Phys. 253 (2000) 73.
[13] H. Wang, E. Miki, S. Re, T. Hiroaki, Inorg. Chim. Acta 340 (2002) 119.
[14] H. Jacobsen, K. Heinze, A. Llamazares, H.W. Schmalle, G. Artus, H. Berke, J. Chem. Soc., Dalton Trans. (1999) 1717.
[15] J.O. Dzięgielewski, B. Machura, T.J. Bartczak, W. Czurak, J. Kusz, J. Warczewski, J. Coord. Chem. 48 (1999) 125.
[16] T.J. Bartczak, W. Czurak, J.O. Dzięgielewski, B. Machura, A. Jankowska, Polyhedron 18 (1999) 2313.
[17] T.J. Bartczak, W. Czurak, J.O. Diêgielewzski, B. Machura, A. Jankowska, J. Kusz, J. Warczewski, J. Coord. Chem. 52 (2001) 361.
[18] B. Machura, J.O. Dzięgielewski, S. Michalik, T.J. Bartczak, R. Kruszynski, J. Kusz, Polyhedron 21 (2002) 2617.
[19] B. Machura, J.O. Dzięgielewski, J. Kusz, Polish J. Chem. 77 (2003) 519.
[20] S. Hirata, M. Head-Gordon, Chem. Phys. Lett. 302 (1999) 375.
[21] R. Andreu, J. Orduna, J. Garín, Tetrahedron 57 (2001) 1358.
[22] E. Brocławik, T. Borowski, Chem. Phys. Lett. 339 (2001) 433.
[23] M.J. Calhorda, M.G.B. Drew, V. Félix, L.P. Fonseca, C.A. Gamelas, S.S.M.C. Godinho, I.S. Gonçavles, E. Hunstock, J.P. Lopes, A.J. Parola, F. Pina, C.C. Romsimao, A.G. Santos, J. Organomet. Chem. 632 (2001) 94.
[24] M.C. Aragoni, M. Arca, T. Cassano, C. Denotti, F.A. Devillanova, F. Isaia, V. Lippolis, D. Natali, L. Niti, M. Sampietro, R. Tommasi, G. Verani, Inorg. Chem. Commun. 5 (2002) 869.
[25] P. Romaniello, F. Lelj, Chem. Phys. Lett. 372 (2003) 51.
[26] P. Norman, P. Cronstrand, J. Ericsson, Chem. Phys. 285 (2002) 207.
[27] J. Bossert, N.B. Amor, A. Strich, C. Daniel, Chem. Phys. Lett. 342 (2001) 617.
[28] C.E. Powell, M.P. Cifuentes, A.M. McDonagh, S.K. Hurst, N.T. Lucas, C.D. Delfs, R. Stranger, M.G. Humphrey, S. Houbrechts, I. Asselberghs, A. Persoons, D.C.R. Hockless, Inorg. Chim. Acta 352 (2003) 9.
[29] J.P. Morral, C.E. Powell, R. Stranger, M.P. Cifuentes, M.G. Humphrey, G.A. Heath, J. Organomet. Chem. 670 (2003) 248.
[30] P. Romaniello, F. Lelj, J. Mol. Struct. Theochem. 636 (2003) 23.
[31] M.J. Frisch, G.W. Trucks, H.B. Schlegel, G.E. Scuseria, M.A. Robb, J.R. Cheeseman, J.A. Montgomery Jr., T. Vreven, K.N. Kudin, J.C. Burant, J.M. Millam, S.S. Iyengar, J. Tomasi, V. Barone, B. Mennucci, M. Cossi, G. Scalmani, N. Rega, G.A. Petersson, H. Nakatsuji, M. Hada, M. Ehara, K. Toyota, R. Fukuda, J. Hasegawa, M. Ishida, T. Nakajima, Y. Honda, O. Kitao, H. Nakai, M. Klene, X. Li, J.E. Knox, H.P. Hratchian, J.B. Cross, C. Adamo, J. Jaramillo, R. Gomperts, R.E. Stratmann, O. Yazyev, A.J. Austin, R. Cammi, C. Pomelli, J.W. Ochterski, P.Y. Ayala, K. Morokuma, G.A. Voth, P. Salvador, J.J. Dannenberg, V.G. Zakrzewski, S. Dapprich, A.D. Daniels, M.C. Strain, O. Farkas, D.K. Malick, A.D. Rabuck, K. Raghavachari, J.B. Foresman, J.V. Ortiz, Q. Cui, A.G. Baboul, S. Clifford, J. Cioslowski, B.B. Stefanov, G. Liu, A. Liashenko, P. Piskorz, I. Komaromi, R.L. Martin, D.J. Fox, T. Keith, M.A. Al-Laham, C.Y. Peng, A. Nanayakkara, M. Challacombe, P.M.W. Gill, B. Johnson, W. Chen, M.W. Wong, C. Gonzalez, J.A. Pople, GAUSSIAN 03, Revision B.03, Gaussian Inc., Pittsburgh, PA, 2003.
[32] A.D. Becke, J. Chem. Phys. 98 (1993) 5648.
[33] C. Lee, W. Yang, R.G. Parr, Phys. Rev. B 37 (1988) 785.
[34] P.J. Hay, W.R. Wadt, J. Chem. Phys. 82 (1985) 299.
[35] N. Psaroudakis, K. Mertis, D.G. Liakos, E.D. Simandiras, Chem. Phys. Lett. 369 (2003) 490.
[36] G. Ciani, D. Giusto, M. Manassero, M. Sansoni, J. Chem. Soc., Dalton Trans. (1975) 2156.
[37] A.A. Batista, C. Pereira, S.L. Queiroz, L.A.A. de Oliveira, R.H. de A. Santos, M.T. de P. Gambardella, Polyhedron 16 (1997) 927.
[38] J.E. Carpenter, F. Weinhold, J. Mol. Struct. Theochem. 169 (1988) 41;
J.P. Foster, F. Weinhold, J. Am. Chem. Soc. 102 (1980) 7211;
A.E. Reed, F. Weinhold, J. Chem. Phys. 78 (1983) 4066;
A.E. Reed, F. Weinhold, J. Chem. Phys. (1983) 1736;
A.E. Reed, R.B. Weinstock, F. Weinhold, J. Chem. Phys. 83 (1985) 735;
A.E. Reed, L.A. Curtiss, F. Weinhold, Chem. Rev. 88 (1988) 899.
[39] M.E. Casida, C. Jamorski, K.C. Casida, D.R. Salahub, J. Chem. Phys. 108 (1998) 4439.
[40] D. Sundholm, Chem. Phys. Lett. 317 (2000) 545.
[41] D. Sundholm, Chem. Phys. Lett. 302 (1999) 480.
[42] B. Machura, M. Jaworska, R. Kruszynski, Polyhedron 23 (2004) 1819.
[43] J.B. Cook, B.K. Nicholson, D.W. Smith, J. Organomet. Chem. 689 (2004) 860.

Available online at www.sciencedirect.com
SCIENCE DIRECT®
Polyhedron 23 (2004) 2373–2379
POLYHEDRON
www.elsevier.com/locate/poly

Dinuclear Pd(II) complexes with the anionic form of 4,5-dihydro-1,2,4-triazolo[1,5-a]pyrimidine-5-one

Mohammad Abul-Haj [a], Miguel Quirós [b,*], Juan M. Salas [b]

[a] Department of Chemistry and Chemical Technology, Al-Quds University, P.O. Box 20002, Abu Dis, Jerusalem, Palestine
[b] Departamento de Química Inorgánica, Facultad de Ciencias, Universidad de Granada, Av. Fuentenueva, s.n., 18071 Granada, Spain

Received 1 April 2004; accepted 12 July 2004
Available online 21 September 2004

Abstract

This article describes the synthesis, spectroscopic characterization and single crystal X-ray structure of several Pd(II) dinuclear complexes with the ligand 4,5-dihydro-1,2,4-triazolo[1,5-a]pyrimidine-5-one (5HtpO) in its anionic form ($5tpO^-$). The synthesis and characterization of the related mononuclear compound $[PdCl_2(5HtpO)_2]$ is also included. This compound is transformed into the dinuclear $[Pd_2(5tpO)_4] \cdot 4H_2O$ by raising the pH, the structure of which indicates a head–tail–head–tail disposition of the heterocycles (D_{2d} symmetry) as a difference with the analogous Cu(II) and Pt(II) clusters. Using the auxiliary ligands bipyridine (bpy), phenanthroline (phen) and *trans*-1,2-diaminocyclohexane (*t*-dach, racemic mixture), dinuclear compounds with the general formula $[Pd_2(5tpO)_2(a–a)_2](NO_3)_2 \cdot nH_2O$ are obtained. The crystal structure of those with a–a = phen and a–a = *t*-dach have been solved showing a head–tail disposition of the organic ligands, in contrast with the NMR data for a–a = bpy, which point to a head–head disposition.
© 2004 Elsevier Ltd. All rights reserved.

Keywords: Triazolopyrimidine; Palladium dimers; Head–head; Head–tail

1. Introduction

The coordination chemistry of 1,2,4-triazolo[1,5-a] pyrimidine derivatives is a research field that has yielded a considerable number of new compounds with interesting structural features [1], which may be considered as model systems for some naturally occurring metal coordination compounds with isomeric purine derivatives. The binding modes of triazolopyrimidines are rather variable and, among these, the bidentante mode through the nitrogen atoms at positions 3 and 4 (corresponding to positions 9 and 3 of purines in the biochemical numbering scheme) is interesting, since it usually gives rise to the formation of dinuclear compounds including one or more eight-member $M_2N_2C_4$ rings. Such compounds have been described for Cu(I) [2], Cu(II) [3], Ag(I) [4], Pd(II) [5] and Pt(II) [6], and there are also examples of heteronuclear Pt–Ag [7] and Pt–Pd complexes [8].

The distance between both metal atoms in the core is forced to be rather short, which makes it possible for a direct metal–metal interaction to take place. In the case of Cu(II), this interaction is observed as a strong antiferromagnetic coupling [3]. Theoretical studies have been performed in order to obtain information about the nature of this interaction and the topological analysis of the calculated charge density (AIM theory [9]) revealed the existence of a bond critical point between the metal atoms for Ag(I) [10], Cu(II) [3] and Pt(II) [6]. The relative disposition of the bridging heterocycles (head–head, head–tail) is also an interesting subject and it has shown to relay more in the kinetic path that leads to the formation of the compound or in the interactions with neighbouring species than in intrinsic electronic reasons [11].

* Corresponding author. Tel.: +34 958 240441; fax: +34 958 248526.
E-mail address: mquiros@ugr.es (M. Quirós).

0277-5387/$ - see front matter © 2004 Elsevier Ltd. All rights reserved.
doi:10.1016/j.poly.2004.07.024

Following this research line, we present in this paper the synthesis, characterization and crystal structures of a number of dinuclear Pd(II) complexes with the anionic form of 4,5-dihydro-1,2,4-triazolo[1,5-a]pyrimidine-5-one (5HtpO), including the mononuclear precursor of one of them. The goal of the study is to extend the results previously obtained for this kind of compound, trying to relate the structural features of the dinuclear clusters with the nature of the metal atoms (Cu, Pd or Pt), the substituents in the bridging ligand and the presence of auxiliary ligands.

2. Experimental

2.1. Synthesis of the complexes

The compound 5HtpO was prepared according to the published method from 3-amino-1,2,4-triazole and ethyl 3,3-diethoxypropionate in NaOEt/EtOH [12]. Other reagents were obtained from commercial sources.

$[PdCl_2(5HtpO)_2]$ (**1**) was obtained by mixing two solutions, 10 mL each, one containing 2 mmol of $K_2[PdCl_4]$ and the other 4 mmol of 5HtpO, both in 1 M HCl. A yellow precipitate immediately appeared, which was filtered, washed with water and ethanol, and dried with ether. Elemental *Anal*. Calc. for $C_{10}Cl_2H_8N_8O_2Pd$: C, 26.7; H, 1.8; N, 24.9. Found: C, 26.9; H, 1.8; N, 24.1%.

$[Pd_2(5tpO)_4] \cdot 4H_2O$ (**2**): 2 mmol of **1** were suspended in 40 ml of water and the pH was raised up to 6.4 by dropwise addition of 0.1 M NaOH. The solid was completely dissolved after this and an orange solution was obtained. After several minutes, an orange precipitate appeared which was filtered and washed with water and ethanol, and then recrystallized in an acetonitrile:ethanol:water 2:2:1 mixture, yielding X-ray suitable orange crystals. Elemental *Anal*. Calc. for $C_{20}H_{20}N_{16}O_8Pd_2$: C, 29.1; H, 2.4; N, 27.1. Found: C, 28.7; H, 2.5; N, 26.7%.

$[Pd_2(5tpO)_2(bpy)_2](NO_3)_2 \cdot 2H_2O$ (**3**), $[Pd_2(5tpO)_2(phen)_2](NO_3)_2 \cdot 4H_2O$ (**4**) and $[Pd_2(5tpO)_2(t\text{-dach})_2](NO_3)_2 \cdot 4H_2O$ (**5**) (where bpy = bipyridine, phen = phenanthroline and *t*-dach = *trans*-diaminocyclohexane): Firstly, the compounds $[PdCl_2(a–a)]$ (a–a = bpy, phen or *t*-dach) were obtained using the procedure previously described for $[PdCl_2(en)]$ [13], changing the ethylenediamine by the appropriate diamine. 2 mmol of $[PdCl_2(a–a)]$ and 4 mmol of $AgNO_3$ were dissolved in 40 ml of water and kept in the dark at 45 °C for an hour. The resulting AgCl was filtered off and the solution was treated with 4 mmol of 5HtpO and kept at 60 °C for 4 h. After this, it was left to stand at room temperature, crystalline solids appearing after several days. The crystals of compound **5** were found to be suitable for X-ray work. **3** and **4** were recrystallized in an acetonitrile:ethanol:water 2:2:1 mixture and the crystals obtained for **4** were also suitable for X-ray work. Elemental analysis data:

Compound **3**: *Anal*. Calc. for $C_{30}H_{26}N_{14}O_{10}Pd_2$: C, 37.7; H, 2.7; N, 20.5. Found: C, 37.8; H, 2.5; N, 20.8%.

Compound **4**: *Anal*. Calc. for $C_{34}H_{30}N_{14}O_{12}Pd_2$: C, 39.3; H, 2.9; N, 18.9. Found: C, 39.0; H, 2.9; N, 19.0%.

Compound **5**: *Anal*. Calc. for $C_{22}H_{42}N_{14}O_{12}Pd_2$: C, 29.1; H, 4.7; N, 21.6. Found: C, 29.0; H, 4.4; N, 21.3%.

2.2. Instrumentation

Microanalysis of C, H and N were performed in a Fisons Instruments EA-1008 analyser. Thermal behaviour was studied under an air flow in Shimadzu TGA-50 and Shimadzu DSC-50 equipment. ^1H and ^{13}C NMR spectra were recorded for dmso-d_6 solutions of the compounds on a Bruker AM-300 spectrometer (all this equipment is sited at the Centre of Scientific Instrumentation of the University of Granada). IR spectra were obtained using a FT MIDAC Prospect 1 spectrophotometer with samples dispersed in KBr pellets.

2.3. Crystallography

Data were collected at room temperature for compounds **2**, **4** and **5** in a Siemens P4 diffractometer with Mo Kα radiation ($\lambda = 0.7107$ Å). The crystals were covered with a drop of paraffin oil to prevent their decomposition. Data were corrected for absorption only for **2** (ψ-scans, transmission range, 0.4251–0.6778). Structures were solved by the heavy atom method and refined in F^2 using SHELXL-97 [14]. The nitrate ion in **4** was disordered into two positions with half occupancy and refined with restrained geometry. Four carbon atoms of each *t*-dach moiety (those in α and γ positions respect to the to N atoms) in **5** are also disordered into two positions, which correspond to the two enantiomers of the auxiliary ligand. Several water molecules in the three structures have been introduced with partial occupancy. Atoms with partial occupancy have been refined isotropically and remaining non-H atoms anisotropically. Hydrogen atoms of the heterocycles were placed in ideal positions and those of water molecules were not introduced. Isotropic thermal parameters of all H atoms were fixed to 1.2 times the equivalent isotropic thermal parameter of their parent atoms. Crystal data for the three structures have been listed in Table 1.

3. Results and discussion

3.1. X-ray structural studies

The main structural blocks of the crystal structures of compounds **2**, **4** and **5** are dinuclear clusters in which

Table 1
Crystal data for compounds **2**, **4** and **5**

	2	**4**	**5**
Empirical formula	$C_{20}H_{20}N_{16}O_8Pd_2$	$C_{34}H_{30}N_{14}O_{12}Pd_2$	$C_{22}H_{40}N_{14}O_{11}Pd_2$
Formula weight	825.32	1039.52	889.48
Crystal dimensions (mm)	$0.4 \times 0.4 \times 0.1$	$0.4 \times 0.2 \times 0.1$	$0.4 \times 0.2 \times 0.1$
Crystal system	orthorhombic	monoclinic	monoclinic
Space group	$C222_1$	C2/c	$P2_1/c$
Unit cell dimensions			
a (Å)	12.864(2)	19.688(12)	10.2842(15)
b (Å)	14.634(2)	14.219(12)	18.920(3)
c (Å)	30.703(3)	14.448(6)	18.450(3)
β (°)		110.02(4)	104.117(10)
V (Å^3)	5779.7(14)	3800(4)	3481.5(9)
Z	8	4	4
$F(000)$	3264	2080	1800
D_{calc} (Mg m^{-3})	1.897	1.817	1.697
Absorption coefficient (mm^{-1})	1.320	1.031	1.106
Unique reflections	5222	5547	4542
Flack parameter	0.12(10)		
wR^2 (all data)	0.1972	0.2325	0.1238
$R(I > 2\sigma(I))$	0.0765	0.0793	0.0487
Largest ΔF peak (e Å^{-3})	1.688	1.733	1.089

both palladium atoms are linked by 5tpO$^-$ moieties, 5tpO$^-$ representing the anionic form of 4,5-dihydro-1,2,4-triazolo[1,5-a]pyrimidine-5-one, which are linked to the metal atoms through the nitrogen atoms at positions 3 and 4. Several examples of this coordination mode have been described for 1,2,4-triazolo[1,5-a]pyrimidine derivatives which lead to dinuclear (or polynuclear, if other bridges are present) compounds of Cu(I), Ag(I), Cu(II), Pd(II) and Pt(II) (see Section 1). The crystal structures are completed by interstitial water molecules and, in the structures of **4** and **5**, by nitrate counteranions balancing the charge of the cationic clusters. Bond distances and angles around the palladium atoms are listed in Table 2.

Four 5tpO$^-$ bridges are present in the molecular structure of compound **2**, building in this way neutral $[Pd_2(5tpO)_4]$ species. Each Pd atom in these species is surrounded in a square-planar fashion by two N3 and two N4 atoms in a *trans* disposition, thus defining the head–tail–head–tail isomer with molecular D_{2d} symmetry. Two crystallographically different but chemically identical $[Pd_2(5tpO)_4]$ molecules are present (Fig. 1), in both cases a crystallographic binary axis runs across the molecule, relating the two equivalent halves of it. In one case (Pd1) the crystal binary axis in the b direction is perpendicular to the Pd–Pd line (C_2' axis of the D_{2d} point group) where in the other (Pd2–Pd3) the crystal binary axis in the a direction crosses through the metal atoms (main axis of D_{2d}).

This kind of cluster with triazolopyrimidine ligands has been previously described for Cu(II) [3] and for Pt(II) [6], but in these two cases the head–head–tail–tail isomer (C_{2h}) was found. For steric reasons, it is expected that the D_{2d} isomer is thermodynamically more stable than the C_{2h} isomer, but the synthetic procedure and the slower Pt(II) kinetics and the presence of a water molecule in the apical position of the Cu(II) compound would explain the presence of the C_{2h} isomer in these

Table 2
Bond distances (Å) and angles (°) around Pd atoms

	2 (Pd1)	**2** (Pd2–Pd3)	**4**	**5**
Bond distances				
Pd–Pd	2.7409(19)	2.7441(18)	3.0031(18)	3.2378(9)
Pd–N3	2.012(11)	2.016(11)	2.026(7)	2.036(6)
	2.037(11)	2.040(14)		2.031(6)
Pd–N4	2.045(11)	2.059(11)	2.018(7)	2.052(6)
	2.062(12)	2.040(13)		2.052(6)
Pd–Na			2.029(6)	2.035(6)
			2.016(6)	2.019(6)
				2.029(6)
				2.024(6)
Bond angles				
N3–Pd–N3	169.2(5)	170.2(7)		
		170.6(10)		
N4–Pd–N4	171.4(5)	169.5(7)		
		169.6(8)		
N3–Pd–N4	88.6(5)	91.2(5)	87.0(3)	93.1(2)
	90.0(4)	87.9(5)		92.8(2)
	89.5(4)	91.9(5)		
	90.3(5)	87.3(5)		
N3–Pd–Na			177.6(3)	173.2(2)
			97.1(3)	90.5(3)
				174.3(3)
				90.5(2)
N4–Pd–Na			174.2(2)	175.7(2)
			94.3(3)	93.1(2)
				176.3(2)
				92.9(2)
Na–Pd–Na			81.5(3)	83.2(2)
				83.8(2)

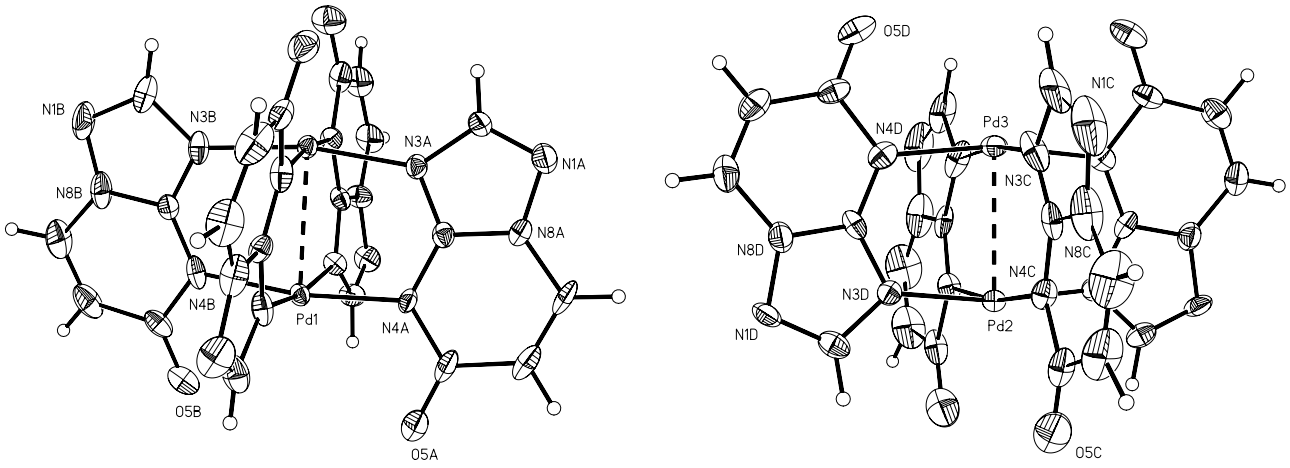

Fig. 1. Crystallographically independent clusters of compound **2** as deduced from X-ray diffraction data. There is a crystallographic binary axis perpendicular to the Pd–Pd line in the cluster on the left side and another one through the metal atoms in the cluster on the right. Non-hydrogen atoms are represented by ellipsoids at the 30% probability level.

cases. None of these reasons are applicable to **2**, so the D_{2d} isomer is obtained.

The N_4 planes are perfectly parallel for the Pd2–Pd3 dimer (imposed by the crystallographic symmetry) and almost so for the Pd1 dimer (interplanar angle, 0.4(3)°). The metal atoms are deviated from these planes by 0.172(2) (Pd1), 0.179(1) (Pd2) and 0.178(1) Å (Pd3), in all cases away from the other Pd atom, as it happens in the above mentioned Cu and Pt compounds. The Pt–Pt distance in the later is almost identical to the Pd–Pd distances in **2**.

We have found only three structures in the literature comprising a $Pd_2N_8C_4$ core, two of them with flexible ligands [15,16] with a Pd–Pd distance shorter than in **2**, these compounds being oxidizable to Pd(II)–Pd(III) species. The only example we have found with the N atoms belonging to a rigid bicyclic heterocycle is a Pd(III) compound [17] with a very short (2.391(2) Å) intermetallic distance.

On the other hand, there are only two bridging 5tpO$^-$ ligands in the dinuclear entities in the crystal structures of **4** and **5**. Each metal atom in these is linked by the N3 atom of one ligand and the N4 atom of the other thus defining the head–tail isomer. The other two coordination sites are occupied by the nitrogen atoms of the bidentate phenanthroline (**4**) or *trans*-diaminocyclohexane (**5**). Figs. 2 and 3 display the structures of these dinuclear cations. Both halves of the cluster in **4** are related by a crystallographic binary axis. Four carbon atoms of each auxiliary ligand in **5** are disordered between two positions, which is clearly due to the presence of both enantiomers (RR and SS) of *t*-dach, randomly distributed across the crystal.

As it happens with structurally analogous compounds [5], the interaction between the auxiliary ligands influences the geometry of the cluster, as indicated by the intermetallic distance (Table 2) and the angle between the N_4 planes (19.2(2)° and 36.5(2)° for **4** and **5** respectively). Stacking takes place between the phen planes, with an angle between them of 1.6(2)° and average interplanar distance of 3.47 Å. The optimization of such an interaction produces the relative rotation of both PdN_4 planes (torsional angles N–Pd–Pd–N, 10.4(3)° and 13.6(3)°) as was observed for the analogous compound with the 7-oxo isomer of the ligand [11].

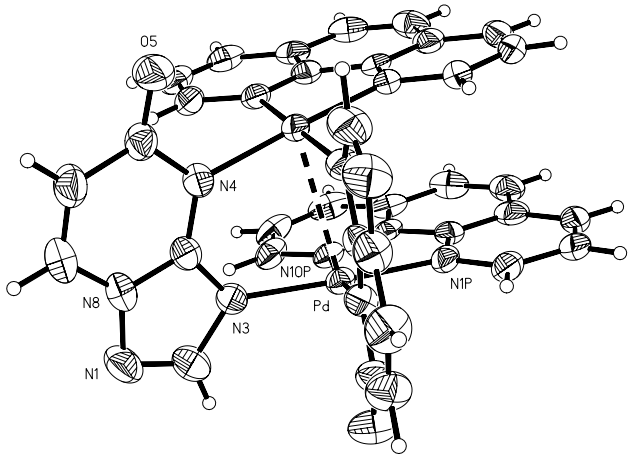

Fig. 2. Structure of the dinuclear cation in **4** according to X-ray analysis. A crystallographic binary axis runs perpendicular to the Pd–Pd line. Non-hydrogen atoms are represented by ellipsoids at the 30% probability level.

3.2. Infrared and thermal studies

The thermal behaviour of these compounds in air has been studied from their TG and DSC plots. Dehydration appears as a well defined weight loss accompanied by the corresponding endothermic effect only for compound **2**, for which a dehydration enthalpy of 49 kJ per mole of water can be calculated. For the remaining

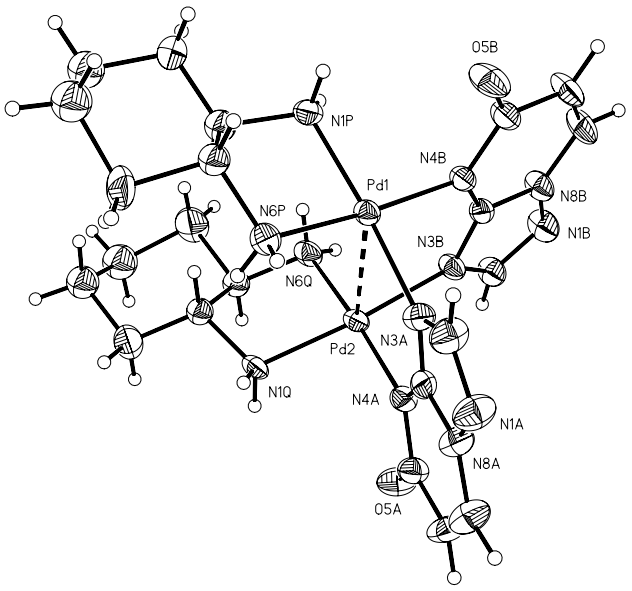

Fig. 3. Structure of the dinuclear cation in **5** according to X-ray analysis. Non-hydrogen atoms are represented by ellipsoids at the 30% probability level.

compounds these effects are poorly defined, showing a loose attachment of water to the structure, which also explain a certain lack of reproducibility of water content in the analysis and partial occupancy of water in the crystal structures. Dehalogenation of **1** is clearly seen from the corresponding weight loss and endothermic effects (peak at 310 °C) which overlap with the beginning of the pyrolysis. The final residue of the pyrolysis is PdO in all cases.

The infrared spectra are not very informative. Those including the anionic form of the ligand show the expected bathochromic effect for the ν(C=O) band that appears between 1645 and 1650 cm^{-1}. The spectrum of **1** displays an acute band at 342 cm^{-1}, assignable to ν(Pd–Cl): the presence of a single band may indicate a *trans* geometry. Most compounds with the $PdCl_2N_2$ chromophore included in the Cambridge Structural Database [18] (excluding of course those with both N atoms belonging to the same ligand) display *trans* geometry (159 *trans* vs. only 3 *cis*), but one of the few with a *cis* geometry include a triazolopyrimidine derivative as a ligand [19].

3.3. NMR studies

^1H and ^{13}C NMR spectra have been recorded for dmso-d_6 solutions of compounds **1**, **2**, **3** and **5**. **4** was found to be insoluble in this solvent. DEPT spectra were also recorded to help in ^{13}C assignments. Both spectra of **1** display two sets of signals, the most intense ones being clearly attributable to free 5HtpO [12], which indicates that **1** extensively decomposes when dissolved in dmso, this decomposition quickly reaches equilibrium since the spectra do not appreciably change with time. The other species (with a concentration of about one third of free 5HtpO), possibly a complex of the type $[PdCl_2(5HtpO)L]$ (L = H_2O or dmso), exhibits the resonances listed in Table 3. Downfield shifts with respect to the free ligand are observed for H2, C5 and C6, and upfield shifts for the remaining signals.

Table 3
^1H and ^{13}C assignments (δ in ppm) for 5HtpO and 5tpO$^-$ moieties

	5HtpO	**1**[a]	**2**	**3**	**5**
H2	8.11	8.32	8.03	8.50	8.14–8.21
H6	6.16	6.11	5.97	6.18	6.04–6.11
H7	8.62	8.38	8.21	8.56	8.35–8.39
J(H6–H7), Hz	7.9	7.6	7.6	7.7	
C2	152.6	148.8	148.5	147.5	148.9–149.5
C3a	150.0	[b]	153.9	154.1	153.9–154.1
C5	161.0	166.2	165.7	165.5	166.4–166.6
C6	108.0	108.7	108.6	109.6	108.5–109.0
C7	136.9	135.3	135.0	135.9	134.9–135.2

[a] Data refer to the minor species: see text.
[b] Not observed.

In both ^1H and ^{13}C spectra of **2**, all organic moieties appear equivalent, indicating that a single species is present, so we may infer that the solid state molecular structure is retained in solution. Nevertheless, the possibility of complete and quick isomerisation to the C_{2h} (head–head–tail–tail) isomer cannot be ruled out, since for compound **3** (see below) the head–tail isomer seems to be more stable in solution and the reasons for stabilizing the HT isomer of **3** could also apply the stabilization of the C_{2h} isomer of **2**.

For **3**, there is clearly a major species in solution, with a single set of resonances for the 5tpO$^-$ moiety (listed in Table 3), which indicates that one of the two possible isomers (head–head, HH or head-tail, HT) is much more stable in solution than the other. Two sets of signals appear for bipyridine, either both bpy are equivalent but the two halves of each molecule are not (HT) or there are two different bpy moieties with equivalent halves (HH). In a previous work with the isomeric 7-oxo derivative as a bridging ligand [11], the position of the signals assigned to Hb protons (see Scheme 1 for the labelling of bpy used in this section) is regarded as diagnostic to distinguish between HH and HT isomers. In compound **3**, the Hb triplets are centred at 7.31 and 7.35 ppm,

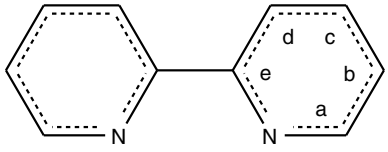

Scheme 1.

overlapping to build an ill-shaped quintet, so it is deduced that they belong to the HH isomer: two well separated triplets would be expected for the HT isomer, as happens with the analogous compound with the 5-methyl-7-oxo derivative [5], for which the HT isomer is much more stable due to the steric repulsion between the methyl groups for the HH isomer. Other ^{1}H resonances of the auxiliary ligand are 7.83 and 8.03 (Ha), 8.08 and 8.17 (Hc) and 8.24 and 8.31 ppm (Hd) with J(Ha-Hb) = 5.6, J(Hb-Hc) = 7.8 and J(Hc-Hd) = 8.1 Hz. ^{13}C resonances of bpy (assigned by comparison with free bpy [20]) appear at 151.3 and 151.5 (Ca), 128.1 and 128.3 (Cb), 141.9 and 142.4 (Cc), 123.8 and 123.9 (Cd) and 154.7 and 154.8 ppm (Ce). Apart from this, we can also see in the ^{1}H spectrum a number of very weak signals attributable to a very small proportion of the HT isomer: in particular, Hb triplets are visible at 7.24 and 7.44 ppm, well separated as expected. Other visible signals for this species are 8.51 (H2), 6.24 (H6), 8.62 (H7) and 7.87 ppm (one of the Ha), the rest being obscured by the intense HH isomer signals.

It is noteworthy that we find that the HH isomer of **3** is much more stable in solution than the HT isomer, a difference from the analogous compound with the 7-oxo isomer as the bridging ligand [11], for which both isomers display analogous stability. This could be explained by the possible presence of a water molecule simultaneously hydrogen-bonded to both carbonyl oxygen atoms keeping in this way the ''heads'' together. There is also a noticeable difference between the molecular structure of **3** in solution and the solid state structure of **4**, which is HT (see above), possibly favoured by crystal packing considerations. Unfortunately, comparisons cannot be done for these compounds since no good single crystals of **3** could be grown and **4** is insoluble in dmso. The coupling pattern of the resonances of the H atoms of phen belonging to the external (benzene) ring would let us unequivocally distinguish between HH and HT isomers [11].

Finally, the spectra of **5** are very complex, due to the presence of both enantiomers (RR and SS) of *trans*-diaminocyclohexane. The existence of four different 5tpO^{-} species can be deduced since there are four signals in the region of the H2 singlet and four signals can also be seen for each carbon of this ligand (the δ ranges are listed in Table 3). At least seven signals (possibly eight), easily assignable (with the aid of the DEPT spectrum) to the CH next to the amino groups of *t*-dach, are visible. If we think that only HH species are present, the presence of four non-equivalent triazolopyrimidine moieties can be explained by the existence of RRRR (and enantiomeric SSSS) and RRSS diasteromers since the symmetry plane that would make the two ''heads'' equivalent is eliminated by the chiral auxiliary ligands. Also, if only HT species are present, four 5tpO^{-} sets are expected, two for asymmetric RRSS and another two for RRRR (+SSSS), for which the two bridging ligands are related by a binary axis but with two non-equivalent possibilities for the disposition of the ligands. Therefore, the spectra are compatible with a major presence of either only HH or only HT species.

4. Supplementary data

The supplementary crystallographic data for this paper have been deposited in the CCDC (Deposition numbers CCDC 234810, CCDC 234811 and CCDC 234812 respectively for **2**, **4** and **5**). These data can be obtained free of charge via www.ccdc.cam.ac.uk/conts/retrieving.html (or from the CCDC, 12 Union Road, Cambridge CB2 1EZ, UK; fax: +44 1223 336033; e-mail: deposit@ccdc.cam.ac.uk).

Acknowledgements

This work was supported by a project of the Ministry of Science and Technology of Spain (BQU 2001-2955-CO2). M. Abul Haj acknowledges TEMPUS program of the European Community for an individual mobility grant.

References

[1] J.M. Salas, M.A. Romero, M.P. Sánchez, M. Quirós, Coord. Chem. Rev. 193 (1999) 1119.
[2] J.G. Haasnoot, T.L.F. Favre, W. Hinrichs, J. Reedijk, Angew. Chem. Int. Ed. Engl. 27 (1988) 901.
[3] M. Abul Haj, M. Quirós, J.M. Salas, J.A. Dobado, J. Molina, M.G. Basallote, M.A. Máñez, Eur. J. Inorg. Chem. (2002) 811.
[4] J.M. Salas, M.A. Romero, A. Rahmani, M. Quirós, Anal. Quím. Int. Ed. 92 (1996) 249.
[5] J.A.R. Navarro, M.A. Romero, J.M. Salas, J. Chem. Soc., Dalton Trans. (1998) 901.
[6] J.A.R. Navarro, M.A. Romero, J.M. Salas, M. Quirós, J. El Bahraoui, J. Molina, Inorg. Chem. 35 (1996) 7829.
[7] M. Abul Haj, M. Quirós, J.M. Salas, R. Faure, Inorg. Chem. Commun. 4 (2001) 254.
[8] J.A.R. Navarro, M.A. Romero, J.M. Salas, M. Quirós, Inorg. Chem. 36 (1997) 3277.
[9] R.F.W. Bader, Chem. Rev. 91 (1991) 893.
[10] M.A. Romero, J.M. Salas, M. Quirós, M.P. Sánchez, J. Molina, J. El Bahraoui, R. Faure, J. Mol. Struct. 354 (1995) 189.
[11] M. Abul Haj, M. Quirós, J.M. Salas, J. Chem. Soc., Dalton Trans. (2002) 4740.
[12] M. Abul Haj, J.M. Salas, M. Quirós, J. Molina, R. Faure, J. Mol. Struct. 519 (2000) 165.
[13] H. Hohmann, R. Van Eldick, Inorg. Chim. Acta 174 (1990) 87.
[14] G.M. Sheldrick, SHELXL-97, University of Göttingen, Germany, 1997.
[15] F.A. Cotton, M. Matusz, R. Poli, X. Feng, J. Am. Chem. Soc. 110 (1988) 1144.

[16] C.L. Yao, L.P. He, J.D. Korp, J.L. Bear, Inorg. Chem. 27 (1988) 4389.
[17] F.A. Cotton, J. Gu, C.A. Murillo, D.J. Timmons, J. Am. Chem. Soc. 120 (1998) 13280.
[18] F.H. Allen, Acta Crystallogr. B 58 (2002) 380.
[19] E. Szlyk, A. Grodzicki, L. Pazderski, A. Wojtezak, J. Chatlas, G. Wrzeszez, J. Sitkowski, B. Kamienski, J. Chem. Soc., Dalton Trans. (2000) 867.
[20] G.A. Naganagowda, K.V. Ramanathan, V. Gayathri, N.M. Nanje Gowda, Magn. Reson. Chem. 38 (2000) 223.

Available online at www.sciencedirect.com
SCIENCE DIRECT®
Polyhedron 23 (2004) 2381–2385
POLYHEDRON
www.elsevier.com/locate/poly

On the complex hedgehog-shaped cluster species containing 368 Mo atoms: simple preparation method, new spectral details and information about the unique formation

Achim Müller *, Bogdan Botar, Samar K. Das, Hartmut Bögge, Marc Schmidtmann, Alice Merca

Faculty of Chemistry, University of Bielefeld, P.O. Box 100131, 33501 Bielefeld, Germany

Received 21 June 2004; accepted 26 July 2004
Available online 11 September 2004

Abstract

The deep-blue compound $Na_{48}[H_xMo_{368}O_{1032}(H_2O)_{240}(SO_4)_{48}] \cdot$ ca. $1000H_2O \equiv Na_{48}$ **1a** $\cdot$ ca. $1000H_2O$ (**1**) exhibiting an unusual nanosized hedgehog-type cluster anion, could now be obtained in good yield – allowing now several materials science studies – in the presence of a high concentration of an electrolyte destroying the hydration shell, in only two days. **1** was characterized by elemental analysis (including redox titrations to determine the (formal) number of Mo^V centers), thermogravimetry and spectroscopic methods (IR, resonance Raman, Vis/NIR). Information about unusual aspects of the formation is reported together with additional spectroscopic details as well as a new crystal structure determination of the very complex system while confirming the earlier one.
© 2004 Elsevier Ltd. All rights reserved.

Keywords: Clusters; Complexity; Nanochemistry; Polyoxomolybdates

1. Introduction

Aesthetically beautiful giant polyoxomolybdates of the type $\{Mo_{11}\}_n$ which are either sphere- ($n = 12$) or wheel-shaped ($n = 14$) can now be obtained by undergraduates in facile syntheses [1,2]. Following our related work other research groups have also reported comparable syntheses of the cluster species [3] and used them e.g., for materials science studies (see below). The mentioned cluster anions, in spite of their completely different overall structure, have formally similar building blocks resulting in the remarkable mentioned equivalent stoichiometry [2e] which is also of importance for the cluster reported here. The related molybdate building units abundant in a unique 'dynamic library' can form – via a type of 'split and/or link process' – a versatility of molecular architectures upon slight variation of the boundary conditions under reduced conditions. This is especially the case for Mo-blue-type solutions [2] from which the above mentioned wheel-type species can be obtained. From this 'library' an even larger and highly reduced cluster anion containing 368 Mo atoms can – under very special conditions – be obtained [4] which shows much more structural complexity than the wheel-type cluster species. As the related earlier published synthetic method requires a rather long time – crystallization occurs only after 2 weeks according to the high solubility – we report here (1) a facile synthesis allowing now several types of studies together with some detailed spectroscopic information for an easy identification of the cluster, (2) a second (crystal) structure

* Corresponding author. Tel.: +49 521 106 6153; fax: +49 521 106 6003.
E-mail address: a.mueller@uni-bielefeld.de (A. Müller).

0277-5387/$ - see front matter © 2004 Elsevier Ltd. All rights reserved.
doi:10.1016/j.poly.2004.07.018

determination for the extremely complex inorganic cluster confirming the earlier published one and (3) further details about the related cluster-formation problem which seems to be interesting.

2. Experimental

The chemicals were purchased from commercial sources and all manipulations were performed using materials as received.

2.1. $Na_{48}[H_xMo_{368}O_{1032}(H_2O)_{240}(SO_4)_{48}] \cdot ca.\ 1000\ H_2O,\ x \approx 16$

To a solution of 6 g $Na_2MoO_4 \cdot 2H_2O$ (24.8 mmol) in 25 ml of water acidified with 100 ml 0.5 M H_2SO_4, 0.18 g $N_2H_6SO_4$ (1.38 mmol) as reducing agent is added under stirring. After stirring for 30 min 1.50 g NaCl (25.6 mmol) is added. The solution is then stored in a closed flask for 2 days and the precipitated deep-blue crystals of **1** are filtered off. Yield: 1.2 g (23% based on Mo). Characteristic IR bands (KBr pellet, cm^{-1}): ν = 1620m ($\delta(H_2O)$), 1199w, 1101w, 1060 (all $\nu_{as}(SO_4)$), 981/958s (ν(Mo=O)), 765s, ≈700sh, 628w, 557m, 462w; characteristic resonance Raman bands (solid/KBr dilution, λ_e = 1064 nm, cm^{-1}): ν = 810m, 681w, 456 m; Vis spectrum (in H_2O, nm): λ = 785(very broad) ($\epsilon = 2.4 \times 10^5$ $mol^{-1}\ dm^3\ cm^{-1}$). *Elemental Anal.* Calc.: Na, 1.39; S, 1.92. Found: Na, 1.5; S, 2.2% (cerimetric titration ≈110 Mo^V centers).

Vibrational spectra were recorded on a Bruker FTIR IFS 66 with a Raman FRA 106 unit spectrophotometer (λ_e = 1064 nm). The Vis spectrum was measured using a Shimadzu UV-3101PC instrument.

3. Results and discussion

By reducing an aqueous molybdate solution acidified with sulfuric acid – the important reagent in the present case, corresponding to [4] – the deep-blue giant mixed-valence cluster anion **1a** (Fig. 1) with the size of hemoglobin is formed and can be crystallized as Na salt. In order to improve the yield of the synthesis and decrease the crystallization time we changed the reaction conditions leading to a decrease of the solubility of **1** due to the presence of a rather high concentration of an electrolyte, which destroys the hydration shell of the giant cluster anion (see Section 2). The presence of the hydration shell caused by the abundance of a large number of H_2O ligands – which are responsible for the high solubility of molybdenum blue type species – prevented the isolation of crystalline Mo-blue type materials for more than 200 years since the times of Scheele and Berzelius [2], see also [5–7].

Compound **1,** which was now obtained with a facile synthesis by decreasing the solubility drastically, was characterized by elemental analysis (including redox titrations to determine the (formal) number of Mo^V centers), thermogravimetry (to determine the actual crystal water content which is important for the analyses), and spectroscopic methods (IR, resonance Raman, Vis/NIR). The data obtained for the new synthesized compound agree with those of the earlier reported substance including the results of the thermogravimetry [4].

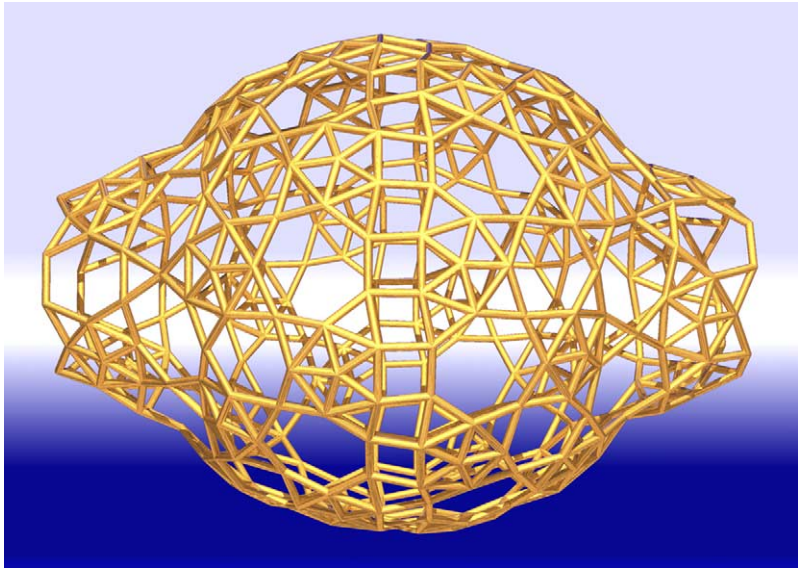

Fig. 1. $\{Mo_{368}\}$ metal atom framework of **1a** in wire-frame representation showing nicely the change from positive via negative to positive curvature at the surface.

$Na_{48}[H_xMo_{368}O_{1032}(H_2O)_{240}(SO_4)_{48}] \cdot$ ca. $1000H_2O \equiv Na_{48}$ **1a** $\cdot$ ca. $1000H_2O$ (**1**). **1a** $\equiv [H_x\{(Mo)Mo_5\}'_8\{(Mo)Mo_5\}''_{32}\{Mo_2\}'_{16}\{Mo_2\}''_8\{Mo_2\}'''_8\{Mo_1\}_{64}]^{48-}$ ($x \approx 16$ corresponding to ≈112 Mo^V-type centers).

Definitions: $\{(Mo)Mo_5\}' \equiv \{Mo_6O_{21}(H_2O)_6\}$; $\{(Mo)Mo_5\}'' \equiv \{Mo_6O_{21}(H_2O)_3(SO_4)\}$; $\{Mo_2\}' \equiv \{Mo_2O_3(H_2O)_2\}$; $\{Mo_2\}'' \equiv \{Mo_2O(t)_2O(br)_3(SO_4)\}$; $\{Mo_2\}''' \equiv \{Mo_2O(t)_4O(br)(SO_4)\}$; $\{Mo_1\} \equiv \{MoO(H_2O)\}$.

Compound **1** crystallizes in the space group *I4mm* and contains in the unit cell two giant hedgehog-like cluster anions **1a** with a central spheroid-shaped fragment $\{Mo_{288}O_{784}(H_2O)_{192}(SO_4)_{32}\}$ = B and two capping units $\{Mo_{40}O_{124}(H_2O)_{24}(SO_4)_8\}$ = C (*note:* the second structure analysis which confirmed the earlier published one was performed with crystals obtained with the earlier reported synthesis [4]). Remarkably, there are three rather large areas, i.e. 2 C + B, with different local symmetries: D_{8d} in the central B part and C_{4v} in the two capping areas C. There is a small error limit for the correlated number of protonations and Mo^V centers.

The comparably large number of different building units of **1a** can be identified from the above given formulae. The two $\{(Mo)Mo_5\}$-type units differ with respect to the abundance of the SO_4^{2-} ligands (32 occur with SO_4^{2-} ligands, and 8 without, located in the C_{4v} areas; the two numbers were erroneously referred to in [4]). The dinuclear units $\{Mo_2\}$ do not only differ with respect to the abundance of bidentate SO_4^{2-} ligands (see formulae): those at the ends of both C caps, i.e., the borderlines, have contrary to the other type two terminal O atoms at both Mo centers, a situation characteristic for stopping growth. The $\{Mo_1\}$ units are of the 'classical' type $\{OMo^V(H_2O)\}^{3+}$ and contribute correspondingly to the highly reduced state of **1a**; the remaining predominantly Mo^V-type centers are distributed over several parts of the large cluster areas and cause a widespread delocalization of Mo (4d) electrons while the capping units C are less reduced (corresponding the size of the cluster and the resolution obtained there are of course limits with respect to the interpretation of the bond valence sum values). This again causes broad peaks in the resonance Raman and electron absorption spectra of **1**. The structure of the cluster anion can be formally considered as a hybrid between the $\{Mo_{176}\}/\{Mo_{154}\}$-type giant molecular wheels and the $\{Mo_{102}\}/\{Mo_{132}\}$-type spherical clusters mentioned above (for details see [4]).

The high reduction state (ca. 112 Mo^V/256 Mo^{VI}), which is much higher than that in the above mentioned Mo-blue type wheel systems (i.e. 28 Mo^V/126 Mo^{VI} for $n = 14$ [2a]), refers to the fact that strong reducing conditions favour cluster growth (see [4]). The largest cluster existing in acidified molybdate solution is – in absence of a reducing agent – the 'rather small' $\{Mo_{36}\}$ anion [2,8,9] which 'starts growing' upon reduction [2a].

Due to the rather short crystallization time of the new synthesis method no suitable crystals for single crystal X-ray diffraction analysis were obtained. Important in this context is that in case of less symmetrical giant species like **1a** nucleus formation is less favoured than in case of more symmetrical and smaller ones (see [10]). A crystal obtained according to the earlier reported synthetic method was again used for a new crystal structure determination. As even the crystals of the latter method are normally obtained in small size, data were collected with an instrument equipped with a rotating anode and an X-ray mirror (see Acknowledgements). The structure analysis confirmed the earlier reported one. [1] Compound **1**, obtained with the new method, could be identified clearly by comparison of the spectroscopic (Figs. 2 and 3) and analytical data with those of the earlier reported compound obtained with the synthesis leading to larger crystals [4]. Especially the IR spectrum of **1** (Fig. 2) is very characteristic and, e.g., different from the compounds containing the other Mo-blue-type species, i.e., the wheel-shaped clusters [1b], and can therefore be easily used for the simple identification. The presence of the bidentate SO_4^{2-} ligands is proven by the IR bands at 1199, 1101, 1060 cm^{-1} originating from the $\nu_3(F_2)$ vibration of discrete SO_4^{2-}.

Some important additional experiments have to be mentioned. If K^+ ions are present in the reaction mixture not the hedgehog-type species is formed but a derivative of the $\{Mo_{176}\}$ wheel-type cluster in which a novel $\{KSO_4\}_{16}$ ring has been integrated [11]. The related unusual species was reported recently in a paper [11] entitled 'Synergetic activation of 'silent receptor' sites leading to a new type of inclusion complex: integration of a 64-membered ring comprising K^+ and SO_4^{2-} ions into a molybdenum oxide-based nanoobject'. The unusual inclusion species $[Mo^{VI}_{114}Mo^{V}_{32}O_{429}(H_2O)_{50}(KSO_4)_{16}]^{30-}$ shows the remarkable 64-membered $\{K(SO_4)\}_{16}$ ring integrated into a wheel-shaped nanocluster host. It is formed by a novel unprecedented reaction type, based on synergetically induced functional complementarity [11]. Furthermore it represents a text-book example of a very complex non-biological material. The K^+ ions have in presence of SO_4^{2-} a direct influence on the activation of the ring-type cluster's silent receptor sites and prevent formation of the $\{Mo_{368}\}$-type cluster having much smaller formation tendency than the more

[1] The structure of **1** was redetermined using crystals prepared according to the earlier reported method [4]. The lattice constants were determined as $a = 43.257(2)$, $c = 68.999(5)$ Å, $V = 129111(13)$ Å^3. The structure could be nicely refined in space group *I4mm* as done in [4], though the situation showed that the partial 'disorder' of a part of the anion could be removed by refining the structure in space group *I*4 assuming that the crystal is merohedrally twinned. The special twin problem will be considered separately at a later date.

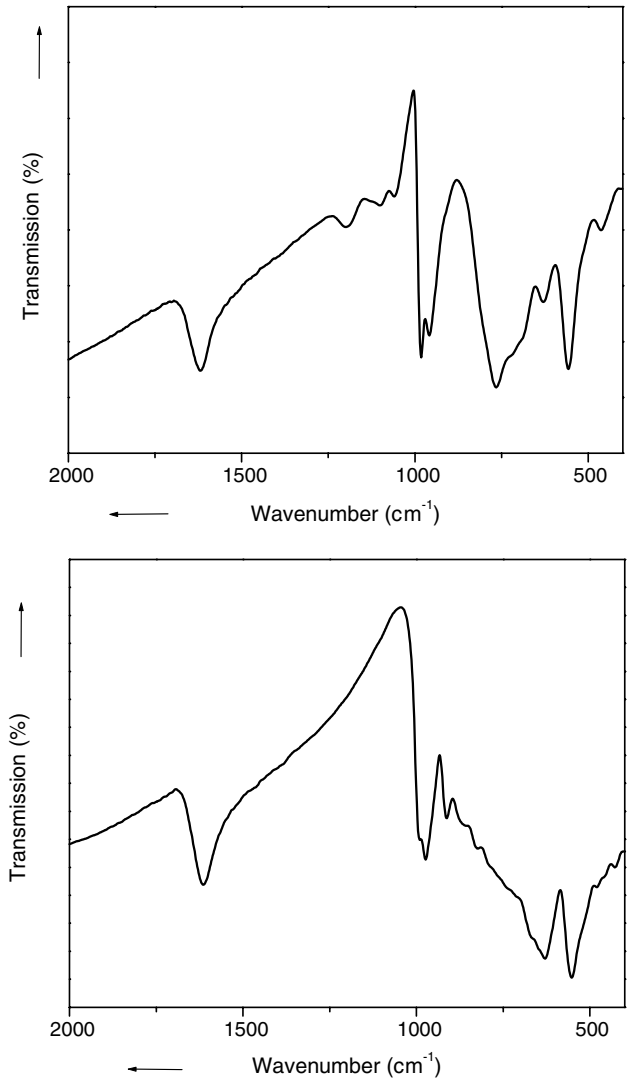

Fig. 2. IR-spectra of **1** (KBr pellets; top) and of the typical wheel-shaped Mo-blue cluster $\{Mo_{154}\}$ (bottom, see [1b], too). (See Section 2 for details.)

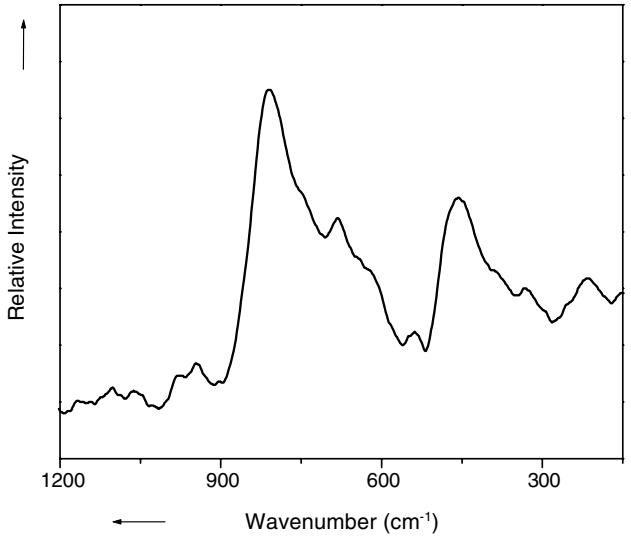

Fig. 3. Solid state resonance-Raman spectrum of **1**. The missing intense lines due to ν(Mo=O) vibrations proves that the corresponding terminal bonds are not involved in the Mo 4d electron delocalization as compared to the $\{Mo_{154}\}$ wheel-type species, where in each of the 14 $\{Mo_5O_6\}$ units two 4d electrons are delocalized (see [2a]). (See Section 2 for experimental details.)

symmetrical one. On the other hand in the presence of Li^+ cations in the reaction mixture also not the hedgehog-type species is formed but the neutral spherical $\{Mo_{102}\}$ ball-type cluster species [12]. The results can be understood, as the wheel- and ball-shaped species have a much higher formation tendency while the formation of the very complex $\{Mo_{368}\}$ cluster, showing in case of the synthesis of **1** an unprecedented symmetry breaking of the surface, really only occurs under very special limited conditions. Note: the role of the Na^+ cations is not understood until now.

The knowledge of the cluster **1a** will probably be the starting point for the syntheses of related other clusters of comparable size. This should be possible in case of the abundance of ligands like 'the medium-ligand-strength' SO_4^{2-} ions generating a large number of building units (for details see [4]) and may be a starting point of an interesting route in nanochemistry. This includes also the option of handling the giant clusters as intact units for instance for the preparation of composites, e.g., with silica or cationic surfactants, which is possible with these types of anionic clusters as was shown before in case of the above mentioned giant ball- and wheel-type species with the generation of micelles, films, monolayers and even liquid crystals [13]. A further option for the future is to study the vesicle formation of the giant cluster which follows unprecedented principles (see [14]).

An important result of the present paper is the formation of an extreme complex structure, showing symmetry breaking at the surface which is very much dependent on the special synthesis conditions in contrary to cases of higher symmetrical species (see [15]).

Acknowledgements

The authors thank Prof. G.M. Sheldrick for collecting data for a single-crystal X-ray structure analysis under the mentioned special conditions. The financial support from the Fonds der Chemischen Industrie, the Deutsche Forschungsgemeinschaft, the Volkswagen Stiftung and the European Union (Brussels) is highly acknowledged. S.K. Das thanks the Alexander von Humboldt-Foundation and A. Merca the 'Graduiertenkolleg Strukturbildungsprozesse', Universität Bielefeld, for their fellowships.

References

[1] (a) L. Cronin, E. Diemann, A. Müller, in: J.D. Woollins (Ed.), Inorganic Experiments, Wiley-VCH, Weinheim, 2003, p. 340;

(b) A. Müller, S.K. Das, E. Krickemeyer, C. Kuhlmann, in: J. Shapley (Ed.), Inorg. Synth., vol. 34, Wiley, New York, 2004, p. 191.
[2] (a) A. Müller, C. Serain, Acc. Chem. Res. 33 (2000) 2;
(b) A. Müller, P. Kögerler, C. Kuhlmann, Chem. Commun. (1999) 1347;
(c) A. Müller, S. Roy, Coord. Chem. Rev. 245 (2003) 153;
(d) N. Hall, Chem. Commun. (2003) 803;
(e) A. Müller, P. Kögerler, H. Bögge, Struct. Bond. (Berlin) 96 (2000) 203.
[3] (a) T. Yamase, P.V. Prokop, Angew. Chem., Int. Ed. 41 (2002) 466;
(b) K. Eda, Y. Sato, Y. Iriki, Chem. Lett. (2002) 952;
(c) C. Jiang, Y. Wei, Q. Liu, S. Zhang, M. Shao, Y. Tang, Chem. Commun. (1998) 1937;
(d) W. Yang, C. Lu, X. Lin, S. Wang, H. Zhuang, Inorg. Chem. Commun. 4 (2001) 245.
[4] A. Müller, E. Beckmann, H. Bögge, M. Schmidtmann, A. Dress, Angew. Chem., Int. Ed. 41 (2002) 1162.
[5] Gmelins Handbuch der anorganischen Chemie, vol. 53 (Mo), Verlag Chemie, Berlin, 1935, pp. 134–147.
[6] Gmelin Handbook of Inorganic Chemistry, vol. B3a, Mo Suppl., Springer-Verlag, Berlin, 1987, pp. 63–65.
[7] Gmelin Handbook of Inorganic Chemistry, vol. B3b, Mo Suppl., Springer-Verlag, Berlin, 1989, pp. 15–16.
[8] M.T. Pope, A. Müller, Angew. Chem., Int. Ed. 30 (1991) 34.
[9] When it was published it was considered as the largest (!) inorganic anion: K.H. Tytko, B. Schönfeld, B. Buss, O. Glemser, Angew. Chem. Int. Ed. Engl. 12 (1973) 330.
[10] A. Müller, E. Diemann, B. Hollmann, H. Ratajczak, Naturwissenschaften 83 (1996) 321.
[11] A. Müller, L. Toma, H. Bögge, M. Schmidtmann, P. Kögerler, Chem. Commun. (2003) 2000.
[12] A. Müller, S.-Q. Nazir-Shah, H. Bögge, M. Schmidtmann, P. Kögerler, B. Hauptfleisch, S. Leiding, K. Wittler, Angew. Chem., Int. Ed. 39 (2000) 1614.
[13] (a) S. Polarz, B. Smarsly, C. Göltner, M. Antonietti, Adv. Mater. 12 (2000) 1503;
(b) S. Polarz, B. Smarsly, M. Antonietti, Chem. Phys. Chem. 2 (2001) 457;
(c) D. Kurth, P. Lehmann, D. Volkmer, A. Müller, D. Schwahn, J. Chem. Soc., Dalton Trans. (2000) 3989 (and relevant literature cited therein);
(d) Yan Zhu, A. Cammers-Goodwin, B. Zhao, A. Dozier, E.C. Dickey, Chem. Eur. J. 10 (2004) 2421.
[14] T. Liu, E. Diemann, H. Li, A.W.M. Dress, A. Müller, Nature 426 (2003) 59.
[15] A. Müller, S.K. Das, H. Bögge, M. Schmidtmann, A. Botar, Chem. Comm. (2001) 657.

Available online at www.sciencedirect.com
SCIENCE DIRECT®
Polyhedron 23 (2004) 2387–2391
POLYHEDRON
www.elsevier.com/locate/poly

A dinuclear Mn(II) chloro-bridged compound with a weak ferromagnetic Mn–Mn interaction Synthesis, structure, EPR and magnetism of $[Mn(\mu\text{-}Cl)(2,2'\text{-bi-imidazoline})_2]_2Cl_2$

Gerard A. van Albada [a], Aminou Mohamadou [b], Willem L. Driessen [a], René de Gelder [c], Stefania Tanase [a], Jan Reedijk [a,*]

[a] Leiden Institute of Chemistry, Gorlaeus Laboratories, Leiden University, P.O. Box 9502, 2300 RA Leiden, The Netherlands
[b] Groupe de Recherche en Chimie Inorganique (GRECI), Faculté des Sciences, Université de Reims Champagne-Ardenne, Moulin de la Housse, BP 1039, 51687 Reims, France
[c] Department of Inorganic Chemistry, University of Nijmegen, Toernooiveld 1, 6525 ED Nijmegen, The Netherlands

Received 30 June 2004; accepted 26 July 2004
Available online 11 September 2004

Abstract

In this study an unusual dinuclear bis-chloride bridged Mn(II) compound, $[Mn(\mu\text{-}Cl)(biz)_2]_2Cl_2$ (in which biz = 2,2′-bi-imidazoline), has been described and characterised. Also the magnetic susceptibility and EPR investigations are made. The distorted octahedral geometry around the Mn(II) ion is formed by four nitrogen atoms of two dichelating biz ligands and two bridging chloride atoms. The lattice is further stabilised by hydrogen bonds between uncoordinating N atoms of the ligand and the coordinating and uncoordinating chloride atoms. Magnetic susceptibility measurements reveal a weak ferromagnetic interaction between the two high-spin Mn(II) ions of $J = 0.33$ cm^{-1}.
© 2004 Elsevier Ltd. All rights reserved.

Keywords: Crystal structure; Manganese; Hydrogen bond; Magnetism; EPR

1. Introduction

The organic ligand 2,2′-bi-imidazoline (abbreviated as biz, see Scheme 1) is an interesting and flexible bifunctional ligand. This heterocyclic didentate ring ligand is of special interest as it deviates from the more "flat" molecules, like bisimidazole, bipyridine or bipyrimidine, due to the fact that the steric effects at the rear side of the molecule are influenced by two acidic hydrogen atoms. These two N–H donor groups can form polymeric aggregates by hydrogen bonding [1,2].

So far X-ray structures with biz and transition metals have only been reported for a few Fe(II), Fe(III) and Co(II), Co(III) compounds [3,4], in which neutral and mono-deprotonated biz are present. Recently, X-ray structures of Cu(II), Ni(II) and Co(II) as transition metal ions with this ligand and the anion dicyanamide and a copper(II) azide compound have been reported by us [1,2]. Furthermore, the ligand is capable to hydrolyse in-situ with a metal ion to form different organic ligands [5,6].

The coordination chemistry of manganese ions with N and/or O containing ligands has been receiving a great deal of attention, because of the variable structures of manganese complexes and the importance of manganese

* Corresponding author. Tel.: +31 71 5274450; fax: +31 71 5274671.
E-mail address: reedijk@chem.leidenuniv.nl (J. Reedijk).

0277-5387/$ - see front matter © 2004 Elsevier Ltd. All rights reserved.
doi:10.1016/j.poly.2004.07.019

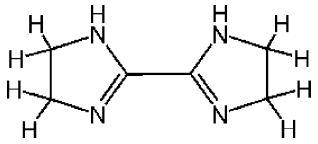

Scheme 1. 2,2′-bi-imidazoline.

enzyme models, the possibility of magnetic coupling interactions, and the application of manganese compounds in industrial catalysis [7,8].

The behaviour of these manganese complexes is mainly dependent on the structure and coordination mode of the ligands in addition to the oxidation number of manganese. Dinuclear chloro-bridged Mn(II) compounds with N/O donor ligands are relatively rare and only a few six-coordinated Mn(II) compounds have been structurally investigated [8–12]. Of these compounds only two have also been magnetically investigated [8,12].

In this study the molecular and X-ray structure of an unusual dinuclear chloro-bridged Mn(II) compound with the formula $[Mn(\mu\text{-}Cl)(biz)_2]_2Cl_2$ is reported along with its EPR and magnetic susceptibility properties.

2. Experimental

2.1. Syntheses

The ligand, 2,2′-bi-imidazoline (biz), was prepared by the method reported in the literature [13]. The title compound was prepared according to the following procedure: 0.24 g (1.2 mmol) of Mn(II) chloride tetrahydrate and 0.33 g (2.4 mmol) ligand were each dissolved in 10 ml of ethanol. The ligand solution was then added slowly to the metal-salt solution and filtered to remove any undissolved material. After a few weeks, the product separated as a crystalline product, which was isolated by filtration and dried in air, and characterised by elemental analysis and spectroscopic methods. Yield 64%. Elemental analysis: found (calc) for $C_{24}H_{40}Cl_4$ Mn_2N_{16} (M_w 804.40): 35.7 (35.8) %C; 4.8 (5.0) %H; 27.6 (27.9) %N.

2.2. Physical measurements

C,H,N determinations were performed on a Perkin Elmer 2400 Series II analyser. Ligand-field spectra were obtained on a Perkin-Elmer Lambda900 spectrophotometer using the diffuse-reflectance technique, with MgO as a reference. X-band powder EPR spectra were obtained on a Jeol RE2x electron spin resonance spectrometer, using DPPH ($g = 2.0036$) as a standard and measured at 4 mW.

Magnetic susceptibility measurement (5–200 K) were carried out using a Quantum Design MPMS-5 5T SQUID magnetometer (measurements carried out at 1 T). Data were corrected for magnetisation of the sample holder and for diamagnetic contributions, which were estimated from Pascal constants.

2.3. Crystal structure determination and refinement of the structures

The reflection intensities were measured on a four-circle Enraf-Nonius CAD-4 diffractometer using graphite-monochromated Cu Kα radiation ($\lambda = 1.54184$ Å). The cell dimensions were determined using 25 independent reflections. Intensity data were corrected for Lorentz and polarization effects. Absorption correction was not applied. The positions of the heavy atoms were determined from a Patterson map (DIRDIF) [14]. The atomic scattering factors were taken from the International tables for X-ray crystallography [15]. The remainder of the non-H atoms were located in subsequent difference Fourier syntheses. Hydrogen atoms were placed at calculated positions (at 0.95 Å) from their parent atoms. Full-matrix least-squares refinement on F using the XTAL3.4 set of programs [16] with the function minimized being $\sum w(|F_o| - |F_c|)^2$ with $w = 1/\sigma^2(F)$. Positional refinement of all non-H atoms, anisotropic for the nonhydrogen atoms, fixed isotropic thermal parameters for the hydrogens. Geometric calculations and molecular graphics were performed with the PLATON package [17] (see Table 1).

Table 1
Crystal data and details of the structure determination

Compound	$C_{24}H_{40}Cl_2Mn_2N_{16}$
Molecular weight	804.40
Crystal system	triclinic
Space group	$P\bar{1}$ (no. 2)
a (Å)	8.9292(5)
b (Å)	9.3363(5)
c (Å)	11.7937(11)
α (Å)	66.627(6)
β (Å)	72.605(5)
γ (Å)	83.767(6)
V (Å^3)	861.18(11)
Z	1
D_{calc} (g cm^{-3})	1.551
F (0 0 0)	414
μ (mm^{-1})	1.088
Crystal size (mm)	$0.25 \times 0.38 \times 0.41$
Temperature (K)	293
θ_{min}, θ_{max}	4.25, 69.88
Total data collected	3439
Independent reflections	3069
No. of refined parameters	208
Final R_1 ($I > 2\sigma(I)$), wR_2	0.059, 0.095
Goodness-of-fit on F^2	0.598
Minimum and maximum residual densities (e Å^{-3})	−0.94, 0.686

3. Results and discussion

3.1. Description of the crystal structure of $[Mn(\mu\text{-}Cl)(biz)_2]_2Cl_2$ (1)

The structure of the dinuclear unit is depicted in Fig. 1. Relevant bond length and bond angle information is given in Table 2. The molecular structure consists of two centro-symmetrically related Mn(II) centres, bridged almost symmetrically by two chloride ions.

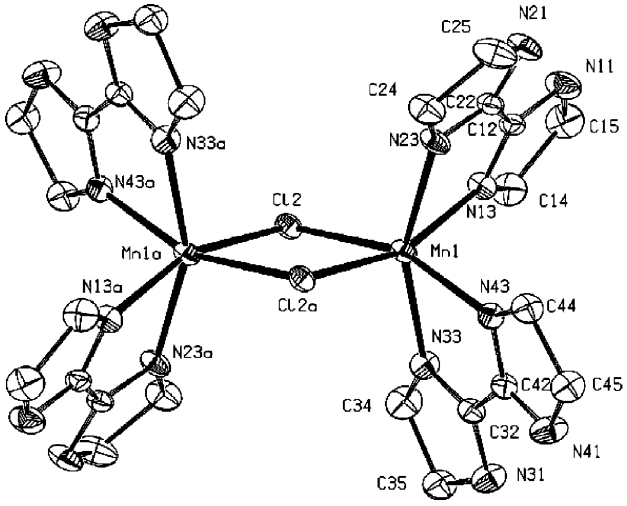

Fig. 1. Thermal ellipsoid plot [17] at 50% probability of $[Mn(\mu\text{-}Cl)(biz)_2]_2Cl_2$ with atom-labelling scheme. Hydrogen atoms are omitted for clarity. Atoms marked with an "a" are generated by an inversion centre.

The octahedral coordination around each Mn atom is formed by four nitrogen atoms of two dichelating biz ligands (with distances which vary from 2.232(4) to 2.262(3) Å) and two bridging chloride atoms with distances of 2.5578(13) and 2.5754(13) Å. The two other chloride atoms are not coordinating. The Mn–Mn distance is 3.740 Å and the Mn–Cl–Mn bridging angle is 93.53(4)°.

The lattice is stabilised through hydrogen bonds between the uncoordinated nitrogen atoms of the biz ligand at the rear side of the molecule and both the uncoordinated and coordinated chloride anions with distances which vary from 3.184(5) to 3.271(5) Å (see Fig. 2 and details of the H-bonding in Table 2). The lattice is further stabilised by ring–ring contacts of imidazoline units (closest ring–ring contacts of 3.960 Å).

3.2. EPR and magnetic properties

The X-band EPR recorded on the powdered solid reveals a spectrum with a broad band around $g \approx 2$ (RT and 77 K give the same spectrum) typical for Mn(II) in a distorted octahedral environment [18] (Fig. 3(a)). The broad signals above and below $g = 2$ are due to the $S = 5/2$ zero-field splitting, as has been reported for distorted mononuclear Mn(II) complexes [19–21], but the same type of spectra are also reported for dinuclear Mn(II) compounds [7,12,22].

The compound measured as a frozen solution in DMF/MeOH (1:1) exhibits a well-resolved six-line signal ($A \sim 90$ G) centred near $g = 2$, consistent with the

Table 2
Selected bond distances (Å), angles (°) and H-bond information for structure $[Mn(\mu\text{-}Cl)(biz)_2]_2Cl_2$ (**1**)

Bond distances			
Mn1–Cl2	2.5578(13)	Mn1–N13	2.232(4)
Mn1–N23	2.255(4)	Mn1–N33	2.253(4)
Mn1–N43	2.262(3)	Mn1–Cl2a	2.5754(13)
Mn1–Mn1a	3.740		
Bond angles			
Cl2–Mn1–N13	90.60(11)	Cl2–Mn1–N23	109.74(11)
Cl2–Mn1–N33	89.52(11)	Cl2–Mn1–N43	160.00(10)
Cl2–Mn1–Cl2a	86.47(4)	N13–Mn1–N23	73.93(15)
N13–Mn1–N33	93.49(16)	N13–Mn1–N43	100.88(14)
Cl2a–Mn1–N13	160.17(11)	N23–Mn1–N33	156.70(16)
N23–Mn1–N43	89.30(14)	Cl2a–Mn1–N23	88.61(11)
Cl2a–Mn1–N33	106.08(12)	Cl2a–Mn1–N43	87.97(10)
Mn1–Cl2–Mn1a	93.53(4)		

$a = -x, -y, -z$

Hydrogen bond distance for structure **1**

	D···A
N(11)–H(11)···Cl(2) [$-x, -y, -z$]	3.233(5)
N(21)–H(21)···Cl(3)	3.184(5)
N(31)–H(31)···Cl(3) [$-1-x, -y, 1-z$]	3.200(5)
N(41)–H(41)···Cl(3) [$-1-x, -y, 1-z$]	3.271(5)

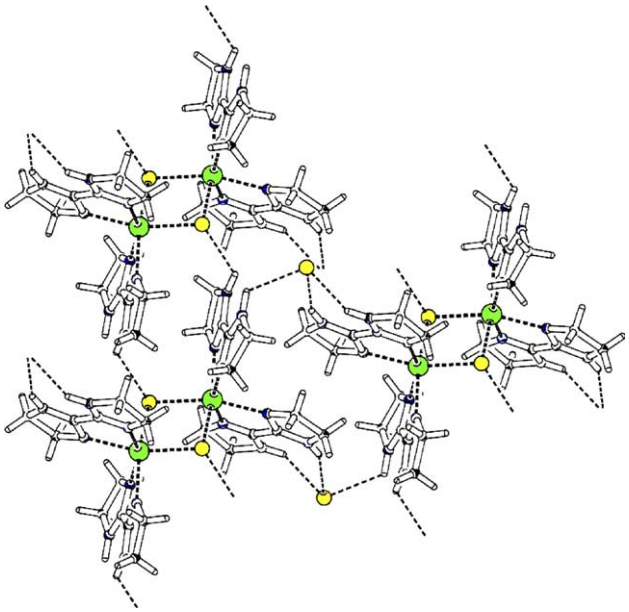

Fig. 2. Hydrogen bonding and packing in the title compound.

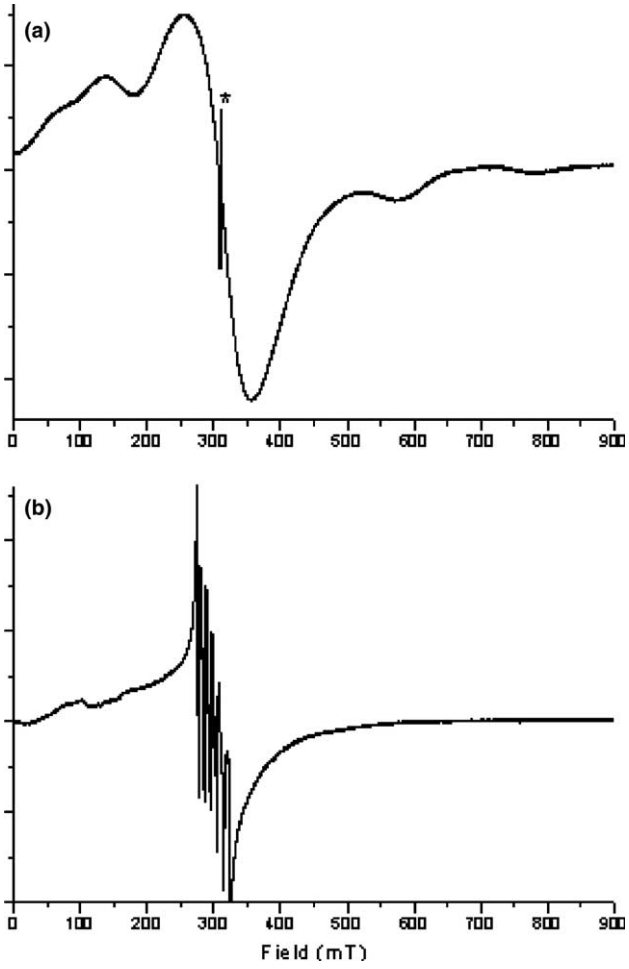

Fig. 3. X-band EPR spectrum of the powdered solid (a; * = dpph reference) and frozen solution (b) in DMF/MeOH in the range from 0–900 mT.

hyperfine splitting due to the coupling of the electron spin with $I = 5/2$ of the ^{55}Mn(II) nucleus [19]. Also the broad signals, albeit weaker, are visible below and above $g = 2$, which are also observed in other Mn(II) dinuclear [8,22] and mononuclear compounds [20] (Fig. 3(b)). So from the point of view of an EPR study alone, it is hard to prove whether a Mn(II) compound is mononuclear or dinuclear [8], as also in most cases a mononuclear impurity is present in dinuclear species (vide infra).

To gain more insight in the magnetic behaviour of the dinuclear compound, magnetic susceptibility measurements were undertaken from 5 to 200 K. The result is depicted in Fig. 4 in the form of X_mT versus T. The X_mT value of the title compound is about 8.5 $cm^3\,K\,mol^{-1}$ (μ_{eff} 8.4 μ_B) per dinuclear unity at 200 K, a value close to the spin-only value for two independent high-spin Mn(II) ions (8.7 μ_B). This value stays almost constant till around 80 K and then increases with decreasing temperature, typical for a ferromagnetic interaction between the pair of high-spin Mn(II) ions. The equation for the magnetic susceptibility per Mn(II) for the dinuclear Mn(II) system based on the isotropic Heisenberg model $\boldsymbol{H} = -J\boldsymbol{S}_1 \cdot \boldsymbol{S}_2$ ($\boldsymbol{S}_1 = \boldsymbol{S}_2 = 5/2$) is given as follows [8,23,24]:

$$\chi_M = \frac{Ng^2\beta^2}{kT} \cdot \frac{x^{28} + 5x^{24} + 14x^{18} + 30x^{10} + 55}{x^{30} + 3x^{28} + 5x^{24} + 7x^{18} + 9x^{10} + 11} + N\alpha \quad (1)$$

where $x = \exp(-J/kT)$, $N\alpha$ = paramagnetic impurity and the other symbols have their usual meanings. No zero-field splitting parameter was needed to obtain a good fit. The magnetic parameters $g = 2.00$, $J = 0.33(1)$ cm^{-1} and $N\alpha = 0.07$ cm^3/mol are obtained from a fit of the experimental data, with $R = 4 \times 10^{-4}$.

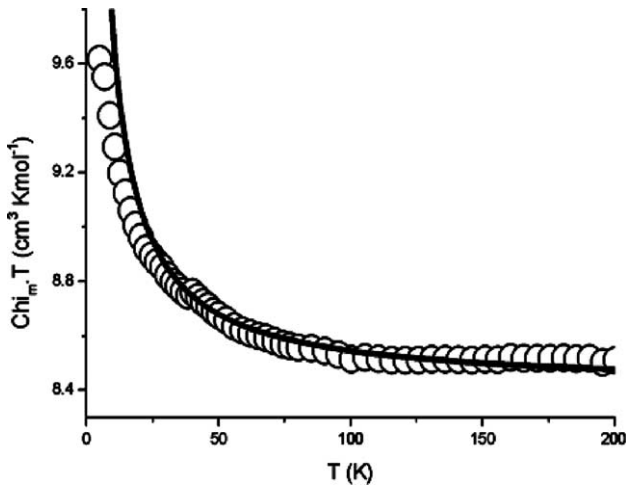

Fig. 4. Temperature dependence of $\chi_M T$ versus T per dinuclear unity. The solid lines is the best fit with $J = 0.33(1)$ cm^{-1}, $g = 2.00$ (see text).

Table 3
Structural and magnetic data for [Mn(II)μ-Cl_2] compounds

Compound[a]	Mn–Mn distance (Å)	Mn–Cl distance (Å)	Mn–Cl–Mn angle (°)	J (cm^{-1})	Reference
$[Mn(\mu\text{-}Cl)(biz)_2]_2Cl_2$	3.740	2.5754(13) 2.5578(13)	93.53(4)	0.33(1)	this work
$[MnCl(\mu\text{-}Cl)(bpea)]_2$	3.786	2.5374(9) 2.4249(8)	95.72(2)	0.34	[12]
$[MnCl(\mu\text{-}Cl)(mpbpa)]_2$	3.8500(6)	2.5684(6) 2.4451(6)	96.426(19)	0.55	[8]

[a] *Abbreviations*: biz = 2,2-bi-imidazoline; mpbpa = *N*-(3-methoxypropyl)-*N*,*N*-bis(pyridin-2-ylmethyl)amine; bpea = *N*,*N*-bis(2-pyridyl methyl)ethylamine.

4. Conclusions

In this study investigations by X-ray, EPR and magnetic susceptibility of a novel dinuclear chloro-bridged Mn(II) compound are reported. The small ferromagnetic exchange interaction of $J = 0.33(1)$ cm^{-1} between the pair of Mn(II) ions is similar in strength to that found for the (few) analogous compounds with the same chromophore, $[MnCl(\mu\text{-}Cl)(bpea)]_2$ and $[MnCl(\mu\text{-}Cl)(mpbpa)]_2$ (see Table 3).

5. Supplementary material

Crystallographic data (excluding structure factors) for the structure in this paper have been deposited with the Cambridge Crystallographic Data Centre as supplementary publication no. CCDC-242535. Copies of the data can be obtained free of charge on application to CCDC, 12 Union Road, Cambridge CB2 1EZ, UK [fax: (internat.) +44(1223)336-033, e-mail: deposit@ccdc.cam.ac.uk, or www at http://www.ccdc.cam.ac.uk].

Acknowledgements

The work described in the present paper has been supported by the Leiden University Study group WFMO (Werkgroep Fundamenteel Materialen Onderzoek) and the Council for Chemical Sciences of the Netherlands Organisation for Scientific Research (CW-NWO). Part of the work has been supported financially by the Graduate Research School Combination Catalysis.

References

[1] A. Mohamadou, G.A. van Albada, H. Kooijman, B. Wieczorek, A.L. Spek, J. Reedijk, New J. Chem. 27 (2003) 983.
[2] A. Mohamadou, G.A. van Albada, A. Mills, A.L. Spek, J. Reedijk, J. Chem. Cryst. 34 (2004) 233.
[3] J.P. Roth, S. Lovell, J.M. Mayer, J. Am. Chem. Soc. 122 (2000) 5486.
[4] J.C. Yoder, J.P. Roth, E.M. Gussenhoven, A.S. Larsen, J.M. Mayer, J. Am. Chem. Soc. 125 (2003) 2629.
[5] G.A. van Albada, A. Mohamadou, J. Reedijk, H. Kooijman, A.L. Spek, Z. Anorg. Allg. Chem. 629 (2003) 2190.
[6] G.A. van Albada, A. Mohamadou, A.M. Manotti Lanfredi, I. Mutikainen, U. Turpeinen, F. Ugozzoli, J. Reedijk, Z. Anorg. Allg. Chem., in press.
[7] J.-Z. Wu, S. Tanase, E. Bouwman, J. Reedijk, A.M. Mills, A.L. Spek, Inorg. Chim. Acta 351 (2003) 278, and references cited therein.
[8] J.-Z. Wu, E. Bouwman, A.M. Mills, A.L. Spek, J. Reedijk, Inorg. Chim. Acta 357 (2004) 2694.
[9] Z.M. Wang, M. Yuan, Z. He, C.-S. Liao, C.-H. Yan, Acta Chim. Sinica 58 (2000) 1615.
[10] M. Goher, M.A.M. Abu-Youssef, F.A. Mautner, Polyhedron 12 (1993) 1751.
[11] A. Garoufis, S. Kasselouri, S. Boyatzis, C.P. Raptopoulou, Polyhedron 18 (1999) 1615.
[12] I. Romero, M.-N. Collomb, A. Deronzier, A. Llobet, E. Perret, J. Pécaut, L. Le Pape, J.-M. Latour, Eur. J. Inorg. Chem. (2001) 69.
[13] J.C. Wang, J.E. Bauman Jr., Inorg. Chem. 4 (1965) 1613.
[14] P.T. Beurskens, G. Admiraal, G. Beurskens, W.P. Bosman, S. Garcica-Granda, R.O. Gould, J.M.M. Smits, C. Smykalla, The DIRDIF program system, Techmical report of the Crystallography Laboratory, University of Nijmegen, Nijmegen, The Netherlands, 1992.
[15] C.J. Wilson, International Tables for X-ray crystallography, vol. C, Kluwer Academic Publishers, Dordrecht, The Netherlands, 1992.
[16] S.R. Hall, G.S.D. King, J.M. Stewart, XTAL 3.4 Users Manual, University of Western Australia and Maryland, 1995.
[17] A.L. Spek, J. Appl. Cryst. 36 (2003) 7.
[18] R.D. Dowsing, B. Nieuwenhuijse, J. Reedijk, Inorg. Chim. Acta 5 (1971) 301.
[19] F.E. Mabbs, D. Collison, Electron Paramagnetic Resonance of d Transition Metal Compounds, Elsevier, Amsterdam, 1992.
[20] S.T. Warzeska, F. Micciché, M.C. Mimmi, E. Bouwman, H. Kooijman, A.L. Spek, J. Reedijk, J. Chem. Soc., Dalton Trans. (2001) 3507.
[21] E. Garribba, G. Micera, M. Zema, Inorg. Chim. Acta 357 (2004) 2038.
[22] B. Albela, M. Corbella, J. Ribas, Polyhedron 15 (1996) 91.
[23] O. Kahn, Molecular Magnetism, Wiley-VCH, New York, 1993.
[24] H. Sakiyama, A. Sugawara, M. Sakamoto, K. Unoura, K. Inoue, M. Yamasaki, Inorg. Chim. Acta 310 (2000) 163.

Available online at www.sciencedirect.com
SCIENCE DIRECT®
Polyhedron 23 (2004) 2393–2404
POLYHEDRON
www.elsevier.com/locate/poly

A spectroscopic investigation of the complexing ability of catecholate or salicylate derivatives towards aluminium(III)

Sébastien Giroux [a], Sabrina Aury [a], Patrice Rubini [a,*], Stéphane Parant [a], Jean-Roger Desmurs [b], Michel Dury [b]

[a] *Groupe de Chimie Physique Organique et Colloïdale, Laboratoire Structure et Réactivité des Systèmes Moléculaires Complexes (UMR CNRS-UHP 7565), Université Henri Poincaré – Nancy 1, BP 239, 54506, Vandœuvre-lès-Nancy Cédex, France*
[b] *Rhodia Recherches, Centre de Recherches de Lyon, 85 rue des Frères Perret, 69192 Saint Fons Cédex, France*

Received 6 May 2004; accepted 27 July 2004
Available online 11 September 2004

Abstract

The coordination of the aluminium(III) cation to 2,3-dihydroxybenzoic acid (2,3-dhba), 5-nitrosalicylic acid (5-nsa), 4-nitrocatechol (4-ncat) and 3,5-dinitrocatechol (3,5-dncat) was studied by pH-potentiometry and by spectroscopic techniques. The stoichiometry of the complexes and their formation constants were determined. NMR spectroscopy allowed us to obtain thermodynamical, dynamical and structural information about the complexes formed in solution. The complexing power of these molecules was compared to that of catechol and salicylic acid. Additionally, the proton exchange rate constant between the phenolic and the phenolate forms of 5-nsa was determined by NMR line-shape analysis. This proton exchange that is usually very fast is considerably slowed down by the formation of an intramolecular hydrogen bond between the carboxylate and the phenolic groups.
© 2004 Elsevier Ltd. All rights reserved.

Keywords: Aluminium(III); Catecholates; Salicylates; Complexation; Proton exchange; NMR

1. Introduction

Many trades are evolving in application domains which resort to the complexation properties of metals by organic molecules. For instance, the surface treatment of metals in electronics, galvanoplasty and electroplating allows to improve the performances, to decorate or to protect against oxidation, respectively. The treatment of water used in heat exchangers or in the detergency domain, is also included in these areas; a large variety (and amount) of complexing molecules is involved in this activity.

There is an important class of compounds: the salicylate and catecholate derivatives, the complexing properties of which are recognised. These compounds are industrially produced in a great quantity. They are not always employed for their complexing ability and could be valorised in fields where this property is required (galvanoplasty, electroplating for instance). Aluminium(III) is concerned by this kind of use.

The study of the complexation of Al(III) by salicylate and catecholate derivatives is also important to understand the phytotoxicity of this element when it is released from the mineral matter and solubilized under acidic conditions [1,2]. The availability of Al in the soils depends on its state: free or in organic complexes. Humic acids are able to complex the aluminium(III) cation and have an influence on its speciation in soils. The complexing parts of these organic macromolecules are constituted by salicylate and catecholate functions. The knowledge of the complexes that are formed in aqueous solution with the Al(III) ion is crucial to evaluate the

* Corresponding author. Tel.: +33 3 83 68 43 27; fax: +33 3 83 68 43 22.
E-mail address: Patrice.Rubini@lesoc.uhp-nancy.fr (P. Rubini).

0277-5387/$ - see front matter © 2004 Elsevier Ltd. All rights reserved.
doi:10.1016/j.poly.2004.07.017

competition with the other organic ligands and to reach the concentration of the different species.

This paper reports the study of the complexation of the Al(III) ion with four ligands: 2,3-dihydroxybenzoic acid (2,3-dhba), 5-nitrosalicylic acid (5-nsa), 4-nitrocatechol (4-ncat) and 3,5-dinitrocatechol (3,5-dncat) in aqueous solutions as a function of pH. The first compound was chosen because of the possible competition between the salicylate and the catecholate coordination modes. The three other compounds have one or two nitro substituants on the aromatic ring that enhance the acidity of the salicylic and catechol functions and consequently induce a modulation of the complexing power of the molecules.

Besides the pH-potentiometric study that allowed us to propose a set of complexes for each Al(III)/ligand system, an extensive spectroscopic investigation was made (IR, UV–visible and especially ^{1}H and ^{13}C NMR) to confirm the potentiometric results and to obtain information on the structure and the dynamics of the complexes. Additionally, the proton exchange kinetics between the OH function and the phenolate form of 5-nsa could be studied; the formation of an intramolecular hydrogen bond, inducing the slowing down of the proton exchange rate, leads to unusual line broadenings in the NMR spectra.

2. Experimental

2.1. Materials

Aluminium(III) chloride (Fluka $\geqslant$99%) was used with no further purification. The concentration of aluminium(III) solutions was determined by a standard procedure using EDTA (Merck).

2,3-Dihydroxybenzoic acid ($\geqslant$99%), 2,4-dihydroxybenzoic acid ($\geqslant$97%), 5-nitrosalicylic acid ($\geqslant$99%) and 4-nitrocatechol ($\geqslant$97%) were purchased from Aldrich without further purification. 3,5-Dinitrocatechol was a Rhodia product.

The ionic strength was adjusted by potassium chloride (BDH AnalaR 99.5%).

pH-metric titration were performed with sodium hydroxide from Prolabo (0.100 mol L^{-1} Titrinorm).

The pH of the solutions was adjusted with hydrochloric acid and sodium hydroxide from Prolabo (1.00 mol L^{-1} Titrinorm).

2.2. pH-potentiometric measurements

The pH-potentiometric titrations were performed in aqueous solutions to investigate the protonation and coordination equilibria of the ligands at $T = 298.0 \pm 0.1$ K and for an ionic strength $I = 0.1$ mol L^{-1} (KCl) under an argon atmosphere. They were recorded using an automatic titration set, including a Metrohm Dosimat 716 DMS Titrino titrator and an Orion 9103SC type combined glass electrode.

The different equilibria were characterised by the following equation:

$$pM + qL + rH = M_pL_qH_r$$

and the corresponding constants are given by:

$$\beta_{pqr} = \frac{[M_pL_qH_r]}{[M]^p \cdot [L]^q \cdot [H]^r},$$

where M denotes the aluminium(III) cation, L the non-protonated ligand and H the proton. For simplicity, charges are omitted in most cases. However, they can be calculated knowing the fully protonated ligand is LH_2, leading to the LH^- and L^{2-} anions by successive deprotonations. A detailed description of the experimental procedure and data evaluation (from the PSEQUAD computer program [3]) was reported earlier [4,5].

The protonation and complex formation constants were determined from 6 to 8 independent titrations (between 30 and 70 data points per titration). The ligand to metal ratios varied from 1/1 to 10/1. The ligand concentration was 0.01 mol L^{-1}, except in the case of 5-nsa (0.004 mol L^{-1}) that is sparingly soluble. The pH-metric data between pH 2 and 11.3 were used for the evaluation, unless precipitation occured.

For the analysis of the titration curves, the formation of the hydroxo complexes MH_{-1}, M_2H_{-2}, M_3H_{-4}, $M_{13}H_{-32}$ and MH_{-4} were taken in account, with the following formation constant values [6]: $\log\beta_{10-1} = -5.52$, $\log\beta_{20-2} = -7.70$, $\log\beta_{30-4} = -13.57$, $\log\beta_{130-32} = -109.1$ and $\log\beta_{10-4} = -23.46$.

2.3. NMR spectroscopy

The ^{1}H and a part of ^{13}C NMR spectra were recorded on a Bruker DRX 400 apparatus at 400 and 100.6 MHz, respectively. The same apparatus was used for recording HMQC ^{13}C-^{1}H correlation maps. Another part of the ^{13}C spectra were recorded on a Bruker AC 200 apparatus at 50.3 MHz. The solutions were mainly prepared in D_2O/H_2O (20/80 v/v) mixtures. The chemical shifts were referenced to dioxane and converted to the TMS scale, knowing that $\delta_{dioxane}(^{13}C) = 67.40$ ppm and $\delta_{dioxane}(^{1}H) = 3.700$ ppm. In the case of the exchange rate measurements, an external capillary tube, filled up with D_2O and dioxane, was used.

The concentration of the ligand varied from 0.1 to 0.001 mol L^{-1}.

2.4. IR spectroscopy

The IR spectra were recorded on a Perkin–Elmer Spectrum One apparatus with an ATR accessory.

The spectra were analysed after the subtraction of the solvent (water) spectrum. The concentration of 2,3-dhba was 0.05 mol L^{-1} and the ligand to metal ratio varied from 1/1 to 5/1. According to ligand spectra, the 1390 and 1232 cm^{-1} vibration bands were attributed to COO^- and to COOH functions, respectively.

3. Results

3.1. pH-potentiometry

The values of the protonation and complexation constants deduced from the pH-potentiometric studies are shown in Table 1.

The acidity constant values are in agreement with those proposed in the literature for 2,3-dihydroxybenzoic acid (2,3-dhba) [7,8], 5-nitrosalicylic acid (5-nsa) [9–11], 4-nitrocatechol (4-ncat) [12,13] and 3,5-dinitrocatechol (3,5-dncat) [14,15] at 25 °C and for a 0.1 mol L^{-1} ionic strength. All the ligands are noted LH_2 with two ionizable functions. The third potential acidity constant of 2,3-dhba could not be determined indicating a pK_a value higher than 12.

The set of complexes for the Al(III)–2,3-dhba system determined in this work is less large than that found by Kiss et al. [7] (25 °C and 0.2 mol L^{-1} KCl) or S. Desroches et al. [8] (37 °C, 0.15 mol L^{-1} NaCl), but the species ML, ML_2, ML_2H_{-1} and $M_2L_2H_{-3}$ are common for all the systems. The additional complexes are ML_2H_{-2} and $M_2L_2H_{-2}$ for the first reference and MLH, M_2L and $M_2L_2H_{-2}$ for the second reference. The comparison of the literature results [7] to our data, both obtained at 25 °C, indicates that the $\log\beta_{pqr}$ values determined in this work are slightly higher, probably because of the presence of less species in our system. For this ligand, the problem of the complexation mode: catecholate or salicylate, arises and will be discussed in the discussion part with the help of the NMR results.

For 5-nsa, the complexes formed with Al(III) are ML, ML_2, ML_3. The formation constants of these complexes are very close to those reported in the literature [9–11]. The structure of these complexes and the existence of different isomers for the ML_2 and ML_3 species have been analysed by NMR spectroscopy and discussed below.

The 4-ncat ligand also leads to the formation of ML, ML_2 and ML_3 complexes with the Al(III) cation. The formation constant for the ML species is comparable to that reported in the literature [12,13] and those for ML_2 and ML_3 are slightly higher.

There is no previous study on the complexation of Al(III) with 3,5-dncat to the best of our knowledge. The pH-potentiometric study shows that ML_2 and ML_3 complexes are formed with $\log\beta$ values equal to 21.80 and 31.68, respectively. Beyond pH = 5, another species appears; it was not possible to determine its stoichiometry.

The distribution curves deduced from the pH-potentiometric measurements are plotted in Fig. 1.

3.2. NMR spectroscopy

The ^1H NMR chemical shifts of all the systems described below are summarised in Table 2.

3.2.1. 2,3-dhba

^1H NMR spectroscopy allowed us to follow the formation of the four complexes detected by pH-potentiometry. Besides the signal due to the free ligand (doublets for the H_4 and H_6, a doublet of doublets for H_5) the signals due to the different complexes successively appear when the pH is increased. For a ligand to metal ratio L/M equal to 5/1, the proportion of ML and ML_2 can be easily quantified by integrating the corresponding NMR signals. The ML_2H_{-1} complex exhibits many peaks that overlap the other signals; its concentration cannot be determined.

For L/M = 3/1 or 1.1/1, the different complexes can be distinguished but the overlapping of the numerous signals is very important preventing the determination of their concentrations.

ML and ML_2 present very similar spectra that are slightly shifted to higher field relatively to the free ligand.

$M_2L_2H_{-3}$ appears in the NMR spectra for low L/M ratio such as 1.1/1. The spectrum presents two patterns similar to that of the free ligand. They are more shifted relatively to the free ligand than those of the ML and ML_2 complexes. The spectrum corresponding to ML_2H_{-1} is composed of many peaks due probably to inequivalences in the complex and/or different isomeric species.

A ^{13}C NMR study was also performed in order to determine the complexation mode with 2,3-dhba. The chemical shifts of all the carbons (the carboxylate carbon is noted C_7) for the LH_2, LH and L forms are summarised in Table 3. A shift amplitude from 4 to 9 ppm is measured from the LH_2 to the L species. When Al(III) is added to the solution, new peaks appear in the spectra corresponding to the formation of the complexes (Table 3). The chemical shifts of these signals do not depend on pH. For the spectra recorded between pH 2.0 and 6.5, two series of "bound" peaks are successively observed.

3.2.2. 5-nsa

As for 2,3-dhba, the chemical shifts of the H_3, H_4 and H_6 aromatic protons depend on the pH. They were measured as a function of pH and the chemical shifts of the species L, LH and LH_2 deduced from these measurements. As mentioned above, the peaks are broad for a pH value around the pK_{a2} value.

Table 1
Protonation constants of the 2,3-dhba, 5-nsa, 4-ncat and 3,5-dncat molecules and complex formation constants with Al(III) at 298 K and for $I = 0.1$ mol L^{-1} compared to those of catechol and salicylic acid ligands

	2,3-dhba	5-nsa	4-ncat	3,5-dncat	Catechol[a]	Salicylic acid[a]
pK_{a1}	2.76 (COOH)	2.07 (COOH)	6.68 (1-OH)	3.39 (2-OH)	9.28	2.79 (COOH)
pK_{a2}	10.03 (3-OH)	9.90 (OH)	10.70 (2-OH)	9.69 (1-OH)	13.02	13.4 (OH)
$\log\beta_{110}(AlL)$	10.62 (10.32[a], 10.50[b])	10.65 (11.11[c], 10.91[d], 11.26[e])	13.89 (13.74[f], 13.75[g])		16.20	13.22
$\log\beta_{120}(AlL_2)$	19.20 (18.26[a], 18.24[b])	19.81 (19.73[c], 19.67[d])	26.33 (25.39[f], 25.44[g])	21.80	29.26	23.73
$\log\beta_{130}(AlL_3)$		25.74 (25.86[c], 25.03[d])	37.08 (34.31[f], 34.38[g])	31.68	37.95	32.55
$\log\beta_{22-3}(Al_2L_2H_{-3})$	10.30 (8.87[a], 9.74[b])				$\log\beta_{22-2}$ 24.05	$\log\beta_{22-2}$ 17.9
$\log\beta_{12-1}(AlL_2H_{-1})$	13.50 (11.56[a], 11.70[b])					
$M + LH_2 = ML + 2H^+$ $\log K_1 = \log\beta_{110} - pK_{a1} - pK_{a2}$	−2.2	−1.3	−3.5		−6.1	−3.0
$M + 2LH_2 = ML_2 + 4H^+$ $\log K_2 = \log\beta_{120} - 2pK_{a1} - 2pK_{a2}$	−6.4	−4.1	−8.4	−4.4	−15.3	−8.7
$M + 3LH_2 = ML_3 + 6H^+$ $\log K_3 = \log\beta_{130} - 3pK_{a1} - 3pK_{a2}$		−10.2	−15.1	−7.6	−29.0	−16.0

[a] Ref. [7], at 25 °C, $I = 0.20$ mol L^{-1} KCl.
[b] Ref. [8], at 37 °C, $I = 0.15$ mol L^{-1} NaCl.
[c] Ref. [9], $I = 0.1$ mol L^{-1} $NaClO_4$.
[d] Ref. [10], at 30 °C, $I = 0.100$ mol L^{-1} KNO_3.
[e] Ref. [11].
[f] Ref. [16].
[g] Ref. [13].

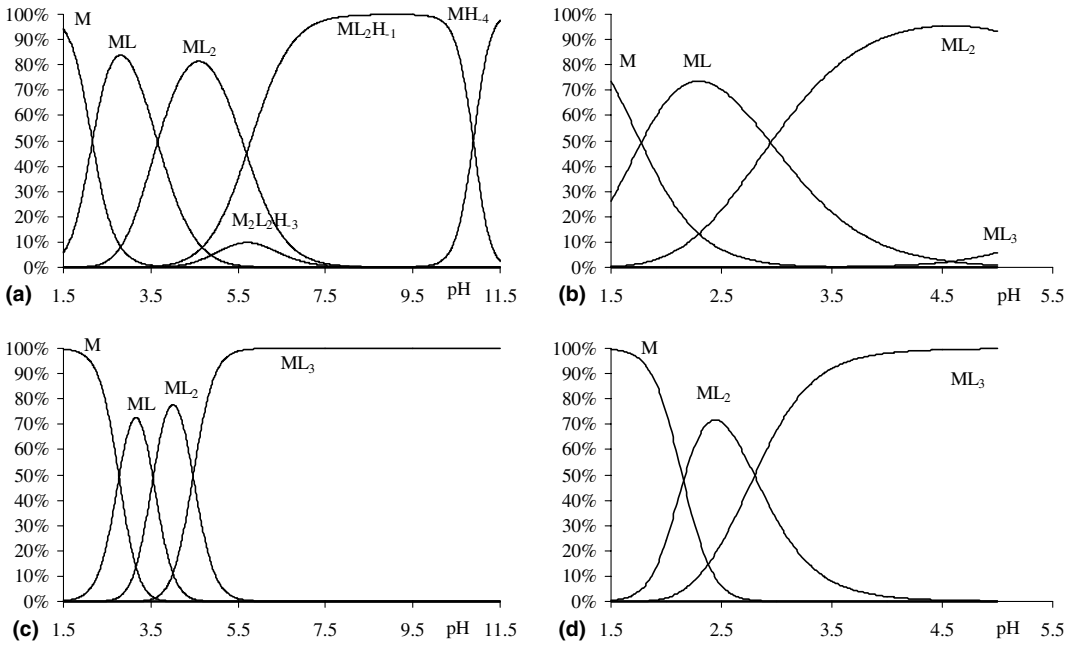

Fig. 1. Distribution diagrams of the complexes formed at 25 °C between aluminium(III) and 2,3-dhba (a), 5-nsa (b), 4-ncat (c), 3,5-dncat (d) as a function of the pH; [ligand] = 0.01 mol L^{-1}, ligand to metal ratio 5/1.

When aluminium(III) is present in solution, new peaks corresponding to the Al-bound ligand molecule merge in the spectra. These different ''bound'' signals are observed when pH is increased and correspond to the formation of the ML, ML_2, and ML_3 complexes. The chemical shift of the ML complex signals is only shifted of a few hundredth ppm. The spectrum of ML_2 is not well resolved at room temperature. At 5 °C, there are two series of signals with similar intensities for this complex.

The fine structure of ML_3 is visible at room temperature and corresponds to four sets of signals with nearly equal intensities (Fig. 2).

3.2.3. 4-ncat

The signals of the free ligand shift according to the pH of the solutions and the knowledge of the chemical shifts for the species LH_2, LH and L are needed to discriminate them from those of the bound ligand molecules. The successive apparition of the complexes is seen when pH is increased. The structures of the patterns corresponding to the bound ligand are similar to that of the free ligand and are shifted to a higher field. H_5 is not very perturbed by the complexation of the ligand to the Al(III) cation. The shift of H_3 is more pronounced and almost corresponds to that of the deprotonated ligand L. H_6 also undergoes an important shift and the shift of the complexes is near to that of the free deprotonated ligand L. For ML_2, the peaks are broadened contrary to those of the ML_3 complex for which only one set of signal is observed.

3.2.4. 3,5-dncat

There are only two aromatic protons in the molecule. H_4 and H_6 give two doublets in the NMR spectra ($J \approx 2.8$ Hz). The chemical shift of these doublets depends on the pH. The pH effect is weak for H_4 (LH_2: $\delta = 8.56$ ppm; LH: $\delta = 8.56$ ppm; L: $\delta = 8.41$ ppm) and much stronger for H_6 (LH_2: $\delta = 7.91$ ppm; LH: $\delta = 7.53$ ppm; L: $\delta = 7.27$ ppm).

For pH $\leqslant$ 5, two species are detected. The determination of their concentrations from NMR spectra and the comparison to those obtained from the potentiometric results allow us to assign the peaks to the ML_2 and ML_3 complexes. The chemical shifts of ML_2 and ML_3 are similar for H_4 whereas those for H_6 are different: 7.42 and 7.58 ppm, respectively. The peaks corresponding to ML_3 are broadened when these two species are present together whereas those of ML_2 remain sharp.

Beyond pH 5, a new complex is detected in the NMR spectra in agreement with the potentiometric results. It gives rise to many peaks (two doublets and a triplet for H_6, for instance) but its structure could not be determined.

3.3. Infrared spectroscopy

In order to study the complexation mode of the 2,3-dhba ligand (salicylate or catecholate), IR spectra were recorded. COO^- and COOH bands can be easily distinguished [17]. The peak at 1390 cm^{-1} corresponds to the carboxylate in an aqueous phase. Another peak at 1232 cm^{-1} is characteristic of the COOH function. Their

Table 2
^{1}H chemical shifts in ppm for 2,3-dhba, 5-nsa, 4-ncat and 3,5-dncat and for most of their Al(III) complexes

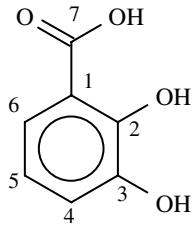

2,3-dhba

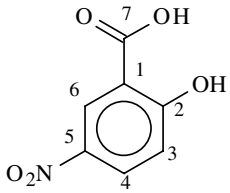

5-nsa

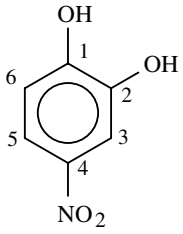

4-ncat

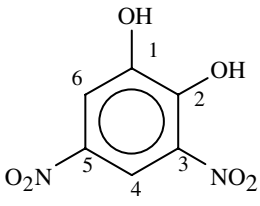

3,5-dncat

		2,3-dhba	5-nsa	4-ncat	3,5-dncat
LH_2	H_3		7.039[c]	7.695[c]	
	H_4	7.107[d]	8.284[d]		8.566[c]
	H_5	6.826[e]		7.740[d]	
	H_6	7.406[d]	8.704[c]	6.930[c]	7.939[c]
LH	H_3		6.978[c]	7.563[c]	
	H_4	6.997[d]	8.229[d]		8.564[c]
	H_5	6.756[e]		7.755[d]	
	H_6	7.321[d]	8.642[c]	6.505[c]	7.552[c]
L	H_3		6.506[c]	7.417[c]	
	H_4	6.686[d]	7.991[d]		8.327[c]
	H_5	6.632[e]		7.723[d]	
	H_6	6.934[d]	8.148[c]	6.448[c]	7.091[c]
ML	H_3		6.796[c]	7.347[c]	
	H_4	6.962[d]	8.155[d]		
	H_5	6.604[e]		7.649[d]	
	H_6	7.297[d]	8.702[c]	6.577[c]	
ML_2	H_3		6.743[c,a] 6.649[c,a]	7.293[c,a]	
	H_4	6.942[d]	8.147[d,a] 8.099[d,a]		8.360[c]
	H_5	6.586[e]		7.629[d,a]	
	H_6	7.309[d]	8.724[c,a] 8.717[c,a]	6.502[c,a]	7.415[c]
ML_3	H_3		6.600[c] 6.565[c] 6.556[c] 6.532[c]	7.214[c]	
	H_4		8.107[d] 8.084[d] 8.048[e] 8.025[e]		8.360[c]
	H_5			7.623[d]	
	H_6		8.702[c] 8.697[c] 8.671[c] 8.656[c]	6.441[c]	7.385[c]
[b]	H_3				
	H_4	6.884[d] 6.654[d]			8.340[c] 8.333[c] 8.323[c]
	H_5	6.793[e] 6.725[e]			
	H_6	7.129[d] 7.082[d]			7.350[c] 7.313[e] 7.294[c]

The spectra were recorded at 400 MHz; coupling constant values: ^{3}J = 9.0 Hz; ^{4}J = 2.8 Hz; T = 298 K.
[a] T = 278 K.
[b] $M_2L_2H_{-3}$ for 2,3-dhba and additional species for 3,5-dncat.
[c] Doublet.
[d] Doublet of doublets.
[e] Triplet.

variations in intensity can be correlated to the proportion of COO^- group compared to that of COOH groups in the solution. The intensity of the peak at 1390 cm^{-1} (COO^-) is proportional to the sum of LH, ML and ML_2 concentrations in solution and not to the alone LH concentration.

4. Discussion

4.1. 2,3-dhba

The ^{1}H NMR study allowed us to confirm the potentiometric results. Four different complexes were

Table 3
^{13}C chemical shifts in ppm for 2,3-dhba and for ML and ML_2 complexes

^{13}C	LH_2	LH	L	ML	ML_2
C_1	114.11	119.47	118.48	[a]	[a]
C_2	150.18	150.17	155.99	153.37	154.10
C_3	145.04	144.88	153.72	148.00	148.27
C_4	122.17	120.15	122.23	117.91	117.81
C_5	120.27	119.20	119.57	116.58	116.02
C_6	122.64	122.52	115.87	122.90	122.88
C_7	173.44	176.44	177.89	[a]	174.61

The spectra were recorded at 400 MHz; $T = 298$ K; the peaks were assigned according to ChemDraw Ultra® Software[b] and to HMQC ^1H–^{13}C correlation maps.

[a] Peak not observed.

[b] ChemDraw Ultra® v 7.0.1 (2002), Chemical Structure Drawing Standard, Cambridge Soft Corporation.

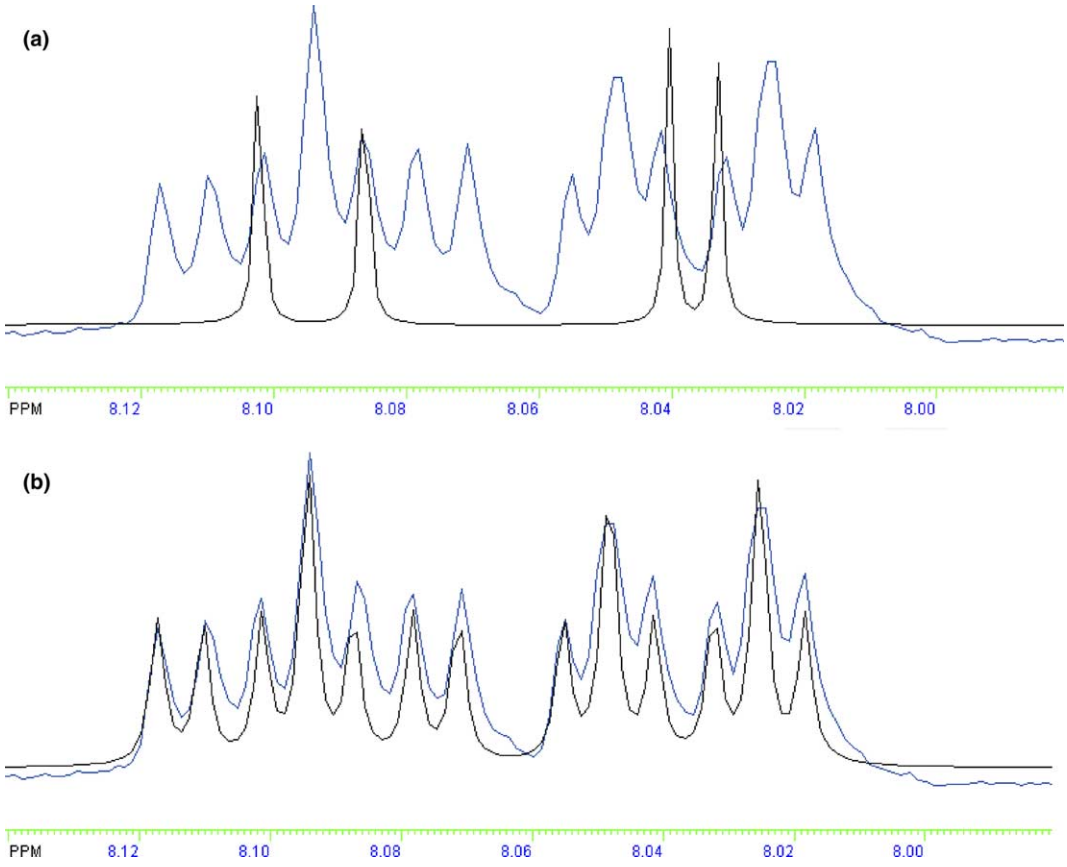

Fig. 2. Simulation (dark lines) of H_4 NMR pattern for $Al(5\text{-nsa})_3$ complex; spectrum (light lines) recorded at 400 MHz: [5-nsa] = 4×10^{-3} mol L^{-1}, [Al(III)] = 1.33×10^{-3} mol L^{-1}, pH 9.7; $T = 278$ K; a: simulation in the absence of coupling (chemical shifts of the four species: 8.103, 8.087, 8.041 and 8.034 ppm); b: simulation with coupling (2.8 Hz with H_6 and 9.2 Hz with H_3).

detected. For L/M = 5/1, we could determine the concentrations of two of them. The values correspond to those deduced from potentiometric results for the ML and ML_2 complexes. The ML_2H_{-1} species gives rise to many peaks that overlap the other NMR signals. For this reason, it was not possible to quantify its concentration. For L/M = 1/1, $M_2L_2H_{-3}$ is the major complex. From the integrals of the NMR spectra, the logβ values could be evaluated: 10.96 and 10.97 at pH 3.0 and 4.0, respectively, for ML; 19.55 and 19.39 at pH 3.0 and 4.0, respectively, for ML_2 and 10.49 at pH 4.0 for $M_2L_2H_{-3}$. These values are similar to those found by pH-potentiometry: 10.62, 19.20 and 10.30 for ML, ML_2 and $M_2L_2H_{-3}$, respectively.

Once the stoichiometry of the species known, the question of the structure and of the coordination mode of the ligand arises. It is well recognised that catecholate

leads to stronger complexes than salicylate. 2,3-dhba can act as both of these ligands. The salicylate complexation mode implies that the less acidic OH function must be deprotonated. The catecholate complexation implies that the carboxylic function be not ionised in the ML and ML_2 complexes in which only two (OH) deprotonations occur. A ^{13}C NMR study was performed to solve this question. Up to pH 3.5, the C_7 carbon gives one signal. From pH 4.5, two signals are observed: one at 176.4 ppm for the free carboxylate and another one at 174.6 ppm for the complex ML_2. This latter value approximately corresponds to the chemical shift of the free COOH ligand. The shifts of the C_2 and C_3 carbons are more important: nearly 3.0 ppm and 4.0 ppm at lowfield for C_2 in ML and ML_2, respectively, and nearly 3.1 ppm and 3.4 ppm at lowfield for C_3 in ML and in ML_2, respectively. These raw results are in favour of a catecholate complexation for which the carboxylic function remains protonated. Nevertheless this observation is inconsistent with the fact that the logβ values for 2,3-dhba are similar to the corresponding one for 5-nsa (Table 1) which is a salicylate-type ligand and very different from the values found for 4-ncat which is a catecholate-type ligand.

This difficulty was solved by an IR study that showed that the intensity of the COO^- band corresponds to the sum of the concentrations of the free ligand, LH, and of the ML and ML_2 complexes, and not to the concentration of LH. Thus, the carboxylate function is deprotonated in the complex: this result proves a salicylate complexation.

This conclusion was reinforced by the ^{13}C NMR study of 2,4-dhba for which the complexation can only be of the salicylate type. The shift of the C_7 carbon of the free 2,4-dhba and that of the C_7 carbon in the complex ML_2 at pH 5.2 are identical to the corresponding ones for 2,3-dhba.

For all these reasons it can be concluded that the complexation of 2,3-dhba with Al(III) occurs through the carboxylate and the deprotonated α-OH function in the ML and ML_2 complexes as for the salicylate ligand.

The stoichiometry of the $M_2L_2H_{-3}$ species supposes that at less one hydroxide ion participates to the coordination of Al(III). The ^1H NMR spectrum of this species shows two sets of peaks with an equal intensity indicating that there is either one complex with two inequivalent ligands or two isomeric forms in which rapid intramolecular ligand exchange occurs.

The ligand can be coordinated to the Al^{3+} in a catecholate manner, so the complex can be more properly written $M_2(LH_{-1})_2(OH)$ in this case.

Mixed catecholate/salicylate coordination modes with two OH^- ions, as already reported in the literature [7], or only salicylate coordination with three OH^- ion can also be evoked.

4.2. 5-nsa (see NMR spectra on Fig. 3)

4.2.1. Kinetics study of the phenolic proton exchange

The NMR study of the ligand leads to the exceptional direct observation of the slow exchange of the OH proton in the LH species between the ligand and the bulk. Indeed, the ^1H and ^{13}C NMR signals are broadened around pH 9.90 (Fig. 3), whereas they are sharp for pH $\leqslant$ pK_{a2} − 1 and for pH $\geqslant$ pK_{a2} + 1. This broadening is due to the observation of an averaged signal between the LH and the L species: the full coalescence is not achieved because of the slow exchange of the OH proton relatively to the NMR time scale. It is effectively known that the intermolecular exchange of this proton between the protonated form of the ligand and a base present in the solution can be slowed down because of the intramolecular hydrogen bond between the carboxylate group and the OH function [18–22]. The NMR study allows the determination of the rate constants for the exchange of the phenolic OH proton between LH^- and L^{2-} or OH^- [23]

$$LH^- + L^{2-} \underset{k}{\overset{k}{\rightleftarrows}} L^{2-} + LH^-$$

$$LH^- + OH^- \underset{k^-}{\overset{k^+}{\rightleftarrows}} L^{2-} + H_2O$$

The exchange rate is the sum of the rates corresponding to these two mechanisms, leading to:

$$k_{NMR} = k[L^{2-}] + k^+[OH^-]$$

For pH = pK_a, the concentration of L^{2-} and LH^- species are equal and it can be written that:

$$k[L^{2-}] + k^+[OH^-] = k[LH^-] + k^-[H_2O].$$

In this case: $k^+[OH^-] = k^-[H_2O] = k'$, since the water concentration is constant. k, k^+ and k^- can be calculated from the measurement of the NMR linewidths for different ligand concentrations.

^{13}C NMR was preferred to ^1H NMR because the chemical shift differences $\Delta\delta$ between the signals corresponding to the acidic and basic forms of the ligand are higher. The chemical shifts for the different carbon atoms in the LH^- and L^{2-} species are summarised in Table 4. $\Delta\delta$ values are particularly important for C_1, C_2 and C_5 carbons (10.7, 7.8 and 6.4 ppm, respectively).

Beyond the coalescence of the LH^- and the L^{2-} signals, at pH = pK_a = 9.90, and consequently for $[LH^-] = [L^{2-}]$, the exchange rate k_{NMR} is given by the formula [23]:

$$(\Delta\nu_{1/2})_{obs} - (\Delta\nu_{1/2})_0 = \frac{\pi(\nu_{LH^-} - \nu_{L^{2-}})^2}{2k_{NMR}}$$

where $(\Delta\nu_{1/2})_{obs}$ is the observed linewidth at half height, $(\Delta\nu_{1/2})_0$, that of the signals not submitted to the exchange and ν, the chemical shift in Hz.

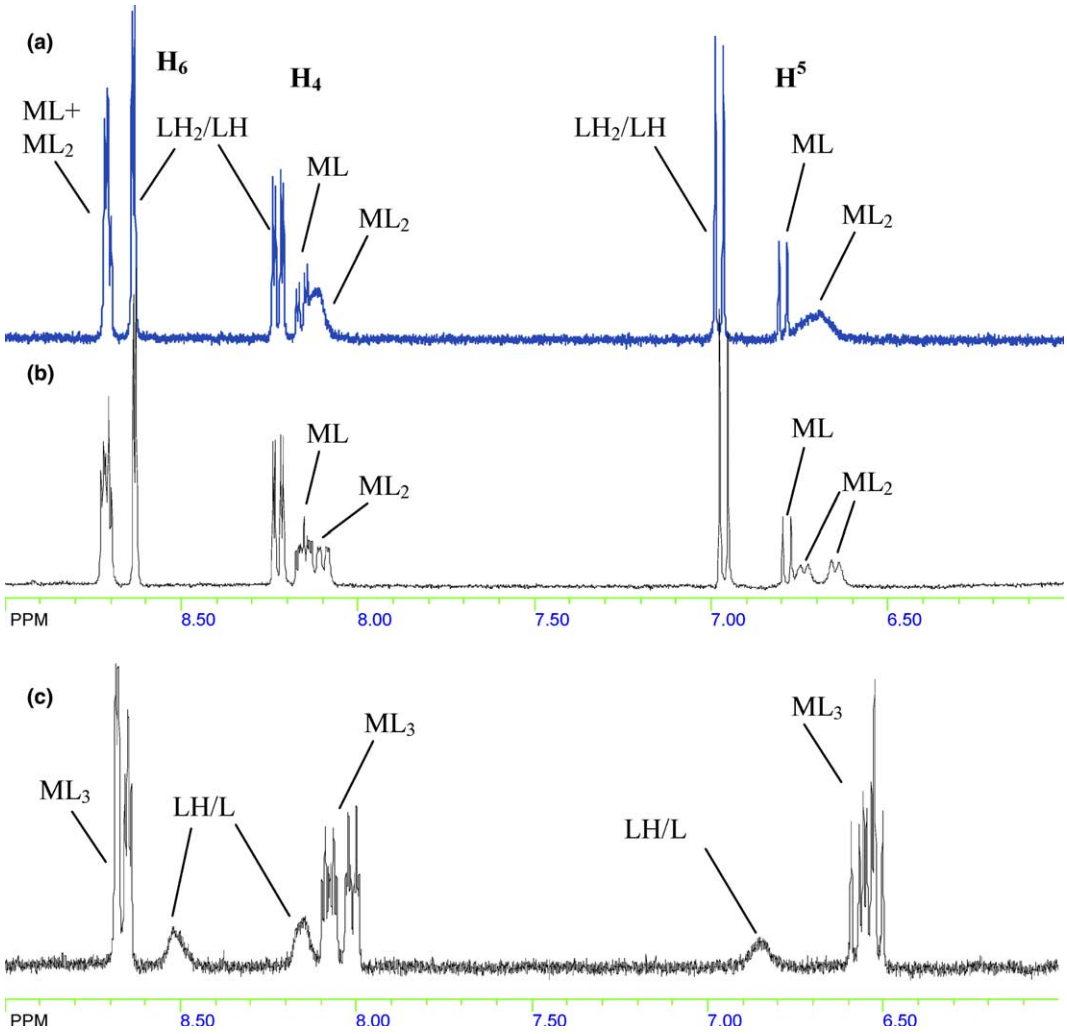

Fig. 3. ^{1}H NMR spectra of aluminium(III)–5-nsa (4×10^{-3} mol L^{-1}) solutions for a ligand to metal ratio 3/1, recorded at 400 MHz in D_2O/H_2O (20/80 v/v); a: $T = 298$ K, pH 3.92, b: $T = 278$ K, pH 4.08 and c: $T = 298$ K, pH 9.80, the peaks corresponding to the LH/L species are broad; this is due to the relatively slow exchange of the phenolic proton.

Table 4
^{13}C chemical shifts (δ) in ppm for 5-nsa, linewidth at half-height of ^{13}C peaks ($(\Delta\nu_{1/2})_0$) in Hz for the LH species; linewidth at half-height of ^{13}C peaks ($(\Delta\nu_{1/2})_{obs}$) in Hz for LH/L mixtures (50/50 mol/mol) at pH = pK_a = 9.9 and for different concentrations

	δ		$(\Delta\nu_{1/2})_0$	$(\Delta\nu_{1/2})_{obs}$		
	LH	L	0.05 mol L^{-1}	0.1 mol L^{-1}	0.05 mol L^{-1}	0.035 mol L^{-1}
C_1	118.66	129.56	1.3	13.9	[a]	[a]
C_2	167.86	175.68	1.7	7.1	14.3	17.0
C_3	118.31	121.45	0.8	1.9	2.8	4.0
C_4	129.83	128.62	0.6	0.8	1.0	1.2
C_5	139.69	133.29	3.3	10.6	12.4	12.3
C_6	127.68	127.30	0.5	0.6	0.6	0.7
C_7	174.12	177.21	0.5	1.6	2.0	1.8

The spectra were recorded at 50 MHz; $T = 298$ K.
[a] Peak too broad to be detected.

k_{NMR} was found to be dependent on [LH$^-$] or [L^{2-}]. For these different concentration values, a straight line was obtained when k_{NMR} is plotted versus [L^{2-}] (Fig. 4). The slope of this line gave a k value equal to 5.7×10^5 L mol^{-1} s^{-1} and $k' = 4.5 \times 10^3$ s^{-1} ($k^+ = 5.7 \times 10^7$ L mol^{-1} s^{-1} and $k^- = 80$ L mol^{-1} s^{-1}).

The k value found in this work with 5-nsa is in the same order of magnitude as the value reported by

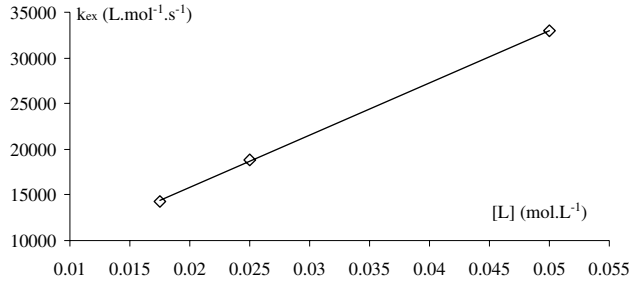

Fig. 4. Exchange constant (k_{ex}) of the phenolic proton in 5-nsa measured by ^{13}C NMR as a function of ligand concentration; $T = 298$ K; pH 9.9.

Diebler et al. [19] for the exchange rate constant corresponding to the exchange of the dinitrosalicylic anion with the NH_3 base. ($k = 1.9 \times 10^6$ L mol^{-1} s^{-1}). The k^+ value is higher than the value obtained for alizarine yellow S [22] ($k^+ = 1.4 \times 10^7$ L mol^{-1} s^{-1}) and comparable to that obtained for the exchange of thiosalicylic acid with OH^- (4.4×10^8 L mol^{-1} s^{-1} [19] or 5.3×10^7 L mol^{-1} s^{-1} at 12 °C [21]). The literature values were obtained from *T*-jump experiments.

4.2.2. Complexation study

^1H NMR spectroscopy confirms the formation of three different complexes when pH is varied. Separate signals from those of the free ligand are observed for each complex. The integration of these signals allows the determination of the logβ values for the ML and ML_2 complexes. Because of the broadness of the free ligand peaks around pH 10.0 (see above) the determination of the logβ values for ML_3 is not possible. The logβ values calculated for ML and ML_2 from NMR spectra at 3 different pH values are close to the values deduced from the potentiometry experiments (11.3 against 10.65 for ML and 20.35 against 19.61 for ML_2).

The NMR spectrum of the ML species is similar to that of the free ligand, but slightly shifted.

The signals of ML_2 are broad at room temperature. By cooling down the solution to 5 °C, two sets of signals with equal intensities are observed for this complex (Fig. 3). This can be due to the non-equivalence of the two ligand molecules in the complex or to two different isomeric forms of equivalent stability. If we consider a cis-complexation of the two salicylate ligands with the hexa-coordinated Al^{3+} cation with two axial water molecules, there are two possible isomers in which the ligands are equivalent (probabilities 1/2–1/2).

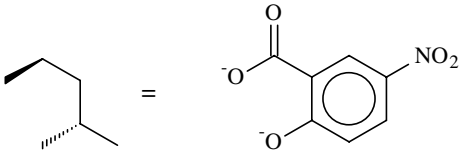

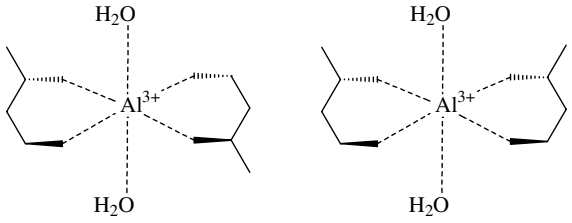

isomers of the cis-ML_2 species

An intramolecular exchange can convert an isomer into another and leads to the partial coalescence of the signals at room temperature.

The signals of the ML_3 complex are sharp at room temperature and present four different patterns of equal intensities (Fig. 2).

The hexa-coordination of Al(III) with the three unsymmetrical chelating ligands leads to the formation of two isomers. In the fully symmetrical isomer, all the three ligands are equivalent. In the other isomer, the hydrogen atoms of each ligand are inequivalent. It can be considered that the stability of the two isomers are close together. Moreover, if the steric effects are weak, the population for the symmetrical and for the other isomer must be 1/4 and 3/4. This leads to four patterns of equal intensities as observed.

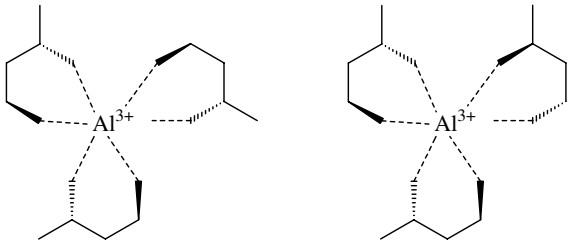

isomers of the ML_3 species

4.3. 4-ncat

^1H NMR allows to follow the formation of three successive complexes. The signals of the first and third species are sharp whereas those of the second complex are broad. When the second species is present, the peaks of the free ligand are also broadened. At 5 °C, these signals become sharper. The integration of the free and bound signals allows the determination of the percentages of all the species present in solution. On the basis of the formation of the ML, ML_2 and ML_3 complexes, the proportions determined by NMR are fully consistent with the results of the potentiometric study. It can be

concluded that the three species which are detected in the ^{1}H NMR spectra are effectively ML, ML_2 and ML_3.

The $\log\beta_{110}$ and $\log\beta_{120}$ for the ML and ML_2 complexes were determined from the ^{1}H NMR spectra. The values found at pH 2.0 and 3.0 (13.96 for ML and 25.62 for ML_2) are very close to that determined from the potentiometric study (13.89 for ML and 26.33 for ML_2). The $\log\beta$ values for ML_3 could not be evaluated because of the quantitative complexation which occurs for the pH range where this species is formed.

It must be mentioned that, from pH 8, additional peaks due to the formation of other species are detected in the ^{1}H NMR spectra but their total concentration do not exceed 4% of the total complex concentration.

The broadening of the ligand and ML_2 signals when the ML_2 complex is formed can be due to the exchange of the LH_2 molecules with the bound L^{2-} ligands:

$$ML_2^- + L^*H_2 = MLL^{*-} + LH_2$$

where the asterisk is only a typographical distinction.

This kind of exchange is not observed for the ML^+ and $ML_3{}^{3-}$ species at the NMR time scale level.

4.4. 3,5-dncat

The NMR results are consistent with the potentiometric results. For pH $\leqslant$ 5.0, the ML_2 and ML_3 complexes are formed in solution. The determination of the formation constants from the NMR experiments is difficult because the poor solubility of the ligand leads to the use of low concentrations. Nevertheless, the average values obtained from six different experiments (two different ligand to metal ratios at three different pH values for each) are 21.2 and 31.7 for $\log\beta_{120}$ and $\log\beta_{130}$, respectively. The values are close to those obtained from the potentiometric experiments: $\log\beta_{120} = 21.80$ and $\log\beta_{130} = 31.68$.

It must be mentioned that these $\log\beta$ values are lower than those obtained for 4-ncat: $\log\beta_{120} = 26.33$ and $\log\beta_{130} = 37.08$. It might be due to the presence of one nitro-substituent in an *ortho*-position relatively to one OH function in the 3,5-dncat ligand leading to a decrease of the negative charge on the phenolate oxygen atom owing to mesomeric effects.

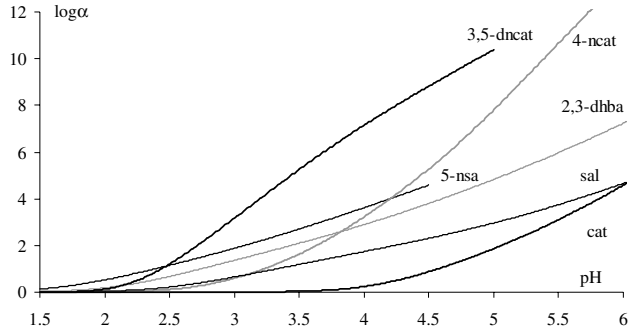

Fig. 5. logα as a function of pH for 2,3-dhba, 4-ncat, 5-nsa, 3,5-dncat, catechol (cat) and salicylic acid (sal); α is the ratio of the total aluminium(III) concentration to that of free aluminium(III); [ligand] = 0.01 mol L^{-1}, ligand to metal ratio 5/1, $I = 0.1$ mol L^{-1}, $T = 298$ K.

5. Conclusion

The spectroscopic investigation of some salicylate or catecholate/aluminium(III) systems allowed us to obtain dynamical, thermodynamical and structural information on the ligands and the complexes formed in aqueous solutions. These results prove that the studied ligands are good complexing agents for the Al(III) cation. This complexing ability can be easily shown by considering the plot of logα versus pH, where α is the ratio of the total cation concentration to that of free cation. A high α value is characteristic of a strong complexation. It can be seen on Fig. 5 that 3,5-dncat is the best ligand from pH $\approx$ 2.5 up to pH $\approx$ 5. 5-nsa and 2,3-dhba have a similar complexing ability. The complexing power of 4-ncat which is the lowest up to pH 3.5, strongly increases from pH 3.5 and becomes comparable to that of 3,5-dncat at pH $\approx$ 5.0. The $\log\beta_{1n0}$ values for the formation of the ML_n complexes are higher for catecholate derivatives than for salicylate compounds but, at low pH values, the complexing ability of salicylate ligand is nevertheless good, owing to low pK_{a1} values. The $\log\beta_{1n0}$ values are lower for 3,5-dncat and 4-ncat, but they are offset by a low pK_{a1} value leading to a very good complexing power.

For systems that do not lead to precipitate formation (4-ncat and 2,3-dhba) beyond pH $\approx$ 5.0, the complexation is challenged by the formation of the aluminate species $Al(OH)_4{}^-$ from pH $\approx$ 6.0.

The $\log\beta_{1n0}$ formation constants for 5-nsa are lower than those for salicylic acid ($\log\beta_{110} = 13.2$, $\log\beta_{120} = 23.7$ for salicylic acid [7]). Similarly, these values for 4-ncat are lower than those for catechol ($\log\beta_{110} = 16.2$, $\log\beta_{120} = 29.3$ and $\log\beta_{130} = 37.95$ [7]). The presence of one nitro-substituant on the aromatic ring decreases the negative charge borne by the phenolate oxygen atoms owing to mesomeric effects. When a second NO_2-substituent is present in an *ortho*-position relatively to the OH function, this effect is enhanced, leading to lower values for the formation constant as noted for 3,5-dncat and 4-ncat. This is true if the interactions between the Al^{3+} cation and the ligand are essentially electrostatic. Theoretical calculations on these systems might allow to precise these points.

Acknowledgements

The authors are grateful to Professor J.-J. Delpuech for helpful discussions about the proton exchange study.

References

[1] G. Guibaud, C. Gauthier, J. Inorg. Biochem. 97 (2003) 16.
[2] S. Hiradate, N.U. Yamaguchi, J. Inorg. Biochem. 97 (2003) 26.
[3] L. Zékány, L. Nagypál, in: D. Leggett (Ed.), Computational Methods for the Determination of Stability Constants, Plenum, New York, 1985 (Chapter 8).
[4] T. Gajda, B. Henry, A. Aubry, J.-J. Delpuech, Inorg. Chem. 35 (1996) 386.
[5] P. Surdy, P. Rubini, N. Buzas, B. Henry, L. Perrito, T. Gajda, Inorg. Chem. 38 (1999) 346.
[6] L. Öhman, L. Sjöberg, Acta. Chem. Scand. A 36 (1982) 47.
[7] T. Kiss, K. Atkári, M. Jezowska-Bojczuk, P. Decock, J. Coord. Chem. 29 (1993) 81.
[8] S. Desroches, F. Biron, G. Berthon, J. Inorg. Biochem. 75 (1999) 27.
[9] L. Lajunen, M. Tikanmäki, Acta Univ. Oul. Chem. A 74 (1978) 8.
[10] A.L.R. Mercê, A.S. Mangrich, B. Szpoganicz, N.M. Levy, J. Felcman, J. Braz. Chem. Soc. 7 (2) (1996) 97.
[11] B. Perlmutter-Hayman, E. Tapuhi, Inorg. Chem. 18 (3) (1979) 875.
[12] P. Häkkinen, Finn. Chem. Lett. (1984) 9.
[13] A.J. Downard, R.J. Lenihan, S.L. Simpson, B. O'Sullivan, K.J. Powell, Anal. Chim. Acta 345 (1997) 5.
[14] V.A. Nazarenko, N.V. Lebedeva, L.I. Vinarova, Zhur. Neorgan. Khimii 15 (3) (1970) 643.
[15] P. Häkkinen, Finn. Chem. Lett. 13 (4) (1986) 85.
[16] P. Häkkinen, Finn. Chem. Lett. (1984) 151.
[17] L.J. Bellamy, The Infra-Red Spectra of Complex Molecules, vol. 1, 3rd ed., Chapman and Hall, London, 1975 (Chapter 10).
[18] W.L. Mock, L.A. Morsch, Tetrahedron 57 (2001) 2957.
[19] H. Diebler, F. Secco, M. Venturini, J. Phys. Chem. 88 (1984) 4229.
[20] M. Eigen, Angew. Chem. Int. Edit. 3 (1) (1964) 1.
[21] M. Eigen, W. Kruse, G. Maass, L. De Maeyer, Prog. React. Kinet. 2 (1964) 286.
[22] M. Eigen, W. Kruse, Zeit. Naturforsch. B 18 (1963) 857.
[23] J.-J. Delpuech, Dynamics of Solutions and Fluid Mixtures by NMR, Wiley, New York, 1995.

Available online at www.sciencedirect.com
SCIENCE DIRECT®
Polyhedron 23 (2004) 2405–2412
POLYHEDRON
www.elsevier.com/locate/poly

The preparation and characterization of tin(IV) complexes of 2-quinolinecarboxaldehyde Schiff bases of *S*-methyl- and *S*-benzyldithiocarbazates and the X-ray crystal and molecular structures of the 2-quinolinecarboxaldehyde Schiff base of *S*-benzyldithiocarbazate (Hqaldsbz) and its tin(IV) complex [Sn(qaldsbz)I_3]

Mohammad Akbar Ali [a,*], Aminul H. Mirza [a], Malai Haniti S.A. Hamid [a], Fatriah Hj Bujang [a], Paul V. Bernhardt [b]

[a] *Department of Chemistry, Universiti Brunei Darussalam, Jalan Tungku Link, Bandar Seri Begawan, BE 1410, Negara Brunei Darussalam*
[b] *Department of Chemistry, The University of Queensland, Brisbane 4072, Australia*

Received 7 June 2004; accepted 27 July 2004
Available online 12 September 2004

Abstract

New tin(IV) complexes of empirical formula, Sn(NNS)I_3 (NNS = anionic forms of the 2-quinolinecarboxaldehyde Schiff bases of *S*-methyl- and *S*-benzyldithiocarbazate) have been prepared and characterized by a variety of physico-chemical techniques. In the solid state, the Schiff bases exist as the thione tautomer but in solution and in the presence of tin(IV) iodide they convert to the thiol tautomer and coordinate to the tin atom in their deprotonated thiolate forms. The structures of the free ligand, Hqaldsbz and its triiodotin(IV) complex, [Sn(qaldsbz)I_3] have been determined by X-ray diffraction. The complex, [Sn(qaldsbz)I_3] has a distorted octahedral structure with the Schiff base coordinated to the tin atom as a uninegatively charged tridentate chelating agent via the quinoline nitrogen atom, the azomethine nitrogen atom and the thiolate sulfur atom. The three iodo ligands are coordinated meridionally to the tin atom. The distortion from an ideal octahedral geometry of [Sn(qaldsbz)I_3] is attributed to the restricted bite size of the tridentate Schiff base ligand.
© 2004 Elsevier Ltd. All rights reserved.

Keywords: Tin(IV) complexes; Dithiocarbazates; 2-Quinolinecarboxaldehyde Schiff bases of *S*-alkyl/aryl dithiocarbazates

1. Introduction

Interest in metal complexes of Schiff bases derived from *S*-alkyl- and *S*-aryl esters of dithiocarbazic acid [1–10] has been stimulated by their interesting physico-chemical properties [3–5] and potentially useful biological activities [6–10]. However, in the past, most work on dithiocarbazates involved their complexes with transition metal ions. Complexes of these ligands with non-transition metal ions such as tin have not received as much attention. In view of the importance of tin compounds in medicinal chemistry and biotechnology [11] and as part of our ongoing work on metal-dithiocarbazates, we report here two new tin(IV) complexes of the 2-quinolinecarboxaldehyde Schiff bases of *S*-methyl- and *S*-benzyl esters of dithiocarbazic acid together with the

* Corresponding author. Tel.: +673 2 2463001x1341; fax: +673 2 461502.
E-mail address: akbar@fos.ubd.edu.bn (M.A. Ali).

0277-5387/$ - see front matter © 2004 Elsevier Ltd. All rights reserved.
doi:10.1016/j.poly.2004.07.015

X-ray crystal structures of the Schiff base, Hqaldsbz and its tin(IV) complex, [Sn(qaldsbz)I_3].

2. Experimental

2.1. Reagents

All chemicals were of analytical reagent grades and used without any further purification. 2-Quinolinecarboxaldehyde was purchased from the Aldrich Chemical Company and tin(IV) iodide was prepared according to the published procedure [17]. Microanalyses for C, H and N were performed by the Elemental Analysis Laboratory, National University of Singapore, Singapore. Molar conductances of ca. 10^{-3} M solutions of the complexes in either DMSO or CH_2Cl_2 were measured by means of a Jenway 4310 conductivity meter. The IR spectra in KBr discs and the electronic spectra either as Nujol mulls or in solution were recorded on a Perkin–Elmer 2000 FT IR spectrometer and a Shimadzu MPC-3100 spectrophotometer, respectively. The ^1H and ^{13}C NMR spectra of the Schiff bases were run in DMSO-d_6 on a Bruker Advance DPX 300K FT NMR spectrometer whereas the ^1H NMR spectra of the tin(IV) complexes were run in $CDCl_3$ on a Bruker DPX 300 MHz spectrometer using TMS as an internal standard.

2.2. Preparation of the ligands

2-Quinolinecarboxaldehyde (0.79 g; 0.01 mol) was dissolved in boiling ethanol (30 ml) and the solution mixed with a solution of the appropriate *S*-alkyldithiocarbazate (0.01 mol; 1.22 g of *S*-methyldithiocarbazate or 1.74 g of *S*-benzyldithiocarbazate) in methanol (35 ml). The mixture was heated on a water bath for ca. 30 min and then left to stand overnight. The yellow product that had formed was filtered off, washed with cold ethanol, dried in a desiccator over silica gel and then recrystallized from chloroform. Yield: Hqaldsbz: 54.3%; m.p. 184–186 °C. Calc. for $C_{18}H_{15}N_3S_2$: C, 64.07; H, 4.48; N, 12.45. Found: C, 64.20; H, 5.11, N, 12.33%. Hqaldsme: Yield: 85.6%; m.p. 194–195 °C. Calc. for $C_{12}H_{11}N_3S_2$: C, 55.15; H, 4.24; N, 16.08. Found: C, 55.20, H, 4.61; N, 16.70%.

2.3. Preparation of the complexes

Tin(IV) iodide (1 mmol; 0.626 g) dissolved in boiling abs. ethanol (20 ml) was mixed with a hot solution of the appropriate Schiff base (1 mmol; 0.337 g of *S*-benzyldithiocarbazate or 0.261 g of *S*-methyldithiocarbazate) in the same solvent (30 ml) and the mixture was then refluxed for one hour. On cooling to room temperature, crystals of the tin complexes were obtained which were filtered off, washed with cold ethanol and dried in a desiccator over silica gel. Yield: 50–60%. Crystals of [Sn(qaldsbz)I_3] suitable for X-ray analysis were obtained during preparation of the complex: [Sn(qaldsbz)I_3]: Calc. for $C_{18}H_{14}N_3S_2SnI_3$: C, 25.87; H, 1.69; N, 5.03. Found: C, 25.73; H, 2.01; N, 5.22%. [Sn(qaldsme)I_3]: Calc. for $C_{12}H_{10}N_3S_2SnI_3$: C, 19.00; H, 1.33; N, 5.53. Found: C, 18.89; H, 1.25; N, 5.38%.

2.4. Crystallography

Cell constants were determined by a least-squares fit to the setting parameters of 25 independent reflections, measured on an Enraf–Nonius CAD 4 four-circle diffractometer using graphite monochromated Mo Kα radiation (0.71073 Å) and operating in the ω–2θ mode within the range $2 < 2\theta < 50°$. Empirical absorption correction (ψ scans) and data reduction were performed with the WINGX [18] suite of programmes. The structures were solved by direct methods with SHELX86 and refined by full-matrix least-squares analysis with SHELXL97 [19]. Non-hydrogen atoms were refined with anisotropic thermal parameters whereas H-atoms were included at estimated positions. Despite absorption correction, significant electron density remained close to the I and Sn atoms in the structure of [Sn(qaldsbz)I_3]. Drawings of each molecule were produced with ORTEP3 [20] or PLUTON [21]. A summary of the crystal data, structure solution and refinement parameters are given in Table 1 and selected bond lengths appear in Tables 4 and 5.

3. Results and discussion

Like thiosemicarbazones and all other Schiff bases derived from *S*-alkyl/aryldithiocarbazates, the 2-quinolinecarboxaldehyde Schiff bases of *S*-methyl- and *S*-benzyldithiocarbazate (Fig. 1(a); R = –SCH_3, *S*-$CH_2C_6H_5$) are also capable of exhibiting thione (**1a**)- thiol (**1b**) tautomerism since they contain the thioamide, -NH–C(=S)S functional group.

However, their IR spectra (Table 2) exhibit broad and weak bands in the 3087–2784 cm^{-1} range attributable to the *sec* NH group of the thione form. The spectra do not show any band at ca. 2700 cm^{-1} that can be assigned to $\bar{\nu}_{SH}$ indicating that, in the solid state, they remain solely as the thione tautomer. However, in solution, they could exist as an equilibrium mixture of both the thione and thiol tautomers. The ^1H NMR spectra of the Schiff bases in DMSO-d_6 (Table 3) show a broad signal at ca. 13.60 ppm attributable to the resonance of the *sec* N(1)H proton. The appearance of the –NH– signal at ~13 ppm and the absence of any signal at ca. 4.00 ppm due to the -SH proton, indicate that in DMSO, both the Schiff bases remain in their thione

Table 1
Crystallographic data

	Hqaldsbz	[Sn(qaldsbz)I_3]
Formula	$C_{18}H_{15}N_3S_2$	$C_{18}H_{14}I_3N_3S_2Sn$
Formula weight	337.45	835.83
Temperature (K)	296	296
Wavelength (Å)	0.71073	0.71073
Crystal system	orthorhombic	triclinic
Space group	$P2_12_12_1$	$P\bar{1}$
Unit cell dimensions		
a (Å)	6.9000(7)	7.518(1)
b (Å)	14.983(3)	10.253(1)
c (Å)	16.521(3)	15.543(3)
α (°)	86.54(1)	
β (°)	86.78(1)	
γ (°)	74.67(1)	
Volume (Å^3)	1708.0(5)	1152.3(3)
Z	4	2
D_{calc} (g cm^{-3})	1.312	2.409
Absorption coefficient (mm^{-1})	0.314	5.318
F(0 0 0)	704	768
Reflections collected	2342	4359
Independent reflections	2164 [R_{int} = 0.0378]	4020 [R_{int} = 0.1103]
Observed reflections [$I > 2\sigma(I)$]	857	1962
Parameters	209	234
Goodness-of-fit on F^2	0.974	0.957
$R_1[I > 2\sigma(I)]$	0.0493	0.0798
w_2 (all data)	0.1116	0.2494
Flack parameter	−0.4(2)	–

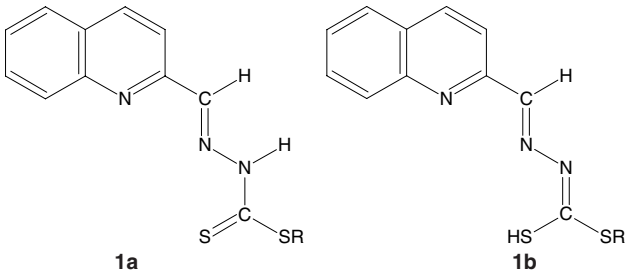

Fig. 1. The thione and thiol forms of the ligands (**1a** – R = CH_3, $CH_2C_6H_5$; thione form), (**1b** – R = CH_3, $CH_2C_6H_5$; thiol form).

forms. The presence of the N(H) signal at ca. 13.60 ppm in the ^{1}H NMR spectra of the Schiff bases also indicates that both Schiff bases remain as the Z isomer with the hydrogen atom on N(1) being intramolecularly H-bonded with the quinoline nitrogen atom similar to that observed in the related 1-quinolinecarboxaldehydethiosemicarbazone [22]. In ethanolic solutions and in the presence of tin(IV) iodide, the ligands quickly convert to the thiol forms with the concomitant formation of tin(IV) complexes of their deprotonated thiolate forms. The ready conversion of a thione tautomer to a thiol form in the presence of a metal ion has been found to be a common property of most Schiff bases derived from *S*-alkyl- and *S*-aryldithiocarbazates [1–10]. Thiosemicarbazones, which are structurally similar to Schiff bases derived from *S*-alkyl- and *S*-aryldithiocarbazates, on the other hand, do not always deprotonate in the presence of metal ions and consequently, complexes of both protonated [18] and deprotonated [19] forms of these ligands have been prepared in neutral media. There are also interesting examples of metal complexes in which both protonated and deprotonated forms of a thiosemicarbazone ligand have been found to be present in the same complex [29]. In contrast with thiosemicarbazones, Schiff bases derived from *S*-alkyl/aryl esters of dithiocarbazic acid, almost invariably coordinate in their deprotonated forms even in the presence of mineral acids.

When tin(IV) iodide was allowed to react with the Schiff bases in boiling abs. ethanol, crystalline tin(IV) complexes of empirical formula, [Sn(NNS)I_3] (NNS = anionic form of the Schiff bases) were readily obtained. These compounds are quite stable at ambient temperature. They are sparingly soluble in weak-donor solvents such as acetonitrile, chloroform and dichloromethane but dissolve readily in donor solvents like DMSO. The molar conductance of Sn(qaldsme)I_3 in dichloromethane is 0.80 Ω^{-1} cm^2 mol^{-1} indicating that it is essentially a non-electrolyte in this solvent [30]. The [Sn(qaldsbz)I_3]

Table 2
IR and electronic spectral data

Compound	IR				UV spectra[a] in CH_2Cl_2 λ_{max} (nm)
	$\bar{\nu}_{NH}$	$\bar{\nu}_{C=N}$	$\bar{\nu}_{N-N}$	$\bar{\nu}_{CSS}$	
Hqaldsme	3087br, w 2918br, w 2784br, w	1617m	1050s	899s	390sh, 360(4.72), 345(4.70), 297(4.52), 247(4.68)
Hqaldsbz	3087br, w 2930br, w 2806br, w	1617m	1047s	901s	385(4.9), 362(5.1), 346(5.0), ca. 325sh, 298(5.0), 252(5.2), 226(5.1)
[Sn(qaldsme)I_3]	–	1585m	1089s	908s, ca. 900sh	[403, 313, ca. 263sh, 203][b]
[Sn(qaldsbz)I_3]	–	1600 1586m	1085s	934s, ca. 925sh	400(4.6), 312(4.3), 260sh, 227(4.8)

[a] Log ε (mol^{-1} dm^3 cm^{-1}) in parentheses.
[b] Spectra run as a saturated solution.

Table 3
NMR spectral data for the Schiff bases and their tin(IV) complexes[a]

Compound	^{1}H NMR				^{13}C NMR			
	–NH–	–CH=N–	quinoline and/or phenyl	–SCH_2/SCH_3	–C=S	–CH=N–	quinoline and/or phenyl	SCH_2/SCH_3
Hqaldsme	13.60 (s, 1H)	8.42 (s, 1H)	8.40 (m, 1H)	2.57 (s, 3H)	200.6	153.7	148.3, 147.2, 137.8, 131.1, 129.8, 128.9 128.5, 118.1	17.8
		7.95–8.10 (m, 3H) 7.75–7.85 (m, 1H) 7.60–7.70 (m, 1H)						
Hqaldsbz	13.65 (s, 1H)	8.40 (s, 1H)	8.36–8.39 (m, 1H)	4.53 (s, 2H)	198.7	153.6	148.3, 147.5 137.8, 137.4 131.1, 130.2, 129.8, 129.4, 128.9, 128.5, 128.2	38.7
		8.00–8.05(m, 3H) 7.76–7.97(t, 1H) 7.61–7.66(t, 1H) 7.44–7.46(m, 2H) 7.25–7.37(m, 3H)						
[Sn(qaldsme)I_3]	–	8.50 (s, 1H)	9.99(d, 1H), 8.63(d, 1H)	2.76 (s, 3H)	–	–	–	–
		8.09–8.14(d, 1H) 8.09–8.14(d, 1H) 7.88–7.95(dd, 1H)						
[Sn(qaldsbz)I_3]	–	8.52 (s, 1H) 8.23–8.29 (dd, 1H) 8.13 (d, 1H),9.99 (d, 1H) 7.90–7.96 (dd, 1H) 7.86 (d, 1H) 7.30–7.45 (m, 5H)	8.64(d, 1H)	4.64 (s, 2H)	–	–	–	–

[a] Because of insufficient solubilities of [Sn(qaldsme)I_3] and [Sn(qaldsbz)I_3] in $CDCl_3$, their ^{13}C NMR spectra could not be recorded in this solvent.

complex was not sufficiently soluble in dichloromethane and so its conductance in this solvent could not be measured. The very low conductance of [Sn(qaldsme)I_3] in dichloromethane is strong evidence that the Schiff base is coordinated to the tin atom as a uninegatively charged ligand and that the three iodo ligands are also coordinated to the tin ion. The complexes, [Sn(qaldsme)I_3] and [Sn(qaldsbz)I_3] however, exhibit molar conductance values 100.5 and 101.0 $\Omega^{-1}\,cm^2\,mol^{-1}$, respectively, in DMSO indicating that there is extensive dissociation of these complexes in DMSO [30]. The high conductances of these complexes in DMSO lend further support to the NMR results (see later) that extensive solvolysis of the complexes occurs in this solvent.

Relevant IR spectral bands of the ligands and their tin complexes together with their assignments are given in Table 2. A comparison of the IR spectra of the ligands with those of their tin complexes indicate that the $\bar{\nu}_{NH}$ bands of the free ligands are absent in the spectra of the complexes supporting deprotonation of the ligand during coordination with the tin ion. The $\bar{\nu}_{C=N}$ bands of the free ligands at 1617 cm^{-1} are shifted to lower wavenumbers (1600–1585 cm^{-1}) in the spectra of the complexes indicating coordination of the ligand to the tin ion via the azomethine nitrogen atoms. Additional support in favor of coordination of the azomethine nitrogen atom to tin is provided by the shift of the $\bar{\nu}_{N-N}$ bands of the free ligands at 1050–1047 cm^{-1} to higher frequency (1089–1085 cm^{-1}) in the spectra of the complexes [31]. The positive shift of the $\bar{\nu}_{N-N}$ band upon coordination with the tin ion is a consequence of the reduction of repulsion between lone pairs of electrons on the nitrogen atoms. The splitting of the $\bar{\nu}_{aCSS}$ band of the ligand at ca. 900 cm^{-1} in the spectra of the complexes indicates coordination of the ligands to the tin ion via one of the sulfur atoms [32].

The electronic spectral data of the Schiff bases and their tin(IV) complexes in dichloromethane are shown in Table 2. The spectra of the ligands exhibit five bands at ~390, 360, 345, 297 and 252 nm of which the band at ca. 390 nm of the free ligands shows a bathochromic shift in the spectra of the complexes and those at ca. 360 and 346 nm disappear in the spectra of the complexes. The electronic spectra of the present tin complexes do not exhibit any band which can be attributed to ligand-to-metal charge transfer transitions. Electronic spectra of metal complexes of Schiff bases derived from *S*-alkyl/aryl esters of dithiocarbazic acid and thiosemicarbazones, invariably exhibit a ligand-to-metal charge transfer (S → M) band [24]. The absence of such a band in the electronic spectra of the present tin(IV) complexes suggests that the metal center is not easily

reduced, i.e. the metal centered orbitals are not accessible by the electrons on the sulfur atom of the ligands.

The ^{1}H and ^{13}C NMR spectral data for the ligands in DMSO-d_6, together with the assignments of the relevant signals, are compiled in Table 3. Because of extensive dissociation of the [Sn(qaldsme)I_3] and [Sn(qaldsbz)I_3] complexes in DMSO, as indicated by the conductance results discussed above, the NMR spepctra of these complexes were recorded in $CDCl_3$. The ^{1}H NMR spectra of the complexes do not contain the signals due to the -NH- protons of the free ligands lending further support to the IR and conductivity results that the ligands are coordinated to the tin atoms in their deprotonated forms. The ^{1}H NMR spectra of the complexes also exhibit downfield shift of the azomethine protons because of the coordination of the ligands via the azomethine nitrogen atom. The quinoline ring protons also exhibit shifts in the complexes relative to that in the free ligands as a result of coordination via the quinoline ring nitrogen atom.

3.1. The crystal structure of Hqaldsbz

A view of the free ligand Hqaldsbz is shown in Fig. 2. The dithiocarbazate moiety shows *E* configurations about the C(1)–N(1), N(1)–N(2) and C(2)–N(2) bonds similar to that exhibited by most semicarbazones [36–38] and thiosemicarbazones [39–41]. The compound contains two planar fragments viz. the quinoline and dithiocarbazate moiety. The planarity in the dithiocarbazate chain is revealed by all dihedral angles along the S(2)–C(1)–N(1)–N(2)–C(2)–C(3) chain being within 2° of 180° (or 0°). All atoms in the quinoline group and those along the S(2)–C(1)–N(1)–N(2)–C(2) chain lie within 0.05 Å of the least-squares plane. The only significant deviations in the dihedral angles from planarity involve the phenyl-methylene bond viz. S(2)–C(12)–C(13)–C(18) 79.8(9)°, which orients the phenyl ring almost orthogonally relative to the best plane defined by the remaining atoms in the molecule.

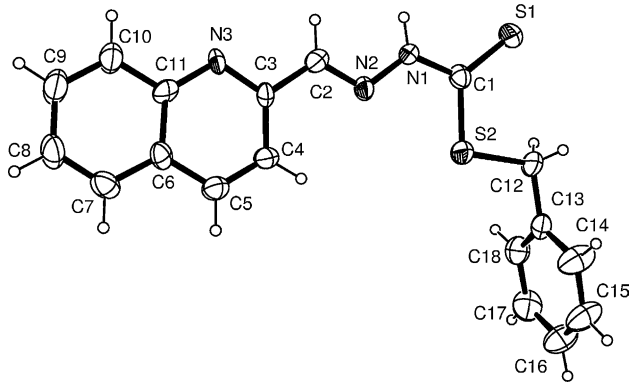

Fig. 2. ORTEP drawing of Hqaldsbz (30% probability ellipsoids).

The bond lengths in the dithiocarbazate chain [NNCSSCH$_2$Ph] (Table 4) are similar to those observed in free dithiocarbazates [31] except that the C(1)–S(1) bond length [1.622(7) Å] (Table 4) in this compound is by far the shortest value observed in this class of ligands indicating that the C–S bond is very close to a double bond and that there is minimal electron delocalization in the C–S bond compared to those in related ligands. However, the C–S bond length still has an intermediate value between 1.82 Å for a single bond and 1.56 Å for a C=S double bond [45]. The C(2)–N(2) distance [1.287(8) Å] corresponds to a double bond whereas the C(1)–N(1) distance [1.352(8) Å] indicates some double bond character. A comparison of the N–N distance [1.372(7) Å] with that in *S*-benzyldithiocarbazate [46] shows that the bond is shorter than a single N–N bond [1.44 Å] indicating that a significant π-charge delocalization occurs along the CNNC moiety. In contrast with *S*-benzyldithiocarbazate, Hqaldsbz has an extensively delocalized group attached to the imino nitrogen atom N(2). The inclusion of resonance forms including the quinoline ring in the ligand would account for the shortening of the N–N distance through extensive electron delocalization.

As is usual in free unsubstituted thiosemicarbazides and *S*-alkyldithiocarbazates, the S atom in Hqaldsbz is *trans* to the azomethine nitrogen atom. The quinoline nitrogen atom and the azomethine nitrogen atoms are also *trans* to each other. Therefore, the configuration of the ligand as observed in the solid state is ill-suited for its coordination with a metal ion as an NNS

Table 4
Selected bond lengths (Å) and angles (°) for Hqaldsbz

Bond lengths (Å)	
C(1)–N(1)	1.352(8)
C(1)–S(2)	1.761(7)
C(12)–S(2)	1.818(7)
C(2)–C(3)	1.450(9)
C(1)–S(1)	1.622(7)
C(12)–C(13)	1.518(9)
C(2)–N(2)	1.287(8)
N(1)–N(2)	1.372(7)
Bond angles (°)	
N(1)–C(1)–S(1)	120.9(6)
S(1)–C(1)–S(2)	126.6(5)
N(2)–C(2)–C(3)	119.0(7)
N(3)–C(3)–C(2)	113.6(7)
C(12)–S(2)–C(1)	99.0(4)
N(1)–N(2)–C(2)	115.9(6)
N(1)–C(1)–S(2)	112.5(5)
C(13)–C(12)–S(2)	110.3(5)
N(3)–C(3)–C(4)	123.9(7)
C(4)–C(3)–C(2)	122.5(7)
C(1)–N(1)–N(2)	122.2(6)
C(12)–C(13)–C(18)	122.1(9)

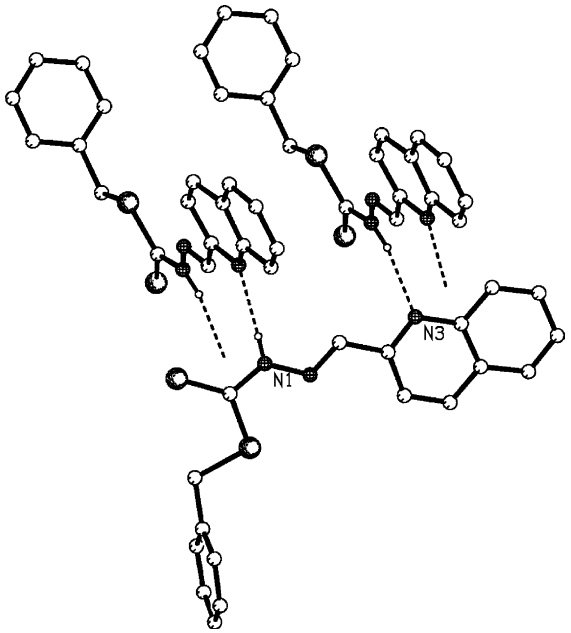

Fig. 3. PLUTON drawing of Hqaldsbz showing the H-bonded chain (amide H-atom shown only).

tridentate chelating agent. However, rotation of the S(2)C(1)S(1) fragment by 180° about the C(1)–N(1) bond and a simultaneous rotation of the quinoline ring by 180° about the C(2)–C(3) bond can place the S(1) atom, the N(2) atom and the quinoline N(3) atom all in the same side thus enabling the ligand to function as an NNS tridentate chelating agent as found for other tridentate thiosemicarbazones [47] and Schiff bases derived from *S*-alkyl/aryl esters of dithiocarbazic acid [35].

A notable feature of the crystal structure of Hqaldsbz is the formation of an intermolecular, H-bonded chain linked through the quinoline nitrogen and the amide NH of an adjacent ligand (N(1)–H(1)···N(3)′ 2.17 Å, 169°, symmetry operation $x + 1/2, -y + 3/2, -z + 1$) (Fig. 3).

3.2. The crystal structure of [Sn(qaldsbz)I_3]

The structure of the [Sn(qaldsbz)I_3] complex, together with atom numbering scheme adopted is depicted in Fig. 4 and selected bond lengths and angles are compiled in Table 5. The structure shows that the complex is

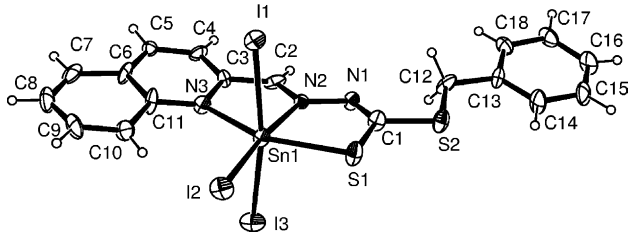

Fig. 4. ORTEP drawing of [Sn(qaldsbz)I_3] (30% probability ellipsoids).

Table 5
Selected bond lengths and bond angles for [Sn(qaldsbz)I_3]

Bond lengths (Å)	
Sn(1)–N(3)	2.377(18)
Sn(1)–I(3)	2.824(2)
Sn(1)–I(2)	2.752(2)
C(2)–C(3)	1.42(3)
N(2)–N(1)	1.38(2)
C(1)–S(1)	1.77(2)
Sn(1)–N(2)	2.198(17)
Sn(1)–I(1)	2.790(1)
Sn(1)–S	2.508(6)
C(2)–N(2)	1.30(3)
C(1)–N(1)	1.28(3)
C(1)–S(2)	1.71(2)
Bond angles (°)	
N(2)–Sn(1)–N(3)	72.0(6)
S(1)–Sn(1)–I(1)	96.46(19)
N(3)–Sn(1)–S(1)	149.1(5)
N(2)–Sn(1)–I(3)	87.8(4)
N(3)–Sn(1)–I(3)	83.1(5)
I(2)–Sn(1)–I(3)	93.44(7)
S(1)–Sn(1)–I(2)	95.22(15)
I(1)–Sn(1)–I(3)	166.98(7)
N(3)–Sn(1)–I(1)	83.9(5)
N(2)–Sn(1)–S(1)	77.1(4)
I(2)–Sn(1)–I(1)	92.52(7)
N(2)–Sn(1)–I(2)	172.3(4)
N(3)–Sn(1)–I(2)	115.7(4)
S(1)–Sn(1)–I(3)	94.51(19)
N(2)–Sn(1)–I(1)	87.8(4)

a monomer in which the tin atom adopts a six-coordinate geometry being ligated to three iodide ions, two nitrogen atoms and one sulfur atom. The Schiff base is coordinated to the tin atom as a uninegatively charged chelating agent in its deprotonated thiolate form via the thiolate sulfur atom, the azomethine nitrogen atom and the quinoline nitrogen atom.

There is an extensive delocalization of the negative charge, which is generated upon deprotonation of the ligand, in the C–N–N–C chain as indicated by the intermediate C(2)–N(2) [1.30(3) Å], N(1)–N(2) [1.38(2) Å] and N(1)–C (1) [1.28(3) Å] bond distances. The two Sn–N distances are close to the sum of the non-polar covalent radii 2.15 Å [50] indicating strong tin-nitrogen interaction. However, as found in other tin(IV) complexes of related tridentate thiosemicarbazone ligands [51], the Sn–N_{azom} bond distance [2.198(17) Å] in the present complex is shorter than the Sn–$N_{quinoline}$ distance [2.377(18) Å]. The stronger coordination of the tin atom to the azomethine nitrogen compared with the quinoline nitrogen atom is consistent with the higher basicity of the azomethine nitrogen atom, and also a consequence of the atom being shared by adjacent five-membered chelate rings. The Sn–S distance is longer than the sum of the covalent radii (2.42 Å) but is considerably shorter than the van der Waals radii (4.0 Å) [52]. A comparison of the Sn–S, Sn–$N_{quinoline}$ and Sn–$N_{azom.}$

distances with those for [Sn(pytsc)Cl_3] [51] which also has a distorted octahedral geometry, shows that the lengths of these bonds compare well with those in [Sn(pytsc)Cl_3] although the Sn–S bond in the present complex is slightly weaker than that in [Sn(pytsc)Cl_3] [51]. In the present tin complex, the Schiff base shows an *E* configuration about both the C(2)–N(2) and C(1)–N(1) bonds similar to those in other complexes of related ligands [51]. The C–S bond distance [1.71(2) Å] is slightly longer than that in the free ligand, but caution should be exercised in drawing comparisons due to the poorer precision of this structure compared with that of the free ligand. However, the apparent lengthening of the C–S bond in the complex is consistent with the ene-thiolate resonance form of the ligand being the major contributor.

An examination of the bond angle data for [Sn(qaldsbz)I_3] (Table 5) indicates that the complex has a distorted octahedral structure in which the iodide ions are meridionally coordinated to the tin(IV) ion. The two *trans*-disposed iodo ligands exhibit slightly longer bonds to tin than the remaining iodo ligand, which is *trans* to the azomethine nitrogen atom. A similar difference in the Sn–Cl bond lengths has also been observed in the related six-coordinate tin(IV) complex [$SnCl_3$(pytsc)] whose structure has been determined by X-ray diffraction [51]. The distortion of [Sn(qaldsbz)I_3] from an ideal octahedral geometry is reflected in all the twelve bond angles subtended at the tin atom which show substantial deviation from that required for an ideal octahedral geometry. The largest deviation from ideal values are observed for the angles S(1)–Sn(1)–N(3) [149.1(5)° versus 180°], N(2)–Sn(1)–S(1) [77.1(4)° versus 90°], N(2)–Sn(1)–N(3) [72.0(6)° versus 90°]. The deviation from octahderal geometry is due to the restricted bite size of the ligand.

4. Conclusions

The 2-quinolinecarboxaldehyde Schiff bases of *S*-methyl- and *S*-benzyldithiocarbazates, like most other Schiff bases derived from *S*-alkyl esters of dithiocarbazic acid, remain as the thione tautomer in the solid state, and remain predominantly in this form in solution but, in the presence of tin(IV) iodide they convert to the iminothiol form, deprotonate and coordinate with the tin atom as uninegatively charged NNS tridentate chelating agents with the elimination of HI. The complexes adopt a distorted octahedral geometry as a result of the strain imposed by the five-membered chelate rings, Sn1–N3–C3–C2–N2 and Sn1–N2–N1–C1–S1. They appear stable in the solid state and in solutions of non-donor solvents such as chloroform and dichloromethane but they are extensively dissociated in donor solvents such as DMSO.

5. Supplementary material

Full crystallographic data (CCDC 239922 for Hqaldsbz and CCDC 239923 for [Sn(qaldsbz)I_3] have been deposited at the Cambridge Crystallographic Data Centre and are available on request from the Director, CCDC, 12 Union Road, Cambridge, CB2 1EZ, UK (fax: +44 1223 336033; e-mail: deposit@ccdc.cam.ac.uk or http://www.ccdc.cam.ac.uk).

Acknowledgements

M. Akbar Ali, A.H. Mirza and Malai Haniti thank Universiti Brunei Darussalam for supporting this work.

References

[1] M. Akbar Ali, A.H. Mirza, M. Nazimuddin, R. Ahmed, L.H. Gahan, P.V. Bernhardt, Polyhedron 22 (2003) 1471.
[2] M. Akbar Ali, A.H. Mirza, C.W. Voo, A.L. Tan, P.V. Bernhardt, Polyhedron 22 (2003) 3433, and references cited therein.
[3] A. Abu-Raqabah, G. Davies, M.A. El-Sayed, A. El-Toukhy, S.N. Shaikh, J. Zubeita, Inorg. Chim. Acta 193 (1992) 43.
[4] S. Al-Shehri, G. Davies, M.A. El-Sayed, A. El-Toukhy, Inorg. Chem. 29 (1990) 1198.
[5] M.T.H. Tarafder, N. Saravanan, K.A. Crouse, A.M. Ali, Transit. Met. Chem. 26 (2001) 613.
[6] Yu-Peng Tian, D. Chung-Ying Dian, Xia-Xeng You, T.C.W. Mak, L. Qing, Z. Jian-Ying, Transit. Met. Chem. 23 (1998) 17.
[7] M.T.H. Tarafder, Teng-Jin Khoo, K.A. Crouse, A.M. Ali, Polyhedron 25 (2002) 27.
[8] M.T.H. Tarafder, M.A. Ali, D.J. Wee, K. Azahari, S. Silong, K.A. Crouse, Transit. Met. Chem. 25 (2000) 456.
[9] M. Akbar Ali, S.E. Livingstone, Coord. Chem. Rev. 13 (1974) 101, and refs. therein.
[10] M. Das, S.E. Livingstone, Br. J. Cancer 37 (1978) 101.
[11] D.X. West, S.B. Padhye, P.B. Sonawane, Struct. Bonding (Berlin) 76 (1991) 1.
[12] M. Akbar Ali, A.H. Mirza, R.J. Butcher, M.T.H. Tarafder, Tan B. Keat, A.M. Ali, J. Inorg. Biochem. 92 (2002) 141.
[13] I. Belsky, D. Gerther, A. Ziluka, J. Med. Chem. 1 (1968) 92.
[14] R.H. Holm, in: G.L. Eichorn (Ed.), Inorganic Biochemistry, vol. 2, Elsevier, Amsterdam, 1974, p. 1137.
[15] L. Abrams, N.E. Bjorklund, B. Gustafsson, M. Johnson, Acta Pharmacol. Toxicol. Suppl. 36 (1975) 93.
[16] K. Joshi, V.N. Pathak, P. Pawar, Agric. Biol. Chem. 41 (1977) 543.
[17] T. Moeller, D.C. Edwards, R.L. Brandt, J. KleinbergInorg. Synth., vol. 4, Robert K. Krieger Publishing, Huntington, NY, 1978, p. 119.
[18] L.J. Farrugia, J. Appl. Crystallogr. 32 (1999) 837.
[19] G.M. Sheldrick, SHELX97. Programs for Crystal Structure Analysis, University of Gottingen, Germany, 1997.
[20] L.J. Farrugia, J. Appl. Crystallogr. 30 (1997) 565.
[21] A.L. Spek, Acta Crystallogr., Sect. A 46 (1990) C34.
[22] I. Antonini, F. Claudi, F. Franchetti, S. Martelli, J. Med. Chem. 20 (1970) 447.
[23] R. Gronbaek-Hazell, Acta Chem. Scand. 26 (1972) 1365.
[24] A. Mohan, P. Sharma, N.K. Jha, Inorg. Chim. Acta 106 (1985) 117.
[25] A. Castneiras, R. Carballo, T. Perez, Polyhedron 20 (2001) 441.

[26] D.X. West, T.J. Tomack, A.E. Liberta, Transit. Met. Chem. 17 (1992) 256.
[27] L. Carvalca, M. Nardelli, G. Fava, Acta Crystallogr. 15 (1962) 1139.
[28] J. Valdez- Martinez, A. Sierra-Ramoco, C. Alvarez-Toledano, R.A. Toscano, H. Garcia-Topia, J. Organomet. Chem. 352 (1983) 321.
[29] P. Souza, A.I. Matesanz, V. Fernandez, J. Chem. Soc., Dalton Trans. (1996) 3011.
[30] W.J. Geary, Coord. Chem. Rev. 7 (1971) 81.
[31] R. Ugo, J. Organomet. Chem. 9 (1967) 395.
[32] P. Pelagatti, A. Venturini, A. Leporati, M. Carcelli, M. Costa, A. Bacchi, G. Pelizzi, C. Pelizzi, J. Chem. Soc., Dalton Trans. (1998) 2715.
[33] M. Akbar Ali, S.M.G. Hossain, S.M.M.H. Majumder, M. Nazimuddin, M.T.H. tarafder, Polyhedron 6 (1987) 1653.
[34] E.W. Ainscough, A.M. Brodied, J.D. Ranford, J.M. Waters, J. Chem. Soc., Dalton Trans. (1991) 2125.
[35] A.G. Bingham, H. Bogge, A. Muller, E.W. Ainscough, A.M. Brodie, J. Chem. Soc., Dalton Trans. (1987) 493.
[36] G.D. Andretti, P. Domino, G. Fava, M. Nardelli, P. Sagarbotto, Acta Crystallogr., Sect. B 26 (1970) 1005.
[37] M. Czulger, A. Kalman, G. Argay, Cryst. Struct. Commun. 2 (1973) 655.
[38] A. Kalman, G. Argay, M. Czulger, Cryst. Struct. Commun. 1 (1972) 375.
[39] M. Mathew, G.J. Palenik, Acta Crystallogr., Sect. B 27 (1971) 59.
[40] R. Restivo, G.J. Palenik, Acta Crystallogr., Sect. B 26 (1970) 1397.
[41] E.J. Gabe, M.R. Taylor, J.P. Glusker, J.A. Minkin, A.L. Patterson, Acta Crystallogr., Sect. B 25 (1969) 1620.
[42] M. Akbar Ali, A.H. Mirza, R.J. Butcher, Polyhedron 20 (2001) 1037.
[43] Yu-Peng Tian, Chun-Ying Duan, Zhong-Lin Lu, Xiao-Zeng You, Hong-Kun Fun, S. Kandasamy, Polyhedron 15 (1996) 2263.
[44] M.T.H. Tarafder, Teng-Jin Khoo, K.A. Crouse, A.M. Ali, B.M. Yamin, H.-K. Fun, Polyhedron 21 (2002) 2691.
[45] L.E. Sutton, Tables of Interatomic Distances & Configurations in Molecules and Ions Supplement, The Chemical Society, London, 1965.
[46] S.S.S. Raj, B.M. Yamin, Y.A. Yusof, M.T.H. Tarafder, H.-K. Fun, K.A. Crousre, Acta Crystallogr., Sect. C 56 (2000) 1236.
[47] J.S. Casas, A. Castíneiras, M.C. Rodríguez-Argüelles, A. Sánchez, S. Sordo, A. Vázquez-López, E.M. Vázquez-López, J. Chem. Soc., Dalton Trans. (2000) 2267.
[48] M. Akbar Ali, R.J. Butcher, J.C. Bryan, Inorg. Chim. Acta 287 (1999) 8.
[49] M. Akbar Ali, S.M.M.H. Majumder, R.J. Butcher, J.P. Jasinski, J.M. Jasinski, Polyhedron 16 (1997) 2794.
[50] R.T. Sanderson, Inorganic Chemistry, Reinhold, New York, 1967, p. 74.
[51] R.S. Barbieri, H.O. Beraldo, C.A.L. Filgueiras, A. Abras, J.F. Nixon, P.B. Hitchcock, Inorg. Chim. Acta 206 (1993) 169.
[52] A. Bondi, J. Phys. Chem. 68 (1964) 441.

Available online at www.sciencedirect.com
SCIENCE DIRECT®
Polyhedron 23 (2004) 2413–2425
POLYHEDRON
www.elsevier.com/locate/poly

Crystalline hydrates and polymeric Ag(I) complexes of isomeric flexible double betaines 1,4-bis(*n*-picolyloxyl)benzene-*N*,*N*′-diacetate (*n* = 2,3,4)

Lin-Ping Zhang, Chi-Keung Lam, Hai-Bin Song, Thomas C.W. Mak *

Department of Chemistry, The Chinese University of Hong Kong, Shatin, New Territories, Hong Kong SAR, PR China

Received 11 May 2004; accepted 2 August 2004
Available online 11 September 2004

Abstract

The isomeric flexible double betaines 1,4-bis(2-picolyloxyl)benzene-*N*,*N*′-diacetate (L^1), 1,4-bis(3-picolyloxyl)benzene-*N*,*N*′-diacetate (L^2) and 1,4-bis(4-picolyloxyl)benzene-*N*,*N*′-diacetate (L^3) were used to react with $AgNO_3$, affording coordination polymeric complexes $\{[Ag_2L^1](NO_3)_2 \cdot 3.5H_2O\}_n$ (**1**), $\{[Ag_2L^1](NO_3)_2 \cdot 6H_2O\}_n$ (**2**) and $\{[Ag_3L^3](NO_3)_3 \cdot 3H_2O\}_n$ (**3**). The crystal structures of the betaine hydrates $L^1 \cdot 8H_2O$, $L^2 \cdot 6H_2O$, $L^3 \cdot 5H_2O$ and the silver(I) complexes have been determined. $L^1 \cdot 8H_2O$ consists of a hydrogen-bonded three-dimensional network, whereas both $L^2 \cdot 6H_2O$ and $L^3 \cdot 5H_2O$ feature hydrogen bonded two-dimensional frameworks. In complex **1**, the Ag(I) ions in the dimeric unit have different coordination environments; through the linkage of L^1 ligands and nitrates, the dimeric units are extended into a polymeric double chain. In complex **2**, each Ag(I) ion of the centrosymmetric dimeric unit adopts a severely distorted tetrahedral coordination geometry; the dimeric subunits are connected by the L^2 ligands, giving an infinite one-dimensional chain, and the chains are further connected through hydrogen bonding to generate an infinite three-dimensional network. In complex **3**, three Ag(I) ions constitute an isosceles triangle consolidated by weak Ag···Ag interactions, and such trinuclear subunits are further connected by the L^3 ligands, nitrate ions and water molecules through coordination and hydrogen bonding, yielding a three-dimensional network.
© 2004 Elsevier Ltd. All rights reserved.

Keywords: Carboxylate; Coordination polymer; Double betaine; Hydrate; Hydrogen bonding; π–π Interaction; Silver nitrate

1. Introduction

Supramolecular assembly has been employed as a powerful tool in the design of metallo-organic based complex molecular architectures [1]. Furthermore, strong, selective and directional hydrogen bonding and π–π interactions have been fully exploited for the generation of metal-organic complexes, and molecular recognition associated with biological activity and the crystal engineering of molecular solids have attracted much recent attention [2]. For some time we have been engaged in the investigation of inorganic polymeric structures using various double betaine ligands each comprising two carboxylate betaine moieties [3]. Recent studies have shown that the variation of double betaine ligands regarding the type of bridging units, the flexibility of the molecular backbone, conformational preference, as well as the metal ions and counter ions employed, has a profound influence on the polymeric structures obtained [4]. In the present work, we report three isomeric double betaine ligands: 1,4-bis(2-picolyloxyl)benzene-*N*,*N*′-diacetate (L^1) [5], 1,4-bis(3-picolyloxyl)benzene-*N*,*N*′-diacetate (L^2) [6] and 1,4-bis(4-picolyloxyl)benzene-*N*,*N*′-diacetate (L^3) (Scheme 1) and determined the structures of their crystalline hydrates $L^1 \cdot 8H_2O$,

* Corresponding author. Tel.: +852 2609 6279; fax: +852 2603 5057.
E-mail address: tcwmak@cuhk.edu.hk (T.C.W. Mak).

0277-5387/$ - see front matter © 2004 Elsevier Ltd. All rights reserved.
doi:10.1016/j.poly.2004.08.002

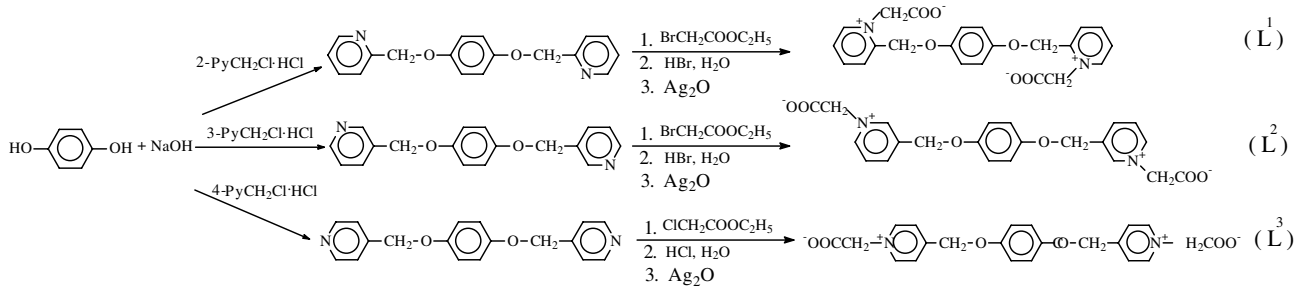

Scheme 1. Synthesis procedure for isomeric ligands.

$L^2 \cdot 6H_2O$ and $L^3 \cdot 5H_2O$ by single crystal X-ray analysis. As Ag(I) is known to exhibit flexible coordination geometries (linear, bent, trigonal planar, T-shaped, tetrahedral, trigonal pyramidal) in its complexes with polydentate ligands [7], we decided to study the coordination behavior of the isomeric double betaine ligands through the synthesis and structural characterization of their silver(I) complexes $\{[Ag_2L^1](NO_3)_2 \cdot 3.5H_2O\}_n$ (**1**), $\{[Ag_2L^2](NO_3)_2 \cdot 6H_2O\}_n$ (**2**) and $\{[Ag_3L^3](NO_3)_3 \cdot 3H_2O\}_n$ (**3**).

Although complex **2** and **3** were synthesized by the same procedure as that for complex **1**, the products differ in regard to their silver(I) coordination modes and overall structures, which may be attributed to the different positions of the betaine moieties in the relevant ligands. Complex **1** and **2** are both binuclear polymers, which are bridged by the carboxylate group in the common *syn–syn* bidentate mode [8]. However complex **3** is trinuclear, being bridged by the carboxylate group in the tridentate μ-*O*,*O*′$_{syn}$-μ-*O*,*O* mode [8].

2. Experimental

2.1. General

All chemicals were obtained commercially (Aldrich) and used without further purification. Elemental analyses of C, H and N were performed by the MEDAC LTD Vrunel Science Centre, United Kingdom. IR spectra were recorded with a Nicolet Impact 420 FT-IR spectrometer using KBr pellets. ^{1}H NMR spectra were taken at 300 Hz with a Bruker-300 spectrometer using D_2O as solvent.

2.2. Synthesis of the hydrate of 1,4-bis(2-picolyloxyl)benzene-N,N′-diacetate ($L^1 \cdot 8H_2O$)

We have reported the synthesis of 1,4-bis(2-picolyloxyl)benzene-*N*,*N*′-diacetate (L^1) previously (Scheme 1) [5]. The light yellow hydrate $L^1 \cdot 8H_2O$ is obtained by re-crystallization of the dehydrated solid of L^1 in water. *Anal.* Calc. for $C_{22}H_{20}N_2O_6 \cdot 8H_2O$: C, 47.82; H, 6.57; N, 5.07. Found: C, 47.69; H, 6.37; N, 5.13%. IR (KBr, cm^{-1}): 3472 brs, 3074 w, 1635 s, 1512 s, 1444 s, 1372 s, 1239 s, 1211 m, 1072 m, 818 m, 775 w, 718 w. ^{1}H NMR (300 Hz, D_2O): δ 5.20 (s, 4H), 5.42 (s, 4H), 7.01 (s, 4H), 8.02 (t, 2H), 8.18 (d, 2H), 8.52 (t, 2H), 8.79 (d, 2H) (Table 1).

2.3. Synthesis of the hydrate of 1,4-bis(3-picolyloxyl)benzene-N,N′-diacetate ($L^2 \cdot 6H_2O$)

1,4-Bis(3-picolyloxyl)benzene-*N*,*N*′-diacetate (L^2) [6] was recrystallized in water to obtain $L^2 \cdot 6H_2O$. *Anal.* Calc. for $C_{22}H_{20}N_2O_6 \cdot 6H_2O$: C, 51.16; H, 6.24; N, 5.42. Found: C, 51.19; H, 6.71; N, 5.44%. IR (KBr, cm^{-1}) 3399 brs, 3073 w, 1639 s, 1508 m, 1451 w, 1373 s, 1231 s, 1059 m, 917 w, 809 w, 769 w, 711 w. ^{1}H NMR (300 Hz, D_2O): δ 5.18 (s, 4H), 5.32 (s, 4H), 7.01 (s, 4H), 8.03 (dd, 2H), 8.56 (d, 2H), 8.68 (d, 2H), 8.83 (s, 2H) (Table 1).

2.4. Synthesis of the hydrate of 1,4-bis(4-picolyloxyl)benzene-N,N′-diacetate ($L^3 \cdot 5H_2O$)

This compound was synthesized in the same way as $L^1 \cdot 8H_2O$, but ethyl chloroacetate was used instead of ethyl bromoacetate and 4-picolylchloride hydrochloride

Table 1
^{1}H NMR spectroscopic data for the series of double betaines L^1, L^2 and L^3

Compound	$\delta_{1,3\text{-H}}$	$\delta_{4\text{-CH}_2\text{–}}$	$\delta_{11\text{-CH}_2\text{–}}$	$\delta_{6\text{-H}}$	$\delta_{7\text{-H}}$	$\delta_{8\text{-H}}$	$\delta_{9\text{-H}}$	$\delta_{10\text{-H}}$
L^1	7.01	5.42	5.20		8.79	8.52	8.02	8.18
L^2	7.01	5.32	5.18	8.83		8.68	8.03	8.56
L^3	7.01	5.43	5.15	8.06	8.66		8.66	8.06

instead of 2-picolylchloride hydrochloride. *Anal.* Calc. for $C_{22}H_{20}N_2O_6 \cdot 5H_2O$: C, 53.01; H, 6.07; N, 5.62. Found: C, 52.80; H, 5.76; N, 5.64%. IR (KBr, cm^{-1}) 3419 brs, 3073 w, 1641 s, 1512 m, 1441 w, 1373 s, 1228 m, 1062 m, 897 w, 829 w, 729 w. ^{1}HNMR (300Hz, D_2O): δ 5.15 (s, 4H), 5.43 (s, 4H), 7.01 (s, 4H), 8.06 (d, 4H), 8.66 (d, 4H) (Table 1).

2.5. Synthesis of $\{[Ag_2L^1](NO_3)_2 \cdot 3.5H_2O\}_n$ (1)

Aqueous solutions of L^1 (dehydrated) (6 ml; 0.08 g, 0.2 mmol) and $AgNO_3$ (4 ml; 0.17 g, 1 mmol) were mixed together and heated at 70 °C for 10 min with continuous stirring, and then filtered. Upon slow evaporation of the filtrate at room temperature, light yellow needle-shaped crystals of **1** were obtained after several weeks (ca. 46% yield based on L^1). *Anal.* Calc. for $C_{22}H_{27}Ag_2N_4O_{15.5}$: C, 32.57; H, 3.35; N, 6.91. Found: C, 32.69; H, 3.51; N, 6.73%. IR (KBr, cm^{-1}): 3429 brs, 3066 w, 1624 s, 1509 m, 1380 s, 1232 m, 1078 w, 910 w, 823 w, 776 w, 715 w, 614 w.

2.6. Synthesis of $\{[Ag_2L^2](NO_3)_2 \cdot 6H_2O\}_n$ (2)

This complex was prepared as colorless needle-like crystals by the procedure described for **1** using L^2 instead of L^1 (ca. 63% yield based on L^2). *Anal.* Calc. for $C_{22}H_{32}Ag_2N_4O_{18}$: C, 30.86; H, 3.77; N, 6.54. Found: C, 30.41; H, 3.46; N, 6.40%. IR (KBr, cm^{-1}): 3432 brs, 3066 w, 1638 s, 1506 m, 1380 s, 1228 m, 1058 w, 910 w, 829 w, 715 w, 628 w.

2.7. Synthesis of $\{[Ag_3L^3](NO_3)_3 \cdot 3H_2O\}_n$ (3)

This complex was prepared as colorless block-like crystals by the procedure described for **1** using L^3 instead of L^1 (ca. 37% yield based on L^3). *Anal.* Calc. for $C_{22}H_{20}Ag_3N_5O_{15}$ (thoroughly dried sample): C, 28.78; H, 2.20; N, 7.63. Found: C, 28.42; H, 2.18; N, 7.34%. IR (KBr, cm^{-1}): 3441 brs, 3046 w, 1633 s, 1508 m, 1381 s, 1232 m, 1058 w, 923 w, 823 w, 715 w, 588 w.

2.8. X-ray crystallography

Intensity data of all compounds were collected on a Bruker SMART 1000 CCD diffractometer with graphite-monochromatized Mo K radiation ($\lambda = 0.71073$ Å) at 293 K [9]. The structures were solved by direct methods and refined by full-matrix least squares based on F^2 using the SHELXTL program package [10]. All the non-hydrogen atoms were refined anisotropically, and the hydrogen atoms were generated geometrically except for those of the water molecules, which were located from the ΔF maps. Complex **3** belongs to non-centric space group $P1$, and the structure is refined as a racemic twin. The crystallographic data of the hydrated ligands and complexes **1**–**3** are summarized in Table 2, and

Table 2
Crystallographic data of hydrated betaines and complexes **1**–**3**

Complex	$L^1 \cdot 8H_2O$	$L^2 \cdot 6H_2O$	$L^3 \cdot 5H_2O$	**1**	**2**	**3**
Empirical formula	$C_{22}H_{36}N_2O_{14}$	$C_{22}H_{32}N_2O_{12}$	$C_{22}H_{30}N_2O_{11}$	$C_{22}H_{27}N_4O_{15.5}Ag_2$	$C_{22}H_{32}N_4O_{18}Ag_2$	$C_{22}H_{26}N_5O_{18}Ag_3$
Formula weight	552.53	516.50	498.48	811.22	856.26	972.09
Crystal size (mm)	$0.64 \times 0.40 \times 0.20$	$0.40 \times 0.03 \times 0.30$	$0.52 \times 0.34 \times 0.32$	$0.24 \times 0.22 \times 0.20$	$0.40 \times 0.20 \times 0.20$	$0.40 \times 0.20 \times 0.10$
Crystal system	triclinic	triclinic	monoclinic	triclinic	monoclinic	triclinic
Space group	$P\bar{1}$ (No. 2)	$P\bar{1}$ (No. 2)	$C2/c$ (No. 15)	$P\bar{1}$ (No. 2)	P_1/c (No. 14)	$P1$ (No. 1)
a (Å)	9.862(4)	4.995(1)	20.581(2)	8.542(2)	5.7407(7)	5.2194(5)
b (Å)	11.981(4)	9.426(2)	9.0156(7)	13.034(4)	16.541(2)	11.069(1)
c (Å)	12.063(4)	13.723(3)	13.2848(9)	14.426(4)	15.913(2)	14.399(1)
α (°)	75.592(8)	83.878(4)	90	64.526(5)	90	73.208(2)
β (°)	80.940(8)	84.934(4)	99.834(2)	78.246(6)	94.749(3)	83.348(2)
γ (°)	89.251(8)	86.101(4)	90	72.686(6)	90	81.145(2)
V (Å^3)	1362.7(8)	638.8(2)	2428.8(3)	1378.9(7)	1505.7(3)	784.7(1)
Z	2	1	4	2	2	1
D_{calc} (g/cm^3)	1.347	1.343	1.363	1.954	1.889	2.057
μ(Mo Kα) (mm^{-1})	0.113	0.110	0.110	1.504	1.389	1.941
F(000)	588	274	1056	810	860	478
Reflections collected	9591	4560	8000	8493	8773	4662
Independent reflections	6468	3055	2925	5656	2954	3803
Observed reflections [$I > 2\sigma(I)$]	3338	1906	1716	3111	1621	2915
Parameters	343	163	164	397	208	443
Goodness-of-fit	1.026	1.008	1.127	0.913	0.8943	0.958
R_1 [$I > 2\sigma(I)$][a]	0.0707	0.0632	0.0569	0.0623	0.0529	0.0527
wR_2 (all data)[b]	0.2253	0.1954	0.1783	0.1729	0.1601	0.1343

[a] $R_1 = \sum||F_o|-|F_c||/\sum|F_o|$.
[b] $wR_2 = [\sum[w(F_o^2 - F_c^2)^2]/\sum[w(F_o^2)^2]]^{1/2}$.

Table 3
Selected bond lengths (Å) and angles (°) for complexes **1**–**3**

*Complex **1***			
Bond lengths			
Ag(1)–O(1)	2.224(5)	Ag(2)–O(8b)	2.660(7)
Ag(1)–O(7)	2.646(5)	Ag(2)–O(9b)	2.698(6)
Ag(1)–O(11)	2.608(7)	O(1)–C(1)	1.232(8)
Ag(1)–O(12)	2.688(8)	O(2)–C(1)	1.260(8)
Ag(1)–O(5a)	2.234(5)	O(5)–C(22)	1.250(8)
Ag(2)–O(2)	2.256(5)	O(6)–C(22)	1.232(8)
Ag(2)–O(6a)	2.253(5)	Ag(2)···Ag(1)	2.873(1)
Bond angles			
O(1)–Ag(1)–O(5a)	165.1(2)	O(6a)–Ag(2)–O(2)	153.9(2)
O(1)–Ag(1)···Ag(2)	84.9(1)	O(6a)–Ag(2)···Ag(1)	82.8(1)
O(2)–Ag(2)–O(8b)	86.6(2)	O(6a)–Ag(2)–O(8b)	114.4(2)
O(2)–Ag(2)–O(9b)	113.7(2)	O(6a)–Ag(2)–O(9b)	92.4(2)
O(8b)–Ag(2)–O(9b)	46.6(2)	O(8b)–Ag(2)–Ag(1)	162.5(1)
O(9b)–Ag(2)–Ag(1)	134.1(1)	O(1)–Ag(1)–O(11)	105.1(2)
O(5a)–Ag(1)–O(11)	88.6(2)	O(1)–Ag(1)–O(7)	95.5(2)
O(5a)–Ag(1)–O(7)	87.7(2)	O(11)–Ag(1)–O(7)	98.8(2)
O(1)–Ag(1)–O(12)	92.1(2)	O(5a)–Ag(1)–O(12)	93.6(2)
O(11)–Ag(1)–O(12)	46.0(2)	O(7)–Ag(1)–O(12)	144.6(2)
O(11)–Ag(1)···Ag(2)	166.7(2)	O(7)–Ag(1)···Ag(2)	88.6(1)
O(12)–Ag(1)···Ag(2)	126.5(1)	O(2)–Ag(2)···Ag(1)	77.8(1)
O(5a)–Ag(1)···Ag(2)	80.6(1)	C(1)–O(2)–Ag(2)	126.0(4)
C(1)–O(1)–Ag(1)	120.1(4)	O(6)–C(22)–O(5)	128.3(6)
O(1)–C(1)–O(2)	128.0(6)	C(22)–O(6)–Ag(2c)	122.2(4)
C(22)–O(5)–Ag(1c)	125.4(4)		
*Complex **2***			
Bond lengths			
Ag(1)–O(1)	2.228(5)	Ag(1)–O(2a)	2.251(4)
Ag(1)–O(1W)	2.378(5)	Ag(1)–O(2W)	2.590(5)
Ag(1)···Ag(1a)	2.826(1)	O(1)–C(1)	1.260(8)
O(2)–C(1)	1.250(8)		
Bond angles			
O(1)–Ag(1)–O(2a)	153.7(2)	O(1)–Ag(1)–O(1W)	105.6(2)
O(2a)–Ag(1)–O(1W)	93.7(2)	O(1)–Ag(1)–O(2W)	97.2(2)
O(2a)–Ag(1)–O(2W)	100.2(2)	O(1W)–Ag(1)–O(2W)	91.1(3)
O(1)–Ag(1)···Ag(1a)	81.5(1)	O(2a)–Ag(1)···Ag(1a)	80.2(1)
O(1W)–Ag(1)···Ag(1a)	172.5(2)	O(2W)–Ag(1)···Ag(1a)	85.8(1)
C(1)–O(1)–Ag(1)	121.8(5)	C(1)–O(2)–Ag(1a)	121.6(4)
O(2)–C(1)–O(1)	126.2(6)		
*Complex **3***			
Bond lengths			
Ag(1)–O(1W)	2.71(2)	Ag(2)–O(2)	2.189(8)
Ag(1)–O(1)	2.398(9)	Ag(2)–O(6)	2.206(9)
Ag(1)–O(7)	2.45(1)	Ag(2)–O(1b)	2.417(8)
Ag(3)–O(2W)	2.26(1)	Ag(3)–O(5)	2.370(9)
Ag(3)–O(6a)	2.505(9)	Ag(3)–O(12)	2.69(1)
Ag(1)···Ag(3)	3.360(2)	Ag(1)···Ag(2)	3.057(1)
O(1)–C(1)	1.24(1)	Ag(2)···Ag(3)	3.090(1)
O(5)–C(22)	1.22(1)	O(2)–C(1)	1.23(1)
O(6)–C(22)	1.26(1)		
Bond angles			
O(1)–Ag(1)–O(7)	125.9(3)	O(2)–Ag(2)–O(6)	174.0(3)
O(1)–Ag(1)–O(1w)	78.2(4)	O(2)–Ag(2)–O(1b)	103.1(3)
O(7)–Ag(1)–O(1w)	107.7(4)	O(6a)–Ag(2)–O(1b)	81.4(3)
O(2W)–Ag(3)–O(5)	166.4(4)	O(5)–Ag(3)–O(6b)	88.8(3)
O(2)–Ag(2)···Ag(1)	82.5(2)	O(6)–Ag(2)···Ag(1)	91.5(2)
O(1W)–Ag(1)···Ag(2)	91.4(3)	O(1b)–Ag(2)···Ag(1)	133.5(2)
O(1)–Ag(1)···Ag(2)	65.5(2)	O(2)–Ag(2)···Ag(3)	99.1(2)

Table 3 (*continued*)

O(7)–Ag(1)···Ag(2)	159.0(4)	O(6)–Ag(2)···Ag(3)	77.8(2)
O(1W)–Ag(1)···Ag(3)	134.4(3)	O(1b)–Ag(2)···Ag(3)	151.8(2)
O(1)–Ag(1)···Ag(3)	59.5(2)	Ag(1)···Ag(2)···Ag(3)	66.26(4)
O(7)–Ag(1)···Ag(3)	110.5(3)	O(2w)–Ag(3)···Ag(2)	98.4(4)
Ag(2)···Ag(1)···Ag(3)	57.35(3)	O(5)–Ag(3)···Ag(2)	70.1(2)
O(2w)–Ag(3)–O(6a)	102.9(5)	O(2w)–Ag(3)···Ag(1)	123.3(3)
O(5)–Ag(3)–O(6a)	88.8(3)	O(5)–Ag(3)···Ag(1)	57.0(3)
O(2w)–Ag(3)–O(12)	94.6(4)	O(6a)–Ag(3)···Ag(1)	60.9(3)
O(5)–Ag(3)–O(12)	81.9(4)	O(12)–Ag(3)···Ag(1)	138.0(3)
O(6a)–Ag(3)–O(12)	132.6(3)	Ag(2)···Ag(3)···Ag(1)	56.39(3)
O(6b)–Ag(3)···Ag(2)	115.5(2)	C(1)–O(1)–Ag(1)	119.7(7)
O(12)–Ag(3)···Ag(2)	104.7(3)	C(1)–O(1)–Ag(2a)	134.1(7)
O(1)–C(1)–O(2)	128(1)	Ag(1)–O(1)–Ag(2a)	101.0(3)
O(5)–C(22)–O(6)	128(1)	C(1)–O(2)–Ag(2)	112.2(7)

Symmetry codes. For **1**: (a) x, $y+1$, $z-1$; (b) $-x+1$, $-y+1$, $-z$; (c) x, $y-1$, $z+1$. For **2**: (a) $-x$, $-y+1$, $-z+1$. For **3**: (a) $x+1$, y, z; (b) $x-1$, y, z.

selected bond distances and angles for **1**–**3** are given in Table 3.

3. Results and discussion

3.1. Supramolecular structures of three isomeric double betaines hydrates

Betaine compounds are good proton acceptors, so they readily form stoichiometric hydrates upon crystallization in water [11].

The crystal structure of $L^1 \cdot 8H_2O$ exhibits a hydrogen-bonded three-dimensional network. There are two independent double betaine molecules (labeled **A** and **B**) each located at an inversion center, and intermolecular π–π overlap occurs between the phenylene ring of one and a pyridyl ring of the other in the "T" fashion, with a separation of 3.846 Å between the ring centers and a dihedral angle of 6.3° (Fig. 1). The two parallel pyridyl rings of each molecule are twisted with respect to the phenylene ring; the dihedral angle is 6.4° for molecule **A** and 5.1° for molecule **B**. The torsion angle C(9)–O(3)–C(8)–C(3) in molecule **A** is 174.2(2)°, and in molecule **B** the torsion angle C(20)–O(6)–C(19)–C(14) is 176.5(2)°. Both carboxymethyl groups of each double betaine molecule lie on opposite sides of the pair of pyridine rings. The oxygen atoms of the carboxylate group are not equidistant to the positively charged nitrogen atom [N(1)···O(1) 2.72, N(1)···O(2) 3.62 Å; N(2)···O(4) 2.72, N(2)···O(5) 3.62 Å], and the C–O bonds are different in length [C(1)–O(1) 1.239(4), C(1)–O(2) 1.246(4) Å; C(12)–O(4) 1.226(3), C(12)–O(5) 1.242(3) Å]. The close proximity of O(1) to N(1) and O(4) to N(2) facilitate internal charge neutralization. The torsion angles O(1)–C(1)–C(2)-N(1) and O(2)–C(1)–C(2)-N(1) are −2.4(4)° and 177.0(3)°, respectively. For molecule **B**, the torsion angles O(4)–C(12)–C(13)–N(2) and O(5)–C(12)–C(13)–N(2) are −5.9(4)° and 174.3(2)°, respectively. In molecule **A**, the plane of the carboxylate group is nearly perpendicular to the pyridine plane (dihedral angle 88.8°), but in molecule **B** the dihedral angle is about 94.0°. The water molecules are joined together by strong O—H···O hydrogen bonds and occupy the hydrophilic region between double betaine molecules. In particular, a pair of independent water molecules O1W and O2W, together with their centrosymmetrically-related partners, connects two centrosymmetrically-related carboxylate oxygen atoms of betaine molecules **A** and **C** by strong O—H···O$^-$ hydrogen bonds to generate a chair-like six-member ring of the type O1W···O2WB···O4B···O1WB···O2W···O(4). This six-member ring is further linked by two pairs of bridging water molecules derived from O3W and O8W to fuse with another pair of non-planar six-member

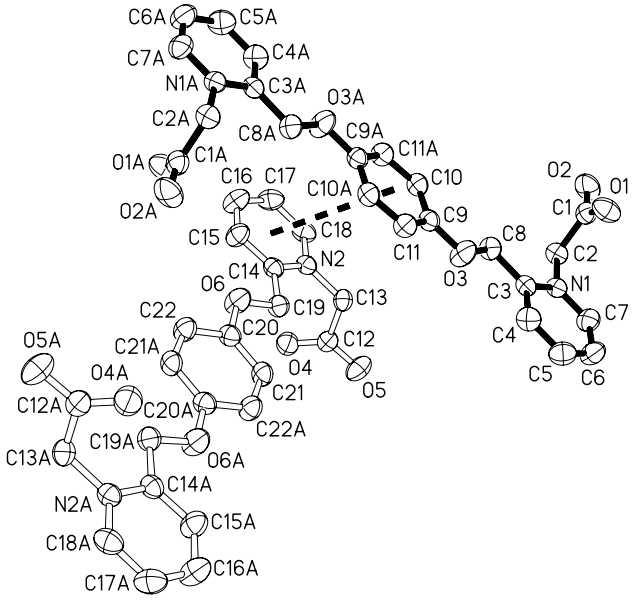

Fig. 1. π–π Interaction between two betaine molecules in the "T" fashion of $L^1 \cdot 8H_2O$. Hydrogen atoms and water molecules are omitted for clarity. Displacement ellipsoids are plotted at the 30% probability level. Symmetry transformations: (A) $-x$, $-y+1$, $-z+1$; (B) $-x+1$, $-y+2$, $-z+1$.

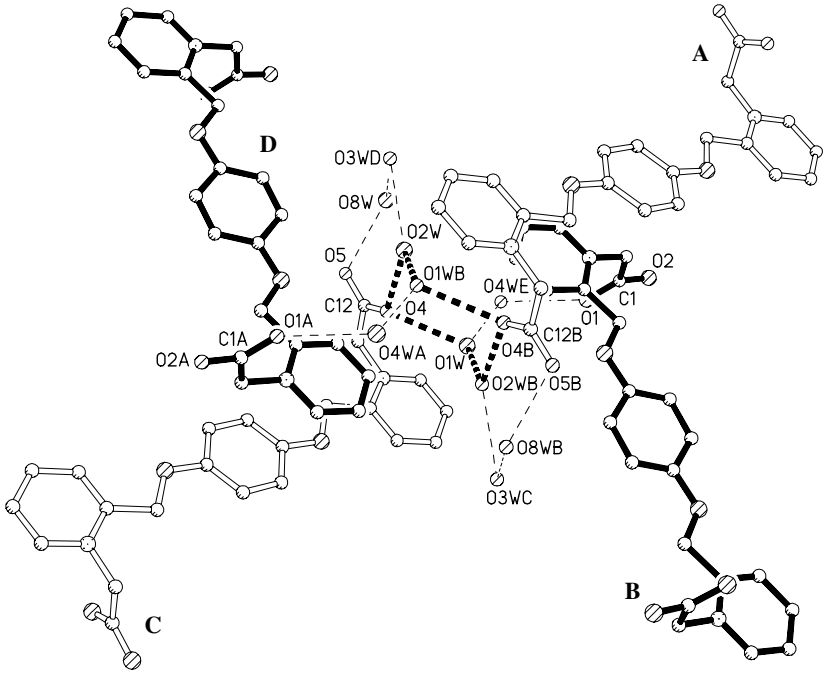

Fig. 2. Scheme of hydrogen bonding in $L^1 \cdot 8H_2O$. Two types of symmetry-related molecules are drawn in different bond types, and the centrosymmetric chair-like six-member ring is highlighted by bold dotted lines. Hydrogen atoms are omitted for clarity. Symmetry transformations: (A) $-x + 1, -y + 1, -z + 1$; (B) $-x + 1, -y + 1, -z + 2$; (C) $-x, -y + 1, -z + 2$ and (D) $x + 1, y, z$.

rings O2W···O(4)—C(12)—O(5)···O8W···O3WD and O2WB···O4B—C12B—O5B···O8WB···O3WC. Another pair of symmetry-related betaine molecules **B** and **D** are joined to this hydrogen-bonded ring system through a pair of bridging water molecules derived from O4W with strong O—H···O^- hydrogen bonds of the type O2W···O4W···O(1) (Fig. 2). In this way, the betaine molecules are alternately bridged by water molecules to produce an infinite three-dimensional network (Fig. 3). Details of the hydrogen bonding scheme are shown in Table 4.

In the crystal structure of $L^2 \cdot 6H_2O$ (Fig. 4), L^2 is located at an inversion center, and each pyridyl ring is twisted by 8.6° with respect to the phenylene ring. The torsion angle C(9)–O(3)–C(8)–C(4) is −172.8(2)°. The oxygen atoms of the carboxylate group are not equidistant to the positively charged nitrogen atom [N(1)···O(1) 2.71, N(1)···O(2) 3.61 Å], and the close proximity of O(1) to N(1) also facilitates internal charge neutralization. The torsion angle O(1)–C(1)–C(2)–N(1) is 6.7(3)°. The plane of the carboxylate group makes a dihedral angle of 77.6° with the pyridine plane. The L^2 betaine molecules are stacked along the *a*-axis and interlinked by strong O—H···O^- hydrogen bonds with water molecules derived from O1W to form an infinite chain (Fig. 5). The remaining two independent water molecules O2W and O3W together with their symmetry-related partners generate a pleated ladder characterized by an alternating arrangement of $R_4^2(8)$ and $R_4^4(8)$ hydrogen bonding motifs (Fig. 6a) running parallel to the *a*-axis. This functions as a wide bridging ribbon to connect adjacent chains of water-bridged double betaines by strong O—H···O^- hydrogen bonds to form a

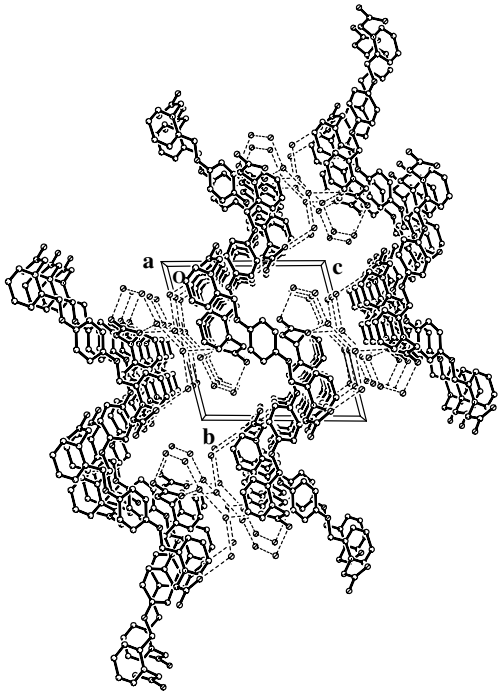

Fig. 3. Three-dimensional framework connected by hydrogen bonds in $L^1 \cdot 8H_2O$. Hydrogen atoms are omitted for clarity. Displacement ellipsoids are plotted at the 30% probability level.

Table 4
Hydrogen bonding parameters (d in Å and θ in °)[a]

D–H···A	d(H···A)	d(D···A)	θ(D–H···A)
$L^1 \cdot 8H_2O$			
O(1W)–H(1WA)···O(4)	1.88	2.794(3)	174.9
O(1W)–H(1WB)···O(2W)^{i}	1.83	2.751(4)	175.5
O(2W)–H(2WA)···O(3W)^{ii}	2.00	2.912(4)	172.8
O(2W)–H(2WB)···O(4)	1.88	2.778(3)	166.0
O(3W)–H(3WA)···O(5W)^{iii}	2.11	3.010(5)	168.1
O(3W)–H(3WB)···O(7W)^{iv}	1.83	2.740(4)	171.5
O(4W)–H(4WA)···O(1)	1.91	2.812(4)	169.2
O(4W)–H(4WB)···O(1W)^{v}	1.89	2.780(4)	162.7
O(5W)–H(5WA)···O(2)	1.75	2.646(4)	165.1
O(5W)–H(5WB)···O(6W)^{vi}	1.97	2.884(5)	172.5
O(6W)–H(6WA)···O(4W)	1.78	2.675(4)	165.6
O(6W)–H(6WB)···O(8W)^{v}	2.47	2.982(5)	115.1
O(7W)–H(7WA)···O(6W)^{vi}	2.05	2.914(5)	156.6
O(8W)–H(8WA)···O(5)	1.80	2.706(4)	166.5
O(8W)–H(8WB)···O(3W)^{ii}	1.94	2.845(4)	167.5
$L^2 \cdot 6H_2O$			
O(1W)–H(1WA)···O(2)	1.98	2.869(3)	162.2
O(1W)–H(1WB)···O(2)^{i}	1.89	2.809(3)	173.3
O(2W)–H(2WA)···O(3W)^{ii}	1.80	2.718(4)	179.1
O(2W)–H(2WB)···O(3W)^{iii}	2.03	2.953(5)	178.2
O(3W)–H(3WA)···O(1)	1.85	2.769(4)	177.5
O(3W)–H(3WB)···O(2W)	1.94	2.826(6)	161.5
$L^3 \cdot 5H_2O$			
O(1W)–H(1WA)···O(1)	1.89	2.803(3)	169.5
O(1W)–H(1WB)···O(2)^{i}	1.90	2.822(3)	175.4
O(2W)–H(2WA)···O(2)	2.23	2.758(3)	116.1
O(2W)–H(2WB)···O(2W)^{ii}	2.36	2.760(6)	105.9
O(3W)–H(3WA)···O(2W)^{iii}	2.33	3.012(7)	130.6
*Compound **1***			
O1W–H1WA···O10	2.188	2.71(1)	115.4
O1W–H1WB···O6^{i}	2.367	3.12(1)	138.5
O2W–H2WA···O6	2.090	2.94(1)	153.9
O2W–H2WB···O2^{ii}	2.221	3.01(1)	144.7
O3W–H3WB···O12	2.124	2.95(2)	148.7
O4W–H4WA···O5^{iii}	2.145	2.98(2)	150.1
*Compound **2***			
O1W–H1WA···O4	2.23	2.89(1)	127.9
O2W–H2WA···O1^{i}	1.88	2.791(8)	170.6
O2W–H2WB···O6^{ii}	1.97	2.79(1)	147.4
O3W–H3WA···O2W^{iii}	2.03	2.91(1)	159.3
O3W–H3WB···O5^{iii}	1.87	2.78(1)	168.1
*Compound **3***			
O2W–H2WB···O14	2.153	2.97(1)	147.0
O2W–H2WB···O13	2.292	2.91(1)	123.3
O2W–H2WA···O13^{i}	2.000	2.724(9)	134.4
O1W–H1WA···O10^{ii}	2.066	2.98(1)	170.2
O1W–H1WA···O11^{ii}	2.529	3.19(1)	129.2
O3W–H3WA···O4W^{i}	2.400	3.05(1)	127.4
O3W–H3WB···O4W	2.433	2.89(1)	111.2

Symmetry codes. For $L^1 \cdot 8H_2O$: (i) $-x+1, -y+1, -z+2$; (ii) $x+1, y, z$; (iii) $-x, -y, -z+1$; (iv) $x, y, z+1$; (v) $x, y, z-1$; (vi) $-x, -y, -z$. For $L^2 \cdot 6H_2O$: (i) $x+1, y, z$; (ii) $x-1, y, -z$; (iii) $-x+1, -y+1, -z+1$. For $L^3 \cdot 5H_2O$: (i) $x, -y+1, z+1/2$; (ii) $-x, -y+1, -z$; (iii) $-x+1/2, -y+1/2-z$. For compound **1**: (i) $-x+1, -y, -z$; (ii) $-x+1, -y, -z+1$; (iii) $x-1, y+1, z-1$. For Compound **2**: (i) $x-1, y, z$; (ii) $-x, y+1/2, -z+3/2$; (iii) $x+1, y, z$. For compound **3**: (i) $x+1, y, z$; (ii) $x, y-1, z$.

[a] d(D–H) is set to 0.92 Å for all compounds.

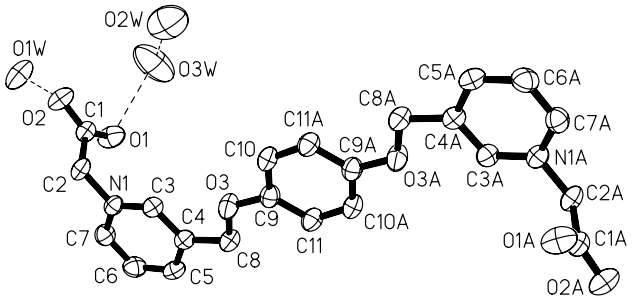

Fig. 4. Asymmetric unit with atom labeling in $L^2 \cdot 6H_2O$. Hydrogen atoms are omitted for clarity.

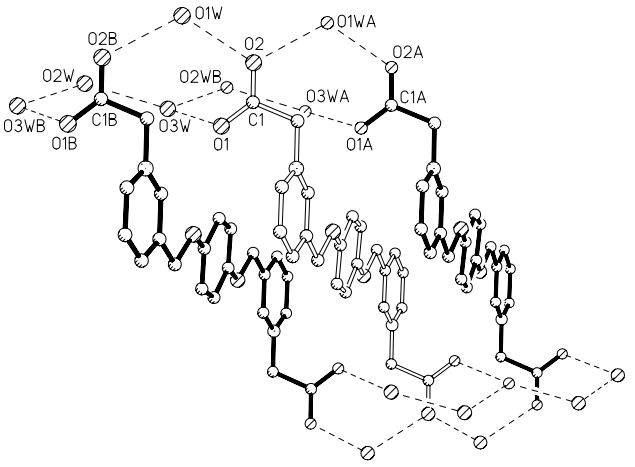

Fig. 5. Perspective diagram showing the hydrogen-bonding interactions between the double betaine and the water molecules in $L^2 \cdot 6H_2O$. Hydrogen atoms are omitted for clarity. Symmetry transformations: (A) $x-1, y, z$ and (B) $x+1, y, z$.

corrugated layer (Fig. 6b) featuring a ten-member ring motif of the type O(1)—C(1)—O(2)···O1W···O2B—C1B—O1B···O3WB···O2W···O3W (Fig. 5). There is no distinct π–π interaction in this structure, and the hydrogen bonds are shown in Table 4.

$L^3 \cdot 5H_2O$ shows the hydrogen bonded two-dimensional network. The molecular backbone of the double betaine L^3 has a twofold axis passing through the mid points of the C(10)–C(10A), C(11)–C(11A) bonds, being different from those of L^1 and L^2 (Fig. 7). The two pyridyl rings are not parallel to each other but make a dihedral angle of 5.3°, and each is twisted by 3.7° with respect to the phenylene ring. The torsion angle C(5)–C(8)–O(3)–C(9) is −178.6(2)°. Both carboxymethyl groups also lie on opposite sides of the two pyridine rings. The two oxygen atoms of the carboxylate group are not equidistant to the positively charged nitrogen atom [N(1)···O(1) 2.73, N(1)···O(2) 3.60 Å], facilitating internal charge neutralization. The torsion angles O(1)–C(1)–C(2)–N(1) and O(2)–C(1)–C(2)–N(1) are 8.8(4)° and −173.0(2)°, respectively. The carboxylate group makes a dihedral angle of 99.4° with the pyridine plane. Water molecules derived from O1W bridge two adjacent

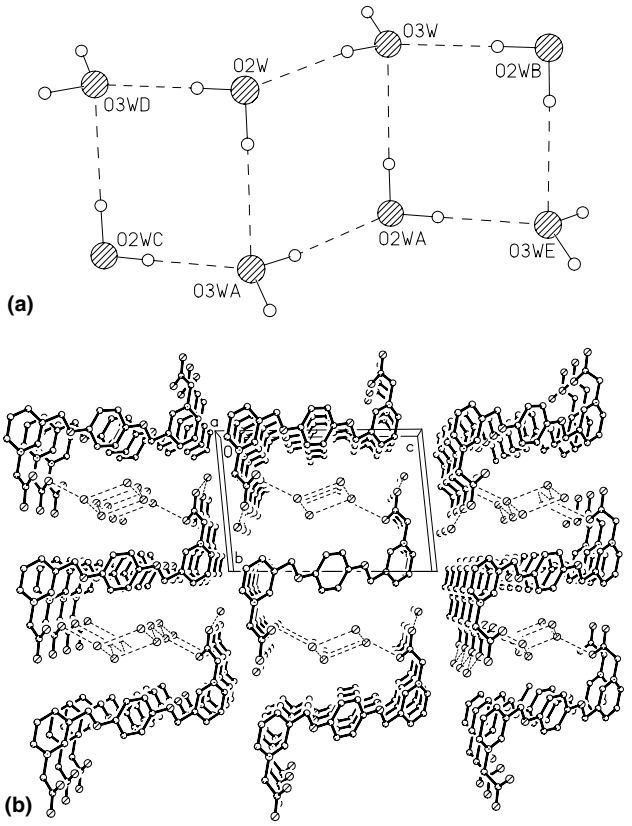

Fig. 6. (a) Water molecules are connected by strong O—H···O hydrogen bonds and form a "water-ladder" running along the *a*-axis in $L^2 \cdot 6H_2O$. Symmetry transformations: (A) $-x+1, -y+1, -z+1$; (B) $x+1, y, z$; (C) $-x, -y+1, -z+1$; (D) $x-1, y, z$ and (E) $-x+2, -y+1, -z+1$. (b) Perspective view of the crystal structure of $L^2 \cdot 6H_2O$ along the *a*-axis showing highly pleated sheets composed of "water-ladders" and double betaine molecules. The sheets are further consolidated by the terminal water molecules.

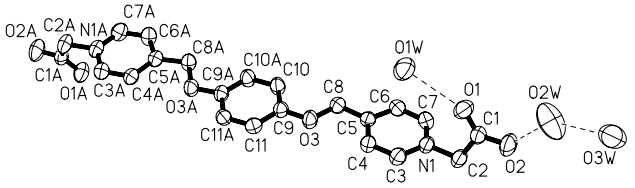

Fig. 7. Asymmetric unit with atom labeling in $L^3 \cdot 5H_2O$. Displacement ellipsoids are plotted at the 30% probability level.

L^3 molecules by pairs of strong O—H···O^- hydrogen bonds. The other two independent water molecules O2W and O3W together with their symmetry-related partners form a zigzag water chain running along the *c*-axis. This zigzag water chain interlinks two neighboring sets of betaines further by strong O—H···O^- hydrogen bonds to generate an infinite two-dimensional network (Fig. 8). The betaine molecules are associated through π–π interactions between the pyridyl and phenylene rings of adjacent molecules with a separation of 3.57 Å between ring centers and a twist angle of 3.7° between the planes. The metric parameters of the hydrogen bonds are shown in Table 4.

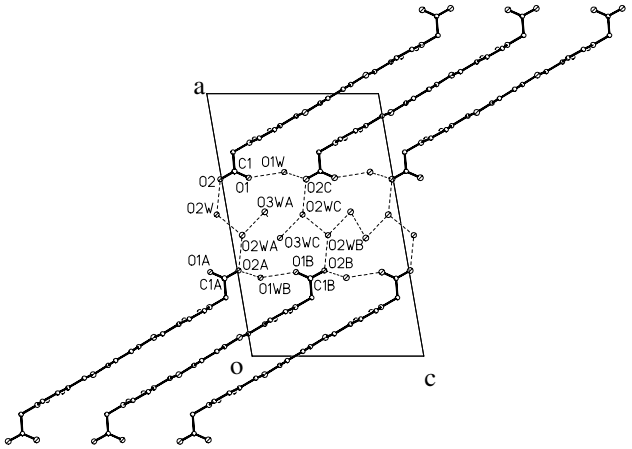

Fig. 8. Two-dimensional network connected by hydrogen bonds in $L^3 \cdot 5H_2O$. Symmetry transformations: (A) $-x$, $-y+1$, $-z$; (B) $-x+1/2$, $-y+1/2$, $-z$; (C) x, $-y+1$, $z+1/2$.

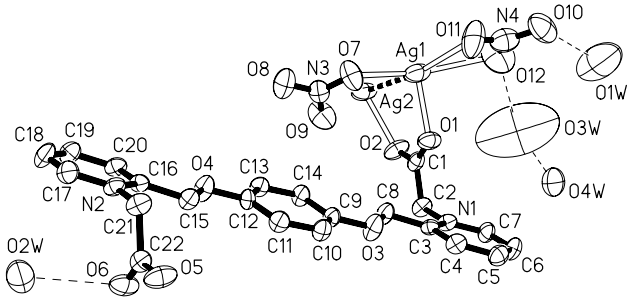

Fig. 9. Asymmetric unit and atom labeling in compound **1** with thermal ellipsoids represented at the 30% probability level. All hydrogen atoms are omitted for clarity.

3.2. Supramolecular structures of Ag(I) complexes of three isomeric double betaines

Molar ratio 5:1 was chosen to carry out the reaction between $AgNO_3$ and the three isomeric double betaine ligands L^1, L^2 and L^3. Excess $AgNO_3$ was used to prevent the deposit of the hydrated ligands. Complexes **1**, **2** and **3** exhibit different polymeric molecular structures, being bridged by the carboxylate groups in bidentate and/or tridentate mode, which may be attributed to the different positions of the betaine moieties in the relevant ligands.

The structure of $\{[Ag_2L^1](NO_3)_2 \cdot 3.5H_2O\}_n$ **1** is a one-dimensional double-chain network containing dimeric subunits (Fig. 9). The Ag···Ag separation (2.873(1)Å) in the dimeric subunit is close to that in metallic silver, indicating a comparable d^{10}–d^{10} closed-shell [12] attractive argentophilic interaction [13]. The two independent silver ions have different coordination environments. The coordination geometry around Ag(1) can be described as a distorted trigonal bipyramid surrounded by two μ_2-carboxylate groups and two nitrate ligands. The Ag(1)–O distances for the μ_2-carboxylate groups are Ag(1)–O(1), 2.224(5) Å and Ag(1)–O(5a), 2.234(5) Å, (a: x, $y+1$, $z-1$). Each Ag(1) atom also makes two intermediate contacts (Ag(1)–O(11), 2.608(7) and Ag(1)–O(12), 2.688(8) Å) with the oxygen atoms of a bidentate chelating nitrate and one bond (Ag(1)–O(7), 2.646(5) Å) to a tridentate nitrate. The Ag(2) atom is coordinated by two oxygen atoms from two different carboxylate groups (Ag(2)–O(2), 2.256(5) Å and Ag(2)–O(6a) 2.253(5) Å) and two oxygen atoms from a tridentate chelating nitrate (Ag(2)–O(8b), 2.2660(7) and Ag(2)–O(9b), 2.698(6) Å; b: $-x+1$, $-y+1$, $-z$), giving a distorted tetragonal pyramidal coordination geometry. The dimeric subunits are extended into an infinite chain in the [0 1 1] direction through the linkage of double betaine ligands L^1. In this compound, the two pyridyl rings of L^1 ligand are not parallel to each other as in its hydrate crystals, but twist 3.7° to bridge the Ag(I) ions. Two adjacent chains are further connected through tridentate nitrate ions (Ag(1)–O(7), Ag(2b)–O(8), Ag(2b)–O(9), generating an infinite double-chain structure, which contains cavities of size 12×6 Å. These double chains are further

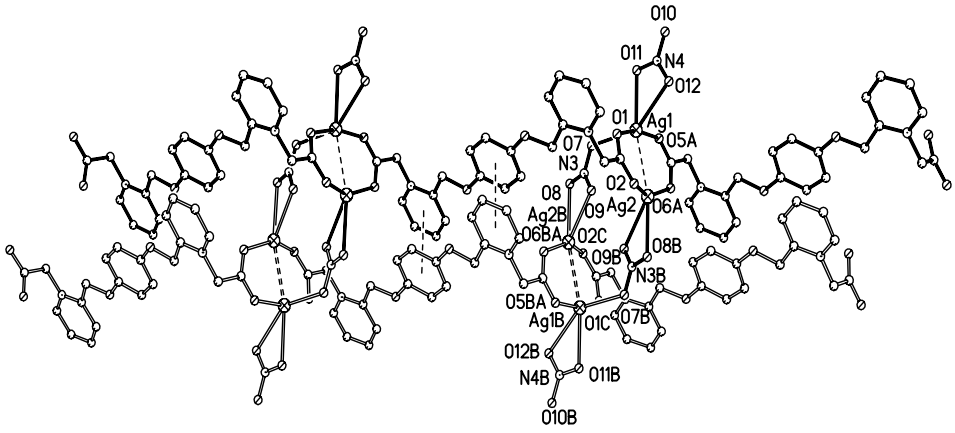

Fig. 10. Double-chain polymeric structure of compound **1**, showing the π–π interactions formed between the ligands and Ag···Ag interactions. Lattice water molecules and all hydrogen atoms are omitted for clarity.

consolidated through π–π stacking interactions between adjacent phenylene rings and pyridyl rings, with centroid-to-centroid distance 3.879 Å and dihedral angle 7.8° (Fig. 10). The lattice water molecules O1W, O2W, O3W and O4W (disorder, with half occupation) are accommodated in the cavities and the space between the double-chain structures, connecting to the chain through hydrogen bonds (Table 4).

Complex **2**, $\{[Ag_2L^2](NO_3)_2 \cdot 6H_2O\}_n$, is also a dimeric complex but different from complex **1**. The asymmetric unit of **2** only contains a silver ion, one half of a centrosymmetric L^2 double betaine ligand, a nitrate ion and three water molecules. The Ag1 ion is tetrahedrally coordinated by two oxygen atoms from two L^2 ligands (Ag(1)–O(1), 2.228(5) Å; Ag(1)–O(2a), 2.251(4) Å; a: $-x$, $-y+1$, $-z+1$) and two aqua ligands (Ag(1)–O1W, 2.378(5) Å; Ag(1)–O2W, 2.590(6) Å). The other Ag1a ion of the dimeric center is generated by the symmetry operator $-x$, $-y+1$, $-z+1$ at a separation of 2.826(1) Å from Ag(1), close to that in metallic silver as in complex **1**. Similarly, the other half of the L^2 ligand is obtained through the symmetry operator ($-x-1$, $-y+2$, $-z+1$) (Fig. 11). The pyridyl ring of ligand L^2 is twisted by 8.8° with respect to the phenylene ring. The combined effect of these connections is to render a series of one-dimensional zigzag chains in the crystal lattice. These chains are further connected by the hydrogen bond O2W–H2WA···O(1b), 170.6°; O2W···O(1b), 2.791(8)Å (b: $x-1$, y, z) (Table 4), generating an infinite two-dimensional layer structure parallel to the *ab*-plane (Fig. 12). The π–π stacking interactions are also found between the pyridyl rings and the phenylene rings of adjacent L^2 ligands in this plane, with an inter-ring distance of 3.92 Å and dihedral angle 8.8°. The layers are extended into a three-dimensional network through the connection of the hydrogen bonds (Table 4, Fig. 13).

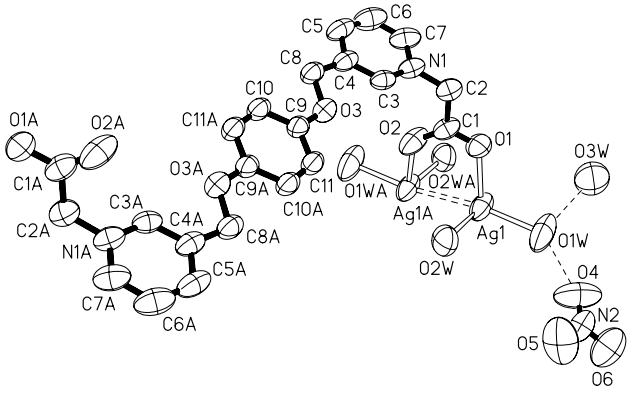

Fig. 11. Asymmetric unit and atom labeling in compound **2** with thermal ellipsoids represented at the 30% probability level. All hydrogen atoms are omitted for clarity.

The asymmetric unit of complex **3**, $\{[Ag_3L^2](NO_3)_3 \cdot 3H_2O\}_n$, consists of three silver atoms at the apices of an isosceles triangle, a L^3 ligand, three nitrate ions, two coordinated and two halves lattice water molecules (Fig. 14). In this compound, the molecular back-

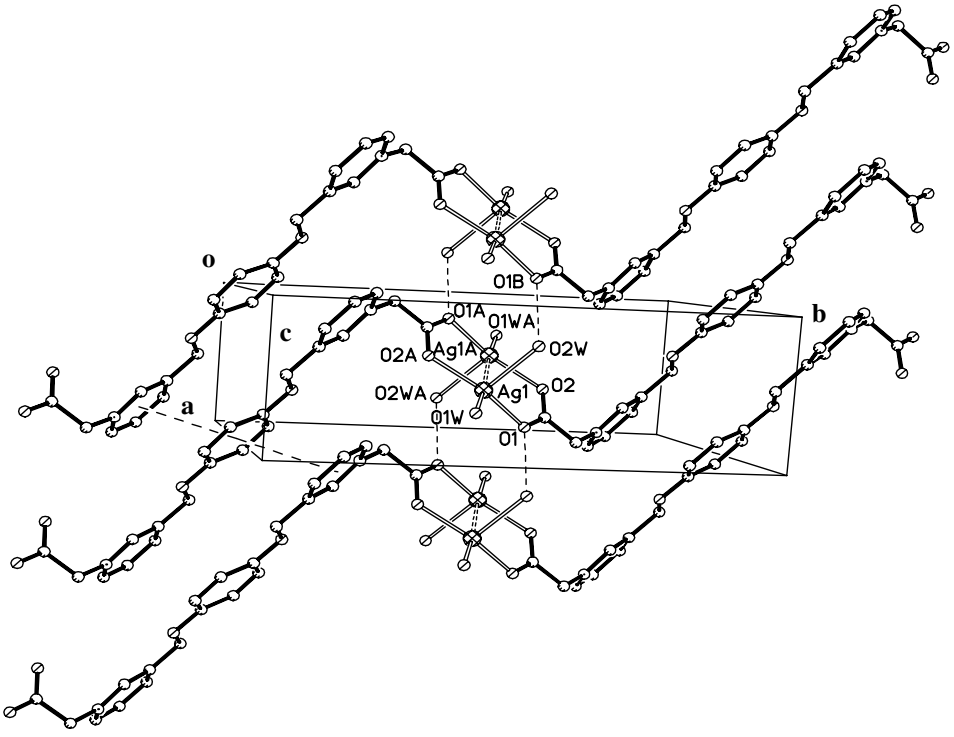

Fig. 12. View of the two-dimensional layer structure in compound **2**, in which the chains are connected through hydrogen bonding and π–π interactions. Lattice water molecules, hydrogen atoms, and all other atoms, which make no contribution to this connection, are omitted for clarity.

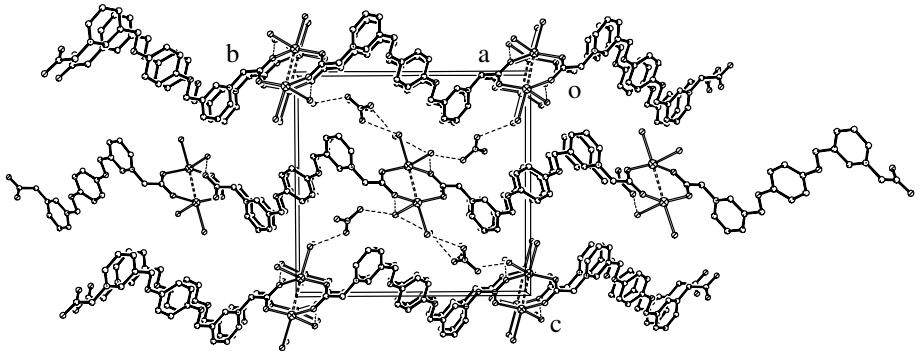

Fig. 13. Three-dimensional network of **2**, which are connected by hydrogen bonds through the nitrate ions.

bone of the double betaine L^3 does not possess C_2 symmetry as in its hydrate, and the two pyridyl rings of ligand L^3 are not parallel to each other, but twisted by 3.1° to link the Ag(I) ions. The triangular Ag(I) cluster is found in this compound with silver–silver distances of 3.057(1), 3.090(1) and 3.360(2) Å, suggesting weak d^{10}–d^{10} interactions. It is notable that the three silver ions have different coordination environment (Fig. 15). Ag(1) exhibits trigonal pyramidal coordination geometry, being coordinated by an aqua ligand (Ag1–O1W, 2.71(2) Å), a nitrate (Ag1–O7, 2.45(1) Å), and a L^3 ligand (Ag1–O1, 2.398(9) Å). Although also coordinated by three oxygen atoms belonging to three different L^3 ligands (Ag(2)–O(2), 2.189(8) Å; Ag(2)–O(6), 2.206(9) Å; Ag(2)–O(1a), 2.417(8) Å; a: $x-1$, y, z), Ag(2) shows a T-shaped coordination geometry. Ag(3) is coordinated by four oxygen atoms, which are provided by an aqua ligand (Ag(3)–O2W, 2.27(1) Å), a nitrate ion (Ag(3)–O(12), 2.69(1) Å) and two L^3 ligands (Ag(3)–O(5), 2.370(9) Å; Ag(3)–O(6b), 2.505(9) Å; b: $x+1$, y, z) in a distorted tetrahedral environment. The carboxyl oxygen atoms of the L^3 ligand coordinate to four different silver ions, linking the triangular silver clusters to generate an infinite two-dimensional network with large cavities (18 × 5 Å) (Fig. 16). The layer structures are further linked through hydrogen bonds (O1W–H1WA···O(10d), 170.2°; O1W···O(10d), 2.98(2) Å; d: x, $y-1$, z) (Table 4), extending to a more complex three-dimensional network (Fig. 17). The remaining nitrate ion,

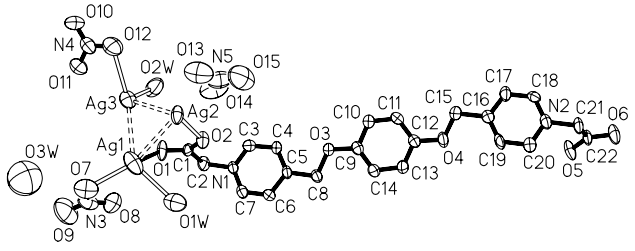

Fig. 14. Asymmetric unit and atom labeling in compound **3** with thermal ellipsoids represented at the 30% probability level. All hydrogen atoms are omitted for clarity.

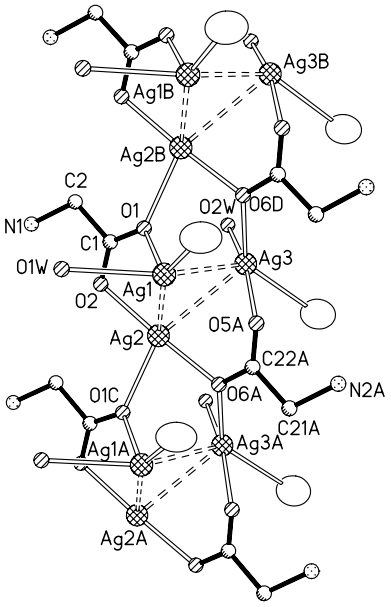

Fig. 15. A section of the polymeric structure of **3**, showing the interactions between the silver atoms of the trinuclear unit and the oxygen atoms of carboxylate, nitrate and aqua ligand. Large open circle represents terminal nitrate group for clarity.

which is not coordinated to silver ions directly, is connected to the network through hydrogen bonds O2W–H2WB···O(13) (Table 4). The lattice water molecules O3W and O4W are accommodated between the layers, and no distinguishable π–π interaction is found in the crystal structure.

4. Concluding remarks

In the crystal structures of the hydrated ligands and silver(I) complexes **1**–**3**, the –CH_2–py–CH_2–O–C_6H_4–O–CH_2–py–CH_2– backbone of the isomeric betaine molecules is nearly planar, the largest dihedral angle between the pyridyl rings being 5.3° in $L^3 \cdot 5H_2O$. Intermolecular π–π interaction between the central phenylene ring and the pyridyl ring of a neighboring betaine molecule exists in $L^1 \cdot 8H_2O$ and $L^3 \cdot 5H_2O$,

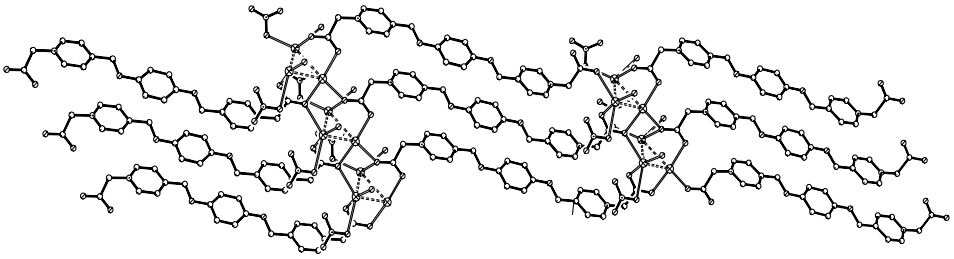

Fig. 16. Layer structure of **3** exhibiting the connection between the trinuclear silver clusters and the L^3 ligands. The parallelogram-like cross-section between the Ag centers and betaine ligands is about 18 Å × 5 Å.

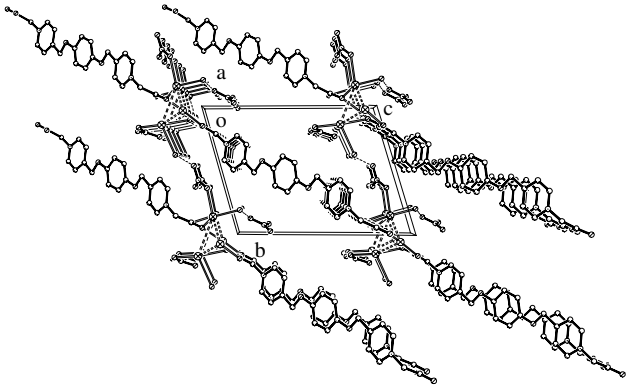

Fig. 17. Three-dimensional network of **3** linked by hydrogen bonding.

as well as in complex **1** and **2**. The dinuclear building block in **1** and **2**, with close Ag···Ag contact comparable to that in metallic silver, exhibits significant argentophilic interaction, whereas in **3** the Ag···Ag distances in the trinuclear unit are longer, suggesting much weaker d^{10}–d^{10} attraction. The structure of **3** is comparable with that of $[Ag_2(O_2C(CH_2)_2CO_2)]$, in which four silver atoms are connected by the more flexible and shorter succinate ligand to give a planar tetrasilver cluster that also exhibits weaker d^{10}–d^{10} attraction [14].

The flexible double betaines L^1 and L^2 are versatile ligands for the generation of novel coordination networks in lanthanum complexes. They can act in the bidentate, tridentate and tetradentate modes to bridge La(III) centers, forming 2D or 3D network with the aid of complementary hydrogen bonding involving coexisting aqua ligands and/or lattice water molecules [6]. Ligand L^1 can also display two principal types of bridging modes (*anti* and *syn*) leading to different metal–metal separations in complexes $[Cu(\mu\text{-}L)Cl_2]_n$ and $\{[Zn(\mu\text{-}L)Cl_2]\cdot 2H_2O\}_n$ [5]. In contrast to L^1 and L^2, as L^3 has its pair of carboxylate groups fully extended to the limit and accordingly possesses a less bulky backbone, it is expected to be best suited to the generation of porous coordination networks.

Acknowledgement

We gratefully acknowledge financial support from the Hong Kong Research Grants Council through Earmarked Grant CUHK 402003.

Appendix A. Supplementary material

Crystallographic data for the crystal structures reported in this paper have been deposited with the Cambridge Crystallographic Data Center (CCDC Nos. 210828–210833). This material can be obtained free of charge from the Director, CCDC, 12 Union Road, Cambridge, CB2 1EZ, UK (fax: +44 1223 336033; e-mail: deposit@ccdc.cam.ac.uk or http://www.ccdc.cam.ac.uk). Supplementary data associated with this article can be found, in the online version, at doi:10.1016/j.poly.2004.08.002.

References

[1] (a) S.R. Batten, B.F. Hoskins, R. Robson, Angew. Chem. Int. Ed. 34 (1995) 820;
(b) S. Dalai, P.S. Mukherjee, E. Zangrando, F. Lloret, N.R. Chaudhuri, J. Chem. Soc., Dalton Trans. (2002) 822;
(c) J. Hamblin, A. Jackson, N.W. Alcock, M.J. Hannon, J. Chem. Soc., Dalton Trans. (2002) 1635.

[2] (a) P.R. Ashton, P.J. Campbell, E.J.T. Chrystal, P.T. Glink, S. Menzer, D. Philp, N. Spencer, J.F. Stoddart, P.A. Tasker, D.J. Williams, Angew. Chem. Int. Ed. 34 (1995) 1865;
(b) C.Y. Su, B.S. Kang, H.Q. Liu, Q.G. Wang, T.C.W. Mak, J. Chem. Soc., Chem. Commun. (1998) 1551;
(c) M.J. Hannon, C.L. Painting, E.A. Plummer, L.J. Childs, N.W. Alcock, Chem. Eur. J. 8 (2002) 2225.

[3] (a) D.-D. Wu, T.C.W. Mak, J. Chem. Crystallogr. 24 (1994) 689;
(b) D.-D. Wu, T.C.W. Mak, J. Mol. Struct. 326 (1994) 193;
(c) D.-D. Wu, T.C.W. Mak, J. Chem. Soc., Dalton Trans. (1995) 2671;
(d) D.-D. Wu, T.C.W. Mak, J. Chem. Crystallogr. 27 (1997) 11.

[4] (a) D.-D. Wu, T.C.W. Mak, J. Mol. Struct. 372 (1995) 187;
(b) P.-R. Wei, Q. Li, B.-M. Wu, T.C.W. Mak, Polyhedron 16 (1997) 153;
(c) J.-G. Mao, T.C.W. Mak, H.-J. Zhang, J.-Z. Ni, S.-B. Wang, J. Coord. Chem. 47 (1999) 145;

(d) X. Zhang, G.-C. Guo, F.-K. Zheng, G.-W. Zhou, J.-G. Mao, Z.-C. Dong, J.-S. Huang, T.C.W. Mak, J. Chem. Soc., Dalton Trans. (2002) 1344.
[5] L.-P. Zhang, H.-B. Song, Q.-M. Wang, T.C.W. Mak, Polyhedron 22 (2003) 811.
[6] L.-P. Zhang, T.C.W. Mak, Polyhedron 22 (2003) 2787.
[7] (a) M. Etienne, Coord. Chem. Rev. 156 (1996) 201;
(b) L.F. Szczepura, L.M. Witham, K.J. Takeuchi, Coord. Chem. Rev. 174 (1998) 5;
(c) V. McKee, J. Nelson, D.J. Speed, R.M. Town, J. Chem. Soc., Dalton Trans. (2001) 3641;
(d) H.-J. Kim, D. Moon, M.S. Lah, J.-I. Hong, Angew. Chem. Int. Ed. 41 (2002) 3174.
[8] (a) M. Munakata, L.-P. Wu, T. Kuroda-Sowa, Adv. Inorg. Chem. 46 (1999) 173;
(b) X.-M. Chen, M.-L. Tong, Daxue Huaxue 12 (1997) 24;
(c) F.A. Cotton, R. Clerac, K.R. Dunbar, E.A. Hillard, C.A. Murillo, M.A. Petrukhina, B.W. Smucker, H.-C. Zhou, Pap. Am. Chem. Soc. 221 (2001) INOR-032.
[9] G.M. Sheldrick, SADABS: Program for Empirical Absorption Correction of Area Detector Data, University of Göttingen, Germany, 1996.
[10] 'G.M. Sheldrick, SHELXTL: Structure Determination Software Programs, Bruker Analytical X-ray System, Inc., Madison, WI, USA, 1997.
[11] (a) K.M. Harmon, G.F. Avci, J. Mol. Struct. 117 (1984) 295;
(b) T.C.W. Mak, J. Mol. Struct. 220 (1990) 13;
(c) E. Alcalde, M. Gisbert, C. Alvarez-Rúa, S. García-Granda, Tetrahedron 52 (1996) 15189.
[12] P. Pyykkö, Chem. Rev. 97 (1997) 597.
[13] (a) G.-C. Guo, T.C.W. Mak, Angew. Chem. Int. Ed. 37 (1998) 3183;
(b) C.-M. Che, M.-C. Tse, M.C.W. Chan, K.-K. Cheung, D.L. Phillips, K.-H. Leung, J. Am. Chem. Soc. 122 (2000) 2464;
(c) M.A. Rawashdeh-Omary, M.A. Omary, H.H. Patterson, J. Am. Chem. Soc. 122 (2000) 10371.
[14] A. Michaelides, V. Kiritsis, S. Skoulika, A. Aubry, Angew. Chem. Int. Ed. 32 (1993) 1495.

Available online at www.sciencedirect.com
SCIENCE DIRECT®
Polyhedron 23 (2004) 2427–2436
POLYHEDRON
www.elsevier.com/locate/poly

Coordination polymers of lead(II) with 4,4′-bipyridine: syntheses and structures

Ali Morsali *, Alireza Mahjoub

Department of Chemistry, School of Science, Tarbiat Modarres University, P.O. Box 14155-4838 Tehran, I.R. Iran

Received 16 May 2004; accepted 3 August 2004
Available online 21 September 2004

Abstract

Lead(II) complexes with the 4,4′-bipyridine (4,4′-bipy) ligand have been synthesized and characterized by CHN elemental analysis, IR, ^{1}H NMR, ^{13}C NMR and ^{207}Pb NMR spectroscopy. The structures of the compounds $[Pb_2(4,4'\text{-bipy})(NO_3)_4]_n$, $[Pb_2(4,4'\text{-bipy})(NCS)_4]_n$ and $[Pb(4,4'\text{-bipy})(NO_3)(SCN)]_n$ have been determined by X-ray crystallography. The single crystal X-ray data shows the $[Pb_2(4,4'\text{-bipy})(NO_3)_4]_n$ complex to be polymeric and the Pb atom has a 10 coordinate geometry, and the $[Pb_2(4,4'\text{-bipy})(NCS)_4]_n$ complex to be polymeric and the Pb atom has an eight coordinate geometry. The single-crystal X-ray data of the compound $[Pb(4,4'\text{-bipy})(NO_3)(SCN)]_n$ shows the complex to be two dimensional polymeric and the Pb atom has an eight coordinate geometry. The lone pair of electrons on lead(II) is active in the complexes $[Pb_2(4,4'\text{-bipy})(NO_3)_4]_n$ and $[Pb_2(4,4'\text{-bipy})(NCS)_4]_n$, and inactive in the complex $[Pb(4,4'\text{-bipy})(NO_3)(SCN)]_n$.
© 2004 Elsevier Ltd. All rights reserved.

Keywords: 4,4′-Bipyridine; Lead(II); Coordination polymers; Lone pair; π–π staking interaction; Crystal structure

1. Introduction

The 4,4′-bipyridine (4,4′-bipy) ligand is widely used for the synthesis of polynuclear complexes with extended structures. In relation to work on different metal ions (Cd^{2+}, Zn^{2+}, Cu^{2+}, Co^{2+}, Ni^{2+}, Fe^{2+}) [1–8] and Pb^{2+} [9] complexes containing the 4,4′-bipyridine bridge ligand described in earlier papers, it is interesting to find further examples of these complexes with the Pb^{2+} ion. The lead(II) complexes are interesting and frequently discussed when considering the coordination and stereo-activity of heavy metals, that is the "stereo-chemical activity" of the valence shell electron lone pairs [10–15]. Extensive recent structural studies on lead (II) compounds [16] in particular have provided a basis for a rather detailed analysis for the evidence of coordination sphere distortions as a consequence of the presence of such lone-pairs. It appears that in complexes of lead(II) (and probably in those of related species such as Tl^{I} [17–19] and Bi^{III} [20–24]), the nature and form of the coordination sphere is generally determined by a number of factors, possibly lone-pair bond-pair repulsions of comparable influence, so that seemingly minor differences in ligands or in the crystal array can have quite marked effects upon the coordination stereochemistry. Since the presence of a lone pair is not directly detected but recognized on the basis of the spatial distribution of the atoms assumed to be donors to the central ion, the identification of these donor atoms is fundamental to the analysis of any particular system. Interestingly, this is not a straightforward process. Building new molecular species and modifying their architectures in order to control their physical properties, has been a topic for many research groups. Different ligands have been used to study the lead(II) complexes. The ligand

* Corresponding author. Tel.: +8 011 001; fax: +8 009 730.
E-mail address: morsali_a@yahoo.com (A. Morsali).

0277-5387/$ - see front matter © 2004 Elsevier Ltd. All rights reserved.
doi:10.1016/j.poly.2004.08.014

4,4′-bipyridine, because of its ability to form polynuclear complexes, is a very good candidate for the investigation of the ''stereo-chemical activity'' of valence shell electron lone pairs in polymeric and supramolecular compounds.

2. Experimental

2.1. Physical measurements

IR spectra were recorded as Nujol mulls using Perkin-Elmer 597 and Nicolet 510P spectrophotometers. Microanalyses were carried out using Heraeus CHN-O-RAPID. The ^{207}Pb solution NMR spectra were recorded on a Bruker DRX-500 AVANCE spectrometer at 104.6 MHz using a 5-mm broadband probe. Lead chemical shifts are reported (ppm) downfield from tetramethyllead using $Pbph_4$ ($\delta_{Pb} = -178.0$ ppm, saturated in $CDCl_3$) as an external standard. Each lead spectrum was acquired over 3–10 h.

2.2. Preparation of $[Pb_2(4,4'\text{-bipy})(NO_3)_4]$

4,4′-Bipyridine (4,4′-bipy) (0.156 g, 1 mmol) was placed in one arm of a branched tube and lead (II) nitrate (0.331 g, 1 mmol) in the other. Methanol was carefully added to fill both arms, the tube sealed and the ligand-containing arm immersed in a bath at 60 °C while the other was at ambient temperature. After 15 days, white crystals had deposited in the cooler arm which were filtered off, washed with acetone and ether, and air dried (0.288 g, yield 60%), m.p. > 320 °C. Calc. for $C_8H_8N_6O_{12}Pb_2$: C, 11.70; H, 1.66; N, 10.24. Found C, 10.87; H, 0.97; N, 11.12%. IR (cm^{-1}) selected bands: 740(s), 1010(s), 1380(vs), 1528(s), 1618(s), 3038(w). ^{1}H NMR (DMSO, δ): 7.80 (m, 2H), 8.70 (m, 2H). ^{13}C–{^{1}H} NMR (DMSO; δ): 124.30, 139.30, 144.50, 149.30. ^{207}Pb NMR (DMSO; δ) −2590.00.

2.3. Preparation of $[Pb(4,4'\text{-bipy})Cl_2]$

4,4′-Bipyridine (4,4′-bipy) (0.156 g, 1 mmol) was placed in one arm of a branched tube and lead (II) chloride (0.28 g,1 mmol) in the other. Methanol was carefully added to fill both arms, then the tube was sealed and the ligand-containing arm immersed in a bath at 60 °C while the other was at ambient temperature (Fig. 1). After 30 days, yellow-white crystals had deposited in the cooler arm, which were filtered off, washed with acetone and ether, and air dried (0.177 g yield 40%), m.p. > 320 °C. Calc. for $C_{10}H_8N_2Cl_2Pb$: C, 27.52; H, 1.83; N, 6.42. Found C, 27.32; H, 1.75; N, 6.55%. IR (cm^{-1}) selected bands: 612(vs), 797(vs), 1209(s), 1396(s), 1583(s), 3015(w). ^{1}H NMR (DMSO, δ): 7.75 (m, 2H), 8.80 (m, 2H). ^{13}C–{^{1}H} NMR (DMSO; δ): 124.30, 139.30, 144.50, 149.30. ^{207}Pb NMR (DMSO; δ) −2556.78.

2.4. Preparation of $[Pb(4,4'\text{-bipy})(CH_3COO)_2]$

4,4′-Bipyridine (4,4′-bipy) (0.156 g, 1 mmol) was placed in one arm of a branched tube and lead (II) acetate (0.36 g,1 mmol) in the other. Methanol was carefully added to fill both arms, then the tube was sealed and the ligand-containing arm immersed in a bath at 60 °C while the other was at ambient temperature (Fig. 1). After 15 days, white crystals had deposited in the cooler arm, which were filtered off, washed with acetone and ether, and air dried (0.240 g yield 50%), m.p. > 320 °C. Calc. for $C_{14}H_{14}N_2O_4Pb$: C, 34.85; H, 2.90; N, 5.80. Found C, 34.61; H, 2.18; N, 5.33%. IR (cm^{-1}) selected bands: 740(s), 1010(s), 1398(vs), 1557(vs), 1618(s), 3040(w). ^{1}H NMR (DMSO, δ): 1.70 (s, 3H), 7.8 (m, 2H), 8.75 (m, 2H). ^{13}C–{^{1}H} NMR (DMSO; δ): 27.30 ($^{13}CH_3$-COO), 124.30, 139.30, 144.50, 149.30, 178.58 (CH_3-^{13}COO). ^{207}Pb NMR (DMSO; δ) −2556.78.

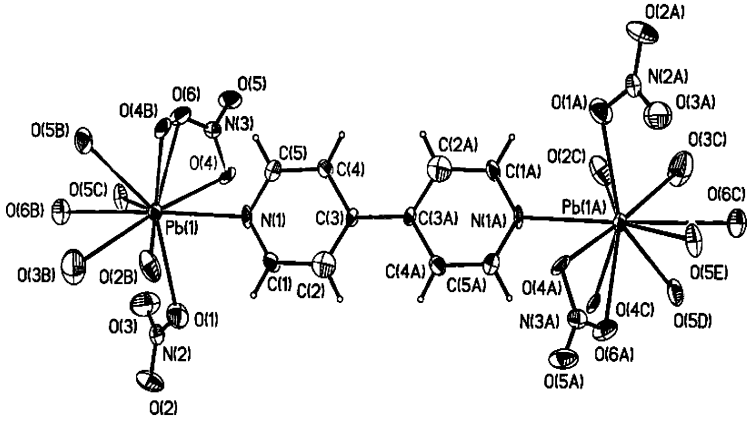

Fig. 1. ORTEP drawing of compound $[Pb_2(4,4'\text{-bipy})(NO_3)_4]$.

2.5. Preparation of $[Pb_2(4,4'\text{-bipy})(SCN)_4]$

4,4′-Bipyridine (4,4′-bipy) (0.156 g, 1 mmol) was placed in one arm of a branched tube and a mixture of lead (II) acetate (0.36 g, 1 mmol) and potassium thiocyanate (1.96 g, 2 mmol) in the other. Methanol was carefully added to fill both arms, then the tube was sealed and the ligand-containing arm immersed in a bath at 60 °C while the other was at ambient temperature. After 10 days, white crystals, m.p. > 320 °C had deposited in the cooler arm, which were filtered off, washed with acetone and ether, and air dried (0.40 g, yield 60%). Calc. for $C_{14}H_8N_6S_4Pb_2$: C, 20.92; H, 0.99; N, 10.46. Found C, 20.41; H, 1.08; N, 10.73%. IR (cm^{-1}) selected bands: 740(s), 1010(s), 1255(s), 1557(s), 1618(s), 2025(vs), 3040(w). ^1H NMR (DMSO, δ): 7.80 (m, 2H), 8.70 (m, 2H). ^{13}C–{^1H} NMR (DMSO; δ): 123.20 ($S^{13}CN$), 124.50, 139.40, 144.50, 149.30. ^{207}Pb NMR (DMSO; δ) −2856.78.

2.6. Preparation of $[Pb(4,4'\text{-bipy})(NO_3)(SCN)]_n$

4,4′-Bipy (0.156 g, 1 mmol) was placed in one arm of a branched tube and mixture of lead(II) nitrate (0.331 g, 1 mmol) and potassium thiocyanate (0.097 g, 1 mmol) in the other. Methanol was carefully added to fill both arms, the tube sealed and the ligand-containing arm immersed in a bath at 60 °C while the other was at ambient temperature. After 10 days, white crystals (m.p. = 220 °C) had deposited in the cooler arm which were filtered off, washed with acetone and ether, and air dried (0.242 g, yield 50%). Calc. for $C_{11}H_8N_4O_3PbS$ C, 27.30; H,1.65; N,11.58. found C, 27.87; H, 1.29; N, 11.25%. IR (cm^{-1}) selected bands: 718(s), 800(s), 1060(m), 1365(vs), 1585(s), 2040(s), 3035(w). ^1H NMR (DMSO, δ): 7.8 (m, 2H), 8.75 (m, 2H). ^{13}C–{^1H}NMR (DMSO, δ): 123.20 ($S^{13}CN$), 124.30, 139.30, 144.50, 149.30. ^{207}Pb NMR (DMSO; δ) −2369.44.

3. Results and discussion

3.1. Synthesis

Reaction between 4,4′-bpy ligand with lead(II) thiocyanate, lead(II) nitrate, lead(II) chlorate, lead(II) acetate and mixture of lead(II) nitrate and potassium thiocyanate provided crystalline materials analyzing as $[Pb_2(4,4'\text{-bipy})(NCS)_4]_n$, $[Pb_2(4,4'\text{-bipy})(NO_3)_4]_n$, $[Pb(4,4'\text{-bipy})(CH_3COO)_2]$, $[Pb(4,4'\text{-bipy})Cl_2]$ and $[Pb(4,4'\text{-bipy})(NO_3)(SCN)]_n$, respectively. Attempts to isolate the 1:1 adduct of lead(II) thiocyanate and lead(II) nitrate with 4,4′-bpy ligand, {$[Pb(4,4'\text{-bipy})(NCS)_2]$ and $[Pb(4,4'\text{-bipy})(NO_3)_2]$}, were not successful and each time the 1:2 (L:M) adduct was isolated.

3.2. Crystal structure of $[Pb_2(4,4'\text{-bipy})(NO_3)_4]_n$

The crystal structure of $[Pb_2(4,4'\text{-bipy})(NO_3)_4]_n$ consists of polymeric units of $[Pb_2(4,4'\text{-bipy})(NO_3)_4]$. The nitrogen atoms of the 4,4′-bipyridine ligand link each lead atom with a Pb–N distance of 2.578(9) Å. The oxygens of two nitrate anions are coordinated with distances of Pb(1)–O(1) = 2.672(11) Å, Pb(1)–O(4) = 2.910(10) Å and Pb(1)–O(6) = 2.731(11) Å, and also six oxygen atoms of neighboring nitrate anions with distances of about 2.6–3.035(11) Å. The coordination number in this complex is 10 (one from the '4,4′-bipy' ligand, nine from nitrate anions) (Fig. 1). The interaction of lead(II) with oxygen atoms of an adjacent molecule produce polymer units in the solid state (Fig. 2). The two lead atoms are bridged by the 4,4′-bipy ligand. Since the inversion center is located at the middle of the C(3)–C(3A) bond, the aromatic rings of the 4,4′-bipy ligand are coplanar. In conclusion, the structure reported here reveals a new type of interpenetration and a rarely observed 2D framework type.

3.3. Crystal structure of $[Pb_2(4,4'\text{-bipy})(NCS)_4]_n$

The crystal structure of $[Pb_2(4,4'\text{-bipy})(NCS)_4]_n$ consists of polymeric units of $[Pb_2(4,4'\text{-bipy})(NCS)_4]$. Each lead atom is linked by the nitrogen atoms of 4,4′-bpy ligand and with a Pb–N distance of 2.675 Å and thiocyanate anions with Pb–N distances of 2.543(8) and 2.590(9) Å. The lead atom also has weak links to one nitrogen atom and four sulfur atoms of neighboring thiocyanate anions. So the coordination number in this complex is three (one from the '4,4′-bpy' ligand and two from thiocyanate ligands) (Fig. 3) and the weak interaction of lead(II) with nitrogen and sulfur atoms of an adjacent molecule produces polymeric units in solid state (Fig. 4). In fact each Pb atom in this structure, along with three normal bonds, forms five "weak" Pb···N and Pb···S bonds and the exact distances are Pb(1)–N(3)#1 = 2.829(9), Pb(1)–S(2)#2 = 3.174(3), Pb(1)–S(1)#3 = 3.192(3), Pb(1)–S(2)#4 = 3.203(3) and Pb(1)–S(1)#5 = 3.376(3) Å (Table 4).

The presence of a lone pair on the lead atom is apparently the reason that the bridging interactions cannot come closer together. If the stereochemically active lone pair was not present, there might be more of an interaction between the bridging atoms of lead (II) with the neighboring sulfur atoms of the thiocyanate ligand, and this phenomenon could lead to more symmetry. The coordination number in this complex would be eight (one from the '4,4′-bpy' ligand, seven from thiocyanate anions) and indeed, interaction of lead (II) with nitrogen and sulfur atoms of an adjacent molecule

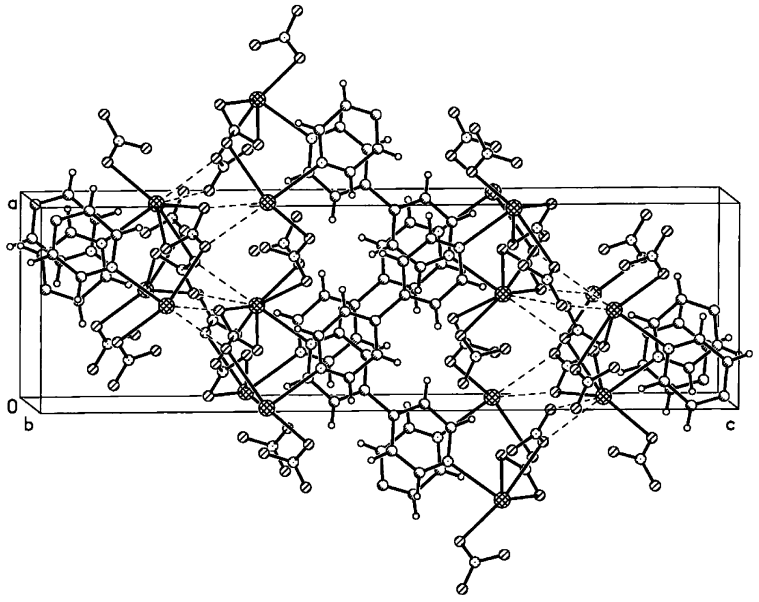

Fig. 2. The unit cell showing the π–π stacking interaction (charge-transfer arrays) between the parallel aromatic rings belonging to adjacent chains in $[Pb_2(4,4'\text{-bipy})(NO_3)_4]$.

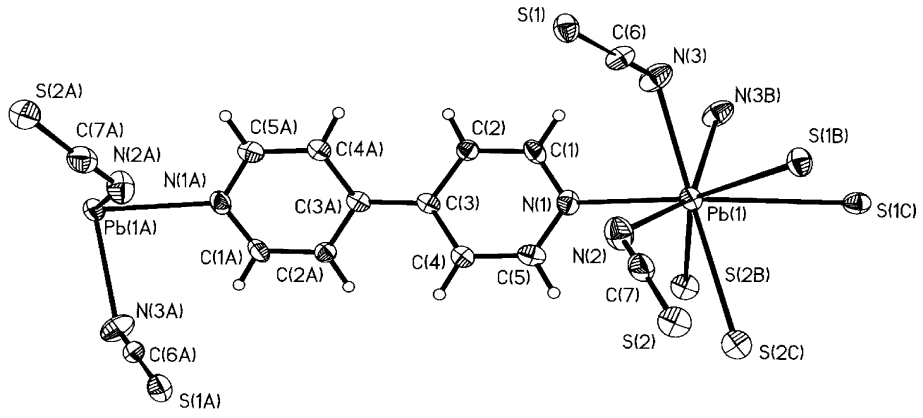

Fig. 3. ORTEP drawing of compound $[Pb_2(4,4'\text{-bipy})(SCN)_4]$.

produces polymer units in solid state. 4,4′-Bipyridine bridges the two lead atoms. Since the inversion center is located at the middle of the C(3)–C(3A) bond, the aromatic rings of 4,4′-bipyridine are coplanar. In conclusion, the structure reported here, analogously to $[Pb_2(4,4'\text{-bipy})(NO_3)_4]_n$, reveals a new type of interpenetration and rarely observed 2D framework type.

3.4. Crystal structure of $[Pb(4,4'\text{-bipy})(NO_3)(SCN)]_n$

The crystal structure of $[Pb(4,4'\text{-bipy})(NO_3)(SCN)]_n$ consists of two dimensional polymeric units of $[Pb(4,4'\text{-bipy})(NO_3)(SCN)]$. The nitrogen atoms of the 4,4′-bipy ligand and the oxygen atoms of the nitrate anion are linked to different lead atoms and the sulfur and nitrogen atoms of the thiocyanate anion are bridged to two lead atoms. Each lead atom is linked by the nitrogen atoms of the 4,4′-bipy ligand with Pb–N distances of 2.664(5) and 2.702(5) Å, the oxygens of nitrate anions with Pb–O distances of 2.724(6), 2.802(6), 2.815(6) and 2.842(6) Å, the nitrogen of the thiocyanate anion with a Pb–N distance of 2.461(6) Å and also the sulfur atom of the thiocyanate anion with a Pb–S distance of 2.909(2) Å. The coordination number in this complex is eight (two from 4,4′-bipy ligands, four from nitrate anions, two from thiocynate anions) (Fig. 5) and the lead atoms are bridged by 4,4′-bipy, nitrate and thiocyanate ligands and produce polymer units in the solid state (Fig. 6). Since the inversion center is not located at the middle of the C(3)–C(3′) bond, the aromatic rings of 4,4′-bipyridine are not coplanar. The two 4,4′-bipyridine ligands are trans and the N(1)–Pb(1)–N(1′A) angle is 162.4(2)°. The thiocyanate and also the nitrate ligands are *cis*. The nitrate anion could be bidentate chelated

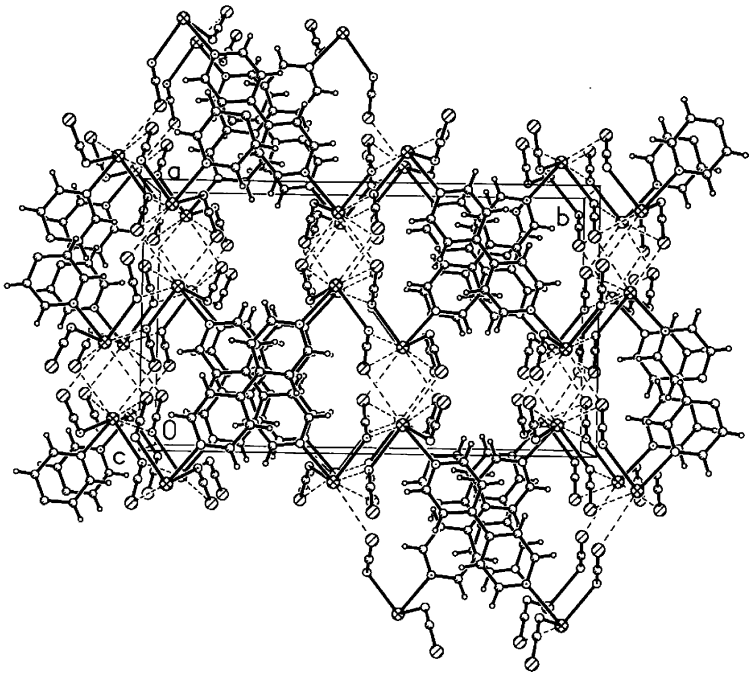

Fig. 4. The unit cell showing the π–π stacking interaction (charge-transfer arrays) between the parallel aromatic rings belonging to adjacent chains in $[Pb_2(4,4'\text{-bipy})(SCN)_4]$.

and also could be bridged, and indeed one of oxygen atoms of this anion is linked to two difference lead atoms (Chart 1).

It is very interesting that the bond lengths of the three N–O bonds and also the three bond angles for the nitrate anion in this complex are different, [N(3)–O(1) = 1.256(8), N(3)–O(2) = 1.232(8) and N(3)–O(3) = 1.231(8) Å; O(2)–N(3)–O(3) = 122.6(6)°, O(2)–N(3)–O(1) = 118.8(6)° and O(1)–N(3)–O(3) = 118.6(6)°]. This point shows that the nitrate anion has been distorted in forming a bridge between the two lead atoms and in producing the polymeric structure, and the result of this phenomena causes the variety of bond lengths and bond angles of the nitrate anion in this complex (Table 5).

The structure of the $[Pb(4,4'\text{-bipy})(NO_3)(SCN)]_n$ compound is interesting in several aspects. The above-mentioned compound is a new rarely observed 2D framework type and a new mixed-ligand complex containing three ligands that have simultaneously been bridged in its crystal structure and also the lone pair in this complex is inactive. The lone pair in most lead (II) complexes is active, and structures with inactive lone pairs are rarely observed [16].

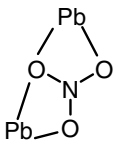

Chart 1.

The arrangement of 4,4′-bipy and nitrate anions do not suggests a gap or hole in the coordination geometry around the metal, indicating the lone pair of electrons on lead (II) is probably inactive in this complex.

The possible stereochemical activity of the lone pair in divalent lead compounds has recently been discussed by Shimoni-Livny et al. [16] based on a thorough review of crystal data available in the Cambridge Structural Database (CSD). They classify lead complex coordination as holodirected which refers to complexes in which the bonds to ligand atoms are placed throughout the surface of the encompassing sphere, while hemidirected refers to those cases in which the bond to ligand atoms are directed to particular parts of the coordination sphere, leaving a gap in the distribution of bonds to ligands. The latter holds for all lead (II) complexes with coordination number 2 to 5, is quite common for coordination numbers 6, 7 and 8, and does not exist in lead complexes with higher coordination numbers where holodirected geometry is the rule (Chart 2).

For the three structures described here, the coordination around the lead atoms is holodirected. It is becoming increasingly clear, however, that it is not necessarily true that one of the effects of the lone pair activity in Pb(II) compounds is to cause a void in the coordination geometry; in fact this geometry can take various forms [25]. Some authors [26] have also suggested that in the holodirected Pb(II) complexes there may be some adjacent short Pb^{II}–X bonds and some other long Pb–X bonds. Such a specific pattern of difference in bond lengths of holodirected complexes has been attributed

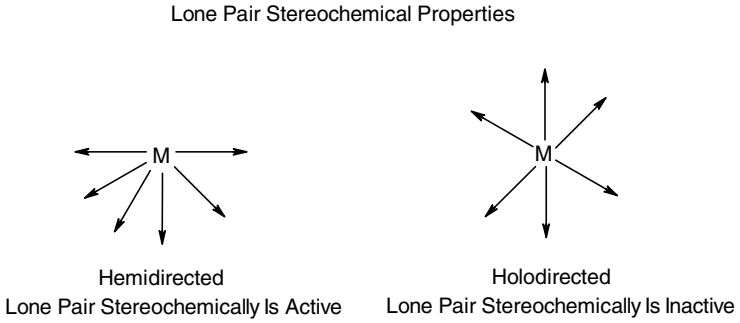

Chart 2.

Table 1
Crystal data and structure refinement for $[Pb(4,4'\text{-bipy})(NO_3)(NCS)]$ and $[Pb_2(4,4'\text{-bipy})(SCN)_2]$

Identification code	$[Pb(4,4'\text{-bipy})(NO_3)(NCS)]$	$[Pb_2(4,4'\text{-bipy})(SCN)_2]$
Empirical formula	$C_{11}H_8N_4O_3PbS$	$C_{14}H_8N_6Pb_2S_4$
Formula weight	483.46	802.88
Temperature (K)	293(2)	293(2)
Wavelength (Å)	0.71073	0.71073
Crystal system	monoclinic	orthorhombic
Space group	$P2_1/n$	$Pccn$
Unit cell dimensions		
a (Å)	9.2367(18)	12.899(2)
b (Å)	8.2303(16)	21.730(4)
c (Å)	19.0120(4)	6.6809(13)
α (°)	90	90
β (°)	103.13(3)	90
γ (°)	90	90
V (Å^3)	1407.6(5)	1872.6(6)
Z	4	4
D_{calc} (Mg/m^3)	2.281	2.848
Absorption coefficient (mm^{-1})	12.146	18.415
$F(000)$	896	1448
Crystal size (mm)	$0.40 \times 0.30 \times 0.30$	$0.40 \times 0.25 \times 0.20$
Θ range for data collection (°)	2.78–27.06	3.16–26.37
Index ranges	$-24 \geqslant h \geqslant 0$	$-3 \geqslant h \geqslant 16$
	$-10 \geqslant k \geqslant 0$	$-3 \geqslant k \geqslant 27$
	$-24 \geqslant l \geqslant 0$	$0 \geqslant l \geqslant 8$
Reflections collected	3164	1873
Independent reflections [R_{int}]	3070 [0.0534]	1821 [0.0127]
Completeness to θ (%)	99.1	95.1
Absorption correction	Ψ-correctional	Ψ-correctional
Maximum and minimum transmission	0.3115 and 0.1508	0.9597 and 0.2178
Refinement method	full-matrix least-squares on F^2	full-matrix least-squares on F^2
Data/restraints/parameters	3070/0/181	1821/6/119
Goodness-of-fit on F^2	0.997	0.971
Final R [$I > 2\sigma(I)$]	indices for 2441 reflections	indices for 1260 reflections
	$R_1 = 0.0326$, $wR_2 = 0.0771$	$R_1 = 0.0385$, $wR_2 = 0.0784$
R indices (all data)	$R_1 = 0.0463$, $wR_2 = 0.0790$	$R_1 = 0.0850$, $wR_2 = 0.0874$
Largest differential peak, hole (e Å^{-3})	1.316, −1.483	2.465, −1.630

by various authors to repulsion involving a stereochemically active lone pair [27]. In two of the reported complexes {1:2 (L:M) adducts, $[Pb_2(4,4'\text{-bipy})(NCS)_4]_n$ and $[Pb_2(4,4'\text{-bipy})(NO_3)_4]_n$}, the bond lengths of the coordination sphere are very difference {2.578–3.035 Å for $[Pb_2(4,4'\text{-bipy})(NO_3)_4]_n$ and 2.543–3.376 Å for $[Pb_2(4,4'\text{-bipy})(NCS)_4]_n$}. This point shows that in the $[Pb_2(4,4'\text{-bipy})(NCS)_4]_n$ and $[Pb_2(4,4'\text{-bipy})(NO_3)_4]_n$ complexes the coordination geometry is holodirected and there is a relatively large difference between the Pb–L distances in the two axial directions so possibly the lone pair is active. In contrast, in the $[Pb(4,4'\text{-bipy})(NO_3)(SCN)]_n$ complex, the coordination geometry is holodirected and the difference between the Pb–L distances is relatively small and the lone pair is likely to be inactive.

The striking similar feature of the three reported complexes here and $[Pb(4,4'\text{-bipy})I_2]$ [9] is that there is

Table 2
Crystal data and structure refinement for $[Pb_2(4,4'\text{-bipy})(NO_3)_4]$

Empirical formula	$C_{10}H_8N_6O_{12}Pb_2$
Formula weight	818.60
Temperature (K)	293 (2)
Wavelength (Å)	0.71073
Crystal system	orthorhombic
Space group	*Pbca*
Unit cell dimensions	
a (Å)	7.9264 (l 6)
b (Å)	8.4573 (17)
c (Å)	26.754 (5)
α (°)	90
β (°)	90
γ (°)	90
V (Å^3)	1793.5 (6)
Z	4
D_{calc} (Mg/m^3)	3.032
Absorption coefficient (mm^{-1})	18.830
$F(000)$	1480
Crystal size (mm)	$0.4 \times 0.3 \times 0.2$
Θ range for data collection (°)	2.99–29.06
Index ranges	$0 \geqslant h \geqslant 10$, $0 \geqslant k \geqslant 11$, $0 \geqslant l \geqslant 36$
Reflections collected	2336
Independent reflections [R_{int}]	2336 [0.0000]
Completeness to $\theta = 30.060$ (%)	97.5
Absorption correction	multi-scan (SADABS)
Maximum and minimum transmission	0.42 and 0.69
Refinement method	full-matrix least-squares on F^2
Data/restraints/parameters	2336/6/137
Goodness-of-fit on F^2	0.999
Final R indices for 1734 reflections [$I > 2\sigma(I)$]	$R_1 = 0.0665$, $wR_2 = 0.1884$
R indices (all data)	$R_1 = 0.0880$, $wR_2 = 0.1968$
Extinction coefficient	0.0035 (5)
Largest differential peak, hole (e Å^{-3})	6.828, −4.171

Table 3
Selected bond lengths (Å) and angles (°) for $[Pb_2(4,4'\text{-bipy})(NO_3)_4]$

Bond lengths	
Pb(1)-N(1)	2.578(9)
Pb(1)–O(2)#1	2.605(12)
Pb(1)–O(1)	2.672(11)
Pb(1)–O(4)#2	2.698(9)
Pb(1)–O(5)#2	2.736(11)
Pb(1)–O(6)	2.731(11)
Pb(1)–O(3)#1	2.849(18)
Pb(1)–O(4)	2.910(10)
Pb(1)–O(6)#3	2.918(10)
Pb(1)–O(5)#3	3.035(11)
Bond angles	
N(2)–Pb(1)–O(1)	78.2(4)
N(1)–Pb(1)–O(6)	87.9(3)
O(2)–Pb(1)–O(6)	141.9(3)
O(1)–Pb(1)–O(6)	138.8(3)
N(1)–Pb(1)–O(4)	68.2(3)
O(1)–Pb(1)–O(4)	94.5(3)
O(4)–Pb(1)–O(4)	98.73(5)
O(6)–Pb(1)–O(4)	44.6(3)

Symmetry codes. #1: $-x-1/2$, $y + 1/2$, z; #2: $-x + 1/2$, $y + 1/2$, z; #3: $x-1/2$, y, $-z + 1/2$.

Table 4
Selected bond lengths (Å) and angles (°) for $[Pb_2(4,4'\text{-bipy})(SCN)_4]$

Bond lengths	
Pb(1)–N(1)	2.543(8)
Pb(1)–N(2)	2.590(9)
Pb(1)–N(3)	2.675(9)
Pb(1)–N(3)#1	2.829(9)
Pb(1)–S(2)#2	3.174(3)
Pb(1)–S(1)#3	3.192(3)
Pb(1)–S(2)#4	3.203(3)
Pb(1)–S(1)#5	3.376(3)
Bond angles	
N(1)–Pb(1)–N(2)	75.7(3)
N(1)–Pb(1)–N(3)	82.8(3)
N(2)–Pb(1)–N(3)	83.3(3)

#1: $-x + 1$, $-y + 1$, $-z-1$; #2: x, y, $z + 1$; #3: $-x + 1$, $-y-1$, $-z-2$; #4: $-x + 1$, y, $z + 1/2$; #5: $x-1/2$, $-y + 1$, $-z-3/2$.

Table 5
Selected bond lengths (Å) and angles (°) for $[Pb(4,4'\text{-bipy})(NO_3)(NCS)]$

Bond lengths	
Pb(1)–N(1)	2.664(5)
Pb(1)–N(2)#1	2.461(6)
Pb(1)–N(1′)#2	2.702(5)
Pb(1)–O(1)	2.724(6)
Pb(1)–O(2)	2.802(6)
Pb(1)–O(3)#3	2.815(6)
Pb(1)–O(1)#3	2.842(6)
N(3)–O(1)	1.256(8)
N(3)–O(2)	1.232(8)
N(3)–O(3)	1.231(8)
Pb(1)–S(1)	2.909(2)
Bond angles	
O(1)–Pb(1)–N(1)	72.7(2)
O(2)–Pb(1)–N(1)	114.67(18)
O(1)–Pb(1)–O(2)	45.57(16)
N(1)–Pb(1)–S(1)	84.37(15)
O(1)–Pb(1)–S(1)	156.75(16)
O(2)–Pb(1)–S(1)	151.52(12)
O(2)–N(3)–O(3)	122.6(6)
O(2)–N(3)–O(1)	118.8(6)
O(1)–N(3)–O(3)	118.6(6)

#1: $-x + 1$, $-y + 1$, $-z$; #: $2x + 1$, $y-1$, z; #3: $-x + 1$, $y-1/2$, $-z + 1/2$.

a π–π stacking [28,29] interaction between the parallel aromatic rings that belong to an adjacent chain in the lead(II) polymer complex, as shown in Figs. 2, 4 and 6. As planar species in which the mean molecular planes are close to parallel and are separated by a distance of ~3.5 Å, they have a close resemblance to the planes in graphite.

The parallel arrays of the planes of the aromatic moieties indicate that these interactions in $[Pb_2(4,4'\text{-bipy})(SCN)_4]_n$, $[Pb(4,4'\text{-bipy})I_2]$ and $[Pb(4,4'\text{-bipy})(NO_3)(NCS)]$ are of the "π-stacking" type, rather than "edge-to-face" or "vertex-to-face" types [30–33]. Projection of the structure perpendicular to the ring plane shows the overall form of "slipped" stacking [30–34],

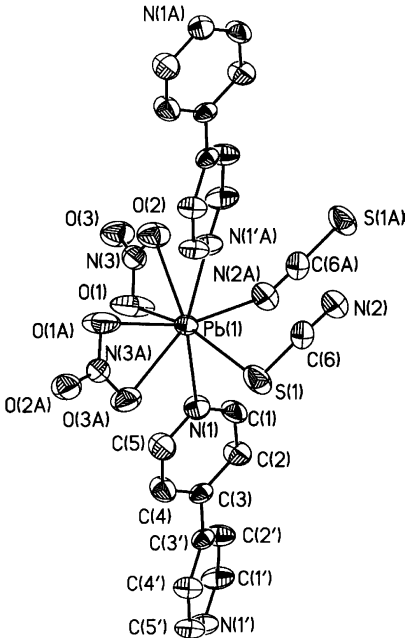

Fig. 5. ORTEP drawing of compound $[Pb(4,4'\text{-bipy})(NO_3)(SCN)]_n$.

which can be rationalized qualitatively in terms of optimizing the attraction between atoms of opposite charges [35]. In the $[Pb_2(4,4'\text{-bipy})(NO_3)_4]_n$ complex the parallel arrays interactions are of the ''edge-to-face'' type.

A simple model to describe the nature of π–π interactions has been developed by Hunter et al. [35]. This model predicts that face-to-face π-stacked interactions will be disfavored due to the dominance of π–π repulsion. However, in offset π-stacked, and edge-on or T-shaped geometries, favourable π–σ attractions dominate. The polarization of aromatic systems through the introduction of heteroatoms, electron-withdrawing groups or electron-donating groups, alters the nature of any π–π interactions. For example, although it is well known that neither benzene [36] nor hexafluorobenzene tend to form stacked arrangements, the adduct between these two molecules adopts a structure comprising of inclined stacks of alternating molecules [37]. Here the hexafluorobenzene π-system is electron-deficient with respect to benzene and this reduces the π–π repulsion, making the formation of offset π-stacked molecules more favorable. The introduction of heteroatoms can lead to a similar perturbation of aromatic interactions [32], specifically nitrogen atoms have been shown to remove electron density from the π-system, and hence have a similar effect to electron-withdrawing groups. It has been shown that electron-deficient aromatic groups interact most strongly with electron-rich aromatic groups. Hence, since the molecules of these complexes include equally or almost equally electron-deficient, or indeed electron-rich, rings, it can be expected that within $[Pb_2(4,4'\text{-bipy})(SCN)_4]_n$, $[Pb(4,4'\text{-bipy})I_2]_n$ and [Pb(4,4′-

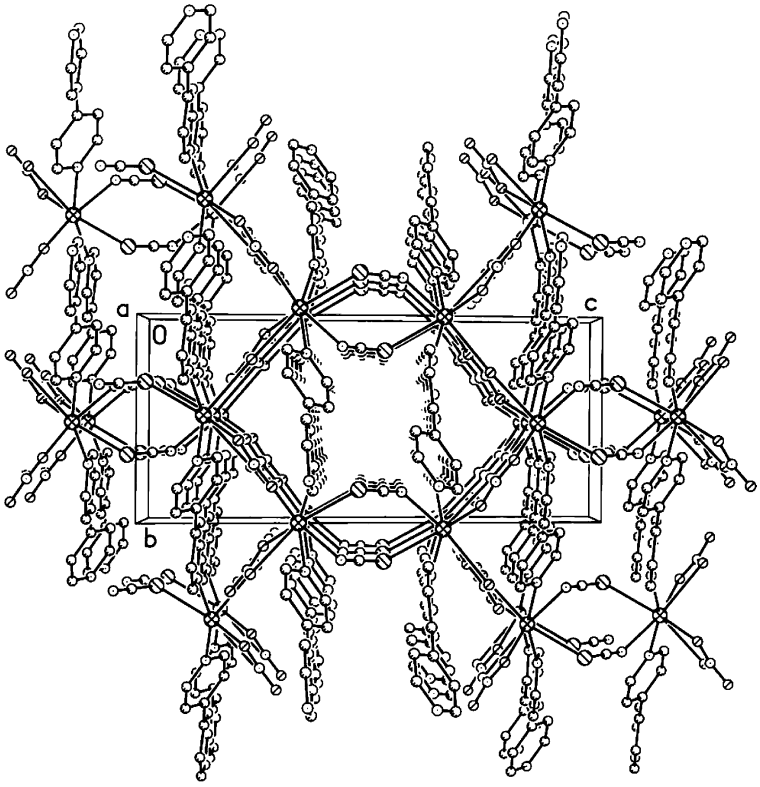

Fig. 6. The unit cell showing the π–π stacking interaction (charge-transfer arrays) between the parallel aromatic rings belonging to adjacent chains in $[Pb(4,4'\text{-bipy})(NO_3)(SCN)]_n$.

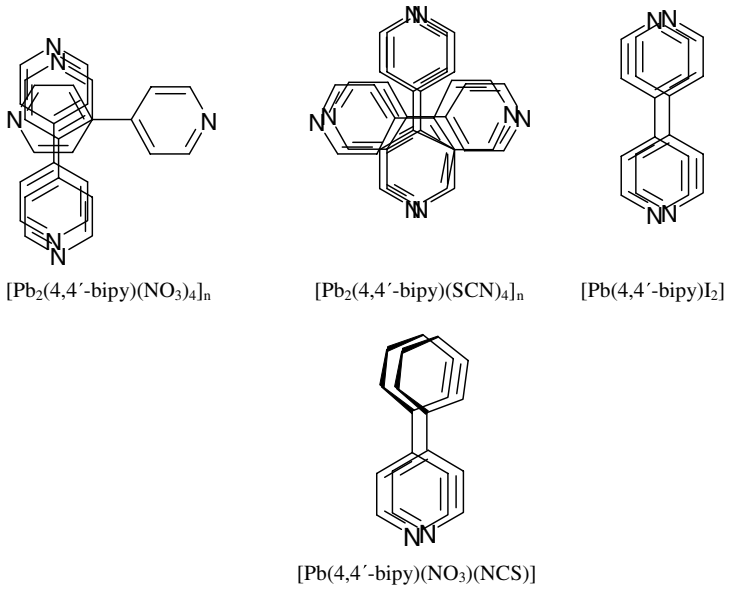

Fig. 7. Projection of nearest neighbour pairs in the π–π stacks of heteroaromatic bases in Pb(II) complexes containing the 4,4′-bipy ligand.

bipy)$(NO_3)(NCS)]_n$ complexes, model face-to-face π-stacked interactions must be disfavored due to the dominance of π–π repulsion and within $[Pb_2(4,4'\text{-bipy})(NO_3)_4]_n$ the edge-to-face model must be favor. This point suggests that the lone pair activity is the most important factor and it may be more important than the π–π repulsion that is formed (Fig. 7).

Thus two factors, lone pair activity and π–π stacking, may control the coordination sphere of this complex. The obvious question then is whether the lone pair activity has stretched coordinate bonds to result in ligand stacking or whether it is the stacking interaction, which has imposed a positioning of the donor atoms for forming gap in the coordination sphere. Since the model face-to-face π-stacked interactions must be disfavored due to the dominance of π–π repulsion, this possibly suggests that lone pair activity may be the most important factor and results in the formation of π–π stacking. Indeed, it is now realized that lone pair activity can also play a significant and predictable structure-determining role in the polymeric structures.

Crystallographic data, selected bond lengths and angles are given in Tables 1–3. Atomic coordinates, anisotropic thermal parameters, observed and calculated structure factors; full lists of bond distances, band angles and torsion angles are given in the supplementary material. A perspective view of ORTEP diagrams and the packing in the unit cells are shown in Figs. 1–6.

4. Supplementary material

Complete bond lengths and angles, co-rdinates and displacement parameters have been deposited at the Cambridge Crystallography Data Centre. Supplementary data are available from the CCDC, 12 Union Road, Cambridge CB2 1EZ, UK (fax: +44-1223-336033; e-mail: deposit@ccdc.cam.ac.uk or www: http://www.ccdc.cam.ac.uk) on request, quoting the deposition number 195034 for $[Pb_2(4,4'\text{-bipy})(NO_3)_2]$, 208614 for $[Pb_2(4,4'\text{-bipy})(SCN)_2]$ and 208613 for [Pb(4,4′-bipy)$(NO_3)(NCS)$].

Acknowledgement

Support of this investigation by Tarbiat Modarres University is gratefully acknowledged.

References

[1] M. Fujita, Y.J. Kwon, S. Washizu, K. Ogura, J. Am. Chem. Soc. 116 (1994) 1151.
[2] R.W. Gable, B.F. Hoskins, R. Robson, J. Chem. Soc. Chem. Commun. (1990) 1677.
[3] L. Carlucci, G. Ciani, D.M. Proserpio, A. Sironi, J. Chem. Soc. Dalton Trans. (1997) 1801.
[4] O.M. Yaghi, G. Li, Angew. Chem. Int. Ed. Engl. 34 (1995) 207.
[5] K. Biradha, K.V. Domasevitch, B. Moulton, C. Sewad, M.J. Zaworotko, Chem Commun. (1999) 1327.
[6] M.-L. Tong, B.-h. Ye, J.-W. Cai, X.-M. Chen, S.W. Ng, Inorg. Chem. 37 (1998) 2645.
[7] Y.-C. Liang, M.-C. Hong, R. Cao, W.-P. Su, Y.-J. Zhao, J.-B. Weng, Polyhedron 20 (2001) 2477.
[8] V. Tudor, V. Kravtsov, M. Julve, F. Lloret, y.A. Simonov, J. Lipkowski, V. Buculei, M. Andruh, Polyhedron 20 (2001) 3033.
[9] Y.J. Shi, Y. Xu, Y. Zhang, B. Huang, D.R. Zhu, C.M. Jin, H.G. Zhu, Z. Yu, X.T. Chen, X.Z. You, Chem. Lett. (2001) 678.

[10] P. Pyykkö, Chem. Rev. 88 (1988) 563.
[11] A. Bashall, M. Mcpartlin, B.P. Murphy, D.E. Fenton, S.J. Kitchen, P.A. Tasker, J. Chem. Soc. Dalton Trans. (1990) 505, and references therein.
[12] P. Schwerdtheger, G.A. Heath, M. Dolg, M.A. Bennett, J. Am. Chem. Soc. 114 (1992) 7518.
[13] K. Byriel, K.R. Dunster, L.R. Gahan, C.H.L. Kennard, J.L. Latten, I.L. Swann, P.A. Duckworth, Polyhedron 11 (1992) 1205.
[14] A. Andres, A. Bencini, A. Garachalios, A. Bianchi, P. Dapporto, E. Garcia-Espna, P. Paoletti, P. Paoli, J. Chem. Soc. Dalton Trans. (1993) 3507.
[15] J.M. Harrowfield, H. Miyamae, B.W. Skelton, A.A. Soudi, A.H. White, Aust. J. Chem. 49 (1996) 1165, and references therein.
[16] L. Shimoni-Livny, J.P. Glusker, C.W. Bock, Inorg. Chem. 37 (1998) 1853.
[17] J.M. Harrowfield, R.P. Sharma, B.W. Skelton, A.H. White, Aust. J. Chem. 51 (1998) 735, and references therein.
[18] R.D. Hancock, A.E. Martell, Chem. Rev. 89 (1989) 1875.
[19] A.R. Mahjoub, A. Morsali, Polyhedron 21 (2002) 2555.
[20] S.W. Schwarz, M.J. Welch, in: J.W. Kelly, T.O. Balldwin (Eds.), Applications of Enzyme Biotechnology, Plenum, New York, 1991.
[21] R.B. Lauffer, Chem. Rev. 87 (1987) 901.
[22] G.F. Baxter, Chem. Br. 28 (1992) 445.
[23] A. Morsali, A. Tadjarodi, R. Mohammadi, A.R. Mahjoub, Z. Kristallogr. NCS 216 (2001) 379.
[24] L.J. Barbour, S.J. Belfield, P.C. Junk, M.K. Smith, Aust. J. Chem. 51 (1998) 337.
[25] S.-W. Ng, J.J. Zuckerman, Adv. Inorg. Chem. Radiochem. 29 (1985) 297.
[26] I.D. Brown, J. Solid State Chem. 11 (1974) 214.
[27] S. Wang, D.B. Mitzi, C.A. Field, A. Guloy, J. Am. Chem. Soc. 117 (1995) 5297.
[28] N.N. Greenwood, A. Earnshaw, Chemistry of the Elements, Pergamon Press, Oxford, 1984, pp. 235–236.
[29] R. Foster, Paul Elek (Eds.), Molecular Complexes, Scientific Books Ltd, London, 1973.
[30] V. Russell, M.L. Scudder, I.G. Dance, J. Chem. Soc. Dalton Trans. (2001) 789, and references therein.
[31] I.G. Dance, M.L. Scudder, J. Chem. Soc. Dalton Trans. (1996) 3755.
[32] C. Janiak, J. Chem. Soc. Dalton Trans. (2000) 3885.
[33] Z.-H. Liu, C.-Y. Duan, J.-H. Li, Y.-J. Liu, Y.-H. Mei, X.-Z. You, New J. Chem. 24 (2000) 1057.
[34] T.M. Barclay, A.W. Cordes, J.R. Mingie, R.T. Oakley, K.E. Preuss, Cryst. Eng. Commun. 80 (15) (2000).
[35] C.A. Hunter, J.K.M. Sanders, J. Am. Chem. Soc. 112 (1990) 5525.
[36] J.M. Steed, T.A. Dixon, W. Klemperer, J. Chem. Phys. 70 (1979) 4940.
[37] J.C. Collings, K.P. Roscoe, E.G. Robins, A.S. Batsanov, L.M. Stimson, J.A.K. Howard, S.J. Clark, T.B. Marder, New J. Chem. 26 (2002) 1740.

Available online at www.sciencedirect.com
SCIENCE DIRECT®
Polyhedron 23 (2004) 2437–2445
POLYHEDRON
www.elsevier.com/locate/poly

Synthesis and reactivity in salt metathesis reactions of trivalent [La(Tp^{Me2})$_2$X] (X = Cl, I) complexes: crystal structures of [La(Tp^{Me2})$_2$Cl] and [La(Tp^{Me2})$_2$(κ^2-pz^{Me2})]

Fábio A. Kunrath [a], Osvaldo L. Casagrande Jr. [*,b], Loic Toupet [c], Jean-François Carpentier [d,*]

[a] *Instituto de Química de Araraquara, UNESP, C.P. 355, Araraquara, SP 14800-900, Brazil*
[b] *Laboratório de Catálise Molecular, Instituto de Quimica-Universidade Federal do Rio Grande do Sul, Av. Bento Goncalves, 9500, Porto Alegre, RS 90501-970, Brazil*
[c] *Groupe Matière Condensée et Matériaux, Cristallochimie, UMR 6626 CNRS-Université de Rennes 1, 35042 Rennes Cedex, France*
[d] *Laboratoire Organométalliques et Catalyse, UMR 6509 CNRS-Université de Rennes 1, 35042 Rennes Cedex, France*

Received 30 July 2004; accepted 27 August 2004
Available online 21 September 2004

Abstract

Reaction of $LaX_3(THF)_n$ (X = Cl, I) with two equiv. of K(Tp^{Me2}) gave good yields of the bis-Tp complexes [La(Tp^{Me2})$_2$X] (X = Cl (**1**); I (**3**)). However, the formation of **1** and **3** is always accompanied by significant amounts of La(Tp^{Me2})$_2$(κ^2-pz^{Me2}) ([pz^{Me2}]$^-$ = 3,5-dimethyl-pyrazolato) (**2**). The pyrazolato complex **2**, which presumably arises from decomposition of the [Tp^{Me2}]$^-$ moiety during salt metathesis, was independently prepared in good yield from **1** and in situ generated [pz^{Me2}]$^-$. The solid-state structures of **1** and **2** were determined by single-crystal X-ray diffraction studies. Subsequent reactions of halogeno-Tp^{Me2} complexes **1** and **3** with various alkali metal salts MR (M = Li, R = CH_2SiMe_3, Ph, $N(SiMe_3)_2$; M = K, R = OAr) gave M(Tp^{Me2}) as the major product. Alternatively, the mono-Tp bis(aryloxide) derivatives [Ln(Tp^{Me2})(OC_6H_2-2,6-^{t}Bu-4-Me)$_2$] (Ln = La (**4**); Nd (**5**)) were obtained in high yields by salt metathesis of [Ln(OC_6H_2-2,6-^{t}Bu-4-Me)$_3$] with one equiv. of K(Tp^{Me2}).
© 2004 Elsevier Ltd. All rights reserved.

Keywords: Tris(pyrazolyl)hydroborate (Tp) ligands; Lanthanum; Neodymium; Salt metathesis; Aryloxide derivatives

1. Introduction

First introduced by Trofimenko [1], tris(pyrazolyl)hydroborate (Tp) ligands is an attractive class of sterically demanding ancillaries for a wide variety of ionic metal centers [2]. Of particular interest is the case of lanthanides and analogous group 3 metals [3], due to their predominant ionic character. Indeed, one of the most attractive features of the Tp ligands is their steric tunability. This is a crucial point in lanthanide chemistry, which is recognized to be largely affected by steric factors [4]. Also, albeit ubiquitous cyclopentadienyl-type ligands are excellent for lanthanides, recent years have witnessed a considerable interest in developing related organolanthanide complexes involving other supporting ligands [5]. This quest for alternative ancillaries originates in large part from the permanent search for new-generation olefin polymerization catalysts, which is a very topical application field of early transition organometallic chemistry [6]. In this regard, the first use of Tp ligands for

* Corresponding author. Tel.: +33 223 235 950; fax: +33 223 236 939.
E-mail address: jean-francois.carpentier@univ-rennes1.fr (J.-F. Carpentier).

0277-5387/$ - see front matter © 2004 Elsevier Ltd. All rights reserved.
doi:10.1016/j.poly.2004.08.013

lanthanide-mediated ethylene polymerization was claimed with yttrium complexes $[Y(Tp^{Me2})R_2(THF)_x]$ (R = CH_2SiMe_3, C_6H_5) and analogous complexes with variously substituted $Tp^{R,R'}$ ligands [1] and lanthanide metal centers [7,8]. Despite the quite poor catalytic activity, the results suggested potentiality for improvement via specific catalyst design [7].

Potential precursors for this purpose include half-sandwich trivalent lanthanide dihalides $[Ln(Tp^R)X_2]$, and the more sterically crowded sandwich monohalides $[Ln(Tp^R)_2X]$ [3]. Relevant examples of such complexes derived from the ubiquitous Tp^{Me2} ligand are the mono-solvated complexes $[Ln(Tp^{Me2})Cl_2(THF)]$ (Ln = Yb [9], Nd [10], Lu [11], Y [10], Sc [12]) and the non-solvated complexes $[Nd(Tp^{Me2})_2X]$ (X = Cl, NPh_2, dpm, OAr, β-dike, H_2BEt_2) [13] and $[Sm(Tp^{Me2})_2X]$ (X = Cl, Br, I) [14]. However, at this early stage, one shall face a first synthetic problem, that is the preparation of these complexes is often hampered by the propensity of the Tp^R ligand, especially Tp^{Me2}, to decompose [15]. A number of degradation products that likely arise from hydrolysis by adventitious water during purification or crystallization, e.g., pyrazole adducts $[Ln(Tp^{Me2})Cl(\mu\text{-}Cl)(Hpz^{Me2})]$ (Ln = Nd, Pr; Hpz^{Me2} = 3,5-dimethylpyrazole) [9] and $[Ln(Tp^{Me2})X_2(Hpz^{Me2})]$ (Ln = La, Y) [10], and dimers $[Ln(Tp^{Me2})(\mu\text{-}BOp^{Me2})]_2$ (Ln = La, Ce, Sm; $BOp^{Me2} = (HBO(pz^{Me2})_2)^{2-}$) [16], have been isolated. Beside those, significant amounts of other products are formed directly from the salt metathesis reactions between LnX_3 and the Tp^R salt, of which the identity remains to be established [16]. Further complications arise for the preparation of potentially active polymerization complexes from the halide lanthanide precursors. For instance, attempts at derivatization of $[Sm(Tp^{Me2})Cl_2(L)]$ (L = coordinating molecule) using such groups as RO^-, Et_2N^-, or R^- failed due to ligand redistribution [17].

This work reports on the synthesis and characterization of new trivalent lanthanum mono-halide complexes incorporating the Tp^{Me2} ligand, and the identification of side-products that originate directly for the salt metathesis reactions. In addition, reactions of these halide precursors with alkoxides, amides and alkyl reagents have been investigated and shown to give mainly undesired products. An alternative synthesis toward diaryloxide lanthanide complexes $[Ln(Tp^{Me2})(OAr)_2]$ (Ln = La, Nd) is proposed.

[1] The abbreviation used for the ligands is that proposed by Trofimenko [2g]: Tp stands for tris(pyrazolyl)borate; R and R′ are substituents at the 3 and 5 positions of the pyrazolyl group, respectively, and a 4-substituent is denoted by the superscript 4R.

2. Experimental

2.1. General procedures

All manipulations were performed under a purified argon atmosphere using standard high vacuum Schlenk techniques or in a glovebox. Solvents were distilled from Na/benzophenone (THF) and Na/K alloy (toluene, pentane and cyclohexane) under nitrogen and degassed thoroughly prior to use. Deuterated solvents (>99.5% D, Eurisotop) were vacuum-transferred from drying agents (benzene-d_6, toluene-d_8, THF-d_8: Na/K; $CDCl_3$: CaH_2). $LaCl_3(THF)_{1.5}$ was obtained after repeated extraction of anhydrous $LaCl_3$ (Strem) from THF. $NdCl_3(THF)_2$ was generously provided by Rhodia. $K(Tp^{Me2})$ [1b], $LaI_3(THF)_n$ [18], $Ln(OC_6H_2\text{-}2,6\text{-}{}^tBu_2\text{-}4\text{-}Me)_3$ (Ln = La, Nd) [19], and $Nd(Tp^{Me2})_2Cl$ [13] were prepared according to literature procedures. $LiCH_2SiMe_3$ (1.0 M solution in pentane, Aldrich), PhLi (1.9 M solution in THF, Aldrich) and *n*-BuLi (1.6 M solution in hexane, Acros) were used as received. NMR spectra were recorded on Bruker DPX-200 and AC-300 spectrometers in Teflon-valved NMR tubes at 20 °C unless otherwise indicated. ^1H and ^{13}C chemical shifts are reported versus $SiMe_4$ and were determined by reference to the residual solvent peaks. Assignment of signals was made from ^1H–^1H COSY, ^1H–^{13}C HMQC and HMBC NMR experiments. Coupling constants are given in Hertz. Elemental analyses (C, H, N) were performed by the Microanalytical Laboratory at the Institute of Chemistry of Rennes and are the average of two independent determinations. IR spectroscopy was carried out on a Nicolet 510 FTIR spectrophotometer and is expressed by wave number (cm^{-1}).

2.2. Synthesis of lanthanide complexes

2.2.1. Salt elimination reaction of $LaCl_3$ and $K(Tp^{Me2})$: synthesis of $[La(Tp^{Me2})_2Cl]$ (1) and $[La(Tp^{Me2})_2(\kappa^2\text{-}pz^{Me2})]$ (2)

$LaCl_3$ (0.900 g, 3.68 mmol) was introduced in a Schlenk flask and THF (70 mL) was added. The suspension was stirred for 12 h at room temperature and $K(Tp^{Me2})$ (2.47 g, 7.35 mmol) was added. The mixture was stirred at 20 °C for 7 days, period over which the amount of insoluble material decreased. Volatiles were removed under vacuum and the residue was extracted with toluene (2 × 40 mL). The colorless filtrate was evaporated under vacuum and the residue washed with pentane (3 × 25 mL) to afford **1** as a white powder (1.88 g, 65%). Crystals of **1** suitable for X-ray diffraction were grown from a 1:2 toluene/pentane solution at −34 °C.

Elemental *Anal.* Calc. for $C_{30}H_{44}B_2ClN_{12}La$ (MW 768.32): C, 46.87; H, 5.77; N, 21.86. Found: C, 47.18; H, 5.93; N, 21.79%.

^{1}H NMR (200 MHz, toluene-d_8): δ 5.60 (s, 6H, 4-H), 2.22 (s, 18H), 2.03 (s, 18H) (3-CH_3 and 5-CH_3).

^{13}C{^{1}H} NMR (50 MHz, toluene-d_8): δ 151.1 (3-C), 145.5 (5-C), 106.9 (4-C), 14.0, 13.6 (3-CH_3 and 5-CH_3).

Evaporation of the final pentane washings (vide supra) left **2** as a white powder (0.49 g, 16%). Crystals of **2** suitable for X-ray diffraction were grown from a toluene/cyclohexane solution at −34 °C.

Elemental *Anal.* Calc. for $C_{35}H_{51}B_2N_{14}La$ (MW 828.01): C, 50.75; H, 6.21; N, 23.67. Found: C, 50.25; H, 6.31; N, 22.66%.

^{1}H NMR (200 MHz, toluene-d_8): δ 5.95 (s br, 1H, 4-H pyrazolato), 5.60 (s, 6H, 4-H pyrazolyl), 2.28 (s, 18H, CH_3 Tp^{Me2}), 1.93 (s br, 6H, 3,5-CH_3 pyrazolylato), 1.75 (s, 18H, CH_3 Tp^{Me2}).

^{13}C{^{1}H} NMR (50 MHz, toluene-d_8): δ 150.4 (3-C), 145.5 (3,5-C pyrazolato), 144.9 (5-C), 106.9 (4-C pyrazolato), 106.4 (4-C Tp^{Me2}), 14.0 (3,5-CH_3 pyrazolato), 13.7, 12.7 (3-CH_3 and 5-CH_3).

2.2.2. Synthesis of $[La(Tp^{Me2})_2Cl]$ (1) and $[La(Tp^{Me2})_2(\kappa^2\text{-}pz^{Me2})]$ (2) from $LaCl_3(THF)_{1.5}$

$LaCl_3(THF)_{1.5}$ (0.560 g, 1.78 mmol) and K(Tp^{Me2}) (1.31 g, 3.56 mmol) were introduced in a Schlenk flask and THF (50 mL) was added. The mixture was stirred at 20 °C for 7 days, period over which the amount of insoluble material decreased. Volatiles were removed under vacuum and the residue was extracted with toluene (2 × 40 mL). The colorless filtrate was evaporated under vacuum and the residue washed with pentane (3 × 25 mL) to afford **1** as a white powder (0.66 g, 48%). Evaporation of the final pentane washings left **2** as a white powder (0.49 g, 33%).

2.2.3. Conversion of $[La(Tp^{Me2})_2Cl]$ (1) to $[La(Tp^{Me2})_2(\kappa^2\text{-}pz^{Me2})]$ (2)

The reaction was performed using a procedure similar to that described by Winter et al. [20]. Complex **1** (0.210 g, 0.275 mmol) and 3,5-dimethylpyrazole (0.080 g, 0.825 mmol) were introduced in a Schlenk flask, with some toluene (15 mL). Under magnetic stirring, NEt_3 (0.12 mL, 0.825 mmol) was added dropwise to the solution by syringe. The solution became immediately turbid. The mixture was stirred for 5 days at 20 °C. After this period, volatiles were removed under vacuum and the residue was analyzed by ^{1}H NMR (C_6D_6), which showed the presence of **1** (36%) and **2** (64%).

2.2.4. $La(Tp^{Me2})_2I]$ (3)

This reaction was performed as described above for **1** starting from $LaI_3(THF)_{0.63}$ (1.76 g, 3.13 mmol) and K(Tp^{Me2}) (2.10 g, 6.26 mmol), with a reaction time of 3 days at 20 °C. Usual workup afforded **2** (0.31 g, 12%) from the final pentane washings and **3** as a white powder insoluble in pentane (1.82 g, 67%).

Elemental *Anal.* Calc. for $C_{30}H_{44}B_2IN_{12}La$: (MW 859.84): C, 41.89; H, 5.16; N, 19.54. Found: C, 41.88; H, 5.45; N, 19.80%.

^{1}H NMR (200 MHz, $CDCl_3$): δ 5.73 (s, 6H, 4-H), 2.38 (s, 18H, CH_3 Tp^{Me2}), 1.88 (s, 18H, CH_3 Tp^{Me2}).

^{13}C{^{1}H}NMR (50 MHz, $CDCl_3$): δ 151.3 (3-C), 146.8 (5-C), 107.0 (4-C), 14.5, 13.8 (3-CH_3 and 5-CH_3).

2.2.5. $La(Tp^{Me2})(OC_6H_2\text{-}2,6\text{-}^tBu_2\text{-}4\text{-}Me)_2]$ (4)

$La(OC_6H_2\text{-}2,6\text{-}^tBu_2\text{-}4\text{-}Me)_3$ (0.560 g, 0.725 mmol) and K(Tp^{Me2}) (0.240 g, 0.725 mmol) were introduced in a Schlenk flask, and toluene (10 mL) was added. The mixture was stirred at 60 °C for 12 h, period over which a white solid precipitated. Pentane (10 mL) was added and the solid was filtered out. Volatiles were removed under vacuum and the residue was heated at 60 °C under ca. 0.1 mm Hg to remove the phenol 2,6-^{t}Bu$_2$-4-Me- C_6H_2OH formed in the reaction, leaving **4** as a pale brown solid (0.514 g, 81%).

Elemental *Anal.* Calc. for $C_{45}H_{68}N_6O_2BLa$: (MW 874.22): C, 61.79; H, 7.84; N, 9.61. Found: C, 62.23; H, 7.52; N, 9.86%.

^{1}H NMR (200 MHz, C_6D_6): δ 7.16 (s, 4H, C_6H_2), 5.48 (s, 3H, 4-H Tp^{Me2}), 2.31 (s, 6H, 4-CH_3 Ar), 2.27 (s, 9H, CH_3 Tp^{Me2}), 2.12 (s, 9H, CH_3 Tp^{Me2}), 1.56 (s, 36H, 2,6-^{t}Bu Ar).

^{13}C{^{1}H} NMR (50 MHz, C_6D_6): δ 150.0, 146.4 (3-C and 5-C pyrazolyl), 136.2 (*ipso*-C Ar), 128.4 (*o*-C Ar), 126.4 (*m*-C Ar), 125.0 (*p*-C Ar), 106.6 (4-C pyrazolyl), 35.3 (C ^{t}Bu), 32.6 ($CH_3{}^t$Bu), 21.7 (4-CH_3 Ar), 14.6, 13.4 (3-CH_3 and 5-CH_3).

2.2.6. $Nd(Tp^{Me2})(OC_6H_2\text{-}2,6\text{-}^tBu\text{-}4\text{-}Me)_2]$ (5)

This complex was synthesized using the same procedure as that described above, starting from $Nd(OC_6H_2\text{-}2,6\text{-}^tBu\text{-}4\text{-}Me)_3$ (0.300 g, 0.376 mmol) and K(Tp^{Me2}) (0.130 g, 0.376 mmol), to afford **5** as a clear blue solid (0.204 g, 88%).

Elemental *Anal.* Calc. for $C_{45}H_{68}N_6O_2BNd$ (MW 879.56): C, 61.41; H, 7.79; N, 9.55. Found: C, 62.14; H, 7.79; N, 9.61%.

2.3. Crystal structure determination of complexes 1 and 2

Suitable single crystals of all investigated compounds were mounted onto glass fibers using the "oil-drop" method. All diffraction data were collected at 120 K using a NONIUS Kappa CCD diffractometer with graphite monochromatized Mo Kα radiation (λ = 0.71073 Å). A combination of ω- and φ-scans was carried out to obtain at least a unique data set. Crystal structures were solved by means of the Patterson method, remaining atoms were located from difference Fourier synthesis, followed by full-matrix least-squares refinement based on F^2 (programs SHELXS-97 and SHELXL-97) [21]. Many hydrogen atoms could be found

Table 1
Summary of crystallographic data for compounds **1** and **2**

Compound	**1**	**2** · (0.5cyclohexane)
Formula	$C_{30}H_{44}B_2ClN_{12}La$	$C_{38}H_{57}B_2N_{14}La$
Formula weight	768.75	870.51
Crystal system	orthorhombic	monoclinic
Space group	$Pna2_1$	$P2_1/n$
a (Å)	18.7985(3)	14.5084(3)
b (Å)	10.2409(1)	18.3523(3)
c (Å)	18.3686(2)	15.8518(3)
α (°)	90.00	90.00
β (°)	90.00	96.8160(10)
γ (°)	90.00	90.00
V (Å^3)	3536.20(8)	4190.91(14)
Z	4	4
ρ_{calc} (g cm^{-3})	1.444	1.380
μ(Mo Kα) (mm^{-1})	1.323	1.065
F(0 0 0)	1568	1800
T (K)	120	120
θ Range (°)	2.17–27.48	2.57–27.48
Crystal size (mm)	0.22 × 0.18 × 0.08	0.32 × 0.22 × 0.22
Collected reflections	4190	9605
Observed data [$I > 2\sigma(I)$]	3702	6909
Goodness-of-fit on F^2	1.058	1.042
R_1 [$I > 2\sigma(I)$]	0.0390	0.0463
wR_2 [$I > 2\sigma(I)$]	0.0987	0.1165
$\Delta\rho_{max}$ (e Å^{-3})	1.92	2.7

from the Fourier Difference. Carbon-bound and boron-bound hydrogen atoms were placed at calculated positions and forced to ride on the attached carbon and boron atoms. The hydrogen atom contributions were calculated but not refined. All non-hydrogen atoms were refined with anisotropic displacement parameters. The locations of the largest peaks in the final difference Fourier map calculation as well as the magnitude of the residual electron densities were of no chemical significance. The cell of **2** was found to contain half a molecule of crystallization cyclohexane. Crystal data and details of data collection and structure refinement are given in Table 1.

3. Results and discussion

3.1. Synthesis and characterization of [La(Tp^{Me2})$_2$X] compounds (X = Cl, I)

The procedure we used to prepare [La(Tp^{Me2})$_2$X] (X = Cl, I) compounds involves the common salt metathesis (elimination) reaction of LaX_3 or the appropriate THF adduct complex $LaX_3(THF)_n$ (X = Cl, n = 1.5; X = I, n = 0.63) with two equiv. of K(Tp^{Me2}) in THF at room temperature. Thus, $LaCl_3$ reacts with K(Tp^{Me2}), over a time period ranging from 3 to 7 days, to give reproducibly a mixture of the lanthanum complexes [La(Tp^{Me2})$_2$Cl] (**1**) and La(Tp^{Me2})$_2$(κ^2-pz^{Me2}) ([pz^{Me2}]$^-$ = 3,5-dimethylpyrazolato) (**2**) (Eq. (1)). The desired chloro complex **1** is easily separated from this mixture due to its insolubility in pentane, in contrast to the pyrazolato complex **2** which is highly soluble in aliphatic hydrocarbons. Compounds **1** and **2** were obtained after workup as white powders in 65% and 16% yields, respectively. It is important to note that the use of different experimental conditions, i.e., temperature, reaction time, and lanthanide precursor, did not avoid the formation of the side-product **2**. [2] For instance, the use of $LaCl_3(THF)_{1.5}$ instead of $LaCl_3$ led reproducibly to a mixture of complexes, from which **1** and **2** were isolated in 48% and 33% yields, respectively. The analogous iodine derivative [La(Tp^{Me2})$_2$I] (**3**) was prepared readily in 67% yield using the same procedure as for **1**. However, the use of the iodide precursor $LaI_3(THF)_{0.63}$ instead of chloride ones did not avoid the formation of complex **2**, which was isolated in 12% yield (Eq. (1)).

$$\begin{aligned} &LaX_3(THF)_n + 2K(Tp^{Me2}) \\ &\xrightarrow[-2KCl]{THF,20^\circ C} [La(Tp^{Me2})_2X]\ (X = Cl, \mathbf{1};\ X = I, \mathbf{3}) \\ &\quad + [La(Tp^{Me2})_2(\kappa^2\text{-}pz^{Me2})]\ \mathbf{2} \end{aligned} \tag{1}$$

The identity of compounds **1**–**3** was established on the basis of elemental analysis, ^{1}H and ^{13}C NMR spectroscopy, and by single-crystal X-ray diffraction studies for **1** and **2**. A noteworthy feature of these complexes, which reflects the steric size of the Tp^{Me2} ligand, is the lack of coordinated THF molecule.

The ^{1}H NMR spectra of complexes **1** and **3** in toluene-d_8 are quite similar, featuring a singlet corresponding to the H-4 of the pyrazolyl ring ($\delta_{H\text{-}4}$ **1**, 5.60; **3**, 5.73 ppm), and two singlets assigned to the both methyl groups at the 3/5-positions of the pyrazolyl ring ($\delta_{Me3,5}$ **1**, 2.22 and 2.03; **3**, 2.38 and 1.88 ppm). The equivalence between the 3/5-methyl groups of the three pyrazolyl rings (one resonance for each) can be attributed to a rapid reorganization of the coordination sphere on the NMR timescale.

The ^{1}H NMR spectrum of **2** in toluene-d_8 contains a set of pyrazolyl resonances ($\delta_{H\text{-}4}$ 5.60; $\delta_{Me3,5}$ 2.28 and 1.75 ppm) similar to those observed for **1** and **3**. The equivalence between the signals relative to the methyl groups of the pyrazolyl rings indicates the ability of the lanthanum atom, thanks to its large ionic radius [22], to accommodate all the ligands in its coordination sphere, without occurrence of important steric hindrance. In addition to those signals, two relatively broad

[2] On the other hand, consistent with Sellas's recent report [13], we observed that the reaction of $NdCl_3(THF)_2$ with 2 equiv. of K(Tp^{Me2}) in THF solution at 20 °C for 4 days is selective for the formation of [Nd(Tp^{Me2})$_2$Cl] (84% isolated yield); no pyrazolato complex was observed in this case, as during the syntheses of the analogous Eu and Sm complexes [14]. Introduction of two Tp^{Me2} ligands appear therefore problematic for large metal centers (La) and small metal centers (Y) where only the half-sandwich complex can be prepared. There appears therefore to be a trade-off between excessive crowding and a bite-angle mismatch.

signals are observed for the H-4 (δ 5.95 ppm) and the methyl groups ($\delta_{Me3,5}$ 1.93 ppm) of the pyrazolato ring.

3.2. Possible pathways for the formation of the pyrazolato complex 2

The relatively low yields obtained in the syntheses of **1** and **3** (up to 65% and 67%, respectively), as compared to Nd, Sm, and Eu analogues, [2] can be rationalized in terms of partial decomposition of the [Tp^{Me2}] moiety to the benefit of the pyrazolato complex **2**. Two pathways are usually proposed to account for decomposition processes involving Tp-lanthanide compounds [16,23]. The first one is related to ligand rearrangements involving either 1,2-borotropic or 1,2-metallotropic shifts; the second one is based on partial or complete decomposition of the Tp ligand within the coordination sphere of the metal centers, in the presence of adventitious protic sources, generating most often free pyrazole which can coordinate to the metal center in the neutral form [9,10]. The latter process is frequently observed for Tp^{Me2} complexes, presumably due to the high steric crowding induced by the presence of the methyl group at 5-position of the pyrazolyl ring.

Only one example of a lanthanide compound containing two Tp ligands and one pyrazolato ligand, i.e., the samarium counterpart of **2**, is reported in the literature [24,25]. The latter was prepared from the chloro precursor and 3,5-dimethylpyrazole in the presence of the strong base $KC_6H_4CH_2NMe_2$. In a separate experiment, we also observed that the chloro complex **1** is selectively converted to the pyrazolato complex **2** by treatment with 3 equiv. of 3,5-dimethylpyrazole in the presence of NEt_3, albeit the reaction proceeds slowly with this weak base (64% conversion after 5 days) (Eq. (2)) [20]. These results give evidence, as simply expected from the formulae, that complex **2** can arise from the substitution of the chloride in **1** by a pyrazolato moiety. In principle, the latter can be generated in situ during the salt metathesis of $LaX_3(THF)_n$ (X = Cl, I) with K(Tp^{Me2}) in two different ways: (i) either as achieved in Eq. (2), from free 3,5-dimethylpyrazole (Hpz^{Me2}) arising from preliminary hydrolysis and acting as both the pyrazolato source and base, or (ii) directly as a transient [pz^{Me2}]$^-$ moiety. The former hypothesis: (i) is unlikely in our case considering the stringent precautions to avoid adventitious protic sources, and the fact that no free Hpz^{Me2} nor adducts of the type [$La(Tp^{Me2})_2Cl(Hpz^{Me2})$] could be detected (NMR) during the reaction course [26]. Rather, we assume that the lanthanum center in $LaX_3(THF)_n$ and/or **1** promotes cleavage of a B–N bond, possibly in K(Tp^{Me2}) or in **1** which features elongated and therefore probably weakened bonds due to twisting of the pyrazolyl rings about the B–N bond (vide infra).

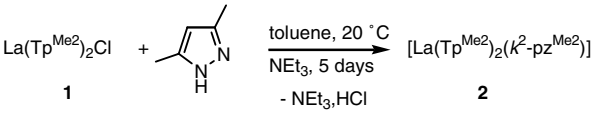

(2)

3.3. Solid-state structures of [$La(Tp^{Me2})_2Cl$] (1) and [$La(Tp^{Me2})_2(\kappa^2\text{-}pz^{Me2})$] (2)

Crystal data for **1** and **2** are summarized in Table 1, refinement details are discussed in Section 2, and selected bond distances and angles are listed in Tables 2 and 3, respectively. Both compounds are very similar to their samarium and neodymium counterparts [13,14,24] and show comparable metrical parameters, allowing for the difference in ionic radius of the metal [22]. We will therefore discuss them briefly.

The molecular structure of **1** features a seven-coordinate monomeric species with a distorted pentagonal bipyramidal geometry (Fig. 1). The average La–N values (2.6485(5) Å) are comparable to those found in similar Tp-lanthanum compounds such as [La(Tp^{Me2})-(μ-BOp^{Me2})]$_2$ (average La–N = 2.6366(1) Å) [16]. The Tp^{Me2} ligands show the typical twisting of the

Table 2
Selected bond lengths (Å) and angles (°) for [$La(Tp^{Me2})_2Cl$] (**1**)

Bond lengths			
La(1)–Cl(1)	2.7402(17)	La(1)–N(7)	2.537(5)
La(1)–N(1)	2.552(5)	La(1)–N(9)	2.743(5)
La(1)–N(3)	2.751(5)	La(1)–N(11)	2.693(5)
La(1)–N(5)	2.615(5)		
Bond angles			
Cl(1)–La(1)–N(1)	112.31(12)	N(1)–La(1)–N(5)	76.44(17)
Cl(1)–La(1)–N(3)	77.57(12)	N(5)–La(1)–N(3)	68.38(16)
Cl(1)–La(1)–N(5)	143.55(13)	N(7)–La(1)–N(11)	78.29(17)
Cl(1)–La(1)–N(7)	93.43(13)	N(7)–La(1)–N(9)	74.52(16)
Cl(1)–La(1)–N(9)	142.04(11)	N(9)–La(1)–N(11)	67.31(15)
Cl(1)–La(1)–N(11)	75.09(12)	N(1)–La(1)–N(7)	152.90(18)
N(1)–La(1)–N(3)	82.48(16)		

Table 3
Selected bond lengths (Å) and angles (°) for [$La(Tp^{Me2})_2(\kappa^2\text{-}pz^{Me2})$] (**2**)

Bond lengths			
La(1)–N(1)	2.742(3)	La(1)–N(11)	2.678(3)
La(1)–N(3)	2.601(3)	La(1)–N(13)	2.514(3)
La(1)–N(5)	2.722(3)	La(1)–N(14)	2.468(4)
La(1)–N(7)	2.748(3)	N(13)–N(14)	1.379(5)
La(1)–N(9)	2.609(3)		
Bond angles			
N(1)–La(1)–N(3)	74.34(10)	N(7)–La(1)–N(11)	66.28(10)
N(1)–La(1)–N(5)	68.89(10)	N(9)–La(1)–N(11)	78.20(10)
N(3)–La(1)–N(5)	73.31(10)	N(13)–La(1)–N(14)	32.13(11)
N(7)–La(1)–N(9)	77.62(10)		

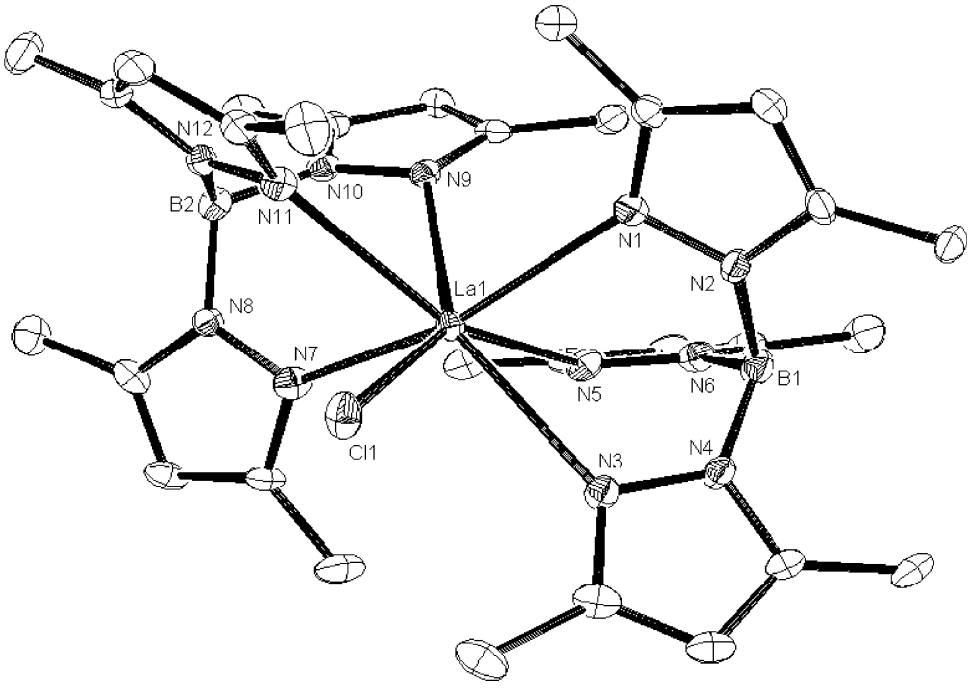

Fig. 1. Molecular structure of compound **1** drawn at the 30% probability level (hydrogen atoms omitted for clarity).

pyrazolyl rings about the B–N bond in consequence of the presence of bulky groups at 3- and 5-positions [16,27]. The extent of this twisting is different for the two Tp ligands of a given $[La(Tp^{Me2})_2X]$ complex, which accounts for the ca. 10° difference between the B–La–Cl angles. The largest B–N–N–La torsion angles is found for B(1)–N(2)–N(1)–La (33.5(6)°). [3] The B–N bond distance associated to the twisted pyrazolyl rings (N(2)–B = 1.557(11) Å) is slightly longer than the other B–N distances (average 1.539(9) Å).

The lanthanum atom in complex **2** is eight-coordinate in a pentagonal bipyramidal geometry, with N(3) and N(9) occupying the apical sites (N(3)–La–N(9) = 157.83(10)°) and considering the center of the N–N bond in the $[pz^{Me2}]^-$ moiety as a monodentate ligand (Fig. 2). The nitrogen atoms of the Tp^{Me2} ligands are bent back with a bond angle B–La–B of 137.4(8)° significantly lower than the one observed in the samarium analogue (146.0 (2)°) [24]. Also, one pyrazolyl group is 35.6° twisted around the B(1)–N(4) bond, a distortion which is slightly larger than the one found in **1** and that can be associated to the increased steric interactions between the pyrazolyl group of the Tp^{Me2} ligands and the pz^{Me2} group. The $[pz^{Me2}]^-$ ligand is bonded to lanthanum in a slightly asymmetric fashion with a difference in La–N bond distance of 0.047 Å.

[3] Additional torsion angles (deg) for 1: La(1)–N(3)–N(4)–B(1) = −1.1(8), La(1)–N(5)–N(6)–B(1) = 23.8(7), La(1)–N(7)–N(8)–B(2) = 20.1(7), La(1)–N(9)–N(10)–B(2) = 23.7(7), La(1)–N(11)–N(12)–B(2) = −4.6(7).

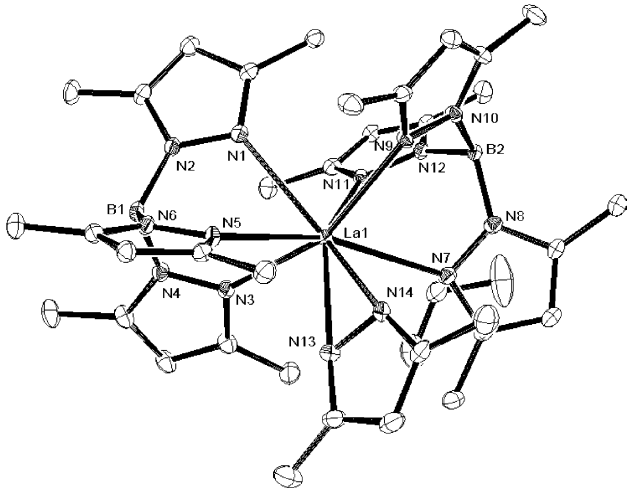

Fig. 2. Molecular structure of compound **2** drawn at the 30% probability level (hydrogen atoms omitted for clarity).

The N–N bond distance (1.379(5) Å) and the bite angle (N(13)–La–N(14) = 32.13(11)°) associated with the $[pz^{Me2}]^-$ ligand are similar to the values found in related group 3 pyrazolato complexes [25].

3.4. Metathesis reactions of $[La(Tp^{Me2})_2X]$ (X = Cl, I) with alkali metal salts

Neutral group 3 metal complexes having a reactive Ln–R bond (R = hydrocarbyl, aryl, amide, aryloxide) have increasingly attracted attention in recent years, in particular to act as single-component initiators for

polymerization of polar and non-polar monomers [5]. We have therefore investigated the possibility to access some $[La(Tp^{Me2})_2R(L)_n]$ (L = coordinating solvent; $n = 0$, 1) derivatives via salt metathesis reactions of the prepared halides **1** and **3** with appropriate alkali metal reagents. This strategy is analogous to that claimed by Bianconi et al. to prepare the yttrium complexes $[Y(Tp^{Me2})(CH_2SiMe_3)_2(THF)]$ and $[Y(Tp^{Me2})Ph_2(THF)]$ from $[Y(Tp^{Me2})Cl_2(THF)]$ [7]. However, we have not been able to reproduce the latter results and found that treatment of $[Ln(Tp^{Me2})_2X]$ (Ln = La, Nd; X = Cl, I) and $[Y(Tp^{Me2})Cl_2(THF)]$ with $LiCH_2SiMe_3$, LiPh, $LiN(SiMe_3)_2$, or $K(OC_6H_2$-2,6-^{t}Bu-4-Me) [4] under a variety of conditions led essentially to the formation of $M(Tp^{Me2})$ (M = Li, K) in 33–90% yield (depending on the starting compound and the alkali metal reagent). Similar displacement of the Tp ligand from chloro-scandium complexes by lithiated reagents has been reported by Piers et al. [12]. In any case, the expected complexes $[Ln(Tp^{Me2})_{3-x}R_x(L)_n]$ could be identified in no more than 10% NMR yield in the crude reaction mixtures. Clearly, other routes to $[Ln(Tp^{Me2})_{3-x}R_x(L)_n]$ complexes are necessary.

3.5. Synthesis of $[Ln(Tp^{Me2})(OC_6H_2$-26-^{t}Bu-4-Me$)_2]$ compounds (Ln = La (**4**), Nd (**5**))

An alternative preparation of Ln-Tp-aryloxide derivatives was developed. The salt metathesis reaction of $[Ln(OC_6H_2$-2,6-^{t}Bu-4-Me$)_3]$ (Ln = La, Nd) with one equiv. of $K(Tp^{Me2})$ in toluene at 60 °C affords the mono-substituted $[Ln(Tp^{Me2})(OC_6H_2$-2,6-^{t}Bu-4-Me$)_2]$ compounds (Ln = La (**4**); Ln = Nd (**5**)) as pale brown and blue solids in 81% and 88% yield, respectively

$$Ln(OC_6H_2\text{-}2,6\text{-}^t\text{Bu-4-Me})_3 + K(Tp^{Me2}) \xrightarrow[60^\circ C,12h\text{-}KOAr]{\text{toluene}} Ln(Tp^{Me2})(OC_6H_2\text{-}2,6\text{-}^t\text{Bu-4-Me})_2] \quad (Ln = La, (\mathbf{4}); Ln = Nd, (\mathbf{5})) \qquad (3)$$

The structures of **4** and **5** were assigned on the basis of elemental analysis, and multinuclear (^{1}H, ^{13}C) NMR for the diamagnetic complex **4**. The ^{1}H NMR spectrum of **4** in benzene-d_6 contains a set of resonances for two equivalent aryloxide groups and one set of resonances for the pyrazolyl moiety (one doublet for 4-H pz and two singlets for the methyl groups) indicating a fluxional behavior that is fast on the NMR time scale.

Complexes **4** and **5** are sensitive to air and moisture, decomposing in solution or in the solid state when exposed to air at room temperature within two days to give the corresponding phenol (2,6-^{t}Bu$_2$-4-Me-C_6H_2OH) and unidentified solid materials. It is noteworthy to mention that the reactions carried out using two equiv. of $K(Tp^{Me2})$ afford only the mono-substituted Tp-Ln complexes **4** and **5**, presumably because of the steric effects between the ^{t}Bu groups at 2- and 6-positions of the bulky aryloxide ligand and the methyl groups of the Tp ligand. This may account, at least in part, for the impossibility to introduce the aryloxide group into $[Ln(Tp^{Me2})_2X]$ (vide supra) [4].

[4] The preparation and structural characterization of Sm-$(Tp^{Me2})_2(OC_6H_2$-2,6-^{t}Bu-4-Me) via a slightly different salt metathesis procedure has been reported; see Ref. [24].

4. Conclusions

The synthesis and characterization of bis-Tp^{Me2}-lanthanum complexes have been described. Besides obtaining of the desired Tp^{Me2}-halogeno-lanthanum complexes, decomposition processes generating a free pyrazole group and a κ^2-pyrazolato group have been evidenced. In general, $[Ln(Tp^{Me2})_{3-x}X_x]$ ($x = 1$, 2) complexes appear to be poor precursors to synthesize via salt metathesis reactions $[Ln(Tp^{Me2})_{3-x}R_x(L)_n]$ (L = coordinating solvent) derivatives with a potentially Ln–R reactive moiety. Alternative efficient syntheses are still required to provide an easy entry to a broad range of such derivatives and thus enable to investigate their true potentialities in (polymerization) catalysis.

5. Supplementary data

Crystallographic data for the structures reported in this paper (excluding structure factors) have been deposited with the Cambridge Crystallographic Data Centre, CCDC No. 237701 for compound **1**, CCDC No. 237702 for **2**. Copies of this information may be obtained free of charge from the Director, CCDC, 12 Union Road, Cambridge CB2 1EZ, UK (fax: +44-1223-336033; e-mail: deposit@ccdc.cam.ac.uk or www: http://www.ccdc.cam.ac.uk).

Acknowledgements

This work was financially supported by the Brazilian-French Capes-Cofecub (Grant 382/02) and the Centre National de la Recherche Scientifique (CNRS).

References

[1] (a) S. Trofimenko, J. Am. Chem. Soc. 89 (1967) 3170;
(b) S. Trofimenko, J. Am. Chem. Soc. 89 (1967) 6288.
[2] (a) S. Trofimenko, Acc. Chem. Res. 4 (1971) 17;
(b) S. Trofimenko, Chem. Rev. 72 (1972) 497;
(c) A. Shaver, J. Organomet. Chem. Libr. 3 (1977) 157;
(d) S. Trofimenko, Progr. Inorg. Chem. 34 (1986) 115;

(e) K. Niedenzu, S. Trofimenko, Top. Curr. Chem. 132 (1986) 1;
(f) P.K. Byers, A.J. Carty, R.G. Honeyman, Adv. Organomet. Chem. 34 (1992) 1;
(g) S. Trofimenko, Chem. Rev. 93 (1993) 943;
(h) N. Kitajima Tolman, W. B. Prog. Inorg. Chem. 43 (1995) 419;
(i) G. Parkin, Adv. Inorg. Chem. 42 (1995) 291;
(j) D.L. Reger, Coord. Chem. Rev. 147 (1996) 571;
(k) S. Trofimenko, Scorpionate: The Coordination Chemistry of Polypyrazolylborate Ligands, Imperial College Press, London, 1998.

[3] N. Marques, A. Sella, J. Takats, Chem. Rev. 102 (2002) 2137.

[4] Recent organolanthanide reviews: (a) H. Schumann, J.A. Meese-Marktscheffel, L. Esser, Chem. Rev. 95 (1995) 865;
(b) R. Anwander, W.A. Herrmann, Top. Curr. Chem. 179 (1996) 1;
(c) F.T. Edelmann, Top. Curr. Chem. 179 (1996) 247;
(d) R. Anwander, in: B. Cornils, W.A. Herrmann (Eds.), Applied Homogeneous Catalysis with Organometallic Compounds, 2, Wiley, Weinheim, 1996, p. 866;
(e) R. Anwander, Top. Organomet. Chem. 2 (1999) 1;
(f) G.A. Molander, E.C. Dowdy, Top. Organomet. Chem. 2 (1999) 119;
(g) S. Arndt, J. Okuda, Chem. Rev. 102 (2002) 1953.

[5] (a) Recent reviews on fundamental "post-metallocene" organogroup 3 chemistry: W.E. Piers, D.J.H. Emslie, Coord. Chem. Rev. 233 (2002) 131;
(b) P. Mountford, B.D. Ward, Chem. Commun. (2003) 1797.

[6] (a) G.J.P. Britovsek, V.C. Gibson, D.F. Wass, Angew. Chem, Int. Ed. Engl. 38 (1999) 428;
(b) V.C. Gibson, S.K. Spitzmesser, Chem. Rev. 103 (2003) 283;
(c) Z. Hou, Y. Wakatsuki, Coord. Chem. Rev. 231 (2002) 1;
(d) J. Gromada, A. Mortreux, T. Chenal, J.W. Ziller, F. Leising, J.-F. Carpentier, Chem. Eur. J. 8 (2002) 3773, and references cited therein;
(e) J. Gromada, J.-F. Carpentier, A. Mortreux, Coord. Chem. Rev. 248 (2004) 397.

[7] D.P. Long, P.A. Bianconi, J. Am. Chem. Soc. 118 (1996) 12453.

[8] Highly efficient ethylene polymerization with scandium alkyls supported by neutral tris(pyrazolyl)methane ligands has been reported: S.C. Lawrence, B.D. Ward, S.R. Dubberley, C.M. Kozak, P. Mountford, Chem. Commun. (2003) 2880.

[9] C. Apostolidis, A. Carvalho, A. Domingos, B. Kanellakopoulos, R. Maier, N. Marques, A. Pires de Matos, J. Rebizant, Polyhedron 18 (1999) 263.

[10] D.P. Long, A. Chandrasekaran, R.O. Day, P.A. Bianconi, A. Rheingold, Inorg. Chem. 39 (2000) 4476.

[11] R. Ball, J.G Matison, J. Takats, in: 190th ACS National Meeting, Chicago, 1985, Abstract 291.

[12] J. Blackwell, C. Lehr, Y. Sun, W.E. Piers, S.D. Pearce-Batchilder, M.J. Zaworotko, V.G. Young, Can. J. Chem. 75 (1997) 702.

[13] J.L. Galler, S. Goodchild, J. Gould, R. McDonald, A. Sella, Polyhedron 203 (2004) 253.

[14] A.C. Hillier, X.W. Zhang, G.H. Maunder, S.Y. Liu, T.A. Eberspacher, M.V. Metz, R. McDonald, A. Domingos, N. Marques, V.W. Day, A. Sella, J. Takats, Inorg. Chem. 40 (2001) 510.

[15] For decomposition of Tp ligands in main-group and transition-metal complexes, see: (a) R. Alsfasser, S. Trofimenko, A. Looney, G. Parkin, H. Vahrenkamp, Inorg. Chem. 30 (1991) 4098;
(b) K. Niedenzu, H. Nöth, J. Serwatowska, J. Serwatowski, Inorg. Chem. 30 (1991) 3249;
(c) M. Ruf, H. Vahrenkamp, Inorg. Chem. 35 (1996) 6571;
(d) P. Ghosh, G. Parkin, Inorg. Chem. 35 (1996) 1429;
(e) C.J. Jones, J.A. McCleverty, A.S. Rothin, J. Chem. Soc., Dalton Trans. 109 (1986);
(f) N. Alobaidi, C.J. Jones, J.A. McCleverty, Polyhedron 8 (1989) 1033;
(g) M.N.T. Khan, P.S. Roy, K. Venkatasubramanian, N.H. Khan, Inorg. Chim. Acta 176 (1990) 49;
(h) N. Kitajima, S. Hikichi, M. Tanaka, Y. Moro-oka, J. Am. Chem. Soc. 115 (1993) 5496;
(i) A. Albinati, M. Bovens, H. Rüegger, L.M. Venanzi, Inorg. Chem. 36 (1997) 5991;
(j) G. Bellachioma, G. Cardaci, V. Gramlich, A. Macchioni, F. Pieroni, L.M. Venanzi, J. Chem. Soc., Dalton Trans. (1998) 947;
(k) S. Minhas, A. Devlin, D.T. Richens, A.T. Benyei, P. Lightfoot, J. Chem. Soc., Dalton Trans. (1998) 953;
(l) H.A. Hinton, H.L. Chen, T.A. Hamor, F.S. McQuillan, C.J. Jones, Inorg. Chim. Acta 285 (1999) 55;
(m) S. Huh, Y. Kim, K.T. Youm, M.J. Jun, Polyhedron 18 (1999) 2625;
(n) L.M.L. Chia, S. Radojevic, I.J. Scowen, M. McPartlin, M.A. Halcrow, J. Chem. Soc., Dalton Trans. (2000) 133;
(o) M.A. Halcrow, J.A. Davies, P.R. Raithby, Polyhedron 16 (1997) 1535.

[16] A. Domingos, M.R.J. Elsegood, A.C. Hillier, G. Lin, S.Y. Liu, I. Lopes, N. Marques, G.H. Maunder, R. McDonald, A. Sella, J.W. Steed, J. Takats, Inorg. Chem. 41 (2002) 6761.

[17] J.M. Carretas, N. Marques, in: First International Conference on f-Elements, Leuven, Belgium, 1990.

[18] (a) P.N. Hazin, J.C. Human, J.V. Bruno, Organometallics 6 (1987) 23;
(b) A.A. Trifonov, P. Van de Weghe, J. Collin, I. Santos, A. Domingos, J. Organomet. Chem. 527 (1997) 225.

[19] (a) P.B. Hitchcock, M.F. Lappert, A. Singh, J. Chem. Soc., Chem. Commun. (1983) 1499;
(b) M.F. Lappert, A. Singh, R.G. Smith, Inorg. Synth. 27 (1990) 164.

[20] C. Yélamos, M.J. Heeg, C.H. Winter, Inorg. Chem. 38 (1999) 1871.

[21] (a) G.M. Sheldrick, SHELXS-97, Program for the Determination of Crystal Structures, University of Göttingen, Germany, 1997;
(b) G.M. Sheldrick, SHELXL-97 Program for the Refinement of Crystal Structures, University of Göttingen, Germany, 1997.

[22] Effective ionic radii for eight-coordinate metal centers: La^{3+}, 1.160 Å; Nd^{3+}, 1.109 Å; Sm^{3+}, 1.079 Å; Y^{3+}, 1.019 Å. R.D. Shannon, Acta Crystallogr., Sect. A A32 (1976) 751.

[23] M. Onishi, N. Nagaoka, K. Hiraki, K. Itoh, J. Alloys Comp. 236 (1996) 6.

[24] I. Lopes, B. Monteiro, G. Lin, A. Domingos, N. Marques, J. Takats, J. Organomet. Chem. 632 (2001) 119.

[25] For κ^2-pyrazolato lanthanide and group 3 complexes see: (a) G. Lin, R. McDonald, J. Takats, Organometallics 19 (2000) 1814;
(b) D. Pfeiffer, B.J. Ximba, L.M. Liable-Sands, A.L. Rheingold, M.J. Heeg, D.M. Coleman, H.B. Schlegel, T.F. Kuech, C.H. Winter, Inorg. Chem. 38 (1999) 4539;
(c) G.B. Deacon, E.E. Delbridge, B.W. Skelton, A.H. White, Eur. J. Inorg. Chem. (1998) 543;
(d) J.E. Cosgriff, G.B. Deacon, G.D. Fallon, B.M. Gatehouse, H. Schumann, R. Weimann, Chem. Ber. 129 (1996) 953;
(e) J.E. Cosgriff, G.B. Deacon, B.M. Gatehouse, H. Hemling, H. Schumann, Angew.Chem., Int. Ed. Engl. 32 (1993) 874;
(f) J.E. Cosgriff, G.B. Deacon, B.M. Gatehouse, H. Hemling, H. Schumann, Aust. J. Chem. 47 (1994) 1223;
(g) J.E. Cosgriff, G.B. Deacon, B.M. Gatehouse, Aust. J. Chem. 46 (1993) 1881.

[26] Displacement of the coordinated THF molecule in $[Y(Tp)_2Cl(THF)]$ has been shown to occur once free molecules of pyrazole are present: D.L. Reger, J.A. Lindeman, L. Lebioda, Inorg. Chem. 27 (1988) 3923.

[27] (a) A.C. Hillier, S-Y. Liu, A. Sella, M.R.J. Elsegood, Inorg. Chem. 39 (2000) 2635;
(b) G.M. Ferrence, R. McDonald, M. Morissette, J. Takats, J. Organomet. Chem. 596 (2000) 95.

Available online at www.sciencedirect.com
SCIENCE DIRECT®
Polyhedron 23 (2004) 2447–2456
POLYHEDRON
www.elsevier.com/locate/poly

Structural confirmation of the 3,5-dinitrosalicylato anion coordination ability to metal ion: crystal structure, spectral and magnetic properties of the $[Cu_3\{3,5\text{-}(NO_2)_2sal^{2-}\}_2\{3,5\text{-}(NO_2)_2sal^{1-}\}_2(H_2O)_4]\cdot 4H_2O$

Dušan Valigura [a,*], Milan Melník [a], Marian Koman [a], Ladislav Martiška [a], Maria Korabik [b], Jerzy Mroziński [b], Tadeusz Glowiak [b]

[a] Department of Inorganic Chemistry, Slovak Technical University, Radlinskeho 9, 81237 Bratislava, Slovakia
[b] Faculty of Chemistry, Wroclaw University, 50-383 Wroclaw, Poland

Received 30 June 2004; accepted 30 August 2004
Available online 21 September 2004

Abstract

Reaction of copper(II) salts with 3,5-dinitrosalicylic acid yields to the complex formation of the composition $[Cu_3\{3,5\text{-}(NO_2)_2sal^{2-}\}_2\{3,5\text{-}(NO_2)_2sal^{1-}\}_2(H_2O)_4]\cdot 4H_2O$ ($3,5\text{-}(NO_2)_2sal^{x-}$ = 3,5-dinitrosalicylate anion). The complex was characterized, by elemental microanalysis, electronic, IR and EPR spectra and magnetic susceptibility measurements. The crystal structure of the complex has been determined and refined to $R = 0.0482$, and $wR = 0.1206$ for 2980 reflections with $I > 2\sigma(I)$ ($R = 0.0724$, and $wR = 0.1283$ for all 4124 reflections. The complex crystallizes in monoclinic system, space group $P2_1/c$, $a = 10.873(2)$, $b = 14.726(3)$, and $c = 13.167(3)$ Å, $\beta = 94.11(3)°$, $V = 2102.8(8)$ Å^3, and $Z = 4$. Structure of the complex comprises of the centrosymmetric $[Cu_3\{3,5\text{-}(NO_2)_2sal^{2-}\}_2\{3,5\text{-}(NO_2)_2sal^{1-}\}_2(H_2O)_4]$ molecules and the water molecules which are held together by system of different types of hydrogen bonds and van der Waals interactions. The Cu(1) atom is centrosymmetrically coordinated by two 3,5-dinitrosalicylato dianions, thus forming the square planar CuO_4 chromophore. Each of the satellite Cu(2) atoms are coordinated by one oxygen atom of bridging 3,5-dinitrosalicylato dianion, two oxygen atoms of chelating 3,5-dinitrosalicylato monoanion (in the phenolato form), and by two water oxygen atoms in the square pyramidal coordination polyhedron. Variable-temperature magnetic susceptibility measurements (1.9–300 K) show occurrence of significant ferromagnetic interactions caused by *syn–anti* conformation of carboxylato bridges within the trimer ($J_{12} = 4.31$, $J_{13} = 0$ cm^{-1}). Bellow 3 K, antiferromagnetic intermolecular interaction between trimeric molecules in the crystal lattice was observed ($zJ' = -0.29$ cm^{-1}). The EPR spectroscopy is in agreement with the molecular structure of the complex and magnetic properties, indicates superposition spectra of copper centres ($S = 1/2$) with square-planar and square pyramidal coordination polyhedrons ($g_\parallel = 2.32$, $g_\perp = 2.05$).
© 2004 Elsevier Ltd. All rights reserved.

Keywords: Copper; 3,5-Dinitrosalicylate complex; Trimer; Crystal structure; Magnetic properties; Spectral properties

1. Introduction

The chemistry of copper compounds has been extensively investigated and the relationship between the structure and reactivity, ranging from industrial catalysis to biomedical activity, is of major importance. The ability of salicylic acid to act as an oxygen donor and to form complexes with different metal atoms is well known [1]. Nitro-derivatives of salicylic acids as a donor in solid state coordination compounds has been studied only sporadically [2] and study of metal complexes with 3,5-dinitrosalicylic acid in solid state is also

* Corresponding author. Tel.: +421 2 5932 5726; fax: +421 2 5249 3198.
E-mail address: dusan.valigura@stuba.sk (D. Valigura).

0277-5387/$ - see front matter © 2004 Elsevier Ltd. All rights reserved.
doi:10.1016/j.poly.2004.08.015

rare [3–5]. Published data concerning copper(II) 3,5-dinitrosalicylates are not consistent, e.g., the EPR study of frozen solutions [4] and/or microcrystalline samples [3] using only stoichiometric metal/anion formulae (e.g., $Cu(2NO_2–SA)_2$) or proposing dimeric structure formula [5] $[Cu(Hdns)_2(H_2O)_2]\cdot 10H_2O$ for substance showing the effective magnetic moment $\mu_{eff} = 2.12$ BM per copper ion at 298 K. In addition to that only the study of stability constants of some nitrosalicylic acids complexes with different metal ions have been done [6–8].

On the other hand, the 3,5-dinitrosalicylato moiety could be relatively frequently found in the CCDC System, mostly as ionic salts with different organic cations (e.g., including *N*-protonized aminobenzoic acids) [9–20] and as the structure of free acid solvates. A logical explanation of that could be related to the pK_a values of 3,5-dinitrosalicylic acid [21] ($pK_1 = 0.45$, and $pK_2 = 7.6$). Very interesting structural feature of 3,5-dinitrosalicylate anion in mentioned structures [9–20] is an existence of all three possible types that in solid state. The phenolato anions (figure (b) of Scheme 1) is more frequent [9–12,16–18] than existence of carboxylato anion [9,13–16,19,20] (figure (a) of Scheme 1). Presence of 3,5-dinitrosalicylato dianions (figure (c) of Scheme 1) were found in the cases of ethylenediamonium 3,5-dinitrosalicylate monohydrate [9]. The 3,5-dinitrosalicylic acid molecules were found in structures [22–24] in spite of the presence of protonizable nitrogen atoms of urea [22], diethylurea [23] and phenazine [24]. This, together with controversial data in the literature, is the aim of the study of the donor properties of the 3,5-dinitrosalicylic acid to the copper(II) atom and our preliminary communication [25] is the first structural example of a 3,5-dinitrosalicylatometal complex. The compound of the composition $[Cu_3\{3,5\text{-}(NO_2)_2sal^{2-}\}_2\{3,5\text{-}(NO_2)_2sal^{1-}\}_2(H_2O)_4]\cdot 4H_2O$ was prepared and characterized by elemental analysis, spectral and magnetic properties. The crystal and molecular structure of the complex was also studied and analyzed in relation to spectral and magnetic properties.

Caution. Metal complexes of 3,5-dinitrosalicylic acid are potentially explosive. Only a small amount of material should be prepared and handled with caution.

2. Experimental

2.1. Synthesis of $[Cu_3\{3,5\text{-}(NO_2)_2sal^{2-}\}_2\{3,5\text{-}(NO_2)_2\text{-}sal^{1-}\}_2(H_2O)_4]\cdot 4H_2O$

Procedure 1. Crystals suitable for X-ray crystal structure analysis were obtained by slow crystallization of the yellow-green reaction mixture containing copper(II) sulphate (0.0926 g $CuSO_4\cdot 5H_2O$, 0.37 mmol), 3,5-dinitrosalicylic acid (0.2811 g, 0.74 mmol) and nicotinamide (0.186 g, 1.52 mmol) in water solution (50 mL), in an Erlenmayer flask at ambient temperature for a few weeks. Mixture of dark green and yellow-orange crystals were collected by filtration, washed with a small amount of water and dried in air. The dark green crystals of title compound and yellow-orange plates of 1*H*-nicotinamidium 3,5-dinitrosalicylate [20] were separated mechanically and used for X-ray structure determination.

Procedure 2. The water solution of copper(II) sulphate (17 mL, $c(CuSO_4) = 0.281$ mol L^{-1}) was under stirring added to water solution of 3,5-dinitrosalicylic acid (2.3532 g, 9.56 mmol in 150 mL) and reaction mixture was left for slow crystallization at ambient temperature in an Erlemayer flask. Crystals were filtered off, washed with water and dried at room temperature. Yields of crystals were found between 30% and 60% (depending on the time of crystalization). *Anal*. Calc. for $C_{28}H_{26}N_8O_{36}Cu_3$: C, 27.10; H, 2.11; N, 9.03, Cu, 15.36. Found: C, 27.5; H, 2.3; N, 9.2; Cu, 15.5%.

2.2. Spectral studies

Electronic spectrum of the complex was measured in Nujol suspension in the region of 190–1100 nm with a SPECORD 200 (Carl Zeiss Jena) spectrophotometer. Infrared spectrum in the region of 4000–100 cm^{-1} was measured with a Nicolet MAGNA 750 IR spectrometer using both KBr pellet and Nujol suspension technics for 4000–400 cm^{-1} region and PE pellet for 400–100 cm^{-1}.

EPR spectra of powdered sample were recorded at room temperature, 77 and 4.5 K, on the spectrometer Bruker ESP 300, operating at X-band equipped with an ER 035M Bruker NMR gaussmeter and a HP 5350B Hewlett–Packard microwave frequency counter.

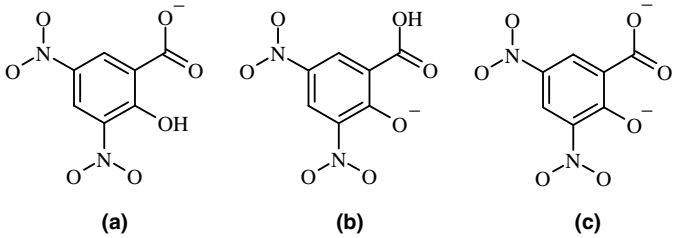

Scheme 1.

The EPR measurements at 4.3 K were performed on a conventional X–band reflection spectrometer equipped with an Oxford Instruments ESR-900 helium flow cryostat.

2.3. Magnetic measurements

Magnetic susceptibility measurements in the temperature range of 1.9–300 K were carried out on powdered samples of complex, at the magnetic field 5 kG, using a Quantum Design SQUID Magnetometer (type MPMS-XL5). Corrections for diamagnetism of the constituting atoms were calculated using the Pascal constants [26], the value of 60×10^{-6} cm^3 mol^{-1} was used as the temperature-independent paramagnetism of copper(II) ion.

2.4. X-ray measurement

Data collection and cell refinement of the complex were carried out using Kuma KM4CCD κ-axis diffractometer (graphite monochromated Mo Kα radiation, $\lambda = 0.71073$ Å) [27]. Crystal was positioned at 65 mm distance from CCD camera; 312 frames were measured at 0.75° intervals with a counting time of 20 s. Accurate cell parameters were determined and refined by the least-squares fit of 6000–7000 of the strongest reflections. Intensity data were corrected for Lorenz and polarization factors. Absorption correction based on least-squares fit to $|F_c| - |F_o|$ differences was also applied [28]. Data reduction and analysis were carried out with the Oxford Diffraction Poland (formerly Kuma Diffraction Wroclaw, Poland) programs. The structure was solved by the heavy atom method with SHELX86 [29], and subsequent Fourier synthesis using SHELXS93 [30]. Geometrical analysis was performed using SHELXL97 [31] (see Table 1) and the structure was drawn using ORTEP-3 for Windows program [32].

Table 1
Crystal data and structure refinement for $[Cu_3\{3,5\text{-}(NO_2)_2sal^{2-}\}_2\{3,5\text{-}(NO_2)_2sal^{1-}\}_2(H_2O)_4]\cdot 4H_2O$

Identification code	lm114
Empirical formula	$C_{14}H_{13}N_4O_{18}Cu_{1.5}$
Formula weight	620.59
Temperature (K)	293(2)
Wavelength (Å)	0.71073
Crystal system	monoclinic
Space group	$P2_1/c$
Unit cell dimensions	
a (Å)	10.873(2)
b (Å)	14.726(3)
c (Å)	13.167(3)
β (°)	94.11(3)
V (Å^3)	2102.8(8)
Z	4
D_{calc} (Mg/m^3)	1.960
Absorption coefficient (mm^{-1})	1.636
$F(000)$	1250
θ range for data collection (°)	3.34–26.00
Index ranges	$-13 < h < 12$ $-18 < k < 15$ $-16 < l < 15$
Reflection collected	14179
Independent reflections	4124
Refinement method	full matrix least squares on F^2
Data/restrains/parameters	4124/0/340
Goodness-of-fit on F^2	0.992
Final R indices [$I > 2\sigma I$)]	$R_1 = 0.0482$, $wR_2 = 0.1206$
R indices (all data)	$R_1 = 0.0724$, $wR_2 = 0.1283$
Largest differential peak and hole (e Å^{-3})	0.91, −1.42

3. Results and discussion

3.1. Complex preparation

The title compound was for the first time prepared by the reaction of copper(II) sulphate with 3,5-dinitrosalicylic acid in presence of nicotinamide in our effort to study the preparation and properties of new copper(II) complexes containing nicotinamide as biologicaly active ligand (see procedure 1 in Section 2). This procedure gave us the mixture of dark green and yellow-orange crystals. The yellow-orange crystals were found as 1*H*-nicotinamidium 3,5-dinitrosalicylate [20]. The preliminary structural parameters of the dark green complex were already published [25]. Later both products were prepared separately. The 1*H*-nicotinamidium 3,5-dinitrosalicylate [20] was obtained by the direct reaction of nicotinamide with 3,5-dinitrosalicylic acid. The reaction of different copper(II) salts with 3,5-dinitrosalicylic acid (e.g., procedure 2) resulted in obtaining the dark green crystals of title compound. Those experiments could be taken as confirmation of two independent chemical reactions were proceeding within the experiment described as procedure 1. Unusual stoichiometry and properties of dark green product could be explained only on the base of the X-ray crystal structure determination.

3.2. Crystal and molecular structure

The atom numbering of $[Cu_3\{3,5\text{-}(NO_2)_2sal^{2-}\}_2\{3,5\text{-}(NO_2)_2sal^{1-}\}_2(H_2O)_4]\cdot 4H_2O$ complex and the structure of complex molecule are illustrated in Fig. 1 and the selected bond distances and angles are listed in Table 2. The complex molecule is centrosymmetric and Cu(1) atom is in the centre of symmetry. The 3,5-dinitrosalicylate dianions are forming with Cu(1) two six-membered metallocyclic rings with the angle O(22)–Cu(1)–O(23) of 90.7(1)°. The carboxylato oxygen atom O(22) and the O(23) phenolato oxygen atom exhibit the Cu(1)–O distances of 1.937(3) and 1.916(3) Å, respectively. The other carboxylato oxygen atom of this dianion O(21) is bonded to the terminal Cu(2) atom with little bit

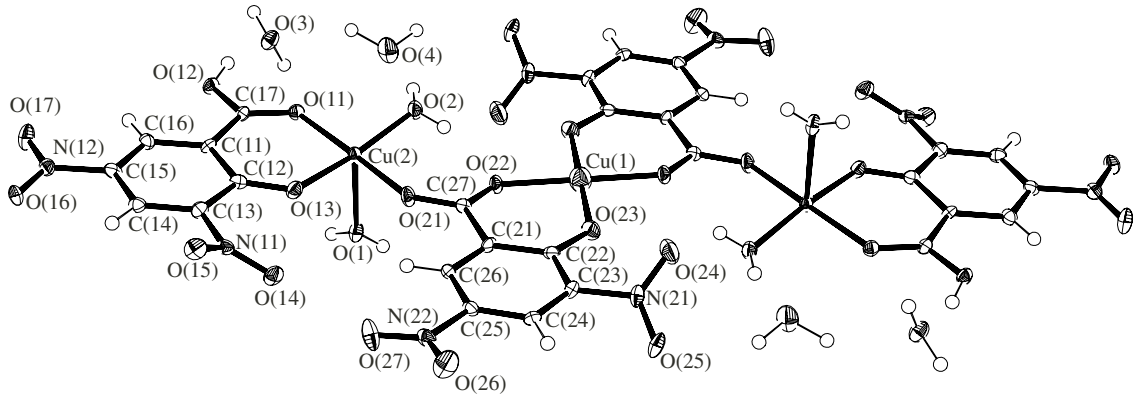

Fig. 1. An ORTEP drawing of the $[Cu_3\{3,5\text{-}(NO_2)_2sal^{2-}\}_2\{3,5\text{-}(NO_2)_2sal^{1-}\}_2(H_2O)_4]\cdot 4H_2O$ with the numbering scheme.

Table 2
Selected intramolecular distances (Å) and bond angles (°) of $[Cu_3\{3,5\text{-}(NO_2)_2sal^{2-}\}_2\{3,5\text{-}(NO_2)_2sal^{1-}\}_2(H_2O)_4]\cdot 4H_2O$

Cu(1)–O(23)	1.916(3)	O(23)–Cu(1)–O(23^{i})	180.0
Cu(1)–O(22)	1.937(2)	O(23)–Cu(1)–O(22)	90.74(11)
Cu(2)–O(13)	1.942(3)	O(23)–Cu(1)–O(22)	89.26(11)
Cu(2)–O(2)	1.953(3)	O(22)–Cu(1)–O(22^{i})	180.0
Cu(2)–O(11)	1.990(2)	O(13)–Cu(2)–O(2)	169.26(11)
Cu(2)–O(21)	2.001(3)	O(13)–Cu(2)–O(11)	92.94(11)
Cu(2)–O(1)	2.382(3)	O(2)–Cu(2)–O(11)	88.53(11)
O(11)–C(17)	1.252(4)	O(13)–Cu(2)–O(21)	81.26(11)
O(12)–C(17)	1.339(4)	O(2)–Cu(2)–O(21)	96.34(11)
O(12)–H(12′)	0.8587	O(11)–Cu(2)–O(21)	172.64(11)
O(13)–C(12)	1.273(4)	O(13)–Cu(2)–O(1)	95.00(10)
O(14)–N(11)	1.249(4)	O(2)–Cu(2)–O(1)	95.59(11)
O(15)–N(11)	1.266(4)	O(11)–Cu(2)–O(1)	91.82(10)
O(16)–N(12)	1.250(4)	O(21)–Cu(2)–O(1)	93.20(10)
O(17)–N(12)	1.258(4)	C(17)–O(11)–Cu(2)	127.4(2)
O(21)–C(27)	1.269(4)	C(17)–O(12)–H(12′)	119.7
O(22)–C(27)	1.285(4)	C(12)–O(13)–Cu(2)	128.5(2)
O(23)–C(22)	1.331(4)	C(27)–O(21)–Cu(2)	132.9(2)
O(24)–N(21)	1.241(4)	C(27)–O(22)–Cu(1)	130.1(2)
O(25)–N(21)	1.256(4)	C(22)–O(23)–Cu(1)	131.2(2)
O(26)–N(22)	1.236(4)		
O(27)–N(22)	1.244(4)		

(i) $-x, -y, -z$.

longer Cu(2)–O(21) distance of 2.000(3) Å, thus forming the bridging *syn–anti* bonding mode of the carboxylato group. The terminal Cu(2) atom exhibits square pyramidal coordination polyhedron formed by the O(21) oxygen atom of the bridging 3,5-dinitrosalicylate dianion, by two oxygen atoms O(11) and O(13) of the terminal chelating 3,5-dinitrosalicylate monoanion, and by two O(2) and O(1) oxygen atoms of the water molecules. The terminal chelating salicylato anion exhibit slightly longer both Cu(2)–O distances (1.990(3) and 1.942(3) Å, respectively) in comparison to those ones of the Cu(1) atom. This elongation is in good relation to the anion charge. The equatorial water molecule exhibit the Cu(2)–O(2) distance 1.953(3) Å, and the apical Cu(2)–O(1) distance is longer (2.382(3) Å).

The terminal 3,5-dinitrosalicylato anion is rather unique from the transition metal coordination chemistry point of view. This is the first example of presence of phenolato monoanion of the salicylic acid bonded as chelate to the 3d transition metal atom. There are only five examples of structures containing this type of salicylato anion – four of them are tungsten complexes $[W(Cl)_2(sal^{1-})]\cdot THF$, $[W_2(\mu_2\text{-}O)(O)_2(sal^{1-})_2(sal^{2-})_2]\cdot CH_2Cl_2$ (where THF = tetrahydrofuran) [33] $[W(Cl)_3(5Cl\text{-}sal^{1-})(\eta^2\text{-dpe})]$, $[W(Cl)_3(sal^{1-})(\eta^2\text{-dpe})]\cdot$18-crown-6 (where dpe = diphenylethenyl anion, 18-crown-6 = $C_{12}H_{24}O_6$ crown ether) [34] and one of them is a molybdenum complex $[pyH]^+[Mo(O)_2(sal^{1-})(sal^{2-})]^-$ [35].

Another structural feature of the trimeric complex under study is the presence of mono- and di-anions of 3,5-dinitrosalicylic acid within one complex molecule [25]. Such complexes were up to now found only for unsubstituted salicylato complexes, the simpliest one is the dimeric $[Bi_2(sal^{1-})_2(sal^{2-})_2(phen)_2]\cdot CH_3Ph$ (where sal^{x-} = salicylato anion, phen = phenantroline, and CH_3Ph = toluene), that has been published recently [36]. The others are higher oligomeric substances, as mixed metal complexes $[Ti_3Bi_2(sal^{1-})_2(sal^{2-})_8]\cdot CH_2Cl_2$, $[Ti_4Bi_2(sal^{1-})_1(sal^{2-})_{10}(i\text{PrO})_1]\cdot i\text{PrOH}\cdot H_2O$, $[Nb_2Bi_2(sal^{1-})_4(sal^{2-})_4(i\text{PrO})_4]$, and $[Ta_2Bi_2(sal^{1-})_4(sal^{2-})_4(i\text{PrO})_4]$ (where $i\text{PrO}^-$ = izopropanoloato anion) [37] and/or nonamanganese complexes $[Mn_9(O)_4(sal^{1-})_2(sal^{2-})_4(PhCO_2)_8(py)_4]\cdot CH_2Cl_2$ (where py = pyridine, $PhCO_2$ = benzoate anion) [38], $[Mn_9(O)_4(sal^{1-})_2(sal^{2-})_4(PhCO_2)_8(py)_4]\cdot xH_2O$ [39] or decazirconium complex $[Zr_{10}(O)_6(OH)_4(sal^{1-})_8(sal^{2-})_8]\cdot$PrOH [40].

A planarity of the complex molecule, with exception of apical O(1) atom and the oxygen atoms (O(14), O(15), O(16), O(17), O(24), O(25), O(26), and O(27), respectively) is another structural feature of studied complex that allows stepwise stacking molecules in solid state. The deviations of the oxygen atoms of nitro-groups from the mentioned plane is due to rotation of nitro-groups along the C–N bond and could be characterized by the angle between the nitro-group plane and the least square plane mentioned above. Those angles are 31.8°, 2.0°, 33.8° and 11.5° for nitro-groups containing the N(11), N(12), N(21) and N(22) atoms, respec-

tively. The difference in rotational position of the individual nitro-groups is in connection with another feature of this structure and this is a system of hydrogen bonds.

Three types of hydrogen bonds – intramolecular, and two types of intermolecular ones – could found in this structure. The intramolecular hydrogen bonds system (Fig. 2) involving the O(12)–H(12)–O(3)–H(42)–O(4)–H(21)–O(2)–H(22)–O(22) might be together with the additional intermolecular hydrogen bonds (Table 3 and text below) a reason of the larger deviation (of 0.150 Å) of the O(22) from the complex molecule plane. The planar trimeric molecules are within the structure coplanar (Fig. 2) each to other and water molecules containing the O(1), O(3) and O(4) atoms are involved in extending intermolecular hydrogen bonds between the neigbouring trimeric molecules (Table 3). The O(4) oxygen atom containing water molecules form intermolecular hydrogen bonds only within the individual plane (Fig. 2), while the O(3) and O(1) water molecules form hydrogen bonds between the planes (Fig. 3). The O(1) water molecules are with oxygen atom and both hydrogen atoms involved in the strong hydrogen bonds only within the neigbouring planes (Figs. 3 and 4) and the relatively short distance Cu(2)–O(1) of 2.382(3) Å consequently gives the relatively short distance between the neigbouring planes, 3.108 Å. The mutual position of neigbouring interplanar molecules is shown in Fig. 4 with Cu(2)–Cu($2^{iv,i}$) distance of 3.718 Å (the O(1)–Cu(2)–Cu($2^{iv,i}$) angle is 155.0°), the distance is shorter than the intramolecular Cu(1)–Cu(2) distance 5.201 Å. This shorter interplanar distance together with the mutual position of trimeric molecules is probably the reason that there is not enough space for another ligands to be bonded to copper atoms and thus increasing the coordination number of copper atoms.

The coordination ability of 3,5-dinotrosalicylato anion firstly proved in this paper allow us to compare coordination Cu–O bond distances of this ligand with those ones for other salicylato complexes of copper (II) and because of uniqueness of terminal salicylato monoanion only comparation for dianion [41–46] could be done. The Cu–O_p (O_p = phenolato oxygen) distances and the Cu–O_c (O_c = carboxylato oxygen) distances of salicylato dianion are in all found examples shorter those ones for the complex under study in this work (Table 4 and text above).

Searching for above structural data brings interesting result in the case of some dimeric copper(II) complexes with ligands containing salicylato-group moiety. When salicylic acid contains another coordinationable substituent, mostly Schiff base fragment, next to hydroxo-group dimeric phenolato bridged complexes could be formed. There are four examples [47–50] of dimeric species containing salicylato-group moiety that exhibit two different coordination polyhedra within each molecule (Scheme 2) and two examples [51,52] containing salicylato-group moiety (Scheme 3) showing the same coordination polyhedra for both copper(II) atoms. There are two main structural differences between those two groups of complexes. The first group of complexes (Scheme 2) shows "planar" organization of the most part of complex molecule with exception of apical water molecule ligand and the "cis" organization of donor atoms sets. In the case of the second group of complexes (Scheme 3) there are longer side arms that are nonplanar

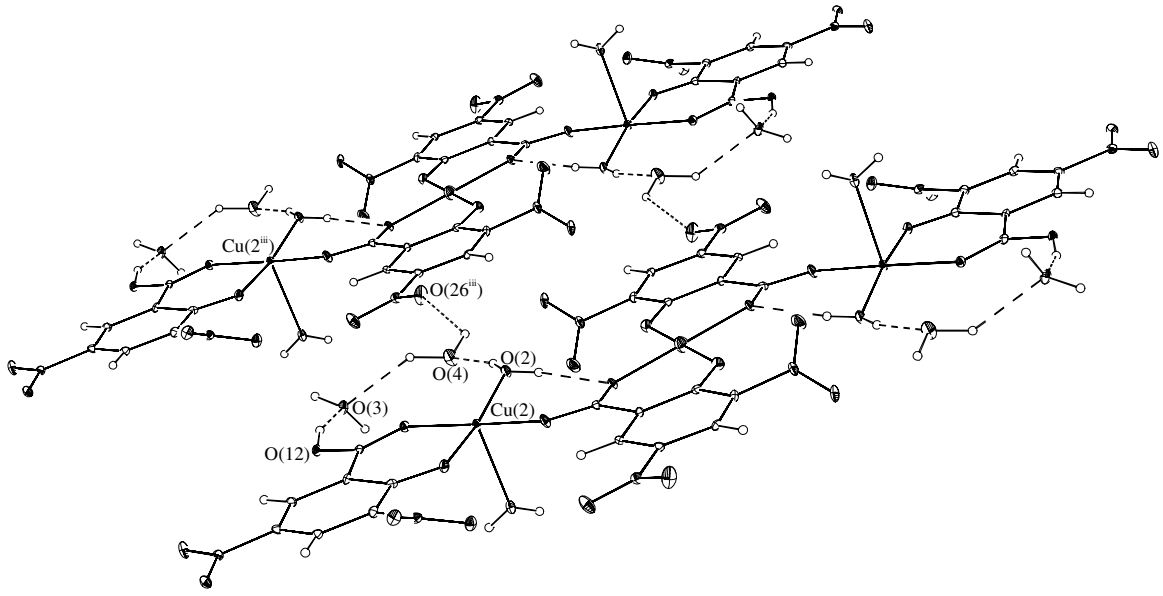

Fig. 2. Drawing of the mutual position of the $[Cu_3\{3,5\text{-}(NO_2)_2sal^{2-}\}_2\{3,5\text{-}(NO_2)_2sal^{1-}\}_2(H_2O)_4]\cdot 4H_2O$ units within the plane showing intramolecular and in plane intermolecular hydrogen bond system (iii $x, y-1, z$).

Table 3
Hydrogen bonds of $[Cu_3\{3,5\text{-}(NO_2)_2sal^{2-}\}_2\{3,5\text{-}(NO_2)_2sal^{1-}\}_2(H_2O)_4]\cdot 4H_2O$

D–H	*d*(D–H)	*d*(H...A)	∠DHA	*d*(D...A)	A
O(2)–H(21)	0.884	1.811	163.87	2.672	O(4)
O(2)–H(22)	0.777	2.124	148.08	2.814	O(22)
O(3)–H(31)	0.934	1.982	154.54	2.854	O(1^{ii})
O(3)–H(32)	0.906	2.109	149.83	2.929	O(13^{iii})
O(3)–H(32)	0.906	2.259	131.01	2.934	O(14^{ii})
O(4)–H(41)	0.963	2.298	129.27	3.002	O(26)
O(4)–H(41)	0.963	2.398	145.15	3.236	O(25)
O(4)–H(42)	0.996	2.061	142.51	2.915	O(3)
O(12)–H(12′)	0.859	1.775	159.70	2.597	O(3)
O(1)–H(11)	0.791	2.167	153.84	2.898	O(17^{iv})
O(1)–H(12)	0.905	2.227	132.65	2.918	O(27^{ii})

(i) $-x, -y, -z$; (ii) $-x-1, y-1/2, -z+1/2$; (iii) $x, y-1, z$; (iv) $x+1, y, z$.

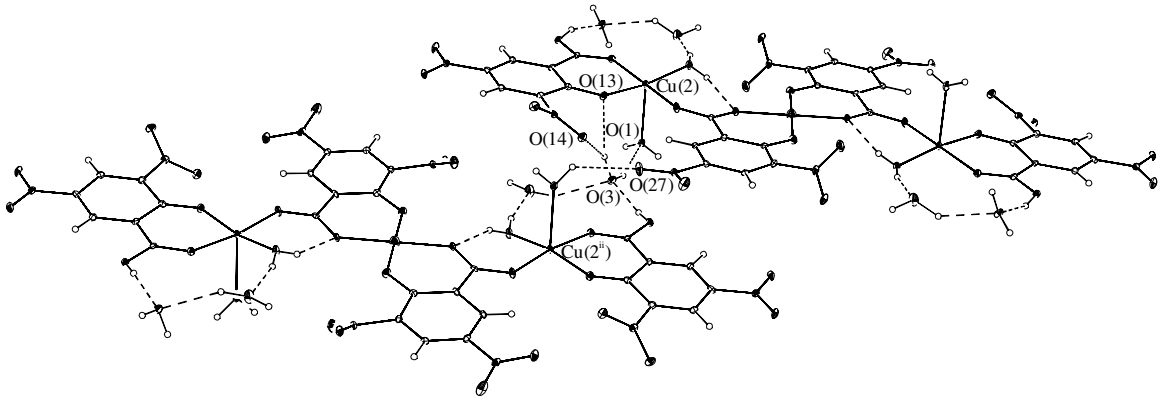

Fig. 3. Drawing of the mutual position of the $[Cu_3\{3,5\text{-}(NO_2)_2sal^{2-}\}_2\{3,5\text{-}(NO_2)_2sal^{1-}\}_2(H_2O)_4]\cdot 4H_2O$ units of the neigbouring planes showing intermolecular hydrogen bond system (^{ii} $-x-1, y-1/2, -z+1/2$).

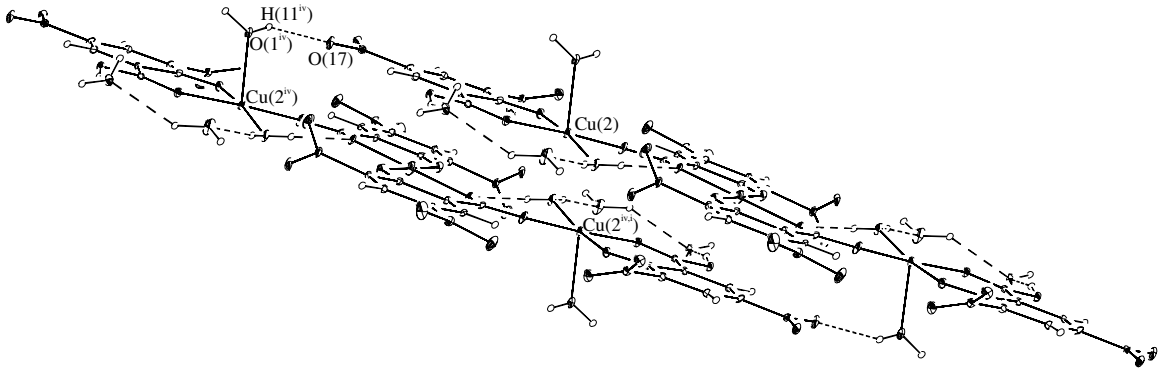

Fig. 4. Drawing of the mutual position of the $[Cu_3\{3,5\text{-}(NO_2)_2sal^{2-}\}_2\{3,5\text{-}(NO_2)_2sal^{1-}\}_2(H_2O)_4]\cdot 4H_2O$ units o the neighbouring planes showing intermolecular hydrogen bond system (^{ii} $-x-1, y-1/2, -z+1/2$; ^{i} $-x, -y, -z$).

Table 4
Coordination mode of salicylates^{2-} in some copper(II) complexes

Compound	Bonding mode	Cu–O_p	Cu–O_c	References
$[Cu(sal^{2-})(tmen)(EtOH)]$	Chelate	1.886	1.915	[41]
$[Cu(sal^{2-})(phen)]\cdot H_2O$	Chelate	1.884	1.884	[42]
$[Cu(sal^{2-})(bipy)]\cdot EtOH$	Chelate	1.899	1.898	[43]
$[Cu(dmen)_2][Cu(sal^{2-})_2]\cdot i$PrOH	Chelate	1.900	1.903	[44]
$[Cu_2(sal^{2-})_2(bipy)_2]\cdot$aspH	Chelate + (bridge O_p)	1.891 (2.413)	1.900	[45]
$[Cu_2(3,5\text{-}(i\text{Pr})_2sal^{2-})_2(bipy)_2]\cdot 3,5\text{-}(i\text{Pr})_2$salH	Chelate + (bridge O_p)	1.922 (2.283)	1.914	[46]
$[Cu_3\{3,5\text{-}(NO_2)_2sal^{2-}\}_2\{3,5\text{-}(NO_2)_2sal^{1-}\}_2(H_2O)_4]\cdot 4H_2O$	Chelate + (bridge O_c)	1.937	1.916 (2.000)	This work

tmen, *N*,*N*,*N*′,*N*′-tetramethylethylenediamine; phen, 1,10-phenantroline; bipy, bipyridine; dmen, 1,1-dimethylethylenediamine; *i*PrOH, 2-propanol; aspH, acetylosalicylic acid; O_p, phenolato oxygen atom; O_c, carboxylato group oxygen atom.

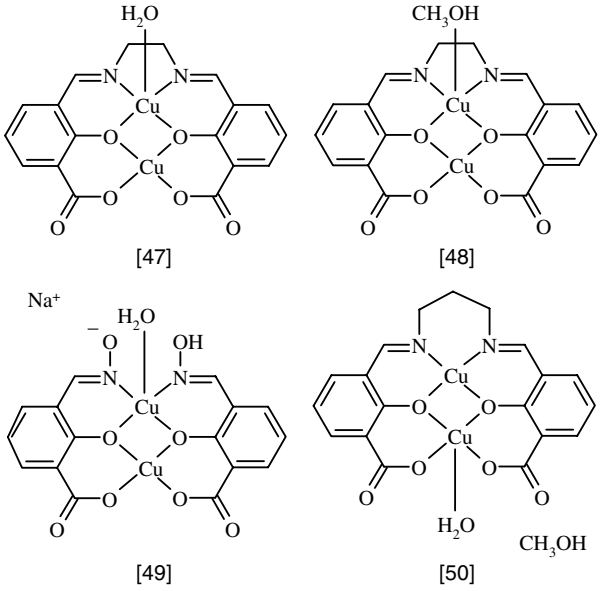

Scheme 2.

with the nearest surrounding of both central atoms and "trans" of donor atoms set is preferred thus both central atoms shows the same coordination atom polyhedra including the apical water molecule. It is interesting that within the first group of complexes (Scheme 2) the complexes containing water molecule as apical ligand show similar organisation of crystal structure packing as it was found in trimeric complex studying – stacking complex molecules one over the other, water molecules involving in hydrogen bond system within neighbouring plane of molecules and some sterical hindrance of the

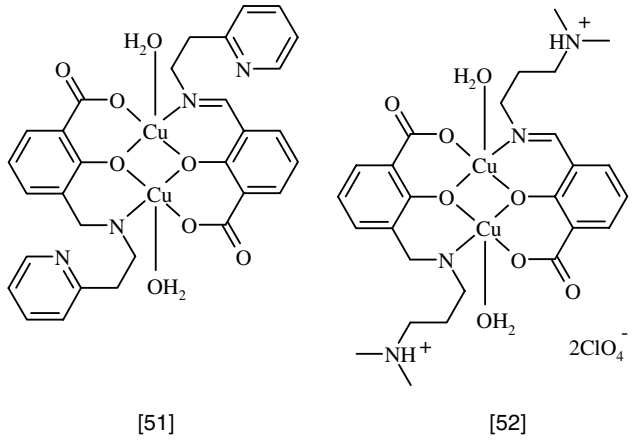

Scheme 3.

square planar coordination polyhedra of copper atom by neighbouring complex molecules.

3.3. Magnetic susceptibility and EPR measurements

Magnetic susceptibility measurements on a polycrystalline sample of the complex between 1.9 and 300 K shows a dependence on the temperature (Fig. 5). Magnetic moment value of 1.80 BM at the 300 K increases with the lowering temperature to 2.13 BM at 3 K. The graphic functions χ_M versus T and $\chi_M T$ versus T, are shown on Fig. 5. The $\chi_M T$ value is 0.406 cm^3 mol^{-1} K at 300 K (it corresponds to non coupled copper(II) atoms, $S = 1/2$ spin-only value). This value increases with the lowering temperature to a maximum 0.568

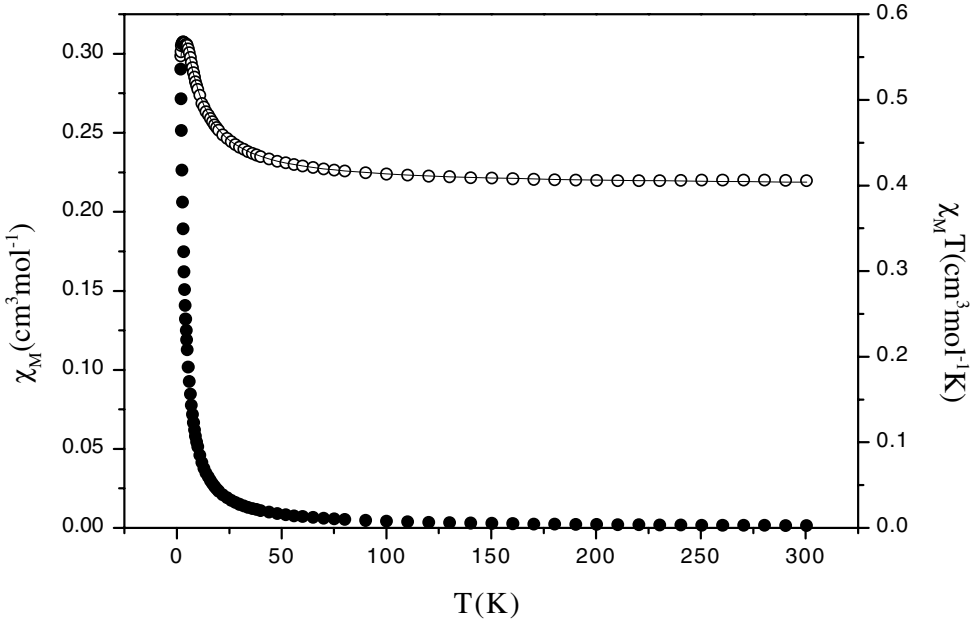

Fig. 5. The plot of the χ_M and $\chi_M T$ product vs. temperature (χ_M – the molar magnetic susceptibility calculated per one copper(II) centre). The solid line was generated from the best-fit magnetic parameters.

$cm^3\ mol^{-1}$ K at about 3 K and decreases upon further cooling. This behavior indicates a weak ferromagnetic interaction between copper(II) atoms. In keeping with the structure, the experimental magnetic susceptibility data were analyzed with Eq. (1)

$$\chi_M = \frac{Ng^2\beta^2}{12kT} \times \frac{10\exp(J_{12}/kT)+\exp(-2J_{12}/kT)+\exp(-2J_{13}/kT)}{2\exp(J_{12}/kT)+\exp(-2J_{12}/kT)+\exp(-2J_{13}/kT)} \quad (1)$$

where χ_M denotes the magnetic susceptibility per mole of copper(II) [53]. The spin Hamiltonian appropriate to describe the exchange interaction in a linear symmetric copper(II) trimmer, based on the isotropic HDvV model may be written

$$H = -2J_{12}(S_1S_2 + S_2S_3) - 2J_{13}S_1S_3. \quad (2)$$

The exchange integral J_{12} refers to two adjacent centres and J_{13} to the interaction between the terminal centres. Linear trimmers with ferromagnetic ground states have been reported and some authors have proposed to negligible interaction between the terminal centres. and accept $J_{13} = 0$ [54–59]. To take into account, the decrease of the $\chi_M T$ value at low temperatures (intertrimer exchange interactions) a molecular field correction term is added to Eq. (1). The equation for the susceptibility then has the form

$$\chi_M = \frac{\chi_C}{1 - (2zJ'/Ng^2\beta^2)\chi_C}, \quad (3)$$

where χ_C is the susceptibility calculated from Eq. (1), J' is the intertrimer exchange parameter and the z is the number of interacting nearest neighbours. The best fitting for the experimental data gives the following parameters: $J_{12} = 3.75\ cm^{-1}$, $J_{13} = 0.56\ cm^{-1}$, $zJ' = -0.32\ cm^{-1}$, and $g = 2.063$. As was shown earlier [59], $J_{13} \neq 0$ gives better agreement between experimental and calculated susceptibility data ($R = 8.866 \times 10^{-4}$) than obtained with constant $J_{13} = 0$: $J_{12} = 4.31\ cm^{-1}$, $zJ' = -0.29\ cm^{-1}$, and $g = 2.061$ ($R = 1.552 \times 10^{-3}$). The agreement factor is defined as

$$R = \frac{\sum_{i=1}^{n}(\chi_i^{exp}T_i - \chi_i^{calc}T_i)^2}{\sum_{i=1}^{n}(\chi_i^{exp}T_i)^2}. \quad (4)$$

The obtained exchange parameters are comparable to those found in other linear trimeric and polymeric *syn–anti* carboxylate copper(II) compounds [54–63].

To understand the ferromagnetic exchange interaction it is necessary to know the factors leading to orthogonal magnetic orbitals on Cu(1) and Cu(2) atoms. This compound represents the first structurally characterized linear trinuclear copper(II) complex containing 3,5-dinitrosalicylate bridges and showing weak ferromagnetic interaction between adjacent copper(II) atoms. Ferromagnetic coupling in the compound is consistent with the nature of the magnetic orbitals (built up from d-orbitals of the metals and the symmetry adapted linear contribution of the ligands orbitals) on Cu(1) and Cu(2) atoms, and the geometrical features of the Cu–O–C–O–Cu bridges. Central Cu(1) atom is, as it was shown above, joined to the other two satelite Cu(2) atoms by two bridging carboxylate groups of 3,5-dinitrosalicylates in a *syn–anti* conformation, resulting in a Cu…Cu separation between the nearest neighbours of 5.201(7) Å. The complex molecule is planar. The plane is formed by: Cu(1), Cu(2), bridging salicylato–dianion (except O atoms of nitro–groups) and terminal salicylato monoanion (except of nitro–groups O atoms) shows average deviation from the plane of 0.0513 Å. The O(22) atom (bridging COO group) exceeds deviation from the respective plane of 0.132(2) Å.

The coordination arrangement of the central Cu(1) atom is nearly square planar – CuO_4 and the two satelite Cu(2) atoms show nearly square-pyramidal coordination – CuO_5 with a tetragonality parameter $\tau \approx 0$ [64]. The magnetic d-orbitals on Cu(1), Cu(2) and Cu(2^i) atoms are delocalized toward the 2p oxygen orbitals of the both COO bridges and then the exchange coupling through the carboxylate groups may be operative [60]. According to Kahn's model [65], the exchange coupling constant J, can be expressed as a sum of both ferromagnetic (J_F) and antiferromagnetic (J_{AF}) contributions $J = J_F + J_{AF}$.

The ferromagnetic contribution is weak when the metal ions are bridged by polyatomic extended ligands whereas the magnitude of the antiferromagnetic one is proportional to the square of the overlap integral between magnetic orbitals centred on nearest-neighbour metal atoms. So, the sign and magnitude of J are primarily governed by the overlap [66]. For the well characterized copper(II) complexes with bridging *syn–anti* carboxylate groups, the magnitudes of the exchange coupling constants are rather small [60] (from −8.5 to 6.5 cm^{-1}). To generalize which factors determine the sign of the exchange coupling many examples are needed. In the present complex the *syn–anti* conformation and the small deviation of bridging O(22) carboxylate atom from the plane would cause the unfavourably orientation of magnetic orbitals centred on Cu(1) and Cu(2), reduce the antiferromagnetic contribution, so the ferromagnetic one would become predominant. Our results confirm suggestion that intramolecular ferromagnetic interaction (positive J constant) is observed when the *syn–anti* bridging mode of the Cu–O–C–O–Cu skeleton deviates from planarity [63]. Structural factors such as Cu–O lengths and Cu…Cu distances seem not to be determining the sign of the exchange coupling [61].

Decreasing of $\chi_M T$, observed below 3 K (Fig. 5) suggests antiferromagnetic intermolecular interaction

[59,65]. Planar molecules of trimers are stacked in the crystal lattice, interplanar distance of neighbouring planes is 3.31 Å and intramolecular hydrogen bond system exists (Figs. 2–4 and text above). Antiferromagnetic component obtained from fitting procedure confirm weak antiferromagnetic intermolecular interaction $zJ' = -0.32\ cm^{-1}$.

The EPR spectra of solid state of this complex, independent of the temperature (293, 77 and 4.5 K) display a pattern consistent with an axially distorted Cu^{II} centre with $g_{\|} = 2.32$, $g_{\perp} = 2.05$ and $g_{av} = 2.14$.

It is in agreement with the molecular structure of the trimer, square-planar and square pyramidal coordination polyhedrons of Cu^{II} [67,68]. The small differences between g values: $g = 2.06$ obtained from the fitting procedure and $g_{av} = 2.14$ from the EPR spectra is often observed and can be attributed to the unresolved axial anisotropy of the EPR spectra and the fact that the g value obtained from the magnetic data are only refined isotropically [69].

3.4. Spectral study

The electronic spectrum of the complex shows a wide asymmetric band at about 1.37 μm^{-1} (730 nm) and a shoulder at about 2.90 μm^{-1} (345 nm). The band at about 1.37 μm^{-1} is due to d–d transitions. Wideness and asymmetry of this d–d band is in connection with known structure showing two types of coordination polyhedra of the copper atoms. The other band may be assigned as a charge-transfer.

All the features of the IR spectrum of the compound are clearly compatible with the structural characteristics of the $[Cu_3\{3,5\text{-}(NO_2)_2sal^{2-}\}_2\{3,5\text{-}(NO_2)_2sal^{1-}\}_2(H_2O)_4]\cdot 4H_2O$. The IR spectrum of the compound shows strong and broad absorption band in the area 3620–3300 cm^{-1} with three maxima around 3095, 3460 and 1577 cm^{-1}, belonging O–H vibrations of water molecules and O–H of protonized carboxylic group. Carboxylate stretching frequencies were found as dublets $\nu_{as}(COO^-)$ at 1624 and 1605 cm^{-1}, and $\nu_s(COO^-)$ at 1448, and 1431 cm^{-1}. The difference between the asymmetric and symmetric stretching vibrations ($\Delta\nu = \nu_{as}(COO^-) - \nu_s(COO^-)$) of 176 and 174 cm^{-1} indicates [70] that the 3,5-dinitrosalicylate anions coordinated as a bidentate chelating, or bridging carboxylic group (see the crystal structure). The nitro-group stretching frequencies were found, $\nu_{as}(NO_2)$ at 1524 cm^{-1}, and $\nu_s(NO_2)$ at 1343 cm^{-1} as wider and unresolved probably triplets.

4. Supplementary material

CCDC-223041 contains the supplementary crystallographic data for this paper. These data can be obtained free of charge at http://www.ccdc.cam.ac.uk/conts/retrieving.html (or from the Cambridge Crystallographic Data Centre, 12, Union Road, Cambridge CB2 1EZ, UK; [fax: +44 (0) 1223/336033; e-mail: deposit@ccdc.cam.ac.uk].

Acknowledgements

This work was supported by the Slovak Ministry of Education, APVT foundation 2001902 and VEGA 1/9251/02 and by the Grant 4T09A 11523 of the Polish Ministry of Science and Computerization.

References

[1] M. Melník, J. Inorg. Nucl. Chem. 40 (1978) 463.
[2] L.H.J. Lajunen, P. Kokkonen, A. Nissi, H. Ruotsalainen, Thermochim. Acta 72 (1984) 219.
[3] Y. Anjaneyulu, N.V.S. Rao, R. Prabhakara Rao, L.N. Murthy, V.G.K.M. Pisipati, Indian J. Pure Appl. Phys. 24 (1986) 256.
[4] Y. Anjaneyulu, N.V.S. Rao, R. Prabhakara Rao, V.G.K.M. Pisipati, Proc. Indian Acad. Sci. 97 (1986) 177.
[5] J.D. Ranford, P.J. Sadler, D.A. Trocher, J. Chem. Soc., Dalton Trans. (1993) 3393.
[6] S.S. Dube, S.S. Dhindsa, J. Indian Chem. Soc. 46 (1969) 838.
[7] V.P. Gupta, J.K. Sthapak, D.D. Sharma, J. Inorg. Nucl. Chem. 43 (1981) 3019.
[8] C.R. Dhat, D.V. Jahagirdar, Indian J. Chem. 21A (1982) 792.
[9] G. Smith, U.D. Wermuth, B.C. Bott, P.C. Healy, J.M. White, Aust. J. Chem. 55 (2002) 349.
[10] G. Smith, U.D. Wermuth, J.M. White, Acta Crystallogr. E57 (2001) o1036.
[11] G. Smith, R.C. Bott, U.D. Wermuth, Acta Crystallogr. E57 (2001) o895.
[12] S.W. Ng, P. Naumov, M.G.B. Drew, G. Wojciechowskid, B. Brezinski, J. Mol. Struct. 595 (2001) 29.
[13] G. Smith, U.D. Wermuth, B.C. Bott, J.M. White, A.C. Willis, Aust. J. Chem. 54 (2001) 165.
[14] G. Smith, U.D. Wermuth, J.M. White, Aust. J. Chem. 54 (2001) 171.
[15] G. Smith, R.C. Bott, U.D. Wermuth, Acta Crystallogr. E57 (2001) o640.
[16] G. Smith, D.E. Lynch, K.A. Byriel, C.H.L. Kennard, Aust. J. Chem. 48 (1995) 1133.
[17] G. Smith, D.E. Lynch, K.A. Byriel, C.H.L. Kennard, Acta Crystallogr. C52 (1996) 231.
[18] G. Smith, U.D. Wermuth, P.C. Healy, Acta Crystallogr. E58 (2002) o845.
[19] G. Smith, U.D. Wermuth, J.M. White, Acta Crystallogr. E58 (2002) o1315.
[20] M. Koman, L. Martiška, D. Valigura, T. Glowiak, Acta Crystallogr. E59 (2003) o441.
[21] J. Aggett, Eng Sin Ow, Aust. J. Chem. 24 (1971) 1839.
[22] G. Smith, D.E. Lynch, K.A. Byriel, C.H.L. Kennard, Aust. J. Chem. 50 (1997) 977.
[23] G. Smith, M.G. Coyne, J.M. White, Aust. J. Chem. 53 (2000) 203.
[24] V.S.S. Kumar, S.S. Kuduva, G.R. Desiraju, Acta Crystallogr. E58 (2002) o865.
[25] D. Valigura, M. Melník, M. Koman, L. Martiška, M. Korabik, J. Mrozinski, T. Glowiak, Inorg. Chem. Commun. 7 (2004) 548.

[26] E. König, Magnetic Properties of Coordination and Organometallic Transition Metal Compounds, Springer-Verlag, Berlin, 1966.
[27] Kuma Diffraction, KM4CCD System Software, Version1.149, Kuma Diffraction Instruments and Université de Lausanne, Switzerland, 1998.
[28] P. Starynowicz, COSABS99: Program for Absorption Correction, University of Wroclaw, Poland, 1999.
[29] G.M. Sheldrick, SHELXS-86, in: G.M. Sheldrick, C. Kruger, R. Goddard (Eds.), Crystallographic Computing 3, Oxford University Press, 1985, pp. 175–189.
[30] G.M. Sheldrick, SHELXL93. Program for Crystal Structure Refinement, University of Göttingen, Germany, 1993.
[31] G.M. Sheldrick, SHELXL97. Program for Crystal Structure Refinement, University of Göttingen, Germany, 1997.
[32] L.J. Farrugia, ORTEP-3 for Windows, J. Appl. Crystallogr. 30 (1997) 565.
[33] V. Kolesnichenko, M.H. Mason, J.B. Botts, A.M. Botts, T.E. Baroni, J.A. Heppert, A.L. Rheingold, L. Liable-Sands, G.P.A. Yap, Inorg. Chem. 40 (2001) 5010.
[34] T.E. Baroni, J.A. Heppert, R.R. Hodel, R.P. Kingsborough, M.D. Morton, A.L. Rheingold, G.P.A. Yap, Organometallics 15 (1996) 4872.
[35] C.F. Edwards, W.P. Griffith, A.J.P. White, D.J. Williams, Polyhedron 11 (1992) 2711.
[36] J.H. Thurston, E.M. Marlier, K.H. Whitmira, Chem. Commun. (2002) 2834.
[37] H. Thurston, K.H. Whitmira, Inorg. Chem. 41 (2002) 4194.
[38] C. Christmas, J.B. Vincent, Hsiu Rong Chang, J.C. Huffman, G. Christou, D.N. Hendrickson, J. Am. Chem. Soc. 110 (1988) 823.
[39] C. Christmas, J.B. Vincent, J.C. Huffman, G. Christou, Hsiu RongChang, D.N. Hendrickson, Angew. Chem., Int. Ed. Engl. 26 (1987) 915.
[40] G. Kickelbick, U. Schubert, J. Chem. Soc., Dalton Trans. (1999) 1301.
[41] A. Pajunen, S. Pajunen, Cryst. Struct. Commun. 11 (1982) 427.
[42] P. Lemoine, B. Viossat, G. Morgant, F.T. Greenaway, A. Tomas, Nguyen-Huy Dung, J.R.J. Sorenson, J. Inorg. Biochem. 89 (2002) 18.
[43] M. Geraghty, V. Sheridan, M. McCann, M. Devereux, V. McKee, Polyhedron 18 (1999) 2931.
[44] H. Muhonen, Acta Crystallogr. B38 (1982) 2041.
[45] P. Lemoine, D. Nguyen-Huy, B. Viossat, J.M. Leger, A. Tomas, Acta Crystallogr. C55 (1999) 2068.
[46] P. Lemoine, A. Mazurier, I. Billy, D. Nguyen-Huy, B. Viossat, Z. Krystallogr. 215 (2000) 523.
[47] M. Gawron, R.C. Palenik, G.J. Palenik, Inorg. Chim. Acta 112 (1986) 71.
[48] J. Galy, J. Jaud, O. Kahn, P. Tola, Inorg. Chim. Acta 36 (1979) 229.
[49] K. Ikeda, M. Ohba, H. Okawa, J. Chem. Soc., Dalton Trans. (2001) 3119.
[50] Ruo-Jie Tao, Shuan-Quan Zang, Jin-Yang Niu, Zhao-Wen Yu, Xu-Ya Zhou, Wuji Huaxue Xuabao(Chin) (Chin. J. Inorg. Chem.) 18 (2002) 409.
[51] F. Tuna, L. Patron, Y. Journaux, M. Andruh, W. Plass, J.C. Trombe, J. Chem. Soc., Dalton Trans. (1999) 539.
[52] F. Tuna, G.I. Pascu, J.-P. Sutter, M. Andruh, S. Golhen, J. Guillevic, H. Pritzkow, Inorg. Chim. Acta 342 (2003) 131.
[53] B.N. Figgis, D.J. Martin, J.Chem. Soc., Dalton Trans. (1972) 2174.
[54] D.B. Brown, J.R. Wasson, J.W. Hall, W.E. Hatfield, Inorg. Chem. 16 (1977) 2526.
[55] T.E. Grigereit, B.L. Ramakrishna, H. Place, R.D. Willett, G.C. Pellacani, T. Manfredini, L. Menabue, A. Bonamartini-Corradi, L.P. Battaglia, Inorg. Chem. 26 (1987) 2235.
[56] I.V. Vasilevsky, R.E. Stenkamp, E.C. Lingafelter, V. Schomaker, R.D. Willett, N.J. Rosse, Inorg. Chem. 28 (1989) 2619.
[57] Jin-Kui Tang, Hong-Mei Wang, Peng Cheng, Xin Liu, Dai-Zheng Liao, Zong-Hui Jiang, Shi-Ping Yan, Polyhedron 20 (2001) 675.
[58] E. Colacio, J.P. Costes, R. Kivekäs, J.P. Laurent, J. Ruiz, Inorg. Chem. 29 (1990) 4240.
[59] E. Colacio, J.M. Dominigues-Vera, J.P. Costes, R. Kivekäs, J.P. Laurent, J. Ruiz, M. Sundberg, Inorg. Chem. 31 (1992) 774.
[60] E. Colacio, J.M. Dominigues-Vera, J.M. Moreno, J. Ruiz, R. Kivekäs, A. Romerosa, Inorg. Chim. Acta 212 (1993) 115, and references therein.
[61] E. Colacio, M. Ghazi, R. Kivekäs, J.M. Moreno, Inorg. Chem. 39 (2000) 2882.
[62] W. Haase, S. Gehring, J. Chem. Soc., Dalton Trans. (1985) 2609.
[63] S. Konar, P.S. Mukherjee, M.G.B. Drew, J. Ribas, N.R. Chaudhuri, Inorg. Chem. 42 (2003) 2545.
[64] A.W. Addison T.N. Rao, J. Reedijk, J. Vanrijn, G.C. Verschoor, J. Chem. Soc., Dalton Trans. (1984) 1349.
[65] O. Kahn, Molecular Magnetism, VCH Publishers, Weinheim, 1993.
[66] M. Julve, M. Verdaguer, A. Gleizes, M. Philoche-Levisalles, O. Kahn, Inorg. Chem. 23 (1984) 3808.
[67] B.J. Hathaway, D.E. Billing, Coord. Chem. Rev. 5 (1970) 87.
[68] B.J. Hathaway, Struct. Bonding (Berlin) 57 (1984) 55.
[69] J.F. Berry, F.A. Cotton, P. Lei, C.A. Murillo, Inorg. Chem. 42 (2003) 377.
[70] K. Nakamoto, Infrared and Raman Spectroscopy of Inorganic and Coordination Compounds, Willey Interscience Publications, New York, 1999.

Available online at www.sciencedirect.com
SCIENCE DIRECT®
Polyhedron 23 (2004) 2457–2464
POLYHEDRON
www.elsevier.com/locate/poly

Copper(II) complexes of new tetradentate NSNO pyridylthioazophenol ligands: synthesis, spectral characterization and crystal structure

Pulak K. Dhara [a], Sadhan Pramanik [a], Tian-Huay Lu [b], Mike.G.B. Drew [c], Pabitra Chattopadhyay [a,*]

[a] *Department of Chemistry, The Burdwan University, Golapbag, Burdwan 713104, W.B., India*
[b] *Department of Physics, National Tsing Hua University, Hsinchu 300, Taiwan, ROC*
[c] *Department of Chemistry, Reading University, Reading RG 66AD, Berks, UK*

Received 26 June 2004; accepted 16 July 2004
Available online 25 September 2004

Abstract

Copper(II) complexes of a series of new tetradentate NSNO ligands were synthesized and characterized spectroscopically. The ligands were also characterized by elemental analyses, IR, ^{1}H NMR, FAB-MS and UV–Vis spectroscopy. The solid-state structures of two complexes **2a** and **4a** were established by X-ray crystallography. The geometry about the copper ion of the complexes is dependent on the counter anion of the copper salt used. The five-coordinated copper ion is distorted square pyramidal when SCN^- or Cl^- ligate with the copper(II) ion, occupying the equatorial position, whereas the geometry about the four-coordinated copper ion is square planar when the counter anion is perchlorate. The electronic spectra of **2** and **3** in methanol show that the distortion of square pyramidal towards trigonal bipyramidal geometry about the copper ion of the complexes in solution is dependent on the presence of the electron withdrawing group. All the complexes exhibit a band for $S(\sigma) \rightarrow Cu(II)$ charge transfer (LMCT) in the range of 380–394 nm. The EPR spectra of complexes **2** and **3** are consistent with the fact that the unpaired electron is predominantly in the $d_{x^2-y^2}$ orbital as $g_{II} > g_I$. The redox behavior of all the complexes in methanol was studied by CV using TBAP as the supporting electrolyte.
© 2004 Elsevier Ltd. All rights reserved.

Keywords: Copper(II) complex; Pyridylthioazophenol ligands; Crystal structure

1. Introduction

The coordination chemistry of transition metal complexes involving nitrogen and sulfur donor ligands has been the cynosure among chemists during recent years due to the application of these chelates in modelling of biomolecules, in the field of chemical and biological reactivity and nuclear medicine. The potential role played by copper ions, being present in the active sites of a large number of metalloproteins having the CuN_2S_2 chromophore [1], has stimulated efforts to design new ligand frames having nitrogen–sulfur donor sets and characterize copper complexes as models for providing a better understanding of the biological system [2]. It has been found that copper(II) chelates, especially of nitrogen–sulfur ligand frames, have antineoplastic activities and interactions with biological systems [3]. Considerable attention has been directed towards the synthesis of copper(II) chelates, especially of nitrogen–sulfur containing ligands, in search of nuclear medicine [4] and anticancer agents present in the hypoxic cell [5]. Again, current research shows that the involvement of both the

* Corresponding author. Tel.: +913422558339; fax: +913422530452.
E-mail address: pabitracc@yahoo.com (P. Chattopadhyay).

0277-5387/$ - see front matter © 2004 Elsevier Ltd. All rights reserved.
doi:10.1016/j.poly.2004.07.023

sulfur-to-copper charge transfer (LMCT) and the copper d–d band in the photosensitization process lead to an efficient DNA cleavage [6].

Herein, we have synthesized three sets of copper(II) complexes of a series of new tetradentate NSNO ligands using different copper(II) salts. In this paper, we present an account on copper(II) complexes of pyridylthioazophenol ligands. The present contribution aims to study the structural chemistry of the copper(II) complexes of the new ligands and the change of the geometry about the copper ion due to the presence of the anions (Cl^-, SCN^- and ClO_4^-) in the copper salts. The complexes **2** and **3** are five-coordinated inner metallic complexes where the fifth coordination number is satisfied by NCS^- or Cl^- being present in the equatorial position and the borderline base pyridine-N of the tetradentate (NSNO) ligands are in the axial site of the distorted square pyramidal geometry. In the cationic copper(II) pyridylthioazophenol complexes (**4**), the counteranion is perchlorate and the geometry about the copper ion is square planar.

2. Experimental

2.1. Materials

All the reagents were obtained from commercial sources and used without further purification. Copper(II) thiocyanate was obtained by adding a saturated solution of potassium thiocyanate to a solution of copper(II) chloride in methanol, followed by removing the precipitate of KCl by filtration. Tetra-*n*-butylammoniumperchlorate was prepared by the addition of sodium perchlorate to a hot solution of tetra-*n*-butylammonium bromide (Aldrich). The product was recrystallized from aqueous ethanol and tested for the absence of bromide. Solvents were distilled from an appropriate drying agent [7].

2.2. Physical measurements

The ^1H NMR spectra were obtained on a Bruker AC300 spectrometer with chemical shifts reported in δ values relative to the residual solvent resonance of $CDCl_3$. IR spectra were obtained on a JASCO FT-IR model 420 spectrometer using KBr disks, UV–Vis on a JASCO UV–Vis/NIR model V-570 spectrometer and mass spectra on a VG system, model 70-250S spectrometer. Microanalyses were performed with the use of a Perkin–Elmer 2400 CHN elemental analyzer and copper analysis was carried out by the iodometric titration method [8]. Molar conductance (Λ_M) were measured in a systronics conductivity meter 304 model using $\sim 10^{-3}$ M solutions in MeOH. Magnetic moments (μ, BM) were obtained from vibrating sample magnetometer PAR 155 model. X-band EPR spectra were taken on a Brucker spectrometer with a variable temperature liquid nitrogen cryostat at NTHU, Hsinchu, Taiwan. The values g_{II} and A_{II} were measured at 77 K. Electrochemical measurements were made with a computer controlled EG&G PAR model 270 VERSTAT electrochemical instrument using Ag/AgCl electrodes. All measurements were made at 298 K in dry MeOH with $[Bu_4N]ClO_4$ as the supporting electrolyte. The experimental solutions were deoxygenated by bubbling with research grade dinitrogen. The reported potentials are uncorrected for junction potential.

2.3. Syntheses of the ligands (HL)

The syntheses of the ligands were carried out following the common procedure of coupling different *para*-substituted phenols with the diazotized 2-(2-pyridylmethylthio)-aniline (Scheme 1). The procedure for the synthesis of 2-hydroxy-4-methyl-2′-(2-picolyl-thio)azobenzene (HL1) is as follows.

At first 2-(2-pyridylmethylthio)-aniline was synthesized following the reported procedure [9]. Then the preparation of 2-(2-pyridylmethylthio)-phenylazo-(4-methyl)-phenolate was carried out. The details are given as follows for **1a**. To an alkaline solution of *p*-cresol (1.0 g, 9.3 mmol) at 5 °C was added a diazotized solution of 2-(2-pyridylmethyl-thio)-aniline (2.0 g, 9.3 mmol) dropwise with continuous stirring. The temperature was controlled at ice-cold conditions. The resulting solution was acidified and the pH was controlled between 6 and 7. The red colored compound so precipitated was filtered and washed with water. Finally the pure recrystallized compound was obtained from ethanol-water. The yield was 65%. The yield of the other ligands varied from 50% to 68% following a similar method. *Anal*. Calc. for **1a**: C, 68.06; H, 5.07; N, 12.53. Found: C, 68.83; H, 4.96; N, 12.74%. Calc. for **1b**: C, 70.02; H, 6.10; N, 11.14. Found: C, 69.63; H, 5.98; N, 11.54%. Calc. for **1c**: C, 60.76; H, 3.94; N, 11.81. Found: C, 60.23; H, 3.81; N, 11.99%. Calc. for **1d**: C, 59.01; H, 3.82; N, 15.30. Found: C, 58.75; H, 3.75; N, 15.48%. Calc. for **1e**: C, 71.16; H, 4.58; N, 11.32. Found: C, 70.92; H, 4.47; N, 11.56%; m.p.(°C): **1a**: 87 ± 1, **1b**: 167 ± 1, **1c**: 118 ± 1, **1d**: 75 ± 1, **1e**: 159 ± 1; ^1H NMR δ (ppm) (in $CDCl_3$): **1a**: 12.58(s, 1H), 8.52(d, 1H), 7.82–6.96 (m, 10H), 4.31(s, 2H), 2.31(s, 3H); **1b**: 12.61(s, 1H), 8.54(d, 1H), 7.78–7.01 (m, 10H), 4.83(s, 2H), 1.40(s, 9H); **1c**: 12.54(s, 1H), 8.50(d, 1H), 7.91–6.75 (m, 10H), 4.45(s, 2H); **1d**: 12.61(s, 1H), 8.54(d, 1H), 8.01–6.96 (m, 10H), 4.50(s, 2H); **1e**: 12.61(s, 1H), 8.51(d, 1H), 7.72–6.23 (m, 13H), 4.48(s, 2H); FAB-MS (FAB^+, $[M+H]^+$): **1a**: 336.11, **1b**: 378.15, **1c**: 356.06, **1d**: 367.10, **1e**: 372.12.

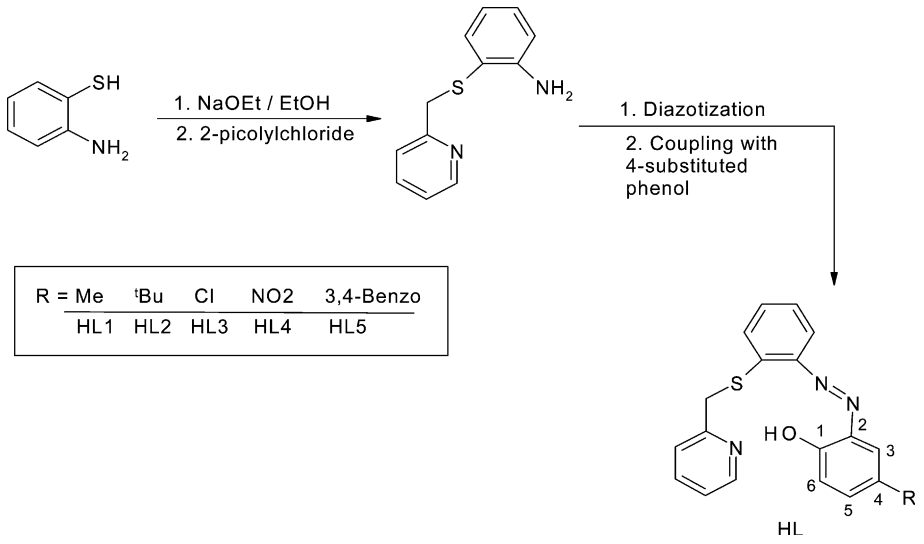

Scheme 1. Synthetic procedure for the ligands.

2.4. Syntheses of Cu(II) complexes of the ligands (HL)

The preparation follows a common procedure. To a methanolic solution (15 mL) of **1a** (0.335 g, 1.0 mmol) the corresponding copper salt (1.0 mmol) solution was added dropwise and the resulting solution stirred for a period of 3 h for **2a**, 2 h for **3a** and 4 h for **4a**. The solution was dried at ambient temperature. The product was collected by washing with cold MeOH–H_2O and dried. The pure reddish-violet colored crystallized product was obtained from dichloromethane. Yield: 80–85%. *Anal*. Calc. for **2a**: C, 52.66; H, 3.69; N, 9.70; Cu, 14.67. Found: C, 52.01; H, 3.59; N, 9.91; Cu, 14.21%. Calc. for **2b**: C, 55.58; H, 4.63; N, 8.84; Cu, 13.36. Found: C, 55.28; H, 4.50; N, 8.97; Cu, 12.98%. Calc. for **2c**: C, 47.63; H, 2.87; N, 9.26; Cu, 14.00. Found: C, 48.01; H, 2.93; N, 9.31; Cu, 13.67%. Calc. for **2d**: C, 46.55; H, 2.80; N, 12.07; Cu, 13.68. Found: C, 46.76; H, 2.78; N, 12.19; Cu, 13.90%. Calc. for **2e**: C, 56.29; H, 3.41; N, 8.96; Cu, 13.54. Found: C, 55.98; H, 3.32; N, 8.98; Cu, 13.39%. Calc. for **3a**: C, 52.69; H, 3.51; N, 12.29; Cu, 13.94. Found: C, 52.12; H, 3.44; N, 12.51; Cu, 13.39%. Calc. for **3b**: C, 55.48; H, 4.42; N, 11.25; Cu, 12.76. Found: C, 55.98; H, 4.30; N, 11.77; Cu, 12.18%. Calc. for **3c**: C, 47.90; H, 2.73; N, 11.76; Cu, 13.34. Found: C, 48.12; H, 2.83; N, 11.99; Cu, 13.69%. Calc. for **3d**: C, 46.86; H, 2.67; N, 14.39; Cu, 13.05. Found: C, 47.01; H, 2.81; N, 14.89; Cu, 12.79%. Calc. for **3e**: C, 56.15; H, 3.25; N, 11.39; Cu, 12.92. Found: C, 56.28; H, 3.30; N, 11.58; Cu, 12.39%. Calc. for **4a**: C, 45.87; H, 3.22; N, 8.45; Cu, 12.78. Found: C, 46.03; H, 3.10; N, 8.71; Cu, 12.81%. Calc. for **4b**: C, 48.98; H, 4.08; N, 7.79; Cu, 11.78. Found: C, 48.89; H, 4.06; N, 7.62; Cu, 11.57%. Calc. for **4c**: C, 41.74; H, 2.51; N, 8.11; Cu, 12.27. Found: C, 41.95; H, 2.63; N, 7.95; Cu, 12.25%. Calc. for **4d**: C, 40.90; H, 2.46; N, 10.60; Cu, 12.03. Found: C, 40.64; H, 2.51; N, 10.79; Cu, 11.79%. Calc. for **4e**: C, 49.53; H, 3.00; N, 7.88; Cu, 11.91. Found: C, 50.04; H, 2.88; N, 7.78; Cu, 11.51%.

2.5. X-ray crystal structure analysis

Single crystals suitable for X-ray work of **2a** were grown by slow evaporation of a solution of the complex **2a** in methanolic:toluene (1:2) at ambient temperature while **4a** was grown by slow diffusion of hexane into a benzene solution of the complex at 298 K. A suitable single crystal of the complex **2a** was mounted on a Bruker SMART CCD diffractometer equipped with graphite monochromated Mo Kα ($\lambda = 0.71073$ Å) radiation. The intensity data were corrected for Lorentz and polarization effects and an empirical absorption correction was also employed using the SAINT program. A total of 10601 [unique data = 4107; $R_{int} = 0.032$] reflections were measured and 2876 reflections were assumed observed the applying the condition $I > 2\sigma(I)$. The structure was solved by Patterson syntheses, followed by successive Fourier and difference Fourier syntheses. Full matrix least squares refinements on F^2 were carried out using SHELXL-97 with anisotropic displacement parameters for all non-hydrogen atoms in all cases. Hydrogen atoms were constrained to ride on the respective carbon atoms with an isotropic displacement parameter equal to 1.2 times the equivalent isotropic displacement parameter of their parent atom. The refinement converged to residual indices $R = 0.0390$; $wR_2 = 0.0927$ with $I > 2\sigma(I)$. The final difference Fourier map showed the maximum and minimum peak heights at 0.43 and -0.27 e Å^{-3}, respectively, having no chemical significance. Complex neutral atom scattering factors [10a] were used throughout. All calculations were carried

out using SHELXS-93 [10b], SHELXL-97 [10c], PLATON-99 [10d] and ORTEP3 [10e] programs. Data of **4a** were measured with Mo Kα radiation using the MARresearch Image Plate System. The crystal was positioned at 70 mm from the Image Plate. 100 frames were measured at 2° intervals with a counting time of 2 min. Data analysis was carried out with the XDS program [11a] to provide 2593 independent reflections. The structure was solved using direct methods with the SHELX-86 program [11b]. Non-hydrogen atoms were refined with anisotropic thermal parameters. The hydrogen atoms bonded to carbon were included in geometric positions and given thermal parameters equivalent to 1.2 times those of the atom to which they were attached. An empirical absorption correction was applied using DIFABS [11c]. The structure was refined on F^2 using SHELXL [11d] with $I > 2\sigma(I)$.

3. Result and discussions

3.1. Synthesis

The ligands 2-(2-pyridylmethylthio)-phenylazo-(4-methyl)phenolates (**1**) were prepared by coupling 4-substituted-phenols with the diazonium ion obtained from 2-(2-pyridylmethylthio)-aniline, which was synthesized from 2-aminothiophenol by reacting it with 2-picolylchloride in presence of a base at the first step. This series of organic moieties act as tetradentate NSNO ligands which are interesting chelators due to the presence of hard donor azo-N and phenolate-O, borderline base pyridine-N and soft thioether S donor centres. The ligands have been spectroscopically characterized. The copper(II) complexes of these ligands were obtained by their reaction with equimolar amounts of the appropriate copper salts in methanol. All the complexes are soluble in common organic solvents.

3.2. Structures of the Cu(II) complexes (*2a* and *4a*)

The ORTEP views of **2a** and **4a** are illustrated in Figs. 1 and 2, respectively, with the atom numbering schemes shown. The selected bond distances and angles are listed in Tables 1 and 2, respectively. The crystal of **2a** is of the monoclinic system with the space group $P2_1/n$. In this monomeric complex **2a**, the copper center is bonded to a tetradentate monobasic NSNO donor pyridylthioazophenolate organic moiety (L1) and a monodentate chloride ligand. The coordination geometry is distorted square pyramidal with two nitrogen, one oxygen and chlorine donor atoms occupying the basal plane. The pyridinic N(1) shows the axial contact at a long distance of 2.2194 (18) Å. The axial Cu–N(1) bond distance (2.2194 (18) Å) is longer than the equatorial Cu–N(2) (1.980 (2) Å) due the geometric position as

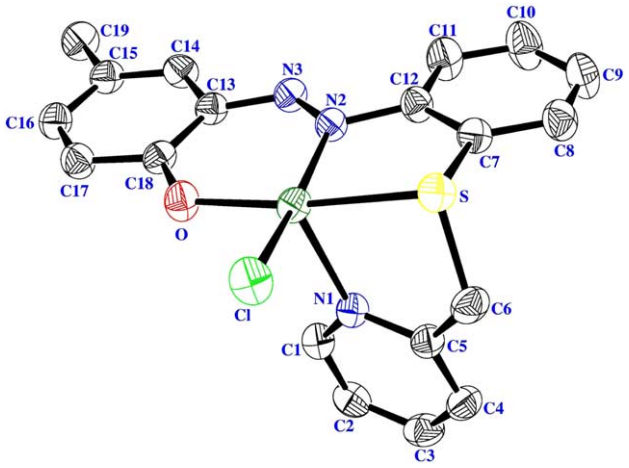

Fig. 1. Solid-state structure of [Cu(L1)Cl] (**2a**) showing the atom labelling scheme.

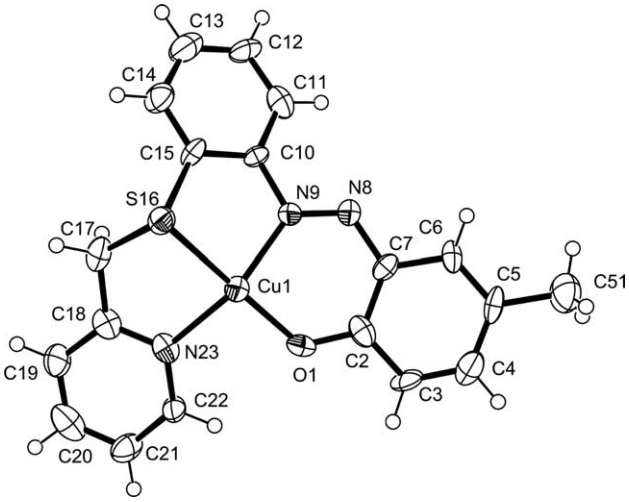

Fig. 2. An ORTEP view of the cation of the complex **4a** with thermal ellipsoids at the 50% probability level and the atom numbering scheme.

usual. The Cu–Cl bond distance is 2.2973(9) Å. The thioether sulfur S is strongly coordinated with copper, being present in the basal plane, and the Cu–S bond distance of 2.3360(8) Å is shorter than axial [12] and moderate in comparison to the usually observed basal Cu–S bond distances in pentacoordinated copper complexes [13]. The structure of **2a** is almost regular square pyramidal as seen from the trigonality index [14] τ of only 0.116 [$\tau = (\beta - \alpha)/60$ where β = O–Cu–S = 172.95(6)° and α = N2–Cu–Cl = 165.99(7)°].

In the complex cation of $[Cu(L1)]ClO_4$ (**4a**), Cu(II) is located in the centre of a square planar environment and the metal atom is bonded to four atoms of the ligand. Here, both coordinating N atoms are at equivalent distances whereas this fact is different in the case of **2a**. The distortion from square planar geometry to tetrahedral geometry is also observed as distances from the donor atoms to the square plane are −0.29, 0.29, −0.27, 0.28

Table 1
Summarized crystallography data for **2a** and **4a**

	2a	**4a**
Empirical formula	$C_{19}H_{16}ClCuN_3OS$	$C_{19}H_{16}ClCuN_3O_5S$
Formula weight	433.42	497.40
Crystal system	monoclinic	monoclinic
Space group	$P2_1/n$	$C2/c$
a (Å)	9.8658(9)	26.15(3)
b (Å)	8.6589(8)	12.047(15)
c (Å)	21.6344(19)	14.179(15)
α (°)	90.00	90.00
β (°)	99.224(2)	117.000(10)
γ (°)	90.00	90.00
V (Å^3)	1824.3(3)	3981(8)
ρ_{calc} (g/cm^3)	1.578	1.660
Z	4	8
Radiation wavelength λ (Å)	0.71073	0.71073
$F(000)$	884	2024
T (K)	293	293
θ (°)	1.9–28.2	2.22–25.98
μ (Mo Kα) (mm^{-1})	1.471	1.471
Number of reflections (total)	10601	5738
Number of reflections (granted)	4107	2593
Observed data ($I > 2\sigma(I)$)	2876	1914
R	0.0390	0.1036
wR	0.0927	0.1347

Table 2
Selected bond distances (Å) and bond angles (°) for **2a** and **4a**

2a		**4a**	
Bond distances			
Cu–O	1.9031(19)	Cu–O1	1.860(9)
Cu–N2	1.980(2)	Cu–N9	1.949(9)
Cu–N1	2.2194(18)	Cu–N23	1.984(10)
Cu–S	2.3360(8)	Cu–S16	2.295(4)
O–C18	1.295(3)	O1–C2	1.321(14)
N3–C13	1.359(3)	C7–N8	1.388(15)
N2–N3	1.283(3)	N8–N9 (azo)	1.267(12)
N2–C12	1.440(4)	N9–C10	1.420(15)
S–C7	1.776(3)	C15–S16	1.799(13)
S–C6	1.812(3)	S16–C17	1.852(13)
Cu–Cl	2.2973(9)	C18–N23	1.353(15)
C1–N1	1.331(3)	C22–N23	1.340(16)
Bond angles			
N1–Cu–S	81.80(6)	O1–Cu–N9	93.5(4)
N1–Cu–N2	92.61(9)	O1–Cu–N23	96.9(4)
N1–Cu–Cl	98.95(6)	N9–Cu–S16	87.7(3)
N1–Cu–O	104.97(8)	N23–Cu–S16	86.2(3)
N2–Cu–S	85.96(7)	O1–Cu–S16	168.0(3)
N2–Cu–O	91.71(9)	N9–Cu–N23	157.8(4)
N2–Cu–Cl	165.99(7)	C2–O1–Cu	123.7(8)
Cl–Cu–S	87.89(3)	N8–N9–Cu	128.1(8)
Cl–Cu–O	92.89(6)	N9–N8–C7	121.1(10)
O–Cu–S	172.95(6)	C10–N9–Cu	114.5(7)
N3–N2–Cu	128.79(18)	C15–S16–Cu	92.9(4)
C6–S–Cu	97.68(9)	C17–S16–Cu	92.3(4)

Å for O(1), N(9), S(16) and N(23), respectively, the copper atom being −0.07 Å from this plane. The perchlorate ion has no close contact to the copper atom.

Both complexes are monomeric but all the corresponding Cu–O, Cu–N and Cu–S distances of **4a** are significantly shorter than those of **2a**. It may be due to the increase in formal charge on **2a** by coordination of chloride and the difference in geometry of the complexes. The Cu–N(pyridinic) distance in **4a** is shorter than that of **2a** by ca. 0.24 Å. This Cu–N bond in **2a** is axial and not in the same plane as the other donor atoms of the ligand, which is different from that in **4a**. This difference in bond lengths for the same ligand frame is due to the flexibility of the Cu(II) coordination geometry.

3.3. Spectral properties

The ligands **1** exhibit medium intense IR bands at ~3300 cm^{-1} (O–H of H bonded phenolic OH) [15] which is absent in all the complexes. This indicates coordination of oxygen to the metal centre [16]. The $\nu_{N=N}$ mode of the free ligand (1495–1505 cm^{-1}) is shifted to lower to wave numbers ($\Delta \sim 20$–30 cm^{-1}) in the complexes, suggesting coordination of the metal ions to the azo function [17]. The $\nu_{N=N}$ band is observed at 1465–1478 cm^{-1} for all the complexes. In addition to this ν_{C-S} at 790 cm^{-1} for the ligands shifts to 760 cm^{-1} for the complexes. Thiocyanato complexes **3** show a characteristic band in the range of 2050–2060 cm^{-1} indicating the presence of N-bonded NCS groups [18]. Infrared spectra of the complexes **4** exhibit an intense band at approximately 1090 cm^{-1} along with a weak band at 625 cm^{-1} which have been assigned to $\nu_{(ClO_4^-)}$. The conductivity measurements of complexes **2** and **3** in methanolic solution show the conductance in the range of 9–20 Λ_0 mol^{-1} cm^{-1} and those of **4** in MeOH are 89–102 Λ_0 mol^{-1} cm^{-1}. The values suggest that the complexes **2** and **3** exist as non-electrolytes and **4** as having 1:1 electrolytic nature in the solution state. Magnetic susceptibility data reveal spin-only values for all the copper complexes as the values are very close to 1.73 BM (in the range of 1.72–1.92 BM).

3.3.1. Electronic spectra

The electronic absorption spectra of the azo ligands and their complexes were recorded at room temperature using MeOH as the solvent, and the results are shown in Table 3. The spectra of the free ligands and the complexes exhibit transitions at lower than 400 nm corresponding to intramolecular $\pi \rightarrow \pi^*$ and $n \rightarrow \pi^*$ transitions [19]. In the case of the complexes, a band around 390 nm is assignable to the $S(\sigma) \rightarrow Cu(II)$ charge transfer (LMCT) transition [6,20]. The copper(II) complexes are characterized by a rather broad d–d absorption band in their solution electronic spectra; often a low- or high-energy shoulder is also present or, occasionally, two distinct absorption maxima are observed. In many cases it has been shown that the presence of a single d–d band with a high energy shoulder

Table 3
UV–Vis spectral, electrochemical and EPR data

Compound	λ nm (ε) (ε, dm^3 mol^{-1} cm^{-1})	Electrochemical data $E^{\circ\prime}$, mV (ΔE_p, mV) [E_{pa}, mV E_{pc}, mV]	EPR data		
			g_{II}	A_{II} (G)	$g_{\perp}$
1a	206 (23385), 254 (11449), 326 (11871), 410 (7244), 458 (3981)				
1b	218 (24231), 252 (12658), 327 (10993), 408 (8012), 456 (3896)				
1c	210 (19952), 251 (10272), 320 (17102), 410 (7562), 472 (4265)				
1d	212 (21158), 236 (11322), 324 (8325), 412 (5822), 486 (3912)				
1e	212 (24271), 260 (12358), 308 (10986), 410 (4375), 494 (8522)				
2a	206 (24268), 260 (11415), 344 (11896), 392 (3854), 528 (6115), 708 (268), 852 (sh, 133)	−65 (150) [10, −140]	2.229	164	2.054
2b	218 (24550), 258 (13381), 346 (16544), 392 (5825), 528 (8182), 708 (270), 850 (sh, 111)	65.8 (148.3) [140, −8.3]	2.234	166	2.060
2c	210 (16886), 260 (9837), 338 (7124), 386 (2967), 528 (4051), 718 (218), 844 (sh, 128)	142.5 (93) [188, 95]	2.230	160	2.052
2d	216 (19982), 262 (10785), 330 (7253), 390 (2598), 528 (3925), 736 (186), 824 (193)	177 (96) [225, 129]	2.221	154	2.052
2e	216 (23245), 258 (16284), 344 (4099), 386 (5127), 528 (8542), 700 (261), 896 (sh, 106)	57.7 (150.6) [133, −17.6]	2.237	168	2.058
3a	206 (22931), 260 (7528), 346 (7531), 394 (2654), 528 (3804), 710 (198), 876 (sh, 97)	−13 (120) [47, −73]	2.231	167	2.040
3b	218 (26822), 258 (17102), 346 (15164), 392 (5165), 528 (8012), 710 (278), 875 (sh, 95)	50 (178) [139, −39]	2.232	172	2.041
3c	208 (17089), 260 (10181), 344 (7201), 392 (3012), 528 (4212), 722 (172), 838 (sh, 92)	130 (108) [184, 76]	2.227	165	2.043
3d	216 (19876), 262 (11108), 330 (7203), 390 (2501), 530 (4125), 730 (140), 820 (138)	165 (134) [232, 98]	2.217	158	2.037
3e	216 (22956), 262 (16203), 338 (4322), 386 (5203), 530 (8433), 714 (201), 912 (sh, 65)	62 (156) [140, −16]	2.238	173	2.045
4a	206 (29604), 260 (14038), 300 (9583), 346 (13671), 390 (5334), 530 (6890), 704 (317)	15 (210) [120, −90]			
4b	216 (25989), 261 (17223), 346 (15003), 390 (5324), 530 (8245), 706 (320)	69 (162) [150, −12]			
4c	208 (17522), 260 (10036), 342 (7112), 392 (4258), 530 (4549), 704 (318)	120 (96) [168, 72]			
4d	216 (19509), 262 (10798), 338 (6978), 391 (3122), 536 (5423), 708 (309)	152.5 (101) [203, 102]			
4e	216 (23203), 258 (16722), 339 (3949), 380 (5344), 536 (8738), 706 (321)	63 (140) [133, −7]			

is typical of a trigonal bipyramidal stereochemistry for copper, whereas an absorption with a low energy shoulder indicates a square pyramidal geometry [21].

On the basis of the above criterion, the observed data of **2** and **3** suggest that the distortion of square pyramidal towards trigonal bipyramidal about the copper ion of the complexes in solution is maximum in case of the complexes **2d** and **3d**. Here, complexes **2d** and **3d** in methanol exhibit two bands of nearly equal intensity between 730 and 824 nm, this pattern suggests that the geometry about the copper ion in solution is between square pyramidal and trigonal bipyramidal. In the case of the complexes **4**, only one broad d–d absorption band around 705 nm and an intense band at 528 nm demon-

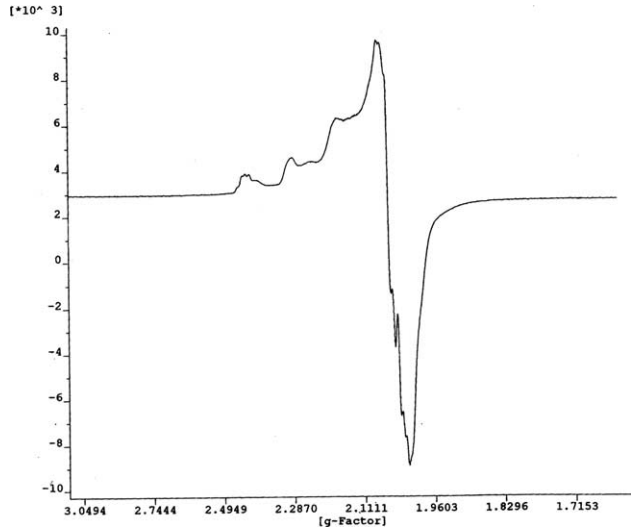

Fig. 3. EPR spectra of [Cu(L1)Cl] (**2a**) in MeOH at 77 K.

strates the square planar geometry around the copper ion.

3.3.2. EPR spectra

EPR spectra of the cupric complexes **2** and **3** have been recorded in MeOH at 300 and 77 K. The data are tabulated in Table 3 and one representative spectra of **2a** is shown in Fig. 3. However, the complexes in the frozen state at 77 K show well-resolved peaks of low intensities in the low-field region and an intense peak in the high field region. No band corresponding to the $M_s = +2$ transition was observed in the spectra, ruling out any Cu–Cu interaction. The complexes **2** and **3** appear to exhibit axial spectra of square pyramidal species with g_{II} varying from 2.217 to 2.238 and A_{II} having a range from 154×10^{-4} to 173×10^{-4} cm^{-1}. The result are in general agreement with the solution electronic spectra, which also suggest the existence of distorted square pyramidal geometries with more distortions in the complexes **2d** and **3d**. From the observed g-tensor values of the Cu(II) complexes it is clear that $g_{II} > g_I$ which dictate that in complexes **2** and **3** the unpaired electron is predominantly in the $d_{x^2-y^2}$ orbital [22] giving $^2B_{1g}$ as the ground state.

3.4. Electrochemistry

Redox properties of the complexes were examined by cyclic voltametry using a Pt-disk working electrode and a Pt-wire auxiliary electrode in dry MeOH and in the presence of [*n*-Bu$_4$N]ClO$_4$ as the supporting electrolyte. The potentials (Table 3, Fig. 4) are expressed with reference to Ag/AgCl electrodes. In solution all compounds displayed a quasi-reversible voltammogram having $i_{pc}/i_{pa} \approx 1$ in the range from −65 to 177 mV with $\Delta E = 96$–210 mV. The influence of the substituents in the ligands is apparent from the data.

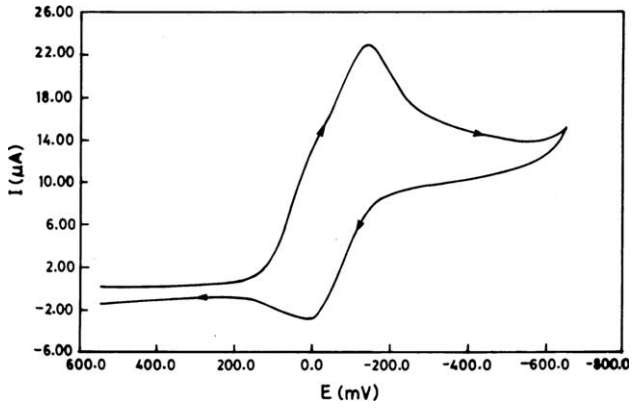

Fig. 4. CV diagram of [Cu(L1)Cl] (**2a**) in MeOH.

4. Supporting material

Crystallographic data for the structural analyses have been deposited with the Cambridge Crystallographic Data Centre, CCDC Nos. 229572 and 224745 for compounds **2a** and **4a**, respectively. Copies of this information are available free of charge on request from CCDC, 12 Union Road, Cambridge, CB2 1EZ, UK (fax: +44 1223 336 033; e-mail: deposit@ccdc.ac.uk or www:http://www.ccdc.cam.ac.uk).

Acknowledgements

We thank the Department of Science and Technology (DST), New Delhi for financial assistance. M.G.B. Drew thanks EPSRC and the University of Reading for funds for the Image Plate system. The author (P.C.) is indebted to Dr. C. Sinha, Department of Chemistry, B.U. for his valuable suggestions and discussions.

References

[1] (a) R.H. Holm, P. Kennepohl, E.I. Solomon, Chem. Rev. 96 (1996) 2239;
(b) M. Rahman, M.A. Ali, P. Bhattacharjee, M. Nazimuddin, Polyhedron 10 (1991) 823, and references therein.
[2] (a) E.I. Solomon, Angew. Chem. Int. Ed. 40 (2002) 4570;
(b) B. Abolmaali, H.V. Taylor, U. Weser, Structure Bond 9 (1998) 91;
(c) W. Kaim, J. Rall, Angew. Chem. 108 (1996) 47;
(d) N. Kitajima, Y. Moro-oka, Chem. Rev. 94 (1994) 737;
(e) N. Kitajima, Adv. Inorg. Chem. 39 (1992) 1;
(f) Y. Nakao, M. Onoda, T. Sakurai, A. Nakahara, I. Kinoshita, S. Ooi, Inorg. Chim. Acta 151 (1988) 55.
[3] (a) D.T. Minkel, A.L. Saryan, D.H. Petering, Cancer Res. 38 (1978) 124;
(b) D.A. Winkelmann, Y. Bermke, D.H. Petering, Bioinorg. Chem. 3 (1974) 261.
[4] P.J. Blower, J.S. Lewis, J. Zweit, Nucl. Med. Biol. 23 (1996) 957.
[5] A.R. Cowley, J.R. Dilworth, P.S. Donnelly, E. Labisbal, A. Sousa, J. Am. Chem. Soc. 124 (2002) 5270.

[6] S. Dhar, D. Senapati, P.K. Das, P. Chattopadhyay, M. Nethaji, A.R. Chakravarty, J. Am. Chem. Soc. 125 (2003) 12118.
[7] D.D. Perrin, W.L.F. Armarego, D.R. Perrin, Purification of Laboratory Chemicals, Pergamon Press, Oxford, 1981.
[8] A.I. Vogel, A Text Book of Quantitative Inorganic Analysis, ELBS & Longmans, London, 1962.
[9] P. Chattopadhyay, Y.H. Chiu, J.M. Lo, C.S. Chung, T.H. Lu, Appl. Radiat. Isot. 52 (2000) 217.
[10] (a) A.J.C. Wilson, International Tables for X-ray Crystallography, Kluwer, Dordrecht, 1992, vol. C, Tables 4.2.6.8 and 6.1.1.4;
(b) G.M. Sheldrick, SHELXS-97: Program for the Solution of Crystal Structure, University of Göttingen, Göttingen, Germany, 1997;
(c) G.M. Sheldrick, SHELXL-97: Program for the Solution of Crystal Structure, University of Göttingen, Göttingen, Germany, 1997;
(d) A.L. Spek, PLATON: Molecular Geometry Program, University of Utrecht, The Netherlands, 1999;
(e) L.J. Farrugia, J. Appl. Crystallogr. 30 (1997) 565.
[11] (a) W. Kabsch, J. Appl. Crystallogr. 21 (1988) 916;
(b) G.M. Sheldrick, SHELX-86, Acta Crystallogr., Sect. A 46 (1990) 467;
(c) N. Walker, D. Stuart, DIFABS program, Acta Crystallogr., Sect. A 39 (1983) 158;
(d) G.M. Sheldrick, SHELXL: Program for Crystal Structure Refinement, University of Göttingen, Göttingen, Germany, 1993.
[12] (a) B.K. Santra, P.A.N. Reddy, M. Nethaji, A.R. Chakravarty, Inorg. Chem. 41 (2002) 1328;
(b) B.K. Santra, P.A.N. Reddy, M. Nethaji, A.R. Chakravarty, J. Chem. Soc., Dalton Trans. (2001) 553.
[13] M. Vaidyanathan, R. Balamurgan, U. Sivagnanam, M. Palaniandavar, J. Chem. Soc., Dalton Trans. (2001) 3498.
[14] A.W. Addision, T.N. Rao, J. Reedijk, J. van Rijn, G.C. Verschoor, J. Chem. Soc., Dalton Trans. (1984) 1349.
[15] M.S. Masoud, A.M. Hindway, A.A. Soayed, Transition Met. Chem. 16 (1991) 372.
[16] (a) P. Chattopadhyay, C. Sinha, Indian J. Chem. Sect. A 34A (1995) 76;
(b) H.H. Freedman, J. Am. Chem. Soc. 63 (1961) 2900.
[17] S. Chattopadhyay, C. Sinha, S.B. Chowdhury, A. Chakravorty, J. Organomet. Chem. 427 (1992) 111.
[18] (a) A.R. Davis, C.J. Murphy, R.A. Plane, Inorg. Chem. 9 (1970) 1081;
(b) R.J.H. Clark, C.S. Williams, Spectrochem. Acta 22 (1966) 1081.
[19] (a) R.M. Silverstein, G.C. Bassler, T.C. Morrill, Spectrometric Identification of Organic Compounds, Wiley, New York, 1981;
(b) B.H. Chen, H.H. Yao, W.T. Huang, P. Chattopadhyay, J.M. Lo, T.H. Lu, Solid-State Sci. t1 (1999) 119.
[20] T. Kita, I. Miura, N. Nakayama, T. Kawata, K. Kano, S. Hirota, M. Kodera, J. Am. Chem. Soc. 123 (2001) 7715.
[21] (a) J. Zubieta, K.D. Karlin, J.C. Hayes, in: K.D. Karlin, J. Zubieta (Eds.), Copper Coordination Chemistry: Biochemical and Inorganic Perspectives, Adenine Press, Albany, NY, 1983, p. 97;
(b) Y. Nakao, M. Onoda, T. Sakurai, A. Nakahara, I. Kinoshita, S. Ooi, Inorg. Chim. Acta 151 (1988) 55;
(c) K.D. Karlin, J.C. Hayes, S. Juen, J.P. Hutchinson, J. Zubieta, Inorg. Chem. 21 (1982) 4106;
(d) A.W. Addison, H.M.J. Hendriks, J. Reedijk, L.K. Thompson, Inorg. Chem. 20 (1981) 103;
(e) M. Duggan, N. Ray, B. Hathaway, G. Tomlison, P. Briant, K. Plein, J. Chem. soc., Dalton Trans. (1980) 1342;
(f) G. Albertin, E. Bordignon, A.A. Orio, Inorg. Chem. 14 (1975) 1411;
(g) B.J. Hathaway, D.E. Billing, Coord. Chem. Rev. 5 (1970) 143;
(h) M. Ciampolini, N. Nardi, Inorg. Chem. 5 (1966) 41.
[22] (a) R.K. Ray, G.R. Hoffman, Inorg. Chim. Acta 173 (1990) 207;
(b) N. Raman, A. Kulandaisamy, K. Jeyasubramanian, Indian J. Chem., Sect. A 41A (2002) 942.

Available online at www.sciencedirect.com
SCIENCE DIRECT®
Polyhedron 23 (2004) 2465–2474
POLYHEDRON
www.elsevier.com/locate/poly

Synthesis and structural characterization of some Schiff bases derived from 4-[{(aryl)imino}ethyl]-3-methyl-1-(4′-methylphenyl)-2-pyrazolin-5-one and spectroscopic studies of their Cu(II) complexes

Rajendra N. Jadeja [a,*,1], J.R. Shah [*,a], E. Suresh [b], Parimal Paul [*,b]

[a] *Department of Chemistry, Sardar Patel University, Vallabh Vidyanagar 388 120, India*
[b] *Analytical Science Division, Central Salt and Marine Chemicals Research Institute, G.B. Marg, Bhavnagar 364 002, India*

Received 20 May 2004; accepted 26 July 2004
Available online 25 September 2004

Abstract

A series of novel bidentate ligands have been synthesized by the condensation of 4-acetyl-2,4-dihydro-5-methyl-2-(4′-methylphenyl)-3H-pyrazol-3-one and various aromatic amines. All of these ligands have been characterized on the basis of elemental analysis, IR, ^{1}H and $^{13}C\{^{1}H\}$ NMR data. The molecular geometries of five of these ligands have been determined by single crystal X-ray study. Crystallographic study reveals that these ligands exist in the amine-one tautomeric form in the solid state. NMR study also suggests the existence of the amine-one form in solution at room temperature. The reaction of these ligands with copper(II) resulted in the formation of mononuclear octahedral complexes of the general formulae $[CuL_2(H_2O)_2]$, with water molecules at the axial positions. These complexes were characterized on the basis of analytical and spectroscopic data. Thermal analyses of these complexes were also carried out. Magnetic moment measurements of these complexes at room temperature correspond to one unpaired electron. An ESR study of all these complexes in solution at room temperature, and also under frozen conditions at liquid nitrogen temperature, is consistent with the distorted octahedral geometry of the metal ion in these complexes. Semi-empirical quantum mechanical calculations (PM3) have been performed on the ligands to get charges over the coordinating atoms. A fairly good linear relation was found between the charges over the coordinating atoms of the ligands and the ligand field transition energies.
© 2004 Elsevier Ltd. All rights reserved.

Keywords: Pyrazolone; Copper(II) complexes; Crystal structures; ESR study

1. Introduction

The chemistry of pyrazolone derivatives has attracted much attention because of their interesting structural properties and applications in diverse areas [1–10]. They are useful reagents for the extraction and separation of various metal ions [11–15]. They can also be used in laser materials, as ^{1}H NMR shift reagents, in chromatographic study and in the petrochemical industry [16–20]. Recently, photochromism of pyrazolone derivatives have also been reported [21]. Many of these ligands exhibit keto enol tautomerism, and because of this they show interesting structural and spectroscopic properties which have been the subject matter of many reports [22,23]. Among these ligands, acyl pyrazolones have been studied extensively owing to their effective properties with respect to extracting metal ions [24,25]. On the other hand pyrazolone-based Schiff base chemistry is less extensive. Our laboratory has been exploring the chemistry of this class of ligand for quite some time [26–30]. Some other groups have also reported lantha-

* Corresponding author. Tel.: +912782561354; fax: +912782-567760.
E-mail address: rajendra_jadeja@yahoo.com (R.N. Jadeja).
[1] Present address: Marine Algae & Marine Environment Discipline, CSMCRI, Bhavnagar 364002, India.

0277-5387/$ - see front matter © 2004 Elsevier Ltd. All rights reserved.
doi:10.1016/j.poly.2004.07.025

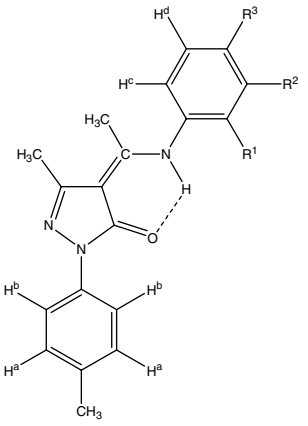

HL^1: $R^1 = H^c$, $R^2 = H^d$, $R^3 = H$

HL^2: $R^1 = CH_3$, $R^2 = H$, $R^3 = H$ HL^5: $R^1 = Cl$, $R^2 = H$, $R^3 = H$

HL^3: $R^1 = H$, $R^2 = CH_3$, $R^3 = H$ HL^6: $R^1 = H$, $R^2 = Cl$, $R^3 = H$

HL^4: $R^1 = H^c$, $R^2 = H^d$, $R^3 = CH_3$ HL^7: $R^1 = H^c$, $R^2 = H^d$, $R^3 = Cl$

Fig. 1. Structural drawing of the ligands with the labelling of the protons.

nide complexes of this class of ligand along with their luminescence properties [31–33].

We were interested to synthesis a new series of pyrazolone-based Schiff base ligands, which can form stable neutral complexes with transition metal ions and may find some application in solvent extraction chemistry. With this view we have synthesized a series of ligands by condensation of acyl pyrazolone with substituted aromatic amines. These ligands are shown in Fig. 1 with the H-numbering scheme (for interpretation of ^1H NMR spectra). Many of these ligands have been characterized crystallographically. We report here synthesis and characterization of these ligands and their Cu(II) complexes. Spectroscopic, magnetic and EPR studies of all the complexes have also been reported.

2. Experimental

2.1. Materials

The compound 3-methyl-1-(4′-methylphenyl)-2-pyrazolin-5-one was obtained from Shree Sidhdhanath Industries, Sachin, India. All of the amines were obtained from Sisco-Chem. Pvt. Ltd., India. The liquid amines were purified by distillation and the solid amines were recrystallised from hot ethanol before use. Dioxane was obtained from E. Merck (India) Ltd., and used after purification following a standard procedure [34]. Absolute alcohol was obtained from Baroda Chem. Industry Ltd. and was used after distillation. Calcium hydroxide and acetyl chloride were obtained from Samir Tech. Chem. Pvt. Ltd. Sodium acetate was obtained from Spectrochem Pvt. Ltd., India. All the chemicals used were of AR grade. Solvents used in this study were purified following the standard procedures.

2.2. Physical measurements

Elemental analyses (C, H, N) were performed on a model 2400 Perkin–Elmer elemental analyzer. Copper was estimated by the titrimetric method using EDTA [35]. FAB mass spectra were recorded on a JEOL SX 102/DA-6000 mass spectrometer using xenon (6 kV, 10 mA) as the FAB gas. The accelerating voltage was 10 kV and the spectra were recorded at room temperature using *m*-nitrobenzyl alcohol as the matrix. Infrared (IR) spectra were recorded on a Nicolet-400D spectrometer as KBr pellets. NMR spectra were recorded on a model DPX 200 Bruker FT-NMR instrument. The electronic spectra were recorded on a model UV160A Shimadzu spectrophotometer. Specific conductivity of the complexes was measured on a model 305 Systronic conductivity bridge. Magnetic moments were measured on a model 7304 Lake Shore Cryotronics vibrating sample magnetometer. The ESR spectra were recorded on a Varian E112 ESR spectrometer.

2.3. Synthesis of ligands

2.3.1. Preparation of 4-acetyl-3-methyl-1-(4′-methylphenyl)-2-pyrazolin-5-one (AMMP)

3-Methyl-1-(4′-methylphenyl)-2-pyrazolin-5-one (20.1 g, 0.1mol) was dissolved in hot dioxane (80 cm^3) in a flask equipped with a stirrer, separating funnel and reflux condenser. Calcium hydroxide (14.81 g, 0.2 mol) was added to this solution, followed by acetyl chloride (7.85 g, 0.1 mol) added dropwise with precaution, as this reaction was exothermic. During this addition the whole mass was converted into a thick paste. After the complete addition, the reaction mixture was refluxed for half an hour and then it was poured into dilute hydrochloric acid (200 cm^3, 2 M). The colored crystals (AMMP) thus obtained were separated by filtration and recrystallized from an acidified methanol–water mixture (HCl:MeOH:H_2O = 1:80:19). Yield: 20.2 g (88%). Melting point (mp): 192 °C. *Anal.* Calc. for $C_{13}H_{14}N_2O_2$: C, 66.06; H, 6.42; N, 12.84. Found: C, 65.78; H, 6.40; N, 12.67%.

2.3.2. General method for the preparation of the ligands

- 4-[{(Phenyl)imino}ethyl]-3-methyl-1-(4′-methylphenyl)-2-pyrazolin-5-one (HL^1).
- 4-[{(2-Methylphenyl)imino}ethyl]-3-methyl-1-(4′-methylphenyl)-2-pyrazolin-5-one (HL^2).
- 4-[{(3-Methylphenyl)imino}ethyl]-3-methyl-1-(4′-methylphenyl)-2-pyrazolin-5-one (HL^3).
- 4-[{(4-Methylphenyl)imino}ethyl]-3-methyl-1-(4′-methylphenyl)-2-pyrazolin-5-one (HL^4).

Table 1
Summary of crystallographic data for the ligands HL^1–HL^5

Compound	HL^1	HL^2	HL^3	HL^4	HL^5
Chemical formula	$C_{19}H_{18}N_3O_1$	$C_{20}H_{21}N_3O_1$	$C_{20}H_{21}N_3O_1$	$C_{20}H_{21}N_3O_1$	$C_{19}H_{18}$ N_3OCl
Formula weight	228.38	319.40	319.40	319.40	339.81
Unit cell dimensions					
a (Å)	7.6866(9)	7.5706(18)	18.391(2)	10.452(7)	7.4237(14)
b (Å)	13.3116(15)	8.501(2)	12.7042(16)	18.961(13)	7.7103(15)
c (Å)	16.965(2)	15.360(4)	7.2652(9)	8.962(6)	15.770(3)
α (°)	69.404(2)	102.217(4)	90.000	90.000	95.593(4)
β (°)	89.794(2)	94.875(4)	91.763(3)	101.590(13)	94.493(4)
γ (°)	87.785(2)	113.910(4)	90.000	90.000	110.373(3)
Z	4	2	4	4	2
V (Å^3)	1623.6(3)	867.0(4)	1696.7(4)	1740(2)	836.1(3)
Crystal system	triclinic	triclinic	monoclinic	monoclinic	triclinic
Space group	$P\bar{1}$	$P\bar{1}$	$P21/c$	$P21/n$	$P\bar{1}$
Radiation used λ (Å)	0.71073	0.71073	0.71073	0.71073	0.71073
$\rho_{calcd.}$ (gcm^{-3})	1.249	1.223	1.250	1.219	1.350
Absorption coefficient μ (cm^{-1})	0.079	0.077	0.079	0.077	0.239
F(000)	644	340	680	680	356
Temperature (°C)	23	23	23	23	23
Goodness-of-fit on F^2	1.044	1.047	0.992	1.012	1.059
$R_1/wR_2([I > 2\sigma(I)])$	0.0541/0.1473	0.0513/0.1463	0.0624/0.1154	0.0604/0.1361	0.0598/ 0.1466
R_1/wR_2 (all data)	0.0745/0.1618	0.0635/0.1566	0.1723/0.1683	0.1073/0.1568	0.0916/0.1694

- 4-[{(2-Chlorophenyl)imino}ethyl]-3-methyl-1-(4′-methylphenyl)-2-pyrazolin-5-one (HL^5).
- 4-[{(3-Chlorophenyl)imino}ethyl]-3-methyl-1-(4′-methylphenyl)-2-pyrazolin-5-one (HL^6).
- 4-[{(4-Chlorophenyl)imino}ethyl]-3-methyl-1-(4′-methylphenyl)-2-pyrazolin-5-one (HL^7).

The compound 4-acetyl-3-methyl-1-(4′-methylphenyl)-2-pyrazolin-5-one (AMMP, 2.30 g, 0.01 mol) was dissolved in ethanol (20 cm^3) and the appropriate amine (0.01 mol, aniline for HL^1, *ortho*-, *meta*- and *para*-toluidine for HL^2–HL^4, respectively, and *ortho*-, *meta*- and *para*-chloroaniline for HL^5–L^7, respectively) was added to this solution. The reaction mixture was refluxed for 2 h. During the reflux a microcrystalline compound was separated, which was isolated by filtration, washed with ethanol and dried in air. Suitable crystals for single crystal X-ray study were grown from acetonitrile.

2.3.3. General method for the preparation of the Copper(II) complexes $[Cu(L)_2(H_2O)_2]$, ($L = L^1$, L^2, L^3, L^4, L^5, L^6 and L^7)

The appropriate ligand (0.01 mol) dissolved in hot DMF (20 cm^3) was added dropwise into an aqueous solution (20 cm^3) of copper(II) nitrate (0.01 mol, 2.41 g) with stirring. After the complete addition, 2.0 g of sodium acetate was added to the solution and the reaction mixture was refluxed for 2 h. The solution thus obtained was concentrated to half of its original volume by evaporation using a hot plate and allowed to cool to room temperature. During this period, a brownish microcrystalline solid was separated, which was isolated by filtration, washed with hot water followed by ethanol and dried in air. Yield: 50–60%.

2.3.4. Single crystal X-ray structure determination of the ligands

Crystallographic data for five of the ligands are summarized in Table 1. The data collections were carried out on a Bruker Mart Apex CCD diffractometer using graphite monochromated Mo Kα (λ = 71073 Å) radiation at 293 K. An absorption correction based on SADABS [36] was also applied. The structures were solved by direct methods (SHELXTL) and refined by least squares methods with atomic anisotropic thermal parameters for all non-hydrogen atoms [37,38]. All hydrogen atoms were either generated geometrically or obtained from the fourier difference map, and were assigned fixed isotropic thermal parameters in the structure factor calculations.

3. Results and discussion

3.1. Characterization of the ligands

All seven ligands, HL^1–HL^7, gave satisfactory elemental analysis (Table 2). A representative FAB mass spectrum, obtained for HL^1, exhibits the largest *m*/*z* isotropic peak at 306, which is in excellent agreement with the calculated value of 305.37 (based on the most common isotope for each element). The molecular structures of these ligands are such that they can exist in three tau-

Table 2
Melting point, elemental analysis (C, H and N)[a] and yield of the ligands

Ligand	Melting point (°C)	%C	%H	%N	Yield %
HL^1	193	75.04 (74.73)	6.26 (6.27)	13.83 (13.76)	75
HL^2	170	75.10 (75.20)	6.60 (6.62)	12.28 (12.38)	70
HL^3	180	67.12 (67.15)	5.32 (5.34)	12.47 (12.37)	60
HL^4	187	74.81 (75.20)	6.13 (6.62)	12.40 (12.38)	78
HL^5	195	67.10 (67.15)	5.24 (5.34)	12.60 (12.37)	55
HL^6	197	75.10 (75.20)	6.13 (6.62)	12.40 (12.38)	60
HL^7	210	67.13 (67.15)	5.20 (5.34)	12.38 (12.37)	62

[a] Calculated values are given in the parentheses.

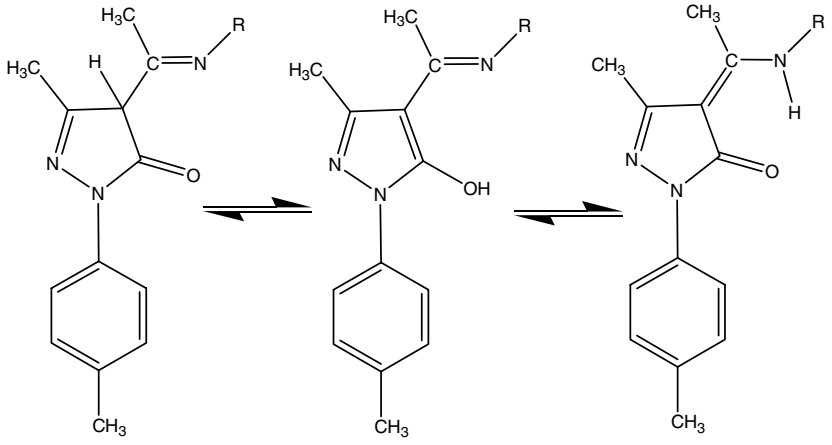

Fig. 2. Tautomeric forms of the ligands.

tomeric forms as shown in Fig. 2. Detailed solution and solid-state studies of these ligands were carried out to establish their geometry. The IR spectra of these ligands exhibit two characteristic bands in the ranges 3228–3241 and 1620–1637 cm^{-1}, which can either be assigned to $\nu_{(O-H)}$ and $\nu_{(C=N)}$, respectively, for the tautomeric imine-ol form (Fig. 2, II) or $\nu_{(N-H)}$ and $\nu_{(C=O)}$ respectively for the amine-one form (Fig. 2, III) of the ligand. We assigned these two peaks to $\nu_{(N-H)}$ and $\nu_{(C=O)}$, respectively for the later form based on the information obtained from crystallographic studies (discussed later).

The ^1H and $^{13}C\{^1H\}$ NMR spectra of all the ligands were recorded in $CDCl_3$ at room temperature and the data are presented in Tables 3 and 4. The signals due to methyl protons (three CH_3 for HL^1 and HL^5–HL^7; and four CH_3 for HL^2–HL^4) appear as singlets in the region δ 2.23–2.41. In some cases signals of two CH_3 groups are overlapped and all of these signals are so closely spaced that it is difficult to assign each signal to a particular methyl group unambiguously. Moreover, such an assignment would not contribute to the establishment of the geometry of the ligands, therefore, no attempt has been made for such an assignment. In the aromatic region, a few doublets and in a few cases some overlapping doublets/multiplets are observed. The appearance of multiplets is mainly because of the different substituents at the *ortho*-, *meta*- and *para*-positions of one of the two benzene rings. The protons marked as 'a' and 'b' (Fig. 1) are common to all ligands and appeared as doublets. The most deshielded doublet in the region δ 7.89–7.91 is assigned to the 'b' protons and the doublet at δ 7.17/7.18 (in a few cases it is overlapped with other signals) is due to 'a' protons. This assignment is on the basis of the substituents in the benzene ring, CH_3 being an electron-donating group is expected to shield the protons attached to the carbon atoms adjacent to it. For the other benzene ring, the spectra are simpler for the ligands with *para*-substituents (HL^4 and HL^7). For HL^4, the 'd' protons appear as a doublet at the same position (δ 7.18) as found for the 'a' protons, this is because of the same substituent at the *para*-position. The 'c' proton for HL^4 appears as a doublet at δ

Table 3
^{1}H NMR spectral data for the ligands recorded in $CDCl_3$

Ligand	CH_3	*a*-H (*J*, Hz)[a]	*b*-H (*J*, Hz)	*c*-H (*J*, Hz)	*d*-H (*J*, Hz)	NH
HL^1	2.32 s, 2.38 s,	7.17 d, $J = 7.4$	7.91 d, $J = 7.8$	7.17 d, $J = 7.4$	7.25–7.43 m (3H)[b]	13.10 s
HL^2	2.23 s, 2.32 s, 2.39 s	7.09–7.26 m	7.91 d, $J = 8.2$	7.09–7.26 m (4H)[c]		12.96 s
HL^3	2.32 s, 2.35 s, 2.38 s	7.08–7.31 m	7.91 d, $J = 7.4$	6.97 d, ($J = 7.8$, 1H), 7.08–7.31 m (3H)[c]		13.06 s
HL^4	2.32 s, 2.36 s, 2.38 s	7.18 d, $J = 6.8$	7.90 d, $J = 7.6$	7.06 d, $J = 7.2$	7.18 d, $J = 6.8$	13.02 s
HL^5	2.30 s, 2.34 s, 2.41 s	7.19 d, $J = 8.4$	7.89 d, $J = 8.4$	7.29–7.36 m (3H), 7.50 (m, 1H)[c]		13.01s
HL^6	2.34 s, 2.35 s, 2.39 s	7.07–7.39 m	7.89 d, $J = 7.4$	7.07–7.39 (m, 4H)[c]		13.12 s
HL^7	2.32 s, 2.38 s	7.18 d, $J = 8.0$	7.89 d, $J = 7.6$	7.11 d, $J = 8.4$	7.37 d, $J = 7.4$	13.05 s

[a] See Fig. 1 for numbering scheme.
[b] The proton at the para position of the ring is overlapped with 'd' protons.
[c] The protons of the benzene ring attached to the imine nitrogen are overlapped and 'c' and 'd' numbering is not applicable to them.

Table 4
$^{13}C\{^1H\}$ NMR spectral data (δ) for the ligands recorded in $CDCl_3$

Ligand	CH_3	>C–N–	Aromatic	>C=N–	>C=O
HL^1	17.3, 17.9, 21.4	100.9	119.5, 125.9, 127.7, 129.7, 129.9, 134.2, 137.1, 147.5	163.5	165.8
HL^2	17.2, 17.9, 18.4, 21.4	100.6	119.7, 127.1, 127.2, 128.4, 129.7, 131.6, 134.2, 134.7, 135.9, 137.1, 147.4	164.1	166.1
HL^3	17.4, 17.9, 21.4, 21.7	100.7	119.5, 122.9, 126.5, 128.5, 129.6, 134.2, 137.1, 137.3, 140.0, 147.5	163.4	165.8
HL^4	17.3, 18.0, 21.4	100.6	119.6, 125.8, 129.6, 130.5, 134.2, 137.5, 137.1, 137.8, 147.4	163.6	165.8
HL^5	17.2, 17.9, 21.4	101.5	119.7, 128.0, 128.5, 129.3, 129.7, 130.9, 131.7, 134.3, 134.9, 137.0, 147.5	163.7	166.0
HL^6	17.3, 17.9, 21.3	101.5	119.6, 124.0, 126.0, 127.8, 129.7, 130.9, 134.4, 135.5, 136.9, 138.5, 147.4	162.7	165.8
HL^7	17.2, 17.9, 21.3	101.2	119.6, 127.1, 129.7, 130.1, 133.4, 134.3, 135.9, 136.8, 147.4	163.1	165.8

7.06. In the case of HL^7 the 'c' and 'd' protons appear at δ 7.11 and 7.37, respectively. For the other five ligands the aromatic protons of the later benzene moiety are overlapped and appear as multiplets in the range δ 7.07–7.43. Another singlet corresponding to one proton for all compounds is observed in the range δ 12.96–13.12. This signal disappeared when a D_2O exchange experiment was carried out. It can be assigned either to OH or NH, in either case it is strongly deshielded because of hydrogen bonding with the other atom (N/O). It may be noted that the integration of this signal perfectly matches with one proton and there is no other fragment(s) of this signal, which suggests that only one tautomeric form of the ligands exist in solution under the experimental conditions. We have not done any temperature dependent experiments. Comparing with the solid state study, we prefer to assign this signal to NH, however, assignment of this peak to OH cannot be ruled out provided solid state structural evidence is not considered.

In the $^{13}C\{^1H\}$ NMR spectra the carbon atoms of the methyl groups appear in the range δ 17.2–21.7 (Table 4). The carbon atoms of the two benzene rings exhibit signals in the range δ 119.5–140.0 and the number of signals varies from seven to ten. Eight signals were observed for HL^4 and HL^7, as expected for the *p*-substituted benzene rings because of symmetry. However, HL^1 shows seven signals, so some of the signals might be overlapped as indicated by the intensity of a few signals. All other ligands, where one of the benzene rings is *ortho*- or *para*-substituted, show ten signals, as expected because of the loss of symmetry. In the low field region, three signals were observed around δ 147.5, 163.5 and 165.8, which are associated with the carbon atoms of the heterocyclic ring. The most deshielded signal (δ 147.5) can be assigned to >C=O and the next signal ($\sim\delta$ 163.5) could be due to >C=N of the heterocyclic ring. The singlet appearing for all compounds in the range δ 100.6–101.5 is assigned to the carbon atom of the >C N- moiety, the significant upfield shift is due to the electron-donating methyl group attached to it.

3.2. Molecular structures of the ligands

The molecular structures of five ligands (HL^1–HL^5) were determined from single crystal X-ray studies. ORTEP diagrams of compounds HL^1 to HL^5 with the atom numbering schemes are shown in Fig. 3. Important bond lengths and angles for all the compounds are listed in Table 5. These structure determinations are quite significant in view of the existence of these compounds in the solid state in different tautomeric forms. An analysis of the structural data shows that the C(10)–O(1) distances in the pyrazol moiety of all the compounds are in the range 1.245–1.261 Å, which are significantly shorter than the distance found for >C–OH in some pyrazolone derivatives, 1.341, 1.346 Å [39] and 1.331 Å [40], however, they are close to the distances found for

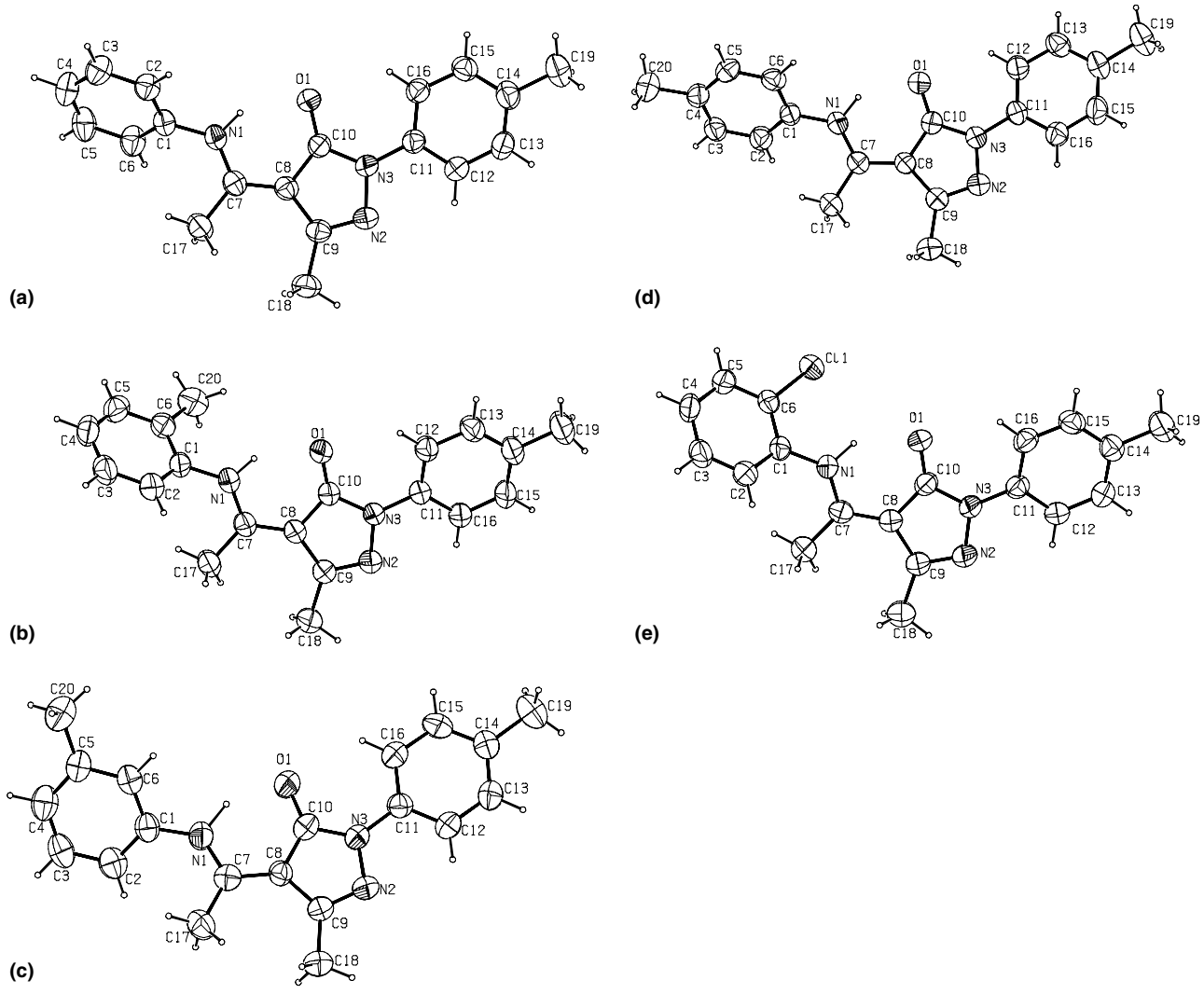

Fig. 3. ORTEP diagram of HL^1 (a), HL^2 (b), HL^3 (c), HL^4 (d) and HL^5 (e).

>C=O in similar compounds, 1.262 Å [39] and 1.254 Å [10]. The C(7)–N(1) distances of the imine moiety are in the range 1.327–1.338 Å, which are significantly longer than that found for C=N in pyrazolone compounds, 1.298 Å [21] and 1.292 Å [10], but similar to that found for >C–N (1.339 Å) [41]. It may be also noted that the proton associated with N(1) is located from the Fourier difference map in all of the five compounds. These three observations clearly establish that these compounds exist in the keto-form in the solid state. However, the N–H proton is strongly hydrogen bonded with the O(1) atom, the N(1)···O(1) distances are in the range 2.664–2.709 Å and ∠N(1)–H(1)···O(1) are in the range 140.35°–145.61° (Table 6). The possibility of the attachment of H(1) with C(8) (imine-one form) is ruled out on the basis of the angles around C(8), the summation of the three angles, ∠C(7)–C(8)–C(10) + ∠C(10)–C(8)–C(9) + C(9)–C(8)–C(7) are in the range 357.00°–360.78°, which is close to the ideal value of 360°, expected from the coplanar C(7), C(8), C(9) and C(10) atoms. Thus, the crystal structure study conclusively proves the existence of these compounds in amine-one form.

The ligand HL^1 crystallizes in the $P\bar{1}$ space group with two molecules in the asymmetric unit. The packing diagram of this compound is shown in Fig. 4. The molecules are associated in pairs by strong C–H···π interactions between the methyl hydrogen atoms and the phenyl rings, and also offset face-to-face π···π interactions between the phenyl rings. The phenyl ring of the first molecule, C(1)–C(6), exhibits strong π···π stacking with the phenyl ring of the second molecule, C(20)–C(25) in the asymmetric unit, forming a layered architecture along the *a*-axis. The various C–H···π interactions of HL^1 are deposited (Table S1) as supplementary material. The ligands HL^2, HL^3 and HL^4, which have *ortho*-, *meta*- and *para*-substituted methyl groups, also exhibit strong intermolecular C–H···π and offset face-to-face π···π stacking interactions forming a novel

Table 5
Selected bond lengths and angles in the ligands HL^1–HL^5

Compunds	HL^1	HL^2	HL^3	HL^4	HL^5
Bond distances (Å) with esd's in parentheses					
N(1)–C(1)	1.428(2)	1.4260(18)	1.425(5)	1.434(3)	1.413(3)
N(1)–C(7)	1.336(2)	1.327(2)	1.344(4)	1.339(3)	1.338(3)
C(7)–C(17)	1.501(2)	1.495(2)	1.494(5)	1.495(3)	1.492(4)
C(7)–C(8)	1.391(2)	1.396(2)	1.393(5)	1.396(3)	1.393(4)
C(10)–C(8)	1.439(2)	1.4389(19)	1.434(5)	1.441(3)	1.432(4)
O(1)–C(10)	1.252(2)	1.2448(17)	1.261(4)	1.253(3)	1.247(3)
N(3)–C(10)	1.379(2)	1.3735(18)	1.364(4)	1.378(3)	1.377(3)
N(3)–N(2)	1.4021(19)	1.4012(16)	1.402(4)	1.408(2)	1.403(3)
N(2)–C(9)	1.304(2)	1.304(2)	1.307(4)	1.307(3)	1.303(4)
C(9)–C(8)	1.433(2)	1.432(2)	1.425(5)	1.432(3)	1.436(4)
Bond angles (°) with esd's in parentheses					
C(7)–N(1)–C(1)	127.75(15)	128.41(13)	130.4(4)	128.06(18)	128.7(2)
N(1)–C(7)–C(17)	119.80(15)	119.21(13)	120.9(4)	119.99(18)	120.5(2)
N(1)–C(7)–C(8)	117.60(16)	117.91(13)	116.5(4)	117.70(19)	116.5(2)
C(8)–C(7)–C(17)	122.59(16)	122.87(14)	122.6(4)	122.3(2)	123.0(2)
C(7)–C(8)–C(10)	122.20(16)	122.04(13)	122.6(3)	123.03(19)	122.7(2)
O(1)–C(10)–C(8)	129.35(16)	129.26(13)	129.0(4)	129.13(19)	129.0(2)
O(1)–C(10)–N(3)	125.68(15)	125.83(13)	125.3(4)	125.74(19)	125.5(2)
C(10)–N(3)–N(2)	111.60(14)	111.81(11)	111.3(3)	111.47(17)	111.1(2)
N(3)–C(10)–C(8)	104.96(14)	104.91(12)	105.6(3)	105.12(18)	105.5(2)
C(9)–N(2)–N(3)	106.48(14)	106.35(11)	106.4(3)	106.34(17)	106.8(2)
N(2)–C(9)–C(8)	111.85(15)	111.78(13)	111.7(3)	111.96(19)	111.5(2)
C(7)–C(8)–C(9)	132.70(16)	132.79(14)	132.4(4)	131.86(19)	132.2(2)

Table 6
N–H···O hydrogen bonding distances and angles

Compound	N(1)–H(1)N(1) (Å)	H(1)N(1)···O(1) (Å)	N(1)···O(1) (Å)	∠N(1)–(1)N(1)···O(1) (°)
HL^1	0.922/0.951	1.878/1.883	2.685/2.699	144.82/143.09
HL^2	0.923	1.871	2.680	145.00
HL^3	1.092	1.681	2.654	145.61
HL^4	0.985	1.868	2.709	141.51
HL^5	0.982	1.833	2.664	140.35

supramolecular architecture. In addition to the stacking interactions of phenyl rings in HL^5, a moderate C–H···Cl interaction is also observed (C(3)–H(3)···Cl(1); C(3)–H(3) = 0.930; H(3)···Cl(1) = 2.804; C(3)–Cl(1) = 3.550 Å; ∠C(3)–H(3)···Cl(1) = 137.88°). The packing diagram of HL^5 showing hydrogen bonding interactions is deposited (Fig. S1) as supplementary material.

3.3. Characterization of the metal complexes

Cu(II) complexes of all the seven ligands have been synthesized by the reaction of $Cu(NO_3)_2$ and the respective ligands in water–DMF (1:1) under reflux conditions in the presence of sodium acetate. The metal and C, H and N analyses of these complexes (Table 7) suggest a molecular formula of the composition $[Cu(L)_2(H_2O)_2]$, where L = deprotonated HL^1, HL^2, HL^3, HL^4, HL^5, HL^6 and HL^7. The IR spectra of the metal complexes exhibit no band for $\nu_{(N-H)}$ (3228 cm^{-1}) of the ligands, indicating deprotonation of the N–H group in metal complexes. The molar conductivity measurements show Λ_M values (Table 7), which are much lower than those expected for 1:1 electrolytes, confirming the non-electrolytic nature of the complexes. The magnetic moment measurements of the complexes show μ_{eff} values of 1.72–1.95 μ_B (Table 7), which corresponds to one unpaired electron and is expected from mononuclear Cu(II) complexes (d^9) with some orbital contribution. On the basis of all these data, the molecular geometry assigned to the metal complexes is shown in Fig. 5. Attempts have been made to grow X-ray quality single crystals of these complexes, however, this has been unsuccessful so far. A FAB mass spectrum of a representative complex $[Cu(L^1)_2(H_2O)_2]$ was recorded and the largest *m/z* isotropic peak appeared at 673, which corresponds to the composition $[Cu(L)_2]$ (672.27, molecular mass – $2H_2O$). Fragmentation of a weakly coordinated molecule/ion in the FAB mass spectrum is not unlikely. To confirm the presence of weakly coordinat-

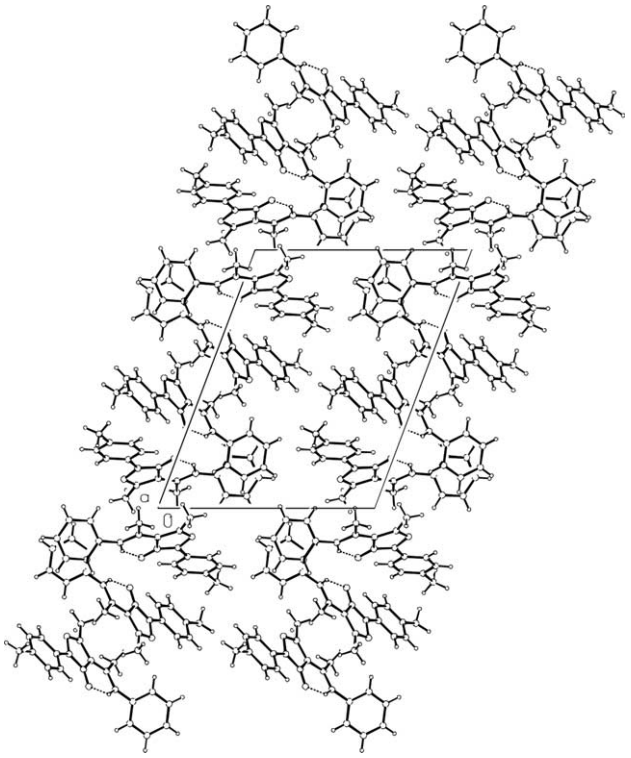

Fig. 4. Packing diagram of HL^1 down the *a*-axis.

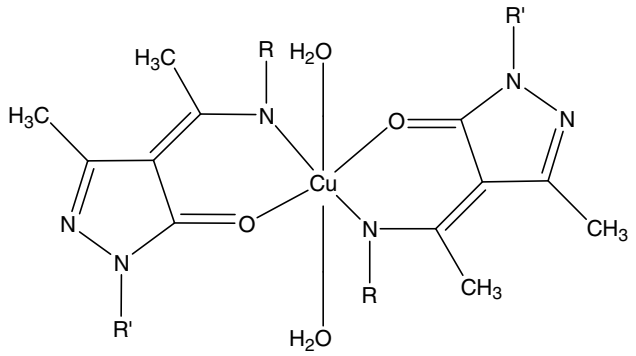

Fig. 5. Structural drawing of the Cu(II) complexes.

ing H_2O molecules in the complex we carried out thermogravimetric analyses of all the complexes. This study shows loss of weight corresponding to two water molecules in the temperature range 130–170 °C, indicating that the water molecules in these complexes are weakly coordinated to the metal ion. The presence of a H_2O molecule in the complexes is also indicated by IR spectra, which show a broad band centered around 3400 cm^{-1} and two sharp bands at 710 and 420 cm^{-1}, the later two can be assigned to the wagging and rocking modes of vibration of the water molecule, respectively [42]. The octahedral geometry of the metal ion in these complexes is also evident from electronic spectra and an EPR study, discussed below.

3.4. Electronic spectra of the metal complexes

The electronic spectra of all the complexes were recorded in DMF and the data are presented in Table 8. All of these complexes exhibit a broad band in the region 659–690 nm and another strong absorption in the region 454–504 nm. In an octahedral geometry, the ^2D state of the free Cu(II) ion (d^9) splits into a lower energy doublet ^2E_g state and a higher energy triplet $^2T_{2g}$ state, from which a $^2T_{2g} \leftarrow {}^2E_g$ d–d transition in the visible re-

Table 8
Electronic spectral data of the Cu(II) complexes

Complex	d–d Transition (λ, nm; ε, $dm^3\,mol^{-1}\,cm^{-1}$)	CT (λ, nm; $\varepsilon\times10^{-4}$, $dm^3\,mol^{-1}\,cm^{-1}$)	Average charge on coordinating atoms[a] (amu)
$[Cu(HL^1)_2(H_2O)_2]$	690.0 (761)	473 (3.0)	
$[Cu(HL^2)_2(H_2O)_2]$	659.3 (527)	458 (2.6)	−0.20065
$[Cu(HL^3)_2(H_2O)_2]$	666.7 (423)	463 (1.8)	−0.20345
$[Cu(HL^4)_2(H_2O)_2]$	660.7 (327)	495 (2.1)	−0.20125
$[Cu(HL^5)_2(H_2O)_2]$	665.7 (545)	471 (2.7)	−0.2019
$[Cu(HL^6)_2(H_2O)_2]$	676.7 (421)	504 (1.9)	−0.2049
$[Cu(HL^7)_2(H_2O)_2]$	670.0 (320)	454 (2.2)	−0.2039

[a] The average charge on coordinating N and O atoms is calculated by semi-empirical quantum mechanical calculations using the PM3 Hamiltonian.

Table 7
Elemental analysis (Cu, C, H and N), molar conductance and magnetic moment data of the Cu(II) complexes

Complex	%Cu	%C	%H	%N	Λ^{Mb}	$\mu_{eff.}$ (μ_B)
$[Cu(L^1)_2(H_2O)_2]$	8.80 (8.97)[a]	66.55 (64.43)	5.27 (5.69)	12.24 (11.87)	4.27	1.78
$[Cu(L^2)_2(H_2O)_2]$	9.25 (8.63)	65.20 (65.24)	6.10 (6.02)	11.40 (11.41)	5.32	1.72
$[Cu(L^5)_2(H_2O)_2]$	8.30 (8.18)	58.80 (58.72)	4.87 (4.93)	10.71 (10.81)	4.98	1.94
$[Cu(L^3)_2(H_2O)_2]$	8.52 (8.63)	65.14 (65.24)	6.10 (6.02)	11.38 (11.41)	5.21	1.82
$[Cu(L^6)_2(H_2O)_2]$	8.17 (8.18)	58.12 (58.72)	4.90 (4.93)	10.72 (10.81)	7.25	1.95
$[Cu(L^4)_2(H_2O)_2]$	8.52 (8.63)	64.89 (65.24)	6.20 (6.02)	11.38 (11.41)	6.22	1.87
$[Cu(L^7)_2(H_2O)_2]$	8.11 (8.18)	58.69 (58.72)	4.90 (4.93)	10.87 (10.81)	8.18	1.86

[a] Calculated values are in parentheses.
[b] $Ohm^{-1}\,cm^2\,mol^{-1}$ in DMF.

gion is expected. However, a complex with the d^9 configuration of the metal ion is expected to experience Jahn–Teller distortion, which leads to further splitting of the ^2E_g and $^2T_{2g}$ levels into $^2B_{1g}$, $^2A_{1g}$ and $^2B_{2g}$, ^2E_g levels, respectively. With this splitting three possible transitions are $^2A_{1g} \leftarrow {}^2B_{1g}$ (ν_1), $^2B_{2g} \leftarrow {}^2B_{1g}$ (ν_2) and $^2E_g \leftarrow {}^2B_{1g}$ (ν_3). The energy difference between these levels depends on the extent of the Jahn–Teller distortion. If the energy difference is not large, then all these three transitions are expected to be close in energy and in this situation these bands may not resolve and may appear as a broad band. Therefore, the broad band in the region 659–690 nm could be due to the combination of these three transitions. The strong absorption found for all complexes in the range 454–504 nm is due to a ligand to copper(II) charge transfer transition.

3.5. Semi empirical calculation of atomic charges and its correlation with the d–d band

The absorption maxima (λ_{max}) of d–d transitions for metal complexes are related to the net atomic charges on the coordinating atoms of the ligands. We were interested to find the correlation between the average atomic charge of the coordinating atoms of the ligands and λ_{max} of the d–d transition. The net atomic charges on the coordinating O and N atoms of the ligands have been calculated using the semi-empirical PM3 Hamiltonian in the MOPAC package [43] and the charges thus obtained have been averaged (Table 8) and plotted against the experimentally obtained λ_{max} of the d–d transition of the complexes (Fig. 6). The plot shows a linear correlation between the net atomic charge and λ_{max}, as the average negative charge of the coordinating atoms increases the absorption maxima shifts towards lower energy. Using the correlation parameters thus obtained (Fig. 6) one can predict the λ_{max} for a similar type of complex by calculating the net atomic charges by semi empirical PM3 on the atoms bound to the metal ion. This method (PM3) is simple compared to the more elaborate calculations (high level ab initio) using quantum mechanical methods and this simple method is quite useful for predicting the absorption maxima of the d–d band for similar classes of metal complexes.

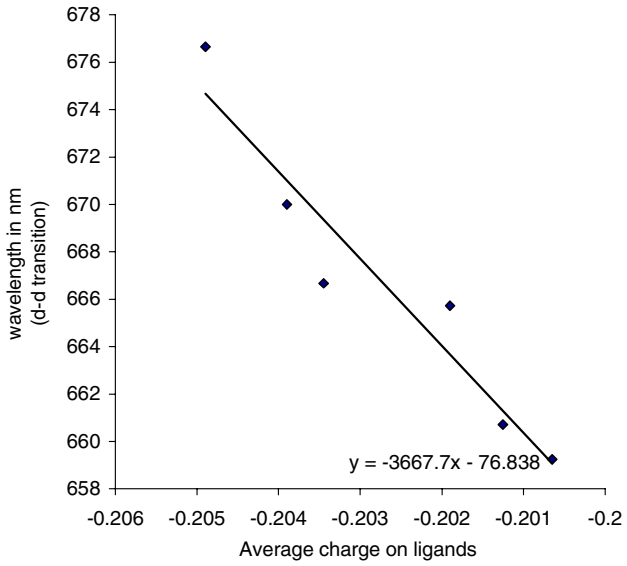

Fig. 6. Plot of the wavelength of d–d transitions vs average charge on the coordinating atoms of the ligands calculated by semi-empirical calculations (PM3 Hamiltonian).

3.6. Electron spin resonance

EPR spectra of all the complexes were recorded in DMF at room temperature (25 °C) and also under frozen conditions at liquid nitrogen temperature. At room temperature all the complexes show four line (equally spaced) spectra, characteristic for mononuclear copper(II) complexes. In frozen solution some hyperfine splitting was observed in the parallel region, however, no such splitting was noted in the perpendicular line. The relevant data are summarized in Table 9. Analysis of these data show that in all cases $g_{II} > g_{\perp}$, which suggest a $d_{x^2-y^2}$ ground state for the Cu(II) ion in these complexes. The axial spectrum with $g_{II} > g_{\perp} > 2.03$ is consistent with a distorted octahedral geometry around the copper(II) ion.

Table 9
ESR spectral data of the Cu(II) complexes

Complex	g_{II}	$g_{\perp}$	g_{av}	$A_{II} \times 10^{-4}$ (cm^{-1})	$A_{\perp}$	A_{av}	α^2_{cu}
$[Cu(L^1)_2(H_2O)_2]$	2.263	2.095	2.150	148.72	27.82	68.12	0.81
$[Cu(L^2)_2(H_2O)_2]$	2.232	2.109	2.150	159.23	21.17	67.19	0.76
$[Cu(L^3)_2(H_2O)_2]$	2.169	2.110	2.130	166.01	17.08	66.72	0.78
$[Cu(L^4)_2(H_2O)_2]$	2.230	2.093	2.139	157.20	21.42	66.68	0.74
$[Cu(L^5)_2(H_2O)_2]$	2.240	2.135	2.170	148.12	10.22	56.19	0.75
$[Cu(L^6)_2(H_2O)_2]$	2.198	2.108	2.138	160.18	13.10	62.13	0.73
$[Cu(L^7)_2(H_2O)_2]$	2.232	2.080	2.131	149.92	21.29	64.17	0.72

Acknowledgements

One of the authors (R.N.J.) is grateful to the Gujarat Government for financial support in the form of a fellowship. The authors are thankful to Shree Sidhdhanath Industries, Sachin, Surat, for providing the free gift sample of the pyrazolone. The micro analytical services at M.S. University of Baroda, Vadodara and RISC, IIT, Chennai are gratefully acknowledged for providing the elemental analyses and ESR facility, respectively. The help of Dr. N.D. Kulkarni, M.S. University of Baroda, Vadodara, India for the theoretical calculations is gratefully acknowledged.

Appendix A. Supporting information available

Intermolecular C–H$\cdots\pi$ interactions in HL^1 (Table S1) and packing diagram of ligand HL^5 (Fig. S1). CCDC 239373–239377 contain the supplementary crystallographic data for the ligands (HL^1–HL^5). These data can be obtained free of charge at www.ccdc.cam.ac.uk/conts/retrievel.html or from the Cambridge Crystallographic Data Center, 12 Union Road, Cambridge CB2 1EZ, UK; fax (internat.) +44 1223/336 033; email: deposit@ccdc.ac.uk. Supplementary data associated with this article can be found, in the online version, at doi:10.1016/j.poly.2004.07.025.

References

[1] D. Gibson, Coord. Chem. Rev. 4 (1969) 163.
[2] J.J. Fortman, R.E. Sivers, Coord. Chem. Rev. 6 (1971) 331.
[3] R.C. Mehrotra, R. Bohra, D.P. Gaur, Metal β-Diketonates and Allied Derivatives, Academic Press, New York, 1978.
[4] M.A. Elmorsi, A.M. Hassanein, Corros. Sci. 41 (1999) 2337.
[5] T. Ito, C. Goto, K. Noguchi, Anal. Chim. Acta 443 (2001) 41.
[6] L. Yang, W. Jin, J. Lin, Polyhedron 19 (2000) 93.
[7] T. Ito, J. Electroanal. Chem. 495 (2001) 87.
[8] C. Pettinari, F. Marchetti, C. Santini, R. Pettinari, A. Drozdov, S. Troyanov, G.A. Battiston, R. Gerbasi, Inorg. Chim. Acta 315 (2001) 88.
[9] F. Marchetti, C. Pettinari, A. Cingolani, R. Pettinari, M. Rossi, F. Caruso, J. Organomet. Chem. 645 (2002) 134.
[10] B. Peng, G. Liu, L. Liu, D. Jia, K. Yu, J. Mol. Struct. 692 (2004) 217.
[11] A. Tong, Y. Akama, S.J. Tanaka, Chromatography 478 (1989) 408.
[12] Y. Akama, A. Tang, S. Ishima, M. Kaijitani, Anal. Sci. 8 (1992) 41.
[13] S. Umetani, H. Freiser, Inorg. Chem. 26 (1987) 3179.
[14] Y.A. Zolotov, N.M. Kuzmin, Metal Extraction with Acylpyrazolones, Izdat Nauka, Moscow, 1977.
[15] E.C. Okafor, B.A. Uzoukwu, Radiochim. Acta 51 (1990) 167.
[16] H. Samelson, A. Lempicki, J. Chem. Phys. 39 (1963) 110.
[17] R.G. Charles, E.P. Riedel, J. Inorg. Nucl. Chem. 28 (1966) 3005.
[18] C.C. Hinkley, J. Am. Chem. Soc. 91 (1969) 5160.
[19] W.DeW Horrrocks Jr., J.P. Sipe III, J. Am. Chem. Soc. 93 (1971) 6800.
[20] E.W. Berg, J.J.C. Acosta, Anal. Chim. Acta 40 (1968) 101.
[21] L. Liu, D.Z. Jia, Y.L. Ji, K.B. Yu, J. Photochem. Photobiol. 154 (2003) 117.
[22] Y. Akama, A. Tong, N. Matsumoto, T. Ikeda, S. Tanaka, Vibr. Spectrosc. 13 (1996) 113.
[23] Y. Akama, A. Tong, Microchem. J. 53 (1996) 34.
[24] D. Zhou, Q. Li, C. Huang, G. Yao, S. Umetani, M. Matsui, L. Ying, A. Yu, X. Zhao, Polyhedron 16 (1997) 1381.
[25] L. Yand, W. Jin, J. Lin, Polyhedron 19 (2000) 93.
[26] N.R. Shah, J.R. Shah, J. Inog. Nucl. Chem. 43 (1981) 1583.
[27] H.K. Soni, J.R. Shah, Bull. Soc. Chim. Fr. 2 (1985) 147.
[28] Y.M. Patel, J.R. Shah, Ind. J. Chem. 24 (1985) 800.
[29] D.S. Raj, P.C. Shah, J.R. Shah, Synth. React. Inorg. Met.-Org. Chem. 22 (1992) 321.
[30] D.S. Raj, N.J. Parmar, J.R. Shah, Synth. React. Inorg. Met.-Org. Chem. 34 (2004) 697.
[31] S. Rao, A.S. Mitra, J. Ind. Chem. Soc. 55 (1978) 420.
[32] R.C. Maurya, M.N. Jayaswal, D.D. Mishra, S. Kovil, Synth. React. Inorg. Met.-Org. Chem. 27 (1997) 49.
[33] I.A. Patel, B.T. Thaker, Indian J. Chem. 38 (1999) 427.
[34] D.D. Perrin, W.L.F. Armarego, D.R. Perrin, Purification of Laboratory Chemicals, 2nd ed., Pergamon Press, New York, 1981.
[35] H.A. Flaschka, EDTA Titrations, Pergamon Press, New York, 1956, p. 78.
[36] G.M. Sheldrick, SADABS, Universität Göttingen, Germany, 1995.
[37] G.M. Sheldrick, SHELXS-97, Program for X-ray Crystal Structure Solution, Göttingen University, Germany, 1997.
[38] G.M. Sheldrick, SHELXL-97, Program for X-ray Crystal Structure Refinement, Göttingen University, Germany, 1997.
[39] F. Bechtel, J. Gaultier, C. Hauw, Cryst. Struct. Commun. 2 (1973) 473.
[40] F. Bechtel, J. Gaultier, C. Hauw, Cryst. Struct. Commun. 2 (1973) 469.
[41] C. Arici, M.N. Tahir, D. Ulku, O. Atakol, Acta Cryst., Sect. C 55 (1999) 1961.
[42] H.B. Suthar, U.G. Deshpande, J.R. Shah, Bull. Soc. Chim. Fr. 1 (1986) 55.
[43] J.J.P. Stewart, J. Comp. Chem. 10 (1989) 209.

Available online at www.sciencedirect.com
SCIENCE DIRECT®
Polyhedron 23 (2004) 2475–2479
POLYHEDRON
www.elsevier.com/locate/poly

Diastereoselective formation of a *meso*-disilane-1,2-diol – a dianionic siloxide ligand for Ti and Zr

C. Krempner [a,b,*], H. Reinke [b], K. Weichert [b], A. Spannenberg [c]

[a] *Department of Chemistry, The Ohio State University, 100 W. 18th Avenue, Columbus, OH 43210, USA*
[b] *Fachbereich Chemie der Universität Rostock, A.-Einstein-Str. 3a, Rostock, 18059, Germany*
[c] *Lebniz-Institut für Organische Katalyse an der Universität Rostock e. V., Buchbinderstr. 11, Rostock 18055, Germany*

Received 24 April 2004; accepted 28 July 2004
Available online 25 September 2004

Abstract

The *meso* form of $(RMeSiOH)_2$ [R = $Si(SiMe_3)_3$] (**2**) was synthesized exclusively by hydrolysis of a diastereomeric mixture of $(RMeSiCl)_2$ (**1**). The novel cyclic metal disiloxides (*E*)-$(RMeSiO)_2Ti(OEt)_2$ (**3**) and $[(Z)\text{-}(RMeSiO)_2]_2Zr \cdot HNEt_2$(**4**) are readily prepared from the reaction of *meso*-**2** with $Ti(OEt)_4$ and $Zr(NEt_2)_4$, respectively. The results of X-ray structure analyses reveal complexes **3** and **4** to be strained five-membered ring compounds forming a dimeric structure and an adduct with diethylamine.
© 2004 Published by Elsevier Ltd.

Keywords: Silanoles; Siloxides; Titanium; Zirconium; Oligosilanes

1. Introduction

The ability of siloxide ligands [1] to act as effective σ- and π-donors enables electronic stabilization of highly electrophilic metal centers, which have found applications in the catalysis of processes such as olefin polymerization [2], olefin metathesis [3] and oxidations [4]. Moreover, siloxide ligands bearing sterically demanding substituents can probably protect the coordination sphere of the metal complexes, thus enforcing coordinative unsaturation and stabilizing reduced early TM centers [5]. Among the various substituted disiloxane-1,3-diols, incompletely condensed polyhedral silsesquioxanes and related compounds mainly consisting of Si–O–Si backbones [6], there are only a few diols that have both an oligosilane backbone and asymmetric silicon centers [7]. These diols might be of interest for the synthesis of stereoregular cyclic metal siloxide complexes. Recently, we reported the preparation of silanols of the general formula $(RMeSiOH)_2$ [R = $Si(SiMe_3)_3$, $Si(SiMe_3)_2Ph$] and we have shown that these derivatives can act as supporting ligands for Cp_2Ti fragments [8]. Herein we report on the first highly diastereoselective formation of a *meso*-disilane-1,2-diol and its utilization for the straightforward synthesis of cyclic titanium and zirconium siloxides in high yields.

2. Results and discussion

The starting point of our investigations was the dichlorohexasilane **1**, which could be synthesized according to the procedure outlined in Scheme 1 [8]. In fact, the reaction of two equiv. of $(Me_3Si)_3Si\text{–}K \cdot 3THF$ with $Cl_2MeSi\text{–}SiMeCl_2$ in pentane at −78 °C gave **1** as a diastereomeric mixture (*rac* and *meso*) in high yield. However, initial efforts to produce one of the two possible diastereomers of diol **2** exclusively by hydrolysis of **1** in the presence of several bases failed. Under the conditions applied only mixtures of both dia-

* Corresponding author. Tel.: +1 614 6883625; fax: +1 614 2920368.
E-mail address: ckrempne@chemistry.ohio-state.edu (C. Krempner).

0277-5387/$ - see front matter © 2004 Published by Elsevier Ltd.
doi:10.1016/j.poly.2004.07.022

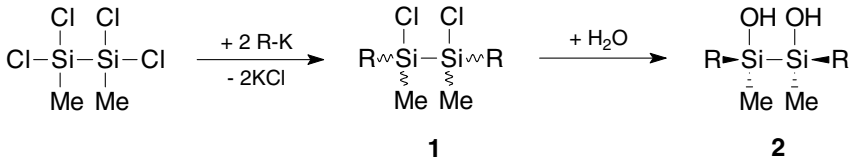

Scheme 1. Synthesis of **2** [R = $Si(SiMe_3)_3$].

stereomers (*rac* and *meso*) were obtained, which had to be separated by column chromatography, limiting the potential application of these ligands in coordination chemistry.

Surprisingly, a very simple hydrolysis of **1** without a base in a two-phase system consisting of water and ether gave the diastereomerically pure *meso*-diol **2** as a colorless crystalline material in 79% yield (Scheme 1). To our knowledge this is the first example of a highly diastereoselective hydrolytic reaction from a diastereomeric mixture of a dichlorodisilane. Compound **2** can be synthesized on a large scale, up to 50 g, and handled in air for months without decomposition; it is stable towards self-condensation and isomerization into the racemic form of **2** [9].

Although the origin of the diastereoselectivity is still unclear, it is reasonable to assume an S_N1 mechanism for the nucleophilic substitution at the silicon centre, since otherwise a diastereomeric mixture would be expected. The fact that the intermediate silylium ion can be sufficiently stabilized by hyperconjugation or σ-conjugation of the oligosilane backbone supports this view.

With the intent to investigate the ability of **2** to act as a supporting dianionic ligand for early transition metals, we extended our studies to the synthesis of novel Ti and Zr siloxide complexes. A suitable entry into the coordination chemistry of Ti and Zr is the use of the corresponding amides and alkoxides as starting materials (Scheme 2).

When $Ti(OEt)_4$ was reacted with one equiv. of **2** in heptane for three hours, a yellow microcrystalline material of what was thought to be the titanium complex **3** could be isolated in a yield of 85%. In contrast, the reaction of **2** with $Zr(NEt_2)_4$ in heptane led to the formation of a colorless solid which could be identified as spirocyclic zirconium complex **4** in a yield of 64%. Whereas **4** is highly moisture sensitive in solution and even in the solid state, **3** is reasonable stable in the solid phase and was unaffected by atmospheric moisture. The proposed structures of the complexes **3** and **4** were confirmed by NMR data and elemental analysis.

Single crystals obtained by slow crystallization from heptane solutions were analyzed by X-ray diffraction. In the case of the titanium compound **3** (Fig. 1, Table 1), the results reveal a dimeric structure in which two titanium diethoxide fragments are linked by two ethoxide groups forming a planar four-membered ring. Distances from the titanium atom to the non-equivalent bridging oxygen centers [2.030(3), 1.984(3) Å], are strongly elongated from the Ti1–O3 distance [1.755(4) Å] indicating only weak interactions in this dimeric structure. The Ti-O distances [1.833(3), 1.820(3) Å] within the ring are comparable to those found in related compounds containing Si–O–Ti units. The coordination geometry around the titanium centers can be regarded as distorted square pyramidal, with the O3 atom and the remaining atoms O1, O2, O4, O4A occupying axial and basal positions, respectively.

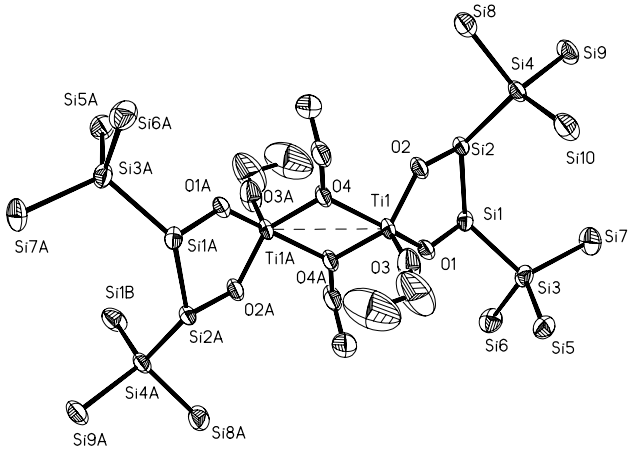

Fig. 1. Thermal ellipsoid plot (30% probability) of **3**. All methyl groups at silicon and one disordered tris(trimethylsilyl)silyl group are omitted for clarity.

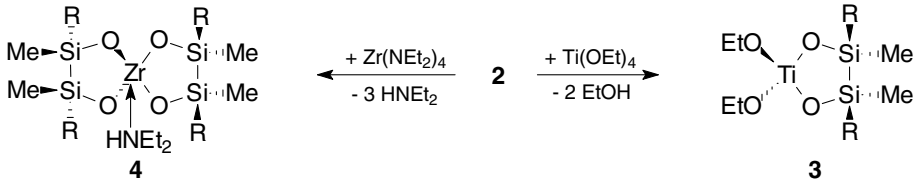

Scheme 2. Synthesis of **3** and **4** [R = $Si(SiMe_3)_3$].

Table 1
Selected bond lengths (Å) and bond angles (°) for **3** and **4**

	3 (M = Ti)	**4** (M = Zr)
Bond lengths		
M–O	1.833(3), 1.820(3)	2.020(2), 1.960(2)
Ti(1)–O(3)	1.755(4)	
Ti–$O_{bridging}$	2.030(3), 1.984(3)	
Zr–N		2.346(6)
Si–O	1.666(3), 1.652(3)	1.674(2), 1.658(2)
Si(1)–Si(2)	2.4368(17)	2.4381(13)
Bond angles		
O–M–O	91.06(12)	88.95 (9)
Si–O–M	131.57(16), 131.23(16)	129.67(12), 123.51(13)
O(1)–Si(1)–Si(2)	92.16(11)	94.16(9)
O(2)–Si(2)–Si(1)	93.70(11)	97.43(9)
Si(3)–Si(1)–Si(2)	136.54(7)	133.95(5)
Si(4)–Si(2)–Si(1)	138.00(7)	137.46(5)

The results of the X-ray analysis of **4** (Fig. 2, Table 1) confirm the expected extensive shielding of the zirconium atom by the two sterically demanding ligands and the diethylamine in which the ethyl groups are disordered. The geometry around the zirconium atom is described best as distorted trigonal bipyramidal with the O2, O2A atoms and the N, O1, O1A atoms occupying axial and apical positions, respectively. Typically, the length of the apical Zr–O1 bond [1.960(2) Å] is somewhat shorter than that of the axial Zr–O2 bond [2.020(2) Å].

Although the geometry and coordination environment around the metal centers are completely different, the structural features of the ligand backbone in **4** are quite similar to those in the titanium complex **3**. The central metal atoms are bonded in a chelate fashion [**3** O–Ti–O 91.06(12)°; **4** O–Zr–O 88.95s(9)°] to both siloxide groups of the ligand, giving a nearly planar five-membered ring. Most of the Si–Si bonds lie unremarkably within the range of 2.34–2.38 Å. But the spatial demand of the two extended hemispherical $(Me_3Si)_3Si$ groups which adopt a (*Z*) position, leads to a significant elongation of the central Si1–Si2 bond in both compounds [**3**; 2.4368(17) Å; **4**; 2.4318(13) Å] and an extreme widening of the central Si–Si–Si angles to values within the range of 134°–138°. Only the Si–O–Ti angles [131.57(16)°, 131.23(16)°] of **3** are somewhat larger than those found in **4** [129.67(12)°, 123.51(13)°] probably due to the fact that the ionic radius of zirconium is larger than that of titanium. In comparison to other cyclic complexes mainly consisting of Si–O–Si backbones the M–O–Si angles and chelate angles of **3** and **4** are remarkably smaller reflecting the exceptionally spatial requirements in these five-membered ring structures. Consequently, it is reasonable to assume that ring strain in both compounds causes only weak oxygen p_π–d_π donation of the siloxide ligand towards the metal center, which makes the metal electrophilic. The fact that **3** adopts a dimeric structure and **4** forms a thermally stable donor adduct with diethylamine can be understood best as a result of coordinative unsaturation of both metals.

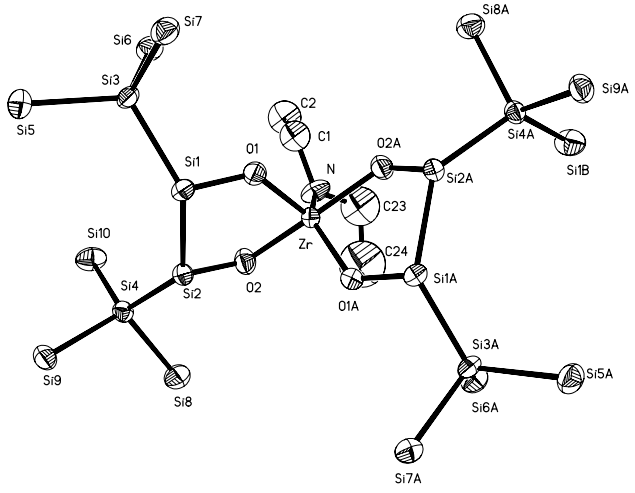

Fig. 2. Thermal ellipsoid plot (50% probability) of **4**. All methyl groups at silicon and one disordered amine ligand are omitted for clarity.

3. Conclusion

In conclusion, *meso*-$(RMeSiOH)_2$ [R = $Si(SiMe_3)_3$] (**2**) was synthesized exclusively by simple hydrolysis of $(RMeSiCl)_2$ (**1**). It has been shown that diol **2** is a supporting dianionic ligand for Ti and Zr fragments, which yields the disiloxides (*E*)-$(RMeSiO)_2Ti(OEt)_2$ (**3**) and [(*Z*)-$(RMeSiO)_2]_2Zr \cdot HNEt_2$(**4**) from the reaction of **2** with $Ti(OEt)_4$ and $Zr(NEt_2)_4$. The results of X-ray analyses reveal disiloxides **3** and **4** to be strained five-membered ring compounds that form a dimeric structure or an adduct with diethylamine, respectively. Studies are underway to examine the electrophilic properties of these disiloxides and their ability to be acceptors towards neutral and anionic donors.

4. Experimental

All manipulations of air- and/or moisture-sensitive compounds were carried out under an atmosphere of argon using standard Schlenk techniques. Solvents were dried using standard procedures. Compound **1** was prepared as previously described [8].

4.1. (meso)-3,4-Dihydroxy-1,1,1,3,4,6,6,6-octamethyl-2,2,5,5- tetrakis(trimethylsilyl)-hexasilane (2)

A mixture of **1** (10 g, 15.3 mmol), 400 ml of ether and 400 ml of water was vigorously stirred at room temperature for one day. The organic phase was separated,

dried with $MgSO_4$, and the solvent was evaporated. The solid residue was recrystallized from heptane at −40 °C to yield crystals of **2** (7.45 g, 79%). The analytical data obtained were in full agreement with those reported [8].

4.2. *Bis-{(Z)-1,2-dimethyl-1,2-bis[tris(trimethylsilyl)-silyl]-η^2-disilanediolato-η^2-diethoxo-η^1-diethoxo-titanium} (**3**)*

Freshly distilled $Ti(OEt)_4$ (0.45 ml, 2.13 mmol) was added to a solution of (*meso*)-2 (1.255 g, 2.04 mmol) in 10 ml heptane at room temperature. After 1 h, a yellow crystalline material started to precipitate from the solution. The mixture was allowed to stand at room temperature for one day and at −40 °C for another day. The resulting yellow crystalline solid 3 (1.15 g) was isolated by filtration, washing with cold heptane, and drying under vacuum. Crystallization from the mother liqueur gave another 0.15 g of 3 (1.3 g, 85%), m.p. 209 °C (decomp.); ^{1}H NMR (500 MHz, C_6D_6): δ 4.77, 4.50 (2m, CH_2CH_3, 2×2H), 1.52, 1.26 (2m, CH_2CH_3, 2×3H), 1.02 (s, OSiMe, 6 H), 0.46 (s, $SiMe_3$, 54H); ^{13}C NMR (125 MHz, C_6D_6): δ 73.6, 71.6 (CH_2CH_3), 18.9, 19.1 (CH_2CH_3), 10.5 (OSiMe), 3.8 ($SiMe_3$); ^{29}Si NMR (60 MHz, C_6D_6): δ −121.1 [*Si*($SiMe_3$)$_3$], −9.7 ($SiMe_3$), 49.0 (OSiMe). *Anal*. Calc. for $C_{24}H_{70}O_4Si_{10}Ti$ (751.53) C, 38.36; H, 9.39. Found: C, 38.63; H, 9.55%.

4.3. *Bis-{(Z)-1,2-dimethyl-1,2-bis[tris(trimethylsilyl)-silyl]-η^2-disilanediolato}-η^1-diethyl-amino-zirconium (**4**)*

$Zr(NEt_2)_4$ (0.3 ml, 1.65 mmol) was added to a stirred solution of (*meso*)-2 (1 g, 1.62 mmol) in 30 ml heptane at room temperature. After stirring for 30 min, a microcrystalline material started to precipitate from the solution and the reaction mixture was refluxed for additional 1 h. The solution was concentrated to a volume of ca. 10 ml and slowly cooled to −40 °C for 2 days to yield colorless crystals of 4 (0.72 g, 64%), m.p. 206 °C (decomp.); ^{1}H NMR (250 MHz, C_6D_6): δ 0.43 (s, 54H, $SiMe_3$), 1.04 (s, 6H, OSiMe); ^{13}C NMR (125 MHz, C_6D_6): δ 4.0 (s, $SiMe_3$), 11.7 (s, OSiMe); ^{29}Si NMR (100 MHz, C_6D_6): δ −122.5 [*Si*($SiMe_3$)$_3$], − 10.1 ($SiMe_3$), −11.7 (OSiMe).

Table 2
Crystal data and structure refinement for **3** and **4**

	3	**4**
Empirical formula	$C_{24}H_{70}O_4Si_{10}Ti$	$C_{44}H_{131}NO_4Si_{20}Zr$
Formula weight	751.60	1391.52
Temperature (K)	293(2)	200(2)
Wavelength of Mo Kα (Å)	0.71073	0.71073
Crystal system	triclinic	orthorhombic
Space group (H.-M.)	$P\bar{1}$	*Aba2*
Space group (Hall)	$\bar{P}1$	*A2-2ac*
a (Å)	10.050(2)	24.643(5)
b (Å)	12.880(3)	18.981(4)
c (Å)	19.930(4)	18.238(4)
α (°)	104.83(3)	90
β (°)	102.39(3)	90
γ (°)	99.81(3)	90
Volume (Å^3)	2365.4(8)	8530.8(31)
Z	2	4
D_{calc} [Mg/m^3]	1.055	1.083
Absorption coefficient (mm^{-1})	0.457	0.441
F(000)	816	3016
Crystal size (mm)	$0.4\times0.3\times0.2$	$0.4\times0.4\times0.3$
Θ range for data collection	2.12–24.20	1.76–24.30
Index ranges	$-10\leqslant h\leqslant11$, $-14\leqslant k\leqslant14$, $-22\leqslant l\leqslant22$	$-28\leqslant h\leqslant0$, $-21\leqslant k\leqslant21$, $-19\leqslant l\leqslant19$
Reflections collected	14748	12512
Independent reflections	6959	6544
R_{int}	0.0886	0.0265
Completeness to θ	24.20°/91.4%	24.3°/95.9%
Absorption correction	none	none
Refinement method	full-matrix least-squares on F^2	full-matrix least-squares on F^2
Data/restraints/parameters	6959/0/401	6544/3/319
Goodness-of-fit on F^2	0.840	0.938
Final *R* indices with $I>2\sigma(I)$	$R_1=0.0528$, $wR_2=0.1207$	$R_1=0.0326$, $wR_2=0.0645$
R indices (all data)	$R_1=0.0960$, $wR_2=0.1333$	$R_1=0.0418$, $wR_2=0.0672$
Largest differential peak/hole [e Å^{-3}]	0.519/−0.312	0.392/−0.302

Anal. Calc. for $C_{44}H_{131}O_4Si_{20}Zr$ (1391.45) C, 37.98; H, 9.47; N, 1.01. Found: C, 38.25; H, 9.83; N, 0.82%.

5. X-ray crystallography

Structure determination and refinement of **3** and **4**. The data collections were done on a STOE IPDS (laser scanned imaging plate) equipped with a molybdenum fine focus X-ray tube and graphite monochromator. The structures were solved by direct methods (Bruker SHELXTL software package). The refinement calculations were performed by the full matrix least-squares method of Bruker SHELXTL [10]. All non-hydrogen atoms were refined anisotropically. The hydrogen atoms were put into theoretical positions and refined according to the riding model (see Table 2).

6. Supplementary material

Crystallographic data (excluding structure factors) for the structures reported in this paper have been deposited with the Cambridge Crystallographic Data Centre as supplementary publication nos. CCDC 236559 (3) and CCDC 236560 (4). Copies of the data can be obtained free of charge on application to The Director, CCDC, 12 Union Road, Cambridge, CB2 1EZ UK (fax: Int. code +44(1223) 336-033; e-mail: deposit@ccdc.cam.ac.uk or on the web: http://www.ccdc.cam.ac.uk).

Acknowledgements

We thank Prof. Dr. H. Oehme for his generous support and we gratefully acknowledge the support of our research by the Fonds der Chemischen Industrie. We thank Prof. M. Michalik for recording the NMR spectra.

References

[1] (a) For recent reviews, see: R. Murugavel, A. Voigt, M.G. Walawalkar, H.W. Roesky, Chem. Rev. 96 (1996) 2205;
(b) L. King, A.C. Sullivan, Coord. Chem. Rev. 189 (1999) 19;
(c) V. Lorenz, A. Fischer, S. Gießmann, J.W. Gilje, Y. Gun'ko, K. Jacob, F.T. Edelmann, Coord. Chem. Rev. 206–207 (2000) 321;
(d) B. Marciniec, H. Maciejewski, Coord. Chem. Rev. 223 (2001) 301;
(e) R. Duchateau, Chem. Rev. 102 (2002) 3525.
[2] (a) H.C.L. Abbenhuis, S. Krijnen, R.A. van Santen, Chem. Commun. (1997) 331;
(b) R. Duchateau, H.C.L. Abbenhuis, R.A. van Santen, S.K.-H. Thiele, M.F.H. van Tol, Organometallics 17 (1998) 5222;
(c) R. Duchateau, H.C.L. Abbenhuis, R.A. van Santen, A. Meetsma, S.K.-H. Thiele, M.F.H. van Tol, Organometallics 17 (1998) 5663;
(d) F.J. Feher, F.J. Walzer, R.L. Blanski, J. Am. Chem. Soc. 113 (1991) 3618;
(e) F.J. Feher, R.L. Blanski, J. Am. Chem. Soc. 114 (1992) 5886.
[3] F.J. Feher, T.L. Tajima, J. Am. Chem. Soc. 116 (1992) 2145.
[4] (a) I.E. Buys, T.W. Hambley, D.J. Houlten, T. Maschmeyer, F.A. Masters, A.K. Smith, J. Mol. Catal. 86 (1994) 309;
(b) M. Crocker, R.H.M. Herold, A.G. Orpen, Chem. Commun. (1997) 2411;
(c) T. Maschmeyer, M.C. Klunduk, C.M. Martin, D.S. Shepard, J.M. Thomas, B.F.G. Johnson, Chem. Commun. (1997) 1847;
(d) M. Crocker, R.H.M. Herold, A.G. Orpen, M.T.A. Overgaag, J. Chem. Soc., Dalton Trans. (1999) 3791.
[5] (a) F.J. Feher, T.A. Budzichowski, Polyhedron 14 (1995) 3239;
(b) P.T. Wolczanski, Polyhedron 14 (1995) 3335.
[6] (a) For recent reviews, see: P.D. Lickiss, Adv. Inorg. Chem. 42 (1995) 147;
(b) P.D. Lickiss, in: Z. Rappoport, Y. Apeloig (Eds.), The Chemistry of Organic Silicon Compounds, 3, John Wiley & Sons, New York, 2001, p. 695.
[7] V.V. Semenov, E. Ladilina, A. Kurskii, S. Korshev, N.P. Makarenko, G.A. Domrachev, L.N. Zakharov, G.K. Fukin, T. Struchkov, Izv. Akad. Nauk, Ser. Khim. 10 (1996) 2550.
[8] D. Hoffmann, H. Reinke, C. Krempner, J. Organomet. Chem. 662 (2003) 1.
[9] M.E. Lee, H.M. Cho, D.J. Kang, J.-S. Lee, J.H. Kim, Organometallics 21 (2002) 4297.
[10] Bruker SHELXTL Version 5.10 SGI/Irix, Copyright 1997 Bruker Analytical X-ray Systems.

Available online at www.sciencedirect.com
SCIENCE DIRECT®
Polyhedron 23 (2004) 2481–2489
POLYHEDRON
www.elsevier.com/locate/poly

Cobalt(II) and zinc(II) compounds with unsaturated ligands derived from 2-aminobenzothiazole

Fabiola Téllez [a], Angelina Flores-Parra [a,*], Norah Barba-Behrens [b], Rosalinda Contreras [*,a]

[a] Departamento de Química, Centro de Investigación y de Estudios Avanzados IPN, A.P. 14-740, México, D.F. 07000, México
[b] Departamento de Química Inorgánica, Facultad de Química, Universidad Nacional Autónoma de México, C.U., Coyoacán, México, D.F. 04510, México

Received 1 June 2004; accepted 4 August 2004
Available online 12 October 2004

Abstract

Four zinc(II) (**6**, **8**, **10** and **12**) and four cobalt(II) (**5**, **7**, **9** and **11**) compounds derived from *N*-(benzothiazol-2-yl)-dithiocarbamic methyl ester (**1**) (**5** and **6**), 1-benzothiazol-2-ylid-3-methyl-thiourea (**2**) (**7** and **8**), 1-benzothiazol-2-yl-2,3-dimethyl-*iso* thiourea (**3**) (**9** and **10**) and *N*-(benzothiazol-2-yl)-*S*,*S*′-dimethyl-dithio-carboimine (**4**) (**11** and **12**) are reported. The complexes were characterized in the solid state by UV–Vis–NIR diffuse reflectance, IR, mass spectrometry and compounds **5**, **9**–**12** by X-ray single crystal diffraction analyses. In all cases two ligand molecules are bonded to a tetracoordinated metal atom. In compounds **5**–**10** the ligand is anionic and bidentate with the metal atom in the center of spirocyclic structures formed by two planar unsaturated six membered rings. In compounds **7**–**10** the metal atom is linked to four nitrogen atoms and in **5** and **6** to two sulfur and two nitrogen atoms. In compounds **11** and **12** the ligand is neutral and monodentate and the metal ion remains coordinated to the chlorine atoms.
© 2004 Elsevier Ltd. All rights reserved.

Keywords: Zinc(II) cobalt(II) compounds from *N*-(benzothiazol-2-yl)-dithiocarbamic methyl ester; 1-Benzothiazol-2-ylid-3-methyl-thiourea; 1-Benzothiazol-2-yl-2,3-dimethyl-*iso*thiourea; *N*-(benzothiazol-2-yl)-*S*,*S*′-dimethyl-dithio-carboimine

1. Introduction

Functionalized benzazoles have many applications as fertilizers, antimicotics, antibiotics, pesticides and neuroprotectors [1–11]. We are interested in unsaturated and planar benzazoles having a framework with alternating sp^2 carbon and heteroatoms such as nitrogen, oxygen and sulfur, and their use as ligands [12–15]. One of our aims is the preparation of benzazoles with coordinative arms in order to give coordination compounds forming planar six membered rings in which the metal atom is included in the electronic unsaturated system. With this idea, we have synthesized metal derivatives of 2-guanidino- and 2-uroylbenzimidazole [7–10]. The molecular structure of the diphenylboron compound derived from 2-guanidinobenzimidazole is particularly remarkable [9], because it does not have the expected structure in which a B–N covalent bond is present for one of the nitrogen atoms and a coordinative bond for the other. The solid state data show that the tetracoordinated boron atom has two similar B–N bond lengths (≈1.56 Å), which could be considered to be between a covalent and a coordinative bond, indicative of a resonance hybrid with a partial negative charge at boron and the positive charge delocalized between the C–N bonds of the ring, Scheme 1. A similar behavior is expected for other Lewis acids and it was found that zinc and nickel compounds derived from 2-guanidinobenzimidazole are

* Corresponding author. Tel.: +55 50613720; fax: +55 57477113.
E-mail address: aflores@mail.cinvestav.mx (A. Flores-Parra).

0277-5387/$ - see front matter © 2004 Elsevier Ltd. All rights reserved.
doi:10.1016/j.poly.2004.08.019

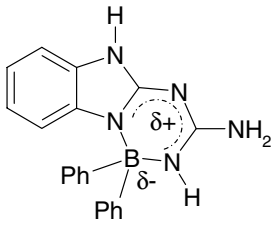

Scheme 1.

some examples in which the ligand is coordinated to the metal with two similar N–M bond lengths [Zn–N 1.996(4); 1.942(4) and Ni–N 1.893(2); 1.867(3) Å] [7].

In this context, we have prepared four compounds derived from 2-aminobenzothiazole with functionalized arms bearing sulfur atoms [15] that could act as ligands: *N*-(benzothiazol-2-yl)-dithiocarbamic methyl ester (**1**), 1-benzothiazol-2-ylid-3-methyl-thiourea (**2**), 1-benzothiazol-2-yl-2,3-dimethyl-*iso*thiourea (**3**) and *N*-(benzothiazol-2-yl)-*S*,*S*′-dimethyl-dithiocarboimine (**4**), Scheme 2. Syntheses of **1** and **4** have been reported by Merchán et al. [16]. The ligands **1**–**4** are complex molecules that can be depicted by several conformers and tautomers, therefore their behavior towards coordination with transition metals is not straightforward. To better understand their reactivity, we have achieved

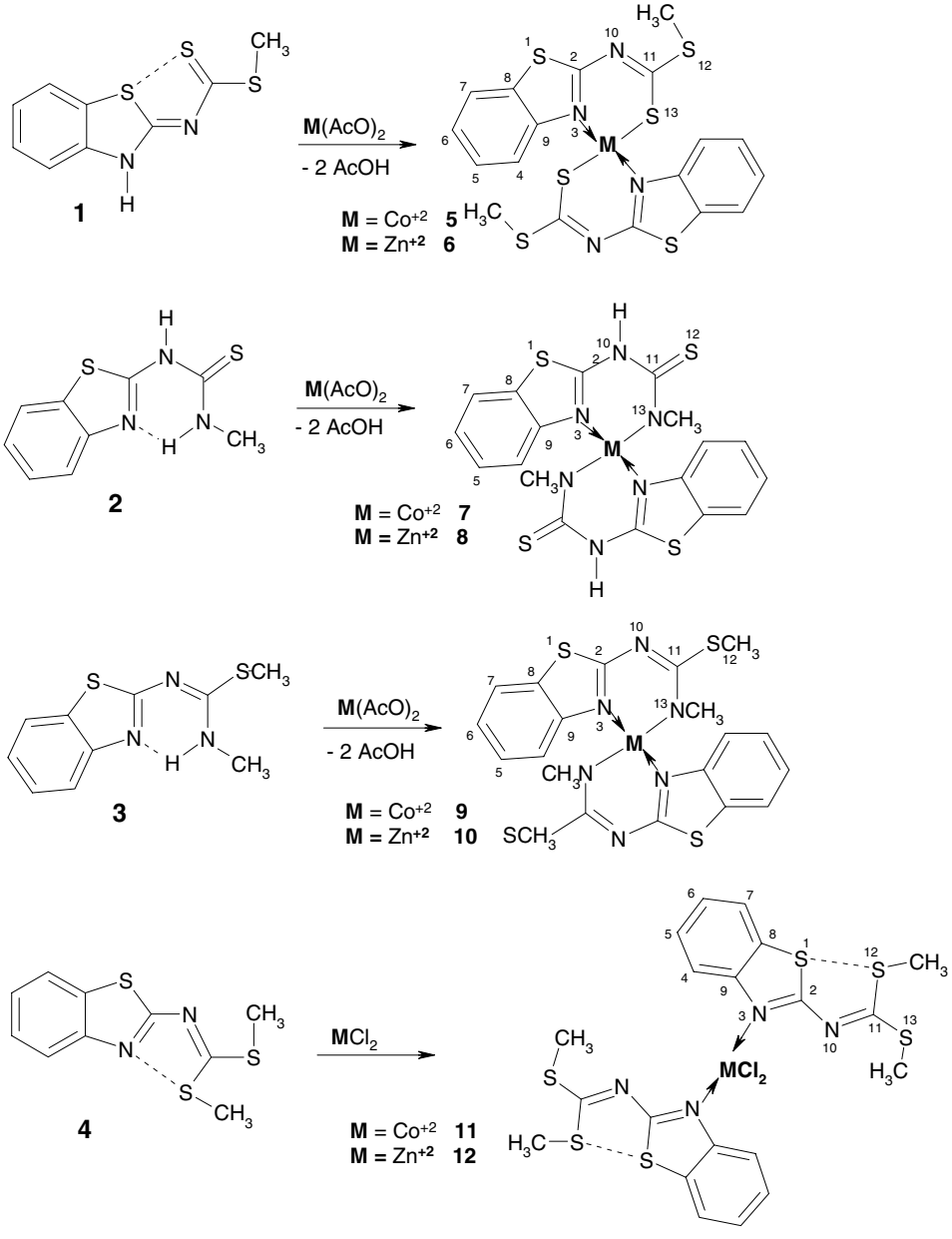

Scheme 2. Reported metal coordination compounds.

a detailed investigation in order to establish their preferred tautomers and conformers [15], and they are depicted in Scheme 2.

The aim of this research was to study the ability of these planar and delocalized ligands towards metal coordination in order to know if they can form the less stable six membered metallocycles in which the metal participates in the delocalization of the π system. Also it is interesting to evaluate the role of the nitrogen and sulfur atoms in the metallic coordination and the preferred arrangement of the ligands.

2. Experimental

2.1. Materials

The metal salts $Co(OAc)_2 \cdot H_2O$, $Zn(OAc)_2 \cdot H_2O$, $CoCl_2 \cdot 6H_2O$ and $ZnCl_2$, methanol (J.T. Baker) and 2-aminobenzothiazole (Aldrich) were used without further purification. Ligands **1**–**4** were prepared as previously described [15,16].

2.2. Synthesis of complexes: general procedure

All coordination compounds were synthesized as described for compound **5**.

2.2.1. Compound **5** *[Co(**1**)$_2$]*

Compound **1** (240 mg, 1 mmol) was dissolved in 40 ml of hot methanol and added to a solution of $Co(OAc)_2 \cdot H_2O$ (98 mg, 0.5 mmol), in 10 ml of methanol. The solution was heated and stirred for 2 h. A light brown precipitate was formed which was filtered and recrystallized from acetone. Single crystals were suitable for diffraction analysis. Yield: 205 mg, 40%, m.p. 210 °C. *Anal*. Calc. for $C_{18}H_{14}N_4S_6Co$: C, 40.21; H, 2.62; N, 10.42. Found: C, 40.23; H, 2.59; N, 10.40%. IR (cm^{-1}): 1464, 1448, 1391. UV–Vis–NIR (cm^{-1}): CT 23427, 17092, 8847. MS: *m/z* 239.

2.2.2. Compound **6**, *[Zn(**1**)$_2$]*

A pale yellow powder was obtained. Yield: 156 mg, 30%, m.p. 218 °C. *Anal*. Calc. for $C_{18}H_{14}N_4S_6Zn$: C, 39.73; H, 2.59; N, 10.30. Found: C, 40.24; H, 2.65; N, 10.37%. IR (cm^{-1}): 1469, 1450, 1407. UV–Vis–NIR (cm^{-1}): CT 24190. MS: *m/z* 239.

2.2.3. Compound 7, *[Co(**2**)$_2$]*

Green powder. Yield: 176 mg, 35%, m.p. 239 °C. *Anal*. Calc. for $C_{18}H_{16}N_6S_4Co$: C, 42.93; H, 3.20; N, 16.69. Found: C, 43.33; H, 3.32; N, 16.67%. IR (cm^{-1}): 1481, 1448, 1387. UV–Vis–NIR (cm^{-1}): CT 24408, 17080, 8684. MS: *m/z* 503 [M^+].

2.2.4. Compound **8**, *[Zn(**2**)$_2$]*

Colorless powder. Yield: 193 mg, 38%, m.p. 130 °C. *Anal*. Calc. for $C_{18}H_{16}N_6S_4Zn$: C, 42.39; H, 3.16; N, 16.48. Found: C, 42.57; H, 3.23; N, 16.48%. IR (cm^{-1}): 1483, 1450, 1386. UV–Vis–NIR (cm^{-1}): CT 26618. MS: *m/z* 508 [M^+].

2.2.5. Compound **9**, *[Co(**3**)$_2$] · 1/2H$_2$O*

Orange powder, recrystallized from DMSO. Crystals were suitable for X-ray diffraction analysis. Yield: 318 mg, 60%, m.p. 192 °C. *Anal*. Calc. for $C_{20}H_{20}N_6S_4Co \cdot 1/2H_2O$: C, 44.41; H, 3.91; N, 15.55. Found: C, 44.42; H, 3.59; N, 15.04%. IR (cm^{-1}): 1463, 1386. UV–Vis–NIR (cm^{-1}): TC 22818, 11663. MS: *m/z* 531 [M^+].

2.2.6. Compound **10**, *[Zn(**3**)$_2$]*

Colorless crystals. Yield: 350 mg, 66%, m.p. 169 °C. *Anal*. Calc. for $C_{20}H_{20}N_6S_4Zn$: C, 44.64; H, 3.75; N, 15.62. Found: C, 44.55; H, 3.70; N, 15.68%. IR (cm^{-1}): 1503, 1469, 1453, 1392. UV–Vis–NIR (cm^{-1}): TC 25158. MS: *m/z* 536 [M^+].

2.2.7. Compound **11**, *[Co(**4**)$_2$Cl$_2$] 1/6C$_6$H$_6$*

Compound **11** was prepared from $CoCl_2 \cdot 6H_2O$ at r.t. for 1 h. A green precipitate was obtained, which was crystallized by liquid–liquid diffusion in methanol–benzene (5:1). Crystals were suitable for X-ray diffraction. Yield: 511 mg, 80%, m.p. 240 °C. *Anal*. Calc. for $C_{20}H_{20}N_4S_6Cl_2Co \cdot 1/6C_6H_6$: C, 38.68; H, 3.25; N, 8.60. Found: C, 38.53; H, 3.13; N, 8.79%. IR (cm^{-1}): 1588, 1514, 1465, 1431. UV–Vis–NIR(cm^{-1}): CT 24318, 16348, 7498. MS: *m/z* 254.

2.2.8. Compound **12** *[Zn(**4**)$_2$Cl$_2$] 1/2C$_3$H$_6$O*

Compound **12** was prepared from $ZnCl_2$ at r.t. for 1 h. Yellow crystals were obtained after several days from the reaction mixture. Yield: 529 mg, 82%, m.p. 238 °C. *Anal*. Calc. for $C_{20}H_{20}N_4S_6Cl_2Zn \cdot 1/2C_3H_6O$: C, 38.28; H, 3.41; N, 8.31. Found: C, 38.06; H, 3.11; N, 8.65%. IR (cm^{-1}): 1516, 1467, 1455, 1432. UV–Vis–NIR (cm^{-1}): CT 25178. MS: *m/z* 254.

2.3. Physical measurements

FT IR spectra were recorded with a (Perkin–Elmer 1600) spectrophotometer using KBr pellets (4000–400 cm^{-1}). The UV–Vis–NIR spectra (diffuse reflectance, 40000–4000 cm^{-1}) were recorded on a Cary-5E (Varian) spectrophotometer. The MS spectra were obtained by direct insertion at 20 eV in an HP 5989 spectrometer. Elemental analyses were carried out with a Fisons EA 1180 analyzer.

2.4. X-ray crystallographic study

Suitable single crystals of compounds **5**, **9**–**12** were mounted on a glass fiber in a small amount of perfluoro ether oil. Data were collected at 293 K. Crystal data and information about the data collection and structure refinement details are given in Tables 1–4. X-ray diffraction studies were performed with ENRAF-Nonius CAD4 and KAPPA-CCD diffractometers. The WINGX [17] software was used. The crystal structures were determined and refined with the SHELXTL-97 [*x*,*y*] system [18]. H atoms were systematically placed in idealized positions and refined with a riding model.

3. Results and discussion

The synthesis of compounds **5**–**12** was carried out from a molar ratio 2:1 ligand:metal salt. Compounds **5**–**10** were obtained by reaction of **1**–**3** with cobalt(II) and zinc(II) acetates, respectively, whereas **11** and **12** were obtained from ligand **4** and cobalt(II) and zinc(II) chlorides, respectively, Scheme 2. Complexes were characterized in the solid state by UV–Vis–NIR diffuse reflectance, IR and mass spectrometry, and compounds **5**, **9**–**12** by X-ray single crystal diffraction analyses (Tables 1–4).

Compounds **5**–**12** are not ionic, **5**–**10** have spirocyclic structures with two deprotonated bidentate ligands for each metal atom, the ligands maintain their planar structure and the metal is included in the six membered unsaturated rings.

From the mass spectra, IR and elemental analyses it is assumed that compounds **5** and **6** have the same structure. Cobalt(II) compound **5** has a light brown color, its magnetic moment μ_{eff} (4.8 BM) is characteristic of a tetrahedral cobalt(II) atom [19], and its electronic spectrum presents two transitions ν_2 8847 cm^{-1} and ν_3 17092 cm^{-1}, and a charge transfer band at 23427 cm^{-1}. The zinc(II) compound **6** is pale yellow, the charge transfer band is found at 24190 cm^{-1}. The experimental data correspond to a distorted geometry and the effect of the planar unsaturated and delocalized ligand.

From the X-ray diffraction study of **5** (Fig. 1), it is known that the metal atom is bonded to the ligands through the sulfur atom of the thione group and is coordinated by the nitrogen atom of the thiazole. This arrangement is different from the preferred structure of the free ligand (**1**, Scheme 2), where the thione group is close to the endocyclic sulfur atom with a stabilizing

Table 1
Crystal data, data collection and refinement details

Chemical formula	$C_{18}H_{14}N_4S_6Co$ (**5**)	$C_{20}H_{20}N_6S_4Co$ (**9**)	$C_{20}H_{20}N_6S_4Zn$ (**10**)	$C_{20}H_{20}N_4S_6Cl_2Co$ (**11**)	$C_{20}H_{20}N_4S_6Cl_2Zn$ (**12**)
Formula weight (g mol^{-1})	537.62	531.59	538.03	638.59	645.03
Crystal size (mm)	$0.40\times0.35\times0.30$	$0.45\times0.35\times0.25$	$0.25\times0.24\times0.20$	$0.33\times0.19\times0.08$	$0.35\times0.25\times0.15$
Crystal system	triclinic	triclinic	triclinic	tetragonal	tetragonal
Space group	$P\bar{1}$	$P\bar{1}$	$P\bar{1}$	I4(1)*cd*	I4(1)*cd*
Unit cell dimensions					
a (Å)	9.283(2)	11.1826(4)	11.1871 (9)	15.950(2)	15.8743(13)
b (Å)	10.779(2)	14.1420(6)	14.0822(11)	15.950(2)	15.8743(13)
c (Å)	11.661(2)	16.223(7)	16.1570(12)	21.021(4)	21.0038(18)
α (°)	77.43(3)	76.238(2)	76.4740(10)	90.00	90.00
β (°)	87.27(3)	73.594(2)	73.575(6)	90.00	90.00
γ (°)	70.53(3)	73.865(2)	74.133(7)	90.00	90.00
V ($Å^3$)	1073.3(4)	2328.6(10)	2314.4(3)	5347.8(14)	5292.8(8)
Z	2	4	4	8	8
D_{calc}	1.663	1.516	1.544	1.586	1.619
μ (mm^{-1})	1.397	1.12	1.44	1.33	1.62
Index range	$-10\leqslant h\leqslant 12$	$-13\leqslant h\leqslant 14$	$0\leqslant h\leqslant 13$	$-19\leqslant h\leqslant 19$	$-20\leqslant h\leqslant 20$
	$-13\leqslant k\leqslant 13$	$-17\leqslant k\leqslant 17$	$-15\leqslant k\leqslant 15$	$0\leqslant k\leqslant 19$	$-21\leqslant k\leqslant 17$
	$-15\leqslant l\leqslant 15$	$-20\leqslant l\leqslant 20$	$-17\leqslant l\leqslant 17$	$0\leqslant l\leqslant 25$	$-26\leqslant l\leqslant 26$
θ (°)	3.58–27.46	3.50–26.71	2.1–25.0	2.55–25.97	2.57–29.18
Reflections collected	17002	15950	8788	5130	14486
Reflections unique (R_{int})	3975 (5.05%)	9677 (4.21%)	8138 (5.57%)	1347 (10.09%)	2984 (7.24%)
Reflections observed	4854	6586	2633	896	2603
Temperature (K)	293(2)	293(2)	293(2)	293(2)	193(2)
No. of variables	262	560	575	163	177
R	0.0332	0.0623	0.0418	0.0339	0.0355
Rw	0.0802	0.1526	0.1427	0.0789	0.0833
Goodness-of-fit	1.067	1.0820	0.941	1.006	1.0250
Maximum Δ/σ	0.00	0.00	0.00	0.00	0.00
$\Delta\rho$ Maximum (e $Å^{-3}$)	0.376	0.6300	0.421	0.37	0.4600
$\Delta\rho$ Minimum (e $Å^{-3}$)	−0.46	−0.4500	−0.700	−0.32	−0.4900

$w^{-1}=\sigma^2F_o^2+(xP)^2+yP;\ P=(F_o^2+2F_c^2)/3;\ P=(F_o^2+2F_c^2)/3.$

Table 2
Selected bond lengths (Å) and angles (°) for **5**

Bond lengths	
Co1–N3A	1.979(1)
Co1–N3	1.988(1)
Co1–S13	2.260(1)
Co1–S13A	2.277(1)
N3–C2	1.323(3)
N10–C2	1.357(3)
N10–C11	1.297(3)
N3–C9	1.405(3)
S13–C11	1.733(2)
S13A–C11A	1.710(2)
S12–C11	1.747(2)
S12A–C11A	1.753(2)
Bond angles	
N3–Co1–S13	96.96(6)
N3A–Co1–S13A	98.64(6)
N3A–Co1–N3	113.69(8)
N3A–Co1–S13	119.95(6)
N3–Co1–S13A	119.40(6)
S13–Co1–S13A	109.56(4)
C11–N10–C2	126.0(2)
C2–N3–Co1	124.9(1)
N10–C11–S13	131.8(2)
N3–C2–N10	131.8(2)

Table 3
Selected bond lengths (Å) and angles (°)

	9	**10**
Bond lengths		
M1–N3	1.971(4)	1.981(6)
M1–N13	1.965(4)	1.935(6)
M1–N3A	1.971(4)	1.961(5)
M1–N13A	1.972(4)	1.983(6)
N3–C2	1.339(6)	1.344(8)
N13–C11	1.334(6)	1.302(9)
N10–C2	1.333(6)	1.309(9)
N10–C11	1.331(6)	1.339(9)
Bond angles		
N3–M1–N13	93.8(2)	94.4(3)
N3A–M1–N13A	92.5(1)	92.8(2)
N13A–M1–N3	112.7(2)	113.0(2)
N3A–M1–N13	112.2(2)	112.4(2)
N3A–M1–N3	127.6(1)	126.5(2)
C2–N3–M1	120.0(3)	117.7(4)
C11A–N13A–M1	124.9(3)	123.1(5)
C15A–N13A–M1	115.9(3)	116.3(4)
C2A–N3A–M1	120.4(3)	120.8(4)
C9A–N3A–M1	127.8(3)	129.5(4)
C8A–S1A–C2A	90.5(2)	89.9(3)

short contact between both sulfur atoms of 2.947 Å [15]; the proton is at N-3, and the S-methyl is pointing to the thione group. The bond lengths Co1–S13 2.260(1) and Co1–S13A 2.2768(9) of compound **5** are characteristic of covalent bonds and it is confirmed by the single bond character of S13–C11 [1.733(2) Å] and S13A–C11A [1.710(2)]. The bond lengths Co1–N3 and Co1–N3A are 1.988(2) and 1.980(2) Å, respectively [6]. Bond

Table 4
Selected bond lengths (Å) and angles (°)

	11	**12**
Bond lengths		
M1–N3	2.033(5)	2.041(2)
M1–Cl1	2.248(2)	2.258(1)
N3–C2	1.36(1)	1.326(4)
N10–C11	1.288(8)	1.282(4)
N10–C2	1.375(8)	1.366(4)
S12–C11	1.737(7)	1.758(3)
S12–C14	1.737(7)	1.804(5)
S13–C15	1.776(9)	1.783(5)
Bond angles		
N3–M1–Cl1	117.2(1)	116.9(1)
N3A–M1–Cl1	97.9(1)	97.7(1)
Cl1A–M1–Cl1	112.4(1)	112.5(1)
N3–M1–N3A	115.4(4)	116.3(1)
Cl1A–M1–Cl1	112.4(1)	112.5(5)
C2–N3–M1	120.3(4)	119.1(2)
C9–N3–M1	126.9(4)	128.3(2)
C11–N10–C2	127.1(5)	125.7(3)
N3–C2–S1	115.8(4)	114.5(2)
N10–C2–S1	124.0(5)	125.2(2)
N10–C11–S13	119.8(5)	120.5(3)
N10–C11–S12	123.7(5)	124.2(2)
S13–C11–S12	116.5(4)	115.3(2)

lengths N3–C2 1.323(3), N10–C2 1.357(3) and N10–C11 1.297(3) Å show that the latter has a stronger double character. The two different orientations for the S–CH_3 groups, one pointing to N10, another to S13A, could be explained by the intermolecular tricentric interaction of the sulfur atom S12A with H7B (2.884 Å)

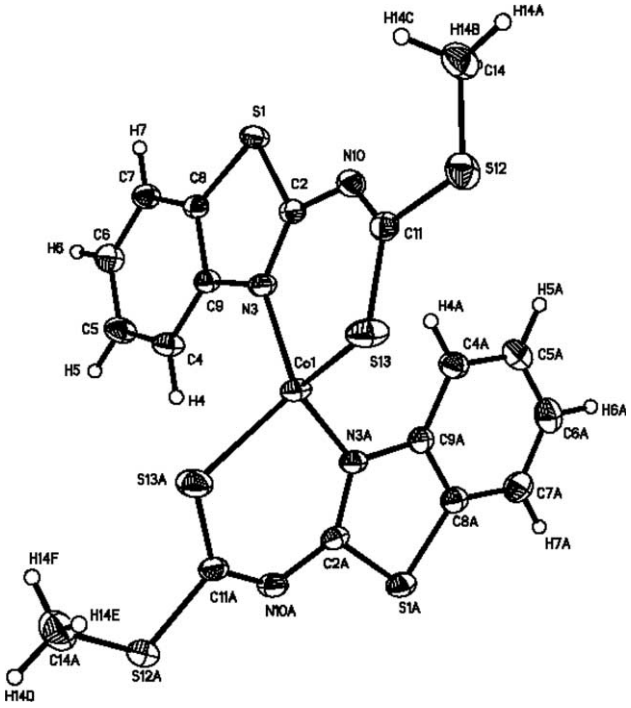

Fig. 1. Molecular structure of compound **5**.

and S1B [3.451 Å] [20]. The ligands are not completely orthogonal, the angle between the planes described by atoms N3–Co1–S13 and N3A–Co1–S13A is 83.54°, Fig. 2.

Compounds **7**–**10** were prepared from **2** and **3**, both ligands have in common a hydrogen bond between two nitrogen atoms forming a six membered ring [15] as it is known from their X-ray diffraction structures and is depicted in Scheme 2. The difference between the two ligands is that **2** has two N–H groups and in **3** one proton is substituted by a methyl group placed at S-12. The mass spectra of compounds **7**–**10** present the molecular ion which indicates the correct formula and the high stability of the compounds.

Compound **7** has a green color with a magnetic moment μ_{eff} of 4.9 BM and UV–Vis–NIR spectrum bands at 8684 and 17080 cm^{-1}, both data indicate a distorted geometry for **7**. The charge transfer band from the metal to the ligand was observed at 24408 cm^{-1} for **7** and at 26618 cm^{-1} for **8**. In compound **9**, the UV–Vis–NIR transitions correspond to distorted cobalt geometry [$^4A_2(F) \rightarrow {}^4T_1(F)$ and $^4A_2(F) \rightarrow {}^4T_1(P)$]. For compounds **9** and **10**, the charge transfer bands are 22818 and 25158 cm^{-1}, respectively.

The X-ray diffraction analyses for compounds **9** and **10**, Figs. 3 and 4, show that the two ligands are bonded to the metal ion by nitrogen atoms which have similar bond lengths in the range of 1.96–1.97 Å for Co–N and 1.93–2.0 Å for Zn–N.

The distorted geometry of the metal atoms is confirmed by the bite angles which for the cobalt compound are 93.8(2)° and 92.5(1)°, while for zinc they are 94.4(3)° and 92.8(2)°; these angles are far from the ideal tetrahedral values of 109° and from the value of 120° for a planar and unsaturated six membered ring. The bond lengths N3–C2, C2–N10, N10–C11, C11–N13 have an average value of 1.33 Å, indicating delocalized π-bonds through the six membered ring. It is noteworthy the unusual orange color of the tetrahedral compound **9** that is in contrast with the green color of compound **7**.

Compounds **11** and **12** were obtained from the reactions of ligand **4** with the cobalt and zinc chlorides, respectively. The metal ions are bonded to two chlorine atoms and to two ligands through the nitrogen atom of the thiazole. They have a C_2 symmetry. The

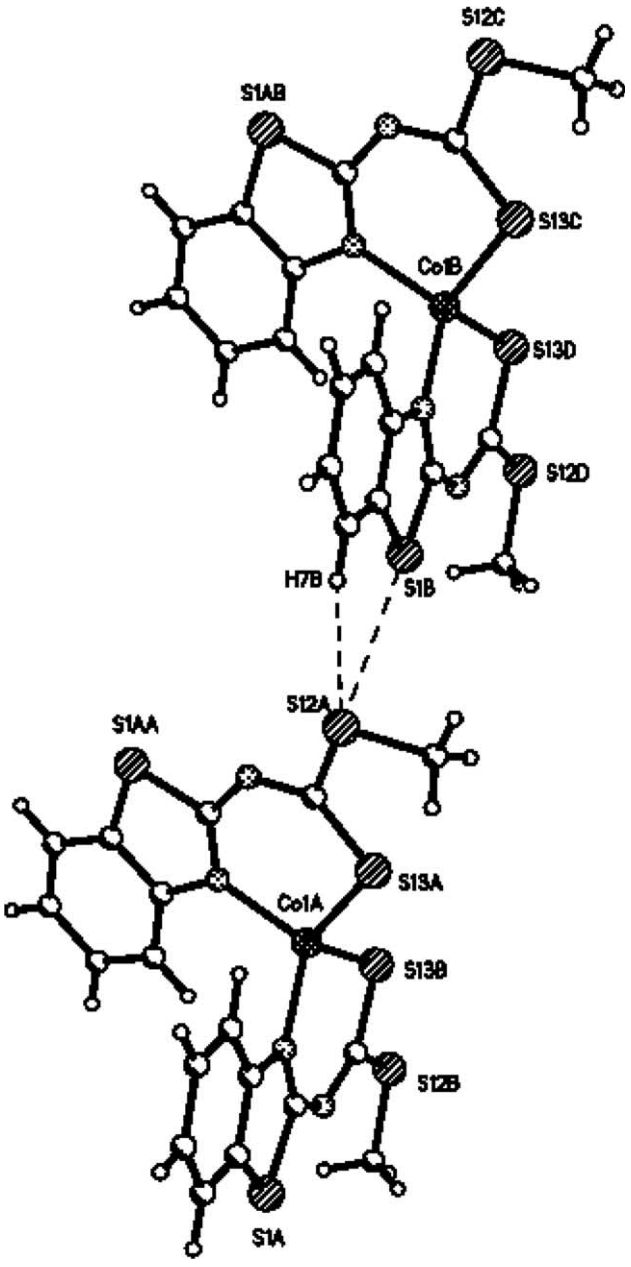

Fig. 2. Intermolecular interactions in compound **5**.

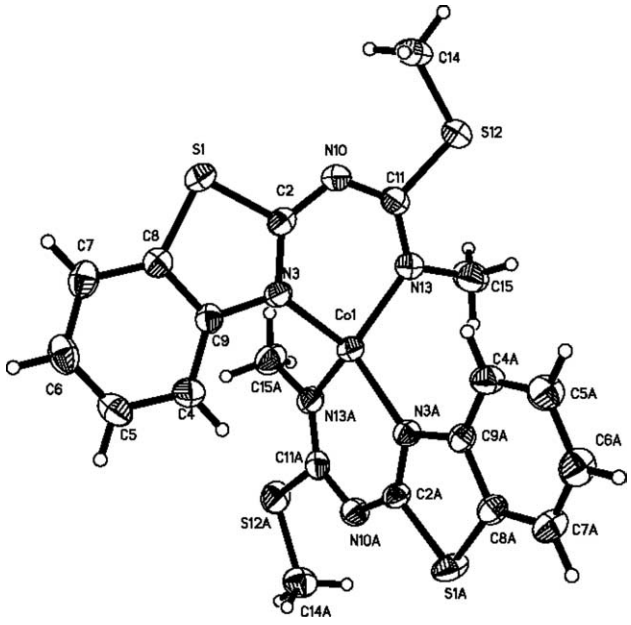

Fig. 3. Molecular structure of compound **9**.

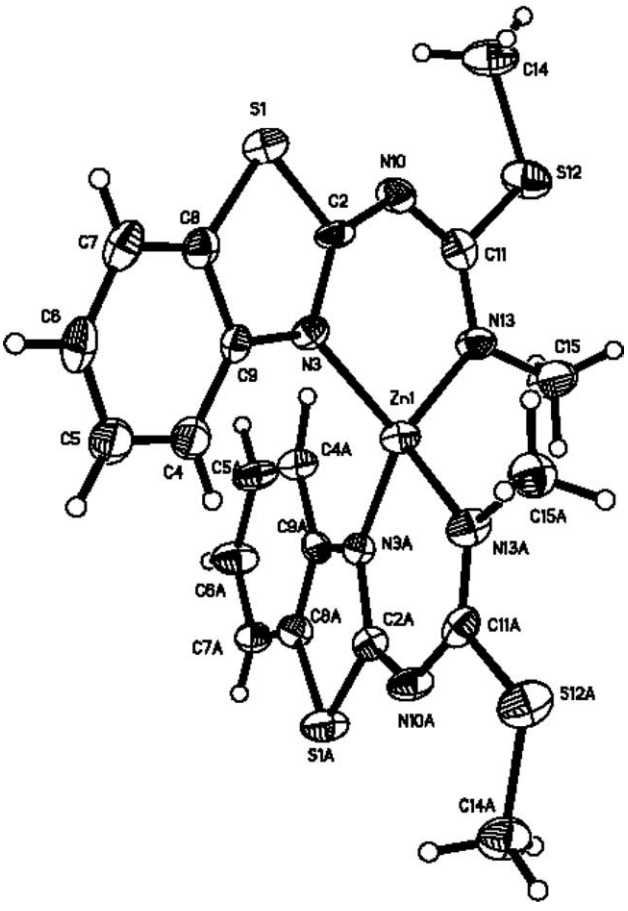

Fig. 4. Molecular structure of compound **10**.

UV–Vis–NIR spectrum bands for **11** are ν_2 7293 cm^{-1} [$^4A_2(F) \rightarrow {}^4T_1(F)$] and ν_3 16313 cm^{-1} [$^4A_2(F) \rightarrow {}^4T_1(P)$] and the value of the magnetic moment is $\mu_{eff} = 4.6$ BM. For **11** and **12**, the bands at 24271 and 25178 cm^{-1} are associated to the metal to ligand charge transfer for cobalt and zinc, respectively. Data are borderline between values for tetrahedral and octahedral geometries and are attributed to the distorted tetrahedral geometry and to the effect of the unsaturated six membered ring. The IR band for the vibration of the C=N bond of the thiazolic ring appears at ν 1514 cm^{-1}, a higher energy value with respect to the free ligand **4** (1510 cm^{-1}) [15], confirms the coordination.

X-ray diffraction analyses of compounds **11** and **12** show that they present the same structure, Figs. 5 and 6. The ligands are coordinated to the metal atom by the nitrogen of the thiazolic ring. It is interesting to observe that the preferred conformation of the free ligand with a short contact between one exocyclic sulfur and N-3 has changed in the complex, where one exocyclic sulfur is pointing to the sulfur of the ring. The ligands are in an *anti* arrangement and their arms are 34.7° (**11**) and 35.6° (**12**) out of the heterocycle plane. This fact indicates that electronic delocalization does not occur, and it is in agreement with the short bond lengths of C2–N3 and

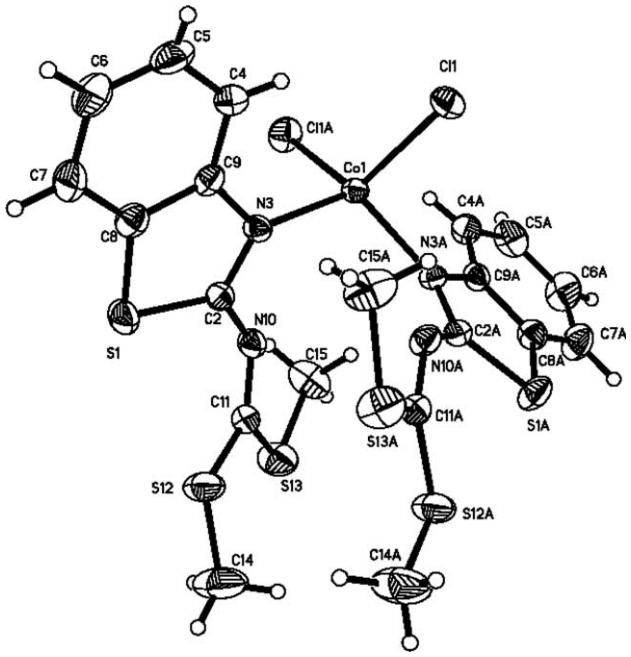

Fig. 5. Molecular structure of compound **11**.

C11–N10 which suggest a stronger double bond character (~1.28–1.32 Å) than those of C2–N10 (~1.37 Å).

Intramolecular interactions occur between H4 and Cl1, and H4a and Cl1A (2.977 Å). Each molecule has two intermolecular π-bonds between two S–CH protons and the double bond N3–C8 (H15B···N3 2.64; H15B···C8 2.63 Å for **11** and H15B···N3 2.58; H15B···C8 2.61 Å for **12**), Fig. 7.

Tricentric intermolecular short contacts are found between S1 and Cl (3.293 Å) and S1 and H7 (2.950 Å),

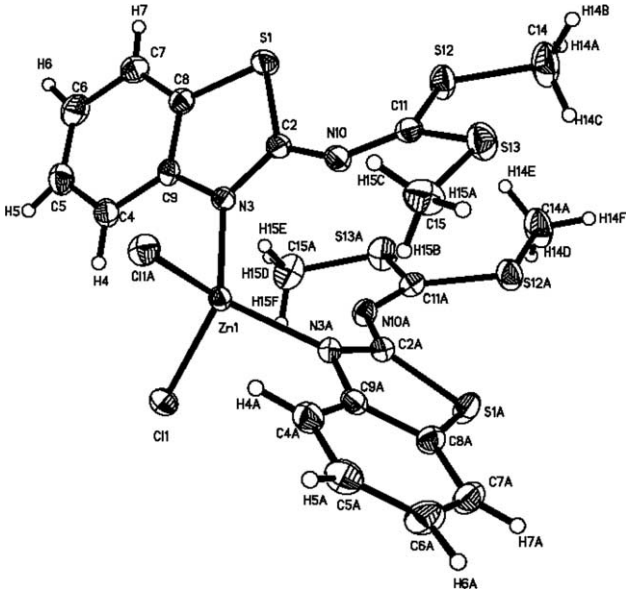

Fig. 6. Molecular structure of compound **12**.

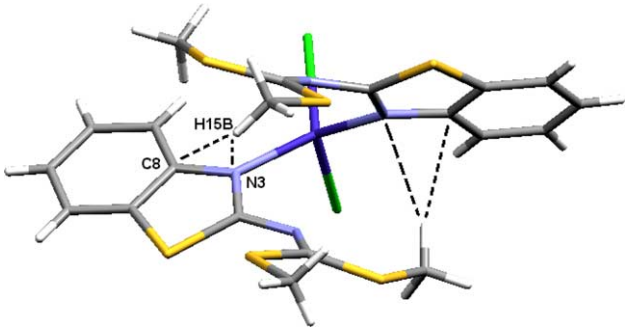

Fig. 7. H···π intramolecular contacts in compound **11**.

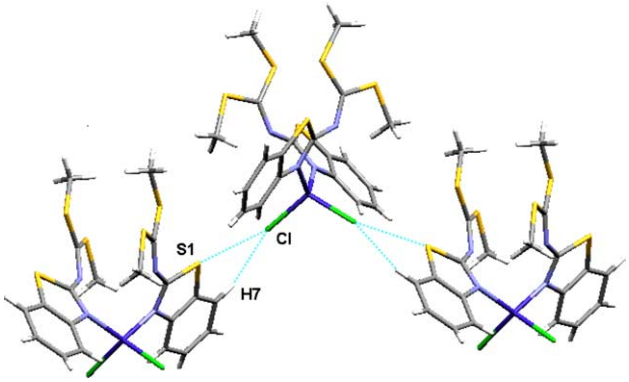

Fig. 8. Tricentric intermolecular short contacts between Cl and S1 and H7, in compound **11**.

Fig. 8. A similar structure was reported for a cobalt derivative of 2-uroylbenzimidazole [10].

4. Summary

New aromatic planar molecules bearing coordinative arms were investigated as ligands. These complex molecules are in equilibrium between different conformers and tautomers, and several coordinative sites of sulfur and nitrogen are possible. It was found that deprotonation of compounds **1**–**3** with the metallic acetate afforded metal spirocyclic molecules. The metal coordination gave planar tricyclic chelates, where the metal is part of six-membered rings. In two compounds sulfur metal covalent bonds were found together with nitrogen coordination. It was found that the cobalt is bonded to the ligands through four similar N–Co bonds indicating a resonance phenomenon which includes the ligand. The six membered rings have four similar C–N bonds for a delocalized unsaturated system. In compounds **5**–**10** the metal atom is tetracoordinated, but with a distorted geometry due to the rigidity of the planar ligands. Compound **4** behaves as a monodentate ligand through N3 and the conformation of the ligand changed in the coordination compound giving S···S intramolecular interactions.

5. Supplementary material

Crystallographic data of the structural analysis (excluding structure factors) have been deposited with the Cambridge Crystallographic Data Centre as supplementary publication numbers CCDC: 230556 (**5**), 230557 (**9**), 230558 (**10**), 230554 (**11**) and 230555 (**12**). Copies of this information may be obtained free of charge from The director, CCDC, 12 Union Road, Cambridge, CB2 1EZ, UK (fax: +44 1223-336-033; e-mail: deposit@ccdc.cam.ac.uk or www:http://www.ccdc.cam.ac.uk).

Acknowledgements

F.T. thanks for the CONACYT scholarship. Financial support by Conacyt (Grant 34714-E) and Cinvestav Mexico is acknowledged. We thank Professor Henrich Nöth for the X-ray data collection of compound **12**.

References

[1] Y. Tanabe, A. Kawai, Y. Yoshida, M. Ogura, H. Okamura, Heterocycles 45 (1997) 11579.
[2] Y. Katsura, S. Nishino, M. Ohno, K. Sakane, Y. Matsumoto, Ch. Morinaga, H. Ishikawa, H. Tagasugi, J. Med. Chem. 42 (1999) 2920.
[3] R.C. Schnur, A.F.J. Fliri, S. Kajiji, V.A. Pollack, J. Med. Chem. 34 (1991) 914.
[4] P. Jimonet, J. Med. Chem. 42 (1999) 2828.
[5] N. Barba-Behrens, A.M. Mutio-Rico, P. Joseph-Nathan, R. Contreras, Polyhedron 10 (1991) 1333.
[6] N. Barba-Behrens, A. Vázquez-Olmos, S.E. Castillo-Blum, R.M. Hernández, S. Meza-Höjer, G. Höjer, R. Vicente, A. Escuer, Transit. Metal Chem. 21 (1996) 31.
[7] N. Andrade-López, A. Ariza-Castolo, R. Contreras, A. Vázquez-Olmos, N. Barba-Behrens, H. Tlahuext, Heteroatom Chem. 8 (1997) 397.
[8] M.-P. Fialon, N. Andrade-López, N. Barba-Behrens, R. Contreras, Heteroatom Chem. 9 (1998) 637.
[9] N. Andrade-López, R. Cartas-Rosado, E. García-Baéz, R. Contreras, H. Tlahuext, Heteroatom Chem. 9 (1998) 399.
[10] M.-P. Fialon, E. García-Baéz, N. Andrade-López, G. Osorio-Monreal, G. Canseco Melchor, I. Velázquez-Montes, N. Barba-Behrens, R. Contreras, Heteroatom Chem. 10 (1999) 577.
[11] E. Quiróz-Castro, S. Bernès, N. Barba-Behrens, R. Tapia-Benavides, R. Contreras, H. Nöth, Polyhedron 19 (2000) 1479.
[12] A.E. Cisneros-Gómez, A. Ramos-Organillo, J. Hernández-Díaz, J. Nieto-Martínez, R. Contreras, S.E. Castillo-Blum, Heteroatom Chem. 11 (2000) 392.
[13] A. Cruz, M. Gayosso, R. Contreras, Heteroatom Chem. 12 (2001) 586.
[14] J.-M. Grevy, F. Téllez, S. Bernès, H. Nöth, N. Barba-Behrens, R. Contreras, Inorg. Chim. Acta 339 (2002) 532.
[15] F. Téllez, A. Cruz, H. López-Sandoval, I. Ramos-García, M. Gayosso, R.N. Castillo-Sierra, B. Paz-Michel, H. Nöth, A. Flores-Parra, R. Contreras, Eur. J. Org. Chem (2004) 4203.

[16] F. Merchán, J. Garín, E. Meléndez, Synthesis 7 (1982) 590.
[17] L.J. Farrugia, J. Appl. Cryst. 32 (1999) 837.
[18] G.M. Sheldrick, SHELX 97-2 Users Manual, University of Göttingen, Germany, 1997.
[19] N.N. Greenwood, A. Earnshaw, Chemistry of the Elements, Pergamon Press, Great Britain, 1986.
[20] M. Lanfranchi, A.M.M. Lanfredi, A. Tiripicchio, A. Monaci, F. Tarli, J. Chem Soc., Dalton Trans. (1980) 1893.

Available online at www.sciencedirect.com
SCIENCE DIRECT®
Polyhedron 23 (2004) 2491–2498
POLYHEDRON
www.elsevier.com/locate/poly

Synthesis, characterization and bioactivity of mixed-ligand Cu(II) complexes containing *S*-methyldithiocarbazate derivatives and saccharinate ligands and the X-ray crystal structure of the copper–saccharinate complex containing *S*-methyl-β-*N*-(6-methylpyrid-2-yl)methylenedithiocarbazate

Thahira B.S.A. Ravoof [a], Karen A. Crouse [a,*], M. Ibrahim M. Tahir [a], Andrew R. Cowley [b], M. Akbar Ali [c]

[a] *Department of Chemistry, Universiti Putra Malaysia, 43400 Serdang, Selangor, Malaysia*
[b] *Chemistry Research Laboratory, University of Oxford, Mansfield Road, Oxford OX1 3TA, UK*
[c] *Department of Chemistry, Universiti Brunei Daussalam, Jalan Tungku Link, BE1410, Brunei Darussalam*

Received 19 May 2004; accepted 9 August 2004
Available online 13 October 2004

Abstract

New mixed-ligand complexes of general empirical formula, [Cu(NNS)(sac)(H_2O)] (NNS′ = *S*-methyl-β-*N*-(6-methylpyrid-2-yl)methylenedithiocarbazate, NNS″ = *S*-methyl-β-*N*-(2-acetylpyrid-2-yl)methylenedithiocarbazate and NNS‴ = *S*-methyl-β-*N*-(2-benzoylpyrid-2-yl) methylenedithiocarbazate, sac = the saccharinate anion) have been synthesized by reacting $[Cu(sac)_2(H_2O)_4]\cdot 2H_2O$ with the appropriate ligands in water–ethanol mixtures and characterized by elemental analysis and conductance, magnetic, IR and electronic spectroscopic measurements. Magnetic and spectral evidence support a five-coordinate geometry for the complexes in which the Schiff bases coordinate as NNS tridentate ligands and the saccharinate anion coordinates as a unidentate N-donor ligand. An X-ray crystallographic structural analysis of [Cu(NNS′)(sac)(H_2O)] shows that the complex has a distorted square-pyramidal structure in which the Schiff base is coordinated to the copper ion as a tridentate NNS chelating agent via the pyridine nitrogen atom, the azomethine nitrogen atom and the thiolate sulfur atom, the fourth and fifth coordination positions of the five-coordinate Cu(II) ion being occupied by the imino nitrogen of the saccharinate anion and oxygen atom of the aqua ligand. The complexes have been evaluated for their biological activities against eight pathogenic microbials and human T-lymphoblastic leukemia cell lines. The complexes exhibit marked cytotoxicity against leukemic cell lines and display moderate activity against pathogenic bacteria and fungi.
© 2004 Published by Elsevier Ltd.

Keywords: Cu(II) complexes; Dithiocarbazate Schiff base; Saccharin complexes; *S*-Methyldithiocarbazate; Tridentate NNS Schiff base

1. Introduction

Saccharin (also known as *o*-sulfobenzoimide) is a polyfunctional ligand [1]. It has a low solubility in most organic solvents but its sodium salt is soluble in these solvents [2]. The sodium salt of saccharin is a synthetic sweetening agent and is commonly used as a sugar substitute in order to reduce caloric intake in the diet and this is of significant use in industry today due to the increased demand of dietary products [3,4]. The chemistry of saccharin had attracted attention in years past as

* Corresponding author. Tel.: +603 8946 6788; fax: +603 8943 5380.
E-mail address: crouse@pc.jaring.my (K.A. Crouse).

0277-5387/$ - see front matter © 2004 Published by Elsevier Ltd.
doi:10.1016/j.poly.2004.08.005

preliminary studies showed that saccharin implanted into the bladders of mice caused urinary bladder carcinomas [5]. The ban that was consequently imposed on saccharin was lifted by the FDA in 1991 when further studies failed to form any conclusive evidence that it was a carcinogen [6].

Reports on the ability of saccharin to act as an inhibitor for certain enzyme reactions have been published [6]. Saccharin complexes have also been reported to have superoxide dismutase-like behaviour (SOD) and the SOD activity of the saccharinate complexes of manganese, iron, cobalt, nickel, copper and zinc have been investigated [7,8].

The structural formula of the saccharinate anion and some of its modes of coordination with metal ions are given in Fig. 1. The saccharinate anion may coordinate to metals through the N, the carbonyl O or both, as shown below [9].

Coordination by N is most commonly observed in complexes of general formula, $[M(C_7H_4SO_3N)_2(H_2O)_4]\cdot 2H_2O$, where M is a first-row transition metal. In these complexes, the saccharinate anions adopt a centrosymmetric arrangement in an octahedral environment [9].

In an attempt to better understand the anticancer properties of Cu(II) complexes of 2-formylpyridinthiosemicarbazone (HL), two saccharin complexes of formula, $[CuL\text{-}(sac)(H_2O)]\cdot 0.5H_2O$ and $[CuL(bipy)(sac)]\cdot 2H_2O$ were synthesized by Ainscough et al. [10]. X-ray crystallographic structure determinations showed that the coordination geometries around the Cu(II) ion varied significantly where the saccharinate anion was coordinated to the central metal ion in one case and not in the other.

As part of our ongoing study of metal complexes of dithiocarbazate derivatives, we report herein the synthesis, characterization and bioactivity of some mixed-ligand ternary Cu(II) complexes of three NNS donor ligands formed by condensation of *S*-methyldithiocarbazate (SMDTC) with 2-acetylpyridine, 2-benzoylpyridine and 6-methyl pyridine-2-aldehyde with the saccharinate anion and water as co-ligands. Since very little work has been reported on metal-saccharinate complexes, the present work is expected to shed some light on the coordination properties of this industrially important sweetener.

2. Experimental

All chemicals and solvents were of analytical grade and were used as received.

2.1. Preparation of the Schiff bases

These were prepared following published procedures [11–13].

2.2. General method of synthesis of $[Cu(sac)_2(H_2O)_4]\cdot 2H_2O$

$[Cu(CH_3COO)_2]\cdot H_2O$ (2.01 g, 0.01 mol) dissolved in boiling water (25 ml) was mixed with a solution of sodium saccharinate monohydrate (4.46 g; 0.02 mol) in water (25 ml) and the mixture heated for 15 minutes to reduce the volume to ca. 30 ml. On standing overnight, the resulting blue solution yielded blue crystals of the $[Cu(sac)_2(H_2O)_4]\cdot 2H_2O$ complex which were filtered off, washed with cold ethanol and dried in a desiccator over anhydrous silica gel. Yield: ca. 90%.

2.3. General method of synthesis of the complexes

$[Cu(sac)_2(H_2O)_4]\cdot 2H_2O$ [2] (0.536 g, 0.001 mol) dissolved in boiling water (25 ml) was mixed with a solution of the appropriate Schiff base (0.001 mol) in ethanol (40 ml) and the resulting mixture was heated on a water bath for 30 minutes. On standing overnight, the mixture yielded crystalline complexes which were filtered off, washed with ethanol and dried in a desiccator over anhydrous silica gel, overnight. Yield: ca. 75%. Crystals of $[Cu(NNS')(sac)(H_2O)]$ suitable for X-ray diffraction analysis were obtained from acetonitrile solution. Some analytical, physical and spectral data on the complexes can be found in Tables 1 and 2.

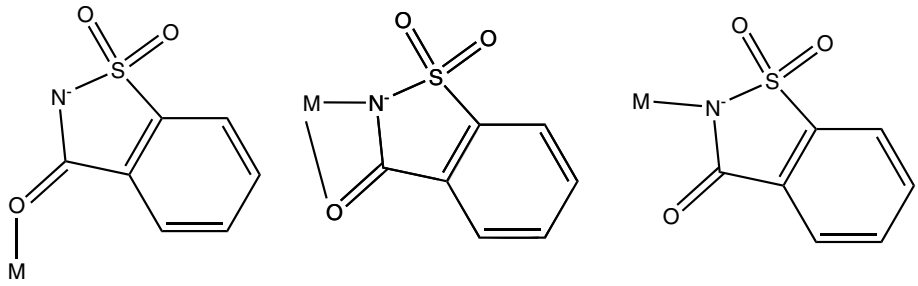

Fig. 1. Different coordination modes of the saccharinate anion.

Table 1
Analytical data and physical properties of the Cu(II) complexes

Compound[a]	Colour	m.p. (°C)	Λ[b]	μ[c]	Analytical data[d] (%)				
					C	H	N	S	Cu
[Cu(NNS′)(sac)(H_2O)]	Green	186.5	0.451	1.59	39.14 (39.38)	3.29 (3.30)	11.74 (11.45)	19.51 (19.66)	12.94 (12.99)
[Cu(NNS″)(sac)(H_2O)]	Green	234	14.91	1.70	39.36 (39.38)	3.17 (3.30)	11.68 (11.48)	20.05 (19.71)	12.94 (13.02)
[Cu(NNS‴)(sac)(H_2O)]	Dark green	246	14.21	1.65	45.31 (45.85)	3.11 (3.30)	10.21 (10.18)	17.73 (17.49)	11.74 (11.55)

[a] NNS′ = *S*-methyl-β-*N*-(6-methylpyrid-2-yl)methylene dithiocarbazate, NNS″ = *S*-methyl-β-*N*-(2-acetylpyrid-2-yl)methylene dithiocarbazate and NNS‴ = *S*-methyl-β-*N*-(2-benzoylpyrid-2-yl)methylene dithiocarbazate.
[b] Molar conductance ($\Omega^{-1}cm^2mol^{-1}$) of ca. 10^{-3} M solutions in DMSO.
[c] Magnetic moments at 298 K.
[d] Calculated values are given in parentheses.

Table 2
Selected IR bands and electronic spectral data for the ligands and their Cu(II)–saccharinate complexes

Compound	IR bands (cm^{-1})[b]							Electronic spectra (in DMSO)[a]
	*ν*NH	*ν*CN	*ν*NN	*ν*CSS	ν_sSO_2	$\nu_{as}SO_2$	*ν*CO	λ_{max} (log ϵ)[c]
HNNS′	3085m	1584s 2917m	1060s	950s				340(5.0)
HNNS″	3150s	1578s 2912s	1062s	950s				337(4.5)
HNNS‴	3050s 2914br	1578s	1050s	948s				354(4.5)
[Cu(NNS′)-(sac)(H_2O)]		1560s	1091s	959s	1154s	1300vs	1641s	690(3.4), 416(4.6)
[Cu(NNS″)-(sac)(H_2O)]		1548s	1088s	952s	1156s	1302vs	1640s	644(2.3), 400(3.9) 326(1.5)
[Cu(NNS‴)-(sac)(H_2O)]		1556s	1062s	966s	1152s	1290vs	1654s	643(2.3) 422(4.0) 336(4.2)

[a] log ϵ (litre $mol^{-1}cm^{-1}$) are given in parentheses.
[b] Wavenumbers are in units of cm^{-1}.
[c] Units of λ_{max} are in nm and units of log ϵ are in L mol^{-1} cm^{-1}.

2.4. Physical measurements

The analyses for carbon, hydrogen, nitrogen and sulfur were carried out using a LECO CHNS-932 instrument. The IR spectra in KBr pellets were recorded on a Perkin–Elmer FT IR 1750X spectrophotometer (4000–400 cm^{-1}). Metal determinations were carried out using a Perkin–Elmer Plasma 1000 Emission Spectrometer. The molar conductance of 10^{-3} M solutions of the metal complexes in DMSO were measured at 29 °C using a Jenway 4310 conductivity meter and a dip-type cell with a platinized electrode. Magnetic susceptibilities at room temperature were measured using a Sherwood Scientific MSB-AUTO magnetic susceptibility balance. The UV–Vis spectra were run on a Shimadzu UV- 2501 PC Recording Spectrophotometer (1000–200 nm).

2.5. X-ray structure determination of [Cu(NNS′)(sac)(H_2O)]

Beautiful dark green crystals of the metal complex were formed after the acetonitrile solution was allowed to slowly evaporate over a few weeks. A dark-green platy single crystal was selected and mounted on a glass fibre using perfluropolyether oil and cooled rapidly to 150 K in a stream of cold N_2 using Oxford Cryosystems CROSTREAM unit. Diffraction data were measured using an Enraf–Nonius Kappa CCD diffractometer (graphite-monochromated Mo Kα radiation, $\lambda = 0.71073$Å). Intensity data were processed using the DENZO-SMN package [14]. The crystal was found to be monoclinic with $a = 14.2347(2)$ Å, $b = 10.7154(2)$ Å, $c = 14.2428(2)$ Å and $\beta = 119.14(1)°$. The structure was solved in the space group $P2_1/n$ using the direct-methods program SIR92 [14] which located all non-hydrogen atoms. Subsequent full-matrix least-squares refinement on F was carried out using CRYSTALS Program Suite [15]. Coordinates and anisotropic thermal parameters of all non-hydrogen atoms were refined. Hydrogen atoms were positioned geometrically after each cycle of refinement. A five-term Chebychev polynomial weighting scheme was applied. Refinement converged satisfactorily to give $R = 0.036$ and $R_w = 0.033$ with residual electron density minimum and maxima of −0.47 and 1.26

e Å^{-3}. Further crystallographic and refinement details are shown in Table 1.

2.6. Bioactivity

2.6.1. Target microorganisms

Eight pathogenic microbials were used to test the biological potential of the complexes. They were Methicillin resistant *staphylococcus* (MRSA), *Bacillus subtilis* wild type (B29), *Subtilis mutant* (mutant defective DNA repair, B28), *Pseudomonas aeruginosa* (60690), *Candida albicans* (C.A.), *Aspergillus ochraceous* (398), *Saccaromyces ceciricaee* (20341) and *Candida lypolytica* (2075).The source of microbes and culture maintenance were as previously described [19].

2.6.2. Qualitative antimicrobial assay

Antimicrobial activity of each sample was qualitatively determined by a modified disc diffusion method [16] as previously detailed [17]. A lawn of microorganisms was prepared by pipetting and evenly spreading inoculum (10^{-4} cm^{-3}), adjusted turbidometrically to 10^5–10^6 cfu cm^{-3} (cfu: colony forming units) on to agar set in Petri dishes, using Nutrient agar (NA) for the bacteria and potato dextrose agar (PDA) for fungi. Whatman No. 1 filter paper discs of 6 mm diameter were impregnated with stock solution of the compound (100 mg cm^{-3}) and dried under sterile conditions. The dried discs were then placed on the previously inoculated agar surface. The plates were inverted and incubated for 24 h at 30 °C for bacteria and 37 °C for fungi. Antimicrobial activity was indicated by the presence of clear inhibition zones around the discs. Commercially available streptomycin (Sigma, USA) was used for the antibacterial control while nystatin (Sigma, USA) was used as the antifungal control.

2.6.3. Quantitative antimicrobial assay

Compounds that showed positive (diameter > 15 mm) anti-microbial inhibition with the disc diffusion assay were subjected to the broth dilution method for the quantitative measurement of microbiostatic (inhibitory) activity as described by Hufford and Clark [18]. The lowest concentration that completely inhibited visible microbial growth was recorded as the minimum inhibitory concentration (MIC, μg, cm^{-3}). Streptomycin and nystatin were used as controls for bacteria and fungi, respectively.

2.6.4. Cytotoxic assay

The HL-60 (human T-lymphoblastic leukemia) cell line was obtained from the National Cancer Institute, U.S.A. The cells were cultured in RPMI-1640 (Sigma) medium supplemented with 10% fetal calf serum, Cytotoxicity was determined using the microtitration of 3-(4, 5-dimethylthiazol-2-yl)-2,5-diphenyltetrazolium bromide (MTT) assay (Sigma, USA) as reported by Mosmann [19]. Controls that contained only cells were included for each sample. Cytotoxicity was expressed as CD_{50}, i.e. the concentration that reduced the absorbance of treated cells by 50% with reference to the control (untreated cells). Doxorubicin and Tamoxifen were used as standard cytotoxins.

3. Results and discussion

The physical and analytical data for the Cu(II) complexes are shown in Table 1. The analytical data agree well with the proposed formulations of the complexes. The complexes are soluble in most organic solvents and appear stable in air. The physical and analytical data for the three Schiff bases used in this work have previously been reported by Akbar Ali et al. [12] and Hossain et al. [13].

3.1. Magnetic and conductivity data

The complexes exhibit room temperature magnetic moments in the 1.6–1.7 B.M. range. Although these values are slightly lower than that expected for a $3d^9$ metal ion (Table 1) [20], they, nevertheless, indicate that the complexes contain the Cu(II) ions. The molar conductance values of the complexes in DMSO (Table 1) fall in the range of 0.45–15 Ω^{-1} cm^2 mol^{-1} indicating that they are essentially non-electrolytes in DMSO. Although some dissociation of the complexes seems to occur, the conductance values are much lower than that expected for a 1:1 electrolytes in this solvent. The conductivity data, therefore, indicate that both the saccharinate anion and the Schiff bases are coordinated to the Cu(II) ion as uninegatively charged ligands [21].

3.2. Electronic and Infrared spectra

The electronic spectra of the complexes in DMSO (Table 2) exhibit an intra-ligand $n \rightarrow \pi^*$ band in the 336–326 nm range, a S → Cu(II) charge transfer band in the 420–450 nm range and a d–d band in the 640–690 nm range. The presence of a S → Cu(II) LMCT band at ca. 420 nm in the spectra of the metal complexes is indicative of the coordination of the Schiff base to the Cu(II) ion via the thiolate sulfur atom [22]. Such LMCT bands are common in the electronic spectra of five-coordinate Cu(II) complexes of related tridentate NNS thiosemicarbazone ligands [23,24]. The presence of a d-d band at ca. 640 nm is consistent with a five-coordinate geometry since such a band has also been observed in the electronic spectrum of the related five-coordinate [Cu(Ap-SBz)NO_3] complex (Ap-SBz is the anionic form of the 2-acetylpyridine Schiff base of S-benzyl-

dithiocarbazate), the structure of which has been established by X-ray diffraction [25].

The IR spectra of the ligands (Table 2) exhibit the ν(C=N), ν(N–N) and (CS) bands at ca. 1580, 1050–1100 and 800–900 cm^{-1}, respectively, which are shifted in the spectra of the complexes, indicating coordination of the ligands to the metal ions via the azomethine nitrogen and the thiolate sulfur atoms. The coordination of the azomethine nitrogen to the Cu(II) ion is indicated by the shift of the ν(C=N) band to lower frequencies along with the occurrence of the ν(N–N) band at higher frequencies. The lowering of the ν(C=N) band is due to the lowering of the C=N bond order as a result of the M–N bond formation. The ν(N–N) bands of all the free ligands were shifted to higher wavenumbers on complexation as a result of a reduction in the repulsion between the lone pairs of electrons on the nitrogen atoms due to coordination via the azomethine nitrogen atom [26]. The splitting of the ν(CSS) band of the free ligands at ca. 950 cm^{-1} in the spectra of the Cu(II) complexes indicates coordination through one of the sulfur atoms. The pyridine ring deformation modes of the free ligands at ca. 600 cm^{-1} are lowered in the spectra of the complexes indicating coordination of the pyridine ring nitrogen atom to the Cu (II) ion. The spectra of the complexes do not exhibit the ν(NH) bands of the free ligands indicating deprotonation of the ligands during coordination to the Cu(II) ion. The IR spectra of the complexes also show the $\nu(SO_2)$ symmetric, $\nu(SO_2)$ asymmetric and ν(C=O) bands of the sac anion at ca. 1150, 1290 and 1640 cm^{-1} [27–29], respectively, confiming the presence of the saccharinate anion in the complexes [17].

3.3. X-ray crystal structure of the Cu(NNS′)(sac)(H_2O)] complex

The ORTEP diagram of the [Cu(NNS′)(sac)(H_2O)] molecule, with the atom numbering scheme is shown in Fig. 2. Selected bond lengths and bond angles are given in Tables 3 and 4. The complex crystallizes as a five-coordinate monomeric species. The structure shows that the complex has a water molecule bonded to the central Cu(II) atom. As inferred by the physicochemical results, the Cu(II) ion has a five-coordinate geometry with the donor atoms of the Schiff base being the pyridyl nitrogen atom, the azomethine nitrogen atom and the mercapto-sulfur atom. The nitrogen from the saccharinate anion and oxygen from the water molecule occupy the fourth and fifth coordination positions of the five-coordinate Cu(II) ion. The Schiff base is coordinated to the Cu(II) ion in its deprotonated iminothiolate form. This form results in delocalisation of the negative charge caused by the deprotonation of the NH proton. The delocalisation is observed in the C–*N*–*N*–C chain as is evident in the interatomic bond distances, C108–N109 [1.290(4) Å], N109–N110 [1.376(3) Å] and C111– N110 [1.318(4) Å]. The C111–S112 bond retains its partial double bond character as its length [1.713(3) Å] is between that of a C–S single bond [1.82 Å] and a C=S double bond [1.62 Å]. It is, however, longer than that found in free methylpyruvate Schiff base of *S*-methyldithiocarbazate [1.652(6) Å] [30] and pyridine-2-carboxaldehydethiosemicarbazone [1.698(3) Å] [31]. The lengthening of the C111–S112 bond in the complex is attributed to the enethiolisation process that occurs when the Schiff base coordinates to the Cu(II) ion. The C–S bond length in the present complex is however close to that found in the [Cu(pysme)(sac)(MeOH)] complex (pysme = *S*-methyl-β-*N*-(pyridine-2-yl)methylenedithiocarbazate) [21]. Other bond lengths, Cu–S [2.3043(8) Å], Cu–N (azomethine) [1.973(2) Å] and Cu–N (py) [2.113(2) Å], are similar to those observed in analogous five-coordinate square-pyramidal Cu(II) complexes (Table 5). Also apparent from the data given in Table 5 is the variation in Cu–N (sac) bond distances of different geometries around the central Cu(II)ion.

Since the Cu(II) ion in [Cu(NNS′)(sac)(H_2O)] is five-coordinate, it can adopt either a square-pyramidal or a trigonal-bipyramidal structure. To determine the more likely structure, the formula of Addison et al.

Table 3
Crystallographic data and structure refinement details for [Cu(NNS′)(sac)(H_2O)]

Empirical formula	$C_{16}H_{14}CuN_4O_4S_3$
Formula weight	486.06
Temperature (K)	150
Wavelength (Å)	0.71073
Crystal system	monoclinic
Space group	$P2_1/n$
Unit cell dimensions	
a (Å)	14.2347(2)
b (Å)	10.7154(2)
c (Å)	14.2428(2)
α (°)	90
β (°)	119.149(1)
γ (°)	90
Volume (A^3)	1897.32(5)
Z	4
ρ_{calc} (g cm^{-3})	1.701
Absorption coefficient (mm^{-1})	1.513
F(000)	988
Crystal size (mm)	$0.04 \times 0.14 \times 0.22$
θ Range for data collection (°)	5–27
Limiting indices	$-18 \leqslant h \leqslant 18$ $-13 \leqslant k \leqslant 13$ $-18 \leqslant l \leqslant 18$
Reflections collected/unique	8570/4323 (R_{int} = 0.0002)
Maximum and minimum transmission	0.94, 0.81
Data/restraints/parameters	3050/0/253
Goodness-of-fit on F^2	1.100
Minimum and maximum residual electron density (e $Å^{-3}$)	−0.47 and 1.26
R,R_w	0.036, 0.033
S	1.0999

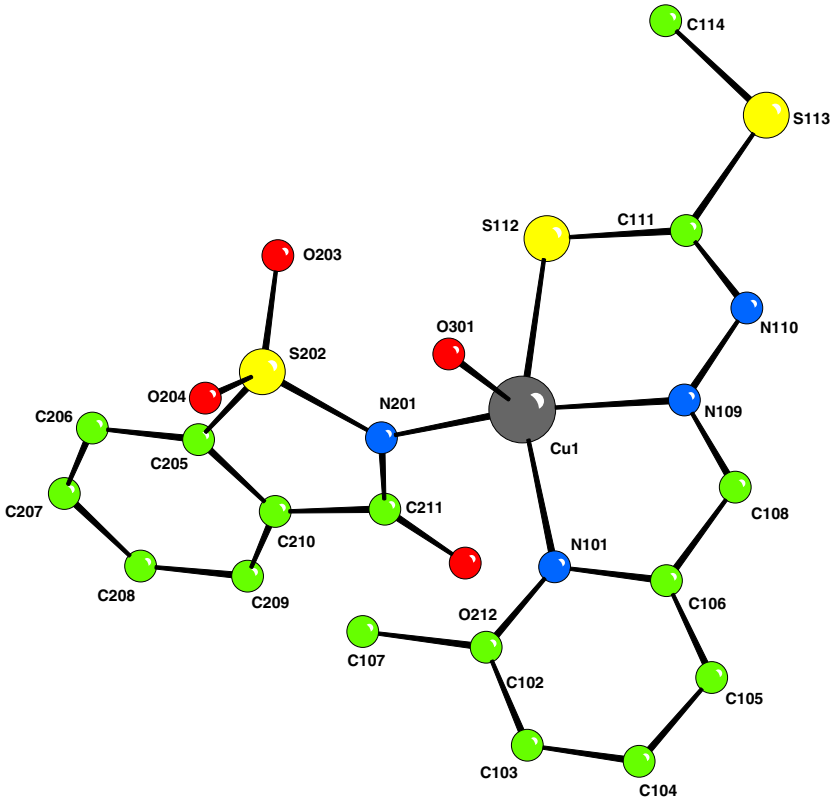

Fig. 2. ORTEP diagram of $C_{16}H_{14}N_4S_3O_4Cu$ (with 50% probability displacement ellipsoids) with atomic numbering scheme.

Table 4
Selected bond lengths (Å) and bond angles for Cu(NNS′)(sac)(H_2O)]

Bond lengths (Å)		Bond angles (°)	
Cu1–O301	2.199(2)	O301–Cu1–S112	98.63(6)
Cu1–N101	2.113(2)	N101–Cu1–S112	161.87(7)
Cu1–N109	1.973(2)	N201–Cu1–S112	92.54(7)
Cu1–S112	2.3043(8)	N109–Cu1–S112	82.74(7)
Cu1–N201	2.004(2)	N101–Cu1–O301	89.81(8)
		N201–Cu1–O301	98.51(9)
		N109–Cu1–O301	105.71(9)
		N201–Cu1–N101	102.11(9)
		N109–Cu1–N101	79.5(1)
		N109–Cu1–N201	155.7(1)

$\tau = (\beta - \alpha)/60 * 100\%$, where β is the larger of the two largest angles subtended at the copper atom, was used [32]. An ideal square pyramid will have $\beta = 180°$ and $\alpha = 180°$ and therefore $\tau = 0\%$, but an ideal trigonal-bipyramidal structure will have $\beta = 180°$ and $\alpha = 120°$ and therefore $\tau = 100\%$. In the current case, the calculated τ of 10.3% is close to that expected for the square-pyramidal structure. However, an examination of the bond angles given in Table 4 leads us to expect a distorted geometry since there is deviation from the ideal values, with the exception of the values for the N101–Cu1–O301 and N201–Cu1–S112 angles. Distor-

Table 5
Comparison of bond lengths (in Å) in some Cu(II) saccharinate complexes

Compound[a]	Cu–N_{sac}	Cu–S	Cu–N_{py}	Cu–N_{azo}	Cu–O_{sac}	Ref.
[Cu(pytsc)(sac)(H_2O)] · 0.5 H_2O	1.974(8)	2.264(3)	2.020(8)	1.956(8)		[10]
[Cu(pysme)(sac)(MeOH)]	1.967(2)	2.295(9)	2.062(2)	1.958(2)		[21]
[Cu(NNS′)(sac)(H_2O)]	2.004(2)	2.3043(8)	2.113(2)	1.973(2)		This work
[Cu(sac)$_2$(mpy)$_2$]	2.335(15)		1.9667(13)			[35]
[Cu(sac)(NH_3)$_4$]					2.113(8)	[36]
[Cu(sac)(PPh_3)$_2$] · CH_2Cl_2	1.933(2)				2.130(2)	[36]
[Cu(sac)(PPh_3)$_2$] · 3/4 $CHCl_3$	1.965(5)					[36]
[Cu(sac)(NH_3)$_4$] · sac · H_2O	2.328(2)				2.715(2)	[36]
	2.309(2)				2.705(3)	[36]
trans-[Cu(sac)$_2$(NH_3)$_4$]	2.508(12)		2.07(12)			[36]
			2.042(12)			
[Cu(sac)$_2$ (H_2O)$_4$] · 2H_2O	2.061(2)					[2]

[a] pytsc = pyridine-2-aldehydethiosemicarbazone, pysme = pyridine-2-aldehyde SMDTC, mpy = 2-pyridylmethanol.

Table 6
Qualitative antimicrobial assay results[a] (diameter in mm)

Compound	MRSA	B29	60690	S-T	C.A	398	20341
[Cu(NNS′)(sac)(H_2O)]	17	17	15	13	14	20	19
[Cu(NNS″)(sac)(H_2O)]	22	23	24	20	20	15	14
[Cu(NNS‴)(sac)(H_2O)]	18	15	15	15	15	13	14
Streptomysin (antibacterial control)	31	30	30	30			
Nystatin (antifungal control)					21	25	24

Methicillin resistant staphylococcus (MRSA); *Bacillus subtilis wild type* (B29), *P. aeruginosa* (60690); *S. typhimurium* (S-T), *C. albicans* (C.A), *A. ochraceous* (398), *S. ceciricaee* (20341).

[a] Diameter of 15 mm and above is considered active.

Table 7
Quantitative antimicrobial assay results[a] (MIC value μg ml^{-3})[b]

Compound	MRSA	B29	60690	S-T	C.A	P.A	20341
[Cu(NNS′)(sac)(H_2O)]	3125	25000					
[[Cu(NNS″)(sac)(H_2O)]	3125	25000	3125	6250	6250	12500	12500
[Cu(NNS‴)(sac)(H_2O)]	6250	25000		25000	12500	12500	
Streptomysin (antibacterial control)	12.2	48.8	12.2				
Nystatin (antifungal control)					3125	3125	6250

[a] *Methicillin resistant staphylococcus* (MRSA); *Bacillus subtilis wild type* (B29), *P. aeruginosa* (60690); *S. typhimurium* (S-T), *C. albicans* (C.A), *P. aspergillus* (P.A), *S. cerevisiae* (20341).

[b] MIC (μg ml^{-3}) = minimum inhibitory concentration, i.e the lowest concentration to completely inhibit microbial growth.

tion from the ideal square-pyramidal geometry can be attributed to the restricted bite angles of the deprotonated tridentate Schiff base ligand.

3.4. Biological activity

3.4.1. Antimicrobial activities

The three Cu(II) complexes are moderately active (inhibitory zones > 15 mm) against all eight bacteria and fungi assayed (Table 6). The values are, however, lower than those observed for both *S*-methyldithiocarbazate and S-benzyldithiocarbazate [33]. The [Cu(NNS″)(sac)(H_2O)] complex shows a higher activity towards the bacteria and fungi than the other two complexes. [Cu(NNS′)(sac)(H_2O)] was completely inactive towards all fungi assayed as compared to the other two complexes. The quantitative assays gave MIC values in the region 3125–25 000 μg ml^{-3} (Table 7).

3.4.2. Cytotoxic activities

When tested against the HL60 cell line (human T-lymphoblastic leukemic cells), all the three Cu(II) complexes exhibited marked activity with CD_{50}(μg cm^{-3}) value of 0.25. This is in contrast with S-benzyldithiocarbazate from which these Schiff bases are derived [34] and also the free salt $CuCl_2 \cdot 2H_2O$ which are inactive. CD_{50} is the cytotoxic dose at 50%, i.e. the concentration required to reduce growth of cancer cells by 50%. CD_{50} values <5.0 μg cm^{-3} indicate that the complex is strongly active whereas CD_{50} values of 5.0–10.0, 10.0–25.0 and >25.0 μg cm^{-3} indicate that the complex is moderately active, weakly active and inactive, respectively. The CD_{50} values for the standards, Doxorubicin and Tamoxifen were 0.1 and 36.0 μg cm^{-3}, respectively.

4. Conclusion

The reaction of $Cu(sac)_2(H_2O)_4] \cdot 2H_2O$ with the tridentate Schiff bases derived from *S*-methyldithiocarbazate and heterocyclic ketones in a methanol–water mixture produces crystalline green complexes in high yields. These were found to be mixed-ligand ternary Cu(II) complexes containing the saccharinate anion, the tridentate NNS^- Schiff base and water as ligands. The complexes display strong cytotoxic activity against the leukemic HL60 cell lines. An X-ray crystal structure determination of [Cu(NNS′)(sac)(H_2O)] shows that it has a five coordinate distorted square pyramidal geometry. In view of the similarity of the IR and electronic spectra of [Cu(NNS″)(sac)(H_2O)] and [Cu(NNS‴)(sac)(H_2O)] with that of [Cu(NNS′)(sac)(H_2O)] it is indeed most expected that the former two complexes also have a distorted square-pyramidal geometry.

5. Supplementary data

Crystallographic data for the structural analysis have been deposited with the Cambridge Crystallographic Data Centre, CCDC No. 237550. A copy of this

information may be obtained free of charge from The Director, CCDC, 12 Union Road, Cambridge, Cb2 1EZ, UK (fax: +44 1223 336033; email: deposit@ccdc.cam.ac.uk or http://www.ccdc.ac.uk).

Acknowledgements

We thank the Department of Chemistry and the Laboratory of Molecular and Cell Biology, Institute of Biosciences, Universiti Putra Malaysia, for the provision of laboratory facilities and University of Oxford for providing X-ray crystallographic services. The research was funded by a grant from the Ministry of Science and Environment, Malaysia, under the Intensification of Research in Priority Areas Scheme (IRPA Grant No. 09-02-04-0296).

References

[1] L.O Nabors, C.G. Robert, Alternative Sweeteners, 2nd ed., Marcel-Dekker, New York, 1991.
[2] S.Z. Haider, K.M.A. Malik, K.J. Ahmad, H. Hess, H. Riffel, M.B. Hursthouse, Inorg. Chim. Acta 72 (1983) 21.
[3] I. Remsen, C. Fahlberg, Ber. 12 (1879) 470.
[4] J. Bykov, Org. Chem. Hist. 2 (1978) 223.
[5] M.J. Allen, E. Bayland, C.E. Dukes, E.S. Horning, J.G. Watson, Brit. J. Cancer 11 (1975) 212.
[6] C.T. Supuran, M.D. Banciu, Rev. Roum. Chim. 36 (1991) 1345.
[7] T. Mann, D. Keilin, Proc. R. Soc. (London) B 126 (1938) 303.
[8] M.C. Apella, R. Totaro, E.J. Baran, Biol. Trace Elem. Res. 37 (1993) 293.
[9] Y. Zhang, Transition Met. Chem. 19 (1994) 446.
[10] E.W. Ainscough, E.N. Baker, A.M. Brodie, R.J. Cresswell, J.D. Ranford, J.M. Waters, Inorg. Chim. Acta 172 (1990) 185.
[11] M. Das, S.E. Livingstone, Inorg. Chim. Acta 19 (1976) 5.
[12] M. Akbar Ali, S.M.M.H. Majumder, R.J. Butcher, J.P. Jasinski, J.M. Jasinski, Polyhedron 16 (1997) 2749.
[13] M. Akbar Ali, A.H. Mirza, M. Nazimuddin, H. Rahman, R.J. Butcher, Polyhedron 20 (2001) 2436.
[14] Z. Otwinowski, W. Minor, in: C.W. Carter, R.M. Sweet (Eds.), Processing of X-ray Diffraction Data Collected in Oscillation Mode, Methods Enzymol., vol. 276, Academic Press, New York, 1997.
[15] P.W. Betteridge, J.R. Carruthers, R.I. Cooper, K. Prout, D.J. Watkin, J. Appl. Cryst. 36 (2003) 1487.
[16] M.T.H. Tarafder, M.A. Ali, N. Saravanan, W.Y. Weng, S. Kumar, N. Umar-Tsafe, K.A. Crouse, Transition Met Chem. 25 (2000) 295.
[17] Zhang Yugeng, Wang Yebin, Yu Heng, Cryst. Res. Technol. 30 (1995) 831.
[18] C.D. Hufford, A.M. Clark, in: A. Ur-Rahman (Ed.), Studies in Natural Product Chemistry, vol. 2, Elsevier, Amsterdam, 1988, p. 421.
[19] T. Mosmann, J. Immunol. Methods 65 (1983) 55.
[20] F.A. Cotton, G.E. Lewis, C.A. Murillo, W. Schwotzer, G. Vale, Inorg. Chem. 23 (1984) 4038.
[21] M.A. Ali, A.H. Mirza, Thahira B.S.A Ravoof, P.V. Bernhardt, Unpublished results.
[22] B.P. Straughan, S. WalkerSpectroscopy, vol. 1, Wiley, USA, 1976.
[23] A.G. Bingham, H. Bogge, A. Muller, E.W. Ainscough, A.M. Brodie, J. Chem. Soc., Dalton Trans (1987) 493.
[24] E.W. Ainscough, A.M. Brodie, N.G. Larson, Inorg. Chim. Acta 60 (1982) 25.
[25] E.W. Ainscough, A.M. Brodie, J.D. Ranford, J.M. Waters, J. Chem. Soc., Dalton Trans. (1991) 2125.
[26] M.T.H. Tarafder, Khoo Teng Jin, K.A. Crouse, A.M. Ali, B.M. Yamin, H.K. Fun, Polyhedron 21 (2002) 2691.
[27] I.G. Binev, B.A. Stamboliyska, E.A. Velceva, Spectrochim. Acta, Part A 52 (1996) 1135.
[28] C. Jovanovski, S. Tancera, B. Soptrajanov, Spectrosc. Lett. 28 (7) (1995) 1095.
[29] V.T. Vilmaz, Synth. React. Inorg Met. Org. Chem. 29 (1999) 621.
[30] M.A. Ali, A.H. Mirza, R.J. Butcher, Polyhedron 20 (2001) 1037.
[31] V.N. Biyushkin, Y.M. Chumakov, N.M. Samers, I.D. Baker, J. Struct. Chem (Eng. Trans.) 28 (1987) 119.
[32] A. Addison, T. Rao, J. Reedjik, J. Van Rijn, G. Verschoor, J. Chem, Soc. Dalton Trans. (1984) 1349.
[33] Chew Kar Beng, K.A. Crouse, M.T.H. Tarafder, A.M. Ali, B.M. Yamin, Unpublished results.
[34] M.T.H. Tarafder, A. Kasbollah, K.A. Crouse, A.M. Ali, B.M. Yamin, H.K. Fun, Polyhedron 20 (2001) 2363.
[35] V.T. Yilmaz, A. Karadag, C. Thoene, J. Coord. Chem. 55 (2002) 609.
[36] L.R. Falvello, J. Gomez, I. Pascual, M. Thomas, E.P. Urriolabeitia, A.J. Schultz, Inorg. Chim. Acta 40 (2001) 4455.

Available online at www.sciencedirect.com
SCIENCE DIRECT®
Polyhedron 23 (2004) 2499–2506
POLYHEDRON
www.elsevier.com/locate/poly

Solid-state studies of the Horner–Wittig reagent $[\{\{Ph_2P(O)\}_2CHLi \cdot (THF)\}_2 \cdot THF]$ and its mixed-anion intermediate $[\{\{Ph_2P(O)\}_2CHLi\}_4 \cdot \{Ph_2P(O)_2Li\}_2 \cdot 8C_6H_6]$ formed by reaction with dioxygen

Roger Nassar, Bruce C. Noll, Kenneth W. Henderson *

Department of Chemistry and Biochemistry, University of Notre Dame, 251 Nieuwland Science Hall, Notre Dame, IN 46556-5670, USA

Received 12 July 2004; accepted 12 August 2004
Available online 13 October 2004

Abstract

Reaction of $Ph_2P(O)_2CH_2$ with one equivalent of RLi (R = Me, Bu) leads to monodeprotonation of the methylene bridge and formation of a Horner–Wittig type reagent. The crystal structure of the resulting lithium complex $[\{\{Ph_2P(O)\}_2CHLi \cdot (THF)\}_2 \cdot THF]$, **1**, reveals a dimeric aggregate, where each lithium is tetracoordinate through bonding to two bridging and one terminally chelating phosphoryl unit, and to a THF molecule. Upon exposing complex **1** to molecular oxygen, an unexpected mixed-anionic species was formed, $[\{\{Ph_2P(O)\}_2CHLi\}_4 \cdot \{Ph_2P(O)_2Li\}_2 \cdot 8C_6H_6]$ **2**. Complex **2** was identified by X-ray crystallography and found to exist in two polymorphic forms that differ only slightly in their metrical parameters. The structure of **2** is an unusual hexalithium cage aggregate containing four Horner–Wittig anions and two diphenyl phosphinate anions. In both complexes **1** and **2** the β-diphosphine oxide anions were found to contain localized P=O double bonds and the negative charge was partially delocalized over the P–C–P fragments. Neither complex displays direct metal–C (anion) contacts but the relative planarity of the individual carbanions show significant variation.
© 2004 Elsevier Ltd. All rights reserved.

Keywords: Alkali metals; Lithium; Phosphorus–carbon bond cleavage; Chelates; O Ligands

1. Introduction

The use of α-stabilized carbanions as synthons in carbon–carbon bond forming reactions continues to be a central feature of modern organic synthesis [1–3]. The synthetic utility of the lithiated derivatives in particular, has led to detailed studies regarding their structure, reactivity and bonding behavior [4]. Our interest in this area has been directed towards a specialized class of these ligands, α,α′-stabilized carbanions, where a methylene group bridges a pair of electron withdrawing groups, e.g., nitriles, phosphonates, sulfonyls [5–8]. During our studies regarding the alkali metal complexes of several unsymmetrical monometallated ligands we have uncovered new structural patterns which contrast with those established for the simple mono-stabilized carbanions [4–8]. This led us to investigate the use of bis(diphenylphosphino)methane dioxide, $\{Ph_2P(O)\}_2CH_2$, as a potentially symmetrically chelating ligand in lithiation reactions. Furthermore, although β-diphosphine oxide Horner–Wittig anionic reagents of the type $\{R_2P(O)\}_2CH^-$ have found widespread use as versatile synthetic units [9–12] the structural elucidation of the metallated intermediates involved has received very limited attention [13]. This deficit is even more surprising considering that these ligands are close analogues to the ubiquitious β-diketonates [14], and the more recently

* Corresponding author. Tel.: +574 631 8025; fax: +574 631 6652.
E-mail address: khenders@nd.edu (K.W. Henderson).

0277-5387/$ - see front matter © 2004 Elsevier Ltd. All rights reserved.
doi:10.1016/j.poly.2004.08.017

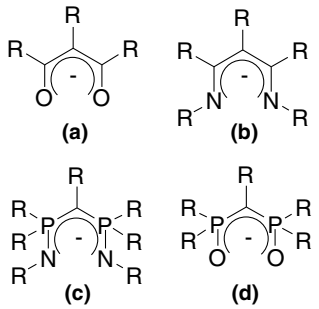

Fig. 1. Generalized (a) β-diketonato, (b) β-diketiminato, (c) β-diphosphiniminato and (d) β-diphosphine oxide anions.

studied β-diketiminates [15] and β-diphosphiniminates [16] (Fig. 1). In comparison, there have been numerous studies of the neutral β-diphosphine oxides as ligands for various transition metal, lanthanide and main group elements [17–27].

Herein, we outline the structural characterization of $[\{\{Ph_2P(O)\}_2CHLi\cdot(THF)\}_2\cdot THF]$, **1**, a lithiated bis(phosphoryl)-stabilized carbanion. In addition, we have identified the unexpected complex $[\{\{Ph_2P(O)\}_2CHLi\}_4\cdot\{Ph_2P(O)_2Li\}_2\cdot 8C_6H_6]$, **2**, which is formed as an intermediate in the oxidation of **1** by dioxygen.

2. Results and discussion

Reaction of $\{Ph_2P(O)\}_2CH_2$ with one equiv. of either BuLi or MeLi in THF solution, followed by recrystallization from *n*-hexane at −45 °C yielded colorless crystalline cubes that were isolated and identified by NMR spectroscopic and X-ray crystallographic studies as **1** (Fig. 2).

The solid-state structure of **1** was found to be a centrosymmetric Li_2O_2 dimer where the metals are tetracoordinate, each binding to a pair of bridging phosphoryl units, a terminally chelating phosphoryl unit and a THF molecule. Two independent dimers are present within the crystalline lattice, however, their core bonding arrangements are similar with the main differences between the structures being in the orientations of the attached phenyl rings (Table 1). THF molecules of crystallization are also present within the lattice but they have no close contacts to the lithiated complex.

The central Li_2O_2 dimeric core within **1** is in accordance with the structures of related mono(phosphoryl)-stabilized carbanions [28,29]. Also, the absence of any direct interactions between the carbanionic carbons and the metals is expected due to the highly electrostatic nature of the bonding present [30]. We have previously observed a similar chelated core arrangement in $[\{LiCl\cdot\{(Pr^iO)_2P(O)\}_2CH_2\}_2]$, [31], where a neutral β-diphosphonate acts as a Lewis base to monomeric LiCl fragments. A distinction in **1** from previously characterized α-phosphoryl carbanions is the position adopted by the hydrogen attached to the carbanion. Usually the carbanionic hydrogen lies in a synperiplanar orientation with respect to the α-phosphoryl group, i.e., the O=P–C–H torsion angles lie close to 0° [28a,c,29a–g,32]. In **1** the O=P–C–H torsion angles are 108.9°, 115.2°, 137.6° and 145.8°, which are closer to antiperiplanar arrangements. This unusual orientation is a consequence of chelation of the ligand to lithium, in turn restricting the flexibility of the P–C(H)–P backbone. This geometry also appears to be retained in solution. The ^1H NMR of **1** in pyridine shows a $^2J_{HP}$ coupling constant for the carbanionic ($P–CH^-$) proton of 4.5 Hz, which is indicative of O=P–C–H torsion angles in the approximate range 120°–180° [33]. The carbanionic carbons in **1** show a significant degree of pyramidalization as can be assessed from: (i) the sum of the angles around the carbanionic C (355.6° and 353.4°), the deviation, Δ_1, of the carbanionic C from the P–H–P plane (0.160 and 0.202 Å); (ii) the pyramidalization angle, χ_1, which is defined as 180° minus the improper P–C–P–H torsion angle (mean for each dimer is 24.2° and 31.0°). Also, the mean P–C distance of 1.714 Å (range 1.708(2)–1.718(3) Å) within the anionic backbone shows significant shorten-

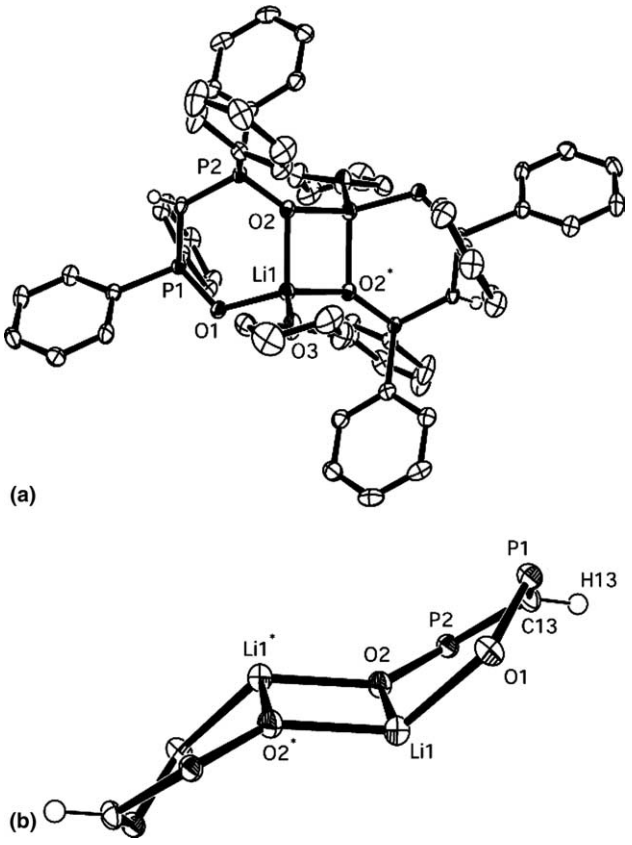

Fig. 2. Molecular structure of one of the two independent dimers of **1** showing: (a) the view perpendicular to the central Li_2O_2 ring; (b) an alternative view of the twisted three fused ring systems. The hydrogens (except those of the carbanions) and the non-bonded THF molecule of crystallization are omitted for clarity.

Table 1
Selected bond distances (Å) and angles (°) in **1**

Dimer (i)			
Bond distances			
Li(1)–O(1)	1.909(4)	Li(1)–O(2)	1.996(4)
Li(1)–O(3)	1.962(5)	Li(1)–O(2)#1	1.931(4)
O(1)–P(1)	1.513 (2)	O(2)–P(2)	1.516(2)
P(1)–C(13)	1.717(3)	P(2)–C(13)	1.711(2)
Bond angles			
O(1)–Li(1)–O(2)#1	127.0(2)	O(1)–Li(1)–O(3)	103.5(2)
O(2)#1–Li(1)–O(3)	116.9(2)	O(1)–Li(1)–O(2)	104.5(2)
O(2)#1–Li(1)–O(2)	90.9(2)	O(3)–Li(1)–O(2)	112.3(2)
P(1)–O(1)–Li(1)	121.4(2)	P(2)–O(2)–Li(1)#1	142.8(2)
P(2)–O(2)–Li(1)	123.4(1)	Li(1)#1–O(2)–Li(1)	89.1(1)
O(1)–P(1)–C(13)	118.1(1)	C(13)–P(1)–C(7)	111.7(1)
O(1)–P(1)–C(7)	106.2(1)	C(13)–P(1)–C(1)	104.8(1)
O(1)–P(1)–C(1)	109.8(1)	O(2)–P(2)–C(13)	114.9(1)
C(7)–P(1)–C(1)	105.6(1)	C(13)–P(2)–C(14)	108.3(1)
O(2)–P(2)–C(14)	110.0(1)	C(13)–P(2)–C(20)	114.4(1)
O(2)–P(2)–C(20)	106.6(1)	C(14)–P(2)–C(20)	101.9(1)
P(2)–C(13)–P(1)	121.7(1)	P(1)–C(13)–H(13)	118(2)
P(2)–C(13)–H(13)	116(2)		
Dimer (ii)			
Bond distances			
Li(2)–O(4)#1	1.920(4)	Li(2)–O(5)	1.923(4)
Li(2)–O(6)	1.971(5)	Li(2)–O(4)	1.991(4)
O(4)–P(3)	1.517(2)	O(5)–P(4)	1.508(2)
P(3)–C(42)	1.708(2)	P(4)–C(42)	1.718(3)
Bond angles			
O(4)#2–Li(2)–O(5)	126.1(2)	O(4)#2–Li(2)–O(6)	118.6(2)
O(5)–Li(2)–O(6)	102.7(2)	O(4)#2–Li(2)–O(4)	90.6(2)
O(5)–Li(2)–O(4)	104.8(2)	O(6)–Li(2)–O(4)	112.3(2)
P(3)–O(4)–Li(2)#2	145.8(2)	P(3)–O(4)–Li(2)	121.8(1)
Li(2)#2–O(4)–Li(2)	89.4(2)	P(4)–O(5)–Li(2)	120.1(1)
O(4)–P(3)–C(42)	114.9(1)	C(42)–P(3)–C(30)	108.8(1)
O(4)–P(3)–C(30)	109.6(1)	C(42)–P(3)–C(36)	114.0(1)
O(4)–P(3)–C(36)	106.1(1)	C(30)–P(3)–C(36)	102.6(1)
O(5)–P(4)–C(49)	106.6(1)	O(5)–P(4)–C(42)	118.8(1)
O(5)–P(4)–C(43)	109.6(1)	C(42)–P(4)–C(49)	111.7(1)
C(49)–P(4)–C(43)	105.1(1)	C(42)–P(4)–C(43)	104.2(1)
P(3)–C(42)–P(4)	121.4(1)	P(4)–C(42)–H(42)	113(2)
P(3)–C(42)–H(42)	119(2)		

Parameters are given for both of the independent dimers present.

ing compared with the free ligand (mean 1.819 Å) [34]. The carbanions can therefore be considered as intermediately hybridized between sp^2 and sp^3. The P═O distances lie in the narrow range 1.508–1.517 Å (mean 1.514 Å) and are only slightly elongated compared to those of the free ligand (mean 1.492 Å). In combination these values indicate relatively localized double bonding in the P═O units and delocalized partial multiple bonding over the P–C–P segment.

A final point of note within the structure of **1** are the highly asymmetrical Li–O distances within the Li_2O_2 central ring. The Li–O bonds resulting from association between non-chelating units are substantially shorter than those of the chelated unit, e.g., Li(1)–O(2*) is 1.931(4), whereas Li(1)–O(2) is 1.996(4). Such asymmetrical bridging of the neutral ligand has previously been observed in $[\{LiCl \cdot \{(Pr^iO)_2P(O)\}_2CH_2\}_2]$ [31] and can be assigned to the limited flexibility of the ligand resulting in relatively long Li–O bonds for the chelated portions.

During our NMR studies of **1** in d_6-benzene, crystals were found to slowly form on the walls of a NMR tube. X-ray crystallographic analysis revealed the formation of the unexpected product $[\{\{Ph_2P(O)\}_2CHLi\}_4 \cdot \{Ph_2P(O)_2Li\}_2 \cdot 8C_6D_6]$, **2**. After a systematic study it was established that complex **2** could be prepared by exposing benzene solutions of **1** to dry air or O_2, followed by recrystallization (Scheme 1).

Several crystalline samples were prepared but these invariably co-precipitated with various unidentified side products (most likely further oxidation products) rendering the purification of **2** problematic. Also, attempts at preparing **2** rationally by the combination of the separately prepared components $[\{Ph_2P(O)\}_2CHLi]$ and $[Ph_2P(O)_2Li]$ or alternatively by the lithiation of a mixture of the neutral ligands were unsuccessful. Aqueous quenching studies of samples of **1** exposed to O_2 did, however, confirm the presence of both the β-diphosphine oxide ligand and diphenylphosphinic acid. It is therefore likely that the formation of **2** is related to its method of preparation, i.e., it is a kinetically stable intermediate formed during the oxidation of a lithiated β-diphosphine oxide. Unfortunately, this limited the unambiguous characterization of **2** to crystallographic analysis. Nevertheless, an interesting outcome of these studies was the identification of a polymorphic variant of **2**, **2a** (the C_6D_6 is replaced by C_6H_6 in this case). Such solid-state polymorphism is notable since it is rarely encountered for lithiated species [35]. The polymorphs **2** and **2a** crystallize in different space groups (triclinic $P\bar{1}$ and monoclinic $P2(1)/n$) and they also contain minor variations in their metrical parameters (Tables 2 and 3). For brevity, only details of complex **2** will be discussed and its molecular structure is depicted in Fig. 3.

Complex **2** is a centrosymmetric, hexalithium aggregate containing four $[\{Ph_2P(O)\}_2CHLi]$ units, similar to those in **1**, and a pair of $[Ph_2P(O)_2Li]$ fragments. Formation of the lithiated diphenylphosphinate group was determined to be via exposure of **1** to molecular oxygen, resulting in P–C bond cleavage. Such P–C bond fission through the oxidation of simple α-stabilized

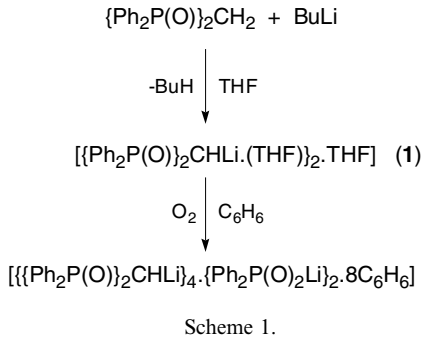

Scheme 1.

Table 2
Selected bond distances (Å) and angles (°) in **2**

Bond distances			
Li(1)–O(1)	1.909(5)	Li(1)–O(6)	1.963(5)
Li(1)–O(2)	1.982(5)	Li(1)–O(5)#1	2.071(5)
Li(2)–O(6)#1	1.981(5)	Li(2)–O(2)	1.941(5)
Li(2)–O(3)	1.894(5)	Li(2)–O(5)	2.053(5)
Li(3)–O(4)	1.874(5)	Li(3)–O(3)	1.994(5)
Li(3)–O(5)	1.963(5)	Li(3)–O(1)#1	1.943(5)
O(1)–P(1)	1.515(2)	O(2)–P(2)	1.527(2)
O(3)–P(3)	1.514(2)	O(4)–P(4)	1.511(2)
O(5)–P(5)	1.515(2)	O(6)–P(5)	1.510(2)
P(1)–C(13)	1.715(3)	P(2)–C(13)	1.722(3)
P(3)–C(38)	1.705(3)	P(4)–C(38)	1.715(3)
Bond angles			
O(1)–Li(1)–O(6)	119.4(2)	O(1)–Li(1)–O(2)	117.1(2)
O(6)–Li(1)–O(2)	114.5(2)	O(1)–Li(1)–O(5)#1	90.4(2)
O(6)–Li(1)–O(5)#1	93.9(2)	O(2)–Li(1)–O(5)#1	116.1(2)
O(3)–Li(2)–O(2)	140.9(3)	O(3)–Li(2)–O(6)#1	103.6(2)
O(2)–Li(2)–O(6)#1	108.7(2)	O(3)–Li(2)–O(5)	92.2(2)
O(2)–Li(2)–O(5)	106.8(2)	O(6)#1–Li(2)–O(5)	93.9(2)
O(4)–Li(3)–O(1)#1	123.5(3)	O(4)–Li(3)–O(5)	124.2(3)
O(1)#1–Li(3)–O(5)	92.8(2)	O(4)–Li(3)–O(3)	106.6(2)
O(1)#1–Li(3)–O(3)	113.6(2)	O(5)–Li(3)–O(3)	92.0(2)
O(1)–P(1)–C(13)	116.6(1)	O(1)–P(1)–C(1)	108.5(1)
C(13)–P(1)–C(1)	106.2(1)	O(1)–P(1)–C(7)	107.2(1)
C(13)–P(1)–C(7)	112.7(1)	C(1)–P(1)–C(7)	105.0(1)
O(2)–P(2)–C(13)	116.6(1)	O(2)–P(2)–C(20)	111.6(1)
C(13)–P(2)–C(20)	107.4(1)	O(2)–P(2)–C(14)	107.4(1)
C(13)–P(2)–C(14)	111.2(1)	C(20)–P(2)–C(14)	101.7(1)
O(3)–P(3)–C(32)	110.3(1)	C(38)–P(3)–C(32)	106.9(1)
O(3)–P(3)–C(26)	105.8(1)	C(38)–P(3)–C(26)	114.2(2)
C(32)–P(3)–C(26)	104.5(1)	O(3)–P(3)–C(38)	114.8(1)
O(4)–P(4)–C(38)	115.9(1)	O(4)–P(4)–C(39)	106.5(1)
C(38)–P(4)–C(39)	112.0(2)	O(4)–P(4)–C(45)	111.0(1)
C(38)–P(4)–C(45)	106.9(2)	C(39)–P(4)–C(45)	103.9(1)
O(6)–P(5)–O(5)	114.1(1)	O(6)–P(5)–C(57)	109.0(1)
O(5)–P(5)–C(57)	110.8(1)	O(6)–P(5)–C(51)	110.5(1)
O(5)–P(5)–C(51)	109.4(1)	C(57)–P(5)–C(51)	102.4(1)
P(1)–O(1)–Li(1)	112.9(2)	P(1)–O(1)–Li(3)#1	158.1(2)
Li(1)–O(1)–Li(3)#1	86.6(2)	P(2)–O(2)–Li(2)	149.3(2)
P(2)–O(2)–Li(1)	111.6(2)	Li(2)–O(2)–Li(1)	97.4(2)
P(3)–O(3)–Li(2)	155.5(2)	P(3)–O(3)–Li(3)	115.6(2)
Li(2)–O(3)–Li(3)	88.8(2)	P(4)–O(4)–Li(3)	117.0(2)
P(5)–O(5)–Li(3)	150.2(2)	P(5)–O(5)–Li(2)	121.4(2)
Li(3)–O(5)–Li(2)	85.3(2)	P(5)–O(5)–Li(1)#1	112.4(2)
Li(3)–O(5)–Li(1)#1	81.7(2)	Li(2)–O(5)–Li(1)#1	82.5(2)
P(5)–O(6)–Li(1)	115.4(2)	P(5)–O(6)–Li(2)#1	126.3(2)
Li(1)–O(6)–Li(2)#1	87.2(2)	P(2)–C(13)–H(13)	117.1(2)
P(1)–C(13)–P(2)	123.8(2)	P(1)–C(13)–H(13)	111(2)
P(3)–C(38)–H(38)	117(2)	P(3)–C(38)–P(4)	122.7(2)
P(4)–C(38)–H(38)	121(2)		

Table 3
Selected bond distances (Å) and angles (°) in **2a**

Bond distances			
Li(1)–O(1)	1.890(6)	Li(1)–O(2)	1.987(6)
Li(1)–O(6)	1.987(6)	Li(1)–O(5)#1	2.110(6)
Li(2)–O(3)	1.904(6)	Li(2)–O(2)	1.930(6)
Li(2)–O(6)#1	1.957(6)	Li(2)–O(5)	2.034(6)
Li(3)–O(4)	1.855(6)	Li(3)–O(1)#1	1.935(6)
Li(3)–O(5)	1.972(6)	Li(3)–O(3)	1.984(6)
O(1)–P(1)	1.518(2)	O(2)–P(2)	1.524(2)
O(3)–P(3)	1.517(2)	O(4)–P(4)	1.508(2)
O(5)–P(5)	1.511(2)	O(6)–P(5)	1.511(2)
P(1)–C(13)	1.706(4)	P(2)–C(13)	1.708(4)
P(3)–C(38)	1.693(4)	P(4)–C(38)	1.713(4)
Bond angles			
O(1)–Li(1)–O(2)	111.7(3)	O(1)–Li(1)–O(6)	118.5(3)
O(2)–Li(1)–O(6)	116.8(3)	O(1)–Li(1)–O(5)#1	91.7(2)
O(2)–Li(1)–O(5)#1	122.8(3)	O(6)–Li(1)–O(5)#1	92.1(2)
O(3)–Li(2)–O(2)	142.1(3)	O(2)–Li(2)–O(6)#1	104.1(3)
O(3)–Li(2)–O(6)#1	108.1(3)	O(2)–Li(2)–O(5)	105.6(3)
O(3)–Li(2)–O(5)	91.0(2)	O(6)#1–Li(2)–O(5)	95.3(2)
O(4)–Li(3)–O(1)#1	114.2(3)	O(4)–Li(3)–O(5)	129.9(3)
O(1)#1–Li(3)–O(5)	94.7(2)	O(4)–Li(3)–O(3)	107.1(3)
O(1)#1–Li(3)–O(3)	119.4(3)	O(5)–Li(3)–O(3)	90.5(2)
O(1)–P(1)–C(13)	117.2(2)	C(1)–P(1)–C(7)	104.6(2)
O(1)–P(1)–C(1)	107.6(1)	C(13)–P(1)–C(1)	108.3(2)
O(1)–P(1)–C(7)	107.4(1)	C(13)–P(1)–C(7)	111.0(2)
O(2)–P(2)–C(20)	110.3(1)	C(13)–P(2)–C(20)	108.2(2)
O(2)–P(2)–C(14)	107.6(1)	C(13)–P(2)–C(14)	111.2(2)
O(2)–P(2)–C(13)	116.1(2)	C(20)–P(2)–C(14)	102.7(2)
O(3)–P(3)–C(38)	113.4(2)	C(32)–P(3)–C(26)	102.5(2)
O(3)–P(3)–C(32)	109.3(1)	C(38)–P(3)–C(32)	109.8(2)
O(3)–P(3)–C(26)	107.8(1)	C(38)–P(3)–C(26)	113.6(2)
O(4)–P(4)–C(38)	116.0(2)	C(45)–P(4)–C(39)	104.9(2)
O(4)–P(4)–C(45)	109.9(1)	C(38)–P(4)–C(45)	106.4(2)
O(4)–P(4)–C(39)	105.6(2)	C(38)–P(4)–C(39)	113.5(2)
O(6)–P(5)–C(51)	112.2(1)	O(5)–P(5)–C(51)	107.9(2)
O(6)–P(5)–C(57)	107.3(1)	O(5)–P(5)–C(57)	112.9(1)
O(6)–P(5)–O(5)	113.1(1)	C(51)–P(5)–C(57)	103.0(2)
P(1)–O(1)–Li(1)	115.7(2)	P(1)–O(1)–Li(3)#1	158.1(2)
Li(1)–O(1)–Li(3)#1	86.1(2)	P(2)–O(2)–Li(2)	145.8(2)
P(2)–O(2)–Li(1)	114.9(2)	Li(2)–O(2)–Li(1)	94.9(2)
P(3)–O(3)–Li(2)	149.8(2)	P(3)–O(3)–Li(3)	121.6(2)
Li(2)–O(3)–Li(3)	88.4(2)	P(4)–O(4)–Li(3)	121.5(2)
P(5)–O(5)–Li(3)	149.9(2)	P(5)–O(5)–Li(2)	124.8(2)
Li(3)–O(5)–Li(2)	85.2(2)	P(5)–O(5)–Li(1)#1	103.9(2)
Li(3)–O(5)–Li(1)#1	79.5(2)	Li(2)–O(5)–Li(1)#1	82.5(2)
P(5)–O(6)–Li(2)#1	134.2(2)	P(5)–O(6)–Li(1)	113.0(2)
Li(2)#1–O(6)–Li(1)	87.7(2)	P(1)–C(13)–P(2)	122.5(2)
P(1)–C(13)–H(13)	117(3)	P(2)–C(13)–H(13)	111(3)
P(3)–C(38)–P(4)	124.8(2)	P(3)–C(38)–H(38)	114(2)
P(4)–C(38)–H(38)	121(2)		

Horner–Wittig reagents has significant precedent and has been assigned to the formation of a peroxide intermediate [36,37]. However, the reaction pathway has generally been interpreted by analysis of products found upon aqueous quenching, as opposed to directly analyzing the organometallic intermediates involved. Furthermore, the identification of such complex mixed-anion intermediates is particularly relevant when considering factors that influence their selectivity in organic synthesis. The benzene solvent of inclusion in **2** and **2a** displays no close contacts with the cage structure. Although incorporation of solvent of crystallization is commonplace the amount present, six benzene molecules per cage, is somewhat unusual.

Viewing the structure of **2** in detail, it can be seen that although each metal is tetracoordinate, there are three distinct lithium environments, Li(1), Li(2) and Li(3). The core of the framework is an atypical tetrametallic cage arrangement (Fig. 3(b)), where a pair of Li_2O_2 rings, Li(1)O(5*)Li(2*)O(6) and Li(1*)O(5)Li(2)O(6*), are connected by two phosphorous centers, P(5) and P(5*), and two phosphoryl groups, O(2) and O(2*). Overall, the cage is composed of two four-membered Li_2O_2 rings and four six-membered LiOLiOPO rings. The framework is then completed by incorporation of a terminal lithium center, Li(3) and Li(3*), at each side of the central cage which, in turn, creates another pair of Li_2O_2 rings, Li(3)O(3)Li(2)O(5) and Li(3)O(1*)-

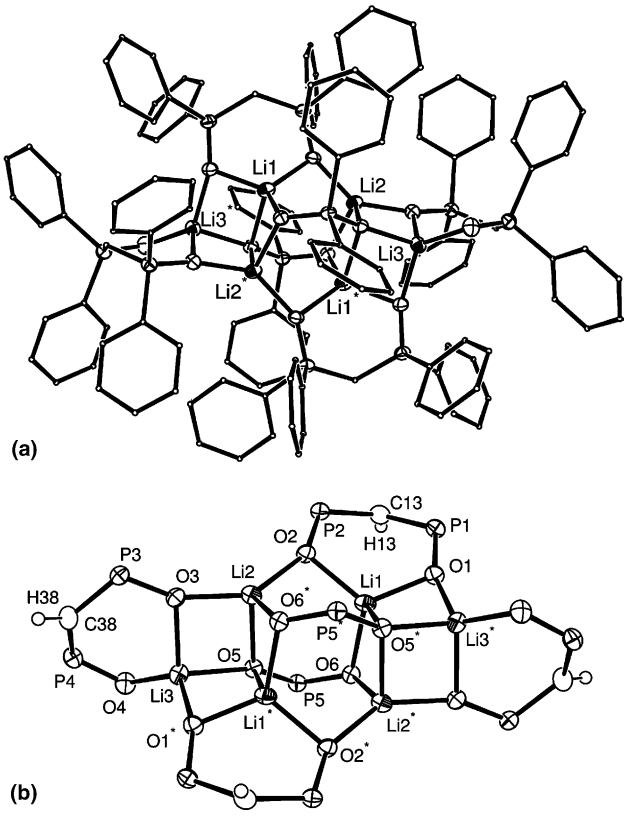

Fig. 3. Molecular structure of **2** showing (a) the complete molecule, and (b) the core framework. Hydrogens, except those of the carbanions in (b), and benzene molecules of solvation are omitted for clarity.

Li(1*)O(5), (and their symmetry equivalents) on each side of the central cage. Although the structure of **2** is somewhat unusual, we were intrigued to find significant similarities with our recently reported structure of the hexasodium β-diphosphonate complex $[\{\{(EtO)_2P(O)\}_2CHNa\}_6]$, **3** [38]. Whereas **2** is a mixed-anion species complex **3** is homoleptic. Nevertheless, the connectivities within the two hexametallic complexes are remarkably similar, with the main difference being the absence of the Li(2)–O(6) and Li(2*)–O(6*) interactions in **2** (Fig. 4).

These additional metal–O interactions in **3** result in a six Na–O rung ladder framework, as opposed to the more open cage core found within **2**. This structural variance is likely due to replacement of the central β-diphosphonate ligands in **3** by the less flexible and smaller phosphinates in **2**. Additionally, the larger sodium cations in **3** can accommodate higher coordination numbers than the lithium centers in **2**, as is required for the six-rung structure.

Turning to the geometric parameters in **2**, the bonding within the β-diphosphine oxide anions is found to follow a similar pattern to those in **1**. The phosphoryl units display relatively localized P=O double bonds (mean P–O 1.522 Å, range 1.516 (2)–1.527 (2) Å) with delocalization over the P–C–P fragment (mean P–C 1.718 Å, range 1.714(3)–1.721(3) Å). Regarding the planarity of the carbanions in **2**, a significant difference is found between the two independent β-diphosphine oxide anions, where the central P(1)–C(13)–P(2) ligand is substantially more pyramidalized compared with the almost planar terminal P(3)–C(38)–P(4) ligand. The sum of the angles around the carbanionic carbons are 350.2° and 360.0°, Δ_1 is 0.225 and 0.007 Å, and χ_1 is 36.3° and 1.2° for these units, respectively. These results clearly indicate that the carbanions in the P–C–P backbone are not necessarily pyramidalized as a consequence of either chelation or due to the presence of localized charge. It is likely that the arrangement adopted at the anionic carbon is dictated by the minimization of torsional strain in the molecule and that its position is a relatively minor effect in energetic terms. Finally, the P–O bond lengths within the phosphinate are essentially identical (1.510(2) and 1.515(2) Å) indicating delocalization over the O–P–O unit [39].

3. Experimental

3.1. X-ray crystallography

Table 4 contains information on the data collection. In all cases (**1**, **2** and **2a**), the crystalline samples were placed in inert oil, mounted on a glass pin and transferred to the cold gas stream of the diffractometer. Crystal data were collected and integrated using a Bruker Apex system, with graphite monochromated Mo Kα (λ = 0.71073 Å) radiation at 100 K. The structure was

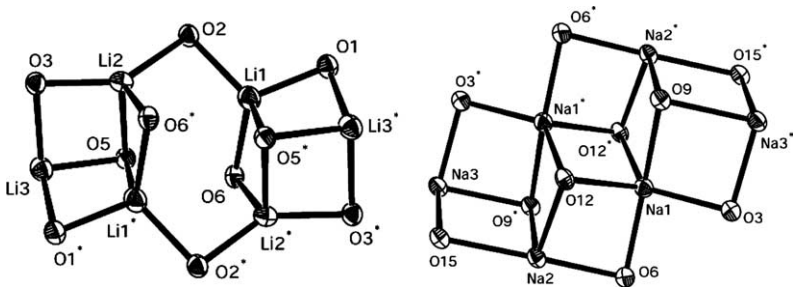

Fig. 4. Core frameworks of **2** and **3** showing their structural relationship to one another.

Table 4
Crystallographic data for **1**, **2** and **2a**

Compound	**1**	**2**	**2a**
Empirical formula	$C_{62}H_{66}Li_2O_7P_4$	$C_{172}H_{104}D_{48}Li_6O_{12}P_{10}$	$C_{172}H_{152}Li_6O_{12}P_{10}$
Formula weight	1060.91	2810.56	2762.42
Temperature (K)	100(2)	100(2)	100(2)
Crystal system	monoclinic	triclinic	monoclinic
Space group	$P2(1)/n$	$P\bar{1}$	$P2(1)/n$
Unit cell dimensions			
a (Å)	19.7789(15)	14.2394 (4)	14.7823 (6)
b (Å)	11.2175 (8)	15.2704 (4)	22.6115 (7)
c (Å)	25.0948(19)	19.5430 (6)	22.7105 (9)
α (°)	90	71.727 (2)	90
β (°)	101.4940 (10)	71.035 (2)	108.527 (2)
γ (°)	90	69.575 (2)	90
Volume (Å^3)	5456.1(7)	3668.85 (18)	7197.6 (5)
Z	4	1	4
D_{calc} (Mg/m^3)	1.292	1.272	1.275
Absorption coefficient (mm^{-1})	0.193	0.179	0.183
$F(000)$	2240	1448	2896
Crystal size (mm)	$0.33 \times 0.26 \times 0.25$	$0.83 \times 0.085 \times 0.085$	
Reflections collected	31 890	54 655	63 833
Independent reflections [R_{int}]	11 408 [0.0880]	14 966 [0.0965]	10 345 [0.1045]
Data/restraints/parameter	11 408/0/684	14 966/1/1010	10 345/0/907
Goodness-of-fit on F^2	0.788	1.042	0.878
R_1	0.0521	0.0591	0.0476
wR_2	0.1131	0.1533	0.1266

solved by direct methods using SHELXS-97 and refined using SHELXL-97 (Sheldrick, G.M., University of Göttingen). Non-hydrogen atoms were refined anisotropically and the carbanionic hydrogens were located from difference Fourier maps and were refined isotropically. The remaining hydrogen atoms were placed at calculated positions and were refined isotropically.

3.2. General synthetic procedures

All experiments were carried out under a dry dinitrogen atmosphere and scrupulously anhydrous conditions using standard Schlenk techniques [40]. The phosphine oxide ligand $\{Ph_2P(O)\}_2CH_2$ was prepared by the oxidation of $(Ph_2P)_2CH_2$ (Aldrich) using H_2O_2. The solvents (except anhydrous benzene that was used as supplied by Aldrich) were purified by passage through copper-based catalyst and molecular sieve columns (Innovative Technology). The *n*-butyl lithium and methyl lithium were supplied by Aldrich as 1.6 M solutions in hexane and diethylether, respectively, and standardized by titration with salicylaldehyde phenylhydrazone directly before use [41]. The NMR experiments were recorded on Varian-300 and -500 spectrometers. ^{1}H and ^{13}C NMR spectra were referenced internally to the protonated portions of the deuterated solvents, whereas ^{31}P NMR spectra were referenced externally to 85% *o*-phosphoric acid. Mass spectra were recorded on 'GCmate' GC–MS instrument and 'Micromass' Triple Quadrupole LC–MS–MS systems. Elemental analyses were performed by the Canadian Microanalytical Service Ltd.

3.2.1. $[\{\{Ph_2P(O)\}_2CHLi\cdot(THF)\}_2\cdot THF]$ (**1**)

The parent phosphine oxide (0.5 mmol) was dissolved in 5 mL of THF and the solution cooled to 0 °C. A solution of alkyllithium reagent (MeLi of BuLi, 0.5 mmol) was added to the reaction mixture via a syringe over several minutes, and the resulting solution was slowly warmed to room temperature. The solvent was then evaporated and 2 ml hexanes were added to dissolve the resultant white solid and the solution stored at −45 °C. After one day, small colorless blocks of **1** precipitated from solution. Yield 85%, m.p. 134 °C, ^{1}H NMR (300 MHz, pyridine-d_5, 25 °C): δ = 1.66 (m, 4H, THF), 2.37 (bt, $^2J_{H,P}$ = 4.5 Hz, 1H, CH^-), 3.69 (m, 4H, THF), 7.28 (m, 3H, *meta* and *para*-Ph), 8.13 (m, 2H, *ortho*-Ph). ^{31}P–{^{1}H} NMR (300 MHz, pyridine-d_5, 25 °C): δ = 37.2 (bs). ^{13}C–{^{1}H} NMR (300 MHz, pyridine-d_5, 25 °C): δ = 131.9, 130.1, 128.4 (Ar–H), 68.3 (OCH_2, THF), 26.3 (CH_2, THF). The ^{1}H NMR spectra indicated loss of the THF of crystallization on isolation. No signal for the carbanionic carbon could be located even after increasing the sample concentration and running extended scans. Elemental *Anal.* for $C_{58}H_{58}Li_2O_6P_4$ (MW 989 based on the integration values obtained from the ^{1}H NMR spectra): Calc. C, 70.45; H, 5.91; N, 0.00. Found: C, 69.96; H, 6.06; N < 0.3%.

3.2.2. $[\{\{Ph_2P(O)\}_2CHLi\}_4\cdot\{Ph_2P(O)_2Li\}_2\cdot 8C_6H_6]$, **2** and polymorph **2a**

The parent phosphine oxide (0.5 mmol) was dissolved in 5 mL of THF and the solution cooled to 0 °C. MeLi in diethyl ether (0.5 mmol) was added to the reaction

mixture via a syringe over several minutes, and the resulting solution was slowly warmed to room temperature. The solution was stirred for three days at room temperature and air was allowed to enter the flask through a $CaCl_2$ tube (or alternatively O_2 from a cylinder). The solvent was then removed in vacuo and benzene (benzene/1 mmol TMEDA mixture in the case of the second polymorph **2a**) was added to dissolve the resultant white solid. After storing the solution at 5 °C for one day, small colorless blocks of **2** (or **2a**) precipitated out of the solution. Unfortunately, **2** and **2a** co-precipitated with other unidentified products, most likely further oxidation species. This resulted in the unambiguous characterization of **2** and **2a** being limited to the solid-state analysis. NMR data proved to be of little value giving broad, ill-defined signals that could be complicated by dynamic processes occurring in solution.

The quenching studies were performed using deionized water, the organic components were extracted into ether and dried over anhydrous $MgSO_4$. The products were identified by ^1H NMR and mass spectroscopy and compared with authentic samples.

3.2.2.1. $Ph_2P(O)CH_2P(O)Ph_2$, L_1. ^1H NMR (300 MHz, pyridine-d_5, 25 °C): $\delta = 4.26$ (t, $^2J_{H-P} = 14.08$ Hz, CH_2), 7.39 (m, 6H, *meta* and *para*-H, Ph), 8.17 (m, 4H, *ortho*-H, Ph). $^{31}P-\{^1H\}$ NMR (300 MHz, pyridine-d_5, 25 °C): $\delta = 24.0$ (s). $^{13}C-\{^1H\}$ NMR (300 MHz, pyridine-d_5, 25 °C): $\delta = 134.9, 132.2, 132.0, 129.1$ (Ar–C, Ph.), 34.4 (t, $^1J_{C,P} = 59.1$ Hz, CH_2). MS (FAB+) $m/z = 417$ $[\mathbf{L_1} + H]^+$, 339 $[\mathbf{L_1} - Ph]^+$. When using ES/MSMS the larger aggregate was observed: $m/z = 839$ $[2\mathbf{L_1} + Li]^+$ and its daughter 423 $[\mathbf{L_1} + Li]^+$.

3.2.2.2. $Ph_2P(O)(OH)$,L_2. ^1H NMR (300 MHz, pyridine-d_5, 25 °C) $\delta = 7.34$ (m, *meta* and *para*-Ar · H), 8.47 (m, *ortho*-Ar · H). $^{31}P-\{^1H\}$ NMR (300 MHz, pyridine-d_5, 25 °C): $\delta = 17.8$ (s). $^{13}C-\{^1H\}$ NMR (300 MHz, pyridine-d_5, 25 °C): $\delta = 132.0$ (d, $J = 10.4$ Hz, Ph), 130.8 (s, Ph), 130.4 (d, $J = 12.2$ Hz) [40]. GC/EI + $m/z = 218.04988$ $[\mathbf{L_2}]^+$ (calculated: 218.04967). ES/MSMS $m/z = 641$ $[\mathbf{L_1} + \mathbf{L_2} + Li]^+$ and its daughter 423 $[\mathbf{L_1} + Li]^+$.

Acknowledgements

We thank the University of Notre Dame for financial support and Dr. Bill Boggess for the mass spectroscopic data.

Appendix A. Supplementary material

Crystallographic data for **1**, **2** and **2a** have been deposited with the Cambridge Structural Data Centre, CCDC Nos. 34322, 34323 and 34324. Copies of this information may be obtained free of charge from The Director, CCDC, 12 Union Road, Cambridge, CB2 1EZ, UK (fax: +44-1223-336033; e-mail deposit@ccdc.cam.ac.uk or www.ccdc.cam.ac.uk). Supplementary data associated with this article can be found, in the online version, at doi:10.1016/j.poly.2004.08.017.

References

[1] B.M. Trost, I. Fleming (Eds.), Comprehensive Organic Synthesis, vols. 1 and 2, Pergamon, Oxford, UK, 1991.
[2] E. Buncel, T. Durst (Eds.), Comprehensive Carbanion Chemistry Part B, Elsevier, Amsterdam, 1984.
[3] A.W. Johnson (Ed.), Ylides and Imines of Phosphorus, Wiley, New York, 1993.
[4] For a structural review see: G. Boche, Angew. Chem., Int. Ed. Engl. 28 (1989) 277.
[5] K.W. Henderson, A.R. Kennedy, A.E. McKeown, D.S. Strachan, J. Chem. Soc., Dalton. Trans. 44 (2000) 4348.
[6] K.W. Henderson, A.R. Kennedy, D.J. MacDougall, D. Shanks, Organometallics 21 (2002) 606.
[7] K.W. Henderson, A.R. Kennedy, D.J. MacDougall, Inorg. Chem. 42 (2003) 2736.
[8] K.W. Henderson, A.R. Kennedy, L. Macdonald, D.J. MacDougall, Inorg. Chem. 42 (2003) 2839.
[9] For examples see: V.K. Issleib, H.P. Abicht, J. Prakt. Chem. 312 (1970) 456.
[10] M.B. Goli, S.O. Grim, Tetrahedron Lett. 32 (1991) 3631.
[11] F. Benvenuti, C. Carlo, M. Marchionna, R. Patrini, A.M.R. Galletti, G. Sbrana, J. Inorg. Organomet. Polym. 7 (1997) 183.
[12] J. Clayden, S. Warren, Angew. Chem., Int. Ed. Engl. 35 (1996) 241.
[13] K. Izod, Chem. Commun. (2002) 2532.
[14] R.C. Mehrotra, R. Bohra (Eds.), Metal β-Diketonate and Allied Derivatives, Academic Press, New York, 1978.
[15] L. Bourget-Merle, M.F. Lappert, J.R. Severn, Chem. Rev. 102 (2002) 3031.
[16] A. Steiner, S. Zacchini, P.I. Richards, Coord. Chem. Rev. 227 (2002) 193.
[17] For representative examples see: J. Fawcett, A.W.G. Platt, Polyhedron 22 (2003) 967.
[18] W. Hewertson, B.T. Kilbourn, R.H.B. Mais, J. Chem. Soc. D (1970) 952.
[19] Y. Ding, P.E. Fanwick, R.A. Walton, Inorg. Chem. Acta 309 (2000) 159.
[20] G. Pelizzi, P. Tarasconi, F. Vitali, C. Pelizzi, Acta Crystallogr., Sect. C 43 (1987) 1505.
[21] J.E. Barclay, D.J. Evans, D.L. Hughes, G.J. Leigh, J. Chem. Soc., Dalton Trans. (1993) 69.
[22] A.M.J. Lees, A.W.G. Platt, Inorg. Chem. 42 (2003) 4673.
[23] S. Bhattacharyya, I. Chakraborty, B.K. Dirghangi, A. Chakravorty, Chem. Commun. (2000) 1813.
[24] C. Pettinari, F. Marchetti, A. Cingolani, R. Pettinari, A. Drozdov, S. Troyanov, Inorg. Chim. Acta 125 (2001) 312.
[25] S. Bhattacharyya, I. Chakraborty, B.K. Dirghangi, A. Chakravorty, Inorg. Chem. 40 (2001) 286.
[26] A. Mendia, E. Cerrada, E.J. Fernandez, A. Laguna, M. Laguna, J. Organomet. Chem. 663 (2002) 289.
[27] F.J. Arnaiz, R. Aguado, M.R. Pedrosa, J. Mahia, M.A. Maestro, Polyhedron 21 (2002) 1635.
[28] (a) W. Clegg, R.P. Davies, L. Dunbar, N. Feeder, S.T. Liddle, R.E. Mulvey, R. Snaith, A.E.H. Wheatley, Chem. Commun. (1999) 1401;
(b) D.R. Armstrong, D. Barr, M.G. Davidson, G. Hutton, P. O'Brien, R. Snaith, S. Warren, J. Organomet. Chem. 529 (1997) 29;

(c) J.E. Davies, R.P. Davies, L. Dunbar, P.R. Raithby, M.G. Russell, R. Snaith, S. Warren, A.E.H. Wheatley, Angew. Chem., Int. Ed. Eng. 36 (1997) 2334;
(d) D.R. Armstrong, R.P. Davies, L. Dunbar, P.R. Raithby, R. Snaith, A.E.H. Wheatley, Phosphorus Sulfur 125 (1997) 51;
(e) D.R. Armstrong, M.G. Davidson, R.P. Davies, H.J. Mitchell, R.M. Oakley, P.R. Raithby, R. Snaith, S. Warren, Angew. Chem., Int. Ed. Eng. 35 (1996) 1942;
(f) I. CraggHine, M.G. Davidson, A.J. Edwards, E. Lamb, P.R. Raithby, R. Snaith, Chem. Commun. (1996) 153.

[29] (a) S.E. Denmark, K.A. Swiss, P.C. Miller, S.R. Wilson, Heteroatom. Chem. 9 (1998) 209;
(b) S.E. Denmark, K.A. Swiss, S.R. Wilson, Angew. Chem., Int. Ed. Eng. 35 (1996) 2515;
(c) C.J. Cramer, S.E. Denmark, P.C. Miller, R.L. Dorow, K.A. Swiss, S.R. Wilson, J. Am. Chem. Soc. 116 (1994) 2437;
(d) S.E. Denmark, K.A. Swiss, S.R. Wilson, J. Am. Chem. Soc. (1993) 3826;
(e) S.E. Denmark, P.C. Miller, S.R. Wilson, J. Am. Chem. Soc. 113 (1991) 1468;
(f) S.E. Denmark, R.L. Dorow, J. Am. Chem. Soc. 112 (1990) 864;
(g) M. Kranz, S.E. Denmark, K.A. Swiss, S.R. Wilson, J. Org. Chem. 61 (1996) 8551;
(h) M. Kranz, S.E. Denmark, J. Org. Chem. 60 (1995) 5867.

[30] For a review on lithium compounds see: A.M. Sapse, P.v.R. Schleyer (Eds.), Lithium Chemistry, A Theoretical and Experimental Overview, Wiley, New York, 1995.

[31] K.W. Henderson, A.R. Kennedy, D.J. MacDougall, D. Strachan, Acta Cryst. Sect. C C59 (2003) m49.

[32] W. Zarges, M. Marsch, K. Harms, F. Haller, G. Frenking, G. Boche, Chem. Ber. 124 (1991) 861.

[33] W.G. Bentrude, W.N. Setzer, in: J.G. Verkade, L.D. Quin (Eds.), Phosphorus-31 NMR Spectroscopy in Stereochemical Analysis, VCH, Deerfield Beach, FL, 1987, p. 380.

[34] M.I. Antipin, I.T. Struchkov, S.A. Pisareva, T.Y. Medved, M.I. Kabachnik, Zh. Strukt. Khim. 21 (1980) 101.

[35] J.F. Allan, R. Nassar, E. Specht, A. Beatty, N. Calin, K.W. Henderson, J. Am. Chem. Soc. 126 (2003) 484.

[36] For example see: M. Mikołajczyk, W. Midura, S. Grzejszczak, Tetrahedron Lett. 25 (1984) 2489.

[37] H. Zimmer, R.E. Koenigkramer, R.L. Cepulis, D.M. Nene, J. Org. Chem. 45 (1980) 2018.

[38] R. Nassar, A.M. Beatty, K.W. Henderson, Eur. J. Inorg. Chem. (2003) 3325.

[39] C.C. Landry, A. Hynes, A.R. Barron, Polyhedron 15 (1996) 391.

[40] D.F. Shriver, M.A. Drezdzonin, The Manipulation of Air-Sensitive Compounds, Wiley, New York, 1986.

[41] B.E. Love, E.G. Jones, J. Org. Chem. 64 (1999) 3755

Available online at www.sciencedirect.com
SCIENCE DIRECT®
Polyhedron 23 (2004) 2507–2513
POLYHEDRON
www.elsevier.com/locate/poly

Mechanistic and spectral investigation of the oxidation of 4-hydroxycoumarin by aqueous alkaline permanganate using the stopped flow technique

R.M. Mulla, Sharanappa T. Nandibewoor *

P.G. Department of Studies in Chemistry, Karnatak University, Dharwad 580 003, India

Received 8 June 2004; accepted 16 August 2004
Available online 14 October 2004

Abstract

The kinetics of the oxidation of 4-hydroxycoumarin (HDC) by permanganate in aqueous alkaline medium at a constant ionic strength of 0.40 mol dm^{-3} was studied spectrophotometrically using a rapid kinetic accessory. The reaction between permanganate and HDC in alkaline medium exhibits 6:1 stoichiometry (permanganate:HDC). The reaction is of first order in [permanganate ion] and has less than unit order in both [HDC] and [alkali]. A decrease in the dielectric constant of the medium increases the rate of reaction. The effect of added products and ionic strength of the reaction medium have been investigated. The oxidation reaction in alkaline medium has been shown to proceed via a permanganate–HDC complex, which decomposes slowly in a rate determining step followed by a fast reaction between a free radical of HDC and five molecules of permanganate species to give the products. The main products were identified by spot test, IR and NMR. A suitable mechanism is proposed. The reaction constants involved in the different steps of the mechanism are calculated. The activation parameters with respect to the slow step of the mechanism are computed and discussed and thermodynamic quantities are determined.
© 2004 Elsevier Ltd. All rights reserved.

Keywords: Kinetics; Permanganate; Oxidation; 4-Hydroxycoumarin

1. Introduction

The permanganate ion (MnO_4^-) oxidises a great variety of substrates and it finds extensive applications in organic synthesis [1,2], especially after the advent of phase transfer catalysis [3,4] which permits the use of solvents such as methylene chloride and benzene. Kinetic studies constitute an important source of mechanistic information on the reaction, as demonstrated by results referring to unsaturated acids in both aqueous [1,3] and non-aqueous media [5].

During oxidation by permanganate, it is evident that the Mn(VII) in permanganate is reduced to various oxidation states in acidic, alkaline and neutral media. Furthermore, the mechanism by which this multivalent oxidant oxidises a substrate depends not only on the substrate but also on the medium [6] used for the study. In strongly alkaline medium, the stable reduction product [7] is the manganate ion, MnO_4^{2-}. It is interesting that the oxidant species (MnO_4^-) requires a pH range 12–13, below which the system becomes disturbed and the reaction will proceed further to give a reduced product of the oxidant as Mn(IV), which slowly develops yellow turbidity. Hence, it becomes apparent that in carrying out this reaction the role of pH in a reaction medium is crucial. No mechanistic information is available to distinguish between a direct one-electron reduction to

* Corresponding author. Tel.: +91 83622747121; fax: +91 8362747884.
E-mail address: stnandibewoor@yahoo.com (S.T. Nandibewoor).

0277-5387/$ - see front matter © 2004 Elsevier Ltd. All rights reserved.
doi:10.1016/j.poly.2004.08.016

Mn(VI) and a mechanism in which a hypomanganate is formed in a two-electron step followed by a rapid reaction [7].

The biological importance of coumarin derivatives as anticoagulants, aflatoxins, mycotoxins and antibiotics has led to a considerable amount of synthetic work in the field of coumarin for their pharmacological evaluation. 4-Hydroxycoumarin (4-hydroxy-2H-1-benzopyran-2-one) is used in the synthesis of pharmaceuticals especially for anticoagulants. It is used in manufacturing fluorescent dyes and rodenticides. Ichikawa et al. [8], reported that 4-hydroxy-3-sulfonamidocoumarins are used as antibacterial and antitubercular agents [9].

A literature survey reveals that there are no reports on the oxidative mechanism of 4-hydroxycoumarin by any oxidant. In view of the medicinal value, the present study deals with the title reaction to investigate the redox chemistry of permanganate in such media and to arrive at a plausible mechanism of the reaction based on kinetic and spectral results.

2. Experimental

2.1. Materials

All chemicals used were of reagent grade. A solution of 4-hydroxycoumarin (M/s. S.S. Antibiotics Pvt. Ltd., Aurangabad, India) was prepared by dissolving an appropriate amount of recrystallised sample in double distilled water. The purity of the sample was checked by TLC and its m.p. 212–214 °C. The preparation of other stock solutions are as given in an earlier paper [7].

2.2. Kinetic measurements

Since the initial reaction was too fast to be monitored by the usual methods, kinetic measurements were performed on a Peltier Accessory (Temperature Control) attached Varian CARY 50 Bio UV–Vis Spectrophotometer connected to a rapid kinetic accessory (HI-TECH SFA-12). All kinetic experiments followed are as given in the previous paper [7].

In the course of measurements, the solution changed from violet to blue and then to green. The spectrum of the green solution was identical to that of MnO_4^{2-}. It is probable that the blue colour originated from the violet of permanganate and the green from the manganate, excluding the accumulation of hypomanganate. The formation of Mn(VI) was also evidenced by a decreasing absorbance of Mn(VII) at 526 nm and an increasing absorbance of Mn(VI) at 608 nm during the course of the reaction (Fig. 1). The effect of dissolved oxygen, added carbonate and surface of the reaction vessel on the kinetics are studied as in the earlier paper [7].

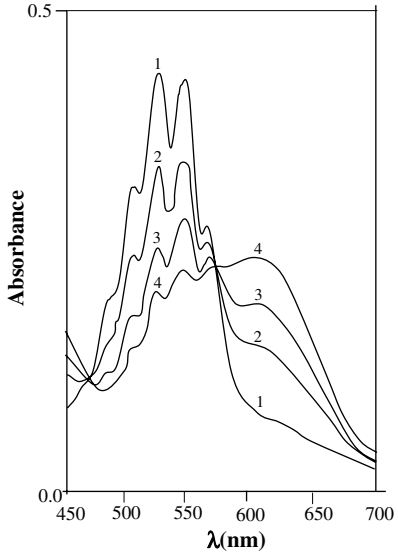

Fig. 1. Spectroscopic changes occurring oxidation of 4-hydroxycoumarin by permanganate with 10^3 [HDC] = 1.0, 10^4 [MnO_4^-] = 1.0, [OH^-] = 0.06 and I = 0.40 mol dm^{-3} at 25 °C, Scanning time interval = 60 s.

3. Results and discussion

3.1. Stoichiometry and product analysis

The reaction mixtures containing an excess of permanganate concentration over 4-hydroxycoumarin, constant 0.06 mol dm^{-3} NaOH and adjusted to an ionic strength of 0.40 mol dm^{-3} were allowed to react for 2 h at 25 ± 0.1 °C. The remaining permanganate was then analysed spectrophotometrically. The results indicated that 6.0 ± 0.2 mol of MnO_4^- were consumed by 1 mol of 4-hydroxy coumarin as given by the following equation:

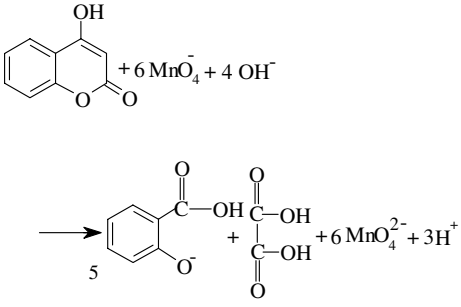

(1)

For identification of products, the reaction mixture containing an excess of 4-hydroxycoumarin was kept for completion of the reaction. The reaction product, salicylic acid, was extracted with ether and recrystallised from aqueous alcohol and the purity was checked by HPLC. This was identified as salicylic acid by its IR spectrum (KBr), which showed a band at (ν) 1701 cm^{-1} due to C=O stretching of the acid, a broad band at 2920 cm^{-1} due to O–H stretching of the acid and

3392 cm^{-1} due to phenolic OH. Salicylic acid was further characterised by its ^1H NMR spectrum ($CDCl_3$ + DMSO-d_6/TMS)δ, 5.74 (s, 1H, phenolic OH, disappeared on D_2O exchange), 7.27–7.82 (m, 4H, 4 aromatic protons), 11.5 (s, 1H, acidic OH, vanished on D_2O exchange). The product Mn(VI) was identified by its visible spectrum showing an absorbance maxima at 608 nm. Oxalic acid, which is highly soluble in water, was identified by a spot test [10]. It was observed that the salicylic acid and oxalic acid did not undergo further oxidation under the present kinetic conditions.

3.2. Reaction orders

The reaction orders were determined from the slopes of log k_{obs} versus log (concentration) plots by varying the concentration of the reductant and alkali in turn while keeping other conditions constant.

The potassium permanganate concentration was varied in the range of 4.0×10^{-5} to 4.0×10^{-4} mol dm^{-3}, and the linearity of plots of log absorbance versus time ($r \geqslant 0.9996$, $S \leqslant 0.0142$) up to 85% completion of the reaction, Fig. 2, indicated a reaction order of unity in [MnO_4^-]. This was also confirmed by variation of [MnO_4^-], which did not result in any change in the pseudo-first order rate constants, k_{obs} (Table 1). The substrate 4-hydroxycoumarin concentration was varied in the range 4.0×10^{-4} to 4.0×10^{-3} mol dm^{-3} at 25 °C while keeping all other reactant concentrations and conditions constant. The k_{obs} values increased with the increase in concentration of 4-hydroxycoumarin indicating an apparent less than unit order dependence on [4-hydroxycoumarin] (Table 1). The effect of alkali on the reaction has been studied at constant concentrations of 4-hydroxycoumarin, potassium permanganate, and a constant ionic strength of 0.40 mol dm^{-3}. The rate constants increased with increasing [alkali] and the order was found to be less than unity (Table 1).

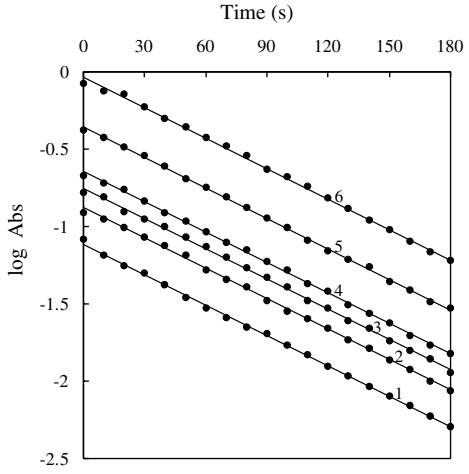

Fig. 2. First-order plots of oxidation of 4-hydroxycoumarin by permanganate aqueous alkaline medium at 25 °C. 10^4 [MnO_4^-] (mol dm^{-3}); (1) 0.4; (2) 0.6; (3) 0.8; (4) 1.0; (5) 2.0; (6) 4.0 (10^3 [HDC] = 1.0, [OH^-] = 0.06 and I = 0.40 mol dm^3).

3.3. Effect of ionic strength and relative permittivity

The effect of ionic strength was studied by variation of the $NaClO_4$ concentration in the reaction medium. The ionic strength was varied from 0.04 to 0.4 mol dm^{-3} at constant concentrations of permanganate, 4-hydroxycoumarin and alkali. It was found that the rate constants increased with increasing concentration of $NaClO_4$. The plot of log k_{obs} versus $I^{1/2}$ was linear with a positive slope (Fig. 3) ($r \geqslant 0.9995$, $S \leqslant 0.0144$).

The effect of relative permittivity (ε_T) on the rate constant has been studied by varying the t-butanol–water content in the reaction mixture with all other conditions being maintained constant. Attempts to measure the relative permittivities were not successful. However, they were computed from the values of pure liquids [11]. No reaction of the solvent with the oxidant occurred under the experimental conditions employed. The rate constant, k_{obs} increased with decreasing relative permittivity of the medium. The plot of log k_{obs} versus $1/\varepsilon_T$ was linear with a positive slope (Fig. 3) ($r \geqslant 0.9994$, $S \leqslant 0.0128$).

3.4. Effect of initially added products

The initially added products, such as manganate, salicylic acid and oxalic acid did not have any significant effect on the rate of the reaction.

3.5. Test for free radicals

The intervention of free radicals in the reaction was examined as follows. The reaction mixture to which a known quantity of acrylonitrile scavenger had been added initially was kept for one hour in an inert atmosphere. On diluting the reaction mixture with methanol, a precipitate resulted, suggesting the possibility of free radical intervention. The blank experiments of either MnO_4^- or 4-hydroxycoumarin with acrylonitrile alone did not induce polymerization under the same conditions as those induced with reaction mixture. Initially added acrylonitrile decreases the rate indicating the free radical intervention, which is the case in earlier work [12].

3.6. Effect of temperature

The rate of reaction was measured at different temperatures under varying 4-hydroxycoumarin concentrations. The rate of reaction increased with the increase of temperature. The rate constants, k of the slow step of Scheme 1 were obtained from intercepts of the plot

Table 1
Effect of variation of [permanganate], [HDC] and [OH^-] on oxidation of 4-hydroxycoumarin by permanganate in aqueous alkaline medium at 25 °C and $I = 0.40$ mol dm^{-3}

10^4 [MnO_4^-](mol dm^{-3})	10^3 [HDC] (mol dm^{-3})	[OH^-] (mol dm^{-3})	10^2 k_{obs} (s^{-1})	
			Found	Calculated
0.4	1.0	0.06	1.52	1.61
0.6	1.0	0.06	1.53	1.61
0.8	1.0	0.06	1.51	1.61
1.0	1.0	0.06	1.50	1.61
2.0	1.0	0.06	1.54	1.61
4.0	1.0	0.06	1.55	1.61
1.0	0.4	0.06	0.76	0.84
1.0	0.6	0.06	1.06	1.15
1.0	0.8	0.06	1.31	1.40
1.0	1.0	0.06	1.50	1.61
1.0	2.0	0.06	2.15	2.31
1.0	4.0	0.06	2.83	2.94
1.0	1.0	0.01	0.04	0.04
1.0	1.0	0.02	0.07	0.07
1.0	1.0	0.04	1.26	1.26
1.0	1.0	0.06	1.50	1.61
1.0	1.0	0.08	1.89	1.87
1.0	1.0	0.10	2.26	2.07

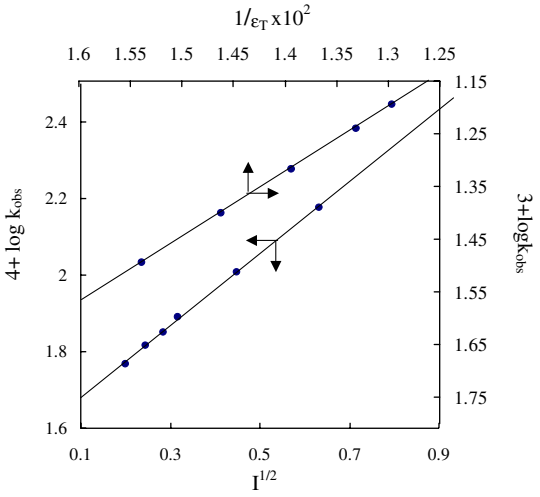

Fig. 3. Plots of log k_{obs} versus $I^{1/2}$ (a) and log k_{obs} versus $1/\varepsilon_T$ (b) (a) 10^3 [HDC] = 1.0, 10^4 [MnO_4^-] = 1.0 and [OH^-] = 0.06 mol dm^{-3} at 25 °C. (b) 10^3 [HDC] = 1.0, 10^4 [MnO_4^-] = 1.0, [OH^-] = 0.06 and $I = 0.40$ mol dm^{-3} at 25 °C.

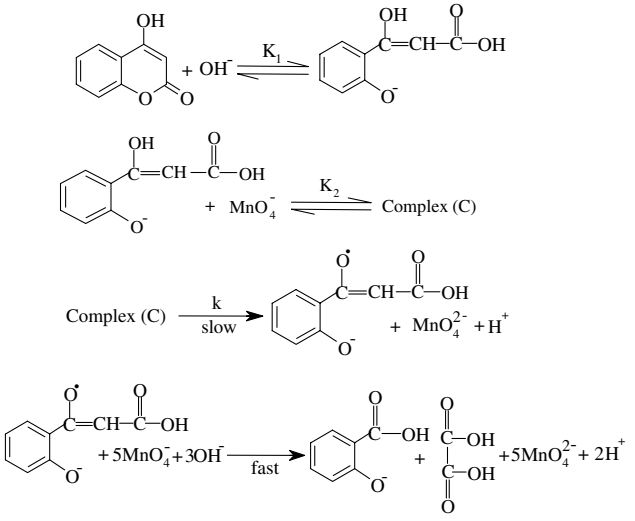

Scheme 1.

of $1/k_{obs}$ versus 1/[4-hydroxycoumarin] ($r \geqslant 0.9993$, $S \leqslant 0.0122$) and were used to calculate the activation parameters. The values of k (s^{-1}) are given in Table 2. The activation parameters corresponding to these constants were evaluated from the plot of log k versus $1/T$ ($r \geqslant 0.9998$, $S \leqslant 0.0134$) and are tabulated in Table 2.

The permanganate ion, MnO_4^-, is a powerful oxidant in an aqueous alkaline medium. As it exhibits many oxidation states, the stoichiometric results and pH of the reaction media play an important role. Under the prevailing experimental conditions at pH > 12, the reduction product of Mn(VII), i.e., Mn(VI), is stable and further reduction of Mn(VI) might be stopped [7]. Diode array rapid scan spectrophotometric (DARSS) studies have shown that at pH > 12, the product of Mn(VII) is Mn(VI) and no further reduction was observed as reported by Simandi et al. [13]. However, on prolonged standing, the green Mn(VI) is reduced to Mn(IV) under our experimental conditions.

The reaction between permanganate and 4-hydroxycoumarin in alkaline medium has a stoichiometry of

Table 2
Thermodynamic activation parameters for the oxidation of 4-hydroxycoumarin by permanganate in alkaline medium with respect to the slow step of Scheme 1

(A) *Effect of temperature*

Temperature (K)	10^2 k (s^{-1})
298	4.06 ± 0.12
303	4.93 ± 0.14
308	5.85 ± 0.18
313	6.98 ± 0.22
318	8.23 ± 0.32

(B) *Activation parameters for the slow step of Scheme 1*

Parameters	Values
$\Delta H^{\#}$ (kJ mol^{-1})	25 ± 1
$\Delta S^{\#}$ (JK^{-1} mol^{-1})	−187 ± 9
$\Delta G^{\#}$ (kJ mol^{-1})	83 ± 4

(C) *Effect of temperature to calculate K_1 and K_2 for the oxidation of 4-hydroxycoumarin by permanganate in alkaline medium*

Temperature (K)	K_1 (dm^3 mol^{-1})	$K_2 \times 10^{-3}$ (dm^3 mol^{-1})
298	1.64 ± 0.06	7.34 ± 0.45
303	2.87 ± 0.08	5.77 ± 0.34
308	4.52 ± 0.18	4.21 ± 0.22
313	8.18 ± 0.22	2.62 ± 0.12
318	13.0 ± 0.28	1.12 ± 0.03

(D) *Thermodynamic quantities using K_1 and K_2*

Thermodynamic quantities	Values from K_1	Values from K_2
ΔH (kJ mol^{-1})	82 ± 4	−71 ± 3
ΔS (JK^{-1} mol^{-1})	278 ± 10	−164 ± 8
ΔG (kJ mol^{-1})	−4.0 ± 0.2	−21 ± 1

6:1 with a first order dependence on the [MnO_4^-] and less than unit order dependence on both the [alkali] and [4-hydroxycoumarin]. No effect of added products was observed. Based on the experimental results, a mechanism can be proposed for which all the observed orders with respect to each constituent such as oxidant, reductant and OH^- may be well accommodated. Here, the 4-hydroxycoumarin reacts with alkali in a prior-equilibrium step to form an anionic form of (2Z)-3-hydroxy-3-(2-hydroxyphenyl)acrylic acid which reacts with one molecule of permanganate species to form a complex (C). This complex (C) decomposes in a slow step to liberate a free radical derived from (2Z)-3-hydroxy-3-(2-hydroxyphenyl)acrylic acid, and the product MnO_4^{2-}. K_2 is the equilibrium constant comprising the equilibrium to bind (2Z)-3-hydroxy-3-(2-hydroxyphenyl)acrylic acid to Mn. This radical in turn reacts with five more molecules of permanganate species in a fast step to yield the products as given in Scheme 1.

Probable structure of the complex (C) is given by

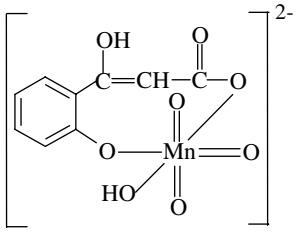

Spectroscopic evidence for the complex formation between oxidant and substrate was obtained from UV–Vis spectra of 4-hydroxycoumarin (1.0×10^{-3} mol dm^{-3}), permanganate (1.0×10^{-4}, [OH^-] = 0.06 mol dm^{-3}) and a mixture of both. A bathochromic shift of about 7 nm from 327 to 334 nm in the spectra of permanganate was observed and hyperchromicity was observed at 334 nm. This was also evident from the Michaelis–Menten plot, $1/k_{obs}$ versus 1/[HDC], (Fig. 4) and such complex formation between substrate and oxidant have also been observed in other studies [14]. Since Scheme 1 is in accordance with the generally well-accepted principle of non-complementary oxidations taking place in sequences of one-electron steps, the reaction between a substrate and oxidant would afford a radical intermediate. A free radical scavenging experiment revealed such a possibility (vide infra). This type of radical intermediate has also been observed in earlier work on the permanganate oxidation of various organic substrates in alkaline medium [15].

Scheme 1 leads to the rate law (5),

$$\text{Rate} = \frac{kK_1K_2[\text{HDC}][\text{MnO}_4^-][\text{OH}^-]}{(1+K_1[\text{OH}^-]+K_1K_2[\text{MnO}_4^-][\text{OH}^-])(1+K_1K_2[\text{HDC}][\text{OH}^-])} \quad (2)$$

In view of the low concentration of [MnO_4^-] used $1 + K_1[OH^-] + K_1K_2[MnO_4^-] \approx 1 + K_1[OH^-]$

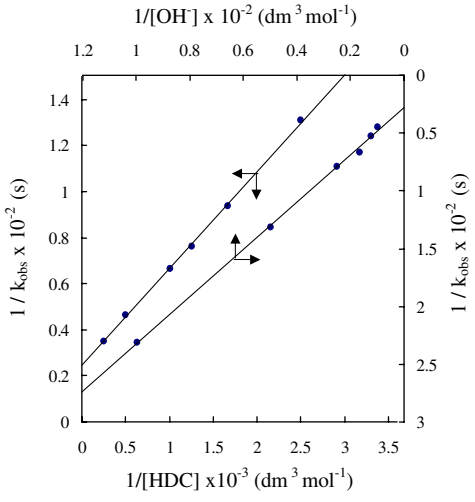

Fig. 4. Verification of rate law (5) in the form of (6) for the permanganate oxidation of 4-hydroxycoumarin in aqueous alkaline medium.

$$\text{Rate} = \frac{kK_1K_2[\text{HDC}][\text{MnO}_4^-][\text{OH}^-]}{(1+K_1[\text{OH}^-])(1+K_1K_2[\text{HDC}][\text{OH}^-])} \quad (3)$$

$$\text{Rate} = \frac{kK_1K_2[\text{HDC}][\text{MnO}_4^-][\text{OH}^-]}{1+K_1K_2[\text{HDC}][\text{OH}^-]+K_1^2K_2[\text{HDC}][\text{OH}^-]^2} \quad (4)$$

Neglecting the square terms in view of the low value compared to unity in the denominator,

$$\frac{\text{Rate}}{[\text{MnO}_4^-]} = k_{\text{obs}} = \frac{kK_1K_2[\text{HDC}][\text{OH}^-]}{1+K_1[\text{OH}^-]+K_1K_2[\text{HDC}][\text{OH}^-]} \quad (5)$$

Eq. (5) can be rearranged to Eq. (6), which is suitable for verification,

$$\frac{1}{k_{\text{obs}}} = \frac{1}{kK_1K_2[\text{HDC}][\text{OH}^-]} + \frac{1}{kK_2[\text{HDC}]} + \frac{1}{k} \quad (6)$$

According to Eq. (6), the plots of $1/k_{\text{obs}}$ versus 1/[4-hydroxycoumarin] ($r \geqslant 0.9993$, $S \leqslant 0.0122$) and $1/k_{\text{obs}}$ versus $1/[\text{OH}^-]$ ($r \geqslant 0.9996$, $S \leqslant 0.0212$) should be linear which is verified in Fig. 4. The slopes and intercepts of such plots lead to the values of K_1, K_2 and k at 25 °C of 1.64 ± 0.06 dm^3 mol^{-1}, $(7.34 \pm 0.45) \times 10^3$ dm^3 mol^{-1} and $(4.06 \pm 0.12) \times 10^{-2}$ s^{-1}, respectively. Using these values, the rate constants under different experimental conditions were calculated and compared with experimental data (Table 1). Experimental and calculated values agree reasonably well, which supplements Scheme 1.

The effect of ionic strength and solvent polarity on the rate of reaction in the present case is entirely different from that of earlier studies. In the case of the L-asparagine–$KMnO_4$ reaction [16], there was no effect of ionic strength and relative permittivity on the rate of reaction. In the case of L-phenylalanine [17] also the rate was independent of ionic strength. But in our present study the effect of increasing ionic strength on the rate explains qualitatively the reaction between two negatively charged ions, as seen in Scheme 1. The effect of solvent on the reaction rate has been described in detail in the literature [18]. Increasing the content of *t*-butanol in the reaction medium leads to an increase in the rate of reaction, which seems to be contrary to the expected interaction between neutral and anionic species in media of lower relative permittivity. However, an increase in the rate of reaction with decreasing relative permittivity may be due to stabilization of the complex (C) at low relative permittivity, which is less solvated than MnO_4^- at higher relative permittivity because of its larger size.

The thermodynamic quantities for the first equilibrium step in Scheme 1 can be evaluated as follows. The 4-hydroxycoumarin and hydroxide ion concentrations (as in Table 1) were varied at different temperatures. The plots of $1/k_{\text{obs}}$ versus 1/[HDC] ($r \geqslant 0.9993$, $S \leqslant 0.0122$) and $1/k_{\text{obs}}$ versus $1/[\text{OH}^-]$ ($r \geqslant 0.9996$, $S \leqslant 0.0212$) should be linear as shown in Fig. 4. From the slopes and intercepts, the values of K_1 are calculated at different temperatures and these values are given in Table 2. A van 't Hoff plot was made for the variation of K_1 with temperature [i.e., log K_1 versus $1/T$ ($r \geqslant 0.9997$, $S \leqslant 0.0201$)] and the values of the enthalpy of reaction ΔH, entropy of reaction ΔS and free energy of reaction ΔG, were calculated. These values are also given in Table 2. A comparison of the latter values with those obtained for the slow step of the reaction shows that these values mainly refer to the rate limiting step, supporting the fact that the reaction before the rate determining step is fairly slow and involves a high activation energy [19].

The negative value of $\Delta S^{\#}$ suggests that the intermediate complex is more ordered than the reactants [20]. The observed modest enthalpy of activation and a higher rate constant for the slow step indicates that the oxidation presumably occurs via an inner-sphere mechanism. This conclusion is supported by earlier observations [21,22]. The existence of two isobestic points as shown in the UV–Vis spectrum (Fig. 1) indicates [23] the presence of two equilibrium steps before the slow step of the mechanism (Scheme 1).

Appendix A

According to Scheme 1

$$\text{Rate} = k[\text{C}] = kK_1K_2[\text{HDC}]_f[\text{MnO}_4^-][\text{OH}^-]_f \quad (\text{I})$$

$$\begin{aligned}[\text{HDC}]_T &= [\text{HDC}]_f + [\text{HDC}^-] + [\text{C}] \\ &= [\text{HDC}]_f + K_1[\text{HDC}][\text{OH}^-] \\ &\quad + K_2[\text{HDC}^-][\text{MnO}_4^-] \\ &= [\text{HDC}]_f(1 + K_1[\text{OH}^-] + K_1K_2[\text{MnO}_4^-][\text{OH}^-])\end{aligned}$$

$$[\text{HDC}]_f = \frac{[\text{HDC}]_T}{1+K_1[\text{OH}^-]+K_1K_2[\text{MnO}_4^-][\text{OH}^-]} \quad (\text{II})$$

$$\begin{aligned}[\text{OH}^-]_T &= [\text{OH}^-]_f + [\text{HDC}^-] + \text{C} \\ &= [\text{OH}^-]_f(1 + K_1[\text{HDC}] + K_1K_2[\text{HDC}][\text{MnO}_4^-])\end{aligned}$$

$$[\text{OH}^-]_f = \frac{[\text{OH}^-]_T}{1+K_1[\text{HDC}]+K_1K_2[\text{HDC}][\text{MnO}_4^-]}$$

In view of the low concentration of $[\text{MnO}_4^-]$ and [HDC] used,

$$[\text{OH}^-]_f = [\text{OH}^-]_T \quad (\text{III})$$

$$\begin{aligned}[\text{MnO}_4^-]_T &= [\text{MnO}_4^-] + [\text{C}] \\ &= [\text{MnO}_4^-] + K_1K_2[\text{HDC}][\text{MnO}_4^-][\text{OH}^-] \\ &= [\text{MnO}_4^-]_f(1 + K_1K_2[\text{HDC}][\text{OH}^-])\end{aligned}$$

$$[MnO_4^-]_f = \frac{[MnO_4^-]_T}{1 + K_1K_2[HDC][OH^-]} \quad \text{(IV)}$$

Substituting Eqs. (II),(III) and (IV) in Eq. (I) (Subscripts T and f stand for total and free)

$$\text{Rate} = (kK_1K_2[HDC]_T[MnO_4^-]_T[OH^-]_T) / ((1 + K_1[OH^-] + K_1K_2[MnO_4^-][OH^-]) \times (1 + K_1K_2[HDC][OH^-]))$$

References

[1] R. Stewart, in: K.B. Wiberg (Ed.), Oxidation in Organic Chemistry, Part A., Academic Press, New York, 1965 (Chapter 1).
[2] A.J. Fatiadi, Synthesis 106 (1987) 85.
[3] D.G. Lee, E.J. Lee, K.C. Brown, Phase Transfer Catalysis, New Chemistry, Catalysts and ApplicationsACS Symposium Series No. 326, American Chemical Society, Washington, DC, 1987, p. 82.
[4] D.G. Lee, in: W.S. Trahanovsky (Ed.), Oxidation in Organic Chemistry, Part D, Academic Press, New York, 1982, p. 147.
[5] J.F. Perez-Benito, D.G. Lee, J. Org. Chem. 52 (1987) 3239.
[6] R. Stewart, K.A. Gardner, L.L. Kuehnert, J.M. Mayer, Inorg. Chem. 36 (1997) 2069.
[7] (a) S.A. Farokhi, S.T. Nandibewoor, J. Chem. Res. (S, M) (2003) 861;
(b) M. Jaky, I.V. Kozhevanikov, E. Hoft, Int. J. Chem. Kinet. 24 (1992) 1055.
[8] (a) M. Ichikawa, H. Ichibagase, Yakugaku Zasshi 86 (11) (1966) 1064;
(b) Chem. Abstr 60 (1967) 104869.
[9] (a) M. Ichikawa, H. Ichibagase, Chem. Pharm. Bull. 17 (11) (1969) 2384;
(b) Chem. Abstr. 72 (1970) 551604;
(c) T. Ichibagase, M. Ichikawa, S. Nagasaki, Jpn. Pat. 7019 (1970) 206;
(d) Chem. Abstr. 73 (1970) 66434.
[10] F. Feigl, Spot Tests in Organic Analysis, Elsevier, Amsterdam, 1975, p. 106.
[11] (a) D.R. Lide (Ed.), CRC Hand Book of Chemistry and Physics, 73 ed., CRC Press, London, 1992, p. 8;
(b) B. Thimme Gowda, M.C. Mary, Indian J. Chem. 40A (2001) 1196.
[12] (a) I.M. Kolthoff, E.J. Meehan, E.M. Carr, J. Am. Chem. Soc. 75 (1953) 1439;
(b) A.A. Frost, R.G. Pearson, Kinetics and Mechanism, Wiley Eastern (P) Ltd., New Delhi, 1970, p. 367.
[13] L.I. Simandi, M. Jaky, C.R. Savage, Z.A. Schelly, J. Am. Chem. Soc. 107 (1985) 4220.
[14] (a) S.V. Rao, V. Jagannadham, React. Kinet. Catal. Lett. 27 (1985) 239;
(b) S.K. Upadyaya, M.C. Agarwal, Indian J. Chem. 19A (1980) 478.
[15] (a) M. Jaky, M. Szeverenyi, L.I. Simandi, Inorg. Chim. Acta. 33 (1991) 186;
(b) D. Laloo, M.K. Mahanti, Polish J. Chem. 60 (1986) 589.
[16] M.R. Kembhavi, A.L. Harihar, S.T. Nandibewoor, Oxi. Commun. 23 (2000) 304.
[17] R.G. Panari, R.B. Chougale, S.T. Nandibewoor, Polish J. Chem. 72 (1998) 99.
[18] (a) E.A. Hughes Moelwyn, Physical Chemistry, 2nd ed., Pergamon Press, New York, 1961;
(b) E.S. Amis, Solvent Effects on Reaction Rates and Mechanisms, Academic Press, New York, 1966.
[19] K.S. Rangappa, M.P. Raghavendra, D.S. Mahadevappa, D. Channegowda, J. Org. Chem. 63 (1998) 531.
[20] (a) A. Weissberger, in: E.S. Lewis (Ed.), Investigation of Rates and Mechanism of Reactions in Techniques of Chemistry, Vol. 4, Wiley, New York, 1974, p. 421;
(b) S.A. Farokhi, S.T. Nandibewoor, Tetrahedron 59 (2003) 7595.
[21] N.N. Halligudi, S.M. Desai, S.T. Nandibewoor, Int. J. Chem. Kinet. 31 (1999) 189.
[22] M. Martinez, M.A. Pitarque, R.V. Eldik, J. Chem. Soc., Dalton Trans. (1996) 2665.
[23] (a) R. Chang, Physical Chemistry with Applications to Biological Systems, MacMillan, New York, 1981, p. 536;
(b) D.N. Sathyanarayana, Electronic Absorption Spectroscopy and Related Techniques, University Press (India) Ltd., Hyderabad, 2001, p. 12.

Available online at www.sciencedirect.com
SCIENCE DIRECT®
Polyhedron 23 (2004) 2515–2522
POLYHEDRON
www.elsevier.com/locate/poly

Model for type 2 Cu(II) oxidase: structure reactivity correlation studies on some mononuclear Cu(X–Salmeen)Im complexes, where X = H, Cl and Im = Imidazole: molecular association, electronic spectra and ascorbic oxidation

P.S. Subramanian *, E. Suresh, P. Dastidar

Analytical Science Division, Central Salt and Marine Chemicals Research Institute, Gijubhai Badgha Marg, Bhavnagar, Gujarat 364 002, India

Received 6 May 2004; accepted 23 August 2004
Available online 14 October 2004

Abstract

The compounds [Cu(Salmeen)(Im)(H_2O)](ClO_4) (**1**) and [Cu(Cl–Salmeen)(Im)(ClO_4)] (**2**), where Salmeen = *N*,*N*-dimethyethylenesalicylidenamine, were synthesized and characterized. The Copper(II) metal in both complexes [Cu(Salmeen)Im(H_2O)](ClO_4) (**1**) and [Cu(Cl–Salmeen)(Im)(ClO_4)] (**2**) possesses square pyramidal geometry, fulfilling the four corners of the square base with the Salmeen moiety and imidazole ligand, while the water and perchlorate anions occupy the axial position of the respective complexes. The weak inter and intra-dimeric H-bonding interactions mediated through heterocyclic nitrogens of imidazole, perchlorate anions and π–π stacking interactions between the aromatic rings and imidazole rings form an interesting supramolecular association. The electronic spectral studies indicate that the existence of weak apical coordination by water and perchlorate ions found in the solid state, is replaced by strong coordinating solvents such as DMSO in solution and thereby the opening of an active site for catalytic reaction is demonstrated with the reduction by the ascorbate dianion (Asc^{2-}) as a model for type-2 Cu(II) ascorbate oxidase. The self-assembled molecular association that favors the electron transfer redox process is demonstrated using UV–Vis electronic spectral studies.
© 2004 Elsevier Ltd. All rights reserved.

Keywords: Copper(II) complex; Ascorbic oxidation; Crystal structure; Imidazole

1. Introduction

Sacconi et al. [1] originally synthesized the Salmeen ligand in 1966. In continuation a number of substituted and modified Cu(II)–Salmeen schiff base complexes were synthesized and investigated for various research interests, due to their interesting geometrical [2], solvatochromic [3] and magnetic properties [2–4]. Monomeric, dimeric and multi-metallic complexes have also been synthesized and investigated for various applications. Szalda et al. [5] have made considerable effort to generalize the determination of the binding site and stereochemistry of the chelate metal system based on the stereo-selective metal ligand and ligand–ligand interactions by keeping the tridentate Salmeen ligand constant and varying purine [5], pyrimidine [6], cytosyine [6], adinine [7], etc. The various intra and intermolecular interactions originating from N-terminus of dimethylamine of ethylenediamine and phenolate oxygen of salicylaldehyde of these complexes were extensively studied [5–7]. In this continuing interest, the present report explores the molecular association in the solid state, the effect

* Corresponding author. Tel.: +912782567930; fax: +912782566970.
E-mail address: siva140@yahoo.co.in (P.S. Subramanian).

0277-5387/$ - see front matter © 2004 Elsevier Ltd. All rights reserved.
doi:10.1016/j.poly.2004.08.020

of substitution on the salicylaldehyde ring and consequent geometrical change in the Cu(II) environment in addition to its synthesis, electronic spectral studies and its reactivity, using ascorbic acid. The existence of weak intra and inter-pair molecular associations of both the complexes in the solid state are explored to favor the catalytic process. The Cu(II) being an ubiquitous bio-element, the present complexes **1** and **2**, possessing $[Cu(Salmeen)Im]^+$ as a common moiety together with square pyramidal geometry (4 + 1) with labile water and perchlorate apical coordination, inspired us to investigate their oxygen transfer process with ascorbic acid. In particular, oxidation of ascorbic acid using Cu(II) and oxygen deserves significant enzymatic importance in bioinorganic chemistry of ascorbic oxidase. Interestingly the ascorbate ion, a two electron donor, readily reduces both the Cu(II) complexes into their Cu(I) counterparts. Ascorbic oxidase has three types of copper centers in which the type-2 site belongs to the functional trinuclear copper cluster [8]. The Cu(II) in AO is coordinated to two histidine molecules and a water molecule. The primary role of the type-2 copper center is electron transfer, in which ascorbate under physiological reaction conditions acts as an electron donor. The reduced Cu(I) sites activate dioxygen and convert it to water involving four electrons and four protons in AO. The present mononuclear square pyramidal Cu(II) complexes possessing labile binding sites are of great importance for modeling the type-2 site of copper oxidases [9].

2. Experimental

Microanalyses of the complexes were done using a Perkin–Elemer PE 2400 series II CHNS/O elemental analyzer. Electronic spectra were recorded in several solvents using a UV–Vis spectrometer (HP Diode array spectrometer model 8452A).

2.1. Materials

The chemicals for the syntheses, ascorbic acid, *N*,*N*-dimethylethylenediamine and salicyladihyde, were received from Sigma–Aldrich and were used without further purification. All solvents were dried and distilled by standard methods prior to use [10].

CAUTION! Perchlorate salts of metal complexes are potentially explosive and should be handled in small quantity with care.

2.2. Preparation of the complexes

2.2.1. [Cu(N,N–Salmeen)(Im)(H_2O)](ClO_4) (**1**)

A schiff base condensation product was obtained by mixing equimolar ethanolic solutions of salicylaldehyde and *N*,*N*-dimethylethylenediamine, followed by constant stirring with gentle heating in a water bath. To this yellow colored oily schiff base product, an equivalent amount of an alcoholic solution of $CuSO_4 \cdot 5H_2O$ (0.5 mmol) was added gradually. An aqueous solution of 0.5 mmol $NaClO_4 \cdot H_2O$ and an ethanolic solution of 0.5 mmol imidazole were added successively. The change in color from yellow to blue and then dark green upon addition of imidazole was observed. *Anal.* Calc. for $CuC_{14}H_{22}N_4O_7Cl$: C, 36.5; H, 4.9; N, 12.8. Found: C, 36.80; H, 4.81; N, 12.26%. UV–Vis [CH_3CN, λ_{max}, nm, (ε, M^{-1}, cm^{-1})], 308(3030), 374(2840), 600(180).

2.2.2. [Cu(Chloro-N,N–Salmeen)(Im)(ClO_4)] (**2**)

The above procedure was repeated except with the addition of 5-Chlorosalicylaldehyde in place of salicylaldehyde. *Anal.* Calc. for $C_{14}H_{18}N_4Cl_2O_5Cu$: C, 36.92; H, 3.95; N, 12.3. Found: C, 36.91; H, 4.14; N, 12.17%. UV–Vis [CH_3CN, λ_{max}, nm, (ε, M^{-1}, cm^{-1})], 306(2700), 384(2600), 602(200).

2.3. X-ray crystallographic analysis

Data collection for both crystals were carried out on an Enraf–Nonius CAD-4 diffractometer with graphite monochromatised Mo Kα radiation (λ = 0.7107 Å). Cell constants and the orientation matrix for data collections for both crystals were obtained from least squares refinement using 25 high angle reflections within the θ range 8–12°. The $\omega - 2\theta$ scan mode, with a maximum θ value being 24.93° and 22.42°, were used to collect the intensity data for complex **1** and complex **2**, respectively. Preliminary data, cell refinement and intensity data collection were carried out using the program CAD4-PC [11] and the data reduction using NRCVAX [12]. The data were corrected for Lorentz Polarization effects but not for absorption. The structure solution was carried out using direct methods with full-matrix least-squares refinement on F^2 using SHELXL-97 [13]. Scattering factors and anomalous dispersion were taken from the International Tables for X-ray Crystallography [14]. Hydrogen atoms were located either from the difference Fourier map or kept fixed using the riding model using the program SHELXL-97.

3. Results and discussion

3.1. Crystal structure and molecular association

ORTEP views along with an atom-numbering scheme for **1** and **2** are shown in Figs. 1 and 2. A summary of the crystallographic data, selected bond lengths and angles for complex **1** and **2** are given in Tables 1 and 2, respectively. The Schiff base ligand obtained by condensation of salicylaldehyde and *N*,*N*-dimethylethylenedi-

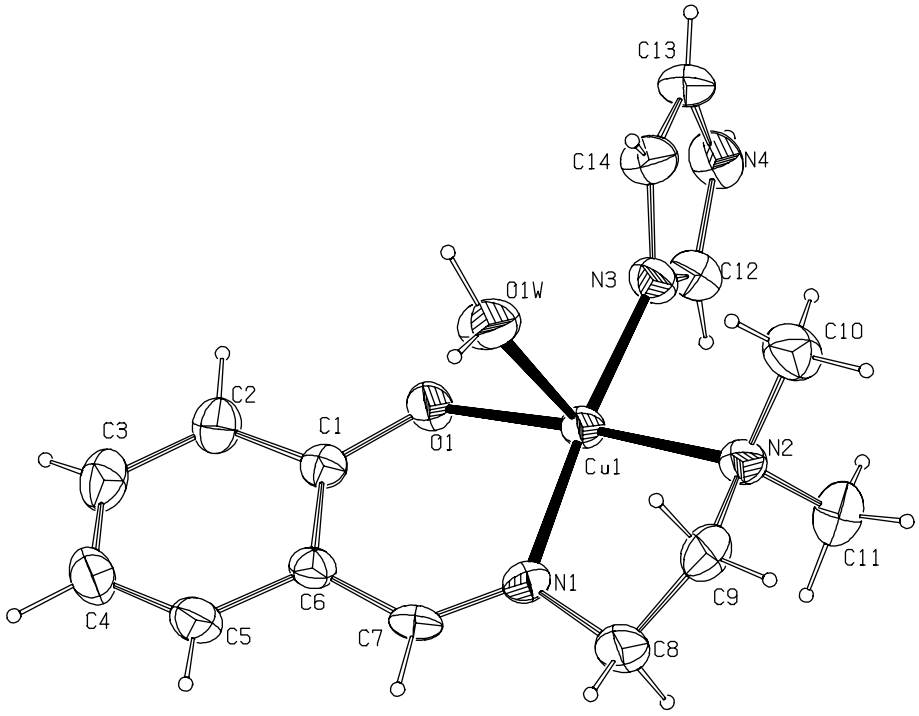

Fig. 1. ORTEP diagram (50% probability for thermal ellipsoids) of complex **1** with the atom numbering scheme.

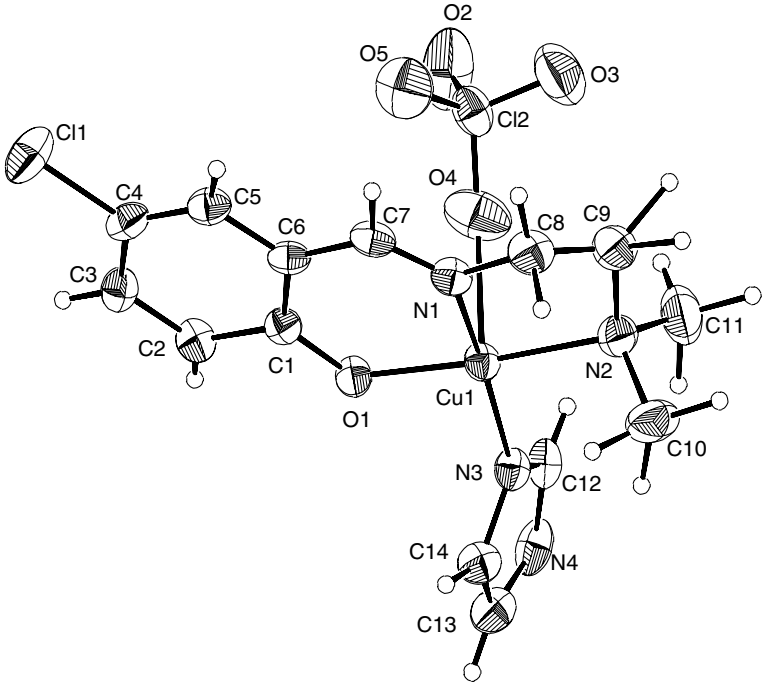

Fig. 2. ORTEP diagram (50% probability for thermal ellipsoids) of complex **2** with the atom numbering scheme.

amine, is basically a mono-anionic tridentate ligand. The metal ion in complexes **1** and **2** forms a square pyramidal geometry and the square base is occupied by the Salmeen and Cl–Salmeen moiety along with imidazole. The longer water coordination in complex **1** (Cu1–O1w = 2.469(5) Å) and perchlorate anion (Cu1–O4 = 2.618 Å) in complex **2** occupies the apical position and completes the N3O2 square pyramidal geometry of the Cu1 atom. The average Cu–N distance (1.991 Å) and Cu–O1 distance (1.936(3) Å) of the square base

Table 1
Summary of crystallographic data for complexes **1** and **2**

Chemical formula	$C_{14}H_{21}Cl_1Cu_1N_4O_6$(**1**)	$C_{14}H_{18}Cl_2Cu_1N_4O_5$ (**2**)
Formula weight	440.34	456.76
a (Å)	8.862(6)	8.476(3)
b (Å)	10.209(6)	12.406(3)
c (Å)	10.976(4)	17.053(2)
α (°)	75.72(4)	90.00
β (°)	78.01(2)	91.05(3)
γ (°)	70.40(5)	90.00
Z	2	4
V (Å^3)	898.1(9)	1792.9(9)
Crystal system	triclinic	monoclinic
Space group	$P\bar{1}$	$P2_1/c$
Radiation used λ (Å)	0.7107 Å	0.7107
$\rho_{calc.}$ (g cm^{-3})	1.628	1.692
Absorption coefficient, μ (cm^{-1})	8.98	15.50
Temperature (K)	300	300
Final $R(F_0^2)$[a]	0.0450	0.0406
Weighted $R(F_0^2)$[b]	0.1299	0.1032

[a] $R = \sum ||F_o| - F_c|| / \sum |F_o|$.
[b] $R_w = [\sum w(F_o^2 - F_c^2)^2] / \sum [w(F_o^2)^2]^{1/2}$; $w = 1/\sigma(F_o)^2$.

Table 2
Selected bond distances and angles for complexes **1** and **2** with estimated standard deviations in the parenthesis

	1	**2**
Bond lengths (Å)		
Cu(1)–N(1)	1.944(4)	1.932(2)
Cu(1)–N(2)	2.092(5)	2.069(3)
Cu(1)–N3	1.985(3)	1.981(3)
Cu(1)–O(1)	1.960(5)	1.936(3)
Cu(1)–O(1W)	2.469(5)	–
Cu(1)–O(4)	–	2.618(4)
Bond angles (°)		
N(1)–Cu(1)–O(1)	92.4(3)	92.77(12)
N(1)–Cu(1)–N(2)	84.9(3)	84.48(13)
N(1)–Cu(1)–N(3)	173.48(12)	168.95(13)
N(3)–Cu(1)–N(2)	94.1(4)	95.09(13)
O(1)–Cu(1)–N(3)	89.4(4)	88.17(11)
O(1)–Cu(1)–N(2)	176.15(11)	176.01(12)
N(1)–Cu(1)–O(1W)	86.90(13)	
O(1)–Cu(1)–O(1W)	90.8(5)	
N(3)–Cu(1)–O(1W)	99.32(14)	
N(2)–Cu(1)–O(1W)	90.15(5)	

coordination for complex **2** is well within the range of reported [Cu(salen)] complexes [15,16]. In complex **1**, the metal center is displaced by 0.057 Å, with a considerable deviation of the coordinated atoms from the N3O plane towards the apically coordinated perchlorate oxygen O4 and the "Sal" unit makes an angle of 7.71(2)° with respect to the N3O2 plane. Both the *trans* atoms, i.e., the atoms from the "Salmeen" moiety N2 and O1 (N2 = 0.100 Å and O1 = 0.150 Å) and imidazole N3 and "Salmeen" N1 (N3 = −0.135 Å and N1 = −0.126 Å) are displaced in the same direction. The degree of distortion on the Cu(II) geometry (τ) in both these square pyramidal complexes can be easily measured by the approach of Addison and coworkers [17], using the distortion parameter (τ). According to Addison and coworkers [17] perfect square pyramidal and trigonal bipyramidal geometries should have τ values ($=\beta - \alpha/60$ where β and α are the *trans* angles, i.e., ∠N(3)–Cu(1)–N(1) = 173.48°; and N(2)–Cu(1)–O(1) = 176.15°) of zero and unity, respectively. The τ values in the present case, calculated as 0.0428 and 0.1177 for **1** and **2**, respectively, indicates that the distortion in the former is negligible, when compared to the perfect square pyramid, resembling the recently reported square pyramidal complexes [Cu(salphe)(bpy)] ($\tau = 0.09$) [18] and $Cu(Salmeen)_2$ ($\tau = 0.098$) [19], while the later compound resembles $Cu(salala)(bpy)\cdot 4H_2O$ ($\tau = 0.10$) [18]. The torsion angle of the ethylenediamine collar of the ligand moiety (torsion angle N1–C8–C9–N2 = −50.14°) shows buckled conformation with displacement of C8 (−0.249 Å) and C9 (+0.250) carbon atoms in the opposite direction from the CuN1N2 plane. The average Cu–N distance is 1.999 Å in complex **1** is similar to that in complex **2,** whereas the Cu1–O1 distance (1.960(5) Å) is longer by 0.024 Å, which may be due to the more numerous and stronger H-bonding interactions of O1 in **2**. The Cu1 atom in **1** is displaced by 0.065 Å from the N3O plane towards the apical coordinated water molecule. The *trans* atoms of the basal plane, O1 and N2 of the "Cl–Salmeen" moiety, are displaced by 0.042 and 0.041 , where as N1 and N3 are displaced by −0.044 and −0.040 Å, respectively, in the opposite direction. The ethylenediamine collar makes a five membered chelate ring with the metal center in a buckled conformation (torsion angle N1–C8–C9–N2 = −47.98°), as observed in **1**, with the C8 and C9 atoms displaced by 0.260 and −0.260 Å, respectively, from the CuN1N2 plane.

The packing diagram for complex **1** viewed down the *a*-axis is shown in Fig. 3. Pairs of the cationic part of the molecules are associated via stacking of the imidazole ring and are arranged along the *b*-axis. The cationic part of the molecules are packed along the *a*-axis with O–H···O and N–H···O H-bonding interactions between O1w, O1 and N4, O1 from adjacent molecules, extending a H-bonded linear chain along the *a*-axis. The perchlorate anions are arranged between the adjacent cationic layers, and the O3 and the O4 perchlorate oxygen atoms act as acceptors in the O–H···O and C–H···O interactions with the cationic moiety to stabilize the molecule in the crystal lattice and connect the adjacent layers along the *c*-axis to form a two dimensional H-bonded network. The nearest Cu···Cu distance between the molecules within the H-bonded linear chain along the *a*-axis is 5.685(2) Å. In addition to the H-bonding interactions, there is a C–H···π interaction of the imidazole hydrogen with the aromatic ring between the neighboring molecule within the layer (C14–

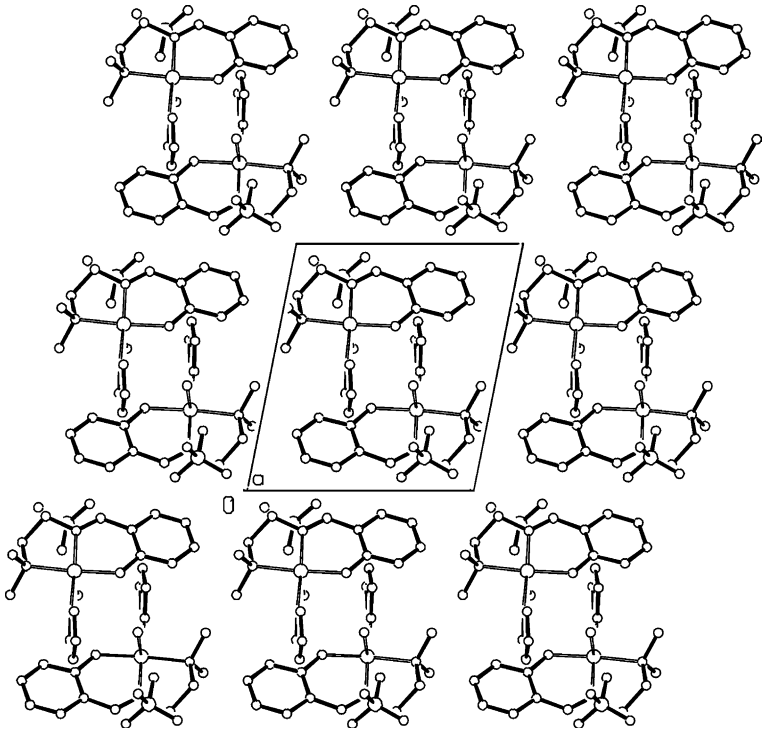

Fig. 3. Packing diagram of complex **1** viewed down the *a*-axis showing the molecular association.

H14···Cg, H14···Cg = 2.768 Å and ∠C14–H14···Cg = 146.63°, where Cg is the center of gravity of the C1–C6 ring). The intra-pair imidazole rings make a significant offset π–π interaction between the C12 carbons (C12–C12 = 3.12 Å) and N3–N4 nitrogens (N3···N4 = 3.648 Å).

The $[Cu(Cl–Salmeen)(Im)]^{+1}$ moiety is associated in pairs due to the intermolecular N–H···O hydrogen bonding interaction between the imidazole nitrogen and the phenolate oxygen (N4···O1 = 2.84(2) Å; ∠N4–H1N4···O1 = 152.9(1)°). Due to this strong H-bonding interaction the imidazole rings make an effective intra pair stacking and the centroid (Cg1)···centroid (Cg1) distance of the stacked imidazole rings is 3.39(2) Å. In addition to the N–H···O H-bonding within the pairs, the pyrrole proton H14 of imidazole is oriented in such a way to make a good C–H···π interaction (H1N4···Cg1 = 3.018 Å; ∠N4–H1N4···Cg1 = 91.2° where C1g is the centroid of the imidazole ring N3 to C14). The Cu···Cu distance within this pair is 7.31 Å. The phenyl rings of the Cl–sal ligand of the hydrogen-bonded pair are involved in π···π offset stacking from either side with the adjacent associated molecules (C2g···C2g = 3.78 Å, where C2g is the centroid of the phenyl ring C1 to C6), extending the pairs to form a one-dimensional corrugated chain along the *b*-axis. These corrugated chains are cross linked along the *c*-axis through C–H···O H-bonding from the perchlorate oxygens O2 and O5 and C–H···Cl interactions with the neighboring chains to form an extended two-dimensional corrugated sheet-like architecture. The various H-bonding interactions with their symmetry codes for compounds **1** and **2** are given in Table 3.

3.2. Electronic spectra

Both these compounds are green in color and are soluble in almost all solvents. The electronic spectral data recorded in various solvents are very similar for compounds **1** and **2** and are shown in Table 4. The characteristic UV peak obtained approximately at 370 nm (ε = 2800–3000) and 600 nm (ε = 120–200) corresponds to the Cu(II) → phenolate MLCT band [20,19] and d–d transition respectively. The peak appearing around 300 nm (ε = 2800–3000) can be attributed to the $\sigma(N) \rightarrow Cu(II)$ LMCT band. The electronic spectra recorded for complexes **1** and **2** in various solvents indicate the effect of solvent with significant red shift in their d–d transition. The bathochromic shift observed for their d–d band follows the Gutmann Donor [21] capacity of the solvent in the ascending order, acetonitrile ⩽ acetone < DMF < water < methanol < DMSO (Table 4). The broad symmetric and metal centered d–d transition appeared approximately at 600 nm in acetonitrile and acetone matches well with the reported UV–Vis values for the square planar geometry [22]. But the existence of square pyramidal geometry in strong coordinating solvents such as DMSO for both the complexes, by replacing the weak water and perchlorate coordination and accommodating the solvent mol-

Table 3
Hydrogen bonding table for complexes **1** and **2**

D–H···A	H···A (Å)	D···A (Å)	∠D–H···A (°)
Complex **1**			
O1w–H1O1···O1[1]	H1O1···O1 = 1.977(1)	O1w···O1 = 2.929(2)	∠O1w–H1O1···O1 = 152.9(1)
O1w–H2O1···O3[1]	H2O1···O3 = 2.175(2)	O1w···O5 = 2.892(1)	∠O1w–H2O1···O3 = 149.8(2)
N4–H1N4···O1[2]	H1N4···O1 = 2.033(2)	N4···O1 = 2.814(2)	∠N4–H1N4···O1 = 170.13(1)
C12–H12···O3[2]	H12···O3 = 2.540(3)	C12···O3 = 3.421(2)	∠C12–H12···O3 = 165.54(2)
C8–H81···O4[3]	H81···O4 = 2.480(2)	C8···O4 = 3.366(2)	∠C8–H81···O4 = 136.91(2)
C9–H92···O5[3]	H103···O5 = 2.471(1)	C10···O5 = 3.519(2)	∠C10–H103···O5 = 162.18(2)
Complex **2**			
N4–H1N4···O1[1]	H4···O1 = 2.161(1)	N4···O1 = 2.835(2)	∠N4–4···O1 = 152.9(1)
C7–H7···O5[2]	H7···O5 = 2.410(2)	C7···O5 = 3.409(1)	∠C7–H7···O5 = 177.9(2)
C9–H92···O2[3]	H92···O2 = 2.404(2)	C9···O2 = 3.513(2)	∠C9–H92···O2 = 151.68(1)
C10–H101···Cl1[4]	H101···Cl1 = 2.588(4)	C10···Cl1 = 3.708(3)	∠C10–H101···Cl1 = 155.65(2)
C10–H103···O5[3]	H103···O5 = 2.471(1)	C10···O5 = 3.519(2)	∠C10–H103···O5 = 162.18(2)

Symmetry code: 1 = 1 − *x*, 1 − *y*, 1 − *z*. 2 = −*x*, 1 − *y*, 1 − *z*. 3 = *x*, 1 + *y*, −1 + *z*.
Symmetry code: 1 = 1 − *x*, −*y*, −*z*. 2 = 1 − *x*, 0.5 + *y*, 0.5 − *z*. 3 = 1 + *x*, *y*, *z*. 4 = 1 − *x*, 1 − *y*, −*z*.

Table 4
Electronic spectral data for compounds [Cu(Salmeen)(Im)(H_2O)](ClO_4) (**1**) and [Cu(Cl–Salmeen)(Im)(ClO_4)] (**2**) in various solvents

Solvent	DN	[Cu(Salmeen)(Im)(H_2O)](ClO_4) (**1**)		[Cu(ClSalmeen)(Im)(ClO_4)] (**2**)	
		Ligand centered transition	d–d transition	Ligand centered transition	d–d transition
CH_3CN	14.1	308(3033), 374(2838)	600(182)	306(2698), 384(2626)	602(200)
Acetone		366(3032)	598(200)	384(2605)	606(182)
DMF	26.6	298(2959), 370(2775)	618(142)	302(2960), 380(2954)	624(163)
Water	18	298(2960), 358(2796)	622(129)	264(2356), 368(1894)	624(62)
MeOH	19.1	302(3015), 370(2841)	622(174)	266(2445), 380(2025)	626(74)
DMSO	29.8	304(2870), 370(2786)	634(148)	304(2535), 380(2508)	636(152)

ecule in its apical position, is evident from the shift of the d–d band from 600 to 636 nm.

The fifth coordination being so labile in strong coordinating solvents such as DMSO has inspired us to investigate their catalytic capability using ascorbic acid.

3.3. Ascorbic oxidase

Ascorbic acid, a common reducing agent such as 3,5-di-*tert*-butyl catechol (DTBC), is an efficient two-electron transfer system. Complexes **1** and **2** are readily reduced to Cu(I) in an aqueous methanolic solution at pH 8.4 by ascorbic acid and form a partially unstable brown Cu(I) species. The complete disappearance of the d–d band as shown in Fig. 4 (complex **1**) and Fig. 5 (complex **2**) upon addition of a methanolic solution of ascorbic acid indicates the stepwise reduction of the vacant d^9 Cu(II) system, becoming a filled d^{10} Cu(I) species. But the partial reappearance of the d–d band after a given time gap indicates that the Cu(I) species, when

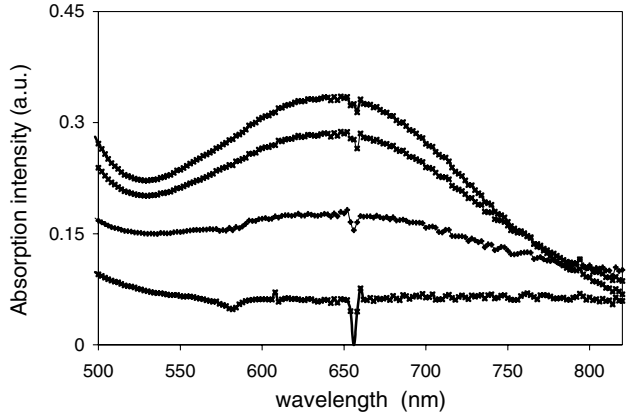

Fig. 4. Electronic spectra for **1** showing the stepwise reduction of Cu(II) to Cu(I) upon addition of ascorbic acid.

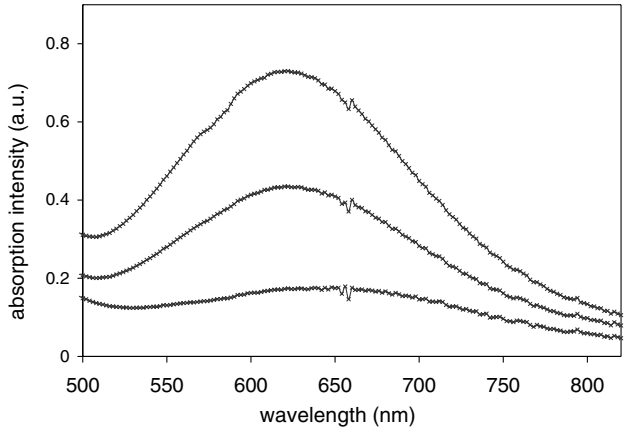

Fig. 5. Electronic spectra for **2** showing the stepwise reduction of Cu(II) to Cu(I) upon addition of ascorbic acid.

exposed to air, takes oxygen and converts into a Cu(II) species as shown below:

$$2[Cu(Salmeen)(Im)(H_2O)](ClO_4) + H_2A \rightarrow 2[Cu(I)(Salmeen)(Im)](ClO_4) + A\cdots \quad (1)$$

$$2[Cu(I)(Salmeen)(Im)](ClO_4) + O_2 + 2H^+ \rightarrow 2[Cu(Salmeen)(Im)(H_2O)](ClO_4) + 2H_2O\cdots \quad (2)$$

The self assembled Cu(II) pairs, as observed in the crystal structure, dissociate into monomeric species and are involved in the electron transfer process. The present complexes **1** and **2** effectively catalyze the ascorbic acid to oxalic acid at a [H_2A]:[complex] mole ratio of 51:1 and 48:1, respectively. The catalytic capability based on the mole ratio of [H_2A]:[complex] indicates that the present compounds are good oxidation catalysts for the oxidation of ascorbic acid compared to the Cu(II) thiosemicarbazone [23] compounds reported by Chakravarty et al, which show a [H_2A]:[complex] mole ratio of 120:1, but a little less effective with respect to [Cu(salgly)(bpy) · $4H_2O$], [Cu(salphe)(bpy)] and [Cu(salala)(bpy) · $4H_2O$] [18] which exhibit ratios of 25:1, 30:1 and 35:1, respectively.

By looking at the molecular association of the solid state, it is obvious that the intra-dimeric H-bonded pairs are dissociated into monomeric species in solution. Ascorbic acid replaces the weak water and perchlorate axial contacts in complexes **1** and **2** in a similar manner to DMSO as indicated in the UV–Vis spectral study (Table 4). Due to the coordination of the imidazole group between the Cu centers in the intra-pair H-bonded association, the intra-pair Cu–Cu distance exceeds more than 7 Å in compound **2** and are not suitable for the binding of the ascorbate as it exceeds the reported optimum distance [24a]. The perpendicular conformational arrangements of the phenyl and imidazole ring and the longer Cu–Cu intra-pair distance jointly forces the ascorbic acid to coordinate with Cu(II) through the inter-pair space available between the phenyl rings by replacing the weak water/perchlorate contacts and thereby facilitate the electron transfer.

3.4. Molecular association and reactivity correlation

The plane of the aromatic benzene ring and the imidazole heterocyclic rings are aligned perpendicular to each other in both complexes. In addition to various other intermolecular interactions, the H-bond connecting the pyrrole nitrogen of the imidazole and phenolate oxygen of the 'Sal' group coordinated to the Cu(II) metal center plays a significant role towards bringing them close, to approximately 2.8 Å *via* ImN(4)–H(1)–O(1)(phenolate). The existence of a π···π stacking interaction between the imidazole rings plays an important role for the formation of intra-pair assembly in both complexes. While an aromatic π–π interaction between the benzene rings stabilize the inter-pair molecular association; the imidazole rings stabilize the intra-pair association through their strong H-bonding network routed through (Im)N–H···O(phenolate). The intra-pair stacking interaction between the imidazole rings ($d_{\pi-\pi}$ = 3.39(2) Å) is found to be more tightly arranged than the inter-pair stacking of the phenyl rings ($d_{\pi-\pi}$ = 3.78(3) Å).

The weak inter-pair π–π stacking association between the benzene rings ($d_{\pi-\pi}$ = 3.78(3) Å) and the intra-pair imidazole rings (d_{Im-Im} = 3.39 Å) play an important role for this novel molecular assembly and facilitates the two-electron transfer catalytic reaction. The Cu–Cu separation calculated through the self-assembled imidazole H-bond spacer exceeds more than 7 Å, while the inter-pair distance between the benzene ring is 3.78 Å.

A detailed analysis carried out by Kao et al. [24a] and other reports [24a–d], show a fine correlation between the optimum geometrical Cu–Cu distance and the catalytic activity of DTBC and ascorbic acid. The dinuclear copper complexes with a Cu–Cu distance between 2.9 and 3.0 Å apparently show higher activity. The approximate Cu–Cu distance of about 3 Å is considered to be the basic criteria for an efficient electron transfer process in ascorbic oxidation and catechol oxidase to take place.

It may be tentatively proposed that the ascorbic acid may approach between the inter-pair stacked phenyl rings assembled by the π–π interaction, thereby replacing the apically coordinated water/perchlorate molecules, and bind the two copper (II) centers to facilitate electron transfer.

4. Conclusion

Compounds **1** and **2** containing *N*,*N*-dimethylethylenesalicyladimine and *N*,*N*-dimethylethylene-chlorosalicyladimine ligands were synthesized and characterized. The self assembled weak intra and inter-pair association, mediated by imidazole and aromatic benzene rings, play a significant role in their catalytic processes upon reduction of ascorbic acid and control the coordination site for catalytic reaction. The intra-pair distance mediated by the imidazole ring, being more than 7 Å, and the perpendicular conformation of the benzene ring and imidazole ring with in the molecule cooperatively adopt the ascorbic acid to coordinate to the Cu(II) centres. However the intra-pair dicopper distance is very close to the expected theoretical value for the binding of ascorbic acid, so it is concluded that the intra-pair assembly is dissociated but the inter-pair association is retained due to the binding of the ascorbic acid in solution, which favors the electron transfer process from ascorbic acid to the Cu(II) active site. The study of the

oxidation of catechol and substituted catechols, such as 3,5-DTBC, to the corresponding quinone is under progress.

5. Supporting information available

CCDC 237638 and 237639 contains the supplementary crystallographic data for these complexes. These data can be obtained free of charge at www.ccdc.cam.ac.uk/conts/retrievel.html or from the Cambridge Crystallographic Data Center, 12, Union Road, Cambridge CB2 1EZ, UK; Fax (internet.). +44-1223/336-033. e-mail: deposit@ccdc.ac.uk.

Acknowledgement

The authors greatly acknowledge Dr. P.K. Ghosh Director of the Central Salt and Marine Chemicals Research Institute for his keen interest and encouragements.

References

[1] (a) L. Sacconi, I. Bertini, Inorg. Chem. 5 (1966) 1520;
(b) M. Calligaris, L. Randaccio, in: G. Wilkinson, R.D. Gillard, J.A. McCleverty (Eds.), Comprehensive Coordination Chemistry, vol. 2, Paragon Press, Oxford, 1987, p. 730 (Chapter 20.1).
[2] T. Tokii, M. Kaneko, K. Yamanaka, Y. Muto, M. Kato, Bull. Chem. Soc. Jpn. 52 (1979) 3751.
[3] (a) T. Tokii, Y. Muto, Bull. Chem. Soc. Jpn. 51 (1978) 139;
(b) T. Tokii, T. Tenhiro, Y. Muto, Bull. Chem. Soc. Jpn 54 (1981) 2217.
[4] R. Sakamoto, M. Ohba, N. Fukita, K. Takahashi, H. Okawa, L.K. Thompson, Bull. Chem. Soc. Jpn. 71 (1998) 2365.
[5] (a) D.J. Szalda, T.J. Kistenmacher, L.G. Marzilli, J. Am. Chem. Soc. 98 (1976) 8371;
(c) T.J. Kistenmacher, D.J. Szalda, C.C. Chiang, M. Rossi, Inorg. Chem. 17 (1978) 2582.
[6] D.J. Szalda, L.G. Marzilli, T.J. Kistenmacher, Inorg. Chem. 14 (1975) 2076.
[7] D.J. Szalda, T.J. Kistenmacher, L. Marzilli, Inorg. Chem. 14 (1975) 2623.
[8] A. Messerschmidt, A. Rossi, R. Landenstein, R. Huber, M. Bolognesi, G. Gatti, A. Marchesini, R. Petruzzelli, A. Finazzi Agro, J. Mol. Biol. 206 (1989) 513.
[9] P.S. Subramanian, E. Suresh, P. Dastidar, S. Waghmode, D. Srinivas, Inorg. Chem. 40 (2001) 4291.
[10] D.D. Perrin, W.L.F. Armarego, D.R. Perrin, Purification of Laboratory Chemicals, Pergamon Press, Oxford, 1980.
[11] CAD4 – PC Software, Version 5, Enraf-Nonius, Delft, 1989.
[12] E.I. Gabe, Y. Le Page, I.P. Charland, F.L. Lee, P.S. White, J. Appl. Cryst. 22 (1989) 384.
[13] G.M. Sheldrick, SHELX-97. Program for Crystal Structure Determination, University of Göttingen, Germany, 1997.
[14] International Tables for X-ray Crystallography, vol. IV, Kynoch Press, Birmingham.
[15] D. Srinivas, M. Bhadbhade, Inorg. Chem. 32 (1993) 6122.
[16] E. Suresh, M. Bhadbhade, D. Srinivas, Polyhedron 15 (1996) 4133.
[17] A.W. Addison, T.N. Rao, Jan Reedijik, J. Van Rijn, G.C. Verschoor, J. Chem. Soc., Dalton Trans. (1984) 1349.
[18] P.A.N. Reddy, M. Nethaji, A.R. Chakravarty, Inorg. Chim. Acta 337 (2002) 450.
[19] P. Bandyopadhyay, P. Ghosh, P.K. Bardwaraj, Indian J. Chem. 37A (1998) 639.
[20] B.P. Kennedy, A.B.P. Lever, J. Am. Chem. Soc. 95 (1973) 6907.
[21] Gutmann Donor (GN) was chosen as a measure of the Lewis basicity of solvent molecules; V. Gutmann, The Donor Acceptor Approach to Molecular Interactions, Plenum press, New York, 1978; V. Gutmann, Coordination Chemistry in Non-aqueous Solutions, Springer, Vienna, 1968.
[22] B.J. Hathaway, in: G. Wilkinson, R.D. Gillard, J.A. McCleverty (Eds.), Comprehensive Coordination Chemistry, vol. 5, Pergamon, Oxford, 1987, p. 558 (Chapter 53).
[23] A.K. Naik, P.A.N. Reddy, M. Nethaji, A.K. Chakravarty, Inorg. Chim. Acta 349 (2003) 149.
[24] (a) C.-H. Kao, H.-H. Wei, Y.-H. Liu, G.-H. Lee, Y. Wang, C.-J. Lee, J. Inorg. Biochem. 84 (2001) 171;
(b) L. Santagostini, M. Gullotti, E. Monzani, L. Casella, R. Dillinger, F. Tuczek, Chem. Eur. J. 6 (2000) 519;
(c) E. Monzani, G. Battaini, A. Perotti, L. Casella, M. Gullotti, L. Santagostini, G. Nardin, L. Randaccio, S. Geremia, P. Zanello, G. Opramolla, Inorg. Chem. 38 (1999) 5359;
(d) S. Torelli, C. Belle, I. Gutier-Luneau, J.L. Pierre, E. Saint-Aman, J.M. Latour, L.Le. Pape, D. Luneau, Inorg. Chem. 39 (2000) 3526;
(e) S. Harmalker, S.E. Jones, D.T. Sawyer, Inorg. Chem. 22 (1983) 2790.

Available online at www.sciencedirect.com
SCIENCE DIRECT®
Polyhedron 23 (2004) 2523–2531
POLYHEDRON
www.elsevier.com/locate/poly

Synthesis, crystal, molecular and electronic structure of the $[ReBr_3(NO)(AsPh_3)(pzH)]$ complex

Barbara Machura [a,*], M. Jaworska [b], R. Kruszynski [c,1]

[a] Department of Inorganic and Radiation Chemistry, Institute of Chemistry, University of Silesia, 9th Szkolna Street, 40-006 Katowice, Poland
[b] Department of Theoretical Chemistry, Institute of Chemistry, University of Silesia, 9th Szkolna Street, 40-006 Katowice, Poland
[c] X-Ray Crystallography Laboratory, Institute of General and Ecological Chemistry, Technical University of Łódź, 116 Żeromski Street, 90-924 Łódź, Poland

Received 27 July 2004; accepted 24 August 2004
Available online 13 October 2004

Abstract

The reaction of the $[ReBr_3(NO)(AsPh_3)_2]$ complex with pyrazole (pzH) has been examined and a new rhenium nitrosyl – $[ReBr_3(NO)(AsPh_3)(pzH)]$ – has been obtained. The crystal, molecular and electronic structure of the $[ReBr_3(NO)(AsPh_3)(pzH)]$ complex has been determined. The geometric parameters of $[ReBr_3(NO)(AsPh_3)(pzH)]$ have been examined using the density functional theory (DFT) method. The UV–Vis spectrum of the complex has been interpreted on the basis of the electronic transitions of $[ReBr_3(NO)(AsPh_3)(pzH)]$ calculated with the time-dependent DFT method.
© 2004 Elsevier Ltd. All rights reserved.

Keywords: Rhenium nitrosyl complexes; Pyrazole; Arsine ligands; X–ray structure; Density functional theory calculations

1. Introduction

For many years much attention has been focused on the synthesis and study of a variety of nitrosyl transition metal complexes, due to their catalytic abilities and uses in the production of organonitrogen compounds or in pollutant control [1–11].

Considering the relation between the coordination mode of the NO group and the reactivity patterns of the MNO unit, the most important aspect of the research on nitrosyl complexes is determination of the bonding nature of nitric oxide to metal centers. Terminal NO ligands may adopt either linear or bent geometries. Historically, the bonding of the M–NO unit has been described by assigning formal oxidation states to the metal centre and the nitrosyl ligand. In such an assignment, a linear M–NO unit is deemed to possess a bound NO^+ ligand, and conversely, a bent M–NO core is deemed to possess a bound NO^- ligand. However, the bonding in the $M(NO)_x$ moieties of metal nitrosyl complexes is largely of covalent nature, and the electron distribution in the M–NO unit is more or less evenly distributed. Enemark and Feltham [1,3,9,11] have proposed the $\{M(NO)_x\}^n$ formalism for metal nitrosyls in which n is taken as the total number of electrons associated with the metal d and π^*(NO).

The chemistry of nitrosyl rhenium complexes arouses particular interest among these compounds, which is connected with the favourable nuclear properties of ^{186}Re and ^{188}Re nuclides, which make the radioisotopes useful for diagnostic nuclear medicine and applications in radioimmunotheraphy [12,13].

Previously, we investigated the reactivity of $[ReOX_3L_2]$ compounds (X = Cl and Br, L = PPh_3 and $AsPh_3$) towards gaseous nitric oxide and we examined the reactions

* Corresponding author. Tel.: +48322582441; fax: +48322599978.
E-mail addresses: bmachura@poczta.onet.pl (B. Machura), mj@tc3.ich.us.edu.pl (M. Jaworska), kruszyna@p.lodz.pl (R. Kruszynski).
[1] A holder of the Foundation for Polish Science (FNP) scholarship.

0277-5387/$ - see front matter © 2004 Elsevier Ltd. All rights reserved.
doi:10.1016/j.poly.2004.08.021

of $[NBu_4]_2[ReX_5(NO)]$ with an excess of triphenylphosphine and triphenylarsine [14–22]. Dependent on the reaction conditions, various products were isolated: $[ReX_3(NO)(OPPh_3)_2]$, $[ReX_3(NO)(PPh_3)_2]$, $[ReX_2(NO)_2(PPh_3)_2]$, $[ReBr_3(NO)(MeCN)(PPh_3)]$, $[ReCl_3(NO)(PPh_3)(OPPh_3)]$, $[ReCl_4(PPh_3)_2]$, $[ReBr_3(NO)(dppe)]$ $[ReBr_4(dppe)]$, $[ReX_3(NO)(OAsPh_3)_2]$, $[ReCl_4(OAsPh_3)_2]$, $[ReCl_3(NO)(AsPh_3)_2][ReCl_4(AsPh_3)_2]$, $[ReBr_3(NO)(AsPh_3)_2]$ and $[ReCl_3(NO)(AsPh_3)_2][ReCl_4(AsPh_3)_2]$.

Here, we present the synthesis, crystal, molecular and electronic structure of a new rhenium nitrosyl with pyrazole (pzH) in the coordination sphere – $[ReBr_3(NO)(AsPh_3)(pzH)]$. The electronic structure of $[ReBr_3(NO)(AsPh_3)(pzH)]$ has been determined based on the results of density functional theory (DFT) calculations. The spin-allowed doublet–doublet electronic transitions of $[ReBr_3(NO)(AsPh_3)(pzH)]$ have been calculated with the time-dependent DFT method (TDDFT), and the UV–Vis spectrum of the title complex has been discussed on this basis.

The calculations with the TDDFT method for open-shell organic, inorganic and organometallic molecules have supported the TDDFT method to be applicable for such systems giving good assignment of experimental spectra [23–26]. There are also several works performed with this method for 5d-metals (including rhenium complexes) in which good correlations between experimental and calculated results have been confirmed [27–33].

2. Experimental

2.1. General procedure

The reaction was carried out under argon atmosphere. All the reagents used in the synthesis of the complex are commercially available and were used without further purification. The $[ReBr_3(NO)(AsPh_3)_2]$ complex was prepared according to the literature method [22].

IR spectra were recorded on a Nicolet Magna 560 spectrophotometer in the spectral range 4000–400 cm^{-1} with the samples in the form of KBr pellets. Electronic spectra were measured on a spectrophotometer Lab Alliance UV–Vis 8500 in the range 800–220 nm in deoxygenated dichloromethane solution. Magnetic susceptibilities were measured at 296 K by the Faraday method. Elemental analyses (C H N) were performed on a Perkin–Elmer CHN-2400 analyzer.

2.2. Preparation of $[ReBr_3(NO)(AsPh_3)(pzH)]$

$[ReBr_3(NO)(AsPh_3)_2]$ (1 g, 0.9 mmol) and pzH (0.54 g, 8 mmol) in chloroform (100 cm^3) were refluxed for 5 h. The volume was condensed to 20 cm^3 and a dark red microcrystalline solid was formed on the addition of 100 cm^3 of diethyl ether. The product was washed with EtOH and cold ether, and dried in vacuo. Crystals suitable for X-ray investigation were obtained by recrystallisation from $CHCl_3$–EtOH. Yield: 70%. IR (KBr, cm^{-1}) 3347 (m), 3137 (w), 3055 (w), 1754 (vs), 1579 (w), 1518 (w), 1482 (s), 1433 (s), 1408 (m), 1351 (m), 1310 (w), 1269 (w), 1182 (w), 1136 (s), 1070 (m), 1051 (s), 1023 (w), 997 (m), 910 (w), 764 (s), 746 (vs), 697 (s), 669 (m), 589 (w), 559 (m), 476(s), 453 (m). Calc. for $C_{21}H_{19}N_3Br_3OAsRe$: C, 30.38; H, 2.31; N, 5.06. Found: C, 30.46; H, 2.40; N, 5.15%.

2.3. Crystal structure determination and refinement

The X-ray intensity data of $[ReBr_3(NO)(AsPh_3)(pzH)]$ was collected on a KM-4-CCD automatic diffractometer equipped with a CCD detector, 30 s exposure time were used and a half of the Ewald sphere was collected. The unit cell parameters were determined from least-squares refinement of the setting angles of 6510 strongest reflections. Details concerning crystal data and refinement are given in Table 1. Lorentz, polarisation and numerical absorption corrections [34] were applied. The structure was solved by means of the Patterson method and subsequently completed by difference Fourier recycling. All the non-hydrogen atoms were refined anisotropically using the full-matrix, least-squares technique. The hydrogen atoms of the phenyl rings were treated as ''riding'' on their parent carbon atoms [d(C–H) = 0.96 Å] and assigned isotropic temperature factors equal to 1.2 times the value of the equivalent temperature factor of the parent carbon atom. SHELXS 97 [35], SHELXL 97 [36] and SHELXTL [37] programs were used for all the calculations. Atomic scattering factors were those incorporated in the computer programs.

2.4. Computational details

The GAUSSIAN03 program [38] was used in the calculations. The geometry optimisation was carried out with the DFT method with the use of the B3LYP functional [39,40]. The electronic spectrum was calculated with the TDDFT method [41].

The LANL2DZ basis set [42] was used on the rhenium, arsenic and bromine atoms, 6-31G(d) on the nitrogen and carbon atoms and 6-31G basis on the hydrogen atoms in the calculations. The arsenic basis set LANL2DZ was used with additional p ($\alpha = 1.0$) and d ($\alpha = 1.0$) functions.

3. Results and discussion

3.1. Preparation

The $[ReBr_3(NO)(AsPh_3)(pzH)]$ complex has been obtained in high yield in the reaction of $[ReBr_3(NO)(AsPh_3)_2]$ with pyrazole.

Table 1
Crystal data and structure refinement for $[ReBr_3(NO)(AsPh_3)(pzH)]$

Empirical formula	$C_{21}H_{19}AsBr_3N_3Ore$
Formula weight	830.24
Temperature (K)	292(2)
Wavelength (Å)	0.71073
Crystal system	monoclinic
Space group	$P2_1/n$
Unit cell dimensions	
a (Å)	11.7199(9)
b (Å)	17.9770(15)
c (Å)	11.8038(11)
β (°)	104.366(8)
Volume (Å^3)	2409.2(4)
Z	4
D_{calc} (Mg/m^3)	2.289
Absorption coefficient (mm^{-1})	11.401
$F(0\,0\,0)$	1548
Crystal size (mm)	$0.49 \times 0.13 \times 0.13$
θ Range for data collection (°)	3.15– 25.11
Index ranges	$-13 \leqslant h \leqslant 13$
	$-21 \leqslant k$ 21
	$-14 \leqslant l \leqslant 13$
Reflections collected	24741
Independent reflections	4284 (R_{int} = 0.0778)
Completeness to 2θ (%)	96.4
Maximum and minimum transmission	0.3254 and 0.0722
Data/restraints/parameters	4284/0/271
Goodness-of-fit on F^2	1.172
Final R indices [$I > 2\sigma(I)$]	R_1 = 0.0456
	wR_2 = 0.0989
R indices (all data)	R_1 = 0.0559
	wR_2 = 0.1039
Largest diff. peak and hole (e Å^{-3})	1.399 and −1.224

$$[ReBr_3(NO)(AsPh_3)_2] + pzH \rightarrow [Re(NO)Br_3(pzH)(AsPh_3)] + AsPh_3$$

The excess of pzH used in the reaction ensures a maximum yield of the product.

3.2. Crystal structure

The complex $[ReBr_3(NO)(AsPh_3)(pzH)]$ crystallises in the monoclinic space group $P2_1/n$ and its structure consists of discrete and well-separated monomers. A thermal ellipsoid plot of $[ReBr_3(NO)(AsPh_3)(pzH)]$ is shown in Fig. 1. The rhenium atom is in a distorted octahedral environment with the bromine ligands in *meridional* geometry and the linear N–O group *trans* to the pyrazole molecule and *cis* to the $AsPh_3$ ligand. The nitrosyl group of the starting complex occupies the *trans* position to one of the bromine ligands. Two intramolecular hydrogen bonds [43–45] linking N(3)–H(3A) ··· Br(1) (D ··· A distance 3.214(8) Å and D–H ··· A angle 115.4°) and C(21)–H(21) ··· Br(3) (D ··· A distance 3.279(9) Å and D–H ··· A angle 114.6°) provide additional stabilisation of the $[ReBr_3(NO)(AsPh_3)(pzH)]$ complex. Except those mentioned above, no other short contacts that can be classified as intra- or intermolecular hydrogen bonds can be found. Table 1 presents the crystal data and structural refinement for $[ReBr_3(NO)(AsPh_3)(pzH)]$. The most important experimental bond lengths and angles for $[ReBr_3(NO)(AsPh_3)(pzH)]$ are reported in Table 2. The Re–NO and N–O bond lengths and the value of the Re–N–O angle confirm the linear coordination of the nitrosyl group and they are compared with values previously found [1,14–22]. In comparison with the starting $[ReBr_3(NO)(AsPh_3)_2]$ complex [Re–N = 1.740(11) and N–O = 1.117(13) Å] [22], the elongation of Re–N and N–O bond lengths is observed in $[ReBr_3(NO)(AsPh_3)(pzH)]$. The Re–As distance [2.5879(9)] is slightly shorter than those found for $[ReBr_3(NO)(AsPh_3)_2]$ [2.5946(9) Å], $[ReCl_4(AsPh_3)_2]$ [2.6023(10) Å] and $[ReCl_3(NO)(AsPh_3)_2]$ [2.6060(11) and 2.6186(11) Å][22]. A *trans* position of the pyrazole ligand to the nitrosyl group explains a significant elongation of the Re–N_{pzH} bond length [2.198(6)] in comparison with $[ReOBr_3(pzH)(OAsPh_3)]$ – 2.089(18) Å [46], but it is comparable with values found for $[Re(CO)_3(pzH)_2Br]$ with a *trans* arrangement of the pyrazole ligands to the carbonyl groups – 2.187(6) and 2.211(3) Å [47].

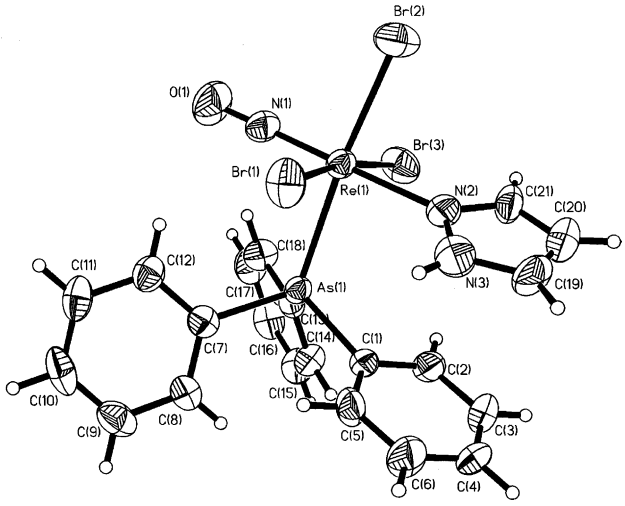

Fig. 1. Thermal ellipsoid plot of $[ReBr_3(NO)(AsPh_3)(pzH)]$ showing the atom numbering scheme (50% probability ellipsoids).

The bond valences were computed as $v_{ij} = \exp[(R_{ij} - d_{ij})/B]$ [48–50], where R_{ij} is the bond-valence parameter (in the formal sense R_{ij} is the single-bond length between i and j atoms [51]). The R_{Re-N}, R_{Re-As}, R_{Re-Br}values were taken as 2.06, 2.54 and 2.45 [48], respectively, and the value of B was taken as 0.37 [49]. The computed bond valences of the rhenium are $v_{Re(1)-N(1)} = 2.28$, $v_{Re(1)-N(2)} = 0.69$, $v_{Re(1)-As(1)} = 0.88$ and $v_{Re(1)-Br(1)} = 0.89$, 0.83, 0.84 v.u. (valence units), thus the NO moiety is bonded more than two times stronger than the rest of the substituents, and the Re–N(1) bond can be formally considered as a double bond.

Table 2
The experimental and optimised bond lengths [Å] and angles [°] for $[ReBr_3(NO)(AsPh_3)(pzH)]$

Bond lengths			Bond angles		
	Experimental	Optimised		Experimental	Optimised
Re(1)–N(1)	1.755(7)	1.760	N(1)–Re(1)–N(2)	178.6(3)	177.1
Re(1)–N(2)	2.198(6)	2.233	N(1)–Re(1)–Br(1)	93.8(2)	94.3
Re(1)–Br(1)	2.4926(9)	2.675	N(2)–Re(1)–Br(1)	85.25(18)	86.7
Re(1)–Br(2)	2.5189(11)	2.605	N(1)–Re(1)–Br(3)	94.5(2)	92.0
Re(1)–Br(3)	2.5151(10)	2.616	N(2)–Re(1)–Br(3)	86.62(18)	87.3
Re(1)–As(1)	2.5879(9)	2.650	Br(1)–Re(1)–Br(3)	170.15(3)	171.4
N(1)–O(1)	1.149(8)	1.171	N(1)–Re(1)–Br(2)	94.1(2)	93.2
			N(2)–Re(1)–Br(2)	84.90(18)	84.1
			Br(1)–Re(1)–Br(2)	93.04(4)	91.4
			Br(3)–Re(1)–Br(2)	91.76(4)	94.0
			N(1)–Re(1)–As(1)	91.4(2)	93.4
			N(2)–Re(1)–As(1)	89.64(18)	89.4
			Br(1)–Re(1)–As(1)	87.74(3)	83.7
			Br(3)–Re(1)–As(1)	86.66(3)	90.11
			Br(2)–Re(1)–As(1)	174.40(3)	172.1
			O(1)–N(1)–Re(1)	178.5(7)	178.0

The triphenylarsine and bromide ligands are bounded with comparable strength, and the pyrazole ligand is bounded distinctly weaker.

3.3. Infrared data and magnetochemical measurements

The IR spectrum of $[ReBr_3(NO)(AsPh_3)(pzH)]$ exhibits a strong band at 1754 cm^{-1} assignable to ν (NO). The value of ν(NO) corresponds to the linear NO range of Haymore and Ibers [52] [ν(NO) above 1620–1610 cm^{-1} were assigned to linear M–N–O systems, while ν(NO) below 1610 cm^{-1} were assigned to bent M–N–O systems]. The considerable lowering of the ν_{NO} of $[ReBr_3(NO)(AsPh_3)(pzH)]$ in comparison with the starting $[ReBr_3(NO)(AsPh_3)_2]$ nitrosyl (1773 cm^{-1}) is consistent with the elongation of the N–O bond length in $[ReBr_3(NO)(AsPh_3)(pzH)]$.

The band (3347cm^{-1}) in the range assignable to N–H vibrations confirms the coordination of the pyrazole in a neutral monodentate form. The characteristic bands of the C=C and C=N stretching modes, observed at 1640 and 1558 cm^{-1}in uncomplexed pyrazole, are shifted to considerable lower frequencies 1579 and 1518 cm^{-1}, respectively. It is consistent with the somewhat longer C=C and C=N bonds in the title complex in comparison with the same distances in the uncomplexed ligand [53].

$[ReBr_3(NO)(AsPh_3)(pzH)]$ is a paramagnetic compound with a room temperature magnetic moment of 1.7 BM, corresponding to one unpaired electron.

3.4. Optimised geometry

The geometry of $[ReBr_3(NO)(AsPh_3)(pzH)]$ was optimised in a doublet state by the DFT method with the B3LYP functional. Table 3 shows the possible electronic configurations and spin multiplicities of the $[ReBr_3(NO)(AsPh_3)(pzH)]$ complex. The doublet state agrees well with the experimental value of the effective magnetic moment for $[ReBr_3(NO)(AsPh_3)(pzH)]$. The optimised geometry is in good agreement with the experimental one, the largest differences are found for the Re–Br bond distances. A similar elongation of the rhenium–halogen bond lengths in the B3LYP with different basis sets has been found in other rhenium complexes [54]. The significant elongation of the calculated Re–Br(1) bond length in comparison with the experimental one can be explained by contribution of Br(1) in the N(3)–H(3A)$\cdots$Br(1) hydrogen bond. The formation of the hydrogen bond causes local deficiency of electron density on the bromine atom and consequently the Br(1) ligand is closer to the rhenium atom in the experimental structure.

3.5. Charge distribution and spin densities

Table 4 presents the atomic charges from the natural population analysis (NPA) and spin densities for $[ReBr_3(NO)(AsPh_3)(pzH)]$. The calculated charge on the nitrogen atom of the nitrosyl group is positive, whereas the oxygen atom is negatively charged. The total charge on the NO group of the title complex is positive, 0.015. The calculated charge on the rhenium atom of $[ReBr_3(NO)(AsPh_3)(pzH)]$ is far from the formal charge +2. It results from charge donation from the bromine ions and triphenylarsine ligand, which act as σ-donors. There is large positive charge on the As atom, and the charges on the bromine ions are significantly smaller than −1. The charge on the

Table 3
The possible oxidation numbers and spin multiplicities of Re and NO in $[ReBr_3(NO)(AsPh_3)(pzH)]$

Re	Spin of Re	NO	Spin of NO	Total spin	Spin multiplicity
Re(II)	5/2, 3/2, 1/2	$NO^+(\pi_1^*)^0(\pi_2^*)^0$	0	5/2, 3/2, 1/2	6, 4, 2
Re(III)	2, 1, 0	$NO(\pi_1^*)^1(\pi_2^*)^0$	1/2	5/2, 3/2, 1/2	6, 4, 2
Re(IV)	3/2, 1/2	$NO^-(\pi_1^*)^1(\pi_2^*)^1$	1	5/2, 3/2, 1/2	6, 4, 2

Table 4
Atomic charges from the natural population analysis (NPA) and spin densities of $[ReBr_3(NO)(AsPh_3)(pzH)]$

Atom	Atomic charge	Spin density
Re	0.382	0.999
Br(1)	−0.392	0.044
Br(2)	−0.321	0.103
Br(3)	−0.332	0.081
As(1)	1.328	−0.029
N(1)	0.241	−0.106
O(1)	−0.225	−0.089
N(2)	−0.370	−0.008
N(3)	−0.312	0.000

pyrazole nitrogen atom bonded with the rhenium is negative – the pyrazole and nitrosyl ligands act as electron acceptors.

In the title complex, there is positive spin density of about 1 on the rhenium atom and small negative spin densities of about −0.1 on the nitrogen and oxygen atoms of the nitrosyl ligand.

3.6. Electronic structure

The energies and characters of several highest occupied and lowest unoccupied molecular orbitals with α- and β-spin for $[ReBr_3(NO)(AsPh_3)(pzH)]$ are presented in Table 5. The selected HOMO and LUMO orbitals of $[ReBr_3(NO)(AsPh_3)(pzH)]$ with α-spin are depicted in Fig. 2. Most of the MOs of $[ReBr_3(NO)(AsPh_3)(pzH)]$ have complicated character. The percent participations of the ligand atomic orbitals in the selected HOMO and LUMO orbitals of mixed character are shown in Table 5.

Table 5
The energy and character of the selected molecular orbitals with α- and β-spin for $[ReBr_3(NO)(AsPh_3)(pzH)]$

	α MO		β MO	
	E (eV)	Character	*E* (eV)	Character
HOMO − 17	−8.670	$\pi_{pzH}(35.1), d_{yz}(23.8) + \pi^*_{NO}(6.1), \pi_{Br}(15.3), \pi_{Ph}(13.8)$	−8.575	$\pi_{pzH}(44.6), d_{yz}(17.1) + \pi^*_{NO}(5.0), \pi_{Br}(16.6), \pi_{Ph}(11.0)$
HOMO − 16	−8.491	$d_{xz}(45.1) + \pi^*_{NO}(20.4), \pi_{Br}(26.5)$	−8.337	$d_{xz}(36.8) + \pi^*_{NO}(23.5), \pi_{Br}(32.8)$
HOMO − 15	−8.187	$\sigma_{Br}(38.2), d_{yz}(16.1) + \pi^*_{NO}(13.1), \pi_{Ph}(14.9), n_{As}(6.4)$	−8.180	$\sigma_{Br}(44.5), d_{yz}(12.4) + \pi^*_{NO}(7.0), \pi_{pzH}(14.0)$
HOMO − 14	−8.081	σ_{Br}	−8.079	$\sigma_{Br}(58.6), d_{yz}(9.1) + \pi^*_{NO}(9.2)$
HOMO − 13	−7.810	π_{pzH}	−8.036	σ_{Br}
HOMO − 12	−7.635	π_{Ph}	−7.736	π_{pzH}
HOMO − 11	−7.475	π_{Br} (40.9), $\pi_{Ph}(41)$	−7.610	π_{Ph}
HOMO − 10	−7.462	π_{Ph}	−7.464	π_{Ph}
HOMO − 9	−7.375	$\pi_{Ph}(49.4), \pi_{pzH}(28.5), d_{yz}(8.4) + \pi^*_{NO}(8.0)$	−7.433	π_{Ph} (44.6),$\pi_{Br}(41.0)$
HOMO − 8	−7.299	π_{Ph} (54.6), $\pi_{Br}(37.0)$	−7.356	$\pi_{Ph}(63.6), \pi_{pzH}(16.4), d_{xz}(5.5) + \pi^*_{NO}(8.1)$
HOMO − 7	−7.289	$\pi_{Ph}(44.4)$, $\pi_{pzH}(27.0)$, $\pi_{Br}(14.4)$	−7.265	$\pi_{Ph}(48.9)$, $\pi_{Br}(33.1)$
HOMO − 6	−7.216	π_{Ph}	−7.244	$\pi_{Ph}(54.3), \pi_{pzH}(21.0), \pi_{Br}(10.0), d_{yz}(7.6) + \pi^*_{NO}(6.1)$
HOMO − 5	−7.076	π_{Ph}	−7.193	π_{Ph}
HOMO − 4	−6.825	π_{Br}, σ_{Br}, n_{As}	−7.007	π_{Ph}
HOMO − 3	−6.571	$\pi_{Br}(59.0), d_{xz}(20.7) + \pi^*_{NO}(14.4)$	−6.715	π_{Br}, σ_{Br}, n_{As}
HOMO − 2	−6.528	π_{Br}	−6.489	$\pi_{Br}(50.9), d_{xz}(19.2) + \pi^*_{NO}(23.4)$
HOMO − 1	−6.343	$\pi_{Br}(72.3), d_{yz}(11.9) + \pi^*_{NO}(9.9)$	−6.280	$\pi_{Br}(70.4), d_{yz}(9.7) + \pi^*_{NO}(13.3)$
HOMO	−6.028	π_{Br} (49.6), $d_{xz}(46.6)$	−6.250	π_{Br}
LUMO	−1.885	$d_{x^2-y^2}(42.9) - \sigma_{Br}(32.1) - \sigma_{As}(11.7)$	−3.520	$d_{xz}(68.1)$, π_{Br} (25.7)
LUMO + 1	−1.775	$\pi^*_{NO}(55.3) - d_{yz}(21.0)$	−1.792	$\pi^*_{NO}(49.9) - d_{yz}(24.9)$
LUMO + 2	−1.713	$\pi^*_{NO}(54.1) - d_{xz}(27.8)$	−1.729	$\pi^*_{NO}(39.3) - d_{xz}(35.6)$
LUMO + 3	−1.046	$\pi_{As}(11.4) + \pi^*_{Ph}(47.1), d_{z^2}(14.3)$	−1.630	$d_{x^2-y^2}(40.5) - \sigma_{Br}(25.2) - \sigma_{As}(11.2)$
LUMO + 4	−0.914	$\pi_{As}(7.9) + \pi^*_{Ph}(77.0), d_{z^2}(5.1)$	−1.168	$\pi_{As}(13.9) + \pi^*_{Ph}(64.4), d_{z^2}(8.1)$
LUMO + 5	−0.702	$\pi_{As}(10.9) + \pi^*_{Ph}(75.1), d_{z^2}(5.0)$	−1.007	$\pi_{As}(4.0) + \pi^*_{Ph}(78.4), d_{z^2}(6.0)$
LUMO + 6	−0.516	π^*_{Ph}	−0.863	$\pi_{As}(9.5) + \pi^*_{Ph}(74.7), d_{z^2}(5.8)$
LUMO + 7	−0.399	$\pi^*_{Ph}(53.8), d_{z^2}(12.6), n_{As}(13.1)$	−0.691	π^*_{Ph}
LUMO + 8	−0.374	π^*_{Ph}	−0.435	π^*_{Ph}
LUMO + 9	−0.285	$\pi^*_{Ph}(45.1), \pi^*_{pzH}(39.2)$	−0.399	π^*_{Ph}
LUMO + 10	0.631	$\pi^*_{pzH}(36.5), \pi^*_{Ph}(31.3)$	−0.336	$\pi^*_{pzH}(60.0), \pi^*_{Ph}(17.3)$

The percent participation of the atomic orbitals is given in round brackets.

The bonding of NO to the rhenium center involves a synergic interaction between the nitrosyl ligand orbitals and the metal orbitals. The Re–NO bond consists of two components (i) a donation of electron density from a σ-type orbital on NO to the metal orbital and (ii) a donation of electron density from the occupied metal d-orbitals into the π* anti-bonding orbitals of the NO ligand. The occupied d_{yz} and d_{xz} rhenium orbitals participate in the back-donation from the central ion to the NO ligand and in the $[ReBr_3(NO)(AsPh_3)(pzH)]$ complex. The π_{Re-NO} bonding interaction makes the largest contribution into HOMO − 16 and HOMO − 15 with α- and β-spin. A substantial contribution of π_{Re-NO} orbitals are also shown in HOMO − 3 and HOMO − 1 with α-spin and HOMO − 2 and HOMO − 1 with β-spin, but the bromine orbitals are the main components of these orbitals (see Table 5). The bonding π_{Re-NO} orbitals with α- and β-spin are localised mainly on the rhenium d orbitals. The LUMO + 1 and LUMO + 2 orbitals with α- and β-spin are of π^*_{Re-NO} anti-bonding character, and they have prevalent NO character. Considering the molecular orbital composition and positive total charge on the NO group, the character of the nitrosyl ligand in $[ReBr_3(NO)(AsPh_3)(pzH)]$ may be described as NO^+.

HOMO − 4 with α-spin and HOMO − 3 with β-spin are mainly localised on the bromine ligands, but they have a substantial contribution from the free electron pair on the arsenic atom of $AsPh_3$ molecule.

The d_{xy} rhenium orbital and π orbitals of bromine ligands in an anti-bonding arrangement make the main contribution into the HOMO with α-spin and LUMO with β-spin. The HOMO with β-spin is mainly localised on the bromine ligands.

The LUMO with α-spin and LUMO + 3 with β-spin are of $d_{x^2-y^2}-\sigma_{Br}-\sigma_{As}$ character. The LUMO + 3 with α-spin and LUMO + 4 with β-spin are mainly localised on the d_{z^2} rhenium orbital. LUMO + 3, LUMO + 4, LUMO + 5 with α-spin and LUMO + 4, LUMO + 5, LUMO + 6 with β-spin present a π interaction of the arsenic orbitals with the π* orbitals of the phenyl groups.

3.7. Electronic spectra

The experimental and calculated electronic spectra of $[ReBr_3(NO)(AsPh_3)(pzH)]$ are presented in Fig. 3. Each calculated transition in Fig. 3(b) was represented by a gaussian function with the height equal to the oscillator strength and width equal to 0.06.

Table 6 shows the spin-allowed doublet–doublet electronic transitions calculated with the TDDFT method for $[ReBr_3(NO)(AsPh_3)(pzH)]$.

The investigated complex is of large size, the number of basis functions is equal to 450. Eighty electron transitions calculated by the TDDFT method do not comprise all the experimental absorption bands. The UV–Vis spectrum of $[ReBr_3(NO)(AsPh_3)(pzH)]$ was calculated only to 265 nm, so the shortest wavelength experimental band cannot be assigned completely to the calculated transitions. Considering that the solution spectra of $AsPh_3$ and pyrazole exhibit intense

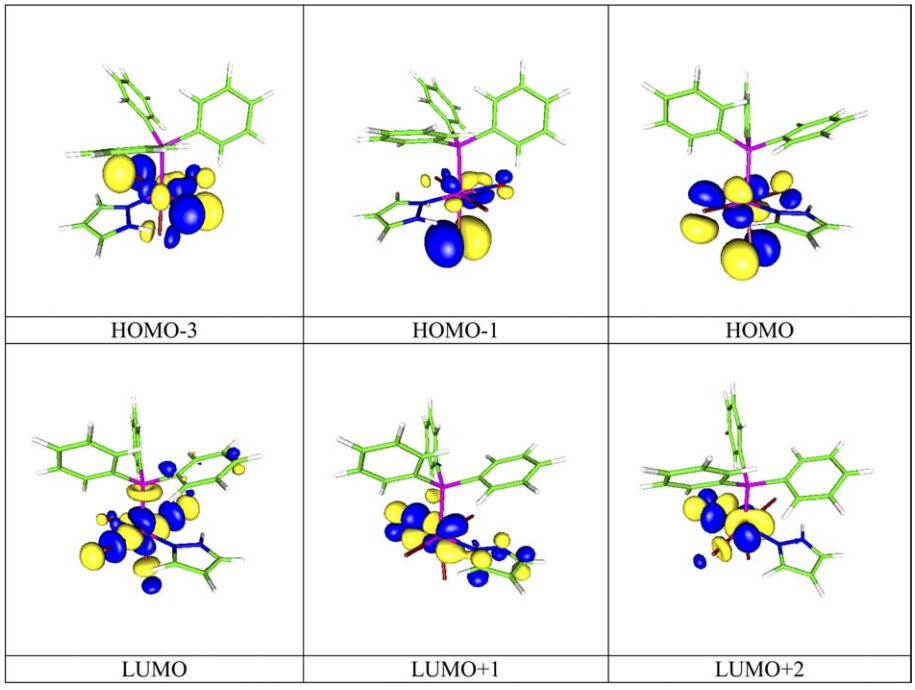

Fig. 2. The selected HOMO and LUMO orbitals with α-spin for $[ReBr_3(NO)(AsPh_3)(pzH)]$. Positive values of the orbital contour are represented in blue (0.04 au) and negative values – in yellow (−0.04 au). (For interpretation of the references to colour in this figure legend, the reader is referred to the web version of this article.)

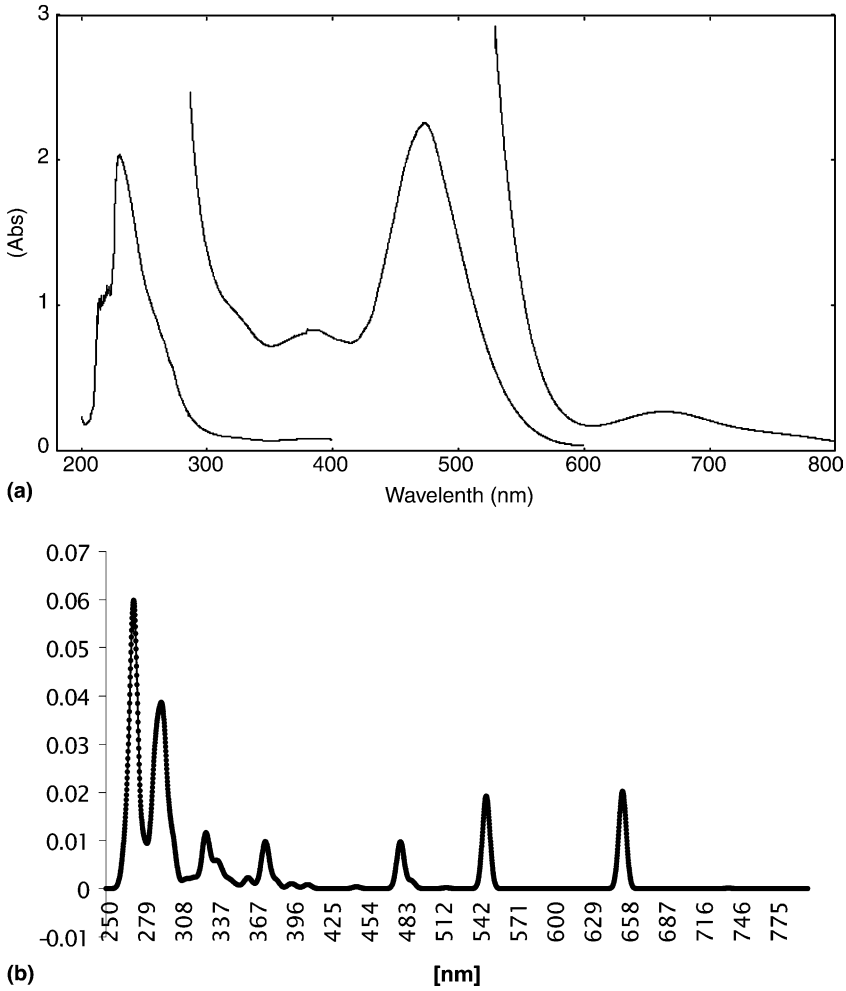

Fig. 3. The experimental (a) and calculated (b) electronic absorption spectrum of $[ReBr_3(NO)(AsPh_3)(pzH)]$.

absorption bands in the 250–200 nm region, some additional intraligand and interligand transitions are expected to be found at higher energies in the calculation.

The calculations result in many transitions with very small oscillator strengths. Except for the electronic transition of $d \rightarrow \pi^*_{NO}$ character and the low energy part of the spectrum, only transitions with oscillator strengths larger than 0.0050 are listed in Table 6.

The assignment of the calculated transitions to the experimental bands is based on the criterion of the energy and oscillator strength of the calculated transitions. In the description of the electronic transitions the main components of the molecular orbital are used. The bonding π_{Re-NO} orbitals are described as d orbitals, and the anti-bonding π^*_{Re-NO} orbitals – as π^*_{NO}.

The longest wavelength experimental band of $[ReBr_3(NO)(AsPh_3)(pzH)]$ (at 765.0 nm) may be attributed to the transitions of $\pi(Br)/d_{xz} \rightarrow d$ character with small oscillator strength, calculated at 737.9 nm.

The next experimental band can be assigned to the calculated transition at 654.8. The transition is of LMCT ($\pi_{Br} \rightarrow d$) character.

The broad experimental band at 476 nm is assigned to the transitions calculated between 548 and 439 nm. Among these electronic transitions are transitions of $d \rightarrow d$ character and transitions of LMCT ($\pi_{Br} \rightarrow d$, $n_{As} \rightarrow d$ and $\pi_{Ph} \rightarrow d$) origin. Considering the large contribution of π bromine orbitals in HOMO – 3 with α-spin and HOMO – 2 with β-spin, character of the transition at 516.7 nm is determined as $d_{xz}/\pi(Br) \rightarrow \pi^*(NO)$.

The next experimental absorption band at 390 nm is attributed to the transitions of LMCT ($\pi_{Br} \rightarrow d$, $\pi_{pzH} \rightarrow d$ and $\pi_{Ph} \rightarrow d$) and MLCT ($d \rightarrow \pi^*_{NO}$) character, calculated between 410 and 345 nm. The electronic transitions from the rhenium d_{xy} orbitals onto π* orbitals of the nitrosyl group are calculated at 408.4 and 405.2 nm. The calculated transitions at 375.1, 358.7, 350.9 and 346.2 nm are of mixed character $d_{xz}/\pi(Br) \rightarrow \pi^*(NO)$. All the transitions from the rhenium d orbitals onto π* orbitals of the nitrosyl group have

Table 6
The energy and molar absorption coefficients of experimental absorption bands and the electronic transitions calculated with the TDDFT method for $[ReBr_3(NO)(AsPh_3)(pzH)]$

The most important orbital excitations	Character	λ [nm]	E [eV]	f	Experimental Λ [nm] (E [eV]) ε
H-2(β) → L(β)	π(Br)/d_{xz} → d	737.9	1.68	*0.0001*	765.0 (1.62) 35
H(β) → L(β)	π(Br) → d	654.8	1.89	*0.0202*	665.8 (1.86) 95
H-3(β) → L(β)	π(Br)/σ(Br)/n(As) → d	548.0	2.26	*0.0192*	476.0 (2.60) 3200
H-3(α) → L + 2(α)	d_{xz}/π(Br) → π*(NO)	516.7	2.40	*0.0002*	476.0 (2.60) 3200
H-2(β) → L + 2(β)					
H(α) → L(α)	d → d	489.4	2.53	*0.0016*	476.0 (2.60) 3200
H(α) → L(α)	d → d	480.8	2.58	*0.0097*	476.0 (2.60) 3200
H-4(β) → L(β)	π(Ph) → d	439.6	2.82	*0.0028*	476.0 (2.60) 3200
H(α) → L + 2(α)	d_{xy} → π*(NO)	408.4	3.04	*0.0008*	390.0 (3.17) 1180
H(α) → L + 1(α)	d_{xy} → π*(NO)	405.2	3.06	*0.0001*	390.0 (3.17) 1180
H-7(β) → L(β)	π(Ph), π(Br) → d	383.3	3.23	*0.0017*	390.0 (3.17) 1180
H-1(α) → L(α)	π(Br)/d_{yz} → d	376.6	3.29	*0.0025*	390.0 (3.17) 1180
H-2(β) → L + 1(β)	d_{xz}/π(Br) → π*(NO)	375.1	3.30	*0.0031*	390.0 (3.17) 1180
H-1(β) → L + 2(β)	d_{yz}/π(Br) → π*(NO)				
H-11(β) → L(β)	π(Ph) → d	374.1	3.31	*0.0047*	390.0 (3.17) 1180
H-12(β) → L(β)	π(pzH) → d				
H-3(α) → L(α)	d_{xz}/π(Br) → d				
H-14(β) → L(β)	σ(Br)/d_{yz} → d	361.4	3.43	*0.0021*	390.0 (3.17) 1180
H-1(α) → L + 2(α)	d_{yz}/π(Br) → π*(NO)	358.7	3.46	*0.0001*	390.0 (3.17) 1180
H-3(α) → L + 1(α)	d_{xz}/π(Br) → π*(NO)	350.9	3.53	*0.0002*	390.0 (3.17) 1180
H-1(β) → L + 2(β)	d_{yz}/π(Br) → π*(NO)				
H-1(α) → L + 1(α)H-1(β) → L + 1(β)	d_{yz}/π(Br) → π*(NO)	346.2	3.58	*0.0011*	390.0 (3.17) 1180
H-2(α) → L(α)	π(Br) → d	328.2	3.78	*0.0110*	330.8 (3.75) 1250
H-3(β) → L + 2(β)	π(Br)/σ (Br)/n(As) → π*(NO)	302.1	4.10	*0.0077*	330.8 (3.75) 1250
H-1(α) → L + 3(α)	(Br)/d_{yz} → π*(Ph)	297.5	4.17	*0.0056*	330.8 (3.75) 1250
H-4(α) → L + 2(α)	π(Br)/σ(Br)/n(As) → π*(NO)	294.6	4.21	*0.0260*	330.8 (3.75) 1250
H-3(β) → L + 3(β)	π(Br)/σ (Br)/n(As) → π*(Ph)				
H-4(α) → L + 1(α)	π(Br)/σ(Br)/n(As) → π*(NO)	291.9	4.25	*0.0071*	330.8 (3.75) 1250
H-4(α) → L + 2(α)	π(Br)/σ(Br)/n(As) → π*(NO)	289.0	4.29	*0.0085*	330.8 (3.75) 1250
H-4(α) → L + 2(α)	π(Br)/σ(Br)/n(As) → π*(NO)	288.6	4.30	*0.0134*	330.8 (3.75) 1250
H-3(α) → L + 3(α)	π(Br)/d_{xz} → π*(NO)				
H-2(α) → L + 3(α)	π(Br) → π*(Ph)	272.9	4.54	*0.0079*	230.6 (5.39) 26,140
H-4(β) → L + 1(β)	π(Ph) → π*(NO)	272.1	4.56	*0.0151*	230.6 (5.39) 26,140
H-4(β) → L + 1(β)	π(Ph) → π*(NO)	272.5	4.57	*0.0312*	230.6 (5.39) 26,140

small oscillator strengths and they do not contribute significantly to the overall shape of the band. They are hidden under the more intense transitions of LMCT ($\pi_{Br} \rightarrow d$ and $\pi_{Ph} \rightarrow d$) character. Such small values of the oscillator strengths seem to be typical of $d \rightarrow \pi^*_{NO}$ transitions, and they have been supported by the calculations for other metal nitrosyls [55,56].

The experimental band at 330.8 nm is assigned to the calculated transition of $\pi_{Br} \rightarrow d$ type (at 328.2 nm) and some transitions ($303 \div 288$ nm) of LLCT character. The LLCT transitions occur from the bromine, phenyl and pyrazole orbitals to the π^*_{NO} or π^*_{Ph} orbitals.

The shortest wavelength experimental band of $[ReBr_3(NO)(AsPh_3)(pzH)]$ (at 230.6 nm) corresponds to the electronic transitions that are of LLCT ($\pi_{Br} \rightarrow \pi^*_{Ph}$ and $\pi_{Ph} \rightarrow \pi^*_{NO}$) character.

4. Supplementary data

Supplementary data for $C_{21}H_{19}AsBr_3N_3ORe$ are available from the CCDC, 12 Union Road, Cambridge CB2 1EZ, UK (fax: +44 1223 336 033; e-mail: deposit@ccdc.ac.uk or www:http://www.ccdc.cam.ac.uk) on request, quoting the Deposition No. 243039.

Acknowledgement

The GAUSSIAN03 calculations were carried out in the Wrocław Centre for Networking and Supercomputing, WCSS, Wrocław, Poland under calculational Grant No. 51/96.

References

[1] G.B. Richter-Addo, P. Legzdins, Metal Nitrosyls, Oxford University Press, Oxford, 1992.
[2] J.A. McCleverty, Chem. Rev. 79 (1979) 53.
[3] J.N. Kukuškin, Reakcionnaja sposobnost koordinacjonnych soedinienij, Chimija, Leningrad, 1987.
[4] J.H. Enemark, R.D. Feltham, Coord. Chem Rev. 13 (1974) 339.
[5] K.G. Caulton, Coord. Chem Rev. 14 (1975) 317.

[6] F. Bottomley, Coord. Chem. Rev. 26 (1978) 7.
[7] K.K. Pandey, Coord. Chem. Rev. 51 (1983) 70.
[8] G. WilkinsonComprehensive Coordination Chemistry, vol. 2, Pergamon Press, Oxford, 1987, p. 100.
[9] G.B. Richter-Addo, P. Legzdins, J. Burstyn, Chem. Rev. 102 (2002) 857.
[10] T.W. Hayton, P. Legzdins, W.B. Sharp, Chem. Rev. 102 (2002) 935.
[11] J.A. McCleverty, Chem. Rev. 104 (2004) 403.
[12] W. Volkert, W.F. Goeckeler, G.J. Ehrhardt, A.R. Ketring, J. Nucl. Med. 32 (1991) 174.
[13] E.A. Deutsch, K. Libson, J.L. Vanderheyden, Technetium and Rhenium in Chemistry and Nuclear Medicine, Raven Press, New York, 1990.
[14] J.O. Dzięgielewski, B. Machura, J. Marek, Polyhedron 15 (1996) 3713.
[15] J.O. Dzięgielewski, B. Machura, T.J. Bartczak, Polyhedron 15 (1996) 2813.
[16] T.J. Bartczak, W. Czurak, J.O. Dzięgielewski, B. Machura, Pol. J. Chem. 72 (1998) 633.
[17] J.O. Dzięgielewski, B. Machura, T. Kupka, T.J. Bartczak, W. Czurak, Pol. J. Chem. 72 (1998) 1009.
[18] J.O. Dzięgielewski, B. Machura, T.J. Bartczak, W. Czurak, J. Kusz, J. Warczewski, J. Coord. Chem. 48 (1999) 125.
[19] T.J. Bartczak, W. Czurak, J.O. Dzięgielewski, B. Machura, A. Jankowska, J. Kusz, J. Warczewski, Polyhedron 18 (1999) 2313.
[20] T.J. Bartczak, W. Czurak, J.O. Dzięgielewski, B. Machura, J. Kusz, J. Warczewski, Pol. J. Chem. 74 (2000) 265.
[21] T.J. Bartczak, W. Czurak, J.O. Dzięgielewski, B. Machura, A. Jankowska, J. Kusz, J. Warczewski, J. Coord. Chem. 52 (2001) 361.
[22] B. Machura, J.O. Dzięgielewski, S. Michalik, T.J. Bartczak, R. Kruszynski, J. Kusz, Polyhedron 21 (2002) 2617.
[23] S. Hirata, M. Head-Gordon, Chem. Phys. Lett. 302 (1999) 375.
[24] R. Andreu, J. Orduna, J. Garín, Tetrahedron 57 (2001) 1358.
[25] E. Brocławik, T. Borowski, Chem. Phys. Lett. 339 (2001) 433.
[26] M.J. Calhorda, M.G.B. Drew, V. Félix, L.P. Fonseca, C.A. Gamelas, S.S.M.C. Godinho, I.S. Gonçavles, E. Hunstock, J.P. Lopes, A.J. Parola, F. Pina, C.C. Romão, A.G. Santos, J. Organomet. Chem. 632 (2001) 94.
[27] M.C. Aragoni, M. Arca, T. Cassano, C. Denotti, F.A. Devillanova, F. Isaia, V. Lippolis, D. Natali, L. Niti, M. Sampietro, R. Tommasi, G. Verani, Inorg. Chem. Commun. 5 (2002) 869.
[28] P. Romaniello, F. Lelj, Chem. Phys. Lett. 372 (2003) 51.
[29] P. Norman, P. Cronstrand, J. Ericsson, Chem. Phys. 285 (2002) 207.
[30] J. Bossert, N.B. Amor, A. Strich, C. Daniel, Chem. Phys. Lett. 342 (2001) 617.
[31] C.E. Powell, M.P. Cifuentes, A.M. McDonagh, S.K. Hurst, N.T. Lucas, C.D. Delfs, R. Stranger, M.G. Humphrey, S. Houbrechts, I. Asselberghs, A. Persoons, D.C.R. Hockless, Inorg. Chim. Acta 352 (2003) 9.
[32] J.P. Morral, C.E. Powell, R. Stranger, M.P. Cifuentes, M.G. Humphrey, G.A. Heath, J. Organomet. Chem. 670 (2003) 248.
[33] P. Romaniello, F. Lelj, J. Mol. Struct. Theochem. 636 (2003) 23.
[34] STOE & Cie, X-RED, Version 1.18, STOE & Cie GmbH, Darmstadt, Germany, 1999.
[35] G.M. Sheldrick, Acta Crystallogr. Sect. A 46 (1990) 467.
[36] G.M. Sheldrick, SHELXL 97. Program For the Solution and Refinement of Crystal Structures, University of Göttingen, Germany, 1997.
[37] G.M. Sheldrick, SHELXTL: Release 4.1 For Siemens Crystallographic Research Systems, 1990.
[38] M.J. Frisch, G.W. Trucks, H.B. Schlegel, G.E. Scuseria, M.A. Robb, J.R. Cheeseman, J.A. Montgomery Jr., T. Vreven, K.N. Kudin, J.C. Burant, J.M. Millam, S.S. Iyengar, J. Tomasi, V. Barone, B. Mennucci, M. Cossi, G. Scalmani, N. Rega, G.A. Petersson, H. Nakatsuji, M. Hada, M. Ehara, K. Toyota, R. Fukuda, J. Hasegawa, M. Ishida, T. Nakajima, Y. Honda, O. Kitao, H. Nakai, M. Klene, X. Li, J.E. Knox, H.P. Hratchian, J.B. Cross, C. Adamo, J. Jaramillo, R. Gomperts, R.E. Stratmann, O. Yazyev, A.J. Austin, R. Cammi, C. Pomelli, J.W. Ochterski, P.Y. Ayala, K. Morokuma, G.A. Voth, P. Salvador, J.J. Dannenberg, V.G. Zakrzewski, S. Dapprich, A.D. Daniels, M.C. Strain, O. Farkas, D.K. Malick, A.D. Rabuck, K. Raghavachari, J.B. Foresman, J.V. Ortiz, Q. Cui, A.G. Baboul, S. Clifford, J. Cioslowski, B.B. Stefanov, G. Liu, A. Liashenko, P. Piskorz, I. Komaromi, R.L. Martin, D.J. Fox, T. Keith, M.A. Al-Laham, C.Y. Peng, A. Nanayakkara, M. Challacombe, P.M.W. Gill, B. Johnson, W. Chen, M.W. Wong, C. Gonzalez, J.A. Pople, GAUSSIAN03. Revision B.03, Gaussian Inc., Pittsburgh, PA, 2003.
[39] A.D. Becke, J. Chem. Phys. 98 (1993) 5648.
[40] C. Lee, W. Yang, R.G. Parr, Phys. Rev. B 37 (1988) 785.
[41] M.E. Casida, in: J.M. Seminario (Ed.), Recent Developments and Applications in Modern Density Functional Theory, Theoretical and Computational Chemistry, vol. 4, Elsevier, Amsterdam, 1996.
[42] P.J. Hay, W.R. Wadt, J. Chem. Phys. 82 (1985) 299.
[43] G.A. Jeffrey, W. Saenger, Hydrogen Bonding in Biological Structures, Springer, Berlin, 1994.
[44] G.R. Desiraju, T. Steiner, The Weak Hydrogen Bond in Structural Chemistry and Biology, Oxford University Press, 1999.
[45] R. Taylor, O. Kennard, J. Am. Chem. Soc. 104 (1982) 5063.
[46] B. Machura, J.O. Dzięgielewski, R. Kruszynski, T.J. Bartczak, J. Kusz, Inorg. Chem. Commun. 6 (2003) 1436.
[47] G.A. Ardizzoia, G. LaMonica, A. Maspero, M. Moret, N. Masciocchi, Eur. J. Inorg. Chem. (1998) 1503.
[48] M. O'Keeffe, N.E. Brese, Acta Crystallogr. Sect. B 47 (1997) 192.
[49] M. O'Keeffe, N.E. Brese, J. Am. Chem. Soc. 113 (1991) 3226.
[50] I.D. Brown, Bond-Length–Bond-Valence Relationship in Inorganic Solids, in: H.B. Burgi, J.D. Dunitz (Eds.), Structure Correlation, Part III, VCH publishers, Weinheim/New York, 1994, pp. 405–429.
[51] L. Sieron, M. Bukowska-Strzyzewska, Acta Crystallogr. Sect. C 55 (1999) 1230.
[52] B.L. Haymore, I.A. Ibers, Inorg. Chem. 14 (1975) 3060.
[53] A. Baldy, J. Elguero, R. Faure, M. Pierrot, E.J. Vincent, J. Am. Chem. Soc. 107 (1985) 5290.
[54] N. Psaroudakis, K. Mertis, D.G. Liakos, E.D. Simandiras, Chem. Phys. Lett. 369 (2003) 490.
[55] S.C. da Silva, D.W. Franco, Spectrochim. Acta 55A (1999) 1515.
[56] S.I. Gorelsky, S.C. da Silva, A.B.P. Lever, D.W. Franco, Inorg. Chim. Acta 300–302 (2000) 698.

Available online at www.sciencedirect.com
SCIENCE DIRECT®
Polyhedron 23 (2004) 2533–2539
POLYHEDRON
www.elsevier.com/locate/poly

Sterically demanding methyl tris(pyrazolyl)borate ligands: synthesis and characterization of thallium(I) complexes supported by $[MeB(3\text{-}(t\text{-}Bu)Pz)_3]^-$ and $[MeB(3\text{-}(Mes)Pz)_3]^-$

H.V. Rasika Dias [a,b,*], Xiaoyu Wang [a]

[a] Department of Chemistry and Biochemistry, The University of Texas at Arlington, Arlington, TX 76019, USA
[b] Institute of Fundamental Studies, Hantana Road, Kandy, Sri Lanka

Received 28 June 2004; accepted 25 August 2004

Abstract

Thallium derivatives of the sterically demanding methyl tris(pyrazolyl)borate ligands $[MeB(3\text{-}(t\text{-}Bu)Pz)_3]^-$ and $[MeB(3\text{-}(Mes)Pz)_3]^-$ have been synthesized using the corresponding pyrazole, $Li[MeBH_3]$ and thallium(I) acetate. Product formation could be followed by ^1H and ^{11}B NMR spectroscopy. $[MeB(3\text{-}(t\text{-}Bu)Pz)_3]Tl$ and $[MeB(3\text{-}(Mes)Pz)_3]Tl$ display monomeric structures. The thallium sites adopt a pyramidal geometry. The crystal structure of 3-(Mes)PzH is also reported. It forms planar, hydrogen bonded tetramers in the solid state.
© 2004 Elsevier Ltd. All rights reserved.

Keywords: Thallium; ^{11}B NMR; B–H coupling; Tris(pyrazolyl)borate; Pyrazole

1. Introduction

Tris(pyrazolyl)borates constitute one of the most widely used group of ligands in chemistry [1,2]. In fact, complexes of tris(pyrazolyl)borates are now known for most of the elements in the periodic table [2]. The vast majority of these involve the use of ligands with a hydride group on the boron atom (e.g., $[HB(Pz)_3]^-$, $[HB(3,5\text{-}(Me)_2Pz)_3]^-$, $[HB(3\text{-}(Mes)Pz)_3]^-$ (**1**), $[HB(3\text{-}(t\text{-}Bu)Pz)_3]^-$). Relatively, few tris(pyrazolyl)borate systems featuring B-alkyl or B-aryl substituents have also been isolated [1]. Most of these ligands, however, are based on the parent pyrazole (e.g., $[PhB(Pz)_3]^-$ (**2**), $[(\eta^5\text{-}C_5H_5)Fe\{\eta^5\text{-}C_5H_4B(Pz)_3\}]^-$).

B-hydride free ligands that also contain sterically demanding substituents at the pyrazolyl moiety 3-position (e.g., $[t\text{-}BuB(3\text{-}(t\text{-}Bu)Pz)_3]^-$ (**3**) and $[PhB(3\text{-}(t\text{-}Bu)Pz)_3]^-$ (**4**)) are rare [3–5]. Such ligands are very attractive because they not only lack the reactive and sometimes problematic B–H functionality, but they also provide excellent protection for labile or reactive metal adducts. In this paper, we describe the synthesis of two methyl tris(pyrazolyl)borate ligands featuring sterically demanding pyrazolyl moieties. X-ray crystal structures of the thallium adducts $[MeB(3\text{-}(t\text{-}Bu)Pz)_3]Tl$ and $[MeB(3\text{-}(Mes)Pz)_3]Tl$ are also reported. Thallium adducts like these serve as excellent ligand transfer agents [6–8].

* Corresponding author. Tel.: +1 817 272 3813.
E-mail address: dias@uta.edu (H.V. Rasika Dias).

0277-5387/$ - see front matter © 2004 Elsevier Ltd. All rights reserved.
doi:10.1016/j.poly.2004.08.023

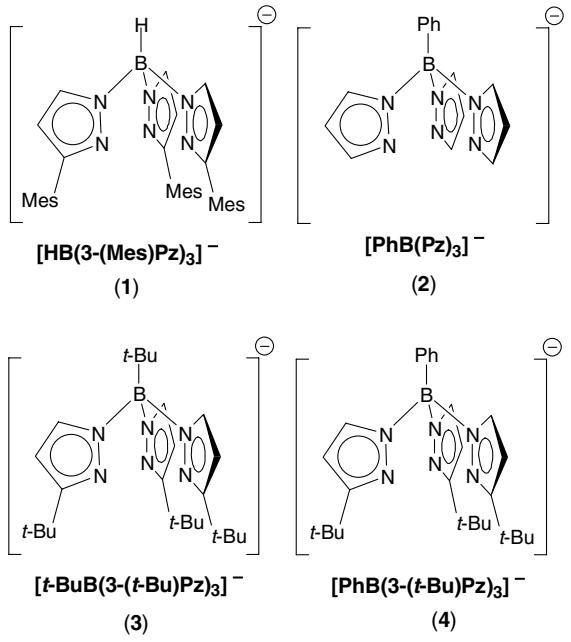

2. Experimental

2.1. General procedures

All manipulations were carried out under an atmosphere of purified nitrogen using standard Schlenk techniques. NMR spectra were recorded at 25 °C on a JEOL Eclipse 500 spectrometer (^{1}H, 500.16 MHz, ^{13}C, 125.78 MHz, ^{11}B, 160.47 MHz). Proton and carbon chemical shifts are reported in ppm versus Me_4Si. ^{11}B NMR spectra were referenced to external $BF_3 \cdot Et_2O$. Melting points were obtained on a Mel-Temp II apparatus and were not corrected. 3-*tert*-Butylpyrazole [9] and 3-mesitylpyrazole [10] were prepared using published methods. TlOAc was purchased from commercial sources.

2.2. Synthesis of Li[MeBH$_3$]

It was synthesized as described using $MeB(OH)_2$ and $LiAlH_4$ in Et_2O, and purified using a slightly modified procedure [11]. A 50-mL Schlenk tube containing a magnetic stirring bar was fitted with a rubber septum and charged with 2,2′-biquinoline (0.002 g) and $LiAlH_4$ (10 mL of a 1.0 M solution in diethylether). The solution became deep blue after stirring for a few minutes. A solution of methylboronic acid (0.395 g, 6.6 mmol) in diethylether (15 mL) was slowly added at 25 °C. After stirring for 1 h, the mixture was filtered, and the filtrate was collected. The solid precipitate was washed with diethylether (3×10 mL), and the washings were combined with the filtrate. Evaporating the solvent from the filtrate under reduced pressure gave Li[$MeBH_3$] as a colorless, oily product. To this, hexane (15 mL) was added and the solution stirred for 10 min. Then the volatile materials were removed under reduced pressure. After repeating this process three times, Li[$MeBH_3$] was obtained as a white powdery product, 0.210 g, 89% yield. ^{11}B NMR (DMSO-d_6): δ −30.7 (qq, $^1J(^{11}B–^1H) = 78.5$ Hz, $^2J(^{11}B–^1H) = 4.8$ Hz). ^{1}H NMR (DMSO-d_6): δ 0.33 (BH_3, quartet of quartets superimposed on a heptet of quartets, $^1J(^{11}B–^1H) = 78.5$ Hz, $^1J(^{10}B–^1H) = 26.5$ Hz, $^3J(^1H–^1H) = 6.5$ Hz); −0.64 (m, BCH_3). See supplementary material for K[BH_4] spectra taken under similar conditions as well as for ^{1}H NMR signals corresponding to BCH_3 protons.

2.3. Synthesis of [MeB(3-(t-Bu)Pz)$_3$]Tl

A mixture of Li[$MeBH_3$] (0.107 g, 3.00 mmol) and 3-*tert*-butylpyrazole (1.127 g, 9.07 mmol) was heated at ca. 220 °C under N_2 for one hour. The product was allowed to cool to room temperature. It was suspended in THF (8 mL), then solid thallium(I) acetate (1.225 g, 4.65 mmol) was added at room temperature and the mixture was stirred overnight. The resulting mixture was filtered and the volatile components were removed from the filtrate by a rotary evaporator giving crude [MeB(3-(*t*-Bu)-Pz)$_3$]Tl as an off-white solid. Pure [MeB(3-(*t*-Bu)Pz)$_3$]Tl was obtained as colorless crystals by crystallization from hexane at −25 °C. Yield: 65%; m.p.: 142–143 °C. ^{1}H NMR ($CDCl_3$): δ 0.95 (s, 3H, BCH_3), 1.36 (s, 27H, $C(CH_3)_3$), 6.05 (d, 3H, $J = 2.0$ Hz, Pz–H) 7.61 (d, 3H, $J = 2.0$ Hz, Pz–H). ^{11}B NMR ($CDCl_3$): δ−0.3 (s). ^{13}C{^{1}H} NMR ($CDCl_3$): δ 31.84 (br), 32.27, 101.28, 133.62, 163.20 (the *C*H_3B-signal could not be clearly detected in the ^{13}C NMR spectrum). *Anal.* Calc. for $C_{22}H_{36}N_6BTl$: C, 44.06; H, 6.05; N, 14.01. Found: C, 43.74; H, 5.88; N, 13.74%.

2.4. Synthesis of [MeB(3-(Mes)Pz)$_3$]Tl

Freshly sublimed 3-mesitylpyrazole (1.690 g, 9.07 mmol) and Li[$MeBH_3$] (0.1074 g, 3.00 mmol) were added into a Schlenk tube containing mesitylene (5 mL). This mixture was stirred for about 5 h at room temperature until the gas evolution ceased. Then it was heated for 48 h at 180 °C. Removal of the solvent by distillation gave the crude product [MeB(3-(Mes)Pz)$_3$]Li. The crude [MeB(3-(Mes)Pz)$_3$]Li and thallium(I) acetate (1.185 g, 4.5 mmol) were mixed in THF (20 mL), and the resulting mixture was stirred overnight at room temperature. The solution was filtered over Celite and the filtrate was collected. Removal of solvent from the filtrate afforded crude [MeB(3-(Mes)Pz)$_3$]Tl. It was washed with methanol to obtain analytically pure [MeB(3-(Mes)Pz)$_3$]Tl (1.766 g). Yield: 75%; m.p.: 245–247 °C; ^{1}H NMR ($CDCl_3$): δ 1.16 (s, 3H), 1.91 (s,

18H), 2.27 (s, 9H), 6.06 (d, 3H, ^3J(H,H) = 1.5Hz), 6.84 (s, 6H), 7.85 (d, 3H, ^3J(H,H) = 1.5Hz); $^{13}C\{^1H\}$ NMR ($CDCl_3$): δ 20.44 (br d, $J = 47$ Hz), 21.19, 104.62, 128.00, 131.11, 133.36, 137.42, 137.54, 150.06 (the CH_3B-signal could not be clearly assigned in the ^{13}C NMR spectrum). ^{11}B NMR ($CDCl_3$): δ 0.0 (s). *Anal.* Calc. for $C_{37}H_{42}N_6BTl$: C, 56.54; H, 5.39; N, 10.69. Found: C, 56.55; H, 5.19; N, 10.62%.

2.5. X-ray structure determinations

X-ray quality crystals of [MeB(3-(*t*-Bu)Pz)$_3$]Tl and [MeB(3-(Mes)Pz)$_3$]Tl were obtained from hexane and THF–hexane solutions at −15 °C, respectively. A suitable crystal of the thallium compound covered with a layer of hydrocarbon oil was selected and mounted with paratone–N oil in (or on) a cryo-loop, and immediately placed in a low-temperature nitrogen stream. The X-ray intensity data were measured at 100(2) K on a Bruker SMART APEX CCD area detector system equipped with a Oxford Cryosystems 700 Series cooler, a graphite monochromator and a Mo Kα fine-focus sealed tube ($\lambda = 0.71073$ Å). The detector was placed at a distance of 5.995 cm from the crystal. The data frames were integrated with the Bruker SAINT-PLUS software package. Data were corrected for absorption effects using the multi-scan technique (SADABS). Structures were solved and refined using the Bruker SHELXTL (Version 6.14) software package. [MeB(3-(*t*-Bu)Pz)$_3$]Tl and [MeB(3-(Mes)Pz)$_3$]Tl crystallize in the *Pnma* and *Cc* space groups, respectively. We have considered the potential ambiguities of the *Cc* space group (e.g., centrosymmetric option) for [MeB(3-(Mes)Pz)$_3$]Tl, but remain confident of the assignment. Some details of the data collection and refinement of [MeB(3-(*t*-Bu)Pz)$_3$]Tl and [MeB(3-(Mes)Pz)$_3$]Tl are given in Table 1. Selected bond distances and angles are presented in Tables 2 and 3. The

Table 2
Selected bond lengths (Å) and angles (°) for [MeB(3-(*t*-Bu)Pz)$_3$]Tl

Bond lengths			
Tl–N(4)	2.5306(17)	N(3)–N(4)	1.374(2)
Tl–N(2A)	2.5496(14)	N(3)–B(1)	1.568(3)
Tl–N(2)	2.5496(14)	B(1)–N(1A)	1.5643(18)
N(1)–N(2)	1.3696(17)	B(1)–C(14)	1.610(3)
N(1)–B(1)	1.5643(18)		
Bond angles			
N(4)–Tl–N(2A)	78.81(4)	N(2A)–Tl–N(2)	74.16(6)
N(4)–Tl–N(2)	78.81(4)	N(1)–B(1)–N(1A)	108.57(17)
N(1)–B(1)–N(3)	110.41(11)	N(1A)–B(1)–C(14)	109.43(11)
N(1A)–B(1)–N(3)	110.41(11)	N(3)–B(1)–C(14)	108.59(17)
N(1)–B(1)–C(14)	109.43(11)		

Table 3
Selected bond lengths (Å) and angles (°) for [MeB(3-(Mes)Pz)$_3$]Tl

Bond lengths			
Tl(1)–N(2)	2.545(4)	N(5)–N(6)	1.355(5)
Tl(1)–N(4)	2.551(4)	N(5)–B(1)	1.553(6)
Tl(1)–N(6)	2.564(4)	N(7)–N(8)	1.364(5)
Tl(2)–N(12)	2.530(4)	N(7)–B(2)	1.562(6)
Tl(2)–N(8)	2.555(3)	N(9)–N(10)	1.367(4)
Tl(2)–N(10)	2.564(3)	N(9)–B(2)	1.554(5)
N(1)–N(2)	1.362(5)	N(11)–N(12)	1.362(5)
N(1)–B(1)	1.557(7)	N(11)–B(2)	1.562(6)
N(3)–N(4)	1.370(5)	C(37)–B(1)	1.618(6)
N(3)–B(1)	1.559(8)	C(74)–B(2)	1.610(5)
Bond angles			
N(2)–Tl(1)–N(4)	72.92(13)	N(5)–B(1)–C(37)	110.4(4)
N(2)–Tl(1)–N(6)	72.10(12)	N(1)–B(1)–C(37)	110.1(4)
N(4)–Tl(1)–N(6)	71.64(11)	N(3)–B(1)–C(37)	110.6(5)
N(12)–Tl(2)–N(8)	71.54(12)	N(9)–B(2)–N(11)	108.9(3)
N(12)–Tl(2)–N(10)	73.63(10)	N(9)–B(2)–N(7)	109.5(3)
N(8)–Tl(2)–N(10)	71.93(11)	N(11)–B(2)–N(7)	107.6(3)
N(5)–B(1)–N(1)	109.7(4)	N(9)–B(2)–C(74)	110.2(3)
N(5)–B(1)–N(3)	107.7(4)	N(11)–B(2)–C(74)	109.8(3)
N(1)–B(1)–N(3)	108.4(4)	N(7)–B(2)–C(74)	110.7(3)

Table 1
Crystal data and structure refinement for [MeB(3-(*t*-Bu)Pz)$_3$]Tl and [MeB(3-(Mes)Pz)$_3$]Tl (there are two molecules of [MeB(3-(Mes)Pz)$_3$]Tl, 0.5 molecule of THF and a molecule of hexane in the asymmetric unit)

Empirical formula	$C_{22}H_{36}BN_6Tl$	$C_{82}H_{102}B_2N_{12}O_{0.5}Tl_2$
Formula weight	599.75	1694.12
Crystal system	orthorhombic	monoclinic
Space group	*Pnma*	*Cc*
Unit cell dimensions		
a (Å)	14.4125(14)	18.951(4)
b (Å)	15.7571(15)	15.197(3)
c (Å)	10.7518(10)	27.750(5)
α (°)	90	90
β (°)	90	92.145(3)
γ (°)	90	90
Volume (Å^3)	2441.7(4)	7986(3)
Z	4	4
Density (calculated) (Mg/m^3)	1.631	1.409
Goodness-of-fit on F^2	1.091	1.074
Final *R* indices [$I > 2\sigma(I)$]	$R_1 = 0.0135$, $wR_2 = 0.0350$	$R_1 = 0.0237$, $wR_2 = 0.0605$
R indices (all data)	$R_1 = 0.0142$, $wR_2 = 0.0353$	$R_1 = 0.0249$, $wR_2 = 0.0610$

X-ray crystal structure of 3-(Mes)PzH was also determined as the solid-state structures of pyrazoles are of interest [12]. Further details and the X-ray crystallographic data for 3-(Mes)PzH are in the cif files.

3. Results and discussion

The thallium derivative of the methyl substituted tris(pyrazolyl)borate $[MeB(3\text{-}(t\text{-}Bu)Pz)_3]^-$ can be synthesized by treating the lithium adduct $[MeB(3\text{-}(t\text{-}Bu)Pz)_3]Li$ (which was obtained from a reaction between $Li[MeBH_3]$ and 3-*tert*-butylpyrazole) with thallium(I) acetate.

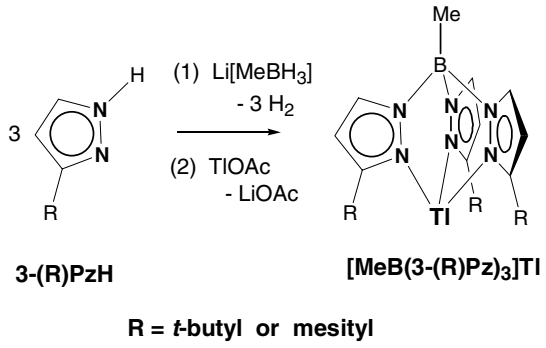

The formation of the final product and the consumption of $Li[MeBH_3]$ could be followed using ^{11}B and ^{1}H NMR spectroscopy. For example, the ^{11}B NMR spectrum of $Li[MeBH_3]$ in d_6-DMSO reveals a quartet of quartets (Fig. 1). The ^{11}B NMR spectrum of the thallium adduct $[MeB(3\text{-}(t\text{-}Bu)Pz)_3]Tl$ shows only a broad singlet. The ^{1}H NMR spectra are also very informative. For example, the BH_3 protons of $Li[MeBH_3]$ appear as a heptet of quartets superimposed on a quartet of quartets (Fig. 2). The heptet (signals show equal intensity as expected) of quartets arises from the coupling between protons of the BH_3 unit with the ^{10}B isotope ($I = 3$, abundance = 19.9%) and methyl protons [13]. The superimposed quartet (peaks have equal intensity) of quartets can be attributed to the splitting caused by the ^{11}B isotope ($I = 3/2$, abundance = 80.1%) and methyl protons. The $^{1}J(^{1}H\text{–}^{11}B/^{1}H\text{–}^{10}B)$ ratio is consistent with the $^{11}B/^{10}B$ nuclear magnetogyric ratio of 2.986 (see supplementary material for $K[BH_4]$ spectra taken under similar conditions) [13]. Protons of the methyl group appear as a complex multiplet (see supplementary material). The ^{1}H NMR spectrum of $[MeB(3\text{-}(t\text{-}Bu)Pz)_3]Tl$, in contrast, shows the presence of signals corresponding to the pyrazolyl units, a broad singlet for B–Me protons and the disappearance of BH_3 related resonances. We did not observe the Tl–H coupling in the ^{1}H NMR (500 MHz) spectrum. However, Tl–H coupling has been observed in the ^{1}H NMR (300 MHz) spectrum of the hydroborato analog, $[HB(3\text{-}(t\text{-}Bu)Pz)_3]Tl$ [14,15]. This somewhat surprising Tl–H (also true for Tl–C) coupling related observation has been attributed to thallium relaxation via chemical shift anisotropy, which is strongly dependent on the external magnetic field strength [15].

The X-ray crystal structure of $[MeB(3\text{-}(t\text{-}Bu)Pz)_3]Tl$ is illustrated in Fig. 3. It contains a crystallographically imposed mirror plane involving Tl, B and one of the pyrazolyl groups. $[MeB(3\text{-}(t\text{-}Bu)Pz)_3]Tl$ exhibits the common symmetric, tridentate coordination of the tris(pyrazolyl)borate ligand. Interestingly, $[HB(3\text{-}(t\text{-}Bu)Pz)_3]Tl$ crystallizes in the same space group and has a very similar structure [14]. The Tl–N (2.582(6), 2.587(9) Å) distances of $[HB(3\text{-}(t\text{-}Bu)Pz)_3]Tl$ are not significantly different from the Tl–N bond lengths of $[MeB(3\text{-}(t\text{-}Bu)Pz)_3]Tl$ (2.5306(17), 2.5496(14) Å). The molecular structure of the B-phenyl analog, however, is very different [4]. The tris(pyrazolyl)borate ligand in $[PhB(3\text{-}(t\text{-}Bu)Pz)_3]Tl$ coordinates to thallium primarily in a bidentate fashion. The third pyrazolyl group, which is rotated by about 90°, shows a contact to thallium, via the nitrogen atom directly bonded to the boron.

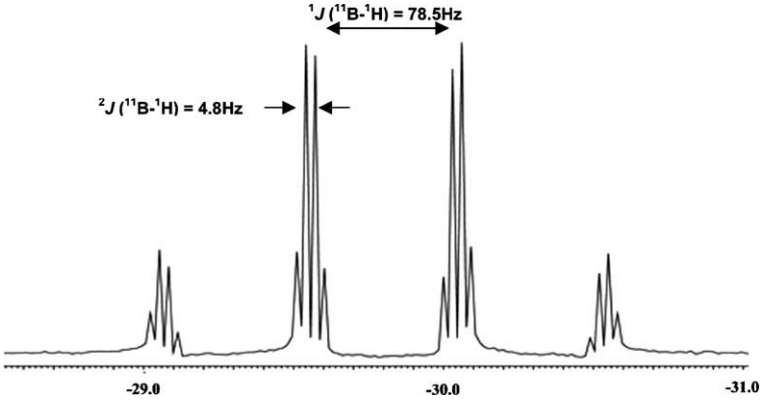

Fig. 1. ^{11}B NMR (160.47 MHz, d_6-DMSO, 25 °C) spectrum of $Li[MeBH_3]$.

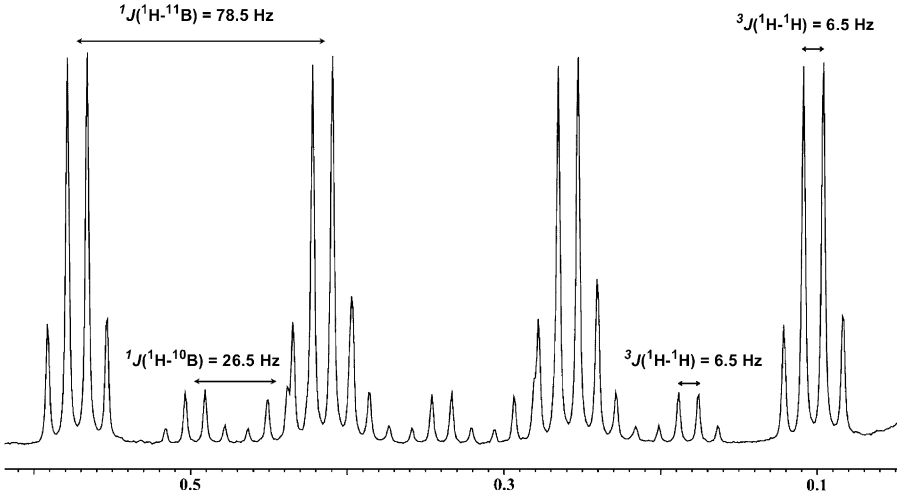

Fig. 2. ^{1}H NMR (500 MHz, d_6-DMSO, 25 °C) spectrum of Li[MeBH$_3$] showing the BH_3-related resonances.

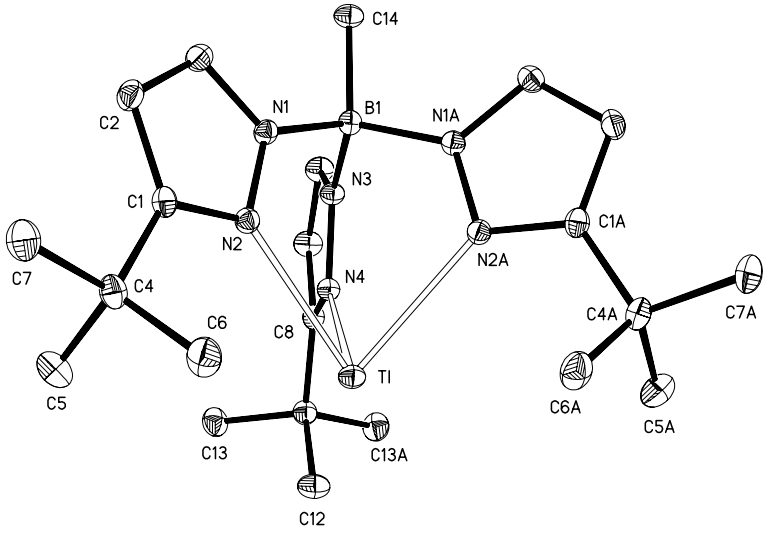

Fig. 3. Crystal structure of [MeB(3-(*t*-Bu)Pz)$_3$]Tl (H-atoms have been omitted for clarity).

The synthesis of [MeB(3-(Mes)Pz)$_3$]Tl was accomplished by using 3-(Mes)PzH, Li[MeBH$_3$] and TlOAc. It was isolated in 75% yield as the only product. Interestingly, the reaction between KBH$_4$ and 3-(Mes)PzH leads to a mixture of isomers [10]. [HB(3-(Mes)Pz)$_3$]Tl, which is closely related to the B–Me analog [MeB(3-(Mes)Pz)$_3$]Tl, was obtained as the minor product whereas the asymmetric species [HB(5-(Mes)Pz)(3-(Mes)Pz)$_2$]Tl is the major product. The X-ray crystal structure of [MeB(3-(Mes)Pz)$_3$]Tl is illustrated in Fig. 4. It crystallizes with two chemically similar but crystallographically different molecules in the asymmetric unit. X-ray data confirm the formation of the isomer with mesityl groups at the pyrazolyl ring 3-positions. The thallium center adopts a pyramidal geometry. The Tl–N distances of 2.530–2.564 Å are in the typical range [6,7].

We have also obtained the X-ray crystal structure of 3-mesitylpyrazole (Fig. 5). It features an interesting planar, tetrameric structure in the solid state due to N–H $\cdots$ N hydrogen bonding [16]. Solid-state structures of pyrazoles are of current interest [12,16–21]. *N*-Unsubstituted pyrazoles display structures ranging from dimers, trimers and tetramers, to polymeric chains. Among these, the tetrameric form is the least common. 3,5-(CF$_3$)$_2$PzH, 3,5-(Ph)$_2$PzH, 3-(CF$_3$),5-(Ph)PzH and 3(5)-phenyl-5(3)-methylpyrazole are some examples of pyrazoles that adopt the tetrameric form in the solid state [16–21].

Overall, we have described the isolation of sterically demanding tris(pyrazolyl)borates with B-methyl groups. Such ligands are rare. The related hydroborato analogs have received significant attention in recent years.

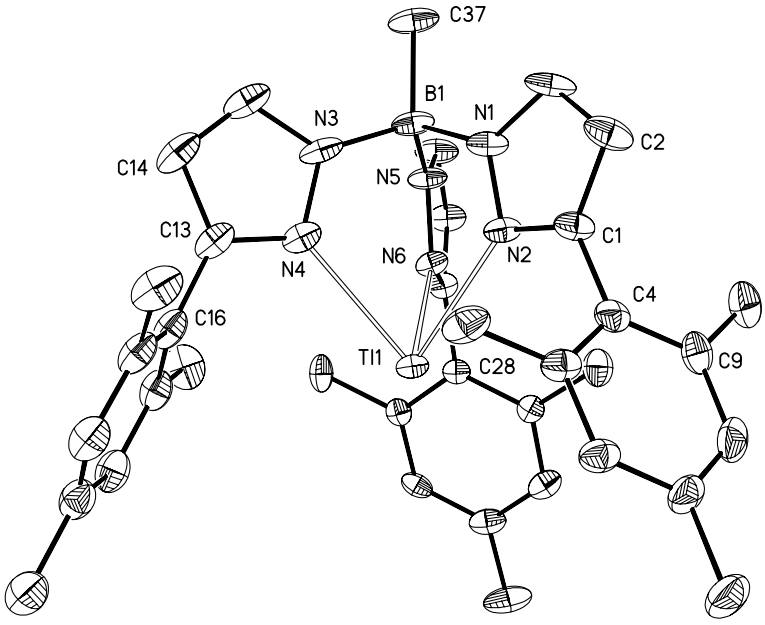

Fig. 4. Crystal structure of $[MeB(3\text{-}(Mes)Pz)_3]Tl$ (only one of the two molecules in the asymmetric unit is shown. H-atoms have been omitted for clarity).

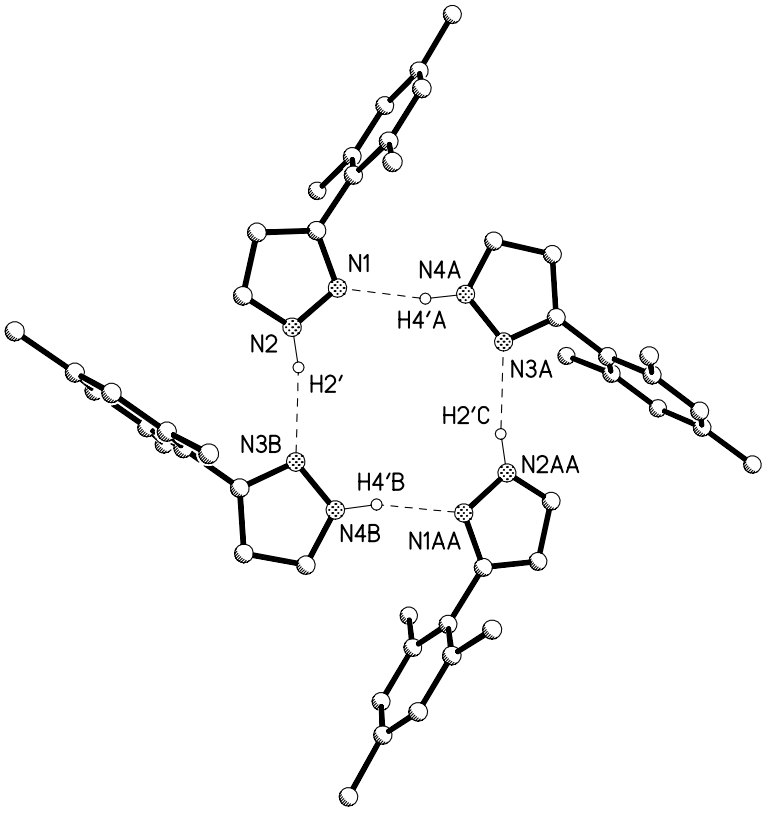

Fig. 5. The structure of 3-(Mes)PzH showing the tetramer (all the hydrogens except those on nitrogen atoms have been omitted for clarity).

[9,10,15,22–34] $[MeB(3\text{-}(t\text{-}Bu)Pz)_3]^-$ and $[MeB(3\text{-}(Mes)Pz)_3]^-$ would be particularly useful for investigating chemistry where B–H units typically create problems. Due to the presence of the B-methyl group, these ligands may also have a somewhat reduced tendency to isomerize (e.g., from the 3,3,3 isomer to the 3,3,5 form) during

reactions [2]. We are currently investigating the coordination chemistry of these B-protected ligand systems. Thallium derivatives are useful in this regard because they serve as good ligand transfer agents [2,6–8]. Preliminary results show that we can synthesize a variety of metal adducts including those involving copper(I). A comparison of IR data of $[MeB(3\text{-}(Mes)Pz)_3]CuCO$ ($\nu_{CO} = 2074$ cm^{-1}) [35] to $[HB(3\text{-}(Mes)Pz)_3]CuCO$ ($\nu_{CO} = 2079$ cm^{-1}) [33] shows that there is no notable electronic effect on the copper(I) center as a result of replacing the hydride on boron with a methyl group [17].

Acknowledgement

This work has been supported by the Robert A. Welch Foundation (Grant Y-1289) and the National Science Foundation (CHE-0314666).

Appendix A. Supplementary material

Selected ^1H and ^{11}B spectroscopic data of $Li[MeBH_3]$ and KBH_4. Crystallographic data for $[MeB(3\text{-}(t\text{-}Bu)Pz)_3]Tl$, $[MeB(3\text{-}(Mes)Pz)_3]Tl$ and 3-(Mes)PzH have been deposited with the Cambridge Crystallographic Data Center, CCDS Nos. 242955–242957. Copies of this information may be obtained free of charge from the Director, Cambridge Crystallographic Data Centre (CCDC), 12 Union Road, Cambridge, CB2 1EZ (Fax: +44 1223 336033; E-mail: deposit@ccdc.cam.ac.uk; or http://www.ccdc.cam.ac.uk). Supplementary data associated with this article can be found, in the online version, at doi:10.1016/j.poly.2004.08.023.

References

[1] C. Pettinari, C. SantiniComprehensive Coordination Chemistry II, vol. 1, 2004, p. 159.
[2] S. Trofimenko, Scorpionates: The Coordination Chemistry of Polypyrazolylborate LigandImperial College, Imperial College, London, 1999.
[3] O. Graziani, L. Toupet, J.-R. Hamon, M. Tilset, Inorg. Chim. Acta 341 (2002) 127.
[4] J.L. Kisko, T. Hascall, C. Kimblin, G. Parkin, J. Chem. Soc., Dalton Trans. (1999) 1929.
[5] J.L. Kisko, T. Hascall, G. Parkin, J. Am. Chem. Soc. 120 (1998) 10561.
[6] H.V.R. DiasComprehensive Coordination Chemistry II, vol. 3, Elsevier, 2004, p. 383.
[7] C. Janiak, Coord. Chem. Rev. 163 (1997) 107.
[8] C. Janiak, Main Group Metal Chem. 21 (1998) 33.
[9] S. Trofimenko, J.C. Calabrese, J.S. Thompson, Inorg. Chem. 26 (1987) 1507.
[10] A.L. Rheingold, C.B. White, S. Trofimenko, Inorg. Chem. 32 (1993) 3471.
[11] B. Singaram, T.E. Cole, H.C. Brown, Organometallics 3 (1984) 774.
[12] J.L.G. de Paz, J. Elguero, C. Foces-Foces, A.L. Llamas-Saiz, F. Aguilar-Parrilla, O. Klein, H.-H. Limbach, Soc. J. Chem., Perkin Trans. 2 (1997) 101.
[13] M. Winter, Available from: http://www.webelements.com/webelements/elements/text/B/nucl.html, 2004.
[14] A.H. Cowley, R.L. Geerts, C.M. Nunn, S. Trofimenko, J. Organomet. Chem. 365 (1989) 19.
[15] P. Ghosh, P.J. Desrosiers, G. Parkin, J. Am. Chem. Soc. 120 (1998) 10416.
[16] S. Trofimenko, A.L. Rheingold, L.M. Liable-Sands, R. Maria Claramunt, C. Lopez, M. Dolores Santa Maria, J. Elguero, New J. Chem. 25 (2001) 819.
[17] H.V.R. Dias, T.K.H.H. Goh, Polyhedron 23 (2004) 273.
[18] C. Foces-Foces, I. Alkorta, J. Elguero, Acta Crystallogr., Sect. B 56 (2000) 1018.
[19] I. Alkorta, J. Elguero, B. Donnadieu, M. Etienne, J. Jaffart, D. Schagen, H.-H. Limbach, New J. Chem. 23 (1999) 1231.
[20] J. Elguero, N. Jagerovic, C. Foces-Foces, F.H. Cano, M.V. Roux, F. Aguilar-Parrilla, H.-H. Limbach, J. Heter. Chem. 32 (1995) 451.
[21] R.G. Raptis, R.J. Staples, C. King, J.P. Fackler Jr., Acta Crystallogr., Sect. C 49 (1993) 1716.
[22] D.L. Reger, T.D. Wright, M.D. Smith, A.L. Rheingold, S. Kassel, T. Concolino, B. Rhagitan, Polyhedron 21 (2002) 1795.
[23] M.H. Chisholm, N.W. Eilerts, J.C. Huffman, S.S. Iyer, M. Pacold, K. Phomphrai, J. Am. Chem. Soc. 122 (2000) 11845.
[24] H. Kunkely, A. Vogler, Chem. Phys. Lett. 327 (2000) 162.
[25] M.H. Chisholm, N.W. Eilerts, J.C. Huffman, Inorg. Chem. 35 (1996) 445.
[26] H.V.R. Dias, L. Huai, W. Jin, S.G. Bott, Inorg. Chem. 34 (1995) 1973.
[27] A. Looney, A. Saleh, Y. Zhang, G. Parkin, Inorg. Chem. 33 (1994) 1158.
[28] K. Michiue, R.F. Jordan, Organometallics 23 (2004) 460.
[29] M.A. Mairena, M.M. Diaz-Requejo, T.R. Belderrain, M.C. Nicasio, S. Trofimenko, P.J. Perez, Organometallics 23 (2004) 253.
[30] F.A. Kunrath, R.F. De Souza, O.L. Casagrande Jr., N.R. Brooks, V.G. Young Jr., Organometallics 22 (2003) 4739.
[31] S. Murtuza, O.L. Casagrande Jr., R.F. Jordan, Organometallics 21 (2002) 1882.
[32] M.M. Diaz-Requejo, A. Caballero, T.R. Belderrain, M.C. Nicasio, S. Trofimenko, P.J. Perez, J. Am. Chem. Soc. 124 (2002) 978.
[33] J.L. Schneider, S.M. Carrier, C.E. Ruggiero, V.G. Young Jr., W.B. Tolman, J. Am. Chem. Soc. 120 (1998) 11408.
[34] C. Lopez, D. Sanz, R.M. Claramunt, S. Trofimenko, J. Elguero, J. Organomet. Chem. 503 (1995) 265.
[35] H.V.R. Dias, X. Wang, unpublished results.

Available online at www.sciencedirect.com
SCIENCE DIRECT®
Polyhedron 23 (2004) 2541–2547
POLYHEDRON
www.elsevier.com/locate/poly

Three dimensional hydrogen-bonding network in a copper complex of 2-hydroxy-1,4-naphthoquinone: structural, spectroscopic and magnetic properties

S. Salunke-Gawali [a,d], S.Y. Rane [a,*], V.G. Puranik [b], C. Guyard-Duhayon [c], F. Varret [d]

[a] Department of Chemistry University of Pune, Pune 411 007, India
[b] National Chemical Laboratory, Pune, India
[c] Laboratoire de Chimie Inorganique et Matériaux Moléculaires, UMR-CNRS-7071, Université Pierre et Marie Curie, 4 place Jussieu, F-75252 Paris Cedex 5, France
[d] Laboratoire de Magnétisme et d'Optique, CNRS-Université de Versailles-Saint-Quentin, 45, Avenue des États-Unis, 78035 Versailles cedex, France

Received 27 July 2004; accepted 25 August 2004
Available online 14 October 2004

Abstract

Supramolecular $[Cu(II)(ONQ)_2(H_2O)_2]_n$ (**1**) a complex of the 2-hydroxy-1,4-naphthoquinone ligand (2HNQ), has been synthesized using $CuCl_2 \cdot 2H_2O$. ONQ is the deprotonated oxidized form of the ligand (viz. 2-oxido-1,4-naphthoquinone). The complex has been characterised by X-ray crystallography, variable temperature magnetic susceptibility measurements (SQUID), EPR and CV studies. The crystal structure of **1** has been solved at 295 and 161 K. The cell volume decreases from 435.3(6) $Å^3$ at 295 K to 427.9(6) $Å^3$ at 161 K. The monomeric units of **1** are linked by three types of intermolecular hydrogen bondings through coordinated ONQ ligands and water molecules, which results in a supramolecular three dimensional hydrogen bonding network. The magnetic susceptibility data of **1** were best fitted with the Bonner Fisher equation with the coupling parameter $J = -3.2\ cm^{-1}$, indicating a weak antiferromagnetic interaction along the chain.
© 2004 Elsevier Ltd. All rights reserved.

Keywords: Lawsone; Quinones; 2-Hydroxy-1, 4-Naphthoquinone; Amine oxidase; Copper complexes; Antiferromagnetic coupling; H-bonding; EPR

1. Introduction

The syntheses and characterization of supramolecular assemblies have been of great interest in recent years due to their potential applications in the crystal engineering of non-linear optical, conducting and molecular ferromagnetic materials [1,2]. They can also be used to build polynuclear assemblies to synthesize bioactive materials having relevance, as chemical models, mimicking biological processes. Intermolecular hydrogen-bonding networks play an important role in the formation of supramolecular structures from smaller molecular units [3]. Such a hydrogen bonding network can also mediate interesting magnetic interactions among the spin centers of assembled molecular materials if they possess unpaired electrons [4,5].

Due to their complicated redox properties, quinone complexes have been of considerable interest for many years [6,7]. Quinones can bind potentially to metal ions in three different oxidation states, viz. (i) quinone, (ii) its one electron reduced form, semiquinone, and (iii) its two electron reduced form, catechol. Coordination complexes of quinones with different oxidation states reflect differences in their structural, magnetic and electrochemical properties [7].

* Corresponding author. Tel.: +912025812183; fax: +91202561728.
E-mail address: syrane@chem.unipune.ernet.in (S.Y. Rane).

0277-5387/$ - see front matter © 2004 Elsevier Ltd. All rights reserved.
doi:10.1016/j.poly.2004.08.022

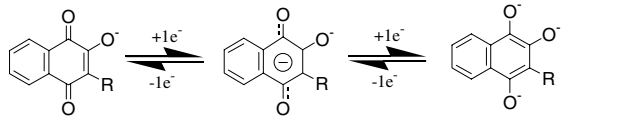

I) Quinone Form (ONQ) **R = H = Lawsone** II) Semi-quinone Form (ONSQ) III) Catechol Form (CAT)

Scheme 1. Various redox forms of 2-hydroxy-1,4-naphthoquinone and its derivatives.

The binding ability of quinones in different oxidation states allows them to play an important role in biological systems. Copper containing oxidases, such as amine oxidase which catalyses the oxidative deamination of primary amines to aldehydes, contain quinone as an active cofactor [8,9]. Another copper containing oxidase enzyme, galactose oxidase, involves the formation of a free radical which is antiferromagnetically coupled with the copper ions. There have been many efforts in recent years to understand the metal–quinone interactions and to mimic the structural and functional models for these enzymes [10,11]. Because of the biological significance of complexes of derivatized hydroxy naphthoquinones [12–14], in this present report we have used 2-hydroxy-1,4-naphthoquinone, viz. 2HNQ or lawsone, for complex **1** to investigate its spectroscopic and magnetic properties. The ligand, 2HNQ, can coordinate (in its deprotonated ONQ form) to metal ions in three different oxidation states, viz. quinone; I, semiquinone; II and catechol; III (Scheme 1).

We report here magnetostructural properties of a synthesized copper complex $[Cu(II)(ONQ)_2(H_2O)_2]_n$ with 2HNQ. We also report the crystal structures at 161 and 295 K. The three-dimensional intermolecular hydrogen-bonding network existing in the structure leads to a weak antiferromagnetic coupling among the copper centers along the *a*-axis.

2. Experimental

2.1. Materials and measurements

All the reagents used in the synthesis were obtained from Aldrich Chemical Co. and are used without further purification. 2-Hydroxy-1,4-naphthoquinone was obtained from Fluka. The polycrystalline EPR spectra were recorded on a Varian E-112 spectrometer using 100 kHz field modulation at X-band (9.5 GHz) and Q-band (35 GHz) frequencies. The magnetization curves are recorded using a SQUID magnetometer (Quantum Design MPMS5) operating in the alternative mode at the Laboratoire de Magnétisme et d'Optique, CNRS/Université de Versailles (UMR 8634) France. The experimental molar magnetic susceptibilities were corrected for the underlying diamagnetic susceptibility using Pascal constants and temperature independent paramagnetism (-60×10^{-6}) cgs units/copper atom [15,16]. The molar magnetic susceptibility data were fitted using a non-linear simplex fitting routine [17]. The function minimized was [18]

$$F=\sum_t \frac{(\chi_t^{\mathrm{obsd}}-\chi_t^{\mathrm{calcd}})^2}{(\chi_t^{\mathrm{obsd}})^2}.$$

Cyclic voltammetry (CV) measurements were performed on BAS-CV-27 assembly in conjunction with an *X–Y* recorder using the three electrode system with direct correction of the uncompensated cell resistance (iR drop). The three-electrode cell includes a glassy carbon working electrode (area 0.23 mm^2) referenced with an Ag|AgCl electrode and platinum wire as an auxiliary electrode. The glassy carbon working electrode was activated according to a procedure by Thorp et al [19]. The solvents used in CV studies were purified according to the literature procedure [20] and were always de-gassed for 10 min before the experiment. 0.1 M tetraethyl ammonium perchlorate (TEAP) in CH_3CN was used as the supporting electrolyte. Before each CV run, the solution in the cell was carefully deareated with purified N_2.

2.2. Synthesis of compound $[Cu(ONQ)_2(H_2O)_2]_n$ (1)

To a solution of $CuCl_2\cdot 2H_2O$ (1 mM) in 15 ml of water, a solution of 2HNQ (1 mM) in 50 ml of methanol, was mixed with constant stirring. This mixture was stirred for 15 min; to this solution solid sodium carbonate (0.5 mM) was added. An orange coloured precipitate was obtained after stirring for 15–20 min; stirring was continued for another 2 h in air for complete precipitation of the orange residue. The yield of this orange precipitate was 20%, and this orange coloured solid was characterised by elemental analysis, infrared spectral studies, thermal and magnetic studies [21] as $[Cu_2(ONQ)_4(\mu\text{-}CO_3)]$ *Anal.* Calc. for $C_{41}H_{20}Cu_2O_{15}$: C, 55.85; H, 2.52; Cu, 14.41. Found : C, 55.64.10; H, 3.28; Cu, 14.10%. The orange precipitate was filtered. Brown crystals of **1** were obtained in a 40% yield from the filtrate after 4 days. *Anal.* Calc. for $C_{20}H_{14}CuO_8$: C, 53.83; H, 3.16; Cu, 14.25. Found: C, 54.10; H, 3.46; Cu, 13.6%. X-ray structures at 295K and 161 K, EPR and magnetic studies were performed on these crystals.

The brown crystals of **1** were also obtained when anhydrous $CuCl_2$ was used as the metal source and the $CuCl_2$:2HNQ ratio was kept as 1:2 at pH 5–6. The X-ray crystal structure of those crystals solved at 300 K [22] using an Enraf-Nonius CAD 4 single crystal X-ray diffractometer showed the same cell parameters as those shown in Table 1.

Table 1
Crystallographic data for $[Cu(C_{10}H_5O_3)_2(H_2O)_2]$ at 295 and 161 K

Formula	$C_{20}H_{14}CuO_8$	$C_{20}H_{14}CuO_8$
Crystal class	triclinic	triclinic
Space group	$P\bar{1}$	$P\bar{1}$
a (Å)	5.027(3)	4.994(5)
b (Å)	9.536(9)	9.532(7)
c (Å)	10.407(5)	10.357(3)
α (°)	63.61(7)	63.19(4)
β (°)	87.26(5)	87.67(6)
γ (°)	77.31(7)	77.08(7)
Volume (Å^3)	435.3(6)	427.9(6)
Z	1	1
λ Mo Kα (Å)	0.710690	0.710690
ρ(g cm^{-3})	1.70	1.73
M (g mol^{-1})	445.86	445.86
μ (cm^{-1})	13.05	13.27
Temperature (K)	295	161
Size (mm)	$0.15 \times 0.25 \times 0.4$	$0.15 \times 0.25 \times 0.4$
Reflections measured	1715	1693
Independent reflections	1523	1504
Reflections used	1455	1416
Number of parameters	135	135
$R = \sum \|\|F_o\| - \|F_c\|\| / \sum \|F_o\|$	0.0497	0.0431
$Rw = [\sum w(\|\|F_o\| - \|F_c\|\|)^2 / \sum wF_o^2]$	0.0577	0.0501

Weighting scheme of the form $w = w'[1 - ((\|F_o\| - \|F_c\|)/6\sigma(F_o))^2]^2$ with $w' = 1/\sum_r A_r T_r(X)$, with coefficients 3.37, 0.94 and 2.27 for a Chebychev series for which $X = F_c/F_c(\max)$ at 295 K.
Weighting scheme of the form $w = w'[1 - ((\|F_o\| - \|F_c\|)/6\sigma(F_o))^2]^2$ with $w' = 1/\sum_r A_r T_r(X)$, with coefficients 2.37, 0.681 and 1.53 for a Chebychev series for which $X = F_c/F_c(\max)$ at 161 K.

2.3. Crystallography

The low temperature and the room temperature crystal structures were solved for the crystals of **1** at the Centre de Resolution de Structures, Université Pierre et Marie Curie, Paris France. Crystals of $[Cu(ONQ)_2(H_2O)_2]$ belong to the triclinic system with space group $P\bar{1}$. The selected crystal was a brown parallel piped of approximate dimensions: $0.15 \times 0.25 \times 0.40$ mm. The crystal was mounted on a glass fiber and data were collected on an Enraf-Nonius CAD4 diffractometer. Cell constants were obtained from a least-squares fit of 25 reflections. Crystal and intensity collection data are summarized in Table 1. A total of 1715 (1693) reflections were recorded to a 2θ (Mo) maximum of 50°. Intensity standards, recorded periodically, showed no significant variations during measurements. Reflections were corrected for Lorentz and polarization effects. 1455 (1416) of the reflections with $I > 3\sigma$ were used in subsequent calculations. Difabs absorption corrections were made.

The structure was solved by direct methods using the SHELXS [23] program and for all other calculations the CRYSTALS [24] program was used. Atomic scattering factors and anomalous dispersion terms were taken from the International Tables for X-ray Crystallography [25]. Full-matrix, least-squares refinement based on $|F|$, and a Chebychev weighting scheme [26] were performed. All non-hydrogen atoms were anisotropically refined. Hydrogen atoms on water molecules were found by difference Fourier techniques. Other hydrogen atoms were introduced in calculated positions. All hydrogen atoms were allocated one overall refinable isotropic thermal parameter. The final refinement minimizing converged to $R = 0.0497$ (0.0431) and $Rw = 0.0577$ (0.0501). The goodness of fit was $S = 1.013$ (1.063) with 1455 (1416) observations and 135 variables.

3. Result and discussion

3.1. Crystal structure of $[Cu(ONQ)_2(H_2O)_2]_n$ (1)

The crystal structure of the complex **1** has been solved at two different temperatures, viz. 161 and 295 K and the cell parameters are given in Table 1. The ORTEP view of complex **1** as a monomeric unit is depicted in Fig. 1, where one half of the molecule generates the other half to give a monomeric unit with the Cu(II) ion lying on the center of inversion. The copper(II) ion is hexa-coordinated with two bidentate ONQ ligands and two water molecules. The basal plane of the complex is occupied by the quinone carbonyl oxygen atoms, O(1) and O(1a) and the phenoxy oxygens O(2) and

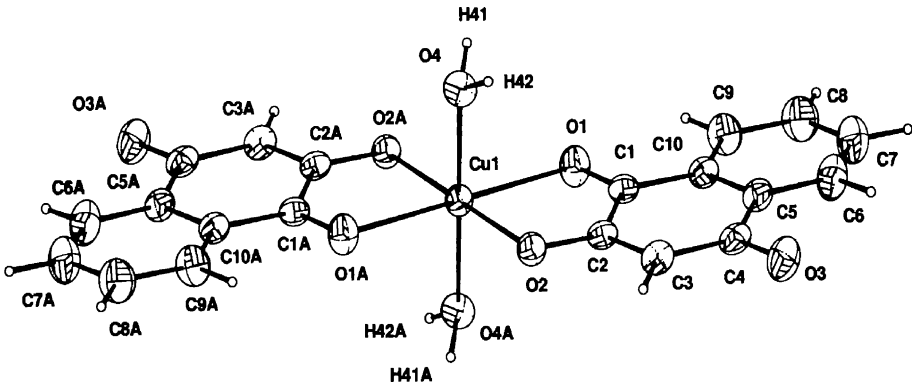

Fig. 1. ORTEP view of monomeric $[Cu(Lw)_2(H_2O)_2]$ at room temperature (showing 50% probability thermal ellipsoids).

O(2a) of ONQ at 2.336(2) Å and 1.954(3) Å, respectively. The apical positions are occupied by the two oxygen atoms of water, viz. O(4) and O(4a) at a distance 2.007(3) Å. The biting angle of the ligand, O(1)–Cu–O(2) is acute (77.05(11)°) while the bond angle between the two biting ligands is 102.95(11)°. The bond angles between the coordinating atoms (O(1) and O(2)) of the ligand ONQ and the oxygen atoms of the coordinating water molecules are nearly at right angles: O(1)–Cu–O(4) = 90.24(13)°, O(1)–Cu(1)–O(4a) = 89.76(13)°, O(2)–Cu(1)–O(4) = 89.04(14)° and O(2)–Cu(1)–O(4a) = 90.96(14)°. Thus, the geometry of the complex can be best described as an axially elongated octahedron. Selected bond distances and angles are given in Table 2. The C(1)–O(1) bond distance (1.216(4) Å) of the coordinating ligand is less than that of chelating semiquinone anions (1.27–1.30 Å) or catecholate (1.34–1.36 Å) [27–30], implying that the ligand 2HNQ is in its fully oxidized deprotonated ONQ form coordinating to a copper(II) ion. The other bond lengths of the coordinated quinone molecule are found to be normal and similar to that of reported metal complexes with the ONQ ligand [31]. The C(2)–O(2) phenoxy distance is similar to that of the phenoxy distance found in iron [31] and manganese[32] complexes with the ONQ form of the ligand.

Table 2
Selected bond distances and angles for $[Cu(Lw)_2(H_2O)_2]$

	295 K	161 K
Bond distances (Å)		
Cu(1)–O(1)	2.336(2)	2.328(2)
Cu(1)–O(2)	1.954(3)	1.953(2)
Cu(1)–O(4)	2.007(3)	1.995(2)
O(1)–C(1)	1.216(4)	1.227(4)
(O2)–C(2)	1.297(4)	1.295(4)
Cu(1)–Cu(1b)	5.03	4.99
Cu(1)–Cu(1c)	9.54	9.53
Bond angles (°)		
O(1)–Cu(1)–O(2)	77.05(11)	77.04(8)
O(1)–Cu(1)–O(2a)	102.95(11)	102.96(8)
O(1)–Cu(1)–O(4)	90.24(13)	90.12(8)
O(1)–Cu(1)–O(4a)	89.76(13)	89.88(8)
O(2)–Cu(1)–O(4)	89.04(14)	89.12(8)
O(2)–Cu(1)–O(4a)	90.96(14)	90.88(8)

a, Symmetry: $1-x, 1-y, 1-z$; b, symmetry: $1+x, y, z$; c, symmetry: $x, y-1, z$.

Formation of supramolecular assemblies via H-bonding is an interesting part of the molecular structure of **1** (Fig. 2). Three types of intermolecular hydrogen bonds exist: (i) between one of the hydrogens of water and the phenoxy oxygen, O(2), of a nearby molecule (symmetry: $-x, 1-y, 1-z$) along the *a*-axis; (ii) between the second hydrogen of water and an oxygen of the uncoordinated carbonyl group of a quinone ring of the next molecule (symmetry: $x, 1+y, z$) along the *c*-axis and (iii) between the uncoordinated quinone oxygen atoms and the H atom at the C3 position of a ONQ quinone group of nearby molecules. Thus, these three types of hydrogen bonding networks with the crystallographic symmetry form an interesting supramolecular hydrogen bonding network assembly. The possible hydrogen bonding distances and angles between the acceptor and donor atoms are summarized in Table 3 and they are in the acceptable range [33]. The nearest Cu–Cu distances are 5.03 and 9.54 Å.

Due to the interesting intermolecular hydrogen bonding networks, we were curious to see the structure of compound **1** at a low temperature. The crystal structure was solved at 161 K and the structure is found to be similar to that of the RT structure (Fig. 1) with some changes in the bond distances and angles. The crystallographic parameters, selected bond distances, angles and

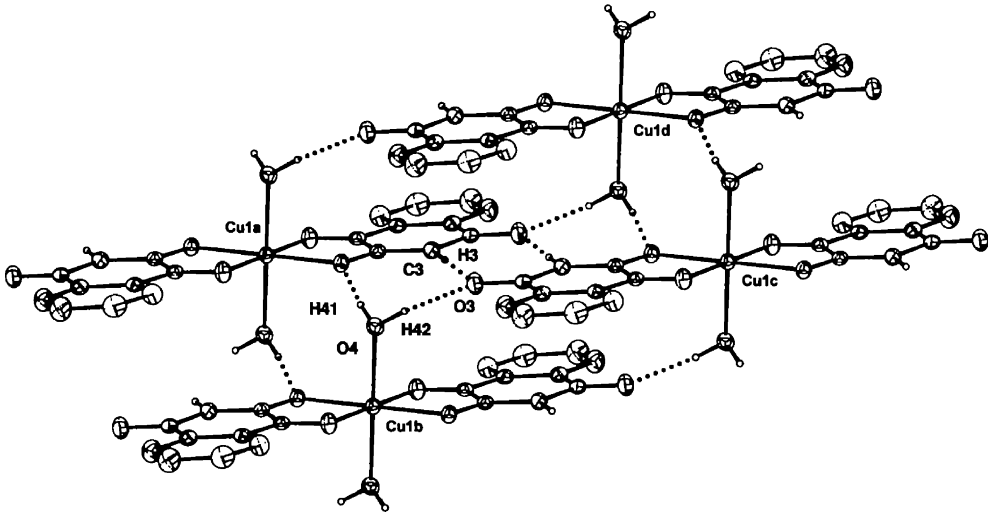

Fig. 2. ORTEP view of the molecular packing of $[Cu(Lw)_2(H_2O)_2]$ showing the possible inter molecular H-bonding networks (showing 30% probability thermal ellipsoids).

Table 3
Possible hydrogen bonding interactions in $[Cu(Lw)_2(H_2O)_2]$ (distances in (Å) and bond angles in (°))

Donor (D)	H	Acceptor (A)	D–H		H···A		D···A		D–H···A	
			296	161	296	161	296	161	296	161
O(4)[a]	H(4)	O(2)	0.93	0.77	1.80	1.94	2.72	2.71	172.46	170.71
O(4)[b]	H(4)	O(3)	0.87	0.80	1.90	1.96	2.75	2.74	168.75	168.28
C(3)[c]	H(3)	O(3)	1.00	1.01	2.51	2.48	3.51	3.48	178.21	177.01

Symmetry (a): $-x$, $1-y$, $1-z$; (b) x, $y+1$, z; (c) $-x$, $-y$, $1-z$.

possible hydrogen bond distances are given in Tables 1–3, respectively, along with the room temperature results for a comparison purpose. There is shrinkage in unit cell length and the volume (see Table 1) due to contraction at the low temperature. As can be seen in Table 2, the bonding parameters are within the estimated error except for the copper ion and the oxygen of the coordinating water molecule, which is 0.01 Å shorter at lower temperature. Similarly, the Cu–Cu distance is ~0.04 Å shorter at lower temperature along the *a*-axis, though there is no difference along the other crystallographic directions. The donor–acceptor distances are also smaller at lower temperatures as indicated in Table 3.

3.2. EPR spectroscopy

X-band polycrystalline EPR spectra recorded at RT and 77 K and Q-band EPR spectra at RT of the present complex are given in Fig. 3. The room temperature X-band EPR spectrum shows a highly anisotropic rhombic pattern where the perpendicular component is not fully resolved, though the unsymmetrical shape is evident. The g_1 (g_z) value appears rather high, indicating the weak ligand field strength. There is no visible signal in the half-field region, indicating absence of a forbidden $\Delta M_s = \pm 2$ transition. At 77 K the features are almost the same except that there is a reduction in the linewidth especially at the $g_\perp$ region. The room temperature Q-band EPR spectrum exhibits a rhombic pattern where the (g_y) and (g_x) signals are resolved. The resolution of $g_\parallel$ and $g_\perp$ into a four line feature results in g_1 to g_4 as 2.399, 2.25, 2.109, 2.0601. Similar features are observed in $[Cu(Lw)_2(H_2O)]_2$ [14b]. This characteristic is in accordance with aggregation of monomeric molecules as seen in the X-ray structure.

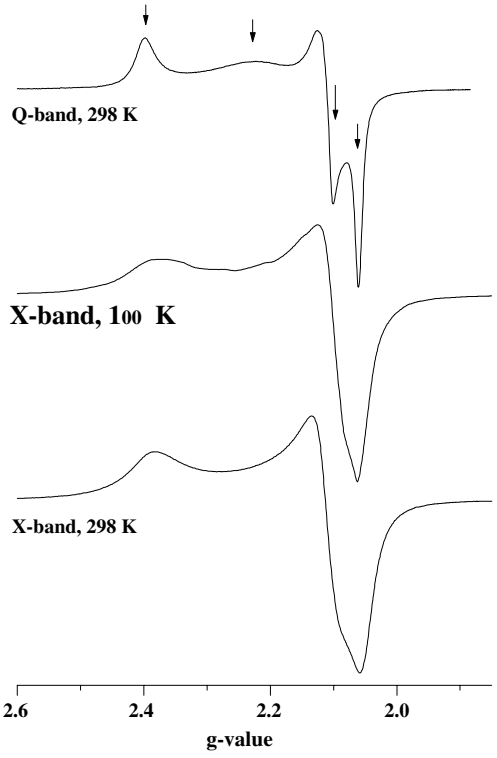

Fig. 3. X-band EPR spectra at 100 and 298 K and Q-band EPR spectrum at 298 K.

3.3. Magnetic properties

Variable temperature magnetic susceptibility measurements (SQUID) for complex **1** were performed on polycrystalline samples in the range 5–300 K. The experimental values of χ_{mol} and μ_{eff} per copper ion are plotted in Fig. 4. At room temperature (300 K) the experimental μ_{eff} value is 1.62 μB, which is less than the spin only value expected for mononuclear copper(II) complexes,

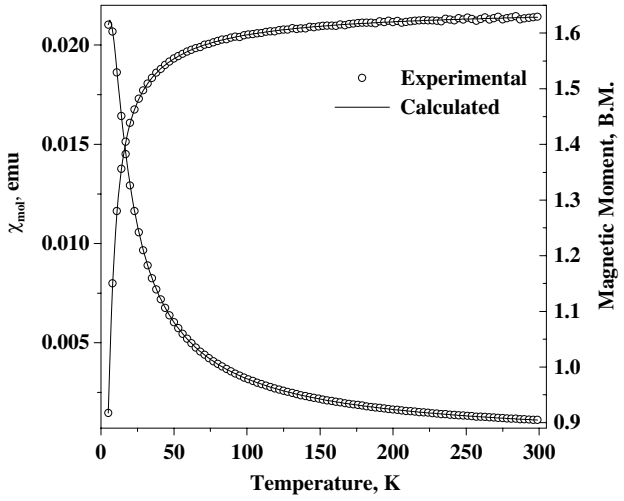

Fig. 4. Experimental and theoretical molar magnetic susceptibility and magnetic moment per copper ion of $[Cu(Lw)_2(H_2O)_2]$. (○○○○, experiment; —-, theoretical). The fit was obtained using Eqs. (1) and (2).

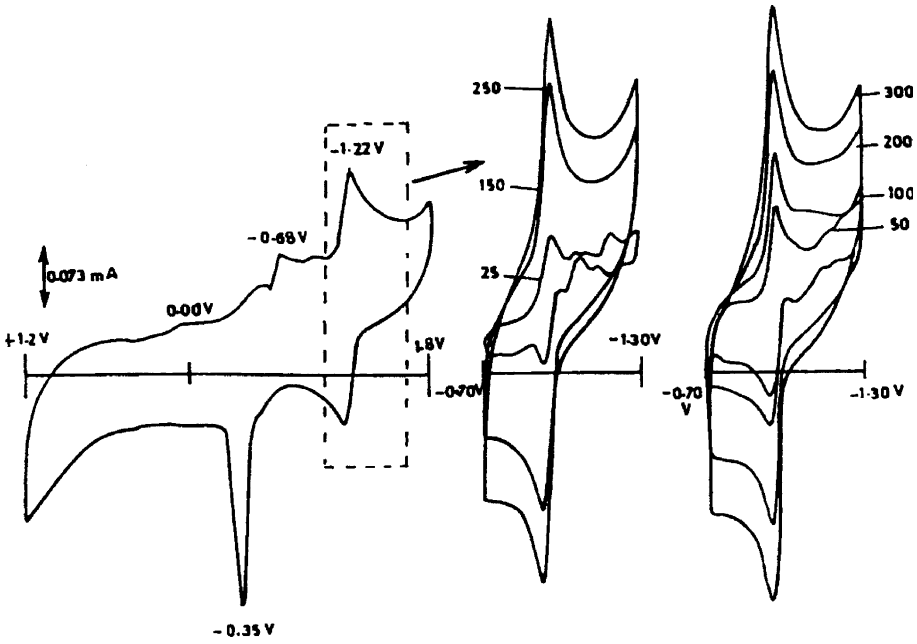

Fig. 5. Cyclic voltammogram of **1** in 0.1 M TEAP in CH_3CN. The dotted line represents the scan rate variations.

and this decreases gradually and steadily with temperature down to 50 K. Below this temperature, the magnetic moment decreases steeply on decreasing the temperature and drops down to 0.9 μB at 5 K. The current magnetic moment behaviour with temperature probably indicates an antiferromagnetic coupling among the copper ion centers. Looking at the structure of compound **1**, there is no direct bonding interaction between the copper ions. So the observed antiferromagnetic behaviour among the copper centers should arise through the intermolecular hydrogen-bondings. It should also be noted that this hydrogen-bonding network brought the copper–copper distance to 4.99 Å along the *a*-axis while the shortest Cu–Cu distance along the other axes is 9.53 Å. The experimental magnetic susceptibility data were best fitted with the Bonner Fisher equation (Eq. (1)) [34] which accounts for the magnetic interaction along the chain and also interactions between chains.

$$\chi_m = Ng^2\beta^2/kT[(0.25 + 0.074975x + 0.07523x^2) /(1.0 + 0.9931x + 0.172135x^2 + 0.757825x^3)], \quad (1)$$

where $x = |J/kT|$, J is the antiferromagnetic coupling parameter, k is the Boltzmann's constant and T is the temperature, g is the gyromagnetic ratio, β is the Bohr-magneton value. The inter-chain exchange (zJ') was estimated following a mean field correction Eq. (2) [16]

$$\chi_m^{corr} = \chi_m/(1 - 2zJ'\chi_m/Ng^2\beta^2). \quad (2)$$

The experimental data were best fitted with the following parameters: $J = -3.26\ cm^{-1}$, $g = 1.9$, $zJ' = 0.01$ and the least-square error: 2.7×10^{-7}.

3.4. Cyclic voltammetric studies

Fig. 5 shows a cyclic voltammogram of **1** and the reactions ascertained with the respective cathodic as well as anodic peak potentials are shown in the following equations.

$$\text{Ligand ONQ} : \text{ONQ} \xrightarrow[1e^-]{-0.51\ V} \text{ONSQ} \underset{1e^-}{\overset{-1.19\ V}{\rightleftharpoons}} \text{CAT}$$

$$\mathbf{1} : \text{ONQ} \xrightarrow[1e^-]{-0.68\ V} \text{ONSQ} \underset{1e^-}{\overset{-1.22\ V}{\rightleftharpoons}} \text{CAT}$$

$$\text{Cu(II)(ONQ)(ONSQ)} \underset{1e^-}{\overset{-0.00\ V}{\rightleftharpoons}} \text{Cu(O)} + 2\text{ONQ}$$

The ligand based peaks in **1** were shifted towards negative potentials compared to the ligand, which suggest weak intramolecular metal–ligand interactions, however the ligand mediated Cu–Cu interaction is observed at 0.00 V [35].

4. Conclusion

Three types of intermolecular H-bondings found in the crystal structure of **1** complex lead to three dimensional network assemblies of $[Cu(ONQ)_2(H_2O)_2]$ units. The magnetic chain of Cu(II) ions in **1** via H-bondings

results in antiferromagnetism with numerical fittings of χ_m with the Bonner and Fisher model.

5. Supplementary material

Crystallographic data (excluding structure factors) for the structures reported in this paper have been deposited with the Cambridge Crystallographic Data Centre as supplementary publication Nos. 212886 and 212887. Copies of the data can be obtained free of charge on application to CCDC, 12 Union Road, Cambridge CB2 1EZ, UK [fax: +44 1223/336 033; E-mail: deposit@ccdc.cam.ac.uk, or http://www.ccdc.cam.ac.uk].

Acknowledgements

S. Gawali Salunke is thankful to UGC for awarding SRF and the Ministry of Research Government of France for awarding a visiting fellowship, S.Y.R. is grateful to the CSIR, New Delhi, India (01(1686)/00/EMR-II) for the Grant.

References

[1] A.D. Burrows, C.W. Chan, M.M. Chaudhary, J.E. McGrady, D.M.P. Mingos, Chem. Soc. Rev. 24 (1995) 329.
[2] A.D. Burrows, D.M.P. Mingos, A.J.P. White, D.J. Williams, J. Chem. Soc., Dalton Trans. (1996) 149.
[3] M. Oh, G.B. Carpenter, D.A. Sweigart, Acc. Chem. Res. 37 (2004) 1.
[4] J. Tercero, C. Diaz, J. Ribas, J. Mahia, M.A. Maestro, Inorg. Chem. 41 (2002) 5373.
[5] C.T. Yang, B. Moubaraki, K.S. Murray, J.D. Ranford, J.J. Vittal, Inorg. Chem. 40 (2001) 5934.
[6] C.G. Pierpont, C. W Lange, Prog. Inorg. Chem. 41 (1994) 331.
[7] C.G. Pierpont, Coord. Chem. Rev. 219–221 (2001) 451.
[8] J.P. Klinman, Biochim. Biophys. Acta 1647 (2003) 131.
[9] W. Kaim, J. Chem. Soc., Dalton Trans. (2003) 761.
[10] P. Chaudhuri, M. Hess, J. Muller, K. Hildenbrand, E. Bill, T. Weyhermuller, K. Wieghardt, J. Am. Chem. Soc. 121 (1999) 9599.
[11] Y. Shimazaki, S. Huth, S. Hirota, O. Yamauchi, Inorg. Chim. Acta 331 (2002) 168.
[12] S.I. Allakhverdiev, M.S. Karacan, G. Somer, N. Karacan, E.M. Khan, S.Y. Rane, S. Padhye, V.V. Klimov, G. Renger, Biochemistry 33 (1994) 12210.
[13] M.S. Karacan, G. Somer, E.M. Khan, S.Y. Rane, S.I. Allkhverdiev, S.B. Padhye, V.V. Kilmov, G. Renger, Z. Naturforsch. C 49 (1994) 587.
[14] (a) S.Y. Rane, E.M. Khan, D.R. Thube, S.B. Padhye, S.K. Date, P.P. Bakare, Indian J. Chem. 39 (2000) 1117;
(b) S.Y. Rane, S.D. Gawali, S.B. Padhye, S.K. Date, P.P. Bakare, Indian J. Chem. 42A (2003) 255;
(c) S. Salunke-Gawali, S.Y. Rane, K. Boukheddaden, E. Codjovi, J. Linares, F. Varret, P.P. Bakare Indian J. Chem. A 43 (2005), to be published.
[15] C.J. O' Connor, Prog. Inorg. Chem. 29 (1982) 203.
[16] O. Kahn, Molecular Magnetism, VCH, Weinheim, Germany, 1993.
[17] J.A. Nelder, R. Mead, J. Comput. 7 (1965) 308.
[18] G.V.R. Chandramouli, C. Balagoplakrishna, M.V. Rajasekharan, P.T. Manoharan, Comput. Chem. 20 (1996) 353.
[19] H.H. Thorp, J.E. Sarneski, G.W. Brudvig, R.H. Crabtree, J. Am. Chem. Soc. 111 (1989) 9249.
[20] D.D. Perrin, W.L. Armarego, D.R. Perrin, Purification of Laboratory Chemicals, Pergamon Press, London, 1966.
[21] (a) S.Y. Rane, S.D. Gawali, S.B. Padhye, A.S. Kumbhar, P.P. Bakare, J. Thermal Anal. Cal. 55 (1999) 24;
(b) S. Salunke-Gawali, S. Rane, R. Dalvi, K. Ahmed, J. Thermal Anal. Cal. 76 (2004) 801;
(c)S.D. Gawali, Magnetostructural studies in synthetic analogs of copper quinoprotiens, Ph.D. Thesis, University of Pune, India, 1999.
[22] S.Y. Rane, S.D. Gawali, S.B. Padhye, A.S. Kumbhar, V.G. Puranik, P.P. Bakare, S.K. Date, Proc. Indian Acad. Sci. (Chem. Sci.) 108 (3) (1996) 289.
[23] G.M. Sheldrick, SHELXS86, Program for the Solution of Crystal Structures, University of Göttingen, Germany, 1986.
[24] D.J. Watkin, C.K. Prout, R.J. Carruthers, P. Betteridge, CRYSTALS, Chemical Crystallography Laboratory, Oxford, UK, 1996 (issue 10).
[25] D.T. CromerInternational Tables for X-ray Crystallography, vol. IV, Kynoch Press, Birmingham, UK, 1974.
[26] J.R. Carruthers, D.J. Watkin, Acta Cryst., Sect. A 35 (1979) 698.
[27] R.M. Buchanan, S.L. Kessel, H.H. Downs, C.G. Pierpont, D.N. Hendrickson, J. Am. Chem. Soc. 100 (1978) 7894.
[28] S.K. Larsen, C.G. Pierpont, G. DeMunno, G. Dolcetti, Inorg. Chem. 25 (1986) 4828.
[29] M.M. Olmstead, P.P. Power, G.A. Sigel, Inorg. Chem. 27 (1988) 580.
[30] S.R. Bonne, G.H. Purser, H.R. Chang, M.D. Lowery, D.N. Hendrickson, C.G. Pierpont, J. Am. Chem. Soc. 111 (1989) 2292.
[31] P. Garge, R. Chikate, S. Padhye, J-M. Savariault, P. de Loth, J.P. Tuchagues, Inorg. Chem. 29 (1990) 3315.
[32] M.P. Mulay, P.L. Garge, S.B. Padhye, R.L. Haltiwanger, L.A. deLearie, C.G. Pierpont, J. Chem. Soc., Chem. Commun. (1987) 581.
[33] J.B.J. Veldhuis, W.L. Driessen, J. Reedijk, J. Chem. Soc., Dalton Trans. (1986) 537.
[34] J.C. Bonner, M.E. Fisher, Phys. Rev. A 135 (1964) 640.
[35] S. Harmalkar, S.E. Jones, D.T. Sawyer, Inorg. Chem. 22 (1983) 2790.

Available online at www.sciencedirect.com
SCIENCE DIRECT®
Polyhedron 23 (2004) 2549–2559
POLYHEDRON
www.elsevier.com/locate/poly

New copper(II) complexes of 2-hydroxyacetophenone *N*(4)-substituted thiosemicarbazones and polypyridyl co-ligands: structural, electrochemical and antimicrobial studies

Rohith P. John [a,1], A. Sreekanth [a,2], V. Rajakannan [b], T.A. Ajith [c], M.R. Prathapachandra Kurup [a,*]

[a] *Department of Applied Chemistry, Cochin University of Science and Technology, Kochi 682022, India*
[b] *Department of Crystallography and Biophysics, Madras University, Chennai 600 025, India*
[c] *Amala Cancer Research Centre, Amala Nagar, Thrissur, Kerala, India*

Received 10 August 2004; accepted 2 September 2004
Available online 13 October 2004

Abstract

Seven new copper(II) complexes of 2-hydroxyacetophenone *N*(4)-substituted thiosemicarbazones (H_2L) and bidentate polypyridyl compounds 2,2′-bipyridine and 1,10-phenanthroline (B) were prepared and characterized. The thiosemicarbazones bind to the metal as dianionic ONS donors (L^{2-}) and yield compounds of the stochiometry [MLB]. The structure of the compound [Cu(L^4)(2,2′-bipy)] (**6**) was investigated by single-crystal X-ray diffraction method. Spin Hamiltonian and bonding parameters of the compounds calculated from the EPR spectra suggest square pyramidal (SPY) structure for the compounds. The *g* values predict geometry of C_{4v} symmetry with B_{1g} ground state. The bonding parameters show significant in-plane π-bonding. The cyclic voltammetric study of the complexes shows irreversible redox peaks corresponding to Cu(II/I) couple and quasi-reversible redox peaks corresponding to copper(II/III) oxidation. The thiosemicarbazones and their copper complexes show significant growth inhibitory activity against bacteria *Escherichia coli*, *Staphylococcus aureus*, and fungi *Candida albicans* and *Aspergillus flavus*.
© 2004 Elsevier Ltd. All rights reserved.

Keywords: Copper(II) complexes; Thiosemicarbazone; 2-Hydroxyacetophenone; EPR; Antimicrobial studies; Cyclic voltammetry; X-ray crystallography

1. Introduction

Thiosemicarbazones constitute an important class of nitrogen sulfur donor ligands, because of the highly interesting chemical, biological and medicinal properties [1,2]. Studies of 2-acetylpyridine *N*(4)-substituted thiosemicarbazones and their copper(II) complexes [3,4] have shown interesting electronic structure and bonding characteristics. Recently, there have been reports of copper(II) complexes of thiosemicarbazones with potential therapeutic properties [5,6]. The coordination chemistry of ONS donor ligands has been of considerable interest due to their remarkable structural and biological properties [7–10]. Interactions between aromatic rings are very important in proteins and protein–DNA systems for protein stabilization and various regulatory processes [11–14]. There has been considerable interest in

* Corresponding author. Tel.: +91 484 2575804; fax: +91 484 2577595.
E-mail addresses: mrp@cusat.ac.in, mrp_k@yahoo.com (M.R. Prathapachandra Kurup).
[1] Present address: Department of Chemistry, Hanyang University, Sa 1 dong, Ansan, Kyongi-do 426 791, Republic of Korea.
[2] Present address: Laboratorium für Physikalische Chemie, Departement Chemie und Angewandte Biowissenschaften ETH-Honggerberg, CH-8093, Zurich, Switzerland.

0277-5387/$ - see front matter © 2004 Elsevier Ltd. All rights reserved.
doi:10.1016/j.poly.2004.09.004

the compounds containing bidentate heterocyclic bases such as phenanthroline and bipyridine because of their versatile self-assembling properties [15]. Multidentate ligands with nitrogen containing heterocycles in general figure prominently as building blocks in the design of metal-ligand networks [16,17]. However, transition metal polypyridyl base adducts containing thiosemicarbazones have not been much investigated. Therefore, in continuation with our studies of polypyridyl adducts of copper(II) [18–20] thiosemicarbazones, we report the synthesis and spectral characterization of a series copper(II) complexes of 2-hydroxyacetophenone *N*(4)-substituted thiosemicarbazones, along with the crystal structure of compound [Cu(L^4)2,2′-bipy] (**6**). Their inhibitory activity against the growth of *Escherichia coli*, *Staphylococcus aureus*, *Candida albicans* and *Aspergillus flavus* was also determined. Primary ligands chosen in this study (Fig. 1) are *N*(4)-substituted thiosemicarbazones of 2-hydroxyacetophenone. 2,2′-bipyridyl (2,2′-bipy) and 1,10-phenanthroline (1,10-phen) were used as co-ligands for coordination with copper metal.

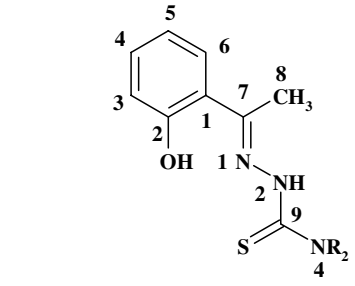

N(4)-substituents

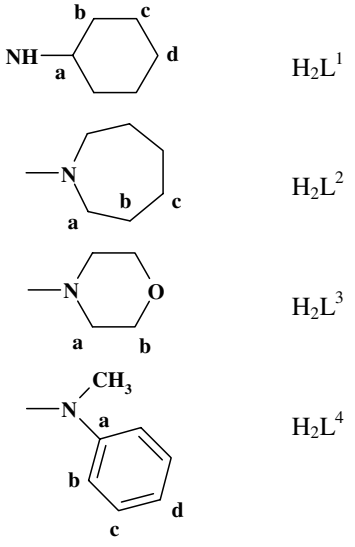

Fig. 1. Formulae of thiosemicarbazone ligands.

2. Experimental

2.1. Materials

All compounds used for the synthesis of thiosemicarbazone ligands and their complexes were purified by standard methods and solvents were purified by distillation. 1,10-Phenanthroline (Merck) and 2,2′-bipyridine (Merck) were used as received. Tetrabutylammonium tetrafluroborate (TBAB) was purchased from Aldrich Chemical Co. Solvents used for cyclic voltammetry were of spectroscopic grade and were used after drying over 4A molecular sieves.

2.2. Synthesis of ligands and their metal complexes

Synthesis of the thiosemicarbazone ligands (except H_2L^4) was carried out as per a modification of the procedure reported by Scovill [21,22]. 4-Methyl-4-phenyl thiosemicarbazone (1 mmol), 2-hydroxyacetophenone (1 mmol) and the respective amines cyclohexylamine/morpholine/hexamethyleneimine (1 mmol) were refluxed in methanol or acetonitrile (20 mL) for 15–60 min. The solution was allowed to cool; the crystalline product formed was filtered, washed with methanol and then with ether and dried over P_4O_{10} in vacuo. For the ligand H_2L^4, 4-methyl-4-phenyl thiosemicarbazone (1 mmol) and 2-hydroxyacetophenone (1 mmol) were refluxed in the presence of a small amount of cyclohexylamine in methanol for 10 min. The crystalline product formed was filtered washed with methanol, ether and then dried over P_4O_{10} in vacuo.

*Synthesis of complexes**1–7***. To a hot solution (20 mL) of the thiosemicarbazone ligand (0.5 mmol) in ethanol is added a 10 mL methanolic solution of the base, bipyridine or phenanthroline (0.5 mmol) while stirring. This is followed by a drop wise addition of about 10 mL of a methanolic solution of copper(II) acetate monohydrate (0.5 mmol). The solution is refluxed for about 2–3 h, allowed to cool, when microcrystals of the respective compounds in decent yield crystallized out. The compounds were filtered off, washed with ethanol, water followed by ether and dried in vacuo over P_4O_{10}.

[Cu(L^1)(2,2′-bipy)] (***1***). Greenish brown, *Anal.* Calc.: C, 58.98; H, 5.35; N, 13.76; Cu, 12.48. Found: C, 59.62; H, 5.50; N, 14.26; Cu, 13.05%. IR (KBr): ν/cm^{-1} 1566, 1592, 1022, 1337, 1439, 1152, 432, 768, 747.

[Cu(L^1)(1,10-phen)] (***2***). Brown, *Anal.* Calc: C, 60.83; H, 5.10; N, 13.14; Cu, 11.92. Found: C, 60.91; H, 5.11; N, 12.74; Cu, 11.53%. IR (KBr): ν/cm^{-1} 1565, 1590, 1028, 424, 1329, 764, 1150, 1431, 725, 845.

[Cu(L^2)(2,2′-bipy)] (***3***). Greenish brown, *Anal.* Calc: C, 58.98; H, 5.35; N, 13.76; Cu, 12.48. Found: C, 59.01; H, 5.42; N, 13.07; Cu, 11.90%. IR (KBr): ν/cm^{-1} 1557, 1592, 1024, 426, 1337, 742, 1204, 1437, 1424, 650.

[Cu(L^3)(2,2′-bipy)] (**4**). Olive green, *Anal.* Calc.: C, 55.58, H, 4.66; N, 14.09; Cu 12.78. Found: C, 55.92; H, 4.74; N, 13.55; Cu, 13.17%. IR (KBr): ν/cm^{-1} 1559, 1592, 1022, 426, 1341, 803, 1132, 1439, 735, 650, 762.

[Cu(L^3)(1,10-phen)] (**5**). Greenish brown, *Anal.* Calc.: C, 57.62; H, 4.45; N, 13.44; Cu, 12.19. Found: C, 57.79; H, 4.48; N, 13.10; Cu, 11.65%. IR (KBr): ν/cm^{-1} 1559, 1593, 1028, 430, 1341, 803, 1138, 1482, 1450, 727, 845.

[Cu(L^4)(2,2′-bipy)] (**6**). Pale brown, *Anal.* Calc.: C, 60.39; H, 4.48; N, 13.54; Cu; 12.29. Found: C, 61.20; H, 4.53; N, 13.16; Cu; 11.77%. IR (KBr)ν/cm^{-1}: 1559, 1593, 1019, 432, 1345, 766, 1142, 756, 745.

[Cu(L^4)(1,10-phen)] (**7**). Olive green, *Anal.* Calc.: C, 62.15; H, 4.28; N, 12.94; Cu, 11.74. Found: C, 62.78; H, 4.22; N, 13.10; Cu, 11.06%. IR (KBr) ν/cm^{-1}: 1563, 1593, 1022, 430, 1340, 750, 1134, 727, 638.

2.3. Physical methods

Elemental analyses were performed on a Heraeus Elemental analyzer. The metal contents were estimated in a Perkin–Elmer AAnalyst 700 Atomic Absorption spectrometer, after decomposing the compounds in conc. HNO_3. Magnetic measurements were performed in the polycrystalline state on a Gouy magnetic balance using $Hg[Co(SCN)_4]$ as a calibrant. Diamagnetic corrections for various atoms and structural units were computed from Pascal's constants. The effective magnetic moments were calculated from the corrected molar susceptibilities of the complexes using Curie's relation. The FT-IR spectra were recorded on a Shimadzu DR 8001 series FTIR spectrometer as KBr pellets and the UV–Vis spectra were recorded on a Shimadzu 160A UV–visible spectrophotometer in DCM solvent. The EPR spectra were recorded on a Varian E-112 Spectrometer using TCNE as the standard. Cyclic voltammetry and chronoamperometry measurements were performed on a BAS Epsilon Electrochemical Workstation equipped with a three-electrode system consisted of a glassy carbon (working), platinum wire (auxiliary) and a silver–silverchloride (reference) electrode on a C3 cell stand. The cyclic voltammetric (CV) measurements were made after degassing (Argon bubbling for 15 min) a dichloromethane solution (10^{-3}M) containing 0.1 M *n*-Bu_4NBF_4 (TEAB) as the supporting electrolyte. A blanket of argon gas was maintained throughout the measurement. The Ag–AgCl reference electrode was standardized for the ferricinium/ferrocene redox couple located at $E_{1/2} = +0.400$ V ($\Delta E_p = 60$ mV). The working electrode was polished fresh before each experiment with an alumina solution. Molar conductance of the complexes was measured in a Century CC-601 Digital Conductivity meter using 10^{-3} M DMF solution.

2.4. X-ray crystallography

A dark brown crystal [3] of the compound **6** having approximate dimensions $0.44 \times 0.38 \times 0.16$ mm was sealed in a glass capillary and intensity data were measured at room temperature (293 K). Accurate unit cell parameters and orientation matrices were obtained by a least-squares fit of several high angle reflections on a Siemens SMART CCD area detector using ω scan mode. Cell refinement and data reduction were carried out using SAINT (Siemens, 1996) [23,24]. A total of 31 541 reflections were collected, resulting in 5886 independent reflections of which 3874 had $I = 2\sigma(I)$ and these were considered as observed. An absorption correction was applied to the data with the maximum and minimum effective transmission factors of 0.867 and 0.510, respectively. Averaging the symmetry equivalent reflections resulted in an R_{int} value of 0.069. The structure was solved by direct methods and the full-matrix least-squares refinement using SHELX97 [25,26] package. The positions of all the non-hydrogen atoms were included in the full-matrix least-squares refinement using SHELXL97 [25,26] program. The final refinement cycle was based on all 5886 reflections and 307 variables, the $R_1 = 0.070$ and $wR_2 = 0.112$. For the subset of data with $I = 2\sigma(I)$ the R_1 value is 0.039 and the wR_2 is 0.098 for 3874 reflections. The maximum and minimum values of the electron densities in the final electron density map were 0.378, −0.671.

3. Results and discussion

3.1. Synthesis of the ligands and complexes

The complexes are readily formed by refluxing a methanolic/ethanolic solutions of the ligand and copper(II) acetate monohydrate. The polypyridyl base 1,10-phen 2,2′-bipy was added as the co-ligand, that also promotes the enolization of the principal thiosemicarbazone ligand and provides the basicity for the medium. Thiosemicarbazones coordinate as a tridentate ligand in the thiolate form (L^{2-}) – as is evident from IR spectra – after double deprotonation. The elemental analyses of the complexes are in agreement with the general formula [MLB]. An X-ray quality single crystal of compound **6** was obtained by slow evaporation of a DMF solution over a period of 8 days.

Since the thiosemicarbazones bind to the metal as a doubly deprotonated anion, it neutralizes +2 oxidation state of the copper(II) ion. The magnetic moment values

[3] The crystal data: Black, slab crystal; dimensions, $0.44 \times 0.38 \times 0.16$ mm; empirical formula, $C_{26}H_{23}CuN_5OS$; orthorhombic, space group Pbca, $a = 21.285(3)$ Å, $b = 9.8755(8)$ Å, $c = 22.609(2)$ Å, $\alpha = \beta = \gamma = 90.0°$, $V = 4752.5(8)$ Å^3, $Z = 8$, $d_{calculated} = 1.445$ g cm^{-3}. θ-range 1.80°–28.32°, completeness 99.4%.

of the complexes are in agreement with the values expected for mononuclear d^9 copper(II) complexes.

3.2. X-ray diffraction studies

An ORTEP plot of the compound **6** along with atom labeling is given in Fig. 2. Selected bond length and bond angles are summarized in Table 1. The copper in the mononuclear complex is five coordinated and is having an approximate square pyramidal (SPY) geometry. The basal coordination positions are occupied by the phenolato oxygen, O(1), azomethine nitrogen, N(1), and thiolate sulfur, S(1), of the thiosemicarbazone and the pyridine nitrogen, N(5), of the base 2,2′-bipy. While the Cu—O bond length is 1.9116 Å the Cu–N equatorial bond length varies between 1.9606 Å (azomethine) to 2.0474 Å (bipyridine). The apical position is occupied by second nitrogen of the base 2,2′-bipy, N(5), with a Cu–N(4) bond length of 2.2278 Å. The shorter Cu–$N_{(azomethine)}$ bond than Cu–$N_{(bipy)}$ bond indicates that the thiosemicarbazone moiety dominates equatorial bonding. The difference in bond lengths can be attributed to the difference in the extent of π-back bonding between the 2,2′-bipyridine and thiosemicarbazone moiety. However, the large bond distance of the axial Cu–N(4) supports the lack of significant out-of-plane π-bonding. This fact is in accordance with the EPR analysis.

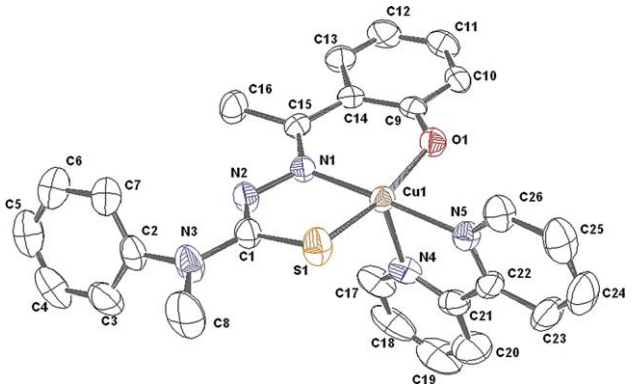

Fig. 2. ORTEP drawing and atomic labelings for compound [Cu(L^4)(2,2′-bipy)] (**6**) with thermal ellipsoids given at 50% probability. Hydrogen atoms are omitted for clarity.

Table 1
Selected bond lengths (Å) and angles (°) of compound [Cu (L^4)(2,2′-bipy)] (**6**)

Atoms	Bond distance	Atoms	Angles
Cu(1)–O(1)	1.9116(15)	O(1)–Cu(1)–N(1)	93.63(6)
Cu(1)–N(1)	1.9606(16)	O(1)–Cu(1)–N(5)	89.40(6)
Cu(1)–N(5)	2.0474(16)	N(1)–Cu(1)–N(5)	176.94(6)
Cu(1)–N(4)	2.2278(18)	O(1)–Cu(1)–N(4)	95.52(7)
Cu(1)–S(1)	2.2729(7)	N(1)–Cu(1)–N(4)	102.39(7)
S(1)–C(1)	1.740(2)	N(5)–Cu(1)–N(4)	76.86(7)
O(1)–C(9)	1.308(2)	O(1)–Cu(1)–S(1)	161.32(5)
N(1)–C(15)	1.307(2)	N(1)–Cu(1)–S(1)	85.91(5)
N(1)–N(2)	1.392(2)	N(5)–Cu(1)–S(1)	91.36(5)
N(2)–C(1)	1.302(2)	*N*(4)–Cu(1)–S(1)	102.83(5)

The four basal atoms are coplanar showing a slight but significant tetrahedral distortion. The central copper atom is slightly displaced from the basal plane in the direction of the axial nitrogen, which is evident from the bond angles of N(1)–Cu–N(5) 176.94°, and O(1)–Cu-S(1) 161.32°. The O(1)–Cu–N(4) bond angle, 95.52°, and S(1)–Cu–N(4) bond angle, 102.83°, indicate a slight tilting of the axial Cu–N(4) bond in the direction of the O(1)–Cu bond and away from S(1)–Cu bond. The small variations in the O(1)–Cu–N(1) (93.63°), O(1)–Cu–N(5) (89.40°), N(1)–Cu-S(1) (85.91°) and S(1)–Cu–N(5) (91.36°) base plane angles from the expected (90°) also contribute to distortion in the SPY geometry. One of the reason for the deviation from an ideal stereochemistry is the restricted bite angle imposed by both the $(L^4)^{2-}$ and 2,2′-bipy ligands. In other complexes involving HL or L coordinated to copper [27], the bite angles around the metal viz., N(1)–Cu–O(1) and N(1)–Cu-S(1) are limited to 80°–85°. Similarly, the bite angle created by the heterocyclic base N(5)–Cu–N(4) of 76.86° (76.2° for compound **3a**) may be considered normal, when compared with an average value of 77° cited in the literature [28–30].

The Cu–N bond lengths of the heterocyclic base are longer than those reported for mononuclear copper(II) complexes [31,32] indicating a weaker binding of the base compared to the thiosemicarbazone. The comparison of the thiosemicarbazone moiety bond distances of the compound **6** to those of the uncoordinated thiosemicarbazone [33–35] shows that coordination lengthen the $^7C{=}^1N$ bond slightly [1.297–1.307 Å] and the $^9C{=}S$ bond length substantially [1.692–1.740 Å], as would be expected on coordination of the azomethine nitrogen and thiolate sulfur.

3.3. IR and electronic spectra

The infrared spectral data of the complexes **1**–**7** are presented in Table 2 with their tentative assignments. The new band found at ca. 1595 cm^{-1} is due to $^2N{=}^9C$ bond resulting from enolization of the principal thiosemicarbazone ligand and the one at ca. 1605 cm^{-1} is due to $C{=}^1N$ of the thiosemicarbazone moiety that shifts to ca. 1560 cm^{-1} upon complexation. Bands in the range 420–470 cm^{-1} are assignable to $\nu_{(Cu-N)}$frequencies [36]. The decrease in the stretching frequency of C–S bond from ca. 830 cm^{-1} in thiosemicarbazones by 60–80 cm_{-1} upon complexation indicates coordination via its thiolate sulfur.

The electronic absorptions of the complexes are presented in Table 3. Two charge transfer (CT) bands are found at ca. 27000 cm^{-1} and 21000–23000 cm^{-1}. In accordance with studies of previous copper(II) complexes the higher energy bands are assignable to $S \rightarrow Cu^{II}$ LMCT transitions, [37,38] tailing into the vis-

Table 2
IR spectral assignments for ligands and their copper complexes (All absorptions are given in units of cm^{-1})

Compound	$\nu(^7C{=}N^1)$	$\nu(^2N{=}C^9)$	$\nu(^1N{-}N^2)$	ν(Cu–N)	ν/δ (C=S)	ν(C–O)	Polypyridyl ring breathing
H_2L^1	1599 s		988 m		1365 m, 826 m	1219 s	
[Cu(L^1)(2,2′-bipy)] (**1**)	1566 m	1592 s	1022 m	432 w	1337 s, 768 m	1152 s	1439 m, 735 m, 747 w
[Cu(L^1)(1,10-phen)] (**2**)	1565 m	1590 s	1028 m	424 w	1329 s, 764 m	1150 s	1431 m, 725 w, 763 m, 845 m
H_2L^2	1603 s		997 m		1383 s, 839 m	1252 s	
[Cu(L^2)(2,2′-bipy)] (**3**)	1557 m	1592 s	1024 m	426 w	1337 m, 742 m	1204 s	1437 m, 1424 m, 650 w, 623 w
H_2L^3	1605 s		1017 m		1374, 835 m	1219 s	
[Cu(L^3)(2,2′-bipy)] (**4**)	1559 m	1592 s	1022 m	426 w	1341 s, 803 m	1132 s	1439 m, 735 m, 650 w, 762 w
[Cu(L^3)(1,10-phen)] (**5**)	1559 m	1593 s	1028 m	430 w	1341 s, 803 m	1138 s	1482 m, 1450 m, 727 m, 845 m
H_2L^4	1601 s		995 m		1375 s, 808 m	1222 s	
[Cu(L^4)(2,2′-bipy)] (**6**)	1559 m	1593 s	1019 m	432 w	1345 m, 766 m	1142 s	756 m, 745 w
[Cu(L^4)(1,10-phen)] (**7**)	1563 m	1593 s	1022 m	430 w	1340 m, 750 m	1134 s	727 m, 638 w

Table 3
Electronic spectral assignments, λ/cm^{-1}(log ε[a]) for the ligands and complexes

Compound	d–d	LMCT	n → π*	π → π*
H_2L^1			30300 (4.05), 32342 sh (4.32)	35000 (4.26)
[Cu(L^1)(2,2′-bipy)] (**1**)	14705(2.03), 16920(2.43)	28531 (3.87) 27100 sh (3.62)	35273 (4.13), 30902 sh (3.96)	42283 (4.11)
[Cu(L^1)(1,10-phen)] (**2**)	14492(1.84), 16750(2.14)	28571 (3.41) 27972 sh (3.38)	32414 (3.92)	43103 (4.22), 37313 sh (4.24)
H_2L^2			30581 (4.19), 32372 sh (4.23)	35587(4.48)
[Cu(L^2)(2,2′-bipy)] (**3**)	15267(2.18), 17699(2.49)	22727 sh (3.19), 27932 (4.24)	35335 (4.34)	41067 (4.37)
H_2L^3			30030 (4.43), 32895 sh (4.41)	42370 (4.25)
[Cu(L^3)(2,2′-bipy)] (**4**)	15151(2.11), 17699(2.46)	22624 (3.29), 28129 sh (4.20)	34843 sh (4.49)	41068 (4.43), 37665 (4.43)
[Cu(L^3)(1,10-phen)] (**5**)	14492(2.11), 17544(2.38)	21739 sh (2.99), 26560 (4.06)	34843 sh (4.43), 31250 sh (4.19)	42644 (4.49), 37665 (4.62)
H_2L^4			30211 sh (4.19), 35524 sh (4.40)	42370 (4.32)
[Cu(L^4)(2,2′-bipy)] (**6**)	14514(2.04), 17361(2.48)	22222 sh (2.90), 28530 (4.16)	30534 (4.06), 35149 sh (4.32)	42105 (4.23), 37879 (4.03)
[Cu(L^4)(1,10-phen)] (**7**)	15267(2.14), 17241(2.37)	21265 (3.02), 26525 (4.20)	31746 sh (4.36), 35026 (4.56)	42735 (4.74), 37807 (4.63)

[a] ε is expressed in 1 mol^{-1} cm^{-1}.

ible region, and the band in 21000–23000 cm^{-1} are assignable to phenolate $O \rightarrow Cu^{II}$ LMCT transitions [39]. The d–d bands of copper(II) complexes are at ca. 14000 and 17000 cm^{-1}, the later being seen as a very weak shoulder in the tail of the CT bands and are similar to copper(II) complexes of S–N donor ligands having a square pyramidal geometry [40,41].

3.4. EPR spectra

The EPR spectra of compounds **1**–**7** in the polycrystalline state at 298 K display different type of geometrical species. Compounds **1** and **6** show typical axial spectra with well-defined $g_\parallel$ and $g_\perp$ features. Compounds **2**, **5** and **7** give signals corresponding to axial symmetry with diffused $g_\parallel$ features. All the above compounds have their g values (Table 4) in conformity with that of a copper(II) species (d^9 system) with a $d_{x^2-y^2}$ ground state. Compounds **3** (Fig. 3) and **5** give three g values viz., g_1, g_2, g_3 indicating slight rhombic distortions in their geometry. The geometric parameter G (R for compounds **3** and **5**) obtained are in the range of 3.5–5.0 (Table 5), indicating that the g values obtained in the polycrystalline samples are near to the molecular g

Table 4
EPR parameters of copper complexes **1**–**7**

Compound	Solid (298 K)		DMF (298 K)			DMF (77 K)				
	$g_0/g_\parallel/g_3$	$g_\perp/g_1$, g_2,	g_0	A(Cu)[a]	A_N[a]	$g_\parallel$	$g_\perp$	g_{av}	$A_\parallel$[a]	$A_\perp$[a] (N)
[Cu(L^1)(2,2′-bipy)] (**1**)	$g_\parallel$ 2.173	$g_\perp$ 2.056	2.096	50.62	20.0	2.193	2.053	2.100	170.0	13.1
[Cu(L^1)(1,10-phen)] (**2**)	g_0 2.124		2.096	51.25	19.0	2.190	2.048	2.095	172.0	14.0
[Cu(L^2)(2,2′-bipy)] (**3**)	g_3 2.120	g_1 2.034 g_2 2.055	2.095	72.33	18.5	2.194	2.052	2.099	170.0	–
[Cu(L^3)(2,2′-bipy)] (**4**)	g_3 2.194	g_1 2.039 g_2 2.061	2.093	71.33	18.5	2.1900	2.052	2.098	170.0	14.2
[Cu(L^3)(1,10-phen)] (**5**)	g_0 2.067		2.095	73.33	15.0	2.190	2.051	2.097	171.7	14.2
[Cu(L^4)(2,2′-bipy)] (**6**)	$g_\parallel$ 2.220	$g_\perp$ 2.07	2.093	70.00		2.190	2.052	2.098	166.7	–
[Cu(L^4)(1,10-phen)] (**7**)	$g_\parallel$ 2.209	$g_\perp$ 2.067	2.106	73.33	19.2	2.174	2.059	2.097	173.3	13.0

[a] All 'A' values are reported in units of Gauss.

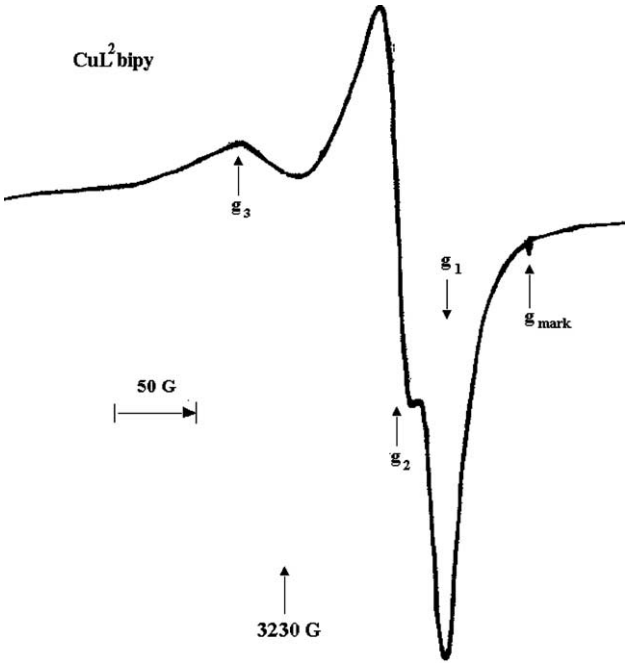

Fig. 3. EPR spectrum of compound **3** in polycrystalline state at 298 K.

values and hence the unit cell of the compounds contain magnetically equivalent sites [42–45].

The solution spectra of complexes at 298 K in DMF show four hyperfine lines. The signal corresponding $M_I = +3/2$ splits into three with a hyperfine coupling constant $A_N \approx 18$ G which indicates that the azomethine nitrogen dominates the bonding in solution. The EPR spectra of the compounds in frozen DMF (77 K) (Figs. 4(a) and (b)) show four hyperfine lines and $g_\parallel$

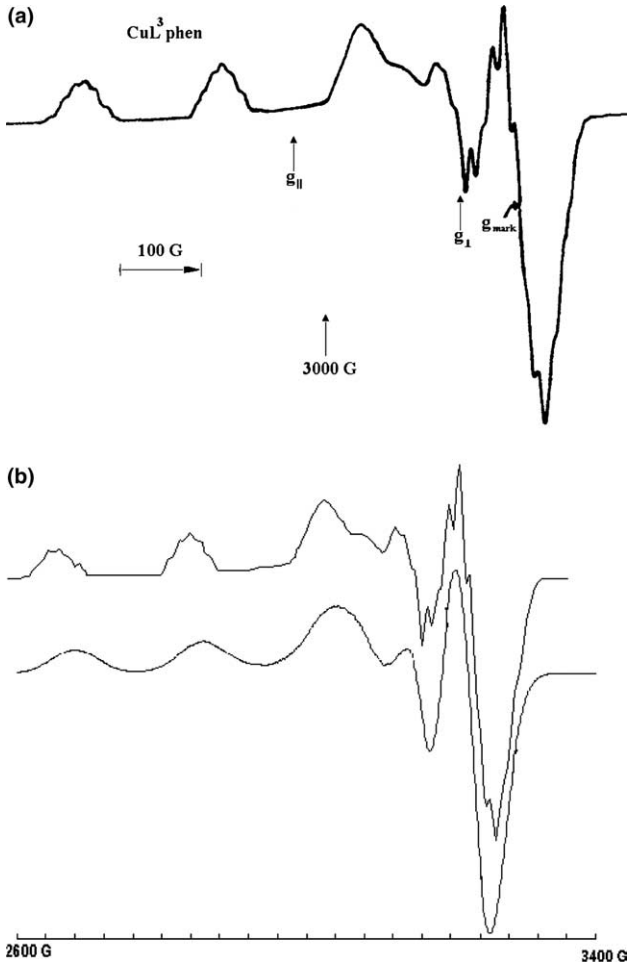

Fig. 4. (a) EPR spectrum of compound **5** in DMF at 77 K. (b) Experimental and simulated best fit pairs of the EPR spectrum of the compound **4** in DMF (77 K).

Table 5
Molecular magnetic and bonding parameters for compounds **1**–**7**

	Compound						
	1	**2**	**3**	**4**	**5**	**6**	**7**
μ(BM)	1.95	1.75	1.88	1.73	1.72	1.93	1.87
$A_\perp$[a]	12.6	14.0		13.6	13.6		12.5
$A_\parallel$[a]	174.1	175.9	174.1	173.8	175.6	170.5	175.9
A_{iso}[a]	49.54	50.17	70.76	69.70	71.74	68.42	72.12
G (77 K)	3.62	3.95	3.72	3.69	3.73	3.64	2.96
G (solid)	3.18		2.76	4.02		3.02	
R[c]			0.326	0.161			
α^2	0.7426	0.7371	0.7265	0.7387	0.7263	0.7352	0.7452
β^2	0.8937	0.8939	0.9143	0.9051	0.8841	0.8901	0.9006
γ^2	0.9588	0.9765	0.9506	0.9303	0.9468	0.9409	0.9889
$K_\parallel$	0.6637	0.6589	0.6643	0.6686	0.6421	0.6544	0.6711
$K_\perp$	0.7120	0.7198	0.6906	0.6872	0.6877	0.6916	0.7369
K_0	0.2644	0.2607	0.3215	0.3192	0.3329	0.3216	0.3413
f[b] (cm)	125.98	124.51	125.86	125.98	124.73	128.48	123.58

[a] Expressed in units of cm^{-1} multiplied by a factor of 10^{-4}.
[b] Parameter $f = g_\parallel/A_\parallel$.
[c] Parameter $R = (g_2 - g_1)/(g_3 - g_2)$.

($\sim$2.19) > $g_\perp$ ($\sim$2.06) values corresponding to monomeric copper(II) species with a square pyramidal geometry. Five superhyperfine (shf) lines in the $g_\parallel$ features ($M_I = -3/2$, or $M_I = -1/2$) of compounds **2**, **3**, **4**, **5**, and **7** evidence the coordination of two coplanar nitrogen atoms [46]. Simulated best-fits [4] of the spectra at 77 K in DMF were used to determine magnetic parameters $g_\parallel$, $g_\perp$, g_{av}, $A_\parallel$ (Cu), $A_\perp$ (Cu) and energies of d–d transitions were used to evaluate the bonding parameters α^2, β^2, γ^2 regarded as measures of covalency of the in-plane σ bonds, in-plane π bonds and out-of-plane π bonds, respectively [47]. The $g_\parallel$ values <2.3 indicate significant covalency in bonding [48,49]. The variation in g_{av} values can be attributed to the variation in the overall geometry and resulting change in the covalency of the bonds, which decreases with increase in covalency.

In all the compounds $g_\parallel > g_\perp > 2.00$ and $G = (g_\parallel - 2)/(g_\perp - 2)$ values are less than 4.4 that are consistent with a copper(II) center in $d_{x^2-y^2}$ ground state having small exchange coupling [50]. The value of in-plane π bonding parameter α^2 was estimated following Maki and McGarvey. All the compounds have $K_\parallel < K_\perp$, which suggests stronger in-plane π bonding [51–53]. The values of the bonding parameters α^2 ($\sim$0.74), β^2 ($\sim$0.89) and γ^2 ($\sim$0.94) < 1.0 (value of 1.0 for 100% ionic character) indicate significant in-plane π-bonding and in-plane σ bonding while the axial bond is more polar in nature. The Fermi contact hyperfine interaction term $K = A_{iso}/P\beta^2 + (g_{av}\text{-}2.0023)/\beta^2$ – a measure of the contribution of the 's' electrons to the hyperfine interaction - is found to be $\sim$0.3 in agreement with general observation. The empirical factor $f = g_\parallel/A_\parallel$ (cm), an index of tetrahedral distortion, is $\sim$126 cm corresponding to a copper(II) center with medium distortion.

3.5. Cyclic voltammetry

Investigations of redox behavior of copper complexes of ONS donor ligands are limited [54] and therefore the mechanistic aspects of redox behavior of most of the copper(II) thiosemicarbazone complexes still remains largely uncovered. Though a few extensive studies were reported most of them are on four-coordinate copper(II) complexes [55,56] where the mechanistic behavior is tractable. Generally, the redox behavior of the complexes depend on a number of factors such as the chelate ring size, axial ligation, degree and distribution of unsaturation and substitution pattern in the chelate ring [57–60]. In our attempt to develop an understanding of the redox behavior of five-coordinate copper(II) complexes of thiosemicarbazones, cyclic voltammetric measurements of compounds **1**–**7** were carried out. Since the complex and products of redox process are susceptible to coordination by coordinating solvents, dichloromethane was chosen as the preferred solvent for cyclic voltammetric studies.

The complexes were scanned at different scan rates ranging from 10 to 2000 mV/s in the potential range of +1000 to −1300 mV. All the cyclic voltammograms are more or less similar with minor variation in the position and appearance of some peaks (Fig. 5). Table 6 shows details of redox couples at 100 mV/s. The irreversible peak ca. −675 mV can be attributed to Cu(II/I) reduction, which is consistent with a previous report of five coordinate O_2N_2S and O_2N_3 copper(II) complexes of dianionic ligands [61]. The subsequent peak ca. −985 mV could be arising out of the ligand conjugate reduction [62]. The three-electron reduction was confirmed by a chronoamperometry experiment.

To confirm the ligand conjugate reduction three of the respective ligands were scanned in the range +1400 to −1300 mV at different scan rates of 50 to 1000 mV/s. During the cathodic sweep except ligand H_2L^4 all others gave two consecutive reduction waves ca. −850 and −1030 mV. These two reduction signals could be inferred as a two-step two-electron reduction process corresponding to the ligand conjugation. However, in the case of ligand H_2L^4 only one signal at −1034 mV was observed. During the anodic sweep a signal of lower intensity was observed for all the ligands at a higher positive potential which gradually increases from H_2L^1 to H_2L^4. This signal was assigned to the re-oxidation of the ligand conjugation.

While complexes containing 2,2′-bipyridine gives rise to an irreversible couple at ca. −675 mV, 1,10′-phenanthroline containing complexes does not give a clear couple. This could be due to the fact that the Cu(II/I) redox couple may be lying close to the conjugate reduction peak ca. −986 mV of the thiosemicarbazone moiety and hence can be buried under it. The irreversible nature of the peaks can be attributed to the formation of a new tetrahedral four coordinate copper(I) complex. Since the addition of the new electron is likely to be occurring in the half-filled $d_{x^2-y^2}$ orbital the bonds in the equatorial region is likely to be destabilized resulting in the weakening and consequent cleavage of one of them. The copper(II/I) reduction peak is followed by the ligand conjugate reduction peak at −986 mV that is shifted to a lower potential compared to the ligand, since the azomethine nitrogen involved in conjugation is bound to copper. The reduction of the ligand conjugation helps flexing of the planar thiosemicarbazone moiety and there by facilitating the formation of a four coordinated pseudo-tetrahedral species. This four coordinate copper(I) species is stabilized in the given condition, which accounts for a high positive irreversible Cu(I/II) re-oxidation signal ca. +485 mV during the reverse anodic sweep. This stability of the resulting copper(I) species

[4] The authors thanks Professor M. V. Rajasekharan, School of Chemistry, Hyderabad Central University for EPR simulation package.

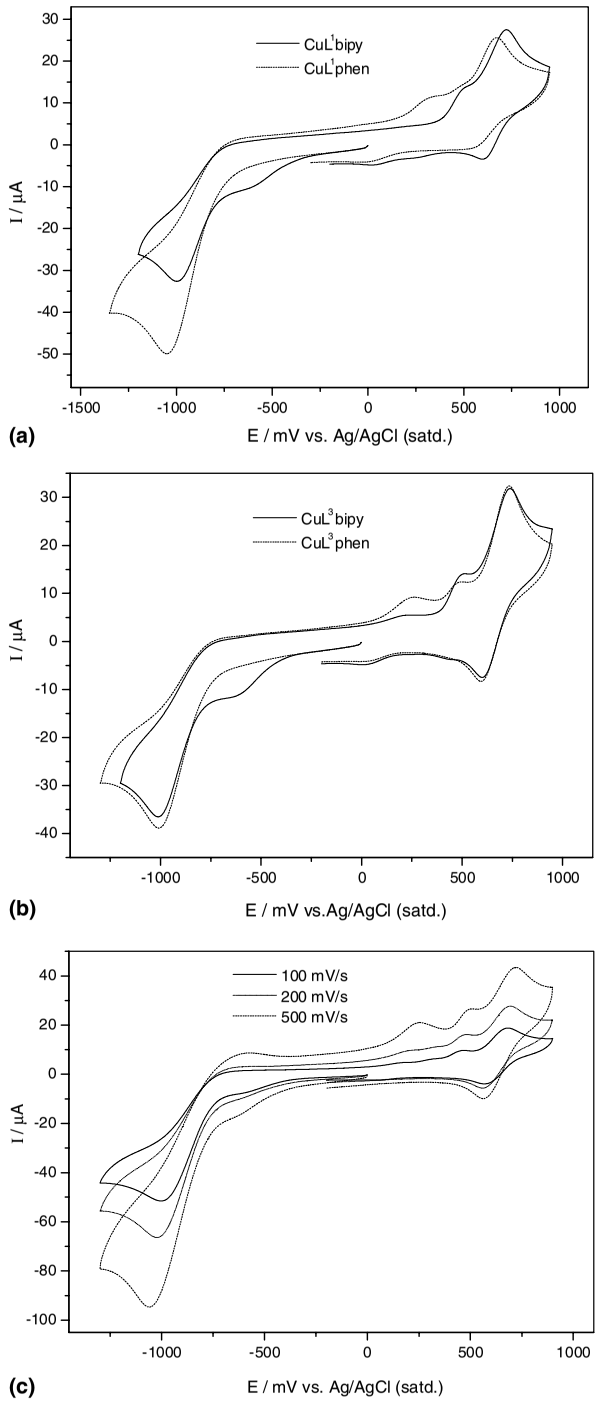

Fig. 5. Cyclic voltammogram of: (a) compound **1** and **2** at 200 mV/s scan rate, (b) compound **4** and **5** at 200 mV/s, (c) compound **6** at different scan rates.

can be attributed to the π-acceptor ability of the coordinated pyridyl groups and stabilization by sulfur donor atoms [63]. A rather diffused peak appears around +360 mV which can be arising out of the re-oxidation of the ligand conjugation. The broad peak cannot be clearly deciphered in the case of compounds **1**, **3**, **3a**, **4** at 100 mV/s, while its gains in intensity at higher scan

Table 6
Electrochemical data for the copper complexes **1**–**7** at 100 mV/s[a]

Complex	Cu(II/I) E_{pc} (mV)	L(conj. redn)	L(conj. oxdn)		Cu(I/II)	Cu(II/III)			
						E_{pa}	E_{pc}	$E_{1/2}$[d]	ΔE_p
H_2L^1		−884, −1029		+284					
[Cu(L^1)bipy] (**1**)	−675[a] (3.7)	−964[a] (14.0)			+502[a] (3.5)	+715[b] (10.8)	+601[b] (4.8)	+658	117
[Cu(L^1)phen] (**2**)		−1020[a] (33.3)		+360[a] (3.6)	+490[a] (4.3)	+648[a] (8.0)			+47[a] (3.0)
[Cu(L^2)bipy] (**3**)	−722[a] (7.9)	−986[a] (11.9)			+433[a] (5.28)	+635[b] (15.3)	+524[b] (11.5)	+680	111
[Cu(L^2)phen] (**3a**)[e]		−985[a] (30.6)			+397[a] (3.3)	+620[b] (14.9)	+504[b] (11.7)	+562	116
H_2L^3		−838, −1065		+376					
[Cu(L^3)bipy] (**4**)	−655[a] (4.8)	−976[a] (15.4)			+500[a] (5.0)	+725[b] (13.2)	+607[b] (7.1)	+666	118
[Cu(L^3)phen] (**5**)		−977[a] (22.7)	+223[a] (2.0)		+485[a] (2.6)	+716[b] (14.0)	+605[b] (7.31)	+661	111
H_2L^4		−1034		+742					
[Cu(L^4)bipy](**6**)	−637[a] (4.9)	−1001[a] (41.9)	+202[a] (1.6)	+344[a] (2.0)	+476[a] (3.4)	+683[b] (9.3)	+568[b] (8.8)	+626	115
[Cu(L^4)phen] (**7**)	−621[a] (1.23)	−979[a] (23.1)	+182[a] (1.1)		+479[a] (3.93)	+696[b] (11.1)	+592[b] (6.6)	+644	104

[a] Current height is indicated in brackets.
[b] Irreversible wave.
[c] quasi reversible.
[d] $E_{1/2} = (E_{pc} + E_{pa})/2$.
[e] Reported elsewhere.

rates viz, 500, 1000 mV/s (see Fig. 5(a) and (b)). In the case of compound **6** two broad peaks can be clearly seen at 100 and 200 mV/s scan rates that corresponds to a two electron re-oxidation of ligand conjugation, but merges at higher scan rates to give a single signal (Fig. 5(c)).

The quasi-reversible signal that appears at ca. +715 mV immediate to the copper(I/II) re-oxidation signal was assigned to a copper(II/III) couple. This value is also in conformity with other reports of four- or five-membered copper(II) complexes of ONS type donor ligands [64]. A scanning from a more positive potential of +900 mV gives an anodic current flow which is indicative of oxidation of copper(II) at potentials higher than +715 mV [65]. This is consistent with our assignment of the couple at E_{pa} = +715 mV arising from copper(II/III) redox process. Conversely, a scanning from a negative potential of −1300 mV gives a cathodic current which is indicative of a reduced species at the potential.

On initial anodic scanning only peak corresponding copper(II/III) oxidation couple is observed at the same potential. This is a further confirmation that the preceding peaks have their origin in post-reduction processes.

The ratio ($I_p/\upsilon^{1/2}$) is practically constant for all the compounds which indicate that the redox process is diffusion controlled. The ΔE_p ($=E_{pc} - E_{pa}$) values vary in the range of 104–118 mV at a scan rate of 100 mV/s, while for individual complexes the variation is between 100 and 237 mV in the scan range 100–1000 mV/s. Except in the case of compound **2** for all other complexes the couple corresponding to Cu(II/III) redox process can be inferred as quasi-reversible one-electron processes on the basis of the above observation. A small intensity peak that appears at a low positive potential is likely to be an unstable species formed during the oxidation couple.

3.6. Antimicrobial studies

All copper complexes (**1**–**7**) along with their parent thiosemicarbazone ligands were screened against two bacterial cultures viz., *E. coli* and *S. aureus*, and two fungal cultures viz., *C. albicans* and *A. flavus*. The 'hole plate diffusion method' [66] was adopted for the activity measurements. The bacterial strains were grown in Nutrient agar slants and fungal strains were grown in Sabouraud dextrose agar slants. The viable bacterial cells were swabbed onto Nutrient agar plates and fungal spores onto Sabouraud dextrose agar plates. The compounds were dissolved in dimethylsulfoxide to a final concentration of 0.1%. A 0.5 cm diameter well was cut in a medium inoculated with the respective cultures, and the solutions of the compounds in different concentrations (5 and 1 μg for bacterial cultures and 50 and 20 μg for fungal cultures) were allowed to stay in the wells. The petri-plates were incubated for 36 h for bacterial cultures and 76 h for the fungal cultures. All the compounds were screened against a standard reference viz., flucanazole for fungal cultures and gentamycin for bacterial cultures, in their standard concentration (200 μg/well). The activity of the compounds was counted by measuring diameter of the inhibition zone around the respective wells. The results are presented in Table 7.

All the copper(II) complexes were found to be more active than uncomplexed thiosemicarbazones at the measured concentrations. The compounds are having potential inhibitory activity to a concentration as low as 1 μg/well for bacterial cultures and 20 μg/well for fungal cultures. The 2-hydroxyacetophenone morpholine-3-thiosemicarbazone (H_2L^3) and its copper-phenanthroline base adduct (compound **5**) are found to be more active against *E. coli*, followed by compound

Table 7
Biological activity measurements of copper(II) complexes[a]

Complex/ligand	*E. coli*		*S. aureus*		*A. flavus*		*C. albicans*	
	5 μg	1 μg	5 μg	1 μg	50 μg	20 μg	50 μg	20 g
H_2L^1	17.2 ± 0.3	15.2 ± 0.5	19.2 ± 0.5	18.0 ± 0.2	09.5 ± 0.3	09.5 ± 0.3	11.1 ± 0.2	10.0 ± 0.4
[Cu(L^1)(2,2′-bipy)] (**1**)	18.0 ± 0.7	16.0 ± 0.3	19.4 ± 0.3	18.2 ± 0.4	11.2 ± 0.5	11.0 ± 0.5	12.0 ± 0.5	11.0 ± 0.3
[Cu(L^1)(1,10-phen)] (**2**)	18.2 ± 0.5	17.4 ± 0.7	23.0 ± 0.4	22.3 ± 0.2	14.0 ± 0.2	13.0 ± 0.4	26.2 ± 0.3	27.0 ± 0.5
H_2L^2	18.0 ± 0.5	17.2 ± 0.2	17.0 ± 0.3	16.0 ± 0.2	15.0 ± 0.3	13.2 0.3	11.0 ± 0.4	12.0 ± 0.3
[Cu(L^2)(2,2′-bipy)] (**3**)	19.2 ± 0.3	17.5 ± 0.3	17.2 ± 0.4	16.3 ± 0.3	18.1 ± 0.4	18.0 ± 0.4	15.0 ± 0.5	13.0 ± 0.4
H_2L^3	19.1 ± 0.2	16.0 ± 0.5	24.2 ± 0.4	22.0 ± 0.3	10.0 ± 0.3	10.0 ± 0.4	11.0 ± 0.3	11.0 ± 0.4
[Cu(L^3)(2,2′-bipy)] (**4**)	19.5 ± 0.7	17.2 ± 0.3	19.1 ± 0.3	18.3 ± 0.4	19.0 ± 0.4	17.0 ± 0.2	23.0 ± 0.5	22.0 ± 0.3
[Cu(L^3)(1,10-phen)] (**5**)	20.3 ± 0.3	19.4 ± 0.3	23.2 ± 0.2	22.5 ± 0.3	15.2 ± 0.4	14.0 ± 0.4	24.0 0.2	25.0 ± 0.4
H_2L^4	15.2 ± 0.2	15.2 ± 0.5	17.0. ± 0.3	16.0 ± 0.5	09.5 ± 0.3	09.5 ± 0.3	10.0 ± 0.3	10.0 ± 0.5
[Cu(L^4)(2,2′-bipy)] (**6**)	15.5 ± 0.5	14.0 ± 0.7	19.2 ± 0.5	17.2 ± 0.3	13.0 ± 0.2	12.2 ± 0.4	22.0 ± 0.4	21.0 ± 0.2
[Cu(L^4)(1,10-phen)] (**7**)	14.4 ± 0.7	13.0 ± 0.5	18.6 ± 0.6	16.5 ± 0.4	16.0 0.3	14.0 ± 0.3	17.0 ± 0.3	16.0 ± 0.4
[Cu(L^2)(1,10-phen)] (**8**)	18.5 ± 0.4	18.1 ± 0.4	23.0 ± 0.5	22.2 ± 0.4	19.0 ± 0.5	19.0 ± 0.5	18.0 ± 0.2	15.0 ± 0.2
Gentamycin/flucanazole[b]	26.0 ± 2.0	26.0 ± 2.0	30.0 ± 2.0	30.0 ± 0.2	20.0 ± 0.5	20.0 ± 0.5	22.0 ± 0.2	22.0 ± 0.2

[a] All measurements are in mm diameter of the inhibition zone (9.0 mm indicates no inhibition).
[b] Commercially available anti-microbial agents.

5, **4**, **3**, **2**, respectively. There are reports that phenathroline and bipyridyl base adducts of copper are less toxic in biological systems [67] than the free ligand. The role of such complicating factors cannot be ruled out which may be responsible for the variation of inhibitory activity in some cases. However, compounds **2**, **4** and **6** are more active against bacteria *S. aureus* among complexes, while H_2L^3 shows better activity among uncomplexed thiosemicarbazones. The inhibitory action of the complexes can be due to their inhibition of the replication of DNA by interacting with enzyme prosthetic group.

Though the complexes are less effective against the fungal culture *A. flavus* compounds **3**, **4** and **5** are found to have better growth inhibitory activity. Compound **2** shows potential growth inhibitory activity against culture *C. albicans*, followed by compounds **5** and **6**. The complexes are found to be more active due to their better membrane penetrating ability. However, the reduced activity of the compounds against fungal cultures can be attributed to their inability to form hydrogen bonds with the cell constituents.

4. Supplementary data

Crystallographic data for the structural analysis have been deposited with the Cambridge Crystallographic Data centre, CCDC 187884 for compound CuL^4bipy. Copies of this information may be obtained free of charge from The Director, CCDC, 12 Union Road, Cambridge, CB2, IEZ, UK (fax: +44-1223-336-033; e-mail: deposit@ccdc.cam.ac.uk or http://www.ccdc.cam.ac.uk)

Acknowledgements

Authors R.P.J. thanks CSIR, New Delhi, Government of India, and A.S. thanks Cochin University of Science and Technology, Kochi, India for the financial assistance. Authors acknowledge Prof. M.S. Lah, Hanyang University for permission to record cyclic voltammogram.

References

[1] D.X. West, S.B. Padhye, P.B. Sonawane, Structure and Bonding, vol. 76, Springer, Heidelberg, 1991, p. 1.
[2] M.J.M. Campbell, Coord. Chem. Rev. 15 (1975) 279.
[3] B.S. Garg, M.R.P. Kurup, S.K. Jain, Y.K. Bhoon, Transition Met. Chem. 13 (1988) 309.
[4] D.X. West, D.A. Bain, R.J. Butcher, J.P. Jasinski, R.Y. Pozdniakiv, R.A. Toscano, S.H. Ortega, Polyhedron 15 (1996) 665.
[5] J.L.J. Dearling, J.S. Lewis, D.W. McCarthy, M.J. Welch, P.J. Blower, Chem. Commun. 2 (1998) 531.
[6] A. Murugkar, S. Padhye, S. Guha-Roy, U. Wag, Inorg. Chem. Commun. 2 (1999) 545.
[7] R.P. John, A. Sreekanth, M.R.P. Kurup, S.M. Mobin, Polyhedron 21 (2002) 2515.
[8] J.S. Casas, M.S. Garcia-Tasende, J. Sordo, Coord. Chem. Rev. 209 (2000) 197.
[9] A. Sreekanth, R.P. John, M.R.P. Kurup, in: XXXVth International Conference on Coordination Chemistry (ICCC 35), P4.005, July 21–26, Heidelberg, Germany, 2002, pp. 543.
[10] R.P. John, M.R.P. Kurup, National Seminar on Newer Vistas in Bio-Active Agents, P55-46, December 20–21, Department of Chemistry, Gandhigram Rural Institute, Gandhigram 624302, Tamil Nadu, India, 1999.
[11] C.A. Hunter, J.K. M Sanders, J. Am. Chem. Soc. 112 (1990) 5525.
[12] Y. Kim, J.H. Geiger, S. Hahn, P.B. Sigler, Nature 365 (1993) 512.
[13] J.L. Kim, D.B. Nikolov, S.K. Burley, Nature 365 (1993) 520.
[14] D.W. Christianson, W.N. Lipscomb, Acc. Chem. Res. 22 (1989) 62.
[15] W.L. Kwik, K.P. Ang, H.S.O. Chan, V. Chebolu, S.A. Koch, J. Chem. Soc., Dalton Trans. (1986) 2519.
[16] G. Filippini, A. Gavezotti, Acta Crystallogr., Sect. B. 49 (1993) 868.
[17] A. Gavezotti, G. Filippini, J. Am. Chem. Soc. 118 (1996) 7153.
[18] P. Bindu, M.R.P. Kurup, Transition Met. Chem. 22 (1997) 578.
[19] P. Bindu, M.R.P. Kurup, T.R. Satyakeerthy, Polyhedron 18 (1999) 321.
[20] R.P. John, A. Sreekanth, M.R.P. Kurup, A. Usman, I.A. Razak, H.K. Fun, Spectrochim. Acta, Part A 59 (2003) 1349.
[21] J.P. Scovill, Phoshorus, Sulfur, Silicon 60 (1991) 15.
[22] B.N. Figgis, R.S. Nyholm, J. Chem. Soc. (1958) 4190.
[23] CAD4 Software, Version 5.0, Delft, The Netherlands, 1989.
[24] Siemens, *SMART* and *SAINT*, Siemens Analytical X-ray Instuments Inc., Madison, WI, 1996.
[25] G.M. Sheldrick, SHELXL 97, Program for the Solution of Crystal Structures, University of Göttingen, Göttingen, Germany, 1997.
[26] G.M. Sheldrick, SHELXS 97, Program for Crystal Structure Refinement, University of Göttingen, Göttingen, Germany, 1997.
[27] (a) B.J. Hathaway, in: G. Wilkinson, R.D. Gillard, J.A. McCleverty (Eds.), Comprehensive Coordination Chemistry, vol. 5, Pergamon Press, Oxford, 1987, p. 533;
(b) J. Cernak, K.A. Abboud, J. Chomic, M.W. Meisel, M. Orendac, A. Orendacova, A. Feher, Inorg. Chim. Acta 311 (2000) 126;
(c) J. Cernak, J. Chomic, P. Graverreau, M. Orendac, A. Orendacova, A. Feher, C. Kappenstein, Inorg. Chim. Acta 281 (1998) 134;
(d) J. Cernak, F. Gerard, J. Chomic, Acta Crystallogr., Sect. C 49 (1993) 1294.
[28] C.B. Castellani, G. Gatti, R. Millini, Inorg. Chem. 23 (1983) 4004.
[29] N.J. Ray, B.J. Hathaway, Acta Crystallogr., Sect. B 34 (1978) 3224.
[30] G. Druhan, B.J. Hathaway, Acta Crystallogr., Sect. B 35 (1979) 344.
[31] D.X. West, R.J. Butcher, Transition Met. Chem. 18 (1993) 449.
[32] D.X. West, H. Gebremethin, R.J. Butcher, J.P. Jasinski, A.E. Liberta, Polyhedron 12 (1993) 2489.
[33] M. Soriano-Garcia, J. Valdez-Martinez, R.A. Toscano, Acta Crystallogr., Sect. C 44 (1988) 1247.
[34] D.X. West, A. Castineiras, E. Bermejo, J. Mol. Struct. 120 (2000) 503.
[35] H. Beraldo, R. Lima, L.R. Teixeira, A.A. Moura, D.X. West, J. Mol. Struct. 559 (2001) 99.
[36] K. Nakamoto, Infrared and Raman Spectra of Inorganic and Coordination Compounds, 5th ed., Wiley, New York, 1997.
[37] M. Mikuriya, H. Okawa, S. Kida, Inorg. Chim. Acta 34 (1979) 13.
[38] E.W. Ainscough, A.M. Brodie, N.G. Larsen, Inorg. Chim. Acta 60 (1982) 25.

[39] M. Mikuriya, H. Okawa, S. Kida, Bull. Chem. Soc. Jpn. 53 (1980) 3717.
[40] A.A.G. Tomilson, B.J. Hathaway, J. Chem. Soc. (1968) 1685.
[41] D.M.L. Goodgame, M. Goodgame, G.W. Canham Rayner, J. Chem. Soc. A (1971) 1923.
[42] I.M. Proctor, B.J. Hathaway, P. Nicholis, J. Chem. Soc. A (1968) 1678.
[43] M.J. Beu, B.J. Hathaway, R.J. Fereday, J. Chem. Soc. A (1972) 1229.
[44] A.A.G. Tomlinson, B.J. Hathaway, J. Chem. Soc. A (1968) 1905.
[45] B.J. Hathaway, J. Chem. Soc., Dalton Trans. (1972) 1196.
[46] J. Jezierska, Asian J. Chem. 4 (1992) 189.
[47] A.H. Maki, B.R. McGarvey, J. Chem. Phys. 29 (1958) 31.
[48] A.H. Maki, B.R. McGarvey, J. Chem. Phys. 29 (1958) 35.
[49] J.R. Wasson, C. Trapp, J. Phys. Chem. 73 (1969) 3763.
[50] M.J. Bew, B.J. Hathaway, R.R. Faraday, J. Chem. Soc., Dalton Trans. (1972) 1229.
[51] D. Kivelson, R. Neiman, J. Chem. Soc., Dalton Trans. 35 (1961) 149.
[52] B.J. Hathaway, in: G. Wilkinson, R.D. Gillard, J.A. McCleverty (Eds.), Comprehensive Coordination Chemistry, vol. 5, Pergamon Press, Oxford, 1987.
[53] U. Sakaguchi, A.W. Addison, J. Chem. Soc., Dalton Trans. (1979) 600.
[54] (a) A.M. Bond, R.L. Martin, Coord. Chem. Rev. 54 (1984) 23;
(b) S. Purohit, A.P. Koley, L.S. Prasad, P.T. Manoharan, S. Ghosh, Inorg. Chem. 28 (1989) 3735;
(c) J. Topic, J.T. Lyon, Polyhedron 3 (1984) 55;
(d) P. Subramanian, J.T. Spence, R. Ortega, J.H. Enemark, Inorg. Chem. 23 (1984) 2564.
[55] (a) M. Juan, G. Fernadez, L. Oscar, R. Ruiz, R.A. Toscano, M.-R. Norma, M.A. Martinez, Transition Met. Chem. 25 (2000) 511;
(b) N. Raman, A. Kulandaisamy, C. Thangaraja, K. Jeyasubramanian, Transition Met. Chem. 28 (2003) 29;
(c) C. Amatore, J.-M. Barbe, C. Bucher, E. Duval, R. Guilard, J.-N. Verpeaux, Inorg. Chim. Acta 356 (2003) 267.
[56] E. Franco, E. Lopez-Torres, M.A. Mendiola, M.T. Sevilla, Polyhedron 19 (2000) 441.
[57] (a) F.V. Lovecchio, E.S. Gore, D.H. Busch, J. Am. Chem. Soc. 96 (1974) 3104;
(b) E.K. Barefield, G.M. freeman, D.G. Van Derveer, Inorg. Chem. 25 (1986) 552.
[58] (a) P.A. Connick, K.A. Macor, Inorg. Chem. 30 (1991) 4654;
(b) A. Botcher, T. Takeuchi, K.I. Hardcastle, T.J. Meade, H.B. Gray, D. Cwikel, M. Kapon, Z. Dori, Inorg. Chem. 36 (1997) 2498.
[59] A.M. Tait, F.V. Lovecchio, D.H. Busch, Inorg. Chem. 16 (1977) 2206.
[60] J.A. Streeky, D.G. Pillsbury, D.H. Busch, Inorg. Chem. 19 (1980) 3148.
[61] P. Zanello, A. CinQuantini, P. Guerriero, S. Tamburini, P.A. Vigato, Inorg. Chim. Acta 117 (1986) 91.
[62] V. Eisner, E. Karowa-Eisner, in: A.J. Bard, H. Lund (Eds.), Encyclopedia of Electrochemistry of the Elements, vol. 13, Marcel Dekker, New York, 1979, p. 348.
[63] (a) E.V. Rybak-akimova, A.Y. Nazerenko, L. Chen, P.W. Kieger, A.M. Herrera, V.V. Tarasov, P.D. Robinson, Inorg. Chim. Acta 324 (2001) 1;
(b) B.R. James, R.J.P. Williams, J. Chem. Soc. A (1961) 2007.
[64] (a) P. Zanello, R. Cini, A. Cinquantini, Inorg. Chim. Acta 74 (1983) 89;
(b) Z. Durackova, M.A. Mendiola, M.T. Sevilla, A. Valent, Bioelectrochem. Bioenerg. 48 (1999) 109.
[65] E. Bouwman, W.L. Driessen, J. Reedijk, C. Smykalla, J.M.M. Smits, P.T. Beurskens, F. Laschi, P. Zanello, Inorg. Chem. 29 (1990) 4881.
[66] C.H. Collins, P.M. Lyne, in: R.D. Gillard, J.A. McCleverty (Eds.), Microbiological Methods, University Park Press, Baltimore, MD, 1970, p. 422.
[67] (a) N.A. Berger, E.S. Johnson, A.M. Skinner Sr., Exp. Cell Res. 96 (1975) 145;
(b) K.H. Falchuk, A. Krishan, Cancer Res. 37 (1977) 2050.

Available online at www.sciencedirect.com
SCIENCE DIRECT®
Polyhedron 23 (2004) 2561–2567
POLYHEDRON
www.elsevier.com/locate/poly

Lanthanide halide and nitrate complexes with potentially tridentate bisphosphine dioxide – ether donors

John Fawcett [a], Andrew W.G. Platt [b,*], Steven Vickers [c], Michael D. Ward [c]

[a] Department of Chemistry, The University of Leicester, Leicester, LE1 7RH, UK
[b] Faculty of Health and Sciences, Staffordshire University, College Road, Stoke-on-Trent ST4 2DE, UK
[c] Department of Chemistry, University of Sheffield, Sheffield S3 7HF, UK

Received 9 August 2004; accepted 10 September 2004
Available online 14 October 2004

Abstract

Complexes of the bisphosphine dioxide ethers, bis[(2-diphenylphosphino)phenyl]ether dioxide (**I**) and 4,5-bis(diphenylphosphino)-9,9-dimethylxanthane dioxide (**II**) with lanthanide chlorides, bromides and nitrates have been synthesised, giving $LnX_3(\mathbf{I})_2(H_2O)_n$ and $LnX_3(\mathbf{II})_2(H_2O)_n$ X = NO_3, Cl, Br. The structures of the complexes of $PrCl_3$ and $NdCl_3$ with (**I**) and $LaCl_3$ and $LaBr_3$ with (**II**) are reported. These complexes are ionic $[LnX_2(\mathbf{I})_2]^+X^-$, $[LnX_2(\mathbf{II})_2]^+X^-$ and show the effect of flexibility in the ligand structure with (**I**) able to coordinate through one of its ether oxygen atoms, whilst (**II**) bonds through the phosphoryl oxygens only. The infrared spectra of the nitrates indicate that $Ln(NO_3)_3(\mathbf{I})_2$ contain monodentate nitrate whilst in $Ln(NO_3)_3(\mathbf{II})_2$ the nitrates are bidentate.
© 2004 Elsevier Ltd. All rights reserved.

1. Introduction

Multidentate phosphine oxide donors to lanthanides have been previously studied with the aim of developing selective extractants [1] and many complexes with f-block metals have been structurally characterised. Ligands in which two phosphine oxide donors flank a third donor atom have recently been extensively reported. Complexes where the third donor is a phenolic OH [2], pyridine [3] and, in particular, pyridine oxide [1,4–8] have received considerable attention and a number of coordination complexes with both lanthanides and actinides have been structurally characterised.

We chose to examine the coordination behaviour of two related ligands (**I**) and (**II**) in which the PO groups surround an ether oxygen donor. Here the potential formation of a six membered O–P–C2–O–Ln chelate ring might be expected to result in tridentate binding of the ligand to the metal. The secondary structure linking the donor sites varies significantly between the two ligands, being more flexible for (**I**), and we felt it of interest to examine the structures of related complexes with a view to assessing the structural effects of ligand backbone rigidity.

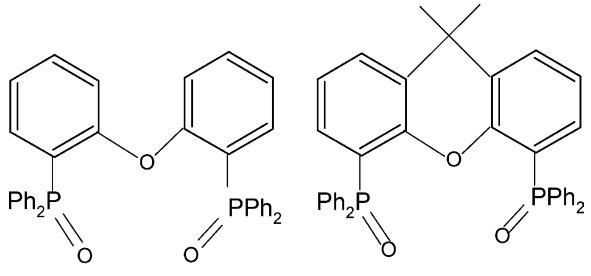

(I) (II)

* Corresponding author. Tel.: +44 1782 29 4784; fax: +44 1782 29 4986.
E-mail address: a.platt@staffs.ac.uk (A.W.G. Platt).

0277-5387/$ - see front matter © 2004 Elsevier Ltd. All rights reserved.
doi:10.1016/j.poly.2004.09.006

2. Results and discussion

2.1. Synthesis

Reaction of lanthanide nitrates and halides with the ligands (**I**) and (**II**) was carried out in hot ethanol or methanol solutions as described in Section 4. Generally all complexes formed with stoichiometries $LnX_3L_2(H_2O)_n$ with the exception of the $Eu(NO_3)_3$ complex of (**II**) for which compositional analysis suggests the formation of a 2:3 complex. This is probably based on an ionic structure $[Eu(NO_3)_2(\mathbf{II})_2][Eu(NO_3)_4(\mathbf{II})]$ which is formed as a result of the slightly higher metal to ligand ratio used in its preparation. We have previously obtained similar complexes with $[Ph_2P(O)]_2CH_2$ [9].

2.2. Solid state structures

Complexes of both ligands could be obtained in a form suitable for X-ray crystallography only with difficulty. Details of crystallisations are given in Section 4. Complexes of (**I**) and (**II**) form with lanthanide nitrates, but to date, we have been unable to obtain crystals of satisfactory quality for structural work. The complexes formed between the ligands and lanthanide chlorides and bromides gave better results and structures of several complexes have been obtained. The structures of $[PrCl_2(\mathbf{I})_2]^+Cl^-$, $[NdCl_2(\mathbf{I})_2]_+[Cl]^-$, $[LaCl_2(\mathbf{II})_2(H_2O)_2]^+ \cdot [Cl]^-$ and $[LaBr_2(\mathbf{II})_2(H_2O)_2]^+ \cdot [Br]^-$ are discussed below. Details of the data collection and refinement are given in Table 1 and selected bond lengths and angles in Table 2.

The structures adopted by the complexes of (**I**) and (**II**) differ significantly and reflect the flexibility of the backbone of the ligand. The structure of $[NdCl_2(\mathbf{I})_2]^+$ is shown in Fig. 1 and that of $[LaBr_2(\mathbf{II})_2(H_2O)_2]^+$ in Fig. 2. Complexes of (**I**) can accommodate, in addition to the two phosphine oxides, the coordination of one of the ether oxygen atoms to give seven coordinate structures based on the cations $[LnCl_2(\kappa^2L)(\kappa^3L)]^+$. The non bonded O(ether)···Ln distances are greater than 4 Å for both the complexes. The coordination geometry about the metal in both complexes of (**I**) can be visualised as a rather distorted pentagonal bipyramid with the chlorine atoms occupying the axial positions. The O–Ln–O angles in the "equatorial plane" are on average 73.7° ± 6.5°, the Cl–Ln–Cl angle is 161.75°

Table 1
Crystal data and refinement

Empirical formula	$C_{76}H_{74}Cl_2O_{11}P_4Pr$	$C_{78}H_{79}Cl_2NdO_{12}P_4$	$C_{39}H_{38}ClLa_{0.50}O_6P_2$	$C_{39}H_{35}Br_{1.50}La_{0.50}O_{4.50}P_2$
Formula weight	1499.04	1547.44	769.54	1653.86
Temperature (K)	150(2)	150(2)	150(2)	150(2)
Wavelength	0.71073	0.71073	0.71073	0.71073
Crystal system	monoclinic	monoclinic	monoclinic	monoclinic
Space group	*C*2/*c*	*C*2/*c*	*C*2/*c*	*C*2/*c*
Unit cell dimensions				
a (Å)	23.4295(11)	23.2903(11)	18.6472(13)	18.513(2)
b (Å)	23.3502(11)	23.1617(11)	19.0071(13)	18.842(2)
c (Å)	28.0868(13)	27.8897(13)	20.2169(14)	20.582(3)
β (°)	91.064(1)	91.238(1)	95.386(2)	85.256(3)
Volume (Å^3)	15363.2(12)	15041.4(12)	7133.8(9)	7149.2(16)
Z	8	8	8	4
D_{calc} (Mg/m^3)	1.296	1.367	1.433	1.537
Absorption coefficient (mm^{-1})	0.842	0.906	0.826	2.421
F(000)	6168	6376	3164	3328
Crystal size (mm)	0.32 × 0.28 × 0.24	0.25 × 0.18 × 0.12	0.24 × 0.14 × 0.13	0.30 × 0.16 × 0.15
θ Range for data collection (°)	1.23–25.00.	1.24–26.00.	1.53–26.00.	1.55–26.00.
Index ranges	$-27 \leqslant h \leqslant 27$, $-27 \leqslant k \leqslant 27$, $-33 \leqslant l \leqslant 33$	$-28 \leqslant h \leqslant 28$, $-28 \leqslant k \leqslant 28$, $-34 \leqslant l \leqslant 34$	$-22 \leqslant h \leqslant 22$, $-23 \leqslant k \leqslant 23$, $-24 \leqslant l \leqslant 24$	$-22 \leqslant h \leqslant 22$, $-23 \leqslant k \leqslant 23$, $-23 \leqslant l \leqslant 25$
Reflections collected	55 589	58 966	27 773	25 654
Independent reflections (R_{int})	13 516 (0.0700)	14 780 (0.0472)	7017 (0.0513)	6968 (0.0497)
Completeness to $\theta = 25.00°$ (%)	99.9	99.8	99.9	99.0
Absorption correction	empirical	empirical	empirical	empirical
Maximum and minimum transmission	0.86 and 0.80	0.81 and 0.71	0.801 and 0.671	0.801 and 0.604
Refinement method	full-matrix least-squares on F^2	full-matrix least-squares on F^2	full-matrix least-squares on F^2	full-matrix least-squares on F^2
Data/restraints/parameters	13 516/0/766	14 780/0/758	7017/0/531	6968/0/440
Goodness-of-fit on F^2	0.593	1.058	1.080	1.002
Final *R* indices [$I > 2\sigma(I)$]	$R_1 = 0.0406$, $wR_2 = 0.0936$	$R_1 = 0.0517$, $wR_2 = 0.1306$	$R_1 = 0.0535$, $wR_2 = 0.1224$	$R_1 = 0.0436$, $wR_2 = 0.1138$
R indices (all data)	$R_1 = 0.0687$, $wR_2 = 0.1075$	$R_1 = 0.0689$, $wR_2 = 0.1391$	$R_1 = 0.0648$, $wR_2 = 0.1307$	$R_1 = 0.0587$, $wR_2 = 0.1206$
Largest differential peak and hole (e Å^{-3})	0.966 and −0.480	1.569 and −0.680	1.433 and −1.537	1.231 and −0.817

Table 2
Selected bond lengths (Å) and angles (°)

	$PrCl_3(\mathbf{I})_2$	$NdCl_3(\mathbf{I})_2$	$LaCl_3(\mathbf{II})_2$	$LaBr_3(\mathbf{II})_2$
Bond distances (Å)				
Ln(1)–O(1)	2.365(2)	2.337(3)	2.448(3)	2.412(2)
Ln(1)–O(2)	2.811(3)	2.786(3)		
Ln(1)–O(3)	2.352(2)	2.349(3)	2.435(3)	2.446(3)
Ln(1)–O(4)	2.324(3)	2.322(3)		
Ln(1)–O(4)(water)			2.615(4)	2.606(3)
Ln(1)–O(6)	2.334(3)	2.315(3)		
Ln(1)–X(1)	2.7568(10)	2.7284(11)	2.9103(14)	3.0978(5)
Ln(1)–X(2)	2.7447(10)	2.7298(11)		
P(1)–O(1)	1.492(3)	1.501(3)	1.480(4)	1.488(3)
P(2)–O(3)	1.497(3)	1.498(3)	1.485(3)	1.485(3)
P(3)–O(4)	1.499(3)	1.493(3)		
P(4)–O(6)	1.491(3)	1.497(3)		
Bond angles (°)				
P(1)–O(1)–Ln(1)	142.40(15)	142.33(18)	149.63(18)	168.81(15)
P(2)–O(3)–Ln(1)	142.58(16)	142.37(18)	166.45(16)	149.90(16)
P(3)–O(4)–Ln(1)	176.10(17)	177.2(2)		
P(4)–O(6)–Ln(1)	176.44(18)	174.94(19)		

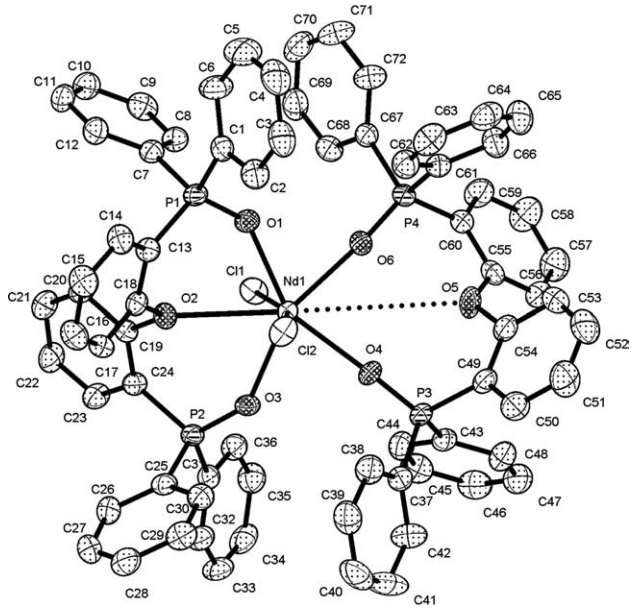

Fig. 1. The structure of $[NdCl_2(\mathbf{I})_2]^+$ showing the atom label scheme and 50% displacement ellipsoids. H atoms and lattice solvent molecules have been omitted for clarity. The dashed distance is 4.156 Å.

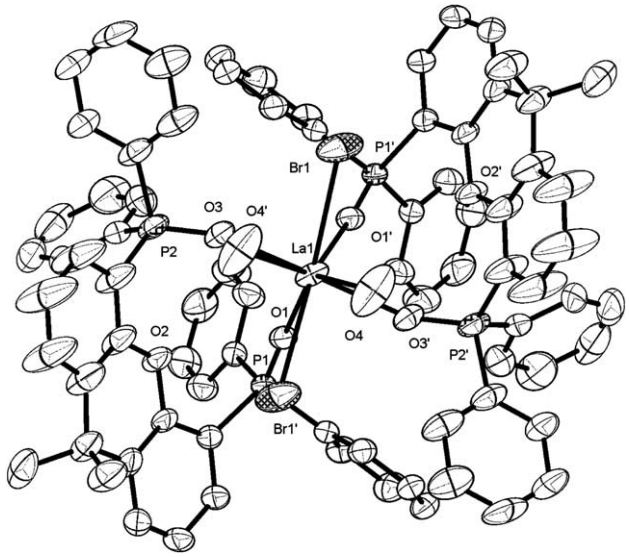

Fig. 2. The full structure of $[LaBr_2(\mathbf{II})_2(H_2O)_2]^+$. The La atom is located on a 2-fold axis and the molecule/ion is completed by symmetry $(1 - x, y, 0.5 - z)$. The Br- is disordered across two sites. Br^-, H atoms and lattice solvent molecules have been omitted for clarity.

and the Cl–Ln–O angles range from 80.45° to 111.81°. The ligand geometry changes depending on whether coordination via the ether oxygen occurs. The main effect is the twisting of the backbone aromatic rings, which increases when the ether oxygen coordinates to the metal from 74.8° to 87.9° (Pr) and from 75.2° to 90.1° (Nd). As expected the C–O distances increase slightly, by up to 0.04 Å, for the tridentate ligand compared to the bidentate. Chelating as a tridentate ligand also forces a narrowing of the C–O–C angle from 123.3(3)° to 114.2(3)° (Pr) and from 122.9(4)° to 114.2(3)° (Nd).

The Ln–O–P angle is strongly dependant on whether the ligand acts as a bidentate or tridentate ligand. In the bidentate chelate the angle approaches linearity which might be expected for unrestrained phosphine oxide donors due to a strong contribution from P^+–O^-, with larger angles reducing repulsion between the positively charged Ln and P centres and seen, for example, in yttrium halide [10] and scandium and lanthanide triflate [11] complexes of Ph_3PO. For the tridentate ligand the angle reduces considerably to around 142° and this in turn increases the Ln–O distances slightly.

The co-planarity of the phenyl rings imposed by the structure of (**II**) restricts the twisting of the ligand around the ether oxygen thus preventing tridentate coordination to the metal. Here the lanthanum ions are eight coordinate bonded to the 4PO, 2Cl (2Br) and $2H_2O$. The complexes of (**II**) both have a distorted square antiprismatic coordination geometry about the metal with the square faces formed by the phosphine oxide oxygen atoms, the halogen and the water oxygen. The angles within each square face range from 84.39° to 97.79° (Cl) and from 86.55° to 97.59° (Br).

Despite the inability of (**II**) to coordinate via the ether oxygen atoms its complexes have higher coordination numbers than those of (**I**). This is probably linked to the relative arrangement of the chelate rings. The angle between the $(P)O_2La$ planes in complexes of (**II**) is around 75°; in comparison the corresponding planes in the Pr and Nd complexes of (**I**) are twisted by only 28.0° (Pr) and 27.6° (Nd). This juxtaposition of the ligands creates a relatively open face of the complex which allows the coordination of additional water molecules. This arrangement is further stabilised by additional hydrogen bonding to non coordinated water and halide ion.

2.3. Infrared spectroscopy

The infrared spectra of the halide complexes show the expected shift in the PO stretching frequency. The two bands at 1197 and 1186 cm^{-1} in (**I**) and 1204 and 1190 cm^{-1} in (**II**) shift to give two bands at around 1160 cm^{-1} in both series of complexes. Similar features are seen in the spectra of the nitrate complexes with additional information from the nitrate absorptions. The spectra of $Ln(NO_3)_3(\mathbf{I})_2$ show two bands assigned to the N–O stretches between 1200 and 1500 cm^{-1}. These occur as a relatively weak band between ~1370 and 1380 cm^{-1} and a stronger absorption between 1295 and 1307 cm^{-1}, the frequencies increasing with the atomic weight of Ln. The splitting of these bands at ~70–80 cm^{-1} is very much smaller than normal range for bidentate nitrates [12]. The small splitting implies that the nitrates are bound as monodentate ligands. Unfortunately this assignment relies only on the infrared data as we have been unable to grow crystals suitable for X-ray diffraction studies. The complexes of (**II**) give spectra which fall into two different classes differing principally in the appearance of the N–O stretches. For the lighter lanthanides (La to Dy), in addition to bands due to (**II**), two intense broad bands between 1464–1485 cm^{-1} and 1290 cm^{-1} can be assigned to nitrate. Here the splitting in the region of 170–190 cm^{-1} is as expected for bidentate nitrates. The spectrum of $[Eu(NO_3)_2(\mathbf{II})_2][Eu(NO_3)_4(\mathbf{II})](H_2O)_4$ is essentially identical to those described above, a similar effect being found for the previously reported complexes with $[Ph_2P(O)]_2CH_2$ [9]. For the heavier lanthanides (Er to

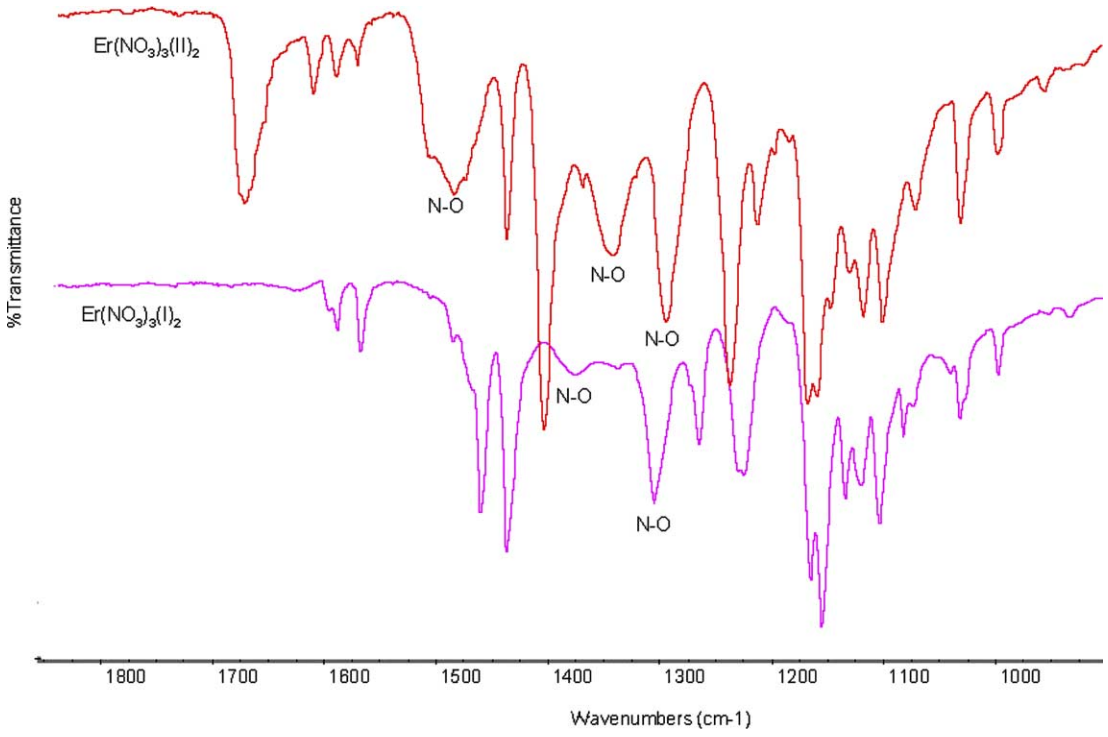

Fig. 3. Infrared spectra of $Er(NO_3)_3$ complexes of (**I**) and (**II**).

Lu) an additional splitting of the lower frequency band occurs $\Delta\nu \sim 50\ cm^{-1}$. This implies some changes to the nitrate coordination as a result of the lanthanide contraction, but in the absence of crystallographic data it is not possible to explain these differences. Fig. 3 shows the spectra of the $Er(NO_3)_3$ complexes of (**I**) and (**II**) with the bands due to nitrate indicated. Other bands are readily assigned to the ligand or water associated with the complex.

The difference in the nitrate coordination mode between the two series of complexes could arise from the ability of (**I**) to act as a tridentate ligand, thus forcing the nitrate to adopt a monodentate coordination mode. As (**II**) is unable to bond with its ether oxygen further coordination sites are available for the nitrates to adopt the bidentate mode.

2.4. Electrospray mass spectra

Mass spectra were obtained on representative complexes in methanol solution. The results are shown in Table 3. The spectra are dominated by strong signals from (**I**) and (**II**) due to $[L + H]^+$ at $m/z = 571$ (**I**) and 611 (**II**), respectively.

Ions produced by ligand redistribution are abundant in most of the spectra with $[LnL_3]^{3+}$ giving rise to the base peak for complexes of both (**I**) and (**II**). Some dependence of abundance on the size of the lanthanide ion is apparent with less sterically congested ions such as $[LnL_2]^{3+}$, $[LnXL_2]^{2+}$ and $[LnX_2L_2]^+$ being favoured over $[LnL_3]^{3+}$ for the heavier lanthanides.

Table 3
Electrospray mass spectra for LnX_3(**I**)$_2$ and LnX_3(**II**)$_2$ in methanol

L = (**I**)	$LnX_2L_2^+$	$LnX_2L_2^{2+}$	LnL_3^{3+}	LnL_2^{3+}
X = NO_3				
La	1403(10)	670(90)	617(100)	426(20)
Nd	1408(30)	673.1(80)	618.3(100)	428(100)
Er	1432(80)	685(100)	626(65)	428(80)
X = Cl				
La	1349(15)	657(100)	617(90)	426(10)
Nd	1354(<5)	660(40)	618(100)	428(<5)
X = Br				
La	1439(<5)	680(20)		426(100)
Ho	1466(<5)	693(15)	626(15)	435(100)
Yb	1474(<5)	697(5)		438(100)
L = (**II**)				
X = NO_3				
Eu	1480(40)	718(15)	661(100)	
Dy	1509(5)	723(<5)	665(100)	
Er	1513(100)	724(<5)	666(25)	
Yb	1519(100)	728(10)		
X = Cl				
Lu				669(100)
X = Br				
La	1520(<5)	720(20)	657(100)	
Ho	1546(<5)	733(100)		

Values of m/z are quoted for the most intense peak in the isotope profile and are within 1 Da of the theoretical values. The relative intensities of the signals are given in parenthesis.

3. Conclusions

The structures of the halide complexes show that with the flexible backbone structure of (**I**) chelation via the ether oxygen becomes possible. A further consequence of this flexibility appears to be the influence on the mode of coordination of the nitrate which from spectroscopic evidence is monodentate in the $Ln(NO_3)_3$ complexes of (**I**), although this remains a tentative conclusion in the absence of crystallographic characterisation.

4. Experimental

4.1. Crystallography

Data for the complexes were measured on a Bruker SMART diffractometer with a 2K CCD area detector. All data were collected using graphite monochromated Mo Kα radiation ($\lambda = 0.71073$ Å). Semi-empirical absorption corrections, based on comparison of Laue equivalents, were applied to the data sets. The structures were solved by Patterson methods and refined by full-matrix least squares cycles on F^2 for all data, using SHELXTL [13]. All non hydrogen atoms were refined with anisotropic displacement parameters and all hydrogen atoms were included in refinement cycles riding on bonded atoms. For both the Pr and Nd complexes the refinement of the metal complexes was straightforward, however peaks in the residual Fourier map satisfactorily modelled as disordered C_2H_5OH and H_2O were not stable to anisotropic refinement. The Pr complex was modelled using the SQUEEZE option of PLATON [14] with disordered atoms excluded. This indicated the presence of 4 symmetry related voids of 886 $Å^3$ at 0, 1/4, 0 and an estimate of 935 electrons/cell due to disordered solvent. The final refinement employed the modified reflection file with the estimated solvent contribution eliminated from the data. The final formula is assumed to include 2EtOH and $3H_2O$ as indicated by the Fourier map, this accounts for 656e of the 935e estimate from the SQUEEZE calculation.

4.2. Mass spectrometry

Electrospray mass spectrometry was carried out on either a Waters 2695 separation module spectra were take on a Micromass/Waters LCT at Sheffield University or at the EPSRC National mass spectrometry service at Swansea University as described previously [15].

4.3. Preparative work

4.3.1. Bis[(diphenylphosphino)phenyl]ether dioxide (**I**)

5.00 g of Bis[(diphenylphosphino)phenyl]ether was suspended in 70 ml acetone and 2.34 g 30% H_2O_2 was added. A thick white precipitate formed during the addition. The mixture was stirred for 30 min at room temperature and heated briefly to boiling and allowed to evaporate to 50 ml at room temperature. The mixture was filtered, washed with diethyl ether and dried at the pump to give 4.94 g (93%) of white solid. Electrospray mass spectrum (methanol) m/z = 571 (100%) $[(\mathbf{I}) + H]^+$, m/z = 593 (60%) $[(\mathbf{I}) + Na]^+$. Principle infrared bands (cm^{-1}) $\nu_{P=O}$ 1184(s).

4.3.2. 4,5-Bis(diphenylphosphino)-9,9-dimethylxanthane dioxide (**II**)

4,5-Bis(diphenylphosphino)-9,9-dimethylxanthane 5.12 g was suspended in 30 ml acetone and 2.23 g 30% H_2O_2 was added in small portions, giving an exothermic reaction on each addition. The mixture was heated to boiling for 1 h, cooled to room temperature and allowed to stand for 16 h. The suspension was filtered and the solid washed with diethyl ether and dried at the pump to give 4.62 g (86%) white powder. Electrospray mass spectrum (methanol) m/z 611 (100%) $[(\mathbf{II}) + H]^+$. Principle infrared bands (cm^{-1}) $\nu_{P=O}$ 1197(s), 1186(s).

4.3.3. $LaBr_3(\mathbf{I})_2(H_2O)_2$

Hot methanolic solutions of hydrated lanthanum bromide (0.10 g, 0.20 mmol) in 3 ml and (**I**) (0.23 g, 0.40 mmol) in 6 ml were mixed. The mixture was evaporated to dryness and the residue recrystallised from ethanol to give 0.23 g (74%) white solid. *Anal.* required: C, 55.59; H, 3.89. Found: C, 55.65; H, 4.19%. Principle infrared bands (cm^{-1}) $\nu_{P=O}$ 1144(s).

4.3.4. $La(NO_3)_3(\mathbf{I})_2(H_2O)_4$

Hot ethanolic solutions of hydrated lanthanum nitrate (0.11 g, 0.25 mmol) in 2 ml was and (**I**) (0.26 g, 0.47 mmol) in 6 ml were mixed. On continued warming a white powder precipitated. The mixture was cooled and the solid filtered and dried at the pump to give 0.28 g (76%). *Anal.* required: C, 56.22; H, 4.19; N, 2.73. Found: C, 55.92; H, 4.08; N, 2.69%. Principle infrared bands (cm^{-1}) ν_{NO} 1373(w), 1295(m) $\nu_{P=O}$ 1149(s).

4.3.5. $Nd(NO_3)_3(\mathbf{I})_2(H_2O)_4$

Solutions of hydrated neodymium nitrate (0.10 g, 0.23 mmol) in 2 ml and (**I**) (0.26 g, 0.47 mmol) in 15 ml ethanol were reacted as for the La complex and gave 0.29 g (85%) of lilac solid. *Anal.* required: C, 56.03; H, 4.18; N, 2.72. Found: C, 55.42; H, 4.16; N, 2.55%. Principle infrared bands (cm^{-1}) ν_{NO} 1373(w), 1295(m), $\nu_{P=O}$ 1147(s).

4.3.6. $Yb(NO_3)_3(\mathbf{I})_2(H_2O)_3$

Hot solutions of hydrated ytterbium nitrate (0.11 g, 0.25 mmol) in 2 ml and (**I**) (0.26 g, 0.47 mmol) in 6 ml ethanol were mixed and led to the immediate formation of a white precipitate. The mixture was heated to boiling, cooled and the solid filtered, washed with ethanol and dried at the pump to give 0.23 g (60%) white solid. *Anal.* required: C, 55.64; H, 4.02; N, 2.70. Found: C, 55.58; H, 4.17; N, 2.53%. Principle infrared bands (cm^{-1}) ν_{NO} 1377(w), 1307(m), $\nu_{P=O}$ 1163(s), 1155(s).

4.3.7. $LaCl_3(\mathbf{II})_2(H_2O)_4$

$LaCl_3 6H_2O$ (0.11 g, 0.31 mmol) in 2.5 ml MeOH was mixed with a solution of (**II**) (0.37 g, 0.61 mmol) in 4 ml MeOH. The mixture was heated to boiling and cooled to room temperature. The solution was evaporated to dryness and the residue recrystallised from MeCN to give 0.25 g (52%) of colourless crystals suitable for X-ray diffraction. *Anal.* required for $LaCl_3(\mathbf{II})_2(H_2O)_4$: C, 60.89; H, 4.72; Cl, 6.91. Found: C, 60.73; H, 4.62; Cl, 6.95%. Principle infrared bands (cm^{-1}) $\nu_{P=O}$ 1172(s), 1165(s).

4.3.8. $LuCl_3(\mathbf{II})_2(H_2O)_3$

$LuCl_3 6H_2O$ (0.10 g, 0.26 mmol) in 1.5 ml MeOH was mixed with a solution of (**II**) (0.34 g, 0.56 mmol) in 6 ml MeOH. The mixture was heated to boiling and cooled to room temperature when a thick suspension formed. This was evaporated to dryness and the resulting solid recrystallised from CH_3CN to give 0.39 g (96%) of colourless crystals. *Anal.* required for $LuCl_3(\mathbf{II})_2(H_2O)_3$: C, 60.18; H, 4.53; Cl, 6.83. Found: C, 60.14; H, 4.30; Cl, 7.13%. Principle infrared bands (cm^{-1}) $\nu_{P=O}$ 1158(s), 1146(s).

4.3.9. $LaBr_3(\mathbf{II})_2(H_2O)_3$

$LaBr_3 6H_2O$ (0.15 g, 0.31 mmol) in 3 ml MeOH was added to a solution of (**II**) (0.38 g, 0.62 mmol) in 7 ml MeOH). After heating to boiling and cooling the solution was evaporated to dryness. The solid residue was recrystallised from MeCN giving very small crystals. A sample suitable for X-ray diffraction was obtained by recrystallising the bulk from MeCN/toluene to give 0.27 g (53%). *Anal.* required for $LaBr_3(\mathbf{II})_2(H_2O)_3{=}C_{78}H_{70}Br_3LaO_9P_4$: C, 56.64; H, 4.27; Br, 14.49. Found: C, 56.40; H, 4.16; Br, 14.97%. Principle infrared bands (cm^{-1}) $\nu_{P=O}$ 1162(s), 1148(s).

4.3.10. $[Eu(NO_3)_3]_2(\mathbf{II})_3(H_2O)_4$

Hot ethanolic solutions of hydrated europium nitrate (0.12 g, 0.27 mmol) in 5 ml and (**II**) (0.26 g, 0.42 mmol) in 5 ml were mixed. On standing at room temperature for 16 h a white precipitate formed. This was filtered, washed with ethanol and dried at the pump to give 0.25 g (72%). *Anal.* required: C, 54.47; H, 4.06; N, 3.26. Found: C, 54.66; H, 3.77; N, 3.26%. Principle

infrared bands (cm^{-1}) ν_{NO} 1464(s), 1297(s), $\nu_{P=O}$ 1155(s).

4.3.11. $Dy(NO_3)_3(\mathbf{II})_2(H_2O)_2$

Hot ethanolic solutions of hydrated dysprosium nitrate (0.11 g, 0.24 mmol) in 5 ml and (**II**) (0.28 g, 0.46 mmol) in 5 ml were mixed. No solid was deposited on standing and the solution was evaporated to dryness and the residue recrystallised from ethanol/toluene to give 0.30 g (78%) colourless powder. *Anal.* required: C, 58.34; H, 4.27; N, 2.62. Found: C, 58.40; H, 4.33; N, 2.62%. Principle infrared bands (cm^{-1}) ν_{NO} 1508(m), 1483(m), $\nu_{P=O}$ 1158(s), 1144(s).

5. Supplementary material

Crystallographic data for the structures reported in this paper have been deposited with the Cambridge Crystallographic Data Centre, CCDC Nos. 237032–237035 for $LaBr_3(\mathbf{II})_2$, $LaCl_3(\mathbf{II})_2$, $NdCl_2(\mathbf{I})_2$ and $PrCl_2(\mathbf{I})_2$ complexes, respectively. Copies of this information may be obtained free of charge from The Director, CCDC, 12 Union Road, Cambridge, CB2 1EZ, UK (fax: +44 1223 336033; e-mail: deposit@ccdc.cam.ac.uk; http://www.ccdc.cam.ac.uk).

Acknowledgements

We are grateful to the Royal Society of Chemistry for support through the research fund and to the EPSRC for the use of the National Mass Spectrometry Service at Swansea University.

References

[1] X. Gan, S. Parveen, W.L. Smith, E.N. Duesler, R.T. Paine, Inorg. Chem. 39 (2000) 4591.
[2] R.T. Paine, Y. Tan, X. Gan, Inorg. Chem. 41 (2001) 7009.
[3] L. Prodi, M. Montalti, N. Zacchweroni, G. Pickaert, L. Charbonniere, R. Ziessel, New J. Chem. 27 (2003) 134.
[4] J.H. Matonic, M.P. Neu, A.E. Enriquez, R.T. Paine, B.L. Scott, J. Chem. Soc., Dalton Trans. (2002) 2328.
[5] X. Gan, E.N. Duesler, R.T. Paine, P.H. Smith, Inorg. Chim. Acta 247 (1996) 29.
[6] B.M. Rapko, E.N. Duesler, P.H. Smith, R.T. Paine, R.R. Ryan, Inorg. Chem. 32 (1993) 2164.
[7] E.M. Bond, E.N. Duesler, R.T. Paine, H. Noth, Polyhedron 19 (2000) 2135.
[8] R.T. Paine, E.M. Bond, S. Parveen, N. Donhart, E.N. Duesler, K.A. Smith, H. Noth, Inorg. Chem. 41 (2002) 444.
[9] A.M.J. Lees, A.W.G. Platt, Inorg. Chem. 42 (2003) 4673.
[10] N.J. Hill, W. Levason, M.C. Popham, G. Reid, M. Webster, Polyhedron 21 (2002) 445.
[11] J. Fawcett, A.W.G. Platt, D.R. Russell, Polyhedron 21 (2002) 287.
[12] K. Nakamoto, Infrared and Raman Spectra of Inorganic and Coordination Compounds, 5th ed., Wiley, New York, 1997.
[13] SHELXTL, An integrated system for solving, refining and displaying crystal structures, Version 5.10, Bruker Analytical X-ray Systems, Madison, WI, USA, 1997.
[14] A.L. Spek, PLATON, Version 1.05 Amulti Purpose Crystallographic Tool, Ultrecht University, Ultrecht, The Netherlands, 2002.
[15] J. Fawcett, A.W.G. Platt, Polyhedron 22 (2003) 967.

Available online at www.sciencedirect.com
SCIENCE DIRECT®
Polyhedron 23 (2004) 2569–2574
POLYHEDRON
www.elsevier.com/locate/poly

Preparation and coordination chemistry of *p*-(xylylenediaminodiphenyl) phosphine

Alexandra M.Z. Slawin, Joanne Wheatley, J. Derek Woollins *

School of Chemistry, University of St. Andrews, St. Andrews, Fife KY16 9ST, UK

Received 17 June 2004; revised 10 September 2004; accepted 20 September 2004

Abstract

Reaction of *p*-xylene diamine with two equivalents of Ph_2PCl in the presence of NEt_3, proceeds in thf to give *p*-(xylylenediaminodiphenyl) phosphine **1** in good yield. **1** was derivatised as the dichalcogenides $Ph_2P(O)NHCH_2(C_6H_4)CH_2NHP(O)Ph_2$, $Ph_2P(S)NHCH_2(C_6H_4)CH_2NHP(S)Ph_2$ and $Ph_2P(Se)NHCH_2(C_6H_4)CH_2NHP(Se)Ph_2$ and the structures of the latter two compounds determined crystallographically. The binuclear compounds $[\{(PEt_3)PtCl_2(Ph_2PNHCH_2)\}_2C_6H_4]$ (**5**), $[\{(PPhMe_2)PtCl_2(Ph_2PNHCH_2)\}_2C_6H_4]$ (**6**), $[\{IrCl_2(\eta^5\text{-}C_5Me_5)(Ph_2PNHCH_2)\}_2C_6H_4]$ (**7**) $[\{RhCl_2(\eta^5\text{-}C_5Me_5)(Ph_2PNHCH_2)\}_2C_6H_4]$ (**8**), $[\{RuCl_2(\eta^6\text{-}p\text{-}MeC_6H_4{}^iPr)(Ph_2PNHCH_2)\}_2C_6H_4]$ (**9**), $[\{Pd(\eta^3\text{-}C_3H_5)Cl(Ph_2PNHCH_2)\}_2C_6H_4]$ (**10**), $[\{RhCl(C_8H_{12})(Ph_2PNHCH_2)\}_2C_6H_4]$ (**11**), $[\{AuCl(Ph_2PNHCH_2)\}_2C_4H_6]$ (**12**) have been prepared and characterised spectroscopically.
© 2004 Elsevier Ltd. All rights reserved.

Keywords: Ligand; Bidentate; Bridging; X-ray; Phosphine

1. Introduction

Bridging ligands are of interest as they can form a number of bi-, tri- and tetra-nuclear species. There are a variety of different ligands that can have bridging properties and these include *o*-, *m*- and *p*-derivatives of benzene or pyridine. For example, $Ph_2PNHC_6H_4PPh_2$ [1,2], (**A**), ($Et_2PN(Me)C_6H_4PEt_2$) [3], (**B**), and 1-(diphenylphosphany)naphtha-2-oxydiphenylphosphane [4], (**C**)

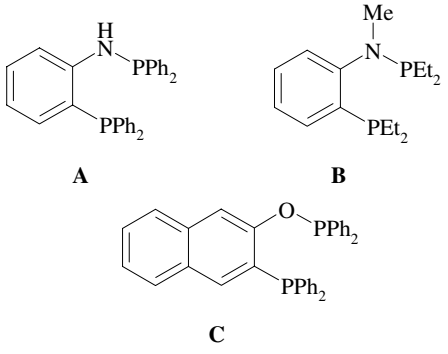

whilst 2,6-bis(diphenylphosphino)pyridine, ($\{Ph_2P\}_2py$), an *o*-bidentate pyridine, has the potential to act as a tridentate PNP ligand [5,6] and was shown to react with a variety of platinum and palladium starting materials to give four different complexes. Gaw et al. [7] recently reported the preparation of the tetradentate (phosphine)amine 1,4-$\{(Ph_2P)_2NCH_2\}_2C_6H_4$. They used this

* Corresponding author. Tel.: +441 334 463 869; fax: +441 334 463 384.
E-mail address: jdw3@st-and.ac.uk (J.D. Woollins).

0277-5387/$ - see front matter © 2004 Elsevier Ltd. All rights reserved.
doi:10.1016/j.poly.2004.09.012

ligand to form a binuclear complex containing two *cis*-$[Mo(CO)_4]$ metal fragments.

Here, we report the preparation of a new phosphine *p*-(xylylenediamonodiphenyl)phosphine which has the potential to act as a bidentate bridging ligand. Illustrative coordination complexes have been prepared.

2. Results and discussion

Reaction of *p*-xylene diamine with two equivalents of Ph_2PCl in the presence of NEt_3, proceeds in thf to give **1** (Eq. (1)) in very good yield (89%) with δ_P 43.3 ppm. The IR spectrum has bands at 3303, 1432 and 997 cm^{-1} that are assigned to ν_{NH}, ν_{PPh} and ν_{PN}, respectively, (ν_{PPh} represents the ν_{CC} of the phosphine aromatic rings). The mass spectrum gave the expected parent ion and fragmentation pattern and microanalysis gave good results.

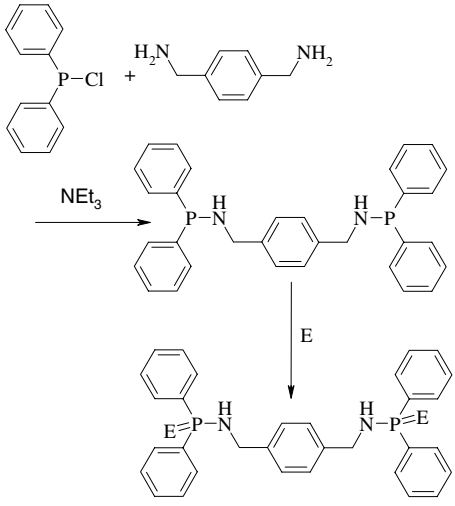

(1)

The oxide (**2**) $Ph_2P(O)NHCH_2(C_6H_4)CH_2NHP(O)Ph_2$ was easily prepared by addition of excess aqueous hydrogen peroxide to **1** in thf whilst the sulfur (**3**) and selenide (**4**) analogues were prepared by the addition of elemental S or Se to **1** in toluene. The EI^+ mass spectral data obtained for these chalcogenides gave the expected parent ions and fragmentation patterns. $^{31}P\{^1H\}$ NMR showed single resonances ($CDCl_3$) at δ_P 24.5 and 60.5 ppm for the oxide and sulfide and at δ_P 58.6 ppm with selenium satellites $^1J(^{31}P–^{77}Se)$ 756 Hz for **4** which is typical for a P=Se group [8].

In the solid state the sulfur and selenide analogues, although not isomorphous, are isostructural, (Fig. 1, Table 1) both have a centre of symmetry; in **3** P(1)–S(1) = 1.9523(11) and P(1)–N(2) = 1.654(3) Å and in **4** P(1)–N(2) = 1.654(5) Å and the P(1)–Se(1) = 2.1198(10) Å which are in the range for previously reported bond lengths [8].

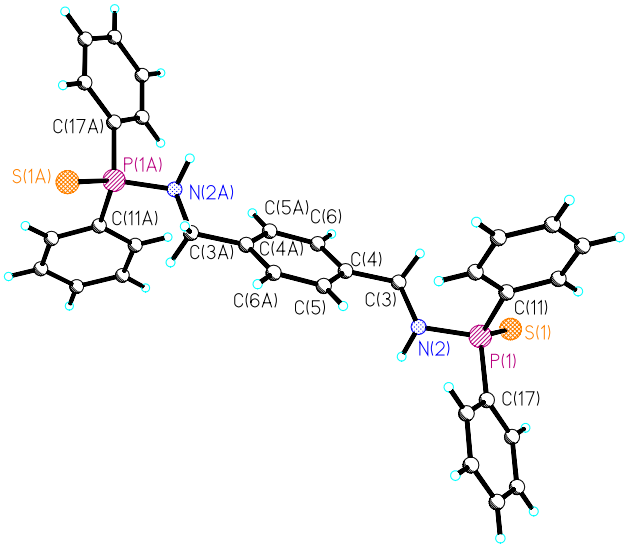

Fig. 1. X-ray structure of *p*-$Ph_2P(S)NHCH_2(C_6H_4)CH_2NHP(S)Ph_2$ (**3**).

Table 1
Selected bond lengths (Å) and angles (°) for *p*-$Ph_2P(S)NHCH_2(C_6H_4)$-$CH_2NHP(S)Ph_2$ (**3**) and *p*-$Ph_2P(Se)NHCH_2(C_6H_4)CH_2NHP(Se)Ph_2$ (**4**). The values in square brackets are for the second independent molecule in **3**

	(3)	(4)
Bond lengths		
P(1)–N(2)	1.654(3)[1.661(2)]	1.654(5)
E(1)–P(1)	1.9523(11) [1.9568(11)]	2.1198(10)
N(2)–C(3)	1.471(4)[1.472(4)]	1.485(7)
P(1)–C(11)	1.811(3)[1.811(3)]	1.797(6)
P(1)–C(17)	1.812(3)[1.812(3)]	1.817(6)
Bond angles		
N(2)–P(1)–C(11)	103.43(13)[103.53(13)]	104.8(3)
N(2)–P(1)–C(17)	101.72(13)[103.36(13)]	104.0(3)
C(11)–P(1)–C(17)	106.39(14)[109.18(14)]	104.5(3)
N(2)–P(1)–E(1)	117.60(10)[116.27(10)]	116.79(19)
C(11)–P(1)–E(1)	112.64(11)[111.87(11)]	113.7(2)
C(17)–P(1)–E(1)	113.74(10)	111.8(2)
P(1)–N(2)–H(2)	109.1(18)[111.3(19)]	110(3)

A range of binuclear compounds were synthesised (Eq. (2)); thus reaction of $[\{PtCl(\mu\text{-}Cl)(PEt_3)\}_2]$ with **1** gives $[\{(PEt_3)PtCl_2(Ph_2PNHCH_2)\}_2C_6H_4]$ (**5**). The EI^+ mass spectrum of (**5**) contains the expected parent ion and fragmentation pattern and the complex displays resonances with platinum satellites in the $^{31}P\{^1H\}$ NMR spectrum (δ_{PA} 34.0 ppm, $^1J\{^{31}P_A–^{195}Pt\}$ 1984 Hz, δ_{PX} 7.5 ppm, $^1J\{^{31}P_X–^{195}Pt\}$ 1715 Hz $^2J\{^{31}P_A–^{31}P_X\}$ 18 Hz). The IR spectrum has ν_{NH} at 3289 cm^{-1}, ν_{PPh} and ν_{PN} at 1435 and 997 cm^{-1}, respectively, and two ν_{PtCl} (symmetric and antisymmetric) bands at 340 and 310 cm^{-1} suggesting a *cis* geometry at the metal. (**6**–**9**) were prepared in a similar way and have comparable spectroscopic properties to **5** (Table 2) see Fig. 2.

Table 2
Characterisation data for $Ph_2PNHCH_2C_6H_4CH_2NHPPh_2$ and its derivatives

	^{31}P-{^1H} NMR	IR (cm^{-1})					Microanalysis % F_{calc}		
	δ_P (ppm)	ν_{PN}	ν_{NH}	ν_{PPh}	$\nu_{P=E}$	ν_{MCl}	C	H	N
$Ph_2PNHCH_2C_6H_4CH_2NHPPh_2 \cdot H_2O$ (**1**)	43.3	997	3303	1432	–	–	73.43 (73.55)	6.39 (6.17)	5.64 (5.36)
$Ph_2P(O)NHCH_2C_6H_4CH_2NHP(O)Ph_2$ (**2**)	24.5	998	3097	1437	1357	–	69.37 (69.31)	5.93 (5.82)	5.38 (5.05)
$Ph_2P(S)NHCH_2C_6H_4CH_2NHP(S)Ph_2$ (**3**)	60.5	997	3180	1437	625	–	65.27 (67.59)	5.35 (5.32)	5.11 (4.93)
$Ph_2P(Se)NHCH_2C_6H_4CH_2NHP(Se)Ph_2$ (**4**)[a]	58.6[a]	996	3177	1435	551	–	57.53 (58.02)	5.14 (4.56)	4.24 (4.23)
[{$(PEt_3)PtCl(Ph_2PNHCH_2)$}$_2C_6H_4$] (**5**)	34.0, 7.5[b]	997	3289	1435	–	340, 310	41.36 (41.52)	5.12 (4.75)	2.36 (2.20)
[{$(PPhMe_2)PtCl(Ph_2PNHCH_2)$}$_2C_6H_4$] (**6**)	35.1, −14.2[c]	998	3300	1435	–	334, 311	44.05 (43.92)	4.17 (3.99)	2.61 (2.13)
[{$IrCl_2(\eta^5\text{-}C_5Me_5)(Ph_2PNHCH_2)$}$_2C_6H_4$] (**7**)	34.4	997	3309	1434	–	289, 268	47.64 (48.00)	4.64 (4.65)	2.35 (2.15)
[{$RhCl_2(\eta^5\text{-}C_5Me_5)(Ph_2PNHCH_2)$}$_2C_6H_4$] $\cdot$ 0.25CH_2Cl_2 (**8**)	66.4[d]	996	3300	1434	–	282, 267	54.76 (54.86)	5.31 (5.33)	2.41 (2.45)
[{$RuCl_2(\eta^6\text{-}p\text{-}MeC_6H_4{}^iPr)(Ph_2$ $PNHCH_2)$}$_2C_6H_4$] (**9**)	61.1	996	3367	1434	–	291, 281	55.53 (55.92)	4.73 (5.23)	2.46 (2.51)
[{$Pd(\eta^3\text{-}C_3H_5)Cl(Ph_2PNHCH_2)$}$_2C_6H_4$] (**10**)	58.1	998	3246	1433	–	276	52.34 (52.44)	4.78 (4.63)	3.45 (3.22)
[{$RhCl(C_8H_{12})(Ph_2PNHCH_2)$}$_2$ C_6H_4] $\cdot$ CH_2 Cl_2 (**11**)	62.3[e]	995	3289	1434	–	279	54.66 (54.37)	5.32 (5.21)	2.89 (2.59)
[{$AuCl(Ph_2PNHCH_2)$}$_2C_4H_6$] (**12**)	61.1	997	3279	1435	–	323	39.98 (39.65)	3.28 (3.12)	2.94 (2.89)

[a] ^1J\{^{31}P–^{77}Se\} 756 Hz.
[b] ^1J\{$^{31}P_A$–^{195}Pt\} 1984 Hz, ^1J\{$^{31}P_X$–^{195}Pt\} 1715 Hz, ^2J\{$^{31}P_A$–$^{31}P_X$\} 18 Hz.
[c] ^1J\{$^{31}P_A$–^{195}Pt\} 1956 Hz, ^1J\{$^{31}P_X$–^{195}Pt\} 1820 Hz, ^2J\{$^{31}P_A$–$^{31}P_X$\} 19 Hz.
[d] ^1J\{^{31}P–^{103}Rh\} 148 Hz.
[e] ^1J\{^{31}P–^{103}Rh\} 157 Hz.

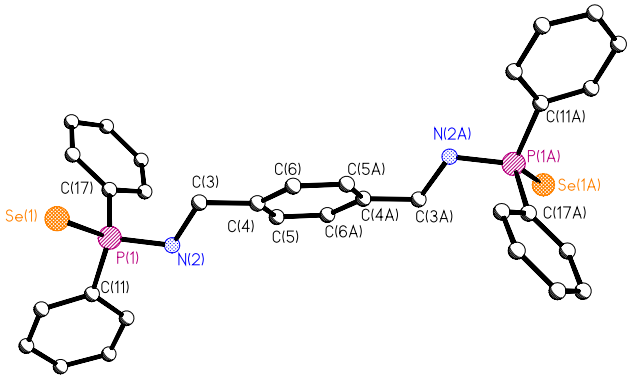

Fig. 2. The X-ray structure of *p*-$Ph_2P(Se)NHCH_2(C_6H_4)CH_2NHP(Se)Ph_2$ (**4**).

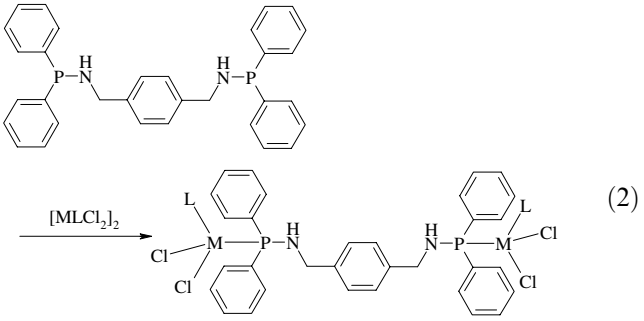

(2)

M= Pt L = PEt_3 **5**, L = PMe_2Ph **6**
M= Ir L= Cp* **7**, M = Rh L= Cp* **8**
M= Ru L= p-cymene **9**

[$(Pd(\eta^3\text{-}C_3H_5)Cl(Ph_2PNHCH_2))_2C_6H_4$] (**10**) was prepared (68%) from [{$Pd(\mu\text{-}Cl)(\eta^3\text{-}C_3H_5)$}$_2$] and **1** in dichloromethane. The microanalysis obtained was satisfactory for the suggested structure and EI^+ mass spectral data gave the expected parent ion and fragmentation pattern. The IR spectrum has bands at 3246, 1433, 998, 276 cm^{-1} that correspond to the ν_{NH}, ν_{PPh}, ν_{PN} and ν_{PdCl} vibrations. The ^{31}P NMR ($CDCl_3$) is a single peak at δ_P 58.1 ppm. Similarly, complex (**11**) was prepared by reaction of [{$Rh(\mu\text{-}Cl)(cod)$}$_2$] and **1** (Eq. (3)).

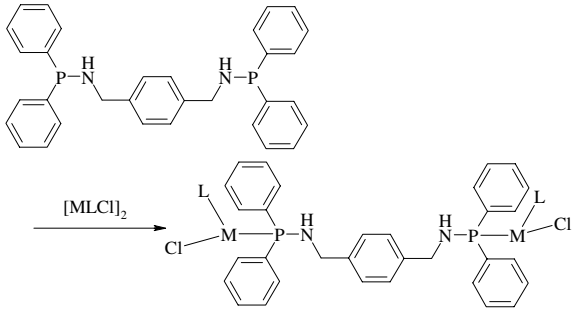

(3)

M=Pd L=allyl **10**, L=Rh L = cod (cyclooctadiene) **11**

Table 3
Details of the X-ray data collections and refinements

	3	**4**
Empirical formula	$C_{32}H_3N_2P_2S_2$	$C_{32}H_3N_2P_2Se_2$
M	568.64	664.46
Crystal system	triclinic	monoclinic
Space group	$P\bar{1}$	$P2_1/n$
Unit cell dimensions		
a (Å)	9.2393(13)	10.950(5)
b (Å)	10.6234(17)	10.964(5)
c (Å)	16.444(3)	12.459(6)
α (°)	92.828(3)	90
β (°)	100.309(3)	96.528(10)
γ (°)	112.799(3)	90
U (Å^3)	1451.3(4)	1468.1(12)
Z	2	2
μ (mm^{-1})	0.318	2.620
Reflections measured	7413	6267
Independent reflections	4150	2100
Final R_1, ωR_2 [$I > 2\sigma(I)$]	0.0402, 0.1035	0.0401, 0.0651

We also prepared a simple bimetallic gold complex **12**. It is clear from the above observations that **1** is readily prepared and able to function as a bridging ligand, but there is no evidence for **1** behaving as a bidentate *trans* ligand (see Table 3).

3. Experimental

Unless otherwise stated, all reactions were carried out under an oxygen-free nitrogen atmosphere using standard Schlenk techniques. Diethyl ether and thf were purified by reflux over sodium-benzophenone and distillation under nitrogen. Dichloromethane was heated to reflux over calcium hydride and distilled under nitrogen. Toluene and hexane were heated to reflux over sodium and distilled under nitrogen. The complexes [AuCl(tht)] (tht = tetrahydrothiophene)[9], $[MCl_2(cod)]$ (M = Pt or Pd; cod = cycloocta-1,5-diene)[10,11], $[\{RuCl(\mu\text{-}Cl)(\eta^6\text{-}p\text{-}MeC_6H_4{}^iPr)\}_2]$[12], $[\{Rh(\mu\text{-}Cl)(cod)\}_2]$[13], $[\{Pd(\mu\text{-}Cl)(\eta^3\text{-}C_3H_5)\}_2]$ $[\{MCl(\mu\text{-}Cl)(\eta^5\text{-}C_5Me_5)\}_2]$ (M = Rh or Ir) [14] $[\{PtCl(\mu\text{-}Cl)(PMe_2Ph)\}_2]$[15] and $[\{PtCl(\mu\text{-}Cl)(PEt_3)\}_2]$ [16] were prepared using the literature procedures. Chlorodiphenylphopshine was distilled prior to use. NEt_3 (99% purity), ^{t}BuOK (95% purity), H_2O_2 (30 wt% in H_2O), *p*-xylylene diamine and reagent grade KBr were used without further purification. Infra-red spectra were recorded as KBr discs in the range 4000–200 cm^{-1} on a Perkin–Elmer 2000 FTIR/RAMAN spectrometer. ^{31}P and ^1H NMR spectra were recorded on a Gemini 2000 spectrometer (operating at 121.4 MHz for ^{31}P and 300 MHz for ^1H) or a JEOL DELTA 270 and are referenced to 85% H_3PO_4 and tetramethylsilane, respectively. Microanalyses were performed by the St. Andrews University service and mass spectra by the Swansea Mass Spectrometer Service.

3.1. $Ph_2PNHCH_2C_6H_4CH_2NHPPh_2$ (1)

To a stirring solution of triethylamine (2.26 g, 22.29 mmol) in thf (100 cm^3) at room temperature was added a thf (50 cm^3) solution of chlorodiphenylphosphine (4.92 g, 22.29 mmol) over 2 h and simultaneously a thf solution of *p*-xylylene diamine (1.52 g, 11.14 mmol) over 2 h. The stirring was continued for a further hour before removing the colourless precipitate that had formed by filtration and the solvent removed to yield a colourless solid which was recrystallised from dichloromethane and hexane to give the desired product as a fine colourless solid that was collected by suction filtration and dried in vacuo. Yield 4.99 g, 89%. ^1H ($CDCl_3$) δ 1.4 (m, 4H, CH_2), 4.1 (br s, 2H, NH), 7.3–7.9 (m, 24H, aromatics). MS: *m/z* 504 $[M]^+$.

3.2. $Ph_2P(O)NHCH_2C_6H_4CH_2NHP(O)Ph_2$ (2)

AqueousHydrogen peroxide (30% w/w, 0.1 cm^3, 0.9 mmol) was added drop wise to a suspension of $Ph_2PNHCH_2C_6H_4CH_2NHPPh_2$ (223 mg, 0.4 mmol) in thf (10 cm^3) and the mixture was stirred for 30 min. The solution was filtered through Celite to remove a small amount of insoluble material and the solvent was removed in vacuo to give viscous oil, which was dissolved in dichloromethane (0.5 cm^3) before precipitating a colourless solid upon addition of diethyl ether (6 cm^3). The product was collected by suction filtration and dried in vacuo. Yield 188 mg, 79%. ^1H NMR ($CDCl_3$): δ 1.4 (m, 4H, CH_2), 4.1 (br s, 2H, NH), 7.3–7.9 (m, 24H, aromatics) ppm. MS: *m/z* 559 $[M + Na]^+$.

3.3. $Ph_2P(S)NHCH_2C_6H_4CH_2NHP(S)Ph_2$ (3)

$Ph_2PNHCH_2C_6H_4CH_2NHPPh_2$ (214 mg, 0.4 mmol) and sulfur (27 mg, 0.8 mmol) were heated to reflux in toluene (15 cm^3) for 4 h. The reaction mixture was filtered through Celite to remove any insoluble material remaining befpre reducing the solvent to yield an off-white solid that was washed with $CHCl_3$ (5 cm^3) and dried in vacuo. Yield 106 mg, 44%. ^1H NMR ($CDCl_3$): δ 1.4 (m, 4H, CH_2), 4.1 (d, 2H, ^2J (^{31}P–^1H) 8 Hz, NH), 7.2–8.0 (m, 24H, aromatics) ppm. MS: *m/z* 591 $[M + Na]^+$.

3.4. $Ph_2P(Se)NHCH_2C_6H_4CH_2NHP(Se)Ph_2$ (4)

$Ph_2PNHCH_2C_6H_4CH_2NHPPh_2$ (198 mg, 0.4 mmol) and grey selenium (62 mg, 0.8 mmol) were heated to reflux in toluene (10 cm^3) for 5 h. The solvent was removed in vacuo and the crude product was taken up in CH_2Cl_2 (5 cm^3) and filtered through Celite to remove a trace of unreacted selenium. The filtrate was evaporated to dryness to yield an off-white solid, which was dried in vacuo overnight. Yield 189 mg, 73%. ^1H NMR ($CDCl_3$): δ 1.4 (m, 4H, CH_2), 4.1 (d, 2H, ^2J (^{31}P–^1H) 8 Hz, NH), 7.2–8.0 (m, 24H, aromatics) ppm. MS: *m/z* 681 $[M + Na]^+$.

3.5. $[\{(PEt_3)PtCl_2(Ph_2PNHCH_2)\}_2C_6H_4]$ (5)

$[\{PtCl(\mu\text{-}Cl)(PEt_3)\}_2]$(39 mg, 0.05 mmol) and ligand (26 mg, 0.05 mmol) were dissolved in dichloromethane (5 cm^3) and stirred overnight. The reaction mixture was filtered through Celite to remove any insoluble material and then reduced to 0.5 cm^3 before addition of diethyl ether (10 cm^3) to precipitate a colourless solid that was isolated by filtration and dried in vacuo. Yield 45 mg, 69%. ^1H ($CDCl_3$) δ 1.0 (m, 18H, CH_3), 1.2 (m, 12H, CH_2), 1.4 (m, 4H, CH_2N), 4.1 (d, 2H, ^2J(^{31}P–^1H) 8 Hz, NH), 7.2–8.0 (m, 24H, aromatics) ppm. MS: *m/z* 1293 $[M + Na]^+$, 1235 $[M - Cl]^+$, 1200 $[M - 2Cl]^+$.

3.6. [{(PPhMe$_2$)PtCl$_2$(Ph$_2$PNHCH$_2$)}$_2$C$_6$H$_4$] (**6**)

[{PtCl(μ-Cl)(PMe$_2$Ph)}$_2$](41 mg, 0.05 mmol) and Ph$_2$PNHCH$_2$C$_6$H$_4$CH$_2$NHPPh$_2$ (26 mg, 0.05 mmol) were dissolved in dry CH_2Cl_2 (5 cm^3) and stirred overnight. The pale yellow solution formed was filtered through Celite to remove any inorganic impurities before reducing the solvent volume to 0.5 cm^3 and addition of diethyl ether (10 cm^3) to precipitate a colourless solid that was isolated by suction filtration and dried in vacuo. Yield 40 mg, 60%. ^{1}H ($CDCl_3$) δ 1.2 (m, 12H, CH_3), 1.4 (m, 4H, CH_2N), 4.1 (d, 2H, ^2J(^{31}P–^{1}H) 8 Hz, NH), 7.2–8.0 (m, 34H, aromatics) ppm. MS: *m/z* 1333 [M + Na]$^+$, 1275 [M − Cl]$^+$, 1239 [M − 2Cl]$^+$.

3.7. [{(IrCl$_2$η^5-C$_5$Me$_5$)(Ph$_2$PNHCH$_2$)}$_2$C$_6$H$_4$] (**7**)

[{IrCl(μ-Cl)(^{5}-ηC$_5$Me$_5$)}$_2$](50 mg, 0.06 mmol) and Ph$_2$PNHCH$_2$C$_6$H$_4$CH$_2$NHPPh$_2$ (32 mg, 0.06 mmol) were dissolved in dry CH_2Cl_2 (5 cm^3) and stirred for 2 h. The orange solution was filtered through Celite to remove a small amount of insoluble material before reducing the volume to 0.5 cm^3 and addition of diethyl ether (20 cm^3) to precipitate an orange solid that was isolated by filtration and dried in vacuo. Yield 60 mg, 73%. ^{1}H ($CDCl_3$) δ 1.3 (s, 30H, CH_3), 1.5 (m, 4H, CH_2N), 4.1 (d, 2H, ^2J (^{31}P–^{1}H) 8 Hz, NH), 7.2–8.0 (m, 24 H, aromatics) ppm MS: *m/z* 1323 [M + Na]$^+$, 1158 [M − 4Cl]$^+$.

3.8. [{RhCl$_2$(η^5-C$_5$Me$_5$)(Ph$_2$PNHCH$_2$)}$_2$C$_6$H$_4$] (**8**)

[{RhCl(μ-Cl)(η^5-C$_5$Me$_5$)}$_2$](48 mg, 0.08 mmol) and Ph$_2$PNHCH$_2$C$_6$H$_4$CH$_2$NHPPh$_2$ (39 mg, 0.08 mmol) were dissolved in dry CH_2Cl_2 (5 cm^3) and stirred for 2 h. The orange solution was filtered through Celite to remove a small amount of insoluble material before reducing the volume to 0.5 cm^3 and addition of diethyl ether (10 cm^3) to precipitate an orange solid that was isolated by filtration and dried in vacuo. Yield 68 mg, 78%. ^{1}H ($CDCl_3$) δ 1.3 (s, 30H, CH_3), 1.5 (m, 4H, CH_2N), 4.1 (d, 2H, ^2J(^{31}P–^{1}H) 8 Hz, NH), 7.2–8.0 (m, 24 H, aromatics) ppm. MS: *m/z* 1145 [M + Na]$^+$, 1087 [M − Cl]$^+$, 1049 [M − 2Cl]$^+$.

3.9. [{RuCl$_2$(η^6-*p*-MeC$_6$H$_4$^{i}Pr)(Ph$_2$PNHCH$_2$)}$_2$C$_6$H$_4$] (**9**)

[{RuCl(μ-Cl)(η^6-*p*-MeC$_6$H$_4$^{i}Pr)}$_2$] (47 mg, 0.08 mmol) and Ph$_2$PNHCH$_2$C$_6$H$_4$CH$_2$NHPPh$_2$ (39 mg, 0.08 mmol) were dissolved in dry CH_2Cl_2 (5 cm^3) and stirred for 1 h. The orange solution was filtered through Celite to remove a small amount of insoluble material before reducing the volume to 0.5 cm^3 and addition of diethyl ether (10 cm^3) to precipitate an orange solid that was isolated by filtration and dried in vacuo. Yield 62 mg, 72%. ^{1}H ($CDCl_3$) δ 0.8 (m, 12H, CH_3), 1.2 (6H, CH_3), 1.9 (m, 4H, CH_2N), 2.5 (m, 2H, CH), 4.1 (d, 2H, ^2J (^{31}P–^{1}H) 8 Hz, NH), 7.2–8.0 (m, 28H, aromatics) ppm. MS: *m/z* 1139 [M + Na]$^+$.

3.10. [{Pd(η^3-C$_3$H$_5$)Cl(Ph$_2$PNHCH$_2$)}$_2$C$_6$H$_4$]. (**10**)

[{Pd(μ-Cl)(η^3-C$_3$H$_5$)}$_2$](61 mg, 0.2 mmol) and Ph$_2$PNHCH$_2$C$_6$H$_4$CH$_2$NHPPh$_2$ (84 mg, 0.2 mmol) were dissolved in dry CH_2Cl_2 (5 cm^3) and stirred overnight. The reaction mixture was filtered through Celite to remove any insoluble inorganic material before reducing the solvent to 0.5 cm^3 and addition of diethyl ether (10 cm^3) to precipitate a yellow microcrystalline solid that was isolated by suction filtration. Yield 98 mg, 68%. ^{1}H ($CDCl_3$) δ 1.3 (m, 8H, CH_2), 1.9 (m, 4H, CH_2N), 2.5 (m, 2H, CH), 4.1 (d, 2H, ^2J (^{31}P–^{1}H) 8 Hz, NH), 7.2–8.0 (m, 24H, aromatics) ppm. MS: *m/z* 835 [M − Cl]$^+$.

3.11. [{RhCl(C$_8$H$_{12}$)(Ph$_2$PNHCH$_2$)}$_2$C$_6$H$_4$] (**11**)

[{Rh(cod)Cl}$_2$](49 mg, 0.1 mmol) and Ph$_2$PNHCH$_2$C$_6$H$_4$CH$_2$NHPPh$_2$ (50 mg, 0.1 mmol) were dissolved in dry toluene (5 cm^3) and stirred for 2 h. The solution was filtered through Celite to remove a small amount of insoluble material before reducing the volume to 0.5 cm^3 and addition of hexane (20 cm^3) to precipitate a yellow solid that was isolated by filtration and dried in vacuo. Recryst from CH_2Cl_2/hexane. Yield 56 mg, 57%. ^{1}H ($CDCl_3$) δ 1.8 (m, 24H, C_8H_{12}), 1.9 (m, 4H, CH_2N), 4.1 (d, 2H, ^2J(^{31}P–^{1}H) 8dz, NH), 7.2–8.0 (m, 24H, aromatics) ppm MS: *m/z* 961 [M − Cl]$^+$.

3.12. [{AuCl(Ph$_2$PNHCH$_2$)}$_2$C$_4$H$_6$] (**12**)

[AuCl(tht)] (116 mg, 0.4 mmol) was dissolved in dry CH_2Cl_2 (5 cm^3) and Ph$_2$PNHCH$_2$C$_6$H$_4$CH$_2$NHPPh$_2$ (91 mg, 0.2 mmol) was added in one portion before stirring for 30 min. The colourless solution was filtered through Celite to remove a small amount of insoluble material before reducing the volume to 2 cm^3 precipitate a colourless solid that was isolated by suction filtration and dried in vacuo. Yield 88 mg, 43%. ^{1}H ($CDCl_3$) δ 1.6 (s, 4H, CH_2N), 4.2 (d, 2H, ^2J(^{31}P–^{1}H) 10 Hz, NH), 7.2–8.0 (m, 24H, aromatics) ppm MS: *m/z* 991 [M + Na]$^+$, 933 [M − Cl]$^+$.

4. Crystallography

X-ray diffraction studies were performed at 125 K using a Bruker SMART diffractometer with graphite-monochromated Mo Kα radiation. The structures were solved by direct methods, non-hydrogen atoms were refined with anisotropic displacement parameters;

hydrogen atoms bound to carbon were idealised, the NH protons were located by a ΔF map. Structural refinements were by the full-matrix least-squares method on F^2 using SHELXTL [17].

Full lists of structure refinement data, atomic coordinates, bond lengths and angles, anisotropic displacement parameters and hydrogen atom parameters have been deposited as supplementary material, CCDC Nos. 239833 and 239834 at the Cambridge Crystallographic Data Centre, 12 Union Road, Cambridge CB2 1EZ, UK [fax: +44-1223-336033; e-mail: deposit@ccdc.cam.ac.uk, or http://www.ccdc.cam.ac.uk].

References

[1] S.M. Aucott, Coordination Chemistry of Aminophosphine Ligands, Ph.D. Thesis, University of Loughborough, 1999.
[2] M.K. Copper, J.M. Downes, P.A. Duckworth, E.R.T. Tiekink, Aust. J. Chem. 45 (1992) 595.
[3] J. Heinicke, A. Tzschach, J. Pract. Chem. 325 (1983) 232.
[4] J. Heinicke, R. Kadryov, M.K. Kindermann, M. Kloss, A. Fischer, P.G. Jones, Chem. Ber. 129 (1996) 1061.
[5] F.E. Wood, M.M. Olmstead, A.L. Balch, J. Am. Chem. Soc. 105 (1983) 6332.
[6] F.E. Wood, J. Hvoslef, H. Hope, A.L. Balch, Inorg. Chem. 23 (1984) 4309.
[7] K.G. Gaw, M.B. Smith, J.W. Steed, J. Organomet. Chem. 664 (2002) 294.
[8] A.M.Z. Slawin, J. Wheatley, M.V. Wheatley, J.D. Woollins, Polyhedron 22 (2003) 1397.
[9] R. Uson, A. Laguna, M. Laguna, Inorg. Synth. 28 (1991) 346.
[10] D. Drew, J.R. Doyle, Inorg. Synth. 28 (1991) 346.
[11] J.X. McDermott, J.F. White, G.M. Whiteside, J. Am. Chem. Soc. 60 (1976) 6521.
[12] M.A. Bennett, T.N. Huang, T.W. Matheson, Inorg. Synth. 21 (1982) 74.
[13] G. Giordano, R.H. Crabtree, Inorg. Synth. 19 (1979) 218.
[14] C. White, A. Yates, P.M. Maitlis, Inorg. Synth. 29 (1992) 228.
[15] W. Baratta, P.S. Pregosin, Inorg. Chim. Acta 209 (1993) 85.
[16] J. Chatt, R.G. Wilkins, J. Chem. Soc. (1952) 273.
[17] SHELXTL, Bruker AXS, Madison, WI, 2001.

Available online at www.sciencedirect.com
SCIENCE DIRECT®
Polyhedron 23 (2004) 2575–2585
POLYHEDRON
www.elsevier.com/locate/poly

Synthesis and coordination of 2-diphenylphosphinothiophenocarboxamide and bis(2,5-diphenylphosphinepicolinamide)

Heather L. Milton, Matthew V. Wheatley, Alexandra M.Z. Slawin, J. Derek Woollins *

School of Chemistry, University of St. Andrews, St. Andrews, Fife KY16 9NB, UK

Received 29 June 2004; accepted 20 September 2004

Abstract

2-Diphenylphosphinothiophenocarboxamide (dpptc) and bis(2,5-diphenylphosphinepicolinamide) (bdpppa) have been prepared and complexed with a variety of metals. Bdpptc behaves as a monodentate P donor ligand and can become bidentate by making use of the C=O site. Bdpppa behaves as a P donor bridging ligand. In many cases, the X-ray structures reveal that the ligand backbone geometry is strongly influenced by intramolecular H-bonding.
© 2004 Elsevier Ltd. All rights reserved.

Keywords: Phosphine; Synthesis; Coordination; X-ray structure

1. Introduction

Hemilabile phosphorus–nitrogen ligands are of great interest and we have recently described the synthesis and coordination of 2-diphenylphosphinopicolinamide (dpppa) and other P–N-based ligands [1,2].

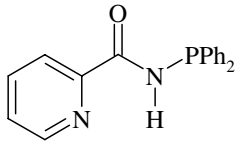

dpppa

There are few known examples of phosphino-thiophenes, and even fewer that act as bidentate phosphino-thiophene ligands. Clot et al. described the major examples in 2000 [3]; 2-(2′-{diphenylphosphino}phenyl)thiophene (dpppth) (**A**) and 3′-diphenylphosphino-2,2′:5′,2″-terthiophene (dppterth) (**B**).

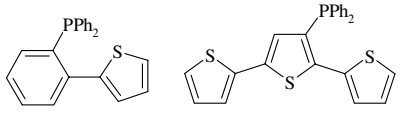

A **B**

These ligands were both shown to bind with a bidentate motif on reaction with $[RuCl_2(PPh_3)_3]$.

Early bridging diphosphines include 2,6-bis(diphenylphosphino)pyridine ($(Ph_2P)_2py$) (**C**), 2,6-(diphenylphosphinomethyl)pyridine (**D**) and *N*,*N*′-bis(diphenylphosphino)-2,6-diaminopyridine (**E**) [4]. These ligands are commonly found as bridging ligands and bidentate ligands with a variety of transition metals.

* Corresponding author. Tel.: +44 133 446 3869; fax: +44 133 446 3384.
E-mail address: jdw3@st-andrews.ac.uk (J.D. Woollins).

0277-5387/$ - see front matter © 2004 Elsevier Ltd. All rights reserved.
doi:10.1016/j.poly.2004.09.014

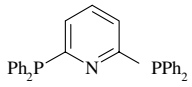

C

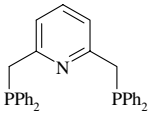

D

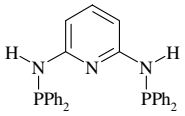

E

Here, we describe two new hemilabile ligands: 2-diphenylphosphinothiophenocarboxamide (dpptc) and bis(2,5-diphenylphosphinepicolinamide) (bdpppa). The coordination properties are compared with dpppa.

2. Results and discussion

The synthesis of dpptc (**1**) is analogous to that of dpppa (Eq. (1)).

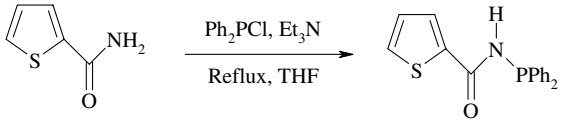

(1)

1

The ligand is readily soluble in chlorinated solvents, acetone, tetrahydrofuran, somewhat less so in toluene, methanol and diethylether. A singlet is observed in the ^{31}P spectrum of dpptc at δ(P) 25.9 ppm; comparable with the value for dpppa. The ^{1}H NMR spectrum does not show the presence of an amide proton, as this resonance is obscured by the main body of the aromatic protons. The IR spectra shows the expected peaks, a weak ν(N–H) band is present at 3265 cm^{-1} together with bands attributable to ν(thCS) and ν(P–N) at 1096 and 996 cm^{-1} respectively, with ν(C–N) coming at 1522 cm^{-1}. The expected ν(C=O) signature is visible at 1624 cm^{-1}.

Only the sulfide of dpptc was synthesised (by reaction of dpptc with elemental sulfur in toluene, dpptc-S (**3**), δ(P) 57.2 ppm) as a representative example of the P(V) form. However, a crystal of the oxide derivative was obtained via air oxidation of the free ligand in a $CDCl_3$ solution (Fig. 1). In the solid state, the molecules adopt a chain line structure as a consequence of hydrogen bonding.

Dpptc reacts with [$PtCl_2$(cod)] in dichloromethane to give *cis*-[$PtCl_2$(dpptc-*P*)$_2$] (**4**), no *trans*-bis(dpptc) or mono-(dpptc) binding was observed. The ^{31}P NMR of **4** is a singlet at δ(P) 27.9 ppm with the expected platinum satellites, $^{1}J_{Pt-P}$ = 3870 Hz, consistent with phosphorus *trans* to chloride. The ^{1}H NMR spectrum

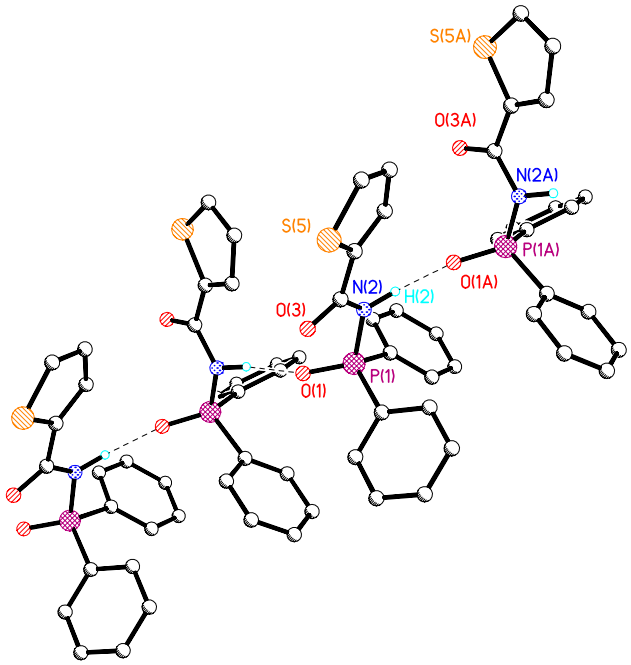

Fig. 1. Crystal structure of dpptc-*O*, **2**, selected bond lengths (Å) and angles (°): P(1)–O(1) 1.456(3), P(1)–N(2) 1.692(3), O(3)–C(3) 1.229(4), N(2)–C(3) 1.373(5), C(3)–C(4) 1.463(5), S(5)–C(4) 1.725(4), C(4)–C(8) 1.365(5), N(2)–O(1) 2.80, N(2)–P(1)–O(1) 115.10(16), C(17)–P(1)–O(1) 112.61(16), N(2)–H(2)···O(1) 171.

displays the anticipated changes from the free ligand. The amine proton is shifted to δ(H) 9.7 ppm, also the coupling constant has increased to $^{2}J_{P-H}$ = 11 Hz. The ν(N–H) vibration in the IR spectrum has shifted to a lower wave number (3214 cm^{-1}), suggesting the possibility of intermolecular hydrogen bonding interactions within the complex. The ν(C=O) also shifts considerably to 1672 cm^{-1} Two Pt-Cl stretches are visible in the spectrum (304 and 273 cm^{-1}), another indication of a *cis*-conformation in **4**.

Reaction of dpptc with [{Pd(μ-Cl)(η^3-C_3H_5)}$_2$] gives the expected monodentate dpptc complex [PdCl(η^3-C_3H_5)(dpptc-*P*)] (**5**), δ(P) 54.3 ppm. The X-ray structure of **5** (Fig. 2) confirms the *P* coordination and displays hydrogen bonding, [N(7)–H(7)···Cl(1) 3.166 Å, with a N(7)–H(7)···Cl(1) 131°], there is no evidence of sulfur coordination.

The mixed phosphine complex [$PtCl_2$($PPhMe_2$)-(dpptc-*P*)] (**6**) was synthesised from [{PtCl(μ-Cl)-($PPhMe_2$)}$_2$] and dpptc in dichloromethane. The ^{31}P NMR of **6** showed two doublets with the appropriate platinum satellites [δ(P) 29.7 ppm, $^{2}J_{P-P}$ = 18.8 Hz, $^{1}J_{Pt-P}$ = 3890 Hz, δ(P) −15.6 ppm, $^{2}J_{P-P}$ = 18.8 Hz, $^{1}J_{Pt-P}$ = 3500 Hz], which are consistent with two phosphorus *cis*- to each other and *trans*- to a chloride (see Fig. 3).

Further monodentate complexes were synthesised (Scheme 1) and these all exhibited the expected spectroscopic properties.

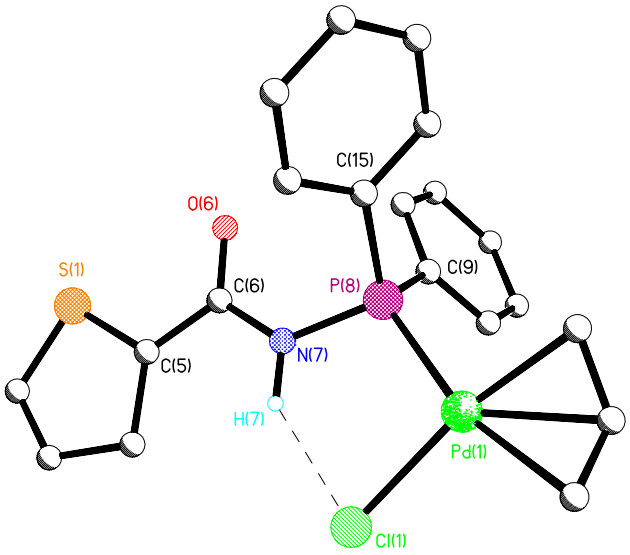

Fig. 2. Crystal structure of [PdCl(η^3-C_3H_5)(dpptc-P)] (**5**), selected bond lengths (Å) and angles (°): P(8)–Pd(1) 2.2937(14), Pd(1)–Cl(1) 2.3780(13), P(8)–N(7) 1.706(4), N(7)–C(6) 1.377(6), O(6)–C(6) 1.227(6) C(6)–C(5) 1.455(8), S(1)–C(5), 1.712(6), N(7)···Cl(1) 3.166(4), P(8)–Pd(1)–Cl(1) 97.18(4), C(15)–P(8)–Pd(1) 116.93(15), N(7)–P(8)–Pd(1) 106.26(14), C(9)–P(8)–Pd(1) 114.06(16), N(7)–H(7)···Cl(1) 131(4).

The X-ray structure of **8** is in space group $P2_12_12_1$ Flack parameter 0.01(3) but we have no evidence there is only one isomer in solution. In **8** there is an interaction between the amide proton and both chlorides attached to the metal and it is worthy of note that there is no interaction involving the oxygen or the sulfur heteroatom in the ring. This could be due to the fact that the sulfur is less likely to form a hydrogen bond, or that the geometry of the five-membered ring as opposed to that of the six-membered ring is less favourable for an N(2)–H(2)···S(5) interaction. These issues and the easy availability of the chlorides account for the chosen motif in this molecule. In the X-ray structure of **9** (Fig. 4), the two hydrogen bonds present are almost identical, showing the favourable motif that can be produced by *trans*-coordination. **10** also has (Fig. 5) H-bond interactions with a N(2)–H(2)···Cl(1) hydrogen bond controlling the ligands geometry, forming a pseudo five-membered ring, similar to the ones we have seen previously; again the sulfur has no part in the bonding motif.

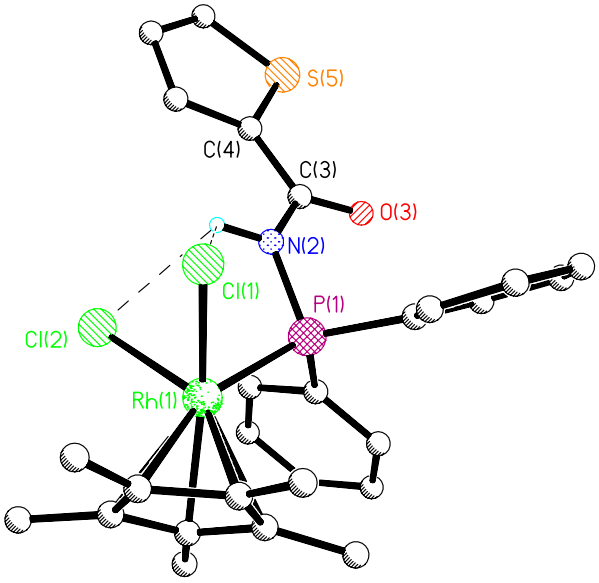

Fig. 3. Crystal structure of [$RhCl_2$(η^5-C_5Me_5)(dpptc-P)] (**8**), selected bond lengths (Å) and angles (°): P(1)–Rh(1) 2.3077(10), Rh(1)–Cl(1) 2.3998(9), Rh(1)–Cl(2) 2.4163(9), P(1)–N(2) 1.695(3), O(3)–C(3) 1.218(4) N(2)–C(3) 1.387(4), N(2)···Cl(1) 3.379(3), N(2)···Cl(2) 3.113(3), P(1)–Rh(1)–Cl(1) 89.44(3), P(1)–Rh(1)–Cl(2) 89.19(3), Rh(1)–P(1)–N(2) 106.88(10), Cl(1)–Rh(1)–Cl(2) 87.96(3), N(2)–H(2)···Cl(1) 112(3), N(2)–H(2)···Cl(2) 121(3).

Dpptc also exhibits bidentate chemistry, though there are significant differences between the chemistry of dpppa and dpptc. Reaction of a halide abstraction reagent with monodentate dpppa complexes gives the *P*,*N* bidentate species. In the case of dpptc, when the same reaction is undertaken one might expect the binding of the thiophene sulfur atom or chelation via the C=O group since thiophene is not an especially good ligand. The coordination mode can be investigated by IR spectroscopy, the frequency of the ν(C=O) vibration indicating chelation through the oxygen. The example investigated was reaction of [$RuCl_2$(*p*-cymene)(dpptc-*P*)] with $AgBF_4$ in CH_2Cl_2, the silver salt was removed by filtration and the product [RuCl(*p*-Cy)(dpptc-*P*,*O*)]BF_4 (**11**) precipitated with diethylether. The ^{31}P NMR displays the expected downfield shift in the spectrum, the peak moves from δ(P) 59.9–100.0 ppm, again the chelate ring effect is responsible for this. The proton spectrum shows some interesting aspects, as the amine proton moves from δ(H) 7.9 ppm in the monodentate complex to δ(H) 10.1 ppm in the bidentate complex and changes from a doublet to a broad singlet, this is typical of extensive hydrogen-bonding being present. The ν(NH) is unchanged in comparison with the monodentate complex at 3216 cm^{-1}. The important IR data is the ν(C=O) – chelation would cause a high frequency shift and this is observed with the band moving to 1561 cm^{-1}, a shift of 104 cm^{-1} from the monodentate complex, typical of C=O bound, bidentate ligand, as described by Braunstein [5]. We also observed the $[BF_4]^-$ counterion in the IR spectrum.

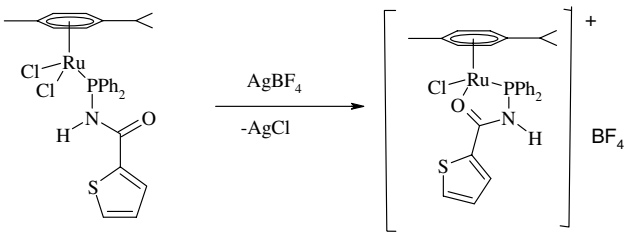

(2)

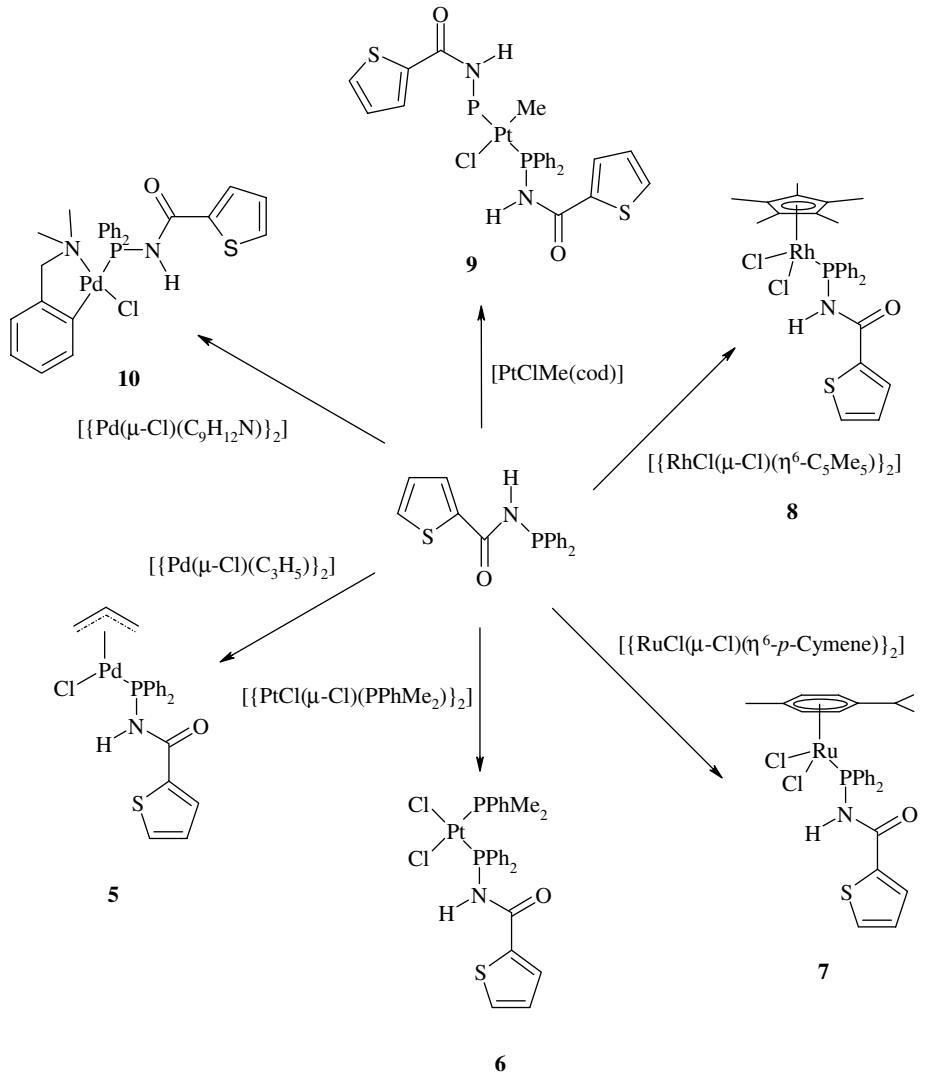

Scheme 1. Formation of monodentate complexes of dpptc.

The synthesis of bdpppa (**12**) is very similar to that of dpppa (Eq. (3)).

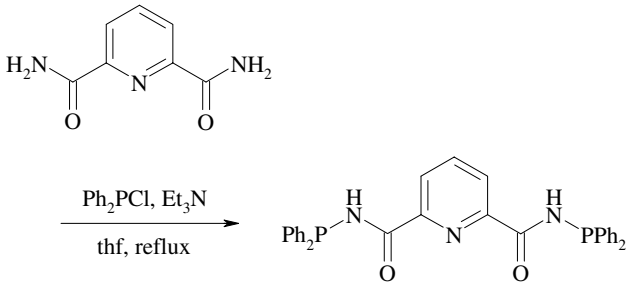

(3)

The expected singlet in the ^{31}P NMR is observed at δ(P) 21.9 ppm. This is extremely close to the value for dpppa (22.0 ppm). We see the same similarities in the proton spectra, the N–H peak appears again as a doublet with a more or less identical shift to dpppa at δ(H) 8.4 ppm, however the coupling constant is significantly larger for bdpppa, being 8 Hz as compared to 4 Hz for dpppa. When one examines the IR spectra for bdpppa we see some significant deviation in the characteristics of bdpppa compared to dpppa. In bdpppa ν(N–H) vibrations are visible at 3345 and 3262 cm^{-1}, this trend continues into the ν(C=O) vibrations – again two are visible at 1665 and 1646 cm^{-1}, the ν(C=N) stretches are also twinned at 1588 and 1571 cm^{-1}. However there is only one ν(P–N) vibration observed at 999 cm^{-1}; from this we could surmise that there is a slight difference in the to 'arms' of the molecule present in the solid state.

The presence of two P^{III} atoms in this molecule provides an opportunity for a variety of oxidation products to be synthesised. Bis(2,6-diphenylphosphino)picolinamide disulfide (**13**) and the diselenide (**14**) were prepared by refluxing bdpppa in toluene with a stoichiometric amount of sulfur or selenium for 1 h, the disulfide has

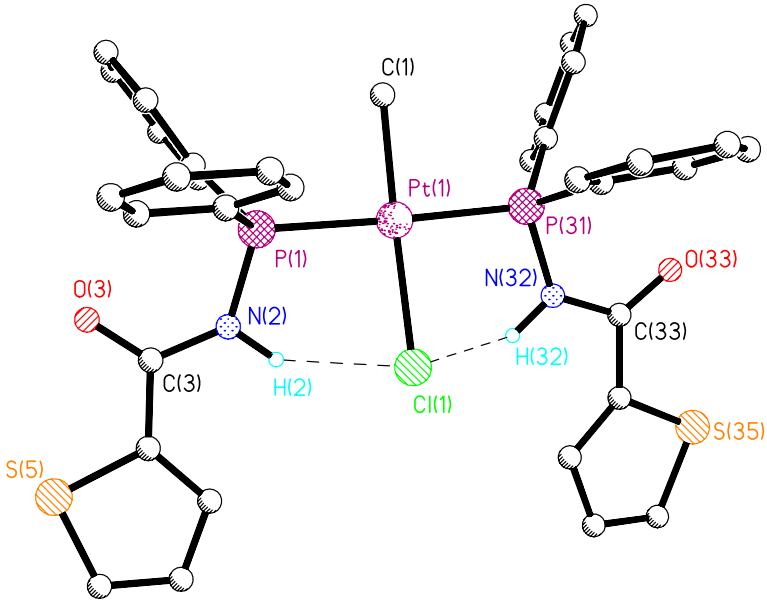

Fig. 4. Crystal structure of [PtMeCl(dpptc-P)$_2$] (**9**), selected bond lengths (Å) and angles (°): P(1)–Pt(1) 2.2902(15), P(31)–Pt(1) 2.2902(15), P(1)–N(2) 1.702(5), P(31)–N(32) 1.700(5), N(2)–C(3) 1.371(8), N(32)–C(33) 1.365(7), C(3)–O(3) 1.227(7), C(33)–O(33) 1.227(7), Pt(1)–Cl(1) 2.4343(16), Pt(1)–C(1) 2.074(6) N(2)···Cl(1) 3.085(6), N(32)···Cl(1) 3.045(5), P(1)–Pt(1)–Cl(1) 91.72(5), P(31)–Pt(1)–Cl(1) 90.34(5), P(1)–Pt(1)–C(1) 89.79(18), N(2)–P(1)–Pt(1) 106.14(18), N(32)–P(31)–Pt(1) 106.14(18), N(2)–H(2)···Cl(1) 139(4), N(32)–H(32)···Cl(1) 139(5).

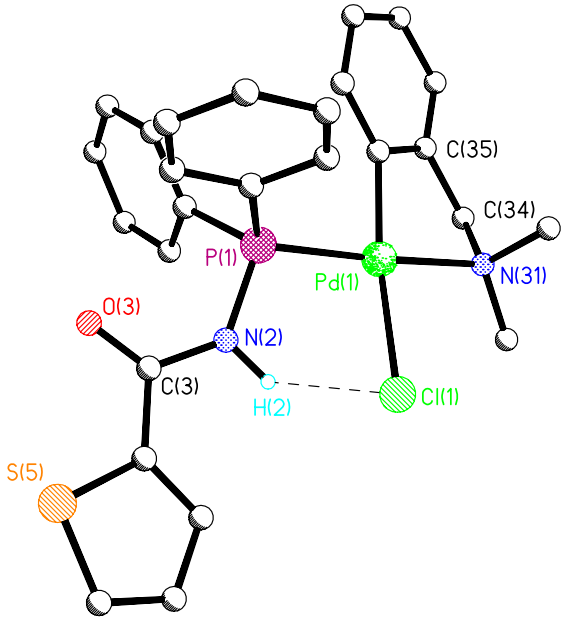

Fig. 5. Crystal structure of [PdCl($C_9H_{12}N$)(dpptc-P)] (**10**), Selected bond lengths (Å) and angles (°): P(1)–Pd(1) 2.2479(12), Pd(1)–N(31) 2.143(4), Pd(1)–Cl(1) 2.4249(12), C(3)–O(3) 1.219(5), N(2)–C(3) 1.382(5), C(4)–S(5) 1.713(4), N(2)···Cl(1) 3.027(4), P(1)–Pd(1)–Cl(1) 93.58(4), P(1)–Pd(1)–N(31) 173.10(10), Cl(1)–Pd(1)–N(31) 91.83(10), N(2)–H(2)···Cl(1) 141(4).

δ(P) 55.1 ppm and the diselenide δ(P) 49.7 ppm with $^1J_{P=Se}$ = 795 Hz. The amide protons in **13** and **14** are shifted to δ(H) 8.9 and 8.8 ppm, respectively, and are both doublets with $^2J_{P-H}$ = 9 Hz, these values are similar to the values observed for the unoxidized ligand. The IR data shows no real variation from the dpppa equivalents, for **13** the ν(N–H) is observed at 3360 cm^{-1} as a sharp peak, however the ν(C=O) is observed at 1697 cm^{-1} with significant line broadening, the ν(P–N) peak remains constant at 999 cm^{-1}. A similar pattern is observed for **14**, with ν(N–H), ν(C=O) and ν(P–N) coming at 3256, 1698 and 998 cm^{-1}, respectively, although the slightly lower value for the ν(N–H) may suggest more extensive hydrogen-bonding in **14** compared to both the disulfide and the free ligand. In the solid state (Fig. 6) **14** adopts a pseudo five-membered ring formed by an interaction of the amide hydrogen's with the pyridyl nitrogen (see Scheme 2).

By making use of the mild conditions involved in synthesis of the sulfur species one can isolate the mono-sulfur derivative of bdpppa, bdpppa-S (**15**). This generates a compound where only one sulfur is bound to phosphorus, leaving one free for further chemistry. The ^{31}P spectrum clearly shows this motif with two singlets being present at δ(P) 56.0 (P=S), and 21.7 ppm (P^{III}). The IR data shows the two now different arms of the molecule clearly, two ν(N–H) vibrations are observed, one at 3345 cm^{-1} which is consistent with bdpppa, and the other at 3262 cm^{-1}, similar to dpppa-S and bdpppa-diS. The same pattern is seen in the ν(C=O), a peak at 1697 cm^{-1} representing the sulfide arm, and a peak at 1665 cm^{-1} represents the P^{III} arm.

As we speculated the mono-oxidised form of bdpppa can use it is unoxidised phosphorus to react further, and reaction with one equivalent of selenium in toluene generates the unsymmetrical bdpppa-S,Se (**16**), δ(P) 55.0

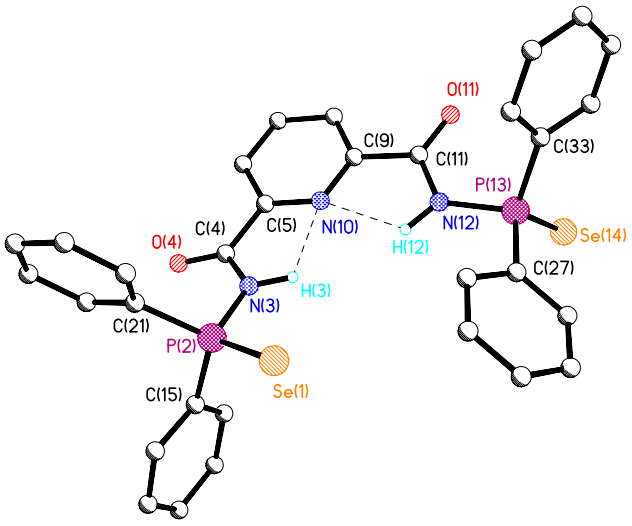

Fig. 6. Crystal structure of bdpppa-diSe (**14**), selected bond lengths (Å) and angles (°): P(2)–Se(1) 2.0974(14), P(13)–Se(14) 2.1014(15), P(2)–N(3) 1.687(4), P(13)–N(12) 1.698(4), N(3)–C(4) 1.374(6), N(12)–C(11) 1.373(6), C(4)–O(4) 1.209(6), C(11)–O(11) 1.207(6), C(4)–C(5) 1.513(6), C(11)–C(9) 1.510(7), C(5)–N(10) 1.334(6), C(9)–N(10) 1.334(16), N(3)···Cl(3) 3.050, N(12)···Cl(3) 3.368, N(3)···N(10) 2.684(5) N(12)···N(10) 2.721(5), Se(1)–P(2)–N(3) 107.68(16), Se(14)–P(13)–N(12) 114.97(16), P(2)–N(3)–H(3) 120(5), N(3)–H(3)···N(10) 113(5), N(12)–H(12)···N(10) 113(5).

ppm (consistent with P=S), δ(P) 49.7 ppm $^{1}J_{P=Se}$ of 795 Hz.. Compound **15** can also be reacted with one equivalent of [AuCl(tht)] in dichloromethane to generate [AuCl(bdpppa-S-*P*)] **17**, δ(P) 55.0 (P=S) and δ(P) 50.2 (P–Au). Reaction of bdpppa with [AuCl(tht)] in dichloromethane gives two products dependant on the stoichiometry of the reaction. One equivalent of [AuCl(tht)] generates the expected product with one phosphorus bound to gold and one remaining unbound (**18**). With two equivalents of [AuCl(tht)] both phosphorus atoms are coordinated (Scheme 3) to give (**19**). In the case of this digold complex, we see the expected singlet in the ^{31}P NMR at 50.0 ppm, this agrees well with the one previous gold complex of dpppa, and the peak seen in **17**. The proton spectrum also displays the characteristics of its dpppa analogue, the amide peak is clearly seen at δ(H) 10.3 ppm with a $^{2}J_{P-H}$ = 16 Hz and the aromatics are all found in the 8.2–7.2 region. The ν(N–H) stretch in the IR spectrum is a broad peak at 3261 cm^{-1}, also the ν(C=O) band is broad, located at 1698 cm^{-1}, both these values correlate well with [AuCl(dpppa-*P*)] (3288 and 1698 cm^{-1}, respectively).

However, when one considers the mono-gold complex it, unlike **15**, does not display two separate peaks in the ^{31}P NMR for P–Au and P^{III}, it displays a singlet at δ(P) 64.3 ppm, at significantly higher chemical shift than anything we have seen earlier, and does not correlate with the shift observed in the mono-sulfide/gold complex. Inspection of the IR data provides further evidence for a single phosphorus environment, with only single peaks being displayed for ν(N–H) and ν(C=O) (3054 and 1698 cm^{-1}, respectively). Also the ^{1}H NMR

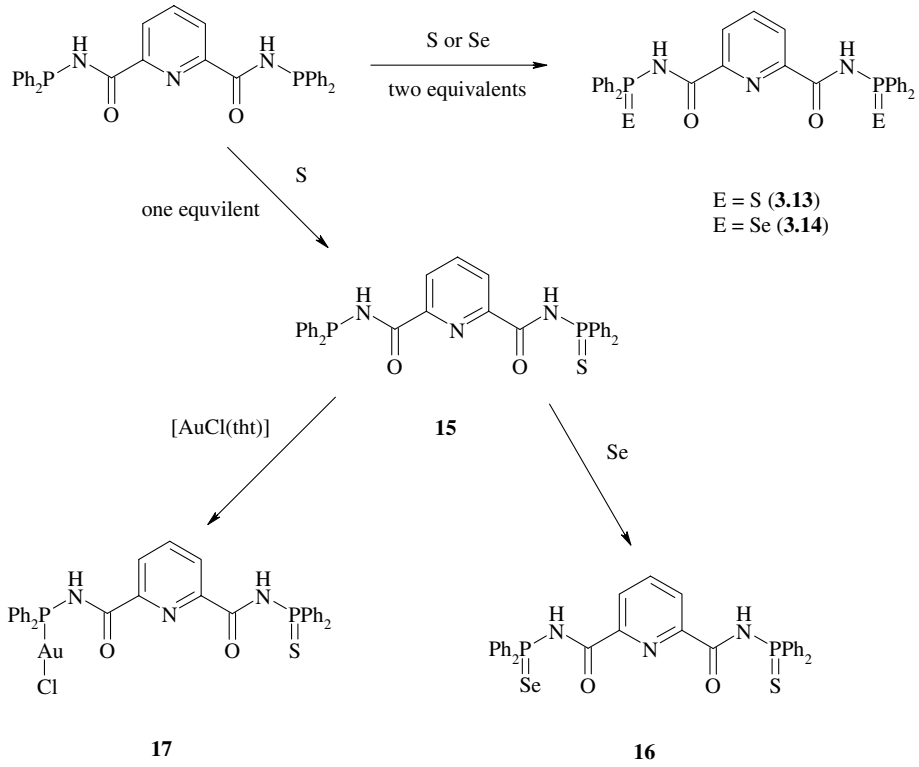

Scheme 2. Reactions of bdpppa and its mono-oxidized derivatives.

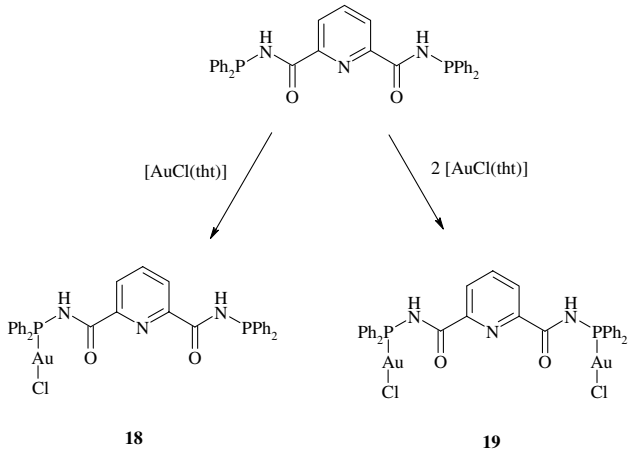

Scheme 3. Reaction of bdpppa with [AuCl(tht)].

data shows a single resonance for the amide proton, a broad singlet at δ(H) 11.0 ppm. The most plausible explanation for these data is for **18** to exist as a dimer, this is not a unique conformation as a similar system has been reported for dppap [13].

Reaction of bdpppa with a range of Pt and Pd dimers generates complexes where the bdpppa ligand bridges two metal atoms. Treatment of bdpppa with one equivalent of $[\{Pd(\mu\text{-}Cl)(\eta\text{-}C_3H_5)\}_2]$, generating $[Pd_2Cl_2(\eta\text{-}C_3H_5)_2$(bdpppa-*P*,*P*)] (**20**). The ^{31}P NMR shows a singlet at δ(P) 55.1 ppm, consistent with the complexes structure when compared to dpppa and dpptc.

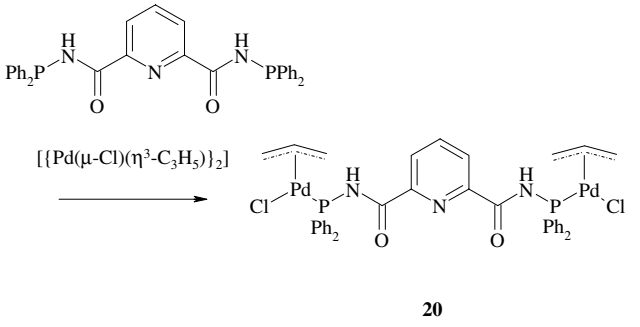

(4)

The analogous reaction with $[\{Pt(\mu\text{-}Cl)(\eta\text{-}C_3H_5)\}_2]$ generated a similar product, $[Pt_2Cl_2(\eta\text{-}C_3H_5)_2$(bdpppa-*P*,*P*)] (**21**), δ(P) 51.7 ppm, $^1J_{Pt-P} = 4730$ Hz. A crystal of **21** was prepared for crystallographic analysis by vapour diffusion of diethylether into a concentrated solution of **21** in $CDCl_3$. Given our conclusions based on **20**, we could imagine the two compounds would be almost analogous in the solid state.

The X-rays structure of **21** (Fig. 7) shows it has an arrangement much like that of **14**, with the amide protons interacting with the pyridyl nitrogen, and if one considers the chlorides to be analogous to the selenium atoms, then we can see that again one is 'in' and one is 'out', of the hole in the centre of the complex. Similar

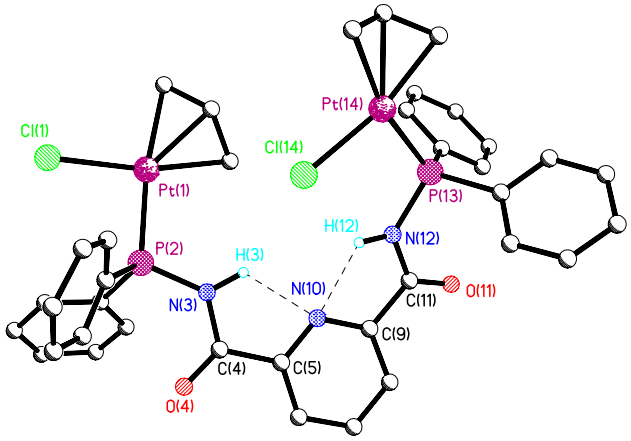

Fig. 7. Crystal structure of $[Pt_2Cl_2(\eta\text{-}C_3H_5)_2$(bdpppa-P,P)] (**21**), selected bond lengths (Å) and angles (°): P(2)–Pt(1) 2.249(2), P(13)–Pt(14) 2.250(2), P(2)–N(3) 1.699(7), P(13)–N(12) 1.720(7), N(3)···N(10) 2.689(10), N(12)···Cl(14) 3.167(7), N(12)···N(10) 2.674(9), Pt(1)–P(2)–N(3) 110.4(2), Pt(14)–P(13)–N(12) 109.9(3), N(3)–H(3)···N(10) 119(7), N(12)–H(12)···N(10) 110(6).

to **14** one can imagine in this scenario that there is probably too much steric bulk involved for both of the chlorides to occupy the 'in' slot as was the case with the selenium atoms.

3. Experimental

All manipulations were carried out in a atmosphere of nitrogen, unless stated otherwise. All solvents were either freshly distilled from an appropriate drying agent (thf, Et_2O, dcm) or obtained as anhydrous grade from Aldrich. ^{1}H and ^{31}P NMR spectra were recorded using a Jeol Delta FT (270 MHz) spectrometer. IR spectra were recorded as KBr discs (prepared in air) on a Perkin–Elmer 2000 FTIR/RAMAN spectrometer. All significant peaks (>800 cm^{-1}) are quoted to serve as a fingerprint. Silver salts, 2-thiophenecarboxamide, 2,6-pyridinedicarboxamide (Aldrich Chemical Co.) and BuLi (2.5 M, Lancaster) were purchased and used as received. Triethylamine and chlorodiphenylphosphine were distilled prior to use. Dimethylaminopyridine (DMAP) was sublimed before use. The various metal starting materials were made by the appropriate literature methods; [AuCl(tht)] [5], $[MCl_2(cod)]$ (M = Pt or Pd; cod = cycloocta-1,5-diene) [6,7], [PtMeCl(cod)] [8], $[\{PtCl(\mu\text{-}Cl)(PMe_2Ph)\}_2]$ [9], $[\{MCl(\mu\text{-}Cl)(Cp^*)\}_2]$ (M = Rh or Ir) [10], $[\{RuCl(\mu\text{-}Cl)(\eta^6\text{-}p\text{-}MeC_6H_4{}^iPr)\}_2]$ [11], $[\{PdCl(\mu\text{-}Cl)(\eta^3\text{-}C_3H_5)\}_2]$ [12–14].

*3.1. 2-(Diphenylphosphino)thiophenecarboxamide (Dpptc) (**1**)*

Chlorodiphenylphosphine (3.53 ml, 20 mmol) was added to a solution of 2-thiophenecarboxamide (2.5 g,

20 mmol), triethylamine (2.88 ml, 20.6 mmol) and DMAP (240 mg, 2 mmol) in THF (100 cm^3) and refluxed overnight. The reaction mixture was filtered to remove a white solid (Et_3NHCl) and washed with THF (50 cm^3). The solvent was removed in vacuo leaving a pale yellow solid. This solid was recrystallised by cooling a concentrated methanol solution in a fridge overnight (yield: 3.28 g, 10.5 mmol, 54%). *Anal.* Calc. $C_{17}H_{14}NOSP$ requires: C, 65.5; H, 4.53; N, 4.50. Found: C, 63.8; H, 4.09; N, 4.70%. ν_{max}/cm^{-1}: 3265, 1624, 1522, 1442, 1270, 1096, 996. ^{31}P NMR (109.3 MHz, $CDCl_3$), δ 25.9. ^1H NMR (270 MHz, $CDCl_3$), 7.6 (2H, m, aromatic), 7.5–7.3 (10H, m, aromatic), 7.1 (2H, m, aromatic).

3.2. 2-(Diphenylphosphino)thiophenecarboxamide sulfide (**3**)

Sulfur (77 mg, 2.4 mmol) was added to a solution of 2-(diphenylphosphino)thiophenecarboxamide (750 mg, 2.4 mmol) in toluene (20 cm^3) and refluxed overnight. The solvent was removed in vacuo leaving an off-white solid. This solid was recrystallised by cooling a concentrated toluene solution at 4 °C overnight (yield: 1.39 g, 93%). *Anal.* Calc. $C_{17}H_{14}NOPS_2$ requires: C, 59.5; H, 4.11; N, 4.08. Found: C, 59.2; H, 3.70; N, 4.48%. ν_{max}/cm^{-1}: 3167, 1624, 1436, 1000. ^{31}P NMR (109.3 MHz, $CDCl_3$), δ 57.2 ppm. ^1H NMR ($CDCl_3$), δ 8.0 (3H, m, aromatic), 7.7–7.3 (6H, m, aromatic), 7.3–7.1 (4H, m, aromatic), 7.0 (1H, d, N–H).

3.3. [$PtCl_2$(dpptc-P)$_2$] (**4**)

Dpptc (166 mg, 0.534 mmol) and [$PtCl_2$(cod)] (100 mg, 0.267 mmol) were weighed into a Schlenk type flask and DCM (5 cm^3) added. The solution was stirred for 10 min and the majority of the solvent removed in vacuo. A white solid was isolated after addition of Et_2O then filtered and washed with further ether (yield: 170 mg, 72%). *Anal.* Calc. $C_{34.5}H_{29}N_2O_2P_2S_2Cl_3Pt$ requires: C, 44.5; H, 3.14; N, 3.01. Found: C, 44.0; H, 3.89; N, 2.95%. ν_{max}/cm^{-1}: 3214, 1672, 1424, 1398, 1042, 304, 273. ^{31}P NMR (109.3 MHz, $CDCl_3$), δ 27.9 ($J_{P–Pt}$ = 3870 Hz). ^1H NMR (270 MHZ, $CDCl_3$), 9.7 (2H, d, J = 11 Hz, N–H), 7.8–6.9 (26H, m, aromatic).

3.4. [PdCl(η^3-C_3H_6)(dpptc-P)] (**5**)

Dpptc (170 mg, 0.54 mmol) and [{Pd(μ -Cl)(η^3-C_3H_5)}$_2$] (100 mg, 0.27mmol) were weighed into a Shlenk type flask and DCM (5 ml) added. The solution was stirred for 10 min and the majority of the solvent removed in vacuo. A white solid was isolated after addition of Et_2O then filtered and washed with further ether (yield: 117 mg, 87%). *Anal.* Calc. $C_{20}H_{20}NOSPClPd$ requires: C, 48.5; H, 4.07; N, 2.83. Found: C, 48.3; H, 2.35; N, 2.82%. ν_{max}/cm^{-1}: 3208, 1671, 1435, 1394, 1010, 277. ^{31}P NMR (109.3 MHz, $CDCl_3$), δ 54.3. ^1H NMR (270 MHz, $CDCl_3$), 9.4 (1H, d, J = 19 Hz, N–H), 7.7 (1H, d, J = 1 Hz, thC[5**]H), 7.7–7.6 (4H, m, aromatic), 7.5–7.3 (7H, m, aromatic) 7.1 (1H, dd, J = 3, 6 Hz, thC[4**]) 5.5 (1H, m, allyl), 4.8 (1H, t, J = 6 Hz, allyl), 3.7 (1H, dd, J = 10, 13 Hz, allyl), 3.3 (1H, obscured, allyl), 2.6 (1H, d, J = 13 Hz, allyl).

3.5. [$PtCl_2$($PPhMe_2$)(dpptc-P)] (**6**)

Dpptc (58 mg, 0.18 mmol) and [{PtCl(μ-Cl)(Me_2PhP)}$_2$] (75 mg, 0.0927 mmol) were weighed into a Schlenk type flask and DCM (5 cm^3) added. The solution was stirred for 10 min and the majority of the solvent removed in vacuo. A yellow solid was isolated after addition of Et_2O then filtered and washed with further ether (yield: 66 mg, 50%). *Anal.* Calc. $C_{25}H_{25}NOSP_2Cl_2Pt$ requires: C, 39.7; H, 4.20; N, 2.01. Found: C, 40.0; H, 3.31; N, 1.72%. ν_{max}/cm^{-1}: 3226, 1671, 1435, 948, 316, 281. ^{31}P NMR (109.3 MHz, $CDCl_3$) δ 29.7 (d, $J_{P–P}$ = 18.78 Hz, $J_{P–Pt}$ = 3890 Hz), -15.6 (d, $J_{P–P}$ = 18.78 Hz, $J_{P–Pt}$ = 3500 Hz). ^1H NMR (270 MHz, $CDCl_3$) δ 11.4 (1H, d, J = 16 Hz, N–H), 8.6 (1H, d, J = 7 Hz, pyC[6]H), 8.2 (4H, m, aromatic), 7.9–7.4 (9H, m, aromatic), 1.6–1.4 (9H, m, Me–H) 1.0–0.8 (6H, m, –CH_2–).

3.6. [$RuCl_2$(p-Cymene)(dpptc-P)] (**7**)

Dpptc (102 mg, 0.326 mmol) and [{RuCl(μ-Cl)(*p*-Cymene)}$_2$] (100 mg, 0.0163 mmol) were weighed into a Schlenk type flask and DCM (5 cm^3) added. The solution was stirred for 10 min and the majority of the solvent removed in vacuo. A red solid was isolated after addition of Et_2O then filtered and washed with further ether (yield: 155 mg, 77%). *Anal.* Calc. $C_{27}H_{28}NOPCl_2Ru$ requires: C, 52.5; H, 4.57; N, 2.27. Found: C, 52.1; H, 3.48; N, 2.19%. ν_{max}/cm^{-1}: 3312, 1665, 1435, 1404, 1091, 288. ^{31}P NMR (109.3 MHz, $CDCl_3$), δ 59.9. ^1H NMR (270 MHZ, $CDCl_3$), 8.0 (5H, m, aromatic) 7.9 (1H, d, J = 14 Hz, N–H), 7.6 (1H, dd, J = 1, 4 Hz), 7.5–7.3 (10H, m, Aromatic), 5.3–5.2 (4H, m, *p*-Cy), 2.5 (1H, m, C–H), 1.9 (3H, s, Me–H), 0.8 (6H, d, J = 7Hz, ^{1}Pr–H).

3.7. [$RhCl_2$(η^5-C_5Me_5)(dpptc-P)] (**8**)

Dpptc (101 mg, 0.326 mmol) and [{RhCl(μ-Cl)(η^5-C_5Me_5)}$_2$] (100 mg,. 0161 mmol) were weighed into a Schlenk type flask and DCM (5 cm^3) added. The solution was stirred for 10 min and the majority of the solvent removed in vacuo. A red solid was isolated after addition of Et_2O then filtered and washed with further ether (yield: 159 mg, 80%). $C_{27.5}H_{30}NSOPCl_3Rh$ requires: C, 49.8; H, 4.56; N, 2.11. Found: C, 50.7; H,

4.17; N, 2.27%. ν_{max}/cm^{-1}: 3299, 1669, 1435, 1097, 246, 231. ^{31}P NMR (109.3 MHz, $CDCl_3$), δ 63.5 ($^1J_{Rh-P}$ = 148 Hz).. ^1H NMR (270 MHZ, $CDCl_3$), 8.2 (1H, d, J = 14 Hz, N–H) 8.1–8.0 (4H, m, aromatic) 7.7 (1H, d, J = 4 Hz, N–H), 7.5–7.3 (7H, m, aromatic), 7.0 (1H, t, J = 8 Hz, aromatic), 1.4 (15H, d, Cp*Me–H).

3.8. [PtClMe(dpptc-P)$_2$] (**9**)

Dpptc (39 mg, 0.12 mmol) and [PtClMe(cod)] (22 mg, 0.06 mmol) were weighed into a Schlenk type flask and DCM (5 cm^3) added. The solution was stirred for 10 min and the majority of the solvent removed in vacuo. A yellow solid was isolated after addition of Et_2O then filtered and washed with further ether (yield: 34 mg, 65%). *Anal.* Calc. $C_{35}H_{31}N_2S_2O_2P_2ClPt$ requires: C, 48.4; H, 3.60; N, 3.23. Found: C, 48.4; H, 3.40; N, 3.17%. ν_{max}/cm^{-1}: 3209, 1671, 1435, 1094. ^{31}P NMR (109.3 MHz, $CDCl_3$), δ 49.1 (J_{P-Pt} = 3220 Hz). ^1H NMR (270 MHZ, $CDCl_3$), 9.7 (2H, t, J_{Pt-H} = 19 Hz, N–H), 7.9 (10H, m, aromatic), 7.6–7.3 (14H, m, aromatic), 7.1 (2H, d, J = 3 Hz, thiophene), 1.5 (3H, s, Me).

3.9. [PdCl($C_9H_{12}N$)(dpptc-P)] (**10**)

Dpptc (79 mg, 0.25 mmol) and [Pd(μ-Cl)($C_9H_{12}N$)]$_2$ (70 mg, 0.13 mmol) were weighed into a Schlenk type flask and DCM (5 cm^3) added. The solution was stirred for 10 min and the majority of the solvent removed in vacuo. A yellow solid was isolated after addition of Et_2O then filtered and washed with further ether (yield: 82 mg, 55%). *Anal.* Calc. $C_{26}H_{26}N_2SOPClPd$ requires: C, 53.0; H, 4.63; N, 4.76. Found: C, 52.3; H, 4.52; N, 4.53%. ν_{max}/cm^{-1}: 3171, 1672, 1438, 1259, 1101, 286. ^{31}P NMR (109.3 MHz, $CDCl_3$), δ 62.4ppm. ^1H NMR (270 MHZ, $CDCl_3$), 10.1 (1 H, bs, N–H) 8.2 (4 H, m, aromatic) 7.2–7.7 (10H, m, aromatic), 7.1 (1H, dd, J = 1, 4 Hz, aromatic) 7.0 (1H, d, J = 6 Hz, aromatic), 6.8 (1H, t, J = 15 Hz, aromatic) 6.4 (2H, m, aromatic) 2.9 (6H, s, N–Me).

3.10. [RuCl(p-Cy)(dpptc-P,O)]BF_4 (**11**)

$AgBF_4$ (22 mg, 0.11 mmol) was added under dark conditions to a solution of [$RuCl_2$(*p*-Cy)(dpptc-*P*)] (70 mg, 0.11 mmol) in DCM (5 cm^3). The solution was stirred overnight and filtered through a celite bed. The majority of the solvent was removed in vacuo. An orange solid was isolated after addition of Et_2O then filtered and washed with further ether (yield: 45 mg, 70%). *Anal.* Calc. $C_{27}H_{28}NRuClOSPBF_4$ requires: C, 48.48; H, 4.21; N, 2.09. Found: C, 48.0; H, 4.07; N, 2.02%. ν_{max}/cm^{-1}: 3216, 1561, 1460, 1433, 1084, 1060, 764. ^{31}P NMR (109.3 MHz, $CDCl_3$) δ 100.0. ^1H NMR (270 MHz, $CDCl_3$) δ 10.1 (1H, s, N–H), 8.3 (1H, d, J = 3Hz, thC[5]H), 8.0 (2H, m, aromatic), 7.7–7.1 (11H, m, aromatic), 5.9 (1H, dd, J = 7 Hz, *p*-Cy-H), 5.6 (1H, dd, J = 6 Hz, *p*-Cy-H), 5.3 (1H, m, *p*-Cy), 5.0 (1H, d, J = 6 Hz, *p*-Cy), 2.6 (1H, m, C–H), 2.1 (3H, s, Me–H), 1.3 (6H, m, Pr^i–H).

3.11. Bis(2,6-diphenylphosphino)picolinamide (bdpppa) (**12**)

Chlorodiphenylphosphine (5.44 cm^3, 30.3 mmol) was added to a solution of 2,6-pyridinedicarboxamide (2.5 g, 30.3 mmol), triethylamine (4.44 cm^3, 32 mmol) and DMAP (370 mg, 3.0 mmol) in thf (100 cm^3) and refluxed overnight. The reaction mixture was filtered to remove a white solid (Et_3NHCl) and washed with thf (50 cm^3). The solvent was removed in vacuo leaving a pale yellow solid. This solid was recrystallised by cooling a concentrated methanol solution at 4 °C overnight (yield: 4.89 g, 61%). *Anal.* Calc. $C_{31.5}H_{26}N_3O_2P_2Cl$ requires: C, 66.0; H, 4.50; N, 7.22. Found: C, 65.7; H, 4.41; N, 7.40%. ν_{max}/cm^{-1}: 3345, 3262, 1665, 1646,, 1588, 1571, 1408, 999. ^{31}P NMR ($CDCl_3$) 21.9. ^1H NMR ($CDCl_3$), 8.42 (2H, d, J = 8 Hz, N–H), 8.00 (3H, m, py), 7.5–7.1 (21H, m, aromatic).

3.12. Bis(2,6-diphenylphosphino)picolinamide disulfide (**13**)

Sulfur (120 mg, 3.7 mmol) was added to a solution of bis(2,6-diphenylphosphino)picolinamide (1 g, 3.7 mmol) in toluene (20 cm^3) and refluxed for 10 min. The solvent was removed in vacuo leaving an off-white solid. This solid was recrystillised by cooling a concentrated toluene solution at 4 °C overnight (yield: 876 mg, 78%). *Anal.* Calc. $C_{31}H_{25}N_3O_2P_2S_2$ requires: C, 63.8; H, 4.32; N, 4.80. Found: C, 64.1; H, 4.46; N, 4.50%. ν_{max}/cm^{-1}: 3360, 1697, 1424, 999. ^{31}P NMR ($CDCl_3$) 55.1 ppm. ^1H NMR ($CDCl_3$), δ 8.9 (2H, d, J = 9 Hz, N–H), 8.3 (2H, d, J = 8 Hz, pyC[3,5]H), 8.1–7.9 (8H, m, aromatic), 7.6–7.4 (10H, m, aromatic), 7.1–7.3 (3H, m, aromatic).

3.13. 2,5-bis(Diphenylphosphino)picolinamide diselenide (**14**)

Selenium (74 mg, 0.9 mmol) was added to a solution of 2,5-bis(Diphenylphosphino)picolinamde (250 mg, 0.47 mmol) in toluene (20 cm^3) and refluxed for 10 min. The solvent was removed in vacuo leaving an off-white solid. This solid was recrystillised by cooling a concentrated toluene solution in a fridge overnight (yield: 263 mg, 81%). *Anal.* Calc. $C_{31}H_{25}N_3O_2P_2Se_2$ requires: C, 53.9; H, 3.64; N, 6.08. Found: C, 53.7; H, 3.24; N, 6.17%. ν_{max}/cm^{-1}: 3256, 1698, 1421, 998. ^{31}P NMR (109.3 MHz, $CDCl_3$), δ 49.6 ($^1J_{P=Se}$ = 795 Hz). ^1H NMR (270 MHz, $CDCl_3$), δ 8.8 (2H, d, J = 9Hz, N–H), 8.3 (1H, d, J = 8Hz, pyC[6]H), 8.0 (8H, m, aromatic), 7.5 (13H, m, aromatic).

3.14. Bis(2,6-diphenylphosphino)picolinamide monosul-fide (**15**)

Sulfur (36 mg, 0.37 mmol) was added to a solution of bis(2,6-diphenylphosphino)picolinamide (600 mg, 0.37 mmol) in toluene (20 cm^3) and refluxed for 10 min. The solvent was removed in vacuo leaving an off-white solid. This solid was recrystallised by cooling a concentrated toluene solution at 4 °C overnight (yield: 415 mg, 65%). *Anal.* Calc. $C_{31}H_{25}N_3O_2P_2S$ requires: C, 65.7; H, 4.46; N, 7.43. Found: C, 67.4; H, 4.47; N, 7.20%. ν_{max}/cm^{-1}: 3345, 3262, 1697, 1665, 1646, 1432, 999. ^{31}P NMR ($CDCl_3$) 56.0 (s, P═S), 21.7 (s, P^{III}). ^1H NMR ($CDCl_3$), δ 8.8 (2H, d, $J = 9$ Hz, N–H), 8.4 (4H, m aromatic), 7.8–8.1 (5H, m, aromatic), 7.0–7.6 (14H, m, aromatic).

3.15. Bis(2,6-diphenylphosphino)picolinamide monosulfide monoselenide (**16**)

Selenium (22 mg, 0.26 mmol) was added to a solution of bis(2,6-diphenylphosphino)picolinamide monosulfide (150 mg, 0.26 mmol) in toluene (10 cm^3) and refluxed for 10 min. The solvent was removed in vacuo leaving an off-white solid. This solid was recrystillised by cooling a concentrated toluene solution at 4 °C overnight (yield: 120 mg, 71%). *Anal.* Calc. $C_{31}H_{25}N_3O_2P_2SSe$ requires: C, 57.7; H, 3.91; N, 6.52. Found: C, 58.8; H, 3.68; N, 6.30%. ν_{max}/cm^{-1}: 3449, 1697, 1421, 997. ^{31}P NMR ($CDCl_3$) 55.0 (s, P═S), 49.7 (s, P═Se, $^1J_{P-Se} = 789$ Hz). ^1H NMR ($CDCl_3$), δ 8.8 (2H, d, $J = 8$ Hz, N–H), 8.3 (2H, dd, $J = 8$, 1 Hz, pyC[3,5]H), 7.9-8.1 (7H, m, aromatic), 7.6–7.4 (14H, m, aromatic).

3.16. [{AuCl}(bdpppa-S)] (**17**)

[AuCl(tht)] (57 mg, 0.17 mmol) and Bis(2,6-diphenylphosphino)picolinamide (100 mg, 0.17 mmol) were added to a round bottomed flask and DCM (5 cm^3) added. The solvent volume was reduced to ~1 cm^3 and the product precipitated with *n*-hexane (20 cm^3). Yield 93 mg, 66%. *Anal.* Calc. $C_{32}H_{26}N_3O_2P_2SAuCl_3$ requires: C, 41.9; H, 2.80; N, 4.58. Found: C, 41.7; H, 2.74; N, 4.69%. ν_{max}/cm^{-1}: 3256, 1697, 1437, 999. ^{31}P NMR ($CDCl_3$) δ(P) 55.0 (s, P═S), 50.2 (s, P–Au). ^1H NMR ($CDCl_3$) δ (H) 10.2 (2H, bs, N–H), 7.0–8.0 (23H, m, aromatic).

3.17. [{AuCl} (bdpppa)] (**18**)

A solution of [AuCl(tht)] (120 mg, 0.37mmol) in DCM (10 cm^3) was dropped into a solution of bis(2,6-diphenylphosphino)picolinamide (200 mg, 0.37 mmol) in DCM (15 cm^3). The solvent volume was reduced to ~1cm^3 and the product precipitated with *n*-hexane (20cm^3). Yield 240 mg, 83%. *Anal.* Calc. $C_{31}H_{25}N_3O_2P_2AuCl$ requires: C, 48.6; H, 3.29; N, 5.49. Found: C, 48.2; H, 2.91; N, 5.48%. ν_{max}/cm^{-1}: 3054, 1698, 1436, 999. ^{31}P NMR ($CDCl_3$) δ(P) 64.3. ^1H NMR ($CDCl_3$) δ(H) 11.0 (2H, bs, N–H), 9.0 (2H, m, aromatic), 7.1–8.1 (21H, m, aromatic).

3.18. [{AuCl}$_2$(bdpppa)] (**19**)

[AuCl(tht)] (84 mg, 0.26 mmol) and bis(2,6-diphenylphosphino)picolinamide (70 mg, 0.13 mmol) were added to a round bottomed flask and DCM (5 cm^3) added. The solvent volume was reduced to ~1 cm^3 and the product precipitated with *n*-hexane (20 cm^3). Yield 125 mg, 95%. *Anal.* Calc. $C_{31}H_{25}N_3O_2P_2Au_2Cl_2$ requires: C, 37.3; H, 2.52; N, 4.21. Found: C, 37.16; H, 2.37; N, 4.12%. ν_{max}/cm^{-1}: 3261, 1697, 1436, 999. ^{31}P NMR ($CDCl_3$) δ(P) 50.0. ^1H NMR ($CDCl_3$) δ(H) 10.2 (2H, d, $J_{H-H} = 16$ Hz, N–H), 8.1 (2H, m, aromatic), 7.9–7.6 (8H, m, aromatic), 7.6–7.1 (13H, m, aromatic).

3.19. [Pd$_2$Cl$_2$(allyl)$_2$(bdpppa-P,P)] (**20**)

Bdpppa (397 mg, 0.7.45 mmol) and [{Pd(μ-Cl)(η^3-C_3H_5)}$_2$] (272 mg, 0.373 mmol) were weighed into a Schlenk type flask and DCM (10 cm^3) added. The solution was stirred for 10 min and the majority of the solvent removed in vacuo. A white solid was isolated after addition of Et_2O then filtered and washed with further ether (yield: 671 mg, 91%). *Anal.* Calc. $C_{37}H_{37}N_3O_2P_2Cl_2Pd_2$ requires: C, 49.3; H, 4.13; N, 4.66. Found: C, 49.23; H, 3.68; N, 4.57%. ν_{max}/cm^{-1}: 3351, 3209, 1698, 1434, 1385, 999. ^{31}P NMR (109.3 MHz, $CDCl_3$), δ 55.1. ^1H NMR (270 MHZ, $CDCl_3$), 10.2 (2H, d, $J = 18$ Hz, N–H), 8.2 (2H, d, $J = 8$ Hz, –pyC[6]H), 8.0–7.8 (10H, m, aromatic), 7.6–7.4 (10H, m, aromatic), 5.5 (4H, quin, $J = 10$ Hz, allyl), 4.7 (4H, t, $J = 7$Hz, allyl), 3.7 (2H, t, $J = 10$ Hz, allyl).

3.20. [Pt$_2$Cl$_2$(allyl)$_2$(bdpppa-P,P)] (**21**)

Bdpppa (59 mg, 0.092 mmol) and [{Pt(μ-Cl)(η^3-C_3H_5)}$_2$] (60 mg, 0.046 mmol) were weighed into a Schlenk type flask and THF (5 cm^3) added. The solution was stirred for 10 min and the majority of the solvent removed in vacuo. A white solid was isolated after addition of Et_2O then filtered and washed with further ether (yield: 43 mg, 43%). *Anal.* Calc. $C_{37}H_{37}N_3O_2P_2Cl_2Pt_2$ requires: C, 41.1; H, 3.46; N, 3.90. Found: C, 40.3; H, 3.59; N, 3.86%. ν_{max}/cm^{-1}: 3360, 3231, 1700, 1434, 1000. ^{31}P NMR (109.3 MHz, $CDCl_3$), δ 51.7 ($^1J_{Pt-P} = 4730$Hz). ^1H NMR (270 MHz, $CDCl_3$), 10.2 (2H, d, $J = 10$ Hz, N–H), 8.2 (2H, d, $J = 8$Hz, pyC[**6]H), 8.0–7.8 (10H, m, aromatic), 7.7–7.3 (12H, m, aromatic), 5.3 (2H, m, allyl), 5.0 (2H, m, allyl), 4.3 (2H, m, allyl), 3.2 (2H, m, allyl), 3.0 (2H, m, allyl), 2.2 (2H, m, allyl).

Table 1
Crystallographic data

	2	5	8	9 · $CHCl_3$	10	14 · $CHCl_3$	21
Formula	$C_{17}H_{14}NO_2PS$	$C_{20}H_{19}NOPSClPd$	$C_{27}H_{29}NOPSCl_2Rh$	$C_{36}H_{32}N_2OP_2S_2ClPt$	$C_{26}H_{26}N_2OPPSClPd$	$C_{32}H_{26}N_3O_2P_2Cl_3Se_2$	$C_{37}H_{35}N_2O_2P_2Cl_2Pt_2$
M	327.32	498.24	620.35	987.59	587.37	810.77	1076.7
Crystal system	monoclinic	monoclinic	orthorhombic	triclinic	triclinic	triclinic	monoclinic
Space group	$P2_1/c$	$P2_1/c$	$P2_12_12_1$	$P\bar{1}$	$P\bar{1}$	$P\bar{1}$	$P2_1/n$
a (Å)	9.617(2)	9.2350(18)	13.616(2)	12.256(1)	10.043(2)	9.617(2)	15.9450(9)
b (Å)	16.571(3)	12.097(2)	11.8190(17)	12.286(1)	10.325(2)	11.620(2)	9.0240(5)
c (Å)	9.877(2)	18.302(4)	16.918(2)	13.613(1)	13.541(3)	15.679(3)	26.5195(19)
α (°)				68.135(1)	87.629(4)	87.463(3)	
β (°)	94.111(4)	100.309(4)		77.150(1)	69.956(3)	74.728(3)	98.818(1)
γ (°)				82.407(1)	70.801(3)	82.062(4	
U (Å^3)	1570.0(6))	2011.5(7)	2722.7(7)	1851.9(3)	1241.7(4)	1673.9(6)	3770.7(4)
Z	4	4	4	2	2	2	4
ρ_{calcd} (g/cm^3)	1.385	1.632	1.513	1.771	1.571	1.609	1.897
μ (mm^{-1})	0.314	1.248	0.980	4.313	1.026	2.579	7.675
Reflections measured	7598	8199	11848	9348	6239	8493	18435
Independent reflections	2219	2780	3864	5256	3522	4727	5409
Final R_1, wR_2 [$I > 2\sigma(I)$]	0.0472, 0.1120	0.0449, 0.1114	0.0235, 0.0557	0.0309, 0.0714	0.0382, 0.0961	0.0393, 0.1223	0.0359, 0.0750

4. Crystallography

Details of the structure determination are given in Table 1. X-ray diffraction measurements were made with graphite-monochromated Mo Kα X-radiation using a Bruker SMART diffractometer. Intensity data were collected using ω/ϕ steps accumulating area detector frames spanning a hemisphere of reciprocal space for all structures. All data were corrected for Lorentz, polarisation and long-term intensity fluctuations. Absorption effects were corrected on the basis of multiple equivalent reflections or by semi-empirical methods. Structures were solved by direct methods and refined by full-matrix least-squares against F^2 (SHELXTL). Hydrogen atoms were assigned isotropic displacement parameters and were constrained to idealised geometries. **8** gave a Flack parameter of 0.01(3). Refinements converged to residuals given in Table 1. All calculations were made with SHELXTL [15].

5. Supplementary material

Atomic coordinates, thermal parameters and bond lengths and angles have been deposited at the Cambridge Crystallographic Data Centre (CCDC Nos. 243091–243097). Any request to CCDC, 12 Union Road, Cambridge, CB2 1EZ, UK (fax: +44 1223 336033; e-mail: deposit@ccdc.cam.ac.uk; http://www.ccdc.cam.ac.uk) for this material should quote the full literature citation and the reference number.

References

[1] S.M. Aucott, A.M.Z. Slawin, H.L. Milton, M.V. Wheatley, J.D. Woollins, Phosph. Sulf. Sili. 179 (2004) 993.
[2] H.L. Milton, M.V. Wheatley, A.M.Z. Slawin, J.D. Woollins, Polyhedron, submitted.
[3] O. Clot, M.O. Wolf, G.P.A. Yap, B.O. Patrick, J. Chem. Soc., Dalton Trans. (2000) 2729.
[4] F.E. Wood, J. Hvoslef, H. Hope, A.L. Batch, Inorg. Chem. 23 (1984) 4309.
[5] P. Giannoccaro, G. Vasapollo, A. Sacco, J. Chem. Soc., Chem. Commun. (1980) 1136.
[6] W. Keim, Chem. Ing. Techn. 56 (1984) 850.
[7] R. Uson, A. Laguna, M. Laguna, Inorg. Synth. 26 (1989) 85.
[8] D. Drew, J.R. Doyle, Inorg. Synth. 28 (1991) 346.
[9] J.X. McDermott, J.F. White, G.M. Whiteside, J. Am. Chem. Soc. 60 (1976) 6521.
[10] H.C. Clark, L.E. Manzer, J. Organomet. Chem. 59 (1973) 411.
[11] W. Baratta, P.S. Pregosin, Inorg. Chem. Acta 209 (1993) 85.
[12] C. White, A. Yates, P.M. Maitlis, Inorg. Synth. 29 (1992) 228.
[13] M.A. Bennett, T.N. Huang, T.W. Matheson, A.R. Smith, Inorg. Synth. 21 (1982) 74.
[14] A.L. Balch, L.S. Benner, Inorg. Synth. 28 (1990) 340.
[15] SHELXTL 6.01, Bruker AXS, Madison, WI, 2001.

Available online at www.sciencedirect.com
SCIENCE DIRECT®
Polyhedron 23 (2004) 2587–2593
POLYHEDRON
www.elsevier.com/locate/poly

Synthesis, characterization and crystal structure of *catena*-bis(1,10-phenanthroline)-μ-chloranilatocadmium(II): a zig-zag polymer based on eight-coordinated square antiprismatic units

Adonis Michaelides, Christos D. Papadimitriou, John C. Plakatouras *, Stavroula Skoulika, Panagiotis G. Veltsistas *

Department of Chemistry, University of Ioannina, 451 10 Ioannina, Greece

Received 29 June 2004; accepted 22 September 2004
Available online 14 October 2004

Abstract

$[Cd(phen)_2(CA)]_n$ (**I**, where phen is 1,10-phenanthroline and CA^{2-} is the dianion of 3,6-dichloro-2,5-dihydroxy-1,4-benzoquinone) has been synthesized and its crystal structure has been determined by single-crystal X-ray diffraction at room temperature. The crystal of **I** is built from infinite chains of chloranilate-bridged cadmium(II) leading to a zig-zag structure, with the phenanthroline ligands being stacked between the chains. These interactions assist the formation of a closely packed 3D structure. The coordination environment of cadmium(II) – very scarce in its chemistry – is square antiprismatic. The polymer was also characterized with spectroscopic (IR, Raman, DRS) and thermogravimetric (TG, DTA) techniques.
© 2004 Elsevier Ltd. All rights reserved.

Keywords: Cadmium(II); Chloranilate anions; Phenanthroline; Square antiprism; Crystal structures; Chain polymers

1. Introduction

The synthesis of coordination polymers is one of the most essential elements in advancing materials chemistry. In general, it remains more of an art than a science, since most new compounds have been synthesized through self-assembly routes and not from controlled synthesis. Research on that area is directed towards the utilization of ligands that maintain their structure in solution and possess more than one well-known coordination sites [1]. Building metal complex – based polymers is an important step to create not only a system to perform optical, electronic and magnetic functions, but also an intercalation system for ion- or molecule-exchange, absorption and catalytic properties (see for example [2,3]).

Substituted dihydroxy benzoquinones, and especially chloranilic acid (CA), hold an important place in the family of bridging ligands [4–15]. This is due to their two allyl systems connected by C–C single bonds, with four partially negatively charged oxygen atoms [16] (Scheme 1). Thus, the chelating effect in addition to the bridging capability of the chloranilate dianion allows the formation of robust frameworks. In addition, the polyoxocarbon molecules have frontier orbitals with energies comparable to those of the transition metal ions and the nature of the reduced and oxidized species depends on the metal ions and the coordination environment [12]. The delocalized π system associated with its planar geometry can provide [9,13] interesting and possibly useful electronic communication between suitable metal centers.

* Corresponding authors. Tel.: +30 26510 98417; fax: +30 26510 44831.
E-mail address: iplakatu@cc.uoi.gr (J.C. Plakatouras).

0277-5387/$ - see front matter © 2004 Elsevier Ltd. All rights reserved.
doi:10.1016/j.poly.2004.09.013

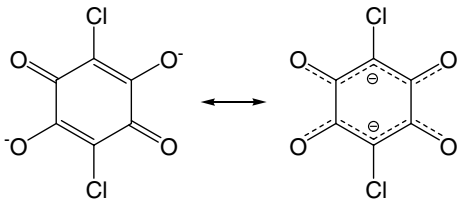

Scheme 1.

Our continuous interest in chloranilate chemistry is stimulated by both its analytical applications and coordination properties. Chloranilic acid can be used for the determination of Mg(II) with FAAS [17], for the construction of electrode membranes [18], and the kinetic determinations of formaldehyde [19] and Mn(II) [20]. Our involvement in the coordination chemistry of the chloranilates have produced several monomeric [21–23] and polymeric [11,24] coordination compounds with interesting structural features. For example, in the case of hydrated sodium chloranilate [11], the ligand can bind four sodium cations using all of its oxygen atoms and one of the organic chlorine atoms, while the number of sodium cations bound to CA is reduced to three when 1,10-phenanthroline is used to block sodium coordination sites.

In the present paper, we present the synthesis, the crystal structure and the spectroscopic and thermal characterization of the chain compound $[Cd(phen)_2(CA)]_n$. The structure is based on rare square antiprismatic CdN_4O_4 polyhedra connected through bis-chelating chloranilato bridges. Stacking interactions provide a 3D supramolecular architecture.

2. Experimental

2.1. Materials

All manipulations were carried out under aerobic conditions. $Cd(CH_3COO)_2 \cdot 2H_2O$ was purchased from Merck, sodium silicate solution, KBr, $BaSO_4$ and organic reagents were purchased from Aldrich. Solvents were of analytical grade and purchased from Lab-Scan Chemical Co.

2.2. Instrumentation

C, H and N analyses were conducted by the University of Ioannina, Greece, Microanalytical Service. IR (4000–370 cm^{-1}) and far-IR (600–30 cm^{-1}) spectra were recorded on a Perkin–Elmer Spectrum GX FT IR System with samples prepared as KBr and polyethylene pellets, respectively. The Raman spectrum was recorded on a SPEX Model 1403 0.85 m double spectrometer, equipped with a Spectra Physics Model 2020 argon ion laser; a spinning cell sample holder was used to avoid thermal degradation of the compound. The excitation was provided by the 514.5 nm line with a laser power of 100 mW, at a resolution of 2 cm^{-1} and signal recording was done using photon counting with an integration time of 1 s. UV/Vis diffuse reflectance spectra were recorded on a Shimadzu UV-2401 PC spectrophotometer with a Shimadzu integration sphere. Thermal studies were carried out on a Shimadzu DTG-60 simultaneous DTA-TG apparatus, under N_2 or forced air flow (50 cm^3 min^{-1}) with a heating rate of 5 °C min^{-1}. Sample sizes were about 5 mg. X-ray powder diffraction patterns were recorded on a Siemens (now Bruker) D8 ADVANCE diffractometer.

2.3. Preparation of the compound

$Cd(CH_3COO)_2 \cdot 2H_2O$ (0.50 g, 1.88 mmol) was dissolved in H_2O (20 cm^3). To this, a solution of 1,10-phenanthroline (0.676 g, 3.75 mmol) in ethanol (10 cm^3) was added. A white solid precipitated readily and dissolved after the addition of 2 cm^3 of glacial acetic acid. Separately, chloranilic acid (0.393 g, 1.88 mmol) was dissolved in water and the pH was adjusted to 7 with an aqueous solution (ca. 0.5 g in 20 cm^3 H_2O) of tris(hydroxymethyl)amino methane. The resulting solution was added to the metal solution to give a dark purple mixture. The mixture was refluxed for 2 h. The dark purple solid which separated upon cooling was filtered, washed with ethanol (3×10 cm^3) and diethylether (3×10 cm^3) and dried under vacuum over silica gel. Yield: 0.97 g (76% based on cadmium).

Slow reaction of an aqueous cadmium acetate solution (0.1 M) with an aqueous solution containing sodium chloranilate (0.05 M) and 1,10-phenanthroline (0.05 M) through a sodium silicate gel (formed after titration of 2 M HNO_3 with a ca. 2 M sodium silicate up to pH $\approx$ 5.3) in a U tube led to large purple crystals suitable for X-ray structural studies.

Anal. Calc. for $C_{30}H_{16}CdCl_2N_4O_4$: C, 53.00; H, 2.38; N, 8.24. Found: C, 52.71; H, 2.63; N, 8.39%. Selected IR (KBr pellet) and far-IR (polyethylene pellet) data (cm^{-1}): 3077w, 3065w, 1624w, 1513vs, 1424ms, 1374m, 1275m, 1207w, 1099w, 1047w, 988w, 841ms, 770w, 728m, 634w, 589w, 573m, 434m, 417m, 377w, 272m, 230s, 215msh, 178w, 156s, 145s, 127s. Selected Raman data (cm^{-1}): 3076w, 1615w, 1521m, 1460s, 1427m, 1346s, 1305s, 1051m, 725s, 586s, 566w, 423m, 312w, 123m. Electronic spectrum (DRS, $BaSO_4$ solution) (nm): 520, 325.

2.4. X-ray crystallography

A suitable single crystal of **I** was selected under a polarizing microscope, cleaned from the gel residues

and glued to a thin glass fibre with cyanoacrylate (super glue) adhesive. X-ray diffraction intensities were collected at room temperature on a Siemens P4 diffractometer employing graphite monochromated Mo Kα radiation, $\lambda = 0.71073$ Å. The WINGX environment was used for the solution and refinement of the structure [25]. The structure was solved by direct methods (SIR-97) [26] and refined by full-matrix least-squares techniques on F^2 (SHELXL-97) [27]. All non-hydrogen atoms were refined anisotropically. All H atoms were located in a difference Fourier map but were introduced in idealized positions and treated as riding on the parent hydrogen atoms. Sources of atomic scattering factors were as in SHELXL-97. Simulated XRPD patterns were produced with PLATON [28].

The details of the final refinements are given in Table 1. Selected bond distances and angles for **I** are given in Table 2.

3. Results and discussion

3.1. Synthesis of the compound

The title compound was initially synthesized in the form of single crystals from slow reaction, through silica gel, of a solution of cadmium(II) acetate with a solution of sodium chloranilate and 1,10-phenanthroline (phen).

Table 1
Crystal data and structure refinement parameters for **I**, $[Cd(CA)(phen)_2]_n$

Empirical formula	$C_{30}H_{16}CdCl_2N_4O_4$
Formula mass	679.77
Crystal system	triclinic
Space group	$P\bar{1}$
a (Å)	9.317(1)
b (Å)	10.773(1)
c (Å)	14.761(2)
α (°)	87.90(1)
β (°)	72.84(1)
γ (°)	69.79(1)
V (Å^3)	1325.0(3)
Z	2
ρ_{calc} (g cm^{-3})	1.704
λ (Mo Kα) (Å)	0.71073
μ (mm^{-1})	1.072
θ Range (°)	2.02–25.00
Total data collected	5573
Index ranges	$-10 \leqslant h \leqslant 11$, $-12 \leqslant k \leqslant 12$, $0 \leqslant l \leqslant 17$
Unique data	4666
Observed data [$I > 2\sigma(I)$]	3346
Refinement method	full-matrix least-squares on F^2
R indices [$I > 2\sigma(I)$]	$R_1 = 0.0444$, $wR_2 = 0.0811$
R indices (all data)	$R_1 = 0.0842$, $wR_2 = 0.0940$[a]
Goodness-of-fit (S)	1.029
Number of variables	370
Largest difference map peak and hole e Å^{-3}	0.534 and −0.661

[a] $w = 1/[\sigma^2(F_o^2) + (0.0274P)^2P]$, where $P = (\max(F_o^2, 0) + 2F_c^2)/3$.

Table 2
Selected bond distances (Å) and angles (°) in **I**, $[Cd(CA)(phen)_2]_n$

Bond distances			
Cd–O(1)	2.415(3)	Cd–O(2)	2.350(3)
Cd–O(3)	2.442(3)	Cd–O(4)	2.386(3)
Cd–N(1A)	2.480(4)	Cd–N(2A)	2.469(4)
Cd–N(1B)	2.470(4)	Cd–N(2B)	2.476(4)
Cl(1)–C(3)	1.738(5)	Cl(2)–C(6)	1.733(5)
O(1)–C(1)	1.248(5)	O(2)–C(2)	1.247(5)
O(3)–C(5)	1.258(5)	C(1)–C(2)	1.543(7)
O(4)–C(4)	1.243(5)	C(4)–C(5)	1.539(7)
C(2)–C(3)	1.391(6)	C(5)–C(6)	1.392(6)
C(1)–C(3)[a]	1.402(6)	C(4)–C(6)[b]	1.389(6)
Cd–Cd[a]	8.61(1)	Cd–Cd[b]	8.69(1)
Bond angles			
O(2)–Cd–O(4)	146.62(12)	O(2)–Cd–O(1)	68.64(11)
O(4)–Cd–O(1)	142.66(12)	O(2)–Cd–O(3)	87.70(11)
O(4)–Cd–O(3)	67.47(11)	O(1)–Cd–O(3)	146.62(11)
O(2)–Cd–N(2A)	80.60(14)	O(4)–Cd–N(2A)	112.52(13)
O(1)–Cd–N(2A)	77.01(13)	O(3)–Cd–N(2A)	76.11(13)
O(2)–Cd–N(1B)	108.44(13)	O(4)–Cd–N(1B)	77.07(12)
O(1)–Cd–N(1B)	78.31(13)	O(3)–Cd–N(1B)	133.21(12)
N(2A)–Cd–N(1B)	148.22(14)	O(2)–Cd–N(2B)	75.83(13)
O(4)–Cd–N(2B)	76.73(13)	O(1)–Cd–N(2B)	117.65(13)
O(3)–Cd–N(2B)	76.15(13)	N(2A)–Cd–N(2B)	144.02(15)
N(1B)–Cd–N(2B)	66.54(15)	O(2)–Cd–N(1A)	138.64(12)
O(4)–Cd–N(1A)	72.79(13)	O(1)–Cd–N(1A)	79.03(12)
O(3)–Cd–N(1A)	107.90(13)	N(2A)–Cd–N(1A)	67.21(15)
N(1B)–Cd–N(1A)	88.70(14)	N(2B)–Cd–N(1A)	144.33(15)
C(1)–C(2)–C(3)	118.1(4)	C(4)–C(5)–C(6)	117.7(4)
C(2)–C(3)–C(1)[a]	123.5(5)	C(2)–C(1)–C(3)[a]	118.3(4)
C(5)–C(6)–C(4)[b]	123.7(4)	C(5)–C(4)–C(6)[b]	118.5(4)
c(2)-c(3)-cl(1)	118.1(4)	C(1)[a]–C(3)–Cl(1)	118.4(4)
C(5)–C(6)–Cl(2)	118.8(4)	C(4)[b]–C(6)–Cl(2)	117.5(4)
O(2)–C(2)–C(3)	124.9(5)	O(3)–C(5)–C(6)	125.4(4)
O(2)–C(2)–C(1)	117.0(4)	O(3)–C(5)–C(4)	116.9(4)
O(1)–C(1)–C(3)[a]	124.0(5)	O(4)–C(4)–C(6)[b]	124.1(5)
O(1)–C(1)–C(2)	117.6(4)	O(4)–C(4)–C(5)	117.4(4)
Cd[a]–Cd–Cd[b]	152.1(2)		

[a] $-x, 1-y, 1-z$.
[b] $1-x, -y, -z$.

The preparation of the compound in larger quantities was proved to be difficult.

When we attempted to prepare the polymer by the direct reaction of its components in various molar ratios and different addition sequences, we systematically isolated solids, which had similar IR spectra with the above mentioned crystals but their XRPD patterns revealed contamination with a second, unknown phase (different from that calculated from the single crystal data). Microanalyses showed that the molar ratio of Cd(II):phen:CA was neither 1:1:1 nor 1:2:1 but, depending on the synthesis, between 1:1.3:1 and 1:1.8:1. Several attempts to synthesize the polymer were made, including use of different counter ions, reaction solvents, temperature, and molar ratios, but reasonably pure products (i.e. having IR spectrum, X-ray powder pattern and stoichiometry with formula $[Cd(CA)(phen)_2]_n$) were isolated only in the case described in Section 2. The XRPD patterns [simulated (for the single crystal) and

experimental (for the separately prepared bulk sample)] are presented in Fig. 1.

We believe that this behavior can be explained in terms of the kinetic and thermodynamic stability of the two products, $[Cd(CA)(phen)]_n$ and $[Cd(CA)(phen)_2]_n$, probably involved in the reaction mixture. Bearing in mind that chloranilate will act as bis-chelating bridging ligand, when in lower concentration than the metal, the 1D polymer $[Cd(CA)(phen)]_n$ would be the initial product, according to Eq. (I). This product must be kinetically stable.

$$n\mathrm{Cd}^{2+} + n\mathrm{CA}^{2-} + n\mathrm{phen} \rightarrow [\mathrm{Cd(CA)(phen)}]_n \qquad \text{(I)}$$

The next, most obvious, step in a successive addition scenario is the addition of the second phen molecule to the coordination sphere of cadmium, which should begin almost simultaneously, and lead to the formation of the thermodynamically stable product as shown in the following equation.

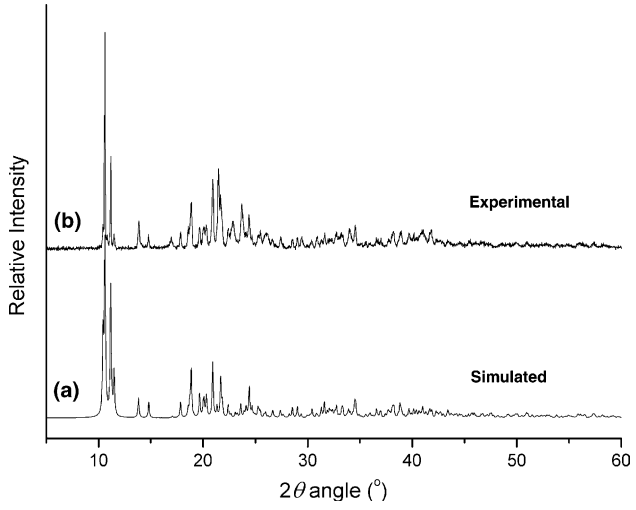

Fig. 1. Experimental (b) and simulated (a) powder XRD patterns for **I**.

$$[Cd(CA)(phen)]_n + n\mathrm{phen} \rightarrow [Cd(CA)(phen)_2]_n \qquad \text{(II)}$$

Though speculative, the mechanism above is supported by two experimental observations: (a) the microanalyses of the insoluble products suggested formulations $[Cd(CA)(phen)_x]$, where $1 < x < 2$ and (b) only after extended heating of the reaction mixture was the desired product isolated.

3.2. Description of the structure

An ORTEP drawing of the asymmetric unit of $[Cd(CA)(phen)_2]_n$ is presented in Fig. 2(a). Selected bond distances (Å) and angles (°) with their standard deviations are presented in Table 2.

The crystal structure of the polymer is built from zigzag chains (type I chain structure), extended along the $[-1, 1, 1]$ direction, accompanied by by stacking interactions (Fig. 3).

The asymmetric unit consists of one cadmium atom, two 1,10-phenanthroline molecules and halves of two different chloranilato ligands (Fig. 2(a)). The coordination sphere of the metal is formed by four nitrogen atoms belonging to two chelating phen ligands, and four oxygen atoms belonging to two different bis-chelating bridging chloranilato ligands.

There are several examples of eight-coordinate cadmium complexes in the literature. They can be separated in two different groups. Those with multidentate ligands (see for example [30–32]) and those with bidentate chelating ligands with small bite angles (see for example [33–35]). To the best of our knowledge the only examples of eight-coordinated Cd(II) complexes with four five-membered chelate rings belong to the family of the oxalate polymers [36–39].

The geometry about Cd(II) can be described as distorted square antiprismatic. As indicated by Drew [40], the values of φ angles, which assess the planarity of the two trapezoids formed in an eight-coordination

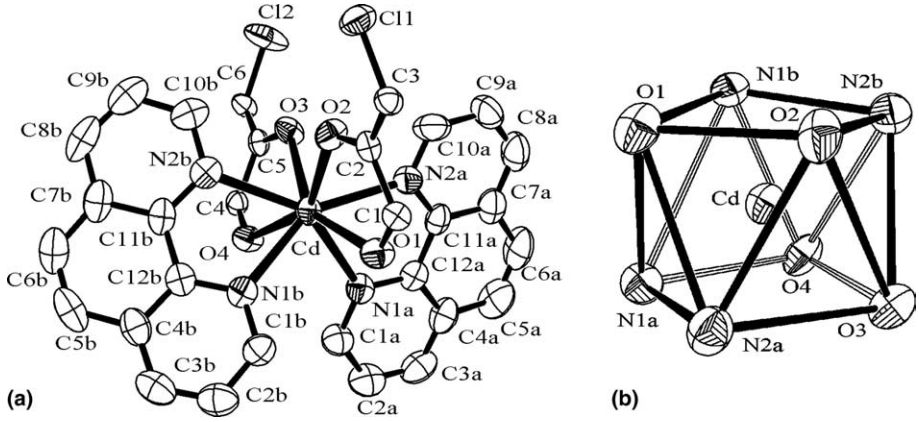

Fig. 2. (a) ORTEP [29] plot of the asymmetric unit of $[Cd(CA)(phen)_2]_n$ (**I**) including the labelling scheme. Hydrogen atoms have been omitted for clarity. (b) The coordination polyhedron about Cd, defined as square antiprism.

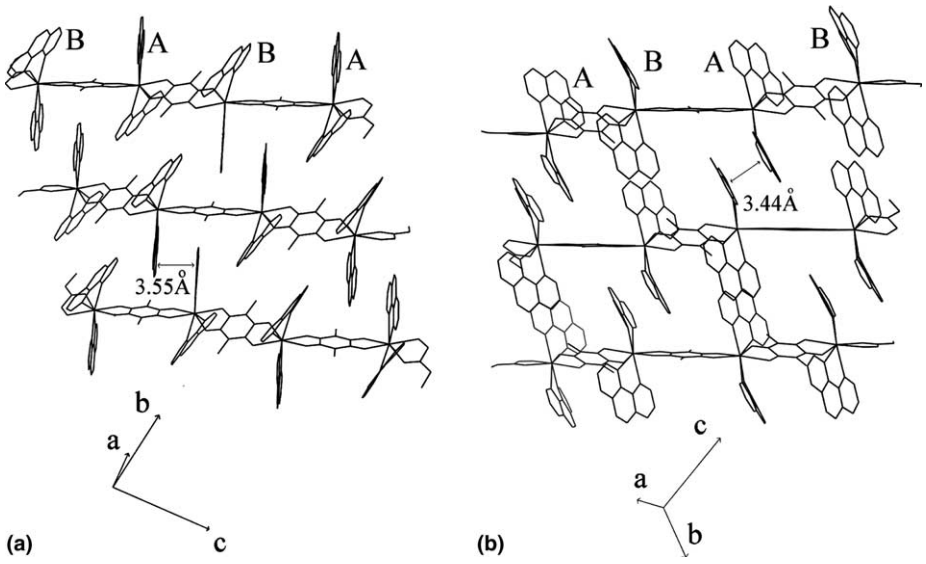

Fig. 3. A part of the 2D sheet (a) formed by stacking interactions of phenanthroline (phen A) molecules. The second phenanthroline (B) forms stacking interactions with the corresponding phen of a neighboring sheet. By this interaction a second sheet intersecting the previous is formed (b). As a result a 3D structure is obtained.

environment, are a good test for the determination of the shape of the coordination polyhedron. The φ angles, calculated by using the hard sphere model (HSM) shape characteristics, are 0.0° and 24.5° for the ideal dodecahedron and the ideal square antiprism, respectively. In our case, the φ values are 26.78° and 29.53°, which indicates that the coordination polyhedron is best described as a distorted square antiprism. The coordination polyhedron is presented in Fig. 2(b). The centroids of the CA moieties are located on inversion centres.

The Cd–N bond distances span the range 2.470(4)–2.481(4) Å and they can be considered long, related to other Cd–phen complexes. A survey of the Cambridge Structural Database shows that there are ca. 40 crystal structures of Cd–phen complexes. None of them has eight-coordinated cadmium, probably due to steric effects. Phen is too large and two of them cannot be easily accommodated in an eight-coordination environment unless other stabilizing interactions (π–π stacking for example) are involved, as well. The coordination number itself can explain the long length of the Cd–N bonds.

The two CA ligands, in the coordination sphere of Cd, are bonded in a slightly different fashion. There are four different Cd–O bond distances in the range 2.350(3)–2.443(3) Å. These distances are well in the range observed in the literature [41,42]. This asymmetry, in addition to the square antiprismatic geometry of course, leads to the formation of the zig-zag chain. As far as the C–O distances are concerned, both of the chloranilates chelate Cd symmetrically (C(1)–O(1), C(2)–O(2), 1.246(5) Å, C(4)–O(4), 1.244(5) Å, C(5)–O(3), 1.256(5) Å). The differences are very small compared with the associated su's. The C–O bond characteristics are similar to those reported for the free chloranilate dianion [43]. The similarity between the C–O bonds is reflected to the C–C bond lengths, connecting the two parts of the chloranilato ligand, as shown in Scheme 1(b). In both chloranilates the distances of the C–C bonds connecting the negatively charged sites are longer than the rest C–C distances (mean values; 1.542, 1.394 Å, respectively). These differences are systematic and suggest extended conjugation between halves of the CA ligands.

Both phen moieties are involved in stacking interactions (Fig. 3) which lead to a 3D supramolecular architecture. Phen A (Fig. 3(a)) utilizes the central ring for π–π interaction with the same ring of a parallel chain. The distance between the least square planes is 3.55 Å, and the offset of the centroids is 0.50 Å. That zipper-like interaction leads to the formation of 2D sheets, which interact with each other through the stacking of the B phen molecule (Fig. 3(b)). Two rings, the central and one external, are involved in this interaction. The distance of the least square planes is 3.44 Å, and the offset of the two ring centroids is 1.36 Å.

3.3. Thermal stability and spectroscopic characterization

The polymer is stable up to 315 °C, when heated in nitrogen atmosphere. A rather complicated decomposition process begins after that temperature, which involves at least four different exothermic steps as shown by the DTA curve. The decomposition proceeds up to 800 °C, where no residue remains. This is probably due to the reduction of Cd(II), from the organic fragments produced by the complex decomposition, and

its subsequent sublimation. When a sample is heated under forced air, the decomposition begins at 275 °C. The decomposition is rather fast, the final plateau is reached at 345 °C and corresponds good to CdO (found 17.5%, calculated 18.9%).

The bands present below 1600 cm^{-1} in the vibrational spectra of the polymer (IR: 1514, 1374; Raman: 1521, 1346 cm^{-1}) are characteristic of symmetry close to D_{2h} for the CA^{2-} ligand, since any other bands above 1600 cm^{-1} are very weak. This is in agreement with its structure. The bands at 434 and 417 cm^{-1} in the far-IR spectrum are assignable to the Cd–O stretches while the Cd–N stretching vibrations appear at 230 and 215 cm^{-1}.

The electronic spectrum of the complex is dominated by two broad bands centered at 520 and 325 nm. These bands are most likely associated with π–π* transitions and their position is in agreement with delocalization of the negative charge over the allyl system. The band at higher energy probably overlaps with phen absorption [44].

4. Concluding remarks

In this work, we have synthesized and characterized a new zig-zag polymer using as bridging ligand the CA^{2-} dianion. In our case CA^{2-} is planar and the charge is delocalized over the two allyl systems presented in Scheme 1(b). Phen forms pairwise offset face-to-face stacking motifs that lead to a 3D supramolecular architecture. We have also described physicochemical and spectroscopic characteristics.

Synthetic attempts to prepare and characterize cadmium(II) chloranilate adducts with Lewis bases other than 1,10-phenanthroline are in progress.

5. Supplementary material

Crystallographic data (excluding structure factors) for the structure reported in this paper have been deposited with the Cambridge Crystallographic Data Centre as supplementary publication No. CCDC 235812. Copies of the data can be obtained free of charge on application to CCDC, 12 Union Road, Cambridge CB2 1EZ, UK (fax: +44 1223 336 033; e-mail: deposit@ccdc.cam.ac.uk, or on the web: http://www.ccdc.cam.ac.uk).

Acknowledgments

The authors thank the Horizontal Laboratory Network of the University of Ioannina for the X-ray (powder and single crystal) measurements. One of the referees is also acknowledged for his helpful comments.

References

[1] O.M. Yaghi, M. O'Keefe, N.W. Ockwig, H.K. Chae, M. Eddaoudi, J.U. Kim, Nature 423 (2003) 705, and references cited therein.
[2] P. Delhaes, M. Drillon (Eds.), Organic and Inorganic Low Dimensional Crystalline Materials, Reidel, Dordrecht, 1987.
[3] D.W. Bruce, D. O'Hare (Eds.), Inorganic Materials, Wiley, New York, 1992.
[4] C.G. Pierpont, L.C. Francesconi, D.N. Hendrickson, Inorg. Chem. 16 (1977) 2367.
[5] P.E. Riley, S.F. Haddad, K.N. Raymond, Inorg. Chem. 22 (1983) 3090.
[6] M.A. Calvo, A.M. Manotti Lanfredi, L.A. Oro, M.T. Pinillos, C. Tejel, A. Tiripicchio, F. Ugozzoli, Inorg. Chem. 32 (1993) 1147.
[7] S. Kawata, S. Kitagawa, M. Kondo, I. Furuchi, M. Munakata, Angew. Chem., Int. Ed. Engl. 33 (1994) 1759.
[8] S. Kawata, S. Kitagawa, H. Kumagai, C. Kudo, H. Kamesaki, T. Ishiyama, R. Suzuki, M. Kondo, M. Katada, Inorg. Chem. 35 (1996) 4449.
[9] M.D. Ward, Inorg. Chem. 35 (1996) 1712.
[10] L.-M. Zheng, H.W. Schmalle, R. Huber, S. Decurtins, Polyhedron 15 (1996) 4399.
[11] C. Papadimitriou, P. Veltsistas, J. Marek, J. Novosad, A.M.Z. Slawin, J.D. Woollins, Inorg. Chem. Commun. 1 (1998) 418.
[12] S. Kawata, S. Kitagawa, H. Kumagai, T. Ishiyama, K. Honda, H. Tobita, K. Adachi, M. Katada, Chem. Mater. 10 (1998) 3902.
[13] B.F. Abrahams, K.D. Lu, B. Moubaraki, K.S. Murray, R. Robson, J. Chem. Soc., Dalton Trans. (2000) 1793.
[14] S. Kitagawa, S. Kawata, Coord. Chem. Rev. 224 (2002) 11.
[15] M. Kawahara, Md.K. Kabir, K. Yamada, K. Adachi, H. Kumagai, Y. Narumi, K. Kindo, S. Kitagawa, S. Kawata, Inorg. Chem. 43 (2004) 92.
[16] S. Kulpe, J. Prakt. Chem. 316 (1974) 353.
[17] D.L. Giokas, E.K. Paleologos, P.G. Veltsistas, M.I. Karayannis, Talanta 56 (2002) 415.
[18] P.G. Veltsistas, M.I. Karayannis, Analyst 112 (1987) 1579.
[19] P.G. Veltsistas, M.I. Karayannis, Quim. Anal. 15 (1996) 334.
[20] P.G. Veltsistas, M.I. Karayannis, Analyst 115 (1990) 741.
[21] H. Burzlaff, J. Lange, R. Spengler, M.I. Karayannis, P.G. Veltsistas, Acta Crystallogr., Sect. C 51 (1995) 190.
[22] A. Bram, G. Bruederl, H. Burzlaff, J. Lange, W. Rothammel, R. Spengler, M.I. Karayannis, P.G. Veltsistas, Acta Crystallogr., Sect. C 50 (1994) 178.
[23] R. Spengler, J. Lange, H. Zimmerman, H. Burzlaff, P.G. Veltsistas, M.I. Karayannis, Acta Crystallogr., Sect. B 51 (1995) 174.
[24] P. Veltsistas, C. Papadimitriou, Y. Arabatzis, A.M.Z. Slawin, J.D. Woolins, Phosphorus Sulfur 125 (1997) 407.
[25] L.J. Farrugia, J. Appl. Crystallogr. 32 (1999) 837.
[26] A. Altomare, M.C. Burla, M. Camalli, G.L. Cascarano, C. Giacovazzo, A. Guagliardi, A.G.G. Moliterni, G. Polidori, R. Spagna, SIR-97, J. Appl. Crystallogr. 32 (1999) 115.
[27] G.M. Sheldrick, SHELX97: Programs for Crystal Structure Analysis (Release 97-2), Institüt für Anorganische Chemie der Universität, Tammanstrasse 4, D-3400 Göttingen, Germany, 1998.
[28] (a) A.L. Spek, Acta Crystallogr., Sect. A 34 (1990) 46; (b) A.L. Spek, J. Appl. Crystallogr. 36 (2003) 7.
[29] L.J. Farrugia, ORTEP3 for Windows, J. Appl. Crystallogr. 30 (1997) 565.
[30] C.B. Smith, A.K.W. Stephens, K.S. Wallwork, S.F. Lincoln, M.R. Taylor, K.P. Wainright, Inorg. Chem. 41 (2002) 1093.
[31] A. Jantti, M. Wagner, R. Suontamo, E. Kolehmainen, K. Rissannen, Eur. J. Inorg. Chem. (1998) 1555.
[32] H. Zhang, X. Wang, H. Zhu, W. Xiao, B.K. Teo, J. Am. Chem. Soc. 119 (1999) 5463.

[33] N.W. Alcock, E.H. Curzon, P. Moore, C. Pierpoint, J. Chem. Soc., Dalton Trans. (1984) 605.
[34] F. Hueso-Urena, S.B. Jimenez-Pulido, M.N. Moreno-Carretero, M. Quiros-Olozabal, J.M. Salas-Peregrin, Inorg. Chim. Acta 277 (1998) 103.
[35] Z.-F. Chen, R.-G. Xiong, B.F. Abrahams, X.-Z. You, C.-M. Che, J. Chem. Soc., Dalton Trans. (2001) 2453.
[36] P.A. Prasad, S. Neeraj, S. Natarajan, C.N.R. Rao, Chem. Commun. (2000) 1251.
[37] E. Jeanneau, N. Audebrand, J.-P. Auffredic, D. Louer, J. Mater. Chem. 11 (2001) 2545.
[38] E. Jeanneau, N. Audebrand, D. Louer, Chem. Mater. 14 (2002) 1187.
[39] R. Vaidhyanathan, S. Natarajan, C.N.R. Rao, J. Solid State Chem. 162 (2001) 150.
[40] M.G.B. Drew, Coord. Chem. Rev. 24 (1977) 179.
[41] A. Tadjarodi, A. Taeb, S.W. Ng, Main Group Met. Chem. 24 (2001) 805.
[42] D. Sun, R. Cao, Y. Liang, Q. Shi, W. Su, M. Hong, J. Chem.Soc., Dalton Trans. (2001) 2335.
[43] E.K. Andersen, Acta Crystallogr. 22 (1967) 191.
[44] J. Chambers, in: S. Patai (Ed.), Chemistry of Quinoid Compounds: Part I, Wiley, New York, 1974.

Available online at www.sciencedirect.com
SCIENCE DIRECT®
Polyhedron 23 (2004) 2595–2596
POLYHEDRON
www.elsevier.com/locate/poly

Preface

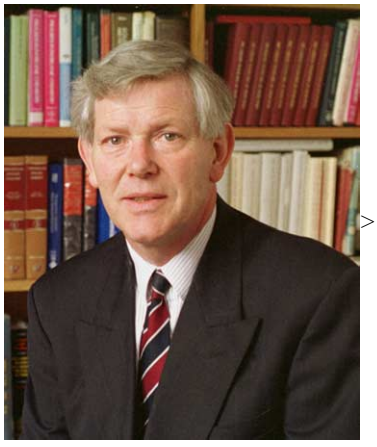

This issue of *Polyhedron* is dedicated to Professor Malcolm L.H. Green on the occasion of becoming an Emeritus Professor at Oxford University, where he was formerly Professor and Head of the Inorganic Chemistry Laboratory.

Malcolm was born in Eastleigh, Hampshire, on the 16th of April, 1936. He received his B.Sc. (Hons) in 1956 from the University of London (Acton Technical College) and his Ph.D. in 1959 from Imperial College of Science and Technology, where he studied under Professor Sir Geoffrey Wilkinson. Following Imperial College, Malcolm moved to Cambridge University in 1960, and finally to Oxford University in 1963, where he was appointed Septcentenary Fellow of Inorganic Chemistry at Balliol College. He was married to Jennifer Green (née Bilham) on the 2nd of January 1965. In 1985 Malcolm was elected to Fellow of the Royal Society and was appointed Professor and Head of the Inorganic Chemistry Laboratory and fellow of St. Catherine's College, Oxford, in 1989. He became a research active Emeritus Professor on the 1st of October 2003, with a current group of 13 researchers.

Malcolm has made numerous outstanding contributions to the field of organometallic chemistry, beginning with his first publication in 1958 on "*Bis*-cyclopentadienylrhenium hydride", resulting from his Ph.D. thesis, entitled "A study of some transition metal hydrides and olefin complexes". To date, he has published more than 600 papers and patents describing synthetic, structural, and mechanistic aspects of the chemistry of virtually every transition element. In view of the great breadth and success of Malcolm's research, it is difficult to single out a specific accomplishment that deserves highlighting over others. Nevertheless, some of the topics that immediately come to mind when prompted by the name Malcolm Green include: (i) the now infamous molybdenocene and tungstenocene systems, (ii) his fundamental studies on α- and β-hydrogen migratory insertion, carbon–hydrogen bond activation, and agostic interactions, and (iii) his development of multigram-scale metal vapor synthesis techniques. Malcolm never stands still and is constantly moving into new and exciting areas: e.g., organometallic intercalation compounds, organometallic chemistry of fullerenes and, most recently, the chemistry of metal complexes in carbon nanotubes. Moreover, his new approach to the formal classification of covalent compounds of the elements (the "MLX scheme") alleviates the problems and pitfalls often associated with oxidation state formalisms,

0277-5387/$ - see front matter © 2004 Elsevier Ltd. All rights reserved.
doi:10.1016/j.poly.2004.09.016

thereby enabling the student (and also researcher!) to understand better the nature of a specific compound.

Without a doubt, Malcolm's enthusiasm and passion has contributed greatly to the excitement that the field of organometallic chemistry has enjoyed over the years and his research has been widely recognized by numerous awards, some of which include: The Royal Society of Chemistry Corday-Morgan Medal and Prize in Inorganic Chemistry (1974); the Chemistry Society Medal in Transition Metal Chemistry (1978); the Royal Society of Chemistry Tilden Lectureship and Prize (1982); The J.C. Bailar Lecture and Medal, University of Illinois (1983); the American Chemical Society Award in Inorganic Chemistry (1984); the Royal Society of Chemistry Medal in Organometallic Chemistry (1986); the Royal Society of Chemistry Sir Edward Frankland Prize (1989); The Karl-Ziegler Prize of the Gesellschaft Deutscher Chemiker (1992); the Davy medal of the Royal Society (1995) ; American Chemical Society award in Organometallic Chemistry (1997) and The Royal Society of Chemistry Sir Geoffrey Wilkinson Medal and Prize (2000). Other recognitions of his work include: University of Western Ontario, Visiting Professor (1971); Ecole de Chimie and Institute des Substances Naturalles, Paris, Visiting Professor (1972); Harvard University, A.P. Sloan Visiting Professor (1973); Pacific West Coast Lecturer in Inorganic Chemistry (1977); Sherman Fairchild Visiting Scholar at the California Institute of Technology (1981); Karl Ziegler Gastprofessor, Max Plank Institute, Mulheim (1983); Hutchinson Lectureship, University of Rochester (1983); The University Lecturer in Chemistry, University of Western Ontario (1984); Debye Lecturer, Cornell University (1985); Wuhan University, PRC, Visiting Professor (1985); Julius Stieglitz Lecturer, University of Chicago (1986); Frontiers of Science Lecturer, Texas A&M University (1987); The DuPont Lecturer, Indiana University (1989/90); The Ida Beam Lecturer, University of Iowa (1990); The Glenn T. Seaborg Lecturer in Inorganic Chemistry at the University of California, Berkeley (1991); The South-East Lecturer in Inorganic Chemistry, USA (1991); The Walter Heiber Gastprofessor, University of Munich (1991); The Pacific Coast Lecturer (1994); The Rayson Huang Visiting Lecturer, Hong Kong (1995); The A.D. Little Lecturer, Massachusetts Institute of Technology (1995); The Stauffer Lecturer, University of Southern California (1996); the Dow Lecturer at the University of Ottowa (1996); and the James Walker Memorial Lecture, University of Edinburgh (1996); Doutor Honoris Causa, University of Lisbon, Portugal (1997); The Frank Dyer Medal, University of New South Wales (1997); The Fred Basolo Medal and Lecture., Northwestern University (1998); Ernest H. Swift Lectureship, California Institute of Technology (1998); Lewis Lecture, Cambridge UK (2001); FMC Lecturer, Princeton (2001); Distinguished Visiting Professor, Hong Kong University (2002); Eastman Company Distinguished Lecturer in Inorganic Chemistry, University of North Carolina (2002); 34th Canille and Henry Dreyfus Lecturer, Dartmouth College (2002); Raymond Siedle Lecturer, Indiana University (2004); Burt Vallee Visiting Professor at Harvard University (2004).

To date, Malcolm has supervised 118 Ph.D. graduate students and about 50 of his alumni now hold academic posts throughout the world. Many of his former students and visiting scientists convened in Oxford on the 20th September 2003 to participate in a symposium to celebrate his career. This special issue of Polyhedron includes contributions from those who have had the privilege of working in his laboratory and from many other colleagues in the organometallic community who hold him in equally high regard.

Gerard Parkin
Department of Chemistry, Columbia University
New York 10027, USA
E-mail address: parkin@chem.columbia.edu

Available online 26 October 2004

Available online at www.sciencedirect.com
SCIENCE DIRECT®
Polyhedron 23 (2004) 2597–2604
POLYHEDRON
www.elsevier.com/locate/poly

On the way to ferrocene-based multiple-decker sandwich complexes ☆

Alireza Haghiri Ilkhechi, Matthias Scheibitz, Michael Bolte, Hans-Wolfram Lerner, Matthias Wagner *

Institut für Anorganische Chemie, J.W. Goethe-Universität Frankfurt, Marie-Curie-Strasse 11, D-60439 Frankfurt (Main), Germany

Received 11 February 2004; accepted 19 May 2004
Available online 15 July 2004

Dedicated to Professor Malcolm L.H. Green on the occasion of his retirement

Abstract

Three ferrocene derivatives, $Li[FcBH_3]$, $Li_2[1,1'\text{-}fc(BMe_3)_2]$ and $Li_2[1,1'\text{-}fc(BMe_2pz)_2]$ [$Fc = (C_5H_5)Fe(C_5H_4)$, $fc = (C_5H_4)_2Fe$, pz = pyrazolyl], have been synthesized and structurally characterized to investigate the interaction of the negatively charged sandwich complex with its Li^+ counterion(s) in the solid state. Single crystals of $Li[FcBH_3]\cdot$(12-crown-4), obtained from a THF solution after addition of 12-crown-4, contain hexacoordinated Li^+ ions, which are bonded to one molecule of crown ether and to two hydrogen atoms of the BH_3 fragment. The compound $Li_2[1,1'\text{-}fc(BMe_3)_2]$ crystallized from THF as solvent-separated ion pairs with each Li^+ being encapsulated by four THF molecules. Single crystals of $Li_2[1,1'\text{-}fc(BMe_2pz)_2]$ were grown from diethyl ether. In this compound, the lithium ions are coordinated by two solvent molecules, the pyrazolyl side-arm and the cyclopentadienyl ring. Thus, $Li_2[1,1'\text{-}fc(BMe_2pz)_2]$ can be regarded as a trinuclear segment of the polymeric structure $[-(C_5H_4R)Li(C_5H_4R)Fe-]_\infty$ with $R = BMe_2pz$.
© 2004 Elsevier Ltd. All rights reserved.

Keywords: Multiple-decker sandwich complex; Ferrocene; Boron; Lithium; Crystal structure

1. Introduction

For more than 30 years, multiple-decker sandwich complexes have been in the focus of attention due to their promising potential as building blocks for nanoscale applications (e.g., one-dimensional wires and spin-chains) [1]. A most remarkable representative of this class of compounds was reported in 1985 by Siebert [2,3], who succeeded in the synthesis of extended columnar structures from Ni ions and η^5,μ-2,3-dihydro-1,3-diborolyl ligands. Later, this one-dimensional system was shown to possess semiconducting properties in the solid state [4–6]. For practical reasons, it would, however, be desirable to substitute simple cyclopentadienyl ligands for the sophisticated boron heterocycle. Numerous triple-decker sandwich complexes of the permethylated cyclopentadienyl derivative $[C_5Me_5]^-$ have already been isolated and structurally characterized [1]. In contrast, the number of known examples featuring exclusively the unsubstituted $[C_5H_5]^-$ ligand is still rather small (e.g., $[Ni_2(C_5H_5)_3]^+$ [7,8], $[Tl_2(C_5H_5)_3]^-$ [9]). Even though Schildcrout [10] reported as early as 1973 the detection of $[Fe_2(C_5H_5)_3]^+$ in the high-pressure electron-impact mass spectrum of ferrocene, this compound has not been isolated yet. However, clusters of the general formula $V_n[Fe(C_5H_5)_2]_{n+1}$ ($n = 1$–3) have recently been generated by two-laser vaporization of vanadium and ferrocene targets. Time-of-flight mass spectra measured with and without the addition of NH_3 gas indicate that these species possess multiple-decker sandwich structures rather than consisting of a central core of vanadium atoms capped by ferrocene molecules [11].

☆ Supplementary data associated with this article can be found, in the online version, at doi:10.1016/j.poly.2004.05.017.

* Corresponding author. Tel.: +49-69-798-29156; fax: +49-69-798-29260.
E-mail address: Matthias.Wagner@chemie.uni-frankfurt.de (M. Wagner).

0277-5387/$ - see front matter © 2004 Elsevier Ltd. All rights reserved.
doi:10.1016/j.poly.2004.05.017

Our group has published the synthesis and X-ray crystal structure analysis of compound **I** (Fig. 1), in which an array of alternating Ga(I) and Fe(II) ions is connected by η^5,μ-$[C_5H_5]^-$ moieties [12]. According to density functional (DFT) calculations, the binding energy of two ferrocenes to Ga^+ is about 80 kJ mol^{-1} higher than that for the formation of $[Ga(C_6H_6)_2]^+$ from Ga^+ and two benzene molecules. Fragment analysis of $\{[Fe(C_5H_5)_2]_2Ga\}^+$ indicated a transfer of 0.4 electrons into the gallium 4p orbitals compared with a zero occupancy for the isolated ion. More detailed insight into the gas phase basicity of ferrocene toward metal cations is provided by a recent DFT study on the ferrocene–Li^+ complex [13]. Two minima have been located on the energy surface: in the lower energy structure, the lithium cation is coordinated on top of one of the cyclopentadienyl rings (cf. **II**; Fig. 1), whereas the second minimum structure **III**, being 33 kJ mol^{-1} higher in energy, has the Li^+ ion bonded laterally to the iron atom. We found a similar structural motif as predicted for the hypothetical aggregate **III** in the [1.1]diborataferrocenophane **IV**, which crystallizes with one lithium cation inside its molecular cavity [d(Fe···Li): 2.4 Å (**III**); 2.706(5), 2.720(6) Å (**IV**)] [14,15]. ^{7}Li NMR spectroscopy shows this ferrocenophane–Li^+ complex to be stable in THF solution even in the presence of excess 12-crown-4.

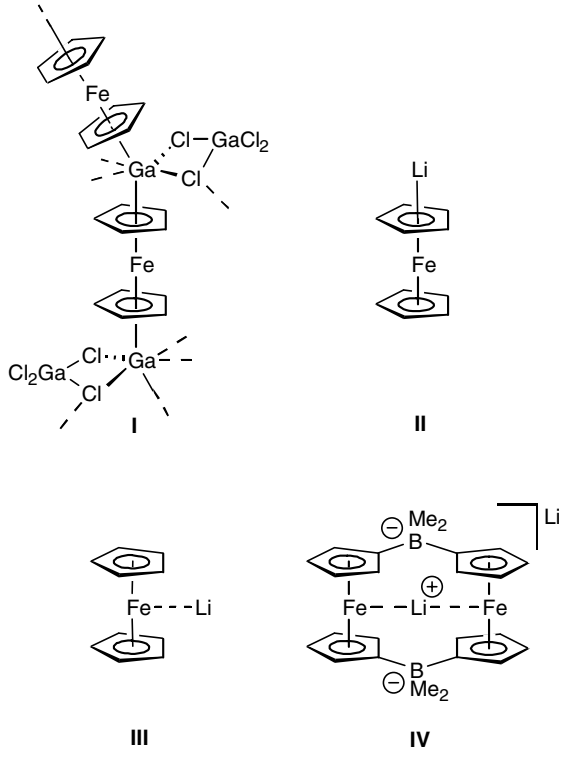

Fig. 1. The Ga^+–ferrocene multiple-decker sandwich complex **I**, the two calculated minimum structures **II** and **III** of the $Li^+\cdots$ferrocene complex in the gas phase, and the lithium [1.1]diborataferrocenophane **IV**.

The purpose of this paper is to describe the synthesis and structural characterization of type-**II** ferrocene–Li^+ adducts, which appears to be a realistic goal given the fact that the ferrocene–Ga^+ fragments in **I** already resemble the geometry of our target structure. It has, however, to be borne in mind that the synthesis protocol leading to **I** is quite unique in that we are starting from the covalent molecule $GaCl_3$ which is readily soluble in non-coordinating solvents. Consequently, there is no competition between the ferrocene donor and Lewis basic solvent molecules for the Ga(I) ion formed in situ in the course of the reaction. Moreover, in the calculated gas phase structure **II** any possible perturbations of the molecular geometry caused by the presence of solvent molecules are necessarily neglected. For a more general approach to ferrocene–metal multiple-decker sandwich complexes, however, we will have to use transition metal salts as starting materials which usually require strongly coordinating solvents as the reaction media. It therefore seemed reasonable to employ ferrocene derivatives equipped with suitable functional groups able to assist the cyclopentadienyl ring in metal ion binding. Such auxiliary substituents will greatly enhance the stability of the ferrocene–metal aggregate but still allow for those metal···Cp interactions that have been theoretically predicted and experimentally proven to exist in the solid state (cf. the unsupported multiple-decker complex **I**).

2. Results and discussion

To bring about close contacts between a lithium cation and the ferrocene cyclopentadienyl ring, we decided to introduce substituents into the ferrocene core that (i) increase the electron density on the organometallic moiety and (ii) bear a negative charge able to attract Li^+ electrostatically. It is important to know in this context, that the Fe(II)/Fe(III) redox potentials of ferrocenylborane-amine adducts have a pronounced shift to cathodic values with respect to the parent ferrocene [cf. $FcBMe_2$–picoline: $E^{0\prime} = -0.33$ V, 1,1′-fc(BMe_2–picoline)$_2$: $E^{0\prime} = -0.56$ V; in CH_2Cl_2 vs. FcH/FcH^+, $Fc = (C_5H_5)Fe(C_5H_4)$, $fc = (C_5H_4)_2Fe$] [16,17]. This effect becomes even stronger when the amine base is replaced by a negatively charged organyl group [14,15]. Thus, tetra-coordinated boryl substituents appear to be particularly well-suited to meet the two requirements outlined above. Starting from the well-known ferrocenylboranes FcB(Br)OEt (**1**) [18] and 1,1′-fc(BMe_2)$_2$ (**2**) [19], three derivatives of ferrocenylborates were chosen for our further investigations (Scheme 1): Li[$FcBH_3$] (**3**), Li_2[1,1′-fc(BMe_3)$_2$] (**4**) and Li_2[1,1′-fc(BMe_2pz)$_2$] (**5**; pz = pyrazolyl), in which the aimed-for Li···Cp coordination may be stabilized by a chelating pyrazolyl side-arm.

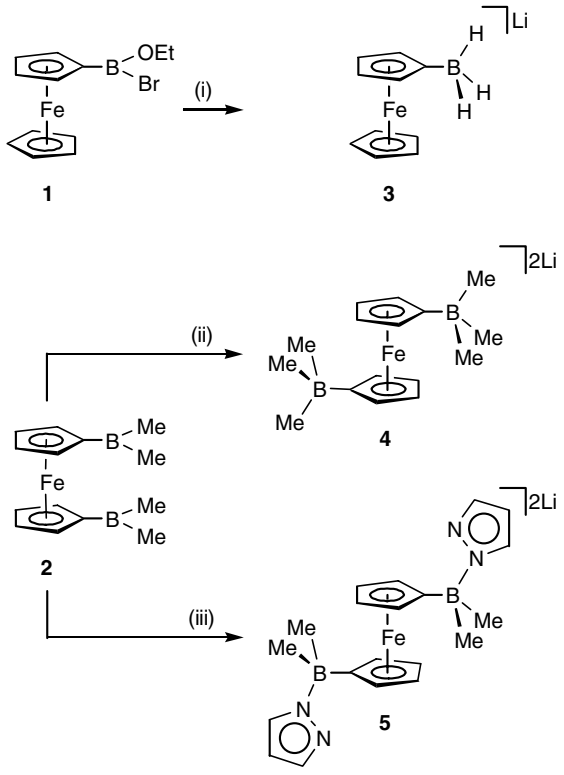

Scheme 1. Syntheses of the lithium ferrocenylborates **3**, **4** and **5**: (i) +Li[AlH_4], Et_2O/C_5H_{12}, 0 °C; (ii) +2LiMe, Et_2O, −78 °C; (ii) +2Lipz, Et_2O, −78 °C.

2.1. Syntheses and NMR spectroscopic characterization

FcB(OEt)Br (**1**) and 1 equiv. of Li[AlH_4] in ether/pentane gave lithium ferrocenylborohydride **3** in excellent yield (Scheme 1). Details of the synthesis procedure and NMR data of **3** have been published elsewhere [20]. Single crystals of Li[$FcBH_3$]·(12-crown-4) were grown by gas phase diffusion of diethyl ether onto a THF solution of **3**, to which a small amount of 12-crown-4 had been added. In the absence of the crown ether, no single crystalline material could be obtained. Reaction of 1,1′-fc(BMe_2)$_2$ (**2**) with either 2 equiv. of LiMe or 2 equiv. of Lipz in diethyl ether at −78 °C gave Li_2[1,1′-fc(BMe_3)$_2$] (**4**) and Li_2[1,1′-fc(BMe_2pz)$_2$] (**5**). The ^{11}B NMR spectra of **4** and **5** show resonances at $\delta = -21.8$ and −9.0, respectively, which agree nicely with those of Li[BMe_4] [$\delta(^{11}B) = -20.2$] [21] on one hand and Na[$B(NH_2)Et_3$] [$\delta(^{11}B) = -9.8$] [22] on the other. The ^{11}B NMR signal of **4** possesses a narrow linewidth ($h_{1/2} = 25$ Hz) testifying to a high local symmetry at the boron atom. In contrast, the less symmetrical boron coordination sphere in **5** results in a significantly broader ^{11}B NMR resonance ($h_{1/2} = 300$ Hz). In the ^{1}H NMR spectrum of **4**, three signals appear at −0.47, 3.55 and 3.75 ppm (integral ratio = 9:2:2), which are assigned to the methyl protons and the two types of magnetically non-equivalent ferrocene hydrogen atoms. In the ^{1}H NMR spectrum of

Table 1
Selected crystallographic data for **3**·(12-crown-4), **4**·$(THF)_8$ and **5**·$(Et_2O)_4$

Compound	**3**·(12-crown-4)	**4**·$(THF)_8$	**5**·$(Et_2O)_4$
Formula	$C_{18}H_{28}BFeLiO_4$	$C_{48}H_{90}B_2FeLi_2O_8$	$C_{36}H_{66}B_2FeLi_2N_4O_4$
Molecular weight	382.00	886.55	710.28
Crystal size (mm)	0.46 × 0.35 × 0.19	0.42 × 0.33 × 0.28	0.41 × 0.36 × 0.33
Crystal system	orthorhombic	orthorhombic	triclinic
Space group	*Pnma*	$Pca2_1$	$P\bar{1}$
Unit cell dimensions			
a (Å)	20.629(5)	17.4302(16)	10.6219(8)
b (Å)	10.3594(15)	17.5219(13)	13.1216(11)
c (Å)	8.6903(11)	17.2759(14)	15.2509(13)
α (°)	90	90	98.722(7)
β (°)	90	90	97.012(7)
γ (°)	90	90	93.914(6)
V (Å^3)	1857.2(6)	5276.2(8)	2077.1(3)
Z	4	4	2
D_c (g cm^{-3})	1.366	1.116	1.136
T (K)	100(2)	173(2)	173(2)
μ(Mo Kα) (mm^{-1})	0.830	0.332	0.402
$2\theta_{max}$ (°)	54.56	51.80	53.08
Measured reflections	6792	22966	33516
Unique reflections (R_{int})	2095 (0.0534)	8934 (0.0638)	8567 (0.0476)
Observed reflections [$I > 2\sigma(I)$]	1252	5285	6765
Parameters refined	167	551	442
R_1 [$I > 2\sigma(I)$; all data]	0.0259; 0.0584	0.1337; 0.1690	0.0577; 0.0709
wR_2 [$I > 2\sigma(I)$; all data]	0.0438; 0.0481	0.3402; 0.3603	0.1645; 0.1718
Goodness-of-fit on F^2	0.568	1.198	1.073
Largest difference peak and hole (e Å^{-3})	0.21 and −0.31	0.52 and −1.01	1.075 and −1.131

5, the corresponding signals are visible at 0.11, 4.05 and 4.19 ppm. This time, an integral ratio of 6:2:2 reveals the presence of only two methyl substituents at each boron atom. Moreover, the electronegative pyrazolyl groups lead to a downfield shift of the methyl and ferrocenyl resonances of **5** compared to **4** and to a pattern of three signals in the aromatic region of the proton spectrum [$\delta(^1H) = 5.95$, 7.01, 7.48]. In the ^{13}C NMR spectrum of **4**, a 1:1:1:1 quadruplet for the methyl groups is observed [$\delta(^{13}C) = 16.4$, $^1J_{BC} = 40$ Hz] as a result of ^{11}B ($I = 3/2$) coupling. The methyl resonance of the less symmetrically substituted derivative **5** [$\delta(^{13}C) = 12.8$] is severely broadened and its multiplet structure was not resolved, which was attributed to the quadrupolar relaxation of the adjacent boron nucleus [22].

2.2. X-ray crystal structure determinations

Selected crystallographic data are summarized in Table 1. Lithium ferrocenylborohydride **3** crystallizes together with 1 equiv. of 12-crown-4 in the orthorhombic space group *Pnma* (Fig. 2). Each Li^+ ion is complexed by four oxygen atoms of a crown ether molecule and establishes close contacts to two hydrogen atoms of the BH_3 fragment [Li(1)–H(1A) = 1.97(2) Å]. The Li···H distance to the third hydrogen atom is almost 1 Å longer [Li(1)···H(1B) = 2.94(2) Å]. Thus, $[FcBH_3]^-$ acts as a bidentate ligand toward the lithium cation. In metal borohydrides, this is the most common binding mode [23]. The coordination geometry of Li^+ in **3** · (12-crown-4) is reminiscent of the structure determined for $Li[BH_4] \cdot 2DME$ in the solid state (DME = dimethoxyethane) [23]. Here, the hexacoordinated Li ion is surrounded by four oxygen atoms of two DME molecules and two hydrogen atoms from a μ_2-$[BH_4]^-$ group. Consequently, the Li–H bond lengths {**3** · (12-crown-4): 1.97(2) Å; $Li[BH_4] \cdot 2DME$: 2.02(2) Å}, as well as the Li–H–B bond angles {**3** · (12-crown-4): 96.4(12)°; $Li[BH_4] \cdot 2DME$: 98.1(9)°} are rather similar in both compounds. A significantly shorter B···Li distance is found in **3** · (12-crown-4) [2.382(4) Å] compared to $Li[BH_4] \cdot 2DME$ [2.470(4) Å]. Using Edelstein's correlation of metal–boron distances as a measure of the denticity of borohydride groups [24], values of 1.6 ± 0.1 and 1.36 ± 0.06 Å are estimated for the ionic radii of bidentate and tridentate borohydride ligands, respectively. Thus, B···Li distances of about 2.50 and 2.26 Å are to be expected for Li-μ_2-BH_3R and Li-μ_3-BH_3R coordination modes [ionic radius of hexacoordinated $Li^+ = 0.90$ Å [25]]. It may therefore be concluded, that the $[BH_4]^-$ ion in $Li[BH_4] \cdot 2DME$ represents the ideal Li-μ_2-BH_3R arrangement, whereas the BH_3 fragment in **3** · (12-crown-4) is slightly tilted in the direction of a Li-μ_3-BH_3R coordination {cf. the distance between Li^+ and the non-coordinating H atom(s) is shorter in **3** · (12-crown-4) than in $Li[BH_4] \cdot 2DME$ with values of 2.94(2) and 3.27(2) Å, respectively}. This effect is most likely caused by steric repulsion between the crown ether ligand and the bulky ferrocenyl substituent in **3** · (12-crown-4).

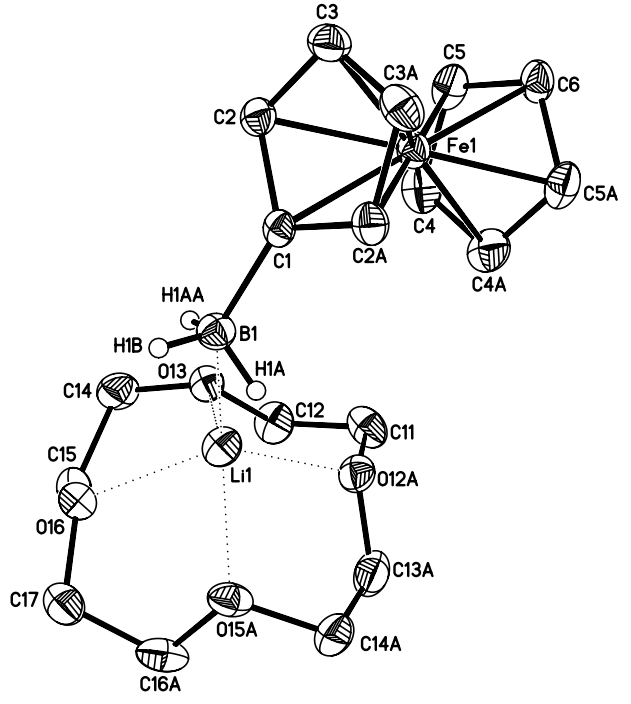

Fig. 2. Molecular structure of compound **3** · (12-crown-4); thermal ellipsoids are shown at the 50% probability level. Selected bond lengths (Å), atom···atom distances (Å), angles (°), torsion angles (°) and dihedral angles (°): B(1)–C(1) = 1.600(4), B(1)···Li(1) = 2.382(4), B(1)–H(1A) = 1.14(2), B(1)–H(1B) = 1.15(3), Li(1)–H(1A) = 1.97(2), Li(1)···H(1B) = 2.94(2); C(2)–C(1)–C(2A) = 104.2(2), C(2)–C(1)–B(1) = 127.8(1), C(1)–B(1)···Li(1) = 141.3(2), C(1)–B(1)–H(1A) = 112.6(10), C(1)–B(1)–H(1B) = 111.6(14), H(1A)–B(1)–H(1B) = 105.1(12), Li(1)–H(1A)–B(1) = 96.4(12); COG–C(1)–B(1) = 176.5; C(2)–C(1)–B(1)···Li(1) = 92.4(2), C(2)–C(1)–B(1)–H(1B) = −87.6(2), C(1)–COG–COG′–C(4A) = −36.1; C(1)C(2)C(3)C(3A)C(2A)//C(4)C(5)C(6)C(5A)C(4A) = 0.2. COG: centre of gravity of a C_5H_4 ring. Symmetry transformation used to generate equivalent atoms: $x, -y + 3/2, z$.

The molecular structure of **3** · (12-crown-4) indicates coordination of Li^+ to the BH_3 group via two hydride bridges to be preferred over $Li^+ \cdots \eta^5$-ferrocene bonding. The system was therefore developed further by replacing the hydrogen substituents with methyl groups, which can be expected to interact less strongly with lithium cations. Moreover, two borate substituents were introduced into the ferrocene core in order to increase the electrostatic attraction of Li^+ ions. Single crystals of the resulting compound **4** were obtained from THF [**4** · $(THF)_8$: orthorhombic, $Pca2_1$; Fig. 3]; addition of 12-crown-4 was not required. The crystal lattice of **4** · $(THF)_8$ consists of solvent-separated ions with each Li^+ being coordinated to four THF molecules in a tetrahedral fashion. The $[1,1'\text{-fc}(BMe_3)_2]^{2-}$ ion adopts a conformation in which the BMe_3 substituents are pointing away from each other [C(11)–COG–COG′–C(21) = 154.1°; COG: centre of gravity of a cyclopentadienyl ring].

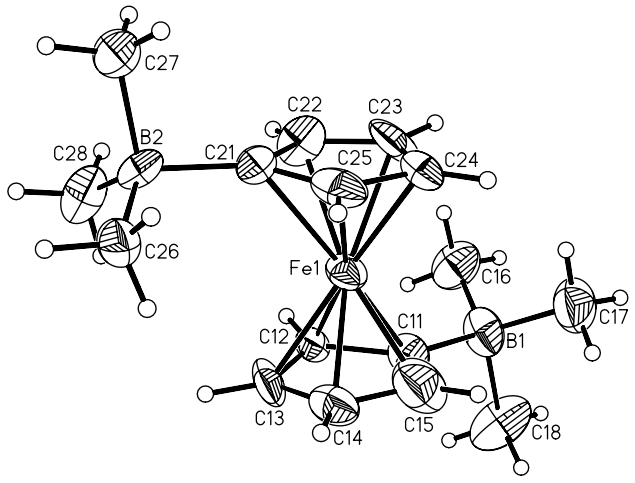

Fig. 3. Molecular structure of the anionic part of compound $\mathbf{4}\cdot(\mathrm{THF})_8$; thermal ellipsoids are shown at the 30% probability level. Selected bond lengths (Å), angles (°), torsion angles (°) and dihedral angles (°): B(1)–C(11) = 1.734(16), B(2)–C(21) = 1.634(16); C(12)–C(11)–C(15) = 102.7(11), C(12)–C(11)–B(1) = 127.6(10), C(15)–C(11)–B(1) = 129.7(13), C(22)–C(21)–C(25) = 101.7(10), C(22)–C(21)–B(2) = 126.4(11), C(25)–C(21)–B(2) = 131.9(11), COG–C(11)–B(1) = 174.9, COG–C(21)–B(2) = 177.7; C(12)–C(11)–B(1)–C(18) = −94.3(14), C(22)–C(21)–B(2)–C(27) = −88.5(13), C(11)–COG–COG′–C(21) = 154.1; C(11)C(12)C(13)C(14)C(15)// C(21)C(22)C(23)C(24)C(25) = 2.2.

Since the desired Li–ferrocene interaction could not be achieved just by increasing the number of negatively charged side-chains, each of the borate groups was equipped with a Lewis-basic pyrazolyl substituent in order to anchor the Li^+ ion via a Li–N adduct bond. The lithium pyrazolylborate **5** crystallizes from diethyl ether together with four solvent molecules in the triclinic space group $P\bar{1}$ [$\mathbf{5}\cdot(Et_2O)_4$; Fig. 4]. This time, each Li^+ ion is bonded to two ether molecules and to the nitrogen lone-pair of the pyrazolyl side-arm [Li(1)–N(32) = 1.998(5), Li(2)–N(42) = 1.999(6) Å], which places it on top of the cyclopentadienyl ring [C(12)–C(11)–B(1)–N(31) = 97.7(3)°, C(22)–C(21)–B(2)–N(41) = −81.3(3)°]. As a consequence, three lithium–carbon contacts [Li(1)–C(11) = 2.646(5), Li(1)–C(12) = 2.395(5), Li(1)–C(13) = 2.910(6), Li(2)–C(21) = 2.475(5), Li(2)–C(22) = 2.496(5), Li(2)–C(25) = 2.730(6) Å] are established by Li(1) as well as Li(2). As the internal angles of the C(Cp)–B–N–N–Li chains do not depart appreciably from the ideal values of 109° [C(11)–B(1)–N(31) = 105.3(2)°, C(21)–B(2)–N(41) = 106.6(2)°] and 120° [B(1)–N(31)–N(32) = 121.9(2)°, N(31)–N(32)–Li(1) = 124.0(2)°, B(2)–N(41)–N(42) = 124.2(2)°, N(41)–N(42)–Li(2) = 122.3(2)°], the molecular framework of the heterotrimetallic aggregate is apparently free of ring strain. Compound **5** is related to the ferrocene-based tris(1-pyrazolyl)borates **V** [26] (Fig. 5), of which several metal complexes [27,28] (including one Li^+ salt) [29] have been synthesized and structurally characterized. In all these cases, the tris(1-pyrazolyl)borate units act as di- or trihapto ligand toward the metal centre, which in turn was never found to interact with the ferrocene backbone. Thus, as is to be expected, Li^+–ferrocene bonding appears to be less favourable than lithium-pyrazolyl adduct formation. Some key structural features of $\mathbf{5}\cdot(Et_2O)_4$ resemble Laguna's coordination polymer **VI** [30] (Fig. 5), consisting of 1,1′-ferrocenediyl bis(dialkyldithiocarbamate) ligands [31] and Ag(I) ions. Here, each silver ion is not only bonded to two sulfur atoms of different ferrocene moieties but also to two cyclopentadienyl rings in an η^2 fashion. In 1998, **VI** represented the first example where an η^5-cyclopentadienyl ring of ferrocene was shared with another metal atom via the π-system.

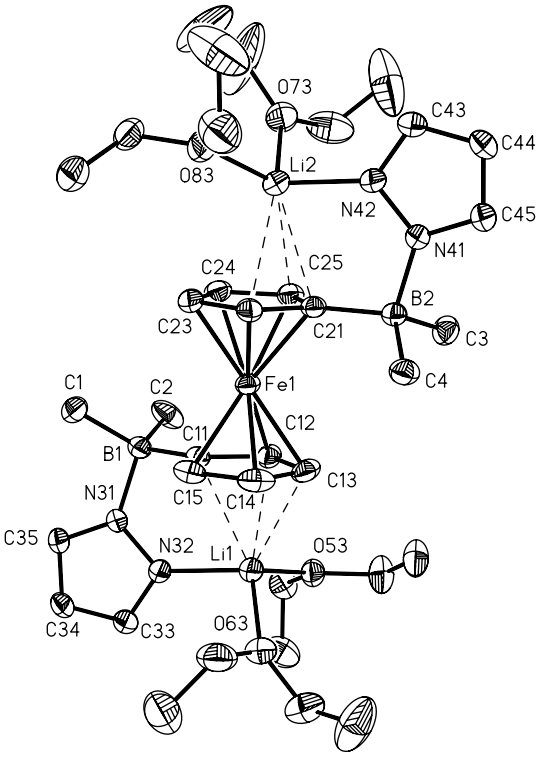

Fig. 4. Molecular structure of compound $\mathbf{5}\cdot(Et_2O)_4$; thermal ellipsoids are shown at the 30% probability level. Selected bond lengths (Å), angles (°), torsion angles (°) and dihedral angles (°): B(1)–C(11) = 1.617(4), B(1)–N(31) = 1.611(3), B(2)–C(21) = 1.621(4), B(2)–N(41) = 1.610(3), Li(1)–N(32) = 1.998(5), Li(1)–C(11) = 2.646(5), Li(1)–C(12) = 2.395(5), Li(1)–C(13) = 2.910(6), Li(2)–N(42) = 1.999(6), Li(2)–C(21) = 2.475(5), Li(2)–C(22) = 2.496(5), Li(2)–C(25) = 2.730(6); C(12)–C(11)–C(15) = 104.5(2), C(12)–C(11)–B(1) = 128.8(2), C(15)–C(11)–B(1) = 126.7(2), C(22)–C(21)–C(25) = 104.9(2), C(22)–C(21)–B(2) = 127.0(2), C(25)–C(21)–B(2) = 128.1(2), C(11)–B(1)–N(31) = 105.3(2), B(1)–N(31)–N(32) = 121.9(2), N(31)–N(32)–Li(1) = 124.0(2), C(21)–B(2)–N(41) = 106.6(2), B(2)–N(41)–N(42) = 124.2(2), N(41)–N(42)–Li(2) = 122.3(2), N(32)–Li(1)–O(53) = 109.0(3), N(32)–Li(1)–O(63) = 106.3(3), O(53)–Li(1)–O(63) = 111.2(2), N(42)–Li(2)–O(73) = 105.4(3), N(42)–Li(2)–O(83) = 109.4(3), O(73)–Li(2)–O(83) = 107.1(2), COG–C(11)–B(1) = 177.5, COG–C(21)–B(2) = 179.3; C(12)–C(11)–B(1)–N(31) = 97.7(3), C(11)–B(1)–N(31)–N(32) = −35.4(3), B(1)–N(31)–N(32)–Li(1) = 14.2(4), C(22)–C(21)–B(2)–N(41) = −81.3(3), C(21)–B(2)–N(41)–N(42) = 4.0(3), B(2)–N(41)–N(42)–Li(2) = −9.2(4), C(11)–COG–COG′–C(21) = −157.9; C(11)C(12)C(13)C(14)C(15)// C(21)C(22)C(23)C(24)C(25) = 1.0.

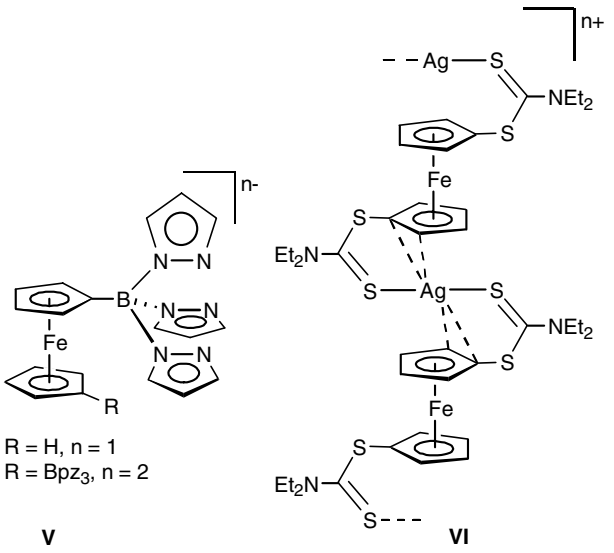

Fig. 5. Ferrocene-based tris(1-pyrazolyl)borate derivatives **V** and a double sandwich silver(I)–ferrocene polymer **VI**.

3. Conclusions

Inspired by a DFT study on the ferrocene–Li^+ complex in the gas phase [13], we synthesized three ferrocene derivatives, $Li[FcBH_3]$, $Li_2[1,1'\text{-fc}(BMe_3)_2]$ and $Li_2[1,1'\text{-fc}(BMe_2pz)_2]$ [Fc = $(C_5H_5)Fe(C_5H_4)$, fc = $(C_5H_4)_2Fe$, pz = pyrazolyl], in order to establish the structural motif of a Li^+ cation located on top of a ferrocene–Cp ring. Our rationale was to stabilize a potential interaction between both components by introducing negatively charged substituents into the ferrocene core. Initially, it appeared to be of prime importance to use anionic side-chains that do *not* possess electron lone pairs able to compete with the cyclopentadienyl π-system for Li^+ coordination. Thus, borate substituents were chosen for all further investigations. A crystal structure analysis of $Li[FcBH_3]\cdot$(12-crown-4), obtained from a THF solution after addition of 12-crown-4, revealed hexacoordinated Li^+ ions bonded to one molecule of crown ether and two hydrogen atoms of the BH_3 fragment. Even a hydridoborate fragment is thus preferred over the Cp π-system for Li^+ coordination. Attempts to block this coordination site by substitution of methyl groups for the hydrogen atoms failed, since the related methylborate crystallized from THF as solvent-separated ion pairs $\{[Li(THF)_4]^+\}_2[1,1'\text{-fc}(BMe_3)_2]^{2-}$. Single crystals of this compound from less strongly coordinating solvents (e.g., diethyl ether) could not be obtained up to now. Contrary to our a priori assumptions, we thus came to the conclusion that a Lewis-basic functionality might be required to stabilize the aimed-for Li^+–ferrocene complex, provided the electron lone pair is part of a side-arm designed to put the Li^+ ion on the cyclopentadienyl ring. From molecular modelling studies, the rigid pyrazolyl ring appeared to be well-suited for this purpose. Single crystals of $Li_2[1,1'\text{-fc}(BMe_2pz)_2]$ were grown from diethyl ether. In this compound, the lithium ions are coordinated by two solvent molecules, the pyrazolyl side-arm and the cyclopentadienyl ring. Thus, $Li_2[1,1'\text{-fc}(BMe_2pz)_2]$ can be regarded as a trinuclear segment of the polymeric structure $[-(C_5H_4R)\text{-}Li(C_5H_4R)Fe-]_\infty$ with R = BMe_2pz. In the future, we are planning to employ the $[1,1'\text{-fc}(BMe_2pz)_2]^{2-}$ ligand in combination with metals other than Li^+ for the synthesis of ferrocene-based multiple-decker complexes.

4. Experimental section

4.1. General remarks

All reactions and manipulations of air-sensitive compounds were carried out in dry, oxygen-free argon using standard Schlenk ware. Solvents were freshly distilled under N_2 from Na–benzophenone (diethyl ether, THF) prior to use. NMR: Bruker DPX 400, Bruker DPX 250. ^{11}B NMR spectra are reported relative to external $BF_3\cdot Et_2O$. Unless stated otherwise, all NMR spectra were run at ambient temperature; abbreviations: s, singlet, d, doublet, vtr, virtual triplet, q, quadruplet, n.r., multiplet expected in the ^1H NMR spectrum but not resolved, n.o., signal not observed. Compounds **1** [18] and **2** [19] were synthesized according to the literature procedures.

4.2. Preparation of *3*

For the synthesis of compound **3** see [20]. Single crystals of **3**·(12-crown-4) were grown by gas phase diffusion of diethyl ether onto a THF solution of **3** to which a small amount of 12-crown-4 had been added. Compound **3** is sensitive to air and moisture. *Anal.* Calc. for $C_{18}H_{28}BFeLiO_4$ [382.00]: C, 56.60; H, 7.39. Found: C, 56.33; H, 7.12%.

4.3. Preparation of *4*

LiMe (1.6 M, 4.42 mL, 7.07 mmol) in Et_2O was added dropwise with stirring at −78 °C to **2** (0.94 g, 3.54 mmol) in Et_2O (20 mL). The mixture was slowly warmed to room temperature and the solvent removed under reduced pressure. The remaining highly viscous oily residue was dissolved in THF (20 ml) and the solution stored at 5 °C overnight, whereupon dark red X-ray quality crystals of **4**·$(THF)_8$ formed. Yield: 2.79 g (89%). ^{11}B NMR (128.4 MHz, d_8-THF): δ −21.8 ($h_{1/2} = 25$ Hz). ^1H NMR (400.1 MHz, d_8-THF): δ −0.47 (s, 18H, CH_3), 3.55, 3.75 (2 × n.r., 2 × 4H, C_5H_4). ^{13}C NMR (100.6 MHz, d_8-THF): δ 16.4 (q, $^1J_{BC} = 40$ Hz, CH_3), 67.8, 70.7 (C_5H_4), n.o. C_5H_4-C_{ipso}. The com-

pound is extremely sensitive to air and the crystals lose THF rapidly when isolated at ambient temperature; a decent elemental analysis was therefore not obtained.

4.4. Preparation of 5

Lipz (0.34 g, 4.60 mmol) in Et_2O (15 mL) was added dropwise with stirring at −78 °C to **2** (0.61 g, 2.30 mmol) in Et_2O (15 mL). The mixture was slowly warmed to room temperature, filtered and the clear yellow filtrate stored at 5 °C overnight, whereupon yellow–orange X-ray quality crystals of $\mathbf{5}\cdot(Et_2O)_4$ formed. Yield: 1.52 g (93%). ^{11}B NMR (128.4 MHz, d_8-THF): δ −9.0 ($h_{1/2}$ = 300 Hz). ^{1}H NMR (400.1 MHz, d_8-THF): δ 0.11 (s, 12H, CH_3), 4.05, 4.19 (2 × vtr, 2 × 4H, $^3J_{HH} = {}^4J_{HH} = 1.6$ Hz, C_5H_4), 5.95 (vtr, 2H, $^3J_{HH} = 1.9$ Hz, pz–H4), 7.01, 7.48 (2 × d, 2 × 2H, $^3J_{HH} = 1.7$, 2.0 Hz, pz–H3,5). ^{13}C NMR (100.6 MHz, d_8-THF): δ 12.8 (n.r., CH_3), 71.0, 72.2 (C_5H_4), 102.8 (pz–C4), 131.9, 135.4 (pz–C3,5), n.o. C_5H_4-C_{ipso}. The compound is sensitive to air and the crystals lose diethyl ether rapidly when isolated at ambient temperature; a decent elemental analysis was therefore not obtained.

4.5. X-ray crystal structure analyses

The crystals of $\mathbf{3}\cdot$(12-crown-4), $\mathbf{4}\cdot(THF)_8$ and $\mathbf{5}\cdot(Et_2O)_4$ were measured on a STOE IPDS II two-circle diffractometer with graphite-monochromated Mo Kα radiation. An empirical absorption correction was performed using the MULABS [32] option in the program PLATON [33]. The structures were solved by direct methods using the program SHELXS [34] and refined against F^2 with full-matrix least-squares techniques using the program SHELXL [35]. The crown ether ring in $\mathbf{3}\cdot$(12-crown-4) is located on a crystallographic mirror plane and therefore disordered over two equally occupied sites. $\mathbf{4}\cdot(THF)_8$ is a racemic twin composed of two domains with an occupancy ratio of 0.70(6)/0.30(6). All non-H atoms of $\mathbf{3}\cdot$(12-crown-4), $\mathbf{4}\cdot(THF)_8$ and $\mathbf{5}\cdot(Et_2O)_4$ were refined with anisotropic displacement parameters. The BH_3 hydrogen atoms of $\mathbf{3}\cdot$(12-crown-4) could be located in the difference Fourier map and were freely refined. All other H atoms were refined using a riding model.

5. Supplementary material

Crystallographic data for the structural analyses have been deposited with the Cambridge Crystallographic Data Centre, CCDC reference numbers: 230425 [$\mathbf{3}\cdot$(12-crown-4)], 230426 [$\mathbf{4}\cdot(THF)_8$], 230427 [$\mathbf{5}\cdot(Et_2O)_4$]. Copies of this information may be obtained free of charge from The Director, CCDC, 12 Union Road, Cambridge, CB2 1EZ, UK (fax: +44-1223-336033; email: deposit@ccdc.cam.ac.uk or www: http://www.ccdc.cam.ac.uk).

Acknowledgements

M.W. is grateful to the Deutsche Forschungsgemeinschaft (DFG) for financial support and to Chemetall for generous gifts of organolithium compounds. M.S. thanks the Fonds der Chemischen Industrie (FCI) and the Bundesministerium für Bildung und Forschung (BMBF) for a Ph.D. grant.

References

[1] N.J. Long, Metallocenes, Blackwell Science, London, 1998.
[2] W. Siebert, Angew. Chem. 97 (1985) 924.
[3] W. Siebert, Angew. Chem., Int. Ed. Engl. 24 (1985) 943.
[4] T. Kuhlmann, S. Roth, J. Rozière, W. Siebert, Angew. Chem. 98 (1986) 87.
[5] T. Kuhlmann, S. Roth, J. Rozière, W. Siebert, Angew. Chem., Int. Ed. Engl. 25 (1986) 105.
[6] M.Y. Lavrentiev, H. Köppel, M.C. Böhm, Chem. Phys. 169 (1993) 85.
[7] A. Salzer, H. Werner, Angew. Chem. 84 (1972) 949.
[8] A. Salzer, H. Werner, Angew. Chem., Int. Ed. Engl. 11 (1972) 930.
[9] D.R. Armstrong, A.J. Edwards, D. Moncrieff, M.A. Paver, P.R. Raithby, M.-A. Rennie, C.A. Russell, D.S. Wright, J. Chem. Soc., Chem. Commun. (1995) 927.
[10] S.M. Schildcrout, J. Am. Chem. Soc. 95 (1973) 3846.
[11] S. Nagao, A. Kato, A. Nakajima, K. Kaya, J. Am. Chem. Soc. 122 (2000) 4221.
[12] S. Scholz, J.C. Green, H.-W. Lerner, M. Bolte, M. Wagner, Chem. Commun. (2002) 36.
[13] A. Irigoras, J.M. Mercero, I. Silanes, J.M. Ugalde, J. Am. Chem. Soc. 123 (2001) 5040.
[14] M. Scheibitz, R.F. Winter, M. Bolte, H.-W. Lerner, M. Wagner, Angew. Chem. 115 (2003) 954.
[15] M. Scheibitz, R.F. Winter, M. Bolte, H.-W. Lerner, M. Wagner, Angew. Chem., Int. Ed. Engl. 42 (2003) 924.
[16] M. Fontani, F. Peters, W. Scherer, W. Wachter, M. Wagner, P. Zanello, Eur. J. Inorg. Chem. (1998) 1453.
[17] M. Fontani, F. Peters, W. Scherer, W. Wachter, M. Wagner, P. Zanello, Eur. J. Inorg. Chem. (1998) 2087.
[18] T. Renk, W. Ruf, W. Siebert, J. Organomet. Chem. 120 (1976) 1.
[19] W. Ruf, T. Renk, W. Siebert, Z. Naturforsch. B 31 (1976) 1028.
[20] M. Scheibitz, J.W. Bats, M. Bolte, H.-W. Lerner, M. Wagner, Organometallics 23 (2004) 940.
[21] R.J. Thompson, J.C. Davis Jr., Inorg. Chem. 4 (1965) 1464.
[22] H. Nöth, B. Wrackmeyer, in: P. Diehl, E. Fluck, R. Kosfeld (Eds.), NMR Basic Principles and Progress, vol. 14, Springer, Berlin, 1978.
[23] H.-H. Giese, H. Nöth, H. Schwenk, S. Thomas, Eur. J. Inorg. Chem. (1998) 941.
[24] N. Edelstein, Inorg. Chem. 20 (1981) 297.
[25] R.D. Shannon, Acta Crystallogr. Sect. A 32 (1976) 751.
[26] F. Jäkle, K. Polborn, M. Wagner, Chem. Ber. 129 (1996) 603.
[27] F. Fabrizi de Biani, F. Jäkle, M. Spiegler, M. Wagner, P. Zanello, Inorg. Chem. 36 (1997) 2103.
[28] E. Herdtweck, F. Peters, W. Scherer, M. Wagner, Polyhedron 17 (1998) 1149.
[29] S.L. Guo, F. Peters, F. Fabrizi de Biani, J.W. Bats, E. Herdtweck, P. Zanello, M. Wagner, Inorg. Chem. 40 (2001) 4928.

[30] O. Crespo, M.C. Gimeno, P.G. Jones, A. Laguna, C. Sarroca, Chem. Commun. (1998) 1481.
[31] B. McCulloch, C.H. Brubaker Jr., Organometallics 3 (1984) 1707.
[32] R.H. Blessing, Acta Crystallogr. Sect. A 51 (1995) 33.
[33] A.L. Spek, Acta Crystallogr. Sect. A 46 (1990) C34.
[34] G.M. Sheldrick, Acta Crystallogr. Sect. A 46 (1990) 467.
[35] G.M. Sheldrick, SHELXL-97. A Program for the Refinement of Crystal Structures, Unversität Göttingen, Göttingen, Germany, 1997.

Available online at www.sciencedirect.com
SCIENCE DIRECT®
Polyhedron 23 (2004) 2605–2610
POLYHEDRON
www.elsevier.com/locate/poly

Synthesis and structure of a new organometallic polyoxomolybdate, $Cp^*_2Mo_6O_{17}$

Edmond Collange [a], Laurent Metteau [a], Philippe Richard [a], Rinaldo Poli [a,b,*]

[a] *Laboratoire de Synthèse et d'Electrosynthèse Organométalliques, Faculté des Sciences ''Gabriel'', Université de Bourgogne, 6 Boulevard Gabriel, 21000 Dijon, France*

[b] *Laboratoire de Chimie de Coordination, UPR CNRS 8241, 205 Route de Narbonne, 31077 Toulouse Cedex, France*

Received 20 February 2004; accepted 17 June 2004
Available online 7 August 2004

Dedicated to M.L.H. Green in recognition of his outstanding contribution to inorganic chemistry

Abstract

Acidic aqueous solutions of the $[Cp^*MoO_2(H_2O)_x]^+$ ion yield single crystals of the novel organometallic polyoxomolybdate $Cp^*_2Mo_6O_{17}$ via a slow protonolysis of the Mo–Cp* bond. This compound has subsequently been obtained selectively and in good yields from the combination of $Cp^*_2Mo_2O_5$ and four equivalents of MoO_4^{2-} under acidic conditions. The X-ray structure of $Cp^*_2Mo_6O_{17}$ is analogous to other hexanuclear polyoxometallate ions but is the most distorted so far reported according to the continuous symmetry measure, the inner $(\mu_6\text{-O})Mo_6$ core featuring a large displacement of the central oxygen atom toward the organometallic moieties and away from the inorganic ones.
© 2004 Elsevier Ltd. All rights reserved.

Keywords: Molybdenum; Polyoxometallate; Aqueous organometallic chemistry; Pentamethylcyclopentadienyl ligands

1. Introduction

We have recently initiated a research program aimed at exploiting the chemistry of high oxidation state organometallic compounds in water. Aqueous organometallic chemistry is attracting growing interest because of its ''green'' impact [1–3] and because of its promise in catalytic [4,5] and biomedical applications [6]. Its development, however, has so far been restricted for the most part to low-valent systems to which hydrophilic functionalities are added on the ligand periphery [7–9], in order to make the systems compatible with an aqueous environment. High oxidation organometallics are now a well established family of compounds [10,11], mostly supported by oxo ligands. Pioneering work in this area was carried out by Cousins and Green [12,13], with the now 40-year old synthesis and subsequent investigations of $Cp_2Mo_2O_5$. Some of these high oxidation state organometallic compounds exhibit interesting catalytic applications [14]. Nonetheless, their investigation has so far mostly involved the use of organic solvents and very little is known about their behaviour in water. The investigation of these materials in water, especially for electroactive metals, offers opportunities for the development of new catalytic and electrocatalytic processes [15]. Our first studies have focused on the speciation [16] and on the electrochemical [17,18] and chemical [19,20] reduction behavior of the Cp^*Mo^{VI} moiety. In particular, we have established that the Cp^*Mo^{VI} species is stable in air and in the entire pH range in a mostly aqueous medium (80% H_2O, 20% MeOH), at least for the time necessary to carry out the speciation studies (several hours at room temperature). While the species is stable in the form of the previously known [21–23] $Cp^*MoO_3^-$ complex at high pH,

* Corresponding author. Tel.: +33 561333195; fax: +33 561553003.
E-mail address: poli@lcc-toulouse.fr (R. Poli).

0277-5387/$ - see front matter © 2004 Elsevier Ltd. All rights reserved.
doi:10.1016/j.poly.2004.06.025

its nature changes to the hitherto unknown cationic complex $Cp^*MoO_2(H_2O)_x^-$ at very low pH (ca. <2) [16]. For the latter species, the hydration status (e.g., whether it contains a coordinated water molecule or not) could not be determined from its spectroscopic characteristics (UV–Vis) nor from its reactivity (kinetics of proton transfer processes). We have therefore attempted to obtain this information from a single crystal X-ray study. The outcome of these attempts have led to the chemistry which is described herein.

2. Experimental

2.1. General part

The compound $Cp^*_2Mo_2O_5$ was prepared as described previously [24]. The infrared spectra were recorded on a Brucker Vector 22 instrument equipped with a Globar (MIR) source. The powder X-ray diffraction spectrum was recorded with a Seifert XRD3000 $\theta/2\theta$ diffractometer using Cu radiation at 40 kV and 30 mA, and equipped with a graphite monochromator. The elemental analysis was carried out by the analytical services of LSEO with Fisons EA 1108 instruments.

2.2. Procedure leading to single crystals of $Cp^*_2Mo_6O_{17}$

To a MeOH solution (2 mL) of $Cp^*_2Mo_2O_5$ (37 mg) was added 2 mL of aqueous HNO_3 (0.2 M) in air. This solution was transferred into a 50 mL Schlenk tube and the oxygen was removed by argon bubbling. The solution was subsequently left undisturbed on the bench. Brown crystals were obtained over a 2.5 month period. One of these crystals was used for the X-ray diffraction analysis.

2.3. Synthesis of $Cp^*_2Mo_6O_{17}$

$Cp^*_2Mo_2O_5$ (54 mg, 0.1 mmole) was dissolved in 2.5 mL of MeOH. Separately, $Na_2MoO_4 \cdot 2H_2O$ (96.8 mg, 0.4 mmol) was dissolved in 2.5 mL of water. The two solutions were mixed with no apparent change. 1 mL of HNO_3 0.1 M was slowly added, forcing the immediate precipitation of an orange solid. The solid was filtered, washed with H_2O, then with MeOH, and finally dried at 70 °C. (Yield 86.5 mg, 77.4%). *Anal.* Calc. for $C_{20}H_{30}Mo_6O_{17}$: C, 21.48; H, 2.70. Found: C, 21.46; H, 2.91%. IR (Nujol mull, cm^{-1}): 978 w, 966 s, ca. 820 sh, 792 s, ca. 770 sh.

2.4. Single crystal X-ray diffraction study

Intensities were collected on an Enraf-Nonius KappaCCD diffractometer at 110 K using Mo Kα radiation. The structure was solved via a Patterson search program [25] and refined with full-matrix least-squares methods [26] based on $|F^2|$ with the aid of the WINGX program [27]. All non-hydrogen atoms were refined with anisotropic thermal parameters. Hydrogen atoms were included with a riding model with isotropic temperature factors fixed to 1.5 times those of the corresponding parent atoms. The essential crystallographic parameters are listed in Table 1 and selected bond distances and angles are collected in Table 2.

3. Results

According to our recent investigation [16], adjusting the pH of a 4:1 H_2O–MeOH solution of $Cp^*_2Mo_2O_5$ to <2 selectively generates the new oxo cation $Cp^*MoO_2(H_2O)_x^+$, where the most likely values of x are 0 and 1. In order to verify the presence of coordinated water in this complex, an acidic aqueous solution of $Cp^*MoO_2(H_2O)_x^+$ was set out for a long term crystal-

Table 1
Crystal data and structure refinement for compound $Cp^*_2Mo_6O_{17}$

Formula	$C_{20}H_{30}O_{17}Mo_6$
M	1118.08
T (K)	110(2)
Crystal system	monoclinic
Space group	$C2/c$
Unit cell dimensions	
a (Å)	8.8927(2)
b (Å)	17.9978(4)
c (Å)	18.4111(6)
β (°)	98.434(1)
V (Å^3)	2914.81(13)
Z	4
$F(000)$	2152
D_{calc} (g/cm^3)	2.548
Diffractometer	Enraf-Nonius KappaCCD
Scan type	mixture of ϕ rotations and ω scans
λ (Å)	0.71073
μ (mm^{-1})	2.580
Crystal size (mm^3)	$0.10 \times 0.05 \times 0.05$
$\sin(\theta)/\lambda_{max}$ (Å^{-1})	0.65
Index ranges	h: −11, 9; k: −23, 20; l: −23, 19
Absorption correction	SCALEPACK
RC = 1 reflection collected	8730
IRC = independent RC	3326 [R(int) = 0.0327]
IRCGT = IRC and [$I > 2\sigma(I)$]	2682
Refinement method	full-matrix least-squares on F^2
Data/restraints/parameters	3326/0/201
R for IRCGT	R_1[a] = 0.0319, wR_2[b] = 0.0706
R for IRC	$R1$[a] = 0.0462, wR_2[b] = 0.0765
Goodness-of-fit[c]	1.035
Largest difference peak and hole (e Å^{-3})	0.86 and −0.91

[a] $R_1 = \sum(||F_o| - |F_c||)/\sum|F_o|$.
[b] $wR_2 = [\sum w(F_o^2 - F_c^2)]^2/\sum[w(F_o^2)^2]^{1/2}$ where $w = 1/[\sigma^2(F_o^2) + (0.028P)^2 + 12.37P]$ where $P = (\mathrm{Max}(F_o^2, 0) + 2 * F_c^2)/3$.
[c] Goodness-of-fit $= [\sum w(F_o^2 - F_c^2)^2/(N_o - N_v)]^{1/2}$.

Table 2
Selected bond lengths (Å) and angles (°) for compound $Cp^*_2Mo_2O_{17}$[a]

Mo(1)–Ct	2.109(5)
Mo(1)–O(1)	2.145(2)
Mo(1)–O(2)	2.029(3)
Mo(1)–O(3)	1.955(3)
Mo(1)–O(5)	1.9430(19)
Mo(1)–O(6)	1.890(3)
Mo(2)–O(7)	1.683(3)
Mo(2)–O(1)	2.3674(5)
Mo(2)–O(2)	1.855(3)
Mo(2)–O(4)	1.871(3)
Mo(2)–O(6)#	1.980(3)
Mo(2)–O(10)#	2.006(3)
Mo(3)–O(9)	1.687(3)
Mo(3)–O(1)	2.542(3)
Mo(3)–O(3)	1.883(3)
Mo(3)–O(4)	1.977(3)
Mo(3)–O(8)	1.9159(17)
Mo(3)–O(10)	1.861(3)
Mo(1)–O(1)–Mo(3)#1	172.33(12)
Mo(1)–O(1)–Mo(1)#	97.78(14)
Mo(1)–O(1)–Mo(2)	93.81(5)
Mo(1)–O(1)–Mo(2)#	93.68(5)
Mo(2)–O(1)–Mo(2)#	168.60(17)
Mo(2)–O(2)–Mo(1)	116.19(13)
Mo(3)–O(3)–Mo(1)	119.93(15)
Mo(2)–O(4)–Mo(3)	119.76(14)
Mo(1)#–O(5)–Mo(1)	112.56(17)
Mo(1)–O(6)–Mo(2)#	116.75(13)
Mo(3)#–O(8)–Mo(3)	121.97(18)
Mo(3)–O(10)–Mo(2)#	120.26(14)
Ct–Mo(1)–O(1)	178.82(13)
Ct–Mo(1)–O(2)	104.62(15)
Ct–Mo(1)–O(3)	102.19(15)
Ct–Mo(1)–O(5)	104.03(16)
Ct–Mo(1)–O(6)	101.51(15)
O(6)–Mo(1)–O(5)	91.07(8)
O(6)–Mo(1)–O(3)	88.94(11)
O(5)–Mo(1)–O(3)	153.22(12)
O(6)–Mo(1)–O(2)	153.75(11)
O(5)–Mo(1)–O(2)	85.03(8)
O(3)–Mo(1)–O(2)	83.25(11)
O(6)–Mo(1)–O(1)	78.26(8)
O(5)–Mo(1)–O(1)	74.83(11)
O(3)–Mo(1)–O(1)	78.97(10)
O(2)–Mo(1)–O(1)	75.67(8)
O(7)–Mo(2)–O(2)	106.89(13)
O(7)–Mo(2)–O(4)	105.67(13)
O(2)–Mo(2)–O(4)	93.30(12)
O(7)–Mo(2)–O(6)#	102.31(13)
O(2)–Mo(2)–O(6)#	86.52(12)
O(4)–Mo(2)–O(6)#	150.77(11)
O(7)–Mo(2)–O(10)#	101.54(13)
O(2)–Mo(2)–O(10)#	150.83(12)
O(4)–Mo(2)–O(10)#	85.16(11)
O(6)#–Mo(2)–O(10)#	81.11(11)
O(7)–Mo(2)–O(1)	173.62(11)
O(2)–Mo(2)–O(1)	73.58(11)
O(4)–Mo(2)–O(1)	80.59(10)
O(6)#–Mo(2)–O(1)	71.32(10)
O(10)#–Mo(2)–O(1)	77.44(9)
O(9)–Mo(3)–O(10)	105.45(13)
O(9)–Mo(3)–O(3)	105.95(13)
O(10)–Mo(3)–O(3)	88.80(12)
O(9)–Mo(3)–O(8)	105.63(13)
O(10)–Mo(3)–O(8)	88.02(9)
O(3)–Mo(3)–O(8)	147.95(12)
O(9)–Mo(3)–O(4)	104.80(13)
O(10)–Mo(3)–O(4)	149.74(11)
O(3)–Mo(3)–O(4)	83.77(12)
O(8)–Mo(3)–O(4)	83.10(8)

[a] Symmetry transformations used to generate equivalent atoms: #$-x+1$, y, $-z+1/2$; Ct, Cp* ring centroid.

lization, as described in Section 2. Salts of various anions such as PF_6^- or BPh_4^- were used, but the procedure typically led to the recovery of crystals of the neutral starting complex, $Cp^*_2Mo_2O_5$. A longer scale crystallization attempt, carried out without added salt, slowly yielded single crystals of a new compound. This turned out to correspond to the title organometallic polyoxometallate.

The title compound is a new member of the family of organometallic polyoxometallates [28]. Once the chemical nature of this compound was revealed by a single crystal X-ray diffraction study (vide infra), a more logical, selective and high yield synthesis was conceived, as illustrated in Eq. (1). Mixing a methanolic solution of the organometallic reagent with an aqueous solution of the inorganic reagents in the appropriate stoichiometry yields a clear solution, from which the desired product rapidly precipitates upon acidification in an analytically pure form. The compound is sparingly soluble in water and only slightly soluble in organic solvents. Unlike the previously reported $[Cp^*Mo_6O_{18}]^-$ analogue [29,30], its solubility in MeCN or DMSO at temperatures up to 80 °C was not sufficient to allow the recording of ^{95}Mo or ^{17}O solution NMR spectra. However, the identity of the bulk sample as obtained from reaction (1) was established by the excellent match of its experimental powder X-ray diffraction pattern with the pattern calculated from the single crystal X-ray data, see Fig. 1 and Table 3

$$Cp^*_2Mo_2O_5 + 4MoO_4^{2-} + 8H^+ \rightarrow Cp^*_2Mo_6O_{17} + 4H_2O \quad (1)$$

The single crystal X-ray analysis shows that the molecule is hexanuclear with the six Mo atoms placed at the vertices of an octahedron, see Fig. 2. Each of the 12 octahedron edges is bridged by an oxygen atom. Four more oxygen atoms are placed on as many Mo atoms in the terminal coordination mode, while the remaining two *cis*-Mo atoms are η^5-bonded to Cp* ligands. The structure is completed by an additional oxygen atom, placed near the center of the octahedron. The molecule sits on

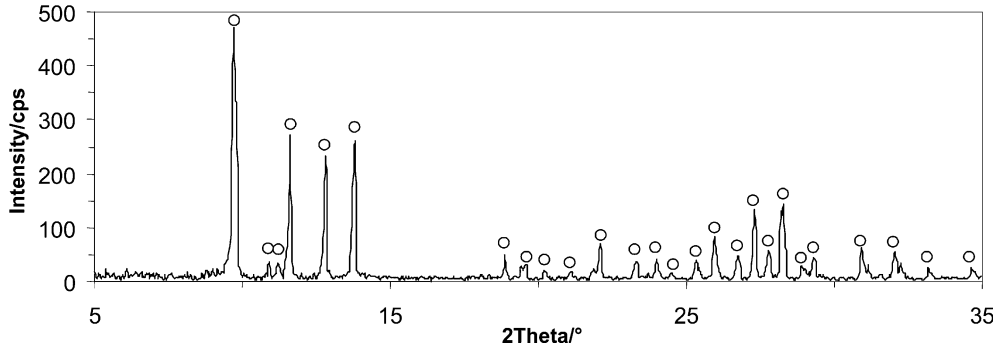

Fig. 1. Powder diffraction spectrum of compound $Cp^*_2Mo_6O_{17}$ obtained from $Cp^*_2Mo_2O_5$ and MoO_4^{2-}. The circles show the diffractions that have been correctly indexed on the basis of the single crystal unit cell (see Table 3).

Table 3
Comparison between experimental (*hkl*) reflections for the powdered sample and the corresponding calculated reflections from the single crystal data

h	*k*	*l*	2θ (obs.)	2θ (calc.)	Δ(2θ)
0	2	0	9.7362	9.7495	0.0133
0	2	1	10.9172	10.8865	−0.0307
−1	1	0	11.2333	11.2073	−0.0260
−1	1	1	11.6057	11.5951	−0.0107
1	1	1	12.7986	12.7973	−0.0012
0	2	2	13.7702	13.7504	−0.0199
1	3	1	18.8771	18.8665	−0.0107
1	1	3	19.5518	19.5597	0.0079
2	0	0	20.2344	20.2545	0.0201
−1	4	1	21.1031	21.1041	0.0010
−1	3	1	22.0832	22.0729	−0.0103
−2	2	2	23.3041	23.3110	0.0069
1	3	3	24.0060	24.0194	0.0133
0	5	0	24.5094	24.5313	0.0219
−1	3	4	25.3254	25.3053	−0.0201
−2	0	4	25.9693	25.9695	0.0002
−1	5	1	26.7528	26.7553	0.0025
1	5	1	27.3104	27.3140	0.0036
1	0	5	27.7927	27.7974	0.0047
1	1	5	28.2441	28.2377	−0.0064
−2	4	2	28.9317	28.9499	0.0182
0	0	6	29.3072	29.3026	−0.0046
0	2	6	30.9357	30.9514	0.0157
2	5	0	32.0447	32.0161	−0.0285
−2	0	6	33.1946	33.1954	0.0008
−2	2	6	34.6695	34.6777	0.0082

a crystallographic twofold axis, which contains the central O(1) and the edge-bridging O(5) and O(8) atoms. The molecular geometry is identical with that of the previously published tungsten analogue, $Cp^*_2W_6O_{17}$, including the relative *cis*-arrangement of the two Cp*-substituted metal atoms [31]. The geometry can also be related to those of the $[Mo_6O_{19}]^{2-}$ and $[Cp^*Mo_6O_{18}]^-$ complexes [29,30,32–34], with which it can be considered isoelectronic and isostructural in light of the isolobal analogy between the terminal Cp^{*-} and O^{2-} ligands.

Selected bond distances and angles are listed in Table 2. The terminal Mo–O distances average 1.685(3) Å,

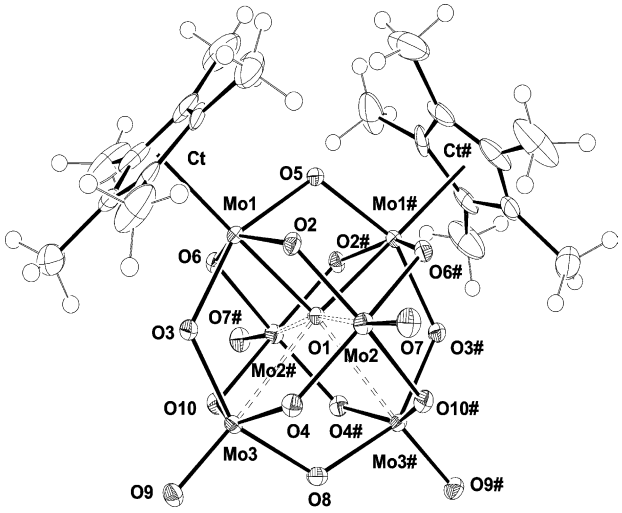

Fig. 2. An ORTEP view of the $Cp^*_2Mo_6O_{17}$ molecule.

which compares with 1.681(8) Å for $[Mo_6O_{19}]^{2-}$ (average over 14 different structures containing this ion available in the CCDC) and with 1.686(11) or 1.66(3) Å in the two different salts of $[Cp^*Mo_6O_{18}]^-$ [29,30]. The edge-bridging Mo–O distances are longer and spread in a rather wide range between 1.855(3) and 2.029(3) Å, showing a certain degree of asymmetry for the octahedral framework, similar to what is commonly found for other polyoxometallate ions [29,35]. Their overall average is 1.93(6) Å, whereas the same average over the 14 different structures of the $[Mo_6O_{19}]^{2-}$ ion in the CCDC is 1.93(3) Å. There is no clear trend depending on the nature of the Mo atom (i.e., inorganic or organometallic). For instance, atoms O(2) and O(3) are closer to the inorganic Mo atom [1.855(3) and 1.883(3) Å] than to the organometallic Mo atom [2.029(3) and 1.955(3) Å], whereas the reverse is true for atom O(6) [1.980(3) versus 1.890(3) Å]. The O atoms bridging two Mo(=O) units [O(4), O(8) and O(10)] also show distances in a relatively wide range [from 1.861(3) to 2.006(3) Å]. The highest degree of asymmetry, however, is exhibited for the μ_6-O atom. The distances are shorter for the

Mo(1) atom, 2.145(2) Å, intermediate for the Mo(2) atom [i.e., *cis* to Mo(1)], 2.3674(5) Å, and longer from the Mo(3) atom [i.e., *trans* to Mo(1)], 2.542(3) Å. A similar, though slightly less pronounced asymmetry was noted for the $[Cp^*Mo_6O_{18}]^-$ ion, where the Mo-(μ_6-O) distances in the two independently determined structures [29,30] are 2.134(9) or 2.14(1) Å to the Cp*Mo atom, 2.343(9) or 2.33(2) Å to the *cis*-Mo atoms, and 2.498(9) or 2.48(1) Å to the *trans*-Mo atom. By comparison, the central oxygen is placed symmetrically in the $[Mo_6O_{19}]^{2-}$ ion, the average over the 14 structures available in the CCDC being 2.318(7) Å. The use of the quantitative ''octahedral symmetry measure'', as defined by Avnir and coworkers [36,37], for the title compound and for the related Cp*-containing polyoxometallates shows that the distortion of the (μ_6-O)M_6 core is systematically and significantly larger than the distortion of the M_6 core and that it is larger for compounds with two Cp* substituents than for those with one. The distortion parameter for the (μ_6-O)M_6 core is by far the largest (0.172) for the title compound (cf. 0.099 for $Cp^*_2W_6O_{17}$, 0.073 and 0.066 for the two salts of $[Cp^*Mo_6O_{18}]^-$ and 0.030 for $[Cp^*TiMo_5O_{18}]^{3-}$). The displacement of the oxygen atom from the octahedron center was previously interpreted in terms of a stronger *trans* influence by the terminal oxo ligand relative to the terminal Cp* ligand. It is possible, however, to provide an alternative rationalization in terms of the greater donor power of the terminal O^{2-} ligand with respect to the terminal Cp^{*-} ligand. Thus, the hypothetical $Cp^*_2Mo_6O_{16}^+$ moiety that is obtained by removal of the central O^{2-} ion would feature a lower electron density for the organometallic Mo atoms. The internal O atom is consequently attracted to a greater extent by these atoms. The metal distance from the Cp* ring centroid, 2.109(4) Å, compares with 2.091(15) Å in the $[Cp^*Mo_6O_{18}]^-$ structure.

4. Discussion

The result of the previous aqueous speciation study of the Cp^*Mo^{VI} moiety seemed to suggest that the Cp*–Mo^{VI} bond is stable in an aqueous environment and in air in the entire pH range. Attempts to grow crystals of salts of the sought acidic $Cp^*MoO_2(H_2O)_x^+$ species, and the consequent formation of the organometallic polyoxomolybdate compound $Cp^*_2Mo_6O_{17}$, show that this is not quite so true. It should be remarked, however, that the crystals were formed over an extended period of time (over 2 months), at pH 1 and in direct summertime sunlight. This proves that the hydrolytic sensitivity of the Cp*–Mo^{VI} bond is not a marked one. Therefore, the possible use the Cp^*Mo^{VI} species for catalytic applications in an aqueous environment at low pH remains promising.

Several other attempts to crystallize salts of the $Cp^*MoO_2(H_2O)_x^+$ ion at low pH over a shorter time scale have systematically resulted in the formation of $Cp^*_2Mo_2O_5$. Our strategy consisted in the diffusion of a liquid (e.g., methanol) perceived as having poor solvent properties with respect to salts, into a solution containing the $Cp^*MoO_2(H_2O)_x^+$ ion and a suitable counterion. However, the solubility product of compound $Cp^*_2Mo_2O_5$ (as a weak electrolyte generating $Cp^*MoO_2(H_2O)_x^+$ and $Cp^*MoO_3^-$) must be very low and the very low concentration of $Cp^*MoO_3^-$ in equilibrium with the cation at pH 1 (the pK_a of $Cp^*MoO_2(OH)$ is 3.65) is sufficient to precipitate the molecular compound. Future efforts at experimentally determining the number of coordinated water ligands in $Cp^*MoO_2(H_2O)_x^+$ will focus on NMR spectroscopy.

5. Conclusions

Our systematic investigation of the aqueous chemistry of Cp^*Mo^{VI} has led to the serendipitous discovery and then to a simple, selective and high-yield synthesis of the organometallic polyoxomolybdate $Cp^*_2Mo_6O_{17}$. This compound is a new member of a relatively small class of cyclopentadienyl containing polyoxometallates, which includes $[CpTiM_5O_{18}]^{3-}$ (M = Mo, W) [35], $[Cp^*Mo_6O_{18}]^-$[29,30] and $Cp^*_2W_2O_{17}$ [31]. The synthetic method shown in Eq. (1) can probably be extended to the synthesis of a wide range of organometallic homo- and heteronuclear polyoxometallates.

6. Supplementary material

Crystallographic data (atomic coordinates, thermal parameters, full lists of bond distances and angles) have been deposited at the Cambridge Crystallographic Data Centre, CCDC No. 231765. Copies of the data can be obtained free of charge from CCDC, 12 Union Road, Cambridge CB2 1EZ, UK (fax: +44-1223-336033; e-mail: deposit@ccdc.com.ac.uk or www: http://www.ccdc.cam.ac.uk).

Acknowledgements

We are grateful to the European Commission for support of this work through the Research Training Network ''AQUACHEM'' (contract No. MRTN-CT-2003-503864). The European COST D29 program (working group 0009-03) and CNRS are also acknowledged for additional financial help. We thank J. Jaud of CEMES (Toulouse) for recording the X-ray powder diffraction pattern of compound $Cp^*_2Mo_6O_{17}$ and Prof. S. Alvarez for the calculation of the octahedral

symmetry measures and for sending us a preprint of [37] prior to publication.

References

[1] T. Chan, L. Li, Y. Yang, W. Lu, ACS Symp. Ser. 819 (2002) 166.
[2] F. Joó, Acc. Chem. Res. 35 (2002) 738.
[3] I.T. Horvath, Acc. Chem. Res. 35 (2002) 685.
[4] D. Sinou, Top. Curr. Chem. 206 (1999) 41.
[5] D. Sinou, Adv. Synth. Catal. 344 (2002) 221.
[6] G.E. Jaouen (Ed.), J. Organomet. Chem., 1999, p. 589 (special issue: bioorganometallic chemistry).
[7] P. Kalck, F. Monteil, Adv. Organomet. Chem. 34 (1992) 219.
[8] B.E. Hanson, Coord. Chem. Rev. 186 (1999) 795.
[9] C. Muller, D. Vos, P. Jutzi, J. Organomet. Chem. 600 (2000) 127.
[10] W.A. Herrmann, E. Herdtweck, M. Flöel, J. Kulpe, U. Küsthardt, J. Okuda, Polyhedron 6 (1987) 1165.
[11] W.A. Herrmann, Comments Inorg. Chem. 7 (1988) 73.
[12] M. Cousins, M.L.H. Green, J. Chem. Soc. (1964) 1567.
[13] M. Cousins, M.L.H. Green, J. Chem. Soc. (A) (1969) 16.
[14] W.A. Herrmann, F.E. Kühn, Acc. Chem. Res. 30 (1997) 169.
[15] R. Poli, Chem. Eur. J. 10 (2004) 332.
[16] E. Collange, J. Garcia, R. Poli, New J. Chem. 26 (2002) 1249.
[17] J. Gun, A. Modestov, O. Lev, D. Saurenz, M.A. Vorotyntsev, R. Poli, Eur. J. Inorg. Chem. (2003) 482.
[18] J. Gun, A. Modestov, O. Lev, R. Poli, Eur. J. Inorg. Chem. (2003) 2264.
[19] F. Demirhan, J. Gun, O. Lev, A. Modestov, R. Poli, P. Richard, J. Chem. Soc., Dalton Trans. (2002) 2109.
[20] F. Demirhan, P. Richard, R. Poli, Inorg. Chim. Acta 347 (2003) 161.
[21] M.S. Rau, C.M. Kretz, L.A. Mercando, G.L. Geoffroy, A.L. Rheingold, J. Am. Chem. Soc. 113 (1991) 7420.
[22] M.S. Rau, C.M. Kretz, G.L. Geoffroy, A.L. Rheingold, Organometallics 12 (1993) 3447.
[23] J. Sundermeyer, U. Radius, C. Burschka, Chem. Ber. 125 (1992) 2379.
[24] D. Saurenz, F. Demirhan, P. Richard, R. Poli, H. Sitzmann, Eur. J. Inorg. Chem. (2002) 1415.
[25] G.M. Sheldrick, SHELXS97. Program for Crystal Structure solution, University of Göttingen, Göttingen, Germany, 1997.
[26] G.M. Sheldrick, SHELXL97. Program for Crystal Structure refinement, University of Göttingen, Göttingen, Germany, 1997.
[27] L.J. Farrugia, J. Appl. Crystallogr. 32 (1999) 837.
[28] P. Gouzerh, A. Proust, Chem. Rev. 98 (1998) 77.
[29] F. Bottomley, J. Chen, Organometallics 11 (1992) 3404.
[30] A. Proust, R. Thouvenot, P. Herson, J. Chem. Soc., Dalton Trans. (1999) 51.
[31] J.R. Harper, A.L. Rheingold, J. Am. Chem. Soc. 112 (1990) 4037.
[32] H. Allcock, E. Bissell, E. Shawl, Inorg. Chem. 12 (1973) 2963.
[33] C. Garner, N. Howlader, A. Mcphail, R. Miller, K. Onan, F. Mabbs, J. Chem. Soc., Dalton Trans. 1978 (1978) 1582.
[34] J. Fuchs, K.F. Jahr, Z. Naturforsch. B: Chem. Sci. 23 (1968) 1380.
[35] T.M. Che, V.W. Day, L.C. Francesconi, M.F. Fredrich, W.G. Klemperer, W. Shum, Inorg. Chem. 24 (1985) 4055.
[36] S. Alvarez, D. Avnir, M. Llunell, M. Pinsky, New J. Chem. 26 (2002) 996.
[37] D. Casanova, J. Cirera, M. Llunell, P. Alemany, D. Avnir, S. Alvarez, J. Am. Chem Soc. 126 (2004) 1755.

Available online at www.sciencedirect.com
SCIENCE DIRECT®
Polyhedron 23 (2004) 2611–2614
POLYHEDRON
www.elsevier.com/locate/poly

Synthesis and structures of tetranuclear rhenium–cobalt mixed metal sulfide clusters $[Re_3CoS_4Cl_6(PMe_2Ph)_4]$

Nobuaki Sakai, Taro Saito *

Department of Chemistry, Faculty of Science and Hightech Research Center, Kanagawa University, Hiratsuka, Kanagawa 259-1293, Japan

Received 23 March 2004; accepted 23 June 2004
Available online 12 August 2004

Abstract

An isomeric pair of the title compounds have been prepared and characterized by NMR spectroscopy and X-ray crystallography. The major isomer contains three dimethylphenylphoshine ligands coordinated to rhenium atoms in the direction of the μ_3-S atom in the starting trinuclear rhenium cluster complex, whereas the minor isomer has a dimethylphenylphosphine ligand in the opposite direction. The temperature of the preparative reactions controls the orientation of the phosphine ligands.
© 2004 Elsevier Ltd. All rights reserved.

Keywords: Rhenium cluster

1. Introduction

Recent development of the chemistry of sulfide and selenide cluster compounds of rhenium has been limited mostly to hexanuclear compounds [1,2]. Only a few trinuclear and tetranuclear rhenium chalcogenide cluster compounds are known [3,4] and mixed metal clusters are even rarer, a single example being a rhenium–nickel complex $[Re_3NiS_4Cl_6(PEt_3)_4]$ [5]. Rhenium is a group 7 metal and its cations are isoelectronic with those of group 6 molybdenum or tungsten in one-electron lower oxidation states [3]. Since there are a number of mixed-metal sulfide clusters of Mo(IV) or W(IV) [6–8], it is anticipated that similar rhenium derivatives can be prepared using Re(V). The starting compounds to prepare rhenium cluster sulfide complexes are rare and $Re_3S_7Cl_7$ [9], isoelectronic with $Mo_3S_7Cl_4$ [10], is useful as a starting compound to lead to either trinuclear [11–13] or higher nuclear mixed-metal cluster compounds [5]. The present paper, describes the preparation of the first tetranuclear rhenium–cobalt mixed metal sulfide cluster complexes coordinated by dimethylphenylphosphine.

2. Experimental

2.1. Materials and methods

All experiments were performed under dinitrogen atmosphere. Solvents were dried and distilled by the reported methods. Electronic spectra were recorded on a JASCO Ubest-570 UV–Vis spectrometer. ^1H and ^{31}P NMR spectra were measured in $CDCl_3$ with a JEOL GX-400 spectrometer.

Rhenium metal, PMe_2Ph and $(PPh_3)_2NCl$ were purchased from Aldrich, while $CoCl_2$ was from WAKO chemicals. These materials were used without further purification. $Re_3S_7Cl_7$ was prepared according to a literature method [9].

2.1.1. $[Re_3CoS_4Cl_6(PMe_2Ph)_4]\cdot(C_2H_5)_2O$, **1**

$[(PPh_3)_2N][Re_3S_4Cl_6(PMe_2Ph)_3]\cdot 3CH_2Cl_2$ [14]: $Re_3S_7Cl_7$ (1.03 g, 0.99 mmol) and PMe_2Ph (0.97 g, 7.02 mmol) in dichloromethane (30 mL) were reacted for 3

* Corresponding author. Tel.: +81 46 359 4111; fax: +81 46 358 9684.
E-mail address: saito-tr@chem.kanagawa-u.ac.jp (T. Saito).

0277-5387/$ - see front matter © 2004 Elsevier Ltd. All rights reserved.
doi:10.1016/j.poly.2004.06.028

days at room temperature. The mixture was filtered and the solvent was removed by evaporation. The residue was washed twice with diethylether and dried. The product was dissolved in dichloromethane (10 mL), and $(PPh_3)_2NCl$ (0.70 g, 1.21 mmol) was added to the solution. The dichloromethane solution was layered with diethylether (30 mL) and then left to stand for 3 days. The crystalline product was obtained by filtration.

A solution of $[(PP_3)_2N][Re_3S_4Cl_6(PMe_2{}^-Ph)_3]\cdot 3CH_2Cl_2$ (0.35 g, 0.16 mmol) in dichloromethane (20 mL) was treated with $CoCl_2$ (0.045 g, 0.34 mmol) and PMe_2Ph (0.1 g, 0.72 mmol) and stirred for 7 days at room temperature and then refluxed for 90 min. The solution was filtered, the solvent was evaporated and the residue was washed with diethylether. The product was dissolved in dichloromethane (10 mL), and diethylether (30 mL) was layered on the solution which was left for 7 days. A black crystalline compound was obtained in 38% yield. *Anal*. Calc. for $C_{32}H_{44}CoCl_6P_4Re_3S_4\cdot 0.4C_4H_{10}O$: C, 25.95; H, 3.16. Found: C, 26.06; H, 3.29%. UV–Vis (CH_2Cl_2): 522 nm (ε 1123 $M^{-1}\,cm^{-1}$), 771 nm (ε 456 $M^{-1}\,cm^{-1}$). ^1H NMR (δ, $CDCl_3$): 1.71 (d, Re–P(CH_3)$_2$(C_6H_5)), 2.10 (dd, Co–P(CH_3)$_2$(C_6H_5)), 2.28 (d, Re–P(CH_3)$_2$(C_6H_5)), 7.22–7.87 (m, P(CH_3)$_2$(C_6H_5)). ^{31}P NMR (δ, $CDCl_3$, 15% H_3PO_4): −24.69 (Re–*P*(CH_3)$_2$(C_6H_5)), 38.77 (Co–*P*(CH_3)$_2$(C_6H_5).

2.1.2. $[Re_3CoS_4Cl_6(PMe_2Ph)_4]$ 2

A solution of $[(PPh_3)_2N][Re_3S_4Cl_6(PMe_2Ph)_3]\cdot 3CH_2Cl_2$ (0.52 g, 0.24 mmol) in dichloromethane (20 mL) was stirred with $CoCl_2$ (0.067 g, 0.56 mmol) for 4 days, following which PMe_2Ph (0.072 g, 0.53 mmol) was added and the mixture was stirred for 3 days at room temperature. The solution was filtered, the solvent was evaporated and the residue was washed with diethylether. The product was dissolved in dichloromethane (10 mL) and chromatographed on a silica gel column with dichloromethane and acetone as eluents. Crystals obtained from the dichloromethane eluate were identical with the cluster **1** and those from the acetone eluate were crystallized from dichloromethane/diethylether to give black crystals **2** in 19% yield. *Anal*. Calc. for $C_{32}H_{44}CoCl_6P_4Re_3S_4$: C, 25.43; H, 2.93. Found: C, 25.36; H, 2.95%. UV–Vis (CH_2Cl_2): 520 nm (ε 1259 $M^{-1}\,cm^{-1}$), 768 nm (ε 452 $M^{-1}\,cm^{-1}$). ^1H NMR (δ, $CDCl_3$): 1.85, 1.87, 2.37 (d, Re–P(CH_3)$_2$(C_6H_5)), 1.92 (d, Co–P(CH_3)$_2$(C_6H_5)), 7.34–8.06 (m, P(CH_3)$_2$(C_6H_5)). ^{31}P NMR (δ, $CDCl_3$, 15% H_3PO_4): −24.80, −26.89, −30.92 (Re–*P*(CH_3)$_2$(C_6H_5)), 33.10 (Co–*P*(CH_3)$_2$(C_6H_5)).

2.1.3. Crystal structures of 1 and 2

Crystals suitable for X-ray crystallography were obtained by recrystallization of the products from dichloromethane and diethylether over a week. Data were collected on a Bruker Smart APEX CCD system with a sealed molybdenum source and graphite monochromator. Crystals were transferred to the goniostat where they were cooled to −100 °C for data collection. The data were collected using 15 s frames with an omega scan of 0.30° and corrected for Lorentz and polarization effects. Data were treated by the Bruker SAINT software and the structures were solved using SHELXTL [15] and Fourier techniques. All hydrogen atoms were placed in calculated positions and included in the final cycles of refinement. Four solvent $(C_2H_5)_2O$ molecules were found in a unit cell of **1**. The final $R_1(wR_2)$ indices for **1** are 0.0345(0.0859) using 12,778 independent reflections. The final $R_1(wR_2)$ indices for **2** are 0.0505(0.0790) using 10,854 independent reflections. Crystallographic data are given in Table 1.

Table 1
Crystallographic data for **1** and **2**

	1	**2**
Formula	$C_{36}H_{54}Cl_6CoOP_4Re_3S_4$[a]	$C_{32}H_{44}Cl_6CoP_4Re_3S_4$
Formule weight (g mol^{-1})	1585.14	1511.02
Crystallographic color	black	black
Crystallographic size (mm^3)	$0.40\times0.10\times0.10$	$0.12\times0.04\times0.02$
Space group	$P2_1/c$	$P2_1/c$
Unit cell dimensions		
a (Å)	17.7793(7)	18.5585(8)
b (Å)	11.5586(5)	11.4916(5)
c (Å)	25.6951(11)	20.6682(8)
α (°)	90	90
β (°)	102.943(1)	96.476(1)
γ (°)	90	90
V ($Å^3$)	5146.3(4)	4379.7(3)
Z	4	4
T (°C)	−100	−100
Radiation (Mo Kα) (Å)	0.71069	0.71069
ρ_{calc} (g cm^{-3})	2.046	2.292
μ (mm^{-1})	7.977	9.365
θ Range (°)	1.18–28.32	1.10–28.28
hkl Index ranges	−20/23	−24/19
	−15/15	−15/12
	−34/23	−23/27
Goodness-of-fit on F^2	1.055	1.039
R indices [$I > 2\sigma(I)$]	$R_1 = 0.0283$,	$R_1 = 0.0396$,
	$wR_2 = 0.0807$	$wR_2 = 0.0744$
R (all data)	$R_1 = 0.0345$,	$R_1 = 0.0505$,
	$wR_2 = 0.0859$	$wR_2 = 0.0790$
Largest differential peak and hole (e $Å^{-3}$)	3.207 and −0.858	1.847 and −0.929

[a] Including a solvate molecule.

3. Results and discussion

3.1. Synthesis

Treatment of $[(PPh_3)_2N][Re_3(\mu_3\text{-}S)(\mu\text{-}S)_3Cl_6(PMe_2Ph)_3]$ with anhydrous cobalt(II) chloride in dichloromethane in the presence of dimethylphenylphosphine formed isomeric rhenium–cobalt mixed metal cluster complexes, $[Re_3Co(\mu_3\text{-}S)_4Cl_6(PMe_2Ph)_4]$ **1** and **2**. ^1H

and ^{31}P NMR spectra showed the presence of two types of cluster compounds in the products obtained from the reaction at room temperature which were isolated by silica-gel column chromatography using dichloromethane (compound **1**) and acetone (compound **2**) as eluents. Only the isomer **1** was obtained from the reaction at room temperature followed by reflux. Single crystals were obtained by slow diffusion of diethyl ether onto the dichloromethane solutions. Although coordination of three bridging sulfurs in the trinuclear rhenium complex to a hetero metal seems to be a facile reaction, only nickel [5] and copper [16] derivatives have been prepared and the present synthesis of the cobalt derivatives gives some clue to the difficulty of the preparation.

3.2. Structures

3.2.1. NMR spectra

^{1}H NMR spectra of **1** show methyl bands at 1.71 (d, Re–P(CH_3)$_2$(C$_6$H$_5$)), 2.10 (dd, Co–P(CH_3)$_2$(C$_6$H$_5$)) and 2.28 (d, Re–P(CH_3)$_2$(C$_6$H$_5$)) ppm with the intensity ratio of 3:2:3. The dimethylphenylphosphine coordinated to three rhenium atoms gives two kinds of methyl signals due to different conformations of the groups. The double doublet signals are assigned to the two methyl groups of dimethylphenylphosphine coordinated to a cobalt atom with slight difference of conformation. ^{31}P NMR spectra of **1** show a band at −24.69 ppm assignable to dimethylphenylphosphine coordinated to rhenium and at 38.77 ppm assignable to the one coordinated to cobalt. ^{1}H NMR spectra of **2** show methyl bands at 1.85 (d, Re–P(CH_3)$_2$(C$_6$H$_5$)), 1.95 (dd, Re–P(CH_3)$_2$(C$_6$H$_5$)), 2.00 (d, Co–P(CH_3)$_2$(C$_6$H$_5$)) and 2.45 (d, Re–P(CH_3)$_2$(C$_6$H$_5$)) with the intensity ratio of 1:1:1:1. ^{31}P NMR spectra of **2** show three bands at −30.92, −26.89 and −24.80 ppm assignable to dimethylphenylphosphine coordinated to rhenium and a band at 33.10 ppm assignable to the one coordinated to cobalt. ^{1}H and ^{31}P NMR spectra indicate the different conformations of the methyl groups of the dimethylphenylphosphine ligands with respect to the Re$_3$ plane and μ_3-S atom. The structures (vide infra) of the isomers indicate that the major isomer has three phosphines directed opposite to μ_3-S and the minor isomer contains a dimethylphenylphosphine in the direction of μ_3-S.

3.2.2. X-ray structures

The crystal of **1** contains a diethylether molecule as a solvate molecule. Both the major product (compound **1**) and minor product (compound **2**) have tetranuclear metal frameworks with three rhenium and one cobalt atom bonded together by four μ_3-S atoms (Figs. 1 and 2).

The Re–Re, Re–Co, Re–S and Co–S interatomic distances in the two isomers are not appreciably different (Table 2).

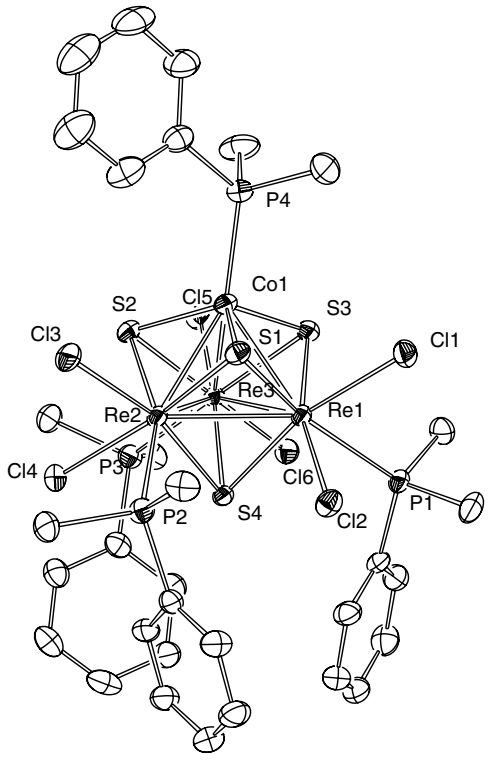

Fig. 1. ORTEP representation of [Re$_3$CoS$_4$Cl$_6$(PMe$_2$Ph)$_4$] **1** at the 50% probability level.

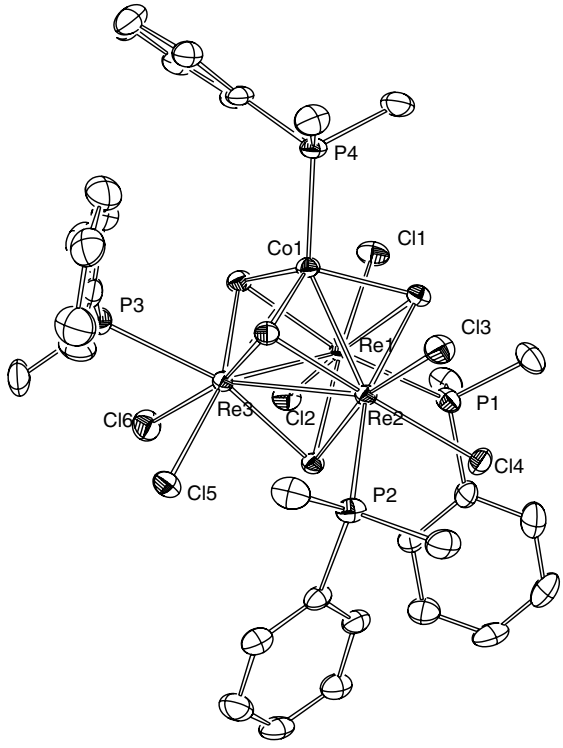

Fig. 2. ORTEP representation of [Re$_3$CoS$_4$Cl$_6$(PMe$_2$Ph)$_4$] **2** at the 50% probability level.

As the Re–Re distances are larger than Re–Co distances, the shapes of the cluster frameworks are flattened tetrahedra. The tetranuclear cluster compounds

Table 2
Selected interatomic distances (Å) and bond angles (°) for **1** and **2**

	1	**2**
Interatomic distances		
Re(1)–Re(2)	2.7720(3)	2.7711(3)
Re(1)–Re(3)	2.7683(3)	2.7647(4)
Re(2)–Re(3)	2.7679(3)	2.7738(3)
Re(1)–Co(1)	2.5970(6)	2.5954(8)
Re(2)–Co(1)	2.5992(6)	2.5990(8)
Re(3)–Co(1)	2.6014(7)	2.6045(8)
Re–S (av)	2.324	2.322
Co–S (av)	2.148	2.144
Re–P (av)	2.553	2.550
Co–P	2.185	2.187
Re–Cl (av)	2.438	2.437
Bond angles		
Re(3)–Re(1)–Re(2)	59.947(6)	60.140(9)
Co(1)–Re(2)–Re(3)	57.882(15)	57.884(19)
Re(1)–Co(1)–Re(3)	64.353(15)	64.238(19)
Co(1)–S(1)–Re(1)	70.68(4)	71.14(5)
Re(2)–S(1)–Re(1)	73.22(4)	73.25(4)
Re(1)–S(4)–Re(2)	73.01(3)	73.24(4)
P(1)–Re(1)–Re(3)	101.32(3)	146.48(4)
P(1)–Re(1)–Re(2)	143.04(3)	101.79(4)
P(4)–Co(1)–Re(3)	141.69(5)	145.96(6)
P(4)–Co(1)–Re(1)	136.27(4)	137.94(6)
Cl(1)–Re(1)–Cl(2)	83.96(4)	84.83(8)
P(1)–Re(1)–Cl(1)	78.41(4)	78.53(6)
P(1)–Re(1)–Cl(2)	79.70(4)	80.20(5)

1 and **2** have 60 valence electrons counted on the basis of neutral atoms (Re7, Co9, S4, Cl1, P2) and the number is common among tetrahedral cluster compounds [17]. The average Re–Re (2.769 Å) and Re–Co (2.599 Å) distances are close enough to invoke Re–Re and Re–Co metal–metal bonding interactions. They are a little shorter than Re–Re (2.806 Å) and Re–Ni (2.710 Å) interatomic distances in $[Re_3NiS_4Cl_6(PEt_3)_4]$, which has 61 valence electrons [5]. The smaller total number of valence electrons (60 vs. 61 e) seems to have a slight influence upon shortening of the metal–metal distances in spite of the fact that different phosphines are coordinated. Each rhenium atom is coordinated by two chlorine atoms and one dimethylphenylphosphine ligand. Compound **1** has three dimethylphenylphosphine ligands in the direction of the original μ_3-S atom in the starting trinuclear cluster, but compound **2** has one dimethylphenylphosphine ligand in the opposite direction. The steric influence of dimethylphenylphosphine ligands upon the capture of the cobalt atom seems to make formation of isomers with two or three dimethylphenylphosphine ligands in the direction opposite to the original μ_3-S atom in the trinuclear cluster less favorable. The cobalt atom is coordinated by a dimethylphenylphosphine ligand. Thus the rhenium atoms are hexa-coordinate and cobalt tetra-coordinate if metal-metal bonds are not taken into account.

The present synthesis of mixed metal Re_3Co sulfide cluster complexes indicates that the conformation of coordinated phosphines in the trinuclear rhenium cluster complex is important to facilitate coordination of μ-S atoms to a hetero atom like cobalt. The fact that the major product **1** contains three dimethylphenylphosphines in the opposite orientation to that in the starting cluster compound necessitates the change of the conformation of chlorine and phosphine ligands during the reaction. It is conceivable that **1**, obtained under reflux, is thermodynamically more stable than **2**.

4. Supplementary material

All the crystallographic data of **1** and **2** have been deposited at the Cambridge Crystallographic Data Centre as supplementary publication Nos. CCDC 232748 and 232749 for **1** and **2**, respectively. These data can be obtained free of charge via www.ccdc.cam.ac.uk/conts/retrieving.html, by emailing data_request@ccdc.cam.ac.uk, or by contacting The Cambridge Crystallographic Data Centre, 12 Union Road, Cambridge CB2 1EZ, UK; fax: +44-1223-336-033.

References

[1] J.-C.P. Gabriel, K. Boubekeur, S. Uriel, P. Batail, Chem. Rev. 101 (2001) 2037.
[2] H.D. Selby, B.K. Roland, Z. Zheng, Acc. Chem. Res. 36 (2003) 933.
[3] T. Saito, J. Chem. Soc., Dalton Trans. (1999) 97.
[4] J. Beck, K. Müller-Buschbaum, Z. Anorg. Allg. Chem. 625 (1999) 1212.
[5] N. Miyake, H. Imoto, T. Saito, Chem. Lett. (1997) 631.
[6] T. Shibahara, Coord. Chem. Rev. 123 (1993) 73.
[7] T. Shibahara, Adv. Inorg. Chem. 37 (1991) 143.
[8] R. Hernandez-Molina, M.N. Sokolov, A.G. Sykes, Acc. Chem. Res. 34 (2001) 223.
[9] N.N. Timoshchenko, V.L. Kolosnichenko, S.V. Volkov, Y.L. Slovokhotov, Y.T. Struchkov, Koord. Khim. 16 (1990) 1062.
[10] J. Marcoll, A. Rabenau, D. Mootz, H. Wunderlich, Revue de Chimie minerale 11 (1974) 607.
[11] S. Yamada, N. Miyake, H. Imoto, T. Saito, Chem. Lett. (1997) 671.
[12] N. Miyake, H. Imoto, T. Saito, Chem. Lett. (1997) 913.
[13] M. Sokolov, H. Imoto, T. Saito, Chem. Lett. (1998) 949.
[14] N. Sakai, T. Sunaga, T. Saito, unpublished.
[15] SHELXTL-NT, v.6.12, Bruker Axis, Inc., Madison, WI., 2001.
[16] T. Sunaga, K. Iijima, N. Sakai, T. Saito, unpublished.
[17] D.M.P. Mingos, D.J. Wales, Introduction to Cluster Chemistry, Prentice-Hall, London, 1990 pp. 11–119.

Available online at www.sciencedirect.com
SCIENCE DIRECT®
Polyhedron 23 (2004) 2615–2623
POLYHEDRON
www.elsevier.com/locate/poly

Hypercoordinate silicon and phosphorus acetylene compounds: crystal structure determinations and fluorescence spectroscopic study

Sergei B. Bushuk [a,*], Francis H. Carré [b], Daniel M.H. Guy [b], William E. Douglas [b], Yulia A. Kalvinkovskya [a], Larissa G. Klapshina [c], Anatoly N. Rubinov [a], Alexander P. Stupak [a], Boris A. Bushuk [a]

[a] B.I. Stepanov Institute of Physics, National Academy of Science of Belarus, F. Skaryna Ave. 68, 220072 Minsk, Belarus
[b] CNRS UMR 5637, Université Montpellier II, 34095 Montpellier cedex 5, France
[c] G.A. Razuvaev Institute of Metallo-organic Chemistry, Russian Academy of Sciences, Tropinin Street 49, GSP-445, Nizhny Novgorod, 603600, Russia

Received 1 April 2004; accepted 17 June 2004
Available online 27 August 2004

Abstract

The steady-state fluorescence, fluorescence excitation spectra and fluorescence lifetime of pentacoordinate [8-(dimethylamino-κ*N*)-1-naphthalenyl-κ*C*]diethynylmethylsilicon as a function of excitation and emission wavelengths were investigated in solvents of various polarities at room temperature. Inhomogeneous spectral broadening and biexponential decay-times ($\tau_1 \sim 1$ ns and $\tau_2 \sim 15$ ns) were associated with the existence of two types of electronic states created as a result of the interaction of the amino group with the π-conjugated system and the $CH_3Si(C{\equiv}CH)_2$ group. The crystal structure of the silicon monomer shows a monocapped tetrahedral geometry in which the N atom is opposite one of the acetylene groups. An interaction between the N and Si atoms is evident, the N–Si distance being less than the sum of the van der Waals radii of the 2 atoms. The crystal structure of the analogous hypercoordinate acetylene phosphorus compound [8-(dimethylamino- κ*N*)-1-naphthalenyl-κ*C*]diphenylethynylphosphorus is similar, the short P–N distance and only slight distortion of the naphthalene ring reflecting the P–N interaction. Oxidation of the phosphorus compound to the corresponding oxide readily occurs on treatment with hydrogen peroxide.
© 2004 Elsevier Ltd. All rights reserved.

Keywords: Silicon; Phosphorus; Hypercoordination; Hypervalency; Spectroscopy; Fluorescence; X-ray crystallography

1. Introduction

The physical–chemical and optical properties of organic polymers are widely investigated due to their potential use in optoelectronics in optical switching, photorefractive and photovoltaic devices. Several conditions have to be fulfilled simultaneously in order to create solid-state organopolymer systems for practical use including polymer films of high optical quality, solubility in organic solvents and molecular structures providing effective intra- and intermolecular charge transfer between donor and acceptor fragments of the organopolymer. From this point of view, silicon-containing organopolymers are very promising compounds giving rise to films of good optical quality by the sol–gel method and with long π-conjugated polymeric chains. The nonlinear optical properties of conjugated silicon-containing polymers have been investigated [1] and it was shown that polymers including pentacoordinate silicon in the main chain exhibit particularly high values of

* Corresponding author. Tel.: +33 467 143 853; fax: +33 467 143 852.
E-mail address: douglas@univ-montp2.fr (S.B. Bushuk).

0277-5387/$ - see front matter © 2004 Elsevier Ltd. All rights reserved.
doi:10.1016/j.poly.2004.06.026

third-order nonlinear susceptibility. Indeed, hypercoordinate silicon [2] and phosphorus [3–5] compounds exhibit very different chemical and electronic behaviour from the tetracoordinate analogues. The spectroscopic characteristics of the molecule with silicon pentacoordination, [8-(dimethylamino-κ*N*)-1-naphthalenyl-κ*C*]diethynylmethylsilicon (**1**), are presented here. Its crystal structure is reported and compared to that of an analogous hypercoordinated acetylene phosphorus compound, [8-(dimethylamino-κ*N*)-1-naphthalenyl-κ*C*]-diphenylethynylphosphorus (**2**). Both molecules contain the 1-(8-dimethylamino)naphthyl ligand, which is known to give stable hypercoordinate species [6].

2. Experimental

All reactions were performed using standard Schlenk-tube techniques under an atmosphere of dry argon. Solvents were distilled from appropriate drying agents and degassed before use. NMR spectra were obtained using a Bruker Avance DPX-200 spectrometer operating at 200 MHz (^{1}H), 50.327 MHz (^{13}C) or 39.763 MHz (^{29}Si), except ^{31}P NMR spectra which were obtained on a Bruker 250 AC spectrometer at 101.202 MHz. ^{1}H, ^{13}C and ^{29}Si NMR chemical shifts are reported relative to Me_4Si, and ^{31}P chemical shifts relative to H_3PO_4. Infrared spectra were obtained in the region 500–4000 cm^1 with a Perkin–Elmer 1600 FT spectrophotometer. Elemental analyses were carried out by the Service Central de Microanalyse du CNRS. [8-(Dimethylamino)-1-naphthalenyl]phosphonous dichloride was prepared as previously described [7].

2.1. Preparation of **1** [8]

Monoacetylene Grignard reagent was prepared by bubbling acetylene through a solution of the Grignard reagent prepared from magnesium (4.4 g, 181.0 mmol) and bromoethane (19.78 g, 181.5 mmol) in THF (350 ml). A solution of [8-(dimethylamino-κ*N*)-1-naphthalenyl-κ*C*]dichloromethylsilicon [9] (17.72 g; 62.3 mmol) in THF (200 ml) was added rapidly to the monoacetylene Grignard reagent at −78 °C. The mixture was allowed to warm to r.t. overnight with stirring. The reaction mixture was pumped to dryness and the residue taken up in diethylether to give a solution which was washed successively with aqueous acetic acid (10%), aqueous sodium bicarbonate and water. The organic layer was dried over $MgSO_4$ and evaporated to give the crude solid product, which was recrystallised from *n*-hexane affording beige crystals (12.5 g; m.p. 102.4–104.3 °C) in 76% yield. IR [nujol, $\bar{\nu}$/cm^{-1}]: 3259vs [ν(≡C–H)], 2036s [ν(C≡C)], 2021s [ν(C≡C)], 1943vw, 1890vw, 1839vw, 1611w, 1588w, 1566m, 1331s, 1284m, 1252s, 1208m, 1164m, 1147w, 1092m, 1072s, 1037m, 1020s, 951s, 882s, 836s, 780s, 742s, 725vs, 714vs, 703vs, 682vs, 672vs, 631vs, 607s, 591vs. ^{1}H NMR ($CDCl_3$): δ 7.4–8.6 (m, 6H, arom.), 2.72 (s, 6H, NCH_3), 2.63 (s, 2H, C≡CH), 0.65 (s, 3H, $SiCH_3$). ^{13}C NMR ($CDCl_3$): δ 152.18, 139.05, 134.69, 134.38, 131.08, 127.91, 126.46, 126.07, 117.33, 93.00 (SiC≡*C*H), 91.34 (Si*C*≡CH), 48.30, 2.47. ^{29}Si NMR ($CDCl_3$): δ −56.65. *Anal.* Calc. for $C_{17}H_{17}NSi$: C, 77.52; H, 6.50; Si, 10.66. Found: C, 77.60; H, 6.18; Si, 10.20%.

2.2. Preparation of **2**

A solution of phenylethynyllithium, prepared from *n*-BuLi in *n*-hexane and phenylacetylene (4.5 ml, 41.0 mmol) in diethylether at −50 °C, was added rapidly to a stirred suspension of [8-(dimethylamino)-1-naphthalenyl]phosphonous dichloride (5.59 g, 20.54 mmol) in diethylether (100 ml) at −50 °C. The mixture was allowed to warm to r.t. and was hydrolysed after being stirred for 20 h. The aqueous phase was extracted with diethylether and the combined organic phase was washed with water. After drying over $MgSO_4$, evaporation afforded a brown oil (8.4 g). Crystallisation from *n*-heptane gave yellow crystals (3 g; m.p. 107.1–107.6 °C) in 36% yield. IR [nujol, $\bar{\nu}$/cm^{-1}]: 3054m, 2177w, 2157s [ν(C≡C)], 1964w, 1894w, 1819w, 1681w, 1592m, 1567m, 1331m, 1290w, 1219m, 1204m, 1182m, 1156w, 1087m, 1072m, 1038m, 1024m, 999w, 970w, 950m, 920m, 875w, 826vs, 801w, 790w, 774vs, 760vs, 743m, 690vs, 668m, 631s, 610s, 602s, 538vs. ^{1}H NMR ($CDCl_3$): δ 7.3–8.8 (m, 16H, arom.), 2.9 (s, 6H, NCH_3). ^{13}C NMR ($CDCl_3$): δ 152–120 (arom.), 103.95 (d, $^2J_{^{31}P^{13}C}$ = 2 Hz, PC≡*C*), 89.20 (d, $^1J_{^{31}P^{13}C}$ = 16.36 Hz, P*C*≡C), 47.55 (CH_3), 47.39 (CH_3). ^{31}P NMR ($CDCl_3$): δ −61.88. *Anal.* Calc. for $C_{28}H_{22}NP$: C, 83.36; H, 5.50; N, 3.47; P, 7.68. Found: C, 83.29; H, 5.79; N, 3.47; P, 7.54%.

2.3. Preparation of [8-(dimethylamino-κN)-1-naphthalenyl-κC]diphenylethynylphosphorus oxide (**3**)

Aqueous hydrogen peroxide (15% w/w, 20 ml, 88 mmol) was added to a solution of **2** (2.00 g, 4.96 mmol) in dichloromethane (20 ml). After the mixture had been stirred at r.t. for 3 h, the aqueous phase was separated and extracted with dichloromethane. The combined organic phases were washed with water and dried over magnesium sulfate. Evaporation afforded a yellow solid (1.82 g, 87%). IR [nujol, $\bar{\nu}$/cm^{-1}]: 2178s [ν(C≡C)], 1610w, 1591m, 1566m, 1335m, 1293w, 1224s, 1199vs, 1182s, 1153s, 1087m, 1082s, 1072m, 1043m, 1026s, 957sw, 916w, 884m, 846vs, 836vs, 790m, 771s, 752vs, 688vs, 653vs, 633s, 604s, 512vs. ^{1}H NMR ($CDCl_3$): δ 7.3–9.0 (m, 16H, arom.), 2.8 (s, 6H, NCH_3). ^{13}C NMR ($CDCl_3$): δ 152–120 (arom.), 101.40 (d, $^2J_{^{31}P^{13}C}$ =

36.64 Hz, PC≡*C*), 87.69 (d, $^2J_{^{31}P^{13}C} = 207.6$ Hz, P*C*≡C), 48.20 (CH_3). ^{31}P NMR ($CDCl_3$): δ −20.29. *Anal.* Calc. for $C_{28}H_{22}NOP$: C, 80.18; H, 5.29; N, 3.34; O, 3.81; P, 7.38. Found: C, 79.98; H, 5.36; N, 3.56; O, 3.83; P, 7.27%.

2.4. Spectroscopic measurements

Spectroscopic-grade solvents (Merck) were used for all investigations. The absorption spectra of the solutions were recorded by using a Cary-500 spectrophotometer. The fluorescence and fluorescence excitation spectra measurements were performed on an SLM-4800 spectrofluorimeter (spectral width of excitation and registration slits were 8 and 4 nm, respectively). The fluorescence decay times were recorded by the single-photon counting method using a thyratron-controlled flash lamp as the excitation source. The instrumental resolution of the device was $\Delta\tau = 0.5$ ns at 400 nm. Fluorescence decay times were obtained from double-exponential decay analysis:

$$I_f(t) = B + A_1 \exp(t/\tau_1) + A_2 \exp(t/\tau_2).$$

The fractional contribution (f_i) of each decay-time was estimated according to:

$$f_i = \frac{A_i\tau_i}{\sum_{j=1}^{2} A_i\tau_i}.$$

All specroscopic measurements were performed at room temperature and a molecular concentration of 1×10^{-5} M.

2.5. Crystal structure determinations

The crystals of **1** and **2** used were found to produce only moderate diffraction intensities. Owing to the small number of observed data, only the silicon, phosphorus and nitrogen atoms were refined anisotropically.

In the case of **1**, the systematic absences revealed either space group $Pca2_1$ or *Pbcm*. Direct methods (SHELXS-86 [10]) solved the structure with space group $Pca2_1$ (No. 29). All the atomic positions appeared in the E-map excepted for atoms C(6) and C(7). A difference Fourier map gave the positions of the remaining atoms. The calculated hydrogen atoms [11] were included in the last stages of the refinement. Convergence occurred for the R_1 value of 0.0480 ($wR_2 = 0.0818$).

In the case of **2**, direct methods [10] solved the structure with the monoclinic space group *C*2/*c* (No. 15). Three carbon atoms [C(34), C(35) and C(36)] were missing but their positions were revealed in a subsequent difference-Fourier synthesis. The hydrogen atoms were positioned by calculation [11] and taken into account in the next refinements. The final R_1 and wR_2 values were 0.0680 and 0.1884, respectively.

3. Results and discussion

3.1. Preparation of complexes

The pentacoordinate silicon-containing monomer **1** (which can be considered as being (4+1) coordinate [12]) was prepared in 76% yield by treating the previously characterised [9] pentacoordinate dichlorosilane with monoethynyl Grignard reagent (Scheme 1). The ^{29}Si NMR spectrum of **1** shows a signal at δ −56.65 whereas that for the hexacoordinate analogue occurs at δ −63.8 [13], and for the tetracoordinate compound $Ph_2Si(C{\equiv}CH)_2$ at δ −48.2 [14]. The IR spectrum exhibits a ν(C≡C) absorbance at 2036 cm^1, between those for the hexacoordinate analogue (2026 cm^{-1}) [13] and $Ph_2Si(C{\equiv}CH)_2$ (2044 cm^{-1}) [15].

The hypercoordinate phosphorus-containing compound **2** was prepared by treatment of [8-(dimethylamino)-1-naphthalenyl]phosphonous dichloride [7] with phenylethynyllithium (Scheme 2). The ^{31}P NMR spectrum of **2** shows a signal at δ −61.88 and the IR spectrum exhibits a ν(C≡C) absorbance at 2157 cm^1. The relative magnitudes of the ^{31}P–^{13}C coupling constants were used to assign the acetylene ^{13}C NMR resonances, δ 103.95 (PC≡*C*) and δ 89.20 (P*C*≡C). As previously observed for such hypercoordinate phosphorus compounds [16], the room temperature solution ^1H NMR spectrum for **2** shows a singlet for the NMe_2 protons, the ^{13}C NMR spectrum exhibiting two signals for the NMe_2 methyls.

Complex **2** is readily transformed into the oxide **3** in 87% yield on treatment of a dichloromethane solution with hydrogen peroxide (Scheme 2). The IR ν(C≡C) absorbance for **3** occurs at higher energy (2178 cm^{-1}) than that for **2** (2157 cm^{-1}), and both acetylene ^{13}C NMR resonances are shifted to higher field.

3.2. Spectroscopic investigations of *1*

In Fig. 1, the absorption (a) and fluorescence (b) spectra of **1** in cyclohexane and dimethylformamide

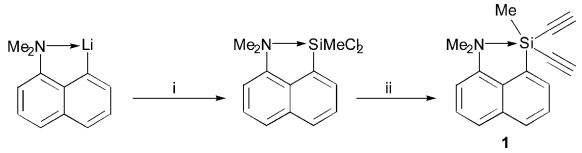

Scheme 1. Reagents and conditions: (i) excess $MeSiCl_3$, Et_2O, room temp., 5 h and (ii) HC≡CMgBr, THF, −78 °C to room temp.

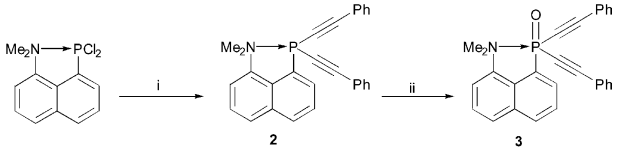

Scheme 2. Reagents and conditions: (i) PhC≡CLi, Et_2O, −50 °C to room temp., 20 h and (ii) H_2O_2, CH_2Cl_2, room temp., 3 h.

(DMF) are displayed. Table 1 shows the spectral characteristics obtained in the set of different polarity solvents. The fluorescence spectra were recorded at excitation into the absorption band maximum. The fluorescence excitation spectra measured with excitation at the fluorescence band maxima correspond well to the absorption spectra regarding both shape and maxima position. As can be seen from the data presented in Table 1, the molecules examined exhibit the following spectral peculiarities: (i) large Stokes shifts between the absorption and fluorescence spectra maxima increasing up to 11 000 cm^{-1} in solvents of high polarity, (ii) the maximum position of the absorption spectrum depends weakly on the solvent polarity and shifts to shorter wavelengths with polarity increase, (iii) the increase in solvent polarity leads to an essentially long wavelength shift of the fluorescence spectrum maximum, (iv) the full width at half maximum (f.w.h.m.) of the fluorescence spectrum depends on the solvent polarity.

The spectral data presented afford evidence of an essential increase of the molecule dipole moment in the excited electronic state (μ_e) with respect to the dipole moment in the ground state (μ_g). It is known that the formation of a charge transfer emitting state includes intramolecular charge transfer during the absorption process and subsequent stabilization of the created electron density distribution by the polar environment [17].

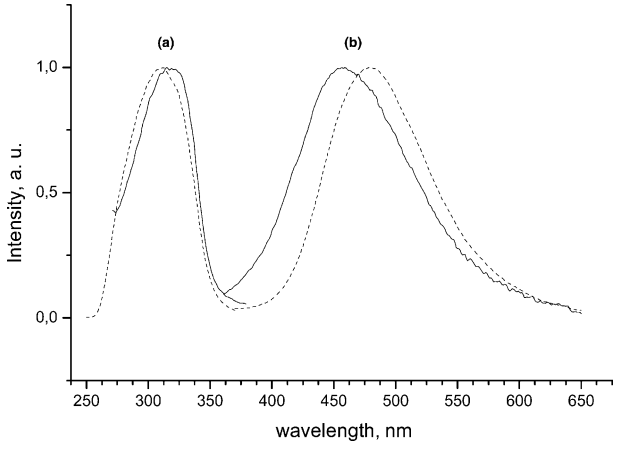

Fig. 1. Absorption (a) and fluorescence (b) spectra of **1** in cyclohexane (bold line) and DMF (dotted line).

To estimate $\Delta\mu = \mu_e - \mu_g$ we used the Bakhshiev equation [18]:

$$hca^3\Delta\nu = 2(\mu_g^2 + \mu_e^2 - 2\mu_g\mu_e\cos\alpha)F(\varepsilon,n)F^2(n), \quad (1)$$

where

$$F(\varepsilon,n) = (\varepsilon-1)/(\varepsilon+2) - (n^2-1)/(n^2+2);$$
$$F^2(n) = (2n^2+1)/(n^2+2)^2,$$

$\Delta\nu = (\nu_a^{max} - \nu_{fl}^{max})$, α is the angle between μ_e and μ_g, ε is the solvent dielectric constant, n is the refractive index (at the sodium d line), c is the velocity of light, a is the Onsager cavity radius. We assume a cavity radius of 3.5 Å, a little higher than that of dimethylaminonaphthalene [19] in view of the presence of the accepting $CH_3Si(C{\equiv}CH)_2$ group in the molecule. The least squares fit analysis of the data based on Eq. (1) is shown in Fig. 2. The slope of the line yields a change of dipole moment of 2.9 D.

To further investigate the nature of the excited electronic state of the molecule, we studied in detail the dependence of the fluorescence spectrum on excitation wavelength. As can be seen from the above results, the maximum position and shape of the fluorescence spectrum do not depend on the excitation wavelength when the excitation is within the region of the first absorption band from 280 to 330 nm in all the solvents used. However, under excitation at the red edge of the absorption spectrum in highly polar solvents a short-wavelength shift of the fluorescence band maximum and an increase of its f.w.h.m. are observed. The fluorescence band spectral characteristics of the DMF solution as a function of excitation wavelength are shown in Table 2. It can be clearly seen from these data that red edge excitation causes the essential transformation of the fluorescence band. The fluorescence excitation spectra measured at various registration wavelengths are depicted in Fig. 3. It follows from these results that the fluorescence excitation spectrum of the molecules forming the short-wavelength part of the fluorescence spectrum shifts to the red side with respect to the absorption spectrum maximum. The set of spectral dependencies obtained gives evidence of essential inhomogeneous broadening of the absorption and fluorescence spectra revealed in high polar solvents at room temperature. The inhomogeneous broadening cannot be caused by

Table 1
Spectral data for compound **1** in various solvents

Solvent	ν_a^{max} (cm^{-1})	ν_{fl}^{max} (cm^{-1})	$\Delta\nu = \nu_a^{max} - \nu_{fl}^{max}$ (cm^{-1})	$\Delta\nu_{1/2}$ f.w.h.m. (cm^{-1})	$F(\varepsilon,n)F^2(n)$
1. Cyclohexane	31 348	21 882	9466	5631	0
2. Chloroform	32 573	21 930	10 643	4914	0.46
3. Dioxane	31 949	21 368	10 581	4844	0.58
4. Dichloromethane	32 468	21 097	11 371	4742	0.74
5. Ethanol	32 787	21 505	11 282	6104	0.99
6. DMF	32 154	30 833	11 321	4170	1.05

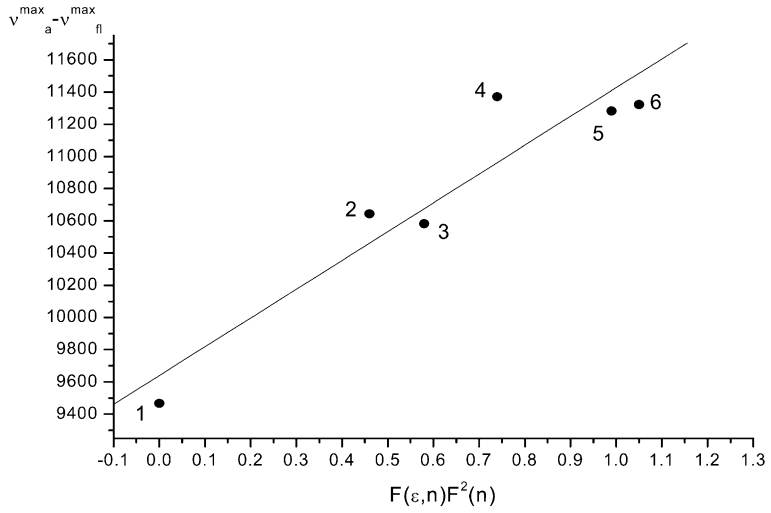

Fig. 2. Plot of Stokes shift ($\nu_a^{max} - \nu_{fl}^{max}$) versus $F(\varepsilon,n)F^2(n)$.

Table 2
Fluorescence band spectral characteristics of compound **1** in DMF at various excitation wavelengths

ν_{ex} (cm^{-1})	ν_{fl}^{max} (cm^{-1})	$\Delta\nu_{1/2}$ f.w.h.m. (emission) (cm^{-1})
34483	20833	4174
32258	20833	4209
29412	20877	4832
28571	21186	5837
27778	22321	5939

the fluctuations of the solvent reactive field or the dynamics of dipole–dipole interactions between solute and solvent molecules because the Debye relaxation time of the solvent used at room temperature is too fast (of the order of picoseconds). On the other hand, electronic spectra inhomogeneous broadening can be of an intramolecular nature as a result of the presence of centres with different electronic state structure in the solution.

Valuable additional information concerning the nature of the emitting state can be obtained from the analysis of time-resolved fluorescence data. These results are presented in Table 3. When a dimethyformamide solution is excited at the short (λ_{ex} = 290 nm) and long wavelength (λ_{ex} = 330 nm) parts of the first absorption band,

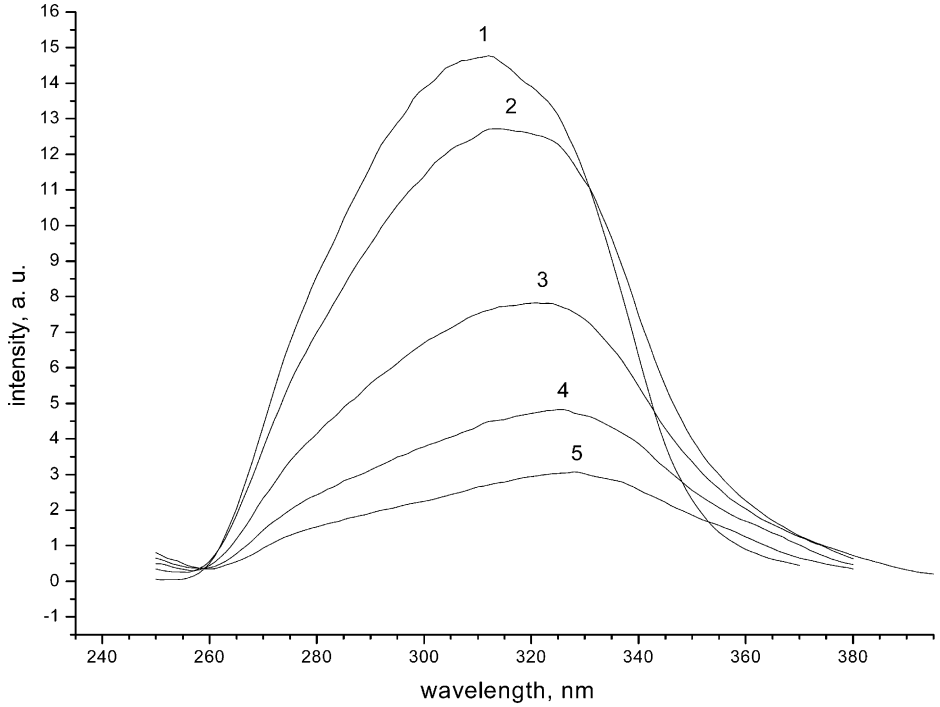

Fig. 3. Fluorescence excitation spectra of **1** in DMF at various recorded wavelengths (1–480, 2–430, 3–420, 4–410 and 5–400 nm).

the fluorescence decay curves are sufficiently well described by two exponents with essentially different decay times ($\tau_1 \sim 1$ ns and $\tau_2 \sim 15$ ns). It should be noted that at red edge excitation the weight contribution of the component with higher decay time increases. The ethanol solution possesses the same spectral and temporal features but both decay times are shorter and the long component weight is essentially higher. Thus, summarizing the above presented frequency dependencies of the fluorescence, fluorescence excitation spectra and biexponential fluorescence decay times one can suggest the existence of two types of electronic transitions in the absorption and fluorescence spectra resulting from the molecular structure. The proposed scheme of electronic levels and the transitions between them are shown in Fig. 4. The absorption spectrum consists of the short wavelength (I) and long wavelength (II) transitions that are separated (Fig. 3) by a sufficiently narrow energy gap ($\sim$3000 cm^{-1}). Intramolecular (non-radiative transition between two excited electronic states) and intermolecular (the interactions between the doped centre and surrounding solvent molecules) processes form two equilibrated excited electronic states S_I^{eq} and S_{II}^{eq}. Both states possess essential charge transfer character due to the large Stokes shift and have different fluorescence lifetimes.

As regards the mechanisms of the excited states formation, we propose the following hypothesis. The crystal structure determination (see below) shows an essentially trigonal bipyramidal geometry at silicon with the amino group lone pair of electrons opposite one of the acetylene groups, both groups lying in the axial positions. The photophysical characteristics of conjugated π-electronic systems containing the electron-donor amino group substituent (including aminonaphthalenes) and the mechanisms of excited state formation have been widely studied [20–22]. It was shown that sp^3-hybridization of the amino group nitrogen and rotation of its hybrid non-shared electron pair with respect to the π-electrons of the ring gave rise to the formation of a charge transfer emitting state. The latter is stabilized by polar solvent molecules. In our case, the presence of the bulky $CH_3Si(C{\equiv}CH)_2$ substituent can cause two additional effects: (i) A change in the orientation of the nitrogen hybrid non-shared electron pair due to additional steric hindrance. This effect results in an alteration of the electronic charge transfer degree from the dimethylamino group into the ring. (ii) The chemistry of silicon is very dependent on coordination number and valency state, and in the case of hypercoordination arising from the 8-dimethylaminonaphthyl group there is extensive evidence of intramolecular coordination of the nitrogen lone pair to the silicon [2]. Quantum-chemical calculations of the electronic charge distribution in tetracoordinated silicon (for silylacetylenes in particular) show the essential decrease of the negative charge at silicon in such structures [23]. This makes for an enhancement of the acceptor properties of silicon in **1**. Thus, the amino group lone pair can interact both with the π-system of the naphthalene ring and with the $CH_3Si(C{\equiv}CH)_2$ group. These interactions can cause inhomogeneous broadening of the absorption spectrum and lead to the possibility of the formation of different excited states. In the case of strong coupling between the nitrogen lone pair and the naphthalene ring π-system, an S_I excited state is formed that corresponds to the dimethylaminonaphthalene local excitation since all the spectral characteristics in various solvents and the decay time value of dimethylaminonaphthalene [19] agree well with the measured features of the S_I state. A decrease of this interaction due to either steric hindrance or direct donor–acceptor interactions between the dimethylamino group nitrogen and silicon leads to the S_{II} state formation. It is seen from the spectral data presented in Table 1 that the importance of the S_{II} state is higher in non-polar cyclohexane, the absorption spectrum maximum shifting towards the red and the fluorescence spectrum f.w.h.m. being larger than that in polar solvents. In the case of polar ethanol solution, one can envisage that the alcohol OH-group provides specific interactions between the nitrogen lone pair and hydrogen on the one hand and between oxygen and silicon

Table 3
Fluorescence decay parameters of compound **1** in DMF and ethanol

Solvent	λ_{ex} (nm)	λ_{reg} = 430 nm		λ_{reg} = 530 nm	
		τ, ns; (weight)	χ^2	τ, ns; (weight)	χ^2
DMF	290	τ_1 = 1.23 (0.72) τ_2 = 14.87 (0.28)	1.026	τ_1 = 1.3 (0.75) τ_2 = 15.98 (0.25)	1.261
	330	τ_1 = 1.06 (0.65) τ_2 = 15.48 (0.35)	1.243	τ_1 = 1.07 (0.65) τ_2 = 15.63 (0.35)	1.081
ethanol	290	τ_1 = 0.49 (0.64) τ_2 = 9.36 (0.36)	1.269		
	330	$_1$ = 0.60 (0.49) τ_2 = 9.54 (0.51)	1.104	τ_1 = 0.48 (0.50) τ_2 = 10.28 (0.50)	0.929

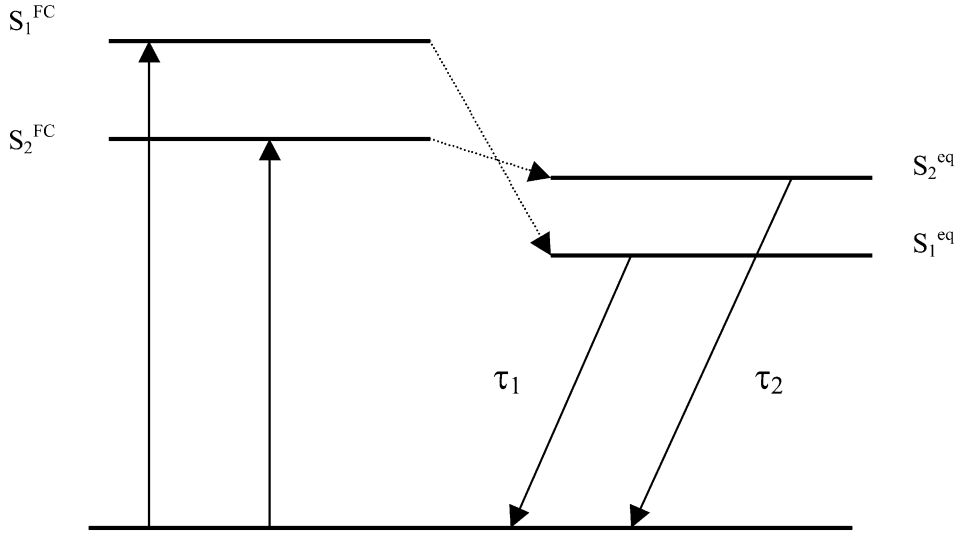

Fig. 4. Schematic energy level diagram for two types of compound **1** electronic states.

on the other. These interactions increase the weighting of the S_{II} state as can be seen from the data shown in Table 3, resulting in a large f.w.h.m. of the fluorescence spectrum in this solvent. Bearing in mind that both ethanol and DMF exhibit electron donor properties and only ethanol interacts with the nitrogen lone pair through H-bonding, one can assume that the orientation of the latter with respect to the ring π-system plays a crucial role in S_{II} state formation.

3.3. Crystal structures

The X-ray crystal structures of **1** (Fig. 5) and **2** (Fig. 6) show a monocapped tetrahedral geometry (including the lone pair in the case of **2**) in which the N atom is opposite one of the acetylene groups, the C(11)–Si–N angle in **1** being 172.3° and the C(11)–P–N angle in **2** being 168.6° (see Table 4 for selected bond lengths and

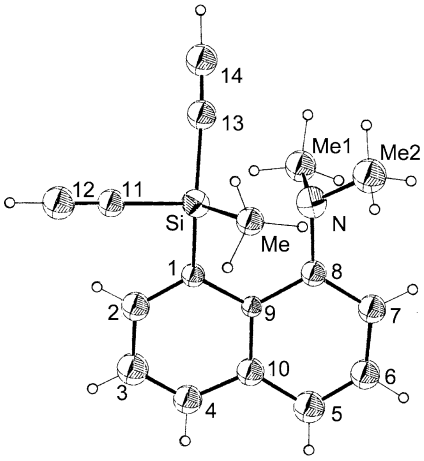

Fig. 5. Molecular structure of **1**; hydrogen atoms have been omitted for clarity. Unaccompanied numbers refer to carbon atoms.

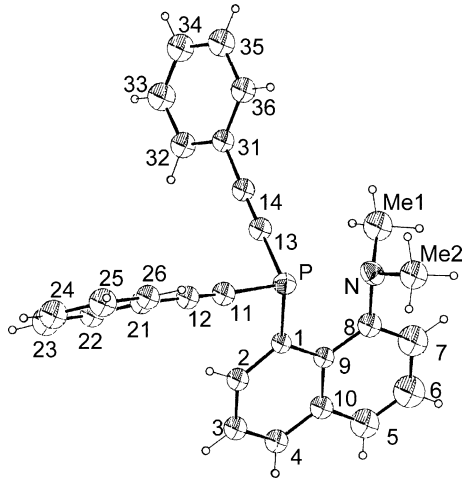

Fig. 6. Molecular structure of **2**; hydrogen atoms have been omitted for clarity. Unaccompanied numbers refer to carbon atoms.

angles and Table 5 for a summary of crystal data, intensity measurements and refinement). The distances in **1** between the Si and the nearest acetylene carbons (Si–C(11) and Si–C(13)) are similar to those for the analogous hexacoordinate compound, being slightly greater than for alkynylsilanes containing tetracoordinate silicon [13]. The distance between the nitrogen and the silicon atoms (2.73 Å) in **1** is less than the sum of the van der Waals radii of the 2 atoms (3.65 Å [24]), thus showing that they interact. Likewise, the distance between the nitrogen and the phosphorus atom (2.59 Å) in **2** is less than the sum of the van der Waals radii of the 2 atoms (3.35 Å [24]), consistent with an interaction [5]. Indeed, the P–N distance is even less than the N–N distance (2.79 Å) in 1,8-bis(dimethylamino)naphthalene [25] despite phosphorus being much larger than nitrogen. Moreover, it should be noted that the naphthalene ring in **2** is distorted out of the plane by only ca. 7° (dihedral

Table 4
Selected interatomic distances (Å) and bond angles (°) for **1** (M = Si) and **2** (M = P)

	1	**2**
Bond distances		
M–C(1)	1.883(6)	1.823(7)
M–C(11)	1.866(8)	1.793(9)
M–C(13)	1.872(8)	1.779(9)
M–Me	1.895(7)	
C(11)–C(12)	1.180(9)	1.185(9)
C(13)–C(14)	1.134(9)	1.183(9)
M···N	2.725(5)	2.594(7)
Bond angles		
N···M–C(11)	172.3(5)	168.6(6)
N···M–C(1)	73.7(5)	78.4(5)
N···M–C(13)	77.9(5)	84.6(6)
N···M–Me	82.6(5)	
C(1)–M–Me	112.4(3)	
C(13)–M–Me	111.6(3)	
C(1)–M–C(13)	123.0(4)	102.4(3)
C(1)–M–C(11)	102.0(4)	100.2(4)
C(13)–M–C(11)	99.6(3)	96.8(4)
C(11)–M–Me	105.3(3)	

Table 5
Summary of crystal data, intensity measurements and refinement for **1** (M = Si) and **2** (M = P)

	1	**2**
Formula	$C_{17}H_{17}NSi$	$C_{28}H_{22}NP$
Crystal system	orthogonal	monoclinic
Space group	$Pca2_1$	$C2/c$
a (Å)	17.460(5)	16.619(4)
b (Å)	7.386(2)	8.743 (3)
c (Å)	11.697(3)	31.875(6)
β (°)		99.78(2)
V (Å^3)	1508.4(7)	4563.8(20)
Molecular weight	263.41	403.46
Z	4	8
d_{calcd} (g cm^{-3})	1.163	1.174
d_{measd} (g cm^{-3})	1.13(3)	1.172(8)
Temperature of data collection (K)	293	293
Crystal size (mm)	$0.21 \times 0.18 \times 0.08$	$0.25 \times 0.20 \times 0.12$
Crystal colour	light yellow	light yellow
Recrystal solvent	heptane	heptane
Melting point (°C)	102.4–104.3	107.1–107.6
Method of data collection	ω,θ	ω,θ
Radiation (graphite) monochromated	Mo Kα	Mo Kα
μ (cm^{-1})	1.33	1.29
2θ limits (°)	4–60	4–40
Number of unique reflections	2041	2033
Number of observed reflections	354	932
Final number of variables	100	139
R_1	0.0490	0.0680
wR_2	0.0766	0.1884
Residual electronic density (e Å^{-3})	0.23 (−0.25)	0.36 (−0.25)

angle between the P–C(1)–C(9)–C(2) and N–C(7)–C(8)–C(9) mean planes) whereas for 1,8-bis(dimethylamino)naphthalene [25] the corresponding angle can be evaluated at 28°. In the case of **1**, the distortion angle is ca. 25° (dihedral angle between the Si–C(1)–C(9)–C(2) and N–C(7)–C(8)–C(9) mean planes). The presence of the lone pair in **2** gives rise to a much smaller angle C(1)–P–C(13) (102.4°) with respect to C(1)–Si–C(13) in **1** (123.0°).

4. Conclusions

1. The crystal structure determinations of compounds **1** and **2** show that both compounds are hypercoordinate with an interaction between the ligand N atom and the Si or P, respectively.
2. The steady-state fluorescence, fluorescence excitation spectra and fluorescence lifetime investigations of **1** as a function of excitation and emission wavelengths in solvents of different polarity at room temperature are consistent with the existence of two types of electronic states created as a result of the interaction of the amino group with the π-conjugated system and the $CH_3Si(C{\equiv}CH)_2$ group.

5. Supplementary data

The crystal structure data (excluding structure factors) have been deposited with the Cambridge Crystallographic Data Centre as supplementary publication nos. CCDC-224849 (**1**) and CCDC-224850 (**2**). Copies of the data can be obtained free of charge on application to CCDC, 12 Union Road, Cambridge CB2 1EZ, G.B. [Fax: +44-1223-336033; e-mail: deposit@ccdc.cam.ac.uk or www: http://www.ccdc.cam.ac.uk].

Acknowledgement

Financial support from INTAS (Brussels) [Open Call 03-51-5959] is gratefully acknowledged.

References

[1] W.E. Douglas, R.E. Benfield, O.L. Antipov, L.G. Klapshina, A.S. Kuzhelev, D.M.H. Guy, R.G. Jones, A. Mustafa, G.A. Domrachev, Phys. Chem. Chem. Phys. 2 (2000) 3195.
[2] C. Chuit, R.J.P. Corriu, C. Reyé, J.C. Young, Chem. Rev. 93 (1993) 1371.
[3] C. Chuit, R.J.P. Corriu, P. Monforte, C. Reyé, J.P. Declercq, A. Dubourg, Angew. Chem., Int. Ed. Engl. 32 (1993) 1430.
[4] M. Chauhan, C. Chuit, R.J.P. Corriu, C. Reyé, J.P. Declercq, A. Dubourg, J. Organomet. Chem. 510 (1996) 173.
[5] C. Chuit, R.J.P. Corriu, P. Monforte, C. Reyé, J.P. Declercq, A. Dubourg, J. Organomet. Chem. 511 (1996) 171.

[6] J.T.B.H. Jastrzebski, C.T. Knaap, G. van Koten, J. Organomet. Chem. 255 (1983) 287.
[7] F.H. Carré, C. Chuit, R.J.P. Corriu, W.E. Douglas, D.M.H. Guy, C. Reyé, Eur. J. Inorg. Chem. 4 (2000) 647.
[8] W.E. Douglas, D.M.H. Guy, A.K. Kar, C.H. Wang, Chem. Commun. (1998) 2125.
[9] F. Carré, R.J.P. Corriu, A. Kpoton, M. Poirier, G. Royo, J.C. Young, C. Belin, J. Organomet. Chem. 470 (1994) 43.
[10] G.M. Sheldrick, SHELXS-86, A Programme for Crystal Structure Solution, Institüt für Anorganische Chemie der Universität Göttingen, FRG, 1986.
[11] G.M. Sheldrick, SHELXL-93, A Programme for Crystal Structure Determination, Institüt für Anorganische Chemie der Universität Göttingen, FRG, 1993.
[12] F. Carré, C. Chuit, R.J.P. Corriu, A. Mehdi, C. Reyé, Angew. Chem., Int. Ed. Engl. 33 (1994) 1097.
[13] K. Boyer-Elma, F.H. Carré, R.J.-P. Corriu, W.E. Douglas, J. Chem. Soc., Chem. Commun. (1995) 725.
[14] R.J.P. Corriu, W.E. Douglas, Z.-X. Yang, J. Polym. Sci. Polym. Lett. Ed. 28 (1990) 431.
[15] C.S. Kraihanzel, M.L. Losee, J. Organomet. Chem. 10 (1967) 427.
[16] C. Chuit, C. Reyé, Eur. J. Inorg. Chem. 2 (1998) 1847.
[17] N. Mataga, in: H. Ratajczak, W.J. Orville-Thomas (Eds.), Molecular Interactions, 2, Wiley, Chichester, 1981.
[18] N.G. Bakhshiev, Opt. Spektrosk. 13 (1962) 43.
[19] S.R. Meech, D.V. O'Connor, D. Phillips, A.G. Lee, J. Chem. Soc., Faraday Trans. 2: Mol. Chem. Phys. 79 (1983) 1563.
[20] W. Rettig, J. Mol. Struct. 84 (1982) 303.
[21] Y. Wang, K.B. Eisenthal, J. Chem. Phys. 77 (1982) 6076.
[22] H. Heitele, F. Poellinger, S. Weeren, M.E. Michel-Beyerle, Chem. Phys. 143 (1990) 325.
[23] M.J.S. Dewar, E.F. Healy, J.J.P. Stewart, J. Friedheim, G. Grady, Organometallics 5 (1986) 375.
[24] A. Bondi, J. Phys. Chem. 68 (1964) 441.
[25] H. Einspahr, J.B. Robert, R.E. Marsh, J.D. Roberts, Acta Crystallogr., Sect. B 29 (1973) 1611.

Available online at www.sciencedirect.com
SCIENCE DIRECT®
Polyhedron 23 (2004) 2625–2630
POLYHEDRON
www.elsevier.com/locate/poly

Mononuclear tantalum (V) pentalene complexes: synthesis of $[Ta\{\eta^8\text{-}C_8H_4(1,4\text{-}Si^iPr_3)_2\}X_3]$ (X = CH_3, Cl, I) and the X-ray crystal structures of $[Ta\{\eta^8\text{-}C_8H_4(1,4\text{-}Si^iPr_3)_2\}(CH_3)_3]$, $[Ta\{\eta^8\text{-}C_8H_4(1,4\text{-}Si^iPr_3)_2\}(CH_3)_2Cl]$, $[Ta\{\eta^8\text{-}C8H_4(1,4\text{-}Si^iPr_3)_2\}(CH_3)Cl_2]$ and $[Ta\{\eta^8\text{-}C_8H_4(1,4\text{-}Si^iPr_3)_2\}I_3]$

F. Geoffrey N. Cloke *, Peter B. Hitchcock, Matthew C. Kuchta, Neil A. Morley-Smith

The Chemistry Department, School of Life Sciences, University of Sussex, Brighton BN1 9QJ, UK

Received 3 April 2004; accepted 10 June 2004
Available online 30 July 2004

Dedicated to Malcolm Green, with deepest thanks for his inspiration and friendship over all the years

Abstract

The reaction between $[TaMe_3Cl_2]$ and the potassium salt of the silylated pentalene dianion $[K_2\{C_8H_4(1,4\text{-}Si^iPr_3)_2\}]$ gives the η^8-pentalene complex $[Ta\{\eta^8\text{-}C_8H_4(1,4\text{-}Si^iPr_3)_2\}(CH_3)_3]$ (**1**). Sequential protonolysis of **1** with $[Et_3NH]Cl$ affords $[Ta\{\eta^8\text{-}C_8H_4(1,4\text{-}Si^iPr_3)_2\}(CH_3)_2Cl]$ (**2**), $[Ta\{\eta^8\text{-}C_8H_4(1,4\text{-}Si^iPr_3)_2\}(CH_3)Cl_2]$ (**3**) and $[Ta\{\eta^8\text{-}C_8H_4(1,4\text{-}Si^iPr_3)_2\}Cl_3]$ (**4**). An alternative and cleaner route to **4** involves treatment of **1** with BCl_3; in an analogous fashion, the reaction of **1** with BI_3 gives $[Ta\{\eta^8\text{-}C_8H_4(1,4\text{-}Si^iPr_3)_2\}I_3]$ (**5**). The X-ray crystal structures of **1**, **2**, **3** and **5** are reported.
© 2004 Elsevier Ltd. All rights reserved.

Keywords: Tantalum; Pentalene; Synthesis; Structures

1. Introduction

Until recently, the organometallic chemistry of the aromatic pentalene dianion, $[C_8H_6]^{2-}$, had only been sporadically studied since the original report of $[C_8H_6]^{2-}$ in 1962 by Katz and Rosenberger [1]. Early work in this area described binuclear transition metal systems which contain the planar pentalene dianion, e.g. $[M_2(\eta^5,\eta^5\text{-}C_8H_6)_2]$ (M = Co, Ni) [2,3], $[(\eta^3\text{-}C_3H_5)\text{-}Ni(\eta^5,\eta^5\text{-}C_8H_6)Ni(\eta^3\text{-}C_3H_5)]$ [4] and $[(\eta^5\text{-}C_5Me_5)\text{-}M(\eta^5,\eta^5\text{-}C_8H_6)M(\eta^5\text{-}C_5Me_5)]$ (M = Fe, Co, Ni) [5], in which the two metal fragments bind to the adjacent 5-membered rings of the pentalene ligand in a *trans* disposition. Binding of two transition metal fragments on the same face of a pentalene ligand was first reported in 1975 by Stone et al., e.g. $[\{Ru(MMe_3)(CO)_2\}_2(\eta^5,\eta^5\text{-}C_8H_6)]$ (M = Si, Ge), $[Ru_3(CO)_8(\eta^5,\eta^5\text{-}C_8H_6)]$ and $[Ru_3(CO)_8(\eta^5,\eta^5\text{-}C_8H_4\{SiMe_3\text{-}1,4\},2)]$ [6]; very recently the binuclear vanadium complex $[\{V(\eta^5\text{-}C_5H_5)\}_2(\eta^5,\eta^5\text{-}C_8H_6)]$ of this general class has also been reported [7]. In addition, we have reported the dimolybdenum bis-pentalene sandwich complex $[Mo\{C_8H_4(1,4\text{-}Si^iPr_3)_2\}]_2$ [8]. In 1997 our group and that of Jonas described the first complexes in which a pentalene ligand binds to a *single* metal centre in an η^8-fashion, viz. $[Ta\{\eta^8\text{-}C_8H_4(1,5\text{-}SiMe_3)_2\}Cl_3]$ [9], $[V(\eta^8\text{-}C_8H_6)(\eta^5\text{-}Cp')]$

* Corresponding author. Tel.: +44-1273-678735; fax: +44-1273-677196.
E-mail address: f.g.cloke@sussex.ac.uk (F. Geoffrey N. Cloke).

0277-5387/$ - see front matter © 2004 Elsevier Ltd. All rights reserved.
doi:10.1016/j.poly.2004.06.015

($Cp' = C_5Me_5$, C_5H_4Me), [V{η^8-C_8H_5(2-Me)}(η^5-C_5H_5)] and [V(η^8-C_8H_6)(η^5-C_9H_7)] [10], [Ti(η^8-C_8H_6)(η^5-C_5H_5)], [M(η^8-C_8H_6)(η^5-C_5H_5)X] (M = Ti, Zr; X = Cl, Br) and [Zr(η^8-C_8H_6)Cl_2(THF)$_2$] [11], and subsequently [Th{η^8-C_8H_4(1,4-Si^{i}Pr$_3$)$_2$}$_2$] [12] and [U(η^5-C_5Me_5){η^8-C_8H_4(1,4-Si^{i}Pr$_3$)$_2$}$_2$] [13]. Of particular interest to us was the formation of the pentalene complex, [Ta{η^8-C_8H_4(1,5-SiMe$_3$)$_2$}Cl_3], from a cyclooctatetraene complex [Ta{η^8-C_8H_6(1,4-SiMe$_3$)$_2$}$(CH_3)_3$] via protonolysis with [Et(^{i}Pr)$_2$NH]Cl and sublimation at 140 °C/10^{-5} mbar [8]. In the light of this unexpected and low yield (ca. 10%) synthesis of [Ta{η^8-C_8H_4(1,5-SiMe$_3$)$_2$}Cl_3], we decided to develop a rational and higher yielding route to Ta(V) pentalene complexes. Here we extend our studies with the Si^{i}Pr$_3$-substituted pentalene ligand [C_8H_4(1,4-Si^{i}Pr$_3$)$_2$]$^{2-}$, and report the synthesis of a trimethyl tantalum pentalene complex, [Ta{η^8-C_8H_4(1,4-Si^{i}Pr$_3$)$_2$}$(CH_3)_3$], and its conversion to the mixed alkyl-halide [Ta{η^8-C_8H_4(1,4-Si^{i}Pr$_3$)$_2$}$(CH_3)_{3-n}Cl_n$] ($n = 1$ and 2) and trihalide [Ta{η^8-C_8H_4(1,4-Si^{i}Pr$_3$)$_2$}X_3] (X = Cl, I) complexes.

2. Results and discussion

2.1. Synthetic studies

The cyclooctatetraene tantalum complexes [Ta(η^8-C_8H_8)Me$_3$] and [Ta{η^8-C_8H_6(1,4-SiMe$_3$)$_2$}$(CH_3)_3$] have been previously prepared by treatment of [$TaMe_3Cl_2$] with the appropriate dilithium cyclooctatetraenide salt [14,8]. In an analogous manner, the η^8-pentalene complex [Ta{η^8-C_8H_4(1,4-Si^{i}Pr$_3$)$_2$}$(CH_3)_3$] (**1**) was prepared in high yield via a direct salt metathesis reaction between the dipotassium salt of the ligand, [K_2{C_8H_4(1,4-Si^{i}Pr$_3$)$_2$}] [15], and [Ta$(CH_3)_3Cl_2$] in toluene (see Scheme 1).

NMR spectra for **1** are typical of complexes containing the η^8-C_8H_6(1,4-SiMe$_3$)$_2$ ligand, in particular the diastereotopic nature of the isopropyl groups of the silyl substituents on the pentalene ring resulting from the facially enantiotopic η^8-bonding mode of the latter. Singlets at δ 0.91 (^{1}H) and δ 50.1 (^{13}C{^{1}H}) ppm can be assigned to the Ta–Me groups.

1 provides a suitable precursor for the synthesis of the mixed alkyl/chloride complexes via the protonolysis of one, two or three of the methyl groups and their replacement by chloride (see Scheme 1). Initially the reaction between [Et_3NH]Cl and **1** in 1:1 and 2:1 ratios in benzene at room temperature gave [Ta {η^8-C_8H_4(1,4-Si^{i}Pr$_3$)$_2$}$(CH_3)_2Cl$] (**2**) and [Ta{η^8-C_8H_4(1,4-Si^{i}Pr$_3$)$_2$}-$(CH_3)Cl_2$] (**3**), respectively. These compounds can be prepared on multigram scales by heating a mixture of the reactants in toluene at ca. 90 °C, and are readily obtained from saturated pentane solutions as yellow crystalline solids. NMR data for **2** and **3** were in accord with the proposed structures. In particular, the ^{1}H NMR of **2** shows the two expected resonances for the Me groups in the prochiral $TaMe_2Cl$ unit bound to the facially enantiotopic pentalene ring. The associated carbons were not readily discernible in the ^{13}C{^{1}H}spectrum, presumably due to quadrupolar broadening by ^{181}Ta (100%, $I = 7/2$). [1]

If three or more equivalents of [Et_3NH]Cl are allowed to react with the trimethyl compound **1** at a higher temperature, instead of the intense yellow solution observed during the synthesis of **2** and **3**, a deep red colour is observed. Workup as per before resulted in a complex mixture of products, by ^{1}H NMR, although the mass spectrum showed the trichloride [Ta{η^8-C_8H_4(1,4-Si^{i}Pr$_3$)$_2$}Cl_3] (**4**) to be one component of the mixture. Sublimation of the mixture at high temperature (160 °C/10^{-6} mbar) gave a pure sample of **4**, but in very low yield. Accordingly, **1** was treated with a slight excess of BCl_3, which resulted in a smooth reaction and facile isolation of **4** in high (82%) yield, as a red-purple crystalline solid. The dark purple tri-iodide analogue [Ta{η^8-C_8H_4(1,4-Si^{i}Pr$_3$)$_2$}I_3] (**5**) was similarly prepared from **1** and boron triiodide.

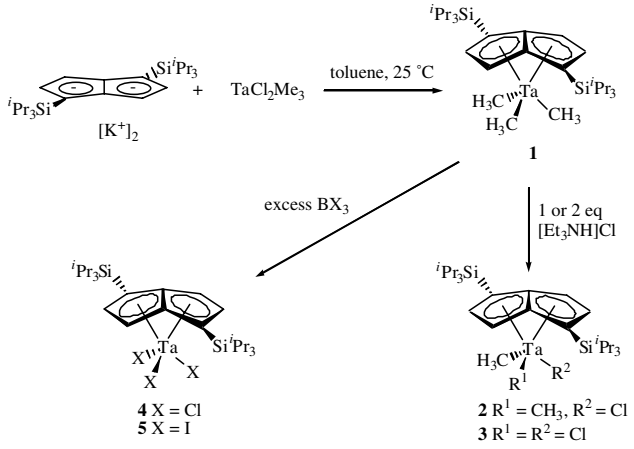

Scheme 1. Synthesis of tantalum η^8-pentalene complexes.

2.2. Structural studies

Although problems with disorder frustrated attempts to determine the X-ray structure of **4**, the molecular structures of **1**, **2**, **3** and **5** have been determined and are shown in Figs. 1–4 respectively, together with selected bond lengths and angles.

All four molecules display the expected three-legged, piano stool structure. An important structural parameter in η^8-mononuclear pentalene complexes is the penta-

[1] Quadrupolar broadening of attached carbons by Ta (100% $I = 9/2$) is rare, but its extent would obviously depend on the electric field gradient at the Ta centre in turn dependent on the symmetry of the molecule (thus it is absent in **1** and **3**).

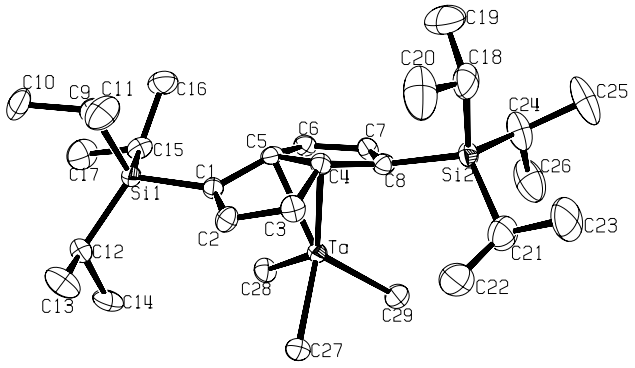

Fig. 1. The molecular structure of **1**. Selected bond lengths (Å) and angles (°): average ring C–C 1.431; Ta–C(1) 2.622(3), Ta–C(2) 2.640(3), Ta–C(3) 2.379(3), Ta–C(4) 2.192(3), Ta–C(5) 2.269(3), Ta–C(6) 2.557(3), Ta–C(7) 2.611(3), Ta–C(8) 2.377(3), Ta–C(27) 2.203(3), Ta–C(28) 2.187(3), Ta–C(29) 2.200(3); C(27)–Ta–C(28) 93.73(14), C(27)–Ta–C(29) 86.03(14), C(28)–Ta–C(29) 87.46(14); fold angle 29.2.

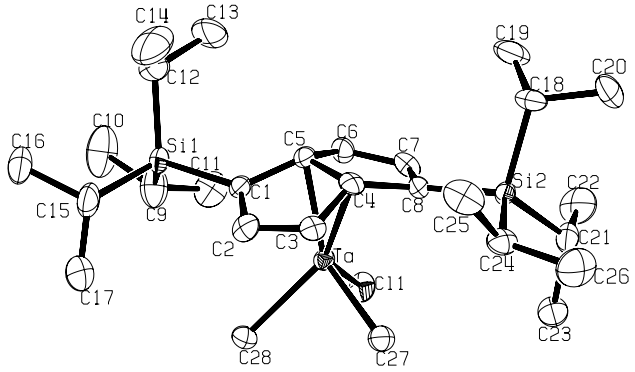

Fig. 2. The molecular structure of **2**. Selected bond lengths (Å) and angles (°) (see footnote 2): average ring C–C 1.427; Ta–C(1) 2.367(6), Ta–C(2) 2.550(6), Ta–C(3) 2.485(6), Ta–C(4) 2.237(6), Ta–C(5) 2.186(6), Ta–C(6) 2.368(6), Ta–C(7) 2.601(6), Ta–C(8) 2.578(6), Ta–Cl(1) 2.355(2), Ta–C(27) 2.199(6), Ta–C(28) 2.326(3); C(27)–Ta–Cl(1) 94.1(2), C(28)–Ta–Cl(1) 84.68(11); pentalene fold angle 31.2.

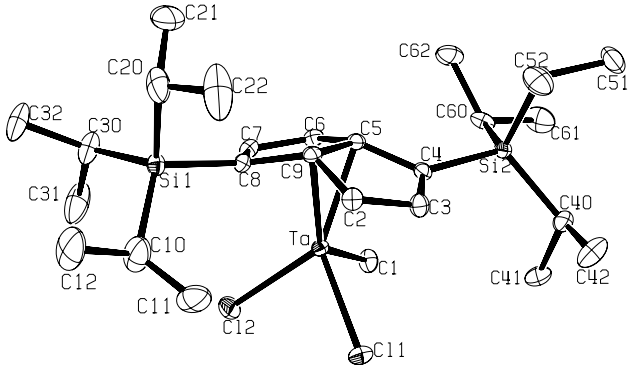

Fig. 3. The molecular structure of **3**. Selected bond lengths (Å) and angles (°): average ring C–C 1.432; Ta–C(2) 2.358(3), Ta–C(3) 2.572(3), Ta–C(4) 2.547(3), Ta–C(5) 2.227(3), Ta–C(6) 2.477(3), Ta–C(7) 2.542(3), Ta–C(8) 2.374(3), Ta–C(9) 2.187(3), Ta–C(l) 2.208(3), Ta–Cl(1) 2.3771(9); Ta–C1(2) 2.3810(9); C(1)–Ta–Cl(1) 92.47(11), C(1)–Ta–Cl(2) 87.45(9), Cl(1)–Ta–Cl(2) 86.27(4); fold angle 32.5.

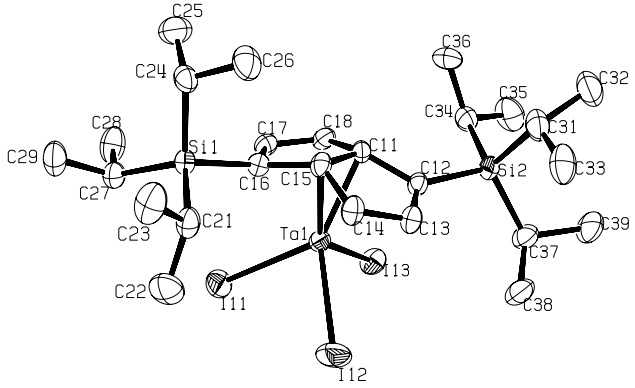

Fig. 4. The molecular structure of **5** (molecule 1). Selected bond lengths (Å) and angles (°): average ring C–C 1.435; Ta–C(11) 2.220(4), Ta–C(12) 2.556(4), Ta–C(13) 2.578(4), Ta–C(14) 2.356(4), Ta–C(15) 2.167(4), Ta–C(16) 2.338(4), Ta–C(l7) 2.537(4), Ta–C(18) 2.485(4), Ta–I(11) 2.7965(4), Ta–I(12) 2.7126(4), Ta–I(13) 2.7662(4); I(11)–Ta–I(12) 86.300(13), I(12)–Ta–I(13) 96.729(14), I(11)–Ta–I(13) 86.220(12); fold angle 32.0.

lene fold angle about the bridge head C–C vector, i.e. the angle between the two 5-membered ring planes. Mononuclear transition metal compounds containing an η^8-pentalene ligand typically have fold angles ranging from 33° to 43° [9–11], inversely related, to a large extent, to the size of the metal. The only previously reported tantalum pentalene complex, [Ta{η^8-C_8H_4(1,4-$SiMe_3$)$_2$}Cl_3], has a fold angle of 33.0° [9]; in **1**, **2** and **3** the fold angles are 29.2°, 31.2° and 32.5°, respectively. Thus there is a small, but discernible increase in fold angle (29.2–33.0°) with increasing chloride substitution (ignoring any effects caused by differing silyl group substitution of the ring). This may be a consequence of sequential substitution of an electron withdrawing chlorine for one of the methyl groups resulting in increasing electron deficiency at the tantalum centre. The tantalum-bridge head carbon distances remain essentially constant (within e.s.d.s.) in **1**, **2** and **3** and [Ta{η^8-C_8H_4(1,4-$SiMe_3$)$_2$}Cl_3] [9] (respectively: 2.192(3), 2.269(3); 2.186(6), 2.237(6); 2.187(3), 2.227(3); 2.182(13), 2.217(12) Å); thus, it appears that, rather than donating electron density from the bridge head C–C bond, the anionic pentalene ligand bends about the bridge head carbons to relieve this electron deficiency. The C–C bond lengths within the pentalene ring system are unexceptional in all three compounds and comparable to those found in [Ta{η^8-C_8H_4(1,4-$SiMe_3$)$_2$}Cl_3] [9].

The tantalum–methyl bond lengths in **1**, **2** and **3** (respectively: 2.203(3), 2.187(3), 2.200(3); 2.199(6), 2.326(3); [2] 2.208(3) Å) are all very similar and are comparable to those found in e.g. [Ta(TBM)$(CH_3)_2$Cl] (TBM = tribenzylidenemethane), which has a tantalum–

[2] In **2** the Cl atom is disordered 0.65:0.35 between the sites labelled Cl(1) and C(28). Therefore bonds and angles involving these two atoms are unreliable.

methyl bond length of 2.149(6) [16]. The tantalum–chlorine bond lengths in **2** and **3** are 2.355(2) Å, [2] and 2.3771(9) and 2.3810(9) Å, respectively; in comparison, Ta–Cl bonds in [{η^8-C_8H_4(1,4-$SiMe_3$)$_2$}$TaCl_3$] lie in the range 2.362(3) to 2.386(3) Å [9].

The triiodide **5** crystallises with two slightly different molecules in the unit cell with fold angles of 31.2 (molecule 1) and 31.6° (molecule 2); the discussion pertains to molecule 1. The Ta-bridge head carbon distances in **5** are 2.220(4) and 2.167(4) Å, very similar to those in **1**, **2** and **3**, and the fold angle of 31.2° fits well with the electron deficiency argument (vide supra), given the relative electronegativities of chlorine and iodine. The average ring C–C distance of 1.435 Å is essentially identical to those in **1**, **2** and **3**.

The tantalum–iodine distances in **5** range from 2.7126(4) to 2.7965(4) Å, slightly shorter than that in the more sterically congested Ta(V) complex [Ta(η^5-C_5H_5)$_2$(η^1-$CHCH_3$)I] (2.8840(7) Å) [17].

3. Experimental

All manipulations were carried out using a combination of standard Schlenk, high vacuum and glovebox techniques. All solvents were distilled from appropriate drying agents and degassed prior to use. K_2[C_8H_4(1,4-Si^iPr_3)$_2$] [15] and [$Ta(CH_3)_3Cl_2$] [18] were prepared according to literature methods. Boron trichloride and boron triiodide were purchased from Aldrich as a 1.0M solution in heptane, and as the solid respectively. NMR spectra were recorded on a Bruker 300DPX Spectrometer operating at 75.475 MHz for ^{13}C and 300.132 MHz for ^{1}H, and at a probe temperature of 295K unless otherwise stated; chemical shifts were referenced to internal solvent resonances. Mass spectra were recorded on a VG Autospec instrument operating in EI mode. Carbon and hydrogen elemental analyses were performed by Mikroanalytisches Labor Pascher (Germany).

3.1. Synthesis of [Ta{η^8-C_8H_4(1,4-Si^iPr_3)$_2$}$(CH_3)_3$] (1)

Toluene (ca. 30 mL) was added to a stirred mixture of K_2[C_8H_4(1,4-Si^iPr_3)$_2$] (1.80 g, 3.65 mmol) and $Ta(CH_3)_3Cl_2$ (1.08 g, 3.64 mmol) at room temperature and the resulting yellow-brown mixture was stirred for ca. 3 h at room temperature. The solvent was removed under reduced pressure, the residue extracted into pentane (ca. 100 mL) and filtered through a bed of Celite supported on a glass frit producing a clear yellow filtrate. The filtrate was concentrated under reduced pressure to a volume of ca. 10 mL and stored overnight at ca. −50 °C. The resulting crop of yellow crystals were isolated by filtration and dried under reduced pressure giving [Ta{η^8-C_8H_4(1,4-Si^iPr_3)$_2$}$(CH_3)_3$] as a yellow solid (1.10 g, 47%). *Anal.* Calc. for $C_{29}H_{54}Si_2Ta$: C, 54.35; H, 8.65. Found: C, 54.46; H, 8.63%. Mass spectrum: m/z = 640 (M^+).

^{1}H NMR (300.132 MHz, C_6D_6): δ 0.91 {Ta(CH_3)$_3$, 9H, s},1.09 {CH(CH_3)$_2$, 18H, d, J_{H-H} = 7.4}, 1.12 {CH(CH_3)$_2$, 18H, d, J_{H-H} = 7.4}, 1.24 {CH(CH_3)$_2$, 6H, sept, J_{H-H} = 7.4}, 5.39 {CH, 2H, d, J_{H-H} = 3.2}, 6.55 {CH, 2H, d, J_{H-H} = 3.2}; ^{13}C NMR (75.475 MHz, C_6D_6): δ 50.1 {Ta(CH_3)$_3$, q, J_{C-H} = 118}, 12.3 {CH(CH_3)$_2$, d, J_{C-H} = 121}, 19.3 {CH(CH_3)$_2$, q, J_{C-H} = 125}, 19.5 {CH(CH_3)$_2$, q, J_{C-H} = 125}, 105.8 {CH, d, J_{C-H} = 171}, 106.5 {C,s},125.5 {C,s}, 130.2 {CH, d, J_{C-H} = 172}.

3.2. Synthesis of [Ta{η^8-C_8H_4(1,4-Si^iPr_3)$_2$}$(CH_3)_2Cl$] (2)

Toluene (ca. 30 mL) was added to a stirred mixture of [Ta{η^8-C_8H_4(1,4-Si^iPr_3)$_2$}$(CH_3)_3$] (0.50 g, 0.78 mmol) and [Et_3NH]Cl (0.10 g, 0.73 mmol) at room temperature and the resulting suspension was stirred for ca. 15 h at ca. 90 °C in a sealed (Teflon stopcock) ampoule. The solvent was removed under reduced pressure, the residue extracted into pentane (ca. 50 mL) and filtered through a bed of Celite supported on a glass frit. The filtrate was concentrated under reduced pressure to a volume of ca. 3 mL giving a crop of yellow crystals which were isolated by filtration and dried under reduced pressure giving [Ta{η^8-C_8H_4(1,4-Si^iPr_3)$_2$}$(CH_3)_2$Cl] as a yellow solid (0.13 g, 27%, based on [Et_3NH]Cl). *Anal.* Calc. for $C_{28}H_{51}Si_2TaCl$: C, 50.86; H, 7.93. Found: C, 50.82; H, 7.84%. Mass spectrum: m/z = 645 ([M − CH_3]$^+$).

^{1}H NMR (300.132 MHz, C_6D_6): δ 0.93 {Ta(CH_3), 3H, s}, 0.94 {Ta(CH_3), 3H, s}, 1.07 {CH(CH_3)$_2$, 18H, d, J_{H-H} = 7.1}, 1.11 {CH(CH_3)$_2$, 18H, d, J_{H-H} = 7.1}, 1.22 {CH(CH_3)$_2$, 6H, sept, J_{H-H} = 7.1}, 5.46 {CH, 2H, d, J_{H-H} = 3.3}, 6.50 {CH, 2H, d, J_{H-H} = 3.3}; ^{13}C NMR (75.475 MHz, C_6D_6): δ 32.6 {Ta(CH_3), br}, 48.4 {Ta(CH_3), br}, 12.2 {CH(CH_3)$_2$, d, J_{C-H} = 124}, 19.3 {CH(CH_3)$_2$, q, J_{C-H} = 121}, 19.5 {CH(CH_3)$_2$, q, J_{C-H} = 121}, 106.4 {CH, d, J_{C-H} = 178}, 108.8 {C,s}, 124.8 {C,s}, 131.2 {CH, d, J_{C-H} = 169}.

3.3. Synthesis of [Ta{η^8-C_8H_4(1,4-Si^iPr_3)$_2$}$(CH_3)Cl_2$] (3)

Toluene (ca. 30 mL) was added to a mixture of [Ta{η^8-C_8H_4(1,4-Si^iPr_3)$_2$}$(CH_3)_3$] (1.00 g, 1.56 mmol) and [Et_3NH]Cl (0.64 g, 4.65 mmol) at room temperature and the resulting suspension was stirred for ca. 20 h at ca. 90 °C in a sealed (Teflon stopcock) ampoule. The solvent was removed under reduced pressure, the residue extracted into pentane (ca. 150 mL) and filtered through a bed of Celite supported on a glass frit producing a clear orange yellow filtrate. The filtrate was concentrated under reduced pressure to a volume of ca. 10

mL resulting in the formation of a crop of yellow crystals which were isolated by filtration and dried under reduced pressure giving [Ta{η^8-C_8H_4(1,4-Si^{i}Pr$_3$)$_2$}-$(CH_3)Cl_2$] as a yellow solid (0.78 g, 73%). *Anal.* Calc. for $C_{27}H_{49}Cl_2Si_2Ta$: C, 47.57; H, 7.24. Found: C, 47.64; H, 7.26%. Mass spectrum: $m/z = 665$ ($[M - CH_3]^+$).

^{1}H NMR (300.132 MHz, C_6D_6): δ 1.28 {Ta(CH_3), 3H, s}, 1.06 {CH(CH_3)$_2$, 18H, d, $J_{H-H} = 7.2$},1.10 {CH(CH_3)$_2$, 18H, d, $J_{H-H} = 7.2$}, 1.27 {CH(CH$_3$)$_2$, 6H, sept, $J_{H-H} = 7.2$}, 5.42 {CH, 2H, d, $J_{H-H} = 3.3$}, 6.42 {CH, 2H, d, $J_{H-H} = 3.3$}; ^{13}C NMR (75.475 MHz, C_6D_6): δ 12.2 {Ta(CH$_3$), q, $J_{C-H} = 128$}, 12.5 {CH(CH$_3$)$_2$, d, $J_{C-H} = 121$}, 19.3 {CH(CH$_3$)$_2$, q, $J_{C-H} = 125$}, 19.4 {CH(CH$_3$)$_2$, q, $J_{C-H} = 125$}, 107.4 {CH, d, $J_{C-H} = 181$}, 111.0 {C,s}, 124.7 {C,s}, 132.6 {CH, d, $J_{C-H} = 174$}.

3.4. Synthesis of [Ta{η^8-C_8H_4(1,4-Si^{i}Pr$_3$)$_2$}Cl_3] (**4**)

Boron trichloride (2.0 mL of a 1.0 M solution in heptane) was added to a yellow solution of [C_8H_4(1,4-Si^{i}Pr$_3$)$_2$]Ta(CH$_3$)$_3$ (0.50 g, 0.78 mmol) in benzene (ca. 5 mL) at room temperature. The resulting red-purple mixture was stirred for ca. 20 min at room temperature and the solvent was removed under reduced pressure. The red purple solid was washed with pentane (ca. 5 mL) giving [Ta{η^8-C_8H_4(1,4-Si^{i}Pr$_3$)$_2$}Cl$_3$] (0.45 g, 82%). *Anal.* Calc. for $C_{26}H_{46}Si_2TaCl_3$: C, 44.48; H, 6.60. Found: C, 44.80; H, 6.78%. Mass spectrum: $m/z = 702$ (M^+).

^{1}H NMR (300.132 MHz, C_6D_6): δ 1.01 {CH(CH_3)$_2$, 18H, d, $J_{H-H} = 7.3$}, 1.12 {CH(CH_3)$_2$, 18H, d, $J_{H-H} = 7.3$}, 1.27 {CH(CH$_3$)$_2$, 6H, sept, $J_{H-H} = 7.3$}, 5.31 {CH, 2H, d, $J_{H-H} = 3.3$}, 6.75 {CH, 2H, d, $J_{H-H} = 3.3$}; ^{13}C NMR (75.475 MHz, C_6D_6): δ 12.1 {CH(CH$_3$)$_2$, d, $J_{C-H} = 113$}, 19.2 {CH(CH$_3$)$_2$, q, $J_{C-H} = 126$}, 19.4 {CH(CH$_3$)$_2$, q, $J_{C-H} = 126$}, 115.2 {CH, d, $J_{C-H} = 183$}, 122.4 {C,s}, 131.8 {C,s}, 136.2 {CH, d, $J_{C-H} = 177$}.

3.5. Synthesis of [Ta{η^8-C_8H_4(1,4-Si^{i}Pr$_3$)$_2$}I_3] (**5**)

Boron triiodide (0.95 g, 2.42 mmol) was added to [C_8H_4(1,4-Si^{i}Pr$_3$)$_2$]TaMe$_3$ in an ampoule, and 15 ml toluene added quickly, resulting in an immediate colour change from orange to deep red. The reaction mixture was stirred at room temperature for 2 h, before removal of the solvent in vacuo. The solid residue was pumped on for 2 h before being redissolved in toluene, and filtered through flame dried Celite on a glass frit. The

Table 1
Selected crystallographic data

Compound	**1**	**2**	**3**	**5**
Empirical formula	$C_{29}H_{55}Si_2Ta$	$C_{28}H_{52}ClSi_2Ta$	$C_{27}H_{49}Cl_2Si_2Ta$	$C_{26}H_{46}I_3Si_2Ta$
Formula weight	640.86	661.3	681.69	976.46
Colour	yellow	yellow	yellow	red-purple
Crystal size (mm)	$0.3 \times 0.2 \times 0.15$	$0.3 \times 0.3 \times 0.3$	$0.2 \times 0.2 \times 0.3$	$01 \times 0.1 \times 0.2$
Crystal system	monoclinic	monoclinic	monoclinic	triclinic
Space group	$P2_1/n$ (No. 14)	$P2_1/n$ (No. 14)	$P2_1/n$ (No. 14)	$P\bar{1}$
Diffractometer	E-N CAD 4	E-N CAD 4	Bruker P4	Bruker P4
λ (Å)	0.71073	0.71073	0.71073	0.71073
Temperature (K)	173(2)	173(2)	203(2)	203(2)
Unit cell dimensions				
a (Å)	14.4566(3)	14.412(4)	14.3940(7)	13.6221(7)
b (Å)	14.7377(4)	14.642(9)	14.7129(7)	14.6816(8)
c (Å)	15.0752(3)	14.999(6)	14.9822(7)	17.7145(10)
α (°)	90.0	90.0	90.0	111.0460(10)
β (°)	105.517(2)	105.96(3)	105.7380(10)	90.7590(10)
γ (°)	90.0	90.	90.0	95.2210(10)
V (Å^3)	3094.8(1)	3043(2)	3053.9(3)	3288.7(3)
Z	4	4	4	4
$D_{calc.}$ (Mg/m^3)	1.38	1.44	1.483	1.972
Absorption coefficient (mm^{-1})	3.64	3.79	3.866	6.244
Reflections collected	19 630	5550	21 008	24 855
Independent reflections	7133	5332	6716	14549
R_{int}	0.045	0.0209	0.0321	0.0233
Reflections with $I > 2\sigma(I)$	5660	3787	5364	12129
Goodness-of-fit on F^2	1.023	1.055	1.040	1.012
Final R indices [$I > 2\sigma(I)$]				
R_1	0.029	0.032,	0.0279	0.0292
wR_2	0.068	0.070	0.0616	0.0643
R indices (all data)				
R_1	0.040	0.055	0.0401	0.0403
wR_2	0.075	0.083	0.0663	0.0688

solvent was removed in vacuo giving [Ta{η^8-C_8H_4(1,4-Si^{i}Pr$_3$)$_2$}I_3] (0.45 g, 82%) as a red-purple solid. *Anal.* Calc. for $C_{26}H_{46}Si_2TaI_3$: C, 31.98; H, 4.75. Found: C, 31.88; H, 4.61%. Mass spectrum: m/z = 849 ($[M-I]^+$).

^{1}H NMR (300.132 MHz, C_6D_6): δ 1.01 {CH(CH_3)$_2$, 18H, d, J_{H-H} = 7.4}, 1.12 {CH(CH_3)$_2$, 18H, d, J_{H-H} = 7.4}, 1.36 {CH(CH$_3$)$_2$, 6H, sept, J_{H-H} = 7.4}, 5.56 {CH, 2H, d, J_{H-H} = 3.1}, 6.07 {CH, 2H, d, J_{H-H} = 3.1}; ^{13}C NMR (75.475 MHz, C_6D_6): δ 12.5 {CH(CH$_3$)$_2$, d, J_{C-H} = 115},19.3 {CH(CH$_3$)$_2$, q, J_{C-H} = 126},19.7 {CH(CH$_3$)$_2$, q, J_{C-H} = 126},111.0 {CH, d, J_{C-H} = 185}, 119.1 {C,s}, 128.9 {C,s}, 134.3 {CH, d, J_{C-H} = 178}.

3.6. X-ray crystallography

See Table 1 for data collection and refinement parameters. In **2** the Cl atom is disordered 0.65:0.35 between the sites labelled Cl(1) and C(28). Therefore bonds and angles involving these two atoms are unreliable.

4. Supplementary material

Crystallographic data for the structural analyses of **1**, **2**, **3** and **5** have been deposited with the Cambridge Crystallographic Data Centre, CCDC Nos. 233912, 233913, 233915 and 233914, respectively. Copies of this information may be obtained free of charge from: The Director, CCDC, 12 Union Road, Cambridge, CB2 1 EZ.

Acknowledgements

This work was supported by EPSRC, NATO and B.P.Chemicals. M.C.K. thanks the NSF-NATO Post-doctoral Fellowship Program for funding (Grant No. DGE-9710868); N.A. M.-S. thanks B.P. Chemicals for financial assistance.

References

[1] T.J. Katz, M. Rosenberger, J. Am. Chem. Soc. 84 (1962) 865.
[2] T.J. Katz, N. Acton, J. Am. Chem. Soc. 94 (1972) 3281.
[3] T.J. Katz, N. Acton, J. McGinnis, J. Am. Chem. Soc. 94 (1972) 6205.
[4] A. Miyake, A. Kanai, Angew. Chem., Int. Ed. Engl. 10 (1971) 801.
[5] E.E. Bunel, L. Valle, N.L. Jones, P.J. Carroll, C. Barra, M. Gonzalez, N. Munoz, G. Visconti, A. Aizman, J.M. Manriquez, J. Am. Chem. Soc. 110 (1988) 6597.
[6] S.A.R. Knox, F.G.A. Stone, Acc. Chem. Res 7 (1974) 321.
[7] S.C. Jones, D. O'Hare, Chem. Commun. (2003) 2208.
[8] F.G.N. Cloke, P.B. Hitchcock, M.C. Kuchta, Organometallics 17 (1998) 1934.
[9] Q.A. Abbasali, F.G.N. Cloke, P.B. Hitchcock, Chem. Commun. (1997) 1541.
[10] K. Jonas, B. Gabor, R. Mynott, K. Angermund, O. Heinemann, C. Kruger, Angew. Chem., Int. Ed. Engl. 36 (1997) 1712.
[11] K. Jonas, P. Kolb, G. Kollbach, B. Gabor, R. Mynott, K. Angermund, O. Heinemann, C. Kruger, Angew. Chem., Int. Ed. Engl. 36 (1997) 1714.
[12] F.G.N. Cloke, P.B. Hitchcock, J. Am. Chem. Soc. 119 (1997) 7899.
[13] F.G.N. Cloke, P.B. Hitchcock, J. Am. Chem. Soc. 124 (2002) 9352.
[14] R.R. Schrock, L.J. Guggenberger, A.D. English, J. Am. Chem. Soc. 98 (1976) 903.
[15] F.G.N. Cloke, M.C. Kuchta, R.M. Harker, P.B. Hitchcock, J.S. Parry, Organometallics 19 (2000) 5795.
[16] G. Rodriguez, J.P. Graham, W.D. Cotter, C.K. Sperry, G.C. Bazan, B.E. Bursten, J. Am. Chem. Soc. 120 (1998) 12512.
[17] R.P. Hughes, S.M. Maddock, A.L. Rheingold, I.A. Guzei, Polyhedron 17 (1998) 1037.
[18] R.R. Schrock, P.R. Sharp, J. Am. Chem. Soc. 100 (1978) 2389.

Available online at www.sciencedirect.com
SCIENCE DIRECT®
Polyhedron 23 (2004) 2631–2636
POLYHEDRON
www.elsevier.com/locate/poly

Ozonolysis for the preparation of high-oxidation state transition metal complexes, and the X-ray crystal structure of $Co(py)_2(OAc)_2(H_2O)_2$

Alan Bailey, William P. Griffith *, David W.C. Leung, Andrew J.P. White *, David J. Williams *

Department of Chemistry, Imperial College London, London SW7 2AZ, UK

Received 5 April 2004; accepted 27 May 2004
Available online 3 September 2004

Dedicated to Malcolm, a great friend ever since our postgraduate students days together (WPG)

Abstract

The use of an ozone/oxygen mixture for the preparation of pyridinecarboxylate complexes of silver(II), $[AgL_2]$, (L = 2-, 3- and 4-pyridinecarboxylate; 2,3-, 2,4-, 2,5- and 3,5-pyridinedicarboxylate), Mn^{III}(picolinate)$_3$, and the heteropolyanion $[Co^{III}W_{12}O_{40}]^{5-}$ are reported. It is shown that previous literature work on oxidation of alcohols with O_3/O_2 using $Co(OAc)_2$ are erroneous in that the latter has no catalytic effect. In the course of this work the title complex was made and its X-ray crystal structure determined.
© 2004 Elsevier Ltd. All rights reserved.

Keywords: Ozone; X-ray crystal structure; Silver(II) complexes; Manganese(III) complexes; Cobalt(III) complexes

1. Introduction

We have shown previously that an ozone/oxygen (O_3/O_2) mixture, produced from dioxygen by a commercial silent electric-discharge ozoniser running from a domestic 13-amp supply, provides a safe and convenient method of producing high oxidation state complexes of iron, ruthenium, osmium, palladium, platinum, gold and cerium under ambient conditions [1,2]. Here we extend this work to show that complexes of silver(II), manganese(III) and cobalt(III) can equally simply be prepared using a similar method. We also report for the first time the single crystal X-ray structure of the new compound $Co(py)_2(OAc)_2(H_2O)_2$ which resulted unexpectedly as a by-product during ozonolysis of a cobalt(II) acetate/pyridine mixture.

In many of the oxidations reported in our earlier work [1] we found that an O_3/O_2 mixture effected oxidations normally carried out with persulfate, unsurprisingly since the oxidation potentials in acid of ozone (+2.07 v.) and persulfate (+2.01 v.) are very close [2]. Ozonolysis is often more convenient since the only by-product is oxygen, giving easier workup, and no heating is required.

2. Experimental

2.1. Materials

Silver nitrate, manganese(II) chloride, cobalt(II) acetate and the pyridinecarboxylic acids were obtained

* Corresponding authors. Tel.: +44 0207 594 5751/5759; fax: +44 0207 594 5804.
E-mail addresses: w.griffith@ic.ac.uk, w.griffith@imperial.ac.uk (W.P. Griffith), ajpw@imperial.ac.uk (A.J.P. White), d.williams01@imperial.ac.uk (D.J. Williams).

0277-5387/$ - see front matter © 2004 Elsevier Ltd. All rights reserved.
doi:10.1016/j.poly.2004.05.020

from Aldrich and used without further purification. The pyridine monocarboxylic acids, HL ($L = C_5H_4N\text{-}COO^-$), were 2-pyridinecarboxylate (pic), 3-pyridinecarboxylate (nic) and 4-pyridinecarboxylate (isonic). The pyridinedicarboxylic acids, H_2L ($L = C_5H_3N\text{-}(COO)_2^{2-}$), were 2,3-pyridinedicarboxylate (quin), 2,4-pyridinedicarboxylate (lut), 2,5-pyridinedicarboxylate (isocinc), 3,4-pyridinedicarboxylate (cinc) and 3,5-pyridinedicarboxylate (dinic).

2.2. Syntheses of compounds

2.2.1. Ozonolysis

This was effected, as in our earlier work [1], with a Tri-Ox model TOG AI ozoniser using 0.02 g of O_3 in 2 dm^3 of O_2 per minute; the O_3 content was determined for various gas flows of O_2 and applied potentials by titration with thiosulfate of iodine released from standard iodide solutions [3].

2.2.2. Silver(II) complexes

The preparation of $Ag(pic)_2$ is typical. To a solution of silver nitrate (0.5 g, 4 mmol, in 25 cm^3 water) was added a solution of picolinic acid (0.72 g, 8 mmol, in 25 cm^3 water). The resultant colourless, gel-like solution was stirred and an O_3/O_2 stream passed through it for 3 h. After 15 min an orange-brown precipitate appeared which was filtered off, washed with 20 cm^3 of water and dried in a vacuum desiccator.

Similar methods were used for the preparation and isolation of $Ag(nic)_2$, $Ag(isonic)_2 \cdot H_2O$, $Ag(quinH)_2 \cdot 2H_2O$, $Ag(lutH)_2 \cdot 3H_2O$, $Ag(isocincH)_2$, $Ag(cincH)_2 \cdot H_2O$ and $Ag(dinicH)_2 \cdot 4H_2O$.

$Ag(pic)_2$. *Anal.* Calc. for $C_{12}H_8N_2O_4Ag$: C, 41.0; H 2.3; N, 7.9. Found: C, 40.8; H, 2.2; N, 7.8%. Magnetic moment μ_{eff} 1.77 B.M. IR (cm^{-1}): 3375b,m, 3061s, 1631vs, 1606vs, 1467m, 1435w, 1392vs, 1337vs, 1287vs, 1263w, 1166m, 1088m, 1042m, 998m, 1088 m, 998m, 838m, 823w, 767s, 747s, 705s, 654m, 624m, 533w. Main FAB peaks 353, 355 ($[Ag(pic)_2H]^+$), 230, 232 ($[Ag(pic)H]^+$), 124 ($[(pic)H]^+$), 230, 232 ($[Ag(pic)H]^+$).

$Ag(isonic)_2 \cdot H_2O$. *Anal.* Calc. for $C_{12}H_{10}N_2O_5Ag$: C, 39.0; H, 2.7; N, 7.6. Found: C, 38.7; H, 2.8; N, 7.5%. Magnetic moment μ_{eff} 1.71 B.M. IR (cm^{-1}): 3407b,m, 3094w, 1603vs, 1550vs, 1232s, 1144w, 1099w, 1046vs, 1028s, 867m, 867m, 844s, 780s, 766vs, 690vs, 511m. Main FAB peaks 353, 355 ($[Ag(isonic)_2H]^+$), 230, 232 ($[Ag(isonic)H]^+$), 124 ($[(isonic)H]^+$).

$Ag(quinH)_2 \cdot 2H_2O$. *Anal.* Calc. for $C_{14}H_{12}O_{10}N_2Ag$: C, 35.3; H, 2.5; N, 5.9. Found: C, 35.4; H, 2.5; N, 5.8%. Magnetic moment μ_{eff} 1.72 B.M. IR (cm^{-1}): 3396vs, 3071m, 1715s, 1668s, 1618s, 1587s, 1412m, 1332vs, 1274s, 1234m, 1169m, 1148m, 1106s, 1064w, 862m, 829s, 761m, 706vs, 600w, 551w, 464m. Main FAB peaks 441, 443 ($[Ag(quinH)_2H]^+$), 274, 276 ($[Ag(quin)H]^+$), 124 ($[(quinH)H]^+$).

$Ag(lutH)_2 \cdot 3H_2O$. *Anal.* Calc. for $C_{14}H_{14}O_{11}N_2Ag$: C, 34.1; H, 2.9; N, 5.7. Found: C, 34.2; H, 2.3; N, 5.6%. Magnetic moment μ_{eff} 1.65 B.M. IR (cm^{-1}): 3491vs, 3300s, 3047m, 1868m, 1774s, 1658s, 1604s, 1566m, 1474m, 1421m, 1364m, 1298vs, 1258vs, 1170s, 970s, 890m, 763s, 714s, 685s, 571m, 513w. Main FAB peaks 441, 443 ($[Ag(lutH)_2H]^+$), 274, 276 ($[Ag(lut)H]^+$), 124 ($[(lutH)H]^+$).

$Ag(isocincH)_2$. *Anal.* Calc. for $C_{14}H_8N_2O_8Ag$: C, 38.2; H, 1.8; N, 6.4. Found: C, 38.4; H, 1.5; N, 614%. Magnetic moment μ_{eff} 1.73 B.M. IR (cm^{-1}): 3439s, 2082s, 3037s, 1716vs, 1609vs, 1588vs, 1485m, 1388vs, 1351s, 1303s, 1242s, 1166m, 1124s, 1042m, 806s, 751s, 683m, 566w, 510s.

$Ag(cincH)_2 \cdot H_2O$. *Anal.* Calc. for $C_{14}H_{10}N_2O_9Ag$: C, 36.7; H, 2.2; N, 6.1. Found: C, 36.9; H, 2.2; N, 5.9%. Magnetic moment μ_{eff} 1.74 B.M. IR (cm^{-1}): 3457s, 3070m, 1703w, 1602vs, 1487w, 1397s, 1273m, 1162w, 1062w, 951w, 801s, 697m, 673s, 610m, 540s. Raman (cm^{-1}): 1632(2), 1594(8), 1542(3), 1485(2), 1376(1), 1277(1), 1227(1), 1163(2), 1118(2), 1059(10), 862(1), 815(7), 670(1), 597(2), 540(1), 457(2), 389(2).

$Ag(dinicH)_2 \cdot 4H_2O$. *Anal.* Calc. for $C_{14}H_{16}N_2O_{12}Ag$: C, 32.8; H, 3.1; N, 5.5. Found: C, 32.0; H, 1.7; N, 5.7%. IR (cm^{-1}): 3315vs, 3080vs, 1698m, 1606s, 1548s, 1418vs, 1221m, 1161w, 1078m, 1043m, 1012m, 994w, 848m, 762s, 698s, 655m, 631m.

2.2.3. Manganese(III) species

$Mn(pic)_3 \cdot 0.5H_2O$. An aqueous solution of $MnCl_2 \cdot 4H_2O$ (0.5 g, 2.5 mmol) was added to an aqueous solution of picolinic acid (1 g, 8 mmol). An ozone/oxygen stream was passed through the resultant colourless solution, which turned clear red within 2 min. Ozone was passed through the solution for a total of 15 min, during which time the solution darkened in colour as crystals were deposited. Further ozonolysis results in over-oxidation and formation of a green precipitate.

Anal. Calc. for $C_{18}H_{13}N_3O_{6.5}$: C, 50.2; H, 2.9; N, 9.8. Found: C, 50.2; H, 2.8; N, 9.7%. IR (cm^{-1}): 3540s, 3449s, 1749vs, 1688vs, 1600s, 1568m, 1472s, 1446s, 1349s, 1253vs, 1230m, 1164m, 1135vs, 1095w, 1042m, 1017m, 862s, 759m, 693m, 642m, 539w, 480s. Raman (cm^{-1}): 1588(7), 1562(3), 1474(2), 1387(2), 1439(2), 1387(2), 1306(2), 1234w, 1142(1), 1087(1), 1043(3), 1010(10), 986(3), 842(3), 698(2), 632(2).

2.2.4. Cobalt(III) and cobalt(II) species

$[Co^{III}W_{12}O_{40}]^{5-}$. Through a solution of $[Co^{II}W_{12}O_{40}]^{6-}$, made as in [4,5], O_3/O_2 was passed for 3 h, during which time the solution turned green and then golden yellow. The Raman spectrum was identical to that of a solution of the authentic sample made as in [4,5].

$Co(py)_2(OAc)_2(H_2O)_2$. This was first made by dissolving $Co(OAc)_2 \cdot 4H_2O$ (1.5 g, 6 mmol) in methanol,

to which pyridine (2 g, 25 mmol) was added, and O_3 passed through for 3 h. Orange crystals of the product were deposited. It was then made non-ozonolytically by reaction of $Co(OAc)_2 \cdot 4H_2O$ (1 g, 4 mmol) dissolved in 95% acetic acid/5% water (total 150 cm^3) and stirred for 30 min. The solvent was then removed and the residue suspended in methanol. Pyridine (0.1 cm^3) was then added and the mixture cooled to 4°C. After two days pale orange crystals were deposited.

$Co(py)_2(OAc)_2(H_2O)_2 \cdot H_2O$. *Anal.* Calc. for $C_{14}H_{22}N_2O_7$: C, 42.7; H, 5.6; N, 7.1. Found: C, 42.9; H, 5.9; N, 7.0%. IR (cm^{-1}): 3315vs, 3080vs, 1698w, 1606s, 1546s, 1418vs, 1321w, 1240w, 1078m, 1042m, 1012m, 934w, 848m, 762s, 698vs, 655m, 631m.

2.2.5. Oxidations of menthol with O_3/O_2

The method of Odinokov et al. [6] was used in an attempt to catalyse the oxidation of menthol to menthone using cobalt(II) acetate as a catalyst. Menthol (1.0 g, 6.4 mmol) and powdered $Co(OAc)_2 \cdot 4H_2O$ (5 mg, 0.02 mmol) were added to ethyl acetate (10 cm^3), and O_3/O_2 passed for 1 h at 0.3 $dm^3\ min^{-1}$, after which a stream of O_2 was continued for 5 min to purge the system of O_3. A solution of sodium thiosulfate was added to the mixture, the organic layer separated and washed with first ether and then with aqueous sodium bicarbonate and sodium chloride solutions, dried and concentrated to give the product mixture which was analysed by gas chromatography. The experiment was repeated in the same way but without cobalt acetate. In both cases the yield of menthone was ca. 33%. A similar lack of catalytic activity was found when dichloromethane was substituted for ethyl acetate.

2.3. Instrumentation

Magnetic moments were measured on a Johnson Matthey Evans magnetic susceptibility balance [7]. FAB measurements in 3-nitrobenzyl alcohol with a primary Cs^+ 25 keV ion beam were recorded using an AutoSpec-Q Micromass FAB+ instrument. Raman spectra were measured on a Dilor LabRam Infinity instrument with 632.8 nm He–Ne excitation of 8 mW at the powdered sample, and IR spectra on a Perkin–Elmer RX-1 spectrometer as discs in KBr (4000–500 cm^{-1}).

2.4. Crystal data for *1*

$C_{14}H_{20}CoN_2O_6$, $M = 371.25$, orthorhombic, *Pbca* (No. 61), $a = 12.5908(10)$, $b = 8.9461(10)$, $c = 15.0180(15)$ Å, $V = 1691.6(3)$ $Å^3$, $Z = 4$ (C_i symmetry), $D_c = 1.458$ g cm^{-3}, μ(Cu Kα) = 8.239 mm^{-1}, $T = 203$ K, pale orange prisms; 1348 independent measured reflections, F^2 refinement, $R_1 = 0.040$, $wR_2 = 0.087$, 926 independent observed absorption corrected reflections [$|F_o| > 4\sigma(|F_o|)$, $2\theta_{max} = 126°$], 116 parameters.

3. Results and discussion

3.1. Silver(II) complexes

A number of such complexes are known, normally made by oxidation of the corresponding silver(I) species with persulfate, but ozonolysis has occasionally been used. Thus the 2,2′-bipyridyl complex $[Ag^{II}(bpy)(NO_3)_2]$ [8] has been so made as have salts of $[Ag(bpy)_2]^{2+}$ [9] and $[Ag(phen)_2]^{2+}$ [10].

We find that ozonolysis at room temperature of a mixture of silver nitrate with the pyridinecarboxylic acids given in Section 2 in a metal:ligand ratio of 1:2 gives good yields of $[Ag^{II}L_2] \cdot nH_2O$. To our knowledge ozonolysis has not been used for such preparations before, most of these silver(II) species having been prepared by reactions involving heating silver nitrate, the ligand and persulfate [11,12]. In our procedure, by contrast, the preparations are simple and are carried out at room temperature.

There are two X-ray structures of such complexes: $Ag(quinH)_2 \cdot 2H_2O$ shows a slightly distorted square planar coordination [13], whilst the silver(II) dipicolinate complex is octahedral with coordination from two tridentate ligands, one neutral and the other dianionic, i.e., $[Ag^{II}(dipic)(dipicH_2)]$ [14,15].

It is clear that all of our AgL_2 complexes contain silver(II) since they are paramagnetic at room temperature with a magnetic moment close to the expected value of 1.73 B.M. Fast-atom bombardment (FAB) studies on $Ag(pic)_2$, $Ag(isonic)_2 \cdot H_2O$, $Ag(quinH)_2 \cdot 2H_2O$ and $Ag(lutH)_2 \cdot 3H_2O$ all show the expected isotope patterns (^{107}Ag 51.8%, ^{109}Ag 48.2%) for the parent ions $[\{AgL_2H\}]^+$, $[\{AgLH\}]^+$ and $[LH]^+$. Their IR spectra are listed in Section 2 and, for the case of $Ag(cincH)_2 \cdot H_2O$, the Raman spectrum; the colours of the other silver(II) complexes precluded recording of Raman spectra. IR spectra for only some of these complexes have been reported previously, and only in the range 1500–1800 cm^{-1} [16].

For pyridine carboxylic acids the simple formula AgL_2 (L = pic, isonic) with square-planar coordination seems likely; $Ag(nic)_2$ was also made but analyses were unsatisfactory. In the cases of the pyridinedicarboxylate ligands, coordination may occur as the dianion (e.g., $quin^{2-}$), the mono-anion (e.g., $quinH^-$) or as the neutral species (e.g., $quinH_2$). We formulate ours as $Ag(LH)_2$ (L = quinH, lutH, isocincH, cincH, dinicH) since the published X-ray crystal structure of $Ag(quinH)_2 \cdot 2H_2O$ [13] shows the anion to be centrosymmetric with coordination from two *trans* $[C_5H_3N(COOH)(COO)]^-$ ligands. The fact that we observe few IR–Raman coincidences

for $Ag(cincH)_2 \cdot H_2O$ also suggests a centrosymmetric structure for this complex.

3.2. Manganese(III) complexes

We have already reported the use of ozone in forming $Mn^{III}(OAc)_3 \cdot 2H_2O$ by ozonolysis of $Mn(OAc)_2$, and in the preparations of the manganese(IV) polyoxometalates $K_6[Mn^{IV}Mo_9O_{32}] \cdot 10H_2O$, $K_8[Mn^{IV}W_6O_{24}] \cdot 6H_2O$ and $(NH_4)_6[Mn^{IV}Mo_6H_6O_{32}] \cdot 10H_2O$; ozonolysis was much more effective in producing these species than was the use of persulfate [1].

We find that reaction of manganese(II) chloride with picolinic acid under an O_3/O_2 stream gave $Mn(pic)_3$ (which has also been made by conventional procedures [11,12]), but our other pyridinecarboxylate complexes, though containing $Mn^{III}L_3$ species, were impure.

3.3. Cobalt(III) and (II) complexes

Salts of $[Co^{III}W_{12}O_{40}]^{5-}$ are normally made by oxidation of $[Co^{II}W_{12}O_{40}]^{6-}$ with persulfate [4,5]. The procedure is tedious; we find that an O_3/O_2 mixture will effect the oxidation of $[CoW_{12}O_{40}]^{6-}$ at room temperature, whilst the persulfate procedure requires heating. Our ozonolytic procedure gave a sample which had an identical Raman spectrum with that of the product made by the procedure of [4,5]. A number of applications of $[Co^{III}W_{12}O_{40}]^{5-}$ as an oxidation catalyst have been described, the most recent of which are its use in the catalytic acetylation and formylation of alcohols [17] and deprotonation of dioxolanes [18].

3.3.1. Oxidation of alcohols by ozone catalysed by $Co(OAc)_2$

We have shown that an O_3/O_2 mixture will epoxidise alkenes to epoxides catalysed by iron(II) porphyrin complexes [19], and we are currently studying other transition-metal catalysed ozonolytic reactions. In 1998 it was claimed that $Co(OAc)_2$ catalysed the ozonolytic oxidation of menthol to menthone, in dichloromethane or ethyl acetate solvents [6] although it has long been known that non-catalysed ozonolysis of alcohols to carbonyl products occurs [20].

We found that, although menthol was indeed oxidised by ozonolysis to menthone in good yield, the presence or absence of $Co(OAc)_2$ had no effect on the yield.

3.3.2. $Co(py)_2(OAc)_2(H_2O)_2$ (1)

In connection with the above oxidation experiments we studied the effect of ozonolysis on solutions of the cobalt(II) acetate with pyridine; there are several reports of the formation of polymeric oxo-centred cobalt(III) species from such a reaction [21,22]. We found that, although some cobalt(III)-containing materials were formed, an orange material $Co(py)_2(OAc)_2(H_2O)_2$ was also present. We subsequently found that this complex could be made without ozone, by direct reaction of cobalt(II) acetate with acetic acid and pyridine. Surprisingly this material seems not to have been reported before, although there is a brief reference to $Co(OAc)_2(py)_2$ [23].

3.3.3. X-ray crystal structure of 1

A single crystal X-ray analysis of **1** showed the complex (Fig. 1) to have crystallographic inversion symmetry and to be isomorphous with its nickel analogue [24]. The pyridine rings are inclined by ca. 61° to the $\{Co,N_2,(OH_2)_2\}$ plane, and the acetate group is rotated by ca. 15° about the Co–O(7) bond, out of the CoO_4 plane. There is an intramolecular O–H···O hydrogen bond between one of the aqua hydrogen atoms and the acetate oxygen atom O(9A), and an intermolecular O–H···O hydrogen bond between the other aqua hydrogen atom and this same oxygen atom in a glide related molecule. These interactions combine to form hydrogen bonded sheets that extend throughout the {0 0 1} plane (Fig. 2). The geometry at cobalt is only slightly distorted octahedral with *cis* angles in the range 87.31(10)°–92.69(10)°. The Co-aqua, –pyridine and –acetate bond lengths (Table 1) all lie within the ranges of values observed in the closely related complexes catena-bis(μ_2-terephthalato-O,O′)-tetra-aqua-tetrapyridine-di-cobalt(II) [25] and catena-(μ_2-4,4′-biphenyldicarboxylato)-diaqua-dipyridine-cobalt(II) [26]. Interestingly, these two literature polymers also have intramolecular aqua···carboxylate hydrogen bonds directly analogous to those observed in **1**.

3.4. Possible mechanism of these oxidations by ozonolysis

We have not carried out any mechanistic studies on the oxidations. However, it seems likely that oxygen-atom transfer is involved, as proposed in our work on

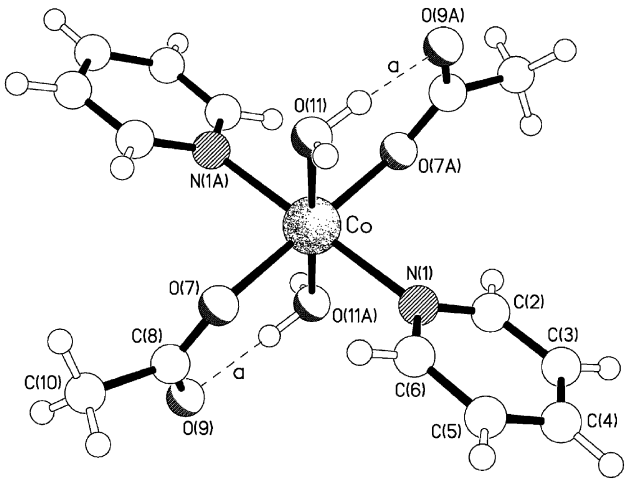

Fig. 1. The molecular structure of **1**.

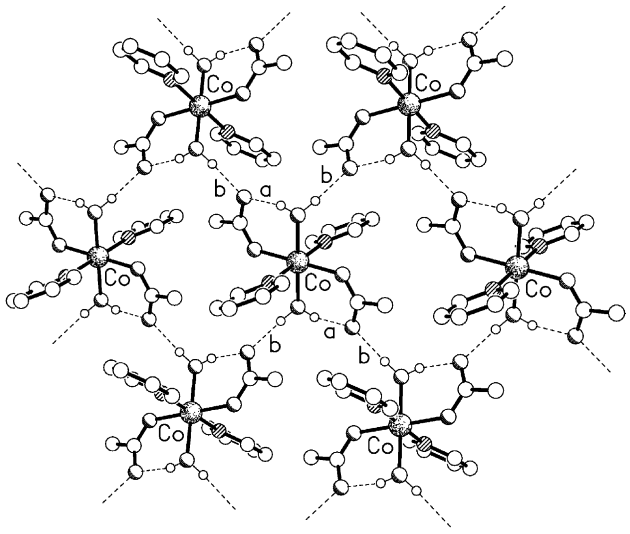

Fig. 2. Part of one of the hydrogen bonded sheets of molecules in the structure of **1**. The hydrogen bonding geometries are: [O···O], [H···O] Å, [O–H···O]°, (a) 2.717(3), 1.84, 165; (b) 2.775(3), 1.88, 172.

Table 1
Selected bond lengths (Å) and angles (°) for **1**

Bond lengths	
Co–N(1)	2.159(3)
Co–O(11)	2.121(2)
Co–O(7)	2.076(2)
Bond angles	
N(1)–Co–O(7)	90.55(10)
N(1)–Co–O(11)	92.69(10)
O(7)–Co–O(11)	88.79(9)
N(1)–Co–O(7A)	89.45(10)
N(1)–Co–O(11A)	87.31(10)
O(7)–Co–O(11A)	91.21(8)

the epoxidation of alkenes by an O_3/O_2 mixture catalysed by iron(II) porphyrins [19]. Such a mechanism has also been proposed for other ozonolytic reactions, notably the reaction of iron(II) species with an O_3/O_2 mixture [2,27].

4. Conclusions

We have shown that simple ozonolysis can be used to prepare complexes of silver(II), manganese(III) and cobalt(III) under ambient conditions, oxidations which can be less conveniently carried out with persulfate. This successful use of ozonolysis in place of more conventional chemical methods as a route to high oxidation state complexes opens up the possibility of preparing other such species by this simple and environmentally friendly technique. It is thought likely that these oxidations involve oxygen atom transfer from the ozone to the metal centre.

During this work, the new complex $Co(py)_2(OAc)_2(H_2O)_2$ was prepared and its X-ray crystal structure determined.

5. Supplementary material

Crystallographic data for complex **1** has been deposited with the Cambridge Crystallographic data centre, CCDC No. 235093. Copies of this data may be obtained free of charge from The Director CCDC, 12 Union Road, Cambridge, CB2 1EZ (fax: +44-1223-336-033 or e-mail: deposit@ccdc.cam.ac.uk or www: http://www.ccdc.cam.ac.uk).

Acknowledgement

We thank John Barton, Imperial College London, for mass spectrometric measurements.

Appendix A. Supplementary data

Supplementary data associated with this article can be found, in the online version at doi:10.1016/j.poly.2004.05.020.

References

[1] A.J. Bailey, W.P. Griffith, S.P. Marsden, A.J.P. White, D.J. Williams, J. Chem. Soc., Dalton Trans. (1998) 3673.
[2] W.P. Griffith, Coord. Chem. Rev. 219–221 (2001) 259.
[3] A. Vogel, Textbook of Quantitative Inorganic Analysis, fourth ed., Longmans, London, 1978, p. 379.
[4] F. Walmsley, J. Chem. Ed. 69 (1992) 936.
[5] L.C.W. Baker, T.P. McCutcheon, J. Am. Chem. Soc. 78 (1956) 4503.
[6] V.N. Odinokov, L.P. Botsman, G.A. Emel'yanova, Russ. Chem. Bull. (Engl. Transl.) 47 (1998) 2021.
[7] D.F. Evans, J. Chem. Soc. A (1967) 1670.
[8] G.W. Bushnell, M.A. Khan, Can. J. Chem. 50 (1972) 315.
[9] A. Malaguti, T. Labianca, Gazz. Chim. Ital. 84 (1954) 976.
[10] J. Selbin, B. Shamburger, J. Inorg. Nucl. Chem. 24 (1962) 1153.
[11] B. Banerjee, P. Rây, J. Ind. Chem. Soc. 34 (1957) 207.
[12] B. Banerjee, P. Rây, J. Ind. Chem. Soc. 33 (1956) 503.
[13] M.G.B. Drew, R.W. Matthews, R.A. Walton, Inorg. Nucl. Chem. Lett. 6 (1970) 277.
[14] M.G.B. Drew, R.W. Matthews, R.A. Walton, J. Chem. Soc., Dalton Trans. (1970) 1405.
[15] M.G.B. Drew, W.G.A. Fowles, R.W. Matthews, R.A. Walton, J. Am. Chem. Soc. 91 (1969) 7769.
[16] G.W.A. Fowles, R.W. Matthews, R.A. Walton, J. Chem. Soc. (A) (1968) 1108.
[17] M.H. Habibi, S. Tangestaninejad, V. Mirkhani, B. Yadollahi, Catal. Lett. 75 (2001) 205.
[18] M.H. Habibi, S. Tangestaninejad, V. Mirkhani, B. Yadollahi, Tetrahedron 547 (2001) 8333.
[19] F.J. Waller, A.J. Bailey, W.P. Griffith, S.P. Marsden, E.H. Smith, J. Mol. Catal. 154A (2000) 85.

[20] W.L. Walters, A.J. Rollin, C.M. Bardwell, J.A. Schneider, T.W. Aanerud, J. Org. Chem. 41 (1976) 889.
[21] S. Uemura, A.S. Spencer, G. Wilkinson, J. Chem. Soc., Dalton Trans. (1973) 2565.
[22] J.K. Beattie, T.W. Hambley, J.A. Klepetko, A.F. Masters, P. Turner, Polyhedron 17 (1998) 1343.
[23] C.B. Kremer, A. Bendich, J. Am. Chem. Soc. 62 (1940) 1279.
[24] J. Drew, M.B. Hursthouse, P. Thornton, J. Chem. Soc., Dalton Trans. (1972) 1658.
[25] R.H. Groeneman, L.R. MacGillivray, J.L. Atwood, Inorg. Chem. 38 (1999) 208.
[26] L. Pan, N. Ching, X. Huang, J. Li, Inorg. Chem. 39 (2000) 5333.
[27] T. Logager, J. Holcman, K. Sehested, T. Pedersen, Inorg. Chem. 31 (1992) 3523.

Available online at www.sciencedirect.com
SCIENCE DIRECT®
Polyhedron 23 (2004) 2637–2644
POLYHEDRON
www.elsevier.com/locate/poly

Synthesis and crystal structure of high and low spin diruthenium complexes with diphenylformamidine and diphenyltriazene ligands

M.C. Barral [a], R. González-Prieto [a], S. Herrero [a], Reyes Jiménez-Aparicio [a,*], J.L. Priego [a], E.C. Royer [a], M.R. Torres [b], F.A. Urbanos [a]

[a] *Departamento de Química Inorgánica, Facultad de Ciencias Químicas, Universidad Complutense, Ciudad Universitaria, 28040 Madrid, Spain*
[b] *Centro de Asistencia a la Investigación de Rayos X, Facultad de Ciencias Químicas, Universidad Complutense, Ciudad Universitaria, 28040 Madrid, Spain*

Received 7 April 2004; accepted 14 May 2004
Available online 15 July 2004

Dedicated to Professor M.L.H. Green

Abstract

The synthesis and structural characterization of the complex $Ru_2(CN)(\mu\text{-DPhF})_4$ (**1**) (DPhF = *N*,*N*′-diphenylformamidinate) is reported. The reactivity of the axial position of $Ru_2Cl(\mu\text{-}O_2CMe)(\mu\text{-DPhF})_3$ is studied and the crystal structures of $Ru_2(N_3)(\mu\text{-}O_2CMe)(\mu\text{-DPhF})_3$ (**2**) and $Ru_2(NCS)(\mu\text{-}O_2CMe)(\mu\text{-DPhF})_3$ (**3**) are described. The isolation of $Ru_2Cl(\mu\text{-}N_3Ph_2)_4$ (**4**) and $Ru_2Cl_2(\mu\text{-}N_3Ph_2)_4$ (**5**), and the crystal structure determination of complex **4**, which constitutes the first example of a chlorotriazenido derivative, are also reported. Each complex forms discrete dinuclear molecules in the solid state, having (each diruthenium unit) one free axial position. The shortest Ru–Ru distance [2.286(2) Å] is observed in the cyano derivative (**1**) and the longest [2.4747(11) Å] is found in the triazenido complex (**4**). The azido (**2**) and isothiocyanato (**3**) derivatives show similar Ru–Ru distances of 2.3182(11) and 2.3159(4) Å, respectively. Complexes **2** and **4** display magnetic moments at room temperature corresponding to three unpaired electrons in agreement with the $\sigma^2\pi^4\delta^2(\pi^*\delta^*)^3$ ground-state configuration, whereas compounds **1** and **3** are low spin complexes with only one unpaired electron. Only very few examples of low spin diruthenium(II,III) species have been previously characterized. The diruthenium(III) compound **5** is diamagnetic.
© 2004 Elsevier Ltd. All rights reserved.

Keywords: Diruthenium compounds; Metal–metal bonds; Triazenido complexes; Formamidinato complexes; Multiple bonds; Low spin complexes

1. Introduction

Diruthenium complexes form a well known class of compounds in which a pair of ruthenium atoms are bridged by four ligands giving a ''paddlewheel'' structure [1–3]. Numerous tetracarboxylatodiruthenium(II,III) and diruthenium(II) complexes are known [3], whereas the analogous diruthenium(III) derivatives have not been isolated [4], although the formation of the cationic complex $[Ru_2(\mu\text{-}O_2CMe)_4(PCy_3)_2]^{2+}$, containing a Ru_2^{6+} unit [5], has been reversibly generated by a cyclic voltammetry technique.

In contrast, with N,N-donor bridging ligands such as formamidinate or aminopyridinate, in addition to the formation of diruthenium(II,III) [1,2,6] and diruthenium(II) complexes [1,2,7], numerous stable diruthenium(III) complexes have been reported [8]. Thus, the reaction of $Ru_2Cl(\mu\text{-}O_2CMe)_4$ with molten formamidines leads to the diruthenium(II,III) derivatives [6b,6c] of the type $Ru_2Cl(\mu\text{-DRF})_4$ (DRF = dialkyl- or diarylformamidinate). We have shown very recently [9] that the similar reaction with *N*,*N*′-diphenylformamidine

* Corresponding author. Tel.: +34-91-394-43-34; fax: +34-91-394-43-52.
E-mail address: qcmm@quim.ucm.es (R. Jiménez-Aparicio).

0277-5387/$ - see front matter © 2004 Elsevier Ltd. All rights reserved.
doi:10.1016/j.poly.2004.05.015

(HDPhF) in refluxing thf leads to the trisubstituted complex $Ru_2Cl(\mu\text{-}O_2CMe)(\mu\text{-}DPhF)_3$, and we have explored its use as a starting material in substitution reactions of the acetato ligand by other carboxylate groups. An analogous behaviour has been observed with the *N*,*N*′-di-*p*-anisylformamidinate ligand (DAniF) [10].

However, the diruthenium chemistry employing triazenide ligands has been little explored [11–14]. Thus, only the preparation and crystal structure determination of two diruthenium(II) complexes of the type $Ru_2(\mu\text{-}N_3R_2)_4$ (R = Ph, C_6H_4-*p*-Me) have been described [12,13]. Some mono- and bis-adducts of these diruthenium(II) complexes such as $Ru_2(\mu\text{-}N_3Ph_2)_4(Bu^tNC)$ or $Ru_2(\mu\text{-}N_3Ph_2)_4(CO)_2$ are also known [11]. These diruthenium(II) complexes can be oxidized with silver salts to diruthenium(II,III) complexes as in the examples $\{Ru_2[\mu\text{-}N_3(C_6H_4\text{-}p\text{-}Me)_2]_4(MeCN)\}BF_4$ [13] and $Ru_2(\mu\text{-}N_3Ph_2)_4(OPF_4)$ [14]. In addition, the chlorotris(triazenido) complex $Ru_2Cl(\mu\text{-}O_2CMe)(\mu\text{-}N_3Ph_2)_3$ has been proposed as an intermediate in the synthesis of $[Ru_2(\mu\text{-}O_2CMe)(\mu\text{-}N_3Ph_2)_3(MeCN)_2]BF_4$, but has not been isolated [15]. To our knowledge there is no example reported of any chloro(triazenido) complex of diruthenium.

In this work we describe the preparation and characterization of some new complexes containing diphenylformamidinate or diphenyltriazenide as bridging ligands. The reactivity of the axial position of $Ru_2Cl(\mu\text{-}O_2CMe)(\mu\text{-}DPhF)_3$ is studied and the crystal structures of $Ru_2(CN)(\mu\text{-}DPhF)_4$, $Ru_2(N_3)(\mu\text{-}O_2CMe)(\mu\text{-}DPhF)_3$, $Ru_2(NCS)(\mu\text{-}O_2CMe)(\mu\text{-}DPhF)_3$ and $Ru_2Cl(\mu\text{-}N_3Ph_2)_4$ are also reported.

2. Results and discussion

2.1. Synthesis and characterization of the complexes

The reaction of $Ru_2Cl(\mu\text{-}DPhF)_4$ with NaCN in thf in air leads to the formation of the diruthenium(III) complex $Ru_2(CN)_2(\mu\text{-}DPhF)_4$ as described previously [6b]. The formation of this complex must occur through the intermediate $Ru_2(CN)(\mu\text{-}DPhF)_4$ which accepts a new CN ligand at the free axial position providing the diruthenium(II,III) anion $[Ru_2(CN)_2(\mu\text{-}DPhF)_4]^-$. This anion is easily oxidized to give the corresponding stable diruthenium(III) complex. Since there was no example of a cyanodiruthenium(II,III) complex well characterized, we undertook the isolation of the intermediate $Ru_2(CN)(\mu\text{-}DPhF)_4$ (**1**).

In a previous paper, we have demonstrated that the substitution of the acetate ligand in $Ru_2Cl(\mu\text{-}O_2CMe)(\mu\text{-}DPhF)_3$ by other carboxylate groups is facile [9]. The axial chloride ligand of this complex can also be removed in thf employing a silver salt such as $AgBF_4$. The addition of NaN_3 to the solution gives the discrete complex $Ru_2(N_3)(\mu\text{-}O_2CMe)(\mu\text{-}DPhF)_3$ (**2**) where the azide ligand is bonded to the axial position. The reaction of $Ru_2Cl(\mu\text{-}O_2CMe)(\mu\text{-}DPhF)_3$ with AgSCN leads directly to $Ru_2(NCS)(\mu\text{-}O_2CMe)(\mu\text{-}DPhF)_3$ (**3**).

Cotton and co-workers [15] have described that the reaction of $Ru_2Cl(\mu\text{-}O_2CMe)_4$ in melted HN_3Ph_2 followed by the removal of the axial chloride ion with $AgBF_4$ gives $[Ru_2(\mu\text{-}O_2CMe)(\mu\text{-}N_3Ph_2)_3(MeCN)_2]BF_4$. We have carried out this reaction in refluxing 2-methoxyethanol without $AgBF_4$ in order to obtain the tetrasubstituted complex. This solvent has proved to be useful for the complete substitution of the acetate groups in $Ru_2Cl(\mu\text{-}O_2CMe)_4$ by amides [16]. However, we have obtained crystals of $Ru_2Cl(\mu\text{-}N_3Ph_2)_4$ (**4**) in low yield (12%). The diruthenium(III) complex $Ru_2Cl_2(\mu\text{-}N_3Ph_2)_4$ (**5**) could be isolated after purifying the mixture by column chromatography.

Complexes **1**–**5** exhibit characteristic bands of the diphenylformamidinate and diphenyltriazenide ligands. The spectrum of **1** shows a sharp and intense band at 2096 cm^{-1} while the azide asymmetric stretching absorption in complex **2** appears as an intense band at 2031 cm^{-1}. Similar values have been found for the diruthenium(III) compounds $Ru_2(DMBA)_4X_2$ (DMBA = *N*,*N*′-dimethylbenzamidinate) where X is a CN or N_3 terminal axial ligand [8b]. Complex **3** presents at 2060 cm^{-1} the absorption corresponding to the SCN group bonded to the ruthenium atom. The shifting of this band with respect to the free SCN group suggests that this ligand is N-bonded to the ruthenium atom, which is corroborated by the crystal structure determination described below.

2.2. Magnetic properties

Complexes **1**–**4** are paramagnetic whereas complex **5** is diamagnetic. Complexes **2** and **4** display magnetic moments at room temperature corresponding to three unpaired electrons in agreement with the $\sigma^2\pi^4\delta^2(\pi^*\delta^*)^3$ ground-state configuration proposed by Norman and co-workers [17] for carboxylatodiruthenium(II,III) complexes. The magnetic moment of complex **2** (4.1 B.M.) is comparable to the parent chloro derivative $Ru_2Cl(\mu\text{-}O_2CMe)(\mu\text{-}DPhF)_3$ (4.0 B.M.), its analogous $Ru_2Cl(\mu\text{-}O_2CMe)(\mu\text{-}DAniF)_3$ (3.8 B.M.) [10] and the rare example $[Ru_2(\mu\text{-}O_2CMe)(\mu\text{-}N,N'\text{-}o\text{-}MeOForm)(\mu\text{-}N,N'\text{-}\eta^2\text{-}N,O\text{-}o\text{-}OMeForm)(\mu\text{-}N,N'\text{-}\eta^2\text{-}N,O\text{-}o\text{-}OMeForm')]$ (3.8 B.M.), where *o*-MeOForm is di(*o*-methoxyphenyl)formamidinate and *o*-MeOForm' is the *o*-demethylation derivative of *o*-MeOForm [18]. Similar magnetic moments are also observed in the chlorotetrakis(formamidinato)diruthenium(II,III) derivatives [6b,6c,19] and in all tetracarboxylatodiruthenium(II,III) derivatives described in the literature [1,3]. As it has been proved, the π^* and δ^* energy levels of the electronic structure of the diruthenium(II,III) units are dependent

on the nature of the bridging and axial ligands [1,3]. Thus, when in diruthenium complexes both bridging acetate and chlore axial ligands are replaced by triazenide groups and MeCN ligands, respectively, the δ^* energy level moves above the π^* level, and their electronic structures become $\sigma^2\pi^4\delta^2\pi^{*3}\delta^{*0}$ [13,15]. As a consequence, a low spin complex is formed as observed in $\{Ru_2[\mu\text{-}N_3(C_6H_4\text{-}p\text{-}Me)_2]_4(MeCN)\}BF_4$ (1.9 B.M.) [13] and $[Ru_2(\mu\text{-}O_2CMe)(\mu\text{-}N_3Ph_2)_3(MeCN)_2]BF_4$ (1.5 B.M.) [15]. These observations are corroborated in the magnetic behaviour of $Ru_2(CN)(\mu\text{-}DPhF)_4$ (**1**) and $Ru_2(NCS)(\mu\text{-}O_2CMe)(\mu\text{-}DPhF)_3$ (**3**), which have at the axial position π-acceptor ligands, showing a magnetic moment of 1.6 and 1.7 B.M., respectively, corresponding to the presence of only one unpaired electron.

On the other hand, the magnetic moment obtained for the first chlorotetrakis(triazenido)diruthenium-(II,III) complex **4** (4.1 B.M.) indicates that the substitution of the carboxylate groups by triazenide ligands is not sufficient to give a low spin complex. Therefore, the substitution of the chloride axial ligand by a good π-acceptor ligand is also needed.

The presence of a high or low spin electronic configuration in diruthenium species is also strongly dependent on the oxidation state of the diruthenium unit. Thus, the chlorotetrakis(formamidinato)diruthenium(II,III) compounds are paramagnetic with a high spin configuration, whereas the analogous diruthenium(II) compounds are diamagnetic [20]. The tetrakis(triazenido)diruthenium(II) complexes [12–14] and many diruthenium(III) compounds, such as complex **5**, are also diamagnetic [8]. According to this diamagnetic behaviour, complex **5** displays a well resolved ^1H NMR spectrum.

2.3. Crystal structures

The structures of complexes **1**–**4** have been determined by X-ray crystallography. Table 1 lists relevant crystallographic data, and selected distances and angles are given in Table 2.

Fig. 1 shows the molecular structure of $Ru_2(CN)(\mu\text{-}DPhF)_4\cdot C_6H_{14}$ (**1** · $\mathbf{C_6H_{14}}$). In this molecule, one axial position is occupied by a CN ligand while the other one remains free. Thus, the first Ru atom has a pseudo-octahedral environment and the second has a square pyramidal geometry. Four bridging diphenylformamidinate ligands form the equatorial planes.

The Ru–Ru distance in **1** · $\mathbf{C_6H_{14}}$ is 2.4747(11) Å, which is significantly longer than in other diruthenium(II,III) complexes, including the parent compound $Ru_2Cl(\mu\text{-}DPhF)_4$ (2.339 Å) [6b] or $Ru_2Cl(\mu\text{-}DtolF)_4$ (DtolF = di-*p*-tolylformamifinate) (2.370(2) Å) [6c], but similar to the value found in $Ru_2(CN)_2(\mu\text{-}DMBA)_4$ (DMBA = *N*,*N*′-dimethylbenzamidinate) (2.4508(9) Å) [8b]. The metal-metal bond distance is even longer (2.539(1) Å) [6b] for the dicyano derivative of diruthenium(III) $Ru_2(CN)_2(\mu\text{-}DPhF)_4$ [6b]. Thus, the Ru–Ru distance in complex **1** · $\mathbf{C_6H_{14}}$ with a theoretical bond order of 2.5, is shorter than that observed in $Ru_2(CN)_2(\mu\text{-}DPhF)_4$, which has a theoretical triple bond order. The shorter Ru–Ru distance in

Table 1
Crystal data for $Ru_2(CN)(\mu\text{-}DPhF)_4\cdot C_6H_{14}$ (**1** · $\mathbf{C_6H_{14}}$), $Ru_2(N_3)(\mu\text{-}O_2CMe)(\mu\text{-}DPhF)_3$ (**2**), $Ru_2(NCS)(\mu\text{-}O_2CMe)(\mu\text{-}DPhF)_3$ (**3**) and $Ru_2Cl(\mu\text{-}N_3Ph_2)_4\cdot 2H_2O$ (**4** · $\mathbf{2H_2O}$)

	1 · $\mathbf{C_6H_{14}}$	**2**	**3**	**4** · $\mathbf{2H_2O}$
Empirical formula	$C_{59}H_{58}N_9Ru_2$	$C_{82}H_{72}N_{18}O_4Ru_4$	$C_{42}H_{36}N_7O_2Ru_2S$	$C_{48}H_{40}ClN_{12}O_2Ru_2$
Formula weight	1095.28	1777.86	904.98	1054.51
Crystal system	tetragonal	triclinic	monoclinic	tetragonal
Space group	$P4/ncc$	$P\bar{1}$	$P2(1)/n$	$P4/ncc$
a (Å)	14.8732(7)	15.334(2)	17.6892(10)	15.3832(8)
b (Å)	14.8732(7)	15.4422(19)	9.9812(6)	15.3832(8)
c (Å)	21.8717(14)	16.970(2)	23.5252(14)	20.1447(14)
α (°)	90	76.004(3)	90	90
β (°)	90	87.709(2)	110.3140(10)	90
γ (°)	90	77.506(3)	90	90
Volume (Å^3)	4838.3(4)	3806.4(8)	3895.3(4)	4767.1(5)
Z	4	2	4	4
D_{calc} (Mg/m^3)	1.504	1.551	1.543	1.469
Absorption coefficient (mm^{-1})	0.676	0.842	0.875	0.741
$F(000)$	2252	1796	1828	2132
θ Range for data collection (°)	1.86–25.00	1.24–23.26	1.25–23.29	1.87–21.96
Reflections collected	23122	17350	16806	17363
Independent reflections [R_{int}]	2141 [0.0722]	10 875 [0.0571]	5607 [0.0514]	1463 [0.1080]
Data/restraints/parameters	2141/0/157	10 875/0/975	5607/0/489	1463/0/146
Goodness-of-fit on F^2	1.060	0.790	0.976	0.983
$R1/wR2$ (final) [$I > 2\sigma(I)$]	0.0422/0.1363	0.0496/0.0850	0.0313/0.0740	0.0816/0.2127
$R1/wR2$ (all data)	0.0774/0.1564	0.1251/0.1073	0.0398/0.0776	0.1261/0.2729
Largest difference peak and hole (e Å^{-3})	1.162 and −0.653	0.766 and −0.416	0.563 and −0.583	1.406 and −2.007

Table 2
Selected bond distances (Å) and angles (°) for $Ru_2(CN)(\mu\text{-DPhF})_4 \cdot C_6H_{14}$ (**1 · C$_6$H$_{14}$**), $Ru_2(N_3)(\mu\text{-}O_2CMe)(\mu\text{-DPhF})_3$ (**2**), $Ru_2(NCS)(\mu\text{-}O_2CMe)(\mu\text{-DPhF})_3$ (**3**) and $Ru_2Cl(\mu\text{-}N_3Ph_2)_4 \cdot 2H_2O$ (**4 · 2H$_2$O**)

1 · C$_6$H$_{14}$		**2**		**3**		**4 · 2H$_2$O**	
Bond distances							
Ru1–Ru2	2.4747(11)	Ru1–Ru2	2.3182(11)	Ru1–Ru2	2.3159(4)	Ru1–Ru2	2.286(2)
Ru1–C1	2.112(11)	Ru1–N7	2.116(8)	Ru1–N7	2.103(3)	Ru1–Cl1	2.418(6)
Ru1–N2	2.061(5)	Ru1–N1	2.064(6)	Ru1–N1	2.083(3)	Ru1–N1	2.110(10)
Ru2–N3	2.034(4)	Ru2–N2	2.015(6)	Ru2–N2	2.038(3)	Ru2–N2	2.037(10)
		Ru1–N3	2.072(7)	Ru1–N4	2.079(3)		
		Ru2–N4	2.039(7)	Ru2–N3	2.042(3)		
		Ru1–N5	2.058(7)	Ru1–N5	2.051(3)		
		Ru2–N6	2.029(7)	Ru2–N6	2.043(3)		
		Ru1–O1	2.075(5)	Ru1–O1	2.078(2)		
		Ru2–O2	2.062(5)	Ru2–O2	2.058(2)		
Bond angles							
C1–N1	1.111(14)	N7–N8	1.173(9)	N7–C6	1.146(4)		
		N8–N9	1.144(10)	C6–S1	1.612(4)		
C1–Ru1–Ru2	180.0	N7–Ru1–Ru2	170.4(2)	N7–Ru1–Ru2	178.16(8)	Cl1–Ru1–Ru2	180.0
N1–C1–Ru1	180.0	N8–N7–Ru1	120.5(7)	C6–N7–Ru1	167.7(3)		
		N7–N8–N9	175.8(11)	N7–C6–S1	179.1(4)		
N2–Ru1–Ru2	86.01(12)	N1–Ru1–Ru2	90.8(2)	N1–Ru1–Ru2	89.08(8)	N1–Ru1–Ru2	85.5(2)
N3–Ru2–Ru1	88.30(11)	N2–Ru2–Ru1	89.0(2)	N2–Ru2–Ru1	90.56(8)	N2–Ru2–Ru1	88.5(3)
		N3–Ru1–Ru2	88.5(2)	N4–Ru1–Ru2	88.15(7)		
		N4–Ru2–Ru1	91.2(2)	N3–Ru2–Ru1	91.33(7)		
		N5–Ru1–Ru2	88.57(19)	N5–Ru1–Ru2	88.15(8)		
		N6–Ru2–Ru1	91.4(2)	N6–Ru2–Ru1	91.64(8)		
		O1–Ru1–Ru2	86.38(16)	O1–Ru1–Ru2	88.45(6)		
		O2–Ru2–Ru1	91.16(17)	O2–Ru2–Ru1	89.03(7)		

diruthenium(II,III) derivatives than in the diruthenium(III) complexes, has been observed previously [6b].

The Ru–C bond length (2.112(11) Å) is longer than the average Ru–C bond distance of 1.971 Å found in $Ru_2(CN)_2(\mu\text{-DPhF})_4$[6b], in accord with the shorter C-N bond distance for **1 · C$_6$H$_{14}$** (1.111(14) Å) in comparison with the dicyano complex (1.148(13) and 1.179(14) Å). The molecule is rotated around the Ru–Ru axis with a N–Ru–Ru–N torsion angle of 14.22(16)°. This torsion angle is analogous to that observed in $Ru_2Cl(\mu\text{-DPhF})_4$ (14.6°) [6b]. The phenyl rings of each ligand are twisted out of the bridging ligand plane (C2–N3–C9–C10 = 36.6(8)° and C2–N2–C3–C8 = 69.9(7)°), similar to $Ru_2Cl(\mu\text{-DPhF})_4$ [6b]. Ru–Ru–C and Ru–C–N are strictly linear.

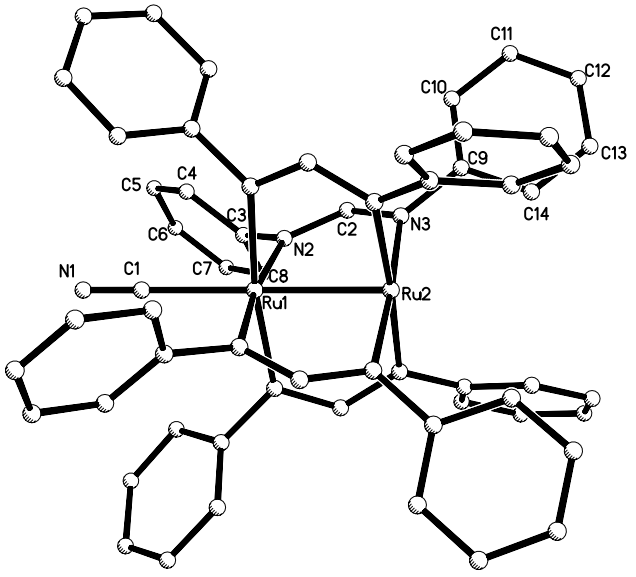

Fig. 1. PLUTO view of **1 · C$_6$H$_{14}$**. Crystallization molecule and hydrogen atoms are omitted for clarity.

Figs. 2 and 3 show a PLUTO view of the structures of $Ru_2(N_3)(\mu\text{-}O_2CMe)(\mu\text{-DPhF})_3$ (**2**) and $Ru_2(NCS)(\mu\text{-}O_2CMe)(\mu\text{- DPhF})_3$ (**3**), respectively. The asymmetric unit of crystal **2** contains two independent molecules (**2a** and **2b**). The differences in the metric parameters of the first coordination spheres of the Ru_2 cores are insignificant except in the torsion angles which are slightly different. Consequently, the metric parameters listed in Table 2 for this complex correspond to one of the two molecules.

The molecular structures of both complexes **2** and **3** are alike. In these derivatives the diruthenium atoms are bridged by three formamidinate ligands and one carboxylate group giving a paddle wheel structure with low values in the torsion angles. The Ru–Ru distances are very similar for **2** and **3**: 2.3182(11) and 2.3159(4) Å, respectively. These distances are comparable to those found in the parent compound $Ru_2Cl(\mu\text{-}O_2CMe)(\mu\text{-DPhF})_3$ [9] and in other trisformamidinato complexes

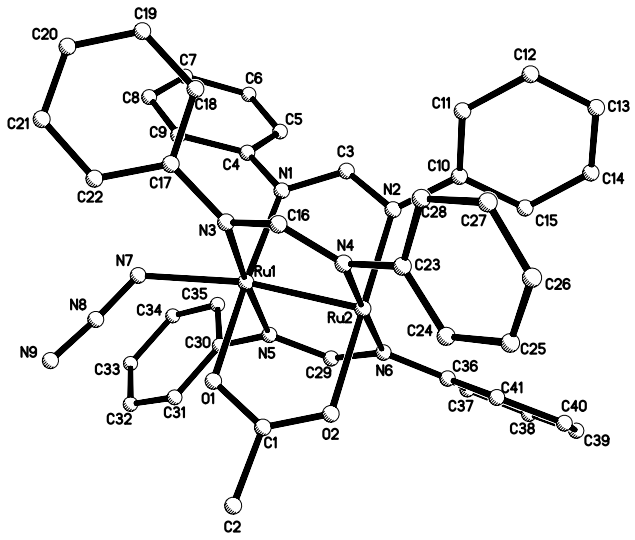

Fig. 2. PLUTO view of **2a**. Hydrogen atoms are omitted for clarity.

[9,10,18]. The Ru–N_{axial} distances are 2.116(8) and 2.103(3) Å for **2** and **3**, respectively, reflecting a similar donor nature for the N_3 and NCS ligands. In the azide ligand the N7–N8 bond length is longer (1.173(9) Å) than the distance N8–N9 (1.144(10) Å). In the NCS ligand the C–N distance is 1.146(4) Å, whereas the C–S distance is 1.612(4) Å. The N_{axial}–Ru–Ru angle in **2** (170.4(2)°) is more acute than the corresponding angle in **3** (178.16(8)°). The azide ligand (N–N–N angle: 175.8(11)°) and the isothiocyanate ligand (N–C–S angle: 179.1(4)°) are both almost linear. However, the N–N–Ru and C–N–Ru angles are very different, being 120.5(7) and 167.7(3)° for **2** and **3**, respectively.

Despite the Ru–Ru bond distance in **2** being very close to that observed in $Ru_2(DMBA)_4(N_3)_2$ (2.3166(7) Å) [8b], the structural parameters of the azide ligands are very different, especially the Ru–N_1 and N_1–N_2

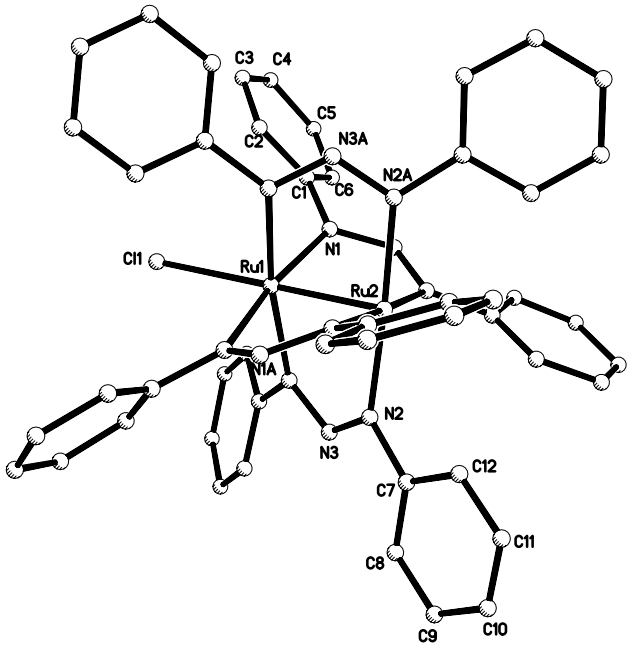

Fig. 4. PLUTO view of $\mathbf{4 \cdot 2H_2O}$. Water molecules and hydrogen atoms are omitted for clarity.

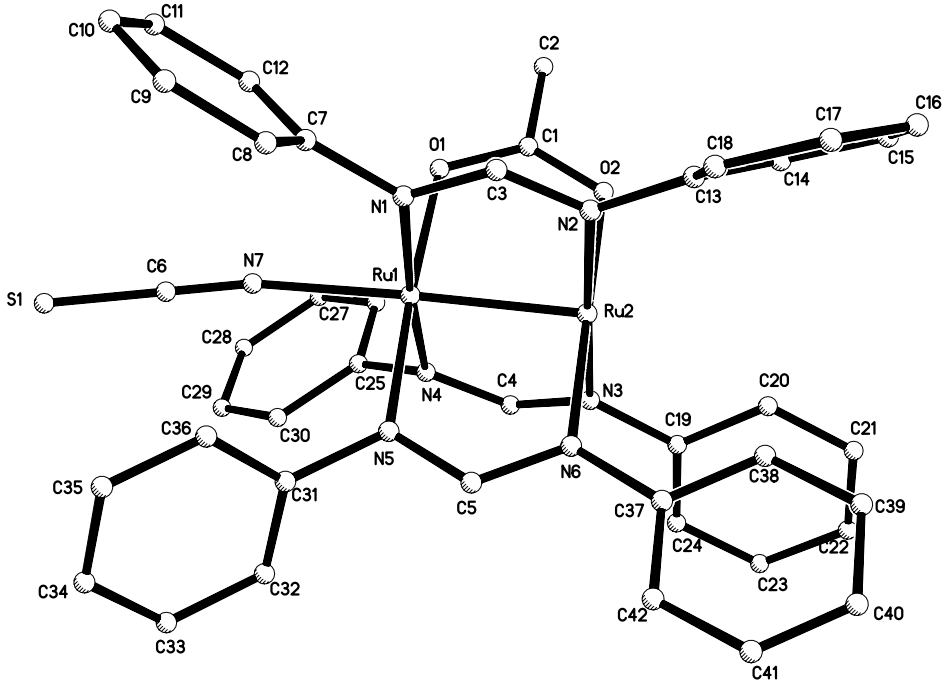

Fig. 3. PLUTO view of **3**. Hydrogen atoms are omitted for clarity.

distances (2.246(4) and 1.036(5) Å) and the Ru–N_1–N_2 angle (153.6(5)°).

The molecular structure of $\mathbf{4 \cdot 2H_2O}$ is shown in Fig. 4. The coordination about Ru1 and Ru2 is essentially octahedral and square pyramidal, respectively, with the four triazenide ligands occupying the equatorial planes. Similarly to compound $\mathbf{1 \cdot C_6H_{14}}$, this complex has elevated torsion angles (23.08°).

The Ru–Ru distance in $\mathbf{4 \cdot 2H_2O}$ (2.286(2) Å) is comparable to tetracarboxylatodiruthenium(II,III) complexes [**1**–**3**], but surprisingly short in comparison with other triazenido or formamidinato complexes: $Ru_2(\mu\text{-}N_3Ph_2)_4(OPF_4)$ (2.385(2) Å) [14], $\{Ru_2[\mu\text{-}N_3(C_6H_4\text{-}p\text{-}Me)_2]_4(MeCN)\}BF_4$ (2.373(2) Å) [13], $[Ru_2(\mu\text{-}O_2CMe)(\mu\text{-}N_3Ph_2)_3(MeCN)_2]BF_4$ (2.3822(8) Å) [15], $Ru_2Cl(\mu\text{-DPhF})_4$ (2.339(1) Å) [6b] and $Ru_2Cl(\mu\text{-DtolF})_4$ (2.370(2) Å) [6c].

3. Conclusions

The preparation of $Ru_2(CN)(\mu\text{-DPhF})_4$ confirms that diruthenium(II,III) complexes with strong π acceptor ligands are stable with suitable bridging ligands. Low spin configurations seem to be preferred for diruthenium(II,III) compounds with this kind of axial ligand. The facile substitution of the axial chloro ligand in $Ru_2Cl(\mu\text{-}O_2CCH_3)(\mu\text{-DPhF})_3$, in addition to the replacement of the carboxylate group, makes this complex very versatile as a starting material to build supramolecular structures.

4. Experimental

Unless otherwise stated, all reactions were routinely carried out under an atmosphere of dry oxygen-free nitrogen. $Ru_2Cl(\mu\text{-}O_2CMe)_4$, $Ru_2Cl(\mu\text{-DPhF})_4$ and $Ru_2Cl(\mu\text{-}O_2CCH_3)(\mu\text{-DPhF})_3$ were prepared as previously reported [21,6b,9]. Other chemicals and solvents were obtained from commercial sources and used without further purification.

Elemental analyses were done by the Microanalytical Service of the Complutense University of Madrid. IR spectra were recorded on a FT ThermoNicolet IR200 spectrometer using KBr pellets. Mass spectra were performed on a Bruker Esquire-LC with electrospray ionization (ESI) using chloroform. The ^1H NMR spectrum was recorded with a Bruker Avance DPX300 using acetone-d_6 as solvent. The magnetic susceptibility data were measured on a Quantum Design MPMS*XL* SQUID (Superconducting Quantum Interference Device) susceptometer. All data were corrected for the diamagnetic contribution of both the sample holder and the compound to the susceptibility. The molar diamagnetic corrections for the complexes were calculated on the basis of Pascal's constants.

4.1. Synthesis of $Ru_2(CN)(\mu\text{-DPhF})_4$ (**1**)

To a violet solution of 0.220 g (0.22 mmol) $Ru_2Cl(\mu\text{-DPhF})_4$ in 20 mL thf was added 0.100 g (2.04 mmol) NaCN with 40 ml thf. The mixture was stirred for 3 days and pumped to dryness to give a solid, which was treated with a mixture of toluene and dichloromethane and stirred overnight. The solid was filtered and 0.060 g (0.06 mmol, 27%) **1** was extracted as the monohydrate with dichloromethane from the residue. *Anal.* Calc. for $Ru_2ON_9C_{53}H_{46}$ ($\mathbf{1 \cdot H_2O}$): C, 61.98; H, 4.51; N, 12.27. Found: C, 61.73; H, 4.50; N, 12.67%. IR (KBr, cm^{-1}): 3435 (m), 3058 (w), 3030 (vw), 2943 (vw), 2096 (w), 1637 (w), 1592 (m), 1533 (s), 1487 (vs), 1450 (w), 1331 (m), 1214 (vs), 1077 (vw), 1027 (w), 933 (m), 779 (m), 760 (s), 696 (vs). MS (ESI^+): *m/z* 984, [**1**-CN]. $\mu_{eff.} = 1.6$ B.M. Crystals of $\mathbf{1 \cdot C_6H_{14}}$ were obtained by layering hexane over a dichloromethane solution of the compound.

4.2. Synthesis of $Ru_2(N_3)(\mu\text{-}O_2CMe)(\mu\text{-DPhF})_3$ (**2**)

To a solution containing 0.200 g (0.23 mmol) $Ru_2Cl(\mu\text{-}O_2CMe)(\mu\text{-DPhF})_3$ in 20 mL thf was added 0.044 g (0.23 mmol) $AgBF_4$. The mixture was stirred overnight and the solid was filtered off using celite. The solution was evaporated to dryness and the residue was dissolved in 10 mL methanol. The addition of 0.015 g (0.23 mmol) NaN_3 to this solution was followed by an immediate precipitation which left the solution almost colourless. After stirring the mixture for half an hour, the solid was filtered, washed with methanol (3 x 4 mL), and dried under vacuum. Yield: 0.170 g (84%). *Anal.* Calc. for $Ru_2O_2N_9C_{41}H_{36}$: C, 55.40; H, 4.08; N, 14.18. Found: C, 55.00; H, 4.09; N, 14.05%. IR (KBr, cm^{-1}): 3060 (vw), 3030 (vw), 2959 (vw), 2031 (vs), 1592 (m), 1537 (vs), 1488 (vs), 1435 (m), 1322 (s), 1219 (s), 1122 (sh), 1080 (w), 1027 (w), 940 (w), 776 (m), 758 (m). MS (ESI^+): *m/z* 878 [MH_2–2N]; 848 [M–N_3]; 834 [M–N_3–CH_2]. $\mu_{eff.} = 4.1$ B.M. Crystals of **2** suitable for X-ray analysis were obtained by layering hexane on a solution of the compound in dichloromethane.

4.3. Synthesis of $Ru_2(NCS)(\mu\text{-}O_2CMe)(\mu\text{-DPhF})_3$ (**3**)

A mixture of 0.200 g (0.23 mmol) $Ru_2Cl(\mu\text{-}O_2CMe)(\mu\text{-DPhF})_3$, 0.039 g (0.24 mmol) AgSCN, and 20 mL thf was stirred overnight. The solid was removed filtering through celite and the solution was evaporated to dryness. The residue was washed with diethyl ether (4×5 mL) and dried under vacuum. Yield: 0.150 g (73%). *Anal.* Calc. for $Ru_2O_2SN_7C_{42}H_{36}$: C, 55.74; H, 4.01; N, 10.83; S, 3.54. Found: C, 55.81; H, 4.09; N, 10.75; S, 3.56%. IR (KBr, cm^{-1}): 3058 (w), 3032 (vw),

2964 (vw), 2060 (vs), 1593 (m), 1533 (vs), 1487 (vs), 1435 (m), 1319 (s), 1219 (s), 1077 (w), 1027 (w), 940 (w), 773 (m), 758 (s), 695 (s). MS (ESI^+): *m/z* 848 [M–NCS] together with *m/z* 847 [M–O_2CMe]. $\mu_{eff.} = 1.7$ B.M. Crystals of **3** were collected after a slow diffusion of hexane into a solution of the complex in thf.

4.4. Synthesis of $Ru_2Cl(\mu\text{-}N_3Ph_2)_4$ (**4**)

A mixture containing 0.200 g (0.42 mmol) $Ru_2Cl(\mu\text{-}O_2CMe)_4$, 0.500 g (2.53 mmol) 1,3-diphenyltriazene, 0.120 g (2.84 mmol) LiCl, 0.4 mL (2.84 mmol) Et_3N and 20 mL 2-methoxyethanol was refluxed for 24 h, giving a dark violet solution. This solution was treated again with fresh 1,3-diphenyltriazene (0.500 g, 2.53 mmol) and Et_3N (0.4 mL, 2.84 mmol) under the same conditions to complete the replacement of the acetate ligands. The solution was evaporated to dryness under vacuum and the dark violet solid obtained was extracted three times with 30 mL toluene. The solvent was removed and the solid left was washed twice with 20 mL petroleum ether (40–60 °C). Yield: 0.052g (12%). *Anal.* Calc. for $Ru_2ClN_{12}C_{48}H_{40}$: C, 56.38; H, 3.94; N, 16.44. Found: C, 56.20; H, 3.89; N, 16.23%. IR (KBr, cm^{-1}): 3065 (w), 2965 (w), 2852 (w), 1590(m), 1483 (vs), 1454 (m), 1409 (w), 1329 (s), 1306 (vs), 1287 (vs), 1220 (m), 1165 (m), 1069(m), 1026 (m), 901 (w), 756 (vs), 688 (vs), 664 (m), 528 (m), 511 (m). MS (ESI^+): *m/z* 988, [M–Cl]. $\mu_{eff.} = 4.1$ B.M. A thf solution of this complex was layered with hexane to give violet single crystals of $Ru_2Cl(\mu\text{-}N_3Ph_2)_4 \cdot 2H_2O$ (**4 · 2H$_2$O**).

4.5. Synthesis of $Ru_2Cl_2(\mu\text{-}N_3Ph_2)_4$ (**5**)

The synthetic procedure is similar to that described for **4**, but the solid obtained was dissolved in toluene and passed through a silica gel chromatographic column and eluted with toluene. Three bands, violet, green and brown, were obtained. The violet one was collected and the spectroscopic characterization revealed that this first band corresponds to $Ru_2Cl_2(\mu\text{-}N_3Ph_2)_4$. Yield: 0.089 g (20%). *Anal.* Calc. for $Ru_2Cl_2N_{12}C_{48}H_{40}$: C, 54.49; H, 3.81; N, 15.89. Found: C, 54.32; H, 3.71; N, 15.73%. IR (KBr, cm^{-1}): 3062 (w), 3034 (w), 1961(w), 1591 (m), 1484 (vs), 1454 (w), 1305 (s), 1290 (s), 1208 (m), 1166 (w), 1073 (w), 1025 (w), 759 (s), 697 (s), 689 (s), 664 (m), 551 (w), 516 (w). MS (ESI^+): *m/z* 988, [M–2Cl]. NMR (acetone-d_6, δ, ppm): 7.75 (m), 7.27 (m), 6.67 (m).

4.6. X-ray crystallography

Single crystals of compounds **1**–**4** were obtained as described above. Details for data collection and crystal structure refinement for these compounds are summarized in Table 1. Representative crystals were mounted on a Bruker Smart-CCD diffractometer with graphite-monochromated Mo Kα ($\lambda = 0.71073$ Å) radiation. In each case data were collected, at 293(2) K, over a hemisphere of the reciprocal space by a combination of three exposures sets. The cell parameters were determined and refined by a least-squares fit of all reflections collected. The structures were solved by direct methods and refined by the full-matrix least-squares method against F^2 of all data. Calculations were performed with the aid of the SHELXS and SHELXL programs [22,23]. The final mixed refinement was undertaken with anisotropic thermal parameters for the non-hydrogen atoms, except for the hexane and water molecules. For **1 · C$_6$H$_{14}$** a massively disordered area of electron density was found, which is presumed to be hexane. The solvent molecule did not refine freely and was refined to convergence with the carbon-carbon bond length restraint in SHELX-76. Similar compounds with the same space group and disordered solvent molecules have been found previously [6b,6c]. For **4 · 2H$_2$O** due to the low quality of the crystal only the good reflections (max. $2\theta = 44°$) have been used in the refinement. In the last cycles of this refinement disordered solvent was found. The best R factor was obtained with two water solvent molecules. It has not been possible to locate the hydrogen atoms in the Fourier synthesis.

5. Supplementary material

Crystallographic data for **1**–**4** have been deposited at the Cambridge Crystallographic Data Centre as a supplementary publication (CCDC Nos. 235127–235130). These data can be obtained free of charge at www.ccdc.cam.ac.uk/conts/retrieving.html or from the Cambridge Crystallographic Data Centre, 12, Union Road, Cambridge CB2 1EZ, UK [Fax: + 44-1223/336-033; e-mail: deposit@ccdc.cam.ac.uk].

Acknowledgements

We are grateful to the Ministerio de Ciencia y Tecnología (Dirección General de Investigación, Project No. BQU2000-0643) and the Universidad Complutense de Madrid (Project No. PR3/04-12426) for financial support.

References

[1] F.A. Cotton, R.A. Walton, Multiple Bonds Between Metal Atoms, second ed., Oxford University Press, Oxford, UK, 1993.
[2] M.C. Barral, R. Jiménez-Aparicio, J.L. Priego, E.C. Royer, F.A. Urbanos, An. Quim. Int. Ed. 93 (1997) 277.
[3] M.A.S. Aquino, Coord. Chem. Rev. 170 (1998) 141.
[4] F.A. Cotton, M. Matusz, B. Zhong, Inorg. Chem. 27 (1988) 4368.

[5] G.G. Briand, M.W. Cooke, T.S. Cameron, H.M. Farrell, T.J. Burchell, M.A.S. Aquino, Inorg. Chem. 40 (2001) 3267.
[6] See, for example (a) K.M. Kadish, L.L. Wang, A. Thuriere, E. Van Caemelbecke, J.L. Bear, Inorg. Chem. 42 (2003) 834;
(b) J.L. Bear, B. Han, S. Huang, K.M. Kadish, Inorg. Chem. 35 (1996) 3012;
(c) F.A. Cotton, T. Ren, Inorg. Chem. 34 (1995) 3190.
[7] See, for example: (a) F.A. Cotton, A. Yokochi, Polyhedron 17 (1998) 959;
(b) F.A. Cotton, Y. Kim, A. Yokochi, Inorg. Chim. Acta 236 (1995) 55;
(c) W.S. Seldrick, M. Mintert, Inorg. Chim. Acta 219 (1994) 23.
[8] See, for example: (a) G.L. Xu, C.G. Jablonski, T. Ren, Inorg. Chim. Acta 343 (2003) 387;
(b) W.Z. Chen, T. Ren, Inorg. Chem. 42 (2003) 8847;
(c) T. Ren, G.L. Xu, Comments on Inorg. Chem. 23 (2002) 355;
(d) G. Xu, T. Ren, J. Organomet. Chem. 655 (2002) 239;
(e) J.L. Bear, Y. Li, B. Han, E. Van Caemelbecke, K.M. Kadish, Inorg. Chem. 40 (2001) 182;
(f) J.L. Bear, Y. Li, J. Cui, B. Han, E. Van Caemelbecke, T. Phan, K.M. Kadish, Inorg. Chem. 39 (2000) 857.
[9] M.C. Barral, S. Herrero, R. Jiménez-Aparicio, M.R. Torres, F.A. Urbanos, Inorg. Chem. Comm. 7 (2004) 42.
[10] P. Angaridis, J.F. Berry, F.A. Cotton, P. Lei, C. Lin, C.A. Murillo, D. Villagrán, Inorg. Chem. Commun. 7 (2004) 9.
[11] A.J. Lindsay, G. Wilkinson, M. Motevalli, M.B. Hursthouse, J. Chem. Soc., Dalton Trans. (1987) 2723.
[12] F.A. Cotton, M. Matusz, J. Am. Chem. Soc. 110 (1988) 5761.
[13] F.A. Cotton, L.R. Falvello, T. Ren, K. Vidyasagar, Inorg. Chim. Acta 194 (1992) 163.
[14] F.A. Cotton, M. Matusz, Chimia 43 (1989) 167.
[15] F.A. Cotton, A. Yokochi, Inorg. Chem. 37 (1998) 2723.
[16] M.C. Barral, I. de la Fuente, R. Jiménez-Aparicio, J.L. Priego, M.R. Torres, F.A. Urbanos, Polyhedron 20 (2001) 2537.
[17] G.J. Norman, G.R. Renzoni, D.A. Case, J. Am. Chem. Soc. 101 (1979) 5256.
[18] T. Ren, V. DeSilva, G. Zou, C. Lin, L.M. Daniels, C.F. Campana, J.C. Alvarez, Inorg. Chem. Commun. 2 (1999) 301.
[19] C. Lin, T. Ren, E.J. Valente, J.D. Zubkowski, J. Organomet. Chem. 579 (1999) 114.
[20] F.A. Cotton, T. Ren, Inorg. Chem. 30 (1991) 3675.
[21] R.W. Mitchell, A. Spencer, G. Wilkinson, J. Chem. Soc., Dalton Trans. (1973) 846.
[22] G.M. Sheldrick, SHELXS-97. Program for the solution of crystal structures, University of Göttingen, Germany, 1997.
[23] G.M. Sheldrick, SHELXL-97. Program for refinement of crystal structures, University of Göttingen, Germany, 1997.

Available online at www.sciencedirect.com
SCIENCE DIRECT®
Polyhedron 23 (2004) 2645–2657
POLYHEDRON
www.elsevier.com/locate/poly

Acetylacetonato, pentachlorophenolato and carboxylato rhodium(I) complexes and their reactivity in the C–C coupling reaction of olefins and diazoalkanes

Helmut Werner *, Norbert Mahr, Michael E. Schneider, Marco Bosch, Justin Wolf

Institut für Anorganische Chemie, Universität Würzburg, Am Hubland, D-97074 Würzburg, Germany

Received 8 April 2004; accepted 8 June 2004
Available online 30 July 2004

Dedicated to Professor Malcolm Green, in honour of his numerous inspiring contributions to Organometallic Chemistry

Abstract

The acetylacetonato complexes [Rh(κ^2-O-O)(C_2H_4)(P*i*Pr$_3$)] (O-O = acac **5**, acac-f$_3$ **6**, acac-f$_6$ **7**) and [Rh(κ^2-O-O)(P*i*Pr$_3$)$_2$] (O-O = acac **10**, acac-f$_6$ **11**) were prepared from either [Rh(κ^2-O-O)(C_2H_4)$_2$] (**2–4**), [Rh(η^3-C_3H_5)(P*i*Pr$_3$)$_2$] (**8**) or [RhCl(P*i*Pr$_3$)$_2$]$_2$ (**9**) as the starting materials. While attempts to obtain the diazoalkane derivatives [Rh(κ^2-O-O)(N_2CR_2)(P*i*Pr$_3$)] (R = Ph, *p*-Tol) failed, treatment of **5–7** with $N_2CC_4Cl_4$ gave the corresponding substitution products [Rh(κ^2-O-O)($N_2CC_4Cl_4$)(P*i*Pr$_3$)] (**12–14**) in good yields. The reaction of **8** with C_6Cl_5OH afforded the square-planar complex [Rh(κ^2-OC_6Cl_5)(P*i*Pr$_3$)$_2$] (**15**), in which the pentachlorophenolato ligand is coordinated in a chelating fashion. From **15** and C_2H_4, O_2 and N_2CPh_2 the 1:1 adducts *trans*-[Rh(κ^1-OC_6Cl_5)(L)(P*i*Pr$_3$)$_2$] (**16–18**) were prepared. Compound **15** catalyzes the reaction of ethene with diaryldiazomethanes to give, instead of 1,1-diarylcyclopropanes, the isomeric olefins $R_2C{=}CHCH_3$ (R = C_6H_5 **1b**, *p*-C_6H_4Me **19**, *p*-C_6H_4Cl **20**) as the main products. The carboxylato complexes [Rh(κ^2-O_2CMe)(P*i*Pr$_3$)$_2$] (**21**) and [Rh(κ^2-O_2CCF_3)(P*i*Pr$_3$)$_2$] (**25**) react with N_2CRR' (R = R′ = C_4Cl_4; R = R′ = Ph; R = H, Ph, R′ = C(O)Ph) by opening the chelate bond to give the four-coordinate 1:1 adducts *trans*-[Rh(κ^1-O_2CMe)(N_2CRR')(P*i*Pr$_3$)$_2$] (**22–24**) and *trans*-[Rh(κ^1-O_2CCF_3)(N_2CRR')(P*i*Pr$_3$)$_2$](**26–28**), respectively. Treatment of **25** with $PhCHN_2$ produced the dinitrogen complex *trans*-[Rh(κ^1-O_2CCF_3)(N_2)(P*i*Pr$_3$)$_2$] (**29**). In contrast to the trifluoracetato compound **25**, which catalyzes the reaction of ethene and diaryldiazomethanes N_2CRR' to give mainly the trisubstituted olefins $R'RC{=}CHCH_3$, the corresponding reaction of C_2H_4 and N_2CRR' with acetato complex **21** as the catalyst affords the isomeric ethene derivatives $CH_2{=}CHCHRR'$ as the major products. A mechanism for this unexpected C–C coupling reaction is discussed.
© 2004 Elsevier Ltd. All rights reserved.

Keywords: Rhodium; Acetylacetonato complexes; Pentachlorophenolato complexes; Carboxylato complexes; Diazoalkane complexes; C–C coupling reactions

1. Introduction

In the context of our studies on the preparation and reactivity of carbenerhodium(I) complexes of the general composition *trans*-[RhCl(=CRR′)(L)$_2$] with L = PR_3, AsR_3 and SbR_3 [1], we observed that upon treatment of [RhCl(C_2H_4)$_2$]$_2$, [Rh(κ^2-acac-f$_6$)(C_2H_4)$_2$] or [RhCl-(P*i*Pr$_3$)$_2$]$_2$ with an excess of ethene and diphenyldiazomethane a catalytic reaction occurred and the trisubstituted olefin 1,1-diphenylpropene (**1b**) was generated as the dominating product [2,3]. The formation of this olefin can be considered, in a formal sense, as the coupling of two carbene fragments :CPh_2 and :CHMe, of which the

* Corresponding author. Tel.: +499318885270; fax: +499318884623.
E-mail address: helmut.werner@mail.uni-wuerzburg.de (H. Werner).

0277-5387/$ - see front matter © 2004 Elsevier Ltd. All rights reserved.
doi:10.1016/j.poly.2004.06.009

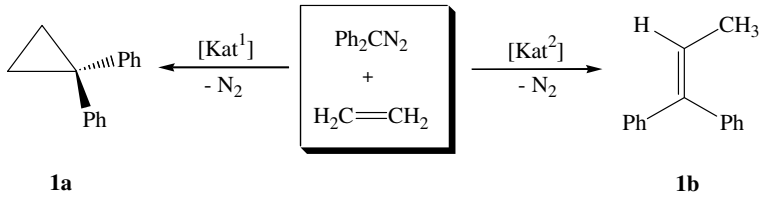

1a **1b**

[Kat^1] : [$Rh_2(O_2CCH_3)_4$], [$Rh_6(CO)_{16}$], [Rh(κ^2-acac)$(C_2H_4)_2$]

[Kat^2] : [$RhCl(C_2H_4)_2]_2$, [$RhCl(PiPr_3)_2]_2$, [Rh(κ^2-acac-f_6)$(C_2H_4)_2$]

Scheme 1.

latter derives from the isomeric ethene. Besides **1b**, only traces of the isomeric disubstituted cyclopropane **1a** could be detected which was surprising insofar as it was well known that dinuclear bis(carboxylato)rhodium(II) compounds such as $[Rh_2(O_2CMe)_4]$ and derivatives thereof [4], some carbonylrhodium(0) clusters [5] and the chelated rhodium(I) complex [Rh(κ^2-acac)$(C_2H_4)_2$] [6] are effective catalysts for the synthesis of cyclopropanes from olefins and diazoalkanes (Scheme 1).

By taking the difference in reactivity of [Rh(κ^2-acac)$(C_2H_4)_2$] on one hand and of $[RhCl(C_2H_4)_2]_2$ and [Rh(κ^2-acac-f_6)$(C_2H_4)_2$] on the other into consideration, it became quite obvious that the anionic ligand of the corresponding rhodium complex has a significant influence on the course of the reaction of ethene and diphenyldiazomethane. Therefore, we set out to prepare some relatives of the above-mentioned chelated rhodium(I) compounds and to study their reactivity, in particular the directing role of the ligands in the C–C coupling reaction. For comparison, we also included in our investigations the mononuclear carboxylato derivatives [Rh(κ^2-O_2CR)$(PiPr_3)_2$] (R = CH_3, CF_3, *p*-C_6H_4OMe, *p*-$C_6H_4NO_2$), the preparation of which was recently reported by our group [7]. Some preliminary results of the present work have already been communicated [8].

2. Results and discussion

The synthetic routes leading to the mono(phosphine) and bis(phosphine) acetylacetonato complexes **5**–**7** and **10**, **11** are outlined in Scheme 2. The preparation of **5** and **7** by ligand exchange from **2** and **4** with an equimolar amount of $PiPr_3$ has previously been described and the spectroscopic data have been reported [9]. Compound **6** with acac-f_3 as an unsymmetrical chelating ligand, was isolated as a mixture of two isomers showing slightly different NMR signals (see Scheme 3). Since the isomers are formed in a ratio of *cis*-**6**:*trans*-**6** = 15:1, the corresponding signals can be easily assigned. The bis(phosphine) compound **11** was initially prepared from **4** and two equivalents of $PiPr_3$ in a modest yield [9]. The preferred pathway is the reaction of **8** with hexafluoroacetylacetone, which gives **11** in 76% yield by elimination of propene.

Quite surprisingly, the acac complex **10** is not accessible either from **2** and excess $PiPr_3$ or from **8** and acacH. However, it can be obtained by salt metathesis

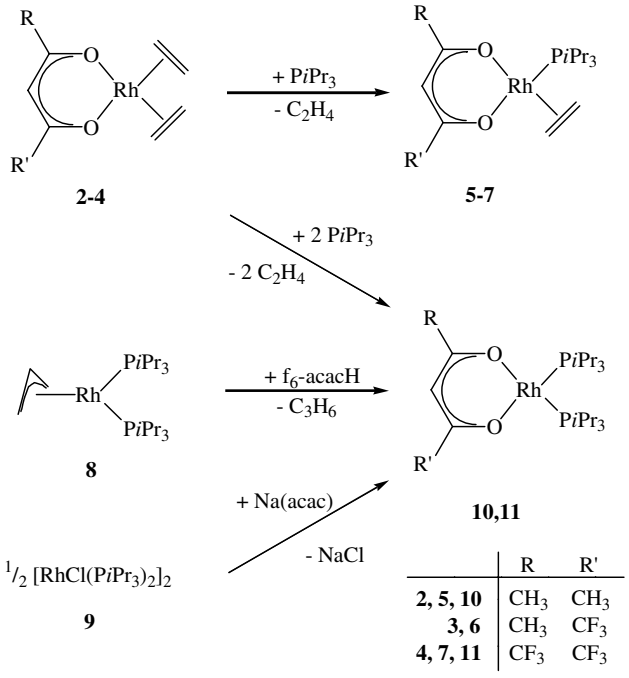

	R	R'
2, 5, 10	CH_3	CH_3
3, 6	CH_3	CF_3
4, 7, 11	CF_3	CF_3

Scheme 2.

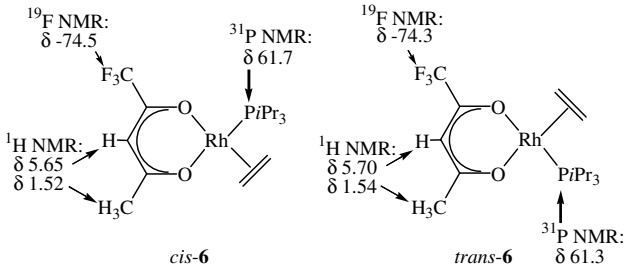

Scheme 3.

from **9** and Na(acac) in a slurry of diethylether. Both **10** and **11** are moderately air-sensitive solids, which are readily soluble in aromatic and chlorinated solvents but almost insoluble in pentane and diethylether. The IR as well as the ^{1}H and ^{13}C NMR data of **10** are similar to those of the bis(tricyclohexylphosphine) compound $[Rh(\kappa^2\text{-acac})(PCy_3)_2]$, the molecular structure of which was determined by X-ray crystallography [10].

While the ethene ligand in the chlororhodium(I) complex *trans*-$[RhCl(C_2H_4)(PiPr_3)_2]$ can be smoothly displaced by diphenyldiazomethane [2], attempts to substitute the olefin in compounds **5**–**7** by N_2CPh_2 failed. Although the formation of a 2:3 mixture of **1a** and **1b** could be detected by GC–MS, the composition of the organometallic product remained obscure.

However, the starting materials **5**–**7** react with $N_2CC_4Cl_4$ in pentane at low temperatures to afford the diazocyclopentadiene complexes **12**–**14** in 58–79% yields (Scheme 4). The greenish air-stable solids were characterized by elemental analysis and mass spectra. Even if they were stored in solution at 20 °C for several days, no conversion to a corresponding carbene derivative occurred by elimination of N_2. The IR spectra of **12**–**14** display the N–N stretching mode at around 1950 cm^{-1}, which is shifted by ca. 150 cm^{-1} to lower frequency compared with uncoordinated $N_2CC_4Cl_4$. Since the signals for the N_2C carbon atom appear in the ^{13}C NMR spectra of **12**–**14** at about the same chemical shift as that of *trans*-$[RhCl(N_2CC_4Cl_4)(SbiPr_3)_2]$ (which was characterized crystallographically) [11], we assume that the $N_2CC_4Cl_4$ ligands in **12**–**14** are bonded end-on to the metal center. In the presence of ethene, compounds **12**–**14** are inert and even upon heating do not undergo a C–C coupling reaction.

The preferred preparative route to obtain the pentachlorophenolato complex **15** is similar to that used for the related compound **11**. Treatment of **8** with an equimolar amount of C_6Cl_5OH in toluene gave **15** (Scheme 5) as a red microcrystalline solid, which is exceedingly air-sensitive and slowly decomposes in solution. The ^{1}H NMR spectrum of **15** shows at room temperature a single resonance for the methyl protons of the isopropyl groups indicating that under these conditions the two

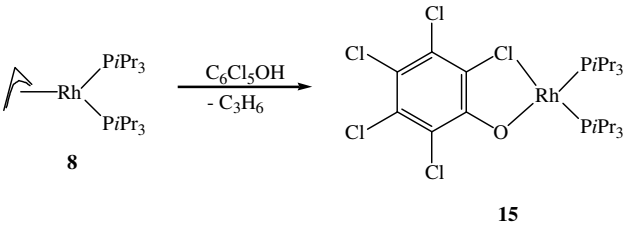

8 **15**

Scheme 5.

$PiPr_3$ ligands are equivalent on the NMR timescale. Accordingly, the ^{31}P NMR spectrum of **15** displays at 295 K one doublet at δ 61.2, which at 213 K splits into two doublets of doublets at δ 60.4 and 59.2. On the basis of these observations, we assume that at room temperature compound **15** is fluxional in solution and that the two identical chelates are transformed into each other via a three-coordinate species as an intermediate (Scheme 6). From the coalescence temperature (228 K in toluene-d_8) and the difference in the chemical shift of the two signals at 213 K in the ^{31}P NMR spectrum, a $\Delta G^{\neq}$ value of 37 kJ/mol can be calculated. We note that the chelating capability of the pentachlorophenolate anion is not unexpected and has also been illustrated in gold(I) [12,13] as well as in ruthenium(II) and osmium(II) chemistry [14].

In agreement with the rather weak interaction between Rh and Cl, compound **15** reacts readily at room temperature with ethene in pentane to give the non-chelate complex **16** in good yield (Scheme 7). The olefinic ligand is only weakly coordinated and thus, during attempts to dry **16** in vacuo, the starting material **15** was regenerated. Under argon at 295 K, or in solution at 223 K in the presence of excess ethene, **16** can be stored without decomposition. The ^{31}P NMR spectrum of **16** in toluene-d_8 shows at 223 K a doublet resonance with a ^{31}P–^{103}Rh coupling constant of 125.0 Hz, which is typical for a *trans*-disposed $PiPr_3$–Rh–$PiPr_3$ moiety [11,15].

More readily than with ethene, compound **15** reacts with O_2 in pentane to form the 1:1 adduct **17**. The brownish compound, the composition of which has been substantiated by elemental analysis, is moderately air-sensitive and decomposes slowly both in solution and

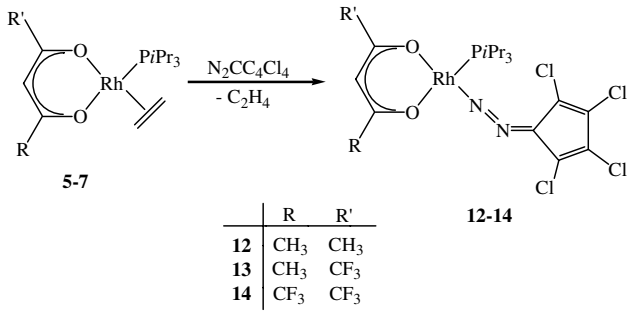

5-7 **12-14**

	R	R'
12	CH_3	CH_3
13	CH_3	CF_3
14	CF_3	CF_3

Scheme 4.

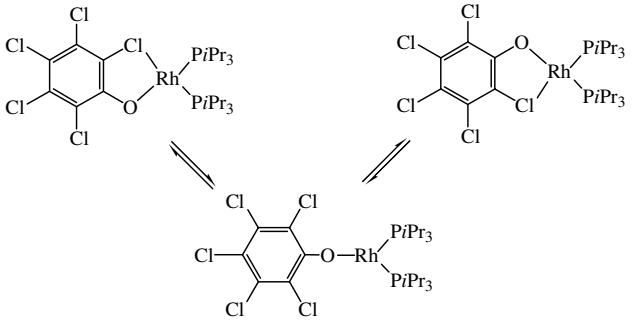

Scheme 6. Dynamics of compound **15** in solution.

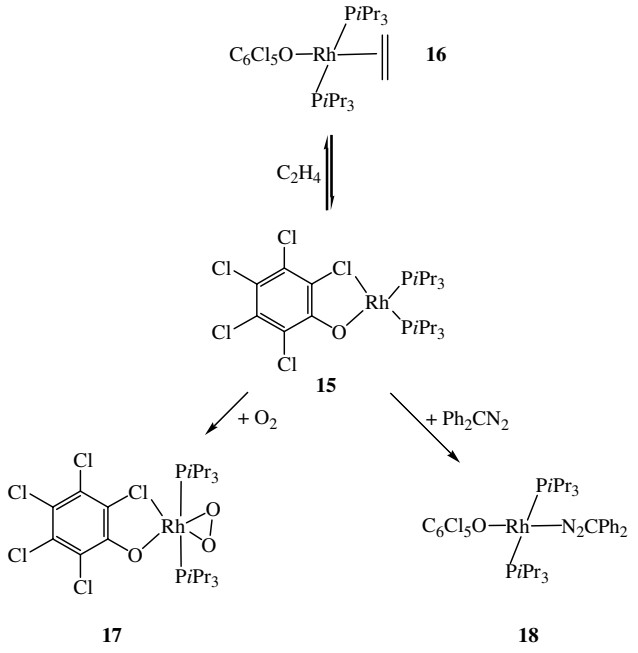

Scheme 7.

as a solid. Among the decomposition products, $OPiPr_3$ could be detected. The increased reactivity of **15** towards O_2 compared with C_2H_4 is illustrated by the fact that the solid–gas reaction with oxygen to give **17** is finished after 1 h at room temperature whereas the analogous reaction with ethene to afford **16** takes 30 h under the same conditions (Scheme 8). In either case, the product is formed in quantitative yield.

Treatment of **15** with diphenyldiazomethane also leads to partial opening of the chelate bond and to the formation of compound **18** (see Scheme 7). Similarly to the chlororhodium(I) derivative *trans*-[RhCl(N_2CPh_2)($PiPr_3$)$_2$], the phenolato complex **18** is a green air-sensitive solid that has been characterized by elemental analysis and spectroscopic techniques. With respect to the bonding mode, the position of the N–N stretching vibration at 2024 cm^{-1} in the IR spectrum suggests an end-on coordination of the N_2CPh_2 unit [16]. In the ^{13}C NMR spectrum, the resonance for the N_2C carbon atom appears at δ 87.1 as a broad singlet, the broadening probably being due to the quadrupole moment of the nitrogen atoms. The ^1H NMR spectrum of **18** displays one doublet of virtual triplets for the PCHCH_3 protons, which indicates that the two phosphine ligands are in a *trans* disposition [15,17].

Although the diazoalkane complex **18** reacts with a saturated solution of ethene in benzene at 40 °C rather slowly to give the olefin **1b**, the precursor **15** catalyzes not only the reaction of C_2H_4 with N_2CPh_2 but also that of ethene with $N_2C(C_6H_4Me\text{-}p)_2$ and $N_2C(C_6H_4Cl\text{-}p)$, respectively (Scheme 9). By monitoring the corresponding reactions by NMR, the exclusive formation of the C–C coupling products **1b**, **19** and **20** has been observed. The turnover number (TON) is ca. 10 and thus is much lower than with [RhCl($PiPr_3$)$_2$]$_2$ or [RhCl(C_2H_4)$_2$]$_2$ as the catalyst [2,3].

To compare the reactivity of **15** with that of the related bis(triisopropylphosphine) analogues [Rh(κ^2-O_2CR)($PiPr_3$)$_2$], the reactions of the previously prepared carboxylato complexes **21** and **25** with various diazoalkanes have been investigated. The results are summarized in Schemes 10 and 11. While the acetato complex **21** reacts with $N_2CC_4Cl_4$ almost instantaneously to give the 1:1 adduct **22** in nearly quantitative yield, the corresponding reactions of **21** with N_2CPh_2 and $N_2C(Ph)C(O)Ph$ lead to equilibria between the starting material and compounds **23**, **24** which could not be completely shifted to the side of the products. Since attempts to separate **21** from **23** or **24** by fractional crystallization or column chromatography failed, the diazoalkane complexes **23** and **24** could only be characterized by IR and NMR spectroscopy. In contrast, the diazocyclopentadiene derivative **22** was isolated as a pale-green solid for which a correct elemental analysis was obtained. The spectroscopic data of **22**–**24** are in agreement with a square-planar arrangement of the four monodentate ligands around the rhodium(I) center and deserve no further comments.

The trifluoracetato compound **25** is significantly more reactive toward diazoalkanes than the counterpart **21** and upon treatment with N_2CPh_2, $N_2CC_4Cl_4$ and $N_2CHC(O)Ph$ in pentane affords the expected 1:1 adducts **26**–**28** in good to excellent yields (Scheme 11). The IR spectra of the green (**26**, **27**) or yellow (**28**) solids display a band for the asymmetric OCO stretching mode

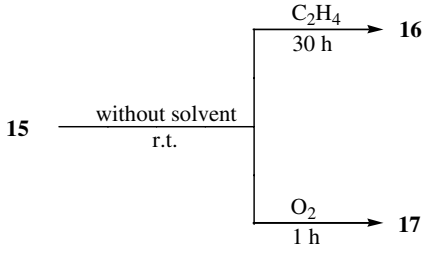

Scheme 8.

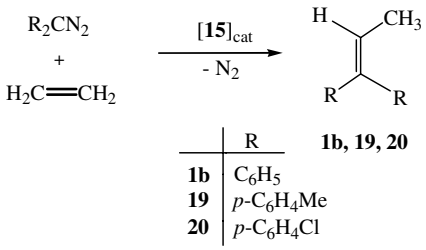

Scheme 9.

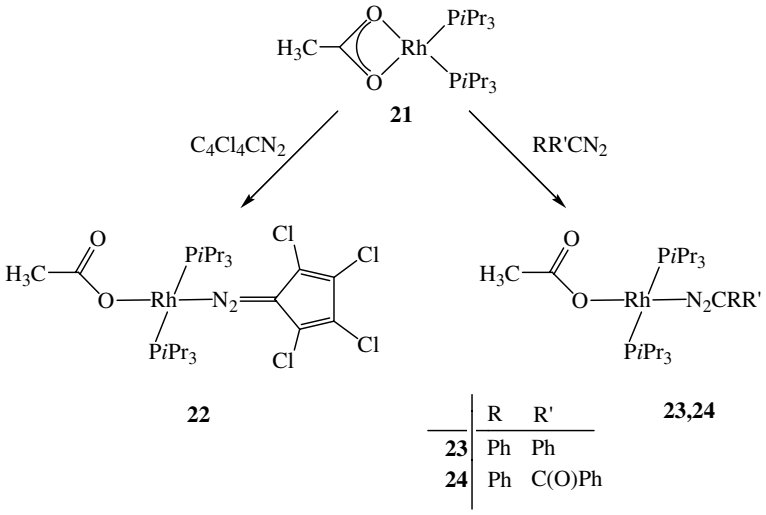

Scheme 10.

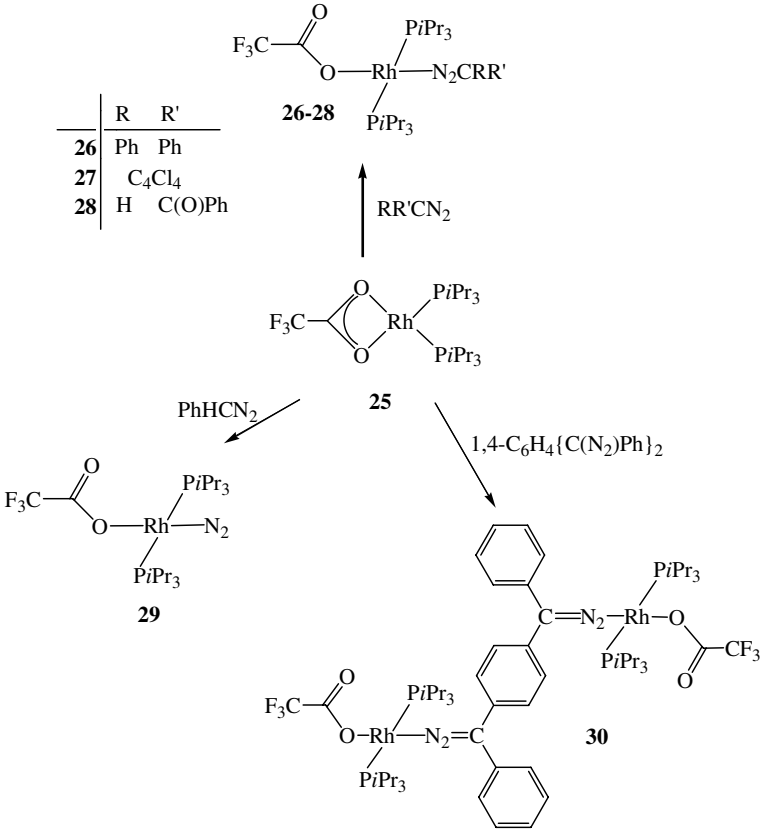

Scheme 11.

at around 1640–1700 cm^{-1}, which is consistent with the monodentate coordination of the trifluoracetato ligand [18]. The bis(diazoalkane) derivative 1,4-C_6H_4-$\{C(N_2)Ph\}_2$ behaves similarly to N_2CPh_2 and reacts with the starting material **25** in diethylether to give the dinuclear complex **30**. The ^{31}P NMR spectrum of **30** shows a doublet at δ 41.9, the chemical shift and the ^{31}P–^{103}Rh coupling constant of which are nearly identical to those of the corresponding signal for **26**.

In contrast to N_2CPh_2, phenyldiazomethane reacts with **25** in pentane to give, instead of *trans*-[Rh(κ^1-O_2CCF_3)(N_2CHPh)($PiPr_3$)$_2$], the dinitrogen complex **29** in 59% yield. Thus, the trifluoracetato compound behaves similarly to [RhCl($PiPr_3$)$_2$]$_2$ which upon treatment

Table 1
Data on the catalytic activity and composition of the product in the reaction of ethene and diaryldiazomethanes N_2CRR' (for details see Section 3)

Catalyst	TON[a]	R,R′	Product[b]
21	10	Ph_2	$CH_2{=}CHCHPh_2$ (**1c**)
21	13	Ph,*p*-C_6H_4Me	$CH_2{=}CHC(Ph)C_6H_4Me$-*p* (**31**)
21	11	Ph,*o*-C_6H_4Me	$CH_2{=}CHC(Ph)C_6H_4Me$-*o* (**32**)
21	10	(*p*-$C_6H_4Me)_2$	$CH_2{=}CHCH(C_6H_4Me$-*p*$)_2$ (**33**)
21	6	(*p*-$C_6H_4OMe)_2$	$CH_2{=}CHCH(C_6H_4OMe$-*p*$)_2$ (**34**)
21	7	(*p*-$C_6H_4Cl)_2$	$CH_2{=}CHCH(C_6H_4Cl$-*p*$)_2$ (**35**)
25	33	Ph_2	$CH_3CH{=}CPh_2$ (**1b**)
25	18	(*p*-$C_6H_4Me)_2$	$CH_3CH{=}C(C_6H_4Me$-*p*$)_2$ (**19**)
25	12	(*p*-$C_6H_4Cl)_2$	$CH_3CH{=}C(C_6H_4Cl$-*p*$)_2$ (**20**)

[a] TON = turnover number = mol product/mol catalyst.
[b] Dominating product, relative amount >94%.

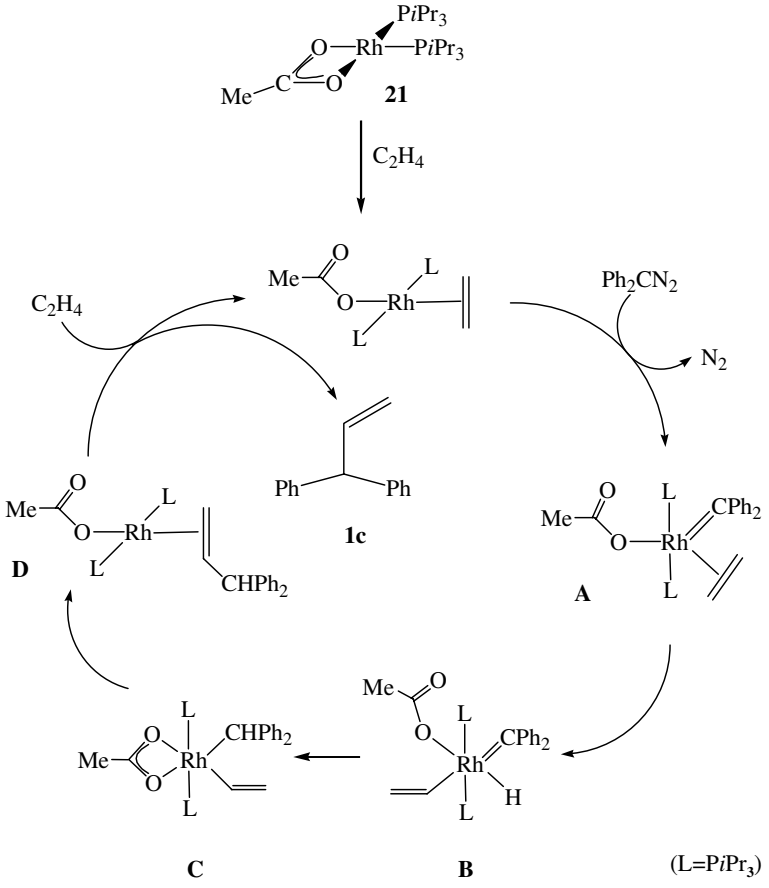

Scheme 12.

with N_2CHPh affords *trans*-[RhCl(N_2)(P*i*Pr$_3$)$_2$] [19,20]. Diagnostic for the coordination of the N_2 ligand in **29** is the $\nu(N_2)$ stretch at 2098 cm^{-1} in the IR spectrum, which is shifted by ca. 160 cm^{-1} to higher frequency compared with the N_2CPh_2 derivative **26**. In solution, compound **29** is less stable than the counterparts **26** and **28** and decomposes slowly to give **25** as the dominating species.

Both the acetato and the trifluoracetato complexes **21** and **25** are also catalysts for the C–C coupling reaction of ethene and diaryldiazomethanes. However, while the catalytic activity is comparable to that of the pentachlorophenolato analogue **15** (see Scheme 9), the substituent of the carboxylato unit has a significant influence on the composition of the coupling product. With **25** as the catalyst, the reaction of C_2H_4 with $N_2C(C_6H_4X)_2$ (X = H, *p*-Me, *p*-Cl) leads almost exclusively to the formation of the trisubstituted olefins **1b**, **19** and **20** with turnover numbers (in toluene at 40 °C) of 33 (X = H), 18 (X = *p*-Me) and 12 (X = *p*-Cl), respectively. At the beginning

of the catalytic processes, the formation of the diazoalkane complexes *trans*-[Rh(κ^1-O_2CCF_3)(N_2CR_2)(P*i*Pr$_3$)$_2$] could be detected by ^{1}H and ^{31}P NMR spectroscopy.

With catalytic amounts of the acetate **21**, the reaction of ethene and diaryldiazomethanes N_2CRR' takes a different course. In this case, the coupling product is neither the disubstituted cyclopropane nor the trisubstituted olefin $CH_3CH{=}CRR'$ but, quite remarkably, the isomeric monosubstituted ethene derivative $CH_2{=}CHCHRR'$. Thus, formally an insertion of the carbene :CRR′ into one of the C—H bonds of ethene occurs. The TON values lie between 6 and 13 (see Table 1) and depend only slightly on the substituents R and R′. If instead of ethene, propene is treated with N_2CPh_2 in the presence of **21** as the catalyst, no reaction occurs under the same conditions. The coupling products $CH_2{=}CHCHRR'$, of which as far as we know those with R = Ph, R′ = *o*-C_6H_4Me, *p*-C_6H_4Me and R = R′ = *p*-C_6H_4(OMe), *p*-C_6H_4Cl have not been described in the literature, were characterized by GC–MS and ^{1}H NMR spectroscopy.

The mechanism of the reaction of ethene and diaryldiazomethanes with **21** as the catalyst to give predominantly the monosubstituted ethene derivative is not clear as yet. As shown in Scheme 12 with N_2CPh_2 as the substrate, we assume that in the initial step, in the presence of a large excess of ethene, the intermediate *trans*-[Rh(κ^1-O_2CCH_3)(C_2H_4)(P*i*Pr$_3$)$_2$] is formed and reacts with diphenyldiazomethane to generate the five-coordinate carbene(olefin) compound **A**. While we have postulated that on this stage, for chloride instead of acetate as the anionic ligand, ring closure occurs to give a metallacyclobutane, alternatively an intramolecular C—H activation could take place to afford the six-coordinate intermediate **B**. Migration of the hydride ligand from the metal to the carbene moiety with concomitant formation of a chelate ring would then give the alkyl(vinyl)rhodium(III) derivative **C**, that rearranges via intramolecular C–C coupling to generate **D**. With excess C_2H_4, the olefinic ligand of **D** could be replaced to produce **1c** (the isomer of **1a** and **1b**) and the ethene compound *trans*-[Rh(κ^1-O_2CCH_3)(C_2H_4)(P*i*Pr$_3$)$_2$], which can start a new catalytic cycle. To explain the rather low TON value for **1c** and the analogous C–C coupling products, we assume that in the course of the reaction either the initially formed ethene complex or one of the postulated intermediates decomposes to give free P*i*Pr$_3$ which reacts with the diazoalkane to form the corresponding phosphorus yield. With regard to the C—H activation step from **A** to **B**, it is worth mentioning that we recently observed, in the presence of L (pyridine or P*i*Pr$_3$), the formation of the hydrido(vinyl)iridium(III) complexes [IrH($CH{=}CH_2$)(κ^2-acac)(L)(P*i*Pr$_3$)] from the etheneiridium(I) precursor [Ir(κ^2-acac)(C_2H_4)(P*i*Pr$_3$)] under either photochemical or thermal conditions [21]. Moreover, in a control experiment we found that upon irradiation of a solution of **21** in C_6D_6, saturated with ethene, a hydridorhodium(III) intermediate is generated that displays in the ^{1}H NMR spectrum a high-field resonance at δ – 20.6, i.e., at a similar chemical shift as for [RhH(κ^1-O_2CCF_3)(κ^2-O_2CCF_3)(P*i*Pr$_3$)$_2$] (δ – 19.0) [22].

In summarizing, the present work extended the series of chelate rhodium(I) complexes with Rh(P*i*Pr$_3$)$_2$ as the core unit. These complexes not only react with ethene but also with diazoalkanes, in particular with N_2CPh_2 and $N_2CC_4Cl_4$, by opening of the chelate bond and formation of four-coordinate rhodium(I) derivatives with the two phosphine ligands in a *trans* disposition. In the presence of excess C_2H_4, compounds such as **15**, **21** and **25** catalyze the reaction of ethene and diaryldiazomethanes N_2CRR' to give, instead of the anticipated 1,1-disubstituted cyclopropane, either $CH_3CH{=}CRR'$ or the isomer $CH_2{=}CHCHRR'$ as the main product. The postulated mechanism for the formation of the terminal olefin, with the acetato complex **21** as the catalyst, involves a stepwise opening and closing of the chelating Rh(κ^2-O_2CCH_3) bond that allows the metal to maintain the preferred coordination number of four for rhodium(I) and six for rhodium(III). The question whether instead of compounds such as **15** and **25** the isolated carbene complexes *trans*-[Rh(OPh)($=CPh_2$)(P*i*Pr$_3$)$_2$] [16] and *trans*-[Rh(κ^1-O_2CCF_3)($=CPh_2$)(P*i*Pr$_3$)$_2$] [23] equally catalyze the reaction of ethene with diphenyldiazomethane to give either **1a**, **1b** or **1c** is currently being investigated in our laboratory.

3. Experimental

3.1. General considerations

All experiments were carried out under an atmosphere of argon by Schlenk techniques. Solvents were purified and degassed by standard procedures. The starting materials **2**–**4** [24], **8** [7], **9** [25], **21** and **25** [7] were prepared as described in the literature. P*i*Pr$_3$ was a commercial product from Strem. IR spectra were recorded on a Perkin–Elmer 1420 infrared spectrometer and NMR spectra were recorded (if not otherwise mentioned) at room temperature (r.t.) on Bruker WH 90, Bruker AC 200 and Bruker AMX 400 instruments. Abbreviations used: s, singlet; d, doublet; t, triplet; q, quartet; m, multiplet; br, broadened signal; vt, virtual triplet; $N = {}^3J(PH) + {}^5J(PH)$ or $^1J(PC) + {}^3J(PC)$. Melting points were determined by Differential Thermal Analysis (DTA). The mass spectra were measured on a Finnigan 90 MAT instrument.

3.2. Preparation of [Rh(κ^2-acac)(C_2H_4)(P*i*Pr$_3$)] (5)

A solution of **2** (60 mg, 0.23 mmol) in 4 ml of pentane was treated with P*i*Pr$_3$ (42 μl, 0.23 mmol) and stirred for

15 min at r.t. The solvent was evaporated in vacuo and the orange residue was recrystallized from 1 ml of acetone at −78 °C: yield 70 mg (81%). The product was characterized spectroscopically by comparison with reference data [9].

3.3. Preparation of [Rh(κ²-acac-f_3)(C_2H_4)($PiPr_3$)] (*cis*- and *trans*-**6**)

This compound was prepared as described for **5**, with 100 mg (0.32 mmol) of **3** and 62 μl (0.32 mmol) of P*i*Pr_3 as starting materials. Orange solid, yield 130 mg (91%), m.p. 86 °C. *Anal*. Calc. for $C_{16}H_{29}F_3O_2PRh$: C, 43.23; H, 6.58. Found: C, 42.89; H, 6.71%. Spectroscopic data for *cis*-**6**: ^{1}H NMR (C_6D_6, 200 MHz): δ 5.65 [s, 1H, CHC(O)], 3.34, 2.76 (both br s, 4H, CH_2), 1.77 (m, 3H, PC*H* CH_3), 1.52 [s, 3H, $CH_3C(O)$], 1.08 [dd, ^3J(PH) = 13.0, ^3J(HH) = 7.2, 18H, PCHC*H*$_3$]. ^{19}F NMR (C_6D_6, 188.2 MHz): δ −74.5 (s, CF_3). ^{31}P NMR (C_6D_6, 81.0 MHz): δ 61.7 [d, ^1J(RhP) = 179.8]. Spectroscopic data for *trans*-**6**: ^{1}H NMR (C_6D_6, 200 MHz): δ 5.70 [s, 1H, CHC(O)], 3.34, 2.76 (both br s, 4H, CH_2), 1.77 (m, 3H, PC*H*CH_3), 1.54 [s, 3H, $CH_3C(O)$], 1.08 [dd, ^3J(PH) = 13.0, ^3J(HH) = 7.2, 18H, PCHC*H*$_3$]. ^{19}F NMR (C_6D_6, 188.2 MHz): δ −74.3 (s, CF_3). ^{31}P NMR (C_6D_6, 81.0 MHz): δ 61.3 [d, ^1J(RhP) = 180.9]. Ratio of *cis*-**6**:*trans*-**6** = 15:1.

3.4. Preparation of [Rh(κ²-acac-f_6)(C_2H_4)($PiPr_3$)] (**7**)

This compound was prepared as described for **5**, with 100 mg (0.27 mmol) of **4** and 64 μl (0.33 mmol) of P*i*Pr_3 as starting materials. Orange solid, yield 118 mg (91%). The product was characterized spectroscopically by comparison with reference data [9].

3.5. Preparation of [Rh(κ²-acac)($PiPr_3$)$_2$] (**10**)

A solution of **9** (241 mg, 0.26 mmol) in 10 ml of diethylether was treated with Na(acac) (150 mg, 1.23 mmol) and stirred for 2 h at r.t. After 30 ml of diethylether were added, the suspension was filtered and the filtrate was brought to dryness in vacuo. The residue was dissolved in 3 ml of boiling acetone and the solution was slowly cooled at −78 °C. Yellow crystals precipitated which were separated from the mother liquor and washed twice with small amounts of pentane: yield 192 mg (70%), m.p. 77 °C (dec.). *Anal*. Calc. for $C_{23}H_{49}O_2P_2Rh$: C, 52.85; H, 9.46; Rh, 19.71. Found: C, 52.39; H, 9.12; Rh, 19.36%. MS (70 eV): *m*/*z* 522 (M^+). IR (KBr): *ν*(N_2) 1958, *ν*(CO) 1579, 1510 cm^{-1}. ^{1}H NMR (C_6D_6, 400 MHz): δ 5.35 [s, 1H, CHC(O)], 2.18 (m, 6H, PC*H*CH_3), 1.74 [s, 6H, $CH_3C(O)$], 1.36 [dd, ^3J(PH) = 12.0, ^3J(HH) = 7.3, 36 H, PCHC*H*$_3$]. ^{13}C NMR (C_6D_6, 100.6 MHz): δ 183.3 (s, CO), 99.8 [s, *C*HC(O)], 27.1 [s, *C*$H_3C(O)$], 24.6 (vt, *N* = 19.1 Hz, P*C*HCH_3), 20.7 (s, PCH*C*H_3). ^{31}P NMR (C_6D_6, 162.0 MHz): δ 59.4 [d, ^1J(RhP) = 192.1].

3.6. Preparation of [Rh(κ²-acac-f_6)($PiPr_3$)$_2$] (**11**)

A solution of **8** (74 mg, 0.16 mmol) in 10 ml of diethylether was treated with hexafluoroacetylacetone (23 μl, 0.16 mmol) and stirred for 20 min at r.t. The solvent was evaporated in vacuo and the residue was dissolved in 4 ml of acetone. After the solution was slowly cooled at −78 °C, orange crystals precipitated which were separated from the mother liquor and washed twice with small amounts of pentane: yield 77 mg (76%), m.p. 88 °C (dec.). *Anal*. Calc. for $C_{23}H_{43}F_6O_2P_2Rh$: C, 43.82; H, 6.87; Rh, 16.32. Found: C, 43.55; H, 6.69; Rh, 15.31%. MS (70 eV): *m*/*z* 630 (M^+). IR (hexane): *ν*(CO) 1541, 1508 cm^{-1}. ^{1}H NMR (C_6D_6, 200 MHz): δ 6.27 [s, 1H, CHC(O)], 2.04 (m, 6H, PC*H*CH_3), 1.22 [dd, ^3J(PH) = 12.8, ^3J(HH) = 7.3, 36H, PCHC*H*$_3$]. ^{13}C NMR (C_6D_6, 100.6 MHz): δ 170.0 [q, ^2J(FC) = 33.2, CO], 119.8 [q, ^1J(FC) = 280.1, CF_3], 91.8 [s, *C*HC(O)], 24.6 (vt, *N* = 21.1 Hz, P*C*HCH_3), 20.3 (s, PCH*C*H_3). ^{19}F NMR (C_6D_6, 188.2 MHz): δ −75.3 (s). ^{31}P NMR (C_6D_6, 81.0 MHz): δ 55.7 [d, ^1J(RhP) = 191.8].

3.7. Preparation of [Rh(κ²-acac)($N_2CC_4Cl_4$)($PiPr_3$)] (**12**)

A solution of **5** (86 mg, 0.22 mmol) in 15 ml of pentane was treated at −78 °C with $N_2CC_4Cl_4$ (101 mg, 0.44 mmol). After the solution was slowly warmed to 0 °C, it was stirred for 10 min. The solvent was evaporated in vacuo, the greenish residue was washed three times with 10 ml portions of pentane (−78 °C) and dried: yield 87 mg (67%), m.p. 61 °C (dec.). *Anal*. Calc. for $C_{19}H_{28}Cl_4N_2O_2PRh$: C, 38.54; H, 4.77; N, 4.73. Found: C, 38.26; H, 4.75; N, 4.47%. IR (hexane): *ν*(N_2) 1958, *ν*(CO) 1579, 1510 cm^{-1}. ^{1}H NMR (C_6D_6, 200 MHz): δ 5.15 [s, 1H, CHC(O)], 2.55 (m, 3H, PC*H*CH_3), 1.92, 1.54 [both s, 3H each, $CH_3C(O)$], 1.20 [dd, ^3J(PH) = 14.2, ^3J(HH) = 7.2, 18H, PCHC*H*$_3$]. ^{13}C NMR ($C_6D_5CD_3$, 50.3 MHz, 233 K): δ 192.0, 182.5 (both s, CO), 109.8, 104.4 (both s, C_4Cl_4), 101.7 [s, *C*HC(O)], 81.7 (br s, N_2C), 27.9, 26.8 [both s, *C*$H_3C(O)$], 23.9 [d, ^1J(PC) = 24.6 Hz, P*C*HCH_3], 19.7 (s, PCH*C*H_3). ^{31}P NMR (C_6D_6, 81.0 MHz): δ 64.0 [d, ^1J(RhP) = 164.7].

3.8. Preparation of [Rh(κ²-acac-f_3)($N_2CC_4Cl_4$)($PiPr_3$)] (*cis*- and *trans*-**13**)

This compound was prepared as described for **12**, with **6** (42 mg, 0.09 mmol) and $N_2CC_4Cl_4$ (43 mg, 0.19 mmol) in 5 ml of pentane as starting materials. Greenish solid; yield 48 mg (79%), m.p. 61 °C (dec.). *Anal*. Calc. for $C_{19}H_{25}Cl_4F_3N_2O_2PRh$: C, 35.32; H, 3.90; N, 4.34. Found: C, 35.25; H, 3.99; N, 4.19%. IR (diethylether):

$\nu(N_2)$ 1950 cm^{-1}. Spectroscopic data for *cis*-**13**: ^1H NMR ($C_6D_5CD_3$, 200 MHz): δ 5.79 [s, 1H, CHC(O)], 2.12 (m, 3H, PC*H*CH_3), 1.87 [s, 3H, $CH_3C(O)$], 1.15 [dd, $^3J(PH) = 14.2$, $^3J(HH) = 6.9$, 18H, PCHC*H*$_3$]. ^{13}C NMR ($C_6D_5CD_3$, 50.3 MHz, 223 K): δ 197.3 [s, $CH_3C(O)$], 162.8 [q, $^2J(FC) = 33.3$, $CF_3C(O)$], 118.1 [q, $^1J(FC) = 283.1$, CF_3], 110.4, 104.6 (both s, C_4Cl_4), 97.7 [s, *C*HC(O)], 84.6 (br s, N_2C), 28.8 [s, *C*$H_3C(O)$], 23.4 [d, $^1J(PC) = 25.0$ Hz, P*C*HCH$_3$], 19.6 (s, PCH*C*H$_3$). ^{31}P NMR ($C_6D_5CD_3$, 81.0 MHz): δ 66.6 [d, $^1J(RhP) = 164.3$]. Selected spectroscopic data for *trans*-**13**: ^1H NMR ($C_6D_5CD_3$, 200 MHz): δ 5.83 [s, 1H, CHC(O)]. ^{31}P NMR ($C_6D_5CD_3$, 81.0 MHz): δ 65.8 [d, $^1J(RhP) = 165.2$].

3.9. Preparation of [Rh(κ^2-acac-f_6)($N_2CC_4Cl_4$)(*PiPr*$_3$)] (**14**)

This compound was prepared as described for **12**, with **7** (144 mg, 0.29 mmol) and $N_2CC_4Cl_4$ (133 mg, 0.58 mmol) in 15 ml of pentane as starting materials. Greenish solid; yield 118 mg (58%), m.p. 67 °C (dec.). *Anal*. Calc. for $C_{19}H_{22}Cl_4F_6N_2O_2PRh$: C, 32.00; H, 3.17; N, 4.00. Found: C, 31.82; H, 3.06; N, 4.03%. MS (70 eV): *m*/*z* 700 (M^+). IR (KBr): $\nu(N_2)$ 1955 cm^{-1}. ^1H NMR (C_6D_6, 200 MHz): δ 6.15 [s, 1H, CHC(O)], 1.77 (m, 3H, PC*H*CH_3), 0.91 [dd, $^3J(PH) = 14.7$, $^3J(HH) = 7.2$, 18H, PCHC*H*$_3$]. ^{13}C NMR ($C_6D_5CD_3$, 100.6 MHz, 223 K): δ 176.5 [q, $^2J(FC) = 35.2$, $CF_3C(O)$], 117.7 [q, $^1J(FC) = 273.6$, CF_3], 111.7, 105.5 (both s, C_4Cl_4), 91.7 [s, *C*HC(O)], 87.6 (br s, N_2C), 23.1 [d, $^1J(PC) = 25.7$, P*C*HCH$_3$], 19.0 (s, PCH*C*H$_3$). ^{31}P NMR (C_6D_6, 81.0 MHz): δ 68.0 [d, $^1J(RhP) = 164.6$].

3.10. Preparation of [Rh(κ^2-OC_6Cl_5)(*PiPr*$_3$)$_2$] (**15**)

A solution of **8** (166 mg, 0.36 mmol) in 10 ml of toluene was treated with a solution of pentachlorophenol (95 mg, 0.36 mmol) in 5 ml of toluene and stirred for 30 min at r.t. The solvent was evaporated in vacuo and the residue was extracted with 20 ml of pentane. The extract was brought to dryness in vacuo and the residue was recrystallized from acetone at −78 °C to give a red microcrystalline solid: yield 179 mg (73%), m.p. 124 °C (dec.). *Anal*. Calc. for $C_{24}H_{42}Cl_5OP_2Rh$: C, 41.85; H, 6.15. Found: C, 42.35; H, 6.80%. ^1H NMR (C_6D_6, 200 MHz): δ 2.02 (m, 6H, PC*H*CH_3), 1.22 [dd, $^3J(PH) = 12.8$, $^3J(HH) = 6.9$, 36 H, PCHC*H*$_3$]. ^{13}C *NMR* (C_6D_6, *50.3 MHz*): δ 161.8 (s, CO), 129.6, 121.9, 114.2 (all s, C_5Cl_5), 26.2 (vt, $N = 20.3$, P*C*HCH$_3$), 20.6 (s, PCH*C*H$_3$). ^{31}P NMR (C_6D_6, 81.0 MHz, 295 K): δ 61.2 [d, $^1J(RhP) = 203.4$]. ^{31}P NMR ($C_6D_5CD_3$, 162.0 MHz, 213 K): δ 60.4 [dd, $^1J(RhP) = 162.8$, $^2J(PP) = 47.0$, P*i*Pr$_3$ *cis* to Cl], 59.2 [dd, $^1J(Rh\ P) = 114.7$, $^2J(PP) = 47.0$, P*i*Pr$_3$ *trans* to Cl].

3.11. Preparation of trans-[Rh(κ^1-OC_6Cl_5)(C_2H_4)(*PiPr*$_3$)$_2$] (**16**)

A slow stream of ethene was passed for 1 min through a solution of **15** (98 mg, 0.14 mmol) in 5 ml of pentane at r.t. A change of colour from red to yellow occurred. After the solution was cooled at −78 °C, light yellow crystals precipitated which were separated from the mother liquor, washed twice with small amounts of pentane (−78 °C) and dried in a stream of argon: yield 72 mg (71%), m.p. 38 °C (dec.). *Anal*. Calc. for $C_{26}H_{46}Cl_5OP_2Rh$: C, 43.57; H, 6.47. Found: C, 43.46; H, 6.39%. ^1H NMR (C_6D_6, 200 MHz, 295 K): δ 2.34 (br s, 4H, C_2H_4), 1.71 (m, 6H, PC*H*CH_3), 1.07 [d, $^3J(HH) = 7.3$, 36H, PCHC*H*$_3$]. ^1H NMR ($C_6D_5CD_3$, 400 MHz, 223 K): δ 2.50 (br s, 4H, C_2H_4), 2.11 (br s, 6H, PC*H*CH_3), 1.25 (br s, 36H, PCHC*H*$_3$). ^{13}C NMR ($C_6D_5CD_3$, 100.6 MHz, 223 K): δ 160.4 (s, CO), 131.7, 123.2, 114.6 (all s, C_5Cl_5), 23.3 (vt, $N = 15.3$, P*C*HCH$_3$), 20.1 (s, PCH*C*H$_3$), signal for C_2H_4 not exactly located. ^{31}P NMR ($C_6D_5CD_3$, 162.0 MHz, 223 K): δ 24.9 [d, $^1J(RhP) = 125.0$]. Compound **16** had alternatively been prepared by storing the starting material **15** in a Schlenk tube under an atmosphere of ethene for 30 h at r.t.; the yield was quantitative.

3.12. Preparation of [Rh(κ^2-OC_6Cl_5)(O_2)(*PiPr*$_3$)$_2$] (**17**)

A slow stream of O_2 was passed for 1 min through a solution of **15** (72 mg, 0.10 mmol) in 6 ml of pentane at r.t. The solution was concentrated to ca. 3 ml in vacuo and then stored at −78 °C for 12 h. A dark brown microcrystalline solid precipitated which was separated from the mother liquor, washed twice with small amounts of pentane (−20 °C) and dried: yield 59 mg (82%), m.p. 48 °C (dec.). *Anal*. Calc. for $C_{24}H_{42}Cl_5O_3P_2Rh$: C, 40.00; H, 5.87. Found: C, 39.73; H, 6.02%. IR (CH_2Cl_2): $\nu(O_2)$ 890 cm^{-1}. ^1H NMR (C_6D_6, 200 MHz): δ 2.50 (m, 6H, PC*H*CH_3), 1.21 [dvt, $N = 13.1$, $^3J(HH) = 7.3$, 18H, PCHC*H*$_3$], 1.13 [dvt, $N = 14.2$, $^3J(HH) = 6.9$, 18H, PCHC*H*$_3$]. ^{13}C NMR (C_6D_6, 50.3 MHz): δ 162.9 (s, CO), 133.5, 131.7, 131.1, 128.3, 123.0 (all s, C_5Cl_5), 22.3 (vt, $N = 19.4$, P*C*HCH$_3$), 19.6, 19.3 (both s, PCH*C*H$_3$). ^{31}P NMR (C_6D_6, 81.0 MHz): δ 32.9 [d, $^1J(RhP) = 98.8$]. Compound **16** had alternatively been prepared by storing the starting material **15** in a Schlenk tube under an atmosphere of oxygen for 1 h at r.t.; the yield was quantitative.

3.13. Preparation of trans-[Rh(κ^1-OC_6Cl_5)(N_2CPh_2)(*PiPr*$_3$)$_2$] (**18**)

A solution of **15** (76 mg, 0.11 mmol) in 10 ml of pentane was treated dropwise at −78 °C with a solution of

diphenyldiazomethane (22 mg, 0.11 mmol) in 2 ml of pentane. While the solution was warmed to r.t., a change of colour first from red to dark brown and then to green occurred. The solution was stirred for 5 min at r.t. and then concentrated to ca. 2 ml in vacuo. After it was stored at −78 °C for 12 h, dark green crystals precipitated which were separated from the mother liquor, washed twice with small amounts of pentane (−20 °C) and dried: yield 70 mg (72%), m.p. 43 °C (dec.). *Anal.* Calc. for $C_{37}H_{52}Cl_5N_2OP_2Rh$: C, 50.33; H, 5.94; N, 3.17. Found: C, 49.97; H, 5.90; N, 2.82.%. IR (hexane): $\nu(N_2)$ 2043 cm^{-1}. ^1H NMR (C_6D_6, 200 MHz): δ 7.30 (m, 4H, C_6H_5), 7.14–6.97 (br m, 6H, C_6H_5), 1.97 (m, 6H, PC*H*CH_3), 1.18 [dvt, $N = 13.2$, $^3J(HH) = 6.2$, 36 H, PCHC*H*$_3$]. ^{13}C NMR (C_6D_6, 50.3 MHz): δ 161.8 (s, CO), 139.8, 132.0, 130.2, 129.7, 129.1, 128.9, 126.7 (all s, C_6H_5 and C_5Cl_5), 87.1 (br s, N_2C), 23.3 (vt, $N = 17.6$, P*C*HCH$_3$), 19.4 (s, PCH*C*H$_3$). ^{31}P NMR (C_6D_6, 81.0 MHz): δ 37.8 [d, $^1J(RhP) = 130.8$].

3.14. Catalytic reaction of ethene with diaryldiazomethanes with compound **15** as a catalyst

In an NMR tube, a slow stream of ethene was passed for 30 s through a solution of **15** (25 mg, 0.03 mmol) and N_2CR_2 (0.10 mmol) (R = Ph, *p*-C_6H_4Me, *p*-C_6H_4Cl) in 0.5 ml of C_6D_6 at r.t. After the solution was warmed to 40 °C, the formation of the olefins **1b** [26], **19** [27], **20** [28] was detected by ^1H NMR spectroscopy. After 30 min, the catalyst decomposed and no Rh-containing product could be characterized.

3.15. Preparation of *trans*-[Rh(κ^1-O_2CCH_3)(N_2C-C_4Cl_4)($PiPr_3$)$_2$] (**22**)

A solution of **21** (38 mg, 0.08 mmol) in 10 ml of pentane was treated at −78 °C with $N_2CC_4Cl_4$ (18 mg, 0.08 mmol). After the solution was slowly warmed to r.t., it was stirred for 10 min. The solvent was evaporated in vacuo and the greenish residue was recrystallized from pentane at −78 °C: yield 45 mg (80%), m.p. 85 °C (dec.). *Anal.* Calc. for $C_{25}H_{45}Cl_4N_2O_2P_2Rh$: C, 47.16; H, 6.37; N, 3.93. Found: C, 48.02; H, 6.67; N, 3.27%. IR (KBr): $\nu(N_2)$ 1930, $\nu(CO_2)$ 1625 cm^{-1}. ^1H NMR (C_6D_6, 200 MHz): δ 2.00 (m, 6H, PC*H*CH_3), 1.73 (s, 3H, CH_3CO_2), 1.13 [dvt, $N = 13.9$, $^3J(HH) = 7.1$, 36H, PCHC*H*$_3$]. ^{13}C NMR (C_6D_6, 50.3 MHz): δ 174.4 (s, CO_2), 102.0, 109.3 (both s, C_4Cl_4), 85.1 (br s, N_2C), 24.4 (vt, $N = 19.0$ Hz, P*C*HCH$_3$), 22.7 (s, *C*H_3CO_2), 19.7 (s, PCH*C*H$_3$). ^{31}P NMR (C_6D_6, 81.0 MHz): δ 46.0 [d, $^1J(RhP) = 117.7$].

3.16. Generation of *trans*-[Rh(κ^1-O_2CCH_3)(N_2CPh_2)-($PiPr_3$)$_2$] (**23**)

A solution of **21** (80 mg, 0.18 mmol) in 30 ml of diethylether was treated at −30 °C with a solution of diphenyldiazomethane (71 mg, 0.36 mmol) in 4 ml of diethylether. A change of colour from red to green occurred. The solution was warmed to r.t., stirred for 10 min, and the solvent was evaporated in vacuo. The residue was dissolved in 10 ml of pentane and the solution was stored at −78 °C for 6 h. A greenish-brown solid precipitated which was separated from the mother liquor, washed with small amounts of pentane (0 °C) and dried. The NMR spectra revealed that a mixture of **21** and **23** in the ratio of 1:2 was isolated. Attempts to separate the two compounds by fractional crystallization or chromatographic techniques failed. If the reaction was repeated by using a 10-fold excess of N_2CPh_2, a mixture of **21** and **23** in the approximate ratio of 1:3 was isolated. Spectroscopic data for **23**: IR (KBr): (N_2) 1950, $\nu(CO_2)$ 1635, 1495 cm^{-1}. ^1H NMR (C_6D_6, 200 MHz): δ 7.40–6.83 (br m, 10H, C_6H_5), 2.06 (m, 6H, PC*H*CH_3), 2.00 (s, 3H, CH_3CO_2), 1.28 [dvt, $N = 13.5$, $^3J(HH) = 6.6$, 36H, PCHC*H*$_3$]. ^{13}C NMR (C_6D_6, 50.3 MHz): δ 174.1 (s, CO_2), 79.4 (br s, N_2C), 24.0 (vt, $N = 17.3$ Hz, P*C*HCH$_3$), 20.6 (s, *C*H_3CO_2), 20.0 (s, PCH*C*H$_3$), signals for phenyl protons were partly covered by the solvent signal. ^{31}P NMR (C_6D_6, 81.0 MHz): δ 42.5 [d, $^1J(RhP) = 130.8$].

3.17. Generation of *trans*-[Rh(κ^1-O_2CCH_3){$N_2C(Ph)$-$C(O)Ph$}($PiPr_3$)$_2$] (**24**)

The reaction of **21** (63 mg, 0.13 mmol) with $N_2C(Ph)C(O)Ph$ (29 mg, 0.13 mmol) in diethylether was carried out as described above with N_2CPh_2 as the substrate. No change of colour occurred. A red solid was isolated which, owing to the NMR spectra, consisted of a mixture of **21** and **24** in the ratio of 1:4. Attempts to separate the two compounds failed. Spectroscopic data for **24**: IR (KBr): $\nu(N_2)$ 1920 cm^{-1}. ^1H NMR (C_6D_6, 400 MHz): δ 7.96, 7.86 (both m, 2H each, C_6H_5), 7.20–6.77 (br m, 6H, C_6H_5), 2.43 (m, 6H, PC*H*CH_3), 1.67 (s, 3H, CH_3CO_2), 1.28, 1.27 [both dvt, $N = 13.4$, $^3J(HH) = 7.0$, 18H each, PCHC*H*$_3$]. ^{13}C NMR (C_6D_6, 100.6 MHz): δ 181.4 (s, CO_2), 158.1 (s, C═O), 108.8 (br s, N_2C), 23.4 (vt, $N = 17.3$ Hz, P*C*HCH$_3$), 20.5 (s, *C*H_3CO_2), 19.9, 19.8 (both s, PCH*C*H$_3$), signals for phenyl protons were partly covered by the solvent signal. ^{31}P NMR (C_6D_6, 162.0 MHz): δ 29.9 [d, $^1J(RhP) = 113.4$].

3.18. Preparation of *trans*-[Rh(κ^1-O_2CCF_3)(N_2CPh_2)-($PiPr_3$)$_2$] (**26**)

A solution of **25** (44 mg, 0.08 mmol) in 10 ml of pentane was treated at −78 °C with a solution of diphenyldiazomethane (18 mg, 0.08 mmol) in 2 ml of pentane. A change of colour from red to green occurred. The solution was warmed to r.t., stirred for 10 min, and the solvent was evaporated in vacuo. The

residue was recrystallized from pentane at −78 °C to give a green microcrystalline solid. This was separated from the mother liquor, washed with small amounts of pentane (−20 °C) and dried: yield 44 mg (73%), m.p. 52 °C (dec.). *Anal*. Calc. for $C_{33}H_{52}F_3N_2O_2P_2Rh$: C, 54.25; H, 7.17; N, 3.83. Found: C, 53.94; H, 7.09; N, 3.50%. IR (KBr): $\nu(N_2)$ 1936, $\nu(CO_2)$ 1640 cm^{-1}. ^1H NMR (C_6D_6, 200 MHz): δ 7.70–6.84 (br m, 10H, C_6H_5), 1.97 (m, 6H, PC*H*CH_3), 1.20 [dvt, $N = 13.5$, $^3J(HH) = 6.9$, 36H, PCHC*H*$_3$]. ^{13}C NMR (C_6D_6, 50.3 MHz): δ 160.6 [q, $^2J(CF) = 35.6$, CO_2], 129.0, 128.8, 125.4, 125.1 (all s, C_6H_5), 120.4 [q, $^1J(CF) = 277.2$, CF_3], 81.0 (br s, N_2C), 23.7 (vt, $N = 17.6$, P*C*HCH$_3$), 19.8 (s, PCH*C*H$_3$). ^{19}F NMR (C_6D_6, 188.3 MHz): δ −74.6 (s). ^{31}P NMR (C_6D_6, 81.0 MHz): δ 42.2 [d, $^1J(RhP) = 126.4$].

3.19. Preparation of trans-[Rh(κ¹-O₂CCF₃)(N₂CC₄Cl₄)(PiPr₃)₂] (27)

This compound was prepared as described for **26**, with **25** (64 mg, 0.12 mmol) and $N_2CC_4Cl_4$ (27 mg, 0.12 mmol) as starting materials. Greenish microcrystalline solid; yield 83 mg (92%), m.p. 111 °C (dec.). *Anal*. Calc. for $C_{25}H_{42}Cl_4F_3N_2O_2P_2Rh$: C, 39.18; H, 5.52; N, 3.65. Found: C, 38.87; H, 5.36; N, 3.38%. IR (KBr): $\nu(N_2)$ 1940, $\nu(CO_2)$ 1700 cm^{-1}. ^1H NMR (C_6D_6, 200 MHz): δ 1.93 (m, 6H, PC*H*CH_3), 1.10 [dvt, $N = 14.1$, $^3J(HH) = 7.1$, 36H, PCHC*H*$_3$]. ^{13}C NMR (C_6D_6, 50.3 MHz): δ 159.6 [q, $^2J(FC) = 36.1$, CO_2], 119.5 [q, $^1J(FC) = 278.3$, CF_3], 110.2, 102.8 (both s, C_4Cl_4), 86.6 (br s, N_2C), 24.1 (vt, $N = 19.4$, P*C*HCH$_3$), 19.8 (s, PCH*C*H$_3$). ^{19}F NMR (C_6D_6, 188.3 MHz): δ −74.4 (s). ^{31}P NMR (C_6D_6, 81.0 MHz): δ 46.5 [d, $^1J(RhP) = 114.8$].

3.20. Preparation of trans-[Rh(κ¹-O₂CCF₃){N₂CH-C(O)Ph}(PiPr₃)₂] (28)

This compound was prepared as described for **26**, with **25** (54 mg, 0.10 mmol) and $N_2CC_4Cl_4$ (27 mg, 0.12 mmol) as starting materials. Yellow microcrystalline solid; yield 62 mg (90%), m.p. 56 °C (dec.). *Anal*. Calc. for $C_{28}H_{50}F_3N_2O_3P_2Rh$: C, 49.27; H, 7.09; N, 4.10. Found: C, 49.48; H, 7.31; N, 3.87%. IR (KBr): $\nu(N_2)$ 1940, ν (CO_2) 1685, ν(C═O) 1625 cm^{-1}. ^1H NMR (C_6D_6, 200 MHz): δ 8.28–7.14 (br m, 5H, C_6H_5), 2.20 (m, 6H, PC*H*CH_3), 1.42 (s, 1H, N_2CH), 1.20 [dvt, $N = 14.6$, $^3J(HH) = 7.6$, 36 H, PCHC*H*$_3$]. ^{13}C NMR (C_6D_6, 50.3 MHz): δ 163.2 [q, $^2J(FC) = 34.7$, CO_2], 150.1 (s, C═O), 136.1, 128.8, 128.1, 126.6 (all s, C_6H_5), 122.6 [q, $^1J(FC) = 287.8$, CF_3], 83.5 (br s, N_2C), 24.0 (vt, $N = 17.8$, P*C*HCH$_3$), 19.6, 19.4 (both s, PCH*C*H$_3$). ^{19}F NMR (C_6D_6, 188.3 MHz): δ −74.1 (s). ^{31}P NMR (C_6D_6, 81.0 MHz): δ 31.5 [d, $^1J(RhP) = 117.1$].

3.21. Preparation of trans-[Rh(κ¹-O₂CCF₃)(N₂)(PiPr₃)₂] (29)

A solution of **25** (59 mg, 0.12 mmol) in 5 ml of pentane was treated at −50 °C with a solution of phenyldiazomethane (13 mg, 0.12 mmol) in 1 ml of pentane. While the solution was warmed to r.t., a brown solid precipitated. The suspension was stirred for 5 min, concentrated to ca. 2 ml in vacuo and then stored for 6 h at −78 °C. A brown microcrystalline solid was obtained, which was separated from the mother liquor, washed with small amounts of pentane (−20 °C) and dried: yield 40 mg (59%), m.p. 91 °C (dec.). *Anal*. Calc. for $C_{20}H_{42}F_3N_2O_2P_2Rh$: C, 42.56; H, 7.50; N, 4.96. Found: C, 43.02; H, 7.21; N, 5.36%. IR (KBr): $\nu(N_2)$ 2098, $\nu(CO_2)$ 1650 cm^{-1}. ^1H NMR (C_6D_6, 200 MHz): δ 2.03 (m, 6H, PC*H*CH_3), 1.22 [dvt, $N = 13.5$, $^3J(HH) = 7.3$, 36 H, PCHC*H*$_3$]. ^{13}C NMR (C_6D_6, 50.3 MHz): δ 159.7 [q, $^2J(CF) = 35.7$, CO_2], 116.5 [q, $^1J(CF) = 255.1$, CF_3], 23.3 (vt, $N = 19.1$, P*C*HCH$_3$), 19.7 (s, PCH*C*H$_3$). ^{19}F NMR (C_6D_6, 188.3 MHz): δ −74.6 (s). ^{31}P NMR (C_6D_6, 81.0 MHz): δ 43.3 [d, $^1J(RhP) = 126.3$].

3.22. Preparation of trans,trans-[{Rh(κ¹-O₂CCF₃)(PiPr₃)₂}{μ-1.4-C₆H₄(C(Ph)N₂)₂}] (30)

A solution of **25** (74 mg, 0.14 mmol) in 5 ml of diethylether was treated dropwise at −78 °C with a solution of 1.4-$C_6H_4(C(Ph)N_2)_2$ (26 mg, 0.08 mmol) in 3 ml of diethylether. A change of colour from red to green occurred. The work-up procedure was the same as described for **26**. A dark green microcrystalline solid was obtained: yield 65 mg (68%), m.p. 46 °C (dec.). *Anal*. Calc. for $C_{60}H_{92}F_6N_4O_4P_4Rh_2$: C, 52.10; H, 7.14; N, 4.05. Found: C, 52.67; H, 7.41; N, 3.91%. IR (KBr): $\nu(N_2)$ 1930, $\nu(CO_2)$ 1630 cm^{-1}. ^1H NMR (C_6D_6, 400 MHz): δ 7.88–6.89 (br m, 14H, C_6H_4 and C_6H_5), 2.00 (m, 12H, PC*H*CH_3), 1.24 [dvt, $N = 13.6$, $^3J(HH) = 6.8$, 72 H, PCHC*H*$_3$]. ^{13}C NMR (C_6D_6, 100.6 MHz): δ 160.3 [q, $^2J(CF) = 35.1$, CO_2], 129.1, 127.9, 125.6, 125.5, 125.3, 124.5 (all s, C_6H_4 and C_6H_5), 122.4 [q, $^1J(CF) = 262.6$, CF_3], 81.2 (br s, N_2C), 23.8 (vt, $N = 17.5$, P*C*HCH$_3$), 19.9 (s, PCH*C*H$_3$). ^{19}F NMR (C_6D_6, 376.5 MHz): δ −74.8 (s). ^{31}P NMR (C_6D_6, 81.0 MHz): δ 42.21.9 [d, $^1J(RhP) = 126.3$].

3.23. Catalytic reaction of ethene with diaryldiazomethanes with compound 21 or 25 as a catalyst

In a typical experiment, a solution of the catalyst (20–30 mg, ca. 0.05 mmol) in 6 ml of toluene was treated dropwise (ca. 10 ml/h) at 40 °C with a 0.1 M solution of N_2CRR' in toluene. While adding the substrate, a slow stream of ethene was passed through the solution. The catalytic reaction was finished when the violet colour of the diazoalkane solution did not disappear on further

addition to the reaction mixture. The solvent was evaporated in vacuo and the oily residue was dissolved in 3 ml of hexane. In order to destroy the excess of N_2CRR' and separate the catalyst, the mixture was filtered through Al_2O_3 (neutral, activity grade III, height of column 4 cm). After removal of the solvent, a colorless oil was isolated from the eluate. The product was analyzed by GC–MS and the dominating olefin (see Table 1) characterized by ^1H NMR spectroscopy. The data for **1b** [26], **1c** [29], **19** [27], **20** [28] and **33** [30] were already reported. ^1H NMR data for N_2CRR' (C_6D_6, 200 MHz): **31**: δ 7.83, 7.77 [both d, $^3J(HH) = 8.2$, 2 H each, C_6H_4], 7.62–7.12 (br m, 5H, C_6H_5), 6.31 [ddd, $^3J(HH)_{trans} = 17.2$, $^3J(HH)_{cis} = 10.2$, $^3J(HH) = 7.3$, 1 H, C*H*=CH_2], 5.22 [ddd, $^3J(HH)_{cis} = 10.2$, $^2J(HH) = 1.5$, $^4J(HH) = 1.1$, 1 H, one H of =CH_2 *trans* to CH], 5.01 [ddd, $^3J(HH)_{trans} = 17.2$, $^2J(HH) = 1.5$, $^4J(HH) = 1.8$, 1 H, one H of =CH_2 *cis* to CH], 4.72 [br d, $^3J(HH) = 7.3$, 1H, C*H*RR′], 2.39 (s, 3H, $C_6H_4CH_3$). **32**: δ 7.31–6.82 (br m, 9H, C_6H_4 and C_6H_5), 6.18 [ddd, $^3J(HH)_{trans} = 16.8$, $^3J(HH)_{cis} = 10.2$, $^3J(HH) = 6.6$, 1H, C*H*=CH_2], 5.12 [ddd, $^3J(HH)_{cis} = 10.2$, $^2J(HH) = 1.5$, $^4J(HH) = 1.5$, 1H, one H of =CH_2 *trans* to CH], 4.81 [br d, $^3J(HH) = 6.6$, 1H, C*H*RR′], 4.75 [ddd, $^3J(HH)_{trans} = 17.2$, $^2J(HH) = 1.5$, $^4J(HH) = 1.8$, 1H, one H of =CH_2 *cis* to CH], 2.18 (s, 3H, $C_6H_4CH_3$). **34**: δ 7.28 [d, $^3J(HH) = 8.4$, 4H, C_6H_4], 7.02 [d, $^3J(HH) = 8.8$, 4H, C_6H_4], 6.44 [ddd, $^3J(HH)_{trans} = 17.2$, $^3J(HH)_{cis} = 10.2$, $^3J(HH) = 6.5$, 1H, C*H*=CH_2], 5.36 [br d, $^3J(HH)_{cis} = 10.2$, 1H, one H of =CH_2 *trans* to CH], 5.14 [ddd, $^3J(HH)_{trans} = 17.2$, $^2J(HH) = 1.5$, $^4J(HH) = 1.4$, 1H, one H of =CH_2 *cis* to CH], 4.82 [br d, $^3J(HH) = 7.3$, 1H, C*H*RR′], 2.94 (s, 3H, OCH_3). **35**: δ 7.90 [d, $^3J(HH) = 8.4$, 4H, C_6H_4], 7.40 (m, 4H, C_6H_4), 6.38 [ddd, $^3J(HH)_{trans} = 17.2$, $^3J(HH)_{cis} = 10.2$, $^3J(HH) = 6.9$, 1H, C*H*=CH_2], 5.42 [ddd, $^3J(HH)_{cis} = 10.2$, $^2J(HH) = 1.5$, $^4J(HH) = 1.2$, 1H, one H of =CH_2 *trans* to CH], 5.14 [ddd, $^3J(HH)_{trans} = 17.2$, $^2J(HH) = 1.5$, $^4J(HH) = 1.2$, 1H, one H of =CH_2 *cis* to CH], 4.85 [br d, $^3J(HH) = 7.3$, 1H, C*H*RR′].

Acknowledgements

Financial support from the Fonds der Chemischen Industrie and BASF AG, Ludwigshafen, is gratefully acknowledged. We also thank Mrs. R. Schedl and Mr. C.P. Kneis for elemental analyses and DTA measurements, Dr. G. Lange and Mr. F. Dadrich for the mass spectrum, and Dr. J. Wolf for valuable advice.

References

[1] (a) P. Schwab, N. Mahr, J. Wolf, H. Werner, Angew. Chem., Int. Ed. Engl. 32 (1993) 1480;
(b) H. Werner, P. Schwab, E. Bleuel, N. Mahr, P. Steinert, J. Wolf, Chem. Eur. J. 3 (1997) 1375.

[2] (a) J. Wolf, L. Brandt, A. Fries, H. Werner, Angew. Chem., Int. Ed. Engl. 29 (1990) 510;
(b) H. Werner, J. Organomet. Chem. 475 (1994) 45.

[3] (a) L. Brandt, Dissertation, Universität Würzburg, 1991;
(b) A. Fries, Dissertation, Universität Würzburg, 1993.

[4] (a) A.J. Anciaux, A.J. Hubert, A.F. Noels, N. Petiniot, P. Teyssie, J. Org. Chem. 45 (1980) 695;
(b) M.P. Doyle, Acc. Chem. Res. 19 (1986) 348;
(c) M.P. Doyle, W.R. Winchester, J.A.A. Hoorn, V. Lynch, S.H. Simonsen, R. Ghosh, J. Am. Chem. Soc. 115 (1993) 9968.

[5] (a) M.P. Doyle, D. van Leusen, W.H. Tamblyn, Synthesis (1981) 787;
(b) M.P. Doyle, W.H. Tamblyn, W.E. Buhro, R.L. Dorow, Tetrahedron Lett. (1981) 1783.

[6] L. Brandt, A. Fries, N. Mahr, H. Werner, J. Wolf, in: H. Werner, A.G. Griesbeck, W. Adam, G. Bringmann, W. Kiefer (Eds.), Selective Reactions of Metal-activated Molecules, Vieweg Verlag, Braunschweig, 1992, p. 171.

[7] H. Werner, M. Schäfer, O. Nürnberg, J. Wolf, Chem. Ber. 127 (1994) 27.

[8] M.E. Schneider, H. Werner, in: 10. International Symposium on Homogeneous Catalysis, Princeton, 1996.

[9] R. Daus, Dissertation, Universität Würzburg, 1990.

[10] M.A. Esteruelas, F.J. Lahoz, E. Onate, L.A. Oro, R. Rodriguez, P. Steinert, H. Werner, Organometallics 15 (1996) 3436.

[11] H. Werner, N. Mahr, J. Wolf, A. Fries, M. Laubender, E. Bleuel, R. Garde, P. Lahuerta, Organometallics 22 (2003) 3566.

[12] L.G. Kuzmina, Yu.T. Struchkov, Koord. Chim. 14 (1988) 1262.

[13] L.G. Kuzmina, Yu.T. Struchkov, Sov. J. Coord. Chem. 14 (1988) 712.

[14] M.A. Tena, O. Nürnberg, H. Werner, Chem. Ber. 126 (1993) 1597.

[15] (a) B. Windmüller, J. Wolf, H. Werner, J. Organomet. Chem. 502 (1995) 147;
(b) B. Windmüller, O. Nürnberg, J. Wolf, H. Werner, Eur. J. Inorg. Chem. (1999) 613.

[16] (a) Inter alia: A. Albini, H. Kisch, Top. Curr. Chem. 65 (1976) 105;
(b) W.A. Herrmann, Angew. Chem., Int. Ed. Engl. 17 (1978) 800;
(c) M. Hidai, Y. Mizobe, M. Sato, T. Kodama, Y. Uchida, J. Am. Chem. Soc. 100 (1978) 5740;
(d) J.A. Ibers, T.R. Gaffney, K.D. Schramm, Coord. Chem. Rev. 21 (1980) 141;
(e) D. Sutton, Chem. Rev. 93 (1993) 995.

[17] R.K. Harris, Can. J. Chem. 42 (1964) 2275.

[18] (a) S.D. Robinson, M.F. Uttley, J. Chem. Soc. (1973) 1912;
(b) G.B. Deacon, R.J. Philips, Coord. Chem. Eev. 33 (1980) 227;
(c) D.A. Tocher, R.O. Gould, T.A. Stephenson, M.A. Bennett, J.P. Ennett, T.W. Matheson, L. Sawyer, V.K. Shah, J. Chem. Soc., Dalton Trans. (1983) 1571.

[19] J. Wolf, unpublished results, 1990.

[20] (a) For the preparation and structural characterization of *trans*-$[RhCl(N_2)(P\textit{i}Pr_3)_2]$ see: C. Busetto, A. D'Alfonso, F. Maspero, G. Perego, A. Zazzetta, J. Chem. Soc., Dalton Trans. (1977) 1828;
(b) D.L. Thorn, T.H. Tulip, J.A. Ibers, J. Chem. Soc., Dalton Trans. (1979) 2022.

[21] B. Papenfuhs, N. Mahr, H. Werner, Organometallics 12 (1993) 4244.

[22] M. Schäfer, J. Wolf, H. Werner, J. Organomet. Chem. 476 (1994) 85.

[23] E. Bleuel, B. Weberndörfer, H. Werner, J. Organomet. Chem. 617–618 (2001) 502.

[24] (a) R. Cramer, J. Am. Chem. Soc. 86 (1964) 217;
(b) A.C. Jesse, H.P. Grijben, P.J. Stufkens, K. Vrieze, Inorg. Chim. Acta 31 (1978) 201;
(c) G. Ingrosso, L. Porri, G. Pantini, R. Rcanelli, J. Organomet. Chem. 84 (1975) 74.

[25] H. Werner, J. Wolf, A. Höhn, J. Organomet. Chem. 287 (1985) 395.
[26] D. Hernandez, G.L. Larson, J. Org. Chem. 49 (1984) 4285.
[27] R. van der Linde, O. Korver, P.K. Korver, P.J. van der Haak, J.U. Veenland, T.J. de Boer, Spectrochim. Acta 21 (1965) 1893.
[28] H. Mayr, R. Pock, Chem. Ber. 119 (1986) 2473.
[29] S. Araki, T. Shimizu, P.S. Johar, S.J. Jin, Y. Butsugan, J. Org. Chem. 56 (1991) 2538.
[30] C.P. Casey, S.R. Marder, R.E. Colborn, P.A. Goodson, Organometallics 5 (1986) 199.

Available online at www.sciencedirect.com
SCIENCE DIRECT®
Polyhedron 23 (2004) 2659–2664
POLYHEDRON
www.elsevier.com/locate/poly

Intramolecular dehydrofluorinative coupling of pentamethylcyclopentadienyl and phosphine ligands in iridium complexes

Ronan M. Bellabarba, Graham C. Saunders *

School of Chemistry, Queen's University Belfast, David Keir Building, Belfast BT9 5AG, UK

Received 13 April 2004; accepted 20 May 2004
Available online 15 July 2004

Dedicated to Prof. Malcolm Green FRS for his guidance and inspiration

Abstract

Cationic iridium(III) complexes of bifunctional $\eta^5,\kappa P$-Cp–P and trifunctional $\eta^5,\kappa P,\kappa L$-Cp–PL ligands may be conveniently prepared by intramolecular dehydrofluorinative carbon–carbon coupling. The iridium(III) complex $[(\eta^5\text{-}C_5Me_5)IrCl(dfppe)]BF_4$ (dfppe = $(C_6F_5)_2PCH_2CH_2P(C_6F_5)_2$) undergoes rapid dehydrofluorinative coupling on addition of proton sponge to produce $[\{\eta^5,\kappa P,\kappa P\text{-}C_5Me_3[CH_2C_6F_4\text{-}2\text{-}P(C_6F_5)CH_2]_2\text{-}1,3\}IrCl]BF_4$. The reaction requires less than the stoichiometric quantity of proton sponge and also occurs on addition of Bu^n_4NF. The cationic phosphine–thioether complex $[(\eta^5\text{-}C_5Me_5)IrCl\{\kappa P,\kappa S\text{-}(C_6F_5)_2PC_6H_4SMe\text{-}2\}]BF_4$ undergoes rapid dehydrofluorinative coupling to $[\{\eta^5,\kappa P,\kappa S\text{-}C_5Me_4CH_2C_6F_4\text{-}2\text{-}P(C_6F_5)C_6H_4SMe\text{-}2\}IrCl]BF_4$ on treatment with proton sponge. NMR studies indicate that on treatment with proton sponge the cations $[(\eta^5\text{-}C_5Me_5)IrCl(CNR)\{PPh_2(C_6F_5)\}]^+$ (R = Ph or ^{t}Bu) undergo coupling to give $[(\eta^5,\kappa P\text{-}C_5Me_4CH_2C_6F_4\text{-}2\text{-}PPh_2)IrCl(CNR)]^+$, but at a much slower rate and less cleanly than for the cations containing chelating ligands. The neutral compound $[(\eta^5\text{-}C_5Me_5)IrCl_2\{PPh_2(C_6F_5)\}]$ does not undergo coupling, indicating that a positive charge is necessary for the reaction. The results are analogous to those for rhodium complexes.
© 2004 Elsevier Ltd. All rights reserved.

1. Introduction

Transition metal complexes of chelating bifunctional $\eta^5,\kappa P$-cyclopentadienyl–phosphine (Cp–P) or trifunctional $\eta^5,\kappa P,\kappa L$-cyclopentadienyl–phosphine-donor (Cp–PL) ligands can possess benefits over the analogous complexes of the unlinked ligands. Enhancement of stability [1–4], reactivity [5,6] and regio and stereo-selectivity in their reactions [7] has been reported, and configurational stability is expected for chiral-at-metal complexes of Cp–PL ligands [8]. Despite the benefits relatively few complexes of Cp–P ligands, and even fewer of Cp–PL ligands, have been reported, primarily due to the lack of convenient synthetic routes [9,10]. Nonetheless a number of rhodium complexes of Cp–P and Cp–PL ligands have been reported [4–6,9,11–14]. In contrast the number of complexes of iridium is limited to those of the Cp–P ligands **1** [15,16] and **2** [17], and **3** [18].

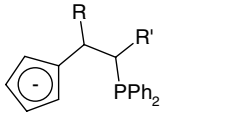

1

R = H, R' = H or *cyclo*-C_6H_{11}
R = Ph, R' = H

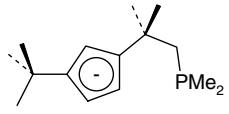

2

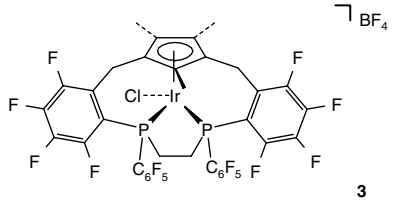

3

* Corresponding author. Tel.: +44-28-90374682; fax: +44-28-90382117/+44-28-90273333.
E-mail address: g.saunders@qub.ac.uk (G.C. Saunders).

0277-5387/$ - see front matter © 2004 Elsevier Ltd. All rights reserved.
doi:10.1016/j.poly.2004.05.014

We have demonstrated that intramolecular dehydrofluorinative carbon–carbon coupling provides a convenient route to cationic rhodium complexes of Cp–P and Cp–PL ligands [12]. The coupling of the pentamethylcyclopentadienyl and fluorophenylphoshphines of cationic complexes of the formula $[(\eta^5\text{-}C_5Me_5)\ RhXL\{PR_2(C_6F_5)\}]^+$ (X = Cl or Br, L = 2-electron donor ligand) may be performed by addition of less than one equivalent of 1,8-bis(dimethylamino)naphthalene (proton sponge) or fluoride ions. The reaction is rapid and quantitative for complexes in which the phosphine is part of a chelating ligand, as in a diphosphine or a phosphine-thioether, but considerably slower for complexes of monodentate phosphines. Alternatively, for cations containing chelating phosphines, heating a solution of the salt in an appropriate solvent yields the coupled product, although not always cleanly [18,19]. The preparation of the complexes of trifunctional cyclopentadienyl–diphosphine ligands containing two linkages has also been accomplished by heating a slurry of a 2:1 mixture of the diphosphine and $[(\eta^5\text{-}C_5Me_5)RhCl(\mu\text{-}Cl)]_2$ in benzene or ethanol [18,20]. The last method has also been found to yield **3** from $[(\eta^5\text{-}C_5Me_5)IrCl(\mu\text{-}Cl)]_2$ and $(C_6F_5)_2PCH_2CH_2P(C_6F_5)_2$ (dfppe) [18]. A mechanism involving formation of an η^4-fulvene by loss of a proton from the pentamethylcyclopentadienyl ligand and intramolecular nucleophilic attack of the methylene carbon on an *ortho* C–F bond has been proposed for cationic rhodium(III) and cobalt(III) complexes [12,21]. The similarity of the chemistry of analogous rhodium(III) and iridium(III) pentamethylcyclopentadienyl complexes suggests that intramolecular dehydrofluorinative carbon–carbon coupling would also provide a convenient route to Cp–P and Cp–PL complexes of iridium. In support η^4-fulvene complexes of iridium have been proposed as nucleophilic intermediates in a number of reactions [22–26] and $[(\eta^4\text{-}C_5Me_4CH_2)IrMe(dppe)]$ has been structurally characterized [27]. However, some differences in reactivity between analogous complexes of iridium and rhodium have been observed. One apposite example is provided by the reactions between $[(\eta^5\text{-}C_5Me_5)MCl(\mu\text{-}Cl)]_2$ and $(C_6H_3\ F_2\text{-}2,6)_2PCH_2CH_2P(C_6H_3F_2\text{-}2,6)$, which yielded the coupled product **4** and the uncoupled bimetallic compound **5** [19]. Therefore, we set out to examine whether the coupling reactions that occur for the cationic rhodium complexes also occur for the analogous complexes of iridium. Here, the results of our study are reported.

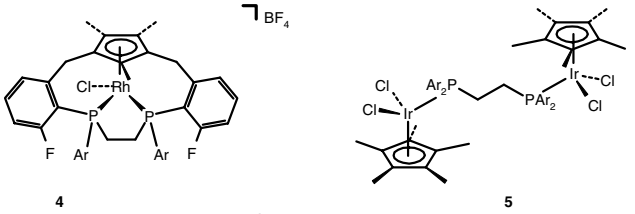

4 **5**

Ar = $C_6H_3F_2$-2,6

2. Experimental

2.1. Physical measurements

The ^1H, ^{19}F and ^{31}P NMR spectra were recorded using a Bruker DPX300 spectrometer. ^1H (300.01 MHz) were referenced internally using the residual protio solvent resonance relative to $SiMe_4$ (δ 0), ^{19}F (282.26 MHz) externally to $CFCl_3$ (δ 0) and ^{31}P (121.45 MHz) externally to 85% H_3PO_4 (δ 0). All spectra were recorded in $CDCl_3$ at 300 K. Data are given as chemical shifts (δ) using the high frequency positive convention, [relative intensity, multiplicity, *J*/Hz, assignment], s, singlet; d, doublet; t, triplet; m, multiplet; br, broad. The IR spectra were recorded on a Perkin–Elmer RX I Fourier transform spectrometer. Mass spectra were recorded on a VG Autospec X series mass spectrometer. Elemental analyses were carried out by A.S.E.P., The School of Chemistry, Queen's University Belfast.

2.2. Materials

The compounds $[(\eta^5\text{-}C_5Me_5)IrCl(\mu\text{-}Cl)]_2$, sodium tetrafluoroborate and proton sponge (Aldrich) were used as supplied. The salt $[(\eta^5\text{-}C_5Me_5)IrCl(dfppe)]BF_4$ [18] and phenylisonitrile [28] were prepared as described. The phosphines $P(C_6F_5)_3$ and $PPh_2(C_6F_5)$ [29] were prepared from PCl_3 and Ph_2PCl as described for similar compounds [30].

2.3. $(C_6F_5)_2PC_6H_4SMe$-2 (**6**)

A solution of Bu^nLi in hexane (3.0 cm^3, 1.6 M) was added to $MeSC_6H_4Br$-2 (1.10 g, 5.4 mmol) in diethyl ether at 0 °C. After stirring for 1 h the solution was added over 10 min to $P(C_6F_5)_3$ (3.12 g, 5.8 mmol) in diethyl ether (100 cm^3) at 0 °C to give a black solution. After stirring for a further 5 min water (100 cm^3) was added. The organic layer was washed with water (100 cm^3). The aqueous layer and washings were extracted with 1:2 ethyl acetate/chloroform (200 cm^3). The combined organic extracts were dried over magnesium sulfate. Filtration and removal of the solvent by rotary evaporation yielded a brown oil comprising $P(C_6F_5)_3$, (**6**) and $(C_6F_5)P(C_6H_4SMe\text{-}2)_2$. Compound **6** was obtained by distillation by kugelrohr at 130–140 °C and 0.03 mm Hg. Yield 0.120 g (4.2%).

2.4. $[(\eta^5\text{-}C_5Me_5)IrCl\{\kappa P,\ \kappa S\text{-}(C_6F_5)_2PC_6H_4SMe\text{-}2\}]BF_4$ (**7**)

Sodium tetrafluoroborate (0.164 g, 1.5 mmol) was added to $[(\eta^5\text{-}C_5Me_5)IrCl(\mu\text{-}Cl)]_2$ (0.175 g, 0.22 mmol) and **6** (0.216 g, 0.44 mmol) in dichloromethane (30 cm^3) and methanol (30 cm^3), and the mixture stirred for 90 min. The solvent was removed by rotary evaporation

and the product extracted into dichloromethane. The extract was filtered and the solvent removed by rotary evaporation to give the product as a yellow solid. Yield 0.351 g (87%). *Anal.* Calc. for $C_{29}H_{22}BClF_{14}PIrS$ (**7**): C, 37.0; H, 2.4. Found: C, 36.9; H, 2.2%. ^{1}H NMR: δ 8.55 (1H, m, C_6H_4), 8.10 (2H, m, C_6H_4), 7.98 (1H, m, C_6H_4), 3.14 (3H, s, SMe), 1.78 (15H, s, Me). ^{19}F NMR: −122.50 (1F, br s, F_o), −127.32 (1F, br s, F_o), −127.55 (1F, br s, F_o), −131.76 (1F, br s, F_o), −141.99 (1F, br s, F_p), −144.65 (1F, br s, F_p), −153.59 (0.8F, s, $^{10}BF_4^-$), −153.64 (3.2F, s, $^{11}BF_4^-$), −155.14 (1F, br s, F_m), −157.24 (1F, br s, F_m), −158.41 (1F, br s, F_m), −160.61 (1F, br s, F_m). $^{31}P\{^1H\}$ NMR: 5.4 (s).

2.5. [{η^5,κP,κS-$C_5Me_4CH_2C_6F_4$-2-P(C_6F_5)C_6H_4SMe-2}IrCl]BF_4 (**8**)

Proton sponge (0.041 g, 0.19 mmol) was added to **7** (0.129 g, 0.14 mmol) in dichloromethane (40 cm^3) and the solution left at ambient temperature for 48 h. The solution was washed with water (50 cm^3), dilute hydrochloric acid (50 cm^3) and water (50 cm^3), and dried over magnesium sulfate. Filtration and removal of the solvent by rotary evaporation gave the product as a yellow solid, which was dried in vacuo. Yield 0.084 g (66.5%). *Anal.* Calc. for $C_{29}H_{21}BClF_{13}PIrS$ (**8**): C, 37.9; H, 2.3. Found: C, 40.05; H, 2.6%. Repeated washing and drying in vacuo failed to give satisfactory analysis ($N < 0.1$%). LSIMS: 831 ($[M-BF_4]^+$) [Found: 831.02980 $C_{29}H_{21}ClF_9^{193}IrPS$ requires 831.02759]. ^{1}H NMR: δ 8.14 (1H, m, C_6H_4), 7.97 (1H, m, C_6H_4), 7.74 (1H, m, C_6H_4), 7.66 (1H, m, C_6H_4), 4.58 [1H, dd, ^2J(HH) 17.9, ^4J(PH) 7.6, CH_2], 3.05 [1H, d, ^2J(HH) 17.9, CH_2], 2.65 (3H, s, SMe), 2.34 [3H, d, ^4J(PH) 6.5, CH_3], 1.87 [3H, d, ^4J(PH) 2.2, CH_3], 1.82 [3H, d, ^4J(PH) 2.9, CH_3], 1.69 (3H, s, CH_3). ^{19}F NMR: δ −119.47 (1F, m), −128.81 (1F, m), −133.22 (1F, m), −133.52 (1F, m), −142.81 (1F, m), −146.05 [1F, t ^3J(FF) 20.7], 151.97 [1F, t ^3J(FF) 22.0, F_p], −153.77 (0.8F, s, $^{10}BF_4^-$), −153.83 (3.2F, s, $^{11}BF_4^-$), −158.85 (2H, m). $^{31}P\{^1H\}$ NMR: δ 31.9 (s).

2.6. [(η^5-C_5Me_5)$IrCl_2${PPh_2(C_6F_5)}] (**9**)

A mixture of [(η^5-C_5Me_5)IrCl(μ-Cl)]$_2$ (0.112 g, 0.14 mmol) and $Ph_2P(C_6F_5)$ (0.099 g, 0.28 mmol) in dichloromethane/methanol (50 cm^3) was left at ambient temperature for 2 h. The solvent was removed by rotary evaporation affording the product as an orange solid, which was recrystallized from dichloromethane. Yield 0.160 g (76.1%). *Anal.* Calc. for $C_{28}H_{27}Cl_2F_5PIr$ (**9**): C, 44.8; H, 3.4. Found: C, 44.5; H, 3.1%. ^{1}H NMR: δ 7.81 (4H, m, C_6H_5), 7.41 (6H, m, C_6H_5), 1.44 [15H, d, ^4J(PH) 2.5, Me]. ^{19}F NMR: δ −120.06 (2F, m, F_o), −148.52 [1F, t, $^3J(F_mF_p)$ 19.8, F_p], −160.22 (2F, m, F_m). $^{31}P\{^1H\}$ NMR: −1.7 (s).

2.7. [(η^5-C_5Me_5)IrCl(CNPh){PPh_2(C_6F_5)}]BF_4 (**10a**)

Sodium tetrafluoroborate (0.110 g, 1.00 mmol) in methanol (30 cm^3) was added to **9** (0.100 g, 0.13 mmol) and phenylisonitrile (0.108 g, 1.05 mmol) in dichloromethane/methanol (30 cm^3), and the mixture stirred for 2 h. The solvent was removed by rotary evaporation and the product extracted into dichloromethane. Concentration by rotary evaporation and addition of hexane precipitated the product as a yellow solid. Yield 0.070 g (59.1%). *Anal.* Calc. for $C_{35}H_{30}BClF_9IrNP.0.5CH_2Cl_2$ (**10a**): C, 44.7; H, 3.9; N, 1.5. Found: C, 45.15; H, 3.15; N, 1.75%. ν(N≡C) 2181 cm^{-1}. ^{1}H NMR: δ 7.85 (2H, m), 7.33 – 7.54 (11H, m), 6.86 (2H, m), 5.30 (1H, s, CH_2Cl_2), 1.80 [15H, d, ^4J(PH) 2.7, Me]. ^{19}F NMR: δ −124.67 (2F, m, F_o), −143.55 (1H, br s, F_p), −153.68 (0.8F, s, $^{10}BF_4^-$), −153.74 (3.2F, s, $^{11}BF_4^-$), −156.93 (2F, br s, F_m). $^{31}P\{^1H\}$ NMR: δ 9.4 (s).

2.8. [(η^5-C_5Me_5)IrCl($CNBu^t$){PPh_2(C_6F_5)}]BF_4 (**10b**)

Compound **9** (0.060 g, 0.08 mmol), ^{t}butylisonitrile (0.009 cm^3, 0.08 mmol) and sodium tetrafluoroborate (0.109 g, 1.00 mmol) were treated as for **10a**. Yield 0.045 g (63.6%). *Anal.* Calc. for $C_{33}H_{34}BClF_9IrNP$ (**10b**): C, 44.8; H, 3.9; N, 1.6. Found: C, 44.5; H, 3.9; N, 1.75%. LSIMS: 798 ($[M-BF_4]^+$), 763 ($[M-BF_4-Cl]^+$) [Found: 798.16367 $C_{33}H_{34}BClF_9^{193}IrNP$ requires 798.16670]. ν(N≡C) 2199 cm^{-1}. ^{1}H NMR: δ 7.79 (2H, m), 7.37 −7.63 (8H, m), 1.72 [15H, d, ^4J(PH) 2.6, Me], 1.29 (9H, s, ^{t}Bu). ^{19}F NMR: δ −124.71 (2F, m, F_o), −144.04 (1H, br s, F_p), −153.87 (0.8F, s, $^{10}BF_4^-$), −153.96 (3.2F, s, $^{11}BF_4^-$), −157.22 (2F, br s, F_m). $^{31}P\{^1H\}$ NMR: δ −9.0 (s).

2.9. [(η^5,κP-$C_5Me_4CH_2C_6F_4$-2-PPh_2)IrCl(CNPh)]BF_4 (**11a**)

Proton sponge (0.005 g, 0.023 mmol) was added to **10a** (0.057 g, 0.063 mmol) in dichloromethane (15 cm^3). After 7 days dichloromethane (85 cm^3) was added and the solution washed with water (3 × 50 cm^3) and dried over magnesium sulfate. Filtration and removal of the solvent by rotary evaporation gave an oily brown solid, which was washed with diethyl ether (10 cm^3) and dried in vacuo. Yield 0.045 g (80.7%). *Anal.* Calc. for $C_{35}H_{29}BClF_8IrNP$ (**11a**): C, 47.5; H, 3.3; N, 1.6. Found: C, 49.4; H, 3.9; N, 1.9%. Repeated washing and drying in vacuo failed to give satisfactory analysis. LSIMS: 798 ($[M-BF_4]^+$), 763 ($[M-BF_4-Cl]^+$) [Found: 798.12522 $C_{35}H_{29}ClF_4^{193}$ IrNP requires 798.12917]. ν(N≡C) 2180 cm^{-1}. ^{1}H NMR: δ 7.05–7.82 (15H, m, C_6H_5), 3.85 [1H, dd, ^2J(HH) 16.9, ^4J(PH) 4.8, CH_2], 3.64 [1H, dd, ^2J(HH) 16.9, ^4J(PH) 4.8, CH_2], 2.30 [3H, d, ^4J(PH) 4.0, CH_3], 1.90 [3H, d, ^4J(PH) 4.3, CH_3], 1.73 [3H, d, ^4J(PH) 4.4, CH_3], 1.51

(3H, s, CH_3). ^{19}F NMR: δ −118.64 (1F, m), −136.29 (1F, m), −145.78 (1F, m), −152.30 (1F, m), −153.05 (0.8F, s, $^{10}BF_4^-$), −153.11 (3.2F, s, $^{11}BF_4^-$). $^{31}P\{^1H\}$ NMR: δ 5.6 (s).

2.10. *[(η^5,κP-$C_5Me_4CH_2C_6F_4$-2-PPh_2)IrCl(CNBu^t)]BF_4 (**11b**)*

A sample was obtained from the reaction between **10b** and proton sponge in an NMR tube. There was insufficient sample for elemental analysis. LSIMS: 778 ($[M-BF_4]^+$), 743 ($[M-BF_4-Cl]^+$) [Found: 778.16394 $C_{33}H_{33}ClF_4^{193}IrNP$ requires 778.160471]. ν(N≡C) 2197 cm^{-1}. ^{19}F NMR: δ −120.71 (1F, m), −136.76 (1F, m), −146.35 (1F, m), −152.45 (1F, m), −153.20 (0.8F, s, $^{10}BF_4^-$), 153.25 (3.2F, s, $^{11}BF_4^-$). $^{31}P\{^1H\}$ NMR: δ 5.1 (s). Important ^1H NMR resonances are given in Section 3 (vide infra).

3. Results and discussion

An in situ NMR experiment in $CDCl_3$ revealed that the salt [($\eta^5C_5Me_5$)IrCl(dfppe)]BF_4 underwent rapid intramolecular dehydrofluorinative carbon–carbon coupling in the presence of less than one equivalent of proton sponge to give **3** [18]. As for the rhodium analogue, the fluoride generated as the by-product acted as a base. An in situ NMR experiment confirmed that the coupling occurred rapidly on addition of tetrabutylammonium fluoride to [(η^5-C_5Me_5)IrCl(dfppe)]BF_4 in acetone. In contrast [(η^5-C_5Me_5)IrCl{κP,κP-[($C_6H_3F_2$-2,6)$_2PCH_2$]$_2$}]BF_4 [20] did not undergo any reaction in the presence of proton sponge in $CDCl_3$ at ambient temperature over 24 h. This observation is consistent with the lack of a coupling reaction of this salt in refluxing ethanol and also when [(η^5-C_5Me_5)IrCl(μ-Cl)]$_2$ and ($C_6H_3F_2$-2,6)$_2PCH_2CH_2P$($C_6H_3F_2$-2,6) are heated in benzene. The rhodium analogue [(η^5-C_5Me_5)RhCl{κP,κP-[($C_6H_3F_2$-2,6)$_2PCH_2$]$_2$}]BF_4 also did not undergo a reaction with proton sponge. This salt also underwent no reaction in refluxing ethanol, but dehydrofluorinative carbon–carbon coupling was observed in the reaction between [(η^5-C_5Me_5)RhCl(μ-Cl)]$_2$ and ($C_6H_3F_2$-2,6)$_2PCH_2CH_2P$($C_6H_3F_2$-2,6) in benzene [20].

We wished to attempt the coupling reaction with an iridium complex of the phosphine-thioether (C_6F_5)$_2$ PC_6H_4SMe-2, (**6**), which possesses only one phosphine functionality. Compound **6** has been prepared by the reaction between $MeSC_6H_4Li$ and (C_6F_5)$_2PBr$ [12], but following the observation that when a mixture of (C_6F_5)PPhCl and (C_6F_5)PPhBr was treated with an excess of $MeSC_6H_4Li$-2 the phosphine $PhP(C_6H_4SMe2)_2$ was formed, consistent with previous reports of P–C_6F_5 bond cleavage by Grignard reagents [31], it was decided to investigate whether **6** could be prepared from $P(C_6F_5)_3$. Addition of one equivalent of $MeSC_6H_4Li$-2 to $P(C_6F_5)_3$ in diethyl ether at 0 °C gave a black solution, consistent with the formation of C_6F_5Li. Following hydrolysis a brown oil was isolated which was shown by NMR spectroscopy to contain $P(C_6F_5)_3$, (**6**) and $(C_6F_5)P(C_6H_4SMe\text{-}2)_2$ in roughly equal amounts. Although the result confirms that the P–C_6F_5 bond can be readily cleaved by organolithium reagents, the reaction is not selective. Further, separating these phosphines proved difficult, although slightly impure **6** was obtained in ca. 4% yield by distillation by kugelrohr at 130–140 °C and 0.03 mm Hg. Thus this method of preparing **6** is inferior to that we have reported previously [12].

Treatment of [(η^5-C_5Me_5)IrCl(μ-Cl)]$_2$ with **6** in the presence of an excess of sodium tetrafluoroborate yielded the salt [(η^5-C_5Me_5)IrCl{κP,κS-(C_6F_5)$_2PC_6H_4SMe$-2}]BF_4, **7**. The ^1H and ^{19}F NMR spectra of **7** are similar to those of the rhodium analogue [11,12]. The ^{19}F NMR spectrum exhibits 10 resonances in addition to those of tetrafluoroborate. Each fluorine atom of the cation is unique due to hindered rotation about the P–C_6F_5 bonds. The $^{31}P\{^1H\}$ spectrum exhibits a singlet at δ 5.4, which is to a lower frequency of the doublet resonance of the rhodium analogue (δ 30.2). This difference is consistent with differences observed between rhodium and iridium analogues of similar compounds [18,20]. There are two stereogenic centres in the cation: the iridium and sulfur atoms. However only one set of resonances is seen in the NMR spectra, in particular there is only one thiomethyl hydrogen resonance, at δ 3.14, strongly suggesting that only one pair of enantiomers are present in solution. It is expected that the $R_{Ir}R_S$ and $S_{Ir}S_S$ pair, in which the methyl group is *trans* to the pentamethylcyclopentadienyl ligand would be the thermodynamically and kinetically preferred products for steric reasons. It is not known whether the exclusive existence of one pair of enantiomers is as a result of kinetics of coordination of the thioether or whether the other stereoisomers are formed and isomerize rapidly. This process can occur by dissociation and re-coordination of the labile thioether or by inversion at coordinated sulfur, which is presumed to have a low activation barrier. In support of the latter, the pyramidal inversion at the sulfur of $PPh(C_6H_4SMe\text{-}2)_2$, κP,κS-coordinated to palladium, has a free energy of activation, $\Delta G^{\ddagger}$, of 40–60 kJ mol^{-1} [32].

An in situ NMR spectroscopic study revealed that on treatment with proton sponge **7** underwent rapid intramolecular dehydrofluorinative coupling to give salt **8** (Scheme 1), which was isolated in 67% yield from a preparative scale reaction. The ^1H and ^{19}F NMR spectra of **8** are similar to those of the rhodium analogue [11,12] and the $^{31}P\{^1H\}$ spectrum exhibits a singlet at δ 31.9. The shift of the phosphorus resonance to higher frequency on coupling of the phosphine to the pen-

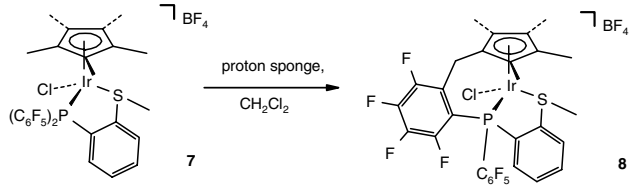

Scheme 1.

tamethylcyclopentadienyl ligand is consistent with previous observations [12,18,20]. The ^{1}H spectroscopic studies show NOE correlation between the thiomethyl hydogen atoms and one aromatic hydrogen, but not between the thiomethyl and pentamethylcyclopentadienyl hydrogen atoms, suggesting that the thiomethyl group is *trans* to the cyclopentadienyl ring, as for the rhodium analogue [11,12]. The cation of **8** contains three stereogenic centres: the iridium, sulfur and phosphorus atoms. In rhodium complexes of Cp–PL ligands the configurations at the metal and phosphorus are fixed relative to each other by the ligand's geometry such that the non-ligating substituent of the phosphine and the halide are on the same side of the plane defined by the metal and phosphorus atoms and the cyclopentadienyl centroid [12]. Presumably the same argument is valid for **8**. This, together with the exclusively *trans* disposition of the thiomethyl and pentamethylcyclopentadienyl groups, leads to the existence of only the $R_{Ir}R_{S}S_{P}$ and $S_{Ir}S_{S}R_{P}$ pair of enantiomers.

Treatment of $[(\eta^5\text{-}C_5Me_5)IrCl(\mu\text{-}Cl)]_2$ with $PPh_2(C_6F_5)$ yielded the neutral complex $[(\eta^5\text{-}C_5Me_5)IrCl_2\{PPh_2(C_6F_5)\}]$ (**9**). Consistent with the rhodium analogue, compound **9** underwent no reaction with proton sponge. The cationic iridium complexes $[(\eta^5\text{-}C_5Me_5)IrCl(CNR)\{PPh_2(C_6F_5)\}]BF_4$ (**10a** R = phenyl; **10b** R = *t*-butyl) were prepared by treatment of **9** with the appropriate isonitrile in the presence of an excess of sodium tetrafluoroborate (Scheme 2). The ^{1}H and ^{19}F NMR spectra of **10a** are similar to those of the rhodium analogue [12] and the $^{31}P\{^{1}H\}$ NMR spectrum exhibits a singlet at δ −9.1. The ^{19}F and $^{31}P\{^{1}H\}$ NMR spectral properties of **10b** are similar to those of **10a**. In situ NMR studies indicate **10a** and **10b** undergo slow reactions in the presence of proton sponge. The NMR data are fully consistent with intramolecular dehydrofluorinative coupling to give **11a** and **11b**. In particular, the ^{19}F NMR spectra show four resonances in addition to those of tetrafluoroborate with values of δ similar to those of the rhodium analogue (−119.22, −136.07, −145.54 and −152.01 [12]). Both $^{31}P\{^{1}H\}$ NMR spectra exhibit a singlet resonance at ca. δ 5. The shift of ca. 15 ppm to higher frequency on coupling is similar to that of 18.3 ppm observed in the rhodium analogue of **11a** [12]. The ^{1}H NMR spectrum of **11a** exhibits the two expected methylene resonances at δ 3.85 (dd) and 3.64 (dd), and four methyl resonances at δ 2.30 (d), 1.90 (d), 1.73 (d) and 1.51 (s), which are at similar chemical shifts to those of the rhodium analogue (δ 2.08, 1.82, 1.71 and 1.52).

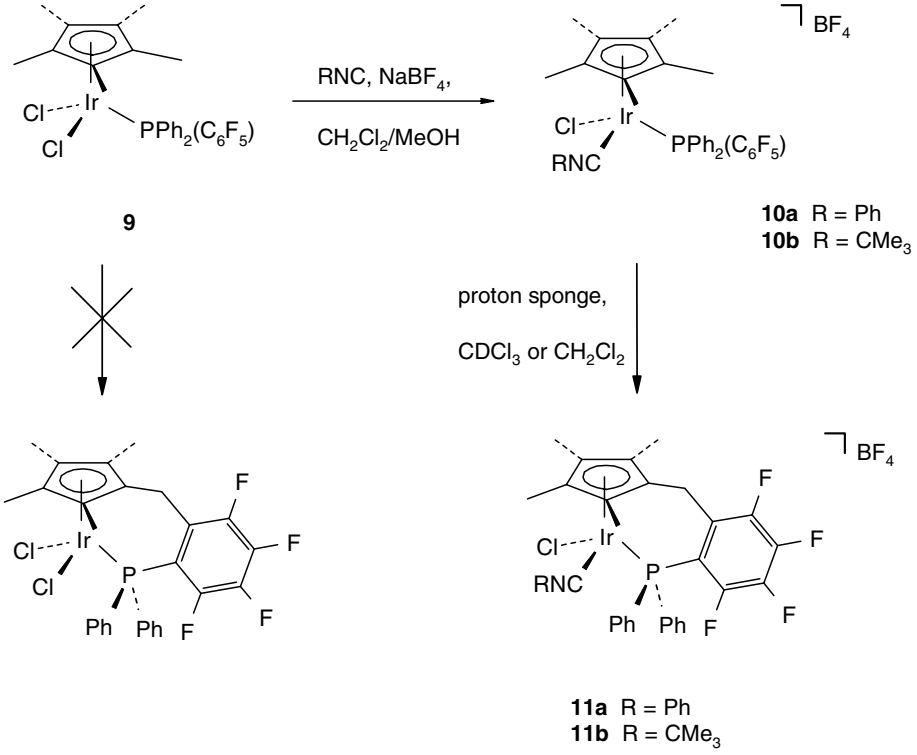

Scheme 2.

Although methylene resonances at δ 3.75 (m) and 3.46 (m), and two methyl resonances at δ 2.18 (d) and 1.85 (d) are evident in the ^{1}H NMR spectrum of **11b**, the other resonances are obscured by other products and the proton sponge resonances. The reaction of **10a** is reasonably clean, but that of **10b** is not and **11b** is produced in ca. 50% yield. The identities of **11a** and **11b** were confirmed by mass spectrometry. The values of ν(N≡C) for **11a** and **11b** were identical within experimental error to those of **10a** and **10b** respectively. The coupling reaction of **10a** was also performed on a preparative scale giving **11a** as a yellow–brown solid in 81% yield.

4. Conclusion

The intramolecular dehydrofluorinative coupling of pentamethylcyclopentadienyl and pentafluorophenylphosphine ligands can be accomplished in cationic iridium complexes by treatment with less than one equivalent of proton sponge. The fluoride generated as the byproduct is sufficient to facilitate the reaction. The reaction occurs slowly for complexes of monophosphines to give bifunctional η^5,κP-Cp–P ligands, but is more successful for complexes of chelating phosphine ligands, which give trifunctional η^5,κP,κL-Cp–PL ligands rapidly. The reported reactions are identical to those of the rhodium analogues.

Acknowledgements

We thank the E.P.S.R.C. for support (to R.M.B.), the Royal Society of Chemistry for a *Grant for International Authors* (to G.C.S.) and Prof. R.P. Hughes for helpful discussion.

References

[1] T.-F. Wang, C.Y. Lai, J. Organomet. Chem. 546 (1997) 179.
[2] M.D. Fryzuk, S.H.S. Mao, M.J. Zaworotko, L.R. MacGillivray, J. Am. Chem. Soc. 115 (1993) 5336.
[3] B.E. Bosch, G. Erker, R. Fröhlich, O. Meyer, Organometallics 16 (1997) 5449.
[4] E.C. McConnell, D.E. Foster, P. Pogorzelec, A.M.Z. Slawin, D.J. Law, D.J. ColeHamilton, J. Chem. Soc., Dalton Trans. (2003) 510.
[5] Y. Kataoka, Y. Iwato, A. Shibahara, T. Yamagata, K. Tani, Chem. Commun. (2000) 841.
[6] Y. Kataoka, A. Shibahara, T. Yamagata, K. Tani, Organometallics 20 (2001) 2431.
[7] K. Onitsuka, N. Dodo, Y. Matsushima, S. Takahashi, Chem. Commun. (2001) 521.
[8] H. Brunner, C. Valerio, M. Zabel, New J. Chem. 24 (2000) 275.
[9] H. Butenschön, Chem. Rev. 100 (2000) 1527.
[10] J. Vogelsgang, A. Frick, G. Huttner, P. Kircher, Eur. J. Inorg. Chem. (2001) 949.
[11] R.M. Bellabarba, M. Nieuwenhuyzen, G.C. Saunders, J. Chem. Soc., Dalton Trans. (2001) 512.
[12] R.M. Bellabarba, M. Nieuwenhuyzen, G.C. Saunders, Organometallics 21 (2002) 5726.
[13] R.M. Bellabarba, M. Nieuwenhuyzen, G.C. Saunders, Organometallics 22 (2003) 1802.
[14] M. Nieuwenhuyzen, G.C. Saunders, J. Organomet. Chem. 595 (2000) 292.
[15] I. Lee, F. Dahan, A. Maisonnat, R. Poilblanc, Organometallics 13 (1994) 2743.
[16] A. Doppiu, U. Englert, V. Peters, A. Salzer, Inorg. Chim. Acta 357 (2004) 1773.
[17] T.A. Mobley, R.G. Bergman, J. Am. Chem. Soc. 120 (1998) 3253.
[18] M.J. Atherton, J. Fawcett, J.H. Holloway, E.G. Hope, A. Karaçar, D.R. Russell, G.C. Saunders, J. Chem. Soc., Dalton Trans. (1996) 3215.
[19] M.J. Atherton, J. Fawcett, J.H. Holloway, E.G. Hope, D.R. Russell, G.C. Saunders, J. Organomet. Chem. 582 (1999) 163.
[20] J. Fawcett, S. Friedrichs, J.H. Holloway, E.G. Hope, V. McKee, M. Nieuwenhuyzen, D.R. Russell, G.C. Saunders, J. Chem. Soc., Dalton Trans. (1998) 1477.
[21] R.P. Hughes, D.C. Lindner, A.L. Rheingold, G.P.A. Yap, Organometallics 15 (1996) 5678.
[22] J.A. Miguel-Garcia, H. Adams, N.A. Bailey, P.M. Maitlis, J. Chem. Soc., Chem. Commun. (1990) 1472.
[23] J.A. Miguel-Garcia, H. Adams, N.A. Bailey, P.M. Maitlis, J. Organomet. Chem. 413 (1991) 427.
[24] J.A. Miguel-Garcia, H. Adams, N.A. Bailey, P.M. Maitlis, J. Chem. Soc., Dalton Trans. (1992) 131.
[25] O.V. Gusev, S. Sergeev, I.M. Saez, P.M. Maitlis, Organometallics 13 (1994) 2059.
[26] J.R. Fulton, T.A. Hanna, R.G. Bergman, Organometallics 19 (2000) 602.
[27] D.S. Glueck, R.G. Bergman, Organometallics 9 (1990) 2862.
[28] J.H. Rigby, S. Laurent, J. Org. Chem. 63 (1998) 6742.
[29] R.D.W. Kemmitt, D.I. Nichols, R.D. Peacock, J. Chem. Soc. A (1968) 2149.
[30] A.H. Cowley, M. Cushner, M. Fild, J.A. Gibson, Inorg. Chem. 14 (1975) 185.
[31] S.A. Sicree, C. Tamborski, J. Fluor. Chem. 59 (1992) 269.
[32] E.W. Abel, J.C. Dormer, D. Ellis, K.G. Orrell, V. Šik, M.B. Hursthouse, M.A. Mazid, J. Chem. Soc., Dalton Trans. (1992) 1073.

Available online at www.sciencedirect.com
SCIENCE DIRECT®
Polyhedron 23 (2004) 2665–2677
POLYHEDRON
www.elsevier.com/locate/poly

Reactions of hydroborating reagents with phosphinorhodium hydride complexes: molecular structures of a Rh_2B_3 metallaborane cluster, an $L_2Rh(\eta^2\text{-}H_2BR_2)$ complex and a mixed valence Rh dimer containing a semi-bridging Bcat (cat = 1,2-$O_2C_6H_4$) group

Stephen A. Westcott [a,*], Todd B. Marder [b,*], R. Thomas Baker [c,d,*], Richard L. Harlow [d], Joseph C. Calabrese [d], King Chung Lam [e], Zhenyang Lin [e,*]

[a] Department of Chemistry, Mount Allison University, 63C York Street, Sackville, NB, E4L 1G8 Canada
[b] Department of Chemistry, Durham University, South Road, Durham DH1 3LE, UK
[c] Los Alamos Catalysis Initiative, Chemical Science and Technology Division, MS J582, Los Alamos National Laboratory, Los Alamos, NM 87545, USA
[d] Central Research and Development, Science and Engineering Laboratories, E.I. du Pont de Nemours and Co., Experimental Station, Wilmington, DE 19880-0262, USA
[e] Department of Chemistry and Open Laboratory of Chirotechnology, Institute of Molecular Technology for Drug Discovery and Synthesis, Hong Kong University of Science and Technology, Clear Water Bay, Kowloon, Hong Kong, China

Received 15 April 2004; accepted 22 May 2004
Available online 27 September 2004

Dedicated to Professor M.L.H. Green on the occasion of his 65th birthday in recognition of his outstanding contributions to chemistry

Abstract

The formation of products derived from competing reactions in Rh-catalyzed alkene hydroborations prompted us to study in situ interactions of several hydroborating reagents with unsaturated phosphinorhodium complexes. The reaction of $[Rh(\mu\text{-}H)(DiPPE)]_2$ (**1**) with borane–dimethylsulfide gave several rhodium–boron containing products including the structurally characterized metallaborane $[RhH(DiPPE)]_2B_3H_7$ (**2**) [DiPPE = 1,2-bis(diisopropylphosphino)ethane]. Addition of thexylborane and 9-H-BBN dimers, containing alkyl groups, to **1** gave the corresponding mononuclear substituted borohydride complexes $Rh(\eta^2\text{-}H_2BRR')(DiPPE)$ (**4**: R = H, R′ = $C(CH_3)_2CH(CH_3)_2$; **5**: R,R′ = bicyclo-[3.3.1]-nonane [C_8H_{14}]). The analogous monodentate phosphine complex $Rh(\eta^2\text{-}H_2BC_8H_{14})(PPr^i_3)_2$ (**6**) was isolated and structurally characterized. Addition of catecholborane (HBcat; cat = 1,2-$O_2C_6H_4$) to **1** gave the unusual dinuclear species $Rh(DiPPE)(\mu\text{-}H)_2(\mu\text{-}Bcat)RhH(DiPPE)$ (**7**) containing a semi-bridging Bcat group, confirmed by single-crystal X-ray diffraction, and zwitterionic $Rh(\eta^6\text{-}catBcat)(DiPPE)$ (**8**). Implications for rhodium-catalyzed hydroborations are addressed.
© 2004 Elsevier Ltd. All rights reserved.

Keywords: Rhodium hydrides; Bridging boryls; Catalyzed hydroborations

1. Introduction

Metal-catalyzed hydroboration of alkenes using dialkoxyboranes, such as catecholborane, HBcat (cat = 1,2-$O_2C_6H_4$), has recently found utility in organic synthesis [1–3]. Organolanthanide-catalyzed alkene hydroborations have been proposed to proceed via a

* Corresponding authors. Tel.: +1-506-364-2372; fax: +1-506-364-2313.
E-mail address: swestcott@mta.ca (S.A. Westcott).

0277-5387/$ - see front matter © 2004 Elsevier Ltd. All rights reserved.
doi:10.1016/j.poly.2004.05.012

'σ-bond metathesis' pathway involving a four-centered transition state between the M–C and B–H bonds [4]. Theoretical calculations suggest that the rate determining step is elimination of the alkylboronate ester product from the metal center to regenerate the metal hydride catalyst [5]. While similar reactions using early transition metal catalysts [6–11] may also proceed by this mechanism, Muhoro and Hartwig [11] have suggested that titanocene-catalyzed alkene hydroborations may employ a catecholborane 'σ complex' as the species that initially interacts with the alkene substrate. The vast majority of metal-catalyzed hydroborations, however, employ late transition metals such as rhodium and have been postulated to proceed via initial oxidative addition of HBcat to the metal center [12] with subsequent insertion of an alkene into either the Rh–H [13,14] or Rh–B bond [15–19]. Reductive elimination of the B–C or C–H bond then affords the alkylboronate ester, whereas β-hydrogen elimination from the Rh–B insertion product can give a vinylboronate ester and a rhodium dihydride which may subsequently afford the alkane. Initial theoretical studies of rhodium phosphine complex-catalyzed alkene hydroboration examined two pathways based on B–H oxidative addition, but the details for the insertion step are incomplete [20] as the two studies employed different boranes [BH_3 versus $HB(OH)_2$] and catalysts [$RhCl(PH_3)$ versus $RhCl(PH_3)_2$] [14,17]. A more recent study showed that both associative and dissociative reaction pathways are energetically accessible and that the associative pathway shows little preference for insertion into the M–H versus the M–B bond [21]. Further theoretical studies are therefore needed to address both the origins of regioselection and the *cis*-bis(phosphine)rhodium model catalyst, as related precursors often generate the most active and selective catalysts for alkene hydroborations. To gain additional insight into the role played by the metal in these transformations, we have examined the stoichiometric reactivity of several common hydroborating agents with bis(phosphine)rhodium hydride complexes and present our findings herein.

2. Experimental

2.1. General procedures

NMR spectra were recorded on General Electric QM-300 (^{1}H at 300 MHz, ^{13}C at 75.4 MHz, ^{31}P at 121 MHz) and Nicolet NMC-300 (^{11}B at 96 MHz) spectrometers in toluene-d_8 unless stated otherwise. ^{1}H NMR chemical shifts are reported in ppm relative to external TMS and were referenced to residual protons in toluene-d_8; coupling constants are in Hz. Multiplicities are reported as (s) singlet, (d) doublet, (t) triplet, (q) quartet, (sext) sextet, (m) multiplet, (br) broad and (ov) overlapping. ^{11}B and ^{31}P chemical shifts are reported in ppm relative to external standards $F_3B\cdot OEt_2$ and 85% H_3PO_4, respectively. THF and toluene were freshly distilled from sodium benzophenone ketyl. Catecholborane (Aldrich Chemical Co.) was distilled under reduced pressure. 1,2-Bis(diisopropylphosphino)ethane (DiPPE) [22] was prepared via literature methods. Reagent purity was ascertained by ^{1}H NMR spectroscopy. $[Rh(\mu\text{-}H)(DiPPE)]_2$ (**1**) [23] and $RhH(N_2)(PPr^i_3)_2$ [24] were prepared by established methods.

2.2. Synthesis

2.2.1. Reaction of $[Rh(\mu\text{-}H)(DiPPE)]_2$ (1) with $H_3B\cdot SMe_2$

To a solution of 73 mg (0.1 mmol) $[Rh(\mu\text{-}H)(DiPPE)]_2$ (**1**) in 1 ml of THF-d_8 in a 5 mm NMR tube was added dropwise 15 mg (0.2 mmol) of $BH_3\cdot SMe_2$. Analysis of the solution by multinuclear NMR spectroscopy indicated a mixture of complexes. Subsequent addition of two 7 mg portions of $BH_3\cdot SMe_2$ was monitored by NMR and eventually gave a mixture of complexes, including **2**. From this solution was obtained an amber crystal of **2** for the X-ray diffraction study. Selected NMR data for complex **2**: (THF-d_8) $^{31}P\{^1H\}$ 106.5, 98.8 (br d), at −80 °C: 106.5 (d d, $J_{PRh} = 169$ Hz, $^2J_{PP} = 29$ Hz), 98.4 (d d, 194, 29 Hz); $^{11}B\{^1H\}$ −26.7; ^{11}B −26.7 (d quint, $J_{BH} = 63$, 62.5 Hz); ^{1}H δ −2.7 (br, 4H, Rh–H–B and terminal B–H), −10.0 (t t t, Rh–H–Rh).

2.2.2. Reaction of $[Rh(\mu\text{-}H)(DiPPE)]_2$ (1) with thexylborane

A solution of thexylborane dimer (10 mg, 0.05 mmol) in 10 ml of toluene was added dropwise to a solution of **1** (73 mg, 0.1 mmol) in 10 ml of toluene. After stirring for 0.5 h, the solution was concentrated in vacuo to 5 ml and cooled at −30 °C for 48 h. The resulting red crystals were filtered, washed with cold pentane and dried in vacuo to yield (**3**), 57 mg (69%). NMR spectroscopic data for **3** (in toluene-d_8): $^{31}P\{^1H\}$ 100.8 (br d, $J_{PRh} = 170$ Hz), at −40 °C, 104.2 (d d, $J_{PRh} = 178$, $^2J_{PP} = 26$ Hz), 97.0 (d d, $J_{PRh} = 169$, $^2J_{PP} = 26$ Hz); $^{11}B\{^1H\}$ 35.9 (br); $^1H\{^{11}B\}$ δ at −40 °C (in THF-d_8) −9.72 (t quint, $J_{HRh} = {}^2J_{HP} = 20$ Hz, 1H, Rh–H–Rh), −3.91 (br, 3H, Rh–H–B and B–H), 0.87 (d, $^3J = 7$ Hz, 6H, $BC(CH_3)_2CH(CH_3)_2$), 0.98 (s, 6H, $BC(CH_3)_2CH(CH_3)_2$), 1.07 (d d, $^3J = 7$, $^3J_{HP} = 12$ Hz, 24H, $PCHCH_3$), 1.17 (d d, $^3J = 7$, $^3J_{HP} = 15$ Hz, 24H, $PCHCH_3$), 1.52 (ov m, 8H, PCH_2CH_2P), 1.88 (sept, $^2J = 7$ Hz, 1H, $BC(CH_3)_2CH(CH_3)_2$), 2.17 (d sept, $^3J = {}^2J_{HP} = 7$ Hz, 8H, $PCHCH_3$). In another experiment, a solution of thexylborane dimer (30 mg, 0.15 mmol) in 1 ml of toluene-d_8 was added dropwise to a solution of **1** (73 mg, 0.1 mmol) in 1 ml of toluene-d_8. The resulting solution was stirred for 1 h and then an-

alyzed by high-field NMR spectroscopy. NMR spectroscopic data for **4** (in toluene-d_8): $^{31}P\{^1H\}$ 112.9 (d, $J_{PRh} = 163$ Hz); $^{11}B\{^1H\}$ 1.7 (br); ^1H δ −80 °C (in THF-d_8) −2.27 (br, 3H, Rh–H–B and B–H), 0.86–0.95 (ov m, 18H, CH_3), 1.21 (ov m, 18H, CH_3), 1.41 (br ov m, 4H, PCH_2CH_2P), 1.55 (m, 1H, $BC(CH_3)_2CH(CH_3)_2$), 1.81 (m, 4H, $PCHCH_3$); $^1H\{^{11}B\}$ −1.53 (d t, $J_{HRh} = 23$, $^2J_{HP} = 15$ Hz). Selected FT-IR data (nujol): 1825, 2515 cm^{-1}.

2.2.3. Reaction of [Rh(μ-H)(DiPPE)]$_2$ (1) with 9-H-BBN

A solution of 9-H-BBN dimer (36 mg, 0.15 mmol) in 1 ml of toluene-d_8 was added dropwise to a solution of **1** (73 mg, 0.1 mmol) in 1 ml of toluene-d_8. The resulting solution was stirred for 1 h and then analyzed by high-field NMR spectroscopy. Selected NMR spectroscopic data for **5** (in toluene-d_8): $^{31}P\{^1H\}$ 111.7 (d, $J_{PRh} = 161$ Hz); $^{11}B\{^1H\}$ 49.6 (br); ^1H δ −4.6 (br, Rh–H–B).

2.2.4. Reaction of trans-RhH(N$_2$)(PPr$^i_3$)$_2$ with 9-H-BBN

A solution of 9-H-BBN dimer (73 mg, 0.3 mmol) in 10 ml of toluene was added dropwise to a solution of *trans*-$RhH(N_2)(PPr^i_3)_2$ (78 mg, 0.2 mmol) in 10 ml of toluene. After stirring for 0.5 h, the solution was concentrated in vacuo to 5 ml and cooled at −30 °C for 48 h. The resulting orange crystals were collected by filtration, washed with cold pentane and dried in vacuo to yield 55 mg of **6** (57%). Selected NMR spectroscopic data for **6** (in toluene-d_8): $^{31}P\{^1H\}$ 71.3 (d, $J_{PRh} = 161$ Hz); $^{11}B\{^1H\}$ 58.5 (br); ^1H δ −7.83 (br, Rh–H–B).

2.2.5. Reaction of [Rh(μ-H)(DiPPE)]$_2$ (1) with HBcat

A solution of HBcat (36 mg, 0.3 mmol) in 1 ml of toluene-d_8 was added dropwise to a solution of **1** (73 mg, 0.1 mmol) in 1 ml of toluene-d_8. The resulting solution was stirred for 1 h and then analyzed by high-field NMR spectroscopy. Selected NMR spectroscopic data (in toluene-d_8): $^{31}P\{^1H\}$ 102.1 (br, major, **7**), 106.9 (d, $J_{PRh} = 209$ Hz, **8**), at −80 °C (in THF-d_8) 114.4 (br, $J_{PRh} = 102$ Hz, **7**); $^{11}B\{^1H\}$ 15.0 (s, **8**), 35.0 (br, **7**); ^1H δ −9.8 (br, Rh–H), 0.93–1.42 (ov m), 1.95 (br), 2.38 (d sept, $^3J = {}^3J_{HP} = 7$ Hz, $CHMe_2$), 4.97 (br), 6.15 (br), 6.6–6.8 (ov m), 7.82 (br d, $J_{HP} = 97$ Hz, **7**), −8.69 (br, **7**), −17.9 (br, **7**).

2.3. Crystallography

Crystals of **2** and **7** suitable for X-ray diffraction studies were obtained by recrystallization from toluene solutions at −30 °C and crystals of **6** from a pentane solution at −30 °C. Diffraction data were collected at low temperatures on an Enraf-Nonius CAD4 diffractometer for **7**, on a Siemens R3m/v diffractometer for **2** using graphite-filtered Mo Kα radiation ($\lambda = 0.71073$ Å) and the ω scan method, and on a Bruker SMART 1K CCD-equipped diffractometer for **6** (see Table 1). Data were reduced in the usual fashion for Lorentz and

Table 1
Crystallographic data collection parameters for **2**, **6**, and **7**

Complex	**2**	**6**	**7**
Formula	$C_{28}H_{73}B_3P_4Rh_2$	$C_{26}H_{58}BP_2Rh$	$C_{34}H_{71}BO_2P_4Rh_2$
Formula weight	772.04	546.38	852.47
Crystal system	orthorhombic	orthorhombic	monoclinic
Space group	$P2_12_12_1$ (No. 19)	$P2_12_12_1$ (No. 19)	$P2_1/c$ (No. 14)
a (Å)	13.773(1)	12.2075(8)	18.024(5)
b (Å)	16.689(4)	12.2333(8)	11.296(2)
c (Å)	16.899(3)	20.0394(13)	21.639(7)
β (°)			109.85(1)
V (Å^3)	3884.4	2992.6	4143.9
Z	4	4	4
ρ_{calc} (Mg m^{-3})	1.320	1.213	1.366
Crystal size (mm)	0.33×0.25×0.39	0.40×0.30×0.42	0.40×0.07×0.50
T (°C)	−70	−100	−70
Radiation, λ (Mo Kα)	0.71073	0.71073	0.71073
μ (cm^{-1})	10.15	6.89	9.62
Maximum 2θ (°)	60.0	66.36	50.0
Total reflections	6010	11 380	7891
Total unique reflections	4279	10 295	3621
Number of variables	370	291	400
Maximum residual density (e Å^{-3})	0.85	0.44	0.59
Goodness-of-fit on F^2	0.91	1.072	0.93
R_1[a] ($I > 2\sigma(I)$)	0.036	0.0239	0.043
wR_2[b] (all data)	0.030	0.0596	0.034

[a] $R_1 = \sum ||F_o| - |F_c|| / \sum |F_o|$.
[b] $wR_2 = (\sum[w(F_o^2 - F_c^2)^2] / \sum[wF_o^2]^2)^{1/2}$.

polarization effects, and corrected for 6% (**6**) decay in intensity versus the standard reflections. When required, data sets were corrected for absorption using azimuthal ψ scan measurements. Heavy atom positions were obtained via automated Patterson analysis (PHASE, **2** and **7**) or direct methods (**6**) and used to phase the reflections for the remaining light atoms via Fourier synthesis. The solution and refinement of the structures were performed on a VAX/IBM cluster system using a local program set or on a Microvax cluster using SHELX. Structures were solved by direct methods (SHELXS and MULTAN) [25]. All refinements were performed using full-matrix least-squares on *F*, with anisotropic thermal parameters for all non-hydrogen atoms, and included anomalous dispersion terms [26] for Rh and P, as well as idealized hydrogen coordinates as fixed atom contributors. The atomic scattering factors were taken from the tabulations of Cromer and Waber [27]. Full details of the structures are given in the Section Supplementary material.

2.4. Computations

Geometry optimization was performed at the Becke3LYP (B3LYP) level [28]. The effective core potentials (ECPs) of Hay and Wadt [29] with a double-ξ valence basis set (LanL2DZ) were used to describe the Pt, Rh and P atoms, while the 6-31G basis set was used for all other atoms [30]. Polarization functions have been added for the P ($\xi_d = 0.340$) atoms [31].

All calculations were performed with the use of the GAUSSIAN-98 package [32] on PC Pentium IV computers. The electron density analysis was carried out with MOPLOT 2.4 [33] and the molecular orbitals obtained from B3LYP calculations were plotted using the MOLDEN 3.7 program [34].

3. Results and discussion

Reactions of 9-H-BBN [$(HBC_8H_{14})_2$] and thexylborane [$(BH_2CMe_2CHMe_2)_2$] with saturated iridium hydride $IrH(PMe_3)_4$ proceed via initial loss of phosphine as the corresponding phosphine–borane adducts ($RR'HB \cdot PMe_3$), followed by oxidative addition of the organoborane B–H bond to the metal center to give the dihydridoiridium boryl complexes *fac*-$IrH_2(BRR')(PMe_3)_3$ [35]. Unfortunately, the analogous chemistry with $RhH(PMe_3)_4$ is more complicated, affording a complex mixture of rhodium complexes containing only one or two phosphines. In order to avoid complications arising from loss of phosphine, we then investigated the reactivity of unsaturated rhodium hydride [Rh(μ-H)(DiPPE)]$_2$ (**1**) [23] with several hydroborating agents.

As one of the most common mechanisms for HBcat degradation during metal-catalyzed hydroborations involves the formation of B_2cat_3 and diborane, or its ligand adducts ($L \cdot BH_3$) [36], it is therefore important to examine what deleterious effects liberated borane would have on the catalyst. We have found that reactions of **1** with $H_3B \cdot SMe_2$ gave a mixture of phosphinorhodium products (as ascertained by multinuclear NMR spectroscopy) in varying yields depending on the B:Rh stoichiometry employed (Scheme 1). Using three equivalents of $H_3B \cdot SMe_2$ per Rh dimer, we generated metallaborane [RhH(DiPPE)]$_2B_3H_7$ (**2**) in good yield (by NMR) and isolated amber crystals suitable for X-ray diffraction studies. The structure of **2** (Fig. 1) is a distorted square-pyramidal cluster analog of pentaborane(9), which is similar to that of [(η^5-C_5Me_5)Rh]$_2B_3H_6Cl$ which was obtained recently by Fehlner and co-workers from the reaction of [(η^5-C_5Me_5)RhCl]$_2$ with $H_3B \cdot THF$ [37]. While the bond distances are somewhat longer in **2** [Rh–Rh = 2.8544(6) Å in **2** versus 2.848(1) Å in the Fehlner cluster, Rh–B_{apical} = 2.166(5), 2.177(5) Å versus 2.07(1), 2.08(1) Å, Rh–B_{eq} = 2.247(6), 2.253(6) Å versus 2.20(1), 2.20(1) Å], the biggest distinction between the two complexes is the lack of symmetry in **2** (see Table 2). Indeed, the two terminal hydrides are on the same side of the equatorial Rh_2B_2 plane, but the bis(phosphine) ligands are on opposite sides.

Owing to the propensity of diborane derivatives to form stable high nuclearity clusters [38], metallaborane **2** arises presumably from a dehydrooligomerization reaction. Thus, addition of three equivalents of borane to **1** affords the *nido*-metallaborane [RhH(DiPPE)]$_2B_3H_7$ (**2**) with loss of dihydrogen. The structure of **2** is in accord with Wade's electron counting rules [39] where each RhH(DiPPE) fragment is isolobal with a B–H vertex, contributing two electrons to cluster bonding. Com-

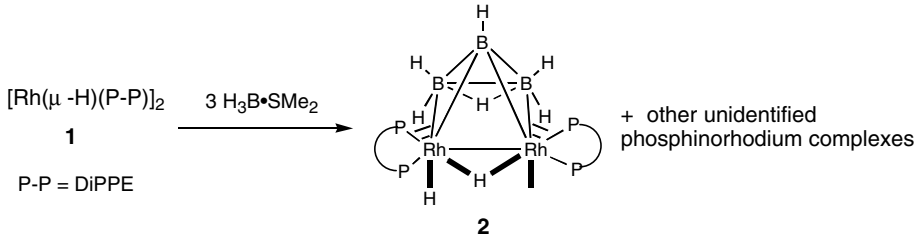

Scheme 1. Reaction of [Rh(μ-H)(DiPPE)]$_2$ (**1**) with $H_3B \cdot SMe_2$.

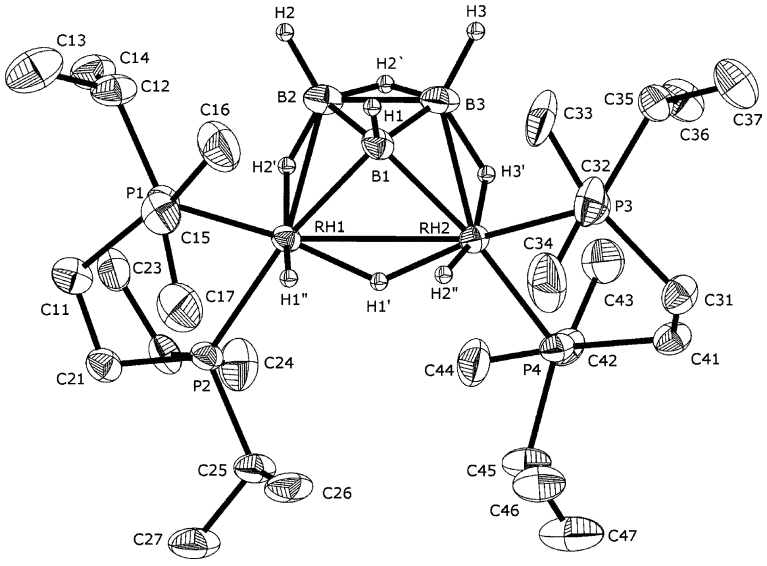

Fig. 1. Molecular structure of $[RhH(DiPPE)]_2B_3H_7$ (**2**) with hydrogen atoms on the DiPPE ligands omitted for clarity.

Table 2
Selected bond lengths (Å) and angles (°) for **2**

Bond distances		Bond angles	
Rh(1)–Rh(2)	2.8544(6)	P(1)–Rh(1)–P(2)	86.88(5)
Rh(1)–P(1)	2.246(1)	P(1)–Rh(1)–B(2)	95.7(2)
Rh(1)–P(2)	2.323(1)	P(1)–Rh(1)–B(1)	100.3(2)
Rh(2)–P(3)	2.245(1)	P(1)–Rh(1)–H(1″)	73(2)
Rh(2)–P(4)	2.303(1)	Rh(2)–Rh(1)–P(1)	144.48(4)
Rh(1)–B(1)	2.166(5)	Rh(2)–Rh(1)–P(2)	122.12(4)
Rh(1)–B(2)	2.253(6)	Rh(2)–Rh(1)–B(2)	76.2(2)
Rh(2)–B(1)	2.177(6)	Rh(2)–Rh(1)–B(1)	49.1(2)
Rh(2)–B(3)	2.247(6)	Rh(2)–Rh(1)–H(1″)	86(3)
Rh(1)–H(1′)	1.69(6)	P(2)–Rh(1)–B(1)	170.8(2)
Rh(1)–H(1″)	1.24(6)	P(2)–Rh(1)–B(2)	138.7(2)
Rh(1)–H(2′)	1.69(5)	P(2)–Rh(1)–H(1″)	89(3)
Rh(2)–H(2″)	1.30(7)	B(2)–Rh(1)–H(1″)	132(3)
Rh(2)–H(3′)	1.53(5)	B(1)–Rh(1)–B(2)	46.9(2)
B(1)–B(2)	1.760(9)	B(1)–Rh(1)–H(1″)	88(3)
B(1)–B(3)	1.744(9)	P(3)–Rh(2)–P(4)	86.61(5)
B(2)–B(3)	1.768(9)	P(3)–Rh(2)–B(1)	103.3(2)
B(1)–H(1)	1.14(4)	P(3)–Rh(2)–B(3)	97.0(2)
B(2)–H(2)	1.18(4)	P(3)–Rh(2)–H(2″)	87(3)
B(2)–H(2*)	1.27(5)	Rh(1)–Rh(2)–P(3)	147.08(5)
B(2)–H(2′)	1.35(5)	Rh(1)–Rh(2)–B(3)	75.9(2)
B(3)–H(3)	1.19(4)	Rh(1)–Rh(2)–B(1)	48.7(1)
B(3)–H(2*)	1.25(5)	Rh(1)–Rh(2)–P(4)	121.98(4)
B(3)–H(3′)	1.45(5)	Rh(1)–Rh(2)–H(2″)	71(3)
		P(4)–Rh(2)–B(1)	170.1(2)
		P(4)–Rh(2)–B(3)	133.1(2)
		P(4)–Rh(2)–H(2″)	105(3)
		B(1)–Rh(2)–H(2″)	76(3)
		B(1)–Rh(2)–B(3)	46.4(2)
		B(3)–Rh(2)–H(2″)	122(3)
		Rh(1)–B(1)–Rh(2)	82.2(2)
		Rh(1)–B(1)–B(2)	69.2(3)
		Rh(2)–B(1)–B(3)	68.9(3)
		B(2)–B(1)–B(3)	60.6(4)
		Rh(1)–B(2)–B(3)	103.5(3)
		Rh(2)–B(3)–B(2)	104.4(3)

pound **2** has a $2n + 4 = 14$ skeletal electron count and is derived from *nido*-B_5H_9 by replacement of two basal BH groups by P_2RhH vertices. The fluxional process observed by NMR spectroscopy for **2** (effective C_s symmetry at 25 °C) may involve a pairwise trigonal twist by the adjacent $RhHP_2$ vertices as more complicated schemes involving terminal and bridging hydrogen exchange can be ruled out. Formation of **2** presumably proceeds via initial insertion of B–H into a Rh–H–Rh bond, analogous to reactions with thexylborane. Oxidative addition of B–H bonds to the metal center during the synthesis of **2** may provide a pathway for the liberation of one equivalent of H_2.

Similar cluster formation was not observed for the reactions of **1** with alkylboranes. We reported previously [40] that addition of 0.5 equivalents of thexylborane to **1** affords red crystals of the dinuclear complex $[Rh(DiPPE)]_2(\mu\text{-}H)\{\eta^2\text{-}H_2BH(thexyl)\}$ (**3**) as the only new phosphinorhodium complex. Further addition of thexylborane gives orange crystals of mononuclear $Rh[\eta^2\text{-}H_2BH(thexyl)](DiPPE)$ (**4**) (Scheme 2). The molecular structure of **3** consists of two distorted 16 electron square-planar Rh(I) centers bridged by hydride and thexylborohydride ligands. The Rh–Rh distance of 2.912 Å is significantly longer than that observed for **1** (2.628(1) Å) [41]. The two square planes are twisted with respect to one another (dihedral angle of 54.8°) to accommodate the disparate bridges. Similar effects have been observed in related structures with bridging $[BH_4]^-$ ligands [42–44].

Complex **3** is fluxional in solution with inequivalent P atoms of the DiPPE ligands, which at −60 °C constitute the A_2A_2' portion of a complicated 10 spin system. These are averaged at 25 °C giving rise to one doublet ^{31}P

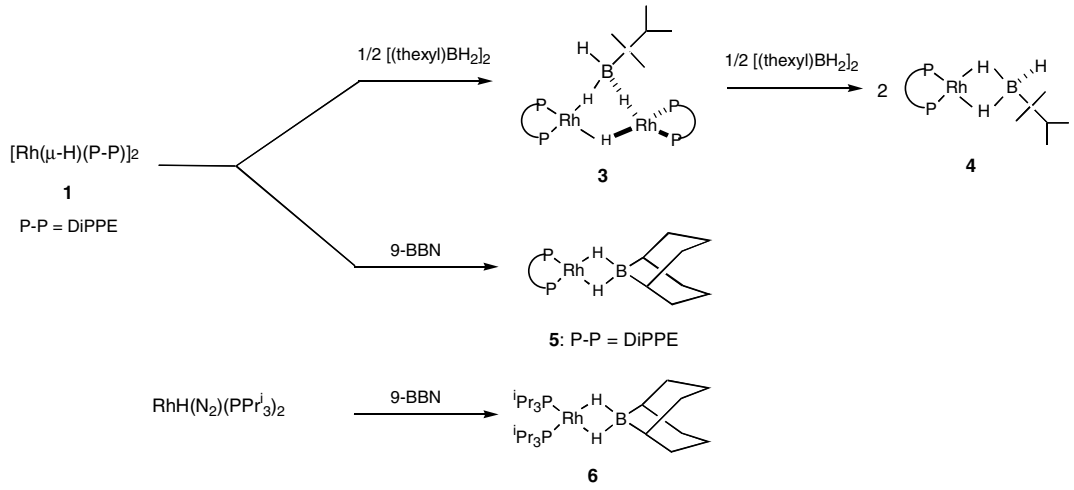

Scheme 2. Reaction of unsaturated phosphinorhodium hydrides with thexylborane and 9-H-BBN dimers.

NMR resonance ($J_{PRh} = 170$ Hz). In the ^{1}H NMR spectrum of **3**, the inequivalent Rh–H–B bridges and the terminal B–H of the thexylborohydride ligand undergo rapid exchange; a single broad resonance at δ −4.0 is observed, even at −100 °C. Slow exchange of the thexylborohydride B–Hs with the Rh–H–Rh bridge was demonstrated qualitatively by proton magnetization transfer experiments at 80 °C. At 25 °C, the Rh–H–Rh bridge is observed as a triplet of quintets at δ −9.63 ($J_{HRh} = {}^2J_{HP} = 20$ Hz).

The ^{1}H NMR spectrum of **4** contains a broad resonance at δ −1.53, which gives rise to a doublet of triplets upon ^{11}B decoupling ($J_{HRh} = 23$, $^2J_{HP} = 15$ Hz). This is assigned to rapidly exchanging terminal and bridging H's of the η^2-thexylborohydride ligand, a significant feature that occurs in almost all covalent metal borohydride complexes [45]. Assignment of the bidentate coordination mode (versus tridentate) of the thexylborohydride ligand is based on the observation of a terminal B–H stretch at 2515 cm^{-1} in the IR spectrum of **4** (versus 1825 cm^{-1} for the Rh–H–B stretch).

Addition of one equivalent of 9-H-BBN to **1** gives the substituted borohydride Rh(η^2-$H_2BC_8H_{14}$)(DiPPE) (**5**) in nearly quantitative yield. A dinuclear intermediate was not detected by multinuclear NMR spectroscopy even at low temperatures (−80 °C). The ^{1}H NMR spectrum of **5** contains a broad resonance at −4.6 ppm attributed to the bridging H's of the η^2-$H_2BC_8H_{14}$ unit. Although we were unable to obtain suitable crystals of **5** for X-ray diffraction studies, addition of 0.5 equivalents of 9-BBN to RhH(N_2)(PPr^i_3)$_2$ [24] gave orange crystals of the analogous complex Rh(η^2-$H_2BC_8H_{14}$)(PPr^i_3)$_2$ (**6**) in 57% yield. The molecular structure of **6** (Fig. 2) consists of a 16 electron square-planar Rh(I) center with the disubstituted borohydride ligand bound to the metal center in an η^2-fashion. The largest deviation from the plane through Rh, both phosphine ligands and B is only 0.007 Å. Similar ruthenium 9-BBN and related exopolyhedral rhodium carborane structures have been reported [46–48] (see Table 3).

Unlike many of the parent tetrahydroborate complexes [45], these alkyl-substituted borohydride compounds are indefinitely stable in solution at room temperature. It is possible that these borohydride complexes may play a vital role in certain metal-catalyzed hydroborations. For example, catalyzed reactions of sterically demanding substrates often results in the degradation of HBcat into B_2cat_3 and 'BH_3' [36], where the latter rapidly hydroborates the organic substrate to give a complicated mixture of alkylboranes. While also severely affecting regioselectivities, the in situ generation of borane and organoboranes may be responsible, in part, for catalyst deactivation. Indeed, no reaction was

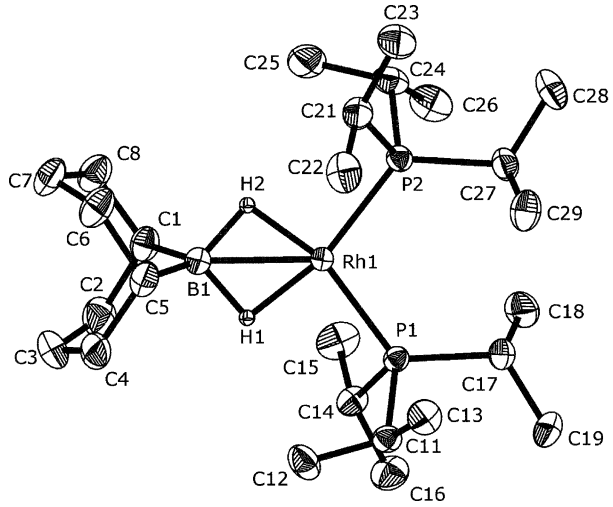

Fig. 2. Molecular structure of Rh(η^2-$H_2BC_8H_{14}$)(PPr^i_3)$_2$ (**6**) with hydrogen atoms omitted for clarity.

Table 3
Selected bond lengths (Å) and angles (°) for **6**

Bond distances		Bond angles	
Rh(1)–P(2)	2.2672(4)	P(1)–Rh(1)–P(2)	108.08(1)
Rh(1)–P(1)	2.2509(3)	P(2)–Rh(1)–B(1)	127.22(4)
Rh(1)–B(1)	2.1700(14)	P(1)–Rh(1)–B(1)	124.69(4)
C(1)–B(1)	1.591(2)	Rh(1)–B(1)–C(1)	127.43(1)
C(5)–B(1)	1.596(2)	Rh(1)–B(1)–C(5)	124.43(1)
		C(1)–B(1)–C(5)	108.24(1)

observed by multinuclear NMR spectroscopy when complex **5** was treated with an excess of 1-octene.

The reactivity of catecholborane with phosphinorhodium hydrides is of singular interest due to the ubiquity of this borane in metal-catalyzed alkene hydroborations. In contrast to reactions with alkylboranes, or recent studies using early transition metal complexes [49], substituted borohydride complexes are not generated from the addition of HBcat to **1**. The room temperature ^{31}P NMR spectrum of the reaction of **1** with two equivalents of HBcat consists of a broad resonance at 102.1 ppm for the novel mixed oxidation state dimer Rh(DiPPE)(μ-H)$_2$(μ-Bcat)RhH(DiPPE) (**7**), which eventually decomposes (24 h) to give a number of unidentified products, along with a sharp doublet at 106.9 ppm assigned to zwitterionic Rh(η^6-catBcat)(DiPPE) (**8**) (Scheme 3).

The ^{31}P NMR spectrum of **7** in THF-d$_8$ at −80 °C contains only a broad doublet-like resonance at 114.4 ppm indicating the overlap of various phosphine signals. The low temperature ^{1}H NMR spectrum, however, consists of three broad resonances at δ −7.82 (br d, J_{HP} = ca. 97 Hz), −8.69, and −17.9, with the latter presumably being a terminal Rh–H. All three resonances broadened considerably upon warming to room temperature, as expected if rapid exchange of the bridging and terminal hydrides is occurring. It is clear from our DFT calculations, vide infra, that other structures are close in energy to the one observed in the solid state.

The molecular structure of **7**, as determined by X-ray diffraction, consists of one Rh(I) center coordinated to a DiPPE group and two bridging hydrides in a square-planar arrangement (Fig. 3). The Rh(III) center is octahedrally coordinated with two bridging hydrides, a terminal hydride, a DiPPE and a σ-bound Bcat ligand. The trigonal-planar boron shows a weak interaction with an apical site on the Rh(I) center, in which the Rh–B distance is 2.444(9) Å. The Rh(III)–B bond distance of 2.057(8) Å is slightly elongated when compared to a length of 1.961(7) Å found in RhHCl(Bcat)(PPr$^i_3$)$_2$ [50]. The strong *trans*-directing effect of the boryl ligand leads to a longer Rh(1′)–P(1′) bond distance (2.324(2) Å) as compared to that with P *trans* to the bridging hydride (Rh(1′)–P(2′) = 2.232(2) Å). The Rh–Rh bonding distance in **7** (2.574(1) Å) is significantly shorter than that observed for **1** [41] (see Table 4). Dinuclear **7** is a rare example of a compound containing a bridging boryl group that has been characterized by both high-field NMR spectroscopy and X-ray diffraction.

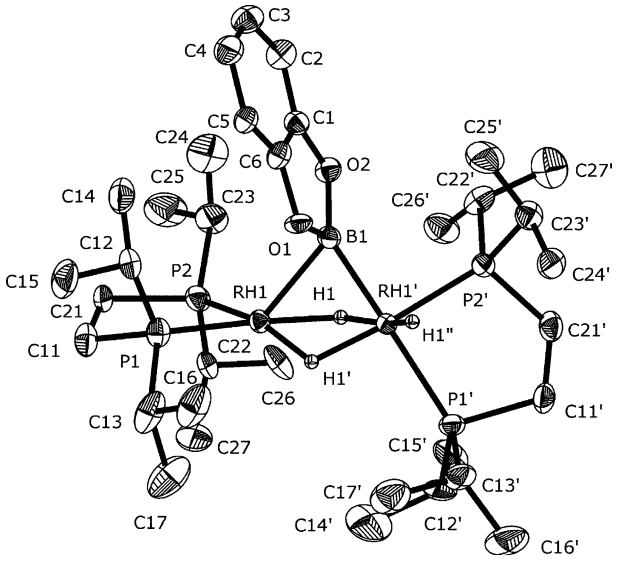

Fig. 3. Molecular structure of Rh(DiPPE)(μ-H)$_2$(μ-Bcat)RhH(DiPPE) (**7**) with hydrogen atoms on the DiPPE and Bcat ligands omitted for clarity.

The only previous structurally characterized examples are the two platinum dimers isolated by Norman and co-workers [51], namely, [Pt$_2$(PPh$_3$)(μ-dppm)$_2$(Bcat)(μ-Bcat)] (**9**) and the analogous compound in which a monodentate, κ^1-dppm ligand replaces the PPh$_3$ group. Another pair of rhodium dimers has also been observed in solution by Brown and co-workers [52]

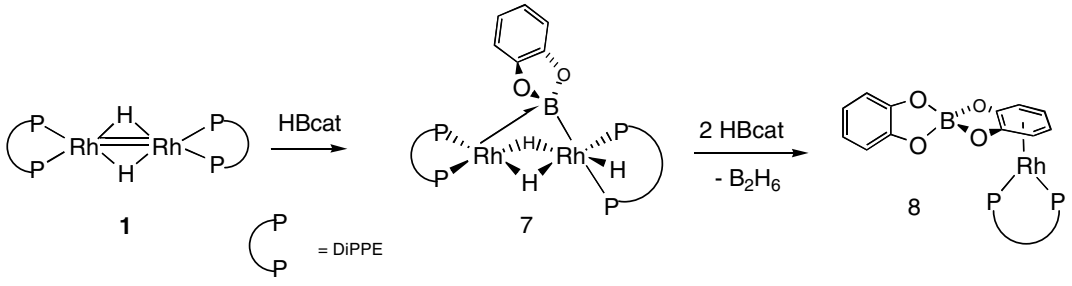

Scheme 3. Reaction of [Rh(μ-H)(DiPPE)]$_2$ (**1**) with HBcat.

Table 4
Selected bond lengths (Å) and angles (°) for **7**

Bond distances		Bond angles	
Rh(1)–Rh(1′)	2.574(1)	Rh(1′)–Rh(1)–P(1)	134.50(6)
Rh(1)–P(1)	2.207(2)	Rh(1′)–Rh(1)–P(2)	140.07(6)
Rh(1)–P(2)	2.212(2)	Rh(1)–Rh(1′)–P(1′)	120.72(6)
Rh(1′)–P(1′)	2.324(2)	Rh(1)–Rh(1′)–P(2′)	136.08(6)
Rh(1′)–P(2′)	2.232(2)	Rh(1′)–Rh(1)–B(1)	48.3(2)
Rh(1)–B(1)	2.444(9)	Rh(1)–Rh(1′)–B(1)	62.5(2)
Rh(1′)–B(1)	2.057(8)	Rh(1′)–Rh(1)–H(1)	45(2)
Rh(1)–H(1)	1.76(5)	Rh(1′)–Rh(1)–H(1′)	39(2)
Rh(1)–H(1′)	1.72(5)	Rh(1)–Rh(1′)–H(1)	43(2)
Rh(1′)–H(1)	1.83(5)	Rh(1)–Rh(1′)–H(1′)	41(2)
Rh(1′)–H(1′)	1.66(5)	Rh(1)–Rh(1′)–H(1″)	126(2)
Rh(1′)–H(1″)	1.54(6)	P(1)–Rh(1)–P(2)	85.19(8)
B(1)–O(1)	1.454(9)	P(1′)–Rh(1′)–P(2′)	87.64(8)
B(1)–O(2)	1.467(9)	P(1)–Rh(1)–B(1)	108.6(2)
		P(2)–Rh(1)–B(1)	125.4(2)
		P(1′)–Rh(1′)–B(1)	171.1(3)
		P(2′)–Rh(1′)–B(1)	94.8(2)
		P(1)–Rh(1)–H(1)	177(2)
		P(1)–Rh(1)–H(1′)	100(2)
		P(2)–Rh(1)–H(1)	95(2)
		P(2)–Rh(1)–H(1′)	163(2)
		P(1′)–Rh(1′)–H(1)	105(2)
		P(1′)–Rh(1′)–H(1′)	97(2)
		P(1′)–Rh(1′)–H(1″)	85(2)
		P(2′)–Rh(1′)–H(1)	101(2)
		P(2′)–Rh(1′)–H(1′)	175(2)
		P(2′)–Rh(1′)–H(1″)	85(2)
		B(1)–Rh(1)–H(1)	74(2)
		B(1)–Rh(1)–H(1′)	69(2)
		B(1)–Rh(1′)–H(1)	83(2)
		B(1)–Rh(1′)–H(1′)	81(2)
		B(1)–Rh(1′)–H(1″)	87(2)
		H(1)–Rh(1)–H(1′)	79(2)
		H(1)–Rh(1′)–H(1′)	79(2)
		H(1)–Rh(1′)–H(1″)	168(3)
		H(1′)–Rh(1′)–H(1″)	95(3)
		Rh(1)–B(1)–Rh(1′)	69.1(3)
		O(1)–B(1)–O(2)	104.9(6)

and structures containing bridging boryl units were proposed on the basis of ^{1}H and ^{31}P NMR data; as the exact nature of these latter compounds are not known, they will be addressed only briefly. With the aid of DFT calculations, we have examined the bonding nature of M1–(μ-B)–M2 and the structural features of the structurally characterized rhodium (**7**) and platinum (**9**) dimers.

In analyzing [Rh(DiPPE)(μ-H)$_2$(μ-Bcat)RhH(DiPPE)], we employed a simplified model complex, [Rh(H$_2$PCH$_2$-PH$_2$)(μ-H)$_2${μ-B(O$_2$C$_2$H$_2$)}RhH(H$_2$PCH$_2$- PH$_2$)]. Selected structural parameters for the calculated model complex, together with the experimental values in parentheses, illustrated in Fig. 4, show that the optimized structure is in good agreement with the observed one. It can be described as two Rh centers bridged by two μ-hydrides and a semi-bridging boryl group. The coordination sphere of Rh1 can be viewed as square planar, as expected for d^8-Rh(I), if the Rh1-B interaction is ignored, whereas Rh2 adopts a distorted octahedral structure, as expected for d^6-Rh(III).

For a square planar 16-electron Rh1 fragment, ignoring initially the interaction with (μ-B) and Rh2, the filled t_{2g} and d_{z^2} orbitals are approximately non-bonding whereas the octahedral 18-electron Rh2 moiety has a filled t_{2g} set of non-bonding orbitals. As the two Rh centers are electronically saturated, their approach (Rh–Rh = 2.574 Å) is a result of two bridging hydrogen atoms rather than direct Rh–Rh attraction.

The Rh1–(μ-B) interaction can be viewed as σ-donation to the vacant p-orbital of the semi-bridging boron from the filled d_{z^2} orbital of Rh1. This is similar to the structurally characterized square pyramidal complex [(PPh$_3$)$_2$Rh(CO)(Cl)(SO$_2$)] in which the bent, apical SO$_2$ moiety is indicative of it functioning as a Lewis acid coordinated to the filled d_{z^2} orbital of Rh rather than as a Lewis base [53]. The relevant MO for the semi-bridging interaction in (**7**) from our B3LYP DFT calculations is illustrated in Fig. 5.

To elucidate further the Rh1–(μ-B)–Rh2 interaction, we have analyzed the Laplacian [54] plot of the electron density ($-\nabla^2\rho$) on the plane defined by [Rh1–(μ-B)–Rh2], shown in Fig. 6. In the contour plot, solid lines represent local electron density concentration ($\nabla^2\rho < 0$) and dashed lines represent local electron density depletion ($\nabla^2\rho > 0$). There are higher electron density concentrations along the (μ-B)–Rh2 direction, with some distorted concentrations around the semi-bridging boron atom in the direction of Rh1. This electron density distortion shows that there is an interaction between Rh1 and (μ-B). The natural bond order (NBO) analyses show that the Wiberg bond indices of Rh1–(μ-B) and Rh2–(μ-B) are 0.3275 and 0.5190, respectively.

The Rh$_2$(μ-H)$_2$ core exhibits a butterfly geometry, as shown in Fig. 4. The importance of the Rh1–(μ-B) interaction in directing the structure is illustrated by our calculations on an isomeric model complex with the μ-boryl group in the equatorial plane and the terminal hydride on Rh2 in an axial position (i.e., interchanging the positions of the μ-boryl and terminal hydride ligands with respect to those found in the X-ray structure). This model would not be expected to exhibit any interaction between the μ-boryl group and Rh1. The calculation indeed yields a planar structure, with the two Rh metal centers and two bridging hydrides in the same plane and an energy which is 1.08 kcal/mol higher than that for the complex with the Rh1–(μ-B) interaction.

We expected to find a related M1–(μ-boryl) interaction in the di-platinum complex (**9**). The bonding in the Pt$_1$-(μ-boryl) system has thus been investigated by DFT calculations on the model complex [Pt$_2$(PH$_3$)(H$_2$-PCH$_2$CH$_2$PH$_2$)$_2$(BO$_2$C$_2$H$_2$)(μ-BO$_2$C$_2$H$_2$)]. The optimized geometry for this model gave a terminal boryl unit which lies approximately orthogonal to the one in the experimental structure which emphasizes the weak π-

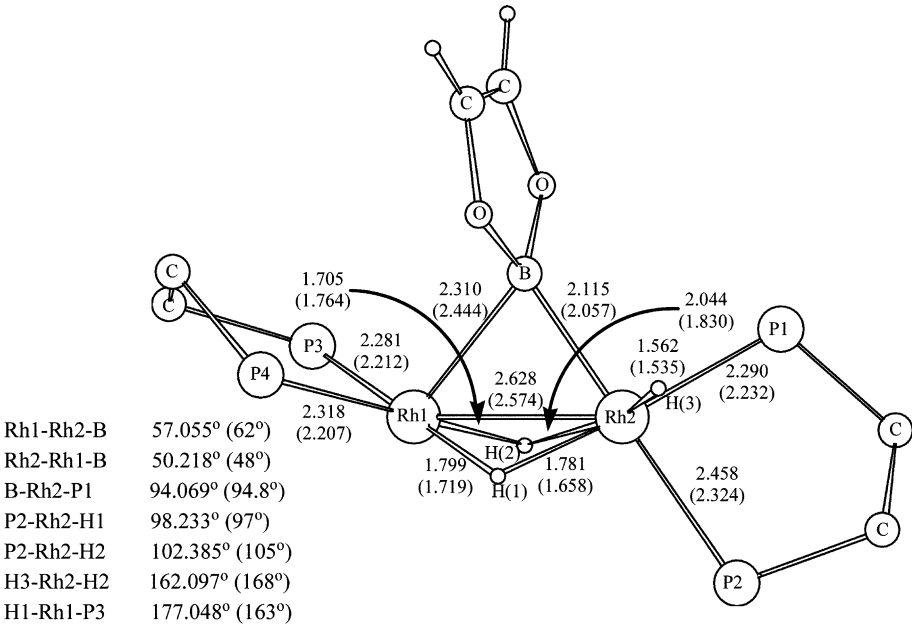

Fig. 4. Selected calculated structural parameters (bond lengths in Å and bond angles in °) for the model complex [Rh($H_2PCH_2CH_2PH_2$)(μ-H)$_2${μ-B($O_2C_2H_2$)}RhH($H_2PCH_2CH_2PH_2$)] together with the experimental structural parameters for [Rh(DiPPE)(μ-H)$_2$(μ-Bcat)RhH(DiPPE)] shown in parentheses. For the purpose of clarity, hydrogen atoms on simplified DiPPE are omitted.

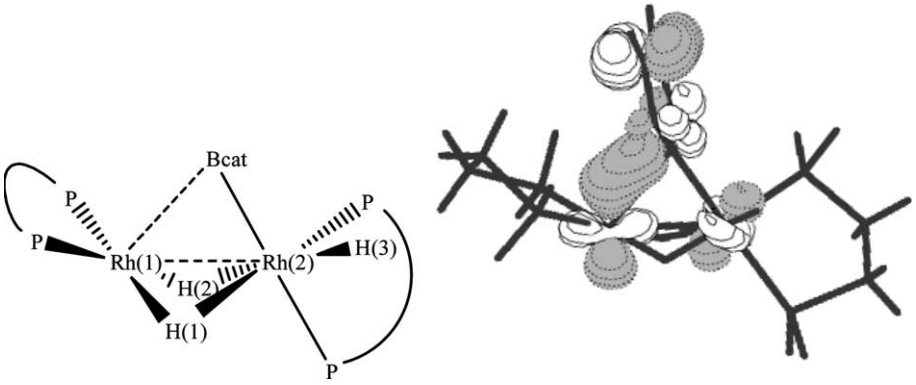

Fig. 5. Spatial plots of the metal–boryl bonding MO for [Rh($H_2PCH_2CH_2PH_2$)(μ-H)$_2${μ-B($O_2C_2H_2$)}RhH($H_2PCH_2CH_2PH_2$)]. The molecular orbital was obtained from the B3LYP calculations.

backbonding to this ligand. This is a known problem with boryl complexes wherein the steric interactions of the experimental ligand set are critical in obtaining the correct orientation for the terminal boryl moiety [50,55]. The di-platinum complex can be described as being composed of a distorted tetrahedral 18-electron, Pt(0) d^{10}-ML_3(boryl) anion coordinated to a T-shaped 14-electron d^8-ML_2(boryl) cation fragment via a donor–acceptor Pt–Pt bond. The spatial plot of the calculated MO corresponding to the Pt-(μ-boryl) interaction between the empty p-orbital on the semi-bridging boryl group and d_{xz} on the Pt1 metal center is illustrated in Fig. 7.

It is interesting that the metal d-orbitals involved in the M1–(μ-B) interaction are different for the Pt and Rh complexes, being d_{xz} for Pt1 and d_{z^2} for Rh1. It is clear that the d-orbital which is utilized depends on the metal–metal bond distance, with d_{xz} preferred for the longer Pt1–Pt2 bond and d_{z^2} preferred for the shorter Rh1–Rh2 bond (Scheme 4). Indeed, the M1–M2–(μ-B) angles (θ) are almost the same in the di-rhodium and di-platinum [1] complexes, being 62.5° and 59.4°, respectively.

The vacant p-orbital on the semi-bridging boryl group can interact not only with a d-orbital on M1 (σ-

[1] We note that some of the angles quoted in Table 2 of [37] are, unfortunately, typographically incorrect, and the experimental ones referred to herein were obtained from the Cambridge Structural Database. N.C. Norman, personal communication.

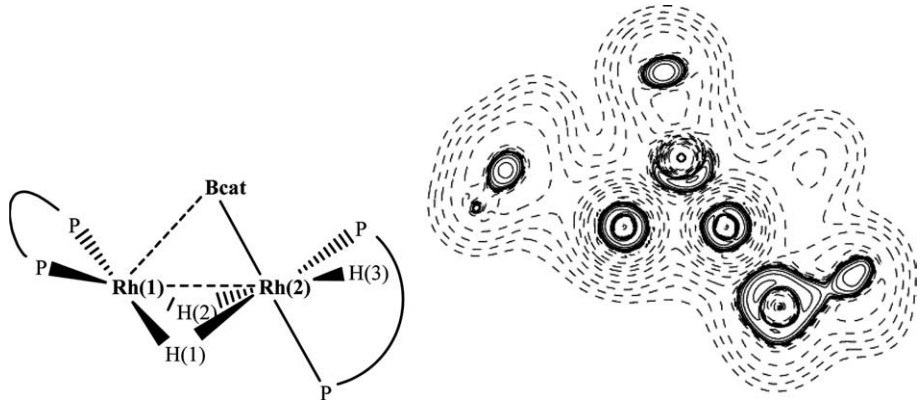

Fig. 6. Plot of the Laplacian of electron density for $[Rh(H_2PCH_2CH_2PH_2)(\mu\text{-}H)_2\{\mu\text{-}B(O_2C_2H_2)\}RhH(H_2PCH_2CH_2PH_2)]$ in a plane defined by the two metal centers and the boron atoms of the bridging boryl ligands.

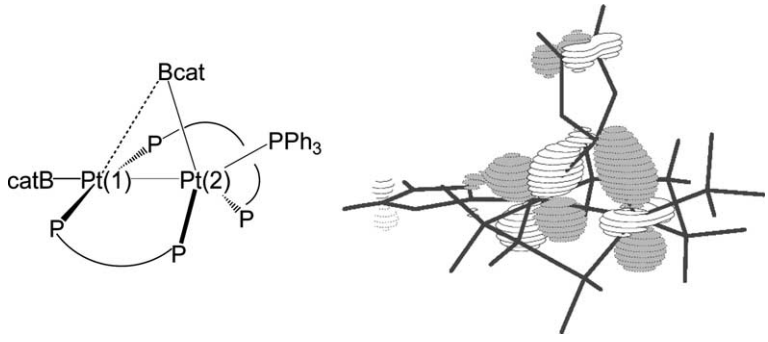

Fig. 7. Spatial plots of the metal–boryl bonding MO for $[Pt_2(PH_3)(\mu\text{-}H_2PCH_2PH_2)_2\{B(O_2C_2H_2)\}\{\mu\text{-}B(O_2C_2H_2)\}]$. The molecular orbital was obtained from the B3LYP calculations.

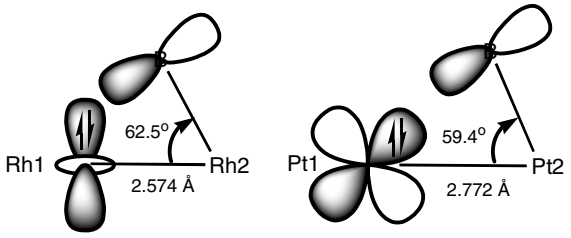

Scheme 4.

donation), but also with a d-orbital on M2 (π-backbonding). The π-accepting property of the boryl group is still controversial but in general, they are believed to be weak π-acceptors at best [49,56]. Here, however, the strong M1–(μ-B)-type interaction shows that the potential electron accepting ability of the B(p-orbital) is strong but that the strength of the interaction depends on the type of interaction (σ or π) [57]. In the present case, we can clearly view the semi-bridging boryl as acting as a Lewis acid to the second metal center.

Finally, it is worth considering the two proposed bridging boryl complexes of Brown and co-workers [52] as illustrated in Fig. 8. Electron counting arguments, along with the details of the above analysis suggest that the two compounds are probably neutral and not dicationic, and that the proposed structures would be unlikely as they are electron deficient. Alternatively, a bridging structure in which the boryl group is terminal to one Rh and O-bound to the other one would satisfy electron counting arguments and would represent yet another type of bridging boryl interaction. Clearly, further synthetic and structural efforts are required to provide additional information on the nature of such novel interactions.

The formation of **7** from dihydride **1** can be rationalized by oxidative addition of one molecule of HBcat to one of the rhodium atoms. Further addition of HBcat eventually affords the novel zwitterion **8**, which has been shown to be a remarkably active and selective catalyst precursor for the hydroboration of a wide variety of alkenes [19]; 'BH_3' production is required for mass balance. Unfortunately, if borane is being liberated in the corresponding catalyzed reactions, this degradation product could compete with HBcat and rapidly hydroborate any unsaturated substrate in solution. As a result, product selectivities could be greatly altered depending upon the amount of borane liberated. Thus, it is useful for catalysis to preform the zwitterionic compounds or to use an alternate mode of generating them in situ [18b,58].

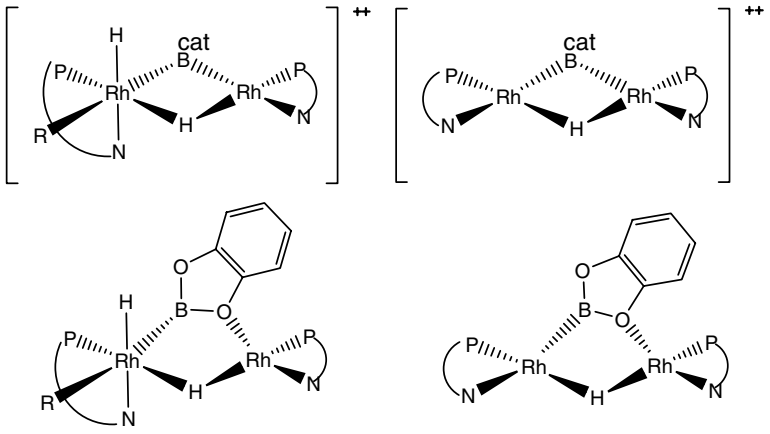

Fig. 8. The two structures at the top were proposed by Brown and co-workers [52] and the ones at the bottom are possible alternatives, which are more consistent with electron counting arguments.

The molecular structure of **8** [59] consists of a chelated bis(phosphine)rhodium cation unsymmetrically coordinated to one of the arene rings of the $[Bcat_2]^-$ anion. There are two unique molecules in the crystallographic asymmetric unit which differ in the rotational orientation and slippage of the P_2Rh moiety with respect to the π-bound arene ring. For instance, the Rh–C bonds (C α to O) in molecule 1 are 2.516(6) and 2.372(6) Å and those for molecule 2 are 2.458(6) and 2.426(7) Å. The potential surfaces for such distortions appears to be quite shallow. Structures and theoretical studies of related zwitterions will be described elsewhere [60]. Significant differences in the Rh–arene carbon bond distances were also observed in the molecular structure of $[Rh\{P(OMe_3)_3\}_2(\eta^6\text{-PhBPh}_3)]$ [61]. The J_{PRh} coupling constant for **8** of 209 Hz is consistent with a P_2Rh fragment π-bound to an arene ring [62]. The formation of **8** involves the redistribution of catecholato groups, which has been observed previously in reactions of HBcat with $NaBH_4$ [63] and tertiary phosphines [36].

4. Conclusions

The nature of the rhodium-containing products observed here demonstrates major reactivity differences between the hydroborating agents employed. Unlike reactions with phosphinoiridium complexes, which give oxidative addition products, addition of borane and alkylboranes to unsaturated rhodium hydride **1** proceeds via initial insertion of B–H into a Rh–H bond to afford stable borohydride complexes. Alkylboranes derived from BH_3 formation (degradation of HBcat) during hydroborations of sterically demanding substrates could result, therefore, in removal of active Rh–H species from the catalytic cycle. The formation of borane in such catalytic reactions also has severe ramifications for product selectivities and for catalyst stability and lifetime due to the formation of metallaborane clusters of undefined activity. Reactions with HBcat are unique, however, in that boron-substituent redistribution products are formed. Addition of HBcat to rhodium hydride **1** gave the novel dinuclear complex $Rh(DiPPE)(\mu\text{-H})_2(\mu\text{-Bcat})RhH(DiPPE)$ (**7**) and, subsequently, zwitterion $Rh(\eta^6\text{-catBcat})(DiPPE)$ (**8**). A single-crystal X-ray diffraction study on **7** shows that the Bcat ligand asymmetrically bridges the two rhodium atoms.

5. Supplementary material

Complete X-ray data collection parameters, bond distances, bond angles, anisotropic thermal parameters, and hydrogen atom coordinates and isotropic thermal parameters for complexes **2**, **6**, and **7**, quoting the deposition numbers CCDC 249353–249355, are available free of charge on request from CCDC, 12 Union Road, Cambridge, CB2 1EZ, UK (fax: +44 1223 336 033; e-mail: deposit@ccdc.ac.uk or www: http://www.ccdc.cam.ac.uk).

Acknowledgements

We thank Tim Onley, Geraldine Direnzo, Nancy Herling, Lou Lardear, John Marcone and Will Marshall for expert technical assistance, Derick Ovenall for $^1H\{^{11}B\}$ NMR spectra, and anonymous reviewers for helpful comments. We also acknowledge support from the Petroleum Research Fund (T.B.M.), administered by the American Chemical Society, the Natural Sciences

and Engineering Research Council of Canada (S.A.W. and T.B.M.), Canadian Foundation for Innovation/ Atlantic Innovation Foundation (S.A.W.), the Leverhulme Trust for a Study Abroad Fellowship (T.B.M.) and the University of Durham for a Sir Derman Christopherson Foundation Fellowship (T.B.M.). Z.L. thanks the Research Grants Council of Hong Kong (HKUST 6087/02P) and the University Grants Committee of Hong Kong, through the Area of Excellent Scheme (AoE), for financial support.

References

[1] K. Burgess, M.J. Ohlmeyer, Chem. Rev. 91 (1991) 1179.
[2] I. Beletskaya, A. Pelter, Tetrahedron 53 (1997) 4957.
[3] C.M. Crudden, D. Edwards, Eur. J. Org. Chem. (2003) 4695, and references therein.
[4] K.N. Harrison, T.J. Marks, J. Am. Chem. Soc. 114 (1992) 9220.
[5] S.A. Kulkarni, N. Koga, Theochem 461–462 (1999) 297.
[6] C.N. Muhoro, X. He, J.F. Hartwig, J. Am. Chem. Soc. 121 (1999) 5033.
[7] D.R. Lantero, D.L. Ward, M.R. Smith III, J. Am. Chem. Soc. 119 (1997) 9699.
[8] G. Desurmont, S. Dalton, D.M. Giolando, M. Srebnik, J. Org. Chem. 62 (1997) 8907.
[9] M.J. Pender, T. Wideman, P.J. Carroll, L.G. Sneddon, J. Am. Chem. Soc. 120 (1998) 9108.
[10] X. He, J.F. Hartwig, J. Am. Chem. Soc. 118 (1996) 1696.
[11] C.N. Muhoro, J.F. Hartwig, Organometallics 19 (2000) 30.
[12] H. Kono, K. Ito, Y. Nagai, Chem. Lett. (1975) 1095.
[13] D. Männig, H. Nöth, Angew. Chem., Int. Ed. Eng. 24 (1985) 878.
[14] A.E. Dorigo, P. von R. Schleyer, Angew. Chem., Int. Ed. Engl. 34 (1995) 115.
[15] K. Burgess, W.A. van der Donk, S.A. Westcott, T.B. Marder, R.T. Baker, J.C. Calabrese, J. Am. Chem. Soc. 114 (1992) 9350.
[16] J.M. Brown, G.C. Lloyd-Jones, J. Chem. Soc., Chem. Commun. (1992) 710.
[17] D.G. Musaev, A.M. Mebel, K. Morokuma, J. Am. Chem. Soc. 116 (1994) 10693.
[18] (a) S.A. Westcott, T.B. Marder, R.T. Baker, Organometallics 12 (1993) 975;
(b) S.A. Westcott, H.P. Blom, T.B. Marder, R.T. Baker, J. Am. Chem. Soc. 114 (1992) 8863.
[19] R.B. Coapes, F.E.S. Souza, R.L. Thomas, J.J. Hall, T.B. Marder, Chem. Commun. (2003) 614.
[20] X. Huang, Z. Lin, in: F. Maseras, A. Lledos (Eds.), Computational Modelling of Homogeneous Catalysis, Kluwer Academic Publishers, Amsterdam, 2002, pp. 189–212.
[21] C. Widauer, H. Grützmacher, T. Ziegler, Organometallics 19 (2000) 209.
[22] M.D. Fryzuk, W.E. Piers, Organomet. Synth. 3 (1986) 128.
[23] M.D. Fryzuk, T. Jones, F.W.B. Einstein, Organometallics 3 (1984) 185.
[24] C. Busetto, A. D'Alfonso, F. Maspero, G. Perego, A. Zazetta, J. Chem. Soc., Dalton Trans. (1977) 1828.
[25] G.M. Sheldrick, SHELX, University of Gottingen, Gottingen, Germany, 1986.
[26] D.T. Cromer, J.A. Ibers, in: International Tables for X-ray Crystallography, vol. IV, Kynoch Press, Birmingham, England, 1974, Table 2.3.2.
[27] D.T. Cromer, J.T. Waber, in: International Tables for X-ray Crystallography, vol. IV, Kynoch Press, Birmingham, England, 1974, Table 2.2B.
[28] (a) A.D. Becke, Phys. Rev. A 38 (1988) 3098;
(b) B. Miehlich, A. Savin, H. Stoll, H. Preuss, Chem. Phys. Lett. 157 (1989) 200;
(c) C. Lee, W. Yang, G. Parr, Phys. Rev. B 37 (1988) 785.
[29] P.J. Hay, W.R. Wadt, J. Chem. Phys. 82 (1985) 299.
[30] (a) M.S. Gordon, Chem. Phys. Lett. 76 (1980) 163;
(b) P.C. Hariharan, J.A. Pople, Theoret. Chim. Acta 28 (1997) 213;
(c) R.C. Binning Jr., L.A. Curtiss, J. Comput. Chem. 11 (1990) 1206.
[31] S. Huzinaga, Gaussian Basis Sets for Molecular Calculations, Elsevier, Amsterdam, 1984.
[32] M.J. Frisch, G.W. Trucks, H.B. Schlegel, G.E. Scuseria, M.A. Robb, J.R. Cheeseman, V.G. Zakrzewski, J.A. Montgomery Jr., R.E. Stratmann, J.C. Burant, S. Dapprich, J.M. Millam, A.D. Daniels, K.N. Kudin, M.C. Strain, O. Farkas, J. Tomasi, V. Barone, M. Cossi, R. Cammi, B. Mennucci, C. Pomelli, C. Adamo, S. Clifford, J. Ochterski, G.A. Petersson, P.Y. Ayala, Q. Cui, K. Morokuma, D.K. Malick, A.D. Rabuck, K. Raghavachari, J.B. Foresman, J. Cioslowski, J.V. Ortiz, B.B. Stefanov, G. Liu, A. Liashenko, P. Piskorz, I. Komaromi, R. Gomperts, R.L. Martin, D.J. Fox, T. Keith, M.A. Al-Laham, C.Y. Peng, A. Nanayakkara, C. Gonzalez, M. Challacombe, P.M.W. Gill, B. Johnson, W. Chen, M.W. Wong, J.L. Andres, C. Gonzalez, M. Head-Gordon, E.S. Replogle, J.A. Pople, GAUSSIAN-98 (Revision A.9), Gaussian, Inc., Pittsburgh, PA, 1998.
[33] Interactive MOPLOT: a package for the interactive display and analysis of molecular wave functions, incorporating the programs MOPLOT (D. Lichtenberger), PLOTDEN (R.F.W. Bader, D.J. Kenworthy, P.M. Beddal, G.R. Runtz, S.G. Anderson), SCHUSS (R.F.W. Bader, G.R. Runtz, S.G. Anderson, F.W. Biegler-Koenig) and EXTREM (R.F.W. Bader, F.W. Bieger-Koenig) by P. Sherwood and P.J. MacDougall, 1989.
[34] G. Schaftenaar, MOLDEN v3.7: CAOS/CAMM Center Nijmegen, Toernooiveld, Nijmegen, Netherlands, 2001.
[35] R.T. Baker, D.W. Ovenall, J.C. Calabrese, S.A. Westcott, N.J. Taylor, I.D. Williams, T.B. Marder, J. Am. Chem. Soc. 112 (1990) 9399.
[36] S.A. Westcott, H.P. Blom, T.B. Marder, R.T. Baker, J.C. Calabrese, Inorg. Chem. 32 (1993) 2175.
[37] X. Lei, M. Shang, T.P. Fehlner, J. Am. Chem. Soc. 115 (1998) 4908.
[38] (a) T.P. Fehlner, in: J.F. Liebman, A. Greenberg, R.E. Williams (Eds.), Advances in Boron and the Boranes, VCH Publishers, New York, 1988, p. 265 (Chapter 12);
(b) P.D. Grebenik, M.L.H. Green, M.A. Kelland, J.B. Leach, P. Mountford, J. Chem. Soc., Chem. Commun. (1989) 1397;
(c) P.D. Grebenik, M.L.H. Green, M.A. Kelland, J.B. Leach, P. Mountford, J. Chem. Soc., Chem. Commun. (1990) 1234.
[39] K. Wade, Adv. Inorg. Radiochem. 18 (1976) 1.
[40] R.T. Baker, D.W. Ovenall, R.L. Harlow, S.A. Westcott, N.J. Taylor, T.B. Marder, Organometallics 9 (1990) 3028.
[41] M.D. Fryzuk, W.E. Piers, F.W.B. Einstein, T. Jones, Can. J. Chem. 67 (1989) 883.
[42] $[(\eta^5\text{-}C_5Me_5)IrH]_2(\mu\text{-}H)(\mu\text{-}H_2BH_2)$: T.M. Gilbert, F.J. Hollander, R.G. Bergman, J. Am. Chem. Soc. 107 (1985) 3508.
[43] $[Mn(CO)_3]_2(\mu\text{-}Ph_2PCH_2PPh_2)(\mu\text{-}H)(\mu\text{-}H_2BH_2)$: R. Carreno, M.A. Ruiz, Y. Jeannin, M. Philoche-Levisalles, J. Chem. Soc., Chem. Commun. (1990) 15.
[44] $[Mn_2(\mu\text{-}BH_4)(\mu\text{-}H)(CO)_5(\mu\text{-}Ph_2PCH_2PPh_2)]$: R. Carreno, V. Riera, M. Ruiz, C. Bois, Y. Jeannin, Organometallics 12 (1993) 1946.
[45] (a) T.J. Marks, J.R. Kolb, Chem. Rev. 77 (1977) 263;
(b) Bulky phosphine ligands can be used to stabilize certain tetrahydroborate complexes of Rh, Ru and Ir, see: J.B. Letts, T.J. Mazanec, D.W. Meek, J. Am. Chem. Soc. 104 (1982) 3898, and references therein.

[46] The molecular structures of related complexes have been reported. [{*exo*-$(R_3P)_2Rh$}(*closo*-$CB_{11}H_{12}$)]: A. Rifat, V.E. Laing, G. Kociok-Köhn, M.F. Mahon, G.D. Ruggiero, A.S. Weller, J. Organomet. Chem. 680 (2003) 127.
[47] Ru[$(\mu$-H)$_2BC_8H_{14}]_2(PCy_3)$: K. Essalah, J.-C. Barthelat, V. Montiel, S. Lachaize, B. Donnadieu, B. Chaudret, S. Sabo-Etienne, J. Organomet. Chem. 680 (2003) 182.
[48] [*exo-nido*-$(Ph_3P)_2$Rh-7-Me-8-Ph-7,8-$C_2B_9H_{10}$] J.A. Long, T.B. Marder, M.F. Hawthorne, J. Am. Chem. Soc. 106 (1984) 3004.
[49] M.R. Smith III, Prog. Inorg. Chem. 48 (1999) 505.
[50] W.H. Lam, S. Shimada, A.S. Batsanov, Z. Lin, T.B. Marder, J.A. Cowan, J.A.K. Howard, S.A. Mason, G.J. McIntyre, Organometallics 22 (2003) 4557.
[51] D. Curtis, M.J.G. Lesley, N.C. Norman, A.G. Orpen, J. Starbuck, J. Chem. Soc., Dalton Trans. (1999) 1687.
[52] A. Korostylev, I. Gridnev, J.M. Brown, J. Organomet. Chem. 680 (2003) 329.
[53] K.W. Muir, J.A. Ibers, Inorg. Chem. 8 (1969) 1921.
[54] R.F.W. Bader, Atoms in Molecules: A Quantum Theory, Oxford University Press, Oxford, 1990.
[55] K.C. Lam, W.H. Lam, Z. Lin, T.B. Marder, N.C. Norman, Inorg. Chem. 43 (2004) 2541.
[56] (a) For recent reviews see: J.F. Hartwig, K.M. Waltz, C.N. Muhoro, X. He, O. Eisenstein, R. Bosque, F. Maseras, in: W. Siebert (Ed.), Advances of Boron Chemistry, Special Publication No. 201, Royal Society of Chemistry, Cambridge, UK, 1997, pp. 373–396;
(b) H. Wadepohl, Angew. Chem., Int. Ed. Engl. 36 (1997) 2441;
(c) G.J. Irvine, M.L.G. Lesley, T.B. Marder, N.C. Norman, C.R. Rice, E.G. Robins, W.R. Roper, G.R. Whittell, L.J. Wright, Chem. Rev. 98 (1998) 2685;
(d) H. Braunschweig, Angew. Chem., Int. Ed. Engl. 37 (1998) 1786;
(e) H. Braunschweig, M. Colling, Coord. Chem. Rev. 223 (2001) 1.
[57] C.E. Webster, Y.B. Fan, M.B. Hall, D. Kunz, J.F. Hartwig, J. Am. Chem. Soc. 125 (2003) 858.
[58] C.Y. Dai, E.G. Robins, A.J. Scott, W. Clegg, D.S. Yufit, J.A.K. Howard, T.B. Marder, Chem. Commun. (1998) 1983.
[59] S.A. Westcott, N.J. Taylor, T.B. Marder, R.T. Baker, N.J. Jones, J.C. Calabrese, J. Chem. Soc., Chem. Commun. (1991) 304.
[60] C.Y. Dai, A.J. Scott, W. Clegg, A.K. Hughes, M.A. Fox, T.B. Marder, unpublished results.
[61] M.J. Nolte, G. Gafner, Acta Crystallogr., Sect. B 30 (1974) 738.
[62] P. Albano, M. Aresta, M. Manassero, Inorg. Chem. 19 (1980) 1069.
[63] D. Männig, H. Nöth, J. Chem. Soc., Dalton Trans. (1985) 1689.

Available online at www.sciencedirect.com
SCIENCE DIRECT®
Polyhedron 23 (2004) 2679–2688
POLYHEDRON
www.elsevier.com/locate/poly

Biphasic hydroformylation catalysis in ionic liquid media

Christian P. Mehnert *, Raymond A. Cook, Nicholas C. Dispenziere, Edmund J. Mozeleski

ExxonMobil Research and Engineering Company, Corporate Strategic Research, Annandale, NJ 08801, USA

Received 15 April 2004; accepted 19 June 2004
Available online 3 September 2004

Dedicated to Prof. M.L.H. Green on the occasion of his retirement from the position of Head of the Inorganic Chemistry Department at Oxford University

Abstract

The ionic liquids 1-butyl-3-methyl-imidazolium tetrafluoroborate ([bmim][BF_4]), 1-butyl-3-methyl-imidazolium hexafluorophosphate ([bmim][PF_6]) and 1,2-dimethyl-3-butyl-imidazolium hexafluorophospate ([bdmim][PF_6]) were investigated as potential media for hydroformylation catalysis in a liquid–liquid biphase reaction environment. The study used the known rhodium/tppti* (tppti* = tri(*m*-sulfonyl) triphenyl phosphine 1,2-dimethyl-3-butyl-imidazolium salt) system as the catalyst and hexene-1 as the substrate, which enabled the produced heptanal to be conveniently isolated from the ionic liquid by phase separation. All catalyst evaluations were carried out in high-purity ionic liquids to avoid any decomposition of the catalyst, substrate and/or ionic liquid. The activity of the biphasic ionic liquid system containing the Rh/tppti* catalyst was approximately one order of magnitude lower than that observed for the conventional Rh/PPh_3 catalyst in toluene. The Rh/tppti* catalyst system showed a decrease of activity in the semicontinuous hydroformylation of hexene-1 due to catalyst deactivation and/or metal loss. The *n*/*i* ratio of the produced heptanal only slightly increased after changing the Rh/P ratio from 1:3 to 1:100 in [bmim][PF_6]. The loss of rhodium metal from the ionic liquid phases appears to be correlated to the solubility characteristics of the ionic liquid and the concentration of the aldehyde in the organic phase. In support of this theory, the ionic liquid [bmim][PF_6] gave the best results due to its very low miscibility with polar substances. A high-pressure NMR (HP-NMR) study revealed that the solution structure of HRh(^{13}CO)(tppts)$_3$ (tppts = tri(*m*-sulfonyl)triphenyl phosphine sodium salt) in [bmim][BF_4] was similar to that of HRh(^{13}CO)(PPh_3)$_3$ in toluene-d^8. The HP-NMR investigation at elevated syngas pressures showed that HRh(^{13}CO)(tppts)$_3$ lies in equilibrium with HRh(^{13}CO)$_2$(tppts)$_2$.
© 2004 Elsevier Ltd. All rights reserved.

Keywords: Hydroformylation; Ionic liquids; Biphase catalysis; High-pressure NMR; Rhodium complexes

1. Introduction

The separation of homogeneous hydroformylation catalysts from reaction mixtures has been a tremendous challenge and continues to be the focus of intense research [1]. Over the last three decades, several elegant approaches have been explored to overcome this limitation including aqueous [2] and fluorous biphase catalysis [3], reactions in supercritical media [4] and catalyst immobilization onto solid support materials [5]. Although some of these novel concepts have successfully been developed into commercial processes, like the Ruhr Chemie Rhône Poulenc Process used in the production of butyraldehyde [2], catalyst recovery continues to be one of the key issues of homogeneous catalysis.

More recently, ionic liquids have been used as alternative reaction media for homogeneous catalysis [6]. Based on their highly charged nature, ionic liquids are

* Corresponding author at: ExxonMobil Chemical Company, Baytown Technology and Engineering Complex, 5200 Bayway Drive, Baytown, TX 77006, USA. Tel.: +1 281 834 1825; fax: +1 281 834 2371.
E-mail address: christian.p.mehnert@exxonmobil.com (C.P. Mehnert).

0277-5387/$ - see front matter © 2004 Elsevier Ltd. All rights reserved.
doi:10.1016/j.poly.2004.06.029

well suited for biphasic reactions with organic substrates. While the first hydroformylation reaction in an ionic liquid (at that time referred to as a molten salt) was performed by Parshall [7] as earlier as 1972, it was not until 1995 that Chauvin et. al. [8] used water-soluble phosphine ligands like the tri(*m*-sulfonyl)triphenyl phosphine sodium salt (tppts) [9] to retain active rhodium complexes in the ionic liquid phases and used them successfully in biphasic hydroformylation catalysis. Since then, a variety of different metal complexes have been investigated for liquid–liquid biphasic hydroformylation reactions in ionic liquid media [10].

As the production of aldehyde is one of the largest volume processes [11] in the chemical industry we have recently attempted to ascertain the viability of ionic liquids for hydroformylation reactions [12]. In this paper, we report our findings on the biphasic hydroformylation catalysis using conventional rhodium catalysts in ionic liquid media, which was encouraged by the initial report of Chauvin et. al. [8]. In this study we have investigated the reactivity of the hydroformylation catalyst $HRh(CO)(P)_3$ (P = phosphine ligand) in imidazolium based ionic liquid derivatives of tetrafluoroborate and hexafluorophosphate. In addition, we have complimented our investigation with a high-pressure NMR (HP-NMR) study of the reaction mixture containing the active rhodium species.

2. Experimental

2.1. General experimental details and materials

All operations were performed in a Vacuum Atmospheres or MBraun dry box under purified nitrogen or using Schlenk techniques under a nitrogen atmosphere. The following chemicals have been purchased from Aldrich and have been used as received: anhydrous heptane, anhydrous toluene, dichloromethane, hexene-1, 1-chlorobutane, 1-methyl-imidazol, 1,2-dimethyl-imidazol, Celite, alumina, activated carbon, sodium tetrafluoroborate, sodium hexafluorophosphate and potassium hexafluorophosphate. The following compounds have been purchased from Strem and have been used as received: tris(*m*-sulfonylphenyl)phosphine sodium salt (tppts) and $Rh(CO)_2(acac)$ (acac = acetylacetonate). The gases CO/H_2 (1:1, UHP grade) and ^{13}CO (UHP grade) were purchased from BOC and MG industries, respectively. NMR spectra were recorded on a Varian Unity 400 spectrometer. Chemical shifts (ppm) were referenced to either an internal standard (e.g. tetramethylsilane) or an external standard (e.g. triphenylphoshite). HP-NMR experiments were performed using single-crystal sapphire NMR tubes [13]. Toluene-d_8 was purchased from Cambridge Isotopes and was degassed and dried over potassium metal. Gas chromatography samples were analyzed using a HP-5890 gas chromatograph with a 30 m Spb-1 capillary column, 0.25 mm i.d. and 0.25 mm film thickness and a HP-6890 GC/MS equipped with a 30 m HP-1 capillary column, 0.25 mm i.d. and 0.25 mm film thickness. Rhodium analyses were performed on an inductively coupled plasma–atomic emission spectrometer (ICP/AES), Jarrell-Ash Model 1100, with argon gas flow and torch alignment. The ICP/AES instrument was calibrated with 10 ppm rhodium solution. Elemental analyses were performed by the Galbraith Laboratory.

2.2. Preparation of the ionic liquids

2.2.1. 1-Butyl-3-methyl-imidazolium tetrafluoroborate – [bmim][BF_4]

A 500 ml round bottom flask was charged under N_2 with 95 g (0.54 mol) 1-butyl-3-methyl-imidazolium chloride [14] and 63 g (0.57 mol) sodium tetrafluoroborate in 250 ml of degassed water. After the reaction was stirred for 15 h at room temperature, the mixture was extracted with dichloromethane (3× 100 ml). The combined organic phases were dried over magnesium sulfate and filtered through a bed of activated carbon and alumina. After the removal of the volatile components under reduced pressure the ionic liquid [bmim][BF_4] was obtained as a colorless liquid in 73% yield. Elemental analysis (%) calculated for $C_8H_{15}N_2BF_4$: C, 42.51; H, 6.69; N, 12.39. Found: C, 42.66; H, 7.12; N, 12.49%.

2.2.2. 1-Butyl-3-methyl-imidazolium hexafluorophosphate – [bmim][PF_6]

A 1000 ml round bottom flask was charged under N_2 with 175 g (1.0 mol) 1-butyl-3-methyl-imidazolium chloride and 190 g (1.03 mol) potassium hexafluorophosphate in 400 ml degassed water. After the reaction was stirred for 15 h at room temperature, the mixture was extracted with dichloromethane (3× 200 ml). The combined organic phases were dried over magnesium sulfate and filtered through a bed of activated carbon and alumina. After the removal of the volatile components under reduced pressure the ionic liquid [bmim][PF_6] was obtained as a colorless liquid in 80% yield. Elemental analysis (%) calculated for $C_8H_{15}N_2PF_6$: C, 33.81; H, 5.32; N, 9.86. Found: C, 33.92; H, 5.64; N, 9.72%.

2.2.3. 1,2-Dimethyl-3-butyl-imidazolium hexafluorophosphate – [bdmim][PF_6]

A 500 ml round bottom flask was charged under N_2 with 56.6 g (0.3 mol) 1,2-dimethyl-3-butyl-imidazolium chloride and 55.4 g (0.33 mol) sodium hexafluorophosphate in 250 ml of degassed water. After the reaction was stirred for 15 h at 40 °C, the mixture was extracted with dichloromethane (3× 100 ml). The combined organic phases were dried over magnesium sulfate and filtered through a bed of activated carbon and alumina.

After the removal of the volatile components under reduced pressure the ionic liquid [bdmim][PF_6] was obtained as a yellow-colored viscous liquid in 70% yield. Elemental analysis (%) calculated for $C_9H_{17}N_2PF_6$: C, 36.25; H, 5.75; N, 9.39. Found: C, 36.27; H, 5.83; N, 9.36%.

2.3. HP-NMR investigation

A solution of 3 mg (0.013 mmol) $Rh(CO)_2(acac)$ and 43 mg (0.075 mmol) tppts in 2 ml of [bmim][BF_4] containing 5 wt% of D_2O was prepared under N_2 and charged into a sapphire NMR tube. The tube was placed into a safety shield container and pressurized to 60 psi with $^{13}CO/H_2$ (1:1). To ensure the formation of $HRh(CO)(tppts)_3$ (**1a**), the tube was shaken at 60 °C for 1 h. After the pressure was released the $^{31}P\{^1H\}$ and $^{13}C\{^1H\}$ NMR spectra were recorded under 15 psi of $^{13}CO/H_2$ (1:1), confirming the presence of **1a**. During the course of the HP-NMR investigation the tube was pressurize up to 2000 psi with $^{13}CO/H_2$ (1:1) and further monitored by NMR spectroscopy.

2.4. Catalyst evaluation

2.4.1. General experimental details for hydroformylation reactions

In a typical experiment carried out in a 300 ml autoclave, catalyst solution was prepared from the ionic liquid, the rhodium precursor $Rh(CO)_2(acac)$ and the phosphine (tppti*) stock solution. The mixture was charged into the reactor under nitrogen and the volatile components removed under reduced pressure (10^{-2} Torr). The reactor was then flushed and pressurized with CO/H_2 (1:1) to ca. 150 psi. The run olefin was charged in a glovebox into a 100 ml injection bomb, which was then mounted into the feed line of the reactor. After the reactor was heated to the run temperature, the reaction was initiated by injecting the olefin into the reactor and the pressure adjusted up to 600 psi CO/H_2 (1:1). The pressure in the reactor was maintained constant by making up the consumed CO/H_2 (1:1) from the PVT tank. The conversion was followed by recording the pressure drop in the PVT tank.

The apparent turnover frequency (TOF) used in the kinetic analysis is defined as the rate of olefin conversion by 1 mol of rhodium and is expressed as the moles of olefin converted to aldehyde per moles of rhodium per minute: $TOF = \{(dn_{olefin}/dt)_t\}/n_{Rh}$. The rate of olefin conversion is calculated from the PVT pressure versus time data. The values for the TOF were determined during the initial 30 min of the gas consumption which corresponds to an approximate olefin conversion of between 10% and 20%.

For the semicontinuous hydroformylation of hexene-1, the autoclave was fitted with a dip leg that reached ca. 5 mm above the heavier ionic liquid phase. At the end of each run, the reactor was cooled to 15 °C, the stirrer was then stopped and the supernatant product phase was removed from the reactor. For metal balance, the concentration of Rh in each product was determined by ICP-AES. For each consecutive run, the catalyst phase was rapidly heated to the reaction temperature and a fresh charge of hexene-1 was injected to initiate the reaction.

For the rhodium analysis, aliquots of the product were ashed with 1 ml of concentrated H_2SO_4 and left in a furnace at 530 °C for at least 8 h. The remaining residue was fused with 0.5 g $K_2S_2O_7$. The resulting mixture was solubilized in a 20% H_2SO_4 solution. The rhodium analysis was performed using ICP/AES instrumentation with matrix-matched standards (3.35 RSD).

2.4.2. Preparation of the tri(m-sulfonyl)triphenylphosphine 1,2-dimethyl-3-butyl-imidazolium salt (tppti*)

A 50 ml round bottom flask was charged under N_2 with 10.1 g (0.017 mol) tri(*m*-sulfonyl)triphenyl phosphine sodium salt (tppts) and 10.0 g (0.053 mol) 1,2-dimethyl-3-butyl-imidazolium chloride in acetonitrile (25 ml). After the reaction was stirred for 3 days at room temperature, the mixture was filtered through a bed of Celite. The filter aid was further washed with acetonitrile (30 ml). The resulting filtrates were combined and used as a stock solution for the tppti* ligand.

2.4.3. Biphasic Hydroformylation using $Rh(CO)_2(acac)$/tppti* in [bmim][BF_4] (Table 2/Entries 1–10)

A mixture of 26 mg (0.1 mmol) $Rh(CO)_2(acac)$ and 3.2 ml (1.0 mmol) tppti* (stock solution) in 60 ml [bmim][BF_4] was stirred at room temperature. After 1 h the yellow solution was charged into a 300 ml autoclave and the volatile components removed under reduced pressure (10^{-2} Torr). The reactor was pressurized with CO/H_2 (1:1) to ca. 150 psi. After the reactor was heated to 100 °C, the reaction was initiated by injecting 61 g (720 mmol) hexene-1 with 300 psi of CO/H_2 (1:1) into the reactor. Due to the extended induction period after the first recycle run the reactor pressure was increased to 600 psi. All further runs were conducted at this run pressure.

2.4.4. Reaction of $Rh(CO)_2(acac)$/tppti* in [bmim][PF_6] (Table 2/Entries 11–20)

A mixture of 26 mg (0.1 mmol) $Rh(CO)_2(acac)$ and 3.2 ml (1.0 mmol) tppti* stock solution in 60 ml [bmim][PF_6] was stirred at room temperature. After 1 h the yellow solution was charged into a 300 ml autoclave and the volatile components removed under reduced pressure (10^{-2} Torr). The reactor was pressurized with CO/H_2 (1:1) to ca. 300 psi. After the reactor was heated to 100 °C, the reaction was initiated by injecting 26 g (307 mmol) hexene-1 in 38 ml of heptane with 600 psi of CO/H_2 (1:1) into the reactor. The

autoclave studies using Rh/P ratios of 1:3 and 1:100 (Table 1/Entries 28, 29) were carried out under the identical conditions.

2.4.5. Reaction of $Rh(CO)_2(acac)$/tppti* in [bdmim][PF_6] (Table 2/Entries 21–27)

A mixture of 26 mg (0.1 mmol) $Rh(CO)_2(acac)$ and 3.2 ml (1.0 mmol) tppti* stock solution in 60 ml [bdmim][PF_6] was stirred at room temperature. After 1 h the yellow solution was charged into a 300 ml autoclave and the volatile components removed under reduced pressure (10^{-2} Torr). The reactor was pressurized with CO/H_2 (1:1) to ca. 300 psi. After the reactor was heated to 100 °C, the reaction was initiated by injecting 25 g (295 mmol) hexene-1 in 38 ml of heptane with 600 psi of CO/H_2 (1:1) into the reactor.

2.4.6. Reaction of $Rh(CO)_2(acac)/PPh_3$ in toluene (Table 2/Entries 30)

A mixture of 6.5 mg (0.025 mmol) $Rh(CO)_2(acac)$ and 66 mg (0.25 mmol) PPh_3 was dissolved in 60 ml toluene and stirred at room temperature. The yellow solution was charged into a 300 ml autoclave and pressurized with CO/H_2 (1:1) to ca. 300 psi. After the reactor was heated to 100 °C, the reaction was initiated by injecting 61 g (720 mmol) hexene-1 at 600 psi of CO/H_2 (1:1) into the reactor.

3. Results and discussion

3.1. Catalyst screening in HP-NMR tubes

We started our study by investigating hydroformylation reactions in ionic liquids under different reaction environments. This initial study was conveniently carried out in sapphire NMR tubes which enabled us to visually follow phase separations and determine solubility limitations. In this investigation the well-established catalyst precursor $Rh(CO)_2(acac)$ (acac = acetylacetonate) was dissolved in the ionic liquid [bmim][PF_6] with (a) no phosphine, (b) triphenylphoshine (PPh_3) and (c) the tri(*m*-sulfonyl)triphenyl phosphine 1,2-dimethyl-3-butyl-imidazolium salt (tppti*). The resulting solutions were loaded into HP-NMR tubes and treated with the substrate hexene-1. The organic phases showed a lower density and therefore generated the top layers while the ionic liquids were confirmed as the bottom phases. After the reaction mixtures were pressurized with CO/H_2 (1:1) to 600 psi the tubes were shaken at 100 °C. The reaction was stopped after 3 h and the tubes were cooled to room temperature. During this time the organic components separated from the ionic liquid phases. While the reaction without a ligand and with the ligand tppti* gave colorless organic phases (upper layer), the experiment using the ligand PPh_3 showed a strong yellow coloration of the organic phase. As the complex $HRh(CO)(PPh_3)_3$ has a yellow coloration in solution, it is a good indication that a substantial amount of the catalyst migrated during the reaction from the ionic liquid into the organic layer. After the pressure was released from the sapphire NMR tubes the organic products were analyzed for their composition and rhodium metal content. In all three cases a significant amount of aldehyde was produced. Concerning the issue of metal leaching, only the reaction mixture using tppti* exhibited a negligible amount of rhodium loss from the ionic liquid, while the other ionic liquid phases suffered from a significant amount of metal loss. On the basis of these initial experiments, the approach of using highly charged ligands like for example tppti* seemed to be a viable method for retaining a rhodium catalyst in an ionic liquid.

One interesting result was that although the organic phase in the reaction using no ligand was colorless, a large amount of rhodium metal was found in this phase. Furthermore, a significant amount of aldehyde was produced in this reaction which indicates that species other than $HRh(CO)(PPh_3)_3$ are active for the hydroformylation of the olefin. Most likely the aldehyde was produced by rhodium-hydrido-carbonyl complexes which tend to form under hydroformylation reaction conditions in the absence of suitable ligands and have been observed in other areas of oxo-catalysis [15]. For this reason, all of our produced aldehyde samples were analyzed for their rhodium content.

Another potentially complicating factor in the evaluation of these ionic liquid media for hydroformylation catalysis are the solubility limitations of the highly charged phosphine ligand. In an early HP-NMR study

Table 1
Selected $^{31}P\{^1H\}$ and $^{13}C\{^1H\}$ NMR data for the Rh/P catalyst system (P = PPh_3, tppts) in [bmim][BF_4], toluene-d^8 and water under varying pressure conditions

Solvent	Pressure[a] (psi)	Complex	$\delta(^{13}CO)$ (ppm)	J_{C-Rh} (Hz)	$\delta(^{31}PR_3)$ (ppm)	J_{P-Rh} (Hz)
[bmim][BF_4]	15	$HRh(^{13}CO)(tppts)_3$	195.2	62	32.2	126
[bmim][BF_4]	2000	$HRh(^{13}CO)_2(tppts)_2$	199.2	61	39.1	137
Toluene-d^8	15	$HRh(^{13}CO)(PPh_3)_3$	206.6	62	37.8	156
Toluene-d^8	1000	$HRh(^{13}CO)_2(PPh_3)_2$	199.9	63	33.8	139
H_2O	15/3000	$HRh(^{13}CO)(tppts)_3$	204.9	55	42.8	156

[a] Syngas $^{13}CO/H_2$ (1:1).

we realized that not all the water-soluble phosphine ligands like the tri(*m*-sulfonyl)triphenyl phosphine sodium salt (tppts) are also automatically soluble in ionic liquid phases. Although the ligand showed excellent solubility in water, it only dissolved in [bmim][BF_4] after the addition of small amounts of water. Even more surprising was the fact that it has negligible solubility in [bmim][PF_6]. To verify this low solubility we charged [bmim][PF_6] together with $Rh(CO)_2$(acac) and tppts (Rh/P ratio 1:10) into a HP-NMR tube. The resulting mixture was stepwise pressurized with CO/H_2 (1:1) to 2000 psi and heated up to 150 °C. During this process we recorded the $^{31}P\{^1H\}$ NMR spectra of the solution and were unable to detect neither coordinated nor free tppts. On the basis of this investigation we synthesized a more soluble derivative of the phoshine ligand. After exchanging the sodium cation of tppts with 1,2-dimethyl-3-butyl-imidazolium we prepared the tri(*m*-sulfonyl)triphenyl phosphine 1,2-dimethyl-3-butyl-imidazolium salt (tppti*) which showed good solubility characteristics in [bmim][PF_6] and was used in all the following catalyst evaluations.

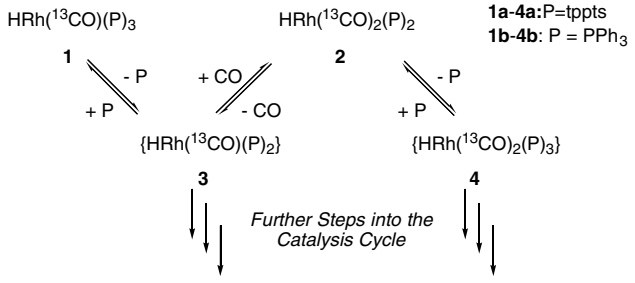

Scheme 1. Initial steps of the hydroformylation mechanism.

3.2. In situ investigation of the rhodium catalyst in ionic liquids

Despite the fact that the mechanism for hydroformylation catalysis is well established in organic [16] and aqueous [17] solvents, we wanted to study the active rhodium species in an ionic liquid environment (Scheme 1). To build upon a recent study focused on the in situ investigation of the rhodium-sulfoxantphos hydroformylation catalyst [18] in ionic liquids, we set out to investigate the rhodium-tppts catalyst system using HP-NMR techniques. In these experiments a mixture consisting of $Rh(CO)_2$(acac), tppts (Rh/P ratio 1:6) and [bmim][BF_4] was pressurized with 60 psi of $^{13}CO/H_2$ (1:1) in a sapphire NMR tube. To ensure the formation of the catalyst species $HRh(^{13}CO)(tppts)_3$ (**1a**) the solution was shaken at 60 °C for 1 h. After the pressure was released the $^{31}P\{^1H\}$ and $^{13}C\{^1H\}$ NMR spectra were recorded (Fig. 1). The $^{31}P\{^1H\}$ NMR spectrum of the catalyst solution showed a doublet at 32.2 ppm for the rhodium bound tppts ligand and a minor resonance at 29.1 ppm for the uncoordinated phosphine oxide species tri(*m*-sulfonyl)triphenylphosphine oxide trisodium (tppts-oxide) (Table 1). A strong signal at −3.7 ppm was apparent for uncoordinated tppts. The corresponding $^{13}C\{^1H\}$ NMR spectrum of the catalyst solution showed a doublet at 195.2 ppm for the metal coordinated carbon monoxide. For a better comparison we also investigated $HRh(^{13}CO)(PPh_3)_3$ **1b** in toluene-d^8 under $^{13}CO/H_2$ (1:1) pressure. Furthermore, we used the HP-NMR study by Horváth et. al. [17] for hydroformylation catalysis in aqueous phases as a reference. Thus, similar to the results of our catalyst investigation in [bmim][BF_4], the $^{31}P\{^1H\}$ NMR spectrum of **1b** in tolu-

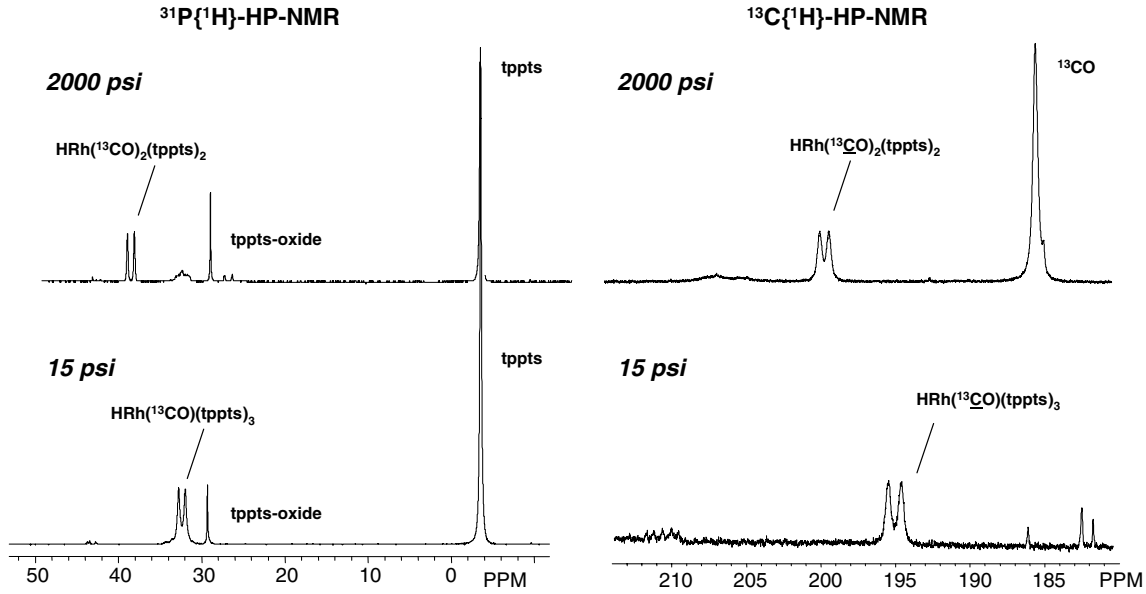

Fig. 1. High-pressure NMR investigation of a rhodium hydroformylation catalyst in the ionic liquid [bmim][BF_4] at 15 and 2000 psi $^{13}CO/H_2$ (1:1).

ene-d^8 showed a doublet at 37.8 ppm for the rhodium bound PPh_3 (Table 1). The corresponding $^{13}C\{^1H\}$ NMR spectrum of the solution exhibited a doublet at 206.6 ppm for the coordinated carbon monoxide ligand. On the basis of these spectroscopic results it can be assumed that the structure of $HRh(^{13}CO)(tppts)_3$ in [bmim][BF_4] is very similar to that of $HRh(^{13}CO)(PPh_3)_3$ in toluene-d^8.

Following this we studied the rhodium catalyst in ionic liquids under elevated syngas pressure. Mechanistic studies [16] of $HRh(^{13}CO)(PPh_3)_3$ (**1b**) and $HRh(^{13}CO)_2(PPh_3)_2$ (**2b**) in toluene have suggested the presence of two coordinatively unsaturated catalyst intermediates $\{HRh(^{13}CO)(PPh_3)_2\}$ (**3b**) and $\{HRh(^{13}CO)_2(PPh_3)\}$ (**4b**). While both of these species are responsible for the production of aldehyde, it is believed that the normal to iso ratio (*n*/*i*) of the aldehyde is largely controlled by the competitive reactions of the olefin with the species **3b** and **4b** resulting in high or low *n*/*i* ratios, respectively. Although we are not able to record the NMR spectra of the reactive intermediates **3b** and **4b**, we can observe the resting state of the catalyst in form of complexes **1b** and **2b**. As the equilibrium between these two complexes is strongly pressure dependent, complex **1b** can readily be converted into complex **2b** at a $^{13}CO/H_2$ (1:1) pressure of less than 300 psi in a toluene-d^8 solution. In contrast, the investigation of $HRh(^{13}CO)(tppts)_3$ **1a** in an aqueous solution showed that applied pressures of $^{13}CO/H_2$ (1:1) as high as 3000 psi did not lead to the formation of $HRh(^{13}CO)_2(tppts)_2$ (**2a**) [17]. Based on this information, we pressurised the complex **1a** in [bmim][BF_4] stepwise with $^{13}CO/H_2$ and recorded the corresponding NMR spectra. The increasing pressure resulted in the formation of new doublets in both the $^{31}P\{^1H\}$ NMR spectrum (39.1 ppm) and the $^{13}C\{^1H\}$ NMR spectrum (199.2 ppm). By going to higher syngas pressures, the intensities of the NMR resonances for **1a** continued to decrease. Finally, at a $^{13}CO/H_2$ pressure of 2000 psi the NMR signals for **1a** disappeared. We believe that the newly formed species in [bmim][BF_4] has the solution structure of $HRh(^{13}CO)_2(tppts)_2$ (**2a**) and corresponds to **2b** which has been observed in toluene-d^8 under elevated pressure. After the ionic liquid sample was depressurized the NMR resonances of **1a** were detected again. It is interesting to note that the NMR signal of the high-pressure species **2a** in [bmim][BF_4] exhibited a down field shift, while the related complex **2b** in toluene-d^8 showed an upfield shift for the corresponding resonances. Although the ionic liquid and toluene samples showed the formation of the high-pressure rhodium species **2a** and **2b**, the chemical environment on the metal center in [bmim][BF_4] seems to be different to that in the toluene-d^8. Finally, it should be noted that the in situ formation of **1a** in [bmim][BF_4] can be accompanied by a series of side reactions. Although it was possible to suppress most of the side reactions through the use of high-purity ionic liquids, we did sometimes observe the formation of unknown species during the investigation of **1a** in ionic liquids.

3.3. Preparation of high-purity ionic liquids

In addition to being important for catalyst lifetime, we also discovered that the purity of the ionic liquid is critical for the stability of the ionic liquid phase itself. In several biphasic hydroformylation experiments we observed the partial decomposition of [bmim][BF_4] and [bmim][PF_6]. After carefully analyzing the purity of these ionic liquids we found that trace amounts of acid were responsible for their decomposition. For this reason, we have used a synthesis procedure which produces high-purity ionic liquids [14]. In our synthesis 1-butyl-3-methyl-imidazolium chloride and 1,2-dimethyl-3-butyl-imidazolium chloride were either treated with $NaBF_4$ or KPF_6 giving [bmim][BF_4], [bmim][PF_6] and [bdmim][PF_6], respectively. The reactions were carried out in water followed by extraction with dichloromethane. The work-up procedure involved the filtration of the extract through a bed of activated carbon and alumina which produced high-purity ionic liquids after the removal of the solvent. The ionic liquids prepared via this route showed a neutral pH value and did not suffer from any substantial decomposition during hydroformylation reactions.

3.4. Evaluation of biphasic hydroformylation catalysis using ionic liquid phases

As a control experiment in the beginning of our study we investigated the reactivity of $Rh(CO)_2(acac)$ in [bmim][PF_6] without a ligand for the hydroformylation of hexene-1. The formed catalyst species produced C_7-aldehyde with a TOF between 21 and 2 min^{-1} and showed an *n*/*i* ratio for the aldehyde of 0.5–1.5 in the five respective runs. The low *n*/*i* ratio between 0.5 and 1.0 for the produced aldehyde is typically observed for rhodium catalysts in the absence of any coordinating ligand [15]. Typically under these reaction conditions, as mentioned earlier, rhodium forms an active rhodium-hydrido-carbonyl complex which readily converts olefin to aldehyde. The active species has no charge and dissolves preferentially in the organic phase. As a result, a substantial amount of the rhodium metal leaches from the ionic liquid into the organic layer. The loss of metal in our control experiment was also confirmed by rhodium metal analysis of the isolated product phases. After the first catalyst run an amount of 119 ppm of rhodium metal was found in the product phase. This amount corresponded to almost 75% of the initial rhodium charge to the reactor. Further runs showed continuous leaching of the metal until >90% of the initial rhodium charge was

removed with the product phase. Corresponding to the loss of active metal species, the conversion of olefin was significantly reduced after every consecutive run. It is therefore not viable to run hydroformylation reactions in ionic liquids with rhodium catalysts which cannot be sufficiently retained in the ionic layer.

Our next investigation focused on the evaluation of $Rh(CO)_2(acac)$ with tppti* in [bmim][BF_4] (Fig. 2/Table 2/Entries 1–10). The initial two runs (Entries 1 and 2) were carried out at a CO/H_2 (1:1) pressure of 300 psi. After we observed an extended induction period of 450 minutes in the first recycle we increased the reactor pressure to 600 psi CO/H_2 (1:1) for all of the consecutive runs. The activity of the catalyst decreased in the following eight runs (Entries 3–10) with their TOF values decreasing from 14 to 4 min^{-1}. The *n*/*i* ratio of the aldehyde remained between 2.6 and 2.1. This ratio is typically observed for a rhodium based hydroformylation catalyst in the presence of a coordinating phosphine ligand (Rh/P ratio 1:10). The analysis of the resulting organic products revealed the presence of low amounts of soluble rhodium species. During the 10 runs almost 10% of the total rhodium charged was removed from the reactor with the product phase. Although the rhodium leaching contributed towards the drop in activity, other catalyst deactivation processes like the formation of rhodium carbonyl clusters are most likely the reason

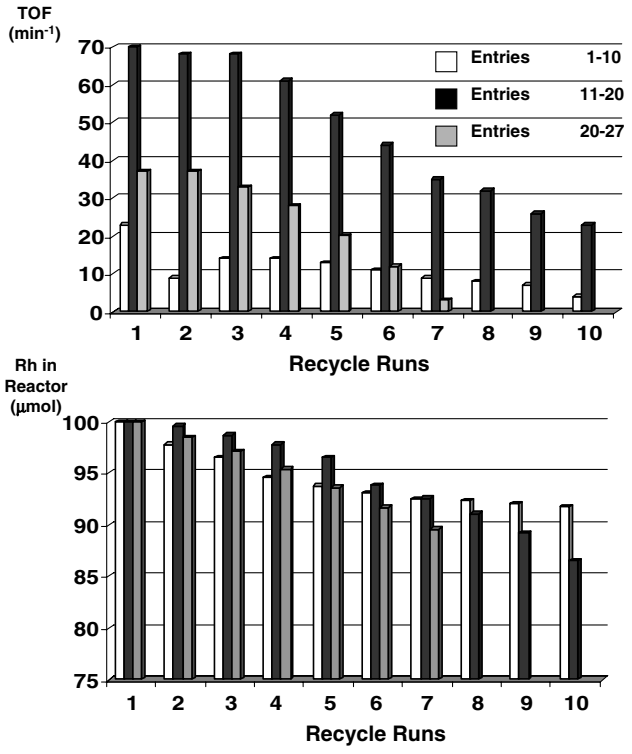

Fig. 2. TOF for biphasic hydroformylation reactions in different ionic liquid phases and rhodium metal content in the reactor during recycle runs.

for the loss in activity. The rhodium leaching from the ionic liquid phase into the organic layer may be associated with the solubility characteristics of [bmim][BF_4]. The ionic liquid has the ability to readily dissolve in water and other polar solvents. Depending on the aldehyde content in the product phase, small amounts of ionic liquid and rhodium complex can become soluble and leach into the organic layer. In one of our investigations (Entry 3) 2.7 ppm rhodium metal was detected in the organic phase at an aldehyde content of 61%. However, when the aldehyde level in the product phase was only 21% the amount of rhodium leaching was reduced to only 0.3 ppm (Entry 10). This trend indicated that the increasing polarity of the organic phase is partially responsible for the metal loss from the ionic liquid phase.

The next investigation focused on the evaluation of [bmim][PF_6]. All reactions were carried out at 600 psi CO/H_2 (1:1) and 100 °C using $Rh(CO)_2(acac)$ and tppti* (Rh/P ratio of 1:10) (Entries 11–20). The TOF values of the catalyst system decreased over the course of the investigation from 70 to 23 min^{-1}. Again the *n*/*i* ratios of the produced aldehydes were observed from 2.6 to 1.8, supporting a phosphine-stabilized rhodium center as the catalytically active species. Although the initial rhodium retention was better than in [bmim][BF_4], after the 6th recycle run the metal leaching became more prominent and surpassed the values obtained for the [bmim][BF_4] system.

To investigate the impact of a changing metal to phosphine ratio we also investigated the [bmim][PF_6] ionic liquid system with a Rh/P ratio of 1:3 and 1:100. As expected the TOF for the reaction carried out with a lower amount of phosphine ligand (1:3) was slightly increased to 75 min^{-1} (Entry 28), while the TOF for the catalysis with the higher loading (1:100) was reduced to 30 min^{-1} (Entry 29). Under both sets of reaction conditions the *n*/*i* ratios remained unchanged at 2.5 and 2.6. However, the higher amount of phosphine ligand helped to better retain the rhodium catalyst and reduced the metal loss to levels below the detection limit.

To broaden the scope of the studied ionic liquids we also investigated [bdmim][PF_6] (Entries 21–27). Although the TOF values were slightly higher than those obtained for [bmim][BF_4], ranging from 37 to 3 min^{-1}, the rhodium leaching was significantly increased. This may indicate that the less polar cation is partially responsible for the higher rhodium loss. Furthermore, the catalyst system showed a drastically reduced activity after the 5th recycle run and we concluded the campaign after the 7th run due to low activity.

In our final study we investigated the conventional homogeneous rhodium catalyst under similar reaction conditions. The reaction was carried out in toluene using $Rh(CO)_2(acac)$ together with PPh_3 (Rh/P ratio of 1:10). The homogeneous catalyst in a monophasic system

Table 2
Evaluation of hydroformylation reactions in ionic liquid media

Entry	Cycle[a]	Ionic liquid[b]	P[c]/Rh ratio	Rh reactor (μmol)	Rh product (ppm)	Time[d] (min)	Induct. (min)	TOF[e] (min^{-1})	*n*/*i*	Selectivity (%)		
										$1-C_6^=$	Ald.	Iso.[f]
1	1[g]	[bmim][BF_4]	10	100.00	4.1	230	40	23	2.2	5	58	37
2	2[g]	[bmim][BF_4]	10	97.79	1.9	700	450	9	1.9	9	54	37
3	3	[bmim][BF_4]	10	96.51	2.7	330	35	14	2.2	4	61	34
4	4	[bmim][BF_4]	10	94.62	1.3	255	0	14	2.4	29	46	25
5	5	[bmim][BF_4]	10	93.75	1.0	265	0	13	2.1	28	47	25
6	6	[bmim][BF_4]	10	93.07	0.8	360	0	11	2.5	32	44	24
7	7	[bmim][BF_4]	10	92.54	0.3	410	0	9	2.5	39	39	22
8	8	[bmim][BF_4]	10	92.34	0.5	365	0	8	2.5	47	34	19
9	9	[bmim][BF_4]	10	92.03	0.4	310	0	7	2.6	55	30	15
10	10	[bmim][BF_4]	10	91.79	0.3	275	0	4	2.6	66	21	13
11	1	[bmim][PF_6]	10	100.00	0.7	100	12	70	2.6	32	63	5
12	2	[bmim][PF_6]	10	99.59	1.4	120	26	68	2.5	10	73	17
13	3	[bmim][PF_6]	10	98.69	1.8	100	13	68	2.4	8	67	25
14	4	[bmim][PF_6]	10	97.77	1.7	100	19	61	2.3	5	62	33
15	5	[bmim][PF_6]	10	96.57	3.9	120	18	52	2.3	8	55	37
16	6	[bmim][PF_6]	10	93.87	1.9	265	25	44	1.9	1	59	40
17	7	[bmim][PF_6]	10	92.57	2.2	240	28	35	1.9	1	54	45
18	8	[bmim][PF_6]	10	91.07	2.9	300	41	32	1.8	1	52	47
19	9	[bmim][PF_6]	10	89.17	3.9	300	50	26	1.8	1	49	50
20	10	[bmim][PF_6]	10	86.57	3.7	300	75	23	1.9	2	44	54
21	1	[bdmim][PF_6]	10	100.00	2.3	180	20	37	2.3	4	37	59
22	2	[bdmim][PF_6]	10	98.5	2.2	180	20	37	2.2	5	57	38
23	3	[bdmim][PF_6]	10	97.1	2.5	210	50	33	2.2	8	53	40
24	4	[bdmim][PF_6]	10	95.4	2.7	180	35	28	2.3	13	45	42
25	5	[bdmim][PF_6]	10	93.6	2.9	250	50	20	2.3	9	41	50
26	6	[bdmim][PF_6]	10	91.7	3.2	360	105	12	2.4	14	39	47
27	7	[bdmim][PF_6]	10	89.6	2.1	500	250	3	2.6	49	17	34
28	1	[bmim][PF_6]	3	100	0.68	150	60	75	2.5	2	81	17
29	1	[bmim][PF_6]	100	100	0.02	200	13	30	2.6	9	87	4
30[i]	1	Toluene	10	25.0	–	120	0	400	2.6	2	95	3

[a] All reactions were carried out in a 300 ml autoclave (2200 rpms) at 100 °C and 600 psi (CO/H_2 ratio 1:1).

[b] Ionic liquid [bmim][BF_4] 1-butyl-3-methyl-imidazolium tetrafluoroborate, [bmim][PF_6] 1-butyl-3-methyl-imidazolium hexafluorophosphate and [bdmim][PF_6] 1,2-dimethyl-3-butyl-imidazolium hexafluorophosphate.

[c] Phosphine ligand tri(*m*-sulfonyl)triphenylphosphine tris(1,2-dimethyl-3-butyl-imidazolium) salt (tppti*).

[d] Full reaction time (including induction period).

[e] TOF defined as mol(aldehyde) per mol(rhodium) per minute (determined during the initial 30 min of gas consumption).

[f] Isomerized $1-C_6^=$ to $2-C_6^=$ and $3-C_6^=$.

[g] Reactor pressure at 300 psi.

[i] Run ligand – triphenylphosphine.

exhibited a significantly higher TOF value of 400 min^{-1} with an *n*/*i* ratio of 2.6 for the produced aldehyde. For comparison the best TOF values obtained for any of the biphasic hydroformylation runs in ionic liquids ranged between 70 and 75 min^{-1} under comparable reaction conditions. Finally the homogeneous catalyst system showed a significantly higher reactivity, however, the biphasic ionic liquid catalyst systems offer the possibility of convenient product separation and easy catalyst recovery.

4. Conclusion

The ionic liquids [bmim][BF_4], [bmim][PF_6] and [bdmim][PF_6] were successfully used for the immobilization of rhodium based hydroformylation catalysts and have been evaluated for the production of aldehyde in a liquid–liquid biphase environment. The purity of the ionic liquids was strictly monitored to avoid any decomposition of the catalyst, substrate and/or ionic liquid. A complimentary HP-NMR study confirmed that the solution structure of $HRh(^{13}CO)(tppts)_3$ (**1a**) in [bmim][BF_4] is similar to that of $HRh(^{13}CO)(PPh_3)_3$ (**1b**) in toluene-d^8. Furthermore, the NMR investigation at elevated syngas pressures showed that **1a** lies in equilibrium with the high-pressure species $HRh(^{13}CO)_2(tppts)_2$ (**2a**). As expected the activity of the biphasic ionic liquid system containing the Rh/tppti* catalyst is approximately one order of magnitude lower than the conventional Rh/PPh_3 catalyst in toluene. The Rh/tppti* catalyst system showed a decrease of activity in the semicontinuous hydroformylation of hexene-1 due to catalyst deactivation and/or metal loss. The *n*/*i* ratio of the produced heptanal only slightly increased after changing the Rh/P ratio from 1:3 to 1:100 in [bmim][PF_6]. The loss of rhodium metal from the ionic liquid phases seemed to be dependent on the solubility characteristics of the ionic liquid and on the concentration of the aldehyde in the organic phase. In this respect, the ionic liquid [bmim][PF_6] was preferred due to its very low miscibility with polar substances. Although ionic liquids offer tremendous opportunities for the development of novel separation technologies, further progress will be necessary to fully establish their potential as a large-volume reaction medium.

Acknowledgements

We thank Dr. H. Freund for carrying out a thermal stability study and Drs. C.A. Costello, J.L. Robbins and R.H. Schlosberg for valuable discussions and their continued support.

References

[1] C.D. Frohning, C.W. Kohlpainter, in: B. Cornils, W.A. Herrmann (Eds.), Applied Homogeneous Catalysis with Organometallic Compounds, Wiley–VCH, Weinheim, 1996, p. 29.
[2] (a) B. Cornils, E.G. Kuntz, in: B. Cornils, W.A. Herrmann (Eds.), Aqueous-Phase Organometallic Catalysis, Wiley–VCH, Weinheim, 1998, p. 271;
(b) J.P. Arhancet, M.E. Davis, J.S. Merola, B.E. Hanson, Nature 339 (1989) 454.
[3] I.T. Horvath, J. Rabai, Science 266 (1994) 72.
[4] (a) P.G. Jessop, T. Ikariya, R. Noyori, Chem. Rev. 99 (1999) 475;
(b) P.G. Jessop, W. Leitner, in: P.G. Jessop, W. Leitner (Eds.), Leitner, Chemical Synthesis using Supercritical Fluids, Wiley–VCH, Weinheim, 1999, p. 351.
[5] (a) F.R. Hartley, Supported Metal Complexes. A New Generation of Catalysts, Kluwer Academic Publishers, Dordrecht, 1985;
(b) M.T. Reetz, G. Lohmer, R. Schwickardi, Angew. Chem., Int. Ed. Engl. 36 (1997) 1526;
(c) W. Keim, B. Driessen-Hölscher, in: G. Ertl, H. Knözinger, J Weitkamp (Eds.), Handbook of Heterogeneous Catalysis, vol. 1, Wiley–VCH, Weinheim, 1997.
[6] (a) T. Welton, Chem. Rev. 99 (1999) 2071;
(b) J.D. Holbrey, K.R. Seddon, Clean Prod. Process. 1 (1999) 223;
(c) P. Wasserscheid, W. Keim, Angew. Chem., Int. Ed. 39 (2000) 3772;
(d) R. Sheldon, Chem. Commun. (2001) 2399;
(e) J. Dupont, R.F. de Souza, P.A.Z. Suarez, Chem. Rev. 102 (2002) 3667;
(f) H. Olivier-Bourbigou, L. Magna, J. Mol. Catal. A 182 (2002) 419;
(g) P. Wasserscheid, in: P. Wasserscheid, T. Welton (Eds.), Ionic Liquids in Synthesis, Wiley–VCH, Weinheim, 2003, p. 213.
[7] G.W. Parshall, J. Am. Chem. Soc. 94 (1972) 8716.
[8] Y. Chauvin, L. Mussmann, H. Olivier, Angew. Chem., Int. Ed. 34 (1995) 2698.
[9] E.G. Kuntz, Chemtech (1987) 570.
[10] (a) J.F. Knifton, J. Mol. Catal. 43 (1987) 65;
(b) J.F. Knifton, J. Mol. Catal. 47 (1988) 99;
(c) N. Karodia, S. Guise, C. Newlands, J.-A. Andersen, Chem. Commun. (1998) 2341;
(d) W. Keim, D. Vogt, H. Waffenschmidt, P. Wasserscheid, J. Catal. 186 (1999) 481;
(e) P. Wasserscheid, H. Waffenschmidt, J. Mol. Catal. A 164 (2000) 61;
(f) C.C. Brasse, U. Englert, A. Salzer, H. Waffenschmidt, P. Wasserscheid, Organometallics 19 (2000) 3818;
(g) P. Wasserscheid, H. Waffenschmidt, P. Machnitzki, K.W. Kottsieper, O. Stelzer, Chem. Commun. (2001) 451;
(h) M.F. Sellin, P.B. Webb, D.J. Cole-Hamilton, Chem. Commun. (2001) 781;
(i) F. Favre, H. Olivier-Bourbigou, D. Commereuc, L. Saussine, Chem. Commun. (2001) 1360;
(j) J. Dupont, S.M. Silva, R.F. de Souza, Catal. Lett. 77 (2001) 131;
(k) R.P.J. Bronger, S.M. Silva, P.C.J. Kamer, P.W.N.M. van Leeuwen, Chem. Commun. (2002) 3044;
(l) O. Stenzel, H.G. Raubenheimer, C. Esterhuysen, J. Chem. Soc., Dalton Trans. (2002) 1132.
[11] S.N. Bizzari, S. Fenelon, M. Ishikawa-Yamaki, Chemical Economics Handbook, SRI International, Menlo Park, 1999, 682.7000A.
[12] C.P. Mehnert, R.A. Cook, N.C. Dispenziere, M. Afeworki, J. Am. Chem. Soc. 124 (2002) 12932.

[13] I.T. Horváth, J.M. Millar, Chem. Rev. 91 (1991) 1339.
[14] (a) P. Bonhôte, A.P. Dias, N. Papageorgiou, K. Kalyanasundaram, M. Grätzeb, Inorg. Chem. 25 (1996) 1168;
(b) J.D. Holbrey, K.R. Seddon, J. Chem. Soc., Dalton Trans. (1999) 2133;
(c) J.H. Davis, C.M. Gordon, C. Hilger, P. Wasserscheid, T. Welton (Eds.), Wiley–VCH, Weinheim, 2003, p. 7.
[15] B. Cornils, in: J. Falbe (Ed.), New Syntheses with Carbon Monoxide, Springer, Berlin, 1980, p. 1.
[16] (a) C. O'Connor, G. Yagupsky, D. Evans, G. Wilkinson, J. Chem. Soc., Chem. Commun. (1968) 420;
(b) D. Evans, G. Yagupsky, G. Wilkinson, J. Chem. Soc. (A) (1968) 2660;
(c) D. Evans, J.A. Osborn, G. Wilkinson, J. Chem. Soc. (A) (1968) 3133;
(d) C.K. Brown, G.J. Wilkinson, J. Chem. Soc. (A) (1970) 2753;
(e) R.L. Pruett, J.A. Smith, J. Org. Chem. 34 (1969) 327;
(f) R.L. Pruett, Adv. Organomet. Chem. 17 (1979) 1;
(g) G. Gregoria, G. Montrasi, M. Tampierei, P. Cavaliezi d'Oro, G. Pagani, A. Andreetta, Chim. Ind. (Milan) 62 (1980) 389;
(h) P. Cavaliezi d'Oro, L. Raimondi, G. Pagani, G. Montrasi, G. Gregorio, A. Andreetta, Chim. Ind. (Milan) 62 (1980) 572;
(i) A.A. Oswald, J.S. Merola, E.J. Mozeleski, R.J. Kastrup, R.V. Reisch, in: L.D. Quin, J.G. Verkade (Eds.), Advances in Chemistry Series, vol. 171, American Chemical Society, Washington (DC), 1981, p. 503;
(j) R.J. Kastrup, J.S. Merola, A.A. Oswald, in: E.C. Alyca, D.W. Mcck (Eds.), Advances in Chemistry Series, vol. 196, American Chemical Society, Washington (DC), 1982, p. 43;
(k) A.A. Oswald, D.E. Hendriksen, R.J. Kastrup, J.S. Merola, Prepr. Pap., Am. Chem. Soc., Div. Pet. Chem. 27 (1982) 292;
(l) J.M. Brown, L.R. Canning, A.G. Kent, P.J. Sidebottom, J. Chem. Soc., Chem. Commun. (1982) 721;
(m) J.M. Brown, A.G. Kent, J. Chem. Soc., Chem. Commun. (1982) 723;
(n) J.M. Brown, A.G. Kent, J. Chem. Soc., Perkin Trans. 2 (1987) 1597;
(o) W.R. Moser, C.J. Papile, D.A. Brannon, R.A. Duwell, S.J. Weininger, J. Mol. Catal. 41 (1987) 271.
[17] I.T. Horváth, R.V. Kastrup, A.A. Oswald, E.J. Mozeleski, Catal. Lett. 2 (1989) 85.
[18] S.M. Silva, R.P.J. Bronger, Z. Freixa, J. Dupont, P.W.N.M. van Leeuwen, New J. Chem. 27 (2003) 1294.

Available online at www.sciencedirect.com
SCIENCE DIRECT®
Polyhedron 23 (2004) 2689–2694
POLYHEDRON
www.elsevier.com/locate/poly

Bis(pentamethylcyclopentadienyl) U(III) oxide and U(IV) oxide carbene complexes

William J. Evans *, Stosh A. Kozimor, Joseph W. Ziller

Department of Chemistry, 516 RowLand Hall, University of California, Irvine, CA 92697 2025, USA

Received 15 April 2004; accepted 25 August 2004
Available online 25 September 2004

Dedicated to Professor Malcolm Green, whose inspiring appetite for discovery has given us such an amazing breadth of new inorganic and organometallic chemistry

Abstract

Oxidation of the sterically crowded complex $(C_5Me_5)_3U$ provides access to two classes of uranium compounds that previously were unknown, a U(III) oxide and a U(IV) carbene, $[(C_5Me_5)_2U]_2(\mu\text{-}O)$ (**1**) and $(C_5Me_5)_2U(O)[C(NMeCMe)_2]$ (**2**), respectively. The structure of **1** allows a direct actinide versus lanthanide comparison within the $[(C_5Me_5)_2M]_2(\mu\text{-}O)$ class. The uranium carbene complex (**2**), represents a rare example of a monometallic uranium mono-oxo-compound. Complex **1** has a 2.094(14) Å U(1)–O(1) bond distance and a 171.5(6)° U(1)–O(1)–U(2) bond angle while the U(1)–O(1) and U(1)–C(21)[C(NMeCMe)$_2$] bond distances in complex **2** are 1.917(6) and 2.673(7) Å, respectively.
© 2004 Published by Elsevier Ltd.

Keywords: Actinide; Lanthanide; Oxides; Carbene; Uranium

1. Introduction

Recent studies of the chemistry of the sterically crowded trivalent uranium complex, $(C_5Me_5)_3U$ [1,2], have shown that it can function as a two or three electron reductant depending on the substrate available, as shown in Eqs. (1) and (2), respectively [3,4].

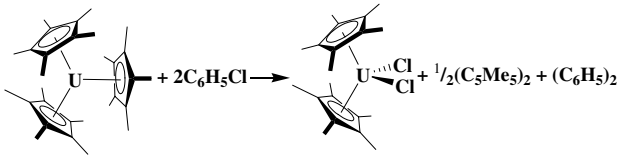

(1)

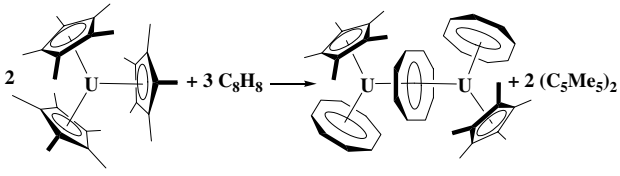

(2)

The reductive reactivity arises not only from the conventional metal-based U(III)/U(IV) redox couple, as is typical for trivalent uranium complexes, but also from $C_5Me_5^{1-}/C_5Me_5$ ligand-based reductions arising from the steric crowding in the system. Since the reductive chemistry of the normally inert $C_5Me_5^{1-}$ ligand appears to be activated by the steric crowding, it has been called sterically induced reduction (SIR) [4].

One reaction common to any type of reductant is oxidation to form oxide products. With organometallic complexes of electropositive metals, this is usually avoided by using rigorously purified inert atmospheres,

* Corresponding author. Tel.: +1 949 824 5174; fax: +1 949 824 2210.
E-mail address: wevans@uci.edu (W.J. Evans).

0277-5387/$ - see front matter © 2004 Published by Elsevier Ltd.
doi:10.1016/j.poly.2004.08.007

solvents, reagents, and in some cases even silylated glassware [5]. Nevertheless, oxide products occasionally arise despite the best efforts to avoid extraneous oxidants [6–10].

When highly reactive organometallic complexes react with oxygen, insoluble oxide products often form that are difficult to characterize. Hence, little is known about the preliminary stages of this common reaction. Only in the occasional cases in which fully characterizable organometallic oxide complexes are obtained as byproducts can such information be obtained [11–15]. In organometallic uranium chemistry, only U(IV), U(V), and U(VI) oxides are familiar. Oxide complexes of uranium in the trivalent state are not generally accessible since oxidation of the metal is likely and this usually results in formation of tetra-, penta-, or hexavalent uranium oxides [16–20].

We report here on two new organometallic uranium oxide products formed from the $(C_5Me_5)_3U$ reduction system. One is unusual in that it is an organometallic U(III) oxide. To our knowledge, this is the first molecular trivalent uranium oxide reported. This complex provides the first opportunity to make direct structural comparisons between $5f^3$ and $4f^3$oxides, a comparison that is of interest in regard to the separation of lanthanide contaminants from highly reactive actinide components in spent nuclear fuel [21–23]. The other compound represents a rare example of a uranium terminal monooxide. Generally uranium oxo-compounds contain the dioxo $(O{=}U{=}O)^{2+}$ unit and few examples of terminal mono-oxides have been reported. Furthermore, this second compound constitutes the first U(IV) *N*-heterocyclic carbene in the literature. The unusual structural aspects of both complexes are discussed.

2. Experimental

2.1. $[(C_5Me_5)_2U]_2(\mu\text{-}O)$ (1)

In an argon-filled glovebox free of coordinating solvents, X-ray quality crystals of **1** were obtained unexpectedly from an NMR sample of a reaction between $(C_5Me_5)_3U$ [1,2] and potassium graphite in toluene. A large blackberry-colored crystal of approximate dimensions $0.20 \times 0.33 \times 0.78$ mm was mounted on a glass fiber and transferred to a Bruker CCD platform diffractometer. The SMART [24] program package was used to determine the unit cell parameters and for data collection (25 s/frame scan time for a sphere of diffraction data). The raw frame data was processed using SAINT [25] and SADABS [26] to yield the reflection data file. Subsequent calculations were carried out using the SHELXTL [27] program. There were no systematic absences. The noncentrosymmetric triclinic space group $P\bar{1}$ was assigned and later determined to be correct ($Z = 1$). The structural parameters for **1** are summarized in Table 1.

The structure was solved by direct methods and refined on F^2 by full-matrix least-squares techniques. The analytical scattering factors [28] for neutral atoms were used throughout the analysis. Hydrogen atoms were included using a riding model. One molecule of toluene solvent was present per formula unit. Attempts to solve the structure using the centrosymmetric space group $P\bar{1}$ were unsuccessful. At convergence, $wR_2 = 0.0859$ and Gof = 1.103 for 452 variables refined against 7845 data (0.80 Å). As a comparison for refinement on F, $R_1 = 0.0351$ for those 7673 data with $I > 2.0\sigma(I)$. The structure was refined using the TWIN and BASF (0.26) instructions [27]. Selected bond distances and angles for **1** and **2** are given in Table 2.

2.2. $(C_5Me_5)_2U(O)[C(NMeCMe)_2]$ (2)

In an argon-filled glovebox free of coordinating solvents, X-ray quality crystals of **2** were obtained from an NMR sample of a reaction between $(C_5Me_5)_3U$ [1,2] and the carbene $C(NMeCMe)_2$ [29] in toluene. A red/brown crystal of approximate dimensions $0.17 \times 0.20 \times 0.22$ mm was mounted on a glass fiber and transferred to a Bruker CCD platform diffractometer. The SMART [24] program package was used to determine the unit cell parameters and for data collection (40 s/frame scan time for a sphere of diffraction data). The raw frame data was processed using SAINT [25] and SADABS [26] to yield the reflection data file. Subsequent calculations were carried out using the SHELXTL [27] program. The diffraction symmetry was 2/*m* and the systematic absences were consistent with the centrosym-

Table 1
X-ray data collection parameters for $[(C_5Me_5)_2U]_2(\mu\text{-O})$ (**1**) and $(C_5Me_5)_2U(O)[C(NMeCMe)_2]$ (**2**)

	1	**2**
Empirical formula	$C_{40}H_{60}OU_2 \cdot C_7H_8$	$C_{27}H_{42}N_2OU$
Formula weight	1125.07	648.66
Crystal system	triclinic	monoclinic
Space group	$P\bar{1}$	$P2_1c$
a (Å)	9.4759(7)	16.1072(14)
b (Å)	10.8487(8)	8.6794(8)
c (Å)	12.5024(14)	18.8631(17)
α (°)	82.1480(10)	90
β (°)	68.5230(10)	90.980(2)
γ (°)	64.4380(10)	90
Volume (Å^3)	1078.60(17)	2636.7(4)
Z	1	4
λ (Å)	0.71073	0.71073
ρ_{calc} (Mg/m^3)	1.732	1.634
Absorption coefficient (mm^{-1})	7.530	6.176
Goodness-of-fit on F^2	1.103	1.062
R^a [$I > 2\sigma(I)$]: R_1	0.0351	0.0457
R^b (all data): wR_2	0.0859	0.1259

Table 2
Selected bond distances (Å) and angles (°) for $[(C_5Me_5)_2U]_2(\mu\text{-}O)$ (**1**) and $(C_5Me_5)_2U(O)[C(NMeCMe)_2]$ (**2**)

	1		**2**
Bond distances			
U–C(C_5Me_5) range	2.676(9)–2.823(9)	U(1)–C(C_5Me_5) range	2.715(9)–2.871(9)
U(1)–O(1)	2.094(14)	U(1)–O(1)	191.7(6)
U(2)–O(1)	2.125(13)	U(1)–C(NCH)	2.637(9)
U–Cnt range	2.455–2.487	U(1)–Cnt range	2.523–2.527
Bond angles			
U(1)–O(1)–U(2)	171.5(6)	O(1)–U(1)–C(21)	93.3(3)
Cnt–U(1)–Cnt	134.5	Cnt–U(1)–Cnt	136.3
Cnt–U(1)–O(1)	110.6	Cnt–U(1)–O(1)	106.4
Cnt–U(2)–O(1)	114.0	Cnt–U(1)–C(21)	104.4

metric monoclinic space group $P2_1/c$ which was later determined to be correct.

The structure was solved by direct methods and refined on F^2 by full-matrix least-squares techniques. The analytical scattering factors [28] for neutral atoms were used throughout the analysis. Hydrogen atoms were included using a riding model. At convergence, $wR_2 = 0.1259$ and Gof = 1.062 for 280 variables refined against 4494 data (0.85 Å). As a comparison for refinement on F, $R_1 = 0.0457$ for those 3299 data with $I > 2.0\sigma(I)$ [27].

3. Results and discussion

3.1. $[(C_5Me_5)_2U]_2(\mu\text{-}O)$ (1)

Complex **1** was isolated from a reaction of $(C_5Me_5)_3U$ with KC_8 in toluene. Formation of **1** in this system is unusual for several reasons. First, the oxide is obtained in a reducing environment. Second, formation of oxides from U(III) organometallic complexes generally gives products in at least the U(IV) oxidation state. For example, stoichiometric addition of oxygen to the less crowded trivalent $(C_5H_5)_3U$ generated the tetravalent product, $[(C_5H_5)_3U]_3(\mu\text{-}O)$ [17]. Similarly, a tetravalent uranium oxide, $\{[C_5H_3(SiMe_3)_2]_2U\}(\mu\text{-}O)_2$, is isolated from hydrolysis of $[C_5H_3(SiMe_3)_2]_3U$ with one equivalent of H_2O, a reaction that goes through a trivalent bridging hydroxide intermediate, $\{[C_5H_3(SiMe_3)_2]_2U\}_2(\mu\text{-}OH)_2$ [20]. In addition, trivalent uranium complexes generally react with oxide delivery agents, such as R_3NO, by the U(III)/U(IV) redox couple [18,19].

Finally, if the oxide is formed by oxidation of a $C_5Me_5^{1-}$ ligand, it would be the first reaction identified in which the SIR involving the $C_5Me_5^{1-}$ reduction precedes the U(III) electron transfer. For example, the reaction of $(C_5Me_5)_3U$ with aryl halides (Eq. (1)) proceeds by reduction with U(III) followed by the $C_5Me_5^{1-}$ based sterically induced reduction [3]. Hence, regardless of the oxygen source, be it O_2, H_2O, or some other oxide delivery agent, a U(IV) product might be expected instead of the U(III) complex isolated here.

Since complex **1** was isolated from the reaction of $(C_5Me_5)_3U$ and KC_8 in toluene, an alternative possibility involves initial reductive cleavage of a $C_5Me_5^{1-}$ ring by KC_8 to form a $[(C_5Me_5)_2U]_2(MeC_6H_5)$ intermediate which subsequently reacts with the oxygen impurity [30–32]. However, attempts to make **1** directly along these lines have been unsuccessful.

The structure of $[(C_5Me_5)_2U]_2(\mu\text{-}O)$, Fig. 1, provides an interesting addition to uranium oxides, Table 2, as well as to the series of $[(C_5Me_5)_2M]_2(\mu\text{-}O)$ oxides previously identified for several trivalent lanthanides (M = La [9], Nd [33], Sm [11], and Y[34]), Table 3. Direct comparisons of analogous lanthanide and actinide complexes and identification of the subtle differences between these elements could provide the basis for effective actinide/lanthanide separation methods [21–23,35–38]. Although several classes of actinide and lanthanide complexes have been compared [39–42], no studies have been published on trivalent organometallic metal oxides since synthetic routes to the U(III) oxide complexes were not available. The structure of **1** allows a direct comparison of U(III) with the trivalent lanthanides and an evaluation of 5f/4f similarities and differences.

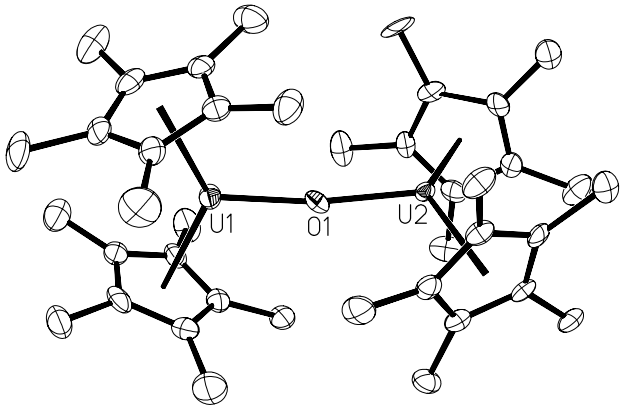

Fig. 1. A thermal ellipsoid plot of **1**, $[(C_5Me_5)_2U]_2(\mu\text{-}O)$, with thermal ellipsoids drawn to 50% probability. The molecule of toluene has been omitted for clarity.

Table 3
Bond distances and ionic radii [44] of $[(C_5Me_5)_2M]_2(\mu\text{-}O)$ (M = U, La [9], Nd [34], Sm [11], Y [35]) complexes

Compound	Ionic radius (Å)	M–O distance (Å)	M–O–M angle (°)	M–C(C_5Me_5) (Å)	M-ring centroid (Å)
$[(C_5Me_5)_2La]_2(\mu\text{-}O)$	1.10	2.1443(3)	180	2.811(3)–2.852(3)	2.561
$[(C_5Me_5)_2U]_2(\mu\text{-}O)$	1.075	2.125(13) 2.094(14)	171.5(6)	2.676(9)–2.823(9)	2.455–2.487
$[(C_5Me_5)_2Nd]_2(\mu\text{-}O)$	1.046	2.101	180	2.739–2.796	2.496
$[(C_5Me_5)_2Sm]_2(\mu\text{-}O)$	1.02	2.094(1)	180	2.72(1)–2.77(1)	2.470
$[(C_5Me_5)_2Y]_2(\mu\text{-}O)$	0.96	2.0525(10)	180	2.656(5)–2.710(5)	2.396

No error limits were available for the Nd structure.

The four structurally characterized lanthanide analogs of **1**, $[(C_5Me_5)_2M]_2(\mu\text{-}O)$ (M = La [9], Nd [33], Sm [11], and Y [34]), display a direct correlation between the M–O bond distances and the ionic radius of the metal. This is as expected for an isomorphous series of complexes in which the bonding is predominantly ionic. Each of these complexes also has a 180° M–O–M angle. This can be rationalized on the basis of steric interactions between the two bulky $[(C_5Me_5)_2M]^+$ units which collectively have the sterically preferred tetrahedral arrangement of the four $C_5Me_5^{1-}$ rings. Alternatively, the linear M–O–M angle could be attributed to multiple bonding between the oxygen and the metals.

Complex **1** is not isomorphous with the other members of the $[(C_5Me_5)_2M]_2(\mu\text{-}O)$ (M = La, Nd, Sm, Y) oxide family and it crystallizes with a molecule of toluene in the cell. The closest approach of the planar toluene molecule to U(1) is 6.73 Å.

On the basis only of ionic radii and extrapolating from the bond distances of the $[(C_5Me_5)_2M]_2(\mu\text{-}O)$ complexes (La, Nd, Sm, and Y [9]), a U–O bond of 2.126 Å would be expected. The 2.094(14) Å U(1)–O(1) and 2.125(13) Å U(2)–O(1) distances in complex **1** are equivalent to this prediction within the experimental error. Hence, an ionic estimation of the U–O bond length based on Shannon radii is close to the observed values [43]. Related to this, Ephritikhine and co-workers [41]have recently observed that U–O distances in the $\{UI_2[OP(C_6H_5)_3]_3\}$ {I} complex can also be predicted based on ionic radii.

Although the U–O distance in **1** is consistent with those of the $[(C_5Me_5)_2M]_2(\mu\text{-}O)$ complexes, the geometry differs slightly in that the U–O–U angle is 171.5(6)° rather than the usual 180°. As shown in the end-on view of Fig. 2, the four $C_5Me_5^{1-}$ ring centroids are still nearly tetrahedral. The (ring centroid)–U(1)–(ring centroid) plane makes a 91.2° angle with the (ring centroid)–U(2)–(ring centroid) plane. In the lanthanide structures, this value is exactly 90° by the crystallographic symmetry.

Associated with this structural distortion, the coordination environments around U(1) and U(2) are not rigorously trigonal planar as in the lanthanide structures. U(1) and U(2) are displaced from the plane defined by their two ring centroids and the oxide by 0.13 and 0.25 Å, respectively. The structure of **1** also differs from the previously characterized $[(C_5Me_5)_2M]_2(\mu\text{-}O)$ complexes in that each uranium atom has one ring in which all of the U–C(C_5Me_5) bond distances are similar, 2.716(9)–2.749(10) Å for U(1)–C(1–5)(C_5Me_5), and one ring that has a wide range of U–C(C_5Me_5) bond distances, 2.676(9)–2.823(9) Å for U(1)–C(11–15)(C_5Me_5). The longest U–C(C_5Me_5) distances are found for the carbons most distant from the oxide and the interior of the structure. In comparison, the values for $[(C_5Me_5)_2Sm]_2(\mu\text{-}O)$ are 2.72(1)–2.77(1) Å for both rings. In both **1** and the lanthanide structures, the rings on each metal are closer to eclipsed than staggered, which is consistent with a sterically crowded environment [44].

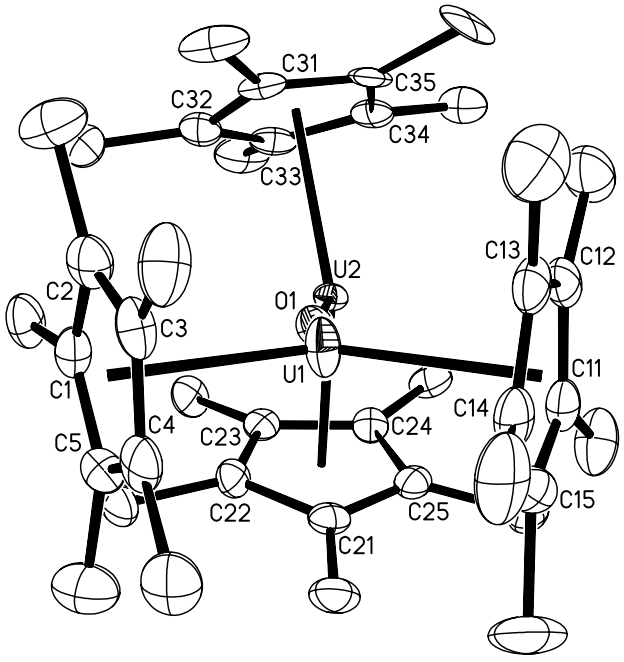

Fig. 2. A thermal ellipsoid plot of **1**, $[(C_5Me_5)_2U]_2(\mu\text{-}O)$, with thermal ellipsoids drawn to 50% probability. The molecule of toluene has been omitted for clarity.

The structure of **1** is unusual in that a more covalent 5f $[(C_5Me_5)_2M]_2(\mu\text{-}O)$ complex might be expected to have more M–O multiple bonding which would generate a shorter M–O distance and a rigorously linear M–O–M

angle. Neither of these structural features are observed in **1**. It is interesting to compare the 2.094(14) and 2.125(13) Å U–O distances as well as the 171.5(6)° U–O–U angle in **1** to those in related organouranium oxide and sulfide structures. The tetravalent uranium oxide complexes $[(C_5H_5)_3U]_2(\mu\text{-O})$ [17] and $[(C_5H_4SiMe_3)_3U]_2(\mu\text{-O})$ [16] both have 180° U–O–U angles and similar 2.0881(4) and 2.1053(2) Å U–O distances, respectively. The sulfur bridged complex, $[(C_5H_4Me)_2U]_2(\mu\text{-S})$, has longer 2.60(1) Å U–S distances that separate the metallocene units to a greater extent than in the oxide and a 164.9(4)° angle is observed [45]. The slightly bent structure of **1** differs from all of these prior examples.

3.2. $(C_5Me_5)_2U(O)[C(NMeCMe)_2]$ (2)

Complex **2** was isolated from a reaction between $(C_5Me_5)_3U$ and the strong sigma bonding N-heterocyclic carbene (NHC) ligand, $C(NMeCMe)_2$ [46–48]. Although a carbene complex was isolated, this was accompanied by unexpected oxidation and complex **2** represents not only the first U(IV) carbene complex, Fig. 3, but also a rare example of a uranium mono-oxide. Although the $[UO_2]^{2+}$ unit is common in uranium chemistry [49–52], only a few reports of uranium terminal mono-oxides are in the literature [18,19,53]. To our knowledge this is the first such example in organometallic U(IV) chemistry.

Complex **2** is assigned a U(IV) oxide structure rather than a U(III)–OH structure on the basis of the short 1.916(6) Å U–O bond length, Table 2. The U–O distance in **2** is shorter than (a) the corresponding distance in bridging U(IV) oxides, i.e. the 2.0881(4) Å in $[(C_5H_5)_3U]_2(\mu\text{-O})$ [17], (b) the 2.145(6) Å U–O(OH) distance in the U(IV) terminal hydroxide complex $U(NN'_3)(OH)(CH_2PMe_3)$ [8], and (c) the 2.44(2) Å U–$O(OH_2)$ distance in the U(VI) terminal H_2O complex $[C_{20}H_{36}O_6][(UO_2)_2(H_2O)_6](ClO_4)_2$ [50]. The U–O bond length in **2** is longer than those in higher valent uranium organometallic terminal mono-oxide complexes: 1.859(6) Å in $(C_5Me_5)_2U^{(V)}(OAr)(O)$ [18], 1.844(4) Å in $(C_5Me_5)_2U^{(VI)}(NAr)(O)$ [19], and 1.76(1) Å in $U^{(VI)}OCl_5^{1-}$ [53]. U–O distances of 1.70–1.76 Å are typical in $U^{VI}O_2$ uranyl compounds [49–52].

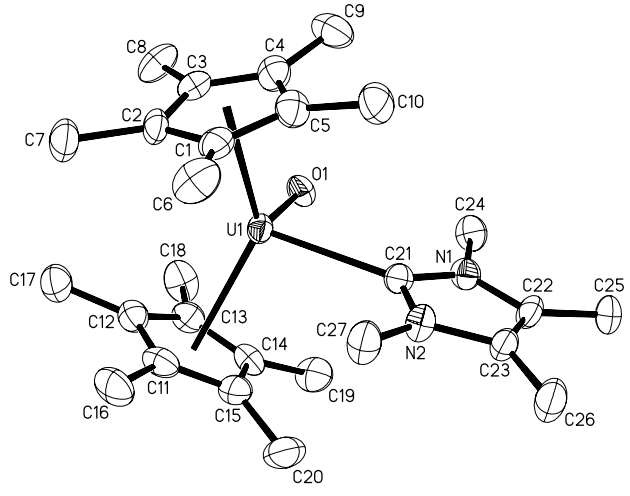

Fig. 3. A thermal ellipsoid plot of **2**, $(C_5Me_5)_2U(O)[C(NMeCMe)_2]$, with thermal ellipsoids drawn to 50% probability.

Recently, NHC ligands have been shown to function as effective sigma bonding ligands in the hexavalent uranium dioxide complexes, $UO_2Cl_2[C(NArCH)_2]_2$ (**3**) and $UO_2Cl_2[C(NArCCl)_2]_2$ (Ar = 2,4,6-$Me_3C_6H_2$) (**4**) [46]. Trivalent uranium carbenes are also known in $[(Me_3Si)_2N]_3U[C(NMeCMe)_2]$ (**5**) and $[(^{Ad}ArO)_3tacn]U[C(NMeCMe)_2]$ (**6**) [55]. The 2.636(9) Å U–C(NHC) distance in tetravalent **2** is indistinguishable from those in hexavalent **3**, 2.626(7) Å, and **4**, 2.609(4) Å [46]. In contrast, the U–C(NHC) distances in trivalent **5** and **6** are 2.672(5) and 2.789(14) Å, respectively [54].

The carbene and oxide donor atoms are not located symmetrically with respect to the $(C_5Me_5)_2U^{2+}$ metallocene unit. The $C_5Me_5^{1-}$ rings are tipped toward the oxide side of the metallocene and away from the sterically bulky carbene. As a result the U–C(C_5Me_5) distances for C(3), C(4), C(13), and C(14) are significantly shorter than the others. These are in the 2.72(1)–2.75(1) Å range, whereas C(2), C(5), C(12), and C(15) range from 2.82(1)–2.83(1) Å. The longest U–C(C_5Me_5) distances are 2.871(9) and 2.858(9) Å for C(1) and C(11), the carbon atoms furthest from the oxide ligand. The 136.3° (ring centroid)–U–(ring centroid) angle is normal and is not in the range of the 120° angle found for the sterically crowded $(C_5Me_5)_3M$ complexes [55].

4. Conclusion

The special reactivity of the sterically crowded $(C_5Me_5)_3U$ has provided synthetic access to the first examples of a U(III) oxide and a U(IV) terminal oxide and carbene complex, compounds that have not been accessible by traditional reactions pathways. The full synthetic utility of the sterically crowded $(C_5Me_5)_3M$ complexes for formation of such compounds remains to be determined. Although additional examples will be required to determine the generality of the structural features of these complexes, they provide the first data for comparison with related analogs.

5. Supporting material

Details on data collection and refinement, fractional atomic coordinates, anisotropic displacement parameters and full list of bond lengths and angles in CIF format has been deposited at the Cambridge Crystallographic

Data Centre, CCDC No. 235982 for compound **1** and CCDC No. 235983 for compounds **2**. Copies of this information may be obtained free of charge from The Director, CCDC, 12 Union Road, Cambridge, CB2 1EZ, UK (fax: +44-1223-336033; e-mail: deposit@ccdc.cam.ac.uk or www.ccdc.cam.ac. uk).

Acknowledgement

For support of this research, we thank the Division of Chemical Sciences of the Office of Basic Energy Sciences of the Department of Energy.

References

[1] W.J. Evans, K.J. Forrestal, J.W. Ziller, Angew. Chem., Int. Ed. 36 (1997) 774.
[2] W.J. Evans, G.W. Nyce, K.J. Forrestal, J.W. Ziller, Organometallics 21 (2002) 1050.
[3] W.J. Evans, G.W. Nyce, M.A. Johnston, J.W. Ziller, J. Am. Chem. Soc. 122 (2000) 12019.
[4] W.J. Evans, G.W. Nyce, J.W. Ziller, Angew. Chem., Int. Ed. 39 (2000) 240.
[5] W.J. Evans, B.L. Davis, J.W. Ziller, Inorg. Chem. 40 (2001) 6341.
[6] G. Lin, W.-T. Wong, Polyhedron 14 (1995) 3167.
[7] G.B. Deacon, G.D. Fallon, C.M. Forsyth, B.M. Gatehouse, P.C. Junk, A. Philosof, P.A. White, J. Organomet. Chem. 565 (1998) 201.
[8] P. Roussel, R. Boaretto, A.J. Kingsley, N.W. Alcock, P. Scott, J. Chem. Soc., Dalton. Trans. (2002) 1423.
[9] W.J. Evans, B.L. Davis, G.W. Nyce, J.M. Perotti, J.W. Ziller, J. Organomet. Chem. 677 (2003) 89.
[10] L. Karmazin, M. Mazzanti, J. Pécaut, Inorg. Chem. 42 (2003) 5900.
[11] W.J. Evans, J.W. Grate, I. Bloom, W.E. Hunter, J.L. Atwood, J. Am. Chem. Soc. 107 (1985) 405.
[12] H. Schumann, E. Palamidis, J. Loebel, J. Organomet. Chem. 384 (1990) C49.
[13] R. Boaretto, P. Roussel, N.W. Alcock, A.J. Kingsley, I.J. Munslow, C.J. Sanders, P. Scott, J. Organomet. Chem. 591 (1999) 174.
[14] W.J. Evans, N.T. Allen, M.A. Greci, J.W. Ziller, Organometallics 20 (2001) 2936.
[15] B.-J. Deelman, M. Booij, A. Meetsma, J.H. Teuben, H. Kooijman, A.L. Spek, Organometallics 14 (1995) 2306.
[16] J.-C. Berthet, J.-F. Le Maréchal, M. Nierlich, M. Lance, J. Vigner, M. Ephritikhine, J. Organomet. Chem. 408 (1991) 335.
[17] M.-R. Spirlet, J. Rebizant, C. Apostolidis, E. Dornberger, B. Kanellakopulos, B. Powietzka, Polyhedron 15 (1996) 1503.
[18] D.S.J. Arney, C.J. Burns, J. Am. Chem. Soc. 115 (1993) 9840.
[19] D.S.J. Arney, C.J. Burns, J. Am. Chem. Soc. 117 (1995) 9448.
[20] W.W. Lukens Jr., S.M. Beshouri, L.L. Blosch, R.A. Andersen, J. Am. Chem. Soc. 118 (1996) 901.
[21] L. Karmazin, M. Mazzanti, C. Gateau, C. Hill, J. Pécaut, Chem. Commun. (2002) 2892.
[22] M.W. Peters, E.J. Werner, M.J. Scott, Inorg. Chem. 41 (2002) 1707.
[23] S. Colette, B. Amekraz, C. Madic, L. Berthon, G. Cote, C. Moulin, Inorg. Chem. 42 (2003) 2215.
[24] SMART Software Users Guide, Version 5.1, Bruker Analytical X-Ray Systems, Inc., Madison, WI, 1999.
[25] SAINT Software Users Guide, Version 6.0, Bruker Analytical X-Ray Systems, Inc., Madison, WI, 1999.
[26] G.M. Sheldrick, SADABS, Version 2.05, Bruker Analytical X-Ray Systems Inc., Madison, WI, 2001.
[27] G.M. Sheldrick, SHELXTL, Version 6.12, Bruker Analytical X-Ray Systems Inc., Madison, WI, 2001.
[28] International Tables for X-Ray Crystallography, Vol. C., Kluwer Academic Publishers, Dordrecht, 1992.
[29] N. Kuhn, T. Kratz, Synthesis (1993) 561.
[30] M.C. Cassani, D.J. Duncalf, M.F. Lappert, J. Am. Chem. Soc. 120 (1998) 12958.
[31] P.L. Diaconescu, P.L. Arnold, T.A. Baker, D.J. Mindiola, C.C. Cummins, J. Am. Chem. Soc. 122 (2000) 6108.
[32] W.J. Evans, S.A. Kozimor, J.W. Ziller, N. Kaltsoyannis, J. Am. Chem. Soc., submitted.
[33] T.D. Tilley, A.L. Rheingold, M.B. Allen, Personal Communication to Cambridge Structure Database, 1996.
[34] S.N. Ringelberg, A. Meetsma, S.I. Troyanov, B. Hessen, J.H. Teuben, Organometallics 21 (2002) 1759.
[35] E.A. Bluhm, N.C. Schroeder, E. Bauer, J.N. Fife, R.M. Chamberlin, K.D. Abney, J.S. Young, G.D. Jarvinen, Langmuir 16 (2000) 7056.
[36] W. Runde, M.P. Neu, C.V. Pelt, B.L. Scott, Inorg. Chem. 39 (2000) 1050.
[37] X.-M. Gan, S. Parveen, W.L. Smith, E.N. Duesler, R.T. Paine, Inorg. Chem. 39 (2000) 4591.
[38] J.L. Sessler, D. Seidel, A.E. Vivian, V. Lynch, B.L. Scott, D.W. Keogh, Angew. Chem., Int. Ed. 40 (2001) 591.
[39] J.G. Brennan, S.D. Stults, R.A. Andersen, A. Zalkin, Organometallics 7 (1988) 1329.
[40] P.G. Allen, J.J. Bucher, D.K. Shuh, N.M. Edelstein, I. Craig, Inorg. Chem. 39 (2000) 595.
[41] J.-C. Berthet, M. Nierlich, M. Ephritikhine, Polyhedron 22 (2003) 3475.
[42] W.J. Evans, S.A. Kozimor, G.W. Nyce, J.W. Ziller, J. Am. Chem. Soc. 125 (2003) 13831.
[43] R.D. Shannon, Acta Crystallogr. A32 (1976) 751.
[44] P.L. Watson, J.F. Whitney, R.L. Harlow, Inorg. Chem. 20 (1981) 3271.
[45] J.G. Brennan, R.A. Andersen, A. Zalkin, Inorg. Chem. 25 (1986) 1761.
[46] W.J. Oldham Jr., S.M. Oldham, B.L. Scott, K.D. Abney, W.H. Smith, D.A. Costa, Chem. Commun. (2001) 1348.
[47] M.-T. Lee, C.-H. Hu, Organometallics 23 (2004) 976.
[48] C. Boehme, G. Frenking, Organometallics 17 (1998) 5801.
[49] A. Navaza, F. Villain, P. Charpin, Polyhedron 3 (1984) 143.
[50] J. Toivonen, R. Laitinen, Acta Crystallogr. C40 (1984) 7.
[51] P.B. Viossat, N.-H. Dung, E.C. Soye, Acta Crystallogr. C39 (1983) 573.
[52] D.L. Clark, S.D. Conradson, R.J. Donohoe, D.W. Keogh, D.E. Morris, P.D. Palmer, R.D. Rogers, C.D. Tait, Inorg. Chem. 38 (1999) 1456.
[53] J.F. de Wet, J.G.H. Su Preez, J. C. S. Dalton (1978) 592.
[54] H. Nakai, X. Hu, L.N. Zakharov, A.L. Rheingold, K. Meyer, Inorg. Chem. 43 (2004) 855.
[55] W.J. Evans, B.L. Davis, Chem. Rev. 102 (2002) 2119.

Available online at www.sciencedirect.com
SCIENCE DIRECT®
Polyhedron 23 (2004) 2695–2707
POLYHEDRON
www.elsevier.com/locate/poly

Synthesis and characterisation of $[(\eta^6\text{-cymene})Ru(L)X_2]$ compounds: single crystal X-ray structure of $[(\eta^6\text{-cymene})Ru(P\{OPh\}_3)Cl_2]$ at 203 K

Emma Hodson, Stephen J. Simpson *

Department of Chemistry and Applied Chemistry, University of Salford, Cockcroft Building, Salford M5 4WT, UK

Received 16 April 2004; accepted 11 June 2004
Available online 6 August 2004

Dedicated to Malcolm Green on his retirement; thank you for teaching me that chemistry should be fun and that the "suck it and see" approach is the most fun of all

Abstract

Treatment of the chloro bridged dimer $\{[(\eta^6\text{-cymene})RuCl]_2(\mu\text{-}Cl)_2\}$ (**1**) with the donor molecules $P(OPh)_3$, $P(OMe)_3$, PPh_3, PMe_3, CO, SMe_2, CN^tBu and CNTos in hot hexane causes bridge splitting reactions that produce the monomeric compounds $[(\eta^6\text{-cymene})Ru(L)Cl_2]$, (**4**)–(**11**), respectively. Use of the chiral isonitrile *S*(−)-α-methylbenzylisonitrile produced the corresponding complex **12**. The diiodo analogues, **13**–**15**, were prepared similarly from $\{[(\eta^6\text{-cymene})RuI]_2(\mu\text{-}I)_2\}$ (**3**) for $P(OPh)_3$, $P(OMe)_3$ and PPh_3, respectively. Insertion of tin(II) chloride into both metal–chlorine bonds was observed for $[(\eta^6\text{-cymene})Ru(P\{OMe\}_3)Cl_2]$ (**5**), while only monosubstitution was observed for $[(\eta^6\text{-cymene})Ru(PPh_3)Cl_2]$ (**6**). Halide abstraction in the presence of a substrate reaction has been used to prepare some selected cationic compounds which contain an asymmetric ligand environment. Reaction of $\{[(\eta^6\text{-cymene})RuCl]_2(\mu\text{-}Cl)_2\}$ with 1,2-bis(diphenylphosphino)-ethane under ionising conditions produced the cation $[(\eta^6\text{-cymene})Ru(dppe)Cl]PF_6$ (**20**). Selected compounds have been examined by $\{^{13}C\text{–}^1H\}$ heteronuclear correlation and $\{^1H\text{–}^1H\}$ COSY and NOESY experiments. The structure of $[(\eta^6\text{-cymene})Ru(P\{OPh\}_3)Cl_2]\cdot CH_2Cl_2$ (**4**) has been determined at −70 °C.
© 2004 Elsevier Ltd. All rights reserved.

Keywords: Cymene; Ruthenium; X-ray

1. Introduction

The chemistry of $(\eta^6$-arene)ruthenium half-sandwich systems has been explored to a lesser extent than that of the isoelectronic $(\eta^5$-cyclopentadienyl)ruthenium systems. This is probably due to the requirement for 1,3- or 1,4-cyclohexadienes as ligand precursors; these are normally obtained by Birch reduction of the appropriate arene. However the diene precursor to $(\eta^6$-cymene)ruthenium compounds, (*R*)-α-Phellandrene, (5-isopropyl-2-methyl-1,3-cyclo-hexadiene) is commercially available and thus the bulk of the reported chemistry to date is of complexes of this arene ligand [1,2]. Other arene ligands such as mesitylene and hexamethylbenzene have generally been introduced by high temperature ligand exchange using the cymene dimer **1** and the free arene.

We have a developing interest in metal complexes which contain chiral at metal centres and/or chiral ligands. The present work describes the development of reaction chemistry designed to generate racemic $(\eta^6$-cymene)ruthenium complexes with an asymmetric ligand environment. These complexes have been examined

* Corresponding author. Tel.: +44-161-295-5978; fax: +44-161-295-5111.
E-mail address: s.j.simpson@salford.ac.uk (S.J. Simpson).

0277-5387/$ - see front matter © 2004 Elsevier Ltd. All rights reserved.
doi:10.1016/j.poly.2004.06.016

by NMR spectroscopy in order to investigate the chemical shift differentiation of the arene ring substituents.

Some of the compounds prepared have been reported previously; **4** and **6** [3–5], **5** and **7** [6], and **10** and **11** [7]. We have improved yields in some cases and provided fuller spectroscopic data in all these cases.

2. Results and discussion

Treatment of a suspension of red {[(η^6-cymene)RuCl]$_2$(μ-Cl)$_2$} (**1**) in hexane with triphenylphosphite, trimethylphosphite, triphenylphosphine or trimethylphosphine under reflux for several hours gave orange or red-orange suspensions of the monomeric compounds [(η^6-cymene)Ru(L)Cl$_2$], (**4**) to (**7**), respectively. The salmon-pink carbonyl compound **8** was prepared from the dimer starting material by stirring the hexane suspension under carbon monoxide (150 psig) for 2 h at 50 °C. An increase in the reaction time to 12 h resulted in the isolation of a small quantity of bright yellow crystals which contained two sharp infrared absorptions at 2080 and 2023 cm^{-1}. This is probably [(η^6-cymene)Ru(CO)$_2$Cl]Cl and was not investigated further. Similarly reactions with dimethylsulfide (SMe$_2$), *tert*-butylisonitrile (CN^{t}Bu) and *p*-toluenesulfonylmethylisonitrile (CNTos), gave the hexane insoluble compounds **9** to **11**, respectively (see Scheme 1).

Subsequent crystallisation of the precipitated products in each case from dichloromethane/petroleum ether provided crystalline products which were used for spectroscopic characterisation. The infrared spectra of **8**, **10** and **11** contain inter alia sharp absorptions at 2042 (ν_{CO}), 2133 (ν_{CN}) and 2162 cm^{-1} (ν_{CN}), indicating only a small degree of π-backbonding from the metal centre to the ligand π^* orbitals in the isonitrile complexes; the free ligand stretching frequencies being 2143, 2131 and 2150 cm^{-1}, respectively.

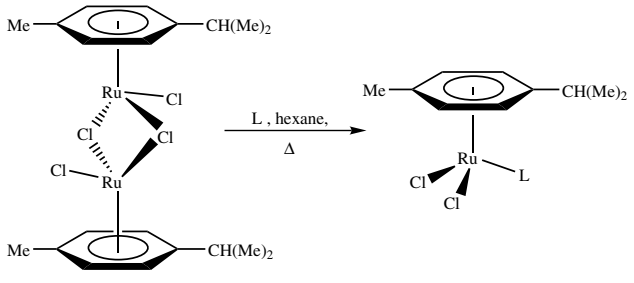

(1)

(4) P(OPh)$_3$
(5) P(OMe)$_3$
(6) PPh$_3$
(7) PMe$_3$
(8) CO
(9) SMe$_2$
(10) CN^{t}Bu
(11) CNTos

Scheme 1.

The diiodo complexes **12**, **13** and **14** were prepared similarly from {[(η^6-cymene)RuI]$_2$(μ-I)$_2$} (**3**) and the ligands in hot heptane solution (see Scheme 2). Treatment of the red dichloro complex **6** with an excess of sodium iodide in moist acetone also produced the purple diiodo complex **14** in 80% yield.

Reaction of anhydrous stannous chloride with **5** in tetrahydrofuran under reflux led to insertion into both ruthenium–chlorine bonds producing orange [(η^6-cymene)Ru(P{OMe}$_3$)(SnCl$_3$)$_2$)] (**15**). The poor solubility of this compound required long acquisition times to obtain NMR spectra and did not allow observation of tin satellites in the ^{31}P{^{1}H} spectrum. The ring protons on the cymene ligand of these complexes formally constitute an AA′BB′ spin system, but in all of the complexes **4**–**15** and the dimer starting materials **1**–**3** they appear as the more simple [AB]$_2$ spin system with J_{AB} being approximately 6 Hz. This is an expected result of both a very small value of $^5J_{HH}$ and rapid ring rotation relative to the [MX$_2$L] fragment; adoption of a static structure like that found in the solid state for [(η^6-cymene)Ru(P{OPh}$_3$)Cl$_2$] (**4**) (vide infra) must lead to two isolated [AB] spin systems. The ring substituent chemical shifts are collected in Table 1, and they do not suggest any correlation with ligand (L) donor or acceptor properties. The ring proton chemical shift differentiation ($\Delta\delta$) is largest for compounds **4**, **11** and **14**, zero for complex **7**, and similar to that of the dimer precursor for the other complexes. The nature of the three ligands is such that the ring protons are differentiated in all rotational conformations but it is likely that there may be some shielding process involving the ring current from a spatially close pendant phenyl ring. A complete assignment of the cymene ring protons in **6** and **12** was made possible by obtaining both COSY and NOESY spectra and demonstrates that the protons *ortho* to the isopropyl substituent (H$_{2,6}$,) are to low-field of those *ortho* to the methyl substituent (H$_{3,5}$). The assignments made in Table 1 assume that this is generally the case for these compounds.

Heteronuclear correlation spectra (^{13}C–^{1}H) were obtained for selected compounds to establish if there was a pattern which would facilitate assignment of the cymene ring chemical shifts for future compounds. Table 2 is a compilation of these data. It is clear from the values of $\Delta(\delta^{13}C)$ that the relative assignment of ^{13}C NMR chemical shifts for the ring methine groups is not predictable; in the free *p*-cymene ligand the chemical shifts are δ 126.3 and δ 129.0 for C$_{2,6}$ and C$_{3,5}$, respectively, while the ^{1}H NMR chemical shifts are isochronous at δ 7.32 [8].

Replacement of one of the two chloro ligands in the symmetrical compounds **4** to **11** would produce compounds which contain an asymmetric centre rendering

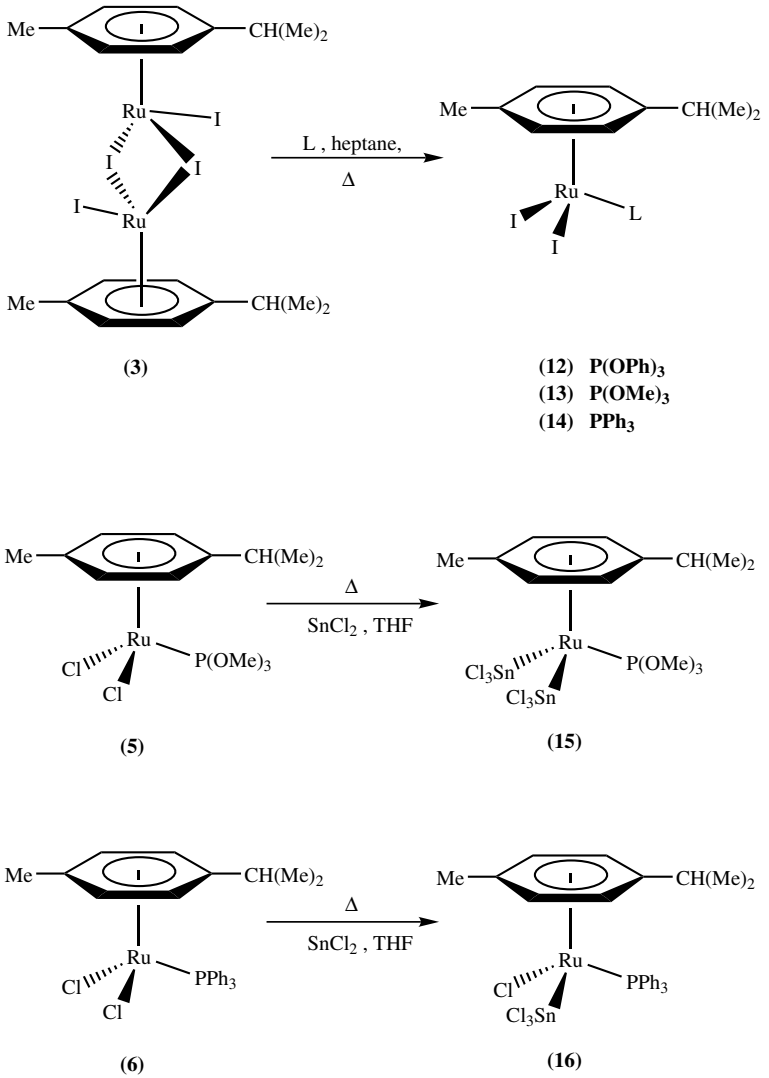

(3)

(12) $P(OPh)_3$
(13) $P(OMe)_3$
(14) PPh_3

(5)

(15)

(6)

(16)

Scheme 2.

all the cymene ring protons inequivalent and also differentiating the isopropyl methyl groups. Such a product would be obtained as a racemic mixture under most reaction conditions and in the Schemes 3–5 only one enantiomer is drawn for clarity.

A valuable synthetic target would be to prepare neutral molecules of the type [(η^6-cymene)Ru(L)(Cl)X] where X is a different halogen; differing metal–halogen bond strengths in subsequent reactions could be exploited. All efforts to replace one chloro ligand with a bromo, cyano or iodo ligand using sodium or potassium salts failed, variation of stoichiometry, solvent, reaction time and temperature gave only mixtures of the symmetrical product, starting material and trace amounts of the required product. Later work with analogues containing more heavily substituted arene ligands has proved more successful [9]. Reaction of [(η^6-cymene)Ru(PPh_3)Cl_2] (**6**) with stannous chloride in tetrahydrofuran gave the orange complex [(η^6-cymene)Ru(PPh_3)($SnCl_3$)(Cl)] (**16**) (see Scheme 2), whose ^{1}H NMR spectrum contained an [AB] system (δ_A 6.11, δ_B 6.01) and two doublets (δ 5.29, 4.95) for the cymene ring protons. The isopropyl group methyl resonances occur as two doublets at δ 1.21, 1.14. The nature of the three ligands is such that the ring protons are differentiated in all rotational conformations but it is likely that the major conformation is one which has a pair of protons in a similar environment and the other pair more strongly differentiated, such as in Fig. 1.

In contrast to **15**, the greater solubility of **16** allowed the observation of the tin satellites in the $^{31}P\{^1H\}$ NMR spectrum; the values of $^2J(^{119}Sn–^{31}P)$ and $^2J(^{117}Sn–^{31}P)$ being 704 and 671 Hz, respectively.

Treatment of the dimer **1** with the chiral isonitrile ligand *S*(−)-α-methylbenzylisonitrile under the conditions used for compounds **10** and **11** gave red microcrystalline **17** (see Scheme 3). The cymene ring protons are all differentiated in the ^{1}H NMR spectrum of **17** as expected when a chiral centre is introduced. The remoteness of

Table 1
^{1}H NMR chemical shifts for the compounds {[(η^6-cymene)RuX]$_2$(μ-X)$_2$} (**1**)–(**3**) and [(η^6-cymene)Ru(L)X$_2$] (**4**)–(**15**)

L	X		$H_{2,6}$	$H_{3,5}$	$\Delta\delta$	Me	$CHMe_2$	$CHMe_2$
	Cl	**1**	5.44	5.30	0.14	2.12	1.24	2.90
	Br	**2**	5.63	5.48	0.15	2.25	1.28	2.78
	I	**3**	5.51	5.41	0.10	2.33	1.22	2.98
$P(OPh)_3$	Cl	**4**	5.39	5.07	0.32	1.80	1.16	2.70
$P(OMe)_3$	Cl	**5**	5.52	5.38	0.14	2.15	1.22	2.90
PPh_3	Cl	**6**	5.17	4.97	0.20	1.84	1.07	2.83
PMe_3	Cl	**7**	5.39	5.39	0.00	2.02	1.18	2.81
CO	Cl	**8**	5.94	5.79	0.15	2.35	1.30	2.87
SMe_2	Cl	**9**[a]	5.61	5.43	0.18	2.18	1.31	2.92
CN^tBu	Cl	**10**	5.53	5.37	0.16	2.26	1.27	2.80
CNTos	Cl	**11**	5.72	5.40	0.32	2.30	1.29	2.92
$P(OPh)_3$	I	**12**	5.32	5.17	0.15	2.11	1.13	3.07
$P(OMe)_3$	I	**13**	5.56	5.38	0.18	2.39	1.23	3.22
PPh_3	I	**14**	5.42	4.90	0.52	1.94	1.06	3.42
$P(OMe)_3$	$SnCl_3$	**15**[b]	6.18	6.02	0.16	2.47	1.30	2.99

Other compounds in $CDCl_3$.
[a] $(CD_3)_2CO$.
[b] CD_2Cl_2.

Table 2
^{13}C–^{1}H correlation data for selected compounds in $CDCl_3$

		$H_{2,6}$	$H_{3,5}$	$C_{2,6}$	$C_{3,5}$	$\Delta(\delta^{13}C)$
{[(η^6-cymene)RuCl]$_2$(μ-Cl)$_2$}	**1**	5.44	5.30	81.20	80.50	0.70
{[(η^6-cymene)RuBrl]$_2$(μ-Br)$_2$}	**2**	5.63	5.48	78.54	78.68	−0.14
{[(η^6-cymene)RuI]$_2$(μ-I)$_2$}	**3**	5.51	5.41	82.02	82.51	−0.49
[(η^6-cymene)Ru(P{OPh}$_3$)(Cl)$_2$]	**4**	5.39	5.07	88.60	88.90	−0.30
[(η^6-cymene)Ru(P{OPh}$_3$)(I)$_2$]	**12**	5.32	5.17	87.85	90.33	−2.48
[(η^6-cymene)Ru(P{OMe}$_3$)(Cl)$_2$]	**5**	5.52	5.38	88.80	89.10	−0.30
[(η^6-cymene)Ru(P{OMe}$_3$)(I)$_2$]	**13**	5.56	5.38	89.31	89.31	0.00
[(η^6-cymene)Ru(PPh_3)(Cl)$_2$]	**6**	5.17	4.97	87.20	89.00	−1.80
[(η^6-cymene)Ru(PPh_3)(I)$_2$]	**14**	5.42	4.90	88.70	88.60	0.10

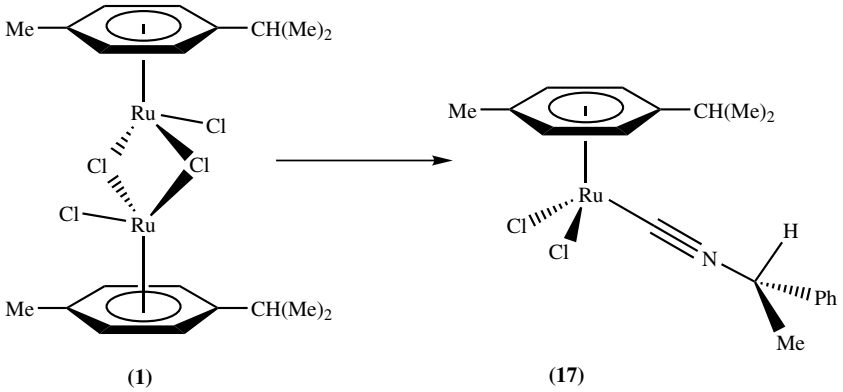

Scheme 3.

the chiral centre from the cymene ring protons induces an equivalence of only 0.02 ppm between the positionally related pairs. The heteronuclear correlation spectrum (^{13}C–^{1}H) established the ((δ_H, δ_C) pairings (5.56, 87.9), (5.54, 87.5), (5.40, 87.6) and (5.38, 87.4) establishing the effect of the remote chiral centre on the cymene ring carbon atoms.

Halide abstraction in the presence of a substrate can also be used to generate asymmetric metal centres; thus the reaction of **4** with dimethylsulfoxide in hot methanol

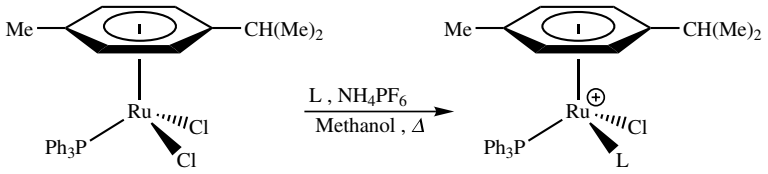

L = SMe_2 (**20**)
CNBu (**21**)
CNTos (**22**)
quinoline (**23**)

Scheme 4.

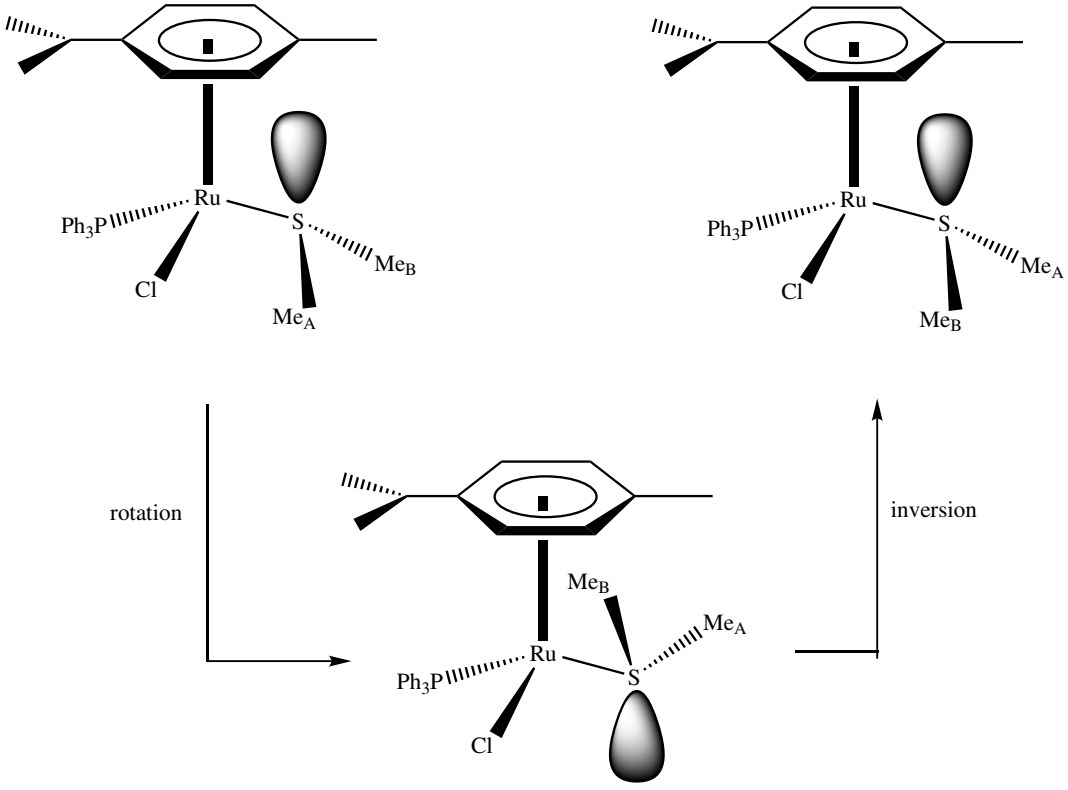

Scheme 5. Rotation–inversion process for the SMe_2 group in **20**.

solutions containing ammonium hexafluorophosphate produced bright yellow [(η^6-cymene)Ru(P{OPh}$_3$)(S{O}Me_2)(Cl)]PF_6 (**18**).

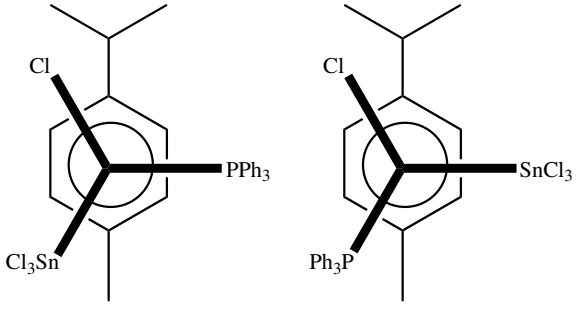

Fig. 1. Possible preferred conformations of **16**.

Similarly compound **5** could be transformed into the cation [(η^6-cymene)Ru(P{OMe}$_3$)(S{O}Me_2)(Cl)]PF_6 (**19**). The infrared spectra of **18** and **19** contained a weak band at 1124 and 1129 cm^{-1}, respectively, indicative of sulfur rather than oxygen coordination. Treatment of **6** with dimethylsulfide, *tert*-butylisonitrile, *p*-toluenesulfonylmethylisonitrile, or quinoline gave the requisite cationic compounds **20** to **23**, respectively, (*see* Scheme 4). The partial ^{1}H NMR chemical shift data for compounds **18** to **23** showing the cymene ring and isopropyl ligand methyl group resonances are collected in Table 3. The assignment of the ring protons is given such that H_A and H_B are mutually coupled and H_C and H_D form the other coupled pair. It seems reasonable to conclude that H_A and H_C are the $H_{2,6}$ pair while H_B and H_D are the $H_{3,5}$ ring protons. The appearance of "AB-roofing"

Table 3
^{1}H NMR chemical shifts for [(η^6-cymene)Ru(L)(L')Cl]PF_6 (**18**)–(**23**)

L	L′		H_A	H_B	H_C	H_D	Me	Me′
$P(OPh)_3$	$S(O)Me_2$	**18**	6.23	6.23	5.78	5.01	1.25	1.12
$P(OMe)_3$	$S(O)Me_2$	**19**[a]	6.53	6.45	6.51	6.27	1.31	1.30
PPh_3	SMe_2	**20**	5.93	5.89	5.45	4.96	1.29	1.28
PPh_3	CN^{t}Bu	**21**	6.09	4.95	5.78	5.59	1.30	1.24
PPh_3	CNTos	**22**[b]	6.13	4.77	6.08	5.95	1.27	1.22
PPh_3	quinoline	**23**[b]	6.01	5.97	5.52	5.33	1.06	1.03

Other compounds are recorded in deuterodichloromethane.
[a] Recorded in deuteroacetone.
[b] Recorded in deuterochloroform.

Table 4
Selected bond lengths (Å) and bond angles (°) for **4**

Ru(1)–C(1)	2.199(3)	Ru(1)–C(2)	2.241(3)
Ru(1)–C(3)	2.246(3)	Ru(1)–C(4)	2.222(3)
Ru(1)–C(5)	2.202(3)	Ru(1)–C(6)	2.177(3)
Ru(1)–Cl(1)	2.4022(8)	Ru(1)–Cl(2)	2.3992(8)
Ru(1)–P(1)	2.2642(8)	P(1)–O(1)	1.596(2)
P(1)–O(2)	1.607(2)	P(1)–O(3)	1.584(2)
Cl(1)–Ru(1)–Cl(2)	87.45(3)	O (1)–P(1)–O(2)	104.74(11)
Cl(1)–Ru(1)–P(1)	87.91(2)	O (1)–P(1)–O(3)	98.70(10)
Cl(2)–Ru(1)–P(1)	85.01(3)	O (2)–P(1)–O(3)	102.06(11)

in the 300 MHz ^{1}H NMR spectra of these compounds has been used to aid this assignment.

These compounds all show inequivalence of the diastereotopic methyl groups of the isopropyl fragment and of the four ring protons. The relative shieldings for some particular complexes, such as **21** and **22**, indicate some preferred conformations leading to differential proximity shielding arising from the π-system of the isonitrile group. The dimethylsulfide group of compound **20** exhibited a broad singlet resonance (δ 2.40) at 294 K which changed into the expected pair of singlets on cooling (δ 2.49, 2.22); the barrier (ΔG_{245}) to this rotation-inversion process was 49.1 kJ mol^{-1} at coalescence (see Scheme 5).

In compounds **18** and **19** where this exchange process is not possible the methyl groups of the dimethylsulfoxide ligands were anisochronous (δ 3.55, 3.37) and (δ 3.55, 3.27), respectively, as required by the lack of molecular mirror planes.

The reaction of the dimer **1** with bis-1,2-(diphenylphosphino)ethane (dppe) and ammonium hexafluorophosphate in 1,2-dichloroethane under reflux produced the symmetrical cation [(η^6-cymene)Ru(dppe)(Cl)]PF_6 (**24**). The conductivity of a dilute nitromethane solution (ca. 5 mM) of this salt was 57.3 Ω^{-1} cm^2 mol^{-1} while that of the very weakly ionized **8** and **9** was 2.0 and 1.3 Ω^{-1} cm^2 mol^{-1}, respectively.

The X-ray single crystal structure of **4** was determined at 203K in order to confirm the disposition of the three metal σ-bound ligands relative to the cymene ligand. The ruthenium–phosphorus bond Ru(1)–P(1) bisects one edge of the cymene ligand, C(5)–C(6), the arrangement expected for minimization of intramolecular repulsions. Selected bond lengths and angles are given in Table 4. The general structure is similar to that

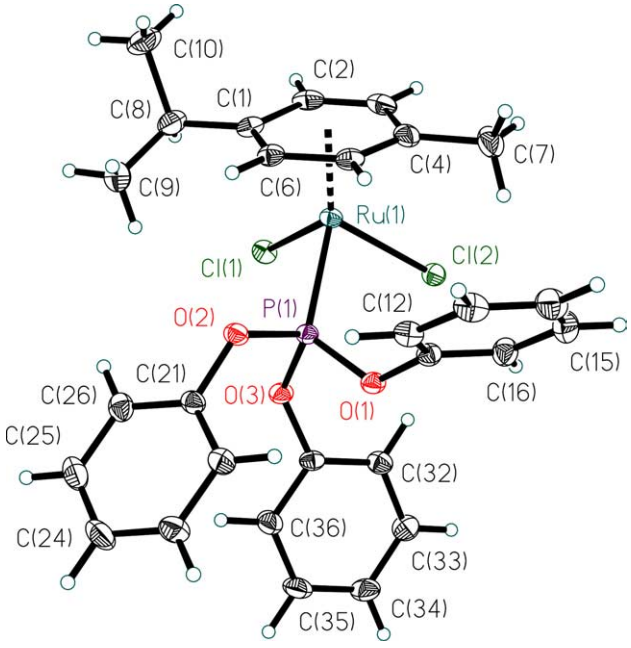

Fig. 2. Structure of the ruthenium containing fragment in **4** showing 25% probability ellipsoids.

found for other [(η^6-cymene)Ru(L)($Cl)_2$] compounds, for example L = PCy_3 [10], L = P(*m*-tolyl)$_3$ [10] and L = $PPh_2{}^tBu$ [11].

Fig. 2 shows the structure obtained of the ruthenium containing fragment and omits the dichloromethane solvent molecule which is also present in the unit cell. The solution structure of **4**, as evidenced by the ^{1}H NMR spectrum, shows that there is free rotation of the cymene ligand about the ruthenium centre and this is consistent with the general disposition of the phenyl rings in the triphenylphosphite ligand.

3. Conclusions

The methine protons of the cymene ligand in these complexes are a sensitive reporter of the auxiliary ligand environment in ^{1}H NMR spectroscopy. Even the presence of a very remote chiral centre in the complex **17** differentiates these ring protons. There does not appear to be a straightforward predictive method of absolutely assigning $\delta(C_{2,6})$ and $\delta(C_{3,5})$ in the ^{13}C NMR spectra of these complexes, the relative ordering being variable unlike the ordering in their ^{1}H NMR spectra. We will report subsequently our results with related compounds possessing planar chiral arene ligands where the asymmetry of the arene ligand facilitates absolute assignment, and also our results concerning the absence of a barrier to rotation of the cymene ring in the compounds [(η^6-cymene)Ru(L)Cl_2] in the range 170–350 K [12].

4. Experimental

All reactions and preparations were carried out on a vacuum/nitrogen line using standard Schlenk-tube techniques. Diethylether was dried over sodium wire. Dichloromethane, hexane, heptane, petroleum ether (40–60 °C) and Analar grade acetone were used as supplied. All solvents were degassed prior to use. All products isolated were dried under reduced pressure, in a hot water bath for at least one hour. Infrared spectra were recorded on a Perkin–Elmer 1710 FTIR instrument, calibrated against polystyrene film; only significant absorption bands are reported. Nuclear magnetic resonance spectra were recorded on Bruker AC300 (300.13 MHz, ^{1}H; 75.47 MHz, ^{13}C; 121.49 MHz ^{31}P) and Bruker Avance 400 (400.13 MHz, ^{1}H; 100.62 MHz, ^{13}C; 161.98 MHz ^{31}P) spectrometers. All ^{1}H and ^{13}C NMR chemical shifts are expressed in ppm relative to $SiMe_4$ (0.00 ppm) and ^{31}P NMR chemical shifts relative to $P(OPh)_3$ (126.5 ppm). All NMR and infrared spectra were measured at room temperature. Standard Bruker microprograms were used for the acquisition of HETCORR, NOESY and COSY-45 spectra. Elemental analyses were obtained at Butterworth Laboratories, London and Manchester University laboratories. Fast Atom Bombardment (FAB) mass spectra were obtained on a Kratos Concept S1 spectrometer. *R*(−)-α-Phellandrene (technical grade) was used as received from Fluka. *Tert*-butylisonitrile and *S*(−)-α-methylbenzylisonitrile were prepared from the respective amines by the phase-transfer Hofmann carbylamine reaction. Compounds **2** and **3** were prepared from **1** by a literature procedure [13].

4.1. Preparation of {[(η^6-cymene)RuCl]$_2$(μ-Cl)$_2$} (*1*)

Hydrated ruthenium trichloride (0.74g, 2.83 mmol) in ethanol (40 ml) was heated under reflux overnight with α-phellandrene (2 ml, 16.4 mmol). The orange precipitate was filtered off, washed with methanol and dried under reduced pressure, yield 0.55 g, 63.5%. ^{1}H NMR [$CDCl_3$]: δa 5.44, δb 5.30 (dd, *J*(HH) ~ 6.0 Hz, 4H, C2,3,5,6-H{ring}), 2.90 (sept, *J*(HH) ~ 7 Hz, H, *CH*(Me)$_2$), 2.12 (s, 3H, CH_3{ring}), 1.24 (d, *J*(HH) ~ 7.0 Hz, 6H, CH(*Me*)$_2$); ^{13}C{^{1}H} NMR [$CDCl_3$]: δ 101.1 (s, $C1_{(quat)}$), 96.7 (s, $C4_{(quat)}$), 81.2 (s, C2,6-H{ring}), 80.5 (s, C3,5-H{ring}), 30.6 (s, *CH*(Me)$_2$), 22.1 (s, CH(*Me*)$_2$), 18.9 (s, Me{ring}).

4.2. Preparation of [(η^6-cymene)Ru(P{OPh}$_3$)Cl_2] (*4*)

A mixture of **1** (0.30 g, 0.49 mmol) and triphenylphosphite (1 ml) in hexane (30 ml) was heated under reflux for 8 h. The reaction mixture yielded a red microcrystalline solid which was filtered warm. The product was washed with light petroleum ether (2 × 10 ml). The crude product was crystallised from dichloromethane and light petroleum ether to give bright red crystals, yield 0.38 g, 62%. ^{1}H NMR [$CDCl_3$]: δ 7.22 (m, 15H, Ph_3), δa 5.39, δb 5.07 (dd, *J*(HH) ~ 6.0 Hz, 4H, C2,3,5,6-H{ring}), 2.70 (sept, *J*(HH) ~ 7.0 Hz, H, *CH*(Me)$_2$), 1.8 (s, 3H, CH_3{ring}), 1.16 (d, *J*(HH) ~ 7.0 Hz, 6H, CH(*Me*)$_2$)); ^{13}C{^{1}H}NMR [$CDCl_3$]: δ 151.44 (d, *J*(PC) ~ 11.0 Hz, C_{ipso}, P{OPh}$_3$), 129.42 (s, C_{ortho}, P{OPh}$_3$), 125.06 (s, C_{para}, P{OPh}$_3$), 121.74 (d, *J*(PC) ~ 4.0 Hz, C_{meta}, P{OPh}$_3$) 109.37 (s, $C1_{(quat)}$), 103.07 (s, $C4_{(quat)}$), 88.92 (d, *J*(PC) ~ 7.0 Hz, C3,5-H{ring}), 88.60 (d, *J*(PC) ~ 6.0 Hz, C2,6-H{ring}), 30.55 (s, *CH*(Me)$_2$), 22.11 (s, CH(*Me*)$_2$), 17.96 (s, Me{ring}); ^{31}P{^{1}H} NMR [$CDCl_3$]: δ 104.2 (s, P{OPh}$_3$).

4.3. Preparation of [(η^6-cymene)Ru(P{OMe}$_3$)Cl_2] (*5*)

A suspension of **1** (0.1 g, 0.16 mmol) and trimethylphosphite (0.1 ml) in hexane (30 ml) was heated under reflux for 4 h. After solvent removal under reduced pres-

sure, fine orange crystals were obtained by crystallising the orange residue at −30 °C from dichloromethane and light petroleum ether overnight, yield 0.14 g, 99.6%. Calc. for $C_{13}H_{23}Cl_2O_3PRu$: C, 36.27; H, 5.34. Found: C, 36.24; H, 5.19%. IR (nujol): ν_{max} 1042 s, 839 w cm^{-1} (PO). ^1H NMR [$CDCl_3$]: δa 5.52, δb 5.38 (dd, J(HH) ~ 6.0 Hz, 4H, C2,3,5,6-H{ring}), 3.77 (d, J(PH) ~ 10.8 Hz, 9H, P{OMe}$_3$), 2.90 (sept, J(HH) ~ 7.0 Hz, H, CH(Me)$_2$), 2.15 (s, 3H, CH_3{ring}), 1.22 (d, J(HH) ~ 7.0 Hz, 6H, CH(Me)$_2$); $^{13}C\{^1H\}$ NMR [$CDCl_3$]: δ 109.9 (s, $C1_{(quat)}$), 101.9 (s, $C4_{(quat)}$), 89.1 (d, J(PC) ~ 6.0 Hz, C2,6-H{ring}), 88.8 (d, J(PC) ~ 6.0 Hz, C3,5-H{ring}), 54.3 (d, J(PC) ~ 6.0 Hz, P(OMe)$_3$), 30.4 (s, CH(Me)$_2$), 22.0 (s, CH(Me)$_2$) 18.3 (s, Me{ring}); $^{31}P\{^1H\}$ NMR [$CDCl_3$]: δ 115.9 (s, P{OMe}$_3$). M.S.[FAB]: m/z 432 {M^+}.

4.4. Preparation of [(η^6-cymene)Ru(PPh_3)Cl_2] (6)

A suspension of **1** (0.4 g, 0.32 mmol) and triphenylphosphine (0.4 g, 1.52 mmol) in hexane (30 ml) was heated under reflux for 5 h. After solvent removal under reduced pressure, bright red crystals were obtained by crystallising the red residue at −30 °C from dichloromethane and light petroleum ether overnight, yield 0.59 g, 80%. ^1H NMR [$CDCl_3$]: δ 7.84−7.24 (m, 15H, PPh_3), δa 5.17, δb 4.97 (2d, 4H, J(HH) ~ 6.0 Hz, C-H{ring}), 2.83 (sept, H, J(HH) ~ 7.0 Hz, CH(Me)$_2$), 1.84 (s, 3H, CH_3{ring}), 1.07 (d, 6H, J(HH) ~ 7.0 Hz, CH(Me)$_2$); $^{13}C\{^1H\}$ NMR [$CDCl_3$]: δ 134.3 (d, J(PC) ~ 10.0 Hz, C_{ortho}, PPh_3), 128.0 (s, C_{para}, PPh_3), 128.0 (d, J(PC) ~ 10.0 Hz, C_{meta}, PPh_3), 111.2 (s, $C1_{(quat)}$), 96.0 (s, $C4_{(quat)}$), 89.0 (s, C2,6-H{ring}), 87.2 (s, C3,5-H{ring}), 30.2 (s, CH(Me)$_2$), 21.9 (s, CH(Me)$_2$), 17.7 (s, Me{ring}); $^{31}P\{^1H\}$ NMR [$CDCl_3$]: δ 23.1 (s, PPh_3). M.S.[FAB]: m/z 568 {M^+}.

4.5. Preparation of [(η^6-cymene)Ru(PMe_3)Cl_2] (7)

A suspension of **1** (0.2 g, 0.32 mmol) and trimethylphosphine (0.15 ml) in hexane (30 ml) was heated under reflux for 4 h. After solvent removal under reduced pressure, fine orange crystals were obtained by crystallising the orange residue at −30 °C from dichloromethane and light petroleum ether overnight, yield 0.22 g, 88%. ^1H NMR [$CDCl_3$]: δ 5.39 (d, 4H, J(HH) ~ 6.0 Hz, C-H{ring}), 2.81 (sept, H, J(HH) ~ 7.0 Hz, CH(Me)$_2$), 2.02 (s, 3H, CH_3{ring}), 1.57 (d, 9H, J(PH) ~ 11.0 Hz, PMe_3), 1.18 (d, 6H, J(HH) ~ 7.0 Hz, CH(Me)$_2$); $^{13}C\{^1H\}$ NMR [$CDCl_3$]: δ 106.8 (s, $C1_{(quat)}$), 93.4 (s, $C4_{(quat)}$), 89.2 (d, J(PC) ~ 3.5 Hz, C-H{ring}), 84.7 (d, J(PC) ~ 5.5 Hz, C-H{ring}), 30.5 (s, CH(Me)$_2$), 21.9 (s, CH(Me)$_2$), 18.2 (s, Me{ring}), 16.3 (d, J(PC) ~ 33.5 Hz, PMe_3); $^{31}P\{^1H\}$ NMR [$CDCl_3$]: δ 3.08 (s, PMe_3). M.S.[FAB]: m/z 382 {M^+}.

4.6. Preparation of [(η^6-cymene)Ru(CO)Cl_2] (8)

A suspension of **1** (0.18 g, 0.29 mmol) in hexane (30ml) was pressurised with carbon monoxide (150 psig.) in a Fischer–Porter bottle and stirred at 50 °C for 2 h. Evaporation of the solvent under reduced pressure produced a salmon pink solid, which upon crystallisation from dichloromethane and petroleum ether afforded bright red microcrystals, yield 0.12 g, 56.0%. Calc. for $C_{11}H_{14}Cl_2ORu$: C, 39.51; H, 4.19. Found: C, 38.34; H, 4.06%. IR (nujol): ν_{max} 2042 s, cm^{-1} (CO); ^1H NMR [$CDCl_3$]: δa 5.94, δb 5.79 (dd, J(HH) ~ 6.5 Hz, 4H, C2,3,5,6-H{ring}), 2.87 (sept, J(HH) ~ 7.0 Hz, H, CH(Me)$_2$), 2.35 (s, 3H, CH_3{ring}), 1.30 (d, J(HH) ~ 7.0 Hz, 6H, CH(Me)$_2$); $^{13}C\{^1H\}$ NMR [$CDCl_3$]: δ 189.7 (s, CO), 114.8 (s, $C1_{(quat)}$), 113.5 (s, $C4_{(quat)}$), 93.4 (s, C2,6-H{ring}), 93.0 (s, C3,5-H{ring}), 31.4 (s, CH(Me)$_2$), 22.5 (s, CH(Me)$_2$) 19.1 (s, Me{ring}).

4.7. Preparation of [(η^6-cymene)Ru(SMe_2)Cl_2] (9)

A suspension of **1** (0.2 g, 0.33 mmol) and dimethylsulfide (0.3 ml) in hexane (30 ml) was heated under reflux in an oil bath overnight. The solvent was removed under reduced pressure. Dissolution in dichloromethane (30 ml), and slow addition of light petroleum ether yielded bright red crystals on storage at −30 °C overnight, yield 0.18 g, 74.8%. Calc. for $C_{12}H_{20}Cl_2SRu$: C, 39.12; H, 5.43. Found: C, 39.09; H, 5.45%. ^1H NMR [$(CD_3)_2$ CO]: δa 5.61, δb 5.43 (dd, J(HH) ~ 6.0 Hz, 4H, C2,3,5,6-H{ring}), 2.92 (sept, J(HH) ~ 7.0 Hz, H, CH(Me)$_2$), 2.29 (s, 6H, SMe_2), 2.18 (s, 3H, CH_3{ring}), 1.31 (d, J(HH) ~ 7.0 Hz, 6H, CH(Me)$_2$); $^{13}C\{^1H\}$ NMR [$(CD_3)_2$ CO]: δ 104.6 (s, $C1_{(quat)}$), 99.4 (s, $C4_{(quat)}$), 84.2 (s, C2,6-H{ring}), 83.8 (s, C3,5-H{ring}), 31.4 (s, CH(Me)$_2$), 22.6 (s, SMe_2), 22.3 (s, CH(Me)$_2$), 18.3 (s, Me{ring}). M.S.[FAB]: m/z 577 {$C_{20}H_{28}Cl_3Ru_2^+$}, 368 {M^+}.

4.8. Preparation of [(η^6-cymene)Ru(CN^tBu)Cl_2] (10)

Tert-butylisonitrile (0.2 ml) was added to a suspension of **1** (0.15 g, 0.25 mmol) in hexane (30 ml) and heated under reflux in an oil bath overnight. Filtration and evaporation under reduced pressure produced an orange residue. Dissolution in dichloromethane and slow addition of light petroleum ether afforded a bright orange microcrystalline solid **10**, yield 0.12 g, 61.5%. Calc. for $C_{15}H_{23}Cl_2NRu$: C, 46.26; H, 5.91. Found: C, 45.95; H, 5.91%. IR (nujol): ν_{max} 2194 s, cm^{-1} (CN). ^1H NMR [$CDCl_3$]: δa 5.53, δb 5.37 (dd, J(HH) ~ 6.0 Hz, 4H, C2,3,5,6-H{ring}), 2.80 (sept, J(HH) ~ 7.0 Hz, H, CH(Me)$_2$), 2.26 (s, 3H, CH_3{ring}), 1.58 (s, CNC(CH_3)$_3$), 1.27 (d, J(HH) ~ 7.0 Hz, 6H, CH(Me)$_2$); *$^{13}C\{^1H\}$ NMR [$CDCl_3$]:* δ 137.0 (s, $CNC(CH_3)_3$), 107.6 (s, $C1_{(quat)}$), 106.3 (s, $C4_{(quat)}$), 87.4 (s, C2,6-H{ring}),

87.2 (s, C3,5-H{ring}), 58.5 (s, CN*C*(CH_3)$_3$), 31.3 (s, *CH*(Me)$_2$), 30.6 (s, CNC(CH_3)$_3$), 22.5 (s, CH(*Me*)$_2$), 18.7 (s, Me{ring}).

4.9. Preparation of [(η^6-cymene)Ru($CNCH_2SO_2C_6H_4Me$)Cl_2] (**11**)

A mixture of **1** (0.15 g, 0.25 mmol) and *p*-toluenesulfonylmethylisocyanide (0.18 g, 0.92 mmol) was suspended in hexane and heated under reflux for 12 h. The product was filtered, washed with petroleum ether and dried under reduced pressure. Dissolution in dichloromethane followed by slow addition of light petroleum ether afforded an orange microcrystalline solid, characterised as **11**, yield 0.15 g, 61.1%. Calc. for $C_{19}H_{23}O_2Cl_2NSRu$: C, 45.50; H, 4.59. Found: C, 43.84; H, 4.61%. IR (nujol): ν_{max} 2162 s, cm^{-1} (CN). ^{1}H NMR [$CDCl_3$]: δa 7.87, δb 7.41 (dd, J(HH) ~ 8.0 Hz, 4H, Me(*C_6H_4*)SO_2CH_2CN), δa 5.72, δb 5.40 (dd, J(HH) ~ 5.5 Hz, 4H, C2,3,5,6-H{ring}), 4.96 (s, 2H, Me(C_6H_4)SO_2CH_2CN), 2.92 (sept, J(HH) ~ 7.0 Hz, H, *CH*(Me)$_2$), 2.43 (s, 3H, Me(C_6H_4)SO_2CH_2CN), 2.30 (s, 3H, Me{ring}), 1.29 (d, J(HH) ~ 7.0 Hz, 6H, CH(*Me*)$_2$)). ^{13}C{^{1}H} NMR [$CDCl_3$]: δ 147.1 (s, $C_{(quat)}$, Me(*C_6H_4*)SO_2CH_2CN), 132.5 (s, $C_{(quat)}$, Me(*C_6H_4*)SO_2CH_2CN), 130.8 (s, Me(*C_6H_4*)SO_2CH_2CN), 129.1 (s, Me(*C_6H_4*)SO_2CH_2CN), 109.9 (s, $C1_{(quat)}$), 108.5 (s, $C4_{(quat)}$), 89.5 (s, C2,6-H{ring}), 89.4 (s, C3,5-H{ring}), 63.6 (s, Me(C_6H_4)SO_2*CH_2*CN), 31.2 (s, *CH*(Me)$_2$), 22.4 (s, CH(*Me*)$_2$) 21.8 (s, *Me*(C_6H_4)SO_2CH_2CN) 18.9 (s, Me{ring}). M.S.[FAB]: *m*/*z* 501 {M^+}.

4.10. Preparation of [(η^6-cymene)Ru(P{*OPh*}$_3$)I_2] (**12**)

A mixture of **3** (0.30 g, 0.49 mmol) and triphenylphosphite (1 ml) in heptane (30 ml) was heated under reflux for 6 h. The reaction mixture yielded a purple microcrystalline solid which was filtered warm. The product was washed with light petroleum ether (2 × 10 ml). The crude product was crystallised from dichloromethane and light petroleum ether to give light purple crystals, yield 0.6 g, 85%. Calc. for $C_{28}H_{29}O_3PI_2Ru$: C, 42.00; H, 3.63. Found: C, 41.88; H, 3.85%. ^{1}H NMR [$CDCl_3$]: δ 7.41 (m, 15H, Ph_3), δa 5.32, δb 5.17 (dd, J(HH) ~ 6.0 Hz, 4H, C2,3,5,6-H{ring}), 3.07 (sept, J(HH) ~ 7.0 Hz, H, *CH*(Me)$_2$), 2.11 (s, 3H, CH_3){ring}), 1.13 (d, J(HH) ~ 7.0 Hz, 6H, CH(*Me*)$_2$)); ^{13}C{^{1}H} NMR [$CDCl_3$]: δ 152.03 (d, J(PC) ~ 12.0 Hz, C_{ipso}, P{OPh}$_3$), 129.48 (s, C_{ortho}, P{OPh}$_3$), 125.00 (s, C_{para}, P{OPh}$_3$), 121.86 (d, J(PC) ~ 4.0 Hz, C_{meta}, P{OPh}$_3$) 114.17 (s, $C1_{(quat)}$), 102.84 (s, $C4_{(quat)}$), 87.85 (d, J(PC) ~ 7.0 Hz, C2,6-H{ring}), 90.33 (d, J(PC) ~ 6.0 Hz, C3,5-H{ring}), 31.69 (s, *CH*(Me)$_2$), 22.49 (s, CH(*Me*)$_2$), 19.93 (s, Me{ring}); ^{31}P{^{1}H} NMR [$CDCl_3$]: δ 105.7 (s, P{OPh}$_3$).

4.11. Preparation of [(η^6-cymene)Ru(P{*OMe*}$_3$)I_2] (**13**)

A suspension of **3** (0.2 g, 0.32 mmol) and trimethylphosphite (0.2 ml) in heptane (30 ml) was heated under reflux for 5 h. Dissolution into dichloromethane, filtration, concentration and slow addition of light petroleum ether yielded deep red/purple crystals on storage at −30 °C, overnight, yield 0.21 g, 80%. Calc. for $C_{13}H_{23}O_3PI_2Ru$: C, 25.41; H, 3.75. Found: C, 25.24; H, 3.69%). ^{1}H NMR [$CDCl_3$]: δa 5.56 δb 5.38 (2d, 2H, J(HH) ~ 6.0 Hz, C-H{ring}), 3.73 (d, 9H, J(PH) ~ 11.0 Hz, P{OMe}$_3$), 3.22 (sept, H, J(HH) ~ 7.0 Hz, *CH*(Me)$_2$), 2.39, (s, 3H, CH_3){ring}), 1.23 (d, 6H, J(HH) ~ 7.0 Hz, CH(*Me*)$_2$); ^{13}C{^{1}H} NMR [$CDCl_3$]: δ 113.31 (d, J(PC) ~ 5.0 Hz, $C1_{(quat)}$), 103.38 (d, J(PC) ~ 3.0 Hz, $C4_{(quat)}$), 89.31 (d, J(PC) ~ 4.0 Hz, C2,6-H{ring}), 89.31 (d, J(PC) ~ 4.0 Hz, C3,5-H{ring}), 55.30 (d, J(PC) ~ 7.0 Hz, P(OMe)$_3$), 31.55 (s, *CH*(Me)$_2$), 22.56 (s, CH(*Me*)$_2$) 20.06 (s, Me{ring}); ^{31}P{^{1}H} NMR [$CDCl_3$]: δ 118.7 (s, P{OMe}$_3$). M.S.[FAB]: *m*/*z* 613 {M^+}.

4.12. Preparation of [(η^6-cymene)Ru(PPh_3)I_2] (**14**)

An acetone solution of **6** (0.22 g) and a large excess of NaI (0.5 g, 3.34 mmol) was heated to 50 °C for 4 h. The solvent was removed under reduced pressure. Dissolution into dichloromethane, filtration, concentration and slow addition of light petroleum ether yielded deep red/purple crystals on storage at −30 °C, overnight, yield 0.20 g, 80%. Calc. for $C_{28}H_{29}PI_2Ru$: C, 44.68; H, 3.89. Found: C, 44.78; H, 4.09%. ^{1}H NMR [$CDCl_3$]: δ 7.77−7.34 (m, 15H, PPh_3), δa 5.42, δb 4.90 (2d, 4H, J(HH) ~ 6.0 Hz, C-H{ring}), 3.42 (sept, H, J(HH) ~ 7.0 Hz, *CH*(Me)$_2$), 1.94 (s, 3H, CH_3){ring}), 1.06 (d, 3H, J(HH) ~ 7.0 Hz, CH(*Me*)$_2$); ^{13}C{^{1}H} NMR [$CDCl_3$]: δ 135.6 (d, J(PC) ~ 47.0 Hz, C_{ipso}, PPh_3), 135.0 (d, J(PC) ~ 8.5 Hz, C_{ortho}, PPh_3), 130.2 (s, C_{para}, PPh_3), 127.6 (d, J(PC) ~ 9.5 Hz, C_{meta}, PPh_3), 112.71 (br.s, $C1_{(quat)}$), 99.5 (s, $C4_{(quat)}$), 88.7, 88.6 (2s, C-H{ring}), 32.0 (s, *CH*(Me)$_2$), 18.9 (s, CH(*Me*)$_2$), 18.1 (s, Me{ring}); ^{31}P{^{1}H} NMR [$CDCl_3$]: δ 21.4 (s, PPh_3).

4.13. Preparation of [(η^6-cymene)Ru(P{*OMe*}$_3$)($SnCl_3$)$_2$] (**15**)

Prior to use $SnCl_2 \cdot 2H_2O$ was dehydrated by stirring vigorously in acetic anhydride (120 g salt for 100 g anhydride) for 1 h. The salt was filtered, washed with dry ether (2 × 50 ml) and dried under reduced pressure. Dehydrated stannous chloride (0.07 g, 0.39 mmol) was then added to a solution of **5** (0.1 g, 0.23 mmol) in THF and heated under refluxing conditions for 4 h. A yellow precipitate formed, concentration and filtration

gave **12** as a yellow solid. Evaporation of the filtrate gave a small amount of a crystalline yellow-orange solid identified as **15** by ^{1}H NMR spectroscopy. Yield 0.12 g, 65%. Calc. for $C_{13}H_{23}PO_3Cl_6Sn_2Ru$: C, 19.27; H, 2.84. Found: C, 20.08; H, 3.20%. ^{1}H NMR [CD_2Cl_2]: δa 6.18 δb 6.02 (2d, 4H, J(HH) ~ 6.5 Hz, C-H{ring}), 3.83 (d, 9H, J(PH) ~ 12.0 Hz, P{OMe}$_3$), 2.99 (sept, H, J(HH) ~ 7.0 Hz, *CH*(Me)$_2$), 2.47 (d, 3H, J(PH) ~ 1.5 Hz, CH_3{ring}), 1.30 (d, 6H, J(HH) ~ 7.0 Hz, CH(*Me*)$_2$); ^{13}C{^{1}H} NMR [CD_2Cl_2]: δ 121.0 (s, C1$_{(quat)}$), 113.8 (br.s, C4$_{(quat)}$), 92.0, 91.8, (2s, C-H{ring}), 56.0 (d, J(PC) ~ 9.5 Hz, P{OMe}$_3$), 31.6 (s, *CH*(Me)$_2$), 23.2 (s, CH(*Me*)$_2$), 20.0 (s, Me{ring}); ^{31}P{^{1}H} NMR [CD_2Cl_2]: δ 127.8 (s, PMe_3). M.S.[FAB]: *m*/*z* 773 {M^+}.

4.14. Preparation of [(η^6-cymene)Ru(PPh$_3$)Cl(SnCl$_3$)] (**16**)

Freshly dehydrated stannous chloride (0.03 g, 0.16 mmol) was added to a solution of **6** (0.1 g, 0.12 mmol) in dry THF (30 ml) and heated under refluxing conditions for 4 h. The solution changed from red to orange. Removal of the solvent under reduced pressure produced an orange solid, which was crystallised from dichloromethane and diethylether. Yield 0.10 g, 71%. Calc. for $C_{28}H_{29}PCl_4SnRu$: C, 44.34; H, 3.83. Found: C, 44.38; H, 3.74%). ^{1}H NMR [CD_2Cl_2]: δ 7.71−7.32 (m, 15H, Ph), δa 6.11 δb 6.01 (2d, 2H, J(HH) ~ 6.0 Hz, C-H{ring}), 5.29 (d, H, J(HH) ~ 6.0 Hz, C-H{ring}), 4.95 (d, H, J(HH) ~ 6.0 Hz, C-H{ring}), 2.45 (sept, H, J(HH) ~ 7.0 Hz, *CH*(Me)$_2$), 1.84 (s, 3H, CH_3{ring}), 1.21, 1.14 (2d, 6H, J(HH) ~ 7.0 Hz, CH(Me)$_2$); ^{13}C{^{1}H} NMR [CD_2Cl_2]: δ 134.9 (s, C$_{ipso}$, PPh_3), 134.2 (d, J(PC) ~ 9.5 Hz, C$_{ortho}$, PPh_3), 131.3 (s, C$_{para}$, PPh_3), 129.0 (d, J(PC) ~ 10.0 Hz, C$_{meta}$, PPh_3), 116.5 (s, C1$_{(quat)}$), 102.8 (s, C4$_{(quat)}$), 92.3, 90.9, 89.3 (3s, C-H{ring}), 89.0 (d, J(PC) ~ 5.0 Hz, C-H{ring}), 30.5 (s, *CH*(Me)$_2$), 22.6, 22.4 (2s, CH(*Me*)(Me′)), 18.1 (s, Me{ring}); ^{31}P{^{1}H} NMR [CD_2Cl_2]: δ 27.7 (s, Sn satellites, ^2J(^{119}Sn–^{31}P) ~ 704 Hz, ^2J(^{117}Sn–^{31}P) ~ 671 Hz, PPh_3). M.S.[FAB]: *m*/*z* 534 {M^+}.

4.15. Preparation of [(η^6-cymene)Ru(CN-(*S*)-CH(Me)(Ph))Cl$_2$] (**17**)

S(−)-α-Methylbenzylisonitrile (0.2 ml) was added to a suspension of **1** (0.15 g, 0.49 mmol) in hexane and heated at 70 °C for 12 h. Filtration and evaporation under reduced pressure produced a red residue. Crystallisation from dichloromethane and petroleum ether (40–60 °C) afforded microcystalline **17**. Yield 0.19 g, 89%. Calc. for $C_{19}H_{23}NCl_2Ru$: C, 52.17; H, 5.26; N, 3.20. Found: C, 52.36; H, 5.46; N, 3.05%. IR (nujol): ν_{max} 2186 (CN) cm^{-1}. ^{1}H NMR [CD_2Cl_2]: δ 7.40–7.24 (m, 5H, Ph), δa 5.56, δb 5.54 (dd, 2H, J(HH) ~ 6.0 Hz, C-H{ring}), δa 5.40, δb 5.38 (2d, 2H, J(HH) ~ 6.0 Hz, C-H{ring}), 5.18 (q, H, J(HH) ~ 7.0 Hz, CHMeNC), 2.72 (sept, J(HH) ~ 7.0 Hz, H, CH(Me)$_2$), 2.22 (s, 3H, CH_3{ring}), 1.72 (d, 3H, J(HH) ~ 7.0 Hz, CHMeNC), 1.19, 1.18 (2d, 6H, J(HH) ~ 7.0 Hz, CH(Me)$_2$); ^{13}C{^{1}H} NMR [CD_2Cl_2]: δ 140.9 ('t', J(NC) ~ 15.0 Hz, CHMeNC), 137.9 (s, C$_{ipso}$, Ph), 129.0 (s, C$_{ortho}$, Ph), 128.5 (s, C$_{para}$, Ph), 125.5 (s, C$_{meta}$, Ph), 107.4 (s, C1$_{(quat)}$), 106.9 (s, C4$_{(quat)}$), 87.9, 87.6, 87.5, 87.4 (4s, C-H{ring}), 53.8 (s, CHMeNC), 31.1 (s, CH(Me)2), 24.8 (s, CHMeNC), 22.3, 22.2 (2s, CH(Me)$_2$), 18.7 (s, Me{ring}). M.S.[FAB]: *m*/*z* 437 {M^+}.

4.16. Preparation of [(η^6-cymene)Ru(P{OPh}$_3$)(SOMe$_2$)Cl]PF$_6$ (**18**)

Dimethylsulfoxide (1 ml) was added to a solution of **4** (0.15 g, 0.24 mmol) and ammonium hexafluorophosphate (0.2 g, 1.22 mmol) in methanol (30 ml) and stirred at 50 °C for 6 h. The solution turned progressively paler. The solvent was removed under reduced pressure to give a bright orange oil. A mixture of dichloromethane (20 ml) and water (5 ml) was added and shaken, the dichloromethane layer was separated and dried with calcium chloride. Filtration and addition of diethylether afforded bright yellow microcrystals, identified as **18**. Yield 0.10 g, 50%. Calc. for $C_{30}H_{35}ClF_6O_4P_2SRu$: C, 41.59; H, 4.04. Found: C, 41.90; H, 4.12%. IR (nujol): ν_{max} 1124, 1054 br, 845 s (PF_6^-) cm^{-1}. ^{1}H NMR [CD_2Cl_2]: δ 7.40−6.89 (m, 15H, Ph), 6.23 (d, 2H, J(HH) ~ 6.5 Hz, C-H{ring}), 5.78, 5.01 (2d, H$_c$, H$_d$, J(HH) ~ 6.5 Hz, C-H{ring}), 3.55, 3.37 (2s, 6H, SO*Me*$_2$), 2.65 (sept, J(HH) ~ 7.0 Hz, H, *CH*(Me)$_2$), 2.07 (s, 3H, CH_3{ring}), 1.25, 1.12 (2d, 6H, J(HH) ~ 7.0 Hz, CH(*Me*)$_2$); ^{13}C{^{1}H} NMR [CD_2Cl_2]: δ 151.0 (d, J(PC) ~ 14.0 Hz, C$_{ipso}$, P{OPh}$_3$), 130.7 (s, C$_{ortho}$, P{OPh}$_3$), 126.9 (s, C$_{para}$, P{OPh}$_3$), 121.4 (d, J(PC) ~ 3.0 Hz, C$_{meta}$, P{OPh}$_3$), 126.1 (s, C1$_{(quat)}$), 108.7 (s, C4$_{(quat)}$), 98.9 (s, C-H{ring}), 97.6 (d, J(PC) ~ 5.0 Hz, C-H{ring}), 93.8 (d, J(PC) ~ 10.0 Hz, C-H{ring}), 89.8 (s, C-H{ring}), 51.6, 51.2 (2s, SO*Me*$_2$) 31.7 (s, *CH*(Me)$_2$), 21.7, 21.6 (2s, CH(*Me*)$_2$), 18.4 (s, Me{ring}); ^{31}P{^{1}H} NMR [CD_2Cl_2]: δ 109.0 (s, P{OPh}$_3$). M.S.[FAB]: *m*/*z* 721 {M^+}.

4.17. Preparation of [(η^6-cymene)Ru(P{OMe}$_3$)(SOMe$_2$)Cl]PF$_6$ (**19**)

NH_4PF_6 (80 mg, 0.49 mmol) was added to a solution of complex **5** (0.15 g, 0.35 mmol) and dimethylsulfoxide (0.2 ml) in methanol (30 ml) and stirred at room temperature for 48 h. The solvent was removed under reduced pressure and the orange residue extracted with dichloromethane. Concentration and slow addition of diethylether afforded bright yellow crystals

on storage in a refrigerator (−30 °C, overnight), yield 0.14 g, 64%. Calc. for $C_{15}H_{29}ClF_6O_4P_2SRu$: C, 29.15; H, 4.70. Found: C, 28.71; H, 4.80%). IR (nujol): ν_{max} 1129, 1064 br (SO), 839 s (PF_6^-) cm^{-1}. ^1H NMR [acetone-d_6]: δa 6.53, δb 6.45, δa 6.51, δb 6.27 (4d, 4H, C-H{ring}), 4.02 (d, 9H, J(PC) ~ 11.0 Hz, P{OMe}$_3$), 3.56, 3.27 (2s, 6H, SOMe_2), 2.89 (sept, H, J(HH) ~ 7.0 Hz, CH(Me)$_2$), 2.26 (s, 3H, CH_3{ring}), 1.31, 1.30 (2d, 6H, J(HH) ~ 7.0 Hz, CH(Me)$_2$); $^{13}C\{^1H\}$ NMR [acetone-d_6]: δ 123.2 (s, C1$_{(quat)}$), 109.2 (s, C4$_{(quat)}$), 98.2, 97.0, 96.9, 91.9 (4s, C-H{ring}), 55.8 (d, J(PC) ~ 8.5 Hz, P{OMe}$_3$), 31.8 (s, CH(Me)$_2$), 21.9, 21.6 (2s, CH(Me)$_2$), 18.4 (s, Me{ring}); $^{31}P\{^1H\}$ NMR [acetone-d_6]: δ 119.8 (s, P{OMe}$_3$). M.S.[FAB]: m/z 473 {M^+}.

4.18. Preparation of [(η^6-cymene)Ru(PPh_3)(SMe_2)Cl] (**20**)

Dimethylsulfide (1 ml) was added to a solution of **6** (0.3 g, 0.53 mmol) and ammonium hexafluorophosphate (0.2 g, 1.22 mmol) in methanol (30 ml) and stirred at 50 °C for 6 h. The solvent was removed under reduced pressure to give a yellow oily solid. Crystallisation from dichloromethane and diethylether gave yellow/orange fluffy microcrystals of **20** yield 0.29 g, 74%. Calc. for $C_{30}H_{35}ClF_6P_2SRu$: C, 48.68; H, 4.47. Found: C, 49.01; H, 4.84%. IR (nujol): ν_{max} 841 s (PF_6) cm^{-1}. ^1H NMR [CD_2Cl_2]: δ 7.58−7.44 (m, 15H, Ph), δa 5.93, δb 5.89 (2d, 2H, J(HH) ~ 7.0 Hz, C-H{ring}), 5.45 (d, H, J(HH) ~ 6.5 Hz, C-H{ring}), 4.96 (dd, H, J(HH) ~ 6.5 Hz, J(PH) ~ 3.0 Hz, C-H{ring}), 2.82 (sept, H, J(HH) ~ 7.0 Hz, CH(Me)$_2$), 2.40 (s, 6H, SMe_2) 1.67 (s, 3H, CH_3{ring}), 1.29, 1.28 (2d 6H, J(HH) ~ 7.0 Hz, CH(Me)$_2$); $^{13}C\{^1H\}$ NMR [CD_2Cl_2]: δ 134.6 (d, J(PC) ~ 9.5 Hz, C_{ortho}, PPh_3), 131.8 (s, C_{para}, PPh_3), 131.3 (d, J(PC) ~ 49.0 Hz, C_{ipso}, PPh_3), 129.0 (d, J(PC) ~ 10.5 Hz, C_{meta}, PPh_3), 122.1 (br.s, C1$_{(quat)}$), 101.5 (s, C4$_{(quat)}$), 93.0 (s, C-H{ring}), 91.0 (s, C-H{ring}), 89.5 (d, J(PC) ~ 7.5 Hz, C-H{ring}), 87.4 (s, C-H{ring}), 31.3 (s, CH(Me)$_2$), 26.3 (s, SMe_2), 22.1, 21.6 (2s, CH(Me)$_2$), 17.9 (s, Me{ring}); $^{31}P\{^1H\}$ NMR [CD_2Cl_2]: δ 29.7 (s, PPh_3). M.S.[FAB]: m/z 595 {M^+}.

4.19. Preparation of [(η^6-cymene)Ru(PPh_3)(CN^tBu)Cl]PF_6 (**21**)

Tert-butylisonitrile (0.5 ml), NH_4PF_6 (0.1 g, 0.61 mmol) and **6** (0.1 g, 0.18 mmol) were dissolved in methanol (30 ml) and stirred at room temperature for 3 h. The solution turned pale yellow after 10 min. Evaporation of the solvent and crystallisation from dichloromethane and diethylether afforded yellow microcrystalline **21**, yield 0.12 g, 75%. Calc. for $C_{33}H_{38}ClF_6NP_2Ru$: C, 52.07; H, 5.00; N, 1.84. Found: C, 52.74; H, 4.91; N, 1.78%. IR (nujol): ν_{max} 2180 (CN), 840 s (PF_6) cm^{-1}. ^1H NMR [CD_2Cl_2]: δ 7.59−7.46 (m, 15H, Ph), δa 6.09, δb 5.78 (2d, 2H, J(HH) ~ 6.5 Hz, C-H{ring}), 5.59, 4.95 (2d, H_c, H_d, J(HH) ~ 6.5 Hz, C-H{ring}), 2.78 (sept, H, J(HH) ~ 7.0 Hz, CH(Me)$_2$), 1.96 (s, 3H, CH_3{ring}), 1.33, 1.24 (2d, 6H, J(HH) ~ 7.0 Hz, CH(Me)$_2$), 1.23 (s, 9H, CNC(Me)$_3$); $^{13}C\{^1H\}$ NMR [CD_2Cl_2]: δ 156.6 (s, CNC(Me)$_3$), 134.2 (d, J(PC) ~ 10.0 Hz, C_{ortho}, PPh_3), 132.0 (s, C_{para}, PPh_3), 131.6 (d, J(PC) ~ 51.5 Hz, C_{ipso}, PPh_3), 129.3 (d, J(PC) ~ 10.5 Hz, C_{meta}, PPh_3), 118.7 (d, J(PC) ~ 5.5 Hz, C1$_{(quat)}$), 113.6 (s, C4$_{(quat)}$), 99.3 (d, J(PC) ~ 5.0 Hz, C-H{ring}), 98.2, 94.5, 91.9 (3s, C-H{ring}), 60.1 (s, CNC(Me)$_3$), 32.2 (s, CH(Me)$_2$), 29.9 (s, CNC(Me)$_3$), 23.7, 21.6 (2s, CH(Me)$_2$), 18.9 (s, Me{ring}); $^{31}P\{^1H\}$ NMR [CD_2Cl_2]: δ 36.1 (s, PPh_3). M.S.[FAB]: m/z 616 {M^+}.

4.20. Preparation of [(η^6-cymene)Ru(PPh_3)(p-$CNCH_2SO_2C_6H_4Me$)Cl]PF_6 (**22**)

p-Toluenesulfonylmethylisocyanide, NH_4PF_6 (0.1 g, 0.61 mmol) and **6** (0.1 g, 0.18 mmol) were dissolved in methanol (30 ml) and stirred at room temperature for 3 h. The solution turned bright yellow after 10 min. Evaporation of the solvent and crystallisation from dichloromethane and diethylether afforded yellow microcrystalline **22**. Yield 0.11 g, 73%. Calc. for $C_{37}H_{38}ClF_6NO_2P_2SRu$: C, 52.07; H, 5.00; N, 1.84. Found: C, 50.91; H, 4.39; N, 1.59%. IR (nujol): ν_{max} 2185 (CN), 842 s (PF_6) cm^{-1}. ^1H NMR [$CDCl_3$]: δa 7.77 (d, J(AB) ~ 8.0 Hz, 4H, Me(C_6H_4)SO_2CH_2CN), 7.48−7.31 (m, 17H, Me(C_6H_4)SO_2CH_2CN + PPh_3), 6.13 (dd, H, J(HH) ~ 6.5 Hz, J(PH) ~ 1.0 Hz, C-H{ring}), δa 6.08, δb 5.95 (2d, 2H, J(AB) ~ 6.5 Hz, C-H{ring}), 5.09 (d, H, J(HH) ~ 15.5 Hz, Me(C_6H_4)-SO_2CH_2CN), 4.77 (d, H, J(HH) ~ 6.5 Hz, C-H{ring}), 4.03 (dd, H, J(HH) ~ 15.5 Hz, J(PH) ~ 2.0 Hz, Me(C_6H_4)SO_2CH_2CN), 2.93 (sept, H, J(HH) ~ 7.0 Hz, CH(Me)$_2$), 2.44 (s, 3H, Me(C_6H_4)SO_2CH_2CN), 1.80 (d, 3H, J(PH) ~ 1.0 Hz, CH_3{ring}), 1.27 (d, 3H, J(HH) ~ 7.0 Hz, CH(Me)(Me′)), 1.22 (d, 3H, J(HH) ~ 7.0 Hz, CH(Me)(Me')); $^{13}C\{^1H\}$ NMR [$CDCl_3$]: δ 150.0 (d, J(PC) ~ 29.0 Hz, Me(C_6H_4)-SO_2CH_2CN), 146.5, 132.7 (2s, C$_{(quat)}$, Me(C_6H_4)-SO_2CH_2CN), 133.9 (d, J(PC) ~ 10.0 Hz, C_{ortho}, PPh_3), 131.6 (s, C_{para}, PPh_3), 130.4 (s, Me(C_6H_4)SO_2CH_2CN), 130.2 (d, J(PC) ~ 53.0 Hz, C_{ipso}, PPh_3), 129.5 (s, Me(C_6H_4)SO_2CH_2CN), 128.8 (d, J(PC) ~ 10.5 Hz, C_{meta}, PPh_3), 121.3 (d, J(PC) ~ 5.0 Hz, C1$_{(quat)}$), 115.6 (s, C4$_{(quat)}$), 1 01.9 (d, J(PC) ~ 5.0 Hz, C-H{ring}), 98.0, 93.7, 92.2 (3s, C-H{ring}), 63.1 (s, Me(C_6H_4) SO_2CH_2CN), 31.6 (s, CH(Me)$_2$), 23.5 (s, CH(Me) (Me′)), 21.8 (s, Me(C_6H_4)SO_2CH_2CN), 21.4 (s, CH(Me)(Me')), 18.6 (s, Me{ring}); $^{31}P\{^1H\}$ NMR [$CDCl_3$]: δ 38.1 (s, PPh_3). M.S.[FAB]: m/z 728 {M^+}.

4.21. Preparation of [(η^6-cymene)Ru(PPh_3)(C_9H_7N)-Cl]PF_6 (**23**)

A red solution of **6** (0.10 g, 0.18 mmol) and KPF_6 in methanol (30 ml) was treated with quinoline (1 ml) and stirred at room temperature for 24 h. A bright yellow solid precipitated out on concentration. The solution was filtered and the yellow solid washed with diethylether. Crystallisation from dichloromethane and diethylether afforded microcrystalline **23**. Yield 0.09 g, 62%. Calc. for $C_{37}H_{36}ClF_6NP_2Ru$: C, 55.05; H, 4.46; N, 1.74; recalc. for 0.5 mol CH_2Cl_2: C, 53.00; H, 4.36; N, 1.65. Found: C, 53.58; H, 4.44; N, 1.63%. IR (nujol): ν_{max} 837 s (PF_6) cm^{-1}. ^1H NMR [$CDCl_3$]: δ 9.41 (s, H, C_9H_7N), 8.67 (d, H, J(HH) ~ 6.5 Hz, C_9H_7N), 7.87–7.47 (m, 22H, Ph, C_9H_7N), 6.01, 5.97, 5.52, 5.33 (4d, 4H, J(HH) ~ 6.0 Hz, C-H{ring}), 2.17 (sept, H, J(HH) ~ 7.0 Hz, CH(Me)$_2$), 1.65 (s, 3H, CH_3{ring}), 1.06, 1.03 (2d, 6H, J(HH) ~ 7.0 Hz, CH(Me)$_2$); $^{13}C\{^1H\}$ NMR [$CDCl_3$]: δ 159.4 (s, C_9H_7N), 147.8 (s, C_9H_7N), 134.0 (s, C_{ortho}, PPh_3), 133.0 (s, C_9H_7N), 131.0 (s, C_{para}, PPh_3), 128.6 (d, J(PC) ~ 8.5 Hz, C_{meta}, PPh_3), 128.6, 128.5 (s, C_9H_7N), 128.2 (s, C_9H_7N), 126.0 (s, C_9H_7N), 123.0 (s, C_9H_7N), 114.1 (d, J(PC) ~ 8.0 Hz, $C1_{(quat)}$), 103.5 (s, $C4_{(quat)}$), 94.7 (d, J(PC) ~ 6.0 Hz, C-H{ring}), 90.2, 88.7, 84.0 (3s, C-H{ring}), 30.8 (s, CH(Me)$_2$), 23.1, 20.9 (2s, CH(Me)$_2$), 18.1 (s, Me{ring}); $^{31}P\{^1H\}$ NMR [$CDCl_3$]: δ 36.6 (s, PPh_3). M.S.[FAB]: m/z 662 {M^+}.

4.22. Preparation of [(η^6-cymene)Ru(dppe)Cl]PF_6 (**24**)

A Schlenk tube was charged with a solution of **1** (0.2 g, 0.33 mmol) in 1,2 dichloroethane (25 ml), NH_4PF_6 (0.3 g, 1.84 mmol), dppe (0.52 g, 1.31 mmol) and a magnetic stirrer bar. The orange solution was stirred under reflux conditions for 16 h. After solvent removal under reduced pressure the yellow residue was extracted in dichloromethane (2 × 15 ml). Concentration followed by addition of light petroleum ether produced yellow microcrystals on storage at −30 °C overnight, yield 0.32 g, 60.2%. H NMR [acetone-d_6]: δ 7.97–7.36 (m, 20H, Ph) δa 6.38, δb 6.24 (dd, J(HH) ~ 6.0 Hz, 4H, C2,3,5,6-H{ring}), 3.12-2.92 (m, 4H, $PPh_2(CH_2)_2PPh_2$) 2.24 (sept, J(HH) ~ 7 Hz, H,$CH(CH_3)_2$), 1.21 (s, 3H, CH_3{ring}), 0.87 (d, J(HH) ~ 7 Hz, 6H, $CH(CH_3)_2$); $^{13}C\{^1H\}$ NMR [acetone-d_6]: δ 136.3 ('t', J(PC) ~ 46.5 Hz, C_{ipso}), 134.7, 133.1 (2s, C_{ortho}, PPh_3), 132.2, 131.9 (2s, C_{para}, PPh_3), 130.0, 129.2 (2'st', J(PC) ~ 10.0 Hz, C_{meta}, PPh_3), 123.5 (s, $C1_{(quat)}$), 101.3 (s, $C4_{(quat)}$), 96.2 (s, C2,6-H{ring}), 92.3 (s, C3,5-H{ring}), 31.1 (s, CH(Me)$_2$), 26.8 (t, J(PC) ~ 22 Hz, $PPh_2(CH_2)_2PPh_2$) 21.4 (s, CH(Me)$_2$) 15.8 (s, Me{ring}). $^{31}P\{^1H\}$ NMR [acetone-d_6]: δ 72.7 (s, $PPh_2(CH_2)_2PPh_2$), 144.1 (sept, PF_6^-). M.S.[FAB]: m/z 669 {M^+}.

4.23. X-ray structure of (**4**)

Well-shaped red cubes were obtained by crystallisation from a dichloromethane/diethylether mixture on cooling to −30 °C. A suitable crystal specimen was mounted on a glass fibre with epoxy resin and cooled on the goniometer head by means of nitrogen gas to 203 K. Precession photographs and intensity data were collected on a Siemens R3m/V diffractometer using graphite monochromatised Mo Kα X-rays.

Crystal data. $C_{28}H_{29}Cl_2O_3PRu\cdot CH_2Cl_2$, M = 701.4, monoclinic, space group $P2_1/n$, a = 12.936(2), b = 16.809(3), c = 13.979(2) Å, β = 98.06(1)°, U = 3009.6(8) Å^3, D_c = 1.548 g cm^{-3} for Z = 4, F(0 0 0) = 1424, μ(Mo Kα) = 9.59 cm^{-1}, T = -70 °C, crystal size 0.45 × 0.45 × 0.50 mm^3. Cell dimensions were obtained from 50 centred reflections with 2θ values from 22.5° to 32.1°. Intensity data in the range 3.5° < 2θ < 58.0° were collected using a 2θ–θ scan technique. The intensities of three reflections measured periodically showed a decrease of less than 1% over the data collection. An empirical absorption correction was applied using azimuthal scan data for twelve selected reflections. A total of 8285 reflections were collected of which 7966 were independent and 6992, for which $I > 2\sigma(I)$, were used in the refinement. The structure was solved by standard heavy atom routines and refined by full matrix least squares methods. All non-hydrogen atoms were given anisotropic temperature factors. Hydrogen atoms were placed in the model at calculated positions and allowed to ride on their respective carbon atoms. The highest peaks in the final difference map were <1.6 e Å^3, at convergence R_1 = 4.55% and wR_2 = 12.73%, $w = [\sigma^2 (F_o) + 0.0822P^2 + 2.0235P]^{-1}$ where $P = (F_o^2 + 2F_o^2)/3$, S = 1.10 for a data/parameter ratio 20.4:1.

5. Supplementary material

CCDC-236210 contains the supplementary crystallographic data for this paper. These data can be obtained free of charge via ccdc.cam.ac.uk/data_request/cif, by emailing data_request@ccdc.cam.ac.uk, or by contacting The Cambridge Crystallographic Data Centre, 12 Union Road, Cambridge, CB2 1EZ, UK; fax +44 1223 336033.

Acknowledgements

We thank the S.E.R.C. for a studentship (E.H.), Johnson–Matthey Chemicals Ltd., for a generous loan of $RuCl_3$, and we acknowledge the use of the EPSRC's Chemical Database Service at Daresbury [14].

References

[1] M.A. Bennett, A.K. Smith, J. Chem. Soc., Dalton Trans. (1974) 233.
[2] F. Faraone, G.A. Loprete, G. Tresoldi, Inorg. Chim. Acta 34 (1979) L251.
[3] A. Demonceau, A.F. Noels, E. Saive, A.J. Hubert, J. Mol. Catal. 76 (1992) 123.
[4] R.A. Zelonka, M.C. Baird, Can. J. Chem. 50 (1972) 3063.
[5] P. Pertici, S. Bertozzi, R. Lazzaroni, G. Vitulli, M.A. Bennett, J. Organomet. Chem. 354 (1988) 117.
[6] S.A. Serron, S.P. Nolan, Organometallics 14 (1995) 4611.
[7] R. Dussel, D. Pilette, P.H. Dixneuf, W.P. Fehlhammer, Organometallics 10 (1991) 3287.
[8] M. Herberhold, H. Yan, W. Milius, J. Organomet. Chem. 598 (2000) 142.
[9] E. Hodson, S.J. Simpson, in preparation.
[10] A. Haffner, A. Muhlebach, P.A. van der Schaal, Angew. Chem. Int. Ed. Engl. 36 (1997) 2121.
[11] G. Bruno, M. Panzalorto, F. Nicolo, C. Grazia Arena, P. Cardiano, Acta Crystallogr. C56 (2000) e429.
[12] E. Hodson, A.M. Boshaala, S.J. Simpson, in preparation.
[13] A. Neels, H. Stoeckli-Evans, L. Plasseraud, E. Garcia Hidalgo, G. Suss-Fink, Acta Crystallogr. C55 (1999) 2030.
[14] The United Kingdom Chemical Database Service, D.A. Fletcher, R.F. McMeeking, D. Parkin, J. Chem. Inf. Comput. Sci. 36 (1996) 746.

Available online at www.sciencedirect.com
SCIENCE DIRECT®
Polyhedron 23 (2004) 2709–2714
POLYHEDRON
www.elsevier.com/locate/poly

NO to NO_2^- conversion by divalent lanthanides: synthesis and crystal structure of $[Sm(Tp^{Me2,4\text{-}Et})_2NO_2]$

Graham H. Maunder, Maria Rosa Russo, Andrea Sella *

Christopher Ingold Laboratories, Department of Chemistry, UCL, 20 Gordon Street, London, WC1H 0AJ, UK

Received 26 May 2004; accepted 27 May 2004
Available online 20 July 2004

Dedicated with affection and gratitude to Malcolm Green on the occasion of his 'retirement'. It's nice being Green

Abstract

The reaction of nitric oxide with the divalent lanthanide complex $[Ln(Tp^{Me2})_2]$ and $[Ln(Tp^{Me2,4\text{-}Et})_2]$ (Ln = Sm, Eu, Yb) gives the corresponding seven-coordinate nitrites $[Ln(Tp^{Me2,X})_2NO_2]$ in a smooth reaction. A possible mechanism is proposed for this NO disproportionation. A single crystal X-ray diffraction study of $[Sm(Tp^{Me2,Et})_2NO_2]$ reveals a dodecahedral metal centre. However, as is customary for these species, the complex is fluxional in solution by NMR even at the lowest accessible temperatures.
© 2004 Elsevier Ltd. All rights reserved.

Keywords: Samarium; Lanthanide; Nitric oxide; Nitrite; Pyrazolylborate; Redox

1. Introduction

Over the past 20 years nitric oxide has come to be seen as a critically important molecule from both an environmental and biological [1] standpoint. While the binding of nitric oxide to transition metals has been explored for many years [2], transition metal-mediated transformations of nitric oxide, disproportionations in particular, have received renewed impetus with the recent discovery of systems capable of stepwise NO conversion [3]. By contrast, we are aware of very few reports of its reactions of the lanthanides [4].

The chemistry of the divalent lanthanides has provided a wealth of reactivity as a result of their unusual combination of reducing power and electrophilicity [5–7]. Much of the work exploring this chemistry has been carried out using cyclopentadienyl ligands as ancillaries, but increasingly other spectator ligands have come to be used [8]. The tris-pyrazolylborate ligand has found increasing application in p-block, transition metal [9,10] and lanthanide [11,12] chemistry because of the range of steric control which can be achieved by varying the substituents on the pyrazolyl groups. The activation of small molecules by the lanthanides continues to generate surprises. Because of the absence of back-bonding, classical complexes of CO are rare [13–16], and complexes of NO [4] and ethylene unknown so far [17,18]. However, an example of σ-only binding of alkyne has been reported [19] and a growing number of examples of side-on binding of dinitrogen to pairs of lanthanide centres have come to light recently [20–27]. The report of the reduction of O_2 by $[Sm(Tp^{Me2})_2]$ [28,29] to yield a thermally stable superoxide complex $[Sm(Tp^{Me2})_2(O_2)]$ [30], in which the O_2^- is enclosed in a steric "pocket" prompted us to examine the corresponding reaction of NO in the hopes of isolating an analogous product.

* Corresponding author. Tel.: +44-20-7679-4687; fax: +44-20-7679-7463.
E-mail address: a.sella@ucl.ac.uk (A. Sella).

0277-5387/$ - see front matter © 2004 Elsevier Ltd. All rights reserved.
doi:10.1016/j.poly.2004.05.018

2. Results

Stirring a suspension of [Sm(Tp^{Me2})$_2$] (**1a**) or a solution of the more soluble [Sm($Tp^{Me2,4-Et}$)$_2$] (**1b**) in THF under 1 atm of NO and warming from −78 °C to room temperature resulted in a bleaching of the purple colour of the starting materials consistent with an oxidative reaction of the metal centre. The resulting white solid could be recrystallized to yield analytically pure [Sm(Tp^{Me2})$_2$NO$_2$] (**2a**) and [Sm($Tp^{Me2,4-Et}$)$_2$NO$_2$] (**2b**), respectively.

The infrared spectrum of **2** is virtually superimposable with that of **1** apart from the appearance of two new bands at 1200 and 1297 cm^{-1}, assigned to the symmetric and antisymmetric stretching vibrations of a chelating O-bound nitrito group [31], and the splitting of many of the peaks in the fingerprint region, consistent with the reduction in symmetry expected with the addition of a new ligand. The frequency difference between the symmetric and antisymmetric stretching bands in the IR spectra of nitrito complexes has been shown to be a good indicator of the difference in N–O bond lengths in the chelate, with values less than 100 cm^{-1} indicating symmetrical binding [32]. The ^{1}H NMR spectrum of **2a** and **2b**, though broadened and shifted by the paramagnetic Sm(III) centre, shows a single set of resonances for the pyrazolyl groups, consistent with a structure containing two equivalent, fluxional $Tp^{Me2-4-Et}$ groups. The B–H protons were visible as a very broad lump in the baseline in the region around δ4. Thus the spectra display none of the complexity of those observed for other eight-coordinate species with symmetrical bidentate ligands such as [Sm(Tp^{Me2})$_2$(S_2CNR_2)] (R = Me, Et) and [Sm(Tp^{Me2})$_2$(S-2-pyr)] [33], and [Sm(Tp^{Me2})$_2$(PhNNPh)] [28] – these display distinct environments for each pyrazole group implying a C_2-symmetric, static coordination sphere. Instead, in **2a** and **2b**, a fast fluxional process occurs which makes all of the pyrazolyl groups equivalent on the NMR timescale. Attempts to slow down these dynamic processes were not successful – the ^{1}H NMR spectra broadened and shifted as the temperature was lowered to −95 °C in toluene-d_8 but the slow exchange limit was not reached. In this respect **2a** and **2b** more closely resemble seven coordinate species.

The synthesis of **2a** by metathesis of [Sm(Tp^{Me2})$_2$Cl] with sodium nitrite

$$[Sm(Tp^{Me2})_2Cl] + NaNO_2 \rightarrow [Sm(Tp^{Me2})_2(NO_2)] + NaCl$$

was also attempted. However the product could not be obtained entirely pure, with evidence of contamination by decomposition products arising from fragmentation of the ligand, which varied in quantity from one prep to another, a credible indicator of adventitious moisture. This is likely due to our failure to obtain sodium nitrate in an entirely anhydrous form in spite of repeated attempts. Lanthanide Tp^{Me2} complexes are notoriously sensitive to hydrolysis, a problem which has dogged this area [34].

The reaction of [Eu($Tp^{Me2-4-Et}$)$_2$] and [Yb($Tp^{Me2-4-Et}$)$_2$] proceeded similarly to give colourless products **3** and **4**, respectively. Complex **3** was NMR silent as expected for a f^6 trivalent europium complex. The ^{1}H NMR spectrum of **4** consisted of four highly shifted peaks with the correct integration ratio, though specific assignment was not possible. The infrared spectra of both compounds were virtually superimposable with those of **2b** although the nitrito bands of **4** were shifted to higher energy. We presume therefore that **3** and **4** are structurally analogous to **2** and that the shift is simply the result of the higher charge to radius ratio of the ytterbium centre.

In order to verify the nature of these complexes, and since we are only aware of one other structure of a lanthanide nitrite in the literature [35], crystals of **2b** suitable for X-ray diffraction were grown by slow evaporation of a solution of **2b** in toluene.

3. X-ray crystallographic study of 2b

Complex **2b** crystallized from toluene in the space group *C2/c*. The structure consists of well-separated discrete molecules of [Sm($Tp^{Me2,4-Et}$)$_2$(κ^2-NO$_2$)] rather similar to the structure of the previously reported [La(Tp^{Me2})$_2$(κ^2-NO$_3$)] [36]. A view of the molecule and the atomic numbering scheme is shown in Fig. 1. The metal centre is eight coordinate with the metal centre and the nitrogen atom of the nitrito group lying on

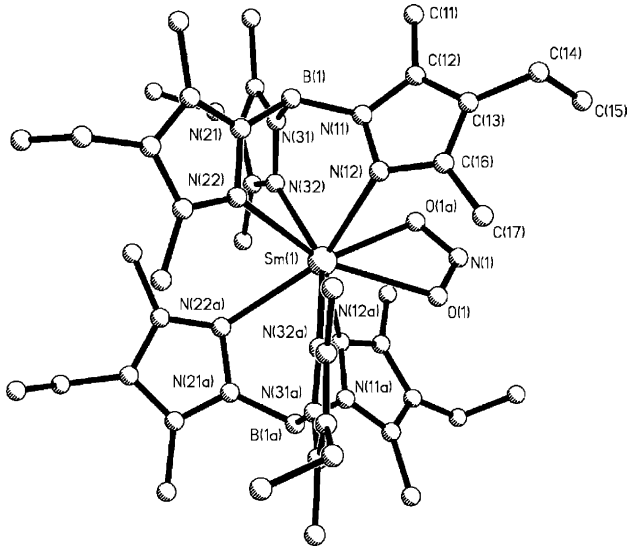

Fig. 1. The molecular structure of **2b** (hydrogen atoms are omitted for clarity). Selected bond angles (Å) and distances (°): Sm(1)–N(12) 2.551(4), Sm(1)–N(22) 2.565(4), Sm(1)–N(32) 2.495(4), Sm(1)–O(1) 2.486(4), Sm(1)–N(1) 2.953(3), O(1)–N(1) 1.263(5), O(1)–N(1)–O(1A) 112.7(6), O(1)–Sm(1)–O(1A) 50.0(2). Symmetry transformations used to generate equivalent atoms: $-x+1, y, -z+\frac{1}{2}$.

the crystallographic C_2 axis, making half of the molecule unique. On the basis of polytopal analysis, the coordination around the metal is best described as being dodecahedral, as shown in Fig. 2, similar to most other eight-coordinate bis-Tp^{Me2} complexes [28,33,36,37]. The two crystallographically planar trapezoids, defined by N12, N22, N12A, N22A and O1, N32, O1A, N32A, intersect at 94°. Thus the polyhedron around the metal is significantly closer to ideality than that observed in $[La(Tp^{Me2})_2(NO_3)]$ where significant distortion towards a bicapped trigonal prismatic arrangement was observed [36].

The two tridentate $Tp^{Me2,4\text{-}Et}$ ligands are mutually staggered and bent back away from the bidentate nitrito group (B1–Sm–B2 = 159.0°). This angle is the largest thus far observed for the Tp^{Me2} type complexes, and presumably reflects the small size of the NO_2 group and its ability to nestle in the gap between the two pyrazolyl groups from opposite ligands. We note however that in $[(SmTp^{Me2})_2(\eta^2\text{-}O_2)]$ the corresponding angle is 144° [30]. However, although the molecule appears analogous to a metallocene, the nitrito group does not lie in the "equatorial plane", but rather is twisted by 45.2° relative to the plane defined by the metal centre and the boron atoms. It therefore lies in the N32–Sm–N32A plane. The $Tp^{Me2,4\text{-}Et}$ ligands deviate significantly from the expected C_3 symmetry. In particular ring 1 shows marked twisting around the B–N bond (51.8° cf. ring 2, 2.7°; ring 3, 14.2°). Thus N11 is drawn in somewhat closer to the samarium (Sm–N11 = 3.166(6) Å cf. Sm–N(21,31) = 3.386(4), 3.336(4) Å) and as a result the pyrazolyl groups lies almost parallel to the orientation of the NO_2 group. The twisting of the ligand serves to enhance the steric protection afforded by the pocket around the nitrito group, pointing to the possibility of the availability of considerable steric control in these systems. But in addition it allows the two Tp ligands to be squeezed together allowing the B–Sm–B angle to increase, as discussed earlier. The distortion may also be thought of as an intermediate structure between normal coordination and the "side-bound" behaviour observed by Takats in $[U(Tp^{Me2})_2I]$ [38], and $[Sm(Tp^{tBu,Me})(\eta\text{-}C_5H_4SiMe_3)]$ [39], by Parkin in $[Tp^{tBu,Me}Tl]$ [40], and by us in $[Sm(Tp^{Me2})_2(SeC_6H_4\text{-}4\text{-}R)]$ (R = H, CH_3) [41]. We note that in $[La(Tp^{Me2})_2(NO_3)]$, which differs effectively only in the ionic radius of the metal (and hence its Lewis acidity), the twisting is much less pronounced. In addition, the distortion results in a Sm–B distance of 3.421 Å, which is much shorter (after correction for ionic radius [42]) than that in $[La(Tp^{Me2})_2(NO_3)]$ (3.681 Å) [36]. Nevertheless, the distortion hardly alters the Sm–N distances which range from 2.495(4) to 2.565(4) Å, very similar to the distances seen in other crystallographically characterized eight-coordinate complexes with this ancillary, $[Sm(Tp^{Me2})_2(\eta^2\text{-}O_2)]$ [30] $[Sm(Tp^{Me2})_2(2\text{-}SC_6H_4N)]$ $[Sm(Tp^{Me2})_2(S_2CNEt_2)]$ [33] and $[Sm(Tp^{Me2})_2(PhNNPh)]$ [28].

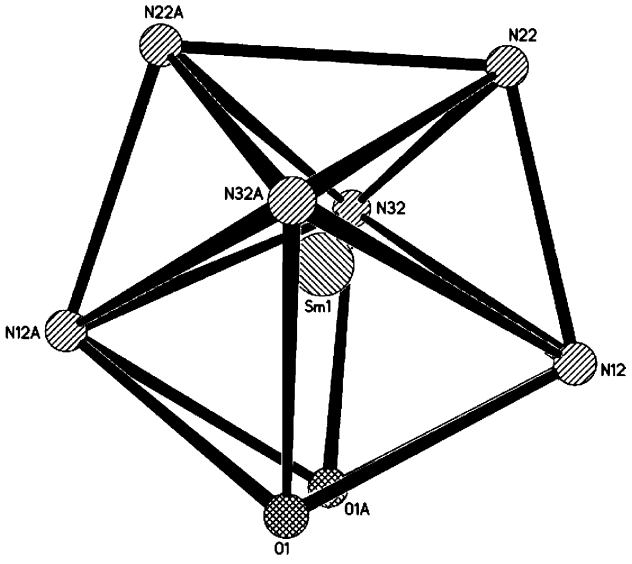

Fig. 2. A view of the dodecahedral coordination polyhedron around the samarium atom in **2b**.

The nitrite group is O-bonded and bidentate, as expected from the infrared spectra. After correcting for ionic radius, the Sm–O distance, 2.487(4) Å, is very similar to that observed in the nitrate $[La(Tp^{Me2})_2(NO_3)]$ but slightly longer than $[YbCp_2(NO_2)(THF)]$ [35]. This difference may reflect the greater steric demand of the pyrazolylborate ligand set compared with the metallocene. Indeed, evidence from related chalcogenolate chemistry suggests that the steric demand of the $(Tp^{Me2})_2Ln$ fragment is similar to that of the more substituted Cp^*_2LnL (L = unidentate ligand) [43]. The N–O distance of 1.263(5) Å is somewhat longer than that observed in $NaNO_2$ (1.24 Å) [35], but is very similar to the binding of nitrito group in transition metal complexes such as $[TpCu(\eta^2\text{-}ONO)]$, for which angles of about 110° and N–O distances of 1.24 Å are typical [44]. The N–O distance observed in **2** is in sharp contrast to those reported for $[YbCp_2(NO_2)(THF)]$ (average 1.10 Å) [35]. The bond length in the latter complex is surprisingly short, being of the order of those observed for the nitronium ion, NO_2^+ (1.123 Å) [45]. This distance, which the authors ascribed to particularly effective π-donation from the antibonding orbital of the nitrito group to the electrophilic lanthanide centre, is not reflected by the vibrational data. Although the electrophilicity increases somewhat on moving from samarium to ytterbium, the shortness of the N–O bond length is surprising. We note that the dataset for $[YbCp_2(NO_2)(THF)]$ appears to have been collected on a particularly poorly diffracting crystal, was refined with a low data:parameters ratio with most atoms in the structure refined isotropically. In addition the authors refer to the possibility of an "un-

resolved disorder'' of the nitrito group. Thus the structure of [$YbCp_2(NO_2)(THF)$] should probably be treated with circumspection.

4. Discussion

Complexes **1a/1b** react with NO to give **2a/2b**, with the more soluble **2b** being isolated in a better yield. This behaviour is in contrast to Evans' report of the behaviour of [$Sm(\eta^5\text{-}C_5Me_5)_2$], which reacts rapidly with NO to give the trivalent μ-oxo complex, [$(Sm(\eta^5\text{-}C_5Me_5)_2)_2(\mu\text{-}O)$], together with several other products [4]. The selectivity in the case of **1** highlights the extent of steric crowding in such systems which restricts the pathways available to the reaction.

No mechanism was proposed for the formation of the samarocene oxo complex. A related zirconium oxo-bridged species, $[Cp_2ZrO]_n$ has been reported to form from the reaction of $[Cp_2Zr(PMe_3)_2]$ with NO. This very fast reaction is accompanied by the formation of N_2 and involves the intermediate formation of N_2O [46]. Hence the samarocene system may also be a stoichiometric reagent for the conversion of NO to N_2. One can envisage a scheme whereby rapid electron transfer to NO yields a transient species ''Cp^*_2SmNO'', in which the NO is presumably side-bound. Dimerization followed by coupling yields a binuclear complex with a bridging $(NO)_2^{2-}$ ligand – Karlin has proposed the intermediacy of a bis-nitrosyl species to account for the conversion of NO to N_2O and oxide in a binuclear copper system [47]. In the case of samarium, the driving force associated with the formation of the bridging oxo ligand can be expected to be considerably larger than for copper, hence the elimination N_2O may be much more favoured. Evans showed that N_2O also reacts rapidly with Cp^*_2Sm to generate the oxo dimer, thereby releasing N_2 and completing the reaction.

The mechanism of the reaction of **1a/1b** with NO is instead presumed to involve a metal-mediated redistribution, as has been reported for a number of transition metal system [3,48–51], and which we presume has the following stoichiometry:

$$[Sm(Tp^{Me2})_2] + 3NO \rightarrow [Sm(Tp^{Me2})_2(NO_2)] + N_2O$$

However, our attempts to identify N_2O in the headspace gas were inconclusive because of the small volumes involved and the difficulty of obtaining NO which we could convince ourselves was entirely free of nitrous oxide as a contaminant.

We presume that NO does bind to the samarium, a process which is accompanied or driven by rapid electron transfer. This may account for the initial yellow colour observed at low temperature. Unfortunately even at these low temperatures it did not prove possible to observe IR or NMR bands consistent with the formation of the adduct [52]. It cannot be surprising that the NO^- ligand, not stabilized by significant covalent interactions, is highly reactive and is presumably attacked rapidly by two further molecules of NO to give **2a/2b** and nitrous oxide. In a similar reaction, Tolman has been able to isolate a terminal nitrosyl species, TpCu(-NO), which, stabilized by back-bonding from the copper centre, subsequently rearranges to give a coordinated nitrito species [3,53]. It is interesting that we have not observed the formation an μ-oxo species, {[$Sm(Tp^{Me2,4\text{-}Et})_2]_2(\mu\text{-}O)$}, analogous to that isolated by Evans. Several attempts have been made to prepare monoatomic bridged species of this type by other routes without success [52,54,55]. These failures may reflect the steric interactions between the ancillary ligands which prevent a close approach in such a dimer, as well as the fragility of the pyrazolyborate which provides several alternative decomposition pathways [34].

5. Conclusions

Nitric oxide appears to be too reactive to bind to low valent lanthanide centres since it undergoes rapid electron transfer followed by disproportionation. Nevertheless it may be possible to form simple adducts of NO to trivalent metal centres with vacant coordination sites and detect this binding by infrared spectroscopy.

6. Experimental

All preparations and manipulations were carried out using standard Schlenk line and dry box techniques in an atmosphere of dinitrogen [56]. Oxygen-free nitrogen was purified by passage over columns containing 3 Å molecular sieves and MnO [57]. All solvents were predried over 5 Å molecular sieves or sodium wire and distilled under nitrogen from the appropriate drying agents {Na (toluene), Na/K alloy (petroleum ether b.p. 30–40 °C, diethyl ether)}, before use.

[$Ln(Tp^{Me2})_2$] and [$Ln(Tp^{Me2,4\text{-}Et})_2$] were prepared by reaction of LnI_2 (Ln = Sm, Yb) with two equivalents of the appropriate KTp reagent, or in the case of Eu by Na/Hg reduction of $[Eu(Tp)_2Cl]$ as previously described [29]. Nitric oxide was either taken from cylinders or was prepared by the action of 7.5 M HNO_3 on copper turnings, and purified by passage through water and then through a trap at −78 °C. Nitric oxide free from N_2O was prepared by the action of HCl on $NaNO_2$ in the presence of $FeSO_4$ [58].

Infrared spectra were recorded as KBr pellets on a Nicolet 205 FTIR spectrometer. NMR spectra were recorded in solution using Varian XL-200 and VXR-400 spectrometers operating at 200 (^1H), 400 (^1H) and 100.6 (^{13}C) MHz. Spectra were calibrated using residual

proton (^{1}H) and solvent resonances (^{13}C), and are reported relative to tetramethylsilane. Elemental analyses were determined by Mr. Alan Stones of the UCL Analytical Services.

6.1. Preparation of $Sm(Tp^{Me2})_2NO_2$ (**2a**)

$Sm(Tp^{Me2})_2$ (0.205 g, 0.275 mmol) was placed in a Schlenk flask. 30/40 petrol (20 cm^3) was added and the solution cooled to −78 °C in a dry ice/acetone bath before being evacuated and then refilled with NO to a pressure of 760 mm Hg (1 atm). No reaction was observed at −78 °C but as the mixture was allowed to warm to room temperature the purple suspension decolourized and a yellow solid was formed. As the solvent was removed under reduced pressure the solid became white. The crude product was extracted into toluene (50 cm^3), filtered and then the solvent removed to yield a white solid.

Yield: 30 mg (14%). *Anal.* Calc. for $C_{30}H_{44}N_{13}B_2O_2Sm$: C, 45.6; H, 5.6; N, 23.0. Found: C, 44.8; H, 5.3; N, 23.8%. ^{1}H NMR (C_6D_6, 298K): 0.35 (s, 18H, Me); 2.41 (s, 18H, Me); 5.50 (s, 6H, 4-CH). IR (KBr pellet, cm^{-1}): ν_{B-H} 2528, ν_{N-O}(a/sym) 1300 (w), ν_{N-O}(sym) 1200 (s).

6.2. Preparation of $Sm(Tp^{Me2-4-Et})_2NO_2$ (**2b**)

$Sm(Tp^{Me2-4-Et})_2$ (0.135 g, 0.148 mmol) was placed in a Schlenk flask. 30/40 petrol (20 cm^3) was added and the solvent frozen in liquid nitrogen. The flask was evacuated and allowed to warm to −78 °C in a dry ice/acetone bath before being filled with NO to a pressure of 760 mm Hg (1 atm). No reaction was observed at −78 °C but as the mixture was allowed to warm to room temperature the purple suspension decolourized and a yellow solid was formed. As the solvent was removed under reduced pressure the solid became white. The crude product was extracted into diethyl ether (50 cm^3), filtered and then the volume reduced by one half. Cooling to −25 °C gave a white microcrystalline solid.

Yield: 50 mg (35%). *Anal.* Calc. for $C_{42}H_{68}N_{13}B_2O_2Sm$: C, 52.6; H, 7.15; N, 18.99. Found: C, 53.3; H, 7.15; N, 18.68%. ^{1}H NMR (C_6D_6, 298K): 1.03 (t, 18H, Me); 1.07 (s, 18H, Me); 2.16 (s, 18H, Me); 2.20 (q, 12H, CH_2); 4.70 (br s, 2H, BH). ^{11}B NMR (C_6D_6, 298K): −9.3. ^{13}C NMR (C_6D_6, 298K): 11.5 (q, 3 or 5 Me); 12.1 (q, 5 or 3 Me); 15.5 (q, 4-Me); 16.9 (6, 4 CH_2); 117.5 (s, 4 C); 141.5 (s, 3 or 5 C); 148.1 (s, 5 or 3 C). IR (KBr pellet, cm^{-1}): ν_{B-H} 2522, ν_{N-O}(a/sym) 1297 (w), ν_{N-O}(sym) 1200 (s).

6.3. Preparation of $Eu(Tp^{Me2-4-Et})_2NO_2$ (**3**)

Complex **3** was prepared by analogy with that of **2**. *Anal.* Calc. for $C_{42}H_{68}N_{13}B_2O_2Eu$: H, 7.13; B, 2.25; C, 52.51; N, 18.95. IR (KBr pellet, cm^{-1}): ν_{B-H} 2522, ν_{N-O}(a/sym) 1298(w), ν_{N-O}(sym) 1202 (s). The compound was NMR silent.

6.4. Preparation of $Yb(Tp^{Me2-4-Et})_2NO_2$ (**4**)

Complex **4** was prepared by analogy with that of **2**. *Anal.* Calc. for $C_{42}H_{68}N_{13}B_2O_2Yb$: H, 6.98; B, 2.2; C, 51.38; N, 18.55. ^{1}H NMR (C_6D_6, 298 K): −6.80 (br s, 18H, Me); −2.2 (t, 18H, Me); 1.04 (q, 18H, CH_2); 14.20 (s, 18H, Me). IR (KBr pellet, cm^{-1}): ν_{B-H} 2522, ν_{N-O}(a/sym) 1303(w), ν_{N-O}(sym) 1210(s).

7. X-ray crystallography

All measurements were made on a Nicolet R3mV four circle diffractometer using Mo Kα ($\lambda = 0.71073$ Å) radiation. Crystallographic calculations were carried out with the SHELX-93 suite of programs on a Pentium computer.

A colourless block of **2**, grown by slow crystallization from toluene, was mounted in a Lindemann capillary under nitrogen in a glove box. The orientation matrix of the crystal and the unit cell determined using 26 reflections chosen from a rotation photograph with 2θ in the range of 11.90–26.95°. Unit cell dimensions were confirmed by axial photographs. Data were collected by ω-2θ scans in a range $5° \leqslant 2\theta \leqslant 50°$. The intensities of three standard reflections monitored every 100 reflections showed no sign of crystal decay. Corrections for Lorentz, polarization and an empirical correction for absorption (using ψ-scans) were applied. The structure of **2** was solved by Patterson methods and developed by alternating cycles of difference Fourier syntheses and full matrix least-squares procedures. Anisotropic thermal parameters were used in the final model for all non-hydrogen atoms. Hydrogen atoms were not located but placed in idealized positions d(C–H) = d(B–H) 0.96 Å and assigned a common isotropic thermal parameter ($U = 0.08$ Å^2).

8. Supplementary material

Details of the experimental conditions appear in Table 1. Final atomic coordinates, thermal parameters, and bond lengths and angles have been deposited at the Cambridge Crystallographic Data Centre (CCDC). Any request to the CCDC for this material should quote the full literature citation and the reference number CCDC 236295.

Acknowledgements

We are grateful to the Royal Society and the University of London Central Research Fund for support, to the EPSRC for a studentship to G.H.M. (GR/H31943)

and for provision of the X-ray diffractometer. We are grateful to Prof. Josef Takats and Dr. Noemia Marques for helpful discussions and to Dr. Derek Tocher for assistance with the X-ray determination.

References

[1] S. Moncada, M.A. Martella, J.B. Hibbs, E.A. Higgs (Eds.), The Biology of Nitric Oxide, Portland Press, London, 1992.
[2] D.M.P. Mingos, D.J. Sherman, Adv. Inorg. Chem. 34 (1989) 293.
[3] C.E. Ruggiero, S.M. Carrier, W.B. Tolman, Angew. Chem., Int. Ed. Engl. 33 (1994) 895.
[4] W.J. Evans, I. Bloom, J.W. Grate, W.E. Hunter, J.L. Atwood, J. Am. Chem. Soc. 107 (1985) 405.
[5] W.J. Evans, Polyhedron 6 (1987) 803.
[6] C. Schaverien, Adv. Organomet. Chem. 36 (1994) 283.
[7] H. Schumann, J.A. Meese-Marktscheffel, L. Esser, Chem. Rev. 95 (1995) 865.
[8] F.T. Edelmann, Angew. Chem., Int. Ed. Engl. 34 (1995) 2466.
[9] S. Trofimenko, Chem. Rev. 93 (1993) 943.
[10] G. Parkin, Adv. Inorg. Chem. 42 (1995) 291.
[11] I. Santos, N. Marques, New J. Chem. 19 (1995) 551.
[12] N. Marques, A. Sella, J. Takats, Chem. Rev. 102 (2002) 2137.
[13] W. Evans, J. Grate, L. Hughes, H. Zhang, J. Atwood, J. Am. Chem. Soc. 107 (1985) 3728.
[14] M. Schultz, C.J. Burns, D.J. Schwartz, R.A. Andersen, Organometallics 20 (2001) 5690.
[15] L. Maron, L. Perrin, O. Eisenstein, R.A. Andersen, J. Am. Chem. Soc. 124 (2002) 5614.
[16] P. Selg, H.H. Brintzinger, M. Schultz, R.A. Andersen, Organometallics 21 (2002) 3100.
[17] W.J. Evans, S.C. Engerer, K.M. Coleson, J. Am. Chem. Soc. 103 (1981) 6672.
[18] M.P. Andrews, A.L. Wajda, Organometallics 7 (1988) 743.
[19] C.J. Burns, R.A. Andersen, J. Am. Chem. Soc. 109 (1987) 941.
[20] W.J. Evans, T.A. Ulibarri, J.W. Ziller, J. Am. Chem. Soc. 110 (1988) 6877.
[21] J. Jubb, S. Gambarotta, J. Am. Chem. Soc. 116 (1994) 4477.
[22] J.-I. Song, S. Gambarotta, Angew. Chem., Int. Ed. Engl. 34 (1995) 2141.
[23] E. Campazzi, E. Solari, C. Floriani, R. Scopelliti, Chem. Commun. (1998) 2603.
[24] W.J. Evans, N.T. Allen, J.W. Ziller, J. Am. Chem. Soc. 123 (2001) 7927.
[25] W.J. Evans, N.T. Allen, J.W. Ziller, Angew. Chem., Int. Ed. Engl. 41 (2001) 359.
[26] W.J. Evans, J. Organomet. Chem. 647 (2002) 2.
[27] W.J. Evans, D.S. Lee, J.W. Ziller, J. Am. Chem. Soc. 126 (2004) 454.
[28] J. Takats, X.W. Zhang, V.W. Day, T.A. Eberspacher, Organometallics 12 (1993) 4286.
[29] A.C. Hillier, X.W. Zhang, G.H. Maunder, S.Y. Liu, T.A. Eberspacher, M.V. Metz, R. McDonald, Â. Domingos, N. Marques, V.W. Day, A. Sella, J. Takats, Inorg. Chem. 40 (2001) 5106.
[30] X.W. Zhang, G.R. Loppnow, R. McDonald, J. Takats, J. Am. Chem. Soc. 117 (1995) 7828.
[31] K. Nakamoto, Infrared and Raman Spectra of Coordination Compounds, Wiley, New York, 1978.
[32] M.A. Hitchens, R. Thomas, J. Chem. Soc., Dalton Trans. (1983) 2273.
[33] I. Lopes, A.C. Hillier, S.Y. Liu, A. Domingos, J. Ascenso, A. Galvao, A. Sella, N. Marques, Inorg. Chem. 40 (2001) 1116.
[34] A. Domingos, M.R.J. Elsegood, A.C. Hillier, G. Lin, S.Y. Liu, I. Lopes, N. Marques, G.H. Maunder, R. McDonald, A. Sella, J.W. Steed, J. Takats, Inorg. Chem. 40 (2001) 5106.
[35] Z. Wu, Z. Xu, X. You, H. Wang, X. Zhou, F. Sheng, J. Hu, J. Organomet. Chem. 455 (1993) 93.
[36] R.J.H. Clark, S.Y. Liu, G.H. Maunder, A. Sella, M.R.J. Elsegood, J. Chem. Soc., Dalton Trans. (1997) 2241.
[37] I. Lopes, B. Monteiro, G.Y. Lin, Â. Domingos, N. Marques, J. Takats, J. Organomet. Chem. 632 (2001) 119.
[38] Y.M. Sun, R. McDonald, J. Takats, V.W. Day, T.A. Eberspacher, Inorg. Chem. 33 (1994) 4433.
[39] G.M. Ferrence, R. McDonald, M. Morissette, J. Takats, J. Organomet. Chem. 596 (2000) 95.
[40] J.L. Kisko, T. Hascall, C. Kimblin, G. Parkin, J. Chem. Soc., Dalton Trans. (1999) 1929.
[41] A.C. Hillier, S.Y. Liu, A. Sella, M.R.J. Elsegood, Inorg. Chem. 39 (2000) 2635.
[42] R.D. Shannon, C.T. Prewitt, Acta Cryst., Sect. B 26 (1976) 1046.
[43] A.C. Hillier, University of London, 1998.
[44] C.E. Ruggiero, S.M. Carrier, W.E. Antholine, J.W. Whittaker, C.J. Cramer, W.B. Tolman, J. Am. Chem. Soc. 115 (1993) 11285.
[45] S. Giese, K. Seppelt, Angew. Chem., Int. Ed. Engl. 33 (1994) 461.
[46] K. McNeill, R.G. Bergman, J. Am. Chem. Soc. 121 (1999) 8260.
[47] P. Paul, K.D. Karlin, J. Am. Chem. Soc. 113 (1991) 6331.
[48] R. Bau, I.H. Sabherwal, A.B. Burg, J. Am. Chem. Soc. 93 (1971) 4926.
[49] P. Gans, J. Chem. Soc., A (1967) 943.
[50] B.F. Hoskins, F.D. Whillans, D.H. Dale, D.C. Hodgkin, J. Chem. Soc., Chem. Commun. (1969) 69.
[51] S. Bhaduri, B.F.G. Johnson, A. Pickard, P.R. Raithby, G.M. Sheldrick, J. Chem. Soc., Chem. Commun. (1977) 354.
[52] J. Takats, personal communication.
[53] J.L. Schneider, S.M. Carrier, C.E. Ruggiero, V.G. Young, W.B. Tolman, J. Am. Chem. Soc. 120 (1998) 11408.
[54] N. Marques, personal communication.
[55] D.L. Deng, Y.H. Zhang, C.Y. Dai, H. Zeng, C.Q. Ye, R. Hage, Inorg. Chim. Acta 310 (2000) 51.
[56] S. McNally, N.J. Cooper, in: A.L. Wayda, M.Y. Darensbourg (Eds.), Experimental Organometallic Chemistry: A Practicum in Synthesis and Characterization, vol. 357, American Chemical Society, Washington, DC, 1987, p. 6.
[57] D.F. Shriver, M.A. Drezdzon, The Manipulation of Air-sensitive Compounds, Wiley, New York, 1986.
[58] G. Fowles, Lecture Experiments in Chemistry, Bell, London, 1948.

Available online at www.sciencedirect.com
SCIENCE DIRECT®
Polyhedron 23 (2004) 2715–2724
POLYHEDRON
www.elsevier.com/locate/poly

Reactions between isocyanides and a binuclear nickel(II) phosphine complex linked by a bridged bis(cyclopentadienyl) ligand. X-ray molecular structure of $[(CN^tBu)(PPh_3)Ni\{\mu\text{-}(\eta\text{-}C_5H_4)CMe_2(\eta\text{-}C_5H_4)\}Ni(PPh_3)(CN^tBu)][PF_6]_2$

Alejandro F.G. Ribeiro [a], Pedro T. Gomes [a,*], Alberto R. Dias [a], João L. Ferreira da Silva [a], M. Teresa Duarte [a], Rui T. Henriques [b], Cristina Freire [c]

[a] *Centro de Química Estrutural, Departamento de Engenharia Química, Instituto Superior Técnico, Av. Rovisco Pais, 1049-001 Lisboa, Portugal*
[b] *Instituto de Telecomunicações – Polo de Lisboa and Departamento de Engenharia Química, Instituto Superior Técnico, Av. Rovisco Pais, 1049-001 Lisboa, Portugal*
[c] *REQUIMTE/Departamento de Química, Faculdade de Ciências, Universidade do Porto, Rua do Campo Alegre, 4169-007 Porto, Portugal*

Received 20 April 2004; accepted 28 June 2004
Available online 11 September 2004

Dedicated to Professor Malcolm L.H. Green

Abstract

The reaction between the binuclear dicationic compound $[(PPh_3)_2Ni\{\mu\text{-}(\eta\text{-}C_5H_4)CMe_2(\eta\text{-}C_5H_4)\}Ni(PPh_3)_2][PF_6]_2$ (**1**) and either 2 or 4 equivalents of isocyanides leads to the substitution of a single PPh_3 ligand per nickel atom. The new binuclear compounds $[(CNR)(PPh_3)Ni\{\mu\text{-}(\eta\text{-}C_5H_4)CMe_2(\eta\text{-}C_5H_4)\}Ni(PPh_3)(CNR)][PF_6]_2$ (R = *S*-(−)-CH(Ph)Me (**2**), cyclohexyl (**3**), *tert*-butyl (**4**) and mesityl (**5**)) were prepared in almost quantitative yields and were fully characterised by elemental analysis, FT-IR and NMR spectroscopies. In the X-ray crystal structure of **4** two crystallographically inequivalent $CpNi(PPh_3)(CN^tBu)$ moieties are observed, where the $Ni(PPh_3)(CN^tBu)$ fragments are positioned on the C_5H_4 faces of the bridging ligand to minimise inter-ring repulsions. Addition of an excess of *S*-(−)-CNCH(Ph)Me to **1** results in the catalytic polymerisation of the isocyanide, yielding polymers of increasing molecular weights when the ratio $[CNR]_o/[Ni]_o$ is increased, consistent with non-living polymerisation. The molecular weights of the poly(*S*-(−)-1-phenylethyl isocyanide) (**6**) obtained with complex **1** are higher than those obtained with the related mononuclear complex $[Ni(\eta\text{-}C_5H_5)(PPh_3)_2]PF_6$ (**8**), which suggests an initiation step involving migratory insertion of isocyanide into the Ni–cyclopentadienyl bonds. An EPR spectrum of the reaction mixture acquired at 77 K, after 10 min of polymerisation at 20 °C, reveals the existence of two pentacoordinated Ni(I) $3d^9$ chain propagating species with trigonal bipyramidal geometry (d_{z^2} ground state). One of the Ni species contains two PPh_3 ligands occupying both axial positions of an axially distorted trigonal bipyramid, whereas the other species contains an axially coordinated PPh_3 and either a PPh_3 coordinated in the equatorial plane or dissociated from the nickel atom.
© 2004 Elsevier Ltd. All rights reserved.

Keywords: Binuclear compounds; Isocyanides; Nickel; Polymerisation; Ring-coupled bis-cyclopentadienyl ligand; X-ray molecular structure

1. Introduction

Despite the great number of NiCp (Cp = η-C_5H_5) compounds reported in the literature, those containing isocyanide ligands (C≡NR) are scarce. In the 1960s,

* Corresponding author. Tel.: +351 218419612; fax: +351 218464455/7.
E-mail address: pedro.t.gomes@ist.utl.pt (P.T. Gomes).

0277-5387/$ - see front matter © 2004 Elsevier Ltd. All rights reserved.
doi:10.1016/j.poly.2004.06.030

Yamamoto et al. [1,2] described the stoichiometric reaction of neutral [Ni(η-C_5H_5)(PPh_3)R′] (R′ = alkyl, aryl) with alkyl isocyanides to yield iminoacyl derivatives of the type [Ni(η-C_5H_5)(CNR){C(=NR)R′}], which were formed by insertion of a coordinated isocyanide into a Ni–R′ bond. According to these authors, the reaction between CN^{t}Bu and [Ni(η-C_5H_5)LX] (L = $P(OPh)_3$, $AsPh_3$; X = Br, I) does not give insertion products, but leads to the formation of cationic compounds of the type [Ni(η-C_5H_5)(CN^{t}Bu)$_2$]$^+X^-$ (X = I, Br). Using analogous compounds [Ni(η-C_5H_5)LX], (L = PPh_3, PEt_3 and X = I) the monosubstituted complexes [Ni(η-C_5H_5)(CNR)L]$^+I^-$ (R = ^{t}Bu, Cy), could be obtained, demonstrating that the selectivity of the cationic products is sensitive to the co-ligands in the coordination sphere.

More recently, Takahashi and co-workers [3] found that the neutral alkynyl derivative [Ni(η-C_5H_5)(PPh_3)(C≡CPh)] is an effective catalyst for the polymerisation of isocyanides [4] and managed to isolate and characterise a PPh_3 free iminoacyl NiCp complex resulting from double insertion, with a proposed structure incorporating a four-membered ring [Ni(η-C_5H_5){C(=N=R)C(=NR)C≡CPh}], which is the first intermediate of multiple insertion reactions. Previous studies on the polymerisation of isocyanides catalysed by nickel complexes comprises the highly active systems based on $Ni(CO)_4$ [5] and $NiCl_2$ [4b,6], and the controlled synthesis of well-defined poly(isocyanides) achieved by Deming and Novak [7]. These authors employed the neutral allyl nickel complex [Ni(η-CH_2CHCH_2)(μ-$OOCF_3$)]$_2$, in which the allyl ligand plays a key role in the rapid initiation of the polymerisation reaction facilitating fast insertion of coordinated isocyanide molecules under living polymerisation conditions. This method enabled the synthesis of elastomeric diblock butadiene–isocyanide [8] and triblock butadiene–isocyanide–butadiene [9] copolymers, the latter being prepared with the bifunctional allyl nickel initiator [(μ-CF_3COO)-Ni{μ-(η-$(CH_2)_2C$)-$(C(CH_2)_2$-η)}Ni(μ-$OOCCF_3$)] (**7**).

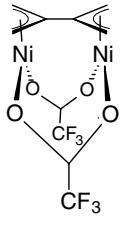

7

We have recently reported the living polymerisation of isocyanides using the cationic allyl nickel complex [Ni(η-$CH_2C(CH_3)CH_2$)(COD)]PF_6 (COD = 1,5-cyclooctadiene) [10]. We demonstrated that indenyl and cyclopentadienyl ligands bound to Ni can also play an important role in the initiation of the isocyanide polymerisation since the cationic allyl, indenyl and cyclopentadienyl nickel derivatives [Ni(η-$CH_2C(Me)CH_2$)(PPh_3)$_2$]PF_6, [Ni(η-C_9H_7)(PPh_3)$_2$]PF_6 and [Ni(η-C_5H_5)(PPh_3)$_2$]PF_6 (**8**) are effective catalysts for this reaction, although in a non-living fashion. Furthermore we have also studied the synthesis and characterisation of ring-coupled cyclopentadienyl and indenyl homobimetallic nickel compounds, including the complex [(PPh_3)$_2$Ni{μ-(η-C_5H_4)CMe_2(η-C_5H_4)}Ni(PPh_3)$_2$][PF_6]$_2$ (**1**) [11]. In this paper, we report the stoichiometric and catalytic reactions between isocyanides and the dicationic binuclear compound **1**.

2. Results and discussion

The reaction between the binuclear compound [(PPh_3)$_2$Ni{μ-(η-C_5H_4)CMe_2(η-C_5H_4)}Ni(PPh_3)$_2$][PF_6]$_2$ (**1**) [11] and stoichiometric amounts of isocyanides (C≡N—R) in *o*-dichlorobenzene at room temperature gives exclusively compounds **2**–**5** [(CNR)(PPh_3)Ni{μ-(η-C_5H_4)CMe_2(η-C_5H_4)}Ni(PPh_3)(CNR)][PF_6]$_2$, where R = *S*-(−)-1-phenylethyl (**2**), cyclohexyl (**3**), *tert*-butyl (**4**) and mesityl (**5**) (Scheme 1). Irrespective of the electronic or stereochemical properties of the isocyanide used and the stoichiometry (2 or 4 equivalents), only the product of a nucleophilic monosubstitution of PPh_3 by CNR at each Ni atom is obtained. These new dicationic binuclear Ni compounds were obtained in almost quantitative yields as green microcrystals (**3**), green lamellar crystals (**4**) or green amorphous powders (**2** and **5**) and all are relatively stable in air. Attempts to synthesise the bis-isocyanide derivative [(CNR)$_2$Ni{μ-(η-C_5H_4)YMe_2(η-C_5H_4)}Ni(CNR)$_2$][PF_6]$_2$ (Y = C or Si) by using an analogous synthetic route to that used for the synthesis of compound **1** [11], from the reaction between [$NiBr_2${*S*-(−)-CNCH(Ph)Me}$_2$] and Li_2[$CMe_2(C_5H_4)_2$] or Li_2[$SiMe_2(C_5H_4)_2$], failed.

Recrystallisation of **4** from CH_2Cl_2–Et_2O gave crystals suitable for a single crystal X-ray diffraction study. The molecular structure of the dication is shown in Fig. 1, and selected distances and angles are listed in Table 1. Unlike the parent compound **1** [11], the molecular structure reveals that dication **4** contains two crystallographically inequivalent CpNi(PPh_3)(CN^{t}Bu) moieties. The Ni(PPh_3)(CN^{t}Bu) fragments are positioned on the C_5H_4 faces of the bridging ligand to minimise inter-ring repulsions. As a consequence there is a long interatomic separation Ni(1)···Ni(2) of 6.659(10) Å, which is, however, shorter than that observed in **1** (6.750(1) Å) [11]. The plane defined by the bridging carbon atoms C(1)—C(6)—C(7) bisects the Cp ring bound to Ni(2) (dihedral angle of 89.4(5)°), whereas the Cp ring connected to Ni(1) shows a 4.9° clockwise rotation in rela-

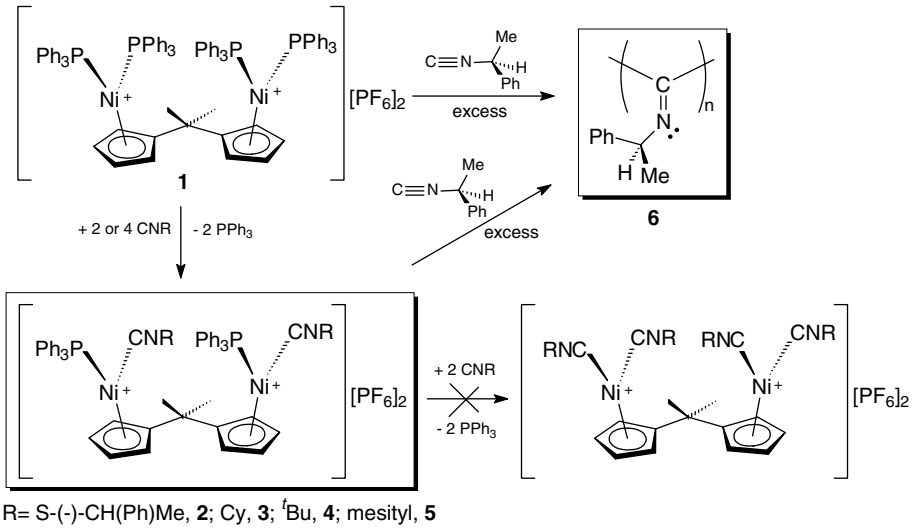

Scheme 1. Reactions between **1** and isocyanides: synthesis of compounds **2**–**5** and polymerisation of *S*-(−)-1-phenylethyl isocyanide catalysed by **1**.

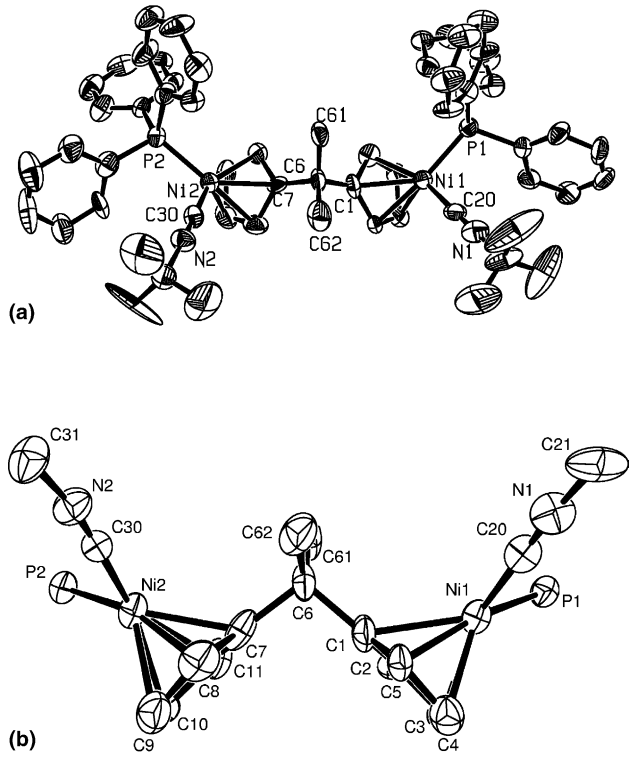

Fig. 1. ORTEPIII diagram of dication **4**, using 30% probability level ellipsoids. (a) Global view. (b) Side view (the hydrogens, the phenyl groups of PPh_3 and the methyl groups of CN^tBu have been omitted for clarity).

tion to the same plane. Geometries at both nickel atoms are trigonal planar (sum of bond angles using Cp ring centroids are 359.6(4)° and 359.5(4)°, respectively, at Ni(1) and Ni(2)), but the Cp planes are deviated slightly from the perpendicular to the corresponding P—Ni—$C_{isocyanide}$ planes (dihedral angles of 83.7(3)° and 84.3(4)°, respectively, for Ni(1) and Ni(2)). This is also observed in the reported structure of binuclear **1** [11] and in other known X-ray structures of monosubstituted nickel cyclopentadienyl complexes [12–14]. The Ni—C_{Cp} distances are within the range of values observed for **1** [11], but the Ni—P distances are shorter than in **1** (2.211(2) and 2.214(2) Å) and similar to the value found in the related indenyl analogue [Ni(η-1-^{i}Pr-C_9H_6)(PPh_3)(CN^tBu)][OSO_2CF_3] (2.1838(9) Å) [15]. This is a consequence of lower steric crowding around the Ni atoms in compound **4**, which have less bulky ligands than **1** (CN^tBu instead of a second PPh_3). The isocyanide ligands are bound to the Ni in a terminal fashion and are essentially linear: Ni(1)—C(20)—N(1) and C(20)—N(1)—C(21) are 179.1(11)° and 175.0(13)°, respectively, while Ni(2)—C(30)—N(2) and N(2)—C(30)—Ni(2) are 176.8(10)° and 175.0(13)°, respectively. These values together with those of Ni(1)—C(20) and Ni(2)—C(30), 1.877(11) and 1.810(10) Å, and C(20)—N(1) and C(30)—N(2), 1.123(13) and 1.124(11) Å, respectively, are within the range of values found for other Ni compounds containing CN^tBu ligands [12,16,17]. The low quality of the crystals precluded a standard refinement, not allowing a reliable discussion of the distortions of the Cp rings according to the classification introduced by Andersen and co-workers [18].

In solution, all the new compounds **2**–**5** exhibit C_{2v} symmetry, which implies the existence of unrestricted rotation of the Ni(PPh_3)(CNR) groups around each Cp—Ni bond. In fact, the ^{1}H NMR spectra of **2**–**5** show single resonances in the range δ 1.53–1.73 for both bridging methyl protons and only two resonances in the ranges δ 5.41–5.49 and 4.91–5.19 for the Cp ring protons, assigned by NOE experiments to the equivalent proximal (H2/H5 – closer to the bridge) and distal (H3′/H4′) protons, respectively. The separation between their chemical shifts ($\Delta = \delta$(H2/H5) – δ(H3/H4) = 0.24–0.50)

Table 1
Selected distances (Å) and angles (°) for the dication $[(CN^tBu)(PPh_3)Ni\{\mu\text{-}(\eta\text{-}C_5H_4)CMe_2(\eta\text{-}C_5H_4)\}Ni(PPh_3)(CN^tBu)]^+$ (**4**)

Distances			
Ni(1)—C(20)	1.877(11)	C(1)—C(2)	1.398(12)
Ni(1)—P(1)	2.172(3)	C(2)—C(3)	1.410(13)
Ni(1)—C(1)	2.191(9)	C(3)—C(4)	1.407(14)
Ni(1)—C(2)	2.087(10)	C(4)—C(5)	1.393(14)
Ni(1)—C(3)	2.080(11)	C(5)—C(1)	1.437(13)
Ni(1)—C(4)	2.122(12)	C(7)—C(8)	1.468(14)
Ni(1)—C(5)	2.113(8)	C(8)—C(9)	1.425(18)
Ni(2)—C(30)	1.810(10)	C(9)—C(10)	1.392(16)
Ni(2)—P(2)	2.175(3)	C(10)—C(11)	1.460(16)
Ni(2)—C(7)	2.141(9)	C(11)—C(7)	1.379(14)
Ni(2)—C(8)	2.086(12)	C(1)—C(6)	1.524(13)
Ni(2)—C(9)	2.142(14)	C(6)—C(7)	1.538(15)
Ni(2)—C(10)	2.106(10)	C(20)—N(1)	1.123(13)
Ni(2)—C(11)	2.104(10)	C(30)—N(2)	1.124(11)
$Ni(1)—Cp_{cent}$	1.747	C(21)—N(1)	1.432(17)
$Ni(2)—Cp_{cent}$	1.734	C(31)—N(2)	1.508(12)
Ni(1)—Ni(2)	6.659(10)		
Nearest Cp carbon (C(5)) to P(1)—Ni(1)—C(20) plane			0.14(1)
Nearest Cp carbon (C(8)) to P(2)—Ni(2)—C(30) plane			0.37(1)
Angles			
C(1)—Ni(1)—C(20)	118.9(4)	N(1)—C(20)—Ni(1)	179.1(11)
C(2)—Ni(1)—C(20)	156.6(4)	C(20)—N(1)—C(21)	175.0(13)
C(3)—Ni(1)—C(20)	150.9(4)	N(2)—C(30)—Ni(2)	176.8(10)
C(4)—Ni(1)—C(20)	113.6(4)	C(30)—N(2)—C(31)	170.9(12)
C(5)—Ni(1)—C(20)	99.4(4)	C(1)—C(6)—C(7)	102.5(8)
P(1)—Ni(1)—C(20)	92.0(3)	C(6)—C(1)—Ni(1)	130.9(8)
C(7)—Ni(2)—C(30)	112.1(4)	C(6)—C(7)—Ni(2)	132.8(7)
C(8)—Ni(2)—C(30)	95.1(5)	$Cp_{cent}—Ni(1)—P(1)$	134.4(4)
C(9)—Ni(2)—C(30)	115.2(5)	$Cp_{cent}—Ni(1)—C(20)$	133.2(4)
C(10)—Ni(2)—C(30)	153.1(5)	$Cp_{cent}—Ni(2)—P(2)$	134.1(4)
C(11)—Ni(2)—C(30)	149.2(5)	$Cp_{cent}—Ni(2)—C(30)$	130.1(4)
P(2)—Ni(2)—C(30)	95.3(3)		
Dihedral angle between Cps			89.6(4)
Dihedral angle between Cp and C(20)—Ni(1)—P(1)			83.7(3)
Dihedral angle between Cp and C(30)—Ni(2)—P(2)			84.3(4)
Dihedral angle between Cp (Ni(1)) and C(1)—C(6)—C(7)			89.4(5)
Dihedral angle between Cp (Ni(2)) and C(1)—C(6)—C(7)			85.1(7)
Dihedral angle between C(1)—C(5)—C(4) and C(4)—C(3)—C(2)—C(1)			5.0(9)
Dihedral angle between C(8)—C(9)—C(10) and C(8)—C(7)—C(11)—C(10)			3.6(9)

are of the same order of magnitude of those verified for other substituted cyclopentadienyl complexes of nickel including $[Ni(\eta\text{-}MeC_5H_4)(dppe)]X$ (X = Cl, I, NCS), with values of Δ between 0.09 and 0.12 [12], or $[Ni(\eta\text{-}RC_5H_4)L_2]BF_4$ (R = Me, ^{t}Bu; L_2 = norbornadiene, 1,5-cyclooctadiene), with Δ varying from 0 to 0.41 [19]. However, this separation is significantly lower than in the binuclear **1** or $[Cl(PPh_3)Ni\{\mu\text{-}(\eta\text{-}C_5H_4)CMe_2(\eta\text{-}C_5H_4)\}Ni(PPh_3)Cl]$ (Δ = 1.82 and 0.77, respectively [11]) or in other mononuclear Ni compounds containing PPh_3 including $[Ni(\eta\text{-}MeC_5H_4)(PPh_3)X]$ (X = Cl, Br, I, NCS), with Δ ranging from 0.90 to 1.66 [12]. The symmetry of **2**–**5** is further confirmed by the $^{13}C\{^1H\}$ spectra that exhibit one methyl resonance in the range δ 29.3–31.1, two peaks at δ 93.0–93.3 (C3/C4) and 95.2–96.0 (C2/C5), and one peak in the range δ 128.1–128.6 corresponding to the Cp *ipso* carbon resonance (C1), and by the ^{31}P spectra showing a single resonance in the range δ 40.7–42.1. In the ^1H NMR spectra, the H2/H5 and H3/H4 resonances multiplicities in compounds **3**–**5** show a deceptively simple AA′XX′ pattern, typical of monosubstituted cyclopentadienyl ligands [20]. However, in compound **2**, these two resonances appear as broadened singlets with no fine structure.

This latter feature exhibited by compound **2**, which reveals a higher lability of this less basic isocyanide ligand, may be eventually related to the difference in reactivity observed for compound **1** towards the presence of an excess of isocyanide. When attempting the synthesis of $[(CNR)_2Ni\{\mu\text{-}(\eta\text{-}C_5H_4)CMe_2(\eta\text{-}C_5H_4)\}Ni(CNR)_2][PF_6]_2$, the addition of an excess of isocyanide to **1** did not lead to a reaction, except in the case of *S*-(−)-1-phenylethyl isocyanide, where **1** caused polymerisation to poly(*S*-(−)-1-phenylethyl isocyanide). Interestingly, the

neutral binuclear compound [Cl(PPh$_3$)Ni{μ-(η-C$_5$H$_4$)CMe$_2$(η-C$_5$H$_4$)}Ni(PPh$_3$)Cl] is not active in the polymerisation of the same isocyanide.

We have very recently reported that the related mononuclear [Ni(η-C$_5$H$_5$)(PPh$_3$)$_2$]PF$_6$ (**8**) is a good catalyst for the polymerisation of *S*-(−)-1-phenylethyl isocyanide, showing an activity similar to that of the corresponding indenyl analogue [Ni(η-C$_9$H$_7$)(PPh$_3$)$_2$]PF$_6$ but lower than that of the 2-methallyl derivative [Ni(η-CH$_2$C(Me)CH$_2$)(PPh$_3$)$_2$]PF$_6$ [10]. In this work, we found out that the polymerisation of *S*-(−)-1-phenylethyl isocyanide catalysed by the binuclear complex **1** also follows an overall second-order kinetic law ($r_p = k_p[Ni]_o[CNR]$). The second-order rate constant k_p obtained is slightly lower than that calculated for the reaction catalysed by the mononuclear **8** (reactions AFP73 versus AFP76 in Table 2), probably due to a higher steric hindrance imposed by the substituted Cp rings of **1** in the polymerisation initiation step. The initiation step will very likely involve the coordination of CNR ligands to **1** followed by insertion into the Ni–η^1–Cp bond giving rise to a Ni-iminoacyl group (vide infra), although the migratory insertion reaction of the cyclopentadienyl ligand is not yet a well-documented reaction [21].

In order to test whether binuclear **1** could give rise to polymers with different molecular weight when compared to **8**, we have carried out a set of polymerisation reactions for each of these catalysts in which the initial concentration ratio [CNR]$_o$/[Ni]$_o$ was varied (Fig. 2). The initial molar concentration of nickel atoms used was exactly the same for both catalysts but, since in **1** two Ni atoms are linked by a bridged bis(cyclopentadienyl) ligand, the molar ratio concentration of complex **8** is double that of **1**. If this was an ideal living polymerisation (very fast initiation: $k_i \gg k_p$, and absence of chain transfer or termination reactions) [22], the theoretical molecular weight expected for the polymerisation catalysed with **1** ($\overline{M}_n = 2M_{CNR}[CNR]_o/[Ni]_o$) would be double that expected with **8** ($\overline{M}_n = M_{CNR}[CNR]_o/[Ni]_o$) (Fig. 3) since the polymer growth would occur at both Ni centres of **1**, and both chains would be chemically linked by the 2,2′-dicyclopentadien-di-yl propane spacer, as shown in Scheme 2. In Fig. 2, it can be seen for both catalysts that the molecular weight polymerisation is not a living polymerisation system and hence chain tranfer and/or slow initiation processes are occurring. Nevertheless, it is clear that at lower [CNR]$_o$/[Ni]$_o$ ratios the binuclear catalyst **1** produces a poly(*S*(−)-1-phenylethyl isocyanide) with higher molecular weight than that obtained with the mononuclear catalyst **8**. We believe these results strongly suggest an initiation step proceeding from the migratory insertion of CNR into the Ni—Cp bond, although at higher ratios, $\overline{M}_n$ values of **1** and **8** become similar, which can be attributed to significant chain transfer reactions.

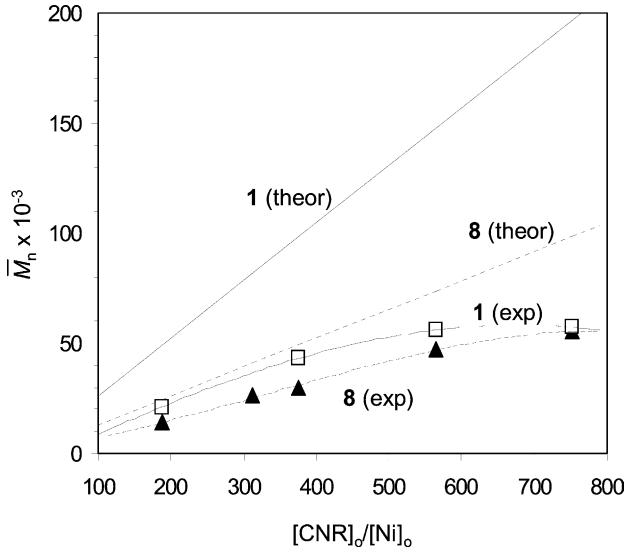

Fig. 2. Plots of the experimental $\overline{M}_n$ values of polyisocyanide *versus* the initial concentration [CNR]$_o$/[Ni]$_o$ obtained after 100% conversion of *S*-(−)-C≡NCH(Ph)Me catalysed by **1** (white squares, continuous line) and **8** (black triangles, dashed line). The straight lines represent the theoretical values expected for living polymerisation. Conditions: 25 °C; under N$_2$; [Ni]$_o$ = 1.44 mM; solvent: CH$_2$Cl$_2$, 4 ml.

Information on the propagation step was obtained by acquiring the EPR spectrum of the reaction mixture of polymerisation of *S*(−)-CNCH(Ph)Me catalysed by **1** after 10 min of reaction. The experimental spectrum obtained at 77 K and three simulated spectra are shown in

Table 2
Catalytic activities of compounds **1** and **8** in the polymerisation of *S*-(−)-C≡NCH(Ph)Me (solv: CH$_2$Cl$_2$ (4 ml); 25 °C; under N$_2$)

Reaction No.	Catalyst	[Ni]$_o$ (mM)	[CNR]$_o$/[Ni]$_o$	Time (min)	Conversion (%)	N_t[d] (min^{-1})	$k_p \pm 0.005$ (l mol^{-1} s^{-1})
AFP73	**1**	1.43	502	32.5	25.1	3.9	0.087
AFP76[a]	**8**	1.27	552	32.5	27.1	4.5	0.096
AFP136[b]	**1**	1.43	502	32.5	24.8	3.8	0.086
AFP137[c]	**1**	1.43	502	32.5	23.8	3.7	0.082

[a] Determined in [10].
[b] Carried out in the presence of 1 equivalent of BHT.
[c] Carried out in the presence of 1 equivalent of galvinoxyl.
[d] Turnover frequency defined as $N_t = ([CNR]_o - [CNR])/([Ni]_o \times \text{time})$.

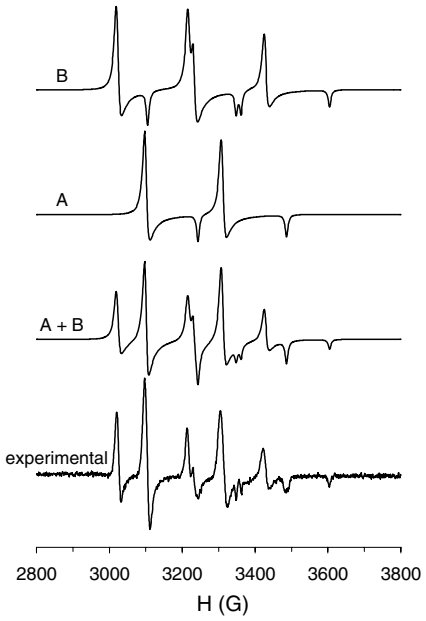

Fig. 3. EPR spectra (77 K) of the reaction mixture of the polymerisation of *S*-(−)-CNCH(Me)Ph catalysed by **1**, after 10 min, at 20 °C, under N_2, and corresponding simulations (**A**, **B** and **A** + **B** – see Scheme 3). Conditions: $[Ni]_o = 1.2 \times 10^{-2}$ M; $[CNR]_o/[Ni]_o = 312$; CH_2Cl_2 (100 μl).

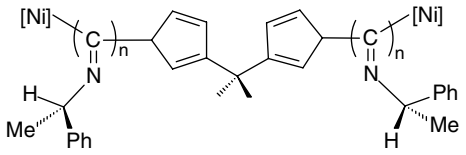

Scheme 2.

Fig. 3. The spectrum suggests the presence of a mixture of two nickel(I) pentacoordinated ($3d^9$) species, presumably **A** and **B** (Scheme 3), both with trigonal bipyramidal geometry and a d_{z^2} ground state [23]. The spectrum of species **A** was simulated with values of $g_\perp = 2.105$ and $g_\parallel = 2.005$ and hyperfine couplings to one phosphorus atom with $A_\perp = 210$ and $A_{||} = 243$ G. The chain propagating species **A** contains at least one coordinated phosphine ligand, which is positioned in the axial position, and the other phosphine ligand is either coordinated in the equatorial plane or dissociated from the metal atom (substituted by an isocyanide). The chain propagating species **B** shows an EPR spectrum that was simulated with $g_\perp = 2.092$ and $g_\parallel = 2.005$ and hyperfine couplings to two inequivalent phosphorus atoms: $A^1_\perp = 210$ and $A^1_\parallel = 256$ G and $A^2_\perp = 196$ and $A^2_\parallel = 243$ G. This result suggests that the two phosphine ligands occupy the axial positions of an axially distorted trigonal bipyramid. These observations are in good agreement with those of Deming and Novak [7] and our own previous results [10] concerning the formation of trigonal bipyramidal (TBP) Ni(I) species during the polymerisation of the same isocyanide catalysed by allyl derivatives of nickel. It was shown that the allyl group acts as a sacrificial ligand, undergoing a fast insertion of isocyanide into the Ni–allyl bond and hence giving rise to a rapid polymerisation initiation step. In the presence of an excess of isocyanide in the polymerisation mixture, the existence of pentacoordinated TBP Ni(II) species is favoured. The latter will be rapidly reduced to Ni(I) tetrahedral species by homolytic cleavage of a Ni—CNR bond in the TBP Ni(II) complex. This can be explained on the basis of the molecular orbital diagrams for TBP d^8 complexes, which show the molecular orbitals centered in e′ ($d_{x^2-y^2}$ and d_{xy}) are anti-bonding in character and thus coordination of strong donor ligands will induce the weakening of the equatorial Ni—CNR bond. [7,23d,24]. The excess of CNR in the reaction mixture induces the coordination of CNR to the Ni(I) tetrahedral complex generating the TBP Ni(I) species, which are clearly detected by EPR. The chain growth (propagation step) occurs by migratory insertion of isocyanide into the nickel–polyiminic chain bond. The mechanism proposed for the initiation and propagation steps of the polymerisation is shown in Scheme 4. A radical mechanism for this polymerisation is ruled out since reactions performed in the presence of 1–5 equivalents of radical traps like BHT or galvinoxyl (a stable free radical) do not change substantially the polymerisation rate constant k_p (reactions AFP136 and 137 versus AFP73 in Table 2). A detailed mechanistic study on the polymerisation of isocyanides with related cationic nickel complexes will be published elsewhere.

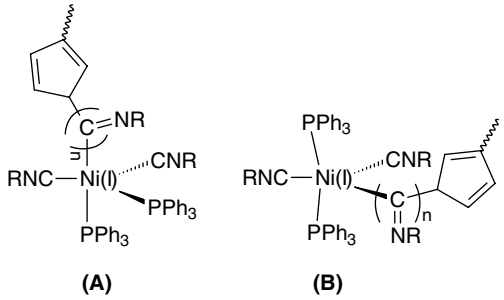

Scheme 3.

3. Experimental

All manipulations of air and/or moisture sensitive materials were carried out under an inert atmosphere using a dual vacuum/nitrogen line and standard Schlenk techniques. Nitrogen gas was supplied in cylinders by Air Liquide, and purified by passage through 4 Å molecular sieves. Solvents and solutions were trans-

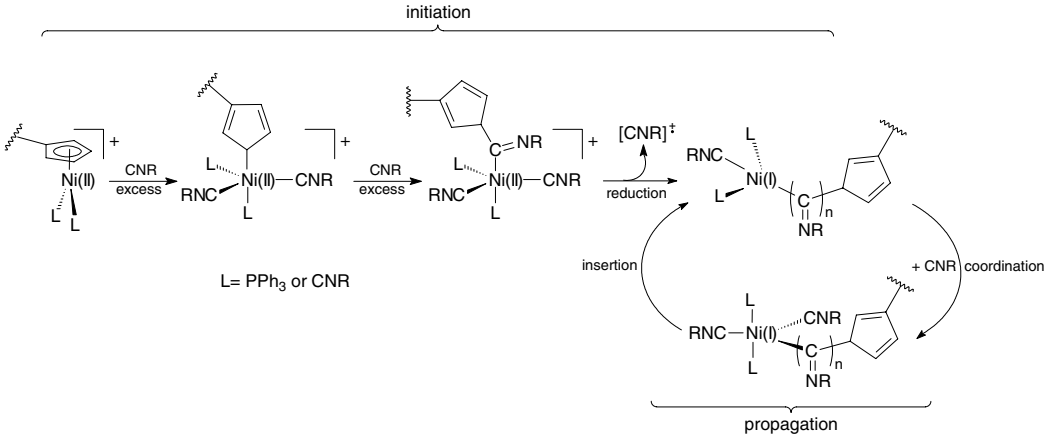

Scheme 4. Mechanism proposal for the initiation and propagation steps of the polymerisation of *S*-(−)-1-phenylethyl isocyanide catalysed by **1**.

ferred using a positive pressure of nitrogen through stainless steel cannulae and mixtures were filtered in a similar way using modified cannulae that could be fitted with glass fibre filter disks. Unless otherwise stated, reagents were purchased from commercial suppliers (Aldrich, Fluka et sim.) and used without further purification. All solvents to be used under inert atmosphere were thoroughly deoxygenated and dehydrated before use. They were dried and purified by refluxing over a suitable drying agent followed by distillation under nitrogen. The following drying agents were used: sodium/benzophenone for toluene, benzene, tetrahydrofuran and diethyl ether; calcium hydride for hexane, dichloromethane and *o*-dichlorobenzene. Deuterated solvents were dried by storage over 4 Å molecular sieves and degassed by the freeze-pump-thaw method.

Nuclear magnetic resonance spectra were recorded on a Varian Unity 300 spectrometer at the following frequencies: ^{1}H at 299.995 MHz; ^{13}C at 75.4296 MHz; ^{31}P at 121.417 MHz. Spectra were referenced internally using the residual protio-solvent resonance relative to tetramethylsilane (^{1}H and ^{13}C, $\delta = 0$) or 85% H_3PO_4 (^{31}P, $\delta = 0$). All chemical shifts are quoted in δ (ppm) and coupling constants are given in Hz. Multiplicities are abbreviated as follows: singlet (s), doublet (d), triplet (t), heptet (h), multiplet (m), broad (br). Assignments were supported by one-dimensional nuclear Overhauser effect experiments and one- and two-dimensional homo- and hetero-correlations, as appropriate. Electron paramagnetic resonance spectra were recorded on a Bruker ESP-300E X-band spectrometer, at 77 K, and were simulated with the programme Win EPR Simfonia (Bruker). The FT-IR spectra were recorded on a Mattson FTIR 1000, either using KBr disks (organometallic compounds) or a NaCl liquid cell with a path length of 0.2 cm (polymerisation kinetics); the IR relative band intensities are abbreviated as follows: very strong (vs), strong (s), medium (m), weak (w). Elemental analyses were obtained from the IST elemental analysis service (Laboratório de Análises do IST). Masses are quoted in grams (g) for quantities above 1 g and milligrams (mg) for smaller amounts.

The compound $[(PPh_3)_2Ni\{\mu\text{-}(\eta\text{-}C_5H_4)CMe_2(\eta\text{-}C_5H_4)\}Ni(PPh_3)_2][PF_6]_2$ (**1**) was prepared following the method described in the literature [11]. Cyclohexyl (R = Cy) [25], mesityl (R = 2,4,6-Me_3-C_6H_2) [25], *S*(−)-1-phenylethyl (R = *S*(−)-CH(Ph)Me) [26] and *tert*-butyl (R = ^{t}Bu) [27] isocyanides (C≡N—R) were synthesised according to the literature procedures, from their corresponding *N*-monosubstituted formamides (RNHCHO) which, in turn, were prepared from reaction of the parent amines with ethyl formate [28].

3.1. Synthesis of $[(S\text{-}(-)\text{-}C{\equiv}NCH(Ph)Me)(PPh_3)Ni\{\mu\text{-}(\eta\text{-}C_5H_4)CMe_2(\eta\text{-}C_5H_4)\}Ni(PPh_3)(S\text{-}(-)\text{-}C{\equiv}NCH(Ph)Me)][PF_6]_2$ (**2**)

A solution of *S*-(−)-1-phenylethylisocyanide (66 μl, 0.48 mmol) in-*o*-dichlorobenzene (2 ml) was added to a brown-yellow solution of $[(PPh_3)_2Ni\{\mu\text{-}(\eta\text{-}C_5H_4)CMe_2(\eta\text{-}C_5H_4)\}Ni(PPh_3)_2][PF_6]_2$ (**1**) (196.5 mg, 0.12 mmol) in *o*-dichlorobenzene ODCB (10 ml). The reaction mixture turned very rapidly to green and, at the end of 2 h, the reaction mixture was concentrated to ca. a third of its volume by partial evaporation of the solvent under vacuum at 35 °C. Addition of Et_2O resulted in the precipitation of a brownish green oil. Filtration of the solvent and dissolution of the oil in CH_2Cl_2 followed by reprecipitation in Et_2O afforded a green powder. Recrystallisation in CH_2Cl_2–Et_2O, by double-layering at −20 °C, gave a green amorphous powder of **2** (160 mg). Yield: 97%. The atom labelling used for the identification of the bridging cyclopentadienyl ^{1}H and ^{13}C NMR resonances in compounds **2**–**5** is shown in the following scheme:

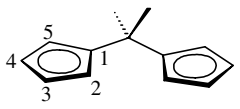

^{1}H NMR (300 MHz, CD_2Cl_2, 23 °C): δ 7.59–7.49 (m, 30H, PPh_3), 7.24–7.15 (m, 6H, $CH(C_6H_5)CH_3$, *meta* and *para*), 6.81 (m, 4H, $CH(C_6H_5)CH_3$, *ortho*), 5.41 (br, 4H, H2 and H5), 5.02 (br, 2H, C*H* $(C_6H_5)CH_3$), 4.91 (br, 4H, H3 and H4), 1.53 (s, 6H, $C(CH_3)_2$), 1.19 (br s, 6H, $CH(C_6H_5)CH_3$); $^{13}C\{^1H\}$ NMR (75.43 MHz, CD_2Cl_2, 23 °C): δ *C*$NCH(C_6H_5)CH_3$ (absent), 136.9 ($CH(C_6H_5)CH_3$, *ipso*), 133.7 (d, $^2J_{CP}$ = 11 Hz, PPh_3, *ortho*), 132.4 (PPh_3, *para*), 130.8 (d, $^1J_{CP}$ = 51 Hz, PPh_3, *ipso*), 129.6 (d, $^3J_{CP}$ = 11 Hz, PPh_3, *meta*), 129.3 ($CH(C_6H_5)CH_3$, *ortho*), 129.1 ($CH(C_6H_5)CH_3$, *para*), 128.6 (C1), 125.9 ($CH(C_6H_5)CH_3$, *meta*), 95.3 (C2 and C5), 93.1 (C3 and C4), 58.3 (*C* $H(C_6H_5)CH_3$), 34.7 (*C* $(CH_3)_2$), 30.4 ($C(CH_3)_2$), 23.0 ($CH(C_6H_5)C$ H_3); $^{31}P\{^1H\}$ NMR (121.44 MHz, CD_2Cl_2, 23 °C): δ 42.1 (s, *P* Ph_3), −143.7 (sept, $^1J_{PF}$ = 712 Hz, *P*F_6^-). FT-IR (KBr disk), cm^{-1}: 2196.2 ($\bar{\nu}$(C≡N), vs), 838.5 ($\bar{\nu}(PF_6^-)$, vs). *Anal.* Calc. for $C_{67}H_{62}F_{12}N_2P_4Ni_2$: C, 58.98; N, 2.05; H, 4.58. Found: C, 58.73; N, 2.11; H, 4.84%.

3.2. Synthesis of [(C≡NCy)(PPh$_3$)Ni{μ-(η-C$_5$H$_4$)CMe$_2$(η-C$_5$H$_4$)}Ni(PPh$_3$)(C≡NCy)][PF$_6$]$_2$ (3)

Following the same procedure as for **2**, a green microcrystalline powder of **3** was obtained. Yield: 96%.

^{1}H NMR (300 MHz, CD_2Cl_2, 23 °C): δ 7.70–7.53 (m, 30H, PPh_3), 5.43 (t, $^3J_{HH}$ = 2.1 Hz, 4H, H2 and H5), 5.02 (t, $^3J_{HH}$ = 2.1 Hz, 4H, H3 and H4), 3.67 (br, 2H, C_6H_{11}, H1′), 1.65 (s, 6H, $C(CH_3)_2$), 1.46 (br, 8H, C_6H_{11}, H2′ and H6′), 1.25–1.00 (m, 12H, C_6H_{11}, H3′, H4′ and H5′); $^{13}C\{^1H\}$ NMR (75.43 MHz, CD_2Cl_2, 23 °C): δ *C* $N(C_6H_{11})$ (absent), 133.9 (d, $^2J_{CP}$ = 10 Hz, PPh_3, *ortho*), 132.4 (PPh_3, *para*), 130.9 (d, $^1J_{CP}$ = 52 Hz, PPh_3, *ipso*), 129.8 (d, $^3J_{CP}$ = 11 Hz, PPh_3, *meta*), 128.4 (C1), 95.3 (C2 and C5), 93.0 (C3 and C4), 56.5 (C_6H_{11}, C1′), 34.7 ($C(CH_3)_2$), 31.7 (C_6H_{11}, C2′ and C6′), 30.5 ($C(CH_3)_2$), 24.7 (C_6H_{11}, C4′), 22.8 (C_6H_{11}, C3′ and C5′); $^{31}P\{^1H\}$ NMR (121.44 MHz, CD_2Cl_2, 23 °C): δ 40.8 (*P*Ph_3), −143.7 (sept, $^1J_{PF}$ = 712 Hz, *P*F_6^-). FT-IR (KBr disk), cm^{-1}: 2202.4 ($\bar{\nu}$(C≡N), vs), 839.2 ($\bar{\nu}(PF_6^-)$, vs). *Anal.* Calc. for $C_{63}H_{66}F_{12}N_2P_4Ni_2$: C, 57.30; N, 2.12; H, 5.04. Found: C, 57.53; N, 2.17; H, 5.03%.

3.3. Synthesis of [(CN^{t}Bu)(PPh$_3$)Ni{μ-(η-C$_5$H$_4$)CMe$_2$(η-C$_5$H$_4$)}Ni(PPh$_3$)(CN^{t}Bu)][PF$_6$] (4)

Following the same procedure as for **2**, lamellar green crystals of **4** were isolated. Yield: 92%. Crystals suitable for X-ray diffraction were available.

^{1}H NMR (300 MHz, CD_2Cl_2, 23 °C): δ 7.75–7.38 (m, 30H, PPh_3), 5.43 (t, $^3J_{HH}$ = 2.3 Hz, 4H, H2 and H5), 5.02 (t, $^3J_{HH}$ = 2.3 Hz, 4H, H3 and H4), 1.65 (s, 6H, $C(H_3)_2$ bridge), 1.01 (s, 18H, $C(CH_3)_3$); $^{13}C\{^1H\}$ NMR (75.43 MHz, CD_2Cl_2, 23 °C): δ *C* $NC(CH_3)_3$ (absent), 133.9 (d, $^2J_{CP}$ = 11 Hz, PPh_3, *ortho*), 132.5 (PPh_3, *para*), 130.9 (d, $^1J_{CP}$ = 52 Hz, PPh_3, *ipso*), 129.8 (d, $^3J_{CP}$ = 11 Hz, PPh_3, *meta*), 128.1 (C1), 95.2 (C2 and C5), 93.2 (C3 and C4), 60.6 s($C(CH_3)_3$), 34.8 ($C(CH_3)_2$ bridge), 30.4 ($C(CH_3)_2$ bridge), 29.3 ($C(CH_3)_3$); $^{31}P\{^1H\}$ NMR (121.44 MHz, CD_2Cl_2, 23 °C): δ 40.8 (*P*Ph_3), −143.7 (sept, $^1J_{PF}$ = 712 Hz, *P*F_6^-). FT-IR (KBr disk), cm^{-1}: 2196.3 ($\bar{\nu}$(C≡N), vs), 840.1 ($\bar{\nu}(PF_6^-)$, vs). *Anal.* Calc. for $C_{59}H_{62}F_{12}N_2P_4Ni_2$: C, 55.87; N, 2.21; H, 4.93. Found: C, 55.42; N, 2.20; H, 4.82%.

3.4. Synthesis of [(CNC$_6$H$_2$-2,4,6-Me$_3$)(PPh$_3$)Ni{μ-(η-C$_5$H$_4$)CMe$_2$(η-C$_5$H$_4$)}Ni(PPh$_3$)(CNC$_6$H$_2$-2,4,6-Me$_3$)][PF$_6$]$_2$ (5)

Following the same procedure as for **2**, a green amorphous powder of **5** was obtained. Yield: 90%.

^{1}H NMR (300 MHz, CD_2Cl_2, 23 °C): δ 7.76–7.51 (m, 30H, PPh_3), 6.80 (s, 4H, mesityl, *meta*), 5.43 (t, $^3J_{HH}$ = 2.1 Hz, 4H, H2 and H5), 5.19 (t, $^3J_{HH}$ = 2.1 Hz, 4H, H3 and H4), 2.23 (s, 6H, mesityl, CH_3 *para*), 1.84 (s, 12H, mesityl, CH_3 *ortho*), 1.71 (s, 6H, $C(CH_3)_2$); $^{13}C\{^1H\}$ NMR (75.43 MHz, CD_2Cl_2, 23 °C): δ *C* N(mesityl) (absent), 135.7 (mesityl, *ipso*), 133.9 (d, $^2J_{CP}$ = 11 Hz, PPh_3, *ortho*), 132.6 (PPh_3, *para*), 130.9 (d, $^1J_{CP}$ = 53 Hz, PPh_3 *ipso*), 130.7 (mesityl, *ortho*), 130.5 (mesityl, *para*), 129.9 (d, $^2J_{CP}$ = 11 Hz, PPh_3 *meta*), 129.1 (mesityl, *meta*), 128.2 (C1), 96.0 (C2 and C5), 93.2 (C3 and C4), 34.7 (*C* $(CH_3)_2$), 31.1 ($C(CH_3)_2$), 21.3 (mesityl, *C*H_3 *para*), 18.2 (mesityl, *C*H_3 *ortho*); $^{31}P\{^1H\}$ NMR (121.44 MHz, CD_2Cl_2, 23 °C): δ 40.7 (*P*Ph_3), −143.7 (sept, $^1J_{PF}$ = 712 Hz, *P*F_6^-); FT-IR (KBr disk), cm^{-1}: 2168.5 ($\bar{\nu}$(C≡N), vs), 839.8 ($\bar{\nu}(PF_6^-)$, vs). *Anal.* Calc. for $C_{69}H_{66}F_{12}N_2P_4Ni_2$: C, 59.51; N, 2.01; H, 4.78. Found: C, 59.80; N, 2.09; H, 4.91%.

3.5. Polymerisation reactions

Polymerisation reactions of *S*(−)-1-phenylethyl isocyanide catalysed by compound **1** were carried out in dried 10 cm^3 crown capped glass vials, sealed with rubber septa, containing a small magnetic stir bar and pump filled with nitrogen atmosphere. The reagents were added through the septa using liquid syringes or cannulae. The reaction mixtures were thermostated to 25 ± 0.5 °C in a water bath and the stirring speed kept constant at 500 rpm.

In a typical experiment, 3 cm^3 of a solution of **1** (5.21 μmol) in CH_2Cl_2 were measured in an inert atmosphere pipette and cannulated to the reaction vial. After ther-

mal equilibration, the reaction was initiated by transferring 2.79 mmol of *S*-(−)-CNCH(Ph)Me (312 μl, 300 mg) with a glass Hamilton syringe. For total conversion, the reaction was quenched after 16 h by the addition of a 0.01 M KOH/MeOH solution. The precipitated polymer was redissolved in CH_2Cl_2 and reprecipitated in MeOH with vigorous stirring. The polymer was filtered on a G5 glass sintered filter, washed several times with MeOH and dried under vacuum.

Kinetic data were obtained by collecting 100 μl aliquots of the reaction mixture at various time intervals, which were then diluted in 5 cm^3 volumetric flasks with $CHCl_3$. The concentration of non-reacted *S*(−)-1-phenylethyl isocyanide was determined by measuring the IR absorbance of these solutions at 2146 cm^{-1} (the wavenumber of the absorption peak of the C≡N stretching band) in NaCl liquid cells with a path length of 0.2 cm. The molar concentration of *S*(−)-1-phenylethyl isocyanide was determined using the experimentally measured molar absorptivity value of $\varepsilon_{2146\,cm^{-1}} = 229 \pm 7$ l mol^{-1} cm^{-1}.

The procedure used in the polymerisation reactions carried out in the presence of radical traps like BHT and galvinoxyl was similar to the one described above except that 2 cm^3 of a solution of **1** in CH_2Cl_2 were introduced in the reaction vial followed by the additions of the isocyanide and finally, after 2 min, 1 cm^3 of a CH_2Cl_2 solution containing 1–5 equivalents of the radical trap in relation to Ni.

3.6. Polymer characterisation

Polymer molecular weights were measured by gel permeation chromatography/size exclusion chromatographyon (GPC/SEC) a Waters 150 CV chromatograph, using a series of three columns Ultrastyragel, HR1, HR3, HR4 (10 μm; 7.8 × 300 mm), at 35 °C, in tetrahydrofuran and at a flow rate of 1 cm^3 min^{-1}; the calibration was made using polystyrene standards (TSK Tosoh Co.). The polymer powders, ranging from pale yellow (higher molecular weights) to deep red (lower molecular weights), could be characterised by FT-IR in the solid (KBr disks) or in $CHCl_3$ solutions (NaCl liquid cells) by the presence of a strong absorption peak corresponding to the C=N iminic bond vibration at 1628–1635 cm^{-1}. Selected polymer samples were characterised by ^1H and $^{13}C\{^1H\}$ NMR spectroscopies and their spectra confirmed to be similar to those reported in the literature for poly(*S*-(−)-1-pheneyletyl isocyanide) [29]. Some of the samples, dissolved in $CHCl_3$ (c = 1 g cm^{-3}), were also analysed by polarimetry, on an Atago Polax-L polarimeter (path length = 1 dm), and circular dichroism (CD) spectroscopy, on a Jasco 720 spectropolarimeter with a 175–800 nm photomultiplier, revealing identical features (negative specific rotations, $[\alpha]_D^{20}$, and CD spectra) to those found in the literature [30].

3.7. X-ray structure determination of *4*

Crystals of **4** suitable for diffraction measurements were sealed in glass capillaries under dinitrogen. Data was collected in a TURBO CAD4 rotating anode equipped with Cu Kα (λ = 1.5418 Å) radiation by the ω–2θ scan mode. Unit cell dimensions were obtained from the refinement of the setting angles of 25 reflections $17° < \theta < 20°$. Data was corrected for Lorentz polarisation and linear decay. No absorption correction was made. The Molen software (Enraf-Nonius) was used in the data reduction.

The structure was solved by direct methods using SIR-97 [31] and refined with SHELXL [32], programs included in WinGX v1.64.05 (PC version) [33]. All non-hydrogen atoms were refined with anisotropic thermal motion parameters based on F^2 and all hydrogen atoms were inserted in idealised positions and refined riding on the parent C atom. The poor diffracting power and low quality of the crystal precluded a better refinement and prevented the structural analysis with the accuracy we expected. All the final R values, as can be seen in Table 3, are very high, but this should be expected due to the

Table 3
Crystal data and structure refinement for compound **4**

Identification code	compound **4**
Empirical formula	$C_{59}H_{62}F_{12}N_2Ni_2P_4$
Formula weight	1268.41
T (K)	293(2)
λ (Å)	1.5418
Crystal system	monoclinic
Space group	$P2_1/c$
Unit cell dimensions	
a (Å)	10.472(6)
b (Å)	10.299(6)
c (Å)	57.29(2)
α (°)	90
β (°)	92.98(2)
γ (°)	90
V (Å^3)	6170(5)
Z	4
D_{calc} (Mg m^{-3})	1.365
Absorption coefficient (mm^{-1})	2.380
$F(000)$	2616
Crystal size (mm)	0.5 × 0.05 × 0.05
θ Range for data collection (°)	4.23–72.8
Limiting indices	$-12 \leqslant h \leqslant 0$, $0 \leqslant k \leqslant 12$, $-68 \leqslant l \leqslant 68$
Reflections collected/unique (R_{int})	11 730/11 115 (0.2104)
Completeness to θ = 72.83° (%)	90.4
Refinement method	full-matrix least-squares on F^2
Data/restraints/parameters	11115/0/713
Goodness-of-fit on F^2	1.022
Final R indices [$I > 2\sigma(I)$]	R_1 = 0.1259, wR_2 = 0.3008
R indices (all data)	R_1 = 0.2361, wR_2 = 0.3842
Extinction coefficient	0.00020(9)
Largest difference peak and hole (e Å^{-3})	1.071 and −0.765

R_{int} value presented. An ORTEPIII [34] diagram with the atomic labelling scheme is presented in Fig. 1.

4. Supplementary data

The supplementary crystallographic data (experimental details, atomic coordinates, full bond lengths and angles, including torsion angles) for this paper have been deposited in the CCDC (Deposition No. CCDC 235842). These data can be obtained free of charge via www.ccdc.cam.ac.uk/conts/retrieving.html (or from the CCDC, 12 Union Road, Cambridge CB2 1EZ, UK; fax: +44 1223 336033; e-mail: deposit@ccdc.cam.ac.uk or www: http://www.ccdc.cam.ac.uk).

Acknowledgements

We thank the Fundação para a Ciência e Tecnologia for financial support (Project POCTI/QUI/42015/2001, co-financed by FEDER) and for the award of a doctoral grant (PRAXIS XXI/BD/5669/95) to A.F.G.R.

References

[1] Y. Yamamoto, H. Yamazaki, N. Hagihara, Bull. Chem. Soc. Jpn. 41 (1968) 532.
[2] Y. Yamamoto, H. Yamazaki, N. Hagihara, J. Organomet. Chem. 18 (1969) 189.
[3] F. Takei, S. Tung, K. Yanai, K. Onitsuka, S. Takahashi, J. Organomet. Chem. 559 (1998) 91.
[4] (a) Reviews on the synthesis and properties of poly(isocyanide)s: F. Millich, in: H.F. Mark, N. Bikales, C.G. Overberger, G. Menges, J.I. Kroschwitz (Eds.), Encyclopedia of Polymer Science and Engineering, vol. 12, Wiley–InterScience, New York, 1988, p. 383;
(b) R.J.M. Nolte, Chem. Soc. Rev. 23 (1994) 11.
[5] (a) Y. Yamamoto, N. Hagihara, Bull. Chem. Soc. Jpn. 39 (1966) 1084;
(b) Y. Yamamoto, T. Takizawa, N. Hagihara, Nippon Kagaku Zasshi 87 (1966) 1355, Chem. Abstr. 67 (1967) 32995c.
[6] W. Drenth, R.J.M. Nolte, Acc. Chem. Res. 12 (1979) 30, and references cited therein.
[7] T.J. Deming, B.M. Novak, J. Am. Chem. Soc. 115 (1993) 9101, and references cited therein.
[8] T.J. Deming, B.M. Novak, Macromolecules 24 (1991) 5478.
[9] T.J. Deming, B.M. Novak, J.W. Ziller, J. Am. Chem. Soc. 116 (1994) 2366.
[10] A.F.G. Ribeiro, P.T. Gomes, A.R. Dias, R.T. Henriques, C. Freire, submitted (2004).
[11] J.R. Ascenso, A.R. Dias, M.T. Duarte, P.T. Gomes, J.N. Marote, A.F.G. Ribeiro, J. Organomet. Chem. 632 (2001) 164.
[12] L. Ballester, S. Perez, A. Gutierrez, M.F. Perpiñan, E. Gutierrez-Puebla, A. Monge, C. Ruiz, J. Organomet. Chem. 414 (1991) 411.
[13] J. Darkwa, R.M. Moutloali, T. Nyokong, J. Organomet. Chem. 564 (1998) 37.
[14] I.L.C. Campbell, F.S. Stephens, J. Chem. Soc., Dalton Trans. (1975) 337.
[15] R Wang, L.F. Groux, D. Zargarian, Organometallics 21 (2002) 5531.
[16] E. Carmona, J.M. Marín, P. Palma, M.L. Poveda, J. Organomet. Chem. 377 (1989) 157.
[17] D. Wilhelm, E. Wenschuh, U. Baumeister, H. Hartung, Z. Anorg. Allg. Chem. 620 (1994) 2114.
[18] P.L. Holland, M.E. Smith, R.A. Andersen, R.G. Bergman, J. Am. Chem. Soc. 119 (1997) 12815.
[19] A. Salzer, T.L. Court, H. Werner, J. Organomet. Chem. 54 (1973) 325.
[20] N.J. Coville, K.E. du Plooy, W. Pickl, Coord. Chem. Rev. 116 (1992) 1.
[21] F.M. Alías, T.R. Belderraín, M. Paneque, M.L. Poveda, E. Carmona, Organometallics 17 (1998) 5620.
[22] (a) G. Wulff, Angew. Chem. Int. Ed. 28 (1989) 21;
(b) S. Penczek, P. Kubisa, R. Szymanski, Makromol. Chem., Rapid Commun. 2 (1991) 59;
(c) S. Penczek, P. Kubisa, in: H.F. Mark, N. Bikales, C.G. Overberger, G. Menges, J.I. Kroschwitz (Eds.), Encyclopedia of Polymer Science and Engineering, Wiley–InterScience, New York, 1990, p. 380 (Suppl. vol.).
[23] (a) W.E. Geiger, C.S. Allen, T.E. Mines, F.C. Senftleber, Inorg. Chem. 16 (1977) 2003;
(b) R. Barbucci, A. Bencini, D. Gatteschi, Inorg. Chem. 16 (1977) 2117;
(c) G.A. Bowmaker, P.D.W. Boyd, G.K. Campbell, J.M. Hope, R.L. Martin, Inorg. Chem. 21 (1982) 1152;
(d) T.A. Albright, J.K. Burdett, M.-H. Whangbo, Orbital Interactions in Chemistry, Wiley, New York, 1985, p. 318.
[24] A.R. Rossi, R. Hoffmann, Inorg. Chem. 14 (1975) 365.
[25] R. Obrecht, R. Hermann, I. Ugi, Synthesis (1985) 400.
[26] R. Appel, R. Kleinstück, K.D. Ziehn, Angew. Chem. Int. Ed. 10 (1971) 132.
[27] G.W. Gokel, R.P. Widera, W.P. Weber, Org. Synth. 6 (1988) 232.
[28] J. Moffat, M.V. Newton, G.J. Papenmeier, J. Org. Chem. 27 (1962) 4058.
[29] M.M. Green, R.A. Gross, F.C. Schilling, K. Zero, C. Crosby, Macromolecules 21 (1988) 1839.
[30] A.J.M. van Beijnen, R.J.M. Nolte, A.J. Naaktgeboren, J.W. Zwikker, W. Drenth, A.M.F. Hezemans, Macromolecules 16 (1983) 1679.
[31] A. Altomare, M.C. Burla, M. Camalli, G. Cascarano, C. Giacovazzo, A. Guagliardi, A.G.G. Moliterni, G. Polidori, R. Spagna, SIR-97: A new tool for crystal structure determination and refinement, J. Appl. Crystallogr. 32 (1998) 115.
[32] G.M. Sheldrick, SHELXL-97: A Computer Program for Refinement of Crystal Structures, University of Göttingen, Göttingen, Germany, 1997.
[33] L.J. Farrugia, WinGX (v1.64.03b), J. Appl. Crystallogr. 32 (1999) 837.
[34] L.J. Farrugia, ORTEP-3 for Windows (v1.076), based on ORTEP-III (v1.0.3) by C.K. Johnson, M.N. Burnett, J. Appl. Crystallogr. 30 (1997) 565.

Available online at www.sciencedirect.com
SCIENCE DIRECT®
Polyhedron 23 (2004) 2725–2731
POLYHEDRON
www.elsevier.com/locate/poly

Incorporation of polybasic aromatic amines into ruthenium(II) chloro complexes

Benjamin G. Harvey, Atta M. Arif, Richard D. Ernst *

Department of Chemistry, University of Utah, 315 South 1400 East, Salt Lake City, UT 84112-0850, USA

Received 20 April 2004; accepted 14 May 2004
Available online 15 July 2004

Abstract

The reactions of $RuCl_2[P(C_6H_5)_3]_3$ with excesses of various aromatic amines led to six coordinate, pseudo-octahedral complexes. Thus, three equivalents of pyridazine or 3-methylpyridazine could be incorporated, or two equivalents of pyrazole or phthalazine, all as monodentate ligands. Reaction with 1,8-naphthyridine led to the incorporation of one bidentate ligand. X-ray structural data were obtained for the pyridazine, phthalazine and 1,8-naphthyridine complexes.
© 2004 Elsevier Ltd. All rights reserved.

1. Introduction

The chemistry involving ruthenium complexes of aromatic amines such as pyridine, 2,2-bipyridine and pyrazine has been remarkably productive, yielding important contributions in a number of areas, including mixed valence compounds and photochemistry [1]. However, in the vast majority of these compounds, the ligand complements do not allow for direct Ru–Ru interactions, although these may easily be generated using a number of other ligands, such as the relatively simple acetate ion and various analogues [2]. We have therefore undertaken the preparations of ruthenium complexes containing aromatic polyamine ligands which could potentially lead to complexes with direct metal–metal interactions. In this study, we have examined reactions of $RuCl_2[P(C_6H_5)_3]_3$ with several relatively simple aromatic diamines, including pyridazine (**1**), 3-methylpyridazine (**2**), phthalazine (**3**), pyrazole (**4**) and 1,8-naphthyridine (**5**).

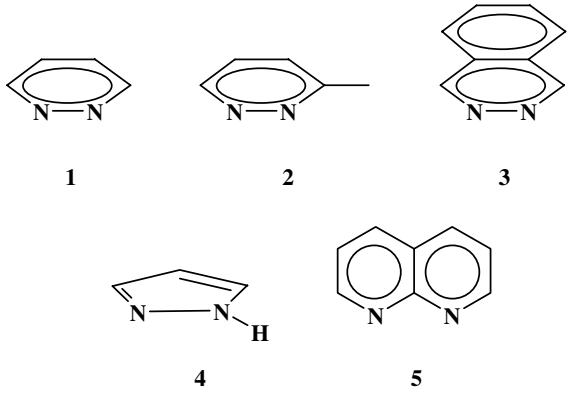

2. Experimental

All reactions were carried out under an atmosphere of nitrogen, using Schlenk techniques and apparatus. Solvents were dried and deoxygenated by distillation from CaH_2 (for CH_2Cl_2) or sodium benzophenone ketyl or by passing through columns of activated alumina, under a nitrogen atmosphere in each case. $RuCl_2[P(C_6H_5)_3]_3$ was prepared by a published procedure [3], while the diamines were all obtained from commercial sources. Elemental analyses were obtained from E&R Microanalytical Laboratories. NMR spectra were obtained as previously described [4].

* Corresponding author. Tel.: +8015818639.
E-mail address: ernst@chem.utah.edu (R.D. Ernst).

0277-5387/$ - see front matter © 2004 Elsevier Ltd. All rights reserved.
doi:10.1016/j.poly.2004.05.016

2.1. Dichlorotris(pyridazine)(triphenylphosphine)ruthenium, $RuCl_2[P(C_6H_5)_3](C_4N_2H_4)_3$ (**6**)

To a magnetically stirred yellow-brown slurry of 1.0 g (1.0 mmol) $RuCl_2(PPh_3)_3$ in 20 ml THF were added 0.40 ml (5.5 mmol) of pyridazine via syringe. The solution rapidly changed color to a bright orange-red. The flask was swirled several times until all solids dissolved and then it was left undisturbed for 18 h. After several hours, bright red crystals began to precipitate from the solution. These crystals were isolated by removing the supernatant, washing with two 20 ml and one 10 ml portions of ether, and drying in vacuo. 0.56 g of product were isolated, corresponding to a yield of 80%. Monoclinic crystals suitable for a single crystal X-ray diffraction study were grown by layering a solution of the compound in CH_2Cl_2 with an equal volume of hexane. A similar procedure using a more concentrated solution led to orthorhombic crystals (space group *Pbca*, $a = 10.2872(3)$, $b = 23.6429(12)$, $c = 33.5918(17)$ Å at 293(1) K), having a higher solvent content, and yielding a similar, but less satisfactory, structural result.

^{1}H NMR (CD_2Cl_2 ambient): δ 10.74 (dt, 2H, H(1,9), $J = 5.7$, 1.4 Hz), 8.81 (dt, 1H, H5, $J = 6.0$, 1.4 Hz), 8.33 (m, 3H, H(4,8,12)), 7.55 (tt, 6H, $H_o(PPh_3)$, $J = 8.1$, 1.2 Hz), 7.43 (ddd, 2H, H(2,10), $J = 8.1$, 7.1, 2.1 Hz), 7.22 (ddd, 2H, H(3,11), $J = 8.0$, 6.5, 1.6 Hz), 7.12 (tq, 3H, $H_p(PPh_3)$, $J = 7.4$, 1.5 Hz), 6.97 (td, 6H, $H_m(PPh_3)$, $J = 7.7$, 1.8 Hz), 6.90 (ddd, 1H, H7, $J = 8.0$, 4.9, 1.5 Hz), 6.45 (ddd, 1H, H6, $J = 8.1$, 6.0, 2.1 Hz).

Anal. Calc. for $C_{30}H_{27}Cl_2PN_6Ru$: C, 53.42; H, 4.03; N, 12.46. Found: C, 53.77; H, 4.02; N, 12.13%.

2.2. Dichlorotris(3-methylpyridazine)(triphenylphosphine)ruthenium, $RuCl_2[P(C_6H_5)_3](3\text{-}CH_3C_4N_2H_3)$

To a stirred yellow-brown slurry of 0.50 g (0.52 mmol) $RuCl_2(PPh_3)_3$ in 20 ml of THF under nitrogen at ambient temperature were added 0.25 g (2.7 mmol) of 3-methylpyridazine via syringe. The reaction mixture rapidly converted to a bright red solution and was stirred overnight. After ca. 18 h, 50 ml of hexane were added with stirring to precipitate the product. The bright red-orange precipitate was collected on a medium frit, washed with 3×10 ml ether, and dried in vacuo. Yield: 285 mg, 75%.

^{1}H NMR ($CDCl_3$ ambient): δ 10.74 (d, 2H, H_o-Mepyd, $J = 5.7$ Hz), 8.52 (d, 1H, H_o-Mepyd, $J = 5.7$ Hz), 7.66 (t, 6H, H_m-PPh_3, $J = 8.4$ Hz), 7.26 (dd, 2H, H_m-Mepyd, $J = 7.8$, 6.0 Hz), 7.09 (t, 3H, H_p-PPh_3, $J = 6.9$ Hz), 7.02–6.90 (m, 8H, H_o-PPh_3 and H_p-Mepyd), 6.68 (d, 1H, H_p-Mepyd, $J = 7.8$ Hz), 6.48 (dd, 1H, H_m-Mepyd, $J = 7.8$, 6.0 Hz), 2.09 (s, 6H, Me), 1.90 (s, 3H, Me).

Anal. Calc. for $C_{33}H_{33}PCl_2N_6Ru$: C, 55.31; H, 4.64; N, 11.73. Found: C, 55.22; H, 4.53; N, 11.51%.

2.3. Dichlorobis(phthalazine)bis(triphenylphosphine)ruthenium, $RuCl_2[P(C_6H_5)_3]_2(C_8N_2H_6)_2$ (**7**)

To a stirred yellow-brown slurry of 0.50 g (0.52 mmol) $RuCl_2(PPh_3)_3$ in 20 ml THF under nitrogen at ambient temperature were added 0.15 g (1.1 mmol) of phthalazine as a solid. The mixture rapidly converted to a bright orange slurry. After 2 h of stirring, 50 ml of hexane were added and the reaction mixture was stirred for an additional 10 min. The resulting bright orange precipitate was collected on a medium frit, washed with 3×10 ml ether and dried in vacuo. The yield is virtually quantitative, with typical isolated yields greater than 90%. Crystals suitable for diffraction studies were grown in a closed system by slow diffusion of ether vapors into a concentrated CH_2Cl_2 solution of the product. A general description of a similar apparatus has been presented [5]; in this application, a solution of the complex was placed in one side and some ether was placed in the other side, thus leading to vapor phase transfer of each solvent to the other side. In other cases, simple evaporation of one solvent may be achieved by placing diphenylmethane in the other side.

Anal. Calc. for $C_{52}H_{42}P_2Cl_2N_4Ru$: C, 65.27; H, 4.42; N, 5.86. Found: C, 65.23; H, 4.82; N, 5.41%.

2.4. Dichloro(1,8-naphthyridine)bis(triphenylphosphine)-ruthenium, $RuCl_2[P(C_6H_5)_3]_2(1,8\text{-}C_8N_2H_6)$ (**8**)

To a stirred yellow-brown slurry of 0.50 g (0.52 mmol) $RuCl_2(PPh_3)_3$ in 20 ml of THF under nitrogen at ambient temperature were added 80 mg (0.61 mmol) of 1,8-naphthyridine as a solid. A rapid color change to bright purple was followed by the precipitation of a purple solid. After stirring for approximately 10 min, the supernatant appeared virtually colorless. The purple precipitate was collected on a medium frit, washed with 3×10 ml ether and dried in vacuo. Yields for this reaction appeared quantitative, with isolated yields typically above 90%. Crystals suitable for diffraction studies were grown in a Schlenk tube by carefully layering hexane onto a concentrated solution of the compound in CH_2Cl_2.

Anal. Calc. for $C_{44}H_{36}P_2Cl_2N_2Ru$: C, 63.93; H, 4.39; N, 3.39. Found: C, 63.85; H, 4.53; N, 3.18%.

2.5. Dichlorobis(pyrazole)bis(triphenylphosphine)ruthenium, $RuCl_2[P(C_6H_5)_3]_2(C_3N_2H_4)_2$ (**9**)

To a magnetically stirred slurry of 0.50 g (0.52 mmol) $RuCl_2(PPh_3)_3$ in 20 ml THF were added 0.10 g (1.5 mmol) of pyrazole. A rapid color change to red was observed, followed by a slower (2–3 min) transition to yellow. The color change to yellow occurred much more rapidly if a large excess of pyrazole was used. The solution was stirred for 18 h and the solvent removed in

vacuo to yield a thick yellow oily solid. The solid was washed with 3×10 ml pentane and dried in vacuo. The powdery residue was extracted with 3×10 ml CH_2Cl_2 and filtered through a coarse frit with a Celite pad. The bright yellow filtrate was concentrated to ca. 10 ml and carefully layered with 50 ml hexane. After the flask had been left undisturbed for 24 h, yellow crystals were deposited on the sides of the flask. The supernatant was removed and the crystals were washed with 3×10 ml ether and dried in vacuo. 0.370 g of product were isolated, corresponding to a yield of 85%. Solutions of the product rapidly turn green upon exposure to air.

^{1}H NMR (chloroform-d_1, ambient): δ 11.70 (s, 2H, N–H), 8.13 (t, 4H, py–H(2,4), $J = 1.5$ Hz), 7.35 (t, 12H, $H_o(PPh_3)$, $J = 8.3$ Hz), 7.17 (t, 6H, $H_p(PPh_3)$, $J = 7.4$ Hz), 7.00 (q, 12H, $H_m(PPh_3)$, $J = 7.0$ Hz), 5.94 (q, 2H, py–H3, $J = 2.2$ Hz).

Anal. Calc. for $C_{42}H_{38}Cl_2P_2N_4Ru$: C, 60.58; H, 4.60; N, 6.73. Found: C, 60.49; H, 4.76; N, 6.49%.

2.6. Crystallographic studies

Single crystals for X-ray diffraction study were fixed to glass fibers using Paratone oil and thereafter transferred to a Nonius Kappa CCD diffractometer for study. Structures were solved using direct method programs provided in the SIR-97 or SHELXL-97 program packages. All non-hydrogen atoms were subjected to anisotropic refinement. For **6**, the hydrogen atoms were refined isotropically, including those in a molecule of solvent CH_2Cl_2. It can be noted that crystals having a higher CH_2Cl_2 content could also be obtained (see Section 2.1), but the solvent was poorly behaved, and a less satisfactory structure was obtained. The hydrogen atoms in **7** were also refined isotropically, except for those associated with the solvent molecules. These atoms were allowed to ride on their respective carbon atoms. Two CH_2Cl_2 molecules, one of half occupancy, were incorporated into this lattice. For **8**, all but one hydrogen atom, H44, could be refined isotropically. That one was refined with a fixed thermal parameter. A summary of crystal and data collection parameters is given in Table 1, while pertinent bonding parameters for **6**–**8** are listed in Tables 2–4.

3. Results and discussion

The reactions of $RuCl_2[P(C_6H_5)_3]_3$ with excesses of pyridazine, 3-methylpyridazine, phthalazine, pyrazole and 1,8-naphthyridine in each case led to a six-coordinate ruthenium(II) complex, as summarized in Scheme 1. The reactions involving pyridazine or 3-methylpyridazine resulted in the incorporation of three equivalents of the ligand, together with expulsion of two phosphine ligands. In contrast, the reactions with phthalazine, pyrazole or 1,8-naphthyridine brought about the loss of only one phosphine ligand, leading only to the incorporation of two phthalazines, two pyrazoles or one (chelating) 1,8-naphthyridine ligand(s). The constitutions of these complexes have been established through analytical data, NMR spectroscopy when solubility permitted, and for **6**–**8**, through single crystal X-ray diffraction studies. In each case where meaningful

Table 1
Crystallographic parameters for $RuCl_2[P(C_6H_5)_3](C_4N_2H_4)_3$, $RuCl_2[P(C_6H_5)_3]_2(C_8N_2H_6)_2$, and $RuCl_2[P(C_6H_5)_3]_2(1,8\text{-}C_8N_2H_6)$

Empirical formula	$C_{31}H_{29}Cl_4N_6PRu$	$C_{53.5}H_{45}Cl_5N_4P_2Ru$	$C_{44}H_{36}Cl_2N_2P_2Ru$
Formula weight	759.44	1084.19	826.66
Temperature (K)	150(1)	150(1)	200(1)
λ (Å)	0.71073	0.71073	0.71073
Crystal system	monoclinic	triclinic	triclinic
Space group	$\underline{P}2_1/\underline{c}$	$\underline{P}\bar{1}$	$\underline{P}\bar{1}$
Unit cell dimensions			
a (Å)	15.5365(3)	11.7277(1)	11.3392(3)
b (Å)	11.7054(3)	13.8433(2)	12.4477(3)
c (Å)	17.4477(3)	17.2485(3)	13.5955(4)
α (°)	90	87.2876(6)	90.0120(12)
β (°)	93.8557(13)	74.6044(6)	82.0268(12)
γ (°)	90	65.5332(10)	74.1443(11)
Volume (Å^3)	3165.87(12)	2451.10(6)	1826.64(8)
Z	4	2	2
D_{calc}	1.593	1.469	1.503
Absorption coefficient (cm^{-1})	9.17	6.99	6.99
θ Range (°)	3.8–27.5	3.5–27.5	2.5–27.9
Limiting indices	$-20 \leqslant h \leqslant 20$, $-14 \leqslant k \leqslant 15$, $-22 \leqslant l \leqslant 22$	$-14 \leqslant h \leqslant 15$, $-17 \leqslant k \leqslant 17$, $-19 \leqslant l \leqslant 22$	$-14 \leqslant h \leqslant 14$, $-16 \leqslant k \leqslant 15$, $-15 \leqslant l \leqslant 17$
Reflections collected	12360	17109	12433
Independent reflections; n: $I > n(I)$	7235; 2	10929; 2	8467; 2
$R(F)$	0.0289	0.0437	0.0469
$R_w(F^2)$	0.0594	0.1052	0.0858
Maximum/minimum difference Fourier peak (e Å^3)	0.41/−0.65	2.07/−1.29	0.64/−0.94

Table 2
Pertinent bonding parameters for $RuCl_2[P(C_6H_5)_3](C_4N_2H_4)_3$ (**6**)

Bond distances (Å)			
Ru–N1	2.0760(17)	Ru–P1	2.2976(5)
Ru–N3	2.0735(17)	Ru–Cl1	2.4309(5)
Ru–N5	2.0604(16)	Ru–Cl2	2.4665(5)
Bond angles (°)			
N1–Ru–N3	93.51(7)	N3–Ru–N5	87.33(7)
N1–Ru–N5	175.72(7)	N3–Ru–P1	97.06(5)
N1–Ru–P1	92.85(5)	N3–Ru–Cl1	172.44(5)
N1–Ru–Cl1	89.45(5)	N3–Ru–Cl2	85.56(5)
N1–Ru–Cl2	85.83(5)	P1–Ru–Cl1	89.73(2)
N5–Ru–P1	91.22(5)	P1–Ru–Cl2	177.14(2)
N5–Ru–Cl1	89.22(5)	Cl1–Ru–Cl2	87.72(2)
N5–Ru–Cl2	90.05(5)	Ru–P1–C19	115.48(7)
Ru–P1–C13	118.82(7)	Ru–P1–C25	116.23(7)

Table 3
Pertinent bonding parameters for $RuCl_2[P(C_6H_5)_3]_2(C_8N_2H_6)_2$ (**7**)

Bond distances (Å)			
Ru–P1	2.4085(7)	Ru–P2	2.3855(7)
Ru–Cl1	2.4421(7)	Ru–Cl2	2.4661(7)
Ru–N1	2.055(2)	Ru–N2	2.057(2)
Bond angles (°)			
N1–Ru–N3	89.16(9)	N3–Ru–P1	95.80(7)
N1–Ru–P1	86.16(7)	N3–Ru–P2	88.17(7)
N1–Ru–P2	94.36(7)	N3–Ru–Cl1	177.21(7)
N1–Ru–Cl1	89.24(7)	N3–Ru–Cl2	87.70(7)
N1–Ru–Cl2	176.22(7)	P1–Ru–P2	176.01(3)
P1–Ru–Cl1	86.37(2)	P2–Ru–Cl1	89.67(2)
P1–Ru–Cl2	92.06(3)	P2–Ru–Cl2	87.65(3)
Cl1–Ru–Cl2	93.98(2)	Ru–P2–C35	112.79(9)
Ru–P1–C17	116.47(10)	Ru–P2–C41	116.23(10)
Ru–P1–C23	112.85(10)	Ru–P2–C47	120.68(10)
Ru–P1–C29	119.76(10)		

Table 4
Pertinent bonding parameters for $RuCl_2[P(C_6H_5)_3]_2(1,8\text{-}C_8N_2H_6)$ (**8**)

Bond distances (Å)			
Ru–P1	2.2819(7)	Ru–P2	2.3040(8)
Ru–Cl1	2.4242(9)	Ru–Cl2	2.4050(9)
Ru–N1	2.217(3)	Ru–N2	2.222(2)
Bond angles (°)			
N1–Ru–N2	60.81(9)	N2–Ru–P1	160.60(7)
N1–Ru–P1	100.96(7)	N2–Ru–P2	101.17(7)
N1–Ru–P2	161.41(7)	N2–Ru–Cl1	86.35(8)
N1–Ru–Cl1	80.95(7)	N2–Ru–Cl2	81.53(7)
N1–Ru–Cl2	85.27(7)	P1–Ru–P2	97.45(3)
P1–Ru–Cl1	97.77(3)	P2–Ru–Cl1	94.09(3)
P1–Ru–Cl2	90.87(3)	P2–Ru–Cl2	97.06(3)
Cl1–Ru–Cl2	164.89(3)	Ru–P1–C9	108.74(9)
Ru–N1–C1	148.6(2)	Ru–P1–C15	125.39(11)
Ru–N1–C8	94.3(2)	Ru–P1–C21	117.42(10)
Ru–N2–C8	94.1(2)	Ru–P2–C27	106.79(11)
Ru–N2–C7	148.8(2)	Ru–P2–C33	124.08(10)
		Ru–P2–C39	119.71(10)

NMR data could be recorded, the spectral results were indicative of the presence of only one isomer, which was also consistent with the structural results.

The product of the reaction with excess pyridazine was found to adopt a *mer,cis* arrangement of ligands in a pseudooctahedral coordination environment (**6**), Fig. 1. A similar structure can be assumed for the 3-methylpyridazine complex, and this would be consistent with the NMR results which revealed two types of amine ligands in a 2:1 ratio. As would be expected, there is some evidence of inter-ligand steric repulsion involving the phosphine ligand, as the P–Ru–N angles all exceed 90° (91.22(5)–97.06(5)°), thereby leading to generally acute N–Ru–Cl2 angles (85.56(5)–90.05(5)°). While other angles also deviate from their ideal values, the presence of six aromatic rings in the complex can be expected to result in C–H/π [6] and/or π/π [7] interactions, whether intramolecular or intermolecular [8], which could play an even larger role than the steric effects and therefore complicate further comparisons.

Although there seem to be no other examples of structurally characterized ruthenium complexes containing both phosphine and the simple pyridazine ligands, and just a few for transition metals generally [9], some comparisons may be made with various more common poly(amine) species. Thus, the Ru–N distances of 2.060(2)–2.076(2) Å in **6** are similar to values of 2.049(2) and 2.084(3) Å in neutral pyridyl-substituted pyridazine complexes [10], as well as to those in a mixed valence Ru(II,III) complex [11], but longer than those in related cationic species (1.986(10)–2.031(7) Å) [12], and shorter than Ru–N bonds in trimetallic carbonyl complexes in which pyridazine coordinates to two adjacent ruthenium(0) centers (2.11(1)–2.136(4) Å) [13]. Likewise, the Ru–Cl distances of 2.4309(5) and 2.4665(5) Å are reasonably similar to values ranging from 2.392(1) to 2.431(1) Å in the related cationic or carbonyl-containing complexes. The Ru–P distance of 2.2976(5) Å may be compared to values in the range of 2.23–2.44 Å found for two modifications of $RuCl_2[P(C_6H_5)_3]_3$ [14].

Notably, the reaction of $RuCl_2[P(C_6H_5)_3]_3$ with phthalazine led only to the incorporation of two equivalents of ligand, rather than three. As the resulting $RuCl_2[P(C_6H_5)_3]_2(C_8H_6N_2)_2$ complex contains an extra phosphine ligand compared to **6**, the additional steric crowding may block access of a third amine ligand to the metal center; alternatively it could be that the lower solubility of this complex compared to its hypothetical pyridazine analogue led to **7**'s precipitation before a third incorporation could take place. Consequently, it could be possible to bring about the third incorporation using other solvents and/or more forcing conditions. A structural determination revealed the complex to have a *cis,trans,cis* pseudooctahedral geometry (Fig. 2), so the chloride ligands have remained *cis* to each other. The two $P(C_6H_5)_3$ ligands are located *trans* to each other, with one phenyl group from each pointed between the two chloride ligands. This results in the other phenyl groups being directed towards the phthalazine ligands,

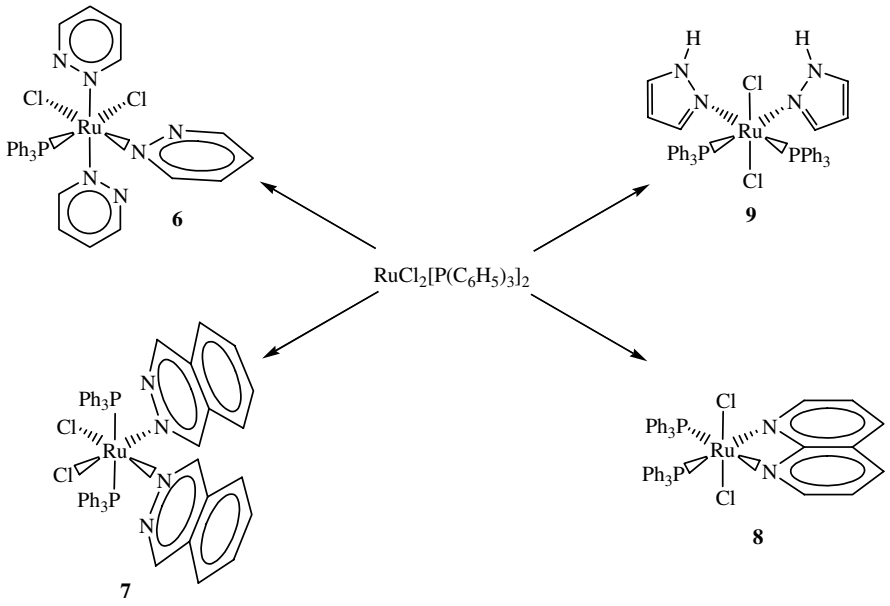

Scheme 1.

presumably in order to optimize C–H/π and π/π interactions. It seems quite possible that these interactions could play a role in stabilizing the observed *cis,trans,cis* isomer, and if the additional fused rings of the phthalazine ligands do not engage in any substantial stabilizing intermolecular interactions, such an arrangement could be found for the analogous pyridazine complex which would be a likely intermediate in the formation of **6**.

While there are no other structurally characterized (phthalazine)ruthenium complexes to compare with **7**, and only a few transition metal complexes containing both phosphine and phthalazine ligands [9c,15], one can note that the Ru–N distances for **7** are slightly shorter than those for **6**. The two Ru–P bonds are lengthened relative to the one in **6**, but are similar to the nearly *trans* Ru–P bonds in $RuCl_2[P(C_6H_5)_3]_3$ [14], whereas as noted before, the unique Ru–P bond in $RuCl_2[P(C_6H_5)_3]_3$ (ca. 2.23 Å) is similar to the Ru–P distance in **6**. The lengthening of the Ru–P bonds in **7** thus appears to be electronic in origin. The Ru–Cl bond distances for **6** and **7** are not significantly different from each other, but are longer than the values of ca. 2.38–2.39 Å in $RuCl_2[P(C_6H_5)_3]_3$.

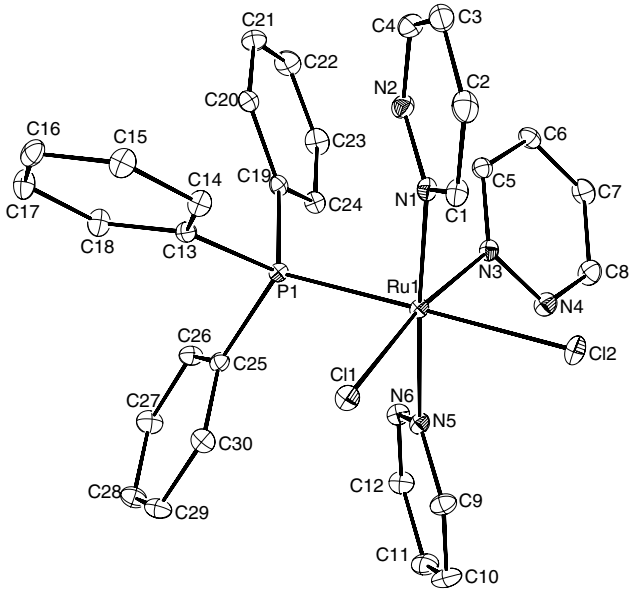

Fig. 1. Perspective view and numbering scheme for $RuCl_2[P(C_6H_5)_3](C_4N_2H_4)_3$ (**6**).

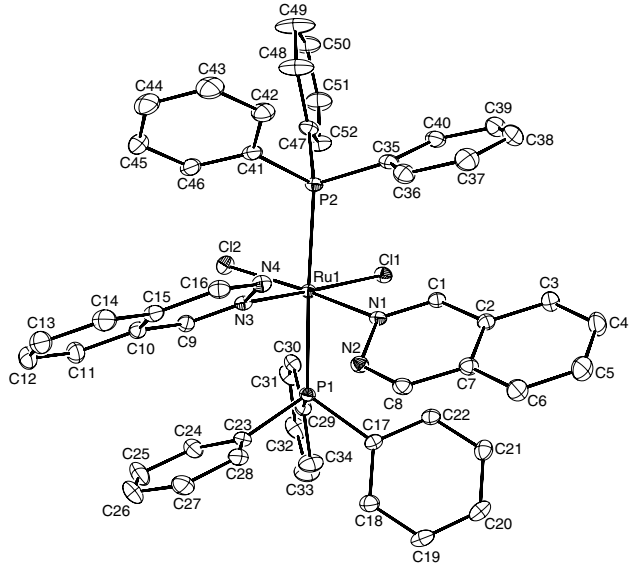

Fig. 2. Perspective view and numbering scheme for $RuCl_2[P(C_6H_5)_3]_2(C_8N_2H_6)_2$ (**7**).

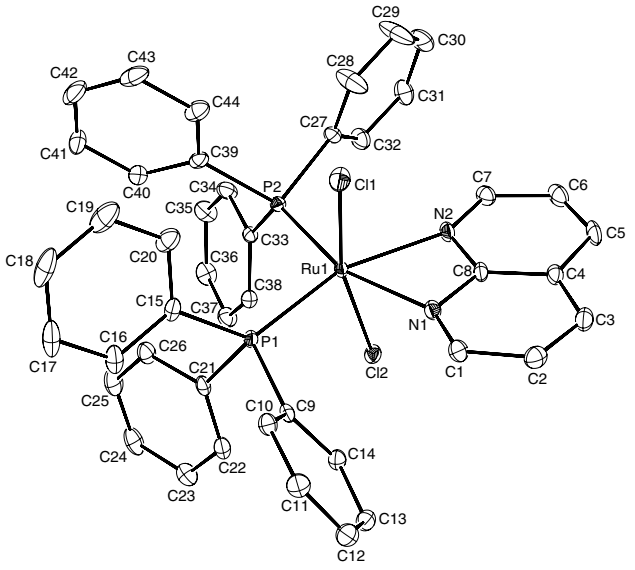

Fig. 3. Perspective view and numbering scheme for $RuCl_2[P(C_6H_5)_3]_2(1,8\text{-}C_8N_2H_6)$ (**8**).

The reaction of $RuCl_2[P(C_6H_5)_3]_3$ with 1,8-naphthyridine was unique in leading to the incorporation of only one ligand, at least under mild conditions, although a bidentate coordination mode was adopted in the product (**8**). Perhaps as a result of the smaller spatial requirements of the chelating diamine as compared to the two phthalazine ligands in **7**, the phosphine ligands in **8** adopt a *cis* rather than *trans* orientation, with the chlorides becoming *trans* (Scheme 1, Fig. 3). Nonetheless, the marked asymmetry in the Ru–P–C angles (Table 3) seems to reveal the presence of some steric interactions between the phosphine ligands. In contrast, the Ru–P–C angles in the other complexes were more regular, although $RuCl_2[P(C_6H_5)_3]_3$ also displays a distortion [14]. In any event, this arrangement leads to an apparently favorable orientation for intramolecular C–H/π interactions between two of the naphthyridine hydrogen atoms and two of the phosphine phenyl groups [6]. The N1–Ru–N2 angle is of necessity quite small, at 60.81(9)°, thereby allowing for the P1–Ru–P2 angle to expand to 97.45(3)°. The chloride ligands are bent away from the phosphines toward the diamine, with a Cl1–Ru–Cl2 angle of 164.89(3)°. Presumably due to the lack of alignment between the nitrogen lone pairs and the metal center, the Ru–N distances in **8** (2.217(3), 2.222(2) Å) are notably longer than those in **6** and **7**. In turn, however, the opposite trend is observed for **8**'s Ru–Cl (2.4050(9), 2.4242(9) Å) and Ru–P bonds (2.2819(7), 2.3040(8) Å).

Although there seem to be no structurally characterized examples of ruthenium complexes containing both phosphine and 1,8-naphthyridine ligands, two reports of chelating (naphthyridine)ruthenium complexes have appeared. The Ru–N distances in $Ru(2,2'\text{-}bpy)_2(1,8\text{-}C_8N_2H_6)^{2+}$ average 2.11(1) Å for the naphthyridine ligand [16], while in a more complicated, amino-substituted 1,8-naphthyridine complex [17], a highly asymmetric coordination is observed, with Ru–N distances of 2.066(6) and 2.377(7) Å. More common than the observed monometallic chelating coordination mode are the monodentate bonding mode (with Ru–N distances to date of 2.078(9)–2.137(6) Å) [16,18] and a bridging mode in which the nitrogen centers are coordinated to different ruthenium centers which generally would be connected by a Ru–Ru bond [17,19,20]. In these cases, the Ru–N distances range from 2.00(3) to 2.21(3) Å. Likewise, the monodentate coordination mode has been observed in phosphine-containing complexes of gold [21] and platinum [22], while the bridging mode has been observed in a dicopper phosphine complex [23].

The reaction of an excess of the five-membered ring ligand pyrazole with $RuCl_2[P(C_6H_5)_3]_3$ led only to the incorporation of two equivalents, and the expulsion of one phosphine ligand, analogous to the reaction involving phthalazine rather than to that of pyridazine. Attempts to incorporate a third equivalent of pyrazole using a large (10 equiv.) excess of pyrazole under reflux conditions did not lead to any observable change. The ^1H NMR spectrum demonstrated that the two phosphine ligands were equivalent, as were the two pyrazoles. The overall complex stoichiometery, $RuCl_2[P(C_6H_5)_3]_2(C_3N_2H_4)_2$, again corresponds to a six-coordinate, pseudo-octahedral complex. A structural study has revealed that it adopts a different arrangement than that of **7** (Scheme 1) [24].

4. Summary

The complex $RuCl_2[P(C_6H_5)_3]_3$ has been found to be a useful starting material for the formation of polybasic aromatic amine complexes of ruthenium. Despite the potential abilities of pyridazine, pyrazole, phthalazine and 1,8-naphthyridine to bridge more than one metal center, none of the complexes involved such bridging, although the 1,8-naphthyridine ligand did chelate a single metal center. Each complex retained one or two of the triphenylphosphine ligands, whose steric bulk may have prevented the formation of dimetallic complexes. To some extent the product that was isolated was determined by solubility considerations, suggesting that additional incorporations could be achieved in some cases. Likewise, for at least pyrazole and pyridazine, it appears possible to limit the extent of incorporation through stoichiometry [24]. Notably, initial attempts to incorporate additional metal centers into the pyridazine complex have tended to lead instead to ligand exchange reactions [24], as has been seen for pyrazine complexes [25]. Possibly the use of less acidic metal centers or the

deprotonation of coordinated pyrazole, which would lead to a more basic ligand that has been successfully employed for preparing heterobimetallic complexes [26], may be used to inhibit such exchanges. It is of final interest to note the recent report of a related Re(III) complex, $ReCl_3[P(C_6H_5)_3]$ $(C_3N_2H_4)_2$ [27].

5. Supplementary material

Crystallographic data for the structural analyses have been deposited with the Cambridge Crystallographic Data Centre, CCDC, Nos. 236487-236489 for compounds **8**, **7** and **6**, respectively. Copies of this information may be obtained free of charge from The Director, CCDC, 12, Union Road, Cambridge CB2 1EZ (fax: +44-1223-336033) or email deposit@ccdc.cam.ac.uk or http://www.ccdc.cam.ac.uk.

Acknowledgements

Support for this research by the Research Corporation and the University of Utah is gratefully acknowledged.

References

[1] (a) W. Keim, A. Klein, M. Glöckle, Acc. Chem. Res. 33 (2000) 755;
(b) H. Durr, S. Bossmann, Acc. Chem. Res. 34 (2001) 905.
[2] F.A. Cotton, R.A. Walton, Multiple Bonds Between Metal Atoms, 2nd ed., Clarendon Press, Oxford, 1993.
[3] T.D. Newbound, L. Stahl, M.L. Ziegler, R.D. Ernst, Organometallics 9 (1990) 2962.
[4] P.S. Hallman, T.A. Stephenson, G. Wilkinson, Inorg. Syn. 12 (1970) 237.
[5] R.J. Neustadt, T.H. Cymbaluk, R.D. Ernst, F.W. Cagle Jr., Inorg. Chem. 19 (1980) 2375.
[6] M. Nishio, M. Hirota, Y. Umezawa, The CH-π interaction, Wiley-VCH, New York, 1998.
[7] (a) C.A. Hunter, K.R. Lawson, J. Perkins, C.J. Urch, J. Chem. Soc., Perkin Trans. 2 (2001) 651;
(b) D. Braga, F. Grepioni, G.R. Desiraju, Chem. Rev. 98 (1998) 1375;
(c) C.A. Hunter, Chem. Soc. Rev. 23 (1994) 101.
[8] (a) M. Scudder, I. Dance, J. Chem. Soc., Dalton Trans. (2000) 2909;
(b) G.R. Lewis, I. Dance, Inorg. Chim. Acta 306 (2000) 160;
(c) V. Kulsomphob, G.C. Turpin, K.-C. Lam, C. Youngkin, W. Trakarnpruk, P. Carroll, A.L. Rheingold, R.D. Ernst, J. Chem. Soc., Dalton Trans. (2000) 3086;
(d) G.C. Turpin, A.L. Rheingold, R.D. Ernst, J. Organometal. Chem. 672 (2003) 109.
[9] (a) A.S. Batsanov, M.J. Begley, M.W. George, P. Hubberstey, M. Munakata, C.E. Russell, P.H. Walton, J. Chem. Soc., Dalton Trans. (1999) 4251;
(b) X.-Y. Yu, M. Maekawa, T. Morita, H.-C. Chang, S. Kitagawa, G.-X. Jin, Polyhedron 21 (2002) 1613;
(c) J.T. Maeyer, T.J. Johnson, A.K. Smith, B.D. Borne, R.D. Pike, W.T. Pennington, M. Krawiec, A.L. Rheingold, Polyhedron 22 (2003) 419;
(d) H.-F. Klein, M. Helwig, U. Koch, U. Flörke, H.-J. Haupt, Z. Naturforsch. 48b (1993) 778;
(e) H.-F. Klein, M. Helwig, M. Karnop, H. König, B. Hammerschmitt, G. Cordier, U. Flörke, H.-J. Haupt, Z. Naturforsch. 48b (1993) 785.
[10] G. De Munno, G. Denti, G. De Rosa, G. Bruno, Acta. Cryst. C 44 (1988) 1193.
[11] A.N. Zhilyaev, I.V. Kuz'menko, T.A. Formina, G.N. Kuznetsova, I.B. Baranovskii, Russ. J. Inorg. Chem. 36 (1991) 1568.
[12] (a) V.J. Catalano, R.A. Heck, A. Öhman, M.G. Hill, Polyhedron 19 (2000) 1049;
(b) V.J. Catalano, R.A. Heck, C.E. Immoos, A. Öhman, M.G. Hill, Inorg. Chem. 37 (1998) 2150.
[13] (a) J.A. Cabeza, R.J. Franco, A. Clamazares, V. Riera, C. Bois, Y. Jeannin, Inorg. Chem. 32 (1993) 4640;
(b) F.A. Cotton, B.E. Hanson, J.D. Jamerson, J. Am. Chem. Soc. 99 (1977) 6588.
[14] (a) S.J. La Placa, J.A. Ibers, Inorg. Chem. 4 (1965) 778;
(b) R.D. Ernst, R. Basta, A.M. Arif, Z. Kristallogr. NCS 218 (2003) 49.
[15] G.W. Bushnell, K.R. Dixon, Can. J. Chem. 56 (1978) 878.
[16] H. Nakajima, H. Nagao, K. Tanaka, J. Chem. Soc., Dalton Trans. (1996) 1405.
[17] M. Mintert, W.S. Sheldrick, J. Chem. Soc., Dalton Trans. (1995) 2663.
[18] (a) T. Mizukawa, K. Tsuge, H. Nakajima, K. Tanaka, Angew. Chem. Int. Ed. 38 (1999) 362;
(b) R.P. Thummel, D. Williamson, C. Hery, Inorg. Chem. 32 (1993) 1587;
(c) S.M. Scott, A.K. Burrell, P.A. Cocks, K.C. Gordon, J. Chem. Soc., Dalton Trans. (1998) 3679.
[19] (a) J.-P. Collin, A. Jouaiti, J.-P. Sauvage, W.C. Kaska, M.A. McLoughlin, N.L. Keder, W.T.A. Harrison, G.D. Stucky, Inorg. Chem. 29 (1990) 2238;
(b) J.A. Cabeza, L.A. Oro, A. Tiripicchio, M. Tiripicchio-Camellini, J. Chem. Soc., Dalton Trans. (1988) 1437;
(c) E. Binamira-Soriaga, N.L. Keder, W.C. Kaska, Inorg. Chem. 29 (1990) 3167;
(d) C.S. Campos-Fernández, L.M. Thomson, J.R. Galán-Mascarós, X. Ouyang, K.R. Dunbar, Inorg. Chem. 41 (2002) 1523.
[20] A.E.M. Boelrijk, M.M. van Velzen, T.X. Neenan, J. Reedijk, H. Kooijman, A.L. Spek, J. Chem. Soc., Chem. Commun. (1995) 2465.
[21] M. Munakata, S.-G. Yan, M. Maekawa, M. Akiyama, S. Kitagawa, J. Chem. Soc., Dalton Trans. (1997) 4257.
[22] G.W. Bushnell, K.R. Dixon, M.A. Khan, Can. J. Chem. 56 (1978) 450.
[23] M. Maekawa, M. Munakata, S. Kitagawa, T. Kuroda-Sowa, Y. Suenaga, M. Yamamoto, Inorg. Chim. Acta 271 (1998) 129.
[24] B.G. Harvey, A.M. Arif, R.D. Ernst, unpublished results.
[25] M. Pizzotti, R. Ugo, C. Dragonetti, E. Annoni, F. Demartin, P. Mussini, Organometallics 22 (2003) 4001.
[26] D. Carmona, J. Ferrer, J.M. Arilla, J. Reyes, F.J. Lahoz, S. Elipe, F.J. Modrego, L.A. Oro, Organometallics 19 (2000) 798.
[27] B. Machura, M. Jaworska, R. Kruszynski, Polyhedron 23 (2004) 1819.

Available online at www.sciencedirect.com
SCIENCE DIRECT®
Polyhedron 23 (2004) 2733–2749
POLYHEDRON
www.elsevier.com/locate/poly

Synthesis and mechanistic investigations of the decomposition of β-hydrogen containing W(VI) dialkyl complexes: β-H elimination vs. β-H abstraction

Shu-Yu S. Wang, Khalil A. Abboud, James M. Boncella *

Department of Chemistry and Center for Catalysis, University of Florida, Gainesville, FL 32611-7200, USA

Received 21 April 2004; accepted 8 September 2004
Available online 22 October 2004

Dedicated to Professor M.L.H. Green

Abstract

The dialkyl complexes containing β-hydrogen atoms:W(NPh)[*o*-$(Me_3SiN)_2C_6H_4$]R_2 (R = Et, *n*-Pr, *i*-Bu, CH_2CH_2Ph) have been prepared.These compounds are indefinitely stable in solution at room temperature in the absence of air and moisture.The diethyl complex reacts with PMe_3 at room temperature ($t_{1/2}$ = 12 min) to give ethane and the W(IV) ethylene complex, W(NPh)[*o*-$(Me_3SiN)_2C_6H_4$](η^2-CH_2CH_2)$(PMe_3)_2$.A mechanistic study of this reaction has revealed that the reaction is first order in W and PMe_3, with $\Delta H^{\ddagger}$ = 5.1(0.6) kcal mol^{-1} and $\Delta S^{\ddagger}$ = −54.9(2.0) cal mol^{-1} K^{-1}.A large primary kinetic isotope effect (k_H/k_D = 6.1(0.5) at 20 °C) was observed for the transformation.These observations are consistent with the reaction proceeding via direct H transfer from the β-carbon of one ethyl group to the α-carbon of the other ethyl group.The (bis)phenethyl complex reacts with PMe_3 at elevated temperature to give ethylbenzene and the W(IV) styrene complex, W(NPh)[*o*-$(Me_3SiN)_2C_6H_4$](η^2-CH_2CHPh)$(PMe_3)_2$.Significantly different activation parameters ($\Delta H^{\ddagger}$ = 13.7(0.8) kcal mol^{-1} and $\Delta S^{\ddagger}$ = −36.7(2.3) cal mol^{-1} K^{-1}) and a phosphine concentration dependent kinetic isotope effect (k_H/k_D = 6.4(5), [PMe_3] = 0 M; k_H/k_D = 4.3(3), [PMe_3] = 0.4 M; k_H/k_D = 2.4(4), [PMe_3] = 0.8 M; extrapolated to room temperature) were observed, suggesting two competing pathways (β-hydride elimination and β-H abstraction) are accountable for the transformation.
© 2004 Published by Elsevier Ltd.

1. Introduction

Over the past 40 years, understanding of the reactivity of transition metal alkyl complexes has grown from the point of view that "the loss of a hydride ion from the β-carbon of suitable transition metal alkyl complexes may well be a general reaction" [1] to a realization that this type of transformation is all pervasive in the chemistry of metal alkyls. Given that transition metal complexes containing metal–carbon bonds play crucial roles in a variety of important catalytic reactions, a detailed understanding of the stability and reactivity of transition metal alkyl complexes remains an important topic in both organometallic chemistry and catalysis [2,41].

For transition metal dialkyl complexes, thermal decomposition often proceeds by intramolecular attack on a C–H bond of an ancillary ligand [3] and several modes of C–H activation, involving α [4], β [5], γ [6], or ε-hydrogen [7] transfer. Among these pathways, the β-elimination process is the most frequently observed thermolysis pathway. Investigating the factors that control the transformation by β-elimination is important to understand the mechanisms of the catalytic processes utilizing transition metal catalysts.

* Corresponding author. Current address: Los Alamos National Laboratory, Nuclear Materials Technlogy Division, P.O. Box 1663, Mail Stop J582, Los Alamos, NM 87545, USA. Tel.: +505-6650795;fax: +505-6679905.
E-mail address: boncella@lanl.gov (J.M. Boncella).

0277-5387/$ - see front matter © 2004 Published by Elsevier Ltd.
doi:10.1016/j.poly.2004.09.002

Recent efforts in our laboratory [8] and others [9–13] have focused on the preparation of complexes of early transition metals in groups 3–6 at their highest oxidation states that contain β-hydrogens in one or more substituents. Mechanistic investigations have also been carried out in order to gain insight into the olefin polymerization reactions in which β-H transfer serves as a key termination step. The majority of these studies suggest that the mechanism of β-H transfer proceeds by one of two mechanisms (Scheme 1). One is the well-known β-H elimination pathway [5] in which the hydrido olefin intermediate is formed followed by reductive elimination of the alkane. The other (less common) pathway proposed is β-H abstraction [8–10] in which the β-hydrogen is transferred directly from the β-carbon to another alkyl group in one step, without the formation of the metal hydride intermediate.

Due to the high reactivities of most β-H containing alkyl complexes, typically these complexes can only be observed as intermediates or when they are coordinatively saturated or can be isolated when sterically protected by bulky groups, such as $[(Me_3SiNCH_2CH_2)_3N]^{3-}$ [10]. Green and co-workers [11], Schrock and co-workers [12], and Bercaw and co-workers [13] have reported that the ethyl complexes of some d^0, early transition metals (Ti, Ta, and Sc), are stabilized by a β-agostic interaction. We now report the preparation and crystal structures of a series of coordinatively unsaturated tungsten(VI) dialkyl complexes containing β-hydrogens, the reactivities of these complexes towards trimethylphosphine, and a mechanistic study of the β-H transfer processes in these compounds, including kinetic activation parameters and deuterium isotope effects, for the formation of olefin complexes from **1a** and **1d**.

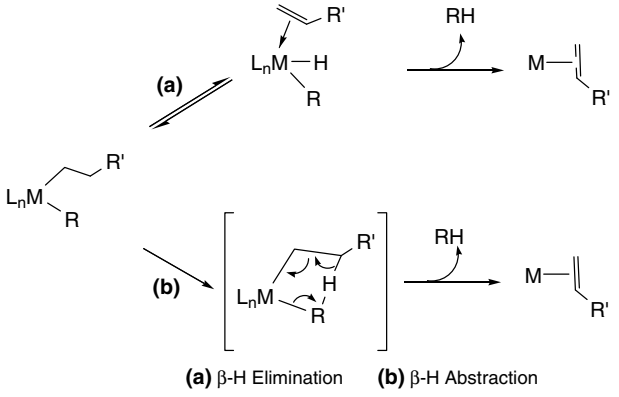

Scheme 1.

As can be seen in Scheme 1, the two pathways proceed through distinct steps that involve that involve C–H bond breaking and bond making. These pathways will result in different amplitudes of H vibration in the transition states involved in each pathway [14]. Therefore, a good way to distinguish these two pathways is by measurement of the primary kinetic isotope effect. β-H elimination followed by reductive elimination involves two steps in which there are C–H bond breaking or bond making. Thus, the isotope effect observed when reductive elimination is rate limiting is the product of the isotope effect for reductive elimination and the isotope effect associated with β-H elimination (which may be an equilibrium isotope effect). The isotope effect for a β-H elimination followed by reductive elimination usually falls into the range 1.4–2.5 at room temperature. Examples include $PdEt_2(PMePh_2)_2$ (KIE = 1.4) [15], $CoEt_2(acac)(PMe_2Ph)_2$ (KIE = 2.3) [16], $PtEt_2(PEt_3)_2$ (KIE = 1.4 to 1.7) [17], $Cp^*_2ScCH_2CH_2Ph$ (KIE = 2.0) [18] and $(CO)(PPh_3)_2IrCH_2CH_2C_6H_{13}$ (KIE = 2.3) [19]. By comparison, the isotope effect for a linear, symmetrical transition state as occurs in the β-H abstraction path is usually found to be 5–8 at room temperature [20]. Experimental data reported for

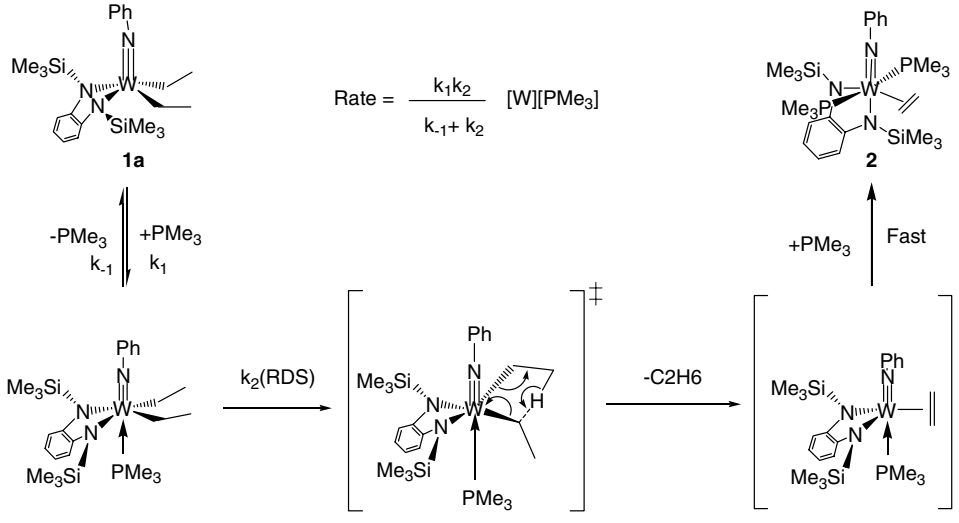

Scheme 2.

$Cp_2Zr(SCH_2Ph)(Me)$ [9], KIE = 5.2, and $[Me_3SiNCH_2CH_2]_3NTa(Et)_2$ [10], KIE = 5.7, are consistent with the proposed near linear transition state for the direct β-hydrogen abstraction pathway.

2. Results

2.1. Synthesis of tungsten(VI) dialkyl complexes

The tungsten(VI) dialkyl complexes **1a**–**1d** were synthesized by addition of two equivalents of Grignard reagent to a diethylether solution of $W(NPh)[o\text{-}(Me_3SiN)_2C_6H_4]Cl_2$ at −78 °C (Eq. (1)) [21]. Removal of solvent under reduced pressure and recrystallization from pentane gives the compounds in good to excellent yields as red-orange crystalline solids (**1c**,**1d**) or as oils (**1a**,**1b**).

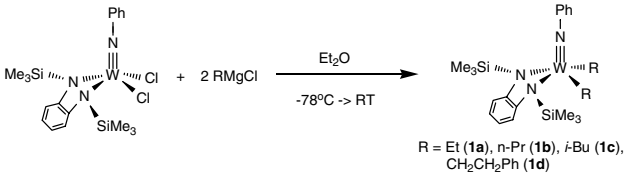

(1)

It is surprising that, despite their coordinative and electronic unsaturation, complexes, **1a**–**1d**, are indefinitely stable at room temperature in the absence of coordinating ligands. All complexes were characterized by ^1H and ^{13}C NMR spectroscopy. Single crystals of **1c** and **1d** that were suitable for X-ray diffraction studies were obtained by slowly cooling pentane solutions of **1c** and **1d** to −20 °C. Thermal ellipsoid plots of **1c** and **1d** are shown in Figs. 1 and 2, respectively. General data collection and refinement data for both **1c** and **1d** are listed in Table 1, while a table of selected bond lengths and angles is shown in Table 2. The coordination geometry about W in both structures is a square pyramid with the imido N in the apical position and the $[o\text{-}(Me_3SiN)_2C_6H_4]^{2-}$ ligand and two alkyl ligands in the basal plane. The W-imido bond lengths (1.738(2) for **1c** and 1.728(4) for **1d**) are consistent with a W–N triple bond [22]. The geometry about the N atoms of the $[o\text{-}(Me_3SiN)_2C_6H_4]^{2-}$ ligand is planar as is observed in silyl amines [23]. Despite the unsaturation of the metal center (14 or $16e^-$, CN = 5), there is no evidence for an agostic interaction between the metal and ligand C–H bonds in either structure.

2.2. Equilibrium between SP and TBP isomers of *1C*

We have reported the crystal structures of related dialkyl complexes [21a] showing that the geometry of these dialkyl complexes is dependent on the size of the alkyl groups. For small alkyls (e.g., methyl), the complex possesses a square pyramidal geometry with the imido N in the apical position. For large alkyls (e.g., neopentyl), the coordination geometry about the metal center is a trigonal bipyramid (TBP) with the imido N and one of the the diamido ligand N atoms in the axial positions. Complexes **1a**, **1b**, and **1d** are all square pyramidal (SP) or are undergoing rapid equilibration

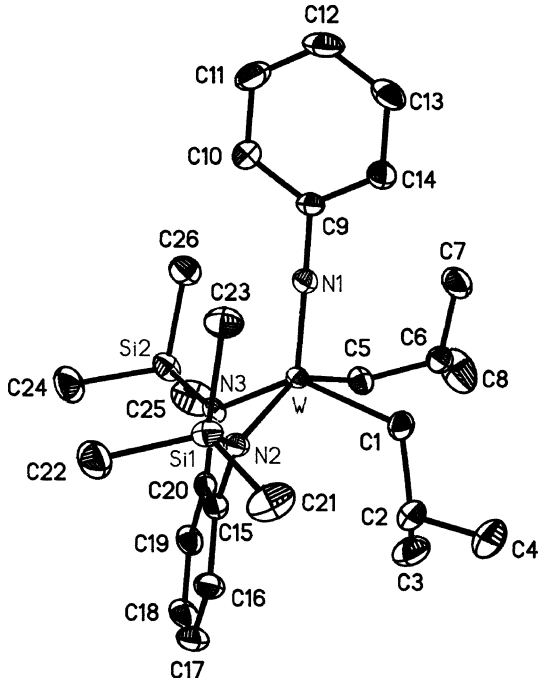

Fig. 1. Molecular structure of $W(NPh)[o\text{-}(Me_3SiN)_2C_6H_4](CH_2CHMe_2)_2$ (**1c**) with 40% probability ellipsoids and showing the atom numbering scheme. All hydrogen atoms are omitted for clarity.

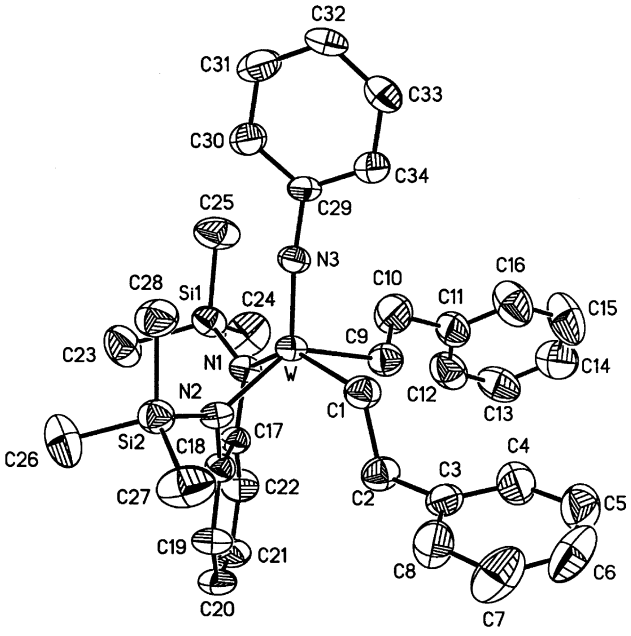

Fig. 2. Molecular structure of $W(NPh)[o\text{-}(Me_3SiN)_2C_6H_4](CH_2CH_2Ph)_2$ (**1d**) with 40% probability ellipsoids and showing the atom numbering scheme. All hydrogen atoms are omitted for clarity.

Table 1
Crystallographic and data collection parameters for W(NPh)[*o*-$(Me_3SiN)_2C_6H_4$]$(CH_2CHMe_2)_2$ (**1c**) and W(NPh)[*o*-$(Me_3SiN)_2C_6H_4$]$(CH_2CH_2Ph)_2$ (**1d**)

	1c	**1d**
A. Crystal data (173 K)		
a (Å)	9.5617(2)	10.0571(4)
b (Å)	10.1808(3)	10.1133(2)
c (Å)	17.2475(4)	19.1479(4)
α (°)	92.220(1)	93.043(1)
β (°)	103.419(1)	99.667(1)
γ (°)	110.999(1)	112.048(1)
V (Å^3)	1510.87(6)	1765.06(5)
d_{calc} (g cm^{-3}) (173 K)	1.406	1.384
Empirical formula	$C_{26}H_{45}N_3Si_2W$	$C_{34}H_{45}N_3Si_2W$
Formula weight (g)	639.68	735.76
Crystal system	triclinic	triclinic
Space group	$\bar{P}$	$\bar{P}$
Z	2	2
F(0 0 0), electrons	648	744
Crystal size (mm)	$0.28 \times 0.27 \times 0.19$	$0.28 \times 0.25 \times 0.21$
B. Data collection (173 K)		
Radiation, λ (Å)	Mo Kα, 0.71073	
Mode	ω–scan	
Scan width & rate	0.3 deg/frame & 30 s/frame	
2θ Range (°)	5–55	3–55
Range of $h\ k\ l$	$-12 \leqslant h \leqslant 11$, $-11 \leqslant k \leqslant 13$, $-22 \leqslant l \leqslant 20$	$-12 \leqslant h \leqslant 8$, $-10 \leqslant k \leqslant 12$, $-23 \leqslant l \leqslant 23$
Total reflections measured	9856	9322
Unique reflections	6643	6519
Absorption coefficient μ(Mo Kα) (mm^{-1})	3.919	3.365
C. Structure refinement		
Refinement method	full-matrix least-squares on F^2	
S, Goodness-of-fit	1.069	0.921
Number of variables	470	362
R_1/Reflections	1.65/6252 > 2$\sigma(I)$	3.40/5292 > 2$\sigma(I)$
wR_2/Reflections	3.94/6643	7.29/6519
R_{int} (%)	1.54	3.64
Maximum shift/esd	0.001	0.001
Minimum peak in difference Fourier map (e Å^{-3})	−0.411	−0.928
Maximum peak in difference Fourier map (e Å^{-3})	0.590	1.013

$R_1 = \hat{A}(||F_o| - |F_c||)/\hat{A}|F_o|, wR_2 = [\hat{A}[w(F_o^2 - F_c^2)^2]/\hat{A}[w(F_o^2)^2]]^{1/2}$.
$S = [\hat{A}[w(F_o^2 - F_c^2)^2]/(n-p)]^{1/2}, w = 1/[s^2(F_o^2) + (0.0370p)^2 + 0.31p], p = [\max(F_o^2, 0) + 2F_c^2]/3$.

of the SP and TBP isomers, as determined by the equivalence of the trimethylsilyl groups in their ^{1}H and ^{13}C NMR spectra from room temperature to −80 °C (though **1d** displays considerable broadening of the Me_3Si resonances at −80 °C).

Complex **1c**, W(NPh)[*o*-$C_6H_4(NSiMe_3)_2$]$(CH_2CHMe_2)_2$, is also square pyramidal, according to the single crystal X-ray study (Fig. 1). However, when dissolved, the complex clearly undergoes an equilibrium between SP and TBP isomers as observed by low temperature NMR spectroscopy (Eq. (2)). The limiting low temperature ^{1}H NMR spectrum (−80 °C) shows a single Me_3Si peak for the SP isomer and two equal intensity Me_3Si peaks for the TBP isomer which integrate to a TPB:SP ratio of 2:3 ($K = 0.67$ (Eq. (2))). A van't Hoff plot of the equilibrium constants from −40 to −80 °C gives values of $\Delta H° = -0.66(3)$ kcal mol^{-1} and $\Delta S° = -4.3(4)$ cal mol^{-1} K^{-1} for the SP/TBP equilibrium (see Table 3). Thus, the TBP isomer is favored enthalpically while entropy favors the SP isomer at higher temperatures. Whether this is due to differences in internal degrees of freedom or solvation effects is unclear.

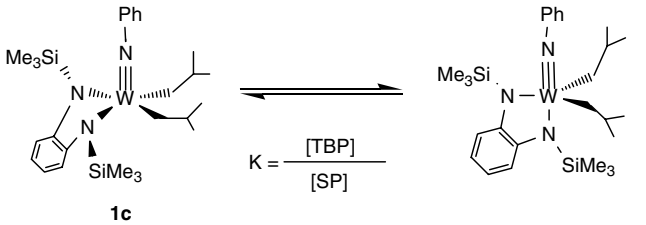

1c **SP** **TBP** (2)

Table 2
Selected bond lengths (Å) and angles (°) for W(NPh)[*o*-(Me_3SiN)$_2$-C_6H_4] (CH_2CHMe_2)$_2$ (**1c**) and W(NPh)[*o*-(Me_3SiN)$_2C_6H_4$](CH_2CH_2-Ph)$_2$ (**1d**)

*W(NPh)[o-(Me$_3$SiN)$_2$C$_6$H$_4$](CH$_2$CHMe$_2$)$_2$ (**1c**)*			
Bond lengths			
W–N(1)	1.738(2)	W–C(1)	2.182(5)
W–N(2)	2.013(2)	W–C(9)	2.195(2)
W–N(3)	2.023(2)		
Bond angles			
N(1)–W–N(2)	114.77(8)	N(3)–W–C(1)	139.31(8)
N(1)–W–N(3)	120.17(8)	N(3)–W–C(5)	83.13(8)
N(1)–W–C(1)	100.35(8)	C(1)–W–C(5)	85.47
N(1)–W–C(5)	101.54(9)	W–N(1)–C(9)	174.9(2)
N(2)–W–N(3)	81.43(7)	W–C(1)–C(2)	120.0(2)
N(2)–W–C(1)	85.09(8)	W–C(5)–C(6)	127.0(2)
N(2)–W–C(5)	143.55(8)		
*W(NPh)[o-(Me$_3$SiN)$_2$C$_6$H$_4$](CH$_2$CH$_2$Ph)$_2$ (**1d**)*			
Bond lengths			
W–N(1)	2.000(4)	W–C(1)	2.189(5)
W–N(2)	2.003(4)	W–C(9)	2.175(5)
W–N(3)	1.728(4)		
Bond angles			
N(1)–W–N(2)	82.9(2)	N(3)–W–C(1)	97.2(2)
N(1)–W–N(3)	117.1(2)	N(3)–W–C(9)	102.6(2)
N(1)–W–C(1)	145.0(2)	C(1)–W–C(9)	80.6(2)
N(1)–W–C(9)	85.1(2)	W–N(3)–C(29)	171.8(3)
N(2)–W–N(3)	120.7(2)	W–C(1)–C(2)	117.6(3)
N(2)–W–C(1)	85.4(2)	W–C(9)–C(10)	117.7(4)
N(2)–W–C(9)	135.8(2)		

2.3. Reactivity of *1a–1d* with trimethylphosphine

Complexes **1a**–**1d** are coordinatively unsaturated tungsten species. It is reasonable to assume that coordination of trimethylphosphine to the d° metal center associated with a color change due to the ligand–metal charge transfer would be facile. However, no PMe_3 adduct was observed for **1a**–**1d** at room temperature. At low temperature, the equilibrium between free and coordinated phosphine is shifted enough so that adducts can be observed by ^{1}H, ^{13}C, and ^{31}P NMR spectroscopy. Previous studies in our group revealed the crystal structure of W(NPh)[*o*-(Me_3SiN)$_2C_6H_4$](PMe_3)Me_2 [21], in which the phosphine coordinates *trans* to the imido ligand (*cis* alkyls) and the molecule has a mirror plane containing the imido N, W and phosphine atoms, resulting in the equivalency of the two trimethylsilyl groups and the two alkyl groups (Eq. (3)).

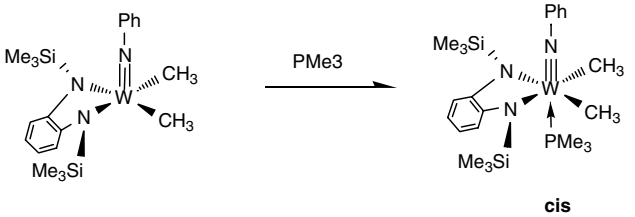

(3)

Table 3
Equilibrium constant (K) and free energy ($\Delta G°$) calculated for the isomerization of **1c**

T (K)	K	$\Delta G°$ (kcal mol^{-1})
233.15	0.49(6)	0.33(6)
223.15	0.52(4)	0.29(3)
193.15	0.66(3)	0.16(2)

Another coordination mode (*trans* alkyls) is found in the case of **1a** and **1d** in which the phosphine coordinates to the metal center between the two alkyls (Eq. (4)). The geometry was verified by observing two trimethylsilyl peaks along with equivalent phenethyl groups in the *trans* isomer in the low temperature ^{1}H and ^{13}C NMR spectra. While other arrangements of the PMe_3 ligand and

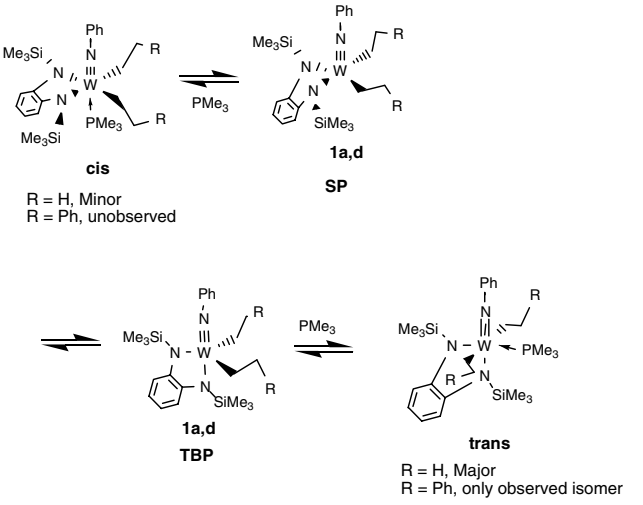

(4)

alkyl groups are possible, the *trans* geometry shown in Eq. (4) is the only one that gives inequivalent $SiMe_3$ groups and equivalent alkyls.

It is worthwhile to note that in the 5-coordinate SP complexes **1a**–**1d**, the LUMO is the d_{xy} orbital (z-axis coincident with the W-imido bond) [24]. Thus, the LUMO is not directed toward the vacant site of the SP isomers suggesting that the coordination of Lewis bases may be somewhat complicated since sterics suggest coordination *trans* to imido while electronics would direct coordination to the LUMO in the basal plane. In the TBP isomers, the LUMO is located in the equatorial plane suggesting that Lewis based should coordinate there. Evidently, the SP/TBP equilibrium plays a major role in directing the coordination of PMe_3 to these complexes. As the alkyl groups get larger, the TBP isomer becomes more favored in solution which apparently leads to a greater propensity to form the *trans* isomer as demonstrated in the bis(phenethyl) example, **1d**. For the dimethyl complex, which has the least propensity to form the TBP isomer, the coordination of PMe_3 occurs at the vacant site of the SP isomer, *trans* to the imido ligand.

Both isomers were observed for the PMe_3 adduct of **1a**, W(NPh)[*o*-$(Me_3SiN)_2C_6H_4$](PMe_3)Et_2. The ^{31}P NMR of a toluene-d_8 solution of **1a** at −80 °C in the presence of 15 eq. of PMe_3 reveals two distinct peaks in a ratio of ca. 20:1 at δ −21.9 ($^1J_{P-W}$ = 240 Hz, major isomer, PMe_3 *cis* to imido and ethyl groups mutually *trans*) and δ −28.1 (broad, minor isomer with PMe_3 *trans* to imido and ethyl groups mutually *cis*). The low temperature ^{13}C NMR spectrum of this mixture is consistent with the proposed structure of the major isomer since two Me_3Si peaks are observed as is expected for the isomer with *trans* alkyl groups.

In the presence of trimethylphosphine, complexes **1a** and **1d** are converted to the ethylene complex, **2**, and the styrene complex, **3**, quantitatively (Eq. (5)). The crystal structure of

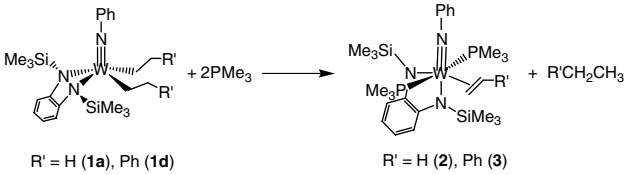

(5)

compound **2** has also been obtained and reported earlier [21b]. The formation of **2** proceeds much faster (<1 h at room temperature) than the formation of **3** (>6 h at 60 °C). Complex **1b** reacts with trimethylphosphine to form the propylene complex in low yield. The reaction between **1c** and trimethylphosphine proceeds at a negligible rate at room temperature and decomposition occurs at elevated temperature with the formation of isobutane and isobutylene. Although isobutylene complexes have been isolated for Hf [25], W [26], and Mo [27a], we were not able to isolate the desired complex, possibly because an isobutylene complex analogous to **2** is unstable at the high temperature needed to induce reaction of **1c**.

2.4. Mechanistic studies

Whitesides [28] proposed a mechanism for the decomposition of Pt(*n*-Bu)$_2$(PPh_3)$_2$ which is initiated by PPh_3 dissociation and illustrated the necessity to increase the stability of the complex by blocking the site for β-elimination by the ligand. Reger [29] also showed that the ligand dissociation to open a coordination site is required for β-elimination in the case of Fe(Cp)(CO)(PPh_3)R. However, the β-H transfer chemistry of **1a**–**1d** is promoted by adding a ligand to the metal center. This behavior is clearly unexpected since it implies that β-H transfer is induced by *increasing the coordination number and electron count of the complex*. To understand the role of PMe_3 and to clarify the mechanism, we have undertaken kinetic studies of the reactions of **1a** and **1d** with PMe_3.

2.5. Kinetics

The kinetics of the thermal decomposition of **1a** and **1d** in toluene-d_8 were examined by following the appearance and disappearance of the trimethylsilyl peaks of starting materials, **1a** and **1d**, and products, **2** and **3** using ^1H NMR spectroscopy in the presence of excess PMe_3. The data points were obtained by plotting the absolute peak intensity with respect to time for more than three half-lives.

Activation parameters for the conversion of **1a** to **2** were determined by reacting toluene-d_8 solutions (0.0486 M) of **1a** with PMe_3 (0.972 M) in the NMR probe at temperatures between 263 and 293 K (three samples at each temperature). Both the appearance of **2** and disappearance of **1a** follow first-order kinetics throughout the reaction with a pseudo first-order rate constant at 293 K of $k = 9.61(82) \times 10^{-4}$ s^{-1} ($t_{1/2}$ = 12 min). Conversion of **1a** to **2** is essentially quantitative and no ^1H NMR signals corresponding to any intermediate were observed. Activation parameters, obtained from an Eyring plot ($\Delta S^{\ddagger} = R$[(intercept) − 23.76]; $\Delta H^{\ddagger} = -R$(slope)), for the formation of **2** from **1a** are $\Delta H^{\ddagger}$ = 5.1(0.6) kcal mol^{-1} and $\Delta S^{\ddagger}$ = −54.9(2.0) cal mol^{-1} K^{-1}, which correspond to $\Delta G^{\ddagger}$ = 21.2 kcal mol^{-1} at 293 K.

The observation that the addition of ethylene has no effect on the rate of thermolysis as well as the large, negative entropy of activation suggests that liberation of ethylene does not occur prior to the rate-determining step in this reaction. The observed value of $\Delta S^{\ddagger}$ is a combination of the PMe_3 binding and the subsequent steps to reach the rate determining step. Values of $\Delta S^{\ddagger}$ between −30 and −40 cal mol^{-1} K^{-1} are often observed in purely associative substitution reactions. Thus, the majority of the observed value of $\Delta S^{\ddagger}$ is accounted for in the binding of PMe_3 [30]. Loss of the remaining 10 – 20 cal mol^{-1} K^{-1} is consistent with the formation of the highly constrained transition state necessary for the proposed β-H transfer [9]. Similar values of $\Delta S^{\ddagger}$ (−10 to −20 eu) have also been observed in direct α-abstraction reactions to form alkylidene complexes [31]. Graphs of representative first-order data and the Eyring plot are shown in Fig. 3.

The kinetics of the formation of **3** from **1d** were carried out by reaction of toluene-d_8 solutions (0.0309M) of **1d** with PMe_3 (0.662 M, 21 equiv.) over a temperature range 333–363 K (three samples at each temperature). The reaction follows first-order kinetics with a pseudo first-order rate constant at 333 K of $k = 6.9(4) \times 10^{-5}$ s^{-1} ($t_{1/2}$ = 167 min). Activation parameters for the formation of **3** from **1d** are $\Delta H^{\ddagger}$ = 13.7(0.8) kcal mol^{-1} and $\Delta S^{\ddagger}$ = −36.6(2.3) cal mol^{-1} K^{-1}, which correspond to $\Delta G^{\ddagger}$ = 25.9 kcal mol^{-1} at 333 K. Graphs of representative first-order data and an Eyring plot are shown in Fig. 4. The observation that the addition of styrene has no effect on the

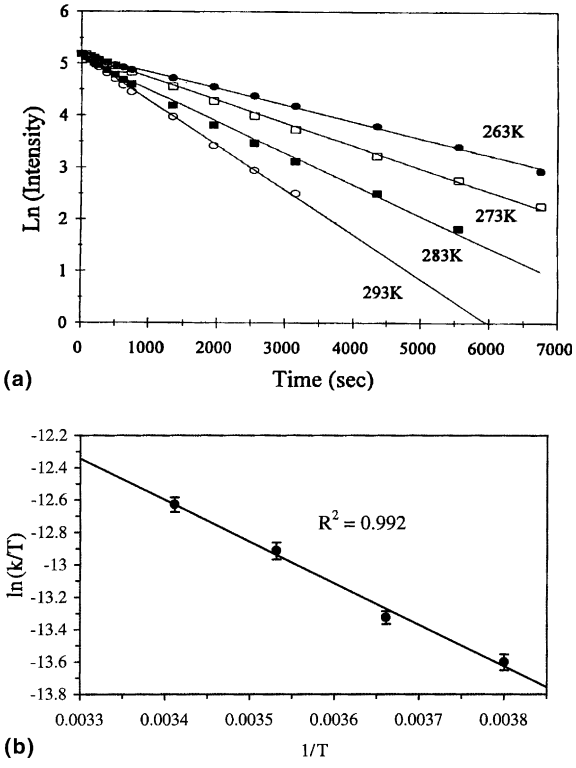

Fig. 3. First-order kinetics (a) and Eyring plot (b) for the formation of **2**.

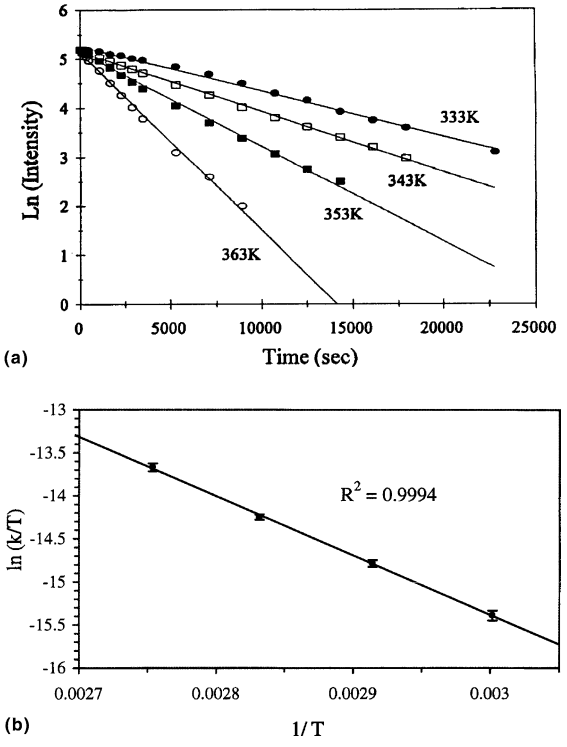

Fig. 4. First-order kinetics (a) and Eyring plot (b) for the formation of **3**.

rate of thermolysis suggests that the liberation of styrene does not occur prior to the rate-determining step in this reaction. The activation parameters in the conversion of **1d** to **3** are significantly different from those of **1a** to **2** ($\Delta\Delta H^{\ddagger} = 8.6$ kcal mol^{-1} and $\Delta\Delta S^{\ddagger} = 18.3$ cal mol^{-1} K^{-1}), suggesting that the two reactions follow different mechanisms. Rate constants obtained for both reactions studied are shown in Table 4. [1]

2.6. Phosphine dependence

The role of trimethylphosphine in the conversion of **1a** to **2** was examined by reacting **1a** (0.0243 M) with PMe_3 (0–1.7 M) at 283 K. In the absence of trimethylphosphine, the diethyl complex, **1a**, is stable in the solution with no decomposition observed within several hours. The rate constants were obtained through the same procedure as described above, but at different PMe_3 concentrations. The reaction is first order in PMe_3, according to the slope of 1.096 obtained from the plot of ln(k) vs. ln[PMe_3] (Fig. 5). Though saturation of the rate at high concentrations of PMe_3 is predicted, we were not able to observe such behavior even at PMe_3 concentrations of 1.7 M.

The phosphine dependence for the formation of **3** from **1d** was measured by examining the reaction of **1d** (0.0309M) with PMe_3 over a range 0–2 M. The reaction exhibits near linear behavior at high phosphine concentrations. However, if the phosphine concentrations are less than ca. 0.6 M (20 equiv.), there is no profound effect on the rate of thermolysis (Fig. 6) and a rate constant of 2.1×10^{-4} s^{-1} (measuring the disappearance of **1d**) was observed when no PMe_3 is added. The data suggests that more than one pathway, in which one of them is phosphine independent, are involved in the reaction. These results exclude the possibility of two parallel pathways where one is phosphine independent and one is first-order phosphine dependent, because the phosphine dependence of the rate constant of such a mechanism would result in a straight line with a positive intercept.

2.7. Deuterium labeling experiments

In order to establish the extent to which the β-elimination pathway, possibly responsible for the formation of olefin complexes, **2** and **3**, is reversible, the β-deuterated analogs of **1a** and **1d**, W(NPh)[*o*-$(Me_3SiN)_2C_6H_4$]-$(CH_2CD_3)_2$, **1a**-d_6 and W(NPh)[*o*-$(Me_3SiN)_2C_6H_4$]-$(CH_2CD_2Ph)_2$, **1d**-d_4 were prepared. If the β-elimination pathway involves a fast equilibrium between β-H elimination and olefin insertion [32] into metal–hydride bond, then scrambling of the deuterium labels [5a,5b,17] from the β-carbon into the α-carbon would give a mixture of d_2–d_6 ethane and a mixture of deuterated ethyl benzenes from **1d**.

[1] Average numbers of three samples at each temperature.

Table 4
Rate constants (average numbers of three samples at each temperature) for the reactions of **1a** and **1d** with PMe_3

[**1a**] = 0.0486 M (T (K))	[PMe3] = 0.972 M ($k \times 10^4$ s^{-1})	[**1d**] = 0.0309M (T (K))	[PMe3] = 0.662 M ($k \times 10^4$ s^{-1})
293.15	9.61 (82)	363.15	4.21 (21)
283.15	6.98 (37)	353.15	2.29 (7)
273.15	4.46 (18)	343.15	1.30 (5)
263.15	3.26 (16)	333.15	0.69 (4)

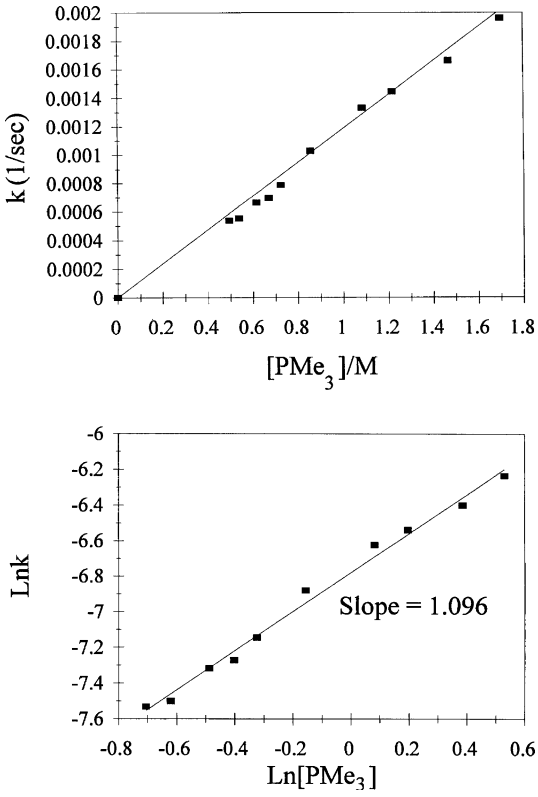

Fig. 5. PMe_3 dependence for the reaction of **1a** with PMe_3.

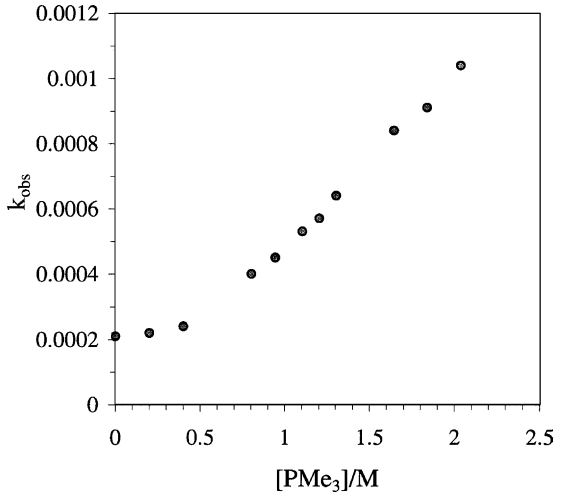

Fig. 6. PMe_3 dependence for the reaction of **1d** with PMe_3.

The conversion of **1a**-d_6 to **2**-d_2 was followed by ^2H NMR in toluene. In both the absence and presence of PMe_3, no scrambling of the deuterium labels among the α- and β-carbons was observed. The products of the reaction are exclusively W(NPh)[*o*-$(Me_3SiN)_2C_6H_4$](η^2-CH_2CD_2)$(PMe_3)_2$, **2**-d_2, and CH_2DCD_3. The formation of CH_2DCD_3 is supported by the observation of a mass peak at 34 *m/e* in EI-MS experiments. The same mass spectrum is also observed for the product of the reaction between CD_3CH_2MgCl and D_2O. The above observations suggest an irreversible β-H abstraction process similar to that proposed by Yamamoto and co-workers [15]. Similar experiments performed on **1d** also suggest that no scrambling occurs.

The kinetic isotope effect for the transformation of **1a** to **2** was determined by reacting **1a**-d_6 with trimethylphosphine under the same conditions at 293 K, giving $k_D = 1.57(4) \times 10^{-4}$ s^{-1}. This corresponds to a k_H/k_D of 6.1(5), which strongly suggests a near linear transition state for the β-H transfer process. This is consistent with the direct transfer of one β-H to the other α-carbon atom as is proposed in Scheme 2. The large KIE in our system is significantly different from those compounds which decompose by β-elimination followed by reductive elimination [15–19]. Buchwald [33], Erker [34], Marks [35] and Schrock [36] have proposed the direct β-hydrogen abstraction process from an sp^2-hybridized carbon in the formation of alkyne/aryne complexes. Similar kinetic isotope effects have also been determined by Marks (6.5) [37] and Teuben (5.1) [38]. The KIE observed in our system is also consistent with those observed for $Cp_2Zr(SCH_2Ph)(Me)$, [9] KIE = 5.2, and $[Me_3SiNCH_2CH_2]_3NTa(Et)_2$, [10] KIE = 5.7, in which the direct β-hydrogen abstraction was proposed to be the most-likely pathway.

The kinetic isotope effect for the transformation of **1d** to **3** was determined by reacting **1d**-d_4 (0.031 M) with PMe_3 (0.8 M) at 343 K, giving $k_D = 0.62(4) \times 10^{-4}$ s^{-1}. This corresponds to a k_H/k_D of 2.1(2) (2.4 when extrapolated to room temperature, assuming linear Arrhenius [40] behavior). This is consistent with the data reported for the β-elimination pathway [15–19]. The unusual rate constants observed at low phosphine concentrations led us to study the kinetic isotope effect at different PMe_3 concentrations. With 0.4 M PMe_3 at 353 K, a kinetic isotope effect of 3.4(3) (4.3 at room temperature) was observed, whereas 4.8(5) (6.4 at room temperature) was observed for the thermolysis of **1d** in the absence

Table 5
KIE for the decomposition of **1d** (0.031 M) under different [PMe_3]

[PMe_3]/M	KIE/Temperature	KIE (extrapolated to room temperature, 298 K)
0	4.8(5)/353 K	6.4
0.4	3.4(3)/353 K	4.3
0.8	2.1(2)/343 K	2.4

of PMe_3. The difference in kinetic isotope effects at different PMe_3 concentrations (Table 5) is clear evidence that there is more than one pathway involved in the transformation. The large number (6.4) observed in the absence of PMe_3 is similar to that of **1a** (6.1), and suggests that the β-abstraction is the dominant pathway at low PMe_3 concentrations.

2.8. Mechanistic study of the formation of 2

Given the experimental data described above, an associative pathway in which the transformation is induced by pre-coordination of a ligand is the mechanism that we propose which accounts for all the observations. A rapid pre-equilibrium coordination of PMe_3 is proposed as the initial step for the transformation of **1a** to **2** due to the first order dependence on PMe_3 and the fact that the PMe_3 adduct, W(NPh)-[*o*-$(Me_3SiN)_2C_6H_4$](PMe_3)Et_2, **1a-P**, has been observed at −50 °C in the presence of excess PMe_3. This adduct exists as a mixture of two isomers as determined by ^{13}C and ^{31}P NMR spectroscopy. The major isomer has *trans* ethyl groups with PMe_3 coordinated *cis* to the imido ligand. The minor isomer has the PMe_3 coordinated *trans* to the imido ligand leaving the ethyl groups mutually *cis*. We suggest that the reaction proceeds through the minor isomer of **1a-P** in which the *cis* disposition of the ethyl groups is retained.

The reaction obeys first-order kinetics in both W and PMe_3. No deuterium scrambling was observed both in the presence and absence of PMe_3, which excludes a β-elimination process in which there is a rapid equilibrium between an olefin-hydride complex and the starting material. The observation of a large kinetic isotope effect (6.1) at 293 K suggests a symmetrical linear transition state, according to Kwart's study [14]. The observed value of $\Delta S^{\ddagger}$ (−54.9 eu) is consistent with the bimolecular nature of this reaction and the highly-ordered transition state, imposed by the geometric requirements of the β-hydrogen to transfer to the α-carbon of the other ethyl group. Evidently, the increased electron density on the metal center in

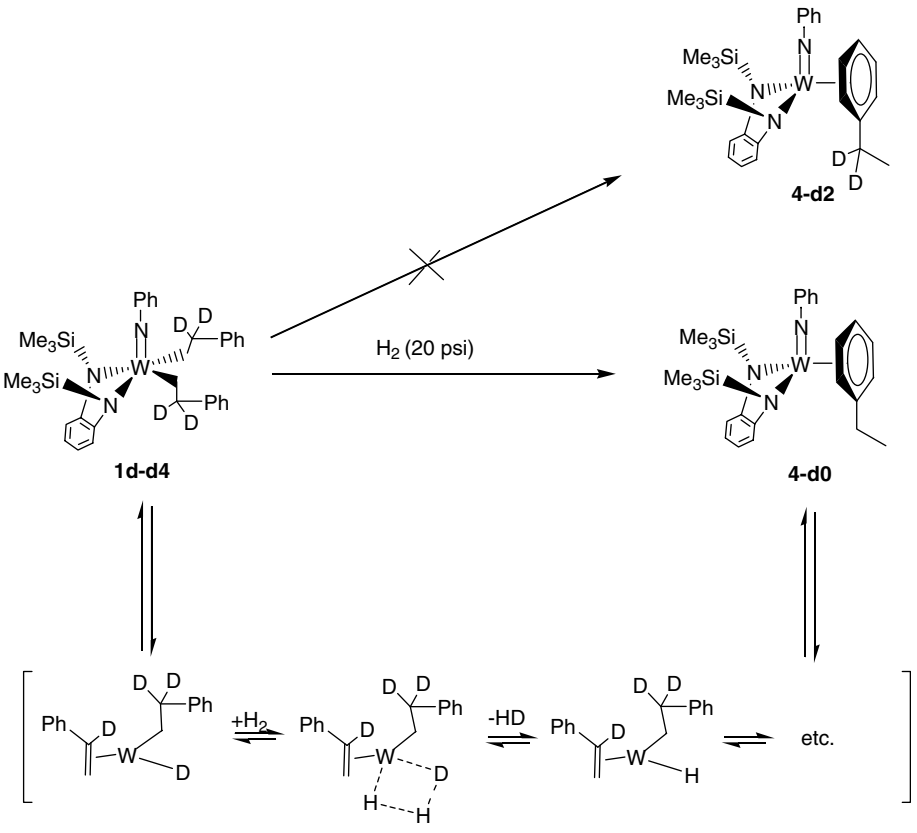

Scheme 3. Hydrogenolysis of W(NPh)[*o*-$(Me_3SiN)_2C_6H_4$]$(CH_2CD_2Ph)_2$ (**1d**-d_4).

$W(NPh)[o\text{-}(Me_3SiN)_2C_6H_4](Et)_2(PMe_3)$ combined with the increased steric congestion induces the rapid β-H abstraction reaction.

2.9. β-H Elimination

The existence of a β-H elimination process, forming a hydrido-styrene intermediate during the conversion of **1d** to **3**, is supported by the observation of trace amounts of free styrene in the ^1H NMR spectrum of **1d** and the study of the hydrogenolysis reaction of **1d**. In the presence of hydrogen, complex **1d** is converted to a W(IV) arene complex $W(NPh)[o\text{-}(Me_3SiN)_2C_6H_4](\eta^6\text{-}C_6H_5Et)$ (**4**) as shown in Eq. (6) [27b].

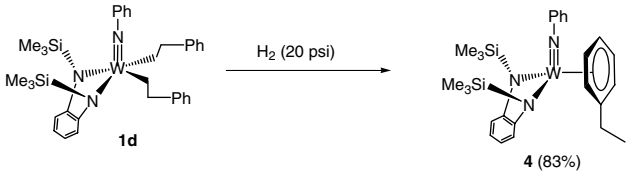

(6)

When **1d**-d_4 was used for the hydrogenolysis reaction, all deuterium labels were washed out by the hydrogen (^2H NMR) and no deuterium label is observed in the product, **4**, that formed. This observation strongly suggests the presence of a hydrido intermediate (Scheme 3), which undergoes H/D exchange with H_2 [42].

2.10. Mechanistic study of the formation of *3*

The transformation of **1d** to **3** proceeds via more complicated pathways than that of **1a** based on the observations mentioned earlier. The near linear PMe_3 dependence at high concentration is similar to the conversion of **1a** to **2**. However, the kinetic isotope effect observed (2.1) implies that the β-H elimination pathway

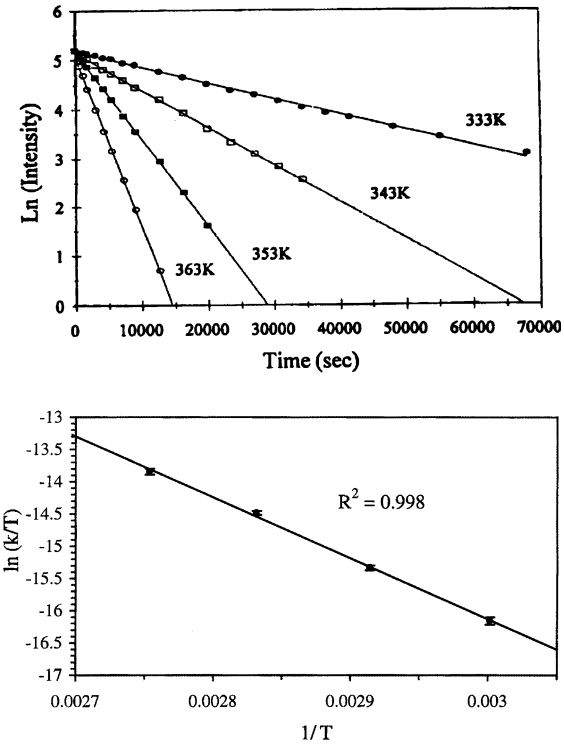

Fig. 7. First-order kinetics (top) and Eyring plot (bottom) for the thermolysis of **1d**.

is more reasonable than a β-H abstraction pathway which gives a k_H/k_D of 6.1 for the transformation of **1a** to **2**.

In the absence of PMe_3, complex **5**, the product of the thermolysis of **1d**, was observed, associated with the ethylbenzene being released from tungsten center. A rate constant of $2.1 \times 10^{-4}\ s^{-1}$ and large kinetic isotope effect (6.4) are observed for the thermolysis of **1d**, suggesting that a similar β-abstraction pathway accounts for this

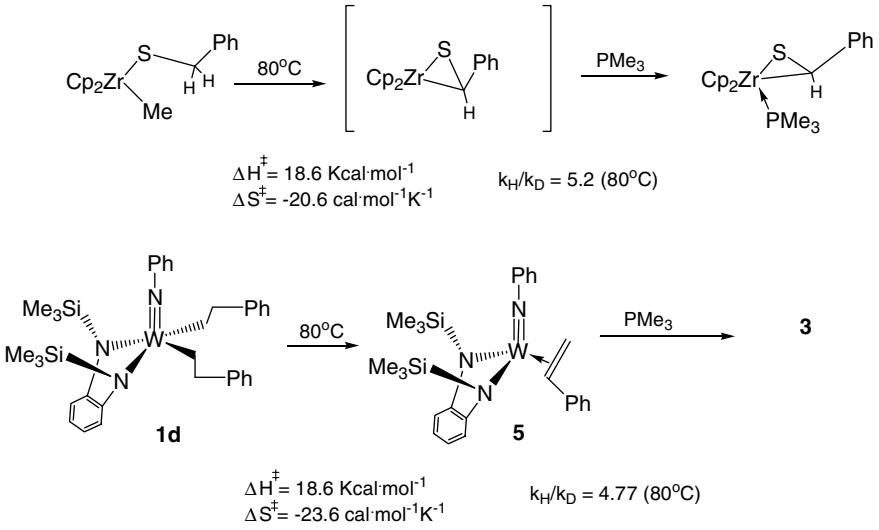

Scheme 4.

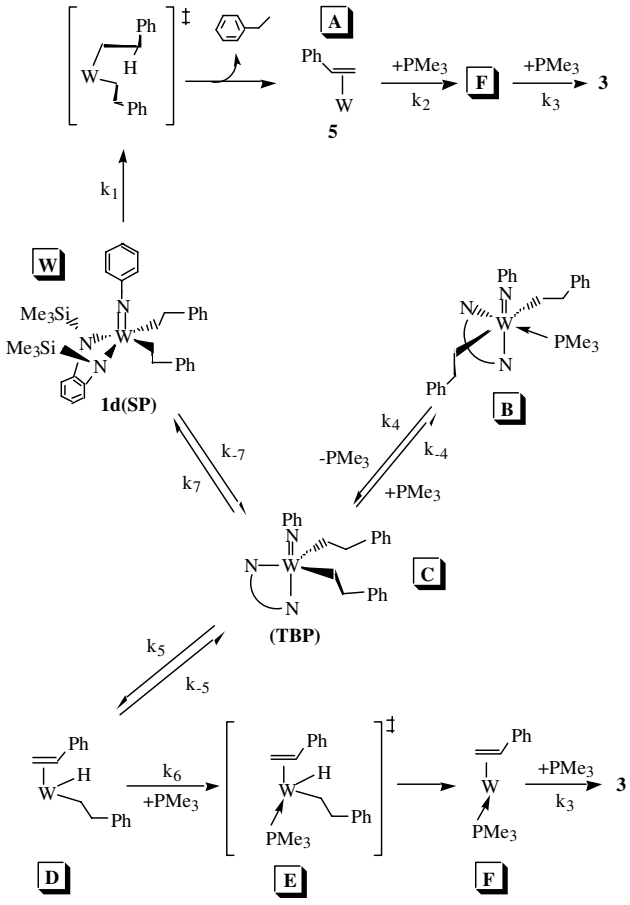

Scheme 5.

reaction. The styrene complex, **5** can be isolated as a dark brown solid. Upon further addition of PMe_3 to **5**, compound **3** is formed quantitatively. The kinetics of the thermolysis of **1d** were also performed (Fig. 7) over a temperature range of 333–363 K and in the absence of PMe_3. The reaction follows first-order kinetics with activation parameters being $\Delta H^{\ddagger} = 18.6(0.6)$ kcal mol^{-1} and $\Delta S^{\ddagger} = -23.3(1.6)$ cal mol^{-1} K^{-1}, which correspond to $\Delta G^{\ddagger} = 26.4$ kcal mol^{-1} at 333 K. The activation parameters obtained here are similar to related studies (Scheme 4) [9].

It should be noted once again that parallel pathways (one being PMe_3 independent and one being first order in PMe_3) *cannot* explain the non-linearity in Fig. 6. The PMe_3-dependent kinetic isotope effect and the deviation from linear PMe_3 dependence at low concentrations suggest that PMe_3 plays a crucial role in determining which pathway the reaction follows. A simple mechanism consisting of phosphine association/dissociation equilibrium followed by β-H elimination does not account for the phosphine dependence observed, since it will result in a linear dependence with a positive intercept in Fig. 6. Furthermore, we have established that the isomerization between trigonal bipyramidal and square pyramidal isomers exists in the solution. Therefore, we propose that the isomerization process shown in Scheme 5 takes place prior to the product forming step.

The *trans* isomer (referred to the *trans* alkyl groups) of the phosphine adduct, W(NPh)[*o*-$(Me_3SiN)_2C_6H_4$]$(PMe_3)(CH_2CH_2Ph)_2$, **B**, is proposed in Scheme 5 because no *cis* isomer has been observed at any temperature and only a small amount of the *cis* isomer of **1a** (which is much less sterically hindered than **1d**) is observed when **1a** is treated with PMe_3. Complex **C** is in equilibrium with the hydrido-styrene intermediate, **D** (which is the source of hydride that exchanges with free H_2). The coordination of PMe_3 to **D** forms a seven-coordinate transition state, **E**. Reductive elimination of ethylbenzene is assisted by the coordination of PMe_3 and is considered the rate limiting step in the second pathway. Reductive elimination from **D** without coordination of PMe_3 is ruled out since it will result in a linear PMe_3 dependence from the calculation of the rate equation. Under these conditions, at high enough concentrations of PMe_3, the rate of the reaction is predicted to be first order in PMe_3 and W with the rate determining step being k_6. With no PMe_3 present, the k_1 path is followed. At intermediate concentrations of PMe_3, a much more complicated set of reactions occurs because PMe_3 is involved in the establishment of the isomerization equilibria between **W**, **B**, **C** and **D**. Furthermore, PMe_3 must dissociate from **B** prior to the product forming step of the PMe_3 dependent pathway.

$$\text{Rate} = \frac{-\mathrm{d}[W]}{\mathrm{d}t} = k_1[W] - k_7[C] + k_{-7}[W]. \tag{7}$$

From Scheme 5, the rate of the reaction can be expressed as Eq. (7). Based on the fact that no intermediate was observed during the reaction, we are able to use the steady-state approximation for the concentration of **B**, **C**, and **D**, which gives the observed rate constant, k_{obs} (Eq. (8)), as a complex dependence on rate constants and phosphine concentrations (Scheme 6). [2]

The complexity of the PMe_3 dependence accounts for the non-linear behavior in Fig. 6. Although we are not able to measure rate constants for each step, an estimation of the rate constants can be made that is consistent with our observations. First, we find no profound effect

[2] $a = k_4k_{-5}k_{-5}k_7k_7; b = 2k_4k_5k_{-5}k_6k_7 + k_4k_{-5}k_6k_7k_7 + k_4k_{-4}k_{-5}k_{-5}k_7 + k_4k_{-5}k_6k_7k_7 - k_4k_{-4}k_{-5}k_6k_7; c = 3k_4k_{-4}k_{-5}k_6k_7 + 2k_{-5}k_6k_7k_7 - k_4k_{-4}k_{-5}k_6k_7; c = 3k_4k_{-4}k_{-5}k_6k_7 + 2k_4k_5k_6k_6k_7 + k_4k_{-4}k_5k_{-5}k_6 + k_4k_5k_5k_6k_6 + k_4k_6k_6k_7k_7 - k_4k_{-4}k_{-4}k_{-5}k_6 - k_4k_{-4}k_5k_6k_6 - k_4k_{-4}k_6 \quad k_6k_7; d = 2k_4k_{-4}k_5k_6k_6 + k_4k_{-4}k_6k_6k_7 + k_4k_{-4}k_{-4}k_{-5}k_6 - k_4k_{-4}k_{-4}k_6k_6; e = k_4k_{-4}k_{-4}k_6k_6; f = k_4k_5k_{-5}k_6k_7 \quad k_{-7} + k_4k_{-4}k_6k_6k_7k_{-7} - 2 \quad k_4k_{-4}k_{-5}k_6k_7k_{-7}; g = 2k_4k_{-4}k_{-5}k_6k_7k_{-7} + k_4k_{-4}k_5k_{-5}k_6k_{-7} + k_4k_5 \quad k_5k_6k_6k_{-7} + k_4k_5k_6k_6k_7k_{-7} - k_4k_{-4}k_{-4}k_{-5}k_6k_{-7} - k_4k_{-4}k_5k_6k_6k_{-7}; h = 2k_4k_{-4}k_5k_6k_6k_{-7} + k_4k_{-4}k_6k_6k_7k_{-7} + k_4k_{-4}k_{-4}k_{-5}k_6k_{-7} - k_4k_{-4}k_{-4}k_6k_6k_{-7}; i = k_4k_{-4}k_{-4}k_6k_6k_{-7}.$

$$\text{Assumption}: \frac{d[B]}{dt} = \frac{d[C]}{dt} = \frac{d[D]}{dt} = 0$$

$$\Rightarrow [B]_{ss} = \frac{k_{-4}[C][PMe_3]}{k_4}$$

$$[C]_{ss} = \frac{k_4[B] + k_{-7}[W] + k_{-5}[D]}{k_{-4}[PMe_3] + k_5 + k_7}$$

$$[D]_{ss} = \frac{k_5[C]}{k_{-5} + k_6[PMe_3]}$$

$$\Rightarrow [C] = [W] * \frac{a'+b'[PMe_3]+c'[PMe_3]^2+d'[PMe_3]^3}{a+b[PMe_3]+c[PMe_3]^2+d[PMe_3]^3+e[PMe_3]^4}$$

(a-e, a'-d': constants)

$$\text{Rate} = k_1[W] - k_{-7}[C] + k_{-7}[W]$$

$$= k_{obs}*[W]$$

$$k_{obs} = k_1 + \frac{f[PMe_3]+g[PMe_3]^2+h[PMe_3]^3+i[PMe_3]^4}{a+b[PMe_3]+c[PMe_3]^2+d[PMe_3]^3+e[PMe_3]^4} \quad (8)$$

(a-i: constants)[45]

Scheme 6. Derivation of the observed rate constant, k_{obs} for the formation of **3**.

on the overall rate in the presence of low concentration of phosphine and the rate only doubles when a large excess (ca. 25 equiv.) of PMe_3 is added. This indicates that rate constants for the phosphine dependent pathway are similar to those of the phosphine independent pathway ($k_1 = 0.00021$). Second, the square pyramidal structure of **1d**, obtained from a single crystal X-ray study, and the inability to observe the trigonal bipyramidal isomer at any temperature suggest that the isomerization process is probably very fast or the equilibrium lies predominantly toward the SP isomer ($k_7 \gg k_{-7}$). Furthermore, if the coordination of phosphines is actually much faster than all other steps, all three species, **1d**, **B**, and **C**, can be considered as one species, which should result in a linear PMe_3 dependence.

Given the complexity of the rate equation in Scheme 6, we have analyzed the rate data using a kinetics simulation program. Rate constants were assigned based on the above discussion and the KINFIT program was used to provide a reaction profile of the concentrations of all species involved in the reaction with respect to time. Rate constants were examined repeatedly until a set of numbers ($k_1 = 0.00021$; $k_4 = 0.04$; $k_{-4} = 0.08$; $k_5 = 0.01$; $k_{-5} = 0.01$; $k_6 = 0.001$; $k_7 = 0.02$; $k_{-7} = 0.002$) was found that fit the experimental results of both the phosphine dependence of k_{obs} (Fig. 8) and that gave a reaction profile that is consistent with the experimental observations (Fig. 9).

The simulation result shows well behaved kinetics with the dominant species being PMe_3, **1d**, **3** and ethylbenzene, which is consistent with the experimental observations. The rate constant obtained from the simulation result (e.g., $k_{obs(calc)} = 0.00023(2)\ s^{-1}$ for the

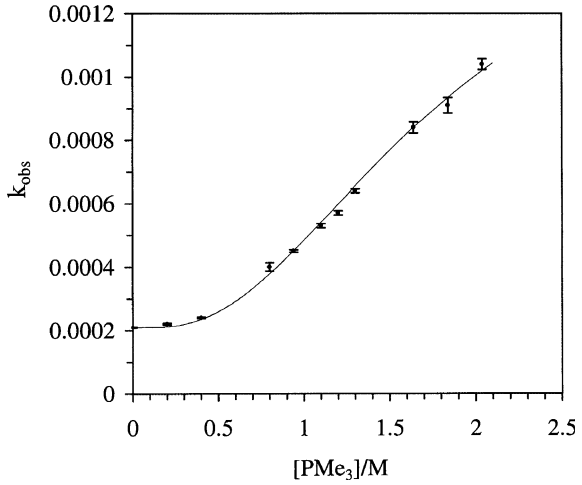

Fig. 8. Fit of the PMe_3 dependence of the observed rate constant, k_{obs}, (Solid line; $k_1 = 0.00021$; $k_4 = 0.04$; $k_{-4} = 0.08$; $k_5 = 0.01$; $k_{-5} = 0.01$; $k_6 = 0.001$; $k_7 = 0.02$; $k_{-7} = 0.002$).

consumption of **1d** and $k_{obs(calc)} = 0.00022(2)\ s^{-1}$ for the formation of **3**; $[PMe_3] = 0.4$ M) is in good agreement with the experimental data ($k_{obs} = 0.00024\ s^{-1}$). In the simulation results (both low and high PMe_3 concentrations), only trace amounts of intermediates are present, which is in accord with the assumptions of the steady-state approximation with k_1 and k_6 being rate limiting steps. The pre-equilibria between **1d**, **B**, **C** and **D** are supported by the noticeable amounts (4–7%) of intermediates **B**, **C** and **D** observed at the early stages of the reaction. However, due to the dynamic properties of these complexes, all of them show up in the ^1H NMR as an averaged peak, which is indistinguishable from the peak of **1d**, causing the intermediates to be "unobservable".

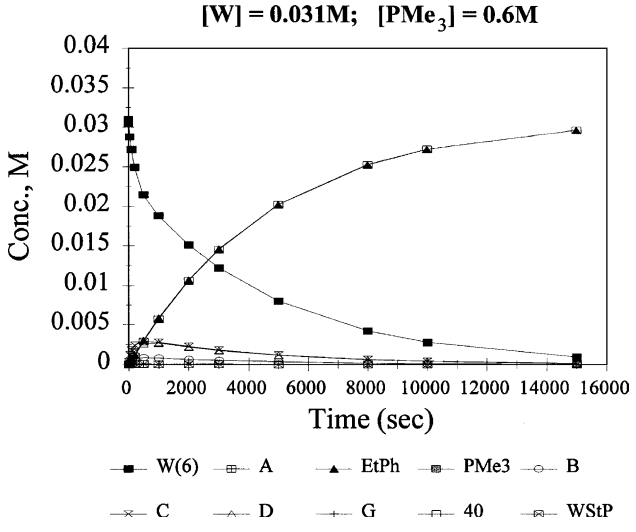

Fig. 9. Simulation of the mechanism proposed for the formation of **3** from **1d**. PMe_3 concentration (~ 0.6M) is out of the scale shown in this plot.

A referee has noted and we agree that this mechanistic simulation is underdetermined. We can only explicitly measure one of the 8 rate constants that are necessary for the simulation and the overall k_{obs} for the phosphine dependent path. Consequently, there is a large uncertainty inherent in the actual values of the rate constants that we calculate and other combinations of rate constants might also lead to reasonable simulations. We are encouraged that the values of the rate constants that we find are consistent with the results of the qualitative arguments given above as well as with the non kinetic mechanistic information.

3. Discussion and conclusion

We have proposed a mechanism for the formation of olefin complexes, **2** and **3**, from stable, coordinatively unsaturated W(VI) dialkyl complexes, **1a** and **1d**, induced by the addition of PMe_3 which accounts for all our observations. An alternative mechanism that involves transfer of the β-H atom to the imido nitrogen followed by α-abstraction of the N-H of the resultant amido group by the remaining ethyl group is also conceivable. While we have no direct evidence that excludes this pathway, we believe that such a mechanism is unlikely because of observations that we have made on the conversion of **1d** to the styrene complex, **3**. The conversion of **1d** to **3** occurs much more slowly ($t_{1/2}$ = 167 min at 333 K) than **1a** is converted to **2** ($t_{1/2}$ = 12 min at 293 K). Furthermore, the data indicates that the conversion of **1d** to **3** proceeds via a different mechanism (KIE = 2.3 at high [PMe_3]) than the conversion of **1a** to **2** (KIE = 6.1).

When complex **1d** binds PMe_3, only the isomer with PMe_3 *cis* to the imido group and the ethyl groups *trans* to one another is observed via low temperature NMR. Apparently, this is responsible for the change in mechanism that occurs when PMe_3 is present because the alkyl groups are no longer *cis* to one another. If transfer of the β-H to the imido is the mechanism that is followed, we would expect that changing the geometry of the PMe_3 adduct in this fashion would not cause such a dramatic change in the reaction rate because the alkyl groups remain *cis* to the imido group regardless of their relationship to one another.

Our observations of a large isotope effect, negative entropy of activation, and no deuterium scrambling are all consistent with the β-H abstraction mechanism proposed for the formation of the ethylene complex, **2**, from **1a** [8a]. We believe that β-H abstraction occurs from the *cis* (minor)isomer of the PMe_3 adduct of **1a** (Eq. (4)). The isotope effect and activation parameters of the transformation of **1d** to the styrene complex in the absence of PMe_3 are also consistent withβ-H abstraction. However, when PMe_3 is added to **1d** only the *trans* isomer of the PMe_3 adduct is observed and reaction of this material follows a different mechanism.

The PMe_3 dependent KIE and non-linear PMe_3 dependence support a change in the mechanism in the transformation of **1d** to **3** with increasing [PMe_3]. The combination of the bimolecular nature of this reaction and the highly-ordered transition state, imposed by the geometric requirements needed for the β-hydrogen transfer account for the large negative entropy value. It is evident that the change in the mechanism of the β-H transfer reaction is brought about by the presence of PMe_3 which effectively catalyzes the isomerization of the starting material. Evidently, β-H elimination is the preferred alkyl decomposition pathway in the TBP isomer and PMe_3 is necessary to induce reductive elimination of ethylbenzene from **D** in Scheme 5 to give the final product.

4. Experimental

4.1. General procedures

All reactions were conducted under dry argon atmosphere using standard Schlenk techniques or in a nitrogen atmosphere dry box. Diethyl ether (Et_2O) was distilled from sodium benzophenone ketyl. Toluene, pentane, and hexane were distilled from sodium. NMR solvents were stored over molecular sieves and degassed prior to use.

^{1}H-NMR spectra were measured at 300 MHz on a Varian Gemini 300 or VXR 300 spectrometer with C_6D_6 or C_7D_8 as solvents. The chemical shifts are reported in parts per million downfield from tetramethylsilane and were measured relative to the residual protons in the deuterated solvents. ^{13}C-NMR spectra were referenced to the central line of the solvents C_6H_6 (δ = 128.0 ppm) and C_7H_8 (δ = 20.4 ppm). The coupling constants (J) are reported in hertz. Elemental analyses (C, H, N) were performed by Atlantic Microlab, Inc., Norcross, GA.

4.2. $W(NPh)[(o\text{-}Me_3SiN)_2C_6H_4](CH_2CH_3)_2$ (**1a**)

$W(NPh)[(o\text{-}Me_3SiN)_2C_6H_4](Cl)_2$ (2.01g, 3.37 mmol) was dissolved in 100 ml of Et_2O and cooled to −78 °C. Two equivalents of EtMgCl (3.37 ml, 6.74 mmol; 2.0 M solution in Et_2O) were then added by a syringe. The reaction was allowed to warm to room temperature and was stirred for 1 h, during which time a brown color appeared and salts precipitated. The solvent was then removed under reduced pressure, and the remaining brown-black oil was dried in vacuo for 3 h. The oil was then extracted with pentane and filtered by filter cannula until filtrate was almost clear. The solvent was then removed under reduced pressure, and the

remaining brown oil was dried in vacuo for 2 h to yield 1.68 g of **1a** as a thick red oil. Yield: 85.3%. ^{1}H NMR: 0.29 (s, 18H, –Si(CH$_3$)$_3$, $^2J_{Si–H}$ = 6.6Hz); 1.86 (t, 6H, –CH$_2$C*H*$_3$); 1.91 (m, 2H, –C*H*$_2$CH$_3$); 2.31 (m, 2H, –C*H*$_2$CH$_3$); 6.86 (t, 1H, *p*-NPh-*H*); 7.04 (m, 2H, aromatic); 7.11 (t, 2H, *m*-NPh-*H*); 7.31 (d, 2H, *o*-NPh-*H*); 7.37 (m, 2H, aromatic). ^{13}C{^{1}H} NMR: 1.5 (–Si(CH$_3$)$_3$, $J_{C–H}$ = 119 Hz); 17.4 (–CH$_2$*C*H$_3$, $J_{C–H}$ = 122 Hz); 58.4 (–*C*H$_2$CH$_3$, $J_{C–H}$ = 120 Hz); 122.3, 123.9, 125.0, 125.6, 128.8, 135.1, 156.2 (aromatic).

4.3. W(NPh)[o-(Me$_3$SiN)$_2$C$_6$H$_4$](CH$_2$CD$_3$)$_2$ (**1a**-d$_6$)

Deuterated analog of **1a** was prepared in the same way as described above. Grignard reagent, CD$_3$CH$_2$MgCl, used for alkylation reaction, was prepared from CD$_3$CH$_2$Cl and Mg^0 metal. ^{1}H NMR: 0.29 (s, 18H, –Si(CH$_3$)$_3$, $^2J_{Si-H}$ = 6.6 Hz); 1.81 (m, 2H, –C*H*$_2$CD$_3$); 2.19 (m, 2H, –C*H*$_2$CD$_3$); 6.85 (t, 1H, *p*-NPh-*H*); 7.03 (m, 2H, aromatic); 7.11 (t, 2H, *m*-NPh-*H*); 7.26 (d, 2H, *o*-NPh-*H*); 7.34 (m, 2H, aromatic).

4.4. W(NPh)[(o-Me$_3$SiN)$_2$C$_6$H$_4$](CH$_2$CH$_2$CH$_3$)$_2$ (**1b**)

W(NPh)[(*o*-Me$_3$SiN)$_2$C$_6$H$_4$](Cl)$_2$ (1.00 g, 1.68 mmol) was dissolved in 100 ml of Et$_2$O and cooled to −78 °C. Two equivalents of *n*-PrMgCl (1.7 ml, 3.4 mmol; 2.0 M solution in Et$_2$O) were then added by a syringe. The reaction was allowed to warm to room temperature and was stirred for 1 h, during which time a brown color appeared and salts precipitated. The solvent was then removed under reduced pressure, and the remaining brown-black oil was dried in vacuo for 3 h. The oil was then extracted with pentane and filtered by filter cannula until filtrate was almost clear. The solvent was then removed under reduced pressure, and the remaining brown oil was dried in vacuo for 2 h. Yield: 78%. ^{1}H NMR: 0.53 (s, 18H, –Si(CH$_3$)$_3$, $^2J_{Si-H}$ = 6.6 Hz); 1.30 (t, 6H, –CH$_2$CH$_2$C*H*$_3$); 1.92 (m, 2H, –CH$_2$C*H*$_2$CH$_3$); 2.06 (d of t, 2H, –C*H*$_2$CH$_2$CH$_3$); 2.16 (m, 2H, –CH$_2$C*H*$_2$CH$_3$); 2.33 (d of t, 2H, –C*H*$_2$CH$_2$CH$_3$); 7.09 (t, 1H, *p*-NPh-*H*); 7.27 (m, 2H, aromatic); 7.34 (t, 2H, *m*-NPh-*H*); 7.53 (d, 2H, *o*-NPh-*H*); 7.57 (m, 2H, aromatic). ^{13}C{^{1}H} NMR: 1.49 (–Si(CH$_3$)$_3$, $J_{C–H}$ = 119.3 Hz); 21.79 (–CH$_2$CH$_2$*C*H$_3$, $J_{C–H}$ = 121.4 Hz); 26.70 (–CH$_2$*C*H$_2$CH$_3$, $J_{C–H}$ = 132.2 Hz); 69.29 (–*C*H$_2$CH$_2$CH$_3$, $J_{C–H}$ = 113.1 Hz); 122.36, 124.08, 125.04, 125.77, 128.64, 134.48, 156.42 (aromatic).

4.5. W(NPh)[(o-Me$_3$SiN)$_2$C$_6$H$_4$](CH$_2$CH(CH$_3$)$_2$)$_2$ (**1c**)

W(NPh)[(*o*-Me$_3$SiN)$_2$C$_6$H$_4$](Cl)$_2$ (1.2 g, 2.01 mmol) was dissolved in 100 ml of Et$_2$O and cooled to −78 °C. Two equivalents of *i*-BuMgCl (2.01 ml, 4.02 mmol; 2.0 M solution in Et$_2$O) were then added by a syringe. The reaction was allowed to warm to room temperature and was stirred for 1 h, during which time a brown color appeared and salts precipitated. The solvent was then removed under reduced pressure, and the remaining brown-black oil was dried in vacuo for 3 h. The oil was then extracted with pentane and filtered by filter cannula until filtrate was almost clear. The solution was concentrated to about 10 ml and cooled to −78 °C for 3 h. The resulting golden-brown solid was isolated by filtration and was dried under reduced pressure for 1 h to yield 0.78 g of **1c** as a brown crystalline solid. Yield: 63.7%. ^{1}H NMR: 0.33 (s, 18H, –Si(CH$_3$)$_3$); 0.93 (d, 6H, –CH$_2$CH(*CH*$_3$)$_2$); 1.10 (d, 6H, –CH$_2$CH(*CH*$_3$)$_2$); 1.72 (m, 2H, –C*H*$_2$CH(CH$_3$)$_2$); 1.94 (m, 2H, –C*H*$_2$CH(CH$_3$)$_2$); 2.55 (m, 2H, –CH$_2$C*H*(CH$_3$)$_2$); 6.84 (t, 1H, *p*-NPh-*H*); 7.01 (m, 2H, aromatic); 7.12 (t, 2H, *m*-NPh-*H*); 7.31 (d, 2H, *o*-NPh-*H*); 7.36 (m, 2H, aromatic). ^{13}C{^{1}H} NMR: 2.20 (–Si(CH$_3$)$_3$, $J_{C–H}$ = 119.3 Hz); 27.33 (–CH$_2$CH(*CH*$_3$)$_2$, $J_{C–H}$ = 125.8 Hz); 29.15 (–CH$_2$CH(*CH*$_3$)$_2$, $J_{C–H}$ = 126.5 Hz); 33.73 (–CH$_2$*C*H-(CH$_3$)$_2$, $J_{C–H}$ = 127.2 Hz); 80.01 (–*C*H$_2$CH(CH$_3$)$_2$); 121.79, 123.60, 125.46, 126.65, 128.62, 133.12, 155.97 (aromatic). *Anal.* Calc. for C$_{26}$H$_{45}$N$_3$Si$_2$W: C, 48.82; H, 7.09; N, 6.57. Found: C, 48.54; H, 7.11; N, 6.50%.

4.6. W(NPh)[(o-Me$_3$SiN)$_2$C$_6$H$_4$](CH$_2$CH$_2$Ph)$_2$ (**1d**)

W(NPh)[(*o*-Me$_3$SiN)$_2$C$_6$H$_4$](Cl)$_2$ (2 g, 3.36 mmol) was dissolved in 150 ml of Et$_2$O and cooled to −78 °C. Two equivalents of PhCH$_2$CH$_2$MgCl (3.4 ml, 3.4 mmol; 2.0 M solution in Et$_2$O) were then added via syringe. The reaction was allowed to warm to room temperature and was stirred for 2 h, during which time a brown color appeared and salts precipitated. The solvent was then removed under reduced pressure, and the remaining brown-orange solid was dried in vacuo for 3 h. The solid was then extracted with pentane and filtered by filter cannula until filtrate was almost clear. The solution was concentrated to about 10 ml and cooled to −78 °C for 3 h. The resulting orange solid was isolated by filtration and were dried under reduced pressure for 1 h to yield 1.68 g of **1d** as a orange crystalline solid. Yield: 68.2%. ^{1}H NMR: 0.30 (s, 18H, –Si(CH$_3$)$_3$); 2.09 (d of t, 2H, –C*H*$_2$CH$_2$Ph); 2.38 (d of t, 2H, –C*H*$_2$CH$_2$Ph); 2.91 (d of t, 2H, –CH$_2$C*H*$_2$Ph); 3.14 (d of t, 2H, –CH$_2$C*H*$_2$Ph); 6.86 (t, 1H, *p*-NPh-*H*); 6.99 (m, 5H, aromatic); 7.02 (m, 2H, aromatic); 7.08 (t, 2H, *m*-NPh-*H*); 7.15 (m, 5H, aromatic); 7.22 (d, 2H, *o*-NPh-*H*); 7.39 (m, 2H, aromatic). ^{13}C{^{1}H} NMR: 1.48 (–Si(CH$_3$)$_3$, $J_{C–H}$ = 118.3 Hz); 39.65 (–CH$_2$*C*H$_2$Ph, $J_{C–H}$ = 123.4 Hz); 65.61 (–*C*H$_2$CH$_2$Ph, $J_{C–H}$ = 119.2 Hz, $J_{W–C}$ = 77.2 Hz); 122.83, 125.01, 125.20, 125.43, 125.58, 128.14, 128.48, 128.62, 132.95, 149.20, 156.22 (aromatic). *Anal.* Calc. for

$C_{34}H_{45}N_3Si_2W$: C, 55.50; H, 6.17; N, 5.71. Found: C, 55.23; H, 6.09; N, 5.75%.

4.7. $W(NPh)[o\text{-}(Me_3SiN)_2C_6H_4](CH_2CD_2Ph)_2$ (**1d-d_4**)

Deuterated analog of **1d** was prepared in the same way as described above using Grignard reagent, $PhCD_2CH_2MgBr$, prepared from $PhCD_2CH_2Br$ and Mg^0. $PhCD_2CH_2Br$ was synthesized from $PhCD_2CH_2OH$ and PPh_3Br_2 in CH_2Cl_2. 2-Phenylethanol-2,2-d_2, $PhCD_2CH_2OH$, was prepared following the literature preparation methods [39]. NMR analysis showed 98% deuteration at the benzylic position. ^{1}H NMR: 0.25 (s, 18H, –Si(CH_3)$_3$); 2.08 (d, 2H, –CH_2CD$_2$Ph, $^2J_{H-H}$ = 12.6Hz); 2.38 (d, 2H, –CH_2CD$_2$Ph, $^2J_{H-H}$ = 12.9Hz); 6.78–7.42 (19H, aromatic). ^{13}C{^{1}H}NMR: 1.45 (s, –Si(CH_3)$_3$, J_{C-H} = 120.7 Hz); 38.93 (–CH_2CD_2Ph); 65.57 (–CH_2CD$_2$Ph, J_{C-H} = 122.3 Hz, J_{W-C} = 76.3 Hz); 122.86, 124.94, 125.22, 125.49, 125.64, 125.94, 128.54, 128.67, 133.04, 149.22, 156.30 (aromatic).

4.8. $W(NPh)[(o\text{-}Me_3SiN)_2C_6H_4](\eta^2\text{-}C_2H_4)(PMe_3)_2$ (**2**)

In a glass tube with a Teflon Young's joint, W(NPh)[(*o*-$Me_3SiN)_2C_6H_4$](CH_2CH_3)$_2$ (**1a**) (1.35 g, 2.32 mmol) was dissolved in 30 mL of pentane. Five equivalents of PMe_3 (1.19 ml, 11.56 mmol) were added via syringe, then the flask was sealed. The reaction was stirred at room temperature for 4 h, during which time the brown solution turned purple and purple crystals precipitated. The mixture was transferred to a Schlenk tube and purple crystals were isolated. The mother liquors were reduced in volume under reduced pressure and cooled to −78 °C to yield more solid. Total yield: 1.44 g, 88.3%. ^{1}H NMR: 0.31 (s, 9H, –Si(CH_3)$_3$); 0.60 (s, 9H, –Si′(CH_3)$_3$); 1.03 (s, 18H, –PMe_3); 1.91 (m, C_2H_4); 2.09 (m, C_2H_4); 6.61–7.42 (aromatic). ^{13}C{^{1}H} NMR: 2.67 (–Si(CH_3)$_3$); 6.34 (–Si′(CH_3)$_3$); 15.78 (s, –PMe_3); 38.13 (s, C_2H_4, J_{C-H} = 156.2Hz); 122.23, 123.13, 124.28, 125.51, 127.23, 128.91, 129.23, 129.78, 158.23 (aromatic); *Anal*. Calc. for $C_{26}H_{49}N_3Si_2P_2W$: C, 44.25; H, 7.00; N, 5.95. Found: C, 43.91; H, 6.79; N, 5.78%.

4.9. $W(NPh)[(o\text{-}Me_3SiN)_2C_6H_4](\eta^2\text{-}CH_2{=}CHCH_3)(PMe_3)_2$

W(NPh)[(*o*-$Me_3SiN)_2C_6H_4$](η^2-CH_2=$CHCH_3$)-(PMe_3)$_2$ can be observed in the reaction of **1b** with PMe_3. ^{1}H NMR: 0.44 (br, s, 18H, –Si(CH_3)$_3$); 1.02 (s, 18H, –PMe_3); 1.62 (d of d, 1H, –CH_2CHCH$_3$); 2.39 (d of d, 1H, –CH_2CHCH$_3$); 2.55 (d, 3H, –CH_2CHCH_3); 2.85 (m, 1H, –CH_2CHCH$_3$); 6.42–7.58 (aromatic).

4.10. $W(NPh)[(o\text{-}Me_3SiN)_2C_6H_4](\eta^2\text{-}CH_2{=}CHPh)(PMe_3)_2$ (**3**)

In a glass tube with a Rotoflo joint, W(NPh)[(*o*-$Me_3SiN)_2C_6H_4$](CH_2CH_2Ph)$_2$ (**1d**) (0.8 g, 1.09 mmol) was dissolved in 50 mL of pentane. Five equivalents of PMe_3 (0.56 ml, 5.45 mmol) were added by a syringe, then the flask was sealed. The reaction was heated to 80 °C and was stirred for 8 h, during which time the solution changed color from brown to purple. The solvent was then removed under reduced pressure and the remaining brown-purple oil was dried overnight. The oil was then redissolved in minimum amount of pentane and cooled to −78 °C for 2 h. The resulting brown-purple solid was isolated by filtration and was dried under reduced pressure for 1 h to give 0.48 g of **3**. Yield: 56.3%. ^{1}H NMR: 0.41 (s, 18H, –Si(CH_3)$_3$); 0.86 (s, 18H, –PMe_3); 2.62 (m, –CH_2CHPh); 2.80 (m, –CH_2CHPh); 3.87 (t, –CH_2CHPh); 6.41–7.24 (aromatic). *Anal*. Calc. for $C_{32}H_{53}N_3Si_2P_2W$: C, 49.16; H, 6.83; N, 5.38. Found: C, 48.80; H, 6.71; N, 5.22%.

4.11. Kinetics study

Samples were prepared by dissolving **1d** and **1d**-d_4 (ca. 10mg) in 0.44 ml of toluene-d_8 solution. The concentration of **1a** samples was obtained from a known concentration of (η^5-C_5H_5)$_2$Fe as internal standard. The samples were sealed and stored at −196 °C immediately after adding desired amount of PMe_3. The NMR probe was equilibrated to the desired temperature and the sample was thawed and well shaken prior to loading into the probe. Approximately 18 spectra were recorded at increasing intervals (more points for early stages of the reaction) over a duration of more than 3 half-lives. Absolute peak intensities of the trimethylsilyl peaks of both starting material and product were recorded for each spectrum. The observed rate constants were obtained from the slope of the plots of ln(Intensity) vs. time. Three samples were performed at each temperature and the rate constants reported were the average of all three runs. Activation parameters were obtained by measuring rate constants at four different temperatures. A plot of ln(k/T) vs. 1/T (T, temperature in Kelvin) results in a line with a slope of $-\Delta E^{\ddagger}/R$ and an intercept of [($\Delta S^{\ddagger}/R$) + 23.76]. Reported errors in the rate constants represent the standard deviation from the least squares fit of the experimental data. Reported errors in the activation parameters are obtained from all experimental data (12 points in the Eyring plot), using 2σ.

4.12. Phosphine dependence

Samples were prepared and experiments were carried out as described above. To determine the dependence of the PMe_3 concentration on the observed rate constants,

a series of experiments were carried out with **1a** and **1d** with various concentrations of PMe_3. Plotting the observed rate constants obtained from these experiments vs. the concentration of added PMe_3 gave a line in the case of **1a** and **1d** (at high concentration). The order in PMe_3 (**1a**) was determined from the slope (1.096) of the plot of ln*k* vs. ln[PMe_3].

4.13. Input for KINFIT simulation of the formation of 3

```
1110
1,W = A + EtPh,0.00021
2,W = C,0.002
3,C = W,0.02
4,B = C + PMe3,0.08
5,C + PMe3 = B,0.04
6,C = D,0.01
7,D = C,0.01
8,D + PMe3 = EtPh + F,0.001
9,F + PMe3 = 40,0.05
10,A + PMe3 = F,0.01
11,F + PMe3 = 40,0.05
END
W,0.031
PMe3,0.6
END
1.0E-30,1.0E-33,1500,0.00345
10,50,100,200,500,1000,
2000,3000,5000,8000,10000,15000
```

4.14. X-ray experimental

Data for compound **1c** and **1d** were collected at 173 K on a Siemens SMART PLATFORM equipped with a CCD area detector and a graphite monochromator utilizing Mo Kα radiation (λ = 0.71073 Å). Cell parameters were refined using up to 8192 and 9856 reflections for **1c** and **1d**, respectively. A hemisphere of data (1381 frames) was collected using the w-scan method (0.3° frame width). The first 50 frames were remeasured at the end of data collection to monitor instrument and crystal stability (maximum correction on *I* was <1%). ψ scan absorption corrections were applied based on the entire data set.

Both structures were solved by the Direct Methods in SHELXTL5 [43], and refined using full-matrix least squares. The non-H atoms were treated anisotropically, whereas the hydrogen atoms were calculated in ideal positions and were riding on their respective carbon atoms. 470 parameters were refined (**1c**) in the final cycle of refinement using 6252 reflections with $I > 2\sigma(I)$ to yield R_1 and wR_2 of 1.65% and 3.94%, respectively. 362 parameters were refined (**1d**) in the final cycle of refinement using 5292 reflections with $I > 2\sigma(I)$ to yield R_1 and wR_2 of 3.40% and 7.29%, respectively. Refinement was done using F^2.

Acknowledgements

We acknowledge the National Science Foundation CHE-9523279 for the support of this work. K.A.A. wishes to acknowledge the National Science Foundation for funding of the purchase of the X-ray equipment.

References

[1] M.L.H. Green, P.L.I. Nagy, J. Organomet. Chem. 1 (1963) 58.
[2] (a) G.W. Parshall, Homogeneous Catalysis, Wiley, New York, 1980;
(b) R.J. CrossThe Chemistry of Metal–Carbon Bond, vol. 2, Wiley, New York, 1985;
(c) J.K. Kochi, Organometallic Mechanism and Catalysis, Academic Press, New York, 1978.
[3] (a) I.P. Rothwell, Polyhedron 4 (1985) 177;
(b) M.L.H. Green, D. O'Hare, Pure Appl. Chem. 57 (1985) 1897.
[4] (a) C. McDade, J.C. Green, J.E. Bercaw, Organometallics 1 (1982) 1629;
(b) A.R. Bulls, W.P. Schaefer, M. Serfas, J.E. Bercaw, Organometallics 6 (1987) 1219;
(c) B.H. Chang, H.S. Tung, C.H. Brubaker Jr., Inorg. Chim. Acta 51 (1981) 143.
[5] (a) S. Komiya, Y. Morimoto, A. Yamamoto, T. Yamamoto, Organometallics 1 (1982) 1528;
(b) G.M. Whitesides, J.F. Gaarch, E.R. Stedronsky, J. Am. Chem. Soc. 101 (1979) 3659;
(c) C.P. Boekel, J.H. Teuben, H.J. De Liefde Meijer, J. Organomet. Chem. 120 (1976) 257;
(d) G. Erker, K. Kropp, J. Am. Chem. Soc. 101 (1979) 3659.
[6] (a) J.M. Bruno, G.M. Smith, T.J. Marks, C.K. Fair, A.J. Schultz, J.M. Williams, J. Am. Chem. Soc. 108 (1986) 40;
(b) S.J. Simpson, H.W. Turner, R.A. Anderson, Inorg. Chem. 20 (1981) 2991.
[7] L.R. Chamberlain, A.P. Rothwell, I.P. Rothwell, J. Am. Chem. Soc. 106 (1984) 1847.
[8] (a) S-Y.S. Wang, K.A. Abboud, J.M. Boncella, J. Am. Chem. Soc. 119 (1997) 11990;
(b) S.-Y.S. Wang, D.D. VanderLende, K.A. Abboud, J.M. Boncella, Organometallics 17 (1998) 2628.
[9] S.L. Buchwald, R.B. Nielsen, J. Am. Chem. Soc. 110 (1988) 3171.
[10] (a) J.S. Freundlich, R.R. Schrock, W.M. Davis, J. Am. Chem. Soc. 118 (1996) 3643;
(b) M.D Fryzuk, S.A. Johnson, S.J. Rettig, J. Am. Chem. Soc. 123 (2001) 1602.
[11] (a) Z. Dawoodi, M.L.H. Green, V.S.B. Mtetwa, K. Prout, J. Chem. Soc., Chem. Commun. (1982) 802;
(b) Z. Dawoodi, M.L.H. Green, V.S.B. Mtetwa, K. Prout, A.J. Schultz, M. Williams, T.F. Koetzle, J. Chem. Soc., Dalton Trans. (1986) 1629.
[12] J.D. Fellmann, R.R. Schrock, D.D. Trificante, Organometallics 1 (1982) 481.
[13] M.E. Thompson, S.M. Baxter, A.R. Bulls, B.J. Burger, M.C. Nolan, B.D. Santarsiero, W.P. Shafer, J.E. Bercaw, J. Am. Chem. Soc. 109 (1987) 203.
[14] H. Kwart, Acc. Chem. Res. 15 (1982) 401.
[15] F. Ozawa, T. Ito, A. Yamamoto, J. Am. Chem. Soc. 102 (1980) 6457.
[16] T. Ikariya, A. Yamamoto, J. Organomet. Chem. 120 (1976) 257.

[17] (a) G.M. Whitesides, Pure Appl. Chem. 53 (1981) 287;
(b) T.J. McCarthy, R.G. Nuzzo, G.M. Whitesides, J. Am. Chem. Soc. 103 (1981) 1676;
(c) T.J. McCarthy, R.G. Nuzzo, G.M. Whitesides, J. Am. Chem. Soc. 103 (1981) 3396;
(d) T.J. McCarthy, R.G. Nuzzo, G.M. Whitesides, J. Am. Chem. Soc. 103 (1981) 3404.
[18] B.J. Burger, M.E. Thompson, W.D. Cotter, J.E. Bercaw, J. Am. Chem. Soc. 112 (1990) 1566.
[19] J. Evans, J. Schwarts, P.W. Urguhart, J. Organomet. Chem. 81 (1974) C37.
[20] (a) K.-T. Smith, M. Tilset, S.S. Kristjansdottir, J.R. Norton, Inorg. Chem. 34 (1995) 6497;
(b) A. Sorokin, A. Robert, B. Meunier, B.J. Am. Chem. Soc. 115 (1993) 7293;
(c) H. Kwart, S.F. Sarnar, J. Slutsky, J. Am. Chem. Soc. 95 (1973) 5242.
[21] (a) J.M. Boncella, S.-Y.S. Wang, D.D. VanderLende, R.L. Huff, K.A. Abboud, W.M. Vaughan, J. Organomet. Chem. 530 (1997) 59;
(b) D.D. VanderLende, K.A. Abboud, J.M. Boncella, Organometallics 13 (1994) 3378.
[22] (a) W.A. Nugent, J.M. Mayer, Metal-Ligand Multiple Bonds, Wiley, New York, 1988;
(b) D.E. Wigley, Prog. Inorg. Chem. 42 (1994) 239.
[23] M.F. Lappert, P.P. Power, A.R. Sanger, R.C. Srivastava, Metal and Metalloid Amides, Wiley, New York, 1980, pp 244–249.
[24] (a) T.A. Albright, J.K. Burdett, M.H. Whangbo, Orbital Interactions in Chemistry, Wiley, New York, 1985;
(b) D. Del Rio, A. Galindo, J. Organomet. Chem. 655 (2002) 16;
(c) A. Galindo, M. Gomez, D. Del Rio, F. Sanchez, Eur. J. Inorg. Chem 16 (2002) 1326;
(d) A. Galindo, A. Ienco, C. Mealli, New J. Chem. 24 (2000) 73;
(e) A. Galindo, A. Ienco, C. Mealli, Comment Inorg. Chem. 23 (2002) 401.
[25] S.L. Buchwald, K.A. Kreutzer, R.A. Fisher, J. Am. Chem. Soc. 112 (1990) 4600.
[26] G.R. Clark, A.J. Nielson, C.E.F. Richard, D.C. Ware, J. Chem. Soc., Dalton Trans. (1990) 1173.
[27] (a) T.M. Cameron, C.G. Ortiz, I. Ghiviriga, K.A. Abboud, J.M. Boncella, Organometallics 20 (2001) 2032;
(b) R.C. Mills, K.A. Abboud, J.M. Boncella, Organometallics 19 (2000) 2953.
[28] G.M. Whitesides, J.F. Gaasch, E.R. Stedronsky, J. Am. Chem. Soc. 94 (1972) 5258.
[29] D.L. Reger, E.C. Culberston, J. Am. Chem. Soc. 98 (1976) 2789.
[30] R.G. Wilkins, Kinetics and Mechanism of Reactions of Transition Metal Complexes, 2nd ed., VCH, New York, NY, 1991.
[31] (a) C.D. Wood, S.J. McLain, R.R. Schrock, J. Am. Chem. Soc. 101 (1979) 3210;
(b) P. Legzdens, J.E. Veltheer, M.A. Young, R.J. Batchelor, F.W.B. Einstein, Organometallics 14 (1995) 407;
(c) W.M. Vaughan, K.A. Abboud, J.M. Boncella, J. Am. Chem. Soc. 117 (1995) 11015.
[32] (a) N.M. Doherty, J.E. Bercaw, J. Am. Chem. Soc. 107 (1985) 2670;
(b) B.J. Burger, B.D. Santarsiero, M.S. Trimmer, J.E. Bercaw, J. Am. Chem. Soc. 110 (1988) 3134;
(c) Burger, M.E. Thompson, W.D. Cotter, J.E. Bercaw, J. Am. Chem. Soc. 112 (1990) 1566;
(d) J. Halpern, T. Okamoto, Inorg. Chim. Acta 89 (1984) L53.
[33] S.L. Buchwald, R.T. Lum, J.C. Dewan, J. Am. Chem. Soc. 108 (1986) 7441.
[34] (a) G. Erker, J. Organomet. Chem. 134 (1977) 189;
(b) G. Erker, K. Kropp, Organometallics 1 (1982) 1246.
[35] P.J. Fagan, J.M. Marinquez, E.A. Maatta, A.M. Seyam, T.J. Marks, J. Am. Chem. Soc. 103 (1981) 6650.
[36] S.J. McLain, R.R. Schrock, P.R. Sharp, M.R. Churchill, W.J. Youngs, J. Am. Chem. Soc. 101 (1979) 263.
[37] L.E. Schock, C.P. Brock, T.J. Marks, Organometallics 6 (1987) 232.
[38] G.A. Luinstra, J.H. Teuben, Organometallics 11 (1992) 1793.
[39] (a) M.J. Raftery, J.H. Bowie, J.C. Sheldon, J. Chem. Soc., Perkin Trans. II (1988) 563;
(b) M. Orfanopoulos, I. Smonou, C.S. Foote, J. Am. Chem. Soc. 112 (1990) 3607.
[40] J.P. Collman, L.S. Hegedus, J.R. Norton, R.G. Finke, Principles and Applications of Organotransition Metal Chemistry, University Science Books, Mill Valley, CA, 1987.
[41] (a) G. Wilkinson, F.G.A. Stone (Eds.), Comprehensive Organometallic Chemistry, vol. 3, Pergamon Press, Oxford, 1982;
(b) G. Wilkinson, F.G.A. Stone (Eds.), Comprehensive Organometallic Chemistry, vol. 5, Pergamon Press, Oxford, 1995.
[42] P.G. Jessop, R.H. Morris, Coord. Chem. Rev. 121 (1992) 155.
[43] G.M. Sheldrick, SHELXTL5, Nicolet XRD Corporation, Madison, WI, 1995.

Available online at www.sciencedirect.com
SCIENCE DIRECT®
Polyhedron 23 (2004) 2751–2768
POLYHEDRON
www.elsevier.com/locate/poly

Complexes obtained by electrophilic attack on a dinitrogen-derived terminal molybdenum nitride: electronic structure analysis by solid state CP/MAS ^{15}N NMR in combination with DFT calculations

Emma L. Sceats [a], Joshua S. Figueroa [a], Christopher C. Cummins [a,*], Nikolaus M. Loening [a,b], Patrick Van der Wel [a,b], Robert G. Griffin [a,b]

[a] *Department of Chemistry, Massachusetts Institute of Technology, 77 Massachusetts Ave., Cambridge, MA 02139, USA*
[b] *Francis Bitter Magnet Laboratory, Massachusetts Institute of Technology, 77 Massachusetts Ave., Cambridge, MA 02139, USA*

Received 25 April 2004; accepted 25 August 2004
Available online 28 October 2004

Abstract

^{15}N Solid state CP/MAS NMR spectroscopy has been used to study a dinitrogen-derived terminal nitride of molybdenum, $^{15}NMo(N[^tBu]Ar)_3$ (Ar = 3,5-$(CH_3)_2C_6H_3$). A number of Lewis acid adducts, including X_3E–$NMo(N[^tBu]Ar)_3$ (X = F, E = B; X = Cl, E = B, Al, Ga, In; X = Br, E = Al; X = I, E = Al) and Cl_2E–$NMo(N[^tBu]Ar)_3$ (E = Ge, Sn), were prepared by the combination of $^{15}NMo(N[^tBu]Ar)_3$ with 1 equiv. of Lewis acid. A series of cationic imido complexes, $[RNMo(N[^tBu]Ar)_3]X$ was prepared by the reaction of electrophiles, RX [R = CH_3, X = I; R = PhC(O) or Me_3Si, X = OTf (OTf = SO_3CF_3)], with $NMo(N[^tBu]Ar)_3$. Deprotonation of $[CH_3NMo(N[^tBu]Ar)_3]I$ by $LiN(SiMe_3)_2$ afforded the ketimide complex $H_2CNMo(N[^tBu]Ar)_3$, which has been shown to undergo a reaction with neat CH_3I to form $[CH_3CH_2NMo(N[^tBu]Ar)_3]I$. ^{15}N solid state CP/MAS NMR spectroscopy was employed in the characterization of each complex. Complementary density functional theory (DFT) studies of $^{15}NMo(N[^t$-$Bu]Ar)_3$ and derivatives enabled a detailed examination of the experimental solid state NMR parameters in terms of electronic structure at the labeled N-atom. Computational analysis demonstrated that significant paramagnetic contributions to the perpendicular components of the chemical shielding tensor (δ_{11} and δ_{22}) were responsible for the huge span of the tensor measured for $^{15}NMo(N[^t$-$Bu]Ar)_3$ (Ω = 1187 ppm). Perturbation of the electronic structure in $^{15}NMo(N[^tBu]Ar)_3$ upon coordination of a Lewis acid or formation of a cationic imido complex was attributed to stabilization of a σ-symmetric orbital. An upfield shift in the perpendicular components of the chemical shift tensor results from the reduced paramagnetic contribution to these tensor components upon increasing the energy gap between the magnetically coupled occupied and virtual orbitals ($e_{occ} - e_{vir}$).
© 2004 Elsevier Ltd. All rights reserved.

Keywords: ^{15}N solid state NMR; DFT calculations; Molybdenum nitride; Imido complexes; Lewis acids

1. Introduction

The use of isotopic labeling of compounds with ^{15}N to probe their structure and bonding by means of solid state NMR spectroscopy is most commonly seen in biological systems and organic molecules [1–9]. In contrast, solid state NMR spectroscopy of spin-active nuclei in transition metal complexes has been underutilized [10–16]. The isotropic chemical shift value determined in solution NMR measurements is the most reported spectroscopic parameter, but a wealth of additional information may be gained through the acquisition of solid state NMR spectra [17,18]. The use of ^{31}P solid state NMR

* Corresponding author. Tel.: +6174522517; fax: +6172585700.
E-mail address: ccummins@mit.edu (C.C. Cummins).

0277-5387/$ - see front matter © 2004 Elsevier Ltd. All rights reserved.
doi:10.1016/j.poly.2004.08.010

spectroscopy to probe the structure and bonding in a terminal molybdenum phosphide, $PMo(N[^tBu]Ar)_3$ (Ar = 3,5-$(CH_3)_2C_6H_3$) was reported previously [19]. The significant anisotropy of the ^{31}P chemical shift tensor and the enormous paramagnetic deshielding of the ^{31}P nucleus when the applied field is oriented perpendicular to the Mo–P triple bond were explained in terms of the magnetic coupling of filled and vacant molecular orbitals.

Herein, we extend our study of structure and bonding through the use of solid state NMR spectroscopy to the analogous terminal nitride of molybdenum, $NMo(N[^tBu]Ar)_3$ (**1**) [20]. The splitting of dinitrogen by a three-coordinate molybdenum(III) complex $Mo(N[^tBu]Ar)_3$ was first reported in 1995 [21]. The ^{15}N-labeled form of **1**, $^{15}NMo(N[^tBu]Ar)_3$ is readily prepared through the use of ^{15}N-isotopically-enriched dinitrogen gas, thereby making this complex amenable to study by ^{15}N NMR spectroscopy [22]. The potential of **1** to serve as a platform in N-atom transfer chemistry is currently under investigation in our laboratories. It is of interest to determine what insight solid state NMR spectroscopy can provide into the electronic structure for a molybdenum complex which is activated toward productive removal of the dinitrogen-derived N-atom into an organic product. The synthesis of several derivatives of **1** and subsequent measurement of their ^{15}N solid state CP/MAS NMR spectra are described.

Complementary density functional theory analyses of **1** and its derivatives were completed utilizing a simplified ligand framework (NH_2 ligands replacing $N[^tBu]Ar$). DFT permits a detailed analysis of experimental solid state NMR parameters (δ_{11}, δ_{22} and δ_{33}) via calculation of the absolute shielding tensors [23–27] together with correlation to calculated molecular orbitals. The validity of our analyses of electronic structure may be assessed by comparison of the experimental tensor values with those determined computationally.

2. Experimental

2.1. General information

Unless stated otherwise, all operations were performed in a vacuum atmospheres drybox under an atmosphere of purified dinitrogen. Diethyl ether, *n*-pentane and dichloromethane were dried and deoxygenated using the method of Grubbs and coworkers [28]. THF was distilled from purple Na/benzophenone ketyl and collected under dinitrogen. C_6D_6 and $CDCl_3$ were degassed and dried over 4 Å molecular sieves. $^{15}N_2$ was purchased from Cambridge Isotope Laboratories (CIL) in 0.1 mL break-seal glass vessels. CH_3I was, freeze–pump–thaw degassed and stored over 4 Å sieves prior to use. $Mo(N[^tBu]Ar)_3$ [20] and benzoyl triflate [29] were prepared according to the literature procedures. Other chemicals were purified and dried by standard procedures [30] or were used as received. Celite, alumina and 4 Å molecular sieves were dried in vacuo for 36 h at ~250 °C. Infrared spectra were recorded on a Bio-Rad 135 Series FT-IR spectrometer.

2.2. X-ray crystal structure determinations

The X-ray data collections were carried out on a Siemens Platform three-circle diffractometer mounted with a CCD or APEX CCD detector and outfitted with a low-temperature, nitrogen-stream aperture. The structures were solved by direct methods, with the exception of **1**-BF_3, which was solved using the Patterson Method, in conjunction with standard difference Fourier techniques and refined by full-matrix least-squares procedures. A summary of crystallographic data is given in Table 1, with full details found in the Supporting Information. The systematic absences in the diffraction data were uniquely consistent with the assigned space groups of $P2_1$ for **3** and $P2_13$ for both [**2b**]OTf and [**2d**]**I** (Flack parameters are 0.01(4), −0.01(4)and 0.00(3), respectively). No symmetry higher than triclinic was indicated in the diffraction data for **1**-BF_3. These choices led to chemically sensible and computationally stable refinements. All hydrogen atoms were placed in calculated positions, with the exception of the ketimide protons of **3**, which were located in the electron density map and refined isotropically. The Mo1–N2–C21 unit of [**2d**]**I** was found to be coincident with a three-fold axis of the $P2_13$ space group, thus imposing three-site positional disorder in the corresponding methyl group (C22). This disorder was modeled and no hydrogen atoms were generated for methylene carbon C21. Complex [**2c**]OTf crystallized in the centrosymmetric space group $P2_1/n$ with two-site positional disorder found for the triflate counter ion. This disorder was modeled to 70:30 occupancy over the two sites as indicated by the refinement statistics and resulted in chemically sensible geometries. Isomorphous **1**-$GeCl_2$ and **1**-$SnCl_2$ were found to crystallize in the centrosymmetric space group $P2_1/c$ and both contained two-site positional disorder of the aryl-ring and ECl_2 residues. Both possible chiral, three-blade propeller orientations of the aryl rings were present and were modeled each with 50% occupancy as indicated by the refinement statistics. Additionally, each aryl-ring orientation corresponded to distinct ECl_2 orientation and was similarly modeled. Only one orientation of **1**-$GeCl_2$ and **1**-$SnCl_2$ is presented in the text. No hydrogen atoms were generated for the aryl rings of **1**-$GeCl_2$ and **1**-$SnCl_2$ due to the disorder. All software for diffraction data processing and crystal-structure solution and refinement are contained in the SHELXTL (v6.14) program suite (G. Sheldrick, Bruker XRD, Madison, WI).

Table 1
Crystallographic data

Compound	**1**-BF_3	**1**-$GeCl_2$	**1**-$SnCl_2$	[**2b**]OTf	[**2c**]OTf	[**2d**]I	3
Crystal data							
Empirical formula	$C_{37}H_{56}N_4MoBCl_2F_3$	$C_{36}H_{54}N_4MoGeCl_2$	$C_{36}H_{54}N_4MoSnCl_2$	$C_{40}H_{63}N_4MoF_3SO_3Si$	$C_{48}H_{67}F_3N_4MoO_5S$	$C_{39}H_{57}N_4MoCl_2I$	$C_{37}H_{56}N_4Mo$
Formula weight	791.51	781.54	828.36	861.03	965.06	875.63	652.80
T (K)	193(2)	193(2)	193(2)	193(2)	193(2)	193(2)	193(2)
Crystal system	triclinic	monoclinic	monoclinic	cubic	monoclinic	cubic	monoclinic
Space group	$P\bar{1}$	$P2_1/c$	$P2_1/c$	$P2_13$	$P2_1/n$	$P2_13$	$P2_1$
Unit cell dimensions							
a (Å)	10.5757(6)	14.803(3)	14.803(3)	16.5578(5)	12.3168(8)	16.3118(6)	11.2145(10)
b (Å)	12.1291(7)	13.711(3)	13.711(3)	16.5578(5)	26.7028(17)	16.3118(6)	11.0462(10)
c (Å)	16.6647(10)	19.132(4)	19.132(4)	16.5578(5)	14.7598(10)	16.3118(6)	14.7723(13)
α (°)	93.3220(10)	90	90	90	90	90	90
β (°)	107.3170(10)	90.12(3)	90.12(3)	90	90.4400(10)	90	94.367(2)
γ (°)	94.7260(10)	90	90	90	90	90	90
Unit cell volume (Å^3)	2026.2(2)	3883.0(13)	3883.0(13)	4539.5(2)	4854.3(6)	4340.2(3)	1824.6(3)
Z	2	4	4	4	4	4	2
Data collection							
λ (Mo Kα) (Å)	0.71073	0.71073	0.71073	0.71073	0.71073	0.71073	0.71073
ρ_{calc} (g cm^{-3})	1.297	1.292	1.370	1.260	1.321	1.340	1.188
μ (mm^{-1})	0.499	1.261	1.131	0.412	0.373	1.166	0.388
Reflections collected	8791	16 135	9171	19 536	20 454	18 731	6978
Independent collections (R_{int})	5282 (0.0355)	5070 (0.0387)	6358 (0.0308)	1988 (0.0601)	6353 (0.0489)	1907 (0.0620)	4511 (0.0592)
Absorption correction	empirical	none	none	empirical	none	none	empirical
Maximum and minimum transmission	0.3804 and 0.3026	na	na	0.2741 and 0.2191	na	na	0.3092 and 0.2137
Structure refinement							
Refinement method	full-matrix least squares on F^2 was used for all complexes						
Observed reflections [$I > 2\sigma(I)$]	5282	5070	6358	1988	6353	1907	4511
Number of parameters	433	552	552	160	572	151	387
Number of restraints	0	0	0	0	0	0	1
Goodness-of-fit on F^2	1.076	1.237	1.217	1.074	1.044	1.068	1.053
$R[I > 2\sigma(I)]$	0.0488	0.0461	0.0620	0.0269	0.0464	0.0314	0.0406
wR_2	0.1264	0.1176	0.1602	0.0658	0.1153	0.0744	0.1063

2.3. NMR measurements

Solution state ^{1}H, ^{13}C and ^{19}F NMR spectra were recorded on a Varian Mercury-300 spectrometer operating at 300 MHz for ^{1}H. Solution state ^{27}Al, ^{11}B and ^{119}Sn NMR spectra were recorded on a Varian INOVA-500 spectrometer operating at 500 MHz for ^{1}H. ^{15}N Solution state NMR spectra were acquired on a Bruker DRX600 spectrometer operating at 600 MHz for ^{1}H (60 MHz for ^{15}N) and equipped with a triple resonance ($^{1}H/^{13}C/^{15}N$) probe. All solution NMR chemical shifts are reported in parts per million (ppm) and coupling constants (J) in Hertz (Hz). ^{1}H and ^{13}C chemical shifts are reported with respect to the internal solvent (C_6D_6, 7.16 and 128.39; THF-d_8, 3.58 and 1.73, 67.57 and 25.37; $CDCl_3$, 7.27 and 77.0). ^{15}N chemical shifts are referenced to external neat CH_3NO_2 (δ = 380.2 ppm with respect to neat liquid NH_3 (0.0 ppm)) [22]. Other nuclei were referenced using an external standard, as follows: ^{19}F spectra were referenced with respect to $CFCl_3$ (0.0 ppm); ^{27}Al spectra were referenced to $Al(D_2O)_6^{3+}$ (1.0 M $AlCl_3$ in D_2O; 0.0 ppm); ^{11}B spectra were referenced to neat $BF_3 \cdot OEt_2$ (0.0 ppm); ^{119}Sn spectra were referenced to 0.5 M $Sn(CH_3)_4$ in CH_2Cl_2 (0.0 ppm). Solid state ^{15}N NMR spectra were acquired using a custom-designed spectrometer operating at 501 MHz for ^{1}H (50.8 MHz for ^{15}N). All spectra were acquired using a triple-resonance ($^{1}H/^{13}C/^{15}N$) magic-angle spinning (MAS) probe from Chemagnetics (Fort Collins, CO) configured for 4.0 mm zirconium rotors. Spinning frequencies of 3–6.5 kHz were used. The identity of the isotropic peak (δ_{iso}) was confirmed by measurement of the spectra at several different spinning speeds. Proton–nitrogen cross-polarization (CP) under the Hartmann–Hahn match was used to enhance the sensitivity of all ^{15}N NMR spectra [31]. Samples were referenced indirectly to the ^{13}C CP/MAS spectrum of adamantane or directly to the ^{15}N CP/MAS spectrum of NH_4Cl (acquired prior to each sample acquisition). Both solution and solid state NMR spectra were acquired at 20 °C. For further details of parameters used in the acquisition of solid state NMR spectra refer to the Supporting Information.

2.4. Simulation and calculation of solid state NMR spectra

The principal components of the chemical shift tensors were determined experimentally by fitting simulated spectra to the experimental data [32,33] using Simpson [34] (a general simulation program for NMR spectroscopy). The residuals between the simulated spectrum and the experimental spectrum could, in most cases, be reduced to <5%. The Simpson program was also used to calculate spectra based on values of the chemical shift tensor (in ppm) that were calculated using ADF. See the Supporting Information. for further details.

2.5. Computational details

Theoretical calculations were carried out using the Amsterdam Density Functional package (version *ADF2002.02*) [35–38]. The Slater-type orbital (STO) basis sets were of triple-ζ quality augmented with two polarization functions (ADF basis TZ2P). Full electronic configuration was used for all atoms. Relativistic effects were included by virtue of the zero order regular approximation (ZORA) [39–41]. The local density approximation (LDA) by Vosko, Wilk and Nusair (VWN) [42] was used together with the exchange correlation corrections of Becke [43] and Perdew [44] (BP-86).

The ^{15}N NMR chemical shielding calculations were performed using a multi-step procedure. First, the geometry of the compound of interest was optimized using X-ray parameters as a starting point. The optimized geometry was then subjected to a single-point calculation incorporating spin–orbit effects. The output of this calculation was used as the input for the ADF NMR utility [45].

Values of the absolute shielding tensor, calculated using density functional methods, were converted to referenced chemical shifts (δ ppm) using the following equation [46]

$$\delta(\mathrm{S},\ \mathrm{calc}) = \sigma(\mathrm{N_2},\ \mathrm{calc}) - \sigma(\mathrm{S},\ \mathrm{calc}) + \delta(\mathrm{N_2},\ \mathrm{ref}), \quad (1)$$

where δ(S, calc) is the calculated chemical shift (ppm) of the compound of interest (S), $\sigma(N_2, \mathrm{calc})$ is the calculated absolute shielding tensor for the reference compound (N_2 gas; $\sigma(N_2, \mathrm{calc}) = -80.012$ ppm), σ(S, calc) is the calculated absolute shielding tensor of S and $\delta(N_2, \mathrm{ref})$ is the experimental chemical shift (ppm) of the reference compound (N_2 gas). The NMR shielding (σ) of N_2 (with reference to neat nitromethane) = + 74.2 ppm, therefore δ (N_2, ref) = 380.2−74.2 = 306 ppm (referenced to liquid NH_3 at 0 ppm) [47,48].

2.6. Synthesis of $^{15}NMo(N[^{t}Bu]Ar)_3$ (*1*)

A 300-mL 3-neck flask fitted with a 0.1 L break-seal flask containing $^{15}N_2$ was charged with KH (3.52 g, 88 mmol). THF (50 mL) was added and the slurry was stirred while sparging with argon for 15 min. Stirring was paused and the headspace of the flask was evacuated. Under a static vacuum the break-seal was opened and the slurry was stirred vigorously as the headspace filled with $^{15}N_2$. In a second flask, $Mo(N[^{t}Bu]Ar)_3$ (5.5 g, 8.8 mmol) was dissolved in THF (35 mL) and the solution was stirred while sparging with argon for 10 min. Addition of the $Mo(N[^{t}Bu]Ar)_3$ solution via syringe to the KH/THF slurry afforded a dark orange mixture. Stirring was continued for 24 h after which time the solution was filtered through Celite. Solvent removal in vacuo gave an orange powder, which upon dissolution in pen-

tane and storage at −35 °C gave amber crystals of the desired terminal nitride complex, $^{15}NMo(N[^tBu]Ar)_3$ (4.72 g, 7.40 mmol, 84%). This procedure is a modification of previously reported syntheses for complex **1** [20,50,51].

2.7. Synthesis of lewis acid adducts *1*-*LA*

A solution of $NMo(N[^tBu]Ar)_3$ in *n*-pentane (5 mL) was prepared in a 20-mL scintillation vial and chilled to −35 °C. In a second vial a solution of the Lewis acid (1 equiv. in 2 mL pentane) was prepared and chilled to −35 °C. The Lewis acid solution was added to the $NMo(N[^tBu]Ar)_3$ solution and stirred at room temperature for 1 h. Upon addition of the Lewis acid a yellow solid precipitated from solution. Filtration of the suspension, washing with pentane and subsequent drying under a dynamic vacuum afforded the desired product. Recrystallization from a concentrated CH_2Cl_2 solution layered with pentane at −35 °C afforded yellow crystals of $X_3E–NMo(N[^tBu]Ar)_3$.

Isolated yield of yellow **1**-$BF_3 \cdot CH_2Cl_2$ (from 0.115 g of **1**): 0.092 g, 0.130 mmol, 72%. *Anal.* Calc. for $C_{36}H_{54}N_4MoBF_3$: C, 61.19; H, 7.70; N, 7.93. Found: C, 60.94; H, 7.76; N, 7.86%. ^1H NMR (300 MHz, CD_2Cl_2, 20 °C) δ: 6.92 (s, 3 H, *para*), 5.71 (br s, 6 H, *ortho*), 2.15 (s, 18 H, ArCH_3), 1.31 (s, 27 H, NC(CH_3)$_3$). ^{13}C *NMR (75.0 MHz, CD_2Cl_2, 20 °C)* δ: 147.8 (*ipso*), 138.4 (*meta*), 129.9 (*ortho*), 129.1 (*para*), 65.95 (N*C*(CH$_3$)$_3$), 32.14 (NC(*C*H$_3$)$_3$), 21.60 (Ar*C*H$_3$). ^{19}F NMR (282 MHz, CD_2Cl_2, 20 °C) δ: 143.7 (m, BF_3). ^{11}B NMR (160 MHz, CD_2Cl_2, 20 °C) δ: −2.83 (m, BF_3). ^{15}N-**1**-BF_3: ^{11}B NMR (160 MHz, $CDCl_3$, 20 °C) δ: −1.72 (br s, $\nu_{1/2}$ = 49 Hz). ^{15}N NMR (60 MHz, $CDCl_3$, 20 °C) δ: 591.9 (s).

Isolated yield of yellow **1**-BCl_3 (from 0.110 g of **1**): 0.104 g, 0.138 mmol, 80%. *Anal.* Calc. for $C_{36}H_{54}N_4MoBCl_3$: C, 57.20; H, 7.20; N, 7.41. Found: C, 57.11; H, 7.14; N, 7.45%. ^1H NMR (300 MHz, CD_2Cl_2, 20 °C) δ: 6.98 (s, 3 H, *para*), 5.7 (br s, 6 H, *ortho*), 2.19 (s, 18 H, ArCH_3), 1.35 (s, 27 H, NC(CH_3)$_3$). ^{13}C *NMR (75.0 MHz, CD_2Cl_2, 20 °C)* δ: 148.0 (*ipso*), 138.2 (*meta*), 130.8 (*ortho*), 128.6 (*para*), 67.56 (N*C*(CH$_3$)$_3$), 31.74 (NC(*C*H$_3$)$_3$), 21.65 (Ar*C*H$_3$). ^{11}B NMR (160 MHz, CD_2Cl_2, 20 °C) δ: 3.91 (s, $\nu_{1/2}$ = 16.5 Hz). ^{15}N-**1**-BCl_3: ^{11}B NMR (160 MHz, CD_2Cl_2, 20 °C) δ: 4.02 (br s, $\nu_{1/2}$ = 36.6 Hz).

Isolated yield of yellow **1**-$AlCl_3$ (from 0.075 g **1**): 0.081 g, 0.104 mmol, 89%. *Anal.* Calc. for $C_{36}H_{54}N_4MoAlCl_3$: C, 55.69; H, 7.01; N, 7.73. Found: C, 55.84; H, 7.11; N, 7.22. ^1H NMR (300 MHz, CD_2Cl_2, 20 °C) δ: 6.95 (s, 3 H, *para*), ~5.6 (br s, 6 H, *ortho*), 2.16 (s, 18 H, ArCH_3), 1.34 (s, 27 H, NC(CH_3)$_3$). ^{13}C NMR (75.0 MHz, CD_2Cl_2, 20 °C) δ: 148.2 (*ipso*), 138.4 (*meta*), 130.1 (*ortho*), 128.9 (*para*), 66.38 (N*C*(CH$_3$)$_3$), 32.40 (NC(*C*H$_3$)$_3$), 21.61 (Ar*C*H$_3$). ^{27}Al NMR (130.1 MHz, CD_2Cl_2, 20 °C) δ: 89.30 (s, $\nu_{1/2}$ = 10 Hz). ^{15}N-**1**-$AlCl_3$: ^{27}Al NMR (130.1 MHz, CD_2Cl_2, 20 °C) δ: 87.76 (m).

Isolated yield of bright yellow **1**-$AlBr_3$ (from 0.070 g **1**): 0.083 g, 0.092 mmol, 84%. *Anal.* Calc. for $C_{36}H_{54}N_4MoAlBr_3$: C, 47.75; H, 6.01; N, 6.19. Found: C, 47.63; H, 5.88; N, 6.12%. ^1H NMR (300 MHz, CD_2Cl_2, 20 °C) δ: 6.95 (s, 3 H, *para*), 5.70 (br s, 6 H, *ortho*), 2.16 (s, 18 H, ArCH_3), 1.35 (s, 27 H, NC(CH_3)$_3$). ^{13}C *NMR (75.0 MHz, CD_2Cl_2, 20 °C)* δ: 148.2 (*ipso*), 138.3 (*meta*), 130.1 (*ortho*), 129.0 (*para*), 66.66 (N*C*(CH$_3$)$_3$), 32.50 (NC(*C*H$_3$)$_3$), 21.62 (Ar*C*H$_3$). presup27Al NMR (130.1 MHz, CH_2Cl_2, 20 °C) δ: 80.17 (br s, $\nu_{1/2}$ = 85 Hz). ^{15}N-**1**-$AlBr_3$: ^{27}Al NMR (130.1 MHz, CH_2Cl_2, 20 °C) δ: 80.18 (br s, $\nu_{1/2}$ = 88 Hz).

Isolated yield of yellow **1**-AlI_3 (from 0.100 g **1**): 0.111 g, 0.106 mmol, 68%. *Anal.* Calc. for $C_{36}H_{54}N_4MoAlI_3$: C, 41.16; H, 5.18; N, 5.71. Found: C, 41.16; H, 5.23; N, 5.26%. ^1H NMR (300 MHz, $CDCl_3$, 20 °C) δ: 6.46 (s, 3 H, *para*), 5.47 (br s, 6 H, *ortho*), 1.83 (s, 18 H, ArCH_3), 1.14 (s, 27 H, NC(CH_3)$_3$). ^{13}C NMR (75.0 MHz, $CDCl_3$, 20 °C) δ: 136.4 (*meta*), 128.1 (*para*), 32.36 (NC(*C*H$_3$)$_3$), 20.70 (Ar*C*H$_3$). ^{27}Al NMR (130.1 MHz, $CDCl_3$, 20 °C) δ: 26.03 (s, $\nu_{1/2}$ = 226 Hz). ^{15}N-**1**-AlI_3: ^{27}Al NMR (130.1 MHz, THF, 20 °C) δ: 24.34 (br s, $\nu_{1/2}$ = 357 Hz).

Isolated yield of bright yellow **1**-$GaCl_3$ (from 0.150 g **1**): 0.174 g, 0.214 mmol, 91%. *Anal.* Calc. for $C_{36}H_{54}N_4MoGaCl_3$: C, 53.06; H, 6.68; N, 6.88. Found: C, 53.20; H, 6.62; N, 6.95%. ^1H NMR (300 MHz, CD_2Cl_2, 20 °C) δ: 6.95 (s, 3 H, *para*), 5.62 (br s, 6 H, *ortho*), 2.16 (br s, 18 H, ArCH_3), 1.33 (s, 27 H, NC(CH_3)$_3$). ^{13}C NMR (75.0 MHz, CD_2Cl_2, 20 °C) δ: 148.0 (*ipso*), 138.4 (*meta*), 130.1 (*ortho*), 128.9 (*para*), 66.26 (N*C*(CH$_3$)$_3$), 32.42 (NC(*C*H$_3$)$_3$), 21.61 (Ar*C*H$_3$).

Isolated yield of yellow **1**-$InCl_3$ (from 0.175 g **1**): 0.198 g, 0.230 mmol, 84%. *Anal.* Calc. for $C_{36}H_{54}N_4MoInCl_3$: C, 50.28; H, 6.33; N, 6.52. Found: C, 50.41; H, 6.38; N, 6.67%. ^1H NMR (300 MHz, $CDCl_3$/THF, 20 °C) δ: 6.59 (s, 3 H, *para*), ~5.6 (br s, 6 H, *ortho*), 1.95 (s, 18 H, ArCH_3), 1.26 (s, 27 H, NC(CH_3)$_3$). ^{13}C NMR (75.0 MHz, $CDCl_3$/THF, 20 °C) δ: 136.7 (*meta*), 128.4 (*ortho*), 32.62 (NC(*C*H$_3$)$_3$), 21.05 (Ar*C*H$_3$).

Isolated yield of yellow **1**-$GeCl_2$ (from 0.075 g **1** and 0.027 g $GeCl_2$.dioxane): 0.069 g, 0.079 mmol, 68%. *Anal.* Calc. for $C_{36}H_{54}N_4MoGeCl_2$: C, 54.99; H, 6.92; N, 7.63. Found: C, 55.21; H, 6.91; N, 7.12. ^1H NMR (300 MHz, $CDCl_3$, 20 °C) δ: 6.88 (s, 3 H, *para*), 5.66 (br s, 6 H, *ortho*), 2.15 (s, 18 H, ArCH_3), 1.37 (s, 27 H, NC(CH_3)$_3$). ^{13}C *NMR (75.0 MHz, $CDCl_3$, 20 °C)* δ: 148.4 (*ipso*), 137.7 (*meta*), 129.2 (*ortho*), 128.8 (*para*), 65.11 (N*C*(CH$_3$)$_3$), 32.66 (NC(*C*H$_3$)$_3$), 21.56 (Ar*C*H$_3$).

Isolated yield of yellow **1**-$SnCl_2$ (from 0.165 g **1**): 0.160 g, 0.193 mmol, 75%. *Anal.* Calc. for $C_{36}H_{54}N_4MoSnCl_2$: C, 51.95; H, 6.54; N, 7.21. Found: C, 52.28; H, 6.53; N, 6.69%. ^1H NMR (300 MHz,

CD_2Cl_2, 20 °C) δ: 6.89 (s, 3 H, *para*), 5.68 (br s, 6 H, *ortho*), 2.14 (s, 18 H, $ArCH_3$), 1.35 (s, 27 H, $NC(CH_3)_3$). *^{13}C NMR (75.0 MHz, CD_2Cl_2, 20 °C)* δ: 144.6 (*ipso*), 138.1 (*meta*), 129.4 (*ortho*), 129.1 (*para*), 64.60 ($NC(CH_3)_3$), 32.93 ($NC(CH_3)_3$), 21.59 ($ArCH_3$). ^{119}Sn NMR (186 MHz, THF, 20 °C) δ: 333 (s, $v_{1/2}$ = 31 Hz). ^{15}N-**1**-$SnCl_2$: ^{119}Sn NMR (186 MHz, THF, 20 °C) δ: 333 (s, $v_{1/2}$ = 57 Hz).

2.8. Synthesis of $[CH_3NMo(N[^tBu]Ar)_3]I$ [**2a**]I

Crystalline **1** (0.120 g, 0.188 mmol) was dissolved in neat CH_3I (0.8 mL, 12.8 mmol) in a 20 mL vial. The solution was stirred at 25 °C for 20 h after which time removal of excess CH_3I in vacuo and a pentane wash afforded a bright yellow powder in 92% yield (0.137 g, 0.173 mmol). ^1H NMR (300 MHz, $CDCl_3$, 20 °C) δ: 6.99 (s, 3 H, *para*), 5.67 (br s, 6 H, *ortho*), 5.16 (s, 3 H, NCH_3), 2.19 (s, 18 H, $ArCH_3$), 1.29 (s, 27 H, $NC(CH_3)_3$). ^{13}C NMR (75.0 MHz, $CDCl_3$, 20 °C) δ: 145.3 (*ipso*), 138.6 (*meta*), 130.8 (*para*), 128.4 (*ortho*), 68.50 ($NC(CH_3)_3$), 65.60 (NCH_3), 32.30 ($NC(CH_3)_3$), 21.70 ($ArCH_3$). NMR data for ^{15}N-[**2a**]I: ^1H NMR (300 MHz, $CDCl_3$, 20 °C) δ: 5.11 (d, $^2J_{N-H}$ 3.3 Hz, 3 H, ^{15}N–CH_3). ^{15}N NMR (60 MHz, $CH_3I/CDCl_3$, 20 °C) δ: 462.6. *Anal.* Calc. for $C_{37}H_{39}D_{18}N_4MoI$: [49] C, 55.63; H, 7.19; N, 7.01. Found: C, 56.13; H, 7.64; N, 6.53%.

2.9. Synthesis of $[(CH_3)_3Si$–$NMo(N[^tBu]Ar)_3][SO_3CF_3]$ [**2b**]OTf

A 20-mL scintillation vial was charged with **1** (0.10 g, 0.157 mmol) and Et_2O (2 mL). In a second vial a solution of trimethylsilyl trifluoromethanesulfonate [$CF_3SO_3Si(CH_3)_3$] (0.174 g, 5 equiv., 0.783 mmol) in Et_2O (1 mL) was prepared. The contents of the two vials were combined and the solution stirred at 25 °C for 10 h. Solvent removal resulted in the isolation of a bright yellow-orange powder; yield 89% (0.120 g, 0.139 mmol). *Anal.* Calc.: C, 55.75; H, 7.32; N, 6.50. Found: C, 55.54; H, 7.75; N, 6.60%. ^1H (300 MHz, $CDCl_3$, 20 °C) δ: 6.91 (s, 3 H, *para*), 5.62 (br s, 6 H, *ortho*), 2.17 (s, 18 H, $ArCH_3$), 1.34 (s, 27 H, $N(CH_3)_3$), 0.69 (s, 9 H, $Si(CH_3)_3$). ^{13}C NMR (75.0 MHz, $CDCl_3$, 20 °C) δ: 147.7 (*ipso*), 137.5 (*meta*), 129.5 (*ortho*), 128.0 (*para*), 66.04 ($NC(CH_3)_3$), 32.44 ($NC(CH_3)_3$), 21.65 ($ArCH_3$), 1.94 ($Si(CH_3)_3$. ^{19}F NMR (282 MHz, $CDCl_3$, 20 °C) δ: −78.44 (s, SO_3CF_3). ^{15}N NMR (60 MHz, $CDCl_3$, 20 °C) δ: 537.

2.10. Synthesis of $[PhC(O)NMo(N[^tBu]Ar)_3]SO_3CF_3$ [**2c**]OTf

Crystalline **1** (0.200 g, 0.31 mmol) was dissolved in CH_2Cl_2 (2 mL) in a 20-mL scintillation vial and chilled to −35 °C. A solution of PhC(O)OTf (0.89 g, 0.37 mmol, 1.2 equiv.) in CH_2Cl_2 was prepared and similarly chilled to −35 °C. The PhC(O)OTf solution was added to the stirred solution of $NMo(N[^tBu]Ar)_3$ and an immediate darkening of the solution to a brown-orange color was noted. The solution was stirred at 25 °C for 1 h before concentration of the solution (to ~0.5 mL) and addition of cold Et_2O caused precipitation of a red powder. The solution was filtered and the precipitate washed with pentane to afford a red-orange powder in 72% yield (0.198 g, 0.225 mmol). Material suitable for elemental analysis and crystallographic characterization was prepared by recrystallization from a concentrated THF solution layered with pentane. *Anal.* Calc.: C, 58.63; H, 6.75; N, 6.36. Found: C, 59.04; H, 6.73; N, 6.20%. IR (KBr plates, THF); $v_{(CO)}$ 1668 cm^{-1}. ^1H NMR (500 MHz, $CDCl_3$, 20 °C) δ: 8.32 (m, 2 H, *meta* Ph), 7.83 (m, 1 H, *para* Ph), 7.77 (m, 2 H, *ortho* Ph), 7.10 (s, 3 H, *para*), 5.74 (br s, 6 H, *ortho*), 2.26 (s, 18 H, $ArCH_3$), 1.34 (s, 27 H, $NC(CH_3)_3$). ^{13}C NMR (125 MHz, $CDCl_3$, 20 °C) δ: 147.7 (*ipso*), 139.1 (*meta*), 136.3 (Ph), 131.5 (Ph), 131.42 (Ph), 130.0 (*para*), 126.8 (*ortho*), 72.0 ($NC(CH_3)_3$), 31.8 ($NC(CH_3)_3$), 21.7 ($ArCH_3$). ^{19}F NMR (282.23 MHz, $CDCl_3$, 20 °C) δ: −78.3.

2.11. Synthesis of $H_2CNMo(N[^tBu]Ar)_3$ (**3**)

To a chilled suspension of $[CH_3NMo(N[^tBu]Ar)_3]I$ (0.098 g, 0.126 mmol) in pentane (5 mL) was added a chilled solution of 1.1 equiv. $LiN[(Si(CH_3)_3]_2$ (0.023 g, 0.138 mmol) in pentane (4 mL). Within a few minutes of adding base the yellow suspension turned bright red. The suspension was stirred for 12 h at 25 °C after which time the solution had turned dark purple and no suspended solids were observed. The solution was filtered through Celite and solvent removed in vacuo to yield a dark red-purple solid. Recrystallization from Et_2O yielded dark red crystals 0.051 g (0.077 mmol, 62%). *Anal.* Calc.: C, 68.017; H, 8.579; N, 8.583. Found: C, 68.22; H, 8.51; N, 8.68%. m.p.: 124 −135 °C (dec). IR (Et_2O solution, cm^{-1}): 1600 (m, v_{NC}), 1587 (s, v_{Ar-CH_3}). ^1H NMR (300 MHz, C_6D_6, 20 °C) δ: 6.69 (s, 3 H, *para*), 6.289 (s, 3 H, *ortho*), 6.287 (s, 3 H, *ortho*), 5.91 (s, 2 H, NCH_2), 2.16 (s, 18 H, $ArCH_3$), 1.41 (s, 27 H, $NC(CH_3)_3$). ^{13}C NMR (75.0 MHz, C_6D_6, 20 °C); δ: 150.2 (*ipso*), 138.9 (NCH_2), 137.4 (*meta*), 129.9 (*ortho*), 127.7 (*para*), 63.1 ($NC(CH_3)_3$), 32.8 ($NC(CH_3)_3$), 22.1 ($ArCH_3$). **3**-^{15}N: ^1H NMR (300 MHz, C_6D_6, 20 °C) δ: 5.90 (d $^2J_{N-H}$ 1.37 Hz, 2 H, $^{15}NCH_2$). ^{13}C NMR (75.0 MHz, C_6D_6, 20 °C) δ: 138.9 (d $^1J_{N-C}$ 5.78 Hz, $^{15}NCH_2$). ^{15}N NMR (60 MHz, C_6D_6, 20 °C) δ: 454.6.

2.12. Synthesis of $[CH_3CH_2NMo(N[^tBu]Ar)_3]I$ [**2d**]I

Crystalline $H_2CNMo(N[^tBu]Ar)_3$ (**3**, 0.074 g, 0.113 mmol) was dissolved in neat CH_3I (0.8 mL) in a 20-mL scintillation vial. The solution was stirred at 25 °C

for 14 h after which time removal of excess CH_3I in vacuo and a pentane wash afforded a bright yellow powder in 96% yield (0.086 g, 0.109 mmol). Recrystallization from a concentrated CH_2Cl_2 solution layered with Et_2O afforded yellow crystals of [**2d**]I · CH_2Cl_2. ^{1}H NMR (300 MHz, $CDCl_3$, 20 °C) δ: 6.98 (s, 3 H, *para*), 5.60 (br s, 6 H, *ortho*), 5.38 (q, 2 H, $^3J_{HH}$ 7.2 Hz, NCH_2CH_3), 2.17 (s, 18 H, $ArCH_3$), 1.95 (t $^3J_{HH}$ 7.2 Hz, 3 H, NCH_2CH_3), 1.27 (s, 27 H, $NC(CH_3)_3$). ^{13}C NMR (75.0 MHz, $CDCl_3$, 20 °C) δ: 145.9 (*ipso*), 138.6 (*meta*), 130.7 (*para*), 128.3 (*ortho*), 77.6 (NCH_2CH_3), 68.1 ($NC(CH_3)_3$), 32.4 ($NC(CH_3)_3$), 21.7 ($ArCH_3$), 17.5 (NCH_2CH_3). *Anal.* Calc.: C, 57.43; H, 7.48; N, 7.55. Found: C, 57.52; H, 7.44; N, 7.89%.

3. Results and discussion

3.1. Synthesis and characterization

The first reported synthesis of $NMo(N[^tBu]Ar)_3$ (**1**) from $Mo(N[^tBu]Ar)_3$ required a 3 d incubation period at −35 °C during which time N_2 uptake takes place [20]. Subsequent work focusing on the redox-catalyzed binding and splitting of dinitrogen by $Mo(N[^tBu]Ar)_3$ has led to the development of a more efficient route to the terminal nitride **1** [50]. Most recently, Lewis bases were found to accelerate the uptake of N_2 by $Mo(N[^tBu]Ar)_3$ enabling its quantitative conversion to **1** within 24 h. Potassium hydride (10 equiv. in THF) was found to be the most efficient base for effecting this conversion (Fig. 1) [51].

Furthermore, the ease of separation of KH from the pentane soluble product (**1**) by filtration makes this route particularly attractive. Complete characterization for complex **1** was reported previously. We will however make note of the ^{15}N solution NMR shift of **1** (840 ppm) for comparison with values reported in the following discussions. While complex **1** has eluded characterization by single crystal X-ray diffraction, the structure of a related compound, $NMo(N[^tBu]Ph)_3$ [20], is pseudo tetrahedral with the Mo≡N bond aligned with a crystallographic C_3 axis.

A number of neutral Lewis acid adducts of formula X_3E–$NMo(N[^tBu]Ar)_3$ (X = F, E = B: X = Cl, E = B, Al, Ga, In; X = Br, E = Al; X = I, E = Al) and Cl_2E–$NMo(N[^tBu]Ar)_3$ (E = Ge, Sn), were prepared by simple combination of **1** with 1 equiv. of Lewis acid (Fig. 2). Yields were generally quite high and in the range of 59–91%. These adducts were typically bright yellow, or sometimes pale orange, exhibiting limited solubility in pentane, benzene and Et_2O. The decomposition of these adducts to starting materials was observed in 0.5–3 h in THF solution at 25 °C.

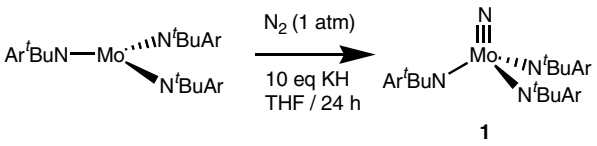

Fig. 1. Formation of complex **1** via the base-catalyzed cleavage of dinitrogen.

Infrared spectroscopy yielded little information with regard to the strength of the Mo–N or N–LA (LA = Lewis acid) interactions as a result of strong absorptions (attributed to the amide ligands) in the relevant regions of the spectrum.

A feature observed in the ^{1}H NMR spectrum of all complexes **1**-LA was significant broadening of the ~5.6 ppm resonance assigned to the six *ortho* protons of the $N[^tBu]Ar$ ligands. This broadening is attributed to hindered rotation about the Mo–N_{amide} bond due to increased steric congestion at the metal center.

As expected, the ^{11}B isotropic chemical shift for **1**-BF_3 (−2.8 ppm) and **1**-BCl_3 (3.9 ppm) showed an upfield shift of each resonance with respect to the uncoordinated Lewis acid (BF_3 = 10.0 ppm, BCl_3 = 46.5 ppm). [1] A similar upfield shift of the ^{27}Al resonance, with respect to the uncoordinated Lewis acid, was observed for the complexes **1**-$AlCl_3$, **1**-$AlBr_3$ and **1**-AlI_3 [52].

The ^{119}Sn NMR spectrum of **1**-$SnCl_2$ displayed a broad singlet at 333 ppm, which is shifted downfield of the resonance for $SnCl_2$ in THF solution (236 ppm) [53]. The ^{119}Sn resonance for **1**-$SnCl_2$ compares with other $SnCl_2$ · N-donor complexes such as $SnCl_2$ · pyridine in which the ^{119}Sn resonance occurs at 295 ppm [54].

In the ^{27}Al, ^{11}B and ^{119}Sn NMR spectra of ^{15}N-**1**-BX_3, ^{15}N-**1**-AlX_3 and ^{15}N-**1**-$SnCl_2$, coupling of the two spin active nuclei (e.g., ^{15}N–^{27}Al) could not be resolved. In each case the resonance for the spin-active Lewis acid center was broadened upon coordination to ^{15}N-**1** (e.g. ^{11}B NMR: ^{14}N-**1**-BCl_3 $\nu_{1/2}$ = 16.5 Hz; ^{15}N-**1**-BCl_3 $\nu_{1/2}$ = 36.6 Hz). Likewise, the ^{15}N solution NMR spectrum measured for ^{15}N-**1**-BF_3 displayed only a broad singlet at 592 ppm. This value is shifted upfield quite considerably (248 ppm) with respect to ^{15}N-**1**.

Crystallographic characterization of **1**-BF_3 confirmed the formation of a σ-bond through donation of the terminal nitride N-lone pair into the vacant p-orbital on the Lewis acidic boron center. [2] The N–B bond distance of 1.609(7) Å is similar to those reported in the literature for other Lewis acid adducts of nitridometal complexes [55–57]. Complex **1**-BF_3 crystallized in the space group $P\bar{1}$ with the B–F bonds of the Lewis acid staggered with

[1] NMR shifts reported in methylcyclohexane solution; referenced to $BF_3 \cdot OEt_2$ at 0.0 ppm.

[2] See Supporting Information for X-ray crystallographic details and an ORTEP plot of **1**-BF_3.

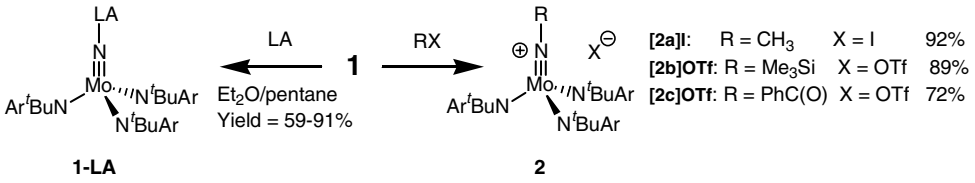

Fig. 2. Syntheses of **1**-LA and the cationic imido complexes [**2a**]I, [**2b**]OTf and [**2c**]OTf.

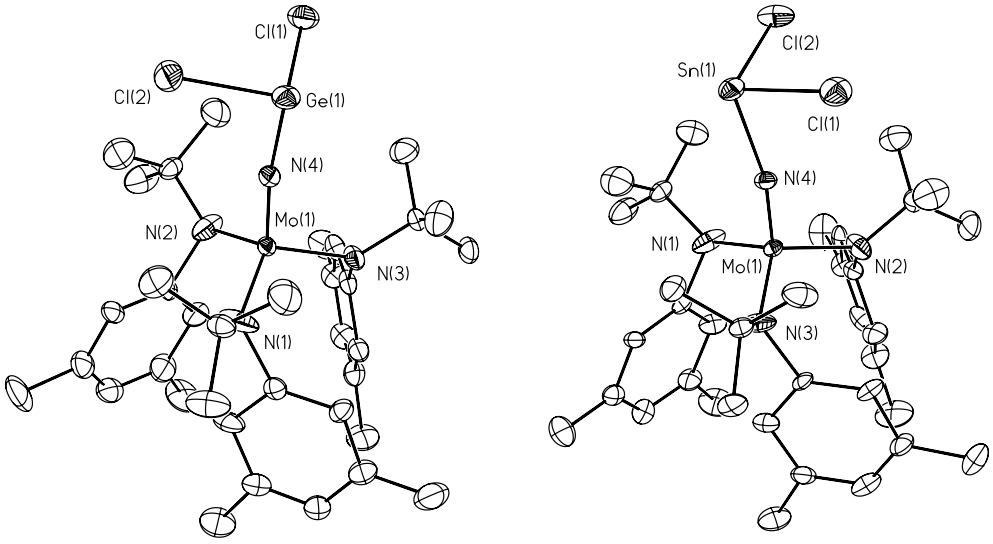

Fig. 3. 35% thermal ellipsoid (ORTEP) representations of **1**-$GeCl_2$ (left) and **1**-$SnCl_2$ (right).

respect to the $Mo–N_{amide}$ bonds. The Mo≡N bond length (1.678(4) Å) in **1**-BF_3 was identical (to within 3σ) to the Mo≡N bond in $NMo(N[^tBu]Ph)_3$ and, as expected, the Mo–N–B bond angle was nearly linear (177.6(4)°).

Complexes **1**-$GeCl_2$ and **1**-$SnCl_2$ were found (by X-ray crystallography) to be isomorphous (Fig. 3). To the best of our knowledge, complexes **1**-$GeCl_2$ and **1**-$SnCl_2$ represent the first examples of coordination at the terminally bound nitrogen in a nitridometal complex by a divalent germanium or tin halide [58,59]. Upon addition of $GeCl_2 \cdot$ dioxane or $SnCl_2$ to **1**, simple Lewis acid adducts analogous to those of the Group 13 **1**-LA complexes were formed. Complexes **1**-$GeCl_2$ and **1**-$SnCl_2$ were characterized by Mo≡N bond lengths of ~1.70 Å and N–Ge (or N–Sn) bond lengths typical of single bonds.

Transition-metal imido complexes containing an Mo≡NR bonding motif are well documented in the literature [60,61]. Reaction of **1** with electrophiles, RX

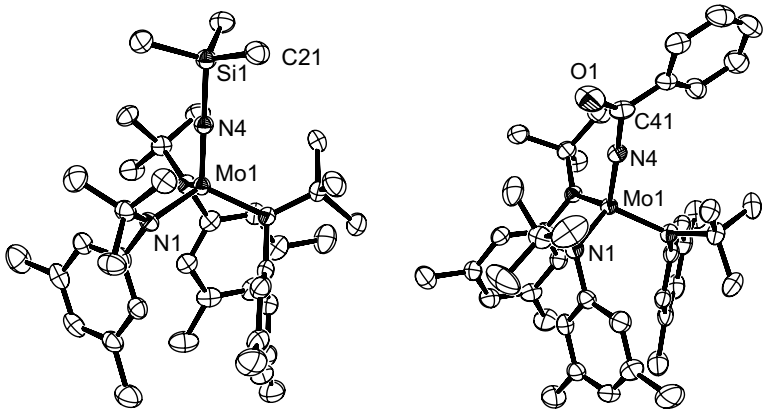

Fig. 4. 50% thermal ellipsoid (ORTEP) representations of cations [**2b**] (left) and [**2c**] (right).

(R = CH_3, X = I and R = Me_3Si, X = SO_3CF_3 = OTf), afforded the imido salts [**2a**]I [49] and [**2b**]OTf as bright yellow, pentane insoluble powders in high yield (92% and 89%, respectively, Fig. 2). In the ^1H NMR spectrum of ^{15}N-[**2a**]I a two-bond coupling ($^2J_{N-H}$) of 3.3 Hz was resolved for the methyl protons ($^{15}N–CH_3$). Solution $^{15}N\{^1H\}$ NMR spectra for [**2a**]I and [**2b**]OTf displayed resonances at 463 and 537 ppm, respectively.

The imido complex [**2b**]OTf crystallized in the cubic space group $P2_13$ (Fig. 4). The Mo–N–Si bond angle is linear as mandated by its alignment with the crystallographic C_3 axis. The Mo≡N bond distance of 1.715(6) Å was lengthened 0.057 Å with respect to the Mo≡N bond distance in **1** while the N–Si bond distance of 1.795(6) Å was slightly longer (~0.08 Å) than might be expected for a single N–Si bond [62]. While complex [**2a**]I has not been structurally characterized, the cation $[CH_3NMo(N[^tBu]Ar)_3]^+$ [**2a**] is presumably a 4-coordinate monomer related to the trimethylsilylimido cation $[(CH_3)_3Si–NMo(N[^tBu]Ar)_3]^+$ [**2b**].

Reaction of benzoyl triflate (PhC(O)OTf) with **1** in CH_2Cl_2 enabled isolation of the red-orange benzoylimido complex $[PhC(O)NMo(N[^tBu]Ar)_3]OTf$ [**2c**]OTf in 72% yield. There have been very few reports of the use of benzoyl triflate in synthetic inorganic chemistry despite this reagent's obvious utility as a potent electrophile [29,63,64]. There are similarly few reports of transition metal complexes containing a benzoylimido moiety i.e., PhC(O)N≡M [65–68]. X-ray crystallographic characterization of [**2c**]OTf showed that the Mo≡N bond is lengthened slightly with respect to the Mo≡N bond in complex **1** (Fig. 4). The N–C bond of 1.422(5) Å is in the range typical for an N–C single bond suggesting that resonance forms involving N–C multiple bond character do not provide added stabilization in this complex.

Dehydrohalogenation of [**2a**]I was achieved using lithium hexamethyldisilazide in pentane (Fig. 5) and resulted in isolation of the purple ketimide complex $H_2CNMo(N[^tBu]Ar)_3$ (**3**). Complex **3** provides a rare example of terminal $–NCH_2$ complexation [69–72], and represents the first example of such ligation to be structurally characterized (Fig. 6). The ketimide N–C bond distance of 1.300(7) Å is consistent with the presence of an N–C double bond. The Mo–N bond distance of 1.777(4) Å is in the range between that of a Mo–N double bond and that of a Mo–N single bond. This multiple bond character is the result of π-donation from a filled Mo d-orbital into the ketimide π*(N–C) molecular orbital and in the perpendicular plane, π-donation from the nitrogen lone pair of electrons into a vacant Mo d-orbital. Complex **3** has a distorted tetrahedral geometry

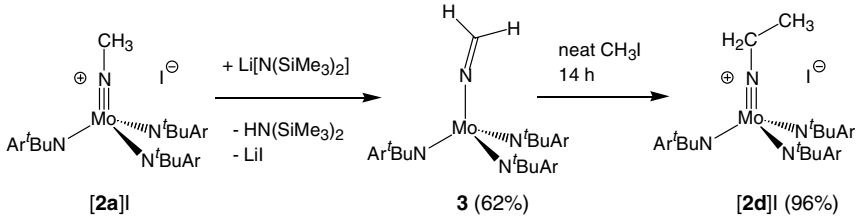

Fig. 5. Dehydrohalogenation of [**2a**]I in the formation of **3** and subsequent reaction with CH_3I to form [**2d**]I.

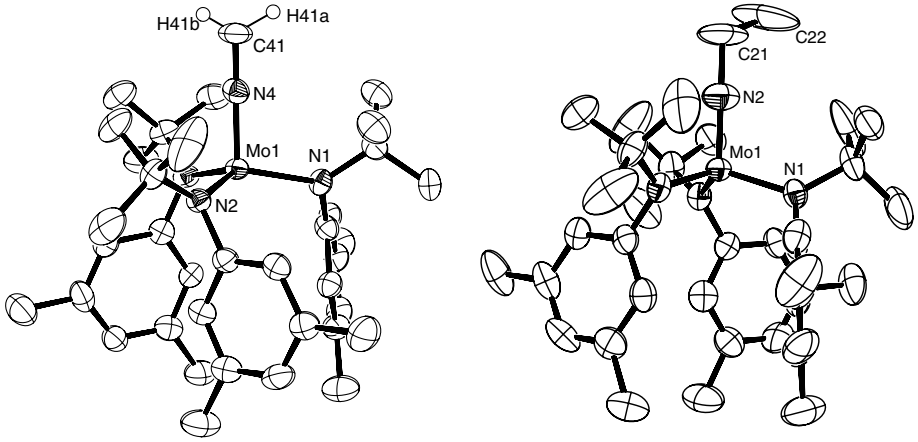

Fig. 6. 50% thermal ellipsoid (ORTEP) representation of **3** (left) and cation [**2d**] (right).

Table 2
Experimental and calculated ^{15}N chemical shielding tensors for **1** and derivatives thereof. δ_{iso} is the isotropic shift, κ is the span defined as $\delta_{11} - \delta_{33}$; κ is the skew of the shielding tensor defined as $[3(\delta_{22} - \delta_{iso})/(\delta_{11} - \delta_{33})]$; $\chi^2 = \sum((\text{obs} - \text{calc})^2)/\text{calc}$

Cplx	Model	Principal components of shielding tensor (ppm)												χ^2
		Experimental						Calculated						
		δ_{iso}	δ_{11}	δ_{22}	δ_{33}	Ω	κ	δ_{iso}	δ_{11}	δ_{22}	δ_{33}	Ω	κ	
1	**1m**	833	1229	1229	42	1187	1	795	1137	1137	113	1024	1	
1-BF_3	**1m**-BF_3	593	836	836	107	729	1	630	878	875	137	741	0.99	12
1-BCl_3	**1m**-BCl_3	558	773	747	152	621	0.92	562	792	791	102	690	1	31
		555	779	733	154	625	0.85							
1-$AlCl_3$	**1m**-$AlCl_3$	602	864	823	119	745	0.89	624	873	872	128	745	1	4
1-$AlBr_3$		599	835	835	126	709	1							
1-AlI_3		598	828	828	139	689	1							
		595	810	810	165	645	1							
		591	809	809	156	653	1							
1-$GaCl_3$	**1m**-$GaCl_3$	590	848	813	110	738	0.90	635	886	885	133	753	1	15
1-$InCl_3$	**1m**-$InCl_3$	608	879	874	72	807	0.99	645	902	902	131	771	1	30
		603	846	846	117	729	1							
1-$GeCl_2$	**1m**-$GeCl_2$	643	918	918	93	825	1	660	930	928	123	807	1	8
1-$SnCl_2$	**1m**-$SnCl_2$	666	955	955	89	866	1	669	944	938	125	819	0.99	11
[**2a**]I	**2a**-m	457	614	614	143	471	1	463	606	603	182	424	0.99	9
		453	611	611	136	475	1							
		441	594	594	137	457	1							
		436	576	576	156	420	1							
[**2b**]OTf	**2b**-m	541	744	716	163	581	0.91	556	758	758	153	605	1	4
[**2c**]OTf	**2c**-m	467	701	493	207	494	0.16	507	695	642	183	512	0.79	41
[**2d**]I	**2d**-m	460	613	613	153	460	1	486	653	637	168	485	0.93	6
3	**3m**-C_3	446	591	591	155	436	1	458	600	563	212	388	0.81	18
	3m-C_s							448	570	457	318	252	0.11	125

(average N–Mo–N_{amide} bond angle 101.7°) with pseudo-C_3 point symmetry courtesy of the nearly linear (178.0(4)°) Mo–N–C bond axis of the ketimide moiety (which lies along the pseudo-C_3 axis).

The overall sequence leading to complex **3** can be viewed as formal carbene (CH_2) addition to **1**. Addition of the Group 14 halides $GeCl_2$ and $SnCl_2$ to **1** did not give products analogous to **3** (i.e., oxidation $Ge/Sn^{II} \rightarrow Ge/Sn^{IV}$ with concomitant formation of a molybdenum(IV) complex $Cl_2E{=}NMo(N[^tBu]Ar)_3$). This observation is consistent with the increased stability of divalent Group 14 species as the group is descended [73].

Synthesis of the ethylimido complex $[CH_3CH_2NMo(N[^tBu]Ar)_3]I$ [**2d**]I, was achieved by reaction of **3** with CH_3I (Fig. 5). This reaction demonstrates the nucleophilicity of the ketimide carbon in **3** and is in direct contrast with organic ketimines ($RN{=}CH_2$) which are electrophilic at carbon [74]. Interestingly, we were unable to generate [**2d**] via the reaction of **1** with a suitable source of $[CH_3CH_2]^+$ (e.g., EtI, EtOTf, $[Et_3O]BF_4$). The inability to generate [**2d**] in this way is consistent with the dramatic decrease in rate observed for other nucleophilic substitution reactions (S_N2) upon increasing the steric bulk at the α-carbon of the alkyl electrophile (methyl ≫ ethyl > propyl) [75]. Crystallographic characterization of [**2d**]I showed that an N–C single bond (1.457(11) Å) and an Mo–N triple bond (1.708(9) Å) are formed upon the reaction of complex **3** with CH_3I.

3.2. ^{15}N Solid state CP/MAS NMR Spectroscopy of $^{15}NMo(N[^tBu]Ar)_3$ (**1**)

Measurement of the ^{15}N solid state CP/MAS NMR spectrum of $^{15}NMo(N[^tBu]Ar)_3$ (**1**) was carried out in order to probe experimentally the electronic structure at nitrogen. The principal components of the chemical shift tensor can be extracted from the experimental data by simulation of the experimental spectrum or by the analysis of the relative intensities of the spinning sidebands [32,33]. The experimentally measured values of the shift tensor components for **1** and each of its derivatives are presented in Table 2.

The experimental, simulated and DFT calculated ^{15}N solid state CP/MAS NMR spectra of **1** (calculated spectrum of complex **1m**) are presented in Fig. 7. In the absence of unusual averaging effects, the shift parameter measured in solution for a given complex is equal to the isotropic chemical shift, which is calculated as the average of the principal components of the chemical shift tensor $[\delta_{iso} = 1/3(\delta_{11} + \delta_{22} + \delta_{33})]$ [76]. Indeed, the isotropic shift (δ_{iso}) of 833 ppm determined for complex **1** from the solid state NMR spectrum is in close agreement with the ^{15}N solution NMR shift of 840 ppm. The axial symmetry of complex **1** constrains the orientation of the principal components of the ^{15}N chemical shift tensor such that the unique axis is aligned along the Mo≡N bond. Our experimental results confirm

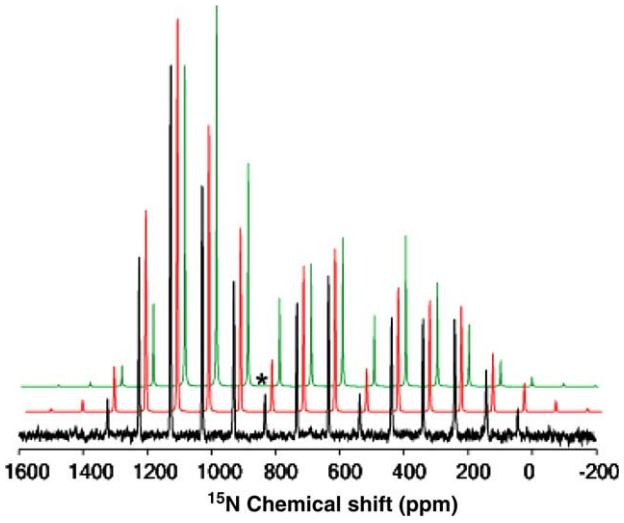

Fig. 7. Experimental (—) and simulated (---) ^{15}N solid state CP/MAS NMR spectra for complex **1** and DFT calculated (---) NMR spectrum for complex **1m**. The simulated and calculated spectra are offset with respect to the experimental spectrum for clarity. The isotropic peak (δ_{iso}) is indicated by an asterisk.

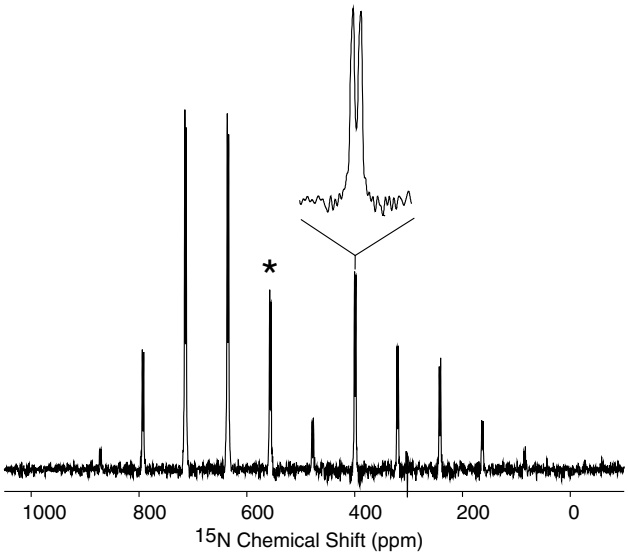

Fig. 8. Experimental ^{15}N solid state CP/MAS NMR spectrum of **1**-BCl_3. The expanded portion of the spectrum shows the multiplicity of one of the spinning sidebands. The isotropic peak is marked with an asterisk.

the axial nature of the chemical shift tensor ($\delta_{11} = \delta_{22} = 1229$ ppm).

A feature of the spectrum that is immediately obvious is the enormous span ($\Omega = \delta_{11}–\delta_{33}$) of the chemical shift anisotropy (CSA) tensor ($\Omega = 1187$ ppm). An understanding of the origin of this significant paramagnetic shift at nitrogen, when the external magnetic field is oriented perpendicular to the Mo≡N bond, was ascertained by analysis of density functional calculations (see Section 4.1) performed on the model complex $NMo(NH_2)_3$ (**1m**).

3.3. ^{15}N solid state CP/MAS NMR spectroscopy of the Lewis acid adducts of 1 (1-LA)

The isotropic shift of **1**-BF_3 ($\delta_{iso} = 593$ ppm) determined from the experimental ^{15}N solid state NMR spectrum is in excellent agreement with δ_{iso} (591 ppm) measured in solution. Complex **1**-BF_3 exhibited an axially symmetric chemical shift tensor wherein $\delta_{11} = \delta_{22} = 836$ ppm. Solid state ^{15}N NMR spectra obtained for complexes **1**-BCl_3, **1**-$AlCl_3$, **1**-$GaCl_3$ and **1**-$InCl_3$ indicate lower symmetry for the geometries of these complexes ($\kappa < 1$). The isotropic shift for the Lewis acid adducts (**1**-LA) studied was shifted upfield by 167 ppm (**1**-$SnCl_2$) to 278 ppm (**1**-BCl_3) with respect to the terminal nitride (**1**). This upfield shift in the magnitude of δ_{iso} can be explained by an increase in the energy gap between occupied frontier molecular orbitals and low-lying virtual molecular orbitals upon coordination of a Lewis acid to the terminally bound N-atom. This information can be extracted from density functional calculations performed on model complexes (**1m**-LA) and is discussed in Section 4.2.

The span (Ω) of the ^{15}N chemical shift tensor was reduced upon coordination of a Lewis acid, from 1187 ppm in **1** to between 866 ppm (**1**-$SnCl_2$) and 621 ppm (**1**-BCl_3). While the magnitude of the most shielded component δ_{33} varied over ca. 90 ppm for **1**-LA, the perpendicular components of the shift tensor, δ_{11} and δ_{22} (referred to as $\delta_\perp$), varied over ca. 180 ppm. Thus, the variation in the span may be attributed primarily to changes in the perpendicular component of the ^{15}N chemical shielding tensor ($\delta_\perp$). Again, this observation can be explained by analysis of the density functional calculations (Section 4.2).

The ^{15}N solid state NMR spectrum of **1**-BCl_3 displayed multiplicity in the isotropic peak and each of the associated spinning sidebands (Fig. 8).

Two unique sets of data, which differed in the magnitude of the isotropic shift (558 and 555 ppm) and the span of the chemical shift tensor (621 and 625 ppm), were obtained on simulation of the experimental spectrum. Similar multiplicity was observed in the spectra acquired for **1**-AlI_3 and **1**-$InCl_3$. This feature could be attributed either to coupling of ^{15}N with the adjacent spin-active nucleus or structural polymorphism [77–79].

3.4. ^{15}N solid state CP/MAS NMR spectroscopy of the imido complexes [2a]I, [2b]OTf, [2c]OTf and [2d]I

The axial symmetry of cation [**2a**] was apparent from the tensor components determined by simulation of the ^{15}N solid state NMR spectrum ($\delta_{11} = \delta_{22}$). The isotropic shift obtained from ^{15}N solid state NMR measurements (457 ppm) was in excellent agreement with δ_{iso} obtained in solution (463 ppm). The spectrum acquired for the

ethylimido complex [**2d**]I was very similar to that of the methylimido complex [**2a**]I in terms of the isotropic shift, span and skew of the chemical shift tensor.

Complex [**2b**]OTf showed unexpected asymmetry in the values of the chemical shift tensor (i.e., $\delta_{11} \neq \delta_{22}$). Interestingly, the spectrum of [**2b**]OTf was more reminiscent of those acquired for the Lewis acid adducts (e.g. **1**-BCl_3) in terms of the magnitude of the chemical shift tensors (δ_{nn}) and the span of the spectrum (Ω) than either of the imido complexes [**2a**]I or [**2d**]I. Again, δ_{iso} obtained for complex [**2b**]OTf from solid state NMR experiments (541 ppm) was in close agreement with the isotropic shift measured in solution (537 ppm).

The acylimido complex [**2c**]OTf is unique in the series of imido complexes that are presented in this study for two reasons: (i) significant asymmetry is present in [**2c**]OTf due to the coordination of the $[PhC(O)]^+$ electrophile to the terminal nitrogen; (ii) the presence of a carbonyl functional group on the fragment coordinated to N provides an opportunity for resonance stabilization of this imido complex. The asymmetric geometry of complex [**2c**]OTf was confirmed by the ^{15}N solid state NMR spectrum for which a rhombic chemical shift tensor ($\delta_{11} \neq \delta_{22} \neq \delta_{33}$) was observed ($\delta_{11} = 701$ ppm, $\delta_{22} = 493$ ppm and $\delta_{33} = 207$ ppm).

The span (Ω) of the ^{15}N chemical shift tensors for the four imido complexes was in the range of 420–581 ppm, which is smaller than for both **1** ($\Omega = 1187$ ppm) and the LA adducts (**1**-LA $\Omega = 866$–621 ppm). This reduction in the span could be attributed (in all four complexes) to the reduced magnitude of the most deshielded component of the chemical shift tensor, δ_{11}. Again, analysis of density functional calculations performed on model complexes enabled a rationalization of this effect in terms of perturbation of the electronic structure of **1** upon coordination of an electrophile (Section 4.3).

Multiplicity in the isotropic peak and the associated spinning sidebands was observed in the ^{15}N solid state NMR spectrum of [**2a**]I. [3] Four isotropic peaks were identified and the span of the chemical shift tensor varied between 420 and 475 ppm. Unlike the Lewis acid adducts (**1**-LA) for which this multiplicity might be attributed to the adjacent spin-active nucleus, complex [**2a**]I is thought to display this multiplicity due to structural polymorphism [77–79].

3.5. ^{15}N NMR spectroscopy of $H_2CNMo(N[^tBu]Ar)_3$ (**3**)

The experimental ^{15}N solid state NMR spectrum of **3** displays a number of noteworthy features. First, the principal components of the chemical shift tensor suggest that complex **3** is axially symmetric ($\delta_{11} = \delta_{22} = 591$ ppm). This symmetry is expected due to the Mo–N multiple bonding in **3** which is attributed to the π-donor/acceptor character of the ketimide (NCH_2) ligand. The isotropic peak in the ^{15}N solid state NMR spectrum was in close agreement with that obtained in solution. Complex **3** has the most shielded value of δ_{11} with respect to all other complexes measured in this study and a narrow span of the shift tensor ($\Omega = 436$ ppm).

4. Chemical shielding: experimental measurement and computational analysis [76]

The measurement of solid state NMR spectra allows for the experimental determination of the principal components (δ_{11}, δ_{22} and δ_{33}) of the chemical shift tensors. To complement our experimental measurements and enable a more complete analysis of these compounds at the electronic level, DFT calculations were performed on model complexes in which the bulky amido ligands N[^{t}Bu]Ar were replaced by three NH_2 ligands (for computational expediency). In most cases, the calculated tensors compared favorably with the experimental data [4] thus discussion of the electronic structure based on DFT calculations can be assumed to be valid. A summary of the analysis of the chemical shielding tensors, together with equations relevant to this analysis, are presented here in brief.

The absolute shielding tensor σ (calculated using DFT), is related to the chemical shift tensor δ

$$\delta = \sigma_{ref} - \sigma, \tag{2}$$

where σ_{ref} is the calculated absolute shielding tensor of the reference compound. NMR calculations based on the density functional method have been used to identify the individual contributions to the total shielding tensor made by the diamagnetic (σ_{dia}), paramagnetic (σ_{para}) and spin orbit (σ_{so}) components

$$\sigma_{total} = \sigma_{dia} + \sigma_{para} + \sigma_{so}. \tag{3}$$

For complexes presented in this study, spin–orbit contributions to the total shielding tensor were included [80,81] but in most cases this contribution was found to be negligible. [5] The diamagnetic contribution is dependent upon the core electron density and acts to reduce the applied magnetic field at the nucleus under observation. In the presence of an applied field σ_{dia} will generally show insignificant variation in its contribution to the total shielding tensor. The paramagnetic contribution

[3] See Supporting Information for experimental, simulated and calculated ^{15}N solid state CP/MAS NMR spectra for [**2a**]I.

[4] Supporting Information: Section 2.15. Plot of the experimental ^{15}N chemical shift tensor (δ_{11}, ppm) vs. Calculated ^{15}N chemical shift tensor (δ_{11}, ppm).

[5] For most of the complexes studied the spin–orbit contribution to the principal components of the chemical shift tensor was <5 ppm.

reinforces the applied field and is determined primarily by magnetic perturbation of the frontier molecular orbitals. Overall, σ_{para} shows the most significant variation in its contribution to the total shielding tensor due to the sensitivity of this term to changes in the electronic environment [82,83]. The paramagnetic contribution to the shielding tensor (σ_{para}) is proportional to the magnetic coupling of high-lying occupied molecular orbitals with low-lying virtual molecular orbitals (M_k) and inversely proportional to the energy difference between these orbitals ($e_{occ} - e_{vir}$). The gauge including atomic orbitals (GIAO) formalism makes it possible to analyze the contributions to the shielding in terms of orbital contributions [84–89]. A molecular orbital analysis of these contributions is contained within the NMR output file of a density functional calculation. [6] This analysis provides a list of the leading contributions to the k^{th} component ($k = 1, 2, 3$) of the magnetic field and includes information about the individual pairs of molecular orbitals (which mix in the applied field), the energy difference between these orbitals ($e_{occ} - e_{vir}$) and the magnitude of the coupling (M_k). Occasionally, one pair of magnetically coupled molecular orbitals is found to provide the major contribution to the paramagnetic deshielding for each component of the magnetic field (k_1, k_2 and k_3).

4.1. Theoretical studies on $^{15}NMo(N[^tBu]Ar)_3$ (1)

The NMR shift calculation for **1m** predicted an axially symmetric chemical shift tensor in which $\delta_{11(calc)} = \delta_{22(calc)} = 1137$ ppm. The primary contributions to $\delta_{11(calc)}$ and $\delta_{22(calc)}$ resulted from rotational mixing in the presence of an applied field of HOMO–3, σ(N p_z–Mo d_z^2) with LUMO, π* (N p_y–Mo d_{yz}) and LUMO + 1, π* (Np_x–Mo d_{xz}). There is a relatively small energy gap ($e_{occ} - e_{vir}$) between the filled N p_z orbital (of A symmetry in the point group C_3), which contains the nitrogen lone pair, and the empty π*(Mo–N) orbitals (a degenerate E set in C_3). Since the paramagnetic contribution to the chemical shielding tensor is proportional to the coupling between these virtual and occupied orbitals and inversely proportional to the energy gap between them, it follows that the components of the shift tensor (δ_{11} and δ_{22}) that are aligned perpendicular to the Mo≡N bond will exhibit extreme paramagnetic shifts.

The large paramagnetic contribution to the perpendicular components of the chemical shift tensor ($\delta_\perp$) is reminiscent of that observed for related terminal phosphide and carbide complexes [19,90]. In all three examples, the principal contributions to $\delta_\perp$ are the result of mixing in the applied field of a high-lying orbital of σ-symmetry with a relatively low-lying doubly degenerate E set of π-symmetry.

For **1** and the derivatives presented in this article, there is a much less significant variation in the magnitude of the most shielded component (δ_{33}) compared to either δ_{11} or δ_{22}. Where as $\delta_{11(expt)}$ varies over 653 ppm (1229–576 ppm), $\delta_{33(expt)}$ varies over a much smaller range of 165 ppm (from 207 to 42 ppm). This can be understood if one considers the chemical shift for a linear molecule. The shift in C_∞ symmetric molecules is dominated by the diamagnetic contribution; the paramagnetic contribution disappears completely along the molecular axis. In **1**, a paramagnetic component to the shift tensor is introduced when the C_∞ symmetry of the Mo≡N axis is broken by the addition of ligands to the metal. This paramagnetic component of δ_{33} is fairly constant for all of the complexes presented herein.

4.2. Theoretical studies on the Lewis acids adducts of 1 (1-LA)

DFT calculations performed on the model complexes **1m**-LA predicted the Lewis acid adducts to be axially symmetric, as evidenced by the calculated skew of the tensor ($\kappa = 1$ or 0.99 in all cases). Experimental ^{15}N solid state NMR spectra for **1**-BCl_3, **1**-$AlCl_3$ and **1**-$GaCl_3$, indicate that the geometry of these complexes is lower than the symmetry to which our DFT calculations converged ($\kappa < 1$). The optimized symmetry of **1m**-BF_3 predicted similar Mo–N and N–B bond lengths to those measured for **1**-BF_3, however, in the model complex the B–F bonds of the Lewis acid were eclipsed with respect to the Mo–N_{amide} bonds. Calculations were performed on model complexes in which either the eclipsed or staggered geometries were enforced in order to gauge the effect of rotation about the N–LA bond on the ^{15}N chemical shift. In general, calculations for the eclipsed and staggered geometries predicted very similar values of the principal components of the ^{15}N chemical shift tensor.

In each of the model Lewis acid adducts (**1m**-LA) the principal contributions to $\delta_\perp$ resulted from rotational mixing in the applied field of an occupied σ-orbital with a vacant π*(Mo–N) orbital. The occupied orbital is characterized by significant N p_z character, involved in donation of the N-lone pair into the vacant orbital on the Lewis acid's central atom. For example, analysis of the DFT calculation performed on **1m**-BCl_3 shows that the principal contributions to δ_{11} and δ_{22} are provided by mixing in the applied field of HOMO − 4, σ(N p_z–B p_z) with LUMO, π*(Np_y–Mo d_{yz}) and LUMO + 1, π*(N p_x–Mo d_{xz}), respectively. [7]

[6] Supporting Information: Section 2.13. Representative input and output files of an NMR calculation.

[7] See Supporting Information 2.17 for selected (calculated) orbitals of **1m**-BCl_3.

The energy gap ($e_{occ} - e_{vir}$) between the occupied σ(N–LA) bonding orbital and the vacant π(Mo–N) orbitals was found to depend principally on the extent to which Lewis acid coordination to the terminal N-atom lowers the energy of the σ(N p_z –LA sp) orbital. In **1**, the occupied (N p_z) orbital contains a non-bonding lone pair of electrons and is at a relatively high energy. Formation of a σ-bond to the Lewis acid lowers the energy of this orbital thereby increasing the energy gap between the magnetically coupled virtual and occupied orbitals ($e_{occ} - e_{vir}$). This in turn reduces the paramagnetic contribution to the perpendicular component of the chemical shift tensor resulting in more upfield shifted values of δ_{11} and δ_{22}.

Complex **1m**-BCl_3 has a smaller energy gap ($e_{occ} - e_{vir}$ = 3.65 eV) compared to **1m**-BF_3 ($e_{occ} - e_{vir}$ = 5.06 eV) but also a reduced paramagnetic contribution to the chemical shift, as evidenced by the more upfield shift of $\delta_{11(calc)}$. This apparently anomalous result can be explained if one accounts for the proportional relationship between the paramagnetic contribution to the chemical shift and the magnitude of the coupling (M_k) of occupied and virtual molecular orbitals in the presence of an applied magnetic field. Analysis of the DFT calculations for these two complexes shows that M_k in **1m**-BF_3 (0.438) is more than twice that calculated for **1m**-BCl_3 (0.206). This suggests that a much larger contribution to the paramagnetic term is made by N-based orbitals in **1m**-BF_3 compared to **1m**-BCl_3.

4.3. Theoretical studies on the imido cations [2a-m], [2b-m], [2c-m] and [2d-m]

Calculations performed on the model cation [**2a-m**] predicted an axially symmetric spectrum ($\delta_{11(calc)} \approx \delta_{22(calc)}$), which was in close agreement with the data obtained experimentally for this complex. Upon formation of an N–C single bond in cation [**2a-m**] there is a more significant lowering in energy of the σ(N–C) molecular orbital compared to that observed for the Lewis acid adducts (**1**-LA) discussed previously. This can be attributed to the build up of positive charge on the complex and the increased bond strength of the σ(N–C) bond compared to the σ(N–LA) bond. All four of the imido complexes exhibit a significant energy gap ($e_{occ} - e_{vir}$) between the filled σ(N–E) orbital to the lowest lying unoccupied orbitals of π-symmetry. The stabilization of this σ(N–E) bonding orbital prohibits its participation in mixing interactions that supplement the paramagnetic contribution to the chemical shift tensor. For the model cation [**2a-m**] the principal contributions to $\delta_{\perp}$ result from rotational mixing in the applied field of two occupied orbitals of π-symmetry (a doubly degenerate *E* set) with a vacant orbital of σ-symmetry (*A* symmetry in C_3). Analysis of the DFT calculation performed on [**2a-m**] shows that the principal contributions to δ_{11} and δ_{22} ($\delta_{11(calc)}$ = 606 ppm, $\delta_{22(calc)}$ = 603 ppm) are provided by mixing in the applied field of HOMO–2, π(Mo d_{xz}–N p_x) and HOMO−3, π(Mo d_{yz}–N p_y) with LUMO + 2, σ*(N p_z–C p_z).

Experimental data acquired for complex [**2b**]OTf displayed a rhombic ^{15}N chemical shift tensor wherein the skew of the shielding tensor κ = 0.91. Since calculations performed on cation [**2b-m**] provided the expected axially symmetric spectrum it is difficult to identify the electronic features of complex [**2b**]OTf that contribute to the asymmetry of the experimental spectrum.

The lack of an axis of symmetry in the optimized geometry for model cation [**2c-m**] is immediately apparent from the calculated values of the chemical shift tensor for [**2c-m**] ($\delta_{11(calc)}$ = 695 ppm, $\delta_{22(calc)}$ = 642 ppm and $\delta_{33(calc)}$ = 183 ppm). Our experimental results for complex [**2c**]OTf displayed greater asymmetry (κ = 0.16) compared to the calculated spectrum (κ = 0.79). Analysis of DFT calculations performed on cation [**2c-m**] shows that the principal contribution to $\delta_{11(calc)}$ is provided by mixing in the applied field of HOMO − 3, σ(N p_z–C p_z) with LUMO + 1, π*(Mo d_{xz}–N p_x). The principal contribution to $\delta_{22(calc)}$ is provided by mixing in the applied field of HOMO − 9, π(Mo d_{xz}–N p_x) with LUMO+2, σ*(N p_z–C p_z). For [**2c-m**] the σ(N p_z–C p_z) orbital is much higher in energy than the σ-orbital comprising the N–C bond in [**2a-m**] and [**2d-m**]. Indeed, the energy ordering of the frontier orbitals in [**2c-m**] is more reminiscent of that seen in the Lewis acid adducts (**1**-LA) than the other imido complexes. This implies that a weaker bonding interaction exists between the terminal N-atom and the electrophilic C-atom of the benzoyl fragment (compared to the interaction in other imido complexes) suggesting that resonance forms do not provide significant stabilization in complex [**2c**]OTf. These facts are consistent with the crystal structure of [**2c**]OTf in which the N–C single bond does not appear to be shortened through additional π-interactions.

4.4. Theoretical studies on $H_2CNMo(N[^tBu]Ar)_3$ (3)

The overall sequence leading to ketimide **3** embodies formal carbene (CH_2) addition to complex **1**, a process that encompasses C=N bond formation along with the reduction of molybdenum from the +6 to the +4 formal oxidation state. [8] Carbene addition to **1** is recognized as a potentially valuable means for the activation of complex **1** in the context of nitrogen atom transfer from N_2 into organic molecules [91]. It was therefore of interest to determine what insight solid state NMR spectroscopy could provide, in conjunction with DFT analysis of the experimental shift tensors into the electronic

[8] ΔH_{RXN} of CH_2 addition to $NMo(NH_2)_3$ is calculated to be −93 kcal mol^{-1}.

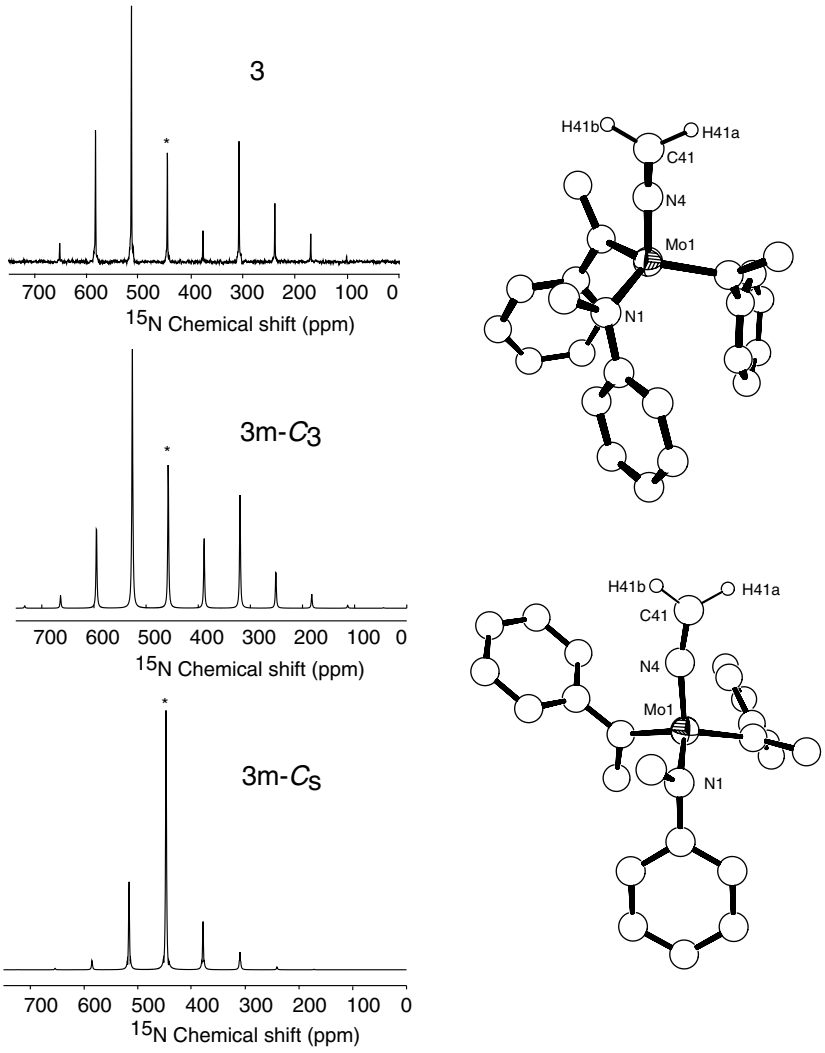

Fig. 9. Optimized geometries for the complexes **3m**-C_3 (top) and **3m**-C_s (bottom) and solid state ^{15}N spectra for complex **3**: experimental (top), calculated **3m**-C_3 (middle) and calculated **3m**-C_s (bottom). The isotropic peak is indicated by an asterisk.

structure at this N-atom which is activated toward productive removal from the molybdenum complex into an organic product.

Interestingly, attempts to use DFT to reproduce the observed ^{15}N solid state CP/MAS NMR spectrum of **3** using $H_2CNMo(NH_2)_3$, (the structure of which converged to near C_s symmetry) as the computational model were not entirely satisfactory. We probed further and found that the larger model $H_2CNMo(N[CH_3]Ph)_3$ (**3m**) converged either to a pseudo-C_s (**3m**-C_s) or to a pseudo-C_3 (**3m**-C_3) conformation depending upon the initial geometry employed. The ^{15}N spectrum calculated for **3m**-C_3 was a good match to the observed spectrum of **3** ($\chi^2 = 18$), while that calculated for **3m**-C_s deviated noticeably ($\chi^2 = 125$) (Fig. 9). The two local minima for **3m** differ with respect to rotation about the Mo–N_{amide} bonds, leading to differing Mo–N_{amide} dπ−pπ overlap, to which the ketimide nitrogen electronic environment is clearly sensitive. Analyses of the NMR calculation performed on **3m**-C_3 reveals that the principal contributions to the most deshielded components of the tensor, $\delta_{11(calc)}$ and $\delta_{22(calc)}$ (600 and 563 ppm, respectively), result from mixing in the applied field of HOMO, π(N–C) with LUMO, π^*(Mo d_{yz}–N p_y) and LUMO + 1, π^*(Mo d_{xz}–N p_x). The same orbitals are responsible for the paramagnetic contributions to $\delta_{11(calc)}$ and $\delta_{22(calc)}$ in **3m**-C_s ($\delta_{11} = 570$ ppm, $\delta_{22} = 457$ ppm) however, the energy gap ($e_{occ} - e_{vir}$) between the HOMO and LUMO orbitals in **3m**-C_3 is appreciably smaller than in **3m**-C_s (1.498 eV versus 1.696 eV). This increased energetic separation of the orbitals in **3m**-C_s reduces the degree of magnetic coupling and results in a more shielded value of δ_{11}.

In addition, the calculated molecular orbitals for **3m**-C_3 show significant p orbital contribution from the ketimide carbon to the HOMO. This indicates that the ketimide carbon has been rendered nucleophilic upon

dehydrohalogenation of the methylimido complex [**2a**]I. Experimental evidence for this is demonstrated by the reaction of **3** with CH_3I to generate the ethylimido complex [**2d**]I.

5. Conclusions

The electronic structure of a dinitrogen-derived terminal molybdenum nitride complex $NMo(N[^tBu]Ar)_3$ (**1**) has been studied by the combined use of ^{15}N solid state CP/MAS NMR spectroscopy and DFT calculations. Parallels may be drawn between the bonding observed in this terminal nitride complex and the analogous terminal phosphide and carbide complexes. Perturbation of the electronic structure in the terminal molybdenum nitride complex (**1**) upon coordination of a Lewis acid can be attributed to stabilization of a σ-symmetric orbital as a result of N–LA bond formation.

Upon formation of a Lewis acid adduct of **1**, the increased energy gap ($e_{occ} - e_{vir}$) between magnetically coupled occupied and virtual orbitals, is seen to correlate with a reduction in the magnitude of the perpendicular components of the chemical shift tensor (δ_{11} and δ_{22}).

The reaction of **1** with electrophiles RX, results in further stabilization of the σ-symmetric orbital containing the N-lone pair of electrons. The paramagnetic contribution to the chemical shift tensor in this series of cationic imido complexes results from rotational mixing in the applied field of high-lying π(Mo–N) orbitals with a low-lying σ(N–E) (E = C, Si) orbital.

Finally, the strength of this combined approach to studying the electronic structure of spin-active nuclei in transition metal complexes is highlighted by our investigations into a ketimide complex, $H_2CNMo(N[^tBu]Ar)_3$ (**3**). Computational studies performed on the model complex $H_2CNMo(N[CH_3]Ph)_3$ (**3**m) identified two geometries to which this complex could converge. The variation in Mo–N dπ–pπ overlap in the two structures is reflected in the calculated chemical shift tensors. A quantitative comparison of the experimental spectrum with the calculated spectra indicates that a closer match is provided by the pseudo-C_3 symmetric model, the optimized geometry of which is in good agreement with X-ray crystallographic data for complex **3**.

Acknowledgements

For support of this work, we are grateful to the US National Science Foundation (CHE 0316823) and the National Institutes of Health (EB002026). Christopher Clough is thanked for his assistance with crystallography. We thank Dr. Christopher D. Incarvito for his crystallographic expertise in the structural refinement of complex **1**-$SnCl_2$. N.M.L. thanks the National Institutes of Health for support via a National Research Service Award post-doctoral fellowship (F32 NS42425-01).

The authors acknowledge the significant contributions made to inorganic and organometallic chemistry by Prof. Malcolm L.H. Green and the inspiration his work has provided to many of his colleagues during the course of his distinguished career.

Appendix A. Supplementary material

Complete crystallographic data for complexes **1**-BF_3 (CCDC-236925), **1**-$GeCl_2$ (CCDC-236927), **1**-$SnCl_2$ (CCDC-236930), [**2b**]OTf (CCDC-236926), [**2c**]OTf (CCDC-236928), [**2d**]I (CCDC-236929) and **3** (CCDC-236924) have been deposited in the Cambridge Structural Database and can be obtained free of charge via www.ccdc.cam.ak/conts/retrieving.htm (or from the Cambridge Crystallographic Data Center, 12 Union Road, Cambridge CB21EZ, UK; (fax: +44-1223-336-033; or deposit@ccdc.cam.ac.uk). Supplementary Information for this article includes the following materials: ORTEP plots, anisotropic displacement parameters, atomic coordinates, bond lengths and angles for complexes **1**-BF_3, **1**-$GeCl_2$, **1**-$SnCl_2$, [**2b**]OTf, [**2c**]OTf, [**2d**]I and **3**; details of DFT calculations including optimized geometries of all model complexes and selected (calculated) orbitals for complexes **1m**, **1m**-BCl_3, [**2b-m**], [**2c-m**] and **3m**-C_3; experimental information for the acquisition of solid state spectra; representative experimental, simulated and calculated solid state ^{15}N CP/MAS spectra. Supplementary data associated with this article can be found, in the online version at doi:10.1016/j.poly.2004.08.010.

References

[1] D.D. Laws, H.-M.L. Bitter, A. Jerschow, Angew. Chem., Int. Ed. 41 (2002) 3096.
[2] R.G. Griffin, Nat. Struct. Biol. 5 (1998) 508.
[3] S.J. Opella, K.M. Morden, in: S.E. Harding, A.J. Rowe (Eds.), Dynamic Properties of Biomolecular Assemblies, The Royal Society of Chemistry, Cambridge, 1989, p. 196.
[4] E.Y. Chekmenev, Q. Zhang, K.W. Waddell, M.S. Mashuta, R.J. Wittebort, J. Am. Chem. Soc. 126 (2004) 379.
[5] S. Luca, H. Heise, M. Baldus, Acc. Chem. Res. 36 (2003) 858.
[6] A. Shoji, S. Ando, S. Kuroki, I. Ando, G.A. Webb, Structural studies of peptides and polypeptides in the solid state by nitrogen-15 NMR, Ann. Rep. NMR Spectrosc. 26 (1993) 55.
[7] C.P. Jaroniec, J. Lansing, B. Tounge, M. Belenky, J. Herzfeld, R.G. Griffin, J. Am. Chem. Soc. 123 (2001) 12929.
[8] A.E. McDermott, T. Polenova, A. Bockmann, K.W. Zilm, G.T. Montellione, J. Biomol. NMR 16 (1999) 209219.
[9] F. Castellani, B. van Rossum, A. Diehl, M. Schubert, K. Rehbein, H. Oschkinat, Nature 420 (2002) 98.
[10] D.L. Bryce, R.E. Wasylishen, Phys. Chem. Chem. Phys. 4 (2002) 3591.
[11] Y. Huang, D.F.R. Gilson, I.S. Butler, J. Chem. Soc., Dalton Trans. (1992) 2881.
[12] R. Salzmann, M. Wojdelski, M. McMahon, R.H. Havlin, E. Oldfield, J. Am. Chem. Soc. 120 (1998) 1349.

[13] G.M. Bernard, R.E. Wasylishen, Phys. Organomet. Chem. 3 (2002) 165.
[14] R. Salzmann, C.J. Ziegler, N. Godbout, M.T. McMahon, K.S. Suslick, E. Oldfield, J. Am. Chem. Soc. 120 (1998) 11323.
[15] N. Godbout, L.K. Sanders, R. Salzmann, R.H. Havlin, M. Wojdelski, E. Oldfield, J. Am. Chem. Soc. 121 (1999) 3829.
[16] R. Gobetto, Mater. Chem. Phys. 29 (1991) 221.
[17] M. Mehring, Principals of High Resolution NMR in Solids, 2nd ed., Springer-Verlag, Berlin, 1983.
[18] M.J. Duer (Ed.), Solid-state NMR: Principals and Applications, Blackwell Science, Oxford, 2002.
[19] G. Wu, D. Rovnyak, M.J.A. Johnson, N.C. Zanetti, D.G. Musaev, K. Morokuma, R.R. Schrock, R.G. Griffin, C.C. Cummins, J. Am. Chem. Soc. 118 (1996) 10654.
[20] C.E. Laplaza, M.J.A. Johnson, J.C. Peters, A.L. Odom, E. Kim, C.C. Cummins, G.N. George, I.J. Pickering, J. Am. Chem. Soc. 118 (1996) 8623.
[21] C.E. Laplaza, C.C. Cummins, Science 268 (1995) 861.
[22] W. von Philipsborn, R. Müller, Angew. Chem., Int. Ed. 25 (1986) 383.
[23] The ADF package utilized in this study allows the calculation of NMR shielding tensors: G. Schreckenbach, T. Ziegler, J. Phys. Chem. 99 (1995) 606.
[24] G. Schreckenbach, T. Ziegler, Int. J. Quantum Chem. 60 (1996) 753.
[25] G. Schreckenbach, T. Ziegler, Int. J. Quantum Chem. 61 (1997) 899.
[26] S.K. Wolff, T. Ziegler, J. Chem. Phys. 109 (1998) 895.
[27] G. Schreckenbach, T. Ziegler, Theor. Chem. Acc. 99 (1998) 71.
[28] A.B. Pangborn, M.A. Giardello, R.H. Grubbs, R.K. Rosen, F.J. Timmers, Organometallics 15 (1996) 1518.
[29] L. Brown, M. Koreeda, J. Org. Chem. 49 (1984) 3875.
[30] D.D. Perrin, W.L.F. Armarego, Purification of Laboratory Chemicals, 3rd ed., Pergamon Press, Oxford, 1988.
[31] Theoretical basis of the cross polarization experiment: S.R. Hartmann, E.L. Hahn, Phys. Rev. 128 (1962) 2042.
[32] M.M. Maricq, J.S. Waugh, J. Chem. Phys. 70 (1979) 3300.
[33] J. Herzfeld, A.E. Berger, J. Chem. Phys. 73 (1980) 6021.
[34] M. Bak, J.T. Rasmussen, N.C. Nielsen, J. Magn. Reson. 147 (2000) 296.
[35] E.J. Baerends, D.E. Ellis, P. Ros, Chem. Phys. 2 (1973) 41.
[36] L. Versluis, T. Ziegler, J. Chem. Phys. 322 (1988) 88.
[37] G. te Velde, E.J. Baerends, J. Comput. Phys. 99 (1992) 84.
[38] C. Fonseca Guerra, J.G. Snijders, G. te Velde, E.J. Baerends, Theor. Chem. Acc. 99 (1998) 391.
[39] J.G. Snijders, E.J. Baerends, P. Ros, Mol. Phys. 38 (1979) 1909.
[40] T. Ziegler, V. Tschinke, E.J. Baerends, J.G. Snijders, W.J. Ravenek, Phys. Chem. 93 (1989) 3050.
[41] E. van Lenthe, E.J. Baerends, J.G. Snijders, J. Chem. Phys. 99 (1993) 4597.
[42] S.H. Vosko, L. Wilk, M. Nusair, Can. J. Phys. 58 (1980) 1200.
[43] A.D. Becke, Phys. Rev. A 38 (1988) 3098.
[44] J.P. Perdew, Phys. Rev. B 33 (1986) 8822.
[45] G. Schreckenbach, T. Ziegler, J. Phys. Chem. 99 (1995) 606.
[46] C. van Wüllen, Phys. Chem. Chem. Phys. 2 (2000) 2137.
[47] W. Witanowski, W. Sicinska, G.A. Webb, Spectroscopy 9 (1991) 55.
[48] C.J. Jameson, A.K. Jameson, D. Oppusunggu, S. Wille, P.M. Burrell, J. Mason, J. Chem. Phys. 74 (1981) 81.
[49] Deuterated isotopomer synthesized by A.J. Johnson, Ph.D. Thesis, Massachusetts Institute of Technology, Cambridge, MA, 1997.
[50] J.C. Peters, J.-P.F. Cherry, J.C. Thomas, L. Baraldo, D.J. Mindiola, W.M. Davis, C.C. Cummins, J. Am. Chem. Soc. 121 (1999) 10053.
[51] Y.-C. Tsai, C.C. Cummins, Inorg. Chim. Acta. 345 (2003) 63.
[52] J.F. Hinton, R.W. Briggs, in: B.E. Mann, R.K. Harris (Eds.), NMR and the Periodic Table, Academic Press, London, 1978, Chapter 9, ^{27}Al NMR (reference $[Al(D_2O)_6]^{3+}$, 0.0 ppm) Al_2Cl_6 (2 M, Et_2O) δ105 ppm; Al_2Br_6 (1.5 M, Et_2O) δ95 ppm; Al_2I_6 (1.5 M, Et_2O) δ40 ppm.
[53] P.C. Lauterbur, J.J. Burke, J. Am. Chem. Soc. 83 (1961) 326.
[54] C.C. Hsu, R.A. Geanangel, Inorg. Chem. 19 (1980) 110.
[55] L.H. Doerrer, A.J. Graham, M.L.H. Green, J. Chem. Soc., Dalton Trans. (1998) 3941.
[56] R. Dantona, E. Schweda, J. Strähle, Z. Naturforsch. B 39 (1984) 733.
[57] U. Abram, B. Schmidt-Brücken, A. Hagenbach, M. Hecht, R. Kirmse, A. Voigt, Z. Anorg. Allg. Chem. 629 (2003) 838.
[58] Tin halide adducts with N-donor molecules: J.D. Donaldson, D.G. Nicholson, Inorg. Nuc. Chem. Lett. 6 (1970) 151.
[59] W.W. Du Mont, H.J. Kroth, Naturforsch. B 35 (1980) 700.
[60] W.A. Nugent, J.M. Mayer, Metal–Ligand Multiple Bonds, Wiley, New York, 1988.
[61] R.A. Eikey, M.M. Abu-Omar, Coord. Chem. Rev. 243 (2003) 83, and references therein.
[62] N–Si single bond distances are typically ca. 1.711 Å: D.R. Lide (Ed.), CRC Handbook of Chemistry and Physics, 86th ed., CRC Press, London, 2003, p. 9.
[63] F. Effenberger, E. Sohn, G. Epple, Chem. Ber. 116 (1983) 1195.
[64] Dissociation tendency of benzoyl triflate: F. Effenberger, G. Epple, J.K. Eberhard, U. Buehler, E. Sohn, Chem. Ber. 116 (1983) 1183.
[65] D.E. Wigley, Prog. Inorg. Chem. 42 (1994) 239.
[66] A.J. Nielson, P.A. Hunt, C.E.F. Rickard, P. Schwerdtfeger, J. Chem. Soc., Dalton Trans. (1997) 3311.
[67] C. Tong, L.A. Bottomley, J. Porphyrins Phthalocyanines 2 (1998) 261.
[68] C.R. Clough, J.B. Greco, J.S. Figueroa, P.L. Diaconescu, W.M. Davis, C.C. Cummins, J. Am. Chem. Soc. 126 (2004) 7742.
[69] N.C. Mösch-Zanetti, R.R. Schrock, W.M. Davis, K. Wanninger, W.S. Seidel, M.B. O'Donoghue, J. Am. Chem. Soc. 119 (1997) 11037.
[70] P.A. Shapley, J.M. Shusta, J.L. Hunt, Organometallics 15 (1996) 1622.
[71] A. Hills, D.L. Hughes, C.J. Macdonald, M.Y. Mohammed, C.J. Pickett, J. Chem. Soc., Dalton Trans. (1991) 121.
[72] J. Chatt, R.J. Dosser, G.J. Leigh, Chem. Commun. (1972) 1243.
[73] N.N. Greenwood, A. Earnshaw, Chemistry of the Elements, 2nd ed., Butterworth-Heinemann, Oxford, 1998, p. 375.
[74] Ketimines undergo reactions with organolithium reagents (R′Li) to form R(Li)N–C(R′)H_2 via addition of nucleophilic $[R']^-$ to the electrophilic carbon of the ketimine: J. Huet, Bull. Soc. Chim. Fr. (1964) 952, p. 960, 967 and 973.
[75] M.B. Smith, J. March, March's Advanced Organic Chemistry, 5th ed., Wiley, New York, 2001, p. 431.
[76] Conventions followed in this paper are defined in the following article: J. Mason, Solid State Nucl. Magn. Reson. 2 (1993) 285.
[77] Polymorphism and characterization by solid state NMR spectroscopy: M. Strohmeier, A.M. Orendt, D.W. Alderman, D.M. Grant, J. Am. Chem. Soc. 123 (2001) 1713.
[78] M.T. Zell, B.E. Padden, D.J. Grant, M.-C. Chapeau, I. Prakash, E.J. Munson, J. Am. Chem. Soc. 121 (1999) 1372.
[79] J. Smith, E. MacNamara, D. Raferty, T. Borchardt, S. Byrn, J. Am. Chem. Soc. 120 (1998) 11710.
[80] Q. Cui, D.G. Musaev, M. Svensson, S. Sieber, K. Morokuma, J. Am. Chem. Soc. 117 (1995) 12366.
[81] K.M. Neyman, V.A. Nasluzov, J. Hahn, C.R. Landis, N. Rösch, Organometallics 16 (1997) 995.
[82] C.J. Jameson, J. Mason, in: J. Mason (Ed.), Multinuclear NMR, Plenum Press, New York, 1987, p. 51.
[83] G. Schreckenback, J. Chem. Phys. 110 (1999) 11936.
[84] Y. Ruiz-Morales, T. Ziegler, J. Phys. Chem. A 102 (1998) 3970.
[85] Y. Ruiz-Morales, G. Schreckenbach, T. Ziegler, J. Phys. Chem. A 101 (1997) 4121.

[86] Y. Ruiz-Morales, G. Schreckenbach, T. Ziegler, Organometallics 15 (1996) 3920.
[87] Y. Ruiz-Morales, G. Schreckenbach, T. Ziegler, J. Phys. Chem. 100 (1996) 3359.
[88] G. Schreckenbach, Y. Ruiz-Morales, T. Ziegler, J. Chem. Phys. 104 (1996) 8605.
[89] A.W. Ehlers, Y. Ruiz-Morales, E.J. Baerends, T. Ziegler, Inorg. Chem. 36 (1997) 5031.
[90] J.B. Greco, J.C. Peters, T.A. Baker, W.M. Davis, C.C. Cummins, G. Wu, J. Am. Chem. Soc. 123 (2001) 5003.
[91] H. Henderickx, G. Kwakkenbos, A. Peters, J. van der Spoel, K. de Vries, Chem. Commun. 16 (2003) 2050.

Available online at www.sciencedirect.com
SCIENCE DIRECT®
Polyhedron 23 (2004) 2769–2777
POLYHEDRON
www.elsevier.com/locate/poly

Near infra-red luminescence from bis-terpyridyl iridium(III) complexes incorporating electron-rich pendants

Wendy Leslie [a], Robert A. Poole [a], Paul R. Murray [b], Lesley J. Yellowlees [b,*], Andrew Beeby [a], J.A. Gareth Williams [a,*]

[a] Department of Chemistry, University of Durham, South Road, Durham DH1 3LE, UK
[b] School of Chemistry, University of Edinburgh, West Mains Road, Edinburgh EH9 3JJ, UK

Received 25 April 2004; accepted 25 August 2004
Available online 25 September 2004

Abstract

Iridium(III) bis-terpyridine complexes have been prepared which incorporate aminobenzene or pyrene substituents at the 4′-position of the terpyridine. The homoleptic complexes, $[Ir(L^1)_2]^{3+}$ and $[Ir(L^2)_2]^{3+}$ {L^1 = 4′-(*p*-Me_2N-C_6H_4)-2,2′:6′,2″-terpyridine; L^2 = 4′-(*p*-Ph_2N-C_6H_4)-2,2′:6′,2″-terpyridine} display an intense absorption band in the visible region, which exhibits slight positive solvatochromism, due to an excited state of intra-ligand charge transfer (ILCT) character, in which the aminobenzene unit acts as the electron donor and the metal-bound terpyridyl unit as the acceptor. The complexes are weakly luminescent in the near infra-red (λ_{max} 750–800 nm); this short-lived, low-energy emission, whose likely origin is an excited state of primarily ILCT character, is in contrast to the long-lived $^3\pi$–π^* luminescence of previously studied bis-terpyridyl iridium complexes. The corresponding ILCT absorption band in the heteroleptic, pyrene-substituted complex, $[Ir(tpy)L^3]^{3+}$ {L^3 = 4′-(1-pyrenyl)-2,2′:6′,2″-terpyridine}, displays negative solvatochromism, owing to the excited state having lower polarity than the ground state. This complex emits weakly at slightly higher energy (710 nm). The switch to ILCT character upon appending the $[Ir(tpy)_2]^{3+}$ core with a pyrene substituent may be compared to the influence of the pyrene unit in $[PtL^3Cl]^+$, but contrasts with the triplet–triplet equilibrium that is established in structurally related ruthenium complexes incorporating pyrene pendants. The electrochemical properties of the pyrene-substituted ligand and complex in solution are also described.
© 2004 Elsevier Ltd. All rights reserved.

Keywords: Iridium; Luminescence; Terpyridine; Near infra-red; Charge-transfer; Intra-ligand charge transfer

1. Introduction

The excited state chemistry of transition metal complexes containing pyridyl-based ligands has long been of interest. A combination of rich photophysical and electrochemical properties makes many compounds of this type potentially appropriate for numerous applications, including photocatalysis, luminescent sensors, electroluminescence and electron transfer reagents for conversion of light to chemical energy [1]. The synthetic challenges associated with the preparation of complexes of iridium(III), particularly the kinetic inertness of this third-row d^6 metal ion with respect to ligand exchange processes, has rather retarded progress with this element compared to its neighbours in the periodic table [2]. However, recent results on the application of *fac*-[Ir(ppy)$_3$] (ppy = 2-phenylpyridyl) as a triplet harvesting agent in organic light emitting devices (OLEDs) has rekindled a great deal of interest in cyclometalated iridium(III) complexes [3]. At the same time, the longer lifetimes associated with derivatives of $[Ir(tpy)_2]^{3+}$,

* Corresponding authors. Tel.: +44 191 334 2124; fax: +44 191 384 4737.
E-mail addresses: l.j.yellowlees@ed.ac.uk (L.J. Yellowlees), j.a.g.williams@durham.ac.uk (J.A. Gareth Williams).

0277-5387/$ - see front matter © 2004 Elsevier Ltd. All rights reserved.
doi:10.1016/j.poly.2004.08.009

containing an N_6 coordination sphere, have initiated studies into their possible application as luminescent sensors or labels amenable to time-resolved detection procedures [4–6].

$[Ir(ppy)_3]$ and $[Ir(tpy)_2]^{3+}$ are, in fact, representative of the two main classes of iridium(III) complexes, in terms of luminescence behaviour. When some of the ligands (normally two or more) are anionic, as in cyclometalated compounds like $[Ir(ppy)_3]$, the emitting excited state usually has significant metal-to-ligand charge transfer (MLCT) character, with lifetimes often of the order of 500–1000 ns in degassed solution [2]. In the presence of exclusively neutral ligands, however, as in $[Ir(tpy)_2]^{3+}$, the electron density at the metal is lower, and metal-centred oxidation is unfavourable. In these cases, the HOMO resides largely on the ligand rather than the metal, the MLCT states are raised in energy, and the emitting state has primarily ligand-centred (LC) character, with longer lifetimes in the microsecond region [2,7,8]. Previous studies on derivatives of $[Ir(tpy)_2]^{3+}$ have shown that the introduction of simple, conjugating aryl substituents (e.g., tolyl) onto the 4′ position of the terpyridine leads to a stabilisation of the LC state and a lengthening of the excited state lifetime, an effect which is even more pronounced for a biphenyl substituent [8,9]. In this contribution, we describe how the introduction of more electron-rich aryl substituents into the same position of the terpyridine unit leads to a switch in the nature of the emission to a third class, namely intra-ligand charge transfer (ILCT).

2. Results and discussion

2.1. Synthesis of ligands and complexes

The complexes investigated in this study are shown in Scheme 1. Most synthetic routes to 4′-aryl-substituted terpyridines are based on the Tschitschibabin pyridine synthesis, involving condensation of the appropriate aryl aldehyde with two equivalents of 2-acetylpyridine, followed by ring closure of the resulting diketone intermediate with ammonia (or an equivalent thereof) at elevated temperatures, to form the central pyridine ring [10]. However, many of the simpler one-pot procedures are satisfactory only for simple aryl substituents, and suffer from low yields and difficult purifications when aryl aldehydes of lower reactivity are employed, including amino-benzaldehydes [11]. We have been exploring the utility of Suzuki cross-coupling of 4′-bromo-terpyridine (tpy-Br) with aryl boronic acids as a divergent and general method for preparing 4′-aryl-terpyridines, and this procedure was employed here to obtain L^1 {4′-(*p*-Me_2N-C_6H_4)-2,2′:6′,2″-terpyridine} in good yield by cross-coupling of tpy-Br with commercially available

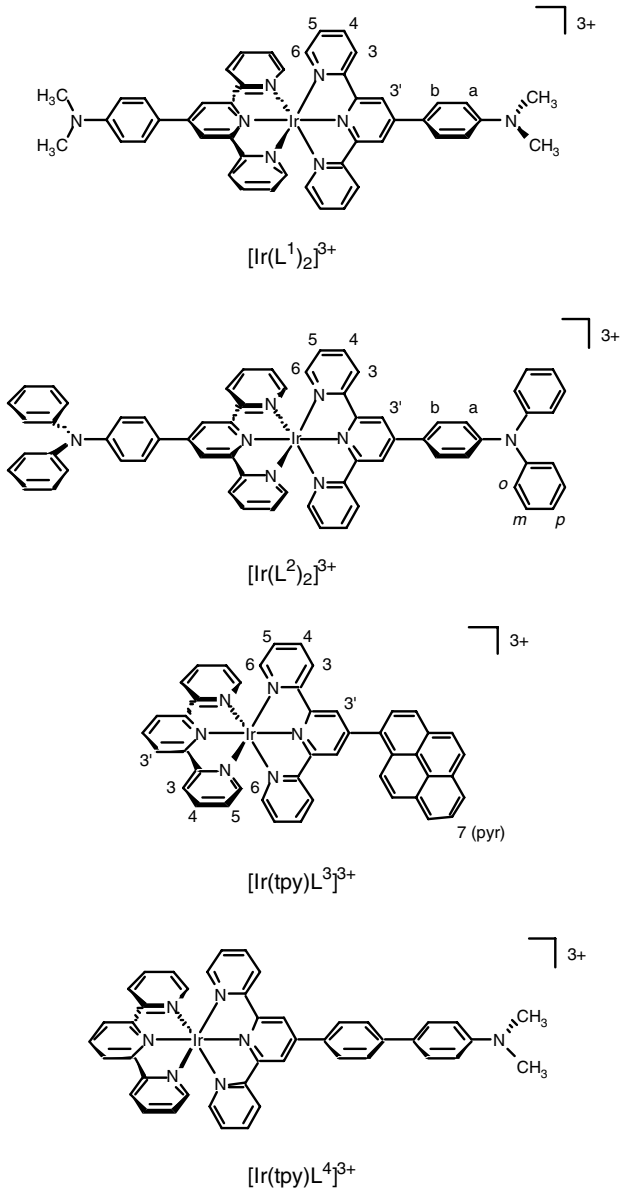

Scheme 1. Structures of the complexes investigated.

4-*N*,*N*-dimethylaminobenzene boronic acid, as reported previously [12–14]. In order to prepare the diphenylamino analogue, L^2, the boronate ester 4-(neopentylglycolatoboron)-*N*,*N*-diphenylaniline was first prepared by palladium-catalysed cross-coupling of 4-bromo-*N*,*N*-diphenylaniline with bis-(neopentylglycolato)diboron, and subsequently coupled with tpy-Br as for L^1 [12,13]. 4′-(1-Pyrenyl)-2,2′:6′,2″-terpyridine L^3 [15] was prepared by condensation methodology, using the procedure of Constable for 4′-anthryl-terpyridine [16]. For these more hindered aryl groups, the enone generated upon treatment of the aryl aldehyde with 2-acetylpyridine is not sufficiently reactive to be attacked directly by the enol form of a second equivalent of 2-acetylpyridine [16]; instead, the latter must be converted to the

more reactive enolate through prior deprotonation with potassium *tert*-butoxide.

The homoleptic iridium(III) complexes $[Ir(L^1)_2](PF_6)_3$ and $[Ir(L^2)_2](PF_6)_3$ were prepared by direct reaction of $IrCl_3 \cdot 3H_2O$ with two or more equivalents of the corresponding ligand, in refluxing ethylene glycol, followed by anion exchange with potassium hexafluorophosphate. Whilst the fomer complex was readily purified by crystallisation, the latter proved more troublesome, requiring chromatography on silica followed by alumina in order to remove all traces of a fluorescent yellow impurity. Both complexes were deep red in colour, in striking contrast to the yellow or pale yellow colours of previously reported bis-terpyridyl iridium complexes, including the parent complex, $[Ir(tpy)_2](PF_6)_3$, and aryl substituted derivatives such as $[Ir(ttpy)_2](PF_6)_3$ (ttpy = 4′-tolylterpyridine). The complex $[Ir(tpy)L^3](PF_6)_3$ was obtained via a two-step strategy: the intermediate compound $[Ir(tpy)Cl_3]$, prepared by reaction of $IrCl_3 \cdot 3H_2O$ with one equivalent of terpyridine as reported previously [8], was first isolated, and then reacted with one equivalent of L^3 in ethylene glycol at reflux for 15 min. Subsequent anion exchange with KPF_6 and column chromatography on silica led to the desired complex as a red solid in 50% yield.

The complexes were characterised by high resolution electrospray ionisation mass spectrometry and by ^1H NMR spectroscopy. A combination of ^1H–^1H NOESY and COSY measurements allowed a full assignment of the ^1H NMR spectra of $[Ir(L^1)_2](PF_6)_3$ and $[Ir(L^2)_2](PF_6)_3$ to be made, with the NOESY data allowing the resonances on the pendent rings to be identified on the basis of through-space coupling between H^b and $H^{3'}$ (see Scheme 1 for atom numbering system). Unsurprisingly, several of the pyrenyl resonances in $[Ir(tpy)L^3](PF_6)_3$ overlap, but the terpyridyl protons are all resolved, providing unambiguous confirmation of the identity of the complex.

2.2. Absorption and fluorescence spectra of the ligands and electrochemistry of L^3

We previously reported on the photophysical properties of ligands L^1 and L^2 [12,13]. These compounds are intensely fluorescent, and their highly solvent-dependent fluorescence emission maxima, which shift to longer wavelengths with increasing solvent polarity, have been interpreted in terms of an intramolecular charge transfer (ICT) excited state. The amino substituent in these ligands raises the energy level of the pendent aryl group to such an extent that the lowest energy excited state corresponds to a π_{Ar}–π^*_{tpy} (ICT) transition, as opposed to the locally excited states (π_{tpy}–π^*_{tpy}) of other 4′-aryl-substituted terpyridines [17].

In the present study, the photophysical properties of the free, pyrene-substituted ligand L^3 have been examined. The absorption spectra in three different solvents of varying polarity are shown in Fig. 1, which show no significant differences in the absorbance maxima. This is consistent with initial excitation to a locally excited state (π_{tpy}–π^*_{tpy}) of similar polarity to the ground state (see also the excitation spectra in Fig. 2). On the other hand, the fluorescence emission maxima undergo significant shifts to longer wavelengths with increasing solvent polarity (Fig. 2), a trend directly analogous to that displayed by the amino substituted compounds L^1 and L^2. This indicates that the pyrene substituent has a similar effect, and that the emission again originates from an ICT state, (where the pyrene unit acts as the electron donor), formed indirectly following excitation to the locally excited state.

These conclusions, particularly regarding the electron-donating character of the pyrene unit in L^3, are supported by the electrochemistry of this ligand. The

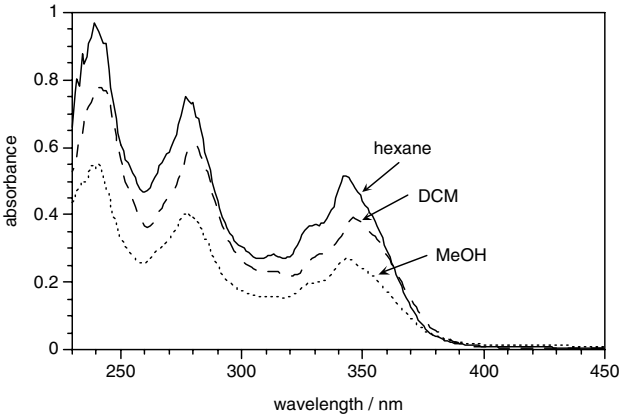

Fig. 1. UV–Vis absorption spectra of L^3 in solution in hexane, dichloromethane and methanol, at 295 K.

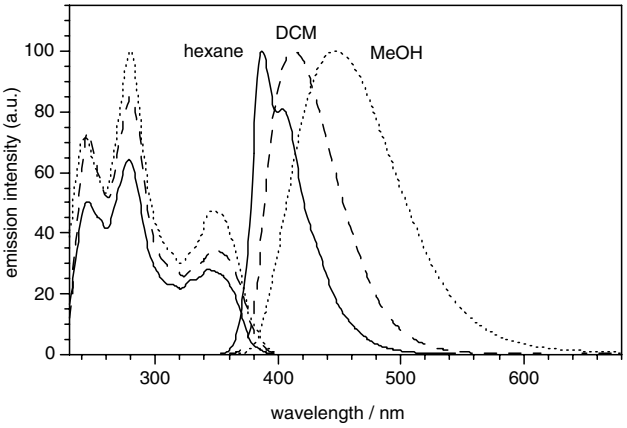

Fig. 2. Corrected fluorescence emission spectra (right) for ligand L^3 in hexane, dichloromethane and methanol (λ_{ex} = 344 nm, excitation and emission bandpasses set to 2.5 nm); and the corresponding fluorescence excitation spectra (λ_{em} set to the maximum in the respective uncorrected emission spectrum); 295 K.

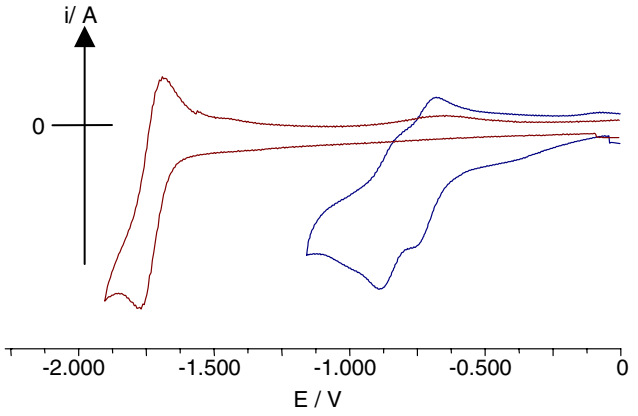

Fig. 3. Cyclic voltammograms of $[Ir(tpy)L^3]^{3+}$, showing the first two reductions, (right), and of ligand L^3 (left), in DMF in the presence of 0.1 M $^tBuN_4BF_4$.

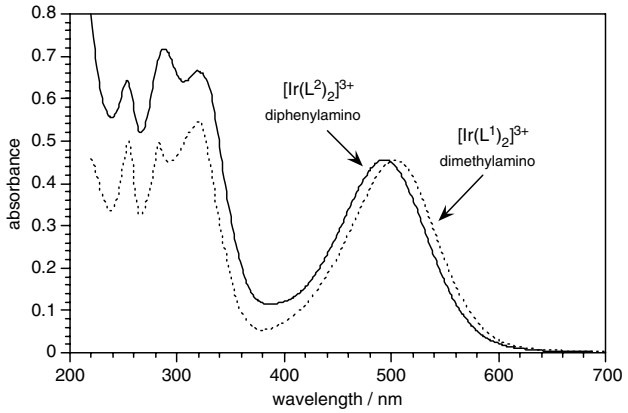

Fig. 4. UV–Vis absorption spectra of $[Ir(L^1)_2]^{3+}$ (dotted line) and $[Ir(L^2)_2]^{3+}$ (solid line) in acetonitrile solution at 295 K.

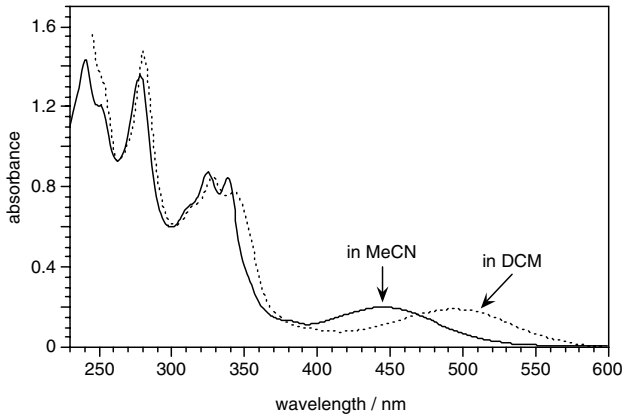

Fig. 5. UV–Vis absorption spectra of $[Ir(tpy)L^3]^{3+}$ in acetonitrile solution (solid line) and in dichloromethane (dotted line) at 295 K.

ligand displays a one-electron reduction process at −1.66 V in solution in DMF at room temperature (Fig. 3 and Table 1). This value is substantially smaller (less negative) than the reduction potentials of both terpyridine and pyrene (which have very similar values to one another, Table 1), indicating that the pyrene-substituted terpyridine is much more readily reduced than either of its two constituent components. Since the reduction is a one-electron process, this demonstrates that the pyrene and terpyridine units are not acting independently, but rather that the electron enters a molecular orbital which is centred over the whole molecule; i.e., the LUMO in L^3 has a considerably extended π-system compared to the two components. In contrast, the oxidation potential of L^3 is very similar to that of pyrene itself (+1.49 and 1.47 V, respectively, Table 1), supporting the conclusion that the pyrenyl unit in L^3 is the site from which charge transfer occurs in the ICT process described above.

2.3. Absorption spectra of the complexes

All three complexes display strong absorption bands in the visible region of the spectrum, (responsible for the intense colours of the compounds), which are not present in the spectra of the free ligands; λ_{max} (CH_3CN)

Table 1
Electrochemical potentials for L^3, $[Ir(tpy)L^3]^{3+}$, pyrene and terpyridine[a]

Compound	$E^{red}_{1/2}$ (V)	$E^{ox}_{1/2}$ (V)
Terpyridine	−1.99	[b]
Pyrene	−1.98	+1.47
L^3	−1.66	+1.49
$[Ir(tpy)L^3]^{3+}$	−0.65, −0.78, −1.23, −1.54	+1.59

[a] In DMF/0.1 M [$^tBu_4N$][BF_4] at room temperature.
[b] No oxidation wave observed within the solvent window (DMF displays a large decomposition peak above +1.8 V).

$[Ir(L^1)_2]^{3+}$ 504 nm, $[Ir(L^2)_2]^{3+}$ 493 nm, $[Ir(tpy)L^3]^{3+}$ 444 nm (Figs. 4 and 5; Table 2). These bands are attributed to an intraligand charge transfer (ILCT) transition, in which the pendent aminobenzene or pyrene group behaves as the donor, and the metal-bound terpyridyl moiety as the electron acceptor. The appearance of such bands in the complexes can be related to the increased acceptor properties of the terpyridyl π* orbitals upon coordination to the metal ion. Previously, we reported on a related, heteroleptic bis-terpyridyl iridium complex, incorporating a terpyridine appended with a *p*-(dimethylamino)-biphenyl unit, $[Ir(tpy)L^4]^{3+}$ (Fig. 1) [9]. This complex also displayed a strong, low-energy band in the same region (λ_{max} 476 nm), similarly assigned to an ILCT transition. In fact, a comparable phenomenon has also been observed upon coordination of zinc(II) to L^1 and L^2, leading to a band at 433 and 426 nm, respectively [13,12]; the longer wavelength of the bands in the iridium complexes can be related to the higher charge density of the iridium(III) ion compared to zinc(II). The bands are also lower in energy than that seen in the iridium chloro complex $[IrL^5Cl_3]$, {L^5 = 4′-(*p*-

Table 2
Absorption and emission data at 295 K for the complexes reported here, with data for the heteroleptic amino-substituted complex $[Ir(tpy)L^4]^{3+}$ for comparison[a]

	$[Ir(L^1)_2]^{3+}$	$[Ir(L^2)_2]^{3+}$	$[Ir(tpy)L^4]^{3+}$	$[Ir(tpy)L^3]^{3+}$
$\lambda_{max}^{abs}(\varepsilon)$ (MeCN)	255 (49 000)	253 (48 800)	251 (38 100)	240 (29 200)
	283 (48 000)	288 (54 800)	278 (29 600)	276 (27 700)
	321 (53 300)	321 (50 600)	322 (31 700)	325 (18 100)
	504 (44 800)	493 (35 100)	476 (9400)	338 (17 400)
				444 (4100)
λ_{max}^{abs} (H_2O)[b]	510	494	420	—[c]
λ_{max}^{abs} (CH_2Cl_2)[b]	502	492	498	492
λ_{max}^{em} (MeCN)	754	784	—[d]	710

[a] Ref. [9].
[b] The wavelength of the lowest energy band in the spectrum is given.
[c] This complex is insoluble in water.
[d] The emission from this complex was too weak to allow a reliable spectrum to be obtained.

Bu_2N-C_6H_4-)-terpyridine}, for which λ_{max} = 465 nm in $CHCl_3$ [18]; again, this is in line with the absence of anionic ligands in the present complexes, in contrast to the chloride ligands in $[IrL^5Cl_3]$, which will serve to counteract partially the positive charge of the metal ion. From Fig. 4, it may be noted that, of the two amino-substituted compounds, the dimethylamino complex displays marginally the lower energy band (by 11 nm), which is consistent with the more strongly electron-donating nature of the Me_2N–C_6H_4– moiety compared to Ph_2N–C_6H_4–, and hence with the ILCT formulation.

In the case of the pyrene-substituted complex, $[Ir(tpy)L^3]^{3+}$, the long wavelength band displays pronounced negative solvatochromism; for example, there is a large red-shift of 50 nm on going from acetonitrile solution (444 nm) to dichloromethane (494 nm) (see Fig. 5). Such negative solvatochromism can be explained in terms of the smaller dipole moment expected in the charge-transfer excited state compared to the ground state, and the fact that the charge-transfer axis is colinear with the dipole axis in this heteroleptic complex (C_{2v} symmetry) [19]. Negative solvatochromism was similarly observed in the aforementioned, heteroleptic amino-substituted complex, $[Ir(tpy)L^4]^{3+}$, described previously (e.g., λ_{max} 476 nm in CH_3CN and 420 nm in H_2O) [9]. In contrast, the bands in the homoleptic amino-substituted complexes display only a very small, positive solvatochromism (e.g., a 2 nm blue-shift for $[Ir(L^1)_2]^{3+}$ on going from acetonitrile to dichloromethane, and a 7 nm red-shift in water). In these homoleptic complexes with D_{2d} symmetry, there is no permanent dipole moment in the ground state, and formation of the ILCT excited state will be accompanied by a small increase in the polarity of the system, leading to the observed behaviour.

2.4. Electrochemistry of $[Ir(tpy)L^3]^{3+}$

The pyrene-substituted complex has a rich redox chemistry. The cyclic voltammogram shows the first two reductions at −0.65 and −0.78 V (Fig. 3) but there are two further reductions at −1.23 and −1.54 V. All reductions are one-electron steps. Thus, compared to the free ligands, complexation to the Ir^{3+} ion has resulted in the ligand-based reductions moving to more positive (less negative) potentials due to the influence of the tri-positive charge. Since L^3 is more readily reduced than terpyridine, as discussed above, it would seem reasonable to suggest that it is the pyrene-substituted ligand that is reduced first, followed by the unsubstituted terpyridine. However, the potential difference between the first two reductions is of the order of that expected for two terpyridine ligands bound to the same metal centre, and hence the site of reduction is ambiguous. In an attempt to identify which ligand is reduced initially, the reduction was probed by spectroelectrochemical methods (UV/vis/nir and epr) at 233 K. Unfortunately, however, the reduced iridium complex is not stable on the timescale of the spectroelectrochemical experiments, even at 233 K.

The complex shows a single, quasi-reversible, one-electron oxidation process at +1.59 V at room temperature. This is in marked contrast to other bis-terpyridyl iridium complexes studied to date, such as $[Ir(tpy)_2]^{3+}$ and $[Ir(ttpy)_2]^{3+}$, which show no oxidation process within the solvent window, supporting the notion that it is the pyrene unit which is the site of oxidation, and hence the origin of the ICT process. The oxidation potential is higher by 0.1 V than that of the free ligand L^3 (Table 1), consistent with the net positive charge on the complex mildly disfavouring oxidation at the remote pyrenyl site.

3. Luminescence of the complexes

3.1. Pyrene-susbtituted complex

Upon excitation into the ILCT band, $[Ir(tpy)L^3]^{3+}$ exhibits very weak red luminescence, centred at 710 nm in acetonitrile solution. The quantum yield was esti-

mated to be of the order of $4(\pm 2) \times 10^{-4}$, using $[Ru(bpy)_3]Cl_2$ as the standard; (the considerable uncertainty in the value stems from the low emission intensity and the poor response of the photomultiplier tube in this region). The emission intensity was too weak to measure the lifetime with available instrumentation; however, on the basis of the observation that the luminescence intensity was only marginally augmented upon degassing the solution, we suspect that the lifetime is short (probably <100 ns), and consistent with an excited state which is subject to severe non-radiative deactivation processes, leading to the low quantum yield. Given that this behaviour contrasts markedly with the long-lived $^3\pi$–π^* luminescence observed in almost all $[Ir(tpy)_2]^{3+}$ derivatives studied hitherto, it seems likely that the origin of the emission is a state comprising significant ILCT character, a hypothesis supported by DFT calculations using B3LYP. It is interesting to compare the behaviour of $[Ir(tpy)L^3]^{3+}$ with that of $[PtL^3Cl]^+$, investigated in detail by McMillin and co-workers [15,20]. In their study of the effect of appending the $[Pt(tpy)Cl]^+$ core with aryl substituents, a complicated yet fascinating picture emerges in the case of a pyrene pendant. Emission arises from two different excited states, of which one (emitting at 645 nm) is assigned as a ^{1}ILCT state and persists under aerated conditions, and the other is attributed to a triplet state (680 nm), probably incorporating both MLCT and ILCT character, and is efficiently quenched by oxygen. The lower energy of the observed emission in the Ir(III) system compared to the Pt(II) complex is fully consistent with the higher positive charge associated with the Ir(III) centre compared to the Pt(II)–Cl unit, stabilising the ILCT state.

The behaviour of the pyrene-substituted iridium compound contrasts with the results of several recent investigations into pyrene-appended $[Ru(bpy)_3]^{2+}$ or $[Ru(phen)_3]^{2+}$ complexes [21]. In such cases, the pyrene unit can act as a ''store'' of the excited state energy, with a triplet–triplet thermal equilibrium being established between the emissive ^{3}MLCT excited state of the ruthenium centre, and the $^3\pi$–π^* state of the pyrene unit. This leads to large augmentations of the observed luminescence lifetime compared to the unsubstituted complexes, for example, up to 148 μs for a *tris*-pyrenyl substituted $[Ru(phen)_3]^{2+}$ derivative [21b]. That the iridium complex does not profit from a similar effect is apparently due to the more highly oxidising nature of the IrN_6^{3+} core compared to RuN_6^{3+}, allowing the former to participate in the ILCT process.

3.2. Amino-substituted complexes

In the case of the amino-substituted complexes, the emission was too red-shifted and too weak to be recorded reliably using the conventional photomultiplier tube of our fluorimeter. However, emission spectra were successfully recorded using a single-photon avalanche detector (Fig. 6), revealing that the complexes do indeed emit in acetonitrile solution, albeit weakly, in the near infra-red region {λ_{max} from uncorrected spectra: $[Ir(L^1)_2]^{3+}$ 754 nm, $[Ir(L^2)_2]^{3+}$ 784 nm}. Again, the presence of oxygen had no effect on the spectral profile and little effect on the intensity of emission, consistent with emission from only one excited state, most probably of predominantly ILCT character. However, an interesting difference between the two compounds emerges in aqueous solution. The diphenylamino-substituted complex, $[Ir(L^2)_2]^{3+}$, emits in water (Fig. 7), with an emission intensity comparable to that observed in acetonitrile (for solutions isoabsorbant at the excitation wavelength of 532 nm). On the other hand, for the dimethylamino-substituted complex $[Ir(L^1)_2]^{3+}$, the emission in aqueous solution was too weak to be measured with the same instrumental set-up. Clearly, an additional non-radiative deactivation process must be operative for the Me_2N-

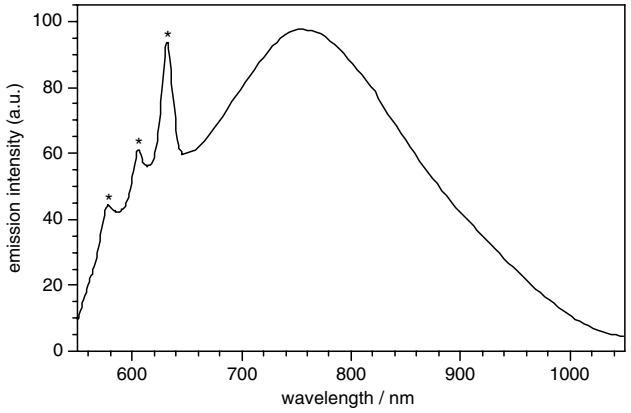

Fig. 6. Emission spectrum of $[Ir(L^1)_2]^{3+}$ in acetonitrile solution; λ_{ex} = 532 nm, 295 K. The bands marked with an asterisk are Raman bands of the solvent (C≡N and two C–H).

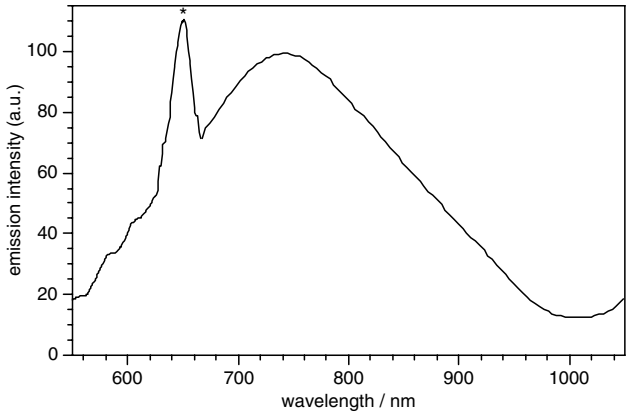

Fig. 7. Emission spectrum of $[Ir(L^2)_2]^{3+}$ in aqueous solution; λ_{ex} = 532 nm, 295 K. The Raman band of water is marked with an asterisk. (The onset of an increased signal at low energy is due to residual 1064 nm radiation in the frequency-doubled output of the Nd:YAG excitation source).

substituted system in water, which is absent (or at least less efficient), in the Ph_2N-analogue. In fact, our previous work on the photophysics of the free ligands revealed a related effect [12,13]. Thus, whilst the fluorescence quantum yield of L^2 in ethanol was comparable to the values in other, non-OH solvents (cyclohexane, THF and DCM), for L^1, in contrast, the emission intensity in ethanol solution was much lower than for the other solvents (e.g., ϕ was 30 times smaller in EtOH than in DCM). Since the fluorescence lifetime did not show a comparable reduction, the small ϕ of L^1 in EtOH was attributed to a reduction in the efficiency of formation of the emissive ICT state, following excitation to the initially populated excited state, as opposed to enhanced non-radiative deactivation. This may be due to hydrogen bonding between the $-NMe_2$ nitrogen atom and the –OH group of the solvent, inhibiting the twisting process that is thought to accompany the formation of the ICT state [22]; such hydrogen bonding will be absent (or only very weak) in the $-NPh_2$ analogue L^2, since triphenylamine is not basic. It is possible that a similar effect operates in the complex, $[Ir(L^1)_2]^{3+}$, reducing the efficiency with which the emissive excited state is formed in this case.

It is also noteworthy that whilst convincing emission spectra could be obtained for these two complexes, the luminescence of the related complex $[Ir(tpy)L^4]^{3+}$, prepared previously [9], is extremely weak, and attempts to obtain a reliable emission spectrum using the same instrumental set-up have met with little success. A possible explanation is that the presence of the additional phenyl ring in $[Ir(tpy)L^4]^{3+}$ (interposed between the metal terpyridyl core and the aminophenyl substituent) promotes non-radiative deactivation pathways, by offering additional C–C stretching vibrations able to act as energy-accepting modes for deactivation of the excited state, and perhaps also by facilitating interaction with the solvent molecules.

4. Conclusions

In summary, we have shown that the introduction of electron-donating amino or pyrenyl substituents into bis-terpyridyl iridium(III) complexes leads to a change in the nature of the lowest-lying excited state, to intramolecular charge transfer (ILCT). Excitation to the ILCT states leads to the appearance of low-energy solvatochromic bands in the absorption spectrum. Unusually, the ILCT states are emissive under ambient conditions (albeit only weakly so), giving rise to broad, structureless bands in the near infra-red. This behaviour contrasts with that of previously studied bis-terpyridyl iridium complexes, which normally display $^3\pi$–π^* luminescence. Given the current interest in near IR-emitting compounds for a variety of applications, complexes of this type may represent an intriguing extension of the future potential of luminescent polypyridyl iridium complexes.

5. Experimental

5.1. Synthetic details

Ligands L^1 and L^2 were prepared by Suzuki cross-coupling methodology from 4′-bromo-terpyridine, as described previously [12,13]. $[Ir(tpy)L^4]^{3+}$ was prepared from $[Ir(tpy)(tpy\text{-}C_6H_4\text{-}Br)]^{3+}$ by an in situ cross-coupling reaction, as described previously [9]. Solvents used were Analar quality or better; THF was distilled from sodium prior to use. Water was purified using the Purite Still-plus system. ^{1}H NMR spectra were recorded on a Varian Mercury-200, Unity-300 or a 500 MHz instrument, and referenced to residual protio-solvent resonances. Coupling constants are in Hertz. Electrospray ionisation mass spectra were acquired on a time-of-flight Micromass LCT instrument; high resolution spectra for accurate mass determinations were carried out either on this instrument or at the EPSRC National Mass Spectrometry Service Centre, Swansea.

3-(Pyren-1-yl)-1-(pyridin-2-yl)-propenone. 2-Acetylpyridine (0.54 g, 4.5 mmol) and 1-pyrenecarboxaldehyde were dissolved in a mixture of ethanol (30 mL) and dichloromethane (15 mL), and sodium hydroxide (0.3 g in 5 mL water) was added dropwise with stirring. The mixture was left for 18 h at room temperature with continuous stirring, and the resulting precipitate was isolated by filtration, and washed with cold ethanol, to give the desired compound as a bright orange solid; 1.1 g, (74%). ^{1}H NMR (500 MHz, $CDCl_3$): δ 9.14 (1H, d, J 16, vinylic H), 8.81 (1H, d, J 4.5, H^6), 8.61 (1H, d, J 16, vinylic H), 8.29 (1H, d, J 7.0, H^3), 8.27–8.00 (9H, m, pyrenyl protons), 7.94 (1H, td, J 7.0, 1.5, H^4), 7.54 (1H, t, J 5.5, H^5). MS (ES+): m/z 334 ($M + H^+$). ν_{max}(KBr) = 3043 (arom C-H), 1660 (C=O), 1588, 1574 cm^{-1} (C=C). $\lambda_{max}{}^{abs}$ (DCM): 270, 311, 340, 391, 425 nm. $\lambda_{max}{}^{em}$ (DCM): 526 nm.

4′-(Pyren-1-yl)-2,2′:6′,2″-terpyridine. The method was based on that described by Constable for 4′-anthryl-terpyridine [16], as also employed by McMillin [15]. 2-Acetylpyridine (0.22 mL, 1.84 mmol) was added to a stirred solution of potassium *tert*-butoxide (0.34 g, 3.00 mmol) in anhydrous THF (40 mL) and stirred at room temperature under nitrogen for 2 h. 3-(Pyren-1-yl)-1-(pyridin-2-yl)-propenone (0.5 g, 1.5 mmol) was added, and the solution stirred at room temperature for 18 h. Ammonium acetate (2.34 g, 30 mmol) and ethanol (40 mL) were added to the deep red solution, and the mixture heated at reflux for 4 h. The solvent was removed under reduced pressure and the residue taken up into a mixture of CH_2Cl_2 and water. The organic layer

was separated, washed with more water, dried over anhydrous K_2CO_3 and the solvent removed. The residue was recrystallised from $CHCl_3$/MeOH to give the desired product as a colourless solid; 0.44 g (68%). ^1H NMR (500 MHz, $CDCl_3$, assigned using ^1H–^1H NOESY and COSY): δ 8.77 (2H, s, $H^{3'}$), 8.76 (2H, d, J 7.2, H^3), 8.70 (2H, d, J 4.1, H^6), 8.09–8.28 (8H, m, pyrenyl protons), 8.04 (1H, t, J 7.5, H^7-pyr), 7.92 (2H, td, J 7.2, 1.5, H^4), 7.36 (2H, ddd, J 7.2, 4.1, 1.0, H^5). MS (ES+): m/z 433 (M^+). Calc. for $C_{31}H_{19}N_3$: C, 85.89, H, 4.42, N, 9.69%. Found C, 85.15, H, 4.89, N, 9.17%.

[Ir(L¹)₂](PF₆)₃. 4′-(*p*-*N*,*N*-Dimethylaminophenyl)-2,2′:6′, 2″-terpyridine (164 mg, 0.47 mmol) and $IrCl_3 \cdot 3H_2O$ (85 mg, 0.24 mmol) were dissolved in ethylene glycol (25 mL) and heated with stirring at 100 °C for 1.5 h, followed by a further 3 h at reflux (oil bath temperature 215 °C). After cooling to ambient temperature, the solution was added to a saturated aqueous solution of KPF_6, to precipitate the crude product as a red solid. Repeated recrystallisation from an acetone/toluene mixture led to the desired complex; 270 mg (83%). TLC (silica): $R_f = 0.6$, in 85% CH_3CN/14% H_2O/1% KNO_3(aq). ^1H NMR (300 MHz, $(CD_3)_2CO$): δ 9.42 (4H, s, $H^{3'}$), 9.14 (4H, d, J 7.8, H^3), 8.32 (12H, overlapping m, H^4, H^6 and H^b), 7.63 (4H, t, J 6.8, H^5), 7.05 (4H, d, J 9.0, H^a), 3.21 (12H, s, CH_3). ^1H NMR (200 MHz, CD_3CN): δ 8.96 (4H, s, $H^{3'}$), 8.70 (4H, d, J 8.0, H^3), 8.20 (4H, m overlapping with following signal, approx. J 7.5, H^4), 8.18 (4H, d, J 9.0, H^b), 7.70 (4H, d, 5.0, H^6), 7.46 (4H, td, J 7.2, 5.0, H^5), 7.04 (4H, d, J 9.0, H^a), 3.18 (12H, s, CH_3). MS (ES+): m/z 521 $(M^{3+} + PF_6^-)^{2+}$, 448 $(M^{3+} - H^+)^{2+}$, 299 (M^{3+}). HRMS (ES+): 1187.2292 $(M^{3+}+2PF_6^-)^+$. Calc. for $C_{46}H_{40}N_8IrP_2F_{12}$: 1187.2289.

[Ir(L²)₂](PF₆)₃. 4′-(*p*-*N*,*N*-Diphenylaminophenyl)-2,2′:6′, 2″-terpyridine (300 mg, 0.63 mmol) and $IrCl_3 \cdot 3H_2O$ (74.1 mg, 0.21 mmol) were dissolved in ethylene glycol (15 mL) and heated with stirring at 90 °C for 2 h, followed by a further 6 h at reflux (bath temperature 215 °C). The solution was then added to a saturated aqueous KPF_6 solution to precipitate the crude product. Unreacted ligand was removed by washing the solid with toluene, and the remaining material was then purified by column chromatography on silica; gradient elution from 100% CH_3CN to 91.6% CH_3CN, 8% H_2O and 0.4% $KNO_{3(aq)}$ followed by ion exchange of fractions containing product, using KPF_6. Further chromatography on a column of alumina was required to remove all traces of an unidentified fluorescent impurity; gradient elution from 100% CH_3CN to 93.4% CH_3CN, 6% H_2O and 0.6% KNO_3(aq). A final ion exchange led to the product as the hexafluorophosphate salt; 55 mg (17%). NMR (500 MHz, $(CD_3)_2CO$): δ 9.48 (4H, s, $H^{3'}$), 9.14 (4H, d, J 8.0, H^3), 8.37 (4H, t, J 7.8, H^4), 8.24 (4H, d, J 5.5, H^6), 8.23 (4H, d, J 8.5, H^b), 7.63 (4H, t, J 6.0, H^5), 7.46 (8H, t, J 8.0, *m*-Ph), 7.26 (16H, overlapping m, *o*-/*p*-Ph and H^a). MS (ES+): m/z 645 $(M^{3+} + PF_6^-)^{2+}$, 572 $(M^{3+} - H^+)^{2+}$. HRMS (ES+): 1435.3161 $(M^{3+} + 2PF_6^-)^+$. Calc. for $C_{66}H_{48}N_8IrP_2F_{12}$: 1435.3158.

[Ir(tpy)L³](PF₆)₃. A mixture of [Ir(tpy)Cl_3], (159 mg, 0.30 mmol, prepared as described previously [8]), and 4′-(pyren-1-yl)-2,2,′:6′,2″-terpyridine (130 mg, 0.30 mmol) in ethylene glycol (10 mL) was heated under vigorous reflux for 15 min (oil bath temperature 215 °C). After allowing to cool to room temperature, the red solution was diluted with water (30 mL). Addition of a saturated aqueous solution of potassium hexafluorophosphate (10 mL) led to a red precipitate, which was separated by centrifugation and washed with water (3×10 mL). The crude product was purified by preparative column chromatography, gradient elution from CH_3CN to 60% CH_3CN/37.5% H_2O/2.5% KNO_3(aq., sat'd). Fractions containing only the desired product were subject to a second anion exchange to give the hexafluorophosphate salt; yield 190 mg (50%). ^1H NMR (500 MHz, CD_3CN): δ 9.21 (2H, s, $H^{3'}$ on L^3), 8.93 (2H, d, J 8.3, $H^{3'}$ on tpy), 8.82 (1H, t, J 8.3, $H^{4'}$ on tpy), 8.65 (2H, d, J 8.0, H^3 on tpy), 8.72–8.63 (4H, m, pyrenyl protons), 8.48 (2H, d, H^3 on L^3), 8.51–8.37 (4H, m, pyrenyl protons), 8.47 (5H, overlapping m, H^7-pyr and H^4 on both ligands), 7.90 (2H, d, J 6.0, H^6 on tpy), 7.67 (2H, d, J 5.7, H^6 on L^3), 7.61 (2H, ddd, J 7.2, 6.0, 1.0, H^5 on tpy), 7.72 (2H, ddd, J 7.3, 5.7, 1.0, H^5 on L^3). MS (ES+): m/z 430 $(M - H)^{2+}$, 286 M^{3+}. HRMS (ES+): 286.4051 (M^{3+}). Calc. for $C_{46}H_{30}N_6Ir$, M^{3+}: 286.4055.

6. Electrochemical measurements

The redox chemistry was investigated using an Autolab Pstat30 potentiostat using GPES version 4.8 software. Cyclic voltammetry was carried out at room temperature in solution in dimethylformamide, in the presence of 0.1 M [^{t}Bu$_4$N][BF_4]. The working electrode was a Pt microdisc electrode, the counter electrode a Pt rod, and a Ag/AgCl electrode was used as the reference. The scan rate was 100 mV s^{-1}. Differential pulse voltammograms were measured under the same conditions, at 20 mV s^{-1}. All solutions studied electrochemically were deoxygenated and kept under an atmosphere of nitrogen. The electrochemical potentials quoted are referenced to the ferrocinium/ferrocene couple, which was measured at 0.55 V using the same experimental conditions.

7. Photophysical measurements

Absorption spectra were measured using a Biotek Instruments XS spectrometer, using matched quartz

cuvettes of 1 cm pathlength. The fluorescence excitation and emission spectra of the ligands and of the pyrene-substituted complex were recorded using a Jobin Yvon FluoroMax-2 spectrofluorimeter, equipped with a Hamamatsu R928 photomultiplier tube. The near infra-red emission spectra of the amino-substituted complexes were obtained by excitation at 532 nm with a frequency-doubled 10 mW CW Nd:YAG laser. The emitted light was passed through a Jobin Yvon Triax-320 monochromator with NIR gratings, and detected using a single photon-counting silicon avalanche photodiode (Perkin–Elmer SPCM-AQR-13). Samples were degassed via a minimum of three freeze–pump–thaw cycles, base pressure $<10^{-3}$ mbar, in 1 cm pathlength quartz cuvettes, modified to allow connection to the vacuum line. All solvents used were HPLC grade or pre-distilled.

Acknowledgements

We thank the University of Durham for a studentship (to W.L.) and the EPSRC National Mass Spectrometry Service Centre, Swansea, for high-resolution mass spectra of the complexes.

References

[1] See, for example, K.S. Schanze, R.H. Schmehl (Eds.), Applications of Inorganic Photochemistry, J. Chem. Educ. 74 (1997) 633 et seq.
[2] A review of the synthesis and photophysical properties of pyridyl-based iridium(III) complexes, up to 2000, is provided by: I.M. Dixon, J.-P. Collin, J.-P. Sauvage, L. Flamigni, S. Encinas, F. Barigelletti, Chem. Soc. Rev. 29 (2000) 385.
[3] M.A. Baldo, S. Lamansky, P.E. Burrows, M.E. Thompson, S.R. Forrest, Appl. Phys. Lett. 75 (1999) 4, and see, for example:; S. Lamansky, P. Djurovich, D. Murphy, F. Abdel-Razzaq, H.-E. Lee, C. Adachi, P.E. Burrows, S.R. Forrest, M.E. Thompson, J. Am. Chem. Soc. 123 (2001) 4304.
[4] M. Licini, J.A.G. Williams, Chem. Commun. (1999) 1943; W. Goodall, J.A.G. Williams, J. Chem. Soc., Dalton Trans. (2000) 2893.
[5] K.K.-W. Lo, C.-K. Chung, D.C.-M. Ng, N. Zhu, New J. Chem. 26 (2002) 81.
[6] K.J. Arm, W. Leslie, J.A.G. Williams, in preparation.
[7] N.P. Ayala, C.M. Flynn Jr., L. Sacksteder, J.N. Demas, B.A. DeGraff, J. Am. Chem. Soc. 112 (1990) 3837.
[8] J.-P. Collin, I.M. Dixon, J.-P. Sauvage, J.A.G. Williams, F. Barigelletti, L. Flamigni, J. Am. Chem. Soc. 121 (1999) 5009.
[9] W. Leslie, A.S. Batsanov, J.A.K. Howard, J.A.G. Williams, Dalton Trans. (2004) 623.
[10] A review of classical methods for synthesising 4′-aryl terpyridines is provided by A.M.W. Cargill Thompson, Coord. Chem. Rev. 160 (1997) 1.
[11] For the preparation of L^1 using the condensation methodology, see T. Mutai, J.-D. Cheon, S. Arita, K. Araki, J. Chem. Soc. Perkin Trans. 2 (2001) 1045.
[12] W. Goodall, K. Wild, K.J. Arm, J.A.G. Williams, J. Chem. Soc., Perkin Trans. 2 (2002) 1669.
[13] W. Goodall, J.A.G. Williams, Chem. Commun. (2001) 2514.
[14] C.J. Aspley, J.A.G. Williams, New J. Chem. 25 (2001) 1136.
[15] J.F. Michalec, S.A. Bejune, D.G. Cuttell, G.C. Summerton, J.A. Gertenbach, J.S. Field, R.J. Haines, D.R. McMillin, Inorg. Chem. 40 (2001) 2193.
[16] G. Albano, V. Balzani, E.C. Constable, M. Maestri, D.R. Smith, Inorg. Chim. Acta 277 (1998) 225; E.C. Constable, D.R. Smith, Supramol. Chem. 4 (1995) 5.
[17] Similar conclusions were drawn for L^1 by Araki et al., supported by semi-empirical MO calculations; see Ref. [11].
[18] D. Roberto, F. Tessore, R. Ugo, S. Bruni, A. Manfredi, S. Quici, Chem. Commun. (2002) 846.
[19] See, for example S.D. Cummings, R. Eisenberg, J. Am. Chem. Soc. 118 (1996) 1949.
[20] J.F. Michalec, S.A. Bejune, D.R. McMillin, Inorg. Chem. 39 (2000) 2708.
[21] (a) A. Harriman, M. Hissler, A. Khatyr, R. Ziessel, Chem. Commun. (1999) 735; (b) D.S. Tyson, J. Bialecki, F.N. Castellano, Chem. Commun. (2000) 2355; (c) A.F. Morales, G. Accorsi, N. Armaroli, F. Barigelletti, S.J.A. Pope, M.D. Ward, Inorg. Chem. 41 (2002) 6711.
[22] The rate of formation of the charge-transfer state in two naphthalene trialkyamines has been shown to be retarded in hydrogen-bonding alcohol solvents. A.M. Brun, A. Harriman, Y. Tsuboi, T. Okada, N. Mataga, J. Chem. Soc. Faraday Trans. 91 (1995) 4047.

Available online at www.sciencedirect.com
SCIENCE DIRECT®
Polyhedron 23 (2004) 2779–2788
POLYHEDRON
www.elsevier.com/locate/poly

New hexanuclear and dodecanuclear Fe(III) clusters with carboxylate and alkoxide-based ligands from cluster aggregation reactions

Muralee Murugesu, Khalil A. Abboud, George Christou *

Department of Chemistry, University of Florida, Gainesville, FL 32611-7200, USA

Received 28 April 2004; accepted 8 July 2004
Available online 11 September 2004

Dedicated to Malcolm L.H. Green on the occasion of his retirement

Abstract

The syntheses, structures and magnetic properties are reported of three new iron(III) clusters $[Fe_6(\mu_3\text{-}O)_2(O_2CH_2)(O_2CCH_2Bu^t)_{12}(py)_2]$ (**1**), $[Fe_6(\mu_3\text{-}O)_2(O_2CCH_2Cl)_6(moe)_6](NO_3)_2$ (**2**) and $[Fe_{12}(\mu_3\text{-}O)_8(\mu\text{-}OMe)_2(O_2CPh)_{12}(pam)_6]$ (**3**). Complex **1** was synthesised from the reaction of $[Fe_3O(O_2CCH_2Bu^t)_6(H_2O)_3](O_2CCH_2Bu^t)$ with pyridine in MeCN. Complex **2** was prepared by treatment of $[Fe_3O(O_2CCH_2Cl)_6(H_2O)_3](O_2CCH_2Cl)$ and $Fe(NO_3)_3$ with methoxyethanol (moeH) in MeCN, and complex **3** was obtained from the reaction of $[Fe_3O(O_2CPh)_6(H_2O)_3](O_2CPh)$, *syn*-2-pyridinealdoxime (pamH) and NaOMe in MeCN. All three compounds can be structurally described as representing different ways of linking or fusing oxide-centered $[Fe_3(\mu_3\text{-}O)]^{7+}$ triangular units. Thus, the Fe_6 core of **1** comprises two such units bridged at one of their edges to give a twisted boat conformation, whereas the Fe_6 core of the cation of **2** comprises two $[Fe_3(\mu_3\text{-}O)]^{7+}$ units face-to-face in a staggered manner to give an Fe_6 octahedron. The more complicated Fe_{12} core of **3** contains a central Fe_6 unit that can be described in various ways, one of which is as four edge-sharing $[Fe_3(\mu_3\text{-}O)]^{7+}$ triangular units and two additional $[Fe_3(\mu_3\text{-}O)]^{7+}$ units attached to the flanks. One particular additional point of interest in **1** is the occurrence of a rare methanediolate group formed in situ and bound in an unusual μ_4-bridging mode. Variable-temperature solid-state magnetic susceptibility studies on complexes **1**–**3** in the temperature range 5.00–300 K reveal that the complexes all possess $S = 0$ ground state spins, consistent with the expected antiferromagnetic exchange interactions between the constituent iron(III) ions.
© 2004 Elsevier Ltd. All rights reserved.

Keywords: Fe(III) carboxylate chemistry; Magnetochemistry; Crystal structures; Cluster complexes

1. Introduction

The synthesis of high nuclearity iron(III) clusters is of interest for a number of reasons. These include the desire to understand and model the assembly of the polynuclear Fe/O core of the iron-storage protein ferritin, and the search for molecular species with unusual or novel magnetic properties. The latter encompasses the currently very active efforts to produce new examples of molecular species that can function as nanoscale magnetic particles, or so-called single-molecule magnets (SMMs), especially since the discovery of iron SMMs [1–5]. In such molecules the presence of a large ground state spin (S) combined with an Ising (or easy-axis) type of magnetoanisotropy (negative zero-field splitting parameter, D) leads to superparamagnet-like slow relaxation of the magnetization at low temperatures, and resulting out-of-phase AC magnetic susceptibility signals and magnetization versus applied DC field hysteresis loops [6,7]. Iron(III) is a good choice for the preparation of high nuclearity clusters given its high charge and resulting propensity to favor

* Corresponding author. Tel.: +1 352 392 6737; fax: +1 352 392 8757.
E-mail addresses: christou@chem.ufl.edu, polyhedron@chem.ufl.edu (G. Christou).

0277-5387/$ - see front matter © 2004 Elsevier Ltd. All rights reserved.
doi:10.1016/j.poly.2004.07.013

oxide-bridged units, and many large iron clusters have been reported, with nuclearities up to 19 [2,8–11]. Indeed, the formation of the Fe/O/OH core of ferritin relies also on this chemistry, and this protein core is effectively a nanoscale Fe/O particle. Thus, there is a continuing search for new synthetic methods that can yield new polynuclear Fe/O clusters. In this paper, we describe some recent results, two of which have resulted from the use of alcohol-based chelate ligands.

The chelates employed are shown in the scheme. The synthetic strategy was to react these organic molecules with the trinuclear $[Fe_3O(O_2CR)_6(H_2O)_3](O_2CR)$ complexes containing the triangular, oxide-centered $[Fe_3(\mu_3\text{-}O)]^{7+}$ core. Such trinuclear species have proven on many occasions to be excellent starting points for the synthesis of higher nuclearity Fe or Mn clusters [12–17]. The 2-methoxyethanol (moeH) [18,19] and *syn*-2-pyridinealdoxime (pamH) [20–22] ligands have been used on several previous occasions for inorganic synthesis, but there are only a very few examples of cluster compounds having been obtained with them. In particular, we are unaware of their use in reactions with $[Fe_3O(O_2CR)_6L_3]$ complexes. As a result, we felt that this approach could yield some interesting new cluster products. Indeed, this has turned out to be the case. We report that the use of moeH and pamH with $[Fe_3O(O_2CR)_6(H_2O)_3](O_2CR)$ species has led to two new high-nuclearity products, Fe_6 and Fe_{12}, respectively, and we describe the syntheses, crystal structures and magnetic properties of these complexes. In addition, we also describe a second Fe_6 complex, obtained from the reaction of $[Fe_3O(O_2CR)_6(H_2O)_3](O_2CR)$ with pyridine in the presence of MeOH. The combined results continue to demonstrate the flexibility and versatility of iron(III) chemistry for the synthesis of unusual high-nuclearity cluster compounds.

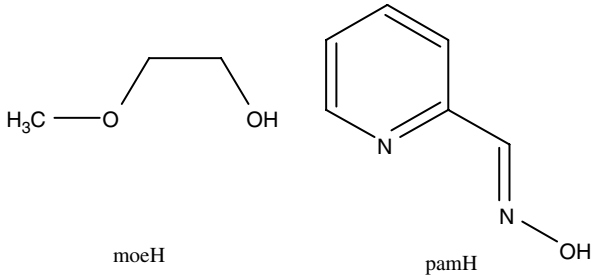

moeH pamH

2. Experimental

2.1. Compound preparations

All manipulations were performed under aerobic conditions using materials and solvents as received. $[Fe_3O(O_2CR)_6(H_2O)_3](O_2CR)$ complexes were prepared using the procedure reported previously [23].

2.1.1. $Fe_6O_2(O_2CH_2)(O_2CCH_2Bu^t)_{12}(py)_2]$ (**1**)

Method A. A solution of $[Fe_3O(O_2CCH_2Bu^t)_6(H_2O)_3](O_2CCH_2Bu^t)$ (0.47 g, 0.50 mmol) and pyridine (0.64 ml, 7.80 mmol) in MeCN/MeOH (45/l5 ml) was stirred for 30 min to give an orange solution. This was layered with diethyl ether and left undisturbed at room temperature. After several weeks, the orange prism-shaped crystals of **1** that had slowly grown were collected in 25% yield. *Anal*. Calc. for **1** ($C_{83}H_{144}Fe_6N_2O_{28}$): C, 51.04; H, 7.43; N, 1.43. Found: C, 51.32; H, 7.11; N, 1.55%. Selected IR data (cm^{-1}): 3446 (br), 2955 (s), 1607 (m), 1557 (s), 1455 (m), 1412 (s), 1369 (m), 1061 (w), 898 (w), 643 (w), 562 (w).

Method B. A solution of $[Fe_3O(O_2CCH_2Bu^t)_6(H_2O)_3](O_2CCH_2Bu^t)$ (0.24 g, 0.25 mmol), py (0.64 ml, 7.80 mmol) and 37% formaldehyde (0.50 ml, 6.6 mmol) in MeCN (45 ml) was stirred for 30 min to give an orange solution. This was left undisturbed at room temperature. After one day, the orange prism-shaped crystals of **1** that had slowly grown were collected by filtration in 75% yield. The material was spectroscopically identical (IR) with that from Method A.

2.1.2. $Fe_6O_2(O_2CCH_2Cl)_6(moe)_6](NO_3)_2$ (**2**)

A solution of $[Fe_3O(O_2CCH_2Cl)_6(H_2O)_3]$ (O_2CCH_2Cl) (0.23 g, 0.25 mmol), $Fe(NO_3)_3 \cdot H_2O$ (0.10 g, 0.25 mmol) and moeH (5 ml, 63 mmol) in MeCN (50 ml) was stirred for 15 min to give a green solution. This was layered with diethyl ether and left undisturbed at room temperature. After 7 days, yellow-green rectangular shaped crystals of **2** were collected in 55% yield based on total Fe. *Anal*. Calc. for **2** ($C_{30}H_{54}Cl_6Fe_6N_2O_{32}$): C, 23.98; H, 3.62; N, 1.86. Found: C, 23.87; H, 3.53; N, 1.55%. Selected IR data (cm^{-1}): 3436 (br), 2946 (s), 1600 (s), 1432 (s), 1384 (m), 1341 (m), 1265 (m), 1079 (s), 1038 (m), 916 (w), 614 (w), 578 (m), 527 (w).

2.1.3. $[Fe_{12}O_8(OMe)_2(O_2CPh)_{12}(pam)_6]$ (**3**)

A solution of $[Fe_3O(O_2CPh)_6(H_2O)_3](O_2CPh)$ (0.26 g, 0.25 mmol) in MeCN (30 ml) was added with stirring to a solution of pamH (0.061 g, 0.50 mmol) and NaOMe (0.054 g, 1.00 mmol) in MeCN (20 ml). The resulting dark red solution was left undisturbed at room temperature. After 7 days, dark red rectangular shaped crystals of $\mathbf{3} \cdot 4MeOH \cdot 2MeCN$ had formed and were collected in 37% yield. *Anal*. Calc. for $\mathbf{3} \cdot 4MeOH$ ($C_{126}H_{112}Fe_{12}N_{12}O_{44}$): C, 47.76; H, 3.56; N, 5.30. Found: C, 47.51; H, 3.23; N, 5.15%. Selected IR data (cm^{-1}): 3446 (br), 1602(s), 1541 (m), 1404 (s), 1122 (w), 1096 (m), 718 (m), 692 (w), 613 (w), 467 (m), 455 (w).

2.2. General and physical measurements

Elemental analyses (C, H and N) were performed in the in-house facilities of the University of Florida Chemistry Department. Infrared spectra in the 400–4000 cm^{-1} range were recorded in the solid state (KBr pellets) on a Nicolet Nexus 670 FTIR spectrometer. Variable temperature dc magnetic susceptibility data down to 5.0 K were collected using a Quantum Design MPMS-XL SQUID susceptometer equipped with a 7-T dc magnet. Pascal's constants were used to estimate the diamagnetic corrections, which were subtracted from the experimental susceptibilities to give the molar magnetic susceptibilities (χ_M). Microcrystalline samples were restrained in eicosane by suspending the solid for 15 min in eicosane maintained at a temperature above its melting point (35–37 °C), and then the temperature was gradually decreased below the melting point to solidify the eicosane.

2.2.1. X-ray crystallography and solution of structures

Data were collected using a Siemens SMART PLATFORM equipped with a CCD area detector and a graphite monochromator utilising Mo Kα radiation ($\lambda = 0.71073$ Å. Suitable crystals of **1**, **2** and **3** · 4MeOH · 2MeCN were attached to glass fibres using silicone grease and transferred to a goniostat where they were cooled to 173 K for data collection. An initial search of reciprocal space revealed monoclinic space group *C*2/*c* for complex **1** and triclinic space group $P\bar{1}$ for both **2** and **3** · 4MeOH · 2MeCN, which were confirmed by the subsequent solution and refinement of the structures. Cell parameters were refined using up to 8192 reflections. A full sphere of data (1850 frames) was collected using the ω-scan method (0.3° frame width). The first 50 frames were re-measured at the end of data collection to monitor instrument and crystal stability (maximum correction on *I* was <1%). Absorption corrections by integration were applied based on measured indexed crystal faces. The structures were solved by direct methods in SHELXTL-6 [24], and refined on F^2 using full-matrix least squares. The non-H atoms were treated anisotropically, whereas the hydrogen atoms were placed in calculated, ideal positions and refined as riding on their respective carbon atoms.

For complex **1**, a total of 557 parameters were included in the structure refinement using 4686 reflections with $I > 2\sigma(I)$. For compound **2**, a total of 448 parameters were included in the structure refinement using 12024 reflections with $I > 2\sigma(I)$. For compound **3**, a total of 907 parameters were included in the structure refinement using 7761 reflections with $I > 2\sigma(I)$. Unit cell data and the final refinement indices R_1 and wR_2 are listed in Table 1.

3. Results and discussion

3.1. Syntheses

As mentioned earlier, the reaction of a $[M_3O(O_2CR)_6L_3]^{0,+}$ (L = py, H_2O, etc.) complex with a chelating ligand represents a commonly employed and convenient synthetic route to a variety of higher nuclearity clusters of Fe and Mn. For example, the use of 2-(hydroxymethyl)pyridine (hmpH) has led to a large variety of products, depending on the precise reaction conditions and ratios, including Mn_7 [14], Mn_{10} [15], Mn_{12} [16], and Fe_6 [17] clusters. The alkoxide arm of the hmp^- ligand normally adopts a bridging mode, fostering formation of higher nuclearity products, and this was the primary reason for choosing to use moeH and pamH in the present work. However, not all the reactions in the present work involved a chelate; we also investigated the long-term stability of the $[Fe_3O(O_2CCH_2Bu^t)_6(H_2O)_3]^+$ complex to MeOH, in the presence also of py as a proton acceptor, seeking the formation higher nuclearity products via methanolysis. Indeed this reaction led to a nuclearity change, although the isolated product contained no methoxide. The reaction slowly turned orange, and layering with Et_2O deposited orange crystals of $[Fe_6O_2(O_2CH_2)(O_2CCH_2Bu^t)_{12}(py)_2]$ (**1**) in 25% yield. Its formation is summarised in Eq. (1).

$$2[Fe_3O(O_2CCH_2Bu^t)_6(H_2O)_3]^+ + 2py + CH_3OH + \tfrac{1}{2}O_2 \rightarrow [Fe_6O_2(O_2CH_2)(O_2CCH_2Bu^t)_{12}(py)_2] + 6H_2O + 2H^+ \quad (1)$$

When the same reaction in MeCN/MeOH was carried out in the presence of triethanolamine ($teaH_3$), the product was instead $[Fe_8O_3(O_2CCH_2Bu^t)_9(tea)(teaH)_3]$, structurally analogous to the benzoate complex $[Fe_8O_3(O_2CPh)_9(tea)(teaH)_3]$ reported recently [12].

The most remarkable feature of the reaction and the resulting structure of **1** (vide infra) is the formation of a rare methanediolate ($^-OCH_2O^-$) group. Such groups are generally unstable but can be formed and trapped in situ [25]. The formation of **1** is not readily amenable to mechanistic studies, but it is reasonable to assume that overall the methanediolate group is formed by iron (III)-promoted oxidation by O_2 of bound MeOH or methoxide, as summarized in Eq. (2), followed by its trapping as a fully deprotonated bridging ligand.

$$CH_3OH + \tfrac{1}{2}O_2 \rightarrow CH_2(OH)_2 \quad (2)$$

Since *gem*-diols are merely hydrated forms of aldehydes or ketones, we wondered whether a higher yield preparation of **1** might be available via a reaction in which formaldehyde (H_2CO) had been deliberately added. This turned out to be the case (Method B of Section 2). Thus, the reaction of $[Fe_3O(O_2CCH_2Bu^t)_6(H_2O)_3]^+$, py and H_2CO in a 1:31:26 ratio in MeCN

Table 1
Crystallographic data for complexes **1**, **2** and **3** · 4MeOH · 2MeCN

Compound	**1**	**2**	**3**
Formula	$C_{83}H_{144}Fe_6N_2O_{28}$	$C_{30}H_{54}Cl_6Fe_6N_2O_{32}$	$C_{130}H_{118}Fe_{12}N_{14}O_{44}$
Formula weight	1953.10	1502.55	3250.58
Space group	*C*2/*c*	$P\bar{1}$	$P\bar{1}$
Unit cell dimensions			
a (Å)	22.8510(16)	11.5721(9)	15.6773(16)
b (Å)	22.1113(15)	11.8411(94)	15.8373(17)
c (Å)	20.3198(14)	12.0082(90)	16.5046(18)
α (°)	90.00	119.497(2)	115.202(2)
β (°)	98.829(2)	101.521(2)	111.135(2)
γ (°)	90.00	98.926(2)	94.183(2)
V (Å^3)	10145.2(12)	1339.88(18)	3331.9(6)
Z	4	1	1
T (°C)	173(2)	173(2)	173(2)
Radiation	Mo Kα	Mo Kα	Mo Kα
ρ_{calc} (g/cm^{-3})	1.279	1.862	1.620
μ (mm^{-1})	0.904	1.975	1.355
R_1[a,b]	6.81	7.72	7.86
wR_2[a,c]	11.68	14.50	15.68

[a] $I > 2\sigma(I)$.
[b] $R_1 = 100\sum(||F_o|-|F_c||)/\sum|F_o|$.
[c] $wR_2 = 100[\sum[w(F_o^2 - F_c^2)^2]/\sum[w(F_o^2)^2]]^{1/2}$, $w = 1/[\sigma^2(F_o^2) + [(ap)^2 + bp]$, where $p = [\max(F_o^2, 0) + 2F_c^2]/3$.

gave an orange solution from which **1** crystallized and was isolated in 75% yield; the absence of MeOH lowers the solubility of **1**, and it crystallizes from MeCN without the addition of Et_2O. This much superior procedure is summarized in Eq. (3).

$$2[Fe_3O(O_2CCH_2Bu^t)_6(H_2O)_3]^+ + 2py + H_2CO \rightarrow [Fe_6O_2(O_2CH_2)(O_2CCH_2Bu^t)_{12}(py)_2] + 5H_2O + 2H^+ \quad (3)$$

The formation of the methanediolate group from formaldehyde is analogous to the more common in situ formation of the *gem*-diol form of di-2-pyridylketone, followed by its trapping as the doubly deprotonated diolate ligand to metal ions [26].

Treatment of an equimolar mixture of $[Fe_3O(O_2CCH_2Cl)_6(H_2O)_3]^+$ and $Fe(NO_3)_3$ in MeCN with an excess of moeH gave a yellow-green solution from which yellow-green rectangular shaped crystals of $[Fe_6O_2(O_2CCH_2Cl)_6(moe)_6](NO_3)_2$ (**2**) were obtained in 55% yield by layering with Et_2O. This is a more typical type of cluster synthesis reaction than the formation of **1**, with no unusual ligand transformations occurring. The formation of the cation of **2** is summarized in Eq. (4).

$$3[Fe_3O(O_2CCH_2Cl)_6(H_2O)_3]^+ + 3Fe^{3+} + 12moeH \rightarrow 2[Fe_6O_2(O_2CCH_2Cl)_6(moe)_6]^{2+} + 6ClCH_2CO_2H + 8H_2O + 8H^+ \quad (4)$$

The reaction contained a large excess of moeH over that required by Eq. (4), indicating that the product **2** is stable to further incorporation of chelate that might lead to smaller nuclearity products, perhaps even $[Fe(moe)_3]$. When the reaction was carried out in MeOH instead of MeCN, a mixture of products was obtained, yellow-green complex **2** and golden crystals of known $[Fe_{10}(OMe)_{20}(O_2CCH_2Cl)_{10}]$ [8]. The latter is a member of the 'ferric wheel' family of wheel-like complexes.

The reaction of $[Fe_3O(O_2CPh)_6(H_2O)_3]^+$, pamH and NaOMe in 1:2:4 ratio in MeCN gave a dark red solution from which dark red rectangular shaped crystals of $[Fe_{12}O_8(OMe)_2(O_2CPh)_{12}(pam)_6]$ (**3**) slowly formed in 37% yield. The reaction is likely a complicated equilibrium involving several species of various nuclearities, and the crystallization of the product directly from the reaction solution is undoubtedly beneficial in providing pure material; the filtrates are still coloured, but we have not pursued isolation of other species. The formation of this novel Fe_{12} cluster is summarised in Eq. (5).

$$4[Fe_3O(O_2CPh)_6(H_2O)_3]^+ + 6pamH + 2MeO^- \rightarrow [Fe_{12}O_8(\mu\text{-}OMe)_2(O_2CPh)_{12}(pam)_6] + 12PhCO_2H + 8H_2O + 2H^+$$

This reaction ratio and solvent represent the combination that was found to give a pure isolated product in reasonable yield. Small changes to the Fe:pamH ratio still gave the same Fe_{12} product. The NaOMe serves both as a base to deprotonate the pamH and also as a source of MeO^- bridges to foster formation of a high-nuclearity product. When NEt_3 or NMe_4OH and a mixed MeCN/MeOH reaction solvent were employed, complex **3** was again obtained but only in very poor isolated yields (<5%). This (and the larger but still relatively low yield of **3** using NaOMe) may be due to the fact that pamH is susceptible to hydrolysis [21]; in these cases, it is difficult to isolate such species in good yields.

3.2. Structural description of $[Fe_6O_2(O_2CH_2)(O_2CCH_2Bu^t)_{12}(py)_2]$ (1)

A labelled ORTEP plot and stereopair of **1** are presented in Fig. 1, and selected bond distances and angles are listed in Table 2. Complex **1** crystallizes in the monoclinic space group *C*2/*c*, with the asymmetric unit containing half the Fe_6 molecule.

The Fe_6 core of **1** has a twisted boat-like topology (Fig. 4(a)), comprising two $[Fe_3(\mu_3\text{-}O)]^{7+}$ oxide-centered triangular moieties linked between one of their edges (Fe2–Fe3 and the symmetry-related partner) by a μ_4-O_2CH_2group and two μ-$O_2CCH_2Bu^t$ groups in their familiar *syn*, *syn* binding mode. This edge of both triangular units is also bridged by a μ-$O_2CCH_2Bu^t$ group. The two remaining edges of each $[Fe_3(\mu_3\text{-}O)]^{7+}$ unit are each bridged by two *syn, syn* μ-$O_2CCH_2Bu^t$ groups. The two pyridine groups complete six-coordination at the end atoms Fe1 and Fe1a. The complex has crystallographic C_2 symmetry, and virtual C_{2v} symmetry if the slight twist in the Fe_6 boat structure is ignored. All Fe atoms are Fe(III) and possess near-octahedral geometries. The overall structure of **1** is similar to those of previously reported $[Fe_6O_2(OH)_2(O_2CBu^t)_{12}]$ [27], $[Fe_6O_2(OH)_2(O_2CPh)_{12}(py)_2]$ [28] and $[Fe_6O_2(OH)_2(O_2CMe)_{10}(C_7H_{11}N_2O)_2]$ [29], but of course differs in possessing the unusual μ_4-O_2CH_2 bridging group (O13, O13a) at the positions occupied by bridging OH^- groups in the above three complexes. The nearest analogue to this μ_4-O_2CH_2 group is found in $[Fe_6O_2(O_2)(O_2CPh)_{12}(H_2O)_2]$ [30] and $[Fe_6O_2(O_2)(O_2CBu^t)_{12}L_2]$ (L = Bu^t- CO_2H or py) [31]. In these

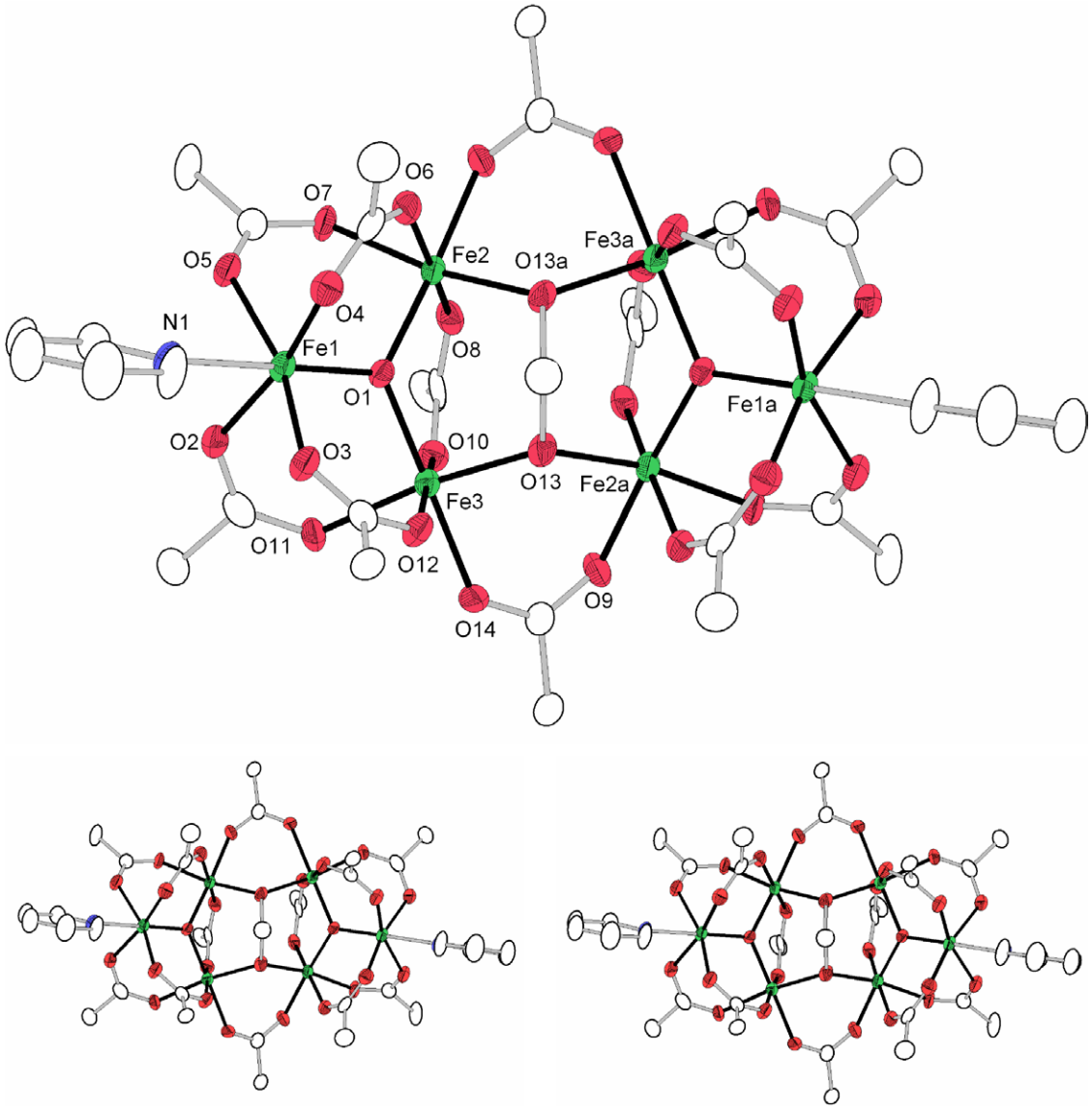

Fig. 1. ORTEP representation and stereopair at the 50% probability level of complex **1**, viewed approximately along the crystallographic C_2 symmetry axis. All H atoms and the Bu^t groups of the $Bu^tCH_2CO_2^-$ groups have been removed for clarity.

Table 2
Selected bond distances (Å) and angles (°) for complex **1**

Bond distances			
Fe1···Fe2	3.286(6)	Fe2–O6	2.058(4)
Fe1···Fe3	3.301(6)	Fe2–O7	2.042(4)
Fe2···Fe3	3.411(6)	Fe2–O8	2.014(4)
Fe2···Fe3a	3.607(6)	Fe2–O9	2.058(4)
Fe1–O1	1.872(4)	Fe2–O13a	1.979(4)
Fe1–O2	2.021(4)	Fe3–O1	1.956(4)
Fe1–O3	2.022(4)	Fe3–O10	1.990(4)
Fe1–O4	2.024(4)	Fe3–O11	2.041(4)
Fe1–O5	2.021(4)	Fe3–O12	2.027(4)
Fe1–N1	2.252(5)	Fe3–O13	1.975(4)
Fe2–O1	1.945(4)	Fe3–O14	2.037(4)
Bond angles			
Fe1–O1–Fe2	118.84(19)	Fe2–O1–Fe3	121.98(18)
Fe1–O1–Fe3	119.10(19)	Fe3–O13–Fe2a	131.7(2)

complexes, there is a central μ_4-O_2^{2-} peroxide group bridging analogously to the methanediolate in **1**, i.e., without the central CH_2 linker between O atoms O13 and O13a. The unusual μ_4-O_2CH_2 group of **1** has itself been seen previously only in a tetranuclear Mo cluster [25], where it bridges the Mo_4 core in the same fashion as that in the central Fe_4 unit of **1**.

3.3. Structural description of $[Fe_6O_2(O_2CCH_2Cl)_6(moe)_6](NO_3)_2$ (**2**)

A labelled ORTEP plot and stereopair of the cation of **2** are presented in Fig. 2, and selected bond distances and angles are listed in Table 3. Complex **2** crystallizes in the triclinic space group $P\bar{1}$, with the Fe_6 cation lying on an inversion centre.

The cation of **2** consists of two triangular $[Fe_3(\mu_3\text{-}O)]^{7+}$ units held together in a face-to-face fashion by six bridging moe^- ligands. Each moe^- group chelates one Fe atom and bridges with its O atom to another Fe atom in the neighboring $[Fe_3O]^{7+}$ unit. All Fe atoms are Fe(III). Each Fe_2 pair within a trinuclear unit is additionally bridged by a $CH_2ClCO_2^-$ group, completing six coordination at each Fe atom. The cation has crystallographic C_i symmetry but virtual S_6 symmetry, with the S_6 axis passing through the μ_3-O^{2-} oxygen atoms (O1, O1a). The Fe_6 cation can be also described as an Fe_6 octahedron (Fig. 4(b)) with two opposite faces bridged by μ_3-O^{2-} ions and six edges bridged by μ-O atoms from moe^- ligands. The Fe···Fe separation within the trinuclear $[Fe_3O]^{7+}$ units (average 3.311 Å) are only slightly shorter than those between $[Fe_3O]^{7+}$ units (average 3.431 Å); thus, the Fe_6 core is almost a regular octahedron. The Fe···Fe separations on the same axis of the octahedron are much longer (average 4.767 Å).

The cation of **2** is the first such cluster with moe^- groups, but the core structure of the cation is similar to those in other Fe_6 species with a recognizable octahedral Fe_6 topology, including $[Fe_6O_2(O_2CCH_2C(CH_3)_3)_6(hmp)_6]^{2+}$ [17] and $[Fe_6O(OMe)_3Cl_6(thme)_3]^{2-}$ [32]; the latter also contains a central μ_6-O^{2-} ion. In contrast, the $[Fe_6O_2(O_2)_3(O_2CMe)_9]^-$ anion contains two face-to-face $[Fe_3(\mu_3\text{-}O)]^{7+}$ units in an eclipsed arrangement giving an Fe_6 trigonal prism [33], rather than the

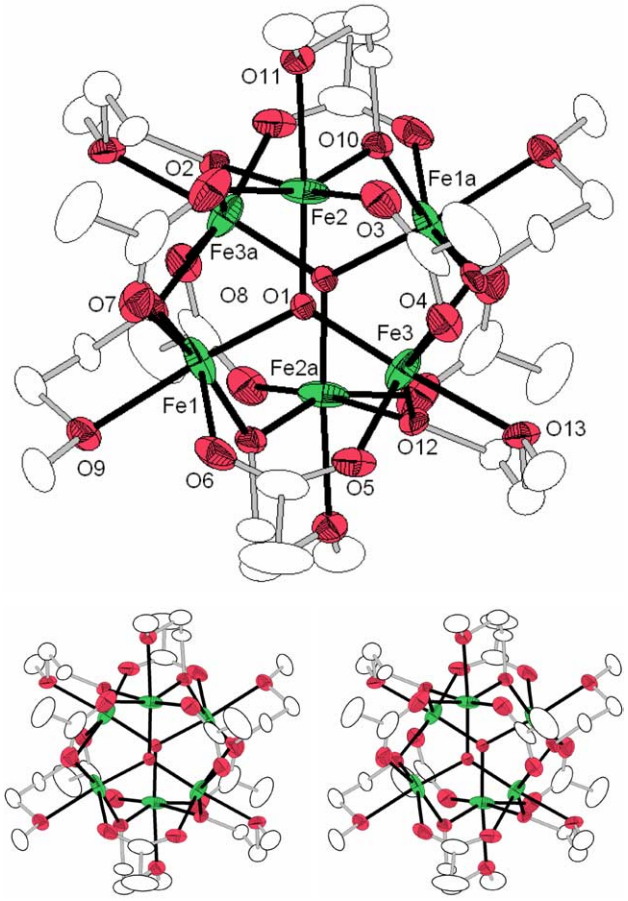

Fig. 2. ORTEP representation and stereopair of the cation of complex **2** at the 50% probability level, viewed almost along the virtual S_6 symmetry axis. All H atoms and the Cl atoms of $CH_2ClCO_2^-$ groups have been removed for clarity.

Table 3
Selected bond distances (Å) and angles (°) for complex **2**

Bond distances			
Fe1···Fe2	3.310(4)	Fe2–O3	2.000(6)
Fe1···Fe3	3.303(4)	Fe2–O10	1.916(6)
Fe2···Fe3	3.320(4)	Fe2–O11	2.215(7)
Fe1–O1	1.919(4)	Fe2–O12a	2.087(7)
Fe1–O6	2.006(6)	Fe3–O1	1.909(4)
Fe1–O7	2.013(6)	Fe3–O4	2.009(6)
Fe1–O8	1.917(7)	Fe3–O5	2.001(5)
Fe1–O9	2.213(7)	Fe3–O8a	2.089(7)
Fe1–O10a	2.087(6)	Fe3–O12	1.920(6)
Fe2–O1	1.909(4)	Fe3–O13	2.191(7)
Fe2–O2	2.009(6)		
Bond angles			
Fe1–O1–Fe2	119.7(2)	Fe1–O10–Fe2a	118.22(7)
Fe1–O1–Fe3	119.3(2)	Fe1–O8–Fe3a	118.04(7)
Fe2–O1–Fe3	120.8(2)	Fe2–O12–Fe3a	117.17(7)

more common staggered arrangement that yields an Fe_6 octahedron.

3.4. Structural description of $[Fe_{12}O_8(OMe)_2(O_2CPh)_{12}(pam)_6]$ (3)

A labelled ORTEP plot and stereopair for complex **3** are presented in Fig. 3, and selected bond distances and angles are listed in Table 4. Complex **3** crystallizes in the triclinic space group $P\bar{1}$, with the Fe_{12} cluster lying on an inversion centre. The unprecedented core of this complex can be described in different ways. The central Fe_6 portion of the core (Fe4, Fe4a, Fe5, Fe5a, Fe6, Fe6a) can be considered as (i) comprising four face-sharing partial cubanes lacking an Fe atom at one vertex; or (ii) as a skewed Fe_6 ladder with μ_3-O atoms of O^{2-} (O4, O4a) or MeO^- (O5, O5a) ions alternately above and below the plane of the ladder; or (iii) as four edge-sharing $[Fe_3(\mu_3\text{-}O)]^{7+}$ triangular units. A similar planar $[Fe_6O_4]^{10+}$ unit has been reported in the cation of

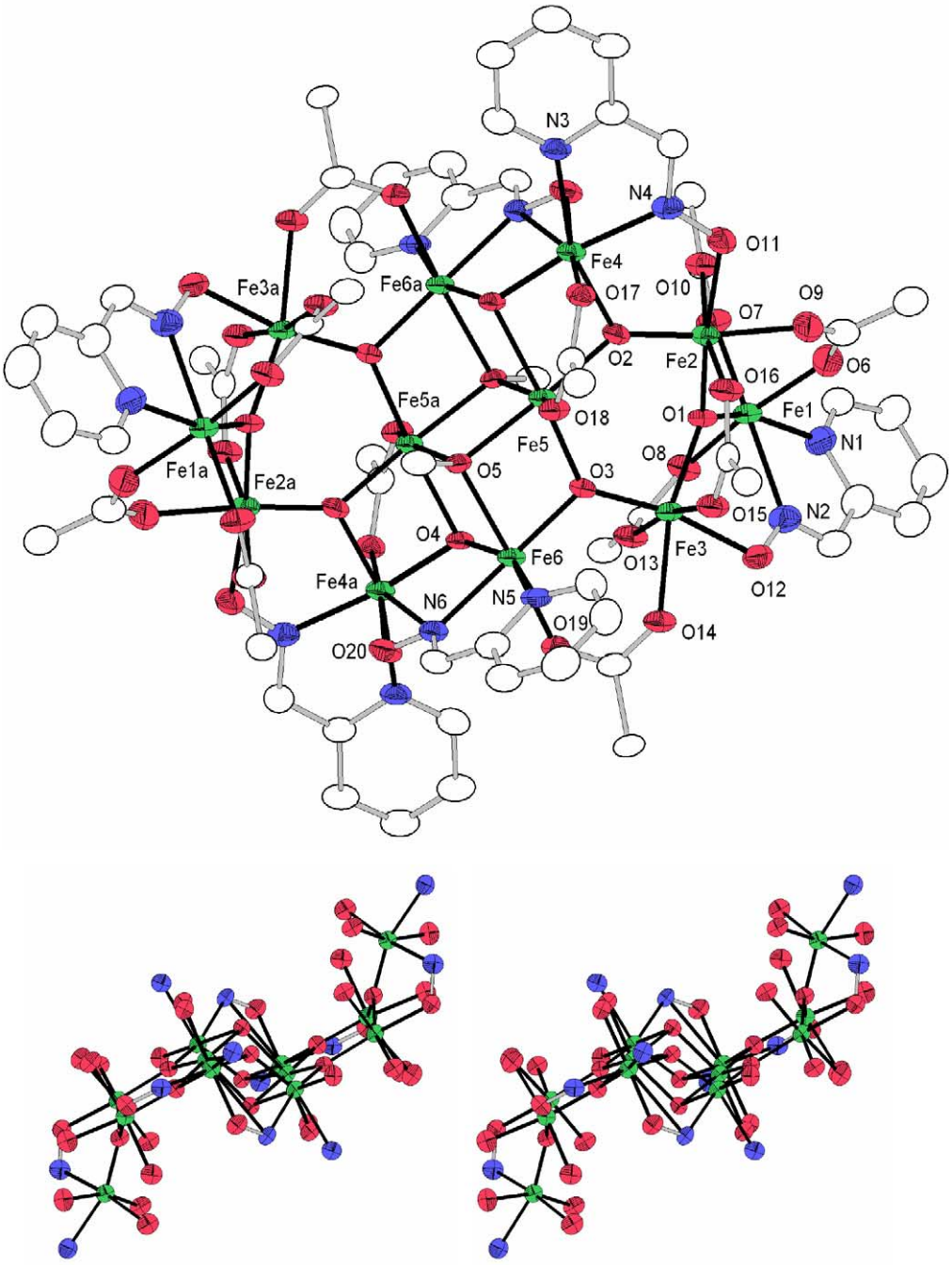

Fig. 3. Labelled ORTEP plot and stereopair at the 50% probability level of complex **3**. H atoms and benzoate phenyl groups have been removed for clarity.

$[Fe_6O_4Cl_4(O_2CPh)_4L_2][FeCl_4]_2$ [31], where however the Fe(III) ions are bridged exclusively via oxide ions. Attached to the central Fe_6 core of **3** by four O^{2-} bridges (O2, O3, O2a, O3a) are two triangular $[Fe_3(\mu_3\text{-}O)]^{7+}$ units (Fe1, Fe2, Fe3 and symmetry equivalents), disposed above and below the central Fe_6 plane. The resulting $[Fe_{12}O_{10}]$ core has an overall chair conformation, as is best seen in Fig. 4(c) where the three cores of **1**–**3** are compared. As is usually the case [2,17], the Fe–O^{2-} bonds (1.853–2.083 Å) are significantly shorter than the Fe–OMe bonds (2.112–2.168 Å). Ligation around the core is provided by the $PhCO_2^-$ and pam^- groups, and every Fe atom consequently has octahedral coordination.

Complex **3** is one of only a very small number of known dodecanuclear iron clusters. Other examples include $[Fe(OMe)_2(dbm)]_{12}$ with a wheel-like structure [37], and $[Fe_{12}O_2(OMe)_{18}(O_2CMe)_6(MeOH)_{4.67}]$ [9], which is mixed-valence 4Fe(III), 8Fe(II).

For all three compounds **1**–**3,** the oxidation states of the Fe atoms and the degree of protonation of O atoms were confirmed by bond valence sum (BVS) calculations, leading to the conclusions described above that all metal centers are Fe(III) and all inorganic O atoms are O^{2-} rather than OH^-. The BVS values obtained were in the 3.05–3.15, 3.10–3.28 and 2.88–3.09 for complexes **1**–**3**, respectively.

Table 4
Selected bond distances (Å) and angles (°) for complex **3** · 4MeOH · 2MeCN

Bond distances			
Fe1···Fe2	3.284(4)	Fe2–O2	1.861(5)
Fe1···Fe3	3.241(4)	Fe2–O9	2.086(6)
Fe2···Fe3	3.410(4)	Fe2–O10	2.100(5)
Fe2···Fe4	3.367(2)	Fe2–O11	2.054(4)
Fe2···Fe5	3.565(4)	Fe2–O16	2.069(5)
Fe3···Fe5	3.540(4)	Fe3–O1	1.938(4)
Fe3···Fe6	3.381(3)	Fe3–O3	1.916(5)
Fe4···Fe5	2.843 (2)	Fe3–O12	2.091(5)
Fe4···Fe6a	3.302 (4)	Fe3–O13	2.069(5)
Fe5···Fe6	3.067 (4)	Fe3–O14	2.099(4)
Fe5···Fe5a	3.328 (4)	Fe3–O15	2.012(5)
Fe5···Fe6a	3.172 (5)	Fe4–O2	1.961(4)
Fe1–O1	1.853(5)	Fe4–O4	1.889(5)
Fe1–O6	2.006(5)	Fe4–O17	2.079(5)
Fe1–O7	2.004(5)	Fe4–O20a	1.991(5)
Fe1–O8	2.028(5)	Fe4–N3	2.192(5)
Fe1–N1	2.222(7)	Fe4–N4	2.148(6)
Fe1–N2	2.149(6)	Fe5–O2	1.920(4)
Fe2–O1	1.956(4)	Fe5–O3	1.950(4)
Fe5–O4	2.083(4)	Fe6–O4a	1.879(5)
Fe5–O5	2.112(4)	Fe6–O19	1.999(4)
Fe5–O5a	2.143(5)	Fe6–O5	2.168(4)
Fe5–O18	2.048(5)	Fe6–N5	2.273(6)
Fe6–O3	1.935(4)	Fe6–N6	2.201(6)
Bond angles			
Fe1–O1–Fe2	119.1(2)	Fe4–O2–Fe5	94.2(2)
Fe1–O1–Fe3	117.5(2)	Fe4–O4–Fe5	91.26(19)
Fe2–O1–Fe3	122.2(2)	Fe4–O4–Fe6a	122.4(2)
Fe2–O2–Fe4	123.5(2)	Fe5–O3–Fe6	104.3(2)
Fe2–O2–Fe5	141.1(2)	Fe5–O4–Fe6a	106.3(2)
Fe3–O3–Fe5	132.6(2)	Fe5–O5–Fe5a	102.90(18)
Fe3–O3–Fe6	122.8(2)	Fe6–O5–Fe5a	94.73(18)

The above structural descriptions of **1**–**3** emphasize that the three clusters can all be structurally related to the parent $[Fe_3O(O_2CR)_6(H_2O)_3]^+$ complexes and can thus all be said to be represent different ways of linking or edge-fusing a number of $[Fe_3(\mu_3\text{-}O)]^{7+}$ triangular units, with the additional incorporation of other bridges such as MeO^-. This point is emphasized by the structural comparison of the three cores provided in Fig. 4.

3.5. Magnetochemistry

Variable-temperature, solid-state magnetic susceptibility (χ_M) studies were performed on microcrystalline samples of **1**–**3** in a 1-kG applied DC magnetic field in the 5.0 – 300 K range. The obtained data for **1** (○), **2** (●) and **3** (▲) are plotted as $\chi_M T$ versus T in Fig. 5. The $\chi_M T$ value for **1** decreases steadily with decreasing temperature from 11.42 $cm^3\,mol^{-1}\,K$ at 300 K to 0.14 $cm^3\,mol^{-1}\,K$ at 5.0 K, consistent with an $S = 0$ ground state. The $\chi_M T$ value at 300 K is well below the spin-only ($g = 2$) value of 26.3 $cm^3\,mol^{-1}\,K$ for six non-interacting Fe(III) ions, indicating strong antiferromagnetic interactions between the Fe(III) centers to give a singlet spin ground state. For complex **2**, the $\chi_M T$ value again decreases steadily with decreasing temperature from 7.13 $cm^3\,mol^{-1}\,K$ at 300 K to 0.11 $cm^3\,mol^{-1}\,K$ at 5.0 K, consistent with an $S = 0$ ground state. The $\chi_M T$ value at 300 K is far below the spin-only value of 26.3 $cm^3\,mol^{-1}\,K$ for six non-interacting Fe(III) ions, indicating even stronger antiferromagnetic interactions between the Fe(III) centers in **2** than in **1**, and again giving an $S = 0$ spin ground state. Similarly, the $\chi_M T$ value for **3** decreases steadily from 12.69 $cm^3\,mol^{-1}\,K$ at 300 K to 0.19 $cm^3\,mol^{-1}\,K$ at 5.0 K, again indicating an $S = 0$ spin ground state. Furthermore, the 300 K $\chi_M T$ value is very far below the spin-only value of 52.5 $cm^3\,mol^{-1}\,K$ for 12 non-interacting Fe(III) ions, which is indicative of very strong antiferromagnetic exchange interactions within this molecule.

The three complexes all thus have $S = 0$ ground states. This is by far the most common ground state for Fe_x clusters with x an even number [10,17,34–36], and is primarily the result of strong antiferromagnetic exchange interactions between $Fe(III)_2$ pairs. Although competing exchange antiferromagnetic interactions and spin frustration effects in higher nuclearity species can occasionally lead to non-zero ground state spins [2,10,29], this is clearly not the case in the present complexes. The $S = 0$ ground states for **1** and **2** can readily be rationalized on the basis of two

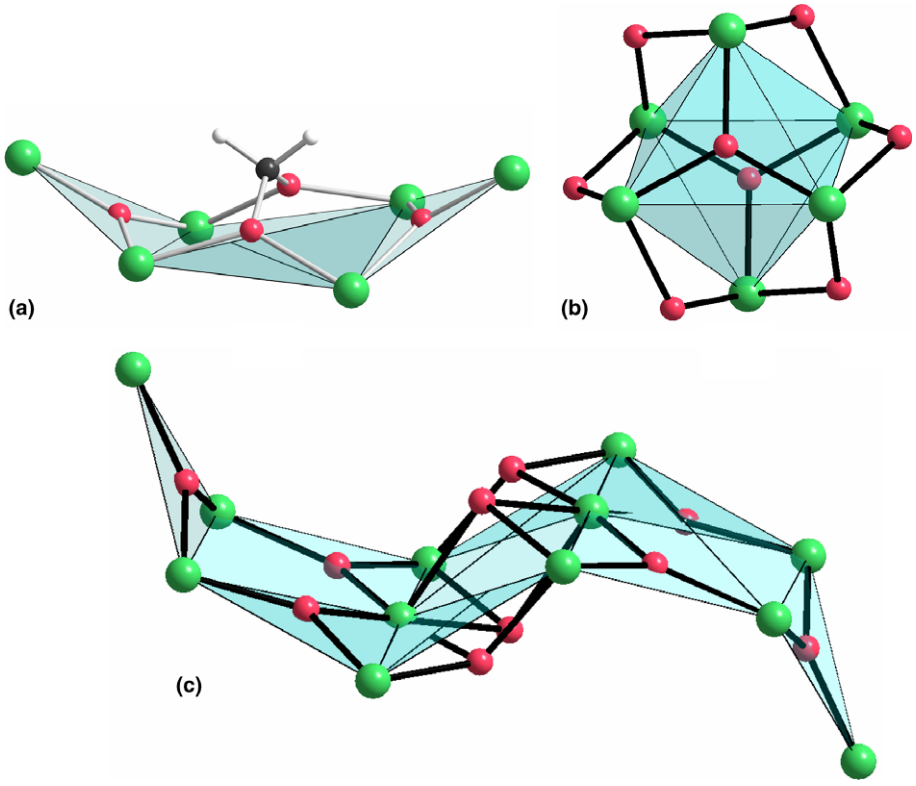

Fig. 4. Comparison of the cores of complexes: **1** (a), **2** (b) and **3** (c), emphasizing the presence of recognizable $[Fe_3O]$ oxide-bridged triangular subunits, and the overall structure of the cores as a twisted boat (a), an octahedron (b), and a chair (c).

$S = 5/2$ $[Fe_3(\mu_3\text{-}O)]^{7+}$ triangular units antiferromagnetically coupled to each other through the bridging ligands connecting them. The ground state for **3** is not so easily rationalized, but the spin of the central Fe_6 unit is likely $S = 0$, as found for other compounds with such a planar, ladder-like Fe_6 topology [38,39], and then the $S = 5/2$ spins of the two $[Fe_3(\mu_3\text{-}O)]^{7+}$ triangular units on the flanks would be coupled antiferromagnetically through the central unit to give an overall $S = 0$ ground state.

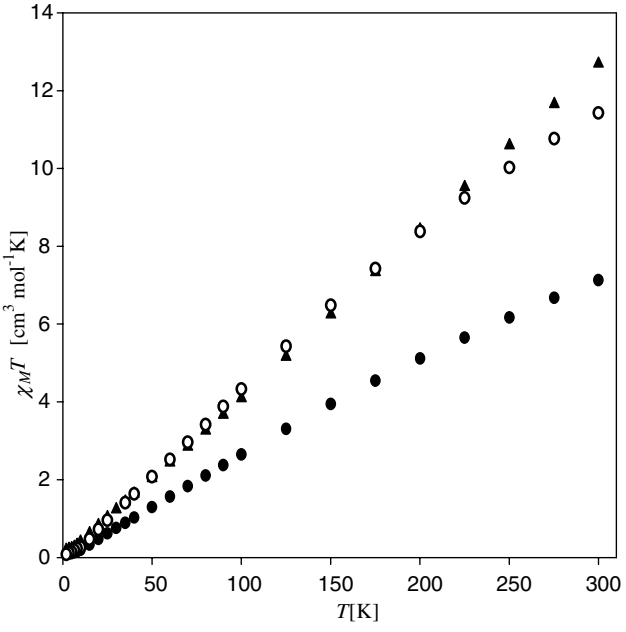

Fig. 5. Plot of $\chi_M T$ vs. T for complexes **1** (○), **2** (●) and **3** (▲).

4. Conclusions

Synthetic methods have been identified that can convert the triangular $[Fe_3O(O_2CR)_6(H_2O)_3]^+$ complexes to new Fe_6 and Fe_{12} products. The structures of the latter can be described as aggregates of Fe_3 triangular units. These results continue to emphasize the utility of small nuclearity clusters as stepping-stones to higher-nuclearity products through the use of alcohol-containing chelate ligands such as the moeH and pamH used in this work, or even by incorporation of methoxide bridges. The magnetic properties of the three complexes described indicate that they all possess $S = 0$ ground states, and this is not surprising given the dominance of antiferromagnetic interactions in high-spin Fe(III) chemistry. Nevertheless, iron(III) carboxylate chemistry continues to surprise with the structural variety and aesthetic beauty of its molecular complexes.

5. Supplementary material

Full crystallographic details have been deposited in CIF format with the Cambridge Crystallographic Data Centre. Copies of the data can be obtained free of charge on request from the CCDC, 12 Union Road, Cambridge CB2 1EZ, UK (fax: +44 1223 336408, e-mail: deposit@ccdc.cam.ac.uk or www at http://www.ccdc.cam.ac.uk) quoting the deposition numbers CCDC 237027 (**1**), 237028 (**2**) and 237029 (**3**).

Acknowledgement

This work was supported by the National Science Foundation.

References

[1] K. Wieghardt, K. Pohl, I. Jibril, G. Huttner, Angew. Chem. 23 (1984) 77.
[2] A.K. Powell, S.L. Heath, D. Gatteschi, L. Pardi, R. Sessoli, G. Spina, F.D. Giallo, F. Pierallill, J. Am. Chem. Soc. 117 (1995) 2491.
[3] A.L. Barra, A. Caneschi, A. Cornia, F. Fabrizi de Biani, D. Gatteschi, C. Sangregorio, R. Sessoli, L. Sorace, J. Am. Chem. Soc. 121 (1999) 5302.
[4] M. Frey, S. Harris, J. Holmes, D. Nation, S. Parsons, P. Tasker, S. Teat, R. Winpenny, Angew. Chem. 37 (1998) 3245.
[5] C. Benelli, J. Cano, Y. Journaux, R. Sessoli, G.A. Solan, R.E.P. Winpenny, Inorg. Chem. 40 (2001) 188.
[6] R. Sessoli, H. Tsai, A.R. Schake, S. Wang, J. Vincent, K. Folting, D. Gatteschi, G. Christou, D.N. Hendrickson, J. Am. Chem. Soc. 115 (1993) 1804.
[7] D. Gatteschi, R. Sessoli, A. Cornia, Chem. Commun. (2000) 725.
[8] K.L. Taft, S. Lippard, J. Am. Chem. Soc. 112 (1990) 9629.
[9] K.L. Taft, G.C. Papaefthymiou, S.J. Lippard, Science 259 (1993) 1303.
[10] D.M. Low, L.F. Jones, A. Bell, E.K. Brechin, T. Mallah, E. Riviere, S.J. Teat, E.J.L. McInnes, Angew. Chem. 42 (2003) 3781.
[11] C. Canada-Vilalta, T.A. O'Brien, M. Pink, E.R. Davidson, G. Christou, Inorg. Chem. 42 (2003) 7819.
[12] M. Murugesu, K.A. Abboud, G. Christou, Dalton Trans. (2003) 4552.
[13] E.K. Brechin, C. Boskovic, W. Wernsdorfer, J. Yoo, A. Yamaguchi, C. Sanudo, T. Concolino, A. Rheingold, H. Ishimoto, D. Hendrickson, G. Christou, J. Am. Chem. Soc. 124 (2002) 9710.
[14] M.A. Bolcar, S.M.J. Aubin, K. Folting, D.N. Hendrickson, G. Christou, Chem. Commun. (1997) 1485.
[15] N.C. Harden, M.A. Bolcar, W. Wernsdorfer, K.A. Abboud, W.E. Streib, G. Christou, Inorg. Chem. 42 (2003) 7067.
[16] C. Boskovic, E.K. Brechin, W.E. Streib, K. Folting, J.C. Bollinger, D.N. Hendrickson, G. Christou, J. Am. Chem. Soc. 124 (2002) 3725.
[17] E.K. Brechin, M.J. Knapp, J.C. Huffmann, D.N. Hendrickson, G. Christou, Inorg. Chem. Acta 297 (2000) 389.
[18] I.A.M. Pohl, L.G. Westin, M. Kritikos, Chem. Eur. J. 7 (2001) 3439.
[19] L.G. Westin, M. Kritikos, Andrea Caneschi, Chem. Commun. (2003) 1012.
[20] R. Clerac, H. Miyasaka, M. Yamashita, C. Coulon, J. Am. Chem. Soc. 124 (2002) 12837.
[21] C.J. Milios, E. Kefalloniti, C.P. Raptopoulou, A. Terzis, A. Escuer, R. Vicente, S.P. Perlepes, Polyhedron 23 (2004) 83.
[22] R.W. Green, M.C.K. Svasti, Aust. J. Chem. 16 (1963) 356.
[23] R.F. Weinland, A. Herz, Ber. Dtsch. Chem. Ges. 45 (1912) 2662.
[24] G.M. Sheldrick, SHELXL-97, Program for Refinement of Crystal Structures, University of Göttingen, Germany, 1997.
[25] V.W. Day, M.F. Fredrich, W.G. Klemperer, R.S. Liu, J. Am. Chem. Soc. 101 (1979) 491.
[26] A.K. Boudalis, B. Donnadieu, V. Nastopoulos, J.M. Clemente-Juan, A. Mari, Y. Sanakis, J. Tuchagues, S.P. Perlepes, Angew. Chem. Int. Ed. 43 (2004) 2266.
[27] A. Batsanov, Y.T. Struchkov, G. Timko, Koord. Khim. 14 (1988) 266.
[28] P.S. Ammala, J.D. Cashion, C.M. Kepert, K.S. Murray, B. Moubaraki, L. Spiccia, B.O. West, J. Chem. Soc., Dalton Trans. (2001) 2032.
[29] C.A. Christmas, H.-L. Tsai, L. Pardi, J.M. Kesselman, P.K. Gantzel, R.K. Chadha, D. Gatteschi, D.F. Jarvey, D.N. Hendrickson, J. Am. Chem. Soc. 115 (1993) 12483.
[30] W. Micklitz, S.G. Bott, J.G. Bentsen, S.J. Lippard, J. Am. Chem. Soc. 111 (1989) 372.
[31] R. Celenligil-Cetin, R.J. Staples, P. Stavropoulos, Inorg. Chem. 39 (2000) 5838.
[32] K. Hegetschweiler, H. Schmalle, H.M. Streit, W. Schneider, Inorg. Chem. 29 (1990) 3625.
[33] I. Shweky, L.E. Pence, G.C. Papaefthymiou, R. Sessoli, J.W. Yun, A. Bino, S.J. Lippard, J. Am. Chem. Soc. 119 (1997) 1037.
[34] S. Watton, P. Fuhrmann, L. Pence, A. Caneschi, A. Cornia, G. Abbati, S.J. Lippard, Angew. Chem. 36 (1997) 2774.
[35] D. Gatteschi, A. Caneschi, R. Sessoli, A. Cornia, Chem. Soc. Rev. 25 (1996) 101.
[36] R.E.P. Winpenny, Acc. Chem. Res. 30 (1997) 89.
[37] G.L. Abbati, A. Caneschi, A. Cornia, A.C. Fabretti, D. Gatteschi, Inorg. Chim. Acta 297 (2000) 291.
[38] E.J. Seddon, J. Yoo, K. Folting, J.C. Huffman, D.N. Hendrickson, G. Christou, J. Chem. Soc., Dalton Trans. (2000) 3640.
[39] C.M. Grant, M.J. Knapp, J.C. Huffman, D.N. Hendrickson, G. Christou, Inorg. Chem. 37 (1998) 6065.

Available online at www.sciencedirect.com
SCIENCE DIRECT®
Polyhedron 23 (2004) 2789–2795
POLYHEDRON
www.elsevier.com/locate/poly

Synthesis and molecular structures of α-diimines and their zinc and palladium dichloride complexes

David N. Coventry, Andrei S. Batsanov, Andres E. Goeta, Judith A.K. Howard, Todd B. Marder *

Department of Chemistry, University of Durham, South Road, Durham DH1 3LE, UK

Received 28 April 2004; accepted 16 June 2004
Available online 3 September 2004

Abstract

Three α-diimines, 2,3-dimethyl-*N,N'*-bis(cyclohexyl)-diaza-1,4-butadiene, Cy-DAD (**1**), (DAD = diaza-1,4-butadiene), bis{2,8-(4-methoxyphenylimino)}acenaphthene, *p*-OMe-BIAN (**3**), (BIAN = 2,8-bis(arylimino)acenaphthene) and bis{2,8-(2,6-di-isopropylphenylimino)}acenaphthene, 2,6-^{i}Pr-BIAN (**4**), were synthesised either via their zinc complexes, as a template, or by the direct reaction of the appropriate primary amine with the diketone. Compound **1** is a non-constrained analogue of the rigid, bidentate nitrogen ligands **3** and **4**. Syntheses of the zinc and palladium complexes of **3** and **4**, namely **2, 5**, **6** and **7**, are also reported herein. All compounds have been characterised spectroscopically, and the molecular structures of **1**, **3**, **4**, $ZnCl_2$(*p*-OMe-BIAN) $\cdot \frac{1}{2}CH_2Cl_2$ (**2**), $PdCl_2$(*p*-OMe-BIAN) (**6**) and $PdCl_2$(2,6-^{i}Pr-BIAN) (**7**) have been determined by single-crystal X-ray diffraction. Compound **1** adopts a *transoid* geometry and possesses a crystallographic inversion centre midway along the N═C–C═N backbone. Compounds **3** and **4** are inherently *cisoidal* and X-ray analysis highlights a twofold axis through the backbone. The Pd(II) centres of **6** and **7** both adopt square planar geometries whilst **6** contains four molecules per asymmetric unit and 1/2 molecule of benzonitrile per Pd atom and complex **7** is isomorphous with the known structure of PdCl(Me)(2,6-^{i}Pr-BIAN). The Zn complex **2** is pseudo tetrahedral as expected for Zn(II).
© 2004 Elsevier Ltd. All rights reserved.

Keywords: X-ray structure; Diimine; Coordination complex; Zinc; Palladium

1. Introduction

Over the past decade there has been considerable interest in alternative ligands to phosphines, for the development of late transition metal catalysts. Examples of this include the substantial development by Brookhart and co-workers [1] of α-diimine ligands for nickel and palladium catalysed olefin polymerisation and recent developments in the zinc catalysed ring-opening polymerisation of epoxides and ε-caprolactone reported by Bochmann and co-workers [2]. Furthermore, other bidentate nitrogen donor ligands have been used in many catalytic studies including the enantioselective carbonylation of olefins [3], hydrogenation and hydrosilylation [4], the borylation of alkanes and alkenes [5], diboration [6] and reduction of nitrobenzene to aniline [7]. Routes to the diimines have been previously developed by Elsevier and co-worker [8a], Fukuda and co-worker [8b] and Dieck and Dietrich [8c].

Whilst most studies of the α-diimines have concentrated on the reactivity of their complexes, very little crystallographic information has been obtained. We report herein the synthesis and structural characterisation of *p*-OMe-BIAN (**3**), 2,6-^{i}Pr-BIAN (**4**), Cy-DAD (**1**), $ZnCl_2$(*p*-OMe-BIAN) $\cdot \frac{1}{2}CH_2Cl_2$ (**2**), $PdCl_2$(*p*-OMe-BIAN) (**6**) and $PdCl_2$(2,6-^{i}Pr-BIAN) (**7**) (shown in

* Corresponding author. Tel.: +44 191 334 2037; fax: +44 191 384 4737.
E-mail address: todd.marder@durham.ac.uk (T.B. Marder).

0277-5387/$ - see front matter © 2004 Elsevier Ltd. All rights reserved.
doi:10.1016/j.poly.2004.06.023

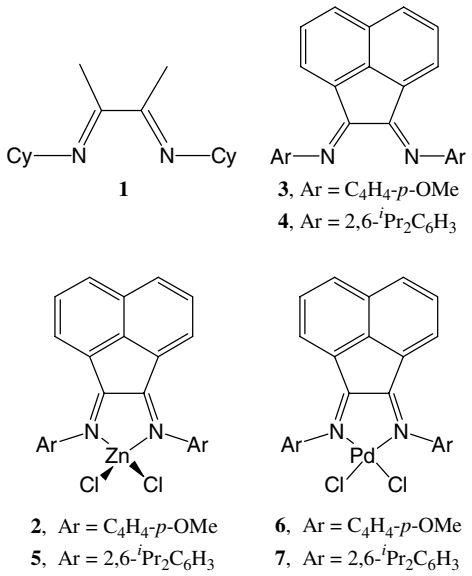

Scheme 1.

Scheme 1). Although the structure of 2,6-^{i}Pr-BIAN has been published previously [9a,9b] we note that the space group reported was wrong [9c].

2. Experimental

2.1. General

All chemicals were commercially available and were used as received. ^{1}H NMR spectra were obtained using a 400 MHz Bruker Avance and Mercury-200, Unity-300 and Inova-500 MHz Varian spectrometers; coupling constants are given in Hz. Mass spectra were obtained with Micromass AutoSpec (EI) and Micromass-LCT (ES) spectrometers. The elemental analyses were carried out with an Exeter Analytical Inc. CE-440 elemental analyser.

2.2. Synthesis of (Cy-DAD) (*1*)

The compound 2,3-dimethyl-*N,N′*-bis(cyclohexyl)-diaza-1,4-butadiene was prepared in a similar manner to that used by Dieck and Dietrich [8c]. Cyclohexylamine (20.25 ml, 180 mmol) was added dropwise to a cooled (0 °C) mixture of butane-2,3-dione (7.8 ml, 90 mmol), molecular sieves (10 g, 4 Å) and formic acid (1 ml, 98%) in chloroform (100 ml). After stirring for one day, the mixture was filtered and the chloroform removed in vacuo. The remaining yellow-white solid was re-crystallised from ethanol yielding colourless plates suitable for X-ray diffraction. Yield: 8.9 g, 40%. (Found: C, 77.40; H, 11.60; N, 11.28. $C_{16}H_{28}N_2$ requires: C, 77.36; H, 11.36; N, 11.28%). ES-MS [*m*/*z*]: 248 $[M]^+$, 205 $[M - C_3H_7]^+$, 166 $[M - C_6H_{10}]^+$. ^{1}H NMR [CD_2Cl_2, 200 MHz]: δ 3.5 (m, 4H, CH_2), 2.05 (s, 6H, CH_3), 1.8 (m, 4H, CH_2), 1.65 (m, 4H, CH_2), 1.4 (m, 8H, CH_2).

2.3. Synthesis of $ZnCl_2$(*p*-OMe-BIAN) · $\frac{1}{2}CH_2Cl_2$ (*2*)

This complex was synthesised in a similar manner to that described in the literature [8a]. A mixture of acenaphthenequinone (2.00 g, 11 mmol), anhydrous $ZnCl_2$ (1.71 g, 12.5 mmol) and 4-methoxyaniline was heated to 170 °C in a closed Young's-tap tube for 4 h. The mixture was then cooled to 20 °C and transferred to a beaker with Et_2O (2 × 50 ml) and glacial acetic acid (2 × 50 ml). Aluminium foil was placed over the beaker and the following day the red precipitate which had formed was collected by filtration and washed with Et_2O (5 × 20 ml). Crystals suitable for X-ray diffraction studies were grown from CH_2Cl_2. Yield: 5.51 g, 95%. (Found: C, 56.49; H, 3.71; N, 5.09. $C_{26}H_{20}Cl_2N_2O_2Zn \cdot \frac{1}{2}CH_2Cl_2$ requires: C, 55.72; H, 3.71; N, 4.90%). This suggests that CH_2Cl_2 may be slowly evaporating from the crystal lattice.) ES-MS [CH_2Cl_2, *m*/*z*]: 528 $[M]^+$, 391 $[M - H - ZnCl_2]^+$. ^{1}H NMR [DMSO; 200 MHz]: δ 8.12 (d, 2H, J = 8.3, $C_{10}H_6$), 7.57 (dd, 2H, J = 8.3, 7.2, $C_{10}H_6$), 7.09 (s, 8H, C_6H_4), 6.96 (d, 2H, J = 7.2, $C_{10}H_6$), 3.85 (s, 6H, OMe).

2.4. Synthesis of *p*-OMe-BIAN (*3*)

Compound **3** was prepared in a similar manner to that described in the literature [8a]. Thus, $ZnCl_2$ (*p*-OMe-BIAN) · $\frac{1}{2}CH_2Cl_2$ (**2**) (3.00 g, 5.25 mmol) was added to a solution of K_2CO_3 (25.00 g, 180 mmol) in water (250 ml) and the mixture was heated at reflux with vigorous stirring. After 17 h, the solid was collected by filtration and washed with water (5 × 30 ml) and then was extracted by soxhlet with ethanol for two days. On cooling, red crystals suitable for X-ray diffraction studies grew from solution. The reaction was filtered and the mother liquor concentrated to half volume to promote the formation of a second crop of crystals. Yield: 1.80 g, 81%. (Found: C, 79.32; H, 5.03; N, 7.17. $C_{26}H_{20}N_2O_2$ requires: C, 79.57; H, 5.14; N, 7.14%), EI-MS [CH_2Cl_2, *m*/*z*]: 391 $[M - 1]^+$, 377 $[M - CH_3]^+$, 361 $[M - OCH_3]^+$. ^{1}H NMR [DMSO; 200 MHz]: δ 8.07 (d, 2H, J = 7.8, $C_{10}H_6$), 7.53 (dd, 2H, J = 7.8, 7.0, $C_{10}H_6$), 7.07 (apparent d, 8H, J = 3.1, C_6H_4), 6.92 (d, 2H, J = 7.0, $C_{10}H_6$), 3.83 (s, 6H, OMe).

2.5. Synthesis of (2,6-^{i}Pr-BIAN) (*4*)

This compound was prepared via a similar method to that of Fukuda and co-workers [8b]. Acenaphthenequinone (1.35 g, 7.4 mmol) was dissolved in acetonitrile (65 ml) and glacial acetic acid (12 ml) and heated

to reflux. 2,6-Diisopropylaniline (3 ml, 16 mmol) was added dropwise and the mixture refluxed for 1.5 h. After cooling to room temperature the yellow solid was filtered, washed with hexane and re-crystallised with hexane/CH_2Cl_2 to yield crystals suitable for X-ray diffraction. Yield: 3.15 g, 85%. (Found: C, 86.20; H, 7.98; N, 5.65 $C_{36}H_{40}N_2$ requires: C, 86.35; H, 8.05; N, 5.59%). EI-MS [CH_2Cl_2, *m/z*]: 500 $[M]^+$, 457 $[M - C_3H_7]^+$, 340 $[M - C_6H_3(C_3H_7)_2 + 1]^+$. ^1H NMR [CD_2Cl_2; 400 MHz]:δ 7.91 (d, 2H, $J = 8.3$, $C_{10}H_6$), 7.58 (dd, 2H, $J = 8.3$, 7.1, $C_{10}H_6$), 7.3 (m, 6H, C_6H_3), 6.69 (d, 2H, $J = 7.1$, $C_{10}H_6$), 2.98 (sept, 2H, $J = 6.8$, $CHCH_3$), 1.30 (d, 6H, $J = 6.8$, CH_3), 1.0 (d, 6H, $J = 6.8$, CH_3).

2.6. Synthesis of $ZnCl_2$(2,6-^{i}Pr-BIAN) (5)

This zinc complex was prepared using a different method to that published by Asselt et al. [8a]. Thus, 2,6-^{i}Pr-BIAN (**4**) (2 g, 3.99 mmol) was added in one portion to a stirring solution of anhydrous $ZnCl_2$ (0.544 g, 3.99 mmol) in glacial acetic acid (50 ml). The yellow-orange solid which formed was collected by filtration, washed with Et_2O (3×30 ml) and dried in air. The product was recrystallised by layering Et_2O over CH_2Cl_2. Yield: 2.34 g, 92%. (Found: C, 67.77; H, 6.33; N, 4.42. $C_{36}H_{40}Cl_2N_2Zn$ requires: C, 67.88; H, 6.33; N, 4.40%). EI-MS [CH_2Cl_2, *m/z*]: 600 $[M - Cl + 1]^+$ 500 $[M - ZnCl_2]^+$, 457 $[M - ZnCl_2 - C_3H_7]^+$, 340 $[M - ZnCl_2 - C_6H_3(C_3H_7)_2 + 1]^+$. ^1H NMR [CD_2Cl_2; 200 MHz]: δ 8.17 (d, 2H, $J = 7.9$, $C_{10}H_6$), 7.58 (dd, 2H, $J = 7.9$, 7.4, $C_{10}H_6$), 7.46 (m, 6H, C_6H_3), 6.75 (d, 2H, $J = 7.4$, $C_{10}H_6$), 3.26 (sept, 2H, $J = 6.8$, $CHCH_3$), 1.36 (d, 6H, $J = 6.8$, CH_3), 0.87 (d, 6H, $J = 6.8$, CH_3).

2.7. Synthesis of $PdCl_2$(*p*-OMe-BIAN)·$\frac{1}{2}C_6H_5CN$ (6)

Cyclooctene (0.341 ml, 2.61 mmol) was added in one portion to a stirring solution of $PdCl_2(NCPh)_2$ (0.5 g, 1.324 mmol) in benzonitrile (10 ml). A solution of *p*-OMe-BIAN (**3**) (1.023 g, 2.608 mmol) in benzonitrile (10 ml) was then added and the reaction was stirred for 2 h. The solid formed was collected by filtration, washed with Et_2O and recrystallised from refluxing CH_2Cl_2/benzonitrile. Yield: 0.511 g, 67%. (Found: C, 56.65; H, 3.64; N, 5.64. $C_{26}H_{20}Cl_2N_2O_2Pd \cdot \frac{1}{2}C_6H_5CN$ requires: C, 57.02; H, 3.65; N, 5.64%). EI-MS [CH_2Cl_2, *m/z*]: 570 $[M]^+$, 391 $[M - PdCl_2 - 1]^+$, 377 $[M - PdCl_2 - CH_3]^+$, 361 $[M - PdCl_2 - OCH_3]^+$. ^1H NMR [DMSO; 300 MHz]: δ 8.27 (d, 2H, $J = 8.4$, $C_{10}H_6$), 7.63 (dd, 2H, $J = 8.4$, 7.3, $C_{10}H_6$), 7.34 (d, 4H, $J = 8.7$, C_6H_4), 7.13 (d, 4H, $J = 8.7$, C_6H_4), 6.73 (d, 2H, $J = 7.3$, $C_{10}H_6$), 3.86 (s, 6H, OMe).

2.8. Synthesis of $PdCl_2$(2,6-^{i}Pr-BIAN) (7)

This complex was prepared and crystallised as for **6** with the following quantities of materials: cyclooctene (0.166 ml, 1.27 mmol), $PdCl_2(NCPh)_2$ (0.244 g, 0.637 mmol) in benzonitrile (10 ml) and 2,6-^{i}Pr-BIAN (0.319 g, 0.637 mmol) in benzonitrile (10 ml). Yield: 0.314 g, 72%. (Found: C, 63.62; H, 5.95; N, 4.13. $C_{36}H_{40}Cl_2N_2Pd$ requires: C, 63.77; H, 5.95; N, 4.13%.) EI-MS [CH_2Cl_2, *m/z*]: 500 $[M - PdCl_2]^+$, 457 $[M - PdCl_2 - C_3H_7]^+$, 340.1 $[M - PdCl_2 - C_6H_3(C_3H_7)_2 + 1]^+$. ^1H NMR [CD_2Cl_2; 200 MHz]: δ 8.18 (d, 2H, $J = 8.4$, $C_{10}H_6$), 7.69 (m, 6H, C_6H_3), 7.41 (dd, 2H, $J = 8.4$, 7.2, $C_{10}H_6$), 6.55 (d, 2H, $J = 7.2$, $C_{10}H_6$), 3.50 (sept, 2H, $J = 6.8$, $CHCH_3$), 1.52 (d, 6H, $J = 6.8$, CH_3), 1.00 (d, 6H, $J = 6.8$, CH_3).

2.9. X-ray crystallography

X-ray diffraction experiments were performed on Bruker 3-circle diffractometers with SMART 6000 CCD area detectors, using graphite-monochromated Mo Kα radiation ($\bar{\lambda} = 0.71073$ Å). The low temperature of the crystals was maintained with Cryostream (Oxford Cryosystems) open-flow N_2 cryostats. The structures were solved by direct methods and refined by full-matrix least squares against F^2 of all reflections, using SHELXTL software [10]. All non-H atoms were refined with anisotropic ADP and all H atoms were located by difference Fourier synthesis and refined isotropically. The absolute structure of **5** has been determined from the anomalous dispersion of sulfur, the Flack parameter converging at 0.26(16) [11]. Crystal data and experimental details are given in Table 1.

3. Results and discussion

3.1. Crystal structures

Molecule **1** (shown in Fig. 1) lies at a crystallographic inversion centre, the C(1)–N=C(7)–C(7′)=N′–C(1′) moiety is planar, and *transoid* with respect to the central C(7)–C(7′) bond; the C(1)–N–C(7)–C(7′) torsion angle is −179.95(7)°. This *E*, s-*trans*-*E* conformation has been observed in CyN=CHCH=NCy [12] and is typical for previously reported 2,3-dimethyl-azabutadienes [13], while their analogues with larger substituents in the 2,3-positions usually adopt *gauche* conformations. The cyclohexyl ring adopts a chair conformation. The bond distances are usual, and indicative of localised C=N double bonds.

In the structure of $\mathbf{2} \cdot \frac{1}{2}CH_2Cl_2$, molecule **2** (Fig. 2) has no crystallographic symmetry, while the CH_2Cl_2 is chaotically disordered around an inversion centre. The

Table 1
Crystal data and experimental parameters

Compound	**1**	**2**	**3**	**4**	**6**	**7**
Formula	$C_{16}H_{28}N_2$	$C_{26}H_{20}N_2O_2Cl_2Zn \cdot \frac{1}{2}CH_2Cl_2$	$C_{26}H_{20}N_2O_2$	$C_{36}H_{40}N_2$	$C_{26}H_{20}N_2O_2Cl_2Pd \cdot \frac{1}{2}C_7H_5N$	$C_{36}H_{40}N_2Cl_2Pd$
Formula weight	248.40	571.17	392.44	500.70	621.30	678.00
T (K)	120(2)	120(2)	120(2)	120(2)	120(2)	120(2)
Crystal system	monoclinic	monoclinic	orthorhombic	monoclinic	monoclinic	orthorhombic
Space group	$P2_1/c$ (# 14)	$P2_1/c$ (# 14)	$Pbcn$ (# 60)	$C2/c$ (# 15)	$P2_1/n$ (# 14)	$Pbca$ (# 61)
a (Å)	14.076(5)	12.402(1)	19.851(4)	15.414(2)	19.360(3)	11.429(1)
b (Å)	5.8507(7)	11.736(1)	8.913(1)	8.860(1)	23.573(4)	21.330(1)
c (Å)	9.222(2)	17.574(2)	10.936(2)	21.452(3)	23.871(4)	26.984(1)
β (°)	93.81(2)	95.99(1)	90	93.56(1)	105.93(1)	90
V (Å^3)	757.8(3)	2543.9(4)	1934.9(6)	2923.8(7)	10476(3)	6578.1(5)
Z	2	4	4	4	16	8
ρ_{calcd} (g cm^{-3})	1.089	1.491	1.347	1.137	1.576	1.369
μ (mm^{-1})	0.06	1.31	0.09	0.07	0.94	0.75
$2\theta_{max}$ (°)	60	60	58	58	60	60
Total reflections	10 161	31 064	30 778	19 346	158 533	86 119
Unique reflections	2211	7424	2569	4261	30 528	9562
Reflections $I > 2\sigma(I)$	2006	5762	2159	3053	18 993	7306
Parameters	138	330	177	181	1349	394
R_{int}	0.071	0.035	0.034	0.059	0.063	0.052
R (F, $I > 2\sigma(I)$)	0.040	0.035	0.038	0.053	0.037	0.033
wR (F^2, all data)	0.119	0.103	0.110	0.156	0.114	0.092

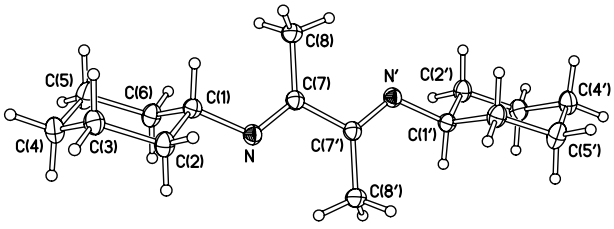

Fig. 1. Molecular structure of **1**. Atoms generated by the inversion centre are primed.

Zn atom has a distorted tetrahedral coordination with two Cl ligands and a nearly-planar chelating diazabutadiene moiety N(1)C(11)–C(12)N(2). In similar complexes with phenyl (and especially substituted phenyl) groups at the N atoms, the phenyl rings usually adopt a perpendicular orientation with respect to the diazabutadiene plane (plane *A*).

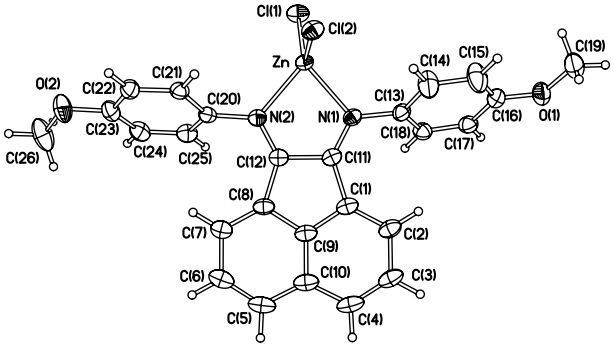

Fig. 2. Molecular structure of **2** in the crystal of **2** · $\frac{1}{2}CH_2Cl_2$.

In **2**, the phenyl rings form angles of 54.1° and 57.7° with the *A* plane and 13.1° between themselves. Thus, the molecule has an approximate mirror plane perpendicular to the acenaphthene plane (violated, however, by opposite orientations of the methyl groups) but loses the mirror plane coinciding with the acenaphthene plane. The two Cl ligands are sterically non-equivalent: Cl(2) faces more overcrowding than Cl(1), with the following results: (i) the Zn–Cl(2) bond is 0.017 Å longer than Zn–Cl(1); (ii) the Zn atom tilts out of the *A* plane by 0.12 Å in the direction of Cl(1); (iii) the N–Zn–Cl(1) angles are wider than N–Zn–Cl(2), averaging 116.5° and 110.2°, respectively; (iv) the naphthalene moiety is tilted out of the *A* plane by 5.1° towards Cl(2), i.e., in the direction of less hindrance on *its* side. Distortions (ii), (iii) and (iv) together make the angle between the acenaphthene plane and the Zn–Cl(2) bond 70.9° compared to 44.5° for Zn–Cl(1).

Molecule **3** lies on a crystallographic twofold axis, passing through atoms C(5), C(6) and the midpoint of the C(7)–C(7′) bond (Fig. 3(a)). The diazabutadiene moiety is planar, and the phenyl rings are inclined to its plane (*A*) by 57.6°; hence, the molecule has no local mirror symmetry but adopts a twisted overall conformation. The *A* and naphthalene planes form an angle $\varphi = 6.0°$, while the N–C(8) bond is tilted out of plane *A* in the opposite direction, with the torsion angles C(7′)–C(7)–N–C(8) 11.0° and C(2)–C(1)···N–C(8) 15.5°.

Molecule **4** also has crystallographic C_2 symmetry (Fig. 3(b)). Bulky ^{i}Pr groups enforce a more perpendicular orientation of the phenyl rings, which are inclined

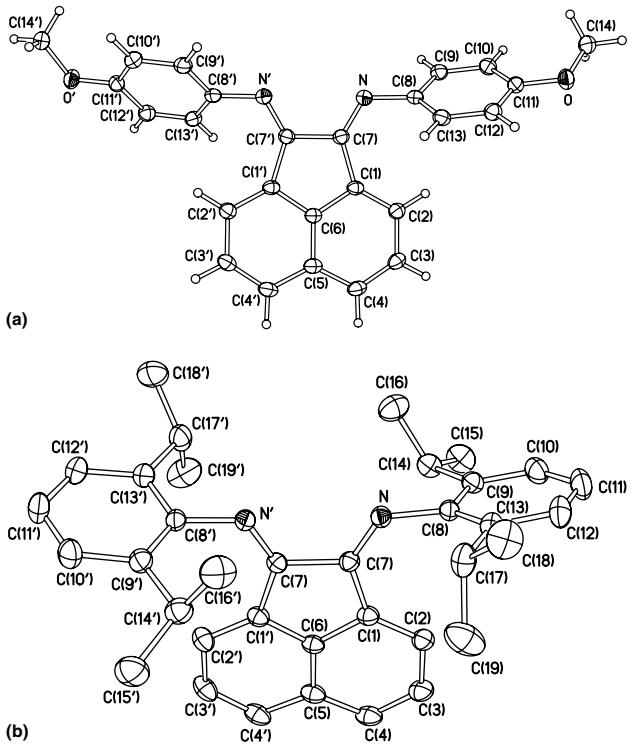

Fig. 3. Molecular structures of **3** (a) and **4** (b). Atoms generated by the twofold axis in each structure are primed.

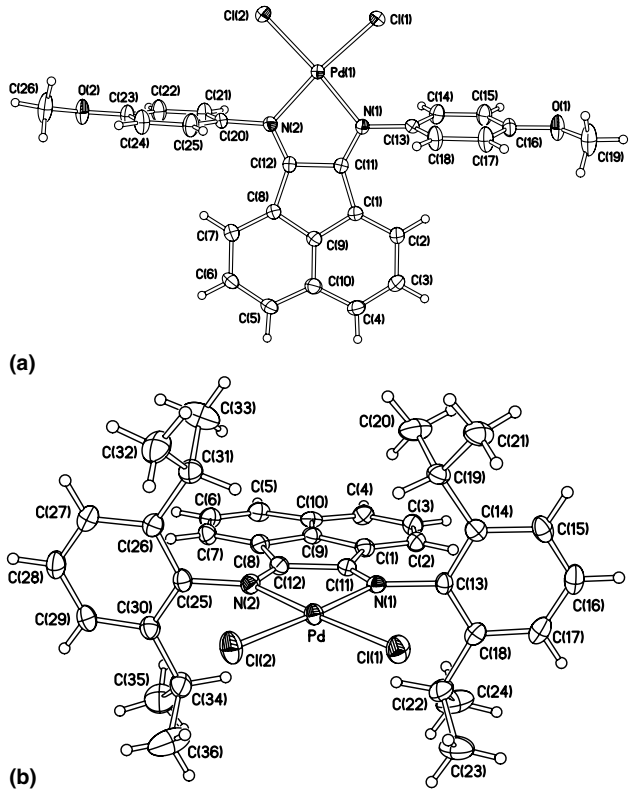

Fig. 4. Molecular structures of **6** (a) (one of the four independent molecules in the crystal of $\mathbf{6}\cdot\frac{1}{2}$PhCN) and **7** (b).

by 78.7° to the *A* plane, and the twist of the molecule is correspondingly smaller than in **3**, with the angles $\varphi = 2.8°$, C(7′)–C(7)–N–C(8) 3.5° and C(2)–C(1)···N–C(8) 5.1°.

While this work was in progress, the crystal structure of **4** was determined [9a,9b] at room temperature in space group *Cc* (No. 9), with the molecule in a general position. The lattice parameters reported, $a = 15.587(2)$ Å, $b = 8.856(2)$ Å, $c = 21.780(7)$ Å, $\beta = 93.85(2)°$, $V = 2999.7$ Å^3, were identical with our results (allowing for thermal expansion). A search for additional symmetry, performed on the atomic coordinates (ref. code WUSLIF) deposited at the CSD, using PLATON software [14], revealed the missing inversion centre with the coordinates (−0.030, 0, −0.212). Thus, the structure [9a,9b] is identical with the one reported herein, in the correct space group *C*2/*c* (No. 15) as already pointed out by Marsh [9c].

The asymmetric unit of $\mathbf{6}\cdot\frac{1}{2}$PhCN comprises four molecules of the complex and two of benzonitrile, all of them devoid of crystallographic symmetry (Fig. 4(a)). Acenaphthene systems of all molecules **6** in the structure are approximately parallel to the (1 0 −1) plane, and the four independent Pd atoms (although not the rest of the molecules) are related by peculiar pseudo-symmetrical operations, viz: (i) *x*, *y*, *z*; (ii) *x*, *y* + 1/2, *z*; (iii) 1/2 − *x*, *y* − 1/4, 1 − *z*; (iv) 1/2 − *x*, *y* − 1/4, 1 − *z*. The geometry and conformation of independent molecules is similar, with square-planar coordination of the Pd atom. Phenyl rings are approximately normal to the diazabutadiene moiety (interplanar angles 74.8°–89.9°). The acenaphthene moiety in molecule (ii) is practically planar and in three others show minor twist, of the same order as in molecule **4**.

The crystal structure of **7** (Fig. 4(b)) is isomorphous with that of chloro-bis{2,8-(2,6-di-isopropylphenylimino)-acenaphthene-N,N)-methylpalladium [5], which differs from **7** by a substitution of a methyl group for one of the chloro-ligands. The asymmetric unit comprises one molecule, without crystallographic symmetry. Molecule **7** is similar to **6** in the nearly perpendicular orientation of the phenyl rings (dihedral angles of 83.3° and 82.6° with plane *A*) and other conformational features.

The ionic radius of square-planar Pd^{2+} (0.64 Å) exceeds that of tetrahedral Zn^{2+} (0.60 Å) [20]. In fact, the Pd–Cl bond distances in **6** and **7** exceed Zn–Cl in **2** by an average of 0.065 Å, while the Pd–N bonds are actually *shorter* than Zn–N, by ca. 0.035 Å (Table 2). This is probably due to $d\pi \rightarrow p\pi$ back donation in the Pd complexes. The resulting π delocalisation in the chelate ring is indicated by small but significant lengthening of C═N bonds and shortening of the intermediate C–C bond in the Pd complexes compared to the free molecules, while coordination with Zn affects these distances insignificantly. It is noteworthy that coordination with

Table 2
Bond distances (Å) in diimine ligands and their complexes

	M–Cl	M–N	C=N	C–C	N···N
1	–	–	1.281(1)	1.510(1)	
2	2.2013(6)	2.085(2)	1.281(3)	1.520(3)	2.713(3)
	2.2180(6)	2.071(2)	1.285(3)	–	–
3	–	–	1.277(1)	1.527(2)	2.815(2)
4	–	–	1.280(1)	1.530(2)	2.812(2)
6					
Minimum	2.2731(7)	2.033(2)	1.275(3)	1.495(3)	2.652(3)
Maximum	2.2817(7)	2.055(2)	1.295(3)	1.499(3)	2.664(3)
Average	2.277(3)	2.041(8)	1.289(6)	1.497(2)	2.660(5)
7	2.2665(5)	2.053(2)	1.293(2)	1.486(3)	2.679(2)
	2.2689(5)	2.051(2)	1.292(2)	–	–

Zn reduces the transannular N···N distance by ca. 0.1 Å compared to free molecules, and coordination with Pd reduces it by 0.15 Å.

3.2. ^1H NMR properties

The ^{1}H NMR spectrum of compound **3** shows three signals at δ 8.07, 7.53 and 6.92 corresponding to positions **A**, **B** and **C**, respectively (see Fig. 5) of the acenaphthenequinone backbone, and an apparent doublet (AB spin system) at δ 7.07 for the C_6H_4 aromatic protons. On complexation to Zn, a very small downfield shift is observed for all of these signals and the apparent doublet collapses to a singlet, i.e., the two chemical environments lead to absolutely coincident signals. When Pd occupies the cavity, a more pronounced effect is observed. The signals relating to protons at positions **A** and **B** move downfield while that of **C** moves upfield. The major difference, however, is the splitting of the C_6H_4 AB signal into two doublets.

These effects may well be due to the Pd–N interaction being stronger than the analogous Zn–N interaction. Very little change is observed in the shift of the methoxy signal. An increase in all of the coupling constants is also observed in complexation of **3** to either Zn or Pd.

The proton signals of compound **4** exhibit very similar behaviour to that observed in **3**. While the ^{1}H signals at positions **A** and **C** move upfield and downfield as described for **3**, the signal for the protons at position **B** does not shift on complexing to Zn but moves upfield when **4** is bound to Pd. As in compound **3**, it is the ^{1}H signals for the aryl side arm that show the most significant shifts. The C_6H_3 signal remains a multiplet regardless of complexation; however, it moves downfield on binding to Zn (0.16 ppm) and Pd (0.39 ppm). This is also the case for the CH of the ^{i}Pr groups. There are two signals present for the methyl groups in compound **4** ($\Delta\delta = 0.3$ ppm), indicative of restricted rotation. The magnitude of separation increases on complexation to Zn ($\Delta\delta = 0.49$ ppm) and Pd ($\Delta\delta = 0.52$ ppm).

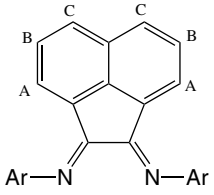

Fig. 5. Assignment of acenaphthenequinone proton positions.

4. Conclusions

Three α-diimines have been synthesised and two of these have been complexed to both $ZnCl_2$ and $PdCl_2$. The ^{1}H NMR spectra have been compared and compounds **1**, **2**, **3**, **4**, **6** and **7** have been structurally characterised by single-crystal X-ray diffraction, revealing the changes resulting from coordination to both tetrahedral Zn(II) and square-planar Pd(II) metal centres.

5. Supplementary material

Crystallographic data for the structural analyses have been deposited with the Cambridge Crystallographic data centre, CCDC Nos. 236150–236155. Copies of this data may be obtained free of charge from The Director CCDC, 12 Union Road, Cambridge, CB2 1EZ (fax: +44-1223-336-033 or e-mail: deposit@ccdc.cam.ac.uk or www: http://www.ccdc.cam.ac.uk).

Acknowledgements

We thank EPSRC for research support and Professor C.J. Elsevier for helpful discussions.

References

[1] S.D. Ittel, L.K. Johnson, M. Brookhart, Chem. Rev. 100 (2000) 1169.

[2] M.D. Hannant, M. Schormann, M. Bochmann, J. Chem. Soc., Dalton Trans. (2002) 4071.

[3] C. Pisano, G. Consiglio, Gazz. Chim. Ital. 124 (1994) 393.

[4] (a) R. van Asselt, C.J. Elsevier, W.J.J. Smeets, A.L. Spek, Inorg. Chem. 33 (1994) 1521;
(b) J.W. Sprengers, M. de Gref, M.A. Duin, C.J. Elsevier, Eur. J. Inorg. Chem. (2003) 3811.

[5] T. Ishiyama, N. Miyaura, J. Organomet. Chem. 680 (2003) 3 (references therein).

[6] N.J. Bell, A.J. Cox, N.R. Cameron, J.S.O. Evans, T.B. Marder, M.A. Duin, C.J. Elsevier, X. Baucherel, A.A.D. Tulloch, R.P. Tooze, Chem. Commun. (submitted).

[7] (a) F. Ragaini, S. Cenini, M. Gasperini, J. Mol. Catal. A, Chem. 174 (2001) 51;
(b) see alsoM. Gasperini, F. Ragaini, Organometallics 23 (2004) 995;
(c) M. Gasperini, F. Ragaini, S. Cenini, Organometallics 21 (2002) 2950;
(d) F. Rangaini, S. Cenini, E. Borsani, M. Dompe, E. Gallo, M. Moret, Organometallics 20 (2001) 3390;
(e) F. Rangaini, S. Cenini, S. Tollari, G. Tummolillo, R. Beltrami, Organometallics 18 (1999) 928.

[8] (a) R. van Asselt, C.J. Elsevier, W.J.J. Smeets, A.L. Spek, R. Benedix, Recl. Trav. Pays-Bas 113 (1994) 88;
(b) A. Paulovicova, U. El-Ayaan, K. Shibayama, T. Morita, Y. Fukuda, Eur. J. Inorg. Chem. 10 (2001) 2641;
(c) H. tom Dieck, J. Dietrich, Chem. Ber. 117 (1984) 694.

[9] (a) U. El-Ayann, A. Paulovicova, Y. Fukuda, J. Mol. Struct. 645 (2003) 205;
(b) U. El-Ayaan, A. Paulovicova, S. Yamada, Y. Fukuda, J. Coord. Chem. 56 (2003) 371;
(c) R.E. Marsh, Acta Crystallogr. Sect. B 60 (2004) 252.

[10] SHELXTL, Ver. 5.10. Bruker AXS, Madison, Wisconsin, USA, 1997.

[11] H.D. Flack, Acta Crystallogr. Sect. A 39 (1983) 876.

[12] J. Keijsper, H. van der Poel, L.H. Polm, G. van Koten, K. Vrieze, P.F.A.B. Seignette, R. Varenhorst, C. Stam, Polyhedron 2 (1983) 1111.

[13] H. tom Dieck, W. Kollvitz, I. Kleinwachter, W. Rohde, L. Stamp, Trans. Met. Chem. 11 (1986) 361.

[14] D.M. Haddeton, M.O. Crossman, B.H. Dana, D.J. Duncalf, A.M. Heming, D. Kukulj, A.J. Shooter, Macromolecules 32 (1999) 2110.

[15] N. Kuhn, M. Steimann, I. Walker, Z. Naturforsch., B 55 (2000) 992.

[16] J.C. Gordon, P. Shulda, A.H. Cowley, J.N. Jones, D.W. Keogh, B.L. Scott, Chem. Commun. (2002) 2710.

[17] L. Gonsalvi, J.A. Gaunt, H. Adams, A. Castro, G.J. Sunley, A. Haynes, Organometallics 22 (2003) 1047.

[18] A.L. Spek, Acta Crystallogr. Sect. A 46 (1990) C34.

[19] A.L. Spek, PLATON, University of Utrecht, The Netherlands, 2002.

[20] R.D. Shannon, Acta Crystallogr. Sect. A 32 (1976) 751.

Available online at www.sciencedirect.com
SCIENCE DIRECT®
Polyhedron 23 (2004) 2797–2804
POLYHEDRON
www.elsevier.com/locate/poly

Pyridinium-derived *N*-heterocyclic carbene ligands: syntheses, structures and reactivity of *N*-(2′-pyridyl)pyridin-2-ylidene complexes of nickel(II), palladium(II) and platinum(II) ☆

Nicholas A. Piro, Jonathan S. Owen, John E. Bercaw *

Arnold and Mabel Beckman Laboratories of Chemical Synthesis, California Institute of Technology, Pasadena, CA 91125, USA

Received 30 April 2004; accepted 14 June 2004
Available online 3 September 2004

Abstract

Pyridinium-derived *N*-heterocyclic carbene complexes $[(i\text{-BIPY})M(acac)]^+[OTf]^-$ (M = Ni (**2a**), Pd (**3a**), Pt (**4a**)) (*i*-BIPY = *N*-(2′-pyridyl)-4-*tert*-butylpyridin-2′-ylidene) are obtained as insoluble microcrystalline powders by cyclometallation of the ligand precursor $[i\text{-BIPY-H}]^+[OTf]^-$ (OTf = trifluormethylsulfonate) to $M(acac)_2$ (acac = acetylacetonate) in chlorobenzene at 160 °C. Consumption of the starting materials in the synthesis of **3a** and **4a** is complete after 18 h, providing (**4a**) and (**5a**) in good yields as analytically pure material after recrystallization. The reaction with $Ni(acac)_2$ is reversible and reaches equilibrium at approximately 75% completion. Removal by distillation of the acetylacetone produced in the cyclometallation drives the reaction to completion furnishing a good yield of pure **6a**. Salt metathesis with sodium tetraphenylborate in methanol yields the tetraphenylborate salts (**2b**–**4b**) that were used to grow X-ray quality crystals. Analysis of the M–O bond lengths confirms the larger *trans*-influence of the carbene donor compared with the pyridine donor. Ratios of the M–O(1)/M–O(2) bond lengths suggest that the carbene–metal bond strength follows the order **4b** ≈ **3b** > **2b**. Protonation of **2a**–**4a** with three equivalents of pyridinium hydrochloride produces $(i\text{-BIPY})MCl_2$ in the case of palladium (**5**) and platinum (**6**), while in the case of nickel it regenerates the starting $[i\text{-BIPY-H}]^+$ and paramagnetic nickel products.
© 2004 Published by Elsevier Ltd.

1. Introduction

Imidazolium-derived *N*-heterocyclic carbenes are useful as ligands for many applications, including ruthenium-mediated olefin metathesis [1] and nickel- and palladium-catalyzed arylhalide cross-couplings [2]. We became interested in developing new carbene ligands based on other *N*-heterocycles, particularly in regard to their relative σ-donating and π-accepting characteristics. We recently reported the preparation of pyridinium-derived *N*-heterocyclic carbene complexes of platinum, e.g., $[(i\text{-BIPY})Pt(CH_3)(DMSO)]^+[B(C_6H_5)_4]^-$ ((*i*-BIPY) = *N*-(2′-pyridyl)pyridin-2-ylidene), using a synthetic strategy that involves loss of methane from dimethylplatinum starting materials [3]. In order to extend the scope of these *N*-heterocyclic carbene complexes to more readily available and easily handled starting materials, we have investigated the cyclometallation of *N*-(2′-pyridyl)-4-*tert*-butylpyridinium triflate with $M(II)(acac)_2$ (acac = acetylacetonate) starting materials. We chose to use the 4-*tert*-butyl substituted ligand precursor (**1**) due to its ease of synthesis, useful ^1H NMR features, and the higher solubilities and stabilities of its complexes. Here we present a scheme for the cyclometallation of this new ligand onto nickel(II), palladium(II) and platinum(II), along with their character-

☆ Honoring a special friend and quite amazing chemist, Malcolm L.H. Green, on the occasion of his retirement.

* Corresponding author. Tel.: +1 6263956577; fax: +1 6265850147.
E-mail address: bercaw@caltech.edu (J.E. Bercaw).

0277-5387/$ - see front matter © 2004 Published by Elsevier Ltd.
doi:10.1016/j.poly.2004.06.021

ization by X-ray crystallography, NMR spectroscopy and electronic absorption spectroscopy.

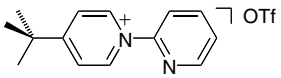

1

2. Experimental

2.1. General

Nickel(II) acetylacetonate hydrate was purchased from Strem and water was removed by heating under vacuum in the presence of P_2O_5 for 3 days. Palladium(II) acetylacetonate and platinum(II) acetylacetonate were purchased from Aldrich and used as received. Chlorobenzene was purchased from Aldrich, dried over calcium hydride, vacuum distilled and stored under argon. *N*-(2′-pyridyl)-4-*tert*-butylpyridinium triflate (**1**) was prepared as previously reported [3]. Reactions were run under argon using standard Schlenk techniques with degassed solvents, while all isolations were performed in air.

2.2. Syntheses

2.2.1. Synthesis of nickel(II)(N-(2′-pyridyl)-4-(tert-butyl)pyridin-2-ylidene)(acetylacetonate) triflate (**2a**)

N-(2′-pyridyl)-4-*tert*-butylpyridinium triflate (725 mg, 2.0 mmol), nickel(II) acetylacetonate (1.027 g, 4.0 mmol) and chlorobenzene (7 mL) were combined in a Schlenk tube, degassed and heated under vacuum to 160 °C for 3 h. Volatiles were removed *in vacuo*, chlorobenzene was added to the solids, and heating continued for another 3 h. Volatiles were again removed, followed by readdition of solvent and heating for 18 h. The reaction mixture was cooled, methylene chloride (10 mL) was added and the mixture was filtered. The solvent was removed in vacuo to give the crude product as a yellow solid. This crude product was recrystallized from hot chlorobenzene to give the desired product (710 mg, 69% yield). ^{1}H NMR (300 MHz, DMSO-d_6): δ 9.34 (d, $J = 6.9$ Hz, 1H), 8.56 (d, $J = 5.5$ Hz, 1H), 8.47 (m, 2H), 7.88 (d, $J = 6.9$ Hz, 1H), 7.83 (s, 1H), 7.75 (m, 1H), 5.80 (s, 1H), 2.10 (s, 6H), 1.35 (s, 9H) ppm. *Anal*. Calc. for $C_{20}H_{23}F_3N_2O_5NiS$: C, 46.33; H, 4.47; N, 5.41. Found: C, 46.37; H, 4.41; N, 5.36%.

2.2.2. Synthesis of nickel(II)(N-(2′-pyridyl)-4-(tert-butyl)pyridin-2-ylidene)(acetylacetonate)tetraphenylborate (**2b**)

2a (520 mg, 1.0 mmol) was dissolved in methanol (50 mL) and a methanol solution (15 mL) of sodium tetraphenylborate (380 mg, 1.1 mmol) was added dropwise to immediately form an orange precipitate. The solution was cooled to −30 °C for 3 h, and the orange precipitate was collected by filtration and dried to give the desired product (655 mg, 95% yield). ^{1}H NMR (500 MHz, CD_2Cl_2): δ 8.54 (dd, $J = 1.6$, 5.9 Hz, 1H), 7.93 (d, $J = 2.1$ Hz, 1H), 7.74 (td, $J = 1.5$, 7.9 Hz, 1H), 7.47 (m, 8H), 7.32 (td, $J = 1.0$, 6.5 Hz, 1H), 7.01 (overlapping, 9H), 6.86 (t, $J = 7.4$ Hz, 4H), 6.28 (d, $J = 8.5$ Hz, 1H), 5.72 (s, 1H), 2.16 (s, 6H), 1.40 (s, 9H) ppm. ^{13}C{^{1}H} NMR(125 MHz, CD_2Cl_2): δ 189.10, 188.90, 175.89, 166.33, 164.66 (q, $J_{B-C} = 49$ Hz), 155.10, 148.13, 143.65, 136.31, 135.76, 129.81, 126.40, 125.34, 122.49, 121.52, 114.06, 102.62, 36.81, 30.11, 26.94, 26.90 ppm. *Anal*. Calc. for $C_{43}H_{43}BN_2NiO_2$: C, 74.92; H, 6.29; N, 4.06. Found: C, 74.61; H, 6.18; N, 3.99%.

2.2.3. Synthesis of palladium(II)(N-(2′-pyridyl)-4-(tert-butyl)pyridin-2-ylidene)(acetylacetonate) triflate (**3a**)

N-(2′-pyridyl)-4-*tert*-butylpyridinium triflate (714 mg, 1.97 mmol), palladium(II) acetylacetonate (600 mg, 1.97 mmol) and chlorobenzene (5 mL) were combined in a Schlenk tube, degassed, and heated under vacuum to 160 °C for 18 h. Filtration through a glass frit and washing with methylene chloride and warm acetonitrile removed palladium metal. The filtrate was dried by removal of solvent in vacuo. The crude product was recrystallized from hot acetonitrile. The desired product was collected as fine, pale yellow needles (825 mg, 74% yield). ^{1}H NMR (300 MHz, DMSO-d_6): δ 9.50 (d, $J = 6.6$ Hz, 1H), 8.74 (dd, $J = 5.5$, 1.6 Hz, 1H) 8.69 (d, $J = 8.8$ Hz, 1H), 8.58 (t, $J = 8.0$ Hz, 1H), 8.03 (overlapping, 2H), 7.93 (t, $J = 6.6$ Hz, 1H), 5.71 (s, 1H), 2.17 (s, 3H), 2.15 (s, 3H), 1.41 (s, 9H) ppm. *Anal*. Calc. for $C_{20}H_{23}F_3N_2O_5PdS$: C, 42.37; H, 4.09; N, 4.94. Found: C, 42.89; H, 4.08; N, 5.62%.

2.2.4. Synthesis of palladium(II)(N-(2′-pyridyl)-4-(tert-butyl)pyridin-2-ylidene)(acetylacetonate) tetraphenylborate (**3b**)

3a (240 mg, 0.35 mmol) was dissolved in methanol (120 mL) and sodium tetraphenylborate (135 mg, 0.40 mmol) was added dropwise as a methanol solution (10 mL). Crystals began to form, and the solution was cooled to −30 °C. The yellow crystalline product was collected after 18 h (240 mg, 93% yield). ^{1}H NMR (300 MHz, CD_2Cl_2): δ 8.75 (dd, $J = 1.6$, 5.5 Hz, 1H), 8.12 (d, $J = 1.6$ Hz, 1H), 7.85 (dt, $J = 1.6$, 8.2 Hz, 1H), 7.47 (dm, 9H), 7.06 (m, 2H), 9.69 (t, $J = 7.4$ Hz, 8H), 6.80 (t, $J = 7.2$ Hz, 4H), 6.34 (d, $J = 8.2$ Hz, 1H), 5.62 (s, 1H), 2.21 (s, 3H), 2.18 (s, 3H), 1.41 (s, 9H) ppm. ^{13}C{^{1}H} NMR(125 MHz, CD_2Cl_2): δ 190.04, 187.92, 174.74, 168.93, 164.72 (q, $J_{B-C} = 49$ Hz) 156.34, 147.93, 143.82, 136.73, 136.30, 128.17, 126.48, 126.28, 122.54, 121.48, 115.41, 102.28, 37.10, 30.10, 27.76,

27.40 ppm. *Anal*. Calc. for $C_{43}H_{43}BN_2O_2Pd$: C, 70.07; H, 5.88; N, 3.80. Found: C, 69.59; H, 5.83; N, 3.87%.

*2.2.5. Synthesis of platinum(II)(N-(2′-pyridyl)-4-(tert-butyl)pyridin-2- ylidene)(acetylacetonate)(triflate) (**4a**)*

N-(2′-pyridyl)-4-*tert*-butylpyridinium triflate (362 mg, 1.0 mmol), platinum(II) acetylacetonate (393 mg, 1.0 mmol) and chlorobenzene (7 mL) were combined in a Schlenk tube, degassed and heated under vacuum to 160 °C for 18 h. The crude reaction mixture was dissolved in methylene chloride and filtered. Solvent was removed in vacuo, the solid was dissolved in hot acetonitrile and the resulting solution was filtered. The product was recrystallized from hot acetonitrile, and a yellow solid was collected by filtration (152 mg, 77% yield). ^{1}H NMR (300 MHz, DMSO-d_6): δ 9.44 (d, J = 7.1 Hz, 1H), 9.04 (d, J = 5.4 Hz, 1H), 8.67 (d, J = 8.2 Hz, 1H), 8.59 (td, J = 1.2, 7.6 Hz, 1H), 8.03 (d, J = 2.0 Hz, 1H), 7.97 (dd, J = 2.0, 7.2 Hz, 1H), 7.91 (t, J = 7.2 Hz, 1H), 5.87 (s, 1H), 2.17 (s, 3H), 2.15 (s, 3H), 1.41 (s, 9H) ppm. *Anal*. Calc. for $C_{20}H_{23}F_3N_2O_5PtS$: C, 36.64; H, 3.54; N, 4.27. Found: C, 36.76; H, 3.59; N, 4.40%.

*2.2.6. Synthesis of platinum(II)(N-(2′-pyridyl)-4-(tert-butyl)pyridin-2-ylidene)(acetylacetonate) tetraphenylborate (**4b**)*

4a (300 mg, 0.46 mmol) was dissolved in methanol (180 mL) and a solution of sodium tetraphenylborate (170 mg, 0.50 mmol) in methanol (10 mL) was added dropwise. This mixture was stored at −30 °C after crystals began to form. The orange crystalline product was collected by filtration and dried (360 mg, 95% yield). ^{1}H NMR (500 MHz, CD_2Cl_2): δ 8.98 (dd, J = 1.5, 5.9 Hz, 1H), 8.08 (d, J = 2.1 Hz, 1H), 7.80 (td, J = 1.6, 8.3 Hz, 1H), 7.46 (bm, 8H), 7.41 (td, J = 1.0, 6.4 Hz, 1H), 7.12 (d, J = 7.3 Hz, 1H), 7.05 (dd, J = 2.4, 7.3 Hz, 1H), 6.97 (t, J = 7.5 Hz, 8H), 6.80 (t, J = 7.6 Hz, 4H), 6.30 (d, J = 8.6 Hz, 1H), 5.71 (s, 1H), 2.17 (s, 3H), 2.17 (s, 3H), 1.42 (s, 9H) ppm. ^{13}C{^{1}H} NMR(125 MHz, CD_2Cl_2): δ 188.49, 186.34, 168.92, 164.7 (q, $J_{B–C}$ = 49 Hz), 161.14, 157.54, 147.14, 143.24, 136.50, 136.34, 127.01, 126.44, 125.65, 122.52, 119.88, 115.51, 103.86, 36.86, 30.07, 27.94, 27.16 ppm. *Anal*. Calc. for $C_{43}H_{43}BN_2O_2Pt$: C, 62.55; H, 5.25; N, 3.39. Found: C, 62.23; H, 5.17; N, 3.34%.

*2.2.7. Synthesis of palladium(II)(N-(2′-pyridyl)-4-(tert-butyl)pyridin-2-ylidene)dichloride (**5**)*

3a (164 mg, 0.29 mmol) and pyridinium chloride (100 mg, 0.87 mmol) were added to a Teflon stoppered Schlenk tube with acetonitrile (10 mL) and heated to 100 °C for 1 h. After cooling the reaction mixture, the yellow precipitate was collected on a glass frit and washed with acetonitrile followed by ether. The yellow powder was dried under vacuum (90 mg, 80% yield). ^{1}H NMR (500 MHz, DMSO-d_6, 85 °C): δ 9.50 (s, 1H), 9.32 (d, J = 6.8 Hz, 1H), 8.79 (s, 1H), 8.52 (d, J = 8.3 Hz, 1H), 8.46 (t, J = 8.1 Hz, 1H), 7.85 (t, J = 6.4 Hz, 1H), 7.80 (dd, J = 7.1, 2.2 Hz, 1H), 1.40 (s, 9H) ppm. ^{13}C{^{1}H} NMR (125 MHz, DMSO-d_6, 85 °C): δ 172.2, 166.5, 156.3, 149.5, 142.0, 137.2, 130.9, 125.5, 119.3, 114.4, 35.9, 28.9 ppm. *Anal*. Calc. for $C_{19}H_{23}N_2O_2PdCl_2$: C, 43.16; H, 4.14; N, 7.19. Found: C, 43.37; H, 4.13; N, 7.18%.

*2.2.8. Synthesis of platinum(II)(N-(2′-pyridyl)-4-(tert-butyl)pyridin-2-ylidene)dichloride (**6**)*

4a (321 mg, 0.50 mmol) and pyridinium chloride (165 mg, 1.43 mmol) were added to a Teflon stoppered Schlenk tube with acetonitrile (10 mL) and heated to 100 °C for 45 min. After cooling the reaction mixture, the yellow precipitate was collected on a glass frit and washed with acetonitrile followed by ether. The bright yellow powder was dried under vacuum to give an orange powder (185 mg, 79% yield). ^{1}H NMR (500 MHz, DMSO-d_6): δ 9.78 (d, J = 5.9 Hz, $J_{Pt–H}$ = 36 Hz, 1H), 9.30 (d, J = 7.3 Hz, 1H), 8.62 (d, J = 2.0 Hz, $J_{Pt–H}$ = 27 Hz, 1H), 8.53 (m, 2H), 7.85 (t, J = 5.9 Hz, 1H), 7.81 (dd, J = 2.1, 6.3 Hz, 1H), 1.37 (s, 9H) ppm. ^{13}C{^{1}H} NMR(125 MHz, DMSO-d_6): δ 167.1, 160.0, 157.5, 148.5, 141.8, 137.3, 128.0, 126.0, 118.1, 115.2, 36.2, 29.3 ppm. *Anal*. Calc. for $C_{19}H_{23}N_2O_2PtCl_2$: C, 35.16; N, 5.86; H, 3.37; Cl, 14.83. Found: C, 34.92; N, 5.89; H, 3.37; Cl, 14.83%.

2.3. X-ray structures

Crystals of **2b** were grown from THF/diethyl ether. Crystals of **3b** and **4b** were grown from dichloromethane/THF/diethyl ether and dichloromethane/THF, respectively. Data for **2b**–**4b** were collected at 100K on a Bruker SMART 1000 using Mo Kα radiation. The structure was solved using SHELXS-97 by direct methods. The hydrogens in **2b** were placed by the difference Fourier map; those of **3b** and **4b** were placed geometrically. The crystals of **3b** appear to contain both water and THF. The water sits near a 4bar symmetry element and was modelled at half occupancy without the hydrogens. The THF molecule sits near a 4-fold axis and was modelled at half occupancy as a flat ring with riding hydrogens. The crystals of **4b** contained sites partially occupied with dichloromethane or THF, both of which were refined anisotropically. Full matrix least squares refinement on F^2 was carried out using SHELXL-97. Refinement of F^2 against ALL reflections. The weighted R-factor (wR) and goodness-of-fit (S) are based on F^2, conventional R-factors (R) are based on F, with F set to zero for negative F^2. The threshold expression of $F^2 > 2\sigma(F^2)$ is used only for calculating R-factors (gt), etc., and is not relevant to the choice of reflections for refinement. R-factors based on F^2 are statistically about

Table 1
Crystal data and structure refinement for **2b**–**4b**

Empirical formula	$[C_{19}H_{23}N_2O_2Ni]^+[B(C_6H_5)_4]^-$	$[C_{19}H_{23}N_2O_2Pd]^+$ $[B(C_6H_5)_4]^- \cdot H_2O \cdot C_4H_8O$	$[C_{19}H_{23}N_2O_2Pt]^+[B(C_6H_5)_4]^- \cdot$ $(CH_2Cl_2)_{0.45} \cdot (C_4H_8O)_{1.45}$
Formula weight	689.31	781.06	973.39
Crystallization solvent	THF/diethylether	dichloromethane/THF/ diethylether	dichloromethane/THF
Crystal habit	block	block	block
Crystal size (mm)	$0.16 \times 0.11 \times 0.11$	$0.33 \times 0.12 \times 0.10$	$0.19 \times 0.16 \times 0.06$
Crystal color	red/orange	yellow	red/orange
Data collection			
Preliminary photos	rotation	rotation	rotation
Type of diffractometer	Bruker SMART 1000	Bruker SMART 1000	Bruker SMART 1000
Wavelength (Å)	0.71073 Mo Kα	0.71073 Mo Kα	0.71073 Mo Kα
Data collection temperature (K)	100(2)	100(2)	100(2)
Reflection used in lattice determination	20388	21364	7031
θ Range for reflections used in lattice determination (°)	2.26–28.15	2.24–27.39	2.39–27.42
Unit cell dimensions			
a (Å)	11.5133(6)	27.5131(11)	13.5043(8)
b (Å)	13.0777(7)	27.5131(11)	13.5841(8)
c (Å)	13.5776(7)	10.2607(6)	14.3311(9)
α (°)	115.9570(10)		65.6340(10)
β (°)	92.5200(10)		84.7180(10)
γ (°)	99.2060(10)		65.8310(10)
Volume (Å^3)	1799.41(16)	7767.0(6)	2175.5(2)
Z	2	8	2
Crystal system	triclinic	tetragonal	triclinic
Space group	$P\bar{1}$	$P4/n$	$P\bar{1}$
D_{calc} (Mg/m^3)	1.272	1.336	1.486
$F(000)$	728	3248	988
Data collection program	Bruker SMART v5.054	Bruker SMART v5.054	Bruker SMART v5.054
θ Range for data collection (°)	1.68–28.24	1.48–28.65	1.66–32.26
Completeness to $\theta = 28.24°$ (2b)/ 28.65 (3b)/(%)	92.50	95.40	
Index ranges	$-15 \leqslant h \leqslant 15$, $-16 \leqslant k \leqslant 16$, $-17 \leqslant l \leqslant 17$	$-36 \leqslant h \leqslant 35$, $-36 \leqslant k \leqslant 35$, $-13 \leqslant l \leqslant 13$	$-19 \leqslant h \leqslant 19$, $-20 \leqslant k \leqslant 18$, $-21 \leqslant l \leqslant 21$
Data collection scan type	ω scans at 7ϕ settings	ω scans at 5ϕ settings	ω scans at 7ϕ settings
Data reduction program	Bruker SAINT v6.45	Bruker SAINT v6.45	Bruker SAINT v6.45
Reflections collected	36729	114354	48593
Independent reflections (R_{int})	8229 (0.0482)	9552 (0.1073)	9403 (0.0420)
Absorption coefficient (mm^{-1})	0.578	0.520	3.32
Absorption correction	none	none	none
Maximum and minimum transmission	0.9391 and 0.9132	0.9498 and 0.8471	0.8257 and 0.5712
Structure solution and refinement			
Structure solution program	SHELXS-97 (Sheldrick, 1990)	SHELXS-97 (Sheldrick, 1990)	SHELXS-97 (Sheldrick, 1990)
Primary solution method	direct methods	direct methods	direct methods
Secondary solution method	difference Fourier map	difference Fourier map	difference Fourier map
Hydrogen placement	difference Fourier map	geometric positions	geometric positions
Structure refinement program	SHELXL-97 (Sheldrick, 1997)	SHELXL-97 (Sheldrick, 1997)	SHELXL-97 (Sheldrick, 1997)
Refinement method	full matrix least-squares on F_2	full matrix least-squares on F_2	full matrix least-squares on F_2
Data/restraints/parameters	8229/0/614	9552/0/463	13078/0/597
Treatment of hydrogen atoms	unrestrained	riding	mixed
Goodness-of-fit on F_2	1.967	2.642	1.123
Final R indices [$I > 2\sigma(I)$, 6974 reflections (**2b**), 5784 reflections (**3b**)], 9403 reflections (**4b**)			
R_1	0.0354	0.0632	0.0420
wR_2	0.0683	0.1071	0.0772
R indices (all data)			
R_1	0.0438	0.1153	0.0691
wR_2	0.0694	0.1094	0.0772

Table 1 (*continued*)

Empirical formula	$[C_{19}H_{23}N_2O_2Ni]^+[B(C_6H_5)_4]^-$	$[C_{19}H_{23}N_2O_2Pd]^+$ $[B(C_6H_5)_4]^- \cdot H_2O \cdot C_4H_8O$	$[C_{19}H_{23}N_2O_2Pt]^+[B(C_6H_5)_4]^- \cdot$ $(CH_2Cl_2)_{0.45} \cdot (C_4H_8O)_{1.45}$
Type of weighting scheme used	sigma	sigma	sigma
Weighting scheme used	$w = 1/\sigma^2(F_o^2)$	$w = 1/\sigma^2(F_o^2)$	$w = 1/\sigma^2(F_o^2)$
Max shift/error	0.002	0.19	0
Average shift/error	0	0.002	0
Largest difference peak and hole (e Å^{-3})	0.972 and −0.356	2.788 and −2.001	2.23 and −1.19

twice as large as those based on *F*, and *R*-factors based on ALL data will be even larger.

All esds (except the esd in the dihedral angle between two l.s. planes) are estimated using the full covariance matrix. The cell esds are taken into account individually in the estimation of esds in distances, angles and torsion angles; correlations between esds in cell parameters are only used when they are defined by crystal symmetry. An approximate (isotropic) treatment of cell esds is used for estimating esds involving l.s. planes. The details of the crystal, data collection and structure refinement are provided in Table 1.

3. Results and discussion

3.1. Synthesis of metal complexes

Ligand cyclometallation is a well precedented reaction and is a reliable way to make M–C bonds. Palladium(II) acetylacetonate and palladium(II) acetate have been used in the cyclometallation of 2-phenylpyridine and its derivatives to produce stable five-membered metallacycles [4]. Initial attempts to cyclometallate **1** with a variety palladium starting materials were plagued by palladium metal deposition, and as a result we tested the more thermally robust palladium(II) acetylacetonate. [1] Heating this commercially available starting material with **1** in chlorobenzene gave rise to the desired palladium(II) *N*-heterocyclic carbene complex **2a**. (Scheme 1). Similarly, reactions of nickel(II) and platinum(II) acetylacetonates afforded the analogous nickel **(3a)** and platinum **(4a)** complexes.

To obtain crystallographic support for the structure of **2–4** the triflate anion was exchanged for tetraphenylborate to improve the solubility and crystallinity. Precipitation of **2b–4b** from methanol by dropwise addition of sodium tetraphenylborate solutions to methanol solutions of **2a–4a** provided complexes suitable for the growth of X-ray quality crystals. Interestingly, in the ^{1}H NMR spectra of **2b–4b** the aromatic resonances showed an average upfield shift of ~1 ppm relative to the triflate salt **2a–4a** suggesting that the triflate ion is closely associated with the cationic coordination complex in DMSO solution.

3.2. Crystal structures

The X-ray diffraction data were able to confirm the identity and predicted geometries of **2b–4b**. ORTEP drawings for the cations of all three structures are shown in Fig. 2, and selected bond lengths and angles are provided in Tables 3–5.

The expected strong *trans*-influence of the carbene donor relative to pyridine is evident from these data, comparing the two *trans* M–O bond lengths. In complex **2b** the bond *trans* to carbene is longer by approximately 0.03 Å while in complexes **3b** and **4b** it is longer by 0.06 Å. The ratio of metal oxygen bond lengths (**4b** ≈ **3b** > **2b**) suggests that the *trans*-influence of the carbene relative to the pyridine increases for Pt ≈ Pd > Ni. These results suggest a stronger bonding interaction in **4b** and **3b** relative to **2b**. Slight shortening of the metal–carbon bond was observed in all cases when compared with M–Ph distances. [2]

3.3. Reactivity

While in the syntheses of the palladium and platinum complexes (Scheme 1), all of the starting pyridinium salt is consumed, reactions with Ni(acac)$_2$ reached equilibrium at ~75% completion upon heating for several days. Distillation of the acetylacetone from the reaction mixture resulted in further consumption of the starting pyridinum salt. In order to probe the equilibrium behavior, acetyl acetone was added to samples of **2b–4b** in

[1] Attempts to prepare complexes from palladium(II)acetate gave little reaction until palladium metal deposition occurred upon heating to higher temperature.

[2] Searching the Cambridge Crystallographic Database for M–Ph complexes showed that the M–C distances in **2b–4b** are in the top 4–6% of metal phenyl distances. The majority of complexes displaying shorter distances contained tridentate chelating ligands where the phenyl ligand is the central donor. Similar M–C distances were reported in [3].

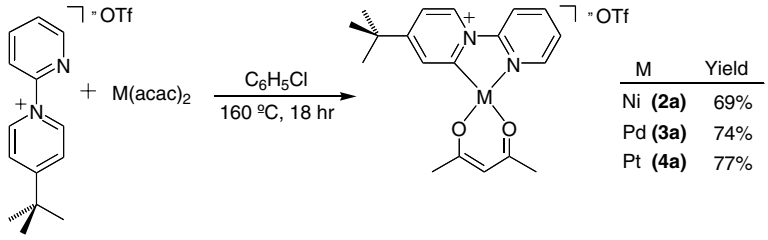

Scheme 1.

Table 2
Electronic absorbance data for **2b**–**4b**

	λ (nm)	ε (M^{-1} cm^{-1})	λ (nm)	ε (M^{-1} cm^{-1})	λ (nm)	ε (M^{-1} cm^{-1})
2b	420	4140	275	24800	240	45500
3b	360	5160	295	22100	230	46400
4b	400	8260	270	26400	230	42100

Table 3
Selected bond lengths (Å) and angles (°) for **2b**

Ni(1)–C(6)	1.8522(15)	C(6)–Ni(1)–N(1)	83.33(6)
Ni(1)–N(1)	1.8830(12)	C(6)–Ni(1)–O(1)	89.36(5)
Ni(1)–O(1)	1.8377(10)	C(6)–Ni(1)–O(2)	175.22(6)
Ni(1)–O(2)	1.8674(10)	O(1)–Ni(1)–N(1)	172.48(5)
		O(2)–Ni(1)–N(1)	92.34(5)
		O(1)–Ni(1)–O(2)	94.91(4)

Table 4
Selected bond lengths (Å) and angles (°) for **3b**

Pd(1)–C(6)	1.942(4)	C(6)–Pd(1)–N(1)	80.71(17)
Pd(1)–N(1)	1.987(4)	C(6)–Pd(1)–O(1)	92.02(18)
Pd(1)–O(1)	1.984(3)	C(6)–Pd(1)–O(2)	174.35(16)
Pd(1)–O(2)	2.039(3)	O(1)–Pd(1)–N(1)	172.53(14)
		N(1)–Pd(1)–O(2)	93.64(15)
		O(1)–Pd(1)–O(2)	93.61(13)

Table 5
Selected bond lengths (Å) and angles (°) for **4b**

Pt(1)–C(1)	1.930(4)	C(1)–Pt(1)–N(1)	80.84(14)
Pt(1)–N(1)	1.983(3)	C(1)–Pt(1)–O(1)	93.06(13)
Pt(1)–O(1)	1.997(2)	C(1)–Pt(1)–O(2)	174.21(13)
Pt(1)–O(2)	2.054(2)	O(1)–Pt(1)–N(1)	173.87(11)
		N(1)–Pt(1)–O(2)	93.81(11)
		O(1)–Pt(1)–O(2)	92.25(10)

$C_2D_2Cl_4$ (used for solvating ability and temperature range) and heated to 100 °C. All samples showed partial disappearance of the metal complex. Complexes **3b** and **4b** each gave rise to their own set of new unidentifiable resonances and, in the case of palladium, deposition of colloidal metal [5]. In the case of **2b**, however, resonances for the free pyridinium salt **1** and obvious broadening of the sample due to the presence of paramagnetic $Ni(acac)_2$ were observed. Furthermore, by heating to 160 °C in $C_2D_2Cl_4$, either $Ni(acac)_2$ with **1**, or **2a** with two equivalents of acetylacetone, broad NMR spectra with peaks for both **1** and **2a** are observed. The relative intensities of the signals for **1** and **2a** are consistent in both experiments with an equilibrium constant of $K_{eq} \approx 3.5 \pm 1$ for the forward reaction [3] [6].

These observations support an equilibrium between the binding of acetylacetone and $[i\text{-BIPY}]^+$. While we cannot rule out such an equilibrium in the case of Pd and Pt, the isolated yields obtained without the distillation of acetylacetone (**3a** 74% and **4a** 77%) and the complete consumption of **1** suggest the reactions to form the desired *N*-heterocyclic carbene complexes are more favorable for Pd and Pt. We believe this is due to the stronger metal–ligand bonding observed for second and third row transition metals, which better support the large ligand field of the carbene donor, thus favoring ligation of *i*-BIPY over acac.

To further probe the stability of the metal's interaction with the carbene and acac ligands, a series of protonolysis experiments were carried out with **2a**–**4a**. Treatment of **2a**–**4a** with pyridinium hydrochloride in acetonitrile at 100 °C results in clean conversion of **3a** and **4a** to the dichlorides (**5** and **6**) (Scheme 2), which can be isolated as yellow and orange solids in 80% yield. In the case of **2a**, rapid protonolysis and de-coordination of the carbene ligand occurs. These results are consistent with the stronger carbene donor interactions for palladium and platinum, relative to nickel.

Studies of arylhalide cross-coupling have shown that monodentate phosphine and carbene ligands furnish the most active catalysts for aryl-halide cross-coupling reactions [7]. Accordingly, we briefly investigated the use of

[3] It should be noted, however, that the NMR tubes both showed some visible signs of solid side products. Further, integration of the peaks in the $Ni(acac)_2$ + **1** reaction is poor due to the very broad peaks.

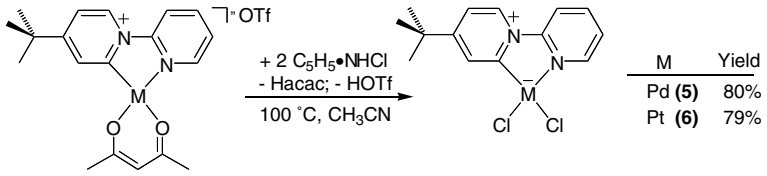

Scheme 2.

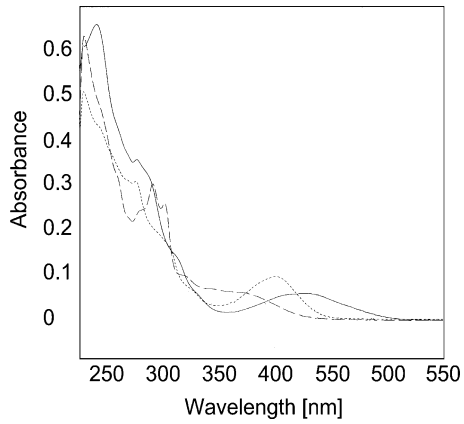

Fig. 1. Electronic absorption spectra for **2b** (–), **3b** (- -) and **4b** (···).

3b in the Heck-coupling of styrene and iodobenzene. The results of these trials indicate that catalysis with **3b** is not significantly faster than with $Pd_2(dba)_3$ [8].

3.4. Electronic absorption spectra

The UV–Vis absorption spectra of **2b**–**4b** in CH_2Cl_2 at concentrations of 10 mg/L were recorded and shown in Fig. 1. These spectra show two principle features: a very intense absorption in the UV ($\sim\lambda < 300$ nm) that is fairly uniform throughout the series, and a weaker absorption in the visible ($350 < \lambda < 450$ nm) that is responsible for the yellow colors of **2b**–**4b**.

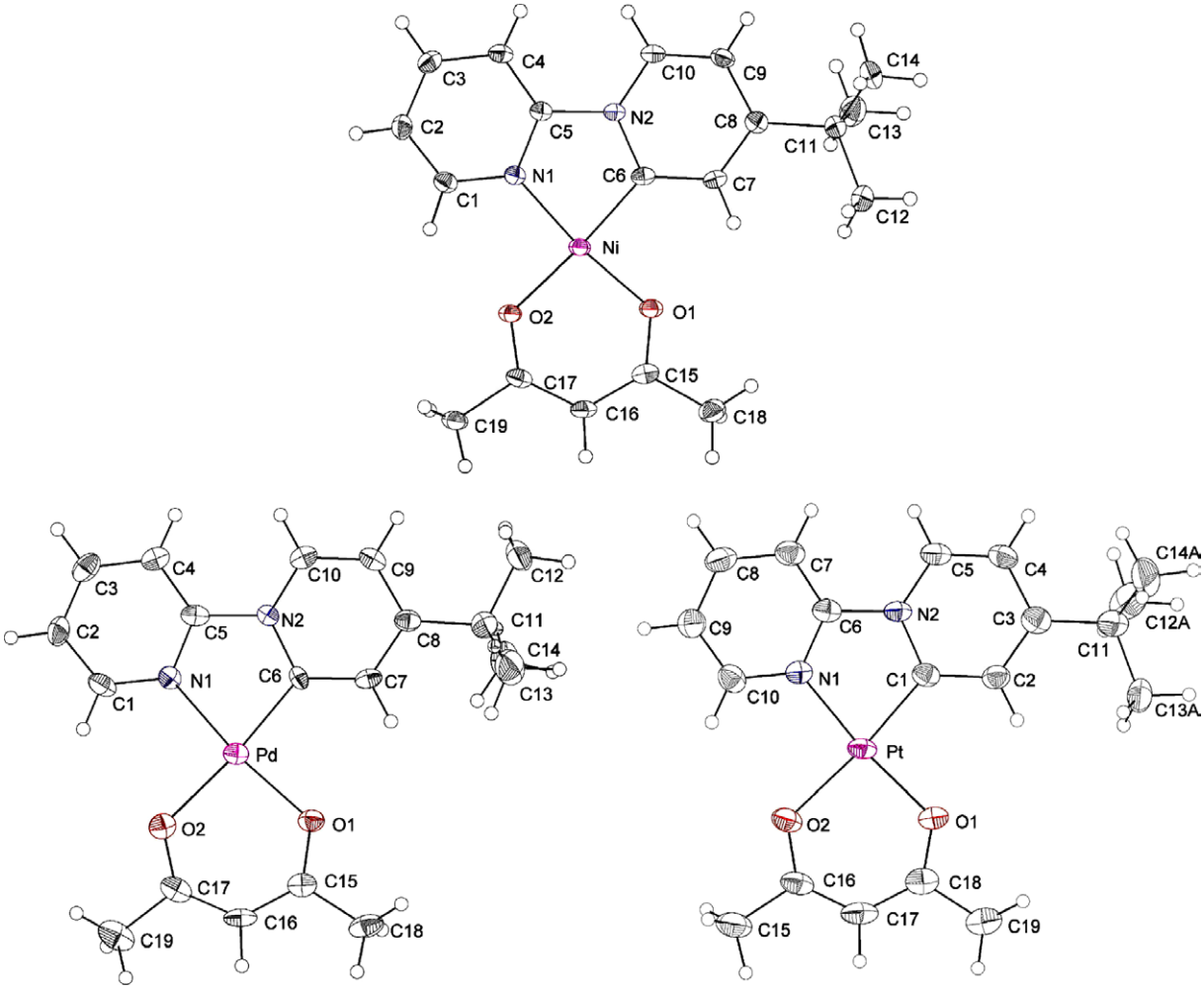

Fig. 2. ORTEP diagrams of **2b**–**4b** with thermal ellipsoids at 50%.

These weaker features have maxima that fall in the order $\nu_{Pd} > \nu_{Pt} > \nu_{Ni}$. This order and the large extinction coefficients of 4100–8300 $(M\ cm)^{-1}$ are consistent with a metal-to-ligand charge transfer (MLCT) assignment (See Table 2). Analogous compounds show similar spectral features where this lower energy transition has been assigned to $d_{z^2} \rightarrow \pi^*$ [9].

4. Conclusions

A series of Group 10 metal complexes with acetylacetonate and (4-*tert*-butyl)-*iso*-bipyridyl ligands can be conveniently obtained by the simple reaction of the pyridyl-pyridinium triflate and the metal(II) acetylacetonates. Structural data provided by X-ray crystal structures of the nickel, palladium and platinum complexes indicate weak π-bonding evidenced by the short metal carbon distances. The ratio of metal oxygen distances (**4b** ≈ **3b** > **2b**) observed in the crystal structures parallels the observed reactivity where the nickel carbene interaction is subject to protonolysis to a greater extent than in the palladium and platinum complexes. These results are consistent with the bond strengths implied from the structural data, though the observed reactivity is not necessarily linked to this ground-state energy difference.

5. Supplementary material

Crystallographic data for **2b** (CCDC 230757), **3b** (CCDC 231159) and **4b** (CCDC 236394) have been deposited with the Cambridge Crystallographic Data Centre. Copies can be obtained free of charge upon request from The Director, CCDC, 12 Union Road, Cambridge CB2 1EZ, UK (fax: +44-1223-336-033 or e-mail: deposit@ccdc.cam.ac.uk or www: http://www.ccdc.cam.ac.uk), by quoting the publication citation and the deposition number.

Acknowledgements

We thank Larry Henling and Michael Day for collection of X-ray data and assistance in solving of the crystal structures. We are also grateful to the Summer Undergraduate Research Fellowship Program for support of N.A.P. and the MC^2 Program sponsored by B.P. for financial support of this research.

References

[1] (a) C.W. Bielawski, R.H. Grubbs, Angew. Chem. Int. Ed. 39 (2000) 2903;
(b) M. Scholl, S. Ding, C.W. Lee, R.H. Grubbs, Org. Lett. 1 (1999) 953;
(c) A.K. Chaterjee, J.P. Morgan, M. Scholl, R.H. Grubbs, J. Am. Chem. Soc. 122 (2000) 3783;
(d) M.S. Sanford, M. Ulman, R.H. Grubbs, J. Am. Chem. Soc. 123 (2001) 749;
(e) M.S. Sanford, M. Ulman, R.H. Grubbs, J. Am. Chem. Soc. 123 (2001) 6543.

[2] (a) W.A. Herrmann, Angew. Chem., Int. Ed. Engl. 41 (2002) 1290;
(b) A.F. Littke, G.C. Fu, Angew. Chem., Int. Ed. Engl. 41 (2002) 4176.

[3] J.S. Owen, J.A. Labinger, J.E. Bercaw, J. Am. Chem. Soc. (2004), in press.

[4] (a) R.P. Thummel, Y. Jahng, J. Org. Chem. 52 (1987) 73;
(b) M.A. Gutierrez, G.R. Newkome, J. Selbin, J. Organomet. Chem. 202 (1980) 342.

[5] (a) Control reactions showed that acetylacetone does not react with **1** at 100 °C in $C_2D_2Cl_4$. Electrospray mass-spectra of the palladium reaction mixture shows evidence of *N*-(2′-pyridyl)-2-phenyl-4-*tert*-butyl-pyridinium (*m*/*z* = 289, 274, 259), the product of reductive elimination from a palladium phenyl complex, presumably generated by activation of tetraphenylborate. Furthermore, in attempts to alkylate **2b** with alkyl aluminum reagents, colloidal metal and alkylated pyridinium salts were observed by mass-spectral analysis. These results, while preliminary, may suggest that reductive elimination reactions involving the carbene carbon are a principal decomposition route. Such behavior has been documented for imidazolium-derived carbene complexes of palladium. For more details see: W.J. Marshall, V.V. Grushin, Organometallics 22 (8) (2003) 1591;
(b) D.S. McGuinness, N. Saenig, B.F. Yates, K.J. Cavell, J. Am. Chem. Soc. 123 (47) (2001) 4029;
(c) D.S. McGuinness, M.J. Green, K.J. Cavell, B.W. Skelton, A.H. White, J. Organomet. Chem. 565 (1998) 165.

[6] It is interesting that the predicted relative bond strengths leads to the postulate that the equilibrium constant should be one for reactions of this type. H.E. Bryndza, L.K. Fong, R.A. Paciello, W. Tam, J.E. Bercaw, J. Am. Chem. Soc. 109 (5) (1987) 1444.

[7] (a) Ligands that support coordinatively unsaturated palladium: M. Yamashita, J.F. Hartwig, J. Am. Chem. Soc. ASAP;
(b) J.P. Stambuli, C.D. Incarvito, M. Buhl, J.F. Hartwig, J. Am. Chem. Soc. 126 (4) (2004) 1184;
(c) A.F. Littke, G.C. Fu, Angew. Chem. Int. Ed. 41 (2002) 4176.

[8] Reactions were conducted under similar conditions to those reported by J.A. Loch, M. Albrecht, E. Peris, J. Mata, J.W. Faller, R.H. Crabtree, Organometallics 21 (2002) 700, Control reactions gave rise to similar turnover frequencies for **3b** or $Pd_2(dba)_3$.

[9] C. Cornioley-Deuschel, A. von Zelewsky, Inorg. Chem. 26 (1987) 3354.

Available online at www.sciencedirect.com
SCIENCE DIRECT®
Polyhedron 23 (2004) 2805–2812
POLYHEDRON
www.elsevier.com/locate/poly

Di- and tetra-bridged diiron(II) complexes with four terphenyl-derived carboxylates and two water molecules

Sungho Yoon, Amy E. Kelly, Stephen J. Lippard *

Department of Chemistry, Massachusetts Institute of Technology, Room 18-498, Cambridge, MA 02139, USA

Received 30 April 2004; accepted 11 June 2004
Available online 25 August 2004

Dedicated to Malcolm Green, an inspiring chemist and friend

Abstract

New diiron(II) complexes having ligated water molecules were prepared and characterized by X-ray crystallography, IR spectroscopy and cyclic voltammetry. The compound $[Fe_2(OH_2)_2(\mu\text{-}O_2CAr^{4F\text{-}Ph})_2(O_2CAr^{4F\text{-}Ph})_2(THF)_2]$ (**1**), where $^{-}O_2CAr^{4F\text{-}Ph}$ is 2,6-di-(*p*-fluorophenyl)benzoate, has two distorted trigonal bipyramidal Fe(II) centers linked by two sterically hindered carboxylate ligands. The related molecules, $[Fe_2(\mu\text{-}OH_2)_2(\mu\text{-}O_2CAr^{Tol})_2(O_2CAr^{Tol})_2(THF)_2]$ (**2**) and $[Fe_2(\mu\text{-}OH_2)_2(\mu\text{-}O_2CAr^{Tol})_2(O_2CAr^{Tol})_2(4\text{-}^{t}BuC_5H_4N)_2]$ (**3**), where $^{-}O_2CAr^{Tol}$ is 2,6-di-(*p*-tolyl)benzoate and 4-^{t}BuC$_5$H$_4$N is 4-*tert*-butylpyridine, contain a tetra-bridged diiron(II) core with a central $Fe_2(OH_2)_2$ planar quadrilateral. Vibrational spectroscopic and electrochemical measurements reveal that the ligated water molecules of **3** are in equilibrium between the bound and free forms.
© 2004 Elsevier Ltd. All rights reserved.

Keywords: Non-heme iron; Water coordination; X-ray structure; Cyclic voltammetry; Sterically hindered carboxylate

1. Introduction

The activation of triplet ground state dioxygen and the hydroxylation of unactivated C–H bonds under ambient conditions by non-heme diiron enzymes are topics of much current interest [1–3]. The hydroxylase component of soluble methane monooxygenase (sMMOH), which utilizes dioxygen to convert CH_4 into CH_3OH, is a well-studied member of this class of enzymes [4]. The enzyme active site contains a diiron core coordinated by four glutamate carboxylate groups and two histidine imidazole ligands [5]. This diiron unit with a carboxylate-rich coordination environment is effectively utilized to bind, activate and transfer an oxygen atom from O_2 to the substrate. Similar diiron cores occur in related multicomponent dioxygen-dependent enzymes, including toluene monooxygenase [6], the R2 subunit of ribonucleotide reductase [7,8] and stearoyl-ACP Δ^9 desaturase [9].

To help understand how these enzymes achieve their physiological roles of O_2 activation and utilization at carboxylate-rich diiron cores, much effort has been devoted to reproducing the structures and functions of their active sites by small model complexes. Recently, our group and others have reproduced the carboxylate-rich composition of these diiron sites with the use of sterically hindered terphenyl-derived carboxylate ligands [10–13]. Although these model complexes are able to hydroxylate benzylic C–H bonds and to oxidize phosphine and sulfide moieties [13–17], the activation of strong C–H bonds, such as that in methane, has not yet been achieved. This situation directed us to revisit the diiron sites in the enzymes to identify features that had not been adequately incorporated into the model complexes. One compositional difference between most of the reported model complexes and the diiron(II) core

* Corresponding author. Tel.: +6172531892; fax: +6172588150.
E-mail address: lippard@lippard.mit.edu (S.J. Lippard).

0277-5387/$ - see front matter © 2004 Elsevier Ltd. All rights reserved.
doi:10.1016/j.poly.2004.06.019

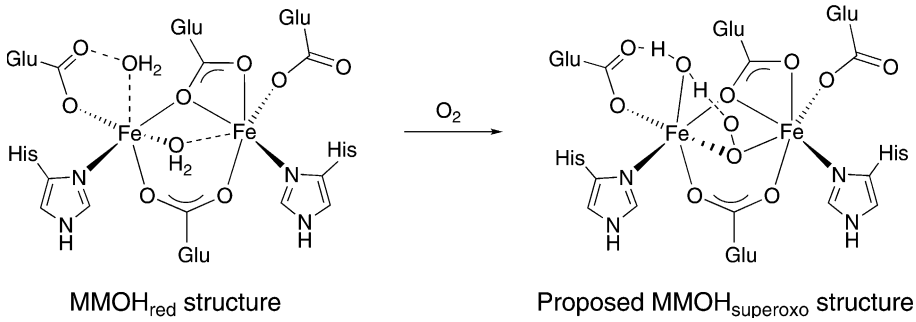

Chart 1.

at the active site of MMOH is the presence of two water molecules in the first and second coordination spheres (Chart 1). In recently published DFT calculations, the utilization of a coordinated H_2O molecule as a hydrogen-bond donor was considered to be a key component in the formation of reactive intermediate(s) upon oxygenation of the diiron(II) site [18–20]. The computational results strongly suggest that the ligated water molecules may be required to reproduce the function of the enzyme in model systems. Accordingly, we have undertaken the synthesis of model complexes containing water molecules in the coordination spheres of their carboxylate-bridged diiron(II) sites. Here, we report the result of our first efforts in this area, in which the synthesis and characterization of diiron(II) complexes with two ligated water molecules and sterically hindered terphenyl-based carboxylates are described.

2. Experimental

2.1. Materials and methods

2.1.1. General considerations

All reagents, including 4-*tert*-butylpyridine (4-^{t}Bu-C_5H_4N), were obtained from commercial suppliers and used as received unless otherwise noted. Dichloromethane, pentane and THF were saturated with argon and purified by passage through activated Al_2O_3 columns under argon [21]. Sodium 2,6-di-(*p*-tolyl)benzoate (NaO_2CAr^{Tol}) [22,23], sodium 2,6-di-(*p*-fluorophenyl)-benzoate ($NaO_2CAr^{4F\text{-}Ph}$) [23], $[Fe_2(\mu\text{-}O_2CAr^{Tol})_2(O_2CAr^{Tol})_2(THF)_2]$ [11] and $[Fe_2(\mu\text{-}O_2CAr^{Tol})_4(4\text{-}^tBuC_5H_4N)_2]$ [11] were prepared as described in the literature. All syntheses and air-sensitive manipulations were carried out under nitrogen in an MBraun glovebox. FT-IR spectra were recorded with a Thermo Nicolet Avatar 360 spectrometer.

2.1.2. $[Fe_2(\mu\text{-}O_2CAr^{4F\text{-}Ph})_2(O_2CAr^{4F\text{-}Ph})_2(THF)_2(OH_2)_2]$ (1)

To a CH_2Cl_2 solution (15 ml) of $NaO_2CAr^{4F\text{-}Ph}$ (528 mg, 1.59 mmol) was added $Fe(BF_4)_2 \cdot 6H_2O$ (268 mg, 0.794 mmol) in THF (5 ml). The resulting suspension was stirred under reflux for 2 days, affording a white precipitate that was filtered through Celite. Colorless blocks of **1** (231 mg, 34% yield) were obtained by layering pentane onto the filtrate followed by slow evaporation, and they were analyzed by X-ray crystallography. FT-IR (KBr, cm^{-1}) 3600 (w, $\nu_{O\text{–}H}$), 3443 (m, br, $\nu_{O\text{–}H}$), 3059 (w), 2979 (w), 1606 (s), 1511 (s), 1455 (s), 1412 (s), 1382 (s), 1300 (w), 1221 (s), 1159 (s), 1095 (m), 1071 (w), 1036 (m), 1013 (w), 845 (m), 835 (m), 808 (s), 792 (m), 772 (m), 738 (w), 714 (m), 700 (m), 554 (s), 529 (s), 463 (m). *Anal.* Calc. for $\mathbf{1} \cdot 0.5(CH_2Cl_2)$ or $C_{84.5}H_{65}Fe_2F_8O_{12}Cl$: C, 64.58; H, 4.17. Found: C, 64.85; H, 4.26%.

2.1.3. $[Fe_2(\mu\text{-}OH_2)_2(\mu\text{-}O_2CAr^{Tol})_2(O_2CAr^{Tol})_2(THF)_2]$ (2)

Method A. To a CH_2Cl_2 solution (9 ml) of NaO_2CAr^{Tol} (100 mg, 308 μmol) was added $Fe(BF_4)_2 \cdot 6H_2O$ (52 mg, 0.15 mmol) in THF (3 ml). The resulting suspension was stirred for a day. The white precipitate was filtered through Celite. Colorless blocks of **2** were obtained by pentane vapor diffusion (7 mg, 6% yield) and analyzed by X-ray crystallography.

Method B. To a portion (45.4 mg, 32.3 μmol) of $[Fe_2(\mu\text{-}O_2CAr^{Tol})_2(O_2CAr^{Tol})_2(THF)_2]$ [11] was added a THF solution (1 ml) containing 10 μl (0.56 mmol) of H_2O. The reaction mixture was stirred for 30 min. Colorless blocks of **2** (34.9 mg, 72% yield), obtained after 2 days by diffusing pentane into the solution, were analyzed by X-ray crystallography. FT-IR (KBr, cm^{-1}) 3555 (m, $\nu_{O\text{–}H}$), 3400 (w, br, $\nu_{O\text{–}H}$), 3051 (w), 3022 (m), 2918 (m), 1588 (s), 1571 (s), 1514 (s), 1454 (s), 1408 (s), 1381 (s), 1305 (w), 1211 (w), 1145 (w), 1070 (w), 1042 (m), 1019 (w), 914 (w), 890 (w), 853 (w), 835 (m), 822 (s), 802 (s), 787 (m), 765 (m), 736 (m), 714 (w), 701 (m), 584 (m), 547 (m), 523 (m). *Anal.* Calc. for $C_{92}H_{88}Fe_2O_{12}$: C, 73.80; H, 5.92. Found: C, 72.98; H, 5.98%.

2.1.4. $[Fe_2(\mu\text{-}OH_2)_2(\mu\text{-}O_2CAr^{Tol})_2(O_2CAr^{Tol})_2(4\text{-}^tBuC_5H_4N)_2]$ (3)

A portion (50.5 mg, 31.8 μmol) of $[Fe_2(\mu\text{-}O_2CAr^{Tol})_4(4\text{-}^tBuC_5H_4N)_2]$ [11] was added to THF (1 ml) containing 10 μl (0.56 mmol) of H_2O. Stirring effected dissolution within 30 min to yield a light yellow solution. Light yellow blocks of **3** (41.6 mg, 76% yield), obtained

by layering pentane onto the solution, were analyzed by X-ray crystallography. FT-IR (KBr, cm^{-1}) 3537 (s, ν_{O-H}), 3425 (w, br, ν_{O-H}), 3052 (m), 3020 (m), 2964 (s), 2919 (s), 2866 (m), 1613 (s), 1587 (s), 1514 (s), 1501 (w), 1451 (s), 1383 (s), 1273 (w), 1071 (m), 1021 (w), 909 (w), 842 (w), 830 (m), 813 (m), 786 (m), 764 (m), 726 (w), 706 (m), 584 (m), 568 (w), 526 (m), 459 (w). *Anal*. Calc. for $C_{102}H_{98}Fe_2N_2O_{10}$: C, 75.46; H, 6.08; N, 1.73. Found: C, 75.26; H, 6.14; N, 1.70%.

2.2. X-ray crystallography

Single crystals were mounted at room temperature on the tips of quartz fibers, coated with Paratone-N oil and cooled under a stream of cold nitrogen. Intensity data were collected on a Bruker (formerly Siemens) APEX CCD diffractometer running the SMART software package, with Mo Kα radiation (λ = 0.71073 Å). Data collection and reduction protocols are described in detail elsewhere [24]. The structures were solved by Patterson and direct methods and refined on F^2 using the SHELXTL software package [25]. Empirical absorption corrections were applied with SADABS [26], part of the SHELXTL program package, and the structures were checked for higher symmetry by the program PLATON [27]. All non-hydrogen atoms were refined anisotropically. In general, hydrogen atoms were assigned idealized positions and given thermal parameters equivalent to either 1.5 (methyl hydrogen atoms) or 1.2 (all other hydrogen atoms) times the thermal parameter of the carbon atom to which they were attached. Hydrogen atoms of O–H of the coordinated water molecule were identified from difference Fourier maps. In the structure of **1**, two CH_2Cl_2 solvent molecules were assigned in the lattice. In the structure of **2** there is slight disorder in the THF molecules that is not modeled. A monoclinic polymorph of **2** has also been observed with unit cell parameters a = 13.509(3) Å, b = 14.260(3) Å, c = 20.278(4) Å, and β = 104.703(3)°. The structure of **3** contains one THF and 0.5 pentane molecules. Data collection and experimental details for the complexes are summarized in Table 1 and relevant interatomic bond lengths and angles are listed in Table 2.

2.3. Electrochemistry

Cyclic voltammetric measurements were performed in an MBraun glovebox under nitrogen with an EG&G model 263 potentiostat. A three-electrode configuration consisting of a platinum working electrode, a $AgNO_3$/Ag (0.1 M in acetonitrile with 0.5 M $Bu_4N(PF_6)$) reference electrode and a platinum mesh auxiliary electrode was used. The supporting electrolyte was 0.5 M $Bu_4N(PF_6)$ in CH_2Cl_2. All cyclic voltammograms were externally referenced to the Cp_2Fe/Cp_2Fe^+ couple.

3. Results and discussion

3.1. Synthesis and characterization of the doubly bridged diiron(II) complex $[Fe_2(OH_2)_2(\mu\text{-}O_2CAr^{4F\text{-}Ph})_2(O_2CAr^{4F\text{-}Ph})_2(THF)_2]$ (1)

Compound **1** was prepared from a reaction between $Fe(BF_4)_2 \cdot 6H_2O$ and 2 equiv of $NaO_2CAr^{4F\text{-}Ph}$ in a

Table 1
Summary of X-ray crystallographic information for $[Fe_2(OH_2)_2(\mu\text{-}O_2CAr^{4F\text{-}Ph})_2(O_2CAr^{4F\text{-}Ph})_2(THF)_2]$ (**1**), $[Fe_2(\mu\text{-}OH_2)_2(\mu\text{-}O_2CAr^{Tol})_2(O_2CAr^{Tol})_2(THF)_2]$ (**2**) and $[Fe_2(\mu\text{-}OH_2)_2(\mu\text{-}O_2CAr^{Tol})_2(O_2CAr^{Tol})_2(4\text{-}^tBuC_5H_4N)_2]$ (**3**)

Compound	**1** · $2CH_2Cl_2$	**2**	**3** · THF · 1/2Pentane
Formula	$Fe_2C_{86}H_{68}O_{12}F_8Cl_4$	$Fe_2C_{92}H_{88}O_{12}$	$Fe_2C_{108.5}H_{112}N_2O_{11}$
formula weight (g/mol)	1698.90	1497.32	1731.70
Space group	$P\bar{1}$	*Pbca*	*C*2/*c*
a (Å)	12.3562(11)	19.884(4)	23.880(6)
b (Å)	13.9639(13)	18.358(4)	17.100(4)
c (Å)	14.0539(13)	20.773(4)	27.078(7)
α (°)	97.189(2)		
β (°)	114.862(2)		112.139(4)
γ (°)	111.331(2)		
V (Å^3)	1935.3(3)	7583(3)	10208(4)
Z	1	4	4
ρ_{calc} (g/cm^3)	1.458	1.312	1.127
T (°C)	−100	−100	−100
μ(Mo Kα) (mm^{-1})	0.596	0.447	0.341
Total number of data	14,443	65007	37,188
Number of unique data	6755	9257	9008
Number of parameters	651	490	616
R (%)[a]	4.55	4.79	6.49
R_w^2 (%)[b]	10.49	10.54	19.35
Maximum and minimum peaks (e/Å^3)	0.370, −0.349	0.636, −0.383	0.768, −0.365

[a] $R = \sum \|F_o\| - |F_c\| / \sum |F_o|$.
[b] $R_w^2 = \{\sum[w(F_o^2 - F_c^2)^2] / \sum[w(F_o^2)^2]\}^{1/2}$.

Table 2
Selected interatomic bond lengths (Å) and angles (°) for $[Fe_2(OH_2)_2(\mu\text{-}O_2CAr^{4F\text{-}Ph})_2(O_2CAr^{4F\text{-}Ph})_2(THF)_2]$ (**1**), $[Fe_2(\mu\text{-}OH_2)_2(\mu\text{-}O_2CAr^{Tol})_2(O_2CAr^{Tol})_2(THF)_2]$ (**2**) and $[Fe_2(\mu\text{-}OH_2)_2(\mu\text{-}O_2CAr^{Tol})_2(O_2CAr^{Tol})_2(4\text{-}^tBuC_5H_4N)_2]$ (**3**)

Compound	**1** · $2CH_2Cl_2$	**2**	**3** · THF · 1/2Pentane
Bond lengths			
Fe1 ··· Fe1A	3.4433(8)	3.0430(7)	3.0548(10)
Fe1–O1	2.157(2)	2.3977(16)	2.292(3)
Fe1A–O1	3.1070(21)	2.3262(15)	2.306(3)
Fe1–O2	2.0391(18)	2.0232(13)	2.043(2)
Fe1–O3	2.0099(18)	2.0322(13)	2.085(2)
Fe1–O4	2.0298(18)	2.0442(13)	2.060(2)
Fe1–L[a]	2.1012(18)	2.1415(15)	2.132(3)
Bond angles			
Fe1–O1–Fe1A	N/A	80.19(5)	83.26(9)
O1–Fe1–O1A	N/A	99.81(5)	96.74(9)
O2–Fe1–O3	138.60(7)	157.21(5)	156.85(9)
O1–Fe1–O4	92.12(8)	87.78(5)	89.06(9)
O1–Fe1–L[a]	176.07(8)	169.88(6)	177.84(11)
O2–Fe1–O4	108.55(7)	105.91(6)	105.68(9)
O3–Fe1–O4	112.85(7)	91.26(5)	93.73(9)
O2–Fe1–L[a]	90.39(7)	89.36(5)	96.02(10)
O3–Fe1–L[a]	89.08(8)	106.48(6)	96.90(10)
O4–Fe1–L[a]	91.46(8)	87.89(5)	88.79(10)
O2–Fe1–O1	90.02(8)	83.05(5)	84.81(10)
O3–Fe1–O1	88.02(8)	82.76(5)	82.99(9)
O2–Fe1–O1A	N/A	85.81(6)	83.60(10)
O3–Fe1–O1A	N/A	79.16(5)	78.40(9)
O4–Fe1–O1A	N/A	166.83(6)	169.52(10)
L[a] –Fe1–O1A	N/A	86.23(5)	85.34(10)
O5 ··· O1	2.608(2)	2.588(2)	2.5519(36)

Numbers in parentheses are estimated standard deviations of the last significant figures.
[a] L is the O-atom of THF in **1** and **2,** and the N-atom of 4-$^tBuC_5H_4N$ in **3**.

THF/CH_2Cl_2 solution. The structure comprises two distorted trigonal bipyramidal iron(II) centers straddling a crystallographic inversion center with an Fe ··· Fe separation of 3.4433(8) Å (Fig. 1). The coordination sites are occupied by two bridging $Ar^{4F\text{-}Ph}CO_2^-$ ligands and the oxygen atoms of THF, water and a monodentate terminal carboxylate group. The water molecule coordinated to Fe(1) with an Fe–O bond length of 2.157(2) Å is 3.107(2) Å from Fe(1A) and thus is not bridging the two iron atoms in this structure. A THF molecule is located trans to the water ligand. Strong intramolecular hydrogen bonding interactions occur between terminal metal-bound carboxylates and water molecules, with O ··· O distances of 2.608(3) Å.

*3.2. Synthesis and characterization of the diaqua-bridged diiron(II) complex $[Fe_2(\mu\text{-}OH_2)_2(\mu\text{-}O_2CAr^{Tol})_2(O_2CAr^{Tol})_2(THF)_2]$ (**2**)*

Although the syntheses of related diaqua-bridged dinickel(II) and dicobalt(II) complexes have been described [28], an iron(II) analogue has not previously been reported. Only monoaqua-bridged diiron(II) complexes, including $[Fe_2(\mu\text{-}OH_2)(O_2CR)_4(tmen)_2]$ [tmen = tetramethylethylenediamine, R = CH_3 and C_6H_5] [29] and $[Fe_2(\mu\text{-}OH_2)(O_2Ac)_5(pyridine)_2]^-$ [30,31], have been characterized. The synthesis of compound **2** was initially achieved by self-assembly from $Fe(BF_4)_2 \cdot 6H_2O$ and 2 equiv of NaO_2CAr^{Tol} in poor yield, as described in Method A in the experimental section. The water molecules in **2** must derive from the iron(II) salt, $Fe(BF_4)_2 \cdot 6H_2O$, used in the synthesis. The reaction may proceed through the intermediate formation of $[Fe_2(\mu\text{-}O_2CAr^{Tol})_2(O_2CAr^{Tol})_2(THF)_2]$ in the reaction. This hypothesis was tested by treating independently synthesized $[Fe_2(\mu\text{-}O_2CAr^{Tol})_2(O_2CAr^{Tol})_2(THF)_2]$ with ~17 equiv of water (Method B), resulting in the isolation of compound **2** in excellent yield.

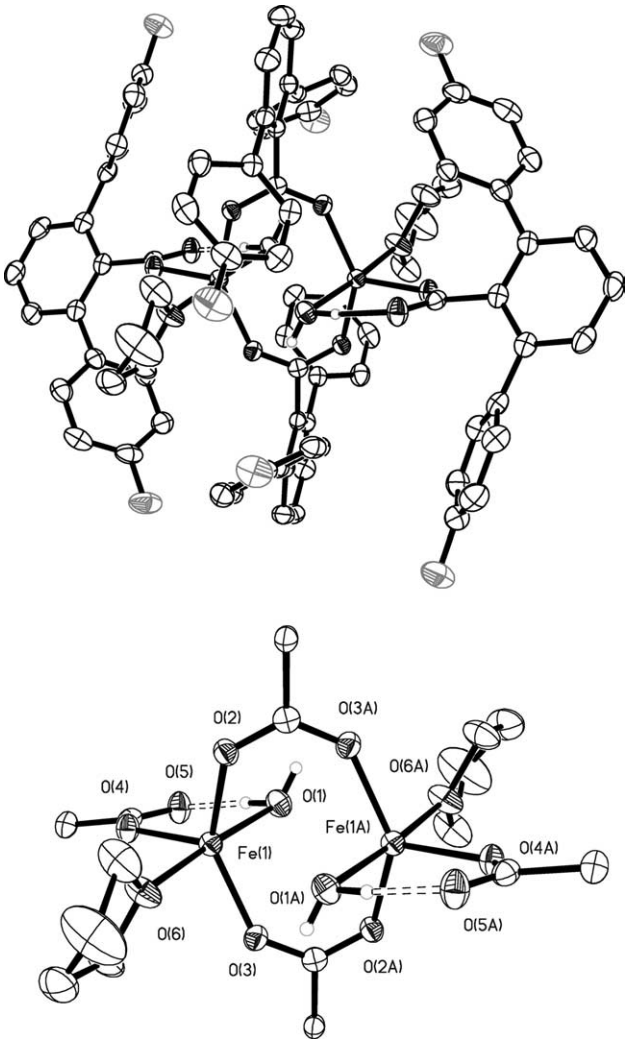

Fig. 1. Top: ORTEP diagram of $[Fe_2(OH_2)_2(\mu\text{-}O_2CAr^{4F\text{-}Ph})_2(O_2CAr^{4F\text{-}Ph})_2(THF)_2]$ (**1**) showing 50% probability thermal ellipsoids for all non-hydrogen atoms. Bottom: Drawing with the aromatic rings of $Ar^{4F\text{-}Ph}CO_2^-$ ligands omitted for clarity.

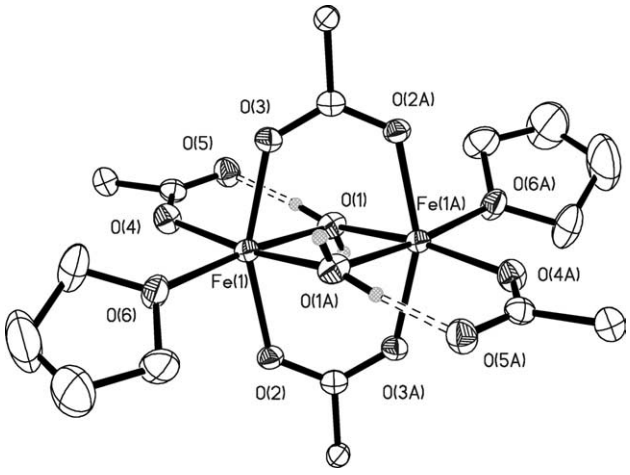

Fig. 2. ORTEP diagram of $[Fe_2(\mu\text{-}OH_2)_2(\mu\text{-}O_2CAr^{Tol})_2(O_2CAr^{Tol})_2(THF)_2]$ (**2**) showing 50% probability thermal ellipsoids for all non-hydrogen atoms. The aromatic rings of the $Ar^{Tol}CO_2^-$ ligands are omitted for clarity.

The structure, displayed in Fig. 2, reveals two pseudo-octahedral iron(II) centers bridged by two carboxylate ligands and two water molecules. The Fe ··· Fe separation of 3.0430(7) Å is shorter by ~0.400 Å than that in **1**, owing to the presence of two additional water bridges. The assignment of these ligands as water rather than hydroxo groups is based on the Fe1-O(aqua) distances, which are 2.3977(16) and 2.3262(15) Å, by the location and refinement of the associated hydrogen atoms in the X-ray structure determination (O–H, 0.80 and 0.94 Å) and by charge considerations. This assignment is further supported by two O–H stretching bands at 3400 and 3555 cm^{-1} in the IR spectrum of **2**. The remaining coordination sites are occupied by THF and monodentate terminal carboxylate ligands. Strong intramolecular hydrogen bonding interactions occur between terminal metal-bound carboxylates and water molecules, with O ··· O distances of 2.588(2) Å.

3.3. Synthesis and characterization of the diaqua-bridged diiron(II) complex $[Fe_2(\mu\text{-}OH_2)_2(\mu\text{-}O_2CAr^{Tol})_2(O_2CAr^{Tol})_2(4\text{-}^tBuC_5H_4N)_2]$ (3)

The compound $[Fe_2(\mu\text{-}O_2CAr^{Tol})_4(4\text{-}^tBuC_5H_4N)_2]$ [11], which has a composition close to those of the MMOH [5], RNR–R2 [8] and ToMOH [6] diiron cores, is one of the better studied model complexes. To address how water in the coordination sphere might affect the properties of this complex, we synthesized a water-containing analogue. Compound **3** was prepared in excellent yield by addition of excess H_2O to $[Fe_2(\mu\text{-}O_2CAr^{Tol})_4(4\text{-}^tBuC_5H_4N)_2]$. The pseudo-octahedrally coordinated iron(II) atoms in **3** are related by a crystallographic inversion center and bridged by two water molecules and two carboxylates, resulting in an Fe ··· Fe distance of 3.0548(10) Å (Fig. 3). Additionally, two hydrogen bonding interactions between terminal carboxylates and bridging water groups further compact the diiron(II) sites. The O ··· O distance of 2.5519 (36) Å indicates a strong interaction. A broad IR band at 3434 cm^{-1} in the spectrum of **3** is consistent with strongly hydrogen-bonded water, and a relatively sharp O–H stretching band at 3573 cm^{-1} originates from the remaining proton on the ligand.

Although the structures of a series of Fe_2(II,II) [32], Fe_2(III,III) [33] and Fe_2(III,IV) [34] complexes having neutral polypyridine ligands and a central 2Fe2O quadrilateral are currently known, only recently have related units with biologically more relevant O-rich metal coordination environments become available (Chart 2) [10]. Compounds **2** and **3** complete one end of the series of diamond cores with O-rich metal coordination environments. As indicated in Chart 2, there are several noteworthy differences between members of the two series. The N-rich diiron complexes tend to have O-atom bridges with fewer protons. Thus, the diiron(II) sites in the neutral O-rich complex **3** are bridged by H_2O molecules, in contrast to the hydroxo bridges in the dicationic diiron(II) complex **A**. Similarly, hydroxo bridges occur in the neutral O-rich diiron(III) compound **E**, compared to the oxo bridges in the N-rich diiron(III) complex **C,** which is a dication. The aqua bridges that occur in the diiron(II) complexes $[Fe_2(\mu\text{-}OH_2)(O_2CR)_4(tmen)_2]$ [29] [R = CH_3 and C_6H_5] and $[Fe_2(\mu\text{-}OH_2)(O_2Ac)_5(pyridine)_2]^-$ [30,31] further substantiate this observation. It is now generally accepted that the diiron(II) sites in deoxyhemerythrin [3], which has a N-rich metal coordination environment, are bridged by a hydroxo moiety rather than water. Bridging H_2O molecule(s) are therefore anticipated in the diiron(II) site ligated by four carboxylates and two histidines in reduced ToMOH, as in MMOH. A second difference noted is the small variation in Fe ··· Fe distance through the O-rich series compared to the N-rich

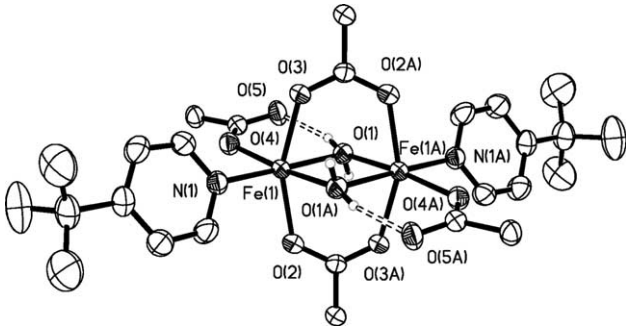

Fig. 3. ORTEP diagram of $[Fe_2(\mu\text{-}OH_2)_2(\mu\text{-}O_2CAr^{Tol})_2(O_2CAr^{Tol})_2(4\text{-}^tBuC_5H_4N)_2]$ (**3**) showing 50% probability thermal ellipsoids for all non-hydrogen atoms. The aromatic rings of $Ar^{Tol}CO_2^-$ ligands are omitted for clarity.

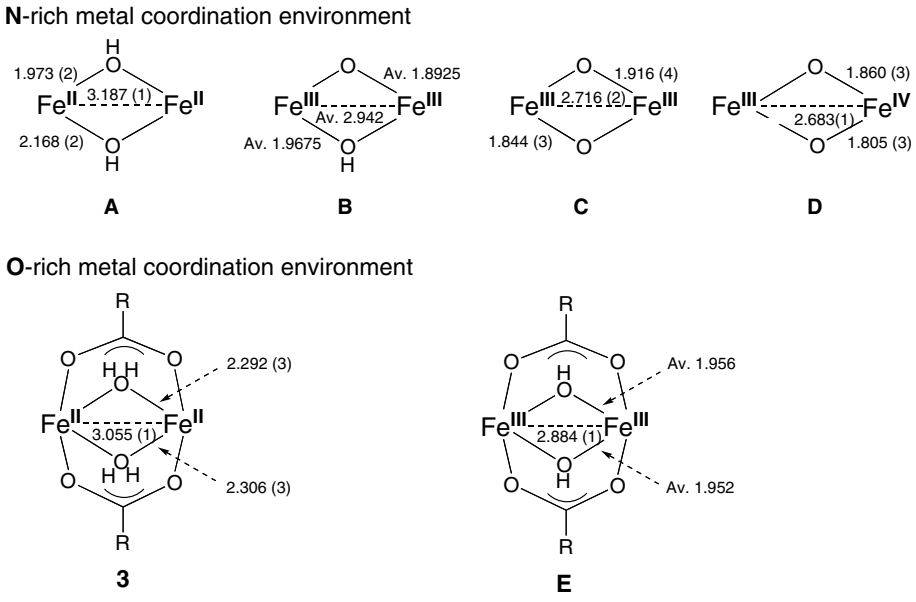

Chart 2.

one. The difference among diiron sites from **3** to **E** is only 0.171 Å, compared to the 0.471 Å spread from **A** to **C**. This property may be attributed to the presence of two additional bridging carboxylates in the O-rich series of compounds.

3.4. Vibrational and electrochemical properties

Fig. 4 displays the infrared spectra of compound **3** before and after heating at 100 °C under a nitrogen atmosphere. The disappearance of bands at 3573 and 3434 cm^{-1} after heating is attributed to the loss of coordinated water molecules in the solid state. The spectrum of **3** after heating matches that of the known compound $[Fe_2(\mu\text{-}O_2CAr^{Tol})_4(4\text{-}^tBuC_5H_4N)_2]$ [11].

The electrochemical properties of **3** were investigated by cyclic voltammetry (Fig. 5). One quasi reversible oxidation at $E_{1/2} = -210$ mV ($\Delta E_p = 140$ mV; $i_{pa}/i_{pc} = 5.9$, scan rate = 50 mV/s) accompanied by a broad reduction wave at ca. −890 mV versus Cp_2Fe^+/Cp_2Fe was observed in CH_2Cl_2 solution. When the voltammogram was re-

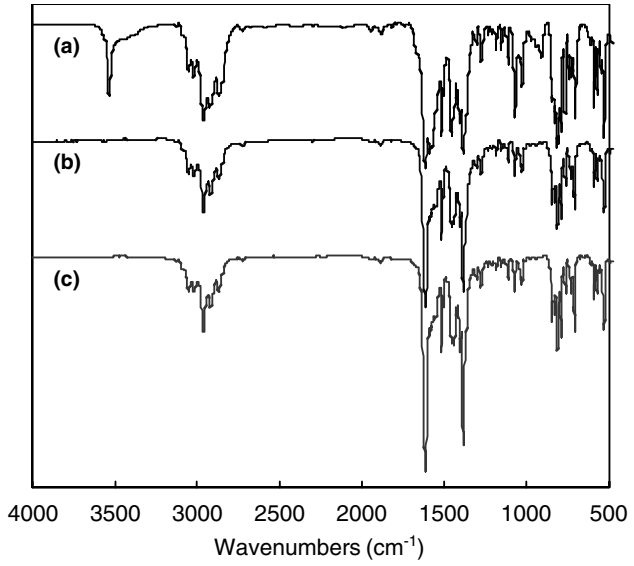

Fig. 4. IR spectra (a and b) of $[Fe_2(\mu\text{-}OH_2)_2(\mu\text{-}O_2CAr^{Tol})_2(O_2CAr^{Tol})_2(4\text{-}^tBuC_5H_4N)_2]$ (**3**), before and after heating, and (c) $[Fe_2(\mu\text{-}O_2CAr^{Tol})_4(4\text{-}^tBuC_5H_4N)_2]$.

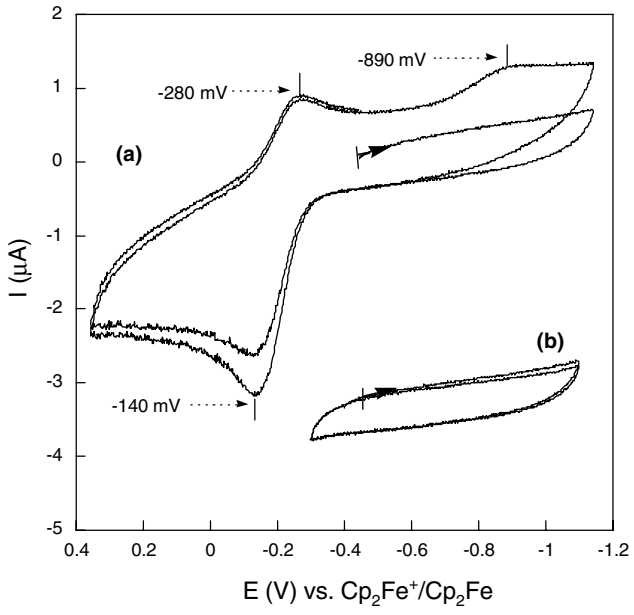

Fig. 5. Cyclic voltammograms of (a and b) $[Fe_2(\mu\text{-}OH_2)_2(\mu\text{-}O_2CAr^{Tol})_2(O_2CAr^{Tol})_2(4\text{-}^tBuC_5H_4N)_2]$ (**3**) in CH_2Cl_2 with 0.5 M $(Bu_4N)PF_6$ as supporting electrolyte and a scan rate of 50 mV/s.

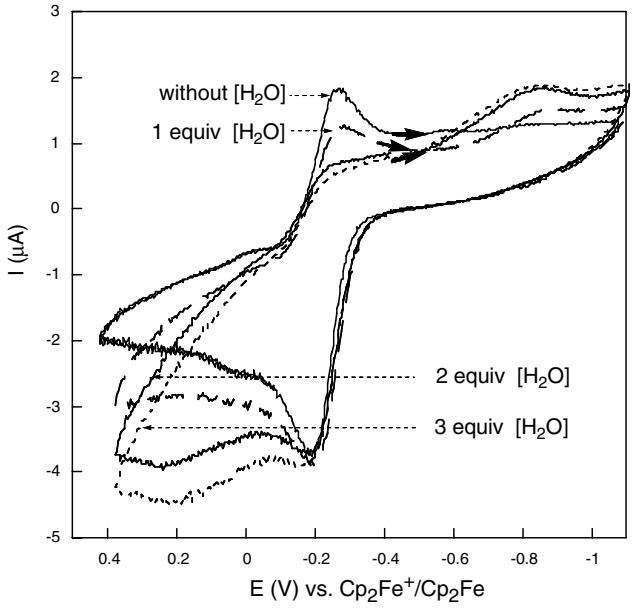

Fig. 6. Cyclic voltammograms of $[Fe_2(\mu\text{-}O_2CAr^{Tol})_4(4\text{-}^tBuC_5H_4N)_2]$ with variable amounts of H_2O in CH_2Cl_2 with 0.5 M $(Bu_4N)PF_6$ as the supporting electrolyte and a scan rate of 50 mV/s.

corded between −343 and −1143 mV, the reduction wave at −890 mV was no longer present (Fig. 5, graph (b)). Similar voltammograms (Fig. 6) were produced by addition of 0, 1, 2 and 3 equiv of H_2O to a CH_2Cl_2 solution of the compound $[Fe_2(\mu\text{-}O_2C\text{-}Ar^{Tol})_4(4\text{-}^tBuC_5H_4N)_2]$. Combined with the IR spectroscopic data, these results can be rationalized in the following manner (Scheme 1). Dehydration of **3** in CH_2Cl_2 can occur to afford two molecules of water and $[Fe_2(\mu\text{-}O_2CAr^{Tol})_4(4\text{-}^tBuC_5H_4N)_2]$, which has a reversible $Fe_2(II,II)/Fe_2(II,III)$ couple at $E_{1/2} = -216$ mV [35]. Oxidation of $[Fe_2(\mu\text{-}O_2C\text{-}Ar^{Tol})_4(4\text{-}^tBuC_5H_4N)_2]$ provides the mixed-valent cation, $[Fe_2(\mu\text{-}O_2CAr^{Tol})_4\ (4\text{-}^tBuC_5H_4N)_2]^+$, which is stable in the absence of water [35]. In presence of water molecules, however, an aquated $[Fe_2(O_2CAr^{Tol})_4(4\text{-}^tBuC_5H_4N)_2\text{-}(OH_2)_X]^+$ species may form, in which x can be one or two. This complex will exhibit different electrochemical behavior, and its reduction may give rise to the wave at ca −890 mV. The complex $[Fe_2(O_2CAr^{Tol})_4(4\text{-}^tBuC_5H_4N)_2(OH_2)_X]$, generated in this manner, would quickly lose water molecules to form $[Fe_2(\mu\text{-}O_2CAr^{Tol})_4(4\text{-}^tBuC_5H_4N)_2]$, resulting in no oxidation wave on the reverse sweep until a potential greater than −300 mV is attained. Uptake of water thus appears to lower the reduction potential of the diiron(II) core by ~610 mV, as might be expected from the addition of good σ donors to the dimetallic center. Both the reported dissociation of water from $[Fe_2(\mu\text{-}OH_2)(O_2CR)_4(tmen)_2]$ in solution by NMR studies [29] and the association/dissociation of water molecules of $\{Co_2(\mu\text{-}OH_2)_2\}^{4+}$ in the solid state [28] are consistent with our observations of reversible water loss from **3** in both the solid and solution states.

The diiron sites in **3** and MMOH both contain four carboxylates, two N-donor ligands and two water molecules. The two water molecules in the first and second coordination spheres of the kinetically labile diiron(II) sites in MMOH may also be in an equilibrium between bound and free forms, like **3**. Dissociation of water molecules in $MMOH_{red}$, together with a carboxylate shift, may generate the open coordination site(s) needed for dioxygen binding and activation [36]. In this respect it is noteworthy that, in the presence of the coupling and reductase components, MMOB and MMOR, the redox potential of the diiron center in MMOH changes significantly [37,38]. The present results suggest that this change may reflect loss of coordinated water molecules. On the other hand, DFT calculations of the MMOH reaction cycle identify an associated water molecule as a key component for generating oxygenated intermediate(s) [18–20]. A more complete understanding of the effects of water association and dissociation at carboxylate-bridged diiron sites, before and after the introduction of dioxygen, is clearly desirable. Although we now have clear evidence that the water molecules in **3** are reversibly bound, exactly when and how they may influence the oxygenation reactivity of diiron(II) sites remains to be determined. Efforts are underway to clarify the effect of water in the oxygenation pathways of model complexes with composition similar to that of MMOH.

4. Summary

The existence of water molecules at the diiron(II) active sites of carboxylate-bridged diiron enzymes directed us to explore water as a ligand in related complexes

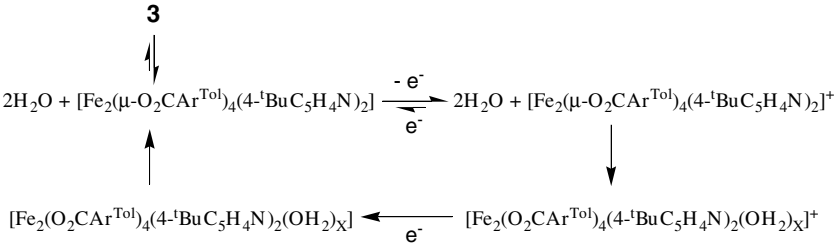

Scheme 1.

supported by sterically hindered carboxylate groups. The first carboxylate rich di(aqua)-bridged diiron(II) complexes have been characterized, completing one end of this series of O-rich diamond core structures. Chemical, IR spectroscopic and electrochemical experiments indicate the reversible generation of the quadruply bridged diiron(II) complex $[Fe_2(\mu\text{-}O_2CAr^{Tol})_4(4\text{-}^tBuC_5H_4N)_2]$ by loss of two water molecules from the compound $[Fe_2(\mu\text{-}OH_2)_2(\mu\text{-}O_2CAr^{Tol})_2(O_2CAr^{Tol})_2(4\text{-}^tBuC_5H_4N)_2]$.

5. Supplementary data

Crystallographic data for the structures reported here have been deposited with Cambridge Crystallographic Data Center (CCDC), 12 Union Road, Cambridge CB2 1EZ, UK (fax: +44-1223-336033; e-mail: deposit@ccdc.cam.ac.uk or www.ccdc.cam.ac.uk), as supplementary publication numbers CCDC 234745, 234746 and 234747 for compounds **1**, **2** and **3**, respectively.

Acknowledgement

This work was supported by a grant from the National Institute of General Medical Sciences.

References

[1] E.Y. Tshuva, S.J. Lippard, Chem. Rev. 104 (2004) 987.
[2] M. Costas, M.P. Mehn, M.P. Jensen, L. Que Jr., Chem. Rev. 104 (2004) 939.
[3] E.I. Solomon, T.C. Brunold, M.I. Davis, J.N. Kemsley, S.-K. Lee, N. Lehnert, F. Neese, A.J. Skulan, Y.-S. Yang, J. Zhou, Chem. Rev. 100 (2000) 235.
[4] M. Merkx, D.A. Kopp, M.H. Sazinsky, J.L. Blazyk, J. Müller, S.J. Lippard, Angew. Chem., Int. Ed. 40 (2001) 2782.
[5] D.A. Whittington, S.J. Lippard, J. Am. Chem. Soc. 123 (2001) 827.
[6] M.H. Sazinsky, J. Bard, A. Di Donato, S.J. Lippard, J. Biol. Chem. 279 (2004) 30600.
[7] J. Stubbe, W.A. van der Donk, Chem. Rev. 98 (1998) 705.
[8] P. Nordlund, H. Eklund, J. Mol. Biol. 232 (1993) 123.
[9] Y. Lindqvist, W. Huang, G. Schneider, J. Shanklin, EMBO J. 15 (1996) 4081.
[10] D. Lee, B. Pierce, C. Krebs, M.P. Hendrich, B.H. Huynh, S.J. Lippard, J. Am. Chem. Soc. 124 (2002) 3993.
[11] D. Lee, S.J. Lippard, Inorg. Chem. 41 (2002) 2704.
[12] J.R. Hagadorn, L. Que Jr., W.B. Tolman, J. Am. Chem. Soc. 120 (1998) 13531.
[13] S.V. Kryatov, F.A. Chavez, A.M. Reynolds, E.V. Rybak-Akimova, L. Que Jr., W.B. Tolman, Inorg. Chem. 43 (2004) 2141.
[14] D. Lee, S.J. Lippard, J. Am. Chem. Soc. 123 (2001) 4611.
[15] D. Lee, S.J. Lippard, Inorg. Chem. 41 (2002) 827.
[16] S. Yoon, S.J. Lippard, Inorg. Chem. 42 (2003) 8606.
[17] E.C. Carson, S.J. Lippard, J. Am. Chem. Soc. 126 (2004) 3412.
[18] B.D. Dunietz, M.D. Beachy, Y. Cao, D.A. Whittington, S.J. Lippard, R.A. Friesner, J. Am. Chem. Soc. 122 (2000) 2828.
[19] B.F. Gherman, B.D. Dunietz, D.A. Whittington, S.J. Lippard, R.A. Friesner, J. Am. Chem. Soc. 123 (2001) 3836.
[20] B.F. Gherman, M.-H. Baik, S.J. Lippard, R.A. Friesner, J. Am. Chem. Soc. 126 (2004) 2978.
[21] A.B. Pangborn, M.A. Giardello, R.H. Grubbs, R.K. Rosen, F.J. Timmers, Organometallics 15 (1996) 1518.
[22] C.-J.F. Du, H. Hart, K.-K.D. Ng, J. Org. Chem. 51 (1986) 3162.
[23] C.-T. Chen, J.S. Siegel, J. Am. Chem. Soc. 116 (1994) 5959.
[24] J. Kuzelka, S. Mukhopadhyay, B. Springler, S.J. Lippard, Inorg. Chem. 43 (2004) 1751.
[25] G.M. Sheldrick, SHELXTL 97-2: Program for the Refinement of Crystal Structures, University of Göttingen, Göttingen, Germany, 1997.
[26] G.M. Sheldrick, SADABS: Area-Detector Absorption Correction, University of Göttingen, Göttingen, Germany, 1996.
[27] A.L. Spek, PLATON, A Multipurpose Crystallographic Tool, Utrecht University, Utrecht, The Netherlands, 1998.
[28] D. Lee, P.-L. Hung, B. Spingler, S.J. Lippard, Inorg. Chem. 41 (2002) 521.
[29] K.S. Hagen, R. Lachicotte, J. Am. Chem. Soc. 114 (1992) 8741.
[30] D. Coucouvanis, R.A. Reynolds III, W.R. Dunham, J. Am. Chem. Soc. 117 (1995) 7570.
[31] R.A. Reynolds III, W.R. Dunham, D. Coucouvanis, Inorg. Chem. 37 (1998) 1232.
[32] V.L. MacMurdo, H. Zheng, L. Que Jr., Inorg. Chem. 39 (2000) 2254.
[33] H. Zheng, Y. Zang, Y. Dong, V.G. Young Jr., L. Que Jr., J. Am. Chem. Soc. 121 (1999) 2226.
[34] H.-F. Hsu, Y. Dong, L. Shu, V.G. Young Jr., L. Que Jr., J. Am. Chem. Soc. 121 (1999) 5230.
[35] D. Lee, J.L. DuBois, B. Pierce, B. Hedman, K.O. Hodgson, M.P. Hendrich, S.J. Lippard, Inorg. Chem. 41 (2002) 3172.
[36] A.C. Rosenzweig, P. Nordlund, P.M. Takahara, C.A. Frederick, S.J. Lippard, Chem. Biol. 2 (1995) 409.
[37] K.E. Liu, S.J. Lippard, J. Biol. Chem. 266 (1991) 12836.
[38] Y. Liu, J.C. Nesheim, K.E. Paulsen, M.T. Stankovich, J.D. Lipscomb, Biochemistry 36 (1997) 5223.

Available online at www.sciencedirect.com
SCIENCE DIRECT®
Polyhedron 23 (2004) 2813–2820
POLYHEDRON
www.elsevier.com/locate/poly

Picoline and pyridine functionalised chelate N-heterocyclic carbene complexes of nickel: synthesis and structural studies

Scott Winston, Neoklis Stylianides, Arran A.D. Tulloch, Joseph A. Wright, Andreas A. Danopoulos *

Department of Chemistry, University of Southampton, Highfield, Southampton SO17 1BJ, UK

Received 30 April 2004; accepted 16 July 2004
Available online 3 September 2004

Honouring a special mentor, amazing chemist and humans Malcolm L.H. Greens on the occasion of his retirement.

Abstract

The first pyridine and picoline functionalised N-heterocyclic carbene complexes of nickel are described in this paper. The nature of the isolated complexes is critically dependent on the bite angle and the substituents of the ligand used and the synthetic method for the introduction of the ligand on the metal. From $NiBr_2$ (DME), DME=1,2-dimethoxyethane, by transmetallation with one equivalent of Ag(C^N)Cl, (C^N) = (3-R^1)[1-(α-picolyl)imidazol-2-ylidene, $R^1 = 2,6\text{-}Pr^i_2\text{-}C_6H_3$, 2,6-$Me_2$-4-$Bu^t$-$C_6H_2$, *tert*-butyl, the tetrahedral Ni(C^N)Br_2 (**1a**), (**1b**) and (**1c**) were obtained, respectively. Substitution of Br^- in (**1a**) by dtc^-, dtc^-=*N*,*N*-diethyldithiocarbamate, gave the derivative [Ni(C^N)(dtc)]Br (**2**). Transmetallation with two equivalents of Ag(C^N)Cl, (C^N) = (3-$Me_3C_6H_2$)[1-(α-picolyl)imidazol-2-ylidene], gave [Ni(C^N)$_2$]Br_2 (**3**). Transmetallation with Ag(C–N)Cl, (C–N) = [3-(2,6-$Pr^i_2C_6H_3$)][1-(2-pyridyl)imidazol-2-ylidene] afforded the bimetallic species [(C–N)$_2$Ni(μ-Br)$_2$ $NiBr_2$] (**4**), containing one octahedral and one tetrahedral nickel centre. Finally, from the reaction of $NiBr_2$ (DME) with free (C–N*), (C–N*) = 3-(2,6-$Pr^i_2C_6H_3$)-1-[2-(3-picolyl)]-imidazol-2-ylidene, good yields of Ni(C–N*)Br_2, (**6**) were obtained. Attempts to alkylate (**1**) were not successful.
© 2004 Elsevier Ltd. All rights reserved.

Keywords: Nickel complexes; Heterocyclic carbenes; Functionalised carbenes; X-ray diffraction

1. Introduction

N-heterocyclic carbene (NHC) complexes of the late transition metals are now numerous and well established [1]. Especially, complexes with catalytically active metals are being investigated intensively. The unique donor and spatial characteristics of the NHC ligands are responsible for some unusual reactivity of the isolated complexes [2]. In recent developments NHCs functionalised with 'classical heteroatom' donors have been used as versatile multidentate spectators on a range of transition metal complexes. In this area we [3] and others [4] have reported pyridine-, picoline- and lutidine-functionalised NHC complexes of Ru, Rh, Ir and Pd. The notable absence of any functionalised NHC complexes of Ni is to be contrasted with the numerous Ni(0) and Ni(II) complexes with simple monodentate or chelating bidentate NHCs that have appeared in the literature [5]. The extensive applications of Ni complexes in catalysis, for example in polymerisation, telomerisation, C–C formation and C–F activation reactions prompted our attempts to explore the synthesis and characterisation of a range of pyridyl and picolyl functionalised NHC complexes of Ni. The compounds described in this paper are summarised in Scheme 1.

* Corresponding author. Tel.: +02380594116; fax: +02380596805.
E-mail address: ad1@soton.ac.uk (A.A. Danopoulos).

0277-5387/$ - see front matter © 2004 Elsevier Ltd. All rights reserved.
doi:10.1016/j.poly.2004.07.002

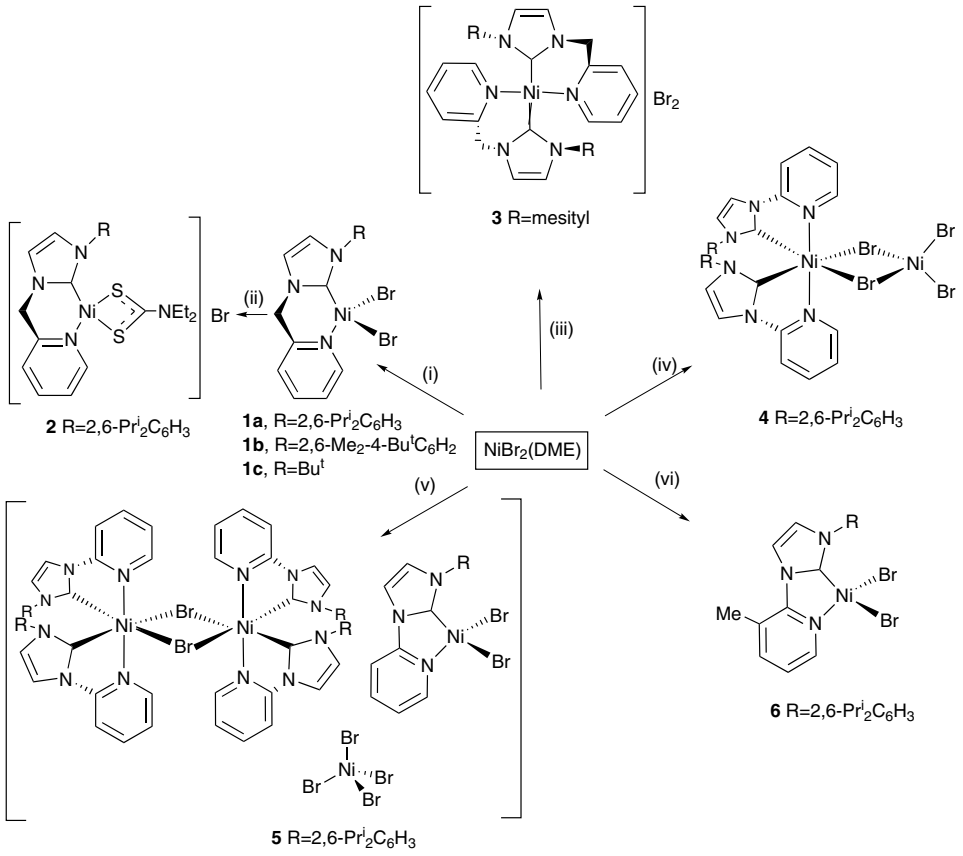

Scheme 1. Complexes described in this paper. Reagents and conditions: (i) 1 equiv. Ag(C^N)Br, CH_2Cl_2 reflux; (ii) $Na(Et_2NCS_2)$, CH_2Cl_2, reflux; (iii) 2 equiv. Ag(C^N)Br, CH_2Cl_2, reflux; (iv) 1 equiv. Ag(C–N)Br, CH_2Cl_2, reflux; (v) 1 equiv. (C–N), THF; (vi) 1 equiv. (C–N*), THF.

2. Experimental

2.1. General methods

Elemental analyses were carried out by the University College, London, microanalytical laboratory. All manipulations were performed under nitrogen in a M. Braun glove-box or using standard Schlenk techniques, unless stated otherwise. Solvents were dried using standard methods and distilled under nitrogen prior use. The light petroleum used throughout had a b.p. 40–60 °C.

The starting imidazolium salts and silver carbene complexes [6] were prepared according to literature procedures. All other materials used were purchased from Aldrich or Lancaster and used without further purification. NMR data were recorded on a Bruker AMX-300. The spectra were referenced internally using the signal from the residual protio-solvent (^{1}H) or the signals of the solvent (^{13}C). Mass spectra (electrospray ionisation) were obtained from acetonitrile solutions on a VG Biotec platform. The calculated isotopic envelopes agree well with the experimentally observed patterns. Magnetic susceptibilities in the solid state were measured at room temperature using a Johnson-Matthey balance. Diamagnetic corrections were ignored.

2.2. 3-(2,6-Di-iso-propylphenyl)-1-(2-pyridyl)]-imidazol-2-ylidene (*C–N*)

The corresponding imidazolium salt precursor was dried azeotropically prior to use using a Dean-Stark apparatus and stored in the glove box. In a Schlenk flask were placed the 3-(2,6-di-*iso*-propylphenyl)-1-(2-pyridyl)]-imidazolium salt (3.00 g, 7.8 mmol) and $KN(SiMe_3)_2$ (1.71 g, 8.6 mmol, 1.2 equiv.) and the solids cooled to −78 °C. Pre-cooled THF (30 cm^3) was added via cannula and the mixture was stirred until the bath temperature rose to −20 °C, and held at this temperature for 3 h. The solution was then allowed to warm to room temperature, and after evaporating the volatiles under reduced pressure, the pale residue was washed with petroleum (2 × 15 cm^3). The product was extracted into toluene (2 × 30 cm^3), filtered through Celite and the solvent removed in vacuo to yield a white crystalline product. Yield: 2.16 g, 90%; m.p. 138–140 °C (dec.). $\delta_H(C_6D_6)$: 1.1, 1.2 [2 × 6H, d, *i*Pr, $CH(CH_3)_2$, J = 7.32 Hz], 2.9 [2H, septet, *i*Pr$CH(CH_3)_2$, J = 7.32 Hz], 6.6 (1H, t, pyridyl *H*), 6.7 and 8.4 (2 × 1H, s, imidazol-2-ylidene backbone), 7.1 (1H, t, pyridyl H), 7.2 (2H, d, *i*Pr$_2$C$_6$*H*$_2$H, 7.44 Hz), 7.3 (1H, t, *i*Pr$_2$C$_6$H$_2$*H*, J = 7.44 Hz), 8.3 (1H, d, 3-pyr H), 8.8 (1H, d, 6-pyr

H). $\delta_C(C_6D_6)$, 22.6, 22.9 [*i*PrCH(C_3)$_2$], 27.1 [*i*Pr *C*(CH_3)$_2$], 113.3, 115.0 (4-,5-imidazol-2-ylidene), 119.8, 121.5, 122.3, 127.7 (*i*Pr$_2C_6H_3$), 136.6, 137.3, 144.8, 146.4, 152.9 (pyridyl) 218.3 (imidazol-2-ylidene). Found: C, 77.62; H, 7.54; N, 13.55. $C_{20}H_{23}N_3$ requires C, 78.65; H, 7.59; N, 13.76%.

2.3. 3-(2,6-di-iso-propyl-phenyl)-1-[2-(3-picolyl)]-imidazol-2- ylidene (*C–N**)

This was prepared following the method described above from the corresponding imidazolium salt (1.00 g, 2.5 mmol) and KN($SiMe_3$)$_2$ (0.55 g, 2.8 mmol). Yield: 0.78 g ca 97%; m.p. 150–155 °C. NMR, $\delta_H(C_6D_6)$: 1.20 and 1.40 [2 × 6H, d, J = 6.89 Hz, CH(CH_3)$_2$], 2.90 (3H, s, methyl H), 3.0 [2H, sept. J = 6.90 Hz, C*H*(CH_3)$_2$], 6.71 (1H, d, J = 1.8 Hz, imidazole backbone) 6.65 (1H, t, J = 4.54 Hz, 4-pyridyl) 7.81 (1H, m, 5-pyridyl), 7.38 (2H, d, J = 7.30 Hz, *m*-$C_6H_3Pr^i_2$), 7.419 (1H, t, J = 7.30 Hz, *p*-$C_6H_3Pr^i_2$), 8.05 (1H, d, 1.8 Hz, imidazole bakbone), 8.30 (1H, d, 4.54 Hz, 6-pyridyl H).

2.4. Preparation of [1-R^1-3-(α-picolyl)imidazol-2-ylidene]nickel dibromide. General method

To the appropriate silver carbene complex in dried dichloromethane (100 cm^3), was added one equivalent of $NiBr_2$ (DME) and the mixture refluxed for 8 h. Silver halide deposits were observed as the reaction progressed. On completion, the reaction mixture was allowed to cool before the solution was filtered through Celite and the solvent removed in vacuo to yield the product. Recrystallisation of samples from dichloromethane layered with petroleum yielded purple crystals.

2.5. 1-(2,6-di-iso-propylphenyl)-3-(α-picolyl)imidazol-2-ylidene]nickel dibromide (*1a*)

It was prepared following the method described above from [1-(2,6-di-*iso*-propylphenyl)-3-α-picolyl)imidazol-2-ylidene]silver bromide (0.16 g, 0.32 mmol) and Ni(DME)Br_2 (0.10 g, 0.32 mmol). Yield: 0.10 g, 59%. Found C, 46.76, H, 4.59, N, 7.36. $C_{21}H_{25}N_3Br_2Ni$ requires C, 46.89, H, 4.68, N, 7.81%. μ_{eff} = 3.3 BM.

2.6. 1-(2,6-dimethyl-4-tert-butyl)-3-(α-picolyl)imidazol-2- ylidene]nickel dibromide (*1b*)

It was prepared following the method described above from the corresponding silver complex (0.15 g, 0.3 mmol) and Ni(DME)Br_2 (0.10 g, 0.3 mmol). Yield: 61%, 0.10 g. MS(ES$^+$) *m*/*z* 320 (Ligand)$^+$. Found C, 46.73, H, 4.57, N, 7.79. $C_{21}H_{25}Br_2N_3Ni$ requires C, 46.89, H, 4.68, N, 7.81%. μ_{eff} = 3.2 BM.

2.7. 1-(tert-butyl)-3-(α-picolyl)imidazol-2-ylidene]nickel dibromide (*1c*)

It was prepared following the method described above from [1-(*tert*-butyl)-3-(α-picolyl)imidazol-2-ylidene]silver bromide (0.30 g, 0.7 mmol) and Ni(DME)Br_2 (0.23 g, 0.8 mmol). Yield: 56%, 0.18 g. Found C, 40.10, H, 4.40, N, 10.79. $C_{13}H_{17}N_3Br_2Ni$ requires C, 35.99, H, 3.95, N, 9.69%. μ_{eff} = 3.2 BM. The X-ray crystal structure shows partial occupation of the halide sites by chloride and bromide, which may account for the deviation between the theoretical and experimental analytical data. The origin of the chloride ion is the silver carbene reagent. Depending of the reaction conditions there is variable incorporation of chloride originating from the chlorinated solvent used during the preparation of the silver complex [6].

2.8. 1-(2,6-di-iso-propylphenyl)-3-(α-picolyl)imidazol-2-ylidene]nickel diethyldithiocarbamate bromide (*2*)

To a solution of **1a** (0.25 g, 0.46 mmol) in dichloromethane (30 cm^3) was added sodium diethyldithiocarbamate (0.87 g, 0.51 mmol) and the solution refluxed overnight. The purple solution changed to pale brown and salt deposits were observed. The supernatant was removed in vacuo and the product extracted into ether, filtered and concentrated to ca. 5 cm^3. On standing at room temperature X-ray quality crystals were formed. Yield: 62%, 0.17 g. MS (ES$^+$) *m*/*z* 525 [Ni(Ligand)(S_2CNEt_2)]$^+$, 320 (Ligand)$^+$. Found C, 50.24, H, 5.32, N, 9.72. $C_{25}H_{35}BrN_4NiS_2$ requires C, 50.53, H, 5.94, N, 9.43%. The ^{1}H NMR spectrum at RT (CD_2Cl_2) consists of broad lines centered at 1.5, [(CH_3)$_2$CH and CH_3CH_2N], 2.6 (CH_3CH_2N) and the aromatic region.

2.9. Bis[1-(2,4,6-trimethylphenyl)-3-(α-picolyl)imidazol-2-ylidene]nickel dibromide salt (*3*)

This was prepared following the general method using [1-(mesityl)-3-(α-picolyl)-imidazol-2-ylidene]silver bromide (0.15 g, 0.33 mmol) and $NiBr_2$ (DME) (0.05 g, 0.16 mmol) in dichloroethane (30 cm^3). The reaction mixture was refluxed overnight. Silver halide precipitated from the green solution. The mixture was filtered through a frit and the resulting pale yellow/green solution was concentrated to ca. 5 cm^3 and cooled to −30 °C giving X-ray quality crystals. Yield: 0.09 g, 74%. $\delta_H(CDCl_3)$: 2.1 (12H, s, *o*-mesityl CH_3), 2.5 (6H, s, *p*-mesityl CH_3), 5.5 (2H, s, CH_2), 6.7 and 7.3 (2 × 2H, s, 4-and 5-imidazol-2-ylidene), 6.9 (2H, s, mesityl H), 7.3 (1H, m, pyr H), 7.5 (1H, m, pyr H), 7.8 (1H, d, J = 8 Hz, pyr H), 8.5 (1H, d, J = 6.9 Hz, pyr H).

2.10. Compound (4)

This was prepared following the general method described above and using 1-(2,6-di-*iso*-propylphenyl)-3-(pyridin-2-yl)-imidazol-2-ylidene silver bromide (0.20 g, 0.4 mmol) and Ni(DME)Br_2 (0.12 g, 0.4 mmol). Yield 0.10 g, 26.5%. Found C, 45.03, H, 4.15, N, 7.55. $C_{40}H_{46}N_6Br_4Ni_2$ requires C, 45.85, H, 4.42, N, 8.02%. X-ray quality crystals were obtained by slow evaporation of dichloromethane solutions.

2.11. Reaction of Ni(DME)Br_2 with (C–N)

To a solution of 1-(2,6-di-*iso*-propylphenyl)-3-(pyridin-2-yl)-imidazol-2-ylidene (0.20 g, 0.65 mmol) in DME (dry, 30 cm^3) at −78 °C, was added Ni(DME)Br_2 (0.22 g, 0.72 mmol) and the reaction stirred for 30 min before being allowed to rise to room temperature. The colour of the solution changed from orange to green to brown. The solvent was removed in vacuo and the resulting brown solid was washed with petroleum (2×10 cm^3). Yield 0.10 g. Found C, 44.26, H, 5.09, N, 7.26. $C_{40}H_{46}N_6Br_4Ni_2$ requires C, 45.85, H, 4.42, N, 8.02%. Green X-ray quality co-crystals (5) were obtained by slow cooling of THF solutions. The product decomposed rapidly in $CDCl_3$ and was insoluble in C_6D_6.

2.12. 1-(2,6-di-iso-propylphenyl)-3-[2-(3-picolyl)]-imidazol-2- ylidene]nickel dibromide (6)

To a suspension of $NiBr_2$ (DME) (0.150 g, 0.485 mmol) in THF (30 cm^3) at −78 °C was added a solution of (C–N*) (0.155 g, 0.485 mmol) in THF precooled at −78 °C. The mixture was allowed to warm to room temperature and was stirred for 2 h. The resulting green solution was filtered and the solvent was then evaporated in vacuo. The green solid was crystallised from THF layered with petroleum. Yield: 0.21 g, 80%. Found C, 46.56, H, 4.59, N, 7.46. $C_{21}H_{25}N_3Br_2Ni$ requires C, 46.88, H, 4.68, N, 7.82%.

2.13. X-ray crystallography

A summary of the crystal data, data collection and refinement for compounds (**1b**), (**2**), (**3**), (**4**), (**C–N***), and (**6**) are given in Table 1. Data related to compounds (**1a**) and (**1c**) and (**C–N**) are included as supplementary information.

All data sets were collected on a Enraf Nonius Kappa CCD area detector diffractometer with rotating anode FR591 and an Oxford Cryosystems low-temperature device operating in omega scanning mode with phi and omega scans to fill the Ewald sphere. The programs used for control and integration were Collect, Scalepack and Denzo [7]. The crystals were mounted on a glass fibre with silicon grease, from Fomblin vacuum oil. All solutions and refinements were performed using the WINGX package [8] and all software packages within. All non-hydrogen atoms were refined using anisotropic thermal parameters and hydrogens were added using a riding model.

3. Results and discussion

The original syntheses of monodentate or bidentate NHC complexes of nickel involved the interaction of a

Table 1
Summary of crystallographic data collections

	1b	2	3	4	6	C–N*
Chemical formula	$C_{21}H_{25}Br_2N_3Ni$	$C_{27}H_{37}BrCl_2N_4NiS$	$C_{38}H_{42}Br_2Cl_4N_6Ni$	$C_{40}H_{46}Br_4N_6Ni_2$	$C_{21}H_{25}Br_2N_3Ni$	$C_{21}H_{25}N_3$
Formula weight	537.97	691.25	943.11	1047.89	537.97	319.44
Crystal system	monoclinic	monoclinic	monoclinic	tetragonal	monoclinic	monoclinic
Space group	*P21/n*	*P21/n*	*P21/n*	*P42/n*	*P21/n*	*P21/c*
a (Å)	7.0347(14)	9.8969(3)	10.669(2)	20.548(3)	9.0549(10)	8.319(3)
b (Å)	23.581(5)	24.1705(10)	10.221(2)	20.548(3)	17.381(3)	10.787(5)
c (Å)	13.633(3)	14.6443(6)	19.561(4)	27.667(6)	13.676(2)	20.628(14)
α (°)	90.00	90.00	90	90	90	90
β (°)	92.98(3)	109.1690(10)	105.41(3)	90	90.884(9)	105.22(5)
γ (°)	90.00	90.00	90	90	90	90
V (Å^3)	2258.5(8)	3308.9(2)	2056.3(8)	11682(3)	2152.1(5)	1786.2(16)
Z	4	4	2	8	4	4
T (K)	120(2)	120(2)	120(2)	100(2)	120(2)	120(2)
μ (mm^{-1})	4.408	2.104	2.710	3.407	4.625	0.071
Number of data collected	17860	20672	12708	33523	21291	20952
Number of unique data	5113	7342	4530	10587	4672	3522
R_{int}	0.0673	0.0811	0.0524	0.1073	0.1865	0.1669
Final $R(\|F\|)$ for $F_0 > 2\sigma(F_0)$	0.0417	0.0524	0.0413	0.0578	0.0589	0.0829
Final $R(F^2)$ for all data	0.0955	0.1081	0.0957	0.1548	0.1003	0.1747

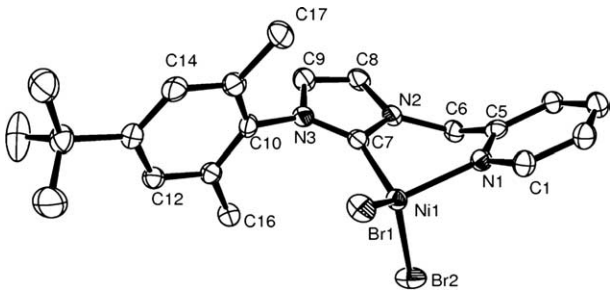

Fig. 1. ORTEP representation of the structure of **1b** showing 50% probability ellipsoids. H atoms are omitted for clarity. Selected bond lengths (Å) and angles (deg) with estimated standard deviations: C(7)–Ni(1) 1.962(3); N(1)–Ni(1) 2.012(3); C(7)–N(2) 1.352(4); C(7)–N(3) 1.341(4); C(7)–Ni(1)–N(1) 93.38(12); Br(1)–Ni(1)–Br(2) 125.92(2).

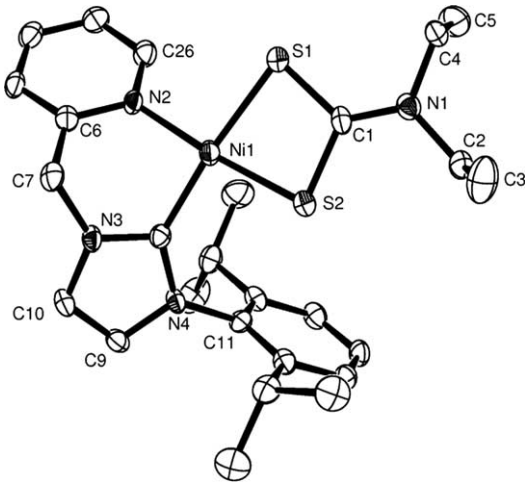

Fig. 2. ORTEP representation of the structure of the cation in **2** showing 50% probability ellipsoids. H atoms are omitted for clarity. Selected bond lengths (Å) and angles (deg) with estimated standard deviations: Ni(1)–S(2) 2.1719(10); Ni(1)–S(1) 2.2324(10); C(8)–Ni(1) 1.880(4); C(8)–N(3) 1.347(4); C(8)–N(3) 1.347(4); N(2)–Ni(1) 1.943(3); C(8)–Ni(1)–N(2) 90.61(13); S(2)–Ni(1)–S(1) 79.08(4).

Ni(II) or Ni(0) precursor with isolated NHCs, prepared by deprotonation of the imidazolium preligands, or by direct metallation of imidazolium salts with $Ni(OAc)_2$. The former method could not be applied successfully to the synthesis of α-picolyl functionalised NHC complexes due to the problematical synthesis and instability of the free ligands at room temperature [3b]. The latter method when used for the synthesis of pyridine- and picoline-functionalised Ni complexes gave intractable mixtures [3d]. We therefore opted for a strategy involving transmetallation of the NHC from silver to nickel, originally reported by Wang and Lin [9a] and applied to the synthesis of palladium and rhodium complexes by us [3a] and [3b] and others [9b]. Reaction of one equivalent of the known silver NHC complexes with $NiBr_2$ (DME) gave selectively good yields of the targeted complexes Ni(C^N)Br_2, (**1a**), (**1b**) and (**1c**), as air stable, purple crystalline materials. The reaction rates were noticeably slower than those of analogous palladium systems as judged by the rate of precipitated silver halide. This may be due to the weaker M–C bonds being formed in the Ni(II) case. Since the products are paramagnetic their characterisation was carried out by analytical and single crystal X-ray diffraction methods. An ORTEP diagram of (**1b**) is shown in Fig. 1; details of the structures of (**1a**) and (**1c**) are included as supplementary information.

All three complexes are distorted tetrahedral [bite angle average 92.70(20)°, Br–Ni–Br average 128.5(4)°]. The Ni–C bond lengths [average 1.969(6) Å] are longer than those previously reported for other Ni(II)–NHC complexes [5]. Attempted substitution of the halide in (**1a**)–(**c**) with a variety of nucleophilic reagents, including alkyl lithium, magnesium and zinc reagents, gave intractable mixtures. However, substitution of one bromide in (**1a**) with pre-dried sodium diethyldithiocarbamate proceeded cleanly giving rise to (**2**) which was unequivocally characterised by analytical and diffraction methods. A diagram of the cation of (**2**) is given in Fig. 2.

In this case the geometry of the nickel centre is best described as square planar. The Ni–C [1.880(4) Å] is shorter than those observed in (**1a**)–(**1c**), and comparable to those reported in the literature for other square planar NHC complexes [5]. The bite angle of (C^N) is reduced to 90.61(13)°, demonstrating the ability of the six membered chelate ring to accommodate different coordination geometries. The dithiocarbamate chelate ring is slightly unsymmetrical due to the increased *trans* influence of the strong σ-donor NHC functional group. The adoption of square planar geometry may be due to the angular constraints imposed by the dtc ligand and the strengthening of metal–ligand σ- and π-bonding in this geometry. Complex (**2**) shows a very broad ^1H NMR spectrum, which may be due to fluxionality or planar–tetrahedral equilibria in solution. Attempts to sharpen the spectrum at lower temperatures (−60 °C) were unsuccessful.

Transmetallation using two equivalents of the silver–NHC complex gave clean products only when the mesityl substituted analogue was employed. In his case complex (**3**) was isolated as brown air stable crystalline material and characterised by analytical, spectroscopic and diffraction methods. A diagram of the cation in (**3**) is given in Fig. 3.

Here too the Ni center adopts a slightly distorted square planar geometry with the two NHC and two pyridine functional groups arranged *trans* to each other. The Ni–C bond lengths [1.908(3) Å] fall in the range typical for other square planar complexes [5]. The carbene

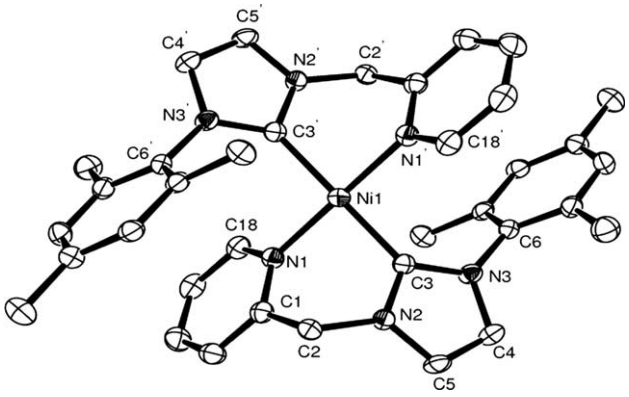

Fig. 3. ORTEP representation of the structure of the cation in **3** showing 50% probability ellipsoids. H atoms are omitted for clarity. Selected bond lengths (Å) and angles (deg) with estimated standard deviations: C(3)–Ni(1) 1.908(3); N(1)–Ni(1) 1.928(2); C(3)–N(2) 1.344(4); C(3)–N(3) 1.365(4); C(3)–Ni(1)–N(1) 87.24(11); C(3)–Ni(1)–N(1)# 1 92.76(11)

heterocyclic ring is twisted by ca. 42° from the coordination plane. In addition, the planes of the aromatic rings of the NHC substituent and the pyridine of the second ligand are almost parallel with short interplanar distances (3.22–3.25 Å).

Attempts to prepare the pyridine functionalised analogues of (**1a**)–(**c**) by either transmetallation or substitution of labile ligands (DME or THF) of Ni(II) precursors by the free (C–N) gave unexpected results.

On refluxing $Ni(DME)Br_2$ with one equivalent of Ag(C–N)Br a deep purple solution was produced, which on cooling formed a light blue precipitate. This could be redissolved on heating giving a purple solution. From the latter on slow cooling light blue crystals of (**4**) precipitated. Complex (**4**) is paramagnetic and its identity was established by analytical and single crystal X-ray diffraction methods. A diagram of the molecule is shown in Fig. 4.

In the solid state (**4**) contains two nickel centres with different coordination geometries. The first, tetrahedral, is coordinated by two terminal and two bridging bromides and the second, octahedral, is hosting two (C–N) ligands and bridged to the other Ni centre through the bromides. The pyridine groups occupy mutually *trans* sites. The Ni–NHC bonds in this complex (2.009–2.019 Å) are longer than those observed with other tetrahedral (1.936–1.957 Å) and square planar (1.880–1.908 Å) examples discussed in this paper and elsewhere [5]. The same trend is observed with the M–pyridine bond lengths as expected. The planes of the aromatic rings of the NHC substituent and the pyridine of the second ligand in the octahedral center are parallel with short interplanar distances (3.15–3.20 Å). The reason for the selective isolation of (**4**) with the (C–N) ligand is not clear. The equilibrium given below is plausible and has been suggested for other Ni(II)/bidentate ligand systems [13]

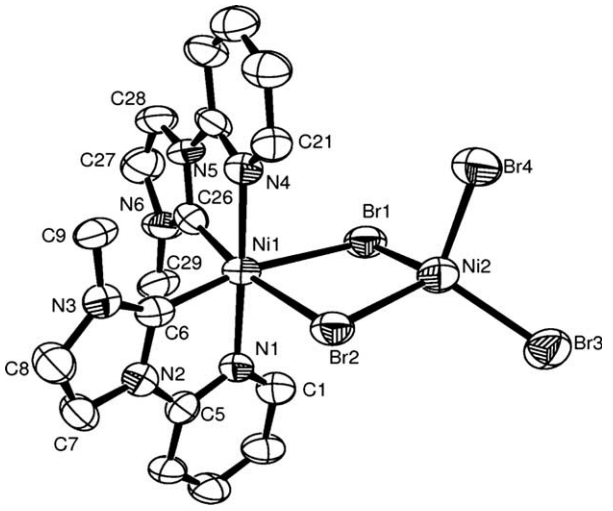

Fig. 4. ORTEP representation of the structure of **4** showing 50% probability ellipsoids. H atoms are omitted for clarity. Selected bond lengths (Å) and angles (deg) with estimated standard deviations: N(1)–Ni(1) 2.103(5); N(4)–Ni(1) 2.102(5); Ni(1)–Br(1) 2.6642(11); Ni(1)–Br(2) 2.6898(12); Ni(2)–Br(4) 2.3525(14); Ni(2)–Br(3') 2.355(2); Ni(2)–Br(3) 2.381(5); Ni(2)–Br(1) 2.4093(13); C(6)–Ni(1) 2.009(7); C(26)–Ni(1) 2.018(7); N(1)–Ni(1) 2.103(5); N(4)–Ni(1) 2.102(5); Ni(1)–Ni(2) 3.597; C(26)–Ni(1)–N(4) 79.3(3); C(6)–Ni(1)–N(1) 80.1(2); C(26)–Ni(1)–N(1) 99.1(2).

$$NiBr_2(DME) \rightleftharpoons NiBr_2(C\text{–}N) \rightleftharpoons NiBr_2(C\text{–}N)_2$$

$$NiBr_2(DME) + NiBr_2(C\text{–}N)_2 \rightleftharpoons Br_2Ni(\mu\text{-}Br)_2Ni(C\text{–}N)_2 + DME$$

It may be speculated that (**4**) formed by dimerisation of $NiBr_2$ (DME) and $NiBr_2$ (C–N) is preferentially crystallising out of solution. Upon dissolving (**4**) to polar donor solvents (e.g., THF) the accompanying colour change could be ascribed to the splitting of the dimeric structure. Attempts to trap the products formed by addition of PMe_3 gave only $NiBr_2$ $(PMe_3)_3$ and white imidazolium salts as precipitates, which may imply dissociation of (C–N) in the presence of PMe_3. The structure of compound (**4**) is a rare example of a binuclear complex of Ni(II) with two centers of different coordination geometries. There are only a few examples of mixed geometry binuclear nickel complexes with extended pre-organised multi-dentate Schiff base ligands [10].

Reaction of $NiBr_2$ (DME) with one equivalent of the free ligand (C–N) gave a complicated reaction mixture from which blue-green crystals were obtained. A detailed X-ray diffraction study was hampered by the small size of the crystals formed, however it revealed the identity of the chemical species that were involved in the crystal. A mixture of the octahedral $\{[Ni(C\text{–}N)_2Br]_2\}^{2+}$, the tetrahedral $Ni(C\text{–}N)Br_2$ and $[NiBr_4]^{2-}$ were all present in the lattice [co-crystal (**5**) in Scheme 1]. Attempts to separate the neutral from the ionic components by selective extraction were not successful. Again the formation of co-crystal (**5**) can be rationalised

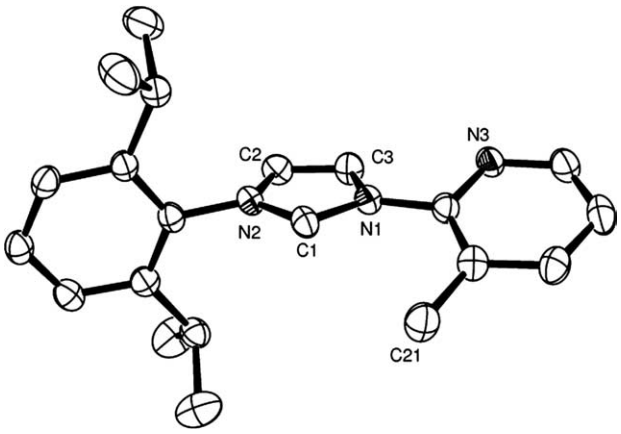

Fig. 5. ORTEP representation of the structure of (**C***–**N**) showing 50% probability ellipsoids. H atoms are omitted for clarity. Selected bond lengths (Å) and angles (deg) with estimated standard deviations: N(1)–C(1) 1.381(4); N(1)–C(3) 1.391(4); N(2)–C(1) 1.357(4); C(2)–C(3) 1.330(4).

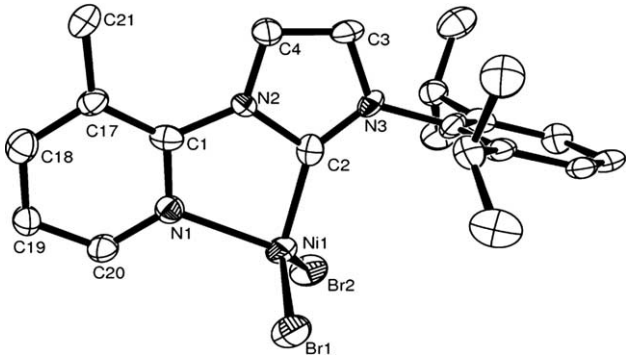

Fig. 6. ORTEP representation of the structure of **6** showing 50% probability ellipsoids. H atoms are omitted for clarity. Selected bond lengths (Å) and angles (deg) with estimated standard deviations: C(2)–N(2) 1.391(7); C(2)–N(3) 1.331(8); C(2)–Ni(1) 1.937(7); N(1)–Ni(1) 2.032(5); Br(2)–Ni(1)–Br(1) 130.35(4); C(2)–Ni(1)–N(1) 81.4(3).

by postulating the establishment of an equilibrium involving mono- and di-substituted Ni containing species as described above for (**4**). It is expected that the position of this equilibrium would be dependent on the electronic and steric factors determining the stability of the species involved.

In an effort to study the effect of nature of the pyridine ring substituents on the electronic properties of the (C–N) ligands, we synthesised a (C–N) analogue with 3-methyl substituted pyridine ring. Following the general method described previously [6] we obtained high yields of the free pyridine functionalised NHC (**C**–**N***), which was characterised by spectroscopic, analytical and diffraction methods. A diagram of the molecule is given in Fig. 5; for comparison purposes the structure of the unsubstituted analogue (**C**–**N**) is also included as supplementary information. Both ligands show very similar metrical data with almost *anti*-arrangement of the pyridine and the NHC lone pairs [the average dihedral angle between the aromatic rings is 21° and 18.5° for (**C**–**N***) and (**C**–**N**), respectively]. Reaction of $NiBr_2$ (DME) with the (**C**–**N***) in THF gave high yields of the tetrahedral [Ni(C–N*)Br_2] **6** (Fig. 6). This was the only identifiable complex in the reaction mixture. A comparison of the structures of (**1a**) and (**6**) shows that both adopt distorted tetrahedral geometries, with the more severe distortions being observed in (**6**); [ligand bite angles 81.4(3)° in (**6**), 92.50° (14) in (**1a**), Br(1)–Ni(1)–Br(2) 130.35(4)° in (**6**), 131.12(3)° in (**1a**)]. The chelating ligand bite angle does not have a significant effect on the Br(1)–Ni(1)–Br(2) angle, the magnitude of which is possibly controlled by the bromide lone pair repulsions. Four coordinate complexes of type [(L–L)Ni(halide)$_2$] are square planar or tetrahedral [11]. The recently reported bidentate bis-NHC complexes [5e,f] invariably adopt square planar geometry. This geometry is also favoured by phosphine complexes of the type $NiBr_2$(L–L) [(L–L) = $R_2P(CH_2)_nPR_2$ n = 1–3, R = aryl, alkyl] [12]. However, Ni[$Me_2P(CH_2)_2PMe_2$]Cl_2 and complexes with large bite angle diphosphines adopt tetrahedral geometry [13].

Preliminary data show that complexes (**1a**), (**1b**) and (**1c**) in the presence of excess of MAO are poor catalysts for the polymerisation of ethylene at room temperature. The polymerisation activity of (**6**) will be reported in the future.

In summary, we have shown that the synthesis of picoline- and pyridine-functionalised NHC complexes of Ni(II) can be accomplished by using transmetallation or substitution synthetic strategies. Transmetallation yields selectively picoline-functionalised tetrahedral complexes of type [(C^N)$NiBr_2$]. Under forcing conditions the square planar [Ni(C^N)$_2$]Br_2 could be obtained. The same methodology when applied to pyridine-functionalised NHC ligands leads to the isolation of octahedral [(C–N)$_2$Ni(μ-Br_2)$NiBr_2$]. However, substitution of the labile DME with the free (C–N*) gave good yields of the tetrahedral [(C–N*)$NiBr_2$]. The preparation of organometallic complexes of [(C–N*)$NiBr_2$] is currently under progress.

Acknowledgement

We thank the EPSRC for a studentship (to S. Winston), Professor M.B. Hursthouse for the provision of X-ray facilities and helpful discussions and Mr. N. Tsoureas for solving the structure of (C–N).

Appendix A. Supplementary material

Supplementary data associated with this article can be found, in the online version, at doi:10.1016/j.poly.2004.07.002.

References

[1] (a) For recent reviews see: W.A. Herrmann, Angew. Chem. Int. Ed. 41 (2002) 1290;
(b) D. Borissou, O. Guerret, F.P. Gabbai, G. Bertrand, Chem. Rev. 100 (2000) 39.

[2] (a) J.C. Green, G. Scurr, P.L. Arnold, F.G.N. Cloke, Chem. Commun. (1997) 1663;
(b) J.A. Mata, A.R. Chianese, J.R. Miecznikowski, M. Poyatos, E. Peris, J.W. Faller, R.H. Crabtree, Organometallics 23 (2004) 1253.

[3] (a) A.A. Danopoulos, A.A.D. Tulloch, S. Winston, G. Eastham, M.B. Hursthouse, J. Chem. Soc., Dalton Trans. (2003) 1009;
(b) A.A. Danopoulos, A.A.D. Tulloch, S. Winston, G. Eastham, M.B. Hursthouse, J. Chem. Soc., Dalton Trans. (2003) 699 and references given there;
(c) A.A. Danopoulos, M.B. Hursthouse, S. Winston, J. Chem. Soc., Dalton Trans. (2002) 3090;
(d) A.A. Danopoulos, unpublished data.

[4] (a) D.S. McGuiness, K.J. Cavell, Organometallics 19 (2000) 741;
(b) S. Grundemann, A. Kovacevic, M. Albrecht, J.W. Faller, R.H. Crabtree, J. Am. Chem. Soc. 124 (2002) 10473.

[5] (a) A.J. Arduengo, S.F. Gamper, J.C. Calabrese, F. Davidson, J. Am. Chem. Soc. 116 (1994) 4391;
(b) P.L. Arnold, F.G.N. Cloke, T. Geldbach, P.B. Hitchcock, Organometallics 18 (1999) 2328;
(c) W.A. Herrmann, G. Gerstberger, M. Spiegler, Organometallics 16 (1997) 2209;
(d) W.A. Herrmann, L.J. Goosen, G.R.J. Artus, C. Köcher, Organometallics 16 (1997) 2472;
(e) R.E. Douthwaite, D. Häussinger, M.L.H. Green, P.J. Silcock, P.T. Gomes, A.M. Martins, A.A. Danopoulos, Organometallics 18 (1999) 4584;
(f) R.E. Douthwaite, M.L.H. Green, P.J. Silcock, P.T. Gomes, Organometallics 20 (2001) 2611;
(g) D.S. McGuiness, W. Mueller, P. Wasserscheid, K.J. Cavell, B.W. Skelton, A.H. White, U. Englert, Organometallics 21 (2002) 175;
(h) C.D. Abernethy, A.H. Cowley, R.A. Jones, J. Organomet. Chem. 596 (2000) 3;
(i) B.R. Dible, M.S. Sigman, J. Am. Chem. Soc. 125 (2003) 872;
(j) R. Dorta, E.D. Stevens, D.S. Hoff, P. Nolan, J. Am. Chem. Soc. 125 (2003) 10490;
(k) N. Clement, K.J. Cavell, C. Jones, C.J. Elsevier, Angew. Chem. Int. Ed. 43 (2004) 1277.

[6] A.A. Danopoulos, G. Eastham, S. Kleinhenz, A.A.D. Tulloch, S. Winston, J. Chem. Soc., Dalton Trans. (2000) 4499.

[7] R. Hooft, COLLECT, Nonius BV, 1997–2000;
Z. Otwinowski, W. Minor, SCALEPACK DENZO, Methods Enzymol. 276 (1997) 307.

[8] L.J. Farrugia, J Appl. Crystallogr. 32 (1999) 83.

[9] (a) H.M.J. Wang, I.J.B. Lin, Organometallics 17 (1998) 972;
(b) A.R. Chianese, X. Li, M.C. Janzen, J.W. Faller, R.H. Crabtree, Organometallics 22 (2003) 1663.

[10] (a) K.K. Nanda, R. Das, K. Ventatsubramanian, P. Paul, K. Nag, J. Chem. Soc., Dalton Trans. (1993) 2515;
(b) S. Brooker, P.D. Croucher, T.C. Davidson, K.S. Dunbar, C.U. Beck, S. Subatamanian, Eur. J. Inorg. Chem. (2000) 169.

[11] F.A. Cotton, G. Wilkinson, 'Advanced Inorganic Chemistry, 5th ed., Wiley Interscience, New York, 1988 p. 746.

[12] J.A.S. Bomfim, F.P. de Souza, C.A.L. Filgueiras, A.G. de Souza, M.T.P. Gambardella, Polyhedron 22 (2003) 1567 and references cited therein.

[13] D.A. Handley, P.B. Hitchcock, G.J. Leigh, Inorg. Chim. Acta 314 (2001) 1.

Available online at www.sciencedirect.com
SCIENCE DIRECT®
Polyhedron 23 (2004) 2821–2829
POLYHEDRON
www.elsevier.com/locate/poly

Acyclic and macrocyclic transition metal dithiocarbamate complexes containing imidazolium moieties for anion binding

Wallace W.H. Wong, Dale E. Phipps, Paul D. Beer *

Inorganic Chemistry Laboratory, Department of Chemistry, University of Oxford, South Parks Road, OX1 3QR Oxford, UK

Received 5 May 2004; accepted 14 June 2004
Available online 3 September 2004

Abstract

The synthesis of acyclic and macrocyclic transition metal dithiocarbamate complexes containing positively charged imidazolium moieties is reported. The assemblies have been characterised by a range of spectroscopic techniques and the ability of these compounds to bind various anions was also examined. UV–Vis spectroscopic binding studies revealed $H_2PO_4^-$ is complexed selectively in preference to F^- and Cl^- for the acyclic transition metal dithiocarbamate complexes containing the *N*-methylimidazolium moiety. Cyclic voltammetric studies demonstrated that the copper(II) dithiocarbamate imidazolium systems can electrochemically sense the binding of Cl^- and $H_2PO_4^-$.
© 2004 Elsevier Ltd. All rights reserved.

1. Introduction

As a consequence of the fundamental roles played by negatively charged species in a range of biological, chemical, medical and environmental processes, there is intense current interest being shown in the syntheses of receptors designed to recognize and sense anions [1]. By incorporating redox- and photo-active transition metal inorganic signaling probes into various acyclic, macrocyclic and calixarene ligand frameworks [2], we have produced a series of selective spectral and electrochemical responsive reagents for anions. In an effort to construct new types of anion redox responsive receptors, we report here the synthesis and preliminary anion coordination investigations of new transition metal dithiocarbamate imidazolium receptor systems, including macrocyclic derivatives, using metal directed self-assembly.

The synthesis of potential macrocyclic anion receptor systems can prove to be problematic as their preparation often requires high dilution conditions and yields can be moderate [3]. Rare examples of using anion templation to circumvent this problem have recently appeared [4]. Metal directed self-assembly synthetic techniques may also be used to aide macrocycle formation [5]. Through careful consideration of ligand and preferred metal coordination geometry, among other factors, complicated and unusual molecular architectures are attainable. The dithiocarbamate (dtc) ligand has proven to be a useful structural motif in the metal directed assembly of a range of supramolecular architectures including nano-sized resorcarene-based assemblies [6], catenanes [7], assorted macrocycles [8], trinuclear cages [9] and cryptands [10]. There is intense current interest in the application of imidazolium compounds in ionic liquids [11] and as precursors to *N*-heterocyclic carbene ligands [12]. The imidazolium moiety has also been employed as an anion binding motif recently [4,13,14]. Combining the dithiocarbamate ligand with positively charged imidazolium moieties followed by transition metal directed assembly has led to the preparation of a series of acyclic

* Corresponding author. Tel.: +44 1865 285 142; fax: +44 1865 272 690 (P.D. Beer).
E-mail addresses: wallace.wong@chem.ox.ac.uk (W.W.H. Wong), paul.beer@chem.ox.ac.uk (P.D. Beer).

0277-5387/$ - see front matter © 2004 Elsevier Ltd. All rights reserved.
doi:10.1016/j.poly.2004.06.020

and macrocyclic receptors with the potential to recognize anionic guest species. Their synthesis, characterization and preliminary anion coordination properties are reported herein.

2. Results and discussion

2.1. Syntheses

The acyclic transition metal dtc complexes containing appended imidazolium moieties were prepared in good yields in four steps (Scheme 1). Condensation of benzaldehyde with *N*-(3-aminopropyl)imidazole (**1**) produced the corresponding imine (**2**), which was alkylated with iodomethane to give the imidazolium-imine ligand (**3**). The imidazolium-amine (**4**) was obtained, with an overall yield of 56%, by reduction of the imidazolium-imine (**3**) with $NaBH_4$. Receptor formation was achieved by metal directed synthesis. Typically, dtc complexes were prepared in a one-pot synthesis from the parent secondary amines by reaction with carbon disulfide, base and an appropriate transition metal salt. Using Ni(II), Cu(II) and Zn(II) acetate salts, crude powders were obtained and anion exchanged with aqueous NH_4PF_6 to afford the analytically pure products (**5a**), (**5b**) and (**5c**) in very good yields (Scheme 1).

The tripodal Co(III) derivative (**6**) was synthesised in 80% yield using cobalt(II) chloride as the transition metal salt (Scheme 1). Macrocyclic transition metal dtc imidazolium receptors (**11**) and (**12**) were prepared by alkylating the imidazole-imine precursor (**2**) with α,α′-dibromo-*p*-xylene and 2,7-bis(bromomethyl)naphthalene, respectively (Scheme 2), followed by dtc ligand formation, addition of the transition metal salt and anion exchange with aqueous NH_4PF_6 to give the pure products in yields of 95% and 81%, respectively (Fig. 1).

An imidazolium dtc cryptand complex was also synthesised (Scheme 3). Alkylation of imidazole imine (**2**) with 1,3,5-tri(chloromethyl)-2,4,6-triethylbenzene [15] followed by reduction of the imine produced the corresponding imidazolium tripod with secondary amine appendages (**14**). Treatment of (**14**) with carbon disulfide and triethylamine in acetonitrile followed by the addition of cobalt(II) chloride gave the cobalt(III) dtc imidazolium cryptand complex (**15**) (Scheme 3) in 82% yield.

All these new transition metal dtc imidazolium derivatives were characterised by a variety of techniques including ^1H NMR, ^{13}C NMR, UV–Vis spectroscopy and elemental analysis (see Section 4).

2.2. Preliminary anion binding studies

2.2.1. UV–Vis spectroscopy

The UV–Vis characterisation data obtained for the nickel(II) (**5a**, **11a** and **12a**), copper(II) (**5b**, **11b** and **12b**), zinc(II) (**5c** and **11c**) dtc complexes and cobalt(III) tripodal dtc systems (**6** and **15**) were comparable to literature values [16,17] of the corresponding transition metal diethyl–dithiocarbamate complexes, respectively (Table 1).

The binding of fluoride, chloride and dihydrogen phosphate anions with the range of transition metal

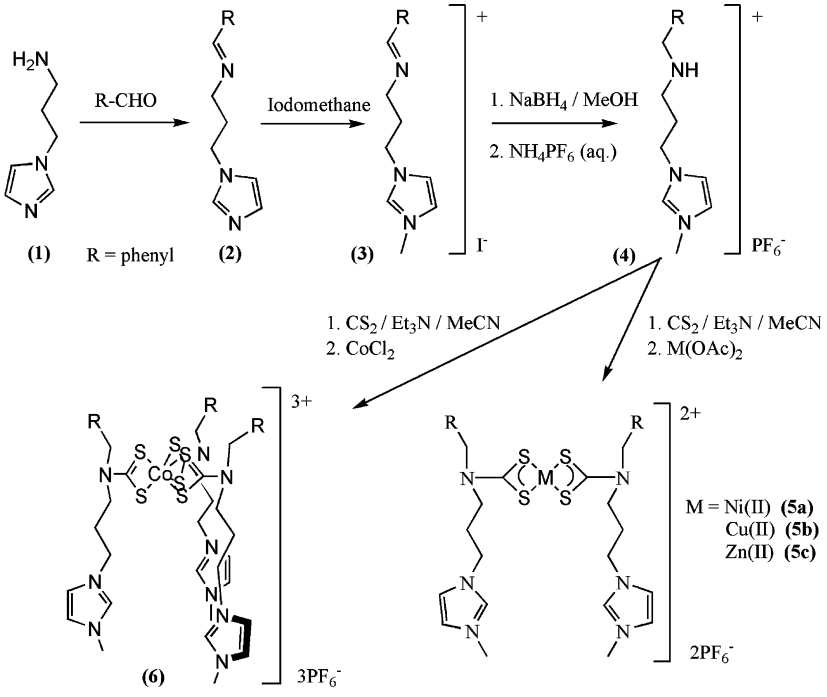

Scheme 1. Synthesis of acyclic transition metal dithiocarbamate imidazolium receptors.

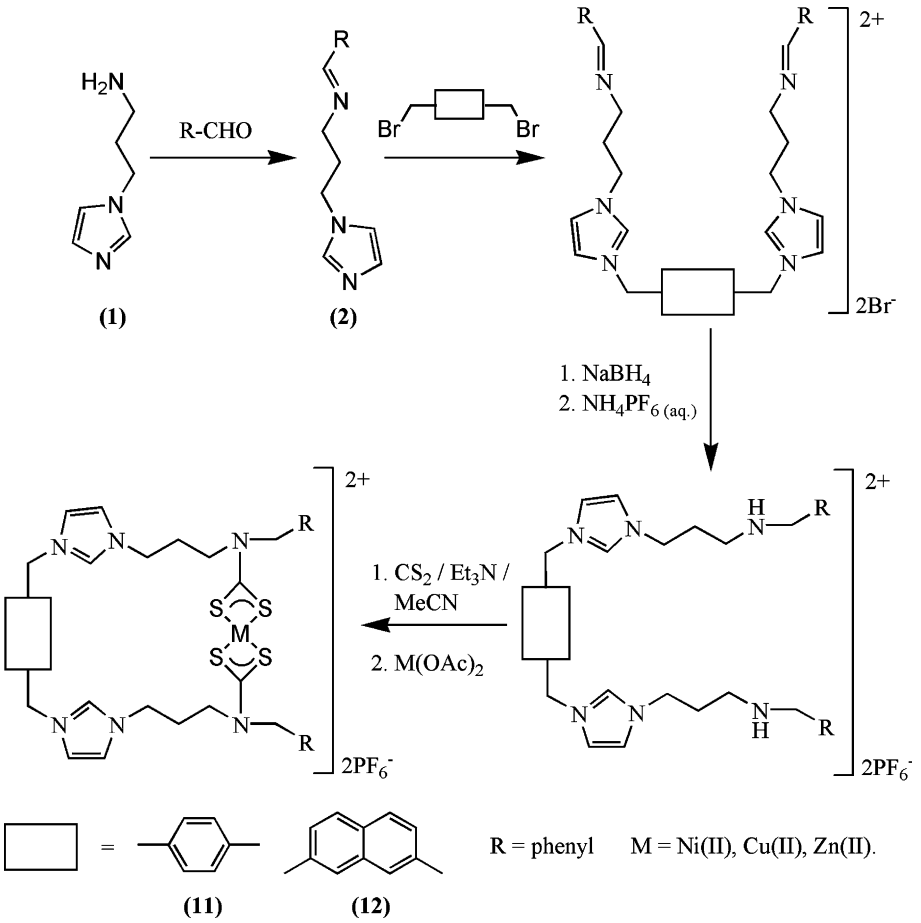

Scheme 2. Synthesis of macrocyclic transition metal dithiocarbamate imidazolium receptors.

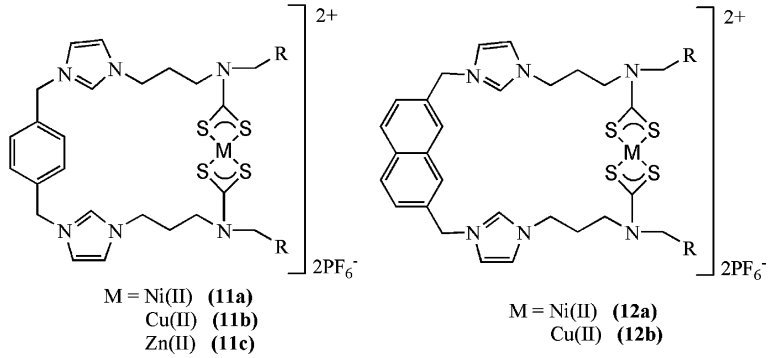

Fig. 1. Macrocyclic transition metal dithiocarbamate imidazolium receptors with xylene and naphthalene spacer groups.

dtc imidazolium derivatives was investigated initially by UV–Vis spectroscopy. Acetonitrile solutions of tetrabutylammonium fluoride, chloride and dihydrogen phosphate were titrated into 10^{-5} M solutions of the metal dtc complexes in acetonitrile, and perturbations in the electronic spectra were analysed using Spectfit [18]. For example, Fig. 2 shows the set of UV–Vis spectra from the titration of dihydrogen phosphate with the acyclic Ni(II) dtc imidazolium receptor (**5a**). The most prominent change in the electronic spectrum seen is the decrease in intensity of the MLCT band at 325 nm; the isobestic points indicate binding stoichiometry is well-behaved.

The acyclic Ni(II), Cu(II) and Zn(II) dithiocarbamate imidazolium receptors (**5a**), (**5b**) and (**5c**) all complexed $H_2PO_4^-$ with no evidence of binding F^- or Cl^-. Job plot analysis indicated 1:1 stoichiometric complexes with $H_2PO_4^-$ in each case. This is in good agreement with anion binding trends observed for an organic imidazolium receptor (**16**) containing a fluorescent anthracene moiety

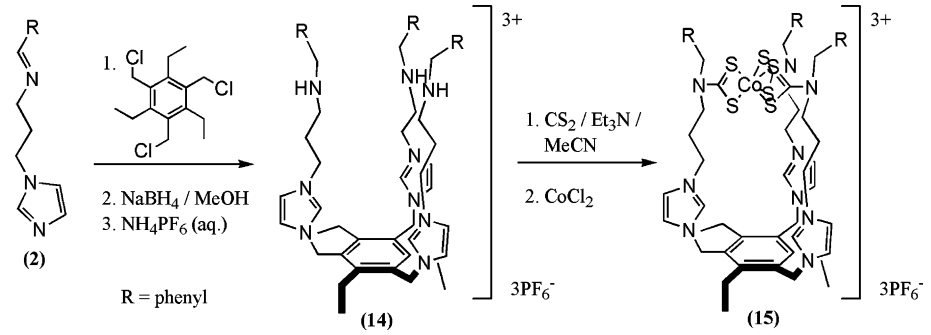

Scheme 3. Synthesis of the cobalt(III) dithiocarbamate imidazolium cryptand receptor.

Table 1
UV–Vis spectroscopic data for the transition metal dithiocarbamate imidazolium complexes

Compound	LC (N–C=S)		MLCT		MLCT	
	Wavelength (nm)	$\varepsilon/10^3$ (M^{-1} cm^{-1})	Wavelength (nm)	$\varepsilon/10^3$ (M^{-1} cm^{-1})	Wavelength (nm)	$\varepsilon/10^3$ (M^{-1} cm^{-1})
5a	246	37.9	325	40.0	395	6.1
11a	245 (245)[a]	34.0	326 (327)[a]	27.1 (33.4)[a]	394 (388)[a]	4.3 (6.7)[a]
12a	228	77.6	326	17.9	395	2.6
	LC (S=C=S)		LC (S=C=S)		MLCT	
5b	272	32.6	290	15.7	434	12.3
11b	272 (272)[b]	49.3 (33.0)[c]	291 (290)[c]	20.9	436 (437)[c]	17.7 (10.6)[c]
12b	268	59.4	292	26.5	441	15.1
	LC		LC			
5c	255	37.8	280	21.8		
11c	263 (263)[c]	25.4 (32.8)[c]	281 (280)[c]	20.3		
	LC		LC		MLCT	
6	249	26	277	24	325 (323)[c]	15(35.4)[c]
15	253	49	275.1	50.3	324	33.1

[a] Literature values for Ni(II) bis(diethyldithiocarbamate) are listed in brackets [16].
[b] Literature values for Cu(II) and Zn(II) bis(diethyldithiocarbamate) are listed in brackets [16].
[c] Literature values for Co(III) tris(diethyldithiocarbamate) are listed in brackets [17].

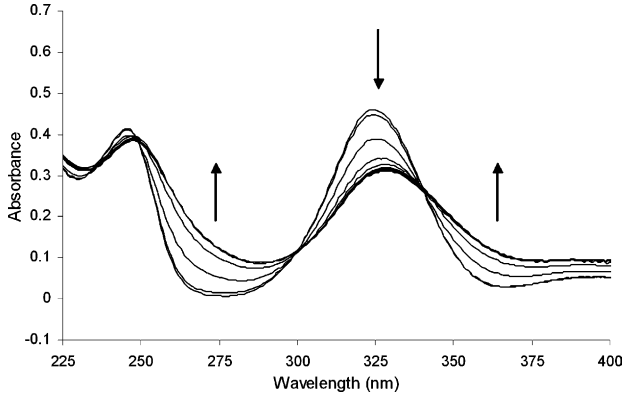

Fig. 2. UV–Vis spectra of the Ni(II) receptor (**5a**) on addition of $H_2PO_4^-$ in MeCN.

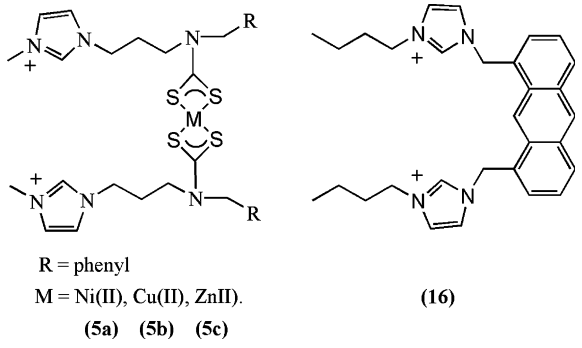

Fig. 3. Transition metal dithiocarbamate imidazolium complexes (**5**) and the anthracene imidazolium receptor (**16**) [13].

(Fig. 3) [13]. For their system, Kim et al. reported preferential binding for $H_2PO_4^-$ over Cl^-, Br^- and I^- as evidenced from fluorescence titration studies in acetonitrile [13].

The determined $H_2PO_4^-$ stability constant values displayed in Table 2 reveal Ni(II) and Cu(II) receptors (**5a**) and (**5b**) bind $H_2PO_4^-$ with similar strength, whereas weaker binding is found with the Zn(II) receptor (**5c**).

Table 2
Stability constant data (log β) for binding $H_2PO_4^-$ in acetonitrile at 298 K

Receptor	Log β
5a	4.3 ± 0.1
5b	3.9 ± 0.2
5c	2.4 ± 0.5

A tentative explanation for this result may be the difference in coordination geometry at the respective metal centre. Ni(II) and Cu(II) dithiocarbamates are known to exhibit square planar geometry whilst Zn(II) dithiocarbamates display distorted tetrahedral stereochemistry. Consequently, the angle between the two imidazolium appendages in these acyclic systems will differ. A square planar geometry at the metal centre apparently favours the tweezer-like binding of $H_2PO_4^-$.

The anion binding properties of macrocyclic systems were also examined by UV–Vis spectroscopy. No changes in the UV–Vis spectra with (**11**) and (**12**) were observed on anion addition which suggests either these systems are incapable of binding anions or anion complexation does not significantly affect the electronic spectra of the receptors.

2.2.2. Electrochemistry

Cyclic voltammetric investigations of the Cu(II) complexes (**5b**), (**11b**) and (**12b**) displayed broadened quasi-reversible Cu(II)/Cu(III) redox couples. (Fig. 4) which appear at more anodic potentials than the Cu(II) bis(diethyldithiocarbamate) system (Table 3).

This anodic displacement of the Cu(II)/Cu(III) redox couple can be attributed to the appended positively charged imidazolium moieties which destabilise the Cu(III) state. Hence, a higher potential is required to oxidise the Cu(II) centers to Cu(III). Cyclic voltammetric studies of the Co(III) complex (**6**) revealed a broadened quasi-reversible Co(III)/Co(IV) redox couple which is anodically shifted compared to the Co(III) tris(diethyldithiocarbamate) complex (Table 3). An irreversible Co(III)/Co(IV) oxidation process was observed at 750 mV for the Co(III) cryptand (**15**) (Table 3).

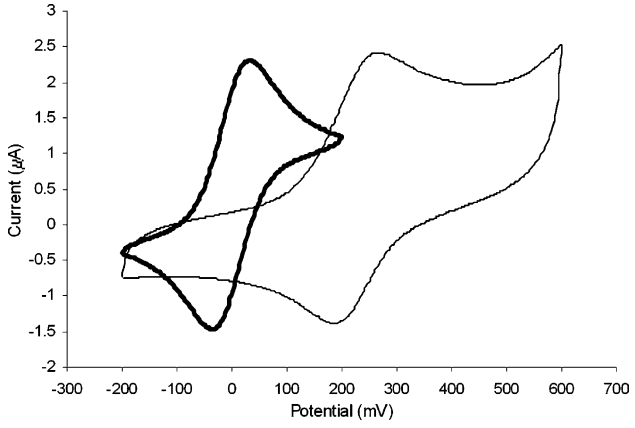

Fig. 4. Cyclic voltammogram of the Cu(II)/Cu(III) redox couple of the Cu(II) bis(diethyl dithiocarbamate) (thick line) and the Cu(II) receptor (**11b**) (fine line). (0.1 M $TBABF_4$/MeCN, 50 mV/s, vs. Ag/Ag^+).

Table 3
Electrochemical data [a]

Receptor	E_{pa} (mV)	E_{pc} (mV)	ΔE	I_{pa}/I_{pc}
Cu(II) bis(diethyl dtc) [b]	32	−36	68	1.07
5b [b]	296	222	74	1.25
11b [b]	272	180	92	1.24
12b [b]	278	166	112	1.13
Co(III) tris(diethyl dtc)	603	529	74	1.33
6 [c]	746	664	82	1.05
15 [b]	790	–	–	–

[a] Conditions: 10^{-4} M solutions of receptor in 0.1 M Bu_4NBF_4 in acetonitrile, scan rate 50 mV s^{-1}, glassy carbon working electrode, $Ag/AgNO_3$ reference electrode. Electrochemical potentials are quoted with errors of ±5 mV.
[b] Cu(II)/Cu(III) dtc redox couple.
[c] Co(III)/Co(IV) dtc redox couple.

The addition of Cl^- and $H_2PO_4^-$ anions to electrochemical solutions of the copper(II) dtc derivatives (**5b**), (**11b**) and (**12b**) resulted in significant cathodic shifts of the respective Cu(II)/Cu(III) redox couple (Table 4). The complexed anion in close proximity to the Cu(II) dtc centre stabilises the Cu(III) redox state, hence lower potentials are required for the oxidation of Cu(II) to Cu(III) [8]. Precipitation problems occurred with (**5b**) and (**6**) on addition of $H_2PO_4^-$ in acetonitrile. Table 4 shows that $H_2PO_4^-$ induced larger magnitudes of cathodic shift in the respective Cu(II)/Cu(III) dtc redox couple compared to Cl^-. This suggests a preferential binding interaction with the $H_2PO_4^-$ anion. It is noteworthy that with the Cu(II) bis(diethyldithiocarbamate) system, no anion induced redox perturbations were observed which suggests the presence of the imidazolium motif is essential for anion complexation. No detectable shifts were observed in the Co(III)/Co(IV) redox couple of the Co(III) dtc cryptand complex (**15**) on addition of anions.

With the diamagnetic transition metal dtc systems, ^1H NMR anion titration experiments were also undertaken. However, precipitation problems were always

Table 4
Electrochemical anion recognition data

Anion	$\Delta E_{1/2}$ (mV) [a]		
	5b	**11b**	**12b**
Cl^-	10	70	40
$H_2PO_4^-$	Precipitation	90	90

[a] Cathodic shifts of the Cu(II)/Cu(III) dtc oxidation potential produced by the presence of 5 equivalents of anion added as the tetrabutylammonium salt. Errors ±10 mV. Conditions: 10^{-4} M solutions of receptor in 0.1 M Bu_4NBF_4 in acetonitrile, scan rate 50 mV s^{-1}, glassy carbon working electrode, $Ag/AgNO_3$ reference electrode.

encountered which prevented the determination of stability constant values.

3. Conclusion

The synthesis of a range of potential acyclic and macrocyclic imidazolium-based anion receptors was achieved by metal directed self-assembly with the dithiocarbamate ligand. The assemblies have been characterised by ^{1}H NMR, ^{13}C NMR, UV–Vis spectroscopy, mass spectrometry and elemental analysis. Evidence for the binding of $H_2PO_4^-$ was observed in UV–Vis spectroscopy for the acyclic transition metal dithiocarbamate imidazolium receptors. In electrochemical studies, significant cathodic shifts of the respective Cu(II)/Cu(III) dtc redox couple of the acyclic and the macrocyclic receptors were observed on addition of Cl^- and $H_2PO_4^-$. Further work is in progress to improve receptor solubility and investigate the binding of a wider range of anions. In addition these systems offer the opportunity to prepare heterobimetallic complexes via *N*-heterocyclic carbene formation from the imidazolium functional groups.

4. Experimental

4.1. General details

NMR spectra were recorded on a Varian 300 MHz spectrometer. Mass spectrometry was carried out on a Micromass LCT electrospray mass spectrometer (ESMS, cone voltage = 20–50 V, desolvation temp = 80 °C, source temp = 60 °C). Elemental analysis was performed at the Inorganic Chemistry Laboratory, Oxford. Electronic spectra were recorded on a Perkin–Elmer Lambda 6 UV–Vis spectrometer. Cyclic and square wave voltammetry were performed on an EG & G Princeton Applied Research potentiostat/galvanostat model 273 linked to a PC via a National Instruments GPIB-PCII/IIA interface and controlled by EG & G Princeton Applied Research Model 270/250 Research Electrochemistry Software. A glassy carbon working electrode, Ag/Ag^+ reference electrode and platinum counter electrode were used in the instrumental setup. Tetabutylammonium tetrafluoroborate was used as the electrolyte.

4.2. Syntheses

4.2.1. Imidazole imine (**2**)

N-(3-aminopropyl)imidazole (3 g) and benzaldehyde (2.5 g) were dissolved in toluene (100 ml) and the solution was refluxed for 2 h using Dean–Stark apparatus. Toluene was removed and the yellow oil (5 g, 98% yield) was dried under vacuum.

^{1}H NMR (300 MHz, $CDCl_3$, 288 K) δ = 8.23 (s, 1H, imine), 7.71 (m, 2H, benzyl), 7.47 (s, 1H, imidazole), 7.40 (m, 3H, benzyl), 7.05 (s, 1H, imidazole), 6.92 (s, 1H, imidazole), 4.04 (t, 7.0 Hz, 2H, N–CH_2–), 3.51 (t, 7.0 Hz, 2H, –CH_2–N), 2.12 (quintet, 7.0 Hz, 2H, –CH_2–). MS (ESI positive ion, MeOH/CH_2Cl_2): *m*/*z* 214 ($M + H^+$).

4.2.2. Compound (**3**)

Compound (**2**) (0.5 g, 1 eqv.) and iodomethane (0.33 g, 1 eqv.) were dissolved in acetonitrile (50 ml) and the solution was stirred under reflux overnight. The solvent was removed and a yellow oily solid (0.5 g, 60% yield) was obtained after drying under vacuum.

^{1}H NMR (300 MHz, CD_3OD, 288 K) δ = 8.77 (s, 1H, imidazolium), 8.35 (s, 1H, imine), 7.73 (m, 2H, aromatic), 7.47 (m, 4H, aromatic), 7.37 (s, 1H, imidazolium), 4.34 (t, 6.9 Hz, 2H, N–CH_2–), 3.79 (s, 3H, CH_3), 3.63 (t, J = 6.9 Hz, 2H, –CH_2–N), 2.21 (m, 2H, CH_2). MS (ESI positive ion, MeOH): *m*/*z* 228 $[M - I^-]^+$.

4.2.3. Compound (**4**)

Compound (**3**) (0.5 g) was dissolved in methanol (50 ml) and sodium borohydride (0.2 g) was added portionwise to the stirring solution. The mixture was allowed to stir under nitrogen for 2 h and a saturated solution of ammonium hexafluorophosphate (10 ml) was added. The volume of methanol was reduced under vacuum and the resulting oil was taken up in CH_2Cl_2 (50 ml) and dried over anhydrous $MgSO_4$. A pale yellow oil (0.5 g, 95% yield) was obtained after solvent removal.

^{1}H NMR (300 MHz, CD_3OD, 288 K) δ = 8.67 (s, 1H, imidazolium), 7.29–7.45 (m, 7H, aromatic), 4.29 (t, 6.9 Hz, 2H, N–CH_2–), 3.82 (s, 5H, benzyl CH_2 and CH_3), 2.68 (t, J = 6.9 Hz, 2H, –CH_2–N), 2.09 (m, 2H, CH_2). MS (ESI positive ion, MeOH): *m*/*z* 230 $[M - PF_6^-]^+$.

4.2.4. Acyclic transition metal dtc imidazolium complexes (**5**)

Compound (**4**) (0.1 g), triethylamine (0.05 g) and carbon disulfide (0.05 g) were dissolved in acetonitrile (50 ml) and stirred for 10 min. The transition metal acetate salt (0.5 eqv.) was added to the solution and the mixture was stirred overnight. The volume of solvent was reduced and a saturated aqueous solution of ammonium hexafluorophosphate (10 ml) was added. The product was extracted with CH_2Cl_2 (50 ml) and a solid was obtained on solvent removal.

(**5a**) Ni: A pale green solid (0.1 g, 78% yield) was collected. ^{1}H NMR (300 MHz, CD_3CN, 288 K) δ = 8.45 (s, 2H, imidazolium), 7.29–7.43 (m, 14H, aromatic), 4.83 (s, 4H, benzyl–CH_2–), 4.14 (t, J = 7.2 Hz, 4H, N–CH_2–), 3.84 (s, 6H, CH_3), 3.57 (t, J = 7.2 Hz, 4H, –CH_2–N),

2.15 (m, 4H, –CH_2–). MS (ESI positive ion, MeCN): *m/z* 813 $[M - PF_6^-]^+$, 334 $[M - 2PF_6^-]^{2+}$. *Anal*. Calc. for $C_{30}H_{38}N_6S_4NiP_2F_{12}$: C, 37.55; H, 3.99; N, 8.76. Found: C, 37.50; H, 4.04; N, 8.70%.

(**5b**) Cu: A brown solid (0.1 g, 78% yield) was collected. MS (ESI positive ion, MeOH): *m/z* 818 $[M - PF_6^-]^+$, 373 $[M]^{2+}$. *Anal*. Calc. for $C_{30}H_{38}N_6S_4CuP_2F_{12}$: C, 37.36; H, 3.97; N, 8.71. Found: C, 36.35; H, 3.54; N, 8.63%.

(**5c**) Zn: A pale yellow solid (0.1 g, 78% yield) was collected. ^{1}H NMR (300 MHz, CD_3CN, 288 K) δ = 8.38 (s, 2H, imidazolium), 7.48 (s, 2H, imidazolium), 7.32–7.41 (m, 12H, aromatic), 5.12 (s, 4H, benzyl–CH_2–), 4.18 (m, 4H, N–CH_2–), 3.85 (m, 4H, –CH_2–N) 3.81 (s, 6H, CH_3), 2.27 (m, 4H, –CH_2–). ^{13}C NMR (300 MHz, CD_3CN, 288 K) δ = 219.5, 137.3, 136.3, 132.8, 131.4, 130.2, 129.4, 128.8, 128.6, 128.1, 125.1, 124.9, 123.5, 58.6, 53.7, 52.1, 48.2, 37.2, 28.0 ppm. MS (ESI positive ion, MeCN): *m/z* 819 $[M - PF_6^-]^+$, 337 $[M - 2PF_6^-]^{2+}$. *Anal*. Calc. for $C_{30}H_{38}N_6S_4ZnP_2F_{12}$: C, 37.29; H, 3.96; N, 8.70. Found: C, 37.02; H, 3.90; N, 8.53%.

4.2.5. Co(III) dtc imidazolium tripodal complex (6)

The same procedure was used as above except $CoCl_2$ was used as the source of cobalt. A green solid (0.1 g, 80% yield) was collected.

^{1}H NMR (300 MHz, CD_3CN, 288 K) δ = 8.47 (s, 1H, imidazolium), 8.42 (s, 1H, imidazolium), 8.39 (s, 1H, imidazolium), 7.31–7.41 (m, 21H, aromatic), 4.93 (m, 6H, benzyl–CH_2–), 4.20 (m, 6H, N–CH_2–), 3.81 (s, 3H, CH_3), 3.80 (s, 3H, CH_3), 3.79 (s, 3H, CH_3), 3.68 (m, 6H, –CH_2–N), 2.17 (m, 6H, –CH_2–). MS (ESI positive ion, MeCN): *m/z* 1264 $[M - PF_6^-]^+$, 559 $[M - 2PF_6^-]^{2+}$, 325 $[M - 3PF_6^-]^{3+}$. *Anal*. Calc. for $C_{45}H_{57}N_9S_6CoP_3F_{18}$: C, 38.33; H, 4.07; N, 8.94. Found: C, 38.38; H, 4.05; N, 8.94%.

4.2.6. Compound (7)

Compound (**2**) (5 g, 2 eqv.) and α,α′-dibromo-*p*-xylene (3.2 g, 1 eqv.) were dissolved in acetonitrile (100 ml) and the solution was stirred under reflux overnight. The solvent was removed and a yellow oily solid (7 g, 86% yield) was obtained after drying under vacuum.

^{1}H NMR (300 MHz, CD_3OD, 288 K) δ = 9.19 (s, 2H, imidazolium), 8.36 (s, 2H, imine), 7.72 (m, 4H, benzyl), 7.70 (m, 4H, aromatic), 7.61 (m, 4H, aromatic), 7.45 (m, 6H, benzyl), 5.38 (s, 4H, xylene–CH_2–), 4.38 (t, 6.9 Hz, 4H, N–CH_2–), 3.67 (t, 6.9 Hz, 4H, –CH_2–N), 2.28 (quintet, 6.9 Hz, 4H, –CH_2–). MS (ESI positive ion, MeOH): *m/z* 611 $[M–Br^-]^+$, 265 $[M–2Br^-]^{2+}$.

4.2.7. Compound (8)

Compound (**2**) (0.68 g, 2 eqv.) and 2,7-bis(bromomethyl)naphthalene (0.5 g, 1 eqv.) were dissolved in acetonitrile (100 ml) and the solution was stirred under reflux overnight. The solvent was removed and a yellow oily solid (1 g, 84% yield) was obtained after drying under vacuum.

^{1}H NMR (300 MHz, CD_3OD, 288 K) δ = 9.12 (s, 2H, imidazolium), 8.35 (s, 2H, imine), 7.4–8.0 (m, 20H, aromatic), 5.5–5.6 (m, 4H, xylene–CH_2–), 4.31 (t, 6.5 Hz, 4H, N–CH_2–), 2.96 (t, 6.5 Hz, 4H, –CH_2–N), 2.23 (m, 4H, –CH_2–). MS (ESI positive ion, MeOH): *m/z* 659 $[M–Br^-]^+$, 290 $[M–2Br^-]^{2+}$.

4.2.8. Compound (9)

Compound (**7**) (7 g) was dissolved in methanol (50 ml) and sodium borohydride (1 g) was added portionwise to the stirring solution. The mixture was allowed to stir under nitrogen for 2 h and a saturated solution of ammonium hexafluorophosphate (10 ml) was added. The volume of methanol was reduced under vacuum and the resulting precipitate was collected, washed with water and dried. A pale yellow solid (7 g, 84% yield) was obtained after drying.

^{1}H NMR (300 MHz, CD_3CN, 288 K) δ = 8.53 (s, 2H, imidazolium), 7.3–7.4 (m, 18H, aromatic), 5.29 (s, 4H, xylene–CH_2–), 4.23 (t, 7.2 Hz, 4H, N–CH_2–), 3.71 (s, 4H, benzyl–CH_2–), 2.56 (t, 7.2 Hz, 4H, –CH_2–N), 1.96 (m, 4H, –CH_2–). ^{13}C NMR (300 MHz, CD_3CN, 288 K) δ = 141.3, 137.0, 136.1, 130.5, 130.2, 129.6, 128.3, 124.3, 123.6, 54.2, 53.5, 48.8, 45.9, 30.2 ppm. MS (ESI positive ion, MeOH): *m/z* 679 $[M - PF_6^-]^+$, 267 $[M - 2PF_6^-]^{2+}$.

4.2.9. Compound (10)

Compound (**8**) (1 g) was dissolved in methanol (50 ml) and sodium borohydride (0.2 g) was added portionwise to the stirring solution. The mixture was allowed to stir under nitrogen for 2 h and a saturated solution of ammonium hexafluorophosphate (10 ml) was added. The volume of methanol was reduced under vacuum and the resulting precipitate was collected, washed with water and dried. A pale yellow solid (1 g, 84% yield) was obtained after drying.

^{1}H NMR (300 MHz, CD_3CN, 288 K) δ = 8.51 (s, 2H, imidazolium), 7.2–8.0 (m, 20H, aromatic), 5.45 (s, 4H, xylene–CH_2–), 4.25 (t, 6.6 Hz, 4H, N–CH_2–), 3.65 (s, 4H, benzyl–CH_2–), 2.53 (t, 6.6 Hz, 4H, –CH_2–N),d 1.97 (m, 4H, –CH_2–). ^{13}C NMR (300 MHz, CD_3CN, 288 K) δ = 142.2, 137.1, 134.3, 133.6, 130.4, 130.2, 130.3, 129.7, 129.6, 129.5, 128.8, 128.1, 124.3, 123.8, 54.4, 54.1, 49.0, 46.0, 30.5 ppm. MS (ESI positive ion, MeOH): *m/z* 729 $[M - PF_6^-]^+$, 292 $[M - 2PF_6^-]^{2+}$.

4.2.10. Macrocyclic transition metal dtc imidazolium complexes with xylene spacer (11)

Compound (**9**) (0.5 g), triethylamine (0.1 g) and carbon disulfide (0.1 g) were dissolved in acetonitrile (50 ml) and stirred for 10 min. The transition metal salt (1 eqv.) was added to the solution and the mixture was stirred overnight. The volume of solvent was reduced and a

saturated aqueous solution of ammonium hexafluorophosphate (10 ml) was added. The resulting precipitate was collected and washed with diethyl ether.

(**11a**) Ni: A pale green solid (0.6 g, 95% yield) was collected. ^{1}H NMR (300 MHz, CD_3CN, 288 K) δ = 8.78 (s, 2H, imidazolium), 7.3–7.5 (m, 14H, aromatic), 7.24 (s, 4H, xylene), 5.37 (s, 4H, xylene–CH_2–), 4.87 (s, benzyl–CH_2–), 4.19 (br, 4H, N–CH_2–), 3.51 (br, 4H, –CH_2–N), 2.16 (br, 4H, –CH_2–). ^{13}C NMR (300 MHz, CD_3CN, 288 K) δ = 208.9, 137.5, 135.8, 135.6, 130.3, 130.0, 129.7, 129.3, 125.1, 123.6, 53.5, 52.9, 47.9, 46.0, 27.9 ppm. MS (ESI positive ion, MeOH): *m/z* 887 $[M - PF_6^-]^+$, 371 $[M - 2PF_6^-]^{2+}$. *Anal.* Calc. for $C_{36}H_{40}N_6S_4NiP_2F_{12}$: C, 41.83; H, 3.90; N, 8.13. Found: C, 42.27; H, 4.01; N, 8.09%.

(**11b**) Cu: A brown solid (0.6 g, 95% yield) was collected. MS (ESI positive ion, MeOH): *m/z* 892 $[M - PF_6^-]^+$, 373 $[M - 2PF_6^-]^{2+}$. *Anal.* Calc. for $C_{36}H_{40}N_6S_4CuP_2F_{12}$: C, 41.64; H, 3.88; N, 8.09. Found: C, 41.59; H, 3.87; N, 8.27%.

(**11c**) Zn: A pale yellow solid (0.6 g, 95% yield) was collected. ^{1}H NMR (300 MHz, CD_3CN, 288 K) δ = 8.68 (s, 2H, imidazolium), 7.3–7.4 (br, 18H, aromatic), 5.32 (s, 4H, xylene–CH_2–), 5.12 (s, benzyl–CH_2–), 4.16 (br, 4H, N–CH_2–), 3.81 (br, 4H, –CH_2–N), 2.22 (br, 4H, –CH_2–). ^{13}C NMR (300 MHz, CD_3CN, 288 K) δ = 209.0, 137.5, 137.1, 135.7, 130.5, 130.1, 129.1, 128.7, 124.9, 123.5, 58.1, 53.6, 51.6, 48.4, 27.8 ppm. MS (ESI positive ion, MeOH): *m/z* 893 $[M - PF_6^-]^+$. *Anal.* Calc. for $C_{36}H_{40}N_6S_4ZnP_2F_{12}$: C, 41.56; H, 3.88; N, 8.08. Found: C, 43.80; H, 4.28; N, 8.34%.

*4.2.11. Macrocyclic transition metal dtc imidazolium complexes with naphthalene spacer (**12**)*

Compound (**10**) (0.15 g), triethylamine (0.05 g) and carbon disulfide (0.05 g) were dissolved in acetonitrile (50 ml) and stirred for 10 min. The transition metal salt (1 eqv.) was added to the solution and the mixture was stirred overnight. The volume of solvent was reduced and a saturated aqueous solution of ammonium hexafluorophosphate (10 ml) was added. The resulting precipitate was collected and washed with diethyl ether.

(**12a**) Ni: A pale green solid (0.15 g, 81% yield) was collected. ^{1}H NMR (300 MHz, CD_3CN, 288 K) δ = 8.56 (s, 2H, imidazolium), 7.2–8.0 (m, 20H, aromatic), 5.48 (br, 4H, naphthyl–CH_2–), 4.79 (br, benzyl–CH_2–), 4.14 (br, 4H, N–CH_2–), 3.53 (br, 4H, –CH_2–N), 2.10 (br, 4H, –CH_2–). MS (ESI positive ion, MeOH): *m/z* 937 $[M - PF_6^-]^+$, 396 $[M]^{2+}$. *Anal.* Calc. for $C_{40}H_{42}N_6S_4NiP_2F_{12}$: C, 44.33; H, 3.91; N, 7.76. Found: C, 44.25; H, 4.39; N, 7.75%.

(**12b**) Cu: A brown solid (0.15 g, 81% yield) was collected. MS (ESI positive ion, MeOH): *m/z* 942 $[M - PF_6^-]^+$, 398 $[M]^{2+}$. *Anal.* Calc. for $C_{40}H_{42}N_6S_4CuP_2F_{12}$: C, 44.14; H, 3.89; N, 7.72. Found: C, 43.87; H, 3.89; N, 8.06%.

*4.2.12. Compound (**13**)*

Compound (**2**) (0.56 g, 3 eqv.) and 1,3,5-tri(chloromethyl)-2,4,6-triethylbenzene [15] (0.3 g, 1 eqv.) were dissolved in acetonitrile (100 ml) and the solution was stirred under reflux overnight. The solvent was removed and a yellow oily solid (0.6 g, 65% yield) was obtained after drying under vacuum.

^{1}H NMR (300 MHz, CD_3OD, 288 K) δ = 9.77 (s, 3H, imidazolium), 8.24 (s, 3H, imine), 7.4–7.4 (m, 21H, aromatic), 5.36 (s, 6H, benzene–CH_2–), 4.42 (t, 7.0 Hz, 6H, N–CH_2–), 3.58 (m, 6H, –CH_2–N), 2.40 (m, 6H, benzene–CH_2–CH_3), 2.12 (m, 6H, –CH_2–), 1.06 (m, 9H, CH_3). MS (ESI positive ion, MeOH): *m/z* 910 $[M - Cl^-]^+$, 438 $[M - 2Cl^-]^{2+}$.

*4.2.13. Compound (**14**)*

Compound (**13**) (0.6 g) was dissolved in methanol (50 ml) and sodium borohydride (0.2 g) was added portionwise to the stirring solution. The mixture was allowed to stir under nitrogen for 2 h and a saturated solution of ammonium hexafluorophosphate (10 ml) was added. The volume of methanol was reduced under vacuum and the resulting precipitate was collected, washed with water and dried. A pale yellow solid (0.5 g, 62% yield) was obtained after drying.

^{1}H NMR (300 MHz, CD_3CN, 288 K) δ = 8.27 (s, 3H, imidazolium), 7.2–7.5 (m, 21H, aromatic), 5.38 (s, 6H, benzene–CH_2–), 4.23 (t, 6.6 Hz, 6H, N–CH_2–), 3.68 (s, 6H, benzyl–CH_2–N), 2.54 (m, 12H, benzene–CH_2–CH_3 and –CH_2–N), 1.12 (m, 6H, –CH_2–), 0.95 (t, 7.2 Hz, 9H, CH_3). ^{13}C NMR (300 MHz, CD_3CN, 288 K) δ = 149.5, 142.1, 136.3, 129.6, 128.1, 124.2, 123.4, 54.4, 49.1, 48.4, 46.1, 30.8, 24.6 ppm. MS (ESI positive ion, MeOH): *m/z* 1136 $[M - PF_6^-]^+$, 495 $[M - 2PF_6^-]^{2+}$.

*4.2.14. Co(III) dtc imidazolium cryptand complex (**15**)*

Compound (**14**) (0.2 g), triethylamine (0.05 g) and carbon disulfide (0.05 g) were dissolved in acetonitrile (50 ml) and stirred for 10 min. Cobalt(II) chloride (0.05 g, 1 eqv.) was added to the solution and the mixture was stirred overnight. The volume of solvent was reduced and a saturated aqueous solution of ammonium hexafluorophosphate (10 ml) was added. The resulting precipitate was collected and washed with diethyl ether. A green solid (0.2 g, 82% yield) was collected.

^{1}H NMR (300 MHz, CD_3CN, 288 K) δ = 7.32 (br, 21H, aromatic), 5.37 (br, 6H, benzene–CH_2–), 4.13 (br, 6H, N–CH_2–), 3.43 (br, 6H, benzyl–CH_2–N), 3.29 (br, 6H, –CH_2–N), 1.95 (br, 6H, –CH_2–), 1.13 (br, 9H, CH_3). MS (ESI positive ion, MeOH): *m/z* 637 $[M - 2PF_6^-]^{2+}$, 377 $[M]^{3+}$. *Anal.* Calc. for $C_{57}H_{69}N_9S_6CoP_3F_{18}$: C, 43.70; H, 4.44; N, 8.05. Found: C, 42.45; H, 4.51; N, 7.75%.

Acknowledgements

We gratefully acknowledge the EPSRC for a studentship (W.W.H.W.).

References

[1] (a) P.D. Beer, P.A. Gale, Angew. Chem., Int. Ed. Engl. 40 (3) (2001) 486;
(b) P.A. Gale, Coord. Chem. Rev. 240 (2003) 191;
(c) F.P. Schmidtchen, M. Berger, Chem. Rev. 97 (1997) 1609;
(d) P.D. Beer, D.K. Smith, Progr. Inorg. Chem. 46 (1997) 1;
(e) J.L. Atwood, K.T. Holman, J.W. Steed, Chem. Commun. (1996) 1401;
(f) A. Bianchi, K. Bowman-James, E. García-Espãna (Eds.), Supramolecular Chemistry of Anions, Wiley-VCH, Chichester, 1997;
(g) P.D. Beer, Acc. Chem. Res. 31 (1998) 71;
(h) A.P. de Silva, H.Q.N. Guarantee, T. Gunnlaugsson, A.J. Huxley, C.P. McCoy, J.T. Rademacher, T.R. Rice, Chem. Rev. 97 (1997) 1515;
(i) S.L. Tobey, E.V. Anslyn, J. Am. Chem. Soc. 125 (48) (2003) 4807;
(j) K.J. Wallace, W.J. Belcher, D.R. Turner, K.F. Syed, J.W. Steed, J. Am. Chem. Soc. 125 (2003) 9699.

[2] (a) P.D. Beer, J. Cadman, Coord. Chem. Rev. 205 (2000) 131;
(b) P.D. Beer, E.J. Hayes, Coord. Chem. Rev. 240 (1–2) (2003) 167.

[3] P.D. Beer, F. Szemes, V. Balzani, C.M. Sala, M.G.B. Drew, S.W. Dent, M. Maestri, J. Am. Chem. Soc. 49 (1997) 11864.

[4] (a) S. Ramos, E. Alcalde, G. Doddi, P. Mencarelli, L. Perez-Garcia, J. Org. Chem. 67 (24) (2002) 8463;
(b) E. Alcalde, S. Ramos, L. Perez-Garcia, Org. Lett. 1 (7) (1999) 1035;
(c) R. Vilar, Angew. Chem., Int. Ed. 42 (13) (2003) 1460.

[5] (a) R.W. Saalfrank, E. Uller, B. Demleitner, I. Bernt, Struct. Bonding 96 (2000) 149;
(b) P.J. Stang, S.R. Seidel, Acc. Chem. Res. 35 (2002) 972;
(c) R.W. Saalfrank, I. Bernt, Curr. Opin. Solid State Mater. Sci. 3 (1998) 407;
(d) M. Fujita, Chem. Soc. Rev. 27 (1998) 417;
(e) S. Leininger, B. Olenyuk, P.J. Stang, Chem. Rev. 100 (2000) 853;
(f) C.J. Jones, Chem. Soc. Rev. 27 (1998) 289.

[6] O.D. Fox, M.G.B. Drew, P.D. Beer, Angew. Chem., Int. Ed. Engl. 39 (2000) 136.

[7] M.E. Padilla-Tosta, O.D. Fox, M.G.B. Drew, P.D. Beer, Angew. Chem., Int. Ed. Engl. 40 (2001) 4235.

[8] (a) P.D. Beer, N. Berry, M.G.B. Drew, O.D. Fox, M.E. Padilla-Tosta, S. Patell, Chem. Commun. (2001) 199;
(b) N.G. Berry, M.D. Pratt, O.D. Fox, P.D. Beer, Supramolecular Chem. 13 (2001) 677.

[9] P.D. Beer, A.G. Cheetham, M.G.B. Drew, O.D. Fox, E.J. Hayes, T.D. Rolls, J. Chem. Soc., Dalton Trans. 4 (2003) 603.

[10] P.D. Beer, N.G. Berry, A.R. Cowley, E.J. Hayes, E.C. Oates, W.W.H. Wong, Chem. Commun. (2003) 2408.

[11] (a) P. Wasserscheid, T. Welton (Eds.), Ionic Liquids in Synthesis, Wiley-VCH, Weinheim, Germany, 2003;
(b) F. Endres, T. Welton, Inorganic Synthesis (2003) 289.

[12] W.A. Herrmann, L.J. Goossen, C. Koecher, G.R.J. Artus, Angew. Chem., Int. Ed. Engl. 35 (1996) 2805.

[13] S.K. Kim, N.J. Singh, S.J. Kim, H.G. Kim, J.K. Kim, J.W. Lee, K.S. Kim, J. Yoon, Org. Lett. 12 (2003) 2083.

[14] S. Yun, H. Ihm, H.G. Kim, C.W. Lee, B. Indrajit, K.S. Oh, Y.J. Gong, J.W. Lee, J. Yoon, H.C. Lee, K.S. Kim, J. Org. Chem. 68 (2003) 2467.

[15] Synthesised by following procedure from K.V. Kilway, J.S. Siegel, Tetrahedron 57 (17) (2001) 3615.

[16] D. Oktavec, B. Siles, J. Stefanec, E. Korgova, J. Garaj, Czechoslov. Chem. Commun. 45 (1980) 791.

[17] (a) R.D. Webster, G.A. Heath, A.M. Bond, J. Chem. Soc., Dalton Trans. (2001) 3189;
(b) C.K. Jorgensen, J. Inorg. Nucl. Chem 24 (1962) 1571.

[18] R.A. Binstead, A.D. Zuberbühler, Specfit Global Analysis, Version 2.90X; Binstead, R.A., Specfit, 32, 2000.

Available online at www.sciencedirect.com
SCIENCE DIRECT®
Polyhedron 23 (2004) 2831–2840
POLYHEDRON
www.elsevier.com/locate/poly

Coordination and reactivity of acetonitrile in tungsten(IV) complexes: oxidation, methylation and dimerization of coordinated acetonitrile

Jeffrey L. Cross, Andrew D. Garrett, Todd W. Crane, Peter S. White, Joseph L. Templeton *

Department of Chemistry, University of North Carolina at Chapel Hill, Chapel Hill, NC 27599-3290, USA

Received 6 May 2004; accepted 10 September 2004
Available online 26 October 2004

We are grateful for the extensive seminal contributions of Malcolm Green to the field of organometallic chemistry. The positive impact of both his documented productivity and his legendary personality is difficult to overestimate

Abstract

Reaction of Tp′W(O)(CO)(I) (**1**) with silver trifluoromethanesulfonate (silver triflate, AgOTf) in dichloromethane generates Tp′W(O)(CO)(OTf) (**2**) with triflate in the coordination sphere. Dissolution of neutral triflate adduct **2** in acetonitrile immediately produces the cationic tungsten(IV) nitrile complex [Tp′W(O)(NCMe)(CO)][OTf] (**3**). Exchange of the triflate anion in **3** for the large, non-coordinating tetrakis[3,5-bis(trifluoromethyl)phenyl]borate anion, $[BAr'_4]^-$, produces the isolable salt [Tp′W(O)(NCMe)(CO)][BAr'_4] (**4**). Photolysis of Tp′W(O)(CO)(I) complex (**1**) in acetonitrile promotes loss of carbon monoxide and generates the neutral tungsten(IV) nitrile complex Tp′W(O)(I)(NCMe) (**5**). Spectroscopic data for **5** is consistent with formation of an η^2-bound nitrile ligand. Chromatography of complex **5** on alumina led to oxidation to form an acylimido complex, Tp′W(O)(I)(NC(O)Me) (**6**). A dimeric complex, Tp′(O)(I)W(NC(Me)C(Me)N)W(I)(O)Tp′ (**7**) resulting from reductive coupling of two nitrile ligands was also isolated following alumina chromatography. Methylation of η^2-nitrile complex **5** by MeOTf generates the cationic η^2-iminoacyl complex [Tp′W(O)(I)(MeNCMe)][OTf] (**9**).
© 2004 Elsevier Ltd. All rights reserved.

Keywords: η^2-nitrile; Tungsten; Oxo; Oxidation; Methylation; Dimerization

1. Introduction

Transition metal nitrile complexes are ubiquitous in organometallic chemistry as versatile precursors for a variety of chemical transformations [1]. Additionally, functionalization of nitrile substrates is a valuable route to nitrogen containing compounds. Activation of an organonitrile molecule by coordination to a metal center is one method for promoting chemical elaboration of nitrile substrates [2]. Stepwise reduction of acetonitrile bound to a metal center is representative of the reaction sequences accessible beginning with coordinated nitrile ligands [3]. Upon coordination to a chiral tungsten metal center, acetonitrile may be systematically reduced by alternate addition of hydride anions and protons to the nitrile ligand to generate intermediates including azavinylidene and imine complexes. Addition to imine ligands has been shown to be stereoselective in multiple cases [4]. The synthesis of chiral amines from nitrile reagents is of widespread importance in organic chemistry [5].

The vast majority of transition metal nitrile complexes display simple σ-coordination of the nitrile ligand to the metal through the nitrogen lone pair [1], but a

* Corresponding author. Tel.: +919 9664575; fax: +919 8438005.
E-mail address: jaetemp@unc.edu (J.L. Templeton).

0277-5387/$ - see front matter © 2004 Elsevier Ltd. All rights reserved.
doi:10.1016/j.poly.2004.09.008

number of complexes exhibiting η^2-coordination of nitrile ligands are also known. Although rare compared to σ-coordination, binding of the nitrile through the N≡C triple bond, in an η^2-coordination, is well established [6–11,15].

When bound to a metal center through the C≡N triple bond, a nitrile ligand may act as both a π-acid ligand and as a π-base ligand in analogy to alkyne ligands [12]. One of the C≡N triple bond π-orbitals may donate electron density into a metal dπ orbital while a perpendicular C≡Nπ* orbital may accept electron density from a different metal dπ orbital [13].

Several insightful early reports identifying η^2-nitrile complexes were based on infrared spectroscopy. While σ-coordination of a nitrile ligand usually causes the frequency of ν(NC) to increase slightly relative to the free ligand [1], upon η^2-coordination to a metal the ν(NC) stretching frequency drops to dramatically lower wavenumbers. A common complication, however, is that the infrared absorption coefficient of η^2-bound nitrile ligands is often small, and frequently the ν(NC) stretch cannot be observed and identified unambiguously in the IR spectrum [7e].

In addition to IR spectroscopy, NMR spectroscopy can help distinguish between nitrile coordination modes. In the ^{1}H NMR spectrum, methyl singlets for σ-bound acetonitrile have typically been observed in the 2–3 ppm range; recall that the signal for the free acetonitrile appears at δ 1.94 ppm. For η^2-bound acetonitrile the methyl resonances may be shifted further downfield, by roughly one or two ppm, so that proton NMR signals for the nitrile methyl group of η^2–acetonitrile complexes are commonly observed between 3 and 4 ppm [6–11]. A nice example is provided by the two isomeric $[MoCl(NCMe)(dmpe)_2]^+$ complexes reported by Wilkinson and co-workers [7e], where the nitrile methyl signal was observed at 2.10 ppm for σ-coordination while the η^2-coordination mode produced a methyl resonance at 3.20 ppm. Because the ranges for σ- and η^2-coordination can overlap significantly in some cases, interpretation of the ^{1}H NMR chemical shift for nitrile ligands should be considered as indicative rather than as definitive. A recent well documented η^2–acetonitrile complex of nickel exhibits a methyl signal at 2.42 ppm, so no simple line of demarcation is provided by ^{1}H NMR spectroscopy [15a]. Supplemental characterization, such as by ^{13}C NMR, is generally required for decisive assignment of nitrile coordination modes.

For transition metal alkyne complexes the ^{13}C NMR chemicals shifts of the coordinated carbons have been used to assess the extent of electron donation from alkyne ligands [12]. Analogous to this technique, ^{13}C NMR spectroscopy may be used to discern nitrile coordination modes and electronic structure in nitrile complexes. In 1991, Green et al. [6c] exploited the utility of ^{13}C NMR spectroscopy for the detection of η^2-nitrile ligands. In complexes with σ-bound nitrile ligands the nitrile carbon resonates in the range of 120–150 ppm. In contrast, complexes possessing η^2-nitrile ligands that act as formal two-electron donors have ^{13}C shifts between δ 160 and 180 [6,7]. Here again the nickel system provides an example near the overlap region in that the nitrile carbon of (dippe)-Ni(η^2-CH_3CN) resonates at 160 ppm, not far from the sigma bond range [15a].

Akin to alkyne ligands, η^2-nitrile ligands may serve as variable electron donors (2–4 electrons). A number of tungsten complexes are known in which the nitrile ligand acts as a formal four-electron donor, and the nitrile carbons in these complexes resonate between 230 and 240 ppm [8–10]. More recently, Etienne [11] has reported η^2-nitrile complexes of niobium in which the η^2-nitrile acts as a formal three-electron donor ligand. Carbon-13 chemical shifts for these three-electron donor ligands are between 175 and 185 ppm [11].

X-ray crystallography remains the definitive characterization technique for identifying η^2-nitrile complexes [7–10,15]. X-ray characterization of $(Cp)_2$ Mo(NCMe) in 1986 showed η^2-coordination of the nitrile moiety in which the nitrile methyl group was bent away from the metal center at an angle of 138° relative to the C≡N bond [7g]. The R–C≡N moiety in this structure resembles the R–C≡C fragments found in η^2-alkyne complexes [12]. Other η^2-nitrile structures display this same type of bent nitrile ligand geometry [7–10,15].

Relatively little is known about the chemistry of transition metal η^2-nitrile complexes. In recent years they have been utilized in the investigation of C–C bond cleavage reactions. Parkin and co-workers [14] formed molybdenum methyl cyanide products from acetonitrile and ansa-molybdenocene reagents. In a particularly complete study, Garcia and Jones [15] have reported equilibria between an η^2-nitrile nickel(0) complex, (dippe)Ni(η^2-ArCN), and a C–C bond cleavage product containing a Ni(Ar)(CN) fragment. Transition metal η^2-nitrile complexes have been suggested as possible intermediates in other C–C bond [16] and C–H bond activation reactions [17].

This paper reports the synthesis and spectroscopic characterization of W(IV) acetonitrile complexes. The acetonitrile ligand in one of these complexes, believed to be η^2-coordinated, is capable of adding oxygen, undergoing reductive C–C bond formation, or serving as a nucleophile toward methyl triflate.

2. Results and discussion

2.1. A cationic tungsten(IV) nitrile complex

Reaction of purple Tp′W(O)(CO)(I) (**1**) with 1 equiv. of AgOTf in methylene chloride over 1 h generates a red

solution containing the triflate complex Tp′W(O)(CO)(OTf) (**2**) (Eq. (1)). Associated with this reaction is a small shift of the carbonyl stretching frequency from ν(CO) = 1991 cm^{-1} for the starting material to ν(CO) = 1996 cm^{-1}. The ^1H NMR displays three methine and six methyl signals consistent with Tp′ bound to a chiral metal center. The ^{19}F NMR shows a singlet for the triflate CF_3 group at −77.1 ppm. The carbonyl carbon and trifluoromethyl carbon appear at 271.4 and 119.6 ppm ($^1J_{CF}$ = 320 Hz), respectively. Under aerobic conditions complex **2** decomposes rapidly in solution, while it decomposes slowly, over a period of days, in the solid state. Under an inert atmosphere the complex is stable in the solid state for weeks. Efforts to purify the triflate complex by chromatography led to decomposition.

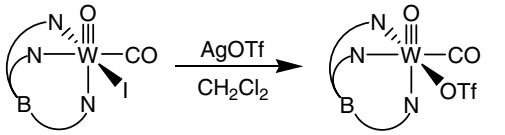

1 **2** (1)

Triflate complex **2** reacts cleanly with acetonitrile. Room temperature dissolution of the red triflate complex **2** in acetonitrile results in a deep purple solution of the cationic nitrile complex [Tp′W(O)(CO)(NCMe)][OTf] (**3**) (Eq. (2)). The IR spectrum of this solution shows a shift of the CO stretching frequency from 1996 cm^{-1} in the starting material to 2023 cm^{-1} in the product, consistent with formation of a cationic complex. The ^1H NMR of the solution shows signals typical of a Tp′ ligand in a chiral environment and an additional methyl signal for acetonitrile at 3.23 ppm.

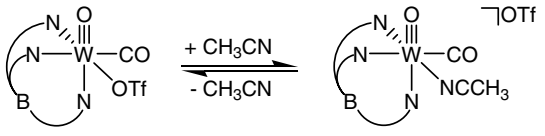

2 **3** (2)

Isolation of this cationic complex has proven difficult. Either removal of solvent by vacuum evaporation or attempts to induce precipitation with non-polar solvents results in regeneration of the precursor triflate complex **2**. Replacement of the triflate anion with a larger and less nucleophilic anion might allow isolation of the cationic complex and allow comparison with independently synthesized [Tp′W(O)(CO)(NCMe)][BAr'_4] [18] prepared by acidification of Tp′W(O)(CO)(Me) in acetonitrile. Indeed, metathesis of the triflate counterion by the large, non-coordinating anion tetrakis-[3,5-bis(trifluoromethyl)phenyl]borate, [BAr'_4]$^-$, yields the readily isolable salt [Tp′W(O)(CO)(NCMe)]-[BAr'_4] (**4**) (Eq. (3)). The IR spectrum of **4** also shows the CO stretching frequency at 2023 cm^{-1}. Proton NMR characterization of **4** immediately after synthesis shows a signal for the nitrile methyl group at 3.07 ppm.

Table 1
Crystallographic data collection parameters

	4	**6**	**7**
Formula	$C_{50}H_{37}B_2N_7O_2F_{24}W$	$C_{34}H_{50}B_2N_{14}O_4I_2W_2$	$C_{34}H_{50}B_2N_{14}O_2I_2W_2$
Molecular weight	1444.32	1361.98	1329.998
Crystal system	triclinic	monoclinic	monoclinic
Space group	$P\bar{1}$	$P2_1/n$	$P2_1/c$
a (Å)	14.12678(3)	13.8320(6)	9.3027(3)
b (Å)	14.2136(3)	15.7885(7)	17.0513(6)
c (Å)	15.7139(3)	25.9304(12)	16.2019(6)
α (°)	73.573(1)	90	90
β (°)	86.318(1)	104.0060(10)	98.221(1)
γ (°)	75.553(1)	90	90
V (Å^3)	2939.18(10)	5494.5(4)	2543.59(15)
Z	2	4	2
$D_{calc.}$ (Mg/m^3)	1.632	1.646	1.954
F(000)	1414.53	2585.21	1426.67
Crystal dimensions (mm)	0.20 × 0.20 × 0.20	0.20 × 0.20 × 0.05	0.10 × 0.10 × 0.10
Temperature (°C)	−100	−100	−100
2θ Range (°)	5–140	5–50	5–50
μ (mm^{-1})	4.75	5.36	5.99
Scan mode	ω	ω	ω
Total number of reflections	39227	28291	11165
Total number of unique reflections	10103	9676	4470
Number of reflections with ($I > 2.5\sigma(I)$)	8858	7567	3913
R_F (%)	0.046	0.059	0.050
R_W (%)	0.061	0.077	0.061
Goodness-of-fit	2.0852	2.79	2.4291

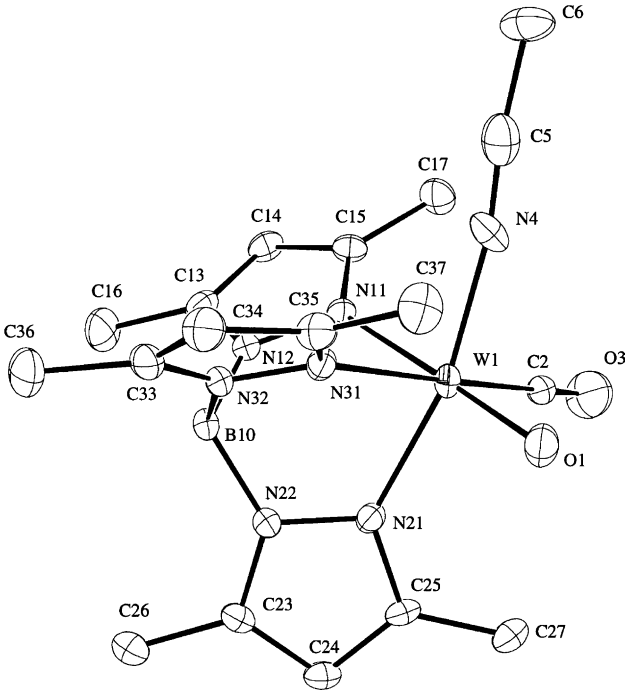

Fig. 1. ORTEP diagram of $[Tp'W(O)(CO)(NCMe)]^+$ (**4**).

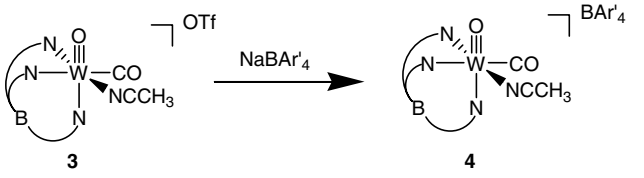

(3)

Crystals suitable for X-ray structural characterization (see Table 1) were grown by diffusion of pentane into a concentrated methylene chloride solution of **4** (Fig. 1). [1] In the solid state structure of **4** the nitrile ligand is coordinated to the tungsten metal center in an σ-fashion, with a nearly linear acetonitrile N(4)–C(5)–C(6) skeleton (173.9°). The W(1)–N(4) and N(4)–C(5) bond lengths are 2.017 and 1.197 Å, respectively (see Table 2). The ^{13}C NMR spectrum of the crystals of **4** show the nitrile carbon at 153.5 ppm. This value is near the border at the low end of the chemical shift range typical of simple nitrile σ-donor ligands, but it is nonetheless consistent with the presence of a σ-bound nitrile ligand, and likewise for the proton signal at 3.07 ppm. Thus for the cationic W(IV) complex only σ-bound acetonitrile has been observed. Replacement of the acetonitrile ligand in **4** by other neutral ligands has not been observed.

2.2. Neutral nitrile complexes

Photolysis of purple-pink W(IV) reagent **1** in acetonitrile for 3 h results in the formation of a dark orange solution that shows no terminal carbonyl absorbances in the IR spectrum. Photolytic excitation, loss of the CO ligand, and subsequent coordination of acetonitrile would yield the neutral tungsten complex, Tp′W(O)(I)(NCMe) (**5**) (Eq. (4)). The ^1H NMR of the orange reaction product shows signals indicative of Tp′ bound to a chiral metal center and an additional signal at 3.85 ppm for a nitrile methyl group (cf. 3.07 ppm for cationic nitrile complex **4**). In the ^{13}C NMR spectrum the nitrile carbon resonates downfield at 184.8 ppm (cf. 153 ppm for cationic nitrile complex **4**). The downfield shift of both the methyl group in the ^1H NMR spectrum and the nitrile carbon in the ^{13}C NMR spectrum point toward η^2-coordination of the acetonitrile.

Table 2
Selected bond distances and angles for $[Tp'W(O)(CO)(NCMe)][BAr'_4]$ (**4**)

Bond distances			
W(1)–O(1)	1.781(4)	W(1)–N(4)	2.017(5)
W(1)–C(2)	2.080(6)	N(4)–C(5)	1.197(10)
C(2)–O(3)	1.067(8)	C(5)–C(6)	1.497(10)
W(1)–N(11)	2.220(4)	W(1)–N(31)	2.145(4)
W(1)–N(21)	2.158(4)		
Bond angles			
O(1)–W(1)–C(2)	91.35(20)	C(2)–W(1)–N(4)	93.64(21)
O(1)–W(1)–N(4)	96.31(19)	N(4)–C(5)–C(6)	173.9(7)

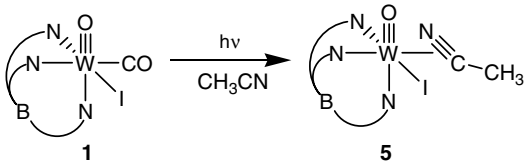

(4)

Reaction chemistry of η^2-nitrile complexes has not yet been extensively probed. As mentioned above, removal of acetonitrile from cationic complex **4** is not easily accomplished. Removal of the nitrile ligand in neutral nitrile complex **5**, however, is facile. Spectroscopic observation of protio-acetonitrile complex **5** in CD_3CN at room temperature reveals slow exchange of the unlabeled nitrile for the deuterated nitrile. In a related W(II) system reported by Young, phenylacetylene displaced acetonitrile in Tp′W(I)(CO)(MeCN) [9a]. For the tungsten(IV) oxo complex **5**, the nitrile ligand may be replaced by phenylacetylene in refluxing THF to give the complementary alkyne complex Tp′W(O)(I)(PhCCH) (**8**) (Eq. (5)). The ^1H NMR spectrum of the reaction mixture, with signature signals for terminal alkyne ligands at 12.3 and 11.0 ppm, shows a 1:1.5 ratio of isomers of complex **8**. These two isomers,related by alkyne rotation, can be separated by column chromatography. Refluxing a single isomer in toluene for two days shows no appreciable conversion to the other isomer, indicating that the barrier to alkyne rotation is >30 kcal/mol. Note that the barrier to alkyne rotation reported for the analogous propyne complex, Tp′W(O)(I)(MeCCH), was 25 kcal/mol [24].

[1] The crystal structure contains the $[BAr'_4]$ anion and disordered pentane with 50% occupancy.

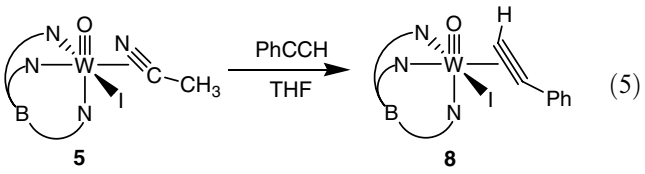

(5)

2.3. Oxidation

Attempts to purify neutral nitrile complex **5** by column chromatography were unsuccessful. However, one red band collected during chromatography on alumina showed signals for a new Tp′ tungsten complex as well as an additional methyl signal intermingled among the Tp′ methyl signals. Crystals of the red complex were grown (see Table 3), and an X-ray structure was obtained (Fig. 2) which identified the unknown complex as the acylimido complex Tp′W(O)(I)(NC(O)Me) (**6**) (Eq. (6)). Since complex **5** does not react with water or alumina under anaerobic conditions, acylimido complex **6** may result from the reaction of **5** with oxygen. The product reflects net addition of a single oxygen atom to the nitrile carbon atom of reagent **5**.

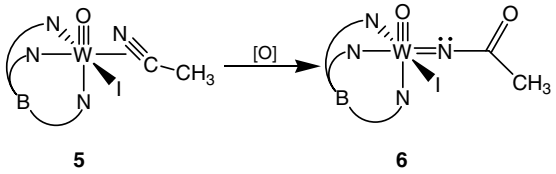

(6)

Young and co-workers [19] previously isolated an acylimido complex of tungsten(IV) which formed via oxidation of coordinated nitrile. Treatment of Tp′W(CO)(I)(η^2-NCMe) with pyridine N-oxide resulted in oxygen atom transfer to the nitrile carbon to form Tp′W(CO)(I)(NC(O)Me) [19]. A similar TpW(CO)(Cl)(NC(O)Me) acylimido tungsten(IV) complex formed by acylation of a terminal nitride ligand has also been reported [20]. Note that the Tp′W(O)(I)(NC(O)Me) product (**6**) formed here is a tungsten(VI) d^0 complex with an oxo ligand in place of the carbonyl ligand present in the acylimido complex prepared by Young [19]. Spectral similarity between some η^2-nitrile ligands and the acylimido fragment in [W=NC(O)CH_3] in both ^{1}H (CH_3 signal around 3–4 ppm) and ^{13}C (acyl C-13 signal around 170–190 ppm) NMR spectra requires caution in differentiating the two ligands.

Table 3
Selected bond distances and angles for Tp′W(O)(I)(NC(O)Me) (**6**)

Bond distances			
W(1)–O(1)	1.690(10)	W(1)–N(2)	1.804(11)
W(1)–I(1)	2.7427(10)	N(2)–C(3)	1.338(18)
C(3)–O(4)	1.219(17)	C(3)–C(5)	1.516(21)
W(1)–N(11)	2.147(10)	W(1)–N(31)	2.306(10)
W(1)–N(21)	2.294(11)		
Bond angles			
O(1)–W(1)–N(2)	102.3(4)	N(2)–C(3)–C(5)	113.5(12)
O(1)–W(1)–I(1)	97.0(3)	N(2)–C(3)–O(4)	123.6(13)
N(2)–W(1)–I(1)	91.6(3)		
Torsion angles			
W(1)–N(2)–C(3)–O(4)	100.5(19)		
W(1)–N(2)–C(3)–C(5)	79.8(17)		

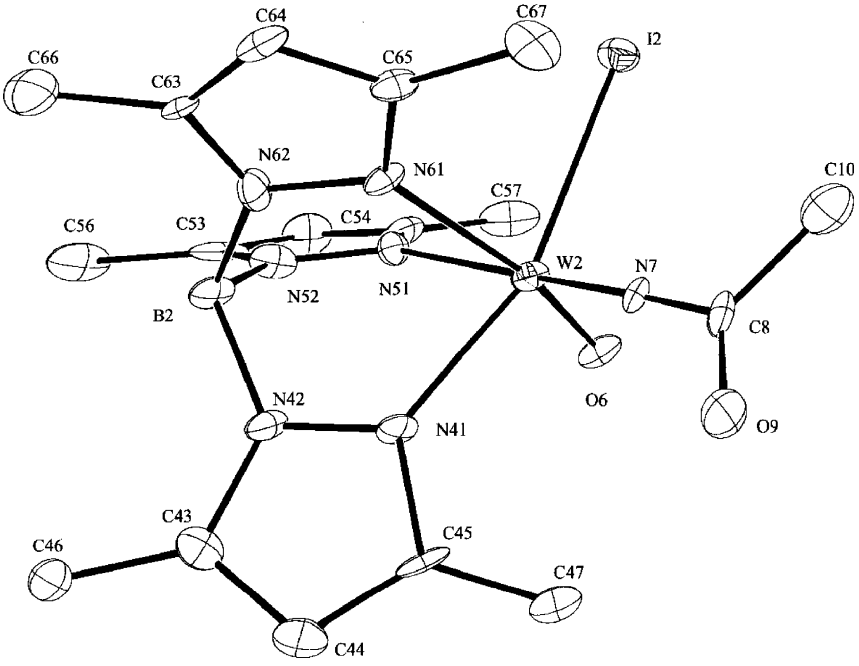

Fig. 2. ORTEP diagram of Tp′W(O)(I)(NC(O)Me) (**6**).

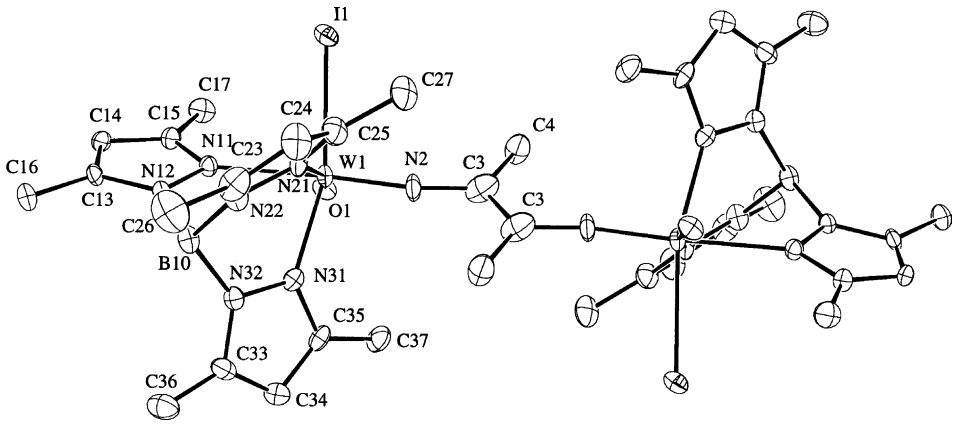

Fig. 3. ORTEP diagram of Tp′(O)(I)W(NC(Me)C(Me)N)W(I)(O)Tp′(**7**).

2.4. Reductive coupling

In addition to the acylimido complex formed during chromatography of neutral complex **5** on alumina, a second complex was identified from the chromatographed reaction mixture by X-ray characterization. This second complex was identified as the tungsten dimer Tp′(O)(I)W(NC(Me)C(Me)N)W(I)(O)Tp′ (**7**) (Fig. 3). [2] Reductive coupling of nitrile ligands has been observed in a number of complexes [21–23]. Dimerization of nitrile complexes can yield a bridging $[NC(Me)]_2$ ligand that has two possible formulations, either [*anti*-butane-2,3-diimino]$^{2-}$, or [(*E*)-butene-2,3-diimido]$^{4-}$ (Fig. 4). The two ligand formulations differ by two electrons and as such are not related by resonance structures. Four-electron reduction to form an enediimido tetraanion linkage from two acetonitrile ligands has been observed more often [22], but there are several examples in the literature of diiminato dianion bridges resulting from two electron reductive coupling of acetonitrile [21,23].

In dinuclear complex **7**, the W(1)–N(2) bond length of 1.791 Å is much shorter than typical W–N single bonds to the Tp′ ligand (2.1–2.3 Å) (Table 4) and is indicative of multiple W–N bond character. The N(2)–C(3) bond length was found to be 1.365(16) Å while the newly formed C(3)–C(3) bond is 1.37(3) Å in length. Based on these bond lengths and compatibility with a W(VI) d^0 formulation, the bridging ligand in **7** is best described as adopting an [(*E*)-butene-2,3-diimido]$^{4-}$ configuration, i.e. a four-electron reductive coupling product.

2.5. Methylation

Addition of 1 equiv. of MeOTf to a methylene chloride solution of neutral nitrile complex **5** generates the cationic iminoacyl complex, [TpW(O)(I)(MeNC-Me)][OTf] (**9**) (Eq. (7)). Complex **9** exists as two isomers in approximately a 5:1 ratio. The major isomer of **9** shows signals for the iminoacyl methyl groups at 4.31 and 3.88 ppm. Two-dimensional NMR spectroscopy indicates that the signal at 4.31 ppm is due to the methyl group bound to the nitrogen while the 3.88 ppm signal is assigned to the methyl group bound to the carbon. In the ^{13}C NMR spectrum, the iminoacyl carbon is observed at 210.6 ppm. The minor isomer of **9** shows the methyl bound to the nitrogen shifted downfield to 4.92 ppm and the methyl group bound to the acyl carbon is shifted upfield to 3.13 ppm.

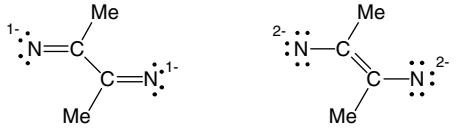

[*anti*-butane-2,3-diimino]$^{2-}$ [(*E*)-butene-2,3-diimido]$^{4-}$

Fig. 4. Possible dimeric configurations for reductive coupling of acetonitrile.

Table 4
Selected bond distances and angles for Tp′(O)(I)W(NC(Me)C-(Me)CN)W(I)(O)Tp′ (**7**)

Bond distances			
W(1)–O(1)	1.763(9)	W(1)–N(2)	1.791(8)
W(1)–I(1)	2.7283(8)	N(2)–C(3)	1.365(16)
W(1)–N(11)	2.292(7)	C(3)–C(4)	1.527(17)
W(1)–N(21)	2.290(8)	C(3)–C(3′)	1.37(3)
W(1)–N(31)	2.150(7)		
Bond angles			
O(1)–W(1)–I(1)	97.7(3)	N(2)–C(3)–C(4)	120.4(11)
O(1)–W(1)–N(2)	101.5(5)	N(2)–C(3)–C(3′)	118.2(12)
N(2)–W(1)–I(1)	99.3(4)	W(1)–N(2)–C(3)	166.1(8)
C(4)–C(3)–C(3′)	121.4(12)		
Torsion angles			
W(1)–N(2)–C(3)–C(4)	172.6(8)		

[2] There is a slight disorder (~10%) in which I(1) and O(1) are reversed. This has been modeled as I(1) 90% occupancy, O(1a) 10% occupancy and O(1) 90% occupancy, I(1a) 10% occupancy.

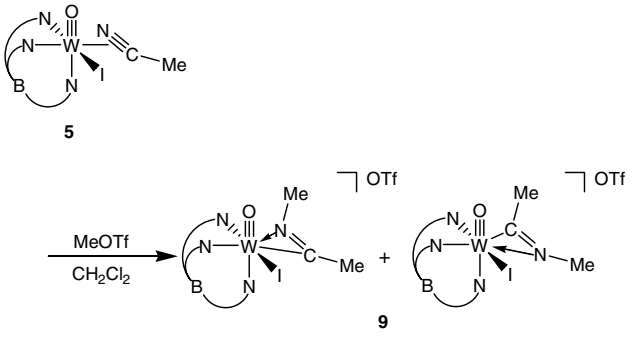

(7)

The iminoacyl ligand is isoelectronic with an alkyne ligand and will coordinate to the d^2 metal center such that the plane of the iminoacyl ligand is perpendicular to the W=O bond (Fig. 5). When bound to the Tp′W(O) fragment the iminoacyl ligand can accept electron density into a C=N π*-orbital from the occupied d_{xy} orbital while donating electron density into the unoccupied d_{xz} orbital from a C≡N π-orbital. In this configuration, perpendicular to the W=O bond, one of the methyl groups of the iminoacyl ligand is placed between two of the pyrazole rings and consequently would experience an upfield shift in the ^{1}H NMR spectrum. Presumably, the major isomer of **9** has the nitrogen methyl group positioned between two of the Tp′ pyrazole rings.

Iminoacyl ligands have been observed in a number of organometallic complexes. Typically these complexes are formed either through the insertion of an isocyanide ligand into a metal–alkyl bond or via electrophilic attack of an alkylating reagent on an isocyanide ligand [25]. The reaction of methyl triflate with an η^2-nitrile reported here is analogous to Parkin's report of methylation of the nitrogen of a π-bound nitrile ligand in the reaction of $(Cp^{t\text{-}Bu})_2Mo(NCMe)$ with MeI to generate the iminoacyl complex $[(Cp^{t\text{-}Bu})_2Mo(MeNCMe)][I]$ [26]. Addition of a proton to an η^2-nitrile three-electron donor ligand was postulated by Etienne as the first step along the route to a metallacyclic product reflecting coupling of the intermediate iminoacyl with an adjacent alkyne ligand [11b].

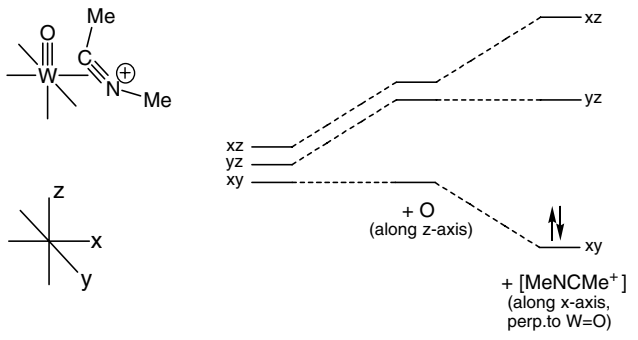

Fig. 5. Qualitative molecular orbital interactions in [Tp′W(O)(I)-(MeNCMe)][OTf] (**9**).

Iminoacyl complex **9** could result either by initial methylation at the metal center to give $[Tp(O)(I)W(Me)(NCMe)]^+$ and subsequent rearrangement to form iminoacyl complex **9** or, more likely, by direct electrophilic attack of the $[Me^+]$ reagent at the nitrile nitrogen. When a nitrile ligand is coordinated in a σ-fashion the nitrogen lone pair is bound to the metal center, and the nitrile carbon is activated towards nucleophilic addition. Less common, but now well established, is electrophilic attack [27] at the nitrile carbon of a σ-bound nitrile ligand. In contrast, when a nitrile ligand is bound in an η^2-fashion the nitrogen lone pair is accessible, and electrophilic attack of the $[Me^+]$ reagent can be easily envisioned.

3. Conclusion

The cationic tungsten(IV) acetonitrile complex $[Tp'W(O)(CO)(NCMe)]^+$ exhibits a σ-bound nitrile ligand and is representative of this large class of transition metal nitrile complexes. In contrast, the neutral tungsten(IV) acetonitrile complex Tp′W(O)(I)(NCMe) exhibits downfield shifts of both the ^{1}H and ^{13}C NMR signals for the acetonitrile ligand which may be indicative of an η^2-bound ligand. Slow displacement of the η^2-nitrile ligand in **5** has been observed with both CD_3CN and phenylacetylene, but more importantly, chromatography of **5** on alumina led to the acylimido complex Tp′W(O)(I)(NC(O)Me) (**6**) and Tp′(O)(I)WNC(Me)C(Me)NW(I)(O)Tp′ (**7**). Additionally, methylation of the nitrile ligand of **5** was accomplished with MeOTf to form the iminoacyl complex [Tp′W(O)(I)(MeNCMe)][OTf] (**9**). The array of reactions reported here suggests that η^2-nitrile ligands will exhibit a rich chemistry not accessible with σ-bound nitrile ligands.

4. Experimental

Reactions were performed under a dry nitrogen atmosphere using standard Schlenk techniques. Hexanes, methylene chloride, and pentane were purified by passage through an activated alumina column under a dry argon atmosphere. Tetrahydrofuran (THF) was distilled from sodium benzophenone ketyl under a dry nitrogen atmosphere. Deuterated solvents were dried using CaH_2 or sodium benzophenone ketyl and deoxygenated using standard freeze–pump–thaw techniques. Acetonitrile was distilled from CaH_2 and stored over 4 Å molecular sieves.

Syntheses of Tp′W(O)(CO)(I) [28] (**1**) and $[Tp'W(O)(CO)(NCMe)][BAr'_4]$ (**4**) [18] have been previously reported. Silver trifluoromethanesulfonate (AgOTf) was obtained and used directly as received

from Aldrich Chemical Company. Sodium tetrakis[3,5-bis(trifluoromethyl)phenyl]borate, ($NaBAr'_4$), was prepared according to literature methods [29].

^1H NMR, ^{13}C NMR, and 2D NMR spectra were recorded on Bruker AMX300, DRX400, AMX400 and Avance500 spectrometers. Infrared spectra were recorded on an ASI Applied Systems ReactIR 1000 FT-IR spectrophotometer. Chemical analyses were performed by Atlantic Microlabs of Norcross, GA.

4.1. Tp′W(O)(CO)(OTf) (2)

In a 100 mL round-bottom flask, Tp′W(O)(CO)(I) (**1**) (0.203 g, 0.311 mmol) was dissolved in 25 mL of methylene chloride. This solution was cannulated into a separate 100 mL round-bottom flask containing AgOTf (0.080 g, 0.311 mmol) stirring in 15 mL methylene chloride. An immediate color change from purple-pink to a red-maroon was accompanied by concomitant precipitation of gray salts. The solution was allowed to stir for 2 h and was cannula filtered to a new flask, leaving behind the gray precipitate. Solvent was removed to yield a dark maroon solid. Yield 0.173 g (83%). IR (CH_2Cl_2): ν(BH) 2308 cm^{-1}, ν(CO) 2001 cm^{-1}, ν(CN) 1544 cm^{-1}. ^1H NMR (CD_2Cl_2): δ 6.19, 6.11, 5.74 (Tp′C*H*), 2.67, 2.54, 2.50, 2.50, 2.29, 2.21 (Tp′CH_3). ^{13}C NMR (CD_2Cl_2): δ 271.4 ($^1J_{WC}$ not observed, *C*O), 154.7, 153.6, 153.3, 148.5, 148.4, 147.4 (Tp′*C*CH_3), 119.7 (q, $^1J_{CF}$ = 320 Hz, O_3SCF_3), 109.0, 108.2, 108.0 (Tp′*C*H), 16.2, 14.7, 14.2, 13.0, 12.7, 11.2 (Tp′*C*H_3). *Anal.* Calc.: C, 30.29; H, 3.29; N, 12.47. Found: C, 30.49; H, 3.47; N, 12.13%.

4.2. [Tp′W(O)(CO)(NCMe)][OTf] (3)

In a 100 mL round-bottom flask, **2** (0.030 g, 0.050 mmol) was dissolved in 15 mL of CH_3CN. The solution immediately became a deep purple color. Removal of the solvent yielded a solid of mixed deep purple and maroon solids. NMR spectroscopy displayed a mixture of **3** and starting material **2**. ^1H NMR (CD_2Cl_2): δ 6.28, 6.19, 5.87 (Tp′C*H*), 3.23 (NCCH_3), 2.76, 2.54, 2.53, 2.49, 2.31, 2.26 (Tp′CH_3).

4.3. NMR observation of (3)

In an NMR tube, triflate complex **2** (0.014 g, 0.021 mmol) was dissolved in 0.7 mL CD_2Cl_2. Acetonitrile (0.005 mL, 5 equiv.) was added via a 10 μL syringe. The tube was shaken to mix the contents. Over a period of 24 h NMR signals for nitrile complex **3** slowly grew with concomitant disappearance of **2**.

4.4. [Tp′W(O)(CO)(NCMe)][BAr′4] (4)

In a 100 mL round-bottom flask, triflate complex **2** (0.121 g, 0.179 mmol) and $NaBAr'_4$ (0.159 g, 0.179 mmol) were dissolved in 15 mL of CH_3CN. The solution immediately became a deep purple color. Cannula filtration of the solution to a new flask and solvent removal yielded a deep purple solid. IR (KBr): ν(CO) 2026 cm^{-1}, ν(CN) 1544 cm^{-1}, ν(WO) 965 cm^{-1}. ^1H NMR (CD_2Cl_2): δ 7.74 (*o*-Ar′), 7.58 (*p*-Ar′) 6.24, 6.18, 5.82 (Tp′C*H*), 3.07 (CH_3CN), 2.64, 2.53, 2.50, 2.48, 2.28, 2.21 (Tp′CH_3). ^{13}C NMR (CD_2Cl_2): δ 248.1 ($^1J_{WC}$ = 190 Hz, *C*O), 162.1 (q, $^1J_{BC}$ = 50 Hz, *ipso* of BAr'_4), 153.5 (CH_3*C*N), 154.0, 152.8, 152.3, 149.4, 149.4, 149.1 (Tp′*C*CH_3), 135.2 (*o*-C of BAr'_4), 129.3 (q, $^2J_{CF}$ = 30 Hz, *m*-C of BAr'_4), 125.0 (q, $^1J_{CF}$ = 270 Hz, *C*F_3), 117.9 (*p*-C of BAr'_4), 109.3, 108.9, 108.8 (Tp′*C*H), 16.3, 15.2, 14.8, 13.0, 12.5, 12.5 (Tp′*C*H_3), 4.9 (*C*H_3CN).

4.5. Tp′W(O)(I)(NCCH3) (5)

In a 100 mL Schlenk tube, **1** (0.450 g, 0.690 mmol) was dissolved in 50 mL of CH_3CN. The purple-pink solution was photolyzed under bubbling nitrogen for 3 h to give a dark orange solution. Solvent was removed to yield an oily dark orange solid. The solid was re-dissolved in 5 mL methylene chloride and mixed with 50 mL hexanes. The orange solution was cannula filtered to remove any insoluble species and solvent was removed to yield a dark orange powder. Yield 0.327 g (71%). ^1H NMR (CD_2Cl_2): δ 6.17, 6.07, 5.61 (Tp′C*H*), 3.87 (CH_3CN), 2.80, 2.52, 2.45, 2.43, 2.30, 1.89 (Tp′CH_3). ^{13}C NMR (CD_2Cl_2) δ 278.6 (*C*O), 184.8 (N*C*CH_3), 155.4, 154.4, 152.5, 146.4, 145.6, 144.6 (Tp′*C*CH_3), 109.1, 108.7, 108.0 (Tp′*C*H), 27.0 (NC*C*H_3), 19.0, 15.9, 15.0, 13.0, 12.8, 12.5 (Tp′C_3).

4.6. Tp′W(O)(I)(NC(O)Me) (6) and Tp′(O)(I)W=NC(CH3)C(CH3)N=W(I)(O)Tp′ (7)

Complex **5** was synthesized as above. Column chromatography of the photolysis reaction product with alumina and CH_2Cl_2/hexanes (25/75) left a deep red band on the column. Addition of ca. 5 mL of THF to 100 mL of the eluent solution removed a red band from the column. Removal of the solvent yields a red powder. Crystals of **6** and **7** suitable for X-ray analysis were grown by diffusion of hexanes into a concentrated methylene chloride solution. **6**:^1H NMR (CD_2Cl_2): δ 6.02, 5.99, 5.88 (Tp′C*H*), 2.78, 2.61, 2.50, 2.50, 2.44, 2.39, 2.38 (Tp′CH_3 and NC(O)CH_3).

4.7. Tp′W(O)(I)(PhCCH) (8)

In a 100 mL round-bottomed flask **5** (0.048 g, 0.070 mmol) was dissolved in 40 mL dry THF. Phenylacetylene (0.079 mL, 10 equiv.) was syringed into the flask and the solution was stirred. The solution was refluxed for 19 h. Solvent was removed to yield a purple solid containing both isomers of **8**. ^1H NMR (CD_2Cl_2): δ

(major) 12.30 ($^2J_{WH}$ = 12 Hz, PhCC*H*), 7.16, 6.48 (m, 5H, *Ph*CCH), 6.11, 5.85, 5.57 (Tp′C*H*), 2.87, 2.49, 2.49, 2.39, 1.79, 1.78 (Tp′CH_3). δ (minor) 11.03 ($^2J_{WH}$ = 12.5 Hz, PhCC*H*), 7.93, 7.59, 7.42 (m, 5H, *Ph*CCH), 6.11, 6.10, 5.62 (Tp′C*H*), 2.87, 2.49, 2.47, 2.33, 2.30, 1.90 (Tp′CH_3). ^{13}C NMR (CD_2Cl_2): δ (major) 162.3 (Ph*C*CH), 157.4 155.7, 154.4, 152.7, 146.1, 145.8, 144.2 (Tp′*C*CH_3 and PhC*C*H), 136.7, 130.6, 129.0, 128.7 (*Ph*CCH), 108.9, 108.7, 108.0 (Tp′*C*H), 19.0, 15.8, 15.7, 13.0, 12.9, 12.6 (Tp′*C*H_3). δ (minor) 173.0 (Ph*C*CH), 155.0, 154.6, 153.5, 152.7, 145.6, 145.5, 144.2 (Tp′*C*CH_3 and PhC*C*H), 138.7, 134.4, 129.7, 128.3 (*Ph*CCH), 108.7, 108.6, 107.6 (Tp′*C*H), 16.6, 15.8, 14.1, 12.9, 12.8, 12.4 (Tp′*C*H_3).

4.8. [Tp′W(O)(I)(MeNCMe)][OTf] (9)

In a 100 mL round-bottom flask **5** (0.200 g, 0.307 mmol) was dissolved in 20 mL methylene chloride. To this orange solution was added MeOTf (0.035 μL, 0.307 mmol). No observable color change was observed. After 2 h, 60 mL of hexanes was added to the solution. The flask was chilled to 0 °C and stirred for 1 h forming a light brown precipitate on the sides of the flask. The solution was cannula filtered to a new flask leaving behind solid **9**. ^{1}H NMR (CD_2Cl_2): δ (major) 6.27, 6.25, 5.79 (TpC*H*), 4.31 (CH_3NCCH$_3$), 3.88 (CH$_3$NCCH_3), 2.77, 2.49, 2.48, 2.36, 2.35, 1.83 (Tp′CH_3). δ (minor) 6.24, 6.24, 5.80 (Tp′C*H*), 4.92 (CH_3NCCH$_3$), 3.13 (CH$_3$NCCH_3), 2.84, 2.48, 2.46, 2.36, 2.32, 1.87 (Tp′CH_3). ^{13}C NMR (CD_2Cl_2): δ 210.6 (CH$_3$N*C*CH$_3$), 157.4, 154.2, 153.0, 148.8, 148.8, 146.7 (Tp′*C*CH_3), 110.2, 110.0, 109.6 (Tp′*C*H), 39.5 (CH$_3$NC*C*H$_3$), 23.0 (*C*H$_3$NCCH$_3$), 19.5, 15.8, 15.5, 13.9, 13.0, 12.6 (Tp′*C*H$_3$). *Anal.* Calc. C, 27.52; H, 3.40; N, 11.83. Found: C, 27.52; H, 3.45; N, 12.50%.

Acknowledgement

We are grateful to the National Science Foundation for support of this research.

References

[1] (a) M.S. Malarek, B.A. Logan, J.M. White, C.G. Young, Organometallics 23 (2004) 4328;
(b) R.A. Michelin, M. Mozzon, R. Bertani, Coord. Chem. Rev. 147 (1996) 299;
(c) B.N. Storhoff, H.C. Lewis, Coord. Chem. Rev. 23 (1977) 1.
[2] V.Y. Kukushkin, A.J.L. Pombeiro, Chem. Rev. 102 (2002) 1771.
[3] S.G. Feng, J.L. Templeton, J. Am. Chem. Soc. 111 (1989) 6477.
[4] (a) N.J. Vogeley, P.S. White, J.L. Templeton, Organometallics 23 (2004) 1378;
(b) N.J. Vogeley, P.S. White, J.L. Templeton, J. Am. Chem. Soc. 125 (2003) 12422;
(c) S.G. Feng, J.L. Templeton, Organometallics 11 (1992) 1295.
[5] (a) S. Kobayashi, H. Ishitani, Chem. Rev. 99 (1999) 1069;
(b) D. Enders, U. Reinhold, Tetrahedron: Asymmetry 8 (1997) 1895.
[6] For some examples of η^2-nitrile complexes without X-ray characterization, see: (a) A.J. Nielson, P.A. Hunt, C.E.F. Rickard, P. Schwerdtfeger, J. Chem Soc., Dalton Trans. (1997) 3311;
(b) D. Lucas, Z. Modarres-Tehrani, Y. Mugnier, A. Antinolo, I. Del Hierro, A. Otero, M. Fajardo, New J. Chem. 20 (1996) 385;
(c) M.L.H. Green, A.K. Hughes, P. Mountford, J. Chem. Soc., Dalton Trans. (1991) 1407;
(d) R.M. Bullock, C.E.L. Headford, S.E. Kegley, J.R. Norton, J. Am. Chem Soc. 107 (1985) 727;
(e) S. Zecchin, G. Zotti, G. Pilloni, Inorg. Chim. Acta 33 (1979) L117;
(f) E.O. Sherman, P.R. Schreiner, J Chem. Soc., Chem. Commun. 1 (1976) 3;
(g) W.R. McWhinnie, J.D. Miller, J.B. Watts, D.Y. Waddan, J. Inorg. Nucl. Chem. 37 (1975) 2329;
(h) J.L. Thomas, J. Am. Chem. Soc. 97 (1975) 5943;
(i) B. Storhoff, A.J. Infante, Inorg. Chem. 13 (1974) 3043;
(j) D.H. Payne, Z.A. Payne, R. Rohmer, H. Frye, Inorg. Chem. 12 (1973) 2540;
(k) D.H. Payne, H. Frye, Inorg. Nucl. Chem. Lett. 9 (1973) 505;
(l) W.J. Bland, R.D.W. Kemmitt, R.D. Moore, J. Chem. Soc., Dalton Trans. (1973) 1292;
(m) M.F. Farona, K.F. Kraus, J. Chem. Soc., Chem. Commun. 513 (1972);
(n) M.F. Farona, K.F. Kraus, Inorg. Chem. 9 (1970) 1700;
(o) S.C. Jain, R. Rivest, Inorg. Chim. Acta 3 (1969) 249;
(p) H. Bock, H. tom Dieck, Chem. Ber 99 (1966) 213.
[7] For some examples of η^2-nitrile complexes with X-ray characterization, see the following in addition to Refs. [8–10] (a) T. Komuro, T. Matsuo, H. Kawaguchi, K. Tatsumi, J. Am. Chem. Soc. 125 (2003) 2070;
(b) M.I. Bruce, B.W. Skelton, A.H. White, N.N. Zaitseva, J. Chem. Soc., Dalton Trans. 3627–3633 (2001);
(c) M.I. Bruce, B.W. Skelton, A.H. White, N.N. Zaitseva, Inorg. Chem. Commun. 4 (2001) 617;
(d) P.A. Chetcuti, C.B. Knobler, M.F. Hawthorne, Organometallics 7 (1988) 650;
(e) S.J. Anderson, F.J. Wells, G. Wilkinson, B. Hussain, M.B. Hurthouse, Polyhedron 7 (1988) 2615;
(f) P.A. Chetcuti, C.B. Knobler, M.F. Hawthorne, Organometallics 5 (1986) 1913;
(g) T.C. Wright, G. Wilkinson, M. Motevalli, M.B. Hurthouse, J. Chem. Soc., Dalton Trans. 2017–2019 (1986).
[8] (a) J. Barrera, M. Sabat, W.D. Harman, Organometallics 12 (1993) 4381;
(b) J. Barrera, M. Sabat, W.D. Harman, J. Am. Chem. Soc. 113 (1991) 8178.
[9] (a) S. Thomas, C.G. Young, E.R.T. Tiekink, Organometallics 17 (1998) 182;
(b) C.G. Young, S. Thomas, R.W. Gable, Inorg. Chem. 37 (1998) 1299;
(c) S. Thomas, E.R.T. Tiekink, C.G. Young, Organometallics 15 (1996) 2428.
[10] (a) J.L. Kiplinger, A.M. Arif, T.G. Richmond, Organometallics 16 (1997) 246;
(b) J.L. Kiplinger, A.M. Arif, T.G. Richmond, J. Chem. Soc., Chem. Commun. (1996) 1691.
[11] (a) M. Etienne, C. Carfagna, P. Lorente, R. Mathieu, D. de Montauzon, Organometallics 18 (1999) 3075;
(b) P. Lorente, C. Carfagna, M. Etienne, B. Donnadieu, Organometallics 15 (1996) 1090.
[12] J.L. Templeton, Adv. Organomet. Chem. 29 (1989) 1.
[13] J.E. Sutton, J.I. Zink, Inorg. Chem. 15 (1976) 675.

[14] D. Churchill, J.H. Shin, T. Hascall, J.M. Hahn, B.M. Bridgewater, G. Parkin, Organometallics 18 (1999) 2403.
[15] (a) J.J. Garcia, A. Arevalo, N.M. Brunkan, W.D. Jones, Organometallics 23 (2004) 3997;
(b) N.M. Brunkan, D.M. Brestensky, W.D. Jones, J. Am. Chem. Soc. 126 (2004) 3627;
(c) J.J. Garcia, N.M. Brunkan, W.D. Jones, J. Am. Chem. Soc. 124 (2002) 9547;
(d) J.J. Garcia, W.D. Jones, Organometallics 19 (2000) 5544.
[16] (a) H. Nakazawa, T. Kawasaki, K. Miyoshi, C.H. Suresh, N. Koga, Organometallics 23 (2004) 117;
(b) F.L. Taw, A.H. Mueller, R.G. Bergman, M. Brookhart, J. Am. Chem. Soc. 125 (2003) 9808;
(c) F.L. Taw, P.S. White, R.G. Bergman, M. Brookhart, J. Am. Chem. Soc. 124 (2002) 4192.
[17] (a) F. Kakiuchi, M. Sonoda, T. Tsujimoto, N. Chatani, S. Murai, Chem. Lett. (1999) 1083;
(b) C.B. Lebrilla, T. Drewello, H. Schwarz, Organometallics 6 (1987) 2450;
(c) D.T. Tsou, J.D. Burrington, E.A. Maher, R.K. Grasselli, J. Mol. Catal. 22 (1983) 29.
[18] J.L. Cross, T.W. Crane, P.S. White, J.L. Templeton, Organometallics 22 (2003) 548.
[19] S. Thomas, P.J. Lim, R.W. Gable, C.G. Young, Inorg. Chem. 37 (1998) 590.
[20] K.R. Powell, P.J. Perez, L. Luan, S.G. Feng, P.S. White, M. Brookhart, J.L. Templeton, Organometallics 13 (1994) 1851.
[21] Y.C. Tsai, F.H. Stephens, K. Meyer, A. Mendiratta, M.D. Gherorghiu, C.C. Cummins, Organometallics 22 (2003) 2902.
[22] (a) R. Duchateau, A.J. Williams, S. Gambarotta, M.Y. Chiang, Inorg. Chem. 30 (1991) 4863;
(b) F.A. Cotton, W.T. Hall, J. Am. Chem. Soc. 101 (1979) 5094;
(c) F.A. Cotton, W.T. Hall, Inorg. Chem. 17 (1978) 3525;
(d) P.A. Finn, M.S. King, P.A. Kilty, R.E. McCarley, J. Am. Chem. Soc. 97 (1975) 220;
(e) R. Gert, W. Perron, J. Less-Common Met. 26 (1972) 369.
[23] (a) C.G. Young, C.C. Phillipp, P.S. White, J.L. Templeton, Inorg. Chem. 34 (1995) 6412;
(b) E.J.M. DeBoer, J.H. Teuben, J. Organomet. Chem. 153 (1978) 53.
[24] T.W. Crane, P.S. White, J.L. Templeton, Organometallics 18 (1999) 1897.
[25] (a) J. Sanchez-Nieves, P. Royo, M.A. Pellinghelli, A. Tiripicchio, Organometallics 19 (2000) 3161;
(b) Z. Wu, J.B. Diminnie, Z. Xue, Organometallics 18 (1999) 1002;
(c) P.J. Daff, A. Monge, P. Palma, M.L. Poveda, C. Ruiz, P. Valerga, E. Carmona, Organometallics 16 (1997) 2263;
(d) A.S. Gamble, P.S. White, J.L. Templeton, Organometallics 10 (1991) 693;
(e) L.D. Durfee, I.P. Rothwell, Chem. Rev. 88 (1988) 1059;
(f) M. Bochmann, L.M. Wilson, M.B. Hursthouse, M. Motevalli, Organometallics 7 (1988) 1148;
(g) A.M. Carrier, J.G. Davidson, E.K. Barefield, D.G. Van Derveer, Organometallics 6 (1987) 454.
[26] J.H. Shin, W. Savage, V.J. Murphy, J.B. Bonanno, D.G. Churchill, G. Parkin, J. Chem. Soc., Dalton Trans. (2001) 1732.
[27] M.F.C.G. da Silva, J.J.R.F. da Silva, A.J.L. Pombeiro, Inorg. Chem. 41 (2002) 219.
[28] S.G. Feng, L. Luan, P. White, M.S. Brookhart, J.L. Templeton, C.G. Young, Inorg. Chem. 30 (1991) 2582.
[29] M. Brookhart, B. Grant, A.F. Volpe, Organometallics 11 (1992) 3920.

Available online at www.sciencedirect.com
SCIENCE DIRECT®
Polyhedron 23 (2004) 2841–2856
POLYHEDRON
www.elsevier.com/locate/poly

Syntheses and electrochemistry of $(p\text{-}XC_6H_4O)_6W$ (1-X, X = H, CH_3, OCH_3, Cl, Br, OH, OCH_2Ph) and $(p\text{-}XC_6H_4O)_5W(OC_6H_4OH)$ (X = H, CH_3, OCH_3, Cl, Br): an approach to electrocatalytic CH bond activation

Orson L. Sydora, Jonas I. Goldsmith, Thomas P. Vaid, Abigail E. Miller, Peter T. Wolczanski *, Hector D. Abruña

Department of Chemistry and Chemical Biology, Baker Laboratory, Cornell University Ithaca, NY 14853, USA

Received 21 May 2004; accepted 25 August 2004
Available online 25 September 2004

Abstract

Alcoholysis of $W(OMe)_6$ afforded $(p\text{-}PhCH_2OC_6H_4O)_6W$ (**1**-OCH_2Ph), which could be hydrogenated (10% Pd/C, 1 atm H_2) to prepare $(p\text{-}HOC_6H_4O)_6W$ (**1**-OH). Related alcoholyses of WCl_6 with HOC_6H_4-*p*-X provided the hexaphenoxides $(p\text{-}XC_6H_4O)_6W$ (**1**-X, X = H, CH_3, OCH_3, Cl, Br) through minor modifications of literature procedures. Acid catalyzed treatment of **1**-X with *p*-$HOC_6H_4OCH_2Ph$ provided a mixture of substitution products $(p\text{-}XC_6H_4O)_{6-x}W(OC_6H_4OCH_2Ph)_x$ ($x = 1$, **5**-X) that could be hydrogenated (10% Pd/C, 1 atm H_2) to a mixture of hydroxylated products. Chromatography permitted isolation of $(p\text{-}XC_6H_4O)_5W(OC_6H_4OH)$ (**6**-X, X = H, 19%; Me, 29%; OCH_3, 19%; Cl, 12%; Br, 11%) in modest yields. Hexaphenoxides **1**-X and **6**-X manifested two electrochemical reduction waves whose positions were a function of *para*-substituent. When oxidized, **6**-X and **1**-OH were proposed to behave as W(V)quinone mimics, albeit at potentials capable of oxidizing hydrocarbons as shown via a thermochemical cycle. If the proposed transients $(p\text{-}XC_6H_4O)_5W(OC_6H_4O)$ (**7**-X) were generated, degradation was apparently competitive with CH bond activation. The structure of oligomeric $\{K[(p\text{-}ClC_6H_4O)_6W]\}_\infty$ (**8**-Cl) is addressed, and comments on the nature of radical CH bond activation in this and related systems are presented.
© 2004 Elsevier Ltd. All rights reserved.

1. Introduction

The direct conversion of alkanes to functionalized products is a tremendously important, yet very difficult chemical transformation facing the organotransition metal community. The stoichiometric activation of carbon–hydrogen bonds has now been achieved in numerous systems [1,2], but the capability to catalyze this reaction concomitant with oxidation of the substrate has rarely been successfully realized [3–14]. To date, only autoxidation processes mediated by cobalt and manganese have been shown to be commercially viable, and these are rather specialized applications (e.g., $^cC_6H_{12} \rightarrow HO_2C(CH_2)_4CO_2H$, $^tBuH \rightarrow {}^tBuOOH$, $p\text{-}MeC_6H_4Me \rightarrow p\text{-}HO_2CC_6H_4CO_2H$, etc.) that have a minimum of selectivity issues [15,16].

Organometallic approaches to C–H bond activation have generated at least one major conceptual advance. In stark contrast to known free radical chemistry, organometallic systems tend to oxidatively or otherwise add stronger CH bonds selectively over weaker. While some have argued for steric interpretations of these events, it seems clear that this CH bond activation selectivity stems from the greater *D*(M–R) derived from

* Corresponding author. Tel.: +1 607 255 7220; fax: +1 607 255 4137.
E-mail address: ptw2@cornell.edu (P.T. Wolczanski).

0277-5387/$ - see front matter © 2004 Elsevier Ltd. All rights reserved.
doi:10.1016/j.poly.2004.08.006

activation of the stronger bond. For example, in Eqs. (1) and (2), if $\Delta G^0_{rxn} \sim \Delta H^0_{rxn}$ and the bonds in L_nMH (Eq. (1)) or L_nMXH (Eq. (2)) are relatively unaffected by R^1 versus R^2, then $\Delta H^0_{rxn} = \{D(M-R^2) - D(MR^1)\} + \{D(R^1H) - D(R^2H)\}$. As long as the *differences* in $D(M–R^n)$ are greater than the *differences* in $D(H–R^n)$ (i.e., $\Delta D(M–R^n)/\Delta D(H–R^n) > 1$), selectivities opposite to that of free radical activations prevail: sp-CH > Ar-H ⩾ sp^2-CH, including ^{c}PrH > MeH > 1°sp^3-CH > 2° sp^3-CH > 3°sp^3-CH, with benzylic and allylic CH bonds often modest exceptions [17–19]. It seems clear that when Green [20] discovered the proclivity of transiently generated tungstenocene to activate arene CH bonds (Eq. (3)), it was this selectivity that was first being witnessed. In most systems involving direct oxidative addition of carbon–hydrogen bonds, this selectivity is modest because binding of R^nH precedes C–H bond cleavage [17,18]. In cases where the actual CH activation is rate-determining [20], there is considerable optimism that problems such as methane to methanol and acetic acid [6,7], and terminal versus internal sp^3-CH activation and functionalization of acyclic alkanes will ultimately be solved [13,14].

$$L_nM(H)R^2 + R^1H \rightleftharpoons L_nM(H)R^1 + R^2H \quad (1)$$

$$L_nM(XH)R^2 + R^1H \rightleftharpoons L_nM(XH)R^1 + R^2H \quad (2)$$

$$Cp_2WH_2 \xrightarrow{h\nu} [Cp_2W] \xrightarrow{PhH} Cp_2W(H)Ph \quad (3)$$

Concerted types of C–H bond activations have been separated into various classes such as σ-bond metathesis, oxidative addition, 1,2-RH-addition and electrophilic activation [1]. While each represents a particular class of reactions, it is clear that electrophilic attack at the C–H bond, whether in a binding or cleavage event, is a common thread among these paths. Free radical and metalaradical (e.g., $L_nM + RH \rightarrow L_nMH + R^{\cdot}$, $L_nMX + RH \rightarrow L_nMXH + R^{\cdot}$, etc.) mechanisms for alkane activation may also yield some control, provided selectivity is built into the metal framework as in nature, or the precise $D(R^nH)$ limits of activation can be controlled and utilized.

Many bioinorganic systems, most notably methane monoxygenase [21], cytochrome P-450 [22], and related oxidases [23–25], have been examined in the context of CH bond activation. Some exciting recent results have been obtained by Que, who has employed the tetramethylcyclam ligand in stabilizing an Fe(IV) oxo complex [26], and has expanded his ligand arsenal to pentadentate ligands whose ligated Fe^{IV}=O groups are capable of hydroxylating cyclohexane and substrates containing weaker CH bonds [27]. Note that the metal functionality (MX) that reacts with RH need not be an oxo or multiple-bonded entity, but the transfer of a hydrogen atom to MX must satisfy certain thermodynamic requirements for it to occur with reasonable facility.

The thermodynamic feasibility of CH bond activation can be predicted with a thermochemical cycle devised by Parker and Tilset that use physically measurable parameters (i.e., E^0_{ox}, pK_a, C) to determine the homolytic bond dissociation energies (BDEs) of X–H species [28]. Fig. 1 illustrates such a cycle in which CH bond activation can be done electrocatalytically [4] provided the reactive intermediate, L_nMX, is generated at a potential positive enough to abstract a hydrogen atom. The sequence gives the BDE (sol) of the X–H bond, which constitutes a reasonable thermodynamic limit of the CH bond that can be broken through H atom abstraction by L_nMX. Mayer [29] has used similar cycles in rationalizing oxidations of permanganate [30] and MMO mimics [31]. Herein is explored the generation of a W^{VI}(semiquinone)/W^{V}(quinone) as a functionality that should be capable of the desired abstraction. Unfortunately, this specific system failed to generate products of CH activation, but a closer look at its features yields some surprises regarding CH bond activations by L_nMX.

2. Results

2.1. Syntheses

2.1.1. $(p\text{-}PhCH_2OC_6H_4O)_6W$ (1-OCH_2Ph) and $(p\text{-}HOC_6H_4O)_6W$ (1-OH)

In an earlier project designed with the synthesis of inorganic dendrimers, the robust character of the hexaaryloxidetungsten coordination environment was exploited as shown in Scheme 1. Treatment of $W(OMe)_6$, prepared from $W(OMe)_4Cl_2$, MeOH and NEt_3 [32], with p-$HOC_6H_4OCH_2Ph$ in toluene for 24 h

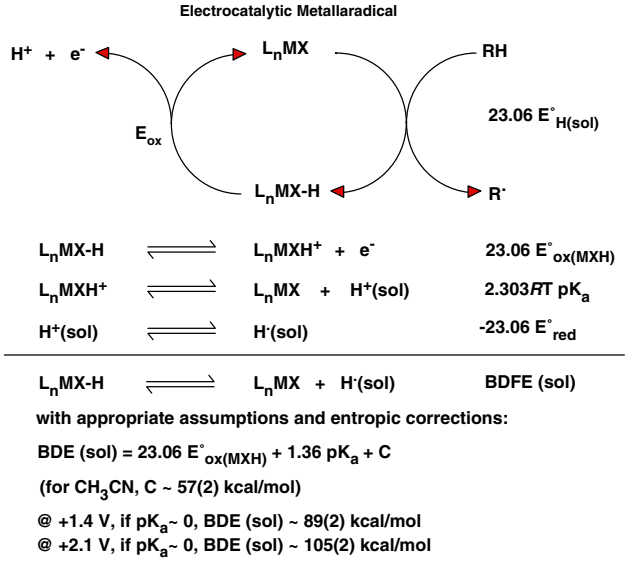

Fig. 1. Electrocatalytic metallaradical.

at 213 °C in a bomb reactor yielded the polybenzyl ether, (p-$PhCH_2OC_6H_4O)_6W$ (**1**-OCH_2Ph, 91%). Deprotection via hydrogenation (H_2 (1 atm), Pd/C) in ethanol/toluene ultimately yielded dark red (p-$HOC_6H_4O)_6W\cdot 2THF\cdot C_6H_6$ ((**1**-OH)$\cdot 2THF\cdot C_6H_6$) upon crystallization from THF/benzene. A structural investigation of (**1**-OH)$\cdot 2THF\cdot C_6H_6$ revealed a dense 3-D hydrogen-bonding network linking phenolic and THF sites. The addition of Lewis bases such as 4,4′-bipyridine and 1,2-di-4-pyridylethane to **1**-OH led to the hexabasic mononuclear complex (4,4′-bipy$\cdot HOC_6H_4O)_6W$ (**2**), the doubly interpenetrating 3-D network [{$W(OC_6H_4OH)_6$}{4,4′-$(NC_5H_4)_2(CH_2CH_2)$}$_2$]$_\infty$ (**3**), and the triply interpenetrating 3-D network [{$W(OC_6H_4OH)_6$}{4,4′-$(NC_5H_4)_2(CH_2CH_2)$}$_3\cdot$THF]$_\infty$ (**4**$\cdot$THF), according to X-ray crystallographic studies [33].

While the network solids were intriguing, the stabilization of pendant hydroxy functionalities on a high valent early transition metal center was a striking observation. Earlier studies of group 4 and 5 derivatives suggested that self-condensation was prevalent, yet no oligomerization chemistry was evident for (p-$HOC_6H_4O)_6W$ (**1**-OH). Now that the hydroxy functional group could be engineered into the W(VI) center, could reactivity other than hydrogen bond formation be exploited?

2.1.2. (p-$XC_6H_4O)_6W$ (**1**-X), (p-$XC_6H_4O)_5W(OC_6H_4OCH_2Ph)$ (**5**-X) and (p-$XC_6H_4O)_5W(OC_6H_4OH)$ (**6**-X, X = H, CH_3, OCH_3, Cl, Br)

para-Substituted tungsten hexaphenoxide complexes were synthesized via modification of methods developed by Beshouri and Rothwell [34], which in turn were modest variants of Funk and Baumann [35], and Mortimer and Strong [36]. Treatment of tungsten hexachloride with ~7 equiv. of p-XC_6H_4OH in refluxing chlorobenzene for 2 d formed (p-$XC_6H_4O)_6W$ (**1**-X, X = H, 82%; CH_3, 60%; OCH_3, 40%; Cl, 87%; Br, 68%) in varying yields.

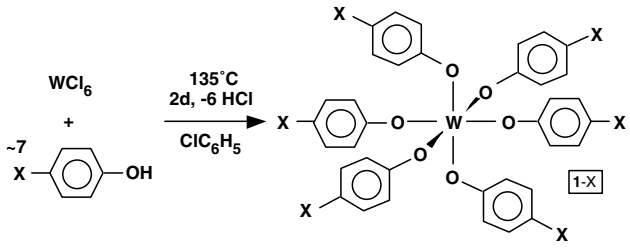

(4)

Since an entire [(p-$XC_6H_4O)_5W$] unit was considered as a tunable group for the ensuing electrochemical study, a protocol for the replacement of one phenoxide from **1**-X was needed. As Scheme 2 reveals, (p-$XC_6H_4O)_6W$ reacted with $HOC_6H_4OCH_2Ph$ in refluxing chlorobenzene with catalytic tosylic acid to yield a mixture of substituted products, (p-$XC_6H_4O)_{6-x}W(OC_6H_4O$-$CH_2Ph)_x$ ($x = 1$, **5**-X), as determined by TLC. The mixture of substituted products was hydrogenated (10% Pd/C, 1 atm H_2) in an EtOH/toluene mixture to a mixture of hydroxylated products, (p-$XC_6H_4O)_{6-x}W(OC_6H_4OH)_x$ ($x = 1$, **6**-X), also determined by TLC. The mono-hydroxylated species **6**-X were separated from the mixture by column chromatography and recrystallized from ethanol (X = H, 19%; Me, 29%; OCH_3, 19%; Cl, 12%; Br, 11%).

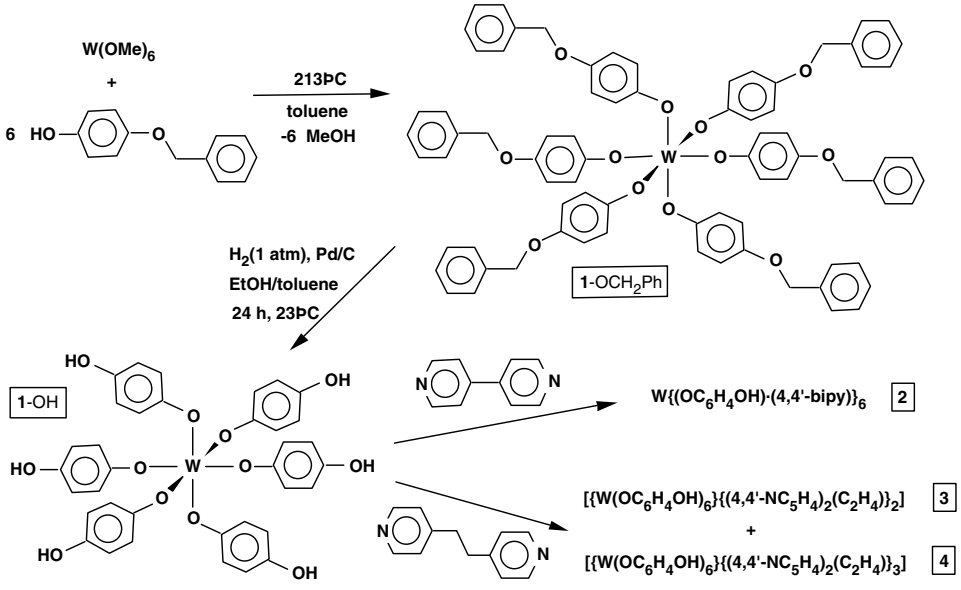

Scheme 1.

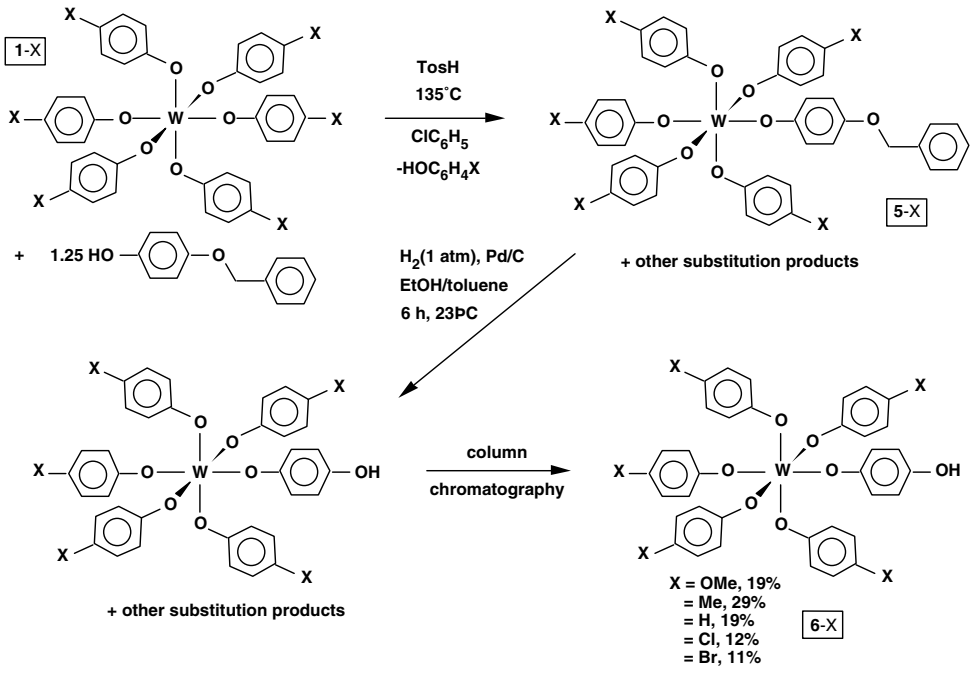

Scheme 2.

2.2. Electrochemistry

2.2.1. Quinone

The 2-electron oxidation of hydroquinone in acetonitrile is irreversible and produces quinone with the release of two protons as shown in Eq. (5) The first step of this oxidation is a one electron oxidation of hydroquinone (**H_2Q**) to the radical cation (**H_2Q^+**, Eq. (6)) followed by rapid proton loss to form the resonance stabilized semiquinodal radical (**HQ**, Eq. (7)) [37,38]. If the $[(p\text{-}XC_6H_4O)_5W]^+$ unit of $(p\text{-}XC_6H_4O)_5W(O\text{-}C_6H_4OH)$ (**6**-X) is considered as a proton ''replacement'', than an analogous one electron oxidation pathway to a W(VI) semiquinone/W(V) quinone species can be envisaged (Eq. (8)).

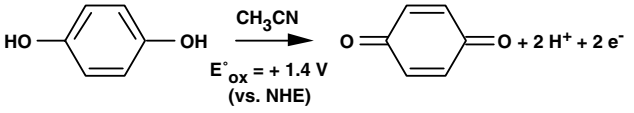

(5)

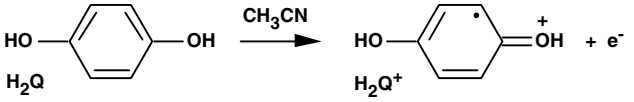

(6)

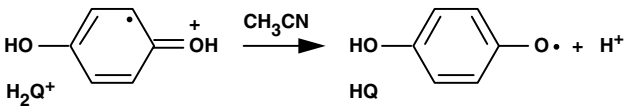

(7)

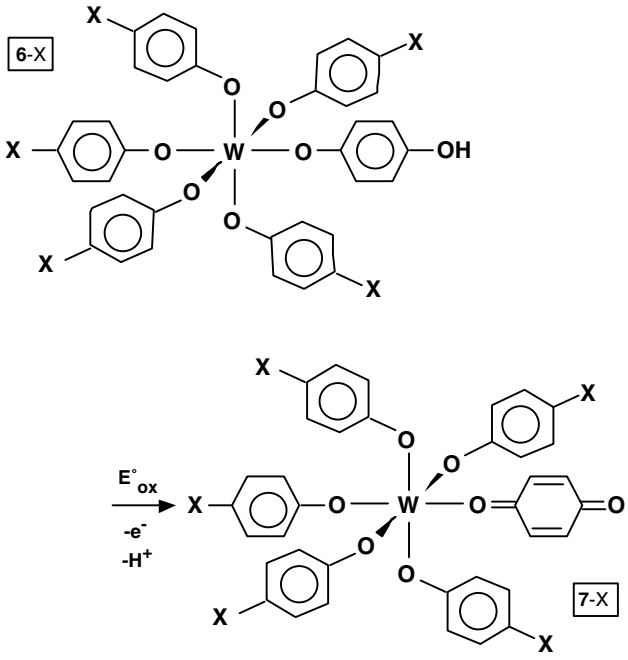

(8)

Application of the cycle shown in Fig. 1 to hydroquinone (HQ = L_nMXH) indicates that HQ ($E^0_{ox} \sim +1.4$ V versus NHE) could activate a CH bond of <89 (2) kcal/mol. However, if the E^0_{ox} potential of a hydroquinone like system could be raised to about +2.1 V (versus NHE), then activation of a 105(2) kcal/mol CH bond is possible. Would the *para*-substituents on **6**-X yield such an increase in oxidation potential?

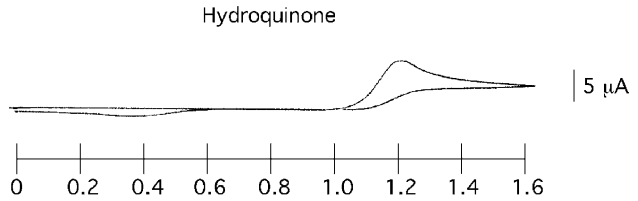

Fig. 2. Cyclic voltammogram of hydroquinone in acetonitrile: 0.5 mM QH_2, 0.1 M TBAH (tetra-*n*-butylammonium hexafluorophosphate), Ag wire reference, 100 mV/s.

Fig. 2 shows the oxidation of hydroquinone at platinum electrodes in acetonitrile. The peak potential of the irreversible oxidation wave (wave I, +1.40 V versus NHE) and irreversible reduction wave (wave II, +0.55 V versus NHE) were similar to the values reported by Chambers and Eggins [37] (wave I, +1.36 V; wave II, +0.37 V versus NHE, 2 V/s), who found that the peak potential and width for wave II was highly dependent on scan rate and pH. Further investigation into the behavior of wave I led to a proposed mechanism whereby reversible one electron oxidation of hydroquinone (**QH_2**) forms the radical cation **QH_2^+** (Eq. (6)) followed by rapid, irreversible deprotonation to the protonated semiquinone **QH** (Eq. (7)). A hemiketal intermediate (**$(QH)_2$**) then forms via **HQ** dimerization (Eq. (9)), followed by disproportionation to yield **Q** and **H_2Q** (Eq. (10))

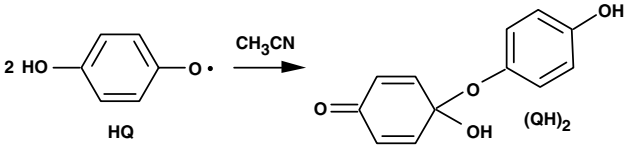

(9)

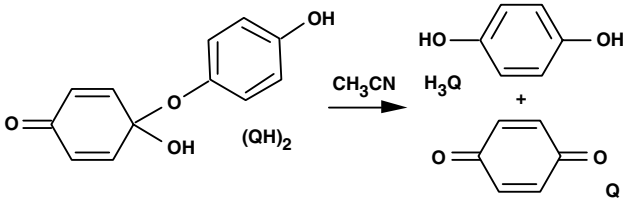

(10)

Wave II is the irreversible two electron reduction of the **Q**/H^+ mixture back to hydroquinone (Eq. (11)) [9]

$$\mathbf{Q} + H^+ + e^- \rightarrow \mathbf{HQ} \overset{e^-}{\rightarrow} \mathbf{QH^-} \overset{H^+}{\rightarrow} \mathbf{QH_2} \qquad (11)$$

2.2.2. Phenols

The oxidation of phenols can lead to a variety of products depending on the oxidant, catalyst, or substitution pattern of the phenol [39]. Treatment of 2,6-xylenol with a copper pre-catalyst in the presence of dioxygen yielded either diphenoquinone or polyphenylene ether depending on the pyridine to cuprous chloride ratio [40]. Lau and coworkers have found that in both water and acetonitrile oxidation of *p*-XC_6H_4OH (X = MeO, ^{t}Bu, Me, Cl, CN, H) by *trans*-$[Ru^{VI}(L)(O)_2]^{2+}$ (L = 1,12-dimethyl-3,4:9,10-dibenzo-1,12-diaza-5,8-dioxacyclopentadecane) proceeds via a hydrogen atom abstraction mechanism. The unstable phenoxy radical was further oxidized to *p*-benzoquinone and 4,4′-biphenoquinone via rapid competing steps [41]. Electrochemical studies on the mechanism of phenol oxidation suggest that the first step is an irreversible one electron oxidation of phenol followed by proton loss forming the resonance stabilized phenoxy radical shown in Eq. (12) [42]

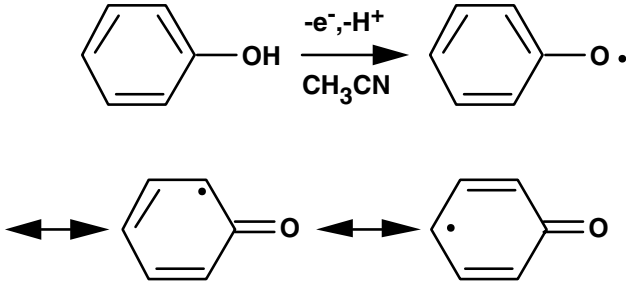

(12)

*2.2.3. (p-$XC_6H_4O)_6W$ (**1**-X, X = H, CH_3, OCH_3, Cl, Br, OH), (p-$XC_6H_4O)_5W(OC_6H_4OH)$, and p-XC_6H_4OH*

The impetus for attempting this project stemmed from three observations. First, cyclic voltammetry on (*p*-$HOC_6H_4O)_6W$ (**1**-OH) revealed multiple irreversible oxidation waves at ~1.29 V (versus NHE) and 1.63 V (Table 1). According to Fig. 1, if these events were indicative of a process such as that in Eq. (8), which is expected to be irreversible in analogy to **H_2Q/Q** electrochemistry, then C–H bonds of considerable strength could conceivably be attacked. In order to simplify the system, and to modulate the oxidation potentials of interest through *para*-substitution, (*p*-$XC_6H_4O)_5W(OC_6H_4OH)$ (**6**-X, X = H, CH_3, OCH_3, Cl, Br) were synthesized. Second, a 0.0–2.3 V (versus Ag wire) cyclic voltammogram of (*p*-$BrC_6H_4O)_5W(O$-$C_6H_4OH)$ (**6**-Br), which was chosen because it possesses a second oxidation wave at ~+1.95 V (versus NHE), showed a pronounced increase in current when excess Ph_3CH (3–10 equiv.; BDE ~ 81 kcal/mol) [43] was added to the solution. In concert with this experiment, the addition of dihydroanthracene (BDE ~ 79 kcal/mol) [31] to a solution of (*p*-$ClC_6H_4O)_5W(OC_6H_4OH)$ (**6**-Cl) caused a similar increase in current at ~+1.9 V (versus NHE) during another 0.0–2.3 V scan.

In view of the possibility of electrocatalytic C–H bond activation, some other cases seemed puzzling. Under similar conditions, no evidence of toluene (BDE ~ 89.8(6) kcal/mol) [43] or acetonitrile

Table 1
E^0_{red} and E^0_{ox} values (V vs. NHE, CH_3CN)[a] for p-XC_6H_4OH, (p-$XC_6H_4O)_6W$ (**1**-X) and (p-$XC_6H_4O)_5W(OC_6H_4OH)$ (**6**-X); X = H, Me, OMe, Cl, Br

Compound vs. NHE (V)	$E_{red}(1)$	$E_{red}(2)$	$E_{ox}(1)$	$E_{ox}(2)$[b]
(p-$BrC_6H_4O)_6W$ (**1**-Br)	−0.17	−1.22	1.88[c]	2.2
(p-$BrC_6H_4O)_5W(OC_6H_4OH)$ (**6**-Br)	−0.16	−1.19	1.32[b]	1.95
p-BrC_6H_4OH	−1.61		2.03	
(p-$ClC_6H_4O)_6W$ (**1**-Cl)	−0.17	−1.28	1.84	2.2
(p-$ClC_6H_4O)_5W(OC_6H_4OH)$ (**6**-Cl)	−0.28	−1.35	1.41	1.91
p-ClC_6H_4OH	−1.25		1.95	
$(C_6H_5O)_6W$ (**1**-H)	−0.4	−1.6	1.83	
$(C_6H_5O)_5W(OC_6H_4OH)$ (**6**-H)	−0.26	[d]	1.45	[d]
C_6H_5OH	−1.89		2.24	
(p-$MeC_6H_4O)_6W$ (**1**-Me)	−0.59	−1.70	1.47	[e]
(p-$MeC_6H_4O)_5W(OC_6H_4OH)$ (**6**-Me)	−0.54	−1.62	1.26	[f]
p-MeC_6H_4OH	−1.85		1.73	
(p-$MeOC_6H_4O)_6W$ (**1**-OMe)	−0.54	−1.5	1.33	1.71[g]
(p-$MeOC_6H_4O)_5W(OC_6H_4OH)$ (**6**-OMe)	−0.56	−1.63	1.17	1.72[g]
p-$MeOC_6H_4OH$	−1.57		1.52	
(p-$HOC_6H_4O)_6W$ (**1**-OH)	−0.58	−1.75	1.29[c]	1.63
p-HOC_6H_4OH	0.55		1.40	

[a] From cyclic volatammetry referenced to Ag wire with 0.1 M added tetra-*n*-butylammonium hexafluorophosphate (TBAH); the tabulated values are vs. NHE because the thermodynamic quantities in Fig. 1 use NHE as a reference. Typical samples were ~0.5 mM, and all scan rates were 100 mV/s.
[b] Appear as shoulders atop a generally featureless, increasing current.
[c] Multiple waves.
[d] Scan was only from −1.6 to +1.8 V.
[e] Possible shoulder at +1.9 V.
[f] Scan to 2.0 V, current still increasing.
[g] Other minor waves visible.

(BDE ~ 94.8(21) kcal/mol) [43] activation by any **6**-X species was noted, despite oxidation potentials that suggested such events were feasible according to the calculations of Fig. 1. It was also plausible that toluene might be activated by hydride transfer, but while a cycle similar to that in Fig. 1 can be constructed [44], not enough thermodynamic parameters are known for $RH \rightarrow R^+ + H^-$ to determine its feasibility. Regardless, cyclic voltammograms of **6**-X in the presence of toluene were unchanged. Finally, Fig. 4 illustrates another CV of (p-$BrC_6H_4O)_5W(OC_6H_4OH)$ (**6**-Br) taken from −2.2 to +2.3 V; when cycled in the presence of Ph_3CH, *this voltammogram was unchanged*. Whatever was generated in Fig. 3 does not persist when the scan is taken to −2.2 V for the longer period associated with it (Fig. 4).

Table 1 lists the electrochemical reduction and oxidation waves attributed to (p-$XC_6H_4O)_6W$ (**1**-X, X = H, CH_3, OCH_3, Cl, Br, OH), (p-$XC_6H_4O)_5W(O$-$C_6H_4OH)$ (**6**-X), and p-XC_6H_4OH. In general, the phenols exhibit an irreversible oxidation wave (two in some cases) that increases in potential according to substituent from π-donors to σ-donors to σ-withdrawing groups: p-X = OH (easiest) < OMe < Me < Cl < Br < H. The oxidation wave appears as a featureless increase in current that is initiated at high potentials. The differences based on substituent are substantial, span 0.84 V, and the parent phenol is oxidized at an anomalously high potential of +2.24 V. Presumably Cl < Br because the former has some π-influence that contradicts its σ-effect. Ignoring hydroquinone and its special characteristics (vide supra), the phenols also exhibit a quasi-reversible reduction wave. Here the inductive contributions appear to play a greater role than any π-effects because the ease of reduction follows p-X = Cl (easiest) > OMe > Br > Me > H, and the range of potentials is 0.64 V. π-Type electrons on substituents are energetically closer to arene π-bonding orbitals than arene π*-orbitals. As a consequence, π-effects play a greater role facilitating oxidation of the phenols. The reduction trend sim-

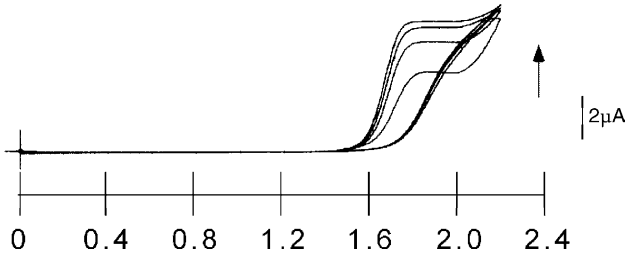

Fig. 3. Cyclic voltammogram of (p-$BrC_6H_4O)_5W(OC_6H_4OH)$ (**6**-Br) in CH_3CN showing the increase in current in successive scans after addition of Ph_3CH (~5 mM): ~0.5 mM **6**-Br, 0.1 M TBAH ($^nBu_4PF_6$), Ag wire reference, 100 mV/s.

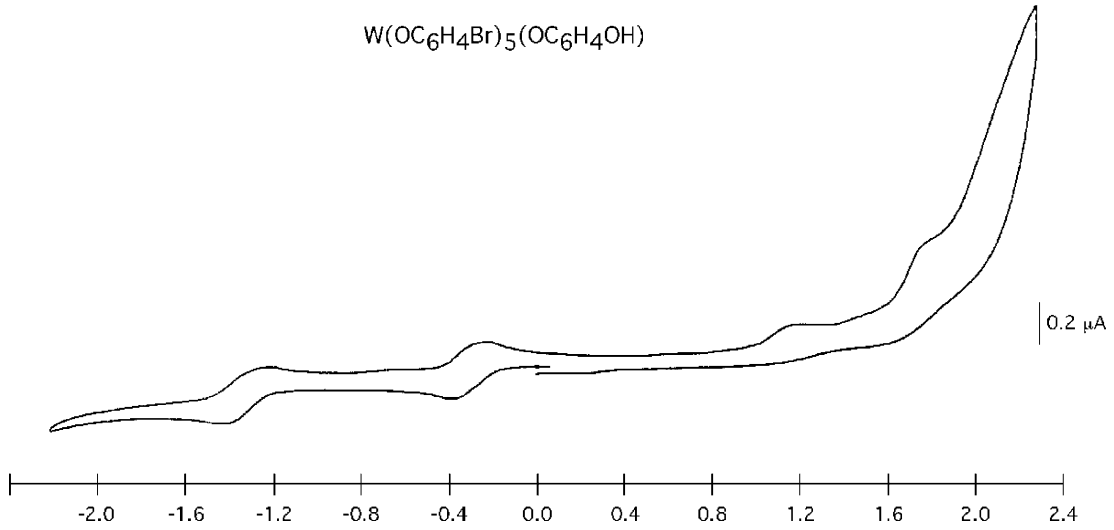

Fig. 4. Cyclic voltammogram of (p-$BrC_6H_4O)_5W(OC_6H_4OH$) (**6**-Br) in acetonitrile from −2.2 to +2.3 V: ~0.5 mM **6**-Br, 0.1 M TBAH (tetra-*n*-butylammonium hexafluorophosphate), Ag wire reference, 100 mV/s.

ply reflects inductive effects, which will tend to lower both the donor π-orbitals and the receptor π*-orbitals of the phenols as the substituents become more electron-withdrawing.

As previously observed for related compounds by Beshouri and Rothwell [34], (p-$XC_6H_4O)_6W$ (**1**-X, X = H, CH_3, OCH_3, Cl, Br, OH) exhibit two reversible reduction waves corresponding to the formation of anions $[\mathbf{1}\text{-X}]^-$ and dianions $[\mathbf{1}\text{-X}]^{2-}$. In contrast to the phenols, these reductions reflect a substantial influence by π-components, which render the reductions more difficult. The trend of ease of the first reduction for **1**-X is p-X = Br ~ Cl (easiest) > H > OMe > OH > Me, and the range of potentials is 0.42 V. Inductively, the oxygenated substituents should be on par with Cl, but their π-donor capability renders them more difficult to reduce. The trend of the second reduction has roughly the same range (0.53 V) and the trend is also similar: p-X = Br (easiest) > Cl > OMe > H > Me > OH. π-Donors increase the π-donating ability of the phenoxides, which results in an increase in energy of the t_{2g} receptor orbitals on the pseudo-octahedral complexes. This counteracts the tendency of σ-withdrawing substituents to lower the t_{2g} set. The reductions can certainly be rationalized as metal in character, and quite different from the phenols.

The oxidations of (p-$XC_6H_4O)_6W$ (**1**-X, X = H, CH_3, OCH_3, Cl, Br, OH) are complicated. A relatively clean irreversible wave ($E_{ox}(1)$) occurs for p-X = OH < OMe < Me < H ~ Cl < Br, which is basically the same trend – corresponding to the same effects – seen for the aforementioned phenol oxidations. The values are slightly less positive by 0.1–0.4 V, consistent with removal of an electron from ligand-based orbitals that are more "phenolate" in character. During and after this oxidation, there is a large increase in current, often with no readily discernable peak. The second oxidation ($E_{ox}(2)$), if it is clear, appears as a wave atop this increase. In the cyclic voltammogram of **1**-Br shown in Fig. 5, both oxidation waves are atop the current increase. The $E_{ox}(2)$ values, when clearly observed, reflect the previous trend. The similarities in $E_{ox}(2)$ and the oxidation waves of the parent phenols strongly suggest that the current increase observed is due to degradation of **1**-X and the release of phenol via phenoxy radical

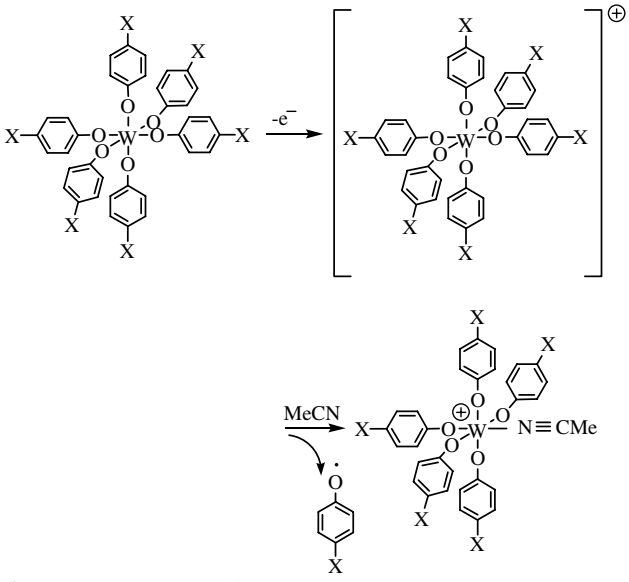

1-X, X = H, CH_3, OCH_3, Cl, Br, OH

(13)

The reductions of (p-$XC_6H_4O)_5W(OC_6H_4OH$) (**6**-X, X = H, CH_3, OCH_3, Cl, Br) are essentially the same as

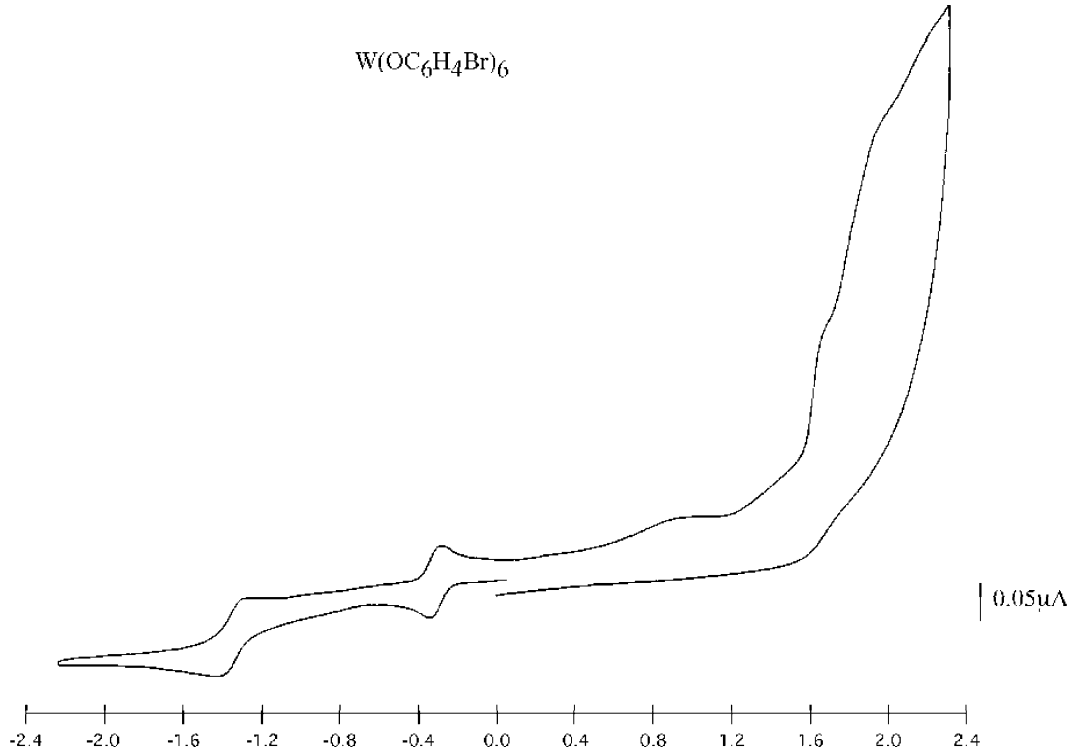

Fig. 5. Cyclic voltammogram of (p-$BrC_6H_4O)_6W$ (**1**-Br) in acetonitrile from −2.2 to +2.3 V: ~0.5 mM **1**-Br, 0.1 M TBAH (tetra-*n*-butylammonium hexafluorophosphate), Ag wire reference, 100 mV/s.

those of **1**-X within 0.1 V. The oxidations appear to reveal the problem in implementing electrocatalytic C–H bond activation. Each complex has an irreversible oxidation around +1.2 to 1.5 V that appears essentially at the onset of a large current increase. This is likely to be the oxidation of the p-HOC_6H_4O-ligand, since it is very close to the oxidations of **1**-OH and that of hydroquinone. The second oxidation, when observed atop the current increase, is near that of $E_{ox}(2)$ of **1**-X and the phenols. It is plausible that initial oxidation occurs at the p-HOC_6H_4O-ligand, perhaps via a process like that revealed in Eq. (8). If the W(V) quinone product (or W(VI) semiquinone) degrades before H atom abstraction can occur to regenerate **6**-X, degradation would lead to phenol loss. While the initial oxidation wave can be attributed to the HOC_6H_4O-ligand, a wave that would correspond to the reduction of free quinone is *not* evident, thus it is likely that protons generated upon oxidation are playing a role in the degradation.

Detection of phenol atop the general increase in current, which probably reflects the production of a number of oxidizable species, is a likely signature of catastrophic degradation.

2.3. Attempted generation of $(XC_6H_4O)_5W(OC_6H_4O)$ (7-X)

Although electrocatalytic C–H bond activation via Fig. 1 was not realized, it was still possible that the W(V) quinone/W(VI) semiquinone complex, (p-$XC_6H_4O)_5W(OC_6H_4O)$ (**7**-X, X = H, CH_3, OCH_3, Cl, Br, OH) was generated yet unstable under the electrochemical conditions. Early work suggested that the in situ preparation of **7**-X could be undertaken by utilizing a W(V) precursor. Funk et al. indicated that the reduction of (p-$XC_6H_4O)_6W$ (**1**-X, X = H, CH_3, Cl) by Raney nickel in the presence of potassium metal produced the five coordinate tungsten(V) aryloxides, "(p-$XC_6H_4O)_5W$" [45]. Despite product characterization that included molecular weight determination, EA, EPR and polarography, a five coordinate complex of this type would seem to be sterically capable of dimerizing to form $[(p\text{-}XC_6H_4O)_4W]_2(\mu\text{-}OC_6H_4X)_2$. Later work by Wilkinson and coworkers [46] showed that reduction of $W(OPh)_6$ by metallic lithium, sodium, or potassium in THF produced the octahedrally coordinated hexaphenoxotungstate(V) ion $[W(OPh)_6]^-$ as $[Li(thf)_2][W(OPh)_6]$, $Na[W(OPh)_6]\cdot NaOPh$, and $K[W(OPh)_6]$, respectively. The monomers $[Et_4N][W(OPh)_6]$, formed by treating $Na[W(OPh)_6]\cdot NaOPh$ with excess $[Et_4N]Br$, and $[Li(thf)_2][W(OPh)_6]$ were structurally characterized. EPR spectra were collected in frozen tetrahydrofuran at 100K for all of the $[W(OPh)_6]^-$ compounds as well as "$(PhO)_5W$", and the values appeared similar. Wilkinson and coworkers [46] proposed that "$(PhO)_5W$" in THF was most likely the axially distorted W^V monomer $W(OPh)_5(thf)$, although no further characterization was reported.

Following the Funk protocol [45], reduction of (p-$ClC_6H_4O)_6W$ (**1**-Cl) with Raney Ni (Et_2O:EtOH; 40:1) generated a red solution that turned yellow-orange upon addition of K^0. The addition of quinone caused an immediate color change to purple-red, and a black solid precipitated. ^1H NMR spectroscopy revealed only the formation of **1**-Cl. Since the solvent system appeared incompatible, the procedure was redone in Et_2O and THF-d_8 with similar results. As Eq. (14) shows, in Et_2O the reduction procedure yields $\{K[(p\text{-}XC_6H_4O)_6W]\}_\infty$ (**8**-X, X = H, 44%; Cl 61%) which can be isolated as orange crystals in 61% yield

$$(p\text{-}xC_6H_4O)_6W\ [\mathbf{1}\text{-}X(X = H, Cl)] \xrightarrow[Et_2O/EtOH(\sim 30:1)]{Raney Ni;K^\circ} \{K[(p\text{-}ClC_6H_4O)_6W]\}_\infty [\mathbf{8}\text{-}X(X = H, Cl)] \quad (14)$$

Attempts to remove one of the phenoxide ligands from $\{K[(p\text{-}ClC_6H_4O)_6W]\}_\infty$ (**8**-Cl) by electrophilic attack with $[Me_3O][BF_4]$ or Me_3SiCl only resulted in oxidation to (p-$ClC_6H_4O)_6W$ (**1**-Cl). The phenoxide ligand resisted substitution by PhCN, but ^1H NMR spectroscopy indicated that benzonitrile breaks up the infinite chain into a monomeric species, $[(p\text{-}ClC_6H_4O)_6W][K(NCPh)_4]$ (**9**-Cl, Eq. (15))

$$\{K[(p\text{-}ClC_6H_4O)_6W]\}_\infty\ (\mathbf{8}\text{-Cl}) \xrightarrow[PhCN]{benzene\text{-}d_6} [(p\text{-}ClC_6H_4O)_6W][K(NCPh)_4]\ (\mathbf{9}\text{-Cl}) \quad (15)$$

2.4. X-ray crystal structure of $\{K[(p\text{-}ClC_6H_4O)_6W]\}_\infty$ (8-Cl)

Crystallographic data for $\{K[(p\text{-}ClC_6H_4O)_6W]\}_\infty$ (**8**-Cl) are presented in Table 2 and pertinent interatomic distances and angles are listed in Table 3 As Fig. 6. reveals, **8**-Cl forms a zig-zag chain of $[(p\text{-}ClC_6H_4O)_6W]^-$ anions and potassium cations. The potassium cation is coordinated by a distorted square plane of oxygen atoms ($\angle O\text{–}K\text{–}O_{cis}$ = 55.8(1)°, 124.2(1)°; $\angle O\text{–}K\text{–}O_{trans}$ = 180°) in addition to axial coordination by two asymmetrically bound aryl rings of two different $[(p\text{-}ClC_6H_4O)_6W]^-$ units (Fig. 7). A small distortion from octahedral coordination is observed in the WO_6 core ($\angle$O1–W1–O2 = 87.8(1)°; $\angle$O1–W1–O3 = 91.4(1)°; $\angle$O2–W1–O3 = 92.4(1)°) (Fig. 8). The average W–O bond distance (1.955(1) Å) is longer than the average distance of normal tungsten(VI) aryloxide bonds (1.889(14) Å) [33,47] reflecting partial population of the π* orbitals of d^1 pseudo-octahedral W(V). A shorter terminal W–O bond distance (1.946(1) Å) is found in comparison to the bridged W–O distances (d(W1–O1) = 1.960(2) Å; d(W1–O2) = 1.959(1) Å).

Table 2
Crystallographic data for triclinic $\{K[(p\text{-}ClC_6H_4O)_6W]\}_\infty$(**8**-Cl)

Formula	$C_{36}H_{24}O_6Cl_6KW$
Formula weight	494.10
Space group	$P\bar{1}$
λ (Å)	0.71073
a (Å)	7.7888 (4)
b (Å)	10.3052 (6)
c (Å)	11.8888 (7)
α (°)	100.7200 (10)
β (°)	105.4990 (10)
γ (°)	96.7620 (10)
V (Å^3)	889.26 (9)
T (K)	173(2)
Z	1
ρ_{calc} (g/cm^3)	1.845
μ (mm^{-1})	3.862
$R[I > 2\sigma(I)]$[a]	0.0218
$w^2[I > 2\sigma(I)]$[b]	0.0558
Goodness-of-fit[c]	1.028
Largest differential peak (e Å^{-3})	1.740
Largest differential hole (e Å^{-3})	−1.188

[a] $R_1 = \sum[|F_o| - |F_c|]/\sum|F_o|$.
[b] $wR_2 = [\sum w(|F_o| - |F_c|)^2/\sum \omega F_o^2]^{1/2}$.
[c] GOF = $[\sum w(|F_o| - |F_c|)^2/(n-p)]^{1/2}$, n = number of independent reflections (5665 of 12570, R_{int} = 0.0237), p = number of parameters (277).

3. Discussion

3.1. Radical CH bond activation

3.1.1. Electrocatalyst lifetime

The premise of this project, electrocatalytic CH bond activation, was not realized. In an electrocatalytic process [4], either reduction or oxidation (this case) serves to regenerate a complex that undergoes a redox process, hence the electrode takes the place of a chemical redox partner that would be consumed (e.g., dioxygen) in the reaction. Rapid degradation of the electrochemically generated W(V) quinone or alternately described W(VI) semiquinone radical intermediate prior to H atom abstraction was considered as one possible cause of failure. In Fig. 3, the short potential range (0.0–2.3V) allowed degradation products (probably phenols) to be regenerated with a H atom source present, whereas the longer potential range in Fig. 4 (−2.2 to 2.3 V) and longer scan time yielded no behavior that could be misconstrued as "electrocatalytic".

In retrospect, the lifetime of the intermediate that must do the H atom abstraction must be substantial, and this factor was underappreciated in this study. For example, according to an Evans–Polanyi plot [48], the activation of dihydroanthracene by transient (p-$XC_6H_4O)_5W$(O-C_6H_4O) (**7**-X, X = H, CH_3, OCH_3, Cl, Br, OH) that was formed from $E^0_{ox} \sim +1.4$ V (Fig. 1) would occur at roughly 10 M^{-1} s^{-1}, hence the lifetime of **7**-X would need to be around a tenth

Table 3
Selected interatomic distances (Å) and angles (°) pertaining to $\{K[(p\text{-}ClC_6H_4O)_6W]\}_\infty$ (**8**-Cl)

Interatomic distances					
W–O1	1.874 (3)	K1–C13	3.139 (2)	K1–C14	3.270 (2)
W–O2	1.926 (3)	K1–C15	3.538 (2)	K1–C16	3.652 (2)
W–O3	1.913 (2)	K1–C17	3.516 (2)	K1–C18	3.257 (2)
$(K–O)_{ave}$	2.904 (2)				
Interatomic angles					
$(O–W1–O)_{trans}$	180	O1–W1–O2	87.8 (1)	O1–W1–O3	91.4 (1)
O2–W1–O3	92.4 (1)	W1–O1–C1	135.0 (1)	W1–O2–C7	139.1 (1)
W1–O3–C13	132.3 (1)	O1–K–O2	55.8 (1)	O1–K–O2′	124.2 (1)

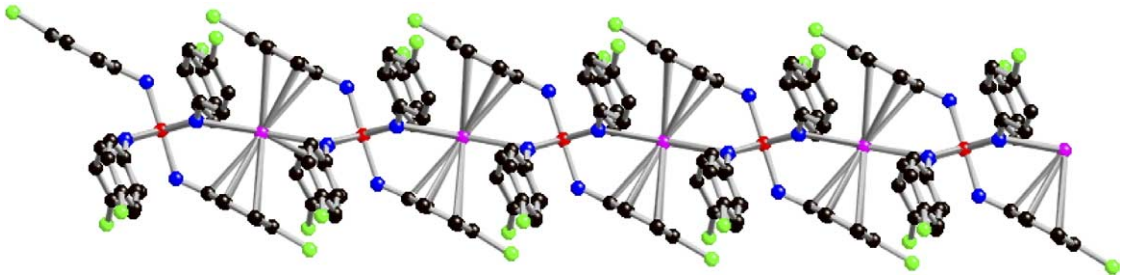

Fig. 6. Molecular view of the extended structure of $\{K[(p\text{-}ClC_6H_4O)_6W]\}_\infty$ (**8**-Cl). W, purple; K, blue; O, red; Cl, green; C, black.

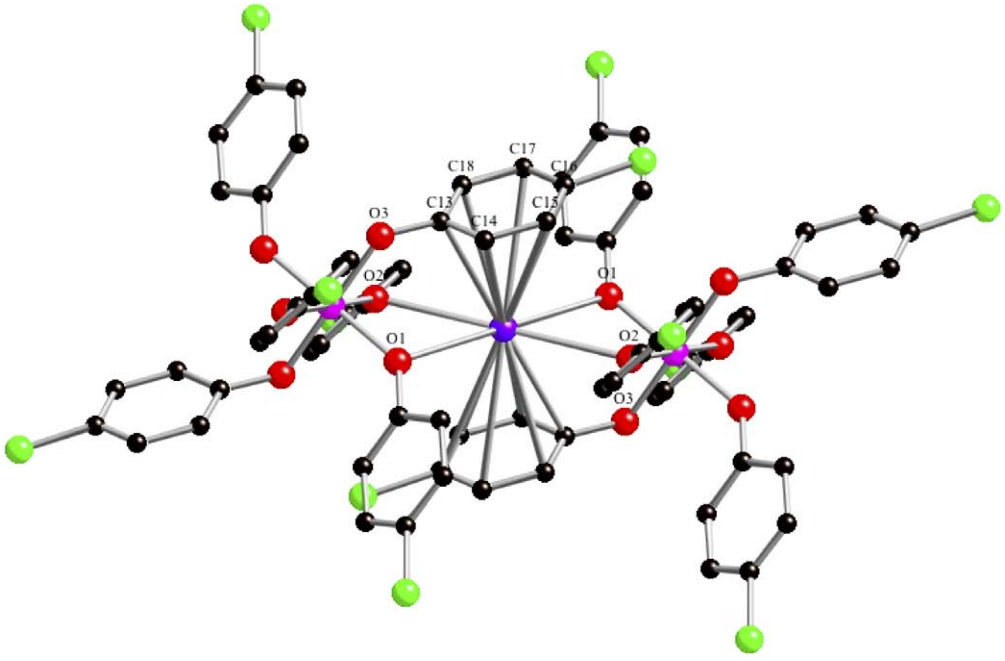

Fig. 7. Coordination environment of K cation in $\{K[(p\text{-}ClC_6H_4O)_6W]\}_\infty$ (**8**-Cl).

of a second; at 2.1 V, activation would occur at $\sim 10^6$ M^{-1} s^{-1} and its lifetime would need to be in the microsecond range. All oxidation waves found for $(p\text{-}XC_6H_4O)_5W(OC_6H_4OH)$ (**6**-X, X = H, CH_3, OCH_3, Cl, Br; X = OH, **1**-OH) on the 100 mV/s timescale were irreversible, and no reproducible reduction waves were ever seen in this region, even at higher scan speeds (100 V/s). Given the failure to achieve activation, no further elucidation of the electrochemistry or product analyses were attempted.

3.1.2. Solvent stability and ionization energy

An attempt at CH bond activation using an electrocatalytic cycle requires the use of a solvent that will support an electrolyte and not suffer activation. One might question the utility of such a process given the rather low BDEs of polar solvents such as acetonitrile (BDE ~ 94.8(21) kcal/mol, ~19 M) [43]. From the calculations in Fig. 1 acetonitrile should have been an excellent substrate for the putative quinone based chemistry projected for **6**-X.

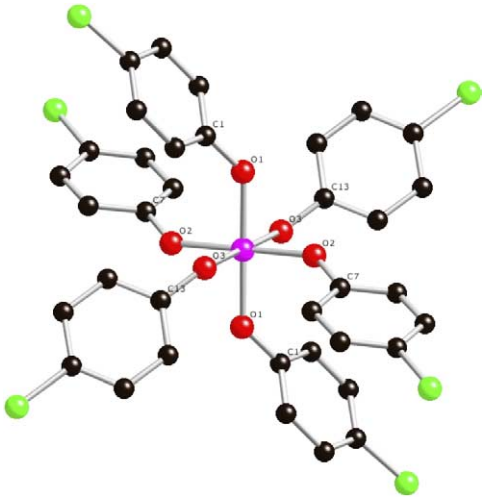

Fig. 8. Molecular view of the $[(p\text{-}ClC_6H_4O)_6W]^-$ ion in $\{K[(p\text{-}ClC_6H_4O)_6W]\}_\infty$ (**8**-Cl).

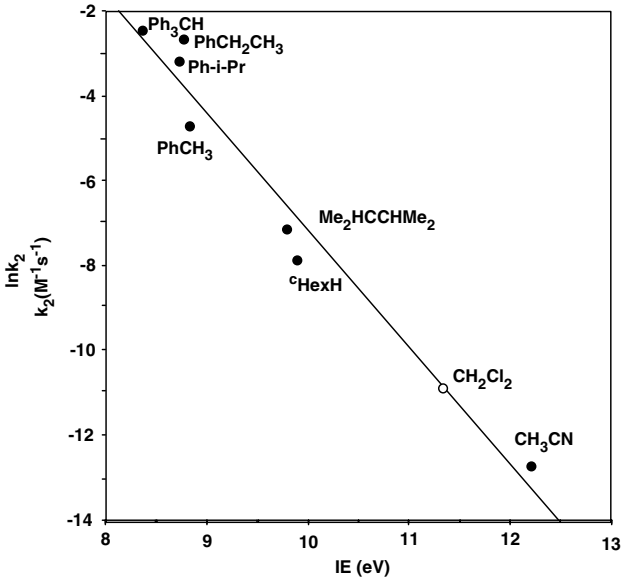

Fig. 9. Correlation of Que et al. hydrocarbon activation rates (k_2 in $M^{-1}\ s^{-1}$) by $[(Bn\text{-}tpen)FeO]^{2+}$ vs. IE (eV), assuming its degradation rate is that of CH_3CN activation. An estimate of methylene chloride activation based on its IE is given as an open circle.

Que has examined the remarkable oxidation of hydrocarbons by non-heme Fe(IV) oxo compounds in acetonitrile, thereby providing evidence to the contrary [27]. Que et al. generate $[\{(pyCH_2)_2NCH_2CH_2N\text{-}(CH_2py)_2\}FeO]^{2+}$ ($[(Bn\text{-}tpen)FeO]^{2+}$) in acetonitrile and measure second-order rate constants for the activation of several hydrocarbons, including cyclohexane, apparently without competition from solvent activation. They correlate the $\log k$(act) versus the BDE(substrate) in the usual fashion, but had acetonitrile been included as a "substrate", it would stand out as a dramatically outlying point. If one estimates the reaction of $[(Bn\text{-}tpen)FeO]^{2+}$ with acetonitrile as the compound's decomposition rate, one can rationalize the inexplicable stability of acetonitrile to H atom abstraction.

Fig. 9 plots the $\ln k_2$ (k_2 in $M^{-1}\ s^{-1}$) versus IE (eV) for the substrates used and acetonitrile, assuming its activation rate is that of the Fe(IV) oxo's degradation in the absence of added substrate [27]. A clean correlation is observed, with $R^2 = 0.955$; CH_2Cl_2, which is not used in Que's study, but has seen use in radical-based systems, is given a predicted activation $\ln k_2$ based on its IE. This plot is a reasonable alternative to the more conventional $\log k_2$ versus BDE employed by Que, and has the obvious advantage of being able to include acetonitrile, yet what is its interpretation?

In Fig. 10, two reaction paths for H atom abstraction are given: one implicates a synchronous transfer of proton and electron, and one reveals a transition state (e.g., the half-way point) that consists of greater electron transfer character than proton transfer. In such an instance, electron withdrawing groups on the substrate, such as the CN on acetonitrile or the chlorides on CH_2Cl_2 can attenuate the susceptibility to H atom abstraction, despite BDEs that would lead one to predict ready activation. Note that a non-synchronous

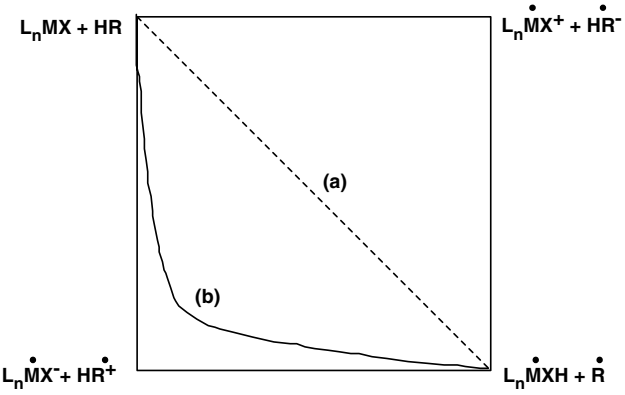

Fig. 10. Reaction coordinate for H atom transfer to L_nMX comparing: (a) direct path where the proton and electron travel simultaneously and (b) a path that possesses more electron transfer character at the transition state.

transfer could lower the frequencies of transition state vibrations that contribute heavily to the kinetic isotope effect (KIE) for H atom transfer (i.e., frequencies of a transition state with $RH^{\cdot+}$ character should be lowered considerably from that of $R^{\cdot}$). It has been shown that such low frequency vibrations are a significant contributor to some anomalously high KIEs [49].

3.2. Phenoxide complexes

The stability of tungsten *para*-hydroxy-phenoxide complexes to degradation via oligomerization and

condensation permitted the synthesis of (p-$XC_6H_4O)_5$-W(O-C_6H_4OH) (**6**-X, X = H, CH_3, OCH_3, Cl, Br; X = OH, **1**-OH) for this study. Their stability to excessive proton-induced ligand exchange, and chromatography conditions verifies their robust character. The complexes and their hexaphenoxide precursors exhibit clean, reversible reductions to anionic and dianionic species, but oxidations were irreversible and induced degradation. It was disappointing that variation of the (p-$XC_6H_4O)_5W$ fragment failed to substantially change the oxidation potential of the –OC_6H_4OH group, which was the first oxidation wave in each **6**-X, despite the wide variation in the oxidation potentials of the parent phenols. It was hoped that the variation in phenol oxidation potential would be transmitted to some extent to the W center and amplified given the five p-XC_6H_4O ligands, but this was not observed.

If one views the WOC_6H_4OH unit as a "phenoxide anion", precedent suggests that the premise of this study was thermodynamically doomed. Cheng et al. calculated several p-hydroquinone anion bond strengths to be ~66–74 kcal/mol, which are values incommensurate with the proposed CH bond activation. This work is certainly consistent with the relatively steady, irreversible $E^0_{ox}(1)$ values for **6**-X, which varied by only 0.28 V.

Clearly, while the concept of electrocatalytic CH bond activation according to Fig. 1. remains apparent, a system possessing higher oxidation potentials and greater stability of the oxidation product is needed for fruition. The more common cycle for Fig. 1 involves the pK_a of L_nMXH and the E^0_{ox} of L_nMX^-, but in this study the compounds were chosen as hydroquinone mimics, hence the pK_a of L_nMXH^+ should be <0, i.e., dissociation should occur spontaneously upon oxidation. Since the 1.36 pK_a factor is rather modest, this was not considered to be a serious detriment to the proposed CH bond activation, but it certainly could be a source of overestimation in terms of limiting the strength of the bonds potentially activated if the pK_a is much less than zero. For another view of this point, consider the more conventional way of estimating the OH bond strength of (p-$XC_6H_4O)_5$W(O-C_6H_4OH) (**6**-X). First, the pK_a of **6**-X would be determined (e.g., the pK_a of **6**-X would be >0), then the oxidation potential of (p-$XC_6H_4O)_5W(OC_6H_4O^-)$ would be measured. It is likely that the oxidation potential for this anionic species would be far less positive than for **6**-X, thereby compensating for the pK_a increase. Unfortunately, attempts to generate a stable anion of **6**-X via deprotonation failed, and mild bases afforded H-bonded coordination networks [33]. It is likely that (p-$XC_6H_4O)_5$W(O-$C_6H_4O^-$), which could also be considered as $[(p\text{-}XC_6H_4O)_5W^{IV}(OC_6H_4O)]^-$, is an unstable species.

4. Experimental

4.1. General considerations

All manipulations were performed using either glovebox or high vacuum line techniques. Hydrocarbon solvents containing 1–2 mL of added tetraglyme, and ethereal solvents were distilled under nitrogen from purple sodium benzophenone ketyl and vacuum transferred from same prior to use. C_6D_6 and acetonitrile were dried over activated 4 Å molecular sieves, vacuum transferred and stored under N_2. All other chemicals were purchased from commercial sources and used as received. All glassware was oven dried, and NMR tubes for sealed tube experiments were additionally flame-dried under dynamic vacuum. All phenols were purchased from Aldrich Chem. Co. and recrystallized prior to use.

NMR spectra were obtained using INOVA-400 and Unity-500 spectrometers, and chemical shifts are reported relative to C_6D_6 (^{1}H, 7.15; $^{13}C\{^1H\}$, 128.39) or acetone-d_6 (^{1}H, 2.05; $^{13}C\{^1H\}$, 29.92). Infrared spectra were recorded on a Nicolet Impact 410 spectrophotometer interfaced to a Gateway PC. Elemental analyses were performed by Oneida Research Services, Whitesboro, NY, or Robertson Microlit Laboratories, Madison, NJ. Magnetic moments were determined in C_6D_6 or thf-d_8 at room temperature using Evans method with an applied diamagnetic correction.

4.2. Procedures

4.2.1. (p-$PhCH_2OC_6H_4O)_6W$ (**1**-OCH_2Ph)

$W(OCH_3)_6$ (1.150 g, 3.11 mmol) and 4-benzyloxyphenol (5.00 g, 25.0 mmol) were combined in a large glass bomb with 40 mL toluene. The bomb was lowered into a salt bath until the solvent level was covered and the temperature settled at 173°C. After 24 h, the reaction was judged incomplete by a TLC using toluene as the eluting solvent. $W(OC_6H_4OCH_2C_6H_5)_6$ has an R_f of 0.70 while the R_f of $W(OC_6H_4OCH_2C_6H_5)_5(OCH_3)$ is 0.65 and other less substituted products have lower R_fs. The temperature was gradually increased, until after 24 h at 213 °C the reaction was complete except for a trace of a lower R_f spot. Toluene was added to the reaction mixture and it was washed with 3×350 mL 5% NaOH (aq). The deep red solution was dried over Na_2SO_4 and the solvent stripped on a rotary evaporator. The resulting dark red, very viscous oil was placed under high vacuum for several hours. ^{1}H NMR showed clean **1**-OCH_2Ph and toluene. The yield of 4.41 g translates to 3.89 g **1**-OCH_2Ph when the presence of toluene was accounted for, giving an actual yield of 91%.

4.2.2. (p-$HOC_6H_4O)_6W$ (**1**-OH)

1-OCH_2Ph (3.85 g, 2.79 mmol) was dissolved in 125 mL toluene/125 mL ethanol along with 500 mg 10% PdC. The

mixture was stirred under 1 atm H_2 and checked periodically by TLC using 100% ethyl acetate as the eluting solvent. Incompletely deprotected products have higher R_fs (0.85 or greater) than the final product ($R_f = 0.80$). After 4 h, the reaction was mostly complete, but required 24 h until only a trace spot at $R_f = 0.85$ remained. The reaction mixture was filtered through celite and the celite washed with ethanol. Volatiles were removed on a rotary evaporator and the product transferred to a 100 mL flask with THF. The THF was stripped and dry THF was added and removed. Dry THF was added and then stripped twice more to remove traces of water. The product was crystallized from 50 mL benzene/3–4 mL THF and dried under vacuum for 12 h (1.778 g, 60% based on $(p\text{-}HOC_6H_4O)_6W\cdot 2THF\cdot C_6H_6$) (**1**-OH·2THF·$C_6H_6$). ^{1}H NMR in acetone-$d_6$ indicated pure **1**-OH with 2.0 equivalents of THF and 0.9 equivalents of benzene. Elemental analysis indicated some loss of solvent before combustion: *Anal.* Calc. for $W(OC_6H_4OH)_6\cdot 1.5$ THF: C, 53.29; H, 4.47. Found: C, 53.11; H, 4.55%.

4.2.3. General (p-$XC_6H_4O)_6W$ (1-X, X = H, CH_3, OCH_3, Cl, Br)

To a 250 mL flask attached to a reflux condenser was added WCl_6 (5 g, 12.6 mmol). A sidearm flask containing p-XC_6H_4OH (81.7 mmol) was connected to the flask, which was attached to an argon line equipped with a bubbler. 100 mL of chlorobenzene was added and the phenol was gradually tapped into the flask and HCl (g) was evolved. The solution was refluxed for 12–24 h followed by an argon purge to remove residual HCl (g). The solution was washed twice with 10% NaOH (aq) and deionized water, then dried over $MgSO_4$. The solvent was removed under reduced pressure, and the product crystallized from petroleum ether (X = Me, Cl, Br) or ethanol (X = OMe, H).

*(a) (p-$MeOC_6H_4O)_6W$ (**1**-CH_3).* TLC (50% ethyl acetate:hexane): $R_f = 0.59$. ^{1}H NMR (acetone-d_6): δ 3.72 (s, Me), 6.78 (d, $J = 9$ Hz, CH), 6.85 (d, $J = 9$ Hz, CH). $^{13}C\{^1H\}$ NMR (acetone-d_6): δ 55.85 (Me), 114.67 (C_m), 121.91 (C_o), 156.71 (C_p), 156.93 (C_{ipso}).

*(b) (p-$MeC_6H_4O)_6W$ (**1**-CH_3).* TLC (25% ethyl acetate:hexane): $R_f = 0.66$. ^{1}H NMR (acetone-d_6): δ 2.33 (s, Me), 6.83 (d, $J = 9$ Hz, CH), 7.05 (d, $J = 9$ Hz, CH). $^{13}C\{^1H\}$ NMR (acetone-d_6): δ 20.69 (Me), 120.96 (C_o), 130.17 (C_m), 133.77 (C_p), 160.78 (C_{ipso}).

*(c) (p-$ClC_6H_4O)_6W$ (**1**-Cl).* TLC (25% ethyl acetate:hexane): $R_f = 0.73$. ^{1}H NMR (acetone-d_6): δ 7.01 (d, $J = 9$ Hz, CH), 7.32 (d, $J = 9$ Hz, CH). $^{13}C\{^1H\}$ NMR (acetone-d_6): δ 122.63 (C_o), 129.81 (C_p), 130.04 (C_m), 160.79 (C_{ipso}).

*(d) (p-$BrC_6H_4O)_6W$ (**1**-Br).* TLC (15% ethyl acetate:hexane): $R_f = 0.68$. ^{1}H NMR (acetone-d_6): δ 6.96 (d, $J = 9$ Hz, CH), 7.47 (d, $J = 9$ Hz, CH). $^{13}C\{^1H\}$ NMR (acetone-d_6): δ 123.07 (C_o), 133.07 (C_m), 161.24 (C_{ipso}), C_p obscured.

*(e) ($C_6H_5O)_6W$ (**1**-H).* TLC (25% ethyl acetate:hexane): $R_f = 0.60$. ^{1}H NMR (acetone-d_6): δ 6.90 (t, $J = 8$ Hz, CH_p), 6.96 (d, $J = 8$ Hz, CH), 7.27 (t, $J = 8$ Hz, CH_m). $^{13}C\{^1H\}$ NMR (acetone-d_6): δ 121.16 (C_o), 124.59 (C_p), 129.81 (C_p), 129.88 (C_m), 162.69 (C_{ipso}).

4.2.4. General (p-$XC_6H_4O)_5W(OC_6H_4OH)$ (6-X, X = OMe, Me, H, Cl, Br)

A 250 mL round bottom flask was charged with **1**-X (5.4 mmol), 4-(benzyloxy)phenol (10 mmol), p-toluenesulfonic acid monohydrate (1.1 mmol), and chlorobenzene (100 mL). The solution was refluxed under an argon atmosphere for 1–3 h and the reaction was monitored by TLC (silica plate) for optimization of the monosubstituted product (p-$XC_6H_4O)_5W(OC_6H_4OCH_2Ph)$ (**5**-X). Toluene (100 mL) was added to reaction solution and the mixture was washed three times with both 5% NaOH(aq) and de-ionized water. It was dried over $MgSO_4$, and the solvent was removed under reduced pressure. The resulting red oil was dissolved in a mixture of toluene (50 mL) and absolute ethanol (50 mL) followed by an argon purge. 10% Palladium on carbon (0.125 g) was added and the heterogeneous solution was stirred under hydrogen (1 atm) for 5 h. Analysis by TLC of the hydrogenated solution versus the starting solution indicated complete hydrogenation. The catalyst was removed by filtration and the volatiles were removed on a rotary evaporator. Purification was accomplished by column chromatography on silica using an appropriate mixture of ethyl acetate and hexane as the mobile phase. Further purification by recrystallization from methanol was performed when possible.

*(a) (p-$MeOC_6H_4O)_5W(O$-$C'_6H'_4OH)$ (**6**-OMe).* TLC(50% ethyl acetate:hexane): $R_f = 0.50$. ^{1}H NMR (acetone-d_6): δ 3.73 (s, 15H, Me), 6.71 (d, $J = 9$ Hz, 2H, H'_o or H'_m), 6.80 (m, 12H, H_m and $C'H'_o$ or $C'H'_m$), 6.86 (m, 10H, CH_o), 8.20 (s, 1H, OH). $^{13}C\{^1H\}$ NMR (acetone-d_6): 55.83 (Me), 114.63 (C_m), 115.98 (C'_m), 121.90 (C_o), 122.02 (C'_o), 154.43 (C'_p), 156.25 (C'_{ipso}), 156.60 (C_p), 156.98 (C_{ipso}). *Anal.* Calc for $C_{41}H_{40}O_{12}W$: C, 54.2; H, 4.5. Found: C, 54.2; H, 4.4%.

*(b) (p-$MeC_6H_4O)_5W(OC'_6H'_4OH)$ (**6**-Me).* TLC (25% ethyl acetate:hexane): R_f(**5**-Me) = 0.44; R_f(**6**-Me) = 0.18. ^{1}H NMR (acetone-d_6): δ2.32(s, 15H, Me), 6.71 (d, $J = 9$ Hz, 2H, $C'H'_o$ or $C'H'_m$), 6.82 (m, 12H, H_o and H'_o or H'_m) 7.05 (d, $J = 9$Hz, 10H, H_m), 8.31 (s, 1H, OH). $^{13}C\{^1H\}$ NMR (acetone-d_6): 20.86 (Me), 115.93 (C'_m), 120.92 (C_o), 122.20 (C'_o), 130.16 (C_m), 133.57 (C_p), 154.81 (C'_p), 156.13 (C'_{ipso}), 160.85 (C_{ipso}). *Anal.* Calc for $C_{41}H_{40}O_7W$: C, 59.4; H, 4.9. Found: C, 59.5; H, 4.8%.

*(c) (p-$BrC_6H_4O)_5W(OC'_6H'_4OH)$ (**6**-Br).* TLC (3% ethyl acetate:hexane): R_f(**5**-Br) = 0.75; R_f(**6**-Br) = 0.44. ^{1}H NMR (acetone-d_6): δ 6.71 (m, 2H, $C'H'_o$ or $C'H'_m$), 6.94 (m, 12H, H_o and $C'H'_o$ or $C'H'_m$) 7.46 (m, 10H, H_m), 8.62 (s, 1H, OH).

*(d) (p-ClC$_6$H$_4$O)$_5$W(OC$'_6$H$'_4$OH) (**6**-Cl).* TLC (3% ethyl acetate:hexane): R_f(**5**-Cl) = 0.70; R_f(**6**-Cl) = 0.41. 4-Chlorophenol could not be separated from **6**-Cl by column chromatography or crystallization and impeded definitive spectroscopic characterization.

*(e) (C$_6$H$_5$O)$_5$W(OC$'_6$H$'_4$OH) (**6**-H).* TLC (25% ethyl acetate:heptane): R_f(**5**-H) = 0.48; R_f(**6**-H) = 0.25. ^{1}H NMR (acetone-d$_6$): δ 6.72 (d, J = 8 Hz, 2H, C$'$H$'_o$ or C$'$H$'_m$), 6.93 (m, 17H, CH$_o$, CH$_m$ and C$'$H$'_o$ or C$'$H$'_m$), 7.26 (m, 10H, d), 8.32 (s, 1H, OH). ^{13}C{^{1}H} NMR (acetone-d$_6$): 115.99 (C$'_m$), 121.09 (C$_o$), 122.30 (C$'_o$), 124.31 (C$_p$), 129.83 (C$_m$), 154.31 (C$'_p$), 155.94 (C$'_{ipso}$), 162.81 (C$_{ipso}$).

4.2.5. {K[(p- ClC$_6$H$_4$O)$_6$W]}$_\infty$ (**8**-Cl)

A 25 mL round bottom flask was charged with **1**-Cl (0.300 g, 0.316 mmol), Raney Nickel (0.075 g, 1.28 mmol), diethyl ether (15 mL), and ethanol (0.40 mL). Potassium metal (0.02 g, 0.5 mmol) was added and the purple-red solution was stirred for 2 h. The resulting heterogeneous orange solution was filtered, and the filtrate layered with pentane yielding the product as orange crystals (0.191 g, 61%). *Anal.* Calc. for $C_{36}H_{24}O_6Cl_6KW$: C, 43.8; H, 2.5; Cl, 21.5. Found: C, 44.0; H, 2.5; Cl, 20.6%.

4.2.6. {K[(C$_6$H$_5$O)$_6$W]}$_\infty$ (**8**-H)

A 25 mL round bottom flask was charged with **1**-H (0.200 g, 0.269 mmol), Raney Nickel (0.050 g, 0.852 mmol), diethyl ether (10 mL), and ethanol (0.30 mL). Potassium metal (0.02 g, 0.5 mmol) was added and the purple-red solution was stirred for 2 h resulting in a yellow precipitate and light yellow solution. The solid was collected by filtration and separated from the remaining Raney Nickel by dissolution in minimal THF followed by filtration and crystallization by slow evaporation (0.093 g, 44%). ^{1}H NMR (thf-d_8): δ 4.96 ($v_{1/2} \sim 20$ Hz, 6H, H$_p$), 6.63 ($v_{1/2} \sim 40$ Hz, 12H, CH), 9.28 ($v_{1/2} \sim 20$ Hz, 12H, CH). The ^{1}H NMR spectrum is similar to that obtained by Wilkinson and coworkers [45] (acetone-d$_6$) for an independent synthesis of KW(OPh)$_6$. μ_{eff}(293K) = 1.5 μ_B (Evans' method in thf-d$_8$).

4.2.7. Preparation of [(p-ClC$_6$H$_4$O)$_6$W][K(PhCN)$_4$] (**9**-Cl)

A 10 mm O.D. glass tube was charged with **8**-Cl (0.081 g, mmol) and benzonitrile (4 mL). The solution was degassed, sealed, and heated at 100 °C for 5 d with no color change. The product was isolated as an orange solid (0.072 g, 63%) after solvent removal followed by trituration with pentane. ^{1}H NMR (thf-d_8): δ 7.12 ($v_{1/2} \sim 160$ Hz, 12H, CH), 7.51 (t, J = 8 Hz, 8H, PhCN H$_p$ or H$_m$), 7.63 (t, J = 8 Hz, 4H, PhCN H$_p$ or H$_m$), 7.69 (d, J = 8 Hz, 8H, PhCN H$_o$), 9.18 ($v_{1/2} \sim 10$ Hz, 12H, CH).

4.2.8. Electrochemistry: general procedure

The working electrode was a 1mm diameter platinum disk electrode sealed in glass. In cases where fast sweep rates were employed, a 75 μm platinum disk electrode, sealed in glass, was used. All measurements were carried out inside a glove-box (Vac. Atmospheres) at 25 °C. Acetonitrile (Burdick & Jackson; distilled in glass) and dried over 4 Å molecular sieves was used as the solvent. Tetra-*n*-butyl ammonium hexafluorophosphate (TBAG; G.F. Smith) used as supporting electrolyte was recrystallized 3× from absolute ethanol and dried under vacuum for 96 h. A Princeton Applied Research Model 173 Potentiostat with a model 175 Programmer were used. Data at sweep rates at or below 500 mV/s were recorded on a Soltec X–Y recorder. At faster sweep rates, data were recorded on a Tektronix digital storage oscilloscope. A background scan of solvent and supporting electrolyte out to the potential limits of the experiment, was always varied out. A sweep rate dependence of the peak current was carried out for all the materials involved and in all cases the current was proportional to the square root of the sweep rate (over a typical range of 50–1000 mV/s) as anticipated for a diffusion controlled process. A silver wire was employed in order to ensure rigorous exclusion of water, especially since experiments were done inside a dry box. Reproducibility of the peak potentials – even those that are irreversible – was roughly ±10–15 mV.

4.2.9. X-ray crystal structure determination: {K[(p-ClC$_6$H$_4$O)$_6$W]}$_\infty$ (8-Cl)

X-ray diffraction quality single crystals were obtained by layering a saturated diethyl ether solution of **8**-Cl with pentane. One orange crystal ($0.3 \times 0.15 \times 0.1$ mm) was selected, coated in polyisobutylene, and placed under a 173 K nitrogen stream on the goniometer head of a Siemens SMART CCD Area Detector system equipped with a fine-focus molybdenum X-ray tube (λ = 0.71073 Å). Preliminary diffraction data revealed a triclinic crystal system. A hemisphere routine was used for data collection. The data was subsequently processed with the Bruker SAINT program and the space group was determined to be $P\bar{1}$. The data was corrected for absorption with SADABS, solved by direct methods, completed by subsequent difference Fourier syntheses and refined by full-matrix least-squares procedures (SHELXTL). All non-hydrogen atoms were refined with anisotropic displacement parameters and hydrogen atoms were included at calculated positions. [1]

[1] Cambridge Crystallographic Data Centre deposition number: CCDC 247677.

Acknowledgements

The National Science Foundation and the Department of Chemistry and Chemical Biology at Cornell University are gratefully acknowledged for support. T.P.V. thanks the NSF for an Inorganic Materials Traineeship. We thank a referee for pointing out the work of Cheng, Handoo, Xue and Parker [50].

References

[1] J.A. Labinger, J.E. Bercaw, Nature 417 (2002) 506–514.
[2] S. Stahl, J.A. Labinger, J.E. Bercaw, Angew. Chem. Int. Ed. Engl. 37 (1998) 2180–2192.
[3] (a) A.E. Shilov, G.B. Shul'pin, Activation and Catalytic Reactions of Saturated Hydrocarbons in the Presence of Metal Complexes, Kluwer Academic Press, Dordrecht, Netherlands, 2000;
(b) A.E. Shilov, A.A. Shteinmann, Coord. Chem. Rev. 24 (1977) 97–143.
[4] M.S. Freund, J.A. Labinger, N.S. Lewis, J.E. Bercaw, J. Mol. Catal. 87 (1994) L11–L16.
[5] M. Lin, C. Shen, E.A. Garcia-Zayas, A. Sen, J. Am. Chem. Soc. 123 (2001) 1000–1001.
[6] R.A. Periana, O. Mironov, D. Taube, G. Bhalla, C.J. Jones, Science 301 (2003) 814–818.
[7] R.A. Periana, D.J. Taube, S. Gamble, H. Taube, T. Satoh, H. Fujii, Science 280 (1998) 560–564.
[8] R.F. Jordan, D.F. Taylor, N.C. Baenziger, Organometallics 9 (1990) 1546–1557.
[9] C.G. Jia, D.G. Piao, J.Z. Oyamada, W.J. Lu, T. Kitamura, Y. Fujiwara, Science 287 (2000) 1992–1995.
[10] T. Matsumoto, R.A. Periana, D.J. Taube, H. Yoshida, J. Mol. Catal. A: Chem. 180 (2002) 1–18.
[11] (a) K.M. Waltz, J.F. Hartwig, J. Am. Chem. Soc. 122 (2000) 11358–11369;
(b) H.Y. Chen, S. Schlecht, T.C. Temple, J.F. Hartwig, Science 287 (2000) 1995–1997;
(c) C.E. Webster, Y.B. Fan, M.B. Hall, D. Kunz, J.F. Hartwig, J. Am. Chem. Soc. 125 (2003) 858–859.
[12] (a) R.E. Maleczka, F. Shi, D. Holmes, M.R. Smith, J. Am. Chem. Soc. 125 (2003) 7792–7793;
(b) J.Y. Cho, M.K. Tse, D. Holmes, R.E. Maleczka, M.R. Smith, Science 295 (2002) 305–308.
[13] C.M. Jensen, Chem. Commun. (1999) 2443–2449.
[14] (a) K.B. Renkema, Y.V. Kissin, A.S. Goldman, J. Am. Chem. Soc. 125 (2003) 7770–7771;
(b) K. Krogh-Jespersen, M. Czerw, N. Summa, K.B. Renkema, P.D. Achord, A.S. Goldman, J. Am. Chem. Soc. 124 (2002) 11404–11416.
[15] G.W. Parshall, S.D. Ittel, Homogeneous Catalysis: The Applications and Chemistry of Catalysis by Soluble Transition Metal Complexes, 2nd ed., Wiley, New York, 1992.
[16] R.A. Sheldon, J.K. Kochi, Metal-catalyzed Oxidations of Organic Compounds, Academic Press, New York, 1981.
[17] W.D. Jones, E.T. Hessell, J. Am. Chem. Soc. 115 (1993) 554–562.
[18] (a) P.O. Stoutland, R.G. Bergman, S.P. Nolan, C.D. Hoff, Polyhedron 7 (1988) 1429–1440;
(b) R.A. Periana, R.G. Bergman, J. Am. Chem. Soc. 108 (1986) 7332–7346.
[19] (a) J.L. Bennett, P.T. Wolczanski, J. Am. Chem. Soc. 119 (1997) 10696–10719;
(b) J.L. Bennett, T.P. Vaid, P.T. Wolczanski, Inorg. Chim. Acta 270 (1998) 414–423.
[20] M.L.H. Green, P.J. Knowles, J. Chem. Soc., Chem. Commun. (1970) 1677.
[21] E.A. Ambundo, R.A. Friesner, S.J. Lippard, J. Am. Chem. Soc. 124 (2002) 8770–8771, and references therein.
[22] M. Newcomb, R. Shen, Y. Lu, M.J. Coon, P.F. Hollenberg, D.A. Kopp, S.J. Lippard, J. Am. Chem. Soc. 124 (2002) 6879–6886, and references therein.
[23] (a) P. Chaudhuri, M. Hess, U. Flörke, K. Wieghardt, Angew. Chem. Int. Ed. 37 (1998) 2217–2220;
(b) P. Chaudhuri, M. Hess, J. Muller, K. Hildenbrand, E. Bill, T. Weyhermüller, K. Wieghardt, J. Am. Chem. Soc. 121 (1999) 9599–9610.
[24] (a) R.C. Pratt, T.D.P. Stack, J. Am. Chem. Soc. 125 (2003) 8716–8717;
(b) Y.D. Wang, J.L. DuBois, B. Hedman, K.O. Hodgson, T.D.P. Stack, Science 279 (1998) 537–540.
[25] C.R. Goldsmith, R.T. Jonas, T.D.P. Stack, J. Am. Chem. Soc. 124 (2002) 83–96.
[26] (a) J.-U. Rohde, J.-H. In, M.H. Lim, W.W. Brennessel, M.R. Bukowski, A. Stubna, E. Münck, W. Nam, L. Que Jr., Science 299 (2003) 1037–1039;
(b) M.H. Lim, J.-U. Rohde, A. Stubna, M.R. Bukowski, M. Costas, R.Y.N. Ho, E. Münck, W. Nam, L. Que Jr., Proc. Natl. Acad. Sci. 100 (2003) 3665–3670.
[27] J. Kaizer, E.J. Klinker, N.Y. Oh, J.-U. Rohde, W.J. Song, A. Stubna, J. Kim, E. Münck, W. Nam, L. Que Jr., J. Am. Chem. Soc. 126 (2004) 472–473.
[28] (a) D.D.M. Wayner, V.D. Parker, Acc. Chem. Res. 26 (1993) 287–294;
(b) M. Tilset, V.D. Parker, J. Am. Chem. Soc. 111 (1989) 6711–6717; M. Tilset, V.D. Parker, J. Am. Chem. Soc. 112 (1990) 2843;
(c) V.D. Parker, K.L. Handoo, F. Roness, M. Tilset, J. Am. Chem. Soc. 113 (1991) 7493–7498.
[29] J.M. Mayer, Acc. Chem. Res. 31 (1998) 441–450.
[30] K.A. Gardner, J.M. Mayer, Science 269 (1995) 1849–1851.
[31] (a) K. Wang, J.M. Mayer, J. Am. Chem. Soc. 119 (1997) 1470–1471;
(b) J.R. Bryant, J.M. Mayer, J. Am. Chem. Soc. 125 (2003) 10351–10361, and references therein.
[32] L.B. Handy, K.G. Sharp, F.E. Brinckman, Inorg. Chem. 11 (1972) 523–531.
[33] T.P. Vaid, O.L. Sydora, R.E. Douthwaite, P.T. Wolczanski, E.B. Lobkovsky, J. Chem. Soc. Chem. Commun. (2001) 1300–1301.
[34] S.M. Beshouri, I.P. Rothwell, Inorg. Chem. 25 (1986) 1962–1964.
[35] H. von Funk, W. Baumann, Z. anorg. Chem. 231 (1937) 264–268.
[36] P.I. Mortimer, M.I. Strong, Aust. J. Chem. 18 (1965) 1579–1587.
[37] B.R. Eggins, J.Q. Chambers, J. Electrochem. Soc. 117 (1970) 186–192.
[38] M.W. Lehmann, D.H. Evans, J. Electroanal. Chem. 500 (2001) 12–20, and references therein.
[39] L. Papouchado, R.W. Sandford, G. Petrie, R.N. Adams, J. Electroanal. Chem. 65 (1975) 275–284.
[40] C. Iwakura, M. Tsunaga, H. Tamura, Electrochem. Acta 17 (1972) 1391–1400.
[41] D.T.Y. Yiu, M.F.W. Lee, W.W.Y. Lam, T.-C. Lau, Inorg. Chem. 42 (2003) 1225–1232.
[42] J.A. Richards, D.H. Evans, J. Electroanal. Chem. 81 (1977) 171–187.
[43] J. Berkowitz, G.B. Ellison, D. Gutman, J. Phys. Chem. 98 (1994) 2744–2765, and references therein.
[44] D.E. Berning, B.C. Noll, D.L. DuBois, J. Am. Chem. Soc. 121 (1999) 11432–11447.
[45] H. Funk, H. Matschiner, H. Naumann, Z. Anorg. Allg. Chem. 340 (1965) 75–81.
[46] J.I. Davies, J.F. Gibson, A.C. Skapski, G. Wilkinson, W.-K. Wong, Polyhedron 1 (1982) 641.
[47] (a) M.L. Listemann, J.C. Dewan, R.R. Schrock, J. Am. Chem. Soc. 107 (1985) 7207–7208;
(b) M.A. Lockwood, P.E. Fanwick, O. Eisenstein, I.P. Rothwell, J. Am. Chem. Soc. 118 (1996) 2762–2763.

[48] (a) J.K. Kochi (Ed.), Free Radicals, Wiley, New York, 1973;
(b) J.H. Knox, in: Z.B. Alfassi (Ed.), Chemical Kinetics of Small Organic Radicals, CRC Press, Boca Raton, FL, 1988.
[49] L.M. Slaughter, P.T. Wolczanski, T.R. Klinckman, T.R. Cundari, J. Am. Chem. Soc. 122 (2000) 7953–7975.
[50] J.-P. Cheng, K.L. Handoo, J. Xue, V.D. Parker, J. Org. Chem. 58 (1993) 5050–5054.

Available online at www.sciencedirect.com
SCIENCE DIRECT®
Polyhedron 23 (2004) 2857–2872
POLYHEDRON
www.elsevier.com/locate/poly

Transfer hydrogenation reduction of ketones, aldehydes and imines using chelated iridium(III) *N*-heterocyclic bis-carbene complexes

John R. Miecznikowski *, Robert H. Crabtree *

Department of Chemistry, Yale University, 225 Prospect Street, New Haven, CT 06520-8107, USA

Received 11 May 2004; accepted 8 July 2004
Available online 27 August 2004

Dedicated to Malcolm Green: not only a great scientist, but also a caring mentor

Abstract

A series of imidazolium and triazolium chelate ligand precursors are metalated with $[Ir(coe)_2Cl]_2$ (coe = cyclooctene) or $[Ir(cod)Cl]_2$ (cod = 1,5-cyclooctadiene) to give iridium(III) *N*-heterocyclic carbene (NHC) chelates [(NHC)(linker)(NHC)IrI_2(OAc)]. The triazolium salts metalate more easily and give less electron donating NHCs as shown by IR spectroscopy on analogous iridium(I) carbonyl derivatives. The iridium(III) complexes show activity for the title catalytic reactions in 2-propanol that is very variable, depending on the nature of the linker and terminal *N*-substituents. Selective reduction of aldehydes over ketones becomes possible with K_2CO_3, an alternative base promoter to the usual KOH. TOFs of up to 1500/h were achieved.
© 2004 Elsevier Ltd. All rights reserved.

Keywords: *N*-Heterocyclic carbenes; Homogenous catalysis; Transfer hydrogenation; Ketones; Aldehydes; Imines

1. Introduction

N-heterocyclic carbenes (NHCs) are sometimes considered phosphine alternatives for homogenous catalysis [1]. As their chemistry becomes better explored, however, differences have continued to emerge. There are many examples of monodentate NHCs, but only a few of chelating bis-carbene ligands [2]. Comparison with phosphine chemistry suggests that having a chelated bis-carbene ligand could be very useful. Chelated carbenes may have higher stability since one possible decomposition pathway, reductive elimination of the carbene, may be slower for this conformationally restricted case. Others [3] and we [4] have published chelating palladium bis-carbene compounds. Meanwhile, Peris and co-workers first synthesized the rhodium species [Rh(III)(bis-carbene)(OAc)I_2], [5] and we have synthesized the iridium species [Ir(III)(bis-carbene)(OAc)I_2] [6]. The rhodium and iridium bis-carbene compounds were subsequently studied for catalysis. We have prepared several iridium(III) bis-carbene complexes which are very active precatalysts under low catalyst loadings for the transfer hydrogenation of ketones and aldehydes [6,7]. These complexes are all very easy to synthesize and air-stable. Furthermore, their catalytic activity was completely unaffected by the presence of air. Most likely, these precatalysts [6] followed a monohydride mechanism, which has been observed before for other complexes [8].

In a variety of rhodium(I) and rhodium(III) chelates we found a strong effect on the chemistry as the linker length was varied [9]. In this paper we prepare robust

* Corresponding authors. Fax: +1 203 432 6144.
E-mail addresses: john.miecznikowski@yale.edu (J.R. Miecznikowski), robert.crabtree@yale.edu (R.H. Crabtree).

0277-5387/$ - see front matter © 2004 Elsevier Ltd. All rights reserved.
doi:10.1016/j.poly.2004.07.001

chelated iridium(III) bis-imidazole and bis-triazole complexes with different linking groups to see how the linker group affects the catalytic activity of these complexes. These complexes are screened for catalytic activity for the transfer hydrogenation of ketones, aldehydes and imines.

Reduction of C=N bonds is of great interest to the pharmaceutical industry because amines are present in many drugs. Reagents such as sodium borohydride or lithium aluminum hydride can of course be used in stoichiometric quantities to reduce ketones and imines. In addition, sodium cyanoborohydride can selectively reduce an imine formed from a ketone and an amine in reductive amination [10].

Catalytic reduction is preferred to stoichiometric reduction for large scale industrial use, and both ketone [11] and imine [12–14] hydrogenation are well known. Hydrogen gas presents considerable safety hazards especially for a large scale reaction [15].

The use of a solvent that can donate hydrogen overcomes these difficulties. 2-propanol is a popular reactive solvent for the transfer hydrogenation reaction since it is easy to handle (b.p. 82 °C), and is relatively non-toxic, environmentally benign, and inexpensive. The volatile acetone product can also be easily removed to shift an unfavorable equilibrium [16]. The formic acid:triethyl amine azeotrope allows reduction of imines under irreversible conditions with formation of carbon dioxide [16]. Noyori [16] has used this azeotrope to reduce imines with high enantiomeric excess under mild conditions. One advantage of 2-propanol is that it does not affect the pH of the reaction solution like formic acid [17]. We previously reported that the formic acid:triethyl amine azeotrope is not optimal for our precatalysts [6]. Imines are more difficult to reduce by homogenous transfer hydrogenation catalysis than ketones and aldehydes, and fewer examples of their transfer hydrogenation are known [18–29] versus ketones [30]. This may well be a result of imine lone pair coordination to the metal partially blocking catalysis.

2. Results and discussion

Robust ligand precursors were prepared with neopentanediyl and *o*-xylene linkers with neopentyl wingtip groups (Fig. 1). This wingtip group was chosen because it gave excellent results for transfer hydrogenation of ketones [6] and aldehydes [7] and also because the neopentyl wingtip group cannot decompose following a Hoffmann elimination pathway [31]. Finally, neopentyl wingtips have previously improved the solubility of the complex and given crystals where disorder problems were minimized.

2.1. Synthesis of ligands and iridium(I) and iridium(III) complexes

Chelating bis-imidazole ligand precursors **1** and **2**, were prepared (Fig. 1). Compound **1** has an *ortho*-xylene

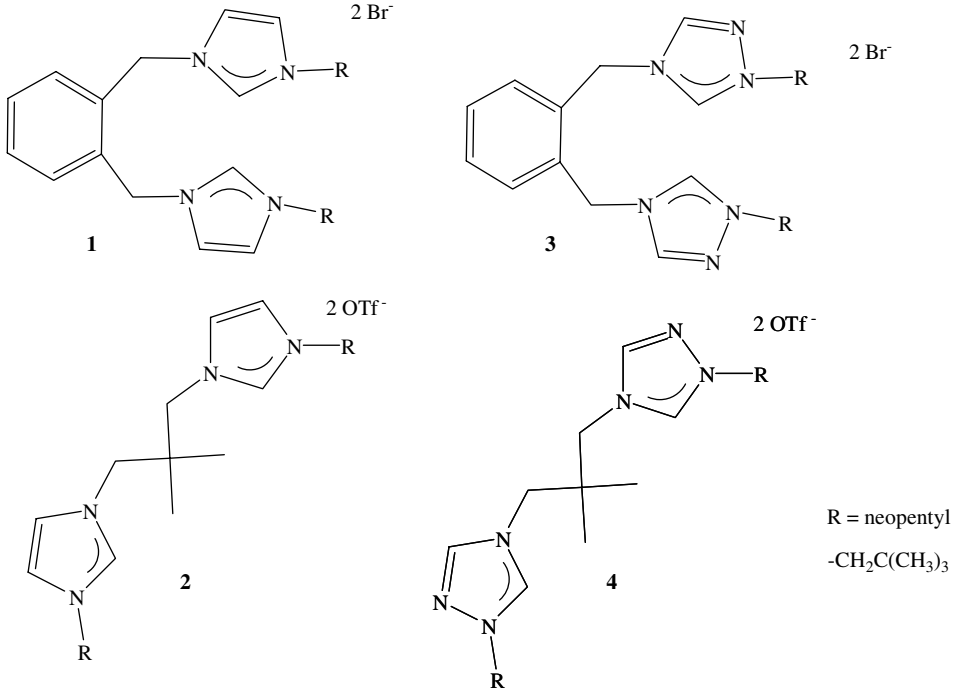

Fig. 1. Robust ligand precursors for iridium (III) bis-carbene complexes.

linker also used for rhodium by Peris and co-workers [32,33] Compound **2** has a neopentanediyl linking group also used by Hahn et al. [34].

In order to vary the electronic effect of the ligand, change of the aromatic core is more efficient than change of substituents at nitrogen, so we have moved to triazole, less electron donating than imidazole [35]. Bis-triazole analogs of **1** and **2** are also given in Fig. 1.

Ligand precursors **1**–**4** could be metalated to form iridium(III) products. It proved hardest to metalate **1** and **2**, but this was finally achieved with $[Ir(cod)Cl]_2$ (cod = 1,5-cyclooctadiene) following Eq. (1) where iridium is oxidized to iridium(III) according to Eq. (2) [32,33]. It seems to be a general pattern that triazole derivatives like **3**–**4** can be metallated more easily than their imidazole analogues.

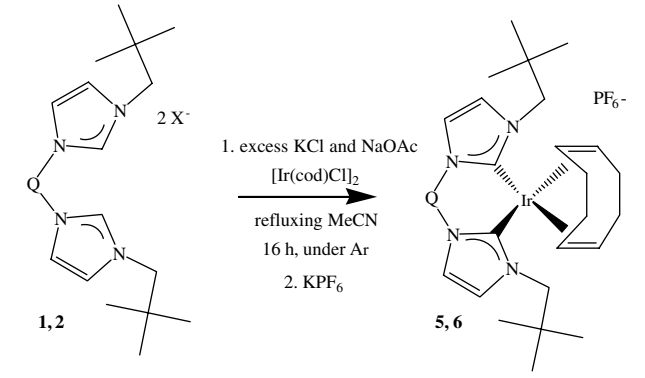

1 (Q = *o*-xylene, X = Br)
2 (Q = neopentanediyl, X = triflate)

5 (Q = *o*-xylene)
6(Q=neopentanediyl)

(1)

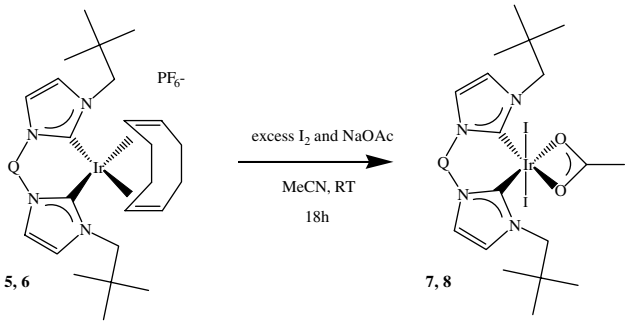

5 (Q = *o*-xylene)
6 (Q = neopentanediyl)

7 (Q = *o*-xylene)
8 (Q = neopentanediyl)

(2)

The iridium(III) products obtained in Eq. (1) followed by (2) were only available via this two step route and not in only one step from compounds **1** or **2**, as has proved possible for other ligand precursors using conditions previously published [5,6]. $[Ir(coe)_2Cl]_2$ (coe = cyclooctene) with more labile coe ligands gave approximately 10% higher yields than $[Ir(cod)Cl]_2$, normally used.

The chelating bis-triazole ligands could also be metalated according to Eq. (3). Unlike the bis-imidazole cases (Eqs. (1) and (2)), only one step was needed to obtain the iridium(III) product. For **9** and **10**, higher yields were again obtained with $[Ir(coe)_2Cl]_2$.

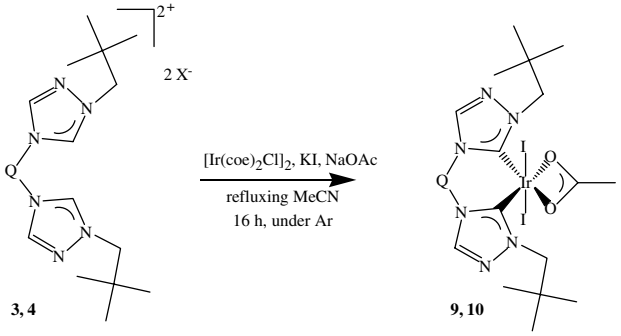

3 (Q = *o*-xylene, X = bromide)
4 (Q = neopentanediyl, X = triflate)

9 (Q = *o*-xylene)
10 (Q = neopentanediyl)

(3)

An iridium(III) compound **11**, was also synthesized from methylenebis(*N*-neopentyl) triazo-ligand precursor (Eq. (4)). This is the triazole analogue of an iridium(III) compound that we previously showed [6] is one of the most active catalysts known for transfer hydrogenation. It was therefore of interest to compare the catalytic activity of **11** to that of the very active prior compound.

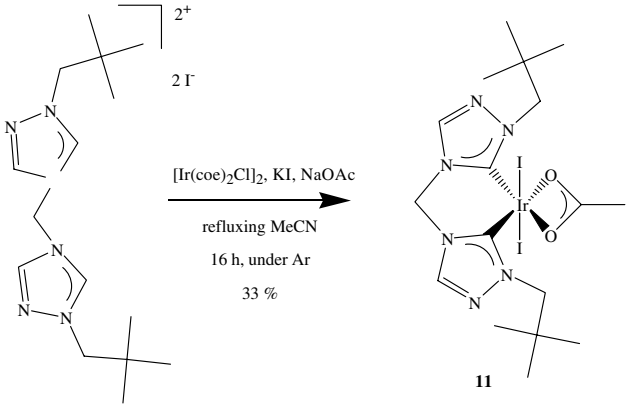

(4)

2.2. Comparison of electron donating ability of bis-imidazole and bis-triazole iridium(I) compounds

Bis-chelating neopentylene imidazole (**12**) and triazole (**14**) iridium(I) compounds with two CO ligands could also be prepared following Eq. (5).

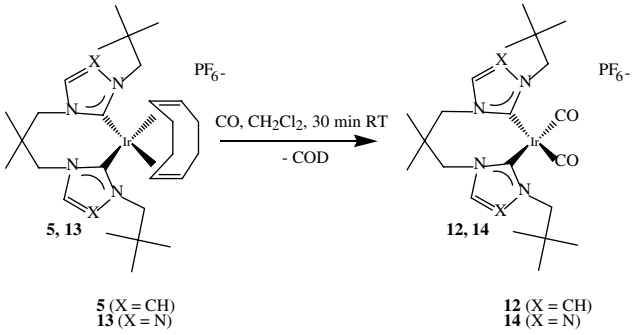

(5)

FT-IR spectra were obtained of **12** and **14**. The iridium(I) compound with a bis-imidazole ligand, **12**, has a CO average stretching frequency of 2036 cm^{-1}, while that with a bis-triazole ligand, **14**, has an average stretching frequency of 2051 cm^{-1}. This comparison, the first to our knowledge, indicates that the triazole compound is less electron donating than the imidazole compound [36]. We also attempted to prepare iridium(I) analogs of **12** and **14** with *n*-butyl wingtips or methyl wingtips, but, we were unable to synthesize the bis-triazole ligands with either *n*-butyl or methyl wingtips and a neopentanediyl linker. Thus, neopentyl wingtip groups are needed to prepare iridium(I) complexes with this linker. This illustrates the utility of the neopentyl wingtip group in facilitating metalation.

All of the iridium (bis-carbene) complexes are soluble in dichloromethane, chloroform, acetone, and tetrahydrofuran, but are insoluble in pentane and diethyl ether.

2.3. Spectroscopy

The structure of the iridium bis-carbene compounds was first deduced from NMR spectroscopy [6,7]. For complex **11**, only one set of signals has been detected for the protons of the carbene chelate. This is consistent with the two halves of the ligand being symmetry related. For the complexes with the less flexible neopentanediyl and *o*-xylene linkers (**5**–**10**), an AB pattern was observed for the protons in the chelate.

For **7**–**11**, in the $^{13}C\{^1H\}$ spectrum there is a low field singlet at approximately δ 132 ppm for the iridium bound carbon. The acetate anion gives rise to the expected NMR signals (δ_H 2.0, δ_C 190 and 25).

In the $^{13}C\{^1H\}$ spectrum the iridium(I) chelating carbene compounds **5**, **6** and **13**, show a low field singlet at approximately δ 179 ppm for the carbene carbon. In the ^1H NMR spectrum, the cyclooctadiene protons appear as three or four broad resonances in the δ 2.3 to 2.0 ppm region.

The iridium(I) biscarbonyl complexes **12** and **14**, show a low field singlet in the $^{13}C\{^1H\}$ spectrum at δ 171 ppm for the iridium bound carbon and the Ir-CO resonance occurs at δ 181 ppm. For complexes **12** and **14**, only one signal for the Ir-CO carbon has been detected indicating that the carbonyls are symmetry related.

2.4. Catalytic transfer hydrogenation of ketones

The iridium bis-carbene complexes **6**, **8**, **9**, **10**, and **11** catalyze the reduction of acetophenone to the corresponding alcohol via hydrogen transfer from the solvent, 2-propanol with potassium hydroxide as promoter (Eq. (6)). The iridium(III) compounds are efficient catalysts at a catalyst/base ratio of 0.2. The excess solvent drives the reaction by mass action.

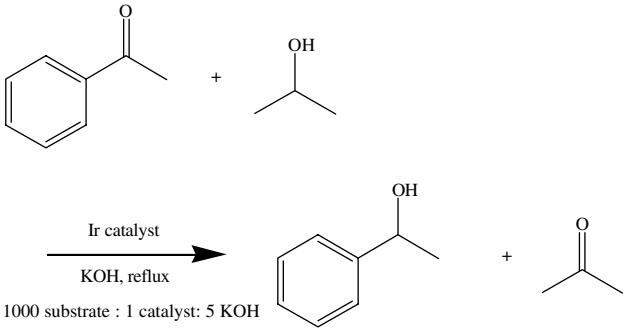

(6)

We have screened the activity of the iridium (bis-carbene) catalysts in transfer hydrogenation using acetophenone as a substrate and substrate/catalyst/base ratio of 1000:1:5. The results in Table 1 show the influence of the linker group and the nature of the azole ring.

The results in Table 1 indicate that the bis-imidazole iridium(III) compounds exhibit higher catalytic activity than the bis-triazole compounds (e.g., entries 2–4 versus 5–7). The order of linker effectiveness is altered, however, methylene being best for imidazole, but neopentanediyl for triazole. The bis-imidazole version of compound **11**, compound **15**, is very active in transfer hydrogenation of acetophenone and other ketones with a maximum TOF (TON h^{-1}) of 50 000 [6]. Entry 8, with a substrate:precatalyst:base ratio of 1000:1:0, indicates that base, KOH, is required as a promoter for the reaction. Entry 9, carried out at 20 °C, shows reflux temperature is required for good activity.

2.5. Use of K_2CO_3 instead of KOH as a base for catalysis

Potassium carbonate, a weaker base than potassium hydroxide and essentially insoluble in 2-propanol, has been used very few times as a base for this reaction [37]. To screen the effectiveness of this base, acetophenone was reduced in the presence of 0.1 mol% catalyst (Eq. (8)). A substrate:precatalyst:base ratio of 1000:1:500 was followed. The results are summarized

Table 1
Influence of the linker group and NHC-ligand in transfer hydrogenation activity of acetophenone[a]

Entry	Catalyst	Linker	Bis-NHC ligand	Time	Yield (%)[b]	TOF[c] (TON h^{-1})
1	none	none	none	24 h	<5	
2	**8**	neopentanediyl	imidazole	20 min	93	2800
3	**7**	*o*-xylene	imidazole	7 h	88	130
4	**15**	methylene	imidazole	4 min	98	15000
5	**10**	neopentanediyl	triazole	1.0 h	98	1000
6	**9**	*o*-xylene	triazole	16.5 h	89	54
7	**11**	methylene	triazole	2.0 h	80	400
8[d]	**10**	neopentanediyl	triazole	17 h	<5	
9[e]	**8**	neopentanediyl	imidazole	24 h	90	38

[a] Reaction conditions for KOH = 1000:1:5 (substrate:precatalyst:base) with 0.2 M substrate in 10 mL of 2-propanol at reflux temperature. The KOH was added as a 10 mM solution in 2-propanol.
[b] The yields were determined using ^{1}H NMR by comparing the amount of starting material and product.
[c] Estimated TOF = (TON/total reaction time).
[d] A substrate:precatalyst:base ratio of 1000:1:0 was used.
[e] Reaction carried out at 20 °C.

Table 2
Potassium carbonate versus potassium hydroxide as a base for transfer hydrogenation of acetophenone[a]

Entry	Catalyst	Linker	Bis-NHC ligand	Base	Time	Yield (%)[b]	TOF[c] (TON h^{-1})
1	**8**	neopentanediyl	imidazole	K_2CO_3	1 h	99	1000
2	**8**	neopentanediyl	imidazole	KOH	20 min	93	2800
3	**15**	methylene	imidazole	K_2CO_3	40 min	97	1500
4	**15**	methylene	imidazole	KOH	4 min	98	15000
5	**10**	neopentanediyl	triazole	K_2CO_3	3 h	98	333
6	**10**	neopentanediyl	triazole	KOH	1 h	98	1000
7	none	none	none	K_2CO_3	3 h	<5	

[a] Transfer hydrogenation of acetophenone. With K_2CO_3, a substrate:precatalyst:base ratio of 1000:1:500 was followed with 0.2 M substrate in 10 mL of 2-propanol at reflux temperature. With KOH, a substrate:precatalyst:base ratio of 1000:1:5 was followed with 0.2 M substrate in 10 mL of 2-propanol at reflux temperature. The KOH was added as a 10 mM solution in 2-propanol.
[b] The yields were determined using ^{1}H NMR.
[c] Estimated TOF = (TON/total reaction time).

in Table 2. For comparison, the catalytic results with potassium hydroxide are also included, where the substrate:precatalyst:base ratio was 1000:1:5.

The results (Table 2) suggest that potassium carbonate can indeed be used as a base for transfer hydrogenation of acetophenone. The reaction occurs faster, though, with potassium hydroxide (Tables 1 and 2). An iridium(I) compound, **6**, was also tested for catalytic activity with potassium carbonate as a promoter but less than 20% of acetophenone was reduced after 20 h. This indicates that an iridium(III) starting material is needed for catalysis.

2.6. Selectivity

Precatalyst **8** catalyzed the transfer hydrogenation reduction of an equimolar mixture of acetophenone and phenylacetaldehyde. Here, a 500:500:1:500 ratio (acetophenone:phenylacetaldehyde:precatalyst **8**:K_2CO_3) was used with 0.2 M total substrate in 10 mL of 2-propanol at reflux temperature. After 1 h, there was complete conversion of phenylacetaldehyde to phenylethyl alcohol but no conversion of acetophenone. Even after 24 h, there was still no further conversion of acetophenone. There was no evidence of aldol products in the proton NMR.

To test intramolecular selectivity, complex **8** was used for the transfer hydrogenation of 4-acetylbenzaldehyde (Eq. (7)).

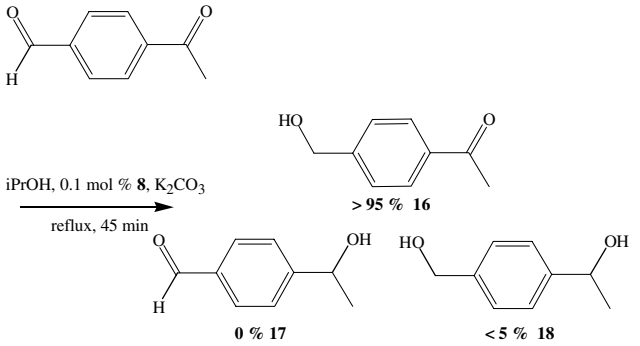

(7)

Of the three possible products possible in Eq. (7) only two are seen in the ^{1}H NMR spectrum with the aldehyde reduction product, **16**, in greater than 95% yield. Precatalyst **8** is therefore also selective for the intramolecular

transfer hydrogenation of aldehydes over ketones. No additional formation of **18** is seen after 90 min.

2.7. Transfer hydrogenation of imines

Because complexes **8**, **10**, and **15** are extremely active catalysts for the transfer hydrogenation of ketones and aldehydes, [6,7] they were also screened for the catalytic transfer hydrogenation of imines (Eq. (8)).

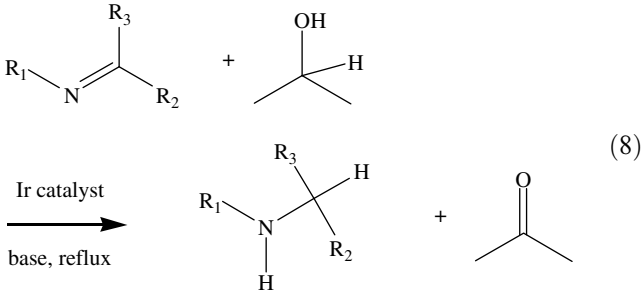

(8)

Precatalyst **15** was screened for catalytic activity in Eq. (9) (Table 3). Either KOH or an alkali carbonate base was utilized, and the products were determined by ^{1}H NMR and compared to authentic material. Prior work suggested that solid alkali carbonates would be useful bases, being milder than the conventional KOH. The imines were either purchased from commercial sources or prepared using known routes [38–40].

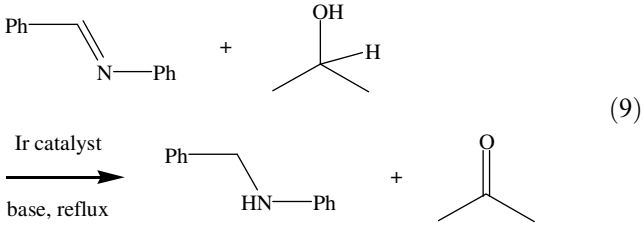

(9)

The results in Table 3 suggest that KOH and K_2CO_3 are the best bases for the transfer hydrogenation of *N*-benzylideneaniline (Eq. (9)). Economy dictates 0.1 mol% as a suitable catalyst loading since in all cases the catalytic reactions were complete within 20 min. For all catalytic reactions discussed below, either KOH or K_2CO_3 will be utilized as a base with either 0.1 or 1.0 mol% catalyst loading. Other imine substrates were subsequently screened for transfer hydrogenation activity (Eq. (8)) and the results are summarized in Table 4.

The results (Tables 3 and 4) suggest that catalyst **15** is only effective for certain types of imine substrates. It appears that bulky substituents must be present at both the carbon and the nitrogen on the imine for successful reduction (Table 3, entries 1–6; Table 4, entries 3–5, 9, 11). The best bases are either KOH or K_2CO_3, and other alkali carbonate bases require longer reaction times.

A low precatalyst loading (0.1 mol%) was sufficient for *N*-benzylideneaniline (PhCH=NPh) (Table 3, entries 1–2) and naphthalen-2-ylmethylene-phenyl-imine (NpCH=NPh) (Table 4, entry 3) but a 1.0 mol% catalyst loading was needed for the other substrates (Table 4, entries 9 and 11). Nevertheless, even higher catalyst loadings were needed for prior catalysts [41]. A very high turnover frequency (TOF) of 3000–6000 (TON h^{-1}) was seen for *N*-benzylideneaniline. Previous precatalysts never gave a TOF greater than 800 (TON h^{-1}) [42].

Precatalysts **8** and **10** also catalyzed transfer hydrogenation of *N*-benzylideneaniline (Table 5 and Eq. (9)).

8 and **10** could also be used as a precatalyst for the transfer hydrogenation reduction of benzylidene aniline but, longer reaction times were needed for this precatalyst when compared to **15** (Tables 3 and 4).

α,β-Unsaturated imines have been reduced previously [43] and one was also prepared according to the method described by Brady and Shieh [44]. These substrates can give several products upon transfer hydrogenation reduction shown in Eq. (10).

Table 3
Transfer hydrogenation of *N*-benzylideneaniline with precatalyst 15

Entry	Catalyst loading (mol%)[a]	Base	Time (min)	Yield (%)[b]	TOF[c] (TON h^{-1})
1	0.1	KOH[d]	10	quantitative	6000
2	0.1	K_2CO_3[e]	20	quantitative	3000
3	1.0	KOH[d]	5	quantitative	1200
4	1.0	K_2CO_3[e]	5	quantitative	1200
5	1.0	Rb_2CO_3[e]	10	quantitative	600
6	1.0	Cs_2CO_3[e]	90	quantitative	67

[a] Transfer hydrogenation of *N*-benzylideneaniline (Eq. (9)). Precatalyst **15** was added as a solution in 0.4 mL of thf.
[b] The yields were determined using ^{1}H NMR.
[c] Estimated TOF = (TON/total reaction time).
[d] Reaction conditions for KOH = 1000:1:5 (substrate:precatalyst:base) with 0.2 M substrate in 10 mL of 2-propanol at reflux temperature. The KOH was added from a 10 mM solution in 2-propanol. Or, 1000:10:50 (substrate:precatalyst:base) with 0.2 M substrate in 10 mL of 2-propanol at reflux. Again, the KOH was added in the form of a 10 mM solution.
[e] The reaction conditions were 1000:1:500 (substrate:precatalyst:base) or 1000:10:500 (substrate:precatalyst:base). Alkali carbonates were added as the solid.

Table 4
Catalytic screening for transfer hydrogenation of imines

Entry	Substrate[a]	Catalyst loading (mol%)[b]	Base	Time	Yield (%)[c]	TOF[d] (TON h^{-1})
1	$Ph_2C{=}NH$	1.0	KOH[e]	1 h	<10	
2	PhCH=NBu	1.0	KOH[e]	1 h	<5	
3	NpCH=NPh	0.1	K_2CO_3[f]	20 min	quantitative	3000
4	NpCH=NPh	1.0	K_2CO_3[f]	4 min	quantitative	1500
5	NpCH=NPh	1.0	KOH[e]	4 min	quant.	1500
6	MesCH=NMes	1.0	K_2CO_3[f]	20 min	14	42
7	*p*-$NO_2C_6H_4$CH=NPh	1.0	K_2CO_3[f]	2 h	36	18
8	*p*-$NO_2C_6H_4$CH=NPh	0.1	K_2CO_3[f]	30 min	<5	
9	*p*-CH_3O-C_6H_4CH=NPh	1.0	K_2CO_3[f]	15 min	quantitative	400
10	PhCH=NC_6H_{11}	1.0	K_2CO_3[f]	20 min	<5	
11	MesCH=NPh	1.0	K_2CO_3[f]	20 min	quantitative	330
12	MesCH=NPh	0.1	K_2CO_3[f]	4 h	79	200
13	PhC(CH_3)=NPh	1.0	K_2CO_3[f]	1 h	<10	
14	PhCH=NCH_2Ph	1.0	KOH[e]	75 min	<5	
15	PhCH=NCH_2 Ph	1.0	K_2CO_3[f]	50 min	<5	

[a] Transfer hydrogenation of imine substrates (Eq. (8)). Ph = phenyl, Bu = *n*-butyl, Np = 2-naphthyl, Mes = mesityl.
[b] Precatalyst **15** was added as a solution in 0.4 mL of thf.
[c] The yields were determined using ^{1}H NMR.
[d] Estimated TOF = (TON/total reaction time).
[e] Reaction conditions for KOH = 1000:1:5 (substrate:precatalyst:base) with 0.2 M substrate in 10 mL of 2-propanol at reflux temperature. The KOH was added as a 10 mM solution in 2-propanol. Or, 1000:10:50 (substrate:precatalyst:base) with 0.2 M substrate in 10 mL of 2-propanol at reflux. Again, the KOH was added in the form of a 10 mM solution.
[f] The reaction conditions were 1000:1:500 (substrate:precatalyst:base) or 1000:1:500 (substrate:precatalyst:base). When potassium carbonate was utilized, it was added as a solid to the reaction flask.

Table 5
Summary of transfer hydrogenation of *N*-benzylideneaniline using precatalysts **8** and **10**s

Entry	Catalyst[a]	Catalyst loading (mol%)	Base	Time	Yield[b]	TOF[c] (TON h^{-1})
1	**8**	1.0	KOH[d]	10 min	quantitative	600
2	**8**	1.0	K_2CO_3[e]	1 h	quantitative	100
3	**8**	0.1	K_2CO_3[e]	2 h	quantitative	500
4	**10**	1.0	KOH[d]	10 min	quantitative	600
5	**10**	1.0	K_2CO_3[e]	3 h	quantitative	17

[a] Transfer hydrogenation of *N*-benzylideneaniline (Eq. (9)). The precatalyst was added to the reaction solution as a solution in 0.4 mL of thf.
[b] The yields were determined using ^{1}H NMR.
[c] Estimated TOF = (TON/total reaction time).
[d] Reaction conditions for KOH = 1000:10:50 (substrate:precatalyst:base) with 0.2 M substrate in 10 mL of 2-propanol at reflux temperature. The KOH was added from a 10 mM solution in 2-propanol.
[e] The reaction conditions were 1000:1:500 (substrate:precatalyst:base) or 1000:10:500 (substrate:precatalyst:base). When potassium carbonate was utilized, it was added as a solid to the reaction flask.

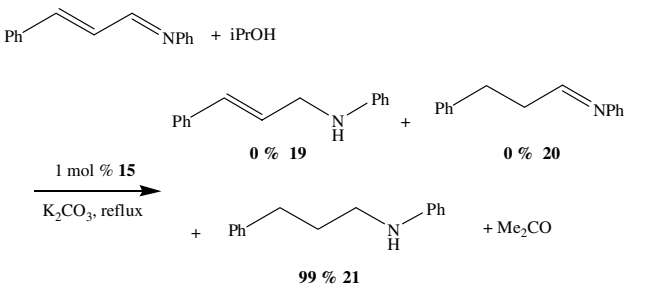

(10)

Precatalyst **15** gave the result shown in Eq. (10), and only the fully reduced product was formed, **21**, in 99% yield. After 30 min, a mixture of **19**–**21** were identified using ^{1}H NMR, an apparent inconsistency here because only **21** is reported in Eq. (10). Again, the products were identified with ^{1}H NMR and compared with authentic material.

Precatalyst **15** can also reduce isolated C=C bonds in amines. For example, the α,β unsaturated imine of Eq. (10) was reduced with sodium borohydride to give amine **19**, which was used as a substrate with precatalyst **15** (1 mol%) to give **21** in quantitative yield after 30 min. Amines often strongly deactivate homogenous catalysts, but this is not the case here. A phenyl substituent may be required on the C=C for amine reduction.

2.8. Competition experiments

Precatalyst **8** gave the transfer hydrogenation reduction of a mixture of acetophenone, phenylacetaldehyde, and *N*-benzylideneaniline (1:1:1 mol. equiv). For this

competition experiment, a 1000:1:500 (sum of substrates:precatalyst **8**:K_2CO_3) was used with 0.2 M total substrate in 10 mL of 2-propanol at reflux temperature. Precatalyst **8** (0.1 mol%) can reduce acetophenone independently in 20 min (Table 1), phenylacetaldehyde independently in 1 h, [45] and *N*-benzylideneaniline independently in 2 h (Table 5). In the competition reaction, after 1 h, there was complete conversion of phenylacetaldehyde to phenylethyl alcohol, but no evidence of *N*-phenylbenzylamine or *sec*-phenylethyl alcohol. After 19 h of total reaction time, there was, in addition, complete conversion of acetophenone to *sec*-phenylethyl alcohol and 73% conversion of *N*-benzylideneaniline to *N*-phenylbenzylamine. Thus, precatalyst **8** is selective for phenylacetaldehyde over acetophenone and *N*-benzylideneaniline. Precatalyst **8** was used instead of **15** because precatalyst **15** cannot reduce phenylacetaldehyde catalytically [7].

Precatalyst **8** catalyzed the transfer hydrogenation reduction of a 1 to 1 mixture of acetophenone and phenylacetaldehyde. Here, 500:500:1:500 (acetophenone:phenylacetaldehyde:precatalyst **8**:K_2CO_3) was used with 0.2 M total substrate in 10 mL of 2-propanol at reflux temperature. After 1 h, there was complete conversion of phenylacetaldehyde to phenylethyl alcohol but no conversion of acetophenone. Even after 24 h, there was still no further conversion of acetophenone.

Precatalyst **8** catalyzed the transfer hydrogenation reduction for a 1 to 1 mixture of phenylacetaldehyde and *N*-benzylideneaniline, with a ratio of 500:500:1:500 (phenylacetaldehyde:*N*-benzylideneaniline:precatalyst **8**:K_2CO_3) and 0.2 M total substrate in 10 mL of 2-propanol at reflux temperature. After 1 h, there was complete conversion of phenylacetaldehyde to phenylethyl alcohol but less than 5% of *N*-phenylbenzylamine. After 17 h, there was 17% of *N*-phenylbenzylamine present. Phenylacetaldehyde is therefore reduced most rapidly in all cases, a rather surprising result, since the imine is the better ligand. The imine no doubt has to attain a π-bound form to be reduced and so strong binding via the N lone pair is a disadvantage. The bulky substituent groups required for efficient imine reduction no doubt help attainment of the π-bound form.

3. Conclusions

We have developed a series of iridium bis-imidazole and bis-triazole precatalysts for the transfer hydrogenation of ketones. The choice of the linker group is important; the best results were obtained with methylene and neopentanediyl linkers. Precatalyst **8**, with a neopentanediyl linker, was selective for the transfer hydrogenation reduction of aldehydes over ketones. The mechanism remains to be defined.

Iridium(III) bis-carbene complexes **8**, **10**, **15** are efficient precatalysts for the transfer hydrogenation reduction of certain imine substrates. Precatalyst **15**, with a methylene linker, is more active than **8** or **10**. Competition experiments show precatalyst **8** is selective for phenylacetaldehyde over acetophenone, and *N*-benzylideneaniline. Further work is in progress.

4. Experimental

$[Ir(cod)Cl]_2$ [46] and $[Ir(coe)_2Cl]_2$ [47] were prepared according to literature procedures; all other reagents are commercially available and were used as received. NMR spectra were recorded at 25 °C on Bruker spectrometers at 400 or 500 MHz (^{1}H NMR or ^{19}F NMR) and 100 or 125 MHz (^{13}C NMR), respectively, and referenced to $SiMe_4$ (δ in ppm, J in Hz). Assignments are based either on distortionless enhancement of polarization transfer (DEPT) experiments or on homo- and heteronuclear shift correlation spectroscopy. Melting points are uncorrected. Elemental analyses were performed by Atlantic Microlab, Inc. (Norcross, GA); solvent of crystallization in the solids has been identified by ^{1}H NMR spectroscopy. Electrospray mass spectra were recorded on a Micromass ZQ instrument using nitrogen as a drying and nebulizing gas. When solvent of crystallization was needed for the analytical data, we verified the presence of that solvent in the sample by ^{1}H NMR spectroscopy. The syntheses of precatalysts **8**, **10**, **15**, complex **6**, ligand precursors **2** and **4**, 1-neopentyl-1,2,4 triazole and neopentanediyl bistriflate have been previously described and were synthesized [6,7].

4.1. Typical procedure for catalytic transfer hydrogenation

Ketone (2.0 mmol), catalyst (0.2 mL of a 10 mM THF solution), base (if KOH is used, it is added to the reaction solution from a 10 mM solution in *i*PrOH) (if alkali carbonate base is used, it is added as a solid to the reaction solution) and *i*PrOH (10 mL) were added in a 50 mL round bottom flask in a preheated oil bath. Aliquots (0.5 mL) were taken at fixed times, diluted in *n*-hexane (10 mL) and filtered through a short path column of SiO_2. The filtrate was evaporated to dryness and analyzed by ^{1}H NMR spectroscopy. The reported yields are a percent conversion of starting material. All data are averages of at least two runs. An internal standard, mesitylene, has been used previously for the transfer hydrogenation reduction of 2-phenylpropionaldehyde and hydrocinnamaldehyde and proton NMR experiments showed no aldehyde after 1 h and the alcohol as

the major product. GC–MS experiments were consistent with this result [7].

Imine (2.0 mmol), precatalyst (0.4 mL in a THF solution), base (if KOH is used, it is added to the reaction solution from a 10 mM solution in *i*PrOH) (if alkali carbonate base is used, it is added as a solid to the reaction solution) and *i*PrOH (10 mL) were added in a 50 mL round bottom flask in a preheated oil bath. The footnotes for each table give the reaction conditions that were followed. Aliquots (0.5 mL) were taken at fixed times, diluted in *n*-hexane (10 mL) and filtered through a short path column of SiO_2. The filtrate was evaporated to dryness and analyzed by ^1H NMR spectroscopy. All data are averages of at least two runs.

4.1.1. Methylenebis(N-neopentyl)triazolium diiodide

A solution of *N*-neopentyl triazole (1.404 g, 10.09 mmol) and CH_2I_2 (1.4084 g, 5.258 mmol) was stirred in refluxing toluene (10 mL) for 3 days. The formed precipitate was collected by filtration and recrystallized from hot MeOH at −20 °C to give the product as an off-white solid. (0.99 g, 36%). ^1H NMR (DMSO-D_6, 400 MHz, $SiMe_4$) δ 10.41 (s, 2H, NC*H*N), 9.40 (s, 2H, NC*H*N), 6.86 (s, 2H, NCH_2N), 4.32 (s, 4H, CH_2CMe_3), 0.98 (s, 18H, C(CH_3)$_3$). $^{13}C\{1H\}$ NMR (DMSO-D_6, 100 MHz, $SiMe_4$) δ 144.55 (NCHN), 143.88 (NCHN), 62.12 (CH_2CMe_3), 55.28 (NCH_2N), 32.24 ($C(CH_3)_3$), 26.57 (C(CH_3)$_3$). *Anal.* Calc. for $C_{15}H_{28}I_2N_6$ (546.23): C, 32.98; H, 5.17; N, 15.39. Found: C, 32.97; H, 5.24; N, 15.44%. Melting point 229–234 °C (dec).

4.1.2. o-Xylenebis(N-neopentyl)imidazolium dibromide (**1**)

A round bottom flask was charged with neopentyl imidazole (0.845 g, 6.11 mmol), α,α′ dibromo-*o*-xylene (0.8084 g, 3.066 mmol), and 1,4 dioxane (10 mL). This reaction solution was heated at reflux for two days after which a brown oil precipitate had formed. The 1,4 dioxane solution was decanted off and the brown oil was washed two times with 1,4 dioxane (10 mL each). The product was then dissolved in methanol (15 mL) and the product was precipitated with diethyl ether. The white flaky solid was collected via vacuum filtration and was washed three times with diethyl ether (40 mL each). Yield 1.3504 g, (82%). ^1H NMR (DMSO-D_6, 500 MHz, $SiMe_4$) δ 9.42 (s, 2H, NCHN), 7.86 (s, 2H, imid-H), 7.82 (s, 2H, imid-H), 7.49 (m, 2H, C_{aryl}-H), 7.28 (m, 2H, C_{aryl}-H), 5.75 (s, 4H, benzyl-CH_2), 4.05 (s, neopentyl-CH_2), 0.93 (s, 18H, neopentyl CH_3). $^{13}C\{^1H\}$ NMR (DMSO-D_6, 125 MHz, $SiMe_4$) δ 137.48 (NCHN), 133.39 (C_{ipso}), 129.98 (C_{aryl}), 129.66 (C_{aryl}), 124.75 (C_{imid}), 122.66 (C_{imid}), 59.98 (neopentyl *C*H_2), 49.42 (benzyl-*C*H_2), 32.27 ($CH_2C(CH_3)_3$), 27.05 ($CH_2C(CH_3)_3$). *Anal.* Calc. for $C_{24}H_{36}Br_2N_4$ (540.38) · $1H_2O$: C, 51.62; H, 6.86; N, 10.03. Found: C, 51.28; H, 6.68; N, 9.90%. Melting point 223–226 °C (dec).

4.1.3. o-Xylenebis(N-neopentyl)triazolium dibromide (**3**)

To a 50 mL schlenk flask, the following were added, neopentyl triazole (1.441 g, 10.35 mmol), α,α′ dibromo-*o*-xylene (1.0099 g, 3.825 mmol) and 1,4-dioxane (15 mL, degassed). This reaction was heated under reflux for 18 h under argon. After allowing the reaction mixture to cool, the white solid was collected via vacuum filtration. This product was washed three times with 1,4-dioxane (30 mL each) and three times with diethyl ether (50 mL each). Yield: 2.05 g (99%). ^1H NMR (DMSO-D_6, 500 MHz, $SiMe_4$) δ 10.54 (s, 2H, NCHN), 9.42 (s, 2H, NCHN), 7.54 (m, 4H, C_{aryl}-H), 5.82 (s, 4H, benzyl-CH_2), 4.25 (s, neopentyl-CH_2), 0.97 (s, 18H, neopentyl CH_3). $^{13}C\{^1H\}$ NMR (DMSO-D_6, 125 MHz, $SiMe_4$) δ 144.52 (NCHN), 143.24 (NCHN), 132.13 (C_{ipso}), 130.51 (C_{aryl}), 130.12 (C_{aryl}), 62.07 (neopentyl *C*H_2), 47.78 (benzyl-*C*H_2), 32.13 (-$CH_2C(CH_3)_3$), 26.77 ($CH_2C(CH_3)_3$). *Anal.* Calc. for $C_{22}H_{34}Br_2N_6$ (542.35): C 48.72, H: 6.32, N 15.50. Found: C, 48.54; H, 6.35; N, 15.27%. Melting point 204–207 °C (dec).

4.1.4. o-Xylenebis(N-neopentyl)imidazole-2-ylidene bis1,5 cyclooctadiene iridium(I) hexafluorophosphate (**5**)

The synthesis of the iridium (I) compound was accomplished by dissolving **1** (0.3120 g, 0.5773 mmol), KCl (0.2986 g, 3.884 mmol), NaOAc (0.3211 g, 3.914 mmol), $[Ir(cod)Cl]_2$ (0.2027g, 0.3018 mmol) in 15 mL of degassed MeCN. This yellow reaction mixture was stirred under argon for 2 min at RT and then stirred at reflux under argon for 18 h. The product solution was orange. The acetonitrile solvent was evaporated off under reduced pressure. The crude product was then purified using column chromatography (SiO_2, KPF_6, CH_2Cl_2/acetone 1:1). Yield: 0.331 g (80%). The product could be recrystallized from slow Et_2O diffusion into CH_2Cl_2. ^1H NMR ($CDCl_3$, 500 MHz, $SiMe_4$) δ 7.61 (m, 2H, aryl-H), 7.45 (m, 2H, aryl-H), 7.15 (s, 2H, imid-H), 7.00 (s, 2H, imid-H), 6.54 (d, J = 14.1 Hz, 2H, CH_2C$(CH_3)_3$), 4.99 (d, J = 14.1 Hz, 2H, CH_2C$(CH_3)_3$), 4.47 (d, J = 13.4 Hz, 2H, benzyl-CH_2), 4.14 (s, broad, 4H, cod C-H), 3.55 (d, J = 13.4 Hz, 2H, benzyl-CH_2), 2.34 (s, broad, 2H, cod-CH_2), 2.24 (s, broad, 2H, cod-CH_2), 2.07 (m, 2H, cod-CH_2), 2.00 (m, 2H, cod-CH_2), 1.08 (s, 18H, $CH_2C(CH_3)_3$). $^{13}C\{^1H\}$ NMR ($CDCl_3$, 125 MHz, $SiMe_4$) δ 177.09 (Ir-C), 134.74 (C_{ipso}), 132.42 (C_{aryl}), 130.35 (C_{aryl}), 121.69 (C_{imid}), 121.09 (C_{imid}), 74.92 (cod-CH), 63.03 (benzyl-CH_2), 51.40 ($CH_2C(CH_3)_3$), 32.37 ($CH_2C(CH_3)_3$), 31.36 (cod-CH_2), 31.27 (cod-CH_2), 28.82 ($CH_2C(CH_3)_3$). *Anal.* Calc. for $C_{32}H_{46}F_6IrN_4P$ (823.92) · $1CH_2Cl_2$: C, 43.61; H, 5.32; N, 6.16. Found: C, 43.92; H, 5.38; N, 6.16%. Melting point 165–170 °C (dec).

4.1.5. o-Xylenebis(N-neopentyl)imidazole-2-ylidene acetate (diiodo) iridium(III) (7)

This iridium(I) product, **5**, (0.1732 g, 0.2418 mmol) was reacted with iodine (0.1795 g, 0.7072 mmol), NaOAc (0.1073, 1.308 mmol) in MeCN (15 mL). This reaction solution was stirred for 4 h at RT. After the reaction was halted, the acetonitrile solvent was removed under reduced pressure. The product was purified using column chromatography. The excess iodine was eluted with (CH_2Cl_2/hexane 1:1), and the product was eluted with CH_2Cl_2. Yield: 0.102 g (48%). The orange product was recrystallized by a slow diffusion of pentane into a CH_2Cl_2 solution. ^{1}H NMR ($CDCl_3$, 500 MHz, $SiMe_4$) δ 7.35 (m, 2H, aryl-H), 7.27 (m, 2H, aryl-H), 7.04 (s, 2H, imid-H), 6.52 (s, 2H, imid-H), 5.18 (d, $J = 14.3$ Hz, $CH_2C(CH_3)_3$), 5.00 (d, $J = 15.6$ Hz, 2H, benzyl CH_2), 3.42 (d, $J = 15.6$ Hz, 2H, benzyl CH_2), 3.75 (d, $J = 14.4$ Hz, $CH_2C(CH_3)_3$), 2.05 (s, 3H, CH_3COO), 1.08 (s, 18H, $CH_2C(CH_3)_3$). $^{13}C\{^1H\}$ NMR ($CDCl_3$, 125 MHz, $SiMe_4$) δ 189.81 (CH_3COO) 136.37 (Ir-C), 130.67 (C_{aryl}), 129.13 (C_{aryl}), 126.68 (C_{ipso}), 123.40 (C_{imid}), 121.07 (C_{imid}), 62.34 ($CH_2C(CH_3)_3$), 54.74 ($CH_2C(CH_3)_2CH_2$), 33.20 ($CH_2C(CH_3)_3$), 28.32 ($CH_2C(CH_3)_3$), 25.94 (CH_3COO). *Anal*. Calc. for $C_{26}H_{37}I_2IrN_4O_2$ (883.62): C, 35.34; H, 4.22; N, 6.34. Found: C, 35.37; H, 4.69; N, 3.66%. Despite several attempts, no better elemental analysis could be obtained. Similar analysis problems with carbene complexes have been reported [48]. Melting point 210–213 °C (dec).

4.1.6. o-xylenebis(N-neopentyl)triazole-3-ylidene acetate (diiodo) iridium(III) (9)

The following were added to a schlenk flask: **3** (0.4694 g, 0.8655 mmol), $[Ir(coe)_2Cl]_2$ (0.3521 g, 0.4364 mmol), KI (0.6323 g, 3.809 mmol), NaOAc (0.4770 g, 5.815 mmol), and MeCN (15 mL). The reaction solution was stirred for 2 min under Ar at RT and then at reflux for 18 h under Ar. After cooling, all volatiles were removed under reduced pressure and the residue was purified using column chromatography. Column chromatography (SiO_2; CH_2Cl_2) gave the product as an orange solid. Yield: 0.214 g, (28%). Crystalline material was obtained by slow pentane diffusion into a CH_2Cl_2 solution of the titled product. ^{1}H NMR ($CDCl_3$, 500 MHz, $SiMe_4$) δ 7.64 (s, 2H, NCHN), 7.43 (m, 2H, C_{aryl}-H), 7.35 (m, 2H, C_{aryl}-H), 5.17 (d, $J = 13.9$ Hz, 2H, neopentyl-CH_2), 5.01 (d, $J = 16.1$ Hz, 2H, benzyl-CH_2), 4.55 (d, $J = 16.1$ Hz, 2H, benzyl-CH_2), 4.01 (d, $J = 13.9$ Hz, 2H, neopentyl-CH_2), 2.01 (s, 3H, CH_3COO), 1.09 (s, 18H, neopentyl CH_3). $^{13}C\{^1H\}$ NMR ($CDCl_3$, 125 MHz, $SiMe_4$) δ 190.76 (CH_3COO), 142.39 (NCHN), 134.60 (C-Ir), 134.41 (C_{ipso}), 131.05 (C_{aryl}), 130.08 (C_{aryl}), 63.69 (neopentyl CH_2), 52.23 (benzyl-CH_2), 33.25 (-$CH_2C(CH_3)_3$), 28.46 ($CH_2C(CH_3)_3$), 25.73 (CH_3COO). *Anal*. Calc. for $C_{24}H_{35}I_2IrN_6O_2$ (885.60) · $1H_2O$: C, 31.90; H, 4.13; N, 9.30. Found: C, 31.52; H, 3.88; N, 8.88%. Melting point 245–248 °C (dec).

4.1.7. Methylenebis(N-neopentyl)triazole-3-ylidene acetate (diiodo) iridium(III) (11)

The following were added to a schlenk flask: Methylenebis(*N*-neopentyl)triazolium diiodide (0.2460 g, 0.4504 mmol), $[Ir(coe)_2Cl]_2$ (0.1860 g, 0.2305 mmol), KI (0.3099 g, 1.866 mmol), NaOAc (0.2397 g, 2.922 mmol), and MeCN (14 mL). The reaction solution was stirred for 2 min under Ar at RT and then at reflux for 18 h under Ar. After cooling, all volatiles were removed under reduced pressure and the residue was purified using column chromatography. Column chromatography (SiO_2; CH_2Cl_2/acetone (9:1)) gave the product as an orange solid. Yield: 0.117 g, (33%). Crystalline material was obtained by slow pentane diffusion into a CH_2Cl_2 solution of the titled product. ^{1}H NMR (acetone-D_6, 400 MHz, $SiMe_4$) δ 8.68 (s, 2H, NC*H*N), 6.66 (s, 2H, NCH_2N), 4.16 (s, 4H, CH_2CMe_3), 1.94 (s, 3H, CH_3COO), 1.08 (s, 18H, $C(CH_3)_3$). ^{13}C1H NMR (acetone-D_6, 100 MHz, $SiMe_4$) δ 190.55 (CH_3COO), 142.88 (NCHN), 133.96 (C-Ir), 63.00 (CH_2CMe_3), 59.65 (NCH_2N), 33.75 ($C(CH_3)_3$), 29.84 ($C(CH_3)_3$), 26.02 (CH_3COO). *Anal*. Calc. for $C_{17}H_{29}I_2N_6O_2$ (795.48): C, 25.67; H, 3.67; N, 10.56. Found: C, 25.80; H, 3.65; N, 10.48%. Melting point 320–323 °C (dec).

4.1.8. Neopentylenebis(N-neopentyl)imidazole-2-ylidene biscarbonyl iridium(I) hexafluorophosphate (12)

To a schlenk flask the following were added, **6** (0.0717 g, 0.0905 mmol) and 15 mL of CH_2Cl_2. CO gas (1 atm) was bubbled through this solution for 30 min and during this time period the solution changed from orange to yellow. 30 mL of *n*-hexane was added to the CH_2Cl_2 solution which was precipitated at −20 °C. The yellow solid was collected via vacuum filtration and washed three times (30 mL each) with diethyl ether. The product was dried in vacuo. Yield: 0.0472 g (70%). ^{1}H NMR (acetone-D_6, 500 MHz, $SiMe_4$) δ 7.44 (s, 2H, imid-H), 7.34 (s, 2H, imid-H), 5.00 (d, $J = 14.4$ Hz, 2H, CH_2), 4.46 (d, $J = 13.4$ Hz, 2H, CH_2), 4.09 (d, $J = 14.3$ Hz, 2H, CH_2), 3.91 (d, $J = 13.4$ Hz, 2H, CH_2), 1.24 (s, 3H, $CH_2C(CH_3)_2CH_2$), 1.09 (s, 18H, $CH_2C(CH_3)_3$), 1.05 (s, 3H, $CH_2C(CH_3)_2CH_2$). $^{13}C\{^1H\}$ NMR (acetone-d_6, 125 MHz, $SiMe_4$) δ 182.80 (Ir-CO), 170.38 (Ir-C), 126.03 (C_{imid}), 123.37 (C_{imid}), 63.12 (CH_2), 62.16 (CH_2), 36.88 ($CH_2C(CH_3)_2CH_2$), 33.48 ($CH_2C(CH_3)_3$), 29.30 ($CH_2C(CH_3)_3$), 29.15 ($CH_2C(CH_3)_2CH_2$), 21.08 ($CH_2C(CH_3)_2CH_2$). *Anal*. Calc. for $C_{23}H_{36}F_6IrN_4O_2P$ (737.74): C, 37.44; H, 4.92; N, 7.59. Found: C, 37.47; H, 4.87; N, 7.59%. Melting point 270–275 °C (dec).

4.1.9. Neopentylenebis(N-neopentyl)triazole-3-ylidene bis1,5 cyclooctadiene iridium(I) hexafluorophosphate (**13**)

First, a schlenk flask was charged with Neopentylenebis(*N*-neopentyl)triazolium bistriflate, (0.3038 g, 0.4698 mmol), KCl (0.3251 g, 4.360 g), NaOAc (0.3258, 3.972 mmol), $[Ir(cod)Cl]_2$ (0.1613 g, 0.2401 mmol) and MeCN (15 mL). The reaction solution was stirred at RT for 2 min under argon and then at reflux under argon for 18 h. The reaction solution changed from yellow to orange in color during this time. After the reaction solution cooled, the solvent was removed under reduced pressure. The residual product was then dissolved in CH_2Cl_2 (40 mL) and this solution was filtered to remove insoluble salts and neopentylenebis(*N*-neopentyl)triazole-3-ylidene bis1,5 cyclooctadiene iridium(I) chloride was isolated. Yield = 0.306 g (95%). ^{1}H NMR ($CDCl_3$, 500 MHz, $SiMe_4$) δ 8.37 (s, 2H, triazole-H), 4.57 (d, J = 14.4 Hz, 2H, CH_2), 4.32 (d, J = 11.5 Hz, 2H, CH_2), 4.29 (d, J = 12.2 Hz, 2H, CH_2), 4.18 (s, broad, 4H, cod C-H), 3.73 (d, J = 13.3 Hz, 2H, CH_2), 2.30 (m, 4H, cod CH_2), 2.20 (m, 2H, cod CH_2), 2.06 (m, 2H, cod CH_2), 1.41 (s, 3H, $CH_2C(CH_3)_2CH_2$), 1.04 (s, 18H, $CH_2C(CH_3)_3$). 0.87 (s, 3H, $CH_2C(CH_3)_2CH_2$). $^{13}C\{^1H\}$ NMR ($CDCl_3$, 125 MHz, $SiMe_4$) δ 180.67 (Ir-C), 145.67 ($C_{triazole}$), 79.35 (cod C-H), 78.01 (cod C-H), 63.25 (CH_2), 58.92 (CH_2), 38.07 ($CH_2C(CH_3)_2CH_2$), 31.73 (cod CH_2), 31.27 (cod CH_2), 28.53 ($CH_2C(CH_3)_3$), 27.24 ($CH_2C(CH_3)_3$), 19.72 ($CH_2C(CH_3)_2CH_2$).

Then, the above product (0.1805 g, 0.2645 mmol) was dissolved in 50 mL CH_2Cl_2 and $AgPF_6$ was added (0.0724 g, 0.2864 mmol). This solution was stirred in the dark for 18 h. The resulting product was then filtered over Celite and the solvent was evaporated under reduced pressure. Yield: 0.208 g, (99%). ^{1}H NMR ($CDCl_3$, 500 MHz, $SiMe_4$) δ 8.20 (s, 2H, triazole-H), 4.65 (d, J = 14.4 Hz, 2H, CH_2), 4.34 (d, J = 13.4 Hz, 2H, CH_2), 4.30 (s, broad, 4H, cod C-H) 4.12 (d, J = 14.5 Hz, 2H, CH_2), 3.83 (d, J = 13.4 Hz, 2H, CH_2), 2.31 (m, 2H, cod CH_2), 2.23 (m, 2H, cod CH_2), 2.17 (m, 2H, cod CH_2), 2.04 (m, 2H, cod CH_2) 1.34, (s, 3H, $CH_2C(CH_3)_2CH_2$), 1.06 (s, 18H, $CH_2C(CH_3)_3$). 0.94, (s, 3H, $CH_2C(CH_3)_2CH_2$). $^{13}C\{^1H\}$ NMR ($CDCl_3$, 125 MHz, $SiMe_4$) δ 181.10 (Ir-C), 146.04 ($C_{triazole}$), 79.90 (cod C-H), 78.62 (cod C-H), 63.25 (CH_2), 58.93 (CH_2), 37.81 ($CH_2C(CH_3)_2CH_2$), 32.45 (cod CH_2), 31.73 ($CH_2C(CH_3)_3$), 31.19 (cod CH_2), 28.55 ($CH_2C(CH_3)_3$), 22.80 ($CH_2C(CH_3)_2CH_2$). *Anal*. Calc. for $C_{27}H_{46}F_6IrN_6P$ (791.88) · $1H_2O$: C, 40.04; H, 5.97; N, 10.38. Found: C, 39.67; H, 5.69; N, 10.13%. Melting point 270–272 °C (dec).

4.1.10. Neopentylenebis(N-neopentyl)triazole-3-ylidene biscarbonyl iridium(I) hexafluorophosphate (**14**)

To a schlenk flask the following were added, **13** (0.1016 g, 0.1169 mmol) and 15 mL of CH_2Cl_2. CO gas (1 atm) was bubbled through this solution for 40 min and during this time period the solution changed from orange to yellow in color. 35 mL of *n*-hexane was added to the CH_2Cl_2 solution which was precipitated at −20 °C. The yellow solid was collected via vacuum filtration and washed three times (40 mL each) with diethyl ether. The product was dried in vacuo. Yield: 0.0780 g (82%). ^{1}H NMR ($CDCl_3$, 500 MHz, $SiMe_4$) δ 8.51 (s, 2H, triazole-H), 4.62 (d, J = 14.5 Hz, 2H, CH_2), 4.30 (d, J = 14.5 Hz, 2H, CH_2), 4.24 (d, J = 14.3 Hz, 2H, CH_2), 3.77 (d, J = 13.1 Hz, 2H, CH_2), 1.36, (s, 3H, $CH_2C(CH_3)_2CH_2$), 1.08 (s, 18H, $CH_2C(CH_3)_3$). 0.95, (s, 3H, $CH_2C(CH_3)_2CH_2$). $^{13}C\{^1H\}$ NMR ($CDCl_3$, 125 MHz, $SiMe_4$) δ 179.88 (Ir-CO), 172.26 (Ir-C), 146.57 ($C_{triazole}$), 64.46 (CH_2), 59.21 (CH_2), 36.71 ($CH_2C(CH_3)_2CH_2$), 33.35 ($CH_2C(CH_3)_3$), 28.18 ($CH_2C(CH_3)_3$), 26.48 ($CH_2C(CH_3)_2CH_2$), 19.57 ($CH_2C(CH_3)_2CH_2$). *Anal*. Calc. for $C_{21}H_{34}F_6IrN_6O_2P$ (739.71) · $1H_2O$: C, 33.29; H, 4.79; N, 11.09. Found: C, 33.48; H, 4.53; N, 10.81%. Melting point 255–260 °C (dec).

^{1}H and ^{13}C NMR spectra have not been reported for **16** and **18** and are reported below:

4.1.11. 1-(4-hydroxymethyl-phenyl)-ethanone (**16**)

This product was characterized after catalytic transfer hydrogenation of 4-acetylbenzaldehyde.^{1}H NMR ($CDCl_3$, 500 MHz, $SiMe_4$) δ 7.88 (d, ^3J = 8.2 Hz, 2H, CH), 7.38 (d, ^3J = 8.1 Hz, 2H, CH), 4.71 (s, 2H, CH_2), 2.54 (s, 3H, CH_3), 1.71 (broad s, 1H, OH). $^{13}C\{^1H\}$ NMR ($CDCl_3$, 125 MHz, $SiMe_4$) δ 196.84 (C=O), 145.16 (C_{ipso}), 135.37 (C_{ipso}), 127.62 (CH), 125.61 (CH), 63.62 (CH_2), 25.63 (CH_3).

4.1.12. 1-(4-hydroxymethyl-phenyl)-ethanol (**18**)

This product was characterized by reducing 4-acetylbenzaldehyde with $NaBH_4$ following a procedure described by Blackburn and Taylor [49]. 4-acetylbenzaldehyde (0.083 g, 0.56 mmol) was stirred at 0 °C in 7 mL of MeOH for 5 min after which, $NaBH_4$ was added (0.037 g, 0.98 mmol). The contents were then stirred for 30 min. at 0 °C, after which the MeOH was removed under reduced pressure. The residue was taken up in about 25 mL of diethyl ether and 25 mL of saturated $NaHCO_3$. The ether layer was collected and the aqueous layer was washed two additional times with diethyl ether. The ether extracts were combined and dried over $MgSO_4$. The ether solution was filtered and the diethyl ether was removed under reduced pressure. Yield: 0.076 g (89%). ^{1}H NMR ($CDCl_3$, 500 MHz, $SiMe_4$) δ 7.27 (m, 4H, CH), 4.81 (quartet, ^3J = 6.4 Hz, 1H, CH), 4.58 (s, 2H, CH_2), 1.98 (broad s, 2H, OH), 1.40 (d, ^3J = 6.5 Hz, 3H, CH_3). $^{13}C\{^1H\}$ NMR ($CDCl_3$, 125 MHz, $SiMe_4$) δ 145.66 (C_{ipso}), 140.49 (C_{ipso}), 70.54 (CH(OH)), 65.40 (CH_2), 25.58 (CH_3).

Modern data are not available for the imines so we report them below.

4.2. Synthesis of imine substrates for catalysis:

4.2.1. Naphthalen-2-ylmethylene-phenyl-imine (NpCH=NPh)

Following the general procedure described by Neuvonen et al. [50], 2-napthaldehyde (0.5564 g, 3.562 mmol) was dissolved in 10 mL of absolute ethanol. To this solution, aniline (0.3375 g, 3.623 mmol) was added. The solution was allowed to stand at room temperature for 15 h after which, an off-white precipitate had formed. The ethanol was removed under reduced pressure. Yield 0.70 g (84 %). Only the *E* isomer was formed. ^{1}H NMR ($CDCl_3$, 500 MHz, $SiMe_4$) δ 8.55 (s, 1H, CHN), 8.14 (s, 1H), 8.10 (m, 1 H), 7.84 (m, 2 H), 7.81 (m, 1H), 7.47 (m, 2H), 7.36 (m, 2H), 7.20 (m, 3 H). $^{13}C\{^1H\}$ NMR ($CDCl_3$, 125 MHz, $SiMe_4$), δ 160.76 (CHN), 152.50 (C_{ipso}), 135.45 (C_{ipso}), 134.35 (C_{ipso}), 133.52 (C_{ipso}), 131.65 (CH), 129.59 (CH), 129.19 (CH), 129.08 (CH), 128.35 (CH), 127.96 (CH), 127.02 (CH), 126.40 (CH), 124.24 (CH), 121.33 (CH). *Anal.* Calc. for $C_{17}H_{13}N$ (231.29): C, 88.28; H, 5.67; N, 6.06. Found: C, 87.73; H, 5.65; N, 6.00%.

4.2.2. (2,4,6-Trimethyl-benzylidene)-(2,4,6-trimethyl-phenyl)-imine (MesCH=NMes)

Following the procedure described by Texier-Boullet [51], mesityl aldehyde (1.4628 g, 9.869 mmol) was dispersed in 2.5368 g of alumina. To this mixture, mesityl amine (1.3374 g, 9.891 mmol) was added, which was dispersed in 2.7830 g of alumina. This mixture was stirred at RT for three days. After this time period, the residue was dissolved in 100 mL of CH_2Cl_2 and filtered. The CH_2Cl_2 was removed under reduced pressure and the product was an orange oil. Yield: 2.60 g (99%). Only the *E* isomer was formed. ^{1}H NMR ($CDCl_3$, 500 MHz, $SiMe_4$) δ 8.67 (s, 1H, CHN), 6.98 (d, ^3J = 8.6 Hz, 4H), 2.64 (s, 6H, CH_3), 2.38 (d, ^3J = 16.0 Hz, 6H, CH_3), 2.29 (s, 6H, CH_3). $^{13}C\{^1H\}$ NMR ($CDCl_3$, 125 MHz, $SiMe_4$), δ 163.68 (CHN), 150.68 (C_{ipso}), 140.24 (C_{ipso}), 139.18 (C_{ipso}), 133.18 (C_{ipso}), 130.97 (CH), 130.729 (CH), 129.27 (CH), 127.17 (C_{ipso}), 21.75 (CH_3), 21.60 (CH_3), 21.14 (CH_3), 19.22 (CH_3).

4.2.3. (2,4,6-trimethyl-benzylidene)-phenyl imine (MesCH=NPh)

Following the procedure described by Texier-Boullet [49], mesityl aldehyde (1.473 g, 9.938 mmol) was dispersed in 2.5466 g of alumina. To this mixture, aniline (0.9294 g, 9.931 mmol) was added, which was dispersed in 2.5249 g of alumina. This mixture was stirred at RT for 15 h. After this time period, the residue was dissolved in 100 mL of CH_2Cl_2 and filtered. The CH_2Cl_2 was removed under reduced pressure and the product was an orange/brown oil that solidified at RT after 2h. Yield: 2.12 g (95%). Only the *E* isomer was formed. ^{1}H NMR ($CDCl_3$, 500 MHz, $SiMe_4$) δ 8.87 (s, 1H, CHN), 7.45 (m, 2H), 7.28 (m, 1H), 7.21 (m, 2H), 6.98 (s, 2H, CH), 2.51 (s, 6H, CH_3), 2.37 (s, 3H, CH_3). $^{13}C\{^1H\}$ NMR ($CDCl_3$, 125 MHz, $SiMe_4$), δ 161.25 (CHN), 153.54 (C_{ipso}), 140.26 (C_{ipso}), 139.05 (C_{ipso}), 130.96 (CH), 130.20 (CH), 129.54 (CH), 125.95 (CH), 121.14 (CH), 21.66 (CH_3), 21.49 (CH_3).

4.2.4. (4-nitro-benzylidene)-phenyl-imine (p-$NO_2C_6H_4$-CH=NPh)

Following the general procedure described by Neuvonen et al. [48], 4-nitrobenzaldehyde (0.7455 g, 4.933 mmol) was dissolved in 10 mL of absolute ethanol. To this solution, aniline (0.4585 g, 4.923 mmol) was added. This solution was allowed to stand at RT for 16 h, and a yellow precipitate formed after this time. The ethanol was removed under reduced pressure. Yield: 1.03 g (93%). The product could be recrystallized from ethanol at −20 °C. Only the *E* isomer was formed. ^{1}H NMR ($CDCl_3$, 500 MHz, $SiMe_4$) δ 8.49 (s, 2H, CHN), 8.25 (AB d, 2H, ^3J = 8.7 Hz), 8.00 (AB d, 2H, ^3J = 8.7 Hz), 7.36 (m, 2H), 7.20 (m, 3H). $^{13}C\{^1H\}$ NMR ($CDCl_3$, 125 MHz, $SiMe_4$), δ 157.74 (CHN), 151.33 (C_{ipso}), 149.70 (C_{ipso}), 141.98 (C_{ipso}), 129.80 (CH), 129.74 (CH), 127.47 (CH), 124.42 (CH), 121.35 (CH). *Anal.* Calc. for $C_{13}H_{10}N_2O_2$ (226.23) C, 69.02; H, 4.46; N, 12.38. Found: C, 69.00; H, 4.47; N, 12.38%.

4.2.5. Benzylidene-cyclohexyl-imine (PhCH=NC_6H_{11})

Following the procedure described by Texier-Boullet [49], benzylaldehyde (1.070 g, 10.08 mmol) was dispersed in 2.5806 g of alumina. To this mixture, cyclohexylamine (0.9986 g, 10.07 mmol) was added, which was dispersed in 2.5700 g of alumina. This mixture was stirred for 15 h at RT. After this time period, the residue was dissolved in 100 mL of CH_2Cl_2 and filtered. The CH_2Cl_2 was removed under reduced pressure and the product was a colorless oil. Yield: 1.84 g (97%). Only the *E* isomer was formed. ^{1}H NMR ($CDCl_3$, 500 MHz, $SiMe_4$) δ 8.35 (s, 1H, CHN), 7.76 (m, 2H, CH), 7.42 (m, 3H, CH), 3.23 (quintet, ^3J = 4.2 Hz, 1H, CH), 1.87 (m, 2H), 1.77 (m, 5H), 1.65 (m, 3H). $^{13}C\{^1H\}$ NMR ($CDCl_3$, 125 MHz, $SiMe_4$), δ 158.98 (NCH), 137.05 (C_{ipso}), 130.72 (CH), 128.92 (CH), 128.80 (CH), 70.42 (CH), 34.80 (CH_2), 26.09 (CH_2), 25.24 (CH_2).

4.2.6. Benzyl-benzylidene-imine (PhCH=NCH_2Ph)

Following the procedure described by Texier-Boullet [49], benzylaldehyde (1.066 g, 10.04 mmol) was dispersed in 2.5348 g of alumina. To this mixture, benzyl amine (1.0798 g, 10.07 mmol) was added, which was dispersed in 2.5344 g of alumina. This mixture was stirred for 18 h at RT. After this time period, the residue was dissolved in 100 mL of CH_2Cl_2 and filtered. The CH_2Cl_2

was removed under reduced pressure and the product was a colorless oil. Yield: 1.86 g (95%). Only the *E* isomer was formed. ^{1}H NMR ($CDCl_3$, 500 MHz, $SiMe_4$) δ 8.47 (s, 1H, CHN), 7.89 (m, 2H, CH), 7.50 (m, 3H, CH), 7.45 (m, 4H, CH), 7.35 (m, 1H, CH), 4.92 (s, 2H, CH_2). $^{13}C\{^1H\}$ NMR ($CDCl_3$, 125 MHz, $SiMe_4$), δ 162.47 (CHN), 139.81 (C_{ipso}), 136.65 (C_{ipso}), 131.27 (CH), 129.10 (CH), 129.00 (CH), 128.79 (CH), 128.48 (CH), 127.50 (CH), 65.55 (CH_2).

4.2.7. Phenyl-(3-phenyl-allylidene)-imine (*PhCH=CH-CH=N-Ph*)

Following the procedure described by Brady and Shieh [52], *trans*-cinnamaldehyde (0.7048 g, 5.332 mmol) was dissolved in 20 mL of anhydrous diethyl ether. Aniline (0.4999 g, 5.367 mmol) was then added in 5mL of anhydrous diethyl ether to the reaction solution. This solution was allowed to stand at RT for 16 h, after which the ether was removed under reduced pressure. The product was a yellow crystalline solid. Yield = 1.04 g (94%). ^{1}H NMR ($CDCl_3$, 500 MHz, $SiMe_4$) δ 8.19 (d, ^3J = 7.2 Hz, 1H, NCH), 7.46 (d, 2H, ^3J = 7.4 Hz), 7.30 (m, 5H), 7.14 (m, 5H). $^{13}C\{^1H\}$ NMR ($CDCl_3$, 125 MHz, $SiMe_4$), δ 162.06 (NCH), 152.12 (C_{ipso}), 144.44 (CH), 136.00 (C_{ipso}), 130.00 (CH), 129.59 (CH), 129.33 (CH), 129.00 (CH), 127.91 (CH), 126.53 (CH), 121.33 (CH).

The products from the catalytic reactions were compared with authentic material using ^{1}H NMR. If the amine products were not commercially available or previously characterized, [16,19] the imines were reduced stoichiometrically using $NaBH_4$ following the procedure described by Blackburn and Taylor [53].

4.3. General procedure for imine reduction using $NaBH_4$

In general, the imine (~0.2 mmol) was stirred at 0 °C in 6 mL of MeOH for 5 min after which, $NaBH_4$ was added (~0.3 mmol). The contents were then stirred for 1 h at 0 °C, after which the MeOH was removed under reduced pressure. The residue was taken up in about 25 mL of diethyl ether and 25 mL of saturated $NaHCO_3$. The ether layer was collected and the aqueous layer was washed two additional times with diethyl ether. The ether extracts were combined and dried over $MgSO_4$. The ether solution was filtered and the diethyl ether was removed under reduced pressure.

4.3.1. Phenyl-(3-phenyl-propyl)-amine (*PhCH$_2$CH$_2$CH$_2$-NHPh*)

^{1}H NMR ($CDCl_3$, 500 MHz, $SiMe_4$) δ 7.14 (m, 7H), 6.51 (m, 1H), 6.49 (d, 2H, ^3J = 0.65 Hz), 3.53 (s, 1H, NH), 3.08 (t, 2H, ^3J = 7.0 Hz, CH_2), 2.66 (t, 2H, ^3J = 7.7 Hz, CH_2), 1.88 (septet, 2H, ^3J = 7.0 Hz, CH_2). $^{13}C\{^1H\}$ NMR ($CDCl_3$, 125 MHz, $SiMe_4$), δ 148.75 (C_{ipso}), 142.06 (C_{ipso}), 129.63 (CH), 128.83 (CH), 128.81 (CH), 126.36 (CH), 117.62 (CH), 113.14 (CH), 43.82 (CH_2), 33.81 (CH_2), 31.48 (CH_2).

4.3.2. Naphthalen-2-ylmethylene-phenyl-amine (*NpCH$_2$NHPh*)

^{1}H NMR ($CDCl_3$, 500 MHz, $SiMe_4$) δ 7.72 (m, 4H), 7.38 (m, 3H), 7.08 (m, 2H), 6.63 (d, ^3J = 9.0 Hz, 1H), 6.57 (d, ^3J, 10.3 Hz, 2H), 4.39 (d, ^3J = 6.7 Hz, 2H, CH_2), 4.21 (s, 1H, NH). $^{13}C\{^1H\}$ NMR ($CDCl_3$, 125 MHz, $SiMe_4$), δ 148.59 (C_{ipso}), 137.36 (C_{ipso}), 133.90 (C_{ipso}), 133.17 (C_{ipso}), 129.69 (CH), 128.77 (CH), 128.16 (CH), 128.10 (CH), 126.55 (CH), 126.31 (CH), 126.13 (CH), 126.12 (CH), 118.03 (CH), 113.34 (CH), 48.90 (CH_2).

4.3.3. (2,4,6-trimethyl-benzyl)-(2,4,6-trimethyl-phenyl)-amine (*MesCH$_2$NHMes*)

^{1}H NMR ($CDCl_3$, 500 MHz, $SiMe_4$) δ 6.79 (s, 2H, CH), 6.73 (s, 2H, CH), 4.00 (s, 2H, CH_2), 2.30 (s, 6H, CH_3), 2.16 (t, ^3J = 7.4 Hz, 12 H, CH_3). $^{13}C\{^1H\}$ NMR ($CDCl_3$, 125 MHz, $SiMe_4$), δ 144.53 (C_{ipso}), 137.56 (C_{ipso}), 137.22 (C_{ipso}), 134.40 (C_{ipso}), 131.31 (C_{ipso}), 129.97 (CH), 129.56 (CH), 129.48 (C_{ipso}), 47.29 (CH_2), 21.30 (CH_3), 20.92 (CH_3), 20.17 (CH_3), 19.16 (CH_3).

4.3.4. (4-nitro-benzyl)-phenyl-amine (*p-NO$_2$C$_6$H$_4$CH$_2$-NHPh*)

^{1}H NMR ($CDCl_3$, 500 MHz, $SiMe_4$) δ 8.11 (d, 2H, ^3J = 10.9 Hz, CH), 7.45 (d, 2H, ^3J = 10.9 Hz, CH), 7.10 (m, 2H), 6.68 (t, ^3J = 9.2 Hz, 1H, CH), 6.50 (d, 2H, ^3J = 9.6 Hz, CH), 4.41 (s, 2H, CH_2), 4.16 (s, 1H, NH). $^{13}C\{^1H\}$ NMR ($CDCl_3$, 125 MHz, $SiMe_4$), δ 147.97 (C_{ipso}), 147.73 (C_{ipso}), 147.60 (C_{ipso}), 129.79 (CH), 128.11 (CH), 124.28 (CH), 118.63 (CH), 113.33 (CH), 48.03 (CH_2).

4.3.5. (4-methoxy-benzyl)-phenyl-amine (*p-MeOC$_6$H$_4$-CH$_2$NHPh*)

^{1}H NMR ($CDCl_3$, 500 MHz, $SiMe_4$) δ 7.18 (d, 2H, ^3J = 8.4 Hz, CH), 7.07 (t, 2H, ^3J = 7.4 Hz, CH), 6.77 (d, 2H, ^3J = 8.6 Hz, CH), 6.62 (t, 1H, ^3J = 7.4 Hz, CH), 6.52 (d, 2H, ^3J = 7.8 Hz, CH), 4.14 (s, 2H, CH_2), 3.83 (broad s, 1H, NH), 3.69 (s, 3H, OCH_3). $^{13}C\{^1H\}$ NMR ($CDCl_3$, 125 MHz, $SiMe_4$), δ 159.29 (C_{ipso}), 148.66 (C_{ipso}), 131.87 (C_{ipso}), 129.68 (CH), 129.23 (CH), 117.91 (CH), 114.45 (CH), 113.28 (CH), 55.70 (CH_3), 48.21 (CH_2).

4.3.6. Benzyl-cyclohexyl-amine (*PhCH$_2$NHC$_6$H$_{11}$*)

^{1}H NMR ($CDCl_3$, 500 MHz, $SiMe_4$) δ 7.23 (m, 4H), 7.15 (m, 1H), 3.73 (s, 2H, CH_2), 2.40 (m, 1H), 1.82 (m, 2H), 1.66 (m, 2H), 1.53 (m, 1H), 1.10 (m, 6H). (1H, NH not observed). $^{13}C\{^1H\}$ NMR ($CDCl_3$, 125 MHz, $SiMe_4$), δ 141.43 (C_{ipso}), 129.52 (CH aromatic), 128.78 (CH aromatic), 128.49 (CH aromatic), 127.31 (CH aromatic), 127.17 (CH aromatic), 56.59 (CH cyclohexyl),

51.47 (CH_2N), 33.99 (CH_2 cyclohexyl), 26.63 (CH_2 cyclohexyl), 25.43 (CH_2 cyclohexyl).

4.3.7. N-Phenyl-(2,4,6-trimethyl-benzylidene)-amine (Mes-CH_2NHPh)

^1H NMR ($CDCl_3$, 500 MHz, $SiMe_4$) δ 7.15 (m, 2H, CH), 6.82 (s, 2H, CH), 6.66 (t, $^3J = 8.0$ Hz, 1H, CH), 6.59 (m, 2H, CH), 4.11 (s, 2H, CH_2), 3.34 (s, 1H, NH), 2.27 (s, 6H, CH_3), 2.24 (s, 3H, CH_3). $^{13}C\{^1H\}$ NMR ($CDCl_3$, 125 MHz, $SiMe_4$), δ 149.01 (C_{ipso}), 137.89 (C_{ipso}), 137.68 (C_{ipso}), 132.59 (C_{ipso}), 129.67 (CH), 129.46 (CH), 117.60 (CH), 112.81 (CH), 42.71 (CH_2), 21.33 (CH_3), 19.81 (CH_3).

4.3.8. Dibenzyl-amine ($PhCH_2NHCH_2Ph$)

^1H NMR ($CDCl_3$, 500 MHz, $SiMe_4$) δ 7.22 (m, 8H, CH), 7.15 (m, 2H, CH), 3.70 (s, 4H, CH_2), (1H, NH, not observed). $^{13}C\{^1H\}$ NMR ($CDCl_3$, 125 MHz, $SiMe_4$), δ 140.80 (C_{ipso}), 128.85 (CH), 128.61 (CH), 127.40 (CH), 53.62 (CH_2).

Acknowledgement

This work was supported by generous funding from the United States Department of Energy, Johnson Mattley and BP. We also thank Prof. Jack Faller for helpful suggestions.

References

[1] (a) A.J. Arduengo III, H.V.R. Dias, R.I. Harlow, M. Kline, J. Am. Chem. Soc. 114 (1992) 5530;
(b) M.F. Lappert, J. Organomet. Chem. 358 (1988) 185;
(c) W.A. Herrmann, C. Köcher, Agnew Chem. Int. Ed. Engl. 36 (1997) 2162;
(d) D. Bourissou, O. Guerret, F.P. Gabbaï, G. Bertrand, Chem. Rev. 100 (2000) 39;
(e) M.S. Sanford, J.A. Love, R.H. Grubbs, J. Am. Chem. Soc. 123 (2001) 6543;
(f) S.R. Stauffer, S. Lee, J.P. Stambuli, S.I. Hauck, J.F. Hartwig, Org Lett. 2 (2000) 1423.

[2] (a) For C, N-bidentate coordinating carbene complexes see: D.S. McGuinness, K.J. Cavell, Organometallics 19 (2000) 741;
(b) M.T. Powell, D.-R. Hou, M.C. Perry, X. Cui, K. Burgess, J. Am. Chem. Soc. 123 (2001) 8878;
(c) S. Gründemann, A. Kovacevic, M. Albrecht, J.W. Faller, R.H. Crabtree, Chem. Commun. (2001) 2274;
(d) A. Kovacevic, S. Gründemann, J.R. Miecznikowski, E. Clot, O. Eisenstein, R.H. Crabtree, Chem. Commun. (2002) 2580;
(e) S. Gründemann, A. Kovacevic, M. Albrecht, J.W. Faller, R.H. Crabtree, J. Am. Chem. Soc. 124 (2002) 10473;
(f) S. Gründemann, M. Albrecht, A. Kovacevic, J.W. Faller, R.H. Crabtree, J. Chem. Soc., Dalton Trans (2002) 2163.

[3] (a) For first-row transition metal complexes containing chelating carbenes see: K. Öfele, W.A. Herrmann, D. Mihalios, M. Elison, E. Herdtweck, T. Priermeier, P. Kiprof, J. Organomet. Chem. 498 (1995) 1;
(b) U. Kernbach, M. Ramm, P. Luger, W.P. Fehlhammer, Angew. Chem. Int. Ed. Engl. 35 (1996) 310;
(c) R. Fränkel, U. Kernbach, M. Bakola-Christianopoulou, U. Plaia, M. Suter, W. Ponikwar, H. Nöth, C. Moinet, W.P. Fehlhammer, J. Organomet. Chem. 617–618 (2001) 530;
(d) R.E. Douthwaite, D. Haussinger, M.L.H. Green, P.J. Silcock, P.T. Gomes, A.M. Martins, A.A. Danopoulos, Organometallics 18 (1999) 4584.

[4] (a) W.A. Herrmann, M. Elison, J. Fischer, C. Köcher, G.R.J. Artus, Angew. Chem. Int. Ed. Engl. 34 (1995) 2371;
(b) W.P. Fehlhammer, T. Bliss, U. Kernbach, I. Brüdgam, J. Organomet. Chem. 490 (1995) 149;
(c) D.S. Clyne, J. Jin, E. Genest, J.C. Gallucci, T.V. RajanBabu, Org. Lett. 2 (2000) 1125;
(d) A.A.D. Tulloch, A.A. Danopoulos, G.J. Tizzard, S.J. Coles, M.B. Hursthouse, R.S. Hay-Motherwell, B.W. Skelton, A.H. White, C.C. Williams, J. Chem. Soc., Dalton Trans. (2001) 111;
(e) S. Gründemann, M. Albrecht, J.A. Loch, J.W. Faller, R.H. Crabtree, Organometallics 20 (2001) 5485;
(f) J.A. Loch, M. Albrecht, J. Mata, E. Peris, J.W. Faller, R.H. Crabtree, Organometallics 21 (2002) 700;
(g) J.R. Miecznikowski, S. Gründemann, M. Albrecht, C. Mégret, E. Clot, J.W. Faller, O. Eisenstein, R.H. Crabtree, Dalton Trans. (2003) 831.

[5] M. Albrecht, R.H. Crabtree, J. Mata, E. Peris, Chem. Commun. (2002) 32.

[6] M. Albrecht, J.R. Miecznikowski, A. Samuel, J.W. Faller, R.H. Crabtree, Organometallics 21 (2002) 3596.

[7] J.R. Miecznikowski, R.H. Crabtree, Organometallics 23 (2004) 629.

[8] (a) O. Pàmies, J.E. Bäckvall, Chem. Eur. J. 7 (2001) 5052;
(b) R. Noyori, M. Yamakawa, S. Hashiguchi, J. Org. Chem. 66 (2001) 7931;
(c) J.S.M. Samec, J.E. Bäckvall, Chem. Eur. J. 8 (2002) 2955;
(d) R. Noyori, S. Hashiguchi, Acc. Chem. Res. 30 (1997) 97;
(e) Y.R.S. Laxmi, J.E. Bäckvall, Chem. Commun. (2000) 611;
(f) W. Leitner, J.M. Brown, H. Brunner, J. Am. Chem. Soc. 115 (1993) 152;
(g) E. Mizushima, M. Yamaguchi, T. Yamagishi, J. Mol. Catal. A 148 (1999) 69;
(h) C.P. Casey, S.W. Singer, D.R. Powell, R.K. Hayashi, M. Kavena, J. Am. Chem. Soc. 123 (2001) 1090.

[9] J.A. Mata, A.R. Chianese, J.R. Miecznikowski, M. Poyatos, E. Peris, J.W. Faller, R.H. Crabtree, Organometallics 23 (2004) 1253.

[10] F.A. Carey, R.J. Sundberg, Advanced Organic Chemistry, third ed., Part B: Reactions and Synthesis, Plenum Press, New York, 1990, p. 232.

[11] (a) Examples of ketone hydrogenation since 1999: J.-P. Genet, Acc. Chem. Res. 36 (2003) 908;
(b) V. Rautenstrauch, X. Hoang-Cong, R. Churlaud, K. Abdur-Rashid, R.H. Morris, Chem. Eur. J. 9 (2003) 4954;
(c) X. Li, H. Weiping, K.F. William, J. Xiao, Org. Lett. 5 (2003) 4559;
(d) C.A. Sandoval, T. Ohkuma, K. Muniz, R. Noyori, J. Am. Chem. Soc. 125 (2003) 13490;
(e) K. Kris, T. Kanger, A.-M. Muurisepp, M. Lopp, Tetrahedron: Asymmetry (2003) 2271;
(f) J. Wu, J.-X. Ji, R. Guo, C.-H. Yeung, A.S.C. Chan, Chem. Eur. J. 9 (2003) 2963;
(g) S. Subongkoj, S. Lange, W. Chen, J. Xiao, J. Mol. Catal. A 196 (2003) 125;
(h) H.-U. Blaser, C. Malan, B. Pugin, F. Spindler, H. Steiner, M. Studer, Adv. Synth. Catal. 345 (2003) 103;
(i) K. Abdur-Rashid, S.E. Clapham, A. Hadzovic, J.N. Harvey, A.J. Lough, R.H. Morris, J. Am. Chem. Soc. 124 (2002) 15104;
(j) R. Hartmann, P. Chen, Angew. Chem. Int. Ed 40 (2001) 3581;
(k) K. Abdur-Rashid, M. Faatz, A.J. Lough, R.H. Morris, J. Am. Chem. Soc. 123 (2001) 7473;

(l) T. Ohkuma, H. Takeno, Y. Honda, R. Noyori, Adv. Synth. Catal. 343 (2001) 369;
(m) K. Abdur-Rashid, A.J. Lough, R.H. Morris, Organometallics 20 (2001) 1047;
(n) R. Noyori, T. Okhuma, Angew. Chem. Int. Ed. 40 (2001) 40;
(o) K. Abdur-Rashid, A.J. Lough, R.H. Morris, Organometallics 19 (2000) 2655;
(p) J.-X. Chen, J.F. Daeuble, J.M. Styker, Tetrahedron 56 (2000) 2789;
(q) S. Naili, I. Suisse, A. Mortreux, F. Agbossou, M.A. Ali, A. Karim, Tetrahedron Lett. 41 (2000) 2867;
(r) R. Noyori, T. Ohkuma, Pure Appl. Chem. 71 (1999) 1493;
(s) N. Kunzle, R. Hess, T. Mallat, A. Baiker, J. Catal. 186 (1999) 239;
(t) V. Penicaud, C. Maillet, P. Janvier, M. Pipelier, B. Bujoli, Eur. J. Org. Chem. (1999) 1745;
(u) R.M. Bullock, Chem. Eur. J. 10 (2004) 2366.

[12] (a) For examples of imine hydrogenation K. Abdur-Rashid, A.J. Lough, R.H. Morris, Organometallics 20 (2001) 1047;
(b) K. Abdur-Rashid, A.J. Lough, R.H. Morris, Organometallics 19 (2000) 2655;
(c) V. Ayala, A. Corma, M. Iglesias, J.A. Rincon, F. Sanchez, J. Catal. 224 (2004) 170;
(d) H.-U. Blaser, C. Malan, B. Pugin, F. Spindler, H. Steiner, M. Studer, Adv. Synth. Catal. 345 (2003) 103;
(e) C.J. Cobley, J.P. Henschke, Adv. Synth. Catal. 345 (2003) 195;
(f) E. Guiu, B. Munoz, S. Castillon, C. Claver, Adv. Synth. Catal. 345 (2003) 169;
(g) P. Marcazzan, B.O. Patrick, B.R. James, Organometallics 22 (2003) 1177;
(h) R. Margalef-Catala, C. Claver, P. Salagre, E. Fernandez, Tetrahedron: Asymmetry 11 (2000) 1469;
(i) A. Martorell, C. Claver, E. Fernandez, Inorg. Chem. Commun. 3 (2000) 132;
(j) V. Tararov, R. Kadyrov, T.H. Riermeier, J. Holz, A. Borner, Tetrahedron: Asymmetry 10 (1999) 4009;
(k) N.D. Jones, K.S. MacFarlane, M.B. Smith, R.P. Schutte, S.J. Rettig, B.R. James, Inorg. Chem. 38 (1999) 3956;
(l) M. Ringwald, R. Stuermer, H.H. Brintzinger, J. Am. Chem. Soc. 121 (1999) 1524;
(m) P. Schnider, G. Koch, R. Pretot, G. Wang, F.M. Bohnen, C. Kruger, A. Pfaltz, Chem. Eur. J. 3 (1997) 887;
(n) R. Sablong, J.A. Osborn, J.W. Faller, J. Organomet. Chem. 527 (1997) 65;
(o) R. Sablong, J.A. Osborn, Tetrahedron: Asymmetry 7 (1996) 3059;
(p) R. Sablong, J.A. Osborn, Tetrahedron Lett. 37 (1996) 4937;
(q) J.M. Buriak, J.A. Osborn, Organometallics 15 (1996) 3161;
(r) Y. Ng Cheong Chan, J.A. Osborn, J. Am. Chem. Soc. 112 (1990) 9400;
(s) Y.N.C. Chan, D. Meyer, J.A. Osborn, J. Chem. Soc., Chem. Commun. (1990) 869;
(t) T. Morimoto, N. Nakajima, K. Achiwa, Synletters (1995) 748;
(u) Z. Zhou, B.R. James, H. Alper, Organometallics 14 (1995) 4209;
(v) J. Bakos, A. Orosz, B. Heil, M. Laghmari, P. Lhoste, D. Sinou, J. Chem. Soc., Chem. Commun. (1991) 1684;
(w) C.J. Longley, T.J. Goodwin, G. Wilkinson, Polyhedron 5 (1986) 1625;
(x) X.-B. Jiang, A.J. Minnaard, B. Hessen, B.L. Feringa, A.L.L. Duchateau, J.G.O. Andrien, J.A.F. Boogers, J.G. deVries, Org. Lett. 5 (2003) 1503.

[13] (a) C.A. Willoughby, S.L. Buchwald, J. Am. Chem. Soc. 116 (1994) 11703;
(b) C.A. Willoughby, S.L. Buchwald, J. Am. Chem. Soc. 116 (1994) 8952;
(c) C.A. Willoughby, S.L. Buchwald, J. Org. Chem. 58 (1993) 7627;
(d) C.A. Willoughby, S.L. Buchwald, J. Am. Chem. Soc. 114 (1992) 7562.

[14] (a) A.G. Becalski, W.R. Cullen, M.D. Fryzuk, B.R. James, G.J. Kang, S.J. Rettig, Inorg. Chem. 30 (1991) 5002;
(b) G.J. Kang, W.R. Cullen, M.D. Fryzuk, B.R. James, J.P. Kutney, J. Chem. Soc., Chem. Commun. (1988) 1466.

[15] R.A.W. Johnstone, A.H. Wilby, I.D. Entwistle, Chem. Rev. 85 (1985) 129.

[16] R. Noyori, S. Hashiguchi, Acc. Chem. Res. 30 (1997) 97.

[17] J.S.M. Samec, J.-E. Bäckvall, Chem. Eur. J. 8 (2002) 2955.

[18] B. Basu, M.M.H. Bhuiyan, P. Das, I. Hossain, Tetrahedron Lett. 44 (2003) 8931.

[19] G.D. Williams, R.A. Pike, C.E. Wade, M. Wills, Org. Lett. 5 (2003) 4227.

[20] S. Kuhl, R. Schneider, Y. Fort, Organometallics 22 (2003) 4184.

[21] C. Saluzzo, M. Lemaire, Adv. Synth. Catal. 344 (2002) 915.

[22] (a) J.S.M. Samec, J.E. Bäckvall, Chem. Eur. J. 8 (2002) 2955;
(b) G.Z. Wang, J.E. Bäckvall, J. Chem. Soc., Chem. Commun. (1992) 980;
(c) J.E. Bäckvall, J. Organomet. Chem. 652 (2002) 105.

[23] J. Mao, J.C. Baker, Org. Lett. 1 (1999) 841.

[24] (a) N. Uematsu, A. Fujii, S. Hashiguchi, T. Ikariya, R. Noyori, J. Am. Chem. Soc. 118 (1996) 4916;
(b) R. Noyori, S. Hashiguchi, Acc. Chem. Res 30 (1997) 97.

[25] A.A. Danopoulos, S. Winston, W.B. Motherwell, Chem. Commun. (2002) 1376.

[26] M. Albrecht, R.H. Crabtree, J. Mata, E. Peris, Chem. Commun. (2002) 32.

[27] (a) E. Mizushima, M. Yamaguchi, T. Yamagishi, J. Mol. Catal. A 148 (1999) 69;
(b) E. Mizushima, M. Yamaguchi, T. Yamagishi, Chem. Lett. (1997) 237.

[28] M.J. Palmer, M. Wills, Tetrahedron: Asymmetry 10 (1999) 2045.

[29] C.P. Casey, S.W. Singer, D.R. Powell, R.K. Hayashi, M. Kavana, J. Am. Chem. Soc. 123 (2001) 1090.

[30] (a) For examples of catalytic transfer hydrogenation of ketones since 1999 J. Hannedouche, G.J. Clarkson, M. Wills, J. Am. Chem. Soc. 126 (2004) 986;
(b) D. Sterk, M.S. Stephan, B. Mohar, Tetrahedron Lett. 45 (2004) 535;
(c) M. Leautey, P. Jubault, X. Pannecoucke, J.-C. Quirion, Eur. J. Org. Chem. (2003) 3761;
(d) I.M. Pastor, P. Vastila, H. Adolfsson, Chem. Eur. J. 9 (2003) 4031;
(e) J.Q. Yu, H.-C. Wu, C. Ramarao, J.B. Spencer, S.V. Ley, Chem. Commun. (2003) 678;
(f) Y. Himeda, N. Onozawa-Komatsuzaki, H. Sugihara, H. Arakawa, K. Kasuga, J. Mol. Catal. A (2003) 95;
(g) M. Wills, J. Hannedouche, Curr. Opin. Drug Discov. Develop. 5 (2002) 881;
(h) M. De Bruyn, D.E. De Vos, P.A. Jacobs, Adv. Synth. Catal. 344 (2002) 1120;
(i) S. Ogo, T. Abura, Y. Watanabe, Organometallics 21 (2002) 2964;
(j) H.Y. Rhyoo, H.-J. Park, W.H. Suh, Y.K. Chung, Tetrahedron Lett. 43 (2002) 269;
(k) J.W. Faller, A.R. Lavoie, Organometallics 20 (2001) 5245;
(l) J. Cossy, F. Eustache, P.I. Dalko, Tetrahedron Lett. 42 (2001) 5005;
(m) T. Thorpe, J. Blacker, S.M. Brown, C. Bubert, J. Crosby, S. Fitzjohn, J.P. Muxworthy, J.M.J. Williams, Tetrahedron Lett. 42 (2001) 4041;
(n) K. Polborn, K. Serverin, Chem. Eur. J. 6 (2000) 4604;
(o) M. Wills, M. Gamble, M. Palmer, A. Smith, J. Studley, J. Kenny, J. Mol. Catal. A 146 (1999) 139;

(p) D.A. Alonso, P. Brandt, S.J.M. Nordin, J. Am. Chem. Soc. 121 (1999) 9580.
[31] Cope.A. C, E.R. Trumbull, Org. React. 11 (1960) 317.
[32] M. Poyatos, E. Mas-Marza, J. Mata, M. Sanau, E. Peris, Eur. J. Inorg. Chem. (2003) 1215.
[33] M. Poyatos, M. Sanau, E. Peris, Inorg. Chem. 42 (2003) 2572.
[34] F.E. Hahn, L. Wittenbecher, D. Le Van, R. Frohlich, Agnew. Chem. Int. Ed. 39 (2000) 541.
[35] (a) A.R. Chianese, A. Kovacevic, B.M. Zeglis, J.W. Faller, R.H. Crabtree, Organometallics 23 (2004) 2461;
(b) E. Clot, R.H. Crabtree, O. Eisenstein, unpublished computational data, 2003.
[36] (a) A.R. Chianese, X. Li, M.C. Janzen, J.W. Faller, R.H. Crabtree, Organometallics 22 (2003) 1663;
(b) A.R. Chianese, A. Kovacevic, B.M. Zeglis, J.W. Faller, R.H. Crabtree, Organometallics 23 (2004) 2461.
[37] (a) G-Z. Wang, J.E. Bäckvall, J. Chem. Soc., Chem. Commun. (1992) 980;
(b) J. Louie, C.W. Bielawski, R.H. Grubbs, J. Am. Chem. Soc. 123 (2001) 11312;
(c) R.K. Rath, M. Nethaji, A.R. Chakravarty, Polyhedron 20 (2001) 2735;
(d) M.L.S. Almeida, M. Beller, G.Z. Wang, J.-E. Backvall, Chem. Eur. J. 2 (1996) 1533.
[38] J.S.M. Samec, J.E. Bäckvall, Chem. Eur. J. 8 (2002) 2955.
[39] F. Texier-Boullet, Synthesis (1985) 679.
[40] K. Neuvonen, F. Fulop, H. Neuvonen, A. Koch, E. Kleinpeter, K. Pihlaja, J. Org. Chem. 68 (2003) 2151.
[41] S. Kuhl, R. Schneider, Y. Fort, Organometallics 22 (2003) 4184.
[42] J.S.M. Samec, J.E. Bäckvall, Chem. Eur. J. 8 (2002) 2955.
[43] K. Abdur-Rashid, A.J. Lough, R.H. Morris, Organometallics 20 (2001) 1047.
[44] W.T. Brady, C.H. Shieh, J. Org. Chem. 48 (1983) 2499.
[45] J.R. Miecznikowski, R.H. Crabtree, Organometallics 23 (2004) 629.
[46] J. Lin, K. Nomiya, R.G. Finke, Inorg. Chem. 32 (1993) 6040.
[47] A. Vander Ent, A.L. Onderdelinden, Inorg. Synth. 28 (1990) 91.
[48] (a) S. Gründemann, M. Albrecht, J.A. Loch, J.W. Faller, R.H. Crabtree, Organometallics 20 (2001) 5485;
(b) M.H. Voges, C. Rømming, M. Tilset, Organometallics 18 (1999) 529.
[49] L. Blackburn, R.J.K. Taylor, Org. Lett. 3 (2001) 1637.
[50] K. Neuvonen, F. Fulop, H. Neuvonen, A. Koch, E. Kleinpeter, K. Pihlaja, J. Org. Chem. 68 (2003) 2151.
[51] F. Texier-Boullet, Synthesis (1985) 679.
[52] W.T. Brady, C.H. Shieh, J. Org. Chem. 48 (1983) 2499.
[53] L. Blackburn, R.J.K. Taylor, Org. Lett. 3 (2001) 1637.

Available online at www.sciencedirect.com
SCIENCE DIRECT®
Polyhedron 23 (2004) 2873–2878
POLYHEDRON
www.elsevier.com/locate/poly

Synthesis and characterization of CpMn(dfepe)(L) complexes (dfepe = $(C_2F_5)_2PCH_2CH_2P(C_2F_5)_2$; L = CO, H_2, N_2): an unusual example of a dihydride to dihydrogen photochemical conversion

Richard K. Merwin [b], Allyn C. Ontko [a], James F. Houlis [b], Dean M. Roddick [b,*]

[a] *Contribution from the School of Pharmacy, University of Wyoming, P.O. Box 3375, Laramie, Wyoming 82071, USA*
[b] *Contribution from the Department of Chemistry, University of Wyoming, P.O. Box 3838, Laramie, Wyoming 82071, USA*

Received 14 May 2004; accepted 11 June 2004
Available online 6 August 2004

In honor of Malcolm Green, on the occasion of his retirement

Abstract

The synthesis and properties of perfluoroalkylphosphine manganese complexes CpMn(dfepe)(L) (dfepe = $(C_2F_5)_2PCH_2CH_2P(C_2F_5)_2$; L = CO, H_2, N_2) are reported. CpMn(dfepe)(CO) (**1**) was prepared by treatment of $CpMn(CO)_2(thf)$ with excess dfepe. The observed ν(CO) (1934 cm^{-1}) and $E_{1/2}$(ox) (+1.09 V) values confirm the very electron-deficient nature of the CpMn(dfepe) moiety. Photolysis of **1** under a H_2 purge produced a 6:1 equilibrium isomeric mixture of the hydride complexes $CpMn(dfepe)(H)_2$ (**2a**) and $CpMn(dfepe)(\eta^2\text{-}H_2)$ (**2b**). Photolysis of a mixture of **2a** and **2b** in benzene resulted in complete conversion of **2a** to **2b**, which slowly thermally reconverted to an equilibrium mixture ($k \sim 2.3 \times 10^{-4}$ s^{-1}). The dihydrogen complex **2b** reacts with N_2 gas to produce $CpMn(dfepe)(N_2)$ (**3**) ($\nu(N_2)$ = 2113 cm^{-1}). Attempts to isolate **3** resulted in production of the corresponding N_2-bridged dimer, $[CpMn(dfepe)]_2(\mu\text{-}N_2)$ (**4**) (Raman: $\nu(N_2)$ = 2015 cm^{-1}).
© 2004 Elsevier Ltd. All rights reserved.

1. Introduction

Cyclopentadienyl "piano-stool" complexes of the general formula $(\eta^n\text{-}C_nR_n)M(L)_x$ are a versatile and extensively examined class of organometallic compounds. Studies which have focused on both vertical (e.g., $CpM(CO)_3(H)$ (M = Cr, Mo, W), $CpM(CO)_2(Me)$ (M = Fe, Ru, Os) and horizontal (e.g., $(arene)M(CO)_3$ (M = Cr, Mo, W), $(arene)M(CO)_3^+$ (M = Mn, Re)) isoelectronic series provide valuable insights on metal–ligand binding trends and form the basis of many classic paradigms in this field of chemistry.

We have previously reported a series of perfluoroalkylphosphine piano-stool systems incorporating the acceptor phosphine chelate $(C_2F_5)_2PCH_2CH_2P(C_2F_5)_2$ ("dfepe"): $(\eta^6\text{-arene})Mo(dfepe)(L)$ (L = CO, N_2, py) [1], $(\eta^5\text{-}C_5R_5)Mo(dfepe)(CF_2)^+$ [2], $(\eta^5\text{-}C_5R_5)Ru(dfepe)(L)^{0,+}$ (L = halide, H, Me; CO, H_2) [3,4], $(\eta^6\text{-arene})Ru(dfepe)$ [5], and $(\eta^6\text{-arene})Ir(dfepe)^+$ [6]. We have generally observed chemical properties which mirror analogues where dfepe is replaced by two carbonyl ligands rather than donor phosphine derivatives. In this report, we present studies detailing the synthesis and properties of cyclopentadienyl manganese complexes, CpMn(dfepe)(L), where L = CO, N_2 or H_2, which are effective electronic equivalents to well-studied $CpMn(CO)_2(L)$ systems. The dihydrogen complex $CpMn(dfepe)(\eta^2\text{-}H_2)$ is found to be in equilibrium

* Corresponding author. Tel.: +1 307 766 2535; fax: +1 307 766 2807.
E-mail address: dmr@uwyo.edu (D.M. Roddick).

0277-5387/$ - see front matter © 2004 Elsevier Ltd. All rights reserved.
doi:10.1016/j.poly.2004.06.017

with the classic dihydride CpMn(dfepe)$(H)_2$. More interestingly, an unusual photochemical conversion of this mixture exclusively to the nonclassical dihydrogen isomer, followed by thermal re-equilibration has been observed.

2. Experimental

2.1. General procedures

All manipulations were conducted under an atmosphere of purified nitrogen using Schlenk, high vacuum and/or glovebox techniques. Dry oxygen-free solvents were purified by vacuum distillation from sodium/benzophenone (tetrahydrofuran, petroleum ether and hexane). C_6D_6 was dried over activated 4 Å molecular sieves. Elemental analyses were performed by Desert Analytics. Infrared spectra were recorded on a Perkin–Elmer 1600 FTIR instrument as Nujol mulls, unless otherwise noted. Raman spectra were collected on a DeltaNu Advantage 200A spectrometer. NMR spectra were obtained with a JEOL JNM-FX270 or GSX-400 instrument. ^{31}P NMR spectra were referenced to an 85% H_3PO_4 external standard. $CpMn(CO)_3$ was prepared following literature methods [7]. Dfepe was prepared as described previously [8].

2.2. Synthesis of CpMn(dfepe)(CO) (1)

A photolysis reaction vessel (Ace Glass Inc.) was charged with 2.519 g (12.29 mmol) $CpMn(CO)_3$. Four-hundred milliliter THF was added and the mixture was cooled to 0 °C. The mixture was photolyzed for 3 h using a 240 W Hanovia mercury vapor lamp in order to generate $CpMn(CO)_2$(thf), at which time 6.97 g (12.3 mmol) dfepe was added under a nitrogen counterflow via syringe. The reaction was then allowed to stir in darkness for 5 h followed by an additional photolysis period. Monitoring the reaction by solution IR indicated that substitution of $CpMn(CO)_2$(thf) by dfepe was complete after 12 h (Note: care must be taken to minimize photolysis time after conversion to CpMn(dfepe)CO is complete, since the monocarbonyl product is itself photosensitive). The reaction was then warmed to ambient temperature and the volatiles were removed, yielding a dark red oil. Trituration of the oily residue with 20 ml petroleum ether yielded a yellow crystalline solid. Recrystallization from petroleum ether afforded 8.80 g (52.1%) of analytically pure **1**. *Anal*. Calc. for $C_{16}H_9F_{20}P_2OMn$: C, 26.91; H, 1.27. Found: C, 27.11; H, 1.17%. IR data (cm^{-1}): 1934(vs), 1211(s), 1100(s), 1033(m), 983(m), 811(m). ^1H NMR (C_6D_6, 400 MHz, 27 °C): δ 4.30 (s, 5H; C_5H_5), 1.85 (m, 2H; PCH_2), 1.60 (m, 2H; PCH_2). $^{31}P\{^1H\}$ NMR (C_6D_6, 161.7 MHz, 27 °C): δ 150.4 (s, br).

2.3. Preparation of CpMn(dfepe)$(H)_2$ (2a) + CpMn(dfepe)(η^2-H_2) (2b) isomeric mixture

A 450 ml jacketed Ace Glass photolysis reaction apparatus was charged with 1.082 g (1.52 mmol) of **1**. Four-hundred milliliter hexane was added and the mixture was cooled to 0 °C. The solution was purged with N_2 for 15 min, followed by a 15 min purging with hydrogen. At this point the solution was cooled to −10 °C, and photolysis was begun under a continuous H_2 purge (Pyrex-filtered 240 W Hanovia mercury lamp). The reaction was monitored by solution IR until the sharp CO band of **1** was no longer present (ca. 24 h total photolysis time). After photolysis completion, the solution was allowed to warm to ambient temperature and was transferred to a 250 ml round bottom flask and the volatiles were removed under vacuum. The resulting dark red/brown oil was slurried in petroleum ether, concentrated to ca. 2 ml, and cold filtered at −78 °C, yielding 258 mg (25%) of low-melting (~30 °C) red/orange crystals (6:1 mixture of **2a** and **2b**). Although the purity was >95% as judged by ^1H NMR, elemental analyses of this product mixture were consistently high in carbon. *Anal*. Calc. for $C_{15}H_{11}P_2F_{20}Mn$: C, 26.18; H, 1.61. Found: C, 27.33; H, 1.71%. ^1H NMR (C_6D_6, 400 MHz, 27 °C). **2a**: δ 4.29 (s, 5H; C_5H_5), 1.46 (m, 4H; PCH_2), −10.64 (t, 101 Hz, 2H; $Mn(H)_2$). **2b**: 4.18 (s, 5H; C_5H_5), 1.34 (m, 4H; PCH_2), −13.28 (br s, 2H; Mn(η^2-H_2)). $^{31}P\{^1H\}$ NMR (C_6D_6, 161.7 MHz, 27 °C). **2a**: δ 144.7 (s, br). **2b**: δ 160.3 (s, br).

2.4. Synthesis of [CpMn(dfepe)]$_2$(μ-N_2) (4)

A 450 ml jacketed Ace Glass photolysis reaction apparatus was charged with 502 mg (0.704 mmol) **1** and 400 ml hexane. The solution was cooled to 0 °C and then purged for 15 min with nitrogen followed by a 15 min hydrogen purge. The reaction mixture was then cooled to −10 °C under a continuous hydrogen purge and photolysis was begun (Pyrex-filtered 240 W Hanovia mercury lamp). The reaction was monitored by solution IR until the sharp CO band of **1** was no longer present. After 24 h the photolysis and hydrogen purge were stopped and the photolysis was resumed under a nitrogen purge. A noticeable N_2 stretch was observed in the IR after 3 h. The remaining solution was cannula transferred to a 250 ml round bottom flask and the volatiles were removed. As the nitrogen was pulled off and the solution concentrated, red needles began to precipitate and existed simultaneously with a dark red oil when all volatiles were absent. This mixture was brought up in petroleum ether and concentrated. Filtration followed by several washings yielded 140 mg (28%) of red crystalline **4**. Spectra of redissolved **4** showed only resonances due to **3**, however the elemental analysis of this sample was unsatisfactory: *Anal*. Calc. for $C_{30}H_{18}F_{40}Mn_2N_2P_4$: C, 25.73; H, 1.30; N, 2.00. Found: C, 22.55; H, 1.37; N,

1.01%. Spectroscopic data for **4**: $\nu(N_2)$ (Raman, cm^{-1}) = 2015. Spectroscopic data for **3**: IR (C_6D_6, cm^{-1}): $\nu(N_2)$ = 2113(s), 1292(s), 1214(vs), 1113(vs), 799(m). ^1H NMR (C_6D_6, 400 MHz, 27 °C): δ 4.18 (s, 5H; C_5H_5), 1.92 (m, 2H; PCH_2), 1.64 (m, 2H; PCH_2). $^{31}P\{^1H\}$ NMR (C_6D_6, 161.7 MHz, 27 °C): δ 154.1 (s, br).

2.5. Electrochemical measurements

Cyclic voltammetry experiments were performed under a nitrogen atmosphere for complex **1** using a BAS 100A electrochemical analyzer. Measurements were taken at a platinum disk working electrode in acetonitrile containing 0.1 M *n*-$Bu_4N^+PF_6^-$ as the supporting electrolyte. $E_{1/2}$(ox) values (taken as $(E_{pa} + E_{p,c})/2$) were operationally referenced to $Ag/AgClO_4(0.4\ M)_{solv}$ and corrected to SCE using a ferrocene/ferrocenium couple as an internal standard. Under our conditions the $E_{1/2}$(ox) value for Cp_2Fe^+/Cp_2Fe was +0.440 V.

3. Results and discussion

3.1. Synthesis of CpMn(dfepe)(CO)

CpMn(dfepe)CO (**1**) was prepared in 52% yield by photolysis of in situ prepared $CpMn(CO)_2$(thf) in the presence of excess dfepe (Eq. (1)). The photolysis was closely monitored by solution IR and was stopped after CO bands due to $CpMn(CO)_2$(thf) at 1921 and 1974 cm^{-1}had disappeared. Exhaustive photolysis led to low yields of **1** due to its own intrinsic photosensitivity. The electron-poor nature of complex **1** is clearly indicated by infrared and electrochemical data. A single ν(CO) band appears in the infrared at 1934 cm^{-1}, higher in energy than reported for the fluorophosphine chelate $CpMn(Me_2NPF_2)_2(CO)$ (1920 cm^{-1}) [9] and substantially higher than typical donor phosphine values ($CpMn(PPh_3)_2(CO)$: 1824 cm^{-1}; $Cp'Mn(Ph_2PCH_2CH_2PPh_2)(CO)$: 1826 cm^{-1}) [10]. A cyclovoltammetric study of **1** showed a fully reversible Mn(I)/Mn(II) redox couple at +1.09 V in dichloromethane versus $Ag^+/AgCl$. This oxidation potential indicates that **4** is nearly as electron-poor as $Cp'Mn(CO)_3$ (+1.28 V) [11] and substantially more electron-poor than the arylphosphine analogue ($CpMn(PPh_3)_2(CO)$; −0.21 V) [10].

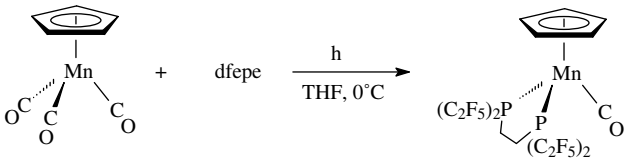

1 (1)

3.2. Synthesis of CpMn(dfepe)H₂

Direct carbonyl displacement reactions were initially examined as potential routes to other CpMn(dfepe)(L) derivatives. No reaction between 1 and 5 equiv. Me_3NO or NH_2OH(HCl) in acetonitrile up to 100 °C was observed. Attempts to reduce the CO ligand with hydride reagents such as KH/THF and $LiAlH_4$ or to produce $CpMn(dfepe)^{2-}$ by reduction with 2 equiv. KC_8 in THF were also unsuccessful. Photochemical substitution reactions have proven more effective. Direct photolytic displacement of CO from **1** under an N_2 purge did not lead to the measurable production of CpMn(dfepe)(N_2), presumably due to an efficient back reaction with photodissociated CO. However, photolysis of **1** in hexane under a purge of hydrogen gas at 0 °C produced a red/orange oil characterized by NMR as a 6:1 isomeric mixture of $CpMn(dfepe)(H)_2$ (**2a**) and CpMn(dfepe)(η^2-H_2) (**2b**) (Eq. (2)). The synthesis of hydride complexes **2a** and **2b** is very sensitive to the reaction parameters and is difficult to reproduce reliably. Synthesis attempts where the H_2 purge rate was insufficient or excessive lead to decomposition and fail to generate significant amounts of the desired product, and very careful monitoring this reaction is essential for success.

Proton spectra of the mixture show two unique cyclopentadienyl resonances (δ 4.29 for **2a**, 4.18 for **2b**) and their associated hydride resonances at δ −10.64 (t, $^2J_{HP}$ = 101 Hz) and −13.28 (br, s), respectively. Variable temperature T_1 measurements at 400 MHz reveal distinctly different T_1 (min) values for the hydride resonances of **2a** (159 ms, 203 K) and **2b** (12 ms, 213 K) which further support the structural assignment. The short T_1 value associated with **2b** falls within the range generally found for nonclassical dihydrogen coordination [12]. While caution must be exercised when interpreting T_1 data for spin-active metal systems such as manganese [13,16d], the R_{HMn} and $R_{Hligand}$ spin relaxation components to R_{obs} for both **2a** and **2b** should be very similar and the distinct difference in T_1 (min) values should therefore be primarily due to relaxation due to H–H dipolar interactions, R_{HH}.

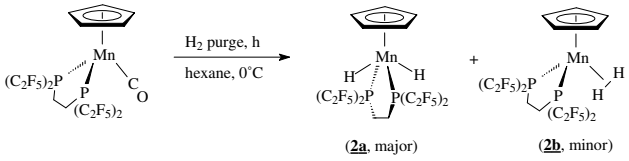

(2)

The related carbonyl complex $CpMn(CO)_2H_2$ [14], originally reported by Leong and Cooper, has been characterized as exclusively the dihydrogen isomer [15]. Other examples of manganese dihydrogen complexes which have been reported include the mixed phosphine–carbonyl cations $(R_3P)_nMn(CO)_{5-n}(\eta^2\text{-}H_2)^+$ [16,17], and the neutral hydride, $(R_2PCH_2CH_2PR_2)_2$-

$Mn(\eta^2\text{-}H_2)H$ (R = Me, Et) [18]. The isomeric mixture of **2** is thermally stable and does not react with excess acids ($HBF_4(Et_2O)$, HOTf) or bases (*n*-BuLi, $NaN(SiMe_3)_2$, NaH) to form the corresponding $CpMn(dfepe)(H)_3^+$ or $CpMn(dfepe)(H)^-$ derivatives. A determination of $^1J_{HD}$ would provide further support for dihydrogen coordination in **2b**. However, addition of stoichiometric or excess DOTf to mixtures of **2a** and **2b** in toluene-d_8 did not lead any significant isotopic scrambling to form $CpMn(dfepe)(\eta^2\text{-}HD)$.

During a series of photolysis studies, it was noticed that the ratio between **2a** and **2b** was time-dependent, with the dihydrogen product **2b** being favored in freshly-photolyzed solutions. Indeed, ^1H NMR monitoring of the photolysis of an equilibrium mixture of **2a** and **2b** in C_6D_6 at 10 °C showed that complete conversion of dihydride **2a** to the dihydrogen complex **2b** occurred after 30 min, followed by a slow ($k \sim 2.3 \times 10^{-4}\ s^{-1}$) first order thermal re-equilibration. To our knowledge, this photochemical control of a dihydride–dihydrogen complex equilibrium is unprecedented. For related $CpRuL_2H_2^+$ chelating phosphine systems, Heinekey has proposed an intramolecular isomerization mechanism whereby the dihydrogen complex's "*cisoid*" phosphine chelate adopts an intermediate equatorial-axial position and subsequently "slides" between the two hydride ligands to form the *transoid* dihydride geometry [19]. However, this equilibration mechanism does not explain why **2a** is selectively driven to **2b** photolytically. An additional photochemical pathway involving photo-assisted chelate dissociation to a 3-legged piano stool geometry (where the hydride ligands must necessarily be *cis*) followed by reassociation of the dangling phosphine end to give the dihydrogen complex is therefore tentatively proposed (Scheme 1).

3.3. Synthesis of $CpMn(dfepe)(N_2)$ and $[CpMn(dfepe)]_2(\mu\text{-}N_2)$

Under an atmosphere of nitrogen, displacement of H_2 from **2b** occurs to form $CpMn(dfepe)(N_2)$ (**3**), identified by the appearance of a strong $\nu(N_2)$ band at 2113 cm^{-1} (Scheme 2). This monomeric dinitrogen complex could not be isolated due to facile loss of N_2 upon

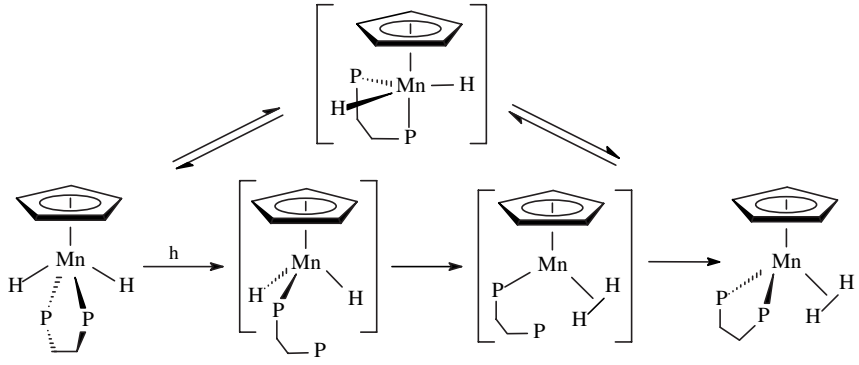

Scheme 1.

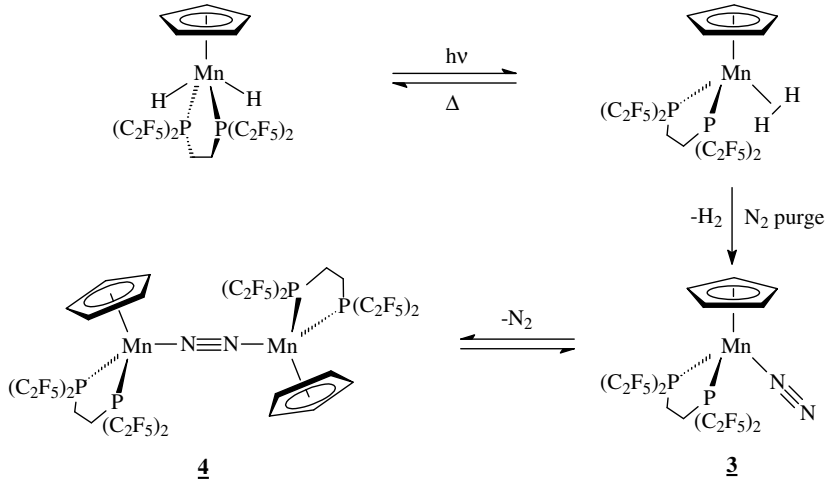

Scheme 2.

solvent concentration to form the corresponding dimer, $[CpMn(dfepe)]_2(\mu\text{-}N_2)$ (**4**), which was isolated as sparingly-soluble red crystals from hexane. The absence of an infrared-active $\nu(N_2)$ band for **4** together with the observation of a Raman-active symmetrical $\nu(N_2)$ mode at 2015 cm^{-1}supports the depicted centrosymmetric dimeric geometry. Redissolving **4** in C_6D_6 under 590 Torr N_2 produces a single solution species with a cyclopentadienyl ^1H resonance at δ 4.18. Solution infrared indicates this species to be essentially pure monomeric **3**.

Photoisomerization of dihydride **2a** to the presumably more thermally labile dihydrogen isomer **2b** suggested a possible one-pot synthesis of **4**. After photolysis of CpMn(dfepe)(CO) at −10 °C under an H_2 purge for 24 h, the reaction mixture was placed under a dinitrogen purge and the photolysis was continued for an additional 3 h. Workup from petroleum ether afforded a modest yield (28%) of **4**.

4. Summary

A comparison of isomeric preferences for the isoelectronic series $(\eta^5\text{-}C_6H_5Me)Mo(dfepe)H_2$, $CpMn(dfepe)H_2$ and $CpRu(dfepe)H_2^+$ is informative. The observed 6:1 $M(H)_2$:$M(H_2)$ coordination preference for manganese falls between the exclusive classic dihydride coordination preference for $(\eta^5\text{-}C_6H_5Me)Mo(dfepe)H_2$ and the 1:6 $M(H)_2$:$M(H_2)$ dihydrogen coordination preference for $CpRu(dfepe)(L)^+$ [4]. For molybdenum, substitution studies with $(\eta^6\text{-}C_6H_5Me)Mo(dfepe)L$ have indicated considerable steric congestion about the metal center [1]. By assuming a "*transoid*" geometry with classical dihydride coordination, steric strain is relieved despite a presumed electronic preference for nonclassical coordination [20]. CpMn(dfepe) and $CpRu(dfepe)^+$ analogues should exhibit an even stronger steric preference for the *transoid* geometry due to decreasing metal size, but it is apparent that the accompanying decrease in metal electron density overcomes the steric preference and favors the dihydrogen isomer as we progress from group six to group eight. Nevertheless, the ready accessibility of a $(\eta^5\text{-}C_6H_5Me)Mo(dfepe)(\eta^2\text{-}H_2)$ intermediate in ligand substitution reactions and the direct observation of both hydride isomers for manganese and ruthenium piano stool complexes suggests that the energetic preferences are very small.

The photochemically-driven isomerization of the classical dihydride isomer **2a** to the nonclassical dihydrogen complex **2b** is similar the that reported for $CpRe(CO)_2(H)_2$ [21]. Both CO and phosphine photolabilization are well established in coordination chemistry [22], so the de-chelation of dfepe proposed in Scheme 1 is a reasonable possibility. Alternatively, Jones has proposed that the active intermediate in phosphine photosubstitution of $CpRe(Ph_3P)_2H_2$ is the allylic intermediate $(\eta^3\text{-}C_5H_7)Re(Ph_3P)_2$ formed via ring-slippage and hydride migration [23]. Further studies will be required to determine the mechanism of dihydride/dihydrogen photoisomerization in this manganese system.

Acknowledgements

This work has been supported by the National Science Foundation (Grant CHE-0093049) and the National Science Foundation EPSCoR Program (Grant EPS-0083030).

Appendix A. Supplementary material

Supplementary data associated with this article can be found, in the online version, at doi:10.1016/j.poly.2004.06.017.

References

[1] M.F. Ernst, D.M. Roddick, Organometallics 9 (1990) 1586.
[2] J.D. Koola, D.M. Roddick, Organometallics 10 (1991) 591.
[3] M.S. Esslinger, J.D. Koola, A.C. Ontko, R.K. Merwin, D.M. Roddick, Organometallics 11 (1992) 3417.
[4] A.C. Ontko, J.F. Houlis, R.C. Schnabel, D.M. Roddick, T.P. Fong, A.J. Lough, R.H. Morris, Organometallics 17 (1998) 5467.
[5] J.D. Koola, D.M. Roddick, J. Am. Chem. Soc. 113 (1991) 1450.
[6] R.C. Schnabel, D.M. Roddick, Organometallics 15 (1996) 3550.
[7] T.S. Piper, F.A. Cotton, G. Wilkinson, J. Inorg. Nucl. Chem. 1 (1955) 165.
[8] M.F. Ernst, D.M. Roddick, Inorg. Chem. 28 (1989) 1624.
[9] R.B. King, W.C. Zipperer, M. Ishaq, Inorg. Chem. 11 (1972) 1361.
[10] N.G. Connelly, M.D. Kitchen, J. Chem. Soc., Dalton Trans. (1977) 931.
[11] The reported potential for $Cp'Mn(CO)_3$ is adjusted +0.13 V based on the cited Cp_2Fe/Cp_2Fe^+ reference couple of +0.31 V. J.K. Kochi, J.W. Hershberger, Polyhedron 2 (1983) 929.
[12] G.J. Kubas, Metal Dihydrogen and σ-Bond Complexes, Kluwer Academic/Plenum Publishers, New York, 2001 (Section 5.5).
[13] P.J. Desrosiers, L. Cai, Z. Lin, R. Richards, J. Halpern, J. Am. Chem. Soc. 113 (1991) 4173.
[14] V.S. Leong, N.J. Cooper, Organometallics 7 (1988) 2080.
[15] J.A. Banister, P.D. Lee, M. Poliakoff, Organometallics 14 (1995) 3876.
[16] (a) X. Fang, J. Huhmann-Vincent, B.L. Scott, G.J. Kubas, J. Organomet. Chem. 609 (2000) 95;
(b) W.A. King, X.-L. Luo, B.L. Scott, G.L. Kubas, K.W. Zilm, J. Am. Chem. Soc. 118 (1996) 6782;
(c) A. Toupadakis, G.J. Kubas, W.A. King, B.L. Scott, J. Huhmann-Vincent, Organometallics 17 (1998) 5315;
(d) W.A. King, B.L. Scott, J. Eckert, G.J. Kubas, Inorg. Chem. 38 (1999) 1069.
[17] G. Albertin, S. Antoniutti, M. Bettiol, E. Bordignon, F. Busatto, Organometallics 16 (1997) 4959.
[18] C. Perthuisot, M. Fan, W.D. Jones, Organometallics 11 (1992) 3622.
[19] M.S. Chinn, D.M. Heinekey, J. Am. Chem. Soc. 112 (1990) 5166.

[20] R.H. Morris, K.A. Earl, R.L. Luck, Inorg. Chem. 26 (1987) 2674.
[21] C.P. Casey, R.S. Tanke, P.N. Hazin, C.R. Kemnitz, R.J. McMahon, Inorg. Chem. 31 (1992) 5474.
[22] (a) T.P.M. Goumans, A.W. Ehlers, M.C. van Hemert, A. Rosa, E.-J. Baerends, K. Lammertsma, J. Am. Chem. Soc. 125 (2003) 3558;
(b) T.J. Burkey, S.K. Nayak, J. Am. Chem. Soc. 115 (1993) 6391;
(c) R.T. Aplin, J. Booth, R.G. Compton, S.G. Davies, S. Jones, J.P. McNally, M.R. Matzler, W.C. Watkins, J. Chem. Soc., Perkin Trans. 2 (1999) 913.
[23] W.D. Jones, G.P. Rosini, J.A. Maguire, Organometallics 18 (1999) 1754.

Available online at www.sciencedirect.com
SCIENCE DIRECT®
Polyhedron 23 (2004) 2879–2900
POLYHEDRON
www.elsevier.com/locate/poly

Theoretical investigation of the metal–metal interaction in dimolybdenum complexes with bridging hydride and methyl ligands

Mu-Hyun Baik [*,a,b], Richard A. Friesner [*,a], Gerard Parkin [a,*]

[a] Department of Chemistry, Columbia University, New York, NY 10027, USA
[b] Department of Chemistry and School of Informatics, Indiana University, Bloomington, Indiana 47405, USA

Received 27 May 2004; accepted 5 August 2004
Available online 16 September 2004

Dedicated to Malcolm L.H. Green for being a tremendous mentor whose enthusiasm and excitement for chemistry, together with his numerous discoveries, have provided inspiration for many

Abstract

DFT calculations on dinuclear molybdenum complexes with bridging hydride and methyl ligands, namely $[CpMo(\mu\text{-}O_2CH)]_2(\mu\text{-}PH_2)(\mu\text{-}H)$ and $[Cp^*Mo(\mu\text{-}O_2CMe)]_2(\mu\text{-}PMe_2)(\mu\text{-}Me)$, indicate that the bonding is best described in terms of: (i) a 2-center-2-electron Mo–Mo single bond and (ii) a 3-center-2-electron Mo–H–Mo or Mo–Me–Mo bond. The presence of a 2-center-2-electron Mo–Mo single bond is in accord with an electron counting procedure that views the bridging hydride and methyl ligands as μ-LX ligands; in contrast, an electron counting procedure which apportions half of the valence electron of the hydrogen atom or methyl radical to each metal dictates a Mo=Mo double bond, a result that is contrary to the theoretical calculations. Consideration of a variety of other bridging hydride complexes indicates that the μ-LX electron counting method provides the best general description of the bonding by clearly distinguishing between the number of 3-center-2-electron M–H–M interactions and direct 2-center-2-electron M–M interactions.
© 2004 Elsevier Ltd. All rights reserved.

1. Introduction

The ability to discern whether or not the proposed structure of a molecule is reasonable is paramount to understanding and predicting its properties, such as stability. While these issues can be addressed by theoretical studies of various levels of sophistication, the first order evaluation is normally performed by the application of simple qualitative and empirical rules, such as the octet rule and those embodied in valence shell electron pair repulsion theory. For example, the chemistry of carbon is dictated by the octet rule and application of this rule successfully predicts the existence of single, double, and triple bonds in ethane, ethylene, and acetylene, respectively. The transition metals, however, with their multiple valence states, are not so readily rationalized by such simple rules. Nevertheless, a notable exception pertains to the organometallic chemistry of the transition elements (and especially for the metals Groups 6–8), for which many structures are governed by the "18-electron rule" [1,2]. By analogy with the octet rule, the successful application of the 18-electron rule merely requires knowledge of how many electrons the ligand array contributes to the valence shell of the metal. For example, the Mn–Mn bond order in $(CO)_5Mn\text{–}Mn(CO)_5$ is predicted to be one on the basis that each $[Mn(CO)_5]$ fragment posseses a 17-electron configuration (cf. the single C–C bond in ethane is a consequence of the fact that each methyl radical possesses a 7-electron configuration). Despite this simplicity, inspection of the literature makes it evident that certain ligands cause confusion with respect to the number of electrons that they contribute to the metal center; bridging hydride and alkyl

* Corresponding authors.
E-mail address: parkin@chem.columbia.edu (G. Parkin).

0277-5387/$ - see front matter © 2004 Elsevier Ltd. All rights reserved.
doi:10.1016/j.poly.2004.08.004

ligands, in particular, are two of the most common ligands for which opinions differ. An important ramification of employing different electron counts for a given bridging ligand is that the inferred bond order between the two metal centers will vary. As an illustration, the molecule $Os_3(CO)_{10}(\mu_2\text{-}H)_2$ [3] has been represented in the literature with no less than five bonding descriptions in which the Os···Os bond order varies from zero to two, including variants with less certain bonding depictions (Fig. 1). Thus, although the formal classification of the bridging ligands and the resulting differences of the formal electron-count may be subjective, the consequences for predicting the electronic structure, of which the most salient feature is the nature of the metal–metal interaction, are significant. Therefore, we address this issue here by performing density functional theory (DFT) [4] electronic structure calculations on a series of dimolybdenum compounds with bridging hydride, methyl and chloride ligands. Specifically, evaluation and comparison of the derived Mo–Mo bond orders provides a means to assess which of the literature electron counting methods for treating symmetrically bridging hydride and methyl ligands is the most apt. The conclusion of this study is that symmetrically bridging hydride and methyl ligands are best represented as 3-center-2-electron interactions, and that electron counting schemes that apportion half of the valence electron of the hydrogen atom or methyl radical to each metal are not appropriate.

2. Results and discussion

2.1. Electron counting and bond order ambiguities

The theoretical calculations that are described in this paper are intended to evaluate which is the most appropriate method for counting electrons in complexes that possess [M(μ-X)M] (X = H, R) 3-center-2-electron interactions [5,6]. To place this work in context, it is pertinent to review the two basic methods for evaluating the number of electrons contributed to each metal center by symmetrically bridging hydride and alkyl ligands.

2.1.1. Method I: the "half-electron" method

This method merely apportions the electrons associated with the isolated hydride and alkyl ligands equally to both metals [7,8]. If one employs a neutral ligand electron counting procedure, this method has the outcome that a bridging hydrogen atom or alkyl radical contributes 0.5 electrons to the electron count at each metal center of a dinuclear complex [9].

2.1.2. Method II: the μ-LX "half-arrow" method

An alternative method to evaluate the number of electrons contributed to the metal center by bridging hydride and alkyl ligands fully recognizes the 3-center-2-electron nature of the [M(μ-X)M] interaction [10]. A simplified molecular orbital representation of the 3-center-2-electron [M(μ-H)M] interaction is illustrated in Fig. 2. An important point to note is that, depending upon the geometry of the system, the amount of direct M–M interaction can vary from being significant to insignificant; such extremes are termed "closed" and "open" 3-center-2-electron interactions and are illustrated in Fig. 3 [11]. As a consequence, while the MO description of the 3-center-2-electron interaction is unambiguous, the schematic depiction of this interaction is not definitive; thus, 3-center-2-electron [M(μ-H)M] bonds have been represented by a variety of means, as illustrated in Fig. 4. Dahl originally formulated [M(μ-H)M] interactions with two solid lines between M and H (**A**) [14,15], but this representation can give the mistaken impression that the two "bonds" at-

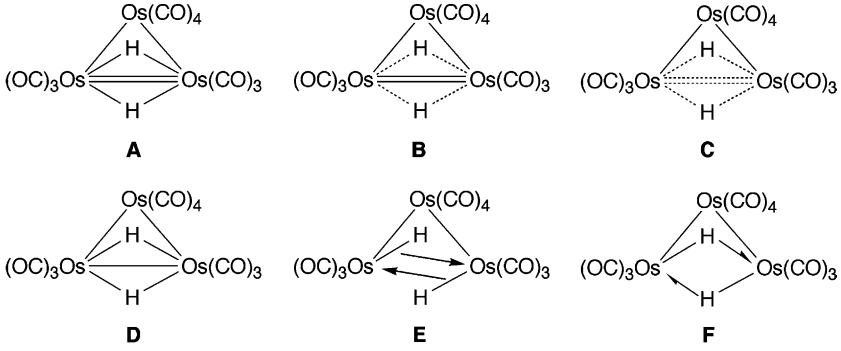

Fig. 1. Structural representations for $Os_3(CO)_{10}(\mu_2\text{-}H)_2$. **A**: (a) Ref. [63c]. (b) M.R. Churchill, H.J. Wasserman, Inorg. Chem. 19 (1980) 2391; (c) F.A. Cotton, G. Wilkinson, Advanced Inorganic Chemistry, 5th ed., Wiley–Interscience, New York, 1988, p. 1057; (d) A.F. Hill, Organotransition Metal Chemistry, Wiley–Interscience, New York, 2002, p. 34. **B**: J.P. Collman, L.S. Hegedus, J.R. Norton, R.G. Finke, Principles and Applications of Organotransition Metal Chemistry, University Science Books, Mill Valley, CA, 1987 p. 37. **C**: Ref. [3b]. **D**: (a) Ref. [60a]. (b) M.G. Karpov, S.P. Tunik, V.R. Denisov G.L. Starova, A.B. Nikolskii, F.M. Dolgushin, A.I. Yanovsky, Y.T. Struchkov, J. Organomet. Chem. 485 (1995) 219; (c) G.O. Spessard, G.L. Miessler, Organometallic Chemistry, Prentice-Hall, Englewood Cliffs, NJ, 1996, p. 454. **E**: (a) R.H. Crabtree, The Organometallic Chemistry of the Transition Metals, 3rd ed., Wiley–Interscience, New York, 2001, p. 373; (b) N.A. Richardson, Y.M. Xie, R.B. King, H.F. Schaefer, J. Phys. Chem. A 105 (2001) 11134. **F**: this work.

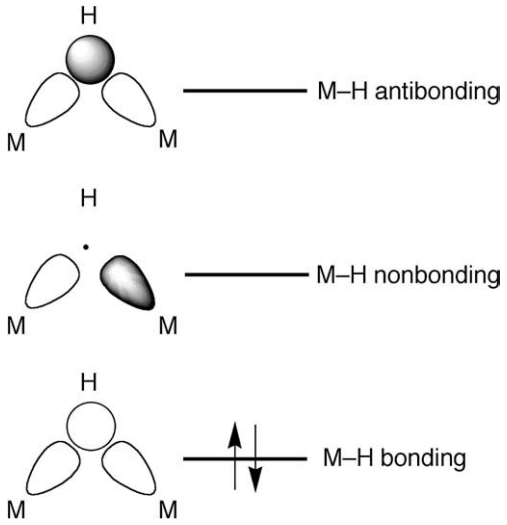

Fig. 2. Simplified MO diagram for a 3-center-2-electron interaction.

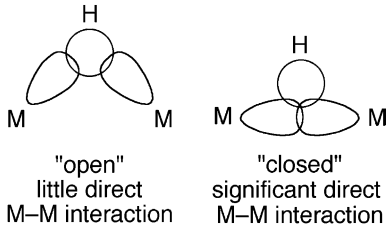

Fig. 3. "Open" and "closed" 3-center-2-electron interactions with varying degrees of M···M interaction.

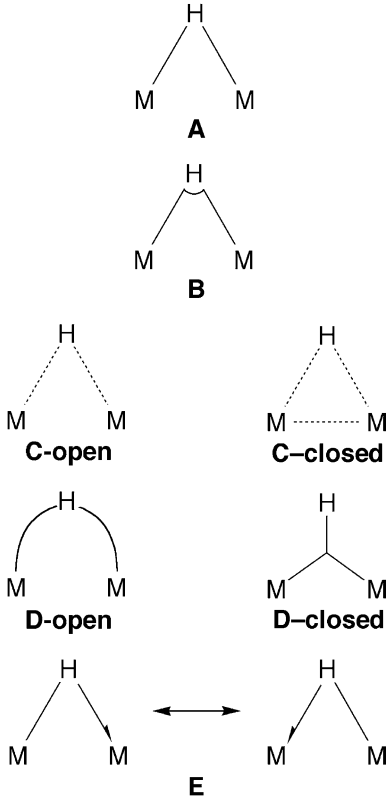

Fig. 4. Representations of 3-center-2-electron M–H–M interactions.

tached to hydrogen are independent 2-center-2-electron bonds. A simple modification of the Dahl representation involves joining the two bonds by a curved line around the hydrogen atom (**B**) to indicate that the two bonds are not independent and thereby emphasize the 3-center-2-electron nature of the interaction [16]. Churchill has employed a "dashed-bond" depiction of the 3-center-2-electron bond that also emphasizes the possible "open" (**C-open**) and "closed" (**C-closed**) nature of the interactions [17,18]. Bau, Koetzle and Kirtley have also proposed representations for "open" and "closed" 3-center-2-electron [M(μ-H)M] interactions by using "bent" (**D-open**) and "Y" (**D-closed**) bonds [12,13], a symbolism that is used in borane chemistry and which is intended to convey the same information portrayed by Churchill's "dashed-bond" depictions. While Churchill's "dashed-bond" depiction of the "closed" 3-center-2-electron [M(μ-H)M] interaction (**B-closed**) is a good representation, Dahl has noted that a problem which has arisen is that others have redrawn the dashed lines as solid lines, thereby implying the incorrect notion that *there is a separate M–M 2-center-2-electron bond in addition to the 3-center-2-electron M–H–M interaction* [15,19]. Another problem associated with each of the representions (**A**) to (**D**) is that they are not particularly useful for electron counting purposes. It is, therefore, significant that Green's μ-LX "half arrow" notation (**E**) (Fig. 4) is of particular benefit in this regard [20,21]. Thus, the representation M–H ⇀ M′ depicts the essence of the valence bond description of the 3-center-2-electron bond in that the pair of electrons associated with the M–H sigma bond (i.e. an "X" type interaction) [21] is donated into a vacant orbital on M′ (i.e. an "L" type interaction) [21], as illustrated in Fig. 5; obviously, by resonance, the bridge (M ↼ H–M′) is symmetric (Fig. 4,**E**). It is important to emphasize that the absence of a "line" between the M atoms bridged by the hydrogen atom in the "half arrow" notation does *not* imply that there is no interaction between

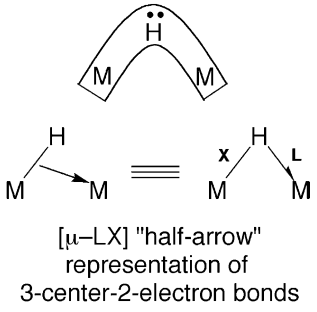

Fig. 5. The [μ-LX] "half-arrow" representation of a 3-center-2-electron M–H–M interaction; the hydrogen atom may be viewed as a μ-LX ligand, where X refers to the one electron contribution to the normal covalent M–H component and L is associated with donation of the pair of electrons associated of the M–H sigma bond into a vacant orbital on M′.

these atoms. Rather, the "half-arrow" notation indicates that any M···M interaction that does exist is one that is mediated by the bridging atom.

The "half arrow" notation is not restricted to M–H–M interactions, but applies equally well to other complexes that exhibit 3-center-2-electron bonds, such as those involving coordination of: (i) C–H bonds, e.g. agostic alkyl complexes [22] and hydrocarbon σ-complexes [M](σ-HR) [23,24], (ii) B–H bonds, e.g. diborane [5], borane adducts [25], and borohydride derivatives [26], and (iii) M–C bonds, e.g. symmetrically bridging methyl ligands.

The existence of two different electron counting procedures causes confusion with respect to the full bonding description of molecules that possess 3-center-2-electron [M(μ-X)M] (X = H, R) interactions, as exemplified by the various bonding descriptions of $Os_3(CO)_{10}(\mu_2\text{-}H)_2$ described above. Furthermore, even though Dahl reported in 1965 the first structure of a transition metal complex with a bridging hydride ligand, namely $[CpMo(CO)_2]_2(\mu\text{-}PMe_2)(\mu\text{-}H)$, and stated that "the bent, three-center Mo–H–Mo bond involving one electron from the two molybdenum atoms and one from the hydrogen accounts for the compound's diamagnetism without the invoking of a separate Mo–Mo bond" [14,15], more than thirty five years later closely related $[CpMo(CO)_2]_2(\mu\text{-}PRR')(\mu\text{-}H)$ derivatives are represented by some chemists with direct Mo–Mo bonds [27]. A further illustration of the confusion that may ensue is illustrated by the description of the bonding in $[(\eta^6\text{-}C_6H_6)Re]_2(\mu\text{-}H)(\mu\text{-}CHR)$. Thus, taking into account the 3-center-2-electron nature of the bonding, $[(\eta^6\text{-}C_6H_6)Re]_2(\mu\text{-}H)(\mu\text{-}CHR)$ was originally assigned a Re–Re single bond, a result that was also confirmed by calculations [28]; a subsequent report, however, does not properly recognize the nature of the bonding and states that the previous assignment is incorrect and that the bond order is three [29]!

To address these issues in more detail, and thereby provide evidence for which of the electron counting methods provides a better description of the bonding in molecules with bridging hydride and methyl ligands, we have used computational methods to investigate the bonding in a series of derivatives with bridging ligands, namely $[Cp^*Mo(\mu\text{-}O_2CMe)]_2(\mu\text{-}PMe_2)(\mu\text{-}Me)$ [30] and $[CpMo(\mu\text{-}O_2CH)]_2(\mu\text{-}PH_2)$ (μ-X) (X = H, Me, Cl).

2.2. The Mo–Mo bond length and bond order in $[Cp^*Mo(\mu\text{-}O_2CMe)]_2(\mu\text{-}PMe_2)(\mu\text{-}Me)$

In contrast to bridging hydride derivatives, complexes with bridging methyl groups are uncommon [31,32]. Bridging methyl ligands also differ from bridging hydride ligands by virtue of the fact that a variety of coordination modes are possible, which may be classified as: (i) symmetric pyramidal, (ii) symmetric trigonal planar, (iii) monohapto agostic [33], (iv) dihapto agostic, and (v) trihapto agostic (Fig. 6) [30,31]. We are aware of only one dimolybdenum complex with a bridging methyl ligand that has been structurally characterized by X-ray diffraction, namely $[Cp^*Mo(\mu\text{-}O_2CMe)]_2(\mu\text{-}PMe_2)(\mu\text{-}Me)$ **1** [30,34], as illustrated in Fig. 7. With chemically equivalent Mo–C bond lengths [2.300(7) and 2.301(7) Å] and an acute Mo–C–Mo bond angle [76.4(2)°], the bridging methyl group in $[Cp^*Mo(\mu\text{-}O_2CMe)]_2(\mu\text{-}PMe_2)(\mu\text{-}Me)$ may be appropriately described as symmetric pyramidal. There is also a short Mo···H separation of 2.02 Å which suggests that some monohapto agostic character to the interaction could be considered, but the equivalence of the Mo–C bond lengths and the acute Mo–C–Mo bond angle is considered to be a more important indicator of the symmetric pyramidal coordination mode [35].

The Mo–Mo interaction in $[Cp^*Mo(\mu\text{-}O_2CMe)]_2(\mu\text{-}PMe_2)(\mu\text{-}Me)$ is predicted to be a single bond using the

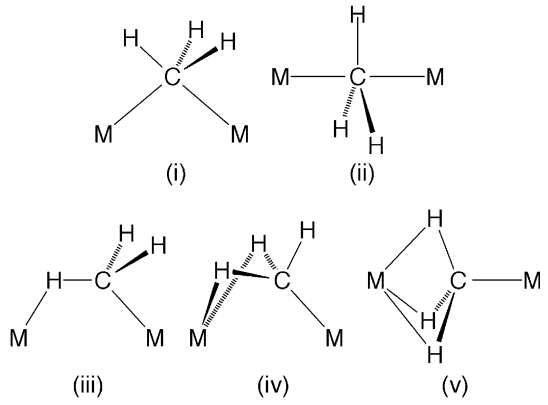

Fig. 6. Coordination modes of bridging methyl complexes.

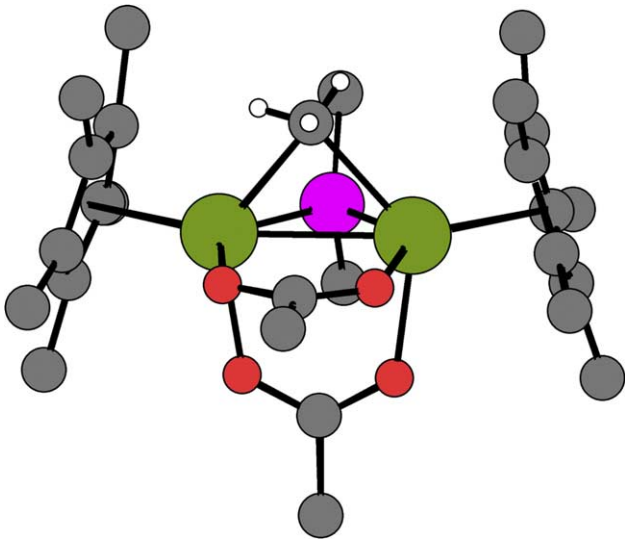

Fig. 7. Experimental molecular structure of $[Cp^*Mo(\mu\text{-}O_2CMe)]_2(\mu\text{-}PMe_2)(\mu\text{-}Me)$.

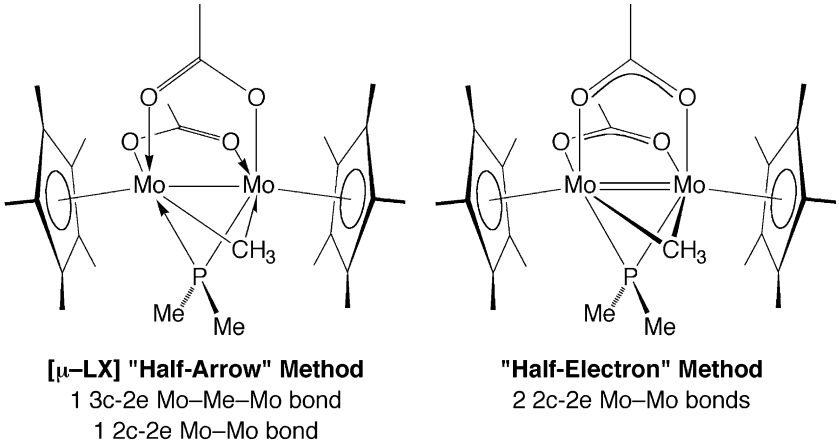

Fig. 8. Predicted Mo–Mo bond orders for $[Cp^*Mo(\mu\text{-}O_2CMe)]_2(\mu\text{-}PMe_2)(\mu\text{-}Me)$ using two different electron counting procedures.

μ-LX "half-arrow" electron counting procedure that recognizes the 3-center-2-electron nature of the interaction, but a double bond using the "half-electron" procedure that does not consider the 3-center-2-electron nature of the interaction, as illustrated in Fig. 8. Specifically, application of the formula [7b]

$$m = (18n - N)/2,$$

where m is the number of 2-center-2-electron M–M bonds, n is the number of M atoms, and N is the total electron count, predicts a Mo=Mo double bond using the "half-electron" method. It is evident from this formula that the higher Mo–Mo bond order for the μ-LX "half-electron" method is merely a consequence of a reduced electron count (N) due to the 3-center-2-electron nature of the interaction not being recognized [7].

Experimental evidence for the Mo–Mo bond order in $[Cp^*Mo(\mu\text{-}O_2CMe)]_2(\mu\text{-}PMe_2)(\mu\text{-}Me)$ could be expected to be procured from the Mo–Mo bond length, in a manner similar to that in which C–C bond distances may be used to distinguish between single (1.53 Å), double (1.32 Å) and triple (1.18 Å) bonds in organic compounds [36]. Indeed, it is evident from the summary of Mo–Mo bond lengths for dinuclear molybdenum complexes provided in Table 1 that Mo–Mo bond lengths span a substantial range; for example, the Mo–Mo single bond in $[CpMo(CO)_3]_2$ [3.235(1) Å] [37] is approximately 1 Å longer than in compounds with Mo≡Mo quadruple bonds, which are typically in the range 2.06–2.17 Å [38]. However, despite this large range of Mo–Mo bond lengths, the presence of bridging ligands creates a significant problem in attempting to correlate metal–metal distances with bond order because the steric and electronic requirements of the bridging group exert an additional influence that causes the metal–metal distance to be either shorter or longer than that in the absence of the bridge [39–42]. For example, complexes with bridging ligands may have Mo–Mo single bonds that are more than 0.5 Å shorter than the Mo–Mo single bond in unbridged $[CpMo(CO)_3]_2$ [3.235(1) Å] [37], as illustrated by $[CpMo(SMe)_2]_2$ [2.603(2) Å] [43], $[Cp^{Pr^i}Mo(\mu\text{-}Cl)_2]_2$ [2.607(1)Å] [44,45], and $[Cp^*Mo(\mu\text{-}I)_2]_2$ [2.708(3) Å] [46,47]. Furthermore, Mo–Mo single bond lengths in complexes with bridging ligands may be comparable to the formal Mo=Mo double bonds in complexes such as $[Cp^*Mo(\mu\text{-}S)(\mu\text{-}SH)]_2$ [2.573(1) Å] [46], $[CpMo(\mu\text{-}S)]_2(\mu\text{-}SPr^i)(\mu\text{-}PPh_2)$ [2.623(2) Å] [27c,48], and $[(Bu^tO)_2Mo_2(\mu\text{-}OBu^t)]_2(\mu\text{-}CO)$ [2.498(1) Å] [49]. Likewise, the Mo=Mo double bond lengths in these complexes are comparable to the formal Mo≡Mo triple bond lengths in $[CpMo(CO)_2]_2$ [2.448(1) Å] [50] and $[IndMo(CO)_2]_2$ [2.500(1) Å] [51,52]. It is, therefore, apparent that assigning a Mo–Mo bond order on the basis of the bond length may be fraught with difficulty. Nevertheless, it is apparent that the Mo–Mo bond length of 2.8447(5) Å for $[Cp^*Mo(\mu\text{-}O_2CMe)]_2(\mu\text{-}PMe_2)(\mu\text{-}Me)$ is much more in accord with that of a Mo–Mo single bond than that of a Mo=Mo double bond. Moreover, the Mo–Mo bond in $[Cp^*Mo(\mu\text{-}O_2CMe)]_2(\mu\text{-}PMe_2)(\mu\text{-}Me)$ is substantially shorter than that in $[CpMo(CO)_2]_2(\mu\text{-}PMe_2)(\mu\text{-}H)$ [3.267(7) Å], a compound that was reported by Dahl as having no direct Mo–Mo bond [14]. As such, these limited bond length comparisons support the notion that electron counting using the μ-LX "half-arrow" method, which recognizes the 3-center-2-electron nature of the interaction, is more appropriate than that of the "half-electron" method. However, in view of the aforementioned caveat, we deemed it essential to establish the Mo–Mo bond order using theoretical methods.

2.3. Geometry optimization of $[Cp^*Mo(\mu\text{-}O_2CMe)]_2(\mu\text{-}PMe_2)(\mu\text{-}Me)$ and related complexes

The geometry optimized structure of $[Cp^*Mo(\mu\text{-}O_2CMe)]_2(\mu\text{-}PMe_2)(\mu\text{-}Me)$ (**1**) is illustrated in Fig. 9 and the derived Mo–Mo bond length (2.88 Å) compares favorably with the experimental value (2.85 Å); likewise,

Table 1
Mo–Mo bond lengths and formal bond orders in dinuclear cyclopentadienyl molybdenum complexes and related derivatives

	$d_{Mo\cdots Mo}$ (Å)	Mo–Mo bond order: [μ-LX] "half-arrow" method	Mo–Mo bond order: "half-electron" method	Ref.
$[CpMo(CO)_2]_2(\mu\text{-}PMe_2)(\mu\text{-}H)$	3.267(2)	0	1	1
$[CpMo(CO)_2]^2(\mu\text{-}PBu^t_2)(\mu\text{-}H)$	3.247(1)	0	1	2
$[CpMo(CO)_2]_2(\mu\text{-}PPh_2)(\mu\text{-}H)$	3.244(1)	0	1	3
$[CpMo(CO)_2]_2(\mu\text{-}PPhEt)(\mu\text{-}H)$	3.278(1)	0	1	4
$[CpMo(CO)_2]_2](\mu\text{-}P\{C_6H_2Bu^t_2CMe_2CH_2\})(\mu\text{-}H)$	3.250(1)	0	1	5
$[CpMo(CO)_3]_2$	3.235(1)	1	1	6
$\{[CpMo(CO)_2]_2(\mu\text{-}PMe_2)\}^-$	3.157(2)	1	1	7
$\{[CpMo(CO)_2]_2(\mu\text{-}PPh_2)\}^-$	3.185(1)	1	1	3
$[Cp^*Mo(\mu\text{-}O_2CMe)]_2(\mu\text{-}PMe_2)(\mu\text{-}Me)$	2.8447(5)	1	2	8
$[Cp^{Pr^i}Mo(\mu\text{-}Cl)_2]_2$	2.607(1)	1	1	9
$[Cp^*Mo(\mu\text{-}Br)_2]_2$	2.643(2)	1	1	10
$[Cp^*Mo(\mu\text{-}I)_2]_2$	2.708(3)	1	1	11
$[(C_5Me_4Et)Mo]_2(\mu\text{-}Cl)_3(\mu\text{-}PPh_2)$	2.6388(8)	1	1	12
$[CpMo(\mu\text{-}SMe)_2]_2$	2.603(2)	1	1	13
$[(Cp^{Me_4Et})Mo(\mu\text{-}SMe)_2]_2$	2.616(1)	1	1	11
$[(Cp^{Me})Mo(\mu\text{-}S)(\mu\text{-}SMe)]_2$	2.582(1)	2	2	14
$[Cp^*Mo(\mu\text{-}S)(\mu\text{-}SH)]_2$	2.573(1)	2	2	11
$[Cp^*Mo(\mu\text{-}S)(\mu\text{-}SMe)]_2$	2.573(1)	2	2	15
$[CpMo(\mu\text{-}S)]_2(\mu\text{-}SPr^i)(\mu\text{-}PPh_2)$	2.623(2)	2	2	16
$[CpMo(CO)_2]_2$	2.448(1)	3	3	17
$[IndMo(CO)_2]_2$	2.500(1)	3	3	18

(1) Ref. [14b].
(2) R.A. Jones, S.T. Schwab, A.L. Stuart, B.R. Whittlesey, T.C. Wright, Polyhedron 4 (1985) 1689.
(3) H. Hartung, B. Walther, U. Baumeister, H.-C. Böttcher, A. Krug, F. Rosche, P.G. Jones, Polyhedron 11 (1992) 1563.
(4) A.J. Bridgmann, M.J. Mays, A.D. Woods, Organometallics 20 (2001) 2076.
(5) Ref. [27a].
(6) Ref. [37].
(7) J.L. Petersen, R.P. Stewart Jr., Inorg. Chem. 19 (1980) 186.
(8) J.H. Shin, G. Parkin, J. Chem. Soc., Chem. Commun. (1998) 1273.
(9) Ref. [44].
(10) J.U. Desai, J.C. Gordon, H.-B. Kraatz, B.E. Owens-Waltermire, R. Poli, A.L. Rheingold, Angew. Chem. Int. Ed. Engl. 32 (1993) 1486.
(11) J.H. Shin, G. Parkin, Polyhedron 13 (1994) 1489.
(12) K. Fromm, E. Hey-Hawkins, Z. Anorg. Allg. Chem. 619 (1993) 261.
(13) Ref. [43].
(14) M. Rakowski DuBois, M.C. VanDerveer, D.L. DuBois, R.C. Haltiwanger, W.K. Miller, J. Am. Chem. Soc. 102 (1980) 7456.
(15) H. Brunner, W. Meier, J. Wachter, P. Weber, M.L. Ziegler, J.H. Enemark, C.G. Young, J. Organomet. Chem. 309 (1986) 313.
(16) Ref. [27c].
(17) Ref. [50].
(18) Ref. [51].

there is good agreement between the calculated (75.3°) and experimental (76.4°) Mo–C–Mo bond angles [30,53]. However, whereas the experimental Mo–CH_3 bond lengths are identical (2.30 Å), the calculation predicts a slight asymmetry of the Mo–CH_3–Mo interaction, with Mo–CH_3 bond lengths of 2.23 and 2.45 Å, indicative of the presence of a weak agostic interaction [22]. We were unable to find a symmetric local minimum where the methyl group is oriented such that there is no agostic interaction. However, although the asymmetric orientation of the methyl group perturbs the shapes of the molecular orbitals, the agostic interaction is quite weak and does not change the overall bonding significantly (vide infra).

To facilitate the interpretation of the theoretical analysis, we have performed additional calculations on simpler derivatives with bridging hydride and chloride ligands, namely $[CpMo(\mu\text{-}O_2CH)]_2(\mu\text{-}PH_2)(\mu\text{-}X)$ (X = H, **2**; Cl, **3**) (Fig. 9). In particular, comparison of the bridging hydride and methyl complexes serves to highlight the electronic similarity of the two systems, while the chloride complex $CpMo(\mu\text{-}O_2CH)]_2(\mu\text{-}PH_2)(\mu\text{-}Cl)$ provides an example of an unambiguous Mo–Mo single bond (in the sense that both electron counting methods predict the same bond order due to the presence of lone pair electrons on chlorine). Comparisons with $\{[CpMo(\mu\text{-}O_2CH)]_2(\mu\text{-}PH_2)\}^-$(**4**$^-$) are also pertinent since the absence of a bridging X ligand results in the molecule possessing a formal Mo=Mo double bond according to both electron counting procedures. Thus, using the electronic structures of $[CpMo(\mu\text{-}O_2CH)]_2(\mu\text{-}PH_2)(\mu\text{-}Cl)$ (**3**) and $\{[CpMo(\mu\text{-}O_2CH)]_2(\mu\text{-}PH_2)\}^-$ (**4**$^-$) as reference points, it is possible to assess critically whether the characteristics of the Mo–Mo interaction in

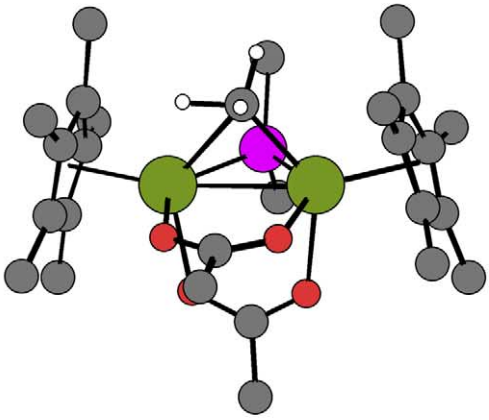

[Cp*Mo(μ-O_2CMe)]$_2$(μ–PMe_2)(μ–Me), **1**

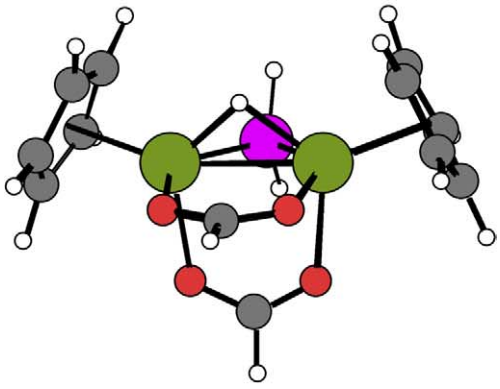

[CpMo(μ-O_2CH)]$_2$(μ–PH_2)(μ–H), **2**

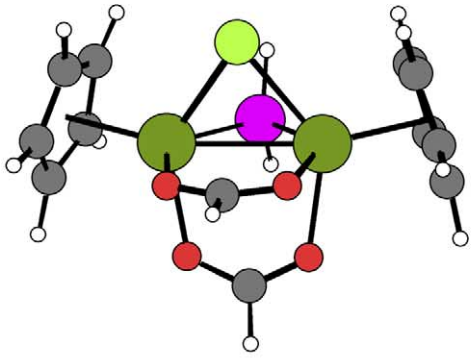

[CpMo(μ-O_2CH)]$_2$(μ–PH_2)(μ–Cl), **3**

Fig. 9. Geometry optimized structures of [Cp*Mo(μ-O_2CMe)]$_2$(μ-PMe_2)(μ-Me), [CpMo(μ-O_2CH)]$_2$(μ-PH_2)(μ-H), and [CpMo(μ-O_2CH)]$_2$(μ-PH_2)(μ-Cl).

[Cp*Mo(μ-O_2CMe)]$_2$(μ-PMe_2)(μ-Me) and [CpMo(μ-O_2CH)]$_2$(μ-PH_2)(μ-H) resemble those of a typical single or double bond.

2.4. Bond orders and bond lengths

Quantum mechanical calculations of the electronic structure of a molecule provide a means for determining bond order. In this regard, although bond orders are not observables in a quantum mechanical sense, such that their derivation is not uniquely defined, a number of protocols have been suggested in the literature [54], of which Wiberg's bond index W is particularly relevant to the goal of the present study [55]. Specifically, Wiberg has shown that the sum of squares of the off-diagonal elements of the density matrix P involving the atomic orbitals of the nuclei that are directly connected to each other gives a good estimate for the bond order

$$W = \sum_{\mu \in A} \sum_{\nu \in B} P_{\mu\nu}^2. \quad (1)$$

A slightly more robust and more generally applicable modification of the Wiberg bond index is the Mayer bond order (M) [56], where the orbital overlap matrix S is also included in the computation of the bond order

$$M = \sum_{\mu \in A} \sum_{\nu \in B} (PS)_{\mu\nu} (PS)_{\nu\mu}. \quad (2)$$

Mayer's protocol has been shown to give bond order values that are in fairly good agreement with intuitive expectations for both organic [57] and inorganic systems [58]. In the following discussion we utilize only the Mayer bond orders and list the Wiberg bond index only for comparison purposes (Table 2).

Examination of the array of complexes shown in Fig. 10 indicates how the computed Mayer bond orders vary as a function of the bridging ligand. Notably, the computed bond order of [Cp*Mo(μ-O_2CMe)]$_2$(μ-PMe_2)(μ-Me) is 0.72, while that of the bridging hydride derivative [CpMo(μ-O_2CH)]$_2$(μ-PH_2)(μ-H) is 0.97. These values are clearly too low to be assigned to a Mo=Mo double bond and more closely correspond to that of a Mo–Mo single bond. A particularly important comparison is with the chloride derivative, [CpMo(μ-O_2CH)]$_2$(μ-PH_2)(μ-Cl), which serves as a reference point for an undisputed formal Mo–Mo single bond since both electron counting methods predict the same bond order. In this regard, the Mayer Mo–Mo bond order of 0.78 for [CpMo(μ-O_2CH)]$_2$(μ-PH_2)(μ-Cl) is comparable to those of [Cp*Mo(μ-O_2CMe)]$_2$(μ-PMe_2)(μ-Me) (0.72) and [CpMo(μ-O_2CH)]$_2$(μ-PH_2)(μ-H) (0.97), thereby indicating that the Mo–Mo interactions are similar and thus support the assignment of a single Mo–Mo bond to each of these complexes.

Further evidence that the Mayer bond orders for the above derivatives correspond to formal Mo–Mo single bonds is provided by comparison with the hypothetical species {[CpMo(μ-O_2CH)]$_2$(μ-PH_2)}$^-$ which is derived by proton abstraction from [CpMo(μ-O_2CH)]$_2$(μ-PH_2)(μ-H). {[CpMo(μ-O_2CH)]$_2$(μ-PH_2)}$^-$ provides a convenient reference point for an undisputed formal Mo=Mo double bond according to both electron counting methods and this is reflected by the Mayer bond order for {[CpMo(μ-O_2CH)]$_2$(μ-PH_2)}$^-$ (1.53) being

Table 2
Comparison of calculated bond orders for a series of dinuclear molybdenum compounds with those predicted by two alternative electron counting methods. In each case, the bond order predicted by the [μ-LX] "half-arrow" method corresponds exactly to that obtained from the calculations, whereas the "half-electron" method fails for the compounds with bridging hydride and methyl ligands

	$d_{Mo\cdots Mo}$ (Å)	Wiberg bond index W	Mayer bond index M	Mo–Mo configuration and calculated bond order	Electron count bond order: [μ-LX] "half-arrow" method	Electron count bond order: "half-electron" method
$\{[CpMo(\mu\text{-}O_2CH)]_2(\mu\text{-}PH_2)(\mu\text{-}H)\}^{2-}$ (**2**$^{2-}$)	3.07	0.39	0.45	$\sigma^2\delta^2\delta^{*2}\pi^{*2}$, BO = 0	0	1
$[Cp^*Mo(\mu\text{-}O_2CMe)]_2(\mu\text{-}PMe_2)(\mu\text{-}Me)$ (**1**)	2.88	0.61	0.72	$\sigma^2\delta^2\delta^{*2}$, BO = 1	1	2
$[CpMo(\mu\text{-}O_2CH)]_2(\mu\text{-}PH_2)(\mu\text{-}H)$ (**2**)	2.77	0.87	0.97	$\sigma^2\delta^2\delta^{*2}$, BO = 1	1	2
$[CpMo(\mu\text{-}O_2CH)]_2(\mu\text{-}PH_2)(\mu\text{-}Cl)$ (**3**)	2.91	0.60	0.78	$\sigma^2\delta^2\delta^{*2}$, BO = 1	1	1
$\{[CpMo(\mu\text{-}O_2CH)]_2(\mu\text{-}PH_2)\}^-$ (**4**$^-$)	2.64	1.41	1.53	$\sigma^2\delta^2\pi^2\delta^{*2}$, BO = 2	2	2
$\{[Cp^*Mo(\mu\text{-}O_2CMe)]_2(\mu\text{-}PMe_2)(\mu\text{-}Me)\}^{2+}$ (**1**$^{2+}$)	2.81	1.02	1.17	$\sigma^2\delta^2$, BO = 2	2	3
$\{[CpMo(\mu\text{-}O_2CH)]_2(\mu\text{-}PH_2)(\mu\text{-}H)\}^{2+}$ (**2**$^{2+}$)	2.67	1.40	1.52	$\sigma^2\delta^2$, BO = 2	2	3
$\{[CpMo(\mu\text{-}O_2CH)]_2(\mu\text{-}PH_2)(\mu\text{-}Cl)\}^{2+}$ (**3**$^{2+}$)	2.83	1.10	1.23	$\sigma^2\delta^2$, BO = 2	2	2
$\{[CpMo(\mu\text{-}O_2CH)]_2(\mu\text{-}PH_2)\}^+$ (**4**$^+$)	2.35	2.17	2.38	$\sigma^2\delta^2\pi^2$, BO = 3	3	3

notably greater than the values for $[Cp^*Mo(\mu\text{-}O_2CMe)]_2(\mu\text{-}PMe_2)(\mu\text{-}Me)$ (0.72), $[CpMo(\mu\text{-}O_2CH)]_2(\mu\text{-}PH_2)(\mu\text{-}H)$ (0.97), and $[CpMo(\mu\text{-}O_2CH)]_2(\mu\text{-}PH_2)(\mu\text{-}Cl)$ (0.78).

An additional comparison is provided by the cation $\{[CpMo(\mu\text{-}O_2CH)]_2(\mu\text{-}PH_2)\}^+$ (**4**$^+$) which is derived by hydride abstraction from $[CpMo(\mu\text{-}O_2CH)]_2(\mu\text{-}PH_2)(\mu\text{-}H)$ and provides a reference point for an undisputed formal Mo≡Mo triple bond according to both electron counting methods. As expected, the Mayer bond order for $\{[CpMo(\mu\text{-}O_2CH)]_2(\mu\text{-}PH_2)\}^+$ (2.38) is substantially greater than that for $\{[CpMo(\mu\text{-}O_2CH)]_2(\mu\text{-}PH_2)\}^-$ (1.53). Thus, consideration of the Mayer bond orders of $[CpMo(\mu\text{-}O_2CH)]_2(\mu\text{-}PH_2)(\mu\text{-}Cl)$ (0.78), $\{[CpMo(\mu\text{-}O_2CH)]_2(\mu\text{-}PH_2)\}^-$ (1.53), and $\{[CpMo(\mu\text{-}O_2CH)]_2(\mu\text{-}PH_2)\}^+$ (2.38), which, respectively, have Mo–Mo single, double and triple bonds according to both electron counting methods, demonstrates that the Mayer bond orders are sensitive to the changes in Mo–Mo interaction in this system. In accord with the increase in Mayer bond order, a corresponding reduction in Mo–Mo bond length is observed for this series of complexes with formal single, double and triple Mo–Mo bonds: $[CpMo(\mu\text{-}O_2CH)]_2(\mu\text{-}PH_2)(\mu\text{-}Cl)$ (2.91 Å), $\{[CpMo(\mu\text{-}O_2CH)]_2(\mu\text{-}PH_2)\}^-$ (2.64 Å), and $\{[CpMo(\mu\text{-}O_2CH)]_2(\mu\text{-}PH_2)\}^+$ (2.35 Å).

While $[CpMo(\mu\text{-}O_2CH)]_2(\mu\text{-}PH_2)(\mu\text{-}Cl)$, $\{[CpMo(\mu\text{-}O_2CH)]_2(\mu\text{-}PH_2)\}^-$, and $\{[CpMo(\mu\text{-}O_2CH)]_2(\mu\text{-}PH_2)\}^+$ provide examples of the changes expected in the Mayer bond order and bond length as a function of the formal Mo–Mo bond order, the comparison is not perfect because the presence of the bridging ligand exerts an intrinsic effect on bond length [39–42]. This problem can be circumvented by consideration of dicationic and dianionic counterparts of $[Cp^*Mo(\mu\text{-}O_2CMe)]_2(\mu\text{-}PMe_2)(\mu\text{-}Me)$, $[CpMo(\mu\text{-}O_2CH)]_2(\mu\text{-}PH_2)(\mu\text{-}H)$, and $[CpMo(\mu\text{-}O_2CH)]_2(\mu\text{-}PH_2)(\mu\text{-}Cl)$. Thus, removal of two electrons from each of the aforementioned complexes is expected to increase the formal bond order by one, while addition of two electrons is expected to reduce the bond order by one (Table 2). As an illustration, the Mayer bond orders for the anionic, neutral, and cationic hydride bridged complexes increase progressively, concomitant with a reduction of Mo–Mo bond length: $\{[CpMo(\mu\text{-}O_2CH)]_2(\mu\text{-}PH_2)(\mu\text{-}H)\}^{2-}$ (**2**$^{2-}$) (0.45, 3.07 Å), $[CpMo(\mu\text{-}O_2CH)]_2(\mu\text{-}PH_2)(\mu\text{-}H)$ (**2**) (0.97, 2.77 Å), and $\{[CpMo(\mu\text{-}O_2CH)]_2(\mu\text{-}PH_2)(\mu\text{-}H)\}^{2+}$ (**2**$^{2+}$) (1.52, 2.67 Å).

2.5. Molecular orbital diagrams

While the Mayer bond orders provide a convenient and quantitative evaluation of the metal–metal interaction, a more detailed picture is required to understand fully the nature of the Mo–Mo interaction. Therefore, we have used the results of DFT calculations to deduce partial molecular orbital (MO) diagrams for the above systems and thereby identify the frontier orbitals that are involved in the Mo–Mo bonding.

Considering initially the hydride bridged complex, $[CpMo(\mu\text{-}O_2CH)]_2(\mu\text{-}PH_2)(\mu\text{-}H)$, it is evident that there are two possible fragmentation patterns for constructing the MO diagram, both of which are useful for understanding the electronic structure of the series of bridged complexes. Thus, the MO diagram can be constructed by using either: (i) an anionic dinuclear fragment, $\{[CpMo(\mu\text{-}O_2CH)]_2(\mu\text{-}PH_2)\}^-$, and the cationic form of the bridging ligand, H^+ or (ii) a cationic dinuclear fragment, $\{[CpMo(\mu\text{-}O_2CH)]_2(\mu\text{-}PH_2)\}^+$, and the anionic form of the ligand, H^-. The MO diagram constructed for the first possibility is illustrated in Fig. 11, where all 10 metal-d dominated MOs are shown as simplified iconic representations. Isosurface plots of the most important MOs are shown in Fig. 12.

It is important to note that the local coordinate system that is used for each molybdenum center is one in which the z-axis is defined as the Mo–Cp_{cent} vector and that these are *not* in alignment with the Mo–Mo

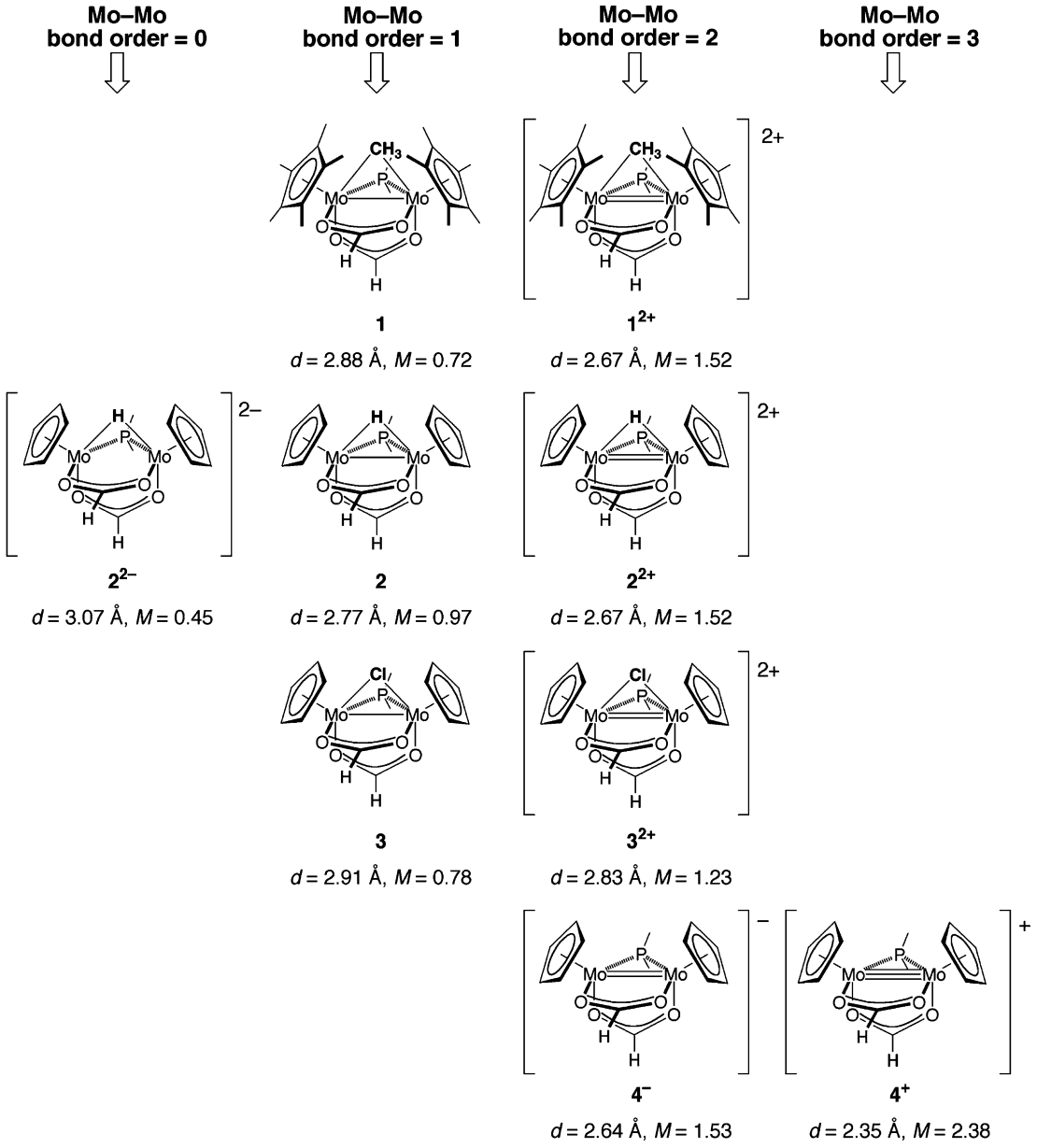

Fig. 10. Metal–metal distances (Å) and Mayer bond orders for a variety of dinuclear complexes. Note that for simplicity the lines between the bridging ligands and the molybdenum centers are only intended to convey connectivity and are not intended to be used for electron counting purposes; in this regard, the resonance structure on the left hand side of Fig. 8 illustrates the appropriate method for counting the bridging ligands.

vector. Thus, whereas the overlap of two d_{xy} orbitals would be expected to give rise to δ and δ* molecular orbitals, the lack of alignment of the Mo–Cp_{cent} and Mo–Mo vectors causes the derived orbitals to have some π-character such that they are best described as "slipped" δ and δ* orbitals. Correspondingly, the overlap of the two d_{xy} orbitals is normally expected to give rise to π and π* molecular orbitals, but the lack of alignment of the Mo–Cp_{cent} vector with the Mo–Mo vector causes these interactions to have some σ-character such that the MOs are best described as "slipped" π and π* orbitals. For brevity, however, we will simply refer to these orbitals as δ/δ* and π/π*, respectively.

The lowest metal-d dominated MO of the $\{[CpMo(\mu\text{-}O_2CH)]_2(\mu\text{-}PH_2)\}^-$ fragment, [σ, MO-⟨57⟩], is an in-phase combination of the Mo-d_{z^2} orbitals and forms the basis of the Mo–Mo σ-bond (left hand side of Fig. 11). The second lowest metal-d dominated MO of the $\{[CpMo(\mu\text{-}O_2CH)]_2(\mu\text{-}PH_2)\}^-$ fragment [δ, MO-⟨58⟩] is derived from overlap of the two Mo-d_{xy} orbitals, while the third lowest MO [π, MO-⟨59⟩] is derived from overlap of the two Mo-d_{xz} orbitals. This orbital is of particular importance with respect to the interaction with the bridging ligands and is therefore marked in red in Fig. 11. The highest occupied molecular orbital (HOMO) of $\{[CpMo(\mu\text{-}O_2CH)]_2(\mu\text{-}PH_2)\}^-$ is the

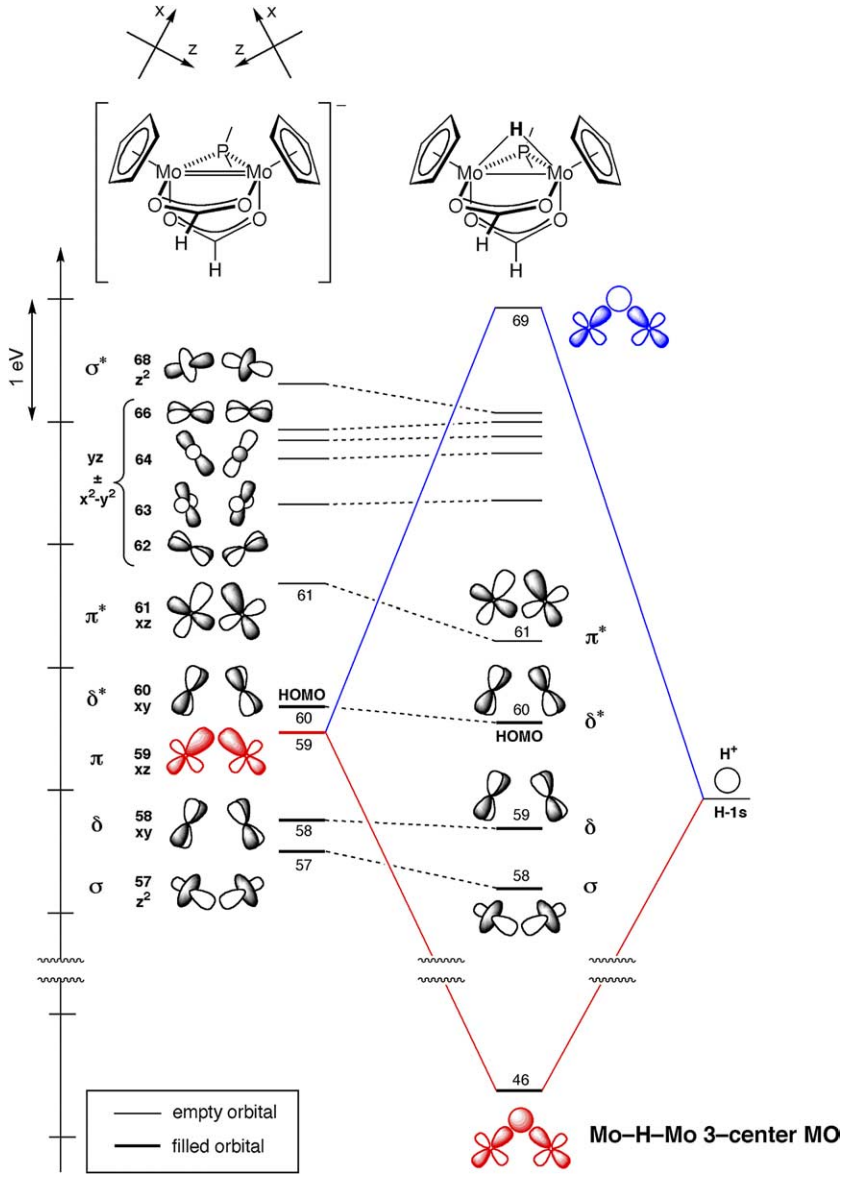

Fig. 11. MO diagram for $[CpMo(\mu\text{-}O_2CH)]_2(\mu\text{-}PH_2)(\mu\text{-}H)$ derived from $\{[CpMo(\mu\text{-}O_2CH)]_2(\mu\text{-}PH_2)\}^-$ and H^+ fragments. The d orbitals listed correspond to the significant component of the molecular orbital.

out-of-phase combination of the metal d_{xy} orbitals [δ*, MO-⟨60⟩], while the lowest unoccupied molecular orbital (LUMO) is the out-of-phase combination of the metal d_{xz} orbitals [π*, MO-⟨61⟩] [59]. With two Mo(II)-d^4 centers in the dinuclear fragment, it is evident that the $\sigma^2(\delta)^2(\pi)^2\text{-}(\delta^*)^2$ configuration corresponds to a formal Mo=Mo double bond in $\{[CpMo(\mu\text{-}O_2CH)]_2(\mu\text{-}PH_2)\}^-$, consisting of one σ and one π bond, which is in accord with the bond order predicted by both electron counting methods.

With respect to construction of the MO diagram for the bridging hydride complex $[CpMo(\mu\text{-}O_2CH)]_2(\mu\text{-}PH_2)(\mu\text{-}H)$ from the $\{[CpMo(\mu\text{-}O_2CH)]_2(\mu\text{-}PH_2)\}^-$ and H^+ fragments, it is only the π orbital [MO-⟨59⟩] of $\{[CpMo(\mu\text{-}O_2CH)]_2(\mu\text{-}PH_2)\}^-$ that has the appropriate symmetry and sufficient overlap with the empty 1s orbital of the proton fragment to give a significant electronic interaction. Thus, the in-phase combination gives rise to a three-center Mo–H–Mo bonding orbital [MO-⟨46⟩, $E = -9.76$ eV] which, as expected for a metal-ligand bonding orbital, is highly dominated by the ligand, i.e. the 1s orbital of hydrogen (Fig. 13). The out-of-phase combination of this interaction [MO-⟨69⟩, $E = -1.76$ eV] has metal based character and is of significantly higher energy (Fig. 14).

As a result of the transfer of electron density from the metal based π orbital to the bridging ligand, only three metal-dominated MOs remain occupied in $[CpMo(\mu\text{-}O_2CH)]_2(\mu\text{-}PH_2)(\mu\text{-}H)$, as shown in Figs. 11 and 14. Of these three MOs, the lowest in energy is the metal–metal

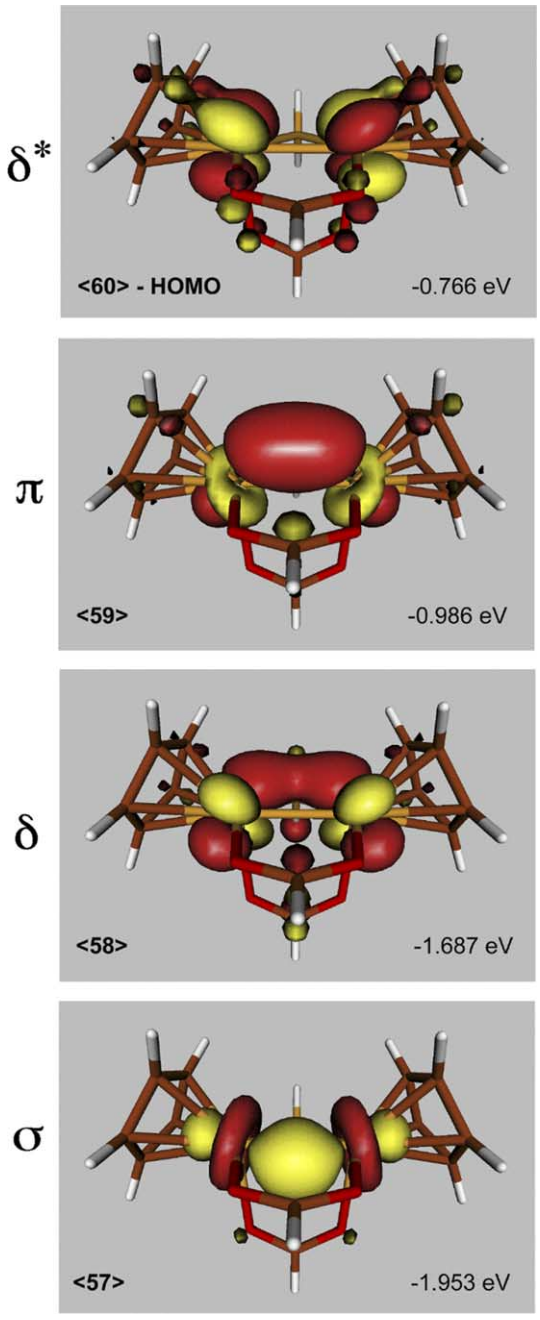

Fig. 12. Isosurface plots of the occupied σ, δ, π and δ* orbitals corresponding to the direct Mo–Mo interaction in $\{[CpMo(\mu\text{-}O_2CH)]_2(\mu\text{-}PH_2)\}^-$. The $\sigma^2(\delta)^2(\pi)^2(\delta^*)^2$ configuration corresponds to a formal Mo=Mo double bond.

σ-bonding orbital [MO-⟨58⟩]. The remaining two orbitals are δ-bonding and δ*-antibonding [MO-⟨59⟩ and MO-⟨60⟩], and since these are both occupied, there is a net zero δ-bonding interaction. Thus, the $\sigma^2(\delta)^2(\delta^*)^2$ configuration for $[CpMo(\mu\text{-}O_2CH)]_2(\mu\text{-}PH_2)(\mu\text{-}H)$ is most consistent with a Mo–Mo single bond. In essence, the π-bond component of the double bond in $\{[CpMo(\mu\text{-}O_2CH)]_2(\mu\text{-}PH_2)\}^-$ is destroyed as a consequence of removal of the π-bond electron density upon protonation.

As indicated above, an alternative approach for constructing the MO diagram for $[CpMo(\mu\text{-}O_2CH)]_2(\mu\text{-}PH_2)(\mu\text{-}H)$ is to employ the cationic dinuclear species $\{[CpMo(\mu\text{-}O_2CH)]_2(\mu\text{-}PH_2)\}^+$ and anionic hydride ligand as the fragments. This approach is chemically more meaningful since the bridging H is usually viewed as a hydride rather than a proton, and it allows for a more intuitive comparison with the bridging chloride derivative since Cl is normally treated as Cl^- rather than Cl^+. While the final MO diagram is, of course, unchanged, it is instructive to consider how the addition of H^- to $\{[CpMo(\mu\text{-}O_2CH)]_2(\mu\text{-}PH_2)\}^+$ causes the formal Mo≡Mo triple bond to be reduced to a single Mo–Mo bond. In essence, there are two factors responsible for the two fold reduction of the Mo–Mo bond order: (i) the Mo–Mo π-bond is eradicated by virtue of the fact that it becomes a component of the three-center Mo–H–Mo interaction, (ii) the additional pair of electrons is elevated to an orbital that is Mo–Mo δ* antibonding (i.e. the LUMO of $\{[CpMo(\mu\text{-}O_2CH)]_2(\mu\text{-}PH_2)\}^+$, [MO-⟨60⟩]), as illustrated in Fig. 15).

To understand in more detail the reason for why addition of H^- causes the formal Mo≡Mo triple bond in $\{[CpMo(\mu\text{-}O_2CH)]_2(\mu\text{-}PH_2)\}^+$ to be reduced to a single Mo–Mo bond, the hypothetical transformation is traced in Fig. 15. Iconic representations of the frontier molecular orbitals of $\{[CpMo(\mu\text{-}O_2CH)]_2(\mu\text{-}PH_2)\}^+$ derived from interactions of the d orbitals are illustrated on the left hand side of Fig. 15, from which it is evident that the $\sigma^2(\delta)^2(\pi)^2$ configuration resulting from the two Mo(III)-d^3 centers predicts a formal Mo≡Mo triple bond in $\{[CpMo(\mu\text{-}O_2CH)]_2(\mu\text{-}PH_2)\}^+$. There are two factors that deserve attention upon the hypothetical coordination of H^- to $\{[CpMo(\mu\text{-}O_2CH)]_2(\mu\text{-}PH_2)\}^+$. Firstly, a significant structural distortion of the $\{[CpMo(\mu\text{-}O_2CH)]_2(\mu\text{-}PH_2)\}^+$ fragment is required to form the hydrogen bridged dimer, $[CpMo(\mu\text{-}O_2CH)]_2(\mu\text{-}PH_2)(\mu\text{-}H)$, with the Mo–Mo bond being required to expand from 2.35 to 2.77 Å upon hydride addition. Secondly, the negative charge density centered on the bridging hydride ligand introduces a purely Coulombic response from the dimetallic fragment. The results of these two changes are illustrated in the MO-correlation diagram shown in Fig. 15: the first step illustrates the consequence of distorting the geometry of the dinuclear $\{[CpMo(\mu\text{-}O_2CH)]_2(\mu\text{-}PH_2)\}^+$ fragment from its equilibrium structure to that of the hydrogen-bridged species $[CpMo(\mu\text{-}O_2CH)]_2(\mu\text{-}PH_2)(\mu\text{-}H)$, while the second step illustrates the result of incorporating a single negative point charge at the position of the hydride bridge. The elongation of the Mo–Mo distance in the first step has the effect of raising the energy of the MOs that are Mo–Mo bonding in character, while stabilizing the MOs that are Mo–Mo antibonding in character. At the distance of 2.77 Å, the HOMO (π) of $\{[CpMo(\mu\text{-}O_2CH)]_2(\mu\text{-}PH_2)\}^+$ in its equilibrium geometry becomes

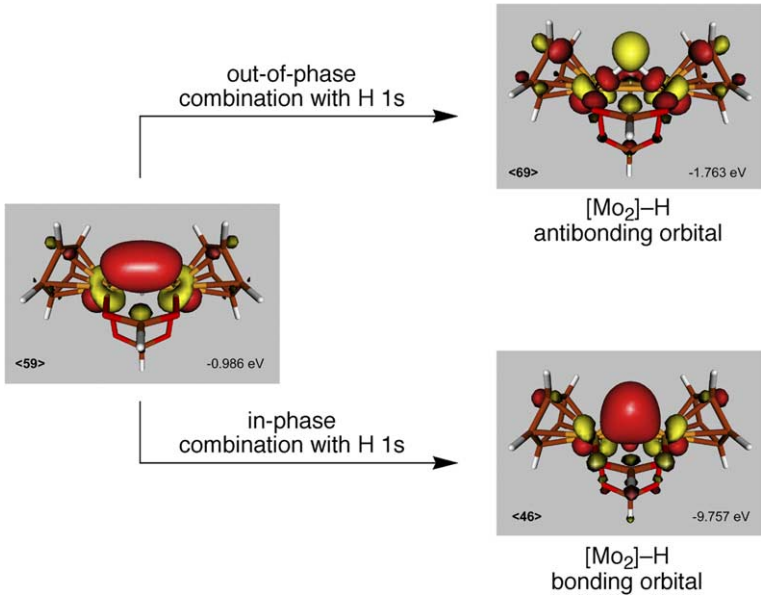

Fig. 13. Mo–H bonding and antibonding orbitals derived by interaction of the H^+ 1s orbital with the Mo–Mo π-bonding orbital of $\{[CpMo(\mu\text{-}O_2CH)]_2(\mu\text{-}PH_2)\}^-$.

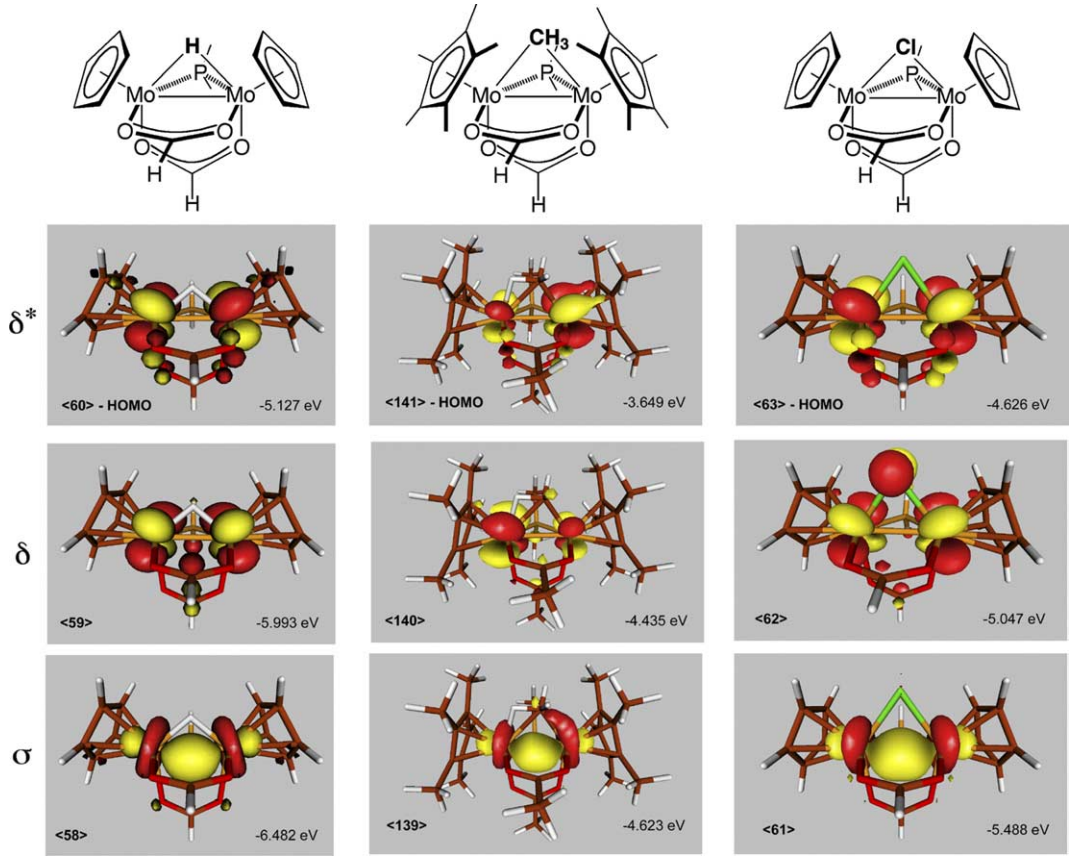

Fig. 14. Comparison of the occupied σ, δ, and δ* orbitals corresponding to the direct Mo–Mo interaction in $[CpMo(\mu\text{-}O_2CH)]_2(\mu\text{-}PH_2)(\mu\text{-}H)$, $[Cp^*Mo(\mu\text{-}O_2CMe)]_2(\mu\text{-}PMe_2)(\mu\text{-}Me)$, and $[CpMo(\mu\text{-}O_2CH)]_2(\mu\text{-}PH_2)(\mu\text{-}Cl)$. The $\sigma^2(\delta)^2(\delta^*)^2$ configuration corresponds to a formal Mo–Mo single bond for each complex.

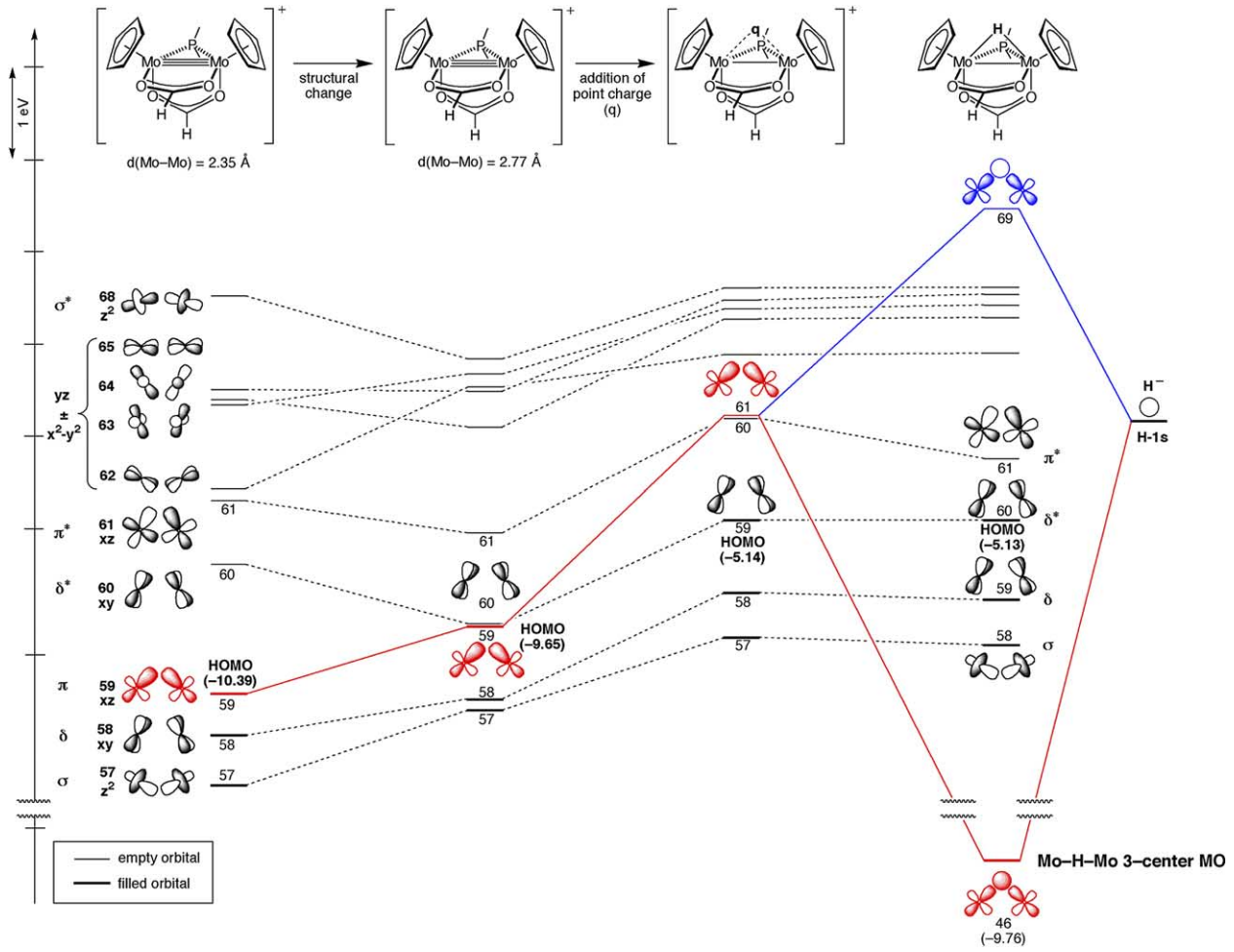

Fig. 15. MO diagram for $[CpMo(\mu\text{-}O_2CH)]_2(\mu\text{-}PH_2)(\mu\text{-}H)$ derived from $\{[CpMo(\mu\text{-}O_2CH)]_2(\mu\text{-}PH_2)\}^+$ and H^- fragments, highlighting the variation in orbital energies of the $\{[CpMo(\mu\text{-}O_2CH)]_2(\mu\text{-}PH_2)\}^+$ fragment resulting from: (i) the change in structure to that of $[CpMo(\mu\text{-}O_2CH)]_2(\mu\text{-}PH_2)(\mu\text{-}H)$ and (ii) the Coulombic response to the negative charge of the hydride ligand.

almost degenerate with its LUMO (δ*). Upon addition of the negative point charge at the hydride site, all the MOs of the $\{[CpMo(\mu\text{-}O_2CH)]_2(\mu\text{-}PH_2)\}^+$ fragment are raised in energy, but especially so for the π HOMO because the shape of this orbital causes it to be fully exposed to the negative charge. As a consequence, the π orbital becomes higher in energy than δ* orbital, such that the latter becomes the HOMO of the hypothetical $\{[CpMo(\mu\text{-}O_2CH)]_2(\mu\text{-}PH_2)\}^+$ fragment. The $\sigma^2(\delta)^2(\delta^*)^2$ configuration thus predicts a formal Mo–Mo single bond for the $\{[CpMo(\mu\text{-}O_2CH)]_2(\mu\text{-}PH_2)\}^+$ fragment with a point charge at the vacant hydride site. The subsequent interaction of this fragment with the 1s orbital of the hydride ligand is primarily with the Mo–Mo π orbital, which is empty as the result of the structural distortion and the presence of the Coulombic potential; this interaction corresponds to the Mo–H–Mo 3-center-2-electron bond, thereby resulting in a $\sigma^2(\delta)^2(\delta^*)^2$ configuration for $[CpMo(\mu\text{-}O_2CH)]_2(\mu\text{-}PH_2)(\mu\text{-}H)$, i.e. a single bond between the two molybdenum centers. As would be expected, the empty π orbital of the $\{[CpMo(\mu\text{-}O_2CH)]_2(\mu\text{-}PH_2)\}^+$ fragment with a negative point charge (q) at the site to be occupied by the hydride ligand corresponds closely to the filled π* orbital of the anionic $\{[CpMo(\mu\text{-}O_2CH)]_2(\mu\text{-}PH_2)\}^-$ fragment that interacts with H^+ (Figs. 11 and 13).

The MO diagram for the chloride derivative $[CpMo(\mu\text{-}O_2CH)]_2(\mu\text{-}PH_2)(\mu\text{-}Cl)$ is illustrated in Fig. 16. Significantly, the $\sigma^2(\delta)^2(\delta^*)^2$ configuration indicates the presence of a Mo–Mo single bond that is formally identical to that of the hydride derivative. Indeed, comparison of the isosurface plots of the most important MOs of $[Cp^*Mo(\mu\text{-}O_2CMe)]_2(\mu\text{-}PMe_2)(\mu\text{-}Me)$, $[CpMo(\mu\text{-}O_2CH)]_2(\mu\text{-}PH_2)(\mu\text{-}H)$ and $[CpMo(\mu\text{-}O_2CH)]_2(\mu\text{-}PH_2)(\mu\text{-}Cl)$ (Fig. 14) indicates that the frontier orbital signatures of these complexes are essentially identical. Thus, even though the slight asymmetry of the bridging mode of the methyl ligand and the presence of high-energy p-orbitals on the chloride ligand give rise to small changes in the shapes of these frontier orbitals, these effects do not have a significant consequence for the qualitative classification of the Mo–Mo interactions.

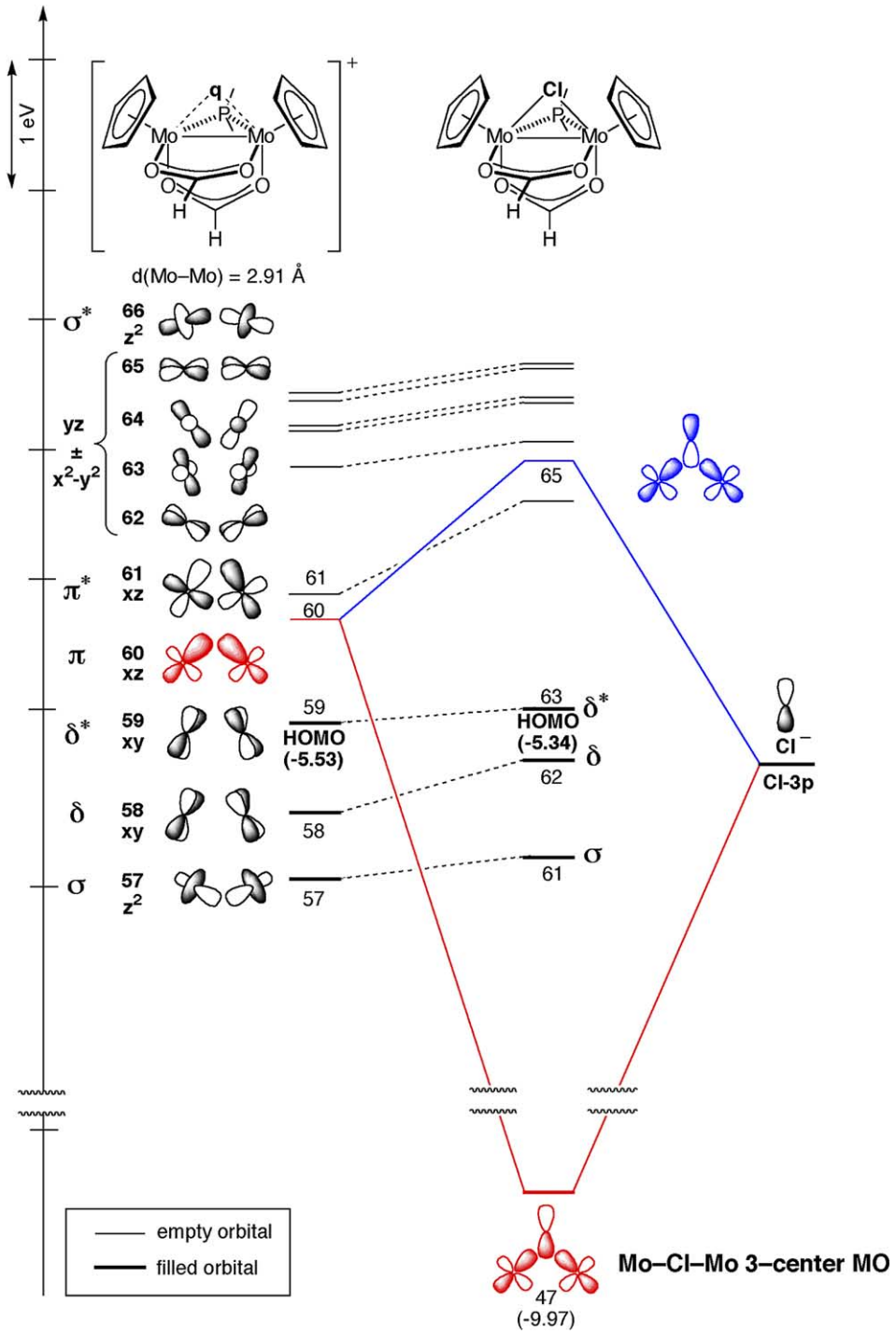

Fig. 16. MO diagram for $[CpMo(\mu\text{-}O_2CH)]_2(\mu\text{-}PH_2)(\mu\text{-}Cl)$ derived from $\{[CpMo(\mu\text{-}O_2CH)]_2(\mu\text{-}PH_2)\}^+$ and Cl^- fragments; the orbital energies for $\{[CpMo(\mu\text{-}O_2CH)]_2(\mu\text{-}PH_2)\}^+$ correspond to the geometry in $[CpMo(\mu\text{-}O_2CH)]_2(\mu\text{-}PH_2)(\mu\text{-}Cl)$ and incorporate the Coulombic response to the negative charge of the chloride ligand.

2.6. Comparison of computed bond orders with those predicted by electron counting methods

Examination of the data in Table 2 indicates that there is qualitative agreement between the computed Wiberg and Mayer bond orders and the bond orders derived by consideration of the molecular orbital electronic configurations. It is also evident that, of the two methods for electron counting, there is a much better correspondence between calculated bond order and the μ-LX "half-arrow" method, i.e. the method that explicitly takes into account the 3-center-2-electron nature of

the interaction involving bridging hydrogen and alkyl groups. For example, while the $\sigma^2(\delta)^2(\delta^*)^2$ configuration of both $[CpMo(\mu\text{-}O_2CH)]_2(\mu\text{-}PH_2)(\mu\text{-}H)$ and $[CpMo(\mu\text{-}O_2CH)]_2(\mu\text{-}PH_2)(\mu\text{-}Cl)$ indicates a Mo–Mo single bond, in accord with the formal single bonds predicted using the μ-LX "half-arrow" method, the formal bond orders derived by using the "half-electron" method differ, with the latter being predicted to have a Mo=Mo double bond rather than a Mo–Mo single bond. Thus, in cases where ambiguities arise in the prediction of the Mo–Mo bond orders by the two electron counting methods, the μ-LX "half-arrow" method provides results that are closer to the theoretically predicted values since it clearly differentiates between the 3-center-2-electron M–H–M interactions and direct 2-center-2-electron M–M interactions.

In addition to the results described here, other studies are also in accord with the μ-LX "half-arrow" representations of bridging hydride ligands. For example, whereas the "half-electron" method predicts an Os=Os double bond in $Os_3(CO)_{10}(\mu\text{-}H)_2$ (Fig. 1A), the μ-LX "half-arrow" method predicts that there is no 2-center-2-electron Os–Os interaction (Fig. 1E and F). Both experimental and theoretical studies are more in accord with the latter description. For example, UV PES studies on $Os_3(CO)_{10}(\mu\text{-}H)_2$ and related bridging hydride complexes have been interpreted with the M(μ-H)M bonding orbital as being localized principally on the hydrogen atom, rather than the metal atoms; [60,61] as such, it would seem inappropriate to describe the Os–Os interaction as that of a Os=Os double bond. Furthermore, MO calculations also indicate that the major interaction between the two osmium centers is via the two 3-center-2-electron Os–H–Os bonds [62,63]. The cyclopentadienyl compound $[Cp^*(CO)Os]_2(\mu\text{-}H)_2$ contains a similar $[Os_2H_2]$ unit that has also been reported to have a Os=Os double bond; [64] by analogy to $Os_3(CO)_{10}(\mu\text{-}H)_2$, however, the direct 2-center-2-electron Os–Os bond order is reduced to zero upon consideration of the 3-center-2-electron nature of the Os–H–Os interactions.

$\{[(CO)_5M]_2(\mu\text{-}H)\}^-$ (M=Cr, Mo, W) [13] provide a classic series of complexes with single 3-center-2-electron M–H–M interactions for which the "half-electron" method predicts a M–M single bond, whereas the μ-LX "half-arrow" method indicates that there is no 2-center-2-electron M–M interaction (Fig. 17); calculations on these complexes also indicate that there is no direct M–M bond and that the interactions are exclusively through the hydride bridge [65]. The closely related complex $\{[(CO)_4W(\mu\text{-}H)]_2\}^{2-}$ [66], with two 3-center-2-electron W–H–W bridges, has also been investigated theoretically, and likewise demonstrates that there is effectively no direct W–W interaction, with the interactions being exclusively through the hydride bridge [67,68]. The results of the calculation are once again

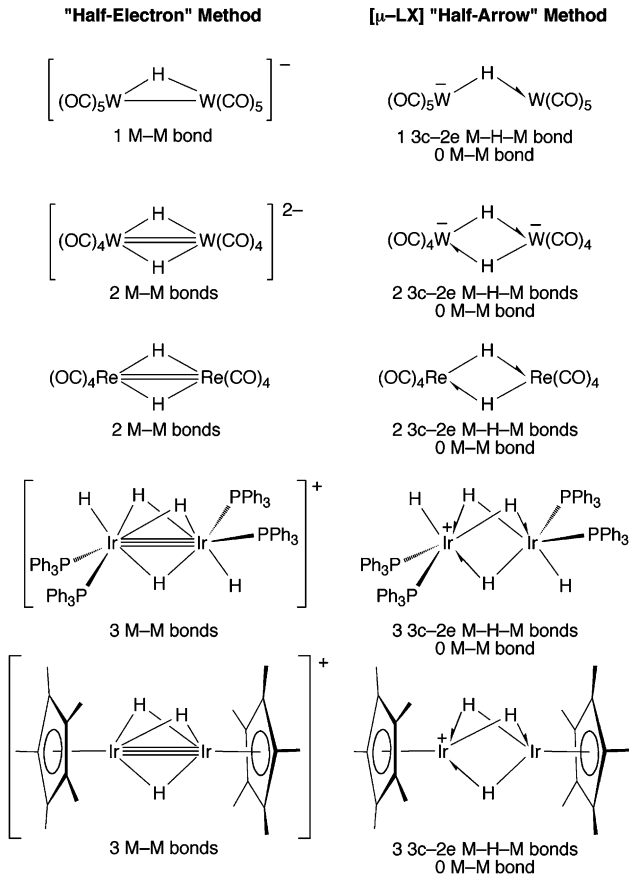

Fig. 17. Different descriptions of the metal–metal bond orders in some dinuclear complexes with bridging hydride ligands according to the electron counting method. The "half-electron" method does not explicitly take into account the 3-center-2-electron nature of the M–H–M interaction and thus results in a greater M–M bond order than would be predicted theoretically. In contrast, the [μ-LX] "half-arrow" method treats the 3-center-2-electron nature of the M–H–M interactions explicitly and thereby predicts a M–M bond order which is in accord with theory.

more in accord with the μ-LX "half-arrow" electron counting method that predicts no 2-center-2-electron W–W interaction, compared to the double bond predicted by the "half-electron" method (Fig. 17). Calculations also indicate that the isostructural neutral rhenium analogue $[(CO)_4Re(\mu\text{-}H)]_2$ [8] is predicted to have effectively no direct Re–Re interaction [67].

The dinuclear iridium complex $\{[(Ph_3P)_2HIr]_2(\mu\text{-}H)_3\}^+$ with three bridging hydride ligands was originally described as possessing a direct Ir≡Ir triple bond to satisfy the 18-electron rule [69]. However, upon recognizing the 3-center-2-electron nature of the interaction it was later realized that there is no direct Ir···Ir interaction and the shortness of the Ir···Ir separation is a geometric consequence of having three bridging hydrogen atoms [70,71] The cyclopentadienyl analogue $\{[Cp^*Ir]_2(\mu\text{-}H)_3\}^+$ was likewise originally reported to possess an Ir≡Ir triple bond [72], but by analogy to $\{[(Ph_3P)_2HIr]_2(\mu\text{-}H)_3\}^+$ can be viewed as possessing no direct Ir–Ir

bond. Structurally related isoelectronic complexes with three bridging hydride ligands that face the same bonding ambiguity description include $\{[(CO)_3Re]_2(\mu\text{-}H)_3\}^-$ [73] and $\{[\{MeC(CH_2PPh_2)_3\}Fe]_2(\mu\text{-}H)_3\}^+$ [74]. Interestingly, while the iron complex was reported to have a Fe≡Fe triple bond, the rhenium complex $\{[(CO)_3Re]_2(\mu\text{-}H)_3\}^-$ was *not* described as possessing a Re≡Re triple bond, but rather described as having 3-center-2-electron Re–H–Re bonds. Hoffmann [75] has analyzed the general class of $[LM]_2(\mu\text{-}H)_3$ molecules theoretically in terms of 3-center-2-electron interactions.

It is important to note that situations arise where the μ-LX "half–arrow" method does *not* predict an 18-electron configuration for both metals in a dinuclear complex with bridging hydrogen atoms. For example, the "half–arrow" method predicts that each of the metal centers in $[Cp^*Re(CO)_2]_2(\mu\text{-}H)_2$, $\{[\{MeC(CH_2AsPh_2)_3\}Co]_2(\mu\text{-}H)_3\}^+$, $[Cp^*Ru]_2(\mu\text{-}H)_4$, and $[(Et_2PhP)_2Re(H)_2]_2(\mu\text{-}H)_4$ would possess a 20-electron configuration (Fig. 18) [76]. However, rather than being a failure of the method, the prediction of a 20-electron configuration is actually a strength of the method since it indicates that the HOMO is an *antibonding* orbital. Occupation of this antibonding orbital thus weakens the bonding interaction that derives from the M–H–M 3-center-2-electron interactions, a notion that has been discussed by Hoffmann and coworkers [77], Dahl [15], and Bursten [78]. As an illustration, consider the hypothetical protonation of a dinuclear system in which there is no formal 2-center-2-electron M–M bond because both bonding and antibonding components are occupied (Fig. 19). The hydrogen 1s orbital interacts specifically with the bonding component, thereby forming the 3-center-2-electron bond. Since the M–M bonding orbital is effectively converted to the M–H–M 3-center-2-electron bond, the pair of electrons that remains in the M–M antibonding orbital constitutes an "antibond". Whereas a bond is conventionally represented by a line between two atoms, an antibond may be depicted by using a crossed-dashed M–×–M representation in which the cross is intended to emphasize that the direct interaction is *antibonding*. Despite the presence of an "antibond", the overall interaction between the two metal centers is favorable because of the stabilization resulting from the formation of the 3-center-2-electron bond. For example, Casey has described the bonding of the $[Re_2H_2]$ unit of $[Cp^*Re(CO)_2]_2(\mu\text{-}H)_2$ as being composed of two 3-center-2-electron Re–H–Re bonds and a Re–×–Re "antibond", such that there is a *net* bond order of one between the two rhenium centers [79].

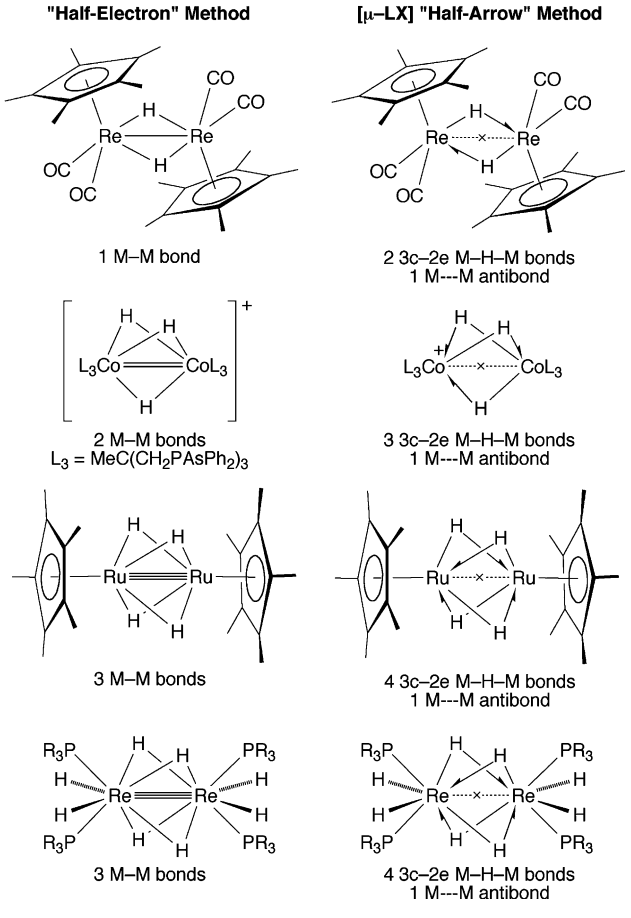

Fig. 18. Examples of compounds that exhibit M–×–M antibonding interactions resulting from a 20-electron configuration that places a pair of electrons in a M–M antibonding orbital. In contrast, the formula employing the "half-electron" method defines each metal center as possessing an 18-electron configuration and so the true nature of the M–M interaction is not evident.

Another illustration is provided by the tetrahydride bridged ruthenium complex $[Cp^*Ru]_2(\mu\text{-}H)_4$ which, on the basis of electron counting according to the "half-electron" method, was proposed to have a Ru≡Ru triple bond [80,81]. However, calculations by Morokuma indicate that the direct Ru–Ru interaction is *repulsive*, and that the two ruthenium centers are only held together by the 3-center-2-electron Ru–H–Ru bonds [82,83]. Again, the μ-LX "half-arrow" method predicts a 20-electron configuration for each ruthenium, thereby correctly suggesting that the direct Ru–Ru interaction is antibonding. An Fe≡Fe triple bond has also been considered as a possibility for the iron counterpart $[Cp^*Fe]_2(\mu\text{-}H)_4$, but has been recognized to be erroneous on the basis of the theoretical study on the ruthenium analogue [84].

$[(Et_2PhP)_2Re(H)_2]_2(\mu\text{-}H)_4$ belongs to the same category of complex that was described as possessing a formal Re≡Re triple bond [85], but the μ-LX "half-arrow" notation would indicate a Re–×–Re antibonding interaction (Fig. 18), which is also in accord with the $\sigma^2(\delta^*)^2(\sigma^*)^2$ electronic configuration that has been calculated for $[(H_3P)_2Re(H)_2]_2(\mu\text{-}H)_4$ [77]. Likewise, the cobalt complex $\{[\{MeC(CH_2AsPh_2)_3\}Co]_2(\mu\text{-}H)_3\}^+$ was proposed to have a double Co=Co bond [74], but is now recognized to have Co–×–Co antibonding interaction (Fig. 18) [77].

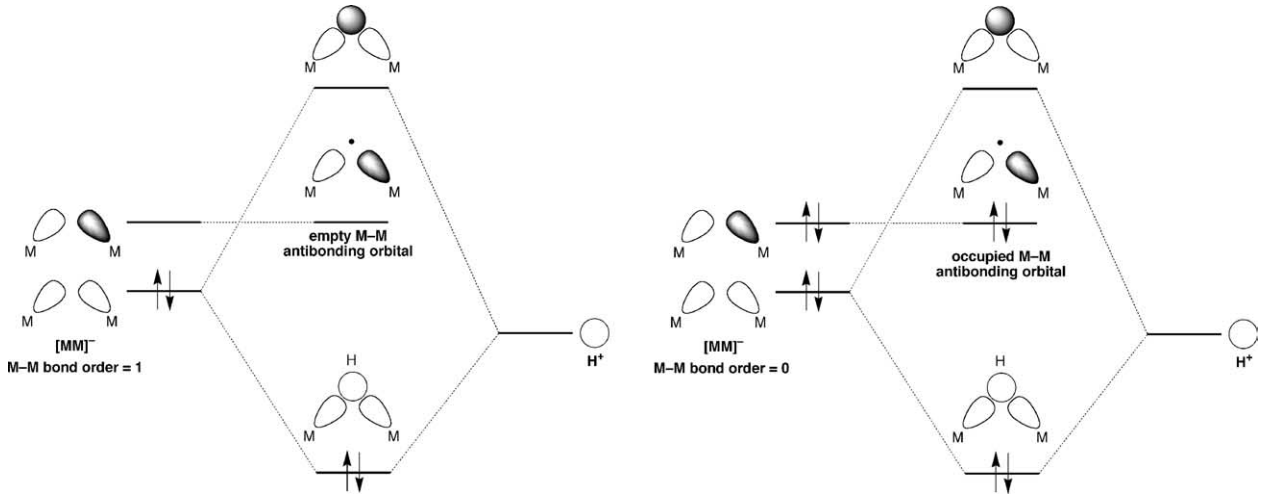

Fig. 19. Molecular orbital description of a M–×–M antibonding interaction in a [MHM] species derived by interaction of $[M_2]^-$ and H^+ fragments in which each atom uses a single orbital. Protonation of the $[M_2]^-$ fragment results in the interaction of the H 1s orbital with the M–M bonding orbital, thereby forming the 3-center-2-electron M–H–M bonding and antibonding orbitals. The M–M antibonding orbital does not have the appropriate symmetry to interact with the H 1s orbital and thus remains M–H nonbonding. If the $[M_2]^-$ fragment possesses two electrons only the M–M bonding orbital is occupied and there is a M–M bond order of one; upon protonation these electrons occupy the 3-center-2-electron M–H–M bonding orbital and the direct M–M bond is eradicated. A similar situation arises for a $[M_2]^-$ fragment that possesses four electrons such that both the M–M bonding and antibonding orbitals are occupied and the M–M bond order is zero; however, in this case, a pair of electrons remains in the M–M antibonding orbital after protonation so that the direct M–M interaction becomes repulsive, i.e. an *antibond*.

Consideration of the above complexes with bridging hydrogen ligands demonstrates that for every 3-center-2-electron M–H–M interaction, the ''half-electron'' method over counts the M–M bond order by one from the value predicted by the μ-LX ''half-arrow'' method. At one level, this is not really an issue once it is recognized that the M–M bond orders derived by the two different electron counting methods are merely *formalisms* and, as such, do not necessarily reflect reality. Problems of this type are commonplace in chemistry. For example, the formal charge [86] on an atom does not necessarily bear any relationship to the actual charge, viz. the formal charge on nitrogen in NH_4^+ is +1, whereas the actual charge is *negative* [87,88]. At another level, the derivation of different M–M bond orders for the same compound is an issue because, from a pedagogical point of view, it causes confusion (as aptly demonstrated by the various descriptions of $Os_3(CO)_{10}(\mu\text{-}H_2)$ shown in Fig. 1). Recognizing that both methods are formalisms, it is more appropriate to adopt the formalism that approximates more closely to the bond orders that are derived theoretically. For all of the examples discussed above, the μ-LX ''half-arrow'' electron counting method provides the best description of the bonding by clearly distinguishing between the number of 3-center-2-electron M–H–M interactions and direct 2-center-2-electron M–M interactions.

Two additional examples serve to point out the inadequacies of electron counting using the ''half-electron'' method. Firstly, the ''half-electron'' method would predict a Zr=Zr double bond in dinuclear $[Cp_2Zr(H)]_2(\mu\text{-}H)_2$ [89] whereas the μ-LX ''half-arrow'' method indicates that each Zr center can attain an 18-electron configuration without forming two 2-center-2-electron Zr–Zr bonds. The latter description is clearly preferable because the Zr center of mononuclear Cp_2ZrH_2 is d^0 and, as such, is incapable of forming a 2-center-2-electron Zr–Zr bond with the Zr center of another molecule. Secondly, the metal–metal bond order predicted by the ''half-electron'' method is *independent* of whether or not the hydrogen atoms bridge the two metals. As an illustration, the three isomers of $[CpReH_3]_2$ with: (i) no bridging hydrogens, $[CpReH_3]_2$, (ii) two bridging hydrogens, $[CpReH_2]_2(\mu\text{-}H)_2$ and (iii) four bridging hydrogens, $[CpReH]_2(\mu\text{-}H)_4$ are each predicted by the ''half-electron'' method to have Re≡Re triple bonds (Fig. 20) [78]. The notion that the Re–Re bond order is not influenced by whether or not the hydrogen atoms bridge is far from intuitive. In contrast, the μ-LX ''half-arrow'' method for counting electrons predicts that the Re–Re bond order decreases from a triple bond in $[CpReH_3]_2$ to a single bond in $[CpReH_2]_2(\mu\text{-}H)_2$, and to an ''antibond'' in $[CpReH_2]_2(\mu\text{-}H)_2$ (Fig. 20). Indeed, calculations by Bursten [78] are in accord with the changes predicted by the μ-LX ''half-arrow'' method. Thus, focusing on the metal-based orbitals: (i) the $\sigma^2(\pi)^4$ electronic configuration for $[CpReH_3]_2$ indicates a direct Re≡Re triple bond, (ii) the $(\sigma/\delta)^2(\pi)^2(\delta^*)^2$ configuration of $[CpReH_2]_2(\mu\text{-}H)_2$ indicates a direct Re–Re single bond, and (iii) the $(\sigma/\delta)^2(\delta^*)^2(\delta^*)^2$ configuration of $[CpReH]_2(\mu\text{-}H)_4$ indicates a direct Re–×–Re antibonding interaction [78].

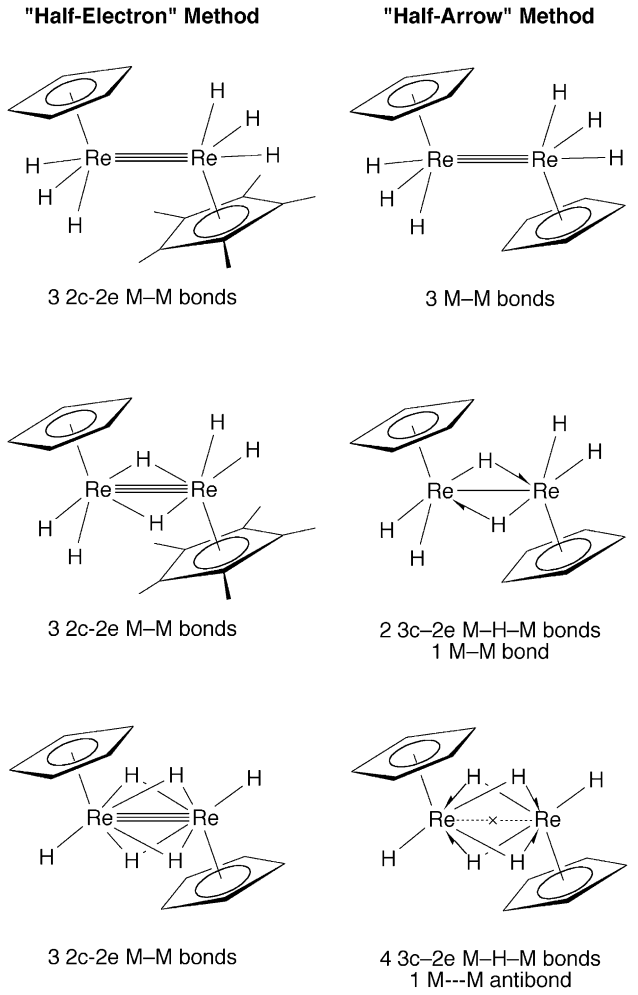

Fig. 20. Three postulated isomeric rhenium hydride complexes for which formal Re≡Re triple bonds were invoked to satisfy the 18-electron rule (left hand side); the corresponding description of their bonding in terms of 3-center-2-electron bonds and direct Re–Re bonds (right hand side).

Why does the "half-electron" method predict the same bond order for the above rhenium complexes regardless of whether or not the hydrogen atoms bridge? This counter-intuitive result is, in essence, a consequence of the "half-electron" method assigning the same number of electrons to bridging and terminal hydride ligands [7]. As such the "half-electron" method fails to address properly the 3-center-2-electron nature of the [M–H–M] bridge.

Hoffmann has aptly concluded that for complexes with 3-center-2-electron bonds "it is best not to argue over whether there is or is not metal–metal bonding in these molecules. The orbitals in question are delocalized and are used to bond a metal atom *both* to its metal partner and to the bridging group" [75]. It is, however, important to emphasize that: (i) the "direct" M···M component for a 3-center-2-electron interaction cannot be viewed as equivalent to that of a normal 2-center-2-electron M–M bond [90], and (ii) there may be additional direct M···M interactions that do not have a significant component from the bridging ligands. These issues are not addressed by the "half-electron" method for counting electrons which merely applies a formula to predict the M–M bond order [7], a formula that does not even require knowledge of the structure of the molecules since the same result is obtained regardless of whether or not the hydrogen atoms bridge. In contrast, the μ-LX "half-arrow" method of counting electrons requires one to draw the structure of the molecule prior to determining the electron count at a metal center from which the M–M bond order is inferred. The μ-LX "half-arrow" method thus provides a more complete picture of the bonding by clearly distinguishing between: (i) the number of 3-center-2-electron M–H–M interactions and (ii) the number of direct 2-center-2-electron M–M interactions. Furthermore, by not forcing an 18-electron count on a metal center (which is *explicitly* forced by the formula employed by the "half-electron" method [7]), the μ-LX "half-arrow" method has the advantage of providing an indication of whether or not a M–M antibonding interaction exists.

One of the significant features of separating the bonding into 3-center-2-electron M–H–M interactions and 2-center-2-electron M–M interactions is that it provides a greater understanding of the bonding. In fact, these two interactions may be viewed as the "*s*" and "*y*" counterparts in Lipscomb's *styx* nomenclature, [91] that has found much use in evaluating the topological structures of boranes [92], and which has also been extended to the structures of metal-hydride clusters [60b].

3. Computational details

All calculations were carried out using density functional theory as implemented in the Jaguar 4.1 suite [93] of quantum chemistry programs, Amsterdam Density Functional 2000.02 package (ADF) [94] and DMOL3 version 2.1 [95,96]. Geometries were optimized using Jaguar and the B3LYP [97] functional with the 6-31G** basis set. Molybdenum was represented using the Los Alamos LACVP** basis [98] that includes relativistic effective core potentials. Vibrational frequency calculation results based on analytical second derivatives at the B3LYP/6-31G** level of theory were used to confirm proper convergence to local minima. Owing to computational cost vibrational frequencies for $[Cp^*Mo(\mu\text{-}O_2CMe)]_2(\mu\text{-}PMe_2)(\mu\text{-}Me)$ and $\{[Cp^*Mo(\mu\text{-}O_2CMe)]_2(\mu\text{-}PMe_2)(\mu\text{-}Me)\}^{2+}$ were not computed. Additional single point calculations on the Jaguar-optimized structures were carried out using ADF to obtain fragment wavefunctions that were helpful for constructing the MO-diagrams. In these calculations, a double-ζ STO basis set was utilized, with one set of polarization

functions as provided in the ADF package (Basis Set III – frozen core), together with the BLYP functional. Relativistic effects on Mo are included using the "zeroth-order regular approximation" (ZORA) [99]. Mayer bond order [56,57] calculations were carried out using DMOL3 [95,97] and the Jaguar-optimized geometries. The BLYP functional was used in combination with the DNP basis set, which corresponds to the 6-31G** basis. Note that the B3LYP functional is not available in "pure DFT" packages, such as ADF and DMOL. Some of the calculations presented above incorporate a point charge placed at appropriate coordinates in space to mimic the electrostatic effect of bridging ligand moieties on the orbitals of the dinuclear metal fragment. In these calculations, the Coulombic potential generated by the point charge in space is included natively in the self-consistent field procedure as implemented in ADF [100].

4. Conclusions

DFT calculations on dinuclear molybdenum complexes with bridging hydride and methyl ligands, namely $[CpMo(\mu\text{-}O_2CH)]_2(\mu\text{-}PH_2)(\mu\text{-}H)$ and $[Cp^*Mo(\mu\text{-}O_2CMe)]_2(\mu\text{-}PMe_2)(\mu\text{-}Me)$, indicate that the bonding is best described in terms of: (i) a 2-center-2-electron Mo–Mo single bond and (ii) a 3-center-2-electron Mo–H–Mo or Mo–Me–Mo bond. The presence of a 2-center-2-electron Mo–Mo single bond is in accord with the prediction of the "half-arrow" electron counting method that views the bridging hydride and methyl ligands as μ-LX ligands. In contrast, the "half-electron" counting procedure, which apportions half of the valence electron of the hydrogen atom or methyl radical to each metal, predicts a Mo=Mo double bond, a result that is contrary to the theoretical calculations. Consideration of the structures of a variety of other bridging hydride complexes indicates that the "half-arrow" electron counting method provides the best general description of the bonding by clearly distinguishing between the number of 3-center-2-electron M–H–M interactions and direct 2-center-2-electron M–M interactions. Several simple examples serve to highlight the failings of the "half-electron" method, namely:

1. The "half-electron" counting procedure predicts a Zr=Zr double bond for $[Cp_2Zr(H)]_2(\mu\text{-}H)_2$. A Zr=Zr double bond is clearly implausible because the Zr center of each Cp_2ZrH_2 fragment is d^0 and is thereby *incapable* of forming a 2-center-2-electron Zr–Zr bond with a second fragment. In contrast, the μ-LX "half-arrow" method predicts that there is no direct Zr–Zr bond in $[Cp_2Zr(H)]_2(\mu\text{-}H)_2$.
2. The M–M bond order predicted by the "half-electron" method is *independent* of whether or not the hydrogen atoms bridge the two metals. As an illustration of this counter-intuitive prediction, the three isomers of $[CpReH_3]_2$ with: (i) no bridging hydrogens, $[CpReH_3]_2$, (ii) two bridging hydrogens, $[CpReH_2]_2(\mu\text{-}H)_2$ and (iii) four bridging hydrogens, $[CpReH]_2(\mu\text{-}H)_4$ are each predicted to have Re≡Re triple bonds by the "half-electron" method. Calculations by Bursten, however, demonstrate that the Re–Re bond orders do indeed vary with the number of bridging hydrogens, in a manner as predicted exactly by the "half-arrow" method.
3. The M–M bond order that is determined by the "half-electron" method is derived by forcing the metal centers to have an 18-electron configuration. In contrast, the M–M bond order derived by the μ-LX "half-arrow" electron counting method does not enforce such a restriction. For example, the μ-LX "half-arrow" electron counting method predicts $[Cp^*Ru]_2(\mu\text{-}H)_4$ to have a 20-electron configuration for each ruthenium. The 20-electron configuration indicates that the HOMO is a Ru–×–Ru *antibonding* orbital which reduces the overall bonding associated with the four Ru–H–Ru 3-center-2-electron interactions. This prediction is in full accord with a theoretical study by Morokuma which indicates that the direct Ru–Ru interaction is *repulsive*, a result that is in marked contrast to the Ru≡Ru triple bond predicted by the "half-electron" method.

In conclusion, the "half-arrow" method is the procedure of choice for counting electrons for complexes that possess 3-center-2-electron M–×–M interactions. In all cases evaluated, the "half-arrow" method provides results that are much more in accord with theoretical calculations than those obtained by the "half-electron" method.

Acknowledgements

We thank the US Department of Energy, Office of Basic Energy Sciences (DE-FG02-93ER14339 to G.P.) and the National Institutes of Health (GM 40526 to R.A.F.) for support of this research.

References

[1] The "18-electron rule" is variously referred to as "effective atomic number rule", "inert gas rule" and "rare gas rule" in the literature. For reviews of the 18-electron rule, see:
(a) P.R. Mitchell, R.V. Parish, J. Chem. Educ. 46 (1969) 811;
(b) D.P. Craig, G. Doggett, J. Chem. Soc. (1963) 4189;
(c) C.A. Tolman, Chem. Soc. Rev. 1 (1972) 337;
(d) P.S. Braterman, Struct. Bond. 10 (1972) 57.
[2] For a discussion of the 18-electron rule in terms of the Complementary Spherical Electron Density Model, see:
(a) D.M.P. Mingos, J. Organomet. Chem. (2004), in press;
(b) D.M.P. Mingos, J.C. Hawes, Struct. Bond. 63 (1985) 1.

[3] For the X-ray and neutron diffraction studies of $Os_3(CO)_{10}(\mu_2\text{-}H)_2$, see:
(a) V.F. Allen, R. Mason, P.B. Hitchcock, J. Organomet. Chem. 140 (1977) 297;
(b) M.R. Churchill, F.J. Hollander, J.P. Hutchinson, Inorg. Chem. 16 (1977) 2697;
(c) A.G. Orpen, A.V. Rivera, E.G. Bryan, D. Pippard, G.M. Sheldrick, K.D. Rouse, J. Chem. Soc., Chem. Commun. (1978) 723;
(d) R.W. Broach, J.M. Williams, Inorg. Chem. 18 (1979) 314.
[4] R.G. Parr, W. Yang, Density Functional Theory of Atoms and Molecules, Oxford University Press, New York, 1989.
[5] For a brief overview of 3-center-2-electron interactions, see: R.L. DeKock, W.B. Bosma, J. Chem. Ed. 65 (1988) 194.
[6] For a recent theoretical analysis of the 3-center-2-electron bonding interaction in B_2H_6, see: R. Ponec, D.L. Cooper, Int. J. Quantum Chem. 97 (2004) 1002.
[7] (a) J.P. Collman, L.S. Hegedus, J.R. Norton, R.G. Finke, Principles and Applications of Organotransition Metal Chemistry, University Science Books, Mill Valley, CA, 1987, pp. 24 and 36;
(b) S.M. Owen, Polyhedron 7 (1988) 253;
(c) C.E. Housecroft, A.G. Sharpe, Inorganic Chemistry, Prentice-Hall, New York, 2001, p. 591.
[8] For a specific example, see: M.J. Bennett, W.A.G. Graham, J.K. Hoyano, W.L. Hutcheon, J. Am. Chem. Soc. 94 (1972) 6232.
[9] An alternative (but mathematically identical) description employing the closed shell method is to apportion the two electrons associated with H^- and R^- ligands equally to each metal, i.e. the anion contributes 1 electron to the electron count of each metal center, both of which bear a +0.5 charge.
[10] See, for example:
(a) R.H. Crabtree, The Organometallic Chemistry of the Transition Metals, 3rd ed., Wiley–Interscience, New York, 2001, p. 70;
(b) C. Elschenbroich, A. Salzer, Organometallics, 2nd ed., VCH, New York, 1992, p. 323.
[11] It should be noted that the "open" and "closed" nomenclature for [M(μ-H)M] is not completely analogous to that used in boron hydride chemistry for B_3 fragments. Specifically, the "open" B–B–B interaction employs a p-orbital on the central boron, such that the outer boron atoms are required by symmetry arguments to exhibit an out-of-phase antibonding interaction. For situations with a bridging hydrogen atom, the two outer atoms will always exhibit a bonding interaction, and the classification of "open" and "closed" relates to the magnitude of the interaction. See [12,13].
[12] J.P. Olsen, T.F. Koetzle, S.W. Kirtley, M. Andrews, D.L. Tipton, R. Bau, J. Am. Chem. Soc. 96 (1974) 6621.
[13] R. Bau, R.G. Teller, S.W. Kirtley, T.F. Koetzle, Acc. Chem. Res. 12 (1979) 176.
[14] (a) R.J. Doedens, L.F. Dahl, J. Am. Chem. Soc. 87 (1965) 2576;
(b) J.L. Petersen, L.F. Dahl, J.M. Williams, J. Am. Chem. Soc. 96 (1974) 6610.
[15] L.F. Dahl, Ann. NY Acad. Sci. 415 (1983) 1.
[16] This notation was first introduced to describe B–H–B interactions. See:
(a) R.W. Parry, G. Kodama, Coord. Chem. Rev. 128 (1993) 245;
(b) R.W. Parry, L.J. Edwards, J. Am. Chem. Soc. 81 (1959) 3554.
[17] (a) M.R. Churchill, S.W.-Y. Ni, J. Am. Chem. Soc. 95 (1973) 2150;
(b) M.R. Churchill, S.W.-Y. Chang, Inorg. Chem. 13 (1974) 2413;
(c) M.R. Churchill, B.G. DeBoer, F.J. Rotella, Inorg. Chem. 15 (1976) 1843.
[18] M.R. Churchill, Adv. Chem. Ser. 167 (1978) 36.
[19] The 3-center-2-electron M–H–M interaction has also been described as a protonated metal–metal bond of the anionic $[M–M]^-$ moiety [17c]. While this is a perfectly good description of the interaction, it must be emphasized that the protonated "metal–metal bond" is no longer the same as that in the hypothetical anionic $[M–M]^-$ fragment.
[20] M. Berry, N.J. Cooper, M.L.H. Green, S.J. Simpson, J. Chem. Soc., Dalton Trans. (1980) 29.
[21] M.L.H. Green, J. Organomet. Chem. 500 (1995) 127.
[22] (a) M. Brookhart, M.L.H. Green, J. Organomet. Chem. 250 (1983) 395;
(b) M. Brookhart, M.L.H. Green, L.L. Wong, Prog. Inorg. Chem. 36 (1988) 1.
[23] J.M. Buchanan, J.M. Stryker, R.G. Bergman, J. Am. Chem. Soc. 108 (1986) 1537.
[24] (a) C. Hall, R.N. Perutz, Chem. Rev. 96 (1996) 3125;
(b) R.H. Crabtree, Chem. Rev. 95 (1995) 987;
(c) R.H. Crabtree, Angew. Chem., Int. Ed. Engl. 32 (1993) 789;
(d) G.J. Kubas, Metal Dihydrogen and σ-Bond Complexes: Structure, Theory, and Reactivity, Kluwer Academic Publishers/Plenum Press, New York, 2001.
[25] R.W. Parry, G. Kodama, Coord. Chem. Rev. 128 (1993) 245.
[26] Z. Xu, Z. Lin, Coord. Chem. Rev. 156 (1996) 139.
[27] See, for example:
(a) M.E. García, V. Riera, M.A. Ruiz, D. Sáez, J. Vaissermann, J.C. Jeffery, J. Am. Chem. Soc. 124 (2002) 14304;
(b) M.E. García, V. Riera, M.A. Ruiz, M.T. Rueda, D. Sáez, Organometallics 21 (2002) 5515;
(c) H. Adams, N.A. Bailey, A.P. Bisson, M.J. Morris, J. Organomet. Chem. 444 (1993) C34.
[28] J.C. Green, M.L.H. Green, D. O'Hare, R.R. Watson, J.A. Bandy, J. Chem. Soc., Dalton Trans. (1987) 391.
[29] See reference [13] in B.-S. Kang, U. Koelle, U. Thewalt, Organometallics 10 (1991) 2569.
[30] J.H. Shin, G. Parkin, J. Chem. Soc., Chem. Commun. (1998) 1273.
[31] For a brief review, see: P. Braunstein, N.M. Boag, Angew. Chem., Int. Ed. Engl. 40 (2001) 2427.
[32] J. Holton, M.F. Lappert, R. Pearce, P.I.W. Yarrow, Chem. Rev. 83 (1983) 135.
[33] For examples, and for a discussion of the factors responsible for the bridging methyl group in $[\{Cp(CO)Fe\}_2(\mu\text{-}CO)(\mu\text{-}Me)]^+$ adopting a monohapto agostic interaction, see: B.E. Bursten, R.H. Cayton, Organometallics 5 (1986) 1051, and references therein.
[34] The bridging methyl compound $[CpMo(CO)]_2(\mu\text{-}PCy_2)(\mu\text{-}CH_3)$ has recently been reported, although it has not been structurally characterized by X-ray diffraction. See: M.E. García, S. Melón, A. Ramos, V. Riera, M.A. Ruiz, D. Belletti, C. Graiff, A. Tiripicchio, Organometallics 22 (2003) 1983.
[35] See, for example: S.D. Stults, R.A. Andersen, A. Zalkin, J. Organomet. Chem. 462 (1993) 175.
[36] D.R. Lide (Ed.), Handbook of Chemistry and Physics, 72nd ed., CRC Press, Boca Raton, FL, 1991, pp. 9-2–9-6.
[37] R.D. Adams, D.M. Collins, F.A. Cotton, Inorg. Chem. 13 (1974) 1086.
[38] F.A. Cotton, L.M. Daniels, E.A. Hillard, C.A. Murillo, Inorg. Chem. 41 (2002) 2466.
[39] M.J. Bennett, J.V. Brencic, F.A. Cotton, Inorg. Chem. 8 (1969) 1060.
[40] F.A. Cotton, Acc. Chem. Res. 11 (1978) 225.
[41] F.A. Cotton, Walton, R.A Multiple, Bonds Between Metal Atoms, 2nd ed., Oxford University Press, Oxford, 1993.
[42] Indeed, the metal–metal separation in dinuclear complexes with bridging ligands and no metal–metal bond may be shorter than unbridged complexes with a metal–metal bond. See, for example: H. Vahrenkamp, Angew. Chem., Int. Ed. Engl. 17 (1978) 379.
[43] N.G. Connelly, L.F. Dahl, J. Am. Chem. Soc. 92 (1970) 7470.

[44] P.D. Grebenik, M.L.H. Green, A. Izquierdo, V.S.B. Mtetwa, K. Prout, J. Chem. Soc., Dalton Trans. (1987) 9.
[45] J.C. Green, M.L.H. Green, P. Mountford, M.J. Parkington, J. Chem. Soc., Dalton Trans. (1990) 3407.
[46] J.H. Shin, G. Parkin, Polyhedron 13 (1994) 1489.
[47] Note that these specific compounds have been selected because the bond order assignment is independent of electron count method used because none of the bridges are involved in 3-center-2-electron interactions.
[48] MO calculations on axially symmetric complexes of the type $[CpMo(\mu\text{-}X)_2]_2$ indicate that the δ* orbital may be lower in energy than the δ orbital. Specifically, the δ orbital interacts with an appropriate combination of p orbitals of the $(\mu\text{-}X)_4$ fragment whereas the δ* orbital does not; if this destabilization of the δ orbital is sufficiently strong, the energies of the δ and δ* orbitals may be reversed. An important consequence of this reversal pertains to "d^2–d^2" dimers such that rather than have a $\sigma^2\delta^2$ configuration, and hence a Mo=Mo double bond, a $\sigma^2\delta^{*2}$ configuration results such that the Mo–Mo bond order is zero. See [45].
[49] M.H. Chisholm, F.A. Cotton, M.W. Extine, R.L. Kelly, J. Am. Chem. Soc. 101 (1979) 7645.
[50] R.J. Klingler, W. Butler, M.D. Curtis, J. Am. Chem. Soc. 97 (1975) 3535.
[51] M.A. Greaney, J.S. Merola, T.R. Halbert, Organometallics 4 (1985) 2057.
[52] It should, however, be noted that compounds with substantially shorter formal Mo≡Mo triple bonds are known for non-cyclopentadienyl derivatives, e.g. $Mo_2(NMe_2)_6$ [2.214(3) Å][a] and $Mo_2(OCH_2CMe_3)_6$ [2.222(2) Å][b]:
(a) M.H. Chisholm, F.A. Cotton, B.A. Frenz, W.W. Reichert, L.W. Shive, B.R. Stults, J. Am. Chem. Soc. 98 (1976) 4469;
(b) M.H. Chisholm, F.A. Cotton, C.A. Murillo, W.W. Reichert, Inorg. Chem. 16 (1977) 1801.
[53] For some calculations on dinuclear chromium complexes with bridging methyl ligands, see:
(a) S.K. Noh, S.C. Sendlinger, C. Janiak, K.H. Theopold, J. Am. Chem. Soc. 111 (1989) 9127;
(b) C. Janiak, J. Silvestre, K.H. Theopold, Chem. Ber. 126 (1993) 631.
[54] G. Frenking, N. Fröhlich, Chem. Rev. 100 (2000) 717.
[55] (a) K.B. Wiberg, Tetrahedron 24 (1968) 1083;
(b) Wiberg's bond index is often denoted as *P*. We use *W* to avoid confusion with the density matrix, which is widely abbreviated as *P*, as we do here.
[56] I. Mayer, Chem. Phys. Lett. 97 (1983) 270.
[57] (a) I. Mayer, Int. J. Quantum Chem. 29 (1986) 477;
(b) I. Mayer, Int. J. Quantum Chem. 29 (1986) 73.
[58] (a) A.J. Bridgeman, G. Cavigliasso, L.R. Ireland, J. Rothery, J. Chem. Soc., Dalton Trans. (2001) 2095;
(b) A.J. Bridgeman, G. Cavigliasso, Polyhedron 20 (2001) 2269.
[59] There are five more unoccupied metal-dominated MOs to complete the set of 10 MOs relevant for the dimetallic complex, all of which are indicated in Fig. 11. However, because they are not of much significance for the goal of this investigation, they are not further discussed.
[60] Specifically, the ionization bands assigned to the M(μ-H)M interactions showed a marked variation in intensity in the HeI and HeII spectra, indicating a significant contribution from the hydrogen 1s orbital which is known to be sensitive to such changes:
(a) J.C. Green, D.M. Mingos, E.A. Seddon, Inorg. Chem. 20 (1981) 2595;
(b) J.C. Green, D.M. Mingos, E.A. Seddon, J. Organomet. Chem. 185 (1980) C20.
[61] M.B. Hall, J.C. Green, Phil. Trans. Roy. Soc. London A 308 (1982) 85.
[62] D.E. Sherwood, M.B. Hall, Inorg. Chem. 21 (1982) 3458.
[63] It should be noted that there is an additional way of describing the structure of 4–membered $[M(\mu\text{-}H)_2M]$ fragments. Specifically, rather than describing the interaction as two 3-centered-2-electron bonds, it is permissible to describe the interaction as one 4-centered-2-electron $[M(\mu\text{-}H)_2M]$ bond and one 2-centered M–M bond. However, a double 2-centered-2-electron M=M interaction is not a viable alternative since there would be no orbitals available on M for interaction with the hydrogen atoms. See, for example:
(a) C. Elschenbroich, A. Salzer, Organometallics, 2nd ed., VCH, New York, 1992, p. 79;
(b) R.W. Broach, J.M. Williams, Inorg. Chem. 18 (1979) 314;
(c) R. Mason, D.M.P. Mingos, J. Organomet. Chem. 50 (1973) 53.
[64] J.K. Hoyano, W.A.G. Graham, J. Am. Chem. Soc. 104 (1982) 3722.
[65] B. Jezowska-Trzebiatowska, B. Nissen-Sobocinska, J. Organomet. Chem. 322 (1987) 331.
[66] M.R. Churchill, S.W.-Y. Chang, Inorg. Chem. 13 (1974) 2413.
[67] B. Jezowska-Trzebiatowska, B. Nissenso-Sobocinska, J. Organomet. Chem. 342 (1988) 215.
[68] For related calculations, see:
(a) B. Jezowska-Trzebiatowska, B. Nissen-Sobocinska, J. Organomet. Chem. 342 (1988) 353;
(b) B. Jezowska-Trzebiatowska, B. Nissen-Sobocinska, L. Natkaniec, J. Organomet. Chem. 376 (1989) 67;
(c) B. Jezowska-Trzebiatowska, B. Nissen-Sobocinska, J. Organomet. Chem. 369 (1989) 69;
(d) B. Nissen-Sobocinska, B. Jezowska-Trzebiatowska, J. Organomet. Chem. 452 (1993) 277.
[69] R.H. Crabtree, H. Felkin, G.E. Morris, T.J. King, J.A. Richards, J. Organomet. Chem. 113 (1976) C7.
[70] R. Crabtree, Acc. Chem. Res. 12 (1979) 331.
[71] M. Bortz, R. Bau, J.J. Schneider, S.A. Mason, J. Clust. Sci. 12 (2001) 285.
[72] R.C. Stevens, M.R. McLean, T. Wen, J.D. Carpenter, R. Bau, T.F. Koetzle, Inorg. Chim. Acta 161 (1989) 223.
[73] A.P. Ginsberg, M.J. Hawkes, J. Am. Chem. Soc. 90 (1968) 5930.
[74] P. Dapporto, S. Midollini, L. Sacconi, Inorg. Chem. 14 (1975) 1643.
[75] R.H. Summerville, R. Hoffmann, J. Am. Chem. Soc. 101 (1979) 3821.
[76] 20-electron compounds, such as Cp_2Ni, are known and their stability requires that a low energy antibonding orbital is available to accept the electrons. In addition to bona fide 20-electron complexes, there are several examples, such as Cp_3ZrX and $W(R_2C_2)_3CO$ where the apparently >18electron count is deceiving because one of the ligand orbital combinations remains nonbonding as a result of there being no metal based orbital of appropriate symmetry with which to interact; the electron count at the metal in such complexes is thus reduced from 20 to 18. See, for example:
(a) H. Jacobsen, H. Berke, T. Brackemeyer, T. Eisenblätter, G. Erker, R. Fröhlich, O. Meyer, K. Bergander, Helv. Chim. Acta 81 (1998) 1692;
(b) W.W. Lukens Jr., R.A. Andersen, Organometallics 14 (1995) 3435;
(c) J.W. Lauher, R. Hoffmann, J. Am. Chem. Soc. 98 (1976) 1729;
(d) R.M. Laine, R.E. Moriarty, R. Bau, J. Am. Chem. Soc. 94 (1972) 1402;
(e) S.Y. Chu, R. Hoffmann, J. Phys. Chem. 86 (1982) 1289;
(f) A. Davison, S.S. Wreford, Inorg. Chem. 14 (1975) 703;
(g) R.J. Strittmatter, B.E. Bursten, J. Am. Chem. Soc. 113 (1991) 552;
(h) M.H. Schofield, T.P. Kee, J.T. Anhaus, R.R. Schrock, K.H. Johnson, W.M. Davis, Inorg. Chem. 30 (1991) 3595;
(i) J.T. Anhaus, T.P. Kee, M.H. Schofield, R.R. Schrock, J. Am. Chem. Soc. 112 (1990) 1642;
(j) Z. Lin, M.B. Hall, Coord. Chem. Rev. 123 (1993) 149.

[77] A. Dedieu, T.A. Albright, R. Hoffmann, J. Am. Chem. Soc. 101 (1979) 3141.
[78] B.E. Bursten, R.H. Cayton, Organometallics 7 (1988) 1349.
[79] C.P. Casey, H. Sakaba, P.N. Hazin, D.R. Powell, J. Am. Chem. Soc. 113 (1991) 8165.
[80] H. Suzuki, H. Omori, D.H. Lee, Y. Yoshida, Y. Moro-oka, Organometallics 7 (1988) 2243.
[81] The structure of $[Cp^*Ru]_2(\mu\text{-}H)_4$ was originally reported in an incorrect space group. See: R.E. Marsh, Organometallics 8 (1989) 1583.
[82] N. Koga, K. Morokuma, J. Mol. Struct. 300 (1993) 181.
[83] This view of the bonding has been accepted by the original authors. See: H. Suzuki, H. Omori, D.H. Lee, Y. Yoshida, M. Fukushima, M. Tanaka, Y. Morooka, Organometallics 13 (1994) 1129.
[84] Y. Ohki, H. Suzuki, Angew. Chem. Int. Ed. 39 (2000) 3120.
[85] R. Bau, W.E. Carroll, R.G. Teller, T.F. Koetzle, J. Am. Chem. Soc. 99 (1977) 3872.
[86] The formal charge (FC) of an atom in a given Lewis structure is the charge it would possess if the electrons in each covalent bond were to be distributed equally between the two bonded atoms such that each partner receives one electron. The notion of formal charge as disussed by Pauling is based on Langmuir's residual charge concept.
(a) L. Pauling, The Nature of The Chemical Bond, 3rd ed., Cornell University Press, Ithaca, NY, 1960, p. 9;
(b) I. Langmuir, Science 54 (1921) 59.
[87] See, for example:
(a) A. Greenberg, R. Winkler, B.L. Smith, J.F. Liebman, J. Chem. Educ. 59 (1982) 367;
(b) E.U. Wurthwein, K.D. Sen, J.A. Pople, P.V. Schleyer, Inorg. Chem. 22 (1983) 496;
(c) J.B. Sorensen, A.H. Lewin, J.P. Bowen, Theochem., J. Mol. Struct. 623 (2003) 145.
[88] Furthermore, it is well known that the charge on an atom generally bears no relationship to oxidation state. For a brief discussion, including the problem with actually calculating the charge, see: R. Hoffmann, Am. Sci. 89 (2001) 311.
[89] Bulky substituents on the cyclopentadienyl rings enable the isolation of monomeric zirconocene hydride complexes. See, for example: P.J. Chirik, M.W. Day, J.E. Bercaw, Organometallics 18 (1999) 1873.
[90] For example, the bona fide B=B double bond in $[H_2B{=}BH_2]^{2-}$ is very different to the "double bond" in $H_2B(\mu\text{-}H)_2BH_2$ that would be predicted using a "half-electron" counting method. The bonding in diborane was initially described as a "protonated double bond". See: K.S. Pitzer, J. Am. Chem. Soc. 67 (1945) 1126.
[91] *s* is the number of BHB bridge bonds, *t* the number of BBB three-center bonds, *y* number of B–B single bonds, and *x* is the number of terminal B–H groups.
[92] I.M. Pepperberg, T.A. Halgren, W.N. Lipscomb, Inorg. Chem. 16 (1977) 363.
[93] Jaguar 4.1; Schrödinger, Inc., Portland, OR, 2000.
[94] G.T. Velde, F.M. Bickelhaupt, E.J. Baerends, C.F. Guerra, S.J.A. Van Gisbergen, J.G. Snijders, T. Ziegler, J. Comput. Chem. 22 (2001) 931.
[95] B. Delley, J. Chem. Phys. 92 (1990) 508.
[96] B. Delley, J. Chem. Phys. 113 (2000) 7756.
[97] (a) A.D. Becke, Phys. Rev. A 38 (1988) 3098;
(b) A.D. Becke, J. Chem. Phys. 98 (1993) 5648;
(c) C.T. Lee, W.T. Yang, R.G. Parr, Phys. Rev. B 37 (1988) 785;
(d) S.H. Vosko, L. Wilk, M. Nusair, Can. J. Phys. 58 (1980) 1200;
(e) J.C. Slater, Quantum Theory of Molecules and SolidsThe Self-Consistent Field for Molecules and Solids, vol. 4, McGraw-Hill, New York, 1974.
[98] (a) P.J. Hay, W.R. Wadt, J. Chem. Phys. 82 (1985) 270;
(b) W.R. Wadt, P.J. Hay, J. Chem. Phys. 82 (1985) 284;
(c) P.J. Hay, W.R. Wadt, J. Chem. Phys. 82 (1985) 299.
[99] (a) E. van Lenthe, E.J. Baerends, J.G. Snijders, J. Chem. Phys. 99 (1993) 4597;
(b) E. van Lenthe, R. van Leeuwen, E.J. Baerends, J.G. Snijders, Int. J. Quantum Chem. 57 (1996) 281.
[100] For example, see:
(a) A.J. Lupinetti, S. Fau, G. Frenking, S.H. Strauss, J. Phys. Chem. (A) 101 (1997) 9551;
(b) A.S. Goldman, K. Krogh-Jespersen, J. Am. Chem. Soc. 118 (1996) 12159.

Available online at www.sciencedirect.com
SCIENCE DIRECT®
Polyhedron 23 (2004) 2901–2913
POLYHEDRON
www.elsevier.com/locate/poly

Structural and spectroscopic studies of three-coordinate copper(I) supported by bis(phosphino)borate ligands

J. Christopher Thomas, Jonas C. Peters *

Contribution from the Division of Chemistry and Chemical Engineering, Arnold and Mabel Beckman Laboratories of Chemical Synthesis, California Institute of Technology, Pasadena, CA 91125, USA

Received 1 July 2004; accepted 25 August 2004
Available online 28 October 2004

Dedicated to Professor Malcolm H. Green, an inspiring organometallic chemist

Abstract

The bis(phosphino)borates [(*p*-^{t}BuPh)$_2$B(CH$_2$PPh$_2$)$_2$][ASN] (**1**[ASN]; ASN = 5-azonia-spiro[4.4]nonane), [Ph$_2$B(CH$_2$P^{i}Pr$_2$)$_2$]-Li(THF)$_2$ (**2**[Li]), and [(3,5-Me$_2$Ph)$_2$B(CH$_2$P^{t}Bu$_2$)$_2$]$^-$ (**3**[Li] and **3**[Tl]) react with copper(I) reagents to generate anionic and neutral complexes. Reaction of **1**[ASN] with CuI provides the 1:1 adduct [[(*p*-^{t}BuPh)$_2$B(CH$_2$PPh$_2$)$_2$]CuI][ASN] (**4**). CuCl reacts with **3**[Li] in THF to afford [[(3,5-Me$_2$Ph)$_2$B(CH$_2$P^{t}Bu$_2$)$_2$]CuCl][Li(THF)$_4$] (**5**), along with a minor byproduct, the three-coordinate bis(phosphine) adduct {(3,5-Me$_2$Ph)B(CH$_2$P^{t}Bu$_2$)$_2$}CuCl (**6**). An analogous neutral complex, {PhB(CH$_2$P^{t}Bu$_2$)$_2$}CuCl (**7**), can be synthesized directly by reacting CuCl with the neutral phosphino borane PhB(CH$_2$P^{t}Bu$_2$)$_2$. Reaction of the substituted copper(I) halide Me$_2$S · CuBr with **3**[Tl] provides the anionic dimer complex [{[(3,5-Me$_2$Ph)$_2$B(CH$_2$P^{t}Bu$_2$)$_2$]Cu}$_2$(μ-Br)]Tl (**8**). The neutral solvent adducts [Ph$_2$B(CH$_2$P^{i}Pr$_2$)$_2$]Cu(NCCH$_3$) (**9**) and [(3,5-Me$_2$Ph)$_2$B(CH$_2$P^{t}Bu$_2$)$_2$]Cu(NCCH$_3$) (**10**) are prepared by the reactions between [Cu(CH$_3$CN)$_4$][PF$_6$] and **2**[Li] or **3**[Li], respectively. Neutral **10** is a useful precursor to several other neutral species via substitution of the labile acetonitrile ligand, including [(3,5-Me$_2$Ph)$_2$B(CH$_2$P^{t}Bu$_2$)$_2$]Cu(PMe$_2$Ph)(**11**), [(3,5-Me$_2$Ph)$_2$B(CH$_2$P^{t}Bu$_2$)$_2$]-Cu(S=PMe$_3$) (**12**), [(3,5-Me$_2$Ph)$_2$B(CH$_2$P^{t}Bu$_2$)$_2$] Cu(2,6-lutidine) (**13**), and [(3,5-Me$_2$Ph)$_2$B(CH$_2$P^{t}Bu$_2$)$_2$]Cu(CN^{t}Bu) (**14**). Attempts to isolate a neutral monocarbonyl adduct, [(3,5-Me$_2$Ph)$_2$B(CH$_2$P^{t}Bu$_2$)$_2$]Cu(CO) (**15**), are frustrated by the high lability of the CO ligand. The solid-state crystal structures of complexes **6**, **8**, **9**, **10**, and **11** have been determined and are described.
© 2004 Elsevier Ltd. All rights reserved.

Keywords: Zwitterions; Monoanionic ligands; Phosphines; Syntheses; Structures; Boron

1. Introduction

Copper(I) complexes play a significant role in many catalytic and stoichiometric processes, including catalytic hydrocarbon functionalization reactions [1], catalytic oxidation reactions [2], and biomimetic dioxygen activation [3]. Several well-defined copper(I) systems have been developed recently using ligands designed to control both steric and electronic factors that dictate overall reactivity profiles. These include modified bis- and tris(pyrazolyl)borates [4], β-diketiminates [5], *N*-heterocyclic carbenes [6], and a host of other nitrogenous ligands [7].

We recently reported the synthesis of a new family of bis(phosphino)borate ligands that are both sterically and electronically tunable [8]. These ligands are anionic relatives to the better known bis(pyrazolyl)borate and β-diketiminate ligands, and their fundamental coordination chemistry is therefore of comparative interest. In this contribution, we introduce a series of well-defined copper(I) complexes supported by monoanionic

* Corresponding author. Tel.: +1 626 395 4036; fax: +1 626 577 4088.
E-mail address: jpeters@caltech.edu (J.C. Peters).

0277-5387/$ - see front matter © 2004 Elsevier Ltd. All rights reserved.
doi:10.1016/j.poly.2004.08.008

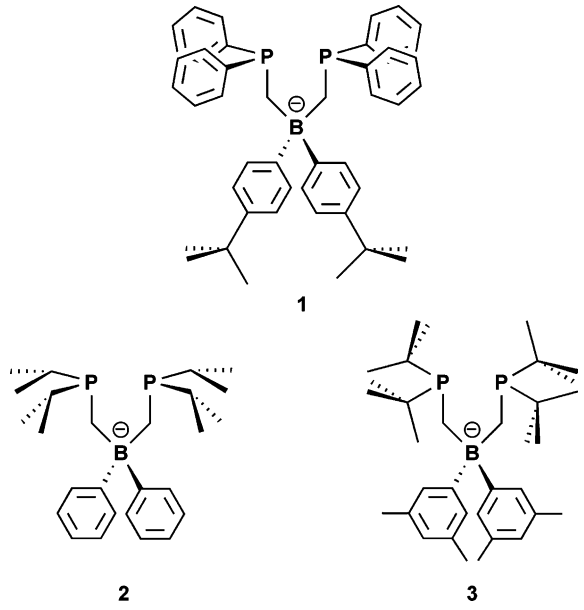

Fig. 1. Bis(phosphino)borate ligands used to prepare copper(I) complexes.

bis(phosphino)borates. The aim of this initial study is to develop reliable protocols for the generation and isolation of these new copper species, to establish their structural characterization, and to assess their ligand substitution chemistry. In this context, we examine the copper(I) coordination chemistry of the three bis(phosphino)borate ligands: $[(p\text{-}^t\text{BuPh})_2\text{B}(\text{CH}_2\text{PPh}_2)_2]$[ASN] (**1**[ASN]), $[\text{Ph}_2\text{B}(\text{CH}_2\text{P}^i\text{Pr}_2)_2]\text{Li}(\text{THF})_2$ (**2**[Li]), and $[(3,5\text{-Me}_2\text{Ph})_2\text{B}(\text{CH}_2\text{P}^t\text{Bu}_2)_2]^-$ (**3**[Li] and **3**[Tl]) (Fig. 1). In particular, we emphasize the use of the sterically encumbered *tert*-butyl phosphine ligand **3** due to its ability to enforce three-coordinate geometries for a host of copper(I) complexes. Our hope is that the complexes described will serve as useful "$[\text{BP}_2]\text{Cu}^\text{I}(\text{L})$" sources in the context of future group transfer studies.

2. Experimental

2.1. General considerations

General procedures were performed according to previously published methods [9]. The compounds $[(p\text{-}^t\text{BuPh})_2\text{B}(\text{CH}_2\text{PPh}_2)_2]$[ASN] (**1**[ASN]), $[\text{Ph}_2\text{B}(\text{CH}_2\text{P}^i\text{Pr}_2)_2]\text{Li}(\text{THF})_2$ (**2**[Li]), $[(3,5\text{-Me}_2\text{Ph})_2\text{B}(\text{CH}_2\text{P}^t\text{Bu}_2)_2]\text{Li}(\text{OEt}_2)$ (**3**[Li]), $[(3,5\text{-Me}_2\text{Ph})_2\text{B}(\text{CH}_2\text{P}^t\text{Bu}_2)_2]\text{Tl}$ (**3**[Tl]), and $\text{Me}_3\text{P}{=}\text{S}$ were prepared by published methods [8]. ^{t}BuNC was distilled under dinitrogen and dried over 3 Å molecular sieves prior to use. 2,6-Lutidine was sparged with dinitrogen and then dried with CaH_2 and distilled under dinitrogen. $\text{PhB}(\text{CH}_2\text{P}^t\text{Bu}_2)_2$ was generated by the addition of PhBCl_2 to a cold ethereal suspension of $\text{LiCH}_2\text{P}^t\text{Bu}_2$.[1] All other reagents were purchased from commercial vendors and used without further purification.

2.2. Syntheses of complexes

2.2.1. $[[(p\text{-}^t\text{BuPh})_2\text{B}(\text{CH}_2\text{PPh}_2)_2]\text{CuI}][\text{ASN}]$ (**4**)

Solid CuI (83.6 mg, 439 μmol) and $[(p\text{-}^t\text{BuPh})_2\text{B}(\text{CH}_2\text{PPh}_2)_2]$[ASN] (351.8 mg, 438.7 μmol) were combined with THF (4 mL) and ethanol (0.3 mL). The reaction mixture was stirred for 2.5 h. Volatiles were removed under reduced pressure. The resulting solids were washed with diethyl ether (3 mL) and dried under reduced pressure, providing analytically pure white **4** (432.8 mg, 99.4%). ^{1}H NMR (300 MHz, acetone-d_6): δ 7.60 (m, 8H), 7.12 (m, 16H), 6.82 (d, 4H), 3.69 (m, 8H), 2.24 (m, 8H), 1.76 (br, 4H), 1.21 (s, 16H). $^{13}\text{C}\{^1\text{H}\}$ NMR (75.4 MHz, acetone-d_6): δ 162.7 (br), 144.55, 141.80 (d, $^1J_{\text{P–C}} = 12.3$ Hz), 141.64 (d, $^1J_{\text{P–C}} = 12.3$ Hz), 133.83, 133.71 (d, $^2J_{\text{P–C}} = 8.0$ Hz), 133.60 (d, $^2J_{\text{P–C}} = 8.0$ Hz), 128.72, 128.49 (d, $^3J_{\text{P–C}} = 4.3$ Hz), 128.43 (d, $^3J_{\text{P–C}} = 4.0$ Hz), 123.51, 63.78 (t, $(\text{CH}_2\textit{C}\text{H}_2)_2\text{N}$, $^1J_{\text{N–C}} = 3.4$ Hz), 34.42 (Ph-$\textit{C}(\text{CH}_3)_3$), 32.15 (Ph-C($\textit{C}\text{H}_3)_3$), 22.84 (($\textit{C}\text{H}_2\text{CH}_2)_2\text{N}$), 22.0 (br, $\text{B}(\textit{C}\text{H}_2\text{PPh}_2)_2$). $^{31}\text{P}\{^1\text{H}\}$ NMR (121.4 MHz, acetone-d_6): δ −13.08. $^{11}\text{B}\{^1\text{H}\}$ NMR (128.3 MHz, acetone-d_6): δ −12.5. *Anal.* Calc. for $\text{C}_{54}\text{H}_{66}\text{BCuINP}_2$: C, 65.36; H, 6.70; N, 1.41. Found: C, 65.08; H, 6.94; N, 1.21%.

2.2.2. $[[(3,5\text{-Me}_2\text{Ph})_2\text{B}(\text{CH}_2\text{P}^t\text{Bu}_2)_2]\text{CuCl}][\text{Li}(\text{THF})_4]$ (**5**)

Solid CuCl (26.5 mg, 268 μmol) was suspended in THF (1.5 mL), stirred vigorously, and a THF solution (4 mL) of $[(3,5\text{-Me}_2\text{Ph})_2\text{B}(\text{CH}_2\text{P}^t\text{Bu}_2)_2]\text{Li}(\text{OEt}_2)$ (166.2 mg, 268.2 μmol) was then added to the stirring suspension. After stirring for 24 h, analysis by $^{31}\text{P}\{^1\text{H}\}$ NMR spectroscopy revealed the formation of one major product, along with two minor byproducts. The reaction mixture was then filtered. The resulting filtrate was concentrated under reduced pressure to 0.5 mL. Vapor diffusion of petroleum ether into the THF solution provided white crystalline solids over several days. The isolated solids were dried under reduced pressure to provide the major product, $[[(3,5\text{-Me}_2\text{Ph})_2\text{B}(\text{CH}_2\text{P}^t\text{Bu}_2)_2]\text{CuCl}][\text{Li}(\text{THF})_4]$ (163.9 mg, 65.5%). ^{1}H NMR (300 MHz, C_6D_6/THF-d_8, 6:1): δ 7.59 (s, 4H, *ortho*-

[1] The synthesis of $\text{PhB}(\text{CH}_2\text{P}^t\text{Bu}_2)_2$ and its use as a ligand building block to other borate ligands will be reported separately (C.M. Thomas, J.C. Peters, manuscript in preparation). Key characterization data for $\text{PhB}(\text{CH}_2\text{P}^t\text{Bu}_2)_2$: ^{1}H NMR (300 MHz, C_6D_6): $\delta = 8.02$ (m, 2H, *o*-Ph), 7.27 (m, 3H, *m*, *p*-Ph), 2.27 (d, $^2J_{\text{P–H}} = 5.7$ Hz, CH_2), 1.12 (d, $^2J_{\text{P–H}} = 10.5$ Hz, 36 H, ^{t}Bu). ^{31}P NMR (300 MHz, C_6D_6): $\delta = 38.4$ (s). *Anal.* Calc. for $\text{C}_{24}\text{H}_{45}\text{BP}_2$: C, 70.93; H, 11.16. Found: C, 69.32; H, 10.60%.

($Me_2C_6H_3)_2B$), 6.62 (s, 2H, *para*-($Me_2C_6H_3)_2B$), 3.54 (m, 16H, ($CH_2CH_2)_2O$) 2.29 (s, 12H, (($CH_3)_2C_6H_3)_2B$), 1.92 (br, 4H, $B(CH_2P^tBu_2)_2$), 1.45 (m, 16H, ($CH_2CH_2)_2O$) 1.32 (d, 18H, $P(C(CH_3)_3)_2$, $^3J_{P-H} = 5.7$ Hz), 1.30 (d, 18H, $P(C(CH_3)_3)_2$, $^3J_{P-H} = 6.3$ Hz). $^{13}C\{^1H\}$ NMR (75.4 MHz, C_6D_6/THF-d_8, 6:1): δ 167.3 (br, *ipso*-($Me_2C_6H_3)_2B$), 134.52 (*meta*-($Me_2C_6H_3)_2B$), 131.89 (*ortho*-($Me_2C_6H_3)_2B$), 124.50 (*para*-($Me_2C_6H_3)_2B$), 68.17 (($CH_2C H_2)_2O$), 34.22 (d, $CH_2P(C(CH_3)_3)_2$, $^1J_{P-C} = 4.6$ Hz), 34.16 (d, $CH_2P(C(CH_3)_3)_2$, $^1J_{P-C} = 4.6$ Hz), 31.05 (br, $CH_2P(C(CH_3)_3)_2$), 30.92 (br, $CH_2P(C(CH_3)_3)_2$), 26.17 (($C H_2CH_2)_2O$), 22.68 ((($CH_3)_2C_6H_3)_2B$), 14.7 (br, BC H_2P). $^{31}P\{^1H\}$ NMR (121.4 MHz, C_6D_6/THF-d_8, 6:1): δ 33.31. $^{11}B\{^1H\}$ NMR (128.3 MHz, C_6D_6/THF-d_8, 6:1): δ −14.0. *Anal*. Calc. for $C_{50}H_{90}BClCuLiO_4P_2$: C, 64.38; H, 9.71. Found: C, 64.30; H, 9.70%.

2.2.3. {(3,5-Me_2Ph)B($CH_2P^tBu_2)_2$}CuCl (6)

Yellow crystals of the minor byproduct, **6**, were isolated from a separate reaction, carried-out in an analogous fashion to that used in the preparation of **5**, by petroleum ether diffusion into a THF solution of the crude reaction mixture. A $^{31}P\{^1H\}$ NMR spectrum of the solution prior to crystallization showed **6** to be present as approximately 15% of the observed diamagnetic phosphorus containing products. $^{31}P\{^1H\}$ NMR (121.4 MHz, THF): δ 23.75. The identity of **6** was established by XRD analysis (see Fig. 2), and by comparison to the spectral properties of independently prepared **7**.

2.2.4. {PhB($CH_2P^tBu_2)_2$}CuCl (7)

Solid $PhB(CH_2P^tBu_2)_2$ 1 (25.4 mg, 62.5 μmol) and CuCl (6.2 mg, 63 μmol) were combined in THF (4 mL) and stirred for 1 h, forming a homogeneous yellow solution. The solution was filtered, and volatiles were removed under reduced pressure, forming microcrystalline yellow {$PhB(CH_2P^tBu_2)_2$}CuCl (30.7 mg, 97.2%). ^1H NMR (300 MHz, C_6D_6): δ 7.88 (m, 2H), 7.28 (m, 3H), 1.73 (br, 4H, $B(CH_2P^tBu)_2$), 1.22 (d, 18H, $P(C(CH_3)_3)_2$, $^3J_{P-H} = 6.3$ Hz), 1.20 (d, 18H, $P(C(CH_3)_3)_2$, $^3J_{P-H} = 6.6$ Hz). $^{13}C\{^1H\}$ NMR (75.4 MHz, C_6D_6): δ 134.60, 133.29, 129.05, 34.47 (m, $CH_2P(C(CH_3)_3)_2$), 29.82 (m, $CH_2P(C(CH_3)_3)_2$), 18.8 (br, BC H_2P). $^{31}P\{^1H\}$ NMR (121.4 MHz, C_6D_6): δ 23.11. $^{11}B\{^1H\}$ NMR (160.4 MHz, C_6D_6): δ 75.2. *Anal*. Calc. for $C_{24}H_{45}BClCuP_2$: C, 57.04; H, 8.98. Found: C, 57.40; H, 8.67%.

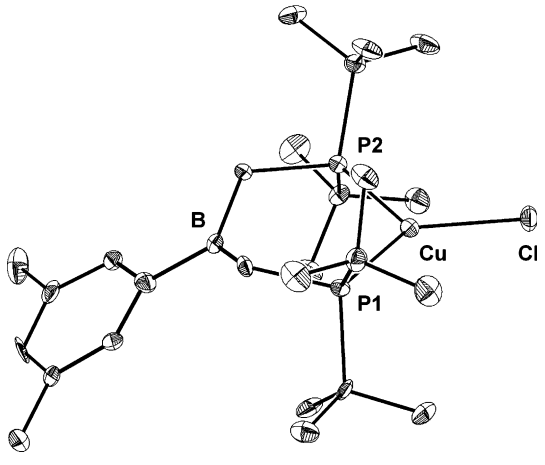

Fig. 2. Displacement ellipsoid representation (50%) of {(3,5-Me_2Ph)B($CH_2P^tBu_2)_2$}CuCl (**6**). Hydrogen atoms are omitted for clarity. Selected interatomic distances (Å) and angles (°): P1–Cu, 2.2433(11); P2–Cu, 2.2481(12); Cl–Cu, 2.2183(12); B–Cu, 3.639(5); P1–Cu–P2, 108.55(5); P1–Cu–Cl, 129.28(5); P2–Cu–Cl, 121.93(5).

2.2.5. [{[(3,5-Me_2Ph)$_2$B($CH_2P^tBu_2)_2$]Cu}$_2$(μ-Br)]Tl (8)

Solid $Me_2S \cdot CuBr$ (16.2 mg, 78.8 μmol) was suspended in THF (3 mL). While stirring, a THF solution (9 mL) of [(3,5-Me_2Ph)$_2$B($CH_2P^tBu_2)_2$]Tl (58.6 mg, 78.8 μmol) was added dropwise. Upon completing the addition, the reaction mixture was stirred for 15 min. The reaction mixture was filtered, removing white and gray solids. The resulting solution was concentrated under reduced pressure to 1 mL. Vapor diffusion of petroleum ether into the THF solution provided colorless crystals over several days. The crystals were dried under reduced pressure to provide **8** (28.7 mg, 48.9%). ^1H NMR (300 MHz, THF-d_8): δ 7.03 (s, 4H, *ortho*-($Me_2C_6H_3)_2B$), 6.34 (s, 2H, *para*-($Me_2C_6H_3)_2B$), 2.11 (s, 12H, (($CH_3)_2C_6H_3)_2B$), 1.53 (br, 4H, $B(CH_2P^tBu)_2$), 1.12 (d, 18H, $P(C(CH_3)_3)_2$, $^3J_{P-H} = 6.3$ Hz), 1.10 (d, 18H, $P(C(CH_3)_3)_2$, $^3J_{P-H} = 6.0$ Hz). $^{13}C\{^1H\}$ NMR (75.4 MHz, THF-d_8): δ 167 (br), 134.58, 131.50, 124.35, 34.34 (d, $CH_2P(C(CH_3)_3)_2$, $^1J_{P-C} = 6.0$ Hz), 34.26 (d, $CH_2P(C (CH_3)_3)_2$, $^1J_{P-C} = 6.4$ Hz), 30.99 (d, $CH_2P(C(CH_3)_3)_2$, $^2J_{P-C} = 4.8$ Hz), 30.77 (d, $CH_2P(C(C H_3)_3)_2$, $^2J_{P-C} = 3.7$ Hz), 22.31 ((($CH_3)_2C_6H_3$)$_2$B), 14.8 (br, BC H_2P). $^{31}P\{^1H\}$ NMR (121.4 MHz, THF-d_8): δ 38.79. $^{11}B\{^1H\}$ NMR (128.3 MHz, THF-d_8): δ −14.4. *Anal*. Calc. for $C_{68}H_{116}B_2BrCu_2P_4Tl$: C, 54.79; H, 7.84. Found: C, 55.17; H, 7.55%.

2.2.6. [$Ph_2B(CH_2P^iPr_2)_2$]Cu($NCCH_3$) (9)

Solid [$Ph_2B(CH_2P^iPr_2)_2$]Li(THF)$_2$ (157.5 mg, 272.2 μmol) and solid [$Cu(CH_3CN)_4$][PF_6] (101.5 mg, 272.3 μmol) were combined in Et_2O (4 mL). The reaction mixture was stirred for 30 min, forming a pale yellow solution. Volatiles were removed under reduced pressure, providing pale yellow solids. The solids were washed with acetonitrile (3 × 0.5 mL). The resulting solids were dissolved in THF (3 mL) and filtered. Removal of volatiles under reduced pressure provided white solids that analyzed as [$Ph_2B(CH_2P^iPr_2)_2$]Cu($NCCH_3$) (62.7 mg, 43.3%). Crystals for an X-ray diffraction experiment were grown by vapor diffusion of petroleum ether into a THF solution of **9**. ^1H NMR (300 MHz, THF-d_8): δ

7.30 (br, 4H), 6.90 (t, 4H, $^3J_{H-H}$ = 7.2 Hz), 6.72 (t, 2H, 6.9 Hz), 2.206 (s, 3H, CH_3CN), 1.73 (m, 4H, P(CH(CH$_3$)$_2$)$_2$), 1.21 (br, 4H, BCH_2P), 1.07 (dd, 12H, P(CH(CH_3)$_2$)$_2$, J = 7.2, 15 Hz), 0.87 (dd, 12H, P(CH(CH_3)$_2$)$_2$, J = 6.9, 13.2 Hz). ^{13}C{^{1}H} NMR (75.4 MHz, THF-d$_8$): δ 166 (br), 133.55, 126.84, 124.24 (CH$_3$$C$N), 123.88, 21.6 (m, P($C$H(CH$_3$)$_2$)), 19.34 P(CH($CH_3$)$_2$), 17.10 (q, B$CH_2$P, $^1J_{B-C}$ = 41 Hz), 1.52 (CH$_3$CN). ^{31}P{^{1}H} NMR (121.4 MHz, THF-d$_8$): δ 17.83. ^{11}B{^{1}H} NMR (160.4 MHz, THF-d_8): δ −14.4. IR: (KBr (s), cm^{-1}) ν_{CN} = 2265 (w). *Anal*. Calc. for $C_{28}H_{45}BCuNP_2$: C, 63.22; H, 8.53; N, 2.63. Found: C, 63.27; H, 8.73, N, 2.84%.

2.2.7. [(3,5-Me$_2$Ph)$_2$B(CH$_2$P^{t}Bu$_2$)$_2$]Cu(NCCH$_3$) (**10**)

White [(3,5-Me$_2$Ph)$_2$B(CH$_2$P^{t}Bu$_2$)$_2$]Li(OEt$_2$) (323.1 mg, 521.4 μmol) and [Cu(CH$_3$CN)$_4$][PF$_6$] (194.4 mg, 521.6 μmol) were combined, and diethyl ether (10 mL) was added. The reaction mixture was stirred vigorously for 40 min. Volatiles were removed under reduced pressure, providing pale yellow solids. The solids were washed with acetonitrile (3 × 0.8 mL), and then dissolved in THF (5 mL) and filtered. The resulting solution was concentrated to dryness under reduced pressure, providing fine white, analytically pure **10** (280.8 mg, 83.6%). Crystals of **10** were grown by vapor diffusion of petroleum ether into a THF solution of **10**. ^{1}H NMR (300 MHz, THF-d$_8$): δ 7.01 (s, 4H, *ortho*-(Me$_2$C$_6$$H_3$)$_2$B), 6.33 (s, 2H, *para*-(Me$_2$C$_6$$H_3$)$_2$B), 2.28 (s, 3H, Cu-NCC$H_3$), 2.11 (s, 12H, ((C$H_3$)$_2C_6H_3$)$_2$B), 1.51 (br s, 4H, B(C$H_2$P^{t}Bu)$_2$), 1.12 (d, 18H, P(C(C$H_3$)$_3$)$_2$), 1.10 (d, 18H, P(C(C$H_3$)$_3$)$_2$). ^{13}C{^{1}H} NMR (75.4 MHz, THF-d_8): δ 166.7 (br q, $^1J_{B-C}$ = 44 Hz), 134.43, 131.59, 124.87 (Cu-NCCH$_3$), 124.27, 34.32 (d, P(C(CH$_3$)$_3$)$_2$, $^1J_{P-C}$ = 6.0 Hz), 34.24 (d, P(C(CH$_3$)$_3$)$_2$, $^1J_{P-C}$ = 6.0 Hz), 30.85 (d, P(C(CH$_3$)$_3$)$_2$, $^2J_{P-C}$ = 4.3 Hz), 30.79 (d, P(C(CH$_3$)$_3$)$_2$, $^2J_{P-C}$ = 4.3 Hz), 22.34 ((CH$_3$)$_2$C$_6$H$_3$)$_2$B, 14.22 (br q, B(CH$_2$P^{t}Bu)$_2$, $^1J_{B-C}$ = 42 Hz), 1.59 (Cu-NCCH$_3$). ^{31}P{^{1}H} NMR (121.4 MHz, THF-d_8): δ 36.4. ^{11}B{^{1}H} NMR (128.3 MHz, THF-d$_8$): δ-14.2. IR: (KBr (s), cm^{-1}) ν_{CN} = 2267 (w). *Anal*. Calc. for $C_{36}H_{61}BCuNP_2$: C, 67.12; H, 9.54; N, 2.17. Found: C, 66.98; H, 9.55; N, 2.43%.

2.2.8. [(3,5-Me$_2$Ph)$_2$B(CH$_2$P^{t}Bu$_2$)$_2$]Cu(PMe$_2$Ph) (**11**)

A THF solution (2 mL) of Me$_2$PPh (12.8 μL, 90.0 μmol) was added to solid **10** (58.0 mg, 90.0 μmol), providing a colorless solution. After 15 min, the solution was concentrated to dryness under reduced pressure. The resulting white solids were washed with petroleum ether (3 × 1 mL) and dried under reduced pressure, providing analytically pure white **11** (61.8 mg, 92.7%). Crystals of **11** were grown by vapor diffusion of petroleum ether into a THF solution of **11**. ^{1}H NMR (300 MHz, C$_6$D$_6$): δ 7.68 (s, 4H, *ortho*-(Me$_2$C$_6$$H_3$)$_2$B), 6.96–7.14 (m, 5H, P(C$_6$$H_5$)), 6.74 (s, 2H, *para*-(Me$_2$C$_6$$H_3$)$_2$B), 2.37 (s, 12H, ((C$H_3$)$_2C_6H_3$)$_2$B), 1.93 (br, 4H, B(C$H_2$P^{t}Bu)$_2$), 1.07 (m, 42H, P(C(C$H_3$)$_3$)$_2$ and P(CH_3)$_2$). ^{13}C{^{1}H} NMR (125.7 MHz, C$_6$D$_6$): δ 166.85 (q, $^1J_{B-C}$ = 54 Hz), 135.33, 131.72, 130.65 (d, J_{P-C} = 12 Hz), 130.12, 129.48 (d, J_{P-C} = 8.3 Hz), 125.30, 34.38 (d, P(C(CH$_3$)$_3$)$_2$, $^1J_{P-C}$ = 6.0 Hz), 34.30 (d, P(C(CH$_3$)$_3$)$_2$, $^1J_{P-C}$ = 6.0 Hz), 31.04 (d, P(C(CH$_3$)$_3$)$_2$, $^2J_{P-C}$ = 4.1 Hz), 30.99 (d, P(C(CH$_3$)$_3$)$_2$, $^2J_{P-C}$ = 4.0 Hz), 22.99 ((CH$_3$)$_2$C$_6$H$_3$)$_2$B), 15.49 (d, P(CH$_3$)$_2$, $^1J_{P-C}$ = 18 Hz), 14.09 (br q, B(CH$_2$P^{t}Bu)$_2$, $^1J_{B-C}$ = 43 Hz). ^{31}P{^{1}H} NMR (121.4 MHz, C$_6$D$_6$): δ 40.81 (d, 2P, CH$_2$$P^tBu_2$, $^2J_{P-P}$ = 79 Hz), −36.22 (t, 1P, P Me$_2$Ph, $^2J_{P-P}$ = 79 Hz). ^{11}B{^{1}H} NMR (128.3 MHz, C$_6$D$_6$): δ −14.4. *Anal*. Calc. for $C_{42}H_{69}BCuP_3$: C, 68.05; H, 9.38. Found: C, 67.87; H, 9.17%.

2.2.9. [(3,5-Me$_2$Ph)$_2$B(CH$_2$P^{t}Bu$_2$)$_2$]Cu(S = PMe$_3$) (**12**)

Solid Me$_3$P = S (8.8 mg, 81 μmol) and **10** (52.1 mg, 80.9 μmol) were dissolved in THF (2 mL). After 15 min, the reaction mixture was filtered and concentrated to dryness under reduced pressure. The resulting white solids were washed with petroleum ether (3 × 1 mL) and dried under reduced pressure, producing analytically pure white **12** (49.2 mg, 85.6%). ^{1}H NMR (300 MHz, C$_6$D$_6$): δ 7.73 (s, 4H, *ortho*-(Me$_2$C$_6$$H_3$)$_2$B), 6.75 (s, 2H, *para*-(Me$_2$C$_6$$H_3$)$_2$B), 2.39 (s, 12H, ((C$H_3$)$_2C_6H_3$)$_2$B), 2.03 (br s, 4H, B(C$H_2$P^{t}Bu)$_2$), 1.29 (m, 36H, P(C(C$H_3$)$_3$)$_2$), 0.90 (d, 9H, S=P(C$H_3$)$_3$, $^2J_{P-H}$ = 13 Hz). ^{13}C{^{1}H} NMR (75.4 MHz, C$_6$D$_6$): δ 134.76, 131.33, 124.71, 34.10 (br, P(C(CH$_3$)$_3$)$_2$), 30.64 (m, P(C(CH$_3$)$_3$)$_2$), 30.25 (d, S = P(CH$_3$)$_3$, $^1J_{P-C}$ = 6.7 Hz), 22.47 ((CH$_3$)$_2$C$_6$H$_3$)$_2$B). ^{31}P{^{1}H} NMR (121.4 MHz, C$_6$D$_6$): δ 35.05 (s, 2P, CH$_2$$P^tBu_2$), 26.48 (s, 1P, S = P Me$_3$). ^{11}B{^{1}H} NMR (128.3 MHz, C$_6$D$_6$): δ −14.3. *Anal*. Calc. for $C_{37}H_{67}BCuP_3S$: C, 62.48; H, 9.49. Found: C, 62.28; H, 9.25%.

2.2.10. [(3,5-Me$_2$Ph)$_2$B(CH$_2$P^{t}Bu$_2$)$_2$]Cu(2,6-lutidine) (**13**)

Solid **10** (51.7 mg, 80.3 μmol) was dissolved in THF (2 mL). An aliquot of 2,6-lutidine (9.6 μL, 83 μmol) was added to the reaction mixture, providing a pale yellow solution. After 15 min, the solution was concentrated to dryness under reduced pressure. The resulting white solids were washed with petroleum ether (3 × 1 mL) and dried under reduced pressure, providing analytically pure pale yellow **13** (48.9 mg, 85.8%). ^{1}H NMR (300 MHz, C$_6$D$_6$): δ 7.67 (s, 4H, *ortho*-(Me$_2$C$_6$$H_3$)$_2$B), 6.76 (t, 1H, *para*-Me$_2$C$_5$$H_3$N, $^3J_{H-H}$ = 7.5 Hz), 6.75 (s, 2H, *para*-(Me$_2$C$_6$$H_3$)$_2$B), 6.32 (d, 2H, *meta*-Me$_2$C$_5$$H_3$N, $^3J_{H-H}$ = 7.5 Hz), 2.50 (s, 6H, (CH_3)$_2$C$_5$H$_3$N), 2.38 (s, 12H, ((CH_3)$_2$C$_6$H$_3$)$_2$B), 1.99 (br s, 4H, B(CH_2P^{t}Bu)$_2$), 1.14 (d, 18H, P(C(CH_3)$_3$)$_2$, $^3J_{P-H}$ = 5.7 Hz), 1.12 (d, 18H, P(C(CH_3)$_3$)$_2$, $^3J_{P-H}$ = 6.3 Hz). ^{13}C{^{1}H} NMR (75.4 MHz, C$_6$D$_6$):

δ 166.2 (br), 156.98, 137.62, 135.12, 132.57, 125.33, 122.55, 34.17 (d, P(C(CH$_3$)$_3$)$_2$, $^1J_{P-C}$ = 5.4 Hz), 34.09 (d, P(C(CH$_3$)$_3$)$_2$, $^1J_{P-C}$ = 5.7 Hz), 31.05 (d, P(C(CH$_3$)$_3$)$_2$, $^2J_{P-C}$ = 4.3 Hz), 31.00 (d, P(C(CH$_3$)$_3$)$_2$, $^2J_{P-C}$ = 4.0 Hz), 26.70 (*o*,*o*-(CH$_3$)$_2$C$_5$H$_5$N), 22.97 (((CH$_3$)$_2$C$_6$H$_3$)$_2$B), 14.88 (br q, B(CH$_2$P^{t}Bu)$_2$, $^1J_{B-C}$ = 40 Hz). ^{31}P{^{1}H} NMR (121.4 MHz, C$_6$D$_6$): δ 36.10. ^{11}B{^{1}H} NMR (128.3 MHz, C$_6$D$_6$): δ −14.1. *Anal.* Calc. for C$_{41}$H$_{67}$BCuNP$_2$: C, 69.33; H, 9.51; N, 1.97. Found: C, 68.94; H, 9.14; N, 2.09%.

2.2.11. [(3,5-Me$_2$Ph)$_2$B(CH$_2$P^{t}Bu$_2$)$_2$]Cu(CN^{t}Bu) (14)

A THF solution (2 mL) of *tert*-butyl isonitrile (11.8 μL, 104 μmol) was added to solid **10** (66.3 mg, 103 μmol), providing a colorless solution. After 15 min, the solution was concentrated to dryness under reduced pressure. The resulting white solids were washed with petroleum ether (3 × 1 mL) and dried under reduced pressure, providing analytically pure white **14** (63.9 mg, 90.4%). ^{1}H NMR (300 MHz, C$_6$D$_6$): δ 7.68 (s, 4H, *ortho*-(Me$_2$C$_6$$H_3$)$_2$B), 6.74 (s, 2H, *para*-(Me$_2$C$_6$$H_3$)$_2$B), 2.38 (s, 12H, (($CH_3$)$_2C_6H_3$)$_2$B), 1.94 (br s, 4H, B(C$H_2$P^{t}Bu)$_2$), 1.24 (d, 18H, P(C(C$H_3$)$_3$)$_2$, $^3J_{P-H}$ = 6.6 Hz), 1.22 (d, 18H, P(C(CH_3)$_3$)$_2$, $^3J_{P-H}$ = 6.0 Hz), 0.77 (s, 9H, Cu-CNC(CH_3)$_3$). ^{13}C{^{1}H} NMR (75.4 MHz, C$_6$D$_6$): δ 166.7 (br q, $^1J_{B-C}$ = 45 Hz), 144.26 (br, Cu-CN^{t}Bu), 135.25, 131.91, 125.30, 57.02 (Cu-CNC(CH$_3$)$_3$), 34.46 (d, P(C(CH$_3$)$_3$)$_2$, $^1J_{P-C}$ = 6.3 Hz), 34.38 (d, P(C(CH$_3$)$_3$)$_2$, $^1J_{P-C}$ = 6.0 Hz), 30.97 (d, P(C(CH$_3$)$_3$)$_2$, $^2J_{P-C}$ = 4.0 Hz), 30.92 (d, P(C(CH$_3$)$_3$)$_2$, $^2J_{P-C}$ = 4.0 Hz), 29.99 (Cu-CNC(CH$_3$)$_3$), 22.98 (((CH$_3$)$_2$C$_6$H$_3$)$_2$B), 12.84 (br q, B(CH$_2$P^{t}Bu)$_2$, $^1J_{B-C}$ = 41 Hz). ^{31}P{^{1}H} NMR (121.4 MHz, C$_6$D$_6$): δ 38.07. ^{11}B{^{1}H} NMR (128.3 MHz, C$_6$D$_6$): δ −13.6. IR: (CH$_2$Cl$_2$/KBr, cm^{-1}) ν_{CN} = 2162 (st). *Anal.* Calc. for C$_{39}$H$_{67}$BCuNP$_2$: C, 68.26; H, 9.84; N, 2.04. Found: C, 68.01; H, 9.81; N, 2.24%.

2.2.12. [(3,5-Me$_2$Ph)$_2$B(CH$_2$P^{t}Bu$_2$)$_2$]Cu(CO) (15)

(a) Solid **10** (11.3 mg, 17.5 μmol) was dissolved in THF-d_8 (0.7 mL) and placed in a J. Young NMR tube. The tube was partially evacuated. CO gas (approximately 1 atm) was introduced to the J. Young tube, and the tube was sealed. The solution was analyzed by NMR spectroscopy. ^{1}H NMR (300 MHz, THF-d$_8$): δ 7.00 (s, 4H, *ortho*-(Me$_2$C$_6$$H_3$)$_2$B), 6.36 (s, 2H, *para*-(Me$_2$C$_6$$H_3$)$_2$B), 2.12 (s, 12H, (($CH_3$)$_2C_6H_3$)$_2$B), 2.03 (s, 3H, C$H_3$CN), 1.53 (br, 4H, B(C$H_2$P^{t}Bu)$_2$), 1.14 (d, 18H, P(C(C$H_3$)$_3$)$_2$, $^3J_{P-H}$ = 6.3 Hz), 1.12 (d, 18H, P(C(CH_3)$_3$)$_2$, $^3J_{P-H}$ = 6.3 Hz). ^{13}C{^{1}H} NMR (125.7 MHz, THF-d$_8$): δ 186.21(*C*O), 165.82 (br q, $^1J_{B-C}$ = 48 Hz), 134.66, 131.48, 124.55, 118.78 (CH$_3$$C$N), 34.70 (d, P($C$(CH$_3$)$_3$)$_2$, $^1J_{P-C}$ = 7.2 Hz), 34.64 (d, P(C(CH$_3$)$_3$)$_2$, $^1J_{P-C}$ = 7.2 Hz), 30.72 (br, P(C(CH$_3$)$_3$)$_2$), 22.28 (((CH$_3$)$_2$C$_6$H$_3$)$_2$B), 12.76 (br q, B(CH$_2$P^{t}Bu)$_2$, $^1J_{B-C}$ = 42 Hz), 1.01 (CH$_3$CN). ^{31}P{^{1}H} NMR (121.4 MHz, THF-d_8): δ 42.33. ^{11}B{^{1}H} NMR (128.3 MHz, THF-d$_8$): δ −13.9.

(b) In a 25 mL Schlenk flask, solid **10** (14.3 mg, 22.2 μmol) was dissolved in THF (1.5 mL) with a stirbar. The solution was stirred under a stream of CO gas until dry, producing pale green solids. ^{1}H NMR (300 MHz, C$_6$D$_6$): δ 7.56 (s, 4H, *ortho*-(Me$_2$C$_6$$H_3$)$_2$B), 6.72 (s, 2H, *para*-(Me$_2$C$_6$$H_3$)$_2$B), 2.35 (s, 12H, (($CH_3$)$_2C_6H_3$)$_2$B), 1.86 (br, 4H, B(C$H_2$P^{t}Bu)$_2$), 1.07 (d, 18H, P(C(C$H_3$)$_3$)$_2$, $^3J_{P-H}$ = 6.3 Hz), 1.12 (d, 18H, P(C(CH_3)$_3$)$_2$, $^3J_{P-H}$ = 6.3 Hz). IR: (THF/KBr, cm^{-1}) ν_{CO} = 2084 (st).

2.3. X-ray crystallography

The general X-ray experimental procedure was performed according previously published methods [9]. Crystallographic information is provided in Table 1. The structures of **8 · THF · pentane** and **10 · 0.56THF · 0.22 pentane** contained sites of disordered solvent molecules.

3. Results and discussion

3.1. Copper(I) complexes containing halides

The formation of low-coordinate copper complexes using bis(phosphino)borate ligands was examined using several Cu(II) precursors, such as CuCl$_2$ · 0.8THF [10], anhydrous Cu(OAc)$_2$, and Cu(OTf)$_2$. As has been observed in previous efforts to develop Cu(II)–phosphine chemistry [11], we found that Cu(II) was easily reduced to Cu(I) in the presence these reducing phosphine ligands to provide ill-defined degradation products. In comparison, copper(I) starting materials provide in many cases clean 1:1 adducts with monoanionic bis(phosphino)borate ligands. Anionic complexes of copper(I) halides were prepared using both the phenyl substituted phosphine ligand [(*p*-^{t}BuPh)$_2$B(CH$_2$PPh$_2$)$_2$]$^-$ (**1**) and the *tert*-butyl substituted phosphine ligand [(3,5-Me$_2$Ph)$_2$B(CH$_2$P^{t}Bu$_2$)$_2$]$^-$ (**3**). For example, reacting **1**[ASN] with CuI in THF/EtOH solution resulted in the near quantitative generation of [[(*p*-^{t}BuPh)$_2$B(CH$_2$PPh$_2$)$_2$]CuI][ASN] (**4**), which could be isolated in high yield (Eq. (1)). Reactions using the [Ph$_2$B(CH$_2$PPh$_2$)$_2$][ASN] ligand [8] provided similar results with CuI and CuCl; however, the presence of *tert*-butyl substituents in the backbone of the ligand framework increases the hydrocarbon solubility of these complexes.

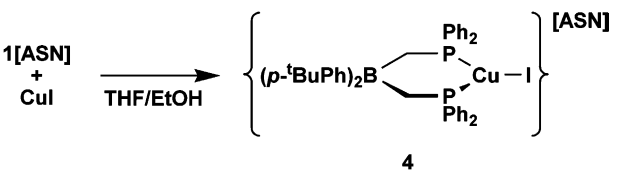

4 (1)

Table 1
X-ray diffraction experimental details for **6**, **8 · THF · pentane**, **9**, **10 · 0.56THF · 0.22pentane**, and **11**

Compound	**6**	**8 · THF · pentane**	**9**	**10 · 0.56THF · 0.22pentane**	**11**
CCDC ID	238116	238119	238120	238118	238117
Empirical formula	$C_{26}H_{49}BClCuP_2$	$C_{68}H_{116}B_2BrCu_2P_4Tl \cdot C_5 \cdot C_4O$	$C_{28}H_{45}BCuNP_2$	$C_{36}H_{61}BCuNP_2 \cdot 0.56(C_4O) \cdot 0.22(C_5)$	$C_{42}H_{69}BCuP_3$
Formula weight	533.39	1490.54 · 124.02	531.94	644.18 · 49.76	741.23
Crystal description	yellow block	colorless rod	colorless block	colorless block	colorless block
Crystal size (mm)	$0.19 \times 0.19 \times 0.19$	$0.33 \times 0.18 \times 0.13$	$0.25 \times 0.21 \times 0.19$	$0.26 \times 0.26 \times 0.19$	$0.34 \times 0.27 \times 0.21$
Crystal system	orthorhombic	monoclinic	monoclinic	monoclinic	triclinic
Space group	$P2_12_12_1$	$P2_1/c$	$P2_1/n$	$P2_1/n$	$P\bar{1}$
Unit cell dimensions					
a (Å)	7.3748(8)	12.3182(11)	13.4206(9)	9.9223(8)	12.6936(12)
b (Å)	11.7329(13)	24.799(2)	15.8317(11)	21.5707(18)	16.8198(16)
c (Å)	33.404(4)	27.773(3)	14.1571(9)	19.7938(17)	20.773(2)
α (°)	90	90	90	90	104.598(2)
β (°)	90	95.881(2)	98.3490(10)	100.6480(10)	92.772(2)
γ (°)	90	90	90	90	90.192(2)
V (Å^3)	2890.4(6)	8439.5(13)	2976.1(3)	4163.5(6)	4286.3(7)
Z	4	4	4	4	4
D_{calc}(g cm^{-3})	1.226	1.271	1.187	1.107	1.149
μ (mm^{-1})	0.971	2.991	0.857	0.628	0.648
T (K)	98	98	98	98	98
Radiation λ (Å)	0.71073	0.71073	0.71073	0.71073	0.71073
Reflections collected	17622	127436	17391	72447	26776
Unique data/parameters	6558/295	20450/775	6028/307	9928/418	18540/883
R_1, wR_2 ($I > 2\sigma(I)$)	0.0565, 0.1037	0.0723, 0.1467	0.0349, 0.0738	0.0530, 0.1100	0.0469, 0.0753
Goodness-of-fit	1.386	2.302	1.401	2.087	1.240
Largest difference peak and hole (e Å^{-3})	0.987 and −0.825	2.510 and −1.144	0.676 and −0.295	0.867 and −0.449	0.808 and −0.559

$R_1 = \sum||F_o| - |F_c||/\sum|F_o|$, $wR_2 = \{\sum [w(F_o^2 - F_c^2)^2]/\sum[w(F_o^2)^2]\}^{1/2}$.

Similar attempts to prepare 1:1 adducts of copper(I) halides using the alkyl substituted phosphine ligands **2**[Li] or **3**[Li] gave more complicated results. For example, the reaction of copper(I) iodide with either **2**[Li] or **3**[Li] resulted in the immediate precipitation of black sediment with concomitant phosphine degradation, ascertained by $^{31}P\{^{1}H\}$ and $^{11}B\{^{1}H\}$ NMR spectroscopies. By contrast, combining copper(I) chloride and **3**[Li] in THF solution provided one major product ($^{31}P\{^{1}H\}$ NMR). Spectroscopic and elemental analysis proved consistent with the formation of [[(3,5-$Me_2Ph)_2B(CH_2P^tBu_2)_2$]CuCl][Li(THF)$_4$] (**5**) (Eq. (2)). The clean preparation of copper(I) halides using the alkyl substituted phosphine ligands **2** and **3** appears to require a less redox susceptible copper(I) synthon (i.e., CuCl instead of CuI).

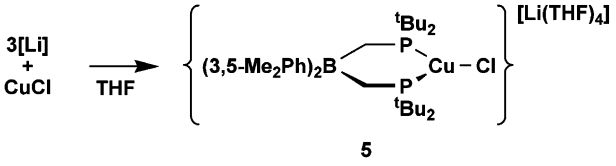

(2)

A significant body of work on {P_2CuX} complexes (P = phosphine, X = Cl, Br, I) shows that their coordination geometry can vary between three-coordinate (P_2CuX) or four-coordinate with bridging halides ($\{P_2Cu(\mu\text{-}X)\}_2$) [12,13]. For some phosphines, such as PPh_3, structural data have been obtained for both forms [12b,12c]. A related example containing the *tert*-butyl substituted chelating bis(phosphine) ligand dtbpe (dtbpe = $^tBu_2PCH_2CH_2P^tBu_2$) provided the dimeric structure $\{(dtbpe)Cu(\mu\text{-}Cl)\}_2$ [14]. It is therefore possible that **4** and **5** exist as either three-coordinate monomers, or four-coordinate, bridged dimers in solution. An equilibrium mixture of the two conformations may also prevail in solution.

The reaction between **3**[Li] and several copper(I) halide reagents provides a common secondary product. For instance, the reaction between **3**[Li] and CuCl provided a mixture of three phosphine containing products ($^{31}P\{^{1}H\}$ NMR). Along with the formation of the dominant product **5** (>80%), two minor products were observed. One of the minor products proved to be isolable by fractional crystallization, and XRD analysis of crystals thus obtained established its identity as {(3,5-$Me_2Ph)B(CH_2P^tBu_2)_2$}CuCl (**6**) (Fig. 2). Neutral **6** results from the loss of an aryl ring from the borate ligand, generating a neutral bis(phosphino)borane ligated to copper(I) chloride. Potentially related examples of (phosphino)borate ligand degradation have been observed previously [15]. In all of these cases, a boron–carbon bond is cleaved at the boron–methylene link. The present example demonstrates that the boron–aryl link is also susceptible to cleavage.

The spectroscopic identification of **6** was supported by the independent synthesis of a structurally analogous species, {$PhB(CH_2P^tBu_2)_2$}CuCl (**7**). The reaction between the neutral borane $PhB(CH_2P^tBu_2)_2$ and CuCl in THF solution provided a high yield route to **7** (97% yield) 1. The phosphine precursor $PhB(CH_2P^tBu_2)_2$ was readily generated by the addition of two equiv of $LiCH_2P^tBu_2$ to $PhBCl_2$ in diethyl ether. Neutral **7** has two important spectroscopic features. First, its $^{11}B\{^{1}H\}$ NMR spectrum (singlet at 75.2 ppm) confirms the three-coordinate nature of the boron atom [16]. Second, the $^{31}P\{^{1}H\}$ NMR chemical shift of **7** (23.11 ppm) is consistent with the resonance ascribed to **6** (23.75 ppm).

To circumvent ligand degradation pathways, alternative copper(I) sources and the use of thallium phosphine reagents were examined. Upon addition of a THF solution of **3**[Tl] to $Me_2S \cdot CuBr$, thallium bromide precipitated from solution. NMR analysis of the reaction solution showed one major product. XRD analysis of crystals obtained from the reaction solution provided the unexpected molecular structure, [{[(3,5-$Me_2Ph)_2B(CH_2P^tBu_2)_2$]Cu}$_2$(μ-Br)]Tl (**8**), shown in Fig. 3. As is evident, only one-half of an equivalent of TlBr is lost in the reaction (Eq. (3)).

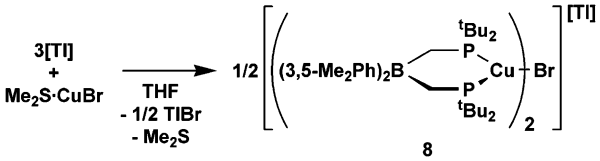

(3)

The structure of **8** shows two copper centers connected by a linear bromide bridge, thus providing a monoanionic dinuclear copper species with one thallium counter-cation. A common plane cuts through each of the phosphine, copper, bromide, and boron atoms of **8**. The chelate phosphine ligand exists in its typical twisted boat conformation [8,17]. In the molecular structure, the thallium atom resides in the pocket formed by the two aryl rings of the borate anion. This thallium coordination environment is similar to that observed in the molecular structure of $[Ph_2B(CH_2PPh_2)_2]Tl$ (**3**[Tl]) [8]. Halide-bridged systems are well known for copper(I), although there are few structurally characterized examples of copper centers bridged by a single halide [18]. This example appears to be structurally unique amongst phosphine-coordinated copper(I) species. In addition, all previous structurally characterized exhibit a copper–halide–copper angle that is significantly bent. The present example contains a linear halide bridge (Cu1–Br–Cu2 = 178.00(6)°). Attempts to induce loss of TlBr in solution by the addition of a donor ligand to **8**, such as PMe_3, pyridine, or acetonitrile, have not been successful.

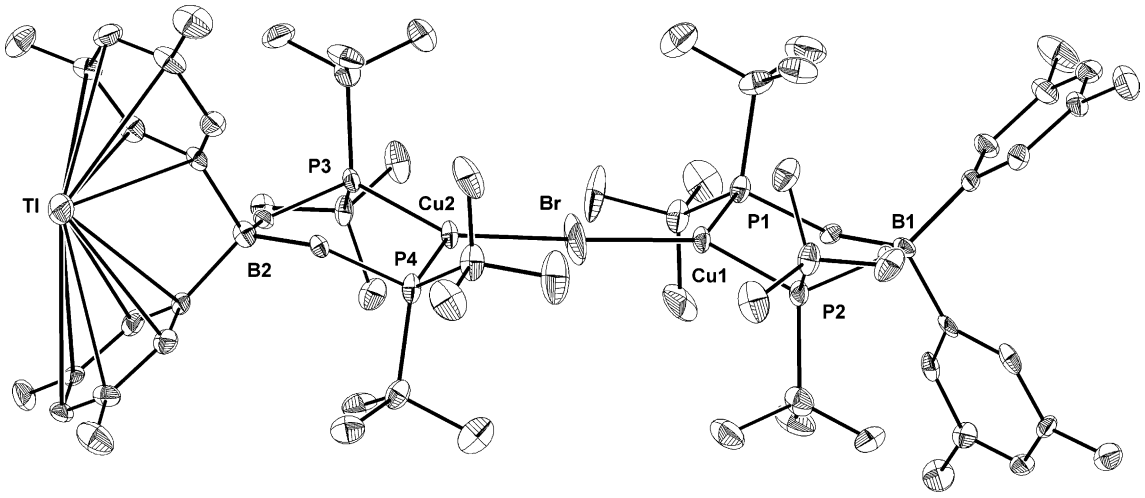

Fig. 3. Displacement ellipsoid representation (50%) of [{[(3,5-$Me_2Ph)_2B(CH_2P^tBu_2)_2$]Cu}$_2$(μ-Br)]Tl · THF · pentane (**8 · THF · pentane**). Hydrogen atoms and solvent molecules are omitted for clarity. Selected interatomic distances (Å) and angles (°): P1–Cu1, 2.238(2); P2–Cu1, 2.230(2); P3–Cu2, 2.235(2); P4–Cu2, 2.231(2); Cu1–Br, 2.3660(12); Cu2–Br, 2.3638(12); B1–Cu1, 3.819(8); B2–Cu2, 3.829(8) and P1–Cu1–P2, 110.67(7); P1–Cu1–Br, 125.55(7); P2–Cu1–Br, 123.78(7); P3–Cu2–P4, 110.60(7); P3–Cu2–Br, 124.63(7); P4–Cu2–Br, 124.70(7); Cu1–Br–Cu2, 178.00(6).

3.2. Neutral three-coordinate acetonitrile copper(I) complexes

To access more substitutionally labile copper(I) complexes, the copper(I) reagent [$Cu(CH_3CN)_4$][PF_6] proved effective. Reaction of the alkyl-substituted phosphine ligands **2**[Li] or **3**[Li] with [$Cu(CH_3CN)_4$][PF_6] in THF solution led to rapid formation of the three-coordinate products [$Ph_2B(CH_2P^iPr_2)_2$]Cu(NCCH $_3$) (**9**) and [(3,5-$Me_2Ph)_2B(CH_2P^tBu_2)_2$]Cu(NCCH$_3$) (**10**) (Eqs. (4) and (5)). Isolated yields of pure **9** were low (ca. 40%) due to the difficulty in separating [Li(solvent)$_x$][PF_6] from **9**. In comparison, **10** was isolated in much higher yield (80%). Both compounds have been thoroughly characterized by NMR spectroscopy and elemental analysis. The IR spectra for **9** and **10** show ν_{CN} bands at 2265 and 2267 cm^{-1}, respectively. These stretches are consistent with acetonitrile acting as a weakly bound σ-donor. Previously reported IR data for phosphine-coordinated copper(I) acetonitrile complexes show a wide range of C≡N stretching frequencies (2268–2361 cm^{-1}), all of which are above the value for the free ligand (CH_3CN, thin film on KBr: 2253 cm^{-1}) [19].

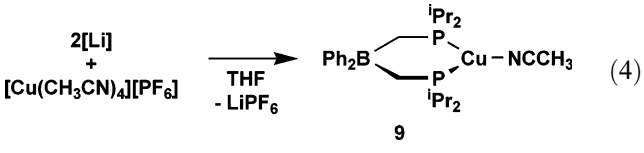

9 (4)

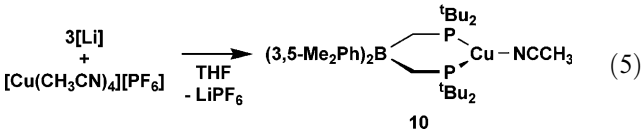

10 (5)

An X-ray diffraction study verified the three-coordinate nature of **9** (Fig. 4). The bis(phosphino)borate ligand is again in a twisted boat conformation. Two parameters of further note from the molecular structure of **9** are the B–Cu distance and the nature of the coordinated acetonitrile ligand. In other structures of transition metal complexes coordinated by bis(phosphino) borate ligands, the B–Cu distance in the twisted-boat conformation has typically been observed at B–M = 3.91–4.12 Å (M = Fe, Co, Rh, Pd, Pt). In the structure of **9** and the other three-coordinate structures presented in the present study, the B–M distance is relatively short (**9**: B–Cu = 3.823(2) Å). This is due to an

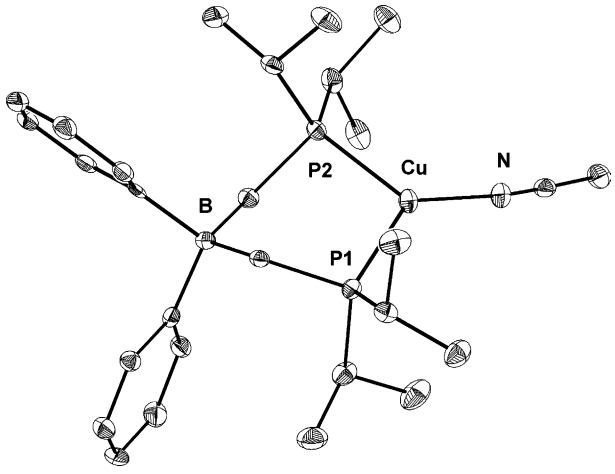

Fig. 4. Displacement ellipsoid representation (50%) of [$Ph_2B(CH_2P^iPr_2)_2$]Cu(NCCH$_3$) (**9**). Hydrogen atoms are omitted for clarity. Selected interatomic distances (Å) and angles (°): P1–Cu, 2.2349(6); P2–Cu, 2.2556(6); Cu–N, 1.934(2); B–Cu, 3.823(2) and P1–Cu–P2, 103.35(2); P1–Cu–N, 133.25(5); P2–Cu–N, 118.98(5).

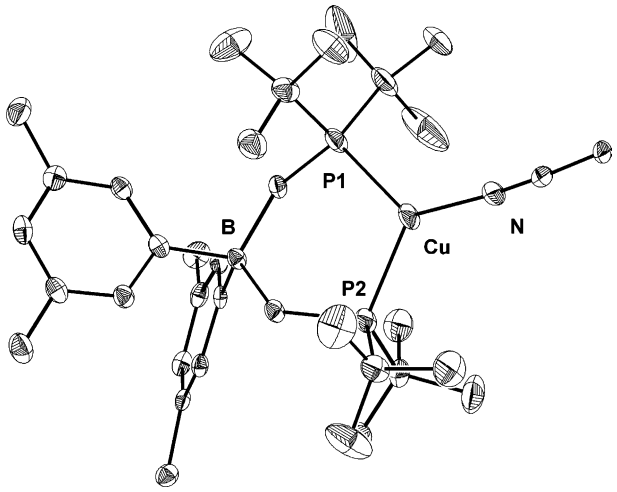

Fig. 5. Displacement ellipsoid representation (50%) of [(3,5-$Me_2Ph)_2B(CH_2P^tBu_2)_2$]Cu($NCCH_3$) · 0.56THF · 0.22pentane (**10 · 0.56 THF · 0.22pentane**). Hydrogen atoms and solvent molecules are omitted for clarity. Selected interatomic distances (Å) and angles (°): P1–Cu, 2.2421(8); P2–Cu, 2.2333(8); Cu–N, 1.930(2); B–Cu, 3.861(3) and P1–Cu–P2, 108.55(3); P1–Cu–N, 124.94(7); P2–Cu–N, 126.49(7).

expansion of the P–M–P angle (103.35(2)°) that results from the three-coordinate structure and the sterically small acetonitrile ligand. The acetonitrile ligand of **9** adopts a distorted coordination mode. Rather than bisecting the P–Cu–P linkage, the nitrile is canted below the plane of these three atoms, favoring one side of the C_2 axis. This is likely a solid-state phenomenon: the solution spectra of **9** are consistent with a molecule that contains a C_2 axis.

An X-ray diffraction study carried out on **10** also shows a trigonal planar three-coordinate copper center (Fig. 5). The structural parameters of **10** are quite similar to those found for **9**, with two minor differences. First, the acetonitrile ligand is coincident with the C_2 axis of the molecule and thus colinear with the B–Cu vector. Second, the P–Cu–P angle is modestly wider (108.55(3)°) than that observed in **9** (103.35(2)°). The slightly wider bite angle of the bis(phosphine) does not result in a corresponding contraction of the B–Cu distance; instead, a slight increase in the B–Cu distance of **10** as compared to **9** (3.861(3) vs. 3.823(2) Å) is observed. The acetonitrile compounds **9** and **10** are structurally distinctive examples of monomeric, phosphine-supported nitrile adducts of 3-coordinate copper(I). A few related examples of phosphine-coordinated copper nitrile complexes have been structurally characterized previously [20]. These examples are each either four-coordinate, or contain multiple metal centers (e.g., Cu_2 or RhCu).

3.3. Substitution chemistry of the sterically encumbered complex *10*

The well-defined three-coordinate acetonitrile complexes **9** and **10** serve as useful precursors to other three coordinate donor adduct complexes. Accordingly, replacement of the labile acetonitrile complex **10** is affected by a variety of donor ligands (Eq. (6)). Reaction of **10** with dimethylphenylphosphine (PMe_2Ph), trimethylphosphine sulfide ($S{=}PMe_3$), 2,6-lutidine, and *tert*-butylisonitrile (^{t}BuNC) in THF solution provides the corresponding complexes [(3,5-$Me_2Ph)_2B(CH_2P^tBu_2)_2$]-Cu($PMe_2Ph$) (**11**), [(3,5-$Me_2Ph)_2B(CH_2P^tBu_2)_2$]-Cu($S{=}PMe_3$) (**12**), [(3,5-$Me_2Ph)_2B(CH_2P^tBu_2)_2$]Cu(2,6-lutidine) (**13**), and [(3,5-$Me_2Ph)_2B(CH_2P^tBu_2)_2$]Cu($CN^t$-Bu) (**14**). All of these products can be isolated in high yield (85–95%) and the reactions are complete in less than 15 min at ambient temperature. In addition to PMe_2Ph, several other phosphine donors were also examined. Triethylphosphine provided a well-defined three-coordinate adduct complex, whereas $PMePh_2$ provided a mixture of the expected three-coordinate adduct complex and also a second, unidentified diamagnetic product. PPh_3 does not substitute the acetonitrile ligand of **10**, presumably due to steric congestion. Addition of the phosphite ligand $P(OPh)_3$ gradually consumes **10**, but results in overall complex degradation to ill-defined products. Substitution reactions of **10** by simple olefins was also surveyed. No reaction was observed (^{1}H and $^{31}P\{^1H\}$ NMR) between **10** and the potentially η^2-donors ethylene, 1-hexene, styrene, and azobenzene (1–10 equiv) in THF solution. This lack of reactivity is consistent with previous literature studies that suggest that copper(I) complexes supported by phosphine ligands do not form stable olefin adducts readily. Those that have been observed have typically required the presence of a large excess of the olefin [21] or chelation effects [22] to provide a Cu-olefin adduct species.

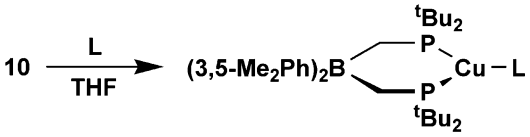

(6)

L = PMe_2Ph, 11; $S{=}PMe_3$, 12; 2,6-lutidine, 13; CN^tBu, 14

The tris(phosphine) complex **11** was structurally characterized by X-ray diffraction, verifying its three-coordinate geometry (Fig. 6). The structural parameters of **11** reflect the incorporation of a more sterically demanding phosphine donor ligand relative to the acetonitrile ligand of **10**. For example, the P–Cu–P angle is reduced (103.87(3)° in **11** versus 108.55(3)° in **10**) and the B–Cu distance is increased (3.972(3) Åin **11** versus 3.861(3) Å in **10**). Also, the average P–Cu bond lengths for the bis(phosphino)borate ligand are modestly longer (2.27 Å in **11** versus 2.24 Å in **10**), likely reflecting the greater electron-releasing nature of PMe_2Ph as compared to acetonitrile.

Neutral **11** is similar to previous structurally characterized P_3Cu complexes (P = trialkyl phosphine). Several

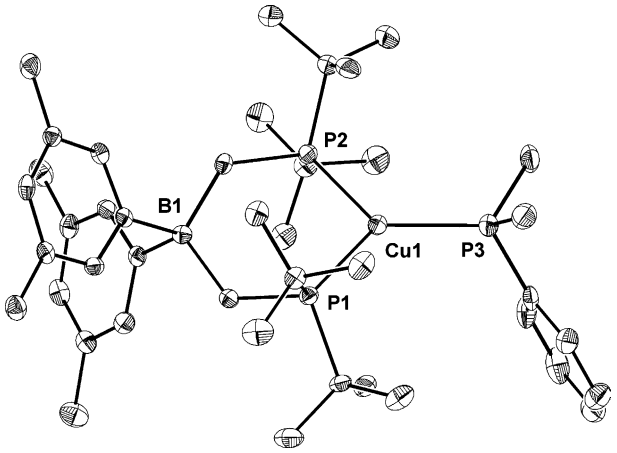

Fig. 6. Displacement ellipsoid representation (50%) of [(3,5-$Me_2Ph)_2B(CH_2P^tBu_2)_2$]Cu($PMe_2Ph$) (**11**). Second molecule in the asymmetric unit and hydrogen atoms are omitted for clarity. Selected interatomic distances (Å) and angles (°): P1–Cu1, 2.2714(8); P2–Cu1, 2.2707(8); Cu1–P3, 2.2477(8); B1–Cu1, 3.972(3) and P1–Cu1–P2, 103.87(3); P1–Cu1–P3, 127.29(3); P2–Cu1–P3, 128.84(3).

structures reported for $[(Ph_3P)_3Cu]^+$ [23] and the related $[\{(p\text{-MeOPh})_3P\}_3Cu]^+$ cation [24] have shown a mean Cu–P length of 2.295 Å and P–Cu–P angles near 120°. Also, Mathey and coworkers reported a macrocyclic P_3-phosphinine ligand system in which a copper center lies in a distorted trigonal planar coordination geometry [25]. Additionally, there are two reports of bimetallic $[Cu_2(\eta^1{:}\eta^1\text{-}L_2)_3]^{2+}$ (L_2 = dmpm, $(Ph_2P)_2py$), where the copper centers are both in highly symmetric trigonal planar environments [26]. The structures of these homoleptic phosphine adducts are relatively C_3 symmetric, whereas the structure of **11** is better described as C_{2v} due to the geometric constraint imposed by the chelated bis(phosphine) ligand. A similarly distorted structure has been reported for dicationic $[\{(dppf)Cu\}_2(\eta^1{:}\eta^1\text{-}dppf)]^{2+}$ [27], which has Cu–P bond lengths of 2.280 Å, 2.283 Å, and 2.260 Å and P–Cu–P angles of 124.6°, 123.4°, and 111.3°.

A complex related to **11** is the phosphine sulfide adduct [(3,5-$Me_2Ph)_2B(CH_2P^tBu_2)_2$]Cu(S=$PMe_3$) (**12**). A structurally related species has been reported: $[\{(dppf)Cu\}_2(\eta^1{:}\eta^1\text{-}dppfS_2)][BF_4]_2$ [28]. Complex **12** exhibits remarkably poor solubility (<5 mg/mL) in benzene and THF solution, distinct from **11**, **13**, and **14**.

Similar to **12**, the lutidine derivative [(3,5-$Me_2Ph)_2B(CH_2P^tBu_2)_2$]Cu(2,6-lutidine) (**13**) contains an uncommon coordination environment for copper(I). The sterically hindered pyridines 2,6-lutidine and 2,4,6-collidine have been used previously to prepare two- and three-coordinate copper complexes [29–32]. In almost all of these cases, the complexes are homoleptic pyridine cations, or include a single halide or pseudo-halide donor [29–31]. One notable exception reported by Omary et al. [32] is the fluorinated bis(pyrazolyl)borate derivative, $[H_2B(3,5\text{-}(CF_3)_2Pz)_2]$Cu(2,4,6-collidine). Similar to **13**, the monoanionic borate-based $[H_2B(3,5\text{-}(CF_3)_2Pz)_2]^-$ provides a neutral, three-coordinate copper(I) center.

The isonitrile complex [(3,5-$Me_2Ph)_2B(CH_2P^tBu_2)_2$]-Cu($CN^tBu$) (**14**) is structurally distinct in that it represents what is to our knowledge the only example of a phosphine-supported, three-coordinate monoisonitrile complex of copper(I). Four-coordinate copper(I) complexes featuring terminal isocyanide ligands more typically feature either three phosphine ligands and one isonitrile ligand, or two phosphines and two isocyanide ligands [33–37]. A key spectroscopic feature of metal-bound isocyanides is their infrared signature. The infrared spectrum of **14** shows a ν_{CN} band at 2162 cm^{-1}. This value is presented in Table 2 along with several other previously reported copper(I) complexes containing a single *tert*-butyl isonitrile ligand [38–43]. As can be seen, most of the examples have ν_{CN} values greater than that observed for free CN^tBu. This increase in the C≡N stretching frequency has been attributed to both poor back-donation from the copper d-orbitals into the ligand π* orbitals, and to a strong σ-donor effect that polarizes the C≡N bond [44,45]. Thus, the isonitrile ligand in **14** can be considered as primarily a strong σ-donor in this context.

We also surveyed the generation of a monocarbonyl copper complex analogous to **14**. To our knowledge, there are as yet no examples of well-defined copper carbonyl complexes supported by phosphine ligands. This is consistent with the observations of related isonitrile complexes, where copper(I) has been characterized as a relatively poor π-donor. We have found that the reaction between **10** and excess CO gas results in the formation of an unstable carbonyl adduct species that can be formulated as [(3,5-$Me_2Ph)_2B(CH_2P^tBu_2)_2$]Cu(CO) (**15**). In THF solution, excess carbon monoxide appears to displace the acetonitrile ligand, resulting in a shift in the $^{31}P\{^1H\}$ NMR resonance from 36.4 to 42.3 ppm. If CO is removed under vacuum, the acetonitrile adduct is

Table 2
Infrared resonances (ν_{CN}) for some copper(I) monoisonitrile complexes

Complex	ν_{CN} (cm^{-1})	Ref.
[HB{3,5-$(CF_3)_2pz\}_3$]Cu(CN^tBu)	2196[a]	[38]
[$(Ph_3P)_3$Cu(CNEt)][BF_4]	2193[b]	[37]
CpCu(CN^tBu)	2170[a]	[39]
[(3,5-$Me_2Ph)_2B(CH_2P^tBu_2)_2$]Cu($CN^tBu$) (**14**)	2162[c]	
[$HB(Pz)_3$]Cu(CN^tBu)	2155[d]	[40]
[$CpCo\{P(OMe)_2O\}_3$]Cu(CN^tBu)	2148[a]	[41]
[κ^3-$B(Pz)_4$]Cu(CN^tBu)	2140[d]	[42]
^tBuNC	2138[e]	[19]
(^tBuO)Cu(CN^tBu)	2102[b]	[43]

[a] KBr.
[b] Nujol.
[c] THF/KBr.
[d] Not reported.
[e] Neat.

regenerated as indicated by the return of the 36.4 ppm resonance. Infrared analysis of green solids isolated by drying a sample of **10** under a stream of CO gas revealed a single infrared band at 2084 cm^{-1}, consistent with a metal-bound monocarbonyl species. The carbonyl species **15** is not stable in the absence of excess CO, apparently decaying to solvent-bound species with concomitant loss of CO. For instance, if a THF solution of **10** is dried under a stream of CO gas, the resulting pale green solids that are isolated display a $^{31}P\{^{1}H\}$ NMR resonance at 44 ppm upon dissolution in benzene-d_6. This resonance gradually disappears unless a blanket of CO is preserved above the NMR sample solution. A single new resonance grows in at 38 ppm, which may be indicative of a benzene solvent adduct of Cu(I). The lability of the putative monocarbonyl species is consistent with previous observations for phosphine-supported copper [20n].

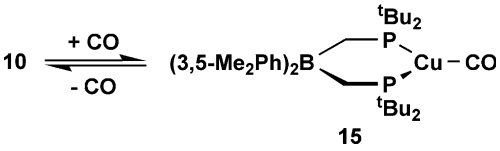

(7)

In summation, we have prepared and characterized several neutral and anionic copper complexes supported by chelating, monoanionic bis(phosphino)borate ligands. In particular, the sterically encumbered *tert*-butyl substituted bidentate phosphine **3** is useful for stabilizing three-coordinate species with a host of donor ligands occupying the third coordination site. The substitution chemistry of the available to the acetonitrile complex **10** is key to the preparation of numerous donor adduct complexes in this series. These synthons should expand the reaction chemistry available to neutral and anionic phosphine-chelated copper(I) systems. In particular, the 3-coordinate systems described may serve as useful entry points to group transfer reactions that would generate $[BP_2]Cu^{III}$ = E species.

4. Supplementary material

Crystallographic data for the structural analyses have been deposited at the Cambridge Crystallographic Data Centre, CCDC numbers 238116 (**6**), 238119 (**8** · THF · pentane), 238120 (**9**), 238118 (**10** · **0.56 THF** · **0.22 pentane**), and 238117 (**11**). Copies of this information may be obtained free of charge from the Director, CCDC, 12 Union Road, Cambridge, CB2 1EZ, UK (fax: +44-1223-336033; e-mail: deposit@ccdc.cam.ac.uk or http://www.ccdc.cam.ac.uk).

Acknowledgements

Financial support from the NSF (CHE-0132216) and the DOE (PECASE) is acknowledged. Larry Henling provided assistance with X-ray crystallography. Christine Thomas generously provided a sample of $PhB(CH_2P^tBu_2)_2$. J.C.T. is grateful to the NSF and to the Moore Foundation for graduate research fellowships.

References

[1] (a) S.V. Ley, A.W. Thomas, Angew. Chem., Int. Ed. 42 (2003) 5400;
(b) A. Caballero, M.M. Diaz-Rodriguez, T.R. Belderrain, M.C. Nicasio, S. Trofimenko, P.J. Perez, J. Am. Chem. Soc. 125 (2003) 1446;
(c) W. Kirmse, Angew. Chem., Int. Ed. 42 (2003) 1088;
(d) P. Müller, C. Fruit, Chem. Rev. 103 (2003) 2905;
(e) T. Rovis, D.A. Evans, Prog. Inorg. Chem. 50 (2001) 1.
[2] (a) I.E. Marko, A. Gautier, R. Dumeunier, K. Doda, F. Philippart, S.M. Brown, C.J. Urch, Angew. Chem., Int. Ed. 43 (2004) 1588;
(b) B.H. Lipshutz, K. Noson, W. Chrisman, A. Lower, J. Am. Chem. Soc. 125 (2003) 8779;
(c) J. Gao, J.H. Reibenspies, A.E. Martell, Angew. Chem., Int. Ed. 42 (2003) 6008;
(d) P. Gamez, P.G. Aubel, W.L. Driessen, J. Reedijk, Chem. Soc. Rev. 30 (2001) 376.
[3] (a) E.A. Lewis, W.B. Tolman, Chem. Rev. 104 (2004) 1047;
(b) E. Kim, E.E. Chufan, K. Kamaraj, K.D. Karlin, Chem. Rev. 104 (2004) 1077;
(c) L.M. Mirica, M. Vance, D.J. Rudd, B. Hedman, K.O. Hodgson, E.I. Solomon, T.D.P. Stack, J. Am. Chem. Soc. 124 (2002) 9332.
[4] (a) Recent examples include: J.L. Schneider, V.G. Young, Jr., W.B. Tolman, Inorg. Chem. 40 (2001) 165;
(b) M.M. Diaz-Requejo, T.R. Belderrain, M.C. Nicasio, S. Trofimenko, P.J. Perez, J. Am. Chem. Soc. 125 (2003) 12078.
[5] (a) Recent examples include: X. Dai, T.H. Warren, Chem. Commun. (2001) 1998;
(b) D.J.E. Spencer, N.W. Aboelella, A.M. Reynolds, P.L. Holland, W.B. Tolman, J. Am. Chem. Soc. 124 (2002) 2108;
(c) D.S. Laitar, C.J.N. Mathison, W.M. Davis, J.P. Sadighi, Inorg. Chem. 42 (2003) 7354;
(d) C. Shimokawa, S. Yokuta, Y. Tachi, N. Nishiwaki, M. Ariga, S. Itoh, Inorg. Chem. 42 (2003) 8395.
[6] (a) Recent examples include: X. Hu, I. Castro-Rodriguez, K. Meyer, J. Am. Chem. Soc. 125 (2003) 12237;
(b) H. Kaur, F.K. Zinn, E.D. Stevens, S.P. Nolan, Organometallics 23 (2004) 1157;
(c) N.P. Mankad, T.G. Gray, D.S. Laitar, J.P. Sadighi, Organometallics 23 (2004) 1191.
[7] (a) Recent examples include:S.B. Harkins, J.C. Peters, J. Am. Chem. Soc. 126 (2004) 2885;
(b) C.X. Zhang, H.-C. Liang, E. Kim, J. Shearer, M.E. Helton, E. Kim, S. Kaderli, C.D. Incarvito, A.D. Zuberbuehler, A.L. Rheingold, K.D. Karlin, J. Am. Chem. Soc. 125 (2003) 634.
[8] J.C. Thomas, J.C. Peters, Inorg. Chem. 42 (2003) 5055.
[9] J.C. Thomas, J.C. Peters, Polyhedron 23 (2003) 489.
[10] J.H. So, P. Boudjouk, Inorg. Chem. 29 (1990) 1592.
[11] (a) F. Tisato, F. Vallotto, G. Pilloni, F. Refosco, C. Corvaja, B. Corain, J. Chem. Soc., Chem. Commun. (1994) 2397, and references therein;
(b) G. Pilloni, G. Bandoli, F. Tisato, B. Corain, Chem. Commun. (1996) 433;
(c) F. Tisato, G. Pilloni, F. Refosco, G. Bandoli, C. Corvaja, B. Corain, Inorg. Chim. Acta 275–276 (1998) 401.

[12] (a) P.H. Davis, R.L. Belford, I.C. Paul, Inorg.Chem. 12 (1973) 213;
(b) G.A. Bowmaker, J.C. Dyason, P.C. Healy, L.M. Engelhardt, C. Pakawatchai, A.H. White, J. Chem. Soc., Dalton Trans. (1987) 1089;
(c) G.L. Soloveichik, O. Eisenstein, J.T. Pouton, W.E. Streib, J.C. Huffman, K.G. Caulton, Inorg. Chem. 31 (1992) 3306;
(d) T. Kräuter, B. Neumüller, Polyhedron 15 (1996) 2851;
(e) T. Kräuter, B. Neumüller, Polyhedron 15 (1996) 2851;
(f) G.A. Bowmaker, S.E. Boyd, J.V. Hanna, R.D. Hart, P.C. Healy, B.W. Skelton, A.H. White, J. Chem. Soc., Dalton Trans. (2002) 2722.

[13] (a) P.G. Eller, G.J. Kubas, R.R. Ryan, Inorg. Chem. 16 (1977) 2454;
(b) D.K. Srivastava, N.P. Rath, L. Barton, Polyhedron 11 (1992) 1251;
(c) G.A. Bowmaker, R.D. Hart, B.E. Jones, B.W. Skelton, A.H. White, J. Chem. Soc., Dalton Trans. (1995) 3063;
(d) É. Balogh-Hergovich, L. Párkányi, G. Speier, Z. Kristall. - New Cryst. Struct. 213 (1998) 265;
(e) E.W. Ainscough, A.M. Brodie, A.K. Burrell, G.H. Freeman, G.B. Jameson, G.A. Bowmaker, J.V. Hanna, P.C. Healy, J. Chem. Soc., Dalton Trans. (2001) 144;
(f) P. Aslanidis, P.J. Cox, S. Divanidis, A.C. Tsipis, Inorg. Chem. 41 (2002) 6875.

[14] E.D. Blue, A. Davis, D. Conner, T.B. Gunnoe, P.D. Boyle, P.S. White, J. Am. Chem. Soc. 125 (2003) 9435.

[15] (a) J.D. Feldman, J.C. Peters, T.D. Tilley, Organometallics 21 (2002) 4050;
(b) L. Turculet, J.D. Feldman, T.D. Tilley, Organometallics 23 (2004) 2488;
(c) C.E. MacBeth, J.C. Thomas, T.A. Betley, J.C. Peters, Inorg. Chem. 43 (2004) 4645;
(d) D.M. Jenkins, J.C. Peters, unpublished results;
(e) J.C. Thomas, J.C. Peters, unpublished results.

[16] H. Nöth, B. Wrackmeyer, Nuclear Magnetic Resonance Spectroscopy of Boron Compounds, in: P. Diehl, E. Flack, R. Kosfeld (Eds.), NMR: Basic Principles and Progress, vol. 14, Springer-Verlag, Berlin, 1978.

[17] (a) J.C. Thomas, J.C. Peters, J. Am. Chem. Soc. 123 (2001) 5100;
(b) C.C. Lu, J.C. Peters, J. Am. Chem. Soc. 124 (2002) 5272;
(c) T.A. Betley, J.C. Peters, Inorg. Chem. 41 (2002) 6541;
(d) J.C. Thomas, J.C. Peters, J. Am. Chem. Soc. 125 (2003) 8870;
(e) T.A. Beltey, J.C. Peters, Angew. Chem., Int. Ed. 42 (2003) 2385.

[18] (a) W. Clegg, S.R. Acott, D. Garner, J. Chem. Soc., Dalton Trans. (1984) 2581;
(b) L. Stamp, H.T. Dieck, Inorg. Chim. Acta 147 (1988) 199;
(c) G.M. Villacorta, P. Rao, S.J. Lippard, J. Am. Chem. Soc. 110 (1988) 3175;
(d) R. Clérac, F.A. Cotton, K.R. Dunbar, C.A. Murillo, X. Wang, Inorg. Chem. 40 (2001) 420.

[19] C.J. Pouchert, The Aldrich Library of FT-IR Spectra, Edition I, Aldrich Chemical Company, Inc., Milwaukee, WI, 1985.

[20] (a) H. El-Amouri, A.A. Bahsoun, J. Fischer, J.A. Osborn, M.-T. Youinou, Organometallics 10 (1991) 3582;
(b) C.-M. Che, Z. Mao, V.M. Miskowski, M.-C. Tse, C.-K. Chan, K.-K. Cheung, D.L. Phillips, K.-H. Keung, Angew. Chem., Int. Ed. 39 (2000) 4084;
(c) H. Liu, M.J. Calhorda, M.G.B. Drew, V. Félix, J. Novosad, L.F. Veiros, F.F. de Biani, P.J. Zanello, J. Chem. Soc., Dalton Trans. (2002) 4365;
(d) M. Herberhold, N. Akkus, W. Milius, Z. Naturforsch. 58B (2003) 528;
(e) W.-H. Chan, S.-M. Peng, C.-M. Che, J. Chem. Soc., Dalton Trans. (1998) 2867;
(f) M.-M. Wu, L.-Y. Zhang, Y.-H. Qin, Z.-N. Chen, Acta Cryst. E 59 (2003) m195;
(g) D. Ferraris, B. Young, C. Cox, W.J. Drury III, T. Dudding, T. Lectka, J. Org. Chem. 63 (1998) 6090;
(h) J.V. Hanna, R.D. Hart, P.C. Healy, B.W. Skelton, A.H. White, J. Chem. Soc., Dalton Trans. (1998) 2321;
(i) J. Liedtke, S. Loss, G. Alcaraz, V. Gramlich, H. Grützmacher, Angew. Chem., Int. Ed. 38 (1999) 1623;
(j) D.J. Darensbourg, E.M. Longridge, E.V. Atnip, J.H. Reibenspies, Inorg. Chem. 30 (1991) 358;
(k) M. Yan, Z.-Y. Zhou, A.S.C. Chan, Chem. Commun. (2000) 115;
(l) J. Diez, M.P. Gamasa, J. Gimeno, A. Tiripicchio, M.T. Camellini, J. Chem. Soc., Dalton Trans. (1987) 1275;
(m) P.F. Barron, J.C. Dyason, L.M. Engelhardt, P.C. Healy, A.H. White, Aust. J. Chem. 38 (1985) 261;
(n) D. Li, Q. Feng, X.-L. Feng, J.-W. Cai, Inorg. Chem. Commun. 6 (2003) 361;
(o) J Green, E. Sinn, S. Woodward, R. Butcher, Polyhedron 12 (1993) 991;
(p) N. Vijayashree, A.G. Samuelson, Curr. Sci. 65 (1993) 57;
(q) K. Osakada, T. Takizawa, T. Koizumi, T. Yamamoto, Chem. Lett. (1997) 325.

[21] (a) M. Håkansson, K. Brantin, S. Jagner, J. Organomet. Chem. 602 (2000) 5;
(b) M. Onishi, K. Hiraki, H. Itoh, H. Eguchi, S. Abe, T. Kawato, Inorg. Chim. Acta 145 (1988) 105;
(c) D.J. Fife, W.M. Moore, K.W. Morse, J. Am. Chem. Soc. 107 (1985) 7077.

[22] (a) J. Thomaier, S. Boulmaâz, H. Schönberg, H. Rüegger, A. Currao, H. Grützmacher, H. Hillebrecht, H. Pritzkow, New J. Chem. 22 (1998) 947;
(b) E.C. Alyea, P.R. Meehan, G. Ferguson, S. Kannan, Polyhedron 16 (1997) 3479;
(c) T. Miyaji, Z. Xi, K. Nakajima, T. Takahashi, Organometallics 20 (2001) 2859.

[23] (a) D.J. Saturnino, A.M. Arif, Inorg. Chem. 32 (1993) 4157;
(b) J.L. Davidson, W.E. Lindsell, K.J. McCullough, C.H. McIntosh, Organometallics 14 (1995) 3497;
(c) G. Doyle, K.A. Eriksen, D. Van Engen, Organometallics 4 (1985) 2201;
(d) P.C. Healy, J.V. Hanna, Acta Cryst. E 59 (2003) m384;
(e) P. Klüfers, U. Wilhelm, J. Organomet. Chem. 421 (1991) 39;
(f) D. Li, R. Li, Z. Qi, X. Feng, J. Cai, X. Shi, Inorg. Chem. Commun. 4 (2001) 483.

[24] A. Baiada, F.H. Jardine, R.D. Willett, K. Emerson, Inorg. Chem. 30 (1991) 1365.

[25] A. Moores, N. Mézailles, N. Maigrot, L. Ricard, F. Mathey, P. le Floch, Eur. J. Inorg. Chem. (2002) 2034.

[26] (a) Z. Mao, H.-Y. Chao, Z. Hui, C.-M. Che, W.-F. Fu, K.-K. Cheung, N. Zhu, Chem. Eur. J. 9 (2003) 2885;
(b) J.S. Field, R.J. Haines, B. Warwick, M.M. Zulu, Polyhedron 15 (1996) 3741.

[27] (a) P. Pinto, M.J. Calhorda, V. Félix, T. Avilés, M.G.B. Drew, Monatsh. Chem. 131 (2000) 1253;
(b) U. Casellato, R. Graziani, G. Pilloni, J. Cryst. Spec. Res. 23 (1993) 571.

[28] G. Pilloni, B. Longato, G. Bandoli, Inorg. Chim. Acta 277 (1998) 163.

[29] T.N. Sorrell, D.L. Jameson, J. Am. Chem. Soc. 105 (1983) 6013.

[30] (a) P.C. Healy, C. Pakawatchai, A.H. White, J. Chem. Soc., Dalton Trans. (1983) 1917;
(b) P.C. Healy, C. Pakawatchai, R.I. Papasergio, V.A. Patrick, A.H. White, Inorg. Chem. 23 (1984) 3769;
(c) L.M. Engelhardt, C. Pakawatchai, A.H. White, P.C. Healy, J. Chem. Soc., Dalton Trans. (1985) 117;
(d) J.C. Dyason, P.C. Healy, C. Pakawatchai, V.A. Patrick, A.H. White, Inorg. Chem. 24 (1985) 1957.

[31] (a) A. Habiyakare, E.A.C. Lucken, G. Bernardinelli, J. Chem. Soc., Dalton Trans. (1991) 2269;
(b) A. Habiyakare, E.A.C. Lucken, G. Bernardinelli, J. Chem. Soc., Dalton Trans. (1992) 2591.
[32] M.H. Omary, M.A. Rawashdeh-Omary, H.V.K. Diyabalanage, H.V.R. Dias, Inorg. Chem. 42 (2003) 8612.
[33] E. Fournier, S. Sicard, A. Decken, P.D. Harvey, Inorg. Chem. 43 (2004) 1491.
[34] J. Diez, M.P. Gamasa, J. Gimeno, M. Lanfranchi, A. Tiripicchio, J. Organomet. Chem. 637-639 (2001) 677.
[35] A. Bell, R.A. Walton, D.A. Edwards, M.A. Poulter, Inorg. Chim. Acta 104 (1985) 171.
[36] G. La Monica, G. Ardizzoia, S. Cenini, F. Porta, J. Organomet. Chem. 273 (1984) 263.
[37] J. Bailey, M.J. Mays, J. Organomet. Chem. 47 (1973) 217.
[38] H.V.R. Dias, H.-L. Lu, J.G. Gorden, W. Jin, Inorg. Chem. 35 (1996) 2149.
[39] T. Saegusa, Y. Ito, S. Tomita, J. Am. Chem. Soc. 93 (1971) 5656.
[40] M.I. Bruce, A.P.P. Ostazewski, J. Chem. Soc., Dalton Trans. (1973) 2433.
[41] B. Lenders, W. Kläui, Chem. Ber. 123 (1990) 2233.
[42] O.M. Abu Salah, M.I. Bruce, J.D. Walsh, Aust. J. Chem. 32 (1979) 1209.
[43] T. Tsuda, H. Habu, S. Horiguchi, T. Saegusa, J. Am. Chem. Soc. 96 (1974) 5930.
[44] L. Malatesta, F. Bonati, Isocyanide Complexes of Metals, Wiley, New York, NY, 1969.
[45] (a) M. Pasquali, C. Floriani, Copper(I)–carbon monoxide chemistry: recent advances and perspectives, in: K.D. Karlin, J. Zubieta (Eds.), Copper Coordination Chemistry: Biochemistry and Inorganic Perspectives, Adenine, Guilderland, NY, 1983, pp. 311–330, For related discussion, see;
(b) A.J. Lupinetti, S.H. Strauss, G. Frenking, Prog. Inorg. Chem. 49 (2001) 1.

Available online at www.sciencedirect.com
SCIENCE DIRECT®
Polyhedron 23 (2004) 2915–2919
POLYHEDRON
www.elsevier.com/locate/poly

Open shell metallocenes and exchange splitting of ligand bands: a reassignment of the photoelectron spectra of manganocene ☆

Jennifer C. Green *, Claire Burney

Department of Chemistry, University of Oxford, Inorganic Chemistry Laboratory, South Parks Road, Oxford OX1 3QR, UK

Received 24 May 2004; accepted 6 July 2004
Available online 12 September 2004

Abstract

Unrestricted density functional calculations on the neutral molecular and ion states of $Mn(\eta\text{-}C_5H_5)_2$ indicate a reassignment of its photoelectron spectrum. The ordering of the occupied spin orbitals is inverted with respect to the normal metallocene orbital ordering with the metal orbitals lying below the ligand e_1 π orbitals. The spin orbitals can be related directly to the observed ion states with one minor reversal of ordering.
© 2004 Elsevier Ltd. All rights reserved.

1. Introduction

Metallocenes were among the early candidates for the application of gas-phase photoelectron spectroscopy (PES) to transition metal compounds [1–4]. Their volatility made them experimentally accessible and their high symmetry theoretically tractable. These studies were fundamental to the development of methods for predicting the number and relative intensity of PE bands of open shell molecules based on fractional parentage coefficients [5]. Also the wealth of data on ion states further informed ligand field treatments of these systems [6].

The availability of experimental data was also a challenge to the development of quantum mechanical methods for predicting ionization energies and hence served as a validation of electronic structure descriptions of transition metal complexes [7].

Variable energy PES, first with He I and II radiation [8], and subsequently with synchrotron sources [9,10], gave valuable information on covalency in metallocenes and confirmed the majority of the assignments.

In spite of all these extensive studies, there remained some paradoxes in the assignment of $MnCp_2$ ($Cp = (\eta^5\text{-}C_5H_5)$). $MnCp_2$ is unusual among the first transition series metallocenes in showing a high spin state with $S = 5/2$. Magnetic measurements demonstrate that this is the ground state when magnetically dilute in $MgCp_2$ [11]. However, ESR has established that the more constrained sites of $FeCp_2$ and $RuCp_2$ promote a low spin state with $S = 1/2$ [12]. In the gas-phase $MnCp_2$ is predominantly high spin with a $^6A_1$ ground state [3,13]. PES has shown that a small amount of a $^2E_2$ low spin state is also present [3]. Assignment of the PE bands [3] (Fig. 1) of the high spin species gave ion states associated with the d ionizations at 7.01 ($^5E_1$a) 10.25 ($^5A_1$c) and 10.50 eV ($^5E_2$d). Application of ligand field theory to these energies leads directly to values of Δ_1 and Δ_2 of 3.24 and 0.25 eV for $[MnCp_2]^+$. The derived value of Δ_1 is very large [14,15]. This is the first puzzle.

The second unresolved question is the presence of an extra unassigned band, x, at 11.1 eV. This is far removed from the ligand band, b, associated with ionization of

☆ This paper is dedicated to Malcolm Green who catalyzed the application of photoelectron spectroscopy to metal complexes in Oxford.

* Corresponding author. Tel.: +44 1865 272637; fax: +44 1865 272690.
E-mail address: jennifer.green@chem.ox.ac.uk (J.C. Green).

0277-5387/$ - see front matter © 2004 Elsevier Ltd. All rights reserved.
doi:10.1016/j.poly.2004.07.011

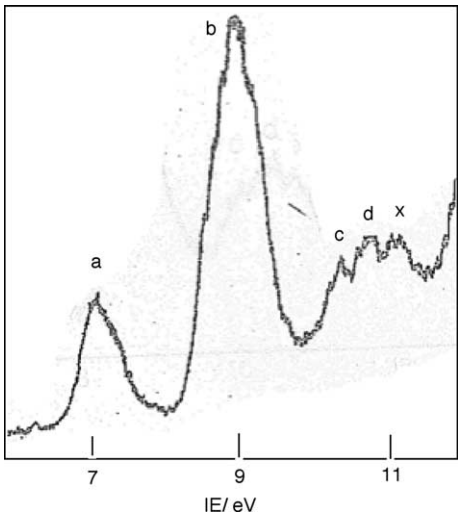

Fig. 1. Low IE region of the He I PE spectrum of $MnCp_2$.

the Cp e_1 π electrons, which is found centred on 8.85 eV, and is redundant to the assignment of the ionization of the d^5 configuration which predicts only three d bands. A very weak band associated with a very small amount of the compound in the low spin state is observed at 6.26 eV, but band x is too intense for this low spin species and is in the wrong IE region. Band x was originally assigned to an impurity [3] but it appears reproducibly in various measurements of $MnCp_2$.

In this paper, we describe unrestricted density functional calculations of the PE spectrum of $MnCp_2$ that account well for all features.

2. Computational methods

Calculations were performed using density functional methods of the Amsterdam Density Functional Package (version 2002.02) [16]. Type V basis sets were used with triple ξ accuracy sets of Slater type orbitals, with a single polarisation function added to the main group atoms. The cores of the atoms were frozen up to 2p for Mn and 1s for C. The generalised gradient approximation (GGA non-local) method was used, using Vosko, Wilk and Nusair's local exchange correlation [17] with non-local exchange corrections by Becke [18] and non-local correlation corrections by Perdew [19,20]. The structure was optimised in an unrestricted calculation. The molecule was assumed to have five unpaired electrons so the spin S was set at 5/2. The calculation therefore placed five more electrons in α spin orbitals than β spin orbitals. A single point restricted calculation was carried out using the optimised structure with S=O with the configuration fixed to the same occupancy as that determined by the unrestricted calculation, namely $1e''_1(4)1e'_1(4)1e'_2(2)1a'_1(1)2e''_1(2)$ (see Fig. 2). Ionisation energies were calculated by direct unrestricted calculations on the molecular ions in their ground and appropriate excited states, and subtraction of the energy of the neutral molecule.

3. Results and discussion

Recent calculations have demonstrated that modern computational methods give good structural and vibrational data for the first row metallocenes [21]. Both pure density functional and hybrid methods were compared for ferrocene and the B3LYP hybrid was selected to model the open shell metallocenes. In these studies we have employed the ADF program suite [16] because of its facility for fixing configurations when calculating energies of excited states. ADF does not support hybrid methods so the BP86 functional was used, which also gave a good account for ferrocene, though pure density functionals are approximate in handling the exchange correlation problem and may overestimate covalency.

The geometry of $MnCp_2$ was optimised with an unrestricted calculation assuming D_{5h} symmetry and a spin of 5/2. The resulting Mn–C and C–C distances of 2.42 and 1.44 Å are in reasonable agreement with the experimental values (2.380(6) and 1.429(2) Å) obtained by gas-phase electron diffraction [13,22].

The energies of the seven highest occupied spin orbitals are given in Table 1 together with their AO composition.

Using the optimised geometry from the unrestricted calculation, a spin restricted calculation was carried out with the same configuration as the unrestricted calculation, namely $1e''_1(4)1e'_1(4)1e'_2(2)1a'_1(1)2e''_1(2)$. These restricted orbitals have AO compositions typical of a metallocene (Table 1). The $1e'_1$ orbitals show a small amount of mixing with the Mn 4p orbitals. The $1a'_1$ and $1e'_2$ are more than 90% metal in character. The largest mixing is between the ligand and Mn e''_1 orbitals resulting in a predominantly ligand bonding orbital, $1e''_1$, and a predominantly metal anti-bonding orbital, $2e''_1$, the latter being the HOMO.

Their energies are represented diagramatically in Fig. 2 and are related to those obtained with the spin unrestricted calculation. In the latter, the metal based $1a'_1$ and $1e'_2$ α spin orbitals are lowered substantially in energy by over 2 eV and are more stable than the primarily ligand levels. The $1e'_1$ orbitals, which have no Mn 3d character, show a small exchange splitting of 0.2 eV and are unshifted in energy. In all these cases the orbital composition is very similar in the two calculations. The e''_1 orbitals show substantial reorganisation. The $2e''_1\alpha$ spin orbital is stabilised by 1.28 eV and becomes more ligand than metal based. The $1e''_1\alpha$ spin orbital is stabilised by 0.94 eV and becomes more metal than ligand based. The $1e'_1$ β spin orbital is slightly raised in energy and increases its ligand character. The consequence

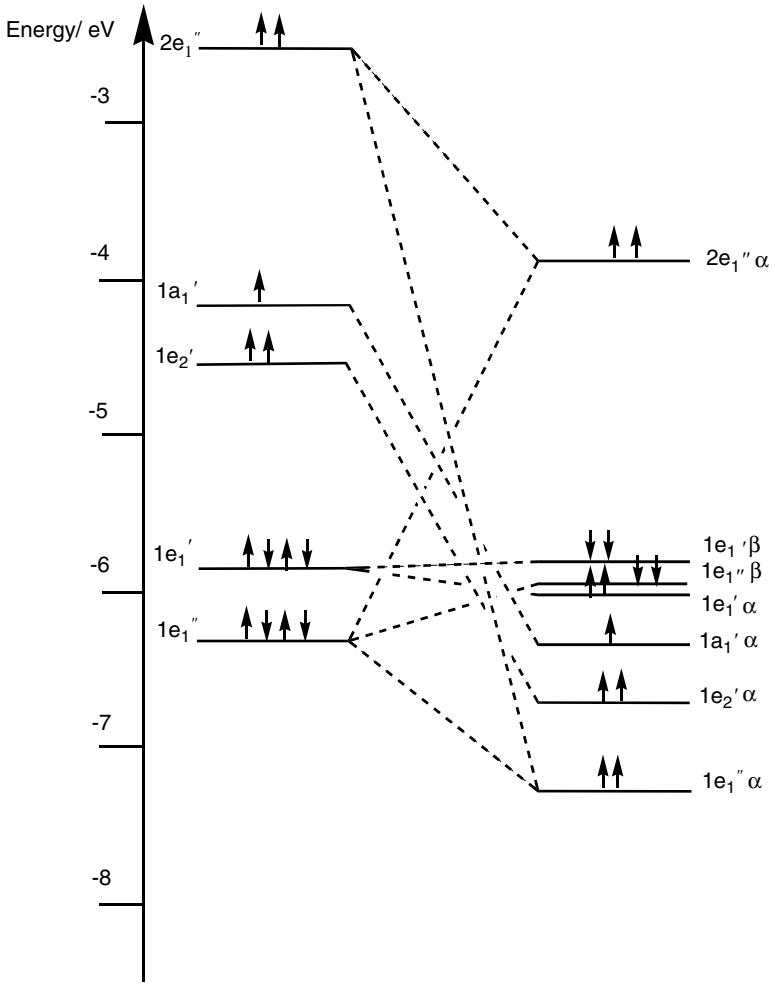

Fig. 2. Correlation of MO energy levels from restricted and unrestricted calculations on $MnCp_2$. On the left the energies of the orbitals from the restricted calculations are given and on the right the spin orbitals energies are shown.

Table 1
DFT calculations on $MnCp_2$ and $MnCp_2^+$ giving energy and composition of orbitals and holes in ion states

	Orbital	Energy	Mn (%)			C (%)	Ion state	Mn (%)			C (%)	IE calc.	IE exp.
			3d	4s	4p	2p		3d	4s	4p	2p		
Unrestricted	$2e_1''\alpha$	−3.87	35			61	$^5E_1''$	26			68	6.52	7.01a
	$1e_1'\beta$	−5.76			8	87	$^7E_1'$			9	86	8.19	8.5 b
	$1e_1'\alpha$	−5.97			12	83	$^5E_1'$	14			81	8.43	8.85 b
	$1e_1''\beta$	−5.96	19			73	$^7E_1''$	24			67	8.52	9.1 b
	$1a_1'\alpha$	−6.34	90	7		1	$^5A_1'$	89	5		4	9.62	10.25 c
	$1e_2'\alpha$	−6.69	97			3	$^5E_2'$	79			14	10.46	11.10 x
	$1e_1''\alpha$	−7.27	58			35	$^5E_1''$	63			28	10.12	10.5 d
Restricted	$2e_1''$	−2.59	65			34							
	$1a_1'$	−4.17	88	12									
	$1e_2'$	−4.58	94			5							
	$1e_1'$	−5.83			9	86							
	$1e_1''$	−6.33	32			59							

is that all predominantly metal orbitals lie below the predominantly ligand orbitals. The exchange stabilisation in this high spin compound is sufficient to invert the normal metal ligand energy ordering [23].

The energies of the ion states associated with the seven spin orbitals were calculated by fixing the configuration with a hole in the associated vacant spin orbital. The resulting state energies are given in Table

1. Calculated ionization energies (IE) are compared with the experimental values in Table 1.

The ion state ordering is very similar to that of the spin orbitals, thus the spin unrestricted calculation gives a good guide to assignment of the PE bands. An exception is that the $^5E_1''$ ion state lies between the $^5A_1'$ and $^5E_2'$ ion states whereas the $1e_1''$ spin orbital is the most stable of the set. The $^5A_1'$ and $^5E_2'$ ion states have a greater energy separation from the E_1' ion states than do the corresponding spin orbitals from each other, indicating additional relaxation of the metal d orbitals in the ion. This is consistent with the reordering suggested by the calculation.

Inspection of the orbital composition of the hole states in the ion state calculations show that the description of the spin orbitals corresponds closely to that of the holes. Thus in this respect too the unrestricted ground state calculation gives a good description of the ionisation process.

Direct mapping of the calculated IE onto the experimental bands reassigns the bands. The principal difference from the original assignment is that the higher $^5E_1''$ ionization is now assigned to band d rather than the ligand band b. Also the $^5E_2'$ state is assigned to band x rather than band d. Thus the origin of the additional band is accounted for.

Both cobaltocene and nickelocene show low intensity bands at higher energies than the main ligand band. As they also have unpaired electrons in $2e_1''$ orbitals it is likely that they have a similar origin to band d of manganocene.

Orbitals with higher d character are expected to show higher He II/He I intensity ratios when the photon energy dependence of the PE spectrum is determined. For $MnCp_2$ the highest He II/He I ratio was found for band a, which we are now assigning as having less than 50% 3d character [8]. In general, PE studies of the He II/He I band intensity ratios of the metallocenes established the ordering for the originating orbitals of $2e_1'' > 1a_1' > 1e_2' > 1e_1'' > 1e_1'$. It was pointed out that these results were in accord with expectations from MO calculations except for the $2e_1''$ ionization band, as this was the anti-bonding partner of the orbital where the greatest metal d – carbon 2p mixing occurs. In this sense the large increase in the intensities of the $2e_1''$ band in the He II spectra of $MnCp_2$, $CoCp_2$ and $NiCp_2$ was deemed anomalous [8]. Further light was thrown on this anomaly by synchrotron studies of the metallocenes. Though $MnCp_2$ was not included in this study, the $2e_1''$ band was studied for both $CoCp_2$ and $NiCp_2$ [10]. Two particular features in the cross section were noted. One was the 3p–3d resonance, generally indicative of a d orbital contribution to the ionizing orbital; the intensity of this feature was less than that found in the a_1' and e_2' based bands in accord with expectations from MO calculations. The second was the presence of a shape resonance around 40 eV. (He II photons have an energy of 40.8 eV.) This was present in all 3d based ionizations and is a general feature of sandwich compounds [24], but was particularly strong in the $2e_1''$ band. Subsequent calculations of the cross sections of $CoCp_2$ reproduced this very strong shape feature and assigned it to excitation to an $f(xz^2)$ wave localised within the molecular potential at this energy [25]. Thus the intensity of the feature is not directly related to d character and the HeII/HeI ratios are non-indicative of metal character.

The inverted ordering found for this high spin molecule means that naïve application of the ligand field model is inappropriate for this system.

4. Conclusions

Unrestricted density functional calculations of $MnCp_2$ lead to a reassignment of its PE spectrum that accounts for all observed features. Agreement between experimental and calculated IE is good, the calculations underestimate the ionization energies by around 0.5 eV. The spin orbitals of an unrestricted calculation of the neutral molecule map directly onto the calculated ion states with one exception. In this calculation the exchange stabilization of the α spin orbitals leads to all predominantly metal orbitals being more stable than the cyclopentadienyl e_1 δ orbitals, an inversion from the normal metallocene ordering.

Acknowledgements

We thank the Oxford Supercomputing Centre for access to its facilities.

References

[1] D.W. Turner, C. Baker, A.D. Baker, C.R. Brundle, Molecular Photoelectron Spectroscopy, Wiley, London, 1970.
[2] S. Evans, M.L.H. Green, B. Jewitt, A.F. Orchard, J. Pygall, J. Chem. Soc., Faraday Trans. II 68 (1972) 1847.
[3] S. Evans, M.L.H. Green, B. Jewitt, G.H. King, A.F. Orchard, J. Chem. Soc., Faraday Trans. II 70 (1974) 356.
[4] J.W. Rabalais, L.O. Werme, T. Bergmark, L. Karlsson, M. Husain, K. Siegbahn, J. Chem. Phys. 57 (1972) 1185.
[5] P.A. Cox, Struct. Bonding 24 (1975) 59.
[6] K.D. Warren, Struct. Bonding 27 (1976) 45.
[7] J.C. Green, Struct. Bonding 43 (1981) 37.
[8] C. Cauletti, J.C. Green, M.R. Kelly, P. Powell, J. Van Tilborg, J. Robbins, J. Smart, J. Electron. Spectrosc. Relat. Phenom. 19 (1980) 327.
[9] G. Cooper, J.C. Green, M.P. Payne, Mol. Phys. 63 (1988) 1031.
[10] J. Brennan, G. Cooper, J.C. Green, M.P. Payne, C.M. Redfern, J. Electron. Spectrosc. Relat. Phenom. 66 (1993) 101.
[11] M.E. Switzer, R. Wang, M.F. Rettig, A.H. Maki, J. Am. Chem. Soc. 96 (1974) 7669.

[12] J.H. Ammeter, R. Bucher, N. Oswald, J. Am. Chem. Soc. 96 (1974) 7833.
[13] A. Haaland, Inorg. Nucl. Chem. Lett. 15 (1979) 267.
[14] K.R. Gordon, K.D. Warren, Inorg. Chem. 17 (1978) 987.
[15] R. Poli, Chem. Rev. 96 (1996) 2135.
[16] E.J. Baerends, Scientific Computing and Modelling NV Vrije Universiteit, Amsterdam, 2002.
[17] S.H. Vosko, L. Wilk, M. Nusair, Can. J. Phys. 58 (1980) 1200.
[18] A.D. Becke, J. Chem. phys. 98 (1993) 5648.
[19] J.P. Perdew, Phys. Rev. B 34 (1986) 7046.
[20] J.P. Perdew, Phys. Rev. B 33 (1986) 8822.
[21] X.-F. Xu, Y. Xie, W.-L. Feng, H.F.I. Schaefer, J. Phys. Chem. A 107 (2003) 2716.
[22] A. Haaland, J. Lusztyk, J. Brunvoll, K.B. Starowieyski, J. Organomet. Chem. 859 (1975) 279.
[23] E.I. Solomon, L. Basumallick, P. Chen, P. Kennepohl, Coord. Chem. Rev., 2004 (in press).
[24] J.C. Green, P. Decleva, Coord. Chem. Rev., 2004 (in press).
[25] G. Fronzoni, M. Stener, S. Furlan, P. Decleva, J. Chem. Phys. 273 (2001) 117.

Available online at www.sciencedirect.com
SCIENCE DIRECT®
Polyhedron 23 (2004) 2921–2928
POLYHEDRON
www.elsevier.com/locate/poly

Five-coordinate iron(II) complexes bearing tridentate nitrogen donor ligands as catalysts for atom transfer radical polymerisation

Rachel K. O'Reilly, Vernon C. Gibson *, Andrew J.P. White, David J. Williams

Department of Chemistry, Imperial College, Exhibition Road, South Kensington, London SW7 2AZ, UK

Received 27 May 2004; accepted 8 September 2004

Dedicated to Malcolm Green for his inspiring contributions to chemistry

Abstract

A series of five-coordinate complexes of iron(II) containing tridentate nitrogen donor ligands has been synthesised and evaluated for the atom transfer radical polymerisation of styrene. The molecular structures of two derivatives are described. Cyclic voltammetric studies show that the redox potential for the Fe(II)/Fe(III) couple strongly depends on the donor capacity of the complexing ligand, and styrene polymerisations reveal that ligands derived from alkyl amine or pyridine groups are the most active for ATRP, although slower than for their four-coordinate relatives due to unfavourable steric interactions. In general, catalyst activity decreases in the order of donor group: alkyl amine ≈ pyridine > alkyl imine ≫ aryl imine > aryl amine, with the aryl derivatives being almost completely inactive in ATRP. The trend in polymerisation activity correlates with the redox potential of the corresponding complexes. Complexes derived from aryl-imine or -amine ligands afford catalytic chain transfer rather than ATRP catalysis.
© 2004 Elsevier Ltd. All rights reserved.

Keywords: Iron; Radical; Styrene; Catalyst; Polymerisation

1. Introduction

Atom transfer radical polymerisation (ATRP) allows the preparation of a wide range of well-defined polymeric materials with controlled molecular weights and complex architectures [1]. Following key reports by Matyjaszewski and Sawamoto in the mid-1990s, of highly efficient ATRP catalysts based on copper(I) and ruthenium(II) respectively, a number of different metal–ligand combinations have been investigated, including systems based on Rh, Pd, Ni and Fe [2–12]. There remains, however, a need to understand the factors important for efficient ATRP catalysis.

Since the process of ATRP is dependent upon the reversible binding of a halogen atom (Scheme 1), it is important that the metal complex has a relatively open coordination sphere, especially in its reduced form, and that neither the reduced nor the oxidised metal species are prone to decomposition. This may, for example, rule out three-coordinate complexes for many metals unless ligands are chosen that would stabilise the low coordination number. However, such ligands tend to be very bulky and not necessarily pre-disposed towards allowing the metal to accept another ligand.

Recently, we described a new family of four coordinate iron-based catalysts stabilised by α-diimine ligands [13,14]. These four-coordinate iron(II) complexes showed evidence for accessible and reversible redox couples to the corresponding iron(III) species depending on the nature of the imine substituents. The high catalytic

* Corresponding author. Tel.: +20 7594 5830; fax: +20 7594 5810.
E-mail address: v.gibson@imperial.ac.uk (V.C. Gibson).

0277-5387/$ - see front matter © 2004 Elsevier Ltd. All rights reserved.
doi:10.1016/j.poly.2004.09.001

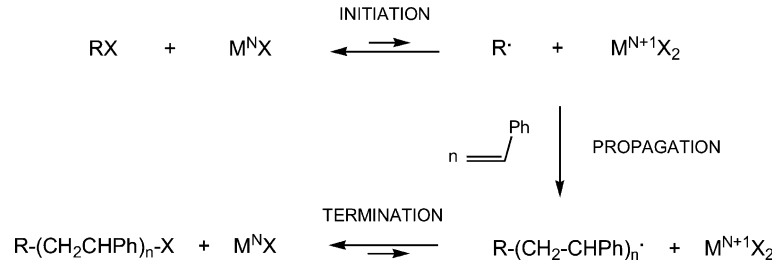

Scheme 1. Generalised mechanism for atom transfer radical polymerisation of styrene.

efficiency of these catalysts may be related to the fact that the reduced Fe(II) species possess a relatively uncluttered tetrahedral geometry and are, therefore, able to accept an additional halogen atom without any severe steric conflict arising between the co-ligands. In the five-coordinate oxidised form, the flexibility in the coordination geometry (via pseudo rotation) may assist the complex in achieving a coordination environment suited to the dissociation of a halogen atom (certain six-coordinate environments, e.g. d^3 and d^6 octahedral systems, have reduced kinetic lability). Thus, the 4–5 coordination manifold might be anticipated to possess important attributes for the efficient functioning of ATRP catalysts.

In order to further probe the effect of coordination geometry on the efficiency of ATRP catalysis, we decided to target a series of five-coordinate Fe(II) chloride complexes bearing tridentate nitrogen ligands and evaluate their performance in ATRP catalysis. These complexes possess an additional nitrogen donor relative to the (α-diimine)$FeCl_2$ catalysts reported recently, and would therefore be expected to afford lower oxidation potentials and render them more electronically suited to ATRP catalysis. However, these catalysts necessarily have to operate by interconverting between five- and six-coordinate species which may lead to increased steric conflict in the oxidised form of the catalyst.

Earlier work by Göbelt and Matyjaszewski examined tridentate bis(imino)pyridine and bis(amino)pyridine ligands bearing *N*-octyl substituents, in conjunction with copper(I) bromide and iron(II) bromide [15]. They found that the bis(imino)pyridine ligand formed an active catalyst in both systems, whereas, the bis(amino)pyridine ligand formed an active catalyst only in conjunction with copper(I) bromide. The use of bromide as the transferable group is recognised to hold advantages in terms of C–halogen bond strengths, though the thermodynamic advantage may be off-set by the increased steric demands of bromine atoms coordinated to the metal centre. In this study we focus on a series of metal–chloride derivatives containing tridentate ligands with a view to obtaining an improved understanding of the factors influencing efficient ATRP catalysis in iron-based systems.

2. Results and discussion

2.1. Synthesis and characterisation

The series of tridentate [NNN] ligands, **I**–**VI**, containing a central pyridine or amine unit and two peripheral imine or amine donors with either *N*-alkyl or *N*-aryl substituents was synthesised (Fig. 1). Ligand **I** (PMDETA) is commercially available, while **II**, **III**, **V** and **VI** were synthesised using literature procedures[16–21]. Ligand **IV** was synthesized by a modification of a literature preparation using $Si(OEt)_4$ and recovered as a yellow solid in 62% yield [22]. Ligands **I**–**VI** were reacted with iron(II) dichloride to afford the corresponding monochelate complexes (**1**–**6**) in good yields.

Complexation of **I** to iron(II) dichloride was first reported in 1966, by Ciampolini and Speroni [23]. At that time, **1** was the first reported high spin five-coordinate iron(II) complex. In 1999, Calderazzo and co-workers [24] structurally characterized **1** and reported a distorted square pyramidal structure with a chlorine atom occupying the apical position. Ligand **II** has previously been

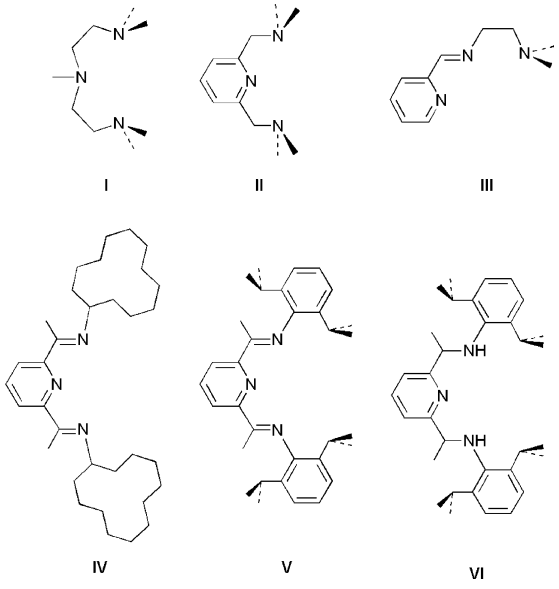

Fig. 1. Ligands **I**–**VI**.

complexed to mid and late transition metals such as ruthenium and zinc by the groups of van Koten and Reinhoudt [18,25]. It was synthesised by reaction of 2,6-bis(bromomethyl)pyridine with dimethylamine and complexed to iron(II) to afford **2**, as a yellow microcrystalline solid. Single crystals of **2** were grown by slowly cooling a saturated solution of **2** in hot tetrahydrofuran. X-ray single crystal analysis revealed the structure (which has molecular C_S symmetry about a plane containing the iron, the two chlorides and the pyridine nitrogen atom) to have a distorted square pyramidal geometry around the iron centre (Fig. 2). The four basal atoms {Cl(1),N(1),N(7),N(8)} are coplanar to within 0.06 Å with the iron lying ca. 0.68 Å out of this plane in the direction of the apical atom Cl(2); the *trans*-basal angles are 136.1(2) and 147.0(2)°, and the apical–basal angles range between 106.2(2) and 111.4(2)°. The Fe–Cl bond lengths are noticeably asymmetric, with that to the apical chloride being significantly shorter [2.291(2) Å] than to its basal counterpart [2.341(2) Å]; the Fe–N distances are unexceptional [21,24,26]. The two five-membered chelate rings both have envelope geometries with in each case the amino nitrogen lying out of the plane of the other four atoms [by ca. 0.57 Å for N(7) and ca. 0.68 Å for N(8)] which are coplanar to within 0.02 Å. The only intermolecular packing interaction of note is a π–π stacking between adjacent pyridyl rings with centroid···centroid and mean interplanar separations of 3.72 and 3.55 Å, respectively. Subsequent to this determination, Grubbs and co-workers [27] reported the room temperature (298 K) structure of the same polymorph of **2** in a private communication; taking into account the 115 K difference in temperature, the unit cells are the same.

Ligand **III** has recently been complexed to late transition metals such as copper and palladium [28,29]. Complex **3** was synthesised by reaction of **III** with iron(II) dichloride in diethyl ether and was isolated as a dark red, microcrystalline solid. This complex was first reported in 1969 and, based on magnetic and spectroscopic techniques, a five-coordinate geometry around the iron centre was proposed [30]. We confirmed this assignment by determining the solid state X-ray structure of crystals of **3** obtained by slow diffusion of an equal volume of heptane into a saturated solution of **3** in dichloromethane. This study revealed **3** to have a structure (Fig. 3) closely related to that of its zinc dibromide analogue [31]. The geometry at iron can be considered as intermediate between square pyramidal, with Cl(2) occupying the apical position, and trigonal bipyramidal with N(1) and N(10) defining the major axis, though being somewhat closer to the latter description. Considered as square pyramidal, the metal centre lies ca. 0.58 Å [0.64 Å] out of the basal plane which is only coplanar to within 0.18 Å [0.30 Å]. Viewed as trigonal bipyramidal, the axial atoms subtend an angle of 147.21(14)° [150.2(2)°] at the metal, and the angles within the equatorial plane range between 108.30(11) and 141.54(11)° [111.8(2) and 133.9(2)°]; the iron lies ca. 0.06 Å [0.04 Å] out of the equatorial plane in the direction of N(10). (The values in square parentheses refer to the zinc dibromide analogue [31].) The five-membered N(1)/N(7) chelate ring is almost planar with the metal lying ca. 0.09 Å [<0.01 Å] out of the plane of the other four atoms which are coplanar to better than 0.01 Å. By contrast, the N(7)/N(10) five-membered chelate ring has a twisted envelope conformation with N(10) displaced by ca. 0.72 Å [0.76 Å] out of the plane of the other atoms, which are coplanar to within 0.08 Å [0.12 Å]. The pattern of bonding around the metal centre is generally the same between the $FeCl_2$ species **3** and its previously reported $ZnBr_2$ analogue, though it is noticeable that, whereas in the $ZnBr_2$ complex the M–N(pyridyl) and M–N(amino) distances are the same [2.245(8) and

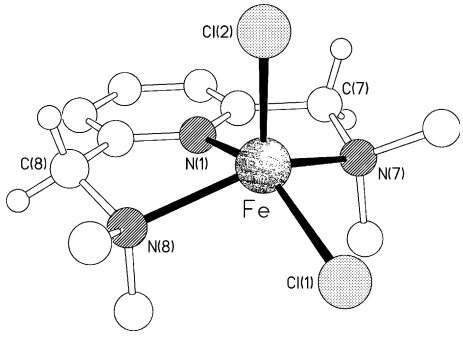

Fig. 2. The molecular structure of **2**. Selected bond lengths (Å) and angles (°); Fe–Cl(1) 2.341(2), Fe–Cl(2) 2.291(2), Fe–N(1) 2.121(6), Fe–N(7) 2.262(6), Fe–N(8) 2.248(6), C(7)–N(7) 1.468(9), C(8)–N(8) 1.474(10), N(1)–Fe–N(8) 74.3(2), N(1)–Fe–N(7) 74.4(2), N(8)–Fe–N(7) 136.1(2), N(1)–Fe–Cl(2) 106.2(2), N(8)–Fe–Cl(2) 106.4(2), N(7)–Fe–Cl(2) 111.4(2), N(1)–Fe–Cl(1) 147.0(2), N(8)–Fe–Cl(1) 95.7(2), N(7)–Fe–Cl(1) 94.1(2), Cl(2)–Fe–Cl(1) 106.84(9).

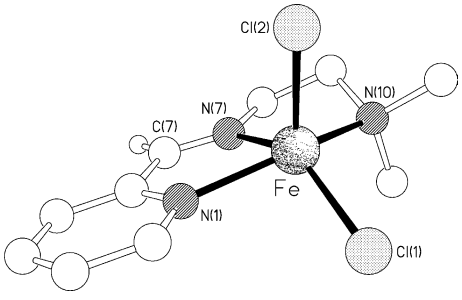

Fig. 3. The molecular structure of **3**. Selected bond lengths (Å) and angles (°); Fe–Cl(1) 2.3034(12), Fe–Cl(2) 2.3361(13), Fe–N(1) 2.185(4), Fe–N(7) 2.129(3), Fe–N(10) 2.236(4), C(7)–N(7) 1.258(6), N(7)–Fe–N(1) 74.04(14), N(7)–Fe–N(10) 75.98(14), N(1)–Fe–N(10) 147.21(14), N(7)–Fe–Cl(1) 141.54(11), N(1)–Fe–Cl(1) 93.79(10), N(10)–Fe–Cl(1) 101.55(10), N(7)–Fe–Cl(2) 108.30(11), N(1)–Fe–Cl(2) 102.39(10), N(10)–Fe–Cl(2) 99.34(11), Cl(1)–Fe–Cl(2) 109.94(5).

2.236(7) Å, respectively], in **3** the M–N(pyridyl) bond length is noticeably shorter [2.185(4) Å] than that to the amino nitrogen [2.236(4) Å]. The Fe–N bond lengths differ noticeably from those in, for example, (2-((2,6-di-*iso*propylphenyl)iminomethyl)-6-(1-(2,6-di-*iso*propylphenylamino)ethyl)pyridine-*N*,*N*′,*N*″)dichloroiron(II) and other related complexes with the bond to the pyridine nitrogen being longer and that to the imino nitrogen shorter [25]. The Fe–Cl bond lengths in **3** are noticeably asymmetric, with that to the pseudo-apical chloride Cl(2) being significantly longer [2.3661(13) Å] than to its pseudo-basal counterpart Cl(1) [2.3034(12) Å]. The only intermolecular packing feature of note is a π–π stacking of the pyridine rings of centrosymmetrically related pairs of molecules; the centroid···centroid and mean interplanar separations are 3.54 and 3.38 Å, respectively. An analogous contact is seen in the zinc dibromide species with centroid–centroid and mean interplanar separations of 3.56 and 3.36 Å, respectively.

Complex **4** was synthesized by a similar route to that reported in the literature for the *N*-aryl derivative, **5** [32]. After washing with diethyl ether and extraction into tetrahydrofuran, **4** was isolated as a dark grey microcrystalline solid. The *N*-aryl pyridine(bis)imino and pyridine(bis)amino complexes, **5** and **6**, have both been reported recently by this group and were synthesized as described in the literature reports [32,33]. Both of these complexes have previously been structurally characterized and found to possess a five-coordinate distorted square pyramidal geometry.

Complexes **1**–**6** are all air-stable paramagnetic solids, with magnetic moments (determined by the Evans' NMR method) in the range 4.9–5.3 μ_B [34–36]. The magnetic moments are consistent with the presence of four unpaired electrons and a quintet ground state ($S = 2$) for the iron(II) centres [37].

2.2. Cyclic voltammetry

Matyjaszewski and co-workers [38] have investigated the structure–activity relationship for a series of tridentate nitrogen donor ligands in copper-based ATRP. The redox properties of these complexes were measured using CV techniques and their electrochemistry was correlated to their activity as ATRP catalysts for styrene and MMA polymerisation [39]. By comparison with Matyjaszewski's findings in copper-based ATRP, it would be predicted that the series of complexes should exhibit the following order of reducing power: **1** < **2** < **3** < **4** ≪ **5** < **6**. Experimentally determined electrochemical parameters for **1**–**6** are collected in Table 1 and confirm this trend. Table 1 also shows the oxidation potentials, E_{ox}, for this series of complexes. Since this parameter can be correlated with the ease of oxidation of the complex, E_{ox} should provide an indication of activities in ATRP catalysis.

Table 1
Cyclic voltammetry results for **1**–**6**

	E_{ox} (mV)	$E_{1/2}$ (mV)	ΔE_p (mV)
1	−370	−280	170
2	−240	−150	170
3	−190	−100	180
4	−150	−70	170
5	180	330	310
6	260	410	320

Complexes **1**–**4** all have low oxidation potentials (−370 to −150 mV) and redox potentials (−280 to −70 mV) indicating that they are easy to oxidise, unlike **5** and **6** whose high oxidation potentials indicate the opposite. Thus, it would be predicted that **1**–**4** should be active ATRP catalysts since they are easily oxidised and possess an accessible and reversible one-electron redox couple. In fact, **1**–**4** have lower redox potentials than the previously reported *N*-alkyl diimine complexes ($E_{1/2}$ ca.−100 mV) and thus would be predicted to be faster ATRP catalysts [13]. However, **5** and **6**, which are supported by ligands possessing *N*-aryl groups have irreversible ($\Delta E_p > 300$ mV) and less accessible ($E_{1/2} > 300$ mV) redox couples and thus would be predicted to have low activity in ATRP.

2.3. Polymerisation results

Complexes **1**–**6** were screened for the ATRP of styrene (200 equiv.) at 120 °C using 1-phenylethyl chloride (1-PECl) as an initiator and the results are presented in Table 2. **1**–**4** polymerised styrene in a controlled manner, with linear kinetics and with molecular weights increasing with monomer conversion [40]. Analysis of the polymer produced using **1**–**4** revealed the presence of a halogen end group by ^{1}H NMR spectroscopy and also by microanalysis [for **2**, M_n = 5100% Cl, found (calc.): 0.64 (0.70)]. The more reducing the complex, the lower the redox potential, and the faster the ATRP catalyst cf. **1** versus **3** (Fig. 4).

However, these complexes are slower ATRP catalysts than their α-diimine counterparts (e.g. for 1,2-bis(cyclo-

Table 2
Results of styrene polymerisations using **1**–**6**

	k_{obs} (h^{-1})	% Conv. in 24 h	$M_{n,calc}$[a]	M_n	M_w/M_n
1	0.04	65	13700	15100	1.62
2	0.03	52	10900	11800	1.53
3	0.02	39	8200	8500	1.59
4	0.02	37	7800	8700	1.56
5		72	15100	2900	2.07
6		45	9500	2100	1.92

Conditions: 120 °C, bulk, $[1\text{-PECl}]_0$:$[\text{catalyst}]_0$:$[\text{styrene}]_0$ = 1:1:200. Control polymerisation of styrene at 120 °C with no catalyst > 90% conversion in 24 h, M_n ca. 200000.

[a] $M_{n,calc}$ is calculated M_n based on degree of conversion.

hexylimino)ethane iron(II) dichloride, $k_{obs} = 0.25\ h^{-1}$, cf. $k_{obs} = 0.04\ h^{-1}$ for **1**), despite their significantly lower redox potentials (for 1,2-bis(cyclohexylimino)ethane iron(II) dichloride, $E_{1/2} = -120$ mV cf. $E_{1/2} = -280$ mV for **1**) [13]. This can be attributed to the less favourable steric environment around the metal in these five-coordinate complexes as compared with the four-coordinate tetrahedral α-diimine complexes. Thus, the rate of Cl atom transfer from RCl to **1**, for example, is slowed due to steric crowding, despite **1** having more favourably disposed redox chemistry. This may also explain the loss of control and broadening of the polydispersity of the polymers produced using these five-coordinate systems compared to their α-diimine relatives.

For **5** and **6**, which both possess *N*-aryl substituents, the polymerisation did not proceed in a controlled manner and low molecular weight polymers were produced throughout, the molecular weight of which were independent of the degree of conversion (Fig. 5). The polymer produced had unsaturated end groups by ^{1}H NMR spectroscopy and zero halide content by microanalysis. Thus, complexes **5** and **6** do not polymerize styrene by an ATRP mechanism, but rather chain propagation is accompanied by catalytic chain transfer (CCT). Here, the polystyrenyl radical reacts with the Fe(II) catalyst to generate an organometallic Fe(III) species which undergoes β-hydrogen elimination to release the polymer chain bearing an unsaturated end-group. This is presumed to occur in an analogous manner to that proposed for the α-diimine catalyst system shown in Scheme 2 [14]. The capacity of the aryl derivatives to support CCT, we believe, is a result of a lower spin ($S = 3/2$) ground state for the oxidised Fe(III) species containing aryl substituents (the alkyl derivatives are all high spin) affording stronger Fe–C bonds and consequently more stable organometallic intermediates.

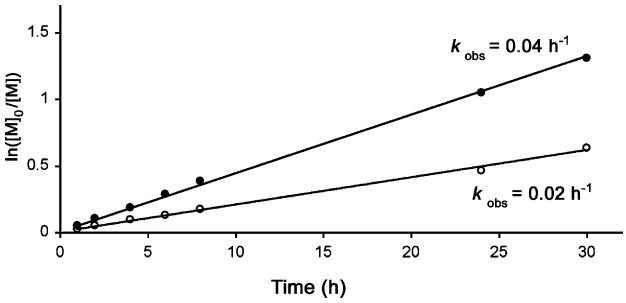

Fig. 4. Plot of $\ln([M]_0/[M])$ vs. time for complexes **1** (•) and **3** (○).

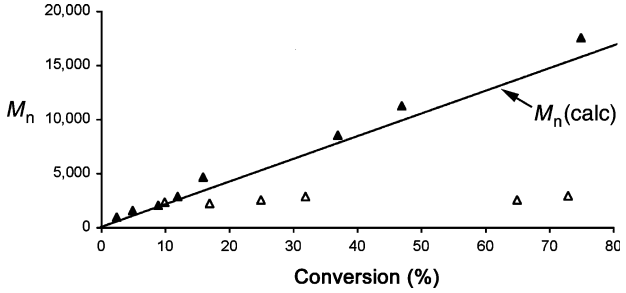

Fig. 5. Plot of M_n vs. conversion for **4** (▲) and **5** (Δ).

3. Conclusions

Iron(II) dichloride complexes containing neutral tridentate [NNN] ligands are found to be active ATRP catalysts, and their activities correlate well with their oxidation potentials. Although their electrochemical properties suggest that they should be more efficient catalysts than four-coordinate α-diimine iron systems, they are in fact much slower. This is explained by the increased steric hindrance at the metal for the oxidised six-coordinate species, which prevents fast and facile atom transfer from occurring. Thus the hypothesis made

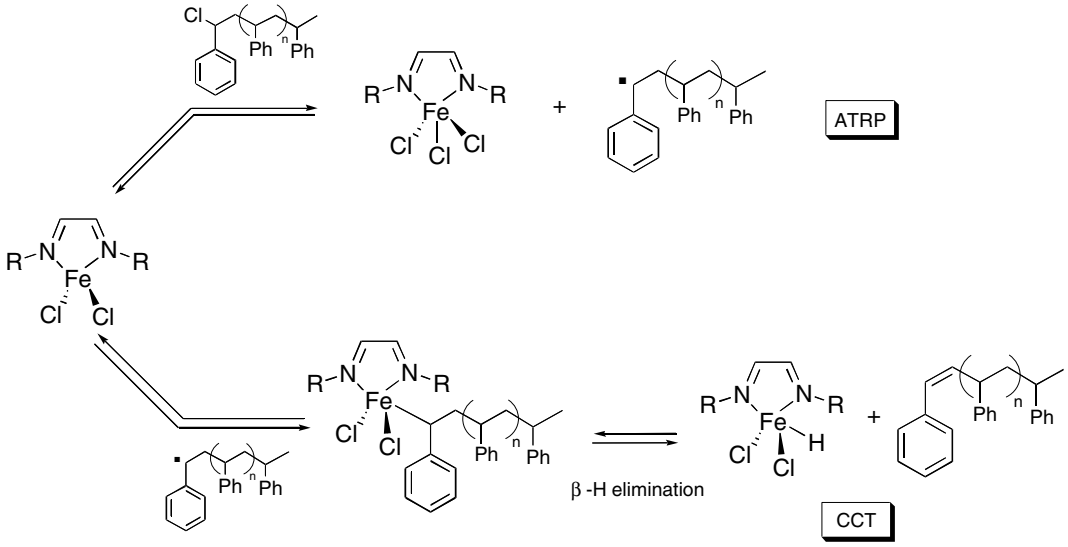

Scheme 2. ATRP vs. CCT pathways for α-diimine iron catalysts.

at the outset of this study, that a four/five-coordinate equilibrium should be more favourable than a five/six-coordinate equilibrium for efficient ATRP catalysis in iron complexes appears to hold.

4. Experimental

4.1. General

All manipulations of water and/or moisture sensitive compounds were performed by means of standard high vacuum Schlenk and cannula techniques. Air sensitive compounds were transferred to a nitrogen filled glovebox and, unless stated otherwise, stored at room temperature. Crystal data were collected on Siemens P4/PC or P4/RA diffractometers. NMR spectra were recorded on a Bruker AC-250 MHz, DRX-400 MHz or AM-500 MHz spectrometers. Infra-red spectra were obtained with thin sample films on NaCl plates or as KBr discs on a Perkin–Elmer 1710X FT-IR spectrometer. Mass spectra were recorded on either a VG Autospec or a VG Platform II spectrometer. Elemental analyses were performed by the microanalytical services of the Chemistry departments of London Metropolitan University and University College London. Magnetic susceptibilities were determined by the Evans NMR method. Gel permeation chromatography (GPC) was performed using Viscotek Trisec software connected to a Knauer differential refractometer. Samples were injected onto two linear 10 μm columns using chloroform as elutant (conventionally calibrated prior to use, using polystyrene standards (PSS Mainz)) at a flow rate of 1.0 $cm^3 min^{-1}$ at room temperature. Cyclic voltammetry (CV) was performed using a MacLab potentiostat operated by EChem 1.3.2. software. The working electrode and reference electrode were purchased from Bioanalytical (ref: MF-2013 and RE-5B).

All solvents were dried by prolonged reflux over a suitable drying agent under an atmosphere of nitrogen, being freshly distilled prior to use. All solvents were degassed prior to use unless otherwise stated. Styrene (St) was purified by vacuum distillation and then stored under an inert atmosphere over 4 Å molecular sieves at −15 °C. 1-PECl was synthesized according to literature methods and purified by column chromatography [41]. All amines and anilines were freshly distilled before use. All other reagents are commercially available and were used without further purification. Compounds **1**[23] **5**[21] and **6**[33] were prepared by literature procedures.

All polymerisations were set up and performed under an atmosphere of oxygen-free, dry dinitrogen using standard Schlenk-line techniques. In an ampoule equipped with a magnetic stirrer bar, were placed in order, monomer, initiator and catalyst in various ratios and the ampoule was then sealed. In all cases the catalyst was soluble in the monomer solution. The ampoules were heated in an oil bath, at 120 °C. After stirring for the allotted period of time, an aliquot (0.1 ml) was removed and quenched with THF (1 ml). Conversion was determined by integration of the monomer versus polymer backbone resonances in the ^1H NMR spectrum of the crude product in $CDCl_3$. After the reaction time, usually 24 h, the contents of the ampoules were dissolved in THF. This solution was added dropwise to an approximately 20-fold excess of rapidly stirred acidified methanol (1% HCl v/v). The precipitate that formed was filtered off and washed with methanol. The precipitate was dried for 24 h in a vacuum oven at 60 °C. Samples were then analysed by GPC.

CV was performed using a sample vial (50 × 24 mm) as a cell. The counter electrode was a section of 0.5 mm platinum wire, the working electrode was a platinum disk electrode and the reference electrode was a Ag/AgCl electrode. Electrolyte ($[^nBu_4N][PF_6]$ (1.00 mmol)) and the complex under study (0.01 mmol) was loaded into the cells before being degassed by evacuation and admission of dinitrogen, acetonitrile (10 cm^3) was then added.

4.2. Preparation of 2,6-bis-[(dimethylamino)methyl]-pyridine) (*II*)

Dimethylamine (6.0 g, 0.133 mol) was quickly added to 30 ml of precooled (ca. 5 °C) C_6H_6 after which a solution of 2,6-bis(bromomethyl)pyridine (3.51 g, 0.013 mol) in 80 ml of C_6H_6 was added dropwise over 30 minutes [12,13]. After stirring at room temperature for 30 min, the reaction mixture was filtered under suction and the residue was washed with Et_2O. The C_6H_6 and Et_2O fractions were combined and reduced in vacuo to yield a pale yellow oil. This oil was vacuum distilled at 60 °C and 8 mm/Hg to afford a colourless oil (2.45 g, 95%). *Anal.* Calc. for $C_{11}H_{19}N_3$: C, 68.4; H, 9.9; N, 21.7. Found: C, 67.7; H, 9.5; N, 21.7%. δ_H ($CDCl_3$) 7.50 (1H, t, *J*(HH) 8 Hz, 1Ar–*H*), 7.15 (2H, d, *J*(HH) 8 Hz, 2Ar–*H*), 3.46 (4H, m, 2CH_2), 2.15 (12H, s, 4CH_3); δ_C (CD_3COCD_3) 159.6 (s, 2Ar–*C*), 137.3 (s, 1Ar–*C*), 121.5 (s, 2Ar–*C*), 66.5 (s, 2*C*H_2), 45.9 (s, 4*C*H_3); MS (CI^+) (*m*/*z*) 194 $[M+H]^+$.

4.3. Preparation of 2,6-bis-(cyclododecylimino)pyridine (*IV*)

A solution of 2,6-diacetylpyridine (5.0 g, 0.03 mol) and cyclododecylamine (13.8 g, 0.075 mol) in $Si(OEt)_4$ (14.05 g, 0.067 mol) with a few drops of concentrated H_2SO_4 was placed in a round bottom flask and attached to a side arm and air condenser which was stoppered with a round bottom flask [18]. The solution was heated overnight with stirring at 130 °C, after which time etha-

nol (ca. 3 ml) had been distilled over from the reaction mixture. The solid reaction mixture was dissolved in CH_2Cl_2, washed with saturated solutions of $NaHCO_3$ (2×10 ml) and brine (2×10 ml) and then dried over $MgSO_4$. The solvent was removed in vacuo to afford a yellow solid. Washing this solid with cold petroleum ether (20 ml) afforded ligand **IV** as a bright yellow solid (9.17 g, 62%). *Anal.* Calc. for $C_{35}H_{55}N_3$: C, 80.3; H, 11.2; N, 8.5. Found: C, 79.6; H, 11.1; N, 8.7%. IR/cm^{-1} (C=N) 1650s; δ_H ($CDCl_3$) 8.03 (2H, d, *J*(HH) 8 Hz, 2Ar-*H*), 7.66 (1H, t, *J*(HH) 8 Hz, Ar–*H*), 3.82 (2H, m, 2C*H*), 2.41 (6H, s, 2CH_3), 1.58–1.25 (44H, br m, 22CH_2); δ_C ($CDCl_3$) 163.9 (s, 2Ar–*C*), 156.7 (s, 2Ar–*C*), 136.4 (s, Ar–*C*), 121.1 (s, 2Ar–*C*), 57.04 (s, 2*C*H), 40.35 (s, 2*C*H_3), 24.7–21.3 (s, 22*C*H_2); MS (CI^+) (*m*/*z*) 494 $[M+H]^+$.

4.4. Preparation of 2,6-bis-[(dimethylamino)methyl]-pyridine) iron(II) chloride (2)

To a solution of $FeCl_2(THF)_{1.5}$ (0.58 g, 0.0025 mol) in toluene (20 ml) was added dropwise, with stirring, ligand **II** (0.48 g, 0.0025 mol) also in toluene (20 ml) and the resulting suspension stirred overnight at room temperature. The mixture was then cooled to 0 °C and filtered; the filtrate was reduced to ca. 10 ml and stored overnight at −10 °C, after which time crystals of **2** had formed. These yellow crystals were isolated by filtration and dried overnight in vacuo. This afforded **2** as a microcrystalline bright yellow solid (0.67 g, 84%). Slow cooling of a solution of **2** in hot THF afforded crystals suitable for X-ray analysis. *Anal.* Calc. for $C_{11}H_{19}N_3Cl_2Fe$: C, 41.2; H, 6.0; N, 13.1. Found: C, 41.2; H, 6.0; N, 13.0%. IR/cm^{-1} 3584m, 3397s, 2349w, 2282w, 1653m, 1559w, 1541w, 1507w, 1457w, 1073w, 666w; MS (CI^+) (*m*/*z*) 319 $[M]^+$; μ_{eff} = 5.05 μ_B.

4.5. Preparation of N,N-dimethyl-N′-pyridin-2-ylmethylene-ethane-1,2-diamino iron(II) chloride (3)

To a suspension of $FeCl_2$ (1.27 g, 0.01 mol) in Et_2O (20 ml) was added dropwise, with stirring *N*,*N*-dimethyl-*N*′-pyridin-2-ylmethylene-ethane-1,2-diamine, **III** (1.77 g, 0.01 mol) in Et_2O (10 ml) [24]. The reaction mixture was stirred overnight at room temperature and then filtered and the filtrate reduced under reduced pressure. The solid residue was extracted into CH_2Cl_2 and then the solvent was removed. The resultant solid was dried in vacuo and this afforded **3** as a purple microcrystalline solid (2.01 g, 66%). Slow diffusion of a solution of **3** in $CH_2Cl_2$with an equal volume of heptane afforded crystals suitable for X-ray analysis. *Anal.* Calc. for $C_{10}H_{15}N_3Cl_2Fe$: C, 39.5; H, 5.0; N, 13.8. Found: C, 39.1; H, 5.0; N, 13.2%. IR/cm^{-1} 3447m, 2966m, 2838w, 1615w, 1568m, 1507w, 1457w, 1279w, 1174w, 1117w, 1026w, 923w, 750w; MS (CI^+) (*m*/*z*) 318 $[M+NH_4]^+$; μ_{eff} = 4.96 μ_B.

4.6. Preparation of 2,6-bis-(cyclododecylimino)pyridine iron(II) chloride (4)

To a suspension of $FeCl_2$ (0.92 g, 0.007 mol) in ^{n}BuOH (20 ml) was added dropwise, with stirring, **IV** (4 g, 0.008 mol) also in ^{n}BuOH (10 ml) and the reaction mixture stirred overnight at 90 °C. After this time it was allowed to cool and the solvent was then removed in vacuo at 60 °C for 4 h. The residue was washed with Et_2O (3×10 ml) and then extracted into THF (20 ml). The solution was reduced to ca. 10 ml and stored at −10 °C overnight. After this time, dark grey crystals of **4** had formed which were isolated by filtration and dried (3.30 g, 73%). *Anal.* Calc. for $C_{33}H_{55}N_3Cl_2Fe$: C, 63.9; H, 8.9; N, 6.8; Cl, 11.4. Found: C, 63.7; H, 8.7; N, 6.8; Cl, 10.3%. IR/cm^{-1} 2938s, 2864s, 2362w, 1703m, 1585w, 1470m, 1446m, 1359w, 1292w, 1268w, 1205w, 1163w, 1075w, 1020w, 994w, 813w, 740w; MS (FAB^+) (*m*/*z*) 584 $[M-Cl]^+$; μ_{eff} = 5.11 μ_B.

4.7. X-ray crystallography

Crystal data for **2**: $C_{11}H_{19}N_3Cl_2Fe$, M = 320.04, tetragonal, $P4_32_12$ (no. 96), a = 10.5887(5), c = 26.080(3) Å, V = 2924.1(4) Å^3, Z = 8, D_c = 1.454 gcm^{-3}, μ(Cu Kα) = 11.491 mm^{-1}, T = 183 K, yellow platy prisms; 2142 independent measured reflections, F^2 refinement, R_1 = 0.054, wR_2 = 0.122, 1720 independent observed absorption-corrected reflections [$|F_o| > 4\sigma(|F_o|)$, $2\theta_{max}$ = 120°], 155 parameters. The absolute structure of **1** was determined by a combination of *R*-factor tests [$R_1^+ = 0.0541$, $R_1^- = 0.1025$] and by use of the Flack parameter [$x^+ = -0.013(14)$]. CCDC 239659.

Crystal data for **3**: $C_{10}H_{15}N_3Cl_2Fe\cdot0.5CH_2Cl_2$, M = 346.46, monoclinic, I 2/*a* (no. 15), a = 14.870(3), b = 10.2360(8), c = 20.545(4) Å, β = 104.216(11)°, V = 3031.4(9) Å^3, Z = 8, D_c = 1.518 gcm^{-3}, μ(Mo Kα) = 1.508 mm^{-1}, T = 293 K, very dark red/brown needles; 2666 independent measured reflections, F^2 refinement, R_1 = 0.046, wR_2 = 0.103, 2011 independent observed absorption-corrected reflections [$|F_o| > 4\sigma(|F_o|)$, $2\theta_{max}$ = 50°], 173 parameters. CCDC 239660.

5. Supplementary material

Full crystallographic details have been deposited in CIF format with the Cambridge Crystallographic Data Centre. Copies of this information may be obtained free of charge from The Director, CCDC, 12 Union Road, Cambridge, CB2 1EZ, UK (fax: +44 1223 336033; e-mail: deposit@ccdc.cam.ac.uk or www: http//www.ccdc.cam.ac.uk).

Acknowledgements

BP Chemicals is thanked for financial support (R.K. O'R). Dr. Jane Boyle is thanked for NMR measurements.

References

[1] (a) For recent reviews see K. Matyjaszewski, J. Xia, Chem. Rev. 101 (2001) 2921;
(b) M. Kamigaito, T. Ando, M. Sawamoto, Chem. Rev. 101 (2001) 3689.
[2] J.S. Wang, K. Matyjaszewski, J. Am. Chem. Soc. 117 (1995) 5614.
[3] M. Kato, M. Kamigaito, M. Sawamoto, T. Higashimura, Macromolecules 28 (1995) 1721.
[4] P. Lêcomte, I. Drapier, P. Dubois, P. Teyssié, R. Jérôme, Macromolecules 30 (1997) 7631.
[5] G. Moineau, C. Granel, P. Dubois, P. Teyssié, R. Jérôme, Macromolecules 31 (1998) 542.
[6] C. Granel, P. Dubois, R. Jêromé, P. Teyssié, Macromolecules 29 (1996) 8576.
[7] T. Ando, M. Kamigaito, M. Sawamoto, Macromolecules 30 (1997) 4507.
[8] K. Matyjaszewski, M. Wei, J. Xia, N.E. McDermott, Macromolecules 30 (1997) 8161.
[9] K. Matyjaszewski, S. Coca, S.G. Gaynor, M. Wei, B.E. Woodworth, Macromolecules 30 (1997) 7348.
[10] M. Teodorescu, S.G. Gaynor, K. Matyjaszewski, Macromolecules 33 (2000) 2335.
[11] T. Sarbu, K. Matyjaszewski, Macromol. Chem. Phys. 202 (2001) 3379.
[12] V.C. Gibson, R.K. O'Reilly, D.F. Wass, A.J.P. White, D.J. Williams, J. Chem. Soc., Dalton Trans. (2003) 2824.
[13] V.C. Gibson, R.K. O'Reilly, D.F. Wass, W. Reed, A.J.P. White, D.J. Williams, Chem. Commun. (2002) 1850.
[14] V.C. Gibson, R.K. O'Reilly, D.F. Wass, A.J.P. White, D.J. Williams, Macromolecules 36 (2003) 2591.
[15] B. Göbelt, K. Matyjaszewski, Macromol. Chem. Phys. 201 (2000) 1619.
[16] M. Newcomb, J.M. Timko, D.M. Walba, D.J. Cram, J. Am. Chem. Soc. 99 (1977) 6392.
[17] B.A. Markies, P. Wijkens, J. Boersma, H. Kooijman, N. Veldman, A.L. Spek, G. van Koten, Organometallics 13 (1994) 3244.
[18] P. Molenveld, W.M.G. Stikvoort, H. Koojiman, A.L. Spek, J.F.J. Engbersen, D.N. Reinhoudt, J. Org. Chem. 64 (1999) 3896.
[19] G. Zahrzewski, G.P. Speroni, Inorg. Chem. 7 (1968) 1034.
[20] F. Guérin, D.H. Mc Conville, J.J. Vittal, Organometallics 15 (1996) 5586.
[21] G.J.P. Britovsek, M. Bruce, V.C. Gibson, B.S. Kimberley, P.J. Maddox, S. Mastroianni, S.J. McTavish, C. Redshaw, G.A. Solan, S. Strömberg, A.J.P. White, D.J. Williams, J. Am. Chem. Soc. 121 (1999) 8728.
[22] B.E. Love, J. Ren, J. Org. Chem. 58 (1993) 5556.
[23] M. Ciampolini, G.P. Speroni, Inorg. Chem. 5 (1966) 45.
[24] F. Calderazzo, U. Englert, G. Pampaloni, E. Vanni, C.R. Acad. Sci. Paris (1999) 311.
[25] I. Del Rio, R.A. Gossage, M.S. Hannu, M. Lutz, A.L. Spek, G. van Koten, Organometallics 18 (1999) 1097.
[26] B.L. Small, M. Brookhart, A.M.A. Bennett, J. Am. Chem. Soc. 120 (1998) 4049.
[27] M.W. Day, B.D. Ward, R.H. Grubbs, Private Communication, CCDC OCUJOL (2001).
[28] M. Costa, P. Pelagatti, C. Pelizzi, D. Rogolino, J. Mol. Catal. A 178 (2002) 21.
[29] P.S. Mukherjee, T.K. Maji, A. Escuer, R. Vicente, J. Ribas, G. Rosair, F.A. Mautner, N.R. Chaudhuri, Eur. J. Inorg. Chem. (2002) 943.
[30] P. Bamfield, R. Price, R.G.J. Millar, J. Chem. Soc. A 9 (1969) 1447.
[31] G. Zakrzewski, E.C. Lingafelter, Inorg. Chim. Acta 4 (1970) 251.
[32] G.J.P. Britovsek, V.C. Gibson, B.S. Kimberley, P.J. Maddox, S.J. McTavish, G.A. Solan, A.J.P. White, D.J. Williams, Chem. Commun. (1998) 849.
[33] G.J.P. Britovsek, V.C. Gibson, S. Mastroianni, D.C.H. Oakes, C. Redshaw, G.A. Solan, A.J.P. White, D.J. Williams, Eur. J. Inorg. Chem. (2001) 431.
[34] D.F. Evans, J. Chem. Soc. (1959) 2003.
[35] D.F. Evans, G.V. Fazakerley, R.F.J. Phillips, J. Chem. Soc. A (1971) 1931.
[36] D.H. Grant, J. Chem. Ed. 72 (1995) 39.
[37] B.N. Figgis, J. Lewis, in: J. Lewis, R.G. Wilkins (Eds.), Modern Coordination Chemistry, Interscience, New York, 1960, p. 400.
[38] K. Matyjaszewski, B. Göbelt, H.-J. Paik, C.P. Horwitz, Macromolecules 34 (2001) 430.
[39] J. Qui, K. Matyjaszewski, L. Thouin, C. Amatore, Macromol. Chem. Phys. 201 (2000) 1625.
[40] A. Goto, T. Fukuda, Prog. Polym. Sci. 29 (2004) 329.
[41] D. Landini, F. Rolla, J. Org. Chem. 45 (1980) 3527.

Available online at www.sciencedirect.com
SCIENCE DIRECT®
Polyhedron 23 (2004) 2929–2936
POLYHEDRON
www.elsevier.com/locate/poly

Synthesis and structural studies of bis-amino-functionalised ferrocene salts and ferrocenium salts

Kenneth D. Camm, Stephen J. Furtado, Andrew L. Gott, Patrick C. McGowan *

School of Chemistry, University of Leeds, Woodhouse Lane, Leeds LS6 3BZ, UK

Received 16 June 2004; accepted 9 July 2004
Available online 26 October 2004

Dedicated to Professor Malcolm L.H. Green – an inspiration to many and a great scientist to all.

Abstract

A number of bis-amino-functionalised ferrocene salts and ferrocenium salts have been synthesised and characterised. There are interesting structural features in the solid state, including N–H···O and N–H···F hydrogen bonds.
© 2004 Elsevier Ltd. All rights reserved.

1. Introduction

There has been interest in the synthesis and properties of ionic ferrocene compounds for their use in asymmetric catalysis [1], sequestering metal ions [2] and molecular recognition [3]. Ferrocenium compounds have been shown to act as mild 1-electron oxidising agents [4] as well as chelating ligands with a redox active centre [5,6]. With respect to biological systems a range of ferrocenium compounds have been reported for their cytotoxic activity, which is thought to be based on their ability to generate oxygen active species [7]. Previous examples of amino–functionalised ferrocenium compounds have also been reported [5,6,8,9]. Primary ferrocenes, such as 1,1-bis(amino)ferrocene [10], have received attention recently from a number of research groups due to their potential as ligands in polymerisation catalysis [5,11–14]. One of the reasons for this renewed activity in the area is due to improvements in the synthesis of 1,1-bis(amino)ferrocenes [5].

We have been interested in the synthesis and bonding of amino-functionalised ferrocene systems [8,15–17]. In this paper, we report the synthesis of primary amino-functionalised ferrocene salts and ferrocenium salts with an alkyl spacer between the cyclopentadienyl (cp) moiety and primary amine. This paper also reports a series of tertiary amino-functionalised ferrocene and ferrocenium salts. We have been also interested also in functionalised cp systems to stabilise metal centres and as a way of making organometallic/coordination compounds water soluble [8,16,18–21].

2. Results and discussion

$NaC_5H_4(CH_2)_2NMe_2$ (**1**) was used in the preparation of the orange oil $Fe\{\eta\text{-}C_5H_4(CH_2)_2NH_2\}_2$ (**2**). Compound **2** was characterised by ^1H and $^{13}C\{^1H\}$ NMR spectroscopy and mass spectrometry.

The compounds $[Fe\{\eta\text{-}C_5H_4(CH_2)_2NH_3\}_2]^{2+}2[CF_3COO]^-$ (**3**) and $[Fe\{\eta\text{-}C_5H_4(CH_2)_3NH_3\}_2]^{2+}2[CF_3COO]^-$ (**4**) were prepared by addition of CF_3COOH to ether solutions of **2** and $Fe\{\eta\text{-}C_5H_4(CH_2)_3NH_2\}_2$ to yield light orange powders (as shown in Scheme 1). The compounds $[Fe\{\eta\text{-}C_5H_4(CH_2)_2NHMe_2\}_2]^{2+}2[CF_3COO]^-$ (**5**) and

* Corresponding author. Tel.: +44 113 343 6404; fax: +44 113 343 6465.
E-mail address: p.c.mcgowan@chem.leeds.ac.uk (P.C. McGowan).

0277-5387/$ - see front matter © 2004 Elsevier Ltd. All rights reserved.
doi:10.1016/j.poly.2004.07.020

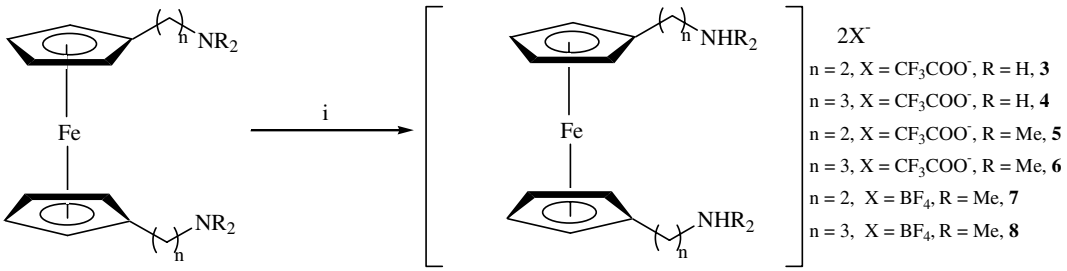

Scheme 1. i = HBF_4 or CF_3COOH in diethyl ether.

$[Fe\{\eta\text{-}C_5H_4(CH_2)_3NHMe_2\}_2]^{2+}2[CF_3COO]^-$ (**6**) were prepared by addition of the corresponding sodium salts $NaC_5H_4(CH_2)_2NMe_2$ and $NaC_5H_4(CH_2)_3NMe_2$ to $FeCl_2$ followed by addition of CF_3COOH (Scheme 1). Compounds **3–6** were characterised by ^1H and ^{13}C NMR spectroscopy, mass spectrometry and elemental analyses and additionally in the case of **6**, by X-ray crystallography. The ^1H and $^{13}C\{^1H\}$ NMR spectra of compounds **3–6** show similarities to those of other bis-functionalised analogues [16].

The compounds $[Fe\{\eta\text{-}C_5H_4(CH_2)_2NHMe_2\}_2]^+2[BF_4]^-$ (**7**) and $[Fe\{\eta\text{-}C_5H_4(CH_2)_3NHMe_2\}_2]^+2[BF_4]^-$ (**8**) were synthesised by addition of two equivalents of the corresponding sodium salts $NaC_5H_4(CH_2)_2NMe_2$ and $NaC_5H_4(CH_2)_3NMe_2$ to $FeCl_2$ followed by addition of $HBF_4 \cdot OEt_2$. The yellow solids were isolated by filtration and washed with petroleum ether (b.p. 40–60 °C). Compounds **7–8** were characterised by ^1H and ^{13}C NMR spectroscopy, mass spectrometry and elemental analyses.

Excess $HBF_4 \cdot OEt_2$ was added to solutions of compounds **2** and $Fe\{\eta\text{-}C_5H_4(CH_2)_3NH_2\}_2$ in diethyl ether in the presence of *p*-benzoquinone, resulting in the formation of $[Fe\{\eta\text{-}C_5H_4(CH_2)_2NH_3\}_2]^{3+}3[BF_4]^-$ (**9**) and $[Fe\{\eta\text{-}C_5H_4(CH_2)_3NH_3\}_2]^{3+}3[BF_4]^-$ (**10**) (as shown in Scheme 2). This procedure was carried out following a method similar to Connelly and Geiger [4]. Repeated attempts at acquiring micro-analytical data for compounds **9** and **10** proved to be unsuccessful. The compounds $[Fe\{\eta\text{-}C_5H_4(CH_2)_2NHMe_2\}_2]^{3+}3[BF_4]^-$ (**11**) and $[Fe\{\eta\text{-}C_5H_4(CH_2)_3NHMe_2\}_2]^{3+}3[BF_4]^-$ (**12**) were synthesised by addition of the corresponding sodium salts $NaC_5H_4(CH_2)_2NMe_2$ and $NaC_5H_4(CH_2)_3NMe_2$ to $FeCl_2$ in the presence of a solution of *p*-benzoquinone and $HBF_4 \cdot OEt_2$ (as shown in Scheme 2). Compounds **11–12** were obtained as blue solids and characterisation of these paramagnetic compounds was achieved using mass spectrometry, elemental analyses and X-ray crystallography.

The bis-functionalised ferrocene compound $[Fe\{C_5H_3\text{-}1\text{-}SiMe_3\text{-}3\text{-}CH(CH_2)_4\ NHMe\}_2]$ has been previously reported [8]. The compound $[Fe\{(C_5H_3\text{-}1\text{-}SiMe_3\text{-}3\text{-}CH(CH_2)_4NHMe\}_2]^{2+}\ 2[CF_3CO_2]^-$ (**13**) was synthesised by addition of $LiC_5H_3\text{-}1\text{-}SiMe_3\text{-}3\text{-}CH(CH_2)_4NMe$ to $FeCl_2$ in THF followed by removal in vacuo and extraction of the product in petroleum ether (b.p. 40–60 °C). Addition of CF_3COOH afforded a yellow precipitate which was washed in petroleum ether (b.p. 40–60 °C), and subsequently isolated. Compound **13** was characterised by ^1H and ^{13}C NMR spectroscopy, mass spectrometry and elemental analyses.

3. Crystallographic data collection and structure analysis

3.1. X-ray crystallography

Data for compounds **6**, **11** and **12** were collected on a Nonius Kappa CCD area-detector diffractometer using graphite monochromated Mo Kα radiation ($\lambda = 0.71073$ Å) using 1.0° ϕ-rotation frames. Pertinent crystallographic details are given in Table 1. The structures of all three compounds were solved by direct methods using SHELXS-86. Refinement by full-matrix least-squares on F^2 using SHELXL-97 was similar for

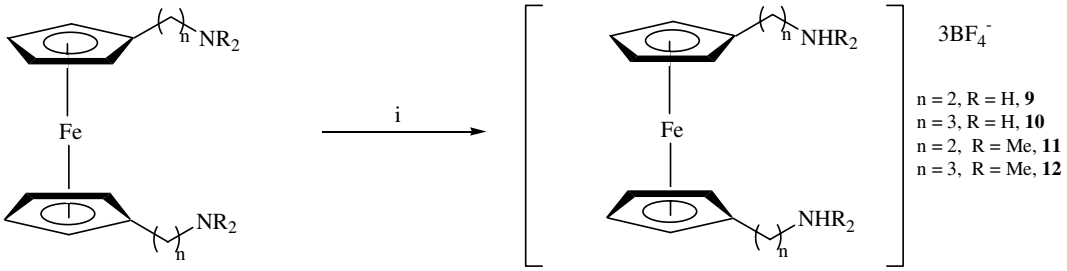

Scheme 2. i = HBF_4 and benzoquinone in diethyl ether.

Table 1
Crystallographic data for compounds **6**, **11** and **12**

	6	**11**	**12**
Formula	$C_{24}H_{34}F_6FeN_2O_4$	$C_{20}H_{34}B_3F_{12}FeN_2$	$C_{18}H_{30}B_3F_{12}FeN_2$
Molecular weight	584.38	618.77	590.72
Crystal system	orthorhombic	triclinic	monoclinic
Space group	$Pca2_1$	$P\bar{1}$	$C2/c$
a (Å)	30.3403(7)	7.7863(2)	14.5482(6)
b (Å)	5.8475(1)	13.8444(3)	7.3020(3)
c (Å)	14.8365(3)	14.3897(4)	22.7391(11)
α (°)	90	65.4302(16)	90
β (°)	90	75.3380(11)	92.4029(19)
γ (°)	90	73.7036(13)	90
V (Å^3)	2632.05(9)	1337.33(6)	2413.43(18)
Temperature (K)	150(2)	150(2)	150(2)
Z	4	2	4
D_{calc} (Mg m^{-3})	1.475	1.537	1.626
μ(Mo Kα) (mm^{-1})	0.648	0.661	0.728
Reflections collected	10455	21748	8319
Independent reflections	5510	5197	2734
R_{int}	0.0803	0.0848	0.0665
$R_1(I > 2\sigma)$	0.0550	0.0669	0.0558
$wR_2(I > 2\sigma)$	0.1304	0.1797	0.1390

all three compounds. Hydrogen atoms were constrained to idealised positions using a riding model (with free rotation for methyl groups).

The molecular structure of $[Fe\{\eta\text{-}C_5H_4(CH_2)_3NHMe_2\}_2]^{2+}2[CF_3CO_2]^-$ (**6**) is shown in Fig. 1 (Table 2 for selected bond lengths and angles) and the cyclopentadienyl rings are eclipsed with the *N*,*N*-dimethylaminopropyl side chains lying *trans* to each other (ca. 180°). There are two trifluoroacetate ions in the asymmetric unit and the fluorine atoms of one of the counter ions are disordered over two sites with a partial occupancy of 0.5. There are two hydrogen bond interactions between the N–H groups and the oxygen atoms of the adjacent trifluoroacetic acid counter ions, for which the bond lengths and angles are shown in Table 3; these have typical values for N–H···O hydrogen bonds.

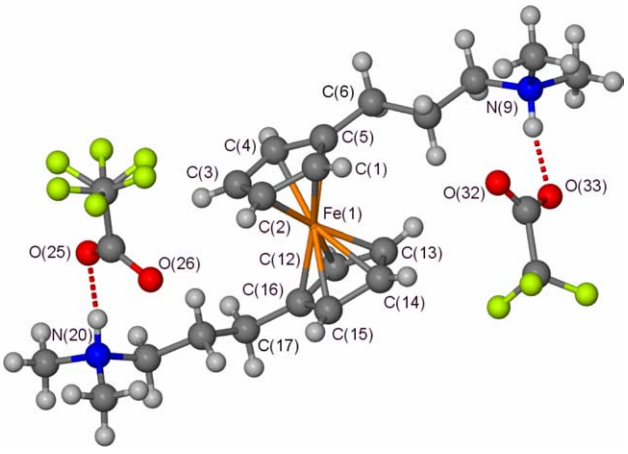

Fig. 1. The molecular structure of compound **6**, showing the hydrogen bonding interactions.

Table 2
Selected interatomic distances (Å) angles between interatomic vectors (°) with estimated standard deviations in parenthesis [M(1) and M(2) denote the centroid of the C_5 rings C(1)–C(5) and C(12)–C(16), respectively] for $[Fe\{\eta\text{-}C_5H_4(CH_2)_3NHMe_2\}_2]^{2+}[2CF_3CO_2]^-$ (**6**)

Interatomic distances			
Fe(1)–C(1)	2.038(5)	C(1)–C(2)	1.447(6)
Fe(1)–C(2)	2.053(5)	C(2)–C(3)	1.437(7)
Fe(1)–C(3)	2.055(5)	C(3)–C(4)	1.406(7)
Fe(1)–C(4)	2.052(5)	C(4)–C(5)	1.450(7)
Fe(1)–C(5)	2.068(5)	C(5)–C(1)	1.412(7)
Fe(1)–C(12)	2.046(5)	C(12)–C(13)	1.426(7)
Fe(1)–C(13)	2.034(5)	C(13)–C(14)	1.438(8)
Fe(1)–C(14)	2.038(5)	C(14)–C(15)	1.430(7)
Fe(1)–C(15)	2.045(5)	C(15)–C(16)	1.425(7)
Fe(1)–C(16)	2.053(5)	C(16)–C(12)	1.429(7)
Average Fe–C	2.048	Fe(1)–M(1)	1.642
Average C–C	1.43	Fe(1)–M(2)	1.654
Interatomic angles			
C(1)–C(2)–C(3)	106.3(4)	C(12)–C(13)–C(14)	107.1(4)
C(2)–C(3)–C(4)	108.8(4)	C(13)–C(14)–C(15)	107.9(4)
C(3)–C(4)–C(5)	108.7(4)	C(14)–C(15)–C(16)	108.5(4)
C(4)–C(5)–C(1)	106.7(4)	C(15)–C(16)–C(12)	107.3(4)
C(5)–C(1)–C(2)	109.4(4)	C(13)–C(12)–C(16)	109.1(4)
Average C–C–C	108		
C(6)–C(5)–M(1)	177.8	C(17)–C(16)–M(2)	177.1

Table 3
Hydrogen bond distances (Å) and angles (°) for compound **6**

D–H	d(D–H)	d(H···A)	–DHA	d(D···A)	A
E					
N(9)–H(9)	0.9300	1.7528	169.62	2.6728	O(33)
N(20)–H(20)	0.9299	1.7540	172.98	2.6793	O(25)

The molecular structure of $[Fe\{\eta\text{-}C_5H_4(CH_2)_2NHMe_2\}_2]^{3+}3[BF_4]^-$ (**11**) shown in Fig. 2 (with bond lengths and angles in Table 4) shows the cyclopentadienyl

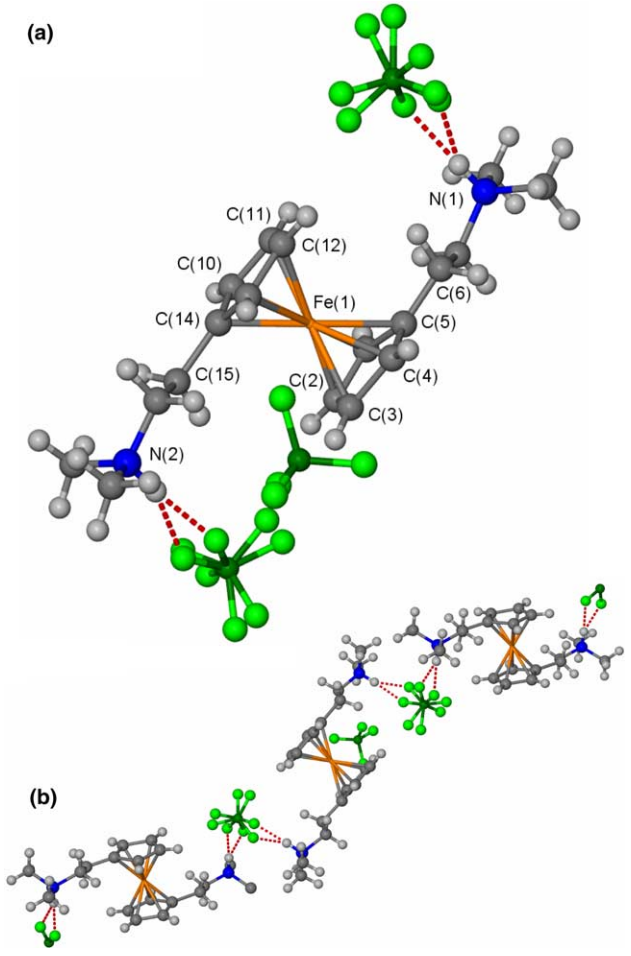

Fig. 2. (a) The molecular structure of compound **11**, showing the hydrogen bonding interactions. (b) The intermolecular hydrogen bonding of compound **11**.

Table 4
Selected interatomic distances (Å) and angles between interatomic vectors (°) with estimated standard deviations in parenthesis [M(1) and M(2) denote the centroid of the C_5 rings C(1)–C(5) and C(10)–C(14), respectively] for $Fe\{\eta\text{-}C_5H_4(CH_2)_2NHMe_2\}_2]^{3+}[3BF_4]^-$ (**11**)

Interatomic distances			
Fe(1)–C(1)	2.068(10)	C(1)–C(2)	1.404(15)
Fe(1)–C(2)	2.049(10)	C(2)–C(3)	1.374(16)
Fe(1)–C(3)	2.050(10)	C(3)–C(4)	1.481(14)
Fe(1)–C(4)	2.077(9)	C(4)–C(5)	1.482(15)
Fe(1)–C(5)	2.129(10)	C(5)–C(1)–	1.444(15)
Fe(1)–C(11)	2.055(10)	C(10)–C(11)	1.388(16)
Fe(1)–C(10)	2.047(12)	C(11)–C(12)	1.372(18)
Fe(1)–C(13)	2.085(9)	C(12)–C(13)	1.438(15)
Fe(1)–C(14)	2.062(10)	C(13)–C(14)	1.377(17)
Fe–M(1)	1.677	C(14)–C(10)	1.384(16)
Fe–M(2)	1.694	Average C–C	1.4144
Average Fe–C	2.069		
Interatomic angles			
C(1)–C(2)–C(3)	110.3(10)	C(10)–C(11)–C(12)	106.2(11)
C(2)–C(3)–C(4)	109.8(10)	C(11)–C(12)–C(13)	108.3(11)
C(3)–C(4)–C(5)	103.7(10)	C(12)–C(13)–C(14)	107.7(11)
C(4)–C(5)–C(1)	107.9(9)	C(13)–C(14)–C(10)	106.4(11)
C(5)–C(1)–C(2)-	108.0(11)	C(14)–C(10)–C(11)	111.3(11)
Average C–C–C	107.96		
C(6)–C(5)–M(1)	171.44	C(15)–C(14)–M(2)	177.08

Table 5
Hydrogen bond distances (Å) and angles (°) for compounds **11**

D–H	*d*(D–H)	*d*(H···A)	–DHA	*d*(D···A)	A
N(1)–H(1)	0.9300	1.9226	175.62	2.8508	F(14A)
N(1)–H(1)	0.9300	1.8286	154.34	2.6972	F(14B)
N(2)–H(2)	0.9300	1.8755	174.93	2.8031	F(11A)
N(2)–H(2)	0.9300	1.8889	157.17	2.7697	F(11B)

rings are staggered with the *N*,*N*-dimethylaminoethyl side chains *trans* to each other (ca. 180°). There are three BF_4^- counter ions associated with each ferrocenium molecule. Two of the BF_4^- counter ions are hydrogen bonded to the N–H groups (hydrogen bond lengths and angles shown in Table 5) as well as being attached to the adjacent ferrocenium fragment in an μ^2 fashion, as shown in Fig. 2(b). The BF_4^- counter ions involved in the hydrogen bonding are disordered with respect to the fluorine atoms which are orientated over two sites with a partial occupancy of 0.5. The third BF_4^- counter ion is not disordered or involved in hydrogen bonding.

The molecular structure of $[Fe\{\eta\text{-}C_5H_4(CH_2)_3\text{-}NHMe_2\}_2]^{3+}3[BF_4]^-$ (**12**) showed two independent half molecules per asymmetric unit on inversion centres of symmetry and is shown in Fig. 3 (with bond lengths and angles in Table 6). The cyclopentadienyl rings are staggered with the *N*,*N*-dimethylaminopropyl side chains lying *trans* to each other (180°). There are three

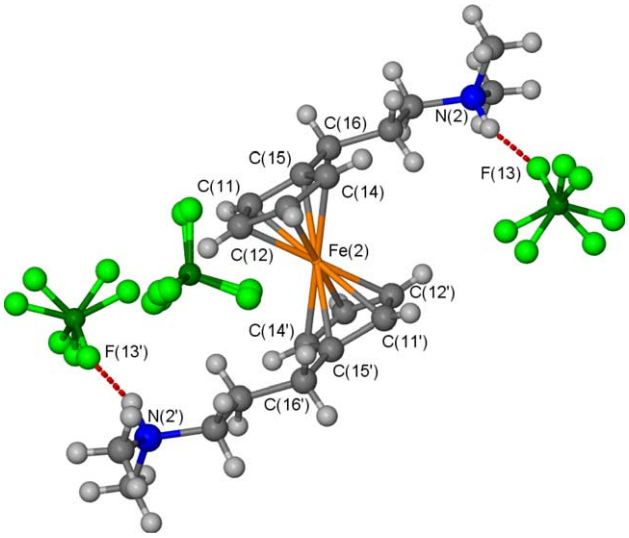

Fig. 3. The molecular structure of compound **12**, showing the hydrogen bonding interactions

BF_4^- counter ions associated with each molecule. In the asymmetric unit, the fluorine atoms of two of the BF_4^- counter ions are disordered over two orientations

Table 6
Selected interatomic distances (Å) and angles between interatomic vectors (°) with estimated standard deviations in parenthesis [M(1) and M(2) denote the centroid of the C_5 rings C(1)–C(5) and C(11)–C(15), respectively] for $[Fe\{\eta\text{-}C_5H_4(CH_2)_3NHMe_2\}_2]^{3+}[3BF_4]^-$ (**12**)

Molecule 1		Molecule 2	
Interatomic distances			
Fe(1)–C(1)	2.090(5)	Fe(2)–C(11)	2.093(4)
Fe(1)–C(2)	2.069(4)	Fe(2)–C(12)	2.071(4)
Fe(1)–C(3)	2.061(4)	Fe(2)–C(13)	2.071(4)
Fe(1)–C(4)	2.080(4)	Fe(2)–C(14)	2.090(4)
Fe(1)–C(5)	2.117(4)	Fe(2)–C(15)	2.118(4)
C(1)–C(2)	1.416(7)	C(11)–C(12)	1.421(7)
C(2)–C(3)	1.396(7)	C(12)–C(13)	1.407(8)
C(3)–C(4)	1.415(7)	C(13)–C(14)	1.419(7)
C(4)–C(5)	1.418(6)	C(14)–C(15)	1.426(6)
C(5)–C(1)	1.424(7)	C(15)–C(11)	1.414(6)
Average C–C	1.414	Average C–C	1.417
Fe(1)–M(1)	1.701	Fe(2)–M(2)	1.705
Average Fe(1)–C	2.083	Average Fe(2)–C	2.089
Interatomic angles			
C(1)–C(2)–C(3)	108.0(4)	C(11)–C(12)–C(13)	108.3(4)
C(2)–C(3)–C(4)	108.5(4)	C(12)–C(13)–C(14)	107.8(4)
C(3)–C(4)–C(5)	108.3(4)	C(13)–C(14)–C(15)	108.4(4)
C(4)–C(5)–C(1)	106.9(4)	C(14)–C(15)–C(11)	107.2(4)
C(5)–C(1)–C(2)	108.3(4)	C(15)–C(11)–C(12)	108.4(4)
Average C–C–C	108	Average C–C–C	108.02
C(6)–C(5)–M(1)	178.46	C(16)–C(15)–M(2)	178.65

Table 7
Hydrogen bond distances (Å) and angles (°) for compounds **11** and **12**

D–H	*d*(D–H)	*d*(H···A)	–DHA	*d*(D···A)	A
N(1)–H(1N)	0.9100	2.0942	149.21	2.9135	F(11)
N(1)–H(1N)	0.9100	2.0879	141.02	2.8533	F(11A)
N(2)–H(2N)	0.9099	1.9761	152.83	2.8164	F(13)

and the other BF_4^- has three disordered fluorine atoms, which have a partial occupancy of 0.5. In a similar fashion to compound **11**, there are hydrogen bond interactions between the N–H groups and the fluorine atoms of two of the three BF_4^- counter ions and the bond lengths and angles are shown in Table 7. A number of reported amino-functionalised ferrocenium salts have been structurally characterised and their bond lengths and angles are similar to these compounds [8,22].

4. Conclusion

In conclusion, this paper reports the synthesis of a number of primary and tertiary bis-amino-functionalised ferrocene and ferrocenium salts. Structural studies have been carried out showing a number of interesting features, including N–H···O and N–H···F hydrogen bonds.

5. Experimental

5.1. General

Standard inert atmosphere techniques were used throughout. Petrol (40-60°), diethyl ether, and THF were distilled from Na/Ph_2CO. NMR solvents were degassed by three freeze–pump–thaw cycles and stored over 3 Å molecular sieves in a dry box. All reagents were purchased in reagent grade and used without further purification.

5.2. Instrumentation

^1H and ^{13}C NMR spectra were recorded on Bruker 250 MHz, 300 MHz and 500 MHz spectrometers. High resolution mass spectrometry was performed by the University of Leeds mass spectral service. Elemental analyses were performed by the University of Leeds microanalytical services.

5.3. $NaC_5H_4(CH_2)_2NH_2$ (*1*)

To a Schlenk tube charged with NaH (1.2 g, 0.005 mol) and THF (100 ml) was added $C_5H_5(CH_2)_2NH_2$ (6.39 g, 0.06 mol) in THF (50 ml) dropwise with stirring. Evolution of a gas and formation of a pale brown precipitate was observed. The reaction mixture was stirred for ca. 24 h. THF was then removed in vacuo and the product was washed with petroleum ether (b.p. 40–60 °C) (3 × 30 ml) to give a pale brown powder. (3.0 g, 0.027 mol, 47%). ^1H NMR (CD_3CN, 300.1 MHz, 300 K) δ 5.42, 5.32 [2 × s, 4H, CH of C_5H_4], 2.64 [t, 2H, $^3J(^1H–^1H)$ = 5.0Hz, CH_2 of $CH_2CH_2NH_2$], 2.44 [t, 2H, $^3J(^1H–^1H)$ = 5.0 Hz, CH_2 of $CH_2CH_2NH_2$] (s, 3H); $^{13}C\{^1H\}$ NMR (CD_3CN, 75.5 MHz, 300K) δ 103.2 [CH of C_5H_4], 102.6 [CH of C_5H_4], 45.0 [CH_2 of $CH_2C_2NH_2$], 33 8 [CH_2 of $C_2CH_2NH_2$].

5.4. $Fe\{\eta\text{-}C_5H_4(CH_2)_2NH_2\}_2$ (*2*)

To a Schlenk tube charged with $FeCl_2$ (0.25 g, 0.002 mol) and THF (50 ml) was added a suspension of **1** (0.59 g, 0.004 mol) in THF (30 ml). The reaction mixture was stirred overnight. The solvent was removed in vacuo. The product was extracted in diethyl ether (3 × 30 ml). The extracts were combined and removal of the solvent afforded the product as a viscous orange oil. (0.38 g, 0.00125 mol, 63%). EI mass spectrum: *m/z* 272.1 – $Fe\{\eta\text{-}C_5H_4(CH_2)_2NH_2\}_2$ ^1H NMR ($CDCl_3$, 500 MHz, 300 K) δ 3.94 [2 × virt. d, 8H, $C_5H_4CH_2CH_2NH_2$], 2.73 [t, 2H, $^3J(^1H–^1H)$ = 6.9 Hz $CH_2CH_2NH_2$], 2.40 [t, 2H, $^3J(^1H–^1H)$ = 6.9 Hz $CH_2CH_2NH_2$], 1.31 [br. S, 2H, $CH_2CH_2NH_2$]; $^{13}C\{^1H\}$ NMR ($CDCl_3$, 500 MHz, 300 K) δ 86.7 [s, $C(CH_2)2NH_2$], 69.4, 68.5 [2 × s, CH of

$C_5H_4(CH_2)_2NH_2]$, 44.0 [s, $CH_2CH_2NH_2$)], 34.2 [s, $C_2CH_2NH_2$].

5.5. $Fe\{\eta\text{-}C_5H_4(CH_2)_2NH_3\}_2]^{2+}2[CF_3CO_2]^-$ (3)

To a Schlenk tube charged with **2** (1.5 g, 0.006 mol) in diethyl ether (100 ml) was added CF_3CO_2H (1.14 g, 0.01 mol). A yellow precipitate was immediately formed. The mixture was allowed to stir (1 h) and stand (5 min). The product was isolated via filtration, washed with diethyl ether (3×15 ml) and dried in vacuo to afford a yellow powder. (1.72 g, 0.003 mol, 65.0%). *Anal*. Calc. for $FeC_{18}H_{22}N_2F_6O_4$: C, 43.2; H, 4.4; N, 5.6. Found: C, 43.0; H, 4.5; N, 5.4%. ^{1}H NMR(CD_3CN, 300.13 MHz, 300 K) δ 4.09 [br.s, 4H, CH of C_5H_4], 4.03 [br.s, 4H, CH of C_5H_4], 3.80 [t, 4H, $^3J(^1H\text{–}^1H) = 9.0$ Hz, $CH_2CH_2NH_3$], 2.80 [t, 4H, $^3J(^1H\text{–}^1H) = 9.0$ Hz, $CH_2CH_2NH_3$]; $^{13}C\{^1H\}$ NMR (CD_3COCD_3, 75.47MHz, 300K) δ 69.2 [2 × CH of C_5H_4], 68.5 [2 × CH of C_5H_4], 48.2 [$CH_2C_2HNH_3$], 28.0 [$C_2HCH_2NH_3$].

5.6. $Fe\{\eta\text{-}C_5H_4(CH_2)_3NH_3\}_2]^{2+}2[CF_3CO_2]^-$ (4)

$Fe\{\eta\text{-}C_5H_4(CH_2)_3NH_2\}_2$ (1.5 g, 0.005 mol) was reacted with CF_3CO_2H (1.14 g, 0.01 mol) in diethyl ether (100 ml). A yellow precipitate was immediately formed. The mixture was allowed to stir (1 h) and stand (5 min). The product was isolated by filtration and washed with diethyl ether (3×15 ml) to give a yellow powder (1.77 g, 0.0034 mol, 67.0%). *Anal*. Calc. for $FeC_{20}H_{26}N_2F_6O_4$: C, 45.5; H, 5.0; N, 5.3. Found: C, 46.8; H, 5.0; N, 6.2%. ^{1}H NMR (CD_3CN, 300 MHz, 300 K) δ 7.4 [br s, 6H, $C_5H_4(CH_2)_3NH_3$], 4.0, 3.9, [2 × virt. t, 8H, $C_5H_4(CH_2)_3NH_3$], 2.9 [t, 4H, $CH_2CH_2NH_3$], 2.3 [m, 4H, $CH_2CH_2CH_2NH_3$], 1.9 [m, 4H, $CH_2CH_2CH_2NH_3$]; $^{13}C\{^1H\}$ NMR (CD_3CN, 300MHz, 300K) δ 88.0 [s, $C(CH_2)_3NH_3$], 68.4, 67.2 [2 × s, CH of $C_5H_4(CH_2)NH_3$], 39.8 [s, CH of $(CH_2)_2C_2NH_3$], 28.3 [s, CH of $CH_2C_2CH_2NH_3$], 25.4 [s, CH of $C_2(CH_2)_2NH_3$].

5.7. $Fe\{\eta\text{-}C_5H_4(CH_2)_2NHMe_2\}_2]^{2+}2[CF_3CO_2]^-$ (5)

To a Schlenk tube charged with $FeCl_2$ (0.80 g, 0.006 mol) and THF (30 ml), $Na(C_5H_4)(CH_2)_2NMe_2$ (2 g, 0.013 mol) in THF (30 ml) was added. The reaction mixture was stirred overnight. The solvent was removed in vacuo and the product extracted in petroleum ether (b.p. 40–60 °C) (3×30 ml). The volume of the resulting orange solution was reduced *in vacuo* (50 ml) and CF_3CO_2H (1.48 g, 0.013 mol, 0.97 ml) was added. Immediately, a yellow precipitate was formed and the reaction mixture was left to stir overnight. The solution was removed by filtration and the solid washed in petroleum ether (b.p. 40–60 °C) (3 30 ml). The resulting solid was dried in vacuo to yield $[Fe\{\eta\text{-}C_5H_4(CH_2)_3NHMe_2\}_2]^{2+}2[CF_3CO_2]^-$ (2.8 g, 0.005 mol, 79%). *Anal*. Calc. for $FeC_{22}H_{30}F_6N_2O_4$: C, 47.5; H, 5.4; N, 5.0. Found: C, 47.6; H, 5.6; N, 5.1%. TOF FAB MS(+) 329.1 ($-2CF_3CO_2H$). ^{1}H NMR (acetone-d_6, 300 MHz, 300 K) δ 4.15, 4.11[2 × m, 8H, C_5H_4], 3.31 [m, 4H, $C_5H_4CH_2CH_2NHMe_2$], 2.90 [s, 12H, $NHMe_2$], 2.85 [m, 4H, $C_5H_4CH_2CH_2NHMe_2$]. $^{13}C\{^1H\}$ NMR (acetone-d_6, 75.5 MHz, 300 K) 85.3 [s, $C_5H_4C(CH_2)_2NHMe_2$], 70.0, 69.6 [2 × s, CH of C_5H_4], 58.8 [s, $C_5H_4CH_2C_2NHMe_2$], 43.2 [s, $NHMe_2$], 25.2 [s, $C_5H_4C_2CH_2NHMe_2$].

5.8. $Fe\{\eta\text{-}C_5H_4(CH_2)_3NHMe_2\}_2]^{2+}\ 2[CF_3CO_2]^-$ (6)

To a Schlenk tube charged with $FeCl_2$ (0.73 g, 0.006 mol) and THF (30 ml), $Na(C_5H_4)(CH_2)_3NMe_2$ (2 g, 0.011 mol) in THF (30 ml) was added. The reaction mixture was stirred overnight. The solvent was removed in vacuo and the product extracted in petroleum ether (b.p. 40–60°C) (3×30 ml). The volume of the resulting orange solution was reduced in vacuo (50 ml) and CF_3CO_2H (1.25 g, 0.011 mol, 0.8 ml) was added. Immediately, a yellow precipitate was formed and the reaction mixture was left to stir overnight. The solution was removed by filtration and the solid washed in petroleum ether (b.p. 40–60 °C) (3×30 ml). The resulting solid was dried in vacuo to yield $[Fe\{\eta\text{-}C_5H_4(CH_2)_3NHMe_2\}_2]^{2+}2[CF_3CO_2]^-$ (2.3 g, 0.004 mol, 66%). *Anal*. Calc. for $FeC_{24}H_{34}F_6N_2O_4$: C, 49.3; H, 5.9; N, 4.8. Found: C, 48.5; H, 5.7; N, 5.0%. ^{1}H NMR ($CDCl_3$, 300 MHz, 300 K) δ 12.0 [br s, 2H, $NHMe_2$], 3.9, 3.85 [2 × m, 8H, C_5H_4], 2.86 [t, 4H, $C_5H_4CH_2CH_2CH_2NHMe_2$], 2.66 [s, 12H, $NHMe_2$], 2.28 [t, 4H, $C_5H_4CH_2CH_2CH_2NHMe_2$], 1.79 [m, 4H, $C_5H_4CH_2CH_2CH_2NHMe_2$]. $^{13}C\{^1H\}$ NMR ($CDCl_3$, 75.5 MHz, 300 K) δ 86.5 [s, $C_5H_4C(CH_2)_3NHMe_2$], 68.9, 68.4 [2 × s, CH of C_5H_4], 57.4 [s, $C_5H_4CH_2CH_2C_2NHMe_2$], 47.2 [s, $NHMe_2$], 26.2 [s, $C_5H_4C_2CH_2CH_2NHMe_2$], 26.0 [s, $C_5H_4CH_2C_2CH_2NHMe_2$].

5.9. $Fe\{\eta\text{-}C_5H_4(CH_2)_2NHMe_2\}_2]^{2+}2[BF_4]^-$ (7)

To a Schlenk tube charged with $FeCl_2$ (0.80 g, 0.006 mol) and THF (30 ml), $Na(C_5H_4)(CH_2)_2NMe_2$ (2 g, 0.013 mol) in THF (30 ml) was added. The reaction mixture was stirred overnight. The solvent was removed in vacuo and the product extracted in diethyl ether (3×30 ml). The volume of the resulting orange solution was reduced in vacuo (50 ml) and $HBF_4 \cdot OEt$ (54% in diethyl ether) (1.14 g, 0.013 mol, 1.5 ml) was added. Immediately, a yellow precipitate was formed and the reaction mixture was left to stir overnight. The solution was removed by filtration and the solid washed in petroleum ether (b.p. 40–60 °C) (3×30 ml). The resulting solid was dried in vacuo to yield $[Fe\{\eta\text{-}C_5H_4(CH_2)_3NHMe_2\}_2]^{2+}2[BF_4]^-$ (2.2 g, 0.0043 mol, 72%). *Anal*. Calc. for $FeC_{18}H_{30}B_2F_8N_2$: C, 42.9; H, 6.0; N, 5.6. Found: C, 43.3; H, 6.1; N, 5.4%. TOF ES MS(+) 329.1 ($-2HBF_4$). ^{1}H NMR (acetone-d_6,

300 MHz, 300 K) δ 7.45 [br s, 2H, N*H* Me_2], 4.16 [br s, 8H, C_5 *H_4*], 3.23 [m, 4H, $C_5H_4CH_2C$*H_2*$NHMe_2$], 2.87 [s, 12H, NH*Me_2*], 2.76 [m, 4H, C_5H_4C*H_2*CH_2NHMe_2]. $^{13}C\{^1H\}$ NMR (acetone-d_6, 75.5 MHz, 300 K) δ 82.7 [s, *C_5H_4C*$(CH_2)_2NHMe_2$], 68.7, 68.4 [2 × s, CH of *C_5H_4*], 58.2 [s, $C_5H_4CH_2$*C_2*$NHMe_2$], 42.8 [s, NH*Me_2*], 23.8 [s, C_5H_4*C_2*CH_2NHMe_2].

5.10. *Fe{η-$C_5H_4(CH_2)_3NHMe_2$}$_2$]$^{2+}$2[BF_4]$^-$ (**8**)*

To a Schlenk tube charged with $FeCl_2$ (0.73 g, 0.006 mol) and THF (30 ml), $Na(C_5H_4)(CH_2)_3NMe_2$ (2 g, 0.011 mol) in THF (30 ml) was added. The reaction mixture was stirred overnight. The solvent was removed in vacuo and the product extracted in diethyl ether (3 × 30 ml). The volume of the resulting orange solution was reduced in vacuo (50 ml) and $HBF_4 \cdot OEt$ (54% in diethyl ether) (0.96 g, 0.011 mol, 1.26 ml) was added. Immediately, a yellow precipitate was formed and the reaction mixture was left to stir overnight. The solution was removed by filtration and the solid washed in petroleum ether (b.p. 40–60 °C) (3 × 30 ml). The resulting solid was dried in vacuo to yield [Fe{η-$C_5H_4(CH_2)_3$-$NHMe_2$}$_2$]$^{2+}$2[BF_4]$^-$ (1.9 g, 0.0036 mol, 60%). *Anal.* Calc. for $FeC_{20}H_{34}B_2F_8N_2$: C, 45.2; H, 6.4; N, 5.3. Found: C, 45.4; H, 6.4; N, 5.3%. TOF FAB MS(+) 532.1. ^1H NMR ($CDCl_3$, 300 MHz, 300 K) δ 4.25 [br s, 2H, N*H*Me_2], 3.96 [m, 8H, C_5*H_4*], 2.93 [t, 4H, $C_5H_4CH_2CH_2C$*H_2*$NHMe_2$], 2.68 [s, 12H, NH*Me_2*], 2.29 [t, 4H, C_5H_4C*H_2*CH_2-CH_2NHMe_2], 1.78 [m, 4H, $C_5H_4CH_2C$*H_2*CH_2NHMe_2]. $^{13}C\{^1H\}$ NMR ($CDCl_3$, 75.5 MHz, 300 K) δ 87.3 [s, *C_5H_4C* $(CH_2)_3NHMe_2$], 68.6, 68.0 [2 s, CH of *C_5H_4*], 57.8 [s, $C_5H_4CH_2CH_2$- *C_2*$NHMe_2$], 43.1 [s, NH*Me_2*], 25.8 [s, C_5H_4 *C_2*CH_2- CH_2NHMe_2], 25.6 [s, $C_5H_4CH_2$*C_2*CH_2NHMe_2].

5.11. *Fe{η-$C_5H_4(CH_2)_2NH_3$}$_2$]$^{3+}$3[BF_4]$^-$ (**9**)*

To a Schlenk tube charged with **2** (1.9 g, 0.004 mol) in diethyl ether (25 ml) was added *p*-benzoquinone (0.4 g, 0.004 mol) with stirring. Excess HBF_4. OEt_2 (54% in diethyl ether) was added dropwise. A blue precipitate was immediately formed. The mixture was allowed to stir (20 min). The precipitate was isolated via filtration, washed in diethyl ether (3 × 10 ml) and dried in vacuo to afford a blue powder. (0.71 g, 0.001 mol, 59%). ES MS (+): *m*/*z* 273.1058 [M^+].

5.12. *Fe{η-$C_5H_4(CH_2)_3NH_3$}$_2$]$^{3+}$3[BF_4]$^-$ (**10**)*

To a Schlenk tube charged with Fe{η-$C_5H_4(CH_2)_3NH_2$}$_2$ (1.72 g, 0.003 mol) in diethyl ether (25 ml) was added *p*-benzoquinone (0.4 g, 0.004 mol) with stirring. Excess HBF_4. OEt_2 (54% in diethyl ether) was added dropwise via syringe. A blue precipitate was immediately formed. The mixture was allowed to stir (20mins). The precipitate was isolated via filtration, washed in diethyl ether (3 × 10 ml) and dried in vacuo to afford a blue powder. (0.83 g, 0.002 mol, 61%). ES MS (+): *m*/*z* 300.1277 [M^+].

5.13. *Fe{η-$C_5H_4(CH_2)_2NHMe_2$}$_2$]$^{3+}$ 3[BF_4]$^-$ (**11**)*

To a Schlenk tube charged with **2** (0.5 g, 0.0009 mol) and diethyl ether (30 ml), *p*–benzoquinone (0.05 g, 0.0005 mol) in diethyl ether (20 ml) was added. To this mixture $HBF_4 \cdot OEt$ (54% in diethyl ether) (0.08 g, 0.0009 mol, 0.07 ml) was added. A blue solid immediately formed and the reaction mixture was left stirring overnight. The solution was removed by filtration and the solid washed in petroleum ether (b.p. 40–60 °C) (2 × 30 ml). The resulting blue solid was dried in vacuo to yield [Fe{η-$C_5H_4(CH_2)_2NHMe_2$}$_2$]$^{3+}$3[BF_4]$^-$ (0.46 g, 0.00078 mol, 86%). *Anal.* Calc. for $FeC_{18}H_{30}B_3F_{12}N_2$: C, 36.6; H, 5.1; N, 4.7. Found: C, 36.7; H, 5.1; N, 4.7%.

5.14. *Fe{η-$C_5H_4(CH_2)_3NHMe_2$}$_2$]$^{3+}$ 3[BF_4]$^-$ (**12**)*

To a Schlenk tube charged with **8** (0.5 g, 0.0008 mol) and dithyl ether (30 ml), *p*-benzoquinone (0.04 g, 0.0004 mol) in diethyl ether (20 ml) was added. To this mixture $HBF_4 \cdot OEt$ (54% in diethyl ether) (0.07 g, 0.0008 mol, 0.06 ml) was added. A blue solid immediately formed and the reaction mixture was left stirring overnight. The solution was removed by filtration and the solid washed in petroleum ether (b.p. 40–60 °C) (2 × 30 ml). The resulting blue solid was dried in vacuo to yield [Fe{η-$C_5H_4(CH_2)_3NHMe_2$}$_2$]$^{2+}$3[BF_4]$^-$ (0.35 g, 0.00056 mol, 70%). *Anal.* Calc. for $FeC_{20}H_{34}B_3F_{12}N_2$: C, 38.8; H, 5.5; N, 4.5. Found: C, 38.6; H, 5.4; N, 4.6%.

5.15. *Fe{C_5H_3-1-$SiMe_3$-3-$CH(CH_2)_4NHMe$}$_2$]$^{2+}$2[CF_3CO_2]$^-$ (**13**)*

To a Schlenk tube charged with $FeCl_2$ (0.40 g, 0.003 mol) and THF (30 ml), LiC_5H_3-1-$SiMe_3$-3-$CH(CH_2)_4NMe$ (1.5 g, 0.006 mol) in THF (30 ml) was added. The reaction mixture was stirred overnight. The solvent was removed in vacuo and the product extracted in petroleum ether (b.p. 40–60 °C) (3 × 30 ml). The volume of the resulting orange solution was reduced in vacuo (50 ml). CF_3CO_2H (0.68 g, 0.006 mol, 0.45 ml) was added. Immediately, a yellow precipitate was formed and the reaction mixture was left to stir overnight. The solution was removed by filtration and the solid washed in petroleum ether (b.p. 40–60 °C) (3 × 30 ml). The resulting solid was dried in vacuo to yield [Fe{η-$C_5H_4(CH_2)_3NHMe$}$_2$]$^{2+}$2[CF_3CO_2]$^-$ (2.96 g, 0.004 mol, 65%). *Anal.* Calc. for $FeC_{32}H_{50}F_6N_2O_4Si_2$: C, 51.1; H, 6.7; N, 3.7. Found: C, 51.0; H, 6.5; N, 3.8%. TOF FAB MS(+) 525.2 (–2CF_3CO_2H). ^1H NMR (acetone-d_6, 300 MHz, 300 K) δ 4.10 [m, 6H,

C_5H_3 ($SiMe_3$)$CH(CH_2)_4NHMe$], 3.46 [m, 4H, C_5H_3 ($SiMe_3$)$CH(CH_2CH_2)_2NHMe$], 2.90 [m, 4H, C_5H_3 ($SiMe_3$)$CH(CH_2CH_2)_2NHMe$], 2.73 [s, 6H, C_5H_3 ($SiMe_3$)$CH(CH_2CH_2)_2NHMe$], 2.45 [m, 2H, C_5H_3 ($SiMe_3$)CH $(CH_2CH_2)_2NHMe$], 2.07 [m, 4H, C_5H_3 ($SiMe_3$)$CH(CH_2CH_2)_2NHMe$], 1.93 [m, 4H, C_5H_3 ($SiMe_3$)$CH(CH_2CH_2)_2NHMe$], 0.19 [s, 18H, C_5H_3($SiMe_3$)$CH(CH_2CH_2)_2NHMe$]. $^{13}C\{^1H\}$ NMR (acetone-d_6, 75.5 MHz, 300 K) 95.0, 94.8, 94.7, 92.1, 92.0 [5× s, $CSiMe_3$], 71.6, 71.5 [2× s, $CCH(CH_2CH_2)_2NHMe$], 72.6, 72.0, 70.2, 67.8, 67.5, 67.4, 66.6, 65.9, 65.8 [9× s, C_5H_3 ($SiMe_3$)$CH(CH_2CH_2)_2NHMe$], 53.8 [s, C_5H_3($SiMe_3$)$CH(C_2C_2)_2NHMe$], 42.5 [s, C_5H_3($SiMe_3$)CH $(CH_2CH_2)_2NHMe$], 32.0, 31.9, 31.8 [3× s, C_5H_3 ($SiMe_3$) $CH(CH_2CH_2)_2NHMe$], 29.8, 29.7, 29.5 [3× s, C_5H_3 ($SiMe_3$)$CH(C_2C_2)_2NHMe$],1.5, 1.2 [2× s, C_5H_3($SiMe_3$) $CH(CH_2CH_2)_2NHMe$].

6. Supplementary material

Crystallographic data for the structural analysis have been deposited with the Cambridge Crystallographic Data Centre, CCDC No. 244344 for compound **6**, 244345 for compound **11** and 244346 for compound **12**. Copies of this information may be obtained free of charge from the Director, CCDC, 12 Union Road, Cambridge, CB2 1FZ, UK (fax: +44-1223-336033; e-mail: deposit@ccdc.cam.ac.uk or www: www.ccdc.cam.ac.uk).

References

[1] H. Dialer, K. Polborn, W. Ponikwar, K. Sunkel, W. Beck, Chem. Eur. J. 8 (2002) 691.
[2] M. Enders, G. Kohl, H. Pritzkow, Organometallics 21 (2002) 1111.
[3] J.D. Carr, S.J. Coles, W.W. Hassan, M.B. Hursthouse, K.M.A. Malik, J.H.R. Tucker, J. Chem. Soc., Dalton Trans. 57 (1999).
[4] N.G. Connelly, W.E. Geiger, Chem. Rev. 96 (1996) 877.
[5] A. Shafir, M.P. Power, G.D. Whitener, J. Arnold, Organometallics 19 (2000) 3978.
[6] B. Neumann, U. Siemeling, H.G. Stammler, U. Vorfeld, J.G.P. Delis, J. Chem. Soc., Dalton Trans. (1997) 4705.
[7] G. Tabbi, C. Cassino, G. Cavigiolio, D. Colangelo, A. Ghiglia, I. Viano, D. Osella, J. Med. Chem. 45 (2002) 5786.
[8] S. Bradley, M.M. Corradi, K.D. Camm, S.J. Furtado, P.C. McGowan, R. Mumtaz, M. Thornton-Pett, J. Organomet. Chem. 656 (2002) 49.
[9] H. Plenio, C. Aberle, Angew. Chem. Int. Ed. 37 (1998) 1397.
[10] A.N. Nesmeyanov, V.N. Drozd, V.A. Sazonova, Dokl. Akad. Nauk SSSR 150 (1963) 321.
[11] V.C. Gibson, N.J. Long, E.L. Marshall, P.J. Oxford, A.J.P. White, D.J. Williams, J. Chem. Soc., Dalton Trans. (2001) 1162.
[12] V.C. Gibson, C.M. Halliwell, N.J. Long, P.J. Oxford, A.M. Smith, A.J.P. White, D.J. Williams, Dalton Trans. (2003) 918.
[13] A. Shafir, J. Arnold, Organometallics 22 (2003) 567.
[14] A. Shafir, J. Arnold, J. Am. Chem. Soc. 123 (2001) 9212.
[15] S.J. Furtado, A.L. Gott, P.C. McGowan, Dalton Trans. (2004) 436.
[16] S. Bradley, K.D. Camm, X.M. Liu, P.C. McGowan, R. Mumtaz, K.A. Oughton, T.J. Podesta, M. Thornton-Pett, Inorg. Chem. 41 (2002) 715.
[17] S. Bradley, P.C. McGowan, K.A. Oughton, M. Thornton-Pett, M.E. Walsh, Chem. Commun. (1999) 77.
[18] P.C. McGowan, R.J. Knox, in: Wo (Ed.), PCT International Applications, University of Leeds, UK, 2004, 23pp.
[19] M.A.D. McGowan, P.C. McGowan, International Patent WO 01/42260, 2001.
[20] P.C. McGowan, C.E. Hart, B. Donnadieu, R. Poilblanc, J. Organomet. Chem. 528 (1997) 191.
[21] S. Bradley, K.D. Camm, S.J. Furtado, A.L. Gott, P.C. McGowan, T.J. Podesta, M. Thornton-Pett, Organometallics 21 (2002) 3443.
[22] B. Neumann, U. Siemeling, H.-G. Stammler, U. Vorfeld, J.G.P. Delis, P.W.N.M. van Leeuwen, K. Vrieze, J. Fraanje, K. Goubitz, F. Fabrizi de Biani, P. Zanello, J. Chem. Soc., Dalton Trans. (1997) 4705.

Available online at www.sciencedirect.com
SCIENCE DIRECT®
Polyhedron 23 (2004) 2937–2942
POLYHEDRON
www.elsevier.com/locate/poly

Synthesis and X-ray structures of metallocenium diamines of iron and cobalt

Sviatoslav Inyushin [a,b], Alexandr Shafir [a,b], John E. Sheats [c,*], Michael Minihane [d], Charles E. Whitten Jr. [d], John Arnold [a,b,*]

[a] Department of Chemistry, University of California, Berkeley, CA 94720-1460, USA
[b] Chemical Sciences Division, Lawrence Berkeley National Laboratory, Berkeley, CA 94720-1460, USA
[c] Department of Chemistry, Rider University, Lawrenceville, NJ 08648, USA
[d] Department of Chemistry, Bowdoin College, Brunswick, ME 04011, USA

Received 30 May 2004; accepted 26 August 2004
Available online 25 September 2004

Dedicated to Professor M.L.H. Green on the occasion of his retirement as Head of the ICL

Abstract

A detailed, reproducible synthesis of 1,1′-diaminocobaltocenium hexafluorophosphate is provided. The compound can be made on gram scales in several steps starting from 1,1′-dimethylcobaltocenium salts. The X-ray structures of 1,1′-diaminocobaltocenium hexafluorophosphate and a related 1,1′-diaminoferrocenium salt, are described.
© 2004 Elsevier Ltd. All rights reserved.

Keywords: Metallocene; Ferrocenium; Cobaltocenium; Crystal structure

1. Introduction

We [1–6], and others [7–16], have recently described a wide assortment of new chemistry based on 1,1′-diaminoferrocene, much of it based on use of this compound to prepare new ligands for use in olefin polymerization catalysts. Extension of this work to the isoelectronic cobalt species was, in our view, a logical synthetic goal. Nevertheless, in contrast to their ferrocene counterparts, relatively little is known regarding the chemistry of 1,1′-substituted diaminocobaltocenium species. The parent cation $(C_5H_4NH_2)_2Co^+$ was first described in the literature many years ago; nevertheless, its synthesis is not well-documented despite the fact that extensive characterization data have appeared [17,18]. These species are of interest since, unlike their ferrocene analogs, cobaltocenium derivatives show strong resistance to oxidation, as well as to electrophilic and radical attack. Also, due to the ionic character of cobaltocenium derivatives, they exhibit good solubility in polar solvents [17].

The purpose of this paper is to provide a detailed, reproducible synthesis of 1,1′-diaminocobaltocenium hexafluorophosphate, to describe its reactivity in comparison to the ferrocene analog, and to present its X-ray crystal structure alongside data for the homologous 17-electron iron(III) counterpart.

2. Results and discussion

Although 1,1′-diaminocobaltocenium hexafluorophosphate was first described 20 years ago, a detailed procedure for its synthesis has not, to the best of our knowledge, been reported. Nevertheless, El Murr reported its characterization by IR, UV, and ^{1}H NMR

* Corresponding authors. Tel.: +51 06 43 5181; fax: +50 84 37 7852.
E-mail address: arnold@berkeley.edu (J. Arnold).

0277-5387/$ - see front matter © 2004 Elsevier Ltd. All rights reserved.
doi:10.1016/j.poly.2004.08.012

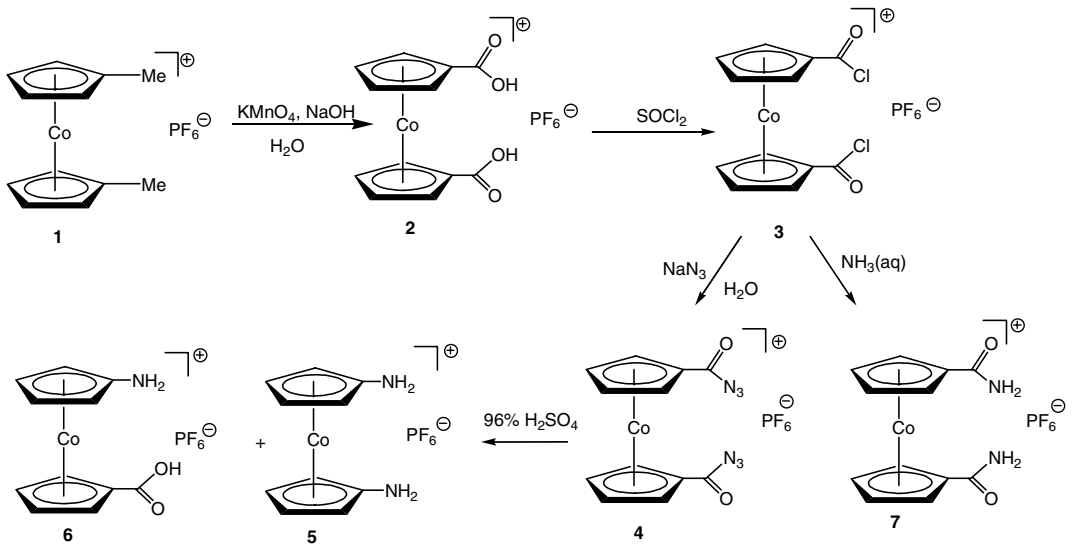

Scheme 1.

spectroscopy, along with its redox behavior in 1976 [17,18]; a general sequence of reaction steps was also given, but with no experimental details (Scheme 1). In contrast, the preparation of monoaminocobaltocenium hexafluorophosphate using related procedures was described in detail.

Following El Murr's outline for the synthesis of the 1,1′-diaminocobaltocenium hexafluorophosphate, the first two steps entailed synthesis of the dimethylcobaltocenium cation **1** from CpLi and $CoCl_2$, followed by oxidation to dicarboxycobaltocenium **2** using potassium permanganate in alkaline aqueous solution. The oxidation reaction was complete in 3 h, affording a reasonable yield of the diacid. The latter was then transformed in high yield into the corresponding diacid chloride **3** by refluxing in thionyl chloride for ca. 5 h. Conversion of the bis(acid chloride) **3** to the bis(azidocarbonyl) **4** was carried out using a 30% aqueous solution of sodium azide in almost quantitative yield.

We caution that while large amounts of the bis(azidocarbonyl) **4** complex have been isolated without incident, the material has been shown to be shock and heat sensitive, especially when dry. Thus, we strongly recommend that the material from this step be taken on to the final step without excessive drying and that appropriate safety precautions be taken when handling this material.

Curtius rearrangement of the bis(azidocarbonyl) was conducted using 96% sulfuric acid, affording the desired 1,1′-diaminocobaltocenium hexafluorophosphate **5** in moderate yields (typically ca. 30%). The reaction mixture included 1-amino-1′-carboxycobaltocenium isolated in 30% yield as well as 10–20% of unreacted diacid. These products presumably arise from the partial or complete hydrolysis of **4** during the reaction.

Attempts to prepare diaminocobaltocenium in higher yield using a Hoffman rearrangement under standard conditions from diamidocobaltocene were tried but were unsuccessful. While diamidocobaltocenium hexafluorophosphate (**7**) was prepared from **3** in good yields, attempts to convert this material to **5** resulted in black tarry mixtures from which no pure products could be isolated.

Schiff-base condensation and silylation reactions with diamine were attempted, in efforts to prepare ligands analogous to those described for ferrocene-based systems [4]. However, due to the strong electron withdrawing nature of the cobaltocenium moiety, diaminocobaltocenium proved to be less reactive than the isoelectronic diaminoferrocene. Schiff-base condensations with aldehydes were unsuccessful under typical acidic or basic catalytic conditions. Efforts to shift the equilibrium of the reaction by removing water with molecular sieves were also unsuccessful.

Attempts to silylate 1,1′-diaminocobaltocinium with trimethylsilylchloride using conditions similar to those employed in the preparation of the ferrocene analog resulted in no reaction [3].

Based on these results, the chemical properties of the NH_2 groups in diaminocobaltocenium would appear to resemble those of iminium moieties rather then of traditional amines (Fig. 1).

This resonance structure is consistent with the low reactivity and low basicity of these amino groups ($pK_b^1 = 13.5$ compared to 10.5 in isoelectronic diaminoferrocene. $pK_b^2 = 18.1$).

X-ray quality crystals of $[(C_5H_4NH_2)_2Co][PF_6]$ were grown from a CD_2Cl_2 solution. The compound crystallized in a chiral space group $P4_32_12$ with the Co and the P atoms residing on a crystallographic C_2 axis. The mol-

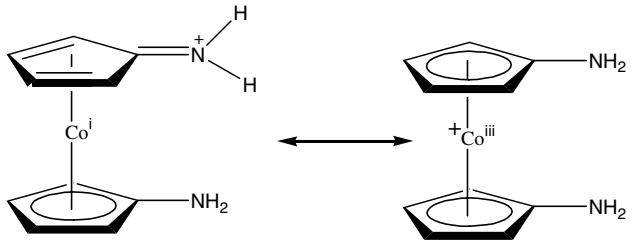

Fig. 1. Resonance structures of 1,1′-diaminocobaltocenium.

ecule adopts an eclipsed synclinal conformation, i.e. the two Cp rings are eclipsed and the amino groups are in the 1 and 2′ positions. An analogous conformation was observed for one of the crystallographically independent molecules of 1,1′-diaminoferrocene [1]. The 1,2′-substitution pattern renders each molecule chiral, which, in this case, translates into a chiral space group. The Co–Cp(centroid) distance of 1.644 is very slightly shorter than the average Fe–Cp(centroid) distance of 1.654 in diaminoferrocene. The C–N distance of 1.373(4) is considerably shorter compared to that in diaminoferrocene, where the C–N distance is 1.412(5). This is consistent with our assumption of contributions from the resonance structure shown in Fig. 2.

As reported earlier [1], cyclic voltammetry of diaminoferrocene exhibited a reversible oxidation wave with $E_{1/2} = -0.602$ V versus $Fc^{0/+}$ couple. Simple chemical oxidation using Ag^+ salts resulted in clean conversion to the paramagnetic (solution $\mu_{eff} = 2.1$ BM) ferrocenium salts (as OTf (**8**) and PF_6 (**9**) salts). In marked contrast to the air-stable cobaltocenium salts, these Fe(III) species are sensitive to oxygen, but exhibit similar solublities, in line with their related structures.

Green crystals of $[Fc(NH_2)_2][OTf]$ (**8**) suitable for X-ray diffraction were grown from a CH_3CN/CH_2Cl_2 solution at −30 °C. The compound crystallizes in the monoclinic space group $P2_1/c$. Two crystallographically independent $Fc(NH_2)_2^+$ cations were located in the asymmetric portion of the unit cell (Fig. 3). Both cations adopt a fully eclipsed synclinal conformation (i.e. the two amino groups are located on the same side of the cation). The oxygen atoms of each triflate anion are hydrogen-bonded to the amino groups of two different $Fc(NH_2)_2^+$ cations. Therefore, discrete "rings" are formed composing of two $Fc(NH_2)_2^+$ cations bridged by two triflate anions. The average Fe–C bonds in **8** [2.079(5) and 2.084(5) Å for two independent cations] are slightly longer that the average Fe–C bond in the neutral diaminoferrocene [2.051(7) and 2.052(8) Å for two independent molecules], although the differences are not very significant in light of the fairly high standard deviations of the Fe–C bond lengths.

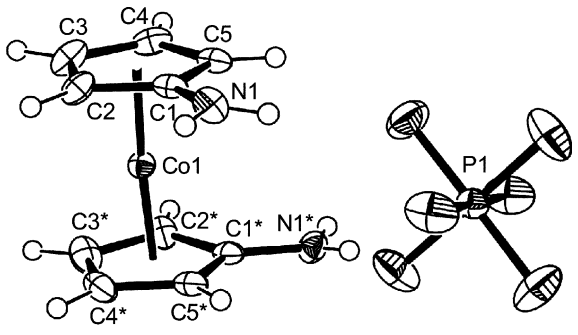

Fig. 2. ORTEP diagram of 1,1′-diaminocobaltocenium hexafluorophosphate shown with 50% thermal ellipsoids.

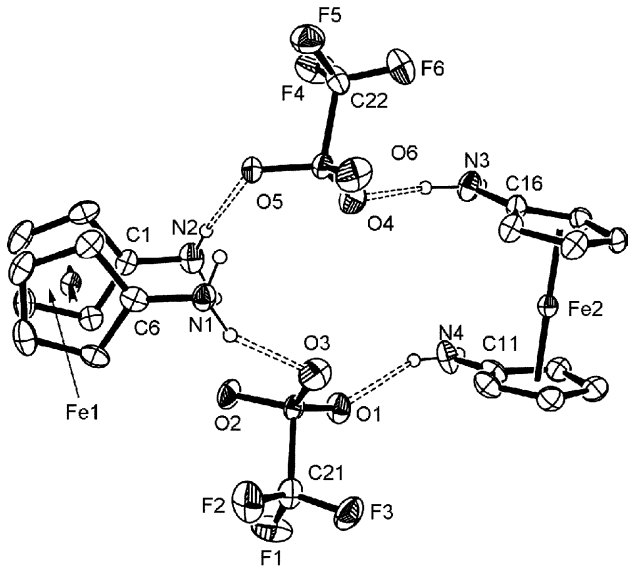

Fig. 3. ORTEP diagram (40% thermal ellipsoids) of $[Fc(NH_2)_2][OTf]$ (**8**) showing the hydrogen-bonded "rings" are formed by two $Fc(NH_2)^{2+}$ cations and two triflate anions. Selected hydrogen bonds are shown as dashed lines. Only the amine hydrogen atoms are shown.

3. Experimental

3.1. General considerations

Standard Schlenk-line and glove box techniques were used unless otherwise indicated. CH_3CN was distilled over CaH_2 under a nitrogen atmosphere. All other solvents were passed through a column of activated alumina and degassed with argon prior to use. $CDCl_3$ and CD_3CN were vacuum transferred from CaH_2. All other chemicals were purchased from Aldrich. Melting points were determined in sealed capillary tubes under nitrogen and are uncorrected. NMR spectra were recorded at ambient temperature on a Bruker AMX-300 or DRX-500 spectrometer. ^1H NMR chemical shifts are given relative to C_6D_5H (7.16 ppm), $CHCl_3$ (7.26 ppm) and CHD_2CN (2.09 ppm). Solution magnetic susceptibilities were determined using Evans NMR method

[19] with CD_3CN as solvent. IR samples were prepared either as Nujol mulls and taken between KBr plates, or as pressed KBR discs. Elemental analyses were determined at the Microanalytical Laboratory of the College of Chemistry, University of California, Berkeley. Single crystal X-ray structure determinations were performed at CHEXRAY, University of California, Berkeley.

3.2. 1,1′-Dimethylcobaltocenium hexafluorophosphate (*1*)

$CoCl_2$ (12.9 g, 0.10 mol) was added to a cooled (−78 °C) solution of $Li(C_5H_4Me)$ (17 g, 0.19 mol) in 250 ml of THF. The black reaction mixture was allowed to warm to room temperature and stirring was continued for an additional 12 h. The solvent was removed under reduced pressure and the resulting residue was dissolved in 250 ml of hot water. The mixture was filtered and washed with diethyl ether (2×100 ml) to remove unreacted organic species. The yellow aqueous phase was cooled and 1,1′-dimethylcobaltocenium was precipitated by dropwise addition of a solution of potassium hexafluorophosphate (40 g, 022 mol) in 150 ml of water. The resulting yellow solid was obtained by filtration. Yield: 17 g (46%). ^{1}H NMR (dmso-d_6, 300 MHz): δ 2.11 (s, 6H), 5.7 (s, 8H).

3.3. 1,1′-Dicarboxycobaltocenium hexafluorophosphate (*2*)

Potassium permanganate (58 g, 0.36 mol), sodium hydroxide (10 g, 0.25 mol) and 1,1′-dimethylcobaltocenium hexafluorophosphate (22 g, 0.06 mol) were mixed in 200 ml of water. The mixture was warmed to 95 °C and was stirred for 3 h. After cooling to room temperature and filtration to remove manganese dioxide, potassium hexafluorophosphate (10 g 0.05 mol) in 50 ml of water was added. The solution was chilled and any unreacted dimethylcobaltocenium complex was filtered off. Dropwise addition of 20 ml (0.12 mol) of 6 M HCl produced a yellow precipitate. Filtration afforded 12 g (55%) of the product in the form of a yellow solid. ^{1}H NMR (dmso-d_6, 300 MHz): δ 6.02 (t, 4H), 6.21 (t, 4H). IR (Nujol; cm^{-1}) 1736 (s), 1163 (m), 833 (s), 558 (m). *Anal.* Calc. for $C_{12}H_{10}O_4PF_6Co$: C, 34.12; H, 2.36. Found: C, 34.44; H, 2.44%.

3.4. 1,1′-Dichlorocarboxycobaltocenium hexafluorophosphate (*3*)

1,1′-Dicarboxycobalticinium hexafluorophosphate (10 g, 0.022 mol) was refluxed in 50 ml (large excess) of thionyl chloride for 5 h. The solution was concentrated to 15 ml and chilled to 0°. The yellow precipitate of the bis-chlorocarbonyl derivative was collected on a sintered glass filter, washed with anhydrous ether and stored in a desiccator. Yield: 8.5 g (83%). IR (Nujol; cm^{-1}) 1773 (s), 1741 (s), 1239 (s), 1056 (m), 944 (s), 843 (s), 559 (s).

3.5. 1,1′-Bis(azidodicarbonyl)cobaltocenium hexafluorophosphate (*4*)

A suspension of 1,1′-bis-chlorocarbonyl cobalticinium hexafluorophosphate (8.5 g, 18.2 mmol) was stirred with 75 ml of 30% aqueous sodium azide for 30 min. When the reaction was complete, the solution was chilled to 0° and the yellow precipitate was collected and washed with anhydrous ether. Yield: 8.7 g (98%) IR (Nujol; cm^{-1}): 3120, 2240, 2200, 2150, 1730, 1680, 1457, 1393, 1370, 1215, 1180 (s), 1065, 1030, 900, 880, 833, 820, 760.

3.6. 1,1′-Diaminocobaltocenium hexafluorophosphate (*5*)

1,1′-Dicarbonylazidocobaltocenium hexafluorophosphate (8.5 g, 0.018 mol) was dissolved in 25 ml concentrated sulfuric acid in a 250 ml round-bottomed flask resulting in evolution of a gas that persisted for ca. 15 min. When gas evolution had ceased, the solution was heated on a steam bath for 2 h, cooled and poured over 100 g ice. The solution was neutralized with concentrated KOH until slightly basic. Ethanol (200 ml) was added and a precipitate of potassium sulfate was collected and extracted with ethanol. The combined ethanol fraction was concentrated to one third of their original volume. The resulting solution was treated with charcoal and filtered. Precipitation of the product was induced by a dropwise addition of a saturated aqueous solution of ammonium hexaflurophosphate. Yield: 1.8 g (28%). ^{1}H NMR (CD_2Cl_2, 300 MHz): δ 4.26 (s, 4H), 4.87 (t, 4H), 4.99 (t, 4H). IR (1% in KBr; cm^{-1}) 3415, 3390, 3118, 1636, 1522, 1379, 1293 1047, 1032, 833, 741, 558. *Anal.* Calc. for $C_{10}H_{12}N_2PF_6Co$: C, 33.0; H, 3.32; N, 7.69. Found: C, 33.46; H, 3.55; N, 8.23%. The mother liquor was acidified to pH 1.0 with 6.0 M HCl and 1-amino-1′-carboxycobalticinium hexafluorophosphate was precipitated by dropwise addition, with stirring, of saturated aqueous NH_4PF_6. Yield: 3.0 g (42%).

3.7. 1,1′-Diamidocobaltocenium hexafluorophosphate (*7*)

A 2.37 g (5.2 mmol) sample of 1,1′-dichlorocarboxycobaltocenium hexafluorophosphate was stirred with 30 ml of saturated aqueous ammonia solution for 3 h. Filtration afforded 1.98 g (72%) of product in the form of a dark-green solid. ^{1}H NMR (dmso-d_6, 300 MHz): δ 5.92 (t, 4H), 6.20 (t, 4H), 7.92 (s, 2H), 8.19 (s, 2H). *Anal.* Calc. for $C_{12}H_{12}O_2N_2PF_6Co$: C, 34.3; H, 2.88; N, 6.67. Found: C, 35.41; H, 2.86; N, 6.66%.

3.8. General procedures for X-ray crystallography

A crystal of appropriate size was mounted on a glass capillary using Paratone-N hydrocarbon oil. The crystal was transferred to a Siemens SMART [20] diffractome-

Table 1
Crystallographic details

	$[(C_5H_4NH_2)_2Co][PF_6]$ (**5**)	$[Fc(NH_2)_2][OTf]$ (**8**)
Molecular formula	$C_{10}H_{12}N_2CoPF_6$	$C_{11}H_{12}N_2F_3O_3SFe$
Formula weight	364.11	365.13
Crystal color, habit	Yellow plate	Dark-green plate
Crystal size (mm)	$0.25 \times 0.11 \times 0.08$	$0.24 \times 0.18 \times 0.13$
Crystal system	tetragonal	monoclinic
Space group	$P4_32_12$	$P2_1/c$
a (Å)	8.4488(4)	12.7632(4)
b (Å)	8.4488(4)	19.7746(6)
c (Å)	17.7001(8)	11.2156(3)
α (°)	90	90
β (°)	90	93.336(1)
γ (°)	90	90
V (Å^3)	1263.47(9)	2825.9(3)
Z	4	8
D_c (g cm^{-1})	1.914	1.716
Temperature (°C)	−140	−116
Radiation, λ (Å)	Mo Kα (0.71069)	Mo Kα (0.71069)
μ (cm^{-1})	15.49	12.58
T_{max}, T_{min}	0.86, 0.52	0.87, 0.46
R_{merge}	0.047	0.055
R, R_w	0.026, 0.029	0.041, 0.043
Goodness-of-fit	0.92	1.15
Largest shift/error	0.00	0.00
Maximum/minium (e Å^{-3})	0.25/−0.39	0.46/−0.76

ter/CCD area detector, centered in the beam, and cooled by a nitrogen flow low-temperature apparatus that had been previously calibrated by a thermocouple placed at the same position as the crystal. Preliminary orientation matrix and cell constants were determined by collection of sixty 10-s frames, followed by spot integration and least squares refinement. An arbitrary hemisphere of data was collected and the raw data were integrated using SAINT [21]. Data were analyzed for agreement and possible absorption using XPREP [22]. An empirical absorption correction based on comparison of redundant and equivalent reflections was applied using SADABS [23]. The data were corrected for Lorentz and polarization effects, but no correction for crystal decay was applied. Cell dimensions were calculated from all reflections with $I > 10\sigma(I)$. The structures were solved and refined with teXsan software package [24]. ORTEP diagrams were created using ORTEP-3 software package [25].

3.9. Crystallographic detail for $[(C_5H_4NH_2)_2Co][PF_6]$ (**5**)

Crystals were grown from CH_2Cl_2 −30 °C. X-ray quality crystals were grown from a CD_2Cl_2 solution. Based on the systematic absences the space group choice was narrowed to the enantiomorphic pair $P4_12_12/P4_32_12$ (#92/96). The structure was solved in $P4_12_12$, but $P4_32_12$ was chosen as the correct space group based on the Flack parameter and a lower R-factor ($R = 4.1\%$ in $P4_12_12$ and 2.6% in $P4_32_12$). All non-hydrogen atoms were refined anisotropically. The amine hydrogen atoms were located in a difference Fourier map and their positional parameters allowed to refine. The remaining hydrogen atoms were included in geometrically calculated positions and were not refined. (See Table 1.)

3.10. Crystallographic detail for $[Fc(NH_2)_2][OTf]$ (**8**)

Crystals were grown from CH_2Cl_2/CH_3CN at −30 °C. Space group $P2_1/c$ was assigned based on the systematic absences. All non-hydrogen atoms were refined isotropically. The amine hydrogen atoms were located in a difference Fourier map and their positional parameters allowed to refine. The remaining hydrogen atoms were included in geometrically calculated positions and were not refined. (See Table 1.)

4. Supplementary material

The crystal structures have been deposited at the Cambridge Crystallographic Data Centre and allocated the deposition numbers CCDC 240121, 240122. These data can be obtained free of charge from the Cambridge Crystallographic Data Centre, 12, Union Road, Cambridge CB2 1EZ, UK; Fax: +44-1223-336-033, e-mail: deposit@ccdc.ac.uk, or on the web: www.ccdc.cam.ac.uk.

Acknowledgement

We are grateful to the DOE for the support of this work (J.A.).

References

[1] A. Shafir, M.P. Power, G.D. Whitener, J. Arnold, Organometallics 19 (2000) 3978.
[2] A. Shafir, J. Arnold, J. Am. Chem. Soc. 123 (2001) 9212.
[3] A. Shafir, M.P. Power, G.D. Whitener, J. Arnold, Organometallics 20 (2001) 1365.
[4] A. Shafir, D. Fiedler, J. Arnold, J. Chem. Soc., Dalton Trans. (2002) 555.
[5] A. Shafir, J. Arnold, Inorg. Chim. Acta 345 (2003) 216.
[6] A. Shafir, J. Arnold, Organometallics 22 (2003) 567.
[7] V.C. Gibson, C.M. Halliwell, N.J. Long, P.J. Oxford, A.M. Smith, A.J.P. White, D.J. Williams, Dalton Trans. (2003) 918.
[8] V.C. Gibson, N.J. Long, E.L. Marshall, P.J. Oxford, A.J.P. White, D.J. Williams, J. Chem. Soc., Dalton Trans. (2001) 1162.
[9] V.C. Gibson, N.J. Long, A.J.P. White, C.K. Williams, D.J. Williams, Organometallics 21 (2002) 770.
[10] M. Herberhold, Angew. Chem., Int. Ed. Engl. 41 (2002) 956.
[11] U. Siemeling, T.C. Auch, O. Kuhnert, M. Malaun, H. Kopacka, B. Bildstein, Z. Anorg. Allg. Chem. 629 (2003) 1334.
[12] A. Tarraga, F. Oton, A. Espinosa, M.D. Velasco, P. Molina, D.J. Evans, Chem. Commun. (2004) 458.
[13] D. van Leusen, B. Hessen, Organometallics 20 (2001) 224.
[14] B. Wrackmeyer, E.V. Klimkina, W. Milius, Inorg. Chem. Commun. 7 (2004) 412.
[15] U. Siemeling, O. Kuhnert, B. Neumann, A. Stammler, H.-G. Stammler, B. Bildstein, M. Malaun, P. Zanello, Eur. J. Inorg. Chem. (2001) 913.
[16] S. Bradley, K.D. Camm, X. Liu, P.C. McGowan, K. Oughton, T.J. Podesta, M. Thornton-Pett, M.E. Walsh, Inorg. Chem. 41 (2002) 715.
[17] N. El Murr, J. Organomet. Chem. 112 (1976) 177.
[18] N. El Murr, J. Organomet. Chem. 112 (1976) 189.
[19] D.F. Evans, J. Chem. Soc. (1959) 2005.
[20] SMART Area-Detector Software package, Madison, WI, 1995.
[21] SAINT: SAX Area Detector Integration Program, Madison, WI, 1995.
[22] XPREP: Part of SHELXTL Crystal Structure Determination Package, Madison, WI, 1995.
[23] SADABS: Siemens Area Detector ABSsorption correction program, George Sheldrick, 1996. Advance copy, private communication.
[24] TeXsan: Crystal Structure Analysis Software Package, Molecular Structure Corporation, The Woodlands, TX, 1992.
[25] L.J. Farrugia, J. Appl. Cryst. 30 (1997) 565.

Available online at www.sciencedirect.com
SCIENCE DIRECT®
Polyhedron 23 (2004) 2943–2954
POLYHEDRON
www.elsevier.com/locate/poly

Aromatic and aldehyde carbon–hydrogen bond activation at cationic Rh(III) centers. Evaluation of electronic substituent effects on aldehyde binding and C–H oxidative addition

Britton K. Corkey [a], Felicia L. Taw [a], Robert G. Bergman [b,*], Maurice Brookhart [a,*]

[a] Department of Chemistry, University of North Carolina at Chapel Hill, CB #3290, Chapel Hill, NC 27599-3290, USA
[b] Department of Chemistry, University of California and Division of Chemical Sciences, Lawrence Berkeley National Laboratory, Berkeley, CA 94720-1460, USA

Received 4 June 2004; accepted 2 September 2004
Available online 26 October 2004

Dedicated to Malcolm L.H. Green for his pathbreaking contributions to organometallic chemistry, his international collegiality, his wit, and his warmth

Abstract

Cationic rhodium methyl complexes, $[Cp^*(PMe_3)Rh(Me)(CH_2Cl_2)]BAr'_4$ (**1**) and $[Cp^*(P(OMe)_3)Rh(Me)(CH_2Cl_2)]BAr'_4$ (**3**), react with benzene to yield the corresponding phenyl complexes, $[Cp^*(PMe_3)Rh(Ph)(CH_2Cl_2)]BAr'_4$ (**6**) and $[Cp^*(P(OMe)_3)Rh(Ph)(CH_2Cl_2)]BAr'_4$ (**7**). First-order rate constants observed in 1.1 M benzene in CD_2Cl_2 at 25 °C are $(2.1 \pm 0.2) \times 10^{-5}$ s^{-1} and $(1.9 \pm 0.2) \times 10^{-5}$ s^{-1}, respectively. Reactions of **1** and **3** with *p*-X-substituted benzaldehydes (X = $-CF_3$, $-CH_3$, and –OMe) initially produce the σ-aldehyde adducts, $[Cp^*(L)Rh(Me)(p\text{-}XC_6H_4CHO)]BAr'_4$ (L = PMe_3 (**15**), $P(OMe)_3$ (**16**)). Exchange of free with bound aldehyde occurs via a dissociative process and quantitative NMR rate measurements show that complexes of **1** exchange faster than those of **3** and that less basic aldehydes exchange faster than more basic aldehydes (*p*-$CF_3C_6H_4CHO$ > *p*-$CH_3C_6H_4CHO$ > *p*-$CH_3OC_6H_4CHO$). The aldehyde adducts undergo C–H bond activation to produce initially methane plus acyl aldehyde adducts, $[Cp^*(L)Rh(C(O)C_6H_4X)(p - XC_6H_4CHO)]BAr'_4$ (L = PMe_3 (**17**), $P(OMe)_3$ (**18**)). Rates of C–H activation are correlated with aldehyde exchange rates; activation barriers of weakly bound aldehydes are lower than more strongly bound aldehydes. In the case of L = PMe_3, decarbonylation of the aldehyde adducts occurs cleanly to form aryl carbonyl complexes, $[Cp^*(PMe_3)Rh(C_6H_4X)(CO)]BAr'_4$. For L = $P(OMe)_3$, decarbonylation is a more complicated process; some intermediates and products have been identified by NMR spectroscopy.
© 2004 Elsevier Ltd. All rights reserved.

Keywords: C–H bond activation; Rhodium(III); Benzene activation; Aldehyde activation

1. Introduction

Early examples of the oxidative addition reactions of alkane C–H bonds, leading to hydrido(alkyl)metal complexes, take place at metal centers in relatively low formal oxidation states. This has led to the general perception that electron-rich complexes are required in order to make this important oxidative addition process exergonic and therefore capable of generating stable products.

However, the platinum-based alkane functionalization reactions observed many years ago by Shilov and his coworkers [1], and the dehydrogenation

* Corresponding authors. Present address: Department of Chemistry, Los Alamos National Laboratory, Mailstop J514, Los Alamos, USA. Tel.: +1 505 6673968; fax: +1 505 6679905.
E-mail address: ftaw@lanl.gov (F.L. Taw).

0277-5387/$ - see front matter © 2004 Elsevier Ltd. All rights reserved.
doi:10.1016/j.poly.2004.09.005

reactions subsequently observed using high-valent iridium and rhenium complexes by the Crabtree [2] and Felkin [3] groups, were early indications that more electron-deficient metal centers could also undergo C–H oxidative addition. More recently, direct observation of C–H oxidative addition reactions at iridium (III) [4], as well as analogous reactions that take place in Pt(II) complexes [5], have made clear that such processes can occur at metal centers that are relatively electrophilic, and in some cases can be overall exergonic. This has given rise to a substantial increase in the number of studies directed toward alkane activation reactions involving higher-valent late transition metal complexes in recent years.

The cationic Ir(III) C–H oxidative addition reactions referred to above lead to relatively rare examples of organometallic positively-charged Ir(V) intermediates [6]. Many of these have been generated only in transient form, but a few have been found to be stable enough to isolate or detect in solution. In contrast to this growing body of research on Ir(III) C–H activation, much less attention has been directed toward the search for analogous reactions at Rh(III). In view of the fact that pentamethylcyclopentadienylrhodium(I) complexes were ultimately discovered to undergo C–H oxidative addition reactions analogous to those of their iridium congeners [7], we felt it would be interesting to look for Rh(III)-to-Rh(V) C–H oxidative addition reactions in related systems as well. This manuscript reports the results of our investigation of C–H bond activations of benzene and aryl aldehydes by $[Cp^*(L)Rh(Me)(CH_2Cl_2)]BAr'_4$ (L = PMe_3 (**1**), $P(OMe)_3$ (**3**)).

2. Results and discussion

2.1. Synthesis of cationic rhodium(III) methyl complexes, $[Cp^*(L)Rh(Me)(CH_2Cl_2)]BAr'_4$ (L = PMe_3 (**1**), $P(OMe)_3$ (**3**), Ar′ = 3,5-$(CF_3)_2C_6H_3$)

Synthesis of $[Cp^*(PMe_3)Rh(Me)(CH_2Cl_2)]BAr'_4$ (**1**) by treatment of Cp*(PMe_3)Rh(Me)(Cl) (**2**) with $NaBAr'_4$ has been previously reported by us [8]. This complex was fully characterized by NMR spectroscopy and X-ray diffraction studies. The phosphite analogue $[Cp^*(P(OMe)_3)Rh(Me)(CH_2Cl_2)]BAr'_4$ (**3**) was synthesized in a similar manner (Eq. (1)). The rhodium methyl chloride complex, Cp*($P(OMe)_3$)Rh(Me)(Cl) (**4**), was prepared by reaction of previously reported Cp*($P(OMe)_3$)$RhCl_2$ [9] with MeLi. The ^{1}H NMR spectrum of **3** in CD_2Cl_2 showed signals at 3.78 (d, $^3J_{P-H}$ = 11.4 Hz) for $P(OMe)_3$, 1.63 ppm (d, $^4J_{P-H}$ = 4.2 Hz) for Cp*, and 1.02 ppm (dd, $^3J_{P-H}$ = 5.5 Hz, $^2J_{Rh-H}$ = 1.5 Hz) for the Rh–CH_3 group. The $^{31}P\{^1H\}$ NMR signal appeared at 126.9 ppm (d, $^1J_{Rh-P}$ = 269 Hz), and the $^{13}C\{^1H\}$ NMR resonance of the Rh–CH_3 group exhibited a signal at 1.19 ppm (dd, $^2J_{P-C}$ = 37.1 Hz, $^1J_{Rh-C}$ = 22.0 Hz).

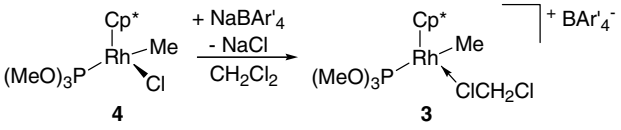

(1)

2.2. Carbon–hydrogen bond activation studies

In contrast to Bergman's cationic iridium (III) complex, $[Cp^*(PMe_3)Ir(Me)(CH_2Cl_2)]BAr'_4$ (**5**) [4b], the analogous rhodium methyl complex **1** does not react with alkanes to any appreciable extent, even at 45 °C. Addition of 500 equivalents of pentane to a CD_2Cl_2 solution of **1** resulted in the observation of only trace amounts of methane (by ^{1}H NMR) over the course of several days at 25 °C. Similar results were obtained with the corresponding Rh phosphite compound **3**. Given the inertness toward alkanes, studies of C–H bond activations using **1** and **3** focused on the more reactive substrates: benzene and aryl aldehydes.

2.3. Carbon–hydrogen bond activation of benzene

Rhodium methyl complexes **1** and **3** react with benzene to yield methane and the cationic rhodium phenyl complexes **6** and **7**, respectively (Eq. (2)). To further verify the structure of product **6**, this compound was independently synthesized and fully characterized by NMR spectroscopy and X-ray diffraction studies (see below). Product **7** was directly isolated from the C–H activation reaction of benzene and characterized by NMR spectroscopy.

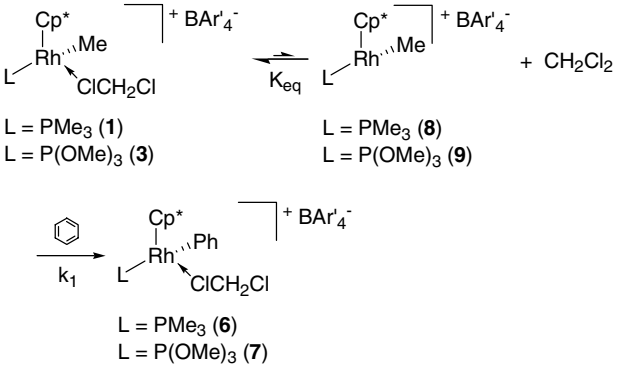

(2)

The rates of these reactions are sufficiently slow that clean conversions can be achieved only by using high ratios of benzene to rhodium complex. Under these conditions, the reactions exhibit clean pseudo-first order kinetics, as determined by integrations of ^{1}H NMR signals. Table 1 summarizes the observed first-order rate

Table 1
First-order rate constants for C–H activation of benzene by **1**, **3**, **5**, and **10**

$[Cp^*(L)M(Me)(CH_2Cl_2)]BAr'_4$	L = PMe_3	L = $P(OMe)_3$	Rate ratio
M = Rh[a]	$(2.1 \pm 0.2) \times 10^{-5}$ s^{-1}	$(1.9 \pm 0.2) \times 10^{-5}$ s^{-1}	(**1/3**) = 1.1
M = Ir[b]	$(8.4 \pm 0.8) \times 10^{-3}$ s^{-1}	$(3.0 \pm 0.3) \times 10^{-4}$ s^{-1}	(**5/10**) = 28.0

[a] 1.1 M C_6H_6 in CD_2Cl_2, 25 ± 2 °C.
[b] 0.26 M C_6H_6 in CD_2Cl_2, 0 °C.

constants for the reactions of **1** and **3** (0.02 M) with 1.1 M benzene in CD_2Cl_2 at 25 ± 2 °C. [1] For comparison, the reported rate constants [10] for the corresponding iridium analogues **5** and $[Cp^*(P(OMe)_3)Ir(Me)(CH_2Cl_2)]BAr'_4$ (**10**) reacting at 0 °C with 0.26 M benzene in CD_2Cl_2 are also listed.

In general, the iridium complexes **5** and **10** are far more reactive toward benzene than rhodium analogues **1** and **3**. Correcting for benzene concentrations, **5** reacts with benzene ca. 10^3 times faster than either **1** or **3** at a considerably lower temperature (0 °C vs. 25 °C). A significant feature of these comparisons is that, in the case of the Ir examples, the PMe_3 complex exhibits a rate ca. 30× that of the $P(OMe)_3$ complex; in contrast, the rates are comparable in the rhodium systems. Bergman has postulated that these reactions occur through the 16-electron species **11** and **12** (Eq. (3)) and that, while the presumably more electrophilic species **12** is expected to be more reactive (k_1 for $P(OMe)_3 > k_1$ for PMe_3), the value of K_{eq} for $P(OMe)_3$ is much less than K_{eq} for (PMe_3), resulting in $K_{eq(PMe_3)}k_{1(PMe_3)} > K_{eq(P(OMe)_3)}k_{1(P(OMe)_3)}$ [10]. In the case of the rhodium complexes, it appears that the $k_{1(PMe_3)} : k_{1(P(OMe)_3)}$ ratio is counterbalanced by the $K_{eq(P(OMe)_3)} : K_{eq(PMe_3)}$ ratio, and the observed rates of benzene activation are essentially equal (see Eq. (2)). The assumptions that Rh phosphite complex **9** is more electrophilic than the Rh phosphine complex **8** and that $K_{eq(PMe_3)} > K_{eq(P(OMe)_3)}$ receive independent support from observations described below in connection with the C–H bond activation of aryl aldehydes.

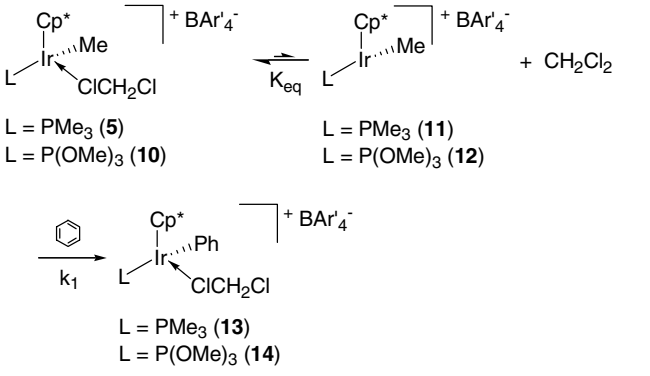

(3)

[1] Reactions of **1** and **3** in 2.2 M benzene in CD_2Cl_2 at 25 ± 2 °C give pseudo first-order rate constants of $(3.2 \pm 0.2) \times 10^{-5}$ s^{-1} and $(3.8 \pm 0.4) \times 10^{-5}$ s^{-1}, respectively. These data establish a clear dependence of the rate on benzene concentration.

2.4. Independent synthesis and characterization of $[Cp^*(PMe_3)Rh(Ph)(CH_2Cl_2)]BAr'_4$ (6)

To verify the identity of the product derived from C–H activation of benzene by rhodium methyl complex **1**, the cationic rhodium phenyl complex (**6**) was independently synthesized by adding $NaBAr'_4$ to a dichloromethane solution of previously reported $Cp^*(PMe_3)Rh(Ph)(Cl)$ [11]. X-ray quality, orange–red crystals of **6** were isolated in 70% yield. This compound is more thermally and air-sensitive than the rhodium methyl complex **1**, but can be stored under inert conditions at −30 °C for extended periods of time. An ORTEP diagram of **6** is shown in Fig. 1, with some selected bond distances and bond angles listed in Table 2. The bond distance between Rh and the ipso aryl carbon of the phenyl ring is 2.026(8) Å, which is shorter than the Rh–CH_3 bond length (2.106(5) Å) of complex **1** [8], as is expected for a metal bonded to an sp^2-hybridized carbon versus an sp^3 carbon. However, the Rh–Cl distance of phenyl complex **6** is 2.512(2) Å and differs only by 0.02 Å relative to the bond distance of 2.488(1) Å observed for the Rh–Cl bond of methyl complex **2** [8].

2.5. Carbon–hydrogen bond activation of aryl aldehydes

Bergman has shown that the iridium (III) complex $Cp^*(PMe_3)Ir(Me)(OTf)$ reacts rapidly with benzaldehyde at −80 °C to form an η^1-(O)-bound aldehyde

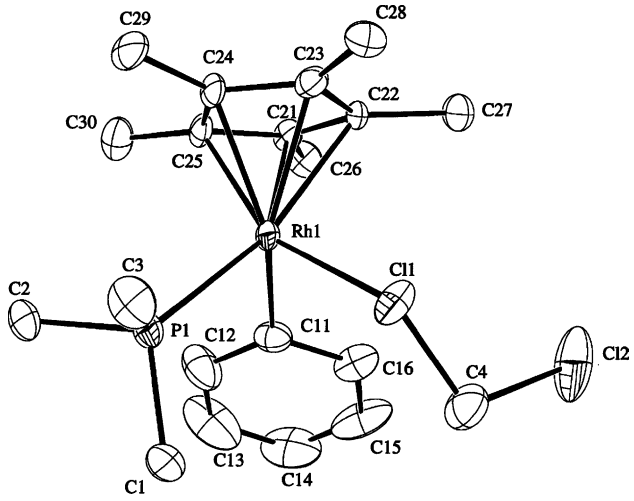

Fig. 1. ORTEP diagram of $[Cp^*(PMe_3)Rh(Ph)(CH_2Cl_2)]^+$ (**6**, BAr'_4^- counterion omitted for clarity).

Table 2
Selected bond distances and bond angles for complex **6**

	Bond distance (Å)		Bond angle (°)
Rh(1)–C(24)	2.195(6)	C(24)–Rh(1)–P(1)	101.5(2)
Rh(1)–P(1)	2.374(2)	C(11)–Rh(1)–Cl(1)	98.3(2)
Rh(1)–C(11)	2.026(8)	P(1)–Rh(1)–C(11)	87.9(3)
Rh(1)–Cl(1)	2.512(2)	P(1)–Rh(1)–Cl(1)	84.9(8)

adduct [12]. Upon warming to −60 °C, the adduct undergoes C–H bond activation and decarbonylation to form the iridium phenyl carbonyl complex, [Cp*(PMe_3)Ir(Ph)(CO)]OTf, and methane. Similarly, the cationic rhodium methyl complexes **1** and **3** react with aryl aldehydes (tolualdehyde, anisaldehyde, and 4-(trifluoromethyl)benzaldehyde) in CD_2Cl_2 at −80 °C to form η^1-aldehyde adducts (Eq. (4)).

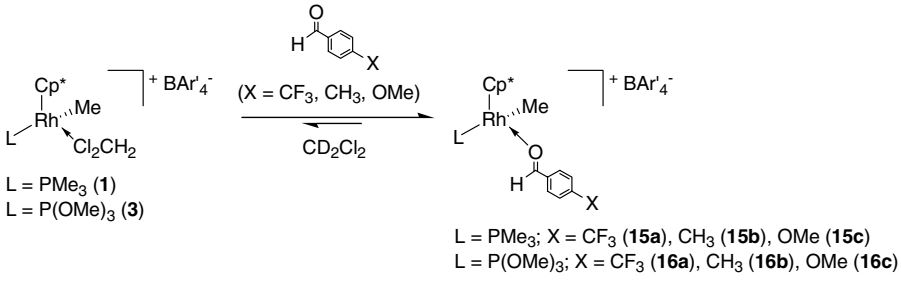

(4)

When reactions with **1** and **3** are carried out using excess aldehyde as substrate, ^{1}H NMR resonances for the aldehydic proton of both the bound and free aldehydes can be detected at low temperatures. The lack of rhodium coupling to the aldehydic hydrogen supports the η^1 structure. Upon warming, these resonances broaden and coalesce. The rates for loss of bound aldehydes from Rh were assessed by measuring the changes in line-width at half-height of the aldehydic protons and applying the slow exchange equation, $k = \pi(\Delta w)$. A key finding is that the linewidth and thus the rate of exchange of the bound aldehyde is *independent* of the concentration of free aldehyde. This clearly indicates the exchange occurs through a dissociative process. Table 3 summarizes the $\Delta G^{\ddagger}$ values obtained from line broadening experiments together with ^{1}H NMR shifts for free and bound aldehyde at −88 °C.

The trends follow the expected electronic effects. For both series **15a**–**15c** and **16a**–**16c** the order of dissociation is *p*-$CF_3C_6H_4CHO$ > *p*-$CH_3C_6H_4CHO$ > *p*-$CH_3OC_6H_4CHO$ which inversely parallels the order of basicity of the aldehydes. In comparing **15a**–**15c** with **16a**–**16c** in each of the three pairs the barrier to dissociation of aldehyde from the more electron-deficient $P(OMe)_3$ complex is ca. 1.7 kcal/mol higher than that for the more electron-rich PMe_3 complex. The strongest Rh(III)-aldehyde interaction is between the more electrophilic phosphite complex **16** and the most electron-rich aldehyde, *p*-$CH_3OC_6H_4CHO$. The weakest interaction is between the less electrophilic PMe_3 complex **15** and the most electron-deficient aldehyde, *p*-$CF_3C_6H_4CHO$.

The C–H activation chemistry of aryl aldehydes by rhodium complexes **1** and **3** is similar to the iridium chemistry but more complex in the case of **3**. Deinsertion products can react with **3** which complicates kinetic measurements and gives rise to a mixture of products. The most definitive kinetic studies were carried out using a large excess of aldehyde. First, this approach ensures that the equilibrium between the methylene chloride adducts **1** and **3** and the aldehyde adducts **15a**–**15c** and **16a**–**16c** lies strongly in favor of the aldehyde adducts. Second, and critical in the case of **3**, the C–H activation reactions result in generation of the Rh acyl aldehyde adducts **17** and **18**. Little deinsertion occurs under these conditions. The aldehyde adduct intermediate **15** or **16** builds up to high concentrations and clean first-order kinetics for conversion to **17** or **18**, respectively, are exhibited over ca. two half-lives (Eq. (5)). Rates and free energies of activation are summarized for these C–H bond activation reactions in Tables 4 and 5.

Table 3
Kinetic parameters for dissociation of bound aldehyde and ^{1}H NMR shifts (in ppm) for free and bound aldehyde at −88 °C

[Cp*(L)Rh(Me)(XC_6H_4CHO)]$^+$(η^1-aldehyde adduct)	k (s^{-1})	T (±2 °C)	$\Delta G^{\ddagger}$ (kcal/mol)	δ CHO (bound)	δ CHO (free)
L = PMe_3, X = CF_3 (**15a**)	50	−58	10.8 ± 0.1	9.38	10.02
L = PMe_3, X = CH_3 (**15b**)	60	−38	11.7 ± 0.2	9.13	9.87
L = PMe_3, X = OMe (**15c**)	75	−28	12.1 ± 0.2	8.97	9.79
L = $P(OMe)_3$, X = CF_3 (**16a**)	115	−18	12.4 ± 0.1	9.33	10.02
L = $P(OMe)_3$, X = CH_3 (**16b**)	105	0	13.4 ± 0.2	9.02	9.86
L = $P(OMe)_3$, X = OMe (**16c**)	110	7	13.7 ± 0.1	8.88	9.79

Table 4
k_{obs} of C–H activation using 50 equivalents of aldehyde (20 ± 2 °C)

$[Cp^*(L)Rh(Me)(XC_6H_4CHO)]^+(\eta^1$-aldehyde adduct)	L = PMe_3 (**15**)	L = $P(OMe)_3$ (**16**)	Rate ratio (**15**/**16**)
X = CF_3 (**a**)	$5.4 \pm 0.4 \times 10^{-4}$ s^{-1}	$5.2 \pm 0.3 \times 10^{-5}$ s^{-1}	10
X = CH_3 (**b**)	$2.1 \pm 0.1 \times 10^{-4}$ s^{-1}	$1.2 \pm 0.4 \times 10^{-5}$ s^{-1}	18
X = OMe (**c**)	$9.0 \pm 0.5 \times 10^{-5}$ s^{-1}	$2.9 \pm 0.3 \times 10^{-6}$ s^{-1}	31

Table 5
$\Delta G^{\ddagger}$ for activation of aldehydic C–H bonds (20 ± 2 °C)

$[Cp^*(L)Rh(Me)(XC_6H_4CHO)]^+(\eta^1$-aldehyde adduct)	L = PMe_3 (**15**)	L = $P(OMe)_3$ (**16**)
X = CF_3 (**a**)	21.5 ± 0.1 kcal/mol	22.9 ± 0.1 kcal/mol
X = CH_3 (**b**)	22.1 ± 0.1 kcal/mol	23.7 ± 0.1 kcal/mol
X = OMe (**c**)	22.6 ± 0.2 kcal/mol	24.6 ± 0.1 kcal/mol

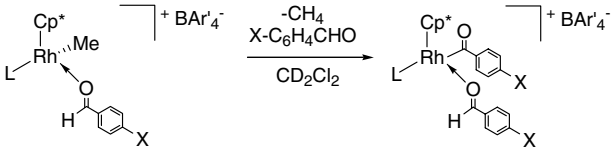

(5)

As noted earlier, C–H bond activation of benzene by **1** and **3** occurs at essentially equal rates. In these cases benzene is a weakly binding substrate and does not compete with CH_2Cl_2. That is, no benzene adduct is observed during the activation reaction. In the case of aryl aldehyde activation, the aldehyde adducts, **15a**–**15c** and **16a**–**16c**, rather than the CH_2Cl_2 adducts, are the more stable species, and as shown in Scheme 1, C–H bond activation is initiated from these species. The rates of C–H bond activation of these complexes correlate qualitatively with the rates of dissociation of the aldehydes. The more electron-rich PMe_3 complexes show higher rates of dissociation and higher rates of C–H bond activation than their $P(OMe)_3$ congeners. Similarly, the more electron-deficient aldehydes show faster rates of dissociation and higher rates of C–H bond activation (**15a** > **15b** > **15c**; **16a** > **16b** > **16c**). These rate trends can be rationalized by considering the expected substituent effects on the ground state aldehyde complexes relative to the transition state for C–H bond activation (Scheme 1). In the σ-aldehyde complexes there will be substantial partial positive charge on the carbonyl carbon due to polarization of the C=O π bond upon binding to the Lewis acidic Rh center. Ground state energies of these σ-complexes will be significantly affected by resonance and inductive effects of *para* substituents. In the four-centered transition state for C–H bond activation, Lewis acidic rhodium will no longer be bound exclusively to oxygen, thus *para*-substituent effects, especially π effects, should be less significant in affecting relative transition state energies. In short, electron-donating substituents will stabilize the aldehyde adducts **15** and **16** more than the corresponding transition states and thus retard the rate of C–H bond activation.

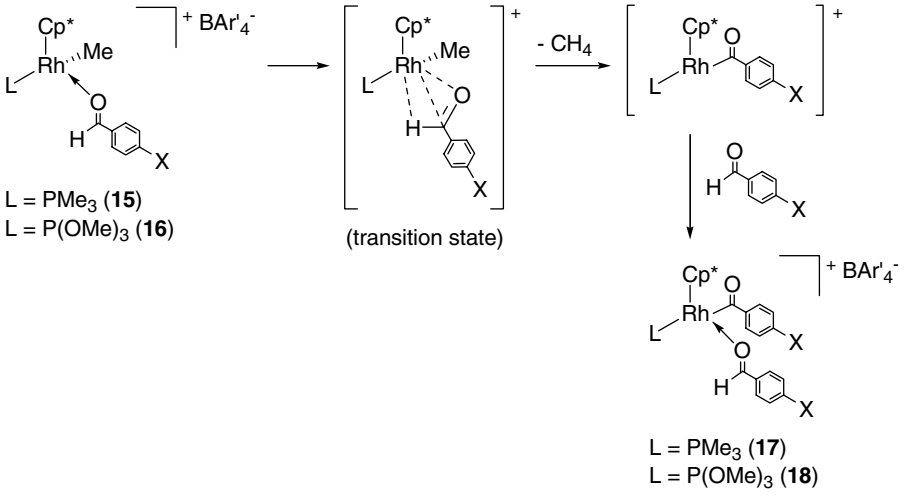

Scheme 1.

When 5 equivalents of tolualdehyde is allowed to undergo reaction with cationic Rh methyl complex **1** at room temperature, facile C–H bond activation and decarbonylation occurs, as evidenced by extrusion of methane and formation of $[Cp^*(PMe_3)Rh(C_6H_4CH_3)(CO)]BAr'_4$ (**19**). X-ray quality orange crystals of **19** were isolated via pentane layering of the reaction mixture. The ORTEP diagram is shown in Fig. 2, with some selected bond distances and bond angles listed in Table 6.

Contrary to the reaction described above between **1** and tolualdehyde, the reactions of Rh phosphite complex **3** with aryl aldehydes do not result in clean formation of decarbonylation products. A variety of species can be detected by ^1H and $^{31}P\{^1H\}$ NMR spectroscopy. The concentrations of these species fluctuate as a function of time, and vary with the particular aldehyde used along with the initial ratio of Rh complex to aldehyde. In the case of the reaction between **3** and tolualdehyde, several reaction products and intermediates have been identified by independent synthesis. Prior to proposing a sequence of reactions for the C–H activation and decarbonylation process, generation of potential intermediates is outlined below.

The ^{13}C-labeled Rh methyl carbonyl complex, $[Cp^*(P(OMe)_3)Rh(Me)(^{13}CO)]BAr'_4$ (**20′**), was readily generated in situ by exposure of a CD_2Cl_2 solution of **3** to ^{13}CO at 25 °C (Eq. (6)).

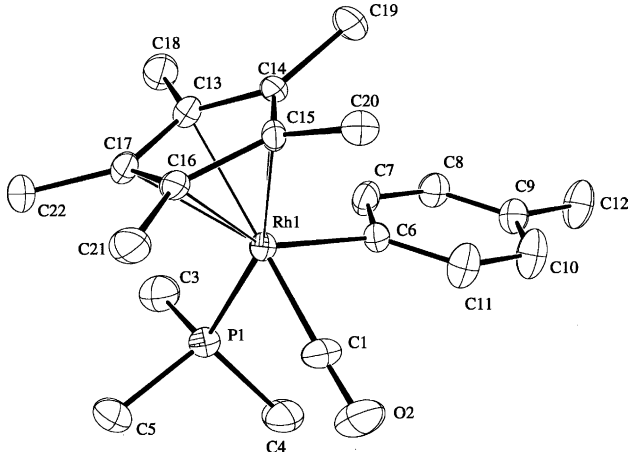

Fig. 2. ORTEP diagram of $[Cp^*(PMe_3)Rh(C_6H_4CH_3)(CO)]^+$ (**19**, BAr'^-_4 counterion omitted for clarity).

Table 6
Selected bond distances and bond angles for complex **19**

	Bond distance (Å)		Bond angle (°)
Rh(1)–C(16)	2.246(7)	C(16)–Rh(1)–P(1)	124.3(2)
Rh(1)–P(1)	2.298(3)	C(6)–Rh(1)–C(1)	89.4(3)
Rh(1)–C(6)	2.091(8)	P(1)–Rh(1)–C(6)	87.2(2)
Rh(1)–C(1)	1.879(8)	P(1)–Rh(1)–C(1)	89.0(3)
C(1)–O(2)	1.134(10)	Rh(1)–C(1)–O(2)	174.6(8)

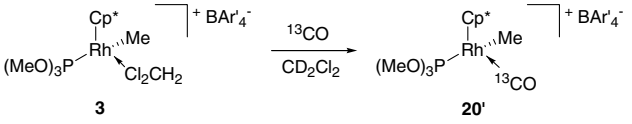

(6)

The corresponding ^{13}C-labeled Rh tolyl carbonyl complex, $[Cp^*(P(OMe)_3)Rh(C_6H_4CH_3)(^{13}CO)]BAr'_4$ (**21′**), was generated by an analogous reaction using $[Cp^*(P(OMe)_3)Rh(C_6H_4CH_3)(CH_2Cl_2)]BAr'_4$ (**22**), as shown in Scheme 2. The independent synthesis and characterization of **22** is detailed in Section 4. Interestingly, formation of **21′** by exposure of a CD_2Cl_2 solution of **22** to ^{13}CO was accompanied by formation of a rhodium acyl carbonyl complex (**23′**), which results from migratory insertion of carbon monoxide from **21′** followed by trapping with additional ^{13}CO (Scheme 2). Addition of excess $P(OMe)_3$ to a mixture of **21′** and **23′** led to the Rh bis-phosphite acyl complex $[Cp^*(P(OMe)_3)_2Rh(^{13}C(O)C_6H_4CH_3)]BAr'_4$ (**24′**). To generate Rh tolyl aldehyde adduct **25**, excess tolualdehyde was added to a CD_2Cl_2 solution of **22** (Scheme 2). NMR parameters for these species, which have been generated in situ, are summarized in Section 4.

Scheme 3 summarizes a proposed reaction sequence which accounts for the various species observed during the C–H activation and decarbonylation process involving cationic Rh methyl **3** and tolualdehyde. This reaction proceeds over the course of several days at room temperature, and was monitored by NMR spectroscopy.

As noted above, treatment of **3** with excess tolualdehyde (25–50 equivalents) results in immediate formation of Rh aldehyde adduct **16b**. After ca. 4 days, the C–H activation product, Rh acyl aldehyde **18b**, is formed as the major species (Scheme 3). Exchange of free aldehyde with bound aldehyde in **18b** is rapid at room temperature, but distinct aldehydic proton resonances for free and η^1-bound aldehyde could be observed by ^1H NMR spectroscopy at −88 °C. Treatment of **18b** with one equivalent of $P(OMe)_3$ results in complete conversion to the Rh bis-phosphite acyl complex $[Cp^*(P(OMe)_3)_2Rh(C(O)C_6H_4CH_3)]BAr'_4$ (**24**). In addition to the presence of **18b** as the major species, the Rh tolyl carbonyl complex $[Cp^*(P(OMe)_3)Rh(C_6H_4CH_3)(CO)]BAr'_4$ (**21**) and the Rh methyl carbonyl complex $[Cp^*(P(OMe)_3)Rh(Me)(CO)]BAr'_4$ (**20**) were also detected, along with small amounts of unidentified rhodium compounds (Scheme 3). Formation of **20** can be attributed to transfer of CO from **21** to either **3** (CO displaces coordinated dichloromethane) or **16b** (CO displaces coordinated aldehyde).

Treatment of **3** with 5 equivalents of tolualdehyde results in formation of **16b**, which decays predominantly to **20** and **21**. In this case we see very little build-up of

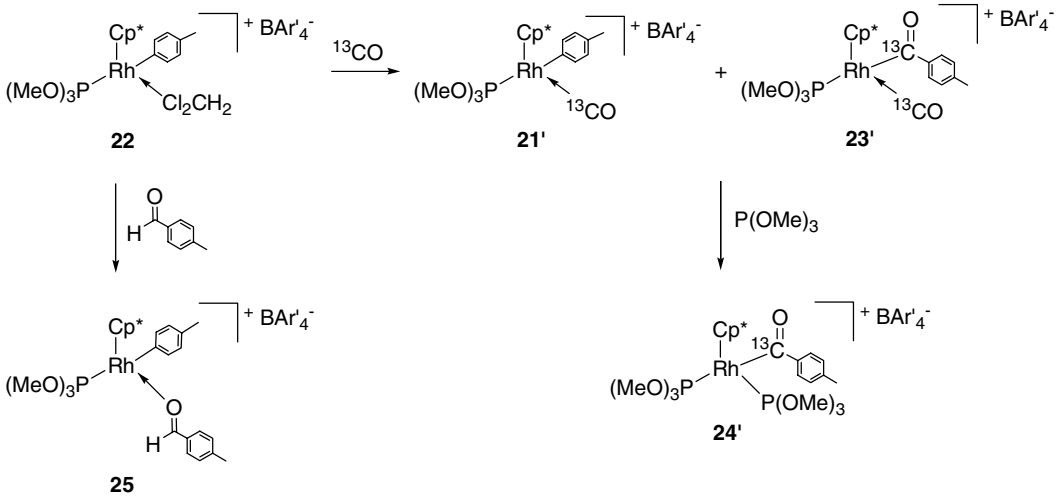

Scheme 2.

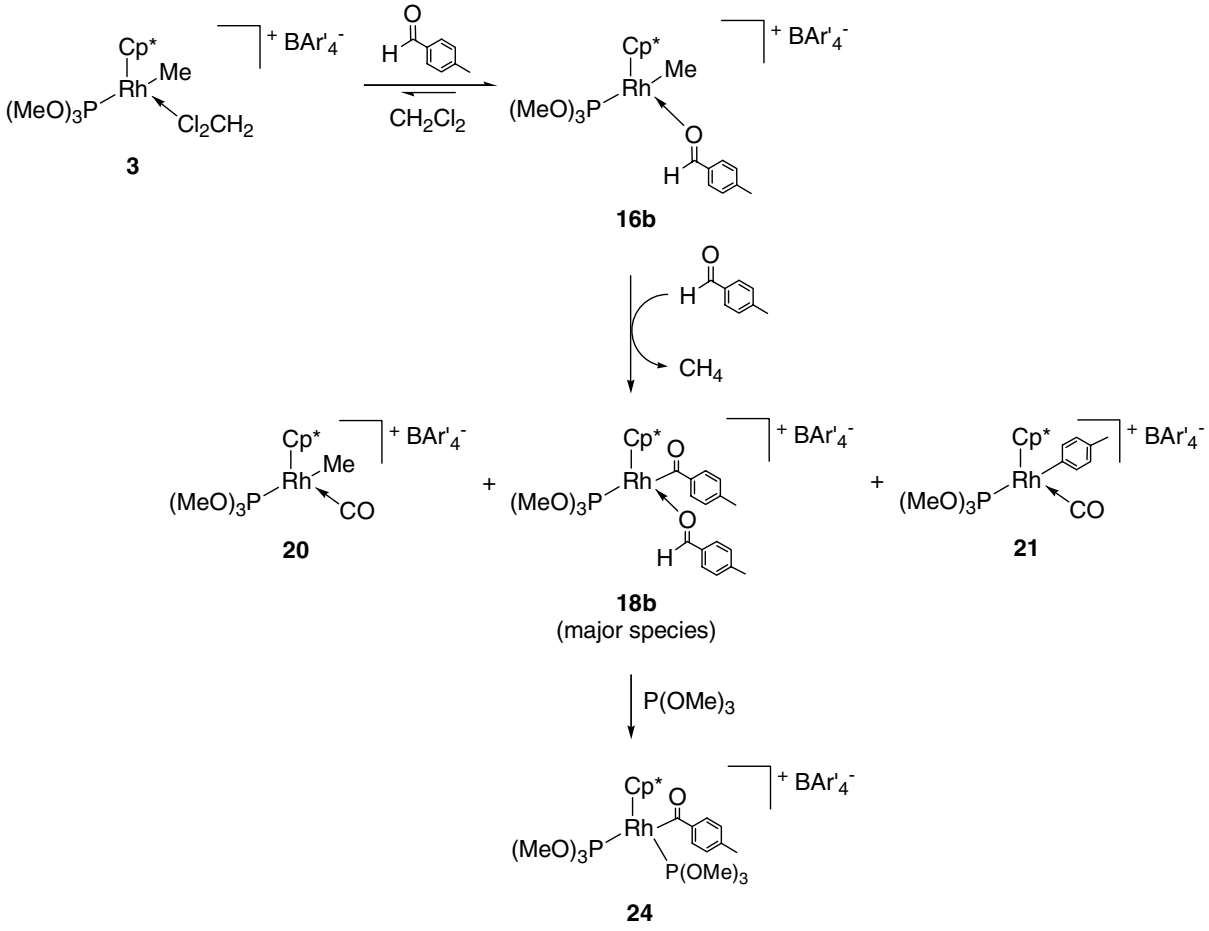

Scheme 3.

18b due to the low concentration of aldehyde present. After 16 days, the only identifiable product remaining is Rh methyl carbonyl **20**, which presumably, is the most stable species. When anisaldehyde or 4-(trifluoromethyl)benzaldehyde are used in the reaction with **3**, similar reactivity patterns emerge. However, the Rh acyl anisaldehyde adduct (the analogue of **18b**) is more stable than the Rh acyl tolualdehyde adduct (**18b**) due to the

tighter binding of the more basic anisaldehyde. The least basic aldehyde, 4-(trifluoromethyl)benzaldehyde, forms the least stable Rh acyl aldehyde adduct.

3. Conclusions

The work described here has provided new insights into the primary steps involved in C–H activation reactions that occur at cationic Group 9 M(III) centers. It has also revealed significant differences between the way such reactions take place at rhodium and iridium. Specifically, the focus on rhodium in this work has allowed us to measure the rates of exchange of free and bound aldehyde in the rhodium aldehyde complexes **15** and **16**. It has also revealed that in the presence of high concentrations of aldehyde, Rh acyl complexes, formed by decarbonylation of aryl aldehydes, can be stabilized by coordination of a second molecule of aldehyde, leading to cationic Rh acyl aldehyde complexes that are stable enough to be characterized in solution.

Our ability to observe the coordination and exchange of aldehyde at cationic Rh(III), and the subsequent C–H activation reaction, has allowed us to examine and compare the electronic effects on both processes. The factors that contribute to strong or weak aldehyde binding to the Rh^+ center appear to be dominated by σ-donation effects, as one would expect for a relatively electrophilic metal center. The rates of exchange and C–H activation are strongly correlated. The primary influence on the overall C–H activation rate is a ground state effect: when the aldehyde is strongly bound to the Rh^+ center, this binding retards its rearrangement to the transition state for C–H activation. Conversely, a more loosely-held aldehyde rearranges more easily to the transition state, facilitating the C–H activation process. Thus this system reflects a property often noted for enzymes: strong coordination of substrate to an active site does not necessarily promote efficient catalysis, and in fact can have the opposite effect [13]. The optimum situation for catalysis involves relatively weak binding of substrate in the ground state, so that this interaction does not counteract the binding energy of the rearranging substrate to the active site in the transition state.

4. Experimental

4.1. General considerations

Unless otherwise noted, all reactions and manipulations were performed using standard high-vacuum, Schlenk, or drybox techniques. Argon and nitrogen were purified by passage through columns of BASF R3-11 catalyst (Chemalog) and 4 Å molecular sieves. ^1H and ^{13}C NMR chemical shifts were referenced to residual ^1H and ^{13}C NMR signals of the deuterated solvents, respectively. ^{31}P NMR chemical shifts were referenced to an 85% H_3PO_4 sample used as an external standard. Elemental analyses were performed by Atlantic Microlab Inc. of Norcross, GA.

4.2. Materials

All solvents were deoxygenated and dried via passage over a column of activated alumina [14]. Deuterated solvents (Cambridge Isotope Laboratories) were purified by vacuum transfer from CaH_2 and stored over 4 Å molecular sieves. Unless otherwise noted, all chemicals were purchased from Aldrich and used without further purification. ^{13}C-labeled CO was purchased from Cambridge Isotope Laboratories. $NaBAr'_4$ was purchased from Boulder Scientific and used without further purification. Solutions of 1.5 M MeLi and PhLi in Et_2O were purchased from Acros and used without further purification. Organometallic complexes **1** [8], **2** [15], Cp*(P(OMe)$_3$)$RhCl_2$ [9], and Cp*(PMe_3)Rh(Ph)(Cl) [11] have been previously reported and were synthesized according to literature procedures.

4.3. Spectral data for BAr'^-_4

The ^1H and ^{13}C NMR resonances of the BAr'_4 (Ar′ = 3,5-$(CF_3)_2C_6H_3$) counteranion in CD_2Cl_2 were essentially invariant for all cationic complexes discussed here and spectroscopic data are not repeated for each compound. ^1H NMR (400 MHz, CD_2Cl_2) δ 7.73 (s, 8 H, H_{ortho}), 7.57 (s, 4 H, H_{para}). $^{13}C\{^1H\}$ NMR (101 MHz, CD_2Cl_2) δ 161.9 (q, $^1J_{C-B} = 49.8$, C_{ipso}), 135.0 (s, C_{ortho}), 129.0 (q, $^2J_{C-F} = 31.4$, C_{meta}), 124.7 (q, $^1J_{C-F} = 272.6$, CF_3), 117.7 (s, C_{para}).

4.4. Synthesis of $[Cp^*(P(OMe)_3)Rh(Me)(CH_2Cl_2)]BAr'_4$ (**3**)

A vial was charged with 172 mg (0.412 mmol) of **4** and 408 mg (0.461 mmol) of $NaBAr'_4$. The reactants were dissolved in 5 mL of CH_2Cl_2 and the resulting mixture was stirred for 5 min. The contents were filtered and stored at −35 °C for 24 h. Red–orange crystals of **3** were isolated in 55% yield. ^1H NMR (300 MHz, CD_2Cl_2) δ 5.33 (s, CH_2Cl_2), 3.78 (d, $^3J_{P-H} = 11.4$ Hz, 9 H, P(OMe)$_3$), 1.63 (d, $^4J_{P-H} = 4.2$ Hz, 15 H, Cp*), 1.02 (dd, $^3J_{P-H} = 5.5$ Hz, $^2J_{Rh-H} = 1.5$ Hz, 3 H, Me). $^{31}P\{^1H\}$ NMR (121.5 MHz, CD_2Cl_2) δ 126.9 (d, $^1J_{Rh-P} = 268.6$ Hz, P(OMe)$_3$). $^{13}C\{^1H\}$ NMR (101 MHz, CD_2Cl_2) δ 103.3 (s, Cp*–Ar), 54.34 (d, $^2J_{P-C} = 8.0$ Hz, P(OMe)$_3$), 54.19 (s, CH_2Cl_2), 9.16 (d, $^3J_{P-C} = 1.4$ Hz, Cp*–Me), 1.19 (dd, $^2J_{P-C} = 37.1$ Hz, $^1J_{Rh-C} = 22.0$ Hz, Me).

4.5. Synthesis of $Cp^*(P(OMe)_3)Rh(Me)(Cl)$ (**4**)

To a flame-dried Schlenk flask under argon, 2.5 g (6.9 mmol) of $Cp^*(P(OMe)_3)RhCl_2$ was dissolved in 100 mL dry ether. The solution was cooled to −78 °C and methyllithium (7.6 mmol in THF) was added to the solution, which was then brought to room temperature. The reaction was opened to air and quenched with 10 mL of water, the ether phase was removed, and the red/orange product isolated by roto-evaporation. The crude product was dissolved in 20 mL CH_2Cl_2 to which hexanes were added (50 mL) until the solution became cloudy. Red–orange crystals were isolated in 50% yield. ^1H NMR (300 MHz, CD_2Cl_2) δ 3.68 (d, $^3J_{P-H}$ = 11.4 Hz, 9 H, $P(OMe)_3$), 1.61 (d, $^4J_{P-H}$ = 4.1 Hz, 15 H, Cp*), 0.73 (dd, $^3J_{P-H}$ = 5.1 Hz, $^2J_{Rh-H}$ = 2.1 Hz, 3 H, Me). $^{31}P\{^1H\}$ NMR (121.5 MHz, CD_2Cl_2) δ 138.36 (d, $^1J_{Rh-P}$ = 259.9 Hz, $P(OMe)_3$). $^{13}C\{^1H\}$ NMR (101 MHz, CD_2Cl_2) δ 100.00 (vt, $^1J_{Rh-C} = {}^2J_{P-C}$ = 4. 2 Hz, Cp*–Ar), 53.00 (d, $^2J_{P-C}$ = 4.38 Hz, $P(OMe)_3$), 8.94 (d, J = 2.25 Hz, Cp*–Me), −2.57 (dd, $^1J_{Rh-C}$ = 22.2 Hz $^2J_{P-C}$ = 20.6 Hz, Me).

4.6. Synthesis of $[Cp^*(PMe_3)Rh(Ph)(CH_2Cl_2)]BAr'_4$ (**6**)

A Schlenk flask was charged with 50 mg (0.117 mmol) of $Cp^*(PMe_3)Rh(Ph)(Cl)$ and 109 mg (0.123 mmol) of $NaBAr'_4$ and sealed with a rubber stopper. The flask was placed in an ice bath and 5 mL of CH_2Cl_2 was introduced via syringe. The contents of the flask were stirred for 5 min and then filtered through Celite supported by a glass frit. The filtrate was concentrated in vacuo and the flask placed in a freezer (−30 °C) for 3 d. Orange–red crystals of **6** (110 mg, 0.082 mmol) were isolated in 70% yield and can be stored at −30 °C for weeks. ^1H NMR (400 MHz, CD_2Cl_2, 0 °C) δ 7.19 (br m, 2 H, Ph), 7.07 (br m, 3 H, Ph), 5.33 (s, CH_2Cl_2), 1.51 (d, $^4J_{P-H}$ = 2.7 Hz, 15 H, Cp*), 1.46 (d, $^2J_{P-H}$ = 10.1 Hz, 9 H, PMe_3). $^{31}P\{^1H\}$ NMR (162 MHz, CD_2Cl_2, 0 °C) δ 1.1 (d, $^1J_{Rh-P}$ = 168.2 Hz, PMe_3). $^{13}C\{^1H\}$ NMR (101 MHz, CD_2Cl_2, 0 °C) δ 158.3 (dd, $^1J_{Rh-C}$ = 32.0 Hz, $^2J_{P-C}$ = 17.5 Hz, Ph–C_{ipso}), 136.2 (d, $^2J_{Rh-C}$ = 4.6 Hz, Ph–C_{ortho}), 130.2 (s, Ph–C_{meta}), 125.1 (s, Ph–C_{para}), 103.1 (s, Cp*–Ar), 54.1 (s, CH_2Cl_2), 15.31 (d, $^1J_{P-C}$ = 32.0 Hz, PMe_3), 9.66 (s, Cp*–Me).

4.7. Synthesis of $[Cp^*(P(OMe)_3)Rh(Ph)(CH_2Cl_2)]BAr'_4$ (**7**)

In a J-Young NMR tube, 15.9 mg (0.01 mmol) of **3** was dissolved in 0.5 mL of 1.1 M benzene in CD_2Cl_2. After 24 h, the volatile materials were removed to yield a light orange powder in quantitative yields. ^1H NMR (400 MHz, CD_2Cl_2) δ 7.30 (m, 5 H, Ph), 3.74 (d, $^3J_{P-H}$ = 11.2 Hz, 9 H, $P(OMe)_3$), 1.56 (d, $^4J_{P-H}$ = 4.4 Hz, 15 H, Cp*). $^{31}P\{^1H\}$ NMR (162 MHz, CD_2Cl_2) δ 121.7 Hz (d, $^1J_{Rh-P}$ = 268.4 Hz, $P(OMe)_3$).

4.8. Generation of $[Cp^*(P(OMe)_3)Rh(Me)(p\text{-}CH_3C_6H_4CHO)]BAr'_4$ (**16b**)

In a J-Young NMR tube 15.0 mg (0.01 mmol) of **3** was dissolved in 0.5 mL CD_2Cl_2, and tolualdehyde (5 equivalents, 6.0 μL, 0.055 mmol) was added to the solution. At −68 °C, **16b** and the aldehydic protons of both the bound and free aldehyde were observable by NMR spectroscopy. ^1H NMR (300 MHz, CD_2Cl_2, −68 °C) δ 9.11 (s, 1 H, $CH_3C_6H_4CO$-*H*), 3.69 (d, $^3J_{P-H}$ = 11.7 Hz, 9 H, $P(OMe)_3$), 1.64 (d, $^4J_{P-H}$ = 4.2 Hz, 15 H, Cp*), 0.96 (dd, $^3J_{P-H}$ = 5.4 Hz, $^2J_{Rh-H}$ = 1.6 Hz, 3 H, Me). $^{31}P\{^1H\}$ NMR (121.5 MHz, CD_2Cl_2, −68 °C) δ 132.1 Hz (d, $^1J_{Rh-P}$ = 266 Hz, $P(OMe)_3$).

4.9. Generation of $[Cp^*(P(OMe)_3)Rh(C(O)C_6H_4CH_3)(p\text{-}CH_3C_6H_4CHO)]BAr'_4$ (**18b**)

In a J-Young NMR tube 15.0 mg (0.01 mmol) of **3** was dissolved in 0.5 mL CD_2Cl_2 and 50 μL of tolualdehyde was added to the solution. After 3 days, the solution was cooled to −68 °C to allow for the resolution (by NMR spectroscopy) of the aldehydic proton of bound aldehyde in **18b**.^1H NMR (300 MHz, CD_2Cl_2, −68 °C) δ 9.58 (s, 1 H, $CH_3C_6H_4CO$–*H*), 3.81 (d, $^3J_{P-H}$ = 11.1 Hz, 9 H, $P(OMe)_3$), 1.71 (d, $^4J_{P-H}$ = 5.3 Hz, 15 H, Cp*). $^{31}P\{^1H\}$ NMR (121.5 MHz, CD_2Cl_2, −68 °C) δ 115.4 Hz (d, $^1J_{Rh-P}$ = 235 Hz, $P(OMe)_3$).

4.10. Synthesis of $[Cp^*(PMe_3)Rh(C_6H_4CH_3)(CO)]BAr'_4$ (**19**)

A Schlenk flask was charged with 30 mg (0.023 mmol) of **1** and 1 mL of dichloromethane. A dichloromethane solution of tolualdehyde (0.115 mmol) was added via syringe and the contents of the flask were allowed to stir overnight. To afford crystals, 1 mL of pentane was added and the flask placed in a freezer at −30 °C. After 6 d, 12 mg (0.0093 mmol) of X-ray quality orange crystals were isolated in 39% yield. ^1H NMR (400 MHz, CD_2Cl_2) δ 6.99 (d, ^3J = 7.7 Hz, 2 H, tolyl-Ar), 6.91 (d, $^3J_{H-H}$ = 7.7 Hz, 2 H, tolyl-Ar), 2.28 (s, 3 H, tolyl-Me), 1.84 (d, $^4J_{P-H}$ = 2.9 Hz, 15 H, Cp*), 1.50 (d, $^2J_{P-H}$ = 10.8 Hz, 9 H, PMe_3). $^{31}P\{^1H\}$ NMR (162 MHz, CD_2Cl_2) δ 4.1 (d, $^1J_{Rh-P}$ = 129.1 Hz, PMe_3). $^{13}C\{^1H\}$ NMR (101 MHz, CD_2Cl_2) δ 188.8 (dd, $^1J_{Rh-C}$ = 72.5 Hz, $^2J_{P-C}$ = 21.9 Hz, CO), 138.5 (br m, C_{ipso} of tolyl-Ar), 136.0 (s, tolyl-Ar), 131.9 (s, tolyl-Ar), 130.1 (s, tolyl-Ar), 107.6 (s, Cp*–Ar), 20.59 (s, tolyl-Me), 16.43 (d, $^1J_{P-C}$ = 35.6 Hz, PMe_3), 9.89 (s, Cp*–Me). *Anal.* Calc. for $C_{53}H_{43}OBF_{24}PRh$: C, 49.10; H, 3.34. Found: C, 48.93; H, 3.12%.

4.11. Synthesis of $[Cp^*(P(OMe)_3)Rh(p\text{-}C_6H_4CH_3)(CH_2Cl_2)]BAr'_4$ (**22**)

In the glove box, a vial was charged with 36 mg (0.075 mmol) of $Cp^*(P(OMe)_3)Rh(C_6H_4\ CH_3)(Cl)$ (see below for synthesis of this compound) and 72 mg (0.081 mmol) of $NaBAr'_4$. The reactants were dissolved in 2 mL of CH_2Cl_2. The contents were filtered and stored at −35 °C for 24 h. An orange powder was isolated in 40% yield. ^1H NMR (300 MHz, CD_2Cl_2) δ 6.95 (d, $J = 8.1$ Hz, 2 H, tolyl-H), 7.26 (d, J = 7.2 Hz, 2 H, tolyl-H), 3.68 (d, $^3J_{P-H} = 10.8$ Hz, 9 H, $P(OMe)_3$), 2.24 (s, 3 H, tolyl-CH_3), 1.48 (d, $^4J_{P-H} = 4.5$ Hz, 15 H, Cp*). $^{31}P\{^1H\}$ NMR (121.5 MHz, CD_2Cl_2) δ 126.8 Hz (d, $^1J_{Rh-P} = 260$ Hz, $P(OMe)_3$). $^{13}C\{^1H\}$ NMR (75.5 MHz, CD_2Cl_2) δ 131.1 (s, tolyl-Ar) 102.6 (s, Cp*–Ar), 54.72 (d, $^2J_{P-C} = 7.6$ Hz, $P(OMe)_3$), 20.44 (s, tolyl-Me), 8.71 (s, Cp*–Me).

4.12. Synthesis of $Cp^*(P(OMe)_3)Rh(C_6H_4CH_3)(Cl)$

To a flame dried Schlenk flask under argon, $Cp^*(P(OMe)_3)RhCl_2$ was dissolved in 40 mL dry THF and the resulting solution was cooled to −78 °C. Tolyl-lithium (2.3 equivalents, 321 mg, 3.28 mmol) [16] was dissolved in 10 mL of THF, and the resulting solution was cooled to −78 °C and cannula-transferred into a stirred solution of $Cp^*(P(OMe)_3)RhCl_2$ at which point the color changed from red to orange. After being brought to room temperature the solvent was removed to yield an orange foam, which was then extracted with 3×20 mL toluene and filtered through celite. Concentration of this solution under vacuum yielded a red oil which, upon addition of pentane and cooling to −78 °C afforded an orange powder in 46% yield. ^1H NMR (300 MHz, CD_2Cl_2) δ 7.36 (d, $J = 7.2$ Hz, tolyl-H), 6.80 (d, $J = 7.6$ Hz, tolyl-H), 3.49 (d, $^3J_{P-H} = 11.4$ Hz, 9 H, $P(OMe)_3$), 2.22 (s, tolyl-Me), 1.50 (d, $^4J_{P-H} = 4.1$ Hz, 15 H, Cp*), $^{31}P\{^1H\}$ NMR (121.5 MHz, CD_2Cl_2) δ 135.56 (d, $^1J_{Rh-P} = 247.0$ Hz, $P(OMe)_3$). $^{13}C\{^1H\}$ NMR (101 MHz, CD_2Cl_2) δ 139.41 (s, tolyl-Ar), 131.97 (s, tolyl-Ar), 128.93 (s, tolyl-Ar), 101.60 (d, $J = 4.6$ Hz, Cp*–Ar), 53.66 (d, $^3J_{P-C} = 4.6$ Hz, $P(OMe)_3$), 21.14 (s, tolyl-*C* H_3), 9.29 (d, $J = 1.61$ Hz, Cp*–Me).

4.13. Synthesis of $[Cp^*(P(OMe)_3)Rh(C_6H_4CH_3)(p\text{-}CH_3C_6H_4CHO)]\ BAr'_4$ (**25**)

In a J-Young NMR tube 15.0 mg (0.010 mmol) of **22** was dissolved in 0.5 mL CD_2Cl_2 and 25 μL of tolualdehyde was added to the solution. The solution was cooled to −68 °C to allow for the resolution of the aldehydic proton of bound aldehyde. ^1H NMR (300 MHz, CD_2Cl_2, −68 °C) δ 8.98 (s, *p*-$CH_3C_6H_4CO$-*H*), 6.95 (d, J = 7.7 Hz, 2 H, tolyl-H), 7.26 (d, partially obscured, 2 H, *m*-Ar–H), 3.68 (d, $^3J_{P-H} = 10.8$ Hz, 9 H, $P(OMe)_3$), 2.13 (s, 3 H, tolyl-CH_3), 1.50 (d, $^4J_{P-H} = 4.5$ Hz, 15 H, Cp*). $^{31}P\{^1H\}$ NMR (121.5 MHz, CD_2Cl_2, −68 °C) δ 126.8 Hz (d, $^1J_{Rh-P} = 260$ Hz, $P(OMe)_3$).

4.14. Generation of $[Cp^*(P(OMe)_3)Rh(Me)(^{13}CO)]BAr'_4$ (**20′**)

In a J-Young NMR tube 15.0 mg (0.011 mmol) of **3** was dissolved in 0.5 mL CD_2Cl_2. The solution was subject to three freeze–pump–thaw cycles, at which point the headspace of the tube was backfilled with ^{13}CO. Upon shaking of the tube, the solution turned from orange to light yellow. ^1H and ^{31}P NMR spectroscopy showed complete conversion of **3** to **20′**. ^1H NMR (300 MHz, CD_2Cl_2) δ 3.77 (d, $^3J_{P-H} = 12.0$ Hz, 9 H, $P(OMe)_3$), 1.87 (d, $^4J_{P-H} = 4.8$ Hz, 15 H, Cp*), 0.78 (dd, $^3J_{P-H} = 3.9$ Hz, $^2J_{Rh-H} = 2.1$ Hz, 3 H, Me). $^{31}P\{^1H\}$ NMR (121.5 MHz, CD_2Cl_2) δ 121.6 Hz (d, $^1J_{Rh-P} = 217$ Hz, $P(OMe)_3$). $^{13}C\{^1H\}$ NMR (101 MHz, CD_2Cl_2) δ 187.1 (dd, $^1J_{Rh-C} = 70.7$ Hz, $^2J_{P-C} = 32.0$ Hz, ^{13}CO).

4.15. Generation of $[Cp^*(P(OMe)_3)Rh(C_6H_4CH_3)(^{13}CO)]BAr'_4$ (**21′**)

A J-Young tube with 35 mg of **22** in 0.5 mL CD_2Cl_2 was freeze–pump-thawed three times and backfilled with ^{13}CO. The solution was shaken, and excess ^{13}CO was evacuated from the headspace and backfilled with argon while the solution was frozen. ^1H, ^{13}C and ^{31}P NMR spectroscopy showed the presence of both **21′** and **23′** (see below) in solution. ^1H NMR (300 MHz, CD_2Cl_2) δ 6.98 (d, $J = 7.8$ Hz, 2 H, tolyl-H), 7.05 (d, J = 7.8 Hz, 2 H, tolyl-H), 3.63 (d, $^3J_{P-H} = 12.0$ Hz, 9 H, $P(OMe)_3$), 2.25 (s, 3 H, tolyl-CH_3), 1.77 (d, $^4J_{P-H} = 4.8$ Hz, 15 H, Cp*). $^{31}P\{^1H\}$ NMR (121.5 MHz, CD_2Cl_2) δ 116.9 Hz (dd, $^1J_{Rh-P} = 215$ Hz, $^2J_{P-C} = 32.8$ Hz, $P(OMe)_3$). $^{13}C\{^1H\}$ NMR (101 MHz, CD_2Cl_2) δ 187.5 (dd, $^1J_{Rh-C} = 68.3$ Hz, $^2J_{P-C} = 38.4$ Hz, ^{13}CO).

4.16. Generation of $[Cp^*(P(OMe)_3)Rh(^{13}C(O)\text{-}C_6H_4CH_3)(^{13}CO)]BAr'_4$ (**23′**)

A J-Young tube charged with 35 mg of **22** in 0.5 mL CD_2Cl_2. The contents were freeze–pump-thawed three times and backfilled with ^{13}CO. The solution was shaken, and excess ^{13}CO was evacuated from the headspace and backfilled with argon while the solution was frozen. ^1H, ^{13}C and ^{31}P NMR spectroscopy showed the presence of both **21′** and **23′** in solution. ^1H NMR (300 MHz, CD_2Cl_2) δ 7.31 (m, 4 H, Ar–H), 3.74 (d, $^3J_{P-H} = 11.7$ Hz, 9 H, $P(OMe)_3$), 2.39 (s, 3 H, tolyl-CH_3), 1.88 (d, $^4J_{P-H} = 3.9$ Hz, 15 H, Cp*). $^{31}P\{^1H\}$ NMR (121.5 MHz, CD_2Cl_2) δ 114.7 (ddd, $^1J_{Rh-P} = 226$ Hz, $^2J_{P-C} = 35.2$ Hz, $^2J_{P-C} = 12.1$ Hz, $P(OMe)_3$). $^{13}C\{^1H\}$ NMR (101 MHz, CD_2Cl_2) δ 223.6 (ddd, $^1J_{Rh-C} =$

23.3 Hz, $^{2}J_{P-C}$ = 10.9,$^{2}J_{C-C}$ = 3.0 Hz, Rh–acyl-^{13}CO), 188.5 (ddd, $^{1}J_{Rh-C}$ = 74.7 Hz, $^{2}J_{P-C}$ = 34.8Hz,$^{2}J_{C-C}$ = 3.0 Hz, Rh–^{13}CO).

4.17. Generation of [Cp*(P(OMe)$_3$)$_2$Rh(^{13}C(O)C$_6$H$_4$CH$_3$)]BAr′$_4$ (24′)

A J-Young tube containing a mixture of **21′** and **23′** in CD_2Cl_2 solution (product from synthesis of **21′**) was brought into the glove box where 3.1 μL of trimethyl phosphite was introduced. After 1 day at room temperature, the resulting yellow solution was decanted from precipitate, at which point **24′** was the only species detected in solution. Alternatively, **24′** can be generated by the addition of trimethyl phosphite to a solution of **18b**. ^{1}H NMR (300 MHz, CD_2Cl_2) δ 7.35 (m, 2 H, tolyl-H$_{ortho}$), 7.19 (d, J = 8.1 Hz, 2 H, tolyl-H$_{meta}$), 3.72 (t, J = 5.7 Hz, 18 H, P(OMe)$_3$), 2.39 (s, 3 H, tolyl-CH$_3$), 1.66 (t, $^{4}J_{P-H}$ = 4.6 Hz, 15 H, Cp*). ^{31}P{^{1}H} NMR (121.5 MHz, CD_2Cl_2) δ 119.1 (dd, $^{1}J_{Rh-P}$ = 244 Hz, $^{2}J_{P-C}$ = 11.9 Hz, P(OMe)$_3$). ^{13}C{^{1}H} NMR (75.5 MHz, CD_2Cl_2) δ 233.21 (dt, $^{1}J_{Rh-C}$ = 29.1 Hz, $^{2}J_{P-C}$ = 12.2 Hz, Rh–^{13}*C*O-tolyl), 142.90 (s, tolyl-Ar), 128.8 (br d, tolyl-Ar), 128.5 (br d, tolyl-Ar), 125.1 (s, tolyl-Ar), 106.1 (m, Cp*–Ar), 55.17 (m, P(OMe)$_3$), 21.27 (tolyl-Me), 9.67 (s, Cp*–Me).

4.18. Kinetics of C–H activation reactions of aldehydes using 1 and 3

Reactions using 10–20 mg of **1** or **3** (0.03 M) with aldehydes (1.5 M) were carried out in J-Young NMR tubes in CD_2Cl_2. Values of k_{obs} were determined by integration of the rhodium–methyl and Cp* peaks relative to the invariant BAr'_4 peaks during reaction of **1** and **3** with 50 equivalents of aldehyde over the course of days at room temperature.

4.19. Determination of $\Delta G^{\ddagger}$ for dissociative exchange of aldehydes in 15 and 16

Solutions of 10 mg of **1** or **3** in CD_2Cl_2 were combined with 5 equivalents of aldehyde and cooled to −88 °C. At this temperature, the natural $w_{1/2}$ of the aldehydic proton was determined. The $w_{1/2}$ was again measured at a temperature where the width had reached 5–10 times the natural line width. Rate constants for exchange and $\Delta G^{\ddagger}$ were calculated from this data using the slow exchange equation $k = \pi(\Delta w)$.

4.20. Crystallographic studies

For complexes **6** and **19**, data were collected at −100 °C on a Bruker SMART diffractometer, using the omega scan mode. Crystal data and collection parameters are given in Table 7. All computations were performed using the NRCVAX suite of programs [17].

Table 7
Crystallographic data and collection parameters for **6** and **19**

	6	19
Empirical formula	$RhPC_{52}H_{43}BF_{24}Cl_2$	$RhPBC_{53}H_{43}F_{24}O$
Formula weight	1339.46	1317.79
Crystal system	monoclinic	triclinic
Space group	$P2_1/c$	$P\bar{1}$
a (Å)	12.5934(22)	12.3960(5)
b (Å)	18.824(3)	12.7232(6)
c (Å)	24.160(4)	18.3440(8)
α (°)	–	76.5570(10)
β (°)	94.260(7)	86.1510(10)
γ (°)	–	84.6820(10)
V (Å^3)	5711.3(15)	2798.67(21)
Z	4	2
D_{calc} (Mg/m^3)	1.558	1.564
Radiation	Mo Kα	Mo Kα
μ (mm^{-1})	0.53	0.47
R_f	0.129	0.098
R_w	0.131	0.086
Goodness-of-fit	1.8114	2.1963

5. Supplementary material

CCDC-240673 (**6**) and -240674 (**19**) contain the supplementary crystallographic data for this paper. These data can be obtained free of charge via www.ccdc.cam.ac.uk/data_request/cif, by emailing data_request@ccdc.cam.ac.uk, or by contacting The Cambridge Crystallographic Data Centre, 12, Union Road, Cambridge CB2 1EZ, UK; fax: +44 1223 336033.

Acknowledgement

B.K.C., F.L.T., and M.B. acknowledge the National Science Foundation (CHE-0107810) for support of this work and R.G.B. acknowledges support by the Director, Office of Energy Research, Office of Basic Energy Sciences, Chemical Sciences Division, of the US Department of Energy under Contract No. DE-AC03-7600098.

References

[1] (a) N.F. Gol'dshleger, V.V. Es'kova, A.E. Shilov, A.A. Shteinman, Zh. Fiz. Khim. 46 (1972) 1353;
(b) A.E. Shilov, A.A. Shteinman, Coord. Chem. Rev. 24 (1977) 97.
[2] (a) R.H. Crabtree, J.M. Mihelcic, J.M. Quirk, J. Am. Chem. Soc. 101 (1979) 7738;
(b) R.H. Crabtree, M.F. Mellea, J.M. Mihelcic, J.M. Quirk, J. Am. Chem. Soc. 104 (1982) 107;
(c) R.H. Crabtree, C.P. Parnell, Organometallics 4 (1985) 519;
(d) M.J. Burk, R.H. Crabtree, D.V. McGrath, J. Chem. Soc., Chem. Commun. 24 (1985) 1829;
(e) M.J. Burk, R.H. Crabtree, J. Am. Chem. Soc. 109 (1987) 8025.
[3] (a) D. Baudry, M. Ephritikhine, H. Felkin, R. Holmes-Smith, J. Chem. Soc., Chem. Commun. 14 (1983) 788;
(b) D. Baudry, M. Ephritikhine, H. Felkin, J. Zakrzewski, Tetrahedron Lett. 25 (1984) 1283;

(c) N. Aktogu, D. Baudry, D. Cox, M. Ephritikhine, H. Felkin, R. Holmes-Smith, J. Zakrzewski, Bull. Soc. Chim. Fr. 3 (1985) 381.
[4] (a) P. Burger, R.G. Bergman, J. Am. Chem. Soc. 115 (1993) 10462;
(b) B.A. Arndtsen, R.G. Bergman, Science 270 (1995) 1970.
[5] (a) R.L. Brainard, W.R. Nutt, T.R. Lee, G.M. Whitesides, Organometallics 7 (1988) 2379;
(b) S.S. Stahl, J.A. Labinger, J.E. Bercaw, J. Am. Chem. Soc. 118 (1996) 5961;
(c) M.W. Holtcamp, J.A. Labinger, J.E. Bercaw, J. Am. Chem. Soc. 119 (1997) 848;
(d) D.D. Wick, K.I. Goldberg, J. Am. Chem. Soc. 119 (1997) 10235;
(e) U. Fekl, K.I. Goldberg, Adv. Inorg. Chem. 54 (2003) 259, and references therein.
[6] (a) P.J. Alaimo, R.G. Bergman, Organometallics 18 (1999) 2707, and references therein;
(b) S.R. Klei, T.D. Tilley, R.G. Bergman, J. Am. Chem. Soc. 122 (2000) 1816.
[7] (a) A.H. Janowicz, R.G. Bergman, J. Am. Chem. Soc. 104 (1982) 352;
(b) J.K. Hoyano, W.A.G. Graham, J. Am. Chem. Soc. 104 (1982) 3723;
(c) W.D. Jones, F.J. Feher, J. Am. Chem. Soc. 104 (1982) 4240;
(d) A.A. Bengali, B.A. Arndtsen, P.M. Burger, R.H. Schultz, B.H. Weiller, K.R. Kyle, C.B. Moore, R.G. Bergman, Pure Appl. Chem. 67 (1995) 281.
[8] F.L. Taw, H. Mellows, P.S. White, F.J. Hollander, R.G. Bergman, M. Brookhart, D.M. Heinekey, J. Am. Chem. Soc. 124 (2002) 5100.
[9] P. Jutzi, M. Söte, B. Neumann, H.G. Stammler, J. Organomet. Chem. 556 (1998) 97.
[10] D.M. Tellers, C.M. Yung, B.A. Arndtsen, D.R. Adamson, R.G. Bergman, J. Am. Chem. Soc. 124 (2002) 1400.
[11] W.D. Jones, F.J. Feher, Inorg. Chem. 23 (1984) 2376.
[12] (a) P.J. Alaimo, B.A. Arndtsen, R.G. Bergman, J. Am. Chem. Soc. 119 (1997) 5269;
(b) P.J. Alaimo, B.A. Arndtsen, R.G. Bergman, Organometallics 19 (2000) 2130.
[13] A. Fersht, Enzyme Structure and Mechanism, 2nd ed., W.H. Freeman, New York, 1985.
[14] (a) A.B. Pangborn, M.A. Giardello, R.H. Grubbs, R.K. Rosen, F.J. Timmers, Organometallics 15 (1996) 1518;
(b) P.J. Alaimo, D.W. Peters, J. Arnold, R.G. Bergman, J. Chem. Educ. 78 (2001) 64.
[15] W.D. Jones, F.J. Feher, Organometallics 2 (1983) 562.
[16] M.P.R. Spee, J. Boersma, M.D. Meijer, M.Q. Slagt, G. van Koten, J.W. Geus, J. Org. Chem. 66 (2001) 1647.
[17] E.J. Gabe, Y. Le Page, J.P. Charland, F.L. Lee, P.S. White, J. Appl. Cryst. 22 (1989) 384.

Available online at www.sciencedirect.com
SCIENCE DIRECT®
Polyhedron 23 (2004) 2955–2958
POLYHEDRON
www.elsevier.com/locate/poly

Rhenium(I) tricarbonyl complexes with photoisomerizable ligands

Oliver S. Wenger *, Lawrence M. Henling, Michael W. Day, Jay R. Winkler *, Harry B. Gray *

Beckman Institute, California Institute of Technology, Pasadena, CA 91125, USA

Received 7 June 2004; accepted 10 September 2004
Available online 26 October 2004

Dedicated to Professor M.L.H. Green

Abstract

The photophysical and photochemical properties of a series of rhenium(I) tricarbonyl complexes with photoisomerizable ligands (styryl and azobenzene substituted 2,2′-bipyridines (bpy); a pyridyl substituted dithienylperfluorocyclopentene (py-DTPCP)) are reported. A complex with a 4,4′-distyryl-bpy ligand exhibits photoswitchable luminescence, but decomposes over time when exposed to the UV wavelengths required for *trans* ↔ *cis* photoisomerization of the styryl moieties. A rhenium(I) tricarbonyl 1,10-phenanthroline(phen) complex with the py-DTPCP ligand in its open form exhibits yellow Re(I)-phen MLCT luminescence. Upon 350-nm irradiation, py-DTPCP photocyclizes, thereby quenching the MLCT emission; 620-nm light triggers the reverse reaction, and the luminescence is fully recovered.
© 2004 Elsevier Ltd. All rights reserved.

1. Introduction

The luminescence and photoredox properties of rhenium(I) tricarbonyl diimines have been extensively investigated over the past 30 years [1–3]. Such complexes are being used as luminescent (redox) probes in proteins [4,5], chemical sensors [6,7] and in new functional materials [8–11]. We have synthesized a series of rhenium(I) tricarbonyl diimines with photoisomerizable ligands and shown that some of them can function as photoswitchable systems (Scheme 1).

2. Experimental

Physical measurements including infrared spectroscopy, mass and ^{1}H NMR spectroscopy, as well as optical absorption and luminescence spectroscopy were performed as described in [12].

1 was crystallized as yellow plates by slow diffusion of pentane into a dichloromethane solution at room temperature. **3** was crystallized as red needles by the same method. X-ray diffraction and structure solution/refinement were performed as described in [12].

2.1. Materials

Trans,*trans*-4,4′-distyryl-2,2′-bipyridine (*tt*-distybpy) was synthesized from 4,4′-dimethyl-2,2′-bipyridine and benzaldehyde as described in [13].

Trans-4-styryl-2,2′-bipyridine (*t*-stybpy) was prepared in an analogous reaction using 4-methyl-2,2′-bipyridine as the starting material. The latter was prepared following a published procedure [14]. ESI-MS *m*/*z*: 259.0 ($M + H^+$), 281.2 ($M + Na^+$). ^{1}H NMR ($CDCl_3$). δ 8.71 (d, 1H, 4.8 Hz), 8.64 (d, 1H, 5.7 Hz), 8.52 (s, 1H), 8.43 (d, 1H, 7.8 Hz), 7.82 (t, 1H, 6.0 Hz),

* Corresponding authors. Tel.: +1 626 395 6500; fax: +1 626 449 4159.
E-mail addresses: wenger@alumni.caltech.edu (O.S. Wenger), winklerj@caltech.edu (J.R. Winkler), hbgray@caltech.edu (H.B. Gray).

0277-5387/$ - see front matter © 2004 Elsevier Ltd. All rights reserved.
doi:10.1016/j.poly.2004.09.009

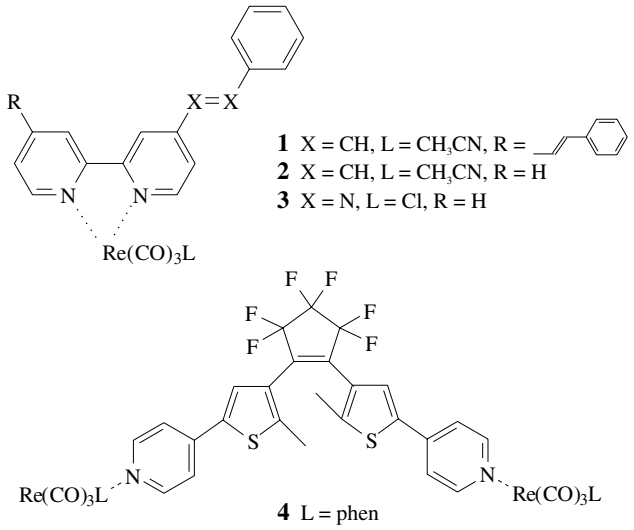

Scheme 1.

7.55 (d, 2H, 7.5 Hz), 7.43 (1H, A of AB, 16.5 Hz), 7.45-7.32 (m, 5H), 7.11 (B of AB, 1H, 16.5 Hz).

4-Phenylazo-2,2′-bipyridine (4-PAbpy) was made from 4-amino-2,2′-bipyridine and nitrosobenzene following a published protocol for the synthesis of phenylazopyridines [15]. 4-Amino-bpy was prepared as described in [16]. ESI-MS *m/z*: 261.0 ($M + H^+$). ^1H NMR ($CDCl_3$). δ 8.86 (d, 1H, 4.8 Hz), 8.82 (s, 1H), 8.74 (d, 1H, 4.5 Hz), 8.47 (d, 1H, 8.1 Hz), 8.00 (d, 2H, 4.2 Hz), 7.85 (t, 1H, 6.9 Hz), 7.57-7.52 (m, 3H), 7.74 (d, 1H, 5.4 Hz), 7.35 (t, 1H, 6.9 Hz).

The dithienylperfluorocyclopentene (py-DTPCP) ligand was synthesized following [17], and the rhenium complexes were prepared from $Re(CO)_5Cl$ as described in [3].

*[Re(tt-distybpy)(CO)$_3$(CH$_3$CN)]BF$_4$ · 2CH$_2$Cl$_2$ (**1**).* ESI-MS *m/z*: 670.2, 672.2 (M^+). IR(NaCl) = 1924, 2031 cm^{-1}. ^1H NMR (CD_3CN): δ 8.91 (d, 2H, 5.7 Hz), 8.74 (s, 2H), 7.88 (A of AB, 2H, 16.5 Hz), 7.78-7.73 (m, 6H), 7.50-7.43 (m, 6H), 7.40 (B of AB, 2H, 16.5 Hz). *Anal.* Calc. for $C_{33}H_{27}N_3O_3BCl_4F_4Re$: C, 49.09; H, 3.06; N, 5.54. Found: C, 49.10; H, 3.20; N, 5.16%.

*[Re(t-stybpy)(CO)$_3$(CH$_3$CN)]BF$_4$ (**2**).* ESI-MS *m/z*: 567.8, 569.8 (M^+). IR(NaCl) = 1922, 2036 cm^{-1}. ^1H NMR (CD_3CN): δ 9.02 (d, 1H, 5.7 Hz), 8.90 (d, 1H, 5.7 Hz), 8.65 (d, 1H, 4.5 Hz), 8.63 (s, 1H), 8.32 (t, 1H, 8.1 Hz), 7.83 (A of AB, 1H, 16.2 Hz), 7.80-7.70 (m, 4H), 7.50-7.40 (m, 3H), 7.38 (B of AB, 1H, 16.2 Hz).

*Re(4-PAbpy)(CO)$_3$Cl (**3**).* ESI-MS *m/z*: 560.5, 562.5 ($M^+ - Cl + CH_3OH$). IR(NaCl) = 1866, 1902, 2029 cm^{-1}. ^1H NMR ($CDCl_3$): δ 9.21 (d, 1H, 6.0 Hz), 9.10 (d, 1H, 5.7 Hz), 8.57 (s, 1H), 8.37 (d, 1H, 7.8 Hz), 8.12 (t, 1H, 8.4 Hz), 8.06 (d, 2H, 6.0 Hz), 7.94 (d, 1H, 6.9 Hz), 7.66–7.56 (m, 4H). *Anal.* Calc. For $C_{19}H_{12}N_4O_3ClRe$: C, 40.32; H, 2.14; N, 9.90. Found: C, 40.16; H, 2.32; N, 9.81%.

*[[Re(phen)(CO$_3$)]$_2$(py-DTPCP)](PF$_6$)$_2$ (**4**).* ESI-MS *m/z*: 1566.5, 1567.5, 1568.5, 1569.5 ($M^{2+} + PF_6^-$), 970.8, 972.9 ($M^+ - Re(phen)(CO)_3$). ^1H NMR (CD_3CN): δ 9.61 (d, 4H, 5.7 Hz), 8.84 (d, 4H, 8.7 Hz), 8.17 (s, 4H), 8.13 (d, 4H, 5.1 Hz), 8.15-8.10 (m, 4H), 7.51 (s, 2H), 7.25 (d, 4H, 6.6 Hz), 1.81 (s, 6H).

3. Results and discussion

Fig. 1 shows the X-ray crystal structure of the BF_4^- salt of **1**. The *tt*-distybpy ligand is nearly planar; the C_7–C_8–C_{18}–C_{19} and C_{12}–C_{13}–C_{26}–C_{31} dihedral angles are 10° and 17°, i.e., *tt*-distybpy shows a high degree of π-conjugation. Nonetheless, the energetic position, bandshape, and lifetime (90 ± 10 ns) of the luminescence of a deaerated acetonitrile solution of **1** (left part of Fig. 2, solid line) are indicative of a lowest excited state with predominant MLCT (metal-to-ligand charge transfer) character. In absorption, the MLCT band is hidden below the more intense *tt*-distybpy π–π* systems. 400-nm irradiation leads to *trans* → *cis* (*t* → *c*) photoisomerization of the styryl moieties on the *tt*-distybpy ligand; ^1H NMR experiments reveal that this isomerization is moderately efficient for the first styryl substituent (*tt* → *tc* quantum yield: 0.23) and inefficient for the second substituent (*tt* → *cc* and *tc* → *cc* quantum yield <0.05). After long irradiation times (30 min; photon flux 8×10^{15} s^{-1}), a steady state comprised of roughly 55% *tt*, 40% *tc*, and 5% *cc* isomers is reached. The absorption spectrum of this solution (Fig. 2, dashed line) shows weaker low energy features and a stronger high energy (>36 000 cm^{-1}) band than the 100% *tt*-isomer solution, consistent with the loss of π-conjugation typically associated with *t* → *c* isomerization in styrene and azoben-

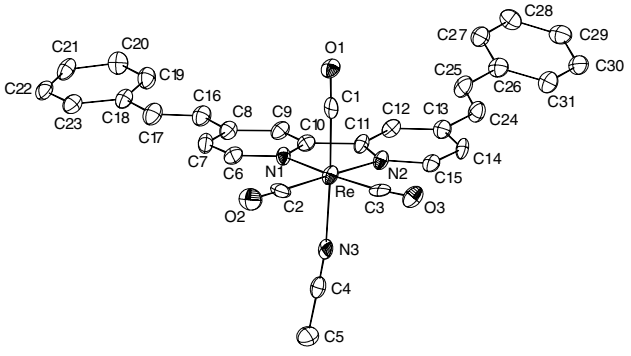

Fig. 1. X-ray crystal structure of the cation of **1**. Displacement ellipsoids are drawn to the 50% probability level. H-atoms are omitted for clarity. Crystal system: triclinic, space group P-1, cell parameters: $a = 10.0913(17)$ Å, $b = 12.606(2)$ Å, $c = 14.528(2)$ Å, $\alpha = 100.985(2)°$, $\beta = 107.128(2)°$, $\gamma = 90.488(2)°$. $V = 1729.7(5)$ Å^3, $Z = 2$, $\rho = 1.783$ g/cm^3. Collection parameters: Mo Kα radiation (0.71073 Å), $T = 100$ K, 27 258 reflections, 7728 independent reflections. Refinement: least-squares fit on F^2, 445 parameters, $R[F^2 > 2\sigma(F^2)]$: 0.0536, R(all data): 0.0872, Goodness-of-fit: 1.887. CCDC deposition number: 214272.

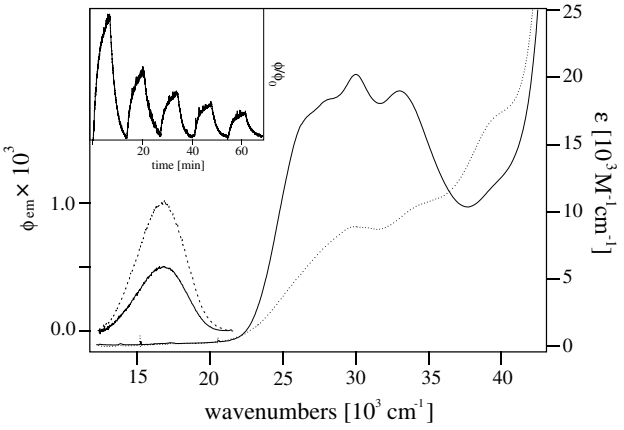

Fig. 2. Luminescence (left) and absorption (right) spectra of a dichloromethane solution of **1** before (solid line) and after (dashed line) 400-nm irradiation. The inset plots the luminescence intensity as a function of irradiation time at 400 nm (increasing intensities) and 260 nm (decreasing intensities).

zene derivatives: in $[Re(phen)(CO)_3(dpe)]^+$, dpe = 1,2-di(4-pyridyl)ethylene, the dihedral angle between the two dpe-pyridyl moieties increases from 16° to 51° upon $t \rightarrow c$ photoisomerization [12], resulting in a ~4000 cm^{-1} blue shift of the lowest dpe π–π* transitions. The $tt \rightarrow tc$ isomerization in **1** is accompanied by a factor of 2 increase in luminescence quantum yield; the lowest excited state of the *tc*-distybpy complex has purer MLCT (less distybpy π–π*) character, and the luminescence is more competitive with nonradiative relaxation than in the *tt*-distybpy complex. The reverse $c \rightarrow t$ styryl isomerizations are induced by irradiating at 260 nm, decreasing the luminescence quantum yield. Repeated 400- and 260-nm irradiations induce luminescence intensity switchings as shown in the inset of Fig. 2. The maximum emission intensity decreases exponentially with the number of on/off cycles; this is attributed to photochemical decomposition of the sample when exposed to 260-nm light.

Complex **2** exhibits similar photoisomerization behavior: 365-nm irradiation induces *trans* → *cis* isomerization of the styryl substituent ($\phi_{tc} = 0.15$), whereas 250-nm light triggers the reverse process as well as photochemical decomposition. The luminescence is blue shifted by 1000 cm^{-1} with respect to **1**, and its quantum yield is about an order of magnitude higher, in accord with the energy-gap law for rhenium(I) tricarbonyl diimines [18]. The luminescence quantum yield is virtually identical for the *t*- and *c*-stybpy complexes; i.e., the luminescence is not photoswitchable. The stybpy π–π* levels are roughly 3000 cm^{-1} higher in energy than those of distybpy and consequently, in **2**, the lowest excited state is relatively pure MLCT and experiences little perturbation upon photoisomerization of the stybpy ligand.

3 is nonluminescent. The PAbpy ligand has low lying *n*-π* levels, from which nonradiative relaxation to the ground state is the most efficient excited state depopulation mechanism. Neither luminescence nor photoisomerization is competitive with this process. In the crystal structure of **3** [19], the dihedral angle between the bpy and phenyl planes is about 53°, but this appears to be caused by crystal packing.

A dichloromethane solution of **4** with the py-DTPCP ligand in its open form (scheme in Fig. 4) exhibits the absorption spectrum shown in Fig. 3(a) (dashed line). The weak shoulder around 25 000 cm^{-1} is the Re(I)-phen MLCT. The more intense bands at higher energy are py-DTPCP (29 000 cm^{-1}) and phen (35 000 cm^{-1}) ligand π–π* absorptions. On 400-nm irradiation, this compound exhibits yellow MLCT emission as shown in Fig. 3(b) (dashed line). Excitation into the py-DTPCP absorption band at 350 nm induces a photocyclization reaction, as schematically shown in Fig. 4. ^1H NMR experiments reveal that this isomerization occurs with a quantum yield of about 0.1, and extended irradiation leads to about 85% conversion of the open to the closed py-DTPCP form (^1H NMR spectra in Fig. 4). The cyclization reaction generates a basically planar DTPCP conformation with extended π-conjugation; the resulting closed form of **4** has an intense π–π* absorption band centered at 16 000 cm^{-1} (Fig. 3(a), solid line). These low lying py-DTPCP localized states quench the Re(I)-phen MLCT emission (Fig. 3(b), solid line). The reverse ring-opening reaction is induced after irradiation into the visible py-DTPCP absorption band at 620 nm; thus **4** is converted completely back to its open form, and the MLCT luminescence is fully recovered. Importantly, the MLCT emission can be switched on and off multiple times (Fig. 3(b), inset), i.e., photodecomposition of **4** is not pronounced. In contrast to the work of Lehn and

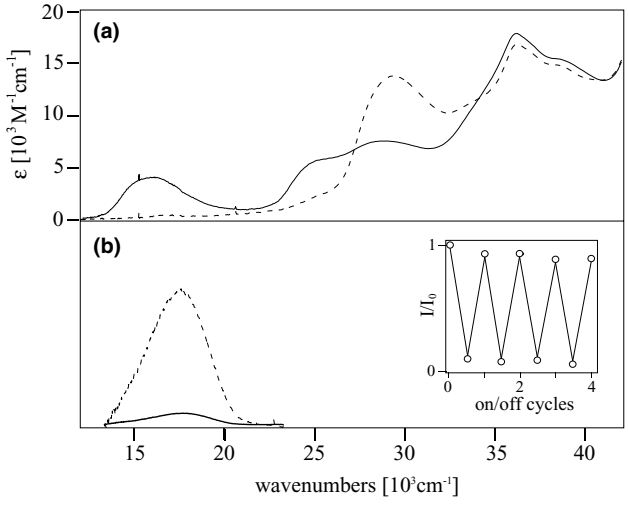

Fig. 3. Absorption (a) and luminescence (b) spectra of a dichloromethane solution of **4** with the py-DTPCP ligand in its open (dashed line) and closed (solid line) forms. The inset illustrates the reversibility of the switching process.

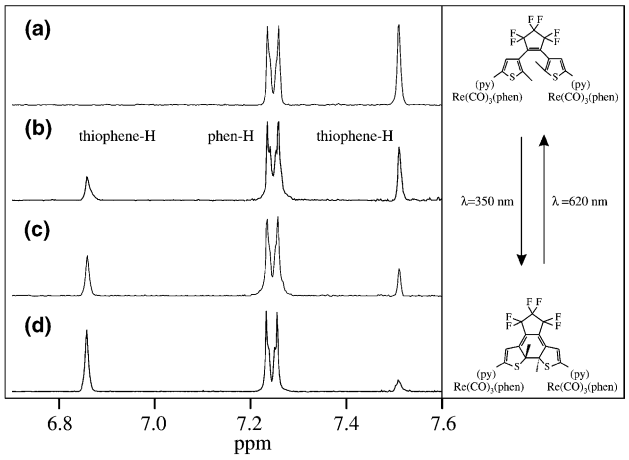

Fig. 4. ^{1}H NMR spectral changes of a CD_3CN solution of **4** during irradiation at 350 nm. Trace a is the spectrum of **4** with the py-DTPCP ligand purely in its open form.

coworkers [20] on similar transition metal/dithienylperfluorocyclopentene systems, we observe MLCT luminescence switching instead of intraligand π–π* emission switching.

4. Summary and conclusions

The behavior of **1** is analogous to that of previously investigated rhenium(I) tricarbonyl complexes with photoisomerizable ligands [12,21,22]: off-switching is induced after irradiation at very short wavelengths (<260 nm), which excites the rhenium(I) complexes into highly dissociative ligand-field excited states, inducing the loss of CO ligands [23]. Photochemical decomposition of **4**, on the other hand, is inefficient for two main reasons: (i) substantially longer irradiation wavelengths (>350 nm) are used to induce photoisomerization; and (ii) photocyclization in dithienylperfluorocyclopentenes is highly reversible [24]. Thus, complex **4** is an example of a reversible luminescent photoswitch.

Acknowledgements

This work was supported by the National Science Foundation. O.S.W. acknowledges a postdoctoral fellowship from the Swiss National Science Foundation.

Appendix A. Supplementary material

Supplementary data associated with this article can be found, in the online version, at doi:10.1016/j.poly.2004.09.009.

References

[1] M. Wrighton, D.L. Morse, J. Am. Chem. Soc. 96 (1974) 998.
[2] D.R. Striplin, G.A. Crosby, Coord. Chem. Rev. 211 (2001) 163.
[3] L. Sacksteder, A.P. Zipp, E.A. Brown, J. Streich, J.N. Demas, B.A. DeGraff, Inorg. Chem. 29 (1990) 4335.
[4] B.R. Crane, A.J. Di Bilio, J.R. Winkler, H.B. Gray, J. Am. Chem. Soc. 123 (2001) 11623.
[5] J.E. Miller, C. Grădinaru, B.R. Crane, A.J. Di Bilio, W.A. Wehbi, S. Un, J.R. Winkler, H.B. Gray, J. Am. Chem. Soc. 125 (2003) 14220.
[6] R.V. Slone, D.I. Yoon, R.M. Calhoun, J.T. Hupp, J. Am. Chem. Soc. 117 (1995) 11813.
[7] S.-S. Sun, A.J. Lees, P.Y. Zavalij, Inorg. Chem. 42 (2003) 3445.
[8] A. Beyeler, P. Belser, L. De Cola, Angew. Chem., Intl. Ed. Engl. 36 (1997) 2779.
[9] S.-S. Sun, E. Robson, N. Dunwoody, A.S. Silva, I.M. Brinn, A.J. Lees, Chem. Commun. (2000) 201.
[10] J.D. Lewis, R.N. Perutz, J.N. Moore, Chem. Commun. (2000) 1865.
[11] V.W.-W. Yam, Y. Yang, J. Zhang, B.W.-K. Chu, N. Zhu, Organometallics 20 (2001) 4911.
[12] O.S. Wenger, L.M. Henling, M.W. Day, J.R. Winkler, H.B. Gray, Inorg. Chem. 43 (2004) 2043.
[13] C.R. Leidner, B.P. Sullivan, R.A. Reed, B.A. White, M.T. Crimmins, R.W. Murray, T.J. Meyer, Inorg. Chem. 26 (1987) 882.
[14] S.A. Savage, A.P. Smith, C.L. Fraser, J. Org. Chem. 63 (1998) 10048.
[15] E.V. Brown, G.R. Granneman, J. Am. Chem. Soc. 97 (1975) 621.
[16] R.A. Jones, B.D. Roney, W.H.F. Sasse, K.O. Wade, J. Chem. Soc. B 2 (1967) 106.
[17] S.L. Gilat, S.H. Kawai, J.-M. Lehn, Chem. -Eur. J. 1 (1995) 275.
[18] J.V. Caspar, T.J. Meyer, J. Phys. Chem. 87 (1983) 952.
[19] Crystallographic data have been deposited at the CCDC, Cambridge CB2 1EZ, UK (fax: +44 1223 336033; e-mail: deposit@ccdc.cam.ac.uk; http://www.ccdc.cam.ac.uk) and copies can be obtained on request, free of charge, by quoting the publication citation and the deposition number 212431.
[20] A. Fernández-Acebes, J.-M. Lehn, Chem. -Eur. J. 5 (1999) 3285.
[21] M.K. Itokazu, A.S. Polo, D.L.A. de Faria, C.A. Bignozzi, N.Y.M. Iha, Inorg. Chim. Acta 313 (2001) 149.
[22] M.K. Itokazu, A.S. Polo, N.Y.M. Iha, J. Photochem. Photobiol. A 160 (2003) 27.
[23] K. Koike, N. Okoshi, H. Hori, K. Takeuchi, O. Ishitani, H. Tsubaki, I.P. Clark, M.W. George, F.P.A. Johnson, J.J. Turner, J. Am. Chem. Soc. 124 (2002) 11448.
[24] M. Irie, Chem. Rev. 100 (2000) 1685.

Available online at www.sciencedirect.com
SCIENCE DIRECT®
Polyhedron 23 (2004) 2959–2965
POLYHEDRON
www.elsevier.com/locate/poly

Synthesis, structure and reactivity of $[Ir(dippe)(\mu\text{-}Cl)]_2$, $[Ir(dippe)_2][Ir(dippe)Cl_2]$ and $[Ir(dippe)_2]Cl$

Stephen S. Oster, William D. Jones *

Department of Chemistry, University of Rochester, Rochester, New York 14627, USA

Received 21 June 2004; accepted 30 June 2004
Available online 2 September 2004

Abstract

$[Ir(COD)(\mu\text{-}Cl)]_2$ reacts with two equivalents of 1,2-bis(diisopropylphosphino)ethane (dippe) to produce $[Ir(dippe)(\mu\text{-}Cl)]_2$ (**1a**) in yields that are dependent upon the solvent. Its single crystal X-ray structure shows a hinge angle θ of 132.2°, which is larger than in other reported iridium analogs, but smaller than in $[Rh(dippe)(\mu\text{-}Cl)]_2$ (**1b**). $[Ir(dippe)_2][Ir(dippe)Cl_2]$ (**2**), whose anion is without literature precedent, is an intermediate species in the conversion of **1a** to $[Ir(dippe)_2]Cl$ (**3**). Complex **3** reacts with dihydrogen to produce $[Ir(dippe)_2H_2]Cl$ (**4**).
© 2004 Elsevier Ltd. All rights reserved.

Keywords: Iridium complexes; Chelating phosphines

1. Introduction

$[Rh(dippe)(\mu\text{-}H)]_2$ is one of a class of $[L_2Rh]_n(\mu\text{-}H)_n$ compounds that was developed by Fryzuk and coworkers in the 1980s [1]. They found that $[Rh(dippe)(\mu\text{-}H)]_2$ reacts with olefins, phenol, *N*-benzylideneaniline, aldimines, silanes, nitriles and dialkylzinc reagents often to form hydrido-X-bridged rhodium dimers, as well as other products. Interest in $[Rh(dippe)(\mu\text{-}H)]_2$ for homogeneous catalysis arises from the fact that it is an electronically and coordinatively unsaturated molecule that, by all evidence, remains a dimer as it reacts with substrates [2].

One salient feature of rhodium and iridium dimers of the type $M_2(\mu\text{-}X)_2$ is that all but one adopt bent conformations as opposed to being planar molecules [3]. This behavior is attributed to d-orbital diffuseness that allows for better p_z/d_{z^2} overlap between the two metal centers in each of the bridged dimers [4]. The choice of the bridging atom influences the degree of bending, as well.

In the course of the investigation of the reactions between $[Rh(dippe)(\mu\text{-}H)]_2$ and dibenzothiophenic substrates [5], we became interested in the unknown iridium analog, $[Ir(dippe)(\mu\text{-}H)]_2$. Consequently, $[Ir(dippe)(\mu\text{-}Cl)]_2$ (**1a**) was synthesized and characterized for the first time [6] with the intent that it would provide a reactive precursor for $[Ir(dippe)(\mu\text{-}H)]_2$. Herein, is a report on the synthesis, structural characteristics and reactivity of $[Ir(dippe)(\mu\text{-}Cl)]_2$, a secondary product that was identified as $[Ir(dippe)_2][Ir(dippe)Cl_2]$, and $[Ir(dippe)_2]Cl$, as well as reactions with dihydrogen.

2. Experimental

All operations were performed under a nitrogen atmosphere unless otherwise stated. Benzene, THF

* Corresponding author. Tel.: +1 585 275 5493; fax: +1 585 276 0205.
E-mail address: jones@chem.rochester.edu (W.D. Jones).

0277-5387/$ - see front matter © 2004 Elsevier Ltd. All rights reserved.
doi:10.1016/j.poly.2004.06.031

and hexanes were distilled from dark purple solutions of benzophenone ketyl/tetraglyme. Acetonitrile and dichloromethane were dried and distilled over CaH_2. $[Ir(COD)(\mu\text{-}Cl)]_2$ was purchased from Strem Chemicals and dried under vacuum before it was used. 1,2-Bis(diisopropylphosphino)ethane was prepared as described in the literature [7]. A Siemens-SMART 3-Circle CCD diffractometer was used for X-ray crystal structure determination (see Supporting Information for experimental details). Elemental analyses were obtained from Desert Analytics and Complete Analysis Laboratories, Inc. All ^1H, ^{31}P and ^{13}C spectra were recorded on a Bruker Avance400 NMR spectrometer. All ^1H chemical shifts are reported relative to the residual proton resonance in the deuterated solvent. All ^{31}P chemical shifts are reported relative to 85% H_3PO_4.

2.1. Preparation of *[Ir(dippe)(μ-Cl)]$_2$* (**1a**)

Dippe (1.35 g, 5.16 mmol) in approximately 4 mL of CH_3CN was added dropwise to a stirred 50 mL CH_3CN solution of $[Ir(COD)(\mu\text{-}Cl)]_2$ (1.65 g, 2.46 mmol). The solution color changed immediately from yellow to dark green. After 30 min, the solvent was evaporated under vacuum to yield a yellow solid. The solid was washed with CH_3CN and then hexanes to remove $[Ir(dippe)_2][Ir(dippe)Cl_2]$ and other unidentified products to leave a bright yellow solid. The solid was redissolved in THF and the resulting solution was chilled at −30 °C to yield bright yellow crystals (1.97 g, yield = 81.6%). ^1H NMR (THF-d_8, 25 °C): δ 2.01 (m, 8H), 1.26 (dd, J = 7.1, 7.5 Hz, 24H), 1.21 (d, J = 9.6 Hz, 8H), 1.05 (dd, J = 7.0, 6.0 Hz, 24H). $^{13}C\{^1H\}$ NMR (THF-d_8, 25 °C): δ 26.28 (d, J = 32.9 Hz), 23.30 (m), 20.17 (s), 18.91 (s). $^{31}P\{^1H\}$ NMR (THF-d_8, 25 °C): δ 67.80 (s). *Anal.* Calc. for $C_{28}H_{64}Ir_2P_4Cl_2$: C, 34.32; H, 6.58. Found: C, 33.85; H, 6.47%.

2.2. Preparation of *[Ir(dippe)$_2$][Ir(dippe)Cl$_2$]* (**2**)

Dippe (1.156 g, 4.41 mmol) in approximately 4 mL of THF was added dropwise to a stirred 50 mL THF solution of $[Ir(COD)(\mu\text{-}Cl)]_2$ (1.41 g, 2.09 mmol). The solvent was evaporated under vacuum to leave a dark red solid. The solid was washed with hexanes to leave a bright orange-red powder. The powder was redissolved in CH_3CN and vacuum-filtered, which left a yellow solid on the frit and a bright orange-red filtrate. The filtrate was concentrated and then chilled at −30 °C to yield a bright orange-red powder (2.00 g, yield = 77.4%). ^1H NMR (THF-d_8, 25 °C): δ 2.60 (sept, J = 6.9 Hz, 8H), 2.27 (oct, J = 7.5 Hz, 4H), 1.89 (m, 8H), 1.27 (m, 64H), 0.99 (m, 12H). $^{13}C\{^1H\}$ NMR (THF-d_8, 25 °C): δ 29.86 (m), 22.45 (s), 20.97 (m), 20.40 (m), 19.78 (s), 19.25 (m), 19.09 (m). $^{31}P\{^1H\}$ NMR (THF-d_8, 25 °C): δ 65.25 (s), 64.59 (s). *Anal.* Calc. for $C_{42}H_{96}Ir_2P_6Cl_2$: C, 40.60; H, 7.79. Found: C, 40.38; H, 8.05%.

2.3. Preparation of *[Ir(dippe)$_2$]Cl* (**3**)

Dippe (45.0 mg, 0.17 mmol) in THF was added dropwise to a stirred 25 mL THF solution of $[Ir(COD)(\mu\text{-}Cl)]_2$ (84.0 mg, 0.125 mmol). The resulting mixture was stirred for approximately 3 h, during which time an orange solid precipitated. The solvent was evaporated under vacuum and the resulting orange solid was washed, first with diethylether and then with hexanes to remove excess dippe, and then dried under vacuum (150.9 mg, yield = 63.9%). ^1H NMR (CD_2Cl_2, 25 °C): δ 2.42 (sept, J = 7.0 Hz, 8H), 1.68 (br t, J = 6.7 Hz, 8H), 1.22 (m, 48H). $^{13}C\{^1H\}$ NMR (CD_2Cl_2, 25 °C): δ 29.36 (pseudo quint, J = 7.4 Hz), 21.98 (s), 20.15 (quint, J = 12.2 Hz), 19.25 (s). $^{31}P\{^1H\}$ NMR (CD_2Cl_2, 25 °C): δ 64.93 (s). *Anal.* Calc. for $C_{29}H_{66}IrP_4Cl_3$ (includes one molecule of CH_2Cl_2): C, 41.60; H, 7.95. Found: C, 41.87; H, 8.14%.

2.4. Preparation of *[Ir(dippe)$_2$H$_2$]Cl* (**4**)

Approximately 760 mm Hg of H_2 was added to a storage flask that contained a degassed CH_3CN solution of **3** (65.5 mg, 0.069 mmol). Within 15 min, the solution color had changed from bright orange to yellow and after one day it was colorless. The solvent was removed under vacuum and a colorless solid was obtained (41.6 mg, yield = 63.3%). ^1H NMR (CD_3CN, 25 °C): δ 2.18 (m, 8H), 1.72 (m, 8H), 1.15 (m, 42H), 0.94 (dd, J = 15.3, 7.0 Hz, 6H), −15.16 (dm, J = 90.8, 16.8 Hz, 2H). $^{13}C\{^1H\}$ NMR (CD_3CN, 25 °C): δ 30.25 (m), 28.18 (m), 26.96 (m), 25.87 (m), 24.80 (m), 23.20 (m), 21.43 (s), 21.08 (s), 19.79 (s), 19.66 (s), 19.06 (m), 18.81 (s), 17.77 (s). $^{31}P\{^1H\}$ NMR (CD_3CN, 25 °C): δ 53.83 (t, J = 7.5 Hz), 26.16 (m). *Anal.* Calc. for $C_{28}H_{66}IrP_4Cl$: C, 44.58; H, 8.82. Found: C, 44.22; H, 8.61%.

2.5. Preparation of *[Rh(dippe)(μ-Cl)]$_2$* (**1b**)

Using a modification of the literature prep [8], 2.1 equiv. of dippe (568 mg, 2.17 mmol) in THF was added dropwise to a rapidly stirred 50 mL THF suspension of $[Rh(COD)(\mu\text{-}Cl)]_2$ (509 mg, 1.03 mmol). The resulting mixture was stirred for 24 h as a portion of the product precipitated out of solution. The solvent was evaporated to dryness under vacuum and the solid was washed three times with hexanes. The solid was then placed under vacuum for three days (502 mg, 60.7%). ^1H NMR (THF-d_8, 25 °C): δ 2.05 (m, 8H), 1.34 (dd, $J_{(H-H)}$ = 7.1 Hz, $J_{(H-P)}$ = 7.7 Hz, 24H), 1.31 (d, $J_{(H-P)}$ = 14.0Hz, 8H), 1.10 (dd, $J_{(H-H)}$ = 7.0 Hz, $J_{(H-P)}$ = 5.6 Hz, 24H). $^{31}P\{^1H\}$ NMR (THF-d_8, 25 °C): δ 102.20 (d, $J_{(P-Rh)}$ = 199.9 Hz).

3. Results

3.1. Synthesis of complexes

The reaction between $[Ir(COD)(\mu\text{-}Cl)]_2$ and two equivalents of dippe to produce $[Ir(dippe)(\mu\text{-}Cl)]_2$ (**1a**) was run in several different solvents under the same experimental conditions (Eq. (1)). The reaction was non-selective in CH_2Cl_2, C_6H_6, THF and acetone in that it produced a large number of phosphorus-containing products as evidenced by ^{31}P NMR spectroscopy. Yet, the reaction was highly selective when conducted in CH_3CN solvent, with a singlet at δ 67.80 in the ^{31}P NMR spectrum for **1a** as the only major product. However, additional side products appeared with increasing reaction times if **1a** was allowed to stir in solution. In CH_2Cl_2, C_6H_6, THF and acetone, both $[Ir(dippe)_2][Ir(dippe)Cl_2]$ (**2**) and $[Ir(dippe)_2]Cl$ (**3**) were formed as prominent secondary products. In THF-d_8, **2** exhibits two singlets at δ 65.25 and 64.54 in the ^{31}P NMR spectrum. The downfield singlet, which corresponds to $[Ir(dippe)_2]^+$, is twice the intensity of the upfield singlet that is produced by the anion. The cation of **3** produces a singlet in the same region of the ^{31}P NMR spectrum at δ 65.25. The choice of solvent also determines the relative amounts of **1a**, **2** and **3** that are formed in this reaction. As Table 1 illustrates, **[3 + 2]**:**1a** is lowest for CH_3CN and highest for acetone. Furthermore, differences in solvent electronic properties fail to account for the observed trend in the ratio of **[3 + 2]** to **1a**.

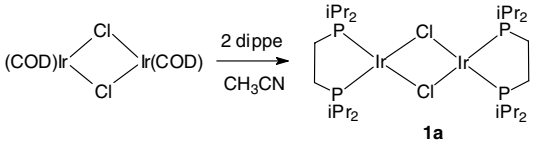

1a (1)

Complex **1a** converts to **3** upon standing in CD_3CN solution. Moreover, **2** appears to be an intermediate species in going from **1a** to **3**. In one experiment, a mixture of **1a**, **2** and **3** in THF-d_8 in a 0.9:1:0.4 ratio was totally converted to **3** when THF-d_8 was removed under vacuum and the mixture was redissolved in CD_3CN. Compound **2** can be synthesized best by adding 1 equiv. of dippe to **1a** (Eq. (2))). Compound **3** can be synthesized cleanly by adding 2 equiv. of dippe to **1a** (Eq. (3)). Complex **2** is sparingly soluble in THF-d_8. Consequently, attempts were made to use CD_3CN and CD_2Cl_2 for the sake of better ^1H and ^{31}P NMR spectra. However, **2** converted to **3** upon dissolution in each of these solvents. Again, this supports the idea that **2** is an intermediate in going from **1a** to **3**.

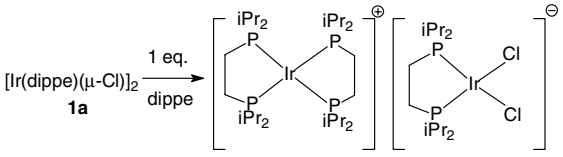

2 (2)

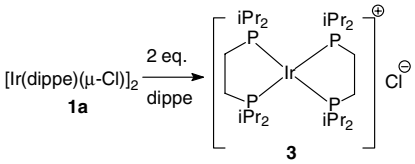

3 (3)

3.2. X-ray structures

Complex **1a** crystallizes from THF at −30 °C in the $P2_1/n$ space group (Fig. 1). Complex **1a** is bent along the Cl–Cl axis, which creates a dihedral angle θ of 132.2°. Moreover, a slight propeller twist exists in the molecule that is brought about by the ethylene backbone of the terminal dippe ligands. For comparison, the structure was determined for the rhodium analog $[Rh(dippe)(\mu\text{-}Cl)]_2$ (**1b**, Fig. 2), which showed a dihedral angle of 137.1°.

The novel complex salt $[Ir(dippe)_2][Ir(dippe)Cl_2]$ (**2**) whose X-ray crystal structure is shown in Fig. 3, is without literature precedent. While a diphos analog of the cation is known [9], the anion is the first of its kind. It crystallizes from THF at −30 °C in the space group $P2_1/c$. Tables 2 and 3 include a list of bond lengths and angles in **2** that are of interest.

The $[Ir(dippe)_2]^+$ cation is a four-coordinate, tetraphosphine iridium(I) complex with an average Ir–P bond length of 2.3185(34) Å (Fig. 4). Its geometry in the solid state is distorted square-planar with a dihedral

Table 1
Solvents used in the synthesis of $[Ir(dippe)\text{-}(\mu\text{-}Cl)]_2$

Solvent	**[(2) + (3)]**:**(1a)**	Dielectric constant ε at 25 °C[a]	Dipole moment, μ (Debye units)[a]
Acetonitrile	0	35.94	3.53
Dichloromethane	0.18	8.93	1.14
Benzene	0.31	2.27	0
Tetrahydrofuran	0.33	7.58	1.75
Acetone	1.05	20.56	2.69

[a] J.A. Riddick, W.B. Bunger, T.K. Sakano, in: Arnold Weissberger (Ed.), Techniques of Chemistry, vol. 2, Organic Solvents: Physical Properties and Methods of Purification, 4th ed., Wiley, New York, 1986.

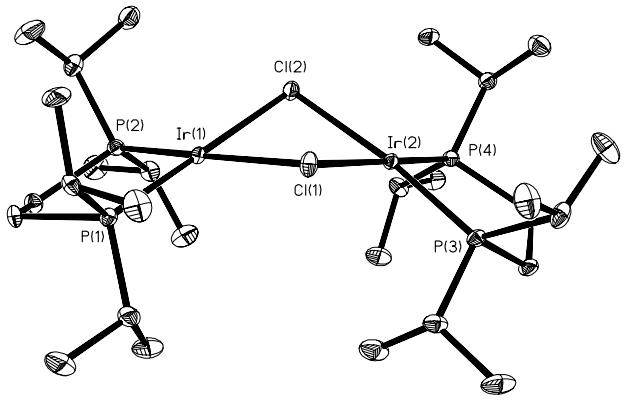

Fig. 1. ORTEP diagram of $[Ir(dippe)(\mu\text{-}Cl)]_2$ (**1a**). Ellipsoids are shown at the 30% probability level. All hydrogen atoms are omitted for clarity. Selected distances (Å): Ir(1)–P(1), 2.1809(13); Ir(1)–P(2), 2.1811(13); Ir(2)–P(3), 2.1844(13); Ir(2)–P(4), 2.1848(13); Ir(1)–Cl(1), 2.4138(13); Ir(1)–Cl(2), 2.4215(13); Ir(2)–Cl(1), 2.4291(13); Ir(2)–Cl(2), 2.4386(13).

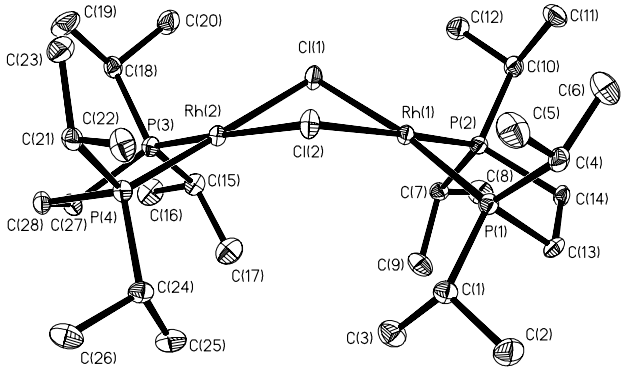

Fig. 2. ORTEP diagram of $[Rh(dippe)(\mu\text{-}Cl)]_2$ (**1b**). Ellipsoids are shown at the 30% probability level. All hydrogen atoms are omitted for clarity. Selected distances (Å): Rh(1)–P(1), 2.1814(13); Rh(1)–P(2), 2.1828(12); Rh(2)–P(3), 2.1859(13); Rh(2)–P(4), 2.1892(12); Rh(1)–Cl(1), 2.4161(12); Rh(1)–Cl(2), 2.4272(12); Rh(2)–Cl(1), 2.4347(12); Rh(2)–Cl(2), 2.4480(12).

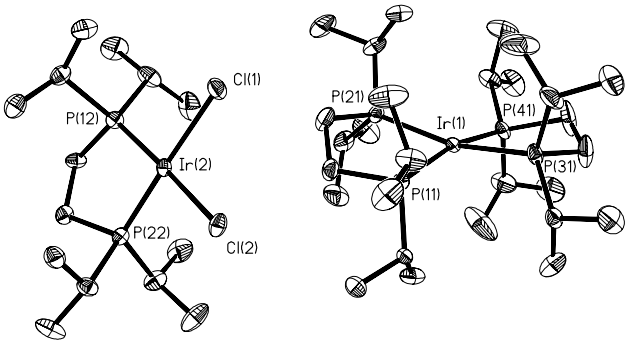

Fig. 3. ORTEP diagram of $[Ir(dippe)_2][Ir(dippe)Cl_2]$ (**2**). Ellipsoids are shown at the 30% probability level. All hydrogen atoms are omitted for clarity.

Table 2
Selected bond lengths (Å) for $[Ir(dippe)_2][Ir(dippe)Cl_2]$ **(2)**

$[Ni(dippe)_2]^+$	
Ir(1)–P(11)	2.3188(17)
Ir(1)–P(21)	2.3135(16)
Ir(1)–P(31)	2.3104(17)
Ir(1)–P(41)	2.3311(18)
$[Ni(dippe)Cl_2]^-$	
Ir(2)–P(12)	2.1710(16)
Ir(2)–P(22)	2.1714(17)
Ir(2)–Cl(1)	2.4096(17)
Ir(2)–Cl(2)	2.4306(15)

Table 3
Selected bond angles (°) for $[Ir(dippe)_2][Ir(dippe)Cl_2]$ **(2)**

$[Ni(dippe)_2]^+$	
P(21)–Ir(1)–P(11)	83.88(6)
P(31)–Ir(1)–P(41)	83.39(6)
P(31)–Ir(1)–P(11)	96.46(6)
P(41)–Ir(1)–P(11)	166.46(6)
P(41)–Ir(1)–P(21)	100.15(6)
P(31)–Ir(1)–P(21)	163.82(7)
$[Ni(dippe)Cl_2]^-$	
P(22)–Ir(2)–P(12)	86.96(6)
P(22)–Ir(2)–Cl(1)	177.09(7)
P(12)–Ir(2)–Cl(1)	92.70(6)
P(22)–Ir(2)–Cl(2)	92.39(6)
P(12)–Ir(2)–Cl(2)	176.16(7)
Cl(1)–Ir(2)–Cl(2)	88.14(6)

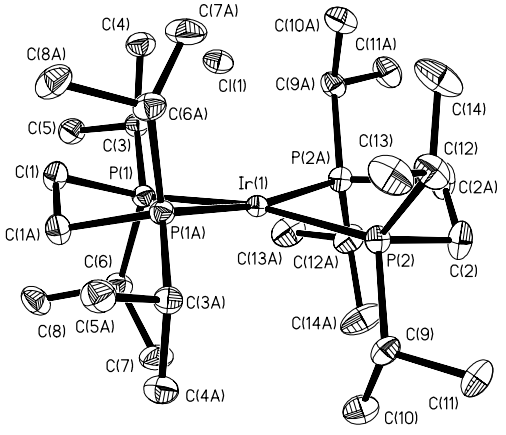

Fig. 4. ORTEP diagram of $[Ir(dippe)_2]Cl$ (**3**). Ellipsoids are shown at the 30% probability level. All hydrogen atoms are omitted for clarity. Selected distances (Å): Ir(1)–P(1), 2.3330(10); Ir(1)–P(2), 2.3220(10).

angle between the P_{11}–Ir–P_{21} and P_{31}–Ir–P_{41} planes of 22.3°. The average dippe bite angle in $[Ir(dippe)_2]^+$ is 83.6°. The cation of **2** displays D_{2h} symmetry upon going from the solid phase into solution, as all isopropyl substituents become equivalent in the ^1H NMR spectrum.

The anion $[Ir(dippe)Cl_2]^-$ has square planar geometry with average Ir–P and Ir–Cl bond lengths of 2.1712(23) and 2.4201(23) Å, respectively. In contrast to $[Ir(dippe)_2]^+$, distortion is minimal. While the iridium center is slightly displaced from the mean IrP_2Cl_2 plane, the greatest deviation, which corresponds to P_{12}, is only −0.0721 Å. Furthermore, the dihedral angle between the P–Ir–P and Cl–Ir–Cl planes is nominal at 4.8°, and the average *trans*-P–Ir–Cl angle is 176.63 (9)°.

The same cation as found in **2** appears in **3**, which has also been structurally characterized. The complex appears as a twisted square plane just as in **2**, with a slightly smaller dihedral angle between the P_1–Ir–P_{1A} and P_2–Ir–P_{2A} planes of 13.8°. The average dippe bite angle in $[Ir(dippe)_2]^+$ is 83.6°, just as in **2**.

3.3. Reaction with dihydrogen

Complex **3** behaves in a like manner to its analog $[Ir(dppe)_2]Cl$ in that it reacts with dihydrogen (Eq. (4)) [9]. Both a crystal structure (CCDC 247139) and ^1H and ^{31}P NMR spectra indicate that the six coordinate Ir^{III} salt $[Ir(dippe)_2H_2]Cl$ (**4**) was formed. The ^1H NMR spectrum in CD_3CN, that is shown in Fig. 5, displays a doublet of multiplets at δ −15.24, which corresponds to the hydride ligands of $[Ir(dippe)_2H_2]^+$. The hydrides couple to the magnetically inequivalent *cis* and *trans* groups of phosphorus atoms. The ^{31}P NMR spectrum in the same solvent consists of a multiplet at δ 53.83 and a broad singlet at δ 26.15.

$$\underset{\mathbf{3}}{[Ir(dippe)_2]Cl} \xrightarrow{H_2} \underset{\mathbf{4}}{[Ir(dippe)_2H_2]Cl} \quad (4)$$

Exposure to UV light labilizes the hydride ligands of $[Ir(dippe)_2H_2]^+$ reversibly to produce $[Ir(dippe)_2]^+$, as illustrated in Scheme 1. The addition of approximately 1 atm of H_2 to a CD_3CN solution of **3** in a resealable NMR tube results in the formation of **4**, which is stable even after the reaction mixture is degassed. When the tube with its contents is irradiated with UV light, the initial orange color returns and is accompanied by the appearance of the singlet at δ 65 in the ^{31}P NMR spectrum, characteristic of **3**. Upon standing, **3** reconverts back to **4**.

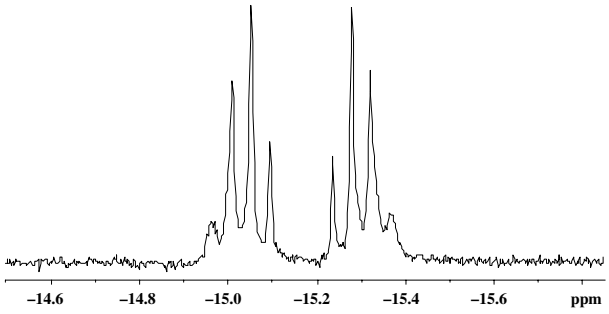

Fig. 5. ^1H NMR spectrum of $[Ir(dippe)_2H_2]Cl$ (**4**) in CD_3CN.

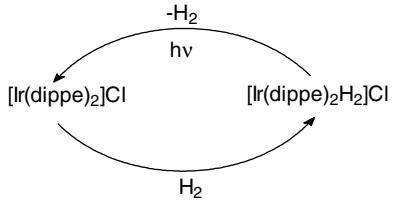

Scheme 1. Labilization of the hydride ligands of $[Ir(dippe)_2H_2]^+$.

4. Discussion

The rhodium dimer $[Rh(dippe)(\mu\text{-}Cl)]_2$ (**1b**) is easily synthesized in high yield from $[Rh(COD)(\mu\text{-}Cl)]_2$, and so it was reasonable to expect similar results for the synthesis of the iridium analog **1a**. In contrast, the synthesis of **1a** from $[Ir(COD)(\mu\text{-}Cl)]_2$ and two equivalents of dippe results in a mixture of products in varying relative amounts that is highly influenced by the choice of solvent. It is especially interesting that two of the products are monomeric salts. The relationship of **1a**, **2** and **3** differ by the dippe:iridium stoichiometry, with ratios of 1:1, 1.5:1 and 2:1, respectively, for these three complexes. The conversion of **1a** to **2** and then **3** has been demonstrated by the addition of dippe. It is interesting, however, that this conversion also occurs if **1a** is allowed to stand in solution, implying that an 'IrCl' fragment is ejected in balancing the stoichiometry for this conversion.

One factor affecting the stability of **1a** is the ability of dippe to stabilize the bridging chloride dimer. For example, EH MO calculations for $[Rh(PH_3)_2(\mu\text{-}Cl)]_2$ and $[Rh(dtbpm)(\mu\text{-}Cl)]_2$ (dtbpm = di-*tert*-butylphosphinomethane) have indicated that P–Rh–P angles that deviate from 90° result in weaker Rh(μ-Cl) bonds. Moreover, experimentally determined Rh(μ-Cl) distances in $[Rh(dtbpm)(\mu\text{-}Cl)]_2$ and $[Rh(P^iPr_3)_2(\mu\text{-}Cl)]_2$, which have P–Rh–P angles of approximately 75° and 105°, respectively, support the theoretical results [10,11]. The former is even known to dissociate into its monomers when it is in solution. Yet, the average bite angle of the dippe ligands in **1a** is only about 4° smaller than the optimal 90°, suggestive that the chelate bite angle is not responsible for the instability of **1a**.

There are other factors that need to be considered, as well, in determining the effect of the terminal dippe ligand on the formation of **1a**. It has been reported that the stabilities of rhodium and iridium $[ML_2(\mu\text{-}X)]_2$ and $[M(LL)(\mu\text{-}X)]_2$ complexes, where X = halide, are affected to a large degree by steric and electronic characteristics of the phosphine. Phosphines that are

sterically demanding and are poor σ-donors favor dimeric products while phosphines that are less sterically demanding and are good σ-donors favor the monomeric products [12]. The cone angle about a phosphorus atom in dippe can be estimated [13] as being between 151° and 160°, rendering it as a sterically demanding ligand that should favor the formation of **1a**. It is worthwhile to note that the syntheses of both $[Ir(dippp)(\mu\text{-}Cl)]_2$ and $[Ir(dtbpp)(\mu\text{-}Cl)]_2$ have been reported, but their X-ray structures were not determined [14].

The hinge angle of **1a** is comparable to those found in other chloro-bridged iridium dimers with terminal phosphines [12,15–17]. A listing of these complexes and their measured hinge angles (θ) is found in Table 4. **1a** possesses the largest angle among the members of the group (132.2°). In regard to other related Ir and Rh analogs that contain a M_2X_2 core, where X = Cl and S, θ has been found to increase by no greater than 1.2° when Rh is replaced with Ir, as illustrated in Table 5. The difference between **1a** and **1b** is larger and in the opposite direction, by about 5° [18–21].

The cation of **2** and **3**, $[Ir(dippe)_2]^+$, bears a resemblance to species such as $[Ir(dppe)_2]^+$, $[Rh(dppe)_2]^+$ and $[Rh(dmpe)_2]^+$ in terms of metal oxidation state, coordination number and connectivity to two bidentate phosphorus ligands [9,22]. Yet, it displays slightly different solid-state structural characteristics when it is a constituent of **3** as opposed to **2**. First, the tetrahedral distortion that is created by the steric interaction between the isopropyl substituents of the dippe ligands is less pronounced for $[Ir(dippe)_2]^+$ in **3** [23,24]. The dihedral angle between the P–Ir–P planes decreases from 22.3° in **2** to 13.8° in **3**. Also, the deviation from the mean Ir–P plane is less in **3**: the iridium center is in the plane while all of the phosphorus atoms are displaced less than 0.2 Å from it. Second, the iridium–phosphorus core of $[Ir(dippe)_2]^+$ is less compact in **3**; the mean Ir–P bond length is approximately 0.05 Å larger.

The fact that the average Ir–P bond length in $[Ir(dippe)_2]^+$ is approximately 0.15 and 0.14 Å longer than the values that are found in the anion of **2** and in **1a**, respectively, can be attributed to two phenomena. First, the longer distance may be a result of the σ-donating ability of dippe that gives rise to a substantially large *trans*-influence. Second, steric interaction between the isopropyl substituents of the dippe ligands may result in the longer bond distances. Evidence for steric repulsion between the isopropyl groups of the opposing dippe ligands is found in the effect that the substitution of one bidentate ligand by two chlorides has on the P–Ir–P angle: the bite angle in $[Ir(dippe)Cl_2]^-$ is approximately 3.4° larger than in $[Ir(dippe)_2]^+$. Furthermore, evidence for a direct relationship between metal–phosphorus bond lengths and phosphine cone angle was found in the study of a series of 19 trialkylphosphine $Cr(CO)_5$ complexes [25]. Of particular relevance to the formation of this anion is the report by Roddick et al. that $[Ir(COD)(\mu\text{-}Cl)]_2$ reacts with silver triflate and dfepe (dfepe = bis-diperfluoroethylphosphinoethane) to give [Ir(dfepe)(COD)] + $[(dfepe)Ir(OTf)]^-$ [26].

The anion, $[Ir(dippe)Cl_2]^-$, is the only example of a Group 9 d^8 metal bisphosphine dichloride complex to be found in the literature. Several rhodium and cobalt bisphosphine dichloride species have been made and structurally characterized, but all of them are neutral with d^7 metal centers [27].

Table 4
Hinge angles, θ, in selected $[IrP_2(\mu\text{-}Cl)]_2$ complexes

Complex	θ (°)	Ref.
$[Ir(dippe)(\mu\text{-}Cl)]_2$	132.2	this work
$[Ir(dtbpm)(\mu\text{-}Cl)]_2$	130	[15]
$[Ir(dfepe)(\mu\text{-}Cl)]_2$	128	[12]
$[Ir(PF_3)_2(\mu\text{-}Cl)]_2$	107	[16]
$[Ir(binap)Cl]_2$	125	[17]

Table 5
Hinge angles, θ, in Rh and Ir analogs with a M_2S_2 core

Complex	Rh	Ir	Ref.
$[M(dippe)(\mu\text{-}Cl)]_2$	137.1	132.2	this work
$[M(COD)(\mu\text{-}SPh)]_2$	114.5	115.0	[18,19]
$[M(COD)(\mu\text{-}S(CH_2)_3NMe_2)]_2$	104.7	105.9	[20,21]

5. Conclusions

In summary, the reaction between $[Ir(COD)(\mu\text{-}Cl)]_2$ and dippe selectively produces **1a** in CH_3CN, but converts to **2** and **3** when allowed to remain in solution. This observed instability is in contrast to its rhodium analog **1b**. The complex salt **2** appears to be an intermediate in going from **1a** to **3**, and is without literature precedent. The salt **3** reacts with dihydrogen to form **4**.

Appendix A. Supplementary material

Tables of complete crystallographic information for compounds **1a**, **1b**, **2**, **3**, and **4** have been deposited with the Cambridge Crystallographic Center, CCDC Nos. 242508–242511 and 247139. Copies of this information may be obtained free of charge from The Director, CCDC, 12 Union Road, Cambridge, CB2, IEZ, UK (fax: +44-1233-336-033, email: deposit@ccdc.cam.ac.uk or www:http//www.ccdc.cam.ac.uk). Supplementary data associated with this article can be found, in the online version, at doi:10.1016/j.poly.2004.06.031.

References

[1] (a) M.D. Fryzuk, T. Jones, F.W.B. Einstein, Organometallics 3 (1984) 185;
(b) M.D. Fryzuk, M.L. Jang, T. Jones, F.W.B. Einstein, Can. J. Chem. 64 (1986) 174;
(c) M.D. Fryzuk, W.E. Piers, Organometallics 7 (1988) 2062;
(d) M.D. Fryzuk, W.E. Piers, Polyhedron 7 (1988) 1001;
(e) M.D. Fryzuk, W.E. Piers, Organometallics 9 (1990) 986;
(f) M.D. Fryzuk, L. Rosenberg, S.J. Rettig, Organometallics 10 (1991) 2537;
(g) M.D. Fryzuk, W.E. Piers, S.J. Rettig, Can. J. Chem. 70 (1992) 2381;
(h) M.D. Fryzuk, D.H. McConville, S.J. Rettig, Organometallics 12 (1993) 2152;
(i) M.D. Fryzuk, L. Rosenberg, S.J. Rettig, Inorg. Chim. Acta 222 (1994) 345;
(j) L. Rosenberg, M.D. Fryzuk, S.J. Rettig, Organometallics 18 (1999) 958.

[2] M.D. Fryzuk, W.E. Piers, F.W.B. Einstein, T. Jones, Can. J. Chem. 67 (1989) 883.

[3] G. Aullón, G. Ujaque, A. Lledós, S. Alvarez, Chem. Eur. J. 5 (1999) 1391.

[4] G. Aullón, G. Ujaque, A. Lledós, S. Alvarez, P. Alemany, Inorg. Chem. 37 (1998) 804.

[5] S.S. Oster, W.D. Jones, Inorg. Chim. Acta 357 (2004) 1836.

[6] The *t*-butyl analog has been reported: A.A. Del Paggio, R.A. Andersen, E.L. Muetterties, Organometallics 6 (1987) 1260.

[7] F.G.N. Cloke, V.C. Gibson, M.L.H. Green, J. Chem. Soc., Dalton Trans. (1988) 2227.

[8] M.D. Fryzuk, W.E. Piers, S.J. Rettig, F.W.B. Einstein, T. Jones, T.A. Albright, J. Am. Chem. Soc. 111 (1989) 5709.

[9] M.C. Hall, B.T. Kilbourn, K.A. Taylor, J. Chem. Soc. (A) (1970) 2539.

[10] P. Hofmann, C. Meier, W. Hiller, M. Heckel, J. Riede, M.U. Schmidt, J. Organomet. Chem. 490 (1995) 51.

[11] P. Binger, J. Haas, G. Glaser, R. Goddard, C. Krüger, Chem. Ber. 127 (1994) 1927.

[12] R.C. Schnabel, D.M. Roddick, Inorg. Chem. 32 (1993) 1513, and references therein.

[13] Using the measured cone angles of P(*i*-Pr)$_2$Et and P(*i*-Pr)$_3$: K.J. Lee, T.L. Brown, Inorg. Chem. 31 (1992) 289.

[14] M.D. Fryzuk, D.H. McConville, S.J. Rettig, J. Organomet. Chem. 445 (1993) 245.

[15] P. Hofmann, C. Meier, A. Maier, O. Steck, V. Sporys, F. Rominger, Z. Kristallogr. 215 (2000) 609.

[16] P.B. Hitchcock, S. Morton, J.F. Nixon, J. Chem. Soc., Dalton Trans. (1985) 1295.

[17] R. Dorta, P. Egli, F. Zurcher, A. Togni, J. Am. Chem. Soc. 119 (1997) 10857.

[18] J. Pursiainen, T. Teppana, S. Rossi, T.A. Pakkanen, Acta Chem. Scand. 47 (1993) 416.

[19] P.J.J. Bonnet, D. De Montauzon, R. Poilblanc, J. Galy, Acta Crystallogr., Sect. B 35 (1979) 832.

[20] A. Polo, C. Claver, S. Castillón, A. Ruiz, J.C. Bayón, J. Real, C. Mealli, D. Masi, Organometallics 11 (1992) 3525.

[21] E. Fernández, A. Ruiz, S. Castillón, C. Claver, J.F. Piniella, A. Alvarez–Larena, G. Germain, J. Chem. Soc., Dalton Trans. (1995) 2137.

[22] J. van den Broeke, M. Lutz, H. Kooijman, A.L. Spek, B. Deelman, B. van Koten, Organometallics 20 (2001) 2114.

[23] C.G. Young, S.J. Rettig, B.R. James, Can. J. Chem. 64 (1986) 51.

[24] W. Clegg, M.R.J. Elsegood, A.J. Scott, T.B. Marder, C. Dai, N.C. Norman, N.L. Pickett, E.G. Robins, Acta Crystallogr., Sect. C 55 (1999) 733, and references therein.

[25] K.J. Lee, T.L. Brown, Inorg. Chem. 31 (1992) 289.

[26] R.C. Schnabel, D.M. Roddick, Organometallics 15 (1996) 3550.

[27] (a) C.A. Ogle, T.C. Masterman, J.L. Hubbard, J. Chem. Soc., Chem. Commun. (1990) 1733;
(b) K.R. Dunbar, S.C. Haefner, Inorg. Chem. 31 (1992) 3676;
(c) R.L. Harlow, D.L. Thorn, R.T. Baker, N.L. Jones, Inorg. Chem. 31 (1992) 993;
(d) T. Rappert, J. Wolf, M. Schulz, H. Werner, Chem. Ber. 125 (1992) 839;
(e) R.L. Carlin, R.D. Chirico, E. Sinn, G. Mennenga, L.J. de Jongh, Inorg. Chem. 21 (1982) 2218;
(f) K. Heinze, G. Huttner, L. Zsolnai, P. Schober, Inorg. Chem. 36 (1997) 5457.

Available online at www.sciencedirect.com
SCIENCE DIRECT®
Polyhedron 23 (2004) 2967–2973
POLYHEDRON
www.elsevier.com/locate/poly

Palladium complexes of novel azo-compounds derived from cycloalkeno-1,2,3-selenadiazoles: X-ray crystal structure of cyclohexeno-1,2,3-selenadiazole

Christopher P. Morley [a,*], Susan Ford [a], Massimo Di Vaira [b]

[a] Department of Chemistry, University of Wales Swansea, Singleton Park, Swansea SA2 8PP, UK
[b] Dipartimento di Chimica, Università degli Studi di Firenze, Via della Lastruccia 3, 50019 Sesto Fiorentino (FI), Italy

Received 6 July 2004; accepted 25 August 2004
Available online 26 October 2004

Abstract

Cycloalkeno-1,2,3-selenadiazoles react with a mixture of $[Pd_2(dba)_3]$ (dba = dibenzylideneacetone) and a trialkylphosphine, in toluene under reflux, to yield the complexes $[PdL(PR_3)]$ ($L = SeC(R^1)=C(R^2)N=NC(R^1)=C(R^2)Se$; $R^1–R^2 = (CH_2)_{n-2}$; $n = 6$, 7, 8; R = Et, Bu), which contain a novel Se, N, Se tridentate ligand formed by the coupling of two 1,2,3-selenadiazole molecules; the structures of cyclohexeno-1,2,3-selenadiazole and the product with R = Bu and $n = 6$ have been determined by X-ray crystallography.
© 2004 Elsevier Ltd. All rights reserved.

Keywords: Palladium; Selenium; Complexes; X-ray

1. Introduction

The use of organoselenium compounds as ligands in transition metal coordination chemistry has increased during the last few years, in part as a result of the recognition that they may confer significantly different properties from their sulfur analogues on the resultant complexes [1]. We have previously demonstrated that 1,2,3-selenadiazoles may serve as precursors to a range of selenium-containing ligands in combination with the cyclopentadienylcobalt moiety [2–5], and also reported on the reaction of cycloocteno-1,2,3-selenadiazole with $[Pt(PPh_3)_4]$ [6]. The palladium compound $[Pd(PPh_3)_4]$ behaves differently from its platinum analogue, yielding novel dinuclear diselenolenes [7]. We have now studied the reactivity of a series of cycloalkeno-1,2,3-selenadiazoles (**1a**–**c**) towards palladium(0) trialkylphosphine complexes, generated in situ from $[Pd_2(dba)_3]$ (dba = dibenzylideneacetone), **2**. A preliminary report of part of this work has previously been published [8].

2. Results and discussion

A toluene solution of **2**, four equivalents of one of the 1,2,3-selenadiazoles **1a**–**c**, and two equivalents of triethylphosphine or tributylphosphine, turns deep purple on heating to reflux for one hour. The intensely coloured product **3a**–**c** or **4a**–**c** may be isolated in good yield by column chromatography (Scheme 1). Compounds **3a**–**c**, **4a**–**c** have the general formula $[PdL(PR_3)]$ and contain the first examples of a new type of formally dianionic ligand $L = SeC(R^1)=C(R^2)N=NC(R^1)=C(R^2)Se$, which may be considered as an alicyclic analogue of an azo-dye.

* Corresponding author. Tel.: +44 1792 295273; fax: +44 1792 295747.
E-mail address: c.p.morley@swan.ac.uk (C.P. Morley).

0277-5387/$ - see front matter © 2004 Elsevier Ltd. All rights reserved.
doi:10.1016/j.poly.2004.08.011

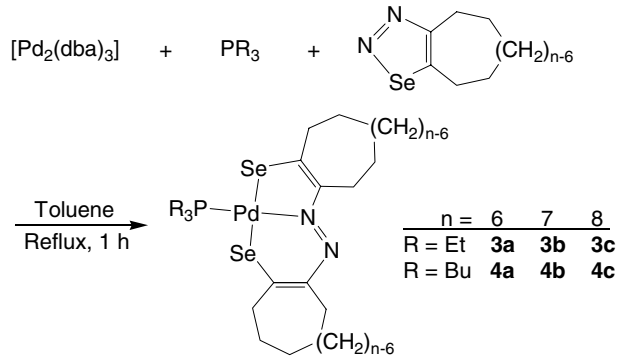

Scheme 1.

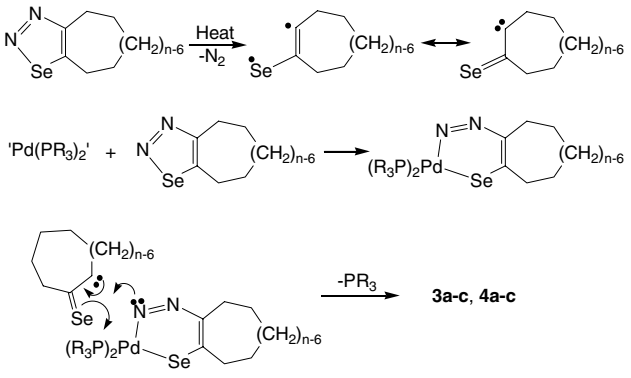

Scheme 2.

Although the detailed mechanism of this reaction has not been determined, some inferences can be drawn on the basis of previous work. Most reactions of 1,2,3-selenadiazoles proceed via the elimination of dinitrogen to yield a selenaketocarbene, the fate of which then determines the outcome of the reaction [9]. As far as we are aware, attack by this fragment on another molecule of intact 1,2,3-selenadiazole is unprecedented. We therefore, postulate insertion of palladium(0) into the selenium–nitrogen bond of a 1,2,3-selenadiazole molecule, followed by 1,3 dipolar addition of a selenaketocarbene to the Pd–N bond of the palladium(II) intermediate thus formed (Scheme 2). It is interesting to note that behaviour analogous to that of $[Pd(PPh_3)_4]$ (i.e., formation of the diselenolene) is not observed. This we ascribe to the greater basicity of the trialkylphosphines used in this study, when compared with that of triphenylphosphine. Oxidative addition of palladium(0) is expected to be more favourable in this case.

The molecular structure of **4a** has been determined by X-ray crystallography and is shown in Fig. 1. Here we add details to the preliminary communication [8], giving the results of the final refinement of the structure. Selected bond lengths and angles are listed in Table 1. The palladium atom is square planar coordinated, with the phosphine *trans*- to a nitrogen atom of the novel tridentate Se, N, Se ligand. The positions of the nitrogen atoms in the azo-group, affected by disorder, have been re-examined, leading to improvements with respect to the previous model [8] (see Section 3). Two orientations

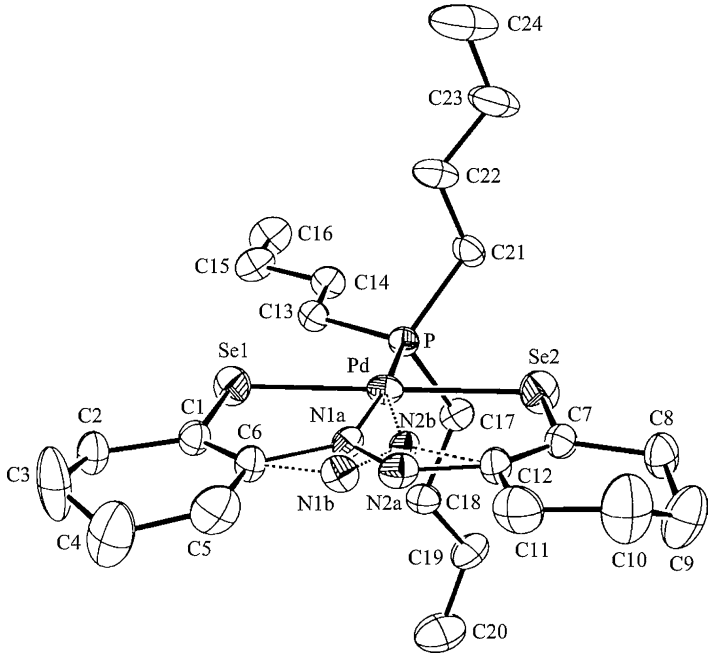

Fig. 1. Molecular structure of $[Pd\{(SeC_6H_8)_2N_2\}(PBu_3)]$, **4a**. 20% probability ellipsoids are shown; H atoms are omitted for clarity. Both the major azo-group orientation (N(1a) and N(2a) sites, thin continuous bonds) and the minor, complementary, orientation (N(1b) and N(2b), dashed bonds) are shown.

Table 1
Selected bond lengths (Å) and angles (°) in the structure of **4a**[a]

Bond lengths			
Pd–Se(1)	2.370(1)	C(7)–C(12)	1.331(10)
Pd–Se(2)	2.371(1)	C(6)–N(1a)	1.49(3)
Pd–P	2.264(2)	C(6)–N(1b)	1.36(4)
Pd–N(1a)	2.102(17)	C(12)–N(2a)	1.40(3)
Pd–N(2b)	2.131(28)	C(12)–N(2b)	1.55(4)
Se(1)–C(1)	1.861(7)	N(1a)–N(2a)	1.29(3)
Se(2)–C(7)	1.864(7)	N(1b)–N(2b)	1.26(4)
C(1)–C(6)	1.315(10)		
Bond angles			
Se(1)–Pd–Se(2)	178.96(4)	Se(1)–C(1)–C(6)	124.3(6)
P–Pd–N(1a)	172.2(7)	Se(2)–C(7)–C(12)	125.5(6)
P–Pd–N(2b)	164.5(1.0)	C(1)–C(6)–N(1a)	111.2(8)
Se(1)–Pd–P	91.69(6)	C(1)–C(6)–N(1b)	148.9(1.4)
Se(1)–Pd–N(1a)	80.8(7)	C(7)–C(12)–N(2a)	143.5(1.0)
Se(1)–Pd–N(2b)	103.6(1.0)	C(7)–C(12)–N(2b)	105.2(1.1)
Se(2)–Pd–P	87.26(6)	C(6)–N(1a)–N(2a)	105(2)
Se(2)–Pd–N(1a)	100.2(7)	C(6)–N(1b)–N(2b)	120(5)
Se(2)–Pd–N(2b)	77.5(1.0)	C(12)–N(2a)–N(1a)	119(3)
Pd–Se(1)–C(1)	98.4(2)	C(12)–N(2b)–N(1b)	105(4)
Pd–Se(2)–C(7)	101.5(2)		

[a] The atom pairs N(1a) and N(2a) and, respectively, N(1b) and N(2b) belong to two complementary fractions of the disordered azo-chain. N(1a) and N(2a) have 0.63(4) population parameter.

of the –N=N– group have been identified, according to which either nitrogen atom is coordinated to the metal, although with different probability, one orientation being about twice as probable than the other. Two mutually exclusive N—Pd bond directions result, forming a 22.8(5)° angle with each other. The present picture appears to be overall more detailed and satisfactory than the previous one, that consisted of a single chain orientation with large effects of thermal motion, although even the present model yields a few non-ideal values of bond angles at the connections between the azo-group and the alicyclic rings, presumably as a residual effect of disorder, difficult to account for in greater detail. This may be associated with a "pedal motion", common in compounds such as stilbenes and azobenzenes [10]. The metal and donor atoms deviate by $\leqslant$0.10(2) Å from their best plane, by far the largest deviations being exhibited by the fractional N sites. The twelve atoms associated with the π-system of the ligand (Se–C(C)=C(C)—N=N—C(C)=C(C)—Se) are also coplanar, with deviations $\leqslant$0.14(1) Å from their least-squares plane (this forms a 3.71(6)° angle with the above coordination plane). This part of the molecule is therefore virtually flat, and visually only the three *n*-butyl groups on the phosphine appear to protrude significantly from the coordination plane. The Pd–Se bond lengths in **4a** [2.370(1), 2.371(1) Å] are almost identical to that in [PdCl($SeCH_2CH_2NMe_2$)(PPh_3)] (2.3710(6) Å [11]), and significantly shorter than most of the one hundred thus far reported in the literature (average value 2.45 Å; see for example [12–14]). In the related complexes [Pd{PhSeNC(4-MeC_6H_4)NNC(4-MeC_6H_4)NSePh}(PPh_3)] [15] and [PdCl{5-MeC_6H_3-2-(N=N-4′-MeC_6H_3-2′-SePh)}] [16] the Pd–Se distances are 2.375(1) Å, and 2.4495(4) Å, respectively. The 2.264(2) Å Pd–P distance in **4a** is within the 2.22–2.29 Å range found for Pd(II) complexes with *trans* PBu_3 phosphorus and nitrogen donor atoms [17–19]. The Pd–N distance, of 2.10(2) or 2.13(3) Å, depending on the arrangement of the azo-group being considered, is rather long (cf. 1.98–2.05 Å values in [15–18]). Larger values (2.139(6) and 2.140(5) Å) than the present ones are found for a dimetal system [19] where geometric coordination constraints may play a role; overall the present values seem to be indicative of a rather weak and not strongly directional Pd–N interaction.

For comparative purposes we have also determined the structure of cyclohexeno-1,2,3-selenadiazole, **1a**, as shown in Fig. 2. Suitable crystals were obtained from a hexane solution of the compound at −20 °C. Table 2 lists selected bond lengths and angles. Although this class of compounds has been known for many years, the only example previously to have been structurally characterised is 4,5,6,10,11,12-hexahydrocyclodeca-(1,2-d:6,7-d′)-bis(1,2,3-selenadiazole), **5** [20]. The bond lengths and angles in the heterocyclic ring of **1a** are almost identical to those observed in **5**, and similar to those found for the coordinating heterocyclic molecule in the metal complex pentacarbonyl(4-methyl-1,2,3-selenadiazole)chromium [21] (bond distances in the heterocyclic ring of **1a** are, overall, 0.018 Å larger than those in the coordinating molecule of the latter compound). The structure of **1a** is essentially planar, with only the outer carbon atoms in the hydrocarbon ring deviating slightly (C(4) by 0.23(2) Å and C(5) by 0.30(2) Å, in opposite directions) from the notional molecular plane.

If features of the five-membered heterocyclic ring present in the structures of both **1a** and **4a** are com-

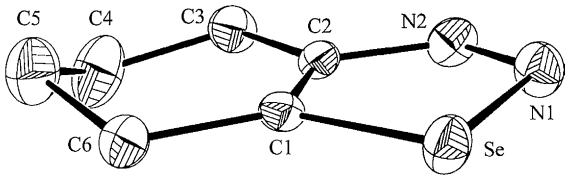

Fig. 2. Molecular structure of cyclohexeno-1,2,3-selenadiazole, **1a**. 20% probability ellipsoids are shown; H atoms are omitted for clarity.

Table 2
Selected bond lengths (Å) and angles (°) in the structure of **1a**

Bond lengths			
C(1)–Se	1.824(11)	Se–N(1)	1.888(10)
N(1)–N(2)	1.260(13)	N(2)–C(2)	1.394(14)
C(1)–C(2)	1.33(2)		
Bond angles			
C(1)–Se–N(1)	86.4(4)	Se–N(1)–N(2)	110.8(7)
N(1)–N(2)–C(2)	116.5(9)	N(2)–C(2)–C(1)	116.0(1.0)
C(2)–C(1)–Se	110.3(8)		

pared, the Se–C bond is found to be 0.04 Å longer and the C=C bond possibly shorter (by 0.01 Å) in **4a**. This may be understood in terms of the loss of the aromatic character of **1a** as well as the larger size of the palladium atom in **4a** compared to the nitrogen atom in **1a**.

The NMR spectroscopic data (Tables 3–5) show that the structure observed in the solid state is maintained in solution for **4a**, and that the structures of **3a**–**c** and **4b**–**c** are similar. The selenium atoms are inequivalent and give rise to two signals in the ^{77}Se NMR spectrum, each of which shows a small splitting (J = 9 Hz) due to coupling to the phosphorus atom in the *cis*-position. This feature is also evident in the ^{31}P NMR spectra, where the single peak has clearly defined ^{77}Se satellites. A second pair of satellites flanks the central ^{31}P resonance due to coupling with the α-carbon atoms of the alkyl chains, ^{1}J (^{13}C–^{31}P) = 30 Hz. For the PBu_3 complexes ^{31}P coupling to the β-carbons is also observed, so that the ^{13}C resonance for these atoms is a doublet with $^{2}J(^{13}C–^{31}P)$ = 14 Hz. No corresponding splitting of the signal for the methyl group occurs in the ^{13}C NMR spectra of the analogous PEt_3 complexes. As expected, for all the compounds, each atom in the two alicyclic rings gives a separate ^{13}C resonance. This asymmetry leads to considerable complexity in the ^{1}H NMR spectra, but a number of features are clear. There are four well-spaced multiplets at relatively low field which may be assigned to the α-CH_2 groups. The methyl groups of the phosphine alkyl chains give rise to a well-defined triplet at higher field, which is further split in the case of the PEt_3 complexes by coupling to phosphorus (the contrast with the absence of ^{13}C–^{31}P coupling for this group is notable).

Table 3
^{1}H NMR spectroscopic data for **3a**–**c**, **4a**–**c** in $CDCl_3$ solution

	3a	3b	3c	4a	4b	4c
CH_3	1.17 (dt)[a]	1.18 (dt)[a]	1.16 (dt)[a]	0.91 (t)[b]	0.91 (t)[b]	0.91 (t)[b]
CH_2P	2.01 (dq)[c]	2.03 (dq)[c]	2.01 (dq)[c]	1.95 (m)	1.96 (m)	1.95 (m)
CH_2CH_2P	–	–	–	1.51 (m)	1.54 (m)	1.52 (m)
$CH_3CH_2CH_2$	–	–	–	1.41 (m)	1.43 (m)	1.41 (m)
$(CH_2)_n$	1.72–1.96	1.50–1.87	1.48–1.89	1.69–1.85	1.69–1.82	1.62–1.95
α-CH_2[d]	2.71 (m)	3.04 (m)	2.91 (m)	2.71 (m)	3.04 (m)	2.91 (m)
	2.89 (m)	3.07 (m)	3.06 (m)	2.88 (m)	3.07 (m)	3.07 (m)
	3.06 (m)	3.24 (m)	3.19 (m)	3.05 (m)	3.23 (m)	3.19 (m)
	3.13 (m)	3.36 (m)	3.41 (m)	3.13 (m)	3.35 (m)	3.41 (m)

[a] $^{4}J(^{1}H–^{31}P)$ = 17.0 Hz; $^{3}J(^{1}H–^{1}H)$ = 7.6 Hz.
[b] $^{3}J(^{1}H–^{1}H)$ = 7.2 Hz.
[c] $^{2}J(^{1}H–^{31}P)$ = 9.2 Hz; $^{3}J(^{1}H–^{1}H)$ = 7.6 Hz.
[d] These resonances generally appear as 'virtual' triplets.

Table 4
^{13}C NMR spectroscopic data for **3a**–**c**, **4a**–**c** in $CDCl_3$ solution

	3a	3b	3c	4a	4b	4c
CH_3	8.3	8.3	8.4	13.7	13.6	13.7
CH_2[a]	17.7	17.9	17.8	25.2	25.4	25.4
CH_2CH_2P[b]	–	–	–	24.2	24.2	24.2
$CH_3CH_2CH_2$	–	–	–	22.7	22.7	22.7
C=C	157.2	163.1	159.6	157.3	163.1	159.6
	144.1	149.5	147.7	144.1	149.8	147.7
	141.8	143.2	143.9	141.9	144.0	144.1
	131.3	134.9	139.3	131.3	135.0	139.3
α-CH_2	36.8	42.6	41.9	36.9	42.5	42.3
	35.8	39.5	39.4	35.9	39.5	39.4
	34.6	37.5	36.5	34.6	37.5	37.1
	30.4	31.8	31.9	30.4	31.7	32.0
β-CH_2	27.0	29.3	30.1	26.3	29.4	29.7
	25.5	27.4	29.2	25.5	27.4	29.4
	24.7	27.2	28.1	24.7	27.2	28.1
	24.0	26.7	27.1	24.0	26.7	27.1
γ-CH_2		26.4	26.6		26.4	26.7
		26.2	26.5		26.3	26.5
			26.4			26.3
			26.0			26.1

[a] $^{1}J(^{13}C–^{31}P)$ = 30 Hz.
[b] $^{2}J(^{13}C–^{31}P)$ = 14 Hz.

Table 5
^{31}P and ^{77}Se NMR spectroscopic data for **3a–c**, **4a–c** in $CDCl_3$ solution

	3a	3b	3c	4a	4b	4c
^{31}P	22.1	21.6	21.4	13.7	13.6	13.4
^{77}Se[a]	548	607	579	548	604	574
	365	397	384	366	395	380

[a] $^{2}J(^{77}Se–^{31}P) = 9$ Hz for both resonances.

Table 6
Yield and mass spectrometric data for **3a–c**, **4a–c**

	3a	3b	3c	4a	4b	4c
Yield (%)	48	36	55	53	46	51
Mass spec.[a]						
M^+	572 (25%)	600 (53%)	628 (44%)	656 (74%)	684 (37%)	712 (39%)
$PR_3 + H^+$	119 (100%)	119 (100%)	119 (100%)	203 (100%)	203 (100%)	203 (100%)

[a] Recorded using FAB; figures are for isotopomers containing ^{80}Se, ^{106}Pd.

The mass spectrometric data are in accord with the proposed formulations (Table 6). In the mass spectrum of each compound there is an intense cluster due to the molecular ion, with the expected isotope distribution, and the base peak corresponds to the protonated trialkylphosphine.

The infrared spectrum of **4a** contains typical absorptions for compounds having aliphatic CH_2 and CH_3 groups. A feature corresponding to the N=N stretch of the azo-group might also have been expected. If seen, it should occur in the range 1350–1600 cm^{-1} [22], but this band is often weak or absent [23]. An unequivocal assignment of the spectrum in this region is not possible. The observation of ν (N=N) has been reported for the related complex $[Pd\{C_6H_4N{=}NCH{=}C(Me)O\}(PPh_3)]$ [24] but no details were given.

Complexes **3a–c** and **4a–c** are an intense purple colour. Examination by ultraviolet/visible spectroscopy showed that their absorption spectra are all very similar (Table 7). There are two intense bands in the ultraviolet, and three weaker bands in the visible region. Only the two lowest energy bands show any dependence on the size of the alicyclic rings, where the shifts in λ_{max} are small (±10 nm) but significant. The nature of the trialkylphosphine appears to have no effect. It may therefore be supposed that the transitions responsible for these absorptions are predominantly ligand-based.

The complexes **3a–c** and **4a–c** may be expected to resemble diselenolenes and dithiolenes in having delocalised metal–ligand bonding. We therefore anticipate rich and varied chemical and physical behaviour for these compounds and their derivatives.

3. Experimental

All reactions were performed using standard Schlenk techniques and pre-dried solvents under an atmosphere of dinitrogen. ^{1}H and ^{13}C NMR spectra: Bruker AC400; tetramethylsilane as internal standard. ^{31}P and ^{77}Se NMR spectra: Bruker WM250; 85% phosphoric acid or dimethyl selenide as external standard. IR spectra: Perkin–Elmer 1725X. UV/VIS spectra: Perkin–Elmer Lambda 9. Mass spectra were recorded by the EPSRC Mass Spectrometry Centre, using Fast Atom Bombardment (FAB).

Cycloalkeno-1,2,3-selenadiazoles (**1a–c**) [8] and $[Pd_2(dba)_3]$.dba (**2**.dba) [25] were prepared by literature methods. Triethyl- and tributylphosphine were obtained commercially and used without further purification.

3.1. Synthesis of *3a–c* and *4a–c*

In a typical experiment, a solution containing $[Pd_2(dba)_3]$.dba, **2**.dba (0.28 g, 0.24 mmol), PBu_3 (0.10

Table 7
Ultraviolet/visible spectroscopic data[a] for **3a–c**, **4a–c**

3a	3b	3c	4a	4b	4c
555 (1300)	570 (2400)	Not recorded	555 (1400)	570 (1800)	565 (1700)
490 (1100)	480 (1900)		490 (1000)	480 (1200)	485 (1300)
390 (240)	390 (320)		390 (300)	390 (290)	390 (310)
290 (4100)	290 (5200)		290 (4500)	290 (4800)	290 (4400)
250 (10,000)	250 (11,000)		250 (9700)	250 (10,000)	250 (10,000)

[a] λ_{max}/nm (ε/dm^3 mol^{-1} cm^{-1}); recorded as 10^{-4} mol dm^{-3} solutions in hexane.

g, 0.50 mmol) and cyclohexeno-1,2,3-selenadiazole, **1a** (0.19 g, 1.00 mmol), in toluene (100 cm^3) was heated under reflux for one hour. After this time the solution had darkened considerably. Removal of the solvent under reduced pressure left an intensely coloured oily solid, which was purified by column chromatography on alumina using a 2:1 mixture of toluene and hexane. Collection of the bright purple band and recrystallisation from hexane gave **4a** as an analytically pure solid. Yield: 0.17 g. IR (ν/cm^{-1}; KBr disk; selected bands only): 2929 vs, 2857 s, 1578 m, 1479 m, 1450 m, 1405 m, 1359 m, 1307 w, 1262 m, 1091 vs, 1050 s, 904 m, 802 s, 720 w.

Yields, spectroscopic and analytical data are summarised in Tables 3–7.

3.2. X-ray crystallography

X-ray data for both **1a** and **4a** were collected at room temperature on an Enraf-Nonius CAD4 diffractometer using graphite-monochromated Mo Kα radiation ($\lambda = 0.71069$ Å). Cell constants were determined by least-squares refinement of the setting angles of 25 reflections with $20° < 2\theta < 30°$. Details of data collection and structure refinement procedures are reported in Table 8. A 15% overall decay in intensities was observed at data collection time for **1a** and was corrected for; no decay was observed for **4a**. An empirical correction for absorption, by ψ scans, was applied to the data of **4a**, but it could not be applied for **1a**, whose crystal was lost soon after data collection, probably as an effect of partial decomposition. In the case of **1a** an empirical correction for absorption with DIFABS [26] was applied after the structure was solved, at isotropic convergence; this procedure was preferred to the use of uncorrected data, which yielded higher R values, more scattered thermal parameters and slightly worse agreement with the values of distances formed by the Se and N atoms in the related structure of [20]. Differences between values of structural parameters from refinements with absorption-corrected, or uncorrected, data for **1a** were, however, small ($<2\sigma$). Both structures were solved by direct methods, with SIR-97 [27], and were extended and refined on F^2 with SHELXL-97 [28]. Repeated effort and improved software facilities [29] with respect to those used for the previous report on **4a** [8] (CCDC deposition No. 182/872, reference code PIJQII), allowed us to improve the model for the azo-chain in the tridentate ligand of that compound. Two orientations of the diatomic group were identified, the more probable one corresponding to the unique arrangement of the previous report. In the least-squares cycles the two fractions were assigned complementary population parameters and were imposed a mild geometrical restraint, forcing the N–N distances to be similar in the two images. Besides being more detailed than the previous model, the present one yielded slightly lower final R values. In the final refinement cycles anisotropic temperature factors were assigned to all non-hydrogen atoms, including those with fractional occupancy factors. Hydrogen atoms were in calculated positions, riding on the respective carrier atom (methyl groups being treated as rigid bodies), with $U_H = 1.2U_C^{eq}$ ($U_H = 1.5U_C^{eq}$ for methyl hydrogens). The highest peaks in the final difference syntheses could not be assigned any chemical significance. Computer programs used included PARST [30] for geometry calculations, and ORTEP [29,31] for graphics.

Table 8
Crystallographic data for compounds **1a** and **4a**

Compound	**1a**	**4a**
Formula	$C_6H_8N_2Se$	$C_{24}H_{43}N_2PPdSe_2$
M_r	187.10	654.90
Crystal system	monoclinic	triclinic
Space group	$P2_1/n$ (No. 14)	$P\bar{1}$ (No. 2)
Unit cell dimensions		
a (Å)	9.525(9)	9.930(2)
b (Å)	7.787(2)	12.044(3)
c (Å)	10.155(16)	13.277(3)
α (°)	90	63.43(2)
β (°)	111.11(14)	83.55(2)
γ (°)	90	81.16(2)
V (Å^3)	702.7(13)	1401.6(6)
Z	4	2
F (000)	368	660
D_c (Mg m^{-3})	1.769	1.552
Crystal size (mm)	$0.30 \times 0.40 \times 0.60$	$0.05 \times 0.50 \times 0.70$
μ (mm^{-1})	5.25	3.33
Absorption correction	empirical	ψ-scan
Minimum and maximum correction factors	0.742, 1.644	0.66, 1.00
Data collected	$\pm h$, $+k$, $+l$	$\pm h$, $\pm k$, $+l$
2θ Range	5–50	5–50
Reflections collected	1247	4956
Unique reflections	1236	4923
Unique observed reflections with $F_o > 4\sigma(F_o)$	909	2936
No. of parameters	82	294
R_1 (all reflections)	0.093	0.109
R_1 (observed reflections)	0.064	0.051
wR_2	0.202	0.134
Goodness-of-fit	1.040	1.032
Largest features (maximum, minimum) in final ΔF map (e Å^{-3})	1.17, −0.95	0.53, −0.54

Acknowledgements

We thank EPSRC for the provision of a research studentship to S.F., Johnson Matthey plc for the loan of palladium salts, and the Ministero dell' Università e della Ricerca Scientifica e Tecnologica for financial support to M.Di V. Last but not least, we are grateful to

Malcolm Green for inspiring a generation of organometallic chemists, C.P.M. included.

Appendix A. Supplementary material

Crystallographic data (excluding structure factors) for the structures reported in this paper have been deposited with the Cambridge Crystallographic Data Centre, 12 Union Road, Cambridge CB2 1EZ, UK (Fax: +44-1223-336033; e-mail: deposit@ccdc.cam.ac.uk, or on the web: http://www.ccdc.cam.ac.uk) and are available on request quoting the deposition numbers CCDC 244070 (**1a**) and CCDC 244069 (**4a**). Supplementary data associated with this article can be found, in the online version, at doi:10.1016/j.poly.2004.08.011.

References

[1] E.G. Hope, W. Levason, Coord. Chem. Rev. 122 (1993) 109.
[2] C.P. Morley, Organometallics 8 (1989) 800.
[3] M.R.J. Dorrity, A. Lavery, J.F. Malone, C.P. Morley, R.R. Vaughan, Heteroatom Chem. 3 (1992) 87.
[4] C.P. Morley, R.R. Vaughan, J. Chem. Soc., Dalton Trans. (1993) 703.
[5] C.P. Morley, R.R. Vaughan, J. Organomet. Chem. 444 (1993) 219.
[6] P.K. Khanna, C.P. Morley, J. Chem. Res. (S) (1995) 64.
[7] S. Ford, P.K. Khanna, C.P. Morley, M. Di Vaira, J. Chem. Soc., Dalton Trans. (1999) 791.
[8] S. Ford, C.P. Morley, M. Di Vaira, Chem. Commun. (1998) 1305.
[9] H. Meier, E. Voigt, Tetrahedron 28 (1972) 187.
[10] J. Harada, K. Ogawa, J. Am. Chem. Soc. 123 (2001) 10884.
[11] S. Dey, V.K. Jain, S. Chaudhury, A. Knoedler, F. Lissner, W. Kaim, J. Chem. Soc., Dalton Trans. (2001) 723.
[12] J.-C. Wang, J.P. Fackler Jr., Acta Crystallogr., Sect. C 45 (1989) 951.
[13] U. Drutkowski, B. Wenzel, P. Strauch, Inorg. Chem. Commun. 1 (1998) 449.
[14] C. Bornet, R. Amardeil, P. Meunier, J.C. Daran, J. Chem. Soc., Dalton Trans. (1999) 1039.
[15] T. Chivers, K. McGregor, M. Parvez, Inorg. Chem. 33 (1994) 2364.
[16] P.G. Jones, M.C. Ramirez de Arellano, J. Chem. Soc., Dalton Trans. (1996) 2713.
[17] M. Fukazawa, M. Kita, N. Nonoyama, Polyhedron 13 (1994) 1609.
[18] F. Hintermaier, F. Kuhlwein, C. Robl, W. Beck, Z. Anorg. Allg. Chem. 621 (1995) 829.
[19] P. Espinet, J.A. Miguel, S. Garcia-Granda, D. Miguel, Inorg. Chem. 35 (1996) 2287.
[20] G.A. Morales, F.R. Fronczek, J. Chem. Cryst. 24 (1994) 811.
[21] V. Batzel, R. Boese, Z. Naturforsch., Teil B 36 (1981) 172.
[22] L.J. Bellamy, third ed.The Infrared Spectra of Complex Molecules, vol. 1, Chapman and Hall, London, 1976.
[23] D.D. Heinrich, J.P. Fackler Jr., P. La Huerta, Inorg. Chim. Acta 116 (1986) 15.
[24] J. Albert, A. Gonzalez, J. Granell, R. Moragas, C. Puerta, P. Valerga, Organometallics 16 (1997) 3775.
[25] Y. Takahashi, T. Ito, S. Sakai, Y. Ishii, J. Chem. Soc., Chem. Commun. (1970) 1065.
[26] N. Walker, D. Stuart, Acta Crystallogr., Sect. A 39 (1983) 158.
[27] A. Altomare, M.C. Burla, M. Camalli, G.L. Cascarano, C. Giacovazzo, A. Guagliardi, A.G.G. Moliterni, G. Polidori, R. Spagna, J. Appl. Cryst. 32 (1999) 115.
[28] G.M. Sheldrick, SHELXL-97, Program for Crystal Structure Refinement, University of Göttingen, Göttingen, 1997.
[29] L.J. Farrugia, J. Appl. Crystallogr. 30 (1997) 565.
[30] M. Nardelli, J. Appl. Crystallogr. 28 (1995) 659.
[31] C.K. Johnson, ORTEP, Report ORNL-5138, Oak Ridge National Laboratory, Oak Ridge, TN, 1976.

Available online at www.sciencedirect.com
SCIENCE DIRECT®
Polyhedron 23 (2004) 2975–2983
POLYHEDRON
www.elsevier.com/locate/poly

On the determination of the structure of ferrocene in solution

John F.C. Turner [a,*], Alan K. Soper [b,*]

[a] Neutron Sciences Consortium and Department of Chemistry, University of Tennessee, Buehler Hall, Knoxville, TN 37996-1600, USA
[b] ISIS Facility, Rutherford Appleton Laboratory, Chilton, Didcot OX11 0QX, UK

Received 15 July 2004; accepted 8 September 2004
Available online 26 October 2004

Dedicated to Prof. M.L.H. Green FRS

Abstract

The molecular structure of ferrocene in toluene solution is examined for the first time, using neutron scattering with hydrogen isotope substitution on the ferrocene hydrogen atoms. The results are interpreted via a computer-simulated model of ferrocene and toluene molecules at the same concentration and density as the experiment. It is found that the solvation shell of ferrocene is highly anisotropic, with concentrations of toluene in the axial and equatorial regions around the ferrocene molecule. In addition these toluene molecules show a strong orientational correlation with their position in the solvation shell of ferrocene. The ferrocene molecule itself can be slightly bent at times (up to about 30° although most molecules are much straighter than this) along the axis joining the centroids of the two cyclopentadienyl rings. There is a weak torsional correlation between the two rings on the ferrocene molecule at the temperature of the present experiment, which is 313 K.
© 2004 Elsevier Ltd. All rights reserved.

1. Introduction

Knowledge of structure is fundamental to the understanding of the nature of bonding, properties and reactivity in chemical systems. Structural determinations are routinely carried out by diffraction of radiation from an appropriate source by a sample, from which information about the interatomic distances and atomic identities can be ascertained [1–5]; the majority of these determinations are conducted in the solid state, using a crystalline sample, either as a single crystal or a microcrystalline powder.

In this paper, we present the results of a set 'proof of concept' experiments that allows the investigation of a structurally complex organometallic in solution, using neutron diffraction augmented with isotopic substitution. It is the first set of experiments of which we are aware in which the scientific focus is the structure of the solute alone.

Elastic neutron scattering is a complementary technique to the more conventional diffraction methods, which use usually X-rays or occasionally electrons. Both X-rays and electrons are scattered by electron density and therefore the scattering intensity is directly coupled to the *chemical identity* of the scattering atom. In contrast, neutron scattering is decoupled from the chemical identity of the atom; for the purposes of this report, neutrons can be considered to be scattered solely by the atomic nucleus and it is the composition of the nucleus that determines the strength of the elastic nuclear scattering cross-section. At current levels of nuclear theory, the a priori prediction of the strength of the scattering interaction for a particular isotope in not possible [6] and empirical scattering parameters are tabulated in the literature [7] and on the World Wide Web [8].

* Corresponding authors. Tel.: +1 865 974 8591; fax: +1 865 974 3454.
E-mail address: jturner@ion.chem.utk.edu (J.F.C. Turner).

0277-5387/$ - see front matter © 2004 Elsevier Ltd. All rights reserved.
doi:10.1016/j.poly.2004.09.003

The determination of chemical structure in the solid state is greatly assisted by the long range order of the crystal, which imposes rigorously defined symmetries on any proposed structure. For a crystalline molecular system, the structure can be defined in either reciprocal or real space via a convolution of the intermolecular structure, P and the structure of the individual structural motifs, a such that $M = a \otimes P$. In a crystalline material, this representation of structure is transparent: P represents the lattice and a the asymmetric unit [1–3]. Interpretation of Bragg diffraction from a crystal is therefore simplified by the inherent periodicity, which truncates the description of the structure, or any property of the crystalline system, allowing, in principle, a tractable yet complete description.

The liquid state is clearly an important chemical milieu and for inorganic systems and the correlation between the solid state structure and the structure in the liquid state is less strong than in an organic system; factors such as fluxionality and dissociation can profoundly affect the structure of an inorganic system. The key problem with the liquid state is the disordered nature of the phase; with a disordered material, i.e. one which lacks the long range order of a crystal, there are no constraints on the structure. The diffraction pattern from a disordered material is much simpler in form as there is no Bragg contribution. However the *interpretation* of that structure is much more ambiguous than in the crystalline case, precisely because of the lack of symmetry and periodicity to impose structural constraints. Real progress in understanding disordered structures is only made by generating a model of the disordered material which includes as much prior knowledge as possible. Ideally, the model will include molecular structure and symmetry, likely minimum distances of approach between atom pairs, possible force models for atom pair interaction, amongst other contributions.

In a liquid sample, all correlations between all pairs of atoms contribute to the interference of the scattered waves, i.e. the diffraction pattern. For a sample containing N atom types, there are $N(N + 1)/2$ site–site correlations between atom pairs. For even a modestly complicated system therefore the diffraction pattern is a weighted average of these correlations, making it difficult to interpret the data directly. In a solution, the inherent problem with the liquid phase is exacerbated by the dominance of both the intra- and intermolecular structure in the diffraction pattern. The unique ability of neutron diffraction is that it can, by means of isotope labelling, dissect the diffraction pattern into subsets of the total set of correlation functions: the scattering cross-section can be perturbed while retaining the structure of the sample through isotopic labelling, because to a good approximation the nuclear nature of the scattering process depends on the isotope of the scattering atom, not on its chemical situation. Through isotopic substitution of specific atoms, the scattering properties of the atom in question are changed, without major changes to the chemical bonding, which highlights the structure around the labelled atom. The most common substitution is that of deuterium for hydrogen, but other isotopic substitutions have also been used [9–13].

In this paper, we apply this technique to solutions of ferrocene, substituting the cyclopentadienyl hydrogen atoms with deuterium, to provide the isotopic contrast, while keeping the isotopic nature of the solvent identical between samples.

In the liquid state, the major methods of structural determination are spectroscopic, either using a vibrational technique, such as infra-red or Raman spectroscopy, or nuclear magnetic resonance. Direct structural information, in terms of interatomic distances and identities on a par with a crystalline diffraction experiment, is therefore necessarily absent using these methods, though their utility in solving inorganic structural problems is not in question. This paper shows that structural information in a solute structure can be accessed using diffraction techniques.

Ferrocene holds a seminal position in the field of organometallics, being the first π-bound organometallic 'sandwich' complex to be identified [14–16]. The discovery of the then unique structure led to an explosion of work in the field and the correct assignment of the structure [17–19] and the subsequent development of the field led to the award of the Nobel Prize in 1973 to Wilkinson [20,21] and Fischer [22,23].

The structure of ferrocene has been determined in the crystalline solid state using both neutron and X-ray diffraction [19,24–27]. The structure in the gas phase has also been determined using gas phase electron diffraction [28–30]. The two symmetrical *extrema*, corresponding to D_{5h} and D_{5d} symmetry, are the eclipsed and staggered conformations around the ring centroid–Fe–ring centroid vector. The interconversion process has been extensively investigated [26–29,31–35] and the height of the barrier is ~4 kJ mol^{-1}.

In this report, the diffraction patterns of h_5-(η–Cp)$_2$Fe and d_5-(η–Cp)$_2$Fe in toluene solution are reported. Analysis of the first order difference between the two diffraction patterns using empirical potential structure refinement (EPSR) [36] reveals the structure of the molecule, together with the structure of the solvation shell around this molecule.

2. Theory

The quantity measured in a neutron diffraction experiment is the differential scattering cross-section, $d\sigma/d\Omega$, where

$$\frac{d\sigma}{d\Omega} = \frac{d\sigma}{d\Omega_{self}} + \frac{d\sigma}{d\Omega_{distinct}} = \sum_{\alpha} c_\alpha b_\alpha^2 (1 + P(Q,\theta)) + F_N(Q). \quad (1)$$

Here $P(Q,\theta)$ is the contribution which arises from inelastic scattering, $F_N(Q)$ is the structure factor arising from the 'distinct scattering', c_α is the atomic concentration and b_α the scattering length of isotope α [37]. The scattering lengths in this and the following equations are averaged over the spin and isotope states for each nucleus. Q is the wave vector change in the scattering experiment.

The words "self" and "distinct" refer, respectively, to scattering by single atoms and scattering by distinct pairs of atoms. Distinct scattering is sometimes also called "interference scattering" which indicates that it contains the important structural information of the material in question, while the self scattering represents a background which needs to be subtracted from the measured data prior to attempting to analyse the distinct scattering. The self scattering also serves a useful function in helping to ensure that the sample composition is as planned: the scattering level from the self scattering is quite sensitive to the detailed sample composition, e.g. if there is any light hydrogen present.

The function $F_N(Q)$ itself splits into two terms, a molecular form factor which corresponds to interference scattering between atoms within the same molecule, sometimes called "intramolecular" correlations $F_{intra}(Q)$, and an intermolecular term which corresponds to interferences between atoms on different molecules, $F_{inter}(Q)$, i.e. $F_N(Q) = F_{intra}(Q) + F_{inter}(Q)$. Since the former consists only of correlations within the same molecule it is straightforward to calculate the orientational average of this quantity, since it will be independent of how the molecule is oriented relative to other molecules

$$F_{intra}(Q) = \sum_j x_j \sum_{\alpha\beta\neq\alpha} b_\alpha^{(j)} b_\beta^{(j)} \frac{\sin Q d_{\alpha\beta}^{(j)}}{Q d_{\alpha\beta}^{(j)}} \exp\left[-\frac{Q^2\sigma_{\alpha\beta}^2}{2}\right], \quad (2)$$

where x_j is the mole fraction of molecules j, $b_\alpha^{(j)}$ is the scattering length for atom α on the j th molecule, and $d_{\alpha\beta}^{(j)}, \sigma_{\alpha\beta}^2$ are the mean separation and standard deviation, respectively, of atoms α and β on this molecule.

For the intermolecular term this simple average is not possible since the orientation of one molecule may well be correlated with its position relative to another. Instead the intermolecular interference term is normally written in terms of the Faber–Ziman partial structure factors, $S_{\alpha\beta}(Q)$, by the following equation:

$$F_{inter}(Q) = \sum_{\alpha,\beta\geqslant\alpha} (2 - \delta_{\alpha\beta}) c_\alpha b_\alpha c_\beta b_\beta [S_{\alpha\beta}(Q) - 1], \quad (3)$$

where c_α is the atomic fraction of component α, and the partial structure factors are related to their corresponding real space site–site radial distribution functions (SSRDF) by Fourier transform

$$S_{\alpha\beta}(Q) - 1 = 4\pi\rho \int_0^\infty r^2 [g_{\alpha\beta}(r) - 1] \frac{\sin Qr}{Qr}\, dr. \quad (4)$$

If there are N distinct atomic types in a material there will be $N(N+1)/2$ distinct partial structure factors needed to define the atomic structure. In the present experiments, use was also made of the ability to isotopically substitute light hydrogen for deuterium on the ferrocene molecule. This changes the neutron scattering length of the hydrogen atoms on the ferrocene molecule only, and enables a "first order difference" to be calculated which only contains correlations which involve the hydrogen atoms on the ferrocene molecule

$$\begin{aligned}\Delta_H(Q) &= F_N^{(D)}(Q) - F_N^{(H)}(Q) \\ &= [b_D - b_H]\left\{\sum_j x_j \sum_{\alpha=H,\beta\neq\alpha} b_\beta^{(j)} \frac{\sin Q d_{\alpha\beta}^{(j)}}{Q d_{\alpha\beta}^{(j)}} \exp\left[-\frac{Q^2\sigma_{\alpha\beta}^2}{2}\right]\right. \\ &\quad \left. + \sum_{\alpha=H,\beta\geqslant\alpha} (2 - \delta_{H\beta}) c_\alpha c_\beta b_\beta [S_{\alpha\beta}(Q) - 1]\right\}, \end{aligned} \quad (5)$$

where the summations over atoms α in (5) includes only those atoms that have been substituted. The first order difference, calculated by subtraction of the diffraction pattern of h_5-$(\eta$–$Cp)_2Fe$ from that of d_5-$(\eta$–$Cp)_2Fe$, therefore contains only that part of the interference function that depends on the labelled site. This partial pattern will therefore contain the internal structure of the molecule and the structure of the solvation sphere, with the bulk solvent correlations being removed as they are unperturbed by the isotopic substitution and are therefore the same in both diffraction patterns.

In the present experiment there are five distinct atom types to be identified. These are C_S and H_S, representing the carbon and hydrogen atoms on the solvent (toluene) molecule, and Fe, C_{Cp} and H_{Cp}, representing, respectively, the iron, carbon and hydrogen atoms of the ferrocene molecule. Only the H_{Cp} atoms were isotopically substituted in this experiment with the remaining hydrogen atoms deuterated. In the present experiment each of the datasets was normalised to the sum of intermolecular weights to give a set of total structure factors:

$$S_N^{(D)}(Q) = \frac{F_N^{(D)}(Q)}{\left(\sum_{\alpha,\beta\geqslant\alpha} (2 - \delta_{\alpha\beta}) c_\alpha c_\beta b_\alpha b_\beta\right)}, \quad (6)$$

$$S_N^{(H)}(Q) = \frac{F_N^{(H)}(Q)}{\left(\sum_{\alpha,\beta\geqslant\alpha} (2 - \delta_{\alpha\beta}) c_\alpha c_\beta b_\alpha b_\beta\right)} \quad (7)$$

and

$$\Delta S(Q) = \frac{\Delta_H(Q)}{\left((b_D - b_H)\sum_{\alpha=H,\beta\geqslant\alpha}(2-\delta_{H\beta})c_H c_\beta b_\beta\right)}. \quad (8)$$

The normalised intermolecular weights outside each partial structure factor are listed in Table 1 for the diffraction datasets from the 0.5 M $(\eta\text{–}d_5\text{Cp})_2\text{Fe}$, 0.5 M $(\eta\text{–}h_5\text{Cp})_2\text{Fe}$, and the first order difference. Notice how by taking the first order difference many of the strongest correlations in the total structure factors are eliminated. The weights for the protiated sample are slightly larger than for the deuterated sample because the negative neutron scattering length for protons compared to neutrons means that the normalisation constant for the protiated sample is slightly smaller than for the deuterated sample. Obviously this normalisation is only done after the first order difference has been calculated.

3. Experimental and data analysis

Neutron diffraction measurements were performed at 40 °C on two solutions of $(\eta\text{–}h_5\text{Cp})_2\text{Fe}$ and $(\eta\text{–}d_5\text{Cp})_2\text{Fe}$ dissolved in d_8-toluene at a concentration of 0.5 M, using the SANDALS diffractometer [38] at the ISIS Pulsed Neutron Facility, the temperature of experiment being chosen to eliminate any possibility of crystalline material being present in the sample. The samples were contained in flat-plate 2 mm internal thickness titanium–zirconium containers of wall thickness 1 mm (each) with a gold O-ring seal. The neutron diffraction data were corrected for container scattering, attenuation, absorption, multiple scattering, and inelastic scattering using standard analysis procedures [39].

Table 1
Normalised neutron weightings for each partial structure factor for the different datasets

Partial structure factor	$S_N^{(D)}(Q)$	$S_N^{(H)}(Q)$	$\Delta S(Q)$
C_S–C_S	0.1639	0.2003	–
C_S–H_S	0.3760	0.4595	–
C_S–Fe	0.0071	0.0086	
C_S–C_{Cp}	0.0493	0.0602	–
C_S–H_{Cp}	0.0495	−0.0339	0.4251
H_S–H_S	0.2157	0.2636	–
H_S–Fe	0.0081	0.0099	–
H_S–C_{Cp}	0.0565	0.0691	–
H_S–H_{Cp}	0.0568	−0.0389	0.4876
Fe–Fe	0.0001	0.0001	–
Fe–C_{Cp}	0.0011	0.0013	–
Fe–H_{Cp}	0.0011	−0.0007	0.0092
C_{Cp}–C_{Cp}	0.0037	0.0045	–
C_{Cp}–H_{Cp}	0.0074	−0.0051	0.0639
H_{Cp}–H_{Cp}	0.0037	0.0014	0.0141

The normalised structure factors defined in (6)–(8) above have been subjected to an EPSR, developed by one of us [43,44]. Briefly, the EPSR performs a standard Monte Carlo computer simulation of the solution in question, starting from physical constraints on the molecular geometry and an assumed reference site–site pair interaction potential. This is then perturbed iteratively for each of the site–site interactions until the simulated total structure factors converge to a satisfactory fit of the diffraction data. This perturbation is called the empirical potential (EP).

After convergence, molecular configurations, compatible with the experimental data, were recorded and the whole set of SSRDF were estimated, as well as other structural properties of interest, which are not available from a direct Fourier transform of the total structure factors. Among these the so called spatial density function (SDF) describes how the molecules of one kind are distributed around those of another at the origin [45]. The orientational correlation functions (OCF) can then be used to explore the relative orientations of the two molecules in specified directions through the SDF. Alternatively one can calculate so called ''bond angle distributions'', which show the angular distribution between pairs of atoms on different molecules, averaged over all directions in the SDF.

The EPSR method has the advantage of fitting all the measured data simultaneously to a single atomistic model of the scattering system, instead of the traditional Fourier transform of individual structure factors. Of course this cannot necessarily be done unambiguously, but the use of a starting potential serves to eliminate physically unreasonable structures, so that any structure that is constructed will not contain unphysical atom overlaps. In that sense the EPSR method can be thought of generating a set of plausible structures which are consistent with a given set of data.

The starting reference potential was generated from a series of site–site Lennard–Jones potentials of the form:

$$U_{\alpha\beta}^{(\mathrm{ref})}(r) = 4\varepsilon_{\alpha\beta}\left[\left(\frac{\sigma_{\alpha\beta}}{r}\right)^{12} - \left(\frac{\sigma_{\alpha\beta}}{r}\right)^{6}\right], \quad (9)$$

where,

$$\varepsilon_{\alpha\beta} = \sqrt{\varepsilon_\alpha \varepsilon_\beta} \quad (10)$$

and

$$\sigma_{\alpha\beta} = \frac{1}{2}(\sigma_\alpha + \sigma_\beta), \quad (11)$$

the so-called Lorentz–Berthelot mixing rules. Table 2 lists the Lennard–Jones parameters used for the present set of simulations. The cubic simulation box was of dimension 33.73 Å and contained 200 toluene molecules and 10 ferrocene molecules. Periodic boundary conditions and the minimum image convention were applied in the usual way, but no correction for the long range

Table 2
Lennard–Jones parameters used for the EPSR simulations on ferrocene in toluene

Atom	ε_α (kJ/mole)	σ_α (Å)
C_S	0.30	3.0
H_S	0.10	1.0
Fe	0.60	3.3
C_{Cp}	0.30	3.0
H_{Cp}	0.10	1.0

part of the potential was made. No Coulombic charges appeared on any of the atoms. There was no particular reason for this particular choice of parameters, other than they gave a reasonable simulated energy and pressure and did not lead to any obvious atomic overlap. At this time there do not appear to have been any previous computer simulations of ferrocene in solution from which to derive a set of starting parameters for the reference potential. Fig. 2 shows the diffraction data and their EPSR fits, using the molecular models for toluene and ferrocene as described in Section 4.

The fits in *r*-space are shown in Fig. 3, where the Fourier transforms are given by

$$G_N^{(D)}(r) = 1 + \frac{1}{2\pi^2\rho}\int_0^\infty r^2 S_N^{(D)}(Q)\frac{\sin Qr}{Qr}\,dr \qquad (12)$$

and

$$\Delta G(r) = 1 + \frac{1}{2\pi^2\rho}\int_0^\infty r^2 \Delta S(Q)\frac{\sin Qr}{Qr}\,dr\Delta(r), \qquad (13)$$

so that these functions are weighted sums of the corresponding SSRDF with the same weights as those given in Table 1.

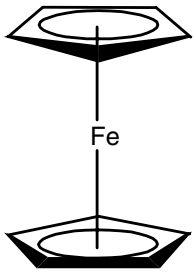

Fig. 1. Schematic structure of Cp_2Fe.

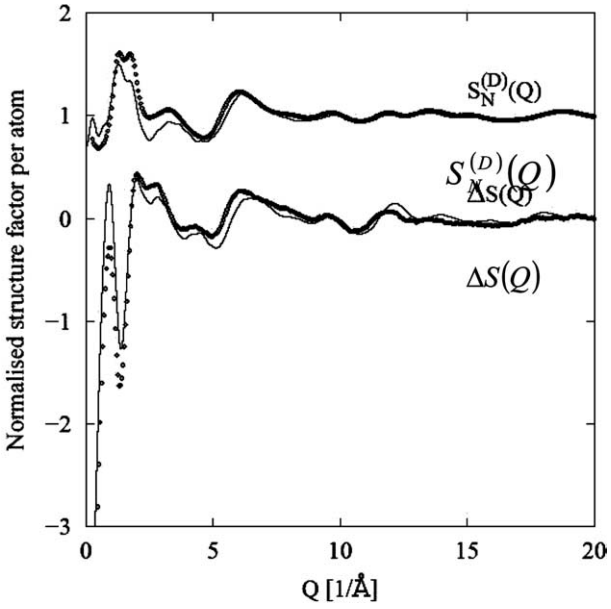

Fig. 2. Normalised structure factors for first order difference $\Delta S(Q)$ (bottom) and total structure factor, $S_N^{(D)}(Q)$, (top, fully deuteriated sample). The diffraction data are shown as the points and the EPSR fits to the data are shown as lines.

4. Results and discussion

4.1. Intramolecular structure

The structure of ferrocene has been determined several times by both neutron [24,40] and X-ray studies [15,19,25] on crystalline samples at varying temperatures. Ferrocene has a classical 'sandwich' structure in which two cyclopentadienyl (Cp) rings are arranged in a coplanar manner, with the Fe atom lying between them on the centroid–centroid vector and equidistant from both rings. The structure is shown schematically in Fig. 1.

For the EPSR simulations in the present work it was necessary to set up a model of the ferrocene and toluene molecules. Ferrocene was constructed from two C_5H_5 pentagonal rings held roughly parallel to one another at a separation of 3.32 Å and perpendicular to a common axis through the centre of each ring (see Fig. 1.). The iron atom was placed on this axis and midway between the two rings. In this model, the C_{Cp}–C_{Cp} near neighbour distance was set to 1.36 Å, the C_{Cp}–H_{Cp} distance was set nominally to 1.08 Å, and the distance between each C_{Cp} atom and the centre of each pentagon was 1.16 Å, these distances being consistent with the diffraction data, though no attempt to actually refine the molecular structure against the data was made. There were no specific torsional forces inhibiting free rotation of one ring relative to the other about the common axis, although the atoms on opposite rings interacted via the usual dispersion and atomic overlap forces. The toluene molecule was modelled starting from a benzene ring with an extra CH_3 group attached to one of the carbons on the ring. The C_S–C_S distance was set to 1.38 Å in all cases, the C_S–H_S distance to 1.08 Å, and the methyl group was allowed to adopt random rotational displacements about the relevant C_S–C_S bond. Again there was no specific attempt to fit the structure of the molecule to the diffraction experiment, although the chosen distances were consistent with those indicated by the data.

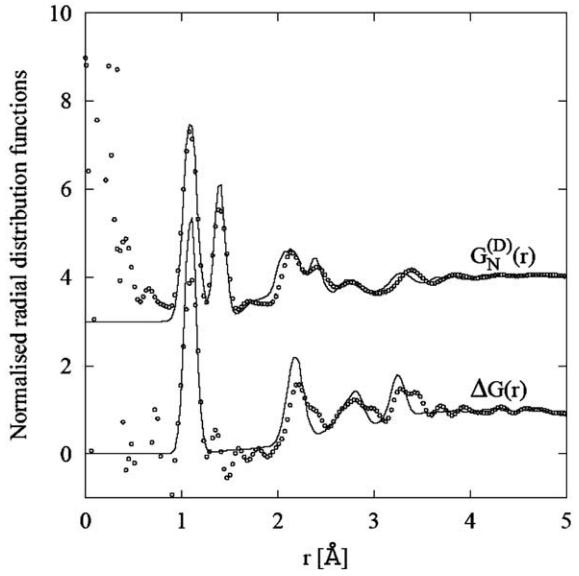

Fig. 3. Fourier transforms of the data shown in Fig. 2, as defined in Eqs. (12) and (13). Fourier transforms of the data are shown as points, while the lines are the EPSR reconstruction using the simulated radial distribution functions.

The cyclopentadienyl rings were assumed to be planar and regular pentagons. The toluene ring was also assumed to be a regular hexagon. However some distortion of the ideal geometries was permitted to reproduce the zero point displacements that would inevitably occur in the real molecules.

Salient intramolecular structural parameters are collated in Table 3. These are comparable with those given in the Cambridge Crystallographic Structure Database [41,42]. However the assumed C–H distance is 1.08 for both the Cp and toluene rings, which is larger than the value of 1.008 given by the Cambridge database. The fits to the short distance data in *r*-space are shown graphically in Fig. 3, and these do not show any obvious discrepancy in the position of the first peak at 1.08, so it is likely the crystallographic values do not represent the true local distances in the liquid state as shown here. Particularly for the first order difference data there appears to be some slight mismatch between the assumed model for ferrocene and the measured data, but overall it is clear that the model has captured the principle features of the molecular structure in both toluene and ferrocene.

Fig. 4 shows the distribution of angles subtended by the iron atom with the centres of the two Cp rings. If the rings were exactly parallel this angle would be $\theta = 180°$ ($\cos\theta = z = -1$). In practice a small deviation from linearity is observed along this axis, with $\cos\theta$ up to −0.88, or $\theta = 151°$, indicating that although the most probable angle is 180° (straight line along the molecular axis) some bending of the axis up to about 30° is observed in a few cases.

Table 3
Average distances for the ferrocene molecule as found in the EPSR simulation, together with their crystallographic counterparts

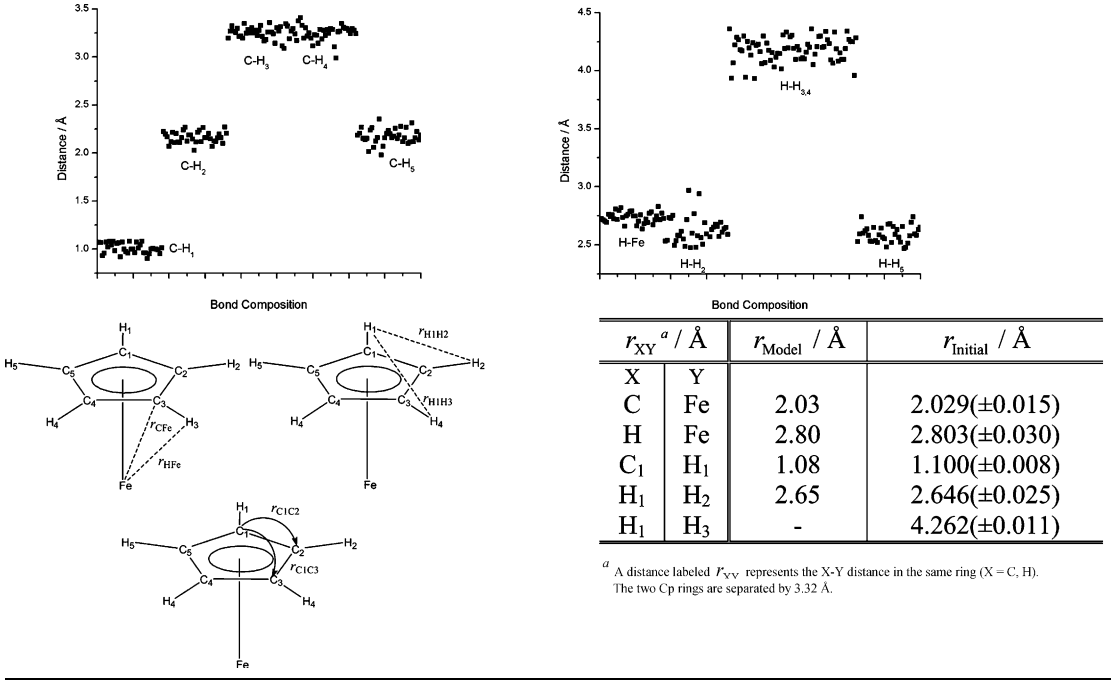

r_{XY} [a] / Å		r_{Model} / Å	$r_{Initial}$ / Å
X	Y		
C	Fe	2.03	2.029(±0.015)
H	Fe	2.80	2.803(±0.030)
C_1	H_1	1.08	1.100(±0.008)
H_1	H_2	2.65	2.646(±0.025)
H_1	H_3	-	4.262(±0.011)

[a] A distance labeled r_{XY} represents the X-Y distance in the same ring (X = C, H). The two Cp rings are separated by 3.32 Å.

Numbers in parenthesis show the r.m.s. deviation of these numbers within the simulation.

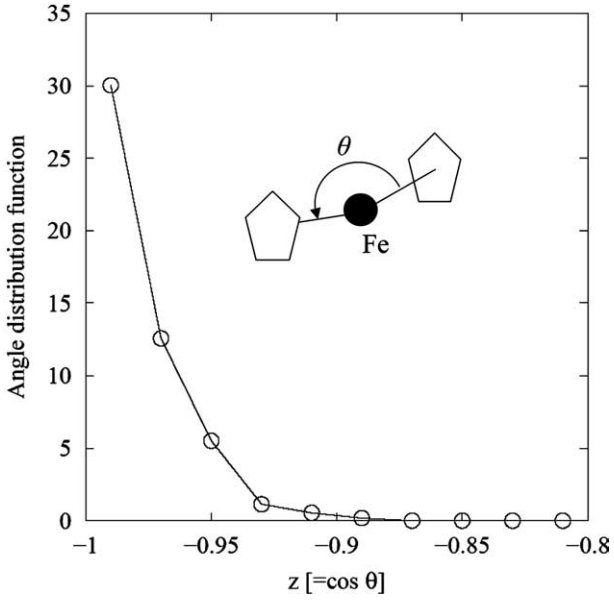

Fig. 4. Angle probability distribution along the axis of a ferrocene molecule. The angle is measured between the vector joining the Fe atom with the centre of one Cp ring and the vector from the Fe atom to the centre of the other Cp ring (see inset). The variable z is defined as $z = \cos\theta$.

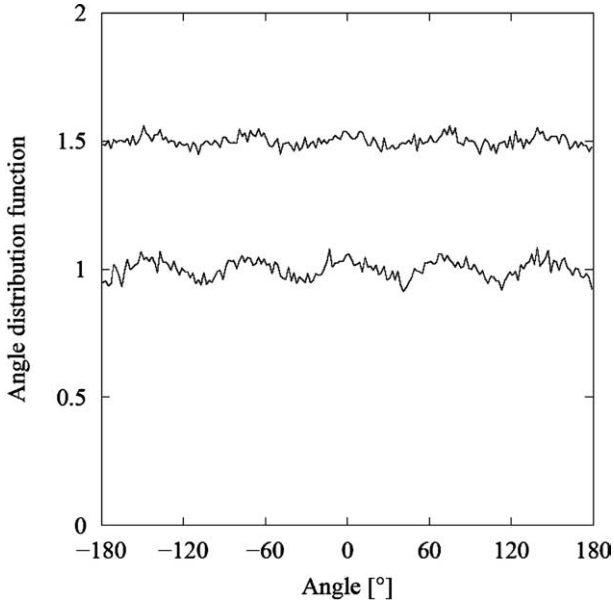

Fig. 5. Torsional angle distribution function for the Cp rings in ferrocene in toluene. The torsional angle is measured as the degree of rotation of one ring relative to the other about the common axis joining their centres. The bottom curve shows the result using the reference potential parameters as listed in Table 2. The top curve shows the effect of increasing σ_{Cp} to 3.4 Å.

A second angle distribution of interest is the distribution of torsional angles along the ferrocene axis. The torsional angle is measured by choosing any pair of carbon atoms on opposite Cp rings and measuring their torsional angle relative to an axis drawn between the centres of the two rings. Thus there are many pairs of carbon atoms that could have been chosen, each of which would give equivalent results. Fig. 5 shows the distribution of torsion angles averaged over some 4000 molecular configurations and over five such pairs of carbon atoms on opposite rings. It can be seen that a small undulation appears in this distribution, with peaks at 0°, ±72°, and ±144°, indicating that the eclipsed configuration is slightly preferred over the staggered configuration, when using the present reference and empirical potentials. The effect is fairly subtle and only appears after accumulating a large number of Monte Carlo configurations. At the present time it is not clear whether the data have sufficient sensitivity to really pick this correlation out, and or whether the assumed reference potential is really responsible for the observed correlation. The relevant average inter-ring distances in the first order difference function are C_{Cp}–H_{Cp} (about 4.1 Å) and H_{Cp}–H_{Cp} (about 4.5 Å) which are sufficiently far out in the correlation function to show no strong correlation, although with the rings separated by about 3.32 Å on average, these distances would range down to about 3.32 Å, depending on the precise orientation of the rings. With the staggered configuration the H_{Cp}–H_{Cp} distance increases to ~3.57 Å. A second reference potential was attempted (see Fig. 5, top curve), with somewhat larger $\sigma_{C_{Cp}}$, to try to make the carbon–carbon potential on opposite rings more repulsive. The chosen value ensured that when in the eclipsed position the C_{Cp} atoms on opposite rings would be inside their repulsive cores. Even so the effect remained, but was weaker, indicating that there may be some weak aspect in the data which requires the rings to adopt the eclipsed configuration marginally more often than the staggered configuration. It is not however a strong contributor to the structure factor, at least at the temperature of the present experiment, 40 °C.

4.2. Solvation structure

Ferrocene has an inter-ring dimension of 3.32 Å, calculated from the assumed Fe–Cp centroid distance of 1.66 Å, and the diameter of the Cp ring is ca. 4 Å. Given that, in solution, the molecule shows no preferred orientation, and is very nearly dimensionally isotropic, the solvation of the molecule might be assumed to be also spherical and the solvation cage should then show little structure in the first coordination sphere. Indeed, the NMR of ferrocene gives no information as to the solvation structure – the ^{13}C and ^{1}H NMR spectra show a singlet at all temperatures in solution. However, from the EPSR analysis of the data, this is found not to be the case. In order to extract the structure of the solvation of the

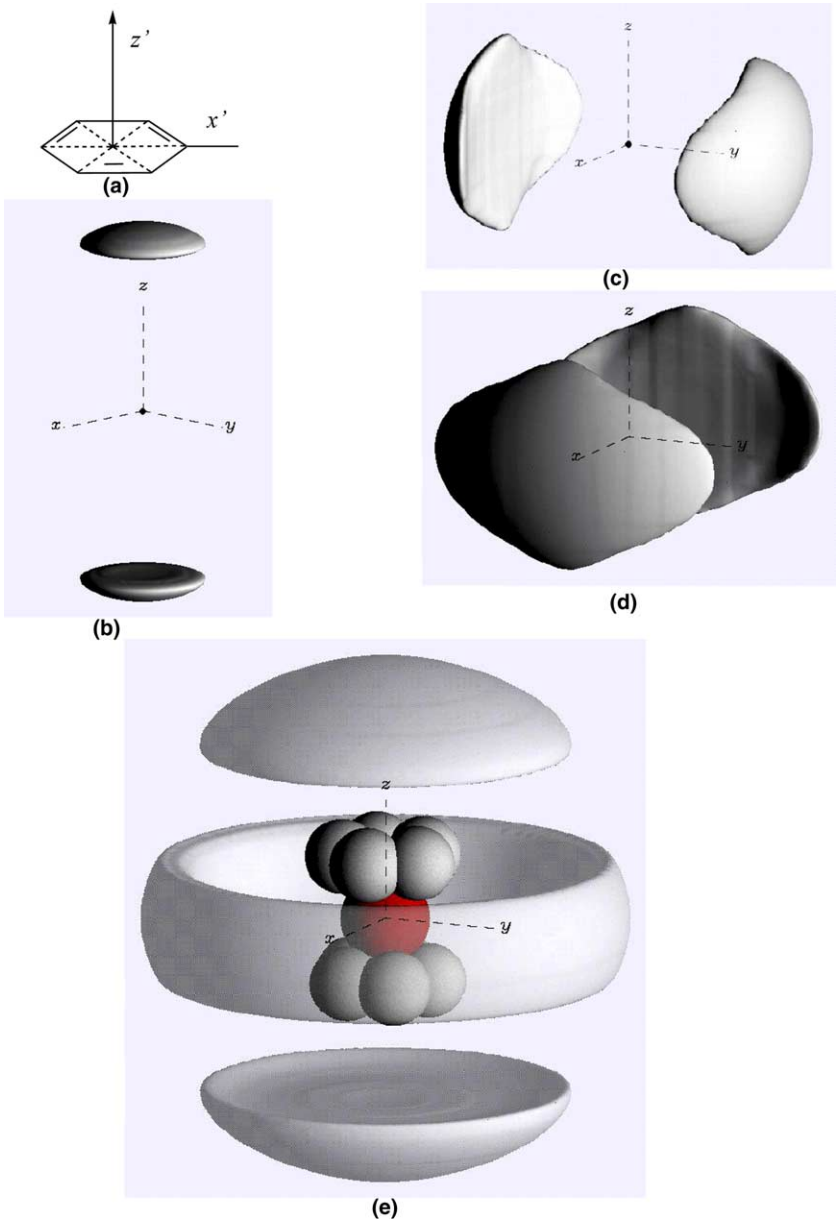

Fig. 6. (a) Internal coordinates of the toluene molecule. The axis is normal to the plane of the aromatic ring of the toluene molecule, while the x' axis passes through the methyl group. The y' axis is normal to both of these axes and points into the paper. (b) The distribution of the orientation of the z' axis about the z axis, with z being defined as the Cp_{cent}–Fe–Cp_{cent} vector, for toluene molecules that lie directly above or below one of the Cp rings. (c) and (d) show the same type of distribution but in the equatorial plane of a central ferrocene molecule along the y and x axes, respectively. (e) shows the total distribution of toluene molecules in the first solvation shell of a ferrocene molecule, averaged over orientations of the toluene molecule. These indicate that toluene prefers to occupy the polar positions above and below the ferrocene molecule and also the equatorial plane between the two Cp rings. However, as plots (b)–(d) demonstrate, in practice the orientation of the toluene molecule is strongly dependent on the direction of the toluene relative to the central ferrocene molecule, indicating there are strong orientational as well as spatial correlations in the first solvation shell.

molecule, the distribution of vectors normal to the plane of the d_8-toluene rings was extracted. Fig. 6 shows the vector used in the extraction of the solvent orientational correlations from the model, together with the distribution of these vectors around the average ferrocene molecule. It is clear that there is a strong orientational correlation in the first solvation shell of ferrocene in toluene solution and that the idea of an isotropically solvated molecule are not supported by the data or the analysis. Moreover, the orientational correlations are intuitively obvious; the aromatic portion of the solvent is preferentially orientated towards the maxima of electron density in the molecule – the Cp rings and the iron atoms, whereas the less polarisable areas – the C–H bonds show less preferential solvation.

5. Conclusion

The study presented is probably the first of its kind of an organometallic compound in solution. We find clear evidence for a non-spherical solvation shell around the ferrocene molecule in toluene solution (Fig. 6), and the toluene molecules show a high degree of orientational correlation in the first solvation shell, tending to lie flat and parallel above or below the Cp rings in ferrocene, but in the equatorial plane they lie mostly vertical, with the plane of the toluene molecule facing the iron of the ferrocene molecule. Some slight torsional correlation is observed between the ends of the ferrocene molecule. It remains to be seen how this develops as the solution temperature is lowered. In addition a slight bending of the Cp centroid to Cp centroid axis about the Fe atom midway is observed.

Given these initial results we expect to study a variety of related compounds in the near future.

Acknowledgements

We thank Dr. A.D. Taylor (ISIS Spallation Neutron Source) for an allocation of Director's Discretionary beam time, Dr. K. Knight for material help with the experiment and EPSRC and the University of Tennessee for funding (JFCT). We also acknowledge the support and input of Prof. C.R.A. Catlow (Royal Institution of Great Britain).

References

[1] C.C. Wilson, first ed.Single Crystal Neutron Diffraction from Molecular Materials, vol. 2, World Scientific, Singapore, 2000.
[2] W.H. Zachariasen, Theory of X-Ray Diffraction in Crystals, Dover Publications, Mineola, NY, 1995.
[3] A. Guinier, X-ray Diffraction: In Crystals, Imperfect Crystals and Amorphous Bodies, Dover Publications, Mineola, NY, 1994.
[4] B.E. Warren, X-ray Diffraction, Dover Publications, Mineola, NY, 1990.
[5] R.W. James, Optical Principles of the Diffraction of X-rays, Ox Bow Press, 1982.
[6] J. Byrne, J.M. Robson, Neutrons, Nuclei and Matter: An Exploration of the Physics of Slow Neutrons, Institute of Physics, Bristol, 1996.
[7] V.J. Sears, Neutron News 3 (1992) 29.
[8] NIST Online Neutron Scattering Parameters. Available from: http://www.ncnr.nist.gov/resources/n-lengths/list.html.
[9] J.E. Enderby, Chem. Soc. Rev. 24 (1995) 159.
[10] P.H.K. de Jong, G.W. Neilson, M.C. Bellissent-Funel, J . Chem. Phys. 105 (1996) 5155.
[11] S. Ansell, J. Dupuy-Philon, J.F. Jal, G.W. Neilson, J. Phys.: Condens. Matter 9 (1997) 8835.
[12] J.C. Wasse, S. Hayama, N.T. Skipper, C.J. Benmore, A.K. Soper, J. Chem. Phys. 112 (2000) 7147.
[13] J.F.C. Turner, C.J. Benmore, C.M. Barker, N. Kaltsoyannis, J.M. Thomas, W.I.F. David, C.R.A. Catlow, J. Phys. Chem. B 104 (2000) 7570.
[14] T.J. Kealy, P.L. Paulson, Nature (London) 168 (1951) 1039.
[15] E.O. Fischer, W. Pfab, Z. Naturforsch. 7b (1952) 377.
[16] S.A. Miller, J.A. Tebboth, J.F. Tremaine, J. Chem. Soc., Abstracts (1952) 632.
[17] G. Wilkinson, M. Rosenblum, M.C. Whiting, R.B. Woodward, J. Am. Chem. Soc. 74 (1952) 2125.
[18] R.B. Woodward, M. Rosenblum, M.C. Whiting, J. Am. Chem. Soc. 74 (1952) 3458.
[19] J.D. Dunitz, L.E. Orgel, Nature (London) 171 (1953) 121.
[20] G. Wilkinson, Angew. Chem. 86 (1974) 664.
[21] M.A. Bennett, A.A. Danopoulos, W.P. Griffith, M.L.H. Green, J. Chem. Soc., Dalton Trans.: Inorg. Chem. (1997) 3049.
[22] E.O. Fischer, R. Jira, J. Organomet. Chem. 637–639 (2001) 7.
[23] E.O. Fischer, Angew. Chem. 86 (1974) 651.
[24] F. Takusagawa, T.F. Koetzle, Acta Crystallogr., Sect. B: Struct. Crystallogr. Cryst. Chem. B35 (1979) 1074.
[25] W. Pfab, E.O. Fischer, Z. Anorg. Allgem. Chem. 274 (1953) 316.
[26] D.C. Levendis, J.C.A. Boeyens, J. Crystallogr. Spectrosc. Res. 15 (1985) 1.
[27] E. Maverick, J.D. Dunitz, Mol. Phys. 62 (1987) 451.
[28] A. Haaland, J.E. Nilsson, Acta Chem. Scand. (1947–1973) 22 (1968) 2653.
[29] A. Haaland, J.E. Nilsson, Chem. Commun. (London) (1968) 88.
[30] E.A. Seibold, L.E. Sutton, J. Chem. Phys. 23 (1955) 1967.
[31] A.B. Gardner, J. Howard, T.C. Waddington, R.M. Richardson, J. Tomkinson, Chem. Phys. 57 (1981) 453.
[32] S. Carter, J.N. Murrell, J. Organomet. Chem. 192 (1980) 399.
[33] F. Rocquet, L. Berreby, J.P. Marsault, Spectrochim. Acta, Part A: Mol. Biomol. Spectrosc. 29 (1973) 1101.
[34] A. Haaland, Acta Chem. Scand. (1947–1973) 23 (1969) 1836.
[35] M. Rosenblum, R.B. Woodward, J. Am. Chem. Soc. 80 (1958) 5443.
[36] A.K. Soper, Chem. Phys. 202 (1996) 295.
[37] G.L. Squires, Introduction to the Theory of Thermal Neutron Scattering, Dover Publications, Mineola, NY, 1997.
[38] SANDALS homepage. Available from: http://www.isis.rl.ac.uk/disordered/.
[39] A.K. Soper, W.S. Howells, A.C. Hannon, ATLAS – analysis of time-of-flight diffraction data from liquid and amorphous samples, RAL-89-046 ISIS Pulsed Neutron Source, Rutherford Appleton Laboratory, Chilton, Didcot, 1989.
[40] C.P. Brock, Y. Fu, Acta Crystallogr., Sect. B: Struct. Sci. B53 (1997) 928.
[41] I.J. Bruno, J.C. Cole, P.R. Edgington, M. Kessler, C.F. Macrae, P. McCabe, J. Pearson, R. Taylor, Acta Crystallogr. B58 (2002) 389.
[42] F.H. Allen, W.D.S. Motherwell, Acta Crystallogr. B58 (2002) 407.
[43] A.K. Soper, Chem. Phys. 202 (1996) 295.
[44] A.K. Soper, Mol. Phys. 99 (2001) 1503.
[45] I.M. Svishchev, P.G. Kusalik, J. Chem. Phys. 99 (1993) 3049.

Available online at www.sciencedirect.com
SCIENCE DIRECT®
Polyhedron 23 (2004) 2985–2991
POLYHEDRON
www.elsevier.com/locate/poly

Isomer distribution in thallium hydrotris(polymethylenepyrazol-1-yl) borates (thallium scorpionates): a multinuclear NMR study

Rosa M. Claramunt [*,a], M. Dolores Santa María [a], José Elguero [b,*], Swiatoslaw Trofimenko [c]

[a] *Departamento de Química Orgánica y Bio-Orgánica, Facultad de Ciencias, UNED, Senda del Rey 9, E-28040 Madrid, Spain*
[b] *Instituto de Química Médica, CSIC, Juan de la Cierva 3, E-28006 Madrid, Spain*
[c] *Department of Chemistry and Biochemistry, University of Delaware, Newark, DE 19716-2522, USA*

Received 19 July 2004; accepted 5 August 2004
Available online 26 October 2004

Abstract

The structure of two thallium scorpionates derived from 3(5),4-trimethylene- and 3(5),4-hexamethylenepyrazole was determined by multinuclear NMR, both in solution and in the solid state. The isomeric distribution is the same in both phases suggesting a kinetic origin. A $^{1}J(^{15}N–^{205}Tl)$ coupling of 862 Hz was measured for $[Tl(Tp^{(3,4-(CH_2)_6)})]$ in the solid state.
© 2004 Elsevier Ltd. All rights reserved.

Keywords: Pyrazolylborates; Thallium; NMR; CPMAS

1. Introduction

When an asymmetric pyrazole, i.e., a pyrazole that has different substituents at positions 3 and 5, reacts with potassium borohydride to afford a tris(pyrazol-1-yl)borate (a scorpionate) [1–3], four different isomers can be obtained (Scheme 1):

Even if the solid compound is formed regioselectively, when dissolved it can rearrange into a mixture of isomers [4]. Related to this are the examples of scorpionates that isomerize during complexation due to a boratropic rearrangement [5–7], for instance, during the preparation of the thallium complexes. In the present paper, we will discuss the case of two new thallium scorpionates, $[Tl(Tp^{(3(5),4-(CH_2)_3)})]$ and $[Tl(Tp^{(3(5),4-(CH_2)_6)})]$ derived from two fused 3(5),4-polymethylene pyrazoles **5** and **6** (Scheme 2).

* Corresponding author. Tel.: +349 141 10874; fax: +349 156 44853.
E-mail address: iqmbe17@iqm.csis.es (J. Elguero).

0277-5387/$ - see front matter © 2004 Elsevier Ltd. All rights reserved.
doi:10.1016/j.poly.2004.08.018

2. Experimental

2.1. Chemical synthesis

2.1.1. 3(5),4-Trimethylenepyrazole (5)

This pyrazole was prepared by the method described below for cyclooctanone but starting from cyclopentanone; it was obtained after distillation in vacuo in 68% yield and was recrystallized from hexane. m.p. 61–62 °C. *Anal.* Calc. for $C_6H_8N_2$ (108.14): C, 66.7; H, 7.41; N, 26.7. Found: C, 66.9; H, 7.53; N, 26.6%. ^{1}H NMR (ppm): $\delta = 2.43$ (m, 2H), 2.64 (t, 2H), 2.71 (t, 2H), 7.14 (s, 1H), 11.6 (s, vb, N–H).

2.1.2. 3(5),4-Hexamethylenepyrazole (6)

A mixture of 300 g (2.38 mol) cyclooctanone and 400 g (5.6 mol) ethyl formate was added in one portion to a rapidly stirred slurry of 129 g (2.38 mol) dry sodium methoxide in 2 L toluene. After a short induction period the slurry turned amber, cleared up,

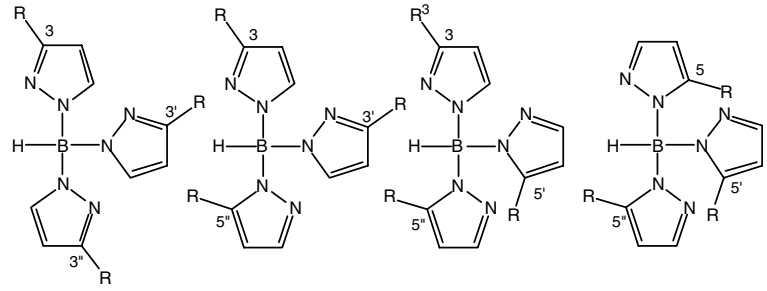

1, the 3,3',3"-regioisomer **aaa**

2, the 3,3',5"-regioisomer **aab**

3, the 3,5',5"-regioisomer **abb**

4, the 5,5',5"-regioisomer **bbb**

Scheme 1.

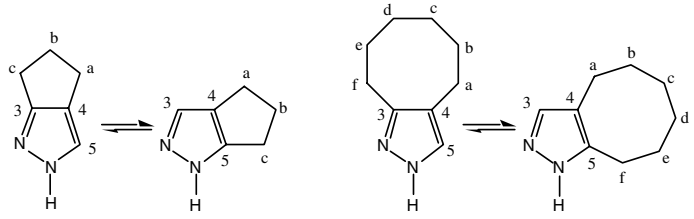

5a, 3,4-trimethylene-pyrazole

5b, 4,5-trimethylene-pyrazole

6a, 3,4-hexamethylene-pyrazole

6b, 4,5-hexamethylene-pyrazole

Scheme 2.

and then the sodium salt precipitated. The salt was extracted with 1.5 L water, and then the extracts were treated with 145 mL (2.38 mol) hydrazine hydrate and 150 mL (2.4 mol) acetic acid. An amber oil separated. It was taken up in methylene chloride, the extracts were separated, stripped, and distilled in vacuo. The main fraction, b.p. 136–140 °C/2.6 Torr, was obtained in 240 g (67%) yield. *Anal.* Calc. for $C_9H_{14}N_2$ (150.12): C, 72.0; H, 9.33; N, 18.7. Found: C, 72.0; H, 9.39; N, 18.6%. ^{1}H NMR (ppm): $\delta = 1.43$ (m, 4H), 1.60 (m, 2H), 1.70 (m, 2H), 2.58 (t, 2H), 2.79 (t, 2H), 7.26 (s, 1H), 12.3 (s, vb, N–H). ^{13}C NMR (ppm): $\delta = 22.1$, 24.3, 25.2, 25.6, 30.5, 117.3, 132.8, 145.5.

2.1.3. Thallium hydrotris(3(5),4-trimethylenepyrazol-1-yl)borate [$Tl(Tp^{3(5),4-(CH_2)_3})$] (7)

This was prepared from 35 g (0.32 mol) 3(5),4-trimethylenepyrazole and 4.8 g (0.090 mol) KBH_4 in 150 mL reluxing 4-methylanisole. Hydrogen evolution was rapid and in 4 h the theoretical amount was evolved. After distilling off the solvent in vacuo, the residue was dissolved in THF and converted to the Tl salt as below. This compound was obtained in 37 g (68%) yield. IR: BH at 2430 cm^{-1}. *Anal.* Calc. for $C_{18}H_{22}BN_6Tl$: C, 40.2; H, 4.10; N, 15.6. Found: C, 40.3; H, 4.19; N, 15.5%.

2.1.4. Thallium hydrotris(3(5),4-hexamethylenepyrazol-1-yl)borate [$Tl(Tp^{3(5),4-(CH_2)_6})$] (8)

A mixture of 48 g (0.32 mol) 3,4-hexamethylenepyrazole and 2.9 g (0.054 mol) KBH_4 was heated in an oil bath, up to 220 °C, at which point the theoretical amount of hydrogen was evolved. The excess pyrazole was distilled off in vacuo. The residue was cooled, dissolved in THF, filtered through Celite, and stirred with excess aqueous $TlNO_3$. The product was extracted with methylene chloride, the extracts were filtered through a bed of alumina, and evaporated to dryness. The residue was stirred with methanol and then filtered yielding, after washing with methanol and drying, 27 g (75%) of the Tl salt. IR: BH 2434 cm^{-1}. *Anal.* Calc. for $C_{27}H_{40}BN_6Tl$: C, 48.9; H, 6.03; N, 12.7. Found: C, 49.1; H, 6.13; N, 12.6%.

2.2. NMR measurements

NMR spectra were recorded on a Bruker DRX 400 (9.4 T, 400.13 MHz for ^{1}H, 100.62 MHz for ^{13}C and 40.56 MHz for ^{15}N) spectrometer. Chemical shifts (δ in ppm) are given from internal solvent $CDCl_3$ 7.26 for ^{1}H and 77.0 for ^{13}C, and for ^{15}N NMR nitromethane was used as external standard. 2D gs-COSY (^{1}H–^{1}H) and 2D inverse proton detected heteronuclear shift correlation spectra, gs-HMQC (^{1}H–^{13}C), gs-HMBC

Table 1
^{1}H NMR data (δ in ppm) of scorpionates **7** and **8** in $CDCl_3$

Compounds	3,4-Polymethylenepyrazoles							4,5-Polymethylenepyrazoles						
	H-5	H-a	H-b	H-c	H-d	H-e	H-f	H-3	H-a	H-b	H-c	H-d	H-e	H-f
7aaa	7.37	2.63	2.44	2.77	–	–	–	–	–	–	–	–	–	–
7aab	7.38	2.63	2.44	2.77	–	–	–	7.24	2.62	2.54	2.86	–	–	–
7abb	7.36	2.63	2.44	2.77	–	–	–	7.24	2.62	2.62	2.86	–	–	–
7bbb	–	–	–	–	–	–	–	7.24	2.62	2.54	2.86			
8aaa	7.32	2.52	1.57	1.42	1.42	1.71	2.84	–	–	–	–	–	–	–
8aab	7.32	2.52	1.57	1.42	1.42	1.71	2.84	7.22	2.52	1.57	1.42	1.30	1.71	2.97
8abb	7.32	2.52	1.57	1.42	1.42	1.71	2.84	7.24	2.52	1.57	1.42	1.30	1.71	2.97

(^{1}H–^{13}C) and gs-HMBC (^{1}H–^{15}N), were obtained using the standard pulse sequences [8]. Solid state ^{13}C (50.32 MHz) CPMAS NMR and ^{15}N (20.28 MHz) CPMAS NMR spectra have been obtained on a Bruker AC-200 spectrometer at 298 K using a 7 mm BRUKER DAB 7 probehead that achieves rotational frequencies of 3.5–4.5 kHz. Samples were carefully packed in ZrO_2 rotors and the standard CPMAS sequence was employed. ^{13}C spectra were originally referenced to a glycine sample and then the chemical shifts were recalculated to Me_4Si (for the carbonyl atom δ(glycine) = 176.1 ppm) and ^{15}N spectra to $^{15}NH_4Cl$ (these were converted to the nitromethane scale using the relationship: δ^{15}N(nitromethane) = δ^{15}N(ammonium chloride) −338.1 ppm) [9].

3. Results and discussion

Before starting the discussion, a few words about the prototropic tautomerism of *N*-unsubstituted pyrazoles and their reactivity [10,11] are given. Pyrazoles such as **5** and **6** exist in solution as rapidly equilibrating mixtures of tautomers **5a/5b** and **6a/6b**. The prototropy is usually so fast that only average signals are observed by NMR. The knowledge of the equilibrium constant is irrelevant on discussing their reactivity: there is a simple relationship between tautomers and *N*-substituted isomers.

These compounds can exist, in principle, in four isomeric forms depending on the substitution pattern (see Scheme 1). Since there are three pyrazoles per scorpionate ligand, in the reaction of the free pyrazole with potassium borohydride, four isomers can be formed: **aaa**, **aab**, **abb** and **bbb**. In a first approximation, the distribution should follow a binomial expression of the form $(\mathbf{a} + \mathbf{b})^3$, for instance, for identical populations (pop. **a** = pop. **b** = 50%), 12.5% of **aaa**, 37.5% of **aab**, 37.5% of **abb** and 12.5% of **bbb** and for the frequent case in which the 3,4-isomer (pop. **a** = 75%) is more stable than the 4,5 one (pop. **b** = 25%), 42.2% of **aaa**, 42.2% of **aab**, 14.1% of **abb** and 1.5% of **bbb**. Remember that here we refer to isomers, not to tautomers.

The NMR data necessary for the discussion are gathered in Table 1 (^{1}H NMR) and Table 2 (^{13}C NMR). The assignment of the signals will be discussed separately for compounds **7** and **8**.

The case of thallium hydrotris[3(5),4-trimethylenepyrazol-1-yl]borate [Tl($Tp^{(3(5),4-(CH_2)_3)}$)] (**7**). The sample used for the NMR study contains 75 mg of **7** in 0.6 mL $CDCl_3$.

In the ^{1}H NMR spectrum the H-3 pyrazole protons of isomers **7aab**, **7abb** and **7bbb** appear as an unique broad signal at 7.24 ppm and the H-5 protons of **7aaa**, **7aab** and **7abb** at 7.37, 7.38 and 7.36 ppm (see Fig. 1(a)). Five groups of signals for the methylene protons at 2.44, 2.54, 2.62, 2.77 and 2.86 ppm appear as multiplets in the spectrum (see Fig. 1(b)), and their assignment has been achieved taking into account the corresponding chemical shift values described for substituted 3,4- or 4,5-trimethylenepyrazoles in which δH-b < δH-a < δH-c [12]. Besides, δH-c in the 4,5-isomers is shifted downfield in comparison to the corresponding one in 3,4-isomers. The integral also shows that several H-b protons of the 4,5-substituted pyrazoles appear together with the H-a protons at 2.62 ppm. (^{1}H–^{1}H) COSY correlations between the following pairs of signals: 2.44 ↔ 2.63, 2.44 ↔ 2.77, 2.54 ↔ 2.62 and 2.54 ↔ 2.86, allows the complete assignment.

The ^{13}C-CPD NMR spectra, gs-HMQC (^{1}H–^{13}C) and gs-HMBC (^{1}H–^{13}C) 2D correlations permitted the assignments shown in Table 2, where the expected relative intensity of the signals according to the populations of the different isomers has also been considered. The pyrazole carbons chemical shifts C-3, C-4 and C-5 are in agreement with those found in substituted 3,4- or 4,5-trimethylenepyrazoles [12,13].

The case of thallium hydrotris[3(5),4-hexamethylenepyrazol-1-yl]borate [Tl($Tp^{(3(5),4-(CH_2)_6)}$)] (**8**). Here again, the sample used for the NMR study contains 75 mg of **8** in 0.6 mL $CDCl_3$.

In the ^{1}H NMR spectrum the H-5 pyrazole protons of isomers **8aaa**, **8aab** and **8abb** appear as an unique broad signal at 7.32 ppm and the H-3 protons of **8aab** and **8abb** at 7.22 and 7.24 ppm (see Fig. 2(a)). For the methylene protons, signals at 1.30 (broad multiplet),

Table 2
^{13}C NMR data (δ in ppm) of scorpionates **7** and **8** in $CDCl_3$

Compounds	3,4-Polymethylenepyrazoles					4,5-Polymethylenepyrazoles				
	C-3	C-4	C-5	C-a C-b C-c	C-d C-e C-f	C-3	C-4	C-5	C-a C-b C-c	C-d C-e C-f
7aaa	161.94	124.16	128.94	22.7 30.44 23.9	– – –	–	–	–	– – –	– – –
7aab	161.88[a]	124.24[b]	129.05	22.7 30.44 23.9	– – –	132.42	124.75	156.07[c]	23.1 30.47 24.4	– – –
7abb	162.01[a]	124.10[b]	128.87	22.7 30.44 23.9	– – –	132.48	124.69	156.13	23.1 30.41 24.4	– – –
7bbb	–	–	–	– – –	– – –	132.56	124.64	156.22[c]	23.1 30.47 24.4	–
8aaa	151.4	117.4	133.9	22.46 30.9 25.7	25.7 29.5 25.34	–	–	–	– – –	– – –
8aab	151.4	117.4	134.1	22.42 30.9 25.7	25.7 29.4 25.29	137.1	117.9	145.1	23.6 31.8 25.8	25.8 28.4 23.2
8abb	151.4	117.4	134.1	22.42 30.9 25.7	25.7 29.4 25.29	137.4	117.9	145.3	23.5 31.6 25.8	25.8 28.5 23.4

In some cases two significant figures are given to show the splitting of the signals.
Pairs of signals marked a, b, c can be reversed.

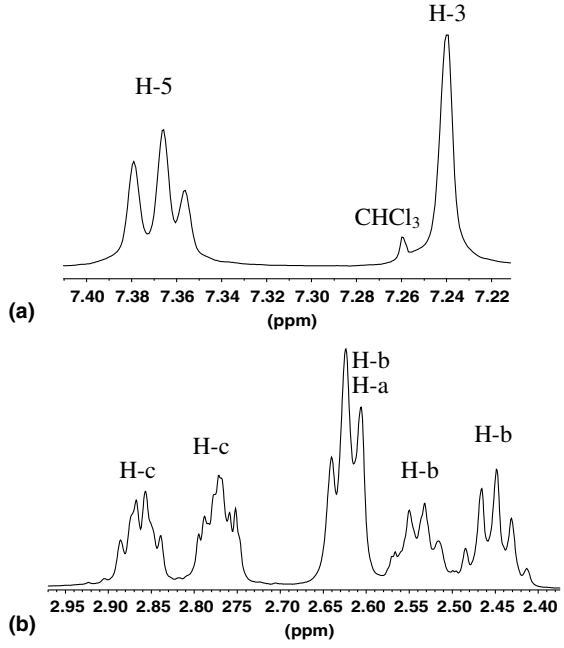

Fig. 1. ^1H NMR of isomers **7**: (a) pyrazole protons; (b) methylene protons.

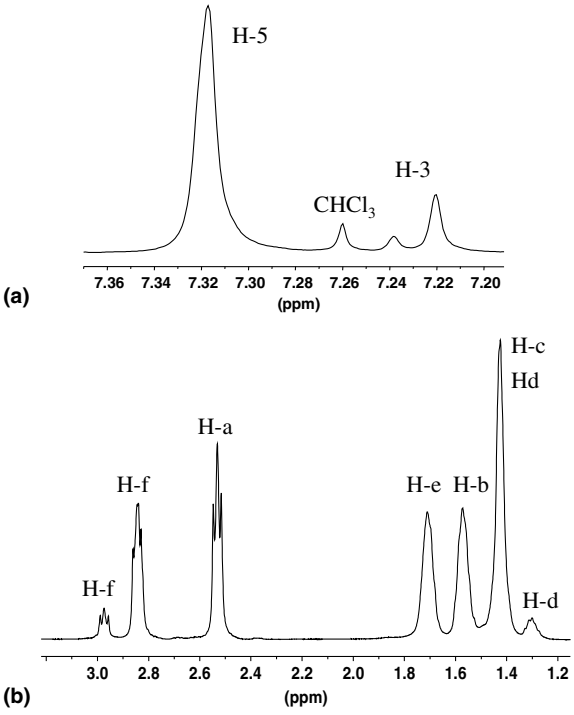

Fig. 2. ^1H NMR of isomers **8**: (a) pyrazole protons; (b) methylene protons.

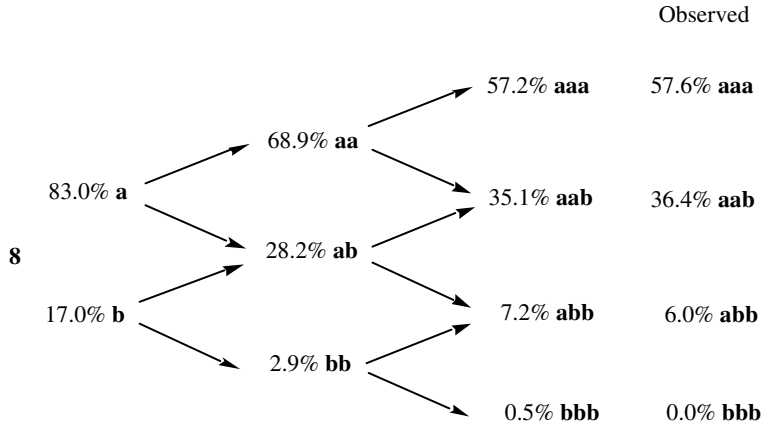

Scheme 3.

1.42 (broad multiplet), 1.57 (broad multiplet), 1.71 (broad multiplet), 2.52 (triplet), 2.84 (triplet) and 2.97 (triplet) ppm are shown (see Fig. 2(b)). The assignment has been achieved taking into account the following: (i) (^{1}H–^{1}H) COSY correlations between the following pairs of signals: 1.30 ↔ 1.42, 1.30 ↔ 1.71, 1.42 ↔ 1.57, 1.42 ↔ 1.71, 1.57 ↔ 2.52, 1.71 ↔ 2.84, 1.71 ↔ 2.97 and 2.62 ↔ 2.86; (ii) the corresponding chemical shift values described for substituted 3,4- or 4,5-hexamethylenepyrazoles in which δH-a < δH-f [12,13]; (iii) the chemical shifts found in isomers of thallium scorpionate **7**.

Once the ^{1}H NMR assignment was established, the relative ratio between the three isomers **8aaa**, **8aab** and **8abb** could be determined as discussed below. ^{13}C NMR chemical shifts gathered in Table 2 were obtained with the help of gs-HMQC (^{1}H–^{13}C) and gs-HMBC (^{1}H–^{13}C) 2D correlations.

In the case of the hexamethylene derivative **8** the populations are 57.6% of **aaa**, 36.4% of **aab** and 6.0% of **abb**; the **bbb** isomer was not observed. This corresponds, almost perfectly, to 83% of **a** and 17% of **b** (Scheme 3).

In the case of the trimethylene derivative **7** the determination of the populations is less precise but, based on a deconvolution treatment of the ^{1}H NMR signals, the following populations have been estimated: 23.0% of **aaa**, 25.0% of **aab**, 37.5% of **abb** and 14.5% of **bbb**. In this case, they do not correspond to an exact binomial distribution, see Scheme 4. Nevertheless, it is clear that the populations of isomers **a** and **b** are less different in this case, probably because the "cyclopentene" ring is less steric demanding than the "cyclooctene" one so both isomers should have similar stabilities. According to Scheme 4, there is an 11% excess of **aaa** and a 12% default of **aab**, probably due to an incomplete equilibration.

It should be noted that the ^{15}N chemical shifts in $CDCl_3$ of N(1) are very similar for both isomers in [Tl(Tp$^{(3(5),4-(CH_2)_6)}$)] (**8**) [−154.2 (**a**) and −150.5 ppm (**b**)] and rather different for [Tl(Tp$^{(3(5),4-(CH_2)_3)}$)] (**7**) [−141.5 (**a**) and −160.3 ppm (**b**)]. This fact has already been reported for simple *N*-methyl derivatives of polymethylenepyrazoles [14] and it has been related to the Mills–Nixon effect [13].

The solid state results are essential to discuss an important aspect of the structure of scorpionates. First hypothesis: the solid compound is a pure regioisomer, for instance **aaa**, and when dissolved in $CDCl_3$ it rearranges into the statistical distribution $(\mathbf{a} + \mathbf{b})^3$. This

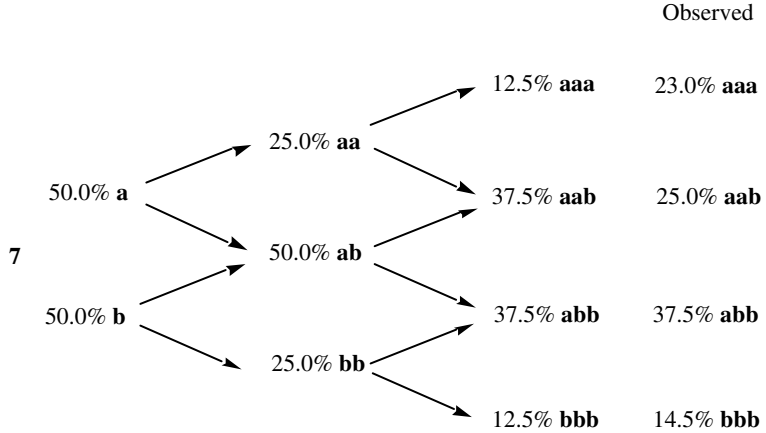

Scheme 4.

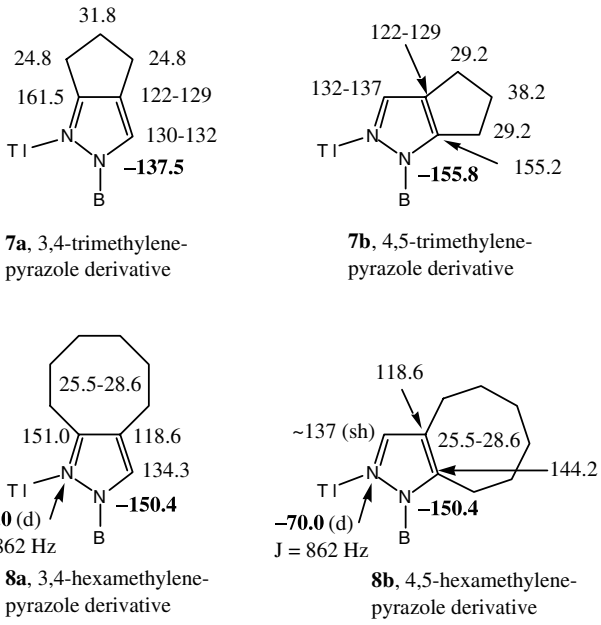

7a, 3,4-trimethylene-pyrazole derivative

7b, 4,5-trimethylene-pyrazole derivative

8a, 3,4-hexamethylene-pyrazole derivative

8b, 4,5-hexamethylene-pyrazole derivative

Scheme 5.

means that the percents correspond to an equilibrium mixture, *a thermodynamic mixture*. Second hypothesis: the solid compound is already a mixture of the three (in the case of **8**) or four regioisomers (in the case of **7**) in the same ratio as in solution, this corresponds to *a kinetic mixture*.

Since ^{1}H CPMAS is not easily obtainable and ^{15}N CPMAS is not useful in some cases, this part must be mainly based on ^{13}C CPMAS NMR. The problem is that the resolution is not good enough to observe the different regioisomers. In the case of compound **8**, in ^{15}N NMR only *one* type of pyrazole is observed (the same for **a** and **b**), while in ^{13}C NMR both are observed *but independent of the remaining pyrazoles* of the scorpionate (for instance, the **a** signals are the same for the **aaa** as for the **aab** regioisomers). The assignments are reported in Scheme 5, the use of the NQS sequence (Non-suppression of Quaternary signals) has been useful for carbons C[3(5)] and C(4) of pyrazoles.

In the case of compound **7**, in ^{13}C NMR the signals of quaternary carbons at 161.5 and 155.2 ppm are of about the same intensity (see Fig. 3) and the same happens for the ^{15}N signals at −137.5 and −155.8 ppm; therefore, in the solid state there is the same amount of **a** and **b** isomers. The trimethylene part of the ^{13}C CPMAS NMR spectrum (see Fig. 4) shows that the signals of the **b** part are very narrow while those of the **a** part are very broad. We assign this difference to a larger conformational mobility of the cyclopentene-like envelope in the case of the latter, less hindered than the former.

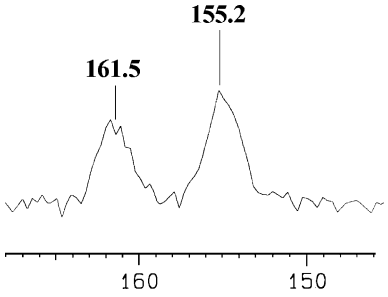

Fig. 3. ^{13}C CPMAS NMR quaternary carbons C-3 and C-5 of isomers **7**.

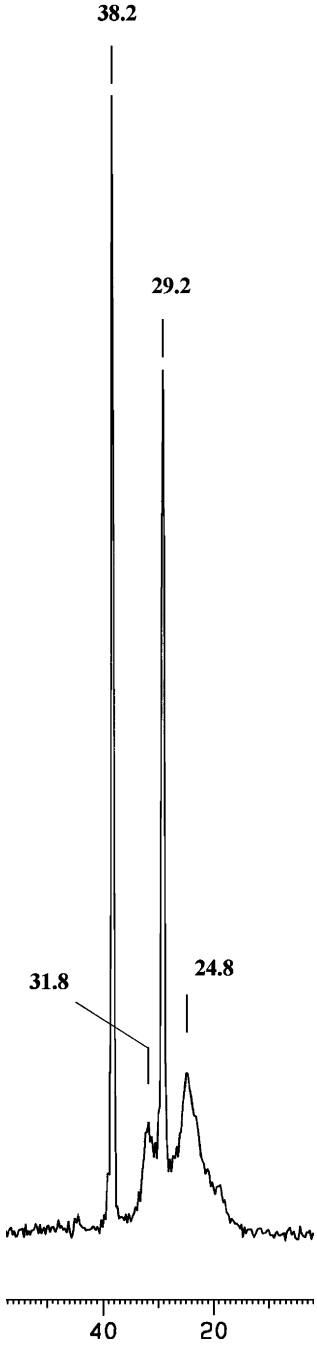

Fig. 4. ^{13}C CPMAS NMR methylene carbons of isomers **7**.

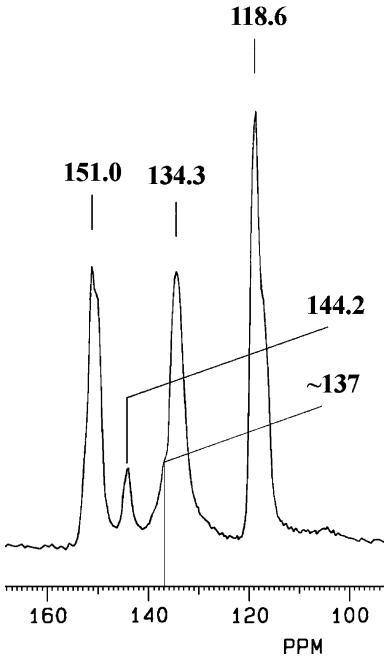

Fig. 5. ^{13}C CPMAS NMR pyrazole carbons of isomers **8**.

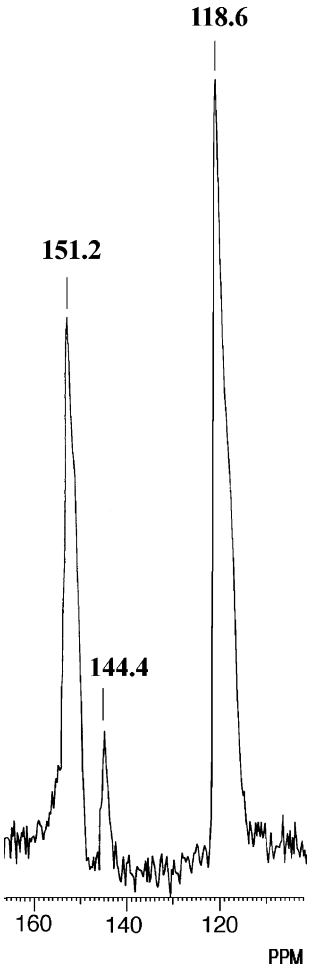

Fig. 6. ^{13}C CPMAS NMR quaternary carbons C-3, C-4 and C-5 of isomers **8**.

In the case of compound **8**, the pyrazole signals of both types of isomers (**a** and **b**) are clearly apparent (see Fig. 5) but the most useful spectrum is the ^{13}C NQS CPMAS one (see Fig. 6): the signals at 151.2 (**a**) and 144.4 (**b**) ppm are in an approximate 90/10% ratio.

4. Conclusions

It appears that the second hypothesis is valid: in the solid state, compound **7** is a mixture of 50% **a** – 50% **b** while compound **8** is much richer in the less hindered isomer **a** (80–90% **a** – 10–20% **b**), these behaviors being maintained in solution. Therefore, if the statistical distribution is not followed, like in the case of the trimethylene derivative, the reason should be that in the purification, the mixture is altered. Finally, it is reasonable to suppose that if a single crystal is obtained for X-ray structure determination, probably it would be formed by a unique regioisomer.

Acknowledgement

Financial support was provided by the Spanish DGI/MCYT (Project No. BQU2000-0252).

References

[1] S. Trofimenko, Scorpionates. The Coordination Chemistry of Polypyrazolylborate Ligands, Imperial College Press, London, 1999.
[2] A.L. Rheingold, C.B. White, S. Trofimenko, Inorg. Chem. 32 (1993) 3471.
[3] C. Janiak, Main Group Met. Chem. 21 (1998) 33.
[4] C. López, D. Sanz, R.M. Claramunt, S. Trofimenko, J. Elguero, J. Organomet. Chem. 503 (1995) 265.
[5] M. Cano, J.V. Heras, S. Trofimenko, A. Monge, E. Gutiérrez, C.J. Jones, J.A. McCleverty, J. Chem. Soc., Dalton Trans. (1990) 3577.
[6] S. Trofimenko, J.C. Calabrese, P.J. Domaille, J.S. Thompson, Inorg. Chem. 26 (1989) 1091.
[7] J.C. Calabrese, P.J. Domaille, J.S. Thompson, S. Trofimenko, Inorg. Chem. 29 (1990) 4429.
[8] S. Braun, H.-O. Kalinowki, S. Berger, 150 and More Basic NMR Experiments, Wiley-VCH, Weinheim, 1998.
[9] R.M. Claramunt, D. Sanz, M.D. Santa María, J. Elguero, S. Trofimenko, J. Organomet. Chem. 689 (2004) 463.
[10] J. Elguero, C. Marzin, A.R. Katritzky, P. Linda, The Tautomerism of Heterocycles, Academic Press, New York, 1976.
[11] V.I. Minkin, A.D. Garnovskii, J. Elguero, A.R. Katritzky, O.V. Denisko, Adv. Heterocycl. Chem. 76 (2000) 157.
[12] J. Elguero, A. Martínez, S.P. Singh, D. Kumar, J. Heterocycl. Chem. 28 (1991) 647.
[13] A. Martínez, M.L. Jimeno, J. Elguero, A. Fruchier, New J. Chem. 18 (1994) 269.
[14] R.M. Claramunt, D. Sanz, C. López, J.A. Jiménez, M.L. Jimeno, J. Elguero, A. Fruchier, Magn. Reson. Chem. 35 (1997) 35.

Available online at www.sciencedirect.com
SCIENCE DIRECT®
Polyhedron 23 (2004) 2993–3002
POLYHEDRON
www.elsevier.com/locate/poly

Theoretical studies of 18-electron $M(C_nH_n)(C_{10-n}H_{10-n})$ (M = Fe, Ru, Os; n = 3, 4, 5) sandwich complexes ☆

Constance M. Brett, Bruce E. Bursten *

Department of Chemistry, The Ohio State University, 100 W 18th Avenue, Columbus, OH 43210, USA

Received 7 September 2004; accepted 13 September 2004
Available online 28 October 2004

Abstract

Density functional theory has been used to explore the energetics and bonding of the symmetric and unsymmetric isomeric sandwich complexes $(\eta^5\text{-}C_5H_5)_2M$, $(\eta^4\text{-}C_4H_4)M(\eta^6\text{-}C_6H_6)$, and $(\eta^3\text{-}C_3H_3)M(\eta^7\text{-}C_7H_7)$ (M = Fe, Ru, Os). For each metal atom, the symmetric "5–5" metallocene was found to be the most stable isomer, with the "4–6" and "3–7" isomers ca. 40 and 80 kcal/mol higher in energy, respectively. Bonding analysis shows that $(\eta^4\text{-}C_4H_4)Fe(\eta^6\text{-}C_6H_6)$ is best considered as a $(\eta^4\text{-}C_4H_4)Fe$ fragment interacting with a C_6H_6 ligand, although the interactions become less separable as the metal is changed to Ru and Os. Similarly, the dominant bonding in $(\eta^3\text{-}C_3H_3)M(\eta^7\text{-}C_7H_7)$ is that of a $M(\eta^7\text{-}C_7H_7)$ perturbed by the interaction with a C_3H_3 ligand.
© 2004 Elsevier Ltd. All rights reserved.

Keywords: Organometallics; Sandwich complex; Metallocene; Bonding; Density functional theory; Orbital analysis

1. Introduction

The name of M.L.H. Green will forever be associated with the keen understanding of how metal–ligand interactions influence the structures, bonding, and reactivity of organometallic complexes. In particular, Green's work has explored the impact of cyclic C_nH_n ligands on organometallic chemistry, from his first paper with Pratt and Wilkinson [1] on the synthesis and properties of Cp_2ReH ($Cp = \eta^5\text{-}C_5H_5$) to his pioneering studies in the use of metal–vapor techniques for the synthesis of sandwich complexes [2] and his explorations of the nature of cycloheptatrienyl complexes [3]. One of the many themes of Green's research has been the comparison of symmetric sandwich complexes, such as the bis(benzene) complexes $(\eta^6\text{-}C_6H_6)_2M$ (M = Cr, Mo, W) with isomeric unsymmetric complexes, such as the CpMCht (Cht = η^7-C_7H_7) systems [4]. These unsymmetric "5–7" sandwich complexes are known for a variety of electron counts, including 16, 17, and 18 electron complexes [5–7].

We have been inspired by this latter aspect of "Green chemistry" to explore the bonding in some seemingly simple 18-electron sandwich complexes that are isomers of the symmetric metallocenes Cp_2M (M = Fe, Ru, Os) and have yet to be synthesized. The synthesis of ferrocene in 1951 by two independent research groups [8,9] and the subsequent independent determinations of the famous sandwich-structure of ferrocene by Wilkinson [10] and Fischer [11] transformed organometallic chemistry. Ferrocene (Cp_2Fe; **1**), ruthenocene (Cp_2Ru; **2**) and osmocene (Cp_2Os; **3**) have since been extensively studied and reviewed [12–15] and the 50th anniversary of the synthesis of ferrocene was widely celebrated [16]. The sandwich bonding in these metallocenes, which rests on the interactions of the π-system of the Cp ligands

☆ In celebration of Prof. Malcolm Leslie Hodder Green, our colleague, our mentor, and, most of all, our friend.

* Corresponding author. Tel.: +1 614 292 1866, fax: +1 614 688 3306.
E-mail addresses: cbrett@chemistry.ohio-state.edu (C.M. Brett), bursten.1@osu.edu (B.E. Bursten).

0277-5387/$ - see front matter © 2004 Elsevier Ltd. All rights reserved.
doi:10.1016/j.poly.2004.09.015

with the *n*d, (*n* + 1)s, and (*n* + 1)p orbitals of the metal atom, now appears in most standard inorganic and organometallic textbooks.

The remarkable stability of the metallocenes is generally attributed to the strong metal–ligand π-bonding and the formulation of the ligand as a Cp^- anion, which is a six π-electron Hückel aromatic system. Since the discovery of the metallocenes, a plethora of sandwich and sandwich-like compounds have been synthesized and studied including half-sandwich complexes, multidecker sandwich complexes, and bent sandwich complexes. Many of these complexes are based on other π-coordinated η^n-C_nH_n rings from (η^3-C_3H_3) to (η^8-C_8H_8), which can all be formulated to be formally Hückel aromatic depending on the formal charge placed on the ring. Whether the rings are charged and the question of the degree of aromaticity in the various complexes formed is still a lively debate [17], and will not be discussed in detail in this work. All of these ring systems are known to bond in a π-fashion to transition metals, however cyclopentadiene and benzene rings are most commonly found as sandwich ligands. Complexes with the unsubstituted cyclic rings are known for all of these ligands except for C_3H_3; the cyclopropenyl complexes reported to date involve substituted C_3R_3 rings with typically Ph or *t*-Bu substituents on the ring, such as (η^5-C_5H_5)Ni(η^3-C_3 Ph_3), (η^3-C_3Ph_3)Co(CO)$_3$, and (η^3-C_3(*t*-Bu)$_3$)M(CO)$_3$ [18–22].

One of the more notable half-sandwich complexes is cyclobutadiene iron tricarbonyl, (η^4-C_4H_4)Fe(CO)$_3$ [23], which in addition to exhibiting unusual binding also serves as a synthon for the unstable and unisolable cyclobutadiene molecule in organic synthesis. Longuet-Higgens and Orgel [24] predicted that cyclobutadiene would be stabilized by transition metals before there was any experimental evidence for cyclic π-system complexes other than the metallocenes. This prediction was soon realized in 1959 with the synthesis of tetraphenylcyclobutadiene iron tricarbonyl, (η^4-$C_4(C_6H_5)_4$)Fe(CO)$_3$ [25] and tetramethylcyclobutadiene nickel chloride dimer, [(η^4-$C_4(CH_3)_4$)$NiCl_2$]$_2$ [26]. The successful synthesis of cyclobutadiene complexes is a nice example of theoretical prediction predating experimental realization, as has been recently reviewed by Seyferth [27].

The existence and properties of unsubstituted CbFe(CO)$_3$ (Cb = η^4-C_4H_4) has stimulated a large number of experimental and theoretical studies of this and other cyclobutadiene complexes [28,29]. Both X-ray [30] and gas-phase electron diffraction [31] studies of CbFe(CO)$_3$ showed that the cyclobutadiene ligand is square-planar and thus appears to be an example of the coordination of an archetypal Hückel antiaromatic molecule. The complex underwent electrophilic substitution and Friedel-Crafts acylation reactions [32] similar to Hückel aromatic organic species as well as ferrocene. In 1979, we coined the term "metalloaromaticity" [33] to describe the seemingly aromatic behavior of the coordinated cyclobutadiene ligand. In essence, the strong π-interactions between the C_4H_4 ligand and the Fe center turned the four π-electron antiaromatic ligand into a six π-electron metalloaromatic system. The concept of metalloaromaticity has recently been extended to describe all-metal analogs of organic systems that exhibit unusual stability [34].

In this paper, we will use density functional theory (DFT) to examine some simple 18-electron mixed-sandwich isomers of the metallocenes. The electronic structures of the group 8 metallocenes have been extensively discussed and we will examine them only briefly to provide evidence that the computational methods used provide accurate results for these types of systems. We will subsequently focus on the structure, energetics, and bonding of the cyclobutadiene metal benzene complexes (η^4-C_4H_4)M(η^6-C_6H_6) (M = Fe, **4**; Ru, **5**; Os, **6**) and cyclopropenyl metal cycloheptatrienyl complexes (η^3-C_3H_3)M(η^7-C_7H_7) (M = Fe, **7**; Ru, **8**; Os, **9**). We will discuss the iron isomers **1**, **4**, and **7** in depth before examining the changes that are observed when progressing down the periodic table. Of the complexes examined in this study, only the metallocenes (**1**, **2**, and **3**) are known experimentally. There has been one previous theoretical study related to **4** by Jemmis et al. [35] who examined the viability of an (η^4-C_4H_4)Fe fragment coordinated to the surface of C_{60} and C_{70} clusters. There has been no experimental evidence for, or against, the existence of group 8 mixed-sandwich isomers, although we would be surprised if there have not been efforts to replace the three CO ligands of CbFe(CO)$_3$ with an arene ligand. Through our investigations we hope to provide insights into the possible viability of these series of complexes in relation to the well-known metallocenes.

2. Computational details

DFT calculations were performed using the Amsterdam density functional (ADF) package, version 2003.01, developed by Baerends et al. [36–38] The frozen-core approximation was applied to all atoms except H. 1s was frozen for C and 1s–2p were frozen for Fe, and 1s–(*n* − 1)d were frozen for Ru and Os. All atoms utilized the ADF Basis TZ2P, which is a core double-zeta, valence triple-ζ Slater-type orbital (STO) doubly polarized basis set. Relativistic effects were included in all calculations containing Ru and Os through the use of the zero-order regular approximation (ZORA) formalism [39,40,41] and ZORA TZ2P Basis. The generalized gradient approximation (GGA) exchange and correlation corrections developed by Perdew and Wang (PW91) [42–44] were used for all calculations. Geometry optimizations were carried out with an integration

parameter of at least 6.0, and were optimized to a maximum gradient of no more than 0.0001 hartree/Å.

3. Results and discussion

3.1. Calculated structures

Studies of the structure, bonding, and properties of ferrocene (**1**) are numerous, and only the salient features will be repeated here for comparison to other $MC_{10}H_{10}$ isomers. It is useful to compare experimental data on the Group 8 metallocenes to the calculated structures and properties to provide a benchmark for the DFT methods used in these studies. A representative calculated structure for $(\eta^5\text{-}C_5H_5)_2M$ (Fe: **1**; Ru: **2**; Os:**3**) is shown in Fig. 1 and selected geometric parameters are given in Table 1. The calculated structures of **1**, **2**, and **3** agree extremely well with the available experimental data [45–49] (Table 2). The barrier to rotation for **1** is calculated to be 1.02 kcal/mol, with the eclipsed structure being the lowest energy structure. The experimentally measured [50] rotation energy of ferrocene is 0.9 ± 0.3 kcal/mol, and after much debate it was finally determined that ferrocene is eclipsed in the gas phase [51], and that the crystal structure was nearly eclipsed at low temperature [52]. The eclipsed structure was also calculated to be the lowest-energy for **2** and **3**, with the difference in energy between the eclipsed and staggered structures of 0.61 and 0.77 kcal/mol, respectively.

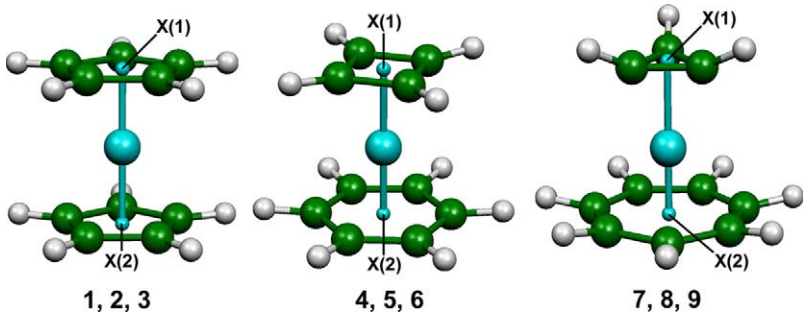

Fig. 1. Representative 3D structures for $MC_{10}H_{10}$ complexes: $(\eta^5\text{-}C_5H_5)_2M$ (M = Fe, **1**; Ru, **2**; Os, **3**), $(\eta^4\text{-}C_4H_4)M(\eta^6\text{-}C_6H_6)$ (M = Fe, **4**; Ru, **5**; Os, **6**), and $(\eta^3\text{-}C_3H_3)M(\eta^7\text{-}C_7H_7)$ (M = Fe, **7**; Ru, **8**; Os, **9**). The centroids of Ring 1 and Ring 2 are labeled X(1) and X(2), respectively.

Table 1
Selected calculated bond distances and angles for $MC_{10}H_{10}$ (M = Fe, Ru, Os) complexes

	$(\eta^5\text{-}C_5H_5)_2M$			$(\eta^4\text{-}C_4H_4)M(\eta^6\text{-}C_6H_6)$			$(\eta^3\text{-}C_3H_3)M(\eta^7\text{-}C_7H_7)$			Notes
	Fe (**1**)	Ru (**2**)	Os (**3**)	Fe (**4**)	Ru (**5**)	Os (**6**)	Fe (**7**)	Ru (**8**)	Os (**9**)	
Distance (Å)										
$M\text{–}X^{(1)}$	1.647	1.822	1.824	1.733	1.887	1.894	1.780	1.896	1.877	
$M\text{–}X^{(2)}$	1.647	1.822	1.824	1.515	1.711	1.713	1.382	1.601	1.626	
$M\text{–}C^{(1)}$	2.048	2.192	2.196	2.016	2.150	2.158	1.962	2.071	2.057	[a]
$M\text{–}C^{(2)}$	2.048	2.192	2.196	2.076	2.232	2.228	2.135	2.286	2.304	[a]
$C^{(1)}\text{–}C^{(1)}$	1.432	1.433	1.438	1.455	1.457	1.464	1.431	1.442	1.459	[a]
$C^{(1)}\text{–}H^{(1)}$	1.085	1.085	1.083	1.085	1.084	1.083	1.082	1.081	1.082	[a]
$C^{(2)}\text{–}C^{(2)}$	1.432	1.433	1.438	1.420	1.422	1.426	1.413	1.417	1.418	[a]
$C^{(2)}\text{–}H^{(2)}$	1.085	1.085	1.083	1.088	1.088	1.086	1.091	1.090	1.088	[a]
Angle (°)										
$M\text{–}X^{(1)}\text{–}C^{(1)}$	0.00	0.00	0.00	0.01	0.00	0.00	0.05	0.02	0.01	[b]
$M\text{–}X^{(2)}\text{–}C^{(2)}$	0.00	0.00	0.00	0.50	0.78	0.96	0.73	1.46	1.74	[b]
$X^{(1)}\text{–}C^{(1)}\text{–}H^{(1)}$	179.32	178.94	179.09	184.24	186.02	186.14	205.79	208.50	210.51	[a]
$X^{(2)}\text{–}C^{(2)}\text{–}H^{(2)}$	179.32	178.94	179.09	176.04	178.12	177.36	171.16	173.35	172.23	[a]
Dihedral (°)										
$C^{(1)}\text{–}C^{(1)}\text{–}C^{(1)}\text{–}C^{(1)}$	0.00	0.00	0.00	−0.02	0.00	0.00				[c]
$C^{(2)}\text{–}C^{(2)}\text{–}C^{(2)}\text{–}C^{(2)}$	0.00	0.00	0.00	1.73	2.57	3.29	5.94	10.85	1.96	[c]
$C^{(1)}\text{–}C^{(1)}\text{–}C^{(1)}\text{–}H^{(1)}$	0.84	1.32	1.13	−5.99	−8.48	−8.65	−44.02	−47.36	−49.70	[a]
$C^{(2)}\text{–}C^{(2)}\text{-}C^{(2)}\text{–}H^{(2)}$	0.84	1.32	1.13	4.57	1.98	3.05	11.20	7.25	8.45	[a]

Atoms are labeled with a superscript (1) or (2) to designate the ring they are a part of, X is the ring centroid (see Fig. 1).

[a] Average value.

[b] Largest deviation from 90°.

[c] Largest deviation from 0° (planarity).

Table 2
Experimental values and the deviation of calculated parameters for $(\eta^5\text{-}C_5H_5)_2M$ (M = Fe, Ru, Os) complexes

$(\eta^5\text{-}C_5H_5)_2M$	Fe (**1**)		Ru (**2**)		Os (**3**)	
	Expt. [45]	Diff.	Expt. [46]	Diff.	Expt. [47]	Diff.
M–X	1.658	−0.011	1.816	0.007	1.804	0.020
M–C	2.056	−0.008	2.186	0.007	2.187	0.009
C–C	1.429	0.003	1.431	0.002	1.453	−0.015
C–H	1.080	0.005	1.080	0.005	1.073	0.011
∠M–X–C	90.000	0.000	90.000	0.000	90.054	−0.054
∠C–C–C	107.999	0.001	108.000	0.000	107.998	0.002

Experimental values for the rotation energies of ruthenocene and osmocene have not yet been accurately determined.

Cyclobutadiene metal benzene $(\eta^4\text{-}C_4H_4)M(\eta^6\text{-}C_6H_6)$ complexes **4**, **5**, and **6** have not been previously reported. A representative calculated structure for **4**, **5**, and **6** is shown in Fig. 1, with geometric parameters given in Table 1. The C_6 ring of the benzene ligand is slightly puckered away from planarity; the average C_a–C_b–C_c/C_b–C_c–C_d dihedral angle, which would be 0° for a perfectly planar ring, is 1.73°, 2.57°, and 3.29° for **4** (Fe), **5** (Ru), and **6** (Os), respectively. By comparison, the C_4 rings of the cyclobutadiene ligands in **4**, **5**, and **6** are rigorously planar, with nearly identical C–C bond lengths in all three complexes. The out-of-plane bending of the C–H bonds on the two rings is more pronounced than in the metallocenes (**1**–**3**) due to the increased hybridization of C atoms to reorient the pπ orbitals for maximum overlap with the metal orbitals. Because of the small size of the C_4H_4 ring, the C–H bonds on the cyclobutadiene ring bend away from the metal in order to cause the pπ orbitals to tip outward (Scheme 1(a)). By comparison, the C–H bonds on the benzene ring show the opposite behavior, bending toward the metal because the ring is slightly too large (Scheme 1(b)). In general, as the size of the metal increases from Fe to Os the ring-size-mismatch with cyclobutadiene becomes larger and increases the C–H bending angle away from the metal, while the mismatch with benzene becomes smaller and decreases the C–H bending angle toward the metal.

The $(\eta^3\text{-}C_3H_3)M(\eta^7\text{-}C_7H_7)$ complexes **7**, **8**, and **9** also have not been previously studied, experimentally or theoretically. In the optimized structures (Fig. 1, Table 1) the out-of-plane bending of the C–H bonds on the C_3H_3 ring is severe (>20° from planarity) due to the large mismatch in size and location of the pπ orbitals relative to the metal orbitals. As the size of the metal increases from Fe to Os, the M–C_3H_3 size mismatch and out-of-plane bending become larger as expected. However, the M–C_7H_7 size mismatch remains relatively constant throughout the series, due in part to the significant deviation from planarity of the C_7 ring of the C_7H_7 ligand: The average dihedral angle within the C_7 ring varies non-monotonically, from 5.94° for **7** (Fe) to 10.85° for **8** (Ru) to 1.96° for **9** (Os).

The data in Table 1 also allow us to examine the changes that occur upon changing the metal from Fe to Ru to Os. As would be expected, for each of the three series of complexes the changes in the metric parameters when replacing Fe with Ru are larger than those when Ru is replaced with Os. This observation is entirely consistent with the more severe change in metal atomic radius from Fe to Ru as compared to Ru to Os.

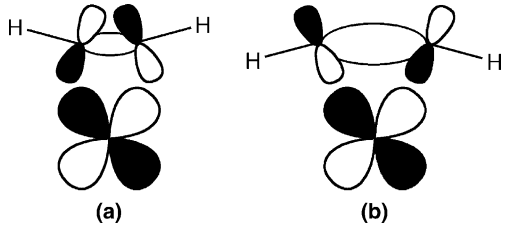

Scheme 1.

3.2. Isomer energies

The calculated relative energies of the Fe, Ru, and Os complexes **1** through **9** are presented in Table 3. We can use these energies to compare the relative energies of the isomers of each metal (Fe: **1**, **4**, **7**; Ru: **2**, **5**, **8**; Os: **3**, **6**, **9**). It is notable that the hypothetical isomerization reactions

$$(\eta^5\text{-}C_5H_5)_2M \rightarrow (\eta^4\text{-}C_4H_4)M(\eta^6\text{-}C_6H_6)$$
$$\rightarrow (\eta^3\text{-}C_3H_3)M(\eta^7\text{-}C_7H_7)$$

are isodesmic processes [53] that should allow for meaningful comparisons of the relative isomer energies.

The data in Table 3 show not surprisingly that for each of the metallocene $(\eta^5\text{-}C_5H_5)_2M$ is the most stable isomer for each of the three metal series. The relative stability of the metallocenes is a consequence of the best ring-size match discussed above and specific orbital interactions, as will be discussed below. The relative energies as one proceeds from the "5–5" to the "4–6" to the "3–7" isomer are roughly the same regardless of the metal – the relative energies rise by approximately

Table 3
Relative energies (kcal/mol) for complexes **1** through **9**

Complex	Relative energy
$FeC_{10}H_{10}$	
1	0.00
4	39.18
7	88.12
$RuC_{10}H_{10}$	
2	0.00
5	39.15
8	86.65
$OsC_{10}H_{10}$	
3	0.00
6	38.48
9	84.52

40 kcal/mol for each –CH unit shifted from one ring to the other. The higher energies of the 4–6 and 3–7 isomers are doubtless due in part to ring strain in the ligands, particularly the C_4H_4 and C_3H_3 rings. Because of the ambiguities in assigning specific charges to the ligands (vida infra), we have not yet attempted to partition the energy differences into metal–ligand bonding and intraligand contributions.

3.3. Bonding analysis – $FeC_{10}H_{10}$

The bonding in **1** is well understood, and we will avoid a detailed reanalysis of the subject here. Under D_{5h} symmetry, the dominant metal–ligand interaction in **1** is donation from the formally filled e_1'' combination of the Cp^- (π_2, π_3) orbitals into the Fe 3dπ (d_{xz}, d_{yz}) orbitals, with lesser donation from the a_1' ligand π-orbital into the Fe 4s orbital. The formally d^6 complex corresponds to an electron configuration of $(d\delta)^4(d\sigma)^2(d\pi)^0$ at the Fe center. Complete molecular orbital diagrams and discussions of the eclipsed and staggered forms may be found in many modern inorganic textbooks [54].

Bonding analyses for the mixed sandwich complexes are necessarily more complex than those of the metallocenes owing to the presence of two different sandwich rings and the concomitant reduction in symmetry. We will discuss the bonding of the iron isomers **4** and **7** in detail first, followed by discussion of any changes in the bonding upon replacing Fe with Ru and Os. For the ligands in our systems it is generally assumed that the σ system of the ring will play a very small role in the bonding, and therefore we only consider the relevant ring π orbitals in our analysis. It is also reasonable to assume that the interaction of each ring with the metal will retain much of the symmetry characteristics of the ring, independent of the overall symmetry of the molecule. For that reason, we will use higher localized pseudo-symmetry than might exist overall in the complex.

Fragment analysis will be used to examine the dominant bonding in **4** to determine whether it should be viewed as a FeC_4H_4 fragment perturbed by a benzene ligand or a FeC_6H_6 fragment perturbed by a cyclobutadiene ligand. We have proposed earlier that the interaction of a cyclobutadiene ligand and an Fe atom arises from a strong covalent π-bonding interaction between the e_g (2π) Cb π orbitals (which are half-filled in neutral square C_4H_4) and the Fe $3d_{xz}$ and $3d_{yz}$ orbitals [33]. We find that the present ADF calculations on (η^4-C_4H_4)Fe yield results similar to those previously reported by Bursten and Fenske on this fragment: as shown in Fig. 2, the Fe 3d orbitals match well energetically with the e_g orbitals of the cyclobutadiene ligand, facilitating a strong covalent π interaction. The π bonding 1e orbital is 48.0% Cb 2π and 38.2% Fe 3dπ, and the π* 2e orbital is 49.1% Fe 3dπ and 33.22% Cb 2π. By comparison, the interaction between a benzene ligand and an Fe atom is due mainly to δ-bonding interactions between the e_{2u} (3π) orbitals of benzene and the Fe $3d_{x^2-y^2}$ and $3d_{xy}$ orbitals, although there is a small π-bonding interaction between the e_{1g} (2π) benzene MOs and the Fe $3d_{xz}$ and $3d_{yz}$ orbitals. The δ-bonding interaction in Fe(η^6-C_6H_6) is weaker than the π-bonding interaction in the (η^4-C_4H_4)Fe fragment because of both the smaller orbital overlap and an energy mismatch between the benzene π orbitals and the iron 3d orbitals.

We previously used the energetic ordering of fragment orbitals to determine whether (η^4-C_4H_4)Fe$(CO)_3$ is better considered as a (η^4-C_4H_4)Fe fragment perturbed by three CO ligands, or as an Fe$(CO)_3$ fragment perturbed by a C_4H_4 ligand – in that case, the C_4H_4–Fe π-bonding interaction dominates and the first description is more appropriate [33]. We have performed a similar orbital analysis for (η^4-C_4H_4)Fe(η^6-C_6H_6) (**4**). If **4** should be viewed as a (η^4-C_4H_4)Fe fragment that has been affected by a benzene ligand, the MO diagram of **4** will have the π-bonding (η^4-C_4H_4)Fe e orbitals below the δ-bonding C_6H_6 orbitals. On the other hand, if this complex is best considered to be an Fe(η^6-C_6H_6) fragment interacting with a cyclobutadiene ligand, the MO diagram of **4** should have the reverse situation – the Fe(η^6-C_6H_6) δ-bonding orbitals should be below the π-bonding C_4H_4 orbitals. Fig. 3 shows the interaction of a (η^4-C_4H_4)Fe fragment with a benzene ligand. The π-bonding orbitals of the FeC_4H_4 fragment are relatively unaffected by the presence of the benzene ligand, although the Fe–C_4H_4 e* antibonding orbitals between are pushed up in energy. There is a stabilization of the $d_{x^2-y^2}$ and d_{xy} orbitals due to the δ-bonding interaction with benzene. Nevertheless, the metal orbital ordering remains similar to that of the (η^4-C_4H_4)Fe fragment, with the π-bonding e orbitals of the (η^4-C_4H_4)Fe fragment below the δ-bonding interaction of Fe with benzene. A similar interaction diagram between a C_4H_4 ligand with a Fe(η^6-C_6H_6) fragment (not shown) shows a large perturbation of the metal-based orbitals of the Fe(η^6–C_6H_6) moiety. Thus, the fragment analysis

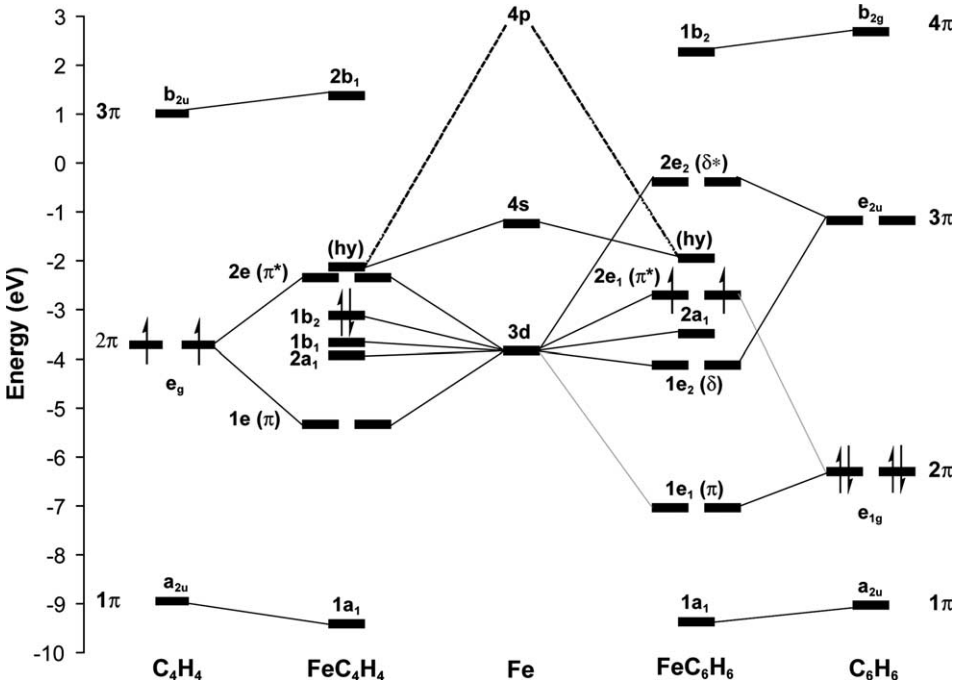

Fig. 2. Orbital interaction diagrams showing the formation of (η^4-C_4H_4)Fe and (η^6-C_6H_6)Fe fragments from the interactions of an Fe atom with the cyclic ligands.

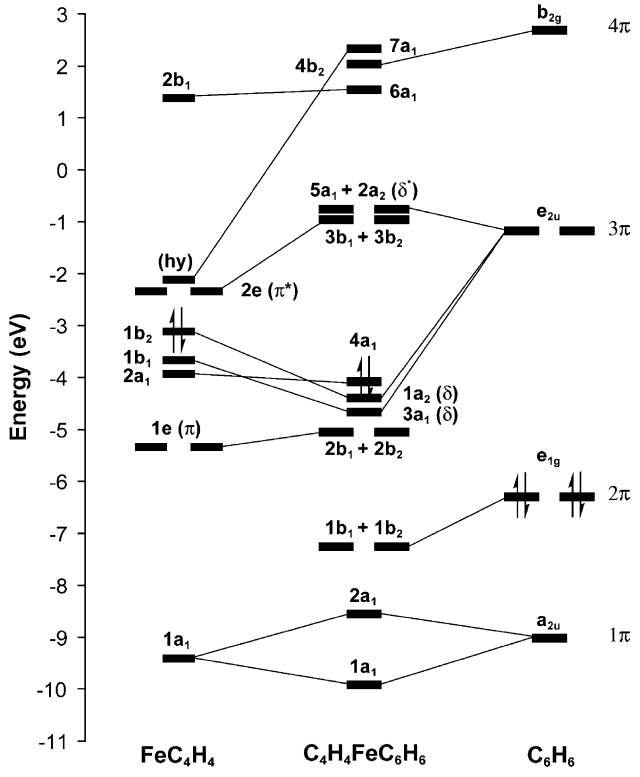

Fig. 3. Interaction diagram showing the development of the orbitals of (η^4-C_4H_4)Fe(η^6-C_6H_6) from (η^4-C_4H_4)Fe and C_6H_6.

clearly indicates that **4** is better viewed as a metalloaromatic (η^4-C_4H_4)Fe fragment interacting with a C_6H_6 ligand, similar to the description of (η^4-C_4H_4)Fe(CO)$_3$. Given that Fe(η^6-C_6H_6) is isolobal to Fe(CO)$_3$ [55], this conclusion is not surprising.

We can apply the same orbital analysis to (η^3-C_3H_3)Fe(η^7-C_7H_7) (**7**). Fig. 4 compares the interactions of an Fe atom with C_3H_3 and C_7H_7 to form (η^3-C_3H_3)Fe and Fe(η^7-C_7H_7), respectively. In the case of (η^3-C_3H_3)Fe, the only significant interaction between Fe and C_3H_3 is a π-bonding interaction between the e″ (2π) orbitals of the ligand and the Fe 3dπ orbitals (Fig. 4). Because the C_3H_3 e″ orbitals are higher in energy than the Fe 3d orbitals, the resultant π-bonding e MO of (η^3-C_3H_3)Fe has greater Fe character than ligand character. In addition, because of the size and orbital orientation mismatch between the C_3H_3 ring and Fe 3d orbitals, there is significant mixing of the Fe $d_{x^2-y^2}$ and d_{xy} orbitals in the π-bonding orbitals as well as significant mixing of the Fe 4p orbitals in the π* orbitals. In contrast, C_7H_7 and Fe have a very small π-bonding interaction because of the large energy mismatch between the C_7H_7 e_1'' (2π) and the Fe 3d orbitals; as shown in Fig. 4, the dominant bonding in Fe(η^7-C_7H_7) is due to the δ interaction between the C_7H_7 e_2'' (3π) orbitals and the Fe 3dδ ($3d_{x^2-y^2}$ and $3d_{xy}$) orbitals. Thus, these metal–ligand interactions lead to distinctly different ordering of the Fe-based MOs of the fragments: The Fe 3dπ MO is the lowest energy metal-based orbital in (η^3-C_3H_3)Fe whereas the Fe 3dδ is lowest in Fe(η^7-C_7H_7).

A comparison of the orbital interactions shows clearly that **7** is better considered as a Fe(η^7-C_7H_7) fragment interacting with a C_3H_3 ligand. Fig. 5 shows these

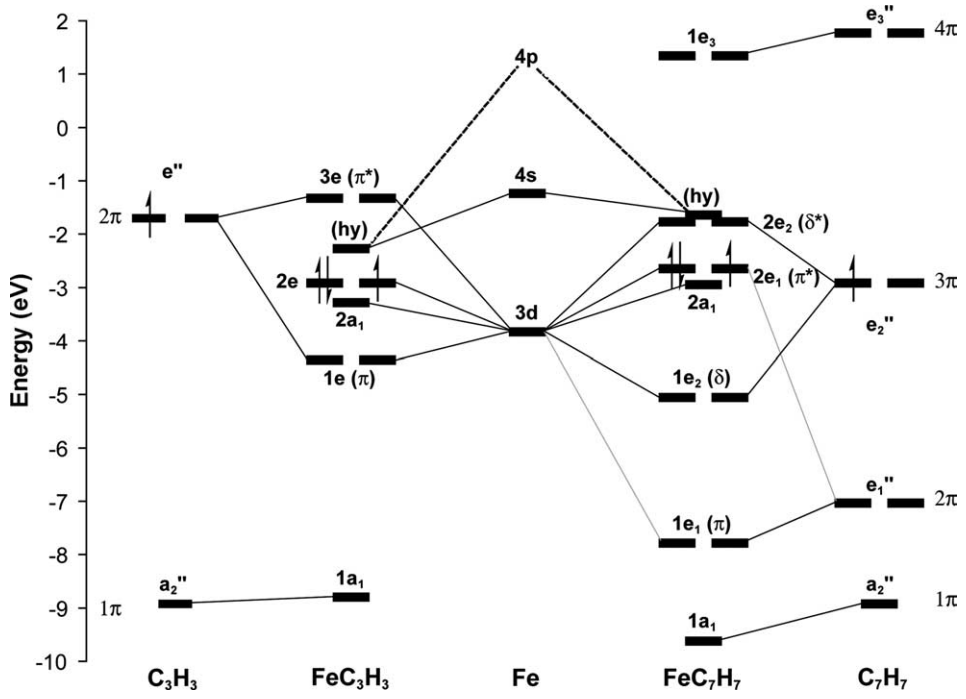

Fig. 4. Orbital interaction diagrams showing the formation of (η^3-C_3H_3)Fe and (η^7-C_7H_7)Fe fragments from the interactions of an Fe atom with the cyclic ligands.

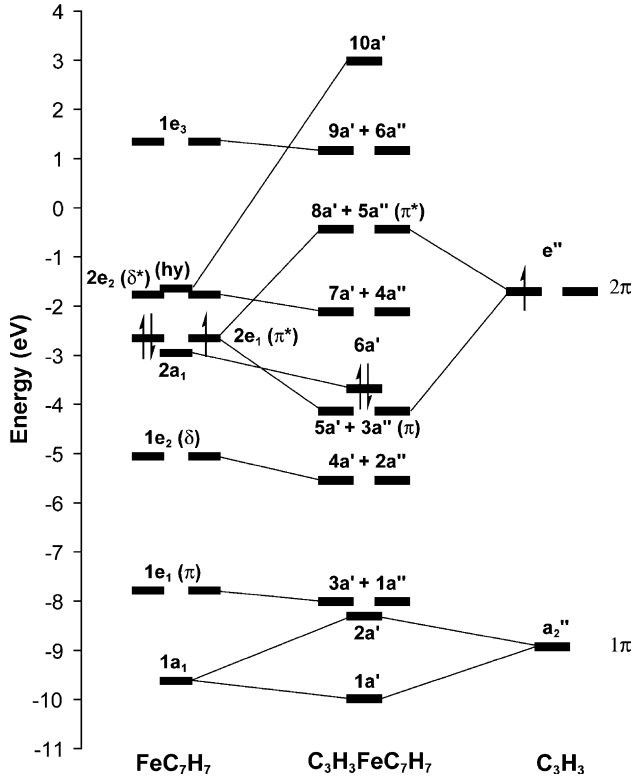

Fig. 5. Interaction diagram showing the development of the orbitals of (η^3-C_3H_3)Fe(η^7-C_7H_7) from (η^7-C_7H_7)Fe and C_3H_3.

orbital interactions and clearly indicates good transferability of the MOs of the Fe(η^7-C_7H_7) fragment to those of **7**; in particular, the lowest metal-based orbital of **7** is the Fe 3dδ MO derived from the Fe(η^7-C_7H_7) fragment. By comparison, the transferability of the (η^3-C_3H_3)Fe fragment onto the overall MO diagram for **7** is poor. The HOMO of **7** is predicted to be the largely unperturbed Fe $3d_{z^2}$ orbital, similar to what has been found experimentally and theoretically by Green et al. [56,57] for 17- and 18-electron unsymmetric (η^5-C_5H_5)M(η^7-C_7H_7) complexes.

The difference in the dominant fragment in complexes **4** and **7** illustrates an important point about mixed sandwich complexes – neither the distance of the ligand centroid from the metal nor the symmetry of the bonding necessarily dictate the dominantly bound fragment. In **4** the dominantly bound fragment is C_4H_4, the centroid of which is further from the metal than that of C_6H_6; in **7** the C_7H_7 ring is the dominant fragment and its centroid is much closer to the metal center than that of C_3H_3. In addition, the dominant fragment is bound in two different ways in these two complexes: in **4** the Fe–C_4H_4 bonding is due primarily to a metal–ligand interaction of π symmetry whereas in **7** the dominant Fe–C_7H_7 interaction has δ symmetry. Although we normally do not consider primary bonding in organometallic species to be of a δ-bonding type, we can see in **7** that the δ-bonding is strong and mainly covalent. This conclusion is in nice accord with that of Green et al., who used variable-photo-energy photoelectron spectroscopy to demonstrate the significance of metal–ligand δ-bonding in Cr(η^6-C_6H_6)$_2$ and Mo(η^6-C_6H_5Me)$_2$ [58]. Frenking et al. [59] have recently reported a computational study

that supports the conclusion that δ-bonding is the dominant bonding type in $Cr(\eta^6\text{-}C_6H_6)_2$.

3.4. Analysis of the formal charges in 1, 4, and 7

Thus far in our discussion, we have avoided assigning formal charges to the cyclic ligands in complexes **1**, **4**, and **7**. We can provide a simple analysis of the formal ligand charges based on the relative orbital energetics presented in Figs. 2 and 4 as well as the usual description of ferrocene. Ferrocene is generally considered to be a complex in which two formally Cp^- ligands are bonded to a d^6 Fe(II) center. This description is consistent with the relative orbital energetics of the Cp ligand and the Fe 3d orbitals, i.e. the e_1'' HOMO of Cp^- is at a lower energy than the Fe 3d orbitals, so the Cp–Fe π-bonding MOs are dominantly Cp in character.

In **4**, the e_g HOMO of neutral C_4H_4 is nearly isoenergetic with the Fe 3d orbitals (Fig. 2), which leads to the strong covalent bonding description we have presented previously [33]. We therefore believe that the C_4H_4-Fe π-bonding is essentially equally shared between the ligand and the metal, which is consistent with considering C_4H_4 as a neutral ligand. The C_6H_6 ligand in **4** is also best considered a neutral ligand inasmuch as all of the filled and empty orbitals of neutral C_6H_6 are lower and higher in energy, respectively, than the Fe 3d orbitals. Thus, this simple analysis suggests that **4** is best considered formally as a d^8 Fe(0) complex with neutral C_4H_4 and C_6H_6 ligands. A similar analysis of **7**, based on Fig. 4, suggests that both C_3H_3 and C_7H_7 be considered cationic ligands: Both the e'' π orbitals of C_3H_3 and the e_2'' π orbitals of C_7H_7 are higher in energy than the Fe 3d orbitals. This observation leads to the unusual proposal that **7** be considered a d^{10} Fe(−2) complex with formal $C_3H_3^+$ and $C_7H_7^+$ ligands, both of which are Hückel aromatic π systems. We are thus left with the intriguing description that the movement of a C–H group from one ring to another in going from **1** to **4** and **4** to **7** is accompanied by a formal two-electron reduction of the Fe center, at least within this simplified, orbital-energy-driven description.

Our proposal that the cht ligand be considered as $C_7H_7^+$ runs counter to convincing experimental and theoretical studies by Green and Kaltsoyannis [56,57]. Based on their studies of 16-, 17- and 18-electron $(\eta^5\text{-}C_5H_5)M(\eta^7\text{-}C_7H_7)$ (M = Ti, V, Nb, Ta, Mo) complexes, these authors concluded that the cht ligand should not be considered as a 1+ nor a 3− ligand – rather it is best described as a seven-electron ligand and that three metal-based electrons are required to form the M-cht bond. We note that the Fe, Ru, and Os complexes examined here involve later metals that are expected to compete more effectively for electrons than do the early metals of these other studies.

Because of the intriguing differences in these descriptions, we have used population analysis to examine the conclusion about the charges on the Fe atom and the ligands in complexes **1**, **4**, and **7.** Table 4 presents the Mulliken and Hirshfeld charges [60] on the Fe atom and on the ligands in **1**, **4**, and **7**. There is reasonable agreement between these two methodologies for partitioning the charge among the portions of the molecules. The Mulliken charge on the Fe monotonically decreases from **1** to **4** to **7**, although the magnitude of the changes are rater small; the Hirshfeld charges on the Fe atom are nearly invariant from one complex to another. Interestingly, the two methods both show that the charges on the C_nH_n ligands become monotonically more positive as n increases, i.e. the C_3H_3 ligand is the most negatively charged whereas the C_7H_7 ligand is the most positively charged. We will be exploring the effects of these charges on the relative energetics of the isomeric complexes further.

3.5. Bonding analysis – $RuC_{10}H_{10}$ and $OsC_{10}H_{10}$

Fig. 6 shows the changes in the metal-based MO energies that occur when progressing down the periodic table from Fe to Os. In the $(\eta^4\text{-}C_4H_4)M(\eta^6\text{-}C_6H_6)$ series (**4**–**6**) the complex has a significant change in bonding: the C_4H_4-M π-interaction is destabilized, and the C_6H_6-M δ-interaction is strengthened from Fe to Os (Fig. 6(a)). In **6** the benzene MOs of δ symmetry and the cyclobutadiene MOs of π symmetry are essentially

Table 4
Mulliken and Hirshfeld charges for the Fe atom and ligands in complexes **1**, **4**, and **7**

Complex	Fragment	Mulliken charge	Hirshfeld charge
$(\eta^5\text{-}C_5H_5)_2Fe$	Fe	0.154	0.040
	$\eta^5\text{-}C_5H_5$	−0.077	−0.020
$(\eta^4\text{-}C_4H_4)Fe(\eta^6\text{-}C_6H_6)$	Fe	0.107	0.035
	$\eta^4\text{-}C_4H_4$	−0.124	−0.070
	$\eta^6\text{-}C_6H_6$	0.017	0.035
$(\eta^3\text{-}C_3H_3)Fe(\eta^7\text{-}C_7H_7)$	Fe	0.066	0.040
	$\eta^3\text{-}C_3H_3$	−0.173	−0.134
	$\eta^7\text{-}C_7H_7$	0.106	0.093

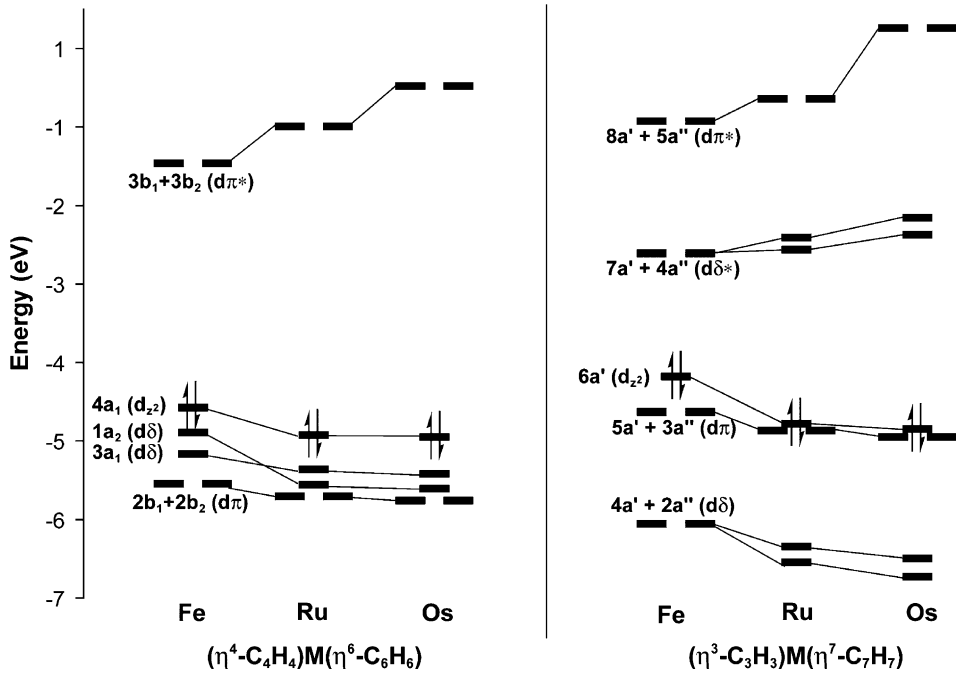

Fig. 6. Correlation diagram showing the energetic changes of the M *n*d-based MOs as M is changed from Fe to Ru to Os. Left: $(\eta^4\text{-}C_4H_4)M(\eta^6\text{-}C_6H_6)$. Right: $(\eta^3\text{-}C_3H_3)M(\eta^7\text{-}C_7H_7)$.

isoenergetic, implying that the bonding of each ligand is competitive with the other – there is no longer a dominantly bound ligand in this complex. The increased size and diffuseness of the Os 5d orbitals, as compared to the Fe 3d orbitals, allow for better π overlap with the benzene e_2'' orbitals and causes a decreased overlap with the cyclobutadiene e″ orbitals (as seen by the increased C–H bending on C_4H_4 in **6**).

Similar effects are seen in the $(\eta^3\text{-}C_3H_3)M(\eta^7\text{-}C_7H_7)$ complexes (**7**–**9**). As the d orbitals increase in size from Fe to Ru to Os, the interaction with the smaller C_3H_3 ligand becomes less effective and that with the larger C_7H_7 ligand increases. In this case, however, the dominant interaction in the complex involves the δ interaction of the metal with the C_7H_7 ligand, Thus, the bonding effects seen in the Fe complex are reinforced in this series of complexes, i.e. the dominance of the $M(\eta^7\text{-}C_7H_7)$ increases as we progress from Fe to Ru to Os.

4. Conclusions

The calculations that we have presented here suggest that the metallocenes are the most stable of the $(\eta\text{-}C_nH_n)M(\eta\text{-}C_{10-n}H_{10-n})$ sandwich complexes examined. In one sense that is a satisfying and sensible conclusion given the central role that the metallocenes play in organometallic chemistry viz-á-viz the nonexistence of the unsymmetric sandwich complexes. Nevertheless, the calculations suggest that the metal–ligand bonding interactions in the "4–6" and "3–7" complexes are, in principle, robust enough to allow these complexes to exist, especially given that there would be no easy route for these to isomerize to the metallocenes.

In future contributions we will look more closely at some of the energetic contributions to the different isomer stabilities. We will also be presenting a similar analysis of sandwich complexes of the type $(\eta\text{-}C_nH_n)M(\eta\text{-}C_{12-n}H_{12-n})$ (M = Cr, Mo, W), the chemistry of which has been indelibly affected by Malcolm L.H. Green.

Acknowledgment

We are grateful to the Ohio Supercomputer Center for a generous grant of computer time.

References

[1] M.L.H. Green, L. Pratt, G. Wilkinson, J. Chem. Soc. (1958) 3916.
[2] See, for example: (a) F.W.S. Benfield, M.L.H. Green, J.S. Ogden, D. Young, J. Chem. Soc., Chem. Commun. (1973) 866;
(b) M.L.H. Green, J. Organomet. Chem. 200 (1980) 119.
[3] See, for example: M.L.H. Green, D.K.P. Ng, Chem. Rev. 95 (1995) 439.
[4] See, for example: (a) J.C. Green, M.L.H. Green, N. Kaltsoyannis, P. Mountford, P. Scott, S.J. Simpson, Organometallics 11 (1992) 3353;
(b) M.L.H. Green, D.K.P. Ng, R.C. Tovey, A.N. Chernega, J. Chem. Soc., Dalton Trans. (1993) 3203.
[5] J.D. Zeinstra, J.L. De Boer, J. Organomet. Chem. 207 (1973) 54.

[6] E.O. Fischer, S. Brietschaft, Chem. Ber. 99 (1966) 2905.
[7] R.B. King, F.G.A. Stone, J. Am. Chem. Soc. 81 (1959) 5263.
[8] T.J. Kealy, P.L. Pauson, Nature (London) 168 (1951) 1039.
[9] S.A. Miller, J.A. Tebboth, J.F. Tremaine, J. Chem. Soc. (1952) 632.
[10] G. Wilkinson, M. Rosenblum, M.C. Whiting, R.B. Woodward, J. Am. Chem. Soc. 74 (1952) 2125.
[11] E.O. Fischer, W. Pfab, Z. Naturforsch. B B7 (1952) 377.
[12] M. Rosenblum, Chemistry of the Iron Group Metallocenes: Ferrocene, Ruthenocene, Osmocene, Interscience, New York, 1965.
[13] R.B. King, Organomet. Chem. Rev. B 4 (1968) 67.
[14] M.I. Bruce, Organomet. Chem. Rev. B 5 (1969) 379.
[15] M.I. Bruce, Organomet. Chem. Rev. B 6 (1970) 665.
[16] See, for example: (a) R.D. Adams (Ed.), 50th Anniversary of the Discovery of Ferrocene, J. Organomet. Chem. 637–639 (2001) 1; (b) R. Dagani, C & E News 79 (2001) 37.
[17] See, for example: (a) R.H. Mitchell, Y. Chen, N. Khalifa, P. Zhou, J. Am. Chem. Soc. 120 (1998) 1785;
(b) P.v.R. Schleyer, B. Kiran, D.V. Simion, T.S. Sorensen, J. Am. Chem. Soc. 122 (2000) 510;
(c) M. Laskoski, W. Steffen, M.D. Smith, U.H.F. Bunz, Chem. Commun. (2001) 691.
[18] M.D. Rausch, R.M. Tuggle, D.L. Weaver, J. Am. Chem. Soc. 92 (1970) 4981.
[19] R.M. Tuggle, D.L. Weaver, Inorg. Chem. 10 (1971) 1504.
[20] T. Chiang, R.C. Kerber, S.D. Kimball, J.W. Lauher, Inorg. Chem. 18 (1979) 1687.
[21] D.L. Lichtenberger, M.L. Hoppe, L. Subramananian, E.M. Kober, R.P. Hughes, J.L. Hubbard, D.S. Tucker, Organometallics 12 (1993) 2025.
[22] R.P. Hughes, D.S. Tucker, A.L. Rheingold, Organometallics 12 (1993) 3069.
[23] G.F. Emerson, L. Watts, R. Pettit, J. Am. Chem. Soc. 87 (1965) 131.
[24] H.C. Longuet-Higgens, L.E. Orgel, J. Chem. Soc. (1956) 1969.
[25] W. Hübel, E.H. Braye, J. Inorg. Nucl. Chem. 10 (1959) 250.
[26] R. Criegee, G. Schröder, Justus Liebigs Ann. Chem. 623 (1959) 1.
[27] D. Seyferth, Organometallics 22 (2003) 2.
[28] A. Efraty, Chem. Rev. 77 (1977) 691.
[29] P.K. Baker, H. Silgram, Trends Organomet. Chem. 3 (1999) 21.
[30] P.D. Harvey, W.P. Schaefer, H.B. Gray, D.F.R. Gilson, I.S. Butler, Inorg. Chem. 27 (1988) 57.
[31] M.I. Davis, C.S. Speed, J. Organomet. Chem. 21 (1970) 401.
[32] L. Watts, J.D. Fitzpatrick, R. Pettit, J. Am. Chem. Soc. 87 (1965) 3253.
[33] B.E. Bursten, R.F. Fenske, Inorg. Chem. 18 (1979) 1760.
[34] See, for example: (a) G.H. Robinson, Acc. Chem. Res. 32 (1999) 773;
(b) H. Masui, Coord. Chem. Rev. 219–221 (2001) 957.
[35] E.D. Jemmis, M. Manoharan, P.K. Sharma, Organometallics 19 (2000) 1879.
[36] G. te Velde, F.M. Bickelhaupt, E.J. Baerends, C.F. Guerra, S.J.A. Van Gisbergen, J.G. Snijders, T. Ziegler, J. Comput. Chem. 22 (2001) 931.
[37] C.F. Guerra, J.G. Snijders, G. Te Velde, E.J. Baerends, Theor. Chem. Acc. 99 (1998) 391.
[38] ADF2003.01, SCM, Theoretical Chemistry, Vrije Universiteit, Amsterdam, The Netherlands. Available from: http://www.scm.com.
[39] E. van Lenthe, E.J. Baerends, J.G. Snijders, J. Chem. Phys. 99 (1993) 4597.
[40] E. van Lenthe, E.J. Baerends, J.G. Snijders, J. Chem. Phys. 101 (1994) 9783.
[41] E. van Lenthe, A.E. Ehlers, E.J. Baerends, J. Chem. Phys. 110 (1999) 8943.
[42] J.P. Perdew, Phys. Rev. B 33 (1986) 8822.
[43] J.P. Perdew, Y. Wang, Phys. Rev. B 45 (1992) 13244.
[44] J.P. Perdew, Y. Wang, Phys. Rev. B 33 (1986) 8800.
[45] P. Seiler, J.D. Dunitz, Acta Cryst. B 38 (1982) 1741.
[46] P. Seiler, J.D. Dunitz, Acta Cryst. B 36 (1980) 2946.
[47] J.C.A. Boeyens, D.C. Levendis, M.I. Bruce, M.L. Williams, J. Crystallogr. Spectrosc. Res. 16 (1986) 519.
[48] A. Haaland, Acc. Chem. Res. 12 (1979) 415.
[49] F. Takusagawa, T.F. Koetzle, Acta Cryst. B 35 (1979) 1074.
[50] A. Haaland, J.E. Nilsson, Acta Chem. Scand. 22 (1968) 2653.
[51] R.K. Bohn, A. Haaland, J. Organomet. Chem. 5 (1966) 470.
[52] P. Seiler, J.D. Dunitz, Acta Cryst. B 35 (1979) 1068.
[53] W.J. Hehre, R. Ditchfield, L. Radom, J.A. Pople, J. Am. Chem. Soc. 92 (1970) 4796.
[54] F.A. Cotton, Chemical Applications of Group Theory, Wiley, New York, 1990.
[55] M. Elian, R. Hoffmann, Inorg. Chem. 14 (1975) 1058.
[56] J.C. Green, N. Kaltsoyannis, K.H. Sze, M. MacDonald, J. Am. Chem. Soc. 116 (1994) 1994.
[57] N. Kaltsoyannis, J. Chem. Soc., Dalton Trans. (1995) 3727.
[58] J.G. Brennan, G. Cooper, J.C. Green, N. Kaltsoyannis, M.A. MacDonald, M.P. Payne, C.M. Redfern, K.H. Sze, Chem. Phys. 164 (1992) 271.
[59] V.M. Rayón, G. Frenking, Organometallics 22 (2003) 3304.
[60] See, for example: (a) R.S. Mulliken, J. Chem. Phys. 23 (1955) 1833;
(b) F.L. Hirshfeld, Theor. Chim. Acta 44 (1977) 129;
(c) C.F. Guerra, J.-W. Handgraaf, E.J. Baerends, F.M. Bickelhaupt, J. Comput. Chem. 25 (2004) 189.

Available online at www.sciencedirect.com
SCIENCE DIRECT®
Polyhedron 23 (2004) 3003–3005
POLYHEDRON
www.elsevier.com/locate/poly

Author Index to Special Issue in Honour of Professor Malcolm L.H. Green

Abboud, K.A., see Wang, S.-Y.S., 2733
Abboud, K.A., see Murugesu, M., 2779
Abruña, H.D., see Sydora, O.L., 2841
Arif, A.M., see Harvey, B.G., 2725
Arnold, J., see Inyushin, S., 2937

Baik, M.-H., Friesner, R.A. and Parkin, G., Theoretical investigation of the metal–metal interaction in dimolybdenum complexes with bridging hydride and methyl ligands, 2879
Bailey, A., Griffith, W.P., Leung, D.W.C., White, A.J.P. and Williams, D.J., Ozonolysis for the preparation of high-oxidation state transition metal complexes, and the X-ray crystal structure of $Co(py)_2(OAc)_2(H_2O)_2$, 2631
Baker, R.T., see Westcott, S.A., 2665
Barral, M.C., González-Prieto, R., Herrero, S., Jiménez-Aparicio, R., Priego, J.L., Royer, E.C., Torres, M.R. and Urbanos, F.A., Synthesis and crystal structure of high and low spin diruthenium complexes with diphenylformamidine and diphenyltriazene ligands, 2637
Batsanov, A.S., see Coventry, D.N., 2789
Beeby, A., see Leslie, W., 2769
Beer, P.D., see Wong, W.W.H., 2821
Bellabarba, R.M. and Saunders, G.C., Intramolecular dehydrofluorinative coupling of pentamethylcyclopentadienyl and phosphine ligands in iridium complexes, 2659
Bercaw, J.E., see Piro, N.A., 2797
Bergman, R.G., see Corkey, B.K., 2943
Bolte, M., see Ilkhechi, A.H., 2597
Boncella, J.M., see Wang, S.-Y.S., 2733
Bosch, M., see Werner, H., 2645
Brett, C.M. and Bursten, B.E., Theoretical studies of 18-electron $M(C_nH_n)(C_{10-n}H_{10-n})$ (M = Fe, Ru, Os; n = 3, 4, 5) sandwich complexes, 2993
Brookhart, M., see Corkey, B.K., 2943
Burney, C., see Green, J.C., 2915
Bursten, B.E., see Brett, C.M., 2993
Bushuk, B.A., see Bushuk, S.B., 2615
Bushuk, S.B., Carré, F.H., Guy, D.M.H., Douglas, W.E., Kalvinkovskya, Y.A., Klapshina, L.G., Rubinov, A.N., Stupak, A.P. and Bushuk, B.A., Hypercoordinate silicon and phosphorus acetylene compounds: crystal structure determinations and fluorescence spectroscopic study, 2615

Calabrese, J.C., see Westcott, S.A., 2665
Camm, K.D., Furtado, S.J., Gott, A.L. and McGowan, P.C., Synthesis and structural studies of bis-amino-functionalised ferrocene salts and ferrocenium salts, 2929
Carré, F.H., see Bushuk, S.B., 2615
Christou, G., see Murugesu, M., 2779
Claramunt, R.M., María, M.D.S., Elguero, J. and Trofimenko, S., Isomer distribution in thallium hydrotris(polymethylenepyrazol-1-yl)borates (thallium scorpionates): a multinuclear NMR study, 2985
Cloke, F.G.N., Hitchcock, P.B., Kuchta, M.C. and Morley-Smith, N.A., Mononuclear tantalum (V) pentalene complexes: synthesis of $[Ta\{\eta^8\text{-}C_8H_4(1,4\text{-}Si^iPr_3)_2\}X_3]$ (X = CH_3, Cl, I) and the X-ray crystal structures of $[Ta\{\eta^8\text{-}C_8H_4(1,4\text{-}Si^iPr_3)_2\}(CH_3)_3]$, $[Ta\{\eta^8\text{-}C_8H_4(1,4\text{-}Si^iPr_3)_2\}(CH_3)_2Cl]$, $[Ta\{\eta^8\text{-}C_8H_4(1,4\text{-}Si^iPr_3)_2\}(CH_3)Cl_2]$ and $[Ta\{\eta^8\text{-}C_8H_4(1,4\text{-}Si^iPr_3)_2\}I_3]$, 2625
Collange, E., Metteau, L., Richard, P. and Poli, R., Synthesis and structure of a new organometallic polyoxomolybdate, $Cp^*_2Mo_6O_{17}$, 2605
Cook, R.A., see Mehnert, C.P., 2679
Corkey, B.K., Taw, F.L., Bergman, R.G. and Brookhart, M., Aromatic and aldehyde carbon–hydrogen bond activation at cationic Rh(III) centers. Evaluation of electronic substituent effects on aldehyde binding and C–H oxidative addition, 2943
Coventry, D.N., Batsanov, A.S., Goeta, A.E., Howard, J.A.K. and Marder, T.B., Synthesis and molecular structures of α-diimines and their zinc and palladium dichloride complexes, 2789
Crabtree, R.H., see Miecznikowski, J.R., 2857
Crane, T.W., see Cross, J.L., 2831
Cross, J.L., Garrett, A.D., Crane, T.W., White, P.S. and Templeton, J.L., Coordination and reactivity of acetonitrile in tungsten(IV) complexes: oxidation, methylation and dimerization of coordinated acetonitrile, 2831
Cummins, C.C., see Sceats, E.L., 2751

Danopoulos, A.A., see Winston, S., 2813
Day, M.W., see Wenger, O.S., 2955
Dias, A.R., see Ribeiro, A.F.G., 2715
Dispenziere, N.C., see Mehnert, C.P., 2679
Douglas, W.E., see Bushuk, S.B., 2615

Elguero, J., see Claramunt, R.M., 2985
Ernst, R.D., see Harvey, B.G., 2725
Evans, W.J., Kozimor, S.A. and Ziller, J.W., Bis(pentamethylcyclopentadienyl) U(III) oxide and U(IV) oxide carbene complexes, 2689

Ferreira da Silva, J.L., see Ribeiro, A.F.G., 2715
Figueroa, J.S., see Sceats, E.L., 2751
Ford, S., see Morley, C.P., 2967
Freire, C., see Ribeiro, A.F.G., 2715
Friesner, R.A., see Baik, M.-H., 2879
Furtado, S.J., see Camm, K.D., 2929

Garrett, A.D., see Cross, J.L., 2831
Gibson, V.C., see O'Reilly, R.K., 2921
Goeta, A.E., see Coventry, D.N., 2789
Goldsmith, J.I., see Sydora, O.L., 2841
Gomes, P.T., see Ribeiro, A.F.G., 2715

doi:10.1016/S0277-5387(04)00416-4

González-Prieto, R., see Barral, M.C., 2637
Gott, A.L., see Camm, K.D., 2929
Gray, H.B., see Wenger, O.S., 2955
Green, J.C. and Burney, C., Open shell metallocenes and exchange splitting of ligand bands: a reassignment of the photoelectron spectra of manganocene, 2915
Griffin, R.G., see Sceats, E.L., 2751
Griffith, W.P., see Bailey, A., 2631
Guy, D.M.H., see Bushuk, S.B., 2615

Harlow, R.L., see Westcott, S.A., 2665
Harvey, B.G., Arif, A.M. and Ernst, R.D., Incorporation of polybasic aromatic amines into ruthenium(II) chloro complexes, 2725
Henling, L.M., see Wenger, O.S., 2955
Henriques, R.T., see Ribeiro, A.F.G., 2715
Herrero, S., see Barral, M.C., 2637
Hitchcock, P.B., see Cloke, F.G.N., 2625
Hodson, E. and Simpson, S.J., Synthesis and characterisation of [(η^6-cymene)Ru(L)X_2] compounds: single crystal X-ray structure of [(η^6-cymene)Ru(P{OPh}$_3$)Cl_2] at 203 K, 2695
Houlis, J.F., see Merwin, R.K., 2873
Howard, J.A.K., see Coventry, D.N., 2789

Ilkhechi, A.H., Scheibitz, M., Bolte, M., Lerner, H.-W. and Wagner, M., On the way to ferrocene-based multiple-decker sandwich complexes, 2597
Inyushin, S., Shafir, A., Sheats, J.E., Minihane, M., Whitten Jr., C.E. and Arnold, J., Synthesis and X-ray structures of metallocenium diamines of iron and cobalt, 2937

Jiménez-Aparicio, R., see Barral, M.C., 2637
Jones, W.D., see Oster, S.S., 2959

Kalvinkovskya, Y.A., see Bushuk, S.B., 2615
Kelly, A.E., see Yoon, S., 2805
Klapshina, L.G., see Bushuk, S.B., 2615
Kozimor, S.A., see Evans, W.J., 2689
Kuchta, M.C., see Cloke, F.G.N., 2625

Lam, K.C., see Westcott, S.A., 2665
Lerner, H.-W., see Ilkhechi, A.H., 2597
Leslie, W., Poole, R.A., Murray, P.R., Yellowlees, L.J., Beeby, A. and Williams, J.A.G., Near infra-red luminescence from bis-terpyridyl iridium(III) complexes incorporating electron-rich pendants, 2769
Leung, D.W.C., see Bailey, A., 2631
Lin, Z., see Westcott, S.A., 2665
Lippard, S.J., see Yoon, S., 2805
Loening, N.M., see Sceats, E.L., 2751

Mahr, N., see Werner, H., 2645
Marder, T.B., see Westcott, S.A., 2665
Marder, T.B., see Coventry, D.N., 2789
Maunder, G.H., Russo, M.R. and Sella, A., NO to NO_2^- conversion by divalent lanthanides: synthesis and crystal structure of [$Sm(Tp^{Me2,4\text{-}Et})_2NO_2$], 2709
McGowan, P.C., see Camm, K.D., 2929
Mehnert, C.P., Cook, R.A., Dispenziere, N.C. and Mozeleski, E.J., Biphasic hydroformylation catalysis in ionic liquid media, 2679
Merwin, R.K., Ontko, A.C., Houlis, J.F. and Roddick, D.M., Synthesis and characterization of CpMn(dfepe)(L) complexes (dfepe = $(C_2F_5)_2PCH_2CH_2P(C_2F_5)_2$; L = CO, H_2, N_2): an unusual example of a dihydride to dihydrogen photochemical conversion, 2873
Metteau, L., see Collange, E., 2605
Miecznikowski, J.R. and Crabtree, R.H., Transfer hydrogenation reduction of ketones, aldehydes and imines using chelated iridium(III) *N*-heterocyclic bis-carbene complexes, 2857
Miller, A.E., see Sydora, O.L., 2841
Minihane, M., see Inyushin, S., 2937
Morley, C.P., Ford, S. and Vaira, M.D., Palladium complexes of novel azo-compounds derived from cycloalkeno-1,2,3-selenadiazoles: X-ray crystal structure of cyclohexeno-1,2,3-selenadiazole, 2967
Morley-Smith, N.A., see Cloke, F.G.N., 2625
Mozeleski, E.J., see Mehnert, C.P., 2679
Murray, P.R., see Leslie, W., 2769
Murugesu, M., Abboud, K.A. and Christou, G., New hexanuclear and dodecanuclear Fe(III) clusters with carboxylate and alkoxide-based ligands from cluster aggregation reactions, 2779

O'Reilly, R.K., Gibson, V.C., White, A.J.P. and Williams, D.J., Five-coordinate iron(II) complexes bearing tridentate nitrogen donor ligands as catalysts for atom transfer radical polymerisation, 2921
Ontko, A.C., see Merwin, R.K., 2873
Oster, S.S. and Jones, W.D., Synthesis, structure and reactivity of [Ir(dippe)(μ-Cl)]$_2$, [Ir(dippe)$_2$][Ir(dippe)Cl_2] and [Ir(dippe)$_2$]Cl, 2959
Owen, J.S., see Piro, N.A., 2797

Parkin, G., Preface, 2595
Parkin, G., see Baik, M.-H., 2879
Peters, J.C., see Thomas, J.C., 2901
Phipps, D.E., see Wong, W.W.H., 2821
Piro, N.A., Owen, J.S. and Bercaw, J.E., Pyridinium-derived *N*-heterocyclic carbene ligands: syntheses, structures and reactivity of *N*-(2′-pyridyl)pyridin-2-ylidene complexes of nickel(II), palladium(II) and platinum(II), 2797
Poli, R., see Collange, E., 2605
Poole, R.A., see Leslie, W., 2769
Priego, J.L., see Barral, M.C., 2637

Ribeiro, A.F.G., Gomes, P.T., Dias, A.R., Ferreira da Silva, J.L., Teresa Duarte, M., Henriques, R.T. and Freire, C., Reactions between isocyanides and a binuclear nickel(II) phosphine complex linked by a bridged bis(cyclopentadienyl) ligand. X-ray molecular structure of [(CN^tBu)(PPh_3)Ni{μ-(η-C_5H_4)CMe_2(η-C_5H_4)}Ni(PPh_3)(CN^tBu)][PF_6]$_2$, 2715
Richard, P., see Collange, E., 2605
Roddick, D.M., see Merwin, R.K., 2873
Royer, E.C., see Barral, M.C., 2637
Rubinov, A.N., see Bushuk, S.B., 2615
Russo, M.R., see Maunder, G.H., 2709

Saito, T., see Sakai, N., 2611
Sakai, N. and Saito, T., Synthesis and structures of tetranuclear rhenium–cobalt mixed metal sulfide clusters [$Re_3CoS_4Cl_6$(PMe_2Ph)$_4$], 2611
Santa María, M.D., see Claramunt, R.M., 2985
Saunders, G.C., see Bellabarba, R.M., 2659
Sceats, E.L., Figueroa, J.S., Cummins, C.C., Loening, N.M., Van der Wel, P. and Griffin, R.G., Complexes obtained by electrophilic attack on a dinitrogen-derived terminal molybdenum nitride: electronic structure analysis by solid state CP/MAS ^{15}N NMR in combination with DFT calculations, 2751
Scheibitz, M., see Ilkhechi, A.H., 2597
Schneider, M.E., see Werner, H., 2645
Sella, A., see Maunder, G.H., 2709
Shafir, A., see Inyushin, S., 2937
Sheats, J.E., see Inyushin, S., 2937
Simpson, S.J., see Hodson, E., 2695
Soper, A.K., see Turner, J.F.C., 2975
Stupak, A.P., see Bushuk, S.B., 2615
Stylianides, N., see Winston, S., 2813
Sydora, O.L., Goldsmith, J.I., Vaid, T.P., Miller, A.E., Wolczanski, P.T. and Abruña, H.D., Syntheses and electrochemistry of (*p*-$XC_6H_4O)_6W$ (1-X, X = H, CH_3, OCH_3, Cl, Br, OH, OCH_2Ph) and (*p*-$XC_6H_4O)_5W(OC_6H_4OH)$ (X = H, CH_3, OCH_3, Cl, Br): an approach to electrocatalytic CH bond activation, 2841

Taw, F.L., see Corkey, B.K., 2943
Templeton, J.L., see Cross, J.L., 2831
Teresa Duarte, M., see Ribeiro, A.F.G., 2715
Thomas, J.C. and Peters, J.C., Structural and spectroscopic studies of three-coordinate copper(I) supported by bis(phosphine)borate ligands, 2901
Torres, M.R., see Barral, M.C., 2637
Trofimenko, S., see Claramunt, R.M., 2985
Tulloch, A.A.D., see Winston, S., 2813
Turner, J.F.C. and Soper, A.K., On the determination of the structure of ferrocene in solution, 2975

Urbanos, F.A., see Barral, M.C., 2637

Vaid, T. P., see Sydora, O.L., 2841
Vaira, M.D., see Morley, C.P., 2967
Van der Wel, P., see Sceats, E.L., 2751

Wagner, M., see Ilkhechi, A.H., 2597
Wang, S.-Y.S., Abboud, K.A. and Boncella, J.M., Synthesis and mechanistic investigations of the decomposition of β-hydrogen containing W(VI) dialkyl complexes: β-H elimination vs. β-H abstraction, 2733
Wenger, O.S., Henling, L.M., Day, M.W., Winkler, J.R. and Gray, H.B., Rhenium(I) tricarbonyl complexes with photoisomerizable ligands, 2955
Werner, H., Mahr, N., Schneider, M.E., Bosch, M. and Wolf, J., Acetylacetonato, pentachlorophenolato and carboxylato rhodium(I) complexes and their reactivity in the C–C coupling reaction of olefins and diazoalkanes, 2645
Westcott, S.A., Marder, T.B., Baker, R.T., Harlow, R.L., Calabrese, J.C., Lam, K.C. and Lin, Z., Reactions of hydroborating reagents with phosphinorhodium hydride complexes: molecular structures of a Rh_2B_3 metallaborane cluster, an $L_2Rh(\eta^2\text{-}H_2BR_2)$ complex and a mixed valence Rh dimer containing a semi-bridging Bcat (cat = 1,2-$O_2C_6H_4$) group, 2665
White, P.S., see Cross, J.L., 2831
White, A.J.P., see O'Reilly, R.K., 2921
White, A.J.P., see Bailey, A., 2631
Whitten Jr., C.E., see Inyushin, S., 2937
Williams, D.J., see O'Reilly, R.K., 2921
Williams, D.J., see Bailey, A., 2631
Williams, J.A.G., see Leslie, W., 2769
Winkler, J.R., see Wenger, O.S., 2955
Winston, S., Stylianides, N., Tulloch, A.A.D., Wright, J.A. and Danopoulos, A.A., Picoline and pyridine functionalised chelate N-heterocyclic carbene complexes of nickel: synthesis and structural studies, 2813
Wolczanski, P.T., see Sydora, O.L., 2841
Wolf, J., see Werner, H., 2645
Wong, W.W.H., Phipps, D.E. and Beer, P.D., Acyclic and macrocyclic transition metal dithiocarbamate complexes containing imidazolium moieties for anion binding, 2821
Wright, J.A., see Winston, S., 2813

Yellowlees, L.J., see Leslie, W., 2769
Yoon, S., Kelly, A.E. and Lippard, S.J., Di- and tetra-bridged diiron(II) complexes with four terphenyl-derived carboxylates and two water molecules, 2805

Ziller, J.W., see Evans, W.J., 2689

Available online at www.sciencedirect.com
SCIENCE DIRECT®
Polyhedron 23 (2004) 3007–3019
POLYHEDRON
www.elsevier.com/locate/poly

Syntheses and crystal structures of three novel Cu(II) coordination polymers of different dimensionality constructed from Cu(II) carboxylates (carboxylate = malonate (mal), 2 acetate (ac), fumarate (fum)) and conformationally flexible 1,4-bis(imidazole-1-yl-methylene)benzene (IX)

S.K. Chawla [a,*], M. Arora [a], Kalle Nättinen [b], K. Rissanen [b], J.V. Yakhmi [c]

[a] *Department of Chemistry, Guru Nanak Dev University, Amritsar 143005, India*
[b] *Department of Chemistry, University of Jyvaskyla, Jyvaskyla, Finland*
[c] *Novel Materials and Structural Chemistry Division, B. A. R. C., Bombay*

Received 14 May 2004; accepted 18 August 2004
Available online 11 November 2004

Abstract

We herein report three new coordination polymers generated from Cu(II) carboxylates (mal, 2ac, fum) and conformationally flexible bifunctional IX as building blocks. All the three complexes adopt unique structures in the solid state. The complex $[Cu_2(mal)_2(IX)_2(H_2O)_6]_n$ crystallizes as orthorhombic co-linear rods with space group P2(1) P2(1) P2(1). Each rod is further formed of two tightly intertwined strings. The second polymer $[Cu_2(ac)_4(IX)_2]_n$ crystallizes with space group P1 which consists of two sets of intersecting 2D sheets composed of parallel rods which interpenetrate to form a fully interlocked 3D structure. In both these complexes IX coordinates in the *anti* mode. The third polymer $[Cu_2(fum)_2(IX)_2(H_2O)_2]_n$ possesses a monoclinic crystal system with space group C_2/c and crystallizes as 1D straps. Cu–fum–Cu forms the base of the string which is alternatively garlanded by a macrocycle derived from $Cu_2(IX)_2$ unit, where IX coordinates in the *syn* fashion. The present study suggests that the use of a rigid building block with a flexible organic ligand leads to a better prediction of the final structure of the polymeric array.
© 2004 Elsevier Ltd. All rights reserved.

Keywords: Flexible; Carboxylates; IX; Coordination polymer; Architecture

1. Introduction

Self-assembly of molecular rods and tubes and their use is a fast growing area of material science [1–12]. Such materials are useful for the study of long distance interaction phenomena particularly electron and energy transfer and magnetic coupling in transition metal ions. Furthermore, molecular rods offer an opportunity to position two active centers at a known distance apart and connect them by spacers with desired properties.

Cu(II) salts or preformed Cu(II) species react with rigid bidentate spacers viz. terephathalate [13–17], 1,4-bis(4-pyridyl)butadiyne [18], piperazine [19], 2,7-diazapyrene [20], 4,4′ bipyridine(bpy) [21–26], 3,4′-bpy [26], 3,3′-bpy [26] and 4,4′-bipyridine dioxide [27] to afford exciting new structures with vast diversity ranging from one dimensional zigzag polymeric chains to interlocked 3D networks. However, all these structures lack any flexibility. Even in nature a slight distortion in angles is prevalent to afford flexibility in structure. Until

* Corresponding author. Tel.: +911832500350; fax: +911832255820.
E-mail address: meenu1410@yahoo.co.in (S.K. Chawla).

0277-5387/$ - see front matter © 2004 Elsevier Ltd. All rights reserved.
doi:10.1016/j.poly.2004.08.025

recently only little attention has been diverted towards the use of flexible and angular bifunctional ligands.The topological isomerism which exists in such ligands, results in different ligand-metal coordination connectivity and introduces an additional ability in such ligands to adopt the most suitable structural architecture. It further offers an opportunity for the construction of polymeric networks with motifs hitherto unknown in the literature. Polymers exhibiting structural isomerism due to more than one isomeric forms and interpenetration of two frameworks with different conformations of the same ligand have been reported in a series of complexes generated from bis(pyridyl)alkane (R = methane, ethane, propane) [28–35]. The situation is further complicated if the complexes are derived from a chiral ligand. A study of structurally similar disulfide ligands such as bis(phenylthio)alkanes (methane and butane) and bis(4-pyridyl)disulfide result in a variety of networks exhibiting both chiral and topological isomerism [36–38]. Currently the greatest challenge of modern inorganic chemistry is to design molecular extended systems possessing original architecture and predictable physical properties. Although with rigid ligands the present state of art is that sufficient data is available to rationalize the final structure of the architecture, more subtle changes are observed with flexible ligands and an extensive study of M-organic reactions using such ligands is demanded to develop proper synthetic strategies to generate designed frameworks with useful functions.

Bifunctional semiflexible angular 1,4-bis(imidazole-1-yl-methylene)benzene can adopt either *syn* or *anti* conformation with imidazole N binding metal ions with angles as diverse as 90° and 180° (Fig. 1). This ligand can assemble into convergent products resulting in discrete architectures or aggregate into extended arrays, which can be viewed as divergent products of similar reactions. However, currently efforts are being made to hybrid the two processes by assembling the discrete molecular products into polymeric arrays by bridging

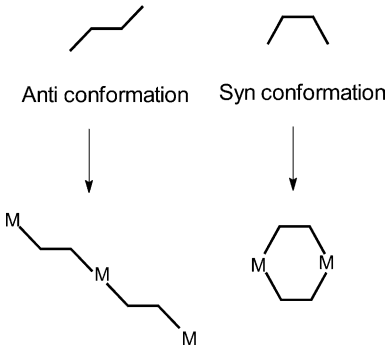

Fig. 1. *Syn* and *anti* conformation of the ligand leading to divergent and convergent products with suitable metal ions.

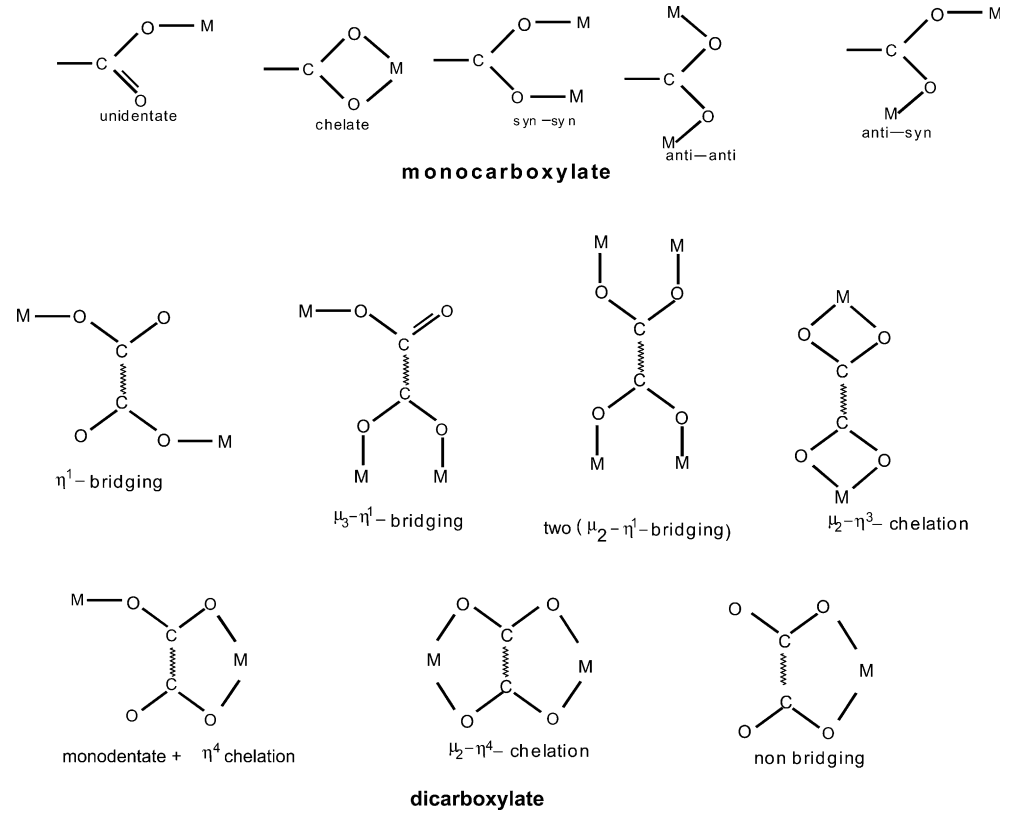

Fig. 2. Various modes of coordination of the carboxylate ligand.

the metal atoms of metallocycles, using suitable bifunctional moieties for which carboxylates fit very well. During the present investigations the selection of Cu carboxylates for generation of assemblies is especially interesting because of many other reasons. They are able to generate robust, neutral and thermally stable frameworks with large pore sizes [39–41]. Assemblies are known in which the original structure of the carboxylate is undisturbed [19]. Moreover, because of their versatility to adopt various bonding modes (non-chelating, chelating and bridging) they generally yield a rich fascinating chemistry (Fig. 2). Nevertheless, polymeric structures employing carboxylate as a coligand with other bifunctional neutral ligands are relatively limited. To explore the influence of the orientation of the carboxylate moiety in these Cu carboxylates on a supramolecular architecture we selected mononuclear copper malonate, dinuclear copper acetate and polymeric copper fumarate. These three metal salts also vary in terms of their flexibility as well as steric hindrance. The combination of conformationally flexible IX and versatility of carboxylate is expected to generate fascinating chemistry. Herein, we report the syntheses and characterization of three polymers $[Cu_2(mal)_2(IX)_2(H_2O)_6]_n$, $[Cu_2(ac)_4(IX)_2]_n$ and $[Cu_2(fum)_2(IX)_2(H_2O)_2]_n$.

2. Experimental

2.1. Materials

Copper malonate was prepared by a known method [42]. Copper acetate, sodium fumarate, *p*-xylene, imidazole and copper chloride were procured from Ranbaxy, Chandigarh and were used as received. All the solvents were A. R. grade and were employed as such without further purification.

2.2. Techniques

Elemental analysis for C, H and N was carried out with a Carlo Erba 1106 microanalyser. The Infrared spectra were recorded using KBr pellets on a FTIR 8101M Shimadzu spectrometer in the 4000–400 cm^{-1} range. TGA-DTA curves were recorded on a simultaneous thermal analyzer Shimadzu DT-40 model. X-ray powder diffraction (XRPD) data were recorded on a PW1710 diffractometer at 3 kV and 20 mA for Cu Kα (λ = 1.54060 Å) radiation with a continuous scan and a step size of 0.5° in 2θ. The sample was subjected to magnetization measurements as a function of temperature, *M* vs *T*, as well as applied field, *M* versus *H*, using a Vibration Sample Magnetometer Model 4500 (EG&G Priceton Applied Research). The temperature dependence of magnetization was studied by carrying out field-cooled magnetization (FCM), zero field-cooled magnetization (ZFCM). FCM data were obtained after cooling the sample in 500 Oe applied field and then recording the magnetization while warming the sample up from 4.5 to 35 K, keeping the field on. The field dependence of the magnetization M versus H plots were recorded at 4.5 K under an applied field of −10 000 to 10 000 Oe. ^1H and ^{13}C NMR spectra of the ligand were recorded on a Bruker A. C. 200MHz instrument in $CDCl_3$. The mass spectrum of the ligand was recorded on a GCMS-QP-2000 mass spectrometer by the EI method.

2.2.1. X-ray data collection

The single-crystal X-ray diffraction was done with a Nonius Kappa CCD diffractometer with graphite monochromatized μ_0Kα (λ = 0.71073 Å) radiation. Collect-software was used in the measurement and DENZO-SMN [43] in processing of the data. The structures were solved and refined by full-matrix least-squares on F^2 with the WINGX-software package [44] utilizing SHELXS-97 [45] and SHELXL-97 [46] modules. Hydrogen atoms were refined by a riding model. The graphic presentations of the structures were created with the software DIAMOND [47].

2.3. Syntheses

2.3.1. Synthesis of IX

The ligand was synthesized by reacting 1,4-dibromobenzene and imidazole in dry acetonitrile under PTC conditions by a known method [48]. Yield 60%; m.p. 74 °C; MS: *m/z* 238 (72.9%, M^+), 171 (86.9%, M^+ − imidazole), 104 (100%, $M^+ - 2$ imidazole), ^1H NMR ($CDCl_3$); δ 7.54 (s, 2H, —N=), 7.09 (dd, 4H), 7.16 (m, 4H), 5.10 (s, 4H); ^{13}C NMR ($CDCl_3$): 50.2 (CH_2), 119.1 (CH), 127.7(CH), 129.9(CH), 136.4(C), 137.2(CH).

2.3.2. $[Cu_2(mal)_2(IX)_2(H_2O)_6]_n$ (1)

To an aqueous solution of $[Cu(mal)]\cdot 2H_2O$ (0.290 g, 1.0 mmol in 5 ml) was added a methanolic solution of IX (0.240 g, 1.0 mmol in 5 ml). A blue complex, in 70% yield (0.320 g) based upon metal, separated out immediately, and was filtered, washed with methanol, water and dried in vacuo. Calc. for $C_{34}H_{44}Cu_2N_8O_{14}$: C, 44.7; H, 4.8; N, 12.2. Found: C, 44.0; H, 4.2; N, 11.9%. Single crystals of the complex were obtained by layering a methanolic solution of IX over an aqueous solution of $[Cu(mal)]\cdot 2H_2O$. Slow evaporation of the resulting solution yielded blue needles.

2.3.3. $[Cu_2(ac)_4(IX)_2]_n$ (2)

A methanolic solution (10 ml) of $Cu(CH_3COO)_2.H_2O$ (0.190 g, 1.0 mmol) and IX (0.240 g, 1.0 mmol) was refluxed for 1 h. The resulting solution upon concentration yielded the desired product in 75% yield (0.315 g). Found: C, 50.9; H, 4.5; N, 13.0 Calc. for $C_{36}H_{40}Cu_2N_8O_8$ C, 51.4; H, 4.76; N, 13.3. Single crystals were

obtained by slow diffusion of ether containing a mixture of $Cu(CH_3COO)_2 \cdot H_2O$ and IX in methanol over a period of one week.

2.3.4. $[Cu_2(fum)_2(IX)_2(H_2O)_2]_n$ (3)

A mixture of $CuCl_2$ (0.017 g, 0.1 mmol) sodium fumarate (0.160 g, 1.0 mmol) and IX (0.230 g, 1.0 mmol) in 10 ml H_2O–CH_3OH(1:1) yielded a blue product which was recrystallized from dilute ammonia. Calc. for $C_{36}H_{36}Cu_2N_8O_{10}$: C, 49.8; H, 4.15; N, 12.9. Found: C, 49.4; H, 4.0; N, 12.5%. Precipitates of **3** dissolved in ammonia solution were left for slow evaporation, which yielded fine needles suitable for X-ray diffraction studies.

3. Results and discussion

The reaction between Cu(II) carboxylates (carboxylate = mal, 2ac, fum) and IX in a 1:1 stoichiometric ratio in CH_3OH–H_2O mixture yielded crystalline products $[Cu_2(mal)_2(IX)_2(H_2O)_6]_n$ (**1**), $[Cu_2(ac)_4(IX)_2]_n$ (**2**) and $[Cu_2(fum)_2(IX)_2(H_2O)_2]_n$ (**3**). The compositions of the complexes remained the same even on employing the reactants in 1:2 (M:L) molar ratio. All the three polymers were insoluble in water and other common organic solvents. Tables 1 and 2 report the crystal data and selected bond lengths and bond angles in the three polymers.

3.1. IR spectra

Selected IR peaks are summarized in Table 3. All the polymers exhibit intense absorption bands in the region, 1600–1620 and 1380–1450 cm^{-1} which are associated with asymmetric and symmetric stretching mode in carboxylates. The Δv values of above 160 cm^{-1} are indicative of the monodentate mode of coordination of carboxylate group in all these complexes.

3.2. Crystal structure of $[Cu_2(mal)_2(IX)_2(H_2O)_6]_n$

Complex 1 consists of a Cu(II)mal-IX adduct in a 1:1 stoichiometric ratio and its elemental analysis corresponds to the formula $C_{34}H_{44}Cu_2N_8O_{14}$. The perspective view of the compound with the numbering scheme is represented in Fig. 3. The geometry around Cu(II) is square pyramidal. Each Cu(II) is coordinated to two nitrogen atoms from imidazoles of different IX ligands (average Cu–N bond distance 1.99 Å), two oxygen atoms from the chelating malonate (average Cu–O distance 1.96 Å) and the apical position is taken up by oxygen of water with a Cu–O distance of 2.21 Å. This apparent axial elongation is attributed to Jahn–Teller distortion. IX acts as a bridging ligand and propagates the chain in a zigzag manner along the 0 0 1 direction. The nearest copper–copper distance within the chain is 10.6 Å. The IX ligand coordinates two Cu(II) ions in *anti* conformation with its phenyl group in a parallel position.

Two strands are twined together to form a co-linear rod-like structure which is composed of parallel IX units. The rod is stabilized by aromatic π-stacking interactions between the phenyl rings of two strands which are nearly parallel as shown in Fig. 4. The distance between the two phenyl rings is 3.4 Å, which is well within the range for π–π interactions. Two water molecules are non-coordinated and are sandwiched by weak and classical hydrogen bonds serving a mediating role in connecting the rods between the two strands. The malonate is chelated to the metal center in a bis-mono-

Table 1
Crystallographic data for the three polymers

	1	2	3
Empirical formula	$C_{34}H_{44}Cu_2N_8O_{14}$	$C_{36}H_{40}Cu_2N_8O_8$	$C_{36}H_{36}Cu_2N_8O_{10}$
Formula weight	911.82	839.84	867.81
Crystal systems	orthorhombic	triclinic	monoclinic
Space group	$P2_12_12_1$ No. 19	$P\bar{1}$	C_2/c
a (Å)	8.5710	8.336Å	29.808
b (Å)	16.0220	10.253Å	8.2874
c (Å)	27.56930	10.893Å	16.608
U (Å^3)	3786.10	925.4A^{-3}	3679.9
D_e (g cm^{-3})	1.600	1.507	1.566
M	1.203	1.212	1.226
F(000)	1880	434	1784
Reflection collected	17 824	5483	11 152
Independent reflection	7111	5483 [R_{iist} = 0.000)	3459] [E_{int} = 0.1439]
Data/restraints/parameters	7111/12/547	5483/3/417	3459/2/259
Goodness of fit of F^2	1.045	1.040	1.036
RA, $WR_2(I > 2\sigma(I))$ all data	0.0446, 0.0823	0.0405,0.0903	0.0614, 0.0891
Absolute structure parameter	0.00	0.0602, 0.1014	0.1281, 0.1069
$(\Delta P)_{max}$, $(\Delta P)_{min}$ (e Å^{-3})	0.550	0.52	0.502, −0.496
Extinction coefficient		0.337, −0.416	

Table 2
Selected bond lengths (in Å) and bond angles (in °) in the three polymers

Polymer **1**	
Bond lengths	
Cu(1)–O(2)	2.277
Cu(28)–O(29)	2.262
Cu(1)–O(3)	1.965
Cu(1)–O(9)	1.955
Cu(1)–N(10)	1.991
Cu(1)–N(26)	2.007
Cu(28)–O(30)	1.955
Cu(28)–O(36)	1.96
Cu(28)–N(37)	1.993
Cu(28)–N(53)	2.007
Bond angles	
O(9)–Cu (1)–O(3)	90.14
O(9)–Cu (1)–N(10)	87.49
O(3)–Cu (1)–N(10)	168.88
O(9)–Cu (1)–N(26)	172.24
O(3)–Cu (1)–N(26)	87.70
N(10)–Cu (1)–N(26)	93.20
O(9)–Cu (1)–O(2)	94.61
O(3)–Cu (1)–O(2)	95.90
N(10)–Cu (1)–O(2)	95.12
N(26)–Cu (1)–O(2)	93.03
O(30)–Cu (28)–O(36)	89.36
O(30)–Cu (28)–N(37)	163.35
O(36)–Cu (28)–N(37)	87.58
O(30)–Cu (28)–N(53)	86.77
O(36)–Cu (28)–N(53)	173.59
N(37)–Cu (28)–N(53)	94.68
O(30)–Cu (28)–O(29)	101.16
O(36)–Cu (28)–O(29)	94.40
N(37)–Cu (28)–O(29)	95.40
N(53)–Cu (28)–O(29)	91.35
Polymer **2**	
Bond lengths	
Cu(1)–N(10)	1.994
Cu(1)–N(25)	2.014
Cu(28)–N(37)	1.949
Cu(28)–N(52)	2.009
Cu(1)–O(2)	1.953
Cu(1)–O(6)	1.956
Cu(28)–O(29)	1.970
Cu(28)–O(33)	1.928
Bond angles	
O(2)–Cu(1)–O(6)	179.3
O(2)–Cu(1)–N(10)	89.8
O(6)–Cu(1)–N(10)	89.7
O(2)–Cu(1)–N(25)	91.8
O(6)–Cu(1)–N(25)	88.7
N(10)–Cu(1)–N(25)	177.7
O(33)–Cu(28)–N(37)	89.9
O(33)–Cu(28)–O(29)	178.8
N(37)–Cu(28)–O(29)	88.9
O(33)–Cu(28)–N(52)	91.2
N(37)–Cu(28)–N(52)	178.9
O(29)–Cu(28)–N(52)	90.0
Polymer **3**	
Bond lengths	
Cu(1)–N(11)	2.021
Cu(1)–N(26)	2.000
Cu(1)–O(2)	2.334
Cu(1)–O(7)	1.988
Bond angles	
O(3)–Cu(1)–O(7)	167.24
O(3)–Cu(1)–N(26)	88.53
O(7)–Cu(1)–N(26)	89.96
O(3)–Cu(1)–N(11)	89.39
O(7)–Cu(1)–N(11)	91.11
N(26)–Cu(1)–N(11)	175.17
O(3)–Cu(1)–O(2)	99.61
O(7)–Cu(1)–O(2)	93.09
N(26)–Cu(1)–O(2)	91.45
N(11)–Cu(1)–O(2)	93.20

Symmetry transformations used to generate equivalent atoms.
For polymer **1**: #1 $-x-3/2$, $-y+1$, $z-1/2$; #2 $-x-1/2$, $-y+1$, $z-1/2$; #3 $-x-3/2$, $-y+1$, $z+1/2$; #4 $-x-1/2$, $-y+1$, $z+1/2$.
For polymer **2**: #1 $x+1$, y, $z-1$; #2 $x+1$, $y-1$, z; #3 $x-1$, y, $z+1$; #4 $x-1$, $y+1$, z.
For polymer **3**: #1 $-x+1/2$, $-y+3/2$, $-z+1$; #2 $-x$, $-y+1$, $-z$.

dentate fashion. The malonate rings are directed above and below the rod in a symmetrical alternate manner. This configuration is imposed by the more stable trans conformation of the ligand. The rods are stacked along the *c*-axis in such a manner that coordinated water molecule as well as malonate of two adjoining threads are interdigitated to maximize the packing.

The packing of rods (Fig. 5) when seen along the *c*-axis reflects that the alkyl parts of IX are pointing inward, in the middle of the two individual dimers of rods, repelled by water molecules between rod-dimers. The malonate carbonyl groups of adjacent dimeric moieties are facing each other with the water molecules situated in between them.

3.3. Structure of $[Cu_2(ac)_4(IX)_2]_n$

Polymer **2** is consistent with the formula $[Cu_2(ac)_4(IX)_2]_n$. The geometry around the Cu(II) ion is essentially square planar. Fig. 6 describes the asymmetric unit together with the labelling scheme. The two acetate groups coordinate in an unidentate mode and are trans to each other. The non-coordinating oxygen of two acetate groups are positioned in an *anti* manner. The other two coordinating sites are occupied by two imidazole nitrogens from different IX ligands. IX acts as a building block connecting two Cu(II) ions. The polymer crystallizes as 1D zigzag chains which run parallel to one another resulting in 2D sheets making an angle of 65.5° with the axis. The metal ions within the sheets are all coplanar and the IX ligand is present in an *anti* conformation. There are two series of 1D polymeric chains extending along the *bc* and *ac* planes which traverse each other at an angle of 45° (Fig. 7a). The sheets interpenetrate to yield a three dimensional network. Fig. 7b

Table 3
Selected IR data for the three complexes

	C=C, C=N	C–H out of plane bending	ν_{as}(COO)	ν_{s}(COO)	$\Delta\nu$
Ligand	1445	695	–	–	–
Polymer **1**	1469	775	1602	1430	172
Polymer **2**	1470	765	1620	1450	170
Polymer **3**	1490	700	1615	1440	175

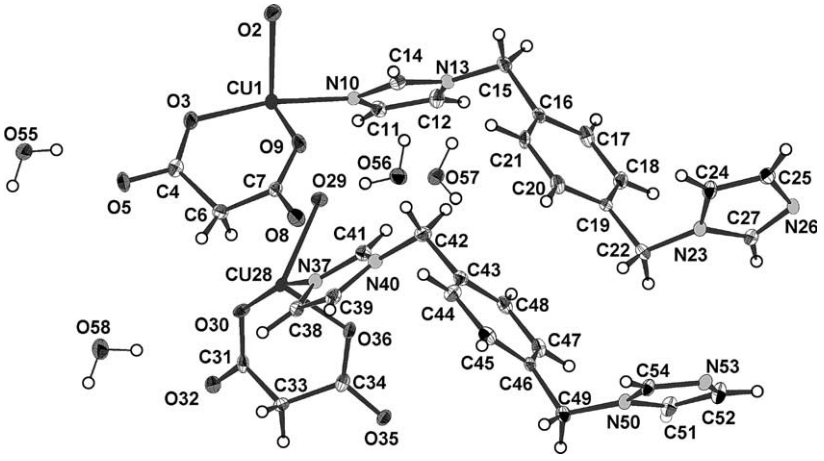

Fig. 3. The asymmetric unit of **1** along with the numbering scheme.

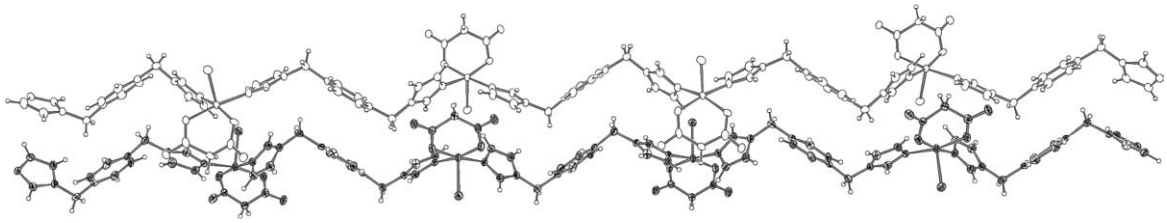

Fig. 4. Thermal ellipsoid representation of the chain formed by twining of two strings in polymer **1**.

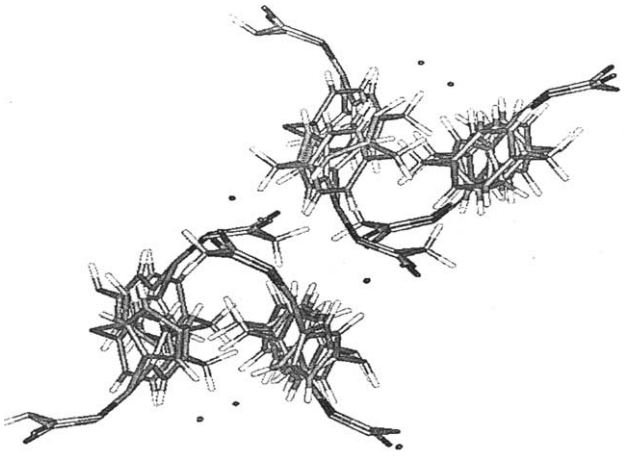

Fig. 5. Stick representation of four rods along the *c*-axis in **1**.

represents the mode of packing with the chains of layer **a** running parallel to the plane of paper and the chains of layer **b** at an approximately 45° angle with respect to it. The horizontal lines of the chains of layer **a** represent the linear part of the chain formed by two imidazoles coordinated to the copper. The diagonal straight lines present the phenyl rings and the angles are the methylene groups providing the *anti* conformation of the ligand units.

The neighboring chains of the same layer are held together by weak hydrogen bonding ($CH_2\ldots O{=}C$ distances ~2.84 Å) and imidazole ring $\pi\ldots\pi$ bonding (distances ~3.65 Å), between the angles where the chains come close to contact. The layers **a** and **b** are held together by interactions between the CH_2 and acetate carbonyls (d = 2.53 Å) as well as $CH\ldots\pi$ interactions between the imidazole rings (d = 3.0 Å).

3.4. Structure of $[Cu_2(fum)_2(IX)_2(H_2O)_2]_n$

Polymer **3** $[Cu_2(fum)_2(IX)_2(H_2O)_2]_n$ can be described as an assembly of ID straps in which Cu(II) is of square pyramidal type with equatorial CuN_2O_2 from two fum-

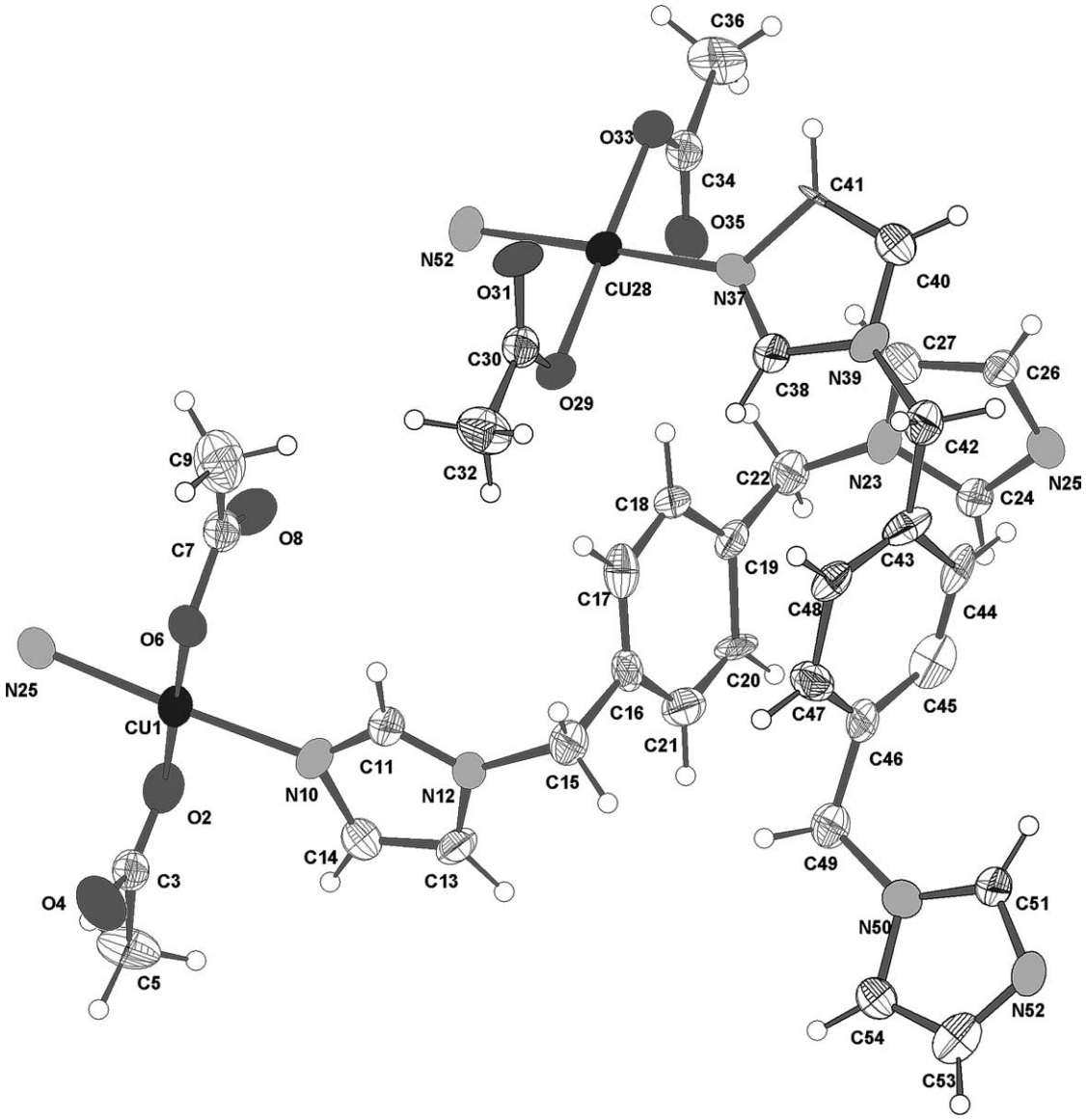

Fig. 6. View of the Cu(II) coordination environment in **2** indicating the labelling scheme adopted.

arate and two IX ligands in trans positions [Cu–O = 1.976 Å (average), Cu–N = 2.01 Å (average)] and a water molecule resides in the apical position (Cu–O = 2.334Å) (Fig. 8). The copper equatorial plane is essentially planar with a maximum bond deviation of 2.580°. Each Cu(II) provides four connecting nodes. The polymer crystallizes in the form of an aggregation of linear rods. Both fumarate and IX act as building sub-units.

The polymer can be viewed as an aggregation of metallocycles which is a convergent product of IX and Cu. Each metallocycle is derived from 2Cu and 2IX units where the Cu is doubly trans bridged by 2-N from imidazole of different IX ligands. The IX coordinates with a convergent *syn* conformation. Each Cu node provides two further linkages for 2 oxygen atoms from two different fumarate groups. The cavity of the macrocycle is being traversed by a fumarate molecule. The Cu–fum–Cu acts as a template around which two IX ligands assemble to form a cycle. Each metallocycle is further linked to another fumarate moiety aggregating the discrete macrocyclic units into a string. Overall, the Cu–fum–Cu forms the base of the string. The coordinating oxygen atoms of fumarate are in an *anti* position with respect to adjacent H atoms. All the Cu(II) ions within the string are essentially co-planar, and overall the string is alternatively garlanded by metallocycles around Cu(II) nodes (Fig. 9).

The various straps runs in the 110 direction and are held together by π–π stacking of phenyl rings of the adjacent strap to form an extended 2D sheet (Fig. 10) in the *ac* plane. The sheet placed immediately above runs along the bc direction (Fig. 11).

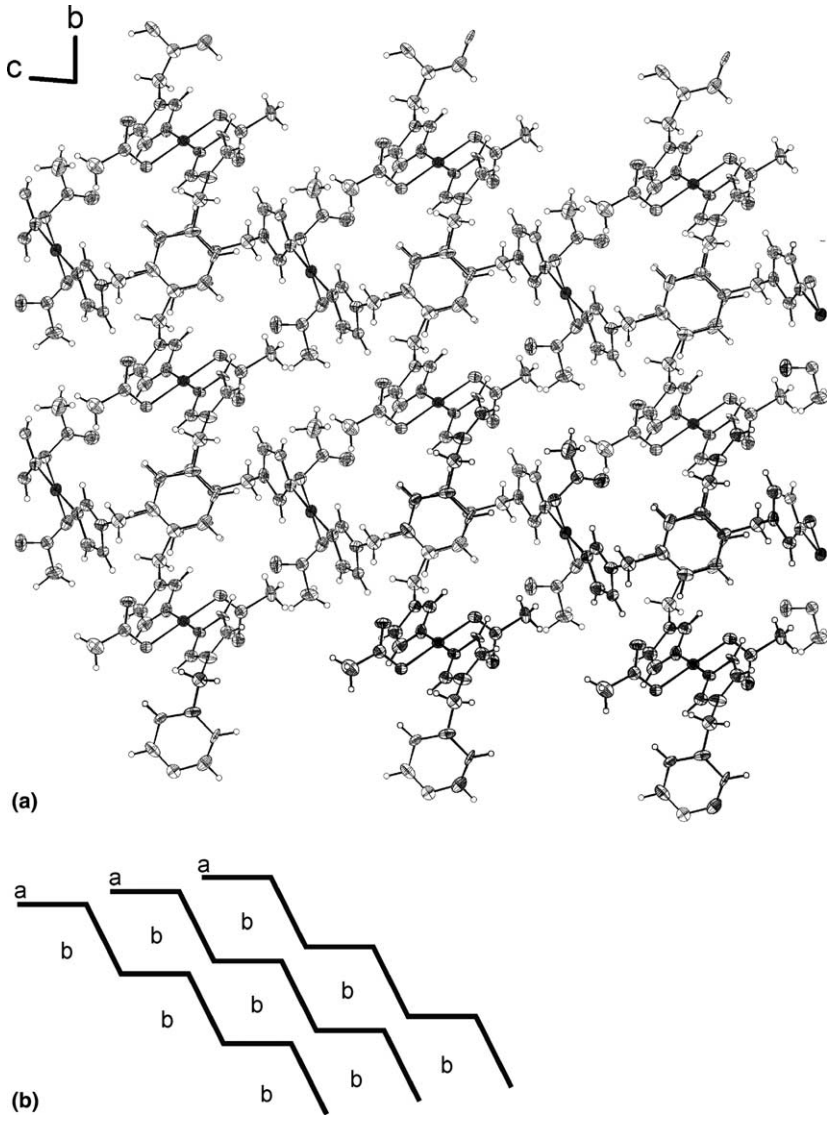

Fig. 7. (a) Schematic representation of packing of chains of $[Cu_2(ac)_4(IX)_2]_n$. (b) Two sheets along the *bc* and *ac* planes traversing at an angle of 45° in polymer **2**.

3.5. Magnetic moment studies

The temperature dependent magnetic moments were measured in the range of 0–200 K. For all the three complexes plots of χ_m versus T indicate that χ_m values increase only slowly and then abruptly as the temperature is lowered, suggesting the existence of ferromagnetic interactions between the metal centers (Fig. 12). Good quality fits were obtained by keeping $g = 2.05$ and $J = 0.005$ cm^{-1} for complexes **1** and **2**, and $g = 2.2$ and $J = 2.75$ cm^{-1} for complex **3**. These values were calculated using Baker's equation

$$\chi_M = \frac{Ng^2\beta^2}{4kT}\left[\frac{N}{D}\right]^{2/3},$$

where $N = 1 + 5.7979916y + 16.902653y^2 + 29.376885y^3 + 29.832959y^4 + 14.036918y^5$; $D = 1 + 2.7979916y + 7.0086780y^2 + 8.653644y^3 + 4.5743114y^4$; and $y = J/kT$.

The parameters β and k have their usual meanings.

Lack of any practical interaction in first two complexes can be attributed to the large Cu–Cu intramolecular distance. The enhanced J value of the fumarate complex may have resulted from magnetic interactions between paramagnetic centers not through IX but through the fumarate bridge. To determine whether these complexes undergo a metamagnetic transition, magnetization versus applied field experiments were carried out. As shown in Fig. 13, the samples do not undergo any magnetic transition up to 10 000 Oe.

3.6. TGA and XRPD of the copper complexes

The TGA curve of complex **1** reveals that loss of first lattice water molecule occurs at 99 °C with a weight loss 3.5% (calc. 3.9%) while the loss of second lattice water

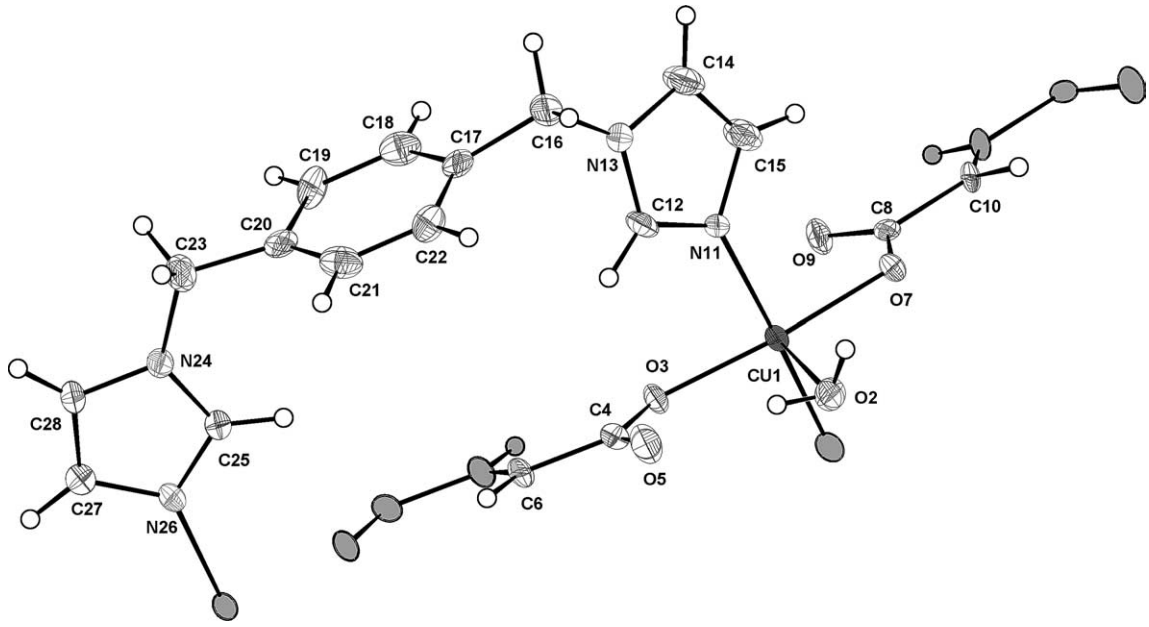

Fig. 8. Thermal ellipsoid presentation and numbering scheme in **3**.

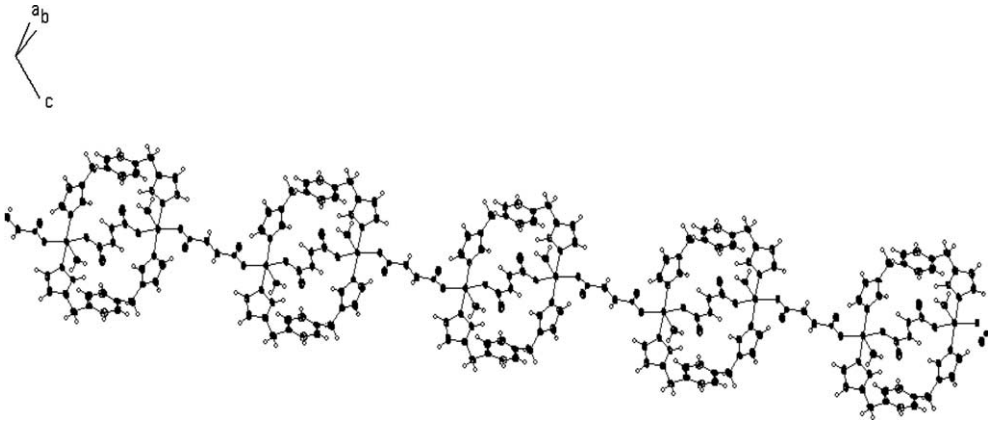

Fig. 9. Individual polymeric strings formed by units of **3**.

molecule is complete at 170 °C. This is followed by the removal of a coordinated water molecule corresponding to another weight loss of 3.9% at 203 °C. Further, the loss of 22.3% corresponds to the decomposition of the malonate molecule with the loss of CO_2 through pyrolysis. Thereafter the complex degrades almost continuously (Fig. 14).

The powder X-ray diffraction data was collected for complex **1** and its dried product at 100 °C and 250 °C (The samples were dried by heating at the desired temperature for 4 h). The XRPD of the sample dried at 100 °C is essentially identical with regard to the intensity, position and line width to that of parent complex. The diffraction pattern yielded by the sample after heating at 250 °C (which corresponds to the loss of all three water molecules) showed significant changes indicating that the structure does not remain stable after the elimination of the coordinated water molecule (Fig. 15).

The loss of only coordinated water molecule from complex **3** is complete at 150 °C (calc. 4.4%; found 4.0%), as suggested by TGA of the complex (Fig. 14). The sample was heated at 150 °C for 4 h to dehydrate it. The XRPD of the original sample and its dried product are identical indicating that the framework maintains its integrity after the removal of the coordinated water molecule (Fig. 16). But above 200 °C the degradation was continued up to 450 °C.

4. Discussion

Three Cu(II) carboxylates [mal, 2ac and fum] of different nuclearity and of different orientation, steric hindrance and flexibility of carboxylate groups have been reacted with angular and conformationally flexible IX. All structures are formed with the same stoichiometry

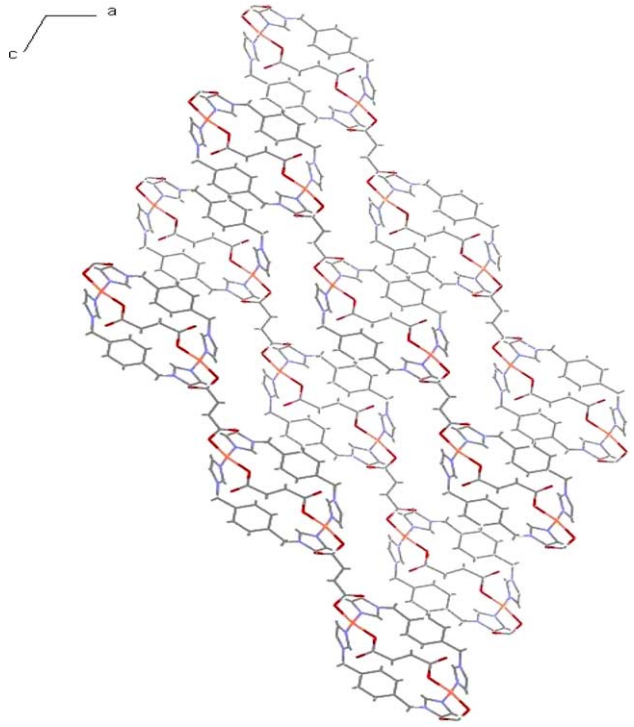

Fig. 10. 1D sheet formation of individual strings of **3** along the ac axis.

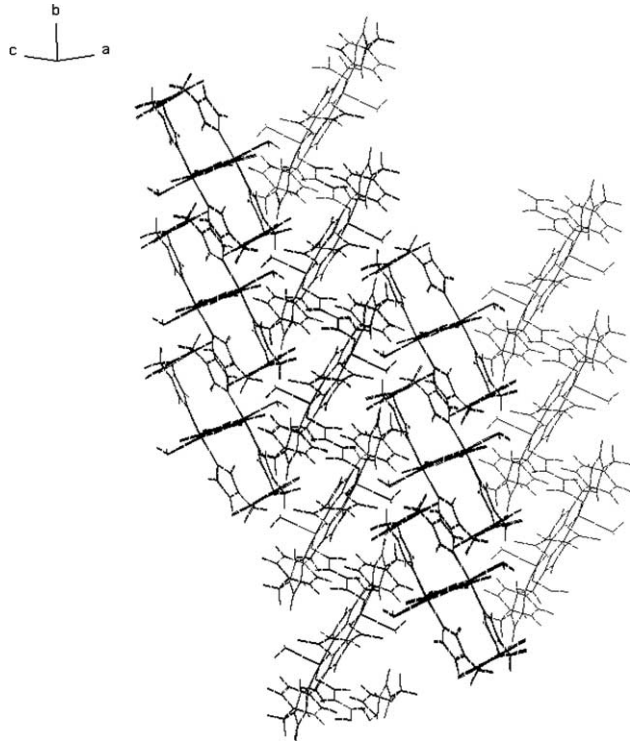

Fig. 11. Packing of strings along the *ac* and *bc* axis in a vertical orientation.

and are rods yet overall display very different and complex structural architectures ranging from 1D to 3D. The synthetic chemistry of coordination polymers has

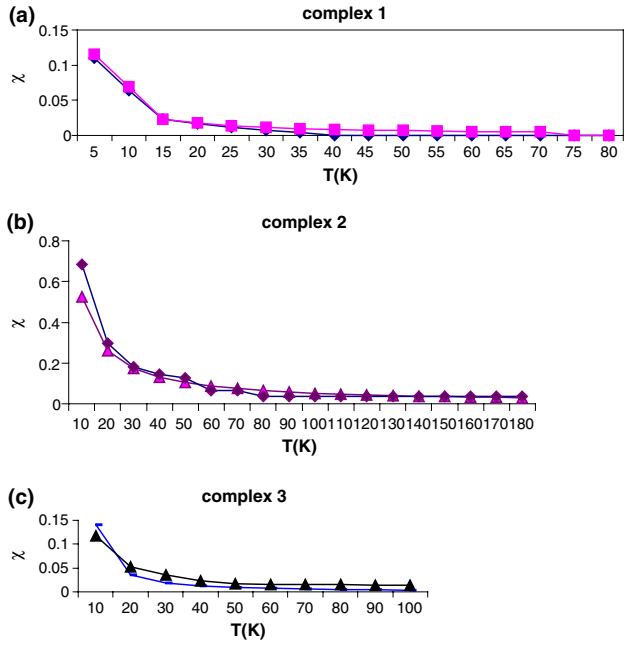

Fig. 12. Temperature dependence of χ_m for (a) complex **1** (b) complex **2** and (c) complex **3**.

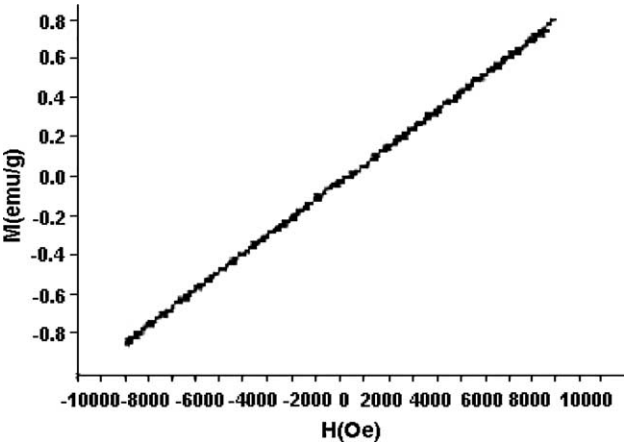

Fig. 13. Magnetization vs. applied field for the three complexes at $T = 4.5$.

so far been mainly focused on the transition metals and rigid organic ligands. The final framework results from the topology and geometry of both organic linear ligand and metal cation and they are regarded as framework builders. The anions used to balance the charge and act as framework regulators. Although sufficient data is available to rationalize the final bulk physical and chemical properties and function of the polymeric array employing linear rigid organic ligands, subtle changes are often observed with their flexible counterparts which make the structural prediction much more cumbersome and uncertain. However, literature survey reveals that polymeric metal halides act both as frame-

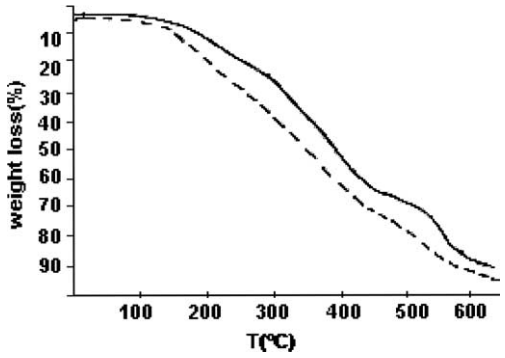

Fig. 14. Thermogravimetric mass loss profiles for complex **1** (—) and complex **3** (----).

work regulators and framework builders and preorganise the system to propagate in a certain direction [49,50].

The present study has been carried out with the aim to examine the effect of rigidity of metal carboxylates on the structure of the polymeric array. However, with monomeric flexible Cu(II) malonate, the malonate group behaves either as a framework builder or a structural regulator. In combination with linear 4,4′-bipyridine, malonate acts as a framework builder and a two dimensional square network enclosing giant cavities of the dimensions 15.776×15.786 Å are generated (Fig. 17) [42]. In our case malonate acts a as framework regulator where the two carboxylate groups of malonate are in the chelate mode and IX and Cu join to build the network as linear rods. The original structure of Cu malonate is retained. The rods only twin successfully placing the alternate malonate on the opposite side of the Cu(II) node which maximizes packing. However, it may be due to the steric influence of malonate group that various rods fail to interpenetrate.

Cu(II) acetate itself exists as a dimer which predisposes the ligand to arrange in a linear manner at the apical position and the original structure of Cu(II) acetate is generally not disturbed. Monodentate ligands coordinate to generate a five coordinate Cu(II) ion and a non-chelating bidentate ligand such as 1,4-diazabicyclo[2,2,2]octane bridges the dimer unit to generate a chain structure [51]. Therefore Cu(II) acetate acts as a framework builder as well as a framework regulator. With IX the dimer breaks to generate monomeric Cu(II) acetate. This may be due to the larger steric bulk of IX. The Cu(II) ion acts as a framework builder and acetate as a framework regulator. The reaction ultimately generates rods which are interlocked in a 3D fashion. Similar effects have been observed with 2,5-bis(4-pyridyl)-1,3,4-oxadiazole which reacts with Cu(II) acetate to yield a monomer [52].

Compound 3 represents a polymeric network with fascinating structural features. With the use of 1D Cu(II) fumarate as a building block, the resulting network is partly locked into place and is tuned to facilitate

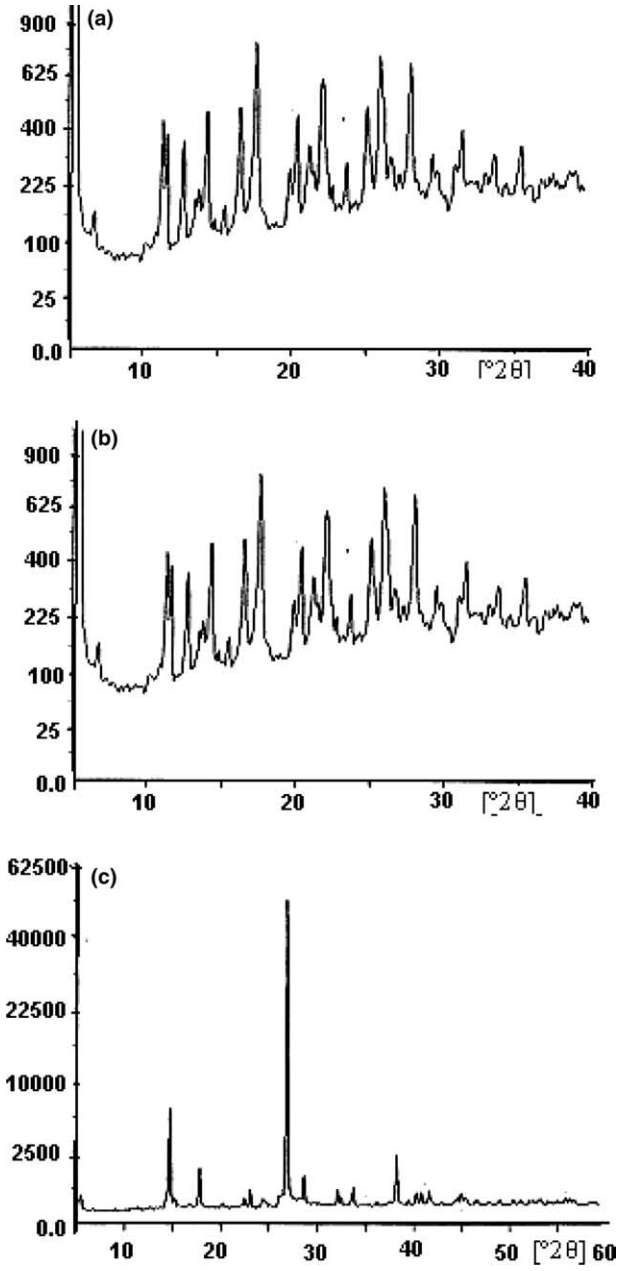

Fig. 15. The XRPD pattern of complex **1**: (a) synthesized material, (b) dried solid at 100 °C and (c) solid resulting from heating at 250 °C.

the bonding of flexible IX in a desired direction resulting in better structural prediction and control of assembly. The IX ligand takes up the less favorable *syn* configuration to generate a cycle around Cu(II) fumarate probably due to size compatibility of the fumarate and IX. It may be regarded as an example of a transition polymer between the convergent metallocycle and the divergent aggregated coordinated polymer. In another similar study by employing polymeric zinc carboxylates (malonate and oxalate) with IX we have demonstrated that it is the preorganization of dicarboxylate which directs the self-assembly to adopt a particular motif [53].

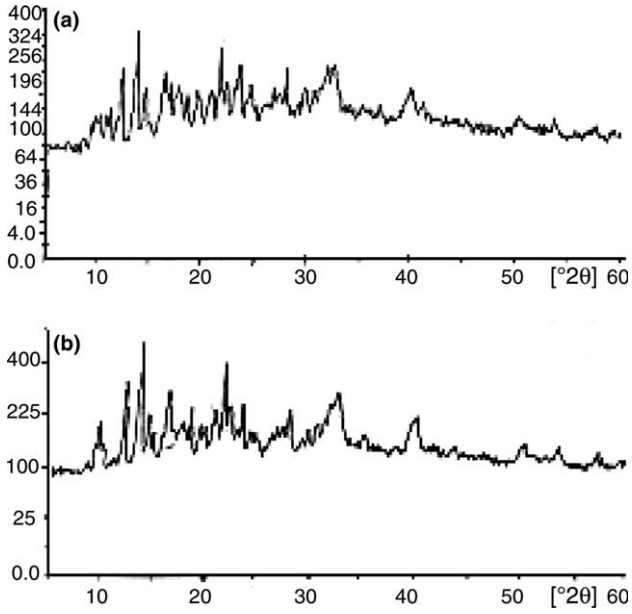

Fig. 16. The XRPD pattern of complex **1**: (a) synthesized material, (b) dried solid at 150 °C.

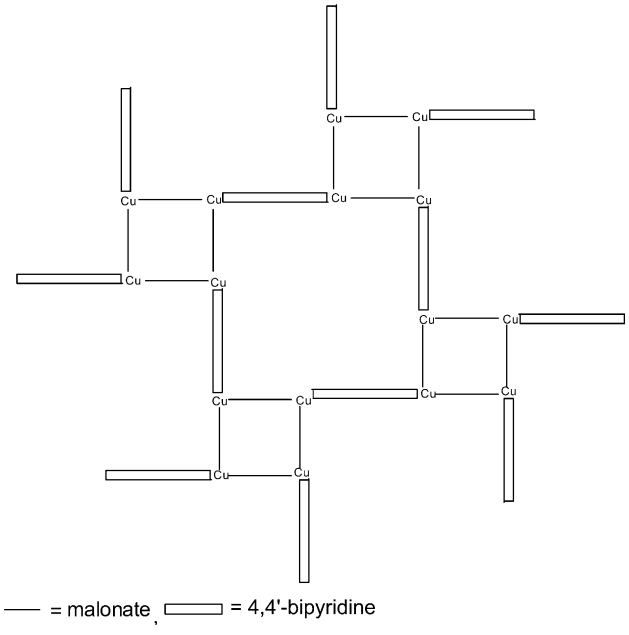

Fig. 17. Stick model representation of $[Cu_2(C_3H_2O_4)_2(H_2O)_2(4,4'\text{-bpy})] \cdot H_2O$.

5. Conclusion

The above study reveals that although due to conformational freedom of flexible ligand the final structure of the architecture becomes much less predictable, the geometry can be better controlled by selecting a combination of a rigid metal building block with a flexible organic ligand.

Acknowledgements

M. Arora is indebted to Guru Nanak Dev University for providing financial assistance and to Dr. Damanjeet Kaur for her useful suggestions, K.R. thanks the Finnish Academy for the financial support and K.N. thanks the Graduate School of Bio organic Chemistry.

Appendix A. Supplementary data

Supplementary data are available from the Cambridge Crystallographic Data Center, 12 Union Road, Cambridge CB2 1EZ, UK (fax: +44 1223 336 033; e-mail: deposit@ccdc.cam.ac.uk or on the web: http://www.ccdc.cam.ac.uk) quoting the deposition numbers 210590, 210592 and 210593. Supplementary data associated with this article can be found, in the online version at doi:10.1016/j.poly.2004.08.025.

References

[1] O.M. Yaghi, H. Li, T.L. Groy, Inorg. Chem. 36 (1997) 4292.
[2] H. Li, C.E. Davis, T.L. Groy, D.G. Kelley, O.M. Yaghi, J. Am. Chem. Soc. 120 (1998) 2186.
[3] S.R. Batten, R. Robson, Angew. Chem. Int. Ed. 37 (1998) 1460.
[4] D. Braga, L. Miani, F. Grepioni, Angew. Chem. Int. Ed. 37 (1998) 2240.
[5] M.J. Zaworotko, Chem. Commun. (2001) 1.
[6] D. Fortin, M. Drouin, P.D. Harvey, J. Am. Chem. Soc. 120 (1998) 5351.
[7] C. Janiak, Angew. Chem. Int. Ed. 36 (1997) 1431.
[8] Y.-Q. Tian, C.-X. Cai, Y. Ji, X.-Z. You, S.-M. Peng, G.-H. Lee, Angew. Chem. Int. Ed. 41 (2002) 1384.
[9] P.J. Hagrman, D. Hagrman, J. Zubieta, Angew. Chem. Int. Ed. 38 (1999) 2638.
[10] M.J. Zawortko, Chem. Soc. Rev. (1994) 283.
[11] O.M. Yaghi, Access Nanoporous Mater. (1995) 111.
[12] M. Hong, Y. Zhao, W. Su, R. Cao, M. Fujita, Z. Zhou, A.S.C. Chan, Angew. Chem. Int. Ed. 39 (2000) 2468.
[13] L. Deakin, A.M. Arif, J.S. Miller, Inorg. Chem. 38 (1999) 5072.
[14] E.G. Bakalbassis, J. Mrozinski, C.A. Tsipis, Inorg. Chem. 25 (1986) 3684.
[15] C.E. Xanthopoulos, M.P. Sigalas, G.A. Katsoulos, C.A. Tsipis, A. Terzis, M. Mentzafos, A. Hountas, Inorg. Chem. 32 (1993) 5433.
[16] P. Chaudhuri, K. Oder, K. Wieghardt, S. Gehring, W. Haase, B. Nuber, J. Weiss, J. Am. Chem. Soc. 110 (1988) 3657.
[17] E. Bakalbassis, P. Bergerat, O. Kahn, S. Jeannin, Y. Jeannin, Y. Dromzee, M. Guillot, Inorg. Chem. 31 (1992) 625.
[18] A.J. Blake, N.R. Champness, A. Khlobystov, D.A. Lemenovskii, W.S. Li, M. Schröder, Chem. Commun. (1997) 2027.
[19] P.S. Mukherjee, S. Dalai, G. Mostafa, E. Zangrando, T.H. Lu, G. Rogez, T. Mallah, N.R. Chaudhuri, Chem. Commun. (2001) 1346.
[20] A.J. Blake, N.R. Champness, A. Khlobystov, D.A. Lemenovskii, W.S. Li, M. Schröder, Chem. Commun. (1997) 1339.
[21] J. Li, H. Zeng, J. Chen, Q. Wang, X. Wu, Chem. Commun (1997) 1213.
[22] M.-L. Tong, H.-J. Chen, X.-M. Chen, Inorg. Chem. 39 (2000) 2235.
[23] S. Dalai, P.S. Mukherjee, E. Zangrando, F. Lloret, N.R. Chaudhuri, J. Chem. Soc., Dalton Trans. (2002) 822.

[24] T.J. Prior, D. Bradshaw, S.J. Teat, M.J. Rosseinsky, Chem. Commun. (2003) 500.
[25] M.-L. Tong, B.-H. Ye, J.W. Cai, X.-M. Chen, S.W. Ng, Inorg. Chem. 37 (1998) 2645.
[26] S. Rarig Jr., R. Lam, P.Y. Zavalij, J.K. Ngala, R.L. LaDuca Jr.^{II}, J.E. Greedan, J. Zubieta, Inorg. Chem. 41 (2002) 2124.
[27] B.-Q. Ma, S. Gao, H. Li Sun, G.-X. Xu, J. Chem. Soc., Dalton Trans. (2001) 130.
[28] L. Carlucci, G. Ciani, M. Moret, D.M. Proserpio, S. Rizzato, Angew. Chem. Int. Ed. 39 (2000) 1506.
[29] B.F. Abrahams, P.A. Jackson, R. Robson, Angew. Chem. Int. Ed. 37 (1998) 2656.
[30] L. Carlucci, G. Ciani, D.W.v. Gudenberg, D.M. Proserpio, Inorg. Chem. 36 (1997) 3812.
[31] M.J. Plater, M.R.St.J. Foreman, T. Gelbrich, M.B. Hursthouse, J. Chem. Soc., Dalton Trans. (2000) 1995.
[32] M.L. Hernandez, M.K. Urtiaga, M.G. Barandika, R. Cortes, L. Lezama, N.d.l. Pinta, M.I. Arriortua, T. Rojo, J. Chem. Soc., Dalton Trans. (2001) 3010.
[33] G.De. Munno, D. Armentano, T. Poerio, M. Julve, J.A. Real, J. Chem. Soc., Dalton Trans. (1999) 1813.
[34] M.L. Hernandez, M.K. Urtiaga, M.G. Barandika, R. Cortes, L. Lezama, N.d.l. Pinta, M.I. Arriortua, T. Rojo, J. Chem. Soc., Dalton Trans. (2000) 79.
[35] X.-H. Bu, W. Chen, W.-F. Hou, M. Du, R.-H. Zhang, F. Brisse, Inorg. Chem. 41 (2002) 3477.
[36] R. Horikoshi, T. Mochida, N. Maki, S. Yamada, H. Moriyama, J. Chem. Soc., Dalton Trans. (2002) 28.
[37] A.J. Blake, N.R. Brooks, N.R. Champness, M. Crew, A. Deveson, D. Fenske, D.H. Gregory, L.R. Hanton, P. Hubberstey, M. Schröder, Chem. Commun. (2001) 1432.
[38] X.-H. Bu, W. Chen, M. Du, K. Biradha, W.-Z. Wang, R.-H. Zhang, Inorg. Chem. 41 (2002) 437.
[39] H. Kumagai, T.M. Akita, K. Inoue, M. Kurmoo, J. Mater. Chem. 11 (2001) 2146.
[40] B.G. Lor, E.G. Puebla, M. Iglesias, M.A. Monge, C.R. Valero, N. Snejko, Inorg. Chem. 41 (2002) 2429.
[41] S.S.Y. Chui, S.M.F. Lo, J.P.H. Charmant, A.G. Orpen, I.D. Williams, Science 283 (1999) 1148.
[42] J. Li, H. Zeng, J. Chen, Q. Wang, X. Wu, Chem. Commun. (1997) 1213.
[43] Z. Otwinowski, W. Minor, Methods in Enzymology, in: C.W. CarterJr., M. Sweet (Eds.), Macromolecular Crystallography, Part A, Academic Press, New York, 1997, pp. 307–326.
[44] L.J. Farrugia, J. Appl. Cryst. 32 (1999) 837.
[45] G.M. Sheldrick, Acta Crystallogr. A 46 (1990) 467.
[46] G.M. Sheldrick, SHELXL-97 – A program for crystal structure refinement, University of Göttingen, Germany, 1997.
[47] DIAMOND – Visual Crystal Structure Information System, Prof. Dr. G. Bergerhoff, Gerhard-Domagk-Str. 1, 53121 Bonn, Germany..
[48] S.K. Chawla, Polyhedron 18 (1999) 1397.
[49] C.B. Aakeröy, A.M. Beatty, K.R. Lorimer, J. Chem. Soc., Dalton Trans. (2000) 3869.
[50] N.S. Persky, J.M. Chow, K.A. Poschmann, N.N. Lacuesta, S.L. Stoll, S.G. Bott, S. Obrey, Inorg. Chem. 40 (2001) 29.
[51] V.M. Rao, D.N. Sathyanararayana, H. Manohar, J. Chem. Soc., Dalton Trans. (1983) 2167.
[52] M. Du, X.-H. Bu, Y.-M. Guo, H. Liu, Inorg. Chem. 41 (2002) 4904.
[53] S.K. Chawla, M. Arora, K. Nättinen, K. Rissanen (communicated).

Available online at www.sciencedirect.com
SCIENCE DIRECT®
Polyhedron 23 (2004) 3021–3032
POLYHEDRON
www.elsevier.com/locate/poly

Synthesis and X-ray crystal structures of six $[TeL_4][MF_6]$ salts, where L is ethylene- or trimethylene-thiourea, and M is Si, Ge or Sn. Five Te(II) complexes with a novel type of structure linked together by unusual N–H···F hydrogen bonds

Olav Foss [a], Steinar Husebye [*,a], Karl W. Törnroos [a,*], Philip E. Fanwick [b]

[a] *Department of Chemistry, University of Bergen, Allégt. 41, N-5007 Bergen, Norway*
[b] *Department of Chemistry, Purdue University, 560 Oval Drive, W. Lafayette, IN 47907-2084, USA*

Received 10 June 2004; accepted 27 August 2004
Available online 5 November 2004

Abstract

The complexes $[Te(etu)_4][SiF_6]$ (**1**), $[Te(etu)_4][SiF_6] \cdot H_2O$ (**2**), $[Te(trtu)_4][SiF_6]$ (**3**), $[Te(etu)_4][GeF_6] \cdot H_2O$ (**4**), $[Te(trtu)_4][GeF_6]$ (**5**) and $[Te(etu)_4][SnF_6]$ (**6**) (etu = ethylenethiourea, trtu = trimethylenethiourea) have been prepared and their crystal structures determined by X-ray crystallographic methods. The crystals of **1**, **3** and **5** are tetragonal; space groups *P*4*cc* (No. 103) with $Z = 4$ for **1**, *P*4*nc* (No. 104) with $Z = 2$ for **3**, and *I*4 (No. 79) with $Z = 2$ for **5**. The crystals of **2**, **4** and **6** are orthorhombic, space group *Pccn* (No. 56) with $Z = 8$ for **2** and **4** and $Z = 4$ for **6**; those of **2** and **4** being isomorphous. The cations contain square planar or slightly distorted square planar TeS_4 coordination groups. In **1**, **3** and **5** the Te atoms are located on fourfold rotation axes; the cations have fourfold rotational symmetry and the four thiourea ligands extend to the same side of the TeS_4 plane. These are the first examples of $[TeL_4]^{2+}$ conformers of this type. In **2** and **4** the Te atoms lie on general positions; the cations are distorted versions of those in **1**, and also in these the four ligands extend to the same side of the TeS_4 plane. In **6** the Te atoms are located on twofold rotation axes, the conformation of the cations corresponds to the point group C_2 with two neighbouring ligands extending to one side of the coordination plane and the remaining two to the opposite side. In **1**–**5** each of the four ligands forms a N–H···F bond to the same F atom in the counter ion. The crystals of **1**–**5** are red, and those of **6** are yellow. The red colour is attributed to interactions of Te and S lone electron pairs caused by ligand TeS_4/TeSC tilt angles markedly different from 90°.
© 2004 Elsevier Ltd. All rights reserved.

Keywords: Te(II) thiourea complexes; Novel conformations; Unexpected colours; X-ray crystallography; Supramolecular associations

1. Introduction

The incentive for the present work was an earlier observation made by one of us (O.F.) in an exploratory experiment on $[Te(etu)_4]^{2+}$ fluorides (etu = ethylenethiourea): when a hydrofluoric acid solution of tellurium dioxide and etu in a molar ratio 1:6 came in contact with glass, a red deposit formed. Crystals of $[Te(etu)_4]^{2+}$ salts are usually yellow. Formation of $[SiF_6]^{2-}$ was possible under these conditions and might somehow be responsible for the unusual colour. It was therefore decided to prepare a series of $[Te(etu)_4]^{2+}$ and $[Te(trtu)_4]^{2+}$ (trtu = trimethylenethiourea) salts with octahedral fluoride anions of the type $[MF_6]^{2-}$, where M = Si, Ge and Sn, and to study their structures in order to find the cause of the red colour.

* Corresponding author. Tel.: +4755583551; fax: +4755589490.
E-mail address: steinar.husebye@kj.uib.no (S. Husebye).

0277-5387/$ - see front matter © 2004 Elsevier Ltd. All rights reserved.
doi:10.1016/j.poly.2004.08.024

2. Experimental

2.1. General

The complex salts were prepared either by the exchange of chloride anions by $[MF_6]^{2-}$ in the complex salts $[Te(stu)_4]Cl_2 \cdot 2H_2O$, where M = Si or Ge, and stu is etu or trtu; or alternatively by the following disproportionation reaction: $Te^{4+} + 6stu + [MF_6]^{2-} = [Te(stu)_4][MF_6] + stu_2^{2+}$, where stu is etu or trtu and M is Si, Ge or Sn. The hexafluorosilicic acid solution used was obtained by saturating 48% hydrofluoric acid with fine-mesh silicon dioxide. The trimethylenethiourea and ethylenethiourea were commercial compounds supplied by Aldrich-Chemie, D-7924 Steinheim, Germany. Operations were performed in polythene beakers.

2.2. Synthesis

2.2.1. The complex $[Te(etu)_4][SiF_6]$ (**1**)

$[Te(etu)_4]Cl_2 \cdot 2H_2O$ (0.50 g, 0.78 mmol) was dissolved under stirring in dimethylformamide (DMF) (15 ml) and methanol (35 ml). The solution was heated gently and 3 ml H_2SiF_6 added. After a few hours at room temperature, the mixture was filtered and the crystals obtained were washed with methanol and then diethyl ether. Yield: 0.34 g (71.7%) of red tetragonal prisms [110]. *Anal.* Calc. for $C_{12}H_{24}F_6N_8S_4SiTe$: C, 21.24; H, 3.57; N 16.52. Found: C, 21.30; H, 3.60; N, 16.57%.

2.2.2. The complex $[Te(etu)_4][SiF_6] \cdot H_2O$ (**2**)

A hot solution of etu (7.0 g, 68.5 mmol) in H_2O (100 ml) was added to TeO_2 (1.6 g, 10.0 mmol) dissolved in HF (48%, 25 g), then 3 ml H_2SiF_6 solution was added. Yield, after standing and treatment as above, 5.0 g (71.6%) of red flat prisms. *Anal.* Calc. for $C_{12}H_{26}F_6N_8OS_4SiTe$: C, 20.70; H, 3.76; N, 16.09. Found: C, 20.80; H, 3.81; N, 16.10%.

2.2.3. The complex $[Te(trtu)_4][SiF_6]$ (**3**)

A hot solution of trtu (7.5 g, 64.5 mmol) in 96% ethanol (70 ml) was added to TeO_2 (1.6 g, 10.0 mmol) in HF (48%, 15 g), and then 3 ml H_2SiF_6 solution was added. After standing overnight and filtering and washing as above, the yield was 7.0 g (95.0%) of red tetragonal prisms 110. The complex also crystallized out when 2 ml H_2SiF_6 solution was added to a solution of $[Te(trtu)_4]Cl_2 \cdot 2H_2O$ (0.50 g, 0.72 mmol) in a mixture of methanol (30 ml) and DMF (2 ml). Yield: 0.49 g (95.2%). *Anal.* Calc. for $C_{16}H_{32}F_6N_8S_4SiTe$: C, 26.17; H, 4.39; N, 15.26. Found: C, 26.82; H, 4.50; N, 15.70%.

2.2.4. The complex $[Te(etu)_4][GeF_6] \cdot H_2O$ (**4**)

A hot mixture of etu (3.5 g, 34.3 mmol) in 40 ml hot H_2O was added to GeO_2 (0.53 g, 5.1 mmol) and TeO_2 (0.80 g, 5.0 mmol) dissolved in HF (48%, 10.0 g). After 2 h at room temperature, the mixture was filtered, the crystals washed with acetone and then diethyl ether. Yield: 2.3 g (61.9%) of red flat prisms. *Anal.* Calc. for $C_{12}H_{26}F_6GeN_8OS_4Te$: C, 19.45; H, 3.54; N, 15.13. Found: C, 21.93; H, 3.77; N, 14.91%.

2.2.5. The complex $[Te(trtu)_4][GeF_6]$ (**5**)

$[Te(trtu)_4]Cl_2 \cdot 2H_2O$ (0.50 g, 0.72 mmol) in warm methanol (15 ml) was added to GeO_2 (0.15 g, 1.43 mmol) dissolved in HF (48%, 5.0 g), and then 10 ml diethyl ether was added. After 2 h in a refrigerator, and then filtering and washing as above (for **4**), the yield was 0.34 g (75.7%) of red tetragonal prisms 110. *Anal.* Calc. for $C_{16}H_{32}F_6GeN_8S_4Te$: C, 24.67; H, 4.14; N, 14.39. Found: C, 25.73; H, 4.20; N, 14.36%.

The red crystals were stable for months when kept in a refrigerator. At room temperature they became yellow and polycrystalline after a few weeks.

2.2.6. The complex $[Te(etu)_4][SnF_6]$ (**6**)

A solution of etu (3.5 g, 34.3 mmol) in hot H_2O (40 ml) was added to TeO_2 (0.80 g, 5.0 mmol) and $(NH_4)_2[SnCl_6] \cdot H_2O$ (2.0 g, 5.2 mmol) in HF (48%, 16 g). This was followed by addition of hot methanol (50 ml). After standing overnight, and treating as above, the yield was 2.4 g (62.2%) of yellow prisms and bipyramids. *Anal.* Calc. for $C_{12}H_{24}F_6N_8S_4SnTe$: C, 18.74; H, 3.15; N, 14.57. Found: C, 18.73; H, 3.24; N, 14.43%.

2.3. Crystal stability

None of the six complexes had normal melting points, instead they all decomposed at higher temperatures yielding black elemental Te and a mostly solid residue. Complexes **1**, **2** and **6** decomposed in the range 170–180 °C. The red complex **5** first slowly converted into a yellow version at room temperature, see above. This was unfit for X-ray analysis. By heating the yellow crystals, decomposition started at 190 °C. Complexes **3** and **4** started to decompose around 130 and 150 °C, respectively.

2.4. Crystallography

Intensities at 293(1) K were recorded on a CAD 4 diffractometer using λ-scans and graphite-monochromated Mo Kα radiation, $\lambda = 0.71073$ Å. Three reference reflections were recorded every 2 h of exposure time. Intensities were corrected for absorption using face-indexing and Gaussian quadrature methods. For **5** intensities were recorded twice on the same crystal and under the same conditions, and the two sets averaged: $R_{int} = 0.018$ for 12 778 reflections, 0.015 for 8211 with $I > 3(\sigma I)$; this gave a noticeable improvement of confidence factors and standard uncertainties.

Crystal data are listed in Table 1. Anisotropic displacement parameters were used for non-hydrogen atoms. Part of the ligand in complex **3** was disordered over two positions, with occupancies of 0.6 and 0.4. Hydrogens were input as riding atoms with C–H(CH_2), N–H(NH) and O–H(O_{water}) distances of 0.97, 0.86 and 0.85 Å, respectively. The isotropic displacement parameters of the H atoms were fixed at 1.2 U_{eq} of their parent atoms.

The structures of complexes **1**–**3** were solved by Patterson and difference Fourier methods, and that of **6** by direct methods. Results and intensity files of the final refinements using the SDP-PLUS program [1] were converted to and re-refined with SHELXL as contained in the SHELXTL package [2]. The latter was used for graphical presentations and PLATON [3] for further geometry calculations.

3. Results and discussion

With $[Te(etu)_4]^{2+}$ or $[Te(trtu)_4]^{2+}$ as cations and $[SiF_6]^{2-}$, $[GeF_6]^{2-}$ or $[SnF_6]^{2-}$ as anions, red crystals of the following salts have been prepared and their X-ray structures at 293(1) K determined: $[Te(etu)_4][SiF_6]$ (**1**), tetragonal, space group *P4cc* with $Z = 4$; $[Te(etu)_4][SiF_6]\cdot H_2O$ (**2**), orthorhombic, space group *Pccn* with $Z = 8$; $[Te(trtu)_4][SiF_6]$ (**3**), tetragonal, space group *P4nc* with $Z = 2$; $[Te(etu)_4][GeF_6]\cdot H_2O$ (**4**), orthorhombic, isomorphous with **2**; $[Te(trtu)_4][GeF_6]$ (**5**), tetragonal, space group *I* 4 with $Z = 2$. Also yellow crystals of $[Te(etu)_4][SnF_6]$ (**6**) were prepared and studied by X-ray crystallographic methods. They are orthorhombic, same space group as **2** and **4** but with $Z = 4$. The TeS_4 coordination groups of the cations of the complexes **1**–**6** are square planar or nearly so, the anions have their usual octahedral shape. In **1**–**5** cation–anion pairs are held together by four N–H···F hydrogen bonds to the same F atom, one from each ligand. Selected bond lengths and angles are listed in Tables 2–8 and the molecular structures of the cations are shown in Figs. 1–5. A cation–anion pair is illustrated in Fig. 6, using **1b** as a model. Supramolecular interactions of representative complex salts are shown in Figs. 7–9 for **2**, **3** and **6** and the hydrogen bond lengths and angles of complexes **1**–**6** are listed in Table 9.

3.1. The tetragonal complexes *1*, *3* and *5*

The Te atom of the cations and three-atom sequences F–Si–F or F–Ge–F of the anions are located on fourfold axes. In **1** there are two crystallographically independent cation–anion units, one on the fourfold axis at $x = 0$, $y = 0$, (**1a**), and the other on the fourfold axis at $x = 1/2$, $y = 1/2$ (**1b**). The three tetragonal structures are closely related. The space groups are polar. The Te···F–Si–F and Te···F–Ge–F sequences on the fourfold axes all point the same way throughout the crystal. With origin at the Te position in **5**, space group *I*4 with $Z = 2$, identical cation–anion units in the same orientations occur at the corners and centre of the cell. In **3**, space group *P4nc* with $Z = 2$, the unit at the centre is reflected by an *n* glide plane. In **1**, space group *P4cc* with $Z = 4$, the *c* axis is nearly doubled compared to **3** and **5**. Every other unit along the axis, Te now at $z \approx 0$ and 1/2, is reflected by a *c* glide plane; the unit at $x = 1/2$, $y = 1/2$ is crystallographically independent, with Te slightly removed from $z = 1/4$, and is likewise reflected, along $x = 1/2$, $y = 1/2$ by a *c* glide plane.

Seen along the fourfold axis of a cation–anion unit of **3**, the directions of the Te–S bonds and equatorial Si–F bonds are almost parallel, the closest S–Te···Si–F torsion angle is 1.33(6)°. In the two crystallographically independent units of **1** these torsion angles are 36.78(5) and 34.42(5)°, for **1a** and **1b**, respectively, and in **5**, with Ge instead of Si, it is 8.96(7)°. In **1b**, at $x = 1/2$, $y = 1/2$, the Te–S bonds point slightly away from the anion, forming F_{axial}···Te–S angles of 95.08(2)°; the distance of Te from the S_4 plane is quite large at 0.237(1) Å making the coordination pyramidally distorted. In **1a**, the F···Te–S angles are 89.61(2)°; the distance of Te from the S_4 plane is 0.018(1) Å, in **3** the corresponding values are 89.93(3)° and 0.003(2) Å, and in **5**, 90.82(3)° and 0.038(2) Å.

3.2. The monohydrates *2* and *4*

In these $[Te(etu)_4]^{2+}$ salts, with $[SiF_6]^{2-}$ as anion in **2** and $[GeF_6]^{2-}$ in **4**, there is no molecular symmetry; all atoms lie in general positions. The cations are distorted versions of those in the tetragonal crystals; also here the four ligands extend to the same side of the TeS_4 plane, toward the anion. The TeS_4 groups are slightly pyramidal, the TeS_1S_2/TeS_3S_4 plane angle in **2** is 8.62(3)° and in **4** 8.50(3)°. The TeS_4 least-squares plane makes an angle of 12.30(1)° with the *c* plane in **2** and 12.09(1)° in **4**, and angles of 14.35(3)° and 13.43(3)°, respectively, with the equatorial $[SiF_6]^{2-}$ and $[GeF_6]^{2-}$ least-squares planes.

3.3. The yellow complex, *6*

The central atoms of the $[Te(etu)_4]^{2+}$ cation and $[SnF_6]^{2-}$ anion both lie on twofold symmetry axes. The cation axis lies in the least-squares TeS_4 plane passing between two sets of neighbouring S atoms. The TeS_4 group here is also slightly pyramidal, by a rotation of ca. 6.5° about the twofold axis of the two halves relative to each other. Although the space groups are different, the structure of the cation in **6** is similar to that in $[Te(etu)_4][TeCl_6]$ [4]. The crystals of the hexachloro analogue of **6**, $[Te(etu)_4][SnCl_6]$, are isomorphous with those of the hexachlorotellurate [5].

Table 1
Crystallographic data

No.	1	2	3	4	5	6
Complex	$[Te(etu)_4][SiF_6]$	$[Te(etu)_4][SiF_6] \cdot H_2O$	$[Te(trtu)_4][SiF_6]$	$[Te(etu)_4][GeF_6] \cdot H_2O$	$[Te(trtu)_4][GeF_6]$	$[Te(etu)_4][SnF_6]$
Formula	$C_{12}H_{24}F_6N_8S_4SiTe$	$C_{12}H_{26}F_6N_8OS_4SiTe$	$C_{16}H_{32}F_6N_8S_4SiTe$	$C_{12}H_{26}F_6GeN_8OS_4Te$	$C_{16}H_{32}F_6GeN_8S_4Te$	$C_{12}H_{24}F_6N_8S_4SnTe$
M	678.32	696.34	734.43	740.84	778.93	768.92
System	tetragonal	orthorhombic	tetragonal	orthorhombic	tetragonal	orthorhombic
Space group	*P*4cc (No. 103)	*Pccn* (No. 56)	*P4nc* (No. 104)	*Pccn* (No. 56)	*I*4 (No. 79)	*Pccn* (No. 56)
a (Å)	10.3001(5)	14.977(2)	10.8605(5)	15.1791(15)	10.6005(13)	10.4401(8)
b (Å)	10.3001(5)	29.187(4)	10.8605(5)	29.474(6)	10.6005(13)	14.213(3)
c (Å)	23.4484(15)	11.718(1)	12.4134(7)	11.7645(10)	13.3321(7)	16.4178(9)
V (Å^3)	2487.7(2)	5122.1(11)	1464.17(13)	5263.3(12)	1498.1(3)	2436.2(5)
Z	4	8	2	8	2	4
D_x (g cm^{-3})	1.811	1.806	1.666	1.870	1.727	2.096
μ (Mo Kα) (mm^{-1})	1.643	1.601	1.403	2.633	2.315	2.630
Crystal size (mm)	$0.22 \times 0.22 \times 0.53$	$0.19 \times 0.34 \times 0.58$	$0.20 \times 0.22 \times 0.36$	$0.19 \times 0.25 \times 0.48$	$0.24 \times 0.24 \times 0.34$	$0.19 \times 0.20 \times 0.51$
Transmission factors	0.694–0.733	0.603–0.750	0.604–0.771	0.526–0.631	0.587–0.628	0.573–0.661
θ Range (°)	1.74–31.96	1.40–27.96	2.49–31.96	1.38–27.96	2.45–35.91	2.42–31.90
hkl Range	h 0 → 15	h 0 → 19	h 0 → 11	h 0 → 20	h 0 → 17	h 0 → 15
	k 0 → 15	k 0 → 38	k 0 → 16	k 0 → 38	h 0 → 17	k 0 → 21
	l 34 → 34	l 0 → 15	l 18 → 18	l 0 → 15	l 22 → 22	l 0 → 24
Unique reflections	4336	6167	2554	6331	3554	4224
No. of variables	152	305	95	305	86	147
Extinction coefficient	0.00289(11)	0.00081(3)		0.000298(13)	0.000352(18)	0.00038(5)
Flack parameter (x)	−0.016(10)	n.a.	−0.04(2)	n.a	−0.018(14)	n.a.
R for I > 2σ(I)/all	0.0225/0.0373	0.0297/0.0561	0.0278/0.0452	0.0255/0.0552	0.0290/0.0514	0.0235/0.0443
R_w for I>2σ(I)/all	0.0431/0.0475	0.0621/0.0786	0.0514/0.0634	0.0482/0.0671	0.0463/0.0666	0.0496/0.0652
S	0.933	1.146	1.094	1.111	1.199	1.148
Max./Min. peak and hole (e Å^{-3})	0.594/−0.205	0.703/−0.443	0.599/−0.299	0.635/−0.608	1.018/−0.956	0.551/−0.723

Table 2
Bond lengths (Å) and angles (°) and ligand tilt and twist angles (°) for the cations, with s.u.'s in parentheses

No. Complex	Te–S	S–C	Te–S–C	Tilt	Twist
1. $[Te(etu)_4][SiF_6]$[a]	2.6847(6)	1.718(2)	98.35(7)	42.82(7)	49.08(8)
	2.6832(7)	1.708(2)	111.10(7)	83.39(9)	17.62(10)
2. $[Te(etu)_4][SiF_6] \cdot H_2O$[b]	2.6240(10)	1.727(3)	98.77(11)	57.12(9)	33.75(16)
	2.7785(12)	1.695(4)	98.44(13)	43.82(12)	55.14(15)
	2.7870(11)	1.712(4)	97.35(12)	30.44(14)	59.70(13)
	2.5802(10)	1.726(4)	104.28(12)	74.44(12)	35.67(18)
3. $[Te(trtu)_4][SiF_6]$	2.6963(8)	1.732(3)	102.75(10)	43.54(10)	41.19(14)
4. $[Te(etu)_4][GeF_6] \cdot H_2O$[b]	2.6180(10)	1.732(4)	99.43(12)	57.86(10)	30.84(17)
	2.7794(13)	1.686(5)	98.78(13)	44.67(12)	52.90(16)
	2.8029(11)	1.712(4)	97.35(13)	30.70(14)	59.53(13)
	2.5831(11)	1.725(4)	104.20(12)	74.08(13)	35.43(18)
5. $[Te(trtu)_4][GeF_6]$	2.6726(10)	1.728(4)	104.03(11)	45.01(12)	45.15(14)
6. $[Te(etu)_4][SnF_6]$	2.6607(7)	1.711(3)	113.00(9)	74.14(10)	22.48(15)
	2.6939(7)	1.717(3)	107.54(8)	70.16(9)	12.00(16)

[a] First and second independent ions.
[b] Te–S(1) to Te–S(4), Te–S(1) *trans* to Te–S(3).

Table 3
Selected bond lengths (Å) and angles (°) in **1**

Te1–S1	2.6847(6)	S1–Te1–S1A	179.22(3)
S1–C1	1.718(2)	S1–Te1–S1B	90
N1–C1	1.316(3)	Te1–S1–C1	98.35(7)
N2–C1	1.318(2)	S1–C1–N1	122.60(15)
		S1–C1–N2	127.23(16)
Te2–S2	2.6832(7)	N1–C1–N2	110.17(19)
S2–C2	1.708(2)		
N3–C2	1.307(3)	S2–Te2–S2A	169.85(3)
N4–C2	1.317(2)	S2–Te2–S2B	89.552(3)
		Te2–S2–C2	111.10(7)
Si1–F1	1.740(2)	S2–C2–N3	122.09(16)
Si1–F2	1.660(3)	S2–C2–N4	127.96(17)
Si1–F3	1.6712(13)	N3–C2–N4	109.93(19)
Si2–F4	1.709(2)	F1–Si1–F2	180
Si2–F5	1.670(3)	F1–Si1–F3	88.08(6)
Si2–F6	1.6733(12)	F2–Si1–F3	91.92(6)
		F4–Si2–F5	180
		F4–Si2–F6	89.36(6)
		F5–Si2–F6	90.64(6)

Table 4
Selected bond lengths (Å) and angles (°) in **2**

Te–S1	2.6240(10)	S1–Te–S2	91.46(4)
Te–S2	2.7785(12)	S1–Te–S3	173.44(3)
Te–S3	2.7870(11)	S1–Te–S4	87.56(4)
Te–S4	2.5802(10)	S2–Te–S3	90.98(4)
S1–C1	1.727(3)	S2–Te–S4	173.77(4)
N1–C1	1.306(4)	S3–Te–S4	90.66(4)
N2–C1	1.317(4)	Te–S1–C1	98.77(11)
S2–C2	1.695(4)	S1–C1–N1	122.2(3)
N3–C2	1.331(5)	S1–C1–N2	127.2(3)
N4–C2	1.310(5)	N1–C1–N2	110.6(3)
S3–C3	1.712(4)	Te–S2–C2	98.44(13)
N5–C3	1.319(5)	S2–C2–N3	126.3(3)
N6–C3	1.316(4)	S2–C2–N4	124.0(2)
S4–C4	1.726(4)	N3–C2–N4	109.7(4)
N7–C4	1.311(4)	Te–S3–C3	97.35(12)
N8–C4	1.302(4)	S3–C3–N5	126.3(3)
		S3–C3–N6	123.9(3)
Si–F1	1.7101(19)	N5–C3–N6	109.8(4)
Si–F2	1.663(2)	Te–S4–C4	104.28(12)
Si–F3	1.666(2)	S4–C4–N7	125.4(3)
Si–F4	1.671(2)	S4–C4–N8	123.0(3)
Si–F5	1.689(2)	N7–C4–N8	111.6(3)
Si–F6	1.693(2)		
		F1–Si–F2	177.94(12)
		F1–Si–F3	90.37(11)
		F3–Si–F5	91.77(12)
		F3–Si–F6	89.91(11)
		F4–Si–F5	89.75(11)
		F4–Si–F6	88.52(11)

3.4. Dimensions of the anions

In the two independent $[SiF_6]^{2-}$ ions in **1** and the one in **3** with F–Si–F on fourfold axes, the F atom of the Si–F bond in the axial Te···F–Si sequence is engaged in four N–H···F hydrogen bonds. This is therefore the longest Si–F bond and the Si–F bond *trans* to it the shortest. The four equivalent equatorial Si–F bonds are intermediate. The lengths of the three bonds, respectively, are as follows: 1.740(2), 1.660(3), 1.6712(13) Å in **1a**, 1.709(2), 1.670(3), 1.6733(12) Å in **1b**, 1.722(3), 1.656(4), 1.6799(16) Å in **3**, the averages are 1.690 Å in **1a**, 1.684 Å in **1b** and 1.686 Å in **3**. In the asymmetric $[SiF_6]^{2-}$ ion in **2** the Si-F bonds vary in a similar way from 1.663(2) to 1.7101(19) Å, with an average of 1.682 Å. These bond lengths may be compared to 1.694(13) Å, an average value found for SiF_6^{2-} anions [6].

In the tetragonal $[GeF_6]^{2-}$ salt **5**, the Ge–F bonds show the same pattern as the Si–F bonds in **1** and **3**: corresponding bond lengths are 1.812(3), 1.786(3), 1.7853(17) Å, average 1.794 Å. In the asymmetric

Table 5
Selected bond lengths (Å) and angles (°) in **3**

Te–S1	2.6963(8)	S1–Te–S1A	179.86(7)
S1–C1	1.732(3)	S1–Te–S1B	90.0
N1–C1	1.319(3)	Te–S1–C1	102.75(10)
N2–C1	1.311(4)	S1–C1–N1	122.9(2)
		S1–C1–N2	117.5(2)
Si–F1	1.722(3)	N1–C1–N2	119.6(3)
Si–F2	1.656(4)		
Si–F3	1.6799(16)	F1–Si–F2	180
		F1–Si–F3	88.93(8)
		F2–Si–F3	91.07(8)
		F3–Si–F3A	177.87(15)

Table 6
Selected bond lengths (Å) and angles (°) in **4**

Te–S1	2.6180(10)	S1–Te–S2	91.48(4)
Te–S2	2.7794(13)	S1–Te–S3	173.56(4)
Te–S3	2.8029(11)	S1–Te–S4	87.60(4)
Te–S4	2.5831(11)	S2–Te–S3	90.64(4)
S1–C1	1.732(4)	S2–Te–S4	173.92(4)
N1–C1	1.306(4)	S3–Te–S4	90.92(4)
N2–C1	1.307(4)	Te–S1–C1	99.43(12)
S2–C2	1.686(5)	S1–C1–N1	121.8(3)
N3–C2	1.327(5)	S1–C1–N2	127.5(3)
N4–C2	1.316(5)	N1–C1–N2	110.7(3)
S3–C3	1.712(4)	Te–S2–C2	98.78(13)
N5–C3	1.325(5)	S2–C2–N3	127.8(3)
N6–C3	1.315(5)	S2–C2–N4	123.3(3)
S4–C4	1.725(4)	N3–C2–N4	108.9(4)
N7–C4	1.318(4)	Te–S3–C3	97.35(13)
N8–C4	1.303(4)	S3–C3–N5	126.4(3)
		S3–C3–N6	123.9(3)
Ge–F1	1.8035(18)	N5–C3–N6	109.7(4)
Ge–F2	1.7702 (19)	Te–S4–C4	104.20(12)
Ge–F3	1.7706(19)	S4–C4–N7	125.0(3)
Ge–F4	1.7906(19)	S4–C4–N8	123.0(3)
Ge–F5	1.7732(19)	N7–C4–N8	111.9(3)
Ge–F6	1.7926(19)		
		F1–Ge–F2	177.76(9)
		F1–Ge–F3	90.31(10)
		F3–Ge–F5	92.23(10)
		F3–Ge–F6	89.83(10)
		F4–Ge–F5	89.27(10)
		F4–Ge–F6	88.61(10)

Table 7
Selected bond lengths (Å) and angles (°) in **5**

Te–S	2.6726(10)	S1–Te–S1A	178.37(6)
S1–C1	1.728(4)	S1–Te–S1B	89.988(1)
N1–C1	1.319(4)	Te–S1–C1	104.03(11)
N2–C1	1.316(4)	S1–C1–N1	122.9(3)
		S1–C1–N2	117.5(3)
Ge–F1	1.812(3)	N1–C1–N2	119.5(3)
Ge–F2	1.786(3)		
Ge–F3	1.7853(17)	F1–Ge–F2	180
		F1–Ge–F3	88.28(6)
		F2–Ge–F3	91.76(6)
		F3–Ge–F3A	176.55(13)

Table 8
Selected bond lengths (Å) and angles (°) in **6**

Te–S1	2.6607(7)	S1–Te–S2	90.39(3)
Te–S2	2.6939(7)	S1–Te–S2A	175.34(2)
S1–C1	1.711(3)	S1–Te–S1A	89.48(4)
N1–C1	1.316(3)	S2–Te–S2A	90.12(3)
N2–C1	1.312(3)	Te–S1–C1	113.00(9)
S2–C2	1.717(3)	S1–C1–N1	121.3(2)
N3–C2	1.315(3)	S1–C1–N2	128.3(2)
N4–C2	1.316(3)	N1–C1–N2	110.4(2)
		Te–S2–C2	107.54(8)
Sn–F1	1.9683(15)	S2–C2–N3	122.52(19)
Sn–F2	1.9501(18)	S2–C2–N4	127.34(19)
Sn–F3	1.9440(19)	N3–C2–N4	110.1(2)
		F1–Sn–F2	87.41(8)
		F1–Sn–F3	89.11(8)
		F2–Sn–F3	89.03(11)
		F1–Sn–F1B	179.57(10)

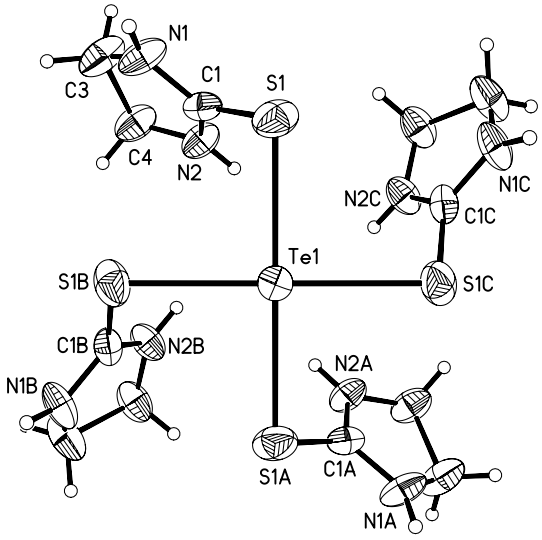

Fig. 1. The structure of the cation of **1a**.

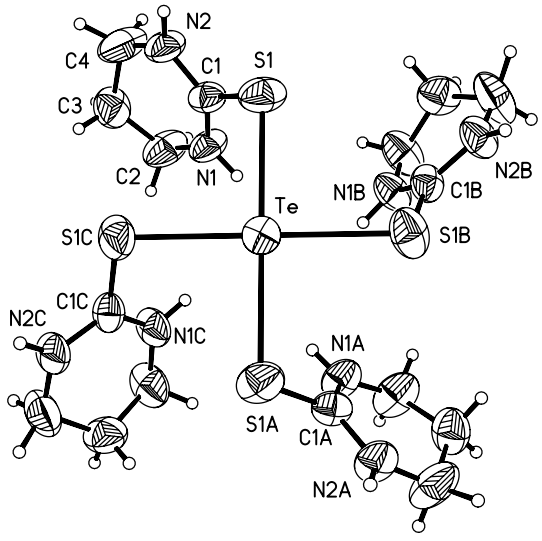

Fig. 2. The structure of the cation of **3**. Only the main component of the disordered ring is shown.

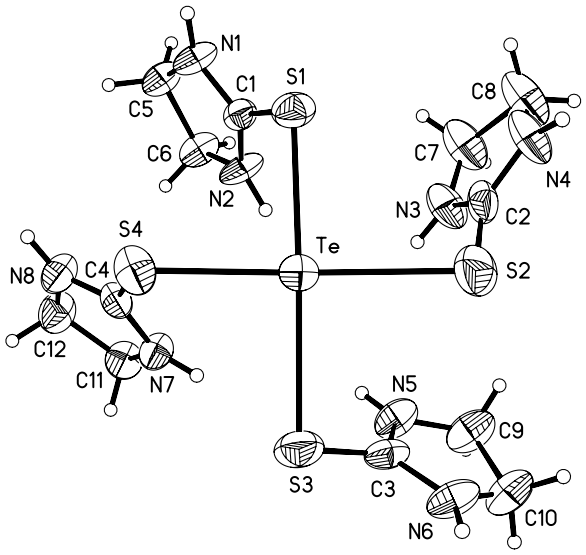

Fig. 3. The structure of the cation of **4** (**2** is isomorphous with **4** and has the same structure).

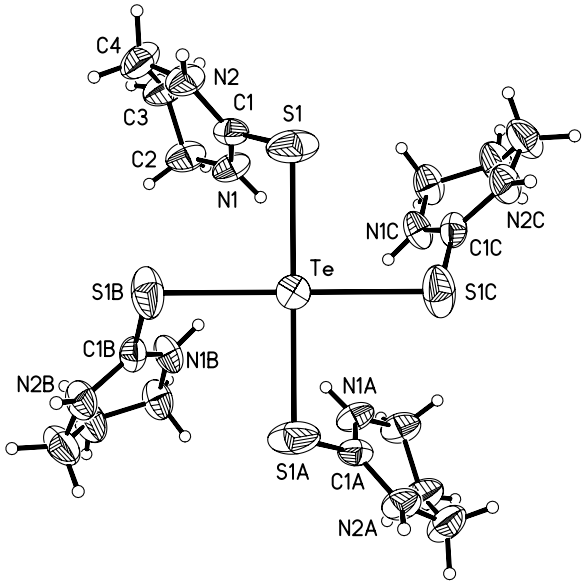

Fig. 4. The structure of the cation of **5**.

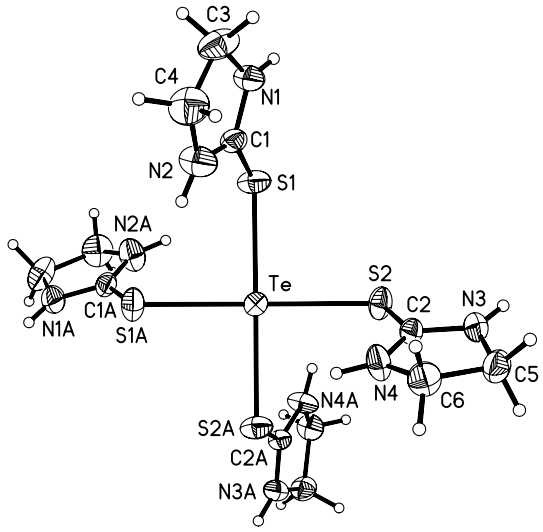

Fig. 5. The structure of the cation of **6**.

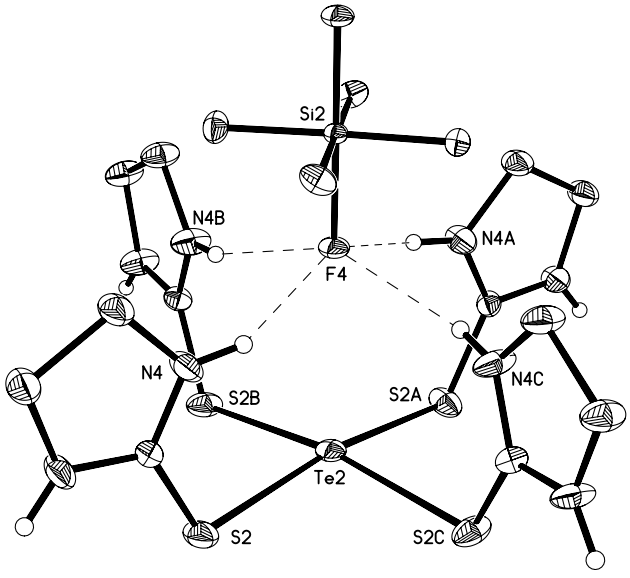

Fig. 6. The structure of the cation–anion pair of **1b** (i.e., the second molecule in the asymmetric unit). Hydrogen bonds are indicated by dashed lines.

$[GeF_6]^{2-}$ ion in **4**, the Ge–F bond lengths vary in the same way as the Si–F bonds in **2**. They range from 1.7702(19) to 1.8035(18) Å; average 1.783 Å. In the $[SnF_6]^{2-}$ salt **6**, the Sn atom lies on a twofold axis, with Sn–F bond lengths of 1.9683(15), 1.9501(18), 1.9440(19) Å; with an average of 1.954 Å.

3.5. Dimensions of the cations

The principal data are shown in Tables 2–8. Tilt and twist angles [7,8] are represented by the TeS_4/TeSC and TeSC/SCN_2 interplanar angles, respectively; the acute angles are listed in Table 2. The TeS_4 and SCN_2 planes are the least-squares planes, except for **6** where the tilt angles refer to the TeS_2 planes of S atoms related by the twofold axis. Where the TeS_4 groups are not exactly planar, as in the present case, the tilt angles for **1**–**5** differ slightly from the *cis*-S–Te–S–C torsion angles, but are close to the average of the acute values of the torsion angles based on each of the two neighbouring sulfur atoms.

The Te–S bond lengths in the tetragonal complexes **1**, **3** and **5** lie in the usual range [9]. In various Te(II) complexes containing centrosymmetric TeS_4 or TeS_2X_2 coordination groups, the three-centre four-electron Te–S bonds vary from 2.651(6) to 2.728(4) Å; the weighted

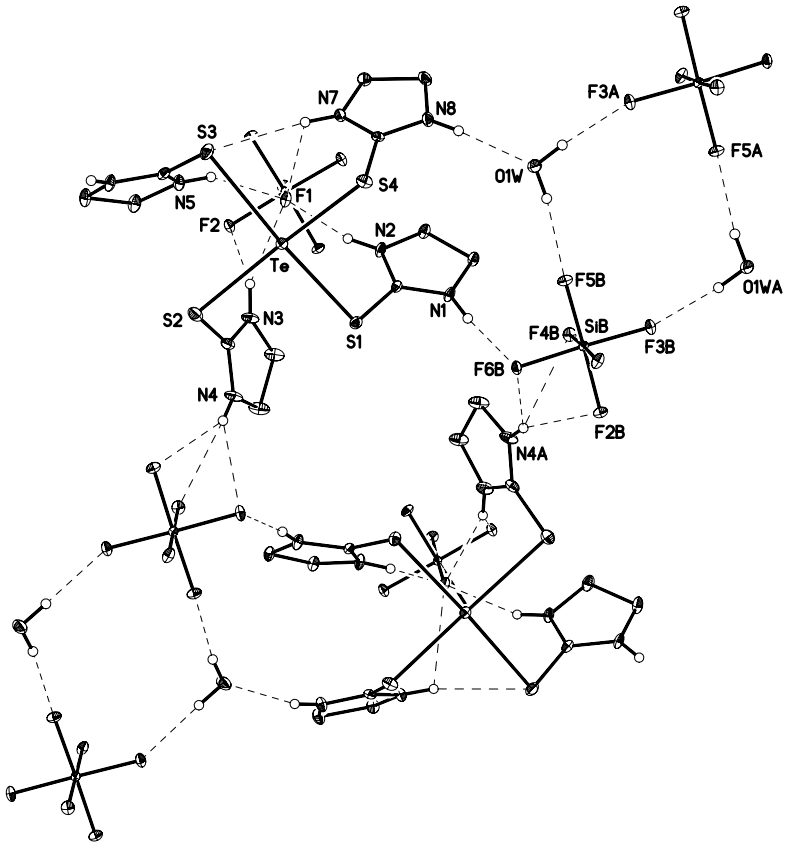

Fig. 7. The molecular packing in **2** with hydrogen bonds indicated by dashed lines.

average of 20 values is 2.682(3) Å. The average Te–S bond length for **1**–**6** is 2.689 Å in good agreement with this. In the centrosymmetric TeS_4 groups of $[Te(etu)_4]Cl_2$ [10], $[Te(trtu)_4]Cl_2 \cdot 2H_2O$ and $[Te(trtu)_4](ClO_4)_2$ [8] the Te–S bond lengths are 2.681(1) and 2.666(1), 2.680(1) and 2.684(1), and 2.667(1) and 2.701(1) Å, respectively. The different Te–S bond lengths in **3** and **5**, 2.6963(8) and 2.6726(10) Å, where the structures are otherwise so similar, remains unexplained. However, this has been observed before in Te complexes with thiourea ligands [11]. The main difference between **1a** and **1b** is found in their Te–S–C angles which differ by nearly 13°; also the TeS_4 group is more planar in **1a** than in **1b** (see above).

In the asymmetric TeS_4 groups of **2** and **4**, the longest and shortest Te–S bonds occur for the smallest and largest tilt angles, respectively. The smaller tilt angles are associated with larger twist angles. A rough correlation between Te–S bond length and thiourea twist angle in centrosymmetric Te(II) complexes has been noted earlier [8].

3.6. The thiourea ligands

All ligands have normal C–S bonds ranging from 1.686(4) to 1.732(4) Å with an average value of 1.716 Å. This may be compared to free thioureas where the average value is 1.681(20) Å [6], and the difference is due to the weakening of the bond upon complexation to Te. In **2** and **4**, the asymmetry in the Te–S bonds is reflected in the corresponding C–S bond length. To a long Te–S bond of average length 2.787 Å, corresponds a short C–S bond of average length 1.701 Å, and to a short Te–S bond of average length 2.601 Å, a long C–S bond of average length 1.728 Å. This asymmetry is further reflected in the C–N bonds, a long C–S bond corresponds to a short C–N bond and vice versa.

The average $C(sp^2)$–N bond length in the thiourea ligands of **1**–**6** is 1.315 Å. This is comparable to 1.326 Å, the average found in some *trans*-dihalodithioureatellurium(II) complexes with similar S–Te–S sequences [12,13]. In free thioureas, the corresponding average is 1.346(23) Å [6]. The C–S and $C(sp^2)$–N bond lengths illustrates the partial double bonding in the central SCN_2 part of the thiourea ligands. The average $C(sp^3)$–N and C–C bond lengths in **1**–**6** are normal at 1.454 and 1.516 Å, respectively (C–C in disordered **3** is not included). The bond angles agree with sp^2 hybridization of the N atoms and of the C atom bonded to S. In the complexes **1**–**5** with the special ion pair formation, the S–C–N angles involving the $N–H\cdots F1_{axial}$ hydrogen bonds between the ion pairs are consistently larger than

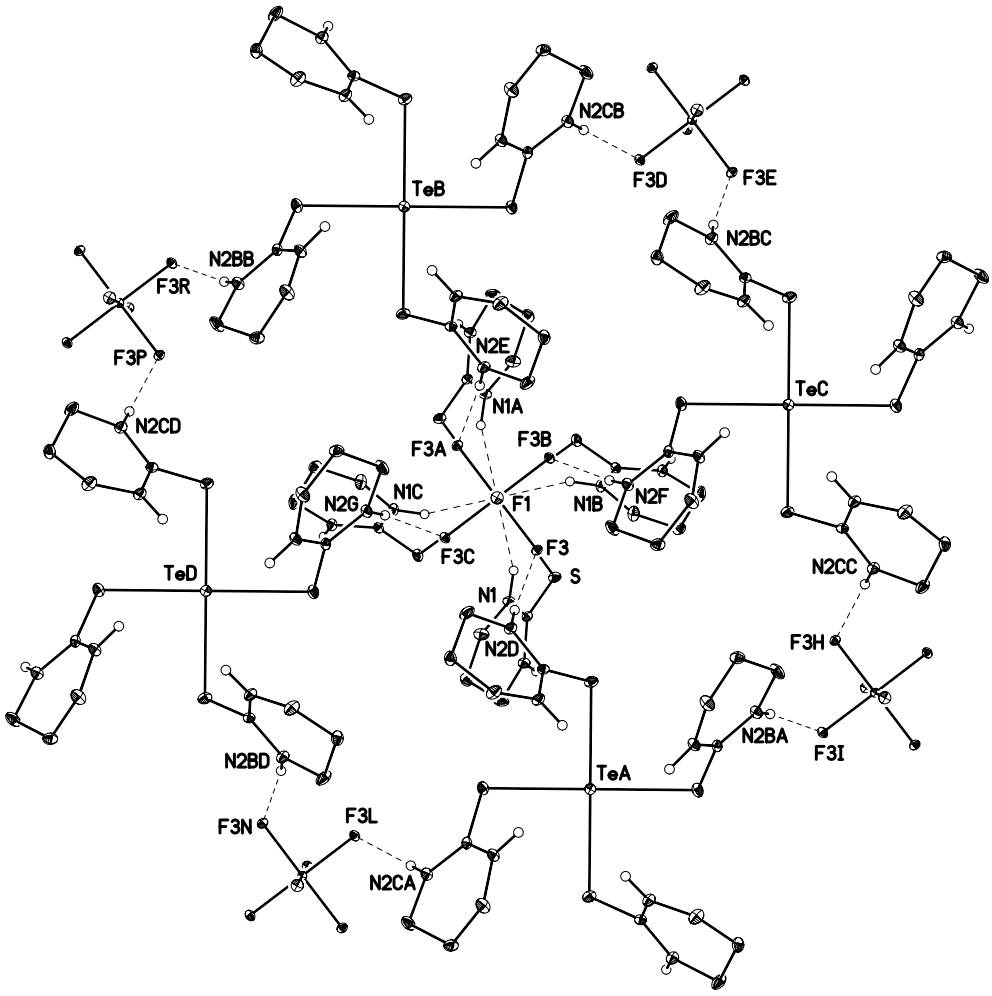

Fig. 8. The molecular packing in **3** with hydrogen bonds indicated as in Fig. 7. The Te atom (not labelled) in the centre lies below atom F1.

the other S–C–N angles. The average difference is ca. 4° and this probably results in an optimal orientation of the ligand with respect to H-bonding and packing.

4. Conformations of the cations

In the $[TeL_4]^{2+}$ cations of the square planar complexes **1**–**5**, the four etu or trtu ligands extend to the same side of the TeS_4 plane. These are the first examples of conformers of this type. In **1**, **3** and **5** the cations have fourfold rotation symmetry, in the isomorphous hydrates **2** and **4** they have a more asymmetric and distorted shape, but the deviations from fourfold symmetry is not great.

Elder et al. [14] determined the crystal structure of $[Te(etu)_4]Cl_2 \cdot 2H_2O$ and discussed the orientations of the etu ligands. In this dihydrate, two independent Te atoms lie on twofold axes, and *cis*-positioned ligands extend to different sides of the TeS_4 plane. The authors regard this, a +−+− conformation in their notation, as the favoured one; it minimizes mutual steric interference of ligands. In ++++ conformers with all four ligands extending to the same side of the TeS_4 plane, and in +++− conformers, "– the steric crowding will be severe and these conformations are unlikely to be observed". However, in the present complexes **1**–**5** ++++ conformers occur, and there are no particularly close inter-ligand contacts.

In complex **6** the Te atoms lie on twofold axes; pairs of *cis*-positioned ligands extend to opposite sides of the TeS_4 plane, in a distorted centrosymmetric ++−− arrangement. In fact, this is the conformation, mostly with the Te atom on a centre of symmetry, that predominates in such complexes [11].

5. Packing and hydrogen bonding

In the Te···F–Si–F and Te···F–Ge–F sequences on the fourfold axes; the Te···F distances are rather short: 3.431(2) and 3.277(2) Å in **1a** and **1b**, 3.378(3) Å in **3** and

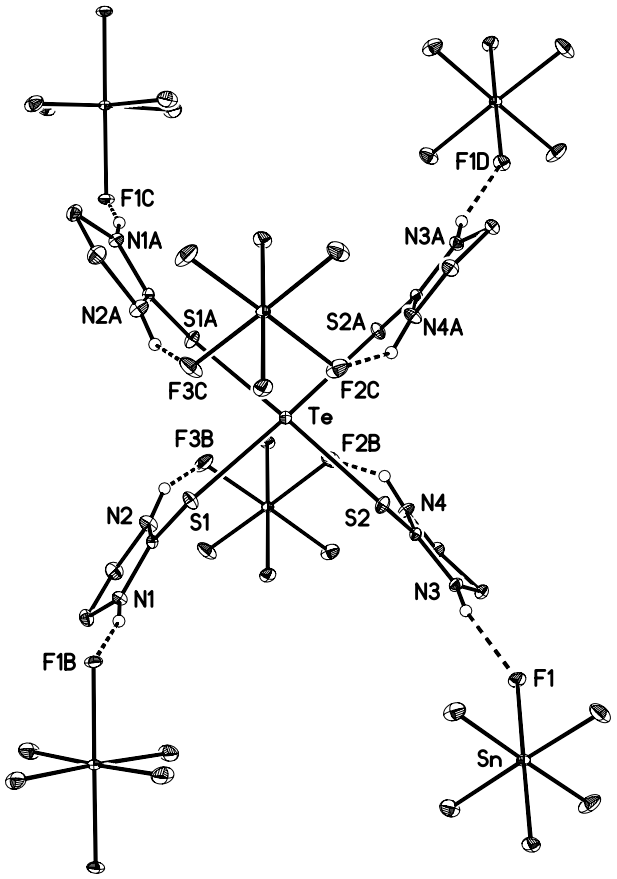

Fig. 9. The molecular packing in **6** with hydrogen bonds indicated as in Fig. 7.

3.348(3) Å in **5**. The cyclic parts of the four etu or trtu ligands of each cation, are all located on the same side of the TeS_4 plane on account of the fourfold axes. Complexes **2** and **4**, in the absence of fourfold symmetry, surprisingly have a similar structure. The closest Te···F distance, on the ligand sides of the TeS_4 plane, is 3.556(2) Å in **2** and 3.544(2) Å in **4**, with S–Te···F angles 81.22(4)° 98.29(4)° in **2** and 81.54(4)° 98.53(4)° in **4.** These Te···F distances are significantly shorter than 3.53 Å, the sum of the van der Waals radii of the respective atoms for **1**, **3** and **5** [15], and this is probably due to the N–H···F hydrogen bonding involving this fluorine atom. For **2** and **4**, the distance is comparable to a van der Waals contact, but here the relevant N–H···F bonding is weaker (Table 9). There are no close Te···F contacts at the other side of the TeS_4 plane in **1**–**5**. The cations of **1**–**5** form basket-like structures with the ligand C, N and H atoms making up the sides of the basket and TeS_4 the bottom with Te in its centre. Into this basket, the lower axial F of the MF_6^{2-} approaches the Te atom. This F atom is now in position to form N–H···F hydrogen bonds with all four ligands of the cationic complex resulting in an unusual situation with the same fluorine atom hydrogen bonded to four different N–H donors, one from each ligand. Such a cation–anion pair is shown in Fig. 6 for **1b**. The N···F distances in these hydrogen bonds range from 2.816(4) to 3.256(4) Å. If one excludes two very weak such bonds, one in **2** and one in **4**, the top of the range becomes 3.105(4) Å (Table 9). Similar N–H···F bonding with the same F atom involved in at least four hydrogen bonds is rare. A search of the Cambridge Crystallographic Data Base show that a single F^- ion can be involved in five and six hydrogen bonds [16,17]. With F bonded to other atoms as in SiF_6^{2-}, the maximum number of hydrogen bonds to F is four [18,19]. The above bonds connect the cation–anion pairs of the asymmetric units in **1**–**5** (Fig. 6). It is probably these interactions between pairs of cations and anions that contribute most to stabilize the unusual ++++ conformations of the complex cations. Why **6** has another structure is difficult to explain. The main difference is the size of the anion as SnF_6^{2-} in **6** is larger than SiF_6^{2-} and GeF_6^{2-} found in **1**–**5**. Thus packing forces may induce a different packing of the complex ions. A further indication that size may be important is that **5** is less stable (loses its red colour and becomes yellow) than **4**. They both share the same anion GeF_6^{2-} which is larger than SiF_6^{2-}, but the thiourea ligand in **5** is trtu which is larger than etu found in **4**. It is also likely that **5** upon its colour change converts its conformation to ++−−.

In addition, there is a series of intermolecular hydrogen bonds connecting the cation–anion pairs in **1**, **3** and **5**. From the second N atom of each ligand, N–H···F hydrogen bonds extend to equatorial F atoms of cation–anion units on neighbouring fourfold axes: 2.967(2) and 2.776(2) Å in **1a** and **1b**, 2.858(3) Å in **3** and 2.803(3) Å in **5**. The hydrogen bonds are listed in Table 9. Fig. 8 shows the supramolecular interactions in **3**, which is fairly representative of these interactions in **1**, **3** and **5**. They connect the ions into an essentially three-dimensional network where layers of anions separate layers of cations. In the isomorphous monohydrate complexes **2** and **4** the intermolecular N–H···F bonding is similar to that found in **1**, **3** and **5**, but there is also a weak N–H···F hydrogen bond involving the second axial F atom. In addition the H_2O molecule takes part in three hydrogen bonds in both complexes. Two O–H···F hydrogen bonds have O···F distances of 2.791(4) and 2.812(4) Å and one N–H···O hydrogen bond has an N···O distance of 2.822(4) Å in **2**. The corresponding distances in **4** are 2.789(4), 2.792(4) and 2.812(5) Å, respectively. These hydrogen bonds connect the cation–anion pairs into a three-dimensional network. There is also an intramolecular N–H···S hydrogen bond in the cations of **2** and **4**, the respective N···S distances being 3.574(3) and 3.569(3) Å. This agrees well with the intramolecular N–H···S bond found in chlorotris (*N*,*N*′-dicyclohexylthiourea)tellurium(II) chloride, where N···S is 3.5618(12) Å [20] and with other N–H···S hydrogen bonds [21]. The supramolecular interactions in **2** are shown in Fig. 7. In **6**, the two etu ligands of the asym-

Table 9
Hydrogen bonds in the complex salts **1**–**6**

Complex H-bond	l_{D-H}	$l_{H\cdots A}$	$l_{D\cdots A}$	∠D–H···A	Symmetry code of A
1. N1–H1A···F6	0.86	2.22	2.967(2)	145	$-y+1, x, z$
N1–H1A···F6	0.86	2.40	3.170(2)	149	none
N1–H1A···F5	0.86	2.59	3.053(2)	115	none
N2–H2A···F1	0.86	2.13	2.924(2)	154	none
N2–H2A···F3	0.86	2.62	3.072(2)	114	$y, -x, z$
N3–H3A···F3	0.86	1.96	2.776(2)	157	$x+1, -y, z+1/2$
N4–H4A···F4	0.86	2.22	3.010(2)	153	none
N4–H4A···F6	0.86	2.55	3.063(2)	119	$-y+1, x, z$
2. N1–H1A···F6	0.86	1.94	2.800(4)	174	$-x-1/2, y, z-1/2$
N2–H2A···F1	0.86	2.00	2.816(4)	158	none
N3–H3A···F1	0.86	2.30	3.105(4)	156	none
N3–H3A···F4	0.86	2.46	3.126(4)	134	none
N4–H4A···F4	0.86	2.35	3.131(4)	152	$x, -y+1/2, z-1/2$
N4–H4A···F6	0.86	2.46	3.217(4)	147	$x, -y+1/2, z-1/2$
N4–H4A···F2	0.86	2.57	3.092(4)	120	$x, -y+1/2, z-1/2$
N5–H5A···F1	0.86	2.06	2.862(4)	155	none
N6–H6A···F4	0.86	2.16	2.933(4)	150	$-x+1/2, y, z-1/2$
N6–H6A···F5	0.86	2.44	3.081(4)	132	$-x+1/2, y, z-1/2$
N7–H7A···S3	0.86	2.79	3.574(3)	152	none
N7–H7A···F1	0.86	2.92	3.247(4)	105	none
N8–H8A···O1W	0.86	2.00	2.822(4)	161	none
O1W–H1W···F5	0.83(3)	2.00(4)	2.791(4)	168(6)	$x-1/2, -y+1, -z+1/2$
O1W–H2W···F3	0.82(4)	2.00(4)	2.812(4)	173(3)	$-x-1/2, y, z-1/2$
3. N1–H1A···F1	0.86	2.16	2.977(3)	157	none
N2–H2A···F3	0.86	2.04	2.858(3)	159	$-y+1/2, -x+1/2, z-1/2$
4. N1–H1A···F6	0.86	1.93	2.783(4)	170	$-x-1/2, y, z-1/2$
N2–H2A···F1	0.86	2.01	2.820(4)	158	none
N3–H3A···F1	0.86	2.26	3.079(4)	159	none
N3–H3A···F4	0.86	2.55	3.179(4)	130	none
N4–H4A···F4	0.86	2.28	3.080(4)	156	$x, -y+1/2, z-1/2$
N4–H4A···F6	0.86	2.55	3.254(4)	140	$x, -y+1/2, z-1/2$
N4–H4A···F2	0.86	2.65	3.150(4)	118	$x, -y+1/2, z-1/2$
N5–H5A···F1	0.86	2.07	2.866(4)	153	none
N6–H6A···F4	0.86	2.17	2.928(4)	147	$-x+1/2, y, z-1/2$
N6–H6A···F5	0.86	2.43	3.074(4)	132	$-x+1/2, y, z-1/2$
N7–H7A···F1	0.86	2.92	3.256(4)	105	none
N7–H7A···S3	0.86	2.79	3.569(3)	152	none
N8–H8A···O1W	0.86	1.99	2.812(5)	160	none
O1W–H1W···F5	0.84(3)	1.95(4)	2.789(4)	177	$x-1/2, -y+1, -z+1/2$
O1W–H2W···F3	0.84(4)	1.96(4)	2.792(4)	176	$-x-1/2, y, z-1/2$
5. N1–H1A···F1	0.86	2.22	3.014(3)	154	none
N2–H2A···F3	0.86	1.96	2.803(3)	165	$-x+1/2, -y+1/2, z+1/2$
6. N1–H1A···F1	0.86	2.06	2.902(3)	165	$-x+1/2, y, z-1/2$
N2–H2A···F3	0.86	2.17	2.832(3)	134	$x-1/2, y-1/2, -z$
N3–H3A···F1	0.86	1.98	2.798(3)	159	none
N4–H4A···F2	0.86	2.14	2.745(3)	126	$x-1/2, y-1/2, -z$

Bond distances are in Å, angles in degrees.
Where the transformation of A is indicated as "none", the hydrogen bonds are between cation–anion pairs within the asymmetric unit.

metric unit each takes part in two N–H···F hydrogen bonds, of lengths 2.902(3), 2.832(3) Å for one ligand and 2.798(3), 2.745(3) Å for the other, the hydrogen bonding is shown in Fig. 9. The N–H···F hydrogen bonds in the present work are relatively weak compared to the strong such bonds observed recently in two fluoromanganates(III) complexes where the N···F distances are 2.657(2) and 2.668(3) Å [22].

6. The red colour

The crystals of complexes **1**–**5** are red, those of **6** yellow; $[Te(etu)_4]^{2+}$ or $[Te(trtu)_4]^{2+}$ salts with colourless anions are usually pale yellow, some with a green tinge [14,23,24]. However, in solution all the six complexes had the same yellow-orange colour. This shows that a conformational change takes place in **1**–**5** upon

crystallization as the special cation–anion pairs form in the solid state.

The "red shift" of disulfides, X–S–S–X, or diselenides, X–Se–Se–X, occurs when the torsion angle at the S–S or Se–Se bond differs from its preferred value of ca. 90°. A smaller torsion angle results in considerable overlap of the two sulfur or selenium lone pair p orbitals to give rise to doubly occupied π and π* molecular orbitals. The red shift results from an electronic transition from the higher lying π* orbital to a σ* molecular orbital, the energy of the first is increasing with decreasing torsion angle while latter is independent of the torsion angle [25–27]. In the crystals of $R_2NC(S)Se–Se(S)CNR_2$ with R = cyclohexyl, the torsion angle at the Se–Se bond is 84.4° and the crystals are yellow, whereas with R = ethyl the torsion angle is 180° and the crystals are red [28].

In the crystals of the $[Te(etu)_4]^{2+}$ and $[Te(trtu)_4]^{2+}$ complex cations a ligand TeS_4/TeSC tilt angle (≈*cis*-S–Te–S–C torsion angle) different from ca. 90° will give rise to overlap of the filled Te 5p orbital, normal to the TeS_4 plane, and the Spπ orbital, with change of energy levels and red shift as in the disulfides and diselenides. A red square planar Te(II) complex containing a planar TeS_4 coordination group has been encountered earlier; the complex of Te dibenzenethiosulfonate with tetramethylthiourea, *trans*-$[Te(S_2O_2Ph)_2(tmtu)_2]$ [29]. The space group is $P2_1/c$ (No. 14) with $Z = 2$; the Te atom lies on a centre of symmetry. Its crystal structure was determined by Åse and Roti [30]. A deviation of 11.51(51)° from the ideal 90° of the S–Te–S angles was found, and this was thought to be a possible cause of the red colour [30]. However, from the given coordinates a TeS_4/TeSC tilt angle as small as 5.9(6)° for the tetramethylthiorea ligand is calculated. Thus the *cis*-S–Te–S–C torsion angle is close to 180°, and this is clearly the cause.

7. Supplementary data

Deposition numbers CCDC 235767–235772 contain the supplementary crystallographic data for this paper. These data can be obtained free of charge via www.ccdc.cam.ac.uk/data_request/cif, or by emailing to data_request@ccdc.cam.ac.uk, or by contacting The Cambridge Crystallographic Data Centre, 12, Union Road, Cambridge CB2 1EZ, UK; fax: +44 1223 336033.

References

[1] Enraf-Nonius Structure Determination Package, Enraf-Nonius, Delft, The Netherlands, 1987.
[2] Bruker AXS, SHELXTL 6.14, Bruker AXS Inc., Madison, WI, USA, 2003.
[3] A.L. Spek, J. Appl. Cryst. 36 (2003) 7.
[4] H.K. Ault, S. Husebye, Acta Chem. Scand. A 32 (1978) 157.
[5] O. Foss, unpublished results.
[6] F.H. Allen, O. Kennard, D.G. Watson, L. Brammer, A.G. Orpen, R. Taylor, J. Chem. Soc., Perkin Trans. II (1987) S1.
[7] D.A. Berta, W.A. Spofford, P. Boldrini, E.L. Amma, Inorg. Chem. 9 (1970) 136.
[8] O. Foss, K. Maartmann-Moe, Acta Chem. Scand. A 41 (1987) 310.
[9] I. Haiduc, R.B. King, M.G. Newton, Chem. Rev. 94 (1994) 301.
[10] O. Foss, K. Maartmann-Moe, K. Marøy, Acta Chem. Scand. A 40 (1986) 685.
[11] S. Husebye, in: F.J. Berry, W.R. McWhinnie (Eds.), Proceedings of the Fourth International Conference on the Organic Chemistry of Selenium and Tellurium, The University of Aston, Birmingham, UK, 1983, p. 298.
[12] S. Husebye, K.W. Törnroos, H. Zhu, Z. Anorg. Allg. Chem. 627 (2001) 1921.
[13] S. Husebye, D. Mughannam, K.W. Törnroos, Phosphorus, Sulfur Silicon 178 (2003) 1825, and 2307.
[14] R.C. Elder, T. Marcuso, P. Boolchand, Inorg. Chem. 16 (1977) 2000.
[15] A. Bondi, J. Phys. Chem. 68 (1964) 441.
[16] J.L. Sessler, M.J. Cyr, V. Lynch, E. McGhee, J.A. Ibers, J. Am. Chem. Soc. 112 (1990) 2810.
[17] L.K. Thompson, C.J. Matthews, L. Chao, M.A. Leech, J.A.K. Howard, J. Chem. Soc., Dalton Trans. (2001) 2258.
[18] Z. Zhang, M. Shao, X. Xu, Y. Tang, Y. Tu, Kexue Tongbao (Chin. Sci. Bull.) 28 (1983) 905, ref. no. BADCIS30 in CCDB.
[19] H. Maluzynska, Acta Cryst. C 50 (1994) 1909.
[20] S. Husebye, K.W. Törnroos, H. Zhu, Acta Cryst. C 57 (2001) 854.
[21] T.K. Venkatashalam, E. Sudbeck, F.M. Uckun, J. Mol. Struct. 687 (2004) 45.
[22] P. Nunez, J.C. Ruiz-Morales, A.D. Lozano-Gorrin, P. Gili, V.D. Rodriguez, J. Gonzales-Platas, T. Barriuso, F. Rodriguez, J. Chem. Soc., Dalton Trans. (2004) 273.
[23] O. Foss, S. Fossen, Acta Chem. Scand. 15 (1961) 1620.
[24] O. Foss, K. Marøy, Acta Chem. Scand. 15 (1961) 1947.
[25] G. Bergson, Arkiv Kemi 12 (1957) 233.
[26] G. Bergson, G. Nordström, Arkiv Kemi 17 (1961) 569.
[27] M. Dötze, G. Klar, J. Chem. Research (S) (1993) 226.
[28] W. Dietzsch, J. Sieler, W. Meiler, W. Robien, Phosphorus Sulfur 38 (1988) 293.
[29] O. Foss, I.-J. Johannessen, Acta Chem. Scand. 15 (1961) 1943.
[30] K. Åse, I. Roti, Acta Chem. Scand. A 28 (1974) 104.

Available online at www.sciencedirect.com
SCIENCE DIRECT®
Polyhedron 23 (2004) 3033–3042
POLYHEDRON
www.elsevier.com/locate/poly

Hydrothermal synthesis and intercalation behavior of a layered titanium phosphate $Ti_2(H_2PO_4)(HPO_4)(PO_4)_2 \cdot 0.5C_6N_2H_{16}$, with an extended γ-phase intercalated into organic amine

Chao Chen, Yu-Lin Yang, Kun-Lin Huang, Zhen-Hua Sun, Wei Wang, Zhuo Yi, Yun-Ling Liu, Wen-Qin Pang *

State Key Laboratory of Inorganic Synthesis and Preparative Chemistry, College of Chemistry, Jilin University, Changchun 130012, P.R. China

Received 23 June 2004; accepted 30 August 2004
Available online 10 November 2004

Abstract

With a hydrothermal technique, a layered titanium phosphate with the formula $Ti_2(H_2PO_4)(HPO_4)(PO_4)_2 \cdot 0.5C_6N_2H_{16}$ (denoted **TP-J2**) has been prepared by treating the $Ti/H_3PO_4/H_2O$/1-methylpiperazine system directly. The as-synthesized products were characterized by powder X-ray diffraction, CP-MAS solid-state ^{31}P NMR spectroscopy, thermogravimetric and differential thermal analyses (TG-DTA). The structure was solved by single-crystal X-ray diffraction analysis and it presents an extended γ-phase intercalated with organic amine. Crystal data: triclinic, $P\bar{1}$, $a = 8.106$ (2) Å, $b = 8.197$ (2) Å, $c = 11.658$ (2) Å. $\alpha = 78.32$ (3)°, $\beta = 80.85$ (3)°, $\gamma = 77.90$ (3)°, $Z = 2$. Additionally, the intercalation behavior of **TP-J2** with *n*-alkyl monoamine ($n = 2$, 3, 4, 6, 8, 10 and 12) was investigated. Owing to the strong brønsted base, *N*,*N*′-dimethylpiperazine, resides in the interlayer, it presented unusual features of **TP-J2** in contrast with that of γ-Tip.
© 2004 Elsevier Ltd. All rights reserved.

Keywords: Hydrothermal; Layered; Titanium phosphate; Intercalation behavior; γ-Phase

1. Introduction

The intercalation chemistry of layered metal (IV) phosphates has been extensively studied because of their special functionalities in the field of photochemistry, electrochemistry, molecular recognition, ion exchange and catalysis [1]. Being members of the layered metal phosphates family, layered titanium phosphates of tetravalent metals have been of considerable interest recently[2]. At the present time, two main types, α- and γ-phase, of layered titanium (IV) phosphates, represented as $Ti(HPO_4)_2 \cdot H_2O$ and $Ti(H_2PO_4)(PO_4) \cdot 2H_2O$ (denote α-Tip and γ-Tip, respectively), are well known. Nevertheless, the number of published papers on the intercalation and the ion-exchange properties of γ-layered phosphates are much fewer than those of the α-phases, though the γ-layers are more rigid, thicker and acidic (owing to the presence of more terminal –OH groups bonded to the phosphorus) to be propitious to intercalate than that of the α-layered phosphates. This is probably due to the fact that structure of the γ-phase was only proposed and not well defined [3]. Therefore, precise structural data of γ-Tip is needed [4].

In recent years, we have devoted efforts towards the hydrothermal and solvothermal syntheses of single crystals of titanium phosphates to obtain possible new types of materials with valuable properties. Up to now, we have prepared 1-D chiral chain titaniumphosphates $[Ti_3P_6O_{27}] \cdot 5[NH_3CH_2CH_2NH_3] \cdot 2[H_3O]$ (JTP-A) and $[NH_3CH_2CH_2NH_3] \cdot [TiO(HPO_4)_2]$ (JTP-B) with zigzag

* Corresponding author. Tel.: +86 431 516 8546; fax: +86 431 516 8624.
E-mail address: wqpang@mail.jlu.edu.cn (W.-Q. Pang).

0277-5387/$ - see front matter © 2004 Elsevier Ltd. All rights reserved.
doi:10.1016/j.poly.2004.08.026

chains under solvothermal conditions [5,6], 2-D layer titaniumphosphates $[H_3NC_2H_4NH_2]TiOPO_4$ (TP-J1) and $Ti_2(HPO_4)_2(PO4)_2 \cdot C_2N_2H_{10}$ [7,8], as well as 3-D open-framework structures $Ti_3(H_2PO_4)(HPO_4)_{3.5}(PO_4)_2 \cdot C_2N_2H_{10}$, $Ti_2(HPO_4)_3(PO_4) \cdot 0.5C_4N_2H_{12}$, $Ti_7(HPO_4)_6(PO_4)_6 \cdot C_6N_2H_{14}$, with unique P/Ti ratios of 6/13, 1/2 and 7/12, respectively [8,9].

In this paper, a lamellar titanium phosphate, $Ti_2(H_2\text{-}PO_4)(HPO_4)(PO_4)_2 \cdot 0.5C_6N_2H_{16}$ denoted **TP-J2** (J=Jilin university), with an extended γ-phase (the arrangement of the macroanionic sheets are similar to that of the γ-phase) intercalated with organic amine, is reported. The structure was determined by single-crystal methods. Additionally, the intercalation behavior of **TP-J2** with *n*-alkyl monoamine ($n = 2$, 3, 4, 6, 8, 10 and 12) was investigated and presented some special features in contrast with that of γ-Tip.

2. Experimental

2.1. Synthesis

TP-J2 was hydrothermally prepared from a mixture of titanium powder (Shanghai Chemical Plant, 99%), phosphoric acid (Beijing Chemical Plant, 85 wt%), 1-methylpiperazine (ACROS, 99%) and distilled water. In a typical synthesis, 0.5 g of titanium powder was dissolved in 10.5 mL of phosphoric acid beforehand by heating, followed by the addition of distilled water and 2.8 mL of 1-methylpiperazine. The molar ratio of the initial mixture was 1.0 Ti:15 H_3PO_4:2.0 1-methylpiperazine:10 H_2O (pH 1.0). The mixture was aged at room temperature for 2 h, followed by transferring to a 16 mL Teflon-lined stainless-steel autoclave and heating under autogenous pressure at 240 °C for 6 days. The resulting products, with colorless plate crystals, were recovered by filtration, washed thoroughly with distilled water and dried overnight at 50 °C.

2.2. Intercalation by n-alkyl monoamine

The intercalation was performed by a batch method. In a typical procedure 300 mg of **TP-J2**, previously ground, was suspended in 10 mL of an aqueous solution of each *n*-alkyl monoamine ($n_c = 2$, 3, 4, 6, 8, 10, 12), ranging in concentration between 0.1 and 1 mol mL^{-1}. For each sample, the solution was stirred for 3–24 h at room temperature. Then the products were separated by centrifugation and dried at 50 °C.

2.3. Characterization

The powder X-ray diffraction (XRD) patterns were collected on a Siemens D5005 diffractometer with Cu Kα radiation ($\lambda = 1.5418$ Å) with a graphite monochromator. The step size was 0.02°, and the count time was 2 s. The elemental analysis was performed on a Perkin–Elmer 2400 analyzer and the inductively coupled plasma (ICP) analysis on a Perkin–Elmer Optima 3300 DV ICP spectrometer. Thermogravimetric (TG) and differential thermal analysis (DTA) were conducted on a Netzsch STA 449C thermogravimetric analyzer in air with a heating rate of 20 °C min^{-1}. CP-MAS solid-state ^{31}P NMR spectra was recorded on a Infinity-plus400WB instrument and referenced to 85% H_3PO_4 as external standard (downfield shifts positive). The pH measurements of the titration were made with a HANNA pH 211 Microprocessor pH Meter.

2.4. Determination of crystal structure

A suitable single crystal was selected for single-crystal XRD analysis. The data were collected on a Rigaku RAXIS RAPID IP diffractometer [λ(Mo Kα) = 0.71073 Å] at -80 ± 2 °C. Data processing was accomplished with the Process-Auto processing program. The structure was solved by direct methods and refined by full-matrix, least squares based on F^2 using the SHELXTL-5.1 [10] software package. The Ti and P atoms were first located, and the C, N and O atoms were found in difference Fourier maps. The hydrogen atoms residing on the amine molecules and inorganic frameworks were placed by geometrical considerations with d(N–H)=0.89 Å, d(C–H) = 0.97 Å and d(O–H) = 0.82 Å. All non-hydrogen atoms were refined anisotropically. Final refinement converged to $R_1 = 0.0284$ and $wR_2 = 0.1221$ ($I > 2\sigma(I)$). Crystal data and details of data collection and refinement are given in Table 1.

3. Results and discussion

3.1. Synthesis and analysis

Generally, γ-Tip is obtained by the reflux method and the product is a powder [11,12]. Recently, Férey and ourselves reported an extended γ-Tip intercalated with ethylenediamine, determined by single-crystal XRD analysis [8,13], but the P atoms were disordered and the structure determination was of poor quality. Herein, with the hydrothermal technique, we obtained an extended γ-Tip intercalated into amine with a rigid structure by treating the Ti/H_3PO_4/H_2O/1-methylpiperazine system directly, and the structure was solved by single-crystal X-ray diffraction analysis. By the structure determination, it is interesting to note that the organic species between the inorganic layers of **TP-J2** is *N*,*N*′-dimethylpiperazine rather than 1-methylpiperazine which was added in the initial reaction mixture. The result was proved by ^{13}C NMR spectra of the as-synthesized products, as shown in supporting information. It is perhaps

Table 1
Crystal data and structure refinement for **TP-J2**

Empirical formula	$C_3H_{11}NO_{16}P_4Ti_2$
Formula weight	536.81
Temperature for data collection (K)	193(2)
Wavelength (Å)	0.71073
Crystal system, space group	triclinic, $P\bar{1}$
Unit cell dimensions	
a (Å)	8.1060(16)
b (Å)	8.1970(16)
c (Å)	11.658(2)
α (°)	78.32(3)
β (°)	80.85(3)
γ (°)	77.90(3)
Volume (Å^3)	736.2(3)
Z	2
D_{calc} (g/cm^3)	2.422
Absorption coefficient (mm^{-1})	1.614
$F(000)$	536
Crystal size (mm)	$0.350 \times 0.240 \times 0.024$
θ Range for data collection (°)	1.80–27.41
Limiting indices	$0 \leqslant h \leqslant 10$, $-10 \leqslant k \leqslant 10$, $-14 \leqslant l \leqslant 15$
Reflections collected/unique (R_{int})	6646/3287 (0.0251)
Completeness to $\theta = 27.41$ (%)	97.7
Maximum and minimum transmission	1.0851 and 0.8256
Refinement method	full-matrix least-squares on F^2
Goodness-of-fit on F^2	0.982
Final R indices [$I > 2\sigma(I)$]	$R_1 = 0.0284$, $wR_2 = 0.1221$
R indices (all data)	$R_1 = 0.0381$, $wR_2 = 0.1301$
Largest differential peak and hole (e Å^{-3})	0.713, −0.759

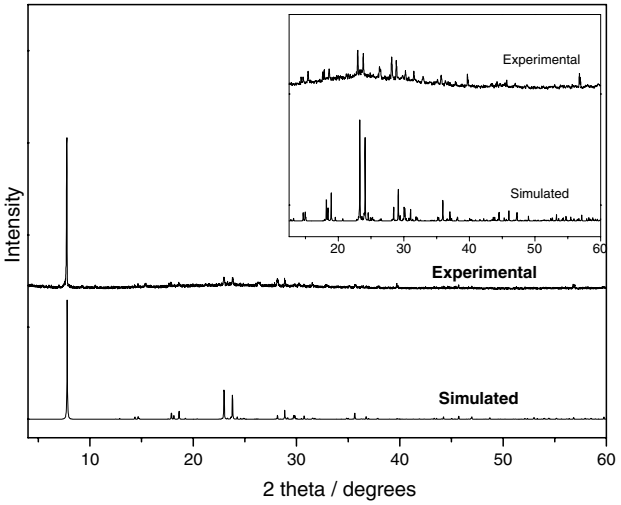

Fig. 1. Experimental XRD curve and simulated XRD curve of **TP-J2**. An enlargement of the 12.5–60° range plot is added at the top right of the figure.

explained that *N*,*N*′-dimethylpiperazine is formed by a decomposed-recomposed process of 1-methylpiperazine under high temperature and pressure conditions (513 K, hydrothermal autogenous pressure conditions), as given by Scheme 1.

The powder XRD pattern of **TP-J2** (Fig. 1) is entirely consistent with that simulated on the basis of the single-crystal structure. The diffraction peaks in both measured and simulated patterns correspond well to each other in position, indicating the phase purity of the as-synthesized sample. The ICP and elemental analysis results show that **TP-J2** contains Ti: 17.21, P: 23.08, C: 6.42, H: 2.72, and N: 2.65 wt%, in good agreement with the calculated values (Ti: 17.84, P: 23.10, C: 6.76, H: 2.05, and N: 2.60 wt%) based on the single-crystal structure formula.

CP-MAS solid-state ^{31}P NMR spectra of the as-synthesized compound are shown in Fig. 2. **TP-J2** gave shifts of −13.64, −17.97, −26.56, −30.03 ppm with equal intensity. On the basis of the previous studies on titanium phosphates and zirconium phosphates [13–15], we assigned the NMR peaks at −13.64 ppm to the H_2PO_4 group and −17.97 ppm to the HPO_4 group. The signals at −26.56 and −30.03 ppm can be attributed to the PO_4 groups. These assignments are all in good agreement with the structure derived from the single-crystal X-ray diffraction. The TG-DTA analyses of **TP-J2** have been performed in the temperature range 25–1000 °C. From Fig. 3, we can see **TP-J2** is thermally stable until 410 °C. A mass loss of 12.6 wt% (cal. 12.48 wt%) at 410–750 °C corresponds to the decomposition of the amine molecules and the partial dehydroxylation (forming of 0.5 mol water). Then the structure collapses and converts to an amorphous phase after calcination at 700 °C, as confirmed by powder X-ray diffraction. Finally, the amorphous phase recrystallizes to form a TiP_2O_7 phase (JCPDS: 38-1468) at 880–950 °C. The

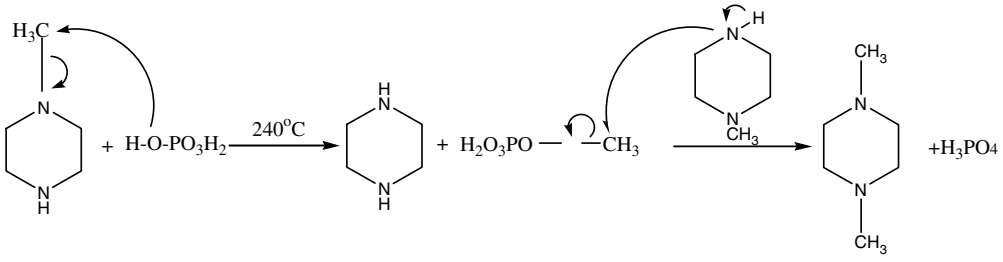

Scheme 1.

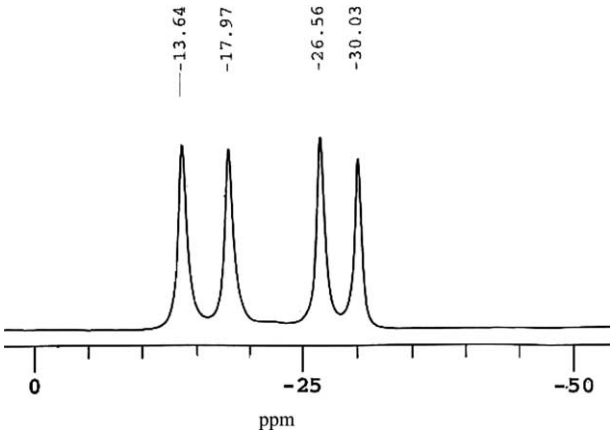

Fig. 2. CP-MAS solid-state ^{31}P NMR spectra for **TP-J2**.

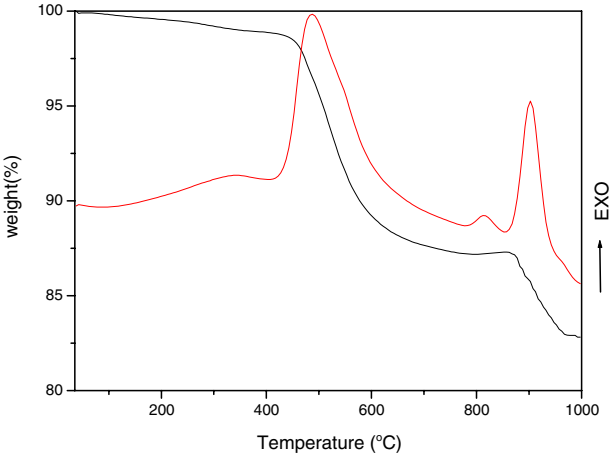

Fig. 3. TG-DTA curves of **TP-J2**.

DTA curve exhibits three exothermic peaks corresponding to the decomposition of the template.

3.2. Structure description of *TP-J2*

The asymmetric unit of **TP-J2** is shown in Fig. 4. It contains two crystallographically distinct Ti sites, each being coordinated octahedrally by oxygen atoms. The Ti–O bond lengths and O–Ti–O bond angles are in the range 1.877(2)–1.994(2) Å and 84.97(10)–178.16(9)°, which are in good agreement with those reported previously for other titanium phosphates. Of the four crystallographically distinct P sites, P(1) and P(2) share four bridging oxygen atoms with adjacent Ti atoms, with the P–O distances varying between 1.507(2) and 1.536(2) Å. P(3) and P(4) both share two bridge oxygens with adjacent Ti atoms, leaving two oxygens on their terminal. But the terminal oxygens of the two phosphate tetrahedron are different. For P(3), the longer bond length of P(3)–O(13) (1.573 (3) Å) indicates that a proton is bonded to O(13). The distance of the P(3)–O(10) bond is slightly shorter (1.527(2) Å), but for charge balance, an H atom must also be bonded to O(10). For P(4), the two terminal P(4)–O bond lengths are 1.502(2) Å (P(4)–O(14)) and 1.567(2) Å (P(4)–O(12)), which imply the presence of one P=O group and one hydroxyl group. The final atomic coordinates, selected bond lengths and angles are listed in Tables 2 and 3, respectively.

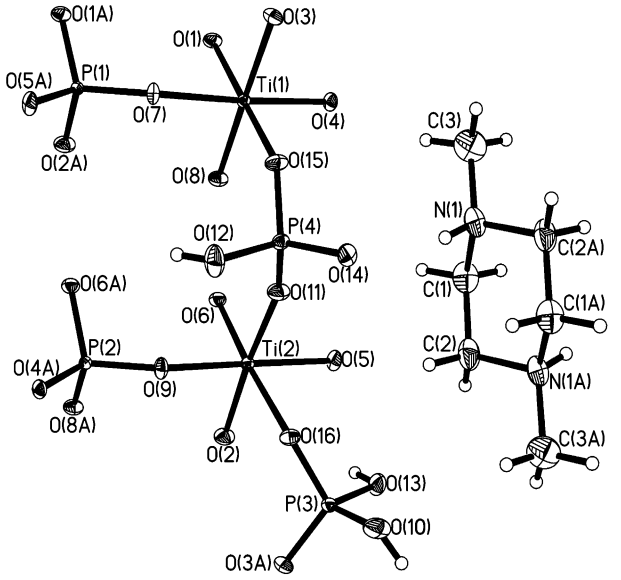

Fig. 4. Thermal ellipsoid plot (50% probability) and atomic labelling scheme for an asymmetric unit of **TP-J2**.

Table 2
Atomic coordinates ($\times 10^4$) and equivalent isotropic displacement parameters ($Å^2 \times 10^3$) for **TP-J2**

Atom	*x*	*y*	*z*	U_{eq}
Ti(1)	5104(1)	2954(1)	8636(1)	7(1)
Ti(2)	170(1)	7842(1)	8671(1)	7(1)
P(1)	2755(1)	32(1)	9457(1)	7(1)
P(2)	−2287(1)	5042(1)	9400(1)	7(1)
P(3)	−1326(1)	11340(1)	7042(1)	10(1)
P(4)	2745(1)	5637(1)	6740(1)	10(1)
O(1)	6046(3)	1506(3)	9996(2)	12(1)
O(2)	−1611(3)	9104(3)	9586(2)	16(1)
O(3)	6842(3)	1794(3)	7548(2)	13(1)
O(4)	6597(3)	4522(3)	8651(2)	11(1)
O(5)	1641(3)	9498(3)	8701(2)	14(1)
O(6)	1043(3)	6499(3)	10061(2)	12(1)
O(7)	3731(3)	1291(3)	8619(2)	11(1)
O(8)	3379(3)	4113(3)	9611(2)	13(1)
O(9)	−1255(3)	6284(3)	8591(2)	12(1)
O(10)	−1069(3)	11986(3)	5714(2)	25(1)
O(11)	1930(3)	6760(3)	7651(2)	16(1)
O(12)	1367(3)	4750(3)	6448(2)	23(1)
O(13)	−181(3)	12224(3)	7599(2)	19(1)
O(14)	3331(3)	6643(3)	5575(2)	15(1)
O(15)	4191(3)	4324(3)	7235(2)	14(1)
O(16)	−637(3)	9451(3)	7273(2)	12(1)
C(1)	4994(5)	9480(5)	6252(3)	27(1)
C(2)	3520(5)	10689(5)	5735(3)	28(1)
C(3)	7375(6)	7081(6)	5949(4)	35(1)
N(1)	5923(4)	8307(4)	5431(3)	22(1)

U_{eq} is defined as one third of the trace of the orthogonalized U_{ij} tensor.

Table 3
Selected bond lengths (Å) and angles (°) for **TP-J2**[a]

Bond lengths			
Ti(1)–O(8)	1.877(2)	P(1)–O(7)	1.528(2)
Ti(1)–O(1)	1.935(2)	P(1)–O(5)#3	1.536(2)
Ti(1)–O(7)	1.937(2)	P(2)–O(4)#4	1.525(2)
Ti(1)–O(15)	1.942(2)	P(2)–O(8)#2	1.528(2)
Ti(1)–O(4)	1.946(2)	P(2)–O(9)	1.531(2)
Ti(1)–O(3)	1.964(2)	P(2)–O(6)#2	1.534(2)
Ti(2)–O(11)	1.895(2)	P(3)–O(3)#5	1.507(2)
Ti(2)–O(2)	1.903(2)	P(3)–O(16)	1.516(2)
Ti(2)–O(6)	1.911(2)	P(3)–O(10)	1.527(2)
Ti(2)–O(9)	1.916(2)	P(3)–O(13)	1.573(3)
Ti(2)–O(16)	1.982(2)	P(4)–O(14)	1.502(2)
Ti(2)–O(5)	1.994(2)	P(4)–O(15)	1.517(2)
P(1)–O(1)#1	1.516(2)	P(4)–O(11)	1.526(2)
P(1)–O(2)#2	1.524(2)	P(4)–O(12)	1.567(3)
Bond angles			
O(8)–Ti(1)–O(1)	91.21(10)	O(6)–Ti(2)–O(5)	88.79(10)
O(8)–Ti(1)–O(7)	91.56(10)	O(9)–Ti(2)–O(5)	178.16(9)
O(1)–Ti(1)–O(7)	88.79(10)	O(16)–Ti(2)–O(5)	84.97(10)
O(8)–Ti(1)–O(15)	90.90(10)	O(1)#1–P(1)–O(2)#2	110.48(13)
O(1)–Ti(1)–O(15)	177.50(9)	O(1)#1–P(1)–O(7)	111.34(13)
O(7)–Ti(1)–O(15)	89.81(10)	O(2)#2–P(1)–O(7)	110.05(13)
O(8)–Ti(1)–O(4)	91.13(10)	O(1)#1–P(1)–O(5)#3	110.06(13)
O(1)–Ti(1)–O(4)	89.31(10)	O(2)#2–P(1)–O(5)#3	108.96(14)
O(7)–Ti(1)–O(4)	176.74(9)	O(7)–P(1)–O(5)#3	105.82(13)
O(15)–Ti(1)–O(4)	91.99(10)	O(4)#4–P(2)–O(8)#2	110.52(13)
O(8)–Ti(1)–O(3)	177.06(10)	O(4)#4–P(2)–O(9)	107.85(13)
O(1)–Ti(1)–O(3)	91.65(10)	O(8)#2–P(2)–O(9)	109.95(13)
O(7)–Ti(1)–O(3)	87.80(10)	O(4)#4–P(2)–O(6)#2	110.93(13)
O(15)–Ti(1)–O(3)	86.23(10)	O(8)#2–P(2)–O(6)#2	109.23(13)
O(4)–Ti(1)–O(3)	89.61(10)	O(9)–P(2)–O(6)#2	108.33(13)
O(11)–Ti(2)–O(2)	174.84(10)	O(3)#5–P(3)–O(16)	113.12(13)
O(11)–Ti(2)–O(6)	93.08(10)	O(3)#5–P(3)–O(10)	111.44(14)
O(2)–Ti(2)–O(6)	91.50(10)	O(16)–P(3)–O(10)	108.69(14)
O(11)–Ti(2)–O(9)	90.82(11)	O(3)#5–P(3)–O(13)	109.95(14)
O(2)–Ti(2)–O(9)	91.33(10)	O(16)–P(3)–O(13)	107.38(13)
O(6)–Ti(2)–O(9)	93.00(10)	O(10)–P(3)–O(13)	105.94(15)
O(11)–Ti(2)–O(16)	88.80(10)	O(14)–P(4)–O(15)	111.52(13)
O(2)–Ti(2)–O(16)	86.39(10)	O(14)–P(4)–O(11)	112.37(14)
O(6)–Ti(2)–O(16)	173.44(10)	O(15)–P(4)–O(11)	109.27(14)
O(9)–Ti(2)–O(16)	93.26(10)	O(14)–P(4)–O(12)	104.10(14)
O(11)–Ti(2)–O(5)	88.64(11)	O(15)–P(4)–O(12)	110.35(14)
O(2)–Ti(2)–O(5)	89.06(10)	O(11)–P(4)–O(12)	109.10(15)

[a] Symmetry transformations used to generate equivalent atoms: #1 $-x+1, -y, -z+2$; #2 $-x, -y+1, -z+2$; #3 $x, y-1, z$; #4 $x-1, y, z$; #5 $x-1, y+1, z$; #6 $x+1, y-1, z$; #7 $x+1, y, z$; # 8 $x, y+1, z$; #9 $-x+1, -y+2, -z+1$.

Although neither unit cells nor space group are correlated, analysis shows the arrangement of the topological structure of **TP-J2** is similar to that of γ-TiP, $[Ti(PO_4)(H_2PO_4)]_2H_2O$. Thus, the individual $[Ti_2(H_2PO_4)(HPO_4)(PO_4)_2]^-$ macroanionic sheet is constructed from infinite corner-sharing 4-ring chains formed by PO_4 tetrahedra and TiO_6 octahedra alternatively. The chains are linked by sharing oxygen atoms so as to form a 2-D network. A highlight of the difference from γ-TiP is the alignment of the terminal P–O groups, located alternatively above and below the sheets. The dihydrogenphosphate groups of γ-TiP are tilted to one side of the adjacent plane, whereas the directions of H_2PO_4 and HPO_4 groups in **TP-J2** are tilted to the left and right relative to the layer by about 30° and 60°, respectively (Fig. 5). The alignment perhaps achieves maximum hydrogen bonding. The diprotonated *N*,*N*′-dimethylpiperazine cations are sandwiched between the sheets which relate to the intercalation of amine into γ-TiP. Extensive H-bonds exist between the organic cations and the framework oxygens. Each proton of the N atoms in the organic cations forms a H-bond with O(14) attached to the phosphate groups (d(N1–H1…O14) = 2.702 Å), and there are strong intralayer H-bonds between O12–H12…O13 = 2.663 Å, O13–H13…O6 = 3.044 Å.

3.3. Intercalation behavior

Owing to the structural similarity of the lamellae between **TP-J2** and γ-TiP, it is essential to investigate the intercalation behavior of **TP-J2**. Herein, a systematic study of the intercalation of **TP-J2** with *n*-alkyl monoamines (n = 2, 3, 4, 6, 8 and 12) has been carried out. There are more differences of intercalation behavior in comparison with that of γ-TiP.

Generally, titration curves of the layered metal phosphates can present the steps of formation of intermediate intercalation compounds and the amount of amine intercalated at various stages of addition can be deduced directly because the added amines are quantitatively intercalated [16]. However, in our preliminary work of intercalation, it was found that the titration curves (present in Fig. 6) increased quickly from the initial pH value of about 3.0 to pH 9.5 where a plateau was presented and the maximum uptake of amine per formula weight of **TP-J2** was only about 0.2 mol, which is far less than that of the previous report (about 1.0–1.5 mol per formula weight of γ-phase at pH >9.0) [17–19]. Furthermore, the pH value declined extremely slowly (over about 12 h) to neutral and the interlayer distance of the final phase was the same as that of initial phase (d_{001} = 13.3 Å). It can be concluded that the added amines did not quantitatively intercalate into **TP-J2** immediately and the titration curve was not suit for this intercalation system. This behavior may be attributed to the difference of the ''guest'' molecules residing in the interlayer. For γ-TiP, the guest molecules are neutral water, a very weak brønsted base. For **TP-J2**, however, the diprontonated *N*,*N*′-dimethylpiperazine cations are anchored between the layers and strong H-bonds exist between the organic cations and the framework oxygens to ensure the stability of the structure (see structure description). It is difficult to exchange the *N*,*N*′-dimethylpiperazine cations or enlarge the interlayer distance to permit the intercalation of the alkylamines. Only if decreasing the energy between the organic cations and the inorganic anions sheet, that is, increasing the additional amine and deprontonating the *N*,*N*′-dimethylpiperazine cations,

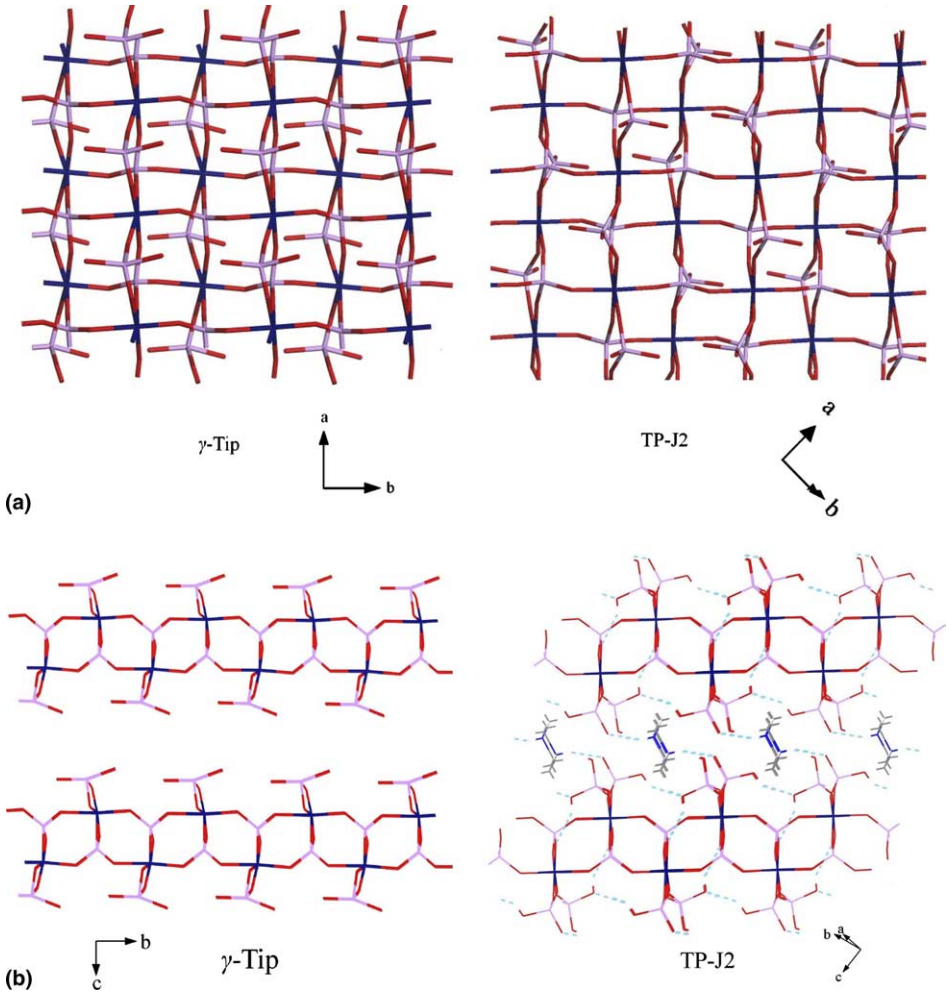

Fig. 5. (a) The sheets of γ-TiP and **TP-J2** viewed along the [0 0 1] direction. (b) Comparison of the structures between γ-TiP and **TP-J2**. Note the difference of orientation of the terminal P–O groups located alternatively above and below the sheets. Hydrogen bonds involving the organic amine molecules and hydroxyl groups of **TP-J2** are marked.

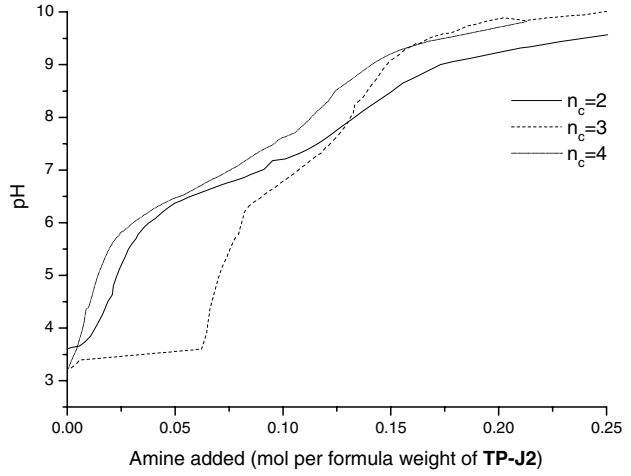

Fig. 6. Potentiometric titration curves for TP-J2 with aqueous solutions of ethylamine, propylamine and butylamine.

can the intercalation behavior proceed. From the titration curves, the plateau present at pH >9.5 and the uptake of amine per formula weight of **TP-J2** higher than 0.2 mol, is the process of deprontonation of the *N*,*N*′-dimethylpiperazine cations. Once the deprontonation of the *N*,*N*′-dimethylpiperazine cations is accomplished, the intercalation phases can be obtained at lower energy.

Consideration of overcoming the energy barrier between the *N*,*N*′-dimethylpiperazine cations and the interlamellae, an excess amount of *n*-alkyl monoamines (about 10 mol amine per formula weight of **TP-J2**) were added into the intercalation system. The final intercalated compounds were expected and characterized by XRD, thermogravimetric and elemental analysis. From XRD patterns, as shown in Fig. 7(a), it can be observed the interlayer distance corresponding to the intercalation compounds of *n*-alkyl monoamine appeared at a lower angle than that ($d = 13.3$) of the host **TP-J2**. As in previous reports, with the exception of the intercalation compound with ethylamine, the interlayer distances increase linearly with the increase of the number of carbon atoms, which suggests that the alkyl monoamines intercalated are regularly

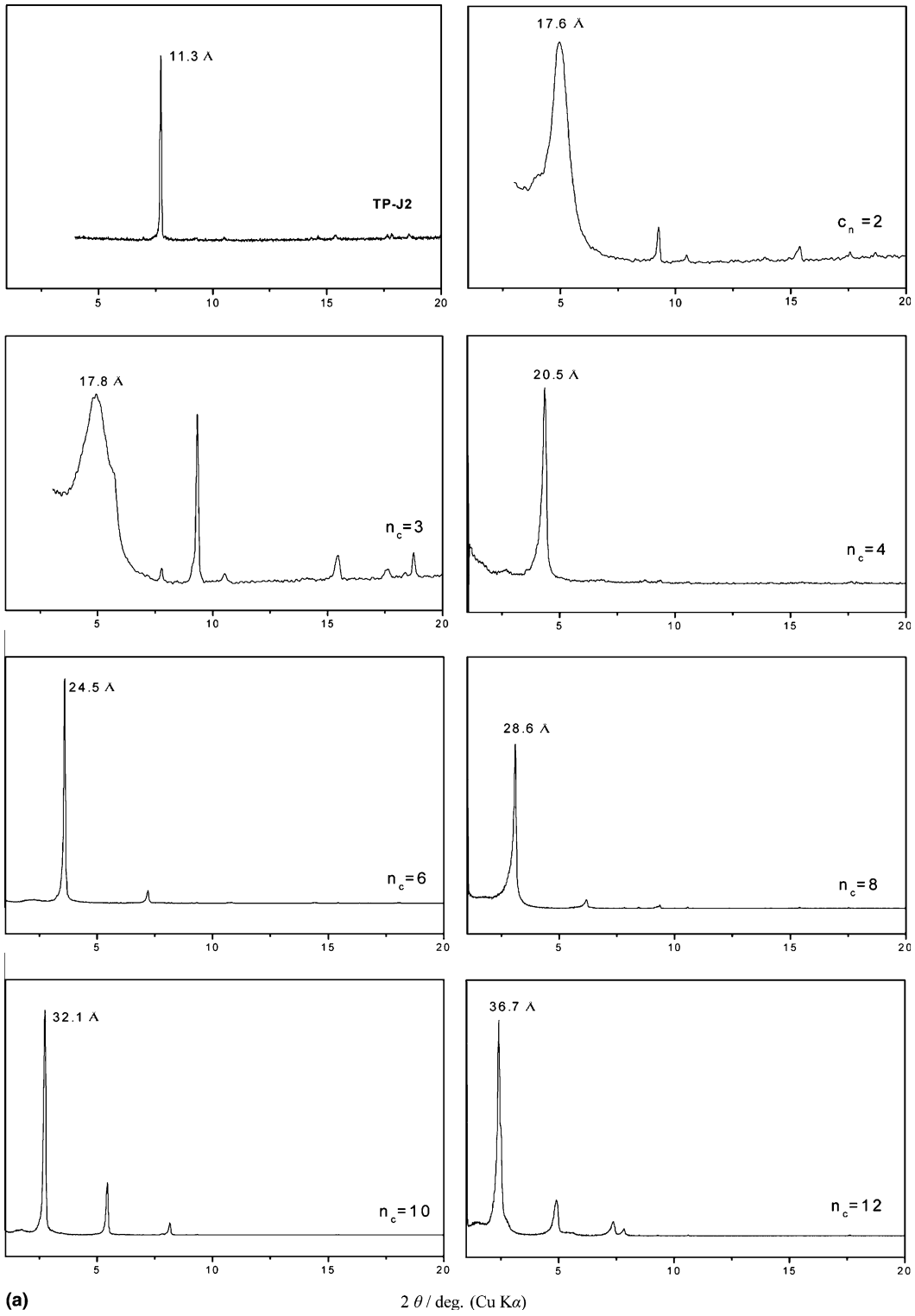

Fig. 7. (a) XRD patterns of **Tp-J2** and intercalation compounds with *n*-alkyl monoamines (*n* = 2, 3, 4, 6, 8 and 12). (b) TGA curves of **Tp-J2** and intercalation compounds with *n*-alkyl monoamines (*n* = 2, 3, 4, 6, 8 and 12).

oriented in the interlayer region of **TP-J2** and the angle to the layer is constant (Fig. 8). In the case of the intercalation compound with ethylamine, the formation of a thin film or membrane through removal of water by slightly heating was observed, and it should be exfoliated in packets of a few lamellae [20]. By elemental and thermogravimetric analysis, the formula is $Ti_2H_{2.75}(PO_4)_4 \cdot 1.25C_2H_5NH_3 \cdot H_2O$, indicating that

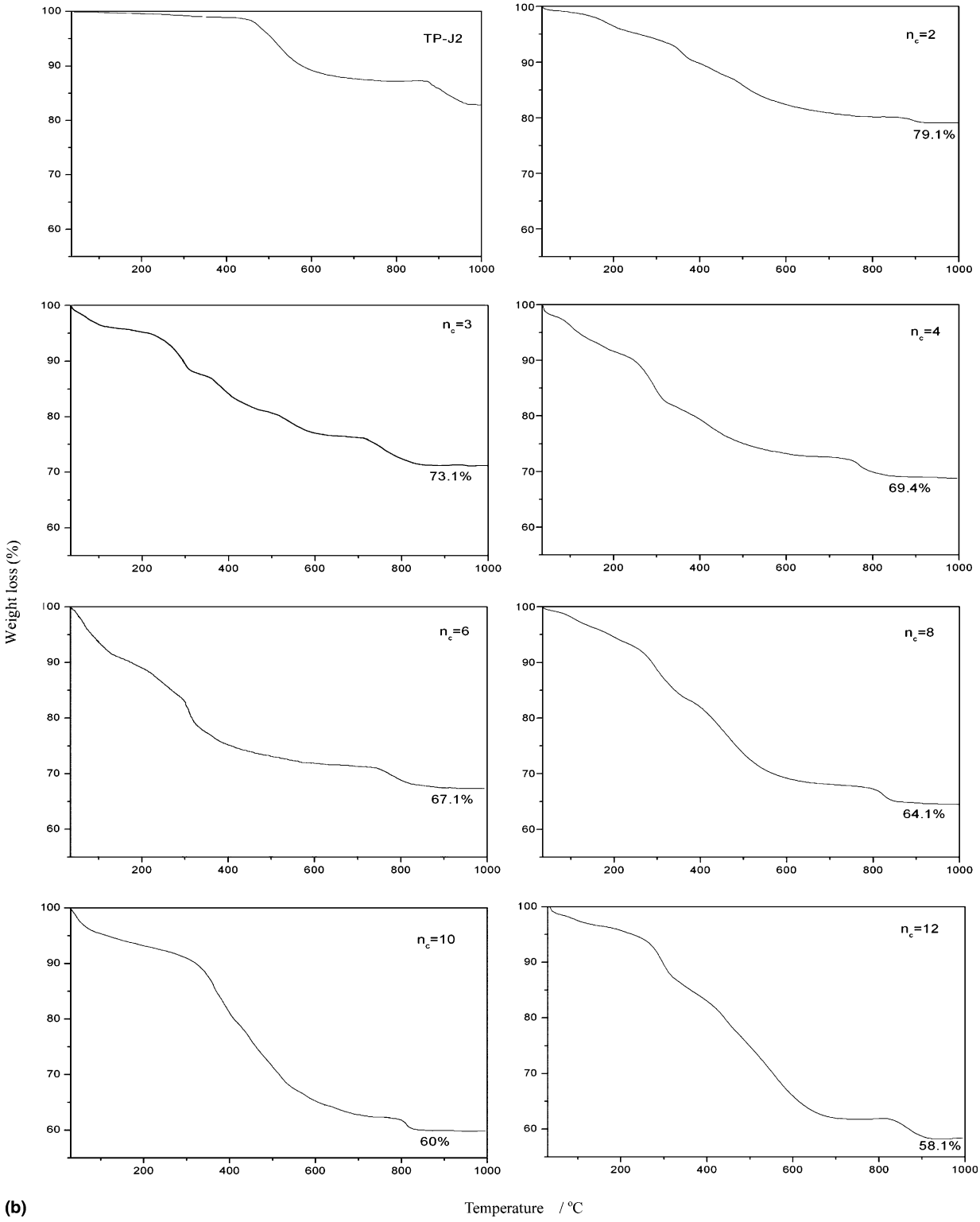

Fig. 7 (*continued*)

the initial *N*,*N*′-dimethylpiperazines were fully displaced by ethylamine. However, for *n*-alkyl mononamines with $n_c = 3$, 4, 6, 8, 10 and 12, the components were more complex. By means of C and N analysis, the C/N ratios corresponding to the intercalation compounds with alkyl chains amines were about 3.0, 3.67, 5.0, 6.33, 7.67 and 9.0, respectively. Nevertheless, the C/N ratios for *n*-alkylmonamine ($n_c = 3$, 4, 6, 8, 10, 12) were equal to their C atom numbers. Therefore, some *N*,*N*′-dimethylpiperazines must remain in the

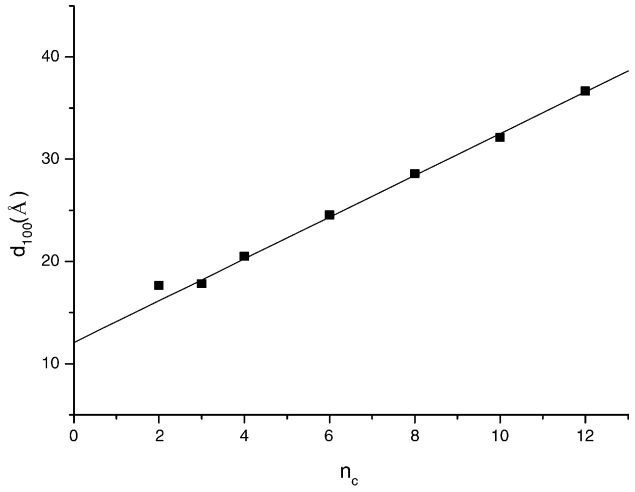

Fig. 8. Interlayer distances of intercalation compounds of **TP-J2** with *n*-alkylamines vs. the number of carbon atoms in the alkyl chain.

interlayer of the intercalated compounds. Considering the C/N ratios, 1/4 mol *N*,*N*′-dimethylpiperazine plus 1 mol $C_nH_{2n+1}NH_3$ is consistent with the experiment values, so it is believed the organic formulas of the intercalated compounds are $[1/4C_6N_2H_{16} + C_nH_{2n+1}NH_3]$. By the thermal decomposition of the intercalation compounds, whose the weight loss curves are shown in Fig. 7(b) and are similar to those reported previously, we can obtain their general formula: $Ti_2(PO_4)_4H_{2.125} \cdot 1.25[0.25C_4N_2H_{16} \cdot C_nH_{2n+1}NH_3] \cdot H_2O$. The experimental and calculated values are in good agreement (see Table 4). The reaction may be represented by Eq. (1).

$$Ti_2(H_2PO_4)(HPO_4)(PO_4)_2 \cdot 0.5C_6N_2H_{16} + 1.25C_nH_{2n+1}NH_2 \rightarrow Ti_2(PO_4)_4H_{2.125} \cdot 1.25[0.25C_4N_2H_{16} \cdot C_nH_{2n+1}NH_3] \cdot H_2O + 0.175C_6N_2H_{14} \quad (1)$$

Table 4
Microanalytical data (C and N) and weight loss at 1000 °C of intercalation compounds

Formula	Experimental				Calculated			
	% C	% N	% Weight loss	n_C/n_N	% C	% N	% Weight loss	n_C/n_N
$Ti_2H_{2.75}(PO_4)_4 \cdot 1.25C_2H_5NH_3 \cdot 0.5H_2O$	5.41	3.19	20.9	1.98	5.49	3.20	18.77	2.0
$Ti_2H_{2.125}(PO_4)_4 \cdot 1.25[0.25C_6N_2H_{16} \cdot C_3H_7NH_3] \cdot H_2O$	10.01	4.20	26.9	2.78	11.10	4.32	27.06	3.0
$Ti_2H_{2.125}(PO_4)_4 \cdot 1.25[0.25C_6N_2H_{16} \cdot C_4H_9NH_3] \cdot H_2O$	14.21	4.44	30.6	3.73	13.18	4.19	29.10	3.67
$Ti_2H_{2.125}(PO_4)_4 \cdot 1.25[0.25C_6N_2H_{16} \cdot C_6H_{13}NH_3] \cdot H_2O$	17.0	3.85	32.9	5.15	17.02	3.97	32.85	5.0
$Ti_2H_{2.125}(PO_4)_4 \cdot 1.25[0.25C_6N_2H_{16} \cdot C_8H_{17}NH_3] \cdot H_2O$	20.29	3.62	35.8	6.50	20.48	3.77	36.23	6.33
$Ti_2H_{2.125}(PO_4)_4 \cdot 1.25[0.25C_6N_2H_{16} \cdot C_{10}H_{21}NH_3] \cdot H_2O$	23.82	3.70	40.0	7.51	23.60	3.59	39.29	7.67
$Ti_2H_{2.125}(PO_4)_4 \cdot 1.25[0.25C_6N_2H_{16} \cdot C_{12}H_{25}NH_3] \cdot H_2O$	25.80	3.54	41.9	8.50	26.44	2.35	42.06	9.0

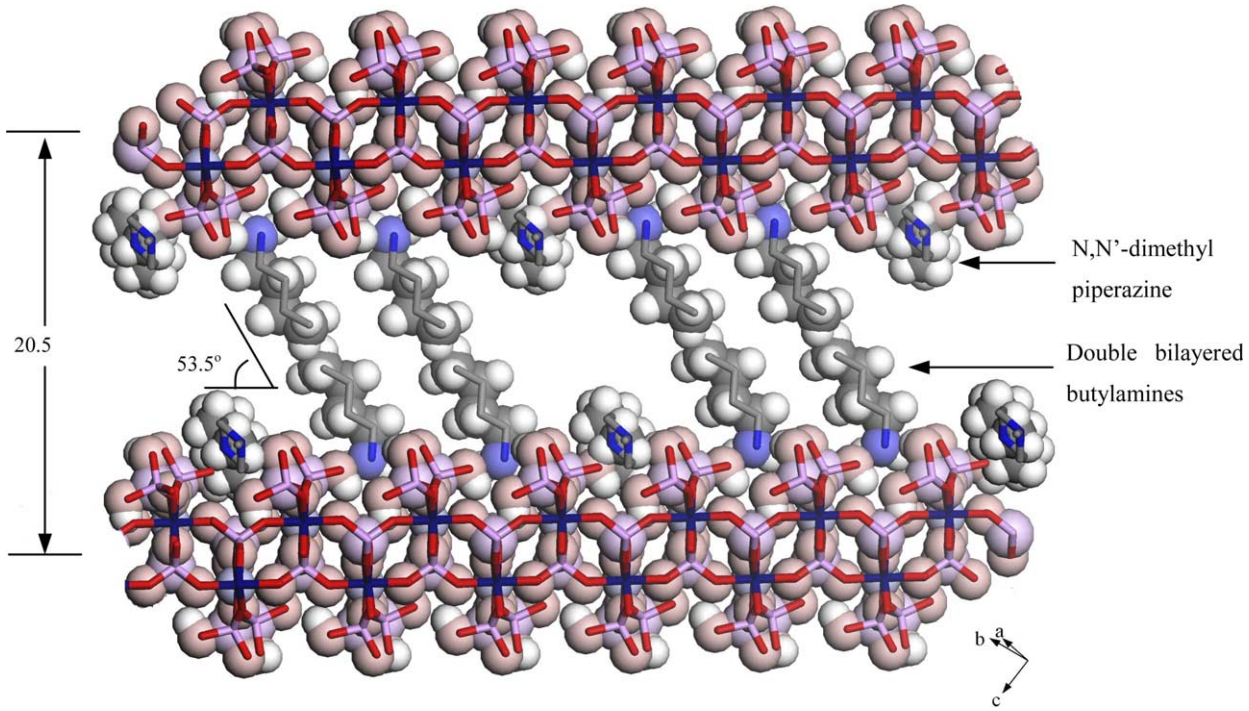

Fig. 9. Schematic model of the arrangement of *N*,*N*′-dimethylpiperazines and butylamines between the lamellae.

The compositions of the final intercalation products indicate that there is only partial exchange of the *N*,*N*′-dimethylpiperazine by the *n*-alkylamines compared with the full intercalation of ethylamine. We tried to increase amount of the additional amine and length of the reaction time of intercalation, but the compositions of the final products were unchanged. A reasonable explanation is that the interaction energy of host–guest in these phases is stronger which makes the structures more stable. Energy calculations and computer models with the help of *Cerius*[2] package are proceeding and will be reported in a separated paper. Herein, a schematic arrangement representation of the intercalation with butlyamine derived from the analysis of the correlation between the interlayer distances and the number of carbon atoms in the alkyl chain is given, as shown in Fig. 9. Between the lamellae, *N*,*N*′-dimethylpiperazines were well-distributed alternatively with double bilayered butylamines. The inclination of the bilayered butylamine chains with respect to the plane is 53.5°, by means of the slope of the straight line of 2.04 pm per carbon atom, expressed in Eq. (2)

$$\alpha = \sin^{-1}(2.04/(2 \times 1.27)) = 53.5^{\circ}. \quad (2)$$

4. Conclusions

TP-J2, $Ti_2(H_2PO_4)(HPO_4)(PO_4)_2 \cdot 0.5C_6N_2H_{16}$, with an extended γ-phase intercalated into organic amine, was prepared directly under hydrothermal conditions. The organic specie was believed to be formed through a decompose-recomposed process of 1-methylpiperazine under high temperature and pressure conditions. The intercalation behavior of TP-J2 was investigated by comparison with that of γ-TiP. There are more differences because of the presence of the *N*,*N*′-dimethylpiperazine cations between the layers of **TP-J2**. The general formula of the final intercalation products was $Ti_2(PO_4)_4H_{2.125} \cdot 1.25[0.25C_4N_2H_{16} \cdot C_nH_{2n+1}NH_3] \cdot H_2O$, and possible arrangements of organic species between the layers were given. The structure and intercalation behavior of **TP-J2** increased our understanding of γ-phase titanium phosphate. The further intercalation of active species and computer models are in progress.

Acknowledgements

The authors acknowledge the financial support of the State Basic Research Project of China (G200077507), the National Natural Science Foundation of China (20233030), and the State Key Laboratory of Inorganic Synthesis and Preparative Chemistry of Jilin University.

Appendix A. Supplementary data

Crystallographic data for the structural analysis have been deposited with the Cambridge Crystallographic Data Center, CCDC No. 241305. Copies of this information may be obtained free of charge from The Director, CCDC, 12 Union Road, Cambridge, CB2 1EZ, UK (fax: +44-1223-336-033; email: deposit@ccdc.cam.ac.uk or www: http://www.ccdc.cam.ac.uk). Supplementary data associated with this article can be found, in the online version, at doi:10.1016/j.poly.2004.08.026.

References

[1] (a) A. Clearfield, U. Costantino, in: G. Alberti, T. Bein (Eds.), Comprehensive Supramolecular Chemistry, vol. 7, Pergamon Press, New York, 1996;
(b) Kunio Ohtsuka, Chem. Mater. 9 (1997) 2039;
(c) G. Cao, H.G. Hong, T.E. Mallouk, Acc. Chem. Res. 25 (1992) 420;
(d) D.P. Vliers, D. Collin, R.A. Schoonheydt, F.C. De Schrijver, Langmuir 2 (1986) 165;
(e) E. Jaimez, R.C.T. Slade, J. Chem. Soc. Dalton Trans. (1997) 1435;
(f) T. Kijima, Y. Matsui, Nature (London) 322 (1986) 533;
(g) C. Ferragina, M.A. Massucci, A.A.G. Tomlinson, J. Mater. Chem. 6 (1996) 645;
(h) M. Danjo, Y. Mizuguchi, Y. Yagita, K. Kakiguchi, Bull. Chem. Soc. Jpn. 70 (1997) 3011.
[2] C. Serre, F. Taulelle, G. Férey, Chem. Commun. (2003) 2755.
[3] A.N. Christensen, E.K. Andersen, I.G.K. Andersen, G. Alberti, M. Nielsen, M.S. Lehmann, Acta Chem. Scand. 44 (1990) 865.
[4] A. Clearfield, U. Costantino, in: G. Alberti, T. Bein (Eds.), Comprehensive Supramolecular Chemistry, vol. 7, Pergamon Press, New York, 1996, p. 140.
[5] Y.H. Guo, Z. Shi, J.H. Yu, J.D. Wang, Y.L. Liu, N. Bai, W.Q. Pang, Chem. Mater. 13 (2001) 203.
[6] Y.H. Guo, Z. Shi, H. Ding, Y. Wei, W.Q. Pang, Chin. Chem. Lett. 12 (2001) 373.
[7] Y.N. Zhao, G.S. Zhu, X.L. Jiao, W. Liu, W.Q. Pang, J. Mater. Chem. 10 (2000) 463.
[8] Y.L. Liu, Z. Shi, Y.L. Fu, W. Chen, B.Z. Li, J. Hua, W.Y. Liu, F. Deng, W.Q. Pang, Chem. Mater. 14 (2002) 1555.
[9] Y.L. Liu, Z. Shi, L.R. Zhang, Y.L. Fu, J.S. Chen, B.Z. Li, J. Hua, W.Q. Pang, Chem. Mater. 13 (2001) 2017.
[10] G.M. Sheldrick, SHELXTL-NT, Version 5.1, Brucker Axs Inc., Madison, WI, 1997.
[11] E. Kobayashi, Bull. Chem. Soc. Jpn. 48 (1975) 3144.
[12] G. Alberti, U. Costantino, M.L.L. Giovagnotti, J. Inorg. Nucl. Chem. 41 (1979) 643.
[13] C. Serre, F. Taulelle, G. Férey, Solid State Sci. 3 (2001) 623.
[14] H. Nakayama, T. Eguchi, N. Nakamura, S. Yamaguchi, M. Danjyo, M. Tsuhako, J. Mater. Chem. 7 (1997) 1063.
[15] H. Sung, J.H. Yu, I.D. Williams, J. Solid State Chem. 140 (1998) 46.
[16] G. Alberti, F. Marmottini, S. Cavalaglio, D. Severi, Langmuir 16 (2000) 4165.
[17] A. Menéndez, M. Bárcena, E. Jaimez, J.R. García, J. Rodríguez, Chem. Mater. 5 (1993) 1078.
[18] L. Beneš, K. Melánová, V. Zima, P. Patrono, P. Galli, Eur. J. Inorg. Chem. (2003) 1577.
[19] A. Espina, F. Menéndez, E. Jaimez, S.A. Khainakov, C. Trobajo, J.R. García, J. Rodríguez, Mater. Res. Bull. 33 (1998) 763.
[20] G. Alberti, S. Cavalaglio, C. Dionigi, F. Marmottini, Langmuir 16 (2000) 7663.

Available online at www.sciencedirect.com
SCIENCE DIRECT®
Polyhedron 23 (2004) 3043–3050
POLYHEDRON
www.elsevier.com/locate/poly

Synthesis, crystal structures and magnetic properties of Cu(II) compounds bridged by the terephthalate ligand and hydrogen bonds

Chang Seop Hong *, Young Sin You

Department of Chemistry and Center for Electro- and Photo-Responsive Molecules, Korea University, Seoul 136-701, Korea

Received 30 July 2004; accepted 1 September 2004

Abstract

A 3D network $[Cu(tmen)(tp)(H_2O)_2]_n$ (**1**) (tmen = *N*,*N*,*N*′,*N*′-tetramethylethylenediamine; tp = terephthalate) and a 2D sheet $[Cu(pyrazole)_2(tp)]_n$ (**2**), featuring 1D chains interwoven by hydrogen bonds, have been prepared and characterized by means of X-ray analyses and magnetic measurements. For **1**, coordinative zigzag chains contain Cu(II) centers capped by the chelate ligand tmen, in which the tetragonal structure is elongated due to Jahn–Teller distortion. Coordinated water molecules are hydrogen-bonded to two free carboxylate oxygens of tp bridges, leading to the observed 3D structure. The use of the non-chelating capping ligand pyrazole produced the covalent-bonded 1D linear compound **2** with hydrogen bonds. A severe octahedral distortion of the Cu(II) center arises from a small bite angle (52.3(1)°) of two carboxylate oxygen atoms of tp, which are in turn hydrogen-bonded to the N–H groups of pyrazole ligands coordinated to Cu(II) atoms in neighboring chains. Magnetic data were fitted with the high-temperature series expansion for the Heisenberg chain spin Hamiltonian $H = -J\sum_i S_i \cdot S_{i+1}$ together with consideration of the molecular field approximation (zJ'). Both compounds interestingly exhibit ferromagnetic interactions with $g = 2.17$, $J = 4.08$ cm^{-1}, $zJ' = -0.28$ cm^{-1} for **1** and $g = 2.09$, $J = 1.47$ cm^{-1}, $zJ' = -0.04$ cm^{-1} for **2**. By taking into account structural parameters of distances between Cu atoms, it is reasonably assigned that the ferromagnetic couplings ($J > 0$) in these systems originate from the hydrogen bonds. The spin density of the $d_{x^2-y^2}$ orbital on a Cu(II) atom in a chain is propagated and induced over the d_{z^2} orbital of another Cu(II) atom in an adjacent chain. This orbital orthogonality gives rise to such interactions. The negative zJ' term suggests that the tp bridges communicate only tiny antiferromagnetic interactions.
© 2004 Elsevier Ltd. All rights reserved.

Keywords: Copper(II) compounds; Crystal structures; Terephthalate ligand; One-dimensional complexes; Magnetic properties

1. Introduction

Molecule-based magnetic materials have been one of the actively studied subjects with the hope of potential applications to magnetic devices [1]. To attain molecular magnets with desirable properties, the fundamental understanding of magnetic interactions between spin centers is an important prerequisite. In this context, a large number of coordination polymers have been prepared and characterized structurally and magnetically [2–4]. They provide useful insights into structure–property relationship, and also confer synthetic strategies how to construct magnetically coupled systems with higher dimensionality that is essentially required for high T_C molecular magnets [5].

To achieve magnetic materials with fascinating characteristics, one of the most basic components considered is ligands to be used as bridges between metal ions. Bridging ligands sit on a central position in the design of magnetically interesting systems because they are in charge of transmitting magnetic interactions between paramagnetic metal ions. The crucial factors for ligands as bridges include multibinding abilility and effectiveness

* Corresponding author. Tel.: +82232903138; fax: +82232903121.
E-mail address: cshong@korea.ac.kr (C.S. Hong).

0277-5387/$ - see front matter © 2004 Elsevier Ltd. All rights reserved.
doi:10.1016/j.poly.2004.09.019

of magnetic exchange coupling. In this vein, the tp ligand is one of the good candidates since it acts in monodentate and bidentate bridging modes, capable of linking up to four metal ions within a metal–metal separation of about 11 Å at the same time [6–9]. The long magnetic pathway through tp enables us to quest for an adequate answer to how far magnetic coupling can propagate. From a magnetic point of view, the tp ligand can mediate weak antiferromagnetic interactions, $J \leqslant -2.2\ cm^{-1}$ based on the Hamiltonian $H = -JS_1 \cdot S_2$, for Cu(II), Ni(II), Co(II) and Mn(II) compounds [10–12]. Some weak ferromagnetic Cu(II) compounds bridged by tp ligands have also been reported [12–15]. Therefore, the weak magnetic interactions via the tp linkage are compatible with those through hydrogen bonds.

To probe the genuine role of the hydrogen bond in magnetic nature we have attempted to make 1D chain Cu(II) compounds bridged by a tp ligand and concurrently connected by hydrogen bonds. Herein we report the synthesis, crystal structures and magnetic properties of two tp-bridged Cu(II) complexes. To obtain structural and magnetic variations, we have utilized chelating (tmen) and non-chelating (pyrazole) capping ligands, producing covalent-linked zigzag $[Cu(tmen)(tp)(H_2O)_2]_n$ (**1**) and linear chain $[Cu(pyrazole)_2(tp)]_n$ (**2**). Both compounds possess hydrogen bonds that interweave adjacent chains, leading to the formation of an extended 3D network (**1**) and a 2D sheet (**2**). Magnetic measurements indicate that the hydrogen bonds communicate ferromagnetic interactions between chains that can be accounted for by the overlap of orthogonal magnetic orbitals, while the tp bridges mediate very weak antiferromagnetic couplings.

2. Experimental

2.1. Materials

All chemicals and solvents were purchased from commercial sources and were used without further purification. Potassium tp was readily prepared by reacting terephthalic acid with a stoichiometric amount of KOH in water.

2.2. Preparation of $[Cu(tmen)(tp)(H_2O)_2]_n$ (*1*)

The bidentate ligand tmen (1.0 mmol) was slowly added by syringe to an aqueous solution (10 ml) of copper(II) perchlorate hexahydrate (1.0 mmol). The resulting solution was treated with an aqueous solution (10 ml) of dipotassium tp (1.0 mmol), immediately forming blue precipitates. After filtration of the solution the filtrate was left undisturbed giving blue crystals of **1** suitable for X-ray crystallography. The total yield corresponds to 65% based on Cu. The reaction of copper nitrate hemipentahydrate with tmen and dipotassium tp gave the same product. *Anal*. Calc. for $C_{14}H_{24}CuN_2O_6$ (**1**): C, 14.3; H, 6.37; N, 7.37. Found: C, 14.6; H, 6.24; N, 7.56%. Selected IR data (cm^{-1}, KBr pellet): 3437 (m), 3262 (m), 3044 (w), 3024 (w), 2984 (w), 2912 (w), 1647 (m, HOH bending), 1585, 1574 (s, tp$\nu_a(CO_2^-)$), 1498 (m), 1470 (m), 1365, 1348 (s, tp$\nu_s(CO_2^-)$), 1297 (m), 1280 (m), 1145 (w), 1122 (w), 1092 (w), 1043 (w), 1016 (m), 1001 (w), 955 (w), 895 (w), 832 (m), 807 (m), 757 (m), 669 (w), 573 (w), 506 (w).

2.3. Preparation of $[Cu(pyrazole)_2(tp)]_n$ (*2*)

A 10 ml aqueous solution of pyrazole (2.0 mmol) was added to an aqueous solution (10 ml) of copper(II) nitrate hemipentahydrate (1.0 mmol) with stirring. A 10 ml aqueous solution of dipotassium tp (1.0 mmol) was mixed with the resulting solution. Immediately, cobalt-violet precipitates were formed and collected by filtration, washed with water, and dried in air. The filtrate was left to stand for several days, providing cobalt-violet single crystals of **2**. The total yield amounts to 87% based on Cu. *Anal*. Calc. for $C_{14}H_{12}CuN_4O_4$: C, 46.2; H, 3.32; N, 15.4. Found: C, 45.9; H, 3.38; N, 15.6%. Selected IR data (cm^{-1}, KBr pellet): 3286 (m), 3125 (w), 1601 (s, tp$\nu_a(CO_2^-)$), 1509 (w), 1466 (w), 1363, 1345 (s, tp$\nu_s(CO_2^-)$), 1251 (w), 1143 (w), 1110 (m), 1067 (m), 1051 (m), 1020 (w), 952 (w), 908 (w), 889 (w), 823 (m), 780 (m), 741 (m), 603 (w), 500 (w).

2.4. Physical measurements

Elemental analyses for C, H and N were performed at the Elemental Analysis Service Center of the Korea Basic Science Institute. Infrared spectra were obtained from KBr pellets with an EQUINOX 55 spectrometer. Magnetic susceptibilities for **1** and **2** were carried out using a Quantum Design MPMS-7 SQUID susceptometer. Diamagnetic corrections of **1** and **2** were estimated from Pascal's Tables.

2.5. X-ray structural analyses

Data were collected at 293 K using an Enraf-Nonius CAD4TSB diffractometer with graphite monochromated Mo Kα radiation ($\lambda = 0.71073$ Å). The unit cell parameters were calculated by least-squares refinement of 25 well-centered reflections. All data were corrected for Lorentz polarization effects. A total of 2782 (**1**) and 1230 (**2**) reflections with a maximum 2θ of 49.94° (**1**) and 49.94° (**2**) were measured and 2470 (**1**) and 1075 (**2**) reflections were assumed to be observed applying the condition $F_o > 4\sigma(F_o)$. Crystallographic data and details of data collection are listed in Table 1.

Table 1
Crystallographic data for **1** and **2**

	1	**2**
Chemical formula	$C_{14}H_{22}N_2O_6Cu$	$C_7H_6N_2O_2Cu_{0.5}$
Formula weight	337.88	181.91
Crystal system	triclinic	triclinic
Space group	$P\bar{1}$	$P\bar{1}$
a (Å)	8.458(1)	5.030(1)
b (Å)	10.615(2)	7.640(1)
c (Å)	11.538(2)	10.180(1)
α (°)	117.06(1)	74.15(1)
β (°)	89.99(1)	77.39(1)
γ (°)	113.45(1)	83.77(1)
V (Å^3)	825.4(2)	366.8(1)
Z	2	2
F(000)	394	185
D_{calc} (g cm^{-3})	1.520	1.647
μ (mm^{-1})	1.354	1.515
Radiation, λ (Å)	Mo Kα, 0.71073	Mo Kα, 0.71073
R_1[a]	0.0454	0.0371
wR_2[b]	0.1167	0.0768

[a] $F_o > 4\sigma(F_o)$, $R_1 = \sum||F_o|-|F_c||/\sum|F_o|$.
[b] $wR_2 = [\sum w(F_o^2 - F_c^2)^2 / \sum w(F_o^2)^2]^{1/2}$.

The structures were solved with the SHELXS-86 program (**1**) and the SIR-92 program (**2**), and refined by least-squares analysis using anisotropic thermal parameters for non-hydrogen atoms with the SHELXL-97 program for **1** and **2** [16–18]. H atoms were calculated at idealized positions ($d_{CH} = 0.970$ for methylene, 0.960 for methyl and 0.930 Å for phenyl) and refined riding on the corresponding carbon atoms with isotropic thermal parameters [$U = 1.2U(C_{methylene})$, $1.5U(C_{methyl})$ and $1.2U(C_{phenyl})$].

3. Results and discussion

3.1. Syntheses and characterization

Compound **1** was prepared by the stoichiometric reaction of the Cu(II) ion with dipotassium tp in the presence of the chelating capping ligand tmen in water. In the IR spectrum, the conspicuous carboxylate stretchings present at 1585 and 1574 cm^{-1} are assignable to the antisymmetric stretching frequency $\nu_a(CO_2^-)$, and those at 1365 and 1348 cm^{-1} are responsible for the symmetric frequency $\nu_s(CO_2^-)$. The binding modes of the carboxylate ligands can be determined based on the difference (Δ) between $\nu_a(CO_2^-)$ and $\nu_s(CO_2^-)$. The calculated Δ value is bigger than 200 cm^{-1}, which compared with the value ($\Delta = 170$ cm^{-1}) of dipotassium tp suggests that the tp ligand in **1** behaves in the monodentate mode [19]. It is also noted that the characteristic broad OH peaks at 3437 and 3262 cm^{-1} indicate the presence of hydrogen bonds.

In order to explore structural and magnetic variations depending on the geometries of the magnetic centers, we prepared a new tp-bridged copper(II) complex (**2**) by employing the non-chelating capping ligand pyrazole, instead of the bidentate tmen. The IR spectrum of **2** reveals that the diagnostic carboxylate stretching vibrations occur at 1601 cm^{-1} for $\nu_a(CO_2^-)$ and 1363, 1345 cm^{-1} for $\nu_s(CO_2^-)$. The difference ($\Delta > 200$ cm^{-1}) supports that the tp bridge in **2** serves as a monodentate ligator, consistent with **1** [19]. The broad band centered at 3286 cm^{-1}, attributable to the N–H stretchings of the pyrazole ligands, denotes the presence of hydrogen bonds, which is confirmed by the X-ray structure below.

3.2. Description of the structures

The structure of **1**, with the asymmetric unit and symmetry related fragments, is shown in Fig. 1a. Selected bond distances and angles are given in Table 2. The inversion centers are placed at the middle of the benzene rings of the tp ligands. The molecular arrangement of the Cu(II) ion is octahedral with a tetragonal distortion. The basal plane consists of two nitrogen atoms of the tmen ligand [Cu1–N1 = 2.072(3), Cu1–N2 = 2.076(3) Å] and two oxygen atoms of two tp ligands [Cu1–O1 = 1.963(2) and Cu1–O3 = 1.962(2) Å], comparable to tp-bridged Cu(II) compounds in a bis-monodentate fashion [20]. The largest deviation from the O1O3N1N2 equatorial least-squares plane is 0.112(2)

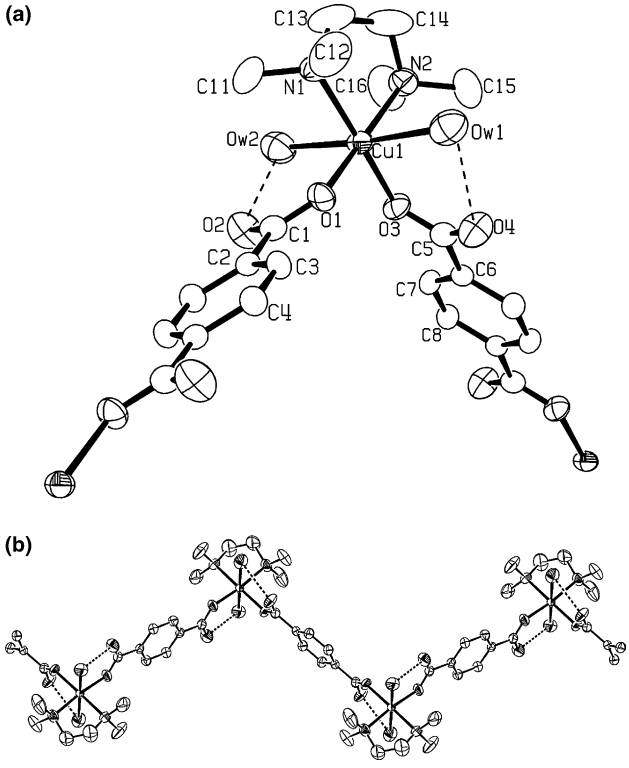

Fig. 1. Molecular structure of **1** showing (a) the asymmetric unit and symmetry-related atoms along with the atom-labelling scheme, and (b) the zigzag chain. The broken lines represent hydrogen bonds.

Table 2
Selected bond distances (Å) and angles (°) for **1**[a]

Bond distances			
Cu1–O3	1.962(2)	Cu1–O1	1.963(2)
Cu1–N1	2.072(3)	Cu1–N2	2.076(3)
Cu1–Ow1	2.613(4)	Cu1–Ow2	2.613(4)
Ow1 ··O4	2.754(5)	Ow2···O2	2.752(5)
Ow1 ···O4d	2.832(5)	Ow2 ···O2a	2.831(5)
Bond angles			
O3–Cu1–O1	94.44(11)	O3–Cu1–N1	172.35(13)
O1–Cu1–N1	90.12(13)	O3–Cu1–N2	90.15(13)
O1–Cu1–N2	172.51(13)	N1–Cu1–N2	85.98(14)
Ow1–Cu1–Ow2	175.44(12)	Ow1–Cu1–O1	86.47(13)
Ow1–Cu1–O3	96.77(13)	Ow1–Cu1–N1	89.66(15)
Ow1–Cu1–N2	87.10(15)	Ow2–Cu1–O1	96.59(13)
Ow2–Cu1–O3	86.38(13)	Ow2–Cu1–N1	86.97(15)
Ow2–Cu1–N3	89.60(15)		

[a] Symmetry code: (a) $-x$, $2-y$, $1-z$ and (d) $-x$, $2-y$, $-z$.

Å at N1 and the Cu1 atom lies −0.002(2) Å out of the plane toward the apical site (Ow2). The two axial positions are occupied by water molecules that are substantially elongated from the Cu center [Cu1–Ow1 = 2.613(4) and Cu1–Ow2 = 2.613(4) Å]. The dihedral angles of carboxylate groups and benzene rings are 2.5° for O1-linked tp and 2.3° for O3-linked tp, which are smaller than that (10.6°) of an en-capped Cu(II) chain compound and similar to that (2.3°–5.5°) of the 1D chain compound Cutp$(H_2O)_2$[13,15]. Two adjacent benzene rings are tilted by 102.3°, forming a 1D zigzag chain structure as seen in Fig. 1b. It is found that the dihedral angles of the basal O_2N_2 plane and the benzene rings for O1-linked tp as well as for O3-linked tp are equal to 98.9° and 98.8°, respectively, larger than those of zigzag tetranuclear or chain complexes with bismonodentate tp bridges [12,13]. The intrachain Cu···Cu distances are 11.224(2) and 11.215(2) Å via the O1- and O3-linked tp bridges, respectively, similar to reported values for tp-bridged Cu(II) systems [6–15,21].

The coordinated water molecules are hydrogen-bonded to the free carboxylate oxygen atoms of tp ligands in a chain [Ow1···O4 = 2.754(5) and Ow2···O2 = 2.752(5) Å], which is completely different from the μ-tp zigzag Cu(II) chain compound where unbound carboxylate oxygen atoms have intermolecular hydrogen bonds to one of amine hydrogen atoms of en [13]. Such N–H···O contacts found in the en-capped Cu system do not exist in **1** due to the absence of amine hydrogen atoms in tmen [13]. In fact, one of the water molecules (Ow2) forms an additional hydrogen bond to a carboxylate oxygen atom (O2a) in an adjacent chain (Ow2···O2a = 2.831(5) Å; a: $-x$, $2-y$, $1-z$), consequently leading to the shortest interchain Cu···Cu distance of 6.539(1) Å, which is longer than that of the en-capped Cu(II) chain, possibly due to the existence of bulky methyl groups on the chelating tmen ligand with respect to the en ligand (Fig. 2) [13]. Thus, two zigzag chains are connected together through intermolecular hydrogen bonds. In the two zigzag chains, the remote Cu–Cu separation of Cu1b···Cu1c (b: x, $-1+y$, z and c: $-1-x$, $1-y$, $-z$) is 12.903(2) Å. The other apical water molecule (Ow1) also has hydrogen bond to a free carboxylate oxygen in another chain (Ow1···O4d = 2.832(5) Å; d: $-x$, $2-y$, $-z$). These hydrogen bonds run along the *c*-axis, finally resulting in a 3D network array as illustrated in Fig. 3.

An ORTEP diagram showing the structure of **2** with the symmetry related fragments and atom-numbering scheme is shown in Fig. 4. Selected bond distances and angles are summarized in Table 3. The Cu(II) atom, with an inversion center, adopts a distorted octahedral geometry comprising two nitrogen atoms of two pyrazole ligands [Cu1–N1 = 1.987(3) Å] and two oxygen atoms of two different tp ligands [Cu1–O1 = 1.932(2) Å]. The N_2O_2 moiety defines the equatorial plane of the octahedron. It is noted that two carboxylate oxygen atoms of two different tp bridges in a chain having very weak bond strength [Cu1–O2 = 2.797(3) Å], larger than that for the tp-bridged Cu(II) binuclear compound [10], are placed at the axial positions of the distorted octahedron. In the equatorial plane, the angles between the *cis*-

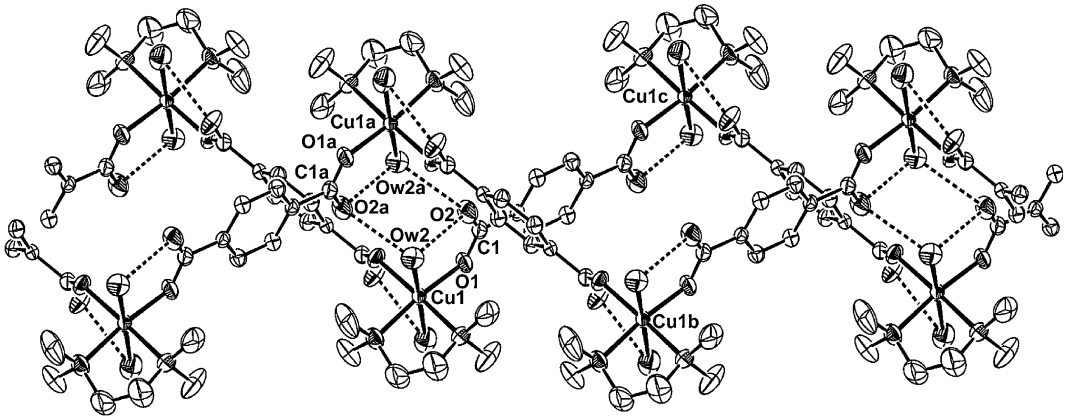

Fig. 2. Perspective molecular representation of **1** showing hydrogen bonds between chains. The broken lines stand for hydrogen bonds. Symmetry code used to generate equivalent atoms: (a) $-x$, $2-y$, $1-z$; (b) x, $-1+y$, z; (c) $-1-x$, $1-y$, $-z$.

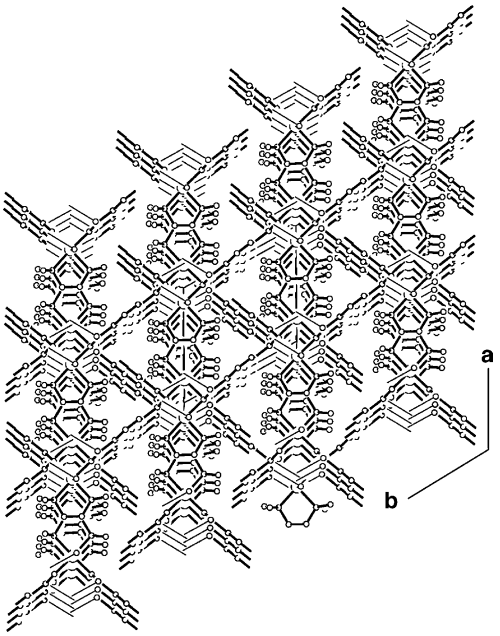

Fig. 3. Extended molecular view of **1** exhibiting 3D network. To illustrate the 3D feature the structure is somewhat slanted from the *ab* plane.

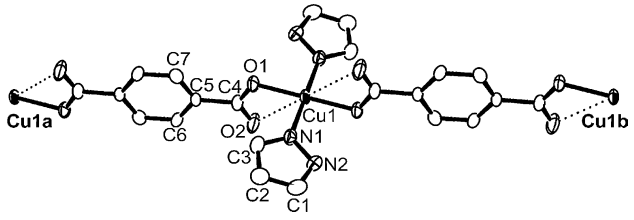

Fig. 4. Molecular structure of **2** with the asymmetric unit and symmetry-related atoms along with the atom-labelling scheme. Symmetry codes used to generate equivalent atoms: (a) x, $1+y$, $1-z$ and (b) x, $-1+y$, $1+z$.

Table 3
Selected bond distances (Å) and angles (°) for **2**[a]

Bond distances			
Cu1–O1	1.932(2)	Cu1–N1	1.987(3)
Cu1–O2	2.797(3)	N2c···O1d	2.878(4)
N2c···O2	2.802(4)		
Bond angles			
O1–Cu1–N1	89.71(12)	O1–Cu1–O2	52.30(10)
O2–Cu1–N1	86.73(11)		

[a] Symmetry code: (c) $1-x$, $-y$, $2-z$ and (d) $1+x$, y, z.

positioned atoms are close to 90° and those of the *trans*-positioned atoms are identical to180° since the Cu atom resides at the inversion center. However, the bite angle (O1–Cu1–O2) of the carboxylate group is acute, 52.3(1)°, significantly deviated from 90°, which gives the main distortion on the octahedral environment. This value is compatible with that of the Cu(II) binuclear compound and smaller than those of Ni(II), Co(II) and Mn(II) binuclear complexes [10]. The dihedral angle of the carboxylate group and benzene ring of tp is found to be 2.5°, which agrees well with that of **1**. The benzene rings of neighboring tp bridges are parallel, while the average dihedral angle of the benzene ring of tp and the pyrazole plane is 96.4°. The intrachain Cu1···Cu1a (a: x, $1+y$, $1-z$) distance via the tp bridge is 10.932(2) Å, shorter than that of **1**. It is worth noting that the use of the non-chelating capping ligand leads to the formation of the linear chain structure (**2**), which is compared with the zigzag chain (**1**) built from the bidentate tmen.

As expected from the IR spectrum, the hydrogen atom in the N–H group of each pyrazole ring serves as a hydrogen donor to the carboxylate oxygen atoms (Fig. 5). The N–H(N2c) unit bound to Cu1d is first hydrogen-bonded to a carboxylate oxygen atom (O1d) within the same chain (N2c···O1d = 2.878(4) Å; c: $1-x$, $-y$, $2-z$; d: $1+x$, y, z). The second hydrogen bond of the N–H moiety is generated with a carboxylate oxygen atom (O2) in a neighboring chain [N2c···O2 = 2.802(4) Å]. Likewise, additional hydrogen bonds between Cu1 and Cu1d are created through the N–H group of the pyrazole ring coordinated to the Cu1 center, which is symmetry-related to the N2c–H event. Consequently, the two Cu centers in the different chains are doubly interconnected via the hydrogen bonds. The overall structure of **2** can be eventually viewed as a 2D sheet made up of the combination of the coordinative 1D chains and the non-covalent forces between them. The shortest interchain Cu···Cu distance is 5.030(1) Å, much shorter than that of **1**.

3.3. Magnetic results

The magnetic susceptibility measurement of **1** is plotted in Fig. 6. At 300 K, the $\chi_m T$ value is 0.44 cm^3 K

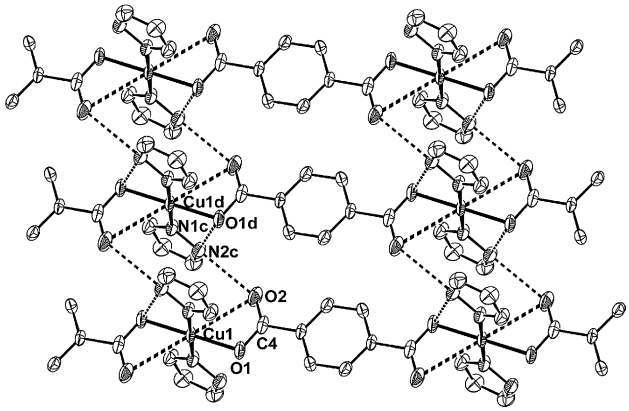

Fig. 5. Extended molecular view of **2** exhibiting hydrogen bonds between chains. The thin broken lines present hydrogen bonds and the thick ones show weak bond interactions between Cu atoms and carboxylate oxygens. Symmetry codes used to generate equivalent atoms: (c) $1-x$, $-y$, $2-z$ and (d) $1+x$, y, z.

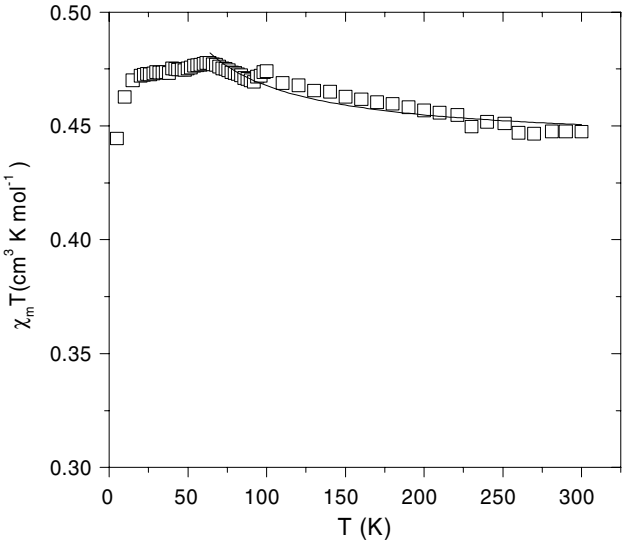

Fig. 6. Plots of χ_m^{-1} and $\chi_m T$ vs. T for **1**. The solid lines denote the best theoretical fits.

mol^{-1}, which is somewhat larger than the value (0.38 cm^3 K mol^{-1}) expected for a non-interacting Cu(II) ion, implying the presence of ferromagnetic interactions in **1**. When the temperature is lowered, $\chi_m T$ rises smoothly to reach a maximum of 0.48 cm^3 K mol^{-1} at 64 K and then decreases down to a value of 0.44 cm^3 K mol^{-1} at 5 K. The variation of the inverse magnetic susceptibility ($1/\chi_m$) with temperature shows a linear dependence down to 64 K and thus follows the Curie–Weiss relation. The calculated parameters of C (Curie constant) = 0.44 cm^3 K mol^{-1} and θ (Weiss constant) = 6.7 K evidence that the magnetic centers in **1** are ferromagnetically coupled.

There are two possible magnetic coupling routes: one is via hydrogen bonds and the other through tp. So, the magnetic data were fit to the high-temperature series expansion derived by Baker et al. for the Heisenberg chain spin Hamiltonian $H = -J\sum_i S_i \cdot S_{i+1}$ together with the consideration of the molecular field correction [22,23]

$$\chi_{chain} = \{Ng^2\beta^2/4kT\}[A/B]^{2/3}$$
$$A = 1.0 + 5.7979916x + 16.902653x^2 + 29.376885x^3 + 29.832959x^4 + 14.036918x^5$$
$$B = 1.0 + 2.7979916x + 7.0086780x^2 + 8.6538644x^3 + 4.5743114x^4 \quad x = J/2kT, \tag{1}$$

$$\chi_m = \chi_{chain}/[1 - (zJ'/Ng^2\beta^2)\chi_{chain}]. \tag{2}$$

The best fit in the high-temperature region 64–300 K yields magnetic parameters of $g = 2.17$, $J = 4.08$ cm^{-1} and $zJ' = -0.28$ cm^{-1}. The measure of the goodness of fit R, defined as $R = \Phi/(n-k)$ where n is the number of data points, k is the number of parameters, and $\Phi = \sum[(\chi_m T)_i^{obs} - (\chi_m T)_i^{calc}]^2$, is equal to 1.0×10^{-5}. The positive J value demonstrates that ferromagnetic interactions in **1** are operative. Kahn and coworkers [20] investigated magnetic properties of tp-bridged binuclear Cu(II) compounds capped by ligands with different bulky groups that brings about the variation of intermolecular Cu···Cu distances, and concluded that intermolecular interactions would play a major role in observed magnetism rather than intramolecular couplings through tp. It is generally accepted that magnetic strength depends on distance between magnetic centers. Thus, the concept of distance–magnetic strength is reasonably applied to this system. Since the shortest intermolecular Cu···Cu distance (6.54 Å) connected with hydrogen bonds is almost half of the intramolecular Cu···Cu length (11.2 Å), sizable magnetic exchange would occur through hydrogen bonds. In view of the magnetic pathways between magnetic centers via hydrogen bonds, the magnetic orbital $d_{x^2-y^2}$ of Cu1 lying in the equatorial plane enables evolvement over two magnetic σ-pathways, that is, Cu1–O1–C1–O2–Ow2a–Cu1a and Cu1–O1–C1–O2–Ow2a–O2a–C1a–O1a–Cu1a skeletons. The first route is shorter and allows the $d_{x^2-y^2}$ spin character on Cu1 to be delocalized through hydrogen bonds and induced on the Cu1b atom, which has d_{z^2} character, hence affording orthogonality between them [24]. Given the total magnetic interaction (J) is divided into an antiferromagnetic term (J_{AF}) and a ferromagnetic term (J_F), J_{AF} can be unequivocally governed by the overlap between the magnetic orbitals. Accordingly, the orthogonality of the relevant orbitals forces J_{AF} to be negligible and as a result the remaining J_F is responsible for the observed overall ferromagnetic behavior in **1** [24–27]. This is in good agreement with the data reported for Cutp systems containing hydrogen bonds [12,15]. The other magnetic pathways giving antiferromagnetic exchange coupling, for instance, Cu1–Ow2–O2a–Ow2a–Cu1a, mediate relatively weak interactions due to the much longer route through the bonds than the major ferromagnetic one. It is thus noted that hydrogen bonds enable the transmission of ferromagnetic interactions in **1**, which are consistent with magnetic results found in organic radicals showing ferromagnetic couplings via hydrogen bonds [28]. As the tp ligand usually exhibits very weak antiferromagnetic interactions, it is appropriate that the calculated zJ' value is assigned to magnetic exchange interactions through the tp linkage, as reported for related metal complexes [10]. The low temperature deviation may arise from antiferromagnetic interactions between Cu(II) ions via hydrogen bonds along the c-axis.

The magnetic susceptibility data for **2** were measured in the temperature range 1.8–300 K, as shown in Fig. 7. The $\chi_m T$ value of 0.41 cm^3 K mol^{-1} at 300 K is slightly larger than the value derived from an isolated Cu(II)

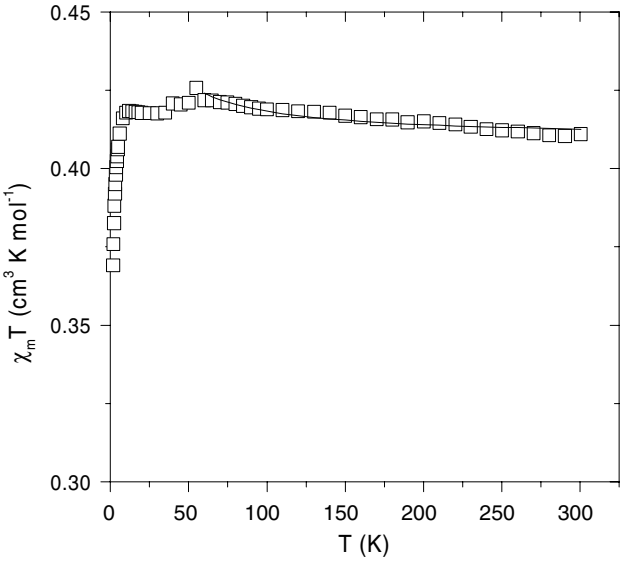

Fig. 7. Plots of χ_m^{-1} and $\chi_m T$ vs. T for **2**. The solid lines indicate the best theoretical fits.

ion. The $\chi_m T$ value increases gradually on cooling, then reaches a value of 0.43 cm^3 K mol^{-1} at 55 K, exhibiting typical ferromagnetic behavior. The inverse magnetic susceptibility data for **2** were fitted to the Curie–Weiss law in the high-temperature region 60–300 K. The parameters determined were equal to $C = 0.41$ cm^3 K mol^{-1} and $\theta = 2.7$ K, supportive of the existence of dominant ferromagnetic interactions as found in **1**.

As shown in Fig. 5, two possible magnetic exchange coupling pathways for **2** are taken into consideration as for **1**: one is via hydrogen bonds and the other through tp. The high-temperature data ($T > 60$ K) were fitted with Eqs. (1) and (2), giving parameters of $g = 2.09$, $J = 1.47$ cm^{-1} and $zJ' = -0.04$ cm^{-1} with $R = 1.6 \times 10^{-6}$. The obtained J value results from exchange coupling between magnetic centers in adjacent chains transmitted by hydrogen bonds since the hydrogen-bonded Cu···Cu separation (5.030 Å) is considerably shorter than the intrachain Cu···Cu distance (10.932 Å) linked by tp. The spin density on the magnetic orbital $(d_{x^2-y^2})$ of Cu1, sitting in the equatorial N_2O_2 plane, is propagated over the $d_{x^2-y^2}$ orbital of Cu1d through the σ-pathway of the Cu1–O1–C4–O2–N2c–(N1c or O1d)–Cu1d backbone. By the way, the more effective route for magnetic interaction is through the Cu1–O2–N2c–(N1c or O1d)–Cu1d backbone owing to the shorter pathway by 0.912 Å. The orbital of Cu1 in the latter route is associated with an admixture of $d_{x^2-y^2}$ and d_{z^2} characters, emanating from the distorted octahedron with the angle (O1–Cu1–O2) of 52.3° deviated from 90°. The main d_{z^2} character along the Cu1–O2 direction is essentially coupled with the $d_{x^2-y^2}$ character in Cu1d, leading to minimal overlap between them [24]. This gives rationale for the ferromagnetic interactions, as manifested in **1** and many oxalato-bridged copper complexes [24–27]. Since the tp ligand is well known to act as a weak magnetic mediator, it is plausible that the zJ' value contributes from the long tp bridge as found in **1** [10]. The drop of $\chi_m T$ at low temperatures is likely attributed to antiferromagnetic interactions between the intersheet Cu(II) centers.

In summary, we have synthesized two tp-bridged Cu(II) compounds showing zigzag and linear structures. It is worth noting that both coordination polymers, with a 3D extended network array (**1**) and a 2D sheet structure (**2**), are formed by incorporating hydrogen bonds into 1D systems. The magnetic data indicate that both complexes exhibit ferromagnetic interactions in the high temperature regime through hydrogen bonds. The magnetic feature can be understood by the fact that the magnetic orbital $(d_{x^2-y^2})$ can propagate through hydrogen bonds and interact with the d_{z^2} orbital by the most effective and shortest pathways. This orthogonality between the orbitals allows antiferromagnetic contribution to be negligible and promotes dominant ferromagnetic couplings. Therefore, it is rationalized that if Cu(II) systems bridged by tp contain hydrogen bonds through which much shorter Cu···Cu separations are established, prevalent magnetic couplings virtually stem not from tp but from hydrogen bonds.

4. Supplementary material

Crystallographic data for the structural analysis have been deposited with the Cambridge Crystallographic Data Center, CCDC Nos. 246238 and 246134 for complexes **1** and **2**, respectively. Copies of this information may be obtained free of charge from The Director, CCDC, 12 Union Road, Cambridge, CB2 1EZ, UK (fax: +44-1223-336-033; email: deposit@ccdc.cam.ac.uk or www: http://www.ccdc.cam.ac.uk).

Acknowledgement

This work is financially supported by the CRM-KOSEF.

References

[1] M.M. Turnbull, T. Sugimoto, L.K. Thompson, Molecule-Based Magnetic Materials, American Chemical Society, Washington, DC, 1996.
[2] T. Kashiwagi, S. Ohkoshi, H. Seino, Y. Mizobe, K. Hashimoto, J. Am. Chem. Soc. 126 (2004) 5024.
[3] D. Armentano, G. De Munno, T.F. Mastropietro, M. Julve, F. Lloret, Chem. Commun. (2004) 1160.
[4] M.A.S. Goher, J. Cano, Y. Journasu, M.A.M. Abu-Youssef, F.A. Mautner, A. Escuer, R. Vicente, Chem. Eur. J. 6 (2000) 778.

[5] M. Ohba, H. Okawa, Coord. Chem. Rev. 198 (2000) 313.
[6] H.X. Zhang, B.-S. Kang, A.-W. Xu, Z.-N. Chen, Z.-Y. Zhou, A.S.C. Chan, K.-B. Yu, C. Ren, J. Chem. Soc., Dalton Trans. (2001) 2559.
[7] K.-Y. Choi, K.-M. Chun, K.-C. Lee, J. Kim, Polyhedron 21 (2002) 1913.
[8] B.-L. Chen, K.-F. Mok, S.-C. Ng, M.G.B. Drew, New J. Chem. 23 (1999) 877.
[9] C.S. Hong, Y. Do, Inorg. Chem. 36 (1997) 5684.
[10] J. Cano, G. De Munno, J.L. Sanz, R. Ruiz, J. Faus, F. Lloret, M. Julve, A. Caneschi, J. Chem. Soc., Dalton Trans. (1997) 1915.
[11] C.S. Hong, Y.S. You, Polyhedron 23 (2004) 1379.
[12] K.-S. Burger, P. Chaudhuri, K. Wieghardt, B. Nuber, Chem. Eur. J. 1 (2000) 583.
[13] E. Bakabassis, A.P. Bozopoulos, J. Mrozinski, P.J. Rentzeperis, C.A. Tsipis, Inorg. Chem. 27 (1988) 529.
[14] C.E. Xanthopoulos, M.P. Sigalas, G.A. Katsoulos, C.A. Tsipis, A. Terzis, M. Mentzafos, A. Hountas, Inorg. Chem. 32 (1993) 5433.
[15] L. Deakin, A.M. Arif, J.S. Miller, Inorg. Chem. 38 (1999) 5072.
[16] G.M. Sheldrick, SHELXS-86 User Guides, University of Göttingen, Göttingen, Germany, 1985.
[17] A. Altomare, G. Cascarano, C. Giacovazzo, A. Guagliardi, M.C. Burla, G. Polidor, M.J. Camallio, J. Appl. Crystalogr. 27 (1994) 435.
[18] G.M. Sheldrick, SHELXL-97 User Guides, University of Göttingen, Göttingen, Germany, 1997.
[19] K. Nakamoto, Infrared and Raman Spectra of Inorganic and Coordination Compounds: Part B: Applications in Coordination, Organometallic, and Bioinorganic Chemistry, 5th ed., Wiley, New York, 1997.
[20] M. Verdaguer, J. Gouteron, S. Jeannin, Y. Jeannin, O. Kahn, Inorg. Chem. 23 (1984) 4291.
[21] H.-D. Bian, J.-Y. Xu, W. Gu, S.-P. Yan, D.-Z. Liao, Z.-H. Jiang, P. Cheng, Inorg. Chem. Commun. 6 (2003) 573.
[22] G.A. Baker, G.S. Rushbrooke, H.E. Gilbert, Phys. Rev. A 135 (1964) 1272.
[23] C.S. Hong, S.-K. Son, Y.S. Lee, M.-J. Jun, Y. Do, Inorg. Chem. 38 (1999) 5602.
[24] H. Oshio, U. Nagashima, Inorg. Chem. 31 (1992) 3295.
[25] O. Castillo, A. Luque, P. Roman, F. Lloret, M. Julve, Inorg. Chem. 40 (2001) 5526.
[26] Y. Akhriff, J. Server-Carrio, A. Sancho, J. Garcia-Lozano, E. Escriva, J.V. Folgado, L. Soto, Inorg. Chem. 38 (1999) 1174.
[27] M.L. Calatayud, I. Castro, J. Sletten, F. Lloret, M. Julve, Inorg. Chim. Acta 300–302 (2000) 846.
[28] F.M. Romero, R. Ziessel, M. Bonnet, Y. Pontillon, E. Ressouche, J. Schweizer, B. Delley, A. Grand, C. Paulsen, J. Am. Chem. Soc. 122 (2000) 1298.

Available online at www.sciencedirect.com
SCIENCE DIRECT®
Polyhedron 23 (2004) 3051–3062
POLYHEDRON
www.elsevier.com/locate/poly

New chiral Schiff base–Cu(II) complexes as cyclopropanation catalysts

Ana L. Iglesias, Gerardo Aguirre, Ratnasamy Somanathan *, Miguel Parra-Hake *

Centro de Graduados e Investigación, Instituto Tecnológico de Tijuana, Tijuana, B.C. 22510, Mexico

Received 17 July 2004; accepted 6 September 2004

Abstract

A series of chiral Schiff base ligands **1**–**4**, derived from (*1R*,*2S*)-(+)-*cis*-1-amino-2-indanol and other chiral amines with substituted salycilaldehydes were synthesized and transformed to the corresponding Cu(II) complexes. Molecular structures of six Cu(II) complexes were determined by X-ray crystallographic studies. The structures show the metal ion in a distorted square planar geometry with dimeric or monomeric structures, depending on the ligand denticity. The potential use of these complexes in asymmetric Cyclopropanation was explored.
© 2004 Elsevier Ltd. All rights reserved.

Keywords: Chiral; Schiff base; Copper; Cyclopropanation; Catalysts; Crystal structures

1. Introduction

Considerable interest exists in the coordination chemistry of transition metals with Schiff bases due to the wide range of applications and structural aspects of the resulting complexes [1–4]. Particular attention has been devoted to salicylidene Schiff base derivatives because they can promote chelation and provide extra stability to the metal centers. Among other applications, this type of complexes have been used as catalysts in reactions such as oxidation of olefins [5–7], polymerization of olefins [8–10], enantioselective epoxidation of olefins [11–13], enantioselective trimethylsilylcyanation of carbonyl compounds [14,15], enantioselective ring opening of meso aziridines [16], asymmetric hetero-Diels Alder reactions [17], and enantioselective Cyclopropanation of olefins [18–20].

A previous report from this laboratory described the use of chiral Schiff base ligands, derived from *cis*-1-amino-2-indanol and salicylaldeydes with titanium(IV) isopropoxide to carry out cyanohydration of benzaldehyde in moderate to very good e.e.'s (enantiomeric excess) [14].

Copper(II) complexes of *N*-substituted salicylideneaminates have been extensively studied as active catalysts in the asymmetric cyclopropanation of olefins [21]. Having had good e.e.'s in the cyanohydration reaction with titanium, we turned our attention to the synthesis and characterization of new Cu(II) complexes with these ligands as well as other less rigid Schiff bases derived from chiral *N*-substituted amines to investigate their use in the enantioselective cyclopropanation of alkenes.

Several structural studies of Cu(II) complexes with non-chiral tetradentate [22,23], tridentate [24,25], and bidentate [26–28] *N*-substituted salicylideneaminate ligands have been reported. However, reports on structures with chiral ligands of this type are rather scarce [19,29–32].

* Corresponding authors. Present address: Chemistry, San Diego State University, 5500 Campanile Dr., San Diego 92182-1030, USA. Tel.: +1 619 594 5264/5595; fax: +1 619 594 4634.
E-mail addresses: somanatha@sundown.sdsu.edu (R. Somanathan), mparra@tectijuana.mx (M. Parra-Hake).

0277-5387/$ - see front matter © 2004 Elsevier Ltd. All rights reserved.
doi:10.1016/j.poly.2004.09.007

We describe here the synthesis and characterization of new Cu(II) complexes derived from chiral ligands **1**–**4**. The molecular structures of complexes **1b-Cu**, **2a-Cu**, **2d-Cu**, **3d-Cu**, **4b-Cu** and **4c-Cu** were determined by X-ray diffraction studies. The potential use of these complexes in the asymmetric cyclopropanation of styrene was explored.

2. Results and discussion

2.1. Ligands

Ligands **1**–**4** were prepared in good yields by condensation of the corresponding substituted salicylaldehydes and chiral amines in refluxing methanol according to a literature procedure [14]. Tridentate ligands **1** are derived from (*1R,2S*)-(+)-*cis*-1-amino-2-indanol. Bidentate ligands **2**–**4** are derived from (*S*)-(−)-α-methylbenzylamine, (*R*)-(+)-1-(1-naphthyl)ethylamine and (*R*)-(−)-1-cyclohexylethylamine, respectively. The main spectroscopic features of these ligands are as follows. In the infrared, an absorption band in the range 1623–1633 cm^{-1}, characteristic of the imine C=N stretching [33], and one broad band at 3454–3425 cm^{-1} due to the phenolic proton hydrogen bonded to the imine nitrogen (O–H···N) [33,34]; in the ^{1}H NMR spectra, a one proton singlet at 7.59–8.59 ppm characteristic of the proton on the imine carbon (H–C=N), a one proton multiplet in the range 3.01–5.60 ppm for the proton on the chiral carbon, and a one proton singlet between 13.5–14.5 ppm for the hydrogen bonded phenolic proton [35]; in the $^{13}C\{^{1}H\}$ NMR spectra, a signal in the range 157.1–177.8 ppm for the imine carbon (C=N), a signal between 149.0 and 161.7 ppm for the phenolic carbon, and a signal between 63.5 and 70.7 ppm for the chiral carbon.

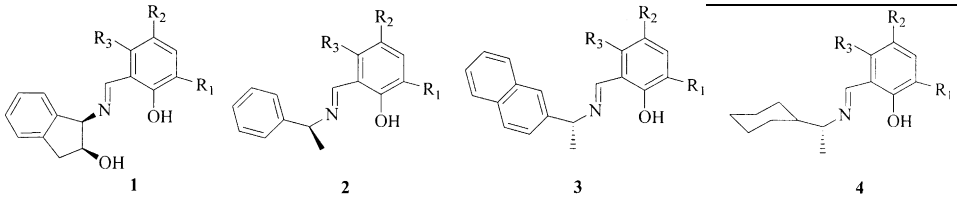

1 2 3 4

a) $R_1 = R_2 = R_3 = H$
b) R_1 = *tert*-Butyl; $R_2 = R_3 = H$
c) $R_1 = R_2$ = *tert*-Butyl; $R_3 = H$
d) $R_1 = H$; R_2, R_3 = Naphthyl

2.2. Synthesis and spectroscopy of complexes

The synthesis of Cu(II) complexes of ligands **1**–**4** is shown in Scheme 1. Combination of a solution of the ligand and triethylamine in dichloromethane with solid copper(II) acetate resulted in the formation of a green to brown solution of the complexes. After work up of the reaction mixture the copper complexes were isolated as green solids in yields ranging from 46% to 99%.

The infrared analysis of the resulting complexes revealed the disappearance of the broad band between 3454 and 3425 cm^{-1} in the free ligand indicating deprotonation of the ligand and replacement by the metal ion [36]. A shift to lower frequencies (1608–1624 cm^{-1}) of the band for the imine group is observed upon metal coordination relative to the free ligand (1623–1633 cm^{-1}), indicating participation of the nitrogen atom in metal complexation [37].

The electronic spectra of the complexes show broad bands in the ranges 218–282 and 324–422 nm attributed to the benzene π–π* transitions [38], and the imine π–π* and *n*–π* transitions [39], respectively. The bands between 592 and 672 nm are assigned to the d–d transitions of the metal, characteristic of tetrahedral distortions of square planar geometries [40]. All the molar absortivities (ε) are about the same order of magnitude (96–295 $1\,cm^{-1}\,mol^{-1}$), which eliminates the possibility of MLCT transitions [41].

2.3. Molecular structures of complexes

The structures of copper(II) complexes with ligands **1b**, **2a**, **2d**, **3d**, **4b** and **4c** were determined by X-ray crystallography. The structure of complex **1b-Cu** is illustrated in Fig. 1. Select bond distances and bond angles are listed in Table 1. Details of the crystal and data collection are outlined in Table 2. The structure of **1b-Cu** consists of two ligands and two copper ions to form a dimeric complex. Each metal is bonded to the ONO coordinating sites of the ligand. Each alkoxy oxygen in the indanol group is bonded to both copper centers forming a bridge for the dimer. The crystal structure of an analogous compound shows the same dimeric structure [19,29]. The molecule has an overall C_2-symmetry with the amino alcohol fragment of both ligands pointing towards the same side of the complex in a *syn* orientation. The copper centers are in a distorted square planar environment defined by the alkoxy oxygen, phenoxy oxygen and the imine nitrogen with the forth coordination position occupied by the bridging alkoxy oxygen from the second ligand. The dihedral angle be-

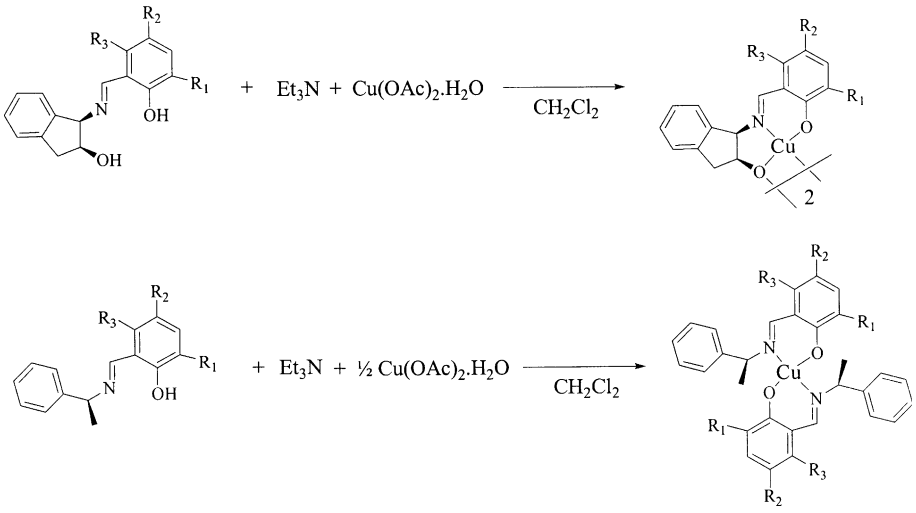

Scheme 1.

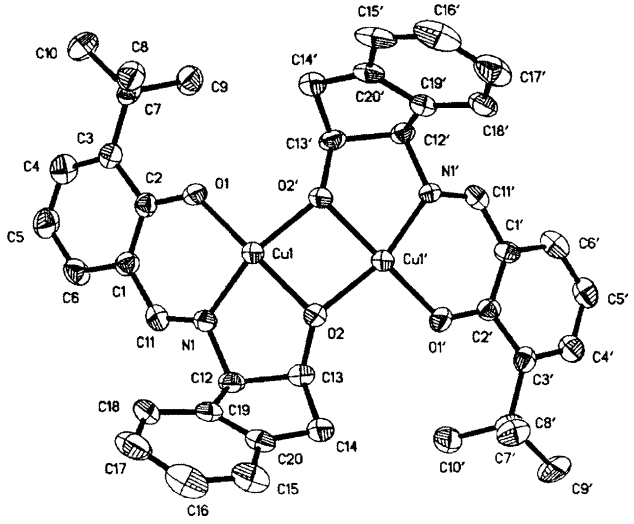

Fig. 1. Structure of **1b-Cu**. Bond distances and angles are given in Table 1.

tween the planes defined by O(2)–Cu(1)–N(1) and O(1)–Cu(1)–O(2′), and by O(2′)–Cu(1′)–N(1′) and O(1′)–Cu(1′)–O(2) are 6.1° and 3.3°, respectively. A deviation from co-planarity of the two units in the dimer is shown by a twist of 43.0° between the planes defined by O(1)–Cu(1)–N(1) and O(1′)–Cu(1′)–N(1′). This distortion may be attributed to the rigidity of the ligand. The O(1)–Cu–O(2), O(1)–Cu–N(1) and N(1)–Cu–O(2) bond angles of 179.4(3)°, 94.3(3)° and 85.4(3)°, respectively, and Cu–O(1), Cu–O(2) and Cu–N(1) bond distances of 1.876(5), 1.948(5) and 1.896(6) Å, respectively, are in agreement with the values in related complexes with a chiral tridentate dianionic Schiff base ligands [29,30].

The structures of complexes **2a-Cu**, **2d-Cu**, **3d-Cu**, **4b-Cu** and **4c-Cu** are illustrated in Figs. 2–6. Select bond distances and angles are listed in Table 3. Details of the crystal data and collection are outlined in Table 4. The structures of these complexes show that the copper ion is bonded to the oxygen and nitrogen donor atoms of the bidentate ligand molecules in the usual *trans* arrangement (O–Cu–N) to form monomeric species with an overall C_2-symmetry. The chiral substituents on the amine fragment are pointing towards the same face of the complex in a *syn* orientation, in contrast with the common *anti* orientation in complexes with non-chiral Schiff base ligands [23,28,42]. As in **1b-Cu**, the copper centers in complexes **2a-Cu**, **2d-Cu**, **3d-Cu**, **4b-Cu** and

Table 1
Selected bond distance (Å) and angles (°) for complex **1b-Cu**

Bond distances	
Cu(1)–Cu(1′)	2.8256(13)
Cu(1)–O(1)	1.876(5)
Cu(1)–O(2)	1.948(5)
Cu(1)–O(2′)	1.918(5)
Cu(1)–N(1)	1.896(6)
Cu(1′)–O(1′)	1.872(5)
Cu(1′)–O(2′)	1.949(5)
Cu(1′)–O(2)	1.951(5)
Cu(1′)–N(1′)	1.900(6)
N(1)–C(11)	1.271(10)
N(1′)–C(H′)	1.274(10)
O(1)–C(2)	1.315(10)
O(1′)–C(2′)	1.307(10)
Bond angles	
O(1)–Cu(1)–O(2)	179.4(3)
N(1)–Cu(1)–O(2′)	164.7(2)
O(1)–Cu(1)–N(1)	94.3(3)
N(1)–Cu(1)–O(2)	85.4(3)
O(2)–Cu(1)–O(2′)	80.6(2)
O(2′)–Cu(1)–O(1)	99.7(2)
O(1′)–Cu(1′)–O(2′)	179.7(3)
N(1′)–Cu(1′)–O(2)	164.5(3)
O(1′)–Cu(1′)–N(1′)	94.7(3)
N(1′)–Cu((1′)–O(2′)	85.0(2)
O(2′)–Cu(1′)–O(2)	79.8(2)
O(2)–Cu(1′)–O(1′)	100.5(2)

Table 2
Crystal data and structure refinement parameters for dinuclear complex **1b-Cu**

Empirical formula	$C_{40}H_{42}Cu_2N_2O_4$
Formula weight	741.84
a (Å)	9.6909(7)
b (Å)	16.0783(13)
c (Å)	23.053(2)
α(°)	90
β(°)	90
γ(°)	90
V (Å^3)	3592.5(5)
Z	4
Space group	$P2_12_12_1$
T (°C)	21
Radiation of Mo Kα, λ (Å)	0.71073
D_{calc} (g cm^{-3})	1.372
μ (nm^{-1})	1.226
Final R indices[a] [$I > 2\sigma(I)$]	$R_1 = 0.0479$, $wR_2 = 0.1096$
R indices (all data)	$R_1 = 0.0938$, $wR_2 = 0.1845$

[a] $R_1 = \sum ||F_o| - |F_c|| / \sum |F_o|$;
$wR_2 = \left[\sum[w(F_o^2 - F_c^2)^2] \Big/ \sum[w(F_o^2)^2]\right]^{1/2}$.

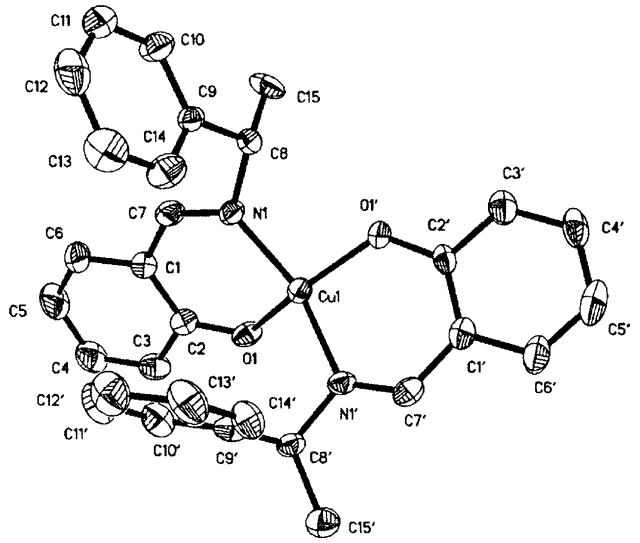

Fig. 2. Structure of **2a-Cu**. Bond distances and angles are given in Table 3.

4c-Cu are in a distorted square planar environment where the dihedral angle between the two coordination planes defined by O(1)–Cu(1)–N(1) and O(1′)–Cu(1)–N(1′) is 38.8°, 28.6°, 38.4° (31.1°), 28.6° and 29.8°, respectively. Bond angles also show that the coordination geometry about the copper atom is distorted square planar, with N–Cu–O angles ranging between 90.6(5)° and 94.8(4)°; O–Cu–O and N–Cu–N angles are in the range 151.0(4)°–159.0(3)° and 150.8(4)°–160.8(6)°, respectively. Cu–O and Cu–N bond lengths are 1.869(9)–1.916(8) and 1.946(8)–1.981(10) Å, respectively, and are in general agreement with similar non-chiral Schiff base complexes [43]. A more pronounced twist from planar toward tetrahedral coordination is observed compared to complex **1b-Cu.** The increased distortion may be attributed to the bulkiness and flexibility of the imine substituent groups.

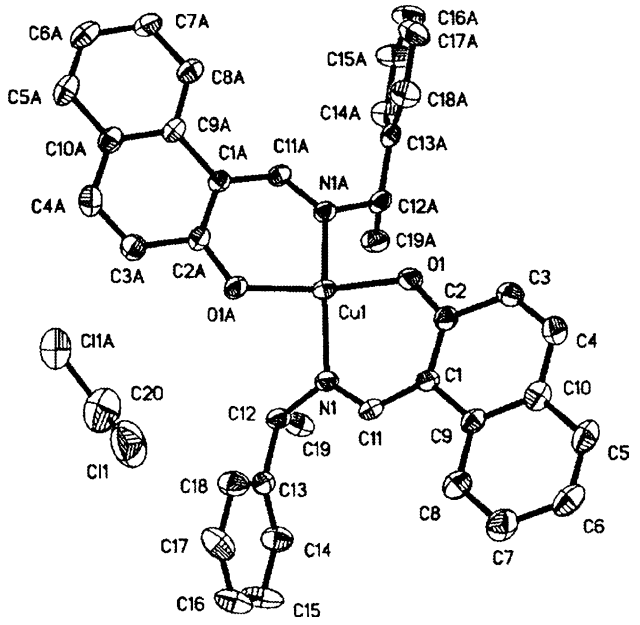

Fig. 3. Structure of **2d-Cu · CH_2Cl_2**. Bond distances and angles are given in Table 3.

The unit cell of **2d-Cu** shows a molecule of CH_2Cl_2, which accounts for the empirical formula found to be $C_{39}H_{32}Cl_2CuN_2O_2$ in the X-ray study. In the unit cell of complex **3d-Cu**, there are two crystallographically independent but very similar molecules differing mainly in the magnitude of the dihedral angle between the two

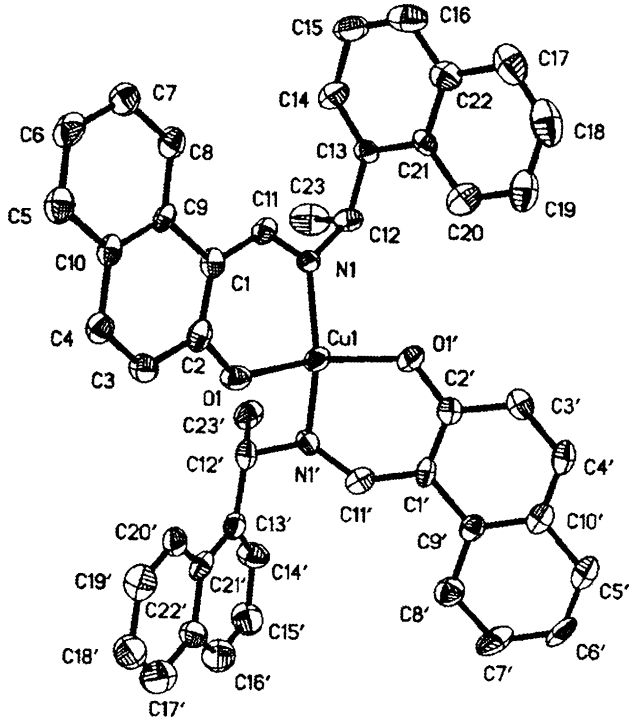

Fig. 4. Structure of **3d-Cu**. Bond distances and angles are given in Table 3.

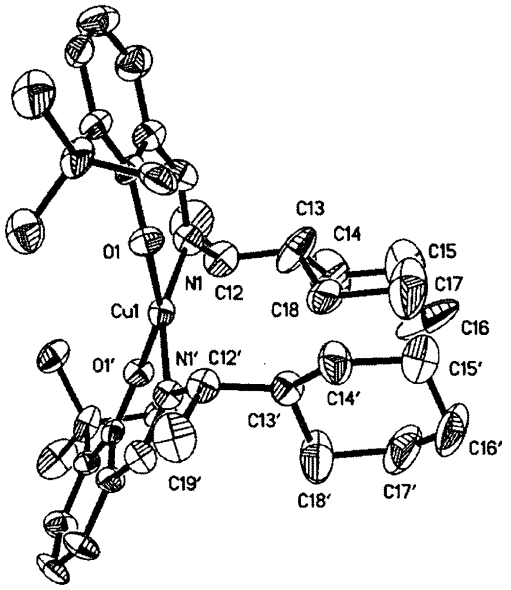

Fig. 5. Structure of **4b-Cu**. Bond distances and angles are given in Table 3.

coordination planes defined by O(1)–Cu(1)–N(1) and O(1′)–Cu(1)–N(1′) of 38.4° in one molecule, and O(1a)–Cu(1a)–N(1a) and O(1b)–Cu(1a)–N(1b) of 31.1° in the other.

One additional feature of these complexes is that a distortion from co-planarity of the aromatic rings on the salicylaldehyde fragment is observed, with twist angles of 57.5° in the dimeric complex **1b-Cu** and in the range 35.7–52.0° in the monomeric complexes **2a-Cu**, **2d-Cu**, **3d-Cu**, **4b-Cu** and **4c-Cu**.

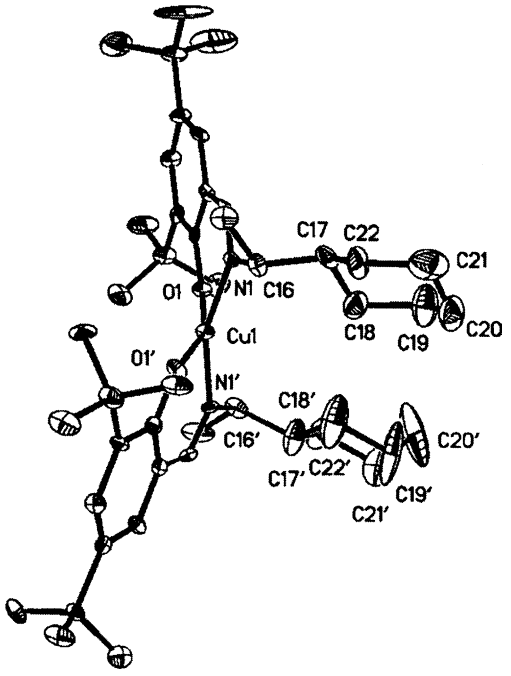

Fig. 6. Structure of **4c-Cu**. Bond distances and angles are given in Table 3.

2.4. Cyclopropanation of styrene

The potential use of these copper(II) complexes as catalyst in the cyclopropanation of styrene using diazoacetates was attempted according to reaction in the following equation. Overall yields, *cis*/*trans* ratios and enantiomeric excess are presented in Table 5. *t*-Butyl diazoacetate was also tested with selected complexes with no substantial improvement on e.e.'s

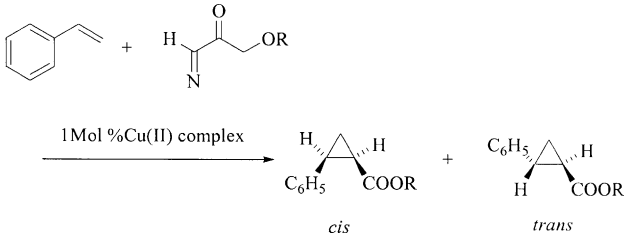

The above cyclopropanation results (high yield and low enantioselectivity) suggest that in the cases examined with Cu(II) complexes with Schiff base ligands, the metal is more open (square planar) and lack steric crowding around the metal to induce any enantioselectivity. As seen in the case of Aratani's Schiff base ligands [19], these complexes probably need conformationally flexible, yet bulky substituents on the amino alcohol portion of the ligand in order to increase the face selection in the cyclopropanation reaction.

2.5. Conclusion

In summary, we have synthesized 16 new Cu(II) complexes with chiral Schiff base ligands, six of which were characterized by X-ray crystallography. The structural studies revealed that tridentate ligands derived from (*1R*,*2S*)-(+)-*cis*-1-amino-2-indanol form dimeric structures of the type M_2L_2 with the alkoxy groups bridging the two metal centers, while those derived from chiral amines yield monomeric complexes of type ML_2. Unexpectedly their catalytic activity in the enantioselective cyclopropanation of styrene was found to be rather poor. Fine tuning of the ligands to improve the catalytic properties of their complexes is currently underway.

3. Experimental

3.1. General

All reactions, except when indicated, were carried out under argon atmosphere using standard Schlenk techniques. Methanol and dichloroethane were dried by

Table 3
Selected bond distances (Å) and angles (°) for complexes **2a-Cu**, **2d-Cu · CH_2Cl_2**, **3d-Cu**, **4b-Cu** and **4c-Cu**

	2a-Cu	**2d-Cu · CH_2Cl_2**	**3d-Cu**		**4b-Cu**	**4c-Cu**
			Molecule 1	Molecule 2		
Bond distances						
Cu(1)–O(1)	1.880(6)	1.896(4)	1.887(8)	1.915(8)	1.919(9)	1.916(8)
Cu(1)–O(1′)	1.889(6)		1.869(9)	1.869(9)	1.900(11)	1.910(8)
Cu(1)–N(1)	1.946(8)	1.970(5)	1.965(9)	1.945(10)	1.96(2)	1.973(9)
Cu(1)–N(1′)	1.965(7)		1.963(9)	1.950(9)	1.959(13)	1.981(10)
N(1)–C(7)	1.288(12)					
N(1′)–C(7′)	1.292(11)					
N(1)–C(11)		1.282(7)	1.290(13)	1.257(13)	1.26(2)	
N(1′)–C(11′)			1.336(14)	1.274(13)	1.29(2)	
N(1)–C(15)						1.26(2)
N(1′)–C(15′)						1.302(14)
O(1)–C(2)	1.318(12)	1.306(7)	1.334(13)	1.305(13)	1.33(2)	1.302(13)
O(1′)–C(2′)	1.323(11)		1.299(13)	1.298(14)	1.27(2)	1.34(2)
Bond angles						
O(1)–Cu(1)–O(1′)	151.8(3)		151.0(4)	155.4(4)	158.1(5)	158.1(4)
O(1)–Cu(1)–O(1A)		159.0(3)				
N(1)–Cu(1)–N(1′)	150.8(4)		153.4(4)	160.4(4)	160.8(6)	159.4(4)
N(1)–Cu(1)–N(1A)		160.1(3)				
O(1)–Cu(1)–N(1)	93.0(3)	91.7(2)	93.0(3)	92.2(4)	91.7(5)	90.6(5)
N(1)–Cu(1)–O(1′)	93.9(3)		94.8(4)	92.1(4)	90.8(6)	91.9(5)
N(1)–Cu(1)–O(1A)		91.9(2)				
O(1′)–Cu(1)–N(1′)	93.9(3)		94.1(4)	91.8(4)	92.3(5)	93.1(5)
O(1A)–Cu(1)–N(1A)		91.7(2)				
N(1′)–Cu(1)–O(1)	93.2(3)		91.2(4)	92.3(3)	92.3(5)	92.2(4)
N(1A)–Cu(1)–O(1)		91.9(2)				

standard methods and stored over molecular sieves 4 Å under argon. All reagents were obtained from commercial suppliers and used without further purification. NMR spectra were recorded on a Varian Gemini 2000-BB FT. ^1H (200 MHz) and $^{13}C\{^1H\}$ NMR (50 MHz) are reported in ppm relative to Me_4Si as an internal standard. Coupling constants J are given in hertz (Hz). IR spectra were recorded on a Perkin–Elmer Model 1605 FT-IR spectrometer. Mass spectra were obtained with a HP-5890 II gas chromatograph (SUPELCO 2-4028, SPβ™-1, and 30 M × 0.25 mm, column #5366-05A) coupled to a HP-5971 mass detector. UV–Vis absorption spectra were measured on a HP 8452 diode array spectrophotometer in dichloromethane solutions with a 1 cm path length cell.

Table 4
Crystal data and structure refinement parameters for mononuclear complexes

Compound	**2a-Cu**	**2d-Cu · CH_2Cl_2**	**3d-Cu**	**4b-Cu**	**4c-Cu**
Empirical formula	$C_{30}H_{28}CuN_2O_2$	$C_{39}H_{32}Cl_2CuN_2O_2$	$C_{92}H_{72}Cu_2N_4O_4$	$C_{38}H_{56}CuN_2O_2$	$C_{46}H_{71}CuN_2O_2$
Formula weight	512.08	695.11	1424.62	636.39	747.59
a (Å)	8.8470(10)	11.2916(11)	14.407(13)	10.7018(9)	10.6804(9)
b (Å)	16.290(3)	15.1471(14)	15.780(3)	12.6995(12)	17.263(4)
c (Å)	17.758(2)	9.8136(10)	15.750(3)	26.531(3)	24.477(5)
α (°)	90	90	90	90	90
β (°)	90	90	99.69(3)	90	90
γ (°)	90	90	90	90	90
V (Å^3)	2559.3(6)	1678.5(3)	5330.3(3)	3605.8(6)	4512.9(14)
Z	4	2	2	4	4
Space group	$P2_12_12_1$	$P2_12_12_1$	$P2_1$	$P2_12_12_1$	$P2_12_12_1$
T (°C)	21	21	21	21	21
Radiation of Mo Kα, λ (Å)	0.71073	0.71073	0.71073	0.71073	0.71073
D_{calc} (g cm^{-3})	1.329	1.375	1.340	1.172	1.100
μ (nm^{-1})	0.883	0.847	0.661	0.639	0.519
Final R indices[a] [$I > 2\sigma(I)$]	$R_1 = 0.0607$, $wR_2 = 0.1329$	$R_1 = 0.0547$, $wR_2 = 0.1150$	$R_1 = 0.0715$, $wR_2 = 0.1592$	$R_1 = 0.0823$, $wR_2 = 0.1597$	$R_1 = 0.0883$, $wR_2 = 0.1384$
R indices (all data)	$R_1 = 0.12887$, $wR_2 = 0.1777$	$R_1 = 0.0865$, $wR_2 = 0.1311$	$R_1 = 0.1373$, $wR_2 = 0.1978$	$R_1 = 0.2552$, $wR_2 = 0.02697$	$R_1 = 0.2354$, $wR_2 = 0.2156$

[a] $R_1 = \sum ||F_o| - |F_c|| / \sum |F_o|$; $wR_2 = \left[\sum[w(F_o^2 - F_c^2)^2] \Big/ \sum[w(F_o^2)^2]\right]^{1/2}$.

Table 5
Results on the asymmetric cyclopropanation of styrene

Catalyst	Yield (%)	*cis*/*trans*	e.e. *cis*	e.e. *trans*
1a	88	31/69	1.46	0.84
1b	60	31/69	1.51	0.65
1c	73	31/69	1.25	0.69
1d	83	31/69	1.52	1.88
2a	88	30/70	11	9
2b	70	30/70	15	13
2c	71	29/71	14	12
2d	76	30/70	10	8
3a	84	30/70	14	13
3b	89	30/70	21	19
3c	60	30/70	12	12
3d	62	30/70	18	16
4b	59	29/71	1.24	3.12
4c	76	29/71	1.78	0.34
4d	89	28/72	1.41	2.93

Optical rotation measurements were determined in CH_2Cl_2 in a 10 cm path length cell using Rudolph Research Flanders automatic polarimeter. Elemental analyses were performed at Inorganic Chemistry Department, Universidad de Alcalá de Henares (ligands) and at NuMega Resonance Labs, Inc. (complexes). All samples for elemental analysis and HRMS were dried under vacuum at room temperature for at least 24 h.

3.2. General procedure for the preparation of Schiff base ligands *1*–*4*

The synthesis of ligands **1** derived from (*1R*,*2S*)-*cis*-1-amino-2-indanol, was reported elsewhere [14]. The condensation of salicylaldehydes with aliphatic or aromatic amines (ligands **2**–**4**) was carried out in the following manner using ligand **2a** as an example: (S)-(−)-α-methylbenzylamine (0.500 g, 4.12 mmol) and 2-hydroxybenzaldehyde (0.503 g, 4.12 mmol) were dissolved in dry methanol (25 ml), and anhydrous sodium sulfate (2 g) was added to the solution as a drying agent. The reaction mixture was refluxed at 65 °C and stirred for 6–24 h. The reaction was followed by TLC. The solution was filtered and the solvent was removed under reduced pressure to afford **2a (S)-(+)-(α-methylbenzyl)-salicylaldimine** as a yellow solid (0.853 g, 91.8%): m.p. 72–74 °C, $[\alpha]_D$ = +159.67 (c 0.04, CH_2Cl_2); IR (cm^{-1}, KBr): 3454, 3023, 2879, 1623, 1577, 1371, 1277, 1080, 761; ^1H NMR (200 MHz, $CDCl_3$): δ 13.50 (s, 1H), 8.33 (s, 1H), 7.30–7.10 (m, 7H), 6.90 (dd, J_1 = 7.6, J_2 = 1.2 Hz, 1H), 6.80 (dt, J = 7.6, 1.2 Hz, 1H), 4.48 (q, J = 6.6 Hz, 1H), 1.56 (d, J = 6.8 Hz, 3H); $^{13}C\{^1H\}$ NMR (50 MHz, $CDCl_3$): δ 163.6, 161.3, 144.0, 132.2, 131.6, 128.9, 128.8, 127.5, 127.4, 126.7, 126.5, 118.9, 117.1, 68.7, 25.2; UV–Vis (CH_2Cl_2, 5×10^{-3} M): λ 218 nm, ε = 44 l cm^{-1} mol^{-1}; λ 328 nm, ε = 599 l cm^{-1} mol^{-1}; λ 338 nm, ε = 591 l cm^{-1} mol^{-1}. MS(EI): *m*/*z* 225 $[M]^+$ (33), 121 (35) 105, (100), 77 (58). *Anal*. Calc. for $C_{15}H_{15}NO$: C, 79.97; H, 6.71. Found: C, 80.29; H, 6.91%.

3.2.1. (S)-(+)-(α-methylbenzyl)-3-t-butylsalicylaldimine (*2b*)

Yellow oil (0.931 g, 80.6%): $[\alpha]$ = +189.52 (c 0.04, CH_2Cl_2); IR (cm^{-1}, neat): 3057, 3028, 2960, 2870, 1627, 1436, 1381, 1265, 741, 700; ^1H NMR (200 MHz, $CDCl_3$): δ 14.20 (s, 1H), 8.46 (s, 1H), 7.50–7.34 (m, 5H), 7.18 (dd, J = 7.7, 1.3 Hz, 2H), 6.92 (t, J = 7.5 Hz, 1H), 4.58 (q, J = 7 Hz, 1H), 1.72 (d, J = 6.8 Hz, 3H), 1.61 (s, 9H); $^{13}C\{^1H\}$ NMR (50 MHz, $CDCl_3$): δ 164.6, 160.7, 144.3, 137.6, 130.2, 129.8, 129.0, 127.6, 126.8, 119.1, 118.3, 68.9, 35.2, 29.8, 25.4; UV–Vis (CH_2Cl_2, 5×10^{-3} M): λ 232 nm, ε = 44 l cm^{-1} mol^{-1}; λ 330 nm, ε = 606 l cm^{-1} mol^{-1}; λ 338 nm, ε = 605 l cm^{-1} mol^{-1}. MS(EI): *m*/*z* 281 $[M]^+$ (52), 176 (32), 162 (35), 134 (40), 105 (100). *Anal*. Calc. for $C_{19}H_{23}NO$: C, 81.09; H, 8.23; N, 4.97. Found: C, 80.86; H, 8.56; N, 4.91%.

3.2.2. (S)-(+)-(α-methylbenzyl)-3,5-di-t-butylsalicylaldimine (*2c*)

Yellow oil (0.618 g, 85.8%): $[\alpha]_D$ = +89.74 (c 0.04, CH_2Cl_2); IR (cm^{-1}, neat): 34 l231, 3052, 2960, 2868, 1630, 1443, 1250, 1172, 824, 765, 702; ^1H NMR (200 MHz, $CDCl_3$): δ 13.8 (s, 1H), 8.40 (s, 1H), 7.38–7.35 (m, 3H), 7.34 (dd, J = 7.94, 1.59 Hz, 2H), 7.27–7.24 (m, 1H), 7.05 (d, J = 2.44 Hz, 1H), 4.53 (q, J = 6.71 Hz, 1H), 1.63 (d, J = 6.72 Hz, 3H), 1.45 (s, 9H), 1.29 (s, 9H); $^{13}C\{^1H\}$ NMR (50 MHz, $CDCl_3$): δ 164.6, 158.0, 144.0, 140.0, 136.6, 128.6, 127.1, 126.9, 126.5, 126.0, 117.9, 68.6, 35.0, 34.1, 31.5, 29.4, 25.0; UV–Vis (CH_2Cl_2, 5×10^{-3} M): λ 332 nm, ε = 607 l cm^{-1} mol^{-1}; λ 352 nm, ε = 545 l cm^{-1} mol^{-1}; λ 414 nm, ε = 40 l cm^{-1} mol^{-1}. MS(EI): *m*/*z* 337 $[M]^+$ (71), 322 (44), 218 (51), 105 (100). *Anal*. Calc. for $C_{23}H_{31}NO$: C, 81.85; H, 9.25; N, 4.15. Found: C, 81.50; H, 9.26; N, 4.14%.

3.2.3. (S)-(+)-(α-methylbenzyl)-2-hydroxy-1-naphthaldimine (*2d*)

Brown solid (1.12 g, 98.5%): m.p. 104–108°C; $[\alpha]_D$ = +114.87 (c 0.04, CH_2Cl_2); IR (cm^{-1}, KBr): 3425, 3023, 2976, 2918, 1625, 1541, 1357, 1185, 747; ^1H NMR (200 MHz, $CDCl_3$): δ 8.35 (s, 1H), 7.81 (d, J = 8.4 Hz, 1H), 7.69 (d, J = 8.8 Hz, 1H), 7.44–7.22 (m, 7H), 6.62 (dd, J = 7.7, 1.2 Hz, 1H), 6.96 (d, J = 9.2 Hz, 1H), 4.65 (q, J = 7.0 Hz., 1H), 1.74 (d, J = 6.6 Hz, 3H); ^{13}C NMR (50 MHz, $CDCl_3$): δ 173.7, 156.5, 142.1, 136.5, 133.0, 128.9, 128.6, 127.6, 127.5, 126.1, 125.9, 123.7, 122.5, 117.7, 63.1, 24.2; UV–Vis (CH_2Cl_2, 5×10^{-3} M): λ 266 nm, ε = 235 l cm^{-1} mol^{-1}; λ 330 nm, ε = 630 l cm^{-1} mol^{-1}; λ 422 nm, ε = 633 l cm^{-1} mol^{-1}. MS(EI): *m*/*z* 275 $[M]^+$ (50), 170 (70), 104 (100), 76 (40). HRMS-FAB: *m*/*z* $[M]^+$ Calc. for $C_{19}H_{17}NO$, 275.1310. Found: 275.1311.

*3.2.4. (R)-(−)-[1-(1-naphthyl)ethyl]salicylaldimine (**3a**)*

Yellow solid (0.251 g, 98.5%): m.p. 83–84 °C; $[\alpha]_D = -336.47$ (c 0.04, CH_2Cl_2); IR (cm^{-1}, KBr): 3435, 3044, 2974, 1626, 1576, 1493, 1277, 1125, 761; ^1H NMR (200 MHz, $CDCl_3$): δ 13.60 (s, 1H), 8.35 (s, 1H), 8.05 (dd, $J = 8.5$, 1.4 Hz, 1H), 7.70 (d, $J = 8.2$, 1H), 7.56 (dd, $J = 6.9$, 1.0 Hz, 1H), 7.52– 7.34 (m, 2H), 7.22 (t, $J = 8.1$, 1.8 Hz, 1H), 7.10 (dd, $J = 7.7$, 1.7 Hz, 1H), 6.90 (d, $J = 8$ Hz, 2H), 6.77 (t, $J = 7.6$, 1.2 Hz, 2H), 5.33 (q, $J = 6.6$ Hz, 1H), 1.71 (d, $J = 6.6$ Hz, 3H); $^{13}C\{^1H\}$ NMR (50 MHz, $CDCl_3$): δ 164.3, 161.3, 139.6, 134.1, 132.4, 131.6, 129.4, 128.2, 126.3, 125.8, 124.2, 123.9, 123.4, 119.1, 117.1, 64.3, 24.7; UV–Vis (CH_2Cl_2, 5×10^{-3} M): λ 224 nm, $\varepsilon = 50\ l\,cm^{-1}\,mol^{-1}$; λ 332 nm, $\varepsilon = 603\ l\,cm^{-1}\,mol^{-1}$; λ 340 nm, $\varepsilon = 593\ l\,cm^{-1}\,mol^{-1}$. MS(EI): *m/z* 275 $[M]^+$ (26), 155 (100), 128 (25), 65 (39). *Anal.* Calc. for $C_{19}H_{17}NO$: C, 82.87; H, 6.22; N, 5.08. Found: C, 82.72; H, 5.93; N, 4.93%.

*3.2.5. (R)-(−)-[1-(1-naphthyl)ethyI]-3-t-butylsalicylaldimine (**3b**)*

Yellow oil (0.390 g, 91.5%): $[\alpha]_D = -327.48$ (c 0.03, CH_2Cl_2); IR (cm^{-1}, neat): 3051, 2960, 2872, 1625, 1436, 1390, 1264, 1144, 798, 779, 739; ^1H NMR (200 MHz, $CDCl_3$): δ 14.19 (s, 1H), 8.35 (s, 1H), 8.05 (d, $J = 7.6$ Hz, 1H), 7.90–7.30 (m, 3H), 7.25–7.15 (m, 3H), 7.23 (dd, $J = 7.6$, 1.6 Hz, 1H), 6.96 (dd, $J = 7.8$, 1.8 Hz, 1H), 6.71 (t, $J = 7.6$ Hz, 1H), 5.27 (q, $J = 6.4$ Hz, 1H), 1.71 (d, $J = 6.6$ Hz, 3H), 1.38 (s, 9H); $^{13}C\{^1H\}$ NMR (50 MHz, $CDCl_3$): δ 164.6, 160.4, 139.6, 137.4, 134.0, 129.9, 129.5, 129.1, 127.8, 126.2, 125.8, 125.6, 124.0, 123.1, 118.9, 117.9, 63.9; UV–Vis (CH_2Cl_2, 5×10^{-3} M): λ 330 nm, $\varepsilon = 606\ l\,cm^{-1}\,mol^{-1}$; λ 422 nm, $\varepsilon = 39\ l\,cm^{-1}\,mol^{-1}$. MS(EI): *m/z* 332 $[M]^+$ (27), 176 (15), 155 (100), 127 (15). *Anal.* Calc. for $C_{23}H_{25}NO$: C, 83.34; H, 7.60. Found: C, 83.70; H, 7.90%.

*3.2.6. (R)-(−)-[1-(1-naphthyl)ethyl]-3,5-di-t-butylsalicylaldimine (**3c**)*

Yellow solid (0.414 g, 66.0%): m.p. 114–117 °C; $\alpha]_D = -273.15$ (c 0.04, CH_2Cl_2); IR (cm^{-1}, KBr): 3051, 2960, 2868, 1628, 1596, 1440, 1362, 1250, 1171, 800, 777; ^1H NMR (500 MHz, $CDCl_3$): δ 13.90 (s, 1H), 8.44 (s, 1H), 8.14 (d, $J = 8.43$ Hz, 1H), 7.88 (dd, $J = 8.37$, 1.22, Hz, 1H), 7.78 (d, $J = 8.18$ Hz, 1H), 7.67 (d, $J = 7.08$ Hz, 1H), 7.54 (dt, $J = 7.69$, 1.46 Hz, 1H), 7.49 (dd, $J = 7.38$, 1.53 Hz, 2H), 7.38 (d, $J = 2.44$, 1H), 7.03 (d, $J = 2.44$ Hz, 1H), 5.41 (c, $J = 6.71$ Hz, 1H), 1.71 (d, $J = 6.6$ Hz, 3H), 1.38 (s, 9H); $^{13}C\{^1H\}$ NMR (50 MHz, $CDCl_3$): δ 165.0, 158.0, 140.0, 139.7, 136.7, 133.9, 130.5, 129.0, 127.7, 127.0, 126.1, 126.0, 125.7, 125.5, 124.0, 123.1, 118.0, 63.8, 35.0, 34.1, 31.5, 29.4, 24.5; UV–Vis (CH_2Cl_2, 5×10^{-3} M): λ 352 nm, $\varepsilon = 551\ l\,cm^{-1}\,mol^{-1}$; λ 336 nm, $\varepsilon = 611\ l\,cm^{-1}\,mol^{-1}$; λ 436 nm, $\varepsilon = 40\ l\,cm^{-1}\,mol^{-1}$. MS(EI): *m/z* 387 $[M]^+$ (31), 155 (100), 128 (16). *Anal.* Calc. for $C_{27}H_{33}NO$: C, 83.67; H, 8.58; N, 3.61. Found: C, 83.36; H, 8.50; N, 3.49%.

*3.2.7. (R)-(−)-[1-(1-naphthyl)ethyl]-2-hydroxy-1-naphthaldimine (**3d**)*

Brown solid (0.424 g, 82.2%): m.p. 87–90 °C, $[\alpha]_D = -366.41$ (c 0.04, CH_2Cl_2); IR (cm^{-1}, KBr): 3444, 3033, 2976, 1624, 1476, 1400, 1125, 776, 753; ^1H NMR (500 MHz, $CDCl_3$): δ 8.90 (s, 1H), 8.12 (d, $J = 8$ Hz, 1H), 7.91 (d, $J = 8$ Hz, 1H), 7.82 (d, $J = 8$ Hz, 1H), 7.74–7.69 (m, 2H), 7.64–7.57 (m, 3H), 7.54–7.48 (m, 2H), 7.34 (dt, $J = 7.7$, 1.22 Hz, 1H), 7.21 (t, $J = 7.7$ Hz 1H), 6.99 (d, $J = 7.0$ Hz, 1H), 5.60 (q, $J = 6.4$ Hz, 1H), 1.71 (d, $J = 6.6$ Hz, 3H), 1.38 (s, 9H); $^{13}C\{^1H\}$ NMR (50 MHz, $CDCl_3$): δ 157.0, 138.2, 137.0, 134.0, 133.6, 130.2, 129.3, 129.2, 128.5, 127.9, 126.7, 126.5, 125.9, 125.7, 124.2, 123.8, 122.9, 122.6, 118.0, 59.1, 23.7; UV–Vis (CH_2Cl_2, 5×10^{-3} M): λ 264 nm, $\varepsilon = 261\ l\,cm^{-1}\,mol^{-1}$; λ 334 nm, $\varepsilon = 625\ l\,cm^{-1}\,mol^{-1}$; λ 422 nm, $\varepsilon = 626\ l\,cm^{-1}\,mol^{-1}$. MS(EI): *m/z* 325 $[M]^+$ (28), 155 (100), 115 (82), 128 (43). *Anal.* Calc. for $C_{23}H_{19}NO$: C, 84.89; H, 5.88. Found: C, 85.17; H, 6.17%.

*3.2.8. (R)-(−)-(1-cyclohexylethyl)salicylaldimine (**4a**)*

Yellow solid (0.786 g, 86.4%): m.p. 28–29°C; $[\alpha]_D = -121.88$ (c 0.04, CH_2Cl_2); IR (cm^{-1}, KBr): 3424, 2972, 2923, 2849, 1629, 1578, 1454, 1279, 1147, 755; ^1H NMR (200 MHz, $CDCl_3$): δ 13.80 (s, 1H), 8.26 (s, 1H), 7.31–7.19 (m, 2H), 6.92 (d, $J = 8.20$ Hz, 1H), 6.84 (t, $J = 7.43$ Hz, 1H), 6.27 (dt, $J = 7.5$, 1.3 Hz, 1H), 3.07 (q, $J = 6.4$ Hz, 1H), 1.76–1.40 (m, 5H), 1.39–0.86 (m, 6H), 1.23 (d, $J = 6.6$ Hz, 3H); $^{13}C\{^1H\}$ NMR (50 MHz, $CDCl_3$): δ 162.8, 161.7, 132.1, 131.2, 118.9, 118.5, 117.2, 70.3, 43.9, 30.0, 29.3, 26.6, 26.5, 26.4, 20.0; UV–Vis (CH_2Cl_2, 5×10^{-3} M): λ 216 nm, $\varepsilon = 110\ l\,cm^{-1}\,mol^{-1}$; λ 332 nm, $\varepsilon = 600\ l\,cm^{-1}\,mol^{-1}$; λ 406 nm, $\varepsilon = 138\ l\,cm^{-1}\,mol^{-1}$. MS(EI): *m/z* 231 $[M]^+$ (36), 148 (100), 130 (41), 76 (30). *Anal.* Calc. for $C_{15}H_{21}NO$: C, 77.87; H, 9.14. Found: C, 78.20; H, 9.43%.

*3.2.9. (R)-(−)-(1-cyclohexylethyl)-3-t-butyl-salicylaldimine (**4b**)*

Yellow oil (1.07 g, 94.6%): $[\alpha]_D = -118.67$ (c 0.14, CH_2Cl_2); IR (cm^{-1}, neat): 3054, 2927, 2853, 1629, 1437, 1383, 1267, 1144, 852, 750; ^1H NMR (200 MHz, $CDCl_3$): δ 8.20 (s, 1H), 7.26 (dd, $J = 8$, 1.7 Hz, 1H), 7.04 (dd, $J = 7.7$, 1.7 Hz, 1H), 6.74 (dd, $J = 7.8$, 1.7 Hz, 1H), 3.01 (q, $J = 6.4$ Hz, 1H), 1.88–1.55 (m, 5H), 1.44–1.32 (m, 3H), 1.39 (s, 9H), 1.30–1.10 (m, 3H), 1.20 (d, $J = 6.4$ Hz, 3H); $^{13}C\{^1H\}$ NMR (50 MHz, $CDCl_3$): δ 163.5, 160.7, 137.4, 129.6, 129.2, 118.8, 117.6, 70.5, 43.8, 34.9, 29.8, 29.6, 29.3, 29.1, 26.4, 20.1, 19.9; UV–Vis (CH_2Cl_2, 5×10^{-3} M): λ 282 nm, $\varepsilon = 329$

l cm^{-1} mol^{-1}; λ 330 nm, ε = 707 l cm^{-1} mol^{-1}; λ 420 nm, ε = 692 l cm^{-1} mol^{-1}. MS(EI): *m/z* 287 [M]$^+$ (71), 245 (100), 162 (93), 54 (98). *Anal*. Calc. for $C_{19}H_{29}NO$: C, 79.39; H, 10.16. Found: C, 79.79; H, 10.51%.

3.2.10. (*R*)-(−)-(1-cyclohexylethyl)-3-5-di-t-butyl-salicylaldimine (**4c**)

Yellow oil (1.19 g, 93.0%): $[\alpha]_D$ = −78.94 (c 0.13, CH_2Cl_2); IR (cm^{-1}, neat): 2957, 2928, 2856, 1629, 1444, 1265, 740; ^{1}H NMR (200 MHz, $CDCl_3$): δ 13.97 (s, 1H), 8.29 (s, 1H), 7.39 (d, J = 2.4 Hz, 1H), 7.09 (d, J = 2.6 Hz, 1H), 3.05 (q, J = 6.4 Hz, 1H), 1.85–1.57 (m, 5H), 1.47 (s, 9H), 1.32 (s, 9H), 1.25 (s, 3H), 1.18–0.97 (m, 6H); ^{13}C{^{1}H} NMR (50 MHz, $CDCl_3$): δ 163.9, 158.5, 140.0, 136.8, 126.7, 125.9, 113.1, 70.7, 44.0, 35.2, 34.3, 31.7, 30.0, 29.7, 29.5, 26.7, 26.5, 26.5, 20.2; UV–Vis (CH_2Cl_2, 5×10^3 M): λ 264 nm, ε = 245 l cm^{-1} mol^{-1}; λ 336 nm, ε = 623 l cm^{-1} mol^{-1}; λ 412 nm, ε = 627 l cm^{-1} mol^{-1}. MS(EI): *m/z* 343 [M]$^+$ (100), 328 (81), 300 (39), 55 (50). *Anal*. Calc. for $C_{23}H_{37}NO$: C, 80.41; H, 10.85. Found: C, 80.76; H, 11.15%.

3.2.11. (*R*)-(−)-(1-cyclohexylethyl)-2-hydroxy-1-naphthaldimine (**4d**)

Brown solid (1.11 g, 91.5%): m.p. 99–101 °C; $[\alpha]_D$ = −144.05 (c 0.04, CH_2Cl_2); IR cm^{-1}, KBr): 3348, 3049, 2983, 2924, 2848, 1633, 1538, 1538, 1361, 832, 749; ^{1}H NMR (200 MHz, $CDCl_3$): δ 14.50 (s, 1H), 8.62 (s, 1H), 7.81 (d, J = 8 Hz, 1H), 7.64 (d, J = 6.2 Hz, 1H), 7.57 (d, J = 9.4 Hz, 1H), 7.40 (dd, J = 8.4, 1.4 Hz, 1H), 7.18 (t, J = 6.8 Hz, 1H), 6.88 (d, J = 7.1 Hz, 1H), 3.30 (q, J = 6.6 Hz, 1H), 1.36 (d, J = 6.8 Hz, 3H), 1.70–1.60 (m, 7H), 1.2–1.0 (m, 4H); ^{13}C{^{1}H} NMR (50 MHz, $CDCl_3$): δ 177.8, 156.2, 137.5, 134.2, 129.5, 128.1, 126.2, 125.5, 122.7, 117.7, 64.4, 43.9, 29.8, 28.9, 26.4, 26.3, 26.3, 19.4; UV–Vis (CH_2Cl_2, 5×10^{-3} M): λ 264 nm, ε = 245 l cm^{-1} mol^{-1}; λ 336 run, ε = 623 l cm^{-1} mol^{-1}. MS(EI): *m/z* 281 [M]$^+$ (17), 198 (47), 181 (23), 55 (100). *Anal*. Calc. for $C_{19}H_{23}NO$: C, 81.09; H, 8.23. Found: C, 81.41; H, 8.55%.

3.3. General procedure for the synthesis of Schiff base–copper(II) complexes

The synthesis of Schiff base–copper(II) complexes is described using ligand **1a** (molar ratio 1:1) as an example. For the complexes with ligands **2**–**4** the same procedure was followed, except that the molar ratio was changed to 2:1. To a solution of Schiff base **1a** (0.150 g, 0.0592 mmol) in dichloromethane (5 ml), was added Et_3N (0.119 g, 1.18 mmol) at room temperature and stirred for 30 min. To the deprotonated ligand solution, solid hydrate copper(II) acetate (0.118 g, 0.0592 mmol) was added and stirred for 1 h. The solution was washed (3×50 ml) with water, and the organic layer dried over anhydrous Na_2SO_4, filtered and the solvent removed under reduced pressure to yield **1a-Cu** {di-μ-oxo-(1*R*,2*S*)-*N*-[2-indanol]-*N*-salicylaldiminato}copper(II) as a green solid (0.183 g, 98.2%): m.p. 138–142 °C; IR (cm^{-1}, KBr): 2023, 2909, 1623, 1528, 1442, 1319, 747; UV–Vis (CH_2Cl_2, 5×10^{-3} M): λ 224 nm, ε = 295 l cm^{-1} mol^{-1}; λ 338 nm, ε = 656 l cm^{-1} mol^{-1}; λ 614 nm, ε = 144 l cm^{-1} mol^{-1}. *Anal*. Calc. for $C_{32}H_{26}N_2O_4Cu_2$: C, 61.04; H, 4.16; N, 4.44. Found: C, 60.90; H, 4.52; N, 4.35%.

3.3.1. {Di-μ-oxo-(1R,2S)-N-[2-indanol]-N-3-terbutylsalicylaldiminato}copper(II) (**1b-Cu**)

Green crystals (0.160 g, 89.0%): m.p. 259–262 °C (dec.); (cm^{-1}, KBr): 3014, 2937, 2889, 1623, 1600, 1542, 1414, 1190, 1147, 861, 747; UV–Vis (CH_2Cl_2, 5×10^{-3} M): λ 246 nm, ε = 229 l cm^{-1} mol^{-1}; λ 328 nm, ε = 685 l cm^{-1} mol^{-1}; λ 602 nm, ε = 209 l cm^{-1} mol^{-1}. HRMS (ES$^+$): *m/z* Calc. for $C_{40}H_{43}Cu_2N_2O_4$ [M + H] 741.1815. Found: 741.1845.

3.3.2. {Di-μ-oxo-(1R,2S)-N-[2-indanol]-N-3′,5′-di-tbutylsalicylaldiminato}copper(II) (**1c-Cu**)

Green solid (0.061 g, 76.8%): m.p. 216–218 ° C (dec); (cm^{-1}, KBr): 3062, 2947, 2899, 1619, 1523, 1428, 1319,1161, 1095, 742, 533; UV–Vis (CH_2Cl_2, 5×10^{-3} M): λ 226 nm, ε = 264 l cm^{-1} mol^{-1}; λ 324 nm, ε = 683 l cm^{-1} mol^{-1}; λ 604 nm, ε = 200 l cm^{-1} mol^{-1} . *Anal*. Calc. for $C_{48}H_{58}N_2O_4Cu_2$: C, 67.50; H, 6.84; N, 3.27. Found: C, 67.40; H, 6.99; N, 3.12%.

3.3.3. {Di-μ-oxo-(1R,2S)-N-[2-indanol]-N-2-oxo-1-naphthaldiminato}copper(II) (**1d-Cu**)

Green solid (0.077 g, 93%): m.p. 218–220 °C (dec); (cm^{-1}, KBr): 3043, 2889, 1619, 1533, 1428, 1395, 1357, 1185, 823, 738; UV–Vis (CH_2Cl_2, 5×10^{-3} M): λ 220 nm, ε = 317 l cm^{-1} mol^{-1}; λ 402 nm, ε = 763 l cm^{-1} mol^{-1}; λ 592 nm, ε = 185 l cm^{-1} mol^{-1}. HRMS (ES$^+$): *m/z* Calc. for $C_{40}H_{30}Cu_2N_2O_2Na$ [M + Na] 751.0695. Found: 751.0670.

3.3.4. Bis[(*S*)-(α-methylbenzyl)-salicylaldiminato]copper(II) (**2a-Cu**)

Green amber crystals (0.123 g, 72.0%): m.p. 137–139 °C; IR (cm^{-1}, KBr): 3023, 2966, 1614, 1533, 1365, 757; UV–Vis (CH_2Cl_2, 5×10^{-3} M): λ 264 nm, ε = 332 l cm^{-1} mol^{-1}; λ 408 nm, ε = 824 l cm^{-1} mol^{-1}; λ 618 nm, ε = 102 l cm^{-1} mol^{-1}. HRMS (ES$^+$): *m/z* Calc. for $C_{30}H_{28}CuN_2O_2Na$ [M + Na] 534.1345. Found: 534.1368.

3.3.5. Bis[(*S*)-(α-methylbenzyl)-3-t-butylsalicylaldiminato]copper(II) (**2b-Cu**)

Brown solid (0.0657 g, 46.3%): m.p. 168–172 °C; IR (cm^{-1}, KBr): 3027, 2953, 2868, 1622, 1593, 1544, 1422,

1313, 1142, 751, 701; UV–Vis (CH_2Cl_2, 5×10^{-3} M): λ 262 nm, $\varepsilon = 341$ l cm^{-1} mol^{-1}; λ 362 nm, $\varepsilon = 824$ l cm^{-1} mol^{-1}; λ 640 nm, $\varepsilon = 201$ l cm^{-1} mol^{-1}. *Anal.* Calc. for $C_{38}H_{44}N_2O_2Cu$: C, 73.10; H, 7.10; N, 4.48. Found: C, 72.96; H, 6.72; N, 4.52%.

3.3.6. *Bis[(S)-(α-methylbenzyl)-3,5-di-t-butylsalicylaldiminato]copper(II)* (**2c-Cu**)

Dark green solid (0.102 g, 93.5%): m.p. 184–186 °C; IR (cm^{-1}, KBr): 3031, 2957, 2866, 1624, 1533, 1456, 1256, 1167, 698; UV–Vis (CH_2Cl_2, 5×10^{-3}M): λ 228 nm, $\varepsilon = 344$ l cm^{-1} mol^{-1}; λ 314 nm, $\varepsilon = 824$ l cm^{-1} mol^{-1}; λ 646 nm, $\varepsilon = 200$ l cm^{-1} mol^{-1}. HRMS (ES$^+$): *m/z* Calc. for $C_{46}H_{61}CuN_2O_2$ [M + H] 736.4129. Found: 736.4096.

3.3.7. *Bis[(S)-(α-methylbenzyl)-2-oxo-1-naphthaldiminato]copper(II)* (**2d-Cu**)

Dark green solid (0.166 g, 90.7%): m.p. 191–194 °C; IR (cm^{-1}, KBr): 3043, 2947, 1614, 1538, 1365, 823, 733; UV–Vis (CH_2Cl_2, 5×10^{-3} M): λ 266 nm, $\varepsilon = 337$ l cm^{-1} mol^{-1}; λ 462 nm, $\varepsilon = 825$ l cm^{-1} mol^{-1}; λ 634 nm, $\varepsilon = 157$ l cm^{-1} mol^{-1}. *Anal.* Calc. for $C_{38}H_{32}N_2O_2Cu$: C,74.55; H, 5.26; N, 4.57. Found: C, 74.54; H, 5.12; N, 4.62%.

3.3.8. *Bis[(R)-[1-(1-naphthyl)ethyl]salicylaldiminato]copper(II)* (**3a-Cu**)

Green solid (0.267 g, 56.2%): m.p. 175–177 °C; IR (cm^{-1}, KBr): 2961, 1615, 1539, 1446, 1323, 1145, 757; UV–Vis (CH_2Cl_2, 5×10^{-3} M): λ 282 nm, $\varepsilon = 349$ l cm^{-1} mol^{-1}; λ 410 nm, $\varepsilon = 824$ l cm^{-1} mol^{-1}; λ 598 nm, $\varepsilon = 141$ l cm^{-1} mol^{-1}. HRMS (ES$^+$): *m/z* Calc. for $C_{38}H_{32}CuN_2O_2Na$ [M + Na] 634.1658. Found 634.1639.

3.3.9. *Bis[(R)-[1-(1-naphthyl)ethyl]-3-t-butylsalicylaldiminato]copper(II)* (**3b-Cu**)

Green solid (0.0602 g, 68.8%): m.p. 227–230 °C; IR (cm^{-1}, KBr): 3046, 2951, 2870, 1618, 1544, 1422, 1336, 1142, 779, 749; UV–Vis (CH_2Cl_2, 5×10^{-3} M): λ 218 nm, $\varepsilon = 348$ l cm^{-1} mol^{-1}; λ 330 nm, $\varepsilon = 823$ l cm^{-1} mol^{-1}; λ 672 nm, $\varepsilon = 267$ l cm^{-1} mol^{-1}. HRMS (ES$^+$): *m/z* Calc. for $C_{46}H_{49}CuN_2O_2$ [M + H] 724.3190. Found: 724.3265.

3.3.10. *Bis[(R)-[1-(1-naphthyl)ethyl]-3,5-di-t-butylsalicylaldiminato]copper(II)* (**3c-Cu**)

Green crystals (0.0494 g, 57.1%): m.p. 218–22 °C; IR (cm^{-1}, KBr): 3048, 2954, 2861, 1618, 1530, 1431, 1316, 1253, 1167, 777; UV–Vis (CH_2Cl_2, 5×10^{-3} M): λ 284 nm, $\varepsilon = 356$ l cm^{-1} mol^{-1}; λ 408 nm, $\varepsilon = 824$ l cm^{-1} mol^{-1}; λ 626 nm, $\varepsilon = 291$ l cm^{-1} mol^{-1}. *Anal.* Calc. for $C_{54}H_{64}N_2O_2Cu$: C, 77.52; H, 7.71; N, 3.34. Found: C, 77.37; H, 7.98; N, 3.36%.

3.3.11. *Bis[(R)-[1-(1-naphthyl)ethyl]-2-oxo-l-naphthaldiminato]copper(II)* (**3d-Cu**)

Green crystals (0.052 g, 82%): m.p. 239–242 °C; IR (cm^{-1}, KBr): 3046, 2961, 2926, 1610, 1539, 1435, 1362, 778, 742; UV–Vis (CH_2Cl_2, 5×10^{-3} M): λ 280 nm, $\varepsilon = 303$ l cm^{-1} mol^{-1}; λ 386 nm, $\varepsilon = 823$ l cm^{-1} mol^{-1}; λ 626 nm, $\varepsilon = 80$ l cm^{-1} mol^{-1}. *Anal.* Calc. for $C_{46}H_{36}N_2O_2Cu$: C, 77.56; H, 5.09; N, 3.93. Found: C, 77.49; H, 4.95; N, 4.03%.

3.3.12. *Bis[(R)-(1-cyclohexylethyl)-salicylaldiminato]copper(II)* (**4a-Cu**)

Bis[(*R*)-(1-cyclohexylethyl)-salicylaldiminato]copper (II) (**4a-Cu**), could not be further purified for characterization.

3.3.13. *Bis[(R)-(1-cyclohexylethyl)-3-t-butyl-salicylaldiminato]copper(II)* (**4b-Cu**)

Dark green solid (0.056 g, 50%): m.p. 165–168 °C; IR (cm^{-1}, KBr)): 3051, 2928, 2851, 1623, 1345, 1425, 1144, 861, 749; UV–Vis (CH_2Cl_2, 5×10^{-3} M): λ 286 nm, $\varepsilon = 367$ l cm^{-1} mol^{-1}; λ 420 nm, $\varepsilon = 825$ l cm^{-1} mol^{-1}; λ 606 nm, $\varepsilon = 142$ l cm^{-1} mol^{-1}. *Anal.* Calc. for $C_{38}H_{56}N_2O_2Cu$: C, 71.71; H, 8.86; N, 4.40. Found: C, 71.41; H, 8.48; N, 4.42%.

3.3.14. *Bis[(R)-(1-cyclohexylethyl)-3,5-di-t-butyl-salicylaldiminato]copper(II)* (**4c-Cu**)

Dark green solid (0.138 g, 96.6%): m.p. 199–203 °C; IR (cm^{-1}, KBr): 2928, 2853, 1621, 1532, 1439, 1255, 1169, 835, 786; UV–Vis (CH_2Cl_2, 5×10^{-3} M): λ 220 nm, $\varepsilon = 353$ l cm^{-1} mol^{-1}; λ 328 nm, $\varepsilon = 824$ l cm^{-1} mol^{-1}; λ 656 nm, $\varepsilon = 177$ l cm^{-1} mol^{-1}. *Anal.* Calc. for $C_{46}H_{72}N_2O_2Cu$: C, 73.80; H, 9.69; N, 3.74. Found: C, 73.59; H, 9.28; N, 3.83%.

3.3.15. *Bis[(R)-(1-cyclohexylethyl)-2-oxo-1-naphthaldiminato]copper(II)* (**4d-Cu**)

Dark green solid (0.099 g, 89%): m.p. 158–160 °C; IR (cm^{-1}, KBr): 3050, 2964, 2924, 2848, 1608, 1539, 1361, 827, 745 745; UV–Vis (CH_2Cl_2, 5×10^{-3} M): λ 286 nm, $\varepsilon = 371$ l cm^{-1} mol^{-1}; λ 348 nm, $\varepsilon = 824$ l cm^{-1} mol^{-1}; λ 632 nm, $\varepsilon = 141$ l cm^{-1} mol^{-1}. *Anal.* Calc. for $C_{38}H_{44}N_2O_2Cu$: C, 73.10; H, 7.10; N, 4.48. Found: C, 73.17; H, 7.08; N, 4.49%.

3.4. *Cyclopropanation of styrene*

Under argon, to a solution of **1a-Cu** (6.3 mg, 0.010 mmol) and styrene (1 ml) in dichloroethane (2 ml), a solution of ethyl diazoacetate (0.114 g, 1.00 mmol) in dichloroethane (2 ml) was added by means of a syringe pump at 60 °C, over a period of 6 h with vigorous stirring. After the addition ceased, the reaction mixture was stirred for another 16 h at room temperature. The crude mixture was directly passed through a short silica gel column eluting with 10 ml of dichloromethane to remove the excess styrene and the catalyst. The % e.e.'s were determined by GC (chiral column β-DEX^{TM} 120, 30×0.25 mm $\times$ 0.25 μm, Column temperature 130°C,

isothermically). The eluant was concentrated under reduced pressure to obtain the *cis* and *trans* cyclopropanes as a mixture of isomers by column flash chromatography on silica gel. The yields were determined based on the weight of the ethyl diazoacetate.

3.5. X-ray crystallographic procedures

Good quality crystals for X-ray structure determination were obtained at room temperature by vapor phase diffusion of CH_2Cl_2/pentane (complexes **1b-Cu**, **2a-Cu**, **2d-Cu** and **3d-Cu)** or by slow evaporation of acetone (**4b-Cu** and **4c-Cu**). Crystals were isolated from the mother liquor and were immersed in epoxy. A crystal was selected for the X-ray diffraction study and mounted on a quartz fiber, and data were collected using a Siemens P4 diffractometer. Corrections for the effects of absorption anisotropy were made. Structure solutions were performed by direct methods and structure refinement was done with the programs SHELXS [44].

4. Supplementary material

Crystallographic data for the structural analysis have been deposited with the Cambridge Crystallographic Data Centre, for **1b-Cu**: CCDC No. 219093; for **2a-Cu**: CCDC No. 219096; for **2d-Cu**: CCDC No. 219092; for **3d-Cu**: CCDC No. 219091; for **4b-Cu**: CCDC No. 219094; for **4c-Cu**: CCDC No. 219095. Copies of this information may be obtained free of charge from The Director, CCDC, 12 Union Road, Cambridge, CB2 1EZ, UK (fax: +44 1223 336033; e-mail: deposit@ccdc.ac.uk or www:http://www.ccdc.cam.ac.uk).

Acknowledgements

This work was supported by Consejo del Sistema Nacional de Educación Tecnológica (COSNET) Grant No. 977.99-P, COSNET Grant No. 498.01-P and by Dirección General de Institutos Tecnológicos (DGIT) Grant No. UR690. Support from Consejo Nacional de Ciencia y Tecnología (CONACYT) in the form of a fellowship for A.L.I. and Proyecto Infraestructura (F264-E9207) for finding of an X-ray diffractometer for Institute Tecnológico de Tijuana is gratefully acknowledged. The authors are indebted to Dr. I. Rivero and Dr. D. Chávez of Instituto Tecnológico de Tijuana and Silvia Calleja of Universidad de Alcalá for analytical support.

References

[1] R.H. Holm, M.J. O'Connor, Prog. Inorg. Chem. 14 (1971) 241.
[2] G.V. Panova, N.K. Vikulova, V.M. Potapov, Russ. Chem. Rev. 49 (1980) 655.
[3] A.D. Garnovskii, A.P. Sadimenko, M.I. Sadimenko, D.A. Garnovskii, Coord. Chem. Rev. 173 (1998) 31.
[4] S. Yamada, Coord. Chem. Rev. 190–192 (1999) 537.
[5] R.M. Wang, C.J. Hao, Y.F. He, Y.P. Wang, S.B. Li, J. Mol. Catal. 147 (1999) 173.
[6] R.M. Wang, C.J. Hao, Y.F. He, C.G. Xia, J. R Wang, Y.P. Wang, J. Appl. Polym. Sci. 75 (2003) 1138.
[7] R.M. Wang, C.J. Hao, Y.F. He, Y.P. Wang, C.G. Xia, Polym. Adv. Technol. 13 (2002) 6.
[8] J. Huang, B. Lian, Y. Qian, W. Zhou, Macromolecules 35 (2002) 4871.
[9] M. Mitani, J. Mohri, Y. Yoshida, J. Saito, S. Ishii, K. Tsuru, S. Matsui, R. Furuyama, T. Nakano, H. Tanaka, S. Cojoh, T. Matsugi, N. Kashiwa, T. Fujita, J. Am. Chem. Soc. 24 (2002) 3327.
[10] V.G. Gibson, S.K. Spitzmesser, Chem. Rev. 103 (2003) 283.
[11] A. Berkessel, M. Frauenkron, T. Schwenkreis, A. Steinmetz, J. Mol. Catal. 117 (1997) 339.
[12] L. Canali, D.C. Sherrington, H. Deleuze, React. Funct. Polym. 40 (1999) 155.
[13] R.I. Kureshy, N.H. Khan, S.H.R. Abdi, S.T. Patel, R.V. Jasra, Tetrahedron: Asymmetr. 12 (2001) 433.
[14] L.Z. Flores-López, M. Parra-Hake, R. Somanathan, P.J. Walsh, Organometallics 19 (2000) 2153.
[15] X.G. Zhou, J.S. Huang, P.H. Ko, K.K. Cheung, C.M. Che, J. Chem. Soc., Dalton Trans. (1999) 3303.
[16] Z. Li, M. Fernández, E.N. Jacobsen, Org. Lett. 1 (1999) 1611.
[17] A.G. Dossetter, T.F. Jamison, E.N. Jacobsen, Angew. Chem., Int. Ed. Engl. 38 (1999) 2398.
[18] H. Nozaki, H. Takaya, S. Moriuti, R. Noyori, Tetrahedron 24 (1968) 3655.
[19] T. Aratani, Pure Appl. Chem. 57 (1985) 1839.
[20] Z. Li, Z. Zheng, H. Cheng, Tetrahedron: Asymmetry 11 (2000) 1157.
[21] H. Lebel, J.F. Marcoux, C. Molinaro, A.B. Charette, Chem. Rev. 103 (2003) 977.
[22] A.D. Garnovskii, A.L. Nivorozhkin, V.I. Minkin, Coord. Chem. Rev. 126 (1993) 1.
[23] A .F. Marinovich, R.S. O'Mahony, J.M. Waters, T.N. Waters, Croatica Chim. Acta 72 (1999) 685.
[24] G. Plesch, V. Kettmann, J. Sivy, O. Švajlenova, C. Friebel, Polyhedron 17 (1998) 539.
[25] S.A. Warda, C. Friebel, J. Sivý, G. Plesch, O. Švajlenova, Acta Crystallogr. C 52 (1996) 2763.
[26] N. Matsumoto, Y. Monaka, S. Kida, Inorg. Chim. Acta 37 (1979) 27.
[27] J.M. Fernández, E. Acevedo-Arauz, R. Cetina-Rosado, R.A. Toscano, Trans. Met. Chem. 24 (1999) 18.
[28] Q. Han, F. Jian, L. Lu, X. Yang, X. Wang, J. Chem. Crystallogr. 31 (2002) 247.
[29] K. Yanagi, M. Minobe, Acta Crystallogr. C 43 (1987) 1045.
[30] S.A. Warda, C. Friebbel, J. Sivý, G. Plesch, M. Bláhová, Acta Crystallogr. C 53 (1997) 50.
[31] S. Bunce, R.J. Cross, L.J. Farrugia, S. Kunchandy, L.L. Meason, K.W. Muir, M. O'Donnell, R.D. Peacock, D. Stirling, S.J. Teat, Polyhedron 17 (1998) 23.
[32] L. Cai, H. Mahmoud, Y. Han, Tetrahedron: Asymmetr. 10 (1999) 411.
[33] M. Calligaris, L. Randaccio, Schiff bases as acyclic polydentate ligands, in: G. Wilkinson, R.D. Gillard, J.A. McCleverty (Eds.), Comprehensive Organometallic Chemistry, vol. 2, Pergamon Press, New York, 1986, p. 715 (Section 20.1).
[34] A. Kriza, A. Reiss, S. Florea, T. Câproiu, J. Ind. Chem. Soc. 77 (2000) 207.
[35] M. Tümer, H. Köksal, M. Kasim, S. Serin, Trans. Met. Chem. 24 (1999) 414.
[36] R.K. Parihari, R.K. Patel, N. Patel, J. Ind. Chem. Soc. 76 (1999) 258.

[37] M. Tümer, C. Çelik, H. Köksal, S. Serin, Trans. Met. Chem. 24 (1999) 525.
[38] M. Tümer, H. Köksal, S. Serin, K. Maras, Synth. React. Inorg. Met-Org. Chem. 27 (5) (1997) 775.
[39] W. Zishen, L. Zhiping, Y. Zhenhuan, Trans. Met. Chem. 18 (1993) 291.
[40] L. Sacconi, M. Ciampolini, J. Chem. Soc. (1964) 276.
[41] J. Losada, I. del Peso, L. Beyer, Inorg. Chim. Acta 321 (2001) 107.
[42] F. Nepveu, J.-P. Laurent, J.-J. Bonnet, Acta Crystallogr. Sect. C 39 (1983) 339.
[43] J.M. Fernández-G., O.L. Rúiz-Ramírez, R.A. Toscano, N. Macías-Ruvalcaba, M. Aguilar-Martínez, Trans. Met. Chem. 25 (2000) 511.
[44] G.M. Sheldrick, SHELXTL PC version 5.03. An integrated system for solving, refining and displaying crystal structures from diffractometer data, Siemens Analytical X-ray Instruments Inc., Madison, WI, 1994.

Available online at www.sciencedirect.com
SCIENCE DIRECT®
Polyhedron 23 (2004) 3063–3068
POLYHEDRON
www.elsevier.com/locate/poly

Metal imidazolato polymers: synthesis, characterization and crystal structure of new silver(I) triphenylphosphine derivatives

G. Attilio Ardizzoia, Stefano Brenna, Fulvio Castelli, Simona Galli *, Girolamo LaMonica, Norberto Masciocchi, Angelo Maspero *

Dipartimento di Scienze Chimiche e Ambientali, Università degli Studi, dell'Insubria, Via Valleggio 11, 22100 Como, Italy

Received 26 May 2004; accepted 6 September 2004
Available online 11 November 2004

Abstract

When the polymeric complex $[Ag(im)]_n$ (Him = imidazole) is reacted with PPh_3 (PPh_3 = triphenylphosphine), it yields the $[Ag_2(\mu_2\text{-im})_2(PPh_3)_3]_n$ and $[Ag(\mu_2\text{-im})(PPh_3)_2]_n$ species, shown to contain wavy chains of metal ions, singly bridged by *N*,*N*′-*exo*-bidentate imidazolate ligands. The former, crystallised as the CH_2Cl_2 solvate, contains two non-equivalent silver(I) ions, differing in the number of coordinated phosphines (one, in trigonal planar stereochemistry, or two, having tetrahedral geometry). The latter has a unique independent silver(I) ion in a tetrahedral environment, with two coordinated PPh_3 ligands. The reactivity of known silver(I) azolates with PPh_3, as well as the solution behaviour and (when available) the crystal structures of the corresponding derivatives are taken into consideration for a due comparison.
© 2004 Elsevier Ltd. All rights reserved.

Keywords: Coordination polymers; Silver; Imidazolate; X-ray structure

1. Introduction

In the recent past, a non negligible number of homoleptic transition metal azolates have been synthesised and shown to possess valuable properties, such as high thermal stability [1], magnetic hysteresis [2] and luminescence [3], as well as anticorrosive [4], sorption [5] and protein staining [6] activities. To highlight both the origin of such properties and their possible optimisation by means of a complete structural insight, we have been actively working to prepare and fully characterise by X-ray powder diffraction (XRPD) manifold 3d-transition metal coordination complexes bearing simple diazaheterocycles: Fe(III), Co(III), Co(II), Ni(II) [7], Cu(I), Ag(I) [8], Zn(II), Cd(II) and Hg(II) [9] pyrazolates, Cu(I), Ag(I) [10] and Cu(II) [11] imidazolates, Co(II), Ni(II), Zn(II) [12], Cu(I) [13] and Ag(I) [14] pyrimidin-2-olates and Co(II), Ni(II) and Zn(II) pyrimidin-4-olates [15].

In the pharmaceutical field, an important role is played by certain silver(I) and gold(I) azolates. Actually, it has been recently discovered that the simple $[Ag(\mu_2\text{-im})]_n$ polymer (Him = imidazole) shows a wide spectrum of antimicrobial activities against bacteria, yeast and even mould [16]. A comparable spectral range against bacteria and yeast, yet not against mould, has been demonstrated by Ag(1,2,4-triz) [17] and Ag(tetz) [18], while a more modest one, involving a few bacteria, has been observed with Ag(1,2,3-triz) [17] (Htriz = triazole, Htetz = tetrazole). The easy rupture of the Ag(I)–N bond upon dissolution has been invoked as one of the key factors of these performances. To better characterise this and other key factors in the quoted (and related) pharmaceutically active silver(I) complexes and to tune

* Corresponding author. Tel.: +39 31 326227/25 314458; fax: +39 31 326230/25 314454.
E-mail address: simona.galli@uninsubria.it (S. Galli).

0277-5387/$ - see front matter © 2004 Elsevier Ltd. All rights reserved.
doi:10.1016/j.poly.2004.09.023

their molecular design, the syntheses, solution behaviour investigation and structural determination of their PPh_3 derivatives (PPh_3 = triphenylphosphine) have been carried out. With this aim, the $Ag(im)(PPh_3)_3$ [19], $[Ag(\mu_2\text{-}1,2,3\text{-triz})(PPh_3)_3]_n$, $[Ag(\mu_2\text{-}1,2,4\text{-triz})(PPh_3)_2]_n$ [17] and $[Ag(\mu_2\text{-tetz})(PPh_3)_2]_n$ [18] species have been prepared and their solution behaviour has been characterised (especially) by variable temperature ^{31}P NMR; as in the case of the previously studied $[Ag_2(\mu_2\text{-pz})_2(PPh_3)_3]$ (Hpz = pyrazole) [20], the concomitant presence of mononuclear species of different $Ag(az)(PPh_3)_n$ formulation (Haz = azole), due to fast PPh_3 dissociation equilibria, has been proved. The pharmaceutical activities of $Ag(im)(PPh_3)_3$ [19], $[Ag(\mu_2\text{-}1,2,3\text{-triz})(PPh_3)]_n$, $[Ag(\mu_2\text{-}1,2,4\text{-triz})(PPh_3)]_n$ [17] and $[Ag(\mu_2\text{-tetz})(PPh_3)_2]_n$ [18] have been properly tested, while a full X-ray structural characterisation has been obtained for the tri- and tetra-azolates only.

Within this context, we report hereafter on the synthesis and the single crystal X-ray structural characterisation of two new derivatives of $[Ag(\mu_2\text{-im})]_n$ with triphenylphosphine, the polymeric $[Ag_2(\mu_2\text{-im})_2(PPh_3)_3]_n$ and $[Ag(\mu_2\text{-im})(PPh_3)_2]_n$ species. A detailed comparison is drawn to the reactivity of Ag(pz), Ag(1,2,3-triz), Ag(1,2,4-triz) and Ag(tetz) with PPh_3, as well as to the solution behaviour and the crystal structure of the corresponding derivatives.

2. Experimental

2.1. General procedures

All reactions were carried out under an atmosphere of dry nitrogen in order to avoid moisture. All chemicals (Aldrich Chemical Co.) were used as supplied. Solvents were purified and dried by standard methods. Elemental analyses were carried out at the Microanalytical Laboratory of this University.

2.2. Synthesis of $[Ag_2(im)_2(PPh_3)_3]_n$ (**1**)

To a suspension of $[Ag(im)]_n$ [10] (0.50 g, 2.9 mmol) in 20 mL of CH_2Cl_2, PPh_3 (1.3 g, 5.0 mmol) was added under stirring. In a few minutes $[Ag(im)]_n$ dissolved, giving a clear solution. The solution was stirred for an additional hour and then evaporated to dryness. The residue was treated with 10 mL of diethyl ether giving a white solid, which was filtered, washed with diethyl ether and dried under vacuum (90% yield). *Anal.* Calc. for $C_{60}H_{51}N_4P_3Ag_2$: C, 63.40; H, 4.49; N, 4.93. Found: C, 63.54; H, 4.50; N, 4.89%. Crystals suitable for X-ray analysis were obtained by slow diffusion of diethyl ether into a dichloromethane solution of **1** containing PPh_3 ($Ag{:}PPh_3$ ratio = 1:1).

2.3. Synthesis of $[Ag(im)(PPh_3)_2]_n$ (**2**)

Complex **2** was obtained in the form of well shaped crystals suitable for X-ray analysis by slow diffusion of a saturated diethyl ether solution of PPh_3 into a dichloromethane solution of **1** (71% yield). *Anal.* Calc. for $C_{39}H_{33}N_2P_2Ag$: C, 66.96; H, 4.72; N, 4.00. Found: C, 70.10; H, 4.68; N, 3.97%. Complexes **1** and **2** are not significantly light sensitive and no particular precautions were taken in order to avoid light exposure. However, direct exposure to intense sunlight for prolonged times (>3 h) causes a superficial darkening of the crystals.

2.4. X-ray crystallography

Suitable colourless flat ($0.25 \times 0.20 \times 0.05$ mm, $\mathbf{1 \cdot CH_2Cl_2}$) and prismatic ($0.13 \times 0.09 \times 0.07$ mm, **2**) crystals were mounted in air on a goniometer head. Data were collected on a Nonius CAD4 diffractometer, equipped with graphite-monochromatised Mo Kα radiation ($\lambda = 0.71073$ Å), by the ω-scan method, acquiring in both cases all unique reflections in the $5° < 2\theta < 50°$ range. Empirical corrections for absorption and Lorentz polarisation effects were applied to the integrated reflections (ψ-scans method [21]). The structures were solved by direct methods [22] and refined with full-matrix least-square calculations on F^2 [23]. Anisotropic temperature factors were assigned to all atoms except hydrogen atoms which were refined riding on their parent atoms with a common isotropic displacement parameter chosen as 1.2 times that of the pertinent parent.

2.4.1. $[Ag_2(im)_2(PPh_3)_3]_n \cdot (CH_2Cl_2)$, ($\mathbf{1 \cdot CH_2Cl_2}$)

$Ag_2(C_3H_3N_2)_2(PPh_3)_3 \cdot (CH_2Cl_2)$, $C_{61}H_{53}Cl_2N_4P_3Ag_2$, $M = 1221.68$ g mol^{-1}; monoclinic, $P2_1/c$, $a = 10.678(1)$, $b = 39.858(12)$, $c = 13.310(2)$ Å, $\beta = 91.31(1)°$, $V = 5663(2)$ Å^3, $Z = 4$; $T = 298(2)$ K, $D_c = 1.43$ g cm^{-3}, μ(Mo Kα) = 0.91 mm^{-1}, $F(000) = 2480$; 644 parameters, no restraints, 9926 unique reflections measured, of which 3633 observed [$I > 2\sigma(I)$]; $R_{obs} = 0.0433$, $wR_{2\ all} = 0.0787$, highest peak and deepest hole = 0.40 and −0.48 e Å^{-3}, GOF = 0.791.

2.4.2. $[Ag(im)(PPh_3)_2]_n$, (**2**)

$Ag(C_3H_3N_2)(PPh_3)_2$, $C_{39}H_{33}N_2P_2Ag$, $M = 699.52$ g mol^{-1}; monoclinic, $P2/_1n$, $a = 14.561(5)$, $b = 9.674(5)$, $c = 24.463(5)$ Å, $\beta = 91.56(2)°$, $V = 3445(1)$ Å^3, $Z = 4$; $T = 298(2)$ K, $D_c = 1.349$ g cm^{-3}, μ(Mo Kα) = 0.71 mm^{-1}, $F(000) = 1432$; 397 parameters, no restraints, 6037 unique reflections measured, of which 4222 observed [$I > 2\sigma(I)$]; $R_{obs} = 0.0263$, $wR_{2\ all} = 0.0685$, highest peak and deepest hole = 0.32 and −0.51 e Å^{-3}, GOF = 0.971.

Relevant bond distances and angles, with estimated standard deviations, are reported throughout the text and are collected in the captions to Figs. 1 and 2.

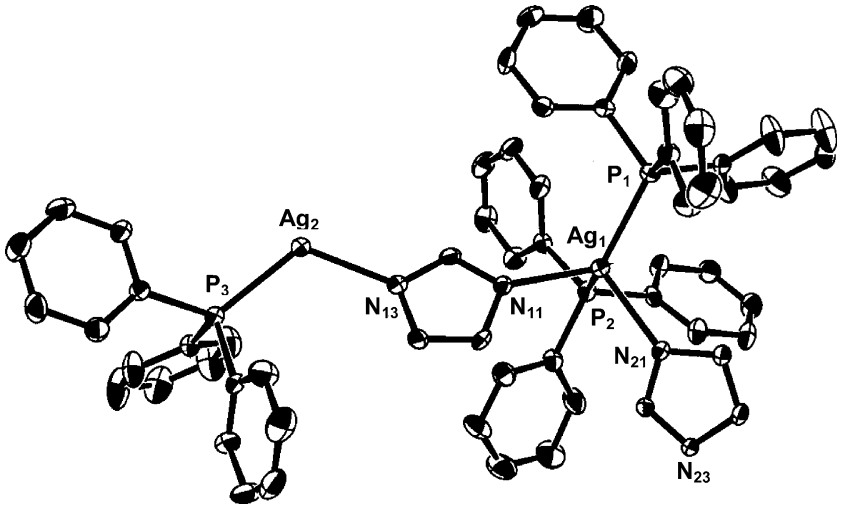

Fig. 1. ORTEP drawing, at 20% probability level, of the asymmetric unit in $[Ag_2(im)_3(PPh_3)_3]\cdot CH_2Cl_2$ (**1 · CH_2Cl_2**). Hydrogen and solvent atoms are omitted for clarity. Significant distances (Å) and angles (°) (e.s.d.'s in parentheses): Ag_1–N_{11} = 2.290(4), Ag_1–N_{21} = 2.301(4), Ag_2–N_{13} = 2.249(5), Ag_2–N_{23} = 2.196(4), Ag_1–P_1 = 2.450(2), Ag_1–P_2 = 2.595(2), Ag_2–P_3 = 2.395(2); N_{11}–Ag_1–N_{21} = 109.25(16), P_1–Ag_1–P_2 = 118.40(5), N_{11}–Ag_1–P_1 = 117.36(12), N_{11}–Ag_1–P_2 = 102.14(12), N_{21}–Ag_1–P_1 = 113.47(13), N_{21}–Ag_1–P_2 = 93.21(12), N_{13}–Ag_2–N_{23} = 109.47(17), N_{13}–Ag_2–P_3 = 118.43(13), N_{23}–Ag_2–P_3 = 131.09(13); $Ag_1\cdots Ag_2$ = 6.433(1) and 6.575(1).

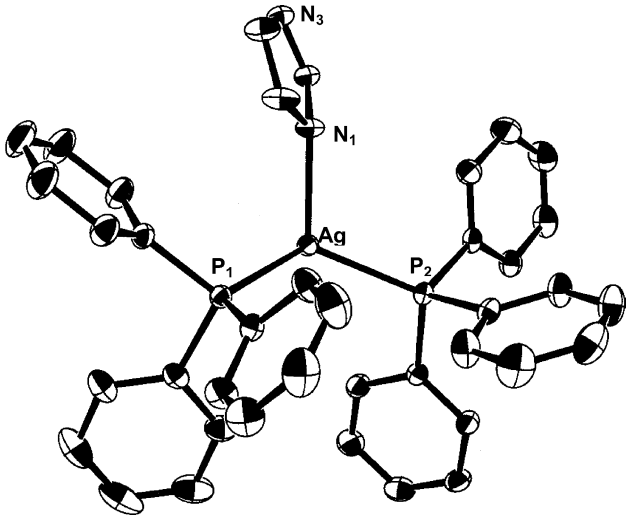

Fig. 2. ORTEP drawing, at 20% probability level, of the asymmetric unit in $[Ag(im)_2(PPh_3)_2]$ (**2**). Hydrogen atoms are omitted for clarity. Significant distances (Å) and angles (°) (e.s.d.'s in parentheses): Ag–N_1 = 2.296(2), Ag–N_3 = 2.294(2), Ag–P_1 = 2.471(1), Ag–P_2 = 2.456(1); N_1–Ag–N_3 = 97.92(8), P_1–Ag–P_2 = 124.22(3), N_1–Ag–P_1 = 105.22(6), N_1–Ag–P_2 = 114.01(6), N_3–Ag–P_1 = 105.78(6), N_3–Ag–P_2 = 106.25(6); Ag···Ag = 6.555(1).

3. Results

3.1. Synthesis and characterization

On reacting the $[Ag(\mu_2\text{-im})]_n$ polymer [10] with PPh_3 in CH_2Cl_2 at room temperature (with an Ag:PPh_3 ratio of 1:1.7) a white product of $Ag_2(im)_2(PPh_3)_3$ formulation, **1**, can be isolated (Eq. (1))

$$2/n[Ag(im)]_n + 3PPh_3 \rightarrow [Ag_2(im)_2(PPh_3)_3]_n \quad (1)$$

On layering diethyl ether over a CH_2Cl_2 solution of **1**, colourless single crystals suitable for X-ray diffraction (**1 · CH_2Cl_2**) are obtained by slow diffusion. At variance, upon layering an excess of PPh_3 dissolved in diethyl ether, the formation of white crystals of a different formulation, $[Ag(im)(PPh_3)_2$, **2**], is observed (Eq. (2))

$$[Ag_2(im)_2PPh_3]_n \overset{PPh_3}{\rightarrow} 2[Ag(im)(PPh_3)_2]_n \quad (2)$$

In both cases, to recover analytically pure products, we found it necessary to operate in a slight excess of PPh_3 with respect to the stoichiometric amount required; only under these conditions is the dissociation of the already coordinated, labile phosphines inhibited. Actually, on suspending **2** in diethyl ether, loss of PPh_3 with concomitant formation of **1** takes place (from IR evidence). Seemingly, to obtain **2**, the required PPh_3 excess lies in the 1:1.7–1:3 range. Actually, on working with a large excess of PPh_3 (i.e., with an Ag:PPh_3 ratio of 1:3 or higher), $Ag(im)(PPh_3)_3$ can be isolated [19].

3.2. Crystallographic aspects

Compound **1 · CH_2Cl_2** is characterised by single-stranded wavy chains of $Ag_2(im)_2(PPh_3)_3$ formulation and clathrated molecules of dichloromethane (Figs. 1 and 3(a)). The chains evolve along **a** with a translation step of 10.678(5) Å (*a*) and pack creating a herringbone motif appreciable down [1 0 0]. Within each chain, two crystallographically independent metal ions [$Ag_1\cdots Ag_2$ = 6.433(1) $Ag_1\cdots Ag_2$ = 6.575(1) Å, $Ag_1\cdots Ag_2\cdots Ag_1$ = 110.3°] are singly bridged by imidazolate anions, which act in their usual *N,N′-exo*-bidentate coordination mode. Both in a general

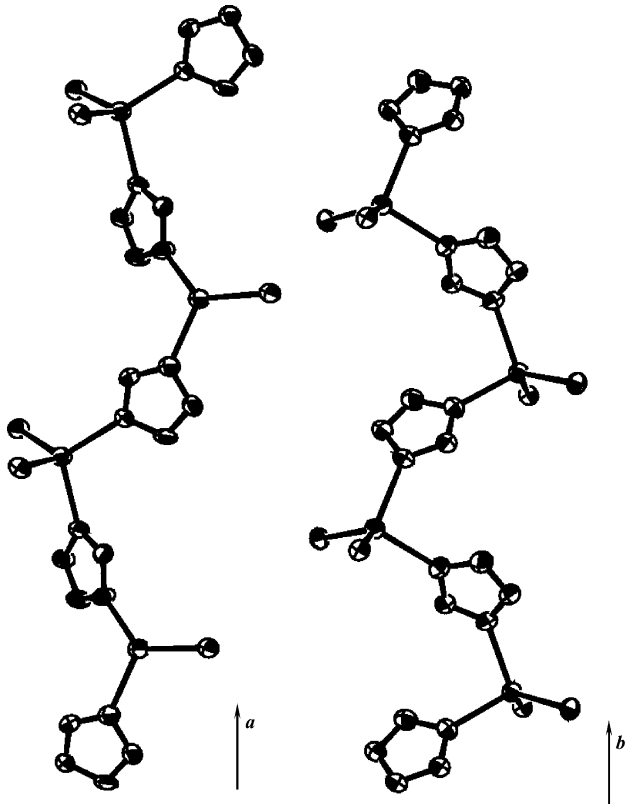

Fig. 3. Schematic representation of the single-stranded chain in $\mathbf{1 \cdot CH_2Cl_2}$ (a) and **2** (b). Phenyl carbons and hydrogen atoms are omitted for clarity.

position, the two metal centres exploit different coordination numbers and geometries: Ag_1, bonded to *two* phosphine ligands, is actually the centre of a distorted $Ag(N)_2(P)_2$ tetrahedral moiety; Ag_2, bonded to just *one* PPh_3 ligand, shows an almost planar trigonal stereochemistry (emerging by 0.06 Å from the plane of the three atoms coordinated to it). A non-negligible distortion of the Ag_1 tetrahedral stereochemistry is highlit by both the discrepancy between $Ag_1–P_{1,2}$ bond distances and the actual spread of the $L–Ag_1–L$ bond angles from the ideal tetrahedral one (L = N or P; see caption to Fig. 1). The observed distortion can be tentatively ascribed to the steric demands of the two PPh_3 ligands, resulting in their different positions with respect to the Ag–N···N–Ag skeleton. Indeed, both ligands point outwards from the polymeric spine: yet $P_2–Ag_1–N$ angles are smaller than those involving P_1 and are compensated by an $Ag_1–P_2$ bond that is longer than $Ag_1–P_1$. This asymmetry is not transferred to the $Ag_1–N$ bonds, $Ag_1–N_{11}$ and $Ag_1–N_{21}$ being almost comparable. Even the Ag_2 stereochemistry is somewhat distorted: its PPh_3 is more proximate to the N_{23}-imidazolate than to the N_{13}-one, this, however, only slightly differentiates $Ag_2–N_{13}$ and $Ag_2–N_{23}$. Solvent molecules are located among the chains and always face the less hindered Ag_2 ions, with a short $Ag_2···Cl_2$ non-bonding contact of 3.567(3) Å.

Even **2** is composed of single-stranded wavy chains (though of $Ag(im)(PPh_3)_2$ formulation) winding up about the monoclinic axis as 2_1 degenerate helices of pitch 9.674(5) Å (see Figs. 2 and 3(b)). The skeleton of each chain is formed by consecutive, non collinear, metal ions [Ag···Ag = 6.555(1) Å and Ag···Ag···Ag = 95.1°], singly bridged by *N*,*N*′-*exo*-bidentate imidazolate ligands. Each metal, in a generic position, is further bonded to *two* independent PPh_3 ligands, thus showing a heavily distorted tetrahedral arrangement due to the steric hindrance of the PPh_3 moieties (see caption to Fig. 2). The crystal packings of both $\mathbf{1 \cdot CH_2Cl_2}$ and **2** show a few C···C contacts between the phenyl rings, the shortest values falling in the usual 3.3–3.4 Å range.

Focusing on the most significant structural aspects, a comparison can be made between $\mathbf{1 \cdot CH_2Cl_2}$ or **2** and related triphenylphosphine derivatives of silver(I) azolates, i.e., the $[Ag(\mu_2\text{-pz})(PPh_3)]_2$ and $[Ag_2(\mu_2\text{-pz})_2(PPh_3)_3]_2$ dimers [20] and the $[Ag(\mu_2\text{-1,2,3-triz})(PPh_3)_2]_n$, $[Ag(\mu_2\text{-1,2,4-triz})(PPh_3)_2]_n$ [17] and $[Ag(\mu_2\text{-tetz})(PPh_3)_2]_n$ [18] polymers.

The pitch characterising the 2_1 helices of **2** is shorter than the translation step of $\mathbf{1 \cdot CH_2Cl_2}$, but almost comparable to those found for the $[Ag(\mu_2\text{-1,2,3-triz})(PPh_3)_2]_n$, $[Ag(\mu_2\text{-1,2,4-triz})(PPh_3)_2]_n$ and $[Ag(\mu_2\text{-tetz})(PPh_3)_2]_n$ polymers [9.119(5), 9.525(6) and 9.471(3) Å, respectively]. Indeed, both the Ag···Ag contacts and the N–Ag–N angles characterising these species (Table 1) confirm the presence of a more 'relaxed' N–Ag···Ag–N skeleton in the crystals of $\mathbf{1 \cdot CH_2Cl_2}$. No reasonable comparison can obviously be made to the metal···metal contacts of the *doubly bridged* $[Ag(\mu_2\text{-pz})(PPh_3)]_2$ and $[Ag_2(\mu_2\text{-pz})_2(PPh_3)_3]_2$ dimers. The latter can be included when considering the Ag–N bond distances. Those departing from tetrahedral centres span the 2.29–2.34 Å range (Table 1), couples of bonds on the same metal ion not always being comparable within experimental error. Noteworthy, is that the quoted range partially overlaps with that spanned by the Ag–N bonds of trigonal metal centres (2.20–2.31 Å, Table 1), thus evidencing, for the Ag–N vectors of the two stereochemistries, a lack of internal consistency. The situation appears somewhat different for Ag–P bond distances, the intervals for tetrahedral and trigonal silver(I) ions being clearly differentiated (2.44–2.59 and 2.37–2.39 Å, respectively; Table 1). Once again, however, couples of bonds on the same metal centre may differ more than allowed by the related e.s.d.'s. The only bond angles showing a certain regularity are N–Ag–N, insisting on three-coordinated metal ions; the other L–Ag–P angles (L = N or P) cover rather wide ranges, though, for a given compound, adhering to the N–Ag–N < N–Ag–P and N–Ag–N < N–Ag–P < P–Ag–P

Table 1
Synoptic collection of chemically relevant distances (Å) and bond angles (°) in the known triphenylphosphine derivatives of silver(I) azolates (e.s.d.'s in parentheses)

Compound	References	Ag···Ag	CN(Ag) = 3[a]				CN(Ag) = 4[a]				
			Ag–N	Ag–P	N–Ag–N	N–Ag–P	Ag–N	Ag–P	N–Ag–N	N–Ag–P	P–Ag–P
$[Ag(pz)(PPh_3)]_2$	20	3.870(1)	2.204(3)	2.376(1)	110.68(10)	124.04(8)					
			2.313(3)			125.24(8)					
$[Ag_2(pz)_2(PPh_3)_3]_2$	20	3.706(1)	2.176(2)	2.370(1)	110.39(8)	117.28(6)	2.295(2)	2.461(1)	100.67(8)	99.38(5)–112.03(6)	121.73(3)
			2.235(2)			132.24(6)	2.323(2)	2.484(1)			
[Ag(1,2,3-triz)$(PPh_3)_2]_n$	17	6.265					2.326(7)	2.460(2)	93.1(3)	108.1(2)–114.3(2)	116.63(8)
							2.327(7)	2.512(2)			
[Ag(1,2,4-triz)$(PPh_3)_2]_n$	17	6.554					2.309(5)	2.441(2)	97.7(2)	101.9(2)–114.8(1)	126.29(7)
							2.321(5)	2.469(2)			
[Ag(tetz)$(PPh_3)_2]_n$	18	6.498					2.316(4)	2.441(1)	94.3(2)	101.5(1)–114.3(1)	127.41(5)
							2.337(3)	2.456(1)			
$[Ag_2(im)_2(PPh_3)_3]_n$	[b]	6.433(1)	2.249(5)	2.395(2)	109.47(17)	118.43(13)	2.290(4)	2.450(2)	109.25(16)	93.21(12)–117.36(12)	118.40(5)
		6.575(1)	2.196(4)			131.09(13)	2.301(4)	2.595(2)			
[Ag(im)$(PPh_3)_2]_n$	[b]	6.555(1)					2.294(2)	2.471(1)	97.92(8)	105.22(6)–114.01(6)	124.22(3)
							2.296(2)	2.456(1)			

For N–Ag–P bond angles on tetrahedral metal centres, only the spanned ranges, not the whole list of values, are reported.
[a] CN(Ag) = coordination number of silver(I).
[b] Present work.

orderings for trigonal and tetrahedral coordinations, respectively (Table 1).

4. Discussion

Already for the long-known $[Ag(\mu_2\text{-pz})]_n$ polymer, the reaction with PPh_3 allows the recovery of different species, $Ag(\mu_2\text{-pz})(PPh_3)$ and $Ag_2(\mu_2\text{-pz})_2(PPh_3)_3$, depending on the Ag:$PPh_3$ ratio employed (1:1.5 and >1:5, respectively) [20]. In the present case, i.e., with the imidazolate analogue, the required excess of PPh_3 not only prevents the dissociation of the already coordinated ligands, but, at an earlier stage of the reaction, also promotes depolymerisation of the starting silver(I) species: actually, as confirmed by single crystal X-ray data collections, both $Ag(\mu_2\text{-pz})(PPh_3)$ and $Ag_2(\mu_2\text{-pz})_2(PPh_3)_3$ consist of truly molecular dinuclear species (their correct formulation being thus $[Ag(\mu_2\text{-pz})(PPh_3)]_2$ and $Ag_2(\mu_2\text{-pz})_2(PPh_3)_3$, respectively). The different amplitude of the *N*,*N*′-*exo*-bidentate coordination bite in imidazolate and pyrazolate suggests the impossibility of forming doubly bridged dinuclear species in the case of **1** · $\mathbf{CH_2Cl_2}$ and **2**, thus suggesting either cyclic oligomers of higher nuclearity, or monodimensional polymers such as $[Ag(\mu_2\text{-1,2,3-triz})(PPh_3)_2]_n$, $[Ag(\mu_2\text{-1,2,4-triz})(PPh_3)_2]_n$ [17] and $[Ag(\mu_2\text{-tetz})(PPh_3)_2]_n$ [18]. In the latter species, N_1 and N_3 (strictly paralleling the reciprocal position of nitrogens in imidazolate), N_1 and N_4, or N_1 and N_3, respectively, are involved in metal bridging, N_2 (retraceable to the only other bite available in pz) being uncoordinated in all three cases. Thus, at least in the solid state, the presence of multiple N donor sites (as in 1,2,3-triz, 1,2,4-triz and tetz) results in *N*,*N*′-*exo*-bidentate (bridging) azolates, strictly avoiding the coordination of adjacent N atoms. The structural features of **1** · $\mathbf{CH_2Cl_2}$ and **2**, established by X-ray single crystals experiments (see above), definitely support these considerations.

The reaction of Ag(az) with PPh_3, depending on the azolate moiety, leads to different products, also on the basis of the Ag:PPh_3 reaction ratios employed, dimeric or polymeric species being typically obtained. The only monomeric tris–triphenylphosphine silver(I) azolate so far isolated is $Ag(im)(PPh_3)_3$; however, variable temperature ^{31}P NMR has shown that, although never recovered from $Ag_2(\mu_2\text{-pz})_2(PPh_3)_3$ solutions, $Ag(pz)(PPh_3)_3$ is stable (in solution) when a large excess of PPh_3 is employed [20]. The existence of other $Ag(az)(PPh_3)_3$ species has been proven, in solution, for az = 1,2,3-triz, 1,2,4-triz (variable temperature ^{31}P NMR) and tetz (r.t. ^{31}P NMR evidences). Noteworthy, with tetz, the Ag:PPh_3 ratio required to obtain $Ag(im)(PPh_3)_3$ (1:3) leads directly to the $[Ag(\mu_2\text{-az})(PPh_3)_2]_n$ polymer [17,18]. Thus, even if "naturally" addressed as a homogeneous set of species, there are still some distinct peculiarities within the $Ag(az)(PPh_3)_n$ family (witnessed, inter alia, by their different pharmacological activity); moreover, among

the missing members of the pyrazolato and imidazolato systems studied in our group, we need to mention $[Ag(\mu_2\text{-pz})(PPh_3)_2]_2$ (with two phosphines per silver(I) ion [20]) and $[Ag(\mu_2\text{-im})(PPh_3)]_n$ [with only one phosphine per silver(I) ion], which could never be prepared, regardless of the $Ag:PPh_3$ ratio applied.

5. Conclusions

Two novel polymeric silver-imidazolate derivatives, $[Ag_2(\mu_2\text{-im})_2(PPh_3)_3]_n$, (**1**), and $[Ag(\mu_2\text{-im})(PPh_3)_2]_n$, (**2**), have been synthesised and characterized, complementing a recent report on the solution and structural chemistry of silver(I) complexes with polyimidazolyl derivatives and tertiary phosphines [24].

Although lacking pharmaceutical investigations, the results herein reported may non-negligibly contribute to the development of pharmaceutically active silver(I) azolates, throwing light on their remarkably different versatility towards phosphorous donor ligands. Actually, Nomiya et al. [17–19] have often remarked that, independently from the solid state organisation, the phosphine derivatives are, once dissolved, markedly less active than the corresponding homoleptic parents, possibly because of the higher affinity of silver(I) toward softer ligands (phosphines vs. azolates). Nevertheless, the stoichiometry, the reactivity and the structural features of the new species presented certainly add significant information on the nature of the complexes which can exist, in equilibrium with the more active species, in physiological conditions.

6. Supplementary material

Crystallographic data (excluding structure factors) have been deposited with the Cambridge Crystallographic Data Centre, supplementary publications Nos. CCDC 235858 and 235859. Copies of this data can be obtained free of charge on application to CCDC, 12 Union Road, Cambridge CB2 1EZ, UK [fax: +44 1223 336 033; e-mail: deposit@ccdc.cam.ac.uk; or on the web: http://www.ccdc.cam.ac.uk].

Acknowledgements

The Italian MIUR (PRIN 2003), the University of Insubria (Progetto di Eccellenza "Sistemi Poliazotati") and the Fondazione Provinciale Comasca are acknowledged for funding. A special acknowledgement is due to Prof. Angelo Sironi (Dipartimento di Chimica Strutturale e Stereochimica Inorganica, Università degli Studi di Milano) for the generous loan of the X-ray single crystal equipment.

References

[1] N. Masciocchi, G.A. Ardizzoia, G. La Monica, A. Maspero, A. Sironi, Eur. J. Inorg. Chem. (2000) 2507.
[2] J. Kröber, E. Codjovi, O. Kahn, F. Grolière, C. Jay, J. Am. Chem. Soc. 115 (1993) 9810;
P. Gütlich, Y. Garcia, H.A. Goodwin, Chem. Soc. Rev. 29 (2000) 419.
[3] G. Yang, R.G. Raptis, Inorg. Chem. 42 (2003) 261.
[4] W.N. Richmond, P.W. Faguy, S.C. Weibel, J. Electroanal. Chem. 448 (1998) 237.
[5] L.C. Tabares, J.A.R. Navarro, J.M. Salas, J. Am. Chem. Soc. 123 (2001) 383;
E. Barea, J.A.R. Navarro, J.M. Salas, N. Masciocchi, S. Galli, A. Sironi, J. Am. Chem. Soc. 126 (2004) 3014.
[6] L. Castellanos-Serra, E. Hardy, Electrophoresis 22 (2001) 864.
[7] N. Masciocchi, G.A. Ardizzoia, S. Brenna, G. LaMonica, A. Maspero, S. Galli, A. Sironi, Inorg. Chem. 41 (2002) 6080.
[8] N. Masciocchi, M. Moret, P. Cairati, A. Sironi, G.A. Ardizzoia, G. La Monica, S. Cenini, J. Am. Chem. Soc. 116 (1994) 7668.
[9] N. Masciocchi, G.A. Ardizzoia, A. Maspero, G. La Monica, A. Sironi, Inorg. Chem. 38 (1999) 3657.
[10] N. Masciocchi, M. Moret, P. Cairati, A. Sironi, G.A. Ardizzoia, G. La Monica, J. Chem. Soc., Dalton Trans. (1995) 1671.
[11] N. Masciocchi, S. Bruni, E. Cariati, F. Cariati, S. Galli, A. Sironi, Inorg. Chem. 40 (2001) 5897.
[12] N. Masciocchi, G.A. Ardizzoia, G. LaMonica, A. Maspero, A. Sironi, Eur. J. Inorg. Chem. 12 (2000) 2507.
[13] N. Masciocchi, G.A. Ardizzoia, G. La Monica, A. Maspero, A. Sironi, Angew. Chem., Int. Ed. Engl. 37 (1998) 3366.
[14] N. Masciocchi, E. Corradi, M. Moret, G.A. Ardizzoia, A. Maspero, G. La Monica, A. Sironi, Inorg. Chem. 36 (1997) 5648.
[15] N. Masciocchi, S. Galli, A. Sironi, E. Barea, J.A.R. Navarro, J.M. Salas, L.C. Tabares, Chem. Mater. 15 (2003) 2153;
E. Barea, J.A.R. Navarro, J.M. Salas, N. Masciocchi, S. Galli, A. Sironi, Inorg. Chem. 43 (2004) 473.
[16] K. Nomiya, K. Tsuda, T. Sudoh, M. Oda, J. Inorg. Biochem. 68 (1997) 39.
[17] K. Nomiya, K. Tsuda, N.C. Kasuga, J. Chem Soc., Dalton Trans. (1998) 1653.
[18] K. Nomiya, R. Noguchi, M. Oda, Inorg. Chim. Acta 298 (2000) 24.
[19] K. Nomiya, K. Tsuda, Y. Tanabe, H. Nagano, J. Inorg. Biochem. 68 (1998) 9.
[20] G.A. Ardizzoia, G. La Monica, A. Maspero, M. Moret, N. Masciocchi, Inorg. Chem. 36 (1997) 2321.
[21] C.T. North, D.C. Phillips, F.S. Mathews, Acta Crystallogr. Sec. A 24 (1968) 351.
[22] A. Altomare, G. Cascarano, C. Giacovazzo, A. Guagliardi, A.G.G. Moliterni, M.C. Burla, G. Polidori, M. Camalli, R. Spagna, SIR97: Package for Structure Solution by Direct Methods, University of Bari, Bari, Italy, 1997.
[23] G.M. Sheldrick, SHELX97: Program for Crystal Structure Refinement, University of Göttingen, Göttingen, Germany, 1997.
[24] Effendy, G.G. Lobbia, M. Pellei, C. Pettinari, C. Santini, B.W. Skelton, A.H. White, J. Chem. Soc., Dalton Trans. (2001) 528, and references therein.

[10–13]. There are also some recent reports on structural studies and spectral characteristics of *N*(4)-phenyl 4-benzoylpyridine thiosemicarbazone [14]. It was found that the presence of a bulky group at the terminal nitrogen *N*(4) considerably increased the activity [15]. We have recently reported structural and spectral studies of copper(II) complexes of 2-benzoylpyridine *N*(4),*N*(4)-(butane-1,4-diyl)thiosemicarbazone [16]. In addition, iron(III) complexes of 2-acetylpyridine-*N*(4),*N*(4)-(butane-1,4-diyl) thiosemicarbazone are also reported [17]. This paper describes the syntheses, structural, spectral and antimicrobial studies of six new Cu(II) complexes of 2-benzoylpyridine *N*(4)-cyclohexyl thiosemicarbazone (HL).

2. Experimental

Cyclohexyl isothiocyanate (Fluka), hydrazine hydrate (Lancaster), 2-benzoylpyridine (Lancaster) were used as received. The HL was prepared by a reported procedure [18].

2.1. Synthesis of complexes

To a methanolic solution of cupric chloride (2 mmol), a methanolic solution of HL (2 mmol) was added and refluxed for 4 h to prepare [CuLCl] (**1**). The resulting solution, on cooling, yielded blue coloured crystals, which were filtered, washed with methanol and ether and dried over P_4O_{10} in vacuo. [{CuLBr}$_2$] (**2**), [CuL-NO_3] (**3**), [CuL_2SO_4]·$2H_2O$ (**6**) were prepared by similar method using the appropriate copper salts. Compounds [CuLNCS] (**4**) and [$CuLN_3$]·$3H_2O$ (**5**) were prepared by a metathetical displacement of the acetate anion of the copper acetate complex by the addition of 1 mmol each of the methanolic solutions of KCNS and NaN_3, respectively, to the reaction mixture containing the ligand and copper acetate in methanol. The resulting solution was refluxed for 3 h and left overnight. The solids, which separated were filtered, washed with methanol and ether and dried over P_4O_{10} in vacuo.

2.2. Physical methods

Carbon, hydrogen and nitrogen analyses of the ligand and the complexes were done on a Heraeus elemental analyser at CDRI, Lucknow, India. The IR spectra were recorded on a Shimadzu DR 8001 series FT-IR instrument using KBr pellets in the range 400–4000 cm^{-1} and far IR spectra were recorded in the range 50–500 cm^{-1} on a Nicolet Magna 550 FT-IR spectrometer using polyethylene pellets at RSIC, IIT, Bombay, India. The solid-state reflectance spectra of the ligand and the complexes were recorded on an Ocean Optics, Inc. SD2000 Fibre Optic Spectrometer. Electronic spectra of the ligand and the complexes in DMF solution were recorded on a Shimadzu 160A UV–Vis. spectrophotometer. The EPR spectra of the complexes were recorded in a Varian E-112 Spectrometer using TCNE as the standard at RSIC, IIT, Bombay. The magnetic susceptibility measurements were carried out at the Indian Institute of Technology, Roorkee, at room temperature in the polycrystalline state on a PAR model 155 Vibrating Sample Magnetometer at 5 K Oersted field strength. The molar conductances of the complexes of the solutions in dimethylformamide (ca. 10^{-3} M) at room temperature were measured using a direct reading conductivity meter.

2.3. X-ray crystallography

Single crystals of compound **1** for X-ray analysis were grown by slow evaporation of the complex in a chloroform–methanol mixture. A deep blue monoclinic crystal of compound [CuLCl] (**1**) was mounted on a glass fibre using epoxy cement. The X-ray diffraction data were measured in frames with increasing θ (width of 0.3°/frame) at room temperature (293 K) using a Bruker SMART APEX CCD diffractometer, equipped with a fine focus sealed tube X-ray source. The SMART software was used for data acquisition and the SAINT software for data extraction [19]. Empirical absorption corrections were made on the intensity data [20]. The structure was solved by the heavy atom method and refined by full-matrix least squares using the SHELX system of programs [21] and the graphics tool was PLATON for windows [22]. All non-hydrogen atoms of the complex cations were refined anisotropically. Few hydrogen atoms were located from the difference Fourier map and the rest were generated, assigned isotropic thermal parameters and refined using a riding model. The hydrogen atoms were used for structure factor calculation only. Similarly, a deep blue crystal of [{CuLBr}$_2$] (**2**) and a light green coloured crystal of [CuLNCS] (**4**) were analysed and the crystallographic data along with the structural refinements are given in Table 2.

2.4. Antimicrobial activity

For antimicrobial activity, two Gram positive and three Gram negative bacteria were used as test organisms. The disc diffusion method was used for screening the antimicrobial property and determining the MIC (minimum inhibitory concentration) of the compounds.

3. Results and discussion

3.1. Synthesis of the complexes

All the complexes were synthesized by refluxing HL with the corresponding copper salt in ethanol. The col-

Table 1
Colours and partial elemental analysis data of the complexes

Compound	Color	Found (Calc.)%			μ (B.M.)
		C	H	N	
[CuLCl] (**1**)	blue	52.62 (52.29)	4.94 (4.82)	12.72 (12.84)	1.52
[{CuLBr}$_2$] (**2**)	blue	47.16 (47.45)	4.55 (4.37)	11.70 (11.65)	1.80
[CuLNO$_3$] (**3**)	green	49.35 (49.29)	4.62 (4.54)	14.73 (15.13)	1.62
[CuLNCS] (**4**)	green	52.40 (52.34)	4.70 (4.58)	15.03 (15.26)	1.94
[CuLN$_3$]·3H$_2$O (**5**)	blue	45.46 (45.96)	4.94 (5.43)	20.14 (19.74)	1.97
[Cu$_2$(L)$_2$SO$_4$]·2H$_2$O (**6**)	dark green	48.87 (48.87)	5.03 (4.93)	11.99 (12.00)	1.66

ours, stoichiometries, elemental analyses and magnetic moments of the Cu(II) complexes are given in Table 1. All the Cu(II) complexes prepared are either blue or green in colour. The elemental analysis data of all the compounds suggest a formula [MLX], where X is Cl, Br, NO_3, NCS, N_3 and L is the deprotonated ligand. However, the sulfato complex is found to have the formula [Cu$_2$(L)$_2$SO$_4$]·2H$_2$O. The compounds **5** and **6** contain water molecules and the IR data suggest that the water molecules are not coordinated, but exist as lattice water [23].

All the complexes are found to be non-conductors in DMF solution. These facts along with the elemental analysis data indicate that the anion and the deprotonated ligand are coordinated to the central Cu(II). Magnetic moments of the complexes are calculated from magnetic susceptibility measurements and the values of all the Cu(II) complexes at room temperature are found to be in the range 1.5–1.9 B.M. The values of the magnetic moments, which are close to the spin only value of 1.7 B.M. indicate the presence of one unpaired electron.

Table 2
Crystal data and structural refinement for the complexes

Parameters	[CuLCl] (**1**)	[{CuLBr}$_2$] (**2**)	[CuLNCS] (**4**)
Empirical formula	$C_{19}H_{21}ClCuN_4S$	$C_{19}H_{22}BrCuN_4S$	$C_{20}H_{21}CuN_5S_2$
Formula weight (M)	436.45	481.92	459.08
Temperature, T (K)	293(2)	293(2)	293(2)
Wavelength, Mo Kα (Å)	0.71073	0.71073	0.71073
Crystal system	monoclinic	triclinic	triclinic
Space group	$P2_1/n$	$P\bar{1}$	$P\bar{1}$
Lattice constants			
a (Å)	13.170(3)	9.642(5)	8.679(5)
b (Å)	8.670(2)	10.714(6)	9.376(5)
c (Å)	35.445(9)	10.899(6)	13.280(7)
α (°)	90.00	72.746(9)	80.761(9)
β (°)	98.00	76.413(9)	81.187(9)
γ (°)	90.00	70.887(8)	76.876(9)
Volume, V (Å^3)	4008.1(18)	1004.1(9)	1031.1(10)
Z	8	2	2
Calculated density, ρ (Mg m^{-3})	1.446	1.5940	13.4787
Absorption coefficient, μ (mm^{-1})	1.337	3.191	1.277
F(000)	1800	488	474
Crystal size (mm)	0.40 × 0.35 × 0.30	0.40 × 0.35 × 0.20	0.45 × 0.40 × 0.35
θ range for data collection	2.82–26	2.5–29.59	2.43–28.08
Limiting indices	$-16 \leqslant h \leqslant 16$, $-10 \leqslant k \leqslant 10$, $-43 \leqslant l \leqslant 43$	$-13 \leqslant h \leqslant 13$, $-14 \leqslant k \leqslant 14$, $-14 \leqslant l \leqslant 14$	$-11 \leqslant h \leqslant 11$, $-12 \leqslant k \leqslant 12$, $-17 \leqslant l \leqslant 17$
Reflections collected	29574	12475	12440
Unique reflections (R_{int})	7862 (0.0498)	9644 (0.0227)	4951 (0.0220)
Completeness to θ	26.00 (99.6%)	29.59 (91.1%)	28.08 (98.5%)
Absorption correction	none	none	none
Maximum and minimum transmission	0.6898 and 0.6168	0.5678 and 0.3617	none
Refinement method	full-matrix least-squares on F^2	full-matrix least-squares on F^2	full-matrix least-squares on F^2
Data/restraints/parameters	7862/0/637	9644/3/529	4951/0/337
Goodness-of-fit on F^2	1.091	0.955	1.050
Final R indices [$I > 2\sigma(I)$]	$R_1 = 0.0555$, $wR_2 = 0.1041$	$R_1 = 0.0362$, $wR_2 = 0.0899$	$R_1 = 0.0406$, $wR_2 = 0.0926$
R indices (all data)	$R_1 = 0.0932$, $wR_2 = 0.1158$	$R_1 = 0.0577$, $wR_2 = 0.1014$	$R_1 = 0.0547$, $wR_2 = 0.0982$
Largest difference peak and hole (e Å^{-3})	0.417 and −0.291	0.736 and −0.499	0.549 and −0.202

3.2. Crystal structures of [CuLCl], [{CuLBr}$_2$] and [CuLNCS]

The structures of [CuLCl] (**1**), [{CuLBr}$_2$] (**2**) and [CuLNCS] (**4**) along with the atom labelling are shown in Figs. 1–3, respectively. Crystal data are given in Table 2 and a comparison of selected bond lengths and bond angles of HL, with compounds **1**, **2** and **4**, is summarized in Table 3.

3.2.1. [CuLCl]

The compound CuLCl (**1**) crystallizes into a monoclinic lattice with a $P2_1/n$ space group symmetry. There are two crystallographically independent molecules, A and B, in the asymmetric unit of the compound, with bond lengths and angles, which agree with each other and are within normal ranges. The compound shows a square planar geometry with the Cu atom lying in an approximate plane with the N1, N3, S1 and Cl1 atoms. Due to coordination, the C13–S1 bond length of the thiosemicarbazone moiety approaches the value corresponding to a C–S single bond, as evident from the increased value of 1.746(3) Å in the complex, compared to 1.675(15) Å in the ligand. The C13–S1 distance in **1** compares well with those reported for the related thiosemicarbazone complexes, in which the coordination by the thiolate tautomers has been definitely established by X-ray structural determinations [24,25]. A slight distortion from the square planar geometry is evidenced by the bond angles, N1–Cu1–N2 (80.31(9)°), N2–Cu1–S1 (84.21(7)°), N1–Cu1–Cl1 (98.15(7)°) and Cl1–Cu1–S1 (97.22(4)°). The bonding parameters reveal that the Cu1–N1 (2.036(2) Å) and Cu1–N2 (1.966(2) Å) bond lengths are much smaller than the Cu1–Cl1 (2.2099(10) Å) bond length. This implies stronger Cu–N bonds compared to the Cu–Cl bond, indicating the domination of the thiosemicarbazone moiety in the bonding. The repeating unit in the crystal packing consists of three molecules where two of them set in an offset fashion are self-assembled by the intermolecular (N2H–S1) hydrogen bonding interactions, while the third molecule is arranged in a face to face manner with the neighbouring molecule. The repeating units are packed in an offset fashion and a three dimensional packing is effected by the π–π stacking, ring–metal and CH–π interactions.

3.2.2. [{CuLBr}$_2$]

Compound **2** is a thiolate bridged copper(II) dimer complex crystallized into a triclinic lattice with $P\bar{1}$ symmetry. Thiolate bridging by sulfur ligands are well reported [26–28], and recently the metal complexes of Schiff bases [29,30] and thiosemicarbazone [31] involving phenolate oxygen bridging are reported. Each CuLBr unit in the molecule assembles into a symmetric binuclear complex by bridging through the thiolate sulfur atom of the adjacent thiosemicarbazone via axial ligation. Thus, the Cu(II) ions reveal a distorted pentacoordinated viz, (4 + 1) (N1N2SBr + S′) square-based pyramidal geometry in the complex. The basal plane is occupied by the thiolate sulfur, azomethine nitrogen, pyridyl nitrogen and the bromine atoms. The bond lengths Cu1–S1 (2.289(2) Å), Cu1–N2 (1.978(4) Å),

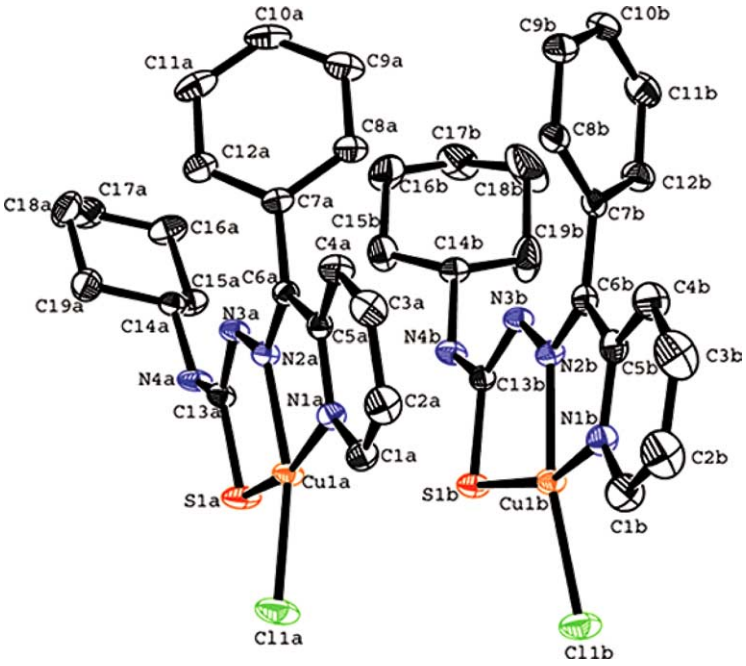

Fig. 1. ORTEP diagram for CuLCl (**1**), displacement ellipsoids are drawn at the 50% probability level and hydrogen atoms are shown as small spheres of arbitrary radii.

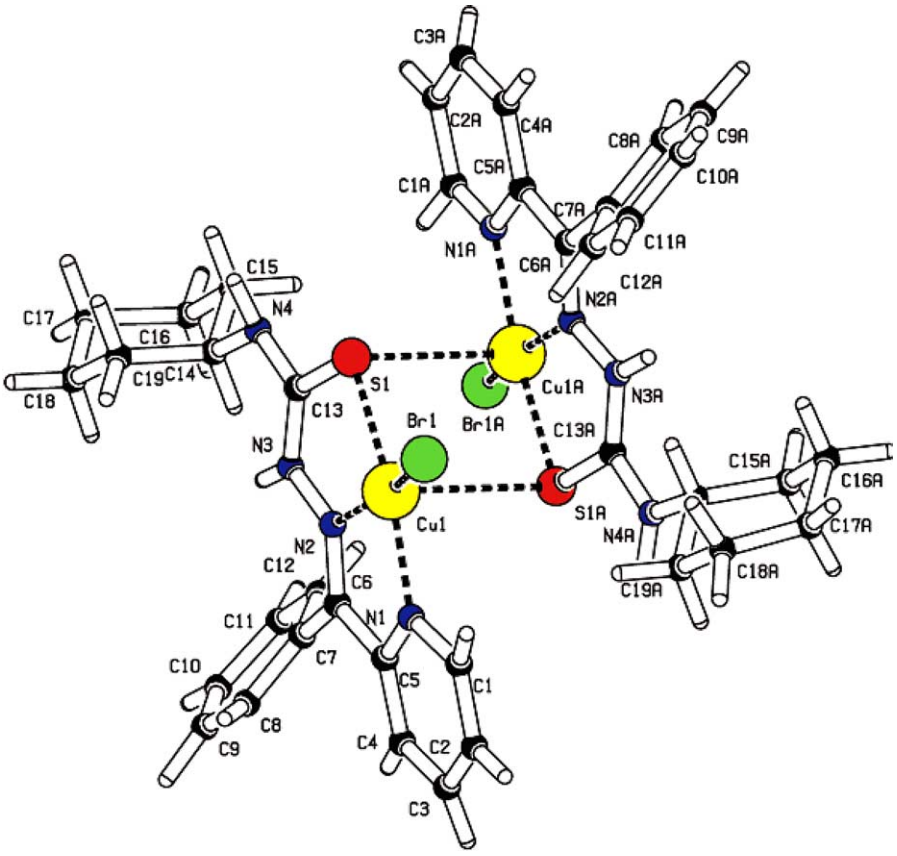

Fig. 2. PLATON diagram for [{CuLBr}$_2$] (**2**).

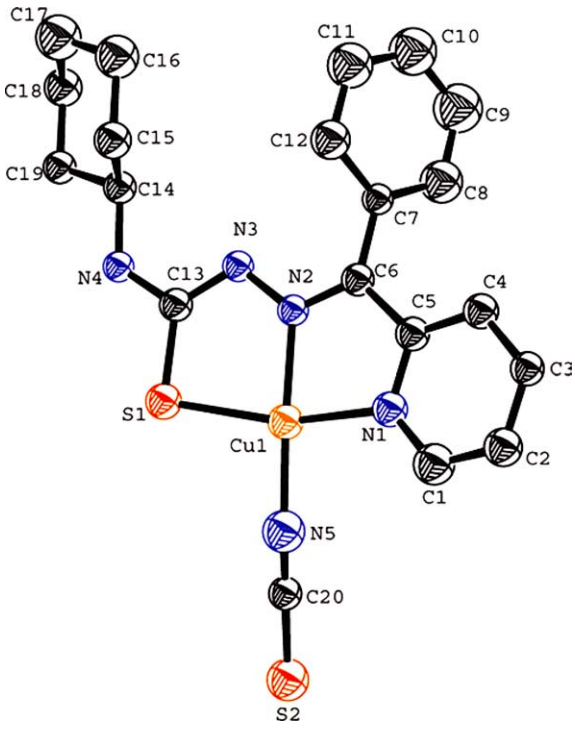

Fig. 3. ORTEP diagram for CuLNCS (**4**), displacement ellipsoids are drawn at the 50% probability level and hydrogen atoms are shown as small spheres of arbitrary radii.

Cu1–N1 (2.028(5) Å) and Cu1–Br1 (2.371(12) Å) are consistent with the other similar bond distances of square pyramidal copper complexes [32]. The apical position of the square pyramid is occupied by the thiolate sulfur of the second unit, at a Cu–Cu distance of ca. 3.523 Å with the Cu1–S1–Cu1A or Cu1–S1A–Cu1A angle being ca. 84.47°. In the Cu_2S_2 plane, the Cu1–S1 or Cu1A–S1A and Cu1–S1A or Cu1A–S1 bond lengths are ca. 2.266 and 2.937 Å, respectively, and the non-equivalent bonds give rise to the asymmetric binuclear thiolate double bridged structure. The basal planes around Cu1 and Cu1A are essentially planar with mean deviations being 0.1905(5) and 0.1891(5) Å, respectively. The significantly longer Cu–S axial bond length of ca. 2.937 Å is likely to reduce the spin–spin coupling between Cu1 and Cu1A centres. The Cu_2S_2 unit in the complex is planar with a mean deviation of 0.0073(5) Å. The Cu_2S_2 plane is observed at angles of 81.76(2)° and 80.60(2)°, respectively, with the basal planes around Cu1 and Cu1A. The crystal packing is effected by the wide network of CH –π interactions and the π–π stacking interactions involving the phenyl, pyridyl and metal chelate rings. The thiolate bridging structure is further stabilized by the comparatively stronger π–π interactions between the centroids Cg(3) and Cg(9) consisting of Cu(1), S(1), Cu(1A), S(1A) and Cu(1A), N(1A),

Table 3
Comparison of selected bond lengths (Å) and bond angles (°) of HL, [CuLCl], [{CuLBr}$_2$] and [CuLNCS]

	HL	[CuLCl]	[{CuLBr}$_2$]	[CuLNCS]
Bond lengths				
C(6)–N(2)	1.290 (18)	1.309 (3)	1.306 (7)	1.299 (3)
N(2)–N(3)	1.367 (17)	1.365 (3)	1.377 (7)	1.366 (2)
N(3)–C(13)	1.364 (18)	1.323 (14)	1.327 (7)	1.325 (3)
S(1)–C(13)	1.675 (15)	1.746 (3)	1.719 (6)	1.746 (2)
C(13)–N(4)	1.328 (19)	1.334 (4)	1.348 (8)	1.339 (3)
Cu(1)–S(1)		2.245 (10)	2.289 (2)	2.261 (12)
Cu(1)–N(1)		2.036 (2)	2.028 (5)	2.016 (2)
Cu(1)–N(2)		1.966 (2)	1.978 (4)	1.962 (19)
Cu(1)–Cl(1)		2.2099 (10)		
Cu(1)–N(5)				1.924 (2)
Cu(1)–Br(1)			2.371 (12)	
Cu(1A)–S(1A)			2.266	
Cu(1A)–S(1A)			2.66 (2)	
Cu(1A)–S(1)			2.937	
Bond angles				
N(1)–C(5)–C(6)	118.25 (13)	115.0 (2)	114.70 (19)	114.60 (5)
N(2)–N(3)–C(13)	118.46 (12)	111.6 (2)	111.45 (17)	112.20 (4)
N(3)–C(13)–S(1)	118.87 (11)	124.9 (2)	125.62 (16)	126.20 (5)
N(1)–Cu(1)–Cl(1)		98.15 (7)		
N(1)–Cu(1)–N(2)		80.31 (9)	79.7 (2)	80.40 (7)
N(2)–Cu(1)–S(1)		84.21 (7)	84.55 (16)	84.43 (6)
S(1)–Cu(1)–Cl(1)		97.22 (4)		
N(2)–Cu(1)–Cl(1)		164.00 (8)		
N(1)–Cu(1)–Br(1)			99.11 (13)	
S(1)–Cu(1)–Br(1)			96.24 (6)	
N(2)–Cu(1)–Br(1)			164.20 (12)	
Cu(1)–S(1)–Cu(1A)			84.11	
Cu(1A)–S(1A)–Cu(1)			84.47	
S(1)–Cu(1A)–S(1A)			95.56	
S(1A)–Cu(1)–S(1)			95.89	
N(1)–Cu(1)–N(5)				97.44 (9)
S(1)–Cu(1)–N(5)				98.15 (7)
N(2)–Cu(1)–N(5)				176.88 (8)

C(5A), C(6A), N(2A), respectively, which is observed at a remarkably shorter distance of 2.7632(3) Å.

3.2.3. [CuLNCS]

The crystal is developed into a triclinic lattice with $P\bar{1}$ symmetry and it reveals a distorted square planar N_3S coordination sphere with the copper centre. The thiosemicarbazone ligand occupies three positions and the thiocyanate nitrogen the fourth position of an approximate square plane. The C13–S1 bond length of 1.675(15) Å in the ligand HL is an evidence for the thione form in the solid state, which is shifted to 1.746(2) Å in the complex, confirming the coordination via the thiolate sulfur in **4**. The N2–N3 bond length of 1.367(17) Å in the uncomplexed thiosemicarbazone is found to remain unchanged in the complex, whereas, the C13–N3 bond length of 1.364(18) Å in HL is shifted to 1.325(3) Å in **4**. This is in support for the shifting of the thione form of the thiosemicarbazone to the thiol form during complexation. The ligand is deprotonated at N3 and the complex carries two five-membered chelate rings. The two planes through Cu1, N1, C5, C6, N2 and Cu1, N2, N3, C13, S1 show that the sets of atoms are almost coplanar, with a dihedral angle of 9.52(2)°. This small deviation from coplanarity would certainly not hinder the delocalization of electrons in the coordination sphere, and the stability of the complex is sustained. The distorted square planar structure is evidenced by the acute value displayed by the thiosemicarbazone bite angles, viz., N1–Cu1–N2 (80.40(7) Å) and N2–Cu1–S1 (84.43(6) Å) [33]. The bond angles of the trans donor atoms, i.e., N1–Cu1–S1 (160.36(6)°) and N5–Cu1–N2 (176.88(8)°) are $\geqslant$160° in **4**, which is consistent with the work on copper(II) complexes of 2-benzoylpyridine *N*(4)-substituted thiosemicarbazones by West et al. [10]. In the crystal lattice, the unit cell contains two molecules and the adjacent molecules are packed in a face to face manner facilitated by the π–π, CH–π and ring-metal interactions. It is also interesting to note that in all three crystals, the torsion angle values and the ring puckering analyses show that the metal chelate ring comprising of Cu1, S1, C13, N3 and N2 adopts an envelope conformation, whereas the cyclohexyl ring exists in the chair form. Atoms C14, C16, C17 and C19 constitute the best-fitting

plane of the cyclohexyl ring, while the atoms C15 and C18 deviate by 1.2415(6) and −1.2491(6) Å, respectively, on either side of the plane.

3.3. Vibrational spectra

The tentative assignments of the significant IR spectral bands of HL and its copper(II) complexes are presented in Table 4. The ν(C=N) band of the thiosemicarbazone at 1582 cm^{-1} is found to be shifted to lower energies in the spectra of the complexes indicating coordination via the azomethine nitrogen. This is confirmed by the bands in the range 440–464 cm^{-1}, which have been assigned to the ν(Cu–N) bond [34]. The ν(N–N) of the thiosemicarbazone is found at 1118 cm^{-1}. The increase in frequency of this band in the spectra of complexes is due to the increase in bond strength, again confirming the coordination via the azomethine nitrogen. In the uncomplexed thiosemicarbazone, a strong band at 833 cm^{-1} is assigned to ν(C=S), whereas in the complexes, this band is found to be shifted to lower frequencies in the range 783–794 cm^{-1}. This negative shift of the ν(C=S) band in the complexes is indicated by the coordination via the thiolate sulfur atom. Strong bands observed in the region 340–353 cm^{-1} have been assigned to the ν(Cu–S) band. In all the copper complexes a strong band is observed in the region 266–280 cm^{-1}, which is consistent with the ν(Cu–N) of pyridine as suggested by Clark and Williams [35]. Based on the above spectral evidences, it is confirmed that the ligand is coordinated to the Cu(II) ion as a tridentate anion, coordinating via the azomethine nitrogen, pyridyl nitrogen and thiolate sulfur. In the chloro complex, a strong band observed at 304 cm^{-1} has been assigned to the ν(Cu–Cl) band. The ν(Cu–Br) frequency is observed at 247 cm^{-1} in the bromo complex. The ν(Cu–Br) and ν(Cu–Cl) frequencies are consistent with terminal chloro and bromo ligands. In the IR spectrum of the complex containing nitrate as the gegenion, the band observed at 268 cm^{-1} can be assigned to ν(Cu–ONO_2), consistent with the bands at 253–280 cm^{-1} reported earlier for Cu–ONO_2 in metal complexes [36]. Moreover, in the nitrato complex of HL, two strong bands at 1280 and 1410 cm^{-1} corresponding to ν_1 and ν_4 modes of nitrato groups with a separation of 130 cm^{-1} indicate the presence of a terminally bonded monodentate nitrate group [23]. In the azido complex, a strong band observed at 2037 cm^{-1} is assigned to ν_a of the azide group, indicative of azide coordination [37]. Other bands due to N_3 such as ν_s(NNN) are difficult to assign because of the richness of the spectrum of the complex. In the thiocyanato complex, the very strong band observed at 2093 cm^{-1} corresponds to ν(C=N). Bands observed at 783, 481 and 461 cm^{-1} are assigned to ν(C=S), δ(NCS) and ν(Cu–N), respectively. These facts indicate that thiocyanate group is N-coordinated to copper [38]. In the sulfato complex, the fourth coordination position is occupied by the oxygen atom of the sulfate ion which belongs to the high symmetry point group T_d. The symmetry of the sulfate is reduced to C_{2v} when it functions as a bidentate ligand in the complex. The IR spectrum of compound **6** contains strong bands at 1002, 1117, 1204 cm^{-1} due to ν_3, 960 cm^{-1} due to ν_1 and 465 cm^{-1} due to ν_2, and these can be assigned to a bridging bidentate sulfato group [23]. This type of bidentate bridging by a sulfato group has been proved by a single crystal X-ray diffraction study for a thiosemicarbazone derived from di-2-pyridyl ketone [39]. According to Stefov et al. [40], coordinated water should exhibit frequencies at 825, 575 and 500 cm^{-1}. The absence of spectral bands in these regions in the spectra of complexes **3** and **6** indicates that the water molecules in these complexes are not coordinated but are present as lattice water.

3.4. Electronic spectra

The energies of the electronic transitions for the thiosemicarbazone HL and its Cu(II) complexes (solid state and DMF solution) are listed in Table 5. The solid-state electronic spectra of the thiosemicarbazone HL consists of a broadband at ca. 29 000 cm^{-1} which is the $n \rightarrow \pi^*$ band of the pyridine ring. Another $n \rightarrow \pi^*$ band of the thiosemicarbazone moiety is present in the 24 000 cm^{-1} region [12]. The molar absorptivity for $n \rightarrow \pi^*$ transitions for the solution spectrum is $>10^4$, which is consistent with the previously studied heterocyclic thiosemicarbazones [10]. The electronic spectra of the Cu(II) complexes consist of a $n \rightarrow \pi^*$ band of the pyridine ring at ca. 30 000 cm^{-1}. Additional bands observed in the range 23 000–25 000 cm^{-1} are assigned to S → Cu

Table 4
IR spectral assignments (cm^{-1}) of HL and the Cu(II) complexes

Compound	ν(C=N)	ν(N–N)	ν(C–S)	ρ(py)	ν(Cu–N)	ν(Cu–Npy)	ν(Cu–S)	ν(Cu–X)
HL	1582m	1118s	1370w, 833m	607w				
[CuLCl]	1582s	1150m	1337m, 785m	642w	460m	280s	349m	304s
[{CuLBr}$_2$]	1544s	1150m	1336m, 794m	644m	443s	282s	353s	247s
[$CuLNO_3$]	1543w	1138m	1279s, 786w	646m	459m	268s	352s	268s
[CuLNCS]	1542s	1138s	1331s, 783w	642m	461s	266m	350s	350s
[$CuLN_3$]·3H_2O	1540m	1131	1324m, 788s	644s	464s	278m	351w	
[$Cu_2(L)_2SO_4$]·2H_2O	1544m	1130s	1332m, 789m	641m	463s	280s	352s	397s

Table 5
Electronic spectral assignments (cm^{-1}) (log ε in parentheses) of HL and the Cu(II) complexes

Compound	Mode	d → d	L → M	n → π*	π → π*
HL	solid			28735, 24390sh	38610
	DMF			29411 (4.13), 26315 (3.32)	39010 (4.20)
[CuLCl]	solid	18691, 15313	24509, 31250sh	30030, 26809sh	38967
	DMF	17452 (2.602)	22830 (4.14)	27624 (3.83)	39062 (4.41)
[{CuLBr}$_2$]	solid	18080sh, 16129	24937	31645	37453sh
	DMF	18080 (2.41)	24860 (3.21)	31620 (4.12)	37560sh (4.25)
[CuLNO$_3$]	solid	16590sh, 15455	24937	32382	35714
	DMF	18350 (2.51)	23510 (4.13)	32310 (4.10)	36810 (4.61)
[CuLNCS]	solid	17761sh, 15308	24213	32362	38314sh
	DMF	17568sh (2.61)	22831 (3.81)	28571 (4.34)	37965 (4.06)
[CuLN$_3$]·3H$_2$O	solid	18691sh, 17123	24213	32362	37453sh
	DMF	17110sh (2.34)	22727 (4.35)	28409 (4.21)	37013sh (4.01)
[Cu$_2$(L)$_2$SO$_4$]·2H$_2$O	solid	17355sh, 15220	24570	31645	37453sh
	DMF	15980 (2.5)	24087 (4.30)	32467 (4.43)	37700 (4.21)

and py → Cu charge-transfer bands [41,42]. In the chloro complex (**1**), a shoulder observed at 31250 cm^{-1} is assigned to the Cl → Cu charge-transfer transition. The solid state spectra of all the Cu(II) complexes have a broadband in the region 15000–19000 cm^{-1}. This is consistent with a broad structured band for square planar complexes in the range 13000–20000 cm^{-1} [43].

3.5. Electron paramagnetic resonance spectra

The EPR spectra of a polycrystalline sample at 298 K and in different solutions at 298 and 77 K were recorded in the X band, using the 100 KHz field modulation; g factors were quoted relative to the standard marker TCNE ($g = 2.00277$). The EPR parameters of the Cu(II) complexes are presented in Table 6. The EPR spectra of CuLCl and Cu$_2$(L)$_2$SO$_4$ in the polycrystalline state at 298 K show only one broad signal at $g = 2.125$ and 2.063, respectively. Such isotropic spectra, consisting of a broad signal, and hence only one g value, arise from extensive exchange coupling through misalignment of the local molecular axes between different molecules in the unit cell (dipolar broadening) and enhanced spin lattice relaxation. These types of spectra unfortunately give no informa-

Table 6
EPR parameters of the Cu(II) complexes of HL

Compound	Solid (298 K)		DMF solution (298 K)		DMF solution (77 K)			
	$g_1/g_2/g_3$	g_{av}	g_{iso}	A_{iso}[a]	$g_1/g_2/g_3$	g_{av}	$A_{\parallel}$[a]	G
[CuLCl]	g_{iso} 2.1257		2.0828	84.13	$g_{\parallel}$ 2.160 $g_{\perp}$ 2.046	2.0854	166.39	3.63
[{CuLBr}$_2$]	g_1 2.0649 g_2 2.0710 g_3 2.1559	2.097	2.1330	79.0	$g_{\parallel}$ 2.1270 $g_{\perp}$ 2.0340	2.065	176.17	3.93
[CuLNO$_3$]	$g_{\parallel}$ 2.1840 $g_{\perp}$ 2.0510	2.095	2.0807	79.46	$g_{\parallel}$ 2.1923 $g_{\perp}$ 2.0532	2.0995	180.7	3.73
[CuLNCS]	g_1 2.037 g_2 2.054 g_3 2.169	2.086	2.1200	88.80	g_1 2.0367 g_2 2.053 g_3 2.1764	2.0887	168.26	4.14
[CuLN$_3$]·3H$_2$O	$g_{\parallel}$ 2.2064 $g_{\perp}$ 2.0993	2.135	2.1456	82.26	$g_{\parallel}$ 2.1276 $g_{\perp}$ 2.0338	2.064	171.1	3.97
[Cu$_2$(L)$_2$SO$_4$]·2H$_2$O	g_{iso} 2.063		2.1152	81.32	$g_{\parallel}$ 2.1826 $g_{\perp}$ 2.0498	2.0940	169.8	3.84

[a] A values are given in 10^{-4} cm^{-1}.

tion on the electronic ground state of the Cu(II) ion present in the complexes. The spectra of [{CuLBr}$_2$] and [CuLNCS] are rhombic with three g values. The spectra of the other compounds show typical axial spectra with well-defined $g_\parallel$ and $g_\perp$ values. The spectra are often broad because of the broadening resulting from the fast spin–lattice relaxation time and exchange coupling. The geometric parameter G, which is a measure of the exchange interaction between copper centres in the polycrystalline compound, is calculated and the value of G is found to be in the range 2.3–4.0. In all the copper(II) complexes $g_\parallel > g_\perp > 2.0023$ and a G value less than 4.1 is consistent with a $d_{x^2-y^2}$ ground state [44,45]. The EPR spectral studies are in agreement with the X-ray diffraction studies for complexes **1**, **2** and **4**. All the complexes in DMF solution at 298 K clearly show four well-resolved hyperfine lines (^{65}Cu, $I = 3/2$). The EPR spectra of the complexes in glassy state at 77 K were recorded in different solvents, such as DMF, $CHCl_3$ and in a 1:1 mixture of $CHCl_3$ and toluene. Solutions of compounds **1** and **2** in chloroform–toluene mixture show well-resolved four hyperfine lines corresponding to monomeric Cu(II) complexes. The spectra have five nitrogen superhyperfine lines on the high field copper hyperfine splitting component, which arise from the coupling of the electron spin with the nuclear spin of the two nitrogen atoms. The EPR spectrum of compound **5** shows four well-resolved hyperfine lines with seven nitrogen superhyperfine lines on the high field copper hyperfine splitting component. The seven superhyperfine lines arise from the coupling of the electron spin with the nuclear spin of the three nitrogen atoms, i.e., one azomethine nitrogen, one nitrogen of pyridine ring and one nitrogen from the azido anion coordinated to the Cu(II) centre. The EPR spectra of compounds **3**, **4** and **6** in DMF solution at 77 K show four hyperfine lines. The EPR spectra of compounds **1** and **5** are given in Figs. 4 and 5, respectively.

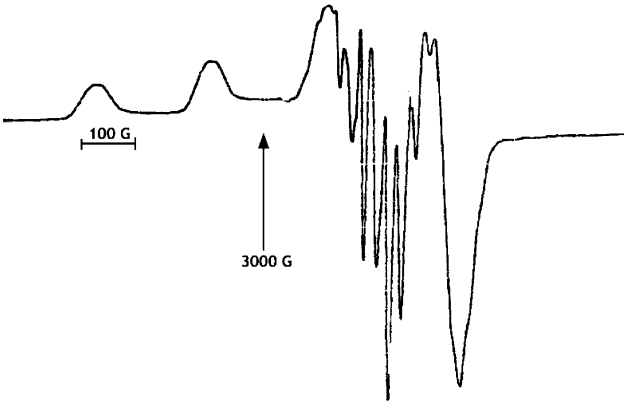

Fig. 4. EPR spectrum of CuLCl (**1**) in DMF solution at 77 K.

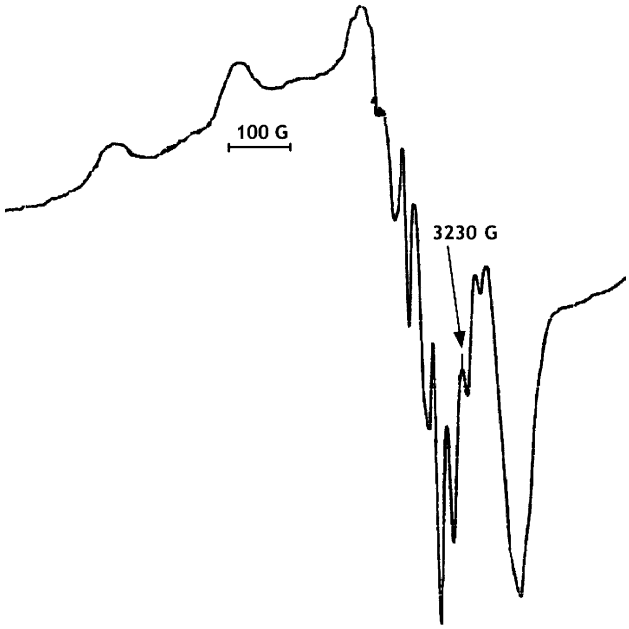

Fig. 5. EPR spectrum of $CuLN_3$ (**5**) in DMF solution at 77 K.

The $g_\parallel$ values of all the compounds are found to be almost the same, which indicates that the bonding is dominated by the thiosemicarbazone moiety. Kivelson and Nieman [46] have reported that $g_\parallel$ values less than 2.3 indicate considerable covalent character to M–L bonds, while a value greater than 2.3 indicate ionic character. The $g_\parallel$ values of all the compounds are found to be less than 2.3, which indicates considerable covalent character to the M–L bond.

The EPR parameters $g_\parallel$, $g_\perp$, g_{av}, $A_\parallel$ (Cu) and $A_\perp$ (Cu) and the energies of the d–d transition were used to evaluate the bonding parameters α^2, β^2 and γ^2, which may be regarded as measures of the covalency of the in-plane σ bonds, in-plane π bonds and out-of-plane π-bonds, respectively (Table 7) [3].

The value of the in-plane sigma bonding parameter α^2 was calculated [44] using the expression

$$\alpha^2 = -A_\parallel/0.036 + (g_\parallel - 2.0023) + 3/7(g_\perp - 2.0023) + 0.04.$$

The orbital reduction factors, $K_\parallel = \alpha^2\beta^2$ and $K_\perp = \alpha^2\gamma^2$ were calculated using the following expressions:

$$K_\parallel^2 = (g_\parallel - 2.0023)E_{d\text{-}d}/8\lambda_0,$$

$$K_\perp^2 = (g_\perp - 2.0023)E_{d\text{-}d}/2\lambda_0,$$

where λ_0 is the spin–orbit coupling constant, with a value of -828 cm^{-1} for a copper(II) d^9 system.

According to Hathaway [44], for pure σ bonding, $K_\parallel \approx K_\perp \approx 0.77$, and for in-plane π bonding, $K_\parallel < K_\perp$; while for out-of-plane π bonding, $K_\perp < K_\parallel$. In all the complexes, it is observed that $K_\parallel < K_\perp$ which indicates

Table 7
Bonding parameters and orbital reduction parameters of the Cu(II) complexes of HL

Compound	α^2	β^2	γ^2	$K_{\parallel}$	$K_{\perp}$	K_0	f
[CuLCl]	0.6810	0.9455	0.9862	0.6439	0.6716	0.3283	129.99
[{CuLBr}$_2$]	0.6667	0.8518	0.8590	0.5687	0.5735	0.3312	120.70
[CuLNO$_3$]	0.7537	0.9250	0.9575	0.6972	0.7217	0.3440	121.32
[CuLNCS]	0.7062	0.9226	0.9643	0.6516	0.6810	0.3581	129.30
[CuLN$_3$]·3H$_2$O	0.6538	0.8750	0.8782	0.5720	0.5742	0.2997	124.43
[Cu$_2$(L)$_2$SO$_4$]·2H$_2$O	0.7165	0.9355	0.9600	0.6658	0.6834	0.3394	128.54

the presence of significant in-plane π bonding. This is further confirmed by the bonding parameters α^2, β^2 and γ^2, which are less than 1.0 expected for purely ionic character of the bonds, and decreases with increasing covalent nature of the bonding. Therefore the evaluated values of α^2, β^2 and γ^2 are consistent with both in-plane σ and in-plane π bonding [47].

The empirical factor $f = g_{\parallel}/A_{\parallel}$ cm^{-1} is an index of tetragonal distortion and its value may vary from 105 to 135 for small to extreme distortion in square planar complexes, and that depends on the nature of the coordinated atom [48]. The f values of the complexes are found to be in the range 121–130, indicating significant distortion from planarity.

Recent studies have shown that biological activity is related to the geometry at the metal sites. Complexes with more tetrahedral distortion are reported to display higher activity [49]. The studies of antimicrobial activity among the six complexes revealed the chloro compound to have the greatest activity, which is consistent with the above statement since compound **1** shows the maximum f value of 129.99. However, compound **4**, with almost the same f value (129.30), is found to be less active.

3.6. Antimicrobial activity

The ligand HL and the Cu(II) complexes were tested for their antimicrobial activity. Test substances which produce a zone of inhibition of diameters 9 mm or more are regarded as positive, i.e. having constructive antimicrobial activity; while in those cases where the diameter is below 9 mm, the bacteria are resistant to the sample tested and the sample is said to have no antimicrobial activity. The following bacteria, isolated from clinical samples, were used as test organisms: (1) *Staphylococcus aureus*, (2) *Bacillus* sp. (Gram positive), (3) *Escherichia coli*, (4) *Salmonella paratyphi*, (5) *Vibrio cholerae O1* (Gram negative).

The disc diffusion method was used for screening the antimicrobial property of the test samples. The MIC (minimum inhibitory concentration) of the compounds showing a positive antimicrobial property was found using the same method. 1% solutions of the samples in DMF were used. The medium used for growing the culture was nutrient agar. The ligand HL was found to be inactive, but all the copper(II) complexes were found to be active (Table 8). The copper(II) complexes **1** and **3** were found to be active against *Bacillus* sp. *V. cholerae O1* and *S. aureus*. Compound **6** was found to be active against *Bacillus* sp., *V. cholerae O1* and *S. paratyphi.* Compound **5** was found to be active against *V. cholerae O1* and *S. paratyphi* and compounds **2** and **4** were found to be active against *V. cholerae O1*. The MIC values of the complexes are given in Table 9.

4. Supplementary data

Crystallographic data for the structural analysis has been deposited with the Cambridge Crystallographic Data centre, CCDC 227455 for compound [CuLCl] (**1**), CCDC 227456 for compound [CuLNCS] (**4**) and CCDC 227457 for compound [{CuLBr}$_2$] (**2**). Copies of this information may be obtained free of charge from The Director, CCDC, 12 Union Road, Cambridge,

Table 8
The antimicrobial activity of the complexes using the disc diffusion method

Compound	Microbial activity inhibition zone				
	Bacillus sp.	*Staphylococcus aureus*	*Vibrio cholera 01*	*Escherichia coli*	*Salmonella paratyphi*
HL					
[CuLCl]	+9 mm	+9 mm	+11 mm		
[{CuLBr}$_2$]			+10 mm		
[CuLNO$_3$]	+11 mm	+10 mm	+11 mm		
[CuL(NCS)]			+10 mm		
[CuLN$_3$]·3H$_2$O			+10 mm		+9 mm
[Cu$_2$(L)$_2$SO$_4$]·2H$_2$O	+10 mm		+14 mm		+9 mm

Table 9
MIC of the Cu(II) complexes

Compound	MIC in μl			
	Bacillus sp.	*Vibrio cholerae O1*	*Salmonella paratyphi*	*Staphylococcus aureus*
[CuLCl]	5	5		4
[{CuLBr}$_2$]		5		
[CuLNO$_3$]	5	5		5
[CuLNCS]		5		
[CuLN$_3$]·3H$_2$O		5	4	
[Cu$_2$(L)$_2$SO$_4$]·2H$_2$O	5	5	5	

CB2, IEZ, UK (fax: +44-1223-336-033; e-mail: deposit@ccdc.cam.ac.uk or http://www.ccdc.cam.ac.uk).

Acknowledgements

The authors are indebted to RSIC, CDRI, Lucknow, India for elemental analyses and IIT Bombay, India for EPR spectral measurements. M.R. P. Kurup and M. Joseph thank Kerala State Council for Science, Technology and Environment, Government of Kerala, for financial assistance.

References

[1] J.P. Scovill, D.L. Klayman, C.F. Franchino, J. Med. Chem. 25 (1982) 1261.
[2] D.X. West, S.B. Padhye, P.S. Sonawane, Struct. Bonding 76 (1991), and references therein.
[3] P. Bindu, M.R.P. Kurup, T.R. Satyakeerty, Polyhedron 18 (1999) 321.
[4] A.C. Sartorelli, K.C. Agarwal, A.S. Tsiftsoglou, E.C. Moore, Adv. Enzyme Reg. 15 (1977) 117.
[5] D.R. Williams, Chem. Rev. 72 (1972) 203, and references therein.
[6] R.A. Finnegan, J.A. Matson, J. Am. Chem. Soc. 94 (1972) 4780.
[7] D.X. West, H. Gebremedhin, T.J. Romack, Transition Met. Chem. 19 (1994) 426.
[8] D.X. West, S.L. Dietrich, I. Thientanavananich, C.A. Brown, Transition Met. Chem. 19 (1994) 195.
[9] B.S. Garg, M.R.P. Kurup, S.K. Jain, Y.K. Bhoon, Transition Met. Chem. 16 (1991) 111.
[10] D.X. West, J.S. Ives, J. Krejct, M.M. Salberg, T.L. Zumbahlen, G.A. Bain, A.E. Liberta, J. Valdes-Martinez, S. Hernandez-Ortiz, R.A. Toscano, Polyhedron 14 (1995) 2189.
[11] H. Beraldo, W. Nacif, A. Rebolledo, R. Costa, J.D. Ardisson, Braz. Meeting Inorg. Chem. (2002).
[12] D.X. West, N.M. Kozub, G.A. Bain, Transition Met. Chem. 21 (1996) 52.
[13] D.X. West, I.S. Billeh, J.P. Jesinski, J.M. Jesinski, R.J. Butcher, Transition Met. Chem. 23 (1998) 209.
[14] H. Beraldo, A.M. Barreto, R.P. Vieira, A.P. Rebolledo, N.L. Speziali, C.B. Pinheiro, G. Chapuis, J. Mol. Struct. 645 (2003) 213.
[15] D.L. Klayman, J.P. Scovill, J.F. Bartosevich, J. Bruce, J. Med. Chem. 26 (1983) 1367.
[16] A. Sreekanth, M.R.P. Kurup, Polyhedron 22 (2003) 3321.
[17] A. Sreekanth, M.R.P. Kurup, Polyhedron 23 (2004) 969.
[18] M. Joseph, V. Suni, C.R. Nayar, M.R.P. Kurup, H.K. Fun, J. Mol. Struct. 705 (2004) 63.
[19] Siemens, SMART and SAINT, Area Detector Control and Integration Software, Siemens Analytical X-ray Instruments Inc., Madison, WI, USA, 1996.
[20] R.H. Blessing, Acta Crystallogr., Sect. A 51 (1995) 33.
[21] G.M. Sheldrick, SHELXS-97, University of Göttingen, Göttingen, Germany, 1997.
[22] A.L. Speck, PLATON, A Multipurpose Crystallographic Tool, Utrecht, Netherlands, 1999.
[23] K. Nakamoto, Infrared and Raman spectra of inorganic and coordination compounds, 5th ed., Wiley, New York, 1997.
[24] E. Ainscough, A.M. Bordie, E.N. Bake, R.J. Cresswell, J. Ranford, J.M. Waters, Inorg. Chim. Acta 172 (1990) 185.
[25] V. Philip, V. Suni, M.R.P. Kurup, M. Nethaji, Polyhedron 23 (2004) 1225.
[26] J.G. Anton, J. Pons, X. Solans, M.F. Bardia, L. Ros, Inorg. Chim. Acta 355 (2003) 87.
[27] V.E. Kaasjager, J. van den Broeke, R.K. Henderson, W.J.J. Smeets, A.L. Spek, W.L. Driessen, E. Bouwman, J. Reedijk, Inorg. Chim. Acta 316 (2001) 99.
[28] M. Cha, J. Sletten, S. Critchlow, J.A. Kovacs, Inorg. Chim. Acta 263 (1997) 153.
[29] K.S. Anjali, Yung-Lin Pui, V. Wing-Wah Yam, J.J. Vittal, Inorg. Chim. Acta 319 (2001) 57.
[30] N. Ancin, S. de, S.G. Ozta, M. Tuzun, J. Mol. Struct. 606 (2002) 45.
[31] E. Labisbal, K.D. Haslow, A. Sousa-Pedrares, J. Valdes-Martinez, S. Hernandez-Ortega, D.X. West, Polyhedron 22 (2003) 2831.
[32] G.J. Palenik, D.F. Rendle, W.S. Carter, Acta Crystallogr., Sect. B 30 (1974) 2390.
[33] M.E. Hossain, M.N. Alam, J. Begum, M.A. Ali, M. Nazimuddin, F.E. Smith, R.C. Hynes, Inorg. Chim. Acta 249 (1997) 207.
[34] M.B. Ferrari, G.G. Fava, M. Lafranchi, C. Pelizzi, P. Tarasconi, Inorg. Chim. Acta 181 (1991) 253.
[35] R.J. Clark, C.S. Williams, Inorg. Chem. 4 (1965) 350.
[36] S.K. Jain, B.S. Garg, Y.K. Bhoon, Spectrochim. Acta 42 A (1986) 701.
[37] R. Raina, T.S. Srivastava, Indian J. Chem. 22A (1983) 701.
[38] D.X. West, G. Ertem, R.M. Makeever, Transition Met. Chem. 10 (1986) 41.
[39] V. Philip, V. Suni, M.R.P. Kurup, M. Nethaji, unpublished results.
[40] V. Stefov, V.M. Petrusevski, B. Soptrajanov, J. Mol. Struct. 293 (1993) 97.
[41] E. Ainscough, A.M. Brodie, N.G. Larsen, Inorg. Chim. Acta 60 (1982) 25.
[42] P.L. Dedert, J.S. Thompson, J.A. Ibers, T.J. Marks, Inorg. Chem. 21 (1982) 969.
[43] A.B.P. Lever, Inorganic Electronic Spectroscopy, 2nd ed., Elsevier, Amsterdam, 1984.
[44] B.J. Hathaway, G. Wilkinson, R.D. Gillard, J.A. McCleverty (Eds.), Comprehensive Coordination Chemistry II, vol. 5, Pergamon, Oxford, 1987.

[45] A.H. Maki, B.R. McGravey, J. Chem. Phys. 28 (1958) 35.
[46] D. Kivelson, R. Neiman, J. Chem. Soc., Dalton Trans. 35 (1961) 149.
[47] R.P. John, A. Sreekanth, V. Rajakannan, T.A. Ajith, M.R.P. Kurup, Polyhedron 23 (2004) 2549.
[48] R. Pogni, M.C. Bartto, A. Diaz, R. Basosi, J. Inorg. Biochem. 79 (2000) 333.
[49] A. Diaz, R. Pogni, R. Cao, R. Basosi, Inorg. Chim. Acta 275 (1998) 552.

procedures before use in electrochemical measurements [15]. The Schiff base ligand HL was prepared by a reported method [16]. The elemental analysis was carried out using a Heraeus CHN-O rapid instrument. The infrared and electronic spectral measurements were recorded using Perkin–Elmer Spectrum One FT-IR and Lambda 55 spectrometers, respectively. The variable temperature magnetic susceptibility measurements in the temperature range 18–300 K were carried out using a George Associates Inc. (Berkeley, CA, USA) Lewis-coil-force magnetometer. $Hg[Co(NCS)_4]$ was used as a standard. Theoretical fitting of the experimental susceptibility data using the Curie-Weiss equation $\chi_M = C/(T-\theta)$ gave a linear fit with a θ value of 3.5 K. Cyclic voltammetric measurements were made at 25 °C on a EG&G PAR 253 VersaStat potentiostat/galvanostat using a three electrode configuration consisting of a glassy carbon working electrode, a platinum wire auxiliary and a saturated calomel reference (SCE) electrode. Ferrocene ($E_{1/2}$ = 0.41 V) and $K_4[Fe(CN)_6]$ ($E_{1/2}$ = 0.18 V) were used as standards in MeCN–0.1 M $[Bu^n_4N]$-ClO_4 (TBAP) and 0.05 M Tris–HCl/0.1 M KCl buffer medium, respectively. Conductivity measurement was made at 25 C using a Control Dynamics conductivity meter. Solution infrared spectral studies were carried out using a silver chloride Quick Cell Kit from Aldrich (USA).

2.2. Synthesis of [Cu(HL)(ClO$_4$)](ClO$_4$) (1)

A 1.6 g quantity (4.3 mmol) of $Cu(ClO_4)_2\cdot 6H_2O$ taken in 20 ml methanol was reacted with 1.15 g (4.3 mmol) Schiff base ligand dissolved in 20 ml methanol under magnetic stirring for 30 min at 60 °C. The reaction mixture was cooled to an ambient temperature and the blue crystalline product thus obtained was separated, washed with cold methanol and dried in vacuum over P_4O_{10} (Yield: 1.6 g, ~70%). Calc. for $C_{16}H_{16}Cl_2CuN_4O_9$: C, 33.9; H, 3.4; N, 10.6. Found: C, 34.2; H, 3.5; N, 10.8%. FT-IR data in KBr phase (cm^{-1}): 3215br, 2928w, 2903w, 1648m, 1596s, 1483w, 1432m, 1318m, 1225m, 1148vs, 1123vs, 1089vs, 1019m, 985w, 786m, 623s, 580w, 520w, 485w, 425w (br, broad; vs, very strong; s, strong; m, medium; w, weak).

2.3. X-ray crystallography

Single crystals of **1** were grown by a diffusion technique using a MeCN solution of the complex and chlorobenzene. A rectangular shaped blue crystal was mounted on a glass fiber with epoxy cement. All geometric and intensity data were collected using an Enraf-Nonius CAD4 diffractometer equipped with graphite monochromated Mo Kα radiation. Intensity data, collected using the $\omega-2\theta$ scan mode, were corrected for Lorentz-polarization effects and for absorption [17]. The structure was solved and refined by full-matrix least-squares techniques using the SHELX system of programs [18]. The lattice perchlorate ion showed positional disorder. The bound perchlorate anion showed high thermal motion. The peaks for the lattice perchlorate ion were modelled for a tetrahedral structure with geometrical restraints using SADI provisions in the SHELX program. The alcoholic OH group of the propanol moiety of the Schiff base showed positional disorder with two peaks and the concerned oxygen atom was refined as O(1) and O(1a) with site occupancy factors of 0.7 and 0.3, respectively. This group showed the presence of intra- and intermolecular weak hydrogen bonding interactions involving the perchlorate ions. The structure refined well giving the highest residual peak of 1.24 e Å^{-3} located at ~0.8 Å from the O(22) atom of the lattice perchlorate ion. The perspective view of the molecule was obtained using ORTEP [19]. Selected crystallographic data are given in Table 1.

3. Results and discussion

3.1. Synthesis and general aspects

Complex **1** is prepared in high yield from the reaction of copper(II) perchlorate with the multidentate Schiff base ligand (HL) (Scheme 1). The complex has been characterized from analytical and physicochemical data (Table 2). Complex **1** is 1:2 electrolytic in nature in MeCN [20]. It shows infrared bands at 1148 and 1123 cm^{-1} for the metal-bound perchlorate ion and at 1089 cm^{-1} for the lattice perchlorate ion. The IR bands at 3215 and 1648 cm^{-1} are assignable to ν(O–H) and ν(C=N), respectively [21]. The complex displays a d–d band at 640 nm in its electronic spectrum in MeCN. The complex exhibits an essentially reversible cyclic voltammetric response at 0.01 V versus SCE (ΔE_p = 74 mV at 50 mV s^{-1} scan rate) in MeCN–0.1 M TBAP due to the copper(II)/copper(I) couple. In 0.05 M Tris–HCl/0.1 M KCl buffer medium, the copper(II)/copper(I) couple is observed at −0.24 V (ΔE_p = 90 mV at 50 mV s^{-1}), indicating better stability of the cupric state in the aqueous medium.

3.2. Crystal structure and magnetic property

The complex crystallizes in the monoclinic space group $P2_{1/C}$ with four molecules in the unit cell. The asymmetric unit consists of a mononuclear complex motif and a lattice perchlorate anion. An ORTEP view of the cationic complex is shown in Fig. 1. Selected bond distances and angles are given in Table 3. The complex forms a one-dimensional coordination polymer in which the {Cu(HL)} units are linked by the perchlorate ligand (Fig. 2). It has a six coordinate (4+2) CuN_4O_2 coordina-

Table 1
Selected crystallographic data[a] for $[Cu(HL)(ClO_4)](ClO_4)$(**1**)

	1
Empirical formula	$C_{16}H_{16}Cl_2CuN_4O_9$
Crystal size (mm)	$0.32 \times 0.2 \times 0.14$
Crystal morphology	rectangular
Crystal system	monoclinic
Space group	$P2_{1/C}$ (No. 14)
Formula weight	530.76
Unit cell dimensions	
a (Å)	14.584(3)
b (Å)	7.216(3)
c (Å)	19.924(6)
$\alpha = \gamma$ (°)	90
β (°)	109.39(2)
V (Å^3)	1977.8(11)
Z	4
D_{calc} (g cm^{-3})	1.782
μ(Mo) (mm^{-1})	1.434
F(000)	1076
λ(Mo Kα) (Å)	0.71073
T (K)	293(2)
Reflections collected	3480
Reflections observed [$I > 2\sigma(I)$]	2615
Parameters	319
$R_{obs.\ data}$ [$R_{all\ data}$]	0.0797 [0.1004]
$R_{w\ obs.\ data}$ [$R_{w\ all\ data}$]	0.2199 [0.2389]
Goodness-of-fit on F^2	0.952
Shift/e.s.d. (maximum)	0.001
Largest differential peak and hole [e Å^{-3}]	1.235; −0.627

[a] $w = [\sigma^2(F_0{}^2) + (0.1339P)^2 + 12.9768P]^{-1}$ where $P = (F_o^2 + 2F_c^2)/3$.

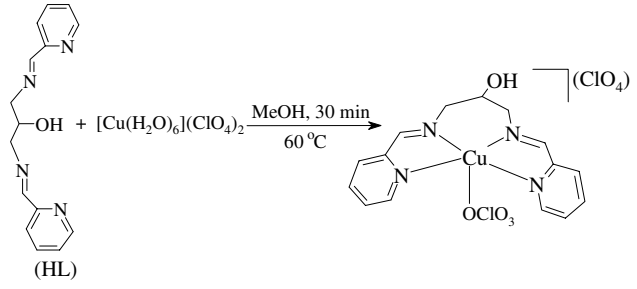

Scheme 1. Synthesis of complex **1**.

Table 2
Physicochemical data for complex **1**

1. IR in KBr phase [$\nu(ClO_4^-)$, cm^{-1}]	1148, 1123, 1089
2. UV–vis in MeCN [λ_{max} nm (ε,M^{-1} cm^{-1})]	640 (90), 289 (15200), 225 (26600)
3. μ_{eff} per copper (μ_B)	1.8 at 298 K; 2.1 at 18 K
4. Conductivity in MeCN [$\Lambda_M(\Omega^{-1}$ cm^2 M^{-1})]	285
5. $E_{1/2}$ (V) vs. SCE [ΔE_p (mV) at 50 mV s^{-1}, i_{pa}/i_{pc}]	
CV in MeCN–0.1 M TBAP	0.01 V [74, 0.9]
CV in 0.05 M Tris–HCl/0.1M KCl (pH 7.8)	−0.24 V [90, 0.8]

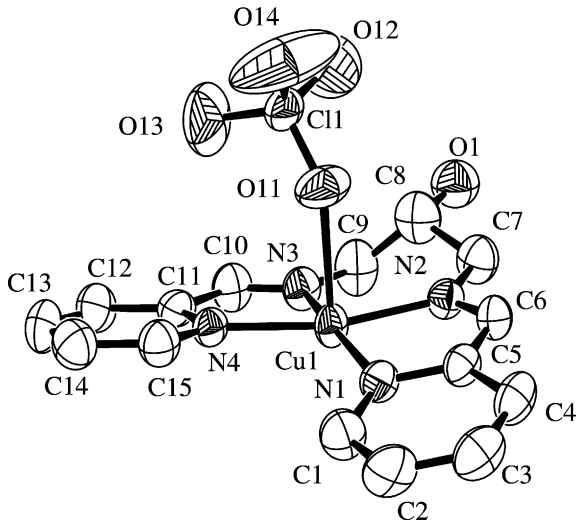

Fig. 1. An ORTEP view of the cationic complex in $[Cu(HL)(ClO_4)](ClO_4)$ (**1**) showing 50% probability thermal ellipsoids and the atom labelling scheme.

Table 3
Selected bond distances (Å) and angles (°) for the polymeric structure of **1**[a]

Bond lengths		Bond angles	
Cu(1)–N(1)	2.028(6)	O(11)–Cu(1)–O(14)#1	160.2(2)
Cu(1)–N(2)	1.989(6)	N(1)–Cu(1)–O(14)#1	79.6(3)
Cu(1)–N(3)	1.976(6)	N(2)–Cu(1)–O(14)#1	110.3(3)
Cu(1)–N(4)	2.020(6)	N(3)–Cu(1)–O(14)#1	94.3(3)
Cu(1)–O(11)	2.528(6)	N(4)–Cu(1)–O(14)#1	81.0(4)
Cu(1)–O(14)#1	2.610(10)	N(1)–Cu(1)–N(2)	81.6(2)
N(2)–C(6)	1.270(10)	N(1)–Cu(1)–N(3)	169.3(3)
N(2)–C(7)	1.485(10)	N(1)–Cu(1)–N(4)	105.8(2)
C(7)–C(8)	1.495(13)	N(1)–Cu(1)–O(11)	91.8(2)
C(5)–C(6)	1.467(11)	N(2)–Cu(1)–N(3)	92.8(3)
N(3)–C(10)	1.248(11)	N(2)–Cu(1)–N(4)	167.8(2)
N(3)–C(9)	1.480(11)	N(2)–Cu(1)–O(11)	85.5(2)
C(10)–C(11)	1.466(12)	N(3)–Cu(1)–N(4)	81.4(3)
O(1)···O(24)#2	2.84(2)	N(3)–Cu(1)–O(11)	96.8(2)
O(1A)···O(12)	2.52(2)	N(4)–Cu(1)–O(11)	84.5(2)
O(1A)···O(23)#2	2.88(2)	Cu(1)–O(11)–Cl(1)	140.6(4)
		Cu(1)–N(2)–C(7)	127.9(5)
		Cu(1)–N(2)–C(6)	113.6(5)
		Cu(1)–N(3)–C(9)	124.1(6)
		Cu(1)–N(3)–C(10)	114.8(6)

[a] symmetry operations #1: $x,y+1,z$ and #2: $-x,-y,-z$.

tion geometry in which the Schiff base binds the copper as a tetradentate ligand at the basal plane with two pyridine nitrogen and two imine nitrogen atoms. The elongated axial site has the perchlorate ligand with a Cu(1)–O(11) distance of 2.528(6) Å. The other axial bond in the polymeric structure, formed by the perchlorate of the adjacent unit, is 2.61(1) Å. The weakness of the axial bonds is evidenced from the 1:2 electrolytic nature of the complex in a solution phase. The bite angles involving the Schiff base pertaining to the 5- and 6-membered chelate rings are ~81.5° and 92.7°, respectively.

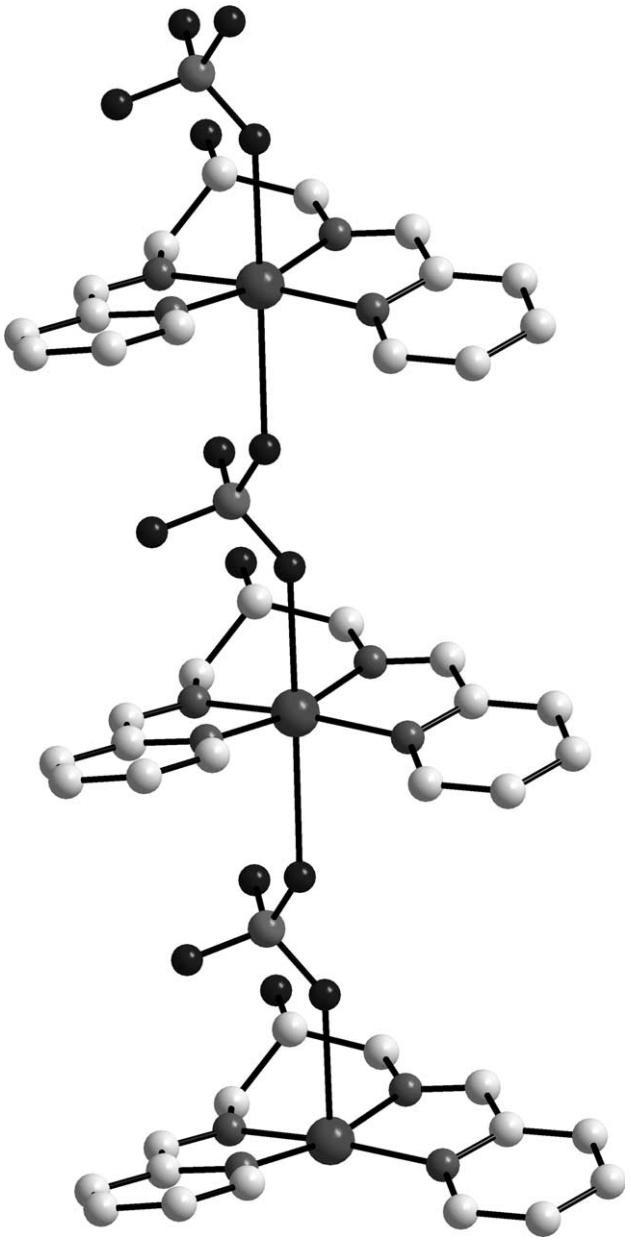

Fig. 2. The perspective view of the one-dimensional coordination polymeric structure of $[Cu(HL)(ClO_4)](ClO_4)$ (**1**). The positional disorder of the hydroxyl group is not shown for clarity.

While the 5-membered ring shows an envelope conformation, the 6-membered ring displays a twist-boat conformation. The complex is one-electron paramagnetic in nature. The 1D chain coordination polymeric structure of **1** does not show any significant magnetic exchange interaction along the chain as evidenced from the linear χ_M^{-1} versus T plot with a θ value of 3.5 K (Fig. 3) [22].

3.3. Imine bond activation

The reaction of the complex with H_2O_2 in an aqueous tetrahydrofuran mixture (1:4 v/v) has been monitored by

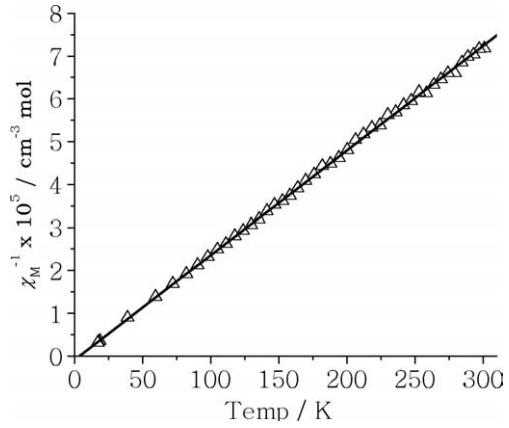

Fig. 3. The χ_M^{-1} vs. T plot for the 1D polymeric complex $[Cu(HL)(ClO_4)](ClO_4)$ (**1**). The solid line is the theoretical fit of the experimental data.

infrared spectroscopy. The spectral traces are shown in Fig. 4. The reaction proceeds with gradual formation of a bis(picolinato)copper(II) species as evidenced from an IR band near 1620 cm^{-1}. An additional band develops near 1685 cm^{-1} with the progress of the reaction. This band is assignable to the amido group formed from the imine moiety. The intensity of this band, however, gets reduced prior to the completion of the reaction, possibly due to conversion of the amido species to the relatively stable picolinic acid. We have isolated the bis(picolinato)copper(II)·dihydrate species in the crystalline form from the reaction of **1** with 30% H_2O_2 in aqueous methanol. The unit cell parameters of the violet colored crystals of the product compare well with the reported crystal data of the picolinato complex which in an aqueous THF medium shows a band at 1638 cm^{-1}, assignable to the carbonyl group of the carboxylate [23]. We have also isolated ammonium perchlorate from the synthetic reaction as a byproduct. It is likely that the

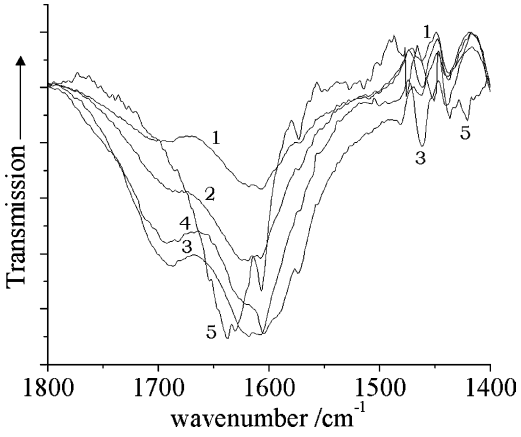

Fig. 4. IR spectral traces of $[Cu(HL)(ClO_4)](ClO_4)$ (**1**) in aqueous tetrahydrofuran (1:4 v/v) on reaction with 30% H_2O_2 at different time intervals: 1, 2 h; 2, 4 h; 3, 6 h; 4, 8 h; 5, pure sample of bis(picolinato)copper(II) complex.

conversion of azomethine to carboxylate promoted by hydrogen peroxide proceeds via formation of the amide bond as an intermediate species giving a reaction sequence: $-CH=N- \rightarrow -C(=O)-NH- \rightarrow -CO_2^- + H_2N-$. In addition, the formation of the amido species as an intermediate is inferred from the observation of a band at 1462 cm^{-1}. This band is assignable to the symmetric valence vibration of the O=C—N moiety of the amide. This band intensity also gets reduced on completion of the reaction (Fig. 4) [23].

4. Conclusions

A new copper(II) complex containing a multidentate Schiff base ligand has been prepared and structurally characterized by X-ray crystallography. The complex shows nearly reversible redox chemistry. It undergoes oxidative conversion to a bis(picolinato)copper(II) species on reaction with hydrogen peroxide through the formation of an intermediate amido species as evidenced from the solution infrared spectral studies.

Acknowledgements

We thank the Department of Science and Technology, Government of India, for financial support. We also thank the Alexander von Humboldt Foundation (Germany) for donation of an electroanalytical system.

Appendix A. Supplementary data

Crystallographic data for the structural analysis of **1** have been deposited with the Cambridge Crystallographic Data Center, CCDC No. 163126. Copies of this information may be obtained free of charge from The Director, CCDC, 12 Union Road, Cambridge, CB2 1EZ, UK (fax: +44-1223-366-033; e-mail: deposit@ccdc.ac.uk or www:http://www.ccdc.cam.ac.uk). Supplementary data associated with this article can be found, in the online version at doi:10.1016/j.poly.2004.09.024.

References

[1] L.A. Tyler, M.M. Olmstead, P.K. Mascharak, Inorg. Chem. 40 (2001) 5408.
[2] G.C. Martin, J.M. Boncella, Organometallics 8 (1989) 2968.
[3] M.A. Cox, P.D. Newman, F.S. Stephens, R.S. Vagg, P.A. Williams, Inorg. Chim. Acta 221 (1994) 191.
[4] G.C. Martin, J.M. Boncella, E.J. Wucherer, Organometallics 10 (1991) 2804.
[5] B.K. Dirghangi, M. Menon, S. Banerjee, A. Chakravorty, Inorg. Chem. 36 (1997) 3595.
[6] P.K. Mascharak, Coord. Chem. Rev. 225 (2002) 201.
[7] V.Y. Kukushkin, A.J.L. Pombeiro, Chem. Rev. 102 (2002) 1771.
[8] R.A. Michelin, M. Mozzon, R. Bertani, Coord. Chem. Rev. 147 (1996) 299.
[9] L.A. Tyler, J.C. Noveron, M.M. Olmstead, P.K. Mascharak, Inorg. Chem. 39 (2000) 357.
[10] A.R. Katritzky, B. Pilarski, L. Urogdi, Synthesis (1989) 949.
[11] P.F.B. Barnard, J Chem. Soc. (A) (1969) 2140.
[12] M.A. Bennett, G.B. Robertson, P.O. Whimp, T. Yoshida, J. Am. Chem. Soc. 95 (1973) 3030.
[13] S. Cacchi, D. Misiti, F. La Torre, Synthesis (1980) 243.
[14] C.A. Grapperhaus, M. Li, A.K. Patra, S. Poturovic, P.M. Kozlowski, M.Z. Zgierski, M.S. Mashuta, Inorg. Chem. 42 (2003) 4382.
[15] D.D. Perrin, W.L.F. Amarego, D.R. Perrin, Purification of Laboratory Chemicals, 2nd ed., Pergamon, Oxford, 1980.
[16] W. Mazurek, K.J. Berry, K.S. Murray, M.J. O'Connor, M.R. Snow, A.G. Wedd, Inorg. Chem. 21 (1982) 3071.
[17] N. Walker, D. Stuart, Acta Crystallogr. 39A (1983) 158.
[18] G.M. Sheldrick, SHELX 97, Programs for Crystal Structure Solution and Refinement, University of Göttingen, Göttingen, Germany, 1997.
[19] M.N. Burnett, C.K. Johnson, ORTEP-III, Report ORNL-6895, Oak Ridge National Laboratory, Oak Ridge, TN, 1996.
[20] A.J. Bard, L.R. Faulkner, Electrochemical Methods: Fundamentals and Applications, Wiley, New York, 1980.
[21] (a) T. Glaser, M. Heidemeier, T. Lügger, J. Chem. Soc., Dalton Trans. (2003) 2381;
(b) M. Lee, H. Kim, H. Rhee, J. Choo, Bull. Korean Chem. Soc. 24 (2003) 205.
[22] O. Kahn, Molecular Magnetism, VCH, Weinheim, Germany, 1993.
[23] P. Segl'a, M. Jamnický, M. Koman, J. Šima, T. Glowiak, Polyhedron 17 (1998) 4525.

In previous papers, VCl_4 and water was used to prepare thin films of V_2O_5 [9] and VO_2 [10] by an APCVD method whereas, $VOCl_3$ and water always produced V_2O_5, which requires further reduction to form VO_2 thin films [9]. In this paper, we describe the APCVD of various phases of vanadium oxide thin films from $VOCl_3$ and water. It was found that the phase of vanadium oxide produced was affected by the substrate temperature and the relative concentrations of the gaseous precursors. Significantly vanadium(IV) oxide could be prepared directly from $VOCl_3$ and water, without the need for a post-production reduction step.

2. Results and discussion

2.1. Film preparation and characterisation

The idealised reaction for the APCVD of VO_2 from $VOCl_3$ and water is given in Eq. (1).

$$VOCl_3 + H_2O \rightarrow VO_2 + 2HCl + 1/2Cl_2 \quad (1)$$

The films produced from $VOCl_3$ and water gave different phases of vanadium oxide depending on the conditions used. A summary of the conditions used and products obtained from the APCVD reaction of $VOCl_3$ and water are given in Table 1. As can be seen from Table 1, most conditions result in orange/yellow V_2O_5 but at higher substrate temperature and with a slight excess of water over the stoichiometric amount idealised in Eq. (1), reduced phases of vanadium oxide could be formed. The reduced phases occurred in two discernable areas. At the leading edge of the substrate a thick, green area consisting of a mixed phase of V_6O_{13} and V_2O_5 was formed. Closer to the exhaust end of the substrate single phase, dark yellow VO_2 was formed. Varying the total gas-flow rate through the CVD reactor could control the relative amount of these two phases, a decrease in total gas-flow rate would decrease the size of the mixed phase V_2O_5/V_6O_{13} region and enable the majority (95%) of the substrate to be coated with VO_2. With total gas-flow rates below 1.0 L min^{-1} the region of mixed phase V_2O_5/V_6O_{13} covered only 1–2 cm of the substrate at the inlet end of the reactor. In all cases the films covered the substrate entirely. The films formed were progressively thinner towards the exhaust end of the substrate suggesting that the film growth may be mass transport controlled. The thickness did not appear to be affected by the variations in temperature across the substrate precluding the kinetic growth mechanism.

The Raman spectra for the vanadium oxide films matched those reported by Barreca [11]. The XRD patterns match database patterns. The Raman spectrum for a vanadium(IV) oxide thin film prepared from $VOCl_3$ and water (Fig. 1(a)) shows bands at 193, 223, 309, 394, 499, 571 and 615 cm^{-1}. The positions of the bands are ±2 cm^{-1} of the bands for literature spectra of vanadium(IV) oxide [12–14].

The Raman spectrum (Fig. 1(b)) for a film prepared from $VOCl_3$ and water and determined by X-ray diffraction (Fig. 2) to be a mixed phase V_6O_{13}–V_2O_5 thin film shows bands at 106, 144, 166, 200, 269, 284, 297, 407, 489, 528, 700, 849, 880, 936, 994, and 1035 cm^{-1}. The bands at 106, 144, 200, 284, 407, 489, 528 and 994 cm^{-1} are the Raman bands of V_2O_5. The Raman spectra of V_2O_5 and V_6O_{13} have similar band positions [15] and overlap of bands will occur in a mixed phase situation. The band at 700 cm^{-1}, when compared to Fig. 1(c), appears to have a shoulder on the low wavenumber side. This is due to the band at 684 cm^{-1} for V_6O_{13}. The same situation occurs for the band at 407 cm^{-1}, with the V_6O_{13} band at 403 cm^{-1} causing broadening of the V_2O_5 band. All bands that show overlap of V_6O_{13} and V_2O_5 are labelled * in Fig. 1(b). The bands at 166, 849, 880, 936 and 1035 cm^{-1}, do not correspond to

Table 1
Experimental conditions for the APCVD of vanadium oxides from $VOCl_3$ and H_2O on glass substrates

Reactor temperature (°C)	Gas-phase ratio $VOCl_3$:H_2O (mol min^{-1})	Total flow (mol min^{-1})	Phase from XRD and Raman
350	1:1.9	2.0	V_2O_5
550	2.2:1	2.7	V_2O_5
550	2.1:1	2.7	V_2O_5
600	3.6:1	3.2	V_2O_5
600	3.8:1	3.2	V_2O_5
650	1.8:1	2.2	V_2O_5
600	2.2:1	3.2	$V_2O_5/V_6O_{13} + V_2O_5$
600	1:2.6	1.9	V_2O_5/V_6O_{13}
650	1:2.4	1.0	$V_2O_5/V_6O_{13} + VO_2$
600	1:6.8	2.4	$V_2O_5/V_6O_{13} + VO_2$
600	1:3.4	1.9	$V_2O_5/V_6O_{13} + VO_2$
630	1:2.7	0.8	$V_2O_5/V_6O_{13} + VO_2$
630	1:2.6	0.9	$V_2O_5/V_6O_{13} + VO_2$
640	1:2.7	0.9	$V_2O_5/V_6O_{13} + VO_2$
640	1:2.9	0.9	$V_2O_5/V_6O_{13} + VO_2$
650	1:2.6	1.1	$V_2O_5/V_6O_{13} + VO_2$

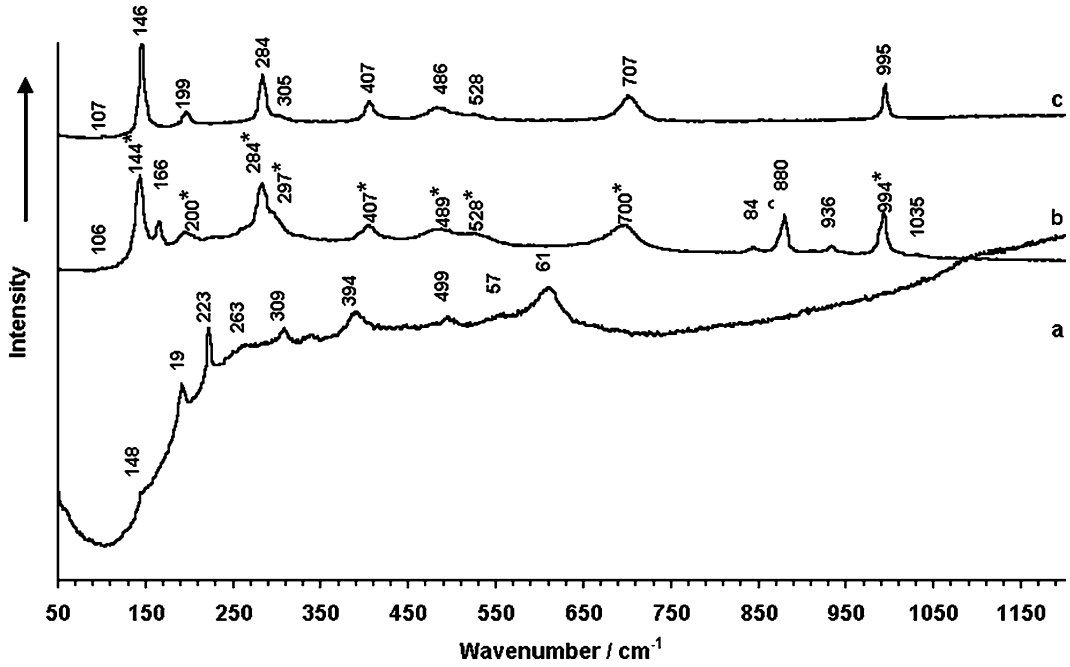

Fig. 1. Raman spectra of: (a) vanadium(IV) oxide; (b) mixed phase V_2O_5/V_6O_{13}; (c) V_2O_5 thin films from the APCVD reaction of $VOCl_3$ and H_2O.

V_6O_{13} or V_2O_5 and may be due to a phase of vanadium oxide not detected in the X-ray diffraction (XRD) pattern. These bands cannot be matched to any of the published Raman spectra for other vanadium oxides (VO_2 [16,14], V_2O_3 [17,18]) so are, at present unassigned.

The Raman spectrum for a vanadium(V) oxide thin film prepared from the APCVD reaction of $VOCl_3$ and water (Fig. 1(c)) show bands at 107, 146, 199, 284, 307, 407, 489, 531, 707 and 995 cm^{-1}, which are ± 2 cm^{-1} of the band positions of literature Raman spectrum for a thin film of vanadium(V) oxide [15].

From the XRD patterns Figs. 2–4, the films appeared to be quite crystalline. Fig. 2 shows the XRD pattern for a mixed phase, V_2O_5/V_6O_{13} film deposited at the leading edge of the substrate when a slight excess of water over $VOCl_3$ is used. Miller indices were assigned by comparison with literature patterns. A weak reflection at 27.8° due the (0 1 1) plane of monoclinic vanadium(IV) oxide is observed in the XRD pattern of the mixed phase deposit. As vanadium(IV) oxide is present further along the substrate, its presence in the partially reduced phase is not surprising.

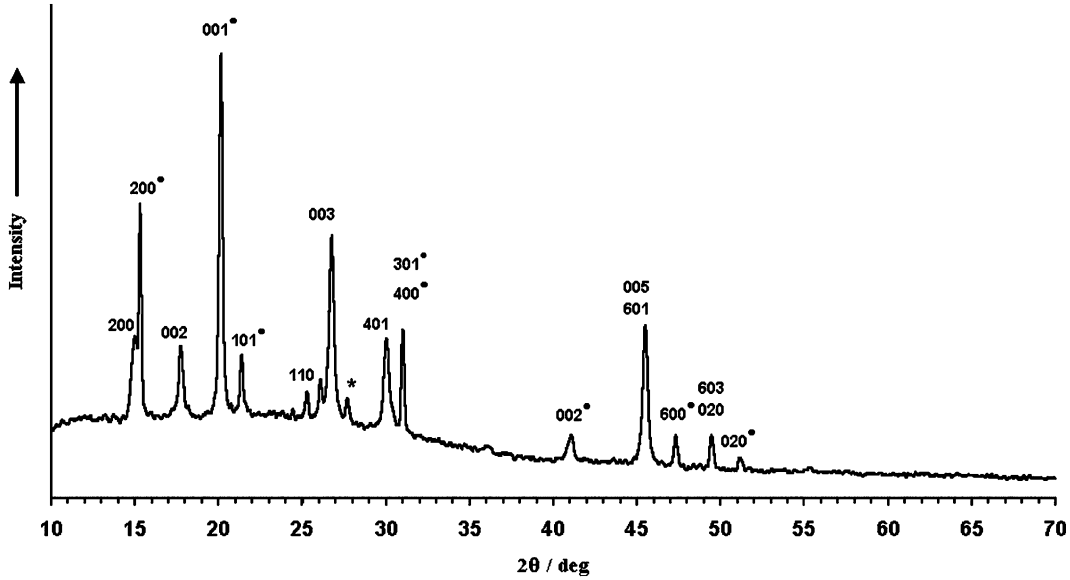

Fig. 2. X-ray diffraction pattern of mixed phase V_6O_{13}–V_2O_5 formed from the APCVD reaction of $VOCl_3$ and H_2O. Reflections marked • are V_2O_5, unmarked reflections are V_6O_{13}. Reflection marked * is assigned to the (0 1 1) reflection of monoclinic vanadium(IV) oxide.

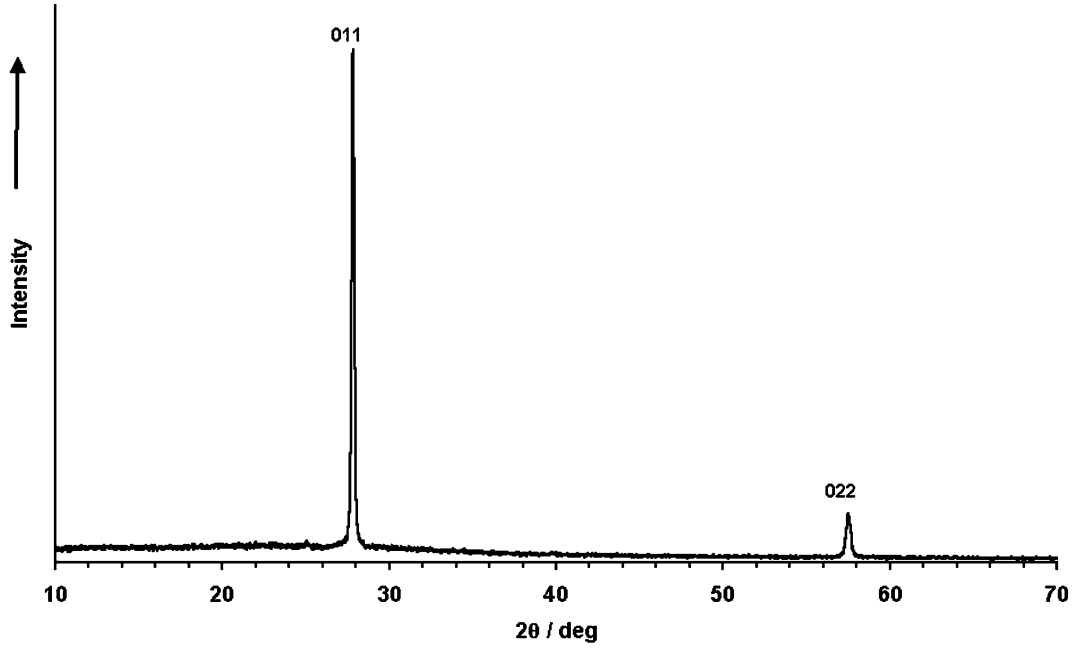

Fig. 3. X-ray diffraction pattern of yellow VO_2 area of film prepared from the APCVD reaction of $VOCl_3$ and H_2O (indexing from JCPDS file 43-0252).

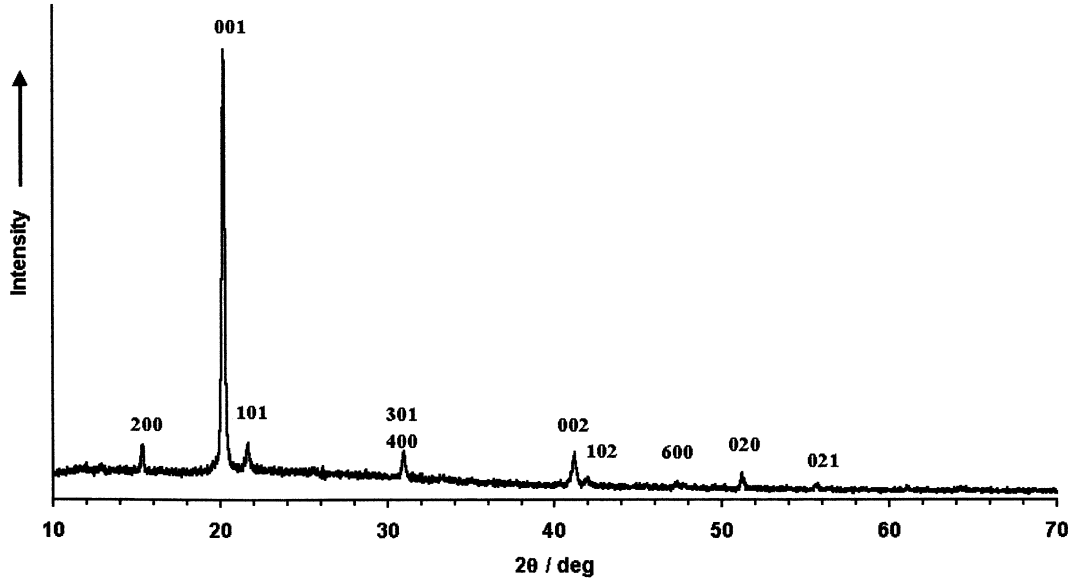

Fig. 4. X-ray diffraction pattern of V_2O_5 film prepared from the APCVD reaction $VOCl_3$ and H_2O.

The VO_2 films formed from $VOCl_3$ showed only one reflection at 27.8° corresponding to the (0 1 1) plane of the monoclinic phase, indicating that the films were potentially preferentially orientated on the substrate. Significantly no reflections due to other phases of vanadium oxide were observed, suggesting a single-phase material was deposited.

The films consisting of V_2O_5 showed no preferential orientation and could be indexed to an orthorhombic unit cell with cell parameters $a = 11.55(2)$ (Å), $b = 9.48(2)$ (Å) and $c = 4.94(2)$ (Å). The b and c cell parameters are slightly larger than those of the literature patterns and is probably due to the limited number of reflections observed in the thin film that incompletely represent the vanadium(V) oxide lattice.

The morphology of thin films of vanadium(IV) oxide grown from $VOCl_3$ and water is shown in Fig. 5. They show what appear to be 50-nm diameter rod-like particles and aggregates growing perpendicular to the substrate, which may account for the preferential orientation observed in the XRD pattern. Growth rates were typically 500 nm min^{-1} at a deposition temperature of 650 °C (as measured from side on SEM studies on glass 3 cm from the reactor inlet).

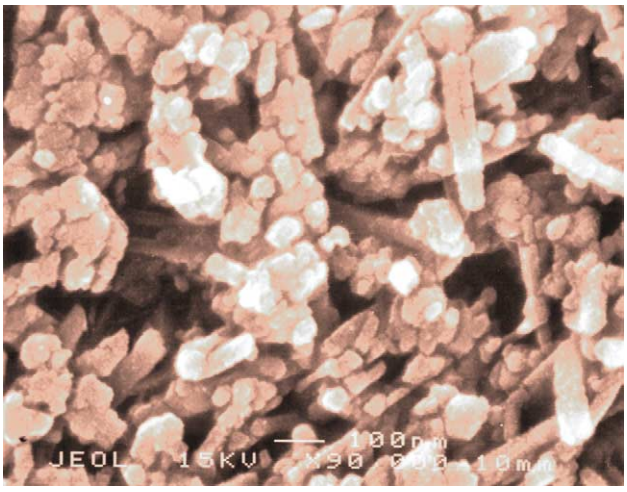

Fig. 5. SEM image of VO_2 thin film from the APCVD reaction of $VOCl_3$ and H_2O.

The films of VO_2 were all a dark yellow colour and could be scratched by a scalpel and removed by wiping with a tissue. Most films passed the Scotch tape test. All of the films were unaffected by organic solvents (toluene, propanone, IMS, dichloromethane) and water but were attacked by oxidising acids (2 mol dm^{-3} HNO_3) non-oxidising acids (2 mol dm^{-3} HCl) and alkali (2 mol dm^{-3} NaOH). The amphoteric nature of vanadium oxides is well known for the bulk materials [19]. The films displayed no significant hydrophilic effect, after 1 h of irradiation with a UV lamp (265 nm), the contact angle measurement for a water droplet of a VO_2 thin film prepared from $VOCl_3$ and water gave a contact angle of 62.8° and a V_2O_5 thin film prepared from VCl_4 and water gave a contact angle of 66.1°. A plain glass substrate gives a water contact angle of 70° indicating no significant hydrophilic effect compared to a plain glass substrate. None of the films displayed photocatalytic activity as shown by the stearic acid test.

In order to further elucidate the composition of the vanadium oxide films and to obtain an insight into the oxidation states of the ions present, a selection of the films were submitted to X-ray photoelectron spectroscopy (XPS) analysis. An analysis of the bulk of the film was obtained by argon ion etching. A broad range survey scan was used as a qualitative measure of the elements present in the film and high resolution scans of the characteristic regions of these elements were used for the quantitative analysis and peak fitting, to determine oxidation states.

For all vanadium oxide films, the elements present on the surface were determined to be V, O, C, Si and N. Nitrogen was a surface contaminant adsorbed from the atmosphere and the inert gas used to fill the sample entry air-lock to the ultra-high vacuum analysis chamber. Most of the contaminant is removed in the ultra-high vacuum but some may still remain due the particulate, high surface area morphology of the films. Carbon contamination can be attributed to atmospheric contamination also, but the major source is saturated hydrocarbons from the oil diffusion pumps in the analysis chamber [20]. The XPS signal due to surface carbon was used as a charge compensation reference peak when assigning binding energies to the regions of the XPS experiment. The surface contaminants could be removed by a single argon ion etching to reveal a clean film surface. The signal assigned to silicon was due to the glass substrate, the films contained a few pinhole defects exposing the glass substrate through the film. No chlorine contamination from the chloride precursors was detected by XPS in any of the vanadium oxide thin films.

Peak fitting analysis of the $V2p_{3/2}$ XPS peak of a thin film prepared from $VOCl_3$ and water (gas-phase molar ratio 1:3) and identified as vanadium(IV) oxide by Raman and XRD analysis, revealed that on the surface of the film some of the vanadium ions were V^{5+}, due to surface oxidation, with the majority present as V^{4+}. As the surface layers were etched and the bulk of the film exposed, the oxidation state of the vanadium ions was determined to be V^{4+} with a binding energy of 515.6 eV, as shown in Fig. 6, confirming the presence of vanadium(IV) oxide. The O1s XPS peak of this level could be deconvoluted to two components. The peak at 532.6 eV was assigned to residual surface contamination of carbon containing species, probably CO_2. The peak at 530.9 eV was assigned to the oxygen of vanadium(IV) oxide. The peak area ratio, corrected for elemental sensitivity factors to give atom% values, of the $V2p_{3/2}$ to O1s (O–V) peak was calculated to be 1.00:2.00, confirming the composition as VO_2. As the film was further etched away some V^{3+} became apparent with a lower $V2p_{3/2}$ binding energy of 515.0 eV, this is most likely due to the preferential removal of lighter elements, especially oxygen, during the sputtering process that will result in reduced forms of vanadium being present in the films.

For a vanadium(V) oxide film, prepared at 500 °C from $VOCl_3$ and water (gas-phase molar ratio 3.5:1), only V^{5+} ions were observed on the surface layer and in the bulk with a binding energy of 517.1 eV, with some reduced species after substantial etching due to preferential sputtering of oxygen. At the surface layers the O1s XPS peak could be deconvoluted to two peaks, one with a binding energy of 532.4 eV could be assigned to carbon containing species contaminating the surface, the second with a binding energy of 530.1 eV was assigned to the oxygen of V_2O_5. Corrected peak area ratios, giving atom% values, for the $V2p_{3/2}$ to O1s for V_2O_5 were 2.0:5.0 confirming the presence of vanadium(V) oxide. Again, this is the expected result and reinforces that the film is single phase V_2O_5.

X-ray photoelectron spectroscopy was also performed on a film at the leading edge of a substrate

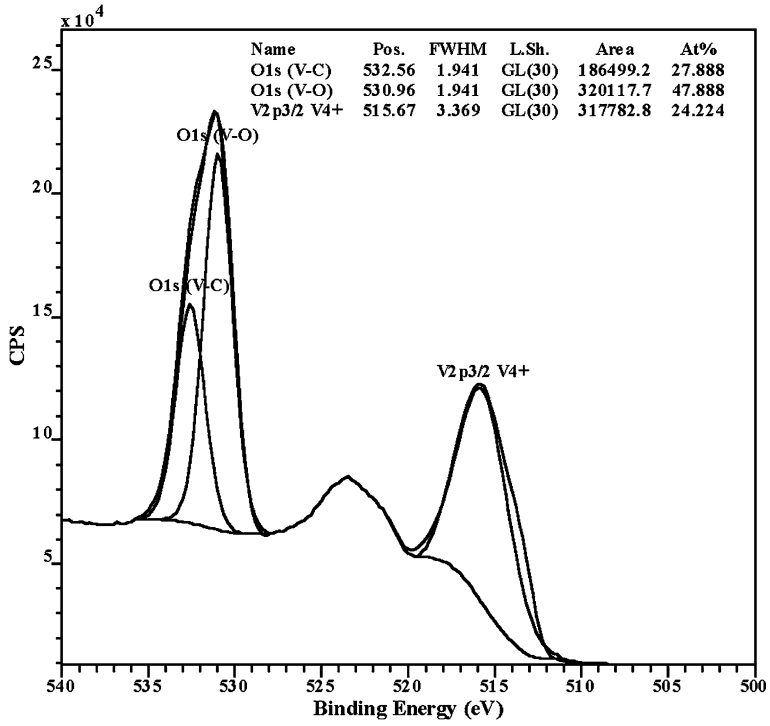

Fig. 6. Deconvoluted XPS spectrum of V2p–O1s region for vanadium(IV) oxide thin film prepared by the APCVD reaction of $VOCl_3$ and H_2O at 650 °C, molar ratio $VOCl_3$:H_2O 1:3.

prepared at 600 °C from $VOCl_3$ and water (gas-phase molar ratio 1:7) and determined to be mixed phase V_6O_{13}–V_2O_5 by Raman and XRD analysis. This film was established to consist of vanadium ions in both the +5 and +4 oxidation states. The V^{5+} XPS peak had a binding energy of 516.9 eV and the V^{4+} XPS peak had a binding energy of 515.5 eV. The O1s XPS peaks close to the surface of the film could be deconvoluted to two peaks. A peak with a binding energy of 532.4 could be assigned to residual carbon containing contaminants for example a carbonate. A second O1s peak with a binding energy of 530.4 eV could be assigned to oxygen bound to vanadium. This again is the expected result as V_2O_5 contains only V^{5+} and V_6O_{13} has V^{4+} and V^{5+} ions. From an analysis of the atom% ratios the V^{4+} and V^{5+} ions there the film consisted of approximately 25% V_6O_{13}. All binding energy assignments were matched to literature [21] and database [22] values.

2.2. Deposition onto silicon

As mentioned in the introduction, thin films of vanadium(IV) oxide have potential uses as infrared modulators in thermal imaging sensors and missile guidance systems. These applications require the deposition of vanadium(IV) oxide onto silicon wafers. Using silicon wafers supplied by Quinetiq, the deposition of vanadium(IV) oxide onto silicon was attempted. The starting point was the conditions found previously to prepare vanadium(IV) oxide on glass.

Raman analysis indicated that single phase vanadium(IV) oxide thin films were deposited at a substrate temperature of 650 and 600 °C (Fig. 7). Raman bands at 144, 191, 222, 260, 283, 307, 337, 388, 441, 499 and 614 cm^{-1} can all be assigned to vanadium(IV) oxide. The bands at 337 and 441 cm^{-1} were very weak in spectra from thin films of vanadium(IV) oxide on glass substrates and were not observed but are observed in spectra from single crystals [13,14,16] and are both assigned to B_g symmetry modes [13]. The band at 571 cm^{-1} is not obvious on the films deposited on silicon, this band not being always observed in spectra from single crystals [16]. This may indicate a more stoichiometric or crystalline phase being produced on the silicon substrates from the APCVD reaction of $VOCl_3$ and water. The ability to prepare vanadium(IV) oxide on silicon substrates is important as it opens up further applications for the APCVD of vanadium(IV) oxide thin films from halide based precursors.

The morphology of the vanadium oxide films deposited onto a silicon substrate (Fig. 8) is also distinct from that of films deposited onto glass. SEM shows that 500-nm long rod-like particles, with a diameter of 50 nm, are deposited above a layer of island growth. The particle appear randomly orientated on the substrate. The layer of island growth directly

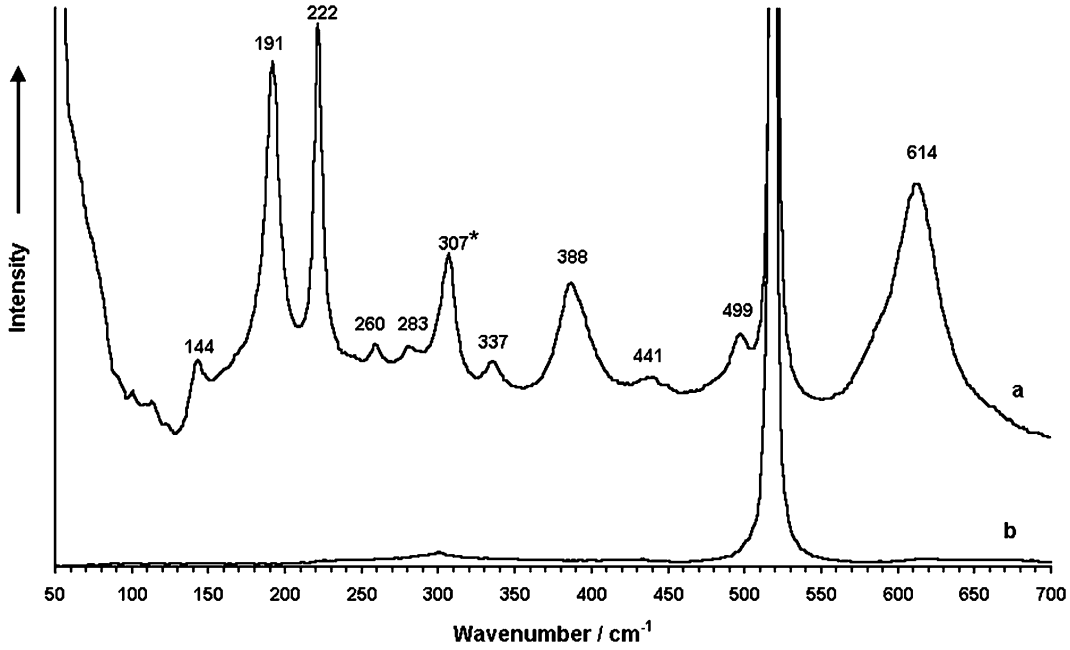

Fig. 7. Raman spectrum of: (a) vanadium(IV) oxide thin film on silicon from the APCVD reaction of $VOCl_3$ and H_2O at 650 °C, gas-phase molar ratio 2:1, (b) silicon substrate.

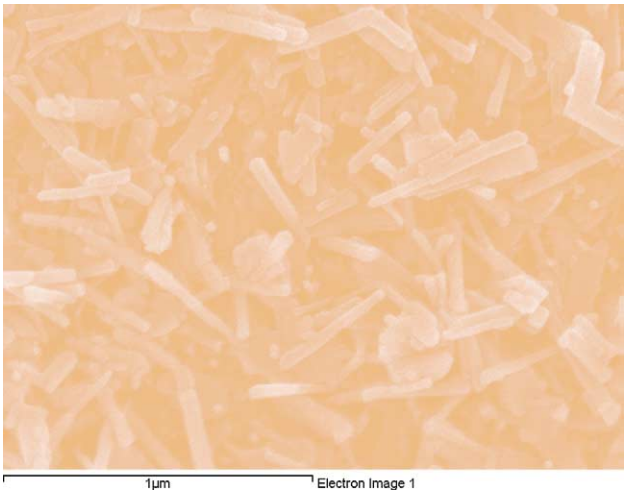

Fig. 8. SEM image of VO_2 thin film deposited on silicon from the APCVD reaction of $VOCl_3$ and H_2O at 650 °C with gas-phase molar ratio $VOCl_3$:H_2O of 2:1.

on the substrate shows particles of approximately 10 nm thickness.

The silicon and glass substrates showed a surprising difference in the morphology of the VO_2 produced. The glass substrate used had a SiO_2 barrier layer (50 nm). It is to be expected that as the Si wafer was not cleaned by any special technique it too would have a thin SiO_2 overlayer (ca. 2 nm). It is probable that the surface structure of the SiO_2 coated glass and wafer derived SiO_2 overlayer would be different – especially as they are formed at different temperatures and on different substrates. This probably accounts for the difference in VO_2 morphology.

2.3. Thermochromic properties of VO_2 thin films on glass substrates

The thermochromic properties of thin films of vanadium(IV) oxide were analysed by two methods, glancing angle XRD and IR transmittance spectroscopy.

The thermochromic transition was studied by glancing angle XRD at different temperature. The (0 1 1) reflection of the monoclinic phase transforming into the (1 1 0) reflection of the tetragonal phase is particularly easy to observe and the results of this study are shown in Fig. 9. The first order transition is well shown in this study, the monoclinic and tetragonal phases of VO_2 are both seen to be present as the transition occurs indicating that different regions undergo the transition at different times. This is a result of the energy involved in the transition being unable to be instantaneously transferred between the system and the environment so mixed-phase regimes are observed. The transition temperature (T_c) is shown to be where the intensities of the reflections for the monoclinic (0 1 1) plane and the tetragonal (1 1 0) plane are approximately equal. This occurs at a temperature of 67 °C on the heating cycle, which agrees with values reported in the literature for single crystals and thin films of pure vanadium(IV) oxide. On the cooling cycle the transition occurs at 54 °C, illustrating the broad hysteresis of the thermochromic transition of the thin films of vanadium(IV) oxide.

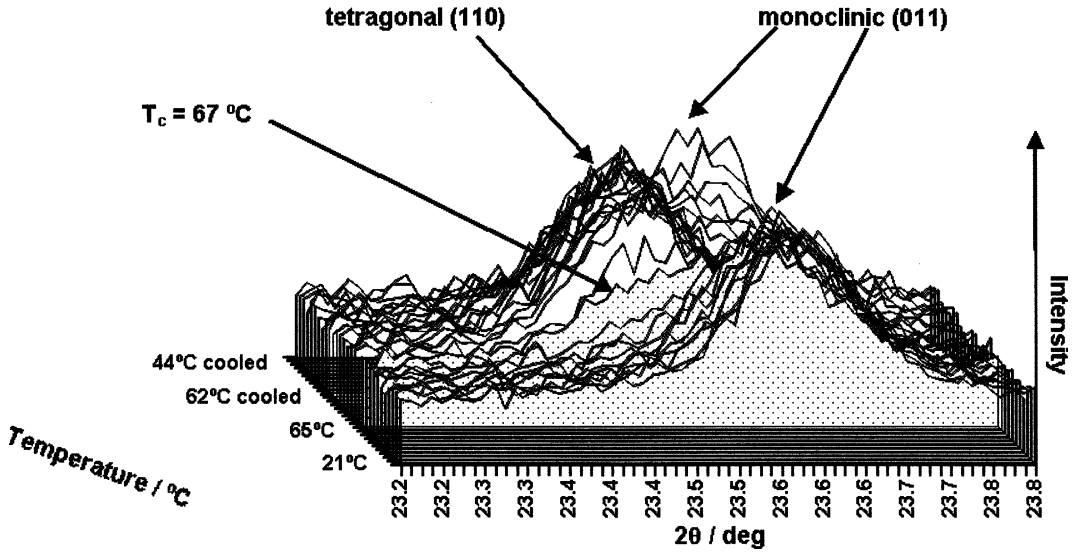

Fig. 9. XRD patterns at different temperatures of monoclinic (0 1 1) reflection to tetragonal (1 1 0) reflection for VO_2 thin film prepared from $VOCl_3$ and water.

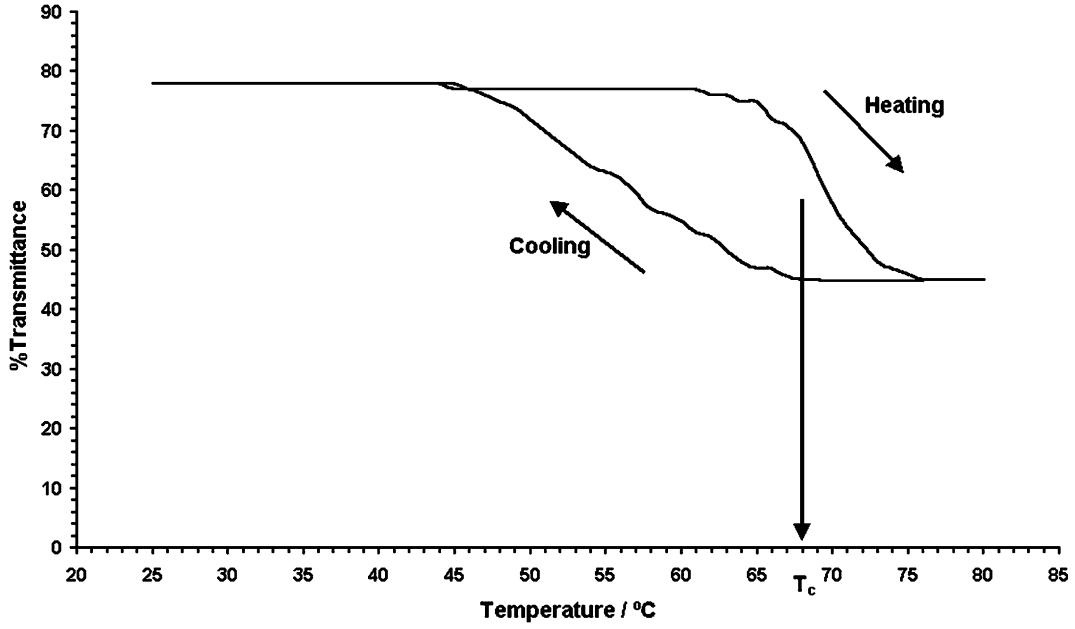

Fig. 10. Hysteresis curve of the IR transmittance at 2.5 μm for a VO_2 thin film on glass substrate.

The hysteresis curve of the transmittance, at 2.5 μm, of a vanadium(IV) oxide thin film is shown in Fig. 10. The optical contrast between the semiconducting and metallic states is particularly large at this wavelength, making its measurement easy and an indication of the effectiveness of the material as an intelligent window coating can be obtained.

The temperature at which the transition occurs on the heating cycle (67 °C) agrees with the result obtained from the XRD study. The hysteresis width is quite broad, which is often observed in thin films of VO_2 and is generally attributed to the polycrystalline nature of the films [23]. The transmittance of the semiconducting phase is 78% which drops to 45% when the temperature is increased to above the MST, this is comparable to the contrast obtained for PVD [23] and sol–gel [24] derived thin films of VO_2.

3. Conclusion

Different phases of vanadium oxide could be prepared from the dual source APCVD reaction of $VOCl_3$ and H_2O. On glass substrates, at reactor temperatures above 600 °C and an excess of water over $VOCl_3$, thermochromic thin films of vanadium(IV) oxide could be pre-

pared. The thin films of VO_2 showed a MST at 67 °C, typical of the material. Under the conditions for VO_2 production, small regions of a mixed phase of V_2O_5 and V_6O_{13} were also produced, the size of which could be controlled by total flow rates through the reactor. Reactor temperatures below 600 °C, or where an excess of $VOCl_3$ over H_2O, where used, V_2O_5 thin films were prepared.

4. Experimental

4.1. Film preparation

The APCVD experiments were performed on a custom built cold-wall apparatus using a previously described procedure [10]. Vanadium(V) oxytrichloride (95%,Strem, UK) was transferred to a bubbler and water was injected into the plain-line gas-flow using a fixed rate syringe driver (1.33 cm min^{-1}). Nitrogen (99.999%, BOC UK) was used as the system gas in all CVD reactions. The substrates were float glass that had a 50-nm thick SiO_2 barrier layer to stop diffusion of ions from the glass into the film (Pilkington Glass, UK), 15 cm × 4.5 cm × 0.3 cm, or 2″silicon wafers broken in half and mounted onto a large glass slide for easy extraction from the CVD reactor.

The substrates were cleaned before use by wiping with a water-soaked tissue and then a propan-2-ol soaked tissue and then rinsed with propan-2-ol. The substrates were allowed to dry in air prior to mounting in the CVD chamber.

A series of films were prepared in which the effect of substrate temperature and gas-phase precursor ratio was investigated. Deposition times were kept constant at one minute per run.

4.2. Film analysis

Analysis of the resulting thin films consisted of XRD, XPS, Raman spectroscopy and scanning electron microscopy with energy dispersive analysis of X-rays (SEM/EDX). X-ray analysis of the films was determined on a Siemens D5000 machine using primary Cu Kα radiation at 1.5418 (Å) in $\theta 2\theta$ mode. Diffraction patterns at different temperatures were obtained at station 2.3 of the CCLRC synchrotron radiation source at Daresbury, UK using 1.2981 (Å) radiation with a 1.5° incident angle. The temperature was controlled using an aluminium temperature cell controlled by *RS* resistive heaters, Eurotherm temperature controllers and k-type thermocouples was used to manipulate sample temperature. Sample temperature was measured by a k-type thermocouple taped to the film surface. X-ray photoelectron spectrometry was performed on a VG ESCALAB 2201 XL instrument using monochromatic Al Kα X-rays with a pass energy of 50 eV. XPS data was analyzed using CasaXPS software version 2.0.11. Raman spectroscopy was performed on a Renishaw 1000 spectrometer using a 632.8-nm laser at 2 mW and 50× magnification, sample temperature was controlled by a Linkam THMS600 variable temperature cell with a liquid nitrogen pump. SEM images to determine film thickness were obtained on a Hitachi S-570 scanning electron microscope at 20 kV accelerating voltage. Samples were prepared by deeply scoring the film side of the substrate to cause shelling of the film and hence a distinct edge between the film and substrate. EDX was performed on a Philips XL30 ESEM instrument using Inca analytical software (Oxford Instruments).

Acknowledgements

The EPSRC is thanked for financial support. Prof. M. Pemble, Prof. D. Sheel and Dr. D. Vernadou are thanked for useful discussion on a related project.

References

[1] F.J. Morin, Phys. Rev. Lett. 3 (1959) 34.
[2] C.G. Granqvist, Thin Solid Films 193/194 (1990) 730.
[3] C.G. Granqvist, Adv. Mater. 15 (2003) 1789.
[4] M.F. Becker, A.B. Buckman, R.M. Walser, T. Lepine, P. Georges, A. Brun, Appl. Phys. Lett. 65 (1994) 1507.
[5] A.W. Smith, Appl. Phys. Lett. 23 (1973) 437.
[6] W.R. Roach, Appl. Phys. Lett. 19 (1971) 453.
[7] M.A. Richardson, J.A. Coath, Opt. Laser Technol. 30 (1998) 137.
[8] D.W. Sheel, M.E. Pemble, private communication.
[9] M.N. Field, I.P. Parkin, J. Mater. Chem. 10 (2000) 1863.
[10] T.D. Manning, I.P. Parkin, R.J.H. Clark, D. Sheel, M.E. Pemble, D. Vernardou, J. Mater. Chem. 12 (2002) 2936.
[11] D. Barreca, L.E. Depero, G.A. Rizzi, L. Sangaletti, E. Tondello, U. Vettori, J. Electrochem. Soc. 146 (1999) 551.
[12] G.I. Petrov, V.V. Yakovlev, Appl. Phys. Lett. 81 (2002) 1023.
[13] P. Schilbe, Phys. B 316–317 (2002) 600.
[14] A.G. Aronov, D.N. Mirlin, I.I. Reshina, F.A. Chudnovskii, Sov. Phys. Solid State 19 (1977) 110.
[15] C. Julien, G.A. Nazri, O. Bergstrom, Phys. Status Solidi 201 (1997) 319.
[16] J.C. Parker, Phys. Rev. B 42 (1990) 3164.
[17] D.N. Mirlin, Sov. Phys. Solid State 19 (1977) 115.
[18] N. Kuroda, H.Y. Fan, Phys. Rev. B 16 (1977) 5003.
[19] F.A. Cotton, G. Wilkinson, Advanced Inorganic Chemistry, 4th ed., Wiley, Chichester, 1980.
[20] A. Wagner, Practical Surface Analysis – Auger and X-Ray Photoelectron Spectroscopy, vol. 2, 2nd ed., Wiley, Chichester, 2003.
[21] J. Mendialdua, R. Casanova, Y. Barbaux, J. Electron Spectrosc. Relat. Phenom. 71 (1995) 249.
[22] C.D. Wagner, A.V. Naumkin, A. Kraut-Vass, J.W. Allison, C.J. Powell, J.R. Rumble, NIST (2003).
[23] W. Burkhardt, T. Christmann, B.K. Meyer, W. Niessner, D. Schalch, A. Scharmann, Thin Solid Films 345 (1999) 229.
[24] F. Béteille, L. Mazerolles, J. Livage, Mater. Res. Bull. 34 (1999) 2177.

evidence that oxophilic uranium can bond to weakly coordinating O-donor anions.

Our attention has now turned to the tetrafluoroborate anion. Coordination of $[BF_4]^-$ to a metal centre is unusual, and the vast majority of these are d-block metal complexes (mainly Cu and Ag) [9]. There is only one crystallographically characterised example of tetrafluoroborate coordinating to an f-block element; $[\{U(\eta^5\text{-}C_5H_3(SiMe_3)_2)_2(\mu\text{-}BF_4)(\mu\text{-}F)\}_2]$ [10], in which two fluorides and two tetrafluoroborate anions bridge two U(IV) centres. $[BF_4]^-$ groups are more commonly used as counter-ions, but despite there being several hundred structurally characterised (mainly d-block) examples listed in the Cambridge Structural Database (CSD) [9], only two of these are actinide complexes; the monomeric, equatorially 5-coordinate uranyl compounds, $[UO_2(dmso)_5][BF_4]_2$ [11] and $[UO_2(dmf)_5][BF_4]_2$ [12].

We report our success in preparing a number of novel complexes from an investigation of $\{UO_2\}^{2+}/[BF_4^-]$/phosphide oxide reaction systems, with triphenylphosphine oxide (TPPO), tri-*n*-butylphosphine oxide (TBPO) or bis(diphenylphosphine oxide)methane ($DPPMO_2$) as organic ligands. However, in no case have we been able to isolate crystalline samples containing $[BF_4]^-$ coordinated directly to $\{UO_2\}^{2+}$, with instead fluoride abstraction by the fluorophilic actinyl dication dominating reactivity.

2. Experimental

Caution. Both natural and depleted uranium were used during the course of these experiments. Uranium is a toxic metal and both ^{235}U and ^{238}U are radioactive isotopes. Good laboratory practices should be employed when working with any uranic material.

2.1. Materials and measurements

UO_3 was obtained from the radiochemical stocks at The Centre for Radiochemistry Research at the University of Manchester. All other chemicals were purchased from standard chemical suppliers. A Carlo Erba Instruments CHNS-O EA1108 Elemental Analyser was used for C, H and N analysis. All metal analysis was measured on a Fisons Horizon Elemental Analysis ICP-OED spectrometer. IR data were collected on a Bruker Equinox 55 spectrometer using a "Golden Gate" ATR (attenuated total reflectance) attachment in the mid – (4000–760 cm^{-1}) and far – (400–240 cm^{-1}) IR regions. A Bruker FRA 106/S Raman instrument with a Coherent laser (1064 nm, 500 mW) was used to collect the Raman scattering from solid samples held in the laser beam path. Solid state diffuse reflectance spectra were recorded on an Ocean Optics SD2000 spectrometer with a fibre optic probe using a deuterium–halogen DH-200 light source over the range 200–1000 nm. $BaSO_4$ was used as a reference.

2.2. Synthesis of $[\{UO_2(\mu\text{-}F)(TPPO)_3\}_2][BF_4]_2$ (**1**)

A solution of TPPO (1.05 mmol, 0.292 g) in hexane (1.5 cm^3) was carefully layered on the surface of a solution containing a stoichiometric amount of UO_3 (0.35 mmol, 0.10 g) dissolved in HBF_4 (0.70 mmol, 0.089 cm^3) and H_2O (1.5 cm^3). Yellow plate crystals formed after two weeks, during which time the solution was kept away from direct sunlight. The crystals were collected and dried in air. Yield: 0.30 g, 70%. (Elemental *Anal*. Calc. for $C_{108}H_{90}O_{10}P_6B_2F_{10}U_2$: C, 53.55; H, 3.72; P, 7.69; B, 0.91; F, 7.85; U, 19.67. Found: C, 53.55; H, 3.74; P, 7.62; B, 1.04; F, 7.31; U, 19.28%).

2.3. Synthesis of $[\{UO_2(\mu\text{-}F)(TBPO)_3\}_2][BF_4]_2$ (**2**)

A solution of TBPO (2.10 mmol, 0.457 g) in hexane (2 cm^3) was added to a solution containing a stoichiometric amount of UO_3 (0.70 mmol, 0.20 g) dissolved in HBF_4 (1.40 mmol, 0.246 cm^3). The resulting sticky yellow precipitate was dissolved in EtOH (5 cm^3) and left to evaporate in air, away from direct sunlight. Irregular yellow crystals coated in a thin layer of viscous oil formed after two weeks. Only a small number of crystals were suitable for single crystal X-ray diffraction and these were removed and dried in air. Yield: 0.02 g, 3%. There was insufficient product to perform elemental analysis.

2.4. Synthesis of $[UO_2(\mu\text{-}F)(F)(DPPMO_2)]_2$ (**3**)

UO_3 (0.35 mmol, 0.10 g) was dissolved in HBF_4 (0.70 mmol, 0.089 cm^3) and evaporated to dryness to produce a yellow solid that was dried in a desiccator. This solid was dissolved in MeOH (4 cm^3) and added to a stirred solution of $DPPMO_2$ (0.70 mmol, 0.291 g) in MeOH (4 cm^3). The solution was left to evaporate in air, away from direct sunlight. Yellow plate crystals formed after 1 week and were collected by filtration and dried in air. Yield: 0.20 g, 80%. (Elemental *Anal*. Calc. for $C_{50}H_{44}O_8P_4F_4U_2$: C, 41.45; H, 3.06; P, 8.55; F, 5.25; U, 32.86. Found: C, 41.98; H, 3.34; P, 8.14; F, 4.92; U, 32.40%).

2.5. X-ray crystallographic analysis

Compound **1** was measured on a Rigaku RAXIS diffractometer at 293 K. Diffraction data for **2** and **3** were measured on a Bruker APEX SMART platform CCD at 100 K. All three structures were solved by direct methods using SIR92 [13] (**1**), SHELXL97[14] (**1**–**3**) and SHELXTL [15] (**2** and **3**). The cell parameters were refined by full-matrix least squares. All non-hydrogen atoms were refined anisotropically, while hydrogen atoms were in-

cluded in calculated positions. Details of the crystal data and refinement for these compounds are collected in Table 1.

As stated previously, the data for **1** were collected using the RAXIS diffractometer, which allows phi rotation only. Although 330° of data were collected, because of the low symmetry of the crystal, only about two-thirds of the data were accessible for recording, the remainder occurring in the blind region.

3. Results and discussion

3.1. Crystallographic characterisation

$[\{UO_2(\mu\text{-}F)(TPPO)_3\}_2][BF_4]_2$ (**1**) is a cationic uranyl complex. The pentagonal bipyramidal uranyl groups are bridged by a pair of μ_2-F anions in a centrosymmetric dimer. The coordination of each U centre is completed by three TPPO groups in the equatorial plane. Two non-coordinating $[BF_4]^-$ anions are present to balance the charge. The structure is shown in Fig. 1 with bond distances and angles given in Table 2. The mean $U–O_{(TPPO)}$ bond length (2.375 Å) compares well with the $U–O_{(eq)}$ distance (2.37(9) Å) quoted by Burns et al. [16], and is similar to the average distances found in the dimeric peroxo-bridged compounds $[\{(UO_2)(TPPO)_3\}_2(\mu\text{-}O_2)][ReO_4]_2$ [7] (2.367 Å) and $[\{(UO_2)(TPPO)_3\}_2(\mu\text{-}O_2)][ClO_4]_2$ [17] (2.368 Å). The difluoride bridge is effectively symmetrical (U–F bond lengths are 2.331(5) and 2.345(5) Å, respectively and F1–U1–F1* is 62.77(16)°), with similar bond lengths and angles being found in the related bridging difluoride compounds $[UO_2(\mu\text{-}F)(F)\{CO(NH_2)_2\}_2]_2$ [18] (2.36(2) and 2.39(2) Å; 65.3(7)°) and *catena*-$[UO_2(\mu\text{-}F_2)(dmso)]$ [19] (2.31(1) and 2.34(1) Å; 65.4(4)°). The uncoordinated tetrafluoroborate is slightly distorted away from tetrahedral geometry, perhaps by anion-cation interactions. This distortion is comparable to that found for uncoordinated $[BF_4]^-$ in both $[UO_2(C_2H_6OS)_5][BF_4]_2$ [11] and $[UO_2(C_3H_7NO)_5][BF_4]_2$ [12]. The uranyl ion is essentially linear (179.8(2)°), unlike analogous bridging peroxo complexes [7,17]. A solid state packing diagram (Supporting data) reveals that the hydrophilic uranyl

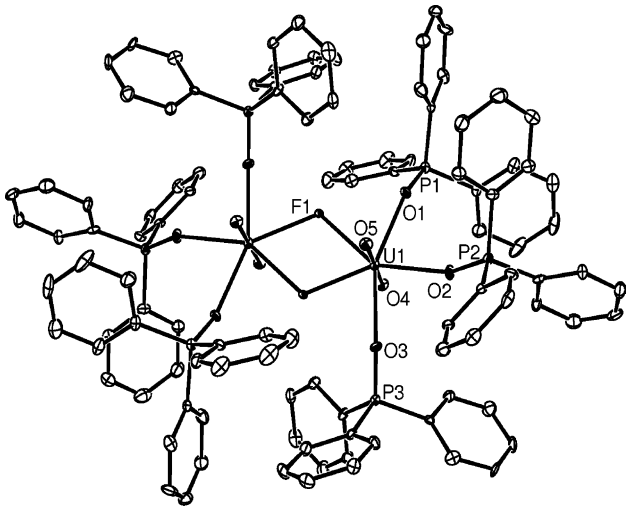

Fig. 1. Molecular structure of $[\{UO_2(\mu\text{-}F)(TPPO)_3\}_2][BF_4]_2$ (**1**). Probability ellipsoids of 30% are shown.

Table 1
Crystal data and structure refinement for $[\{UO_2(\mu\text{-}F)(TPPO)_3\}_2][BF_4]_2 \cdot {}^nC_6H_{14}$ (**1**), $[\{UO_2(\mu\text{-}F)(TBPO)_3\}_2][BF_4]_2$ (**2**) and $[UO_2(\mu\text{-}F)(F)(DPPMO_2)]_2 \cdot 2MeOH$ (**3**)

	1	**2**	**3**
Empirical formula	$C_{57}H_{52}BF_5O_5P_3U$	$C_{36}H_{81}BF_5O_5P_3U$	$C_{26}H_{26}F_2O_5P_2U$
Formula weight	2507.47	2061.52	1510.86
Temperature (K)	293(2)	100(2)	100(2)
Wavelength (Å)	0.71069	0.71069	0.71069
Crystal system	triclinic	monoclinic	monoclinic
Space group	$P\bar{1}$	$P2_1/n$	$P2_1/n$
Unit cell dimensions			
a (Å)	10.515(10)	11.9988(13)	10.8869(10)
b (Å)	16.27(3)	18.5194(19)	17.8195(15)
c (Å)	16.94(3)	21.861(2)	13.6627(12)
α (°)	64.03(9)	90	90
β (°)	83.23(6)	94.449(2)	97.872(2)
γ (°)	77.38(8)	90	90
Volume (Å^3)	2542(7)	4843.2(9)	2625.6(4)
Z	2	2	2
Absorption coefficient (mm^{-1})	3.355	3.504	6.353
F (0 0 0)	1242	2096	1444
Crystal size (mm)	$0.20 \times 0.05 \times 0.01$	$0.20 \times 0.15 \times 0.10$	$0.15 \times 0.15 \times 0.08$
Reflections collected/unique	49782/5861	27680/9888	15107/5360
Final R indices [$I > \sigma(I)$]	$R_1 = 0.0368$, $wR_2 = 0.0672$	$R_1 = 0.0380$, $wR_2 = 0.0836$	$R_1 = 0.0239$, $wR_2 = 0.0534$
R indices (all data)	$R_1 = 0.0672$, $wR_2 = 0.0611$	$R_1 = 0.0572$, $wR_2 = 0.0914$	$R_1 = 0.0309$, $wR_2 = 0.0559$

Table 2
Selected bond lengths (Å) and angles (°) for [{UO_2(μ-F)$(TPPO)_3$}$_2$][BF_4]$_2$ (**1**)

Bond lengths			
U(1)–O(5)	1.765(4)	U(1)–O(3)	2.374(6)
U(1)–O(4)	1.778(4)	B(1)–F(2)	1.341(10)
U(1)–F(1)	2.331(5)	B(1)–F(3)	1.355(11)
U(1)–F(1)*	2.345(5)	B(1)–F(4)	1.360(10)
U(1)–O(1)	2.389(6)	B(1)–F(5)	1.379(10)
U(1)–O(2)	2.363(5)		
Bond angles			
O(5)–U(1)–O(4)	179.8(2)	P(1)–O(1)–U(1)	146.6(2)
O(5)–U(1)–F(1)	86.68(17)	P(2)–O(2)–U(1)	147.6(2)
O(4)–U(1)–F(1)	93.24(17)	P(3)–O(3)–U(1)	156.0(2)
O(5)–U(1)–F(1)*	87.79(19)	U(1)–F(1)–U(1)*	117.23(16)
O(4)–U(1)–F(1)*	91.96(19)	F(2)–B(1)–F(3)	109.8(9)
O(4)–U(1)–O(1)	86.3(2)	F(2)–B(1)–F(4)	108.8(8)
O(4)–U(1)–O(2)	94.89(18)	F(3)–B(1)–F(4)	107.5(8)
O(4)–U(1)–O(3)	86.54(19)	F(2)–B(1)–F(5)	112.1(8)
F(1)–U(1)–F(1)*	62.77(16)	F(3)–B(1)–F(5)	107.1(7)
F(1)–U(1)–O(2)	146.11(15)	F(4)–B(1)–F(5)	111.4(7)
F(1)*–U(1)–O(2)	149.35(14)		

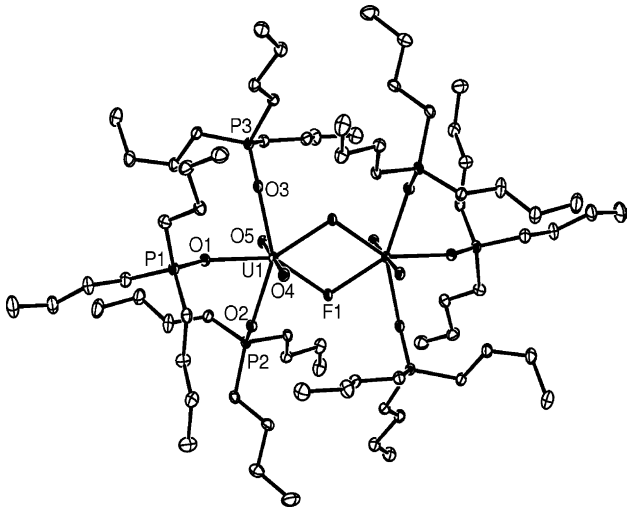

Fig. 2. Molecular structure of [{UO_2(μ-F)$(TBPO)_3$}$_2$][BF_4]$_2$ (**2**). Probability ellipsoids of 30% are shown.

moieties are partially surrounded by their organic ligands while two $[BF_4]^-$ anions lie against the outside of this hydrophobic TPPO "shell". The stacking of molecules on top of one another in a zig–zag arrangement allows TPPO groups to help to complete the hydrophobic "shells" of adjacent molecules. Hydrophilic $[BF_4]^-$ anions in the lattice are encapsulated by the TPPO groups of the cation, and those from neighbouring molecules. The lattice appears to be held together by strong interatomic interactions between F-atoms on the $[BF_4]^-$ groups and H-atoms from TPPO groups on neighbouring molecules, which have F–H distances of 2.158(7) Å at the closest point.

[{UO_2(μ-F)$(TBPO)_3$}$_2$][BF_4] (**2**) is a cationic uranyl complex of similar structural type to **1**, although the TPPO ligands are replaced by three monodentate TBPO ligands in the equatorial coordination sphere of $\{UO_2\}^{2+}$. The structure is shown in Fig. 2 with bond distances and angles given in Table 3. The equatorial plane of each U centre accommodates 2 long (2.375(3) and (2.369(3) Å) and 1 short (2.352(3) Å) U–$O_{(TBPO)}$ bonds, only the shortest bond being comparable to that in *trans*-[$UO_2(NO_3)_2(TBPO)_2$] [20] (2.347(6) Å). The three U–O–P bond angles are all different and are less obtuse (130.97(19)°, 140.16(18)° and 145.14(19)°) compared to those in [$UO_2(NO_3)_2(TBPO)_2$] [20] (average 146.0(5)°). The unsymmetrical difluoride bridge contains two different U–F bond lengths (2.329(2) and 2.340(2) Å), the average being comparable to bond distances found in **1**, [UO_2(μ-F)(F){$CO(NH_2)_2$}$_2$]$_2$ [18] (2.36(2) and 2.39(2) Å) and *catena*-[UO_2(μ-F_2)(dmso)] [19] (2.31(1) and 2.34(1) Å). The F1–U1–F1* angle of 64.01(10)° is within the range previously observed in **1** and related compounds [18,19] (62.77(16)°–65.4(4)°). The uncoordinated $[BF_4]^-$ is slightly distorted away from tetrahedral geometry with F–B–F bond angles of 108.4(5)°–111.8(5)°, although the B–F bond lengths are all the same within error (average 1.368 Å), and are similar to those in **1** (average 1.359 Å) and [$UO_2(C_2H_6OS)_5$][$(BF_4)_2$] [11] (averages 1.35 and 1.37 Å). Molecules pack in a zig–zag arrangement, similar to **1**, allowing TBPO groups to form a hydrophobic "shell" around the hydrophilic uranyl groups. We believe that strong interactions between the F-atoms of $[BF_4]^-$ and H-atoms of neighbouring TBPO groups (2.366(4) Å at the closest point) hold the lattice together, a situation similar to that in **1**.

[UO_2(μ-F)(F)$(DPPMO_2)$]$_2$ (**3**) is a neutral uranyl complex with some structural similarities to **1** and **2**. As with compounds **1** and **2**, two pentagonal bipyrami-

Table 3
Selected bond lengths (Å) and angles (°) for [{UO_2(μ-F)$(TBPO)_3$}$_2$][BF_4]$_2$ (**2**)

Bond lengths			
U(1)–O(4)	1.764(3)	U(1)–F(1)	2.340(2)
U(1)–O(5)	1.777(3)	U(1)–F(1*)	2.329(2)
U(1)–O(1)	2.375(3)	B(1)–F(2)	1.377(7)
U(1)–O(2)	2.369(3)	B(1)–F(3)	1.366(7)
U(1)–O(3)	2.352(3)	B(1)–F(4)	1.352(8)
		B(1)–F(5)	1.377(7)
Bond angles			
O(4)–U(1)–O(5)	179.51(15)	U(1)–F(1)–U(1*)	115.99(10)
O(4)–U(1)–F(1)	90.04(12)	P(1)–O(1)–U(1)	145.14(19)
O(5)–U(1)–F(1)	89.92(11)	P(2)–O(2)–U(1)	130.97(19)
O(4)–U(1)–F(1*)	89.96(12)	P(3)–O(3)–U(1)	140.16(18)
O(5)–U(1)–F(1*)	90.46(12)	F(2)–B(1)–F(3)	111.8(5)
F(1)–U(1)–F(1*)	64.01(10)	F(2)–B(1)–F(4)	109.5(5)
O(4)–U(1)–O(1)	87.01(13)	F(3)–B(1)–F(4)	109.1(6)
O(4)–U(1)–O(2)	94.02(13)	F(2)–B(1)–F(5)	108.9(5)
O(4)–U(1)–O(3)	93.46(13)	F(3)–B(1)–F(5)	108.4(5)
F(1)–U(1)–O(1)	147.46(10)	F(4)–B(1)–F(5)	109.3(6)
F(1*)–U(1)–F(1*)	148.28(9)		

dal uranyl groups are bridged by a pair of μ_2-F anions in a centrosymmetric dimer. However, in **3**, equatorial coordination at each U centre is completed by a bidentate $DPPMO_2$ ligand and a monodentate F anion, whereas in **1** and **2**, equatorial coordination is completed by 3 monodentate P=O donor ligands yielding cationic complexes. There are two identical complexes in the unit cell accompanied by four molecules of MeOH remote from the U coordination spheres. The structure is shown in Fig. 3 with bond distances and angles given in Table 4. Three $\{UO_2\}^{2+}$ complexes with chelating $DPPMO_2$ have been previously structurally characterised, $[UO_2(Cl)(DPPMO_2)_2]$ and $[UO_2(ReO_4)(DPPMO_2)_2]$ [5] as well as $[UO_2(NO_3)_2(DPPMO_2)]$ [21].

Unlike $[UO_2(ReO_4)(DPPMO_2)_2[ReO_4]$ [5] and the related Fe and Ni d-transition metal complexes [22,23], **3** has two similar U–$O_{(DPPMO2)}$ bond distances (2.417(3) and 2.420(2) Å). Symmetrical $DPPMO_2$ groups are not uncommon, and are observed in $[TlCl_2(DPPMO_2)_2][TlCl_4] \cdot 2thf$ [24] (2.321(13) and 2.355(14) Å) and $[Na(DPPMO_2)_3]Cl \cdot 2H_2O \cdot C_6H_6$ [25] (2.4566(14) Å) as well as in $[UO_2(NO_3)_2(DPPMO_2)]$ [21] (2.370(9) and 2.407(10) Å). The U–$O_{(DPPMO2)}$ bonds are long in comparison to those in $[UO_2(ReO_4)(DPPMO_2)_2[ReO_4]$ (average 2.386 Å), but comparable to the U–$O_{(DPPMO2)}$ bonds in $[UO_2(NO_3)_2(DPPMO_2)]$ [21]. The bite angle of the $DPPMO_2$ ligand is fairly normal (71.55(8)°) and comparable to the $DPPMO_2$ bite angles in $[UO_2(ReO_4)(DPPMO_2)_2[ReO_4]$ (73.1(2)° and 72.9(2)°) [5] and bite angle in $[UO_2(NO_3)_2(DPPMO_2)]$ (71.5(4)°) [21]. The fluoride bridge is effectively symmetrical and has bond lengths (average 2.322 Å) and an F1–U1–F1* angle (65.69(9)°) similar to those found in **1**, **2** and related uranyl difluoride-bridged compounds [18,19]. The terminal fluorine atom has a U1–F2 bond distance of 2.199(2) Å, which is comparable to terminal F-atoms in $[UO_2(\mu\text{-}F)(F)\{CO(NH_2)_2\}_2]_2$ [18] (2.23(2) Å) and $[U_2O_4F_6(C_4N_2H_{12})]$ [26] (2.196(8) Å). The mean U=O distance is 1.772 Å, similar to the mean distances found in **1** and **2** (1.768 and 1.770 Å). The uranyl bond angle (178.50(12)°) is within the range expected [16], but is significantly more bent than the essentially linear $\{UO_2\}^{2+}$ in **1** and **2** (179.8(2)° and 179.51(15)°). The solid state packing of the molecule appears to be heavily influenced by F–H interatomic interactions. The $DPPMO_2$ groups are not large enough to encapsulate much of the diuranyl core of the molecule, but a zig–zag packing arrangement exists in a situation similar to that in **1** and **2**. Intermolecular interactions between H-atoms of neighbouring organic ligands and terminal F-atoms (closest separation = 2.292(2) Å) aid the formation of a hydrophobic "shell" around the diuranyl centre, which also incorporates MeOH solvent molecules in the lattice and $DPPMO_2$ groups from neighbouring molecules.

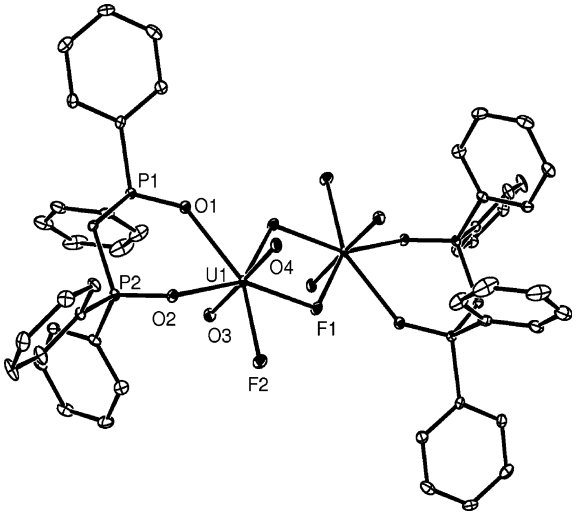

Fig. 3. Molecular structure of $[UO_2(\mu\text{-}F)(F)(DPPMO_2)]_2 \cdot 2MeOH$ (**3**). Probability ellipsoids of 30% are shown.

Table 4
Selected bond lengths (Å) and angles (°) for $[UO_2(\mu\text{-}F)(F)(DPPMO_2)]_2$ (**3**)

Bond lengths			
U(1)–O(3)	1.773(3)	U(1)–F(1)	2.319(2)
U(1)–O(4)	1.771(3)	U(1)–F(1*)	2.326(2)
U(1)–O(1)	2.417(3)	U(1)–F(2)	2.199(2)
U(1)–O(2)	2.420(2)		
Bond angles			
O(3)–U(1)–O(4)	178.50(12)	F(1)–U(1)–O(1)	137.79(8)
O(3)–U(1)–F(1)	90.62(10)	F(1)–U(1)–O(2)	150.66(8)
O(4)–U(1)–F(1)	90.75(10)	F(1)–U(1)–F(2)	74.75(8)
O(3)–U(1)–F(1*)	88.76(10)	F(1*)–U(1)–O(1)	72.10(8)
O(4)–U(1)–F(1*)	91.24(11)	F(1*)–U(1)–O(2)	143.65(8)
F(1)–U(1)–F(1*)	65.69(9)	F(1*)–U(1)–F(2)	140.34(8)
O(2)–U(1)–O(1)	71.55(8)	U(1)–F(1)–U(1*)	114.31(9)
O(3)–U(1)–O(1)	88.44(11)	P(1)–O(1)–U(1)	143.04(15)
O(3)–U(1)–O(2)	90.30(11)	P(2)–O(2)–U(1)	134.87(14)
O(3)–U(1)–F(2)	88.96(11)		

3.2. Spectroscopic characterisation

The mid/far infra-red and Raman spectra of **1** and **3** were recorded. Due to the low yield of compound **2** only

Table 5
Selected infra-red and Raman vibrations (cm^{-1}) for compounds **1**–**3**

Vibration	Technique	**1**	**2**	**3**
ν_1(U=O)	IR	843 w	–	841 w
	Raman	848 m	–	843 s
ν_3(U=O)	IR	926 s	921 s	918 s
ν_1(B–F)	IR	779 sh	772 vw	x
	Raman	764 vw	–	x
ν_2(B–F)	IR	376 w	–	x
ν_3(B–F)	IR	1082 sh	–	x
ν(U–F)$_{(terminal)}$	IR	x	x	381 m
ν(P=O)$_{(coord)}$	IR	1072 sh	1080 s	1100 m

Notes: 'x', not applicable; '–', not observed; 's', strong; 'm', medium; 'w', weak; 'sh', shoulder; 'v', very.

the mid-IR spectra was recorded. Table 5 lists selected IR and Raman vibrations for **1**–**3** with the spectra and the remaining P=O donor ligand bands given in the Supporting data. Bands could be assigned to coordinated P=O (shifting to lower energy on coordination by 118, 75 and 86 cm^{-1}, respectively, for **1**–**3**) and U=O [27], B–F [28] and U–F [29] vibrations. Due at least in part to overlapping P=O donor ligand vibrations identifying bands to $[BF_4]^-$ vibrations proved challenging. The presence of formally IR inactive B–F stretches for unccordinated $[BF_4]^-$ (principally ν_1) in the IR spectra of **1** and **3** can probably be attributed to distortion in the T_d geometry of uncoordinated anion, as discussed previously. Tomlinson et al. [30] have cautioned against the use of IR spectroscopy for the determination of coordinated versus uncoordinated tetrafluoroborate. Diffuse reflectance visible spectra for **1** and **3** display the fine structure typical of the uranyl ion (see Supporting data) [1].

3.3. Summary

Three novel, equatorially 5-coordinate uranyl complexes have been structurally and spectroscopically characterised. Two of these (**1** and **2**) have very similar structures; dimeric uranyl groups bridged by a pair of μ_2-F anions, 3 monomeric phosphine oxide ligands coordinated to each U(VI) centre, and 2 tetrafluoroborate groups remote from the U coordination sphere balancing the charge. Compound **3** is also a U(VI) dimer, bridged by a pair of μ_2-F anions, but the equatorial coordination sphere of each U centre is completed by a bidentate phosphine oxide ligand, and a monodentate F^- anion, which balances the charge. The elemental analysis and supporting spectroscopic data are consistent with the single crystal X-ray structural characterisations.

The syntheses of compounds **1** and **2** were similar, in that the phosphine oxide was added to a solution of UO_3 dissolved in HBF_4, from which crystalline material was isolated. Compound **3** was synthesised by reacting the phosphine oxide with a dried yellow solid (prepared from the dissolution of UO_3 in HBF_4) in MeOH. The fluorophilicity of uranium is well known [1], and the bond dissociation energies of U–F and B–F bonds (at 298 K) are close enough (659 and 757 kJ mol^{-1}, respectively [31]) to assume that under these reaction conditions, the affinity of U for F is sufficient to break B–F bonds. The propensity of fluorine to bridge between metal centres is well known [18,19,26], and allows the 3 complexes to achieve an equatorially 5-coordinate geometry around the U(VI) centre. It is, however, interesting to note that both $[UO_2(dmso)_5][BF_4]_2$ [11] and $[UO_2(dmf)_5][BF_4]_2$ [12] were obtained as single crystals suitable for X-ray diffraction from aqueous dmso or aqueous dmf respective, following addition of HBF_4 to UO_3. In contrast, **1**–**3** were obtained as bulk crystalline samples from aqueous hexane and neat ethanol and methanol solutions, respectively.

4. Conclusions

Our attempts to prepare $\{UO_2\}^{2+}$ complexes with coordinated $[BF_4]^-$ through similar synthetic strategies to those employed for the synthesis of complexes with $\{UO_2\}^{2+}/[ReO_4]^-/P{=}O$ donor ligand have proved unsuccessful. In each case the fluorophilicity of $\{UO_2\}^{2+}$ has led to fluorine abstraction from $[BF_4]^-$ and the resultant formation of dimeric complexes with bridging fluorides. In the case of **1** and **2** the +2 charge on the cationic complexes is balanced by two $[BF_4]^-$ counter anions, which do not displace P=O donor ligand (TPPO and TBPO, respectively) coordinated to the uranyl centres. In **3**, additional terminal fluoride coordination results in the formation of a neutral complex. Clearly any further attempts to coordinate $\{UO_2\}^{2+}$ to $[BF_4]^-$ would require a different synthetic approach.

Acknowledgements

We thank the EPSRC and BNFL for funding.

Appendix A. Supplementary material

Supplementary data associated with this article can be found, in the online version, at doi:10.1016/j.poly.2004.09.010.

References

[1] J.J. Katz, G.T. Seaborg, L.R. Morss, The Chemistry of the Actinide Elements, second ed., Chapman and Hall, London, 1986.
[2] (a) M.J. Sarsfield, M. Helliwell, J. Am. Chem. Soc. 126 (2004) 1036;
(b) D.L. Clark, S.D. Conradson, R.J. Donohoe, D.W. Keogh, D.E. Morris, P.D. Palmer, R.D. Rodgers, C.D. Tait, Inorg. Chem. 38 (1999) 1456.
[3] (a) M.R. Rosenthal, J. Chem. Educ. 50 (1973) 331;
(b) W. Beck, K. Sünkel, Chem. Rev. 93 (1993) 927.
[4] I.S. Denniss, A.P. Jeapes, in: P.D. Wilson (Ed.), The Nuclear Fuel Cycle, BNFL plc, Oxford University Press, Oxford, 1996, p. 116.
[5] A.D. Sutton, G.H. John, M.J. Sarsfield, J.C. Renshaw, I. May, L.R. Martin, A.J. Selvage, D. Collison, M. Helliwell, Inorg. Chem. 43 (2004) 5480.
[6] G.H. John, The chemistry of uranium and neptunium perrhenate compounds, PhD Thesis, The University of Manchester, Manchester, 2003.
[7] G.H. John, I. May, M.J. Sarsfield, H.M. Steele, D. Collison, M. Helliwell, J.D. McKinney, Dalton Trans. (2004) 734.

[8] (a) J.–C. Berthet, M. Nierlich, M. Ephritikhine, C. R. Chim. 5 (2002) 81;
(b) J.–C. Berthet, M. Lance, M. Nierlich, M. Ephritikhine, Eur. J. Inorg. Chem. (2000) 1969;
(c) J.–C. Berthet, M. Lance, M. Nierlich, M. Ephritikhine, Eur. J. Inorg. Chem. (1999) 2005.
[9] F.H. Allen, J.E. Davies, J.J. Galloy, O. Johnson, O. Kennard, C.F. Macrae, E.M. Mitchell, G.F. Mitchell, J.M. Smith, D.G. Watson, J. Chem. Inf. Comp. Sci. 31 (1991) 187.
[10] P.B. Hitchcock, M.F. Lappert, R.G. Taylor, J. Chem. Soc. Chem. Commun. (1984) 1082.
[11] L. Deshayes, N. Keller, M. Lance, M. Nierlich, D. Vigner, Acta Crystallogr. Sect. C 48 (1992) 2209.
[12] L. Deshayes, N. Keller, M. Lance, M. Nierlich, D. Vigner, Acta Crystallogr. Sect. C 48 (1992) 1660.
[13] SIR92: A. Altomare, G.L. Cascarano, C. Giacovazzo, A. Guagliardi, J. Appl. Crystallogr. 26 (1993) 343.
[14] SHELXL97: G.M. Sheldrick, Program for Crystal Structure Refinement, The University of Göttingen, Germany, 1997.
[15] SHELXTL: SHELX-PC Package Bruker Analytical X-ray Systems, Madison, WI, USA, 1998.
[16] P.C. Burns, R.C. Ewing, F.C. Hawthorne, Can. Mineral. 35 (1997) 1551.
[17] I.A. Charushnikova, N.N. Krot, Z.A. Starikova, Radiokhimiya 43 (2001) 448.
[18] Yu.N. Mikhailov, S.B. Ivanov, I.M. Orlova, G.A. Podnebesnova, V.G. Kuznetsov, R.N. Shchelokov, Koord. Khim. 2 (1976) 1570.
[19] J.C. Dewan, A.J. Edwards, D.R. Slim, J.E. Guerchais, R. Kergoat, J. Chem. Soc., Dalton Trans. (1975) 2171.
[20] J.H. Burns, Inorg. Chem. 20 (1981) 3868.
[21] S. Kannan, N. Rajalakshmi, K.V. Chetty, V. Venugopal, M.G.B. Drew, Polyhedron 23 (2004) 1527.
[22] J.E. Barclay, D.J. Evans, D.L. Hughes, G.J. Leigh, J. Chem. Soc., Dalton Trans. (1993) 69.
[23] E. Bermejo, A. Castiñeiras, R. Domínguez, C. Schüle, J. Coord. Chem. 33 (1994) 353.
[24] C.J. Carmalt, L.J. Farrugia, N.C. Norman, Main Group Chem. 1 (1996) 339.
[25] Y. Ding, P.E. Fanwick, R.A. Walton, Inorg. Chim. Acta 309 (2000) 159.
[26] S. Allen, S. Barlow, P.S. Halasyamani, J.F.W. Mosselmans, D. O'Hare, S.M. Walker, R.I. Walton, Inorg. Chem. 39 (2000) 3791.
[27] S.P. McGlynn, J.K. Smith, W.C. Neely, J. Chem. Phys. 35 (1961) 105.
[28] A.S. Quist, J.B. Bates, G.E. Boyd, J. Chem. Phys. 54 (1971) 4896.
[29] M. Gál, P.L. Goggin, J. Mink, Spectrochim. Acta 48A (1992) 121.
[30] A.A.G. Tomlinson, M. Bonamico, G. Dessy, V. Fares, L. Scaramuzza, J. Chem. Soc., Dalton Trans. (1972) 1671.
[31] R.C. Weast (Ed.), CRC Handbook of Chemistry and Physics, 58th ed., CRC Press Inc., Boca Raton, FL, 1978.

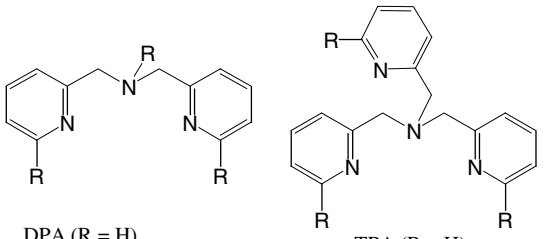

Fig. 1. DPA and TPA ligands and their derivatives.

2. Results and discussion

2.1. Reaction of MCl_2 with TPA

Treatment of anhydrous MCl_2 with one equivalent of TPA in *n*-BuOH at 90 °C afforded [(TPA)MCl_2] (M = Co (**1**), Fe (**2**)) and [(TPA)CoCl]Cl (**3**) in good yield (Scheme 1). All products have been characterised by FAB mass spectrometry, magnetic susceptibility and by elemental analysis (see Table 1). In addition, crystals of **1**–**3** have been subject to single-crystal X-ray diffraction studies.

Crystals of **1** and **2** · MeCN were grown by the slow cooling of a hot acetonitrile solution of each complex. The structures are similar and will be discussed together. The molecular structure of **1** is shown in Fig. 2; selected bond distances and angles are listed for both **1** and **2** · MeCN in Table 2. The discrete molecules consist of a single metal(II) centre bound by a TPA ligand coordinated in a tripodal, tetradentate fashion, with the two other coordination sites filled by terminally bound chloride ligands. The metal centres in each complex adopt an approximately octahedral geometry with Cl(1) *trans* to the tertiary amine [N(1)] and Cl(2) *trans* to one of the pyridine moieties. The angles between Cl(1) and its *cis*-neighbours are significantly larger than 90° [Cl(1)–M(1)–Cl(2) 96.579(17)° (**1**), 97.86(3)° (**2**); Cl(1)–M(1)–N(2) 101.86(4)° (**1**), 102.18(5)° (**2**); Cl(1)–M(1)–N(3) 102.65(4)° (**1**), 107.20(5)° (**2**); Cl(1)–M(1)–N(4) 93.86(4)° (**1**), 93.80(5)° (**2**)]. The metal nitrogen distances range from 2.1205(15) to 2.2191(14) Å in **1** and 2.1885(17)–2.2841(18) Å in **2**, with the tertiary amine nitrogen–metal distance [N(1)–M(1) 2.2191(14) Å (**1**), 2.2841(18) Å (**2**)] the most elongated in each case. Amongst the three M–N(pyridyl) distances, the pyridine group *trans* to Cl(2) has the longest distance [M(1)–N(4) 2.1691(15) (**1**), 2.2162(17) (**2**) *vs.* M(1)–N(3) 2.1205(15) (**1**), 2.1885(17) (**2**) and M(1)–N(2) 2.1363(14) (**1**), 2.1912(17) (**2**) Å], presumably as a consequence of the *trans* effect of the chloride. Notably, in the non-solvated form of **2**, the *trans* effect of the chloride leads to Fe–

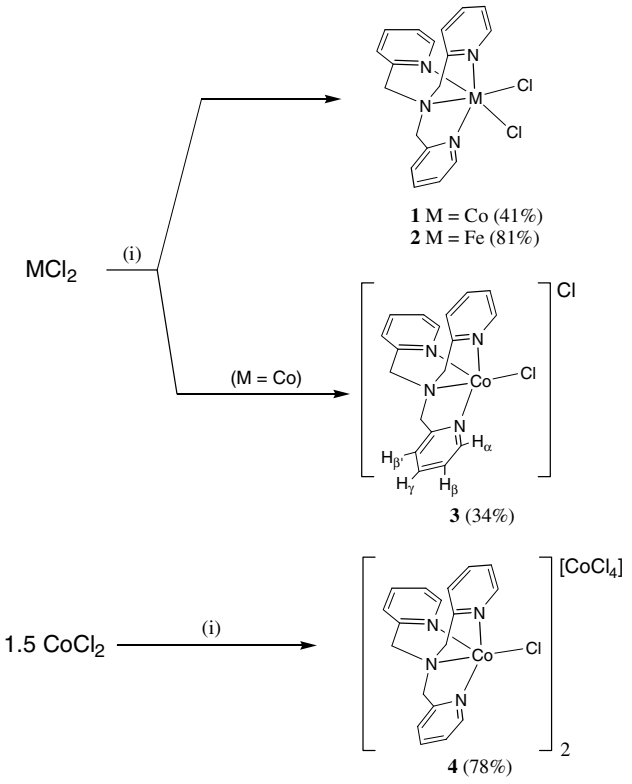

Scheme 1. Reagents and conditions: (i) TPA, *n*-BuOH, 90 °C.

Table 1
Spectroscopic and analytical data for complexes **1**–**8**

Compound	μ_{eff} (BM)[a]	FAB mass spectrum	Microanalysis (%)[b]		
			C	H	N
1	4.4	384 $(M - Cl)^+$	51.31 (51.45)	4.25 (4.32)	13.27 (13.33)
2	4.8	417 $(M)^+$, 381 $(M - Cl)^+$	51.97 (51.80)	4.39 (4.32)	13.30 (13.43)
3	4.2	384 $(M - Cl)^+$	51.39 (51.45)	4.40 (4.32)	13.40 (13.33)
4	3.7	384 $((M - CoCl_4)/2)^+$	44.48 (44.57)	3.82 (3.74)	11.51 (11.55)
6	7.4[c]	616 $(M - Cl)^+$ 290 $(M/2 - Cl)^+$	44.20 (44.17)	3.95 (3.99)	12.97 (12.88)
7	4.4	492 $(M - Cl)^+$ 455 $(M - 2Cl)^+$	54.39 (54.55)	4.96 (4.92)	15.83 (15.91)
8	1.2	489 $(M - Cl)^+$ 453 $(M - 2Cl)^+$	54.91 (54.86)	4.89 (4.95)	15.85 (16.00)

[a] Recorded on an Evans Balance at room temperature.
[b] Calculated values are shown in parentheses.
[c] SQUID value at 298 K.

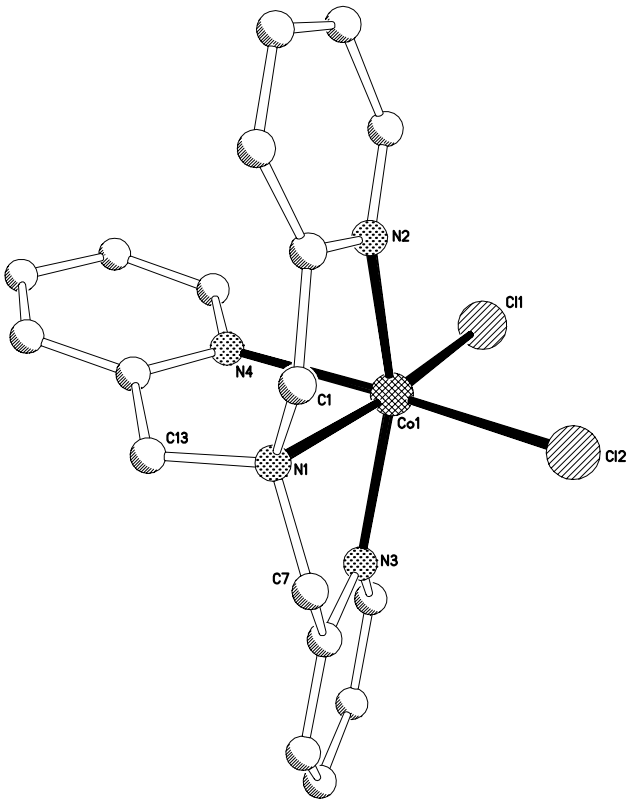

Fig. 2. Molecular structure of **1** including the atom numbering scheme. All the hydrogen atoms have been omitted for clarity.

N(pyridyl) distance being marginally longer than the Fe–N(tertiary) distance [8]. The metal chloride distances are also asymmetric with M(1)–Cl(2) distance being the longest in each case [2.4500(5) (**1**), 2.4573(7) (**2**) Å].

Table 2
Selected bond distances (Å) and angles (°) for **1** and **2** · MeCN

	M = Co (**1**)	M = Fe (**2**)
Bond distances		
M(1)–N(1)	2.2191(14)	2.2841(18)
M(1)–N(2)	2.1363(14)	2.1912(17)
M(1)–N(3)	2.1205(15)	2.1885(17)
M(1)–N(4)	2.1691(15)	2.2162(17)
M(1)–Cl(1)	2.3546(5)	2.3426(6)
M(1)–Cl(2)	2.4500(5)	2.4573(7)
Bond angles		
N(1)–M(1)–N(2)	78.58(5)	74.53(6)
N(1)–M(1)–N(3)	76.30(6)	74.97(7)
N(1)–M(1)–N(4)	78.39(6)	76.17(6)
N(2)–M(1)–N(3)	154.74(6)	149.29(6)
N(2)–M(1)–N(4)	82.74(5)	86.10(6)
N(3)–M(1)–N(4)	89.59(6)	83.29(6)
N(1)–M(1)–Cl(1)	172.15(4)	169.54(5)
N(2)–M(1)–Cl(1)	101.86(4)	102.18(5)
N(3)–M(1)–Cl(1)	102.65(4)	107.20(5)
N(4)–M(1)–Cl(1)	93.86(4)	93.80(5)
N(1)–M(1)–Cl(2)	91.24(4)	92.32(5)
N(2)–M(1)–Cl(2)	91.70(4)	94.33(4)
N(3)–M(1)–Cl(2)	91.50(5)	90.38(5)
N(4)–M(1)–Cl(2)	169.00(4)	167.96(4)

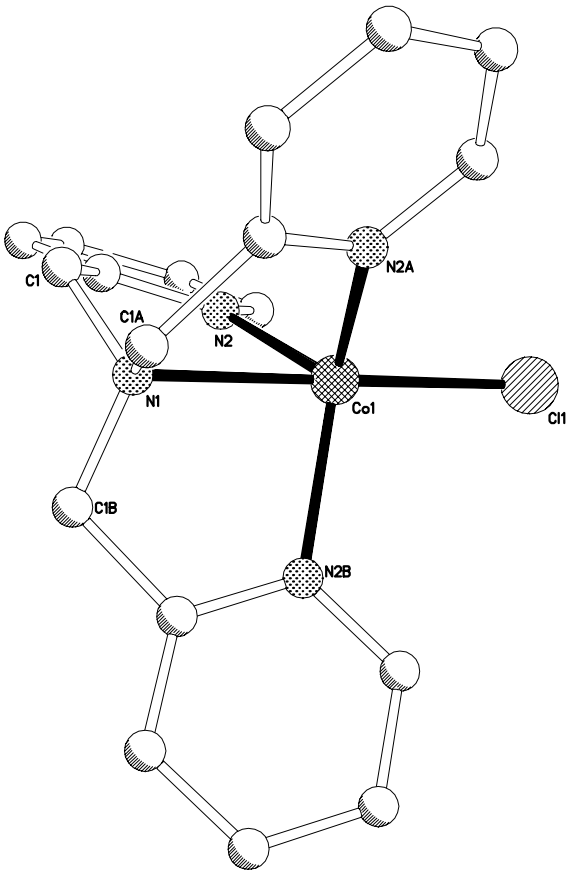

Fig. 3. Molecular structure of the cationic unit in **3** including the atom numbering scheme. All the hydrogen atoms have been omitted for clarity. N(1), Co(1) and Cl(1) are located on a 3-fold axis; N2A, N2B are generated by the symmetry operations (+*z*, +*x*, +*y* and +*y*, +*z*, +*x*).

Crystals of **3** were grown by the slow cooling of a hot acetonitrile solution containing the complex. The molecular structure of **3** is shown in Fig. 3; selected bond distances and angles are given in Table 3. The structure reveals **3** to be composed of a discrete cationic unit along with a chloride counterion. The cationic unit displays a distorted trigonal bipyramidal geometry for the Co(II) ion with the three pyridyl groups in the equatorial plane [N(2)–Co(1)–N(2A) 115.23(2)°] and the amine and the chloride ligands in the apical positions. As with **1**, the tertiary amine nitrogen–metal distance [N(1)–Co(1) 2.2122(18) Å] is

Table 3
Selected bond distances (Å) and angles (°) for **3**

Bond distances	
Co(1)–N(1)	2.2122(18)
Co(1)–N(2)	2.0649(11)
Co(1)–Cl(1)	2.2759(6)
Bond angles	
N(1)–Co(1)–N(2)	77.19(3)
N(2)–Co(1)–N(2A)	115.23(2)
N(2)–Co(1)–Cl(1)	102.81(3)

the most elongated, while the M–N(pyridyl) distances, as a result of the threefold symmetry axis, are all identical [Co(1)–N(2) 2.0649(11) Å]. The cationic unit in **1** resembles closely the five coordinate geometries found in the independent cations in $[(TPA)CoCl]_2[CoCl_4]$ (**4**) and, indeed, the Co–ligand distances are identical within experimental error [10].

The formation of **4** as the sole product from the reaction of cobalt dichloride with one equivalent of TPA in methanol or ethanol at room temperature has been previously reported [9,10]. It is unclear as to the reason why only **1** and **3** are generated when the reaction is performed with equimolar quantities of reagents in *n*-BuOH. Notably, if the reaction is carried out with an excess of $CoCl_2$ in *n*-BuOH, **4** can be isolated in high yield (Scheme 1).

The Fe and Co complexes exhibit different electronic environments. All of the complexes are paramagnetic with the Fe(II) complex (**2**) affording a magnetic moment of 4.8 BM, consistent with four unpaired electrons ($S = 2$), while the Co(II) complexes (**1**, **3** and **4**) have moments ca. 4.1 BM consistent with three unpaired electrons ($S = 3/2$) (Table 1).

The paramagnetic behaviour of **1**–**4** in the solid state is also observed in solution (acetonitrile-d_3) with broad paramagnetically shifted peaks. The spectrum of **2** · MeCN is as described by Mandon et al. [8] for the non-solvated form. Equally, the spectrum for **4** is in agreement with that previously reported [10] and, interestingly, essentially identical to that for six-coordinate **1** and five-coordinate **3** (see Section 4). It would seem therefore likely that **1** in solution can readily undergo chloride dissociation to give **3**.

2.2. Reaction of MCl_2 with DPA

The reaction of DPA was found to be highly dependent on the stoichiometry of the starting materials. Thus, addition of one equivalent of DPA to a solution of MCl_2 in *n*-BuOH at 90 °C gave, on crystallisation from hot acetonitrile, $[(fac\text{-DPA})MCl(\mu\text{-}Cl)]_2$ (M = Co (**5**), Fe (**6**)) in good yield. On the other hand, introduction of two equivalents of DPA gave, following crystallisation, the bis(ligand) complexes $[(fac\text{-DPA})_2M]Cl_2$ (M = Co (**7**), Fe (**8**)) (Scheme 2). Needless to say, mixtures of **5** and **7** or **6** and **8** were obtained when 1.5 equivalents of DPA was employed. X-ray diffraction studies have been performed on **6**–**8**.

Single crystals of $\mathbf{6} \cdot 1\frac{2}{3}CH_2Cl_2$ suitable for the study were grown by the prolonged standing of a solution of the complex in dichloromethane. The molecular structure of **6** is shown in Fig. 4; selected bond distances and angles are listed in Table 4. The structure consists of a dimeric unit in which the iron centres are bridged by two chloride ligands and bound terminally by a chloride and a DPA ligand to give a distorted octahedral geometry at each metal centre. The DPA ligands adopt *facial* bonding modes such that the central amines are *trans* to a terminal chloride and the pyridyl groups *trans* to the bridging chlorides. At each metal centre the pyridyl nitrogen–iron distances [Fe(1)–N(1) 2.174(3), Fe(1)–N(2) 2.181(3) and Fe(2)–N(4) 2.143(3) Å, Fe(2)–N(5) 2.167(3) Å] are marginally shorter than the corresponding iron–secondary amine distances [Fe(1)–N(1) 2.185(2), Fe(2)–N(6) 2.175(3) Å], but not as significantly as that observed in $[(N\text{-Et-DPA})FeCl(\mu\text{-}Cl)]_2$ [11]. The Fe–μ-Cl distances are similar [2.501(1), 2.499(1),

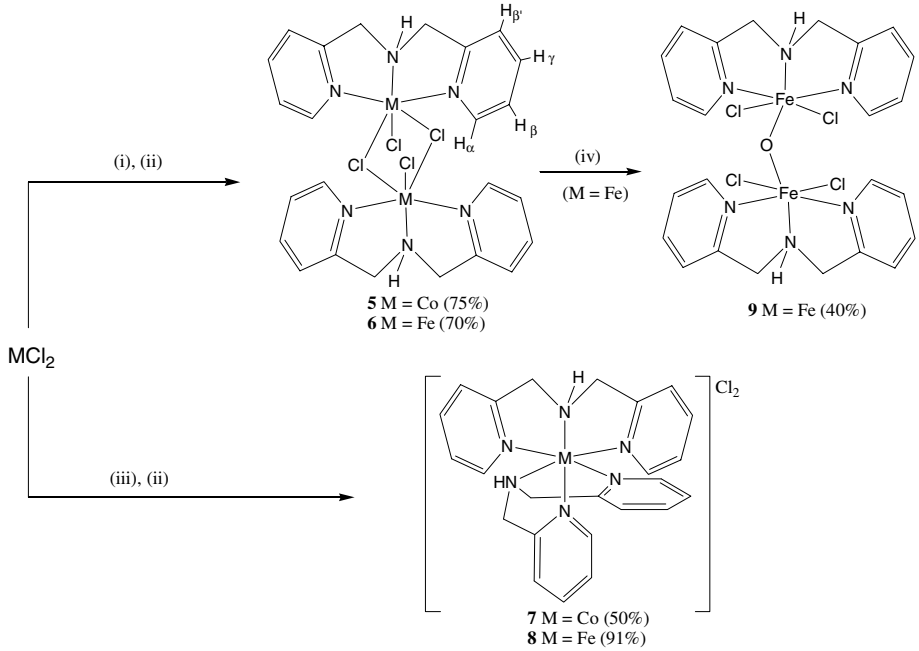

Scheme 2. Reagents and conditions: (i) DPA, *n*-BuOH, 90 °C; (ii) MeCN; (iii) 2 DPA, *n*-BuOH, 90 °C; (iv) air, MeCN.

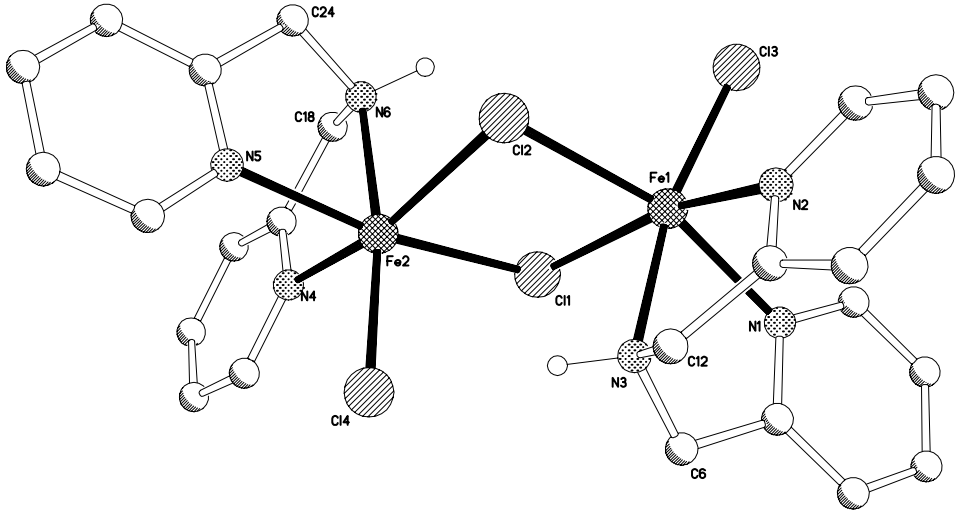

Fig. 4. Molecular structure of **6** including the atom numbering scheme. All hydrogen atoms except for H3 and H6 have been omitted for clarity.

2.500(1), 2.490(1) Å] and fall at the top end of the range found for related complexes [11,13–16]. As expected, the Fe–Cl(terminal) bond distances [Fe(1)–Cl(3) 2.306(1), Fe(2)–Cl(4) 2.315(1) Å] are shorter than those seen for the bridging chlorides but at the top end of the range observed in structurally related complexes [11,13–16]. The $ClFe(\mu\text{-}Cl)_2FeCl$ motif has been found in a number of crystallographically characterised complexes with the transannular Fe···Fe separation in **6** [3.713(1) Å] amongst the longest [11,13–16].

In **6**, the room temperature magnetic moment is observed at 7.4 BM and consistent with two non-interacting high spin Fe(II) centres (Table 1). Indeed, lowering the temperature of the measurement shows little variation in the value [17]. The ^{1}H NMR spectrum of **6** (recorded in acetonitrile-d_3) supports its paramagnetic nature with broad and shifted peaks between 117 and 7 ppm. Assignment of the spectrum for **6** is possible on comparison with previously reported high spin polypyridyl ferrous compounds [8,18,19]. Thus, H_α, $H_\beta/H_{\beta'}$ and H_γ protons of the coordinated pyridyl arms are found at δ 116.5, 54.7/51.8 and 7.8 while the methylene protons are seen at δ 70.8. The spectroscopic data for **5** is essentially as previously reported [10]. However, the FAB mass spectrum does show fragmentation peaks corresponding to the loss of chloride ions from the parent ion for both mono- and di-meric species and in a similar manner to that observed for **6**; we have therefore tentatively ascribed **5** as a dimeric structure.

Crystals of **7** · 3MeCN and **8** · 3MeCN were grown by the slow cooling of a hot acetonitrile solution of each complex. The structures are similar and will be discussed

Table 4
Selected bond distances (Å) and angles (°) for **6** · $1\frac{2}{3}CH_2Cl_2$

Bond distances			
Fe(1)–N(1)	2.174(3)	Fe(2)–N(4)	2.143(3)
Fe(1)–N(2)	2.181(3)	Fe(2)–N(5)	2.167(3)
Fe(1)–N(3)	2.185(2)	Fe(2)–N(6)	2.175(3)
Fe(1)–Cl(1)	2.499(1)	Fe(2)–Cl(1)	2.500(1)
Fe(1)–Cl(2)	2.501(1)	Fe(2)–Cl(2)	2.490(1)
Fe(1)–Cl(3)	2.306(1)	Fe(2)–Cl(4)	2.315(1)
Fe(1)···Fe(2)	3.713(1)		
Bond angles			
N(1)–Fe(1)–N(2)	89.28(9)	N(4)–Fe(2)–N(5)	85.06(9)
N(1)–Fe(1)–Cl(1)	89.38(7)	N(4)–Fe(2)–Cl(1)	90.25(7)
N(1)–Fe(1)–Cl(3)	96.23(8)	N(4)–Fe(2)–Cl(4)	98.06(8)
N(1)–Fe(1)–N(3)	76.77(10)	N(4)–Fe(2)–N(6)	76.99(10)
N(1)–Fe(1)–Cl(2)	163.96(8)	N(4)–Fe(2)–Cl(2)	160.98(8)
N(2)–Fe(1)–Cl(1)	163.28(7)	N(5)–Fe(2)–Cl(1)	166.05(7)
N(2)–Fe(1)–Cl(3)	93.79(7)	N(5)–Fe(2)–Cl(4)	95.31(7)
N(2)–Fe(1)–N(3)	76.22(9)	N(5)–Fe(2)–N(6)	77.20(10)
N(2)–Fe(1)–Cl(2)	93.14(7)	N(5)–Fe(2)–Cl(2)	96.28(7)
N(3)–Fe(1)–Cl(1)	87.26(7)	N(6)–Fe(2)–Cl(1)	88.95(7)
N(3)–Fe(1)–Cl(2)	88.40(7)	N(6)–Fe(2)–Cl(2)	84.79(7)
N(3)–Fe(1)–Cl(3)	167.71(7)	N(6)–Fe(2)–Cl(4)	171.26(7)
Cl(1)–Fe(1)–Cl(2)	83.76(3)	Cl(1)–Fe(2)–Cl(2)	83.96(3)
Cl(1)–Fe(1)–Cl(3)	102.92(3)	Cl(1)–Fe(2)–Cl(4)	98.35(3)

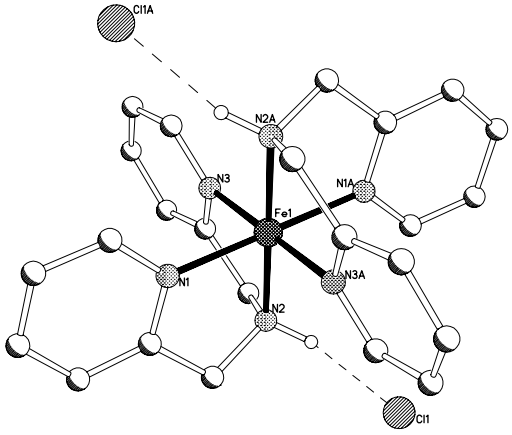

Fig. 5. Molecular structure of **8** showing the atom numbering scheme. All the hydrogen atoms except for H2 have been omitted for clarity.

together. The molecular structure of **8** is shown in Fig. 5; selected bond distances and angles are listed for both **7** and **8** in Table 5. The metal(II) centres in **7** and **8** are surrounded by two DPA ligands, each coordinating in a tridentate fashion to give pseudooctahedral dicationic units. The anionic units are made up of two chloride ions which undergo weak hydrogen bonding interactions with the secondary amine moieties of the DPA ligands [H(2)···Cl(1) 2.269(3) Å (**7**), 2.313(3) Å (**8**)]. The DPA ligands are facially coordinated such that the central amines are mutually *trans* in each complex (i.e., *trans–facially* coordinated). In both cases the pyridyl nitrogen–metal distances [Co(1)–N(1) 2.140(1), Co(1)–N(3) 2.124(1) Å (**7**); Fe(1)–N(1) 1.986(2) Å, Fe(1)–N(3) 1.981(2) Å (**8**)] are shorter than the metal–secondary amine distances [M(1)–N(2) 2.149(1) Å (**7**), 2.020(3) Å (**8**)], presumably as a consequence of some dπ–pπ overlap between metals and pyridyl nitrogen atoms. Crystallographically characterised complexes containing two facially coordinated DPA ligands have been reported for divalent Mn [20], Fe [21], Ni [22],

Table 5
Selected bond distances (Å) and angles (°) for **7** · 3MeCN and **8** · 3MeCN

	M = Co (**7**)	M = Fe (**8**)
Bond distances		
M(1)–N(1)	2.140(1)	1.986(2)
M(1)–N(2)	2.149(1)	2.020(3)
M(1)–N(3)	2.124(1)	1.981(2)
Bond angles		
N(1)–M(1)–N(2)	79.9(1)	83.3(1)
N(2)–M(1)–N(3)	80.0(1)	83.2(1)
N(1)–M(1)–N(3)	85.7(1)	86.0(1)

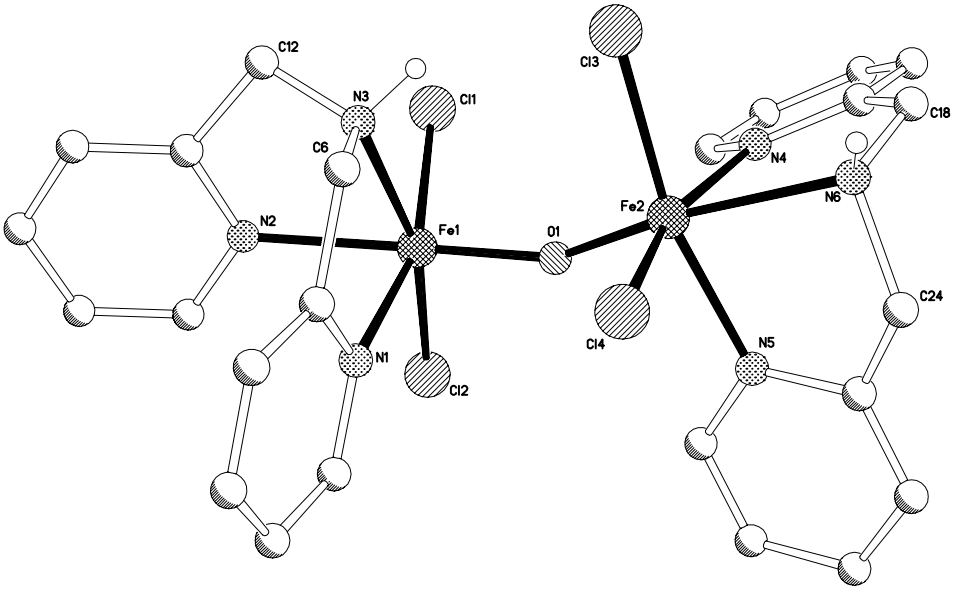

Fig. 6. Molecular structure of **9** including the atom numbering scheme. All the hydrogen atoms, except for H3 and H6, have been omitted for clarity.

Table 6
Selected bond distances (Å) and angles (°) for **9**

Bond distances			
Fe(1)–N(1)	2.182(13)	Fe(1)–Cl(1)	2.350(10)
Fe(1)–N(2)	2.199(13)	Fe(1)–Cl(2)	2.310(12)
Fe(1)–N(3)	2.27(3)	Fe(1)–O(1)	1.805(17)
Fe(2)–N(4)	2.186(16)	Fe(2)–Cl(3)	2.342(11)
Fe(2)–N(5)	2.159(14)	Fe(2)–Cl(4)	2.373(9)
Fe(2)–N(6)	2.28(2)	Fe(2)–O(1)	1.794(17)
Bond angles			
N(1)–Fe(1)–N(2)	76.8(6)	Cl(3)–Fe(2)–Cl(4)	93.3(3)
N(2)–Fe(1)–N(3)	74.1(7)	Cl(1)–Fe(1)–N(1)	162.5(5)
N(1)–Fe(1)–N(3)	79.1(8)	Cl(2)–Fe(1)–N(3)	165.8(6)
N(4)–Fe(2)–N(5)	84.4(7)	Cl(3)–Fe(2)–N(5)	167.1(6)
N(5)–Fe(2)–N(6)	80.6(8)	Cl(4)–Fe(2)–N(4)	162.7(6)
N(4)–Fe(2)–N(6)	74.8(8)	Fe(1)–O(1)–Fe(2)	150.0(11)
Cl(1)–Fe(1)–Cl(2)	97.1(3)		

Table 7
Crystallographic and data processing parameters for complexes **1**, **2** · MeCN, **3**, **6** · $1\frac{2}{3}CH_2Cl_2$, **7** · 3MeCN,**8** · 3MeCN and **9**

Complex	**1**	**2**	**3**	**6**	**7**	**8**	**9**
Formula	$C_{18}H_{18}Cl_2CoN_4$	$C_{18}H_{18}Cl_2FeN_4 \cdot MeCN$	$C_{18}H_{18}Cl_2CoN_4$	$C_{38}H_{39}Cl_6Fe_3N_9 \cdot 2.5CH_2Cl_2$	$C_{24}H_{26}Cl_2CoN_6 \cdot 3MeCN$	$C_{24}H_{26}Cl_2FeN_6 \cdot 3MeCN$	$C_{24}H_{26}Cl_4Fe_2N_6O$
Molecular weight	420.19	458.17	420.19	1190.34	651.50	648.42	668.01
Crystal size (mm)	$0.14 \times 0.15 \times 0.05$	$0.08 \times 0.12 \times 0.16$	$0.29 \times 0.34 \times 0.37$	$0.28 \times 0.24 \times 0.07$	$0.24 \times 0.24 \times 0.07$	$0.17 \times 0.16 \times 0.03$	$0.24 \times 0.24 \times 0.07$
T (K)	150(2) K	160(2) K	150(2) K	160(2)	150(2)	150(2)	150(2)
Crystal system	monoclinic	orthorhombic	cubic	monoclinic	monoclinic	monoclinic	monoclinic
Space group	$P2_1/c$	$Pnn2$	$P2_13$	$C2/c$	$C2/c$	$C2/c$	$P2_1/n$
Lattice parameters							
a (Å)	13.1037(8)	14.984(3)	12.3978(3)	40.645(6)	20.493(1)	20.425(5)	11.15(2)
b (Å)	9.1929(5)	15.312(3)	12.3978(3)	10.579(2)	9.518(1)	9.535(2)	16.92(3)
c (Å)	15.7386(9)	9.1634(17)	12.3978(3)	22.098(3)	16.864(1)	16.656(4)	14.64(3)
α (°)	90	90	90	90	90	90	90
β (°)	92.5490(10)°	90	90	100.41(1)	105.73(1)	107.38(1)	96.40(4)°
γ (°)	90	90	90	90	90	90	90
V (Å^3)	1894.01(19)	2102.3(7)	1905.61(8)	9346(2)	3166.4(3)	3095.8(13)	2747(9)
Z	4	4	4	8	4	4	4
D_{calc} (Mg m^{-3})	1.474	1.448	1.465	1.692	1.367	1.391	1.615
$F(000)$	860	944	860	4824	1356	1352	1360
μ (Mo Kα) (mm^{-1})	1.196	0.987	1.189	1.590	0.746	0.696	1.476
Reflections collected	15544	16933	16095	38649	12058	10766	19225
Independent reflections	4130	4578	1400	10196	3108	2729	4830
R_{int}	0.0336	0.0320	0.0299	0.042	0.0192	0.0471	0.7045
Parameters/restraints	226/0	254/1	76/0	555/0	229/0	229/0	132/0
Final R indices [$I > 2\sigma(I)$]	$R_1 = 0.0290$, $wR_2 = 0.0734$	$R_1 = 0.0247$, $wR_2 = 0.0507$	$R_1 = 0.0166$, $wR_2 = 0.0448$	$R_1 = 0.042$, $wR_2 = 0.103$	$R_1 = 0.029$, $wR_2 = 0.088$	$R_1 = 0.049$, $wR_2 = 0.130$	$R_1 = 0.1462$, $wR_2 = 0.3127$
Final R indices (all data)	$R_1 = 0.0351$, $wR_2 = 0.0746$	$R_1 = 0.0288$, $wR_2 = 0.0512$	$R_1 = 0.0167$, $wR_2 = 0.0448$	$R_1 = 0.061$, $wR_2 = 0.106$	$R_1 = 0.033$, $wR_2 = 0.090$	$R_1 = 0.058$, $wR_2 = 0.136$	$R_1 = 0.4107$, $wR_2 = 0.4981$
Goodness-of-fit on F^2 (all data)	0.979	0.913	1.095	0.944	1.083	1.067	0.767

Data in common: graphite-monochromated Mo Kα radiation, $\lambda = 0.71073$ Å; $R_1 = \sum||F_o| - |F_c||/\sum|F_o|$, $wR_2 = [\sum w(F_o^2 - F_c^2)^2/\sum w(F_o^2)^2]^{1/2}$, $w^{-1} = [\sigma^2(F_o)^2 + (aP)^2]$, $P = [\max(F_o^2, 0) + 2(F_c^2)]/3$, where a is a constant adjusted by the program; goodness − of − fit $= [\sum(F_o^2 - F_c^2)2/(n-p)]^{1/2}$, where n is the number of reflections and p the number of parameters.

Cu [23], Zn [20], Cd [20,24] and Hg [25]. Notably, in [(*fac*-DPA)$_2$Fe](BF$_4$)$_2$ [21] the DPA ligands are *cis-facially* coordinated as compared to the *trans–facial* coordination mode adopted in **8**; the metal–nitrogen bond lengths in each isomer fall in the same range.

As has previously been reported by Nelson and Rodgers [12], complex **8** adopts a low spin configuration at ambient temperature and the non-zero value for the magnetic moment can be attributed to a paramagnetic impurity [probably iron(III)]. In contrast, the magnitude of the magnetic moment (4.4 BM) for **7** suggests a high spin configuration ($S = 3/2$). Further support for the difference in spin configuration between the iron complexes **8** and **6** can be seen by comparison of the Fe–N bond lengths. In **8** the average Fe–N distance is ca. 0.2 Å shorter than in **6**, an observation that is consistent with **8** being low spin and **6** high spin [18].

All the iron complexes **2**, **6** and **8** studied in the work have proved air sensitive. Notably for **6**, red crystals of the Fe(III) species [{(*fac*-DPA)FeCl$_2$}$_2$(μ-O)] (**9**) have been isolated on prolonged standing of an acetonitrile solution of **6** (Scheme 2). The molecular structure of **9** is shown in Fig. 6; selected bond distances and angles are listed in Table 6. The structure consists of a discrete dimeric unit with the two metal centres linked by an oxo group. The approximately octahedral geometry at each metal centre is completed by two chloride ligands and a facially bound DPA ligand. The coordination environments at each metal centre differ, however, with the bridging oxide *trans* to a pyridyl nitrogen [N(2)] at Fe(1) while at Fe(2), the bridging oxide is *trans* to the secondary amine nitrogen [N(6)]. The Fe–O–Fe angle [150.0(11)°] falls in the mid-range for related iron(III)–oxo dimeric complexes [26].

3. Conclusions

In summary, simple halide complexes of iron and cobalt containing TPA and DPA have been prepared and fully characterised. In all the cases the TPA ligands bind to metal centres in a tetradentate fashion and the DPA ligands in a tridentate facial fashion. Dissociation of chloride ligands to form chloride-salts is a feature for both TPA and DPA systems.

4. Experimental

4.1. General

All reactions were carried out under an atmosphere of dry, oxygen-free nitrogen, using standard Schlenk techniques or in a nitrogen purged glove box. Solvents were distilled under nitrogen from appropriate drying agents and degassed prior to use [27]. The infrared spectra were recorded as Nujol mulls between 0.5 mm NaCl plates on a Perkin–Elmer 1600 series. The FAB mass spectra were recorded using a Kratos Concept spectrometer with methanol or NBA as the matrix. ^{1}H NMR spectra were recorded on Bruker ARX spectrometers (250 or 300 MHz); chemical shifts (ppm) are referred to the residual protic solvent peaks and relaxation times (τ_1) are in seconds. Magnetic Susceptibility studies were performed using an Evans Balance (Johnson Matthey) at room temperature. The magnetic moment was calculated following standard methods [28] and corrections for underlying diamagnetism were applied to data [29,30]. Elemental analyses were performed at the Department of Chemistry, University of North London by Dr. S. Boyer.

The metal dichlorides were purchased from Aldrich Chemical Co. and used without further purification. The compounds DPA [31] and TPA [32] were prepared according to previously reported procedures. All other chemicals were obtained commercially and used without further purification.

4.2. Syntheses of [(TPA)CoCl$_2$] (**1**) and [(TPA)CoCl]Cl (**3**)

An oven-dried Schlenk flask equipped with a magnetic stir bar was evacuated and backfilled with nitrogen. The flask was charged with $CoCl_2$ (0.035 g, 0.27 mmol) and dissolved in *n*-butanol (10 cm^3) at 90 °C. TPA (0.079 g, 0.27 mmol) was introduced and the blue solution stirred at 90 °C for 1 h. On cooling to room temperature the reaction mixture was concentrated and hexane added to induce precipitation. The suspension was filtered, washed with hexane (2×30 cm^3) and dried under reduced pressure to give a mixture of [(TPA)CoCl$_2$] (**1**) and [(TPA)CoCl]Cl (**3**) as a blue powder. Recrystallisation from a hot acetonitrile solution gave dark green crystals of **1** and purple crystals of **3** suitable for single-crystal X-ray structure determination. **1**: Yield: 41% (0.046 g, 0.11 mmol). **3**: Yield: 34% (0.038 g, 0.09 mmol). Complex **1**: ^{1}H NMR (acetonitrile-d$_3$, 293 K): δ 131.0 (0.6 ms, H$_\alpha$), 106.1 (1.1 ms, NCH$_2$), 58.4 (17.9 ms, H$_\beta$), 46.2 (10.0 ms, H$_{\beta'}$), −2.0 (29.3 ms, H$_\gamma$). Complex **3**: ^{1}H NMR (acetonitrile-d$_3$, 293 K) δ 131.1 (0.6 ms, H$_\alpha$), 106.3 (1.1 ms, NCH$_2$), 58.4 (16.2 ms, H$_\beta$), 46.3 (9.5 ms, H$_{\beta'}$), −2.2 (22.7 ms, H$_\gamma$).

4.3. Synthesis of [(TPA)FeCl$_2$] · MeCN (**2** · MeCN)

Using the same procedure and molar ratios of reagents as in Section 4.2 using TPA (0.070 g, 0.24 mmol) and $FeCl_2$ (0.030 g, 0.24 mmol), gave [(TPA)FeCl$_2$] (**2**) as an orange powder. Recrystallisation from hot acetonitrile gave orange crystals of **2** · MeCN suitable for sin-

gle-crystal X-ray structure determination. Yield: 81% (0.091 g, 0.23 mmol).

4.4. Synthesis of [(TPA)CoCl]$_2$ [CoCl$_4$] (4)

Using the same procedure as in Section 4.2 using TPA (0.079 g, 0.27 mmol) and 1.5 equivalents of $CoCl_2$ (0.050 g, 0.41 mmol) gave [(TPA)CoCl]$_2$[CoCl$_4$] (**4**) as a blue solid. Recrystallisation from a hot acetontrile solution gave blue crystals of **4** suitable for single-crystal X-ray structure determination. Yield: 78% (0.075 g, 0.18 mmol).

4.5. Syntheses of [(DPA)CoCl(μ-Cl)]$_2$ (5) and [(DPA)$_2$Co]Cl$_2$ (7)

(a) An oven-dried Schlenk flask equipped with a magnetic stir bar was evacuated and backfilled with nitrogen. The flask was charged with $CoCl_2$ (0.100 g, 0.50 mmol) in *n*-butanol (10 cm^3) at 90 °C and a solution of DPA (0.094 g, 0.47 mmol) in *n*-butanol was introduced. After being stirred at 90 °C for 1 h, the reaction was allowed to cool to room temperature. The reaction mixture was concentrated and hexane was added to induce precipitation of [(DPA)CoCl(μ-Cl)]$_2$ (**5**) as a purple solid. Yield: 75% (0.125 g, 0.19 mmol). Compound **5**: IR/cm^{-1}, 3242w (N–H). All other spectroscopic data for **5** are as previously reported [10].

(b) Using an analogous procedure as above in (a) employing DPA (0.242 g, 1.56 mmol) and $CoCl_2$ (0.100 g, 0.78 mmol) gave [(DPA)CoCl]Cl**$_2$** (**7**) as a blue solid. Recrystallisation from hot acetonitrile solution gave golden crystals of **7** suitable for a single-crystal X-ray structure determination. Yield: 50% (0.205 g, 0.39 mmol).

4.6. Syntheses of [(DPA)FeCl(μ-Cl)]$_2$ (6) and [(DPA)$_2$Fe]Cl$_2$ (8)

(a) An oven-dried Schlenk flask equipped with a magnetic stir bar was evacuated and backfilled with nitrogen. The flask was charged with $FeCl_2$ (0.060 g, 0.47 mmol) in *n*-butanol (10 cm^3) at 90 °C and a solution of DPA (0.094 g, 0.47 mmol) in *n*-butanol was introduced to form a yellow solution. After being stirred at 90 °C for 1 h, the reaction was allowed to cool to room temperature. The reaction mixture was concentrated and hexane was added to induce precipitation of [(DPA)FeCl(μ-Cl)]$_2$ (**6**) as a yellow solid. The suspension was stirred overnight, filtered, washed with hexane (2×30 cm^3) and dried under reduced pressure. Recrystallisation by slow cooling of a hot acetonitrile solution or prolonged standing of a dichloromethane solution of the complex gave yellow crystals of **6** suitable for a single-crystal X-ray structure determination. Yield: 70% (0.120 g, 0.18 mmol). Complex **6**: ^{1}H NMR (acetonitrile-d$_3$, 293 K) δ 116.5 (0.4 ms, H_α), 107.0 (1.3 ms, N*H*), 70.8 (1.1 ms, CH_2), 54.7 (10.1 ms, H_β), 51.8 (9.1 ms, $H_{\beta'}$), 7.8 (H_γ). IR/cm^{-1}, 3238w (N–H).

(b) Using an analogous procedure as above in (a) employing DPA (0.187 g, 0.94 mmol) and $FeCl_2$ (0.060 g, 0.47 mmol) gave [(DPA)$_2$Fe]Cl$_2$ (**8**) as a red solid. The suspension was stirred overnight, filtered, washed with hexane (2×30 cm^3) and dried under reduced pressure. Recrystallisation by slow cooling of a hot acetonitrile solution gave red crystals of **8** suitable for a single-crystal X-ray structure determination. Yield: 91% (0.225 g, 0.43 mmol).

4.7. Synthesis of [{(fac-DPA)FeCl$_2$}$_2$(μ-O)] (9)

Prolonged standing of a solution of **6** (0.010 g, 0.016 mmol) in acetonitrile (1 cm^3) gave **9** as red crystals. Yield: 40% (0.004 g, 0.006 mmol).

4.8. Crystallography

Data for **1**, **2** · MeCN, **3**, **6** · $1\frac{2}{3}$CH$_2$Cl$_2$, **7** · 3MeCN, **8** · 3MeCN and **9** were collected on a Bruker APEX 2000 CCD diffractometer. Details of data collection, refinement and crystal data are listed in Table 7. The data were corrected for Lorentz and polarisation effects and empirical absorption corrections applied. Structure solution by Patterson methods and structure refinement on F^2 employed SHELXTL version 6.10 [33,34]. Hydrogen atoms were included in calculated positions (C–H = 0.96 Å) riding on the bonded atom with isotropic displacement parameters set to 1.5 U_{eq}(C) for methyl H atoms and 1.2 U_{eq}(C) for all other H atoms. All non-H atoms were refined with anisotropic displacement parameters. For **6** · $1\frac{2}{3}$CH$_2$Cl$_2$ there are 1.5 metal complex molecules in the asymmetric unit, one on a general position and the other on an inversion centre $(-x, -y, 1-z)$.

5. Supplementary data

Crystallographic data for the structural analyses have been deposited with the Cambridge Crystallographic Data Centre, CCDC Nos. 243697–243703. Copies of this information may be obtained free of charge from The Director, CCDC, 12 Union Road, Cambridge, CB2 1EZ (fax: +44 1223 336033; e-mail: deposit@ccdc.cam.ac.uk or at www: http://www.ccdc.cam.ac.uk).

Acknowledgements

We thank the EPSRC (to C.J.D.) and ExxonMobil (to C.J.D.) for financial assistance. Financial and

equipment support form the Department of Chemistry at the University of Leicester are also gratefully acknowledged.

References

[1] E.I. Solomon, T.C. Brunold, M.I. Davis, J.N. Kemsley, S.-K. Lee, N. Lehnert, F. Neese, A.J. Skulan, Y.S. Yang, J. Zhou, Chem. Rev. 1000 (2000) 235.
[2] K. Chen, M. Costas, L. Que Jr., J. Chem. Soc., Dalton Trans. (2002) 672.
[3] B.J. Wallar, J.D. Lipscomb, Chem. Rev. 96 (1996) 2625.
[4] P. Gutlich, Y. Garcia, H.A. Goodwin, Chem. Soc. Rev. 29 (2000) 419.
[5] P. Gutlich, A. Hauser, H. Spiering, Angew. Chem., Int. Ed. Engl. 33 (1994) 2024.
[6] A. Deiebold, K.S. Hagen, Inorg. Chem. 37 (1998) 215, and references therein.
[7] A.W. Addison, S. Burman, C.G. Wahlgren, O.A. Rajan, T.M. Rowe, E. Sinn, J. Chem. Soc., Dalton Trans. (1987) 2621.
[8] D. Mandon, A. Machkour, S. Goetz, R. Weller, Inorg. Chem. 41 (2002) 5364.
[9] Z. He, D.C. Craig, S.B. Colbran, J. Chem. Soc., Dalton Trans. (2002) 4224.
[10] T.M. Kooistra, K.F.W. Hekking, Q. Knijnenburg, B. de Bruin, P.H.M. Budzelaar, R. de Gelder, J.M.M. Smits, A.W. Gal, Eur. J. Inorg. Chem. (2003) 648.
[11] M. Ito, Y. Takita, K. Sakai, T. Tubomura, Chem. Lett. (1998) 1185.
[12] S.M. Nelson, J. Rodgers, J. Chem. Soc. (A) (1968) 272.
[13] E.S. Raper, A. Miller, T. Glowiak, M. Kubiak, Transition Met. Chem. 14 (1989) 319.
[14] D.A. Handley, P.B. Hitchcock, T.-H. Lee, G.J. Leigh, Inorg. Chim. Acta 314 (2001) 14.
[15] S. Kasselouri, A. Garoufis, S.P. Perlepes, F. Lutz, R. Bau, S. Gourbatsis, N. Hadjiliadis, Polyhedron 17 (1998) 1281.
[16] V.C. Gibson, R.K. O'Reilly, D.F. Wass, A.J.P. White, D.J. Williams, Dalton Trans. (2003) 2824.
[17] C.J. Davies, A. Harrison, G.A. Solan, unpublished results.
[18] A. Diebold, K.S. Hagen, Inorg. Chem. 37 (1998) 215.
[19] Y. Zang, J. Kim, Y. Dong, E.C. Wilkinson, E.H. Appelman, L. Que Jr., J. Am. Chem. Soc. 119 (1997) 4197.
[20] J. Glerup, P.A. Goodson, D.J. Hodgson, K. Michelsen, K.M. Nielsen, H. Weike, Inorg. Chem. 31 (1992) 4611.
[21] R.J. Butcher, A.W. Addison, Inorg. Chim. Acta 158 (1989) 211.
[22] M. Velusamy, M. Palaniandavar, K.R.J. Thomas, Polyhedron 17 (1998) 2179.
[23] (a) G.-S. Huang, J.-K. Lai, C.-H. Ueng, C.-C. Su, Transition Met. Chem. 25 (2000) 84;
(b) M. Palaniandavar, R.J. Butcher, A.W. Addison, Inorg. Chem. 35 (1996) 467.
[24] D.C. Bebout, S.W. Stokes, R.J. Butcher, Inorg. Chem. 38 (1999) 1126.
[25] D.C. Bebout, A.E. Delanoy, D.E. Ehmann, M.E. Kastner, D.A. Parrish, R.J. Butcher, Inorg. Chem. 37 (1998) 2952.
[26] D.M. Kurtz Jr., Chem. Rev. 90 (1990) 585.
[27] W.L.F. Armarego, D.D. Perrin, Purification of Laboratory Chemicals, 4th ed., Butterworth–Heinemann, London, 1996.
[28] F.E. Mabbs, D.J. Machin, Magnetism and Transition Metal Complexes, Chapman & Hall, London, 1973.
[29] C.J. O'Connor, Prog. Inorg. Chem. 29 (1982) 203.
[30] C.J. O'Connor, in: R.C. Weast (Ed.), Handbook of Chemistry and Physics, 70th ed., CRC Press, Boca Raton, FL, 1990, p. E134.
[31] H.J. Horn, P. de Joode, W.L. Driessen, J. Reedijk, Recueil des Travaux. Chim. Des. Pays-Bas. 115 (1996) 191.
[32] Z. Tyeklar, R.R. Jacobson, N. Wei, N.N. Murthy, J. Zubieta, K.D. Karlin, J. Am. Chem. Soc. 115 (1993) 2685.
[33] G.M. Sheldrick, SHELXS-97: Program for Crystal Structure Solution, University of Göttingen, Göttingen, Germany, 1993.
[34] G.M. Sheldrick, SHELXL-97: Program for Crystal Structure Refinement, University of Göttingen, Göttingen, Germany, 1993.

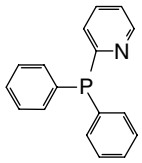

Fig. 1.

(M = Rh, Ir) dimers [10]. In a continuation of our previous work, we report in this communication the syntheses of neutral and chiral amine complexes of *p*-cymene ruthenium as well as hexamethylbenzene ruthenium complexes with the diphenyl(2-pyridyl)phosphine ligand.

2. Experimental

All the solvents were dried and distilled before use following the standard procedures. $RuCl_3 \cdot 3H_2O$ was purchased from Arora Matthey Ltd. and used as received. α-Phellandrene (Fluka), hexamethylbenzene (Acros Organics), benzylamine (Merck), diphenyl(2-pyridyl)phosphine (Aldrich) and 1,1-diphenyl-2-propyn-1-ol (Aldrich) were used as received. The precursor complexes [{(η^6-arene)Ru(μ-Cl)Cl}$_2$] [arene = *p*-cymene (**1**), hexamethylbenzene (**7**)] and [(η^6-*p*-cymene)Ru(PPh_3)Cl_2] (**3**) were prepared according to the literature procedures [11,12]. Elemental analyses were performed in a Perkin–Elmer 2400 CHN/O analyzer. Infrared spectra were recorded on a Perkin–Elmer Model 983 spectrophotometer with samples prepared as KBr and CsI pellets. Electronic spectra were recorded on a Hitachi-300 spectrophotometer. NMR spectra were taken on Bruker AMX-400 (400 MHz) and Bruker ACF-300 (300 MHz) spectrometers with tetramethylsilane as an internal standard. ^{31}P {^1H} NMR chemical shifts are reported relative to H_3PO_4 (85%).

2.1. Preparation of [(η^6-*p*-cymene)Ru($NH_2CH_2C_6H_5$)Cl_2] (**2**)

A mixture of [{(η^6-*p*-cymene)Ru(μ-Cl)Cl}$_2$] (**1**) (0.1 g, 0.163 mmol) and benzylamine (0.44 g, 0.408 mmol) in dichloromethane (20 ml) was stirred at room temperature for 3 h. The orange solution was concentrated under reduced pressure. The residue was extracted with dichloromethane and filtered through a short silica gel column. The resulting solution was reduced in volume to about 2 ml and hexane (20 ml) was added to give an orange-yellow compound, which was recrystallized from the mixture of dichloromethane and hexane to give orange crystals.

Yield: 89.62% (0.12 g). Elemental *Anal*. Calc. (%) for $C_{17}H_{23}RuNCl_2$: C, 49.39; H, 5.61; N, 3.38. Found: C, 49.41; H, 5.94; N, 3.34%.

^1H NMR ($CDCl_3$, δ): 1.30 (d, 6H, J_{H-H} = 6.96 Hz, CH_3), 2.23 (s, 3H, CH_3), 2.98 (sep, 1H), 3.17 (b, 2H, NH_2), 4.14 (t, 2H, J_{H-H} = 7.64 Hz, CH_2), 5.22 (d, 2H, J_{H-H} = 5.88 Hz, cymene), 5.39 (d, 2H, J_{H-H} = 5.88 Hz, cymene), 7.31–7.38 (m, 5H, Ph).

IR (KBr pellets, cm^{-1}): *v*(N–H) 3287 (s), 3221 (s). IR (CsI pellets, cm^{-1}): *v*(Ru–Cl) 286 (s).

UV–vis (CH_2Cl_2): λ_{max} = 393 nm.

2.2. Preparation of chiral complexes

2.2.1. Preparation of [(η^6-*p*-cymene)Ru(PPh_3)($NH_2CH_2C_6H_5$)Cl]PF_6 (**4a**)

A mixture of [(η^6-*p*-cymene)Ru(PPh_3)Cl_2] (**3**) (0.1 g, 0.175 mmol), benzylamine (0.028 g, 0.263 mmol) and NH_4PF_6 (0.043 g, 0.263 mmol) in dichloromethane and methanol (2:1) (15 ml) mixture was stirred at room temperature for 2 h. The orange-yellow solution was concentrated to dryness. The residue was dissolved in dichloro-methane and filtered to remove NH_4Cl. The filtrate was concentrated to 2 ml, and addition of excess hexane gave an orange-yellow complex. The complex was filtered and washed with diethylether and dried under vacuum.

Yield: 71.01% (0.098 g). Elemental *Anal*. Calc. (%) for $C_{35}H_{38}RuNClP_2F_6$: C, 53.54; H, 4.87; N, 1.78. Found: C, 53.51; H, 4.66; N, 1.82%.

^1H NMR ($CDCl_3$, δ): 1.19 (d, 3H, J_{H-H} = 6.36 Hz, CH_3), 1.34 (d, 3H, J_{H-H} = 6.76 Hz, CH_3), 2.17 (s, 3H, CH_3), 2.72 (b, 2H, NH_2), 2.98 (sep, 1H, CH), 4.08 (t, 2H, J_{H-H} = 10.4 Hz, CH_2), 5.29 (d, 2H, J_{H-H} = 5.64 Hz, cymene), 5.42 (d, 2H, J_{H-H} = 5.64 Hz, cymene), 7.54–7.17 (m, 20H, Ph).

^{31}P {^1H} NMR ($CDCl_3$, δ): 36.05 (s).

IR (KBr pellets, cm^{-1}): *v*(N–H) 3287 (s), 3224 (s), *v*(P–F) 839 (s). IR (CsI pellets, cm^{-1}): *v*(Ru–Cl) 276 (s).

2.2.2. Preparation of [(η^6-*p*-cymene)Ru(PPh_3)($NH_2C_6H_4$-*p*-Cl)Cl]BF_4 (**4b**)

A mixture of [(η^6-*p*-cymene)Ru(PPh_3)Cl_2] (**3**) (0.1 g, 0.175 mmol), *p*-chloroaniline (0.044 g, 0.35 mmol) and NH_4BF_4 (0.037 g, 0.35 mmol) in methanol was refluxed for 2 h. The solvent was removed under reduced pressure. The residue was dissolved in CH_2Cl_2 and then filtered. The solution was concentrated to 2 ml and an excess of hexane was added for precipitation. The orange compound was washed with diethylether and dried under vacuum.

Yield: 70.23% (0.092 g). Elemental *Anal*. Calc. (%) for $C_{34}H_{35}RuNCl_2PBF_4$: C, 54.64; H, 4.72; N, 1.87. Found: C, 54.61; H, 4.68; N, 1.84%.

^1H NMR ($CDCl_3$, δ): 1.10 (d, 3H, J_{H-H} = 6.92 Hz, CH_3), 1.25 (d, 3H, J_{H-H} = 6.92 Hz, CH_3), 2.16 (s, 3H, CH_3), 2.87 (sep, 1H, CH), 4.90 (s, 2H, NH_2), 4.98 (d, 2H, J_{H-H} = 5.84 Hz, cymene), 5.03 (d, 2H, J_{H-H} = 5.4 Hz), 5.08 (d, 2H, J_{H-H} = 5.84 Hz, cymene), 5.23 (d, 2H, J_{H-H} = 6.08 Hz), 7.31–7.88 (m, 15H, Ph).

^{31}P {^1H} NMR ($CDCl_3$, δ): 21.25 (s).

IR (KBr pellets, cm^{-1}): ν(N–H) 3429 (s), 3239 (s), ν(B–F) 1096 (s). IR (CsI pellets, cm^{-1}): ν(Ru–Cl) 273 (s).

2.2.3. Preparation of [(η^6-p-cymene)Ru(PPh_3)(NH_2-C_6H_4-p-NO_2)Cl]BF_4 (**4c**)

A mixture of [(η^6-*p*-cymene)Ru(PPh_3)Cl_2] (**3**) (0.1 g, 0.175 mmol), *p*-nitroaniline (0.048 g, 0.35 mmol) and NH_4BF_4 (0.037 g, 0.35 mmol) in methanol was stirred at room temperature for 14 h. A yellow colored product separated out. The complex was washed with diethylether and dried under vacuum.

Yield: 71.42% (0.095 g). Elemental *Anal*. Calc. (%) for $C_{34}H_{35}RuN_2O_2ClPBF_4$: C, 53.88; H, 4.65; N, 3.69. Found: C, 53.82; H, 4.56; N, 3.71%.

^{1}H NMR ($CDCl_3$, δ): 1.12 (d, 3H, J_{H-H} = 7.56 Hz, CH_3), 1.31 (d, 3H, J_{H-H} = 6.92 Hz, CH_3), 2.19 (s, 3H, CH_3), 2.95 (sep, 1H, CH), 4.40 (s, 2H, NH_2), 5.37 (d, 2H, J_{H-H} = 5.96 Hz), 5.50 (d, 2H, J_{H-H} = 5.88 Hz, cymene), 6.69 (d, 2H, J_{H-H} = 5.86 Hz, cymene), 7.68–7.34 (m, 15H, Ph), 8.10 (d, 2H, J_{H-H} = 8.96 Hz).

^{31}P {^{1}H} NMR ($CDCl_3$, δ): 26.54 (s).

IR (KBr pellets, cm^{-1}): ν(N–H) 3317 (s), 3246 (s), $\nu(NO_2)$ 1520 (s), 1341 (s), ν(B–F) 1096 (s). IR (CsI pellets, cm^{-1}): ν(Ru–Cl) 283 (s).

2.3. Preparation of [(η^6-p-cymene)Ru(PDA)Cl]BF_4 (**5**) (PDA = 1,2-phenylenediamine)

A suspension of the complex [{(η^6-*p*-cymene)Ru(μ-Cl)Cl}$_2$] (**1**) (0.1 g, 0.163 mmol) in methanol (20 ml) was treated with 1,2-phenylenediamine (0.035 g, 0.326 mmol) and NH_4BF_4 (0.05 g, 0.489 mmol) and allowed to stir at room temperature for 10 h. The solvent was removed under reduced pressure. The orange mass was dissolved in dichloromethane and filtered. The filtrate was concentrated to 2 ml and an excess of hexane added for precipitation. The orange-colored product was washed with diethylether and dried under vacuum.

Yield: 58.55% (0.089 g). Elemental *Anal*. Calc. (%) for $C_{16}H_{22}RuN_2ClBF_4$: C, 41.26; H, 4.76; N, 6.01. Found: C, 41.42; H, 4.93; N, 5.96%.

^{1}H NMR ($CDCl_3$, δ): 0.86 (d, 3H, J_{H-H} = 2.45 Hz, CH_3, cymene), 1.15 (d, 3H, J_{H-H} = 2.91 Hz, CH_3, cymene), 2.26 (s, 2H, CH_3, cymene), 3.00 (sep, 1H), 5.00 (d, 4H, J_{H-H} = 12.23 Hz, NH_2), 5.70 (d, 2H, J_{H-H} = 5.76 Hz, cymene), 5.93 (d, 2H, J_{H-H} = 5.76 Hz, cymene), 7.16 (dd, 2H, 2.27 Hz), 8.37 (d, 2H, 8.58 Hz).

IR (KBr pellets, cm^{-1}): ν(N–H) 3346 (s), 3232 (s), ν(B–F) 1082 (s).

2.4. Preparation of [(η^6-p-cymene)Ru(PPh_3)(PDA)](BF_4)$_2$ (**6**)

This complex was prepared by following the above-mentioned procedure (**5**), except that the complex [(η^6-*p*-cymene)Ru(PPh_3)Cl_2] (**3**) was used in place of complex [{(η^6-*p*-cymene)Ru(μ-Cl)Cl}$_2$] (**1**). The complex was isolated as an orange-red micro-crystalline solid.

Yield: 70.8% (0.097 g). Elemental *Anal*. Calc. (%) for $C_{34}H_{37}RuN_2PB_2F_8$: C, 52.40; H, 4.78; N, 3.59. Found: C, 52.06; H, 4.82; N, 3.37%.

^{1}H NMR ($CDCl_3$, δ): 0.93 (d, 3H, J_{H-H} = 6.69 Hz, CH_3), 1.11 (d, 3H, J_{H-H} = 6.67 Hz, CH_3), 2.20 (s, 3H, CH_3), 2.87 (sep, 1H), 4.61 (d, 4H, J_{H-H} = 10.74 Hz, NH_2), 5.63 (d, 2H, J_{H-H} = 5.85 Hz, cymene), 5.86 (d, 2H, J_{H-H} = 5.85 Hz, cymene), 6.92 (d, 2H, J_{H-H} = 6.46 Hz), 7.16–7.76 (m, 17H, Ph).

IR (KBr pellets, cm^{-1}): ν(N–H) 3326(s), 3192(s), ν(B–F) 1089(s).

2.5. Preparation of [(η^6-C_6Me_6)Ru(PPh_2Py)Cl_2] (**8**)

A mixture of [{(η^6-C_6Me_6)Ru(μ-Cl)Cl}$_2$] (**7**) (0.1 g, 0.149 mmol) and diphenyl(2-pyridyl)phosphine (PPh_2Py) (0.098 g, 0.374 mmol) in dichloromethane (20 ml) was stirred at room temperature for 1 h. The orange solution was concentrated to 3 ml and an excess of hexane was added for precipitation. The orange microcrystalline product was washed with diethylether and dried under vacuum.

Yield: 79.21% (0.141 g). Elemental *Anal*. Calc. (%) for $C_{29}H_{32}RuNCl_2P$: C, 58.29; H, 5.39; N, 2.34. Found: C, 58.32; H, 5.36; N, 2.39%.

^{1}H NMR ($CDCl_3$, δ): 1.76 (s, 18H, HMB), 7.13–8.11 (m, 13H), 8.57 (d, 1H, J_{H-H} = 6.24 Hz).

^{31}P {^{1}H} NMR ($CDCl_3$, δ): 25.88 (s). IR (CsI pellets, cm^{-1}): ν(Ru–Cl) 286 (s).

2.6. Preparation of [(η^6-C_6Me_6)Ru(PPh_2Py)Cl]BF_4 (**9**)

Method 1: A mixture of [{(η^6-C_6Me_6)Ru(μ-Cl)Cl}$_2$] (**7**) (0.1 g, 0.149 mmol), diphenyl(2-pyridyl)phosphine (PPh_2Py) (0.196 g, 0.748 mmol) and NH_4BF_4 (0.078 g, 0.748 mmol) in methanol were stirred at room temperature for 2 h. The yellow solution was concentrated under reduced pressure. The yellow residue was dissolved in dichloro-methane and filtered. The filtrate was concentrated to 2 ml and an excess of hexane was added for precipitation. The yellow-colored product was washed with diethylether and dried under vacuum.

Yield: 82.47% (0.16 g). Elemental *Anal*. Calc. (%) for $C_{29}H_{32}RuNClPBF_4$: C, 53.68; H, 4.97; N, 2.15. Found: C, 53.61; H, 5.01; N, 2.03%.

^{1}H NMR ($CDCl_3$, δ): 2.08 (s, 18H, HMB), 7.09–7.79 (m, 11H), 7.89 (t, 1H, J_{H-H} = 4.36 Hz), 8.01 (t, 1H, J_{H-H} = 4.42 Hz), 8.67 (d, 1H, J_{H-H} = 5.12 Hz).

^{31}P {^{1}H} NMR ($CDCl_3$, δ): −11.25 (s).

IR (KBr pellets, cm^{-1}): ν(B–F) 1089 (s). IR (CsI pellets, cm^{-1}): ν(Ru–Cl) 280 (s).

Method 2: A mixture of the complex [(η^6-C_6Me_6)Ru(PPh_2Py)Cl_2] (**8**) (0.1 g, 0.167 mmol) and NH_4BF_4 (0.052 g, 0.501 mmol) in methanol (15 ml) was stirred at room temperature for 4 h. The clear orange yellow

solution was then rotary evaporated. The residue was extracted with dichloromethane and filtered to remove insoluble material. The filtrate was then reduced to about 2 ml and addition of excess hexane gave a yellow solid.

Yield: 80.41% (0.156 g).

2.7. Preparation of $[(\eta^6\text{-}C_6Me_6)Ru(PPh_2Py)(NCCH_3)](BF_4)_2$ (**10**)

A mixture of complex **9** (0.06 g, 0.092 mmol) and NH_4BF_4 (0.019 g, 0.184 mmol) was refluxed in acetonitrile (15 ml) under a nitrogen atmosphere for 2 h, and the yellow solution turned light yellow in color. The solvent was rotary evaporated. The yellow solid was dissolved in CH_2Cl_2 and filtered. The filtrate was concentrated to 2 ml and an excess of hexane was added for precipitation. The light yellow product was washed with diethylether and dried under vacuum.

Yield: 78.07% (0.089 g). Elemental *Anal*. Calc. (%) for $C_{31}H_{35}RuN_2PB_2F_8$: C, 50.23; H, 4.75; N, 3.78. Found: C, 50.46; H, 4.57; N, 3.92%.

^{1}H NMR ($CDCl_3$, δ): 2.06 (s, 18H, HMB), 2.18 (s, 3H, CH_3), 7.69–8.01 (m, 13H, Ph), 8.76 (d, 1H).

^{31}P $\{^1H\}$ NMR ($CDCl_3$, δ): −13.57 (s).

IR (KBr pellets, cm^{-1}): ν(B–F) 1082 (s).

2.8. Preparation of $[(\eta^6\text{-}C_6Me_6)Ru(PPh_2Py)\{=C=C=C(Ph)_2\}](BF_4)_2$ (**11**)

A mixture of complex **9** (0.06 g, 0.092 mmol), 1,1-diphenyl-2-propyn-1-ol (0.048 g, 0.23 mmol) and NH_4BF_4 (0.029, 0.27 mmol) was refluxed in methanol (15 ml) under a nitrogen atmosphere for 3 h, the yellow suspension gradually turning brown in color. The solvent was removed under reduced pressure. The brown solid was dissolved in CH_2Cl_2 and filtered. The filtrate was concentrated to 2 ml and an excess of hexane was added for precipitation. The brown colored product was washed with diethylether and dried under vacuum.

Yield: 76.83% (0.063 g). Elemental *Anal*. Calc. (%) for $C_{44}H_{42}RuNPB_2F_8$: C, 59.35; H, 4.75; N, 1.57. Found: C, 59.43; H, 4.69; N, 1.59%.

^{1}H NMR ($CDCl_3$, δ): 1.83 (s, 18H, HMB), 7.15–7.71 (m, 14H), 8.05–8.08 (m, 6H), 8.29–8.31 (m, 3H), 8.95 (d, 1H, J_{H-H} = 5.97 Hz).

^{31}P $\{^1H\}$ NMR ($CDCl_3$, δ): −15.32 (s).

IR (KBr pellets, cm^{-1}): ν(C=C=C) 1964(s), ν(B–F) 1082(s).

3. Crystallographic investigations

X-ray quality crystals of complex **2** were grown by slow diffusion of hexane into a dichloromethane solution of the complex, while those of complex **8** were grown by slow diffusion of diethyl ether into a dichloromethane solution. Crystals of complex **9** were grown by slow diffusion of hexane into an acetone solution. The orange crystals of complexes **2** and **8** and the yellow crystals of complex **9** were mounted on a Bruker Apex CCD diffractometer in a full reciprocal sphere equipped with a CCD detector, and were used for data collection.

Table 1
Crystal data and structure refinement details for complexes **2**, **8** and **9** acetone

Formula	$C_{17}H_{23}Cl_2NRu$	$C_{29}H_{32}Cl_2NPRu$	$C_{32}H_{38}BClF_4NOPRu$
M_r	413.33	597.5	706.93
T (K)	293 (2)	293 (2)	293 (2)
Wavelength (Å)	0.71073	0.71073	0.71073
Crystal system	monoclinic	monoclinic	monoclinic
Space group	$P2_1/c$	$C2/c$	$P2_1$
a (Å)	11.8414(7)	15.6052(19)	13.0710(11)
b (Å)	10.0786(6)	8.7978(11)	8.1669(7)
c (Å)	15.1580(8)	37.107(5)	15.2210(12)
β (°)	102.817 (1)	90.476 (2)	94.782 (1)
V (Å^3)	1763.95(17)	5094.4(11)	1619.2(2)
Z	4	8	2
Crystal size (mm)	0.5 × 0.3 × 0.2	0.3 × 0.2 × 0.2	0.3 × 0.2 × 0.2
D_{calc} (g cm^{-3})	1.556	1.558	1.450
F(000)	840	2448	724
θ (°)	1.76–28.27	1.10–24.85	1.34–28.30
Reflections collected	14969	14468	14227
Independent reflections (R_{int})	4103 (0.0174)	4104 (0.0497)	7272 (0.0283)
Completeness to θ	28.27° – 93.8%	24.85° – 92.7%	28.30° – 95.0%
μ (Mo Kα) (mm)	1.185	0.908	0.665
Data/parameters	4103/0/173	4104/0/253	7272/1/327
Goodness-of-fit on F^2	1.033	1.257	1.077
R_1 [$I > 2\sigma(I)$], wR_2	0.0274, 0.0692	0.0661, 0.1498	0.0515, 0.1232
R_1, wR_2 (all data)	0.0299, 0.0705	0.0809, 0.1625	0.0594, 0.1278
Largest difference peak and hole (e Å^{-3})	0.856 and −0.695	1.152 and −0.795	1.249 and −0.451

X-ray intensity data were collected with graphite monochromated Mo Kα radiation at 293(2) K, with the 0.3°ω scan mode and 10 s per frame. The intensity data were corrected for Lorentz and polarization effects. Absorption correction was done using the SAINT program [13]. A summary of the crystal data, data collection parameters and convergence results is compiled in Table 1. An empirical absorption correction was made by modeling a transmission surface by spherical harmonics employing equivalent reflections with $I > 3\sigma(I)$ (program SADABS) [14]. The structure was solved by direct methods [15]. All the non-hydrogen atoms were refined anisotropically using the full-matrix least-squares technique on F^2 using the SHELXL-97 software [16]. All the hydrogen atoms were found from difference Fourier synthesis after four cycles of an isotropic refinement and as per the ''riding'' model. Figs. 2–4 display the ORTEP [17] representations of the molecules with 50% probability thermal ellipsoids. Refinement converged at final R_1 values of 0.0274, 0.0661 and 0.0515 (for observed data F) for complexes **2**, **8** and **9**, respectively.

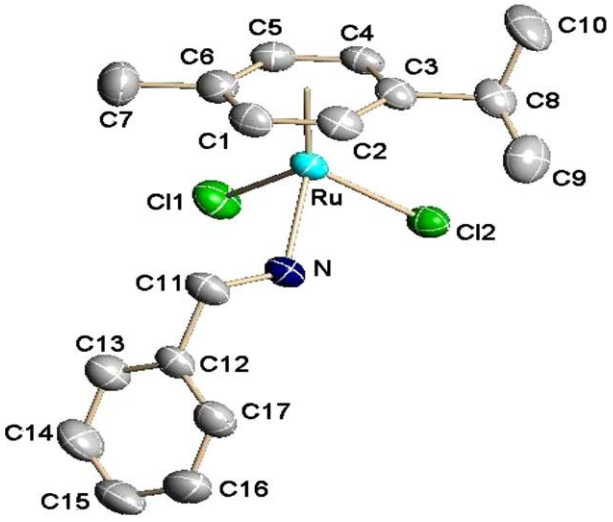

Selected bond lengths (Å) and bond angles (°)	
Bond lengths (Å)	
Ru–N	2.1445(18)
Ru–Cl(1)	2.4282(6)
Ru–Cl(2)	2.2497
N–C(11)	1.484(3)
Ru–C*	1.670
Bond angles (°)	
N–Ru–Cl(2)	80.65(5)
N–Ru–Cl(1)	80.97(6)
Cl(1)–Ru–Cl(2)	87.66(2)

*Ruthenium to centroid of *p*-cymene.

Fig. 2. ORTEP diagram of complex **2** with 50% probability thermal ellipsoids. Hydrogens are omitted for clarity.

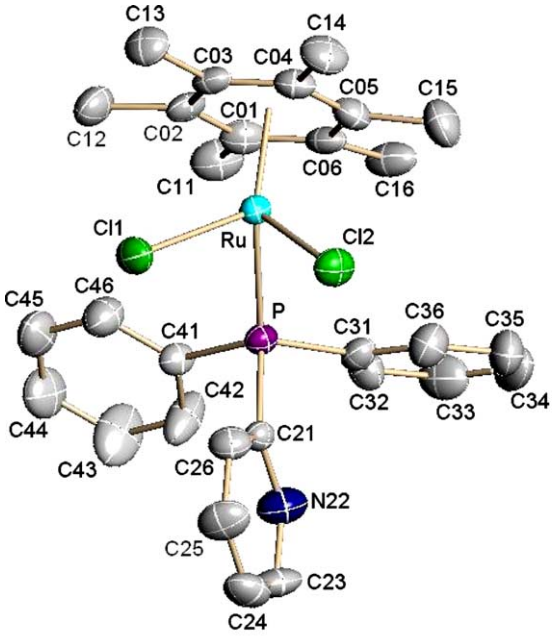

Selected bond lengths (Å) and bond angles (°)	
Bond lengths (Å)	
Ru–Cl(1)	2.417(2)
Ru–Cl(2)	2.422(2)
Ru–P	2.3573(19)
P–C(31)	1.825(3)
P–C(41)	1.834(3)
P–C(21)	1.845(3)
C(21)–N(22)	1.3900
Ru–C*	1.740
Bond angles (°)	
Cl(1)–Ru–Cl(2)	86.41(8)
P–Ru–Cl(1)	88.51(7)
P–Ru–Cl(2)	88.2(7)

*Ruthenium to centroid of HMB.

Fig. 3. ORTEP diagram of complex **8** with 50% probability thermal ellipsoids. Hydrogens are omitted for clarity of the figure.

4. Results and discussion

4.1. Amine complexes

The dinuclear complex $[\{(\eta^6\text{-}p\text{-cymene})Ru(\mu\text{-}Cl)Cl\}_2]$ (**1**) undergoes a bridge cleavage reaction with benzylamine to yield neutral complex **2** (Scheme 1). The complex $[(\eta^6\text{-}p\text{-cymene})Ru(PPh_3)Cl_2]$ (**3**) reacts with amines resulting in the formation of chiral complexes (Scheme 2). Complexes **1** and **3** also react with 1,2-phenylenediamine (PDA) giving the cationic complexes $[(\eta^6\text{-}p\text{-cymene})Ru(PDA)Cl]^+$ (**5**) and $[(\eta^6\text{-}p\text{-cymene})Ru(PPh_3)(PDA)]^{2+}$ (**6**) (Scheme 1, reaction (1)). These complexes are stable in air and are soluble in polar solvents such as dichloromethane and acetone, but insoluble in non-polar solvents such as pentane and hexane. The infrared spectra of these complexes show strong bands in the range 3221–3429 cm^{-1} for the ν_{N-H} mode of the amine group [5b] and a strong band in the range 273–286

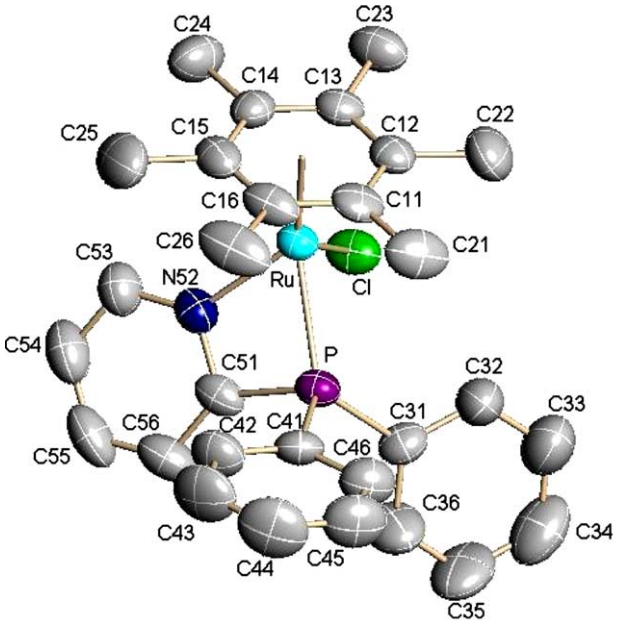

Selected bond lengths (Å) and bond angles (°)	
Bond lengths (Å)	
Ru–Cl	2.3981(14)
Ru–P	2.3412(13)
Ru–N(52)	2.107(2)
P–C(31)	1.818(2)
P–C(41)	1.828(2)
P–C(51)	1.792(2)
N(52)–C(53)	1.3900
Ru–C*	1.705
Bond angles (°)	
P–Ru–Cl	86.97(5)
N(52)–Ru–Cl	82.95(7)
N(52)–Ru–P	67.72(6)

*Ruthenium to centroid of HMB.

Fig. 4. ORTEP diagram of complex **9** with 50% probability thermal ellipsoids. Hydrogens are omitted for clarity.

cm^{-1} for the ν_{Ru-Cl} mode [5b]. All these complexes (**4–6**) exhibit a strong band at 1089 cm^{-1} due to the ν_{B-F} mode of the BF_4 group.

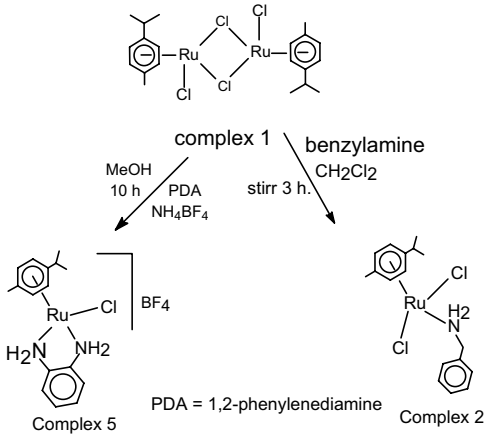

Scheme 1.

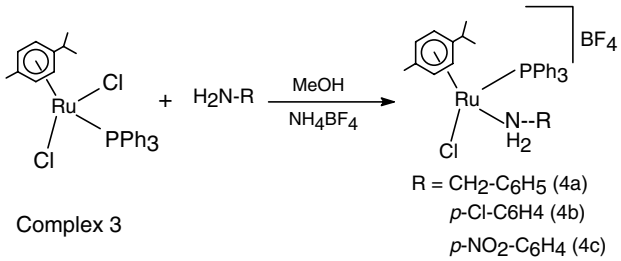

Scheme 2.

The ^{1}H NMR spectrum of complex **2** exhibits a doublet at 1.30 ppm (J = 6.96 Hz) while a septet at 2.98 ppm is observed for the isopropyl group protons. The two doublets observed at 5–6 ppm correspond to the aromatic *p*-cymene ring CH protons. The phenyl group of the benzylamine ligand gives multiplets in the range 7.31–7.40 ppm. The ^{1}H NMR spectra of the mononuclear complexes **4** exhibit two doublets for the methyl protons of the isopropyl group. This is due to the diastereotopic nature of these complexes (**4a–c**) (Scheme 2) since the ruthenium metal is a chiral center. The complexes **5** and **6** also exhibit two doublets for the methyl groups of the *p*-cymene ligand due to the steric nature of the bulky 1,2-phenylenediamine ligand.

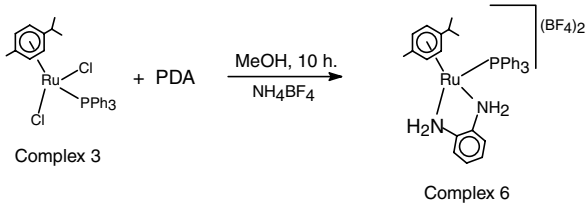

(1)

The ^{1}H NMR spectrum of complex **5** exhibits two doublets at 7.16 and 8.23 ppm for the ring protons of 1,2-phenylenediamine. In the case of complex **6**, the signals for these protons merge with those for the phenyl group protons of the triphenylphosphine ligand, thereby exhibiting multiplets in the range 6.93–7.76 ppm. Both

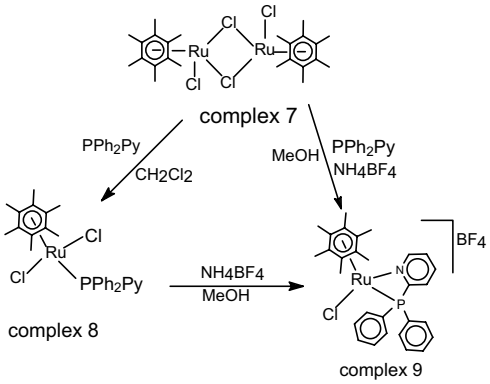

Scheme 3.

the complexes show broad peaks around 4.5–5.0 ppm due to the coordinated NH_2 group. The structure of complex **2** is shown in Fig. 2.

The electronic spectrum of complex **2** in dichloromethane features a UV–vis pattern similar to the analogous ruthenium polypyridyl complexes [18], which arises from the metal-to-ligand charge transfer at 393 nm.

4.2. Complexes of diphenyl-2-pyridylphosphine (*8–11*)

The reaction of $[\{(\eta^6\text{-}C_6Me_6)Ru(\mu\text{-}Cl)Cl\}_2]$ (**7**) with diphenyl(2-pyridyl)phosphine in dichloromethane yields the neutral P-coordinated complex **8**. However, in methanol, the P,N-chelated cationic complex $[(\eta^6\text{-}C_6Me_6)Ru(PPh_2Py)Cl]^+$ (**9**) is isolated as the tetrafluoroborate salt **9**$[BF_4]$. Complex **8** with an excess of NH_4BF_4 in methanol gives the complex **9**$[BF_4]$ (Scheme 3). These complexes are stable in air and soluble in polar solvents such as chloroform and dichloromethane, but are insoluble in non-polar solvents such as hexane and pentane.

The spectroscopic data clearly suggests the coordination of the ligand to the metal as evident from the shift of the phosphorus and proton resonance compared to the starting complex **7**. The ^1H NMR spectrum of complex **8** shows a singlet at 1.76 ppm for the hexamethylbenzene protons (an upfield shift compared to the starting compound) and also in the aromatic region at 7.13–8.11 ppm for the phosphine ligand. The ^{31}P NMR shows one singlet at 25.88 ppm for the phosphine ligand, where a significant downfield shift is observed after coordination to the metal as compared to the free ligand (−3.43 ppm). The far IR spectrum shows a strong band at 286 cm^{-1} for the Ru–Cl stretching vibration mode.

The ^1H NMR spectrum of complex **9** shows a pattern of signals different from the spectrum of complex **8**. The pyridine ring protons appear as two triplets at 7.89 and 8.01 ppm and one doublet at 8.67 ppm. The phenyl group protons appear as a multiplet in the aromatic region at 7.09–7.79 ppm. The singlet at 2.08 ppm for the hexamethyl-benzene protons indicates a downfield shift compared to complex **8**. The ^{31}P $\{^1H\}$ NMR spectrum of complex **9** exhibits a singlet at −11.25 ppm (upfield compared to complex **8**). The far IR spectrum shows a band at 280 cm^{-1}, which is assigned to the terminal stretching vibration of ν_{Ru-Cl}. In addition, the IR spectrum contains a strong band at 1089 cm^{-1} due to the ν_{B-F} mode of the BF_4 group. However, we do not observe formation of a pyridylphosphine-coordinated complex of the type $[Ru(PPh_2Py)_2Cl_2]$ in these reactions, as was the case for the *p*-cymene ruthenium dimer [19].

Treatment of the complex $[(\eta^6\text{-}C_6Me_6)Ru(PPh_2Py)Cl]BF_4$ (**9**) with acetonitrile and 1,1-diphenyl-2-propyn-1-ol ligands generated the cationic complexes **10** and **11** (reactions (2) and (3)), which can be isolated in good yield as their BF_4 salts. Formation of the allenylidene complex **11** is confirmed by the appearance of the ν(C═C═C) absorption mode (asymmetric stretching vibration) as a strong band at 1964 cm^{-1} [20]. The ^1H NMR spectrum of complex **10** shows a singlet for the acetonitrile methyl protons at 2.18 ppm. The phenyl protons appear in the aromatic region in the range of 7.15–8.95 ppm for both complexes. HMB protons are observed at 2.06 ppm for complex **10** and at 1.83 ppm for complex **11**. The ^{31}P $\{^1H\}$ NMR spectrum of complexes exhibits a sharp peak at 13.57 ppm for complex **10** and at 15.32 ppm for complex **11**.

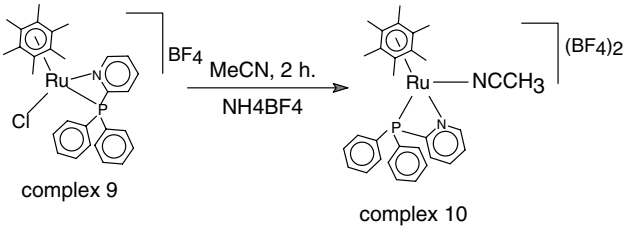

complex 9 complex 10

(2)

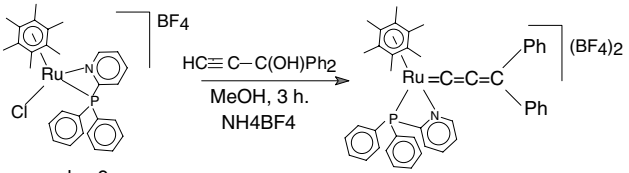

complex 9 complex 11

(3)

5. Molecular structures

In order to confirm the structures suggested by the spectroscopic data, molecular structures of complexes **2**, **8** and **9** were determined using single-crystal X-ray diffraction studies. The summary of the single-crystal X-ray structure analyses is shown in Table 1. ORTEP drawings of the complexes **2**, **8** and **9** are shown in Figs. 2–4, respectively.

The structure of complex **2** consists of a ruthenium atom η^6-coordinated to a *p*-cymene molecule, two chlorine atoms and one benzylamine ligand (through the N atom) leading to the usual 'three-legged piano stool' structure. The complex $[(\eta^6\text{-}p\text{-cymene})Ru(NH_2CH_2C_6H_5)Cl_2]$ (**2**) crystallizes in the monoclinic space group $P2_1/c$ (Fig. 2). The average Ru–C bond distance is 2.1726 Å, whereas the distance between the ruthenium atom and the centroid of the ring is 1.670 Å at the axis $x = 0.3938$, $y = 0.3638$ and $z = 0.1334$. These bond lengths are closely related to those in other reported complexes [21]. The Ru–N bond length involving benzylamine is 2.1445(18) Å, which is within the usual range of Ru–N bond distances [22]. The Ru–Cl bond lengths are 2.4282(6) and 2.4297(6) Å, well in accord with the

literature values [23]. The geometry of the complex is octahedral with a piano-stool structure and is marked by the nearly 90° value for the bond angles between the non-*p*-cymene ligands at the metal centre, viz., Cl(1)–Ru–Cl(2) (87.66(2)°), N–Ru–Cl(1) (80.97(6)°) and N–Ru–Cl(2) (80.65(5)°).

Complex **8** crystallizes in the monoclinic space group *C*2/*c*. The geometry around the ruthenium atom in complex **8** is octahedral where the hexamethylbenzene occupies three-coordination positions. Complex **8** also has a 'three-legged piano stool' type structure. Fig. 3 shows an ORTEP representation of complex **8**. The Ru–Cl(1) and Ru–Cl(2) bond distances (2.417(2) and 2.422(2) Å) are closely related to other reported values (2.4299 Å) [24]. The Ru–P bond distance 2.3573(19) Å is within the range of the literature values [24a]. The average bond distance between ruthenium and hexamethylbenzene is 2.227 Å, and the distance between ruthenium and the centroid of the ring is 1.740 Å. The bond angles P–Ru–Cl(1), P–Ru–Cl(2) and Cl(1)–Ru–Cl(2) are 88.51(7)°, 88.20(7)° and 86.41(8)°, respectively, indicating a piano stool type structure.

Complex **9** crystallizes with one molecule of acetone; the complex cation and the BF_4^- anion are joined by coulombic forces. Complex **9** contain a ruthenium atom η^6-coordinated to a hexamethylbenzene ring and bonded to a chlorine atom and a bidentate PPh_2Py ligand through the P and N atoms. Fig. 4 is an ORTEP representation of complex **9**. Complex **9** crystallizes in the monoclinic space group $P2_1$. The Ru–P bond distance 2.3412(13) Å is shorter than in complex **8**. This is because the diphenyl(2-pyridyl)phosphine ligand restricts the bite angle of the four-membered chelating ring using both the P and N atoms. The Ru–Cl and Ru–N(52) bond distances 2.3981(14) and 2.107(2) Å fall within the range of reported values [25]. The bond angles around the ruthenium are P–Ru–Cl 86.97(5)° and N(52)–Ru–Cl 82.95(7)°. The rigid bond distance between the nitrogen and phosphorus atoms (P∩N) of pyridylphosphine is approximately 3.1 Å, whereas the rigid narrow angle N(52)–Ru–P in complex **9** is 67.72(6)°. The average bond distance between ruthenium and the hexamethylbenzene carbons is 2.204 Å, while that between the centroid of the arene and the metal atom is 1.705 Å.

6. Concluding remarks

We have prepared some new η^6-arene ruthenium(II) complexes containing amines and diphenyl(2-pyridyl)phosphine ligands. The *p*-cymene ruthenium dimer $[(\eta^6\text{-}C_{10}H_{14})RuCl_2]_2$ with diphenyl(2-pyridyl)phosphine in the presence of methanol under refluxing conditions yields two types of products – one having an organic fragment, viz., $[(\eta^6\text{-}p\text{-cymene})Ru(PPh_2Py)Cl]BF_4$, and the other without an organic fragment, viz., $[RuCl_2(PPh_2Py)_2]$ [19]. The hexamethylbenzene ruthenium(II) dimer $[(\eta^6\text{-}C_6Me_6)RuCl_2]_2$ under the same conditions gave only one product having an organic fragment, viz., $[(\eta^6\text{-}C_6Me_6)Ru(PPh_2Py)Cl]BF_4$. This is a clear indication that hexamethylbenzene binds to the metal quite strongly for the latter case due to the high electron-donating ability of the $\eta^6\text{-}C_6Me_6$ moiety relative to the η^6-*p*-cymene in these ruthenium complexes.

Acknowledgements

K.M.R. and P.G. thank the Sophisticated Instruments Facility (SIF), Indian Institute of Science, Bangalore, for providing the NMR facility. We thank Prof. R.H. Duncan Lyngdoh for help in preparing the manuscript.

Appendix A. Supplementary data

Crystallographic data for the structural analyses have been deposited at the Cambridge Crystallographic Data Centre (CCDC), CCDC No. 246203 for complex **2**, CCDC No. 246204 for complex **8**, and CCDC No. 246205 for complex **9**. Copies of this information may be obtained free of charge from The Director, CCDC, 12 Union Road, Cambridge, CB2 1EZ, UK (fax: +44 1223 336 033; e-mail: deposit@ccdc.cam.ac.uk or www: http://www.ccdc.cam.ac.uk). Supplementary data associated with this article can be found, in the online version at doi:10.1016/j.poly.2004.09.031.

References

[1] H.L. Bozec, D. Touchard, P.H. Dixneuf, Adv. Organomet. Chem 29 (1989) 163.
[2] C.S. Hauser, C. Slugove, K. Mereiter, R. Schimid, K. Kirchner, L. Xiao, W. Weissenteiner, J. Chem. Soc., Dalton Trans. (2001) 2989.
[3] (a) A. Frstner, M. Picquet, C. Bruneau, P.H. Dixneuf, Chem. Commun. (1998) 1315;
(b) B.C.G. Soderberg, Coord. Chem. Rev. 241 (2003) 147.
[4] (a) C.S. Allardyce, P.J. Dyson, D.J. Ellis, S.L. Heath, Chem. Commun. (2001) 1396;
(b) H. Chen, J.A. Parkinson, S. Parsons, R.A. Coxall, R.O. Gould, P.J. Sadler, J. Am. Chem. Soc. 124 (2003) 3064;
(c) R.E. Aird, J. Cummings, A.A. Ritchie, M. Muir, R.E. Morris, H. Chen, P.J. Sadler, D.I. Jodrell, Br. J. Cancer 86 (2002) 1652;
(d) R.E. Morris, R.E. Aird, P.D.S. Murdoch, H. Chen, J. Cummings, N.D. Hughes, S. Parsons, A. Parkin, G. Boyd, D.I. Jodrell, P.J. Sadler, J. Med. Chem. 44 (2001) 3616.
[5] (a) P. Govindaswamy, H.P. Yennawar, M.R. Kollipara, J. Organomet. Chem. 689 (2004) 3108;
(b) R.S. Bates, M.J. Begley, A.H. Wright, Polyhedron 9 (1990) 1113.
[6] (a) M.R. Kollipara, P. Sarkhel, S. Chakraborty, R. Lalrempuia, J. Coord. Chem. 56 (2003) 1085;

(b) P. Govindaswamy, Y.A. Mozharivskyj, M.R. Kollipara, J. Organomet. Chem. 689 (2004) 3265.
[7] C.J. Schaverien, Adv. Organomet. Chem. 36 (1994) 283.
[8] (a) N.W. Alcock, P. Moore, P.A. Lampe, K.F. Mock, J. Chem. Soc., Dalton Trans. (1982) 207;
(b) M.M. Olmstead, A. Maisonnat, J.P. Farr, A.L. Balch, Inorg. Chem. 20 (1981) 4060;
(c) Y. Inoguchi, B. Milewski-Marla, H. Schmidbauer, Chem. Ber. 115 (1982) 3085;
(d) J.P. Parr, M.M. Olamstead, F.E. Wood, A.L. Balch, J. Am. Chem. Soc. 97 (1983) 77;
(e) H.J. Wasserman, D.C. Moody, R.T. Paine, R.R. Ryan, K.V. Salazar, J. Chem. Soc., Chem. Commun. (1984) 533.
[9] (a) F.E. Hong, Y.C. Chang, R.E. Chang, C.C. Lin, S.L. Wang, F.L. Liao, J. Organomet. Chem. 588 (1999) 160;
(b) F.E. Wood, M.M. Olamstead, J.P. Farr, A.L. Balch, Inorg. Chim. Acta 97 (1985) 77;
(c) U. Abram, R. Alberto, J.R. Dilworth, Y. Zheng, K. Ortner, Polyhedron 18 (1999) 2995.
[10] P. Govindaswamy, M.R. Kollipara (unpublished work).
[11] M.A. Bennett, A.K. Smith, J. Chem. Soc., Dalton Trans. (1974) 233.
[12] (a) M.A. Bennett, T.N. Huang, T.W. Matheson, A.K. Smith, Inorg. Synth. 21 (1982) 74;
(b) M.A. Bennett, T.W. Matheson, G.B. Robertson, A.K. Smith, P.A. Tocker, Inorg. Chem. 19 (1980) 1014.
[13] D. Becke, J. Chem. Phys. 98 (1993) 5648.
[14] XRD: Single-crystal software; Bruker Analytical X-ray Systems, Madison, WI, USA, 2002.
[15] G.M. Sheldrick, SHELXS-86: Program for Crystal Structure Solution, University of Göttingen, Göttingen, Germany, 1986.
[16] M. Sheldrick, SHELXS-97: Program for Crystal Structure Refinement, University of Göttingen, Göttingen, Germany, 1997.
[17] C.K. Johnson, ORTEP II: A Fortran thermal Ellipsoid Plot Program for Crystal Structure Illustrations, ORNL–5138, 1976.
[18] C.D. Nunes, M. Pillinger, A. Hazell, J. Jepsen, T.M. Santos, J. Madureira, A.D. Lopes, I.S. Goncalves, Polyhedron 22 (2003) 2799.
[19] R. Lalrempuia, P.J. Carroll, M.R. Kollipara, J. Chem. Sci. 116 (2004) 21.
[20] (a) S. Jung, I. Kerstin, C.D. Brandt, J. Wolf, H. Werner, J. Chem. Soc., Dalton Trans. (2002) 318;
(b) J.P. Selegue, Organometallics 1 (1982) 217.
[21] R. Baldwin, M.A. Bennett, D.C.R. Hockless, P. Pertici, A. Verrazzani, G.U. Barretta, F. Marchetti, P. Salvadori, J. Chem. Soc., Dalton Trans. (2002) 4488.
[22] J.A. Cabeza, I.D. Rio, M.E. Navarro, S.G. Granda, Acta Crystallogr., Sect. E 57 (2001) m162.
[23] Y. Yamamoto, H. Nakamura, J.F. Ma, J. Organomet. Chem. 640 (2001) 10.
[24] (a) B. Therrien, G.S. Fink, Inorg. Chim. Acta 357 (2004) 219;
(b) B. Therrien, T.R. Ward, Angew. Chem., Int. Ed. 38 (1999) 405;
(c) F.B. McCormick, W.B. Gleason, Acta Crystallogr., Sect. C 44 (1988) 603.
[25] I. Moldes, E.D.L. Encarnacion, J. Ros, A.A. Larena, J.F. Piniella, J. Organomet. Chem. 566 (1998) 165.

dichloride products of 5,14-dihydro-6,8,15,17-tetramethyldibenzo[b,I][1,4,8,11]tetraazacyclotetradecine which were subsequently reacted with the appropriate amine to yield the desired amino complex in good yields. The amino complexes formed are explained in terms of nucleophillic attack of the amine on the carbonyl carbon within the *meso* substituents of the macrocycle. It is clear the the diallylamine group is potentially capable of interesting transformations.

We have an ongoing interest in hemilabile ligands [10–14] and bis(diphenylphosphino)amines [15] are of interest since they relate to the well known ligand bis(diphenylphosphino)methane, $Ph_2PCH_2PPh_2$ (dppm) [16–18]. Coordination of dppm to metal centres can occur through the lone pair of electrons at one or both of the phosphorus centres as well as by deprotonation of the methylene(or NH) group to form a tridentate ligand (see Fig. 1).

However, diphosphinoamines have received significantly less attention [19,20] and we have a program of study into the synthesis of P–N–P phosphines [21–30]. Here we report the preparation new phosphine and disphosphine that contains the diallyl and allyl group and have the potential to act as a hemilabile ligand. Selected coordination complexes have also been prepared.

2. Results and discussion

Reaction of diallylamine with one equivalent of Ph_2PCl in the presence of NEt_3 proceeds in thf to give **1** (Eq. (2), 83% yield), δ_P 64.3 ppm. In the IR spectrum bands are observed at 1638, 1433 and 993 cm^{-1}, which are assigned to $\nu_{C=C}$, ν_{PPh2} and ν_{PN} respectively. The microanalysis gave satisfactory results.

The oxide (**2**) $Ph_2P(O)N(C_3H_5)_2$ was easily prepared by addition of urea hydrogen peroxide to a dichloromethane solution of **1**, whilst the sulfur (**3**) and seleno (**4**) analogues were prepared by the addition of elemental S or Se to the ligand in toluene. Satisfactory microanalysis was obtained for the **4** though only fairly satisfactory results were obtained for **3** and **4** possible due to difficulties in purifying the oily products formed and the EI^+ mass spectral data gave the expected parent ion and fragmentation patterns. The $^{31}P\{^1H\}$ NMR show single resonances ($CDCl_3$) at δ_P 31.3 and 69.8 ppm for the oxide and sulfide respectively. The seleno analogue exhibits a single $^{31}P\{^1H\}$ NMR resonance ($CDCl_3$) at δ_P 58.1 ppm with selenium satellites $^1J(^{31}P–^{77}Se)$ 756 Hz which is typical for a P=Se group.

Reaction of $[PtCl_2(cod)]$ with $Ph_2PN(C_3H_5)_2$ gave interesting results. Reaction of $[PtCl_2(cod)]$ with three equivalents of $Ph_2PN(C_3H_5)_2$ gives $[Pt\{Ph_2PN(C_3H_5)_2\}_3][Cl_2]$ (**5**). The FAB mass spectrum of **5** contains the expected parent ion and fragmentation pattern and the complex exhibits three different resonances (Fig. 2) with platinum satellites in the $^{31}P\{^1H\}$ NMR spectrum ($\delta(P_A)$ 83.7 ppm, $^1J\{^{31}P_A–^{195}Pt\}$ 4800 Hz; $\delta(P_X)$ 74.5 ppm, $^1J\{^{31}P_X–^{195}Pt\}$ 2052 Hz, $^2J\{^{31}P_A–^{31}P_X\}$ 9 Hz, $^2J\{^{31}P_X–^{31}P_Y\}$ 44 Hz; $\delta(P_Y)$ 47.9 ppm, $^2J\{^{31}P_Y–^{195}Pt\}$ 281 Hz) which indicates the presence of three phosphorus ligands around the platinum centre, and by comparison of the chemicals shifts and coupling constants we propose the structure shown in Eq. (2). If the reaction was performed with a 2:1 ligand/metal molar ratio, $^{31}P\{^1H\}$ NMR indicated the presence of **5** and another complex. Reaction of $[PtCl_2(cod)]$ with one equivalent of $Ph_2PN(C_3H_5)_2$ gives the second product observed in the 2:1 reaction, $[PtCl_2\{Ph_2PN(C_3H_5)_2\}]$ (**6**), in good yield (65%). Microanalysis gave satisfactory results for the formation of the chelate complex and FAB mass spectral analysis gives the expected parent ion and fragmentation pattern. The complex displays a single resonance with platinum satellites in the $^{31}P\{^1H\}$ NMR spectrum (δ_P 701. ppm, $^1J(^{31}P–^{195}Pt)$ 3491 Hz) and the IR spectrum has ν_{PPh2} and ν_{PN} vibrations at 1434 and 1010 cm^{-1}, respectively and two ν_{PtCl} bands at 317 and 295 cm^{-1} which suggest a *cis* geometry. $[PdCl_2(cod)]$ behaved slightly differently to $[PtCl_2(cod)]$; a 2:1 ratio reaction [ligand:metal] gave two products, however, in the presence of three equivalents of **1** only the 2:1 complex, $[PdCl_2\{Ph_2PN(C_3H_5)_2\}_2]$ (**7**) is obtained. The $^{31}P\{^1H\}$ NMR of **7** has two signals [δ_P 109.2

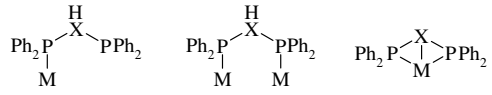

Fig. 1. Coordination modes of dppm, dppa and their respective anions (X=CH or N).

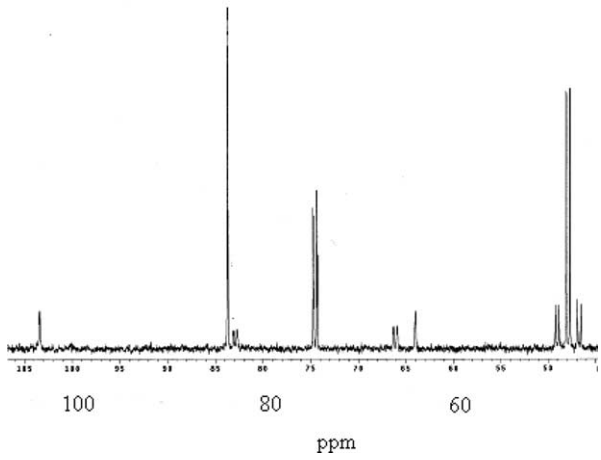

Fig. 2. ^{31}P NMR from the crude the reaction of three equivalents of $Ph_2PN(C_3H_5)_2$ with $[PtCl_2(cod)]$.

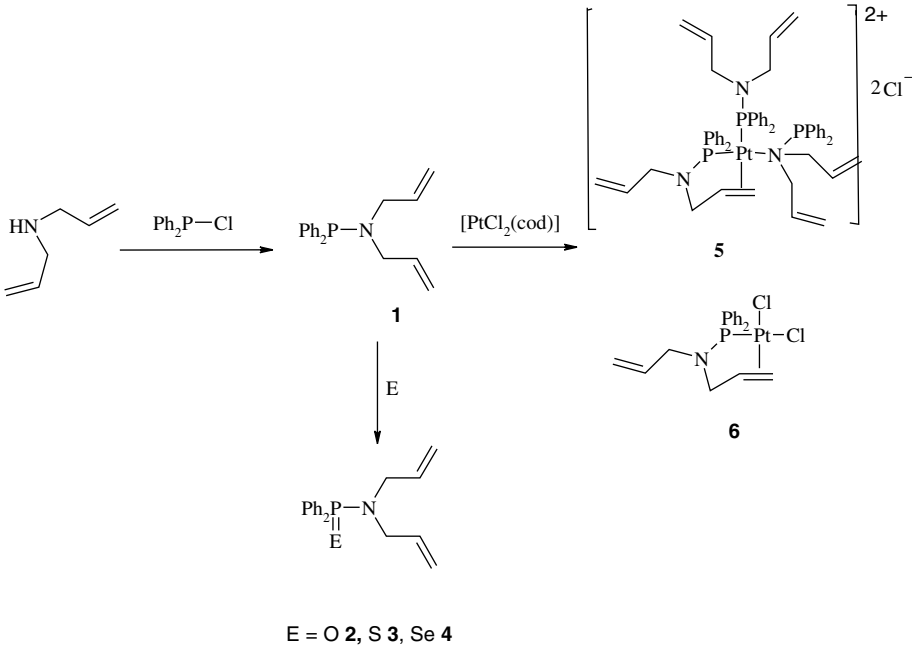

(2)

and 44.7 ppm, $^{2}J\{^{31}P_{A}–^{31}P_{X}\}$ 18 Hz] indicating two phosphorus environments within the complex. The FAB mass spectrum gives the expected parent ion and microanalysis is found to be fairly satisfactory. The IR spectrum has bands at 1435 and 995 cm^{-1} that correspond to ν_{PPh2} and ν_{PN}, respectively and two ν_{PdCl} bands at 292 and 277 cm^{-1}. As might be anticipated, the reaction of one equivalent of $Ph_2PN(C_3H_5)_2$ with [$PdCl_2$ (cod)] gives [$PdCl_2\{Ph_2PN(C_3H_5)_2\}$] (**8**) in good yield. The crystal structure of **8** (Fig. 3) shows that the molecule is *cis*-square planar. The ligand is bound to the palladium metal via phosphorus [P(1)–Pd(1) 2.2247(6) Å] and one of the olefinic arms of the ligand.

The reaction of [$PtMe_2$(cod)] with one equivalent of **1** gave the expected chelate complex, [$PtMe_2\{Ph_2PN$ $(C_3H_5)_2\}$ (**9**). The FAB mass spectral data obtained gave the expected parent ion and in the IR spectrum $\nu_{C=C}$, ν_{PPh2} and ν_{PN} vibrations were observed at 1636, 1432 and 992 cm^{-1}, respectively. The $^{31}P\{^{1}H\}$ NMR (CD_2Cl_2) showed a single resonance with platinum satellites (δ_P 90.7 ppm, $^{1}J\{^{31}P–^{195}Pt\}$ 1937 Hz).

Reaction of **1** with [$Mo(CO)_4$(nbd)] gives [Mo $(CO)_4\{Ph_2PN(C_3H_5)_2\}$] (**10**) as a yellow solid. Monodentate *P*-[$RuCl_2\{Ph_2PN(C_3H_5)_2\}(\eta^6$-*p*-$MeC_6H_4{}^{i}Pr)$] (**11**) was prepared from [{RuCl(α-Cl)(η^6-*p*-Me-$C_6H_4{}^{i}Pr)_2\}_2$] and **1**. [RhCl{$Ph_2PN(C_3H_5)_2$}] (**12**) was obtained from [{Rh(α-Cl)(cod)}$_2$]. The $^{31}P\{^{1}H\}$ NMR ($CDCl_3$) shows a two resonances with rhodium satellites ($\delta(P_A)$ 115.5 ppm, $^{1}J(^{31}P_{A}–^{103}Rh)$ 154 Hz. $\delta(P_X)$ 84.7 ppm, $^{1}J\{^{31}P_{X}–^{103}Rh\}$ 114 Hz. $^{2}J\{^{31}P_{A}–^{31}P_{X}\}$ 25 Hz). The IR spectrum has bands at 1433, 990 and 251 cm^{-1} that correspond to ν_{PPh2} and ν_{PN} and ν_{RhCl} vibrations, respectively.

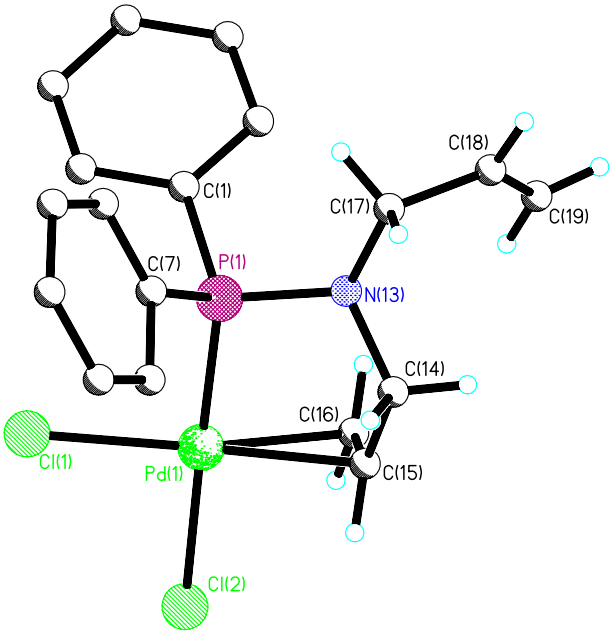

Fig. 3. The X-ray structure of [$PdCl_2\{Ph_2PN(C_3H_5)_2\}$] (**8**), selected bond lengths (Å) and angles (°) : Pd(1)–Cl(1) 2.2983(7), Pd(1)–Cl(2) 2.3641(7), Pd(1)–P(1) 2.2247(6), Pd(1)–C(15) 2.192(2), Pd(1)–C(16) 2.177(3), P(1)–N(13) 1.6719(19), N(13)–C(14) 1.465(3), N(13)–C(17) 1.466(3), C(15)–C(16) 1.361(4). P(1)–Pd(1)–Cl(1) 88.07(2), N(13)–P(1)–M(1) 103.54(7), P(1)–M(1)–Cl(2) 178.67(20).

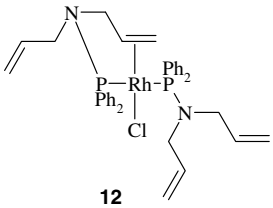

12

Reaction of allylamine with two equivalents of Ph_2PCl in the presence of NEt_3 proceeds in thf to give **13** in good yield, δ_P 62.9 ppm. The IR spectrum has bands observed at 1635, 1434 and 993 cm^{-1}, which are assigned to $\nu_{C=C}$, ν_{PPh} and ν_{PN}, respectively.

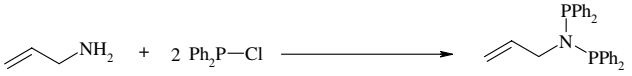

(3)

Reaction of $[MCl_2(cod)]$ with $(C_3H_5)N(PPh_2)_2$ gives $[PtCl_2\{(C_3H_5)N(PPh_2)_2\}]$ (M=Pt **14,** Pd **15**) in good yield. The FAB^+ mass spectrum showed the expected parent ion and the complex has δ_P 19.1 ppm, $^1J\{^{31}P–^{195}Pt\}$ 3296 Hz. The IR spectrum showed bands at 1635, 1435, 995, 291 and 245 cm^{-1}, which are assigned to $\nu_{C=C}$, ν_{PPh}, ν_{PN} and two ν_{PtCl} vibrations respectively.

The crystal structure of **14** (Fig. 4) shows that it is approximately square planar at platinum. The bite angle of the chelating phosphine is significantly lower than the ideal 90° {P(2)–Pt(1)–P(1) 72.03(8)°}.

We prepared a number of other simple complexes of **13**, thus $[Mo(CO)_4\{(Ph_2P)_2N(C_3H_5)\}]$ (**16**) $[\{(C_3H_5)N(PPh_2)_2\}(AuCl)_2]$ (**17**), $[RuCl_2\{(Ph_2P)_2N(C_3H_5)\}_2]$ (**18**), $[RhCl(\alpha\text{-}Cl)(\eta^5\text{-}C_5Me_5)\{(Ph_2P)_2N(C_3H_5)\}]$ (**19**) and $[IrCl(\alpha\text{-}Cl)(\eta^5\text{-}C_5Me_5)\{(Ph_2P)_2N(C_3H_5)\}]$ (**20**) were all obtained. The crystal structure of **18** (Fig. 5) reveals bidentate coordination [bite angle P(2)–Pt(1)–P(1) 69.10(3)°].

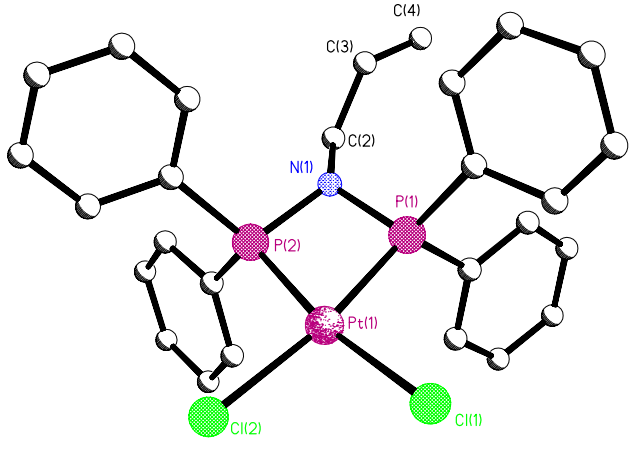

Fig. 4. The X-ray structure of $[PtCl_2\{(C_3H_5)N(PPh_2)_2\}]$ (**14**). Selected bond lengths and angles: Pt(1)–Cl(1),2.352(2), Pt(1)–Cl(2) 2.347(2), Pt(1)–P(1) 2.201(2), Pt (1)–P(2) 2.197(2), P(1)–N(1) 1.696(7), P(2)–N(1) 1.703(7) Å, P(2)–Pt(1)–P(1) 72.10(8), P(2)–Pt(1)–Cl(1) 97.44(9), P(1)–Pt(1)–Cl(2) 98.73(9), Cl(2)–Pt(1)–Cl(1) 91.78(9), P(2)–N(1)–P(1) 99.2(4)°.

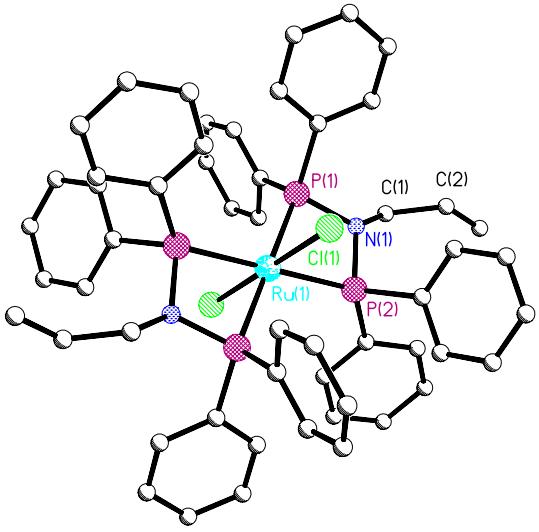

Fig. 5. The X-ray structure of $[RuCl_2\{(Ph_2P)_2N(C_3H_5)\}_2]$ (**18**). Selected bond lengths and angles: Ru(1)–Cl(1) 2.4189(7), Ru(1)–P(2) 2.3585(8), Ru(1)–P(1) 2.3356(7), P(2)–N(1) 1.721(2), P(1)–N(1) 1.710(2) Å P(2)–Ru(1)–P(1) 69.10(3), P(2)–Ru(1)–Cl(1) 85.65(2), P(1)–Ru(1)–Cl(1) 89.65(2), P(2)–N(1)–P(1) 101.78(12)°.

This work clearly demonstrates the ability of allyl aminophosphines to bind using a variety of motifs.

3. Experimental

3.1. $[Ph_2PN(C_3H_5)_2]$ (1)

Diallylamine (2.841 g, 29.2 mmol) and triethylamine (3.107 g, 30.7 mmol) were added together in dry thf (50 cm^3). Chlorodiphenylphosphine (6.453 g, 29.2 mmol) in dry thf (50 cm^3) was added dropwise with stirring overnight. Triethylamine hydrochloride was removed by filtration under nitrogen and the solvent removed in vacuo to yield a colourless oil. Yield: 6.840 g, 83%. Microanalysis: Found (calculated for $C_{18}H_{20}NP$): C, 74.47 (76.85); H, 7.79 (7.17); N, 4.72 (4.98)%. $^{31}P\{^1H\}$ NMR ($CDCl_3$): 64.3 ppm. ^1H NMR ($CDCl_3$) δ 7.5 (m, 10 H, Ph), 5.65 (m, 2H, $CH{=}CH_2$), 5.05 (m, 4H, CH_2), 3.45 (m, 4H, CH_2) ppm. IR (thin film): 1638, 1433, 933 cm^{-1}.

3.2. $Ph_2P(O)N(C_3H_5)_2$ (2)

$Ph_2PN(C_3H_5)_2$ (256 mg, 0.9 mmol) was dissolved in CH_2Cl_2 (20 cm^3) and cooled to 0 °C before addition of urea hydrogen peroxide (86 mg, 0.9 mmol) was added and the reaction mixture was stirred overnight. The product was extracted from the CH_2Cl_2 by addition of distilled water, washed with CH_2Cl_2 (3×5 cm^3), dried

over magnesium sulfate and evaporated to dryness to yield a colourless oil. Yield: 254 mg, 94%. Microanalysis: Found (calculated for $C_{18}H_{20}NOP$): C, 68.61 (72.71); H, 6.58 (6.78); N, 4.46 (4.71)%. $^{31}P\{^{1}H\}$ NMR ($CDCl_3$): 31.3 ppm. ^{1}H ($CDCl_3$) δ 7.55 (m, 10H, Ph), 5.65 (m, 2H, CH=CH_2), 5.05 (m, 4H, CH_2), 3.45 (m, 4H, CH_2) ppm. EI^+ MS: *m/z* 297 $[M]^+$. IR (thin film): 1635, 1433, 1181, 992 cm^{-1}.

3.3. $Ph_2P(S)N(C_3H_5)_2$ (**3**)

$Ph_2PN(C_3H_5)_2$ (766 mg, 2.7 mmol) and elemental sulfur (87 mg, 2.7 mmol) were dissolved in dry toluene (10 cm^3) to yield a yellow solution which was stirred overnight. The reaction mixture was cooled to room temperature and the solvent removed before addition of CH_2Cl_2 (2 cm^3) and filtering through Celite to remove any remaining inorganic solid. After removing the CH_2Cl_2 colourless oil was yielded. Yield: 753 mg, 88%. Microanalysis: Found (calculated for $C_{18}H_{20}NPS$): C, 66.03 (68.98); H, 7.48 (6. 43); N, 4.80 (4.47)%. $^{31}P\{^{1}H\}$ NMR ($CDCl_3$): 69.8 ppm. ^{1}H NMR ($CDCl_3$) δ 7.55 (m, 10H, Ph), 5.65 (m, 2H, CH=CH_2), 5.05 (m, 4H, CH_2), 3.45 (m, 4H, CH_2) ppm. EI^+: *m/z* 273 $[M]^+$. IR (thin film): 1638, 1434, 997, 689 cm^{-1}.

3.4. $Ph_2P(Se)N(C_3H_5)_2$ (**4**)

$Ph_2PN(C_3H_5)_2$ (235 mg, 1.0 mmol) and grey selenium (77 mg, 1.0 mmol) were refluxed in dry toluene (10 cm^3) for 1 h before cooling to room temperature and filtering through a Celite plug to remove any insoluble material. The solvent was reduced to 1 cm^3 to yield a colourless solid that was isolated by suction filtration and dried in vacuo. Yield: 269 mg, 86%. Microanalysis: Found (calculated for $C_{18}H_{20}NPSe$): C, 59.93 (60.01); H, 6.80 (5.60); N, 4.28 (3.89)%. $^{31}P\{^{1}H\}$ NMR ($CDCl_3$): 58.1 ppm $^{1}J(^{31}P–^{77}Se)$ 756 Hz. ^{1}H NMR ($CDCl_3$) δ 7.55 (m, 10H, Ph), 5.65 (m, 2H, CH=CH_2), 5.05 (m, 4H, CH_2), 3.45 (m, 4H, CH_2) ppm. EI^+ MS: *m/z* 361 $[M + H]^+$. IR (KBr disc): 1636, 1435, 995, 573 cm^{-1}.

3.5. $[Pt\{Ph_2PN(C_3H_5)_2\}_3][Cl_2^-]$ (**5**)

$Ph_2PN(C_3H_5)_2$ (165 mg, 0.6 mmol) and $[PtCl_2(cod)]$ (73 mg, 0.2 mmol) were dissolved in CH_2Cl_2 (5 cm^3) to yield a pale yellow solution that was stirred for 30 min. The solvent was reduced to 1 cm^3 before precipitating a colourless solid upon addition of diethyl ether (cm^3) that was isolated by suction filtration. Yield: 140 mg, 64%. Microanalysis: Found (calculated for $C_{54}H_{60}P_3N_3PtCl_2$): C, 58.84 (58.43); H, 5.38 (5.45); N, 3.73 (3.79)%. $^{31}P\{^{1}H\}$ NMR ($CDCl_3$): $\delta(P_A)$ 83.7 (d) ppm, $^{1}J(^{31}P_A–^{195}Pt)$ 4800 Hz. $\delta(P_X)$ 74.5 ppm, $^{1}J(^{31}P_X–^{195}Pt)$ 2052 Hz. $^{2}J(^{31}P_A–^{31}P_X)$ 9 Hz. $^{2}J(^{31}P_Y–^{31}P_X)$ 44 Hz. $\delta(P_Y)$ 47.9 (d) ppm, $^{2}J(^{31}P_Y–^{195}Pt)$ 281 Hz. ^{1}H NMR ($CDCl_3$) δ 7.55 (m, 30H, Ph), 5.65 (m, 4H, CH=CH_2), 5.05 (m, 2H, chelate CH=CH_2), 4.85 (m, 8H, CH_2), 4.45 (m, 4H, chelate CH_2), 3.45 (m, 12H, CH_2) ppm. FAB^+ MS: *m/z* 1075 $[M – Cl]^+$. IR (KBr disc): 1637, 1436, 997, 296 cm^{-1}.

3.6. $[PtCl_2\{Ph_2PN(C_3H_5)_2\}]$ (**6**)

$Ph_2PN(C_3H_5)_2$ (197 mg, 0.7 mmol) in CH_2Cl_2 (5 cm^3) was added dropwise to a CH_2Cl_2 (5 cm^3) solution of $[PtCl_2(cod)]$ (262 mg, 0.7 mmol) over 2.5 h. The solvent was reduced to 1 cm^3 before addition of hexane (10 cm^3) to yield an off white sticky solid on reduction of solvent. The sticky solid was subsequently dissolved in CH_2Cl_2 (0.5 cm^3) before addition of petroleum ether (40–60) (10 cm^3) to yield a colourless solid that was isolated by suction filtration. Yield: 248 mg, 65%. Microanalysis: Found (calculated for $C_{18}H_{20}NPPtCl_2$): C, 40.02 (39.50); H, 3.50 (3.68); N, 3.41 (2.56)%. $^{31}P\{^{1}H\}$ NMR ($CDCl_3$): 70.1 ppm $^{1}J(^{31}P–^{195}Pt)$ 3491 Hz. ^{1}H NMR ($CDCl_3$) δ 7.6 (m, 10H, aromatic), 5.3 (m, 2H, CH), 5.1 (m, 2H, CH_2), 4.7 (d, 1H, $^{3}J\{^{195}Pt–^{1}H\}$ 54 Hz, $^{2}J\{^{31}P–^{1}H\}$ 8 Hz, CH_2), 4.1 (d, 1H,$^{3}J\{^{195}Pt–^{1}H\}$ 59 Hz, $^{2}J\{^{31}P–^{1}H\}$ 13 Hz, CH_2) 3.5 (m, 4H, NCH_2) ppm. FAB^+ MS: *m/z* 569 $[M + Na]^+$, 547 $[M + H]^+$, 511 $[M – Cl]^+$, 474/6 $[M – 2Cl]^{2+}$. IR (KBr disc): 1634, 1434, 1010, 317, 295 cm^{-1}.

3.7. $[PdCl_2\{Ph_2PN(C_3H_5)_2\}_2]$ (**7**)

$(Ph_2P)_2N(C_3H_5)_2$ (124 mg, 0.4 mmol) and $[PdCl_2(cod)]$ (42 mg, 0.1 mmol) were dissolved in CH_2Cl_2 (5 cm^3) to yield an orange solution that was stirred for 30 min. The solvent was reduced to 1 cm^3 before precipitating a pale yellow solid upon addition of diethyl ether (20 cm^3) that was isolated by suction filtration. Yield: 100 mg, 92%. Microanalysis: Found (calculated for $C_{36}H_{40}P_2N_2PdCl_2$): C, 57.56 (58.43); H, 5.22 (5.45); N, 3.40 (3.79)%. $^{31}P\{^{1}H\}$ NMR ($CDCl_3$): $\delta(P_A)$ 109.2 ppm. $\delta(P_X)$ 44.7 ppm. $^{2}J\{^{31}P_A–^{31}P_X\}$ 18 Hz. ^{1}H NMR ($CDCl_3$) δ 7.55 (m, 20H, Ph), 5.65 (m, 3H, CH=CH_2), 5.05 (m, 1H, chelate CH=CH_2), 4.85 (m, 6H, CH $_2$), 4.45 (m, 2H, chelate CH_2), 3.45 (m, 8H, CH_2) ppm. FAB^+ MS: *m/z* 704 $[M – Cl]^+$, 667/8 $[M – 2Cl]^{2+}$. IR (KBr disc): 1638, 1435, 995, 292, 277 cm^{-1}.

3.8. $[PdCl_2\{Ph_2PN(C_3H_5)_2\}]$ (**8**)

$Ph_2PN(C_3H_5)_2$ (111 mg, 0.4 mmol) in CH_2Cl_2 (5 cm^3) was added dropwise to CH_2Cl_2 (5 cm^3) solution of $[PdCl_2(cod)]$ (112 mg, 0.4 mmol). After stirring for 30 min the solvent was reduced in vacuo to 0.5 cm^3 before precipitating a yellow microcrystalline solid upon addition of hexane (10 cm^3) and isolation by suction

filtration. Yield: 164 mg, 91%. Microanalysis: Found (calculated for $C_{18}H_{20}PNPdCl_2$): C, 46.76 (47.14); H, 4.18 (4.40); N, 2.70 (3.05)%. $^{31}P\{^1H\}$ NMR ($CDCl_3$): 101.3 ppm. ^1H NMR ($CDCl_3$) δ 7.55 (m, 10H, Ph), 5.65 (m, 1H, CH=CH_2), 5.05 (m, 1H, chelate CH=CH_2), 4.85 (m, 2H, CH_2), 4.45 (m, 2H, chelate CH_2), 3.45 (m, 4H, CH_2) ppm. FAB^+ MS: *m/z* 422 $[M - Cl]^+$, 386 $[M - 2Cl]^{2+}$. IR (KBr disc): 1634, 1435, 999, 317, 290 cm^{-1}.

3.9. $[PtMe_2\{Ph_2PN(C_3H_5)_2\}]$ (**9**)

$Ph_2PNH(C_3H_5)_2$ (96 mg, 0.3 mmol) in CH_2Cl_2 (5 cm^3) was added dropwise to a CH_2Cl_2 (5 cm^3) solution of [$PtMe_2$(cod)] (114 mg, 0.3 mmol) over 2.5 h. The solvent was reduced to 1 cm^3 before addition of hexane (10 cm^3) to yield an off white sticky solid on reduction of solvent. The sticky solid was subsequently dissolved in CH_2Cl_2 (0.5 cm^3) before addition of petroleum ether (40–60) (10 cm^3) to yield a colourless solid that was isolated by suction filtration. Yield: 92 mg, 53%. Microanalysis: Found (calculated for $C_{20}H_{26}NPPt$) C, 46.90 (47.42); H, 4.46 (5.18); N, 2.35 (2.77)%. $^{31}P\{^1H\}$ NMR (CD_2Cl_2): 90.7 ppm $^1J(^{31}P–^{195}Pt)$ 1937 Hz. ^1H NMR (CD_2Cl_2) δ 7.55 (m, 10H, aromatic), 5.3 (m, 2H, CH), 5.1 (m, 2H, CH_2), 4.7 (d, 1 H, $^3J(^{195}Pt–^1H)$ 54 Hz, $^2J\{^{31}P–^1H\}$ 8 Hz, CH_2), 4.1 (d, 1H,$^3J\{^{195}Pt–^1H\}$ 59 Hz, $^2J\{^{31}P–^1H\}$ 13 Hz, CH_2) 3.5 (m, 4H, NCH_2) ppm. FAB^+ MS: *m/z* 490 $[M - Me]^+$, 476 $[M - 2Me]^{2+}$. IR (KBr disc): 1636, 1432, 992 cm^{-1}.

3.10. $[Mo(CO)_4\{Ph_2PN(C_3H_5)_2\}]$ (**10**)

To a CH_2Cl_2 (10 cm^3) solution of [$Mo(CO)_4$(nbd)] (184 mg, 0.6 mmol) was added dropwise a CH_2Cl_2 (10 cm^3) solution of $(Ph_2P)N(C_3H_5)_2$ (172 mg, 0.6 mmol). After stirring for 30 min the solvent was reduced to 2 cm^3 before addition of petroleum ether (b.p. 40–60) (20 cm^3) and storing overnight at −18 °C. The yellow solid precipitated was isolated by filtration and dried in vacuo. Yield: 95 mg, 32%. Microanalysis: Found (calculated for $C_{22}H_{20}PNO_4Mo$): C, 54.04 (54.00); H, 3.16 (4.12); N, 2.76 (2.86)%. $^{31}P\{^1H\}$ NMR ($CDCl_3$): 116.2 ppm. ^1H NMR ($CDCl_3$) δ 7.3 (m, 10H, aromatic), 5.3 (m, 1H, CH), 5.0 (m, 2H, CH_2), 4.7 (m, 1H, CH), 4.0 (m, 2H, chelate CH_2), 3.5 (m, 4H, NCH_2) ppm. FAB^+ MS: *m/z* $[M]^+$, $[M - CO]^+$, $[M - 2CO]^+$, $[M - 3CO]^+$ 523 $[M - 4CO]^+$. IR (KBr disc): 1893, 1434, 987 cm^{-1}.

3.11. $[RuCl_2\{Ph_2PN(C_3H_5)_2\}(\eta^6\text{-}p\text{-}MeC_6H_4{}^iPr)]$ (**11**)

$(Ph_2P)N(C_3H_5)_2$ (122 mg, 0.4 mmol) and [RuCl(α-Cl)(η^6-*p*-$MeC_6H_4{}^iPr)_2$] (133 mg, 0.2 mmol) were dissolved in CH_2Cl_2 (5 cm^3) to yield a dark red solution. The solvent was reduced to 1 cm^3 before addition of diethyl ether (10 cm^3) to precipitate an orange solid that was isolated by suction filtration. Yield: 118 mg, 92%. Microanalysis: Found (calculated for $C_{28}H_{34}PNRuCl_2$): C, 57.33 (57.24); H, 5.65 (5.83); N, 2.21 (2.38)%. $^{31}P\{^1H\}$ NMR ($CDCl_3$): 74.1 ppm. ^1H NMR ($CDCl_3$) δ 7.3 (m, 14H, aromatic), 5.9 (m, 2H, CH), 4.8 (m, 4H, CH_2), 3.5 (m, 4H, NCH_2), 2.7 (m, 1 H, CH), 1.9 (s, 3H, $ArCH_3$), 1.2 (m, 6H, CH_3) ppm. FAB^+ MS: *m/z* 552 $[M - Cl]^+$, 515/7 $[M - 2Cl]^{2+}$. IR (KBr disc): 1637, 1432, 994, 299, 278 cm^{-1}.

3.12. $[RhCl\{Ph_2PN(C_3H_5)_2\}_2]$ (**12**)

$(Ph_2P)N(C_3H_5)_2$ (148 mg, 0.5 mmol) and [{Rh(α-Cl)(cod)}$_2$] (65 mg, 0.1 mmol) were dissolved in CH_2Cl_2 (5 cm^3) to yield a dark red solution. The solvent was reduced to 1 cm^3 before addition of diethyl ether (10 cm^3) to precipitate an orange solid that was isolated by suction filtration. Yield: 88 mg, 96%. Microanalysis: Found (calculated for $C_{36}H_{40}P_2N_2RhCl$): C, 61.00 (61.70); H, 6.12 (5.75); N, 3.83 (4.00) $^{31}P\{^1H\}$ NMR ($CDCl_3$): $\delta(P_A)$ 115.5 (d) ppm, ^1J ($^{31}P_A–^{103}Rh$) 154 Hz. $\delta(P_X)$ 84.7 (d) ppm, $^1J(^{31}P_X–^{103}Rh)$ 114 Hz. $^2J(^{31}P_A–^{31}P_X)$ 25 Hz. ^1H NMR ($CDCl_3$) δ 7.3 (m, 20H, aromatic), 5.9 (m, 4H, CH), 4.8 (m, 8H, CH_2), 3.5 (m, 8H, NCH_2) ppm. FAB^+ MS: *m/z* 665 $[M - Cl]^+$. IR (KBr disc): 1638, 1433, 990, 251 cm^{-1}.

3.13. $(Ph_2P)_2N(C_3H_5)$ (**13**)

Allylamine (2.319 g, 40.6 mmol) and triethylamine (8.219 g, 81.2 mmol) were dissolved in thf (50 cm^3). Chlorodiphenylphosphine (17.922 g, 81.2 mmol) in thf (50 cm^3) was added dropwise with stirring overnight to yield triethylamine hydrochloride that was isolated by filtration. The solvent was removed in vacuo to yield a colourless solid that was dried in vacuo. Yield: 13.434 g, 78%. Microanalysis: Found (calculated for $C_{27}H_{25}P_2N$): C, 75.19 (76.22); H, 6.20 (5.92); N, 3.34 (3.29)%. $^{31}P\{^1H\}$ NMR ($CDCl_3$): 62.9 ppm. ^1H NMR ($CDCl_3$) δ 7.3 (m, 20H, aromatic), 5.3 (m, 1H, CH), 4.8 (m, 2H, CH_2), 3.9 (m, 2H, NCH_2) ppm. EI^+ MS: *m/z* 424 $[M]^+$. IR (KBr disc): 1635, 1434, 993 cm^{-1}.

3.14. $[PtCl_2\{(Ph_2P)_2N(C_3H_5)\}]$ (**14**)

$(Ph_2P)_2N(C_3H_5)$ (88 mg, 0.2 mmol) and [$PtCl_2$(cod)] (77 mg, 0.2 mmol) were dissolved in CH_2Cl_2 (10 cm^3) to yield a pale yellow solution that was stirred for 30 min. The solvent was reduced to 1 cm^3 before precipitating a colourless solid upon addition of diethyl ether (20 cm^3) that was isolated by suction filtration. Yield: 101 mg, 71%. Microanalysis: Found (calculated for $C_{27}H_{25}P_2NPtCl_2$): C, 47.81

(46.90); H, 2.53 (3.64); N, 1.56 (2.03)%. $^{31}P\{^{1}H\}$ NMR ($CDCl_3$): 19.1 ppm, $^{1}J(^{31}P–^{195}Pt)$ 3296 Hz. ^{1}H NMR ($CDCl_3$) δ 7.3 (m, 20H, aromatic), 5.3 (m, 1H, CH), 4.9 (m, 2H, CH_2), 3.5 (m, 2H, NCH_2) ppm. FAB^+ MS: *m/z* 713/4 $[M + Na]^+$, 691 $[M]^+$, 656 $[M - Cl]^+$, 621 $[M - 2Cl]^{2+}$. IR(KBr disc): 1635, 1435, 995, 302, 291 cm^{-1}.

3.15. $[PdCl_2\{(Ph_2P)_2N(C_3H_5)\}]$ (**15**)

$(Ph_2P)_2N(C_3H_5)$ (104 mg, 0.2 mmol) and $[PdCl_2(cod)]$ (70 mg, 0.2 mmol) were dissolved in CH_2Cl_2 (10 cm^3) to yield an orange solution that was stirred for 30 min. The solvent was reduced to 1 cm^3 before precipitating a pale yellow solid upon addition of diethyl ether (20 cm^3) that was isolated by suction filtration. Yield: 125 mg, 85%. Microanalysis: Found (calculated for $C_{27}H_{25}P_2NPdCl_2$): C, 52.65 (53.80); H, 4.11 (4.18); N, 2.15 (2.32)%. $^{31}P\{^{1}H\}$ NMR ($CDCl_3$): 33.1 ppm. ^{1}H NMR ($CDCl_3$) δ 7.3 (m, 20 H, aromatic), 5.3 (m, 1H, CH), 4.9 (m, 2H, CH_2), 3.6 (m, 2H, NCH_2) ppm. FAB^+ MS: *m/z* 568 $[M - Cl]^+$, 531 $[M - 2Cl]^{2+}$. IR(KBr disc): 1638, 1435, 995, 329, 286 cm^{-1}.

3.16. $[Mo(CO)_4\{(Ph_2P)_2N(C_3H_5)\}]$ (**16**)

To a CH_2Cl_2 (10 cm^3) solution of $[Mo(CO)_4(nbd)]$ (100 mg, 0.3 mmol) was added dropwise a CH_2Cl_2 (10 cm^3) solution of $(Ph_2P)_2N(C_3H_5)$ (141 mg, 0.3 mmol). After stirring for 30 min the solvent was reduced to 2 cm^3 before addition of petroleum ether (b.p. 40–60) (20 cm^3) and storing overnight at −18 °C. The yellow solid precipitated was isolated by filtration and dried in vacuo. Yield: 127 mg, 60%. Microanalysis: Found (calculated for $C_{31}H_{25}P_2NO_4Mo$): C 58.44 (58.78), H 3.83 (3.98), N 2.18 (2.21)%. $^{31}P\{^{1}H\}$ NMR ($CDCl_3$): 92.1 ppm. ^{1}H NMR ($CDCl_3$) δ 7.3 (m, 20H, aromatic), 5.3 (m, 1H, CH), 4.7 (m, 2H, CH_2), 3.5 (m, 2H, NCH_2) ppm. FAB^+ MS: *m/z* 635 $[M]^+$, 579 $[M - 2CO]^+$, 523 $[M - 4CO]^+$. IR (KBr disc): 1887, 1434, 999 cm^{-1}.

3.17. $[\{(C_3H_5)N(PPh_2)_2\}(AuCl)_2]$ (**17**)

$(Ph_2P)_2N(C_3H_5)$ (21 mg, 0.05 mmol) and [AuCl(tht)] (32 mg, 0.1 mmol) were dissolved in $CHCl_3$ (2 cm^3) to yield a colourless solution. Diethyl ether (15 cm^3) was added to precipitate a colourless solid that was isolated by suction filtration. Yield: 20 mg, 45%. Microanalysis: Found (calculated for $C_{27}H_{25}P_2NAu_2Cl_2$): C, 36.22 (36.43); H, 2.67 (2.83); N, 1.55 (1.57)%. $^{31}P\{^{1}H\}$ NMR ($CDCl_3$): 83.8 ppm. ^{1}H NMR ($CDCl_3$) δ 7.3 (m, 20H, aromatic), 5.3 (m, 1H, CH), 4.8 (m, 2H, CH_2), 3.9 (m, 2H, NCH_2), ppm. FAB^+ MS: *m/z* 853 $[M - Cl]^+$, 819 $[M - 2Cl]^{2+}$. IR (KBr disc): 1655, 1436, 997, 282 cm^{-1}.

3.18. $[RuCl_2\{(Ph_2P)_2N(C_3H_5)\}_2]$ (**18**)

$(Ph_2P)_2N(C_3H_5)$ (150 mg, 0.4 mmol) and $[RuCl(\alpha\text{-}Cl)(\eta^6\text{-}p\text{-}MeC_6H_4{}^{i}Pr)_2]$ (54 mg, 0.1 mmol) were dissolved in CH_2Cl_2 (5 cm^3) to yield a dark red solution. The solvent was reduced to 1 cm^3 before addition of diethyl ether (10 cm^3) to precipitate a red solid that was isolated by suction filtration. Yield: 57 mg, 63%. Microanalysis: Found (calculated for $C_{54}H_{50}P_4N_2RuCl_2$) C 62.64 (63.41), H 5.39 (4.93), N 2.90 (2.74)%. $^{31}P\{^{1}H\}$ NMR ($CDCl_3$): 79.7 ppm. ^{1}H NMR ($CDCl_3$) δ 7.3 (m, 40H, aromatic), 5.9 (m, 2H, CH), 4.8 (m, 4H, CH_2), 3.5 (m, 4H, NCH_2) ppm. FAB^+ MS: *m/z* 1022 $[M]^+$, 987 $[M - Cl]^+$, 951 $[M - 2Cl]^{2+}$. IR (KBr disc): 1637, 1434, 998, 289, 273 cm^{-1}.

3.19. $[RhCp^*Cl_2\{(Ph_2P)_2N(C_3H_5)\}]$ (**19**)

$(Ph_2P)_2N(C_3H_5)$ (67 mg, 0.2 mmol) and $[\{RhCl(\alpha\text{-}Cl)(\eta^5\text{-}C_5Me_5)\}_2]$ (49 mg, 0.1 mmol) were dissolved in CH_2Cl_2 (5 cm^3) to yield a blood red solution. The solvent was reduced to 0.5 cm^3 before addition of diethyl ether (20 cm^3) to precipitate an orange solid that was isolated by suction filtration. Yield: 97 mg, 84%. Microanalysis: Found (calculated for $C_{37}H_{40}P_2NRhCl_2.0.25CH_2Cl_2$): C, 58.71 (59.20); H, 5.36 (5.40); N, 1.90 (1.85)%. $^{31}P\{^{1}H\}$ NMR ($CDCl_3$): 70.9 ppm, $^{1}J\{^{31}P–^{103}Rh\}$ 120 Hz. ^{1}H NMR ($CDCl_3$) δ 7.3 (m, 20H, aromatic), 5.5 (m, 1H, CH), 4.9 (m, 2H, CH_2), 3.8 (m, 2H, NCH_2), 1.6 (m, 15H, Cp*) ppm. FAB^+ MS: *m/z* 733 $[M]^+$, 698 $[M - Cl]^+$. IR (KBr disc): 1629, 1434, 997, 297, 273 cm^{-1}.

3.20. $[IrCp^*Cl_2\{(Ph_2P)_2N(C_3H_5)\}]$ (**20**)

$(Ph_2P)_2N(C_3H_5)$ (54 mg, 0.1 mmol) and $[\{IrCl(\alpha\text{-}Cl)(\eta^5\text{-}C_5Me_5)\}_2]$ (51 mg, 0.05 mmol) were dissolved in CH_2Cl_2 (10 cm^3) to yield a yellow solution. The solvent was reduced to 0.5 cm^3 before addition of diethyl ether (20 cm^3) to precipitate a yellow solid that was isolated by suction filtration and dried in vacuo. Yield: 76 mg, 72%. Microanalysis: Found (calculated for $C_{37}H_{40}P_2NIrCl_2.0.5CH_2Cl_2$): C, 51.64 (51.99); H, 4.54 (4.77); N, 1.59 (1.62)%. $^{31}P\{^{1}H\}$ NMR ($CDCl_3$): 37.3 ppm. ^{1}H NMR ($CDCl_3$) δ 7.3 (m, 20H, aromatic), 5.3 (m, 1H, CH), 4.8 (m, 2H, CH_2), 3.9 (m, 2H, NCH_2), 1.6 (m, 15H, Cp*) ppm. FAB^+ MS: *m/z* 823 $[M]^+$, 788 $[M - Cl]^+$. IR (KBr disc): 1629, 1434, 997, 310, 304 cm^{-1}.

4. Crystal data

Single crystal X-ray diffraction studies on crystals were performed using a Bruker SMART diffractometer with graphite-monochromated Mo Kα radiation (λ = 0.71073 Å). The structures were solved by direct

methods, the non-hydrogen atoms were refined with anisotropic displacement parameters; hydrogen atoms were fixed. Structural refinements were by the full-matrix least-squares method on F^2 using SHELXTL. **8** $C_{18}H_{20}Cl_2NPPd$, $M = 458.62$, Monoclinic, $a = 8.5139(2)$, $b = 10.6276(2)$, $c = 20.3072(1)$ Å, $\beta = 90.214(1)°$. $U = 1837.4(1)$ Å^3, $T = 125$ K, space group $P2_{1/c}$, $Z = 4$, ∞(Mo Kα) = 1.386 mm^{-1}. Of 7708 measured data, 2624 were unique, to give $R_1[I > 2\sigma(I)] = 0.0187$, wR 0.0460. **14** $C_{27}H_{25}NP_2Cl_2Pt$, $M = 691.41$, monoclinic, $a = 10.8188(16)$, $b = 14.661(2)$ $c = 16.563(2)$ Å, $\beta = 94.512(2)°$, $U = 2618.9(7)$ Å^3, space group $P2_{1/n}$, $Z = 4$, ∞(Mo Kα) = 5.700 mm^{-1}. Of 12 794 measured data, 3717 were unique to give $R_1[I > 2\sigma(I)] = 0.0430$ and $wR_2 = 0.1032$. **18** $C_{54}H_{50}N_2P_4Cl_2Ru$, $M = 1022.81$, triclinic, $a = 10.1826(17)$, $b = 11.1207(19)$ $c = 12.597(2)$ Å, $\alpha = 111.490(3)°$, $\beta = 95.557(3)°$, $\gamma = 113.376(3)°$, $U = 1168.3(3)$ Å^3, space group $P2_{1/n}$, $Z = 4$, ∞(Mo Kα) = 0.627 mm^{-1}. Of 5901 measured data, 3306 were unique to give $R_1[I > 2\sigma(I)] = 0.0288$ and $wR_2 = 0.0701$.

5. Supplementary material

Crystallographic Data for the structural analyses has been deposited with the Cambridge Crystallographic data centre, CCDC Nos. 242186–242188. Copies of this information may be obtained free of charge from The Director CCDC, 12 Union Road, Cambridge, CB2 1EZ UK. (Fax: +44 1223 336-033 or E-mail deposit@ccdc.cam.ac.uk or www:http://www.ccdc.cam.ac.uk.

References

[1] M.G. Andreu, A. Zapf, M. Beller, Chem. Commun. (Cambridge) (2000) 2475.
[2] H-P. Wu, R. Aumann, R. Froehlich, E. Wegelius, Organometallics 20 (2001) 2183.
[3] K. Hiraki, T. Matsunaga, H. Kawano, Organometallics 13 (1994) 1878.
[4] J.M. Moretó, S. Ricart, J. Organomet. Chem. 617-618 (2001) 334.
[5] J. Pares, J.M. Moretó, S. Ricart, J. Barluenga, F.J. Fananas, J. Organomet. Chem. 586 (1999) 247.
[6] J.M. Moretó, S. Ricart, K.-H. Dotz, E. Molins, Organometallics 20 (2001) 62.
[7] (a) R. Aumann, B. Jasper, M. Lage, B. Krebs, Chem. Ber. 127 (1994) 2475;
(b) R. Aumann, B. Jasper, R. Frolich, Organometallics 14 (1995) 231.
[8] M. Baya, P. Crochet, M.A. Esteruelas, E. Onate, Organometallics 20 (2001) 240.
[9] J. Eilmes, M. Ptaszek, K. Wozniak, Polyhedron 21 (2002) 7.
[10] S.M. Aucott, M.L. Clarke, A.M.Z. Slawin, J.D. Woollins, J. Chem. Soc. Dalton Trans. (2001) 972.
[11] S.M. Aucott, A.M.Z. Slawin, J.D. Woollins, J. Organomet. Chem. 582 (1999) 83.
[12] M.L. Clarke, A.M.Z. Slawin, M.V. Wheatley, J.D. Woollins, J. Chem. Soc., Dalton Trans. (2001) 3421.
[13] A.M.Z. Slawin, M. Wainwright, J.D. Woollins, New J. Chem. 24 (2000) 69.
[14] A.M.Z. Slawin, M. Wainwright, J.D. Woollins, J. Chem. Soc. Dalton Trans. (2002) 513.
[15] P. Bhattacharyya, J.D. Woollins, Polyhedron 14 (1995) 3367.
[16] R.J. Puddephatt, Chem. Soc. Rev. (1983) 99.
[17] I. Haiduc, I. Silaghi-Dumitrescu, Coord. Chem. Rev. 74 (1986) 127.
[18] B. Chaudret, B. Delavaux, R. Poilblanc, Coord. Chem. Rev. 86 (1988) 191.
[19] M.S. Balakrishna, V. Sreenivasa Reddy, S.S. Krishnamurthy, J.F. Nixon, J.C.T.R. Burckett St Laurent, Coord. Chem. Rev. 129 (1994) 1.
[20] H.C. Clark, L.E. Manzer, J. Organomet. Chem. 59 (1973) 411.
[21] A.M.Z. Slawin, M. Wainwright, J.D. Woollins, New J. Chem. 24 (2000) 69.
[22] A.M.Z. Slawin, J.D. Woollins, Q. Zhang, Inorg. Chem. Comm. 2 (1999) 386.
[23] S.M. Aucott, A.M.Z. Slawin, J.D. Woollins, J. Chem. Soc. Dalton Trans. (2000) 2559.
[24] A.M.Z. Slawin, J.D. Woollins, Q. Zhang, J. Chem. Soc. Dalton Trans. (2001) 621.
[25] S.M. Aucott, A.M.Z. Slawin, J.D. Woollins, J. Chem. Soc. Dalton Trans. (2001) 2279.
[26] A.M.Z. Slawin, M. Wainwright, J.D. Woollins, J. Chem. Soc. Dalton Trans. (2001) 2724.
[27] Z. Fei, A.M.Z. Slawin, J.D. Woollins, Polyhedron 20 (2001) 3355.
[28] A.M.Z. Slawin, J. Wheatley, M.V. Wheatley, J. Woollins, Polyhedron 22 (2003) 1397.
[29] Q. Zhang, G. Hua, P. Bhattacharyya, A.M.Z. Slawin, J.D. Woollins, Eur. J. Inorg. Chem (2003) 2426.
[30] D.K. Dutta, J.D. Woollins, A.M.Z. Slawin, D. Konwar, P. Das, M. Sharma, P. Bhattacharyya, S.M. Aucott, J. Chem. Soc. Dalton Trans. (2003) 2674.

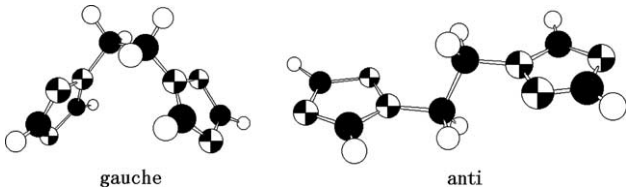

Chart 1. Structures of the *gauche* and *anti* conformations of the bte molecule.

(bte) and cadmium(II) salts with different anions NO_3^-, NO_2^-, ClO_4^- and NCS^-, and the structural characterization of five cadmium complexes, $\{[Cd(bte)_3](NO_3)_2\}_n$ (**1**), $\{[Cd(bte)_2(H_2O)_2](NO_3)_2\}_n$ (**2**), $\{[Cd(bte)(NO_2)_2]\}_n$ (**3**), $\{[Cd(bte)_2(H_2O)_2](H_2O)_2(ClO_4)_2\}_n$ (**4**) and $[Cd(bte)(NCS)_2]_n$ (**5**).

2. Experimental

2.1. General procedures

The flexible ligand 1,2-bis(1,2,4-triazol-1-yl)ethane (bte) was synthesized according to the literature method [12]. All other reagents and solvents employed were commercially available and used as received without further purification. The C, H, N microanalyses were carried out with a Perkin–Elmer 240C analyser. IR spectra were obtained for KBr pellets on a Nicolet 170SX FT-IR spectrophotometer in the 4000–400 cm^{-1} region. Thermogravimetric data were collected on Thermal Analyst 2100 TA Instrument and SDT 2960 Simutaneous TGA-DTA Instrument in flowing dinitrogen at a heating rate 10 °C/min.

2.2. Preparation of the complexes

2.2.1. $\{[Cd(bte)_3](NO_3)_2\}_n$ (*1*)

This compound was prepared under hydrothermal conditions. $Cd(NO_3)_2 \cdot 3H_2O$ (0.093 g, 0.3 mmol) and bte (0.148 g, 0.90 mmol) in the molar ratio of 1:3 in 16 ml H_2O were heated at 140 °C for three days. After cooling, the resultant solution was filtered and well-shaped colorless single crystals of **1** were obtained after the filtrate was allowed to stand at room temperature for two weeks. Yield: 0.142 g, 65%. *Anal.* Calc. $C_{18}H_{24}CdN_{20}O_6$: (728.97): C, 29.66; H, 3.32; N, 38.44. Found: C, 29.69; H, 3.37; N, 38.50%. IR data (cm^{-1}): 3109m, 1516s, 1462w, 1385vs, 1281s, 1211m, 1126s, 1015w, 984w, 961w, 884w, 694w, 683w, 656w.

2.2.2. $\{[Cd(bte)_2(H_2O)_2](NO_3)_2\}_n$ (*2*)

A methanolic solution (10 ml) of bte (0.098 g, 0.60 mmol) was added to an aqueous solution (10 ml) of $Cd(NO_3)_2 \cdot 3H_2O$ (0.093 g, 0.3 mmol) with stirring. The colorless single crystals of **2** were obtained after the mixture was allowed to stand for two weeks. Yield: 0.101 g, 56%. *Anal.* Calc. $C_{12}H_{20}CdN_{14}O_8$ (600.82): C, 23.99; H, 3.36; N, 32.65. Found: C, 24.01; H, 3.39; N, 32.71%. IR data (cm^{-1}): 3383m, 3113m, 1628w, 1528s, 1385vs, 1335s, 1285s, 1219w, 1138s, 1022w, 1007w, 899w, 833w, 675w, 656m.

2.2.3. $\{[Cd(bte)(NO_2)_2]\}_n$ (*3*)

An aqueous solution (2 ml) KNO_2 (0.077g, 0.9 mmol) was added to an aqueous solution (2 ml) of $Cd(ClO_4)_2 \cdot 6H_2O$ (0.126 g, 0.3 mmol) with stirring. The resultant solution was filtered. A methanolic solution (10 ml) of bte (0.098 g, 0.60 mmol) was added to the filtrate with stirring. The colorless single crystals of **3** were obtained after the mixture was allowed to stand for one week. Yield: 0.057 g, 51%. *Anal.* Calc. $C_6H_8CdN_8O_4$: (368.60): C, 19.55; H, 2.19; N, 30.41. Found: C, 19.56; H, 2.23; N, 30.47%. IR data (cm^{-1}): 3129m, 1528s, 1466w, 1354w, 1277s, 1215vs, 1130vs, 1011w, 988w, 899w, 853w, 675w, 648w.

2.2.4. $\{[Cd(bte)_2(H_2O)_2](H_2O)_2(ClO_4)_2\}_n$ (*4*)

A methanolic solution (10 ml) of bte (0.098 g, 0.6 mmol) was added slowly to an aqueous solution (10 ml) of $Cd(ClO_4)_2 \cdot 6H_2O$ (0.126 g, 0.3 mmol) with stirring. The mixture was stirred at room temperature and the resultant solution was filtered. After the filtrate was allowed to stand for three days, colorless single crystals of **4** were obtained. Yield: 0.113 g, 53%. *Anal.* Calc. $C_{12}H_{24}CdCl_2N_{12}O_{12}$: (711.74): C, 20.25; H, 3.40; N, 23.62. Found: C, 20.27; H, 3.45; N, 23.68%. IR data (cm^{-1}): 3438m, 3110m, 3090m, 1519s, 1474w, 1273s, 1216m, 1125vs, 1089vs, 1009m, 984m, 891w, 682m, 627m.

2.2.5. $[Cd(bte)(SCN)_2]_n$ (*5*)

A H_2O/MeOH (1:1, v/v) solution (15 ml) of $Cd(NO_3)_2 \cdot 3H_2O$ (0.154 g, 0.5 mmol) and KSCN (0.097 g, 1 mmol) was added to one side of a "H-shape" tube equipped with a frit, and 15 ml H_2O/MeOH solution (1:1, v/v) of bte (0.082 g, 0.5 mmol) was added to the another side of the "H-shape" tube. After about one month, well-shaped colorless single crystals of **5** were obtained. Yield: 0.071 g, 36%. *Anal.* Calc. $C_8H_8CdN_8S_2$: (392.74): C, 24.47; H, 2.05; N, 28.54. Found: C, 24.50; H, 2.07; N, 28.59%. IR data (cm^{-1}): 3118w, 2110vs, 1524s, 1445w, 1386w, 1288m, 1208w, 1135s, 1010w, 984w, 904w, 872w, 707w, 674w, 644w.

2.3. X-ray crystallography

All data collections were performed at a temperature of 193.15 K on a Rigaku Mercury CCD diffractometer with the ω-scan technique. The structures were solved by direct methods and refined with the full-matrix

Table 1
Crystallographic data for the complexes **1**–**5**

	1	**2**	**3**	**4**	**5**
Empirical formula	$C_{18}H_{24}CdN_{20}O_6$	$C_{12}H_{20}CdN_{14}O_8$	$C_6H_8CdN_8O_4$	$C_{12}H_{24}CdCl_2N_{12}O_{12}$	$C_8H_8CdN_8S_2$
Formula weight	728.97	600.82	368.60	711.74	392.74
Temperature (K)	193.15	193.15	193.15	193.15	193.15
Wavelength (Å)	0.71073	0.71073	0.71073	0.71073	0.71073
Crystal system	trigonal	monoclinic	monoclinic	triclinic	triclinic
Space group	$R\bar{3}$	$P2_1/c$	$P2_1/c$	$P\bar{1}$	$P\bar{1}$
a (Å)	19.410(3)	8.708(5)	14.079(4)	8.311(2)	5.904(2)
b (Å)	19.410(3)	12.403(7)	4.4526(13)	8.601(2)	6.530(2)
c (Å)	7.5413(15)	10.477(6)	18.532(6)	10.341(3)	8.993(3)
α (°)	90.000	90.000	90.000	66.367(10)	104.303(7)
β (°)	90.000	100.629(7)	96.308(7)	76.888(13)	98.978(9)
γ (°)	120.000	90.000	90.000	77.197(12)	96.373(7)
V (Å^3)	2460.5(7)	1112.2(12)	1154.7(6)	652.5(3)	327.8(2)
Z	3	2	4	1	1
F(0 0 0)	1104	604	720	358	192
ρ (Mg m^{-3})	1.476	1.794	2.120	1.811	1.990
μ (mm^{-1})	0.730	1.055	1.919	1.121	1.982
Data/restrain/parameters	1237/5/111	2521/3/168	2593/0/172	2845/6/212	1417/0/88
Goodness-of-fit S	1.093	1.230	1.056	1.028	1.034
R_1 [$I > 2\sigma(I)$]	0.0324	0.0360	0.0490	0.0365	0.0169
wR_2 [all data]	0.0890	0.0743	0.1318	0.0990	0.0447

least-squares technique using the SHELXS-97 and SHELXL-97 programs [13]. Anisotropic thermal parameters were assigned to all non-hydrogen atoms. The hydrogen atoms of the bte ligands were generated geometrically. The hydrogen atoms of the water molecules were located from the difference Fourier maps. The crystallographic data for **1**–**5** are listed in Table 1. The selected bond lengths and angles for **1**–**5** are listed in Table 2.

3. Results and discussion

3.1. Preparation of the complexes

The hydrothermal reaction of bte and $Cd(NO_3)_2 \cdot 3H_2O$ resulted in a double interpenetrating three-dimensional α-poloniumn cubic network, **1**. Direct treatment of bte and cadmium salts with poor coordination ability anions, NO_3^- and ClO_4^-, under the same reaction conditions produced a two-dimensional (4,4) network, **2**, and an infinite double chain, **4**. For compounds **2** and **4**, we found that they both have a Cd/bte molar ratio of 1:2. The different structures of **2** and **4** show that the supramolecular topologies are highly influenced by the counteranions. The key factor governing the structural topologies of **1** and **2** is the Cd/bte molar ratio (1:3 in **1** and 1:2 in **2**). As NO_2^- and NCS^- not only can act as counteranions to sustain neutral charge, but also have various coordination modes, and thus can provide a suitable "building block" for assembling novel inorganic/organic hybrid materials. We want to introduce these anion ligands into the Cd/bte reaction mixture as co-ligands in order to prepare some novel bte/Cd complexes. Mixing of $Cd(ClO_4)_2 \cdot 6H_2O$, KNO_2 and bte with a molar ratio of 1:2:1 in $MeOH/H_2O$ solution resulted in a two-dimensional rhombic network, **3**, via nitrato bridging and a Cd/bte molar ratio of 1:1. $Cd(NO_3)_2 \cdot 3H_2O$ and KNCS react with bte with a molar ratio of 1:2:1 or 1:2:2 in $MeOH/H_2O$ solution through the slow diffusion method to produce a two-dimensional rhombic network, **5**, via NCS^- bridging.

3.2. Crystal structures

The X-ray analysis revealed that **1** is composed of a $[Cd(bte)_3]_n^{2n+}$ macrocation and disordered NO_3^- anions. Each cadmium(II) atom is located on a $\bar{3}$ position with an octahedral geometry (Fig. 1). Each cadmium(II) atom is coordinated by six exodentate nitrogen atoms at the 4-position of the triazole rings from the six individual bte ligands, all of which are equivalent. The N–Cd–N bond angles are close to 90° [89.14(7)° and 90.86(7)°]. Each bte ligand adopts the *anti* conformation and bridges two adjacent cadmium(II) atoms, building up polymers to an open three-dimensional α-poloniumn cubic network (Fig. 2(a)). The Cd···Cd separation is 12.2825(15) Å through the bte ligand. There are double interpenetrating α-poloniumn cubic networks in the crystal (Fig. 2(b)) and channels with dimensions of approximately 6×6 Å are formed, which are filled by disordered NO_3^- anions.

The structure of **2** consists of a two-dimensional (4,4) network, which is obviously different from the open three-dimensional α-poloniumn cubic network in **1**. The key factor governing the structural topologies of **1**

Table 2
Selected bond lengths (Å) and angles (°) for complexes **1**–**5**

1			
Bond lengths			
Cd(1)–N(3)	2.3473(19)	Cd(1)–N(3)^{i}	2.3473(19)
Cd(1)–N(3)^{ii}	2.3473(19)	Cd(1)–N(3)^{iii}	2.3473(19)
Cd(1)–N(3)^{iv}	2.3473(19)	Cd(1)–N(3)^{v}	2.3473(19)
Bond angles			
N(3)–Cd(1)–N(3)^{i}	90.86(7)	N(3)–Cd(1)–N(3)^{ii}	89.14(7)
N(3)–Cd(1)–N(3)^{iii}	179.998(1)	N(3)^{i}–Cd(1)–N(3)^{iv}	180.0
N(3)^{ii}–Cd(1)–N(3)^{v}	180.0	N(3)^{iii}–Cd(1)–N(3)^{v}	89.15(7)
2			
Bond lengths			
Cd(1)–O(1)	2.299(2)	Cd(1)–O(1A)	2.299(2)
Cd(1)–N(3)	2.314(2)	Cd(1)–N(3A)	2.314(2)
Cd(1)–N(6B)	2.335(2)	Cd(1)–N(6C)	2.335(2)
Bond angles			
N(3)–Cd(1)–N(3A)	180.00(12)	N(3)–Cd(1)–N(6C)	90.56(8)
N(3)–Cd(1)–N(6B)	89.44(8)	N(6B)–Cd(1)–N(6C)	180.00(14)
O(1)–Cd(1)–O(1A)	180.0(2)	O(1)–Cd(1)–N(3)	91.14(10)
O(1)–Cd(1)–N(6B)	92.40(9)	O(1)–Cd(1)–N(6C)	87.60(9)
3			
Bond lengths			
Cd(1)–N(3)	2.271(4)	Cd(1)–N(6)	2.291(4)
Cd(1)–O(1)	2.384(5)	Cd(1)–O(2)	2.509(5)
Cd(1)–O(3)	2.359(6)	Cd(1)–O(4)	2.426(8)
Cd(1)–O(1A)	2.425(5)		
Bond angles			
N(3)–Cd(1)–N(6)	165.09(15)	O(1)–Cd(1)–O(2)	50.84(19)
O(1)–Cd(1)–O(3)	107.6(2)	O(1)–Cd(1)–O(4)	67.9(4)
O(1)–Cd(1)–O(1A)	135.6(3)	O(2)–Cd(1)–O(3)	157.1(2)
O(2)–Cd(1)–O(4)	116.2(3)	O(3)–Cd(1)–O(4)	48.4(3)
O(1A)–Cd(1)–O(2)	85.39(19)	O(3)–Cd(1)–O(1A)	114.1(2)
O(1A)–Cd(1)–O(4)	155.6(5)	N(3)–Cd(1)–O(1)	99.36(16)
N(3)–Cd(1)–O(1A)	83.08(16)	N(3)–Cd(1)–O(2)	87.00(15)
N(3)–Cd(1)–O(3)	106.40(18)	N(3)–Cd(1)–O(4)	86.5(3)
N(6)–Cd(1)–O(1)	88.01(17)	N(6)–Cd(1)–O(1A)	82.62(16)
N(6)–Cd(1)–O(2)	87.71(16)	N(6)–Cd(1)–O(3)	83.35(17)
N(6)–Cd(1)–O(4)	108.3(3)		
4			
Bond lengths			
Cd(1)–O(1)	2.346(3)	Cd(1)–O(1)^{i}	2.346(3)
Cd(1)–N(3)	2.313(2)	Cd(1)–N(3)^{i}	2.313(2)
Cd(1)–N(6)^{ii}	2.333(3)	Cd(1)–N(6)^{iii}	2.333(3)
Bond angles			
N(3)–Cd(1)–N(3)^{i}	180.00(10)	N(3)–Cd(1)–N(6)^{ii}	94.17(9)
N(3)–Cd(1)–N(6)^{iii}	85.83(9)	N(6)^{ii}–Cd(1)–N(6)^{iii}	180.00(12)
O(1)–Cd(1)–O(1)^{i}	180.00(13)	O(1)–Cd(1)–N(3)	90.21(11)
O(1)^{i}–Cd(1)–N(3)	89.79(11)	O(1)–Cd(1)–N(6)^{ii}	93.11(11).
5			
Bond lengths			
Cd(1)–N(3)	2.3189(15)	Cd(1)–N(3A)	2.3189(15)
Cd(1)–N(4)	2.3034(17)	Cd(1)–N(4A)	2.3034(17)
Cd(1)–S(1B)	2.7565(8)	Cd(1)–S(1C)	2.7565(8)
Bond angles			
N(3)–Cd(1)–N(3A)	180.0	N(3)–Cd(1)–N(4)	88.68(6)
N(3)–Cd(1)–N(4A)	91.32(6)	N(4)–Cd(1)–N(4A)	180.00(11)

Table 2 (*continued*)

S(1B)–Cd(1)–S(1C)	180.000(19)	N(3)–Cd(1)–S(1B)	91.34(4)
N(3)–Cd(1)–S(1C)	88.66(4)	N(4)–Cd(1)–S(1B)	87.25(5)

Symmetry codes: Complex **1**: (i) $-x+y$, $-x+1$, z, (ii) $y-1/3$, $-x+y+1/3$, $-z+1/3$ and (iii) $-x+2/3$, $-y+4/3$, $-z+1/3$ (iv) x-$y+2/3$, $x+1/3$, $-z+1/3$ and (v) $-y+1$, $x-y+1$, z.

Complex **2**: (A) $-x$, $-y$, $-z$, (B) $-x$, $y-0.5$, $-z-0.5$ and (C) x, $-y+0.5$, $z+0.5$.

Complex **3**: (A) x, $y+1$, z.

Complex **4**: (i) $-x$, $-y$, $-z$, (ii) $-x$, $-y+1$, $-z$ and (iii) x, $y-1$, z.

Complex **5**: (A) $-x$, $-y$, $-z$ (B) $x-1$, y, z and (C) $-x+1$, $-y$, $-z$.

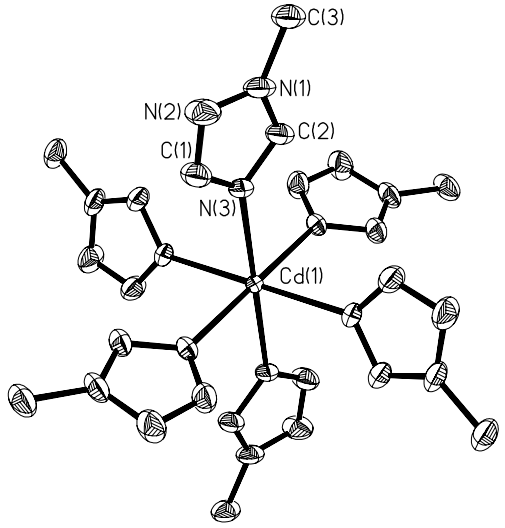

Fig. 1. ORTEP drawing of **1** with the atom numbering, showing the cadmium(II) coordination environment.

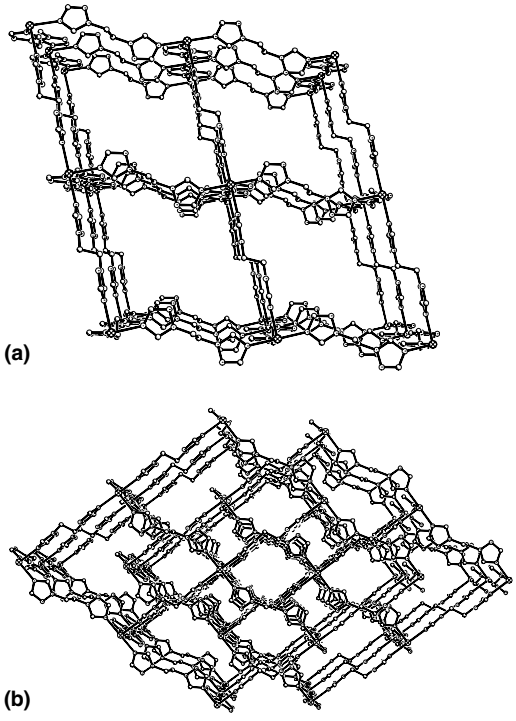

Fig. 2. (a) View of the three-dimensional α-poloniumn cubic network in **1** showing the channels and (b) view of the double interpenetrating three-dimensional α-poloniumn cubic networks in **1**.

and **2** is the Cd/bte molar ratio (1:3 in **1** and 1:2 in **2**). The local geometry of the cadmium(II) atom in **2** is a distorted octahedral arrangement with two water molecules in *trans* positions and four triazole nitrogen atoms from the four bte ligands in the basal plane (Fig. 3). Each bte ligand connects two cadmium(II) atoms to form a two-dimensional (4,4) network containing square $Cd_4(bte)_4$ units (Fig. 4(a)). The two-dimensional network structure consists of puckered rhombus grids with dimensions of 8.1×8.1 Å. The most intriguing feature of the structure is that the basic grid of the two-dimensional network is puckered [14] (Fig. 4(b)), which is different from those observed in the previous grid-like structures where the basic grids are usually coplanar or quasi-coplanar [15]. The puckered shape of the basic grid in **2** is understandable because the bte ligand exhibits the *gauche* conformation in **2**. We note that the ultimate structure of a two-dimensional network is wave-like with a tightly puckered structure containing nitrate anions. There are hydrogen bonding interactions between the hydrogen atoms of the coordination water molecules and the oxygen atoms of the nitrate anions [O(1)–H(WA)···O(3) (x, $-y+0.5$, $z+0.5$), 2.722 Å and O(1)–H(WB)···O(4), 2.850 Å].

The structure of **3** is composed of a two-dimensional rhombic network. The coordination geometry of the cadmium(II) atom is a distorted pentagonal–bipyramid with two nitrogen atoms from the two bte ligands in

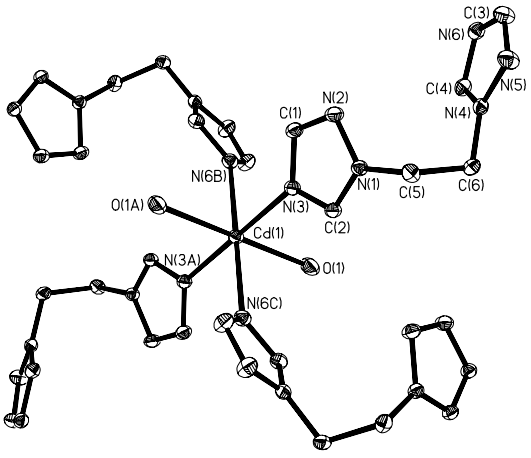

Fig. 3. ORTEP drawing of the cadmium(II) coordination environment in **2** and the atom numbering scheme.

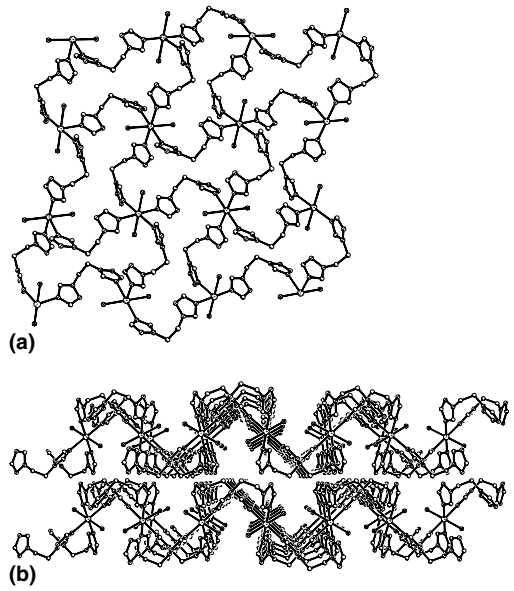

Fig. 4. (a) View of the two-dimensional (4,4) network in **2** along the *a* direction and (b) view of the tightly packed structure in **2** along the *c*-direction, only two layers are shown for clarity.

axial positions and five oxygen atoms from the three nitrite anions in the basal plane (Fig. 5(a)). This cadmium(II) coordination geometry is similar to that of di(nitrito)bis(isonicotonamide)aquacadmium, in which the cadmium(II) atom is in a distorted pentagonal–bipyramidal coordination with the two bidentate NO_2^- groups and one H_2O molecule in the equatorial plane and two nitrogen atoms from the two monodentate isonicotinamide ligands occupying the apexes [16]. There are two kinds of nitrite anions in **3**. One is a disordered nitrite anion with the end-to-end $\mu_{1,3}$-ONO-bridging mode, which is common in nitrite compounds [17]. An occupancy factor of 0.5 was assigned to the N(8), N(9), O(3), O(4), O(5) and O(6) atoms for the disordered nitrite. The other is a tridentate nitrite anion $\mu_{1,3}$-ONO chelating one cadmium(II) atom and one oxygen atom bridging two cadmium(II) atoms. This tridentate nitrite coordination, which was first reported by Kahn in $[Ni(en)_2(NO_2)]_2[B(C_6H_5)_4]$ [17b], has not been observed before in cadmium compounds. The tridentate nitrite anions link the cadmium(II) atoms and form a one-dimensional linear chain with a Cd···Cd distance of 4.453(3) Å. Each bte ligand has an *anti* conformation and links two cadmium(II) atoms with Cd···Cd distances of 12.357(3) and 12.457(3) Å, building up the one-dimensional chains to form a two-dimensional rhombic network with dimensions of 4.4×12.4 Å (Fig. 5(b)).

The structure of **4** is a one-dimensional double chain. The coordination geometry of the cadmium(II) atom in **4** is a distorted octahedral, in the equatorial plane of which is located four nitrogen atoms from the four bte ligands, and the axial positions are occupied by two oxygen atoms from the two water molecules (Fig. 6(a)), which is similar to the coordination geometry of the cadmium(II) atom in **2**. The Cd/bte molar ratios are both

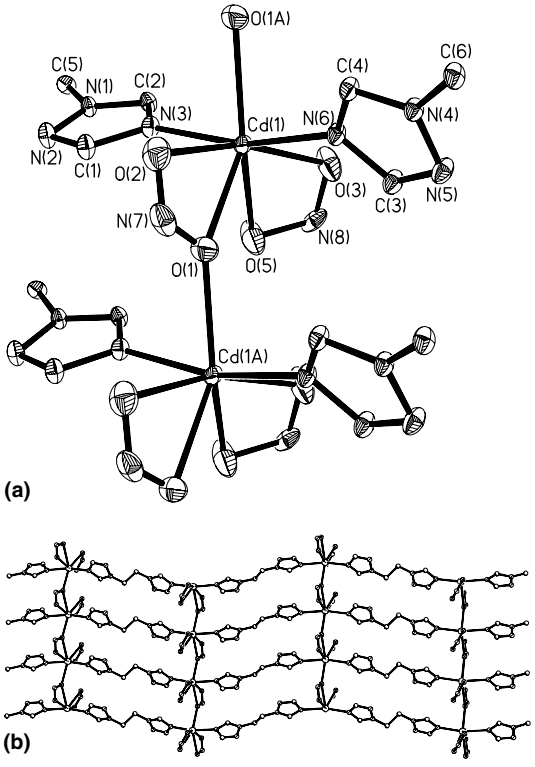

Fig. 5. (a) Drawing of the cadmium(II) coordination environment in **3** and the atom numbering scheme and (b) view of the two-dimensional rhombic network in **3**.

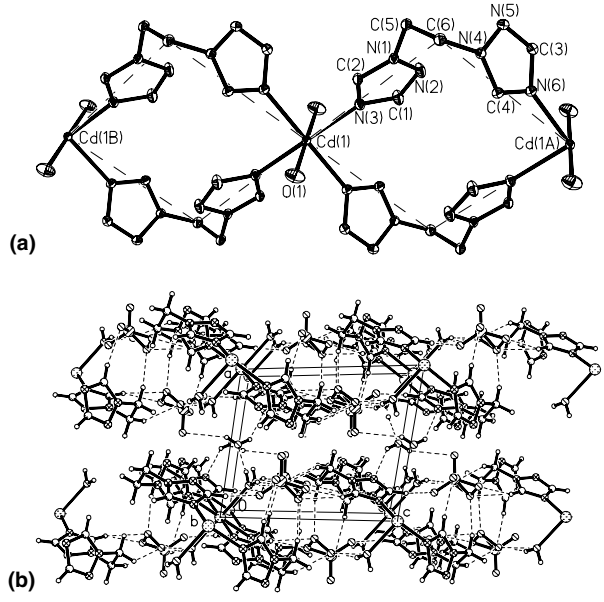

Fig. 6. (a) Drawing of the cadmium(II) coordination environment in **4** and the atom numbering scheme and (b) view of the cell stacking in **4**.

1:2 for compounds **2** and **4**. The differences between **4** and **2** are that one bte ligand bridges two equivalent cadmium(II) atoms in **2** while two bte ligands bridge two equivalent cadmium(II) atoms in **4**. So **4** forms a one-dimensional double chain while **2** forms a two-dimensional (4,4) network. The different structures of **2** and **4** show that the supramolecular topologies are highly influenced by the counteranions. The bte ligand exhibits the *gauche* conformation in **4**. Two bte ligands are wrapped around each other and are held together by cadmium(II) atoms forming a one-dimensional double chain. A rhombic network with a size of 6.6×5.8 Å is formed. As in other double-stranded chain complexes [4c,5b,8,10a,10c,14,18], each chain consists of 18-membered rings, $[Cd_2(bte)_2]$, in which two cadmium(II) atoms are joined by two bte molecules. The Cd···Cd separation across the bte ligand is 8.601(2) Å, which is similar to the Cd···Cd separation of 8.118(2) Å in **2**.

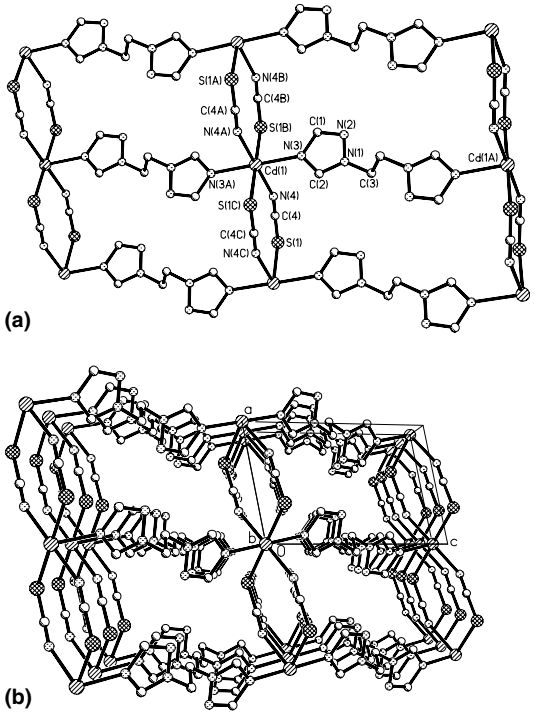

Fig. 7. (a) Drawing of the cadmium(II) coordination environment in **5** and the atom numbering scheme and (b) view of the stacking layers in **5** along the *b*-direction.

There are hydrogen bonding interactions between the coordination water molecules and the solvent water and the perchlorate anions [O(1)–H(W1)···O(8) ($x + 1$, $y - 1$, z) 2.687 Å; O(1)–H(W2)···O(7), 2.690 Å] (Fig. 6(b)). These are also hydrogen bonding interactions between the solvent water molecule and the perchlorate anion and the uncoordinated nitrogen atom of the triazole rings of the bte ligand [O(8)–H(W3)···O(2) ($-x$, $-y + 1$, $-z$) 3.185 Å, O(8)–H(W4)···N(2) 2.978 Å].

The crystal structure of **5** is a two-dimensional rhombic network. Each cadmium(II) atom in **5** is located on an inversion center and coordinated by two thiocyanate nitrogen atoms [Cd–N(SCN), 2.3082(18) Å] and two thiocyanate sulfur atoms [Cd–S(SCN), 2.7560(8) Å] in a *trans* geometry in the equatorial plane, resulting in a two-dimensional network containing eight-membered $[Cd_2(SCN)_2]$ rings (Fig. 7(a)). The μ-SCN-*N*,*S* coordination mode for the cadmium(II) atom is one of the usual coordination fashions [19] since the cadmium(II) atom is between hard base and soft base according to the hard–soft acid–base concept. Two nitrogen atoms of two bte ligands complete the remaining two axial positions around the six-coordinate cadmium(II) center in the distorted octahedron [Cd–N(bte), 2.3237(16) Å]. The bte ligands exhibit the *anti* conformation in **5**. The cadmium(II) atoms are bridged by the bte ligands and the double μ-NCS^- anions, resulting in the two-dimensional rhombic network. The Cd···Cd distances bridged via the μ-NCS^- anions and the bte ligands are 5.904(2) and 12.350(3) Å, respectively. The rhombic network is composed of Cd_4 units with dimensions of 12.35 Å $\times$ 5.90 Å. The parallel two-dimensional network sheets stack on each other along the *b*-direction and the distance between adjacent sheets is 6.529(2) Å (Fig. 7(b)).

The conformations of the bte ligands, the $N_{triazoe}$–$(C–C)_{ethane}$–$N_{triazole}$ torsion angles, the dihedral angles between the two triazole rings of the bte ligands and the Cd···Cd distances through the bte ligands in the five complexes are listed in Table 3. The bte ligands act in the *anti* conformation in **1**, **3** and **5** and in the *gauche* conformation in **2** and **4**. The torsion angles and the dihedral angles show great differences between the bte ligands with the *gauche* and *anti* conformations. The torsion angles and the dihedral angles of the bte ligands

Table 3
The dihedral angles (°) of the two triazole rings and the N–$(C–C)_{ethane}$–N torsion angle (°) of the bte ligands and Cd···Cd separations through the bte ligands (Å) for the five complexes

Complexes	Dihedral angle of the two triazole planes	Torsion angle $N_{triazole}$–$(C–C)_{ethane}$–$N_{triazole}$	Cd···Cd separations *through* the bte ligands
1	0.00	180.00	12.2825(15)
2	35.37(13)	67.38(28)	8.118(2)
3	0.00	180.00	12.357(3), 12.457(3)
4	56.54(15)	63.39(34)	8.601(2)
5	0.00	180.00	12.350(3)

with the *anti* conformation are 180.0° and 0.0°, respectively, in **1**, **3** and **5**. The torsion angles of the bte ligands with the *gauche* conformation show slight differences, 67.38(28)° in **2** and 63.39(34)° in **4**, but the dihedral angles of the bte ligands with the *gauche* conformation show large differences, 35.37(13)° in **2** and 56.54(15)° in **4**, which may be ascribed to the different coordination modes of the bte ligands. The Cd···Cd distances through the bte ligands with the *gauche* conformation are 8.118 Å in **2** and 8.601(2) Å in **4**, and the Cd···Cd distances through the bte ligands with the *anti* conformation are 12.2825(15) Å in **1**, 12.357(3), 12.457(3) Å in **3** and 12.350(3) Å in **5**. The structural data shows the flexibility of the bte ligand in the five coordination polymers.

3.3. IR and thermogravimetric analysis

The very strong absorption at 1385 cm^{-1} in **1** and **2** is attributed to the free nitrate anions. The very strong absorption bands at 1215 and 1130 cm^{-1} and weak absorption at 853 cm^{-1} in **3** suggest two coordinating mode of the nitrite anions [17], which was confirmed by the X-ray diffraction analysis. The very strong absorption bands at 1125vs and 1089vs in **4** are attributed to the perchlorate anions. The very strong C≡N stretching vibration of the thiocyanate anions in **5** at 2110 cm^{-1} suggests a bridging mode [20].

Thermal analysis of **1** shows that **1** is stable up to 252 °C. Thermal analysis of **2** shows that the coordinated water molecules are lost in a continuous fashion (Obsd. 6.3; Calcd. 6.0%) between 110 and 170 °C, then the bte ligands begin to be lost in a continuous fashion. **3** is stable up to 240 °C. Thermal analysis of **4** shows that the water molecules are lost in a continuous fashion in 60–120 °C (Obsd. 10.2; Calc. 10.1%) and the bte ligands begin to be lost above 322 °C. Complex **5** is stable up to 180 °C.

4. Conclusion

In spite of the similarity of the building blocks used, the products display quite different structures. The isolated five coordination complexes include a double interpenetrating three-dimensional α-poloniumn cubic network (**1**), a two-dimensional (4,4) network (**2**), a two-dimensional rhombic network (**3** and **5**), and a one-dimensional double chain (**4**) formed by coordination bonds. The variety of the observed structural motifs confirms that the rationalization of the resulting topologies is still difficult. Many factors play a role in the formation of the final products: (i) the counterions effects (NO_3^- in **1** and **2**, NO_2^- in **3**, ClO_4^- in **4** and NCS^- in **5**); (ii) the conformational flexibility of the bte ligand (the *anti* conformation in **1**, **3** and **5**, the *gauche* conformation in **2** and **4**); (iii) the synthesis methods (direct reaction of $Cd(NO_3)_2 \cdot 3H_2O$ with the bte ligand) resulted in the two-dimensional (4,4) network **2**, while the hydrothermal reaction of $Cd(NO_3)_2 \cdot 3H_2O$ and the bte ligand resulted in the three-dimensional α-poloniumn cubic network **1**; (iv) the molar ratios of the metal: ligand (1:3 in **1**, 1:2 in **2** and **4**, 1:1 in **3** and **5**). The results demonstrate the feasibility of achieving various polymeric frameworks by self-assembly of the flexible bis(triazole) ligand and metal salts and may provide useful information for crystal engineering.

Acknowledgments

This work was supported by the Natural Science Foundation of the University of Jiangsu Province (Grant No. 03KJB150118), the Funds of the State Key Laboratory of Coordination Chemistry and the Funds of the Key Laboratory of Organic Synthesis of Jiangsu Province, PR China.

Appendix A. Supplementary data

Crystallographic data for the structural analysis have been deposited with the Cambridge Crystallographic Data Centre, CCDC Nos. 234269–234273 (for compounds **1** to **5**, respectively). These data can be obtained free of charge via www.ccdc.cam.ac.uk/conts/retrieving.html (or from the Cambridge Crystallographic Center, 12 Union Road, Cambridge CB2 1EZ, UK; Fax: (+44)1223-336033; or deposit@ccdc.cam.ac.uk). Supplementary data associated with this article can be found, in the online version at doi:10.1016/j.poly.2004.09.025.

References

[1] (a) S.R. Batten, R. Robson, Angew. Chem. Int. Ed. 37 (1998) 1460;
(b) M.J. Zaworotko, Chem. Soc. Rev. (1994) 283;
(c) O.M. Yaghi, H. Li, C. Davis, D. Richardson, T.L. Groy, Acc. Chem. Res. 31 (1998) 474.
[2] (a) M. Fujita, Y.J. Kwon, S. Washizu, K. Ogura, J. Am. Chem. Soc. 116 (1994) 1151;
(b) S.I. Noro, R. Kitaura, M. Kondo, S. Kitagawa, T. Ishii, H. Matsuzaka, M. Yamashita, J. Am. Chem. Soc. 124 (2002) 2568.
[3] (a) C. He, B.G. Zhang, C.Y. Duan, J.H. Li, Q.J. Meng, Eur. J. Inorg. Chem. (2000) 2549;
(b) G.J. Halder, C.J. Kepert, B. Moubaraki, K.S. Murray, J.D. Cashion, Science 298 (2002) 1762.
[4] (a) Q.T.L. Hennigar, D.C. Macquarrie, P. Losier, R.D. Rogers, M.J. Zaworotko, Angew. Chem. Int. Ed. 36 (1997) 972;
(b) L. Carlucci, G. Ciani, D.M. Proserpio, S. Rizzato, Chem. Commun. (2000) 1319;
(c) M. Fujita, Y.J. Kwon, M. Miyazawa, K. Ogura, J. Chem. Soc., Chem. Commun. (1994) 1977.

[5] (a) L. Carlucci, G. Ciani, M. Moret, D.M. Proserpio, S. Rizzato, Angew. Chem. Int. Ed. 39 (2000) 1506;
(b) M.T. Bujaci, X. Wang, S. Li, C. Zheng, Inorg. Chim. Acta 333 (2002) 152;
(c) M.L. Tong, Y.M. Wu, J. Ru, X.M. Chen, H.C. Cheng, S. Kitagawa, Inorg. Chem. 41 (2002) 4846.
[6] (a) A.M. Schuitema, M. Engelen, I.A. Koval, S. Gorter, W.L. Driessen, J. Reedijk, Inorg. Chim. Acta 324 (2001) 57;
(b) K. Flinzner, A.F. Stassen, A.M. Mills, A.L. Spek, J.G. Haasnoot, J. Reedijk, Eur. J. Inorg. Chem. (2003) 671.
[7] (a) Effendy, F. Marchetti, C. Pettinari, R. Pettinari, B.W. Skelton, A.H. White, Inorg. Chem. 42 (2003) 112;
(b) L.F. Tang, Z.H. Wang, J.F. Chai, W.L. Jia, Y.M. Xu, J.T. Wang, Polyhedron 19 (2000) 1949.
[8] (a) G.A.V. Albada, R.C. Guijt, J.G. Haasnoot, M. Lutz, A.L. Spek, J. Reedijk, Eur. J. Inorg. Chem. (2000) 121;
(b) Q.H. Zhao, H.F. Li, X.F. Wang, Z.D. Chen, New J. Chem. 26 (2002) 1709.
[9] B.Z. Li, X. Zhu, B.L. Li, Y. Zhang, J. Mol. Struct. 691 (2004) 159.
[10] (a) J.H. Zhou, X. Zhu, Y.N. Zhang, Y. Zhang, B.L. Li, Inorg. Chem. Commun. 7 (2004) 949;
(b) X. Zhu, B.Z. Li, J.H. Zhou, B.L. Li, Y. Zhang, Acta Crystallogr., Sect. C 60 (2004) 191;
(c) B.L. Li, B.Z. Li, X. Zhu, L.M. Zhu, Y. Zhang, Acta Crystallogr., Sect. C 59 (2003) 350;
(d) B.L. Li, J.Z. Zou, C.Y. Duan, Y.J. Liu, X.W. Wei, Z. Xu, Acta Crystallogr., Sect. C 55 (1999) 165;
(e) B.L. Li, Z. Xu, Z.B. Cao, L.M. Zhu, K.B. Yu, Transition Met. Chem. 24 (1999) 622.
[11] (a) O.K. Jung, Y.J. Kim, Y.A. Lee, H.K. Chae, H.G. Jang, J. Hong, Inorg. Chem. 40 (2001) 2105;
(b) O.S. Jung, Y.J. Kim, Y.A. Lee, K.M. Park, S.S. Lee, Inorg. Chem. 42 (2003) 844;
(c) M. Du, X.H. Bu, Z. Huang, S.T. Chen, Y.M. Guo, Inorg. Chem. 42 (2003) 552;
(d) M.A. Withersby, A.J. Blake, N.R. Champness, P. Hubberstey, W.S. Li, M. Schröder, Angew. Chem. Int., Ed. Engl. 36 (1997) 2327;
(e) L. Carlucci, G. Ciani, P. Macchi, D.M. Proserpio, S. Rizzato, Chem.-Eur. J. 5 (1999) 237.
[12] J. Torres, J.L. Lavandera, P. Cabildo, R.M. Claramunt, J. Elguero, J. Heterocycl. Chem. 25 (1988) 771.
[13] G.M. Sheldrick, SHELXS-97 and SHELXL-97, University of Göttingen, Germany, 1997.
[14] J.H. Luo, M.C. Hong, R.H. Wang, D.Q. Yuan, R. Cao, L. Han, Y.Q. Xu, Z.Z. Lin, Eur. J. Inorg. Chem. (2003) 3623.
[15] (a) K. Biradha, M. Fujita Soc., J. Chem., Dalton Trans. (2000) 3805;
(b) K. Biradha, M. Fujita, Chem. Commun. (2001) 15;
(c) K. Biradha, Y. Hongo, Fujita, Angew. Chem. Int. Ed. 39 (2000) 3843.
[16] M.I. Matsaberidze, A.S. Batsanov, Y.T. Struchkov, G.V. Tsintsadze, Koord. Khim. 111 (1985) 1550.
[17] (a) A. Escuer, R. Vicente, X. Solans, J. Chem. Soc., Dalton Trans. (1997) 531;
(b) A. Gleizes, A. Meyer, M.A. Hitchman, O. Kahn, Inorg. Chem. 21 (1982) 2257;
(c) U. Florke, H.J. Haupt, P. Chaudhuri, J. Chem. Soc., Dalton Trans. (1998) 3801;
(d) M.A. Hitchman, G. Rowbottom, Coord. Chem. Rev. 42 (1982) 55.
[18] (a) M.L. Hernández, M.G. Barandika, M.K. Urtiaga, R. Cortés, L. Lezama, M.I. Arriotua, T. Rojo, J. Chem. Soc., Dalton Trans. (1999) 1401;
(b) O.S. Jung, S.H. Park, D.C. Kim, K.M. Lin, Inorg. Chem. 37 (1998) 610.
[19] (a) H. Zhang, X.M. Wang, K.C. Zhang, B.K. Teo, Coord. Chem. Rev. 183 (1999) 157;
(b) J.H. Luo, M.C. Hong, R.H. Wang, R. Cao, Q. Shi, J.B. Weng, Eur. J. Inorg. Chem. (2003) 1778;
(c) S. Sailaja, K.R. Reddy, M.V. Rajasekharan, C. Hureau, E. Riviere, J. Cano, J.J. Girerd, Inorg. Chem. 42 (2003) 180.
[20] K. Nakamoto, Infrared and Raman Spectra of Inorganic and Coordination Compounds, 4th ed., Wiley, New York, 1986.

$[NH_4]_2[MoS_4]$, $[NH_4]_2[WS_4]$ [12], and 3,5-dimethylpyrazole [13] were prepared by published methods. The infrared spectra (4000–400 cm^{-1}) were recorded from KBr disks with a BOMEN MB102 FT-IR spectrometer. UV–Vis spectra of the ligands and complexes were recorded on a JASCO model 7850 spectrophotometer. ^1H NMR spectra were obtained using a Bruker DRX 500 AVANCE spectrometer. Elemental analyses were performed on a Carlo-Erba 1106 elemental analyser.

2.2. Preparation of $MoS_4Cu_4(pz^{Me2})_6Cl_2$ (1)

$[n\text{-}Bu_4N]_2[MoS_4Cu_4Cl_4]$ (1.104 g, 1 mmol) was dissolved in acetone (25 ml). Excess 3,5-dimethylpyrazole (0.672 g, 7 mmol) was added to the solution and the mixture was stirred at room temperature for 12 h. After filtration, the filtrate was vacuum evaporated to dryness, and the residue was washed with distilled water (2×2 ml), ethanol (2×2 ml) and diethyl ether (2×5 ml) and dried in vacuo to give a brown powder. Yield: 65%. Dark purple crystals were obtained after two days by slow evaporation of a saturated solution of the complex in acetone. *Anal.* for (**1**): C, 31.90; H, 4.25; N, 14.80. Calc. C, 32.00; H, 4.30; N, 14.93%.

2.3. Preparation of $WS_4Cu_4(pz^{Me2})_6(Cl/Br)_2$ (2)

n-Bu_4NBr (0.805 g, 2.5 mmol) was added to a suspension of $[NH_4]_2[WS_4]$ (0.348 g, 1 mmol) in analar acetone (30 ml) and the mixture was stirred for 1 h. CuCl (0.398 g, 4 mmol) was added to this solution and the mixture was stirred for another 3 h. After addition of excess 3,5-dimethylpyrazole (0.672 g, 7 mmol), the solution was stirred for an additional 12 h at room temperature. The precipitated NH_4Br was removed by filtration and the filtrate was vacuum evaporated to dryness, leaving a residue that was washed with distilled water (2×5 ml), ethanol (2×2 ml) and diethyl ether (2×5 ml) and dried in vacuo to give a dark red powder. Yield: 60%. Red crystals of the compound were obtained in the same way as for $MoS_4Cu_4(pz^{Me2})_6Cl_2$. *Anal.* for (**2**): C, 29.00; H, 3.90; N, 13.65. Calc. C, 28.84; H, 3.87; N, 13.45%, for the composition established by crystallographic refinement.

2.4. X-ray crystallography

Crystal data and other information on the structure determinations are listed in Table 1. All measurements were made on Bruker–Nonius SMART (**1**) and KappaCCD (**2**) diffractometers with narrow-frame ω scans. Mo Kα radiation ($\lambda = 0.71073$ Å) was employed for data collection at 150 K. Absorption corrections were based on the high redundancy of symmetry-equivalent and repeated reflections. The structures were solved by direct methods and refined by full-matrix least-squares on all F^2 values. Non-hydrogen atoms were refined with anisotropic displacement parameters. Hydrogen atoms were included in calculated positions and refined with isotropic displacement parameters, riding on their parent atoms, except that those bonded to N were refined freely. In the structure of **2** the Cl atoms are randomly substituted by Br in the proportion 0.6:0.4, arising from the use of *n*-Bu_4NBr in the synthesis. A common position was refined for Cl and Br, as it proved impossible to refine them independently. Programs were standard Bruker–Nonius control and integration software, SADABS [14] and SHELXTL [15].

3. Result and discussion

3.1. Infrared spectra

The IR spectra of $MS_4Cu_4(pz^{Me2})_6X_2$ exhibit characteristic strong bands at 447 and 420 cm^{-1} for compound **1** and 437 and 419 cm^{-1} for compound **2**, assigned to stretching vibrations of the MS_4 group [16]. In general, attachment of copper atoms to the $[MS_4]^{2-}$ anion to form an MS_4Cu_n ($n = 1$–4) core shifts the M–S stretching frequencies to lower values as n increases; this is consistent with the longer $M–S_b$ bonds, as confirmed by X-ray crystallography. The ν(N–H) and ν(C–H, aliphatic) stretching vibrations of the pz^{Me2} ligands appear as multiple bands in the region 2858–3351 cm^{-1}. The other absorption peaks of the pz^{Me2} ligands appear at 1700–650 cm^{-1}.

3.2. Electronic spectra

The UV–Vis spectra of the two compounds in DMF are similar in profiles, wavelength and intensity to the electronic spectra of $[Et_4N]_2[MS_4Cu_4(SCN)_2(2\text{-pic})_4]$ (M = W, Mo) [17] in the same solvent. They have absorption bands at 286 and 506 nm for the Mo cluster **1**, and at 256 and 426 nm for the W cluster **2**. The first of these in each case may be attributed to charge transfer from the ligand to Cu, and the other can be assigned as a charge-transfer band of the type $(\pi)S \rightarrow (d)M$ (M = Mo, W), arising from the MS_4 moiety, which is red-shifted compared to that for the free $[MS_4]^{2-}$ anion (397 nm for W and 472 nm for Mo).

3.3. ^1H NMR spectra

The ^1H NMR spectrum of $MoS_4Cu_4(pz^{Me2})_6Cl_2$ in $CDCl_3$ solution at room temperature exhibits three signals, as expected for pz^{Me2} ligands. The resonance at 2.346 ppm is associated with the methyl protons in the 3- and 5-positions of the pyrazole rings, indicating that all of these protons are magnetically equivalent. There are two other signals at 5.941 and 9.787 ppm (br), asso-

Table 1
Crystallographic data

	1	2
Chemical formula	$C_{30}H_{48}Cl_2Cu_4MoN_{12}S_4$	$C_{30}H_{48}Br_{0.81}Cl_{1.19}Cu_4N_{12}S_4W$
Formula weight	1126.0	1250.2
Crystal system	orthorhombic	orthorhombic
Space group	*Pbcn*	*Pbcn*
Unit cell dimensions		
a (Å)	16.691(2)	16.797(2)
b (Å)	14.0722(17)	14.1432(14)
c (Å)	18.400(2)	18.511(2)
V (Å^3)	4321.7(9)	4397.5(8)
Z	4	4
D_{calc} (g cm^{-3})	1.731	1.888
μ (mm^{-1})	2.574	5.550
Crystal size (mm)	0.32 × 0.22 × 0.18	0.60 × 0.20 × 0.10
θ_{max} (°)	25.1	27.5
Reflections collected	28,395	36,222
Independent reflections (R_{int})	3809 (0.0520)	5018 (0.0555)
Transmission	0.551–0.742	0.136–0.607
No. of parameters	258	259
R (F, $F^2 > 2\sigma$)	0.0333	0.0261
R_w (F^2 all data)	0.0780	0.0564
Goodness-of-fit on F^2	1.194	1.124
Elemental density extremes (e Å^{-3})	0.73 and −0.62	0.98 and −1.04

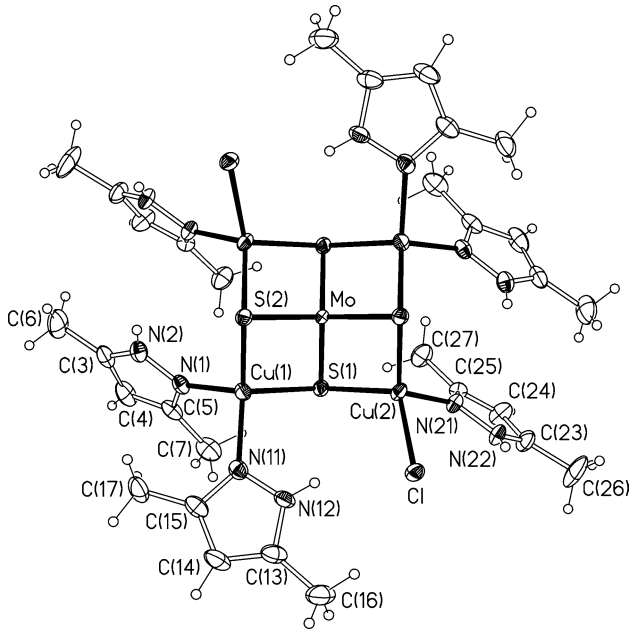

Fig. 1. A perspective view of the structure of the neutral cluster $MoS_4Cu_4(pz^{Me2})_6Cl_2$ (**1**). Non-hydrogen atoms of the asymmetric unit are labelled. Displacement ellipsoids are drawn at the 50% probability level, and H atoms are represented as spheres of arbitrary radius.

ciated with the H_4 and H_1 protons of the pz^{Me2} rings. As for compound **1**, the ^{1}H NMR spectrum of $WS_4Cu_4(pz^{Me2})_6X_2$ (**2**) also shows three signals, at 2.223, 5.907 and 11.619 ppm, due to the methyl protons in the 3- and 5-positions, and the H_4 and H_1 protons; these resonances are in the ratio 6:1:1. This result indicates that rapid exchange is occurring between coordinated copper and the H_1 proton of the pyrazole ring (Scheme 1).

3.4. Crystal structures

The solid-state molecular structure of the pentanuclear neutral cluster **1** is shown in Fig. 1; that of compound **2** is very similar, and the two compounds are isomorphous. Selected bond lengths and angles are in Table 2. The description here concentrates on the details for compound **1**. The structures are similar to those of $MS_4Cu_4(SCN)_2(NC_5H_5)_6$ (M = Mo, W) [18].

The structural core consists of one Mo, four Cu and four μ_3-S atoms in an MoS_4Cu_4 aggregate. The neutral cluster lies on a crystallographic twofold rotation axis, which is perpendicular to the mean plane of the five metal atoms. The four Cu atoms bridge four of the six edges of the central MoS_4 tetrahedron, selected symmetrically in a way that generates two Cu–S bonds for each sulfur atom and places the Cu atoms as far apart as possible.

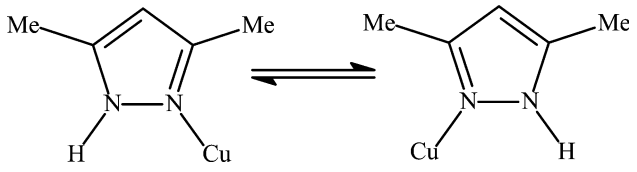

Scheme 1.

The Mo and Cu atoms are tetrahedrally coordinated. The geometry around Mo does not deviate markedly from ideal tetrahedral, and the Mo–S bonds are somewhat longer than those of the free $[MoS_4]^{2-}$ anion, as expected [2.17 Å in the ammonium salt]. The Cu atoms are of two types, with pairs of equivalent Cu atoms lying opposite each other. Cu(1) is coordinated by two μ_3-S atoms and two nitrogen atoms of pz^{Me2} rings, giving a distorted tetrahedral CuS_2N_2 arrangement, while Cu(2) is coordinated by two μ_3-S atoms, one nitrogen atom of pz^{Me2}, and one terminal Cl ligand, producing a distorted tetrahedral CuS_2NCl unit. The Cu–S bonds of Cu(2) are longer than those of Cu(1), while Cu(2) has a shorter Cu–N bond than those of Cu(1). The bond lengths involving Cu are comparable to those found in the related compounds $[Et_4N]_2[(Bp')CuMoS_4Cu_2(\mu\text{-}Bp')_2Cu_2MoS_4Cu(Bp')]$ [19] (mean Cu–S = 2.27 Å, Cu–N = 2.04 Å) and $[Et_4N]_2[MoS_4Cu_2(\mu\text{-}Bp')_2]\cdot CH_3CN$ [20] [$Bp' = H_2B(3,5\text{-}Me_2pz)_2$] (mean Cu–S = 2.27 Å, Cu–N = 2.08 Å). The angle between the two terminal ligands at Cu(1) is rather larger than that at Cu(2), as a result of the greater steric bulk of the pz^{Me2} ligand compared with chloride.

The N–H groups of the three independent pz^{Me2} ligands act as donors in intramolecular and intermolecular

Table 2
Selected bond lengths (Å) and angles (°)

	Compound **1** (M = Mo)	Compound **2** (M = W)
Bond lengths		
M–S(1)	2.2292(11)	2.2354(9)
M–S(2)	2.2426(11)	2.2452(8)
Cu(1)–S(1)	2.2755(12)	2.2946(9)
Cu(1)–S(2)	2.2691(12)	2.2875(10)
Cu(2)–S(1)	2.2796(12)	2.2985(9)
Cu(2)–S(2A)	2.2845(12)	2.3044(10)
Cu(1)–N(1)	2.040(4)	2.040(3)
Cu(1)–N(11)	2.036(4)	2.046(3)
Cu(2)–N(21)	2.009(4)	2.013(3)
Cu(2)–X	2.3728(12)	2.4548(7)
Bond angles		
S(1)–M–S(1A)	108.42(6)	108.52(5)
S(1)–M–S(2)	107.80(4)	107.90(3)
S(1)–M–S(2A)	109.71(4)	109.96(3)
S(2)–M–S(2A)	113.30(6)	112.54(5)
S(1)–Cu(1)–S(2)	105.32(4)	104.48(3)
S(1)–Cu(1)–N(1)	111.04(11)	110.47(9)
S(1)–Cu(1)–N(11)	105.22(10)	106.50(8)
S(2)–Cu(1)–N(1)	109.25(11)	110.10(9)
S(2)–Cu(1)–N(11)	119.90(11)	119.66(9)
N(1)–Cu(1)–N(11)	106.00(15)	105.48(12)
S(1)–Cu(2)–S(2A)	106.48(4)	105.72(3)
S(1)–Cu(2)–N(21)	106.28(11)	106.60(9)
S(1)–Cu(2)–X	116.62(4)	116.12(3)
S(2A)–Cu(2)–N(21)	122.01(11)	122.55(9)
S(2A)–Cu(2)–X	106.86(4)	106.57(3)
N(21)–Cu(2)–X	99.18(10)	99.91(8)
M–S(1)–Cu(1)	73.50(3)	73.82(3)
M–S(1)–Cu(2)	72.07(3)	72.30(3)
Cu(1)–S(1)–Cu(2)	115.91(5)	116.06(4)
M–S(2)–Cu(1)	73.37(3)	73.78(3)
M–S(2)–Cu(2A)	71.74(3)	72.01(3)
Cu(1)–S(2)–Cu(2A)	108.51(5)	108.59(4)

hydrogen bonds to Cl and S atoms, with N···Cl and N···S distances between 3.206(4) and 3.595(4) Å, and with angles at hydrogen deviating by up to 32° from linearity.

4. Supplementary material

Crystallographic data for the structural analyses have been deposited with the Cambridge Crystallographic Data Centre, CCDC Nos. 238321 for compound **1** and 238322 for compound **2**. Copies of this information may be obtained free of charge from The Director, CCDC, 12 Union Road, Cambridge CB2 1IZ, UK (fax: +44 1223 336033; e-mail: deposit@ccdc.cam.ac.uk or www: http://www.ccdc.cam.ac.uk).

Acknowledgments

We thank the EPSRC (UK) and Shahid Chamran University for financial support.

References

[1] A. Müller, E. Diemann, R. Jostes, H. Bögge, Angew. Chem., Int. Ed. Engl. 20 (1981) 934.
[2] M.P. Croughan, Molybdenum and Molybdenum-containing Enzymes, Pergamon Press, Oxford, 1980.
[3] A. Müller, E. Krickemeyer, A. Hildebrand, H. Bögge, K. Schneider, M. Lemke, J. Chem. Soc., Chem. Commun. (1991) 1685.
[4] J.T. Goodman, T.B. Rauchfuss, Angew. Chem., Int. Ed. Engl. 36 (1997) 2083.
[5] J.G. Li, X.Q. Xin, Z.Y. Zhou, K.B. Yu, J. Chem. Soc., Chem. Commun. (1991) 249.
[6] S.W. Du, N.Y. Zhu, P.C. Chen, X.T. Wu, Angew. Chem., Int. Ed. Engl. 31 (1992) 1085.
[7] E.A. Pruss, B.S. Snyder, A.M. Stacy, Angew. Chem., Int. Ed. Engl. 32 (1993) 256.
[8] Q. Huang, X.T. Wu, Q.M. Wang, T.L. Sheng, J.X. Lu, Angew. Chem., Int. Ed. Engl. 35 (1996) 868.
[9] Q. Huang, X.T. Wu, Q.M. Wang, T.L. Sheng, J.X. Lu, Inorg. Chem. 35 (1996) 893.
[10] J. Guo, X.T. Wu, W.J. Zhang, T.L. Sheng, Q. Huang, P. Lin, Q.M. Wang, J.X. Lu, Angew. Chem., Int. Ed. Engl. 36 (1997) 2464.
[11] F. Sécheresse, S. Bernès, F. Robert, Y. Jeanin, J. Chem. Soc., Dalton Trans. (1991) 2875.
[12] (a) A.G. Sykes, Adv. Inorg. Chem. 36 (1991) 377;
(b) E.I. Solomon, K.W. Penfield, D.E. Wilcox, Struct. Bond. 53 (1983) 1.
[13] R.W. Parry, Inorganic Syntheses, Vol. 12, McGraw-Hill, New York, 1970.
[14] G.M. Sheldrick, SADABS, Program for Correction of CCD Data, University of Göttingen, Germany, 1997.
[15] G.M. Sheldrick, SHELXTL User Manual, Bruker AXS Inc., Madison, WI, USA, 1997.
[16] C. Zhang, G.-C. Jin, J.-X. Chen, X.-Q. Xin, K.-P. Qian, Coord. Chem. Rev. 213 (2001) 51.
[17] C. Zhang, Y. Song, G.-C. Jin, G. Fang, Y. Wang, S. Shanmuga Sundara Raj, H.-K. Fun, X.-Q. Xin, J. Chem. Soc., Dalton Trans. (2000) 1317.
[18] H.-G. Zheng, W.-L. Tan, W. Ji, W.-H. Leung, I.D. Williams, D.-L. Long, J.-S. Huang, X.-Q. Xin, Inorg. Chim. Acta 294 (1999) 73.
[19] A. Beheshti, W. Clegg, M. Hosaini Sadr, Polyhedron 20 (2002) 179.
[20] A. Beheshti, W. Clegg, M. Hosaini Sadr, Inorg. Chim. Acta 335 (2002) 21.

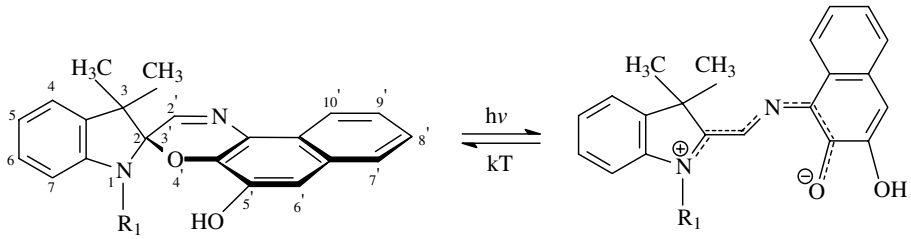

(SO) **(MC)**

Scheme 1.

2. Experimental

2.1. Materials

The photochromic molecules were two spiro[indolinonaphthooxazines]: 1,3,3-trimethyl-5′-hydroxyspiro-(indoline-2,3′-[3H]naphth[2,1-b][1,4]oxazine) (**1**) and 1-butyl-3,3-dimethyl-5′-hydroxyspiro(indoline-2,3′-[3H] naphth[2,1-b][1,4]oxazine) (**2**). The compounds were recently prepared and characterized in our laboratory [18,19]. The p.a. grade metal salts were obtained from Fluka and were used without further purification. The solvents were used after distillation.

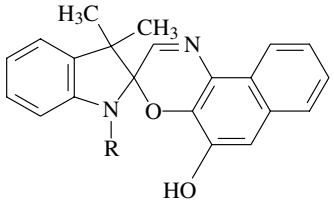

1: R = CH_3

2: R = C_4H_9

2.2. Instrumentation

Absorption spectra were recorded on a SPECORD UV–Vis (Carl Zeiss, Jena) spectrophotometer using quartz cells. For absorption measurements at varying temperatures the reaction cell was enclosed in a thermostatic water jacket placed inside the spectrophotometer sample chamber. A 250 W medium-pressure mercury lamp was used for producing the coloured form. Photochemical reactions were carried out in the spectrophotometric quartz cell with a homogeneously spread light on the cell window to avoid stirring [20,21]. Measurements were made on aerated solutions. EPR spectra were taken at 77 K on an X-band BRUKER B-ER 420 spectrometer using 100 kHz modulation of the magnetic field.

2.3. Kinetics measurements

The effects of metal ions on the **SO** ⇌ **MC** process were studied in 1:1 aqueous/acetone or aqueous/ethanol mixtures at a constant spironaphthooxazine concentration of 5×10^{-5} M and varying the ratio between the **SO** and the metal ion from 2:1 to 1:20.

The kinetics of the thermal colouration in the presence of metal ions was measured at different temperatures in the range 20–50 °C, ca. 30 min after having set the temperature control in order to allow the initial solutions to reach the appropriate temperature in separate vessels. The absorbance was measured at the wavelength of maximum absorption (λ_{max}) directly in the sample cell at 30 s intervals after the insertion of 10 equiv. of aqueous metal ion solution in ethanol solutions of **1** or **2**. First order build up rate constants were obtained from the linear dependences of ln A versus time. The activation energies along with the frequency factors of thermal ring opening were determined from Arrhenius plots.

In the photocolouration experiment the cuvette was irradiated for several seconds after thermal equilibration of the reaction mixture containing **SO** and the metal ion in 1:1 aqueous/ethanol. Trial and error experiments enabled the optimum exposure time to be determined for maximum build-up of the complex. The ring-closure reaction after photocolouration was monitored directly after the removal of the light, scanning at the wavelength of maximum absorption of the complex between the **MC** form and the metal ion (λ_{compl}) at 15 s intervals over a period of 30–50 min at room temperature. First order rate constants of thermal re-equilibration were obtained from the linear ln A versus time descending curves. by extrapolation of the obtained ln A/t plots to zero time, the absorbance A_o of the complexes at $t = 0$ was related to their "colourabilities" [21–24] using the expression $A_o/c_{\mathbf{SO}}b$ in which $c_{\mathbf{SO}}$ was the initial concentration of **SO** and b was the optical path length.

3. Results and discussion

The colourless spiro compounds **1** and **2** give no complexes with the metal ions. However, their merocyanines form complexes with Cu(II), Fe(II) and Al(III) in polar solvents, while Cr(III), Mn(II), Ni(II), Co(II), Ba(II) and Mg(II) do not affect the equilibrium between **SO** and **MC** in Scheme 1.

3.1. Absorption spectra

Visible spectra of photomerocyanines, obtained upon UV illumination of **1** or **2** in polar solvents [19], are characterized by an absorption in the range 600–620 nm which remains unchanged upon UV illumination in the presence of Cr(III), Mn(II), Ni(II), Co(II), Ba(II) and Mg(II). Irradiation of **1** and **2** in the presence of 1 equiv. of Cu(II), Fe(II) or Al(III) generates a new photo-reversible absorption band in the range 540–600 nm, with band intensity dependent on the [M(II),(III)]/[**SO**] ratio and highest effectiveness obtained at 10 equiv. of added metal ion. Less effective is irradiation in the presence of Zn(II) and Pb(II), with absorption bands appearing between 600 and 592 nm. The observed λ_{max} values (Table 1) are slightly blue-shifted and the same is observed at a 10-fold molar excess of M(II),(III). It is obvious that UV irradiation of **SO** in the presence of the appropriate metal ion yields a **MC**–M(II),(III) complex and this process is considered as photoinduced complexation.

Thermal coordination to the metal ion also takes place, giving a complex which is spectroscopically identical to the photoinduced product. The colouration obtained in the dark becomes more intense upon UV illumination and reverses back to its initial level after removing of the light. The time needed for re-establishing equilibria is sensitive to the metal ion and is substantially prolonged compared to the non-complexed merocyanine.

Photoirradiation of the parent unsubstituted spiroindolinonaphthooxazine (Scheme 2) in the presence of a metal salt [25] induces irreversible photo-degradation without any complexation, indicating that the nitrogen atom at the 1′ position in the naphthooxazine moiety takes no part in chelation.

3.2. EPR spectra

Fig. 1 shows a typical EPR spectrum of the photoinduced **MC**–Cu(II) complex in ethanol immediately frozen at 77 K after irradiation. The spin-Hamiltonian parameters: $A_{\parallel} = 112 \pm 2$ G, $g_{\parallel} = 2.317 \pm 0.002$ and $g_{\perp} = 2.010 \pm 0.002$ indicate a strong anisotropy, consistent with the Jahn–Teller deformation of the molecule to a square-planar geometry [26]. The isotropic value $g_o = 2.112 \pm 0.002$, calculated by using the $g_{\parallel}$ and $g_{\perp}$ parameters, seems to be the average of the *g*-values [27,28] of bis(acetylacetonato)Cu(II) with the chromophore CuO_4 ($g_o = 2.219 \pm 0.002$) and bis(8-quinolinolato)Cu(II) with the chromophore CuO_2N_2 ($g_o = 2.105 \pm 0.002$). Since the unpaired electron occupies a 'group' orbital with the participation of Cu and four donor atoms, these results indicate an averaged covalence within the chromophore of **MC**–Cu(II) as compared to CuO_4 and CuO_2N_2. Following the 'additive rule' [28,29] we suggest the chromophore CuO_3N for **MC**–Cu(II), i.e. the formation of a mixed-ligand complex (**3** in Scheme 3) with one chelate ligand and two ethanol molecules coordinated in the *xy*-plane. For comparison, the spin-Hamiltonian parameters of the EPR spectrum (77 K) of an ethanol solution of $CuCl_2$ are $A_{\parallel} = 115 \pm 2$ G, $g_{\parallel} = 2.26$ and $g_{\perp} = 2.06$ [30].

Table 1
Absorption maxima of the complexes obtained upon UV illumination of 5×10^{-5} M solutions of **1** and **2** in the presence of 1 equiv. of metal ion

SO	Solvent	λ_{compl} (nm)			
		None*	Cu(II)	Al(III)	Fe(II)
1	EtOH/H_2O	610	595	585	546
	CH_3COCH_3/H_2O	600	590	580	540
2	EtOH/H_2O	620	600	580	546
	CH_3COCH_3/H_2O	600	590	580	540

* From [19].

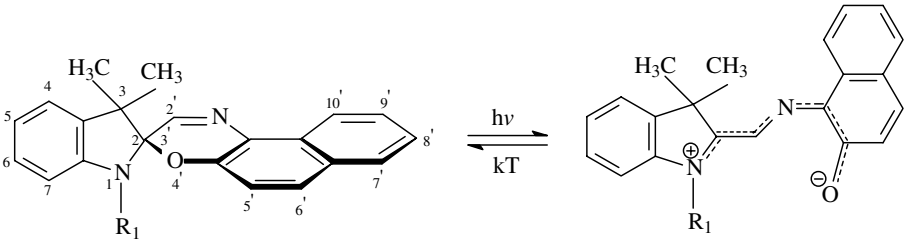

Scheme 2.

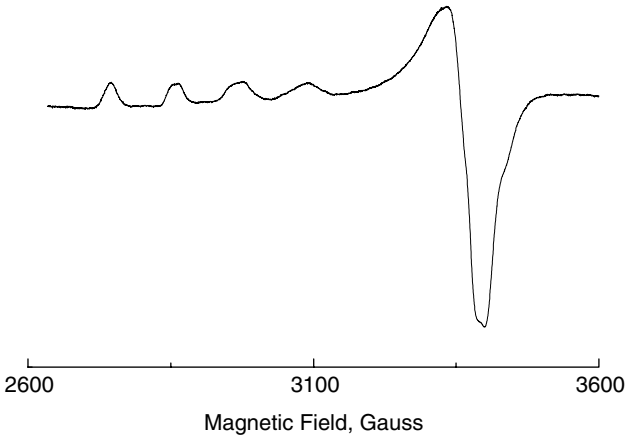

Fig. 1. Typical EPR spectrum of Cu(II)-**MC** in ethanol, 77 K.

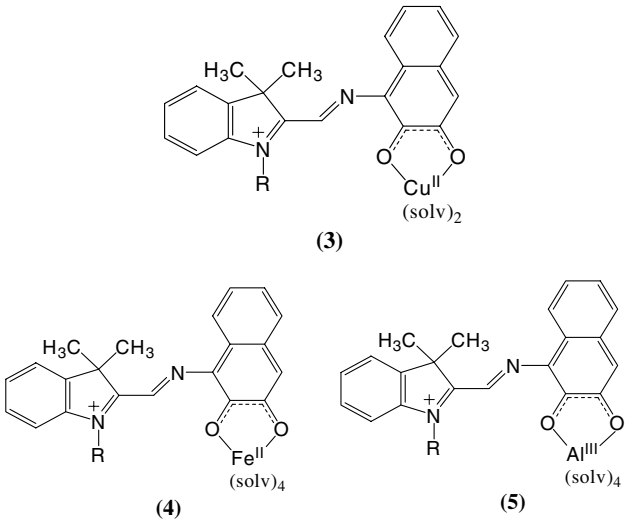

Scheme 3.

By analogy with **MC**–Cu(II), for the cases of higher metal ion concentration than that of **SO,** we suggest one merocyanine and four ethanol molecules as ligands for Fe(II) or Al(III) in Scheme 3. The spectral and kinetic data (Figs. 1–5) also indicate this possibility for [**SO**] ≈ [M(II),(III)]. Job's [31], which is commonly used for determination of the stoichiometry, cannot be applied to our case since the ligand **MC** concentration cannot be varied independently of [M(II),(III)].

3.3. Thermal colouration and decolouration in the presence of metal ions

Typical spectral changes obtained in a few minutes after mixing 1×10^{-4} M ethanol solutions of **1** or **2** with 0.5–10 equiv. of aqueous Al(III), Fe(II) or Cu(II) are given in Fig. 2(a) and (b). The observed changes correspond to the thermal conversion of **SO** to a **MC**–Al(III) complex as indicated by the position of the visible absorption. It seems that chelation affects the thermal equilibrium **SO** ⇌ **MC** and promotes the formation of the open form at room temperature in the absence of light, according to one of the following pathways [32]:

$$\mathbf{SO} \rightleftharpoons \mathbf{MC} + \mathrm{M(II),(III)} \rightarrow \mathbf{MC} - \mathrm{M(II),(III)} \qquad \text{(a)}$$

$$\mathbf{SO} + \mathrm{M(II),(III)} \rightleftharpoons \mathbf{SO} - \mathrm{M(II),(III)} \rightarrow \mathbf{MC} - \mathrm{M(II),(III)} \qquad \text{(b)}$$

$$\mathbf{SO} \rightarrow \mathbf{MC} + \mathrm{M(II),(III)} \rightleftharpoons \mathbf{MC} - \mathrm{M(II),(III)} \qquad \text{(c)}$$

Fig. 2(a) and (b) depicts only a slow increase of intensity of the **MC**–Al(III) absorption band of **2**, getting a saturation after 15–20 min in the dark. The concentration of the metal ion has no effect on the rate of chelation, but the time for saturation and the amount of the obtained

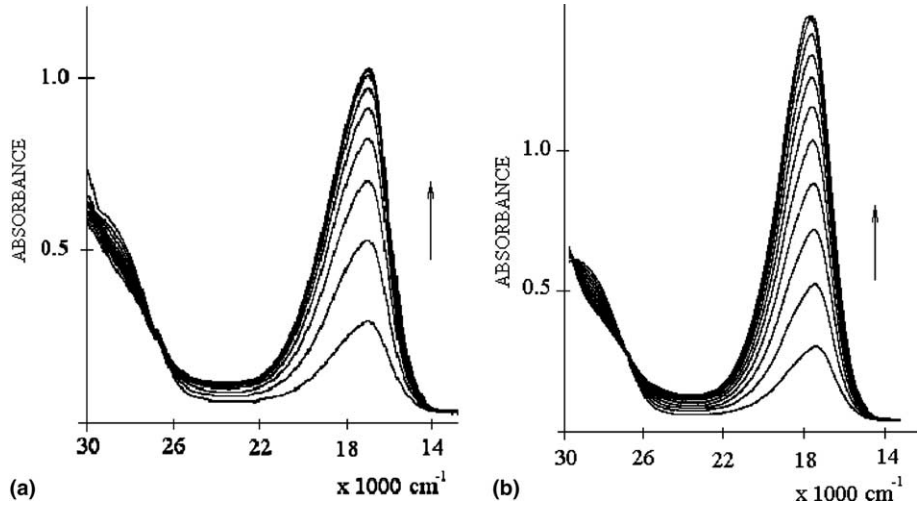

Fig. 2. Visible absorption spectra of an ethanol solution of **2** taken every 2 min in the dark after insertion of: 0.5 (a) and 10 (b) equiv. of aqueous Al(III); $c_{\mathbf{SO}} = 5 \times 10^{-5}$ M.

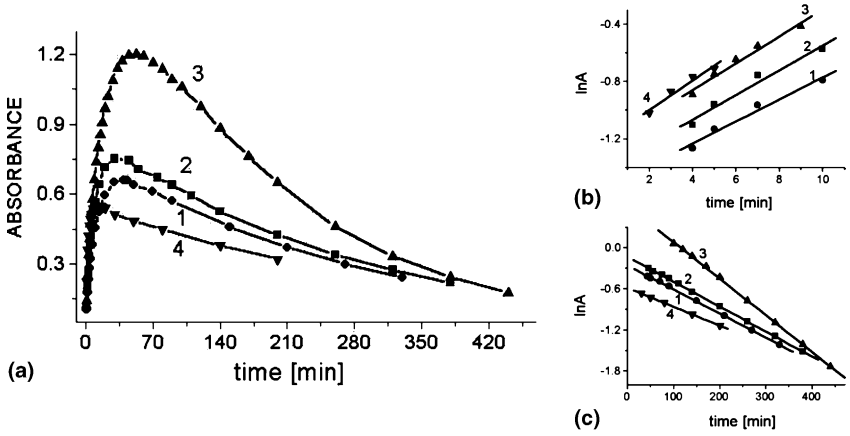

Fig. 3. (a) Kinetic runs at λ_{compl} of 5×10^{-5} M ethanol solution of **2** taken in the dark after insertion of aqueous: Al(III) 1, 2 and 10 equiv. (plots 1–3) or Cu(II) 10 equiv. (plot 4) at 20 °C; (b,c) ln A vs. time dependence.

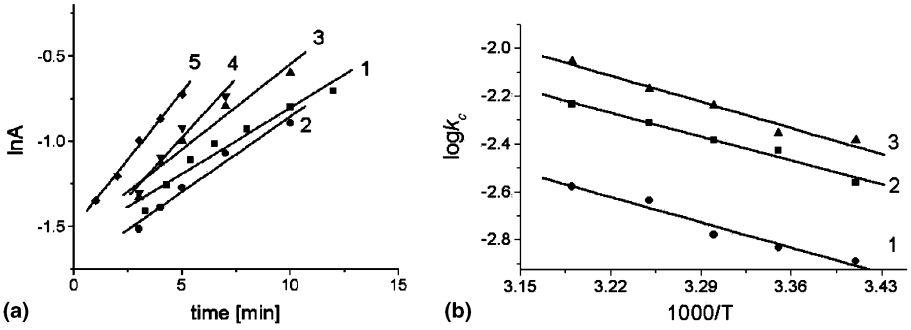

Fig. 4. (a) Plots of ln A vs. time at 585 nm obtained in the dark after insertion of 10 equiv. of aqueous Al(III) in 5×10^{-5} M ethanol solution of **1** at 20 (1), 25 (2), 30 (3), 35 (4) and 40 °C (5); (b) Arrhenius plots of: (1) **MC**–Al(III) using the data of (a); (2) **MC**–Cu(II) and (3) **MC**–Fe(II) under the same experimental conditions.

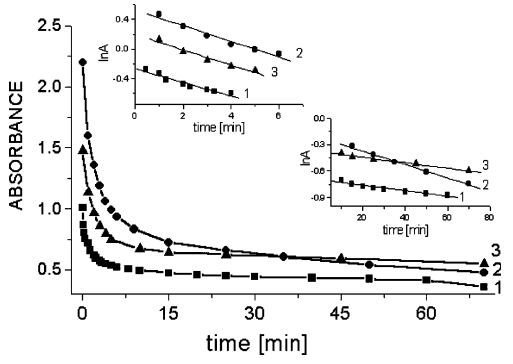

Fig. 5. Absorbance changes at 600 nm following 15 s UV illumination of an ethanol solution of **1** after insertion of: (1) 0.5 or (2) 10 equiv. of Cu(II) in ethanol and (3) 10 equiv. of aqueous Cu(II). Insets: ln A vs. time plots, initial (0.5–6 min) and final (10–70 min).

complex are higher at a larger metal ion excess. After reaching a saturation, the colouration slowly bleaches with longer reaction times (Fig. 3(a)).

Kinetic plots (1)–(3) of **MC**–Al(III) and (4) of **MC**–Cu(II) in Fig. 3(a) are typical of the colouration and decolouration processes of all studied systems. The plots of the linear dependences of ln A versus time at λ_{compl} (Fig. 3(b)), analysed by the least squares method, give k_c values of ca. $(1–2) \times 10^{-3}$ s^{-1} at 20 °C for the rate constants of chelation of all complexes, without any effect of the metal ion. It seems from these data that route (c) is the reaction pathway of chelation since for (a) and (b) the rate constants will depend on the nature of the metal ions, while for (c) metal ions react readily with the coloured form **MC** as it is formed thermally from **SO**.

The first order build-up kinetics of **MC**–Al(III) studied in the range 20–40 °C in 1:1 aqueous/ethanol (Fig. 4(a)) gives the plot (1) of log k_c versus $1/T$ in Fig. 4(b) and similar kinetics runs of **MC**–Fe(II) and **MC**–Cu(II) under the same experimental conditions give the plots (2) and (3). From the linear dependences in Fig. 4(b), the activation energies (E_a) of chelation and the pre-exponential factors are derived. The pre-exponential factors for **3**–**5** vary from 10^{12} to 10^{14} s^{-1}, but the values for E_a are 27–30 kJ mol^{-1} showing no effect of the metal ion, as the process of thermal ring opening of the spiro-form is the rate limiting step of chelation. Thermal

degradation of the complexes (Fig. 3(c)) is also a first order reaction with a metal-dependant rate constant k_d of ca. $(5–9) \times 10^{-5}$ s^{-1}.

3.4. Effect of chelation on the photocolouration and on the thermal re-equilibration of photomerocyanines

In the absence of metal ion, the first order decay of the photomerocyanines of **1** and **2** occurs with $k_r \sim 0.1$ s^{-1} [19] and their relaxation time in acetone and ethanol is $\tau_{\mathbf{MC–SO}} \sim 10$ s. Taking into account that the colouring and fading times are important characteristics of the photochromic systems, we have studied the effect of chelation on the kinetics of photochromic transformations of spironaphthooxazines. In contrast to the lack of effect of Cr(III), Mn(II), Ni(II), Co(II), Ba(II) or Mg(II) on the decolouration of the free **MC** forms of **1** and **2**, Cu(II), Fe(II) and Al(III) have a significant effect on the ring closure reaction and the light enhanced colouration disappears much slower after illumination.

A typical picture of bleaching after irradiation of **1** and **2** in the presence of Al(III), Cu(II) or Fe(II) is depicted in Figs. 5 and 6. Kinetic runs in Fig. 5 followed at λ_{compl} immediately after illumination of ethanol (plots 1 and 2) or 1:1 aqueous/ethanol (plot 3) solutions indicate that the photoinduced **MC**–Cu(II) complex of **1** undergoes spontaneous thermal decolouration which is first order in the concentration of the starting complex, as the plots of ln A versus time (initial inset in Fig. 5) are linear ($\rho > 0.98$) about 50% of reaction completion and similar changes are observed in Fig. 6 for the **MC**–Cu(II) complex of **2**. The strongly descending part of the curves associated with the thermal spironaphthooxazine ring closure, analysed by the least squares method, give metal-dependant values of the re-equilibration rate constant k_r ranging from 1.5 to 2.6×10^{-3} s^{-1} at 20 °C.

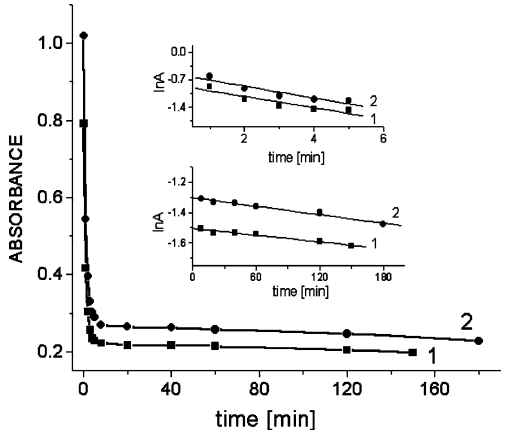

Fig. 6. Absorbance changes at 600 nm following 15 s UV illumination of an ethanol solution of **2** after insertion of: (1) 0.5 or (2) 1 equiv. of aqueous Cu(II). Insets: ln A vs. time plots, initial (1–5 min) and final (10–180 min).

Relaxation times ($\tau_{com–\mathbf{SO}}$) of 5–10 min were obtained using the expression $\tau = 1/k_r$. Data obtained about all the studied systems suggest that complexation with Cu(II), Fe(II) and Al(III) strongly inhibits thermal reversion of **MC** to **SO**.

From the absorbances A_o obtained by extrapolation to $t = 0$ of the room temperature linearly descending kinetic curves ln A/t of spironaphthooxazine ring closure immediately after UV irradiation (Figs. 5 and 6) are calculated "colourability" [21–24] values up to 34 000.

Kinetic runs at larger reaction times in Figs. 5 and 6 are much slower. The rate constants calculated by the least squares method from the final ln A versus time linear plots ca. 5×10^{-5} s^{-1} for **1** and 1×10^{-5} s^{-1} for **2** in 1:1 aqueous/ethanol (up to 1×10^{-4} s^{-1} in ethanol) are near to the obtained k_d values of thermal degradation.

These observations suggest two parallel reactions of the photoinduced complexes proceeding simultaneously (Scheme 4):

- thermal relaxation (k_r ca. 10^{-3} s^{-1}) approaching the steady state concentration of the complex **C** in polar solvents.
- thermal degradation (k_d ca. 10^{-5} s^{-1}) of the complex yielding the product D.

Special experiments were carried out to check the reversibility of the photocolouration. Kinetic runs in Fig. 7(a) depict the increasing intensity with time of the **MC**–Cu(II) absorption band at 600 nm (spectra 1–5), reaching a saturation (spectra 4–5) on keeping its 1:1 aqueous/ethanol solution in the dark. The consequent increase in intensity upon 10 and 30 s UV illuminations is given in Fig. 7(b) (spectra 6–7) together with the kinetic runs of thermal decolouration on keeping the irradiated sample for 0.5, 1, 2 and 3 h in the dark (spectra 8–11) due to the parallel relaxation and degradation processes in Scheme 4. Spectrum 12 in Fig. 7(b), obtained after a further 20 s photoirradiation of the final solution, clearly indicates a reversible photocolouration of **SO**, remaining unaffected by degradation. Similar changes are obtained with **MC**–Fe(II) and **MC**–Al(III).

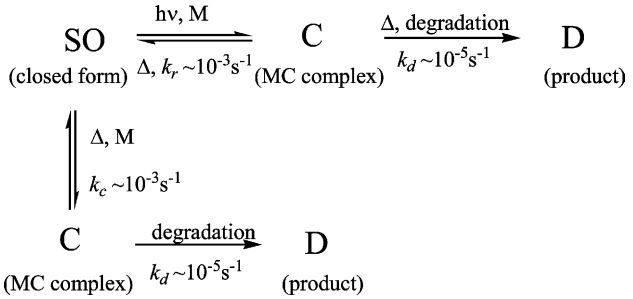

Scheme 4.

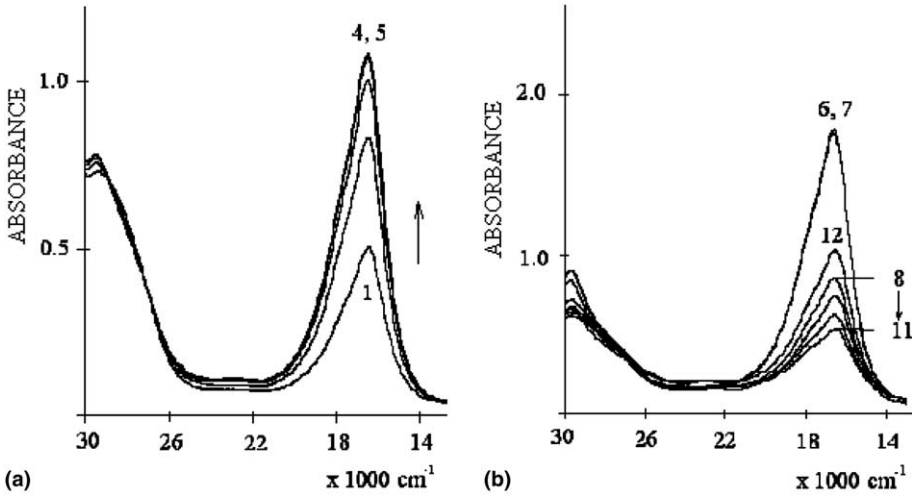

Fig. 7. Visible absorption spectra taken after insertion of 2 equiv. of aqueous Cu(II) into a 5×10^{-5} M ethanol solution of **1**: (a) – every 2 min in the dark (1–5); (b) – (5) upon consecutive 10 and 30 s UV illuminations (6–7); (7) kept for 0.5, 1, 2 and 3 h in the dark (8–11); (11) after a new 20 s UV illumination (12).

4. Conclusions

Coordination of Al(III), Fe(II) and Cu(II) with the open **MC** form of two 5′-(hydroxy)spiroindolinonaphthooxazines takes place both thermally (slowly) and photochemically in ethanol, acetone and their 1:1 water mixtures giving a reversibly photochromic complex. The thermal build-up reaction ($\sim 10^{-3}$ s^{-1}) is independent of the metal ion thus implying that the ring opening is the rate determining step. Chelation induces a 10–45 nm hypsochromic shift of the visible absorption band of the photomerocyanine and drastically slows down its thermal re-equilibration in the dark.

References

[1] N.Y.C. Chu, in: H. Durr, H. Bouas-Laurent (Eds.), Photochromism: Molecules and Systems, Elsevier, Amsterdam, 1990, p. 879.
[2] R. Guglielmetti, in: H. Durr, H. Bouas-Laurent (Eds.), Photochromism: Molecules and Systems, Elsevier, Amsterdam, 1990, p. 855.
[3] I. Willner, B. Willner in: H. Morrison (Ed.), Bioorganic Photochemistry, vol. 2, Biological Applications of Photochemical Switches, New York, 1993, p. 1.
[4] J. D. Winkler, K. DeShayes, B. Shao, in: H. Morrison (Ed.), Bioorganic Photochemistry, vol. 2, Biological Applications of Photochemical Switches, New York, 1993, p. 167.
[5] J.D. Phillips, A. Mueller, F. Przystal, J. Am. Chem. Soc. 87 (1965) 4020.
[6] L.D. Taylor, J. Nicholson, K.B. Davis, Tetrahedron Lett. (1967) 1585.
[7] M. Le Baccon, R. Guglielmetti, J. Chem. Res. (S) (1979) 154.
[8] J.-W. Zhou, Y.-T. Li, X.-Q. Song, J. Photochem. Photobiol., A: Chem. 87 (1995) 37.
[9] H. Görner, A.K. Chibisov, J. Chem. Soc., Faraday Trans. 94 (1998) 2557.
[10] J.T.C. Wojtyk, P.M. Kazmaier, E. Buncel, Chem. Commun. (1998) 1703.
[11] G.E. Collins, L.-S. Choi, K.J. Ewing, V. Michelet, C.M. Bowen, J.D. Winkler, Chem. Commun. (1999) 321.
[12] L.S. Atabekyan, A.K. Chibisov, High Energy Chem. 32 (1998) 30.
[13] H. Nishikiori, R. Sasai, N. Arai, K. Takadi, Chem. Lett. (2000) 1142.
[14] M.J. Preigh, Fu-Tyan Lin, K.Z. Ismail, J. Chem. Soc., Chem. Commun. (1995) 2091.
[15] T. Tamaki, Y. Kawanishi, T. Sehi, M. Sakuragi, K. Ichimura, T. Yamaguchi, J. Photopolymer Sci. Technol. 3 (1990) 85.
[16] T. Tamaki, K. Ichimura, J. Chem. Soc., Chem. Commun. (1989) 1447.
[17] H. Oda, Chem. Express 8 (1993) 629.
[18] T. Deligeorgiev, S. Minkovska, B. Jeliazkova, S. Rakovsky, Dyes Pigments 53 (2002) 101.
[19] S. Minkovska, B. Jeliazkova, E. Borisova, L. Avramov, T. Deligeorgiev, J. Photochem. Photobiol., A: Chem. 163 (2004) 121.
[20] F. Wilkinson, J. Hobley, M. Naftaly, J. Chem. Soc., Faraday Trans. 88 (1992) 1511.
[21] G. Favaro, V. Malatesta, U. Mazzucato, G. Ottavi, A. Romani, J. Photochem. Photobiol., A: Chem. 87 (1995) 235.
[22] S. Kawauchi, H. Yoshida, N. Yamashina, M. Ohira, S. Saeda, M. Irie, Bull. Chem. Soc. Jpn. 63 (1990) 267.
[23] J.-L. Pozzo, A. Samat, R. Guglielmetti, D. de Keukeleire, J. Chem. Soc., Perkin Trans. 2 (1993) 1327.
[24] V. Pimienta, C. Froutė, M.H. Deniel, D. Lavabre, R. Guglielmetti, J.C. Micheau, J. Photochem. Photobiol., A: Chem. 122 (1999) 199.
[25] S. Minkovska, K. Kolev, B. Jeliazkova, T. Deligeorgiev, Dyes Pigments 39 (1998) 25.
[26] B.J. Hathaway, D.E. Billig, Coord. Chem. Rev. 5 (1970) 143.
[27] H.A. Kuska, M.T. Rogers, in: E.T. Kaiser, L. Kevan (Eds.), Radical Ions, Wiley, New York, 1968.
[28] N.D. Yordanov, V. Alexiev, Commun. Dep. Chem. Bulg. Acad. Sci. 16 (1983) 214.
[29] K. Wuetrich, Helv. Chim. Acta 48 (1965) 1012.
[30] N.D. Yordanov, V. Terziev, D. Shopov, Compt. rendue Acad. Sci. Bulg. 27 (1974) 1529.
[31] F.R. Hartley, C. Burgess, R.M. Alcock, Solution Equilibria, Wiley, New York, 1980.
[32] J.-W. Zhou, Y.-T. Li, X.-Q. Song, J. Photochem. Photobiol., A: Chem. 87 (1995) 37.

or phthalonitrile to an insoluble polymer, making it react with a different diiminoisoindoline and, after removal of the symmetric phthalocyanine, releasing the unsymmetrical phthalocyanine from the polymer support. A third method has been described by Kobayashi and co-workers [16,17] and involves the ring expansion of a subphthalocyanine to a phthalocyanine using a phthalonitrile unit which bears a different type of substituent to that on the subphthalocyanine.

Over the past few years, palladium catalysed cross-coupling reactions provide a further and important means of functionalising the phthalocyanine ring with interesting grouping. This has produced various derivatives that include alkynyl and alkenyl functionalised phthalocyanines including some unsymmetrical phthalocyanines. Examples of some of these compounds and related structures have interesting NLO effects [18,19].

We have previously reported peripherally substituted symmetrical and unsymmetrical phthalocyanines [20–22]. The incorporation of macrocyclic groups such as dioxadiaza and triaza-macrocycles has enhanced the solubility of these compounds [23,24]. A consequence of incorporating a sulfanyl function on the periphery has been a shift of the Q-band absorption to longer wavelengths [25]. This is preferred for a number of applications such as with IR absorbers and photosensitizers. In the present work, we report on the synthesis and characterization of unsymmetrical metallophthalocyanines which carry two peripheral hexylthio substituents on each of three of the benzenoid groups while the fourth one carries two phenylethynyl groups.

2. Experimental

IR spectra were recorded on a Mattison 1000 FTIR spectrophotometer using KBr pellets, electronic spectra on a Unicam UV2 spectrophotometer. Elemental analyses were performed by the Instrumental Analysis Laboratory of the TUBITAK Marmara Research Centre. ^{1}H NMR spectra were recorded on a Bruker 250 MHz spectrometer using TMS as an internal reference. All reagents and solvents were of reagent grade quality obtained from commercial suppliers. The homogeneity of the products was tested in each step by TLC. 4,5-Dichlorophthalonitrile (**1**) [26] and 4,5-di(hexylthio)phthalonitrile (**2**) [27] were synthesized according to published methods.

Electrochemical techniques were carried out with a Princeton Applied Research Model 273 potentiostat/galvanostat controlled by an external PC using the computer program HEADSTRT and utilising a three-electrode configuration at 25 ± 1 °C. An Origin 6.0 graph program was used to evaluate Headstrt software data, to draw voltammograms, and to analyse them. A Pt spiral wire served as the counter electrode. A saturated calomel electrode (SCE) was employed as the reference electrode. The working electrode was a Pt plate with an area of 1.0 cm^2. Electrochemical grade tetrabutylammonium-perchlorate (TBAP) in extra pure DCM was employed as the supporting electrolyte at a concentration of 0.1 mol dm^{-3}. High purity N_2 was used for deaeration and to maintain a nitrogen blanket for at least 15 min prior to each run. For controlled potential coulometric (CPC) studies, a Pt gauze working electrode (10.5 cm^2 surface area), a Pt gauze counter electrode separated with a double bridge, a saturated calomel reference electrode (SCE) and a model 377/12 Synchronous stirrer were used. The potential of the working electrode was set to the E_p value obtained in the CV experiments. Then the solution was electrolysed with efficient stirring.

2.1. 4,5-Di(phenylethynyl)phthalonitrile (3)

To a solution of 1 g (5.10 mmol) of **1** dissolved in 100 ml of triethylamine was added 0.20 g (0.30 mmol) of bis(triphenylphosphine)palladium(II)chloride, 0.04 g (0.20 mmol)of copper(I)iodide and then 3.34 ml (30.45 mmol) of phenylacetylene. The reaction mixture was heated to 90 °C for 24 h under N_2. As the reaction proceeded, a dark brown precipitate was formed. The resulting suspension was filtered off and the brown solid collected was washed with hexane. The yellow product was obtained by column chromatography with silica gel using $CHCl_3$/hexane (50:1) as eluent. Yield: 0.67 g, 40%; m.p. 190 °C. IR (KBr), ν (cm^{-1}): 3080 (Ar–H), 2238(C≡N), 2212 (C≡C), 1600, 1523, 1446, 911, 782, 706 cm^{-1}; ^{1}H NMR ($CDCl_3$):δ: 7.92 (s, 2H, Ar–H), 7.59 (d, 4H, Ar–H), 7.42 (m, 6H, Ar–H); UV–Vis λ_{max} (nm) (log ε) in $CHCl_3$: 279 (4.62), 307 (4.70), 349 (4.34). *Anal*. Calc. for $C_{24}H_{12}N_2$: C, 87.79; H, 3.68; N, 8.53. Found: C, 87.07, H, 3.66; N, 8.33%.

2.2. 2,3,9,10,16,17-Hexakis(hexylthio)-23,24-bis(phenylethynyl)-29H, 31H-phthalocyaninato zinc (II) (4)

A mixture of 0.16 g of **2** (0.49 mmol), 0.53 g of **3** (1.46 mmol), 0.09 g of anhydrous $Zn(CH_3COO)_2$ (0.49 mmol), 32 μl of DBU and 5 ml of anhydrous *n*-pentanol was refluxed with stirring for 24 h under N_2. The dark green mixture was cooled to room temperature and then diluted with ethanol until the crude product precipitated. The precipitate was filtered off and washed several times with hot ethanol and methanol to remove unreacted materials. Finally, the green precipitate was chromatographed on silica gel and eluted with $CHCl_3$/CH_3OH (50:1). Yield: 0.10 g, 14%; m.p. > 200 °C. IR (KBr), ν (cm^{-1}): 3080 (H–Ar), 2987–2870 (alkyl CH), 2212 (C≡C) 1600, 1523, 1421, 1395, 1089, 987, 757, 706 cm^{-1}; ^{1}H NMR ($CDCl_3$): δ: 0.94 (t, 18H, CH_3), 1.62 (m, 36H, CCH_2C), 1.88 (qnt, 12H, $SCCH_2$), 3.18 (t, 12H, SCH_2),7.42–7.90 (m, 18H, Ar–H); UV–Vis λ_{max}

(nm) (log ε) in $CHCl_3$: 277 (4.68), 329 (4.80), 727 (4.93). *Anal.* Calc. for $C_{84}H_{96}N_8S_6Zn$: C, 68.41; H, 6.51; N, 7.60. Found: C, 68.28; H, 6.49; N, 7.47%.

2.3. 2,3,9,10,16,17-Hexakis(hexylthio)-23,24-bis(phenylethynyl)-29H,31H-phthalocyaninatonickel (II) (5)

A mixture of 0.40 g of **2** (1.22 mmol), 1.32 g of **3** (3.66 mmol), 0.16 g of anhydrous $NiCl_2$ (1.22 mmol) and 80 μl of DBU was refluxed in 13 ml of anhydrous *n*-hexanol with stirring for 36 h under N_2. The resulting suspension was cooled to room temperature and the crude product was precipitated by addition of ethanol. It was filtered off and washed first with hot ethanol, then with methanol. The green product was isolated on a silica gel column first with hexane/THF (5:1) and then with THF/DMF (5:1) as eluent. Yield 0.09 g, 5%. Melting point > 200 °C. IR (KBr), *v* (cm^{-1}): 3080 (H–Ar), 2987–2870 (alkyl CH), 2212 (C≡C) 1600, 1523, 1421, 1395, 1089, 989, 756, 706 cm^{-1}; ^1H NMR ($CDCl_3$ 250 MHz): 0.97 (t, 18H, CH_3), 1.66 (m, 36H, CCH_2C), 1.93 (qnt, 12H, $SCCH_2$), 3.22 (t, 12H, SCH_2), 7.38–7.91 (m, 18H, Ar–H), 7.78 (s, 2H); UV–Vis λ_{max} (nm) (log ε) in $CHCl_3$: 322 (4.89), 703 (4.83). *Anal.* Calc. for $C_{84}H_{96}N_8S_6Ni$: C, 68.72; H, 6.54; N, 7.63. Found: C, 68.53; H, 6.41; N, 7.33%.

2.4. 2,3,9,10,16,17-Hexakis(hexylthio)-23,24-bis(phenylethynyl)-29H,31H-phthalocyaninatocobalt (II) (6)

A mixture of 0.30 g of **2** (0.92 mmol), 0.99 g of **3** (2.75 mmol), 0.12 g of anhydrous $CoCl_2$ (0.92 mmol) was refluxed in 10 ml anhydrous *n*-pentanol in the presence of 60 μl of DBU under N_2 with stirring for 24 h. The reaction mixture was cooled and the crude product was precipitated by addition of ethanol. It was filtered off and washed several times with hot ethanol and acetone. The green product was chromatographed on silica gel with hexane/THF (2:1) as eluent. Yield 0.11 g, 8%. Melting point > 200 °C. IR (KBr), *v* (cm^{-1}): 3080m (H–Ar), 2987–2870 (alkyl CH), 2212 (C≡C) 1600, 1523, 1421, 1395, 1089, 987, 757, 706 cm^{-1}; UV–Vis λ_{max} (nm) (log ε) in $CHCl_3$: 270 (3.98), 329 (4.19), 711 (4.00). *Anal.* Calc. for $C_{84}H_{96}N_8S_6Co$: C, 68.71; H, 6.54; N, 7.63. Found: C, 68.35; H, 6.36; N, 7.50%.

3. Results and discussion

3.1. Synthesis and characterisation

Different strategies to synthesise unsymmetrically substituted phthalocyanines (A_3B) have been reported, the most common one being the statistical condensation reaction between two different phthalonitriles or diiminoisoindolines. Statistical considerations predict that reaction of two different phthalonitriles of the same reactivity in a 3:1 ratio will afford a mixture of products in the following percentages: A_4 (33%), A_3B (44%), other cross-condensation products (23%) [14]. Using phthalonitriles with different solubility characteristics may permit separation of the unsymmetrical phthalocyanines by virtue of the different solubilities of the compounds present in the resulting statistical mixture. The attachment of alkylthio groups at the peripheral positions of one of the starting compounds facilitates the isolation of the A_3B product, as this substituent confers solubility in organic solvents and disfavours aggregation of the macrocycles [28].

4,5-Di(hexylthio) phthalonitrile (**2**) and 4,5-di(phenylethynyl)phthalonitrile (**3**) were chosen as starting materials for this study. **2** was prepared from 4,5-dichlorophthalonitrile and hexanethiol in DMF. K_2CO_3 was used as the base for this nucleophilic aromatic displacement [27]. Leznoff and Suchozak [29] have reported the synthesis of **3** from 4,5-diiodophthalonitrile. In the present work, **3** was synthesised from 4,5-dichlorophthalonitrile which is easily obtained from commercially available 4,5-dichloro-1,2-benzenedicarboxylic acid in four steps [26]. Under typical Sonogashira reaction conditions [30], the cross-coupling reaction between an excess of phenylacetylene and 4,5-dichlorophthalonitrile in triethylamine with bis(triphenylphosphine)palladium(II)chlorideand copper(I)iodide as catalysts at 90 °C under nitrogen atmosphere produced **3** in 40% yield.

Mixed condensation of 4,5-di(phenylethynyl)phthalonitrile with 4,5-di(hexylthio) phthalonitrile in the presence of the corresponding metal(II) salt afforded the unsymmetrical zinc-, nickel- and cobalt-substituted complexes **4**–**6**. Some experiments with different molar ratios were carried out to raise the yield of the desired unsymmetrically substituted phthalocyanines **4**–**6**. A 1:3 ratio of the two precursors was found to be the most appropriate for dinitriles **2** and **3**. The unsymmetrical phthalocyanines were separated by column chromatography from the corresponding totally symmetrical octahexylthiophthalocyanine formed in the statistical condensation. The unsymmetrical phthalocyanines **4**–**6** show good solubility in common organic solvents such as dichloromethane, chloroform and tetrahydrofuran (see Scheme 1).

The spectroscopic characterisation of the newly synthesised compounds included ^1H NMR, IR and UV–Vis. Spectral investigations and the results are in accord with the proposed structures. In the IR spectrum of **3** the intense absorption band at 2238 cm^{-1}, corresponding to C≡N vibrations, disappears after its conversion into the phthalocyanines. The ^1H NMR spectrum of **3** indicates aromatic protons at δ 7.92, 7.59 and 7.42 ppm.

The ^1H NMR spectra of the unsymmetrical phthalocyanines **4** and **5** are in excellent agreement with the

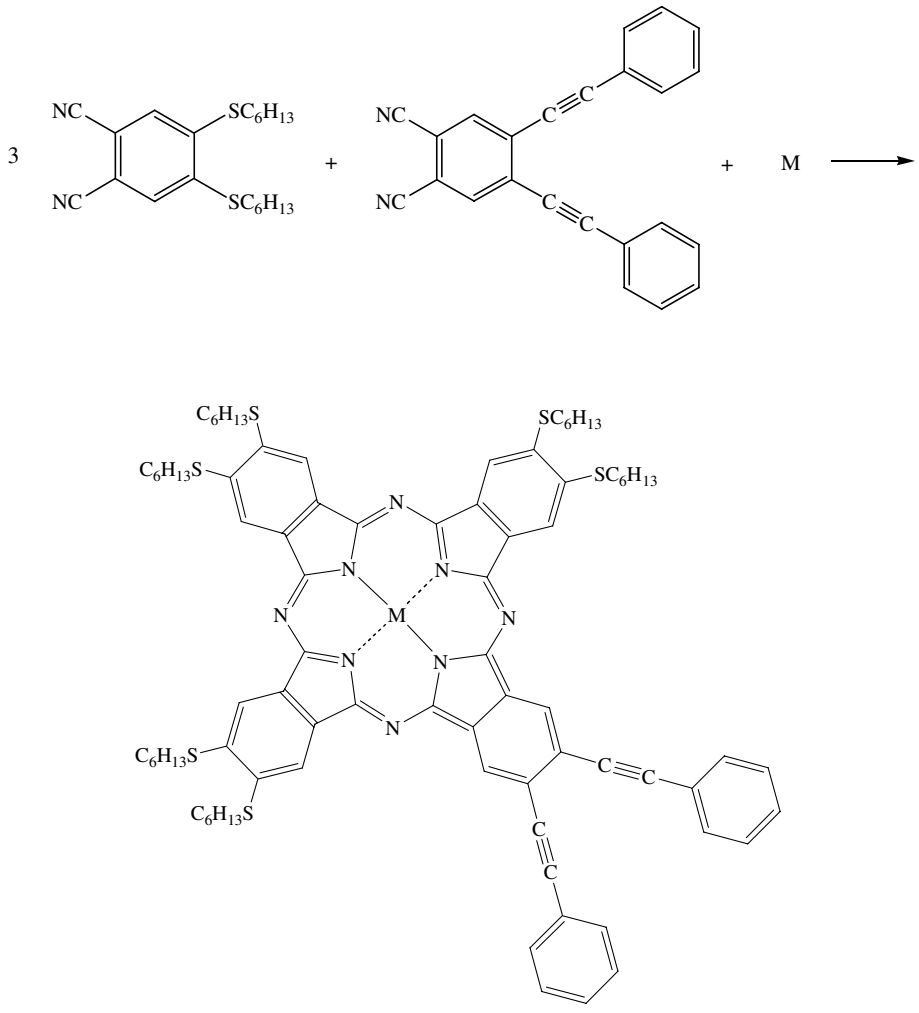

	4	5	6
M	Zn^{2+}	Ni^{2+}	Co^{2+}

Scheme 1.

proposed structures. The dominant features in the NMR spectra of **4** and **5** are the hexylthio group resonances. These resonances are shifted downfield by the phthalocyanine ring current relative to the precursor compound **2** [27]. ^{1}H NMR spectrum of **4** exhibited the aromatic protons at around δ 7.42–7.90 ppm as multiplets, the SCH_2, $SCCH_2$ protons at δ 3.18 and 1.88 ppm as a triplet and a quintet, respectively, and the aliphatic CH_3 protons as a triplet at δ 0.94 ppm. The ratio of aromatic to aliphatic protons appears to show that the benzo groups with two different substituents are present in a 3:1 ratio. The presence of alkylthio side chains in **4** was also confirmed by IR spectroscopy which showed an intense aliphatic C–H stretching at 2987–2870 cm^{-1}. The ^{1}H NMR spectrum of **5** is similar to that of **4**.

The UV–Vis spectra of **4–6** recorded in chloroform show the typical pattern of phthalocyaninatometal complexes. They are dominated by the π–π^* transitions within the heteroaromatic 18-π-electron system. The electronic absorption spectra of **4–6** exhibit a Q band absorption at 727, 703 and 711 nm, respectively. B bands of these phthalocyanines appear in the UV region at about 329 nm. The Q-bands of octakis alkylthio-substituted phthalocyanines are above 700 nm [27], the replacement of one of the benzenoid rings by a phenylethynyl ring gives rise to a bathochromic shift. The different Q band absorptions of **4–6** are attributable to the nature of the central metal ion.

In conclusion, unsymmetrical metallophthalocyanines **4–6** substituted with one phenylethynyl and three

hexylthio groups were synthesised by a statistical condensation route. Their spectral properties in a given solvent depends strongly on the central metal ion.

3.2. Electrochemical measurements

The electrochemical properties of metallophthalocyanine (MPc) complexes are well known [31–44]. Reduction and oxidation reactions can occur at either the Pc ring or central metal or both. Oxidation at the Pc ring in MPc(−2) occurs by successive loss of one or two electrons from the highest occupied molecular orbital (HOMO) resulting in the formation of the $[MPc(-1)]^{+}$ or $[MPc(0)]^{+2}$ cations, respectively. Reduction of the Pc ring occurs by the successive gain of one to four electrons by the lowest unoccupied molecular orbital (LUMO) of the MPc complex, resulting in the formation of MPc(−3), MPc(−4), MPc(−5) and MPc(−6) species, as commonly shown to indicate the oxidation states of the phthalocyanine ligand in the literature related with the electrochemistry of this compounds [1,6,31,40–44].

It has been demonstrated that substituents on the periphery of the phthalocyanine ligand strongly influence the solution redox chemistry of these materials. Electron-donating groups lead to a negative shift of the redox potentials and electron-withdrawing groups to a positive shift. This has been observed with both redox inactive metals like nickel, copper and zinc and redox active metals like cobalt [1].

Cyclic voltammograms of CoPc (**6**) (Fig. 1) show four well-defined redox couples (I–IV) within the available potential range of the TBAP/DCM solvent system at −0.313 and 0.644 V, easily attributed to Co^{II}/Co^{I} (I) and Co^{II}/Co^{III} (IV), and at 0.327 and −1.247 V at 0.100 V s^{-1} scan rate easily attributed to Pc^{2-}/Pc^{3-} (II) and Pc^{2-}/Pc^{1-} (III) redox couples, respectively. It is clearly indicated that first-row transition metallophthalocyanines differ from those of the main-group metallophthalocyanines due to the fact that metal "d" orbitals may be positioned between the HOMO and LUMO of the phthalocyanine (Pc^{2-}) ligand. This has been well established by several papers published by Lever et al. [1,42–44]. According to these studies, electrochemistry of metallophthalocyanines containing a redox active metal center such as Mn, Fe and Co can conveniently be split into two sections, that referring to non-donor solvents, and that referring to donor solvents. For CoPc complexes, donor solvents or coordinating counter anions strongly favour Co(III)Pc by coordinating along the axis to form a six-coordinate $L_2Co(III)Pc$ species. If a donor solvent is not present, such as DCM used in this study, then oxidation to Co(III)Pc is inhibited and ring oxidation occurs first. So in this study, it is possible to assign the first oxidation of the CoPc species at 0.33 V to the ring oxidation and the second one at 0.64 V to the metal center. According to this behaviour of CoPc in DCM, the electron transfer sequence would be [Co(III)/(II)]Pc(1−) > Co(II)[Pc(1−)/(2−)] > [Co(II)/(I)] Pc(2−) > Co(I)[Pc(2−)/(3−)].

The separation between the first reduction and first oxidation processes (640 mV) of **6**, which reflects the HOMO–LUMO gap of the complexes, is smaller than that in the reported CoPc papers [1,31–44]. This is not very surprising since extended π-conjugation of **6** may cause a decrease in the HOMO–LUMO gap of the complex. This voltammetric data was confirmed by the shifting of the Q band towards a longer wavelength in the

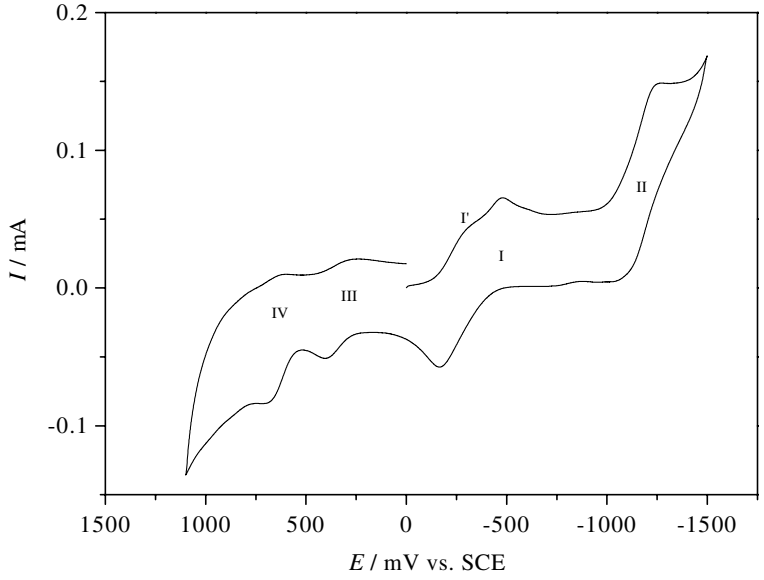

Fig. 1. Cyclic voltammogram of 1.0×10^{-3} mol dm^{-3} CoPc (**6**) in 0.1 mol dm^3 TBAP/DCM at 100 mV s^{-1} scan rate.

Table 1
The cyclic voltammetric data of the complexes with the related MPc derivatives reported in the literature

Complex	Redox processes [e]												Solvent	Reference
	IV			III			I			II				
	[a]$E_{1/2}$ (mV)	[b]ΔE_p (mV)	[c]I_{pc}/I_{pa}	[a]$E_{1/2}$ (mV)	[b]ΔE_p (mV)	[c]I_{pc}/I_{pa}	[a]$E_{1/2}$ (mV)	[b]ΔE_p (mV)	[c]I_{pc}/I_{pa}	[a]$E_{1/2}$ (mV)	[b]ΔE_p (mV)	[c]I_{pc}/I_{pa}		
ZnPc (**4**)	814	98	0.94	633	75	1.1	−780	149	1.2	−1027	191	0.75	DCM	tw
NiPc (**5**)	837	109	0.97	576	87	0.60	−817	186	0.98	−1032	154	0.93	DCM	tw
CoPc (**6**)	644	92	0.78	327	147	0.57	−313	287	1.1	−1247[a]	157	0.58	DCM	tw
$ZnPc(SC_6H_4CH_3)_8$				750			−680			−1050			DMF	45
$ZnPc(SC_4H_9)_8$				620			−830			−1180			DMF	45
$ZnPc(OC_6H_4C(CH_3)_3)H_7$				550			−1080			−1560			DMF	46
$ZnPc(SC_6H_{13})_8$	850			645			−830			−1150			DCM	31
$CoPc(CH_3OC_6H_{13})_8$[d]	730			−160			−490			−670			DMSO	32
$ZnPc(SC_6H_4NH_2)_4Cl_4$[d]							−713			−1105			DMSO	33
$CoPc(SC_6H_4NH_2)_4Cl_4$[d]	950			605			−609			−1037			DMSO	33
$NiPc(SC_6H_4NH_2)_4Cl_4$[d]							−615			−1210			DMSO	33
$ZnPc(SC_4H_9)_8$	1270			620			−830			−1180			DMF	34
$CoPc(SC_2H_4OH)_8$							−340			−1220			DCM	35

[a] Cathodic peak potential for reduction, anodic peak potential for oxidation for irreversible processes.
[b] $\Delta E_p = E_{pa} - E_{pc}$ at 0.100 V s^{-1} scan rate.
[c] I_{pa}/I_{pc} for reduction, I_{pc}/I_{pa} for oxidation at 0.100 V s^{-1} scan rate.
[d] Complexes also have extra reduction and oxidation couples.
[e] For CoPc (6) and study in [35], redox processes; I: M(II)Pc(−2)/M(I)Pc(−2), II: M(I)Pc(−2) M(II)Pc(−3), III: M(II)Pc(−2)/M(II)Pc(−1), IV: M(II)Pc(−1)/M(III)Pc(−1). For CoPc complexes studied in [32,33], redox processes; I: M(II)Pc(−2)/M(I)Pc(−2), II: M(I)Pc(−2)/M(II)Pc(−3), III: M(II)Pc(−2)/M(III)Pc(−2), IV: M(III)Pc(−2)/M(III)Pc(−1). For all ZnPc and NiPc complexes, redox processes;I:M(II)Pc(−2)/M(II)Pc(−3), II: M(II)Pc(−3)/M(II)Pc(−4), III: M(II)Pc(−2)/(II)Pc(−1), IV: M(II)Pc(−1)/M(II)Pc(0).

UV–Vis spectrum of the complex. The separation between the metal based reduction and the ring reduction was found to be 0.930 V, which is in agreement with the separation reported for CoPc's [31–45]. In Table 1, the CV data, cathodic to anodic peak separation (ΔE_p) and peak current ratios (I_{pa}/I_{pc}) of **6** are listed together with those of ZnPc (**4**), NiPc (**5**) and MPc's containing a similar metal centre and substituents reported in the literature.

The observation of two closely spaced reduction peaks (I′ and I) has been attributed to the presence of both the aggregated and unaggregated forms of **6** in solution. At the concentration employed for voltammetric studies in this work, aggregation of the CoPc derivatives is expected and was confirmed by a shoulder of the Q band in the UV–Vis spectra of **6** [46]. Characterisation of this couple could not be done as a result of the splitting of the reduction peak. The process II recorded at −1.247 V was quasi-reversible in that it shows a more enhanced forward (cathodic) peak compared to the return (anodic) peak and a large ΔE_p value (200 mV at 100 mV s^{-1}). Peak current ratios (I_{pa}/I_{pc}) of this couple were smaller than unity at slow scan rates and approached unity with increasing scan rates. This behaviour of the process indicated the existence of a chemical reaction following the electron transfer reaction (EC mechanism) [47–49]. Both of the oxidation processes (III and IV) of **6** exhibited a quasi-reversible peak character with moderate ΔE_p values (157 and 147 mV at 100 mV s^{-1}, respectively). For these processes, the anodic peak currents increased linearly with the square root of the scan rates for scan rates ranging from 10 to 500 mV s^{-1}, indicating that the electrode reaction is purely diffusion-controlled. For both the III and IV couple, peak current ratios (I_{pa}/I_{pc}) were smaller than unity at slow scan rates, but move towards unity by increasing the scan rates, indicating the complication of the mass transport mechanism of the complex probably with a proceeding or succeeding chemical reaction.

Complex **4** and **5** exhibited very similar voltammetric behaviours. Fig. 2 shows the cyclic voltammograms of**4** recorded at 100 mV s^{-1} scan rate. As shown in the figure, two well-defined reduction processes, (I and II) at −0.780 and −1.027 V attributed to the Pc^{2-}/Pc^{3-} and Pc^{3-}/Pc^{-4} redox couples, and two well-defined oxidation processes, (III and IV) at 0.633 and 0.814 V attributed to the Pc^{2-}/Pc^{1-} and Pc^{1-}/Pc^{0} redox couples, are observed. Since the central Zn(II) metal is redox inactive, all oxidation and reduction processes observed are ring-based [38]. Ring-based redox potentials of complex **4** are considerably different to those of complex **6**. The potential of the [Pc(2−)/(1−)] couple of complex **4** is shifted to positive potentials compared with that of complex **6**. The potential of the [Pc(2−)/(1−)] couple of complex **4** is 0.63 V and the [Pc(2−)/(1−)] couple of **6** is 0.33 V. Similar behaviour was observed for the ring reduction potentials of the complexes. The [Pc(2−)/(3−)] couple of **4** is shifted to a more positive potential compared with that of the **6**. The difference between the first

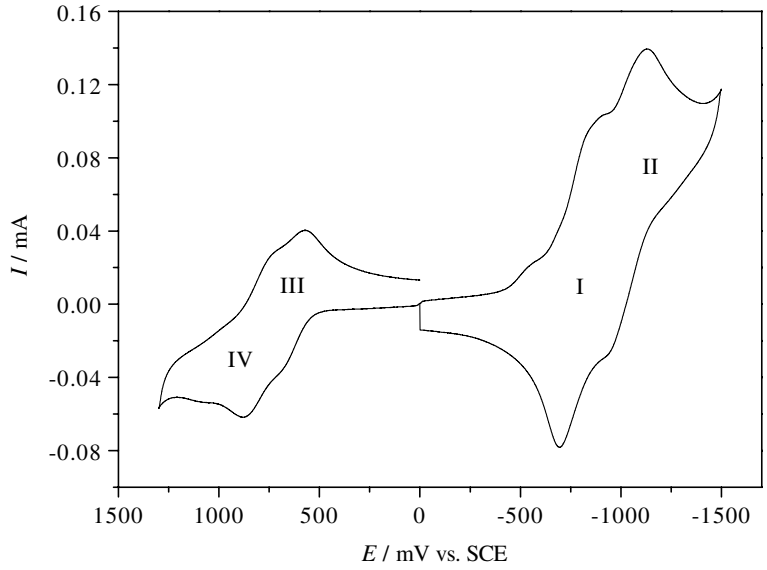

Fig. 2. Cyclic voltammogram of 1.0×10^{-3} mol dm^{-3} ZnPc (**4**) in 0.1 mol dm^3 TBAP/DCM at 100 mV s^{-1} scan rate.

and second reduction processes for **4** is 0.244 V, which is compatible with the average value for the separation of the first and second reduction processes of similar metal phthalocyanine complexes [1]. The potential separation between the first ring oxidation and the first ring reduction (ΔE), which corresponds to the magnitude of the energy difference between the HOMO and LUMO, is approximately between 1.5 and 1.8 V [1,31]. However, the ΔE value of ~1.413 V for **4** is smaller than the range reported for similar complexes. Exchange of one hexylthio substituent of ZnPc bearing an octakis(hexylthio) substituent (ΔE value = 1.475 V) [31] with the diphenylethynylgroup cause a decrease in the ΔE value of **4** of about 62 mV.This is perhaps the result of the decreasing HOMO–LUMO gap by the effect of the extended π-conjugation of the complex. The cyclic voltammograms of **5** also gave two one-electron diffusion controlled quasi-reversible reduction processes at −0.817 and −1.032 V vs. SCE, attributed to the Pc^{2-}/Pc^{3-} and Pc^{3-}/Pc^{-4} redox couples, and two one-electron diffusion controlled quasi-reversible oxidation processes at 0.536 and 0.837 V, attributed to the Pc^{2-}/Pc^{1-} and Pc^{1-}/Pc^{0} redox couples. The difference between the first and second reduction processes (0.215 V) and the small ΔE value (1.393 V) for **5** is compatible with those of **4**. Moreover, the individual potentials for the first reduction and the first oxidation of **4** and **5** varied remarkably due to the function of the polarising power of the central metal ion. In general the more polarising the central metal ions, the easier it is to reduce the ring, and the more difficult to oxidise the ring.

During controlled potential coulometric (CPC) studies, complete electrolysis of the solution at the working electrode at constant potential (E_{pc} of the redox couple) was achieved, and the time integration of the electrolysis current was recorded. The electroactive species in the solution were depleted during the electrolysis, and the charge, Q, at the end of the electrolysis was calculated using the current–time response of solution. *Faraday*'s law was used to estimate the number of electrons transferred. The CPC studies indicated that the number of electrons transferred for all electron transfer reactions of the compounds studied is one.

Acknowledgement

This work was supported by the Research Fund of the Technical University of Istanbul.

References

[1] C.C. Leznoff, A.B.P. Lever (Eds.), Phthalocyanines Properties and Applications, 1–4, VCH, Weinheim, 1989–1996.
[2] N.B. McKeown, Phthalocyanine Materials, Cambridge University Press, Cambridge, 1998.
[3] S. Vagin, M. Hanack, Eur. J. Org. Chem. (2003) 2661.
[4] Ö. Bekaroğlu, Appl. Organomet. Chem. 10 (1996) 605.
[5] Y. Gök, H. Kantekin, I. Degirmencioglu, Supramol. Chem. 15 (2003) 335.
[6] M. Kandaz, M.N.U. Yarasir, A. Koca, Ö. Bekaroğlu, Polyhedron 21 (2002) 255.
[7] Z.A. Bayır, E. Hamuryudan, Ö. Bekaroğlu, J. Chem. Res. (S) (1999) 702.
[8] R. Öztürk, A. Gül, Tetrahedron Lett. 45 (2004) 947.
[9] E.M. Maya, E.M. Garcia-Frutos, P. Vazquez, T. Torres, G. Martin, G. Rojo, F. Agullo-Lopez, R.H. Gonzalez-Jonte, V.R. Ferro, J.M.G. Vega, I. Ledoux, J. Zyss, J. Phys. Chem. A 107 (2003) 2110.

[10] K. Oda, S. Ogura, I. Okura, J. Photochem. Photobiol. B: Biol. 59 (2000) 20.
[11] S. Kudrevich, N. Brasseur, C. LaMadeleine, S. Gilbert, J.E. Vanlier, J. Med. Chem. 40 (1997) 3897.
[12] G.J. Clarkson, N.B. McKeown, K.E. Treacher, J. Chem. Soc., Perkin Trans. I 14 (1995) 1817.
[13] M.J. Cook, N.B. McKeown, J.M. Simmons, A.J. Thomson, M.F. Daniel, K.J. Harrison, R.M. Richardson, S.J. Roser, J. Mater. Chem. 1 (1991) 121.
[14] G. de la Torre, C.G. Claessens, T. Torres, Eur. J. Org. Chem. (2000) 2821.
[15] C.C. Leznoff, T.W. Hall, Tetrahedron Lett. 23 (1982) 3023.
[16] N. Kobayashi, R. Kondo, S.I. Nakajima, T. Osa, J. Am. Chem. Soc. 112 (1990) 9640.
[17] S. Dabak, A. Gül, Ö. Bekaroglu, Chem. Ber. 127 (1994) 2009.
[18] M.J. Cook, Chem. Record 2 (2002) 225.
[19] G. de la Torre, P. Vasquez, F. Agullo-Lopez, T. Torres, J. Mater. Chem. 8 (1998) 1671.
[20] Z.A. Bayır, E. Hamuryudan, A.G. Gurek, Ö. Bekaroğlu, J. Porphyr. Phthalocya. 1 (1997) 349.
[21] S. Gursoy, Z.A. Bayır, E. Hamuryudan, Ö. Bekaroğlu, Monatsh. Chem. 131 (2000) 287.
[22] A. Kalkan, Z.A. Bayır, Monatsh. Chem. 134 (2003) 1555.
[23] E. Hamuryudan, Z.A. Bayır, Ö. Bekaroğlu, Dyes Pigments 43 (1999) 77.
[24] Z.A. Bayır, E. Hamuryudan, Ö. Bekaroğlu, J. Chem. Res. (S) (1999) 702.
[25] E. Hamuryudan, S. Merey, Z.A. Bayır, Dyes Pigments 59 (2003) 263.
[26] D. Wöhrle, M. Eskes, K. Shigehara, A. Yamada, Synthesis (1993) 194.
[27] A.G. Gurek, Ö. Bekaroglu, J. Chem. Soc., Dalton Trans. (1994) 1419.
[28] Z.A. Bayır, S. Merey, E. Hamuryudan, Monatsh. Chem. 134 (2003) 1027.
[29] C.C. Leznoff, B. Suchozak, Can. J. Chem. 79 (2001) 878.
[30] K. Sonagashira, in: F. Diederich, P.J. Stang (Eds.), Metal-Catalyzed Cross-Coupling Reactions, Wiley-VCH, Weinheim, 1998, pp. 203–229.
[31] A.R. Ozkaya, A.G. Gürek, A. Gül, Ö. Bekaroğlu, Polyhedron 16 (1997) 1877.
[32] K. Sakamoto, E.O. Okumura, J. Porphyr. Phthalocya. 3 (1999) 634.
[33] M. Kandaz, M.N.U. Yaraşır, A. Koca, Ö. Bekaroğlu, Polyhedron 21 (2002) 255.
[34] K. Takahashi, M. Kawashima, Y. Tomita, M. Itoh, Inorg. Chim. Acta 232 (1995) 69.
[35] A.R. Özkaya, E. Hamuryudan, Z.A. Bayır, Ö. Bekaroğlu, J. Porphyr. Phthalocya. 7 (2000) 689.
[36] G. Rojo, G. Torre, J. Garcýa-Ruiz, I. Ledoux, T. Torres, J. Zyss, F. Agullo-Lopez, Chem. Phys. 245 (1999) 27.
[37] R. Jung, K.H. Schweikart, M. Hanack, Synth. Met. 453 (2000) 111.
[38] K.M. Kadish, L.A. Bottamley, J.S. Cheng, J. Am. Chem. Soc. 100 (1978) 2731.
[39] M. Kimura, Y. Sugihara, T. Muto, K. Hanabusa, H. Shirai, N. Kobayashi, Chem. Eur. J. 5 (1999) 3495.
[40] K. Sakamoto, E. Ohno, Prog. Org. Coat. 31 (1997) 139.
[41] A. Koca, M. Şahin, A. Gül, R.Z. Uslu, Monatsh. Chem. 133 (2002) 1135.
[42] A.B.P. Lever, P.C. Minor, Inorg. Chem. 20 (1980) 4015.
[43] A.B.P. Lever, Adv. Inorg. Chem. Radiochem. 7 (1965) 27.
[44] A.B.P. Lever, S. Licoccia, K. Magnell, P.C. Minor, B.S. Ramaswamy, Adv. Chem. Ser. 201 (1982) 237.
[45] K.I. Ozoemena, T. Nyokong, Microchem. J. 75 (2003) 241.
[46] P. Matlaba, T. Nyokong, Polyhedron 21 (2002) 2463.
[47] P.T. Kissinger, W.R. Heineman, Laboratory Techniques in Electroanalytical Chemistry, 2nd ed., Marcel Dekker, New York, 1996.
[48] A. Koca, Ö.G. Sağlam, A. Gül, Monatsh. Chem. 134 (2003) 11.
[49] E. Gileadi, E. Kirowa-Eisner, J. Penciner, Interfacial Electrochemistry, Addison-Wesley, Reading, MA, 1975.

catalyze the hydrogenation of styrene and imines with practically 100% conversion is described in the literature [4,5]. Thus the high efficiency of these complexes as pre-catalysts in hydrogenation reactions assumes crucial importance in finding out simple routes for their synthesis.

Face-sharing bi-octahedral complexes are of great importance due to two facts: (1) these species are potential catalysts in hydrogenation reactions [4,5]; (2) at least three different oxidation states can be generated in solution [6]. Due to these facts binuclear ruthenium phosphine complexes containing a face-sharing bioctahedral Ru–(μ-Cl)$_3$–Ru core have received considerable attention [1,2,6–8].

In this work, we present the synthesis of a series of binuclear complexes based on the reactivity of the *mer*-[RuCl$_3$(P–P)H$_2$O] complexes and their synthesis is summarized in Eq. (1):

$$[RuCl_3(P\text{–}P)H_2O] + [RuCl_2(P\text{–}P)'PR_3] \rightarrow [(P\text{–}P)ClRu\text{–}(\mu\text{-}Cl)_3\text{–}RuCl(P\text{–}P)'] + H_2O + PR_3 \quad (1)$$

PR$_3$ = PPh$_3$ (triphenylphosphine), P-ptol$_3$ (tri-*p*-tolylphosphine); (P–P) = dppb (1,4-bis(diphenylphosphino)butane) or *S*-diop ((2S–2S)-*o*-isopropylidene-2,3-dihydroxy-1,4-bis(diphenylphosphino)butane); (P–P)′ = dppb, *S*-diop, *S*-binap ((S)-2,2′-bis (diphenylphosphino)1,1′-binaphthyl), dppn (1,5-bis(diphenylphosphino) pentane), (PPh$_3$)$_2$, (P-ptol$_3$)$_2$ or (SbPh$_3$)$_2$ (triphenylstibine).

2. Experimental

2.1. Materials and instrumentation

All manipulations were carried out under purified Ar using standard Schlenk techniques. Reagent grade solvents were appropriately distilled and dried before use. RuCl$_3 \cdot n$H$_2$O, dppb, PPh$_3$, P-ptol$_3$, dppn, *S*-diop, *S*-binap, dpae (1,2-bis(diphenylarsino)ethane), dppe (1,2-bis(diphenylphosphino)ethane), 1,3-cyclohexadiene, benzonitrile (PhCN) were used as received from Aldrich. Imines were prepared by condensation of the appropriate aldehyde and amines [5] and stored under Ar in the dark. *mer*-[RuCl$_3$(dppb)H$_2$O] (**1**) [1], *mer*-[RuCl$_3$(*S*-diop)H$_2$O] (**2**) [1], [RuCl$_2$(*S*-diop)PPh$_3$] [9], [RuCl$_2$(*S*-Binap)PPh$_3$] [10], [RuCl$_2$(dppb)PPh$_3$] [11], [RuCl$_2$(PPh$_3$)$_3$] [12], [Ru$_2$Cl$_4$(dppn)$_3$] [13], [RuCl$_2$(P-ptol$_3$)$_3$] [14], [RuCl$_2$(SbPh$_3$)$_3$] [12] and [(η^6-C$_6$H$_6$)RuCl(dpae)]Cl [15] were prepared according to the above mentioned literature procedures.

Hydrogenation reactions were carried out in a stainless steel autoclave equipped with a high-pressure regulator and connected to a vacuum line. Oxygen was removed from the system by evacuating the autoclave and refilling it up with Ar three times, and purging three times with H$_2$ before adjusting it to the desired pressure. Conversions of imines to amines were determined by ^{1}H NMR experiments.

IR spectra (cm^{-1}) were recorded as CsI pellets in the 4000–200 cm^{-1} region, on a Bomen–Michelson 102 instrument; UV–Visible (UV–Vis) and near-infrared (NIR) spectra were recorded in solution on a Hewlett-Packard 8452A diode array or Cary 500 spectrophotometers, respectively, and are presented as λ_{max}(nm)/ε_{max} (M^{-1} cm^{-1}). Cyclic voltammetry (CV) experiments were carried out at room temperature in CH$_2$Cl$_2$ containing 0.10 mol l^{-1} Bu$_4$N$^+$ClO$_4^-$ (TBAP) (Fluka Purum) using a BAS-100B/W Bioanalytical Systems Instruments. The working and auxiliary electrodes were stationary Pt foils, and the reference electrode was Ag/AgCl, 0.10 mol l^{-1} TBAP in CH$_2$Cl$_2$, a medium in which ferrocene is oxidized at 0.43 V (Fc$^+$/Fc).

All NMR experiments were run on BRUKER, DRX400 9.4 Tesla equipment, in a BBO 5 mm probe at 298 K, using CDCl$_3$ (^{1}H) and CH$_2$Cl$_2$(^{31}P{^{1}H}) as a solvent, TMS and H$_3$PO$_4$ 85% for internal and external reference for ^{1}H and ^{31}P, respectively. Effective magnetic moments (μ_{eff}) were determined at room temperature (~25 °C) by the Gouy method using a Johnson Matthey magnetic susceptibility balance.

Elemental analyses were performed in the Chemistry Department of Universidade Federal de São Carlos.

2.2. X-ray crystallographic analysis of [(dppb)ClRu–(μ-Cl)$_3$–RuCl(dppb)] (5) and [(η^6-C$_6$H$_6$)Ru–(μ-Cl)–RuCl-(dppb)] (11)

X-ray data of crystals of compounds (**5**) and (**11**) were measured on an Enraf-Nonius Kappa-CCD diffractometer with graphite monochromated Mo Kα (λ = 0.71073 Å) radiation. Data were collected up to 50° in 2θ, with a redundancy of 4. The final unit cell parameters were based on all reflections. Data collections were carried out using the COLLECT program [16]. Integration and scaling of the reflections were performed with the HKL Denzo-Scalepack system of programs [17]. Absorption corrections were carried out using the multi-scan method [18].

The structures were solved by direct methods with SHELXS-97 [19]. Models were refined by full-matrix least-squares on F^2 using SHELXL-97 [20]. All hydrogen atoms were stereochemically positioned and refined with the riding model [21].

Data collection and experimental details for complexes (**5**) and (**11**) are summarized in Table 1. Relevant interatomic bond lengths and bond angles are listed in Table 2. ORTEP projections of the structures are shown in Figs. 1 and 2.

Table 1
Crystallographic data for complexes (**5**) and (**11**)

	(**5**)	(**11**)
Empirical formula	$C_{56}H_{56}P_4Cl_5Ru_2$	$[C_{34}H_{34}P_2Cl_4Ru_2]\cdot C_2H_4Cl_2$
Formula weight	1232.28	947.44
Temperature (K)	120(2)	120(2)
Wavelength (Å)	0.71073	0.71073
Crystal system	monoclinic	triclinic
Space group	$P2_1/c$	$P\bar{1}$
Unit cell dimensions		
a (Å)	13.2450(4)	10.4240(1)
b (Å)	20.3790(7)	12.5350(1)
c (Å)	23.0640(8)	15.6530(2)
α (°)	–	100.467(1)
β (°)	117.912(1)	96.164(1)
γ (°)	–	112.293(1)
Volume (Å^3)	5501.2(3)	1825.67(3)
Z	4	2
D_{calc} (Mg/m^3)	1.488	1.724
Absorption coefficient (mm^{-1})	0.944	1.381
F (0 0 0)	2500	948
Crystal size (mm)	$0.20\times0.04\times0.01$	$0.28\times0.10\times0.02$
θ range for data (°)	2.53–25.00	1.35–25.00
Collection index ranges	$-15\leqslant h\leqslant 15$, $-20\leqslant k\leqslant 24$, $-27\leqslant l\leqslant 27$	$-12\leqslant h\leqslant 12$, $-14\leqslant k\leqslant 14$, $-18\leqslant l\leqslant 18$
Reflections collected	17,640	12,205
Independent reflections	9613 (R_{int} = 0.0523)	6442 (R_{int} = 0.0178)
Completeness to θ = 25.00° (%)	99.5	100.0
Absorption correction	Multiscan	Multiscan
Maximum and minimum transmission	0.9906 and 0.8336	0.9729 and 0.6984
Refinement method	full-matrix least-squares on F^2	full-matrix least-squares on F^2
Data/parameters	9613/604	6442/433
Goodness-of-fit on F^2	1.096	1.143
Final R indices [$I > 2\sigma(I)$]	R_1 = 0.0443, wR_2 = 0.1000	R_1 = 0.0291, wR_2 = 0.0878
R indices (all data)	R_1 = 0.0862, wR_2 = 0.1347	R_1 = 0.0358, wR_2 = 0.1106
Largest differential peak and hole (eÅ^{-3})	0.497 and −0.717	0.842 and −1.519

2.3. Reactivity of mer-[$RuCl_3$(dppb)H_2O] with other Ru(II) or Ru(III) complexes

The procedure for the preparation of binuclear complexes is similar to that used for complex (**3**):

2.3.1. [(*S*-diop)ClRu–(μ-Cl)$_3$–RuCl(dppb)] (**3**)

A suspension of (**1**) (0.0848 g, 0.1301 mmol) and [$RuCl_2$(*S*-diop)PPh_3] (0.1214 g, 0.1301 mmol) in CH_2Cl_2 (50 ml) was stirred at room temperature for 3 h. The solution volume was reduced to ~5 ml and addition of *n*-hexane (10 ml) precipitated a brown solid, which was collected, washed well with methanol and *n*-hexane, and dried under vacuum. Yield (0.1528 g, 90%). *Anal.* Calc. for $C_{59}H_{60}O_2Cl_5P_4Ru_2$: C, 54.33; H, 4.64. Found: C, 54.34; H, 4.64%. UV–Vis (CH_2Cl_2): 372 (3400), 448 (1930), 525 (1380). μ_{eff} 1.80 μ_B/dimer.

2.3.2. [(*S*-binap)ClRu–(μ-Cl)$_3$–RuCl(dppb)] (**4**)

Complex (**1**) (0.0294 g, 0.0450 mmol) and [$RuCl_2$(*S*-Binap)PPh_3] (0.0476 g, 0.0450 mmol). Yield (0.0488 g, 76%). *Anal.* Calc. for $C_{72}H_{60}Cl_5P_4Ru_2$: C, 60.54; H, 4.23. Found: C, 60.39; H, 4.56%. UV–Vis (CH_2Cl_2): 340 (3440), 398 (2840), 534 (1780). μ_{eff} 1.95 μ_B/dimer.

2.3.3. [(dppb)ClRu–(μ-Cl)$_3$–RuCl(dppb)] (**5**)

Complex (**1**) (0.0353 g, 0.0542 mmol) and [$RuCl_2$(dppb)PPh_3] (0.0466 g, 0.0542 mmol). Yield (0.0467 g, 70%). *Anal.* Calc. for $C_{56}H_{56}Cl_5P_4Ru_2$: C, 54.58; H, 4.58. Found: C, 54.51; H, 4.77%. UV–Vis (CH_2Cl_2): 374 (3500), 436 (2730), 550 (1850). μ_{eff} 2.01 μ_B In this case to a dichloromethane solution of (**5**) *n*-hexane was added until cloudiness and it was left undisturbed in a freezer. After 2 days a crop of reddish-brown crystals suitable for X-ray analysis were recovered.

2.3.4. [(PPh_3)$_2$ClRu–(μ-Cl)$_3$–RuCl(dppb)] (**6**)

Complex (**1**) (0.0450 g, 0.0690 mmol) and [$RuCl_2(PPh_3)_3$] (0.0662 g, 0.0690 mmol). Yield (0.0615 g, 67%). *Anal.* Calc. for $C_{64}H_{58}Cl_5P_4Ru_2$: C, 57.78; H, 4.39. Found: C, 57.90; H, 4.66%. UV–Vis (CH_2Cl_2): 378 (3650), 444 (1930), 536 (1720). μ_{eff} 1.78 μ_B/dimer.

Table 2
Selected bond distances (Å) and bond angles (°) of the [(dppb)ClRu–(μ-Cl)$_3$–RuCl(dppb)] (**5**) and [(η^6-C$_6$H$_6$)Ru–(μ-Cl)$_3$–RuCl(dppb)] · C$_2$H$_4$Cl$_2$ (**11**) complexes

(**5**)		(**11**)	
Bond distances			
Ru(1)–Ru(2)	3.174(6)	Ru(1)–Ru(2)	3.314(1)
Ru(1)–Cl(11)	2.3627(15)	Ru(1)–Cl(1)	2.3865(7)
Ru(1)–Cl(1)	2.3402(15)	Ru(1)–Cl(2)	2.4936(8)
Ru(1)–Cl(2)	2.4607(14)	Ru(1)–Cl(3)	2.4343(8)
Ru(1)–Cl(3)	2.4422(14)	Ru(1)–Cl(4)	2.5960(8)
Ru(2)–Cl(21)	2.3927(14)	Ru(2)–Cl(2)	2.4144(8)
Ru(2)–Cl(1)	2.4877(15)	Ru(2)–Cl(3)	2.4208(8)
Ru(2)–Cl(2)	2.3729(15)	Ru(2)–Cl(4)	2.4231(8)
Ru(2)–Cl(3)	2.4829(13)	Ru(2)–C(21)	2.158(4)
Ru(1)–P(1)	2.3293(16)	Ru(2)–C(25)	2.176(3)
Ru(1)–P(2)	2.3236(15)	Ru(2)–C(26)	2.164(4)
Ru(2)–P(3)	2.2957(15)	Ru(1)–P(1)	2.2777(8)
Ru(2)–P(4)	2.2809(16)	Ru(1)–P(2)	2.2463(8)
Bond angles			
P(2)–Ru(1)–P(1)	95.33(6)	P(2)–Ru(1)–P(1)	93.58(3)
P(3)–Ru(2)–P(4)	93.02(5)	P(2)–Ru(1)–Cl(1)	98.30(3)
P(2)–Ru(1)–Cl(1)	91.83(5)	P(1)–Ru(1)–Cl(1)	88.36(3)
P(1)–Ru(1)–Cl(1)	96.76(5)	P(2)–Ru(1)–Cl(3)	94.86(3)
P(2)–Ru(1)–Cl(11)	98.00(5)	P(1)–Ru(1)–Cl(3)	101.44(3)
P(1)–Ru(1)–Cl(11)	87.62(6)	Cl(1)–Ru(1)–Cl(3)	163.07(3)
P(2)–Ru(1)–Cl(3)	91.45(5)	Cl(1)–Ru(1)–Cl(2)	88.42(3)
P(1)–Ru(1)–Cl(3)	172.65(6)	Cl(3)–Ru(1)–Cl(2)	80.92(2)
Cl(1)–Ru(1)–Cl(11)	168.85(6)	P(2)–Ru(1)–Cl(4)	165.09(3)
Cl(1)–Ru(1)–Cl(3)	85.82(5)	P(1)–Ru(1)–Cl(4)	99.54(3)
Cl(11)–Ru(1)–Cl(3)	88.65(5)	Ru(2)–Cl(2)–Ru(1)	84.94(2)
Ru(1)–Cl(1)–Ru(2)	82.14(5)	Ru(2)–Cl(3)–Ru(1)	86.10(3)

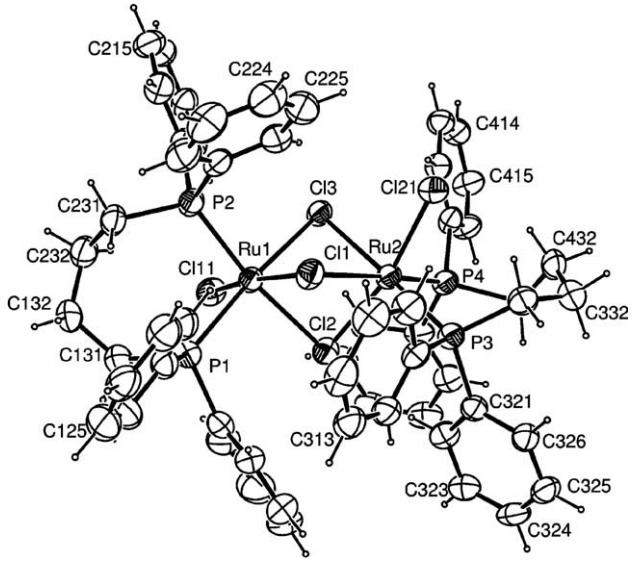

Fig. 1. ORTEP view of the complex [(dppb)ClRu–(μ-Cl)$_3$–RuCl(dppb)] (**5**), showing the atom labelling and the 50% probability ellipsoids.

*2.3.5. [(dppn)ClRu–(μ-Cl)$_3$–RuCl(dppb)] (**7**)*

Complex (**1**) (0.1035 g, 0.1588 mmol) and [Ru$_2$Cl$_4$(dppn)$_3$] (0.1322 g, 0.0794 mmol). Yield (0.1583 g, 80%). *Anal.* Calc. for C$_{57}$H$_{58}$Cl$_5$P$_4$Ru$_2$: C, 54.93; H, 4.69. Found: C, 55.34; H, 4.73%. UV–Vis (CH$_2$Cl$_2$): 380 (2390), 445 (1750), 525 (1040). μ_{eff} 1.83 μ_B/dimer.

*2.3.6. [(P-ptol$_3$)$_2$ClRu–(μ-Cl)$_3$–RuCl(dppb)] (**8**)*

Complex (**1**) (0.0125 g, 0.0192 mmol) and [RuCl$_2$(P-ptol$_3$)$_3$] (0.0208 g, 0.0192 mmol). Yield (0.0190 g, 70%). *Anal.* Calc. for C$_{70}$H$_{70}$Cl$_5$P$_4$Ru$_2$: C, 59.43; H, 4.99. Found: C, 59.29; H, 4.66%. UV–Vis (CH$_2$Cl$_2$): 379 (3820), 437 (2840), 527 (1710). μ_{eff} 1.79 μ_B/dimer.

*2.3.7. [(SbPh$_3$)$_2$ClRu–(μ-Cl)$_3$–RuCl(dppb)] (**9**)*

Complex (**1**) (0.0958 g, 0.1470 mmol) and [RuCl$_2$(SbPh$_3$)$_3$] (0.1809 g, 0.1470 mmol). Yield (0.1166 g, 75%). *Anal.* Calc. for C$_{64}$H$_{58}$Cl$_5$Sb$_2$P$_2$Ru$_2$: C, 50.84; H, 3.87. Found: C, 51.02; H, 3.98%. UV–Vis (CH$_2$Cl$_2$): 379 (3470), 443 (2340), 530 (1470). μ_{eff} 1.85 μ_B/dimer.

*2.3.8. [(**S-diop**)**ClRu–(μ-Cl)**$_3$–RuCl(S-diop)] (**10**)*

Complex (**2**) (0.0250 g, 0.0345 mmol) and [RuCl$_2$-(*S*-diop)PPh$_3$] (0.0322 g, 0.0345 mmol). Yield (0.0356 g, 75%). *Anal.* Calc. for C$_{62}$H$_{64}$O$_4$Cl$_5$P$_4$Ru$_2$: C, 54.10; H, 4.69. Found: C, 54.15; H, 4.67%. UV–Vis (CH$_2$Cl$_2$): 377 (3350), 446 (1950), 540 (1390). μ_{eff} 1.79 μ_B/dimer.

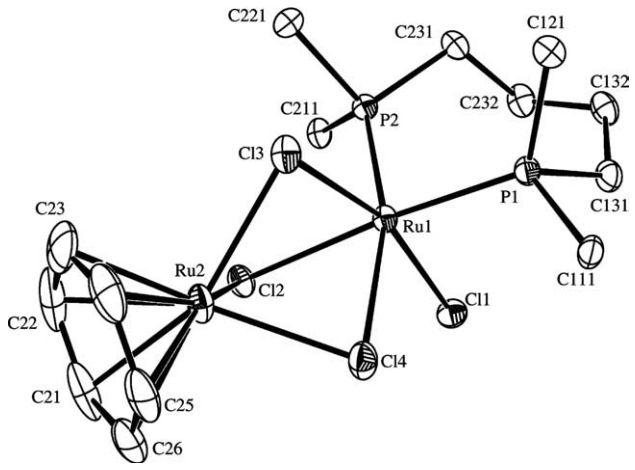

Fig. 2. ORTEP view of the complex $[(\eta^6\text{-}C_6H_6)Ru\text{–}(\mu\text{-}Cl)_3\text{–}RuCl(dppb)]$. $C_2H_4Cl_2$ (**11**), showing the atom labelling and the 50% probability ellipsoids.

2.3.9. *[(η⁶-C₆H₆)Ru–(μ-Cl)₃–RuCl(dppb)] (**11**)*

A suspension of (**1**) (0.0200 g, 0.0307 mmol) and $[(\eta^6\text{-}C_6H_6)RuCl(dpae)]Cl$ (0.0226 g, 0.0307 mmol) in 1, 2-dichloroethane (30 ml) was refluxed for 24 h. Surprisingly, a crop of red crystals was obtained during the reaction and crystals suitable for X-ray analysis were separated from the solution Addition of *n*-hexane to the solution yielded a brown solid that was washed well with *n*-hexane and dried under vacuum. The red crystals and the brown solid are the same compound as proved by $^{31}P\{^1H\}$, ^1H NMR and elemental analysis.

Yield (0.0208 g, 80%). *Anal.* Calc. for $C_{34}H_{34}Cl_4P_2Ru_2$: C, 48.13; H, 4.04. Found: C, 48.17; H, 4.08%. $^{31}P\{^1H\}$, ppm: δ P_B 54.00 (s). ^1H ($CDCl_3$): δ 1.27 (br, s, 2H, CH_2), 1.81 (br, m, 2H, CH_2), 2.04 (br, m, 2H, CH_2), 3.12 (br, m, 2H, CH_2), 6.20 (s, 6H, $\eta^6\text{-}C_6H_6$), 7.20–7.65 (m, 20H, Ph).

2.4. Reactivity of mer-[RuCl₃(dppb)H₂O] with dihydrogen

2.4.1. *[(dppb)ClRu–(μ-Cl)₂–RuCl(dppb)] (**12**)*

A suspension of (**1**) (0.0990 g, 0.1519 mmol) in CH_2Cl_2 (20 ml) and methanol (5 ml) was stirred under H_2 (1 atm) for 48 h at room temperature (RT). The volume of the orange solution was reduced (~10 ml) and addition of methanol (30 ml) precipitated an orange solid that was collected, washed well with methanol and dried under vacuum. Yield (0.0907 g, >99%). *Anal.* Calc. for $C_{56}H_{56}Cl_4P_4Ru_2$: C, 56.20; H, 4.72. Found: C, 56.12; H, 4.60%. $^{31}P\{^1H\}$, ppm: δ P_A 55.30 (d), P_B 63.50 (d) ($^2J P_AP_B$ 30 Hz).

^1H ($CDCl_3$): δ 1.35 (br, m, 4H, CH_2), 1.64 (br, m, 4H, CH_2), 2.05 (br, m, 4H, CH_2), 2.62 (br, m, 4H, CH_2), 6.9–7.7 (m, 40H, Ph).

2.4.2. *[(dppb)(CO)Ru–(μ-Cl)₃–RuCl(dppb)] (**13**)*

A suspension of (**1**) (0.083 g, 0.1273 mmol) in N,N′-dimethylacetamide (20 ml) was stirred under H_2 (1 atm) for 24 h, at room temperature. To the obtained orange solution methanol (30 ml) was added and stirred under H_2 for 3h. An orange solid was collected and washed well with methanol and dried under vacuum. Yield (0.0741 g, 95%). *Anal.* Calc. for $C_{57}H_{56}OCl_4P_4Ru_2$: C, 55.89; H, 4.61. Found: C, 55.35; H, 4.67%. IR (cm^{-1}) 1970 ν(CO). $^{31}P\{^1H\}$, ppm: δ P_A 53.90 (d), P_B 53.35 (d) ($^2J P_AP_B$ 45 Hz), P_C 47.71 (d), P_D 35.07 (d) ($^2J P_CP_D$ 30 Hz).

2.4.3. *[H₂NEt₂][(dppb)ClRu–(μ-Cl)₃–RuCl(dppb)] (**14**)*

A suspension of (**1**) (0.100 g, 0.1534 mmol) in CH_2Cl_2 (10 ml) and an excess of triethylamine (1 ml) was stirred under H_2 (1 atm) for 24 h, at room temperature. The orange solution volume was reduced (~5 ml) and passed through a Celite®. Addition of *n*-hexane precipitated a brown solid that was collected, washed well with methanol and dried under vacuum. Yield (0.0862 g, 86%). *Anal.* Calc. for $C_{60}H_{68}NCl_5P_4Ru_2$: C, 55.16; N, 1.07; H, 5.24. Found: C, 55.23; N, 1.07; H, 5.15%. $^{31}P\{^1H\}$, ppm: δ 49 (s). ^1H ($CDCl_3$): δ 1.22 (br, s, 6H, $CH_3H_2NEt_2$), 1.35 (br, m, 4H, CH_2), 1.64 (br, m, 4H, CH_2), 2.05 (br, m, 4H, CH_2), 2.82 (br, m, 4H, CH_2), 2.92 (br, m, 4H, $CH_2H_2NEt_2$), 6.9–7.5 (m, 40H, Ph), 7.9 (br, s, 2H, NH_2).

3. Results and discussion

The magnetic moments of the mixed-valent complexes (**3–10**) μ_{eff} = 1.78–2.01 are consistent with one unpaired electron per molecule.

The X-ray structure of (**5**) (Fig. 1) shows that the Ru cation is in an approximate C_2 environment, as was reported by Nicholson [22] for $[(P^nBu_3)_2ClRu\text{–}(\mu\text{-}Cl)_3\text{–}RuCl(P^nBu_3)_2]$; this local symmetry is lower than that in [(chiraphos)ClRu–(μ-Cl)$_3$–RuCl(chiraphos)], previously determined [23], which belongs to an approximate C_{2v} point group in which one octahedron was rotated by 120° about the Ru–Ru vector, as compared with the situation in the complex (**5**). The bridging chlorides *trans* to the phosphorus atoms (Ru(2)–Cl(1) = 2.4877(15); Ru(2)–Cl(3) = 2.4839(13); Ru(1)–Cl(2) = 2.4607(14) and Ru(1)–Cl(1) = 2.4422(14) Å) show longer Ru–Cl distances than the bridging chlorides *trans* to the terminal chlorides (Ru(1)–Cl(1) = 2.3402(15) and Ru(2)–Cl(2) = 2.3729(15) Å). This fact can be attributed to the strong *trans* influence of the phosphine ligands. The Ru–Ru distance (3.174(6) Å) is well outside of the range (2.28–2.95 Å) usually found for a Ru–Ru bond [24–30] and shorter than that found for the chiraphos analog (3.25 Å) [23]. The Ru–Cl–Ru bond angles

(81.48°, average) are larger than the expected value for two octahedra sharing one face (70.5°). The bond angles P(1)–Ru–P(2) = 95.33(6)° and P(3)–Ru–P(4) = 93.02(2)° are within the range of other Ru(dppb) core complexes [31,32].

The X-ray structure of (**5**) is similar to the [(dcypb)ClRu–(μ-Cl)$_3$–RuCl(dcypb)] [33] complex, which adopts the same approximate C_2 point group (considering the local symmetry only). As observed for complex (**5**) [(dcypb)ClRu–(μ-Cl)$_3$–RuCl(dcypb)] also presents longer Ru–Cl bond lengths for chlorides *trans* to phosphorus than for chlorides *trans* to chlorides. The Ru–Ru distance for [(dcypb)ClRu–(μ-Cl)$_3$–RuCl(dcypb)] (3.278 Å) is higher than for complex (**5**).

The reaction of *mer*-[RuCl$_3$(dppb)H$_2$O] (**1**) and [(η^6-C$_6$H$_6$)RuCl(dpae)]Cl produces the binuclear complex (**11**). The possible mechanism for this reaction involves the formation of the intermediate ''RuCl$_2$(dppb)'' since the reduction of the *mer*-[RuCl$_3$(dppb)H$_2$O] (**1**) complex by the dpae ligand generates this Ru(II) species which can be dimerized forming the binuclear [(dppb)ClRu–(μ-Cl)$_2$–RuCl(dppb)] [2] (**12**) complex, similar to that found for the dissolution of [RuCl$_2$(dppb)(PPh$_3$)] [11], which once in solution dissociates PPh$_3$ and dimerizes. The ^{31}P{^{1}H} NMR spectrum of the triply chloride-bridged [(η^6-C$_6$H$_6$)Ru–(μ-Cl)$_3$–RuCl(dppb)] complex shows only a singlet at δ 54.0 ppm in CDCl$_3$.

The electrochemical behavior of (**1**) is well documented and the products formed after partial and exhaustive electrolysis were described elsewhere by our research group and collaborators [1]. This reaction is similar to the one of [RuCl$_2$(dppb)(PPh$_3$)] with [(η^6-cymene)RuCl$_2$]$_2$ producing [(η^6-cymene)ClRu–(μ-Cl)$_3$–RuCl(dppb)] [32], which strongly confirms our suggestion regarding the mechanism involved in our reaction.

The binuclear arene complex (**11**) presents two distorted octahedra sharing one face as in [(dppb)ClRu–(μ-Cl)$_3$–RuCl(dppb)]. The Ru–P bond lengths (2.2463(8) and 2.2777(8) Å) are slightly smaller than those found for complex (**5**) and are in the expected range for Ru(II)–P bond lengths [32–35]. The Ru–Cl bond lengths for the bridged chlorides are longer than for terminal ones (see Table 2).

The most relevant manifestation of metal–metal interaction is the separation of electrochemical couples [36–38]. In complexes with similar donor atoms coordinated to both metal centers this separation is related to the comproportionation constant (K_c). In binuclear complexes with apparent similar donor atoms in both metal sites, an increase in the metal–metal interaction is accompanied by increasing separation of electrochemical couples. Separation of electrochemical couples $\Delta E_{1/2}$ of about 0.60 V [39] (for complexes with a similar coordination sphere) show a strong metal–metal interaction and high comproportionation constant and can be considered as belonging to the Class III classification [40].

The cyclic voltammetric studies of mixed-valence complexes (**3–10**) synthesized in this work only reveal two reversible one-electron transfer processes, which correspond to the couples designated in Eq. (2).

$$[\mathrm{Ru(II)–Cl_3–Ru(II)}^-] \underset{E_{1/2}(1)}{\overset{+e^-}{\rightleftharpoons}} [\mathrm{Ru(II)–Cl_3–Ru(III)}] \underset{E_{1/2}(2)}{\overset{-e^-}{\rightleftharpoons}} [\mathrm{Ru(III)–Cl_3–Ru(III)}^+] \quad (2)$$

The observation of only two redox processes in complexes such as [(PPh$_3$)$_2$ClRu–(μ-Cl)$_3$–RuCl(dppb)] avoid the possibility of the presence of two symmetrically mixed-valence complexes [(PPh$_3$)$_2$ClRu–(μ-Cl)$_3$–RuCl(PPh$_3$)$_2$] and [(dppb)ClRu–(μ-Cl)$_3$–RuCl(dppb)]. Of note is the electrochemical behavior of [(SbPh$_3$)$_2$ClRu–(μ-Cl)$_3$–RuCl(dppb)] (discussed below) in which only two redox processes are observed with a separation $\Delta E_{1/2}$ = 0.21 V. If two symmetrically mixed-valence complexes had been formed, the observation of well separated ($\Delta E_{1/2}$ = 0.62 V) redox processes due to [(dppb)ClRu–(μ-Cl)$_3$–RuCl(dppb)] in addition to the observed processes should be expected, but this is not the case. The same argument can be used for the complex [(*S*-diop)ClRu–(μ-Cl)$_3$–RuCl(dppb)].

Fig. 3 shows the cyclic voltammogram of the [(dppb)ClRu–(μ-Cl)$_3$–RuCl(dppb)] (**5**) complex. The separations between half-wave potential $E_{1/2}$(1) and $E_{1/2}$(2) for the complexes in Table 3 are small when compared with those found for unsymmetric complexes such as [(PPh$_3$)$_2$(CO)Ru–(μ-Cl)$_3$–RuCl$_2$(PPh$_3$)] [7] (1.57 V) and [(AsPh$_3$)$_2$(CO)Ru–(μ-Cl)$_3$–RuCl$_2$(AsPh$_3$)] [8] (1.66 V). This observation suggests that in symmetric species (same donor atoms) there is a stronger contribution of the metal–metal interaction, increasing the half-wave potential separations; for unsymmetric complexes (different donor atoms) such as [(PPh$_3$)$_2$(CO)Ru–(μ-Cl)$_3$–RuCl$_2$(PPh$_3$)] this separation is mainly due to the ligand characteristics since the orbital energies of the metal centers are different, the metal–metal interactions are weak and each metal center behaves as a monomer.

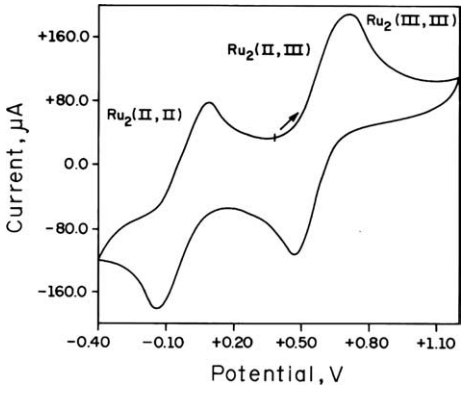

Fig. 3. Cyclic voltammetry of (**5**). CH$_2$Cl$_2$, 0.10 mol l^{-1} (TBAP) $E_{1/2}$ vs Ag/AgCl.

Table 3
Electrochemical data for the mixed-valence complexes

Complexes	$E_{1/2}$ 1(V)	$E_{1/2}$ 2(V)	$\Delta E_{1/2}$ (V)	K_c
[(*S*-diop)ClRu–(μ-Cl)$_3$–RuCl(dppb)] (**3**)	0.0	0.58	0.58	6.8×10^9
[(S-binap)ClRu–(μ-Cl)$_3$–RuCl(dppb)] (**4**)	0.09	0.69	0.60	1.5×10^{10}
[(dppb)ClRu–(μ-Cl)$_3$–RuCl(dppb)] (**5**)	0.08	0.70	0.62	3.2×10^{10}
[(PPh$_3$)$_2$ClRu–(μ-Cl)$_3$–RuCl(dppb)] (**6**)	0.09	0.67	0.58	6.8×10^9
[(dppn)ClRu–(μ-Cl)$_3$–RuCl(dppb)] (**7**)	0.0	0.56	0.56	3.1×10^9
[(P-ptol$_3$)$_2$ClRu–(μ-Cl)$_3$–RuCl(dppb)] (**8**)	0.08	0.66	0.58	6.8×10^9
[(SbPh$_3$)$_2$ClRu–(μ-Cl)$_3$–RuCl(dppb)] (**9**)	0.40	0.61	0.21	3.1×10^3
[(*S*-diop)ClRu–(μ-Cl)$_3$–RuCl(*S*-diop)] (**10**)	0.18	0.79	0.61	2.2×10^{10}

The electrochemical behaviors of the mixed valence complexes are similar to those found in the literature with the general formula [L$_2$ClRu–(μ-Cl)$_3$–RuClL$_2$] (L = arsines and phosphines) [41,42]. The separation of the half-wave potentials (Table 3) are ca. 0.60 V which give K_c values in the range (10^9–10^{10}), greater than the value for the classical Creutz-Taube mixed valence ions type of complexes (7–10^3) [38,43]. Complex (**9**) is the only one in our series that shows a different behavior where the separation between half-wave potentials ($\Delta E_{1/2}$ = 0.21 V) is too small; this can be attributed to the fact that for each metal center there are different donor atoms coordinated. This behavior is also reflected in the intervalence charge transfer energy detected in the near infrared region (Table 4), where the intervalence charge transfer bands are shifted to higher energy values.

These binuclear complexes show two intervalence charge transfer absorptions in the near-IR spectra. One suggestion for this behavior in this kind of triply-chlorine-bridged mixed valence di-ruthenium(II,III) compound was given by James et al. [23], who proposed that the second absorption at higher energy is due to the presence of a tetranuclear species in solution. We do not believe that this applies to our case as the structure proposed for the tetranuclear species is very different from the dimer and if tetramers were formed in solution a different behavior in the cyclic voltammetry experiments would be expected, a fact we did not observe. Another suggestion based on the work developed by Heath et al. [6] ascribes the presence of the second absorption in the near-IR spectra to another transition in binuclear complexes of the type [(R$_3$P)$_3$Ru–(μ-Cl)$_3$–Ru(PR$_3$)$_3$], described as $\sigma \rightarrow \sigma^*$ and $\delta^* \rightarrow \sigma^*$.

We are thus inclined to suggest that the two absorptions observed in our experiments belong to the same complexes in solution.

The presence of donor solvents as methanol, acetonitrile, dimethylsulfoxide make the intervalence charge transfer bands (near-infrared region) disappear due to disproportionation of the dimers into Ru(II) and Ru(III) species and this behavior was previously observed for similar systems [23].

3.1. Reactivity of *mer*-[RuCl$_3$(dppb)H$_2$O] with dihydrogen

The reactivity of *mer*-[RuCl$_3$(dppb)H$_2$O] (**1**) with H$_2$ is dependent upon the reaction conditions. Thus, the reaction in CH$_2$Cl$_2$/MeOH leads to the formation of the known [2] complex [(dppb)ClRu–(μ-Cl)$_2$–RuCl(dppb)] (**12**) (identified by ^{31}P{^{1}H} NMR and elemental analysis). The AB quartet [δ P$_A$ 55.30 (d) and δ P$_B$ 63.50 (d); ^2JP$_A$P$_B$, 30 Hz] for the doubly chloride-bridged [(dppb)ClRu–(μ-Cl)$_2$–RuCl(dppb)] (**12**) complex is in agreement with those reported in the literature [2]. In this case the P$_B$ phosphorus atom is *trans* to the bridged chloride (see Fig. 4).

An "in situ" ^{31}P{^{1}H} NMR experiment was done using complex *mer*-[RuCl$_3$(dppb)H$_2$O] (**1**) in CH$_2$Cl$_2$/MeOH (1:1) and H$_2$ (1 atm). After 24 h of reaction, a mixture of complexes was detected by ^{31}P{^{1}H} NMR experiments, namely [(dppb)ClRu–(μ-Cl)$_2$–RuCl(dppb)] (**12**) [2] (δ_{PA} = 63.5, δ_{PB} = 55.3 ppm; $^2J_{AB}$ = 30 Hz), [(dppb)(η^2-H$_2$)Ru–(μ-Cl)$_3$–RuCl(dppb)] [3] (δ_{PA} = 55.8, δ_{PB} = 40.6; $^2J_{AB}$ = 34 Hz; δ_{PC} = 54.2, δ_{PD} = 52.1 ppm; $^2J_{CD}$ = 45 Hz) and [(dppb)ClRu–(μ-Cl)$_3$–RuCl(dppb)]$^-$

Table 4
Near infrared spectral data for the mixed-valence complexes in CCl$_4$

Complexes	λ_{max} (nm)	ε (M^{-1} cm^{-1})
[(*S*-diop)ClRu–(μ-Cl)$_3$–RuCl(dppb)] (**3**)	1860/961	940/930
[(S-binap)ClRu–(μ-Cl)$_3$–RuCl(dppb)] (**4**)	1900/980	780/720
[(dppb)ClRu–(μ-Cl)$_3$–RuCl(dppb)] (**5**)	1856/980	1180/890
[(PPh$_3$)$_2$ClRu–(μ-Cl)$_3$–RuCl(dppb)] (**6**)	1856/978	740/880
[(dppn)ClRu–(μ-Cl)$_3$–RuCl(dppb)] (**7**)	1736/967	520/495
[(P-ptol$_3$)$_2$ClRu–(μ-Cl)$_3$–RuCl(dppb)] (**8**)	1889/970	770/728
[(SbPh$_3$)$_2$ClRu–(μ-Cl)$_3$–RuCl(dppb)] (**9**)	1648/849	640/665
[(*S*-diop)ClRu–(μ-Cl)$_3$–RuCl(*S*-diop)] (**10**)	1858/968	1145/890

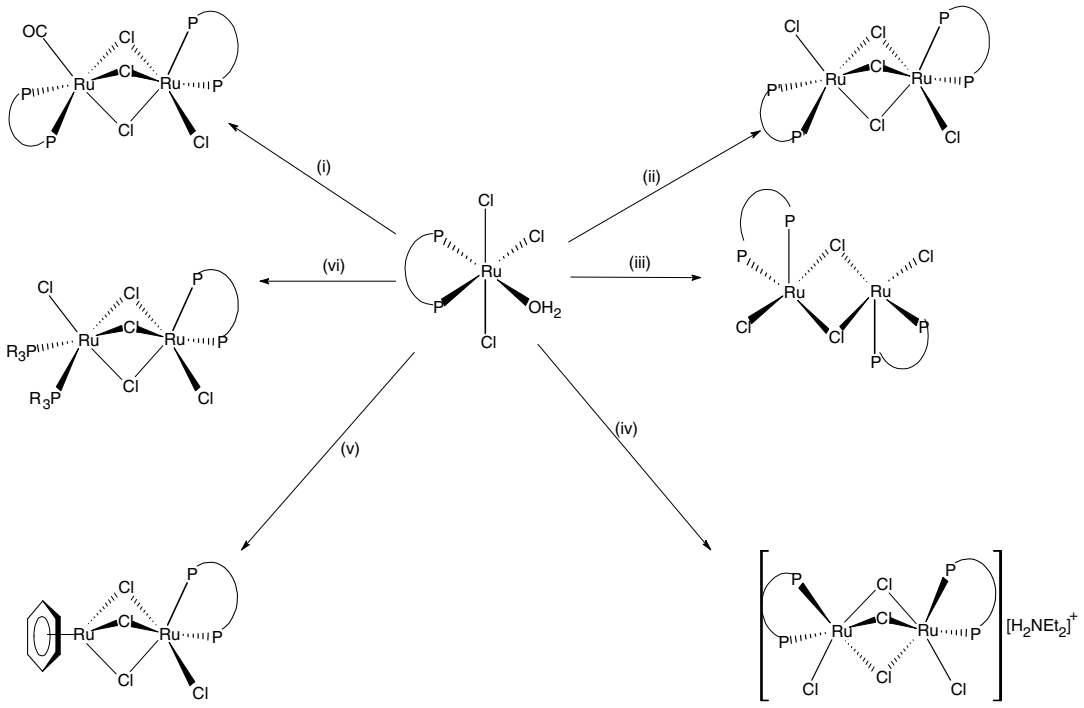

Fig. 4. General scheme for the reactivity of *mer*-[$RuCl_3$(dppb)H_2O] (**1**): (i) in DMA (24 h, RT); (ii) [$RuCl_2$(dppb)(PPh_3)] in CH_2Cl_2 (3 h, RT); (iii) H_2 in CH_2Cl_2/MeOH (48 h, RT); (iv) H_2 in CH_2Cl_2 and NEt_3 (excess, 24 h, RT); (v) [$RuCl(\eta^6$-$C_6H_6)$(dpae)] in $ClCH_2CH_2Cl$ under reflux; (v) [$RuCl_2(PR_3)_3$] in CH_2Cl_2 (3 h, RT).

(**14**) [3] ($\delta_{PA,B}$ = 49 ppm). Evacuation of H_2 from the NMR tube and refilling it with Ar led to the observation of the presence of [(dppb)ClRu–(μ-Cl)$_2$–RuCl(dppb)] (**12**) and [(dppb)ClRu–(μ-Cl)$_3$–RuCl(dppb)]$^-$ (**14**). Complex (**12**) was also identified as being key in the reactivity of *mer*-[$RuCl_3$(dppb)H_2O] (**1**) in the formation of [(dppb)(CO)Ru–(μ-Cl)$_3$–RuCl(dppb)] (**13**) [2], since in a short reaction time (2–3 h) of (**1**) with H_2, complex (**12**) appears as a by-product, while keeping the reaction going for a longer period (24 h) only complex (**13**) was obtained. In the [(dppb)(CO)Ru–(μ-Cl)$_3$–RuCl(dppb)] complex ν(CO) at 1972 cm^{-1} is present in the IR spectrum and an AB quartet is present in the $^{31}P\{^1H\}$ NMR spectrum. For this complex the signals at δ P_A 53.90 (d), δ P_B 53.35 (d) ($^2J_{PAPB}$ 45 Hz) can be assigned to the resonances of the (μ-Cl)$_3$–RuCl(dppb)] side of the molecule while δ P_C 47.71 (d), δ P_D 35.07 (d) ($^2J_{PCPD}$ 30 Hz) belong to the [(dppb)(CO)Ru–(μ-Cl)$_3$ part of the same molecule. On the other hand, stirring complex (**14**) in methanol leads to the formation of (**12**) (under these conditions chloride dissociation is observed).

Similar reactivity of (**1**) was found upon electrochemical reduction [1,44]. Complex (**12**) is obtained in quantitative yield and in this case the mixed-valence compound (**5**) is the intermediate, as proved by partial electrolysis.

Complex (**14**) can be synthesized in high yield by the reaction of *mer*-[$RuCl_3$(dppb)H_2O] with H_2 in CH_2Cl_2 and triethylamine (excess). This procedure has advantages over the published synthesis [3], since it uses mild conditions, short reaction time, gives a high yield and the resulting solution is phosphine free. The symmetric [H_2NEt_2][(dppb)ClRu–(μ-Cl)$_3$–RuCl(dppb)] complex, as expected, shows only a singlet at δ 49.00 ppm.

We have tried to synthesize complex (**12**) as described by James et al. [2] using the reaction of the mixed valence complex (**5**) with H_2 in DMA. In this case the product obtained quantitatively was the carbonyl species (**13**), formed by DMA decarbonylation. Similar behavior was found as described before for complex (**1**) under the same conditions. The desired penta-coordinated double chloride-bridged (**12**) was synthesized from complex (**1**) or (**5**) in a solvent mixture (CH_2Cl_2/MeOH) and H_2. We found that this route was clean since complex (**12**) was obtained quantitavely.

Reactivity of *mer*-[$RuCl_3$(dppb)(H_2O)] is sumarized in Fig. 4.

3.2. Homogeneous hydrogenation of imines

We have performed studies on the hydrogenation of imines catalyzed by some of the complexes described in this work. Hydrogenation of imines is less studied than for alkenes and carbonyl substrates and as a consequence is less understood. Yet, it is an important pathway for the synthesis of amines and is particularly important for the enantioselective reductions of imines that are only achieved in good enantiomeric excess employing homogeneous catalysts [45].

Table 5
Hydrogenation of the imines Ph–CH_2–N=CH–Ph (**15**) and Ph–N=CH–Ph (**16**)

Entry	Complexes	Yield(%) (**15**)[a]	Yield(%) (**16**)[a]
1	[(dppb)ClRu–(μ-Cl)$_3$–RuCl(dppb)] (**5**)	99	49
2	[$(PPh_3)_2$ClRu–(μ-Cl)$_3$–RuCl(dppb)] (**6**)	99	nd[b]
3	[(dppn)ClRu–(μ-Cl)$_3$–RuCl(dppn)] (**7**)	nd[b]	15
4	[$(P\text{-ptol}_3)_2$ClRu–(μ-Cl)$_3$–RuCl(dppb)] (**8**)	100	23
5	*mer*-[$RuCl_3$(dppb)H_2O] (**1**)	93	40
6	[(dppb)(4-Phpy)Ru–(μ-Cl)$_3$–RuCl(dppb)][c]	75	24
7	[(dppb)(PhCN)Ru–(μ-Cl)$_3$–RuCl(dppb)][c]	80	22

[a] 1000 psi H_2, MeOH (10 ml), [Ru] = 1.3×10^{-4} mol l^{-1}, [Ru]/[imine] = 1/200, 24 h, rt.
[b] Not determined.
[c] Synthesized as described in [9].

In Table 5 the results for the hydrogenation of N-benzylidene-benzylamine (Ph–CH_2–N=CH–Ph) and N-benzylidene-aniline (Ph–N=CH–Ph) are presented. It is evident that for the mixed valence Ru(II)–Ru(III) complexes (Entries 1 and 4) the Ph–CH_2–N=CH–Ph (**15**) is reduced at a higher rate than Ph–N=CH–Ph (**16**). A similar behavior is presented by (**1**) (entry 5) which in a first step generates (**5**) under the reaction conditions. Considering the results for the hydrogenation of (**16**) (entries 1, 3 and 4), the ligand dppb seems to be important on the stabilization/activity of the catalytic system as its substitution by dppn decreased the yield of the hydrogenated products.

For the reduction of the aldimines R–N=CHPh; R = methyl, isopropyl, cyclohexyl, benzyl (**15**), phenyl (**16**), catalyzed by (**5**) James et al. [5] have found that the rate of hydrogenation decreased in the order benzyl > methyl > isopropyl ~ cyclohexyl > phenyl. It has been pointed out that the rate of hydrogenation decreased with the bulkiness of R. Since the rate of the reduction of (**15**) was higher than the reduction of CH_3N=CHPh [5], this suggests that the electronic effects play an important role in the process. Indeed, another correlation can be done: as the positive inductive effect of R increased, the rate of hydrogenation decreased. A distinct interpretation should be given for (**16**) as the lone electron pair on nitrogen is conjugated to the aromatic ring (negative mesomeric effect). Thus, even though the mixed valence complexes are reduced to Ru(II) complexes in the presence of dihydrogen and a base (imine), it seems that the Ru(III) centre plays an important role for the hydrogenation of the imines studied.

A more detailed study taking into account not only the catalyst role, but also the role of the substrate should be carried out in order to elucidate these effects.

4. Conclusions

We have shown in this study the versatility in the reactivity of *mer*-[$RuCl_3$(P–P)H_2O] complexes. These complexes are good precursors for inorganic synthesis and there are at least three reasons for this: (1) the ruthenium(III) species are air stable and easy to handle, (2) they can be easily reduced chemically or electrochemically leading to chloride dissociation [1,44], and (3) products will not be contaminated with free triphenylphosphine.

A wide range of binuclear mixed valence diruthenium(II,III) complexes can be synthesized from them and some of their derivatives present high activity in imines hydrogenation.

Asymmetric hydrogenation of imines and ketones studies using (**3**), (**4**) and (**2**) and other chiral ruthenium complexes are currently ongoing in our laboratory.

5. Supplementary material

Coordinates and other crystallographic data have been deposited with the CCDC, deposition number CCDC 203371 for complex (**5**) and CCDC 203372 for complex (**11**). Copies of this information may be obtained free of charge from The Director, CCDC, 12 Union Road, Cambridge, CB2 1EZ (fax: +44 1223 336033; e-mail: deposit@ccdc.cam.ac.uk or at www: http://www.ccdc.cam.ac.uk).

Acknowledgements

We thank CNPq (Conselho Nacional de Desenvolvimento Científico e Tecnológico) and FAPESP (Fundação de Amparo à Pesquisa do Estado de São Paulo) for financial support.

References

[1] L.R. Dinelli, A.A. Batista, K. Wohnrath, M.P. de Araujo, S.L. Queiroz, M.R. Bonfadini, G. Oliva, O.R. Nascimento, P.W. Cyr, K.S. MacFarlane, B.R. James, Inorg. Chem. 38 (1999) 5341.
[2] A.M. Joshi, I.S. Thorburn, S.J. Rettig, B.R. James, Inorg. Chim. Acta 198–200 (1992) 283.

[3] K.S. MacFarlane, I.S. Thorburn, P.W. Cyr, D.E.K.Y. Chau, S.J. Rettig, B.R. James, Inorg. Chim. Acta 270 (1998) 130.
[4] A.M. Joshi, K.S. MacFarlane, B.R. James, J. Organomet. Chem. 488 (1995) 161.
[5] D.E. Fogg, B.R. James, M. Kilner, Inorg. Chim. Acta 222 (1994) 85.
[6] B.D. Yeomans, D.G. Humphrey, G.A. Heath, J. Chem. Soc., Dalton Trans. (1997) 4153.
[7] A.A. Batista, O.M. Porcu, O.R. Nascimento, V. Barbosa, G. Oliva, J. Coord. Chem. 30 (3–4) (1993) 345.
[8] M.P. de Araujo, A.A. Batista, O.M. Porcu, G. Oliva, D.H.F. Souza, M. Bonfadini, O.R. Nascimento, J. Coord. Chem. 54 (2001) 81.
[9] D.E. Fogg, B.R. James, Inorg. Chem. 36 (1997) 1961.
[10] A. Mezzetti, L. Costella, A. Del Zotto, P. Rigo, G. Consiglio, Gazz. Chim. Ital. 123 (1993) 155.
[11] C.W. Jung, P.E. Garrou, P.R. Hoffman, K.G. Caulton, Inorg. Chem. 23 (1984) 726.
[12] T.A. Stephenson, G. Wilkinson, J. Inorg. Nucl. Chem. 28 (1966) 945.
[13] D.K.W. Wang, Ph.D Thesis, The University of British Columbia, Canada, 1978.
[14] W.H. Knoth, J. Am. Chem. Soc. 94 (1972) 104.
[15] F. Faraone, G.A. Loprete, G. Tresoldi, Inorg. Chim. Acta 34 (1979) L251.
[16] Enraf-Nonius, Collect, Nonius, Delft, The Netherlands, 1997–2000.
[17] Z. Otwinowski, W. Minor, in: C.W. CarterJr., R.M. Sweet (Eds.), Methods in Enzimology, vol. 276, Academic Press, New York, 1997, p. 307.
[18] R.H. Blessing, Acta Cryst. A51 (1995) 33.
[19] G.M. Sheldrick, SHELXS-97. Program for Crystal Structure Resolution, University of Göttingen, Göttingen, Germany, 1997.
[20] G.M. Sheldrick, SHELXL-97. Program for Crystal Structures Analysis, University of Göttingen, Göttingen, Germany, 1997.
[21] L.J. Farrugia, ORTEP3 for Windows, J. Appl. Cryst. 30 (1997) 565.
[22] J.K. Nicholson, Angew. Chem. Intern. Ed. 6 (1967) 264.
[23] I.S. Thorburn, S.J. Rettig, B.R. James, Inorg. Chem. 25 (1986) 234.
[24] O.S. Mills, J.P. Nice, J. Organomet. Chem. 9 (1967) 339.
[25] R. Belford, M.I. Bruce, M.A. Cauns, M. Green, H.P. Taylor, P. Woodward, J. Chem. Soc., Chem. Comm. 18 (1970) 1159.
[26] R. Mason, K.M. Thomas, D.F. Gill, B.L. Shaw, J. Organomet. Chem. 40 (1972) C67.
[27] B.M. Mattson, J.R. Herman, L.H. Pignolet, Inorg. Chem. 15 (1976) 564.
[28] H. Schumann, J. Opitz, J. Pickardt, J. Organomet. Chem. 128 (1977) 253.
[29] M.B. Hursthouse, R.A. Jones, K.M.A. Matik, G. Wilkinson, J. Am. Chem. Soc. 101 (1979) 4128.
[30] R.A. Jones, G. Wilkinson, I.J. Colquohoun, W. McFarlane, A.M.R. Galas, M.B. Hursthouse, J. Chem. Soc., Dalton Trans. 12 (1980) 2480.
[31] M. Schroder, T.A. Stephenson, in: G. Wilkinson, R.D. Gillard, J.A. McCleverty (Eds.), Comprehensive Coordination Chemistry, vol. 4, Pergamon, Oxford, 1987 (Chapter 45).
[32] A.C. Silva, H. Piotrowski, P. Mayer, K. Polborn, K. Severin, Eur. J. Inorg. Chem. 3 (2001) 685.
[33] D. Amoroso, G.P.A. Yap, D.E. Fogg, Can. J. Chem. 79 (2001) 958.
[34] T. Ohta, Y. Tonomura, K. Nozaki, H. Takaya, K. Mashima, Organometalics 15 (1996) 1521.
[35] O.M. Akotsi, K. Metera, R.D. Reid, R. McDonald, S.H. Bergens, Chirality 12 (2000) 514.
[36] C. Creutz, Prog. Inorg. Chem. 30 (1983) 1.
[37] R.J. Crutchley, Adv. Inorg. Chem. Radiochem. 41 (1994) 273.
[38] M.D. Ward, Chem. Soc. Rev. 24 (1995) 121.
[39] G.A. Heath, personal communication.
[40] M.B. Robin, P. Day, Adv. Inorg. Chem. RadioChem. 10 (1967) 248.
[41] F.A. Cotton, R.C. Torralba, Inorg. Chem. 30 (1991) 2196.
[42] G.A. Heath, A.J. Lindsay, T.A. Stephenson, D.K. Vattis, J. Organomet. Chem. 233 (1982) 353.
[43] R.C. Rocha, H.E. Toma, Polyhedron 21 (2002) 2089.
[44] K. Wohnrath, M.P. de Araujo, A.A. Batista, L.R. Dinelli, I.S. Moreira, E.E. Castellano, J. Ellena, J. Chem. Soc., Dalton Trans. 19 (2000) 3383.
[45] B.R. James, Catal. Today 37 (1997) 209.

ligand-to-ligand charge transfer (MMLLCT) or ligand-to-ligand charge transfer (LLCT). In all these cases the LUMO is predominantly centered on the diimine ligand.

Square-planar complexes containing both easily oxidisable and reducible ligands were found to show a LLCT transition [16]. These transitions were highly solvatochromic, of which some of them exhibit the remarkable property of being luminescent in solution [17]. Metal complexes possessing such a transition have become the focus for numerous photochemical studies due to large molar absorptivity of the transition [16]. The LLCT excited states had previously been noted in some Zn(II) and Pt(II) complexes containing both diimine and aromatic thiolate (dithiolate) ligands [16c,16f]. Dance and Miller [16a] described the observation of a LLCT band for the first time in a Ni(II) complex containing α-diimine and dithiolate. In general, both electron-donating substituents on the thiolate and electron-withdrawing substituents on the diimine ligands would lower the LLCT transition energy. On the contrary, electron-withdrawing groups on the thiolate and electron-donating substituents on the diimine increase the transition energy. Thus, selective fine tuning of this excited state could be achieved by altering the ligands (diimine or dithiolate) or changing the substituents on the ligand(s) or the metal ion(s) [16,17].

The LLCT transitions have also been reported for a variety of d^8 metal complexes with catecholate and α-diimine ligands [18], where the charge transfer takes place from the catecholate ligand to the diimine ligand. Here too, the electron-withdrawing substituents on the diimine and the electron-donating substituents on the catechol lower the LLCT transition energy and electron-donating substituents on the diimine and the electron-withdrawing substituents on the catechol increase the LLCT transition energy. However, the solution-state emission from these complexes has not been reported. Many of them were found to be potential candidates for generation of singlet molecular oxygen ($^1O_2$) since they produce $^1O_2$ upon irradiation at the LLCT band [18b,18c]. Here we report, for the first time, the solution-state luminescence of such complexes. We also report the spectral and electrochemical behaviour of these complexes. An attempt to make a correlation between redox potentials and the energy of the absorption maxima is made. In addition, we synthesized two dinuclear complexes for comparison of the electronic properties since dinuclear complexes have been known to luminesce at higher wavelength compared to related monomers. It has been shown that dinuclear complexes possess a low-lying excited state due to a large decrease in the energy of the lowest π* orbital of the bridging ligands upon complexation [3]. We also report the solvatochromic LLCT transition and solution state luminescence of these complexes.

The various diimines used are 4,7-diphenyl-1,10-phenanthroline, 2,2′-bipyridine, 2,2′-biquinoline and 1,10-phenanthroline. The metal ions used are Pt(II) and Pd(II). 3,4-Dihydroxybenzaldehyde and 3,4-dihydroxybenzoic acid are used as the dianionic ligand. 3,3′,4,4′-Tetrahydroxybenzaldazine is used as the tetraanionic ligand to synthesise the dinuclear complexes.

2. Experimental

2.1. Starting materials

Potassium tetrachloroplatinate(II), palladium chloride, 1,10-phenanthroline monohydrate, 4,7-diphenyl-1,10-phenanthroline (Loba-Chemie Indoauatranal Co., India), 2,2′-biquinoline, potassium hydroxide (Merck, India), 3,4-dihydroxybenzoic acid, 3,4-dihydroxybenzaldehyde (Fluka AG, Switzerland), hydrazine hydrochloride, ammonia, acetic acid (s.d.fine-CHEM Ltd., India) and 2,2′-bipyridine (Glaxo Industries, India) were bought, of reagent grade and used as such. The reagent grade solvents were purified before use by standard procedures [19]. Solvents of spectroscopic grade were used for cyclic voltammetry and spectroscopic measurements.

2.2. Physical measurements

The chemical analyses of carbon, hydrogen and nitrogen for the complexes were performed using a Carlo Erba Strumentazion Elemental Analyzer, Model 1106, at R.S.I.C., Central Drug Research Institute, Lucknow. The IR spectra of the complexes in KBr pellets were recorded with a Nicolet 170-Sx FT-IR spectrophotometer in the region 4000–600 cm^{-1}. Electronic absorption spectra of the complexes in various solvents were obtained using a Shimadzu UV-265 UV–VIS spectrophotometer. The proton nuclear magnetic resonance (^1H NMR) spectra of the complexes were acquired using a Varian VXR-300s NMR spectrometer in deuterated dimethyl sulfoxide [$(CD_3)_2SO$]. Tetramethylsilane was used as the internal reference. All the spectra were recorded in the range of 0–11 ppm. The cyclic voltammograms of the complexes in acetonitrile ($\sim 10^{-3}$ M) containing 0.1 M tetra(*n*-butyl)ammonium hexafluorophosphate as supporting electrolyte were obtained on a Model CV-IB Bioanalytical Cyclic Voltammetry apparatus equipped with an Omnigraphic 2000 Recorder. A single compartment cell was employed with an Ag/AgCl reference-electrode (−0.041 V versus standard calomel electrode, SCE), a platinum wire counter electrode and a platinum working electrode (6 mm outer diameter). The scan rate used was 200 mV/s. The solutions were degassed for 15 min before recording the cyclic voltammogram. Room-temperature excitation and

luminescence spectra of the metal complexes were recorded in a Spex spectrofluorimeter equipped with a Hamamadzu R928 photomultiplier tube (PMT). The PMT was cooled externally by circulating cold water. The emission spectra were corrected for excitation lamp intensity variation and solvent emission. The fluorescence quantum yields were measured by an optically dilute method [24] using tryptophan in water as a standard [25]. The quantum yield values were corrected for solvent refractive index. Fluorescence lifetime measurements were carried out by the single photon counting technique using a nanosecond fluorescence spectrometer from Applied Photophysics (model SP-170) with a bright and stable nanosecond flash-lamp operating at frequencies up to 200 kHz. The lamp was filled with nitrogen gas. The PMT type XP 2020Q was used for photodetection. Output of the multichannel analyzer was analyzed for single, double or multi exponential decay functions. The solutions were excited at 296, 316 or 337 nm. Phosphorescence measurements were made using a SPEX 1934C phosphorimeter with a RCA C13034 photomultiplier attachment having the facility to provide corrected emission spectra. Metal complexes dissolved in EPA mixture (10^{-6} M) were frozen in liquid nitrogen (77 K) in a 10 mm quartz cuvette and the spectra were recorded using different wavelengths of excitation.

2.3. Synthetic procedures

[M(N-N)Cl_2] {where M = Pd(II) or Pt(II) and N-N is 2,2′-bipyridine (BPY), 2,2′-biquinoline (BIQ), 4,7-diphenyl-1,10-phenanthroline (DPP) and 1,10-phenanthroline (PHEN)} were prepared by the reported procedures [20] and characterized by the methods from the literature [21,22].

2.3.1. [Pd(BPY)(DHB)] (1)

0.2 mmol of [Pd(BPY)Cl_2] was dissolved in 25 cm^3 of hot acetonitrile (60 °C). The solution was filtered while hot to remove any undissolved material. To this 0.2 mmol of H_2DHB dissolved in 1.6 cm^3 of 0.25 N KOH in methanol was added slowly and stirred for 30 min at the same temperature. Then the solution was cooled to room temperature and kept in a refrigerator overnight to obtain crystals of the complex. The compound was filtered and washed with small amounts of cold acetonitrile, water and methanol successively and dried in a vacuum desiccator over anhydrous calcium chloride. The compound was recrystallized from DMF and 70% yield was obtained. ^{1}H NMR [$(CD_3)_2SO$]: 8.58 (d, 2H, 3, 3′), 8.36 (dt, 2H, 4, 4′), 7.81 (t, 2H, 5, 5′), 8.64 (d, 2H, 6, 6′), 6.92 (dd, 1H, B), 6.77 (d, 1H, C), 6.46 (d, 1H, A), 9.5 (s, 1H, D). *Anal.* Calc. for $C_{17}H_{12}N_2O_3Pd$: C, 51.21; H, 3.03; N, 7.02. Found: C, 50.87; H, 3.05; N, 6.98%.

2.3.2. [Pd(PHEN)(DHB)] (2)

[Pd(PHEN)Cl_2] (0.2 mmol) was dissolved in 50 cm^3 of DMF. To this, 0.2 mmol of H_2DHB dissolved in 1.6 cm^3 of 0.25 N KOH in methanol was added slowly. The solution was stirred for 30 min. Then the solution was evaporated to 5 cm^3 and cooled overnight. The precipitate formed was filtered and recrystallized from DMF and dried in a vacuum desiccator over anhydrous $CaCl_2$. The yield obtained was 45%. ^{1}H NMR [$(CD_3)_2SO$]: δ 8.85 (d, 2H, 2, 9), 8.91 (d, 2H, 4, 7), 8.23 (s, 2H, 5, 6), 8.08 (m, 2H, 3, 8), 6.64 (d, 1H, B), 6.68 (s, 1H, C), 6.39 (d, 1H, A), 9.5 (s, 1H, D). *Anal.* Calc. for $C_{19}H_{12}N_2O_3Pd$: C, 53.98; H, 2.86; N, 6.63. Found: C, 53.54; H, 2.85; N, 6.59%.

2.3.3. [Pd(BIQ)(DHB)] (3)

This complex was prepared according to the protocol given for **1**, replacing [Pd(BIQ)Cl_2] with [Pd(BPY)Cl_2]. The yield obtained was 60%. ^{1}H NMR [$(CD_3)_2SO$]: δ 9.35 (d, 1H, 3), 9.25 (d, 1H, 3′), 9.01 (d, 2H, 4, 4′), 8.85 (d, 2H, 5, 5′), 8.23 (d, 2H, 6, 6′), 7.89 (t, 2H, 7, 7′), 8.07 (m, 2H, 8, 8′), 6.92 (dd, 1H, B), 6.82 (d, 1H, C), 6.51 (d, 1H, A), 9.55 (s, 1H, D). *Anal.* Calc. for $C_{25}H_{16}N_2O_3Pd$: C, 60.19; H, 3.23; N, 5.62. Found: C, 59.80; H, 3.25; N, 5.66%.

2.3.4. [Pd(DPP)(DHB)] (4)

The complex was prepared by the procedure described for **2** using [Pd(DPP)Cl_2] in place of [Pd(PHEN)Cl_2]. The yield obtained was 52%. ^{1}H NMR [$(CD_3)_2SO$]: δ 8.89 (m, 2H, 2, 9), 7.74 (s, 2H, 4, 7), 7.88 (s, 2H, 5, 6), 7.66 (m, 2H, 3, 8), 6.66 (d, 1H, B), 6.49 (s, 1H, C), 6.17 (d, 1H, A), 9.40 (s, 1H, D). *Anal.* Calc. for $C_{31}H_{20}N_2O_3Pd$: C, 64.76; H, 3.51; N, 4.87. Found: C, 64.96; H, 3.49; N, 4.86%.

2.3.5. [Pt(BPY)(DHB)] (5)

[Pt(BPY)Cl_2] (0.2 mmol) was dissolved in 25 cm^3 of DMF and filtered. To this 0.2 mmol of H_2DHB dissolved in 1.6 cm^3 of 0.25 N KOH in methanol was added. The solution was stirred for 24 h at 60 °C, then the solvent was evaporated at 40 °C. The crude product obtained was recrystallized from chloroform and dried in a vacuum desiccator over anhydrous calcium chloride. The yield obtained was 62%. ^{1}H NMR [$(CD_3)_2SO$]: 8.55 (d, 2H, 3, 3′), 8.38 (dt, 2H, 4, 4′), 7.78 (t, 2H, 5, 5′), 9.08 (d, 2H, 6, 6′), 6.96 (d, 1H, B), 6.94 (s, 1H, C), 6.64 (d, 1H, A), 9.6 (s, 1H, D). *Anal.* Calc. for $C_{17}H_{12}N_2O_3Pt$: C, 41.89; H, 2.48; N, 5.75. Found: C, 41.60; H, 2.45; N, 5.79%.

2.3.6. [Pt(PHEN)(DHB)] (6)

This complex was prepared by the method described for **5** using [Pt(PHEN)Cl_2] instead of [Pt(BPY)Cl_2]. The yield obtained was 42%. ^{1}H NMR [$(CD_3)_2SO$]: δ 9.59 (d, 2H, 2, 9), 8.99 (d, 2H, 4, 7), 8.23 (s, 2H, 5, 6), 8.12 (q,

2H, 3, 8), 6.94 (d, 1H, B), 6.90 (s, 1H, C), 6.60 (d, 1H, A), 9.62 (s, 1H, D). *Anal.* Calc. for $C_{19}H_{12}N_2O_3Pt$: C, 44.62; H, 2.37; N, 5.48. Found: C, 45.21; H, 2.35; N, 5.48%.

2.3.7. [Pt(BIQ)(DHB)] (7)

Preparation of this complex was made possible by following the procedure given for **5** using $[Pt(BIQ)Cl_2]$ instead of $[Pt(BPY)Cl_2]$. The yield obtained was 62%. ^1H NMR $[(CD_3)_2SO]$: δ 9.49 (d, 2H, 3), 9.40 (d, 1H, 3′), 8.94 (d, 2H, 4, 4′), 8.19 (d, 2H, 5, 5′), 8.03 (d, 2H, 6, 6′), 7.85 (dt, 2H, 7, 7′), 8.64 (m, 2H, 8, 8′), 6.96 (d, 1H, B), 6.94 (s, 1H, C), 6.64 (d, 1H, A), 9.63 (s, 1H, D). *Anal.* Calc. for $C_{25}H_{16}N_2O_3Pt$: C, 51.11; H, 2.75; N, 4.77. Found: C, 51.27; H, 2.75; N, 4.80%.

2.3.8. Pt(DPP)(DHB) (8)

The complex was prepared according to the procedure described for **5** using $[Pt(DPP)Cl_2]$ in place of $[Pt(BPY)Cl_2]$. The yield obtained was 48%. ^1H NMR $[(CD_3)_2SO]$: δ 9.09 (t, 2H, 2, 9), 7.79 (s, 12H, 4, 7, 3, 8), 7.79 (s, 2H, 5, 6), 6.83 (m, 2H, B, C), 6.47 (d, 1H, A), 9.56 (s, 1H, D). *Anal.* Calc. for $C_{31}H_{20}N_2O_3Pt$: C, 56.11; H, 3.04; N, 4.22. Found: C, 55.96; H, 3.01; N, 4.18%.

2.3.9. Synthesis of 3,3′,4,4′-tetrahydroxybenzaldazine (H_4THB)

A solution of H_2DHB (276 mg, 2 mmol in 10 cm^3 of methanol) was added dropwise to a solution containing a mixture of 0.05 cm^3 of hydrazinehydrochloride, 9 cm^3 of distilled water and 1.5 cm^3 of concentrated ammonia solution. The contents were stirred for 3h at room temperature, then the solution was neutralized with 1N acetic acid to remove excess ammonia and cooled to get yellow crystals of the compound. The product was recrystallized from 50% methanol and the yield was 62%. The purity of the compound was checked using TLC. ^1H NMR $[(CD_3)_2SO]$: δ 9.54 (s, 2H, E, E′), 9.25 (s, 2H, F, F′), 8.46 (s, 2H, D), 7.29 (d, 2H, C), 7.08 (dd, 2H, B), 6.81 (d, 2H, A). *Anal.* Calc. for $C_{14}H_{12}N_2O_4$: C, 61.76; H, 4.44; N, 10.29. Found: C, 62.02; H, 2.49; N, 10.21%.

2.3.10. $[Pd_2(BPY)_2(THB)]$ (9)

This complex was prepared according to the method reported for **1** by adding 0.1 mmol of H_4THB instead of 0.2 mmol of H_2DHB. The compound was recrystallized twice from acetonitrile and dried in a vacuum desiccator over anhydrous calcium chloride. The yield was 25%. ^1H NMR $[(CD_3)_2SO]$: δ 8.52 (d, 2H, 3, 3′), 8.31 (dt, 4H, 4, 4′), 7.78 (m, 4H, 5, 5′), 8.59 (d, 4H, 6, 6′), 6.87 (dd, 2H, B), 6.72 (d, 2H, C), 6.41 (d, 2H, A), 9.52 (s, 2H, D). *Anal.* Calc. for $C_{34}H_{24}N_6O_4Pd_2$: C, 51.47; H, 3.05; N, 10.59. Found: C, 51.27; H, 3.05; N, 10.57%.

2.3.11. $[Pt_2(BPY)_2(THB)]$ (10)

$[Pt(BPY)Cl_2]$ (0.2 mmol) was dissolved in 25 cm^3 DMF and filtered. To this 0.1 mmol of H_4THB dissolved in 1.6 cm^3 of 0.25 N KOH in methanol was added. The solution was stirred for 24 h at 60 °C, then the solvent was evaporated at 40 °C. The crude product obtained was recrystallized from chloroform and dried in a vacuum desiccator over anhydrous calcium chloride. The yield obtained was 62%. ^1H NMR $[(CD_3)_2SO]$: δ 8.58 (d, 2H, 3, 3′), 8.40 (d, 4H, 4, 4′), 7.83 (m, 4H, 5, 5′), 9.48 (d, 4H, 6, 6′), 6.94 (dd, 2H, B), 6.65 (d, 2H, C), 6.65 (d, 2H, A), 9.6 (s, 2H, D). *Anal.* Calc. for $C_{34}H_{24}N_6O_4Pt_2$: C, 42.07; H, 2.49; N, 8.66. Found: C, 41.89; H, 2.53; N, 8.72%.

The complexes [Pt(BPY)(DHBA)] (**11**), [Pt(PHEN)(DHBA)] · H_2O (**12**) [Pt(BIQ)(DHBA)] (**13**) and [Pt(DPP)(DHBA)] · H_2O (**14**) were prepared and characterized as reported in the literature [23].

3. Results and discussion

3.1. Syntheses and characterization

Eight complexes of the formula, [M(N-N)(DHB)] {where M = Pd(II) or Pt(II), N-N = 2,2′-bipyridine (BPY), 2,2′-biquinoline (BIQ), 4,7-diphenyl-1,10-phenanthroline (DPP), 1,10-phenanthroline (PHEN) and DHB = dianion of 3,4-dihydroxybenzaldehyde (H_2DHB)} were prepared and characterized. In general these complexes were prepared by reacting stoichiometric quantities of the starting material, $[M(N\text{-}N)Cl_2]$ with H_2DHB in the presence of an appropriate amount of KOH under a nitrogen atmosphere. An illustrative example of the synthesis of [M(BPY)(DHB)] is shown in Scheme 1.

The various complexes prepared are [Pd(BPY)(DHB)] (**1**), [Pd(PHEN)(DHB)] (**2**), [Pd(BIQ)(DHB)] (**3**), [Pd(DPP)(DHB)] (**4**), [Pt(BPY)(DHB)] (**5**), [Pt(PHEN)(DHB)] (**6**), [Pt(BIQ)(DHB)] (**7**) and [Pt(DPP)(DHB)] (**8**).

The tetradentate ligand H_4THB was synthesized by coupling two molecules of H_2DHB with hydrazinehydrochloride in the presence of liquid ammonia as depicted in Scheme 2.

Two complexes of the formula $[M_2(BPY)_2(THB)]$ {where M is Pd(II) or Pt(II) and BPY is 2,2′-bipyridine and THB is the tetraanion of tetrahydroxy benzaldazine} were prepared using the starting material H_4THB. The complexes prepared were $[Pd_2(BPY)_2(THB)]$ (**9**) and $[Pt_2(BPY)_2(THB)]$ (**10**). Four more platinum complexes, namely [Pt(BPY)(DHBA)] (**11**), [Pt(PHEN)(DHBA)] · H_2O (**12**), [Pt(BIQ)(DHBA)] (**13**) and [Pt(DPP)(DHBA)] · H_2O (**14**) were prepared for luminescence studies, according to the reported procedure [23].

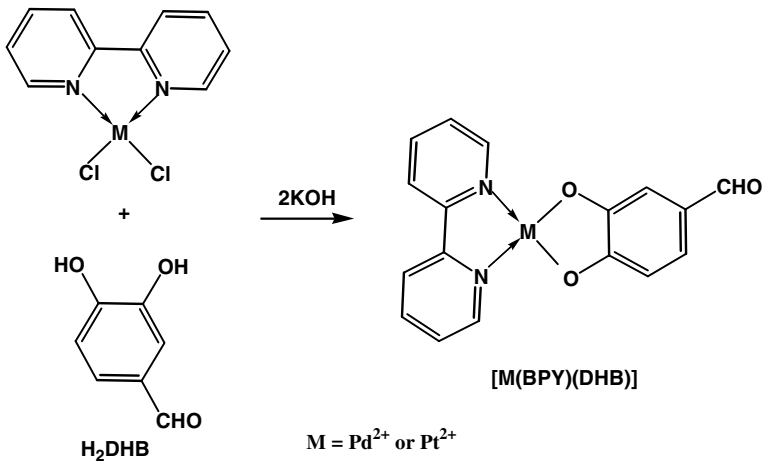

Scheme 1. Synthesis of [M(N-N)(DHB)] complexes.

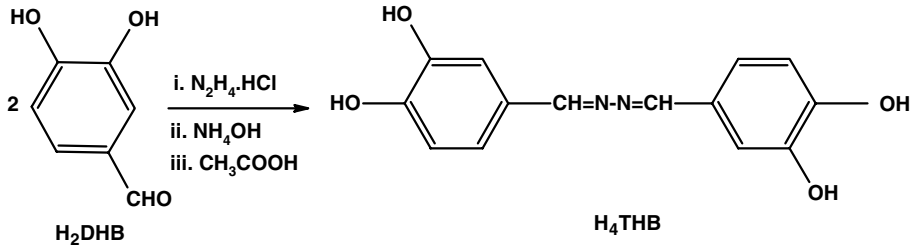

Scheme 2. Synthesis of H_4THB.

Changes in the IR spectra in the ligand segment of the [M(N-N)(DHB)] complexes are compared with that of the parent chloro compounds of the formula [M(N-N)Cl_2], as well as with the free ligands. The ring frequency of the α-diimine moiety is shifted to higher frequency on complexation as compared to the free ligand. The presence of two additional sharp bands around 1250 and 1460 cm^{-1} confirms the bonding of DHB to the metal ion through ionized hydroxyl groups [26,27]. The band at 1460 cm^{-1} is due to the skeletal stretching vibration of the aromatic ring of DHB and the band at 1250 cm^{-1} corresponds to the C–O stretching vibration of DHB. In the case of binuclear complexes, the IR spectra show a peak around 1560 cm^{-1} due to the –CH=N– group. There are strong peaks at 1275 cm^{-1} (which is due to the –C–O– stretching) and around 1475 cm^{-1} (which is due to the aromatic ring stretching of THB). Observation of these two peaks indicates the binding of THB to the metal ion through the $–O^-$ group.

The ^1H NMR spectra of the complexes are compared with the parent dichloro compounds in order to determine the bonding mode and stoichiometry of the complexes. The signals are assigned on the basis of chemical shifts and spin-spin interaction. The structure and numbering scheme of the ligand protons of the complexes are given in Figs. 1 and 2. The α-diimine protons of the complexes generally experience upfield shifts when compared to the parent chloro compound. This could be due to stronger binding of DHB to the metal ion than the chloride ions, or more back bonding from the metal d-orbital to π* orbitals of the α-diimine ligands as compared to chloride ions [20c,28]. The upfield shift is remarkable (0.48 and 0.93 ppm for **1** and **5**, respectively) for the $H_{6,6'}$ protons of [M(BPY)(DHB)] complexes. The $H_{2,9}$ protons of [M(PHEN)(DHB)] complexes experience maximum upfield shift (0.51 and 0.1 ppm for **2** and **6**, respectively). A similar trend is also observed in [M(DPP)(DHB)] complexes. The $H_{2,9}$ protons of **4** and **8** show upfield shifts of 0.52 and 0.66 ppm, respectively. The phenyl protons in the fourth and seventh positions experienced little upfield shifts when compared to their parent chloro compounds. In the ^1H NMR spectra of [M(BIQ)(DHB)] complexes, all the protons of BIQ experience up- or downfield shifts except the $H_{6,6'}$ protons. The protons $H_{4,4'}$ and $H_{8,8'}$ of **3** experience downfield shifts of 0.25 and 0.33 ppm, respectively, whereas the $H_{5,5'}$ and $H_{7,7'}$ protons experience upfield shifts of 0.09 and 0.26 ppm correspondingly as compared to the parent chloro compound. The protons H_3 and $H_{3'}$ of complexes **3** and **6** appear as two separate doublets rather than a single doublet as in the parent chloro compound. This could be due to the fact that the compound lacks planarity in solution which

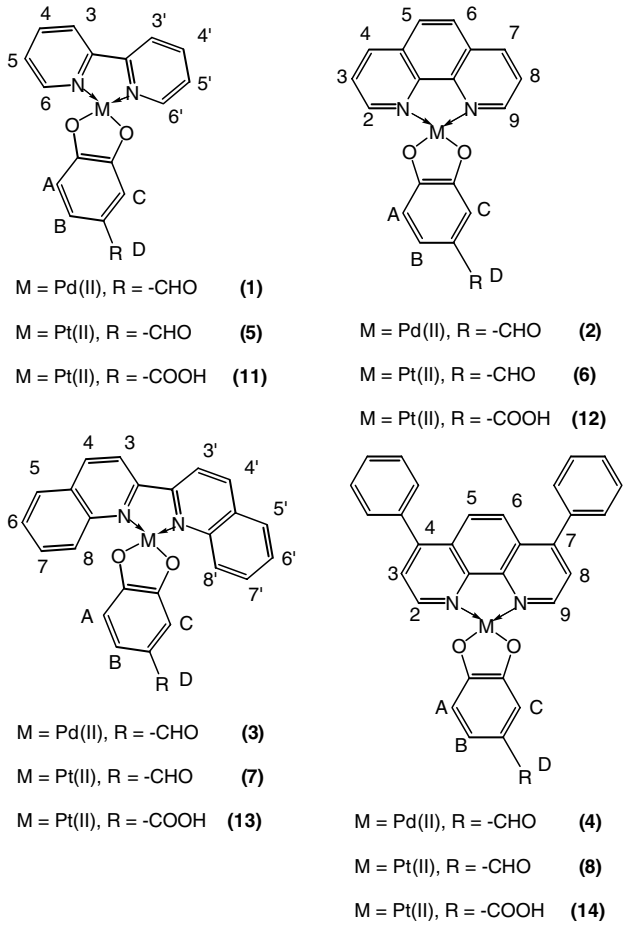

Fig. 1. Structure and numbering scheme of the protons of [M(N-N)(DHB)] and [Pt(N-N)(DHBA)] complexes.

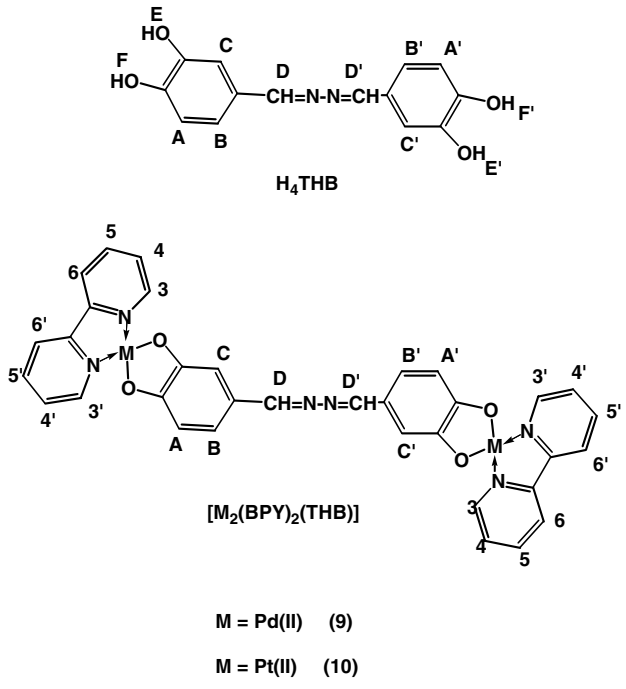

Fig. 2. Structure and numbering scheme of the protons of H_4THB and $[M_2(BPY)_2(THB)]$ complexes.

makes the protons have different electronic environments. Thus, the protons H_3 and $H_{3'}$ could resonate at different frequencies. Similar behaviour was observed earlier in the case of [M(BIQ)(DHBA)] [23]. The free ligand, 3,4-dihydroxybenzaldehyde shows two peaks at 10.11 and 9.55 ppm due to the phenolic –OH protons, but they are absent in the metal complexes. All other protons (H_A, H_B, H_C and H_D) experience upfield shifts in the complexes as compared to the free ligand, indicating the bonding of DHB to the metal ions. Similarly, H_4THB shows two peaks for the four phenolic –OH protons at 9.54 and 9.29 ppm. These two peaks are absent in the metal complexes. The protons H_D, H_C and H_B experienc considerable upfield shifts in the complex as compared to the free ligand. The structure and numbering scheme of the protons in the ligand and complexes are given in Figs. 1 and 2. The ^3J (^{195}Pt–^1H) couplings in these complexes have not been observed due to a decrease of chemical shielding anisotropy with an increase in the magnetic field strength [28].

These data suggest that both ligands are bonded to the metal ion in the mixed-ligand complexes. The integrated areas obtained for the protons of α-diimine and DHB indicate the stoichiometry of these complexes corresponds to [M(N-N)(DHB)]. Similarly, the proton ratio of BPY and THB indicate a stoichiometry of $[M_2(BPY)_2(THB)]$. The sharp ^1H NMR spectral signals observed in these complexes suggest them to be diamagnetic. The proton NMR spectral, the IR and the elemental analysis data confirm the synthesis and the structures assigned to them as shown in Figs. 1 and 2.

3.2. Electronic absorption spectra

The electronic absorption spectral data of these complexes are given in Table 1. A representative spectrum is shown in Fig. 3. The chloro complexes of the formula, $[M(N\text{-}N)Cl_2]$ show four bands (bands are numbered in increasing order of energy), whereas the complexes of the formula [M(N-N)(DHB)] show five band maxima. The bands in the UV region have been assigned on the basis of band assignments of chloro complexes [20c,29,30]. Thus, the bands 2 and 4 have been assigned to charge-transfer transitions from a metal d-orbital to π-antibonding orbitals of the α-diimine (MLCT). Bands 3 and 5 are assigned as the intra-ligand π–π* transition of the α-diimine (IL). In addition, these complexes exhibit a band in the visible region, which is strongly dependent on the polarity of the solvent (band 1). The absorption maximum of this band is found to shift with a change of solvent. The energy of this band increases with an increase in the polarity of the solvent (hydroxylic as well as non-hydroxylic). The observed shift in band maxima to higher energy in solvents of increasing polarity is indicative of a polar ground state and non-polar excited state as reported by Cummings and Eisen-

Table 1
Electronic absorption spectral data of [M(N-N)(DHB)], [Pt(N-N)(DHBA)] and [$M_2(BPY)_2(THB)$] complexes in DMF at 298 K

Complex	Band maxima (λ_{max}/nm)				
	Band 1	Band 2	Band 3	Band 4	Band 5
1	478 (3.73)[a]	364 (17.49)	316 (21.50)	304 (26.20)	266 (46.12)
2	476 (3.07)	363[b] (14.48)		300 (17.80)	270 (40.66)
3	598 (2.42)	372 (38.57)	360 (38.57)	300 (19.62)	267 (72.60)
4	492 (4.17)	350 (19.76)	325 (sh)[c]	293 (51.18)	267 (37.30)
5	496 (8.22)	361 (17.39)	322 (16.87)	310 (sh)	272 (35.95)
6	475 (1.65)	360 (25.24)	300 (sh)	271 (8.93)	264 (9.31)
7	622 (2.86)	374 (18.30)	339 (28.62)	314 (28.96)	267 (51.75)
8	518 (8.97)	360 (sh)	344 (21.75)	296 (45.82)	269 (47.12)
9	465 (7.041)	362 (33.52)	316 (44.53)	304 (51.17)	266 (83.51)
10	510 (5.66)	388 (17.99)	326 (34.85)	313 (32.97)	280 (65.59)
11	510 (7.15)	330 (22.42)	305 (sh)	289 (35.63)	259 (29.03)
12	512 (3.14)	325 (27.49)		280 (34.39)	265 (47.12)
13	640 (1.74)	377 (36.50)	360 (sh)	327 (28.00)	266 (59.59)
14	531 (1.45)	410 (sh)	333 (sh)	309 (sh)	274 (sh)

[a] Molar absorptivity in $\varepsilon \times 10^{-3}$ L mol^{-1} cm^{-1} is given in parentheses.
[b] Broad band.
[c] Shoulder.

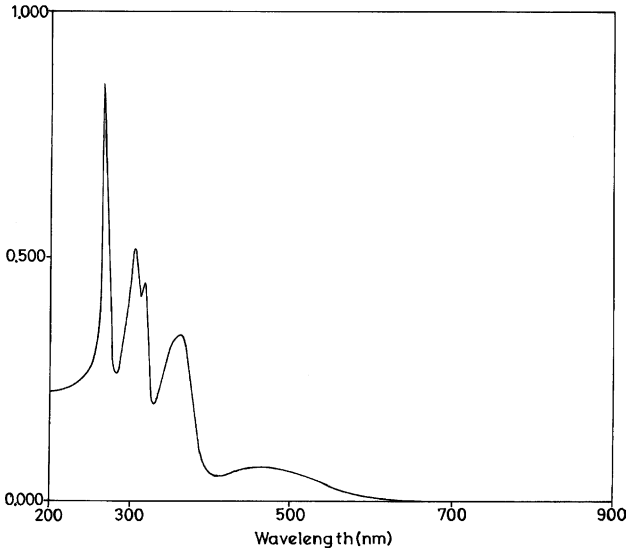

Fig. 3. Electronic absorption spectrum of **6** in DMF.

berg [12b]. This is in contrast to the small degree of solvatochromism observed for the MLCT band of transition metal diimine complexes such as $[Ru(bpy)_3]^{2+}$ and related systems [8]. The effect of various solvents on the λ_{max} of this band is given in Table 2. An excellent correlation of absorption band energy with solvent polarity was found using Reichardt's scale [31]. The plots of Reichardt's parameter (E_T) of the solvents against absorption maxima gave two separate lines, one for hydroxylic solvents and the other for non-hydroxylic solvents [18,29,30]. A typical plot for **2** is given in Fig. 4. This band was not observed in a solution containing a 1:1 mixture of [M(N-N)Cl_2] and H_2DHB.

The energy of this band decreases when the α-diimine is changed from BPY to BIQ. However, small changes were observed when N-N was replaced from BPY to PHEN or DPP. An increase in energy of this band was observed when compared to [M(N-N)(DHBA)] [23] and [M(N-N)(CAT)] [32]. Based on these observations this band has been assigned as a LLCT transition from the HOMO of DHB to the LUMO of α-diimine via the metal [23,32]. The observed trends in the energy of this band can also be explained based on the above assignment. Thus, the decrease in energy of [M(BIQ)(DHB)] complexes when compared to [M(BPY)(DHB)] complexes can be explained to be due to the additional fused rings on the bipyridine, which pulls down the LUMO to lower energy. The two phenyl groups are perpendicular to the plane of 1,10-phenanthroline in the DPP complexes and are therefore not expected to contribute much to conjugation in the complex [33]. Hence, there is a small change in the energy of transition between PHEN and DPP complexes. Because of the electron-withdrawing group (–CHO) on the phenyl ring of DHB, the HOMO of the complexes, [M(N-N)(DHB)] further drops to lower energy. Thus, the energy of transition for [M(N-N)(DHB)] complexes increases when compared to the unsubstituted catechol complexes, [M(N-N)(CAT)] or those substituted with a carboxylic group, [M(N-N)(DHBA)] complexes [23]. This band assignment is supported by the solvent studies. With the increase in polarity of the solvent, the HOMO is stabilized more and leads to an increase in the energy of transition [29,30]. The LLCT band of palladium complexes is at higher energy as compared to the platinum counterparts. This is due to increase in the ligand field of Pt(II) by 30–50% when compared to Pd(II).

The electronic spectra of the dinuclear complexes are similar to the mononuclear complexes. There is a little change in the position of the LLCT band but the molar

Table 2
Effect of hydroxylic and non-hydroxylic solvents on the LLCT band of [M(N-N)(DHB)] complexes

Solvent	Band maxima (λ_{max}/nm)							
	1	**2**	**3**	**4**	**5**	**6**	**7**	**8**
Ethylene glycol	416 (24.06)[a]	426 (23.49)	544 (18.38)	427 (23.43)	430 (23.26)	431 (23.19)	541 (18.48)	429 (23.33)
Methanol	421 (23.74)	431 (23.18)	555 (18.03)	440 (22.71)	437 (22.87)	433 (23.08)	559 (17.90)	483 (20.71)
Ethanol	444 (22.53)	439 (22.78)	568 (17.60)	448 (22.34)	454 (22.03)	443 (22.57)	581 (17.20)	492 (20.34)
n-Propanol	451 (22.16)	454 (22.01)	603 (16.58)	459 (21.81)	473 (21.16)	454 (22.01)	608 (16.45)	505 (19.81)
Acetonitrile	459 (21.80)	450 (22.23)	578 (17.31)	481 (20.79)	491 (20.35)	450 (22.23)	587 (17.03)	485 (20.62)
N,*N*-Dimethyl sulfoxide	468 (21.36)	464 (21.54)	588 (17.01)	484 (20.66)	478 (20.91)	464 (21.54)	602 (16.61)	510 (19.62)
N,*N*-Dimethyl formamide	478 (20.90)	476 (20.99)	598 (16.71)	492 (20.33)	496 (20.15)	476 (21.03)	622 (16.09)	518 (19.31)
Acetone	485 (20.61)	482 (20.76)	600 (16.68)	497 (20.14)	500 (20.01)	482 (20.76)	638 (15.68)	526 (19.00)
Dichloromethane	502 (19.94)	495 (20.20)	622 (16.09)	504 (19.83)	502 (19.94)	495 (20.20)	663 (15.09)	513 (19.51)
Chloroform	510 (19.61)	498 (20.07)	638 (15.68)	506 (19.78)	510 (19.61)	498 (20.07)	681 (14.68)	522 (19.16)

[a] Band maxima in kK mol^{-1} is given in parentheses.

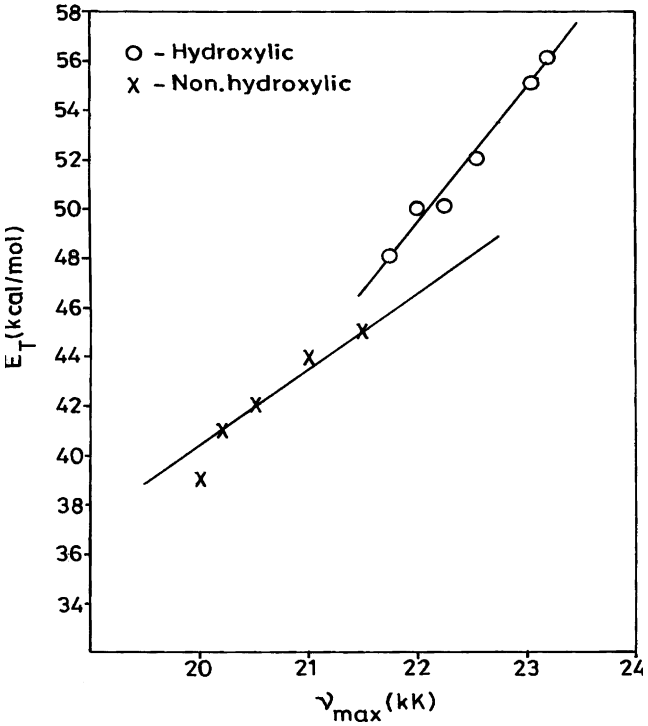

Fig. 4. Plot of E_T vs. ν_{max} for the LLCT band of **2**.

extinction coefficient of this band is higher for the dimer as compared to the monomer, and the position of the MLCT band is considerably red-shifted in the dimer. Since the binuclear complexes were found be soluble in very few solvents, a complete solvent-studies could not be made.

3.3. Electrochemical studies

The cyclic voltammetric data of complexes **1**–**8** are given in Table 3. In general these complexes show diffuse, irreversible and successive two one-electron reductions and one quasi-reversible one-electron oxidation. Irreversibility of the reduction peaks was confirmed by the absence of the peak in the reversible scan or by the large difference in potentials between two counter peaks. The general electron transfer series for the complexes can be represented by the following equations:

Table 3
Electrochemical data of [M(N-N)(DHB)] complexes in CH_3CN at 298 K

Complex	Reduction		Oxidation	
	I	II	I	II
1	−0.825[a]	−1.213	0.750	0.950
2	−0.838	−1.250	0.725	0.950
3	−0.850	−1.250	0.700	
4	−0.950	−1.275	0.750	
5	−0.985	−1.270	0.725	
6	−0.900	−1.450	0.700	
7	−0.915	−1.250	0.780	
8	−0.875	−1.350	0.650	

[a] Potentials in volts vs. Ag/AgCl.

$$[M(N\text{-}N)(DHB)]^{+} \underset{-e^-}{\overset{+e^-}{\rightleftharpoons}} [M(N\text{-}N)(DHB)]^{0} \quad (1)$$

$$[M(N\text{-}N)(DHB)]^{0} \underset{-e^-}{\overset{+e^-}{\rightleftharpoons}} [M(N\text{-}N)(DHB)]^{-1} \quad (2)$$

$$[M(N\text{-}N)(DHB)]^{-1} \underset{-e^-}{\overset{+e^-}{\rightleftharpoons}} [M(N\text{-}N)(DHB)]^{-2} \quad (3)$$

The formation of a charge transfer to the α-diimine excited state formally involves the oxidation of the HOMO and reduction of the α-diimine-based LUMO [12b]. Thus, the potentials of the first reduction and oxidation of the complexes can be related to the nature of the orbitals in these redox processes. These orbitals are the LUMO, consisting exclusively of α-diimine [34,35], and the HOMO of DHB, and they are involved in the charge-transfer transition (band 1) as described above. The first reduction potential of [M(BIQ)(DHB)] complexes lies at lower values as compared to [M(BPY)(DHB)] complexes. This can be explained in terms of the electron-withdrawing effect with increased delocalizing effect of additional fused rings in the former

compared to the latter. Similarly, the oxidation potentials of [M(BIQ)(DHB)] are higher than that of the [M(BPY)(DHB)] counter parts. The [M(DPP)(DHB)] complexes have a much smaller negative value for the first reduction potential than [M(PHEN)(DHB)] complexes. This could be due to the electron-withdrawing nature of the substituted phenyl groups in DPP [33]. However, only a small change was noticed in the position of the absorption bands (band 1) of [M(PHEN)(DHB)] and [M(DPP)(DHB)]. The observed difference in redox potentials of an electron transfer process is normally controlled by both kinetic and thermodynamic parameters [36,37], whereas the absorption band position is purely thermodynamically controlled. Similar observations were found for another series of complexes [23]. Cyclic voltammograms on the dinuclear complexes could not be recorded due to insufficient solubility of these complexes in acetonitrile.

3.4. Luminescence studies

The luminescence studies of the complexes were carried out in acetonitrile at room temperature. These complexes do not show emission on excitation at the LLCT band at room temperature. However, these complexes were found to be luminescent at room temperature on excitation at the MLCT/ILCT band. Only the platinum derivatives were found to show emission at room temperature. This may be due to the lack of structural rigidity of the Pd(II) complexes as compared to the Pt(II) complexes. The parent dichloro complexes of Pt(II) did not show emission at room temperature. The luminescence band maxima of these complexes are given in Table 4. Representative luminescence and excitation spectra are given in Fig. 5(a) and (b). The energies of the MLCT (band 2) and IL (band 3) lie very close to each other in the electronic spectra of these complexes. On excitation at these bands, these complexes show luminescence at room temperature. The energy of the emission maxima of these complexes lies in the following order: **4** ~ **8** > **6** ~ **10** > **5** ~ **7** ~ **9**. This order can be explained in terms of π-conjugation. The difference in energy between **5**, **7** and **9** is very small. This may be due to the only one additional double bond present in **5** and **9** as compared to **7**. The difference in energy between **6**, **10** and **5**, **9** can be attributed to the presence of two additional phenyl groups in DPP. Similar behaviour has earlier been observed by Watts and Crosby [38] for ruthenium complexes. In the case of **4** and **8** the larger red shift in emission maximum is due to the additional fused rings in the BIQ system. The large Stokes shift observed in the excitation spectra of these complexes indicates that the ground state geometry of these complexes differs largely with the excited state. The quantum yields of luminescence (ϕ_L) of these complexes are included in Table 4. The ϕ_L values were determined with reference to tryptophan in water [25]. The DPP derivative is found to show a larger quantum yield than any other complex. Similar behaviour was earlier reported for DPP complexes of ruthenium [39].

Table 4
Photophysical data of [Pt(N-N)(DHB)], [Pt(N-N)(DHBA)] and $[Pt_2(BPY)_2(THB)]$ complexes in CH_3CN

Complex	Luminescence maxima (λ_{max}/nm)	Luminescence excitation maxima (λ_{max}/nm)	τ[a] (ns)	Φ_L[a] ($\times 10^2$)
5	364	294	2.40 8.68	0.188
6	368	291	2.80 7.30	0.278
7	419	333	4.28 4.29	0.295
8	416 398	355 319 284	3.49 10.70	0.409
10	470 422	370 336 295	9.20	0.204
11	364	291	1.40 8.77	0.881
12	363	290	1.53 8.74	0.232
13	422	332	3.80 5.60	0.292
14	414 394	350 319 299	4.80 12.20	2.788

[a] Experimental error is less than 5%.

Two of the complexes were tested for phosphorescence at low temperature. Both complexes **1** and **5** were found to show phosphorescence at 77 K. They were excited at various wavelengths to obtain the same spectrum. The phosphorescence spectrum of **5** is shown in Fig. 6. The phosphorescence spectrum of **5** shows a band around 600 nm which is due to the emission from the lowest excited state, namely the LLCT state as reported earlier for a similar complex [40].

The fluorescence lifetime measurements were done in acetonitrile. The fluorescence lifetime shows a bi-exponential decay. The multiple lifetimes found for these complexes suggest the possibility of more than one emitting state for these complexes. Multiple state luminescence has been reported for a number of metal complexes [41]. Hence, it is concluded that there is a mixing of MLCT and IL excited states as proposed by Balzani and co-workers [42] for a different set of Pt(II) complexes.

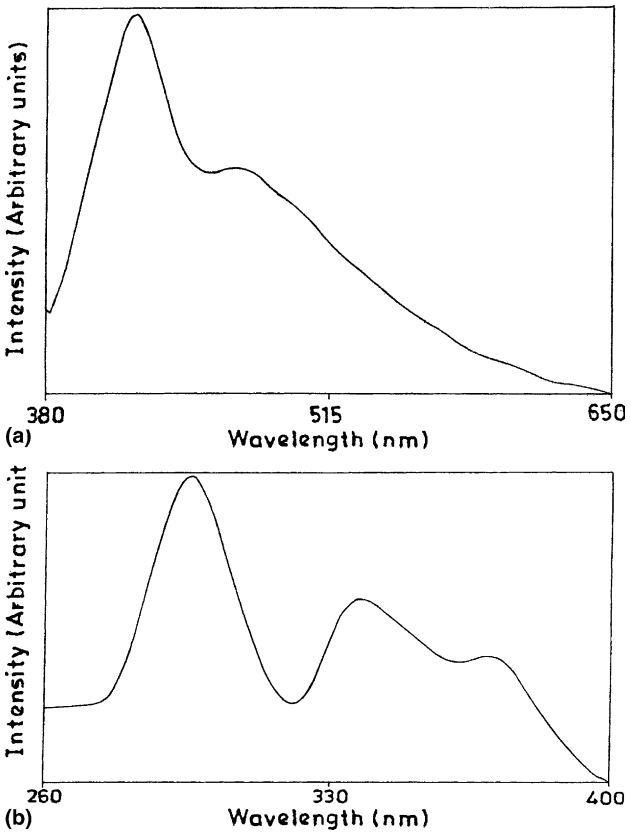

Fig. 5. (a) Luminescence spectrum of **7** in acetonitrile at 298 K. (b) Excitation spectrum of **7** in acetonitrile at 298 K.

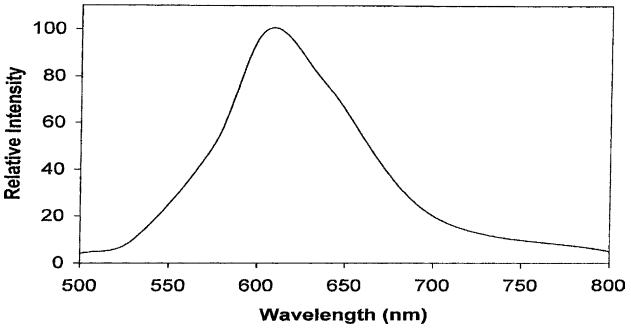

Fig. 6. Phosphorescence spectrum of **5** in EPA glass at 77 K.

4. Conclusion

This study shows that various mixed-ligand complexes of Pt(II) and Pd(II) can exhibit a LLCT band. The platinum complexes of this series were found to emit from a low-energy state at low temperature and a high-energy state at room temperature.

Appendix A. Supplementary data

A representative lifetime trace is available from the publishers. Supplementary data associated with this article can be found, in the online version at doi:10.1016/j.poly.2004.09.029.

References

[1] (a) J.P. Paris, W.W. Brandt, J. Am. Chem. Soc. 81 (1959) 5001;
(b) J.N. Demas, G.A. Crosby, J. Mol. Spectrosc. 26 (1968) 72;
(c) M. Wrighton, D.L. Morse, J. Am. Chem. Soc. 96 (1974) 998;
(d) T.J. Meyer, Prog. Inorg. Chem. 87 (1983) 952;
(e) A.J. Lees, Chem. Rev. 87 (1987) 711;
(f) A. Juris, V. Balzani, F. Barigelletti, S. Campagna, P. Belser, A. von Zelewsky, Coord. Chem. Rev. 84 (1988) 85;
(g) J.A. Zuleta, M.S. Burberry, R. Eisenberg, Coord. Chem. Rev. 97 (1990) 47;
(h) A.L. Balch, V.J. Catalano, M.M. Olmstead, Inorg. Chem. 29 (1990) 585;
(i) C.B. Blanton, Z. Murtaza, R.J. Shaver, D.P. Rillema, Inorg. Chem. 31 (1992) 3230;
(j) W.B. Connick, V.M. Miskowski, V.H. Holding, H.B. Gray, Inorg. Chem. 39 (2000) 2582.
[2] T.J. Meyer, Acc. Chem. Res. 22 (1989) 163.
[3] V. Balzani, F. Scandola, Supramolecular Photochemistry, Ellis Horwood, Chichester, 1991.
[4] E. Pelizzetti, N. Serpone (Eds.), Homogeneous and Heterogeneous Photocatalysis, Reidel, Dordrecht, Holland, 1985.
[5] L-T. Cheng, W. Tam, D.F. Eaton, Organometallics 9 (1990) 2865.
[6] P.N. Prasad, B.A. Reinhardt, Chem. Mater. 2 (1990) 660.
[7] A.E. Friedman, J.-C. Chambron, J.-P. Sauvage, N.J. Turro, J.K. Barton, J. Am. Chem. Soc. 112 (1990) 4960.
[8] (a) J.P. Sauvage, J.P. Collin, J.C. Chambron, S. Guillerez, C. Coudret, V. Balzani, F. Barigelletti, L. De Cola, L. Flamigni, Chem. Rev. 94 (1994) 993;
(b) V. Balzani, A. Juris, M. Venturi, S. Campagna, S. Serroni, Chem. Rev. 96 (1996) 759;
(c) V. Anbalagan, K. Rosa, D.P. Rillema, Coord. Chem. Rev. (communicated).
[9] (a) V.M. Miskowski, V.H. Holding, Inorg. Chem. 28 (1989) 1529;
(b) D.L. Web, L.A. Rosiello, Inorg. Chem. 10 (1971) 2213;
(c) V.M. Miskowski, V.H. Holding, C.M. Che, Y. Wang, Inorg. Chem. 32 (1993) 2518;
(d) F.D. Camassea, F. Castelli, L.A. Rosiello, J. Lumin. 8 (1973) 71;
(e) M. Martin, M.-B. Krough-Jesperson, M. Hsu, J. Tewksbury, M. Laurent, K. Viswanath, H. Patterson, Inorg. Chem. 22 (1983) 647.
[10] J. DePriest, G.Y. Zheng, N. Goswami, D.M. Eichorn, C. Woods, D.P. Rillema, Inorg. Chem. 39 (2000) 1955, and references therein.
[11] M. Maestri, D. Sandrani, v. Balzani, A. von Zelewsky, C. Deuschel-Corniolev, P. Jolliet, Helv. Chim. Acta 71 (1988) 1053.
[12] (a) J.A. Zuleta, C.A. Chesta, R. Eisenberg, J. Am. Chem. Soc. 111 (1989) 8916;
(b) S.D. Cummings, R. Eisenberg, J. Am. Chem. Soc. 118 (1996) 1949;
(c) W. Paw, S.D. Cummings, M.A. Mansour, W.B. Connick, D.K. Geiger, R. Eisenberg, Coord. Chem. Rev. 171 (1998) 125;
(d) W.B. Connick, D. Geiger, R. Eisenberg, Inorg. Chem. 38 (1999) 3264;
(e) M. Hissler, J.E. McGarrah, W.B. Connick, D.K. Geiger, S.D. Cummings, R. Eisenberg, Coord. Chem. Rev. 208 (2000) 115.
[13] C.W. Chan, L.K. Cheng, C.M. Che, Coord. Chem. Rev. 132 (1994) 87.
[14] Y. Zhang, K.D. Ley, K.S. Schanze, Inorg. Chem. 35 (1996) 7102.
[15] W.B. Connick, H.B. Gray, J. Am. Chem. Soc. 119 (1997) 11620.
[16] (a) I.G. Dance, R.T. Miller, J. Am. Chem. Soc. 95 (1973) 6970;

(b) L. Kumar, K.H. Puthraya, T.S. Srivastava, Inorg. Chim. Acta 86 (1984) 173;
(c) R. Benedix, D. Pitsch, K. Schone, H. Hennig, Z. Anorg. Allg. Chem. 42 (1986) 102;
(d) G.E. Matsubayashi, M. Hirao, T. Tanaka, Inorg. Chim. Acta 144 (1988) 217;
(e) T.A. Perkins, D.B. Pourreau, T.L. Netzel, K. Schanze, J. Phys. Chem. 93 (1989) 4511;
(f) R. Benedix, H. Hennig, H. Kunkely, A. Vogler, Chem. Phys. Lett. 175 (1990) 483.
[17] H. Hennig, D. Rehorek, R.D. Archer, Coord. Chem. Rev. 65 (1985) 1.
[18] (a) V. Anbalagan, T.S. Srivastava, J. Photochem. Photobiol. A 66 (1992) 345;
(b) V. Anbalagan, T.S. Srivastava, J. Photochem. Photobiol. A 89 (1995) 113;
(c) V. Anbalagan, T.S. Srivastava, J. Photochem. Photobiol. A 77 (1994) 141.
[19] B.S. Furniss, A.J. Hannaford, V. Roger, P.W.G. Smith, A.R. Tachell, Vogel's Textbook of Practical Organic Chemistry, 4th ed., Longman, London, 1978, pp. 264–279.
[20] (a) F.A. Palacsay, J.V. Rund, Inorg. Chem. 8 (1969) 524;
(b) V. Kumar, M.M. Rao, N. Ahmed, Indian J. Chem. 17 (1979) 217;
(c) S.S. Kamath, V. Uma, T.S. Srivastava, Inorg. Chim. Acta 161 (1989) 49;
(d) B.J. Malormiek, E.N. Joyes Jr., R.I. Kaplan, Inorg. Synth. 13 (1971) 217.
[21] P.M. Gidney, R.D. Gillard, B.T. Heaton, J. Chem. Soc., Dalton Trans. (1973) 132.
[22] L.A. Rosiello, Gazz. Chim. Ital. 97 (1967) 1177.
[23] V. Anbalagan, T.S. Srivastava, Polyhedron 13 (1994) 291.
[24] J.N. Demas, G.A. Crosby, J. Am. Chem. Soc. 93 (1971) 2841.
[25] O. Kalisky, J. Feitelson, M. Ottolenghi, Biochemistry 20 (1981) 2051.
[26] D.G. Brown, J.T. Reiprecht, G.C. Vogel, Inorg. Nucl. Chem. Lett. 12 (1976) 399.
[27] P.A. Wiklund, D.G. Brown, Inorg. Chem. 15 (1976) 396.
[28] P.S. Pregosin, Annu. Rep. NMR Spectrosc. 17 (1986) 285.
[29] A.B.P. Lever, Inorganic Electronic Spectroscopy, 2nd ed., Elsevier, Amsterdam, 1984, pp. 203–376.
[30] J. Burgess, Spectrochim. Acta 23 (1970) 506.
[31] C. Reichardt, Angew. Chem., Int. Ed. Engl. 4 (1965) 29.
[32] S.S. Kamath, V. Uma, T.S. Srivastava, Inorg. Chim. Acta 166 (1989) 91.
[33] S. Musumeli, E. Rizzareth, F. Fragala, S. Summaratano, R.P. Bonomo, Inorg. Chem. Acta 7 (1973) 660.
[34] A. Vogler, H. Kunkely, J. Hlavatch, A. Merz, Inorg. Chem. 23 (1984) 506.
[35] P.S. Braterman, J. Song, F.M. Wimmer, S. Wimmer, W. Kaim, A. Klein, R.D. Peacock, Inorg. Chem. 31 (1992) 5084.
[36] J.A. Davies, V. Uma, J.G. Mierzwink, J. Electroanal. Chem. 196 (1985) 239.
[37] M.K. DeArmound, K.W. Hamok, D.W. Wertz, Coord. Chem. Rev. 64 (1985) 65.
[38] R.J. Watts, G.A. Crosby, J. Am. Chem. Soc. 93 (1971) 3184.
[39] G.D. Hager, R.J. Watts, G.A. Crosby, J. Am. Chem. Soc. 97 (1975) 7037.
[40] S.S. Kamath, S. Shukla, T.S. Srivastava, Bull. Chem. Soc. Jpn. 64 (1991) 1351.
[41] (a) M.M. Glezen, A.J. Lees, J. Am. Chem. Soc. 110 (1988) 6243;
(b) M.K. DeArmound, C.M. Carlin, Coord. Chem. Rev. 36 (1981) 325.
[42] M. Maestri, D. Sandrani, V. Balzani, A. Von Zewlesky, C. Deuschel-Corniolev, P. Joliet, Helv. Chim. Acta 71 (1988) 1053.

1. Introduction

The biogeochemical cycle of Al is so dominated by abiotic events that less than 0.001% of cycled Al is found in biota at any one time [1]. The relative paucity of Al in biota is explained by neither its high abundance in the lithosphere, for example, calcium is present at half the abundance of Al whereas almost 35% of cycled calcium is present in biota, nor its lack of biological essentiality, for example, the non-essential metal cadmium is approximately seven times more abundant in biota than in the Earth's crust. It is, in fact, a consequence of the extremely efficient cycling of Al through increasingly insoluble, and biologically unavailable, mineral phases.

Hydroxyaluminosilicates (HAS) which are formed by the reaction of Al with $Si(OH)_4$ are probably the major secondary mineral phase controlling Al solubility in natural environments [2–6]. They have been studied for at least the last 50 years [7] and recent research has determined the structure and stoichiometry of two discrete forms, HAS_A which is formed in solutions in which $[Al] \geqslant [Si(OH)_4]$ and HAS_B which is only formed when $[Si(OH)_4] > [Al]$ [6]. These 'synthetic' HAS were shown to be structurally similar to the naturally occurring HAS, protoimogolite (HAS_A) and protoimogolite/allophane (HAS_B) [8]. Neither HAS_A nor HAS_B will form in solutions which are undersaturated with respect to $Al(OH)_{3(s)}$ [9] and this has prompted the suggestion that the mechanism of their formation includes the competitive condensation of $Si(OH)_4$ at an aluminium hydroxide template [10]. In nature HAS are most likely formed in the constrained environments of soil waters where concentrations of $Si(OH)_4$ could be as high as 1 mmol/L. In spite of the abundance of $Si(OH)_4$ in soil waters there have been only a few attempts to include the formation and dissolution of HAS in predictions of Al solubility control [2,5,11–15]. Many have chosen to ignore the contribution of HAS in Al solubility control and this may stem from a lack of reliable thermodynamic data to describe both their formation and solubilities. In the majority of soil waters the non-stoichiometric dissolution of aluminosilicate minerals [16] combined with the dissolution of other silicates will ensure that the concentration of $Si(OH)_4$ will be in excess of Al and, therefore, that the major HAS phase formed will be HAS_B. Herein, we have made the first attempt to derive a solubility expression for this phase and, in particular, we have highlighted both the assumptions which were required to enable its determination and the constraints which must be considered in its application in modelling Al solubility control in the natural environment.

2. Experimental

2.1. Preliminary investigations

A classic method to determine the solubility of an ionic solid would involve the addition of the solid to a known volume of solvent to form a saturated solution. We used this simple technique to investigate the dissolution of precipitates of HAS_A, HAS_B and $Al(OH)_{3(s)}$ each of which had been previously prepared and characterised structurally in our laboratory [6]. A known mass of each precipitate was suspended in a dialysis chamber (MWCO 1000 Da) which was immersed in a known volume of 0.1 mol/L KNO_3 (and 0.1% NaN_3 to prevent the growth of micro-organisms) adjusted to pH 6.5 and stored at 4 °C (Table 1). The dialysis chamber had a volume of 0.5 mL, was fully permeable to $Si(OH)_4$ and monomeric Al and was used to ensure that the original HAS material could not be present in the bulk volume. The dissolution of duplicate precipitates was followed over an 18 month period by measuring $[Si(OH)_4]$ and [Al] in the bulk volume. No attempt was made to control the pH of the bulk solutions during this time (Table 1). Neither of the HAS appeared to form a saturated solution during the 18 month period of dissolution. The concentration of $Si(OH)_4$ which was in quasi-equilibrium with HAS_B increased steadily from 5 months of ageing (19.4 and 21.2 μmol/L), through 8 (24.9 and 28.3 μmol/L) and 12 (41.0 and 45.5 μmol/L) to 18 (59.9 and 66.0 μmol/L) months. Al (0.15 and 0.34

Table 1
The concentrations of both $Si(OH)_4$ and total Al in the bulk solution following dissolution of duplicate precipitates of HAS_A, HAS_B and $Al(OH)_3$ after 18 months incubation in 0.1 mol/L KNO_3 at 4 °C

Solid phase	Si:Al of solid phase	Solid phase added (mg)	Solution volume (mL)	Final solution pH	$[Si(OH)_4]$ (μmol/L)	[Al] (μmol/L)
HAS_A (1)	0.36	30	100	6.33	21.1	0.65
HAS_A (2)	0.33	46	120	5.93	15.5	0.61
HAS_B (1)	1.03	30	100	6.34	59.9	0.15
HAS_B (2)	1.04	30	100	6.19	66.0	0.34
$Al(OH)_3$ (1)		45	120	6.07		1.12
$Al(OH)_3$ (2)		44	120	6.10		1.03

μmol/L) was only detected in bulk volumes after 18 months ageing. A similar trend for $[Si(OH)_4]$ in quasi-equilibrium with solid phase was also observed for HAS_A with $[Si(OH)_4]$ increasing from 5 months of ageing (7.9 and 11.2 μmol/L), through 8 (10.2 and 15.7 μmol/L) and 12 (14.2 and 14.4 μmol/L) to 18 (21.1 and 15.5 μmol/L) months. Al was detected in bulk volumes at 12 (0.15 and 0.58 μmol/L) and 18 (0.65 and 0.61 μmol/L) months. $Al(OH)_{3(s)}$ was also slow to dissolve and Al was only detected after 12 (0.54 and 0.33 μmol/L) and 18 (1.12 and 1.03 μmol/L) months of ageing.

These simple experiments showed that the dissolution of both HAS was non-stoichiometric in that $Si(OH)_4$ was released steadily over the 18 month period with almost no release of Al over the same period. It was interesting that the $[Si(OH)_4]$ in bulk volumes were proportional to the Si content of the original solid phases. The non-stoichiometric release of $Si(OH)_4$ for both HAS may have resulted in the formation of Al-enriched surfaces [16] which would then become the predominant determinants of Al solubility and hence explain the release of Al after 12–18 months. Of course, as the [Al] released approached saturation for $Al(OH)_{3(amorphous)}$ the formation of HAS_B would occur and this might then limit any further dissolution of Al. Alternatively, $Si(OH)_4$ might condense across hydroxy-aluminium groups at the surface of the dissolving precipitate and hence limit further the dissolution of both $Si(OH)_4$ and Al. Whilst the outcome of these experiments was ambiguous they did confirm that the dissolution of HAS, like other aluminosilicate phases [16], were non-stoichiometric and that an alternative experimental approach would be required to derive a quantitative solubility expression for $HAS_{B(s)}$.

The ability of HAS to limit the biological availability of Al (i.e., to control the concentration of monomeric and other rapidly equilibrating forms of Al, hereafter denoted as fast reacting Al or Al_r) will depend upon both their formation and, critically, their aggregation towards a kinetically stable solid phase. The attainment of this quasi-equilibrium between solid phase $HAS_{B(s)}$ and the solution phase could be followed by measuring the change in concentration of Al_r against time and the quasi-equilibrium $[Al_r]$ could then be used in combination with the appropriate formation/dissolution equation to derive a solubility expression. This approach was adopted for $HAS_{B(s)}$ and $Al(OH)_{3(s)}$ when prepared under identical experimental conditions.

2.2. The solubility expression

HAS_B will be the only HAS formed when $[Si(OH)_4]$ is significantly in excess (>2-fold) of [Al] and it will have an idealised stoichiometry of Si:Al of 1.0 [6]. HAS are formed via the competitive condensation of $Si(OH)_4$ at an aluminium hydroxide template [10] and so the dissolution of $HAS_{B(s)}$ might be described by the following idealised equation:

$$HAS_{B(s)} \leftrightarrow 2Al^{3+}_{(aq)} + 2Si(OH)_{4(aq)} + 6OH^- \quad (1)$$

This equation can be used to derive a solubility expression for HAS_B

$$K^*HAS_B = [Al^{3+}]^2[Si(OH)_4]^2[OH^-]^6 \quad (2)$$

K^*HAS_B is written in the form of a solubility product at thermodynamic equilibrium. However, the equation in this form is not directly applicable to the solubility of HAS_B as the solubility of this secondary mineral phase will not be defined by $[Al^{3+}]$ but by $[Al_r]$. It will be this fraction of Al which will be in quasi-equilibrium with $HAS_{B(s)}$ and this will be a precise estimate of how effectively the biological availability of Al is controlled by this solid phase. The determination of $K^*HAS_{B(s)}$ will require the measurement of solution pH, $[Si(OH)_4]$ and $[Al^{3+}]$ ($[Al_r]$). An experimental protocol was designed in which solution pH were determined by a non-invasive buffer, the $[Si(OH)_4]$ were in huge excess such that their concentrations were unaffected by the dissolution of $HAS_{B(s)}$ and $[Al^{3+}]$ ($[Al_r]$) could be estimated using the fluor, morin.

2.3. The measurement of $[Al^{3+}]$ as $[Al_r]$

There are no direct means whereby submicromolar concentrations of Al^{3+} can be measured. We need to obtain a best estimate (Al_r) using as non-invasive a method as is possible and we have used the formation and measurement of the fluorescent morin-Al complex (AlM) for this purpose [17]. We have previously shown that AlM is an excellent estimate of Al_r, the biologically available fraction of Al [18].

The experimental solutions were prepared in ultrapure water (0.067 μS/cm; Elga, High Wycombe, UK) and included a background electrolyte of 100 mmol/L KNO_3. The solutions were buffered at pH 6.5 ± 0.05 using PIPES and included a range of [Al] (0–6 μmol/L) and either 0, 100, 1000 or 2000 μmol/L $Si(OH)_4$. All solutions were prepared at room temperature (20 °C) and pressure using an established method [19]. $Si(OH)_4$ was prepared by cation exchange of a 2 mmol/L Na_4SiO_4 solution and was then substituted for ultrapure water to prepare solutions which contained 100, 1000 or 2000 μmol/L $Si(OH)_4$. Al was added from a certified standard solution (Perkin–Elmer, Beaconsfield, UK). Sodium azide was added to each solution at 0.05% w/v to prevent growth of microorganisms during storage. The solutions were stored in the dark for 12 weeks during which time their AlM fluorescence

was monitored every week using the following protocol. A new morin (2,3,4,5,7-pentahydroxyflavone) stock solution (125 μmol/L) was prepared as required and was added to a 5 mL aliquot of the solution in question to give a morin concentration of 12.5 μmol/L. The concentrations of morin in the stock and experimental solutions were carefully chosen to ensure that only 1:1 complexes of AlM were formed and that the fluorescence signal ($\lambda_{ex} = 420$ nm, $\lambda_{em} = 500$ nm) was optimal for the range of [Al] used [17]. Preliminary experiments showed that the formation of the fluorescent AlM complex plateaued 10–15 min after addition of morin and so the fluorescence intensity of AlM in each solution was measured after 15 min incubation with morin. The time-dependent formation of AlM was indicative of small changes in solution equilibria and further exemplified that what was being measured in the solutions was a fast reactive form of Al (Al_r) and not Al^{3+}. In all of the aged solutions, and particularly so in those which included 2000 μmol/L $Si(OH)_4$, the fluorescence intensity of AlM reached a plateau within the 12 week incubation period.

Following the determination of AlM fluorescence each sample was acidified to 1% concentrated HNO_3 (in the cuvette) and its total [Al] was measured by GFAAS using matrix-matched standards [20]. The procedure of acidifying the sample in the quartz cuvette directly after the measurement of its AlM fluorescence enabled each AlM fluorescence to be directly equated with an absolute (as opposed to nominal) total [Al] and circumvented a number of problems associated with sampling potentially inhomogeneous solutions.

The next step towards obtaining reliable estimates of [Al_r] in equilibrium with $HAS_{B(s)}$ (and $Al(OH)_{3(s)}$) was to convert the measured fluorescence intensities (AlM) into concentrations of morin-available Al (i.e., [Al^{3+}] in the solubility expression and [Al_r] in reality). This was achieved by preparing a calibration curve of AlM versus total [Al] such that the chosen [Al] were all undersaturated with respect to $Al(OH)_{3(amorphous)}$ at pH 6.5 [21]. The latter prerequisite was important in that AlM measured for each total [Al] would be a direct reflection of the proportion of the total morin-available Al or [Al_r]. It is this concept of proportionality which enabled the use of a calibration curve to estimate [Al_r] in each of the samples. Al standards of nominal concentrations 0.1, 0.2, 0.3, 0.4 and 0.5 μmol/L (absolute [Al] were determined by GFAAS following acidification in the cuvette) were prepared in triplicate at pH 6.5 and their corresponding AlM were measured. Linear regression analysis was then applied to AlM recorded for each combination of [Al] and [$Si(OH)_4$] to obtain best estimates of [Al_r] in equilibrium with $HAS_{B(s)}$ and $Al(OH)_{3(s)}$ (Table 2).

Table 2
Concentrations of Al_r (μmol/L) in quasi-equilibrium with solid phases ($Al(OH)_{3(s)}$ and $HAS_{B(s)}$) formed in the presence of 0, 100, 1000 and 2000 μmol/L $Si(OH)_4$ after equilibration for 12 weeks at pH 6.5 and 20 °C and the estimated solubility constants (K^*) for each of the solid phases

[$Si(OH)_4$] (μmol/L)	0	100	1000	2000
	0.250	0.068	0.027	0.018
	0.182	0.088	0.032	0.021
	0.191	0.073	0.027	0.017
	0.236	0.095	0.034	0.016
	0.249			0.017
	0.229			0.018
	0.234			0.017
				0.015
				0.019
				0.016
				0.018
				0.018
				0.017
				0.017
				0.016
				0.014
				0.017
$K^* \pm$ SD	$10^{-30.8 \pm 0.27}$	$10^{-40.3 \pm 0.31}$	$10^{-40.2 \pm 0.20}$	$10^{-40.6 \pm 0.15}$
N	7	4	4	17

3. Results

After 12 weeks ageing at a solution pH of 6.5 and in the absence of added $Si(OH)_4$ [Al_r] in quasi-equilibrium with $Al(OH)_{3(s)}$ increased up to a plateau concentration (mean ± SD; 224.4 ± 27.15 nmol/L; $n = 7$) which was reached at between 2.0 and 4.0 μmol/L total Al (Fig. 1 and Table 2). The presence of 2000 μmol/L $Si(OH)_4$ completely abolished any dose-response to increasing total [Al] and the equilibrium [Al_r] reached a plateau (mean ± SD; 17.2 ± 1.57 nmol/L; $n = 17$) from the low-

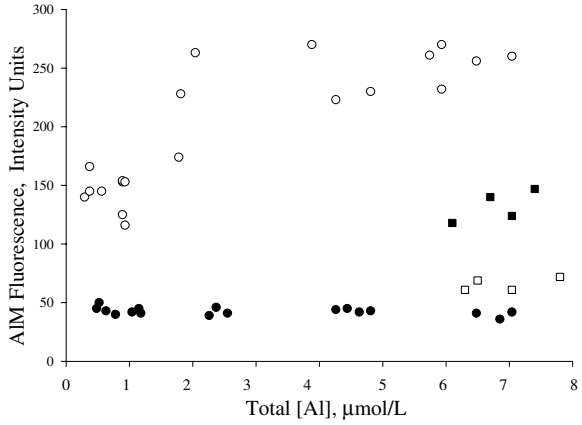

Fig. 1. Morin-available Al (AlM) in quasi-equilibrium with total Al at pH 6.5 in the presence of; 0 (open circles); 100 (closed squares); 1000 (open squares) and 2000 (closed circles) μmol/L $Si(OH)_4$ after 12 weeks ageing.

est measured total [Al]. Thus, relative to a system in which hydroxide was the major ligand for Al, the additional presence of $Si(OH)_4$ significantly reduced the concentration of [Al_r] at each of the [Al] tested (Fig. 1 and Table 2). A limited number of additional solutions in which the initial [Al] was ca. 6.0 μmol/L and [$Si(OH)_4$] were 100 and 1000 μmol/L resulted in quasi-equilibrium [Al_r] of 80.9 ± 12.25 ($n = 4$) and 30.2 ± 3.38 ($n = 4$) nmol/L, respectively, and showed that the quasi-equilibrium [Al_r] was dependent upon [$Si(OH)_4$].

The individual data for each of the solutions used to compute the mean equilibrium [Al_r] were then used to determine the solubilities (K^*) for $Al(OH)_{3(s)}$ (0 $Si(OH)_4$) and $HAS_{B(s)}$ (100, 1000 and 2000 μmol/L $Si(OH)_4$). When these data were substituted into the 'classical' solubility expression for $HAS_{B(s)}$ (i.e., Eq. (2)) the computed K^*s were extremely low (10^{-60}) and unrealistically so in comparison to K^* computed for $Al(OH)_{3(s)}$ (10^{-25}). Whilst the raw data confirmed that $HAS_{B(s)}$ was less soluble than $Al(OH)_{3(s)}$ the difference could not be by the orders of magnitude suggested by the computed K^*s. The value for $K^*HAS_{B(s)}$ was, in particular, heavily biased by the contribution of OH^- from the assumed dissolution of two moles of $Al(OH)_{3(s)}$ via the prior dissolution of only one mole of $HAS_{B(s)}$ (see Eq. (1)). It was clear from the fluorescence data that $HAS_{B(s)}$ was significantly more insoluble than $Al(OH)_{3(s)}$ since it reduced the quasi-equilibrium [Al_r] from ca. 224 to 17 nmol/L. The problem was in attributing a realistic K^* to the observed decrease in solubility. The solution may reside in not treating the solubility of $HAS_{B(s)}$ in the orthodox manner described in Eqs. (1) and (2) but to write a solubility expression which will take into account the incongruent dissolution of $HAS_{B(s)}$. In particular, that $HAS_{B(s)}$ initially dissolved to release only one solution species ($Si(OH)_4$) and that it would be the environmental concentration of this species, via the common ion effect, which would dictate $HAS_{B(s)}$ solubility at any one pH. Thus, a solubility expression was required which would include the contribution of [$Si(OH)_4$] and an estimate of [Al_r] at the experimental pH.

If $HAS_{B(s)}$ was treated as an hydroxide of an aluminosilicate the following hypothetical dissolution equation could be written:

$$Al_2Si_2O_5(OH)_4 \leftrightarrow Al_2O^{4+} + 2SiO_2 + 4OH^- \quad (3)$$

Whilst neither Al_2O^{4+} nor SiO_2 are true products of the dissolution of $HAS_{B(s)}$ these theoretical forms are convenient in that they can be substituted for [Al^{3+}] and [$Si(OH)_4$] in the 'classical' solubility expression without sacrificing electroneutrality and they better reflect the known non-stoichiometric dissolution of $HAS_{B(s)}$. The latter is further supported by the inclusion of only four moles of OH^- which again, will accurately reflect that the dissolution of $HAS_{B(s)}$ would not necessarily involve the further dissolution of two moles of $Al(OH)_{3(s)}$.

The solubility expression might now be written as

$$K^*Al_2Si_2O_5(OH)_4 = [Al_2O^{4+}][SiO_2]^2[OH^-]^4 \quad (4)$$

or, substituting in Al_r and $Si(OH)_4$

$$K^*HAS_B = [Al_r][Si(OH)_4]^2[OH^-]^4 \quad (5)$$

This solubility expression is neither balanced stoichiometrically nor electrically neutral, however, when this expression was applied to data for [Al_r] estimated in the presence of each of the [$Si(OH)_4$] at pH 6.5 (see Table 2) the computed solubility product for 2000 μmol/L $Si(OH)_4$ was $10^{-40.6 \pm 0.15}$ ($n = 17$) (20 °C/$I = 0.1$ mol/L) and those for 1000 and 100 μmol/L were not significantly different to this value (Table 2). The fact that the K^*s for each [$Si(OH)_4$] were not significantly different from each other does suggest that the unorthodox manner by which they were computed may have some validity. However, the validity of the method would be further supported if it also predicted a reliable estimate for the solubility of $Al(OH)_{3(s)}$. Applying the same criteria (i.e., $Al(OH)_{3(s)}$ is treated as the hydroxide of an hypothetical dimeric aluminium oxide) to data for [Al_r] in the absence of added $Si(OH)_4$ at pH 6.5

$$Al_2O(OH)_4 \leftrightarrow Al_2O^{4+} + 4OH^- \quad (6)$$

We get the solubility expression for $Al(OH)_{3(s)}$

$$K^*Al_2O(OH)_4 = [Al_2O^{4+}][OH^-]^4 \quad (7)$$

This gives a $K^* = 10^{-30.8 \pm 0.27}$ ($n = 7$) (20 °C/$I = 0.1$ mol/L) which considering it is for an aluminium hydroxide phase which has been aged for only 12 weeks is reassuringly similar to the literature value for $Al(OH)_{3(gibbsite)}$ of $10^{-33.9}$ [22].

4. Discussion

When the solubilities of Al at pH 6.5 in the presence and absence of a significant excess of $Si(OH)_4$ were compared it was found that the solid phase formed in the presence of $Si(OH)_4$ was significantly less soluble. Al solubility appeared to be related to [$Si(OH)_4$] such that solubility was reduced at higher concentrations of $Si(OH)_4$. The insoluble phase formed in the presence of $Si(OH)_4$ was an HAS which we have previously called HAS_B [6]. The task was to ascribe a credible solubility (K^*) to $HAS_{B(s)}$ based upon the experimental data. The difficulty was in writing a dissolution equation for $HAS_{B(s)}$ which would accurately reflect the non-stoichiometric dissolution of this secondary mineral and enable the formulation of a representative solubility expression. In particular, the solubility expression must have included a component which took strict account of the influence

of $[Si(OH)_4]$ on the measured Al solubility. The chosen solubility expression (see Eq. (4)) was based upon a dissolution equation which though it included hypothetical dissolution products (Al_2O^{4+}, SiO_2) was considered to be a good estimate of the stoichiometries (1:2:4) of the expected dissolution products (Al_r, $Si(OH)_4$, OH^-). In particular, the solubility expression emphasised the relative importance of $[Si(OH)_4]$ over $[Al_r]$ and the computed K^* for $HAS_{B(s)}$ of $10^{-40.6\pm0.15}$ ($n = 17$) was found to be independent of $[Si(OH)_4]$ (Table 2). Further validation of this unconventional approach towards the computation of the solubility of secondary mineral phases was offered by the value computed for $Al(OH)_{3(s)}$ of $10^{-30.8\pm0.27}$ ($n = 7$) which was in line with the literature value for $Al(OH)_{3(gibbsite)}$ of $10^{-33.9}$ [22]. For example, for a solution at pH 5.0, the solubility expression used herein to describe the dissolution of $Al(OH)_{3(s)}$ and the corresponding computed K^* predict a soluble [Al] of ca. 37.0 μmol/L as compared to the literature values of ca. 50.1 μmol/L and 1.6 μmol/L for $Al(OH)_{3(amorphous)}$ ($K_{Sol} = 10^{10.7}$) and $Al(OH)_{3(gibbsite)}$ ($K_{Sol} = 10^{9.2}$), respectively [21].

The concentration of Al which was in quasi-equilibrium with either $Al(OH)_{3(s)}$ or $HAS_{B(s)}$ was measured by its interaction with an excess of morin over a 15 min period of incubation. Denoted herein as $[Al_r]$ it was only an estimate of $[Al^{3+}]$ and so could not be used to derive a solubility product (K_{SP}) which, conventionally, would require that $[Al^{3+}]$ at thermodynamic equilibrium was known. The solubility expressions for $Al(OH)_{3(s)}$ and $HAS_{B(s)}$ determined using $[Al_r]$ are likely to over estimate their solubilities at thermodynamic equilibrium though they may still be useful in predicting solubility control by secondary mineral phases in the natural environment where thermodynamic equilibrium is rarely approached. For example, if K^*HAS_B was used to predict Al solubility control in the natural environment we would find a strict reliance upon the environmental $[Si(OH)_4]$. For example, in a soil solution at pH 4.0, a fall in $[Si(OH)_4]$ from 2000 through 1000 to 100 μmol/L would predict an increase in soluble [Al] from ca. 4.0 through 15.0 to 1500.0 μmol/L. The latter [Al] is approximately equivalent to that predicted by $Al(OH)_{3(gibbsite)}$ at the same pH and this is a good demonstration of how the environmental $[Si(OH)_4]$ may contribute towards the solubility of $HAS_{B(s)}$. At a soil pH of 5.0 the same reductions in $[Si(OH)_4]$ would result in the soluble [Al] increasing from ca. 0.4 through 1.5 to 150 nmol/L. The latter [Al] is ten times lower than that predicted by $Al(OH)_{3(gibbsite)}$ (ca. 1.6 μmol/L) and this is an excellent demonstration of how the influence of $[Si(OH)_4]$ can be reinforced at less acidic pH.

It should be possible to test the validity of our estimate of the solubility of $HAS_{B(s)}$ in the natural environment. If we consider that this phase will form in any environment in which $[Si(OH)_4] \gg [Al]$ then it should be the predominant secondary mineral phase for Al in all but the most acidified catchments, such as those impacted by acidic deposition. We are not aware from the literature of other reported solubility products for an HAS with a Si:Al ratio of 1.0 and so we have nothing to compare it with. There have been a number of attempts to ascribe an equilibrium constant to the solubility of imogolite-like phases [23] in which the Si:Al ratio is 0.5 (similar to HAS_A) and these have predicted a solubility somewhere between $Al(OH)_{3(amorphous)}$ and $Al(OH)_{3(gibbsite)}$. This type of HAS will only be formed in environments in which $[Si(OH)_4] \leqslant [Al]$ and so it will only be important in limiting the solubility of Al in, for example, environments undergoing a progressive acidification. We found that the dissolution of HAS_A was, like HAS_B, also incongruent (see Table 1) and that the solubility of Al was initially dependent upon the release of $Si(OH)_4$. For this reason it is probable that previous measurements based upon solubility equations expressing stoichiometric dissolution of $Si(OH)_4$ and Al will have under-estimated the insolubility of HAS_A, though this remains to be confirmed by experiment.

$K^*HAS_{B(s)}$ cannot be used to predict the formation of HAS in the natural environment. For example, at pH 4.0 it is not possible to make a saturated solution of HAS_B by adding Al to a 2000 μmol/L $Si(OH)_4$ solution such that the total [Al] > 4.0 μmol/L. The formation of both HAS_A and HAS_B will require as a prerequisite the formation of an $Al(OH)_3$ template and as such is dependent upon the prior formation of a saturated solution of $Al(OH)_3$. At pH 4.0 the latter will only form at [Al] greater than 1000 μmol/L and only then in the absence of competitive ligands such as organic acids [24] or inorganic anions such as fluoride and phosphate.

It is clear from our attempts to quantify the solubility of $HAS_{B(s)}$ that this is neither a trivial task nor one that is immediately accessible to conventional solubility expressions. Our unconventional approach in which we have tried to take account of the incongruent dissolution of HAS has used the concentration of a fast-reactive form of Al (Al_r) at a predefined quasi-equilbrium to determine a solubility expression for $HAS_{B(s)}$ which may prove to be useful in identifying Al solubility control (and hence, the biological availability of Al) in the natural environment. HAS are integral to the cycling and recycling of Al in the lithospheric cycle [1] and only where the environmental $[Si(OH)_4]$ is significantly depleted, such as will happen during catchment acidification [10], will this geochemical control of the biological availability of Al be lost to allow the accumulation of Al in biota.

Acknowledgements

This research was funded by EPSRC, NERC and The Royal Society.

References

[1] C. Exley, J. Inorg. Biochem. 97 (2003) 1.
[2] T. Pačes, Geochim. Cosmochim. Acta 42 (1978) 1487.
[3] V.C. Farmer, W.J. McHardy, L. Robertson, A. Walker, M.J. Wilson, J. Soil Sci. 36 (1985) 87.
[4] C. Neal, R.J. Williams, J. Hydrol. 97 (1988) 347.
[5] J.P. Gustafsson, D. Berggren, M. Simonsson, M. Zysset, J. Mulder, Eur. J. Soil Sci. 52 (2001) 655.
[6] F.J. Doucet, C. Schneider, S.J. Bones, A. Kretchmer, I. Moss, P. Tekely, C. Exley, Geochim. Cosmochim. Acta 65 (2001) 2461.
[7] C. Exley, C. Schneider, F.J. Doucet, Coord. Chem. Rev. 228 (2002) 127.
[8] P. Cradwick, V.C. Farmer, J. Russell, C. Masson, K. Wada, N. Yoshinaga, Nat. Phys. Sci. 240 (1972) 187.
[9] F.J. Doucet, M. Rotov, C. Exley, J. Inorg. Biochem. 87 (2001) 71.
[10] C. Exley, J. Inorg. Biochem. 69 (1998) 139.
[11] J.P. Gustafsson, D.G. Lumsdon, M. Simonsson, Clay Miner. 33 (1998) 77.
[12] V.C. Farmer, Eur. J. Soil Sci. 50 (1999) 713.
[13] M. Zysset, P. Blaser, J. Luster, A. Gehring, Soil Sci. Soc. Am. J. 63 (1999) 1106.
[14] V.C. Farmer, D.G. Lumsdon, Eur. J. Soil Sci. 52 (2001) 177.
[15] F. Gerard, M. Francois, J. Ranger, Geoderma 107 (2002) 197.
[16] H.W. Nesbitt, I.J. Muir, Nature 334 (1988) 336.
[17] B.A. Browne, J.G. McColl, C.T. Driscoll, J. Environ. Qual. 19 (1990) 65.
[18] C. Exley, J.D. Birchall, J. Inorg. Biochem. 63 (1996) 241.
[19] C. Exley, J.D. Birchall, Polyhedron 12 (1993) 1007.
[20] C. Schneider, C. Exley, J. Inorg. Biochem. 87 (2001) 45.
[21] R.B. Martin, Clin. Chem. 32 (1986) 1797.
[22] H.M. May, P.A. Helmke, M.L. Jackson, Geochim. Cosmochim. Acta 43 (1979) 861.
[23] D.G. Lumsdon, V.C. Farmer, Eur. J. Soil Sci. 46 (1995) 179.
[24] D. Berggren, J. Mulder, Geochim. Cosmochim. Acta 59 (1995) 4167.

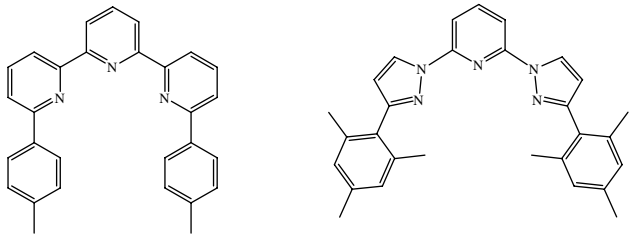

L^1 L^2

Scheme 1. Ligands examined in this study.

potassium salt of *p*-Me-acetophenone in THF, before addition of ammonium acetate and acetic acid, suitable work-up and recrystallisation from dichloromethane/hexane afforded the product as an off-white powder (Scheme 2).

Reaction of L^1 with $FeCl_2$ in THF at room temperature yielded an almost insoluble grey-purple powder whose elemental analysis and infrared spectrum ($\nu_{Fe-Cl} = 304\ cm^{-1}$) are consistent with the formulation L^1FeCl_2. Attempts to recrystallize this powder from warm THF under an inert atmosphere did lead to violet crystals with the same infrared spectrum than the starting material ($\nu_{Fe-Cl} = 304\ cm^{-1}$) formed just over the solution and an orange microcrystalline complex in the solution. The two different crystals were however unsuitable for X-ray analysis. The orange microcrystalline complex seems to result in fact from the conversion of the violet one, and its formation looks reversible. It gives rise to two ν_{Fe-Cl} absorptions at 326 and 307 cm^{-1}, as well as additional bands assignable to bound THF ($\nu_{C-O} = 1028\ cm^{-1}$), and corresponds probably to the THF adduct $L^1FeCl_2(THF)$. In an attempt to obtain better crystals for an X-ray investigation, we heated the orange microcrystalline complex in THF over a longer period of time and at higher temperatures. Thus bigger orange crystals were obtained with other products. The strong IR absorption at 378 cm^{-1}, character-

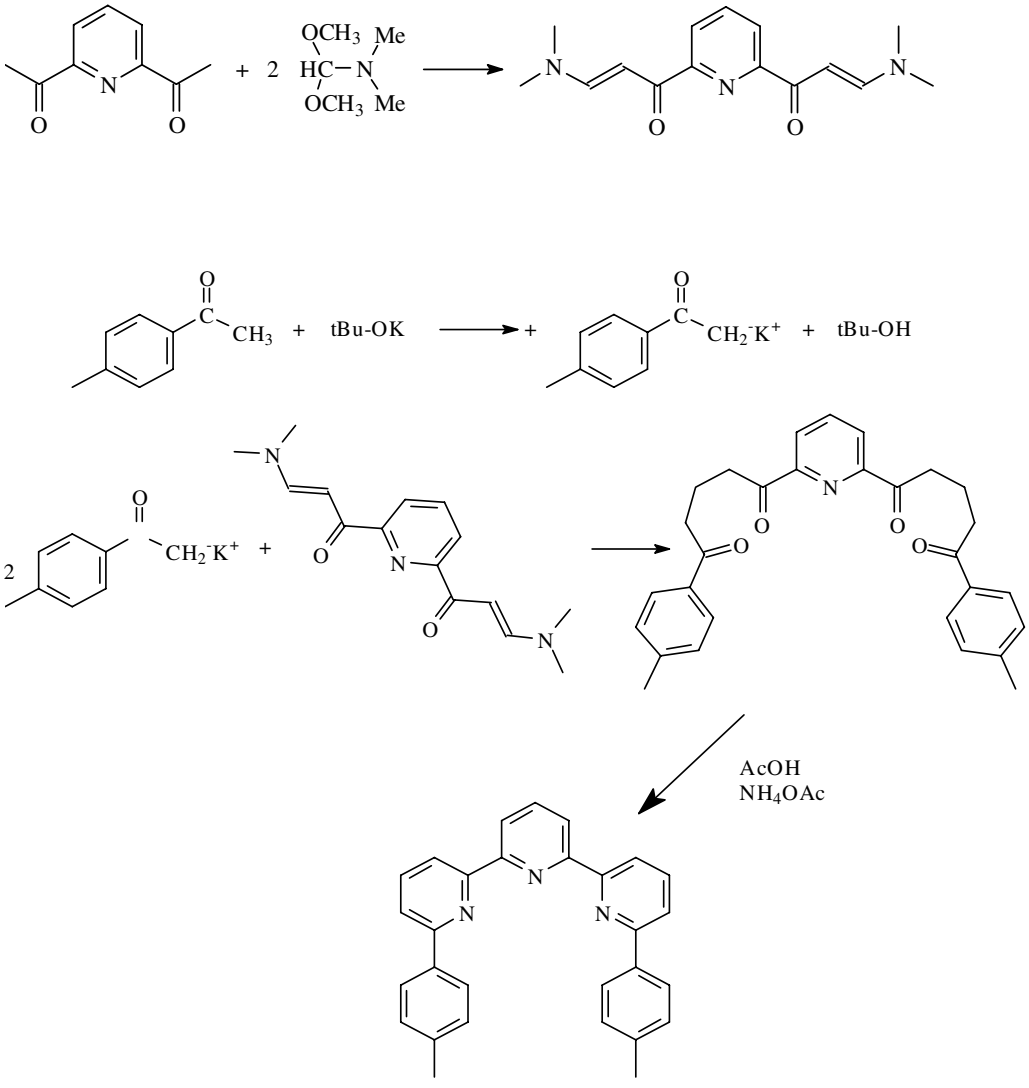

Scheme 2. Synthesis of L^1.

istic of the iron (III) anion $FeCl_4^-$ [5], indicated that we were in the presence of a third complex. An X-ray diffraction study allowed us to confirm this conclusion and to identify this complex as $(L^1)_2Fe^{2+}(FeCl_4^-)_2$. The highly distorted and compressed molecular structure of the iron (II) cation (Fig. 1) is close to that of the analogous complex containing ligands 6,6″-diphenyl-2,2′:6′,2″-terpyridine [6]. Most notably, the long iron–nitrogen bonds are indicative of a high-spin complex and the observation of two even longer distances of 2.422 Å between iron and the nitrogen atom of one of the two lateral pyridyl units of each terpyridine ligand suggests that these two ligands may be considered as only bidentate. Extensive intramolecular π-stacking of the phenyl and pyridyl rings is also remarkable [6]. The structure of the $FeCl_4^-$ anions is unexceptional [5]. The oxidizing agent at the origin of their formation could not be identified. In our case, partial oxidation by accidental air introduction could be favoured by the longer heating period. The presence of the paramagnetic $FeCl_4^-$ counter anion obviously only little modifies the ^1H NMR spectrum of the paramagnetic cationic complex, which remains close to that of the previously reported analogous species that had diamagnetic perchlorate counteranions [6].

Ligand 2,6-bis(3-Mes-*N*-pyrazolyl)pyridine (L^2) [7] was synthesized following the methods reported previously and coordinated to iron (II) chloride by the procedure described for L^1. This afforded a yellow precipitate. The iron-chlorine stretching vibration is found at 308 cm^{-1} for the yellow complex obtained, for which formula L^2FeCl_2 can hence be assigned with some confidence. Again, however, dissolution in MeCN (r.t.) or in THF (70 °C) leads to conversion of this neutral complex into its ionic form $(L^2)_2Fe^{2+}FeCl_4^{2-}$. No important colour change is observed in this case, but the IR absorption assigned to iron–chlorine stretching is shifted to 282 cm^{-1} (the approximate position of the $FeCl_4^{2-}$ anion [5]) for the yellow crystalline solid obtained from these solutions.

The precise nature of complex $(L^2)_2Fe^{2+}FeCl_4^{2-}$ was established by X-ray crystallography at room temperature because a lower temperature destroys the crystal. We could not find a greater symmetry for this crystal so we are in presence of the not centered Pn group not either chiral these explains the rather bad xflack value obtained. The unit cell contains two independent dications whose octahedral coordination geometry and overall structural parameters (Fig. 2) are similar to those of the corresponding cobalt (II) [8a], nickel (II) [8a] and copper (II) [8b] complexes and recently the iron analogue has been described with PF_6^- as the counter anion [8c]. In particular, the two mesityl rings of each ligand are π-stacked with the pyridine ring of the other ligand.

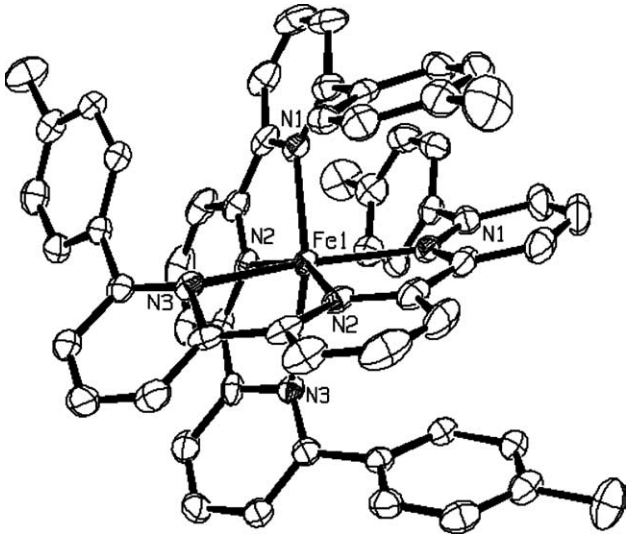

Fig. 1. Ortep view and numbering scheme of the C_2-symmetric cationic part of compound $(L^1)_2Fe^{2+}(FeCl_4^-)_2$ at 173 K (50% probability thermal ellipsoids). Hydrogen atoms are omitted for clarity. Selected bond lengths (Å) and bond angles (°): Fe1–N1 = 2.227(3), Fe1–N2 = 2.100(3), Fe1–N3 = 2.422(3), N1–Fe1–N1 = 89.0(2), N1–Fe1–N2 = 75.1(1), N1–Fe1–N2 = 124.2(1), N1–Fe1–N3 = 147.3(1), N1–Fe1–N3 = 103.3(1), N2–Fe1–N2 = 155.3(2), N2–Fe1–N3 = 73.0(1), N2–Fe1–N3 = 88.4(1), N3–Fe1–N3 = 82.6(1).

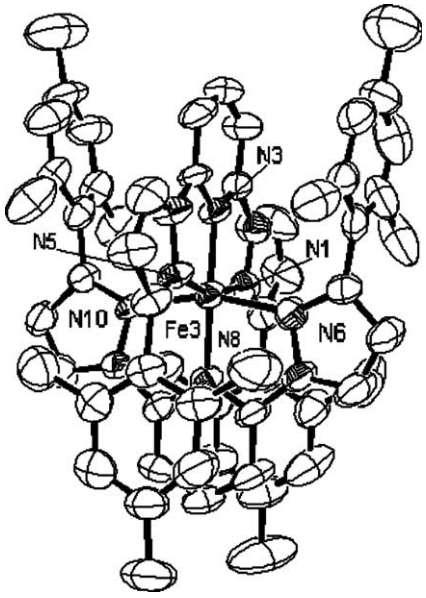

Fig. 2. Ortep view and numbering scheme of one of the two independent dications in the crystal of $(L^2)_2Fe^{2+}FeCl_4^{2-}$ at 293 K (50% probability thermal ellipsoids). Hydrogen atoms are omitted for clarity. Selected bond lengths (Å) and bond angles (°): Fe3–N1 = 1.987(8), Fe3–N3 = 1.874(7), Fe3–N5 = 1.999(8), Fe3–N6 = 2.015(6), Fe3–N8 = 1.883(7), Fe3–N10 = 1.962(6), N1–Fe3–N3 = 81.2(4), N1–Fe3–N5 = 161.7(3), N1–Fe3–N6 = 91.7(3), N1–Fe3–N8 = 98.0(3), N1–Fe3–N10 = 91.3(3), N3–Fe3–N5 = 80.6(4), N3–Fe3–N6 = 99.2(3), N3–Fe3–N8 = 178.7(3), N3–Fe3–N10 = 99.9(3), N5–Fe3–N6 = 90.0(3), N5–Fe3–N8 = 100.2(3), N5–Fe3–N10 = 93.0(3), N6–Fe3–N8 = 79.8(3), N6–Fe3–N10 = 160.9(3), N8–Fe3–N10 = 81.1(3).

Much shorter Fe–N bond distances than in $(L^1)_2Fe^{2+}$ (Fig. 1) indicate however that this complex is low-spin [9], while the cobalt complex is high-spin over a wide temperature range. Furthermore, the parent iron (II) complex containing two non-substituted ligands 2,6-bis(*N*-pyrazolyl)pyridine is low-spin only at low temperature and if the counteranion is BF_4^-, and becomes high-spin at room temperature [10]. The low-spin nature of complex $(L^2)_2Fe^{2+}$ is hence rather unexpected since incorporation of sterically demanding substituents adjacent to the ligand donor atoms, as well as higher temperatures, are known to favour high-spin states [5,11]. The paramagnetic counteranions $FeCl_4^{2-}$ play possibly an important role in this behaviour. By comparison with the crystal structure of the low-spin parent complex [10a], it can be concluded that the introduction of the mesityl substituents on the pyrazolyl rings only slightly lengthens the Fe–N_{pz} bonds (+0.011 Å average) and shortens the Fe–N_{py} bonds (−0.014 Å average).

Although of very similar geometry, the two independent dications show distinctive distortions that are visualized in Fig. 3. In the one already presented in Fig. 2, the two bispyrazolylpyridine ring systems are nearly planar, the three π-stacked aryl rings are almost perfectly eclipsed, and one ligand is coordinated much more asymmetrically than the other (Fe3–N6 = 2.015(6) Å, Fe3–N10 = 1.962(6) Å, Fig. 2). This latter difference is less pronounced in the second molecule, in which a slight deviation from planarity is indeed observed for both bispyrazolylpyridine ring systems. The individual aromatic rings remain planar, but the two pyrazolyl rings of a given ligand are twisted towards each side of the adjacent pyridine plane. The average dihedral angle between the pyrazolyl planes and the pyridine ones is 5.1°. This causes the corresponding mesityl substituents and the pyridine ring with which they are π-stacked to become significantly staggered (Fig. 3). Finally, the $FeCl_4^{2-}$ high-spin dianion [12] exists as well as two independent molecules that show ca. 0.11 Å longer Fe–Cl bond distances than the $FeCl_4^-$ anions of complex $(L^1)_2Fe^{2+}(FeCl_4^-)_2$. One of them is also more dissymmetric than the other.

Reacting ligand L^2 with iron (III) chloride (1 equiv) in MeCN is followed by partial reduction of the metal centers and formation of the same dicationic iron (II) complex in combination with the iron (III) counteranions $FeCl_4^-$. No neutral precursor could be detected, and a fraction (≈1/3) of the initial ligand L^2 remains uncomplexed in the reaction mixture. We obtained this result when the reaction was carried out at 70 °C and we verified that the same result is obtained when the reaction was done at room temperature. Brown-red crystals of the solvated complex $(L^1)_2Fe^{2+}(FeCl_4^-)_2(THF)_4$ were obtained when the crude product is dissolved in THF at room temperature, nice crystals were produced, and were analyzed by infrared spectroscopy (ν_{Fe-Cl} = 380 cm^{-1}) and X-ray crystallography.

All these complexes (mono or bis ligands) were tested for the polymerization of ethylene in the presence of methylaluminoxane. Although for the bis ligand complexes the results were in some way expected [13], none of them produced polymers.

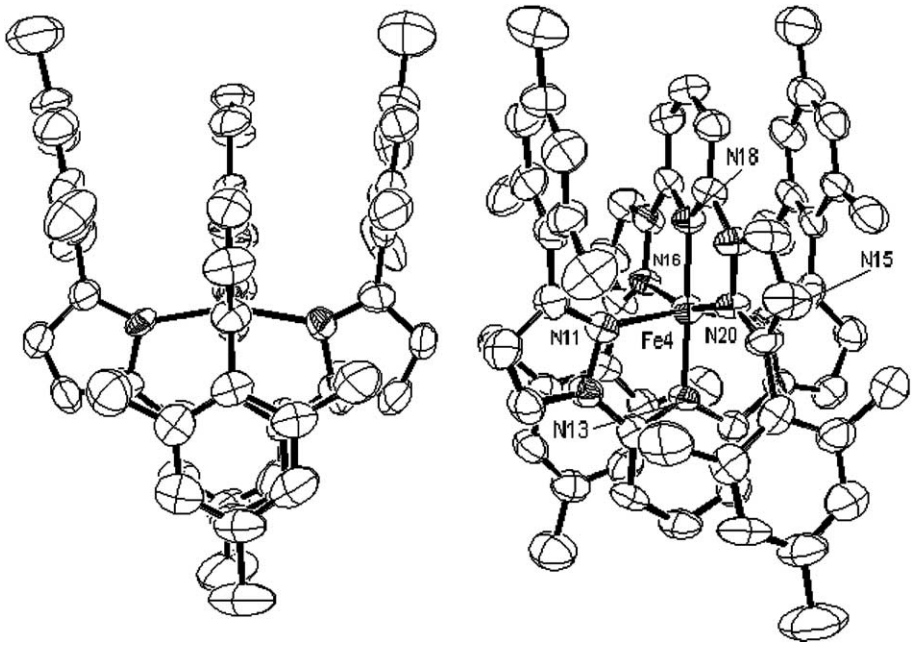

Fig. 3. Ortep view of the two independent dications in the crystal of $(L^2)_2Fe^{2+}FeCl_4^{2-}$ at 293 K (50% probability thermal ellipsoids). Hydrogen atoms are omitted for clarity. The left hand molecule is the one already shown in Fig. 2. Selected bond lengths (Å) for the right hand molecule: Fe4–N11 = 1.998(7), Fe4–N13 = 1.893(7), Fe4–N15 = 1.983(7), Fe4–N16 = 1.988(6), Fe4–N18 = 1.889(6), Fe4–N20 = 1.967(6).

3. Experimental

3.1. General

As the inorganic compounds described herein are air-sensitive, all experiments were performed in a glove box under controlled nitrogen atmosphere. THF, diethyl ether, pentane were dried over Na-benzophenone and acetonitrile over CaH_2 before distillation under nitrogen. Anhydrous $FeCl_2$ (Strem) and $FeCl_3$ were used as purchased. Ligand L^2 was synthesized according to procedures described previously in the literature [8]. ^1H NMR spectra were recorded on Bruker AC-200 or Avance-300 spectrometers at ambient temperature, chemical shifts are reported in parts per million versus $SiMe_4$ and were determined by reference to the residual solvent peaks. The infrared spectra were recorded on a Perkin–Elmer 1650 FT instrument. Mass spectrum was performed by the Service de Spectrométrie de Masse de l'Institut Le Bel (Strasbourg) and elemental analysis by the Service de Microanalyse de l'Institut Charles Sadron (Strasbourg).

3.2. Synthesis

3.2.1. Synthesis of ligand L^1

tert-BuOK (2 g, 17.8 mmol) and *p*-methylacetophenone (1 g, 7.4 mmol) were dissolved in 40 mL of THF at room temperature. After 2 h, 2,6-bis(3-chlorodimethylaminium-1-oxopropyl)pyridine (1 g, 3.7 mmol) was added. After 8 h, 10 g of ammonium acetate, and 14 mL of acetic acid were added to the red solution to yield a yellow solution. The solution was refluxed for 24 h. The solvent was evaporated under vacuum and the acid was neutralized by addition of an aqueous saturated solution of sodium hydrogenocarbonate. The product was extracted with dichloromethane (three times 100 mL) and filtered over a neutral alumina column. After evaporation of the solvent, the solid residue was recrystallized from CH_2Cl_2/hexane to afford a greyish powder. Yield 600 mg (40%). ^1H NMR ($CDCl_3$, 300 MHz): δ 8.70 (2H, d, J 8 Hz, H^3), 8.59 (2H, d, J 8 Hz, $H^{3'}$), 8.09 (4H, d, J 8 Hz, H^0), 8.01 (1H, t, J 8 Hz, H^4), 7.92 (2H, t, J 8 Hz, $H^{4'}$), 7.78 (2H, d, J 8 Hz, $H^{5'}$), 7.33 (4H, d, J 8 Hz, H^m) 2.44 (6H, s, Me). IR (CsI, Nujol) ν (cm^{-1}): 1567.5, 1461.8, 1377.0, 794.7. MS (FAB) m/z: 414.2.

3.2.2. Synthesis of $FeCl_2[L^1]$

$FeCl_2$ (32 mg, 0.25 mmol) and one equivalent of L^1 (103 mg, 0.25 mmol) were maintained under magnetic stirring in 12 mL of THF at room temperature for 24 h. The dark suspension was then isolated and washed with 2 mL of THF affording 107 mg (80%, yield) of a dark powder. IR ν_{Fe-Cl}: 304 cm^{-1}. *Anal.* Calc. for $C_{29}N_3H_{23}FeCl_2$: C, 64.47; H, 4.29; N, 7.78. Found: C, 64.44; H, 4.31; N, 7.65%.

3.2.3. Synthesis of $FeCl_2[L^1][THF]$

$FeCl_2$ [L^1] (50 mg, $9.25.10^{-2}$ mmol) of a dark powder very sparingly soluble with 10 mL of THF were heated at 90 °C in an oil bath in a 50 mL closed screw cap bottle and PTFE-faced rubber liner. Two kinds of crystals were produced by this way, none of them were suitable for an X-ray study. Ones were very small orange crystals attributed to $FeCl_2[L^1][THF]$, with ν_{Fe-Cl}: 307 and 326 cm^{-1} and ν_{C-O}(THF): 1028 cm^{-1}. The other ones were violet crystals produced at the interface of the liquid and were identical to the starting product.

3.2.4. Synthesis of $Fe[L^1]_2^{2+}[FeCl_4]_2^-$

In order to obtain crystals suitable for an X-ray investigation, five tightly closed flasks containing each 10 mg of the complex $FeCl_2[L^1][THF]$ with 2 mL of THF were heated at 120 °C over a long period of time (several days). At this temperature, only a little part of the complex was in solution which was only very slightly colored. By this way, big enough orange crystals were obtained that revealed to be $Fe[L^1]_2{}^{2+}[FeCl_4]_2{}^-$ of the same color than the starting complex that was still present in some amount (confirmed by infrared), as well as other compounds that could not be characterized.

^1H NMR (CDCl3, 300 MHz): δ: 77.45 (2H, s, H^3/H^5), 67.62 (2H, s, $H^{3\prime}$), 58.19 (2H, s, H^3/H^5), 14.42 (2H, s, H^4), 1.87 (6H, s, Me), 0.78 (8H, large, Ar_{tol}), −19.21 (1H, s, $H^{4'}$). IR (CsI, Nujol) ν_{Fe-Cl}: 378 cm^{-1}. ES+MS in $CHCl_3$: gives the isotopic pattern with the corresponding intensities for the dicationic fragment in good agreement with the simulation: $[FeN_6C_{58}H_{46}]^{2+}$: m/z: 440.15, 440.65, 441.15, 441.65, 442.15, and 442.65.

3.2.5. Synthesis of $FeCl_2[L^2]$

$FeCl_2$ (32 mg, 0.25 mmol) and one equivalent of L^2 (112 mg, 0.25 mmol) were maintained under magnetic stirring in 12 mL of THF at room temperature for 12 h. The amorphous yellow complex in suspension were then isolated and washed with 2 mL of THF affording 125 mg (87%, yield) of a yellow powder. IR ν_{Fe-Cl}: 308 cm^{-1}.

3.2.6. Synthesis of $Fe[L^2]_2^{2+}[FeCl_4]_2^-$

About 100 mg of the yellow powder $FeCl_2[L^2]$ was heated up in 10 mL of THF at 80 °C for 4 h.The solution is only slightly colored and an almost quantitative amount of orange crystals are formed. IR ν_{Fe-Cl}: 282 cm^{-1}.

3.2.7. Synthesis of $Fe[L^2]_2^{2+}[FeCl_4]_2^- \cdot 4THF$

$FeCl_3$ (40 mg, 0.25 mmol) was poured into 20 mL of acetonitrile, then one equivalent of L^2 (112 mg, 0.25 mmol) was added and the mixture was maintained under magnetic stirring for 2 h. Some product remained insoluble. Heating at 80 °C completed the dissolution. After cooling, a product crystallized, the IR revealed the unreacted ligand L^2. After separation of excess L^2 and evaporation of the solvent under vacuum a yellow

Table 1
X-ray experimental data for compounnds $(L^1)_2Fe^{2+}(FeCl_4^-)_2$, $(L^2)_2Fe^{2+}FeCl_4^{2-}$ and $(L^2)_2Fe^{2+}(FeCl_4^-)_2 \cdot 4(THF)$

	$(L^1)_2Fe^{2+}(FeCl_4^-)_2$	$(L^2)_2Fe^{2+}FeCl_4^{2-}$	$(L^2)_2Fe^{2+}(FeCl_4^-)_2 \cdot 4(THF)$
Empirical formula	$C_{58}H_{46}Fe_3N_6Cl_8$: $C_{58}H_{46}FeN_6 2FeCl_4$	$C_{58}H_{58}Fe_2N_{10}Cl_4$: $C_{58}H_{58}FeN_{10}FeCl_4$	$C_{74}H_{90}Cl_8Fe_3N_{10}O_4$: $C_{58}H_{58}FeN_{10}2FeCl_4 4C_4H_8O$
Formula weight	1278.22	1148.68	1634.77
Temperature (K)	173	293	173
Crystal system	monoclinic	monoclinic	monoclinic
Space group	*C*12/*c*1	*P*1*n*1	*C*1*c*1
a (Å)	26.5117(4)	11.3497(2)	14.9889(3)
b (Å)	14.1544(2)	23.8420(4)	23.9306(5)
c (Å)	15.9627(3)	21.0341(5)	21.7798(4)
β (°)	110.183(5)	99.606(5)	94.106(5)
V (Å^3)	5622.3(2)	5612.0(2)	7792.2(3)
Z	4	4	4
Color	orange	orange	brown
Crystal size (mm)	$0.20 \times 0.15 \times 0.08$	$0.16 \times 0.12 \times 0.10$	$0.16 \times 0.12 \times 0.09$
$D_{calc.}$(g cm^{-3})	1.51	1.36	1.39
F(000)	2600	2384	3400
Absorption coefficient (mm^{-1})	1.189	0.755	0.879
Index ranges	$-36 \leqslant h \leqslant 36$, $-17 \leqslant k \leqslant 19$, $-21 \leqslant l \leqslant 21$	$-13 \leqslant h \leqslant 13$, $-30 \leqslant k \leqslant 28$, $-27 \leqslant l \leqslant 27$	$0 \leqslant h \leqslant 20$, $0 \leqslant k \leqslant 32$, $-29 \leqslant l \leqslant 29$
θ Range (°)	2.5–29.12	2.5–27.46	2.5–29.08
Reflections collected	13617	21543	10620
Reflections observed [$I > 3\sigma(I)$]	4793	4725	6318
Number of variables	339	1331	890
Trans. min and max	0.9613/1.1570	0.884/0.927	0.8950/1.0000
R	0.050	0.034	0.046
R_w	0.087	0.035	0.067
Goodness-of-fit on F^2	1.531	1.007	1.261
Largest difference peak and hole (e Å^{-3})	0.502	0.191	0.200

brown compound was obtained. The IR revealed ν_{Fe-Cl}: 386 cm^{-1}. The crude product was then dissolved in a minimum of THF (2 mL) and after a while nice brown crystals were formed. The IR revealed the same ν_{Fe-Cl}: 386 cm^{-1} and supplementary bands at 1052 and 897 cm^{-1} attributed to THF. The crystals are suitable for an X-ray analysis. ES + MS in $CHCl_3$: gives the isotopic pattern with the corresponding intensities for the dicationic fragment in good agreement with the simulation: $[FeN_{10}C_{58}H_{58}]^{2+}$: *m*/*z*: 474.21, 474.71, 475.21, 457.71, 476.21, and 476.71.

3.3. X-ray crystallography

Data were collected on a Nonius Kappa CCD diffractometer (graphite Mo Kα radiation, 0.71073 Å). The structure was solved using the Nonius OpenMoleN package and refined by full matrix least-squares with anisotropic thermal parameters for all non-hydrogen atoms. Data collection parameters, solution and refinements results are given in Table 1.

4. Supplementary material

Crystallographic data for structural analysis have been deposited with the Cambridge Crystallographic Data Centre, CCDC Nos. 203433, 203434, 203435 for $(C_{58}H_{58}Cl_4Fe_2N_{10})$ $\{(L^2)_2Fe^{2+}FeCl_4^{2-}\}$, $(C_{58}H_{46}Cl_8Fe_3N_6)$ $\{(L^1)_2Fe^{2+}(FeCl_4^-)_2\}$ and $(C_{74}H_{90}Cl_8Fe_3N_{10}O_4)$ $\{(L^2)_2Fe^{2+}(FeCl_4^-)_2(THF)_4\}$, respectively. These data can be obtained free of charge via www.ccdc.cam.ac.uk/data_request/cif, by emailing data_request@ccdc.cam.ac.uk, or by contacting The Cambridge Crystallographic Data Centre, 12, Union Road, Cambridge CB2 1EZ, UK; fax: +44 1223 336033.

Acknowledgements

We are grateful to Mrs. Michelle Martigneaux from the Service Commun NMR and Caroline Dietrich-Schneider from the Service de Spectrométrie de Masse at the University Louis Pasteur Strasbourg.

References

[1] (a) B.L. Small, M. Brookhart, A.M.A. Bennett, J. Am. Chem. Soc. 120 (1998) 4049;
(b) B.L. Small, M. Brookhart, J. Am. Chem. Soc. 120 (1998) 7143;
(c) G.J.P. Britovsek, V.C. Gibson, B.S. Kimberley, P.J. Maddox, S.J. McTavish, G.A. Solan, A.J.P. White, D.J. Williams, Chem. Commun. (1998) 849;

(d) G.J.P. Britovsek, M. Bruce, V.C. Gibson, B.S. Kimberley, P.J. Maddox, S. Mastroianni, S.J. McTavish, C. Redshaw, G.A. Solan, S. Strömberg, A.J.P. White, D.J. Williams, J. Am. Chem. Soc. 121 (1999) 8728.

[2] (a) V.C. Gibson, S.K. Spitzmesser, A.J.P. White, D.J. Williams, Dalton Trans. (2003) 2718;
(b) D.M. Dawson, D.A. Walker, M. Thornton-Pett, M. Bochmann, J. Chem. Soc., Dalton Trans. (2000) 459;
(c) G.J.P. Britovsek, V.C. Gibson, S. Mastroianni, D.C.H. Oakes, C. Redshaw, G.A. Solan, A.J.P. White, D.J. Williams, Eur. J. Inorg. Chem. (2001) 431;
(d) L. LePichon, D.W. Stephan, X. Gao, Q. Wang, Organometallics 21 (2002) 1362;
(e) C. Amort, M. Malaun, A. Krajete, H. Kopacka, K. Wurst, M. Christ, D. Lilge, M.O. Kristen, B. Bildstein, Appl. Organomet. Chem. 16 (2002) 506.

[3] F. Kröhnke, Synthese (1976) 1.

[4] P. Gamez, R.H. Steensma, W.L. Driessen, J. Reedijk, Inorg. Chim. Acta 333 (2002) 51.

[5] (a) K. Nakamoto, Infrared and Raman Spectra of Inorganic and Coordination Compounds, 4th ed., 1986;
(b) J.S. Avery, C.D. Burdbridge, D.M.L. Goodgame, Spectrochim. Acta 24A (1968) 1721;
(c) T.J. Kistenmacher, G.D. Stucky, Inorg. Chem. 7 (1968) 2150.

[6] E.C. Constable, G. Baum, E. Bill, R. Dyson, R. van Eldik, D. Fenske, S. Kaderli, D. Morris, A. Neubrand, M. Neuburger, D.R. Smith, K. Wieghardt, M. Zehnder, A.D. Zuberbühler, Chem. Eur. J. 5 (1999) 498.

[7] N.K. Solanki, E.J.L. McInnes, F.E. Mabbs, S. Radojevic, M. McPartlin, N. Feeder, J.E. Davies, M.A. Halcrow, Angew. Chem., Int. Ed. 37 (1998) 2221.

[8] (a) J.M. Holland, C.A. Kilner, M. Thornton-Pett, M.A. Halcrow, Polyhedron 20 (2001) 2829;
(b) N.K. Solanki, M.A. Leech, E.J.L. McInnes, J.P. Zhao, F.E. Mabbs, N. Feeder, J.A.K. Howard, J.E. Davies, J.M. Rawson, M.A. Halcrow, J. Chem. Soc., Dalton Trans. (2001) 2083;
(c) J.M. Holland, S.A. Barrett, C.A. Kilner, M.A. Halcrow, Inorg. Chem. Commun. 5 (2002) 328.

[9] E. König, Prog. Inorg. Chem. 35 (1987) 527.

[10] (a) J.M. Holland, J.A. McAllister, Z. Lu, C.A. Kilner, M. Thornton-Pett, M.A. Halcrow, Chem. Commun. (2001) 577;
(b) J.M. Holland, J.A. McAllister, C.A. Kilner, M. Thornton-Pett, A.J. Bridgeman, M.A. Halcrow, J. Chem. Soc., Dalton Trans. (2002) 548.

[11] P. Gütlich, Y. Garcia, H.A. Goodwin, Chem. Soc. Rev. (2000) 419.

[12] J.W. Lauher, J.A. Ibers, Inorg. Chem. 14 (1975) 348.

[13] Y. Chen, C. Qian, J. Sun, Organometallics 22 (2003) 1231.

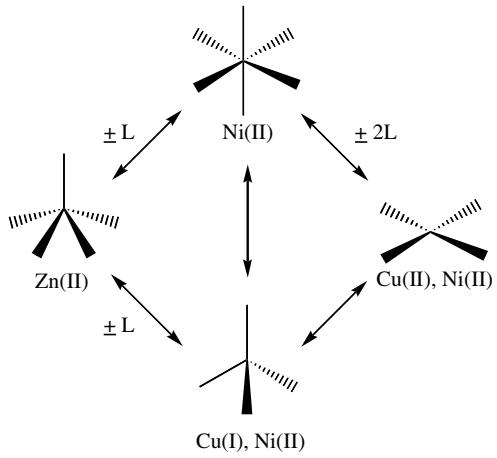

Fig. 1. The geometries available to tetradentate Schiff's base ligands coordinated to the late transition metals, nickel, copper and zinc. Td: tetrahedral; Oh: Octahedral; Sbp: square based pyramid and Sp: square planar.

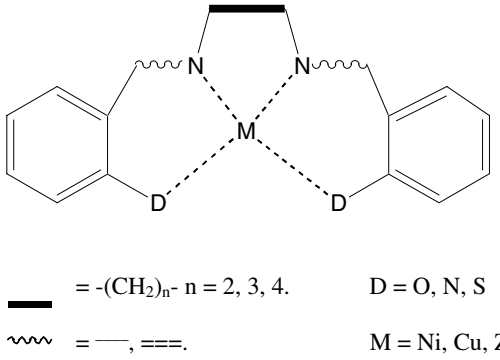

Fig. 2. Design of the simple unsubstituted parent complexes. Conformational flexibility is induced by the systematic expansion of the polymethylene chain between the two internal nitrogen donors (—), and the hydrogenation of the imine bond (〰).

copper and zinc complexes using the salen family of ligands have been carried out previously [9–17].

Square planar nickel complexes of salen and *N*,*N*′-bis-(salicylidene)-1,3-diaminopropane (salpr) have been structurally characterised [18,19]. A red diamagnetic complex of *N*,*N*′-bis-(salicylidene)-1,4-diaminobutane (salbut) has been reported [20] as has a four coordinate green paramagnetic form [21]. The appearance of two isomers of Nisalbut demonstrates that with a longer methylene backbone the structures can shift from the planar towards a more tetrahedral motif. Furthermore, in the presence of additional donors (MeOH, DMF, DMSO) salpr and salbut would seem to support the formation of trimetallic species such as bis-((μ^2-acetato)-(*N*,*N*′-bis-(*o*-salicylidene)-1,3-diaminopropane)(methanol) nickel)nickel ({[Ni(Salpr)(HOCH$_3$)]$_2$(μOAc)$_2$Ni}) and bis-((μ^2-acetato)-(*N*,*N*′-bis-(*o*-salicylidene)-1,4-diaminobutane)(dimethylformamido)nickel)-nickel ({[Ni(Salbut)(DMF)]$_2$(μOAc)$_2$Ni}) where the nickel atoms adopt an octahedral geometry [17,21]. In contrast to salpr, salbut is considerably more flexible thus allowing the additional two donors in the octahedral motif (Fig. 1) to adopt both *cis* and *trans* configurations [17].

The effect of the flexibility of the larger methylene chains on geometry is also observed in the series of copper(II)N_2O_2 Schiff's base complexes where a shift from square planar to a tetrahedrally distorted geometry is observed [12,13]. A similar effect is observed for an analogous series of Cu(I)N_2S_2 species where a shift from distorted square planar to tetrahedral geometry is seen [22]. However, although it has been shown that increasing the backbone length can lead to a wide variety of geometries, work on the related unsubstituted N_2S_2 and N_4 donor ligands remains incomplete. As part of our on-going interest in geometric flexibility we wished to establish a structural basis for these beginning here with a study on nickel.

Several Ni(II) complexes with N_2D_2 donor sets (D = N, S) and backbones with two to four methylene units have been structurally characterised and the structures of many others have also been proposed based on spectroscopic and magnetic data [8,18,19,23–25]. Of the three previously prepared [8] tetradentate N_4 complexes (Fig. 2) desired for this study, (*N*,*N*′-bis-(*o*-amidobenzilidene)-1,2-diaminoethane)nickel (Niamben), (*N*,*N*′-bis-(*o*-amidobenzilidene)-1,3-diaminopropane)nickel (Niambpr) and (*N*,*N*′-bis-(*o*-amidobenzilidene)-1,4-diaminobutane)nickel (Niambut), only the structure of Niamben has been reported [23]. Although visible, NMR and electronic absorption spectroscopy and magnetic susceptibility studies suggest the Niambpr and Niambut complexes also have the planar monomeric structure, a more detailed understanding of their structural parameters remains important to us.

Nickel (N_2S_2) complexes have been of interest recently since nickel centres with sulfur coordination environments have been found to be central to the activity of a wide range of important enzymes [26]. Since the heterobimetallic nature of the active site of these systems was revealed [27], modelling has centred on the design and synthesis of bimetallic complexes. This has left the structural characterisation of four coordinate Ni(II) N_2S_2 complexes incomplete, which in turn suggests that our interpretation of more sophisticated systems may be less than comprehensive.

A second related class of complexes are the hydrogenated Schiff's bases. The effects of hydrogenation on flexibility and therefore the wider range of geometries available to the metal complexes have not been thoroughly investigated and as yet no simple unsubstituted complexes have been structurally characterised. As such we have structurally characterised the corresponding nickel complexes of two hydrogenated ligands namely *N*,*N*′-bis-(*o*-aminobenzyl)-1,2-diaminoethane (H_4amben) and *N*,*N*′-bis-(*o*-aminobenzyl)-1,3-diaminopropane (H_4ambpr).

2. Experimental

All chemicals were commercially obtained and used without further purification. *o*-Amino-benzaldehyde was prepared by published methods [28]. All NMR spectra were recorded on a Bruker DPX400 instrument operating at 400.1 MHz for ^{1}H and 100 MHz for ^{13}C. The spectra were referenced to internal solvent peaks and thus to TMS. Mass spectrometry was carried out on a ThermoFinnigan LCQ mass spectrometer with ESI ionisation, spray voltage 4.5 kV, capillary temperature 200 ° C. Samples were dissolved in MeOH/H_2O 0.1% formic acid.

Crystals were coated in mineral oil and mounted on glass fibres. Data were collected at 123 K on a Nonius Kappa CCD diffractometer using graphite monochromated Mo Kα radiation. The heavy atom positions were determined by Patterson methods and the remaining atoms located in difference electron density maps. Full matrix least-squares refinement was based on F_2, with all non-hydrogen atoms anisotropic. While hydrogen atoms were mostly observed in the difference maps, they were placed in calculated positions riding on the parent atoms except those involved in hydrogen bonding which were refined isotropically. The structure solution and refinement used the programs SHELX-97 [29] and SIR-92 [30] and the graphical interface WinGX [31]. A summary of the crystallographic parameters is given in Table 1. Selected metrical parameters are reported in Table 2.

2.1. Preparation of N,N′-bis-(o-aminobenzilidene)-1,3-diaminopropane (ambpr) and N,N′-bis-(o-aminobenzilidene)-1,4-diaminobutane (ambut)

Ambpr and ambut were prepared according to reported methods [8,28]. Briefly: *o*-nitrobenzaldehyde (0.04 moles), ferrous sulphate (0.38 moles) and conc. HCl (0.5 ml) were suspended in water (175 ml) and heated to 90 °C. Concentrated ammonia solution (25 ml) was added followed by three further 10 ml portions of concentrated ammonia solution at 1-min intervals, and the product retrieved by steam distillation as a creamy yellow suspension. Precipitation was completed by the addition of saturated aqueous NaCl at 0 °C. The *o*-aminobenzaldehyde was collected by filtration, washed with water and dried. The product is prone to self-condensation and is best used immediately.

The Schiff's base compounds ambpr and ambut were prepared by refluxing *o*-aminobenzaldehyde (20 mmol) with the appropriate amine (10 mmol) in ethanol (100 ml) for 1 h. The solution was cooled and the volume reduced yielding a white powder, which was recrystallised from ethanol. Yields typically better than 40% (based on *o*-nitrobenzaldehyde) were obtained for both species.

Ambpr. *Anal*. Calc. for $C_{17}H_{20}N_4$: C, 72.82; H, 7.20; N, 19.98. Found: C, 72.66; H, 7.30; N, 19.74%. δ_H ($CDCl_3$) 8.37 (s, 2H, –CH=), 7.12 (dt, 4H, arom), 6.66 (m, 4H, arom), 6.38 (br s, 4H, NH_2), 3.69 (t, 4H, –NCH_2–), 2.09 (p, 2H, –CH_2–). δ_C ($CDCl_3$) 165, 149, 134, 131, 118, 116 (arom), 115 (C=N), 60 (∼N–CH_2–), 33 (–CH_2–); m.p. 111–112 °C.

Ambut. *Anal*. Calc. for $C_{18}H_{22}N_4$: C, 73.43; H, 7.53; N, 19.03. Found: C, 73.23; H, 7.61; N, 18.80%. δ_H ($CDCl_3$) 8.34 (s, 2H, –CH=), 7.14 (dt, 4H, arom), 6.66 (dt, 4H, arom), 6.36 (br s, 4H, NH_2), 3.61 (t, 4H, –NCH_2–), 1.78 (p, 4H, –CH_2–). δ_C ($CDCl_3$) 164, 149, 134, 131, 118, 116 (arom), 115 (–C=N), 62 (–NCH_2–), 29 (–CH_2–); m.p. 136–138 °C.

2.2. Preparation of (N,N′-bis-(o-amidobenzilidene)-1,3-diaminopropane)nickel(II) (Niambpr) and (N,N′-bis-(o-amidobenzilidene)-1,4-diaminobutane)nickel(II) (Niambut)

Nickel acetate (0.09 g, 0.36 mmol) was added to a refluxing solution of the desired ligand (0.36 mmol) in methanol (20 ml) resulting in a green solution. On addition of NaOH (0.04 g, 1 mmol) the solution turned brown. The solution was refluxed for 90 mins., hot filtered and allowed to cool overnight. A dark red powder and dark red/brown prisms formed, the latter being used for crystallographic analysis. The powders were recrystallised by slow diffusion of hexane into a THF solution of the product.

Ni(II)ambpr. *Anal*. Calc. for $C_{17}H_{18}N_4Ni$: C, 60.57; H, 5.38; N, 16.62. Found: C, 60.02; H, 5.46; N, 16.32%. δ_H ($CDCl_3$) 7.54 (s, 2H, –CH=), 7.16 (d, 4H, arom), 6.57 (s, 2H, arom), 6.26 (s, 2H, arom), 3.64 (s, 4H, –NCH_2–), 1.98 (s, 2H, –CH_2–).

Ni(II)ambut. *Anal*. Calc. for $C_{18}H_{20}N_4Ni$: C, 61.57; H, 5.74; N, 15.96. Found: C, 60.51; H, 5.66; N, 15.51%. δ_H ($CDCl_3$) 7.74 (s, 2H, –CH=), 7.01 (d, 4H, arom), 6.70 (s, 2H, arom), 6.27 (s, 2H, arom), 3.72 (s, 4H, –NCH_2–), 1.88 (s, 4H, –CH_2–).

2.3. Preparation of N,N′-bis(o-aminobenzyl)-1,2-diaminoethane (H_4amben) and N,N′-bis(o-aminobenzyl)-1,3-diaminopropane (H_4ambpr)

Hydrogenation of the imine bonds was carried out by slight modification of Fournea's method [32]. $NaBH_4$ (0.45 g, 12 mmol) was added in small portions to a stirred mixture of the desired ligand (3 mmol) in methanol (50 ml) under an N_2 atmosphere. The solution was stirred at room temperature for 65 h after which time the solvent was carefully removed under reduced pressure to yield an off white solid. The solid was resuspended in water (50 ml), made alkaline by the addition of a pellet of sodium hydroxide and extracted into chloroform (3×50 ml). The chloroform extracts were combined,

Table 1
Experimental details of the crystal structure determination of [Niambpr], [Niambut], [Nitsalbut], [Ni(H_4amben)($MeCN)_2$][BF_4]$_2$, [Ni(H_4amben)($OAc)_2$] and [Ni(H_4ambpr)($OAc)_2$]

	Niambpr	Niambut	Nitsalbut·0.25 dioxan	NiH_4amben(μ-$MeCN)_2\cdot 2BF_4$	NiH_4ambpr(μ-$OAc)_2\cdot H_2O\cdot(CO_2(CH_3CH_2)_2)_{0.5}$	NiH_4amben(μ-$OAc)_2\cdot H_2O$
Molecular formula	$C_{17}H_{18}N_4Ni$	$C_{18}H_{20}N_4Ni$	$C_{19}H_{22}N_4NiO_{0.5}S_2$	$C_{20}H_{28}B_2F_8N_6Ni$	$C_{24}H_{32}N_4Ni_1O_{5.5}$	$C_{20}H_{30}N_4Ni_1O_5$
F_W	337.05	351.33	407.2	578.73	523.24	465.19
T (K)	123	123	298	123	123	123
Crystal system	orthorhombic	monoclinic	monoclinic	monoclinic	monoclinic	monoclinic
Space group	*Pnma*	P_12_1/n	P_12_1/a	C_12/c	$P2_1/n$	P_12_1/c
a (Å)	7.65650(10)	10.42560(10)	14.0696(16)	16.2053(5)	13.5203(3)	9.8671(7)
b (Å)	24.3457(5)	19.6348(3)	14.0895(16)	12.6234(4)	8.9415(2)	12.5672(8)
c (Å)	7.80280(10)	15.9594(3)	19.188(2)	13.0175(4)	21.0725(4)	17.4230(12)
α (°)	90.000	90.000	90.000	90.000	90	90
β (°)	90.000	99.9480(10)	100.128(3)	108.1492(18)	97.9240(10)	95.2929(14)
γ (°)	90.000	90.000	90.000	90.000	90	90
V (Å^3)	1454.4	3217.84(8)	3744.3(7)	2530.45(14)	2523.17(9)	2151. 3(3)
Z	8	4	8	8	4	4
μ_{calc} (mm^{-1})	1.335	1.210	1.265	0.847	0.812	0.941
Crystal dimensions (mm)	$0.3\times0.2\times0.15$	$0.4\times0.4\times0.3$	$0.22\times0.18\times0.10$	$0.25\times0.\ 25\times0.12$	$0.6\times0.14\times0.12$	$0.9\times0.6\times0.2$
Reflections measured	3063	15010	13838	7182	24801	6208
Unique reflections	1698	7671	7188	3703	12324	3408
Observed reflections	1444	6625	4524	2901	6339	3127
R ($I>2\sigma(I)$)[a]	0.0257	0.0315	0.0548	0.037	0.049	0.033
R_W (all reflections)[b]	0.0622	0.0773	0.1411	0.078	0.130	0.089
Number of parameters	141	431	442	169	307	305

[a] $R = \sum||F_o|-|F_c||/\sum|F_o|$.
[b] $R_W = \{\sum[w(F_o^2 - F_c^2)^2]/\sum[w(F_o^2)^2]\}^{1/2}$.

washed with water and dried over anhydrous sodium sulphate. The solution was filtered and the solvent removed to give an off-white solid H_4amben and a yellow oil H_4ambpr. The products were recrystallised from chloroform/diethyl-ether by vapour diffusion (Yield 80%).

H_4amben δ_H ($CDCl_3$) 7.12 (t, 2H, arom), 7.03 (d, 2H, arom), 6.69 (m, 4H, arom), 3.79 (s, 4H, –$PhCH_2$–), 2.78 (s, 4H, –NCH_2–). δ_C (100MHz; solvent $CDCl_3$) 147, 130, 129, 124, 118, 116 (arom), 53 (–$PhCH_2$–), 33 (–NCH_2–). Mass Spec (LC direct) *m/e* 271.1; $[H_4amben]^+$.

H_4ambpr. *Anal*. δ_H ($CDCl_3$) 7.11 (t, 2H, arom), 7.08 (d, 2H, arom), 6.69 (dt, 4H, arom), 4.63 (br s, 4H, NH_2), 3.81 (s, 4H, –$PhCH_2$–), 2.70 (t, 4H, –NCH_2–), 1.70 (p, 2H, –CH_2–), 1.31 (br s, 2H, NH). δ_C (100 MHz; solvent $CDCl_3$) 147, 130, 129, 124, 118, 116 (arom), 53 (–$PhCH_2$–), 48 (–NCH_2–), 30 (–CH_2–). Mass Spec (LC direct) *m/e* 285.1; $[H_4ambpr]^+$.

2.4. Preparation of {bis-O-acetato-(N,N′-bis-(o-aminobenzyl)-1,2- diaminoethane)}nickel(II) [Ni(H_4amben)($OAc)_2$] and {bis-O-acetato- (N,N′-bis-(o-aminobenzyl)-1,3-diaminopropane)}nickel(II) [Ni(H_4ambpr)($OAc)_2$]

Nickel acetate (0.125 g, 0.5 mmol) and the desired ligand (0.5 mmol) were refluxed gently for 1 h in methanol (25 ml) giving brown solutions. The solvent was removed under reduced pressure yielding a purple/brown powder [Ni(H_4amben)($OAc)_2$] and in the case of [Ni(H_4ambpr)($OAc)_2$] a red/brown oil.

Diethyl-ether (5 ml) was added to the oil [Ni(H_4ambpr)($OAc)_2$] and the solution sonicated for 5 min precipitating a pale brown powder which was collected by filtration. Crystals suitable for crystallographic analysis were grown by vapour diffusion, using chloroform/diethyl-ether to produce blue crystals of [Ni(H_4ambpr)($OAc)_2$], and methanol/diethyl-ether to produce pink crystals of [Ni(H_4amben)($OAc)_2$].

[Ni(H_4amben)($OAc)_2\cdot H_2O$]. *Anal*. Calc. for $C_{20}H_{30}N_4NiO_5$: C,51.64; H, 6.50; N, 11.94. Found: C, 51.33; H, 6.68; N, 12.04%.

[Ni(H_4ambpr)][$OAc]_2\cdot 2H_2O$. *Anal*. Calc. for $C_{21}H_{30}N_4NiO_4$cdot$2H_2O$: C, 50.73; H, 7.43; N, 11.27. Found: C, 51.33; H, 6.58; N, 10.68%.

2.5. Preparation of {bis-acetonitrile-(N,N′-bis-(o-aminobenzyl)-1,2- diaminoethane)nickel(II)} tetrafluoroborate [Ni(H_4amben)($NCMe)_2$][$BF_4]_2$

$Ni(BF_4)_2\cdot 6H_2O$ (0.20 g, 0.5 mmol) and H_4amben (0.135 g, 0.5 mmol) were refluxed in methanol (25 ml) for 1 h giving a brown solution. The solution was hot filtered and the solvent removed to leave a red/brown oil. The oil was resuspended in a small volume of acetonitrile (5 ml) and the mixture filtered through celite. Purple/pink crystals suitable for X-ray analysis were obtained by slow diffusion of the acetonitrile solution with diethyl-ether (Yield 80%).

[Ni(H_4amben)($NCMe)_2$][$BF_4]_2$. *Anal*. Calc. for $C_{20}H_{28}B_2F_8N_6Ni$: C, 41.07; H, 4.82; N, 14.37. Found: C, 41.06; H, 4.86; N, 14.26%.

2.6. Preparation of (N,N′-bis-(o-thiobenzylidine)1,4-diaminobutane)nickel(II) (Nitsalbut)

Nitsalbut was prepared through modification of Eichorn's synthesis of Nitsalen [33], i.e., the reaction of 2,2'-dithiobenzaldehyde (DTDB) and 1,4-butanediaminenickel(II)dichloride.

DTDB was prepared by the method of Kasmai and Mischke [34]. Briefly: $LiAlH_4$ (2.12 g, 55.1 mmol) was dissolved in dry THF (50 ml), to which a solution of thiosalicylic acid (3.4 g, 22.0 mmol) in dry THF (80 ml) was added dropwise with cooling. The reaction was stirred under nitrogen for 24 h. Ethylacetate (10 ml) was added, followed by the dropwise addition (care!) of a 10% aqueous solution of H_2SO_4 (100 ml). The mixture was filtered, the organic layer separated and dried over anhydrous sodium sulphate. The solvent was removed under reduced pressure to yield 2-(hydroxymethyl)benzenethiol as a pale yellow oil (Yield 93.8%). The 2-(hydroxymethyl)benzenethiol was dissolved in dry toluene (220 ml) under nitrogen. Excess MnO_2 was added and the reaction stirred at room temperature for 24 h. The solution was filtered and the MnO_2 washed with toluene. The solvent was evaporated to yield a pale yellow powder (Yield 30%).

(1,4-Butanediamine)nickel(II) dichloride was prepared using the method of State for the preparation of tris(ethylenediamine)nickel(II) chloride [35]. Briefly: a 70% aqueous solution of 1,4-diaminobutane (3.2 ml, 31.8 mmol) was added to a solution of $NiCl_2\cdot 6H_2O$ (1.59 g, 6.7 mmol) in H_2O (15 ml). A pale green precipitate formed on the addition of the diamine. The solution was heated to 110 °C and 2 drops of 1,4-diaminobutane added. The solvent was allowed to evaporate and the product recrystallised from ethanol (Yield 35%).

(1,4-Butanediamine)nickel(II) dichloride (47.2 mg, 0.22 mmol) was dissolved in ethanol (5–10 ml) and brought to reflux. A solution of DTDB (0.20 g, 0.73 mmol) in the minimum volume of dichloromethane was added to the solution whereupon it turned brown. The reaction was refluxed for 1 h, allowed to cool and the solvent removed under reduced pressure. The brown solid was resuspended in chloroform and filtered through a silica gel filter stick (3 cm × 0.5 cm) using further aliquots of chloroform. The bulk of the chloroform was removed and the product crystallised by vapour diffusion with diethyl ether (Yield 85 % based on DTDB). Crystals suitable for X-ray analysis were obtained by slow diffusion of cyclohexane into a dioxane solution of the product obtained above.

Anal. Calc. for $C_{18}H_{18}N_2NiS_2\cdot(C_4H_8O_2)_{0.5}$: C, 55.96; H, 5.17; N, 6.52. Found C, 55.15; H, 4.43; N, 6.61%. δ_H ($CDCl_3$) 7.87 (s, 2H, –CH=), 7.70 (d, 2H, arom), 7.21 (d, 2H, arom), 7.15 (t, 2H, arom), 7.01 (t, 2H, arom), 3.88 (t, 4H, d $–NCH_2–$), 1.97 (p, 4H, $–CCH_2–$).

3. Results and discussion

Previous studies on copper(II) *N*,*N*′-bis-(salicylidene)-diamine [13,14,19] complexes have demonstrated how increasing the number of methylene units between the imines allows the complex to move from a planar towards a distorted tetrahedral motif. For transition metals capable of adopting higher coordination numbers, such as nickel, the ability of the larger ring sizes generated by *N*,*N*′-bis-(salicylidene)-1,3-diaminopropane (salpr) and *N*,*N*′-bis-(salicylidene)-1,4-diaminobutane (salbut) complexes would seem to support the formation of a wider range of geometries [17]. In the belief that similar trends may be observed with different donor sets (Fig. 2, D = N, S) we have prepared and structurally characterised the three complexes (*N*,*N*′-bis-(*o*-amidobenzilidene)-1,3-diaminopropane)nickel (Niambpr), (*N*,*N*′-bis-(*o*-amidobenzilidene)-1,4-diaminobutane)nickel (Niambut) and (*N*,*N*′-bis-(*o*-thiobenzilidine)-1,4-diaminobutane)nickel(II) (Nitsalbut), thus completing the series of nickel complexes with 1,2-ethane, 1,3-propane and 1,4-butane backbones with N_2N_2 and N_2S_2 donor sets. The three new structures are shown in Fig. 3, the key bond lengths and angles for the complete series of six complexes being given in Table 2. Consistent with the reported structure of Niamben [23] and the spectroscopic data of Niambpr and Niambut [8,24] the amines deprotonate on chelation and the structures obtained for N_2N_2 are amides.

The *trans* N–Ni–D angles (Table 2) obtained from the six related complexes indicate that they all adopt a square planar geometry. As might be expected the complexes derived from 1,4-diaminobutane show the great-

Table 2
Selected bond lengths and angles for the nickel complexes of amben [23], ambpr and ambut, H_4amben and H_4ambpr (D = N), tsalen [48,49], tsalpr [25,50] and tsalbut. (D = S)

Complex	*Trans* N–Ni–D plane angles (°)	N–Ni and D–Ni Bond lengths Å				∠CN–NC torsion angle (°)
		N–Ni	N–Ni	D–Ni	D–Ni	
NiAmben [23]	176.6(7) 174.7(6)	1.87(1)	1.86(1)	1.88(1)	1.83(1)	21.34
NiAmbpr	174.70(6) 174.70(6)	1.9289(13)	1.9289(13)	1.8615(14)	1.8615(14)	0
NiAmbut	172.14(6) 168.22(7)	1.9268(15)	1.9037(14)	1.8468(15)	1.8684(15)	50.7
	172.67(6) 168.11(6)	1.9299(15)	1.9097(15)	1.8511(16)	1.8769(15)	−55.7
NitSalen [48]	173.0(1) 174.5(1)	1.876(4)	1.883(4)	2.155(2)	2.145(2)	Disordered −29.7, 21.4
	178.3(2) 177.9(2)	1.885(5)	1.892(5)	2.150(2)	2.155(2)	28.4
NitSalen [49]	176.92 178.63	1.86	1.85	2.174	2.139	−27.1
Nitsalpr [25]	170.86(4) 169.35(4)	1.9140(14)	1.9307(15)	2.1760(5)	2.1574(5)	−65.9
NitSalpr [50]	169.55(7) 172.48(7)	1.909(2)	1.916(2)	2.1733(8)	2.1454(8)	61.04
	174.39(7) 172.20(7)	1.919(2)	1.913(2)	2.1610(9)	2.1686(9)	61.89
NitSalbut	165.57(11) 166.89(11)	1.916(4)	1.914(4)	2.1655(13)	2.1636(14)	−78.1
	162.05(11) 162.02(11)	1.910(3)	1.902(4)	2.1477(15)	2.1644(13)	80.9
$NiH_4amben(\mu\text{-}MeCN)_2(BF_4)_2$	93.69(5) 93.69(5)	2.0753(13)	2.0753(13)	2.1310(13)	2.1310(13)	42.8
$NiH_4amben(\mu\text{-}OAc)_2\cdot H_2O$	173.50(11) 173.79(11)	2.081(3)	2.057(3)	2.106(3)	2.113(3)	−33.9
$NiH_4ambpr(\mu\text{-}OAc)_2$	176.61(6) 173.55(6)	2.1044(17)	2.1106(15)	2.1344(17)	2.1473(15)	0.3

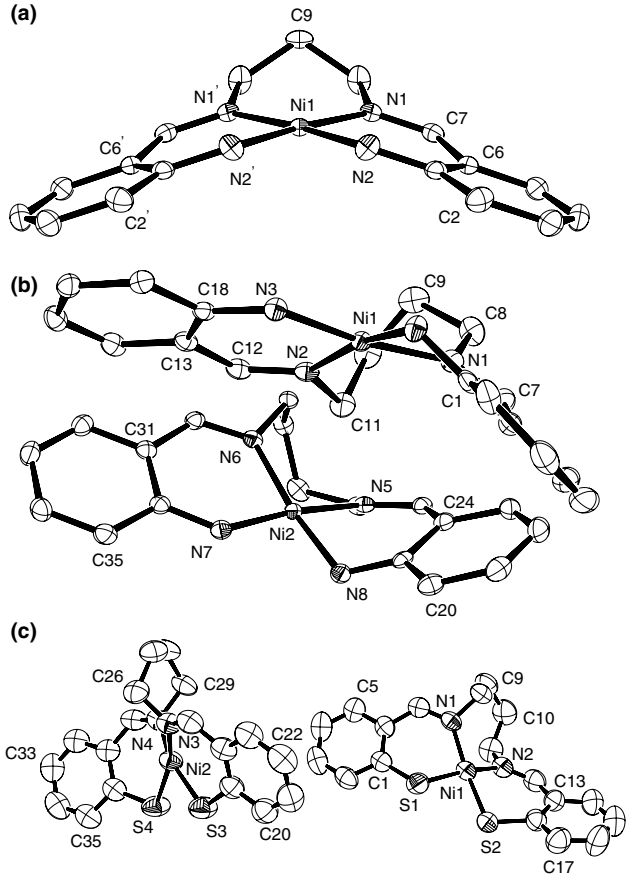

Fig. 3. The X-ray crystal structures of (a) (*N*,*N*′-bis-(*o*-amidobenzilidene)-1,3-diamino-propane)nickel (Niampr), (b) (*N*,*N*′-bis-(*o*-amidobenzilidene)-1,4-diamino-butane)nickel (Niambut) and (c) (*N*,*N*′-bis-(*o*-thiobenzilidine)-1,4-diamino-butane)nickel (Nitsalbut). Hydrogens omitted for clarity; thermal ellipsoids are at 50%, the latter was collected at room temperature.

est distortion (162.02(11)–172.67(6)°). Whilst the square planar nature of the N_2N_2 complexes have been previously proposed [8,24] it is interesting to see how these ligands are able to cope with the geometric preference of the metal centre. As the chain length increases past two methylene units the Ni–$N_{iminato}$ bond lengths (Table 2) increase in order to accommodate the larger backbones. Whereas the 1,3-propanediimine can adopt an apposite chair conformation, the butane backbone is heavily buckled and is positioned out of the plane of the rest of the molecule in comparison with the arrangements in Nitsalbut (Fig. 3(c)) and Cu(II)salbut [36], where the backbone traverses the metal ligand plane in an S-shape allowing the geometry at the metal centre to be slightly tetrahedrally distorted.

The N_2S_2 complexes do not maintain the square planar geometry (178.63°–162.02(11)°) quite as effectively as the N_2N_2 complexes (176.6(7)°–168.11(6)°) as the backbone is lengthened. There is a greater shift towards a tetrahedral distortion, however, this is still small in comparison with the shifts observed in the Cu(II)salen series [17]. There is only very small lengthening of the imine metal bonds, and by allowing a slightly greater distortion from square planar the backbones are not under as much strain, particularly in the butane complex. This probably arises from the subtle differences in the π-contribution in the Ni–S and Ni–NH interactions.

An alternative way of introducing additional flexibility into the polymethylene backbone is to hydrogenate the imine moieties, thus allowing some rotation at the internal nitrogen donors. In the belief that this freedom would be more evident with ligands containing shorter backbones, nickel complexes of *N*,*N*′-bis(*o*-aminobenzyl)-1,2-diaminoethane (H_4amben) and *N*,*N*′-bis-(*o*-aminobenzyl)-1,3-diaminopropane (H_4ambpr) were prepared and isolated (Fig. 4).

In the presence of non-coordinating anions ($[BF_4]^-$) octahedral complexes, e.g., $[Ni(H_4amben)(MeCN)_2]^{2+}$ are formed in which the solvents (acetonitrile) occupy the two remaining sites (Fig. 4(a)). In contrast to the parent imine species the hydrogenated ligand twists to such an extent that the peripheral amine donors are found *trans* to one another (175.58(8)°) and the solvents cis (86.65(8)°). Without the electron withdrawing influence of the conjugated π-system, the pK_a of the external amines rise and they fail to deprotonate thus producing cationic amino complexes (cf. the neutral amido complexes Niamben etc). These differences account for the shorter N–Ni bond distances in the amido complexes (e.g., Niamben) compared to their respective amino complex (NiH_4amben, Table 2).

Synthesising these species from the acetate, we obtained a neutral complex with coordinated acetate ligands in the *trans* arrangement (Fig. 4(b)), and the tetradentate ligand occupying the meridial plane. Close inspection of the structure indicates that hydrogen bonds form between the acetates and the terminal NH_2 groups and it is clear that it is these interactions which define the conformation adopted. However, even when confined to the meridial plane the hydrogenated ligand still shows a slight tetrahedral distortion of the nitrogen donors out of the plane. This distortion extends out towards the aromatic rings where they adopt positions above and below the plane, as apposed to the umbrella arrangement seen in the imine complex (Fig. 3).

Although there are a few notable exceptions (didentate ligands [37,38], multiple bonds [39,40] and bulky ligands [41–43]), typically unidentate ligands predominantly adopt axial positions in the parent ethylenediamine based tetradentate Schiff's base complexes. However a picture is emerging which suggests the analogous hydrogenated species may prefer the additional ligands to adopt a cis conformation [44,45]. Again there are exceptions to this [46,47]. Crucially the acetate complexes give us an insight into just how delicate the balance between the choice of conformation, i.e., *cis* (Fig. 4(a)) and *trans* (Fig. 4(b)), can be and alludes to

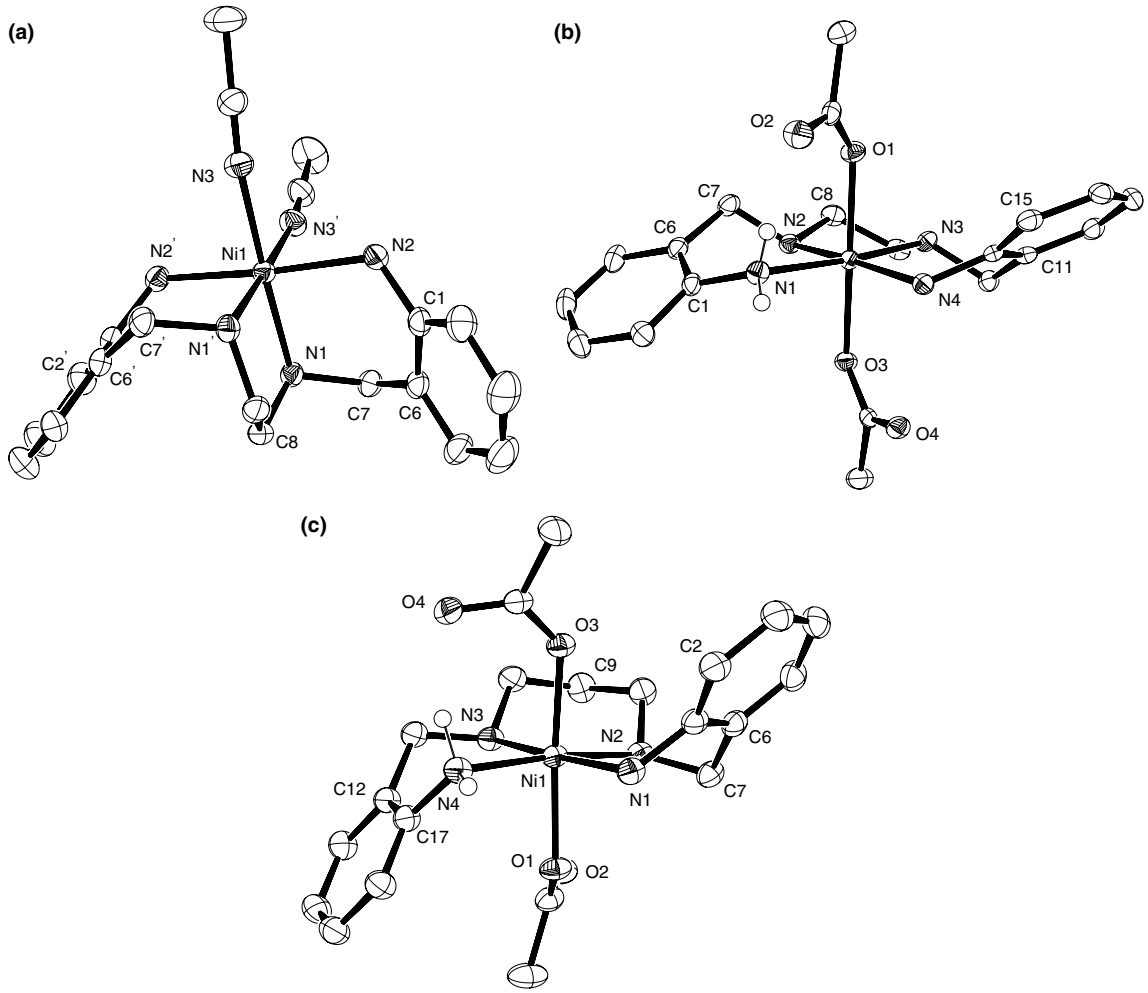

Fig. 4. The X-ray crystal structure of (a) {(bis-acetonitrile)}(*N*,*N*′-bis-(*o*-aminobenzyl)-1,2-diaminoethane)nickel tetrafluroborate, (b) {bis-*O*-acetato-(*N*,*N*′-bis-(*o*-aminobenzyl)-1,2-diaminoethane)}nickel(II) and (c) {(bis-*O*-acetato)}(*N*,*N*′-bis-(*o*-aminobenzyl)-1,3-diaminopropane)nickel. Hydrogens omitted for clarity, except those involved in hydrogen bonding to the acetates (NH—O Å; ethane 2.043, propane 1.921); thermal ellipsoids are at 50%.

the possibility of exchange between them (Fig. 1) during chemical reactions.

4. Supplementary data

Crystallographic data have been deposited with the Cambridge Crystallographic data Centre, CCDC Nos. 249874–249879. Copies of this information may be obtained free of charge from The Director, CCDC, 12 Union Road, Cambridge, CB2 1EZ, UK (fax: +44-1223-336033; e-mail: deposit@ccdc.cam.ac.uk or http://www.ccdc.cam.ac.uk).

Acknowledgements

M.K.T. thanks the University of Strathclyde for funding. M.K.T. also thanks Alan Kennedy and Mark Spicer for their assistance with the X-ray analysis. J.R. thanks the Cunningham Trust, Scotland for financial support.

References

[1] S. Yamada, Coord. Chem. Rev. 192 (1999) 537.
[2] A. Bottcher, H. Elias, L. Muller, H. Paulus, Angew. Chem. 31 (1992) 623.
[3] A. Bottcher, H. Elias, E.G. Jager, H. Langfelderova, M. Mazur, L. Muller, H. Paulus, P. Pelikan, M. Rudolph, M. Valko, Inorg. Chem. 32 (1993) 4131.
[4] S. Zolezzi, E. Spodine, A. Decinti, Polyhedron 21 (2002) 55.
[5] S. Djebbar-Sid, O. Benali-Baitich, J.P. Deloume, Polyhedron 16 (1997) 2175.
[6] S. Djebbar-Sid, O. Benali-Baitich, J.P. Deloume, J. Mol. Struct. 569 (2001) 121.
[7] C. Freire, B.D. Castro, J. Chem. Soc. Dalton Trans. (1998) 1491.
[8] M. Green, P.A. Tasker, J. Chem. Soc. (A) (1970) 2531.
[9] J. Csaszar, Acta Chim. Hung. 128 (1991) 255.
[10] G.V. Panova, V.M. Potapov, I.M. Turovets, E.G. Golub, J. Gen. Chem. USSR Eng. Trans. (1983) 1452.

[11] S.J. Gruber, C.M. Harris, E. Sinn, J. Inorg. Nucl. Chem. 30 (1968) 1805.
[12] G.E. Batley, D.P. Graddon, Aust. J. Chem. 21 (1968) 1473.
[13] L.C. Nathan, Polyhedron 22 (2003) 887.
[14] G.E. Batley, D.P. Graddon, Aust. J. Chem. 885 (1967) 891.
[15] J. Beretka, B.O. West, M.J. O'Connor, Aust. J. Chem. 17 (1964) 192.
[16] J. Reglinski, S. Morris, D.E. Stevenson, Polyhedron 21 (2002) 2175.
[17] J. Reglinski, S. Morris, D.E. Stevenson, Polyhedron 21 (2002) 2167.
[18] A.G. Manfredotti, C. Guatini, Acta Crystallogr. Sect. C 39 (1983) 863.
[19] M.G.B. Drew, R.N. Prasad, R.P. Sharma, Acta Crystallogr. Sect. C 41 (1985) 1755.
[20] R.W. Asmussen, Ph.D., Kopenhagen, as reported by R.H. Holm J. Am. Chem. Soc. 82 (1960) 5632.
[21] R.H. Holm, J. Am. Chem. Soc. 82 (1960) 5632.
[22] M.K. Taylor, J. Reglinski unpublished results.
[23] G. Brewer, J. Jasinski, W. Mahany, L. May, S. Prytkov, Inorg. Chim. Acta 232 (1995) 183.
[24] B.M. Higson, E.D. McKenzie, J. Chem. Soc. Dalton Trans. (1972) 269.
[25] M.K. Taylor, J. Reglinski, D. Wallace, Acta Crystallogr. Sect. E 60 (2004) m850.
[26] L. Gomes, E. Pereira, B. de Castro, J. Chem. Soc. Daltons Trans. 8 (2000) 1373.
[27] A. Volbeda, M.H. Charon, C. Piras, E.C. Hatchikian, M. Frey, J.C. Fontecilla-camps, Nature 373 (1995) 580.
[28] L.I. Smith, J.W. Opie, Org. Synth. Coll. III (1955) 56.
[29] G.M. Sheldrick, SHELXL-97. Programs for Crystal Structure Analysis (Release 97-2), Institut fur Anorganische Chemie der Universitat, Tammanstrasse 4, D-3400 Gottingen, Germany, 1998.
[30] A. Altomare, G. Cascarano, C. Giacovazzo, A. Guagliardi, J. Appl. Crystallogr. 26 (1993) 343.
[31] L.J. Farrugia, J. Appl. Crystallogr. 32 (1999) 837.
[32] J.P. Fourneau, A. Funke, Bull. Soc. Chim. 9 (1942) 806.
[33] D.M. Eichorn, N. Goswami, Inorg. Chem. 38 (1999) 4329.
[34] H.S. Kasmai, S.G. Mischke, Synthesis (1989) 763.
[35] H.M. State, Inorg. Synth. 6 (1960) 200.
[36] D. Ulku, L. Tatar, O. Atakol, M. Aksu, Acta Crystallogr. Sect. C 57 (2001) 273.
[37] Y. Kushi, T. Tada, H. Yoneda, Bull. Chem. Soc. Jpn. 55 (1982) 1834.
[38] R.B. Lauffer, R.H. Heistand II, L. Que, Inorg. Chem. 22 (1983) 50.
[39] M. Gullotti, A. Pasini, G.M. Zanderighi, G. Ciano, A. Sironi, J. Chem. Soc. Dalton Trans. (1981) 902.
[40] M. Motevalli, B.C. Parkin, R. Ramnauth, A.C. Sullivan, J. Chem. Soc. Dalton Trans. (2000) 2661.
[41] O. Runte, T. Priermeier, R. Anwander, Chem. Comunm. (1996) 1385.
[42] J.P. Corden, W. Errington, P. Moore, M.G.H. Wallbridge, Chem. Commun. (1999) 323.
[43] J.R. Dilworth, P. Jopanputra, R.M. Thompson, D.C. Povey, C.M. Archer, J.D. Kelly, J. Chem. Soc. Dalton Trans. (1994) 1251.
[44] R. Garcia-Zarracino, J. Ramos-Quiones, H. Hopfl, J. Organomet. Chem. 664 (2002) 188.
[45] E.Y. Tshuva, I. Goldberg, M. Kol, J. Am. Chem. Soc. 122 (2000) 10706.
[46] L.M. Liable-Sands, C. Incarvito, A.L. Rheingold, C. Jin Qin, A.L. Gavrilova, B. Bosnich, Inorg. Chem. 40 (2001) 2147.
[47] D.A. Atwood, J.A. Jegier, D. Rutherford, J. Am. Chem. Soc. 117 (1995) 6779.
[48] N. Goswami, D.M. Eichorn, Inorg. Chim. Acta 303 (2000) 271.
[49] T. Yamamura, M. Tadokoro, M. Hamaguchi, R. Kuroda, Chem. Lett. (1989) 1245.
[50] L. Gomes, E. Pereira, B. De Castro, Acta Crystallogr. Sect. C 55 (1999) 1061.

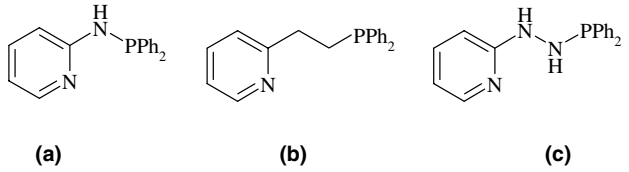

Fig. 1. Pyridylphosphines.

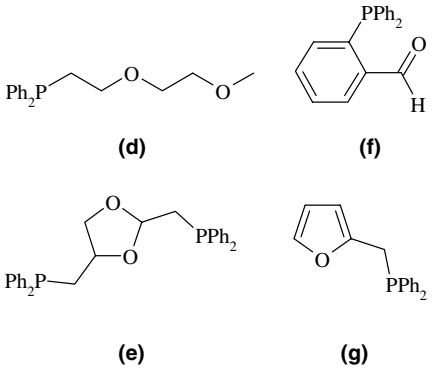

Fig. 2. Phosphorus–oxygen ligands.

Dpppa was recrystallised from boiling methanol to give a colourless crystalline solid in a tolerable yield (55%) and is relatively air stable; however exposure to air for prolonged periods resulted in degradation. It is readily soluble in chlorinated solvents, acetone, thf, somewhat less so in toluene, methanol and diethyl ether. A singlet is observed in the ^{31}P spectra of dpppa (in $CDCl_3$) at δ(P) 22.0 ppm. The ^{1}H NMR clearly shows the presence of an amide proton at δ(H) 8.65 ppm, as a doublet $^2J_{P-H} = 4$ Hz. The IR spectra shows a weak ν(N–H) band at 3297 cm^{-1}, and bands attributable to ν(pyCN) and ν(P–N) at 1452 and 996 cm^{-1} respectively. The expected ν(C=O) signature is visible at 1691 cm^{-1}. Satisfactory microanalysis was also obtained. The crystal structure of dpppa (Table 1 and Fig. 3) reveals that the P(1)–N(2)–C(3)–O(3) backbone is essentially planar

Table 1
Selected bond lengths (Å) and angles (°) for dpppa, dppaO and dppaS

	Dpppa **1**	DpppaO **2**	DpppaS **3**
Bond lengths			
P–O/S		1.478(2)	1.9475(9)
P(1)–N(2)	1.702(3)	1.683(2)	1.699(2)
N(2)–C(3)	1.355(5)	1.370(4)	1.378(3)
C(3)–C(4)	1.500(6)	1.506(4)	!.502(5)
C(3)–O(3)	1.221(5)	1.217(3)	1.219(3)
N(2)···N(5)	2.67(5)	2.65(5)	2.65
Bond angles			
C(3)–N(2)–P(1)	126.1(3)	124.09(19)	125.33(18)
N(2)–C(3)–C(4)	116.2(4)	114.4(2)	114.1(2)
O(3)–C(3)–N(2)	122.1(4)	123.1(3)	123.4(2)
O(3)–C(3)–C(4)	121.7(4)	122.6(3)	122.6(2)
N(2)–H(2)···N(5)	129(3)	109(3)	111(2)

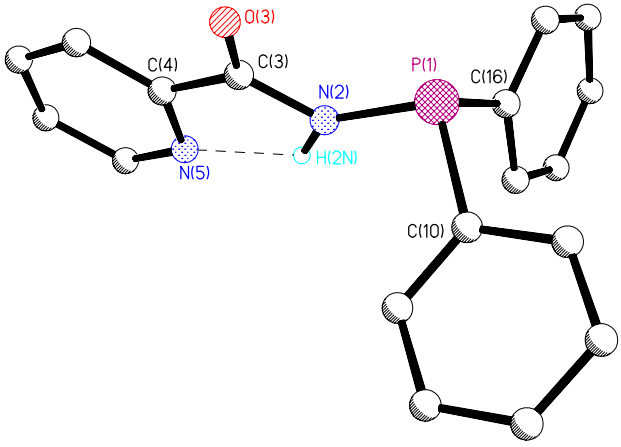

Fig. 3. The crystal structure of dpppa (**1**).

with an intramolecular hydrogen bond between the amide proton and the pyridyl nitrogen, generating an effective five-membered ring that is almost planar [N(2)–N(5) 2.67 Å] The phosphorus–nitrogen bond length of 1.702(3) Å is well within acceptable boundaries previously established in aminophosphine chemistry.

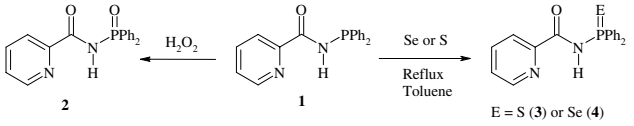

(2)

The oxide, sulfide and selenide of dpppa were also synthesised as seen in Eq. (2). The expected downfield shift is found in the ^{31}P NMR spectra of all three compounds (Table 2), the $^1J_{P-Se}$ is 788 Hz which is typical for a phosphorus–selenium double bond.

In **2**, the P–N bond is somewhat shorter than in dpppa (Table 1 and Fig. 4), the C(4)–C(3)–N(2)–P(1) backbone is essentially planar [mean deviation of 0.0391 Å] and as in **1** there is an H-bonded five-membered ring linking N(5) and H(2) [N(2)–N(5) is 2.653 Å, N(2)–H(2)···N(5) 109°]. It has been shown that the oxides and sulfides of phosphorus(III) ligands can display different solid state motifs [17]. We found that the sulfide **3** crystallises in a dimer arrangement rather than favouring the internal bonding seen in the oxide. The backbone of the molecule remains mostly planar, with the N(2) and N(5) distance [2.65 Å] indicating that the N(2)–H(2)···N(5) hydrogen bond interaction is retained (Table 1 and Fig. 5).

We formed a number of monodentate complexes, thus dpppa reacts with [$PtCl_2$(cod)] in dichloromethane to give *cis*-[$PtCl_2$(dpppa-P_2)] (**5**) as a white crystalline solid in good yield [80%] which is in marked contrast to 2-(diphenylphosphino)aminopyridine (dppap) which is reported to give [PtX(Ph_2PNHpy-*P*,*N*)(Ph_2 PNHpy-*P*)][Cl] (X = Cl or Me) [1–3]. The ^{31}P NMR ($CDCl_3$) of **5** is a singlet at δ(P) 31.2 ppm [$^1J_{Pt-P} = 3984$ Hz],

Table 2
Spectroscopic data for $Ph_2P(E)C(O)NHpy$

Compound	$\delta(^1H)$		$\delta(^{31}P)$	IR (cm^{-1})			
	NH	Aromatics	P	P=E	C=O	NH	CN(py)
1	8.7	8.5–7.2	22.0	N/A	1691	3297	1452
2	9.4	8.5–7.3	22.1	1215	1694	3302	1451
3	9.3	8.6–7.4	54.4	837	1689	3268	1447
4	9.3	8.6–7.1	48.7[a]	Obscured	1698	3288	1391

[a] $^1J_{P-Se}$ = 788 Hz.

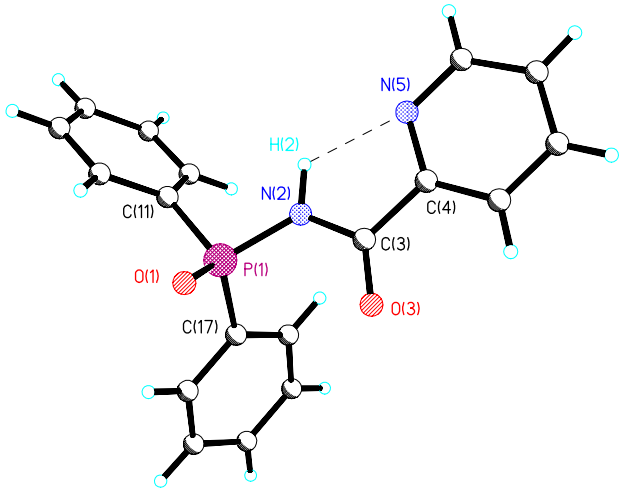

Fig. 4. The crystal structure of dpppaO (**2**).

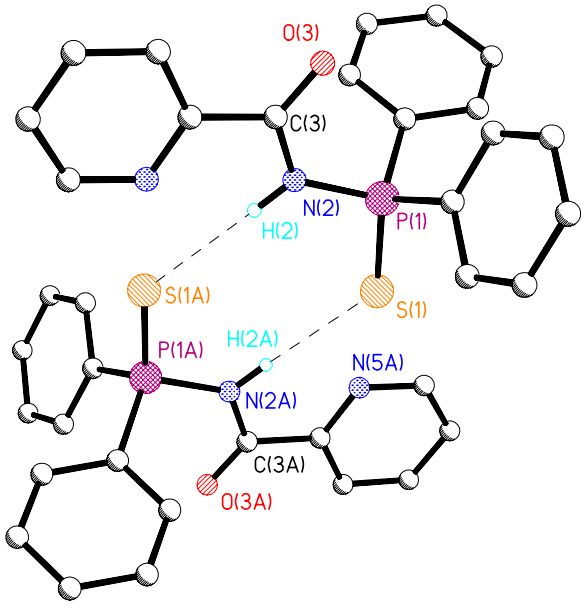

Fig. 5. Crystal structure of dpppaS (**3**).

whilst in the ^1H NMR it displays some significant changes from the free ligand. The amine proton is shifted to δ(H) 10.7 ppm, and $^2J_{P-H}$ at 15 Hz is significantly increased Two Pt–Cl stretches are visible in the IR spectrum (320 and 302 cm^{-1}), further evidence of a *cis*-conformation for **5**. In contrast, reaction of $[PdCl_2(cod)]$ with dpppa gives $[PdCl_2(dpppa\text{-}P)_2]$ (**6**), which is insoluble and displays only one Pd–Cl stretch (310 cm^{-1}), suggesting a *trans*-arrangement, the other expected IR peaks are observed clearly, ν(N–H) at 3232, ν(C=O) at 1694, ν(P–N) at 997 cm^{-1}. This *trans*-arrangement is consistent with previous examples of pyridylaminophosphines found in the literature [1–3].

A series of palladium complexes were synthesised bearing only one dpppa monodentate bound via the phosphorus (Fig. 6). Complexes $[PdCl(allyl)(dpppa\text{-}P)]$ (**7**), $[PdCl(C_{10}H_6NO)(dpppa\text{-}P)]$ (**8**), $[PdCl(C_9H_{12}N)(dpppa\text{-}P)]$ (**9**), $[PdCl(C_{12}H_{12}N)(dpppa\text{-}P)]$ (**10**), were all synthesised via bridge cleavage reactions of the respective dimer starting materials. Complex **7** is a yellow solid which shows the expected singlet at δ(P) 54.5 ppm. The amide proton is shifted downfield in the ^1H NMR spectra ($CDCl_3$), to δ(H) 10.7 ppm, this mirrors the shift of the amide proton in **5**, and also in common with **5** the $^2J_{P-H}$ coupling constant is enlarged, stretching to 22 Hz. The IR spectrum shows the ν(N–H) stretch has shifted to a much greater extent than seen in **5**, this could be due to much stronger hydrogen bonding interaction being present in **7**, and once again the ν(C=O) is relatively unmoved in comparison with the free ligand being found at 1686 cm^{-1}. In the solid state (Table 3 and Fig. 7), complex **7** has a hydrogen-bonds between H(2)–N(5) and H(2)–Cl(1) [N(2)–Cl(1) 3.204 Å and N(2)–N(5) 2.67(8) Å]. The interaction with Cl(1) causes the five-membered ring to distort with a N(5)–C(4)–C(3)–N(2) torsion angle of −15.08°.

Complexes **8**, **9** and **10** are similar and display the expected spectroscopic properties.

Complexes of ruthenium, rhodium and iridium were synthesised to further investigate the coordination of dpppa. $[RuCl_2(p\text{-Cymene})(dpppa\text{-}P)]$ (**11**) was generated by reaction of $[RuCl(\mu\text{-}Cl)(p\text{-Cymene})]_2$ with dpppa and isolated as a red solid. The rhodium and iridium complexes were synthesised by reaction with $[MCl(\mu\text{-}Cl)(\eta^5\text{-}C_5Me_5)]_2$ (where M = Rh or Ir), and dpppa, to give complexes of the type $[MCl_2(\eta^5\text{-}C_5\ Me_5)(dpppa\text{-}P)]$ (where M = Rh (**12**) or Ir (**13**)). Crystals of **12** and **13** proved to be isomorphous; here we will only consider **13** (Table 3 and Fig. 8). On inspection of the ligand

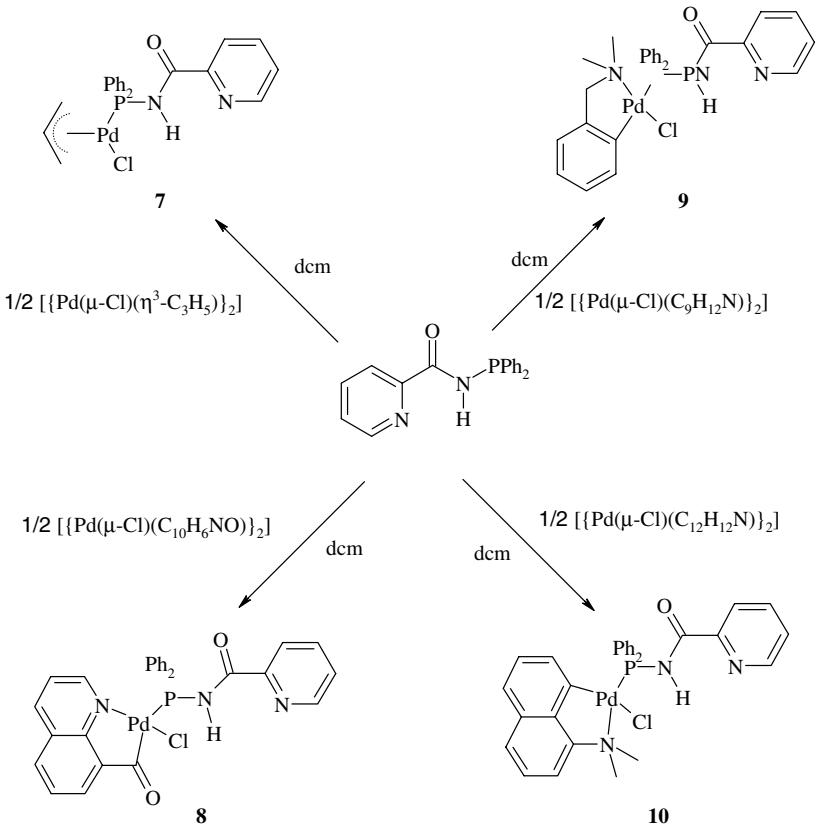

Fig. 6. Reaction of dpppa with palladium dimers.

Table 3
Selected bond lengths (Å) and angles (°) for monodentate complexes of dpppa: [PdCl(allyl)(dpppa-*P*)] (**7**), [$IrCl_2(\eta^5\text{-}C_5Me_5)$(dpppa-*P*)] (**13**), [$PtCl_2$(dpppa-*P*)($PEt_3$)] (**15**) and [AuCl(dpppa-*P*)] (**17**)

	7	13	15	17
Bond lengths				
P(1)–M(1)	2.2786(8)	2.287(2)	2.2389(14)	2.2168(18)
M(1)–Cl(1)	2.3800(8)	2.4126(19)	2.3446(14)	2.2993(17)
M(1)–Cl(2)		2.4034(18)	2.3554(13)	
P(1)–N(2)	1.703(3)	1.699(7)	1.693(4)	1.694(5)
N(2)–C(3)	1.366(4)	1.379(10)	1.377(7)	1.395(8)
C(3)–C(4)	1.512(4)	1.494(11)	1.507(8)	1.495(9)
O(3)–C(3)	1.216(4)	1.233(9)	1.211(6)	1.215(8)
N(2)···Cl	3.204(7)	3.403(6)	3.011(5)	
N(2)···N(5)	2.67(8)	2.71(1)	2.64(7)	2.64(7)
Bond angles				
P(1)–M(1)–Cl(1)	96.52(3)	88.49(7)	175.94(5)	177.82(6)
P(1)–M(1)–Cl(2)		87.72(7)	91.05(5)	
Cl(1)–M(1)–Cl(2)		87.57(7)		
C(3)–N(2)–P(1)	130.3(2)	129.0(5)	126.6(4)	125.6(4)
O(3)–C(3)–N(2)	124.5(3)	123.3(7)	124.3(5)	124.1(6)
O(3)–C(3)–C(4)	121.4(3)	122.1(7)	122.6(5)	122.6(6)
N(2)–C(3)–C(4)	114.1(3)	114.6(6)	113.1(5)	113.3(6)

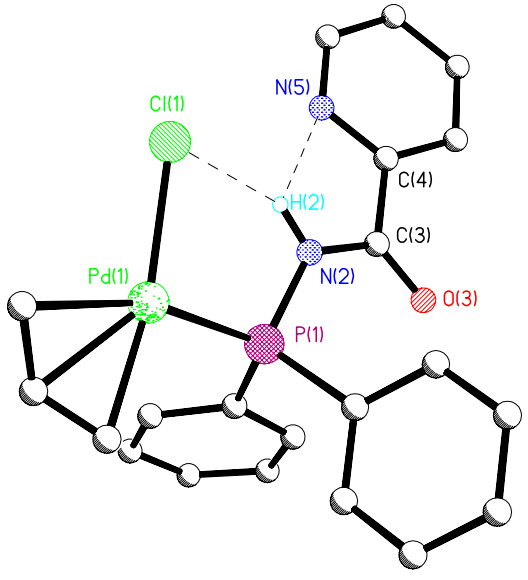

Fig. 7. Crystal structure of [PdCl(allyl)(dpppa-*P*)] (**7**).

backbone, we observe a modest shift out of plane, with the mean deviation of C(3)–N(2)–P(1)–Ir(1) being 0.1160Å, this is the highest deviation seen so far with monodentate dpppa complexes but is not unexpected the analogous complex formed with 2-(diphenylphosphino)hydrazinopyridine displays a similar deviation [18]. Also as seen with the 2-(diphenylphosphino)hydrazinopyridine example there are two types of hydrogen bonding displayed, the first is between the amine proton and one of the chlorides [N(2)···Cl(2) 3.403 Å]. The second type of hydrogen bonding observed in the complex is of

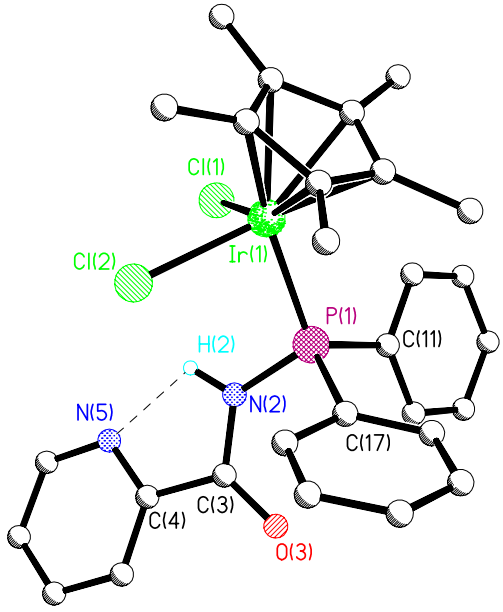

Fig. 8. Crystal structure of [IrCl2(η^5-C_5Me_5)(dpppa-*P*)] (**13**).

a similar motif to that found in the free ligand, oxide and sulfide [N(2)–N(5) 2.71(1) Å].

Dpppa reacts with [{PtCl(μ-Cl)(PR_3)}$_2$](PR_3=PMe_2Ph or PEt_3), to give complexes of the type *cis*-[$PtCl_2$(dpppa-*P*)(PR_3)](PR_3=PMe_2Ph (**14**) or PEt_3 (**15**)). Monodentate binding was the only observed mode of coordination in both instances. The ^{31}P NMR shows the expected AM spectra and the large $^1J_{Pt-P}$ coupling constants and the small $^2J_{P-P}$ couplings are consistent with a *cis*-arrangement of phosphorus around the platinum centre.

In **15** (Table 3 and Fig. 9), the C(3)–N(2)–P(1)–Pt(1) backbone is essentially planar, with a mean deviation of 0.0334 Å, which is consistent with the other structures

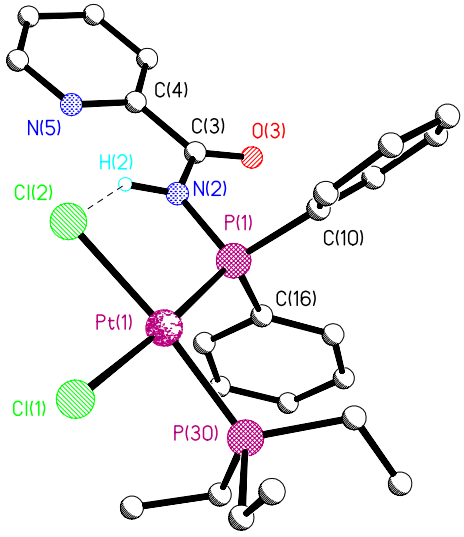

Fig. 9. Crystal structure of [$PtCl_2$(dpppa-*P*)(PEt_3)] (**15**).

described above. Two different hydrogen bonding motifs are again observed within the complex [N(2)–Cl(2) 3.011, N(2)–N(5) 2.64(7) Å]

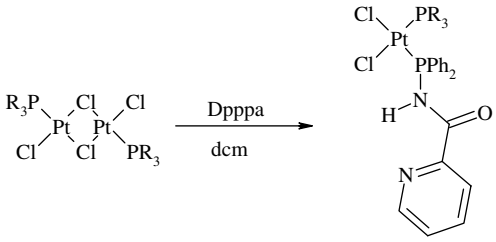

(3)

PR_3 = Me_2PhP (**14**) or Et_3 (**15**)

Reaction of dpppa with [RhCl(cod)]$_2$ in dichloromethane gave [RhCl(cod)(dpppa-*P*)] (**16**) as a yellow solid in average yield (63%), (P) 58.3 $^1J_{Rh-P}$ = 162 Hz.

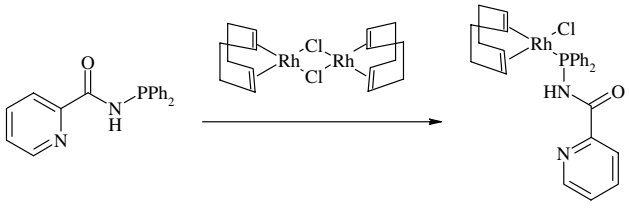

16

(4)

When dpppa was reacted with [AuCl(tht)] in dichloromethane the anticipated monodentate [AuCl(dpppa-*P*)] (**17**) complex was generated as a colourless solid, δ(P) 53.5 ppm, On inspection of the crystal data (Table 3 and Fig. 10), we see the now familiar hydrogen-bonding pattern [N(2)···N(5) 2.64 Å, N(2)–H(2)–N(5) 114°].

Chelation of dpppa was achieved by reaction of a chloride containing monodentate complex with BuLi

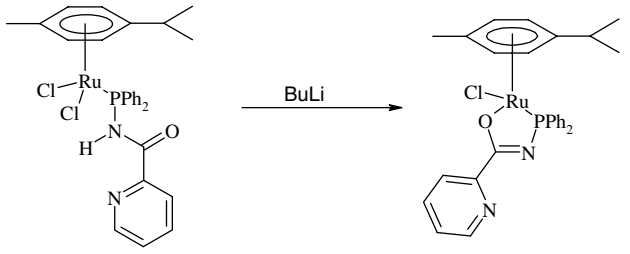

11 **18**

(5)

As can be seen this generates a five-membered 'true' heterocycle, with the oxygen binding to the metal centre. The ^{31}P NMR shows a downfield shift in the complex, to δ(P) 101.5 ppm, indicating chelation. As expected the amide proton disappears from the ^{1}H spectrum, and the pyC[6]H shift and coupling constant is relatively unchanged. The IR spectrum also confirms the loss of the amide proton, and shows a ν(C–O) stretch at 1351 cm^{-1}, confirming C–O is present and not C=O. Acceptable microanalytical data was obtained. The five-membered

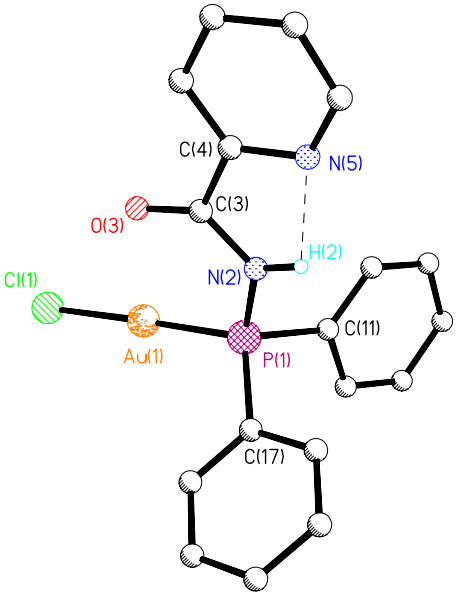

Fig. 10. Crystal structure of [AuCl(dpppa-*P*)] (**17**).

ring that is formed is essentially planar (Fig. 11 and Table 4), the Ru–O and Ru–P bond lengths within the ring are normal whilst the angles are typical for a five membered ring.

A second mode of chelation [via the pyridyl nitrogen] is possible for dpppa. This was facilitated by reaction of the appropriate monodentate complex with a halide abstractor [$AgBF_4$ or $AgClO_4$] generating the cationic species [RuCl(*p*-Cymene)(dpppa-*P*,*N*)][ClO_4] (**19**) and [RhCl(η^5-C_5Me_5)(dpppa-*P*,*N*)][BF_4] (**20**) in good yield (93% and 74%, respectively). The ^{31}P NMR shows the downfield shift generated by chelate ring formation with δ(P) 98.1 and 85.2 ppm for **19** and **20**, respectively, also the amine proton is shifted back toward the free ligand

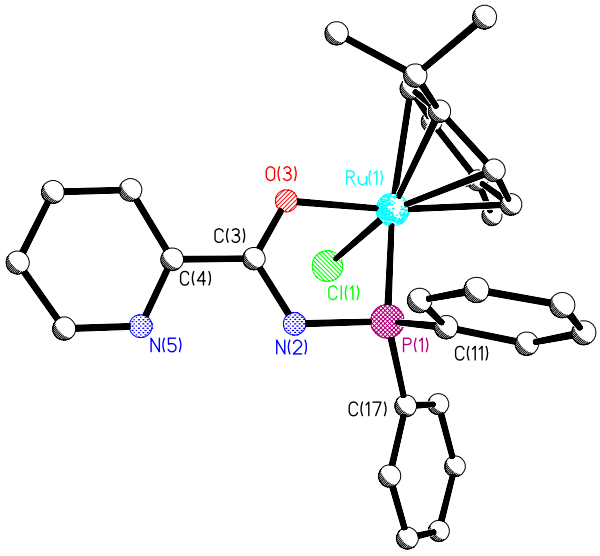

Fig. 11. Crystal structure of [RuCl(p-Cymene)(dpppa-*P*,*O*)] (**18**).

Table 4
Selected bond lengths (Å) and angles (°) for *P*, *O* bidentate [RuCl(*p*-Cymene)(dpppa-*P*,*O*)] (**18**)

Bond lengths			
P(1)–Ru(1)	2.2812(19)	Ru(1)–O(3)	2.097(5)
P(1)–N(2)	1.715(6)	N(2)–C(3)	1.380(10)
C(3)–O(3)	1.276(9)	C(3)–C(4)	1.465(10)
C(4)–C(9)	1.423(10)	C(4)–N(5)	1.315(9)
Ru(1)–Cl(1)	2.3910(18)		
Bond angles			
P(1)–Ru(1)–O(3)	80.28(14)	P(1)–Ru(1)–Cl(1)	86.32(6)
O(3)–Ru(1)–Cl(1)	81.53(14)		
Ru(1)–P(1)–N(2)	101.2(2)	P(1)–N(2)–C(3)	116.3(5)
N(2)–C(3)–O(3)	120.6(6)	C(3)–O(3)–Ru(1)	120.0(5)
N(2)–C(3)–C(4)	117.5(7)	O(3)–C(3)–C(4)	121.9(7)
C(3)-C(4)–C(9)	119.2(7)	C(3)–C(4)–N(5)	117.0(7)
C(9)–C(4)–N(5)	123.8(7)		

value at δ(H) 8.6 ppm in both cases [$^2J_{P-H}$ of 5 and 4 Hz, respectively].

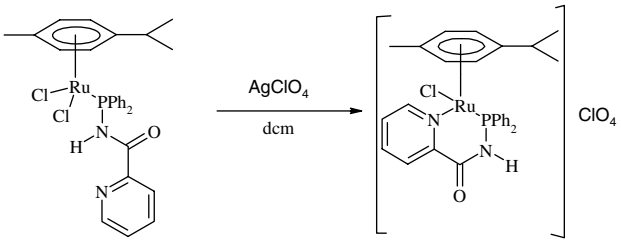

11 **19**

(6)

3. Experimental

3.1. General conditions

All manipulations were carried out in an atmosphere of nitrogen, unless stated otherwise. All solvents were either freshly distilled from an appropriate drying agent (thf, Et_2O from sodium, CH_2Cl_2 from calcium hydride) or obtained as anhydrous grade from Aldrich. ^{1}H and ^{31}P NMR spectra were recorded using a Jeol Delta FT (270 MHz) spectrometer. IR spectra were recorded as KBr discs (prepared in air) on a Perkin–Elmer 2000 FTIR/Raman spectrometer. All significant peaks (>800 cm^{-1}) are quoted to serve as a fingerprint. Silver salts, 2-picolinamide (Aldrich Chemical Co.) and BuLi (2.5 M, Lancaster) were purchased and used as received. Triethylamine and chlorodiphenylphosphine were distilled prior to use. Dimethylaminopyridine (DMAP) was sublimed before use. The various metal starting materials were made by the appropriate literature methods; [AuCl(tht)] [19], [MCl_2(cod)] (M = Pt or Pd; cod = cycloocta-1,5-diene) [20,21], [PdCl(L–L)]$_2$ dimers [22], [{PtCl(μ-Cl)(PMe_2 Ph)}$_2$] [23], [{MCl(μ-Cl)-(Cp*)}$_2$] (M = Rh or Ir) [24], [{Rh(μ-Cl)(cod)}$_2$] [25],

$[\{RuCl(\mu\text{-}Cl)(\eta^6 p\text{-}MeC_6H_4^iPr)\}_2]$ [26], $[\{PdCl(\mu\text{-}Cl)(\eta^3\text{-}C_3H_5)\}_2]$ [27].

3.1.1. 2-Diphenylphosphinopicolinamide (*1*)

Chlorodiphenylphosphine (3.7 cm^3, 20 mmol) was added to a solution of 2-picolinamide (2.5 g, 20 mmol), triethylamine (3.0 cm^3, 21 mmol) and DMAP (240 mg, 2.0 mmol) in thf (100 cm^3) and refluxed overnight. The reaction mixture was filtered to remove a white solid (Et_3NHCl) and washed with thf (50 cm^3). The solvent was removed in vacuo leaving a pale yellow solid. This solid was recrystallised by cooling a concentrated methanol solution at 4 °C overnight (yield: 3.38 g, 55%). *Anal.* Calc. for $C_{18}H_{15}N_2OP$: C, 70.6; H, 4.9; N, 9.1. Found: C, 70.29; H, 4.58; N, 8.95%. ν_{max}/cm^{-1}: 3297, 1691, 1452, 1412, 996. ^{31}P NMR δ 22.0 ppm ^1H NMR ($CDCl_3$), 8.65 (1H, d, $J = 4$ Hz, N–H), 8.54 (1H, d, $J = 5$ Hz, pyC[6]H), 8.26 (1H, d, $J = 8$ Hz, pyC[3]H), 7.85 (1H, t, $J = 8$ Hz, pyC[5]H), 7.6–7.2 (11H, m, aromatic).

3.1.2. 2-Diphenylphosphinopicolinamide oxide (*2*)

Aqueous H_2O_2 (30% w/w, 0.0071 cm^3, 0.065 mol) was added dropwise over 5 min to a solution of dpppa (200 mg, 0.065 mol) in thf (10 cm^3) and the mixture stirred for 30 min and then reduced to dryness. The residue was dissolved in CH_2Cl_2, and filtered while hot and subsequently dried over $MgSO_4$. The filtrate was stored at −4 °C during which time a crystalline solid was deposited and filtered and dried. Yield: 85 mg, 41%. *Anal.* Calc. for $C_{18}H_{15}N_2O_2P$: C, 67.1; H, 4.69; N, 8.69. Found: C, 66.7; H, 4.26; N, 8.41%. ν_{max}/cm^{-1}: 3302, 1694, 1451, 1403, 1215, 998. ^{31}P NMR δ 22.1 ppm. ^1H NMR ($CDCl_3$), δ 9.46 (1H, d, $J = 9$ Hz, N–H), 8.58 (1H, d, $J = 4$ Hz, pyC[6]H), 8.1–7.7 (6H, m, aromatic), 7.5–7.2 (7H, m, aromatic).

3.1.3. 2-Diphenylphosphinopicolinamide sulfide (*3*)

Sulfur (105 mg, 3.3 mmol) was added to a solution of 2-diphenylphosphinopicolinamde (1 g, 3.3 mmol) in toluene (100 cm^3) and refluxed overnight. The solvent was removed in vacuo leaving an off-white solid. This solid was recrystallised by cooling a concentrated toluene solution at 4 °C overnight (yield: 900 mg, 82%). *Anal.* Calc. for $C_{18}H_{15}N_2OPS$: C, 63.9; H, 4.47; N, 8.28. Found: C, 63.6; H, 4.22; N, 8.26%. ν_{max}/cm^{-1}: 3268, 1689, 1387, 997. ^{31}P NMR δ 54.4 ppm. ^1H NMR ($CDCl_3$), δ 9.3 (1H, d, $J = 11$ Hz, N–H), 8.6 (1H, d, $J = 1$ Hz, pyC[6]H), 8.1–7.8 (6H, m, aromatic), 7.6–7.4 (7H, m, aromatic).

3.1.4. 2-Diphenylphosphinopicolinamide selenide (*4*)

Selenium (52 mg, 0.65 mmol) was added to a solution of 2-diphenylphosphinopicolinamde (200 mg, 0.65 mmol) in toluene (5 cm^3) and refluxed overnight. The solvent was removed in vacuo leaving an off-white solid. This solid was recrystallised by cooling a concentrated toluene solution at 4 °C overnight (yield: 105 mg, 48%). *Anal.* Calc. for $C_{18}H_{15}N_2OPSe$: C, 56.1; H, 3.92; N, 7.27. Found: C, 56.4; H, 3.77; N, 7.05%. ν_{max}/cm^{-1}: 3288, 1698, 1391, 998. ^{31}P NMR ($CDCl_3$) δ 47.8, $^1J_{P-Se} = 788$ Hz. ^1H NMR ($CDCl_3$), δ 9.3 (1H, d, $J = 13$ Hz, N–H), 8.6 (1H, d, $J = 1$ Hz, pyC[6]H), 8.2–7.7 (6H, m, aromatic), 7.5–7.3 (7H, m, aromatic).

3.1.5. $[PtCl_2(dpppa\text{-}P)_2]$ (*5*)

Dpppa (50 mg, 0.16 mmol) and $[PtCl_2(cod)]$ (30 mg, 0.08 mmol) were weighed into a schlenk type flask and CH_2Cl_2 (5 cm^3) added. The solution was stirred for 10 min and the majority of the solvent removed in vacuo. A white solid was precipitated after addition of Et_2O (20 cm^3) then isolated by filtration and washed with further ether (10 cm^3) (yield: 57 mg, 80%). *Anal.* Calc. for $C_{36}H_{30}N_4O_2P_2Cl_2Pt(CH_2Cl_2)_{0.5}$: C, 47.6; H, 3.39; N, 6.08. Found: C, 47.5; H, 3.20; N, 5.81%. ν_{max}/cm^{-1}: 3251, 1692, 1446, 1391, 998, 320, 302. ^{31}P NMR ($CDCl_3$) δ 31.2 ppm, $^1J_{Pt-P} = 3984$ Hz. ^1H NMR ($CDCl_3$), 10.7 (2H, d, $J = 15$ Hz, N–H), 8.5 ((2H, d, $J = 4$ Hz), pyC[6]H), 7.7–7.2 (26H, m, aromatic).

3.1.6. $[PdCl_2(dpppa\text{-}P)_2]$ (*6*)

Dpppa (258 mg, 0.86 mmol) and $[PdCl_2(cod)]$ (120 mg, 0.43 mmol) were weighed into a schlenk type flask and CH_2Cl_2 (10 cm^3) added. The solution was stirred for 10 min. This resulted in precipitation of the desired product, which was filtered and washed with ether (10 cm^3). Yield: 307 mg, 92%. *Anal.* Calc. for $C_{36}H_{30}N_4O_2P_2Cl_2Pd$: C, 54.6; H, 3.83; N, 7.09. Found: C, 53.9; H, 3.64; N, 6.85%. ν_{max}/cm^{-1}: 3232, 1694, 1446, 1392, 997, 310.

3.1.7. $[PdCl(allyl)(dpppa\text{-}P)]$ (*7*)

Reaction followed as for **5**. Dpppa (84 mg, 0.27 mmol) and $[\{Pd(\mu\text{-}Cl)(\eta^3\text{-}C_3H_5)\}_2]$ (50 mg, 0.13 mmol) gave a pale yellow solid, (yield: 117 mg, 87%). *Anal.* Calc. for $C_{21}H_{20}N_2OPClPd$: C, 51.5; H, 4.12; N, 5,72. Found: C, 51.8; H, 3.93; N, 5.61%. ν_{max}/cm^{-1}: 3193, 1686, 1446, 1396, 1103, 998. ^{31}P NMR ($CDCl_3$) δ 54.5 ppm. ^1H NMR ($CDCl_3$), 10.5 (1H, d, $J = 22$ Hz, N–H), 8.7 (1H, d, $J = 4$ Hz, pyC[6]H), 7.8–7.4 (12H, m, aromatic), 5.5 (1H, m, allyl), 4.7 (1H, t, $J = 7$ Hz, allyl), 3.7 (1H, t, $J = 13$ Hz, allyl), 3.3 (1H, d, $J = 7$ Hz, allyl), 2.6 (1H, d, $J = 13$ Hz, allyl).

3.1.8. $[PdCl(C_{10}H_6NO)(dpppa\text{-}P)]$ (*8*)

Dpppa (205 mg, 0.66 mmol) and $[Pd(\mu\text{-}Cl)(C_{10}H_6NO)]_2$ (200 mg, 0.33 mmol) were weighed into a schlenk type flask and CH_2Cl_2 (10 cm^3) added. The solution was stirred for 10 min. This resulted in precipitation of the desired product, which was filtered and washed with ether (10 cm^3) (yield: 371 mg, 95%). *Anal.* Calc. for $C_{28}H_{21}N_3O_2PClPd$: C, 55.6; H, 3.50; N, 6.95.

Found: C, 55.7; H, 3.18; N, 6.04%. ν_{max}/cm^{-1}: 3231, 1673, 1446, 1394, 996, 322. FAB MS: *m/z* 568 ($[M - Cl]^+$).

3.1.9. [PdCl(C9H12N)(dpppa-P)] (9)

Dpppa (223 mg, 0.72 mmol) and $[Pd(\mu\text{-}Cl)(C_9H_{12}N)]_2$ (200 mg, 0.36 mmol) gave a yellow solid, (yield: 136 mg, 64%). *Anal.* Calc. for $C_{27}H_{25}N_3OPClPd(CH_2Cl_2)_{0.5}$: C, 52.9; H, 4.51; N, 6.73. Found: C, 54.3; H, 4.46; N, 6.07%. ν_{max}/cm^{-1}: 3187, 1683, 1449, 1391, 997. ^{31}P NMR ($CDCl_3$) δ 63.3 ppm. ^1H NMR ($CDCl_3$) δ 10.9 (1H, d, $J = 19$ Hz, N–H), 8.6 (1H, d, $J = 4$ Hz, pyC[6]H), 8.1 (1H, m, aromatic), 8.0 (1H, m, aromatic), 7.8 (1H, m, aromatic), 7.4 (8H, m, aromatic) 7.0, (1H, m, aromatic), 6.8 (1H, m, aromatic), 6.4 (1H, m, aromatic), 3.4 (2H, d $J = 3$ Hz, CH_2) 2.8 (6H, d, $J = 3$ Hz, NMe–H). FAB MS: *m/z* 546 ($[M - Cl]^+$).

3.1.10. [PdCl(C12H12N)(dpppa-P)] (10)

Reaction followed as for **5**. Dpppa (197 mg, 0.64 mmol) and $[Pd(\mu\text{-}Cl)(C_{12}H_{12}N)]_2$ (200 mg, 0.32 mmol) gave a yellow/green solid, (yield: 176 mg, 44%). *Anal.* Calc. for $C_{30}H_{27}N_3OPClPd$: C, 58.2; H, 3.40; N, 6.80. Found: C, 58.09; H, 2.92; N, 6.62%. ν_{max}/cm^{-1}: 3203, 1678, 1446, 1388, 997. ^{31}P NMR ($CDCl_3$) δ 64.3 ppm. ^1H NMR ($CDCl_3$) 11.3 (1H, d, $J = 18$ Hz, N–H), 8.7 (1H, d, $J = 5$ Hz, pyC[6]H), 8.2 (4H, m, aromatic), 8.0 (1H, d, aromatic), 7.8 (1H, d, aromatic), 7.6 (1H, d, aromatic), 7.5–7.4 (10H, m, aromatic), 6.7 (1H, m, aromatic), 6.5 (1H, m, aromatic), 3.5 (6H, d, $J = 3$ Hz, NMe–H).

3.1.11. [RuCl2(p-Cymene)(dpppa-P)] (11)

Prepared as for **5**. Dpppa (200 mg, 0.66 mmol) and $[\{RuCl(\mu\text{-}Cl)(p\text{-Cymene})\}_2]$ (200 mg, 0.33 mmol) gave a red solid, (yield: 324 mg, 84%). *Anal.* Calc. for $C_{28}H_{29}N_2OPCl_2Ru$: C, 54.9; H, 4.77; N, 4.57. Found: C, 55.8; H, 4.82; N, 4.07%. ν_{max}/cm^{-1}: 3261, 1684, 1449, 1406, 997, 292. ^{31}P NMR ($CDCl_3$) δ 59.3 ppm.. ^1H NMR ($CDCl_3$) δ 9.6 (1H, d, $J = 18$ Hz, N–H), 8.6 (1H, d, $J = 7$ Hz, pyC[6]H), 8.0 (6H, m, aromatic), 7.8 (1H, m, aromatic), 7.6 (1H, m, aromatic) 7.4 (4H, m, aromatic), 7.2 (1H, m, aromatic), 5.3 (2H, m, aromatic [*p*-Cymene]), 5.2 (2H, m, aromatic [*p*-Cymene]), 2.6 (1H, m, Pr^i-H), 1.8 (3H, m, Me–H), 0.8 (6H, d, $J = 7$ Hz, Pr^i–Me).

3.1.12. [RhCl2(η5-C5Me5)(dpppa-P)] (12)

Prepared as for **5**. Dpppa (198 mg, 0.65 mmol) and $[\{RhCl(\mu\text{-}Cl)(\eta^5\text{-}C_5Me_5)\}_2]$ (200 mg, 0.32 mmol) gave a orange solid, (yield: 363 mg, 91%). *Anal.* Calc. for $C_{28}H_{30}N_2OPCl_2$ Rh: C, 54.6; H, 4.91; N, 4.55. Found: C, 54.0; H, 4.65; N, 4.40%. ν_{max}/cm^{-1}: 3298, 1678, 1449, 1410, 997, 282. ^{31}P NMR ($CDCl_3$) δ 62.8 ppm, J_{RhP} 150 Hz. ^1H NMR ($CDCl_3$) δ 9.9 (1H, d, $J = 18$ Hz, N–H), 8.6 (1H, d, $J = 5$ Hz, pyC[6]H), 8.1 (4H, m, aromatic), 7.9 (1H, d, aromatic), 7.7 (1H, m, aromatic), 7.5 (7H, m, aromatic), 7.3 (1H, m, aromatic), 1.4 (15H, d, $J = 12$ Hz, Cp*–H).

3.1.13. [IrCl2(η5-C5Me5)(dpppa-P)] (13)

Prepared as for **5**. Dpppa (77 mg, 0.25 mmol) and $[\{IrCl(\mu\text{-}Cl)(\eta^5\text{-}C_5Me_5)\}_2]$ (100 mg, 0.13 mmol) gave a yellow/orange solid, (yield: 162 mg, 91%). *Anal.* Calc. for $C_{28}H_{30}N_2OPCl_2Ir$: C, 47.6; H, 4.29; N, 3.98. Found: C, 47.1; H, 4.27; N, 3.83%. ν_{max}/cm^{-1}: 3288, 1678, 1450, 1412, 997. ^{31}P NMR ($CDCl_3$) δ 32.7 ppm. ^1H NMR ($CDCl_3$) δ 10.2 (1H, d, $J = 17$ Hz, N–H), 8.6 (1H, d, $J = 4$ Hz, pyC[6]H), 8.1–7.7 (6H, m, aromatic), 7.4 (6H, m, aromatic), 1.4 (15H, d, $J = 2$ Hz, Cp*–H).

3.1.14. [PtCl2(Me2PhP)(dpppa-P)] (14)

Prepared as for **5**. Dpppa (76 mg, 0.25 mmol) and $[\{PtCl(\mu\text{-}Cl)(PMe_2Ph)\}_2]$ (100 mg, 0.12 mmol) gave a white solid, (yield: 114 mg, 65%). *Anal.* Calc. for $C_{26}H_{26}N_2OP_2Cl_2Pt$: C, 44.0; H, 3.69; N, 3.95. Found: C, 43.77; H, 3.61; N, 3.82%. ν_{max}/cm^{-1}: 1686, 1447, 1384, 1107. ^{31}P NMR ($CDCl_3$) δ 30.9 ($^1J_{Pt-P} = 3930$), −14.5 ($^1J_{Pt-P} = 3500$), $^2J_{P-P} = 19$ Hz. ^1H NMR ($CDCl_3$) δ 11.1 (1H, d, $J = 15$ Hz, N–H), 8.6 (1H, d, $J = 4$ Hz, pyC[6]H), 8.0–7.7 (6H, m, aromatic), 7.5–7.0 (12H, m, aromatic), 1.6–1.5 (6H, d, $J = 11$ Hz, Me–H).

3.1.15. [PtCl2(Et3P)(dpppa-P)] (15)

A solution of $[\{PtCl(\mu\text{-}Cl)(PEt_3)\}_2]$ (50 mg, 0.07 mmol), in CH_2Cl_2 (10 cm^3) was added dropwise to a solution of dpppa (40 mg, 0.13 mmol) in CH_2Cl_2 (10 cm^3). The solution was stirred for 10 min and the majority of the solvent removed in vacuo. A white solid was precipitated after addition of Et_2O then isolated by filtration and washed with further ether (10 cm^3) (yield: 55 mg, 66%). *Anal.* Calc. for $C_{24}H_{30}N_2OP_2Cl_2Pt$: C, 41.9; H, 4.38; N, 4.06. Found: C, 42.8; H, 3.60; N, 4.15%. ν_{max}/cm^{-1}: 3162, 1687, 1446, 1385, 998, 310. ^{31}P NMR ($CDCl_3$) δ 30.0 ($^1J_{Pt-P} = 4010$), 7.6 ($^1J_{Pt-P} = 3360$), $^2J_{P-P} = 19$ Hz. ^1H NMR ($CDCl_3$) δ 11.4 (1H, d, $J = 16$ Hz, N–H), 8.7 (1H, d, $J = 1$ Hz, pyC[6]H), 8.2 (2H, m, aromatic), 7.9–7.7 (5H, m, aromatic), 7.5–7.3 (3H, m, aromatic), 7.1 (1H, m, aromatic), 1.5 (6H, m, $-CH_2-$), 0.9 (9H, m, Me–H).

3.1.16. [RhCl(cod)(dpppa-P)] (16)

Dpppa (125 mg, 0.41 mmol), and $[\{Rh(\mu\text{-}Cl)(cod)\}_2]$ (100 mg, 0.20 mmol) were weighed into a schlenk type flask and toluene (5 cm^3) added. The solution was stirred for 10 min and the majority of the solvent removed in vacuo. A yellow solid was precipitated after addition of *n*-hexane (20 cm^3) then isolated by filtration and washed with further hexane (10 cm^3) (yield: 142 mg, 63%). *Anal.* Calc. for $C_{26}H_{27}N_2OPClRh$: C, 56.5; H, 4.92; N, 5.07. Found: C, 56.05; H, 4.76; N, 4.90%. ν_{max}/cm^{-1} : 3194, 1698, 1448, 1407, 997. ^{31}P NMR

($CDCl_3$) δ 58.3 ($^1J_{Rh-P}$ = 162 Hz). ^1H NMR (270 MHz, $CDCl_3$) δ 10.4 (1H, d, J = 21Hz, N–H), 8.6 (1H, d, J = 2Hz, pyC[6]H), 8.0–7.8 (6H, m, aromatic), 7.6–7.2 (6H, m, aromatic), 2.3 (4H, br.s, cod), 2.0 (8H, br.s, cod).

3.1.17. [AuCl(dpppa-P)] (17)

Prepared as for **5**, Dpppa (67 mg, 0.021 mmol) and [AuCl(tht)] (70 mg, 0.021 mmol) reacted in CH_2Cl_2 gave a white solid, (yield: 78 mg, 70%). *Anal.* Calc. for $C_{15}H_{15}N_2OPClAu$: C, 40.0; H, 2.80; N, 5.20. Found: C, 39.5; H, 2.75; N, 5.09%. ν_{max}/cm^{-1} : 3288, 1698, 1391, 998. ^{31}P NMR ($CDCl_3$) 53.5 ppm. ^1H NMR ($CDCl_3$) 9.1 (1H, d, J = 13 Hz, N–H), 8.6 (1H, d, J = 1 Hz, pyC[6]H), 8.2–7.5 (13H, m, aromatic).

3.1.18. [RuCl(p-Cymene)(dpppa-P,O)] (18)

A solution of BuLi (65 μ l,. 0.16 mmol) in THF (2 cm^3) was added dropwise to a solution of [$RuCl_2$-(*p*-Cymene)(dpppa-*P*)] (100 mg, 0.16 mmol) in THF (5 cm^3) at 0 °C. The solution was stirred for 10 min and allowed to reach room temperature, and filtered through a bed of celite. The majority of the solvent removed in vacuo. A dull beige solid was precipitated after addition of Et_2O then isolated by filtration and washed with further ether (10 cm^3) (yield: 47 mg, 52%). Recryst from CH_2Cl_2/hexane. *Anal.* Calc. for $C_{28}H_{28}N_2OPCl$-$Ru(CH_2Cl_2)$: C, 52.7; H, 4.57; N, 4.24. Found: C, 51.9; H, 4.00; N, 4.38%. ν_{max}/cm^{-1}: 3312, 1351, 249. ^{31}P NMR ($CDCl_3$) δ 101.5. ^1H NMR (270 MHz, $CDCl_3$) δ 8.4 (1H, d, J = 8 Hz, pyC[6]H), 7.9–7.7 (3H, m, aromatic), 7.6–7.2 (10H, m, aromatic), 6.0 (1H, d, J = 6 Hz, *p*-Cy-H), 5.7 (1H, d, J = 4 Hz, *p*-Cy-H), 5.4 (1H, d, J = 6 Hz, *p*-Cy-H), 5.0 (1H, d, J = 4 Hz, *p*-Cy-H), 2.5 (1H, m, C–H), 2.0 (3H, s, Me–H), 1.1 (6H, d, J = 10 Hz, Pr^i-H).

3.1.19. [RuCl(p-Cymene)(dpppa-P,N)][ClO_4] (19)

$AgClO_4$ (33 mg, 0.16 mmol) was added under dark conditions to a solution of [$RuCl_2$(*p*-Cy)(dpppa-*P*)] (100 mg, 0.16 mmol) in CH_2Cl_2 (5 cm^3). The solution was stirred overnight and filtered through a celite bed. The majority of the solvent was removed in vacuo. An orange solid was precipitated after addition of Et_2O then isolated by filtration and washed with further ether (10 cm^3) (yield: 87 mg, 0.15 mmol, 93%). *Anal.* Calc. for $C_{28}H_{28}N_2O_5PCl_2Ru(CH_2Cl_2)_{0.5}$: C, 47.6; H, 4.21; N, 3.90. Found: C, 47.2; H, 4.00; N, 3.89%. ν_{max}/cm^{-1}: 1482, 1084. ^{31}P NMR ($CDCl_3$) δ 98.1 ppm. ^1H NMR ($CDCl_3$) δ 8.6 (1H, d, J = 5 Hz, N–H), 8.2 (1H, d, J = 8 Hz, pyCH), 8.0 (1H, t, J = 8 Hz, pyCH), 7.8 (2H, m, aromatic), 7.7–7.5 (10H, m, aromatic), 5.8 (2H, m, *p*-Cymene-H), 5.6 (2H, m, *p*-Cymene-H), 2.8 (1H, m, C–H), 2.1 (3H, s, Me–H), 1.3 (6H, t, J = 6 Hz, Pr^i-H).

Table 5
Crystallographic data for complexes **1**, **2**, **3**, **7**, **13**, **15**, **17** and **18**

	1	**2**	**3**	**7**	**13**	**15**	**17**	**18**
	Mercury/293K/Cu	Smart/125K/Mo	Smart/125K/Mo	Smart/125K/Mo	Smart/125K/Mo	Smart/125K/Mo	Smart/298K/Mo	Smart/125K/Mo
Formula	$C_{18}H_{15}N_2OP$	$C_{18}H_{15}N_2O_2P$	$C_{18}H_{15}N_2OPS$	$C_{21}H_{20}N_2OClPPd$	$C_{28}H_{30}N_2OPCl_2Ir$	$C_{24}H_{30}N_2OP_2Cl_2Pt$	$C_{18}H_{15}N_2OPClAu$	$C_{29}H_{30}N_2OPCl_3Ru$
M	306.29	322.29	338.35	489.21	704.61	690.43	538.71	660.94
Crystal system	triclinic	monoclinic	triclinic	triclinic	orthorhombic	monoclinic	monoclinic	orthorhombic
Space group	$P\bar{1}$	$P2(1)/c$	$P\bar{1}$	$P\bar{1}$	$P(2)1(2)1(2)1$	$P2(1)/c$	$P2(1)/c$	$Pca2(1)$
a (Å)	8.4419(17)	8.4497(1)	8.7701(17)	9.9452(12)	8.2751(16)	15.771(2)	13.271(4)	17.576(3)
b (Å)	10.271(2)	17.369(3)	9.0319(17)	15.3618(19)	17.750(3)	10.4905(16)	12.119(4)	9.0772(15)
c (Å)	10.416(2)	11.264(2)	11.043(2)	15.7040(19)	17.892(4)	17.092(3)	11.111(4)	17.593(3)
α (°)	110.94(3)		77.738(3)	118.018(2)				
β (°)	103.74(3)	108.389(3)	85.554(3)	101.038(2)		113.589(2)	102.124(6)	
γ (°)	90.27(3)		72.540(3)	95.688(2)				
U (Å) [8–10]	815.3(3)	1568.8(5)	815.3(3)	2028.7(4)	2628.1(9)	2591.6(7)	1747.1(10)	2806.8(8)
Z	2	4	2	4	4	4	4	4
ρ_{calcd} (g/cm^3)	1.248	1.365	1.378	1.602	1.781	1.770	2.048	1.564
μ (mm^{-1})	1.511	0.186	0.302	1.138	5.369	5.764	8.672	0.927
Reflections measured	6683	6672	4092	10246	11,347	10858	7308	13398
Independent reflections	2850	2230	2273	5783	3757	3699	2484	3965
Final R_1, wR_2 [$I > 2\sigma(I)$]	0.0881, 0.2260	0.0461, 0.1141	0.0393, 0.1018	0.0273, 0.0731	0.0297, 0.0674	0.0277, 0.641	0.0301, 0.0695	0.0447, 0.1002

*3.1.20. [RhCl(η⁵-C₅Me₅)(dpppa-P,N)][BF₄] (**20**)*

$AgBF_4$ (31 mg, 0.16 mmol) was added under dark conditions to a solution of $[RhCl_2(\eta^5\text{-}C_5Me_5)$(dpppa-*P*)] (100 mg, 0.16 mmol) in CH_2Cl_2 (5 cm^3). The solution was stirred overnight and filtered through a celite bed. The majority of the solvent was removed in vacuo. An orange solid was precipitated after addition of Et_2O then isolated by filtration and washed with further ether (10 cm^3) (yield: 70 mg, 0.12 mmol, 74%). *Anal.* Calc. for $C_{28}H_{30}N_2OPClRhBF_4$: C, 50.4; H, 4.54; N, 4.20. Found: C, 49.8; H, 4.25; N, 4.04%. ν_{max}/cm^{-1}: 1684, 1477, 1421. ^{31}P NMR ($CDCl_3$) δ 85.2 ppm. ^1H NMR ($CDCl_3$) δ 8.6 (1H, d, $J = 4$ Hz, pyC[6]H), 8.3 (1H, d, $J = 8$ Hz, pyC[3]H), 8.0 (1H, t, $J = 8$ Hz, pyC[5]H), 7.8 (2H, m, aromatic), 7.6 (8H, m, aromatic), 1.6 (15H, d, $J = 4$ Hz, Cp*-H).

4. X-ray crystallography

Details of the structure determination are given in Table 5. X-ray diffraction measurements were made with graphite-monochromated Mo Kα X-radiation using a Bruker SMART diffractometer or with Cu Kα radiation and a Rigaku Mercury diffractometer. In both cases, intensity data were collected using ω/ϕ steps accumulating area detector frames spanning a hemisphere of reciprocal space for all structures. All data were corrected for Lorentz, polarisation and long-term intensity fluctuations. Absorption effects were corrected on the basis of multiple equivalent reflections or by semi-empirical methods. Structures were solved by direct methods and refined by full-matrix least-squares against F^2 (SHELXTL). Hydrogen atoms were assigned isotropic displacement parameters and were constrained to idealised geometries. Complex **7** contains some disorder; in both **7** and **18** not all of the protons could be included in the final refinement. Refinements converged to residuals given in Table 5. All calculations were made with SHELXTL [28].

5. Supplementary material

Atomic coordinates, thermal parameters and bond lengths and angles have been deposited at the Cambridge Crystallographic data centre (CCDC) Nos 238211–238218. Any request to CCDC for this material should quote the full literature citation and the reference number. Copies of this information may be obtained free of charge from The Director, CCDC, 12 Union Road, Cambridge, CB2 1EZ (fax: +44 1223 336033; e-mail: deposit@ccdc.cam.ac.uk or at www: http://www.ccdc.cam.ac.uk).

References

[1] S.M. Aucott, A.M.Z. Slawin, J.D. Woollins, J. Chem. Soc., Dalton Trans. (2000) 2559.
[2] S.M. Aucott, M.L. Clarke, A.M.Z. Slawin, J.D. Woollins, J. Chem. Soc. Dalton (2001) 972.
[3] S.M. Aucott, A.M.Z. Slawin, J.D. Woollins, J. Organomet. Chem. 582 (1999) 83.
[4] E. Uhlig, M. Maaser, Z. Anorg. Allg. Chem. 334 (1966) 205.
[5] M.R.i. Zubiri, A.M.Z. Slawin, M. Wainwright, J.D. Woollins, Polyhedron 21 (2002) 1729.
[6] M.R.i. Zubiri, M.L. Clarke, D.F. Foster, D.J. Cole-Hamilton, A.M.Z. Slawin, J.D. Woollins, J. Chem. Soc. Dalton (2001) 969.
[7] M.R.i. Zubiri, H.L. Milton, D.J. Cole-Hamilton, A.M.Z. Slawin, J.D. Woollins, Polyhedron 23 (2004) 693.
[8] M.L. Clarke, A.M.Z. Slawin, M.V. Wheatley, J.D. Woollins, J. Chem. Soc., Dalton Trans. (2001) 3421.
[9] A.M.Z. Slawin, M. Wainwright, J.D. Woollins, New J. Chem. 24 (2000) 69.
[10] A.M.Z. Slawin, M. Wainwright, J.D. Woollins, J. Chem. Soc. Dalton (2002) 513.
[11] T. Okano, M. Yamamoto, T. Noguchi, H. Konishi, J. Kiji, Chem. Lett. (1982) 977.
[12] D. Lafont, D. Sinou, G. Descotes, Nouv. J. Chim. 7 (1983) 283.
[13] P. Bhattacharyya, J. Novosad, J. Phillips, A.M.Z. Slawin, D.J. Williams, J.D. Woollins, J. Chem. Soc., Dalton Trans. (1995) 1607.
[14] P. Bhattacharyya, A.M.Z. Slawin, D.J. Williams, J.D. Woollins, J. Chem. Soc., Dalton Trans. (1995) 3189.
[15] P. Bhattacharyya, M.B. Smith, A.M.Z. Slawin, J.D. Woollins, Inorg. Chem. 35 (1996) 3675.
[16] E. Lindner, C. Scheytt, P. Wegner, J. Organomet. Chem. 308 (1986) 311.
[17] D.J. Birdsall, A.M.Z. Slawin, J.D. Woollins, Polyhedron 20 (2001) 125.
[18] A.M.Z. Slawin, J. Wheatley, M.V. Wheatley, J.D. Woollins, Polyhedron 22 (2003) 1397.
[19] R. Uson, A. Laguna, M. Laguna, Inorg. Synth. 26 (1989) 85.
[20] D. Drew, J.R. Doyle, Inorg. Synth. 28 (1991) 346.
[21] J.X. McDermott, J.F. White, G.M. Whiteside, J. Am. Chem. Soc. 60 (1976) 6521.
[22] C.A. O'Mahoney, I.P. Parkin, D.J. Williams, J.D. Woollins, Chem. Soc., Dalton Trans. (1989) 1179.
[23] W. Baratta, P.S. Pregosin, Inorg. Chim Acta 209 (1993) 85.
[24] C. White, A. Yates, P.M. Maitlis, Inorg. Synth. 29 (1992) 228.
[25] G. Giordano, R.H. Crabtree, Inorg. Synth. 19 (1979) 218.
[26] M.A. Bennett, T.N. Huang, T.W. Matheson, A.R. Smith, Inorg. Synth. 21 (1982) 74.
[27] L. Porri, M.C. Gallazzi, A. Colombo, G. Allegra, Tetrahedron Lett. 47 (1965) 4187.
[28] SHELXTL 6.10, 2002, Bruker AXS, Madison, WI, USA.

Available online at www.sciencedirect.com
SCIENCE DIRECT®
Polyhedron 23 (2004) 3221–3242
POLYHEDRON
www.elsevier.com/locate/poly

Author Index to Volume 23

Abboud, K.A., see Murugesu, M., 2779
Abboud, K.A., see Wang, S.-Y.S., 2733
Abdel-Halim, H.M., see Kettunen, M., 1649
Abruña, H.D., see Sydora, O.L., 2841
Abrutis, A., see Pasko, S., 735
Abu-Surrah, A.S., see Kettunen, M., 1649
Abu-Youssef, M.A.M., see Goher, M.A.S., 2349
Abu-Youssef, M.A.M., see Mautner, F.A., 1217
Abul-Haj, M., Quirós, M. and Salas, J.M., Divalent transition metal complexes of the anionic form of 4,7-dihydro-1,2,4-triazolo[1,5-*a*]pyrimidine-7-one: crystal structure of the zinc(II) compound, 743
Abul-Haj, M., Quirós, M. and Salas, J.M., Dinuclear Pd(II) complexes with the anionic form of 4,5-dihydro-1,2,4-triazolo[1,5-a]pyrimidine-5-one, 2373
Abuskhuna, S., McCann, M., Briody, J., Devereux, M. and McKee, V., Synthesis and structure of Mn(II), Cu(II) and Zn(II) complexes containing bis-imidazole ligands, 1731
Abuskhuna, S., Briody, J., McCann, M., Devereux, M., Kavanagh, K., Fontecha, J.B. and McKee, V., Synthesis, structure and antifungal activity of dimeric Ag(I) complexes containing bis-imidazole ligands, 1249
Aguado, R., see Arnáiz, F.J., 537
Aguirre, G., see Iglesias, A.L., 3051
Ahlgren, M., see Kettunen, M., 1649
Ahmad, S., see Fettouhi, M., 1
Ahmed, M., Schwendt, P., Marek, J. and Sivák, M., Synthesis, solution and crystal structures of dinuclear vanadium(V) oxo monoperoxo complexes with mandelic acid: $(NR_4)_2[V_2O_2(O_2)_2(mand)_2]\cdot xH_2O$ [R=H, Me, Et; mand=mandelato(2−)=$C_8H_6O_3^{2-}$], 655
Ahsen, V., see Yılmaz, F., 1931
Ai, C.-C., see Yin, M.-C., 529
Ainscough, E.W., Brodie, A.M., Burrell, A.K., Derwahl, A., Jameson, G.B. and Taylor, S.K., Platinum(II) and palladium(II) complexes containing a mixed donor 'P_2N' multidentate ligand, 1159
Airoldi, C., see Sales, J.A.A., 719
Ajith, T.A., see John, R.P., 2549
Akbar Ali, M., Mirza, A.H., Ravoof, T.B.S.A. and Bernhardt, P.V., Synthetic, spectroscopic and X-ray crystallographic structural study of the monomeric [Cu(pysme)(sac)(MeOH)] and dimeric $[Cu(6mptsc)(sac)]_2$ complexes [pysme=anion of the pyridine-2-carboxaldehyde Schiff base of *S*-methyldithiocarbazate, 6mptsc=the anion of the 6-methyl-2-pyridinecarbaldehydethiosemicarbazone and sac=the sacchari-nate anion], 2031
Akiba, M., see Mochida, K., 177
Akilan, P., see Thirumavalavan, M., 519
Akita, M., see Takahashi, Y,, 225
Akiyama, E., see Asaji, T., 1605
Aktaş, B., see Gonca, E., 1845
Al-Allaf, T.A.K., see Amin, O.H., 2013
Al-Hayaly, L.J., see Amin, O.H., 2013
Al-Jibori, S.A., see Amin, O.H., 2013
Al-Sogair, F.M., see Sulfab , Y., 583
Alam, T.M., see Coker, E.N., 1739
Alberti, M., see Šedo, O., 1199
Ali, M.A., Mirza, A.H., Tan, A.L., Wei, L.K. and Bernhardt, P.V., The preparation and characterization of seven-coordinate tin(IV) complexes of the 2,6-diacetylpyridine Schiff bases of S-alkyl/aryl-dithiocarbazates and the X-ray crystal structure of the $[Sn(dapsme)I_2]$ complex (dapsme=doubly deprotonated form of the 2,6-diacetylpyridine Schiff base of *S*-methyldithiocarbazate), 2037
Ali, A.M., see Chew, K.-B., 1385
Ali, M.A., see Ravoof, T.B.S.A., 2491
Ali, M.A., Mirza, A.H., Hamid, M.H.S.A., Bujang, F.H. and Bernhardt, P.V., The preparation and characterization of tin(IV) complexes of 2-quinolinecarboxaldehyde Schiff bases of *S*-methyl- and *S*-benzyldithiocarbazates and the X-ray crystal and molecular structures of the 2-quinolinecarboxaldehyde Schiff base of *S*-benzyldithiocarbazate (Hqaldsbz) and its tin(IV) complex $[Sn(qaldsbz)I_3]$, 2405
Ali, A.M., see Crouse, K.A., 161
Alleyne, B.D., see Li, J., 419
Allis, D.G., Burkholder, E. and Zubieta, J., A new octamolybdate: observation of the θ-isomer in $[Fe(tpyprz)_2]_2[Mo_8O_{26}]\cdot 3.7H_2O$ (tpyprz=tetra-2-pyridylpyrazine), 1145
Almeida, M., see Belo, D., 1351
Alvarez, H.M., Tanski, J.M. and Rabinovich, D., Poly(mercaptoimidazolyl)borate chemistry and the predominance of κ^3-*S*,*S*,*H* over κ^2-*S*,*S* or κ^3-*S*,*S*,*S* coordination modes: unexpected formation of square pyramidal Ni(II) complexes, 395
Alvarez, H.M., Gillespie, P.A., Gause, C.D., Rheingold, A.L., Golen, J.A. and Rabinovich, D., Thallium(I) bis(mercaptoimidazolyl)borates, 617
Amada, K., see Mochida, K., 177
Amin, O.H., Al-Hayaly, L.J., Al-Jibori, S.A. and Al-Allaf, T.A.K., Heterobimetallic complexes of palladium(II) and platinum(II) bridged by the ligand 5-phenyl-1,3,4-oxadiazole-2-thione, 2013
Amudha, P., see Thirumavalavan, M., 519
Anacona, J.R., see Marquez, V.E., 1317
Anagnostis, J. and Turnbull, M.M., Rotational barriers in dialkylaminochlorophosphines: methyl-substituted piperidinochlorophenylphosphines, 125
Anbalagan, V. and Srivastava, T.S., Spectral and photophysical properties of mono and dinuclear Pt(II) and Pd(II) complexes: An unusual emission behaviour, 3173
Andruh, M., see Pascu, M., 673
Anpilova, E.L., see Garnovskii, A.D., 1909
Aranyos, V., Hagfeldt, A., Grennberg, H. and Figgemeier, E., Electropolymerisable bipyridine ruthenium(II) complexes: synthesis, spectroscopic and electrochemical characterisation of 4-((2-thienyl) ethenyl)- and 4,4′-di((2-thienyl) ethenyl)-2, 2′-bipyridine ruthenium complexes, 589

doi:10.1016/S0277-5387(04)00439-5

Arce, H., Montero, M.L., Sáenz, A. and Castaño, V.M., Effect of pH and temperature on the formation of hydroxyapatite at low temperatures by decomposition of a Ca–EDTA complex, 1897
Ardisson, J.D., see de Castro, V.D., 63
Ardisson, J.D., see Menezes, D.C., 2103
Ardizzoia, G.A., Brenna, S., Castelli, F., Galli, S., LaMonica, G., Masciocchi, N. and Maspero, A., Metal imidazolato polymers: synthesis, characterization and crystal structure of new silver(I) triphenylphosphine derivatives, 3063
Arevalo, I., see Gómez, M., 611
Arif, A.M., see Harvey, B.G., 2725
Arnáiz, F.J., Aguado, R., Pedrosa, M.R. and Maestro, M.A., Dioxomolybdenum(VI) thionates: molecular structure of dioxo-bis(pyridine-2-thiolate-*N*,*S*)molybdenum(VI), 537
Arnold, J., see Inyushin, S., 2937
Arora, M., see Chawla, S.K., 3007
Arul Prakasam, B., Ramalingam, K., Saravanan, M., Bocelli, G. and Cantoni, A., Effect of free and chelating phosphine coordination environments on the NiS_2P_2 chromophore: synthesis, NMR and other spectral studies. Crystal and molecular structures of (*N*,*N*-dipropyldithiocarbamato)di(triphenylphosphine)nickel(II) perchlorate and (*N*,*N*-dipropyldithiocarbamato)1,2-bis((diphenylphosphino)ethane)nickel(II) tetraphenylborate, 77
Arvin, M.E., see Joshi, H.K., 429
Asaji, T., Akiyama, E., Tajima, F., Eda, K., Hashimoto, M. and Furukawa, Y., Salts of tetrachloroauric acid with pyridine *N*-oxide having various base/acid ratios of 1/1, 4/3, 3/2 and 2/1: crystal structures, ^{35}Cl NQR and phase transitions, 1605
Ataç, A., see Can, N., 1109
Atilla, D., see Yılmaz, F., 1931
Aury, S., see Giroux, S., 2393
Ayala, J.D., see de Castro, V.D., 63

Badr, A.M.A., see Goher, M.A.S., 2349
Bai, G., Vidovic, D., Roesky, H.W. and Magull, J., A novel potassium-centered highly symmetrically polynuclear zirconium complex: $K[\{(Cp^*Zr)_3(\mu_3\text{-}N)(\mu_3\text{-}NH)(\mu\text{-}NH_2)_3\}_4(NH_2)_5(NH_3)_7]$, 1125
Baik, M.-H., Friesner, R.A. and Parkin, G., Theoretical investigation of the metal–metal interaction in dimolybdenum complexes with bridging hydride and methyl ligands, 2879
Bailey, A., Griffith, W.P., Leung, D.W.C., White, A.J.P. and Williams, D.J., Ozonolysis for the preparation of high-oxidation state transition metal complexes and the X-ray crystal structure of $Co(py)_2(OAc)_2(H_2O)_2$, 2631
Bailey Walsh, R.D., see Bose, D., 2045
Baitalik, S., Dutta, B. and Nag, K., Spectroscopic and redox properties of $Rh^{III}Ru^{II}$ and $Ru^{II}Ru^{II}$ complexes derived from 2,2′-bipyridine, pyrazole-3,5-bis(benzimidazole) and 1,2,4-triazole-3,5-dicarboxylic acid as bridging ligands, 913
Bajpai, S., see Srivastava, P.C., 1629
Bajpai, S.M., see Srivastava, P.C., 1629
Baker, R.T., see Westcott, S.A., 2665
Bandyopadhyay, S., Das, A., Mukherjee, G.N., Cantoni, A., Bocelli, G., Chaudhuri, S. and Ribas, J., Synthesis, X-ray crystal structures, physicochemical and magnetic studies on copper(II) *N*-(2-carboxyphenyl) iminodiacetate polymers, 1081
Banerjee, J., see Bose, D., 2045
Baran, M., see Ryazanov, M., 879
Baranovski, V.I. and Korolkov, D.V., Electron density distribution, polarizability and bonding in the octahedral clusters $[Mo_6S_8(CN)_6]^{6-}$, $[Re_6S_8(CN)_6]^{4-}$ and $Rh_6(CO)_{16}$, 1519
Barba-Behrens, N., see Téllez, F., 2481
Barba-Behrens, N., see López-Sandoval, H., 1837
Barbosa, M., see Díaz, C., 1027
Bardak, F., see Can, N., 1109
Baril-Robert, F. and Beauchamp, A.L., Preparation and crystal structure of (2,2′-bibenzimidazole)dihalobis(triphenylphospine)rhenium(III) halides, 1139
Bark, T., see Dias, S.I.G., 1011
Barquín, M., González Garmendia, M.J., Pacheco, S., Pinilla, E., Seco, J.M. and Torres, M.R., Synthesis, spectroscopic, magnetic and EPR results and crystal structure of di-μ-(*N*-methyl-*N*-methoxy-2-pyridinamine)bis[(2,2′-bipyridine)copper(II)]hexaflourophosphate, 1695
Barral, M.C., González-Prieto, R., Herrero, S., Jiménez-Aparicio, R., Priego, J.L., Royer, E.C., Torres, M.R. and Urbanos, F.A., Synthesis and crystal structure of high and low spin diruthenium complexes with diphenylformamidine and diphenyltriazene ligands, 2637
Barros-García, F.J., Bernalte-García, A., Higes-Rolando, F.J., Luna-Giles, F. and Pedrero-Marín, R., X-ray and spectroscopic characterisation of cobalt(III) and nickel(II) complexes with 2-(2-pyridyl)iminotetrahydro-1,3-thiazine hydrochloride water (1/2) ($PyTzHCl \cdot 2H_2O$) in the solid state and study of its interaction with cobalt(II) and nickel(II) in aqueous solution, 1453
Barszcz, B., Głowiak, T., Jezierska, J. and Tomkiewicz, A., Synthesis of new pyrazole-containing binuclear and mononuclear Cu(II) complexes: crystal structure, EPR, magnetic and spectroscopic properties, 1309
Bartczak, T.J., see Małecki, J.G., 885
Basu Baul, T.S., Lycka, A., Butcher, R. and Smith, F.E., Synthesis, X-ray crystal structures and multinuclear NMR characterization of Hg(II) complexes of 2-[(*E*)-2-(aryl)-1-diazenyl]pyridine, 2323
Batista, A.A., see de Araujo, M.P., 3163
Batsanov, A.S., see Coventry, D.N., 2789
Batsanov, A.S., see Venkatasubramanian, U., 629
Bau, R., see Li, J., 419
Bayır, Z.A., see Kalkan, A., 3155
Beauchamp, A.L., see Baril-Robert, F., 1139
Beeby, A., see Leslie, W., 2769
Beer, P.D., see Wong, W.W.H., 2821
Beheshti, A., Brooks, N.R., Clegg, W. and Sichani, S.E., Synthesis, crystal structures and spectroscopic characterization of two neutral heterobimetallic clusters $MS_4Cu_4(pz^{Me2})_6X_2$ (where M=Mo (**1**) or W (**2**), X=Cl (**1**) or disordered Cl/Br (**2**) and pz^{Me2}=3,5-dimethylpyrazole), 3143
Bellabarba, R.M. and Saunders, G.C., Intramolecular dehydrofluorinative coupling of pentamethylcyclopentadienyl and phosphine ligands in iridium complexes, 2659
Belo, D., Santos, I.C. and Almeida, M., 5,6-Dicyano-2,3-dithiopyrazine (dcdmp) chemistry: synthesis and crystal structure of Au(III)$(dcdmp)_2$ complexes and 2,3,7,8-tetracyano-1,4,6,9-tetraazothianthrene, 1351
Bentiss, F., Lagrenée, M., Vezin, H., Wignacourt, J.-P. and Holt, E.M., Syntheses and crystal structures of two mononuclear Zn(II) complexes with the 2,5-bis(2-pyridyl)-1,3,4-thiadiazole ligand, 1903
Bercaw, J.E., see Piro, N.A., 2797
Bergman, R.G., see Corkey, B.K., 2943
Bermejo, M.R., see Sanmartín, J., 963
Bermejo, E., Castiñeiras, A., Fostiak, L.M., Santos, I.G., Swearingen, J.K. and West, D.X., Spectral and structural studies of Zn and Cd complexes of 2-pyridineformamide N(4)-ethylthiosemicarbazone, 2303
Bernalte-García, A., see Barros-García, F.J., 1453
Bernhard, G., see Koban, A., 1793
Bernhardt, P.V., Dyahningtyas, T.E., Han, S.C., Harrowfield, J.M., Chool Kim, Il., Kim, Y., Koutsantonis, G.A., Rukmini, E. and Thuéry, P., Stereocontrol in complexes of cyclam-like macrocycles – influences of chirality, 869
Bernhardt, P.V., see Ali, M.A., 2405
Bernhardt, P.V., see Ali, M.A., 2037
Bernhardt, P.V., see Akbar Ali, M., 2031

Bhat, S.G., see Joseph, M., 3069
Bhattacherjee, A., see Saha, S., 1811
Bicherov, A.V., see Garnovskii, A.D., 1909
Bindu, P., Kingston, J.V. and Sudheendra Rao, M.N., Dianionic silicate derivatives of transition metals: synthesis by a facile ion exchange route, characterization and thermolysis studies, 679
Bird, P.H., see Thompson, L.K., 1175
Blackman, A.G., see Polson, M.I.J., 1427
Blackman, A.G., see Lundin, N.J., 97
Blanco, L.M., see Garnovskii, A.D., 1909
Boča, R., Boča, M., Gembický, M., Jäger, L., Wagner, C. and Fuess, H., Versatile coordination mode of dicyanamide in nickel(II) complexes containing polyamines as blocking ligands, 2337
Boča, M., see Boča, R., 2337
Bocelli, G., see Arul Prakasam, B., 77
Bocelli, G., see Bandyopadhyay, S., 1081
Bögge, H., see Müller, A., 2381
Bolte, M., see Ilkhechi, A.H., 2597
Bombieri, G., see de Castro, V.D., 63
Boncella, J.M., see Wang, S.-Y.S., 2733
Booncoon, S., see Youngme, S., 1685
Borah, R., see Sarmah, S., 1097
Borodkin, G.S., see Garnovskii, A.D., 1909
Borowiec, J., Trojnar, I. and Wołowiec, S., Mono- and dizinc complexes of diporphyrins with flexible spacers of variable length, 33
Bosch, M., see Werner, H., 2645
Bose, D., Banerjee, J., Rahaman, S.H., Mostafa, G., Fun, H.-K., Bailey Walsh, R.D., Zaworotko, M.J. and Ghosh, B.K., Polymeric end-to-end bibridged cadmium(II)thiocyanates containing monodentate and bidentate N-donor organic blockers: supramolecular synthons based on π–π and/or C–H···π interactions, 2045
Bose, D., Rahaman, S.H., Mostafa, G., Walsh, R.D.B., Zaworotko, M.J. and Ghosh, B.K., Synthesis, structure and properties of $[Zn(dpa)(N_3)_2]$ and $[Zn(dpa)(N_3)(NO_3)]_2$ (dpa=2,2′-dipyridylamine): composition tailored architectures, 545
Botar, B., see Müller, A., 2381
Boudalis, A.K., Raptopoulou, C.P., Terzis, A. and Perlepes, S.P., 2,2′-Bipyrimidine (bpym) in iron(III) carboxylate chemistry: preparation and characterization of $[Fe_2O(O_2CMe)_2(bpym)_2(H_2O)_2](ClO_4)_2$ and the influence of weak interactions in the formation of metal clusters, 1271
Bouyagui Tamboura, F., Marcel Haba, P., Gaye, M., Salam Sall, A., Hamady Barry, A. and Jouini, T., Structural studies of bis-(2,6-diacetylpyridine-bis-(phenylhydrazone)) and X-ray structure of its Y(III), Pr(III), Sm(III) and Er(III) complex, 1191
Bowen, R.J., Caddy, J., Fernandes, M.A., Layh, M. and Mamo, M.A., Synthesis of phosphine stabilised group 11 1-azaallyl complexes; molecular structure of $bu^i_3PAuCH(R)C(bu^t)=NR$ ($R = SiMe_3$), 2273
Boyd, L.A., see Venkatasubramanian, U., 629
Boyle, T.J., see Coker, E.N., 1739
Bradford, F.E., Connor, L.P., Kilner, C.A. and Halcrow, M.A., Iron complexes of 3-(pyrazinyl)-1,2,4-triazole ligands, 2141
Brandow, S.L., see Schull, T.L., 1375
Bravic, G., see Karmakar, R., 949
Bravo, J., see Rodríguez, M.C., 1045
Brbot-Šaranović, A., see Cindrić, M., 1859
Bregadze, V., see Semioshkin, A., 2135
Brellochs, B., see Semioshkin, A., 2135
Brenna, S., see Ardizzoia, G.A., 3063
Brett, C.M. and Bursten, B.E., Theoretical studies of 18-electron $M(C_nH_n)(C_{10-n}H_{10-n})$ (M = Fe, Ru, Os; n = 3, 4, 5) sandwich complexes, 2993
Breza, M., see Brudíková, K., 2235
Bridgewater, B.M., see Docrat, A., 481
Briody, J., see Abuskhuna, S., 1731
Briody, J., see Abuskhuna, S., 1249
Brodie, A.M., see Ainscough, E.W., 1159
Brookhart, M., see Corkey, B.K., 2943
Brooks, N.R., see Beheshti, A., 3143
Brożyna, A., see Drożdżewski, P., 1785
Brudíková, K. and Breza, M., MP2 studies of the bis(methoxycarbimido)amine ligand and its anion, 2235
Brusko, V.V., see Zabirov, N.G., 2243
Brylev, K.A., see Naumov, N.G., 599
Bucher, E., see Mautner, F.A., 1217
Bujang, F.H., see Ali, M.A., 2405
Burkholder, E., see Allis, D.G., 1145
Burkut Koçak, M., see Yilmaz, I., 1279
Burlov, A.S., see Garnovskii, A.D., 1909
Burney, C., see Green, J.C., 2915
Burrell, A.K., see Polson, M.I.J., 1427
Burrell, A.K., see Ainscough, E.W., 1159
Bursten, B.E., see Brett, C.M., 2993
Burzlaff, N., see Peters, L., 245
Bushuk, B.A., see Bushuk, S.B., 2615
Bushuk, S.B., Carré, F.H., Guy, D.M.H., Douglas, W.E., Kalvinkovskya, Y.A., Klapshina, L.G., Rubinov, A.N., Stupak, A.P. and Bushuk, B.A., Hypercoordinate silicon and phosphorus acetylene compounds: crystal structure determinations and fluorescence spectroscopic study, 2615
Butcher, R.J., see Pramanik, N.R., 1595
Butcher, R., see Schull, T.L., 1375
Butcher, R.J., see Srivastava, P.C., 1629
Butcher, R., see Basu Baul, T.S., 2323
Butcher, R.J., see Sau, D.K., 5
Butler, J.M., Gray, G.M. and Claude, J.P., Synthesis, characterization and X-ray crystallography of a metallacrown ether complex containing a $Ru^{II}(bpy)_2^{2+}$ chromophore and its $Mo(CO)_4$ analog, 1719
Byabartta, P., see Jasimuddin, S., 727
Byington, L.K., see Schull, T.L., 1375

Caballero, A., Carrión, M.C., Espino, G., Jalón, F.A. and Manzano, B.R., Ruthenium hydride complexes with a heteroscorpionate ligand derived from methane: 2-phenoxy-bis(pyrazol-1-yl)methane. The hemilabile role of the ligand in substitution and proton transfer reactions, 361
Caddy, J., see Bowen, R.J., 2273
Cai, R.-F., see Luo, J., 1243
Calabrese, J.C., see Westcott, S.A., 2665
Camm, K.D., Furtado, S.J., Gott, A.L. and McGowan, P.C., Synthesis and structural studies of bis-amino-functionalised ferrocene salts and ferrocenium salts, 2929
Campello, M.P.C., see Paulo, A., 331
Campo, J.A., see Criado, R., 301
Can, N., Sözerli Can, S.E., Ataç, A. and Bardak, F., Structural characterization and luminescence properties of an isonicotinic acid N-oxide Mn(II) complex, 1109
Cano, M., see Criado, R., 301
Cantoni, A., see Bandyopadhyay, S., 1081
Cantoni, A., see Arul Prakasam, B., 77
Cao, L.-H., see Zhu, Q.-Y., 2259
Carballo, R., Castiñeiras, A., Covelo, B., García-Martínez, E., Niclós, J. and Vázquez-López, E.M., Solid state coordination chemistry of mononuclear mixed-ligand complexes of Ni(II), Cu(II) and Zn(II) with α-hydroxycarboxylic acids and imidazole, 1505
Carducci, M.D., see Joshi, H.K., 429
Carlos Galvez-Ruíz, J., see López-Sandoval, H., 1837
Carpentier, J.-F,, see Kunrath, F.A., 2437
Carrano, C.J., see Shirin, Z., 239
Carré, F.H., see Bushuk, S.B., 2615

Carrión, M.C., see Caballero, A., 361
Casagrande Jr., O.L., see Kunrath, F.A., 2437
Castaño, V.M., see Arce, H., 1897
Castellano, E.E., see Silva, W.C., 1063
Castellano, E.E., see Scarpellini, M., 511
Castellano, E.E., see Soares, L.F., 205
Castellano, E.E., see de Araujo, M.P., 3163
Castelli, F., see Ardizzoia, G.A., 3063
Castiñeiras, A., see Carballo, R., 1505
Castiñeiras, A., see Bermejo, E., 2303
Cataldo, F., Polyynes: a new class of carbon allotropes. About the formation of dicyanopolyynes from an electric arc between graphite electrodes in liquid nitrogen, 1889
Chadha, R.K., see Shankar, R., 71
Chaichit, N., see Youngme, S., 1685
Chaichit, N., see Youngme, S., 1641
Chailuecha, C., see Youngme, S., 1641
Chakraborty, S., see Maiti, D., 831
Chakravarty, A.R., see Gupta, S., 643
Chakravarty, A.R., see Mukherjee, A., 3081
Chakravarty, A.R., see Mukherjee, A., 2177
Chan, T.-L., see Lu, W.-J., 1089
Chan, H.-S., see Lu, W.-J., 1089
Chand, B., Ray, U., Mostafa, G., Lu, T.-H. and Sinha, C., 2D Extended supramolecular structures via π–π interactions of 1D coordination polymers of cadmium(II) complexes of arylazoimidazole using azido and thiocyanato bridging ligands, 1669
Chanda, N., see Maiti, D., 831
Chao, H., see Hong, X.-L., 815
Chapman, P.A., see Scales, S.J., 2169
Chattopadhyay, P., see Dhara, P.K., 2457
Chaudhuri, S., see Sau, D.K., 5
Chaudhuri, S., see Bandyopadhyay, S., 1081
Chawla, S.K., Arora, M., Nättinen, K., Rissanen, K. and Yakhmi, J.V., Syntheses and crystal structures of three novel Cu(II) coordination polymers of different dimensionality constructed from Cu(II) carboxylates (carboxylate=malonate (mal), 2 acetate (ac), fumarate (fum)) and conformationally flexible 1,4-bis(imidazole-1-yl-methylene)benzene (IX), 3007
Chen, J.-X., Liu, S.-X. and Gao, E.-Q., Syntheses, structures and fluorescence of three novel 3D coordination polymers $[Cd_3(TMA)_2(H\text{-}PRZ)(H_2O)_3(OH)]\cdot H_2O$, $Cd_2Na_2(TMA)_2(H_2O)_4$ and $[Cd_2Co(TMA)_2\ (H_2O)_4]\cdot 2H_2O$ (TMA=trimesic acid, PRZ=piperazine), 1877
Chen, C., Yang, Y.-L., Huang, K.-L., Sun, Z.-H., Wang, W., Yi, Z., Liu, Y.-L. and Pang, W.-Q., Hydrothermal synthesis and intercalation behavior of a layered titanium phosphate $Ti_2(H_2PO_4)(HPO_4)(PO_4)_2\cdot 0.5C_6N_2H_{16}$, with an extended γ-phase intercalated into organic amine, 3033
Chen, W., see Cheng, J., 1075
Chen, J.-D., see Yeh, C.-W., 1947
Chen, C., see Yang, Y., 1535
Chen, Lijuan, see Zhang, Q., 1975
Chen, S., see Zhang, Q., 1975
Chen, H.-B., Zhang, H., Yang, J.-M. and Zhou, Z.-H., Transformation of maleato manganese(II): temperature effect and coordination modes, 987
Cheng, P., see Liang, M., 2203
Cheng, J.-K., Zhang, J., Kang, Y., Qin, Y.-Y., Li, Z.-J. and Yao, Y.-G., Syntheses, structures and photoluminescent properties of 1D, 2D, 3D silver (I) coordination polymers with flexible long-chain dinitriles and tetranitriles, 2209
Cheng, P., see Sun, Y.-J., 211
Cheng, J., Cui, D., Chen, W., Tang, T. and Huang, B., Syntheses and crystal structures of bis(tetrahydrofurfurylindenyl) lanthanocene chlorides $(C_4H_7OCH_2C_9H_6)_2LnCl$ (Ln=La, Lu), 1075
Cherkasov, R.A., see Zabirov, N.G., 2243
Chetty, K.V., see Kannan, S., 1527
Chew, K.-B., see Crouse, K.A., 161
Chew, K.-B., Tarafder, M.T.H., Crouse, K.A., Ali, A.M., Yamin, B.M. and Fun, H., Synthesis, characterization and bio-activity of metal complexes of bidentate N–S isomeric Schiff bases derived from *S*-methyldithiocarbazate (SMDTC) and the X-ray structure of the bis[*S*-methyl-β-*N*-(2-furyl-methylketone)dithiocarbazato]-cadmium(II) complex, 1385
Cho, I.-K., see Kim, J., 1333
Choi, K.Y., see Kim, J., 1333
Choi, K.-Y., Jeon, Y.-M., Ryu, H., Oh, J.-J., Lim, H.-H. and Kim, M.-W., Synthesis and characterization of *syn–anti* carboxylate-bridged one-dimensional copper(II) complexes with bis(2-pyridylmethyl)-amino acids, 903
Choi, S.-N., Jung, W.-S., Lee, M.-J., Lee, Y.-M. and Kim, Y.-I., Synthesis and physicochemical properties of charge transfer compounds derived from the reaction of tetrathiafulvalene with copper(II), 2111
Chool Kim, Il., see Bernhardt, P.V., 869
Choudhury, C.R., see Karmakar, R., 949
Christopher Thomas, J. and Peters, J.C., Structural and spectroscopic studies of three-coordinate copper(I) supported by bis(phosphino)borate ligands, 2901
Christou, G., see Murugesu, M., 2779
Chung, Y.K., see Joung, U.G., 1587
Churchill, D.G., see Docrat, A., 481
Chutia, P., Kumari, N., Sharma, M., Derek Woollins, J., Slawin, A.M. Z. and Kumar Dutta, D., Ruthenium(II) carbonyl complexes containing tertiary phosphine chalcogenide ligands of the type Ph_3PX; X=O, S, Se, 1657
Cian, A.D., see Pelascini, F., 3193
Cindrić, M., Vrdoljak, V., Kajfež Novak, T., Strukan, N., Brbot-Šaranović, A., Novak, P. and Kamenar, B., Synthesis, characterization and crystal structures of molybdenum(VI) and (V) complexes with differently N-substituted β′-hydroxy-β-enaminones, 1859
Cingolani, A., see Pettinari, C., 451
Císařová, I., see Štěpnička, P., 921
Ciunik, Z., see Pruchnik, F.P., 103
Ciunik, Z., see Galani, A., 2021
Ciunik, Z., see Ruman, T., 219
Claramunt, R.M., Santa María, M.D., Elguero, J. and Trofimenko, S., Isomer distribution in thallium hydrotris(polymethylenepyrazol-1-yl)borates (thallium scorpionates): a multinuclear NMR study, 2985
Claude, J.P., see Butler, J.M., 1719
Clegg, W., see Hossaini Sadr, M., 637
Clegg, W., see Beheshti, A., 3143
Clegg, W., see Gibson, V.C., 189
Cloke, F.G.N., Hitchcock, P.B., Kuchta, M.C. and Morley-Smith, N.A., Mononuclear tantalum (V) pentalene complexes: synthesis of $[Ta\{\eta^8\text{-}C_8H_4(1,4\text{-}Si^iPr_3)_2\}X_3]$ (X = CH_3, Cl, I) and the X-ray crystal structures of $[Ta\{\eta^8\text{-}C_8H_4(1,4\text{-}Si^iPr_3)_2\}(CH_3)_3]$, $[Ta\{\eta^8\text{-}C_8H_4(1,4\text{-}Si^iPr_3)_2\}(CH_3)_2Cl]$, $[Ta\{\eta^8\text{-}C_8H_4(1,4\text{-}Si^iPr_3)_2\}(CH_3)Cl_2]$ and $[Ta\{\eta^8\text{-}C_8H_4(1,4\text{-}Si^iPr_3)_2\}I_3]$, 2625
Coker, E.N., Boyle, T.J., Rodriguez, M.A. and Alam, T.M., Structurally characterized magnesium carboxylates with tuned melting points, 1739
Cole-Hamilton, D.J., see Zubiri, M.R.I., 693
Collange, E., Metteau, L., Richard, P. and Poli, R., Synthesis and structure of a new organometallic polyoxomolybdate, $Cp^*_2Mo_6O_{17}$, 2605
Collison, D., see John, G.H., 3097
Connor, L.P., see Bradford, F.E., 2141
Constable, E.C., Handel, R., Housecroft, C.E., Neuburger, M., Schofield, E.R. and Zehnder, M., Efficient syntheses of 4′-(2-

thienyl)- and 4′-(3-thienyl)-2,2′:6′,2″-terpyridine: preparation and characterization of Fe(II), Ru(II), Os(II) and Co(II) complexes, 135
Contreras, R., see López-Sandoval, H., 1837
Contreras, R., see Téllez, F., 2481
Cook, R.A., see Mehnert, C.P., 2679
Cooper, G.J.T., see Pickering, A.L., 2075
Copley, R.C.B., see Venkatasubramanian, U., 629
Corkey, B.K., Taw, F.L., Bergman, R.G. and Brookhart, M., Aromatic and aldehyde carbon–hydrogen bond activation at cationic Rh(III) centers. Evaluation of electronic substituent effects on aldehyde binding and C–H oxidative addition, 2943
Correia, J.D.G., see Paulo, A., 331
Coutsolelos, A.G., see Raptopoulou, C., 1777
Covelo, B., see Carballo, R., 1505
Coventry, D.N., Batsanov, A.S., Goeta, A.E., Howard, J.A.K. and Marder, T.B., Synthesis and molecular structures of α-diimines and their zinc and palladium dichloride complexes, 2789
Cowley, A.R., see Ravoof, T.B.S.A., 2491
Coxall, R.A., see Smith, A.A., 1557
Crabtree, R.H., see Miecznikowski, J.R., 2857
Crane, T.W., see Cross, J.L., 2831
Creighton, M.A., see Rudd, M.D., 1923
Criado, R., Cano, M., Campo, J.A., Heras, J.V., Pinilla, E. and Torres, M.R., Mono and binuclear rhodium dicarbonyl complexes containing the hydridotris(3-*p*-chlorophenylpyrazol-1-yl)borate ligand (Tp^{PhCl}). X-ray structures of the binuclear complex $[(OC)_2Rh(\mu{:}\kappa^2,\kappa^1\text{-}Tp^{PhCl})Rh(Cl)(CO)_2]$ and of three isomers of $[Rh(\kappa^2\text{-}Tp^{PhCl})(CO)_2]$, 301
Cronin, L., see Pickering, A.L., 2075
Cross, J.L., Garrett, A.D., Crane, T.W., White, P.S. and Templeton, J.L., Coordination and reactivity of acetonitrile in tungsten(IV) complexes: oxidation, methylation and dimerization of coordinated acetonitrile, 2831
Crouse, K.A., Chew, K.-B., Tarafder, M.T.H., Kasbollah, A., Ali, A.M., Yamin, B.M. and Fun, H.-K., Synthesis, characterization and bio-activity of *S*-2-picolyldithiocarbazate (S2PDTC), some of its Schiff bases and their Ni(II) complexes and X-ray structure of *S*-2-picolyl-β-*N*-(2-acetylpyrrole)dithiocarbazate, 161
Crouse, K.A., see Chew, K.-B., 1385
Crouse, K.A., see Ravoof, T.B.S.A., 2491
Cruz, A., see López-Sandoval, H., 1837
Cui, Y.-J., see Meng, H., 2357
Cui, D., see Cheng, J., 1075
Cui, K., see Zhu, H.-B., 1131
Cummins, C.C., see Sceats, E.L., 2751
Cusack, J., Drew, M.G.B. and Spalding, T.R., Syntheses and spectroscopy of diamine complexes of Zn(II) and Cd(II) ethylxanthates and the molecular structures of $[M(S_2COEt)_2TMEDA]$: formation of CdS nanoparticles from $[Cd(S_2COEt)_2]$ and $[Cd(S_2COEt)_2TMEDA]$, 2315

Daff, P.J., see Etienne, M., 379
Dahan, F., see Etienne, M., 379
Dai, J.-C., see Xia, S.-Q., 1003
Dai, J., see Zhu, Q.-Y., 2259
Dai, J., Yang, W., Ren, Z.-G., Zhu, Q.-Y. and Jia, D.-X., Copper(I) and palladium(II) complexes of 4,5-bis(methylthio)-1,3-dithiole-2-thione, coordination and S···S contact assembled ribbon structures, 1447
Dai, Z.-Y., see Zhu, H.-B., 1131
Dai, J., see Jia, D.-X., 937
Dang, D.-B., see Zou, Y., 2253
Dang, D.-B., see Liu, W.-L., 2125
Daniele, S., see Guillon, H., 1467
Danopoulos, A.A., see Winston, S., 2813
Daphnomili, D., see Raptopoulou, C., 1777
Das, S.K., see Madhu, V., 1235
Das, A. and Mukhopadhyay, S., Kinetics of oxidation of glyoxylic acid by [ethylenebis(biguanide)]silver(III) in aqueous media, 895
Das, A., see Bandyopadhyay, S., 1081
Das, S.K., see Müller, A., 2381
Dastidar, P., see Subramanian, P.S., 2515
Davies, C.J., Solan, G.A. and Fawcett, J., Synthesis and structural characterisation of cobalt(II) and iron(II) chloride complexes containing bis(2-pyridylmethyl)amine and tris(2-pyridylmethyl)-amine ligands, 3105
Day, M.W., see Wenger, O.S., 2955
de Almeida Neves, E.F., see Scarpellini, M., 511
de Araujo, M.P., Valle, E.M.A., Ellena, J., Castellano, E.E., dos Santos, E.N. and Batista, A.A., *mer*-$[RuCl_3(P\text{–}P)H_2O]$ (P–P=dppb or diop) as a starting material for the synthesis of binuclear complexes. Crystallographic structures of $[(dppb)ClRu\text{–}\mu(Cl)_3\text{–}RuCl(dppb)]$ and $[(\eta^6\text{-}C_6H_6)Ru\text{–}\mu(Cl)_3\text{–}RuCl(dppb)]$. Imine hydrogenation using mono- and binuclear ruthenium complexes, 3163
De Bellis, V.M., see Oliveira, M.R.L., 1153
de Castro, B., see Sousa, C., 1401
de Castro, V.D., de Lima, G.M., Porto, A.O., Siebald, H.G.L., de Souza Filho, J.D., Ardisson, J.D., Ayala, J.D. and Bombieri, G., Synthesis, structural characterisation and thermal decomposition of $[\{Pt(dppf)(2\text{-}SPy)\}\{BF_4\}]$ (dppf = 1,1′-bisdiphenylphosfi- noferrocene and 2-SPy = 2-mercaptopyridine) – a source for a Fe–Pt containing alloy, 63
de Faria Franca, E., see Oliveira, M.R.L., 1153
de Gelder, R., see Mohamadou, A., 1969
de Lima, G.M., see Menezes, D.C., 2103
de Lima, G.M., see de Castro, V.D., 63
de Souza, V.R., see Raimondi, A.C., 2069
de Souza Filho, J.D., see de Castro, V.D., 63
Decken, A., see Scales, S.J., 2169
Decken, A., see He, X.-F., 155
Decurtins, S., see Liu, S.-X., 1185
Deligeorgiev, T., see Minkovska, S., 3147
Demertzis, M.A., see Galani, A., 2021
Derek Woollins, J., see Zubiri, M.R.I., 693
Derek Woollins, J., see Chutia, P., 1657
Derek Woollins, J., see Rodriguez i Zubiri, M., 865
Derrah, E.J., see Scales, S.J., 2169
Derwahl, A., see Ainscough, E.W., 1159
Desmurs, J.-R., see Giroux, S., 2393
Devereux, M., see Abuskhuna, S., 1249
Devereux, M., see Abuskhuna, S., 1731
Dhara, P.K., Pramanik, S., Lu, T.-H., Drew, M.G.B. and Chattopadhyay, P., Copper(II) complexes of new tetradentate NSNO pyridylthioazophenol ligands: synthe- sis, spectral characterization and crystal structure, 2457
Di Vaira, M., see Raptopoulou, C., 1777
Dias, A.R., see Ribeiro, A.F.G., 2715
Dias, H.V.R. and Wang, X., Sterically demanding methyl tris(pyrazolyl)borate ligands: synthesis and characterization of thallium(I) complexes supported by $[MeB(3\text{-}(t\text{-}Bu)Pz)_3]^-$ and $[MeB(3\text{-}(Mes)Pz)_3]^-$, 2533
Dias, S.I.G., Heirtzler, F., Bark, T., Labat, G. and Neels, A., Helical zinc complexes of pyrazine–pyridine hybrids, 1011
Díaz, C., Barbosa, M. and Godoy, Z., Monobranched and hyperbranched dendrimers based on cyclophosphazene containing nitrile and phosphine donors and their Fe and Ru organometallic derivatives, 1027
Dinda, J., Jasimuddin, Sk., Mostafa, G., Hung, C.-H. and Sinha, C., Silver(I) complexes of the naphthyl-azoimine function: single crystal X-ray structure of bis-[1-ethyl-2-(naphthyl-α-azo)imidazole]silver(I) perchlorate, 793
Ding, H., see Meng, H., 2357

DiPasquale, A.G., see Soper, J.D., 323
Dispenziere, N.C., see Mehnert, C.P., 2679
diTargiani, R.C., see Karambelkar, V.V., 471
Djuran, M.I., see Radanović, D.D., 2183
Djurovich, P.I., see Li, J., 419
Docrat, A., Morlok, M.M., Bridgewater, B.M., Churchill, D.G. and Parkin, G., N–H···O hydrogen bonding interactions in tetrahedral [ZnS_4] complexes of relevance to zinc enzymes: the synthesis, structures and reactivity of *tris*(2-mercapto-1-arylimidazolyl)hydroborato zinc(2-mercapto-1-arylimidazole) complexes, {[Tm^{Ar}]Zn(mim^{Ar})} [ClO_4] (Ar=Ph, *p*-Tol), 481
Dodds, C.A., Jagoda, M.,Reglinski, J. and Spicer, M.D., Soft scorpionate complexes of the fourth and fifth period elements arsenic and tin, 445
Dokorou, V., see Galani, A., 2021
Dong, S.-J., see Guo, Q.-L., 1461
Donnadieu, B., see Etienne, M., 379
Donnici, C.L., see Menezes, D.C., 2103
Donohoe, D.J., see Venkatasubramanian, U., 629
Doriguetto, A.C., see Menezes, D.C., 2103
Doriguetto, A.C., see Soares, L.F., 205
dos Santos, E.N., see de Araujo, M.P., 3163
Doucet, F., see Schneider, C., 3185
Douglas, W.E., see Bushuk, S.B., 2615
Drago, V., see Fernandes, C., 1419
Drašković, N.S., see Radanović, D.D., 2183
Dressick, W.J., see Schull, T.L., 1375
Drew, M.G.B., see Cusack, J., 2315
Drew, M.G.B., see Kannan, S., 1527
Drew, M.G.B., see Dhara, P.K., 2457
Driessen, W.L., see Mohamadou, A., 1969
Driessen, W.L., see van Albada, G.A., 2387
Drożdżewski, P., Brożyna, A. and Kubiak, M., Synthesis, X-ray crystal structure and vibrational spectra of a polymeric copper(II) complex with 2-thiopheneacetic acid, 1785
Du, G.-H., see Yu, L., 823
Du, W.-X., see Xia, S.-Q., 1003
Du, M., see Zhang, L.-P., 857
Durivage, J.C., see Joshi, H.K., 429
Dury, M., see Giroux, S., 2393
Dutta, B., see Baitalik, S., 913
Dyahningtyas, T.E., see Bernhardt, P.V., 869
Dzięgielewski, J.O., see Małecki, J.G., 885

Eagle, A.A., Gable, R.W., Thomas, S., Sproules, S.A. and Young, C.G., Sulfur atom transfer reactions of tungsten(VI) and tungsten(IV) chalcogenide complexes, 385
Eda, K., see Asaji, T., 1605
Eichhorn, D.M., see Siemer, C.J., 235
El-Sayed, L., see Iskander, M.F., 23
Elguero, J., see Claramunt, R.M., 2985
Ellena, J., see Soares, L.F., 205
Ellena, J., see Menezes, D.C., 2103
Ellena, J., see de Araujo, M.P., 3163
Ellena, J., see Oliveira, M.R.L., 1153
Ellis, D., see Venkatasubramanian, U., 629
Elsegood, M.R.J., see Gibson, V.C., 189
Emseis, P., Failes, T.W., Hibbs, D.E., Leverett, P. and Williams, P.A., Intramolecular NH–π and π–π interactions in ternary cobalt(III) complexes of aromatic aminoacids: a structural and NMR study, 1749
Enemark, J.H., see Joshi, H.K., 429
Ephritikhine, M., see Salmon, L., 623
Ephritikhine, M., see Villiers, C., 1613
Ernst, R.D., see Harvey, B.G., 2725
Escuer, A., Mautner, F.A., Sanz, N. and Vicente, R., New examples of the unusual X-phenylcyanamido bridging ligands. Crystal structure and magnetic properties of Mn^{II} derivatives, 1409
Escuer, A., see Milios, C.J., 83
Espino, G., see Caballero, A., 361
Etienne, M., Hierso, J.-C., Daff, P.J., Donnadieu, B. and Dahan, F., Mono and dinuclear hydrotris(3,5-dimethylpyrazolyl)borato tantalum complexes, 379
Evans, W., Kozimor, S.A. and Ziller, J.W., Bis(pentamethylcyclopentadienyl) U(III) oxide and U(IV) oxide carbene complexes, 2689
Exley, C., see Schneider, C., 3185

Fabbrizzi, L., Licchelli, M., Poggi, A., Sacchi, D. and Zampa, C., A chromogenic penta-aza scorpionand for nickel(II) and copper(II) ions, 373
Fachinetti, G., see Pardey, A.J., 1677
Failes, T.W., see Emseis, P., 1749
Fang, J., see Yao, J., 1169
Fanwick, P.E., see Foss, O., 3021
Faria, F.P., see Sales, J.A.A., 719
Fawcett, J., Platt, A.W.G., Vickers, S. and Ward, M.D., Lanthanide halide and nitrate complexes with potentially tridentate bisphosphine dioxide – ether donors, 2561
Fawcett, J., see Davies, C.J., 3105
Fedieva, M., see Minkovska, S., 3147
Fedorov, V.E., see Naumov, N.G., 599
Fenske, D., see Naumov, N.G., 599
Fernandes, M.A., see Bowen, R.J., 2273
Fernandes, C., Wardell, J.L., Horn Jr., A., Skakle, J.M.S. and Drago, V., Reactions of [{bis(2-pyridylmethyl)amine}trichloroiron(III)] with $(HOCH_2)_3CNHCO(CH_2)_nCONHC(CH_2OH)_3$ $(n = 0 - 2)$: crystal structures of (μ-oxo)bis{(oxalato){[bis(pyridylmethyl)amine]iron(III)} and $(HOCH_2)_3CNHCO(CH_2)_2CONHC(CH_2OH)_3$, 1419
Ferreira da Silva, J.L., see Ribeiro, A.F.G., 2715
Ferrence, G.M., see Morissette, M., 263
Fettouhi, M., Wazeer, M.I.M., Ahmad, S. and Isab, A.A., X-ray structure and ^{77}Se, ^{31}P and ^{13}C MAS NMR of the dinuclear complex 1,2-*bis*(selenourea)-1\κSe,2\κSe-1,2-*bis*(trimethylphosphine)digold(I) chloride, 1
Fiedler, J., see Knödler, A., 701
Figgemeier, E., see Aranyos, V., 589
Figueroa, J.S., see Sceats, E.L., 2751
Firman, T.K., see Hay, B.P., 145
Flood, A.H., see Polson, M.I.J., 1427
Flores-Parra, A., see Téllez, F., 2481
Flores-Parra, A., see López-Sandoval, H., 1837
Fondo, M., see Sanmartín, J., 963
Fontecha, J.B., see Abuskhuna, S., 1249
Ford, S., see Morley, C.P., 2967
Foro, S., see Iskander, M.F., 23
Foss, O., Husebye, S., Törnroos, K.W. and Fanwick, P.E., Synthesis and X-ray crystal structures of six [TeL_4][MF_6] salts, where L is ethylene- or trimethylene-thiourea and M is Si, Ge or Sn. Five Te(II) complexes with a novel type of structure linked together by unusual N–H···F hydrogen bonds, 3021
Fostiak, L.M., see Bermejo, E., 2303
Fox, M.A., see Venkatasubramanian, U., 629
Franco, D.W., see Silva, W.C., 1063
Franco, D.W., see Scarpellini, M., 511
Freijanes, E., see Rodríguez, M.C., 1045
Freire, C., see Sousa, C., 1401
Freire, C., see Ribeiro, A.F.G., 2715
Friesner, R.A., see Baik, M.-H., 2879
Fromm, K.M. and Gueneau, E.D., Structures of alkali and alkaline earth metal clusters with oxygen donor ligands, 1479
Fu, R.-B., see Zhang, J.-J., 2265

Fu, Z.-Y., see Xia, S.-Q., 1003
Fuess, H., see Boča, R., 2337
Fun, H.-K., see Bose, D., 2045
Fun, H., see Chew, K.-B., 1385
Fun, H.-K., see Crouse, K.A., 161
Funaioli, T., see Pardey, A.J., 1677
Furtado, S.J., see Camm, K.D., 2929
Furukawa, Y., see Asaji, T., 1605

Gable, R.W., see Eagle, A.A., 385
Gahan, L.R., see Sharrad, C.A., 2217
Galani, A., Kovala-Demertzi, D., Kourkoumelis, N., Koutsodimou, A., Dokorou, V., Ciunik, Z., Russo, U. and Demertzis, M.A., Organotin adducts of indomethacin: synthesis, crystal structures and spectral characterization of the first organotin complexes of indomethacin, 2021
Galler, J.L., Goodchild, S., Gould, J., McDonald, R. and Sella, A., Tris-pyrazolylborate complexes of redox inactive lanthanides – the structures of $[(Tp^{Me2})_2NdX]$ (X=Cl, NPh_2, dpm, H_2BEt_2), 253
Galli, S., see Ardizzoia, G.A., 3063
Gameiro, P., see Sousa, C., 1401
Gamez, P., see Song, Y., 1769
Gao, S., see Luo, J., 1243
Gao, S., see Zheng, X.-J., 1257
Gao, E.-Q., see Chen, J.-X., 1877
Gao, S., see Zou, Y., 2253
Gao, M.Z., see Gao, J., 59
Gao, J., Zingaro, R.A. and Gao, M., A silica immobilized cobalt complex: absorption of dioxygen and the redox ability in aqueous solution, 59
García-Deibe, A.M., see Sanmartín, J., 963
García-Fontán, S., see Rodríguez, M.C., 1045
García-Martínez, E., see Carballo, R., 1505
Gardinier, J.R., see Reger, D.L., 291
Garnovskii, A.D., Kharisov, B.I., Anpilova, E.L., Bicherov, A.V., Korshunov, O.Yu., Burlov, A.S., Méndez-Rojas, M.A., Blanco, L.M., Borodkin, G.S., Uflyand, I.E. and Ortiz Méndez, U., New β-aminovinylketonates with annealated 1,2-benzothiazine-1,1-dioxide fragment, 1909
Garrett, A.D., see Cross, J.L., 2831
Gatterer, K., see Mautner, F.A., 1217
Gaubeur, I., Guekezian, M., Terra, L.H.S. Ávila, Moraes, M.C.B., Lago, C.L., Matos, J.R. and Suárez-Iha, M.E.V., Synthesis, characterization, thermodynamic and thermal studies of Zn(II) complexes with di-2-pyridyl ketone salicyloylhydrazone, 2095
Gause, C.D., see Alvarez, H.M., 617
Gaye, M., see Bouyagui Tamboura, F., 1191
Gelder, R. de, see van Albada, G.A., 2387
Gembický, M., see Boča, R,, 2337
Gennari, M,, Giannetto, M., Lanfranchi, M., Marchiò, L., Pellinghelli, M.A. and Tegoni, M., Synthesis, structure and electrochemical properties of a nickel complex with the hydrotris[thioxotriazolyl-3-(2-pyridyl)]borate podand ligand, 1829
Ghosh, B.K., see Bose, D., 2045
Ghosh, B.K., see Bose, D., 545
Ghosh, S., see Pramanik, N.R., 1595
Giannetto, M., see Gennari, M., 1829
Gibson, V.C., see O'Reilly, R.K., 2921
Gibson, V.C., Redshaw, C., Clegg, W., Elsegood, M.R.J., Siemeling, U. and Türk, T., Synthesis and X-ray crystal structures of hydridotris(3,5-dimethylpyrazolyl)borate (Tp′) molybdenum(VI) bis(imido) complexes, 189
Gil de Muro, I., Lezama, L., Insausti, M. and Rojo, T., Layered $[BaMn_{1-x}M_x(C_3H_2O_4)_2(H_2O)_4]$ (M = Fe, Co or Cu) solid solutions: thermal, spectroscopic and magnetic properties, 929
Giles, B.T., see Venkatasubramanian, U., 629
Gillespie, P.A., see Alvarez, H.M., 617
Gipson, S.L., see Kim, J., 1371
Giroux, S., Aury, S., Rubini, P., Parant, S., Desmurs, J.-R. and Dury, M., A spectroscopic investigation of the complexing ability of catecholate or salicylate derivatives towards aluminium(III), 2393
Głowiak, T., see Barszcz, B., 1309
Glowiak, T., see Valigura, D., 2447
Glowiak, T., see Stachová, P., 1303
Godinho, S.S.M.C., Royo, B., Lobato, M.T., Herdtweck, E. and Romão, C.C., Synthesis and structure of diphenylphosphine derivatives of molybdenocene, 1263
Godoy, Z., see Díaz, C., 1027
Goeta, A.E., see Coventry, D.N., 2789
Goh, T.K.H.H., see Rasika Dias, H.V., 273
Goher, M.A.S., Hafez, A.K., Abu-Youssef, M.A.M., Badr, A.M.A., Gspan, C. and Mautner, F.A., New metal(II) complexes containing monodentate and bridging 3-aminopyridine and azido ligands, 2349
Goher, M.A.S., see Mautner, F.A., 1217
Goldberg, D.P., see Karambelkar, V.V., 471
Goldsmith, J.I., see Sydora, O.L., 2841
Golen, J.A., see Alvarez, H.M., 617
Gomes, P.T., see Ribeiro, A.F.G., 2715
Gómez, M., Peris, E., Teruel, H., Arevalo, I., Mata, J.A. and Muller, G., Novel ferrocenyl-oxazoline ligands: first preparation of non-symmetrical bis(oxazoline), 611
Gonca, E., Köseoğlu, Y., Aktaş, B. and Gül, A., Octakis(1-naphthylmethylthio) substituted porphyrazine derivatives, 1845
González Garmendia, M.J., see Barquín, M., 1695
González-Prieto, R., see Barral, M.C., 2637
Goodchild, S., see Galler, J.L., 253
Gordon, K.C., see Polson, M.I.J., 1427
Gott, A.L., see Camm, K.D., 2929
Gou, S.-H., see Zhu, H.-B., 1131
Gou, S., see Yao, J., 1169
Gould, J., see Galler, J.L., 253
Govindaswamy, P., see Lalrempuia, R., 1069
Govindaswamy, P., Mozharivskyj, Y.A. and Rao Kollipara, M., Synthesis and characterization of cyclopentadienylruthenium(II) complexes containing *N*,*N*′-donor Schiff base ligands: crystal and molecular structure of $[(\eta^5\text{-}C_5H_5)Ru(C_5H_4N\text{-}2\text{-}CH{=}N\text{–}C_6H_4\text{–}p\text{-}OCH_3)(PPh_3)]PF_6$, 1567
Govindaswamy, P., Mozharivskyj, Y.A. and Kollipara, M.R,, New neutral and cationic η^6-arene ruthenium complexes with phosphine and amine ligands: syntheses and molecular structures of $[(\eta^6\text{-}p\text{-cymene})Ru(NH_2CH_2C_6H_5)Cl_2]$, $[(\eta^6\text{-}C_6Me_6)Ru(PPh_2Py)Cl_2]$ and $[(\eta^6\text{-}C_6Me_6)Ru(PPh_2Py)Cl]^+$, 3115
Grant, G.J., Patel, K.N., Helm, M.L., Mehne, L.F., Klinger, D.W. and VanDerveer, D.G., Heteroleptic platinum(II) complexes with crown thioethers and diimine ligands: the crystal structures of [Pt(9S3)(2,2′-bipy)]$(PF_6)_2$ and [Pt(9S3)(4,4-dimethyl-2,2′-bipy)]-$(PF_6)_2{\cdot}2.5CH_3NO_2$, 1361
Gray, G.M., see Butler, J.M., 1719
Gray, H.B., see Wenger, O.S., 2955
Green, J.C. and Burney, C., Open shell metallocenes and exchange splitting of ligand bands: a reassignment of the photoelectron spectra of manganocene, 2915
Grennberg, H., see Aranyos, V., 589
Griffin, R.G., see Sceats, E.L., 2751
Griffith, W.P., see Bailey, A., 2631
Grove, H., see Thompson, L.K., 1175
Gruhn, N.E., see Joshi, H.K., 429
Gspan, C., see Goher, M.A.S., 2349
Gspan, C., see Mautner, F.A., 1217
Gu, Xiao-Mei, see Jia, D.-X., 937
Guekezian, M., see Gaubeur, I., 2095
Gueneau, E.D., see Fromm, K.M., 1479

Guilardi, S., see Oliveira, M.R.L., 1153
Guillon, H., Daniele, S., Hubert-Pfalzgraf, L.G. and Letoffe, J.M., Synthesis, characterisation and thermal decomposition study of cerium(IV) 2-(2′-hydroxyphenyl)-2-oxazoline derivatives, 1467
Guinesi, L.S., see Júnior, G.C., 1953
Guo, W., Peng, Z., Li, D. and Zhou, Y., Synthesis and structural characterization of zinc(II) and cadmium(II) complexes with 2-oxo-1,3-dithiole-4,5-dithiolate and 1,10-phenanthroline, 1701
Guo, Q.-L., Zhu, W.-X., Ma, S.-L., Dong, S.-J. and Xu, M.-Q., Assembly of superanion capsules of *p*-sulfonatothiacalix[4]arenes with transition metal ions and diaza-crown ether, 1461
Guo, Q.-L., Zhu, W.-X., Liu, Y.-C., Yuan, D.-Q., Zhang, J., Ma, S.-L., Anionic capsules of p-sulfonatothiacalix[4]arene with trivalent lanthanide ions and diaza-crown ether, 2055
Gül, A., see Yasemin Yenilmez, H., 787
Gül, A., see Gonca, E., 1845
Gupta, S., Mukherjee, A., Nethaji, M. and Chakravarty, A.R., An angular trinuclear copper(II) complex as a model for the active site of multicopper oxidases, 643
Gurešić, D.M., see Radanović, D.D., 2183
Gütlich, P.p, see Saha, S., 1811
Guy, D.M.H., see Bushuk, S.B., 2615
Guyard-Duhayon, C., see Salunke-Gawali, S., 2541

Haase, W., see Iskander, M.F., 23
Hafez, A.K., see Goher, M.A.S., 2349
Hagfeldt, A., see Aranyos, V., 589
Halcrow, M.A., see Bradford, F.E., 2141
Hamady Barry, A., see Bouyagui Tamboura, F., 1191
Hamamci, S., see Yilmaz, V.T., 841
Hamid, M.H.S.A., see Ali, M.A., 2405
Hamilton, I.G., see Lundin, N.J., 97
Han, S., see Kim, J., 1333
Han, S.C., see Bernhardt, P.V., 869
Han, Y., see Ma, C., 1207
Handel, R., see Constable, E.C., 135
Harlow, R.L., see Westcott, S.A., 2665
Harrison, A., see Smith, A.A., 1557
Harrowfield, J.M., see Bernhardt, P.V., 869
Hartshorn, C.M., see McMorran, D.A., 1055
Harvey, B.G., Arif, A.M. and Ernst, R.D., Incorporation of polybasic aromatic amines into ruthenium(II) chloro complexes, 2725
Hasegawa, T., see Raimondi, A.C., 2069
Hashimoto, M., see Asaji, T., 1605
Hata, Y., see Kitano, T., 283
Haufe, S., see Morissette, M., 263
Havel, J., see Šedo, O., 1199
Hay, B.P., Uddin, J. and Firman, T.K., Eight-coordinate stereochemistries of U(IV) catecholate and aquo complexes, 145
Hazarika, P., see Sarmah, S., 1097
Hazell, A., Is bipyridine planar in metal complexes?, 2081
He, X., see Zhang, Q., 1975
He, X.-F., Vogels, C.M., Decken, A. and Westcott, S.A., Pyridyl benzimidazole, benzoxazole and benzothiazole platinum complexes, 155
He, X., Zhang, P., Song, T.-Y., Mu, Z.-C., Yu, J.-H., Wang, Y. and Xu, J.-N., Hydrothermal synthesis and structure of a molybdenum(VI) phosphate cluster and a three dimensional cobalt molybdenum(V) phosphate, 2153
Heirtzler, F., see Dias, S.I.G., 1011
Helliwell, M., see Smith, A.A., 1557
Helliwell, M., see John, G.H., 3097
Helm, M.L., see Grant, G.J., 1361
Henderson, K.W., see Nassar, R., 2499
Henling, L.M., see Wenger, O.S., 2955
Henriques, R.T., see Ribeiro, A.F.G., 2715
Heras, J.V., see Criado, R., 301
Herdtweck, E., see Godinho, S.S.M.C., 1263
Herrero, S., see Barral, M.C., 2637
Heu, M., see Kim, J., 1333
Hey-Hawkins, E., see Karakus, M., 2281
Hey-Hawkins, E., see Höcher, T., 1393
Hibbs, D.E., see Emseis, P., 1749
Hierso, J.-C., see Etienne, M., 379
Higes-Rolando, F.J., see Barros-García, F.J., 1453
Higgins, K.A., see Nordell, K.J., 2161
Hikichi, S., see Takahashi, Y., 225
Hill, M.S., Hitchcock, P.B. and Smith, N., Routes to titanium tetrazole complexes, 801
Hitchcock, P.B., see Cloke, F.G.N., 2625
Hitchcock, P.B., see Hill, M.S., 801
Hitchcock, P.B., see López-Sandoval, H., 1837
Ho, N.N., see Li, J., 419
Höcher, T., Salisbury, B.A., Theopold, K.H. and Hey-Hawkins, E., Phosphanylalkylcyclopentadienyl ligands: synthesis, molecular structures and catalytic properties of [{(η^5-C_5H_4)CMe_2PHR}$CrCl_2(PMe_2Ph)$] (R = Ph, ^{t}Bu), 1393
Hodson, E. and Simpson, S.J., Synthesis and characterisation of [(η^6-cymene)Ru(L)X_2] compounds: single crystal X-ray structure of [(η^6-cymene)Ru(P{OPh}$_3$)Cl_2] at 203 K, 2695
Holt, E.M., see Bentiss, F., 1903
Hong, C.S. and You, Y.S., Synthesis, crystal structures and magnetic studies of terephthalato-bridged binuclear nickel(II) complexes, 1379
Hong, C.S. and You, Y.S., Synthesis, crystal structures and magnetic properties of Cu(II) compounds bridged by the terephthalate ligand and hydrogen bonds, 3043
Hong, X.-L., Chao, H., Yao, J.-H., Li, H. and Ji, L.-N., Synthesis, characterization, electrochemistry and solvatochromic studies of $[Ru(dppt)\text{-}(dien)]^{2+}$ and $[Ru(pta)(dien)]^{2+}$, 815
Horn Jr., A., see Fernandes, C., 1419
Hossaini Sadr, M., Clegg, W. and Reza Bijhanzade, H., Synthesis and characterization of two pentanuclear complexes $(NEt_4)_2[MS_4(CuBp)_4]$ (M=Mo, W; Bp=H_2B(pyrazolyl)$_2$) and crystal structure determination of $(NEt_4)_2[WS_4(CuBp)_4]$, 637
Hou, H.-W., see Mao, H.-Y., 1961
Hou, H.-W., see Liu, H.-L., 1799
Hou, H.-W., see Liu, H.-L., 943
Houlis, J.F., see Merwin, R.K., 2873
Housecroft, C.E., see Constable, E.C., 135
Howard, J.A.K., see Venkatasubramanian, U., 629
Howard, J.A.K., see Coventry, D.N., 2789
Howell, S.L., see Polson, M.I.J., 1427
Howie, R.A., Moura, M.V.H., Wardell, J.L. and Wardell, S.M.S.V., Further study of tris(cyclohexyl)stannane compounds, Cy_3SnX. Syntheses of the compounds with X=Br, I, N_3 and NCS and redetermination of the crystal structures of Cy_3SnX (X=Br and I), 2331
Hu, X.-L., Li, Y.-Z. and Luo, Q.-H., Characterization and crystal structure of lanthanide cryptates of a ligand derived from 2,6-diformyl-pyridine, 49
Hu, H.-L., see Yeh, C.-W., 1947
Hu, J.-J., see Yu, L., 823
Hu, S.-M., see Zhang, J.-J., 2265
Hu, X.-Y., see Shi, Y.-C., 567, 749
Hu, Sheng-Min, see Xia, S.-Q., 1003
Hu, X.-Y., see Shi, Y.-C., 15
Huang, W., see Yao, J., 1169
Huang, H., Yu, H.-B. Liu, S.-Y. and Shi, M., Neutral coordination frameworks with host–guest properties constructed by dicopper(II) units and 4,7-phenanthroline, 55
Huang, K.-L., see Chen, Chao, 3033
Huang, W., see Zhu, H.-B., 1131
Huang, B., see Cheng, J., 1075

Hubert-P., L.G., see Pasko, S., 735
Hubert-Pfalzgraf, L.G., see Guillon, H., 1467
Hung, C.-H., see Dinda, J., 793
Hursthouse, M.B., Levason, W., Ratnani, R., Reid, G., Synthesis and spectroscopic properties of Mo(VI) complexes with phosphine oxide ligands and the crystal structures of $[MoO_2X_2(OPMe_3)_2]$ (X=Cl or Br) and $[MoO_2Br_2\{o\text{-}C_6H_4(P(O)Ph_2)_2\}]\cdot 2CH_2Cl_2$, 1915
Husebye, S., see Foss, O., 3021

Iglesias, A.L., Aguirre, G., Somanathan, R., Parra-Hake, M., New chiral Schiff base–Cu(II) complexes as cyclopropanation catalysts, 3051
İhsan Okur, A., see Yasemin Yenilmez, H., 787
Ilkhechi, A.H., Scheibitz, M., Bolte, M., Lerner, H.-W. and Wagner, M., On the way to ferrocene-based multiple-decker sandwich complexes, 2597
Incarvito, C.D., see Voo, Janis K., 405
Incarvito, C.D., see Karambelkar, V.V., 471
Incarvito, C.D., see Niu, W., 1019
Incarvito, C.D., see Pariya, C., 439
Insausti, M., see Gil de Muro, I., 929
Inyushin, S., Shafir, A., Sheats, J.E., Minihane, M., Whitten Jr., C.E. and Arnold, J., Synthesis and X-ray structures of metallocenium diamines of iron and cobalt, 2937
Isab, A.A., see Fettouhi, M., 1
Iskander, M.F., El-Sayed, L., Salem, N.M.H., Haase, W., Linder, H.J. and Foro, S., Synthesis, characterization and magnetochemical studies of some copper(II) complexes derived from *n*-salicylidene-*n*-alkanoylhydrazins: X-ray crystal and molecular structure of bis [monochloro(μ-*n*-salicylidenemyristoylhydrazine)ono(−1)] dicopper(II), 23
Islam, N.S., see Sarmah, S., 1097

Jadeja, R.N., Shah, J.R., Suresh, E. and Paul, P., Synthesis and structural characterization of some Schiff bases derived from 4-[{(aryl)-imino}ethyl]-3-methyl-1-(4′-methylphenyl)-2-pyrazolin-5-one and spectroscopic studies of their Cu(II) complexes, 2465
Jäger, L., see Boča, R., 2337
Jagoda, M., see Dodds, C.A., 445
Jalón, F.A., see Caballero, A., 361
Jameson, G.B., see Ainscough, E.W., 1159
Jasimuddin, Sk., Byabartta, P., Mostafa, G., Lu, T. and Sinha, C., Synthesis, spectral studies, crystal structure and redox properties of homoleptic tris-chelated ruthenium(II)-arylazoimidazoles, 727
Jasimuddin, Sk., see Dinda, J., 793
Jasmin, C., see Sreeja, P.B., 575
Jaworska, M., see Małecki, J.G., 885
Jaworska, M., see Machura, B., 1819
Jaworska, M., see Machura, B., 2523
Jaworska, M., see Machura, B., 2005
Jeffery Leigh, G., see López-Sandoval, H., 1837
Jeliazkova, B., see Minkovska, S., 3147
Jeon, Y.-M., see Choi, K.-Y., 903
Jeong, J.H., see Roh, S.G., 2063
Jezierska, J., see Kurzak, B., 1939
Jezierska, J., see Barszcz, B., 1309
Jeżowska-Bojczuk, M., see Kurzak, B., 1939
Ji, L.-N., see Hong, X.-L., 815
Jia, D.-X., Dai, J., Zhu, Q.-Y., Zhang, Y. and Gu, X.-M., Syntheses, crystal structures and thermo analyses of thiostannates $[Ni(en)_3]_2Sn_2S_6$ and $[Ni(dien)_2]_2Sn_2S_6$, 937
Jia, D.-X., see Dai, J., 1447
Jia, D.-X., see Zhu, Q.-Y., 2259
Jiang, Q., see Ma, C., 779
Jiang, Z.-H., see Liang, M., 2203
Jiang, Z.-H., see Sun, Y.-J., 211
Jiménez-Aparicio, R., see Barral, M.C., 2637
Jin, L.-P., see Zheng, X.-J., 1257
Jin, L.-P., see Sun, C.-Y., 2227
Jin, L.-P., see Sun, C.-Y., 2085
Joe, D.J., see Joung, U.G., 1587
John, R.P., Sreekanth, A., Rajakannan, V., Ajith, T.A. and Kurup, M.R.P. New copper(II) complexes of 2-hydroxyacetophenone *N*(4)-substituted thiosemicarbazones and polypyridyl co-ligands: structural, electrochemical and antimicrobial studies, 2549
John, G.H., May, I., Collison, D. and Helliwell, M., Synthesis, structural and spectroscopic characterisation of three di-μ-fluoro-bis[dioxouranyl] complexes, 3097
Jones, W.D., see Oster, S.S., 2959
Jones, W.D., see Vetter, A.J., 413
Joseph, M., Suni, V., Prathapachandra Kurup, M.R., Nethaji, M., Kishore, A. and Bhat, S.G., Structural, spectral and antimicrobial studies of copper(II) complexes of 2-benzoylpyridine *N*(4)-cyclohexyl thiosemicarbazone, 3069
Joshi, H.K., Arvin, M.E., Durivage, J.C., Gruhn, N.E., Carducci, M.D., Westcott, B.L., Lichtenberger, D.L. and Enemark, J.H., Photoelectron spectra of potassium salts of hydrotris(pyrazol-1-yl)borates: electronic structure of the electron withdrawing scorpionates $Tp^{(CF_3)_2}$, Tp^{*Cl} and comparison to Tp* and Tp, 429
Jouini, T., see Bouyagui Tamboura, F., 1191
Joung, U.G., Kim, T.H., Joe, D.J., Lee, B.Y., Shin, D.M. and Chung, Y.K., Pyridineenolato and pyridineenamido complexes of zirconium, titanium and aluminum, 1587
Jung, W.-S., see Choi, S.-N., 2111
Júnior, G.C., Silva, A.P.S. and Guinesi, L.S., Synthesis, characterization and electropolymerization of a new polypyrrole iron(II) Schiff-base complex, 1953

Kafarski, P., see Kurzak, B., 1939
Kahol, P.K., see Siemer, C.J., 235
Kaim, W., see Knödler, A., 701
Kajfež Novak, T., see Cindrić, M., 1859
Kala, U.L., see Sreekanth, A., 41
Kalita, D., see Sarmah, S., 1097
Kalkan, A., Koca, A. and Bayır, Z.A., Unsymmetrical phthalocyanines with alkynyl substituents, 3155
Kalvinkovskya, Y.A., see Bushuk, S.B., 2615
Kamenar, B., see Cindrić, M., 1859
Kandaswamy, M., see Thirumavalavan, M., 519
Kandaswamy, M., see Saravanakumar, D., 665
Kandaz, M., Koca, A. and Özkaya, A.R., A new redox-active multisite ligand: synthesis, spectroscopy and electrochemistry of its mono and dinuclear complexes and the interaction of (*E*,*E*)M (M=Ni) complex with Pd^{II} and Ag^{I}, 1987
Kang, Y., see Cheng, J.-K., 2209
Kannan, S., Rajalakshmi, N., Chetty, K.V., Venugopal, V. and Drew, M.G.B., Complexes of the uranyl ion with bis(diphenylphosphino)methane dioxide, 1527
Kannappan, R., Tanase, S., Tooke, D.M., Spek, A.L., Mutikainen, I., Turpeinen, U. and Reedijk, J., Separation of actinides and lanthanides: crystal and molecular structures of *N,N*′-bis(3,5-di-*t*-butylsalicylidene)-4,5-dimethyl-1,2-phenylenediamine and its uranium complex, 2285
Karakus, M., Lönnecke, P. and Hey-Hawkins, E., Zwitterionic ferrocenyldithiophosphonates: the molecular structure of $[FcP(S)S(OCH_2CH_2NH_2Me)]$ $[Fc=Fe(\eta^5\text{-}C_5H_4)(\eta^5\text{-}C_5H_5)]$, 2281
Karamalides, A., see Raptopoulou, C., 1777
Karambelkar, V.V., diTargiani, R.C., Incarvito, C.D., Zakharov, L.N., Rheingold, A.L., Stern, C.L. and Goldberg, D.P., Multiple bonding modes exhibited by heteroscorpionate N_2S(alkylthiolate) ligands with Zn(II) and Fe(II), 471
Karmakar, R., Choudhury, C.R., Bravic, G., Sutter, J.-P. and Mitra, S., A novel manganese(III) quadridentate Schiff-base dimeric complex: synthesis, crystal structure and magnetic properties, 949

Kasbollah, A., see Crouse, K.A., 161
Kautz, J.A., see Rudd, M.D., 1923
Kavanagh, K., see Abuskhuna, S., 1249
Kefalloniti, E., see Milios, C.J., 83
Keita, B., see Lu, Y.-W., 1579
Kelly, A.E., see Yoon, S., 2805
Kessler, V.G., see Starikova, Z.A., 109
Kettunen, M., Abu-Surrah, A.S., Abdel-Halim, H.M., Repo, T., Leskelä, M., Laine, M., Mutikainen, I. and Ahlgren, M., Synthesis, spectroscopy and molecular structures of new salicylketiminato nickel(II) complexes, 1649
Kharisov, B.I., see Garnovskii, A.D., 1909
Kilner, C.A., see Bradford, F.E., 2141
Kim, Y.-I., see Choi, S.-N., 2111
Kim, Y., see Bernhardt, P.V., 869
Kim, J. and Gipson, S.L., Oxidatively induced one-electron reductive elimination of pentafluorophenyl from $[Mo(C_6F_5)(CO)_5]^-$, 1371
Kim, M.-W., see Choi, K.-Y., 903
Kim, J., Han, S., Cho, I.-K., Choi, K.Y., Heu, M., Yoon, S. and Suh, B.J., Synthesis of a cyano-bridged Fe_2Mn linear unit and a Fe_2Mn_2 square unit by using the [*fac*-Fe{HB(pz)$_3$}(CN)$_3$]$^-$ building block, 1333
Kim, T.H., see Joung, U.G., 1587
Kingston, J.V., see Bindu, P., 679
Kirk, M.L. and Peariso, K., Ground and excited state spectral comparisons of models for sulfite oxidase, 499
Kishore, A., see Sreeja, P.B., 575
Kishore, A., see Joseph, M., 3069
Kitano, T., Sohrin, Y., Hata, Y., Mukai, H., Wada, H. and Ueda, K., Highly selective extraction of Cu(II) and Zn(II) using $[B(3\text{-iPrpz})_4]^-$ (iPrpz=isopropylpyrazolyl), 283
Klapshina, L.G., see Bushuk, S.B., 2615
Klinger, D.W., see Grant, G.J., 1361
Knödler, A., Fiedler, J. and Kaim, W., Characterization of the mixed-valent intermediate (n=3) of the complex series $\{(\mu,\eta^3\text{: }\eta^3\text{-L})[(Ru(terpy)]_2\}^{n+}$ with the unsaturated bridging ligand *N*,*N*′-bis(α-picolinoyl)hydrazido(2−)=L^{2-}, 701
Knight, D.A., see Schull, T.L., 1375
Koban, A. and Bernhard, G., Complexation of uranium(VI) with glycerol 1-phosphate, 1793
Koca, A., see Kandaz, M., 1987
Koca, A., see Kalkan, A., 3155
Kodai, I., see Wen, M., 2117
Kollipara, M.R., see Govindaswamy, P., 3115
Kollipara, M.R., see Lalrempuia, R., 1069
Koman, M., see Valigura, D., 2447
Koman, M., see Stachová, P., 1303
Koner, S., see Saha, S., 1811
Kopel, P., Trávníček, Z., Marek, J. and Mrozinski, J., Syntheses and study on nickel(II) complexes with thiodiglycolic acid and nitrogen-donor ligands. X-ray structures of $[Ni(bpy)(tdga)(H_2O)] \cdot 4H_2O$ and $[(en)Ni(\mu\text{-tdga})_2Ni(en)] \cdot 4H_2O$ (tdgaH_2=thiodiglycolic acid), 1573
Kopel, P., Trávníček, Z., Zbořil, R. and Marek, J., Synthesis, X-ray and Mössbauer study of iron(II) complexes with trithiocyanuric acid (ttcH_3). The X-ray structures of $[Fe(bpy)_3](ttch) \cdot 2bpy \cdot 7H_2O$ and $[Fe(Phen)_3](ttch_2)(ClO_4) \cdot 2CH_3OH \cdot 2H_2O$, 2193
Korabik, M., see Stachová, P., 1303
Korabik, M., see Valigura, D., 2447
Koreneva, O.V., see Tretyakov, E.V., 763
Korolkov, D.V., see Baranovski, V.I., 1519
Korshunov, O.Yu., see Garnovskii, A.D., 1909
Köseoğlu, Y., see Gonca, E., 1845
Kourkoumelis, N., see Galani, A., 2021
Koutsantonis, G.A., see Bernhardt, P.V., 869
Koutsodimou, A., see Galani, A., 2021
Koval, I.A., see Song, Y., 1769
Kovala-Demertzi, D., see Galani, A., 2021
Kowalski, K., Zakrzewski, J. and Rybarczyk-Pirek, A., $[(\eta^5\text{-}C_5H_5)Fe(CO)_2](Fp)$-complexes of the parabanic acid mono- and dianion: synthesis, X-ray structures and reactivity of the heterocyclic ligand, 1441
Kozimor, S.A., see Evans, W.J., 2689
Krempner, C., Reinke, H., Weichert, K. and Spannenberg, A., Diastereoselective formation of a *meso*-disilane-1,2-diol – a dianionic siloxide ligand for Ti and Zr, 2475
Kress, J., see Pelascini, F., 3193
Krisyuk, V.V., Turgambaeva, A.E. and Rhee, S.-W., Homobinuclear copper(I) hexafluoroacetylacetonate complexes with non-cyclic diene ligands, 809
Krivolapov, D.B., see Zabirov, N.G., 2243
Kruszynski, R., see Małecki, J.G., 885
Kruszynski, R., see Machura, B., 2523
Kruszynski, R., see Machura, B., 2005
Kruszynski, R., see Machura, B., 1819
Kubiak, M., see Drożdżewski, P., 1785
Kuchta, M.C., see Cloke, F.G.N., 2625
Kumar, R., see Srivastava, P.C., 1629
Kumar, M., see Shankar, R., 71
Kumar Dutta, D., see Chutia, P., 1657
Kumar Lahiri, G., see Maiti, D., 831
Kumara Swamy, K.C., see Satish Kumar, N., 979
Kumari, N., see Chutia, P., 1657
Kunrath, F.A., Casagrande Jr., O.L., Toupet, L. and Carpentier, J.-F., Synthesis and reactivity in salt metathesis reactions of trivalent $[La(Tp^{Me2})_2X]$ (X=Cl, I) complexes: crystal structures of $[La(Tp^{Me2})_2Cl]$ and $[La(Tp^{Me2})_2(\kappa^2\text{-}pz^{Me2})]$, 2437
Kuroda-Sowa, T., see Wen, M., 2117
Kurup, M.R.P., see John, R.P., 2549
Kurup, M.R.P., see Sreekanth, A., 969
Kurzak, B., Woźna, A., Jezierska, J., Jeżowska-Bojczuk, M., Szczepanik, W. and Kafarski, P., Copper(II) complexes of several monophosphono dipeptides: the role of phosphonic oxygen and thioether sulfur in complex stabilization, 1939
Kuzmina, N., see Ryazanov, M., 879
Kyritsakas, N., see Pelascini, F., 3193

Labat, G., see Dias, S.I.G., 1011
Lago, C.L., see Gaubeur, I., 2095
Lagrenée, M., see Bentiss, F., 1903
Laine, M., see Kettunen, M., 1649
Lalrempuia, R., Govindaswamy, P., Mozharivskyj, Y.A. and Kollipara, M.R., Reactivity studies of cyclopentadienyl bis(triphenylphosphine)ruthenium(II) complex towards some polypyridyl ligands, 1069
Lam, C.-K., see Zhang, L.-P., 2413
Lam, K.C., see Westcott, S.A., 2665
Lamač, M., see Štěpnička, P., 921
LaMonica, G., see Ardizzoia, G.A., 3063
Lanfranchi, M., see Gennari, M., 1829
Larrazábal, G., see Parada, J., 1341
Lath, R., see Srivastava, P.C., 1629
Latorre, R.O., see Paredes-García, V., 1869
Layh, M., see Bowen, R.J., 2273
Leban, I., see Popović, Z., 1293
Lee, B.Y., see Joung, U.G., 1587
Lee, T.-W., Po-Kwan Lau, J. and Wong, W.-T., Synthesis and characterization of coordination polymers of Zn(II) with 1,3-bis(4-pyridyl)propane and 4,4′-pyridine ligands, 999
Lee, M.-J., see Choi, S.-N., 2111
Lee, H.-J., see Nam, H.J., 115
Lee, Y.-M., see Choi, S.-N., 2111
Lerner, H.-W., see Ilkhechi, A.H., 2597
Leskelä, M., see Kettunen, M., 1649

Leslie, W., Poole, R.A., Murray, P.R., Yellowlees, L.J., Beeby, A. and Williams, J.A.G., Near infra-red luminescence from bis-terpyridyl iridium(III) complexes incorporating electron-rich pendants, 2769
Letoffe, J.M., see Guillon, H., 1467
Leung, D.W.C., see Bailey, A., 2631
Levason, W., Matthews, M.L., Patel, B., Reid, G. and Webster, M., Titanium(IV) iodide complexes with phosphine and arsine donor ligands and the crystal structures of the iron(II)/(III) redox pair $[FeI_2\{o\text{-}C_6H_4(AsMe_2)_2\}_2]^{0/+}$, 605
Levason, W., see Hursthouse, M.B., 1915
Lever, A.B.P., see Thompson, L.K., 1175
Leverett, P., see Emseis, P., 1749
Lezama, L., see Gil de Muro, I., 929
Li, J.-S., see Yu, L., 823
Li, L.-C., see Zheng, X.-J., 1257
Li, G., see Mao, H.-Y., 1961
Li, F.-F., see Ma, J.-F., 553
Li, Y.-Z., see Liu, W.-L., 849
Li, W.-F., Sun, H.-M., Shen, Q., Zhang, Y. and Yu, K.-B., Synthesis, structural characterization and catalysis of ethyl-substituted indenylnickel (II) halides, 1473
Li, L., see Ma, J.-F., 553
Li, G., see Liu, H.-L., 943
Li, D., see Ma, C., 1207
Li, Z.-J., see Cheng, J.-K., 2209
Li, Y.-R., see Luo, J., 1243
Li, Y., see Lu, J., 755
Li, H., see Hong, X.-L., 815
Li, Y.-Z., see Hu, X.-L., 49
Li, Y.-Z., see Liu, W.-L., 2125
Li, Y., see Liang, H., 1619
Li, J., Djurovich, P.I., Alleyne, B.D., Tsyba, I., Ho, N.N., Bau, R. and Thompson, M.E., Synthesis and characterization of cyclometalated Ir(III) complexes with pyrazolyl ancillary ligands, 419
Li, X., see Liang, H., 1619
Li, D., see Guo, W., 1701
Li, B., Zhu, X., Zhou, J., Peng, Y. and Zhang, Y., Syntheses and structures of five cadmium(II) coordination polymers from 1,2-bis(1,2,4-triazol-1-yl)ethane, 3133
Li, Y.-M., see Zhang, J.-J., 2265
Li, G.-H., see Meng, H., 2357
Liang, M., Wang, Q.-L., Yu, L.-H., Liao, D.-Z., Jiang, Z.-H., Yan, S.-P. and Cheng, P., A novel 3D malonato-bridged compound $Cu(mal)(pz)_2$: synthesis, spectroscopy, crystal structure and magnetism, 2203
Liang, H., Liu, J., Li, X. and Li, Y., Synthesis, structure and norbornene polymerization behavior of neutral palladium complexes, 1619
Liao, D.-Z., see Sun, Y.-J., 211
Liao, D.-Z., see Liang, M., 2203
Licchelli, M., see Fabbrizzi, L., 373
Lichtenberger, D.L., see Joshi, H.K., 429
Lim, H.-H., see Choi, K.-Y., 903
Lin, Z., see Westcott, S.A., 2665
Lin, H.-H., see Zhu, Q.-Y., 2259
Linder, H.J., see Iskander, M.F., 23
Lippard, S.J., see Yoon, S., 2805
Litvinov, I.A., see Zabirov, N.G., 2243
Liu, Y.-H., see Shi, Y.-C., 1541
Liu, L., see Meng, H., 2357
Liu, Y., see Yang, Y., 1535
Liu, Y., see Huang, H., 55
Liu, W.-L., Zou, Y., Lu, C.-S., Dang, D.-B., Li, Y.-Z., Yao, Y.-G. and Meng, Q.-J., Self-assembly, structure and magnetic properties of carboxylate-bridged Cu(II)–M(II) (M=Mg, Ca, Sr, Ba) complexes with a new metalloligand as a building block, 2125
Liu, Y.-C., see Guo, Q.-L., 2055
Liu, W.-L., Zou, Y., Ni, C.-L., Ni, Z.-P., Li, Y.-Z., Yao, Y.-G. and Meng, Q.-J., Synthesis and characterization of copper(II) Schiff base complexes derived from salicylaldehyde and glycylglycylglycine, 849
Liu, W.-L., see Zou, Y., 2253
Liu, R.-C., see Yu, L., 823
Liu, J., see Zhang, Q., 1975
Liu, H.-L., see Mao, H.-Y., 1961
Liu, S.-X., Neels, A., Stoeckli-Evans, H., Pilkington, M., Wallis, J.D. and Decurtins, S., Organosulfur donor with hydroxy groups and its conducting salt: crystal structures and physical properties, 1185
Liu, J.-F., see Ma, J.-F., 553
Liu, H.-L., Mao, H.-Y., Zhang, H.-Y., Xu, C., Wu, Q.-A., Li, G., Zhu, Y. and Hou, H.-W., Two novel heterometallacrowns: syntheses and crystal structures of two copper(II) complexes with malonate and *o*-pthalate, 943
Liu, H.-L., Mao, H.-Y., Xu, C., Zhang, H.-Y., Hou, H.-W., Wu, Q.-A., Zhu, Y., Ye, B.-X. and Yuan, L.-J., Four novel sulfur-rich complexes: syntheses, crystal structures of three nickel(II) and one cobalt(II) complex with derivatives of Lawesson's Reagent, 1799
Liu, Y.-L., see Chen, C., 3033
Liu, J., see Liang, H., 1619
Liu, S.-X., see Chen, J.-X., 1877
Lobato, M.T., see Godinho, S.S.M.C., 1263
Lobbia, G.G., see Pettinari, C., 451
Loening, N.M., see Sceats, E.L., 2751
Long, D.-L., see Pickering, A.L., 2075
Longo, C., see Pardey, A.J., 1677
Lönnecke, P., see Karakus, M., 2281
López-Sandoval, H., Richaud, A., Contreras, R., Jeffery Leigh, G., Hitchcock, P.B., Flores-Parra, A., Carlos Galvez-Ruíz, J., Cruz, A., Nöth, H. and Barba-Behrens, N., Triangulo-μ_3-sulfido-trinickel(II) cone-shaped clusters and anion traps: structural characterization, 1837
Loroño, D., see Marquez, V.E., 1317
Lu, T.-H., see Dhara, P.K., 2457
Lu, T., see Jasimuddin, Sk., 727
Lü, C.-H., see Lu, J., 755
Lu, W.-J., see Zhang, L.-P., 169
Lu, W.-J., Zhang, L.-P., Chan, H.-S., Chan, T.-L. and Mak, T.C.W., Di-protonated 1,4,8,11-tetramethyl-1,4,8,11-tetraazacyclotetradecane tetra-*N*-oxide, a bulky di-cation that induces the assembly of unusual lanthanide(III) complexes, 1089
Lu, W.-J., see Zhang, L.-P., 857
Lu, C.-S., see Liu, W.-L., 2125
Lu, Y.-W., Keita, B. and Nadjo, L., Rational approach of the stoichiometries of lanthanide complexes with α_2-$[P_2W_{17}O_{61}]^{10-}$ heteropolytungstate in aqueous solution, 1579
Lu, J., Lü, C.-H., Yu, J.-H., Xu, J.-Q., Li, Y., Zhang, X., Wang, T.-G. and Yang, Q.-X., Syntheses, structures and third-order nonlinear optical properties of heterometal and homometal clusters containing iron, 755
Lu, C.-S., see Zou, Y., 2253
Lu, T.-H., see Chand, B., 1669
Lu, C., see Zhang, Q., 1975
Luna-Giles, F., see Barros-García, F.J., 1453
Lundin, N.J., Hamilton, I.G. and Blackman, A.G., Synthesis and hypodentate Cu(II) complexes of new tripodal tetraamine ligands incorporating a long pendant arm, 97
Luo, J., Zhou, X.-G., Gao, S., Weng, L.-H., Shao, Z.-H., Zhang, C.-M., Li, Y.-R., Zhang, J. and Cai, R.-F., Synthesis and characterization of copper(II) azide complexes containing polyamines as co-ligands, 1243
Luo, Q.-H., see Hu, X.-L., 49
Lutz, P.J., see Pelascini, F., 3193
Lycka, A., see Basu Baul, T.S., 2323

Ma, J.-F., Yang, J., Zheng, G.-L., Li, L., Zhang, Y.-M., Li, F.-F. and Liu, J.-F., Four new coordination polymers of Cu(II) with 1,1′-(1,4-butanediyl)bis(imidazole), 553
Ma, Y.-Q., see Yu, L., 823
Ma, S.-L., see Guo, Q.-L., 1461
Ma, C., Han, Y. and Li, D., Synthesis and crystal structures of diorganotin dicyanoethylene-1,2-dithiolate compounds and their derivatives with 4,4′-Bipy or Phen, 1207
Ma, C., Jiang, Q. and Zhang, R., Syntheses, characterizations and crystal structures of new organotin complexes with 2-mercapto-6-nitrobenzothiazole, 779
Ma, C. and Sun, J., Hydrogen bonding and π–π stacking interaction in the coordination of sulfur and nitrogen donor heterocycle to organotin(IV): syntheses and crystal structures of di- and triorganotin(IV) derivatives with 1-(4-hydroxyphenyl)-1*H*-tetrazole-5-thiol, 1547
Ma, C., Zhang, J. and Zhang, R., Syntheses, characterizations and crystal structures of new triorgano-tin or -germanium complexes with 1H-5-mercapto-1,2,3-triazolato, 1981
Ma, S.-L., see Guo, Q.-L., 2055
Małecki, J.G., Dzięgielewski, J.O., Jaworska, M., Kruszynski, R. and Bartczak, T.J., Synthesis, molecular, crystal and electronic structures of $[(C_6H_6)RuCl(HPz)_2]Cl$ and $[(C_6H_6)RuCl_2(Me_2HPz)]$, 885
Macgregor, S.A., see Venkatasubramanian, U., 629
Machura, B., Jaworska, M. and Kruszynski, R., X-ray and electronic structure of the $[ReCl_3(pzH)_2(PPh_3)]$ and $[ReCl_3(3,5\text{-}Me_2pzH)_2(PPh_3)]$ complexes, 1819
Machura, B., Jaworska, M. and Kruszynski, R., Synthesis, crystal, molecular and electronic structure of the $[ReBr_3(NO)(AsPh_3)(pzH)]$ complex, 2523
Machura, B., Electronic structure and UV–Vis spectroscopy of $[Re(NO)Br_3(PPh_3)_2]$ and $[Re(NO)Br_3(OPPh_3)_2]$ complexes, 2363
Machura, B., Jaworska, M. and Kruszynski, R., DFT calculation and X-ray structure of the $[ReCl_3(pzH)_3]$ complex, 2005
Madhu, V. and Das, S.K., Near-IR absorption due to supramolecular electronic interaction in an extended 3D hydrogen-bonding network material: synthesis, crystal structure and properties of $[4,4'\text{-}H_2bpy][Cu(mnt)_2]$, 1235
Maekawa, M., see Wen, M., 2117
Maestro, M.A., see Arnáiz, F.J., 537
Magull, J., see Neculai, A.M., 183
Magull, J., see Bai, G., 1125
Mahjoub, A., see Morsali, A., 2427
Mahr, N., see Werner, H., 2645
Maiti, D., Paul, H., Chanda, N., Chakraborty, S., Mondal, B., Puranik, V.G. and Kumar Lahiri, G., Synthesis, structure, spectral and electron-transfer properties of octahedral-$[Co^{III}(L)_2]^+$/$[Zn^{II}(L)_2]$ and square planar-$[Cu^{II}(L)\{OC(=O)CH_3\}]$ complexes incorporating anionic form of tridentate bis(8-quinolinyl)amine $[N^1C_9H_6\text{–}N^2\text{–}C_9H_6N^3, L^-]$ ligand, 831
Mak, T.C.W., see Zhang, L.-P., 2413
Mak, T.C.W., see Zhang, L.-P., 857
Mak, T.C.W., see Lu, W.-J., 1089
Mak, T.C.W., see Zhang, L.-P., 169
Mal, D., see Saha, S., 1811
Mamo, M.A., see Bowen, R.J., 2273
Mandal, S.S., see Pramanik, N.R., 1595
Mangrich, A.S., see Raimondi, A.C., 2069
Manning, T.D. and Parkin, I.P., Vanadium(IV) oxide thin films on glass and silicon from the atmospheric pressure chemical vapour deposition reaction of $VOCl_3$ and water, 3087
Manzano, B.R., see Caballero, A., 361
Mao, H.-Y., see Liu, H.-L., 943
Mao, H.-Y., see Liu, H.-L., 1799
Mao, H.-Y., Shen, X.-Q., Li, G., Zhang, H.-Y., Xu, C., Liu, H.-L., Wang, E.-B., Wu, Q.-A., Hou, H.-W. and Zhu, Y., Novel hydrogen-bonded and π–π interaction networks generated from the reaction of copper(II) chloride hydrates with heterocyclic diimines (2,2′-bipyridine, 1,10-phenanthroline) and bidentate diamine (ethylene-diamine), 1961
Mao, H.-Y., see Shen, X.-Q., 1851
Marcel Haba, P., see Bouyagui Tamboura, F., 1191
Marchetti, F., see Pettinari, C., 451
Marchiò, L., see Gennari, M., 1829
Marder, T.B., see Westcott, S.A., 2665
Marder, T.B., see Coventry, D.N., 2789
Marek, J., see Ahmed, M., 655
Marek, J., see Kopel, P., 2193
Marek, J., see Kopel, P., 1573
Marquez, V.E., Anacona, J.R. and Loroño, D., Crystal structure and electrochemistry of copper(II) macrocycles containing terpyridine, 1317
Martini, D., see Pettinari, C., 451
Martiška, L., see Valigura, D., 2447
Mascarenhas, Y.P., see Soares, L.F., 205
Masci, B., see Thuéry, P., 649
Masciocchi, N., see Ardizzoia, G.A., 3063
Maspero, A., see Ardizzoia, G.A., 3063
Mata, J.A., see Gómez, M., 611
Matković-Čalogović, D., see Popović, Z., 1293
Matos, J.R., see Gaubeur, I., 2095
Matsuo, H., Miyazaki, Y., Takemura, H., Matsuoka, S., Sakashita, H. and Yoshimura, K., ^{11}B NMR study on the interaction of boric acid with Azomethine H, 955
Matsuoka, S., see Matsuo, H., 955
Matthews, M.L., see Levason, W., 605
Maunder, G.H., Russo, M.R. and Sella, A., NO to NO_2^- conversion by divalent lanthanides: synthesis and crystal structure of $[Sm(Tp^{Me2,4\text{-}Et})_2NO_2]$, 2709
Mautner, F.A., see Escuer, A., 1409
Mautner, F.A., see Goher, M.A.S., 2349
Mautner, F.A., Gspan, C., Gatterer, K., Goher, M.A.S., Abu-Youssef, M.A.M., Bucher, E. and Sitte, W., Synthesis and characterization of three 5-(4-pyridyl)tetrazolato complexes obtained by reaction of 4-cyanopyridine with metal azides from aqueous solutions, 1217
May, I., see John, G.H., 3097
Mayer, J.M., see Soper, J.D., 323
McCann, M., see Abuskhuna, S., 1249
McCann, M., see Abuskhuna, S., 1731
McDonald, R., see Galler, J.L., 253
McDonald, R., see Morissette, M., 263
McGowan, P.C., see Camm, K.D., 2929
McKee, V., see Abuskhuna, S., 1249
McKee, V., see Abuskhuna, S., 1731
McMorran, D.A., Hartshorn, C.M. and Steel, P.J., Copper(II) complexes of bis- and tetrakis-(2-pyridylsulfanylmethyl)benzenes, 1055
McRory, C.P., see Scales, S.J., 2169
Mehne, L.F., see Grant, G.J., 1361
Mehnert, C.P., Cook, R.A., Dispenziere, N.C. and Mozeleski, E.J., Biphasic hydroformylation catalysis in ionic liquid media, 2679
Melník, M., see Stachová, P., 1303
Melník, M., see Valigura, D., 2447
Méndez-Rojas, M.A., see Garnovskii, A.D., 1909
Menezes, D.C., de Lima, G.M., Porto, A.O., Donnici, C.L., Ardisson, J.D., Doriguetto, A.C. and Ellena, J., Synthesis, characterisation and thermal decomposition of tin(IV) dithiocarbamate derivatives – single source precursors for tin sulfide powders, 2103
Menezes, D.C., see Soares, L.F., 205
Meng, Q.-J., see Liu, W.-L., 2125
Meng, Q.-J., see Liu, W.-L., 849
Meng, H., Li, G.-H., Xing, Y., Yang, Y.-L., Cui, Y.-J., Liu, L., Ding, H. and Pang, W.-Q., Hydrothermal synthesis and characterization

of a new 3D iron phosphatooxalate templated by organo-amine, 2357
Meng, Q.-J., see Zou, Y., 2253
Merca, A., see Müller, A., 2381
Merwin, R.K., Ontko, A.C., Houlis, J.F. and Roddick, D.M., Synthesis and characterization of CpMn(dfepe)(L) complexes (dfepe = $(C_2F_5)_2PCH_2CH_2P(C_2F_5)_2$; L = CO, H_2, N_2): an unusual example of a dihydride to dihydrogen photochemical conversion, 2873
Metteau, L., see Collange, E., 2605
Michaelides, A., Papadimitriou, C.D., Plakatouras, J.C., Skoulika, S. and Veltsistas, P.G., Synthesis, characterization and crystal structure of *catena*-bis(1,10-phenanthroline)-μ-chloranilatocadmium(II): a zig-zag polymer based on eight-coordinated square antiprismatic units, 2587
Miecznikowski, J.R. and Crabtree, R.H., Transfer hydrogenation reduction of ketones, aldehydes and imines using chelated iridium(III) *N*-heterocyclic bis-carbene complexes, 2857
Milios, C.J., Kefalloniti, E., Raptopoulou, C.P., Terzis, A., Escuer, A., Vicente, R. and Perlepes, S.P., 2-Pyridinealdoxime [(py)CHNOH] in manganese(II) carboxylate chemistry: mononuclear, dinuclear, tetranuclear and polymeric complexes and partial transformation of (py)CHNOH to picolinate(−1), 83
Miller, A.E., see Sydora, O.L., 2841
Miller, D.O., see Thompson, L.K., 1175
Milton, H.L., see Rodriguez i Zubiri, M., 865
Milton, H.L., Wheatley, M.V., Slawin, A.M.Z. and Woollins, J.D., Synthesis and coordination of 2-diphenylphosphinothiophenocarboxamide and bis-(2,5-diphenylphosphinepicolinamide), 2575
Milton, H.L., see Slawin, A.M.Z., 3125
Milton, H.L., see Zubiri, M.R.I., 693
Milton, H.L., Wheatley, M.V., Slawin, A.M.Z. and Woollins, J.D., Synthesis and coordination of 2-diphenylphosphinopicolinamide, 3211
Minihane, M., see Inyushin, S., 2937
Minkovska, S., Fedieva, M., Jeliazkova, B. and Deligeorgiev, T., Thermally activated and light-induced metal ion complexation of 5′-(hydroxy)spiroindolinonaphthooxazines in polar solvents, 3147
Mironov, Y.V., see Naumov, N.G., 599
Mirza, A.H., see Ali, M.A., 2405
Mirza, A.H., see Akbar Ali, M., 2031
Mirza, A.H., see Ali, M.A., 2037
Mitra, S., see Karmakar, R., 949
Miyazaki, Y., see Matsuo, H., 955
Mochida, K., Amada, K., Sugimoto, H., Akiba, M. and Sato, K., Preparation of polystyrene-supported hydrogermanes and their reduction of organic halides, 177
Mohamadou, A., see van Albada, G.A., 2387
Mohamadou, A., van Albada, G.A., Driessen, W.L., de Gelder, R. and Reedijk, J., Crystal structures, spectroscopy and EPR of two distortion isomers of Cu(II) perchlorate with 2,2′-bi-imidazoline, 1969
Mondal, B., see Maiti, D., 831
Mondal, S., see Saha, S., 1811
Montero, M.L., see Arce, H., 1897
Moraes, M.C.B., see Gaubeur, I., 2095
Morissette, M., Haufe, S., McDonald, R., Ferrence, G.M. and Takats, J., Steric saturation of the ytterbium coordination environment: $(Tp^{tBu,Me})Yb(OMes)$, a four coordinate, monomeric, base-free divalent lanthanide complex, its solvation with tetrahydrofuran and comparison to the β-diketonate complex, $(Tp^{tBu,Me})Yb(dpm)$, 263
Morley, C.P., Ford, S. and Vaira, M.D., Palladium complexes of novel azo-compounds derived from cycloalkeno-1,2,3-selenadiazoles: X-ray crystal structure of cyclohexeno-1,2,3-selenadiazole, 2967
Morley-Smith, N.A., see Cloke, F.G.N., 2625
Morlok, M.M., see Docrat, A., 481
Moro-oka, Y., see Takahashi, Y., 225
Morsali, A. and Mahjoub, A., Coordination polymers of lead(II) with 4,4′-bipyridine: syntheses and structures, 2427
Mostafa, G., see Dinda, J., 793
Mostafa, G., see Chand, B., 1669
Mostafa, G., see Jasimuddin, Sk., 727
Mostafa, G., see Bose, D., 2045
Mostafa, G., see Bose, D., 545
Moura, M.V.H., see Howie, R.A., 2331
Mozeleski, E.J., see Mehnert, C.P., 2679
Mozharivskyj, Y.A., see Govindaswamy, P., 1567
Mozharivskyj, Y.A., see Govindaswamy, P., 3115
Mozharivskyj, Y.A., see Lalrempuia, R., 1069
Mroziński, J., see Stachová, P., 1303
Mrozinski, J., see Kopel, P., 1573
Mrozińsky, J., see Valigura, D., 2447
Mu, Z.-C., see He, X., 2153
Mukai, H., see Kitano, T., 283
Mukherjee, A., Saha, M.K., Nethaji, M. and Chakravarty, A.R., Dicopper(II) Schiff base aminobenzoates with discrete molecular and 1D-chain polymeric structures, 2177
Mukherjee, M., see Saha, S., 1811
Mukherjee, G.N., see Bandyopadhyay, S., 1081
Mukherjee, A., see Gupta, S., 643
Mukherjee, A., Nethaji, M. and Chakravarty, A.R., Synthesis, crystal structure and imine bond activation of a copper(II) Schiff base complex, 3081
Mukhopadhyay, A. and Pal, S., Complexes of nickel with tetradentate ligands formed by ring opening of 1-benzoyl-3,5-dimethyl-5-(1′-benzoylhydrazido)pyrazoline, 1997
Mukhopadhyay, S., see Das, A., 895
Mulla, R.M. and Nandibewoor, S.T., Mechanistic and spectral investigation of the oxidation of 4-hydroxycoumarin by aqueous alkaline permanganate using the stopped flow technique, 2507
Muller, G., see Gómez, M., 611
Müller, A., see Pascu, M., 673
Müller, A., Botar, B., Das, S.K., Bögge, H., Schmidtmann, M. and Merca, A., On the complex hedgehog-shaped cluster species containing 368 Mo atoms: simple preparation method, new spectral details and information about the unique formation, 2381
Munakata, M., see Wen, M., 2117
Murray, P.R., see Leslie, W., 2769
Murugesu, M., Abboud, K.A. and Christou, G., New hexanuclear and dodecanuclear Fe(III) clusters with carboxylate and alkoxide-based ligands from cluster aggregation reactions, 2779
Mutikainen, I., see Kettunen, M., 1649
Mutikainen, I., see van Albada, G.A., 993
Mutikainen, I., see Song, Y., 1769
Mutikainen, I., see Kannappan, R., 2285

Nadjo, L., see Lu, Y.-W., 1579
Nag, K., see Baitalik, S., 913
Nam, H.J., Lee, H.-J. and Noh, D.-Y., Novel mercury(II) complexes of 1,3-dithiole-2-thiones containing the 2-pyridyl moiety: syntheses, X-ray crystal structures and solution behavior, 115
Nandibewoor, S.T., see Mulla, R.M., 2507
Narula, S.P., see Shankar, R., 71
Nassar, R., Noll, B.C. and Henderson, K.W., Solid-state studies of the Horner–Wittig reagent $[\{\{Ph_2P(O)\}_2CHLi \cdot (THF)\}_2 \cdot THF]$ and its mixed-anion intermediate $[\{\{Ph_2P(O)\}_2CHLi\}_4 \cdot \{Ph_2P(O)_2Li\}_2 \cdot 8C_6H_6]$ formed by reaction with dioxygen, 2499
Nättinen, K., see Chawla, S.K., 3007
Naumov, N.G., Brylev, K.A., Mironov, Y.V., Virovets, A.V., Fenske, D. and Fedorov, V.E., Synthesis and structures of new octahedral water-soluble heterometal rhenium–molybdenum clusters, 599
Navarro, D., see Sanmartín, J., 963
Nayar, C.R., see Sreekanth, A., 41

Neculai, D., see Neculai, A.M., 183
Neculai, A.M., Neculai, D., Roesky, H.W. and Magull, J., Synthesis and structure of $LLnBr_2$ ($L = Et_2N\ CH_2CH_2NC(Me)CHC(Me)NCH_2CH_2NEt_2$; Ln = Y, Sm and Yb), 183
Neels, A., see Dias, S.I.G., 1011
Neels, A., see Liu, S.-X., 1185
Nethaji, M., see Mukherjee, A., 2177
Nethaji, M., see Philip, V., 1225
Nethaji, M., see Gupta, S., 643
Nethaji, M., see Joseph, M., 3069
Nethaji, M., see Mukherjee, A., 3081
Neuburger, M., see Constable, E.C., 135
Neves, A., see Scarpellini, M., 511
Newlands, M.J., see Thompson, L.K., 1175
Ni, C.-L., see Liu, W.-L., 849
Ni, Z.-P., see Liu, W.-L., 849
Niclós, J., see Carballo, R., 1505
Niel, V., see Thompson, L.K., 1175
Nikiforov, G.B., Roesky, H.W., Noltemeyer, M. and Schmidt, H.-G., Reactivity of $Ti(bipy)_3$ and preparation of the $Li(THF)_4[Al(bipy)_2]$ complex with the dinegative bipy ligand, 561
Niu, J.-Y., Wang, Z.-L. and Wang, J.-P., Hydrothermal synthesis and structure characterization of a Keggin tungstocobaltate $[Co(2,2'\text{-bipy})_3]_2H_2[CoW_{12}O_{40}]\cdot 9.5H_2O$, 773
Niu, W., Wong, E.H., Weisman, G.R., Zakharov, L.N., Incarvito, C.D. and Rheingold, A.L., Copper(II) and zinc(II) complexes of amide pendant-armed cross-bridged tetraamine ligands, 1019
Noh, D.-Y., see Nam, H.J., 115
Noll, B.C., see Nassar, R., 2499
Noltemeyer, M., see Nikiforov, G.B., 561
Nordell, K.J., Schultz, K.N., Higgins, K.A. and Smith, M.D., Hydrothermal synthesis of two new lead-containing coordination polymers: $^2_\infty[PbCl_2(4,4'\text{-bipy})]$ and $^2_\infty[Pb_2(NO_3)_4(H_2O)_2(4,4'\text{-bipy})_2](4,4'\text{-bipy})_2$, 2161
Nöth, H., see López-Sandoval, H., 1837
Novak, P., see Cindrić, M., 1859
Nunes, F.S., see Raimondi, A.C., 2069

Oh, J.-J., see Choi, K.-Y., 903
Okamoto, K.-I., see Saha, S., 1811
Okawa, H., see Saravanakumar, D., 665
Oliveira, M.R.L., Rubinger, M.M.M., Guilardi, S., de Faria Franca, E., Ellena, J. and De Bellis, V.M., Preparation, crystal structure and spectroscopic characterization of novel N-*R*-sulfonyldithiocarbimate platinum(II) complexes, 1153
Oñate, E., see Rodríguez, M.C., 1045
Ontko, A.C., see Merwin, R.K., 2873
O'Reilly, R.K., Gibson, V.C., White, A.J.P. and Williams, D.J., Five-coordinate iron(II) complexes bearing tridentate nitrogen donor ligands as catalysts for atom transfer radical polymerisation, 2921
Ortiz Méndez, U., see Garnovskii, A.D., 1909
Oster, S.S. and Jones, W.D., Synthesis, structure and reactivity of $[Ir(dippe)(\mu\text{-}Cl)]_2$, $[Ir(dippe)_2][Ir(dippe)Cl_2]$ and $[Ir(dippe)_2]Cl$, 2959
Ovcharenko, V.I., see Tretyakov, E.V., 763
Owen, J.S., see Piro, N.A., 2797
Özçeşmeci, İ., see Yasemin Yenilmez, H., 787
Özkaya, A.R., see Kandaz, M., 1987

Pacheco, S., see Barquín, M., 1695
Pal, S., see Mukhopadhyay, A., 1997
Pang, W.-Q., see Meng, H., 2357
Pang, W., see Yang, Y., 1535
Pang, W.-Q., see Chen, C., 3033
Papadimitriou, C.D., see Michaelides, A., 2587
Parada, J. and Larrazábal, G., The origin of optical activity in complexes of the type $[Co(diimine)_2carbohydrate]^{2+}$, 1341
Parant, S., see Giroux, S., 2393
Pardey, A.J., Longo, C., Funaioli, T. and Fachinetti, G., Hydrocarboxylation and stepwise alternating oligomerization of carbon monoxide and ethylene catalyzed by *cis*-$[Rh(CO)_2(amine)_2](PF_6)$ complexes in a wet liquid tetrabutylammonium hydrogensulfate, 1677
Paredes-García, V., Latorre, R.O. and Spodine, E., Electronic and magnetic properties of iron (III) dinuclear complexes with carboxylate bridges, 1869
Pariya, C., Incarvito, C.D., Rheingold, A.L. and Theopold, K.H., Preparation and ligand substitution reactions of $Tp^{Ms}Ru(COD)H$ including intramolecular ligand metalation, 439
Parkin, I.P., see Manning, T.D., 3087
Parkin, G., Preface, 2595
Parkin, G., see Baik, M.-H., 2879
Parkin, G., see Docrat, A., 481
Parra-Hake, M., see Iglesias, A.L., 3051
Parsons, S., see Smith, A.A., 1557
Pascu, M., Andruh, M., Müller, A. and Schmidtmann, M., Binuclear coordination compounds as building-blocks in designing polynuclear complexes, 673
Pasko, S., Hubert-Pfalzgraf, L.G., Abrutis, A. and Vaissermann, J., Synthesis and molecular structures of cobalt(II) β-diketonate complexes as new MOCVD precursors for cobalt oxide films, 735
Patel, K.N., see Grant, G.J., 1361
Patel, B., see Levason, W., 605
Paul, H., see Maiti, D., 831
Paul, P., see Jadeja, R.N., 2465
Paulo, A., Correia, J.D.G., Campello, M.P.C. and Santos, I., A short ride on scorpionates: from d- to f-elements, 331
Pavlović, G., see Popović, Z., 1293
Peariso, K., see Kirk, M.L., 499
Pedrero-Marín, R., see Barros-García, F.J., 1453
Pedrosa, M.R., see Arnáiz, F.J., 537
Pelascini, F., Wesolek, M., Peruch, F., Cian, A.D., Kyritsakas, N., Lutz, P.J. and Kress, J., Iron complexes of terdentate nitrogen ligands: formation and X-ray structure of three new dicationic complexes, 3193
Pellei, M., see Pettinari, C., 451
Pellinghelli, M.A., see Gennari, M., 1829
Peng, Y., see Li, B., 3133
Peng, Z., see Guo, W., 1701
Peris, E., see Gómez, M., 611
Perlepes, S.P., see Boudalis, A.K., 1271
Perlepes, S.P., see Milios, C.J., 83
Peruch, F., see Pelascini, F., 3193
Peters, J.C., see Christopher Thomas, J., 2901
Peters, L. and Burzlaff, N., Complexes bearing an enantiopure *N,N,O* scorpionate ligand derived from (−)-menthone, 245
Peters, J.C., see Thomas, J.C., 489
Petriček, S., Syntheses of lanthanide bromide complexes from oxides and the crystal structures of $[LnBr_3(DME)_2]$ (Ln=Pr, Nd, Sm, Eu), $[LnBr_3(THF)_4]$ (Ln=Pr, Sm) and $[EuBr_2(THF)_5][EuBr_4(THF)_2]$, 2293
Pettinari, C., Cingolani, A., Lobbia, G.G., Marchetti, F., Martini, D., Pellei, M., Pettinari, R. and Santini, C., Copper and silver derivatives of scorpionates and related ligands, 451
Pettinari, R., see Pettinari, C., 451
Philip, V., Suni, V., Prathapachandra Kurup, M.R. and Nethaji, M., Structural and spectral studies of nickel(II) complexes of di-2-pyridyl ketone N^4,N^4-(butane-1,4-diyl) thiosemicarbazone, 1225
Phipps, D.E., see Wong, W.W.H., 2821
Phuengphai, P., see Youngme, S., 1685
Pickering, A.L., Cooper, G.J.T., Long, D.-L. and Cronin, L., Facile synthesis and structures of infinite one-dimensional silver(I) coordination polymers, 2075
Pilkington, M., see Liu, S.-X., 1185
Pinilla, E., see Barquín, M., 1695
Pinilla, E., see Criado, R., 301

Piro, N.A., Owen, J.S. and Bercaw, J.E., Pyridinium-derived *N*-heterocyclic carbene ligands: syntheses, structures and reactivity of *N*-(2′-pyridyl)pyridin-2-ylidene complexes of nickel(II), palladium(II) and platinum(II), 2797
Plakatouras, J.C., see Michaelides, A., 2587
Platt, A.W.G., see Fawcett, J., 2561
Po-Kwan Lau, J., see Lee, T.-W., 999
Poggi, A., see Fabbrizzi, L., 373
Poli, R., see Collange, E., 2605
Polson, M.I.J., Howell, S.L., Flood, A.H., Burrell, A.K., Blackman, A.G. and Gordon, K.C., Synthesis and electronic properties of mononuclear osmium(II) and rhenium(I) complexes containing ligands derived from [2,3-a:3′,2′-c]dipyridophenazine (ppb), 1427
Poole, R.A., see Leslie, W., 2769
Popović, Z., Roje, V., Pavlović, G., Matković-Čalogović, D., Rajić, M. and Leban, I., Complexes of zinc(II) halides with *N*-benzyl- and *N*-*p*-tolyl-2-oxo-1-naphthylideneamine – preparation and characterization, 1293
Porto, A.O., see de Castro, V.D., 63
Porto, A.O., see Menezes, D.C., 2103
Prado, A.G.S., see Sales, J.A.A., 719
Pramanik, S., see Dhara, P.K., 2457
Pramanik, N.R., Ghosh, S., Raychaudhuri, T.K., Ray, S., Butcher, R.J. and Mandal, S.S., Synthesis, characterization and crystal structure of oxomolybdenum (VI) and (IV) complexes of some tridentate ONS donor ligands, 1595
Prathapachandra Kurup, M.R., see Joseph, M., 3069
Prathapachandra Kurup, M.R., see Sreeja, P.B., 575
Prathapachandra Kurup, M.R., see Philip, V., 1225
Prathapachandra Kurup, M.R., see Sreekanth, A., 41
Priego, J.L., see Barral, M.C., 2637
Priyadarshni, G., see Saravanakumar, D., 665
Pruchnik, M., see Pruchnik, F.P., 103
Pruchnik, F.P., Ciunik, Z. and Pruchnik, M., New one- and two-dimensional rhodium–tin polynuclear complexes, synthesis, properties and structural characterization, 103
Puranik, V.G., see Salunke-Gawali, S., 2541
Puranik, V.G., see Maiti, D., 831

Qin, Y.-Y., see Cheng, J.-K., 2209
Quirós, M., see Abul-Haj, M., 743
Quirós, M., see Abul-Haj, M., 2373

Rabinovich, D., see Alvarez, H.M., 395
Rabinovich, D., see Alvarez, H.M., 617
Radanović, D.D., Rychlewska, U., Djuran, M.I., Warżajtis, B., Drašković, N.S. and Gurešić, D.M., Alkaline earth metal complexes of the edta-type with a six-membered diamine chelate ring: crystal structures of $[Mg(H_2O)_6][Mg(1,3\text{-pdta})] \cdot 2H_2O$ and $[Ca(H_2O)_3Ca(1,3\text{-pdta})(H_2O)] \cdot 2H_2O$: comparative stereochemistry of edta-type complexes, 2183
Rahaman, S.H., see Bose, D., 545, 2045
Raimondi, A.C., de Souza, V.R., Toma, H.E., Mangrich, A.S., Hasegawa, T. and Nunes, F.S., An unusual vanadium(II) promoted hydrogenation of a magnesium tetraiminediphenolate compound yielding an asymmetric oxovanadium(IV) macrocyclic complex, 2069
Rajakannan, V., see John, R.P., 2549
Rajalakshmi, N., see Kannan, S., 1527
Rajić, M., see Popović, Z., 1293
Ramalingam, K., see Arul Prakasam, B., 77
Rane, S.Y., see Salunke-Gawali, S., 2541
Rao Kollipara, M., see Govindaswamy, P., 1567
Raptopoulou, C.P., see Milios, C.J., 83
Raptopoulou, C.P., see Boudalis, A.K., 1271
Raptopoulou, C., Daphnomili, D., Karamalides, A., Di Vaira, M., Terzis, A. and Coutsolelos, A.G., Perhalogenated porphyrinic derivatives with indium and thallium: the X-ray structures of (β-Cl_4TPP)Tl(Cl), (β-Cl_4TPP)In(Cl) and (T*p*FTPP)Tl(Cl), 1777
Rasika Dias, H.V. and Goh, T.K.H.H., Fluorinated tris(pyrazolyl)-borates. Syntheses and characterization of sodium and copper complexes of $[HB(3\text{-}(CF_3),5\text{-}(Ph)Pz)_3]^-$, 273
Ratnani, R., see Hursthouse, M.B., 1915
Ravoof, T.B.S.A., Crouse, K.A., Tahir, M.I.M., Cowley, A.R. and Ali, M.A., Synthesis, characterization and bioactivity of mixed-ligand Cu(II) complexes containing *S*-methyldithiocarbazate derivatives and saccharinate ligands and the X-ray crystal structure of the copper–saccharinate complex containing *S*-methyl-β-*N*-(6-methylpyrid-2-yl)methylenedithiocarbazate, 2491
Ravoof, T.B.S.A., see Akbar Ali, M., 2031
Ray, S., see Pramanik, N.R., 1595
Ray, U., see Chand, B., 1669
Raychaudhuri, T.K., see Pramanik, N.R., 1595
Redshaw, C., see Gibson, V.C., 189
Reedijk, J., see Song, Y., 1769
Reedijk, J., see Kannappan, R., 2285
Reedijk, J., see van Albada, G.A., 993
Reedijk, J., see van Albada, G.A., 2387
Reedijk, J., see Mohamadou, A., 1969
Reger, D.L., Smith, D.M.C., Shimizu, K.D. and Smith, M.D., Syntheses and solid state structures of europium and terbium complexes of *N,N′*-bis(2-pyridylmethyl)urea and *N,N′*-bis(3-pyridylmethyl)oxalamide, 711
Reger, D.L., Gardinier, J.R. and Smith, M.D., Synthesis of *meta*-$C_6H_4[C(1\text{-pyrazolyl})_2(2\text{-pyridyl})]_2$, a fixed geometry bitopic heteroscorpionate and the crystal structure of its unusual square planar silver(I) complex, 291
Reglinski, J., see Taylor, M.K., 3201
Reglinski, J., see Dodds, C.A., 445
Reid, G., see Hursthouse, M.B., 1915
Reid, G., see Levason, W., 605
Reinke, H., see Krempner, C., 2475
Ren, Z.-G., see Dai, J., 1447
Repo, T., see Kettunen, M., 1649
Reza Bijhanzade, H., see Hossaini Sadr, M., 637
Rezai-Adaryani, M., see Salavati-Niasari, M., 1325
Rhee, S.-W., see Krisyuk, V.V., 809
Rheingold, A.L., see Voo, J.K., 405
Rheingold, A.L., see Pariya, C., 439
Rheingold, A.L., see Karambelkar, V.V., 471
Rheingold, A.L., see Alvarez, H.M., 617
Rheingold, A.L., see Niu, W., 1019
Rhile, I.J., see Soper, J.D., 323
Ribas, J., see Bandyopadhyay, S., 1081
Ribeiro, A.F.G., Gomes, P.T., Dias, A.R., Ferreira da Silva, J.L., Teresa Duarte, M., Henriques, R.T. and Freire, C., Reactions between isocyanides and a binuclear nickel(II) phosphine complex linked by a bridged bis(cyclopentadienyl) ligand. X-ray molecular structure of $[(CN^tBu)(PPh_3)Ni\{\mu\text{-}(\eta\text{-}C_5H_4)CMe_2(\eta\text{-}C_5H_4)\}Ni(PPh_3)(CN^t\text{-}Bu)][PF_6]_2$, 2715
Richard, P., see Collange, E., 2605
Richaud, A., see López-Sandoval, H., 1837
Riordan, C.G., see Voo, J.K., 405
Rissanen, K., see Chawla, S.K., 3007
Robertson, S., see Venkatasubramanian, U., 629
Roddick, D.M., see Merwin, R.K., 2873
Rodríguez, M.C., Bravo, J., Freijanes, E., Oñate, E., García-Fontán, S. and Rodríguez-Seoane, P., Synthesis and reactivity of $[Re(ClCH_2Cl)(CO)_3L][A]$ and $[Re(OSO_2CF_3)(CO)_3L]$ ($L=Ph_2PO(CH_2)_2OPPh_2$; $A=BF_4$, $[B\{3,5\text{-}(CF_3)_2C_6H_3\}_4]$): the crystal structure of $[Re(OSO_2CF_3)(CO)_3L]$ and $[Re(NCCH_3)(CO)_3L][BF_4]$, 1045
Rodríguez-Seoane, P., see Rodríguez, M.C., 1045
Rodriguez, M.A., see Coker, E.N., 1739

Rodriguez i Zubiri, M., Milton, H.L., Slawin, A.M.Z. and Derek Woollins, J., The preparation and coordination of 1,3-C_6H_4-$\{C(O)N(PPh_2)CH_2Ph\}_2$ – a new multidentate ligand, 865
Roesky, H.W., see Neculai, A.M., 183
Roesky, H.W., see Bai, G., 1125
Roesky, H.W., see Nikiforov, G.B., 561
Roh, S.G., Yoon, J.U. and Jeong, J.H., Synthesis and characterization of a chiral Zn(II) complex based on a *trans*-1,2-diaminocyclohexane derivative and catalytic reduction of acetophenone, 2063
Roje, V., see Popović, Z., 1293
Rojo, T., see Gil de Muro, I., 929
Romanenko, G.V., see Tretyakov, E.V., 763
Romão, C.C., see Godinho, S.S.M.C., 1263
Rosair, G.M., see Venkatasubramanian, U., 629
Royer, E.C., see Barral, M.C., 2637
Royo, B., see Godinho, S.S.M.C., 1263
Rubinger, M.M.M., see Oliveira, M.R.L., 1153
Rubini, P., see Giroux, S., 2393
Rubinov, A.N., see Bushuk, S.B., 2615
Rudd, M.D., Creighton, M.A. and Kautz, J.A., Synthesis and characterization of chalcogenoic aminophosphines: X-ray structures of $Bu^t_2P(E)NHPr^n$ (E=Se, Te), $Ph_2P(Se)$-$NHPr^n$ and $\{Et_2P(Se)\}_2NPr^n$, 1923
Rukmini, E., see Bernhardt, P.V., 869
Ruman, T., Ciunik, Z. and Wołowiec, S. Complexes of heteroscorpionate trispyrazolylborate ligands. Part XII. Variable hapticity of hydrobis(3-phenyl-5-isopropylpyrazolyl)(3,5-dimethylpyrazolyl)borate in its rhodium(I) complexes with COD and NBD, 219
Russo, M.R., see Maunder, G.H., 2709
Russo, U., see Galani, A., 2021
Ryazanov, M., Troyanov, S., Baran, M., Szymczak, R. and Kuzmina, N., Synthesis, crystal structure and magnetic properties of dinuclear manganese(II) diketonate with cyanopyridine-N-oxide bridging ligands $[Mn(hfac)_2(4\text{-cpyNO})]_2$, 879
Rybarczyk-Pirek, A., see Kowalski, K., 1441
Rychlewska, U., see Radanović, D.D., 2183
Ryu, H., see Choi, K.-Y., 903

Sacchi, D., see Fabbrizzi, L., 373
Sáenz, A., see Arce, H., 1897
Saha, S., Mal, D., Koner, S., Bhattacherjee, A., Gütlich, P., Mondal, S., Mukherjee, M. and Okamoto, K.-I., Synthesis, X-ray structure and magnetic properties of the azido adducts of quadridentate Schiff base manganese(III) complexes, 1811
Saha, N., see Sau, D.K., 5
Saha, M.K., see Mukherjee, A., 2177
Saito, T., see Sakai, N., 2611
Sakai, N. and Saito, T., Synthesis and structures of tetranuclear rhenium–cobalt mixed metal sulfide clusters $[Re_3CoS_4Cl_6(PMe_2Ph)_4]$, 2611
Sakashita, H., see Matsuo, H., 955
Salam Sall, A., see Bouyagui Tamboura, F., 1191
Salas, J.M., see Abul-Haj, M., 743
Salas, J.M., see Abul-Haj, M., 2373
Salavati-Niasari, M. and Rezai-Adaryani, M., Template condensation reactions of formaldehyde with amines and 2,3-butanedihydrazone: preparation and properties of nickel(II) complexes of 18-membered decaaza macrocycles, 1325
Saleh, M.T., see Scales, S.J., 2169
Salem, N.M.H., see Iskander, M.F., 23
Sales, J.A.A., Faria, F.P., Prado, A.G.S. and Airoldi, C., Attachment of 2-aminomethylpyridine molecule onto grafted silica gel surface and its ability in chelating cations, 719
Salisbury, B.A., see Höcher, T., 1393
Salmon, L., Thuéry, P. and Ephritikhine, M., Crystal structure of the first octanuclear uranium(IV) complex with compartmental Schiff base ligands, 623
Salunke-Gawali, S., Rane, S.Y., Puranik, V.G., Guyard-Duhayon, C. and Varret, F., Three dimensional hydrogen-bonding network in a copper complex of 2-hydroxy-1,4-naphthoquinone: structural, spectroscopic and magnetic properties, 2541
Sambasiva Rao, P., see Srinivasan, R., 1115
Sanmartín, J., García-Deibe, A.M., Fondo, M., Navarro, D. and Bermejo, M.R., Synthesis and crystal structure of a mononuclear iron(III) (η^2-acetato) complex of a β-*cis* folded salen type ligand, 963
Santa María, M.D., see Claramunt, R.M., 2985
Santini, C., see Pettinari, C., 451
Santos, I.C., see Belo, D., 1351
Santos, I.G., see Bermejo, E., 2303
Santos, I., see Paulo, A., 331
Sanz, N., see Escuer, A., 1409
Saravanakumar, D., Sengottuvelan, N., Priyadarshni, G., Kandaswamy, M. and Okawa, H., Synthesis of unsymmetrical 'end-off' phenoxo and oximinato di bridged copper(II) and nickel(II) complexes: spectral, electrochemical and magnetic properties, 665
Saravanan, M., see Arul Prakasam, B., 77
Sarmah, S., Kalita, D., Hazarika, P., Borah, R. and Islam, N.S., Synthesis of new dinuclear and mononuclear peroxovanadium(V) complexes containing biogenic co-ligands: a comparative study of some of their properties, 1097
Satish Kumar, N. and Kumara Swamy, K.C., Synthesis and structures of unsymmetrical bis- and tris-cyclotriphosphazenes, 979
Sato, K., see Mochida, K., 177
Sau, D.K., Butcher, R.J., Chaudhuri, S. and Saha, N., Synthesis and spectroscopic characterization of new cobalt(III) complexes with 5-methyl-3-formyl pyrazole 3-hexamethyleneiminyl thiosemicarbazone (HMPz3Hex): X-ray crystallographic identification of HMPz3Hex and $[Co(MPz3Hex)_2]Br \cdot H_2O$ with evidence for unusual rotation about the azomethine double bond of the ligand on complexation with cobalt(III), 5
Saunders, G.C., see Bellabarba, R.M., 2659
Scales, S.J., Zhang, H., Chapman, P.A., McRory, C.P., Derrah, E.J., Vogels, C.M., Saleh, M.T., Decken, A. and Westcott, S.A., Synthesis, characterization and cytotoxi-cities of palladium(II) and platinum(II) complexes containing fluorinated pyridinecarboxaldimines, 2169
Scarpellini, M., Neves, A., Castellano, E.E., de Almeida Neves, E.F. and Franco, D.W., A structural model for oxidized type II copper nitrite reductase with a polyimidazole tripodal ligand, 511
Sceats, E.L., Figueroa, J.S., Cummins, C.C., Loening, N.M., Van der Wel, P. and Griffin, R.G., Complexes obtained by electrophilic attack on a dinitrogen-derived terminal molybdenum nitride: electronic structure analysis by solid state CP/MAS ^{15}N NMR in combination with DFT calculations, 2751
Scheibitz, M., see Ilkhechi, A.H., 2597
Schmidt, H.-G., see Nikiforov, G.B., 561
Schmidtmann, M., see Pascu, M., 673
Schmidtmann, M., see Müller, A., 2381
Schneider, C., Doucet, F., Strekopytov, S. and Exley, C., The solubility of an hydroxyaluminosilicate, 3185
Schneider, M.E., see Werner, H., 2645
Schofield, E.R., see Constable, E.C., 135
Schull, T.L., Butcher, R., Dressick, W.J., Brandow, S.L., Byington, L.K. and Knight, D.A., *Cis*-$[PtCl_2(p\text{TPPTP}(H)_7)_2]Cl_2 \cdot 4H_2O \cdot (CH_3\text{-}CH(OH)\ CH_3)$: a platinum phosphine complex exhibiting both inter- and intra-molecular hydrogen bonding, 1375
Schultz, K.N., see Nordell, K.J., 2161
Schultz, F.A., see Sheets, J.R., 1037
Schwendt, P., see Ahmed, M., 655
Seco, J.M., see Barquín, M., 1695

Šedo, O., Voráč, Z., Alberti, M. and Havel, J., Laser ablation synthesis of new phosphorus and phosphorus-sulfur clusters and their TOF mass spectrometric identification, 1199
Seisenbaeva, G.A., see Starikova, Z.A., 109
Sella, A., see Maunder, G.H., 2709
Sella, A., see Galler, J.L., 253
Semioshkin, A., Brellochs, B. and Bregadze, V., Reactions of *closo*-$[B_{12}H_{12}]^{2-}$ anion with aromatic acylchlorides: synthesis of novel 1,2-disubstituted dodecaborates $[1\text{-HO-2-ArCOB}_{12}H_{10}]^{2-}$, 2135
Sengottuvelan, N., see Saravanakumar, D., 665
Shafir, A., see Inyushin, S., 2937
Shah, J.R., see Jadeja, Rajendra N., 2465
Shankar, R., Kumar, M., Chadha, R.K. and Narula, S.P., Reactivity behavior of (hydroxy)diorganotin(IV)methanesulfonates with ionic nucleophiles – synthesis and structural characterization of novel diorganostannate salts, $[R_2Sn(\mu\text{-OH})(OSO_2Me)(ONO_2)]_2\ 2Bu_4N$, 71
Shao, Z.-H., see Luo, J., 1243
Sharma, M., see Chutia, P., 1657
Sharrad, C.A. and Gahan, L.R., Synthesis and characterization of cobalt(III) complexes with sinambic amplector ligands, 2217
Sheats, J.E., see Inyushin, S., 2937
Sheets, J.R. and Schultz, F.A., Coupled electron-transfer and spin-exchange reactions of metal–bis[tris(pyrazolyl)methane] complexes, 1037
Shen, Q., see Li, W.-F., 1473
Shen, X.-Q., Zhong, H.-J., Zheng, H., Zhang, H.-Y., Zhao, G.-H.,Wu, Q.-A., Mao, H.-Y., Wang, E.-B. and Zhu, Y., Crystal structure, thermal decomposition kinetics and antimicrobial activities of $[Zn(eatz)_2(OAc)_2]$ (eatz=5-ethyl-2-amino-1,3,4-thiadiazole), 1851
Shen, X.-Q., see Mao, H.-Y., 1961
Shen, P.-W., see Sun, Y.-J., 211
Shen, W.-B., see Shi, Y.-C., 15
Shen, W.-B., see Shi, Y.-C., 749
Shen, W.-Z., see Sun, Y.-J., 211
Shi, Y.-C., Yang, H.-M., Song, H.-B. and Liu, Y.-H., Syntheses and crystal structures of a ferrocene-containing enaminone and its copper complex, 1541
Shi, Y.-C., Yang, H.-M., Song, H.-B., Yan, C.-G. and Hu, X.-Y., Syntheses and crystal structures of the potential tridentate ligand formed from condensation of ferrocenoylacetone and S-benzyldithiocarbazate and its bivalent metal complexes, 567
Shi, M., see Huang, H., 55
Shi, Y.-C., Yang, H.-M., Shen, W.-B., Yan, C.-G. and Hu, X.-Y., Syntheses and crystal structures of ferrocene-containing enaminones and their copper complexes, 15
Shi, Y.-C., Reactions of Mo–Mo singly-bonded complexes $[(\eta^5\text{-}RC_5H_4)_2Mo_2(CO)_6]$ with diphenylditelluride in the presence of $^nBu_4NI$. Crystal structures of complexes $[(\eta^5\text{-}C_5H_5Mo(CO)_3Te]$ and *cis*/ae-$[(\eta^5\text{-}C_2H_5O_2CC_5H_4)_2Mo_2(\mu\text{-Te})_2\ (\mu\text{-TePh})_2]$, 1663
Shi, Y.-C., Shen, W.-B., Yang, H.-M., Song, H.-B. and Hu, X.-Y., Copper and nickel complexes of the tetradentate ligand derived from the condensation of ferrocenoylacetone with 1,2-diaminoethane, 749
Shimizu, K.D., see Reger, D.L., 711
Shin, D.M., see Joung, U.G., 1587
Shirin, Z. and Carrano, C.J., New heteroscorpionate ligands with hydrogen bond donor and acceptor groups: synthesis, characterization and reactivity with divalent Co, Zn and Ni ions, 239
Shvedenkov, Yu.G., see Tretyakov, E.V., 763
Sichani, S.E., see Beheshti, A., 3143
Siebald, Helmuth G.L., see de Castro, V.D., 63
Siemeling, U., see Gibson, V.C., 189
Siemer, C.J., VanStipdonk, M.J., Kahol, P.K. and Eichhorn, D.M., A coordination polymer from a cyanoscorpionate complex, 235
Silva, W.C., Castellano, E.E. and Franco, D.W., Structural and reactivity changes in ruthenium ammines induced by the NO ligand, 1063
Silva, R.M., see Soares, L.F., 205
Silva, A.P.S., see Júnior, G.C., 1953
Simpson, S.J., see Hodson, E., 2695
Sinha, ., see Dinda, J., 793
Sinha, C., see Chand, B., 1669
Sinha, C., see Jasimuddin, Sk., 727
Sitte, W., see Mautner, F.A., 1217
Sivák, M., see Ahmed, M., 655
Skakle, J.M.S., see Fernandes, C., 1419
Skoulika, S., see Michaelides, A., 2587
Slawin, A.M.Z., see Zubiri, M.R.I., 693
Slawin, A.M.Z., see Milton, H.L., 2575
Slawin, A.M.Z., see Chutia, P., 1657
Slawin, A.M.Z., see Rodriguez i Zubiri, M., 865
Slawin, A.M.Z., Milton, H.L., Wheatley, J. and Woollins, J.D., Preparation and coordination chemistry of *N*-diallylaminodiphenylphosphine and *N*-allylaminobis(diphenyl)phosphine, 3125
Slawin, A.M.Z., Wheatley, J. and Woollins, J.D., Preparation and coordination chemistry of *p*-(xylylenediaminodiphenyl) phosphine, 2569
Slawin, A.M.Z., see Milton, H.L., 3211
Smith, F.E., see Basu Baul, T.S., 2323
Smith, David K., see Stone, D.L., 1709
Smith, A.A., Coxall, R.A., Harrison, A., Helliwell, M., Parsons, S. and Winpenny, R.E.P., High-temperature synthesis of polynuclear iron oxo-hydroxy complexes, 1557
Smith, M.D., see Nordell, K.J., 2161
Smith, D.M.C., see Reger, D.L., 711
Smith, N., see Hill, M.S., 801
Smith, M.D., see Reger, D.L., 711
Smith, M.D., see Reger, D.L., 291
Soares, L.F., Menezes, D.C., Silva, R.M., Doriguetto, A.C., Ellena, J., Mascarenhas, Y.P. and Castellano, E.E., Potassium tetrakis(2-mercaptothiazolyl)borate; an open-framework material: synthesis and X-ray structure analysis, 205
Sohrin, Y., see Kitano, T., 283
Solan, G.A., see Davies, C.J., 3105
Somanathan, Ratnasamy, see Iglesias, Ana L., 3051
Song, H.-B., see Shi, Y.-C., 567
Song, Y., Koval, I.A., Gamez, P., van Albada, G.A., Mutikainen, I., Turpeinen, U. and Reedijk, J., Solution studies and structure of a dinuclear-based double-stranded helicate of $[Cu_2\text{-}(p\text{-xysal})_2]$ (H_2-*p*-xysal=bis(hydroxylbenzyl)diaminoxylene), 1769
Song, H.-B., see Shi, Y.-C., 749
Song, H.-B., see Shi, Y.-C., 1541
Song, T.-Y., see He, X., 2153
Song, H.-B., see Zhang, L.-P., 2413
Soper, J.D., Rhile, I.J., DiPasquale, A.G. and Mayer, J.M., Oxidation of $TpOs^{III}(NH_2Ph)Cl_2$ to $TpOs^{IV}(NHPh)Cl_2$ by O_2, 323
Soper, A.K., see Turner, J.F.C., 2975
Sougandi, I., see Srinivasan, R., 1115
Sousa, C., Gameiro, P., Freire, C. and de Castro, B., Nickel(II) and copper(II) Schiff base complexes bearing benzo-15-crown-5 functionalities as probes for spectroscopic recognition of lanthanide ions, 1401
Sözerli Can, S.E., see Can, N., 1109
Spalding, T.R., see Cusack, J., 2315
Spannenberg, A., see Krempner, C., 2475
Spek, A.L., see Kannappan, R., 2285
Spicer, M.D., see Dodds, C.A., 445
Spodine, E., see Paredes-García, V., 1869
Sproules, S.A., see Eagle, A.A., 385
Sreeja, P.B., Prathapachandra Kurup, M.R., Kishore, A. and Jasmin, C., Spectral characterization, X-ray structure and biological

investigations of copper(II) ternary complexes of 2-hydroxyacetophenone 4-hydroxybenzoic acid hydrazone and heterocyclic bases, 575
Sreekanth, A., see John, R.P., 2549
Sreekanth, A., Kala, U.L., Nayar, C.R. and Prathapachandra Kurup, M.R., Cobalt(III) complexes of 2-hydroxyaceto- phenone N(4)-phenyl semicarbazone containing heterocyclic coligands: syntheses, structure and spectral studies, 41
Sreekanth, A. and Kurup, M.R.P., Synthesis, EPR and Mössbauer spectral studies of new iron(III) complexes with 2-benzoylpyridine-N(4), N(4)-(butane-1,4-diyl) thiosemicarbazone (HBpypTsc): X-ray structure of $[Fe(BpypTsc)_2]FeCl_4{\cdot}2H_2O$ and the free ligand, 969
Srinivasan, R., Sougandi, I., Velavan, K., Venkatesan, R., Verghese, B. and Sambasiva Rao, P., Synthesis and characterization of $[Cu_2(L)_2(OCOCH_3)(OCH_3)]ClO_4$ {L=2-[(4-methyl-pyridin-2-ylimino)-methyl]-phenol}: EPR and X-ray studies, 1115
Srivastava, P.C., Bajpai, S., Lath, R., Bajpai, S.M., Kumar, R. and Butcher, R.J., Molecular aggregates, zig-zag 2D-stairs, -ribbons and 3D-supramolecular networks of cyclic telluranes assisted by intermolecular Te···Cl and Te···Br secondary bonding, 1629
Srivastava, T.S., see Anbalagan, V., 3173
Stachová, P., Valigura, D., Koman, M., Melník, M., Korabik, M., Mroziński, J. and Glowiak, T., Crystal structure, magnetic and spectral properties of tetrakis(2-nitrobenzoato)di- (aqua)dicopper(-II)dihydrate, 1303
Starikova, Z.A., Kessler, V.G., Turova, N.Y., Tcheboukov, D.E., Suslova, E.V., Seisenbaeva, G.A. and Yanovsky, A.I., New polynuclear aluminium oxoalkoxides: molecular structures of $Al_{11}(\mu_4\text{-}O)_2(\mu_3\text{-}O)_2(\mu\text{-}O)_2(\mu\text{-}OPr^n)_{10}(\mu\text{-}OPr^i)_2(\mu\text{-}ROH)_2(OPr^i)_8(OR)$, $R = Pr^{n,i}$ and $Al_5Mg_4(\mu_4\text{-}O)_2(\mu_3\text{-}O)(\mu\text{-}OH)_3(\mu\text{-}OPr^i)_8(\mu,\eta^2\text{-}acac)_4(\eta^2\text{-}acac)_2$, 109
Steel, P.J., see McMorran, D.A., 1055
Stern, C.L., see Karambelkar, V.V., 471
Štěpnička, P., Lamač, M. and Císařová, I., Preparation, structure and catalytic activity of palladium(II) complexes with a carboxyferrocenylphosphine and an ortho-metallated C,N-ligand, 921
Stoeckli-Evans, H., see Liu, S.-X., 1185
Stone, D.L., Smith, D.K. and Whitwood, A.C., Copper amino-acid complexes – towards encapsulated metal centres, 1709
Strekopytov, S., see Schneider, C., 3185
Strukan, N., see Cindrić, M., 1859
Stupak, A.P., see Bushuk, S.B., 2615
Stylianides, N., see Winston, S., 2813
Suárez-Iha, M.E.V., see Gaubeur, I., 2095
Subramanian, P.S., Suresh, E. and Dastidar, P., Model for type 2 Cu(II) oxidase: structure reactivity correlation studies on some mononuclear Cu(X–Salmeen)Im complexes, where X=H, Cl and Im=Imidazole: molecular association, electronic spectra and ascorbic oxidation, 2515
Sudheendra Rao, M.N., see Bindu, P., 679
Suen, Maw-Cherng, see Yeh, Chun-Wei, 1947
Suenaga, Yusaku, see Wen, Ming, 2117
Sugimoto, H., see Mochida, K., 177
Suh, B.J., see Kim, J., 1333
Sulfab, Y. and Al-Sogair, F.M., Kinetics and mechanism of reduction of 3,9-diethyl-4,8-diaza-3,8-undeca-2,10-dionedioximatocopper-(III) complex by *p*-methoxyphenol, 1,2-dihydroxybenzene, 1,4-dihydroxybenzene and some of its derivatives in aqueous acidic solutions, 583
Sun, C.-Y. and Jin, L.-P., Hydrothermal synthesis and characterization of the first examples of lanthanide(III) isoorotates with a 3D supramolecular network, 2085
Sun, J., see Ma, C., 1547
Sun, Y.-J., Shen, W.-Z., Cheng, P., Yan, S.-P., Liao, D.-Z., Jiang, Z.-H. and Shen, P.-W., Synthesis, structure and spectroscopic properties of novel half-sandwich nickel(II) complexes with less hindered hydrotris(pyra-zolyl)borate ligand, 211
Sun, C.-Y. and Jin, L.-P., Three-dimensional porous frameworks constructed by transition metal ions and isoorotic acid, 2227
Sun, J.-T., see Yin, M.-C., 529
Sun, H.-M., see Li, W.-F., 1473
Sun, Z.-H., see Chen, C., 3033
Suni, V., see Philip, V., 1225
Suni, V., see Joseph, M., 3069
Suresh, E., see Subramanian, P.S., 2515
Suresh, E., see Jadeja, R.N., 2465
Suslova, E.V., see Starikova, Z.A., 109
Süss-Fink, G., see Vieille-Petit, L., 687
Sutter, J.-P., see Karmakar, R., 949
Swearingen, J.K., see Bermejo, E., 2303
Sydora, O.L., Goldsmith, J.I., Vaid, T.P., Miller, A.E., Wolczanski, P.T. and Abruña, H.D., Syntheses and electrochemistry of $(p\text{-}XC_6H_4O)_6W$ (1-X, X = H, CH_3, OCH_3, Cl, Br, OH, OCH_2Ph) and $(p\text{-}XC_6H_4O)_5W(OC_6H_4OH)$ (X = H, CH_3, OCH_3, Cl, Br): an approach to electrocatalytic CH bond activation, 2841
Szczepanik, W., see Kurzak, B., 1939
Szymczak, R., see Ryazanov, M., 879

Tahir, M.I.M., see Ravoof, T.B.S.A., 2491
Tajima, F., see Asaji, T., 1605
Takahashi, Y., Hikichi, S., Moro-oka, Y. and Akita, M., Oxygenation of a series of cationic aquoruthenium complexes, $Tp^{iPr2}\text{-}Ru(OH_2)_nL_{3-n}{\cdot}CF_3SO_3{\cdot}(THF)_x$, leading to mono- and dinuclear aquo-hydroxo complexes supported by unique hydrogen bonding networks, 225
Takats, J., see Morissette, M., 263
Takemura, H., see Matsuo, H., 955
Tan, A.L., see Ali, M.A., 2037
Tanase, S., see van Albada, G.A., 2387
Tanase, S., see Kannappan, R., 2285
Tang, T., see Cheng, J., 1075
Tanski, J.M., see Alvarez, H.M., 395
Tarafder, M.T.H., see Crouse, K.A., 161
Tarafder, M.T.H., see Chew, K.-B., 1385
Taw, F.L., see Corkey, B.K., 2943
Taylor, S.K., see Ainscough, E.W., 1159
Taylor, M.K., Reglinski, J. and Wallace, D., Coordination geometry of tetradentate Schiff's base nickel complexes: the effects of donors, backbone length and hydrogenation, 3201
Tcheboukov, D.E., see Starikova, Z.A., 109
Tegoni, M., see Gennari, M., 1829
Téllez, F., Flores-Parra, A., Barba-Behrens, N. and Contreras, R., Cobalt(II) and zinc(II) compounds with unsaturated ligands derived from 2-aminobenzothiazole, 2481
Templeton, J.L., see Cross, J.L., 2831
Templeton, J.L., see Vogeley, N.J., 311
Teresa Duarte, M., see Ribeiro, A.F.G., 2715
Terra, L.H.S.A., see Gaubeur, I., 2095
Teruel, H., see Gómez, M., 611
Terzis, A., see Raptopoulou, C., 1777
Terzis, A., see Boudalis, A.K., 1271
Terzis, A., see Milios, C.J., 83
Theopold, K.H., see Höcher, T., 1393
Theopold, K.H., see Pariya, C., 439
Therrien, B., see Vieille-Petit, L., 687
Thirumavalavan, M., Akilan, P., Amudha, P. and Kandaswamy, M., Compartmental unsymmetrical lateral macrobicyclic ligands with an aromatic backbone providing a phenoxo bridge: synthetic, spectral, magnetic, electrochemical and kinetic features of mono and binuclear copper(II) complexes, 519
Thomas, S., see Eagle, A.A., 385

Thomas, J.C. and Peters, J.C., Platinum-alkyl and hydride complexes supported by a tris(phosphino)borate ligand: structural and spectroscopic studies, 489
Thompson, M.E., see Li, J., 419
Thompson, L.K., Niel, V., Grove, H., Miller, D.O., Newlands, M.J., Bird, P.H., Wickramasinghe, W.A. and Lever, A.B.P., Cobalt and nickel complexes of a tetradentate phthalazine ligand – mononuclear, dinuclear and trinuclear derivatives, 1175
Thöne, C., see Yilmaz, V.T., 841
Thuéry, P., see Villiers, C., 1613
Thuéry, P., see Bernhardt, P.V., 869
Thuéry, P., see Salmon, L., 623
Thuéry, P. and Masci, B., Hetero(tri- and tetra-)nuclear complexes of uranyl and alkali metal (Li^+, K^+) ions with *p-tert*-butylhexahomotrioxacalix[6]arene, 649
Toma, H.E., see Raimondi, A.C., 2069
Tomkiewicz, A., see Barszcz, B., 1309
Tooke, D.M., see Kannappan, R., 2285
Törnroos, K.W., see Foss, O., 3021
Torres, M.R., see Criado, R., 301
Torres, M.R., see Barral, M.C., 2637
Torres, M.R., see Barquín, M., 1695
Toupet, L., see Kunrath, F.A., 2437
Trávníček, Z., see Kopel, P., 2193
Trávníček, Z., see Kopel, P., 1573
Tretyakov, E.V., Koreneva, O.V., Romanenko, G.V., Shvedenkov, Yu.G. and Ovcharenko, V.I., Synthesis, structure and magnetism of $M(hfac)_2$ complexes with spin labelled amides, 763
Trofimenko, S., Scorpionates: genesis, milestones, prognosis, 197
Trofimenko, S., see Claramunt, R.M., 2985
Trojnar, I., see Borowiec, J., 33
Troyanov, S., see Ryazanov, M., 879
Tsyba, I., see Li, J., 419
Tulloch, A.A.D., see Winston, S., 2813
Turgambaeva, A.E., see Krisyuk, V.V., 809
Türk, T., see Gibson, V.C., 189
Turnbull, M.M., see Anagnostis, J., 125
Turner, J.F.C. and Soper, A.K., On the determination of the structure of ferrocene in solution, 2975
Turova, N.Y., see Starikova, Z.A., 109
Turpeinen, U., see Song, Y., 1769
Turpeinen, U., see van Albada, G.A., 993
Turpeinen, U., see Kannappan, R., 2285

Uddin, J., see Hay, B.P., 145
Ueda, K., see Kitano, T., 283
Uflyand, I.E., see Garnovskii, A.D., 1909
Urbanos, F.A., see Barral, M.C., 2637

Vaid, T.P., see Sydora, O.L., 2841
Vaira, M.D., see Morley, C.P., 2967
Vaissermann, J., see Pasko, S., 735
Valigura, D., see Stachová, P., 1303
Valigura, D., Melník, M., Koman, M., Martiška, L., Korabik, M., Mrozińsky, J. and Glowiak, T., Structural confirmation of the 3,5-dinitrosalicylato anion coordination ability to metal ion: crystal structure, spectral and magnetic properties of the $[Cu_3\{3,5\text{-}(NO_2)_2sal^{2-}\}_2\{3,5\text{-}(NO_2)_2sal^{1-}\}_2(H_2O)_4]\cdot 4H_2O$, 2447
Valle, E.M.A., see de Araujo, M.P., 3163
van Albada, G.A., see Mohamadou, A., 1969
van Albada, G.A., Mutikainen, I., Turpeinen, U. and Reedijk, J., Synthesis, spectroscopy, crystal structure and magnetism of tetrakis(2-aminopyrimidine) bis(μ-methoxo)bis(perchlorato)dicopper(II): a rare case of distortion isomerism, 993
van Albada, G.A., Mohamadou, A., Driessen, W.L., de Gelder, R., Tanase, S. and Reedijk, J., A dinuclear Mn(II) chloro-bridged compound with a weak ferromagnetic Mn–Mn interaction, Synthesis, Structure, EPR and magnetism of $[Mn(\mu\text{–}Cl)(2,2'\text{-biimidazoline})_2]_2Cl_2$, 2387
van Albada, G.A., see Song, Y., 1769
Van der Wel, P., see Sceats, E.L., 2751
VanDerveer, D.G., see Grant, G.J., 1361
VanStipdonk, M.J., see Siemer, C.J., 235
Varret, F., see Salunke-Gawali, S., 2541
Vázquez-López, E.M., see Carballo, R., 1505
Velavan, K., see Srinivasan, R., 1115
Veltsistas, P.G., see Michaelides, A., 2587
Venkatasubramanian, U., Donohoe, D.J., Ellis, D., Giles, B.T., Macgregor, S.A., Robertson, S., Rosair, G.M., Welch, A.J., Batsanov, A.S., Boyd, L.A., Copley, R.C.B., Fox, M.A., Howard, J.A.K. and Wade, K., The synthesis and molecular and crystal structures of 1-methyl-2-carboxy-1,2-dicarba-*closo*-dodecaborane(12), 1-phenyl-2-carboxy-1,2-dicarba-*closo*-dodecaborane(12) and 1-phenyl-2-benzoyl-1,2-dicarba-*closo*-dodecaborane(12), 629
Venkatesan, R., see Srinivasan, R., 1115
Venugopal, V., see Kannan, S., 1527
Verat, A.Y., see Zabirov, N.G., 2243
Verghese, B., see Srinivasan, R., 1115
Vetter, A.J. and Jones, W.D., Carbon–hydrogen bond activation of chloroalkanes by a rhodium trispyrazolylborate complex, 413
Vezin, H., see Bentiss, F., 1903
Vicente, R., see Milios, C.J., 83
Vicente, R., see Escuer, A., 1409
Vickers, S., see Fawcett, J., 2561
Vidovic, D., see Bai, G., 1125
Vieille-Petit, L., Therrien, B. and Süss-Fink, G., 2,3,4,7-Tetrahydro-1*H*-inden-2-ol: synthesis, molecular structure and coordination chemistry, 687
Villiers, C., Thuéry, P. and Ephritikhine, M., Crystal structure of first- and second-sphere complexes of uranyl nitrate with 1,2- and 1,4-diols, 1613
Virovets, A.V., see Naumov, N.G., 599
Vogeley, N.J. and Templeton, J. L., Interconversions of simple monodentate nitrogen donor ligands bound to Tp′ tungsten fragments, 311
Vogels, C.M., see Scales, S.J., 2169
Vogels, C.M., see He, X.-F., 155
Voo, J.K., Incarvito, C.D., Yap, G.P.A., Rheingold, A.L. and Riordan, C.G., Tris(imidazolyl) cadmium and zinc complexes: structural and spectroscopic characterization of $M\text{–}OH_2$ motifs, 405
Voráč, Z., see Šedo, O., 1199
Vrdoljak, V., see Cindrić, M., 1859

Wada, H., see Kitano, T., 283
Wade, K., see Venkatasubramanian, U., 629
Wagner, C., see Boča, R., 2337
Wagner, M., see Ilkhechi, A.H., 2597
Wallace, D., see Taylor, M.K., 3201
Wallis, J.D., see Liu, S.-X., 1185
Walsh, R.D.B., see Bose, D., 545
Wang, Z.-L., see Niu, J.-Y., 773
Wang, E.-B., see Mao, H.-Y., 1961
Wang, W., see Yang, Y., 1535
Wang, G.-C., see Yu, L., 823
Wang, Y., see He, X., 2153
Wang, W., see Chen, C., 3033
Wang, Q.-L., see Liang, M., 2203
Wang, C.-W., see Yin, M.-C., 529
Wang, J.-P., see Niu, J.-Y., 773

Wang, E.-B., see Shen, X.-Q., 1851
Wang, T.-G., see Lu, J., 755
Wang, J.-C., see Yeh, C.-W., 1947
Wang, S.-Y.S., Abboud, K.A. and Boncella, J.M., Synthesis and mechanistic investigations of the decomposition of β-hydrogen containing W(VI) dialkyl complexes: β-H elimination vs. β-H abstraction, 2733
Wang, C.-H., see Yin, H.-D., 1805
Wang, X., see Dias, H.V.R., 2533
Ward, M.D., see Fawcett, J., 2561
Wardell, S.M.S.V., see Howie, R.A., 2331
Wardell, J.L., see Fernandes, C., 1419
Wardell, J.L., see Howie, R.A., 2331
Warżajtis, B., see Radanović, D.D., 2183
Wazeer, M.I.M., see Fettouhi, M., 1
Webster, M., see Levason, W., 605
Wei, L.K., see Ali, M.A., 2037
Weichert, K., see Krempner, C., 2475
Weisman, G.R., see Niu, W., 1019
Welch, A.J., see Venkatasubramanian, U., 629
Wen, M., Munakata, M., Suenaga, Y., Kuroda-Sowa, T., Maekawa, M. and Kodai, I., Dinuclear silver(I) complexes of *N,N′*-dibenzyl-4,13-diaza-18-crown-6-ether and dibenzo-24-crown-8-ether, 2117
Weng, L.-H., see Luo, J., 1243
Wenger, O.S., Henling, L.M., Day, M.W., Winkler, J.R. and Gray, H.B., Rhenium(I) tricarbonyl complexes with photoisomerizable ligands, 2955
Werner, H., Mahr, N., Schneider, M.E., Bosch, M. and Wolf, J., Acetylacetonato, pentachlorophenolato and carboxylato rhodium(I) complexes and their reactivity in the C–C coupling reaction of olefins and diazoalkanes, 2645
Wesolek, M., see Pelascini, F., 3193
West, D.X., see Bermejo, E., 2303
Westcott, B.L., see Joshi, H.K., 429
Westcott, S.A., see He, X.-F., 155
Westcott, S.A., see Scales, S.J., 2169
Westcott, S.A., Marder, T.B., Baker, R.T., Harlow, R.L., Calabrese, J.C., Lam, K.C. and Lin, Z., Reactions of hydroborating reagents with phosphinorhodium hydride complexes: molecular structures of a Rh_2B_3 metallaborane cluster, an $L_2Rh(\eta^2\text{-}H_2BR_2)$ complex and a mixed valence Rh dimer containing a semi-bridging Bcat (cat=1,2-$O_2C_6H_4$) group, 2665
Wheatley, M.V., see Milton, H.L., 3211
Wheatley, J., see Slawin, A.M.Z., 2569
Wheatley, M.V., see Milton, H.L., 2575
Wheatley, J., see Slawin, A.M.Z., 3125
White, P.S., see Cross, J.L., 2831
White, A.J.P., see O'Reilly, R.K., 2921
White, A.J.P., see Bailey, A., 2631
Whitten Jr., C.E., see Inyushin, S., 2937
Whitwood, A.C., see Stone, D.L., 1709
Wickramasinghe, W.A., see Thompson, L.K., 1175
Wignacourt, J.-P., see Bentiss, F., 1903
Williams, D.J., see Bailey, A., 2631
Williams, J.A.G., see Leslie, W., 2769
Williams, P.A., see Emseis, P., 1749
Williams, D.J., see O'Reilly, R.K., 2921
Winkler, J.R., see Wenger, O.S., 2955
Winpenny, R.E.P., see Smith, A.A., 1557
Winston, S., Stylianides, N., Tulloch, A.A.D., Wright, J.A. and Danopoulos, A.A., Picoline and pyridine functionalised chelate N-heterocyclic carbene complexes of nickel: synthesis and structural studies, 2813
Wolczanski, P.T., see Sydora, O.L., 2841
Wolf, J., see Werner, H., 2645
Wołowiec, S., see Borowiec, J., 33
Wołowiec, S., see Ruman, T., 219
Wong, E.H., see Niu, W., 1019
Wong, W.W.H., Phipps, D.E. and Beer, P.D., Acyclic and macrocyclic transition metal dithiocarbamate complexes containing imidazolium moieties for anion binding, 2821
Wong, W.-T., see Lee, T.-W., 999
Woollins, J.D., see Milton, H.L., 3211
Woollins, J.D., see Slawin, A.M.Z., 2569
Woollins, J.D., see Slawin, A.M.Z., 3125
Woollins, J.D., see Milton, H.L., 2575
Woźna, A., see Kurzak, B., 1939
Wright, J.A., see Winston, S., 2813
Wu, Q.-A., see Liu, H.-L., 1799
Wu, Q.-A., see Liu, H.-L., 943
Wu, Q.-A., see Mao, H.-Y., 1961
Wu, Q.-A., see Shen, X.-Q., 1851
Wu, X.-T., see Xia, S.-Q., 1003
Wu, X.-T., see Zhang, J.-J., 2265
Wu, X., see Zhang, Q., 1975

Xia, C., see Zhang, Q., 1975
Xia, S.-Q., see Zhang, J.-J., 2265
Xia, S.-Q., Hu, S.-M., Dai, J.-C., Wu, X.-T., Fu, Z.-Y., Zhang, J.-J. and Du, W.-X., Syntheses and structures of 1D, 2D, 3D cadmium(II) coordination polymers with oxalate and aromatic co-ligands, 1003
Xiang, S.-C., see Zhang, J.-J., 2265
Xing, Y., see Meng, H., 2357
Xing, Q.-J., see Yin, H.-D., 1805
Xu, C., see Liu, H.-L., 943
Xu, C., see Mao, H.-Y., 1961
Xu, X., see Zhang, Q., 1975
Xu, M.-Q., see Guo, Q.-L., 1461
Xu, C., see Liu, H.-L., 1799
Xu, J.-N., see He, X., 2153
Xu, J.-Q., see Lu, J., 755

Yakhmi, J.V., see Chawla, S.K., 3007
Yamin, B.M., see Chew, K.-B., 1385
Yamin, B.M., see Crouse, K.A., 161
Yan, S.-P., see Liang, M., 2203
Yan, C.-G., see Shi, Y.-C., 15
Yan, C.-G., see Shi, Y.-C., 567
Yan, Y., see Zhang, Q., 1975
Yan, S.-P., see Sun, Y.-J., 211
Yang, H.-M., see Shi, Y.-C., 567
Yang, Y., Liu, Y., Chen, C., Wang, W., Yi, Z. and Pang, W., Hydrothermal synthesis and characterization of an organically templated gallophosphate JGP-5, 1535
Yang, W., see Dai, J., 1447
Yang, W., see Zhang, Q., 1975
Yang, H.-M., see Shi, Y.-C., 15
Yang, H.-M., see Shi, Y.-C., 749
Yang, J., see Ma, J.-F., 553
Yang, Q.-X., see Lu, J., 755
Yang, J.-M., see Chen, H.-B., 987
Yang, Y.-L., see Meng, H., 2357
Yang, Y.-L., see Chen, C., 3033
Yang, H.-M., see Shi, Y.-C., 15
Yanovsky, A.I., see Starikova, Z.A., 109
Yao, Y.-G., see Liu, W.-L., 849
Yao, J.-H., see Hong, X.-L., 815
Yao, J., Huang, W., Zhu, H., Fang, J. and Gou, S., A novel tetranuclear copper(II) complex with 3,5-pyridinedicarboxylate bridges, 1169
Yao, Y.-G., see Liu, W.-L., 2125
Yao, Y.-G., see Cheng, J.-K., 2209

Yap, G.P.A., see Voo, J.K., 405
Yasemin Yenilmez, H., Özçeşmeci, İ., İhsan Okur, A. and Gül, A., Synthesis and characterization of metal-free and metallo phthalocyanines with four pendant naphthoxy-substituents, 787
Ye, B.-X., see Liu, H.-L., 1799
Yeh, C.-W., Suen, M.-C., Hu, H.-L., Chen, J.-D. and Wang, J.-C., Synthesis and structural characterization of two new chiral coordination polymers of Cu(nicotinate)$_2$(H_2O) and Co(nicotinate)$_2$, 1947
Yellowlees, L.J., see Leslie, W., 2769
Yi, Z., see Yang, Y., 1535
Yi, Z., see Chen, C., 3033
Yılmaz, F., Atilla, D. and Ahsen, V., Synthesis and liquid-crystalline behaviour ofNi(II) and Zn(II) phthalocyanines with peripheral monoazacrown ethers, 1931
Yilmaz, I. and Burkut Koçak, M., Electrochemical, spectroelectrochemical and pyridine binding properties of tetrathia macrocycle-bridged dimeric cobalt phthalocyanine, 1279
Yilmaz, V.T., Hamamci, S. and Thöne, C., Cobalt(II) complexes of 2-methanol-, 2,6-dimethanol- and 2-ethanolpyridines: syntheses, spectroscopic, thermal and structural characterizations of $[Co_2(\mu\text{-}Cl)_2(mpy)_4]Cl_2{\cdot}2H_2O$, $[Co(dmpy)_2]Cl_2$ and $[Co(Cl)_4](Hpyet)_2$ (mpy = 2-methanolpyridine; dmpy = 2,6-dimethanolpyridine and Hpyet = 2-ethanolpyridinium), 841
Yin, H.-D., Wang, C.-H. and Xing, Q.-J., Synthesis and characterization of triphenyltin esters of heteroaromatic carboxylic acids and the crystal structure of $[Ph_3SnO_2CC_5H_4N\cdot 0.5H_2O]_\infty$, 1805
Yin, M.-C., Yuan, L.-J., Ai, C.-C., Wang, C.-W., Yuan, E-T. and Sun, J.-T., Synthesis, structure and luminescence properties of europium and zinc ionic complexes, 529
Yoon, J.U., see Roh, S.G., 2063
Yoon, S., see Kim, J., 1333
Yoon, S., Kelly, A.E. and Lippard, S.J. Di- and tetra-bridged diiron(II) complexes with four terphenyl-derived carboxylates and two water molecules, 2805
Yoshimura, K., see Matsuo, H., 955
You, Y.S., see Hong, C.S., 1379
You, Y.S., see Hong, C.S., 3043
Young, C.G., see Eagle, Aston A., 385
Youngme, S., Chailuecha, C. and Chaichit, N., The novel dinuclear doubly and triply bridged copper(II) compound with monoatomic bridges, 1641
Youngme, S., Phuengphai, P., Booncoon, S. and Chaichit, N., The crystal structure and electronic properties of a *cis*-distorted octahedral CuN_4O_2 chromophore: $[Cu(dpyam)_2(OXO)]^+$, OXO= ONO^-, O_2CH^- and ONO_2^-, 1685
Yu, Y., see Zhang, Q., 1975
Yu, L., Ma, Y.-Q., Liu, R.-C., Wang, G.-C., Li, J.-S., Du, G.-H. and Hu, J.-J., Synthesis, characterization and in vitro antitumor activity of some arylantimony ferrocenylcarboxylate derivatives and thecrystal structures of $[C_5H_5FeC_5H_4C\text{-}(CH_3){=}CHCOO]_2Sb(C_6H_4F\text{-}4)_3$ and $[4\text{-}(C_5H_5FeC_5H_4)C_6H_4COO]_2Sb(C_6H_4F\text{-}4)_3$, 823
Yu, J.-H., see Lu, J., 755
Yu, K.-B., see Li, W.-F., 1473
Yu, L.-H., see Liang, M., 2203
Yu, J.-H., see He, X., 2153
Yu, H.-B., see Huang, H., 55
Yuan, L.-J., see Liu, H.-L., 1799
Yuan, D.-Q., see Guo, Q.-L., 2055
Yuan, L.-J., see Yin, M.-C., 529
Yuan, E-T., see Yin, M.-C., 529

Zabirov, N.G., Brusko, V.V., Verat, Alexander Y., Krivolapov, D.B., Litvinov, I.A. and Cherkasov, R.A., Synthesis and crystal structure of complexes of bipodal thiophosphorylated thioureas with divalent transition metals, 2243
Zakharov, L.N., see Karambelkar, V.V., 471
Zakharov, L.N., see Niu, W., 1019
Zakrzewski, J., see Kowalski, K., 1441
Zampa, C., see Fabbrizzi, L., 373
Zaworotko, M.J., see Bose, D., 545
Zaworotko, M.J., see Bose, D., 2045
Zbořil, R., see Kopel, P., 2193
Zehnder, M., see Constable, E.C., 135
Zhang, J., see Ma, C., 1981
Zhang, R., see Ma, C., 1981
Zhang, Q., Lu, C., Yang, W., Chen, S., Yu, Y., He, X., Yan, Y., Liu, J., Xu, X., Xia, C., Chen, L. and Wu, X., Synthesis and characterization of vanadium-(IV)–M (M=Mn, Zn) and vanadium(IV)–Ln (Ln=La, Nd) complexes with nitrilotriacetate ligands: $\{(NH_4)_2[(V^{IV}O)_2(\mu_2\text{-}O)(nta)_2\ M(H_2O)_4]\cdot 2H_2O\}_n$ and $NH_4[Ln(H_2O)_9]$ $[(V^{IV}O)_2(\mu_2\text{-}O)(nta)_2]$ 1975
Zhang, H.-S., see Zhang, J.-J., 2265
Zhang, H.-Y., see Mao, H.-Y., 1961
Zhang, H.-Y., see Shen, X.-Q., 1851
Zhang, Y., see Jia, D.-X., 937
Zhang, H.-Y., see Liu, H.-L., 943
Zhang, H., see Chen, H.-B., 987
Zhang, Y., see Li, B., 3133
Zhang, L.-P., see Lu, W.-J., 1089
Zhang, J.-J., see Xia, S.-Q., 1003
Zhang, Y., see Li, W.-F., 1473
Zhang, J., see Luo, J., 1243
Zhang, C.-M., see Luo, J., 1243
Zhang, H.-Y., see Liu, H.-L., 1799
Zhang, R., see Ma, C., 779
Zhang, L.-P., Lam, C.-K., Song, H.-B. and Mak, T.C.W., Crystalline hydrates and polymeric Ag(I) complexes of isomeric flexible double betaines 1,4-bis(*n*-picolyloxyl)benzene-*N*,*N*′-diacetate (*n*=2,3,4), 2413
Zhang, H., see Scales, S.J., 2169
Zhang, J., see Cheng, J.-K., 2209
Zhang, P., see He, X., 2153
Zhang, L.-P., Du, M., Lu, W.-J. and Mak, T.C.W., Porous coordination networks generated from lanthanum trifluoromethanesulfonate and single/mixed N-oxide spacer linkers, 857
Zhang, L.-P., Lu, W.-J. and Mak, T.C.W., Construction of lanthanide(III) coordination polymers with 1,2-bis(4-pyridyl) ethane-*N*, *N*′-dioxide and *trans*-1,2-bis(4-pyridyl)ethene-*N*,*N*′-dioxide, 169
Zhang, X., see Lu, J., 755
Zhang, Y.-M., see Ma, J.-F., 553
Zhang, J., see Guo, Q.-L., 2055
Zhang, J.-J., Xiang, S.-C., Hu, S.-M., Xia, S.-Q., Fu, R.-B., Wu, X.-T., Li, Y.-M. and Zhang, H.-S., Syntheses and characterizations of a series of heptanuclear octahedral polyhedra $\{LnNi_6\}$ with different amino acids as ligands in aqueous media, 2265
Zhao, G.-H., see Shen, X.-Q., 1851
Zheng, G-L., see Ma, J.-F., 553
Zheng, H., see Shen, X.-Q., 1851
Zheng, X.-J., Li, L.-C., Gao, S. and Jin, L.-P., Hydrothermal syntheses, structures and magnetic properties of two transition metal coordination polymers with a square grid framework, 1257
Zhong, H.-J., see Shen, X.-Q., 1851
Zhou, J., see Li, B., 3133
Zhou, Y., see Guo, W., 1701
Zhou, X.-G., see Luo, J., 1243
Zhou, Z.-H., see Chen, H.-B., 987
Zhu, Q.-Y., see Dai, J., 1447
Zhu, W.-X., see Guo, Q.-L., 1461
Zhu, C.-J., see Zhu, H.-B., 1131
Zhu, Y., see Shen, X.-Q., 1851

Zhu, H.-B., Dai, Z.-Y., Huang, W., Cui, K., Gou, S.-H. and Zhu, C.-J., Chiral copper(II) complexes of optically active Schiff bases: syntheses, crystal structure and asymmetric oxidation of methyl phenyl sulfide with hydrogen peroxide, 1131
Zhu, Q.-Y., Dai, J., Jia, D.-X., Cao, L.-H. and Lin, H.-H., $\pi\cdots\pi$ Interaction assembled silver(I) complexes with the ligand 4′,5′-diaza-9′-(4,5-disubstituted-1,3-dithiol-2-ylidene)fluorene, 2259
Zhu, Y., see Liu, H.-L., 943
Zhu, Y., see Liu, H.-L., 1799
Zhu, X., see Li, B., 3133
Zhu, Q.-Y., see Jia, D.-X., 937
Zhu, H., see Yao, J., 1169
Zhu, W.-X., see Guo, Q.-L., 2055
Zhu, Y., see Mao, H.-Y., 1961
Ziller, J.W., see Evans, W.J., 2689
Zingaro, R.A., see Gao, J., 59
Zou, Y., see Liu, W.-L., 849
Zou, Y., Liu, W.-L., Gao, S., Lu, C.-S., Dang, D.-B. and Meng, Q.-J., Synthesis, structure and magnetic properties of carboxylate-bridged polynuclear copper-(II)–lanthanide(III) rings: $[Ln(H_2O)_5(CuL)_2][CuL]\cdot 8H_2O$ (Ln=La, Ce), 2253
Zou, Y., see Liu, W.-L., 2125
Zubieta, J., see Allis, D.G., 1145
Zubiri, M.R.I., Milton, H.L., Cole-Hamilton, D.J., Slawin, A.M.Z. and Derek Woollins, J., Bis(phosphine) derivatives of diamines, 693

Available online at www.sciencedirect.com
SCIENCE DIRECT®
Polyhedron 23 (2004) 3243–3273
POLYHEDRON
www.elsevier.com/locate/poly

Subject Index to Volume 23

Absorption spectra
Carbohydrate, Cobalt complex, Circular dichroism, Optical activity, 1341
Absorption spectra
Complexation, Kinetics, Photochromism, Spiroindolinonaphthooxazines, 3147
Acetate ligands
Iron complexes, η^2-Coordination modes, Schiff bases, β-Cis arrangements, 963
Acetonitrile reduction
Amine oxidation, Imido, Metal-nitrogen pi bonding, Regioselectivity of nucleophile and electrophile additions, 311
Acetylacetonato complexes
Rhodium, Pentachlorophenolato complexes, Carboxylato complexes, Diazoalkane complexes, C–C coupling reactions, 2645
Actinide
Lanthanide, Oxides, Carbene, Uranium, 2689
Adducts
Cobalt, Oxide, β-diketonates, Structures, MOCVD, 735
Adsorption
Silica gel, Immobilization, 2-Aminomethylpyridine, Epoxide, Thermodynamic, 719
AFM
Schiff-base, Polypyrrole, Electropolymerization, Iron complex, Polymer, 1953
Aldehyde activation
C–H bond activation, Rhodium(III), Benzene activation, 2943
Aldehydes
N-Heterocyclic carbenes, Homogenous catalysis, Transfer hydrogenation, Ketones, Imines, 2857
Aliphatic amino ligands
One-dimensional, Silver(I), Coordination polymers, Tubes, Topology, Supramolecular chemistry, Self assembly, Nanotubes, 2075
Alkali metal ions
Uranyl ion, Calixarenes, Homooxacalixarenes, Crystal structures, 649
Alkali metals
Alkoxides, Enolates, β-Diketonates, Carboxylates, Alkaline earth metals, Cluster compounds, 1479
Alkali metals
Lithium, Phosphorus–carbon bond cleavage, Chelates, O Ligands, 2499
Alkaline earth metal complexes
Crystal structures, 2183
Alkaline earth metals
Alkoxides, Enolates, β-Diketonates, Carboxylates, Alkali metals, Cluster compounds, 1479
Alkaline earth metals
Self-assemble, Carboxylate bridges, Copper complexes, Dipeptides, Magnetic properties, 2125
Alkoxides
Lanthanides, Neodymium, X-ray structures, Pyrazolylborates, Borohydrides, 253
Alkoxides
Enolates, β-Diketonates, Carboxylates, Alkali metals, Alkaline earth metals, Cluster compounds, 1479
Alkylation
Zinc, Enzyme, Thiolate, 481
Alkylation
Parabanic acid, Iron, Cyclopentadienyl, Carbonyl, Thallium, Gold (I) complex, 1441
Alkylthiolate
Heteroscorpionate, Tripodal, Imidazole, Iron, Zinc, 471
Alkyne complex
Hydrotris(pyrazolyl)borate, Scorpionate ligands, Tantalum, Metal–metal multiple bond, Tetrahydrothiophene complex, 379
Aluminium
Oxoalkoxides, Precursor hydrolysis, X-ray, Structure studies, 109
Aluminium
Hydroxyaluminosilicate, Silicic acid, Aluminium solubility, Aluminium biological availability, 3185
Aluminium biological availability
Hydroxyaluminosilicate, Aluminium, Silicic acid, Aluminium solubility, 3185
Aluminium solubility
Hydroxyaluminosilicate, Aluminium, Silicic acid, Aluminium biological availability, 3185
Aluminium(III)
Catecholates, Salicylates, Complexation, Proton exchange, NMR, 2393
Aluminum
Bipyridine, Titanium, Coordination compound, Crystal structure, 561
Aluminum
Enolato, Enamido, Zirconium, Titanium, 1587
Amide
Nitronyl nitroxide, Imino nitroxide, Manganese complexes, Copper complexes, Cobalt complexes, 763
Amine oxidase
Lawsone, Quinones, 2-Hydroxy-1, 4-Naphthoquinone, Copper complexes, Antiferromagnetic coupling, H-bonding, EPR, 2541
Amine oxidation
Acetonitrile reduction, Imido, Metal-nitrogen pi bonding, Regioselectivity of nucleophile and electrophile additions, 311
Amines
Hexamethylbenzene, *p*-Cymene, Diphenyl-2-pyridylphosphine, Ruthenium complexes, 3115
Amino acid
Copper, Dendrimers, Electrochemistry, Electron spin resonance, Ligand, 1709
Amino acid
Nickel(II), Lanthanides(III), Heptanuclear, Cluster compound, 2265
Amino acid containing peroxovanadates
Dinuclear peroxovanadate, Peroxo-bridged divanadate, Peroxidative bromination, Heteroligand peroxovanadate, 1097
2-Aminomethylpyridine
Silica gel, Immobilization, Epoxide, Adsorption, Thermodynamic, 719
Aminopolycarboxylate
Copper(II), Ferromagnetic coupling, π–π stacking, Cylindrical channels, 1081
3-Aminopyridine
Mn(II) and Cd(II) complexes, Azides, Synthesis, Spectra, X-ray structures, Thermal properties, 2349
Ammonolysis
Liquid ammonia/toluene two-phase system, Potassium, Zirconium, 1125
Aniline
Dioxygen, Osmium, Oxidation, Electron transfer self-exchange, 323

doi:10.1016/S0277-5387(04)00440-1

Anion exchange
Pseudoephedrine, Nickel, Triangulo, Cluster, 1837
Anion role
Cadmium complex, Bis(triazole) ligand, Crystal structure, 3133
Anisotropic approximation
EDAX analyses, Cluster anions, Heterometal cluster complexes, 599
Anti-fungal
Bis-imidazole, Bis(imidazol-2-yl)methane, X-ray structures, Silver(I), Argentophilicity, Candida albicans, 1249
Antiferromagnetic coupling
Lawsone, Quinones, 2-Hydroxy-1, 4-Naphthoquinone, Amine oxidase, Copper complexes, H-bonding, EPR, 2541
Antiferromagnetic dimer
Copper dimer, Magnetic properties, Crystal structure, 1695
Antiferromagnetic interaction
Macrobicylic ligands, Compartmental, Copper(II) complexes, Electrochemistry, Catalytic study, 519
Antimicrobial activity
Copper(II) complexes, 2-Benzoylpyridine, Thiosemicarbazone, EPR, Crystal structure, 3069
Antimicrobial studies
Copper(II) complexes, Thiosemicarbazone, 2-Hydroxyacetophenone, EPR, Cyclic voltammetry, X-ray crystallography, 2549
Antimony
Ferrocenylcarboxylate, Crystal structures, Antitumor activity, 823
Antitumor activity
Antimony, Ferrocenylcarboxylate, Crystal structures, 823
Aqueous organometallic chemistry
Molybdenum, Polyoxometallate, Pentamethylcyclopentadienyl ligands, 2605
Aquo complex
Hydrotris(pyrazolyl)borate, Ruthenium, Hydrogen bond, Oxidation, 225
Architecture
Flexible, Carboxylates, IX, Coordination polymer, 3007
Arene ligand
Ferrocene carboxylic acid, Ferrocene derivative, Ruthenium, 687
Argentophilicity
Bis-imidazole, Bis(imidazol-2-yl)methane, X-ray structures, Silver(I), Anti-fungal, Candida albicans, 1249
Aromatic aminoacidate
Cobalt(III), Non-covalent interactions, Octahedral inversion, Tetradentate ligands, NMR, 1749
Arsenazo III
Dawson lacunary heteropolyanion, Complex formation constants, Lanthanides, 1579
Arsine
Titanium iodide, Phosphine, Iron iodide, Crystal structures, 605
Arsine ligands
Rhenium nitrosyl complexes, Pyrazole, X–ray structure, Density functional theory calculations, 2523
2-[(*E*)-2-(aryl)-1-diazenyl]pyridine
Hg(II) complexes, NMR, Crystal structures, 2323
Arylazoimidazoles
Cadmium(II) complexes, End-on and end-to-end bridging, X-ray structure, 1D chain, Sheet structure, 1669
Aryloxide
Lanthanides, Ytterbium, Crystal Structures, Tris(pyrazolyl)borate, Divalent, 263
Aryloxide derivatives
Tris(pyrazolyl)hydroborate (Tp) ligands, Lanthanum, Neodymium, Salt metathesis, 2437
Ascorbate oxidase model
Tricopper(II) complex, Schiff bases, Crystal structure, Magnetic properties, 643
Ascorbic oxidation
Copper(II) complex, Crystal structure, Imidazole, 2515
Assembly
Sulfonatothiacalixarene, Capsules, Diaza-Crown ether, Transition metal ions, 1461
Asymmetric oxidation
Chiral copper(II) complexes, Schiff base, Sulfide, Seven-membered, 1131
Aurates
S ligands, Coordination chemistry, Thianthrenes, 1351
Aza ether
Phthalocyanine, Metallo phthalocyanine, Liquid crystal, Metallo mesogen, Crown ether, 1931
1-azaallyls
Group 11 phosphine complexes, X-ray crystallography, Iminoalkyl bonding mode, 2273
Azide
Manganese(III), N,O ligands, X-ray structure, Magnetochemistry, Dimer, 1811
Azides
Polyamines, Copper(II) complexes, Crystal structures, Magnetic properties, Coordination polymers, 1243
Azides
Mn(II) and Cd(II) complexes, 3-Aminopyridine, Synthesis, Spectra, X-ray structures, Thermal properties, 2349
Azoimidazoles
Ruthenium(II)-tris-chelates, X-ray structure, Electrochemistry, 727
Azomethine H
Borate complex, Boric acid, Complexation, ^{11}B NMR, 955

^{11}B NMR
Thallium, B–H coupling, Tris(pyrazolyl)-borate, Pyrazole, 2533
B–H coupling
Thallium, ^{11}B NMR, Tris(pyrazolyl)borate, Pyrazole, 2533
^{11}B NMR
Borate complex, Azomethine H, Boric acid, Complexation, 955
Back-bonding
Crystal structure, Ruthenium complex, NO, Reactivity, Molecular, 1063
Benzene activation
C–H bond activation, Rhodium(III), Aldehyde activation, 2943
Benzimidazole
Platinum, Imine, Benzoxazole, Benzothiazole, Pyridine, 155
N-(benzothiazol-2-yl)-*S*,*S*′-dimethyl-dithiocarboimine
Zinc(II) cobalt(II) compounds from *N*-(benzothiazol-2-yl)-dithiocarbamic methyl-ester, 1-Benzothiazol-2-ylid-3-methyl-thiourea, 1-Benzothiazol-2-yl-2,3-dimethyl-*iso*-thiourea, 2481
Benzimidazole
Rhenium, Bibenzimidazole, Crystal structure, Paramagnetic NMR, 1139
Benzothiazole
Platinum, Imine, Benzimidazole, Benzoxazole, Pyridine, 155
1-Benzothiazol-2-yl-2,3-dimethyl-*iso*thiourea
Zinc(II) cobalt(II) compounds from *N*-(benzothiazol-2-yl)-dithiocarbamic methyl ester, 1-Benzothiazol-2-ylid-3-methyl-thiourea, *N*-(benzothiazol-2-yl)-*S*,*S*′-dimethyl-dithio-carboimine, 2481
1-Benzothiazol-2-ylid-3-methyl-thiourea
Zinc(II) cobalt(II) compounds from *N*-(benzothiazol-2-yl)-dithiocarbamic methyl ester, 1-Benzothiazol-2-yl-2,3-dimethyl-*iso*thiourea, *N*-(benzothiazol-2-yl)-*S*,*S*′-dimethyl-dithio-carboimine, 2481
2-Benzoylpyridine
Copper(II) complexes, Thiosemicarbazone, EPR, Antimicrobial activity, Crystal structure, 3069
Benzoxazole
Platinum, Imine, Benzimidazole, Benzothiazole, Pyridine, 155
Bibenzimidazole
Rhenium, Benzimidazole, Crystal structure, Paramagnetic NMR, 1139
Bicapped trigonal prism
Eight-coordinate, Stereochemistry, Dodecahedron, Square antiprism, Molecular mechanics, 145
Bidentate
Ligand, Bridging, X-ray, Phosphine, 2569
Bidentate chelate
Bis(diphenylphosphino)methane dioxide, Uranyl nitrate, Uranyl bis(β-diketonates), Monodentate, Bridging bidentate, Coordination modes, 1527
Bidentate diamine
$Cu^{II}N_4Cl$ chromophores, Bidentate diimine, π–π Interactions, Hydrogen bonding, Magnetic property, 1961
Bidentate diimine
$Cu^{II}N_4Cl$ chromophores, Bidentate diamine, π–π Interactions, Hydrogen bonding, Magnetic property, 1961

Bidentate donors
2-Diphenylphosphinopicolinamide (dpppa 1), Coordination chemistry, Monodentate donors, 3211
Bidentate ligand
Dinuclear copper(II) complex, Magnetic properties, Crystal structure, UV–Vis, EPR and IR spectra, 1309
Bidentate NS Schiff base
S-2-picolyldithiocarbazate (Hydrazine carbodithioic acid pyridinium-2-yl methyl ester chloride), Tridentate NNS and NSS Schiff bases, Ni(II) complexes, Dithiocarbazate derivative, 161
Binuclear complexes
Nickel(II) compounds, Crystal structures, Terephthalate ligand, Magnetic properties, 1379
Binuclear compounds
Isocyanides, Nickel, Polymerisation, Ring-coupled bis-cyclopentadienyl ligand, X-ray molecular structure, 2715
Binuclear copper complex
EPR, Half-field, Superhyperfine, X-ray, Electrochemical, 1115
Binuclear ruthenium complexes
Mixed valent Ru(II)/Ru(III) complexes, Catalysis, Imine hydrogenation, 3163
Bioactivity
1,3,4-thiadiazole, Zinc, Crystal structure, Thermal decomposition, Kinetics, 1851
Biphase catalysis
Hydroformylation, Ionic liquids, High-pressure NMR, Rhodium complexes, 2679
Bipodal ligands
P,*S*-metallocycles, Supramolecular chemistry, Crystal structures, Macrocycles, Phosphorylated urea complexes, 2243
Bipyridine
Titanium, Aluminum, Coordination compound, Crystal structure, 561
Bipyridine
Distortions, 2081
2,2′-Bipyridine
Hydrazones, Copper(II) hydrazonate complexes, 1,10- Phenanthroline, X-ray single crystal structure, EPR, 575
2,2′-Bipyrimidine complexes
Iron(III) carboxylate complexes, Oxo-bridged iron(III) complexes, π–π stacking interactions, X-ray crystal structure, 1271
4,4′-Bipyridine
Lead(II), Coordination polymers, Lone pair, π–π staking interaction, Crystal structure, 2427
4,4′-Bipyridyl
Diorganotin, Dicyanoethylene-1,2-dithiolate, 1,10-Phenanthroline, X-ray crystal structure, Co-crystallization, 1207
Bis(2-pyridylmethyl)amine
Iron(II) complexes, Cobalt(II) complexes, X-ray crystal structures, Tris(2-pyridylmethyl)amine, 3105
Bis(2-pyridylmethyl)amino acids
Self-assembly, Crystal structures, Ferromagnetism, One-dimensional chains, Copper(II) complexes, 903
Bis(8-quinolinyl)amine
Cobalt, Copper, Zinc, Structures, 831
Bis(diphenylphosphino)methane dioxide
Uranyl nitrate, Uranyl bis(β-diketonates), Monodentate, Bidentate chelate, Bridging bidentate, Coordination modes, 1527
Bis(ethylenedithio)tetrathiafulvalene (ET)
Radical salts, Crystal structures, Electrical conductivity, 1185
Bis(imidazol-2-yl)methane
Bis-imidazole, X-ray structures, Silver(I), Argentophilicity, Anti-fungal, Candida albicans, 1249
Bis(imido)
Tris(pyrazolyl)borate, Molybdenum, Synthesis, Structures, 189
Bis(mercaptoimidazolyl)borate complexes
Nickel, Tris(mercaptoimidazolyl)borate complexes, Diphosphine, Hydrogenases, Crystal structure, 395
Bis(mercaptoimidazolyl)borate complexes
Thallium, Crystal structure, 617
Bis(methoxycarbimido)amine
MP2 geometry optimization, Topological analysis of electron density, 2235
Bis(triazole) ligand
Cadmium complex, Crystal structure, Anion role, 3133
Bis-(2-pyridylmethyl)amine
Iron, (μ-O)di-iron complex, Oxalato, Hydrogen bonding, Mössbauer spectra, 1419
Bis-imidazole
Bis(imidazol-2-yl)methane, X-ray structures, Silver(I), Argentophilicity, Anti-fungal, Candida albicans, 1249
Bis-imidazole
Metal complexes, X-ray structures, Manganese(II), Copper(II), Zinc(II), 1731
Bis[monochloro(μ-*N*-salicylidenemyristoylhydrazine) ONO′(−1)]dicopper(II)
N-salicylidene-*n*-alkanoylhydrazines, Copper(II) complexes, Magnetochemical studies, X-ray crystal and molecular structure, 23
Bis[tris(pyrazolyl)methane] complexes
Electron-transfer reactions, Spin-exchange reactions, Low-spin configurations, High-spin configurations, 1037
1,3-Bis(4-pyridyl)propane
Zinc, 4,4′-Pyridine, Polymeric network, X-ray crystallography, 999
2,3-Bis(α-pyridyl)pyrazine
Ruthenium, Cyclopentadienyl, 1,3,5-Tris (pyridyl)-2,4,6-triazine, 2,3,5,6-Tetrakis (pyridyl)pyrazine, 1069
2,5-Bis(2-pyridyl)-1,3,4-thiadiazole
Zinc, Energy minimization, Crystal structures, Monomeric complexes, 1903
Bitopic heteroscorpionate ligand
Square planar silver complex, 291
Boat conformations
Iridium, Cyclometalated Ir(II) complexes, Pyrazolyl ancillary ligands, Luminescent, Electroluminescence, 419
Bond cleavage
Molybdenum complexes, Carbonyl complexes, Pentafluorophenyl, Oxidation, Reductive elimination, 1371
Bond valence
Ruthenium arene complexes, Pyrazole, Dimethylpyrazole, X-ray structure, 885
Bonding
Organometallics, Sandwich complex, Metallocene, Density functional theory, Orbital analysis, 2993
Borate complex
Azomethine H, Boric acid, Complexation, ^{11}B NMR, 955
Boric acid
Borate complex, Azomethine H, Complexation, ^{11}B NMR, 955
Borohydrides
Lanthanides, Neodymium, X-ray structures, Alkoxides, Pyrazolylborates, 253
Boron
Multiple-decker sandwich complex, Ferrocene, Lithium, Crystal structure, 2597
Boron
Zwitterions, Monoanionic ligands, Phosphines, Syntheses, Structures, 2901
Boron neutron capture therapy
closo-Dodecaborate, Hydroxy and acyl derivatives, Disubstituted functional derivatives, 2135
Bridging
Iron (III), Dinuclear, Carboxylate, Complexes, Mössbauer, 1869
Bridging
Ligand, Bidentate, X-ray, Phosphine, 2569
Bridging bidentate
Bis(diphenylphosphino)methane dioxide, Uranyl nitrate, Uranyl bis(β-diketonates), Monodentate, Bidentate chelate, Coordination modes, 1527
Bridging boryls
Rhodium hydrides, Catalyzed hydroborations, 2665
Bridging Tp ligands
κ^2-Tp ligands, Rhodium dicarbonyl complexes, Isomers, X-ray structure, 301
Bromotrimethylsilane
Lanthanide oxides, O-donor ligands, Complexes of lanthanide bromides, Crystal structure, Coordination number, 2293
Building block approach
Octamolybdate, Hydrothermal synthesis, Three-dimensional oxide, Organic–inorganic hybrid, Hartree–Fock calculations, 1145

^{59}Co NMR
Multidentate ligand, Cobalt(III), Sinambic, 2217
C–C coupling reactions
Rhodium, Acetylacetonato complexes, Pentachlorophenolato complexes, Carboxylato complexes, Diazoalkane complexes, 2645
C–H activation
Trispyrazolylborate, Rhodium, 413

C–H activation
Ruthenium, Scorpionate, Tris(pyrazolyl)-borate, Hydride, 439
C–H bond activation
Rhodium(III), Benzene activation, Aldehyde activation, 2943
Cadmium
Coordinate, Polymers, Ligands, Supramolecular, 1003
Cadmium
Thiosemicarbazone, 2-pyridineformamide, Crystal structure, Zinc, 2303
Cadmium
Xanthate, Diamine, Zinc, CdS, Nanoparticles, 2315
Cadmium complex
Zinc complex, 2-Oxo-1,3-dithiole-4,5-dithiolate, Synthesis, Crystal structure, Density functional calculation, 1701
Cadmium complex
Bis(triazole) ligand, Crystal structure, Anion role, 3133
Cadmium(II)
Calcium(II), Manganese(II), Synthesis, Crystal structures, Tetrazolate complexes, 1217
Cadmium(II)
Chloranilate anions, Phenanthroline, Square antiprism, Crystal structures, Chain polymers, 2587
Cadmium(II) complexes
Arylazoimidazoles, End-on and end-to-end bridging, X-ray structure, 1D chain, Sheet structure, 1669
Cadmium(II)thiocyanate
Polymer, Schiff base, Imidazole, Supramolecular synthon, 2045
Cage complexes
Rotational barriers, Polyphosphoxane, Cone angles, 125
Calcium phosphates
Hydroxyapatite, Complex, EDTA, Hydrothermal, Low temperature, 1897
Calcium(II)
Cadmium(II), Manganese(II), Synthesis, Crystal structures, Tetrazolate complexes, 1217
Calixarenes
Uranyl ion, Alkali metal ions, Homooxacalixarenes, Crystal structures, 649
Candida albicans
Bis-imidazole, Bis(imidazol-2-yl)methane, X-ray structures, Silver(I), Argentophilicity, Anti-fungal, 1249
Capsules
Sulfonatothiacalixarene, Diaza-Crown ether, Transition metal ions, Assembly, 1461
Capsules
Sulfonatothiacalixarene, Diaza-18-crown-6, Lanthanide ions, 2055
Carbene
Actinide, Lanthanide, Oxides, Uranium, 2689
Carbohydrate
Cobalt complex, Absorption spectra, Circular dichroism, Optical activity, 1341
Carbon allotropes
Polyynes, Carbyne, Dicyanopolyynes, Cyanopolyynes, Electric arc, Graphite, Liquid nitrogen, 1889
Carbon monoxide
Hydrocarboxylation, Oligomerization, Catalysis, Rhodium complexes, Ethylene, 1677
Carbonyl
Sodium, Copper, Tris(pyrazolyl)borate, Fluorinated, 273
Carbonyl
Parabanic acid, Iron, Cyclopentadienyl, Thallium, Gold (I) complex, Alkylation, 1441
Carbonyl complexes
Molybdenum complexes, Pentafluorophenyl, Oxidation, Bond cleavage, Reductive elimination, 1371
Carborane
Spectroscopy, DFT calculations, X-ray crystallography, 629
Carboxylate
Iron (III), Dinuclear, Complexes, Bridging, Mössbauer, 1869
Carboxylate
Coordination polymer, Double betaine, Hydrate, Hydrogen bonding, π–π Interaction, Silver nitrate, 2413
Carboxylate bridge
Cu(II)–Ln(III) complexes, Dipeptides, Hexanuclear cations, Crystal structures, Magnetic properties, 2253
Carboxylate bridges
Self-assemble, Copper complexes, Dipeptides, Alkaline earth metals, Magnetic properties, 2125
Carboxylates
Alkoxides, Enolates, β-Diketonates, Alkali metals, Alkaline earth metals, Cluster compounds, 1479
Carboxylates
Flexible, IX, Coordination polymer, Architecture, 3007
Carboxylato complexes
Rhodium, Acetylacetonato complexes, Pentachlorophenolato complexes, Diazoalkane complexes, C–C coupling reactions, 2645
Carbyne
Carbon allotropes, Polyynes, Dicyanopolyynes, Cyanopolyynes, Electric arc, Graphite, Liquid nitrogen, 1889
Catalysis
Ligand, X-ray structure, Complex, 693
Catalysis
Synthesis, Crystal structures, Indenyl ligand, Nickel complex, 1473
Catalysis
Hydrocarboxylation, Oligomerization, Rhodium complexes, Ethylene, Carbon monoxide, 1677
Catalysis
Mixed valent Ru(II)/Ru(III) complexes, Binuclear ruthenium complexes, Imine hydrogenation, 3163
Catalyst
Neutral palladium(II) complex, X-ray crystallography, Methylaluminoxane, Norbornene, Vinylic polymerizaition, 1619
Catalyst
Iron, Radical, Styrene, Polymerisation, 2921
Catalysts
Chiral, Schiff base, Copper, Cyclopropanation, Crystal structures, 3051
Catalytic enantioselective reduction
trans-1,2-Diaminocyclohexane, Crystal structure, Zinc complex, 2063
Catalytic study
Macrobicylic ligands, Compartmental, Copper(II) complexes, Electrochemistry, Antiferromagnetic interaction, 519
Catalyzed hydroborations
Rhodium hydrides, Bridging boryls, 2665
Catecholates
Aluminium(III), Salicylates, Complexation, Proton exchange, NMR, 2393
CdS
Xanthate, Diamine, Zinc, Cadmium, Nanoparticles, 2315
Cerium
Oxazolines, Chiral, Thermal decomposition, MOCVD, β-ketoesterates, 1467
Chain polymers
Cadmium(II), Chloranilate anions, Phenanthroline, Square antiprism, Crystal structures, 2587
Charge transfer
Ion pair complex, Hydrogen bonding network, Non-covalent interaction, Near-IR absorption, 1235
Charge transfer compounds
Tetrathiafulvalene, Copper(II), Electrical conductivity, 2111
Charge-transfer
Iridium, Luminescence, Terpyridine, Near infra-red, Intra-ligand charge transfer, 2769
Chelates
Alkali metals, Lithium, Phosphorus–carbon bond cleavage, O Ligands, 2499
Chelating phosphines
Iridium complexes, 2959
Chemical vapour deposition
Thermochromism, Thin films, Vanadium dioxide, 3087
Chiral
Cyclophosphazenes, Spirocyclic, X-ray structure, 979
Chiral
Cerium, Oxazolines, Thermal decomposition, MOCVD, β-ketoesterates, 1467
Chiral
Coordination polymers, Nicotinate, Open channel, Grid, 1947
Chiral
Schiff base, Copper, Cyclopropanation, Catalysts, Crystal structures, 3051
Chiral copper(II) complexes
Asymmetric oxidation, Schiff base, Sulfide, Seven-membered, 1131

Chirality
Scorpionate ligands, Tripod ligands, Prochirality, Menthone, 245
Chirality
Tetra-azamacrocycles, Template reaction, Pendent arm, Conformational isomers, 869
Chloranilate anions
Cadmium(II), Phenanthroline, Square antiprism, Crystal structures, Chain polymers, 2587
Chromium complexes
Phosphanylalkylcyclopentadienyl ligands, Polymerisation studies, 1393
Chromophores
Scorpionands, Copper(II), Macrocycles, Nickel(II), 373
β-Cis arrangements
Iron complexes, Acetate ligands, η^2-Coordination modes, Schiff bases, 963
Circular dichroism
Carbohydrate, Cobalt complex, Absorption spectra, Optical activity, 1341
Cluster
Uranium, Schiff base, Crystal structure, 623
Cluster
Pseudoephedrine, Nickel, Triangulo, Anion exchange, 1837
Cluster anions
EDAX analyses, Anisotropic approximation, Heterometal cluster complexes, 599
Cluster complexes
Fe(III) carboxylate chemistry, Magnetochemistry, Crystal structures, 2779
Cluster compound
Nickel(II), Lanthanides(III), Amino acid, Heptanuclear, 2265
Cluster compounds
Alkoxides, Enolates, β-Diketonates, Carboxylates, Alkali metals, Alkaline earth metals, 1479
Clusters
Phosphorus, Sulfur, Phosphorus sulfides, Laser ablation synthesis, TOF mass spectrometry, 1199
Clusters
Electron density distribution, Polarizability, Spherical potential well, Finite electric field, 1519
Clusters
Complexity, Nanochemistry, Polyoxomolybdates, 2381
Clusters
Crystal structures, Copper, Molybdenum, Tungsten, Nitrogen heterocycle ligands, Pyrazole, 3143
Co(II) and Ni(II) complexes
Isoorotic acid, Hydrothermal synthesis, Hydrogen bonds, Supramolecular frameworks, 2227
Co-crystallization
Diorganotin, Dicyanoethylene-1,2-dithiolate, 4,4′-Bipyridyl, 1,10-Phenanthroline, X-ray crystal structure, 1207
Cobalt
Oxide, β-diketonates, Adducts, Structures, MOCVDf, 735
Cobalt
Polyoxometalates, Hydrothermal synthesis, Crystal structure, Keggin, 773
Cobalt
Phthalocyanine, Zinc, Nickel, Naphthalene, 787
Cobalt
Copper, Zinc, Bis(8-quinolinyl)amine, Structures, 831
Cobalt
Porphyrazine, EPR, Naphthalene, Copper, Zinc, 1845
Cobalt complex
Carbohydrate, Absorption spectra, Circular dichroism, Optical activity, 1341
Cobalt complexes
Nitronyl nitroxide, Imino nitroxide, Amide, Manganese complexes, Copper complexes, 763
Cobalt(II) complex
Lawesson's Reagent, Thiophosphoryl compound, Sulfur-rich complex, Nickel(II) complex, 1799
Cobalt(II) complexes
Immobilization, Silica support, H_2O_2, 59
Cobalt(II) complexes
2-Methanolpyridine, 2,6-Dimethanolpyridine, 2-Ethanolpyridinium, Crystal structures, 841
Cobalt(II) complexes
Iron(II) complexes, X-ray crystal structures, Bis(2-pyridylmethyl)amine, Tris(2-pyridylmethyl)amine, 3105
Cobalt(III)
Semicarbazone, 2-Hydroxyacetophenone, NMR spectra, IR spectra, Electronic spectra, X- ray crystal structure, 41
Cobalt(III)
Aromatic aminoacidate, Non-covalent interactions, Octahedral inversion, Tetradentate ligands, NMR, 1749
Cobalt(III)
Multidentate ligand, Sinambic, ^{59}Co NMR, 2217
Cobalt(III) complex
Crystal structure, Thiazine, Nickel(II) complex, Pyridine, 1453
Cobalt(III) complexes
Synthesis, Spectroscopy, Pyrazolyl thiosemicarbazone, X-ray crystallography, 5
Cobalt(III) complexes
Ozone, X-ray crystal structure, Silver(II) complexes, Manganese(III) complexes, 2631
Cobaltocenium
Metallocene, Ferrocenium, Crystal structure, 2937
Compartmental
Macrobicylic ligands, Copper(II) complexes, Electrochemistry, Antiferromagnetic interaction, Catalytic study, 519
Complex
Ferrocene, Enaminone, Ligand, Copper, X-ray crystallography, 15
Complex
Ferrocene, Dithiocarbazate, Ligand, Tin, Crystal structure, 567
Complex
Ligand, Catalysis, X-ray structure, 693
Complex
Hydrazones, Lanthanide, X-ray, Spectroscopy, Crystal structures, 1191
Complex
Crystal structure, Molecular assembly, 1,3-Dithiole-2-thione, 1447
Complex
Ferrocene, Enaminone, Ligand, Copper, X-ray crystallography, 1541
Complex
Hydroxyapatite, EDTA, Hydrothermal, Low temperature, Calcium phosphates, 1897
Complex formation
Uranium, Glycerol phosphate, Potentiometric titration, TRLFS, 1793
Complex formation constants
Dawson lacunary heteropolyanion, Lanthanides, Arsenazo III, 1579
Complexation
Borate complex, Azomethine H, Boric acid, ^{11}B NMR, 955
Complexation
Aluminium(III), Catecholates, Salicylates, Proton exchange, NMR, 2393
Complexation
Absorption spectra, Kinetics, Photochromism, Spiroindolinonaphthooxazines, 3147
Complexation
Terpyridine, Pyridyl bispyrazolyl, Iron, Rearrangement, X-ray structures, 3193
Complexes
Ferrocene, Enaminone, Ligands, X-ray crystallography, 749
Complexes
Iron (III), Dinuclear, Carboxylate, Bridging, Mössbauer, 1869
Complexes
Palladium, Selenium, X-ray, 2967
Complexes of lanthanide bromides
Lanthanide oxides, Bromotrimethylsilane, O-donor ligands, Crystal structure, Coordination number, 2293
Complexity
Clusters, Nanochemistry, Polyoxomolybdates, 2381
Cone angles
Rotational barriers, Polyphosphoxane, Cage complexes, 125
Conformational isomers
Chirality, Tetra-azamacrocycles, Template reaction, Pendent arm, 869
Coordinate
Cadmium, Polymers, Ligands, Supramolecular, 1003
Coordination
Phosphine, Synthesis, X-ray structure, 2575

Coordination chemistry
Scorpionates, Polypyrazolylborates, Nitrogen ligands, 197
Coordination chemistry
S ligands, Aurates, Thianthrenes, 1351
Coordination chemistry
2-Diphenylphosphinopicolinamide (dpppa 1), Monodentate donors, Bidentate donors, 3211
Coordination complex
X-ray structure, Diimine, Zinc, Palladium, 2789
Coordination compound
Bipyridine, Titanium, Aluminum, Crystal structure, 561
Coordination environment
Nickel(II) complexes, Crystal structures, Hydrotris(pyrazolyl)borate complexes, Scorpionates, 211
Coordination framework
Copper, 4,7-Phenanthroline, Host–guest properties, Polymers, Extended structures, 55
Coordination geometry
Nickel, Schiff's bases, Hydrogenated Schiff's bases, X-ray crystal structures, Polymethylene chains, 3201
Coordination modes
Bis(diphenylphosphino)methane dioxide, Uranyl nitrate, Uranyl bis(β-diketonates), Monodentate, Bidentate chelate, Bridging bidentate, 1527
η^2-Coordination modes
Iron complexes, Acetate ligands, Schiff bases, β-Cis arrangements, 963
Coordination number
Lanthanide oxides, Bromotrimethylsilane, O-donor ligands, Complexes of lanthanide bromides, Crystal structure, 2293
Coordination polymer
Lanthanide nitrate, N,N′-dioxide, Self-assembly, 169
Coordination polymer
Crystal structure, Hydrogen bonds, Copper(II), 553
Coordination polymer
Europium, Hydrogen bonds, Luminescence, Supramolecular, Terbium, 711
Coordination polymer
Lanthanum trifluoromethanesulfonate, Isonicotinic acid, N-oxide, Mixed ligands, 857
Coordination polymer
Manganese maleate, Temperature effect, Helical architecture, Hydrogen bonds, π–π interactions, 987
Coordination polymer
Copper, *N*-ligands, Thioethers, Multi-armed ligands, X-ray structures, 1055
Coordination polymer
Hydrothermal synthesis, Magnetic property, Transition metal, Square grid structure, 1,4-Naphthalenedicarboxylic acid, 1257
Coordination polymer
Lead, Hydrothermal synthesis, X-ray structure determination, 2161
Coordination polymer
Carboxylate, Double betaine, Hydrate, Hydrogen bonding, π–π Interaction, Silver nitrate, 2413
Coordination polymer
Flexible, Carboxylates, IX, Architecture, 3007
Coordination polymer
Copper(II) complex, Schiff base, X-ray structure, Imine activation, 3081
Coordination Polymers
Polypyrazolylborate complexes, Copper complexes, Rhodium complexes, Scorpionates, Nitrile coordination, 235
Coordination polymers
Azides, Polyamines, Copper(II) complexes, Crystal structures, Magnetic properties, 1243
Coordination polymers
Chiral, Nicotinate, Open channel, Grid, 1947
Coordination polymers
One-dimensional, Silver(I), Aliphatic amino ligands, Tubes, Topology, Supramolecular chemistry, Self assembly, Nanotubes, 2075
Coordination polymers
Copper(II) complex, Crystal structure, Magnetic properties, 2203
Coordination polymers
4,4′-Bipyridine, Lead(II), Lone pair, π–π staking interaction, Crystal structure, 2427
Coordination polymers
Silver, Imidazolate, X-ray structure, 3063
Copper
Ferrocene, Enaminone, Ligand, Complex, X-ray crystallography, 15
Copper
4,7-Phenanthroline, Coordination framework, Host–guest properties, Polymers, Extended structures, 55
Copper
Sodium, Tris(pyrazolyl)borate, Fluorinated, Carbonyl, 273
Copper
Tetrakis(3-isopropylpyrazolyl)borate, Solvent extraction, Single-crystal X-ray diffraction, Zinc, 283
Copper
Cobalt, Zinc, Bis(8-quinolinyl)amine, Structures, 831
Copper
Structure, Magnetism, Dinuclear, EPR, 993
Copper
N-ligands, Thioethers, Multi-armed ligands, X-ray structures, Coordination polymer, 1055
Copper
Crystal structure, Dimer, Spectral properties, Magnetic properties, 1303
Copper
Nickel, Zinc, Imidazole, α-Hydroxycarboxylato complexes, Thermal behaviour, Crystal structures, 1505
Copper
Ferrocene, Enaminone, Ligand, Complex, X-ray crystallography, 1541
Copper
Amino acid, Dendrimers, Electrochemistry, Electron spin resonance, Ligand, 1709
Copper
Self-assembly, N,O-ligands, Dinuclear, EPR, 1769
Copper
Porphyrazine, EPR, Naphthalene, Zinc, Cobalt, 1845
Copper
Structure, Infrared, Hydrogen bonds, Distortion isomers, 1969
Copper
3,5-Dinitrosalicylate complex, Trimer, Crystal structure, Magnetic properties, Spectral properties, 2447
Copper
Chiral, Schiff base, Cyclopropanation, Catalysts, Crystal structures, 3051
Copper
Crystal structures, Clusters, Molybdenum, Tungsten, Nitrogen heterocycle ligands, Pyrazole, 3143
Copper complexes
Polypyrazolylborate complexes, Rhodium complexes, Scorpionates, Coordination Polymers, Nitrile coordination, 235
Copper complexes
Crystal structures, Zinc complexes, Molecular rectangles, 673
Copper complexes
Nitronyl nitroxide, Imino nitroxide, Amide, Manganese complexes, Cobalt complexes, 763
Copper complexes
Schiff base complexes, Tripeptide complexes, 849
Copper complexes
Di-2-pyridylamine, Nitrito complexes, Plasticity effect, *cis*-Distorted octahedron, Fluxional behaviour, 1685
Copper complexes
Self-assemble, Carboxylate bridges, Dipeptides, Alkaline earth metals, Magnetic properties, 2125
Copper complexes
Lawsone, Quinones, 2-Hydroxy-1, 4-Naphthoquinone, Amine oxidase, Antiferromagnetic coupling, H-bonding, EPR, 2541
Copper dimer
Magnetic properties, Antiferromagnetic dimer, Crystal structure, 1695
Copper dimers
Triazolopyrimidine, Zn complexes, EPR, 743
Copper(I) complexes
Tetrathiomolybdate, Tetrathiotungstate, Dihydridobis(pyrazolyl)borate, Crystal structure, Model compounds, 637
Copper(I) complexes
Hexafluorocetylacetonate, Olefin complexes, Divinyl organics, Crystal structure, Thermal analysis, 809

Copper(II)
Scorpionands, Chromophores, Macrocycles, Nickel(II), 373
Copper(II)
Coordination polymer, Crystal structure, Hydrogen bonds, 553
Copper(II)
Aminopolycarboxylate, Ferromagnetic coupling, π–π stacking, Cylindrical channels, 1081
Copper(II)
Bis-imidazole, Metal complexes, X-ray structures, Manganese(II), Zinc(II), 1731
Copper(II)
Tetrathiafulvalene, Charge transfer compounds, Electrical conductivity, 2109
Copper(II) complex
Crystal structure, Magnetic properties, Coordination polymers, 2203
Copper(II) complex
Pyridylthioazophenol ligands, Crystal structure, 2457
Copper(II) complex
Ascorbic oxidation, Crystal structure, Imidazole, 2515
Copper(II) complex
Schiff base, X-ray structure, Imine activation, Coordination polymer, 3081
Copper(II) complexes
N-salicylidene-*n*-alkanoylhydrazines, Magnetochemical studies, Bis[monochloro-(μ-*N*-salicylidenemyristoylhydrazine) ONO′(−1)]dicopper(II), X-ray crystal and molecular structure, 23
Copper(II) complexes
Macrobicylic ligands, Compartmental, Electrochemistry, Antiferromagnetic interaction, Catalytic study, 519
Copper(II) complexes
Self-assembly, Crystal structures, Bis(2-pyridylmethyl)amino acids, Ferromagnetism, One-dimensional chains, 903
Copper(II) complexes
Azides, Polyamines, Crystal structures, Magnetic properties, Coordination polymers, 1243
Copper(II) complexes
Crystal structure, Dihydroxo-bridged, Roof-shaped, Triply bridged, 1641
Copper(II) complexes
Thioether ligands, Stability constants, Monophosphono dipeptides, Potentiometry, Vis, CD, EPR spectroscopy, 1939
Copper(II) complexes
Dithiocarbazates, Saccharin complexes, 2031
Copper(II) complexes
Pyrazolone, Crystal structures, ESR study, 2465
Copper(II) complexes
Thiosemicarbazone, 2-Hydroxyacetophenone, EPR, Antimicrobial studies, Cyclic voltammetry, X-ray crystallography, 2549
Copper(II) complexes
2-Benzoylpyridine, Thiosemicarbazone, EPR, Antimicrobial activity, Crystal structure, 3069
Copper(II) compounds
Crystal structures, Terephthalate ligand, One-dimensional complexes, Magnetic properties, 3043
Copper(II) hydrazonate complexes
Hydrazones, 1,10- Phenanthroline, 2,2′-Bipyridine, X-ray single crystal structure, EPR, 575
Copper(III)
Imine-oxime ligand, Diols, Kinetics, Mechanism, Electron transfer, 583
CPMAS
Pyrazolylborates, Thallium, NMR, 2985
Crown ether
Ion recognition, Schiff base complexes, UV–Vis, Lanthanides, 1401
Crown ether
Phthalocyanine, Metallo phthalocyanine, Liquid crystal, Metallo mesogen, Aza ether, 1931
Crown thioethers
Thioether complexes, Platinum complexes, Trithiacyclononane, Platinum nuclear magnetic resonance, Diimine complexes, 1361
Cryptate
Lanthanide, Crystal structure, ES-MS, 49
Crystal engineering
Zinc(II)azide, Mononuclear, Dinuclear, 2,2′-Dipyridylamine, Luminescence, 545
Crystal engineering
Supramolecular chemistry, Self-assembly, Polymers, Transition metal, 1877
Crystal structure
Gold complex, Selenourea, MAS NMR, 1
Crystal structure
Lanthanide, Cryptate, ES-MS, 49
Crystal structure
Hypodentate, Tripodal amine ligand, Cu(II) complexes, Five-coordinate, 97
Crystal structure
Nickel, Bis(mercaptoimidazolyl)borate complexes, Tris(mercaptoimidazolyl)borate complexes, Diphosphine, Hydrogenases, 395
Crystal structure
Ionic complex, Rheological phase reaction, Photoluminescence, Europium, Zinc, 529
Crystal structure
Coordination polymer, Hydrogen bonds, Copper(II), 553
Crystal structure
Bipyridine, Titanium, Aluminum, Coordination compound, 561
Crystal structure
Ferrocene, Dithiocarbazate, Ligand, Complex, Tin, 567
Crystal structure
Thallium, Bis(mercaptoimidazolyl)borate complexes, 617
Crystal structure
Uranium, Schiff base, Cluster, 623
Crystal structure
Tetrathiomolybdate, Tetrathiotungstate, Dihydridobis(pyrazolyl)borate, Copper(I) complexes, Model compounds, 637
Crystal structure
Tricopper(II) complex, Schiff bases, Ascorbate oxidase model, Magnetic properties, 643
Crystal structure
Vanadium(V) peroxo mandelato complex, IR spectra, ^{51}V NMR spectra, 655
Crystal structure
Polyoxometalates, Hydrothermal synthesis, Keggin, Cobalt, 773
Crystal structure
2-Mercapto-6-nitrobenzothiazole, Organotin(IV), Non-bonded interaction, X-ray crystallography diffraction, 779
Crystal structure
Copper(I) complexes, Hexafluorocetylacetonate, Olefin complexes, Divinyl organics, Thermal analysis, 809
Crystal structure
Dimeric complex, Manganese(III), Ferromagnetic behaviour, 949
Crystal structure
Back-bonding, Ruthenium complex, NO, Reactivity, Molecular, 1063
Crystal structure
Tetrahydrofurfurylindenyl, Lanthanide chlorides, Ionic radius, 1075
Crystal structure
Mn(II) complex, Isonicotinic acid, N-oxide, Luminescence, 1109
Crystal structure
Rhenium, Benzimidazole, Bibenzimidazole, Paramagnetic NMR, 1139
Crystal structure
Platinum, Palladium, Phosphorus–nitrogen donor, 1159
Crystal structure
Copper, Dimer, Spectral properties, Magnetic properties, 1303
Crystal structure
Dinuclear copper(II) complex, Magnetic properties, Bidentate ligand, UV–Vis, EPR and IR spectra, 1309
Crystal structure
Molecular assembly, 1,3-Dithiole-2-thione, Complex, 1447
Crystal structure
Thiazine, Cobalt(III) complex, Nickel(II) complex, Pyridine, 1453
Crystal structure
Phase transition, Isotope effect, Hydrogen bond, NQR, Tetrachloroaurate(III), 1605
Crystal structure
Copper(II) complexes, Dihydroxo-bridged, Roof-shaped, Triply bridged, 1641
Crystal structure
Ph_2Te_2, Metal–metal bond, Molybdenum complex, Mo_2Te_4 complex, 1663
Crystal structure
Copper dimer, Magnetic properties, Antiferromagnetic dimer, 1695
Crystal structure
Zinc complex, Cadmium complex, 2-Oxo-1,3-dithiole-4,5-dithiolate, Synthesis, Density functional calculation, 1701

Crystal structure
2-Thiopheneacetic acid, Polymeric copper(II) complex, Vibrational spectra, Metal isotope effect, 1785
Crystal structure
Heteroaromatic carboxylic acid, Triphenyltin, Synthesis, 1805
Crystal structure
1,3,4-thiadiazole, Zinc, Thermal decomposition, Kinetics, Bioactivity, 1851
Crystal structure
1H-5-mercapto-1,2,3-triazolato, Organotin, Organogermanium(IV), X-ray crystallography, 1981
Crystal structure
trans-1,2-Diaminocyclohexane, Zinc complex, Catalytic enantioselective reduction, 2063
Crystal structure
Iron, Spin-crossover, Magnetic measurements, 2141
Crystal structure
Transformation, Molybdenum phosphate, Hydrothermal synthesis, 2153
Crystal structure
Dicopper(II) complex, 1D Coordination polymer, Magnetic properties, Schiff base, 2177
Crystal structure
Copper(II) complex, Magnetic properties, Coordination polymers, 2203
Crystal structure
Uranium, N, O donor ligands, 2285
Crystal structure
Lanthanide oxides, Bromotrimethylsilane, O-donor ligands, Complexes of lanthanide bromides, Coordination number, 2293
Crystal structure
Thiosemicarbazone, 2-pyridineformamide, Zinc, Cadmium, 2303
Crystal structure
Nickel(II) complexes, MagnetismPseudohalides,, 2337
Crystal structure
Hydrothermal synthesis, Iron phosphatooxalate, Template, Oxalate acid, Piperazine, 2357
Crystal structure
Manganese, Hydrogen bond, Magnetism, EPR, 2387
Crystal structure
4,4′-Bipyridine, Lead(II), Coordination polymers, Lone pair, π–π staking interaction, 2427
Crystal structure
Copper, 3,5-Dinitrosalicylate complex, Trimer, Magnetic properties, Spectral properties, 2447
Crystal structure
Copper(II) complex, Pyridylthioazophenol ligands, 2457
Crystal structure
Copper(II) complex, Ascorbic oxidation, Imidazole, 2515
Crystal structure
Multiple-decker sandwich complex, Ferrocene, Boron, Lithium, 2597
Crystal structure
Metallocene, Ferrocenium, Cobaltocenium, 2937
Crystal structure
Copper(II) complexes, 2-Benzoylpyridine, Thiosemicarbazone, EPR, Antimicrobial activity, 3069
Crystal structure
Cadmium complex, Bis(triazole) ligand, Anion role, 3133
Crystal structure of Cd(II) complex
S-methyldithiocarbazate (SMDTC), NS Schiff base, Dithiocarbazate derivatives, 1385
Crystal structures
Manganese(II) carboxylate chemistry, Magnetochemistry, Metal-assisted reactions, 2-Pyridinealdoxime complexes, 83
Crystal structures
Nickel(II) complexes, Hydrotris(pyrazolyl)borate complexes, Coordination environment, Scorpionates, 211
Crystal Structures
Lanthanides, Ytterbium, Aryloxide, Tris(pyrazolyl)borate, Divalent, 263
Crystal structures
Titanium iodide, Phosphine, Arsine, Iron iodide, 605
Crystal structures
Uranyl ion, Alkali metal ions, Calixarenes, Homooxacalixarenes, 649
Crystal structures
Copper complexes, Zinc complexes, Molecular rectangles, 673
Crystal structures
Antimony, Ferrocenylcarboxylate, Antitumor activity, 823
Crystal structures
2-Methanolpyridine, 2,6-Dimethanolpyridine, 2-Ethanolpyridinium, Cobalt(II) complexes, 841
Crystal structures
Manganese(II) hexafluoroacetylacetonate, 4-cyanopyridine-N-oxide, Magnetic properties, Ferromagnetic interactions, 879
Crystal structures
Self-assembly, Bis(2-pyridylmethyl)amino acids, Ferromagnetism, One-dimensional chains, Copper(II) complexes, 903
Crystal structures
Solvothermal synthesis, Thiostannates, Nickel, Thermoanalysis, 937
Crystal structures
Rhenium(I), Phosphinite ligands, Dichloromethane complexes, 1045
Crystal structures
Dithiocarbimates, Platinum complexes, 1153
Crystal structures
Radical salts, Bis(ethylenedithio)tetrathiafulvalene (ET), Electrical conductivity, 1185
Crystal structures
Hydrazones, Complex, Lanthanide, X-ray, Spectroscopy, 1191
Crystal structures
Cadmium(II), Calcium(II), Manganese(II), Synthesis, Tetrazolate complexes, 1217
Crystal structures
Azides, Polyamines, Copper(II) complexes, Magnetic properties, Coordination polymers, 1243
Crystal structures
Zinc complexes, Schiff-bases, IR, UV and NMR spectroscopy, Thermal analysis, 1293
Crystal structures
Nickel(II) compounds, Terephthalate ligand, Binuclear complexes, Magnetic properties, 1379
Crystal structures
Manganese, Pheylcyanamide, Magnetic properties, 1409
Crystal structures
Synthesis, Indenyl ligand, Nickel complex, Catalysis, 1473
Crystal structures
Nickel, Copper, Zinc, Imidazole, α-Hydroxycarboxylato complexes, Thermal behaviour, 1505
Crystal structures
Hydrothermal syntheses, Gallophosphates, Templating effect, 1535
Crystal structures
1-(4-Hydroxyphenyl)-1H-tetrazole-5-thiol, Organotin(IV), Hydrogen bonding, π–π stacking interaction, X-ray crystallography, 1547
Crystal structures
Uranyl ions, Diols, Hydrogen bonding, 1613
Crystal structures
2,5-Bis(2-pyridyl)-1,3,4-thiadiazole, Zinc, Energy minimization, Monomeric complexes, 1903
Crystal structures
Indomethacin, Diorganotin, Spectroscopic studies, 2021
Crystal structures
Alkaline earth metal complexes, 2183
Crystal structures
Iron(II) complexes, Trithiocyanuric acid, Mössbauer spectra, Spectroscopic properties, DFT calculations, 2193
Crystal structures
P,*S*-metallocycles, Supramolecular chemistry, Bipodal ligands, Macrocycles, Phosphorylated urea complexes, 2243
Crystal structures
Cu(II)–Ln(III) complexes, Dipeptides, Carboxylate bridge, Hexanuclear cations, Magnetic properties, 2253
Crystal structures
Diaza-fluorene, Silver complexes, Intermolecular interactions, Electronic spectra, 2259
Crystal structures
2-[(*E*)-2-(aryl)-1-diazenyl]pyridine, Hg(II) complexes, NMR, 2323
Crystal structures
Tris(cyclohexyl)tin, Halostannanes, 2331

Crystal structures
Pyrazolone, Copper(II) complexes, ESR study, 2465
Crystal structures
Cadmium(II), Chloranilate anions, Phenanthroline, Square antiprism, Chain polymers, 2587
Crystal structures
Fe(III) carboxylate chemistry, Magnetochemistry, Cluster complexes, 2779
Crystal structures
Copper(II) compounds, Terephthalate ligand, One-dimensional complexes, Magnetic properties, 3043
Crystal structures
Chiral, Schiff base, Copper, Cyclopropanation, Catalysts, 3051
Crystal structures
Clusters, Copper, Molybdenum, Tungsten, Nitrogen heterocycle ligands, Pyrazole, 3143
Crystalline structure
Cu-NIRs, Model complex, Tripodal ligand, Polyimidazole ligand, 511
Cu(II) complexes
Hypodentate, Tripodal amine ligand, Crystal structure, Five-coordinate, 97
Cu(II) complexes
Herometallacrown, Malonate, *o*-Pthalate, 943
Cu(II) complexes
Dithiocarbazate Schiff base, Saccharin complexes, *S*-Methyldithiocarbazate, Tridentate NNS Schiff base, 2491
Cu(II)–Ln(III) complexes
Dipeptides, Carboxylate bridge, Hexanuclear cations, Crystal structures, Magnetic properties, 2253
Cu-NIRs
Model complex, Crystalline structure, Tripodal ligand, Polyimidazole ligand, 511
$Cu^{II}N_4Cl$ chromophores
Bidentate diimine, Bidentate diamine, π–π Interactions, Hydrogen bonding, Magnetic property, 1961
Cyanide bridged clusters
Iron(III) complex, Tris(pyrazolyl)borate, Magnetic properties, 1333
Cyanopolyynes
Carbon allotropes, Polyynes, Carbyne, Dicyanopolyynes, Electric arc, Graphite, Liquid nitrogen, 1889
4-cyanopyridine-*N*-oxide
Manganese(II) hexafluoroacetylacetonate, Crystal structures, Magnetic properties, Ferromagnetic interactions, 879
Cyclic telluranes
Metathetical reactions, Intermolecular, Secondary bonding, Supramolecular networks, 1629
Cyclic voltammetry
Macrocyclic complexes, X-ray crystallography, Imidazole, 1317
Cyclic voltammetry
Nickel complex, Tripodal ligand, 1829
Cyclic voltammetry
Copper(II) complexes, Thiosemicarbazone, 2-Hydroxyacetophenone, EPR, Antimicrobial studies, X-ray crystallography, 2549
Cyclic voltammetry
Non-heme iron, Water coordination, X-ray structure, Sterically hindered carboxylate, 2805
Cyclic voltammetry
Phthalocyanine, Unsymmetrical, Phenylacetylene, 3155
Cycloaddition
Titanium, Tin, Tetrazole, Nitride precursor, 801
Cyclometalated Ir(II) complexes
Iridium, Pyrazolyl ancillary ligands, Boat conformations, Luminescent, Electroluminescence, 419
Cyclooctadiene
Polypyrazolylborate, Rhodium(I), Norbornadiene, Structure, NMR, 219
Cyclopentadienyl
Ruthenium, 2,3-Bis(α-pyridyl)pyrazine, 1,3,5-Tris(pyridyl)-2,4,6-triazine, 2,3,5,6-Tetrakis(pyridyl)pyrazine, 1069
Cyclopentadienyl
Indenyl, Phosphino, Phosphido, Molybdenum, Metallocenes, 1263
Cyclopentadienyl
Parabanic acid, Iron, Carbonyl, Thallium, Gold (I) complex, Alkylation, 1441
Cyclopentadienyl
Schiff bases, Pyridine-2-carboxaldehyde, Ruthenium, 1567
Cyclophosphazene
Dendrimers, Metal–nitrile complexes, Iron complexes, 1027
Cyclophosphazenes
Chiral, Spirocyclic, X-ray structure, 979
Cyclopropanation
Chiral, Schiff base, Copper, Catalysts, Crystal structures, 3051
Cylindrical channels
Copper(II), Aminopolycarboxylate, Ferromagnetic coupling, π–π stacking, 1081
Cymene
Ruthenium, X-ray, 2695
p-Cymene
Hexamethylbenzene, Diphenyl-2-pyridylphosphine, Amines, Ruthenium complexes, 3115
Cytotoxicity
Pyridinecarboxaldimine, Platinum, Palladium, Fluorine, 2169

2D antiferromagnets
Malonate complexes, Weak ferromagnetism, 929
1D, 2D, 3D topological structure
Silver coordination complex polymers, Multi-nitriles, 2209
Dawson lacunary heteropolyanion
Complex formation constants, Lanthanides, Arsenazo III, 1579
Decaazacyclooctadecane
Template synthesis, Nickel(II) complexes, Macrocycle, 1325
Dendrimers
Cyclophosphazene, Metal–nitrile complexes, Iron complexes, 1027
Dendrimers
Amino acid, Copper, Electrochemistry, Electron spin resonance, Ligand, 1709
Density functional calculation
Zinc complex, Cadmium complex, 2-Oxo-1,3-dithiole-4,5-dithiolate, Synthesis, Crystal structure, 1701
Density functional theory
Organometallics, Sandwich complex, Metallocene, Bonding, Orbital analysis, 2993
Density functional theory calculations
Rhenium nitrosyl complexes, Pyrazole, Arsine ligands, X–ray structure, 2523
1D chain
Arylazoimidazoles, Cadmium(II) complexes, End-on and end-to-end bridging, X-ray structure, Sheet structure, 1669
1D Coordination polymer
Dicopper(II) complex, Crystal structure, Magnetic properties, Schiff base, 2177
DFT calculations
Carborane, Spectroscopy, X-ray crystallography, 629
DFT calculations
Rhenium complexes, Pyrazole ligand, X-ray structure, 1819
DFT calculations
Rhenium complexes, Pyrazole ligand, X-ray structure, 2005
DFT calculations
Iron(II) complexes, Trithiocyanuric acid, Mössbauer spectra, Crystal structures, Spectroscopic properties, 2193
DFT calculations
Rhenium, Nitrosyls, Phosphine complexes, 2363
DFT calculations
^{15}N solid state NMR, Molybdenum nitride, Imido complexes, Lewis acids, 2751
(μ-O)di-iron complex
Iron, Bis-(2-pyridylmethyl)amine, Oxalato, Hydrogen bonding, Mössbauer spectra, 1419
Di-2-pyridyl ketone
Thiosemicarbazone, Ni(II) thiosemicarbazone complex, Electronic spectra, IR spectra, X-ray crystal structure, 1225
Di-2-pyridyl ketone salicyloylhydrazone
Zinc(II) complexes, Stability constants, Spectroscopy, Thermal analysis, 2095
Di-2-pyridylamine
Copper complexes, Nitrito complexes, Plasticity effect, *cis*-Distorted octahedron, Fluxional behaviour, 1685
2,6-diacetylpyridine Schiff bases of S-alkyldithiocarbazates
Tin(IV) complexes, Dithiocarbazates, Seven-coordinate tin(IV) complexes, 2037

Diamine
Xanthate, Zinc, Cadmium, CdS, Nanoparticles, 2315
Diaza-18-crown-6
Sulfonatothiacalixarene, Capsules, Lanthanide ions, 2055
Diaza-Crown ether
Sulfonatothiacalixarene, Capsules, Transition metal ions, Assembly, 1461
Diaza-fluorene
Silver complexes, Crystal structures, Intermolecular interactions, Electronic spectra, 2259
Diazoalkane complexes
Rhodium, Acetylacetonato complexes, Pentachlorophenolato complexes, Carboxylato complexes, C–C coupling reactions, 2645
Dichloromethane complexes
Rhenium(I), Phosphinite ligands, Crystal structures, 1045
Dicopper(II) complex
1D Coordination polymer, Crystal structure, Magnetic properties, Schiff base, 2177
Dicyanoethylene-1,2-dithiolate
Diorganotin, 4,4′-Bipyridyl, 1,10-Phenanthroline, X-ray crystal structure, Co-crystallization, 1207
Dicyanopolyynes
Carbon allotropes, Polyynes, Carbyne, Cyanopolyynes, Electric arc, Graphite, Liquid nitrogen, 1889
Diethylenetriamine
Ruthenium(II) complexes, Polypyridine ligands, 815
Differential pulse voltammetry
Electropolymerisation, Ru-complexes, Thiophene, 4-((2-Thienyl)-ethenyl)-2,2′-bipyridine, Redox-polymers, 589
Dihydridobis(pyrazolyl)borate
Tetrathiomolybdate, Tetrathiotungstate, Copper(I) complexes, Crystal structure, Model compounds, 637
Dihydroxo-bridged
Copper(II) complexes, Crystal structure, Roof-shaped, Triply bridged, 1641
Diimine
X-ray structure, Coordination complex, Zinc, Palladium, 2789
Diimine complexes
Thioether complexes, Platinum complexes, Trithiacyclononane, Platinum nuclear magnetic resonance, Crown thioethers, 1361
Diiminediaminediphenolate macrocycle
Vanadium, Magnetochemistry, EPR, FTIR, Spectroelectrochemistry, 2069
Diketiminato
Lanthanides, Yttrium, 183
β-diketonates
Cobalt, Oxide, Adducts, Structures, MOCVD, 735
β-Diketonates
Alkoxides, Enolates, Carboxylates, Alkali metals, Alkaline earth metals, Cluster compounds, 1479
2,6-Dimethanolpyridine
2-Methanolpyridine, 2-Ethanolpyridinium, Cobalt(II) complexes, Crystal structures, 841
Dimer
Copper, Crystal structure, Spectral properties, Magnetic properties, 1303
Dimer
Manganese(III), N,O ligands, X-ray structure, Magnetochemistry, Azide, 1811
Dimeric complex
Manganese(III), Crystal structure, Ferromagnetic behaviour, 949
Dimerization
η^2-nitrile, Tungsten, Oxo, Oxidation, Methylation, 2831
Dimethylpyrazole
Ruthenium arene complexes, Pyrazole, X-ray structure, Bond valence, 885
3,5-Dinitrosalicylate complex
Copper, Trimer, Crystal structure, Magnetic properties, Spectral properties, 2447
Dinuclear
Zinc(II)azide, Mononuclear, 2,2′-Dipyridylamine, Luminescence, Crystal engineering, 545
Dinuclear
Copper, Structure, Magnetism, EPR, 993
Dinuclear
Self-assembly, Copper, N,O-ligands, EPR, 1769
Dinuclear
Iron (III), Carboxylate, Complexes, Bridging, Mössbauer, 1869
Dinuclear complex
Silver(I) complexes, Mononuclear complex, 2117
Dinuclear copper(II) complex
Magnetic properties, Bidentate ligand, Crystal structure, UV–Vis, EPR and IR spectra, 1309
Dinuclear peroxovanadate
Peroxo-bridged divanadate, Peroxidative bromination, Heteroligand peroxovanadate, Amino acid containing peroxovanadates, 1097
Diols
Copper(III), Imine-oxime ligand, Kinetics, Mechanism, Electron transfer, 583
Diols
Uranyl ions, Hydrogen bonding, Crystal structures, 1613
Diorganostannate
Methanesulfonate, Ionic metathesis, Organotin oxide, 71
Diorganotin
Dicyanoethylene-1,2-dithiolate, 4,4′-Bipyridyl, 1,10-Phenanthroline, X-ray crystal structure, Co-crystallization, 1207
Diorganotin
Indomethacin, Crystal structures, Spectroscopic studies, 2021
N,*N*′-dioxide
Lanthanide nitrate, Self-assembly, Coordination polymer, 169
Vic-dioximes
Thiazolidine, Ferrocene, Transition metal complexes, Electrochemistry, 1987
Dioxomolybdenum (VI) and oxomolybdenum (IV) complexes
Dithiocarbazate, Schiff bases, X-ray structures, 1595
Dioxomolybdenum(VI) thionates
Oxotransfer catalysts, 537
Dioxygen
Osmium, Aniline, Oxidation, Electron transfer self-exchange, 323
Dipeptides
Self-assemble, Carboxylate bridges, Copper complexes, Alkaline earth metals, Magnetic properties, 2125
Dipeptides
Cu(II)–Ln(III) complexes, Carboxylate bridge, Hexanuclear cations, Crystal structures, Magnetic properties, 2253
2-Diphenylphosphinopicolinamide (dpppa 1)
Coordination chemistry, Monodentate donors, Bidentate donors, 3211
Diphenyl-2-pyridylphosphine
Hexamethylbenzene, *p*-Cymene, Amines, Ruthenium complexes, 3115
Diphosphine
Nickel, Bis(mercaptoimidazolyl)borate complexes, Tris(mercaptoimidazolyl)borate complexes, Hydrogenases, Crystal structure, 395
Diporphyrins
Zinc(II) complexes, Nitrogen base ligation, Stability constants, 33
2,2′-Dipyridylamine
Zinc(II)azide, Mononuclear, Dinuclear, Luminescence, Crystal engineering, 545
Diruthenium compounds
Metal–metal bonds, Triazenido complexes, Formamidinato complexes, Multiple bonds, Low spin complexes, 2637
Diruthenium(II)
Rhodium(III) Ruthenium(II), Heterodinuclear complexes, Polypyridine complexes, Electrochemistry, 913
Dispersion processing
Magnesium carboxylate, Meltable, Thermal properties, 1739
cis-Distorted octahedron
Copper complexes, Di-2-pyridylamine, Nitrito complexes, Plasticity effect, Fluxional behaviour, 1685
Distortion isomers
Copper, Structure, Infrared, Hydrogen bonds, 1969
Distortions
Bipyridine, 2081
Disubstituted functional derivatives
closo-Dodecaborate, Hydroxy and acyl derivatives, Boron neutron capture therapy, 2135
Dithiocarbamate
Nickel, PPh_3, Dppe, X-ray crystal structure, NMR, 77
Dithiocarbazate
Ferrocene, Ligand, Complex, Tin, Crystal structure, 567

Dithiocarbazate
Dioxomolybdenum (VI) and oxomolybdenum (IV) complexes, Schiff bases, X-ray structures, 1595
Dithiocarbazate derivative
S-2-picolyldithiocarbazate (Hydrazine carbodithioic acid pyridinium-2-yl methyl ester chloride), Bidentate NS Schiff base, Tridentate NNS and NSS Schiff bases, Ni(II) complexes, 161
Dithiocarbazate derivatives
S-methyldithiocarbazate (SMDTC), NS Schiff base, Crystal structure of Cd(II) complex, 1385
Dithiocarbazate Schiff base
Cu(II) complexes, Saccharin complexes, *S*-Methyldithiocarbazate, Tridentate NNS Schiff base, 2491
Dithiocarbazates
Copper(II) complexes, Saccharin complexes, 2031
Dithiocarbazates
Tin(IV) complexes, 2,6-diacetylpyridine Schiff bases of S-alkyldithiocarbazates, Seven-coordinate tin(IV) complexes, 2037
Dithiocarbazates
Tin(IV) complexes, 2-Quinolinecarboxaldehyde Schiff bases of *S*-alkyl/aryl dithiocarbazates, 2405
Dithiocarbimates
Platinum complexes, Crystal structures, 1153
1,3-Dithiol-2-thione
Mercury(II), Pyridyl, ^{1}H NMR, Solid UV, 115
1,3-Dithiole-2-thione
Crystal structure, Molecular assembly, Complex, 1447
Divalent
Lanthanides, Ytterbium, Aryloxide, Crystal Structures, Tris(pyrazolyl)borate, 263
Divalent metals
Heteroscorpionate ligands, Hydrogen bond, X-ray crystallography, 239
Divinyl organics
Copper(I) complexes, Hexafluorocetylacetonate, Olefin complexes, Crystal structure, Thermal analysis, 809
closo-Dodecaborate
Hydroxy and acyl derivatives, Disubstituted functional derivatives, Boron neutron capture therapy, 2135
Dodecahedron
Eight-coordinate, Stereochemistry, Square antiprism, Bicapped trigonal prism, Molecular mechanics, 145
Double betaine
Carboxylate, Coordination polymer, Hydrate, Hydrogen bonding, π–π Interaction, Silver nitrate, 2413
Dppe
Nickel, Dithiocarbamate, PPh_3, X-ray crystal structure, NMR, 77

EDAX analyses
Anisotropic approximation, Cluster anions, Heterometal cluster complexes, 599
EDTA
Hydroxyapatite, Complex, Hydrothermal, Low temperature, Calcium phosphates, 1897
EHMO
Naphthylazoimidazole, Silver(I) complexes, Helical structure, 793
Eight-coordinate
Stereochemistry, Dodecahedron, Square antiprism, Bicapped trigonal prism, Molecular mechanics, 145
Electric arc
Carbon allotropes, Polyynes, Carbyne, Dicyanopolyynes, Cyanopolyynes, Graphite, Liquid nitrogen, 1889
Electrical conductivity
Radical salts, Bis(ethylenedithio)tetrathiafulvalene (ET), Crystal structures, 1185
Electrical conductivity
Tetrathiafulvalene, Copper(II), Charge transfer compounds, 2109
Electrochemical
Binuclear copper complex, EPR, Half-field, Superhyperfine, X-ray, 1115
Electrochemistry
Macrobicylic ligands, Compartmental, Copper(II) complexes, Antiferromagnetic interaction, Catalytic study, 519
Electrochemistry
Magnetic properties, Oximinato monocopper(II) and mononickel(II) complexes, Unsymmetrical oximinato dicopper(II) complexes and unsymmetrical oximinato dinickel(II) complexes, 665
Electrochemistry
Ruthenium(II)-tris-chelates, Azoimidazoles, X-ray structure, 727
Electrochemistry
Diruthenium(II), Rhodium(III) Ruthenium(II), Heterodinuclear complexes, Polypyridine complexes, 913
Electrochemistry
Phthalocyanine, Spectroelectrochemistry, Pyridine binding, 1279
Electrochemistry
Amino acid, Copper, Dendrimers, Electron spin resonance, Ligand, 1709
Electrochemistry
Vic-dioximes, Thiazolidine, Ferrocene, Transition metal complexes, 1987
Electroluminescence
Iridium, Cyclometalated Ir(II) complexes, Pyrazolyl ancillary ligands, Boat conformations, Luminescent, 419
Electron density distribution
Clusters, Polarizability, Spherical potential well, Finite electric field, 1519
Electron spin resonance
Amino acid, Copper, Dendrimers, Electrochemistry, Ligand, 1709
Electron transfer
Copper(III), Imine-oxime ligand, Diols, Kinetics, Mechanism, 583
Electron transfer self-exchange
Dioxygen, Osmium, Aniline, Oxidation, 323
Electron-transfer reactions
Spin-exchange reactions, Bis[tris(pyrazolyl)methane] complexes, Low-spin configurations, High-spin configurations, 1037
Electronic spectra
Cobalt(III), Semicarbazone, 2-Hydroxyacetophenone, NMR spectra, IR spectra, X- ray crystal structure, 41
Electronic spectra
Di-2-pyridyl ketone, Thiosemicarbazone, Ni(II) thiosemicarbazone complex, IR spectra, X-ray crystal structure, 1225
Electronic spectra
Diaza-fluorene, Silver complexes, Crystal structures, Intermolecular interactions, 2259
Electronic structure
Sulfite oxidase, Pyranopterin molybdenum enzymes, Molybdenum complexes, MCD (Magnetic Circular Dichroism), EPR (Electron Paramagnetic Resonance), 499
Electropolymerisation
Ru-complexes, Thiophene, Differential pulse voltammetry, 4-((2-Thienyl)-ethenyl)-2,2′-bipyridine, Redox-polymers, 589
Electropolymerization
Schiff-base, Polypyrrole, Iron complex, AFM, Polymer, 1953
Enamido
Enolato, Zirconium, Titanium, Aluminum, 1587
Enaminone
Ferrocene, Ligand, Copper, Complex, X-ray crystallography, 15
Enaminone
Ferrocene, Ligands, Complexes, X-ray crystallography, 749
Enaminone
Ferrocene, Ligand, Copper, Complex, X-ray crystallography, 1541
Enaminones
Molybdenum(VI) complexes, Molybdenum(V) complexes, Pyrone, X-ray crystal structure, NMR spectra, 1859
End-on and end-to-end bridging
Arylazoimidazoles, Cadmium(II) complexes, X-ray structure, 1D chain, Sheet structure, 1669
Energy minimization
2,5-Bis(2-pyridyl)-1,3,4-thiadiazole, Zinc, Crystal structures, Monomeric complexes, 1903
Enolates
Alkoxides, β-Diketonates, Carboxylates, Alkali metals, Alkaline earth metals, Cluster compounds, 1479
Enolato
Enamido, Zirconium, Titanium, Aluminum, 1587
Enzyme
Zinc, Thiolate, Alkylation, 481
Epoxide
Silica gel, Immobilization, 2-Aminomethylpyridine, Adsorption, Thermodynamic, 719

EPR
Hydrazones, Copper(II) hydrazonate complexes, 1,10-Phenanthroline, 2,2′-Bipyridine, X-ray single crystal structure, 575
EPR
Triazolopyrimidine, Zn complexes, Copper dimers, 743
EPR
Copper, Structure, Magnetism, Dinuclear, 993
EPR
Binuclear copper complex, Half-field, Superhyperfine, X-ray, Electrochemical, 1115
EPR
Self-assembly, Copper, N,O-ligands, Dinuclear, 1769
EPR
Porphyrazine, Naphthalene, Copper, Zinc, Cobalt, 1845
EPR
Vanadium, Diiminediaminediphenolate macrocycle, Magnetochemistry, FTIR, Spectroelectrochemistry, 2069
EPR
Crystal structure, Manganese, Hydrogen bond, Magnetism, 2387
EPR
Lawsone, Quinones, 2-Hydroxy-1, 4-Naphthoquinone, Amine oxidase, Copper complexes, Antiferromagnetic coupling, H-bonding, 2541
EPR
Copper(II) complexes, Thiosemicarbazone, 2-Hydroxyacetophenone, Antimicrobial studies, Cyclic voltammetry, X-ray crystallography, 2549
EPR
Copper(II) complexes, 2-Benzoylpyridine, Thiosemicarbazone, Antimicrobial activity, Crystal structure, 3069
EPR (Electron Paramagnetic Resonance)
Sulfite oxidase, Pyranopterin molybdenum enzymes, Electronic structure, Molybdenum complexes, MCD (Magnetic Circular Dichroism), 499
EPR spectra
Iron(III) complexes, Thiosemicarbazone, Single crystal X-ray diffraction, Mössbauer spectra, IR spectra, 969
EPR spectroscopy
Hydrazido ligand, Mixed-valence, Ruthenium complexes, Spectroelectrochemistry, 701
ES-MS
Lanthanide, Cryptate, Crystal structure, 49
ESR study
Pyrazolone, Copper(II) complexes, Crystal structures, 2465
2-Ethanolpyridinium
2-Methanolpyridine, 2,6-Dimethanolpyridine, Cobalt(II) complexes, Crystal structures, 841
Ethylene
Hydrocarboxylation, Oligomerization, Catalysis, Rhodium complexes, Carbon monoxide, 1677
Europium
Ionic complex, Rheological phase reaction, Crystal structure, Photoluminescence, Zinc, 529
Europium
Coordination polymer, Hydrogen bonds, Luminescence, Supramolecular, Terbium, 711
Extended structures
Copper, 4,7-Phenanthroline, Coordination framework, Host–guest properties, Polymers, 55

Fe(III) carboxylate chemistry
Magnetochemistry, Crystal structures, Cluster complexes, 2779
Ferrocene
Enaminone, Ligand, Copper, Complex, X-ray crystallography, 15
Ferrocene
Dithiocarbazate, Ligand, Complex, Tin, Crystal structure, 567
Ferrocene
Enaminone, Ligands, Complexes, X-ray crystallography, 749
Ferrocene
Palladium, Phosphine, Suzuki–Miyaura coupling, Ortho-metallated complexes, X-ray crystallography, 921
Ferrocene
Enaminone, Ligand, Copper, Complex, X-ray crystallography, 1541
Ferrocene
Vic-dioximes, Thiazolidine, Transition metal complexes, Electrochemistry, 1987
Ferrocene
Multiple-decker sandwich complex, Boron, Lithium, Crystal structure, 2597
Ferrocene carboxylic acid
Arene ligand, Ferrocene derivative, Ruthenium, 687
Ferrocene derivative
Arene ligand, Ferrocene carboxylic acid, Ruthenium, 687
Ferrocenes
Oxazolines, Non-symmetrical ligands, X-ray diffraction, 611
Ferrocenium
Metallocene, Cobaltocenium, Crystal structure, 2937
Ferrocenylcarboxylate
Antimony, Crystal structures, Antitumor activity, 823
Ferromagnetic behaviour
Dimeric complex, Manganese(III), Crystal structure, 949
Ferromagnetic coupling
Copper(II), Aminopolycarboxylate, π–π stacking, Cylindrical channels, 1081
Ferromagnetic interactions
Manganese(II) hexafluoroacetylacetonate, 4-cyanopyridine-N-oxide, Crystal structures, Magnetic properties, 879
Ferromagnetism
Self-assembly, Crystal structures, Bis(2-pyridylmethyl)amino acids, One-dimensional chains, Copper(II) complexes, 903
Finite electric field
Clusters, Electron density distribution, Polarizability, Spherical potential well, 1519
Five-coordinate
Hypodentate, Tripodal amine ligand, Cu(II) complexes, Crystal structure, 97
Flexible
Carboxylates, IX, Coordination polymer, Architecture, 3007
Fluorescence
Silicon, Phosphorus, Hypercoordination, Hypervalency, Spectroscopy, X-ray crystallography, 2615
Fluoride
Uranyl, Phosphine oxide ligands, Structural study, Spectroscopic characterisation, 3097
Fluorinated
Sodium, Copper, Tris(pyrazolyl)borate, Carbonyl, 273
Fluorine
Pyridinecarboxaldimine, Cytotoxicity, Platinum, Palladium, 2169
Fluoroionophore
Ruthenium, X-ray, Metallacrown, 1719
Fluxional behaviour
Copper complexes, Di-2-pyridylamine, Nitrito complexes, Plasticity effect, *cis*-Distorted octahedron, 1685
Formamidinato complexes
Diruthenium compounds, Metal–metal bonds, Triazenido complexes, Multiple bonds, Low spin complexes, 2637
FTIR
Vanadium, Diiminediaminediphenolate macrocycle, Magnetochemistry, EPR, Spectroelectrochemistry, 2069
Functionalised carbenes
Nickel complexes, Heterocyclic carbenes, X-ray diffraction, 2813

Gallophosphates
Hydrothermal syntheses, Crystal structures, Templating effect, 1535
Glycerol phosphate
Uranium, Complex formation, Potentiometric titration, TRLFS, 1793
Glyoxylic acid
Kinetics, Mechanism, Redox, Silver, 895
Gold (I) complex
Parabanic acid, Iron, Cyclopentadienyl, Carbonyl, Thallium, Alkylation, 1441
Gold complex
Crystal structure, Selenourea, MAS NMR, 1
Graphite
Carbon allotropes, Polyynes, Carbyne, Dicyanopolyynes, Cyanopolyynes, Electric arc, Liquid nitrogen, 1889
Grid
Chiral, Coordination polymers, Nicotinate, Open channel, 1947
Group 11 phosphine complexes
1-azaallyls, X-ray crystallography, Iminoalkyl bonding mode, 2273

H-bonding
Lawsone, Quinones, 2-Hydroxy-1, 4-Naphthoquinone, Amine oxidase, Copper complexes, Antiferromagnetic coupling, EPR, 2541
^{1}H NMR
Mercury(II), 1,3-Dithiol-2-thione, Pyridyl, Solid UV, 115
H_2O_2
Immobilization, Silica support, Cobalt(II) complexes, 59
Half-field
Binuclear copper complex, EPR, Superhyperfine, X-ray, Electrochemical, 1115
Halostannanes
Tris(cyclohexyl)tin, Crystal structures, 2331
Hartree–Fock calculations
Octamolybdate, Hydrothermal synthesis, Three-dimensional oxide, Organic–inorganic hybrid, Building block approach, 1145
Head–head
Triazolopyrimidine, Palladium dimers, Head–tail, 2373
Head–tail
Triazolopyrimidine, Palladium dimers, Head–head, 2373
Helical architecture
Manganese maleate, Coordination polymer, Temperature effect, Hydrogen bonds, π–π interactions, 987
Helical structure
Naphthylazoimidazole, Silver(I) complexes, EHMO, 793
Hemilabile
Phosphine, X-ray structure, 3125
Hemilabile ligands
Heteroscorpionates, Ruthenium, Hydrides, Phosphine complexes, 361
Heptanuclear
Nickel(II), Lanthanides(III), Amino acid, Cluster compound, 2265
Herometallacrown
Malonate, *o*-Pthalate, Cu(II) complexes, 943
Heteroaromatic carboxylic acid
Triphenyltin, Synthesis, Crystal structure, 1805
Heterobimetallic
Palladium, Platinum, Phosphine, Oxadiazole ligand complexes, 2013
N-Heterocyclic carbenes
Homogenous catalysis, Transfer hydrogenation, Ketones, Aldehydes, Imines, 2857
Heterocyclic carbenes
Nickel complexes, Functionalised carbenes, X-ray diffraction, 2813
Heterodinuclear complexes
Diruthenium(II), Rhodium(III) Ruthenium(II), Polypyridine complexes, Electrochemistry, 913
Heteroligand peroxovanadate
Dinuclear peroxovanadate, Peroxo-bridged divanadate, Peroxidative bromination, Amino acid containing peroxovanadates, 1097
Heterometal cluster complexes
EDAX analyses, Anisotropic approximation, Cluster anions, 599
Heteroscorpionate
Tripodal, Alkylthiolate, Imidazole, Iron, Zinc, 471
Heteroscorpionate ligands
Hydrogen bond, X-ray crystallography, Divalent metals, 239
Heteroscorpionates
Ruthenium, Hydrides, Phosphine complexes, Hemilabile ligands, 361
Hexafluorocetylacetonate
Copper(I) complexes, Olefin complexes, Divinyl organics, Crystal structure, Thermal analysis, 809
Hexamethylbenzene
p-Cymene, Diphenyl-2-pyridylphosphine, Amines, Ruthenium complexes, 3115
Hexanuclear cations
Cu(II)–Ln(III) complexes, Dipeptides, Carboxylate bridge, Crystal structures, Magnetic properties, 2253
Hg(II) complexes
2-[(*E*)-2-(aryl)-1-diazenyl]pyridine, NMR, Crystal structures, 2323
High-pressure NMR
Hydroformylation, Ionic liquids, Biphase catalysis, Rhodium complexes, 2679
High-spin configurations
Electron-transfer reactions, Spin-exchange reactions, Bis[tris(pyrazolyl)methane] complexes, Low-spin configurations, 1037
Homogenous catalysis
N-Heterocyclic carbenes, Transfer hydrogenation, Ketones, Aldehydes, Imines, 2857
Homooxacalixarenes
Uranyl ion, Alkali metal ions, Calixarenes, Crystal structures, 649
Host–guest properties
Copper, 4,7-Phenanthroline, Coordination framework, Polymers, Extended structures, 55
Hydrate
Carboxylate, Coordination polymer, Double betaine, Hydrogen bonding, π–π Interaction, Silver nitrate, 2413
Hydrazido ligand
EPR spectroscopy, Mixed-valence, Ruthenium complexes, Spectroelectrochemistry, 701
Hydrazones
Copper(II) hydrazonate complexes, 1,10-Phenanthroline, 2,2′-Bipyridine, X-ray single crystal structure, EPR, 575
Hydrazones
Complex, Lanthanide, X-ray, Spectroscopy, Crystal structures, 1191
Hydride
Ruthenium, Scorpionate, Tris(pyrazolyl)-borate, C–H activation, 439
Hydrides
Heteroscorpionates, Ruthenium, Phosphine complexes, Hemilabile ligands, 361
Hydrides
Zwitterions, Monoanionic ligands, Syntheses, Structures, Methyl, 489
Hydrocarboxylation
Oligomerization, Catalysis, Rhodium complexes, Ethylene, Carbon monoxide, 1677
Hydroformylation
Ionic liquids, Biphase catalysis, High-pressure NMR, Rhodium complexes, 2679
Hydrogen bond
Hydrotris(pyrazolyl)borate, Ruthenium, Oxidation, Aquo complex, 225
Hydrogen bond
Heteroscorpionate ligands, X-ray crystallography, Divalent metals, 239
Hydrogen bond
Crystal structure, Phase transition, Isotope effect, NQR, Tetrachloroaurate(III), 1605
Hydrogen bond
Crystal structure, Manganese, Magnetism, EPR, 2387
Hydrogen bonding
Iron, (μ-O)di-iron complex, Bis-(2-pyridylmethyl)amine, Oxalato, Mössbauer spectra, 1419
Hydrogen bonding
1-(4-Hydroxyphenyl)-1H-tetrazole-5-thiol, Organotin(IV), π–π stacking interaction, Crystal structures, X-ray crystallography, 1547
Hydrogen bonding
Uranyl ions, Diols, Crystal structures, 1613
Hydrogen bonding
$Cu^{II}N_4Cl$ chromophores, Bidentate diimine, Bidentate diamine, π–π Interactions, Magnetic property, 1961
Hydrogen bonding
Vanadium complexes, Nitrilotriacetate, X-ray crystal structure, 1975
Hydrogen bonding
Carboxylate, Coordination polymer, Double betaine, Hydrate, π–π Interaction, Silver nitrate, 2413
Hydrogen bonding network
Ion pair complex, Non-covalent interaction, Charge transfer, Near-IR absorption, 1235
Hydrogen bonds
Coordination polymer, Crystal structure, Copper(II), 553
Hydrogen bonds
Coordination polymer, Europium, Luminescence, Supramolecular, Terbium, 711
Hydrogen bonds
Manganese maleate, Coordination polymer, Temperature effect, Helical architecture, π–π interactions, 987
Hydrogen bonds
Tetranuclear copper(II) complex, Structural elucidation, 1169
Hydrogen bonds
Copper, Structure, Infrared, Distortion isomers, 1969

Hydrogen bonds
Lanthanide(III) complexes, Hydrothermal syntheses, Isoorotic acid, Supramolecule, 2085
Hydrogen bonds
Isoorotic acid, Co(II) and Ni(II) complexes, Hydrothermal synthesis, Supramolecular frameworks, 2227
Hydrogenases
Nickel, Bis(mercaptoimidazolyl)borate complexes, Tris(mercaptoimidazolyl)borate complexes, Diphosphine, Crystal structure, 395
Hydrogenated Schiff's bases
Nickel, Schiff's bases, Coordination geometry, X-ray crystal structures, Polymethylene chains, 3201
Hydrogermane
Polystyrene supported, Reduction, Recycle, 177
Hydrothermal
Hydroxyapatite, Complex, EDTA, Low temperature, Calcium phosphates, 1897
Hydrothermal
Layered, Titanium phosphate, Intercalation behavior, γ-Phase, 3033
Hydrothermal syntheses
Crystal structures, Gallophosphates, Templating effect, 1535
Hydrothermal syntheses
Lanthanide(III) complexes, Isoorotic acid, Hydrogen bonds, Supramolecule, 2085
Hydrothermal synthesis
Polyoxometalates, Crystal structure, Keggin, Cobalt, 773
Hydrothermal synthesis
Octamolybdate, Three-dimensional oxide, Organic–inorganic hybrid, Building block approach, Hartree–Fock calculations, 1145
Hydrothermal synthesis
Coordination polymer, Magnetic property, Transition metal, Square grid structure, 1,4-Naphthalenedicarboxylic acid, 1257
Hydrothermal synthesis
Transformation, Molybdenum phosphate, Crystal structure, 2153
Hydrothermal synthesis
Lead, Coordination polymer, X-ray structure determination, 2161
Hydrothermal synthesis
Isoorotic acid, Co(II) and Ni(II) complexes, Hydrogen bonds, Supramolecular frameworks, 2227
Hydrothermal synthesis
Crystal structure, Iron phosphatooxalate, Template, Oxalate acid, Piperazine, 2357
Hydrotris(pyrazol-1-yl)borates
Scorpionates, Polypyrazolylborates, Photoelectron spectra, 429
Hydrotris(pyrazolyl)borate
Ruthenium, Hydrogen bond, Oxidation, Aquo complex, 225
Hydrotris(pyrazolyl)borate
Scorpionate ligands, Tantalum, Metal–metal multiple bond, Alkyne complex, Tetrahydrothiophene complex, 379
Hydrotris(pyrazolyl)borate complexes
Nickel(II) complexes, Crystal structures, Coordination environment, Scorpionates, 211
Hydroxy and acyl derivatives
closo-Dodecaborate, Disubstituted functional derivatives, Boron neutron capture therapy, 2135
2-Hydroxyacetophenone
Cobalt(III), Semicarbazone, NMR spectra, IR spectra, Electronic spectra, X- ray crystal structure, 41
2-Hydroxyacetophenone
Copper(II) complexes, Thiosemicarbazone, EPR, Antimicrobial studies, Cyclic voltammetry, X-ray crystallography, 2549
Hydroxyaluminosilicate
Aluminium, Silicic acid, Aluminium solubility, Aluminium biological availability, 3185
Hydroxyapatite
Complex, EDTA, Hydrothermal, Low temperature, Calcium phosphates, 1897
4-Hydroxycoumarin
Kinetics, Permanganate, Oxidation, 2507
α-Hydroxycarboxylato complexes
Nickel, Copper, Zinc, Imidazole, Thermal behaviour, Crystal structures, 1505
2-Hydroxy-1
Lawsone, Quinones, 4-Naphthoquinone, Amine oxidase, Copper complexes, Antiferromagnetic coupling, H-bonding, EPR, 2541
1-(4-Hydroxyphenyl)-1H-tetrazole-5-thiol
Organotin(IV), Hydrogen bonding, π–π stacking interaction, Crystal structures, X-ray crystallography, 1547
Hypercoordination
Silicon, Phosphorus, Hypervalency, Spectroscopy, Fluorescence, X-ray crystallography, 2615
Hypervalency
Silicon, Phosphorus, Hypercoordination, Spectroscopy, Fluorescence, X-ray crystallography, 2615
Hypodentate
Tripodal amine ligand, Cu(II) complexes, Crystal structure, Five-coordinate, 97

Imidazolate
Coordination polymers, Silver, X-ray structure, 3063
Imidazole
Heteroscorpionate, Tripodal, Alkylthiolate, Iron, Zinc, 471
Imidazole
Macrocyclic complexes, Cyclic voltammetry, X-ray crystallography, 1317
Imidazole
Nickel, Copper, Zinc, α-Hydroxycarboxylato complexes, Thermal behaviour, Crystal structures, 1505
Imidazole
Cadmium(II)thiocyanate, Polymer, Schiff base, Supramolecular synthon, 2045
Imidazole
Copper(II) complex, Ascorbic oxidation, Crystal structure, 2515
Imido
Acetonitrile reduction, Amine oxidation, Metal-nitrogen pi bonding, Regioselectivity of nucleophile and electrophile additions, 311
Imido complexes
^{15}N solid state NMR, DFT calculations, Molybdenum nitride, Lewis acids, 2751
Imine
Platinum, Benzimidazole, Benzoxazole, Benzothiazole, Pyridine, 155
Imine activation
Copper(II) complex, Schiff base, X-ray structure, Coordination polymer, 3081
Imine hydrogenation
Mixed valent Ru(II)/Ru(III) complexes, Binuclear ruthenium complexes, Catalysis, 3163
Imine-oxime ligand
Copper(III), Diols, Kinetics, Mechanism, Electron transfer, 583
Imines
N-Heterocyclic carbenes, Homogenous catalysis, Transfer hydrogenation, Ketones, Aldehydes, 2857
Imino nitroxide
Nitronyl nitroxide, Amide, Manganese complexes, Copper complexes, Cobalt complexes, 763
Iminoalkyl bonding mode
Group 11 phosphine complexes, 1-azaallyls, X-ray crystallography, 2273
Immobilization
Silica support, Cobalt(II) complexes, H_2O_2, 59
Immobilization
Silica gel, 2-Aminomethylpyridine, Epoxide, Adsorption, Thermodynamic, 719
Indenyl
Cyclopentadienyl, Phosphino, Phosphido, Molybdenum, Metallocenes, 1263
Indenyl ligand
Synthesis, Crystal structures, Nickel complex, Catalysis, 1473
Indium
Metalloporphyrins, Thallium, 1777
Indomethacin
Diorganotin, Crystal structures, Spectroscopic studies, 2021
Infrared
Copper, Structure, Hydrogen bonds, Distortion isomers, 1969
π–π interactions
Manganese maleate, Coordination polymer, Temperature effect, Helical architecture, Hydrogen bonds, 987
π–π Interactions
$Cu^{II}N_4Cl$ chromophores, Bidentate diimine, Bidentate diamine, Hydrogen bonding, Magnetic property, 1961
π–π Interaction
Carboxylate, Coordination polymer, Double betaine, Hydrate, Hydrogen bonding, Silver nitrate, 2413
Intercalation behavior
Hydrothermal, Layered, Titanium phosphate, γ-Phase, 3033

Intermolecular
Cyclic telluranes, Metathetical reactions, Secondary bonding, Supramolecular networks, 1629
Intermolecular interactions
Diaza-fluorene, Silver complexes, Crystal structures, Electronic spectra, 2259
Intra-ligand charge transfer
Iridium, Luminescence, Terpyridine, Near infra-red, Charge-transfer, 2769
Ion exchange
Six coordinate silicates, Transition metals, Ligand environment, Thermal studies, Magnetism, 679
Ion pair complex
Hydrogen bonding network, Non-covalent interaction, Charge transfer, Near-IR absorption, 1235
Ion recognition
Schiff base complexes, Crown ether, UV–Vis, Lanthanides, 1401
Ionic complex
Rheological phase reaction, Crystal structure, Photoluminescence, Europium, Zinc, 529
Ionic liquids
Hydroformylation, Biphase catalysis, High-pressure NMR, Rhodium complexes, 2679
Ionic metathesis
Diorganostannate, Methanesulfonate, Organotin oxide, 71
Ionic radius
Tetrahydrofurfurylindenyl, Lanthanide chlorides, Crystal structure, 1075
IR
Zinc complexes, Schiff-bases, Crystal structures, UV and NMR spectroscopy, Thermal analysis, 1293
IR spectra
Cobalt(III), Semicarbazone, 2-Hydroxyacetophenone, NMR spectra, Electronic spectra, X- ray crystal structure, 41
IR spectra
Crystal structure, Vanadium(V) peroxo mandelato complex, ^{51}V NMR spectra, 655
IR spectra
Iron(III) complexes, Thiosemicarbazone, Single crystal X-ray diffraction, Mössbauer spectra, EPR spectra, 969
IR spectra
Di-2-pyridyl ketone, Thiosemicarbazone, Ni(II) thiosemicarbazone complex, Electronic spectra, X-ray crystal structure, 1225
Iridium
Cyclometalated Ir(II) complexes, Pyrazolyl ancillary ligands, Boat conformations, Luminescent, Electroluminescence, 419
Iridium
Luminescence, Terpyridine, Near infrared, Charge-transfer, Intra-ligand charge transfer, 2769
Iridium complexes
Chelating phosphines, 2959
Iron
Heteroscorpionate, Tripodal, Alkylthiolate, Imidazole, Zinc, 471
Iron
(μ-O)di-iron complex, Bis-(2-pyridylmethyl)amine, Oxalato, Hydrogen bonding, Mössbauer spectra, 1419
Iron
Parabanic acid, Cyclopentadienyl, Carbonyl, Thallium, Gold (I) complex, Alkylation, 1441
Iron
Spin-crossover, Crystal structure, Magnetic measurements, 2141
Iron
Radical, Styrene, Catalyst, Polymerisation, 2921
Iron
Terpyridine, Pyridyl bispyrazolyl, Complexation, Rearrangement, X-ray structures, 3193
Iron (III)
Dinuclear, Carboxylate, Complexes, Bridging, Mössbauer, 1869
Iron clusters
Solid-state reactions, Third-order nonlinear optical properties, 755
Iron complex
Schiff-base, Polypyrrole, Electropolymerization, AFM, Polymer, 1953
Iron complexes
Acetate ligands, η^2-Coordination modes, Schiff bases, β-Cis arrangements, 963
Iron complexes
Dendrimers, Cyclophosphazene, Metal–nitrile complexes, 1027
Iron iodide
Titanium iodide, Phosphine, Arsine, Crystal structures, 605
Iron phosphatooxalate
Hydrothermal synthesis, Crystal structure, Template, Oxalate acid, Piperazine, 2357
Iron–platinum compounds
Pyrolysis, Organometallic compounds, 63
Iron(II) complexes
Trithiocyanuric acid, Mössbauer spectra, Crystal structures, Spectroscopic properties, DFT calculations, 2193
Iron(II) complexes
Cobalt(II) complexes, X-ray crystal structures, Bis(2-pyridylmethyl)amine, Tris(2-pyridylmethyl)amine, 3105
Iron(III) carboxylate complexes
2,2′-Bipyrimidine complexes, Oxo-bridged iron(III) complexes, π–π stacking interactions, X-ray crystal structure, 1271
Iron(III) complex
Cyanide bridged clusters, Tris(pyrazolyl)-borate, Magnetic properties, 1333
Iron(III) complexes
Thiosemicarbazone, Single crystal X-ray diffraction, Mössbauer spectra, EPR spectra, IR spectra, 969
Isocyanides
Binuclear compounds, Nickel, Polymerisation, Ring-coupled bis-cyclopentadienyl ligand, X-ray molecular structure, 2715
Isomers
κ^2-Tp ligands, Bridging Tp ligands, Rhodium dicarbonyl complexes, X-ray structure, 301
Isonicotinic acid
Lanthanum trifluoromethanesulfonate, N-oxide, Mixed ligands, Coordination polymer, 857
Isonicotinic acid
Mn(II) complex, N-oxide, Crystal structure, Luminescence, 1109
Isoorotic acid
Lanthanide(III) complexes, Hydrothermal syntheses, Hydrogen bonds, Supramolecule, 2085
Isoorotic acid
Co(II) and Ni(II) complexes, Hydrothermal synthesis, Hydrogen bonds, Supramolecular frameworks, 2227
Isotope effect
Crystal structure, Phase transition, Hydrogen bond, NQR, Tetrachloroaurate(III), 1605
IX
Flexible, Carboxylates, Coordination polymer, Architecture, 3007

Keggin
Polyoxometalates, Hydrothermal synthesis, Crystal structure, Cobalt, 773
β-ketoesterates
Cerium, Oxazolines, Chiral, Thermal decomposition, MOCVD, 1467
Ketones
N-Heterocyclic carbenes, Homogenous catalysis, Transfer hydrogenation, Aldehydes, Imines, 2857
Kinetics
Copper(III), Imine-oxime ligand, Diols, Mechanism, Electron transfer, 583
Kinetics
Mechanism, Redox, Silver, Glyoxylic acid, 895
Kinetics
1,3,4-thiadiazole, Zinc, Crystal structure, Thermal decomposition, Bioactivity, 1851
Kinetics
Permanganate, Oxidation, 4-Hydroxycoumarin, 2507
Kinetics
Absorption spectra, Complexation, Photochromism, Spiroindolinonaphthooxazines, 3147

Lanthanide
Cryptate, Crystal structure, ES-MS, 49
Lanthanide
Hydrazones, Complex, X-ray, Spectroscopy, Crystal structures, 1191
Lanthanide
Actinide, Oxides, Carbene, Uranium, 2689
Lanthanide
Samarium, Nitric oxide, Nitrite, Pyrazolylborate, Redox, 2709
Lanthanide chlorides
Tetrahydrofurfurylindenyl, Crystal structure, Ionic radius, 1075

Lanthanide complex
Proton sponge, Macrocyclic tetramine, 1,4,8,11-tetramethyl-1,4,8,11-tetraazacyclotetradecane, 1089
Lanthanide ions
Sulfonatothiacalixarene, Capsules, Diaza-18-crown-6, 2055
Lanthanide nitrate
N,*N*′-dioxide, Self-assembly, Coordination polymer, 169
Lanthanide oxides
Bromotrimethylsilane, O-donor ligands, Complexes of lanthanide bromides, Crystal structure, Coordination number, 2293
Lanthanide(III) complexes
Hydrothermal syntheses, Isoorotic acid, Hydrogen bonds, Supramolecule, 2085
Lanthanides
Yttrium, Diketiminato, 183
Lanthanides
Neodymium, X-ray structures, Alkoxides, Pyrazolylborates, Borohydrides, 253
Lanthanides
Ytterbium, Aryloxide, Crystal Structures, Tris(pyrazolyl)borate, Divalent, 263
Lanthanides
Ion recognition, Schiff base complexes, Crown ether, UV–Vis, 1401
Lanthanides
Dawson lacunary heteropolyanion, Complex formation constants, Arsenazo III, 1579
Lanthanides(III)
Nickel(II), Amino acid, Heptanuclear, Cluster compound, 2265
Lanthanum
Tris(pyrazolyl)hydroborate (Tp) ligands, Neodymium, Salt metathesis, Aryloxide derivatives, 2437
Lanthanum trifluoromethanesulfonate
Isonicotinic acid, N-oxide, Mixed ligands, Coordination polymer, 857
Laser ablation synthesis
Phosphorus, Sulfur, Clusters, Phosphorus sulfides, TOF mass spectrometry, 1199
Lawesson's Reagent
Thiophosphoryl compound, Sulfur-rich complex, Nickel(II) complex, Cobalt(II) complex, 1799
Lawsone
Quinones, 2-Hydroxy-1, 4-Naphthoquinone, Amine oxidase, Copper complexes, Antiferromagnetic coupling, H-bonding, EPR, 2541
Layered
Hydrothermal, Titanium phosphate, Intercalation behavior, γ-Phase, 3033
Lead
Coordination polymer, Hydrothermal synthesis, X-ray structure determination, 2161
Lead(II)
4,4′-Bipyridine, Coordination polymers, Lone pair, π–π staking interaction, Crystal structure, 2427
Lewis acids
^{15}N solid state NMR, DFT calculations, Molybdenum nitride, Imido complexes, 2751
Ligand
Ferrocene, Enaminone, Copper, Complex, X-ray crystallography, 15
Ligand
Ferrocene, Dithiocarbazate, Complex, Tin, Crystal structure, 567
Ligand
Catalysis, X-ray structure, Complex, 693
Ligand
Ferrocene, Enaminone, Copper, Complex, X-ray crystallography, 1541
Ligand
Amino acid, Copper, Dendrimers, Electrochemistry, Electron spin resonance, 1709
Ligand
Bidentate, Bridging, X-ray, Phosphine, 2569
Ligand environment
Six coordinate silicates, Ion exchange, Transition metals, Thermal studies, Magnetism, 679
Ligand oxidation
Nickel complexes, Pyrazoline, Ring opening, Structures, 1997
Ligands
Ferrocene, Enaminone, Complexes, X-ray crystallography, 749
Ligands
Cadmium, Coordinate, Polymers, Supramolecular, 1003
N-ligands
Copper, Thioethers, Multi-armed ligands, X-ray structures, Coordination polymer, 1055
Liquid ammonia/toluene two-phase system
Ammonolysis, Potassium, Zirconium, 1125
Liquid crystal
Phthalocyanine, Metallo phthalocyanine, Metallo mesogen, Crown ether, Aza ether, 1931
Liquid nitrogen
Carbon allotropes, Polyynes, Carbyne, Dicyanopolyynes, Cyanopolyynes, Electric arc, Graphite, 1889
Lithium
Alkali metals, Phosphorus–carbon bond cleavage, Chelates, O Ligands, 2499
Lithium
Multiple-decker sandwich complex, Ferrocene, Boron, Crystal structure, 2597
LLCT
Luminescence, Phosphorescence, Pt(II) and Pd(II), 3173
Lone pair
4,4′-Bipyridine, Lead(II), Coordination polymers, π–π staking interaction, Crystal structure, 2427
Low spin complexes
Diruthenium compounds, Metal–metal bonds, Triazenido complexes, Formamidinato complexes, Multiple bonds, 2637
Low temperature
Hydroxyapatite, Complex, EDTA, Hydrothermal, Calcium phosphates, 1897
Low-spin configurations
Electron-transfer reactions, Spin-exchange reactions, Bis[tris(pyrazolyl)methane] complexes, High-spin configurations, 1037
Luminescence
Zinc(II)azide, Mononuclear, Dinuclear, 2,2′-Dipyridylamine, Crystal engineering, 545
Luminescence
Coordination polymer, Europium, Hydrogen bonds, Supramolecular, Terbium, 711
Luminescence
Mn(II) complex, Isonicotinic acid, N-oxide, Crystal structure, 1109
Luminescence
Iridium, Terpyridine, Near infra-red, Charge-transfer, Intra-ligand charge transfer, 2769
Luminescence
LLCT, Phosphorescence, Pt(II) and Pd(II), 3173
Luminescent
Iridium, Cyclometalated Ir(II) complexes, Pyrazolyl ancillary ligands, Boat conformations, Electroluminescence, 419

Mössbauer spectra
Iron(II) complexes, Trithiocyanuric acid, Crystal structures, Spectroscopic properties, DFT calculations, 2193
Mössbauer
Iron (III), Dinuclear, Carboxylate, Complexes, Bridging, 1869
Mössbauer spectra
Iron(III) complexes, Thiosemicarbazone, Single crystal X-ray diffraction, EPR spectra, IR spectra, 969
Mössbauer spectra
Iron, (μ-O)di-iron complex, Bis-(2-pyridylmethyl)amine, Oxalato, Hydrogen bonding, 1419
Macrobicylic ligands
Compartmental, Copper(II) complexes, Electrochemistry, Antiferromagnetic interaction, Catalytic study, 519
Macrocycle
Template synthesis, Decaazacyclooctadecane, Nickel(II) complexes, 1325
Macrocycles
Scorpionands, Chromophores, Copper(II), Nickel(II), 373
Macrocycles
P,*S*-metallocycles, Supramolecular chemistry, Bipodal ligands, Crystal structures, Phosphorylated urea complexes, 2243
Macrocyclic complexes
Cyclic voltammetry, X-ray crystallography, Imidazole, 1317
Macrocyclic tetramine
Proton sponge, Lanthanide complex, 1,4,8,11-tetramethyl-1,4,8,11-tetraazacyclotetradecane, 1089

Magnesium carboxylate
Meltable, Dispersion processing, Thermal properties, 1739
Magnetic measurements
Iron, Spin-crossover, Crystal structure, 2141
Magnetic properties
Tricopper(II) complex, Schiff bases, Ascorbate oxidase model, Crystal structure, 643
Magnetic properties
Electrochemistry, Oximinato monocopper(II) and mononickel(II) complexes, Unsymmetrical oximinato dicopper(II) complexes and unsymmetrical oximinato dinickel(II) complexes, 665
Magnetic properties
Manganese(II) hexafluoroacetylacetonate, 4-cyanopyridine-N-oxide, Crystal structures, Ferromagnetic interactions, 879
Magnetic properties
Azides, Polyamines, Copper(II) complexes, Crystal structures, Coordination polymers, 1243
Magnetic properties
Copper, Crystal structure, Dimer, Spectral properties, 1303
Magnetic properties
Dinuclear copper(II) complex, Bidentate ligand, Crystal structure, UV–Vis, EPR and IR spectra, 1309
Magnetic properties
Cyanide bridged clusters, Iron(III) complex, Tris(pyrazolyl)borate, 1333
Magnetic properties
Nickel(II) compounds, Crystal structures, Terephthalate ligand, Binuclear complexes, 1379
Magnetic properties
Manganese, Pheylcyanamide, Crystal structures, 1409
Magnetic properties
Nickel(II), Thiodiglycolic acid complexes, X-ray structures, 1573
Magnetic properties
Copper dimer, Antiferromagnetic dimer, Crystal structure, 1695
Magnetic properties
Self-assemble, Carboxylate bridges, Copper complexes, Dipeptides, Alkaline earth metals, 2125
Magnetic properties
Dicopper(II) complex, 1D Coordination polymer, Crystal structure, Schiff base, 2177
Magnetic properties
Copper(II) complex, Crystal structure, Coordination polymers, 2203
Magnetic properties
Cu(II)–Ln(III) complexes, Dipeptides, Carboxylate bridge, Hexanuclear cations, Crystal structures, 2253
Magnetic properties
Copper, 3,5-Dinitrosalicylate complex, Trimer, Crystal structure, Spectral properties, 2447
Magnetic properties
Copper(II) compounds, Crystal structures, Terephthalate ligand, One-dimensional complexes, 3043
Magnetic property
Hydrothermal synthesis, Coordination polymer, Transition metal, Square grid structure, 1,4-Naphthalenedicarboxylic acid, 1257
Magnetic property
$Cu^{II}N_4Cl$ chromophores, Bidentate diimine, Bidentate diamine, π–π Interactions, Hydrogen bonding, 1961
Magnetism
Six coordinate silicates, Ion exchange, Transition metals, Ligand environment, Thermal studies, 679
Magnetism
Copper, Structure, Dinuclear, EPR, 993
Magnetism
Crystal structure, Manganese, Hydrogen bond, EPR, 2387
Magnetism
Crystal structure, Nickel(II) complexes, Pseudohalides, 2337
Magnetochemical studies
N-salicylidene-*n*-alkanoylhydrazines, Copper(II) complexes, Bis[monochloro(μ-*N*-salicylidenemyristoylhydrazine) $ONO'(-1)$]dicopper(II), X-ray crystal and molecular structure, 23
Magnetochemistry
Crystal structures, Manganese(II) carboxylate chemistry, Metal-assisted reactions, 2-Pyridinealdoxime complexes, 83
Magnetochemistry
Manganese(III), N,O ligands, X-ray structure, Dimer, Azide, 1811
Magnetochemistry
Vanadium, Diiminediaminediphenolate macrocycle, EPR, FTIR, Spectroelectrochemistry, 2069
Magnetochemistry
Fe(III) carboxylate chemistry, Crystal structures, Cluster complexes, 2779
Malonate
Herometallacrown, *o*-Pthalate, Cu(II) complexes, 943
Malonate complexes
2D antiferromagnets, Weak ferromagnetism, 929
Manganese
Pheylcyanamide, Magnetic properties, Crystal structures, 1409
Manganese
Crystal structure, Hydrogen bond, Magnetism, EPR, 2387
Manganese complexes
Nitronyl nitroxide, Imino nitroxide, Amide, Copper complexes, Cobalt complexes, 763
Manganese maleate
Coordination polymer, Temperature effect, Helical architecture, Hydrogen bonds, π–π interactions, 987
Manganese(II)
Cadmium(II), Calcium(II), Synthesis, Crystal structures, Tetrazolate complexes, 1217
Manganese(II)
Bis-imidazole, Metal complexes, X-ray structures, Copper(II), Zinc(II), 1731
Manganese(II) carboxylate chemistry
Crystal structures, Magnetochemistry, Metal-assisted reactions, 2-Pyridinealdoxime complexes, 83
Manganese(II) hexafluoroacetylacetonate
4-cyanopyridine-N-oxide, Crystal structures, Magnetic properties, Ferromagnetic interactions, 879
Manganese(III)
Dimeric complex, Crystal structure, Ferromagnetic behaviour, 949
Manganese(III)
N,O ligands, X-ray structure, Magnetochemistry, Dimer, Azide, 1811
Manganese(III) complexes
Ozone, X-ray crystal structure, Silver(II) complexes, Cobalt(III) complexes, 2631
MAS NMR
Crystal structure, Gold complex, Selenourea, 1
MCD (Magnetic Circular Dichroism)
Sulfite oxidase, Pyranopterin molybdenum enzymes, Electronic structure, Molybdenum complexes, EPR (Electron Paramagnetic Resonance), 499
Mechanism
Copper(III), Imine-oxime ligand, Diols, Kinetics, Electron transfer, 583
Mechanism
Kinetics, Redox, Silver, Glyoxylic acid, 895
Meltable
Magnesium carboxylate, Dispersion processing, Thermal properties, 1739
Menthone
Scorpionate ligands, Tripod ligands, Chirality, Prochirality, 245
Mercury(II)
1,3-Dithiol-2-thione, Pyridyl, ^1H NMR, Solid UV, 115
2-Mercapto-6-nitrobenzothiazole
Organotin(IV), Non-bonded interaction, Crystal structure, X-ray crystallography diffraction, 779
1H-5-mercapto-1,2,3-triazolato
Organotin, Organogermanium(IV), Crystal structure, X-ray crystallography, 1981
Metal complexes
Bis-imidazole, X-ray structures, Manganese(II), Copper(II), Zinc(II), 1731
Metal isotope effect
2-Thiopheneacetic acid, Polymeric copper(II) complex, Crystal structure, Vibrational spectra, 1785
Metal–metal bond
Ph_2Te_2, Molybdenum complex, Mo_2Te_4 complex, Crystal structure, 1663
Metal–metal bonds
Diruthenium compounds, Triazenido complexes, Formamidinato complexes,

Multiple bonds, Low spin complexes, 2637
Metal–metal multiple bond
Hydrotris(pyrazolyl)borate, Scorpionate ligands, Tantalum, Alkyne complex, Tetrahydrothiophene complex, 379
Metal–nitrile complexes
Dendrimers, Cyclophosphazene, Iron complexes, 1027
Metal-assisted reactions
Crystal structures, Manganese(II) carboxylate chemistry, Magnetochemistry, 2-Pyridinealdoxime complexes, 83
Metal-nitrogen pi bonding
Acetonitrile reduction, Amine oxidation, Imido, Regioselectivity of nucleophile and electrophile additions, 311
Metallacrown
Ruthenium, Fluoroionophore, X-ray, 1719
Metallo mesogen
Phthalocyanine, Metallo phthalocyanine, Liquid crystal, Crown ether, Aza ether, 1931
Metallo phthalocyanine
Phthalocyanine, Liquid crystal, Metallo mesogen, Crown ether, Aza ether, 1931
Metallocene
Ferrocenium, Cobaltocenium, Crystal structure, 2937
Metallocene
Organometallics, Sandwich complex, Bonding, Density functional theory, Orbital analysis, 2993
Metallocenes
Cyclopentadienyl, Indenyl, Phosphino, Phosphido, Molybdenum, 1263
P,*S*-metallocycles
Supramolecular chemistry, Bipodal ligands, Crystal structures, Macrocycles, Phosphorylated urea complexes, 2243
Metalloporphyrins
Indium, Thallium, 1777
Metathetical reactions
Cyclic telluranes, Intermolecular, Secondary bonding, Supramolecular networks, 1629
Methanesulfonate
Diorganostannate, Ionic metathesis, Organotin oxide, 71
2-Methanolpyridine
2,6-Dimethanolpyridine, 2-Ethanolpyridinium, Cobalt(II) complexes, Crystal structures, 841
Methyl
Zwitterions, Monoanionic ligands, Syntheses, Structures, Hydrides, 489
Methylaluminoxane
Neutral palladium(II) complex, X-ray crystallography, Catalyst, Norbornene, Vinylic polymerizaition, 1619
Methylation
η^2-nitrile, Tungsten, Oxo, Oxidation, Dimerization, 2831
S-Methyldithiocarbazate
Cu(II) complexes, Dithiocarbazate Schiff base, Saccharin complexes, Tridentate NNS Schiff base, 2491
S-methyldithiocarbazate (SMDTC)
NS Schiff base, Crystal structure of Cd(II) complex, Dithiocarbazate derivatives, 1385
Mixed ligands
Lanthanum trifluoromethanesulfonate, Isonicotinic acid, N-oxide, Coordination polymer, 857
Mixed valent Ru(II)/Ru(III) complexes
Binuclear ruthenium complexes, Catalysis, Imine hydrogenation, 3163
Mixed-valence
EPR spectroscopy, Hydrazido ligand, Ruthenium complexes, Spectroelectrochemistry, 701
Mn(II) and Cd(II) complexes
Azides, 3-Aminopyridine, Synthesis, Spectra, X-ray structures, Thermal properties, 2349
Mn(II) complex
Isonicotinic acid, N-oxide, Crystal structure, Luminescence, 1109
Mo_2Te_4 complex
Ph_2Te_2, Metal–metal bond, Molybdenum complex, Crystal structure, 1663
MOCVD
Cobalt, Oxide, β-diketonates, Adducts, Structures, 735
MOCVD
Cerium, Oxazolines, Chiral, Thermal decomposition, β-ketoesterates, 1467
Model complex
Cu-NIRs, Crystalline structure, Tripodal ligand, Polyimidazole ligand, 511
Model compounds
Tetrathiomolybdate, Tetrathiotungstate, Dihydridobis(pyrazolyl)borate, Copper(I) complexes, Crystal structure, 637
Molecular
Crystal structure, Back-bonding, Ruthenium complex, NO, Reactivity, 1063
Molecular assembly
Crystal structure, 1,3-Dithiole-2-thione, Complex, 1447
Molecular mechanics
Eight-coordinate, Stereochemistry, Dodecahedron, Square antiprism, Bicapped trigonal prism, 145
Molecular rectangles
Crystal structures, Copper complexes, Zinc complexes, 673
Molecular structures
Zwitterionic ferrocenyldithiophosphonates, 2281
Molybdenum
Tris(pyrazolyl)borate, Bis(imido), Synthesis, Structures, 189
Molybdenum
Cyclopentadienyl, Indenyl, Phosphino, Phosphido, Metallocenes, 1263
Molybdenum
^{95}Mo NMR, X-ray structures, Phosphine oxide, 1915
Molybdenum
Polyoxometallate, Aqueous organometallic chemistry, Pentamethylcyclopentadienyl ligands, 2605
Molybdenum
Crystal structures, Clusters, Copper, Tungsten, Nitrogen heterocycle ligands, Pyrazole, 3143
Molybdenum complex
Ph_2Te_2, Metal–metal bond, Mo_2Te_4 complex, Crystal structure, 1663
Molybdenum complexes
Sulfite oxidase, Pyranopterin molybdenum enzymes, Electronic structure, MCD (Magnetic Circular Dichroism), EPR (Electron Paramagnetic Resonance), 499
Molybdenum complexes
Carbonyl complexes, Pentafluorophenyl, Oxidation, Bond cleavage, Reductive elimination, 1371
Molybdenum nitride
^{15}N solid state NMR, DFT calculations, Imido complexes, Lewis acids, 2751
Molybdenum phosphate
Transformation, Hydrothermal synthesis, Crystal structure, 2153
Molybdenum(V) complexes
Enaminones, Molybdenum(VI) complexes, Pyrone, X-ray crystal structure, NMR spectra, 1859
Molybdenum(VI) complexes
Enaminones, Molybdenum(V) complexes, Pyrone, X-ray crystal structure, NMR spectra, 1859
^{95}Mo NMR
Molybdenum, X-ray structures, Phosphine oxide, 1915
Monoanionic ligands
Zwitterions, Syntheses, Structures, Methyl, Hydrides, 489
Monoanionic ligands
Zwitterions, Phosphines, Syntheses, Structures, Boron, 2901
Monodentate
Bis(diphenylphosphino)methane dioxide, Uranyl nitrate, Uranyl bis(β-diketonates), Bidentate chelate, Bridging bidentate, Coordination modes, 1527
Monodentate donors
2-Diphenylphosphinopicolinamide (dpppa 1), Coordination chemistry, Bidentate donors, 3211
Monomeric complexes
2,5-Bis(2-pyridyl)-1,3,4-thiadiazole, Zinc, Energy minimization, Crystal structures, 1903
Mononuclear
Zinc(II)azide, Dinuclear, 2,2′-Dipyridylamine, Luminescence, Crystal engineering, 545
Mononuclear complex
Silver(I) complexes, Dinuclear complex, 2117
Monophosphono dipeptides
Copper(II) complexes, Thioether ligands, Stability constants, Potentiometry, Vis, CD, EPR spectroscopy, 1939
MP2 geometry optimization
Bis(methoxycarbimido)amine, Topological analysis of electron density, 2235

Multi-armed ligands
Copper, *N*-ligands, Thioethers, X-ray structures, Coordination polymer, 1055
Multi-nitriles
Silver coordination complex polymers, 1D, 2D, 3D topological structure, 2209
Multidentate ligand
Cobalt(III), Sinambic, ^{59}Co NMR, 2217
Multiple bonds
Diruthenium compounds, Metal–metal bonds, Triazenido complexes, Formamidinato complexes, Low spin complexes, 2637
Multiple-decker sandwich complex
Ferrocene, Boron, Lithium, Crystal structure, 2597

^{15}N solid state NMR
DFT calculations, Molybdenum nitride, Imido complexes, Lewis acids, 2751
N, O donor ligands
Uranium, Crystal structure, 2285
N,O ligands
Manganese(III), X-ray structure, Magnetochemistry, Dimer, Azide, 1811
N,O-ligands
Self-assembly, Copper, Dinuclear, EPR, 1769
N-oxide
Lanthanum trifluoromethanesulfonate, Isonicotinic acid, Mixed ligands, Coordination polymer, 857
N-oxide
Mn(II) complex, Isonicotinic acid, Crystal structure, Luminescence, 1109
Nanochemistry
Clusters, Complexity, Polyoxomolybdates, 2381
Nanoparticles
Xanthate, Diamine, Zinc, Cadmium, CdS, 2315
Nanotubes
One-dimensional, Silver(I), Aliphatic amino ligands, Coordination polymers, Tubes, Topology, Supramolecular chemistry, Self assembly, 2075
Naphthalene
Phthalocyanine, Cobalt, Zinc, Nickel, 787
Naphthalene
Porphyrazine, EPR, Copper, Zinc, Cobalt, 1845
1,4-Naphthalenedicarboxylic acid
Hydrothermal synthesis, Coordination polymer, Magnetic property, Transition metal, Square grid structure, 1257
4-Naphthoquinone
Lawsone, Quinones, 2-Hydroxy-1, Amine oxidase, Copper complexes, Antiferromagnetic coupling, H-bonding, EPR, 2541
Naphthylazoimidazole
Silver(I) complexes, Helical structure, EHMO, 793
Near infra-red
Iridium, Luminescence, Terpyridine, Charge-transfer, Intra-ligand charge transfer, 2769
Near-IR absorption
Ion pair complex, Hydrogen bonding network, Non-covalent interaction, Charge transfer, 1235
Neodymium
Lanthanides, X-ray structures, Alkoxides, Pyrazolylborates, Borohydrides, 253
Neodymium
Tris(pyrazolyl)hydroborate (Tp) ligands, Lanthanum, Salt metathesis, Aryloxide derivatives, 2437
Neutral palladium(II) complex
X-ray crystallography, Catalyst, Methylaluminoxane, Norbornene, Vinylic polymerizaition, 1619
Ni(II) complexes
S-2-picolyldithiocarbazate (Hydrazine carbodithioic acid pyridinium-2-yl methyl ester chloride), Bidentate NS Schiff base, Tridentate NNS and NSS Schiff bases, Dithiocarbazate derivative, 161
Ni(II) thiosemicarbazone complex
Di-2-pyridyl ketone, Thiosemicarbazone, Electronic spectra, IR spectra, X-ray crystal structure, 1225
Nickel
Dithiocarbamate, PPh_3, Dppe, X-ray crystal structure, NMR, 77
Nickel
Bis(mercaptoimidazolyl)borate complexes, Tris(mercaptoimidazolyl)borate complexes, Diphosphine, Hydrogenases, Crystal structure, 395
Nickel
Phthalocyanine, Cobalt, Zinc, Naphthalene, 787
Nickel
Solvothermal synthesis, Thiostannates, Crystal structures, Thermoanalysis, 937
Nickel
Copper, Zinc, Imidazole, α-Hydroxycarboxylato complexes, Thermal behaviour, Crystal structures, 1505
Nickel
Pseudoephedrine, Triangulo, Cluster, Anion exchange, 1837
Nickel
Binuclear compounds, Isocyanides, Polymerisation, Ring-coupled bis-cyclopentadienyl ligand, X-ray molecular structure, 2715
Nickel
Schiff's bases, Hydrogenated Schiff's bases, Coordination geometry, X-ray crystal structures, Polymethylene chains, 3201
Nickel complex
Synthesis, Crystal structures, Indenyl ligand, Catalysis, 1473
Nickel complex
Tripodal ligand, Cyclic voltammetry, 1829
Nickel complexes
Pyrazoline, Ring opening, Ligand oxidation, Structures, 1997
Nickel complexes
Heterocyclic carbenes, Functionalised carbenes, X-ray diffraction, 2813
Nickel(II)
Scorpionands, Chromophores, Copper(II), Macrocycles, 373
Nickel(II)
Thiodiglycolic acid complexes, X-ray structures, Magnetic properties, 1573
Nickel(II)
Lanthanides(III), Amino acid, Heptanuclear, Cluster compound, 2265
Nickel(II) complex
Crystal structure, Thiazine, Cobalt(III) complex, Pyridine, 1453
Nickel(II) complex
Lawesson's Reagent, Thiophosphoryl compound, Sulfur-rich complex, Cobalt(II) complex, 1799
Nickel(II) complexes
Crystal structures, Hydrotris(pyrazolyl)-borate complexes, Coordination environment, Scorpionates, 211
Nickel(II) complexes
Template synthesis, Decaazacyclooctadecane, Macrocycle, 1325
Nickel(II) complexes
Schiff bases, Salicylketimine ligands, X-ray crystallography, 1649
Nickel(II) complexes
Crystal structure, MagnetismPseudohalides,, 2337
Nickel(II) compounds
Crystal structures, Terephthalate ligand, Binuclear complexes, Magnetic properties, 1379
Nicotinate
Chiral, Coordination polymers, Open channel, Grid, 1947
Nitric oxide
Samarium, Lanthanide, Nitrite, Pyrazolylborate, Redox, 2709
Nitride precursor
Titanium, Tin, Tetrazole, Cycloaddition, 801
η^2-nitrile
Tungsten, Oxo, Oxidation, Methylation, Dimerization, 2831
Nitrile coordination
Polypyrazolylborate complexes, Copper complexes, Rhodium complexes, Scorpionates, Coordination Polymers, 235
Nitrilotriacetate
Vanadium complexes, X-ray crystal structure, Hydrogen bonding, 1975
Nitrite
Samarium, Lanthanide, Nitric oxide, Pyrazolylborate, Redox, 2709
Nitrito complexes
Copper complexes, Di-2-pyridylamine, Plasticity effect, *cis*-Distorted octahedron, Fluxional behaviour, 1685
Nitrogen base ligation
Diporphyrins, Zinc(II) complexes, Stability constants, 33
Nitrogen heterocycle ligands
Crystal structures, Clusters, Copper, Molybdenum, Tungsten, Pyrazole, 3143

Nitrogen ligands
Scorpionates, Polypyrazolylborates, Coordination chemistry, 197
Nitronyl nitroxide
Imino nitroxide, Amide, Manganese complexes, Copper complexes, Cobalt complexes, 763
Nitrosyls
Rhenium, Phosphine complexes, DFT calculations, 2363
NMR
Nickel, Dithiocarbamate, PPh_3, Dppe, X-ray crystal structure, 77
NMR
Polypyrazolylborate, Rhodium(I), Cyclooctadiene, Norbornadiene, Structure, 219
NMR
Pyrazine, Pyridine, X-ray, Stacking, Twist, 1011
NMR
Aromatic aminoacidate, Cobalt(III), Non-covalent interactions, Octahedral inversion, Tetradentate ligands, 1749
NMR
2-[(*E*)-2-(aryl)-1-diazenyl]pyridine, Hg(II) complexes, Crystal structures, 2323
NMR
Aluminium(III), Catecholates, Salicylates, Complexation, Proton exchange, 2393
NMR
Pyrazolylborates, Thallium, CPMAS, 2985
NMR spectra
Cobalt(III), Semicarbazone, 2-Hydroxyacetophenone, IR spectra, Electronic spectra, X- ray crystal structure, 41
NMR spectra
Enaminones, Molybdenum(VI) complexes, Molybdenum(V) complexes, Pyrone, X-ray crystal structure, 1859
NO
Crystal structure, Back-bonding, Ruthenium complex, Reactivity, Molecular, 1063
Non-bonded interaction
2-Mercapto-6-nitrobenzothiazole, Organotin(IV), Crystal structure, X-ray crystallography diffraction, 779
Non-covalent interaction
Ion pair complex, Hydrogen bonding network, Charge transfer, Near-IR absorption, 1235
Non-covalent interactions
Aromatic aminoacidate, Cobalt(III), Octahedral inversion, Tetradentate ligands, NMR, 1749
Non-heme iron
Water coordination, X-ray structure, Cyclic voltammetry, Sterically hindered carboxylate, 2805
Non-symmetrical ligands
Ferrocenes, Oxazolines, X-ray diffraction, 611
Norbornadiene
Polypyrazolylborate, Rhodium(I), Cyclooctadiene, Structure, NMR, 219
Norbornene
Neutral palladium(II) complex, X-ray crystallography, Catalyst, Methylaluminoxane, Vinylic polymerizaition, 1619
Novel conformations
Te(II) thiourea complexes, Unexpected colours, X-ray crystallography, Supramolecular associations, 3021
NQR
Crystal structure, Phase transition, Isotope effect, Hydrogen bond, Tetrachloroaurate(III), 1605
NS Schiff base
S-methyldithiocarbazate (SMDTC), Crystal structure of Cd(II) complex, Dithiocarbazate derivatives, 1385

O Ligands
Alkali metals, Lithium, Phosphorus–carbon bond cleavage, Chelates, 2499
O-donor ligands
Lanthanide oxides, Bromotrimethylsilane, Complexes of lanthanide bromides, Crystal structure, Coordination number, 2293
Octahedral inversion
Aromatic aminoacidate, Cobalt(III), Non-covalent interactions, Tetradentate ligands, NMR, 1749
Octahedral structure
Ruthenium(II) carbonyl complexes, Tertiary phosphine chalcogenides, ''Soft–Hard'' and ''Soft–Soft'' interactions, X-ray crystal structure, 1657
Octamolybdate
Hydrothermal synthesis, Three-dimensional oxide, Organic–inorganic hybrid, Building block approach, Hartree–Fock calculations, 1145
Olefin complexes
Copper(I) complexes, Hexafluorocetylacetonate, Divinyl organics, Crystal structure, Thermal analysis, 809
Oligomerization
Hydrocarboxylation, Catalysis, Rhodium complexes, Ethylene, Carbon monoxide, 1677
Oligosilanes
Silanoles, Siloxides, Titanium, Zirconium, 2475
One-dimensional
Silver(I), Aliphatic amino ligands, Coordination polymers, Tubes, Topology, Supramolecular chemistry, Self assembly, Nanotubes, 2075
One-dimensional chains
Self-assembly, Crystal structures, Bis(2-pyridylmethyl)amino acids, Ferromagnetism, Copper(II) complexes, 903
One-dimensional complexes
Copper(II) compounds, Crystal structures, Terephthalate ligand, Magnetic properties, 3043
One-dimensional compounds
Organotin complexes, Organorhodium complexes, Organorhodiumtin complexes, Two-dimensional compounds, Rhodium carbonyl complexes, 103
Open channel
Chiral, Coordination polymers, Nicotinate, Grid, 1947
Open frame material
S,N ambidentate borate ligands, Synthesis, X-ray structure, 205
Optical activity
Carbohydrate, Cobalt complex, Absorption spectra, Circular dichroism, 1341
Orbital analysis
Organometallics, Sandwich complex, Metallocene, Bonding, Density functional theory, 2993
Organic–inorganic hybrid
Octamolybdate, Hydrothermal synthesis, Three-dimensional oxide, Building block approach, Hartree–Fock calculations, 1145
Organogermanium(IV)
1H-5-mercapto-1,2,3-triazolato, Organotin, Crystal structure, X-ray crystallography, 1981
Organometallic compounds
Pyrolysis, Iron–platinum compounds, 63
Organometallics
Sandwich complex, Metallocene, Bonding, Density functional theory, Orbital analysis, 2993
Organorhodium complexes
Organotin complexes, Organorhodiumtin complexes, One-dimensional compounds, Two-dimensional compounds, Rhodium carbonyl complexes, 103
Organorhodiumtin complexes
Organotin complexes, Organorhodium complexes, One-dimensional compounds, Two-dimensional compounds, Rhodium carbonyl complexes, 103
Organotin
1H-5-mercapto-1,2,3-triazolato, Organogermanium(IV), Crystal structure, X-ray crystallography, 1981
Organotin complexes
Organorhodium complexes, Organorhodiumtin complexes, One-dimensional compounds, Two-dimensional compounds, Rhodium carbonyl complexes, 103
Organotin derivatives
Pyrolysis, Tin sulfide, 2102
Organotin oxide
Diorganostannate, Methanesulfonate, Ionic metathesis, 71
Organotin(IV)
2-Mercapto-6-nitrobenzothiazole, Non-bonded interaction, Crystal structure, X-ray crystallography diffraction, 779
Organotin(IV)
1-(4-Hydroxyphenyl)-1H-tetrazole-5-thiol, Hydrogen bonding, π–π stacking interaction, Crystal structures, X-ray crystallography, 1547
Ortho-metallated complexes
Palladium, Ferrocene, Phosphine, Suzuki–Miyaura coupling, X-ray crystallography, 921
Osmium
Dioxygen, Aniline, Oxidation, Electron transfer self-exchange, 323

Osmium
Rhenium, Polypyridyl, Synthesis, Spectroscopy, 1427
Oxadiazole ligand complexes
Palladium, Platinum, Heterobimetallic, Phosphine, 2013
Oxalate acid
Hydrothermal synthesis, Crystal structure, Iron phosphatooxalate, Template, Piperazine, 2357
Oxalato
Iron, (μ-O)di-iron complex, Bis-(2-pyridylmethyl)amine, Hydrogen bonding, Mössbauer spectra, 1419
Oxazolines
Ferrocenes, Non-symmetrical ligands, X-ray diffraction, 611
Oxazolines
Cerium, Chiral, Thermal decomposition, MOCVD, β-ketoesterates, 1467
Oxidation
Hydrotris(pyrazolyl)borate, Ruthenium, Hydrogen bond, Aquo complex, 225
Oxidation
Dioxygen, Osmium, Aniline, Electron transfer self-exchange, 323
Oxidation
Molybdenum complexes, Carbonyl complexes, Pentafluorophenyl, Bond cleavage, Reductive elimination, 1371
Oxidation
Kinetics, Permanganate, 4-Hydroxycoumarin, 2507
Oxidation
η^2-nitrile, Tungsten, Oxo, Methylation, Dimerization, 2831
Oxide
Cobalt, β-diketonates, Adducts, Structures, MOCVDf, 735
Oxides
Actinide, Lanthanide, Carbene, Uranium, 2689
Oximinato monocopper(II) and mononickel(II) complexes
Electrochemistry, Magnetic properties, Unsymmetrical oximinato dicopper(II) complexes and unsymmetrical oximinato dinickel(II) complexes, 665
2-Oxo-1,3-dithiole-4,5-dithiolate
Zinc complex, Cadmium complex, Synthesis, Crystal structure, Density functional calculation, 1701
Oxo
η^2-nitrile, Tungsten, Oxidation, Methylation, Dimerization, 2831
Oxo-bridged iron(III) complexes
2,2′-Bipyrimidine complexes, Iron(III) carboxylate complexes, π–π stacking interactions, X-ray crystal structure, 1271
Oxoalkoxides
Aluminium, Precursor hydrolysis, X-ray, Structure studies, 109
Oxotransfer catalysts
Dioxomolybdenum(VI) thionates, 537
Ozone
X-ray crystal structure, Silver(II) complexes, Manganese(III) complexes, Cobalt(III) complexes, 2631

^{31}P NMR
Phosphine chalcogenides, X-ray structure, Tellurium, Selenium, 1923
Palladium
Ferrocene, Phosphine, Suzuki–Miyaura coupling, Ortho-metallated complexes, X-ray crystallography, 921
Palladium
Crystal structure, Platinum, Phosphorus–nitrogen donor, 1159
Palladium
Platinum, Heterobimetallic, Phosphine, Oxadiazole ligand complexes, 2013
Palladium
Pyridinecarboxaldimine, Cytotoxicity, Platinum, Fluorine, 2169
Palladium
X-ray structure, Diimine, Coordination complex, Zinc, 2789
Palladium
Selenium, Complexes, X-ray, 2967
Palladium dimers
Triazolopyrimidine, Head–head, Head–tail, 2373
Parabanic acid
Iron, Cyclopentadienyl, Carbonyl, Thallium, Gold (I) complex, Alkylation, 1441
Paramagnetic NMR
Rhenium, Benzimidazole, Bibenzimidazole, Crystal structure, 1139
Pendent arm
Chirality, Tetra-azamacrocycles, Template reaction, Conformational isomers, 869
Pentachlorophenolato complexes
Rhodium, Acetylacetonato complexes, Carboxylato complexes, Diazoalkane complexes, C–C coupling reactions, 2645
Pentafluorophenyl
Molybdenum complexes, Carbonyl complexes, Oxidation, Bond cleavage, Reductive elimination, 1371
Pentalene
Tantalum, Synthesis, Structures, 2625
Pentamethylcyclopentadienyl ligands
Molybdenum, Polyoxometallate, Aqueous organometallic chemistry, 2605
Permanganate
Kinetics, Oxidation, 4-Hydroxycoumarin, 2507
Peroxidative bromination
Dinuclear peroxovanadate, Peroxo-bridged divanadate, Heteroligand peroxovanadate, Amino acid containing peroxovanadates, 1097
Peroxo-bridged divanadate
Dinuclear peroxovanadate, Peroxidative bromination, Heteroligand peroxovanadate, Amino acid containing peroxovanadates, 1097
Ph_2Te_2
Metal–metal bond, Molybdenum complex, Mo_2Te_4 complex, Crystal structure, 1663
γ-Phase
Hydrothermal, Layered, Titanium phosphate, Intercalation behavior, 3033
Phase transition
Crystal structure, Isotope effect, Hydrogen bond, NQR, Tetrachloroaurate(III), 1605
1,10-Phenanthroline
Hydrazones, Copper(II) hydrazonate complexes, 2,2′-Bipyridine, X-ray single crystal structure, EPR, 575
1,10-Phenanthroline
Diorganotin, Dicyanoethylene-1,2-dithiolate, 4,4′-Bipyridyl, X-ray crystal structure, Co-crystallization, 1207
Phenanthroline
Cadmium(II), Chloranilate anions, Square antiprism, Crystal structures, Chain polymers, 2587
4,7-Phenanthroline
Copper, Coordination framework, Host–guest properties, Polymers, Extended structures, 55
Phenylacetylene
Phthalocyanine, Unsymmetrical, Cyclic voltammetry, 3155
Pheylcyanamide
Manganese, Magnetic properties, Crystal structures, 1409
Phosphanylalkylcyclopentadienyl ligands
Chromium complexes, Polymerisation studies, 1393
Phosphido
Cyclopentadienyl, Indenyl, Phosphino, Molybdenum, Metallocenes, 1263
Phosphine
Titanium iodide, Arsine, Iron iodide, Crystal structures, 605
Phosphine
Palladium, Ferrocene, Suzuki–Miyaura coupling, Ortho-metallated complexes, X-ray crystallography, 921
Phosphine
Phosphonic acid, Platinum, 1375
Phosphine
Palladium, Platinum, Heterobimetallic, Oxadiazole ligand complexes, 2013
Phosphine
Ligand, Bidentate, Bridging, X-ray, 2569
Phosphine
Synthesis, Coordination, X-ray structure, 2575
Phosphine
Hemilabile, X-ray structure, 3125
Phosphine chalcogenides
X-ray structure, ^{31}P NMR, Tellurium, Selenium, 1923
Phosphine complexes
Heteroscorpionates, Ruthenium, Hydrides, Hemilabile ligands, 361
Phosphine complexes
Rhenium, Nitrosyls, DFT calculations, 2363
Phosphine oxide
Molybdenum, ^{95}Mo NMR, X-ray structures, 1915

Phosphine oxide ligands
Uranyl, Fluoride, Structural study, Spectroscopic characterisation, 3097
Phosphines
Zwitterions, Monoanionic ligands, Syntheses, Structures, Boron, 2901
Phosphinite ligands
Rhenium(I), Dichloromethane complexes, Crystal structures, 1045
Phosphino
Cyclopentadienyl, Indenyl, Phosphido, Molybdenum, Metallocenes, 1263
Phosphonic acid
Phosphine, Platinum, 1375
Phosphorescence
LLCT, Luminescence, Pt(II) and Pd(II), 3173
Phosphorus
Sulfur, Clusters, Phosphorus sulfides, Laser ablation synthesis, TOF mass spectrometry, 1199
Phosphorus
Silicon, Hypercoordination, Hypervalency, Spectroscopy, Fluorescence, X-ray crystallography, 2615
Phosphorus sulfides
Phosphorus, Sulfur, Clusters, Laser ablation synthesis, TOF mass spectrometry, 1199
Phosphorus–carbon bond cleavage
Alkali metals, Lithium, Chelates, O Ligands, 2499
Phosphorus–nitrogen donor
Crystal structure, Platinum, Palladium, 1159
Phosphorylated urea complexes
P,*S*-metallocycles, Supramolecular chemistry, Bipodal ligands, Crystal structures, Macrocycles, 2243
Photochromism
Absorption spectra, Complexation, Kinetics, Spiroindolinonaphthooxazines, 3147
Photoelectron spectra
Hydrotris(pyrazol-1-yl)borates, Scorpionates, Polypyrazolylborates, 429
Photoluminescence
Ionic complex, Rheological phase reaction, Crystal structure, Europium, Zinc, 529
Phthalocyanine
Cobalt, Zinc, Nickel, Naphthalene, 787
Phthalocyanine
Electrochemistry, Spectroelectrochemistry, Pyridine binding, 1279
Phthalocyanine
Metallo phthalocyanine, Liquid crystal, Metallo mesogen, Crown ether, Aza ether, 1931
Phthalocyanine
Unsymmetrical, Phenylacetylene, Cyclic voltammetry, 3155
S-2-picolyldithiocarbazate (Hydrazine carbodithioic acid pyridinium-2-yl methyl ester chloride)
Bidentate NS Schiff base, Tridentate NNS and NSS Schiff bases, Ni(II) complexes, Dithiocarbazate derivative, 161
Piperazine
Hydrothermal synthesis, Crystal structure, Iron phosphatooxalate, Template, Oxalate acid, 2357
Plasticity effect
Copper complexes, Di-2-pyridylamine, Nitrito complexes, *cis*-Distorted octahedron, Fluxional behaviour, 1685
Platinum
Imine, Benzimidazole, Benzoxazole, Benzothiazole, Pyridine, 155
Platinum
Crystal structure, Palladium, Phosphorus–nitrogen donor, 1159
Platinum
Phosphine, Phosphonic acid, 1375
Platinum
Palladium, Heterobimetallic, Phosphine, Oxadiazole ligand complexes, 2013
Platinum
Pyridinecarboxaldimine, Cytotoxicity, Palladium, Fluorine, 2169
Platinum complexes
Dithiocarbimates, Crystal structures, 1153
Platinum complexes
Thioether complexes, Trithiacyclononane, Platinum nuclear magnetic resonance, Diimine complexes, Crown thioethers, 1361
Platinum nuclear magnetic resonance
Thioether complexes, Platinum complexes, Trithiacyclononane, Diimine complexes, Crown thioethers, 1361
Polarizability
Clusters, Electron density distribution, Spherical potential well, Finite electric field, 1519
Polyamines
Azides, Copper(II) complexes, Crystal structures, Magnetic properties, Coordination polymers, 1243
Polyimidazole ligand
Cu-NIRs, Model complex, Crystalline structure, Tripodal ligand, 511
Polymer
Schiff-base, Polypyrrole, Electropolymerization, Iron complex, AFM, 1953
Polymer
Cadmium(II)thiocyanate, Schiff base, Imidazole, Supramolecular synthon, 2045
Polymeric copper(II) complex
2-Thiopheneacetic acid, Crystal structure, Vibrational spectra, Metal isotope effect, 1785
Polymeric network
Zinc, 1,3-Bis(4-pyridyl)propane, 4,4′-Pyridine, X-ray crystallography, 999
Polymerisation
Binuclear compounds, Isocyanides, Nickel, Ring-coupled bis-cyclopentadienyl ligand, X-ray molecular structure, 2715
Polymerisation
Iron, Radical, Styrene, Catalyst, 2921
Polymerisation studies
Phosphanylalkylcyclopentadienyl ligands, Chromium complexes, 1393
Polymers
Copper, 4,7-Phenanthroline, Coordination framework, Host–guest properties, Extended structures, 55
Polymers
Cadmium, Coordinate, Ligands, Supramolecular, 1003
Polymers
Supramolecular chemistry, Self-assembly, Transition metal, Crystal engineering, 1877
Polymethylene chains
Nickel, Schiff's bases, Hydrogenated Schiff's bases, Coordination geometry, X-ray crystal structures, 3201
Polyoxometalates
Hydrothermal synthesis, Crystal structure, Keggin, Cobalt, 773
Polyoxometallate
Molybdenum, Aqueous organometallic chemistry, Pentamethylcyclopentadienyl ligands, 2605
Polyoxomolybdates
Clusters, Complexity, Nanochemistry, 2381
Polyphosphoxane
Rotational barriers, Cage complexes, Cone angles, 125
Polypyrazolylborate
Rhodium(I), Cyclooctadiene, Norbornadiene, Structure, NMR, 219
Polypyrazolylborate complexes
Copper complexes, Rhodium complexes, Scorpionates, Coordination Polymers, Nitrile coordination, 235
Polypyrazolylborates
Scorpionates, Coordination chemistry, Nitrogen ligands, 197
Polypyrazolylborates
Hydrotris(pyrazol-1-yl)borates, Scorpionates, Photoelectron spectra, 429
Polypyridine complexes
Diruthenium(II), Rhodium(III) Ruthenium(II), Heterodinuclear complexes, Electrochemistry, 913
Polypyridine ligands
Ruthenium(II) complexes, Diethylenetriamine, 815
Polypyridyl
Osmium, Rhenium, Synthesis, Spectroscopy, 1427
Polypyrrole
Schiff-base, Electropolymerization, Iron complex, AFM, Polymer, 1953
Polystyrene supported
Hydrogermane, Reduction, Recycle, 177
Polyynes
Carbon allotropes, Carbyne, Dicyanopolyynes, Cyanopolyynes, Electric arc, Graphite, Liquid nitrogen, 1889
Porphyrazine
EPR, Naphthalene, Copper, Zinc, Cobalt, 1845

Potassium
Ammonolysis, Liquid ammonia/toluene two-phase system, Zirconium, 1125
Potentiometric titration
Uranium, Glycerol phosphate, Complex formation, TRLFS, 1793
Potentiometry
Copper(II) complexes, Thioether ligands, Stability constants, Monophosphono dipeptides, Vis, CD, EPR spectroscopy, 1939
PPh_3
Nickel, Dithiocarbamate, Dppe, X-ray crystal structure, NMR, 77
Precursor hydrolysis
Oxoalkoxides, Aluminium, X-ray, Structure studies, 109
Prochirality
Scorpionate ligands, Tripod ligands, Chirality, Menthone, 245
Proton exchange
Aluminium(III), Catecholates, Salicylates, Complexation, NMR, 2393
Proton sponge
Macrocyclic tetramine, Lanthanide complex, 1,4,8,11-tetramethyl-1,4,8,11-tetraazacyclotetradecane, 1089
Pseudoephedrine
Nickel, Triangulo, Cluster, Anion exchange, 1837
Pseudohalides
Crystal structure, Nickel(II) complexes, Magnetism, 2337
Pt(II) and Pd(II)
LLCT, Luminescence, Phosphorescence, 3173
o-Pthalate
Herometallacrown, Malonate, Cu(II) complexes, 943
Pyranopterin molybdenum enzymes
Sulfite oxidase, Electronic structure, Molybdenum complexes, MCD (Magnetic Circular Dichroism), EPR (Electron Paramagnetic Resonance), 499
Pyrazine
Pyridine, X-ray, NMR, Stacking, Twist, 1011
Pyrazole
Ruthenium arene complexes, Dimethylpyrazole, X-ray structure, Bond valence, 885
Pyrazole
Rhenium nitrosyl complexes, Arsine ligands, X–ray structure, Density functional theory calculations, 2523
Pyrazole
Thallium, ^{11}B NMR, B–H coupling, Tris(pyrazolyl)borate, 2533
Pyrazole
Crystal structures, Clusters, Copper, Molybdenum, Tungsten, Nitrogen heterocycle ligands, 3143
Pyrazole ligand
Rhenium complexes, X-ray structure, DFT calculations, 1819
Pyrazole ligand
Rhenium complexes, X-ray structure, DFT calculations, 2005
Pyrazoline
Nickel complexes, Ring opening, Ligand oxidation, Structures, 1997
Pyrazolone
Copper(II) complexes, Crystal structures, ESR study, 2465
Pyrazolyl ancillary ligands
Iridium, Cyclometalated Ir(II) complexes, Boat conformations, Luminescent, Electroluminescence, 419
Pyrazolyl thiosemicarbazone
Synthesis, Spectroscopy, Cobalt(III) complexes, X-ray crystallography, 5
Pyrazolylborate
Samarium, Lanthanide, Nitric oxide, Nitrite, Redox, 2709
Pyrazolylborates
Lanthanides, Neodymium, X-ray structures, Alkoxides, Borohydrides, 253
Pyrazolylborates
Thallium, NMR, CPMAS, 2985
Pyridine
Platinum, Imine, Benzimidazole, Benzoxazole, Benzothiazole, 155
4,4′-Pyridine
Zinc, 1,3-Bis(4-pyridyl)propane, Polymeric network, X-ray crystallography, 999
Pyridine
Pyrazine, X-ray, NMR, Stacking, Twist, 1011
Pyridine
Crystal structure, Thiazine, Cobalt(III) complex, Nickel(II) complex, 1453
2-Pyridinealdoxime complexes
Crystal structures, Manganese(II) carboxylate chemistry, Magnetochemistry, Metal-assisted reactions, 83
Pyridine binding
Phthalocyanine, Electrochemistry, Spectroelectrochemistry, 1279
Pyridine-2-carboxaldehyde
Cyclopentadienyl, Schiff bases, Ruthenium, 1567
Pyridinecarboxaldimine
Cytotoxicity, Platinum, Palladium, Fluorine, 2169
2-pyridineformamide
Thiosemicarbazone, Crystal structure, Zinc, Cadmium, 2303
Pyridyl
Mercury(II), 1,3-Dithiol-2-thione, ^1H NMR, Solid UV, 115
Pyridyl bispyrazolyl
Terpyridine, Iron, Complexation, Rearrangement, X-ray structures, 3193
Pyridylthioazophenol ligands
Copper(II) complex, Crystal structure, 2457
Pyrolysis
Organometallic compounds, Iron–platinum compounds, 63
Pyrolysis
Organotin derivatives, Tin sulfide, 2102
Pyrone
Enaminones, Molybdenum(VI) complexes, Molybdenum(V) complexes, X-ray crystal structure, NMR spectra, 1859
Quinones
Lawsone, 2-Hydroxy-1, 4-Naphthoquinone, Amine oxidase, Copper complexes, Antiferromagnetic coupling, H-bonding, EPR, 2541
2-Quinolinecarboxaldehyde Schiff bases of *S*-alkyl/aryl dithiocarbazates
Tin(IV) complexes, Dithiocarbazates, 2405

Radical
Iron, Styrene, Catalyst, Polymerisation, 2921
Radical salts
Bis(ethylenedithio)tetrathiafulvalene (ET), Crystal structures, Electrical conductivity, 1185
Reactivity
Crystal structure, Back-bonding, Ruthenium complex, NO, Molecular, 1063
Rearrangement
Terpyridine, Pyridyl bispyrazolyl, Iron, Complexation, X-ray structures, 3193
Recycle
Polystyrene supported, Hydrogermane, Reduction, 177
Redox
Kinetics, Mechanism, Silver, Glyoxylic acid, 895
Redox
Samarium, Lanthanide, Nitric oxide, Nitrite, Pyrazolylborate, 2709
Redox-polymers
Electropolymerisation, Ru-complexes, Thiophene, Differential pulse voltammetry, 4-((2-Thienyl)-ethenyl)-2,2′-bipyridine, 589
Reduction
Polystyrene supported, Hydrogermane, Recycle, 177
Reductive elimination
Molybdenum complexes, Carbonyl complexes, Pentafluorophenyl, Oxidation, Bond cleavage, 1371
Regioselectivity of nucleophile and electrophile additions
Acetonitrile reduction, Amine oxidation, Imido, Metal-nitrogen pi bonding, 311
Rhenium
Scorpionate ligands, Technetium, Uranium, 331
Rhenium
Benzimidazole, Bibenzimidazole, Crystal structure, Paramagnetic NMR, 1139
Rhenium
Osmium, Polypyridyl, Synthesis, Spectroscopy, 1427
Rhenium
Nitrosyls, Phosphine complexes, DFT calculations, 2363
Rhenium cluster, 2611
Rhenium complexes
Pyrazole ligand, X-ray structure, DFT calculations, 1819
Rhenium complexes
Pyrazole ligand, X-ray structure, DFT calculations, 2005

Rhenium nitrosyl complexes
Pyrazole, Arsine ligands, X–ray structure, Density functional theory calculations, 2523
Rhenium(I)
Phosphinite ligands, Dichloromethane complexes, Crystal structures, 1045
Rheological phase reaction
Ionic complex, Crystal structure, Photoluminescence, Europium, Zinc, 529
Rhodium
Trispyrazolylborate, C–H activation, 413
Rhodium
Acetylacetonato complexes, Pentachlorophenolato complexes, Carboxylato complexes, Diazoalkane complexes, C–C coupling reactions, 2645
Rhodium carbonyl complexes
Organotin complexes, Organorhodium complexes, Organorhodiumtin complexes, One-dimensional compounds, Two-dimensional compounds, 103
Rhodium complexes
Polypyrazolylborate complexes, Copper complexes, Scorpionates, Coordination Polymers, Nitrile coordination, 235
Rhodium complexes
Hydrocarboxylation, Oligomerization, Catalysis, Ethylene, Carbon monoxide, 1677
Rhodium complexes
Hydroformylation, Ionic liquids, Biphase catalysis, High-pressure NMR, 2679
Rhodium dicarbonyl complexes
κ^2-Tp ligands, Bridging Tp ligands, Isomers, X-ray structure, 301
Rhodium hydrides
Bridging boryls, Catalyzed hydroborations, 2665
Rhodium(I)
Polypyrazolylborate, Cyclooctadiene, Norbornadiene, Structure, NMR, 219
Rhodium(III)
C–H bond activation, Benzene activation, Aldehyde activation, 2943
Rhodium(III) Ruthenium(II)
Diruthenium(II), Heterodinuclear complexes, Polypyridine complexes, Electrochemistry, 913
Ring opening
Nickel complexes, Pyrazoline, Ligand oxidation, Structures, 1997
Ring-coupled bis-cyclopentadienyl ligand
Binuclear compounds, Isocyanides, Nickel, Polymerisation, X-ray molecular structure, 2715
Roof-shaped
Copper(II) complexes, Crystal structure, Dihydroxo-bridged, Triply bridged, 1641
Rotational barriers
Polyphosphoxane, Cage complexes, Cone angles, 125
Ru-complexes
Electropolymerisation, Thiophene, Differential pulse voltammetry, 4-((2-Thienyl)-ethenyl)-2,2′-bipyridine, Redox-polymers, 589
Ruthenium
Hydrotris(pyrazolyl)borate, Hydrogen bond, Oxidation, Aquo complex, 225
Ruthenium
Heteroscorpionates, Hydrides, Phosphine complexes, Hemilabile ligands, 361
Ruthenium
Scorpionate, Tris(pyrazolyl)borate, Hydride, C–H activation, 439
Ruthenium
Arene ligand, Ferrocene carboxylic acid, Ferrocene derivative, 687
Ruthenium
Cyclopentadienyl, 2,3-Bis(α-pyridyl)pyrazine, 1,3,5-Tris(pyridyl)-2,4,6-triazine, 2,3,5,6-Tetrakis(pyridyl)pyrazine, 1069
Ruthenium
Cyclopentadienyl, Schiff bases, Pyridine-2-carboxaldehyde, 1567
Ruthenium
Fluoroionophore, X-ray, Metallacrown, 1719
Ruthenium
Cymene, X-ray, 2695
Ruthenium arene complexes
Pyrazole, Dimethylpyrazole, X-ray structure, Bond valence, 885
Ruthenium complex
Crystal structure, Back-bonding, NO, Reactivity, Molecular, 1063
Ruthenium complexes
EPR spectroscopy, Hydrazido ligand, Mixed-valence, Spectroelectrochemistry, 701
Ruthenium complexes
Hexamethylbenzene, *p*-Cymene, Diphenyl-2-pyridylphosphine, Amines, 3115
Ruthenium(II) carbonyl complexes
Tertiary phosphine chalcogenides, ''Soft–Hard'' and ''Soft–Soft'' interactions, X-ray crystal structure, Octahedral structure, 1657
Ruthenium(II) complexes
Polypyridine ligands, Diethylenetriamine, 815
Ruthenium(II)-tris-chelates
Azoimidazoles, X-ray structure, Electrochemistry, 727

N-salicylidene-*n*-alkanoylhydrazines
Copper(II) complexes, Magnetochemical studies, Bis[monochloro(μ-*N*-salicylidene-myristoylhydrazine) ONO′(−1)]dicopper(II), X-ray crystal and molecular structure, 23
S ligands
Coordination chemistry, Aurates, Thianthrenes, 1351
S,N ambidentate borate ligands
Synthesis, X-ray structure, Open frame material, 205
Saccharin complexes
Copper(II) complexes, Dithiocarbazates, 2031
Saccharin complexes
Cu(II) complexes, Dithiocarbazate Schiff base, *S*-Methyldithiocarbazate, Tridentate NNS Schiff base, 2491
Salicylates
Aluminium(III), Catecholates, Complexation, Proton exchange, NMR, 2393
Salicylketimine ligands
Nickel(II) complexes, Schiff bases, X-ray crystallography, 1649
Salt metathesis
Tris(pyrazolyl)hydroborate (Tp) ligands, Lanthanum, Neodymium, Aryloxide derivatives, 2437
Samarium
Lanthanide, Nitric oxide, Nitrite, Pyrazolylborate, Redox, 2709
Sandwich complex
Organometallics, Metallocene, Bonding, Density functional theory, Orbital analysis, 2993
Schiff base
Uranium, Cluster, Crystal structure, 623
Schiff base
Asymmetric oxidation, Chiral copper(II) complexes, Sulfide, Seven-membered, 1131
Schiff base
Cadmium(II)thiocyanate, Polymer, Imidazole, Supramolecular synthon, 2045
Schiff base
Dicopper(II) complex, 1D Coordination polymer, Crystal structure, Magnetic properties, 2177
Schiff base
Chiral, Copper, Cyclopropanation, Catalysts, Crystal structures, 3051
Schiff base
Copper(II) complex, X-ray structure, Imine activation, Coordination polymer, 3081
Schiff base complexes
Copper complexes, Tripeptide complexes, 849
Schiff base complexes
Ion recognition, Crown ether, UV–Vis, Lanthanides, 1401
Schiff bases
Tricopper(II) complex, Ascorbate oxidase model, Crystal structure, Magnetic properties, 643
Schiff bases
Iron complexes, Acetate ligands, η^2-Coordination modes, β-Cis arrangements, 963
Schiff bases
Cyclopentadienyl, Pyridine-2-carboxaldehyde, Ruthenium, 1567
Schiff bases
Dioxomolybdenum (VI) and oxomolybdenum (IV) complexes, Dithiocarbazate, X-ray structures, 1595
Schiff bases
Nickel(II) complexes, Salicylketimine ligands, X-ray crystallography, 1649
Schiff's bases
Nickel, Hydrogenated Schiff's bases, Coordination geometry, X-ray crystal structures, Polymethylene chains, 3201
Schiff-base
Polypyrrole, Electropolymerization, Iron complex, AFM, Polymer, 1953

Schiff-bases
Zinc complexes, Crystal structures, IR, UV and NMR spectroscopy, Thermal analysis, 1293
Scorpionands
Chromophores, Copper(II), Macrocycles, Nickel(II), 373
Scorpionate
Ruthenium, Tris(pyrazolyl)borate, Hydride, C–H activation, 439
Scorpionate ligands
Tripod ligands, Chirality, Prochirality, Menthone, 245
Scorpionate ligands
Technetium, Rhenium, Uranium, 331
Scorpionate ligands
Hydrotris(pyrazolyl)borate, Tantalum, Metal–metal multiple bond, Alkyne complex, Tetrahydrothiophene complex, 379
Scorpionates
Polypyrazolylborates, Coordination chemistry, Nitrogen ligands, 197
Scorpionates
Nickel(II) complexes, Crystal structures, Hydrotris(pyrazolyl)borate complexes, Coordination environment, 211
Scorpionates
Polypyrazolylborate complexes, Copper complexes, Rhodium complexes, Coordination Polymers, Nitrile coordination, 235
Scorpionates
Hydrotris(pyrazol-1-yl)borates, Polypyrazolylborates, Photoelectron spectra, 429
Secondary bonding
Cyclic telluranes, Metathetical reactions, Intermolecular, Supramolecular networks, 1629
Selenium
Phosphine chalcogenides, X-ray structure, ^{31}P NMR, Tellurium, 1923
Selenium
Palladium, Complexes, X-ray, 2967
Selenourea
Crystal structure, Gold complex, MAS NMR, 1
Self assembly
One-dimensional, Silver(I), Aliphatic amino ligands, Coordination polymers, Tubes, Topology, Supramolecular chemistry, Nanotubes, 2075
Self-assemble
Carboxylate bridges, Copper complexes, Dipeptides, Alkaline earth metals, Magnetic properties, 2125
Self-assembly
Lanthanide nitrate, *N*,*N*′-dioxide, Coordination polymer, 169
Self-assembly
Crystal structures, Bis(2-pyridylmethyl)amino acids, Ferromagnetism, One-dimensional chains, Copper(II) complexes, 903
Self-assembly
Copper, N,O-ligands, Dinuclear, EPR, 1769
Self-assembly
Supramolecular chemistry, Polymers, Transition metal, Crystal engineering, 1877
Semicarbazone
Cobalt(III), 2-Hydroxyacetophenone, NMR spectra, IR spectra, Electronic spectra, X- ray crystal structure, 41
Seven-coordinate tin(IV) complexes
Tin(IV) complexes, Dithiocarbazates, 2,6-diacetylpyridine Schiff bases of S-alkyldithiocarbazates, 2037
Seven-membered
Asymmetric oxidation, Chiral copper(II) complexes, Schiff base, Sulfide, 1131
Sheet structure
Arylazoimidazoles, Cadmium(II) complexes, End-on and end-to-end bridging, X-ray structure, 1D chain, 1669
Silanoles
Siloxides, Titanium, Zirconium, Oligosilanes, 2475
Silica gel
Immobilization, 2-Aminomethylpyridine, Epoxide, Adsorption, Thermodynamic, 719
Silica support
Immobilization, Cobalt(II) complexes, H_2O_2, 59
Silicic acid
Hydroxyaluminosilicate, Aluminium, Aluminium solubility, Aluminium biological availability, 3185
Silicon
Phosphorus, Hypercoordination, Hypervalency, Spectroscopy, Fluorescence, X-ray crystallography, 2615
Siloxides
Silanoles, Titanium, Zirconium, Oligosilanes, 2475
Silver
Kinetics, Mechanism, Redox, Glyoxylic acid, 895
Silver
Coordination polymers, Imidazolate, X-ray structure, 3063
Silver complexes
Diaza-fluorene, Crystal structures, Intermolecular interactions, Electronic spectra, 2259
Silver coordination complex polymers
1D, 2D, 3D topological structure, Multinitriles, 2209
Silver nitrate
Carboxylate, Coordination polymer, Double betaine, Hydrate, Hydrogen bonding, π–π Interaction, 2413
Silver(I)
Bis-imidazole, Bis(imidazol-2-yl)methane, X-ray structures, Argentophilicity, Antifungal, Candida albicans, 1249
Silver(I)
One-dimensional, Aliphatic amino ligands, Coordination polymers, Tubes, Topology, Supramolecular chemistry, Self assembly, Nanotubes, 2075
Silver(I) complexes
Naphthylazoimidazole, Helical structure, EHMO, 793
Silver(I) complexes
Dinuclear complex, Mononuclear complex, 2117
Silver(II) complexes
Ozone, X-ray crystal structure, Manganese(III) complexes, Cobalt(III) complexes, 2631
Sinambic
Multidentate ligand, Cobalt(III), ^{59}Co NMR, 2217
Single crystal X-ray diffraction
Iron(III) complexes, Thiosemicarbazone, Mössbauer spectra, EPR spectra, IR spectra, 969
Single-crystal X-ray diffraction
Tetrakis(3-isopropylpyrazolyl)borate, Solvent extraction, Zinc, Copper, 283
Six coordinate silicates
Ion exchange, Transition metals, Ligand environment, Thermal studies, Magnetism, 679
Sodium
Copper, Tris(pyrazolyl)borate, Fluorinated, Carbonyl, 273
"Soft–Hard" and "Soft–Soft" interactions
Ruthenium(II) carbonyl complexes, Tertiary phosphine chalcogenides, X-ray crystal structure, Octahedral structure, 1657
Solid UV
Mercury(II), 1,3-Dithiol-2-thione, Pyridyl, ^{1}H NMR, 115
Solid-state reactions
Iron clusters, Third-order nonlinear optical properties, 755
Solvent extraction
Tetrakis(3-isopropylpyrazolyl)borate, Single-crystal X-ray diffraction, Zinc, Copper, 283
Solvothermal synthesis
Thiostannates, Nickel, Crystal structures, Thermoanalysis, 937
Spectra
Mn(II) and Cd(II) complexes, Azides, 3-Aminopyridine, Synthesis, X-ray structures, Thermal properties, 2349
Spectral properties
Copper, Crystal structure, Dimer, Magnetic properties, 1303
Spectral properties
Copper, 3,5-Dinitrosalicylate complex, Trimer, Crystal structure, Magnetic properties, 2447
Spectroelectrochemistry
EPR spectroscopy, Hydrazido ligand, Mixed-valence, Ruthenium complexes, 701
Spectroelectrochemistry
Phthalocyanine, Electrochemistry, Pyridine binding, 1279
Spectroelectrochemistry
Vanadium, Diiminediaminediphenolate macrocycle, Magnetochemistry, EPR, FTIR, 2069
Spectroscopic characterisation
Uranyl, Fluoride, Phosphine oxide ligands, Structural study, 3097
Spectroscopic properties
Iron(II) complexes, Trithiocyanuric acid, Mössbauer spectra, Crystal structures, DFT calculations, 2193

Spectroscopic studies
Indomethacin, Diorganotin, Crystal structures, 2021
Spectroscopy
Synthesis, Pyrazolyl thiosemicarbazone, Cobalt(III) complexes, X-ray crystallography, 5
Spectroscopy
Carborane, DFT calculations, X-ray crystallography, 629
Spectroscopy
Hydrazones, Complex, Lanthanide, X-ray, Crystal structures, 1191
Spectroscopy
Osmium, Rhenium, Polypyridyl, Synthesis, 1427
Spectroscopy
Di-2-pyridyl ketone salicyloylhydrazone, Zinc(II) complexes, Stability constants, Thermal analysis, 2095
Spectroscopy
Silicon, Phosphorus, Hypercoordination, Hypervalency, Fluorescence, X-ray crystallography, 2615
Spherical potential well
Clusters, Electron density distribution, Polarizability, Finite electric field, 1519
Spin-crossover
Iron, Crystal structure, Magnetic measurements, 2141
Spin-exchange reactions
Electron-transfer reactions, Bis[tris(pyrazolyl)methane] complexes, Low-spin configurations, High-spin configurations, 1037
Spirocyclic
Cyclophosphazenes, Chiral, X-ray structure, 979
Spiroindolinonaphthooxazines
Absorption spectra, Complexation, Kinetics, Photochromism, 3147
Square antiprism
Eight-coordinate, Stereochemistry, Dodecahedron, Bicapped trigonal prism, Molecular mechanics, 145
Square antiprism
Cadmium(II), Chloranilate anions, Phenanthroline, Crystal structures, Chain polymers, 2587
Square grid structure
Hydrothermal synthesis, Coordination polymer, Magnetic property, Transition metal, 1,4-Naphthalenedicarboxylic acid, 1257
Square planar silver complex
Bitopic heteroscorpionate ligand, 291
Stability constants
Diporphyrins, Zinc(II) complexes, Nitrogen base ligation, 33
Stability constants
Copper(II) complexes, Thioether ligands, Monophosphono dipeptides, Potentiometry, Vis, CD, EPR spectroscopy, 1939
Stability constants
Di-2-pyridyl ketone salicyloylhydrazone, Zinc(II) complexes, Spectroscopy, Thermal analysis, 2095
Stacking
Pyrazine, Pyridine, X-ray, NMR, Twist, 1011
π–π stacking
Copper(II), Aminopolycarboxylate, Ferromagnetic coupling, Cylindrical channels, 1081
π–π stacking interactions
2,2′-Bipyrimidine complexes, Iron(III) carboxylate complexes, Oxo-bridged iron(III) complexes, X-ray crystal structure, 1271
π–π stacking interaction
1-(4-Hydroxyphenyl)-1H-tetrazole-5-thiol, Organotin(IV), Hydrogen bonding, Crystal structures, X-ray crystallography, 1547
π–π staking interaction
4,4′-Bipyridine, Lead(II), Coordination polymers, Lone pair, Crystal structure, 2427
Stereochemistry
Eight-coordinate, Dodecahedron, Square antiprism, Bicapped trigonal prism, Molecular mechanics, 145
Sterically hindered carboxylate
Non-heme iron, Water coordination, X-ray structure, Cyclic voltammetry, 2805
Structural elucidation
Tetranuclear copper(II) complex, Hydrogen bonds, 1169
Structural study
Uranyl, Fluoride, Phosphine oxide ligands, Spectroscopic characterisation, 3097
Structure
Polypyrazolylborate, Rhodium(I), Cyclooctadiene, Norbornadiene, NMR, 219
Structure
Copper, Magnetism, Dinuclear, EPR, 993
Structure
Copper, Infrared, Hydrogen bonds, Distortion isomers, 1969
Structure studies
Oxoalkoxides, Aluminium, Precursor hydrolysis, X-ray, 109
Structures
Tris(pyrazolyl)borate, Bis(imido), Molybdenum, Synthesis, 189
Structures
Zwitterions, Monoanionic ligands, Syntheses, Methyl, Hydrides, 489
Structures
Cobalt, Oxide, β-diketonates, Adducts, MOCVDf, 735
Structures
Cobalt, Copper, Zinc, Bis(8-quinolinyl)amine, 831
Structures
Nickel complexes, Pyrazoline, Ring opening, Ligand oxidation, 1997
Structures
Tantalum, Pentalene, Synthesis, 2625
Structures
Zwitterions, Monoanionic ligands, Phosphines, Syntheses, Boron, 2901
Styrene
Iron, Radical, Catalyst, Polymerisation, 2921
Sulfide
Asymmetric oxidation, Chiral copper(II) complexes, Schiff base, Seven-membered, 1131
Sulfite oxidase
Pyranopterin molybdenum enzymes, Electronic structure, Molybdenum complexes, MCD (Magnetic Circular Dichroism), EPR (Electron Paramagnetic Resonance), 499
Sulfonatothiacalixarene
Capsules, Diaza-Crown ether, Transition metal ions, Assembly, 1461
Sulfonatothiacalixarene
Capsules, Diaza-18-crown-6, Lanthanide ions, 2055
Sulfur
Phosphorus, Clusters, Phosphorus sulfides, Laser ablation synthesis, TOF mass spectrometry, 1199
Sulfur-rich complex
Lawesson's Reagent, Thiophosphoryl compound, Nickel(II) complex, Cobalt(II) complex, 1799
Superhyperfine
Binuclear copper complex, EPR, Half-field, X-ray, Electrochemical, 1115
Supramolecular
Coordination polymer, Europium, Hydrogen bonds, Luminescence, Terbium, 711
Supramolecular
Cadmium, Coordinate, Polymers, Ligands, 1003
Supramolecular associations
Te(II) thiourea complexes, Novel conformations, Unexpected colours, X-ray crystallography, 3021
Supramolecular chemistry
Self-assembly, Polymers, Transition metal, Crystal engineering, 1877
Supramolecular chemistry
One-dimensional, Silver(I), Aliphatic amino ligands, Coordination polymers, Tubes, Topology, Self assembly, Nanotubes, 2075
Supramolecular chemistry
P,*S*-metallocycles, Bipodal ligands, Crystal structures, Macrocycles, Phosphorylated urea complexes, 2243
Supramolecular frameworks
Isoorotic acid, Co(II) and Ni(II) complexes, Hydrothermal synthesis, Hydrogen bonds, 2227
Supramolecular networks
Cyclic telluranes, Metathetical reactions, Intermolecular, Secondary bonding, 1629
Supramolecular synthon
Cadmium(II)thiocyanate, Polymer, Schiff base, Imidazole, 2045
Supramolecule
Lanthanide(III) complexes, Hydrothermal syntheses, Isoorotic acid, Hydrogen bonds, 2085
Suzuki–Miyaura coupling
Palladium, Ferrocene, Phosphine, Orthometallated complexes, X-ray crystallography, 921

Syntheses
Zwitterions, Monoanionic ligands, Structures, Methyl, Hydrides, 489
Syntheses
Zwitterions, Monoanionic ligands, Phosphines, Structures, Boron, 2901
Synthesis
Spectroscopy, Pyrazolyl thiosemicarbazone, Cobalt(III) complexes, X-ray crystallography, 5
Synthesis
Tris(pyrazolyl)borate, Bis(imido), Molybdenum, Structures, 189
Synthesis
S,N ambidentate borate ligands, X-ray structure, Open frame material, 205
Synthesis
Cadmium(II), Calcium(II), Manganese(II), Crystal structures, Tetrazolate complexes, 1217
Synthesis
Osmium, Rhenium, Polypyridyl, Spectroscopy, 1427
Synthesis
Crystal structures, Indenyl ligand, Nickel complex, Catalysis, 1473
Synthesis
Zinc complex, Cadmium complex, 2-Oxo-1,3-dithiole-4,5-dithiolate, Crystal structure, Density functional calculation, 1701
Synthesis
Heteroaromatic carboxylic acid, Triphenyltin, Crystal structure, 1805
Synthesis
Mn(II) and Cd(II) complexes, Azides, 3-Aminopyridine, Spectra, X-ray structures, Thermal properties, 2349
Synthesis
Phosphine, Coordination, X-ray structure, 2575
Synthesis
Tantalum, Pentalene, Structures, 2625

Tantalum
Hydrotris(pyrazolyl)borate, Scorpionate ligands, Metal–metal multiple bond, Alkyne complex, Tetrahydrothiophene complex, 379
Tantalum
Pentalene, Synthesis, Structures, 2625
Te(II) thiourea complexes
Novel conformations, Unexpected colours, X-ray crystallography, Supramolecular associations, 3021
Technetium
Scorpionate ligands, Rhenium, Uranium, 331
Tellurium
Phosphine chalcogenides, X-ray structure, ^{31}P NMR, Selenium, 1923
Temperature effect
Manganese maleate, Coordination polymer, Helical architecture, Hydrogen bonds, π–π interactions, 987
Template
Hydrothermal synthesis, Crystal structure, Iron phosphatooxalate, Oxalate acid, Piperazine, 2357
Template reaction
Chirality, Tetra-azamacrocycles, Pendent arm, Conformational isomers, 869
Template synthesis
Decaazacyclooctadecane, Nickel(II) complexes, Macrocycle, 1325
Templating effect
Hydrothermal syntheses, Crystal structures, Gallophosphates, 1535
Terbium
Coordination polymer, Europium, Hydrogen bonds, Luminescence, Supramolecular, 711
Terephthalate ligand
Nickel(II) compounds, Crystal structures, Binuclear complexes, Magnetic properties, 1379
Terephthalate ligand
Copper(II) compounds, Crystal structures, One-dimensional complexes, Magnetic properties, 3043
Terpyridine
Iridium, Luminescence, Near infra-red, Charge-transfer, Intra-ligand charge transfer, 2769
Terpyridine
Pyridyl bispyrazolyl, Iron, Complexation, Rearrangement, X-ray structures, 3193
Tertiary phosphine chalcogenides
Ruthenium(II) carbonyl complexes, "Soft–Hard" and "Soft–Soft" interactions, X-ray crystal structure, Octahedral structure, 1657
2,3,5,6-Tetrakis(pyridyl)pyrazine
Ruthenium, Cyclopentadienyl, 2,3-Bis(α-pyridyl)pyrazine, 1,3,5-Tris(pyridyl)-2,4,6-triazine, 1069
1,4,8,11-tetramethyl-1,4,8,11-tetraazacyclotetradecane
Proton sponge, Macrocyclic tetramine, Lanthanide complex, 1089
Tetra-azamacrocycles
Chirality, Template reaction, Pendent arm, Conformational isomers, 869
Tetrachloroaurate(III)
Crystal structure, Phase transition, Isotope effect, Hydrogen bond, NQR, 1605
Tetradentate ligands
Aromatic aminoacidate, Cobalt(III), Non-covalent interactions, Octahedral inversion, NMR, 1749
Tetrahydrofurfurylindenyl
Lanthanide chlorides, Crystal structure, Ionic radius, 1075
Tetrahydrothiophene complex
Hydrotris(pyrazolyl)borate, Scorpionate ligands, Tantalum, Metal–metal multiple bond, Alkyne complex, 379
Tetrakis(3-isopropylpyrazolyl)borate
Solvent extraction, Single-crystal X-ray diffraction, Zinc, Copper, 283
Tetranuclear copper(II) complex
Structural elucidation, Hydrogen bonds, 1169
Tetrathiafulvalene
Copper(II), Charge transfer compounds, Electrical conductivity, 2111
Tetrathiomolybdate
Tetrathiotungstate, Dihydridobis(pyrazolyl)borate, Copper(I) complexes, Crystal structure, Model compounds, 637
Tetrathiotungstate
Tetrathiomolybdate, Dihydridobis(pyrazolyl)borate, Copper(I) complexes, Crystal structure, Model compounds, 637
Tetrazolate complexes
Cadmium(II), Calcium(II), Manganese(II), Synthesis, Crystal structures, 1217
Tetrazole
Titanium, Tin, Nitride precursor, Cycloaddition, 801
Thallium
Bis(mercaptoimidazolyl)borate complexes, Crystal structure, 617
Thallium
Parabanic acid, Iron, Cyclopentadienyl, Carbonyl, Gold (I) complex, Alkylation, 1441
Thallium
Metalloporphyrins, Indium, 1777
Thallium
^{11}B NMR, B–H coupling, Tris(pyrazolyl)-borate, Pyrazole, 2533
Thallium
Pyrazolylborates, NMR, CPMAS, 2985
Thermal analysis
Copper(I) complexes, Hexafluorocetylacetonate, Olefin complexes, Divinyl organics, Crystal structure, 809
Thermal analysis
Zinc complexes, Schiff-bases, Crystal structures, IR, UV and NMR spectroscopy, 1293
Thermal analysis
Di-2-pyridyl ketone salicyloylhydrazone, Zinc(II) complexes, Stability constants, Spectroscopy, 2095
Thermal behaviour
Nickel, Copper, Zinc, Imidazole, α-Hydroxycarboxylato complexes, Crystal structures, 1505
Thermal decomposition
Cerium, Oxazolines, Chiral, MOCVD, β-ketoesterates, 1467
Thermal decomposition
1,3,4-thiadiazole, Zinc, Crystal structure, Kinetics, Bioactivity, 1851
Thermal properties
Magnesium carboxylate, Meltable, Dispersion processing, 1739
Thermal properties
Mn(II) and Cd(II) complexes, Azides, 3-Aminopyridine, Synthesis, Spectra, X-ray structures, 2349
Thermal studies
Six coordinate silicates, Ion exchange, Transition metals, Ligand environment, Magnetism, 679
Thermoanalysis
Solvothermal synthesis, Thiostannates, Nickel, Crystal structures, 937
Thermochromism
Chemical vapour deposition, Thin films, Vanadium dioxide, 3087

Thermodynamic
Silica gel, Immobilization, 2-Aminomethylpyridine, Epoxide, Adsorption, 719
Thianthrenes
S ligands, Coordination chemistry, Aurates, 1351
Thiazine
Crystal structure, Cobalt(III) complex, Nickel(II) complex, Pyridine, 1453
Thiazolidine
Vic-dioximes, Ferrocene, Transition metal complexes, Electrochemistry, 1987
1,3,4-thiadiazole
Zinc, Crystal structure, Thermal decomposition, Kinetics, Bioactivity, 1851
4-((2-Thienyl)-ethenyl)-2,2′-bipyridine
Electropolymerisation, Ru-complexes, Thiophene, Differential pulse voltammetry, Redox-polymers, 589
2-Thiopheneacetic acid
Polymeric copper(II) complex, Crystal structure, Vibrational spectra, Metal isotope effect, 1785 Thin films
Chemical vapour deposition, Thermochromism, Vanadium dioxide, 3087
Thiodiglycolic acid complexes
Nickel(II), X-ray structures, Magnetic properties, 1573
Thioether complexes
Platinum complexes, Trithiacyclononane, Platinum nuclear magnetic resonance, Diimine complexes, Crown thioethers, 1361
Thioether ligands
Copper(II) complexes, Stability constants, Monophosphono dipeptides, Potentiometry, Vis, CD, EPR spectroscopy, 1939
Thioethers
Copper, *N*-ligands, Multi-armed ligands, X-ray structures, Coordination polymer, 1055
Thiolate
Zinc, Enzyme, Alkylation, 481
Thiophene
Electropolymerisation, Ru-complexes, Differential pulse voltammetry, 4-((2-Thienyl)-ethenyl)-2,2′-bipyridine, Redox-polymers, 589
Thiophosphoryl compound
Lawesson's Reagent, Sulfur-rich complex, Nickel(II) complex, Cobalt(II) complex, 1799
Thiosemicarbazone
Iron(III) complexes, Single crystal X-ray diffraction, Mössbauer spectra, EPR spectra, IR spectra, 969
Thiosemicarbazone
Di-2-pyridyl ketone, Ni(II) thiosemicarbazone complex, Electronic spectra, IR spectra, X-ray crystal structure, 1225
Thiosemicarbazone
2-pyridineformamide, Crystal structure, Zinc, Cadmium, 2303
Thiosemicarbazone
Copper(II) complexes, 2-Hydroxyacetophenone, EPR, Antimicrobial studies, Cyclic voltammetry, X-ray crystallography, 2549
Thiosemicarbazone
Copper(II) complexes, 2-Benzoylpyridine, EPR, Antimicrobial activity, Crystal structure, 3069
Thiostannates
Solvothermal synthesis, Nickel, Crystal structures, Thermoanalysis, 937
Third-order nonlinear optical properties
Iron clusters, Solid-state reactions, 755
Three-dimensional oxide
Octamolybdate, Hydrothermal synthesis, Organic–inorganic hybrid, Building block approach, Hartree–Fock calculations, 1145
Tin
Ferrocene, Dithiocarbazate, Ligand, Complex, Crystal structure, 567
Tin
Titanium, Tetrazole, Nitride precursor, Cycloaddition, 801
Tin sulfide
Pyrolysis, Organotin derivatives, 2102
Tin(IV) complexes
Dithiocarbazates, 2,6-diacetylpyridine Schiff bases of S-alkyldithiocarbazates, Seven-coordinate tin(IV) complexes, 2037
Tin(IV) complexes
Dithiocarbazates, 2-Quinolinecarboxaldehyde Schiff bases of *S*-alkyl/aryl dithiocarbazates, 2405
Titanium
Bipyridine, Aluminum, Coordination compound, Crystal structure, 561
Titanium
Tin, Tetrazole, Nitride precursor, Cycloaddition, 801
Titanium
Enolato, Enamido, Zirconium, Aluminum, 1587
Titanium
Silanoles, Siloxides, Zirconium, Oligosilanes, 2475
Titanium iodide
Phosphine, Arsine, Iron iodide, Crystal structures, 605
Titanium phosphate
Hydrothermal, Layered, Intercalation behavior, γ-Phase, 3033
TOF mass spectrometry
Phosphorus, Sulfur, Clusters, Phosphorus sulfides, Laser ablation synthesis, 1199
Topological analysis of electron density
MP2 geometry optimization, Bis(methoxycarbimido)amine, 2235
Topology
One-dimensional, Silver(I), Aliphatic amino ligands, Coordination polymers, Tubes, Supramolecular chemistry, Self assembly, Nanotubes, 2075
κ^2-Tp ligands
Bridging Tp ligands, Rhodium dicarbonyl complexes, Isomers, X-ray structure, 301
trans-1,2-Diaminocyclohexane
Crystal structure, Zinc complex, Catalytic enantioselective reduction, 2063
Transfer hydrogenation
N-Heterocyclic carbenes, Homogenous catalysis, Ketones, Aldehydes, Imines, 2857
Transformation
Molybdenum phosphate, Hydrothermal synthesis, Crystal structure, 2153
Transition metal
Hydrothermal synthesis, Coordination polymer, Magnetic property, Square grid structure, 1,4-Naphthalenedicarboxylic acid, 1257
Transition metal
Supramolecular chemistry, Self-assembly, Polymers, Crystal engineering, 1877
Transition metal complexes
Vic-dioximes, Thiazolidine, Ferrocene, Electrochemistry, 1987
Transition metal ions
Sulfonatothiacalixarene, Capsules, Diaza-Crown ether, Assembly, 1461
Transition metals
Six coordinate silicates, Ion exchange, Ligand environment, Thermal studies, Magnetism, 679
Triangulo
Pseudoephedrine, Nickel, Cluster, Anion exchange, 1837
Triazenido complexes
Diruthenium compounds, Metal–metal bonds, Formamidinato complexes, Multiple bonds, Low spin complexes, 2637
Triazolopyrimidine
Zn complexes, Copper dimers, EPR, 743
Triazolopyrimidine
Palladium dimers, Head–head, Head–tail, 2373
Tricopper(II) complex
Schiff bases, Ascorbate oxidase model, Crystal structure, Magnetic properties, 643
Tridentate NNS and NSS Schiff bases
S-2-picolyldithiocarbazate (Hydrazine carbodithioic acid pyridinium-2-yl methyl ester chloride), Bidentate NS Schiff base, Ni(II) complexes, Dithiocarbazate derivative, 161
Tridentate NNS Schiff base
Cu(II) complexes, Dithiocarbazate Schiff base, Saccharin complexes, *S*-Methyldithiocarbazate, 2491
Trimer
Copper, 3,5-Dinitrosalicylate complex, Crystal structure, Magnetic properties, Spectral properties, 2447
Tripeptide complexes
Copper complexes, Schiff base complexes, 849
Triphenyltin
Heteroaromatic carboxylic acid, Synthesis, Crystal structure, 1805
Triply bridged
Copper(II) complexes, Crystal structure, Dihydroxo-bridged, Roof-shaped, 1641
Tripod ligands
Scorpionate ligands, Chirality, Prochirality, Menthone, 245

Tripodal
Heteroscorpionate, Alkylthiolate, Imidazole, Iron, Zinc, 471
Tripodal amine ligand
Hypodentate, Cu(II) complexes, Crystal structure, Five-coordinate, 97
Tripodal ligand
Cu-NIRs, Model complex, Crystalline structure, Polyimidazole ligand, 511
Tripodal ligand
Nickel complex, Cyclic voltammetry, 1829
1,3,5-Tris(pyridyl)-2,4,6-triazine
Ruthenium, Cyclopentadienyl, 2,3-Bis(α-pyridyl)pyrazine, 2,3,5,6-Tetrakis(pyridyl)pyrazine, 1069
Tris(2-pyridylmethyl)amine
Iron(II) complexes, Cobalt(II) complexes, X-ray crystal structures, Bis(2-pyridylmethyl)amine, 3105
Tris(cyclohexyl)tin
Halostannanes, Crystal structures, 2331
Tris(mercaptoimidazolyl)borate complexes
Nickel, Bis(mercaptoimidazolyl)borate complexes, Diphosphine, Hydrogenases, Crystal structure, 395
Tris(pyrazolyl)borate
Bis(imido), Molybdenum, Synthesis, Structures, 189
Tris(pyrazolyl)borate
Lanthanides, Ytterbium, Aryloxide, Crystal Structures, Divalent, 263
Tris(pyrazolyl)borate
Sodium, Copper, Fluorinated, Carbonyl, 273
Tris(pyrazolyl)borate
Ruthenium, Scorpionate, Hydride, C–H activation, 439
Tris(pyrazolyl)borate
Cyanide bridged clusters, Iron(III) complex, Magnetic properties, 1333
Tris(pyrazolyl)borate
Thallium, ^{11}B NMR, B–H coupling, Pyrazole, 2533
Tris(pyrazolyl)hydroborate (Tp) ligands
Lanthanum, Neodymium, Salt metathesis, Aryloxide derivatives, 2437
Trispyrazolylborate
C–H activation, Rhodium, 413
Trithiacyclononane
Thioether complexes, Platinum complexes, Platinum nuclear magnetic resonance, Diimine complexes, Crown thioethers, 1361
Trithiocyanuric acid
Iron(II) complexes, Mössbauer spectra, Crystal structures, Spectroscopic properties, DFT calculations, 2193
TRLFS
Uranium, Glycerol phosphate, Complex formation, Potentiometric titration, 1793
Tubes
One-dimensional, Silver(I), Aliphatic amino ligands, Coordination polymers, Topology, Supramolecular chemistry, Self assembly, Nanotubes, 2075
Tungsten
η^2-nitrile, Oxo, Oxidation, Methylation, Dimerization, 2831
Tungsten
Crystal structures, Clusters, Copper, Molybdenum, Nitrogen heterocycle ligands, Pyrazole, 3143
Twist
Pyrazine, Pyridine, X-ray, NMR, Stacking, 1011
Two-dimensional compounds
Organotin complexes, Organorhodium complexes, Organorhodiumtin complexes, One-dimensional compounds, Rhodium carbonyl complexes, 103

Unexpected colours
Te(II) thiourea complexes, Novel conformations, X-ray crystallography, Supramolecular associations, 3021
Unsymmetrical
Phthalocyanine, Phenylacetylene, Cyclic voltammetry, 3155
Unsymmetrical oximinato dicopper(II) complexes and unsymmetrical oximinato dinickel(II) complexes
Electrochemistry, Magnetic properties, Oximinato monocopper(II) and mononickel(II) complexes, 665
Uranium
Scorpionate ligands, Technetium, Rhenium, 331
Uranium
Schiff base, Cluster, Crystal structure, 623
Uranium
Glycerol phosphate, Complex formation, Potentiometric titration, TRLFS, 1793
Uranium
Crystal structure, N, O donor ligands, 2285
Uranium
Actinide, Lanthanide, Oxides, Carbene, 2689
Uranyl
Fluoride, Phosphine oxide ligands, Structural study, Spectroscopic characterisation, 3097
Uranyl bis(β-diketonates)
Bis(diphenylphosphino)methane dioxide, Uranyl nitrate, Monodentate, Bidentate chelate, Bridging bidentate, Coordination modes, 1527
Uranyl ion
Alkali metal ions, Calixarenes, Homooxacalixarenes, Crystal structures, 649
Uranyl ions
Diols, Hydrogen bonding, Crystal structures, 1613
Uranyl nitrate
Bis(diphenylphosphino)methane dioxide, Uranyl bis(β-diketonates), Monodentate, Bidentate chelate, Bridging bidentate, Coordination modes, 1527
UV and NMR spectroscopy
Zinc complexes, Schiff-bases, Crystal structures, IR, Thermal analysis, 1293
UV–Vis
Ion recognition, Schiff base complexes, Crown ether, Lanthanides, 1401
UV–Vis, EPR and IR spectra
Dinuclear copper(II) complex, Magnetic properties, Bidentate ligand, Crystal structure, 1309

^{51}V NMR spectra
Crystal structure, Vanadium(V) peroxo mandelato complex, IR spectra, 655
Vanadium
Diiminediaminediphenolate macrocycle, Magnetochemistry, EPR, FTIR, Spectroelectrochemistry, 2069
Vanadium complexes
Nitrilotriacetate, X-ray crystal structure, Hydrogen bonding, 1975
Vanadium dioxide
Chemical vapour deposition, Thermochromism, Thin films, 3087
Vanadium(V) peroxo mandelato complex
Crystal structure, IR spectra, ^{51}V NMR spectra, 655
Vibrational spectra
2-Thiopheneacetic acid, Polymeric copper(II) complex, Crystal structure, Metal isotope effect, 1785
Vinylic polymerizaition
Neutral palladium(II) complex, X-ray crystallography, Catalyst, Methylaluminoxane, Norbornene, 1619
Vis, CD, EPR spectroscopy
Copper(II) complexes, Thioether ligands, Stability constants, Monophosphono dipeptides, Potentiometry, 1939

Water coordination
Non-heme iron, X-ray structure, Cyclic voltammetry, Sterically hindered carboxylate, 2805
Weak ferromagnetism
Malonate complexes, 2D antiferromagnets, 929

X–ray structure
Rhenium nitrosyl complexes, Pyrazole, Arsine ligands, Density functional theory calculations, 2523
X- ray crystal structure
Cobalt(III), Semicarbazone, 2-Hydroxyacetophenone, NMR spectra, IR spectra, Electronic spectra, 41
X-ray
Oxoalkoxides, Aluminium, Precursor hydrolysis, Structure studies, 109
X-ray
Pyrazine, Pyridine, NMR, Stacking, Twist, 1011
X-ray
Binuclear copper complex, EPR, Halffield, Superhyperfine, Electrochemical, 1115
X-ray
Hydrazones, Complex, Lanthanide, Spectroscopy, Crystal structures, 1191

X-ray
Ruthenium, Fluoroionophore, Metallacrown, 1719
X-ray
Ligand, Bidentate, Bridging, Phosphine, 2569
X-ray
Cymene, Ruthenium, 2695
X-ray
Palladium, Selenium, Complexes, 2967
X-ray crystal and molecular structure
N-salicylidene-*n*-alkanoylhydrazines, Copper(II) complexes, Magnetochemical studies, Bis[monochloro(μ-*N*-salicylidenemyristoylhydrazine) ONO′(−1)]dicopper(II), 23
X-ray crystal structure
Nickel, Dithiocarbamate, PPh_3, Dppe, NMR, 77
X-ray crystal structure
Diorganotin, Dicyanoethylene-1,2-dithiolate, 4,4′-Bipyridyl, 1,10-Phenanthroline, Co-crystallization, 1207
X-ray crystal structure
Di-2-pyridyl ketone, Thiosemicarbazone, Ni(II) thiosemicarbazone complex, Electronic spectra, IR spectra, 1225
X-ray crystal structure
2,2′-Bipyrimidine complexes, Iron(III) carboxylate complexes, Oxo-bridged iron(III) complexes, π–π stacking interactions, 1271
X-ray crystal structure
Ruthenium(II) carbonyl complexes, Tertiary phosphine chalcogenides, ''Soft–Hard'' and ''Soft–Soft'' interactions, Octahedral structure, 1657
X-ray crystal structure
Enaminones, Molybdenum(VI) complexes, Molybdenum(V) complexes, Pyrone, NMR spectra, 1859
X-ray crystal structure
Vanadium complexes, Nitrilotriacetate, Hydrogen bonding, 1975
X-ray crystal structure
Ozone, Silver(II) complexes, Manganese(III) complexes, Cobalt(III) complexes, 2631
X-ray crystal structures
Iron(II) complexes, Cobalt(II) complexes, Bis(2-pyridylmethyl)amine, Tris(2-pyridylmethyl)amine, 3105
X-ray crystal structures
Nickel, Schiff's bases, Hydrogenated Schiff's bases, Coordination geometry, Polymethylene chains, 3201
X-ray crystallography
Synthesis, Spectroscopy, Pyrazolyl thiosemicarbazone, Cobalt(III) complexes, 5
X-ray crystallography
Ferrocene, Enaminone, Ligand, Copper, Complex, 15
X-ray crystallography
Heteroscorpionate ligands, Hydrogen bond, Divalent metals, 239
X-ray crystallography
Carborane, Spectroscopy, DFT calculations, 629
X-ray crystallography
Ferrocene, Enaminone, Ligands, Complexes, 749
X-ray crystallography
Palladium, Ferrocene, Phosphine, Suzuki–Miyaura coupling, Ortho-metallated complexes, 921
X-ray crystallography
Zinc, 1,3-Bis(4-pyridyl)propane, 4,4′-Pyridine, Polymeric network, 999
X-ray crystallography
Macrocyclic complexes, Cyclic voltammetry, Imidazole, 1317
X-ray crystallography
Ferrocene, Enaminone, Ligand, Copper, Complex, 1541
X-ray crystallography
1-(4-Hydroxyphenyl)-1H-tetrazole-5-thiol, Organotin(IV), Hydrogen bonding, π–π stacking interaction, Crystal structures, 1547
X-ray crystallography
Neutral palladium(II) complex, Catalyst, Methylaluminoxane, Norbornene, Vinylic polymerizaition, 1619
X-ray crystallography
Nickel(II) complexes, Schiff bases, Salicylketimine ligands, 1649
X-ray crystallography
1H-5-mercapto-1,2,3-triazolato, Organotin, Organogermanium(IV), Crystal structure, 1981
X-ray crystallography
Group 11 phosphine complexes, 1-azaallyls, Iminoalkyl bonding mode, 2273
X-ray crystallography
Copper(II) complexes, Thiosemicarbazone, 2-Hydroxyacetophenone, EPR, Antimicrobial studies, Cyclic voltammetry, 2549
X-ray crystallography
Silicon, Phosphorus, Hypercoordination, Hypervalency, Spectroscopy, Fluorescence, 2615
X-ray crystallography
Te(II) thiourea complexes, Novel conformations, Unexpected colours, Supramolecular associations, 3021
X-ray crystallography diffraction
2-Mercapto-6-nitrobenzothiazole, Organotin(IV), Non-bonded interaction, Crystal structure, 779
X-ray diffraction
Ferrocenes, Oxazolines, Non-symmetrical ligands, 611
X-ray diffraction
Nickel complexes, Heterocyclic carbenes, Functionalised carbenes, 2813
X-ray molecular structure
Binuclear compounds, Isocyanides, Nickel, Polymerisation, Ring-coupled bis-cyclopentadienyl ligand, 2715
X-ray single crystal structure
Hydrazones, Copper(II) hydrazonate complexes, 1,10- Phenanthroline, 2,2′-Bipyridine, EPR, 575
X-ray structure
S,N ambidentate borate ligands, Synthesis, Open frame material, 205
X-ray structure
κ^2-Tp ligands, Bridging Tp ligands, Rhodium dicarbonyl complexes, Isomers, 301
X-ray structure
Ligand, Catalysis, Complex, 693
X-ray structure
Ruthenium(II)-tris-chelates, Azoimidazoles, Electrochemistry, 727
X-ray structure
Ruthenium arene complexes, Pyrazole, Dimethylpyrazole, Bond valence, 885
X-ray structure
Cyclophosphazenes, Chiral, Spirocyclic, 979
X-ray structure
Arylazoimidazoles, Cadmium(II) complexes, End-on and end-to-end bridging, 1D chain, Sheet structure, 1669
X-ray structure
Manganese(III), N,O ligands, Magnetochemistry, Dimer, Azide, 1811
X-ray structure
Rhenium complexes, Pyrazole ligand, DFT calculations, 1819
X-ray structure
Phosphine chalcogenides, ^{31}P NMR, Tellurium, Selenium, 1923
X-ray structure
Rhenium complexes, Pyrazole ligand, DFT calculations, 2005
X-ray structure
Phosphine, Synthesis, Coordination, 2575
X-ray structure
Diimine, Coordination complex, Zinc, Palladium, 2789
X-ray structure
Non-heme iron, Water coordination, Cyclic voltammetry, Sterically hindered carboxylate, 2805
X-ray structure
Coordination polymers, Silver, Imidazolate, 3063
X-ray structure
Copper(II) complex, Schiff base, Imine activation, Coordination polymer, 3081
X-ray structure
Phosphine, Hemilabile, 3125
X-ray structure determination
Lead, Coordination polymer, Hydrothermal synthesis, 2161
X-ray structures
Lanthanides, Neodymium, Alkoxides, Pyrazolylborates, Borohydrides, 253
X-ray structures
Copper, *N*-ligands, Thioethers, Multiarmed ligands, Coordination polymer, 1055
X-ray structures
Bis-imidazole, Bis(imidazol-2-yl)methane, Silver(I), Argentophilicity, Anti-fungal, Candida albicans, 1249
X-ray structures
Nickel(II), Thiodiglycolic acid complexes, Magnetic properties, 1573

X-ray structures
Dioxomolybdenum (VI) and oxomolybdenum (IV) complexes, Dithiocarbazate, Schiff bases, 1595
X-ray structures
Bis-imidazole, Metal complexes, Manganese(II), Copper(II), Zinc(II), 1731
X-ray structures
Molybdenum, ^{95}Mo NMR, Phosphine oxide, 1915
X-ray structures
Mn(II) and Cd(II) complexes, Azides, 3-Aminopyridine, Synthesis, Spectra, Thermal properties, 2349
X-ray structures
Terpyridine, Pyridyl bispyrazolyl, Iron, Complexation, Rearrangement, 3193
Xanthate
Diamine, Zinc, Cadmium, CdS, Nanoparticles, 2315

Ytterbium
Lanthanides, Aryloxide, Crystal Structures, Tris(pyrazolyl)borate, Divalent, 263
Yttrium
Lanthanides, Diketiminato, 183

Zinc
Tetrakis(3-isopropylpyrazolyl)borate, Solvent extraction, Single-crystal X-ray diffraction, Copper, 283
Zinc
Heteroscorpionate, Tripodal, Alkylthiolate, Imidazole, Iron, 471
Zinc
Enzyme, Thiolate, Alkylation, 481
Zinc
Ionic complex, Rheological phase reaction, Crystal structure, Photoluminescence, Europium, 529
Zinc
Phthalocyanine, Cobalt, Nickel, Naphthalene, 787
Zinc
Cobalt, Copper, Bis(8-quinolinyl)amine, Structures, 831
Zinc
1,3-Bis(4-pyridyl)propane, 4,4′-Pyridine, Polymeric network, X-ray crystallography, 999
Zinc
Nickel, Copper, Imidazole, α-Hydroxycarboxylato complexes, Thermal behaviour, Crystal structures, 1505
Zinc
Porphyrazine, EPR, Naphthalene, Copper, Cobalt, 1845
Zinc
1,3,4-thiadiazole, Crystal structure, Thermal decomposition, Kinetics, Bioactivity, 1851
Zinc
2,5-Bis(2-pyridyl)-1,3,4-thiadiazole, Energy minimization, Crystal structures, Monomeric complexes, 1903
Zinc
Thiosemicarbazone, 2-pyridineformamide, Crystal structure, Cadmium, 2303
Zinc
Xanthate, Diamine, Cadmium, CdS, Nanoparticles, 2315
Zinc
X-ray structure, Diimine, Coordination complex, Palladium, 2789
Zinc complex
Cadmium complex, 2-Oxo-1,3-dithiole-4,5-dithiolate, Synthesis, Crystal structure, Density functional calculation, 1701
Zinc complex
trans-1,2-Diaminocyclohexane, Crystal structure, Catalytic enantioselective reduction, 2063
Zinc complexes
Crystal structures, Copper complexes, Molecular rectangles, 673
Zinc complexes
Schiff-bases, Crystal structures, IR, UV and NMR spectroscopy, Thermal analysis, 1293
Zinc(II)
Bis-imidazole, Metal complexes, X-ray structures, Manganese(II), Copper(II), 1731
Zinc(II) cobalt(II) compounds from *N*-(benzothiazol-2-yl)-dithiocarbamic methyl ester
1-Benzothiazol-2-ylid-3-methyl-thiourea, 1-Benzothiazol-2-yl-2,3-dimethyl-*iso*thiourea, *N*-(benzothiazol-2-yl)-*S*,*S*′-dimethyl-dithio-carboimine, 2481
Zinc(II) complexes
Diporphyrins, Nitrogen base ligation, Stability constants, 33
Zinc(II) complexes
Di-2-pyridyl ketone salicyloylhydrazone, Stability constants, Spectroscopy, Thermal analysis, 2095
Zinc(II)azide
Mononuclear, Dinuclear, 2,2′-Dipyridylamine, Luminescence, Crystal engineering, 545
Zirconium
Ammonolysis, Liquid ammonia/toluene two-phase system, Potassium, 1125
Zirconium
Enolato, Enamido, Titanium, Aluminum, 1587
Zirconium
Silanoles, Siloxides, Titanium, Oligosilanes, 2475
Zn complexes
Triazolopyrimidine, Copper dimers, EPR, 743
Zwitterionic ferrocenyldithiophosphonates
Molecular structures, 2281
Zwitterions
Monoanionic ligands, Syntheses, Structures, Methyl, Hydrides, 489
Zwitterions
Monoanionic ligands, Phosphines, Syntheses, Structures, Boron, 2901

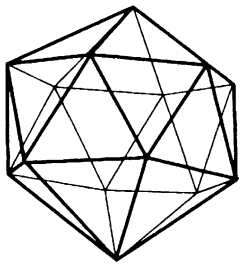

POLYHEDRON

The International Journal for Inorganic and Organometallic Chemistry

Founding Editor: **Sir Geoffrey Wilkinson**✠

Executive Editors

The Americas

G. Christou
Department of Chemistry, University of Florida, Gainesville, FL 32611-7200, USA
E-mail: christou@chem.ufl.edu

Rest of the world

C.E. Housecroft
Department of Chemistry, University of Basel, CH-4056 Basel, Switzerland
E-mail: poly-chemie@unibas.ch

Associate Regional Editor for China

T.C.W. Mak
Department of Chemistry, University Science Centre, The Chinese University of Hong Kong, Shatin NT, Hong Kong, People's Republic of China
E-mail: tcwmak@cuhk.hk

Polyhedron Reports

G. Christou
Department of Chemistry, University of Florida, Gainesville, FL 32611-7200, USA
E-mail: christou@chem.ufl.edu

Symposia-in-print

G.F. Parkin
Department of Chemistry (Box 3115), Columbia University, 3000 Broadway, New York, NY 10027, USA
E-mail: parkin@chem.columbia.edu

Editorial Board

N.Y. Barba-Behrens *(Mexico, DF, Mexico)*
D.C. Bradley *(London, UK)*
D. Braga *(Bologna, Italy)*
A. Brodie *(Palmerston North, New Zealand)*
A. Castiñeiras *(Santiago de Compostela, Spain)*
M.H. Chisholm *(Columbus, OH, USA)*
E.C. Constable *(Basel, Switzerland)*
E. Coronado *(Valencia, Spain)*
W.J. Evans *(Irvine, CA, USA)*
M. Fujita *(Tokyo, Japan)*
L.R. Gahan *(Brisbane, Qld., Australia)*
C.D. Garner *(Nottingham, UK)*
J.F. Harrod *(Montreal, Que., Canada)*
D.N. Hendrickson *(La Jolla, CA, USA)*
L. Hubert-Pfalzgraf *(Villeurbanne, France)*
M.B. Hursthouse *(Southampton, UK)*
T. Kiss *(Szeged, Hungary)*
T. Marder *(Durham, UK)*
P.P. Power *(Davis, CA, USA)*
T.B. Rauchfuss *(Urbana, IL, USA)*
J. Reedijk *(Leiden, The Netherlands)*
A.L. Rheingold *(La Jolla, CA, USA)*
F.G.A. Stone *(Waco, TX, USA)*
A.G. Sykes *(Newcastle upon Tyne, UK)*
L.K. Thompson *(St John's, NF, Canada)*
M.D. Ward *(Bristol, UK)*
R.E.P. Winpenny *(Manchester, UK)*

ELSEVIER

Amsterdam — Boston — Jena — London — New York — Oxford — Paris — Philadelphia — San Diego — St Louis

Available online at www.sciencedirect.com
SCIENCE DIRECT®
Polyhedron 23, issue 18, 2 December 2004
POLYHEDRON
www.elsevier.com/locate/poly

Contents

Papers

S.K. Chawla, M. Arora, Kalle Nättinen, K. Rissanen, J.V. Yakhmi

Polyhedron 23 (2004) 3007

Syntheses and crystal structures of three novel Cu(II) coordination polymers of different dimensionality constructed from Cu(II) carboxylates (carboxylate = malonate (mal), 2 acetate (ac), fumarate (fum)) and conformationally flexible 1,4-bis(imidazole-1-yl-methylene)benzene (IX)

Three new coordination polymers $[[Cu_2(mal)_2(IX)_2(H_2O)_6]_n$, $Cu_2(ac)_4(IX)_2]_n$ and $[Cu_2(fum)_2(IX)_2(H_2O)_2]_n$ are generated by employing Cu(II) carboxylates (mononuclear mal, binuclear 2ac, polynuclear fum) and conformationally flexible bifunctional IX as building blocks. The advantage of using the discrete framework of the building blocks in the form of metal carboxylates with a flexible ligand is demonstrated.

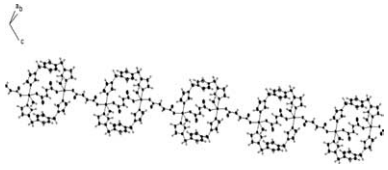

Olav Foss, Steinar Husebye, Karl W. Törnroos, Philip E. Fanwick

Polyhedron 23 (2004) 3021

Synthesis and X-ray crystal structures of six $[TeL_4][MF_6]$ salts, where L is ethylene- or trimethylene-thiourea, and M is Si, Ge or Sn. Five Te(II) complexes with a novel type of structure linked together by unusual N–H···F hydrogen bonds

Six novel tellurium(II) complex salts $[Te(etu)_4][SiF_6]$ (**1**), $[Te(etu)_4][SiF_6] \cdot H_2O$ (**2**), $[Te(trtu)_4][SiF_6]$ (**3**), $[Te(etu)_4][GeF_6] \cdot H_2O$ (**4**), $[Te(trtu)_4][GeF_6]$ (**5**) and $[Te(etu)_4][SnF_6]$ (**6**) (etu = ethylenethiourea, trtu = trimethylenethiourea) have been prepared and characterized, mainly by X-ray crystallographic methods. All the Te(II) complex cations are square planar, but **1**–**5** have an unusual conformation as all four thiourea ligands are extending to the same side of the coordination plane. This conformation is probably stabilized by the supramolecular interactions shown in the figure. The red colour of **1**–**5** is also surprising and is explained on the basis of the *cis*-S–Te–S–C torsion angles near to 180°, which results in a red shift in the UV–Vis spectrum. In **6** this torsion angle is close to 90° and the colour is yellow.

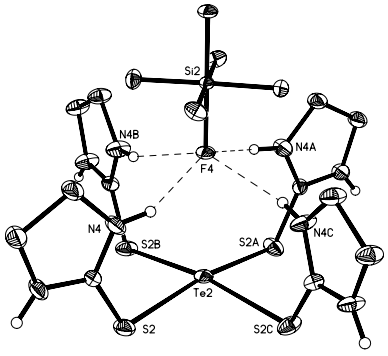

Chao Chen, Yu-Lin Yang, Kun-Lin Huang, Zhen-Hua Sun, Wei Wang, Zhuo Yi, Yun-Ling Liu, Wen-Qin Pang

Polyhedron 23 (2004) 3033

Hydrothermal synthesis and intercalation behavior of a layered titanium phosphate $Ti_2(H_2PO_4)(HPO_4)(PO_4)_2 \cdot 0.5C_6N_2H_{16}$, with an extended γ-phase intercalated into organic amine

The structure exhibits an extended γ-phase intercalated into organic amine, but the interaction behavior presented unusual features because of the presence of *N*,*N*′-dimethylpiperazine cations between the layers.

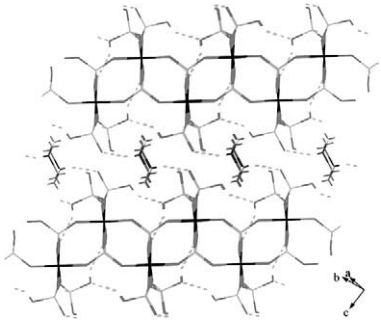

Elsevier Ltd.

Chang Seop Hong, Young Sin You

Polyhedron 23 (2004) 3043

Synthesis, crystal structures and magnetic properties of Cu(II) compounds bridged by the terephthalate ligand and hydrogen bonds

Two tp-bridged Cu(II) compounds, $[Cu(tmen)(tp)(H_2O)_2]_n$ (**1**) (tmen = *N*,*N*,*N*′,*N*′-tetramethylethylenediamine; tp = terephthalate) and $[Cu(pyrazole)_2(tp)]_n$ (**2**), showing coordinative zigzag and linear structures, respectively, were characterized by means of X-ray crystallography and magnetic measurements. Both coordination polymers, with a 3D extended network array (**1**) and a 2D sheet structure (**2**), are formed by incorporating hydrogen bonds into 1D chains. Magnetic data indicate that they exhibit weak ferromagnetic interactions through hydrogen bonds and weak antiferromagnetic couplings via tp ligands.

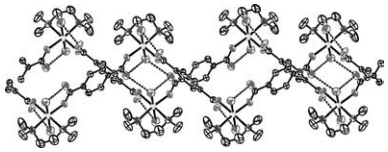

Ana L. Iglesias, Gerardo Aguirre, Ratnasamy Somanathan, Miguel Parra-Hake

Polyhedron 23 (2004) 3051

New chiral Schiff base–Cu(II) complexes as cyclopropanation catalysts

A series of chiral Schiff base ligands and their Cu(II) complexes have been synthesized. X-ray structures show the metal ion in a distorted square planar geometry with dimeric or monomeric structures, depending on the ligand denticity. Unexpectedly the analysis of their catalytic capacity in asymmetric cyclopropanation reactions resulted in rather poor e.e.'s (enantiomeric excess).

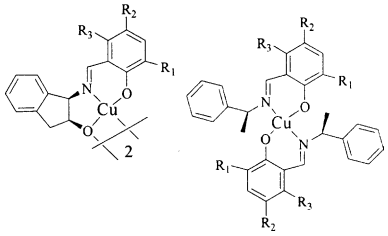

G. Attilio Ardizzoia, Stefano Brenna, Fulvio Castelli, Simona Galli, Girolamo LaMonica, Norberto Masciocchi, Angelo Maspero

Polyhedron 23 (2004) 3063

Metal imidazolato polymers: synthesis, characterization and crystal structure of new silver(I) triphenylphosphine derivatives

On reacting polymeric $[Ag(im)]_n$ (Him = imidazole) with different amounts of PPh_3, the $[Ag_2(\mu_2\text{-im})_2(PPh_3)_3]_n$ and $[Ag(\mu_2\text{-im})(PPh_3)_2]_n$ species, containing wavy chains of metal ions, singly bridged by *N*,*N*′-*exo*-bidentate imidazolate ligands but differing in the number of coordinated phosphines thus in the stereochemistry, are obtained.

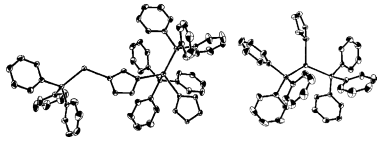

Marthakutty Joseph, V. Suni, Maliyeckal R. Prathapachandra Kurup, Munirathinam Nethaji, Archana Kishore, Sarita G. Bhat

Polyhedron 23 (2004) 3069

Structural, spectral and antimicrobial studies of copper(II) complexes of 2-benzoylpyridine *N*(4)-cyclohexyl thiosemicarbazone

Six new copper(II) complexes of 2-benzoylpyridine *N*(4)-cyclohexyl thiosemicarbazone (HL) have been synthesized and characterized by different physicochemical techniques. Five of the complexes have been found to possess the stoichiometry [CuLX]. The complex prepared from copper sulfate has the composition $[Cu_2L_2SO_4]\cdot(H_2O)_2$. The metal–ligand bonding parameters evaluated from the EPR spectra indicate strong in-plane σ and in-plane π bonding. The antimicrobial activity of the ligand and the copper complexes were tested against five types of bacteria isolated from clinical samples.

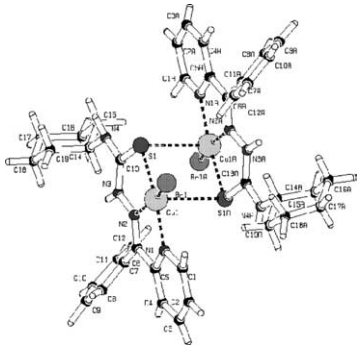

Arindam Mukherjee, Munirathinam Nethaji, Akhil R. Chakravarty

Polyhedron 23 (2004) 3081

Synthesis, crystal structure and imine bond activation of a copper(II) Schiff base complex

A new copper(II) complex $[Cu(HL)(ClO_4)](ClO_4)$ containing a tetradentate Schiff base has been synthesized and structurally characterized by X-ray crystallography. It undergoes oxidative activation of the azoimine moiety through an amido intermediate on reaction with H_2O_2 to form a bis(picolinato)copper(II) species.

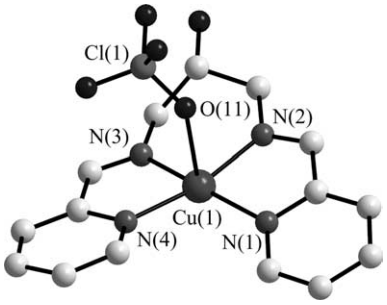

Troy D. Manning, Ivan P. Parkin

Polyhedron 23 (2004) 3087

Vanadium(IV) oxide thin films on glass and silicon from the atmospheric pressure chemical vapour deposition reaction of $VOCl_3$ and water

The dual source atmospheric pressure chemical vapour deposition reaction of $VOCl_3$ and H_2O was used to prepare thin films of vanadium oxides on glass and silicon substrates. Reactor temperatures below 600 °C or with a gas-phase excess of $VOCl_3$ over water, V_2O_5 thin films were produced. Vanadium(IV) oxide thin films were prepared at 600 °C. These films show a thermochromic transition temperature of 67 °C.

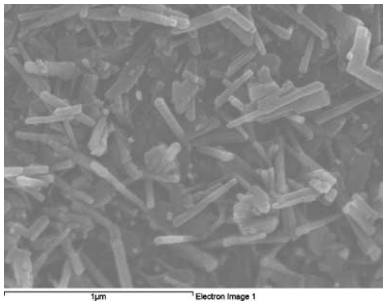

Gordon H. John, Iain May, David Collison, Madeleine Helliwell

Polyhedron 23 (2004) 3097

Synthesis, structural and spectroscopic characterisation of three di-μ-fluoro-bis[dioxouranyl] complexes

We report the synthesis and structural characterisation of three novel dimeric uranyl complexes with organic phosphine oxide ligands and bridging fluorides. Two of the complexes, $[\{UO_2(\mu\text{-}F)(TPPO)_3\}_2][BF_4]_2 \cdot C_6H_{14}$ and $[\{UO_2(\mu\text{-}F)(TBPO)_3\}_2][BF_4]_2$, are dicationic, charge balanced by two uncoordinated tetrafluoroborate anions each. The third complex, $[UO_2(\mu\text{-}F)(F)(DPPMO_2)]_2 \cdot 2MeOH$, is neutral with terminal fluoride also coordinated to both metal centres.

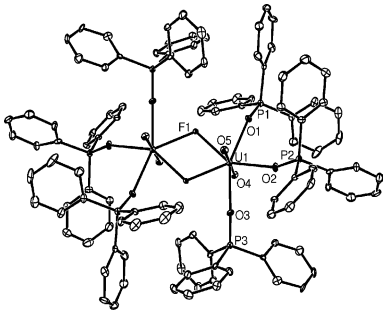

Christopher J. Davies, Gregory A. Solan, John Fawcett

Polyhedron 23 (2004) 3105

Synthesis and structural characterisation of cobalt(II) and iron(II) chloride complexes containing bis(2-pyridylmethyl)amine and tris(2-pyridylmethyl)amine ligands

Divalent cobalt and iron chloride complexes of the type $[LMCl_2]_n$ (n = 1 or 2), $[LMCl]Cl$, $[LMCl]_2[MCl_4]$ and $[L_2M]Cl_2$ are accessible on treatment of L [L = bis (2-pyridylmethyl)-amine (DPA) and tris(2-pyridylmethyl)amine-(TPA)] with anhydrous MCl_2 in n-BuOH at elevated temperatures; complex $[(DPA)FeCl_2]_2$ undergoes oxidation in air to give the oxo-bridged species, $[\{(DPA)FeCl_2\}_2(\mu\text{-}O)]$. All the complexes have been spectroscopically and structurally characterised.

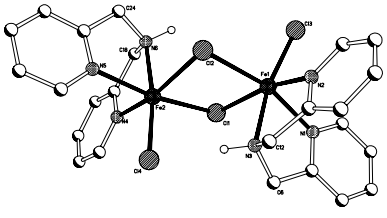

P. Govindaswamy, Yurij A. Mozharivskyj, Mohan Rao Kollipara

Polyhedron 23 (2004) 3115

New neutral and cationic η^6-arene ruthenium complexes with phosphine and amine ligands: syntheses and molecular structures of $[(\eta^6\text{-}p\text{-cymene})Ru(NH_2CH_2C_6H_5)Cl_2]$, $[(\eta^6\text{-}C_6Me_6)Ru(PPh_2Py)Cl_2]$ and $[(\eta^6\text{-}C_6Me_6)Ru(PPh_2Py)Cl]^+$

The dimeric complex $[(\eta^6\text{-}C_6Me_6)Ru(\mu\text{-}Cl)Cl]_2$ reacts with diphenyl-2-pyridyl-phosphine to yield a neutral P-coordinated ruthenium(II) complex $[(\eta^6\text{-}C_6Me_6)Ru(PPh_2Py)Cl_2]$ as well as a cationic P,N-chelating complex $[(\eta^6\text{-}C_6Me_6)Ru(PPh_2Py)Cl]$ The monomeric complex $[(\eta^6\text{-}p\text{-cymene})Ru(PPh_3)Cl_2]$ can react with amine ligands to yield chiral complexes. Representative complexes have been characterized by single-crystal X-ray study.

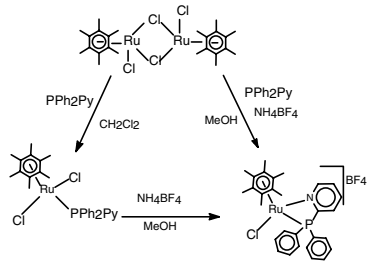

Alexandra M.Z. Slawin, Heather L. Milton, Joanne Wheatley, J. Derek Woollins

Polyhedron 23 (2004) 3125

Preparation and coordination chemistry of *N*-diallylaminodiphenylphosphine and *N*-allylaminobis(diphenyl)phosphine

N-diallylaminodiphenylphosphine coordinates using P, N or C=C whereas *N*-allylaminobis(diphenylphosphine)phosphine is a simple P donor.

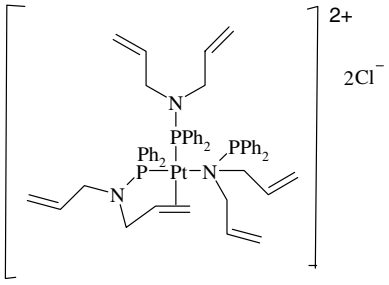

Baolong Li, Xia Zhu, Junhui Zhou, Yanfen Peng, Yong Zhang

Polyhedron 23 (2004) 3133

Syntheses and structures of five cadmium(II) coordination polymers from 1,2-bis(1,2,4-triazol-1-yl)ethane

Five structually distinct cadmium(II) coordination polymers based on 1,2-bis(1,2,4-triazol-1-yl)ethane have been synthesized and structurally characterized.

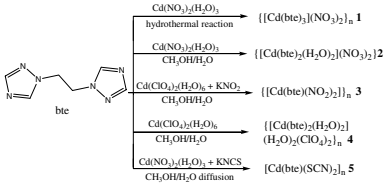

Azizolla Beheshti, Neil R. Brooks, William Clegg, Saeedeh Ebad Sichani

Polyhedron 23 (2004) 3143

Synthesis, crystal structures and spectroscopic characterization of two neutral heterobimetallic clusters $MS_4Cu_4(pz^{Me2})_6X_2$ (where M = Mo (**1**) or W (**2**), X = Cl (**1**) or disordered Cl/Br (**2**), and pz^{Me2} = 3,5-dimethylpyrazole)

The title complexes each contain five coplanar metal atoms; Mo or W is tetrahedrally surrounded by triply-bridging S atoms. Each Cu atom has distorted tetrahedral coordination involving two bridging sulfides, but two Cu atoms additionally have two substituted pyrazole ligands while the other two have one pyrazole and one halide ligand.

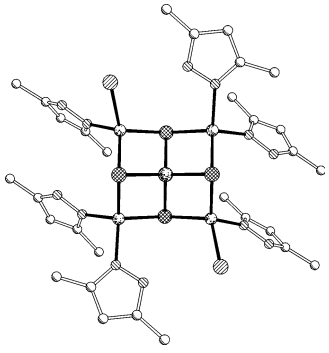

Stela Minkovska, Monika Fedieva, Bojana Jeliazkova, Todor Deligeorgiev

Polyhedron 23 (2004) 3147

Thermally activated and light-induced metal ion complexation of 5′-(hydroxy)spiroindolinonaphthooxazines in polar solvents

Coordination of Cu(II), Fe(II) or Al(III) with the open form of 5′-(hydroxy)spiroindolinonaphthooxazines takes place thermally (slowly) and photochemically in acetone, ethanol and their 1:1 aqueous mixtures resulting a reversibly photochromic complex. Chelation induces a slight hypsochromic shift of the visible absorption of the photomerocyanine and drastically slows down its thermal bleaching in the dark.

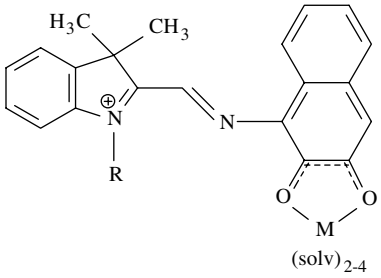

M = Cu(II), Fe(II) or Al(III)

Ayfer Kalkan, Atıf Koca Zehra, Altuntaş Bayır

Polyhedron 23 (2004) 3155

Unsymmetrical phthalocyanines with alkynyl substituents

We report on the synthesis and characterisation of unsymmetrical metallophthalocyanines (M = Zn, Ni, Co) which carry two peripheral hexylthio substituents on each of three of the benzenoid groups, while the fourth one carries two phenylethynyl groups.

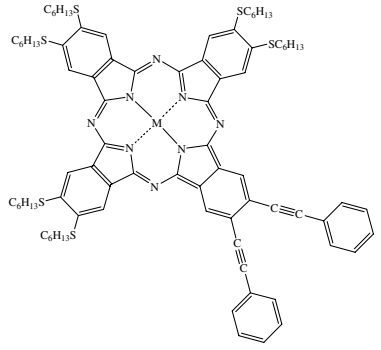

Márcio P. de Araujo, Eliana M.A. Valle, Javier Ellena, Eduardo E. Castellano, Eduardo N. dos Santos, Alzir A. Batista

Polyhedron 23 (2004) 3163

mer-[$RuCl_3$(P–P)H_2O] (P–P = dppb or diop) as a starting material for the synthesis of binuclear complexes. Crystallographic structures of [(dppb)ClRu–μ$(Cl)_3$–RuCl(dppb)] and [(η^6-C_6H_6)Ru–μ$(Cl)_3$–RuCl(dppb)]. Imine hydrogenation using mono- and binuclear ruthenium complexes

In this work the reactvity of *mer*-[$RuCl_3$(P–P)H_2O] (P–P = chiral and achiral chelating ditertiary phosphine) with H_2, ruthenium(II) and ruthenium(III) complexes was studied. Several new and known complexes (Ru_2(II,II) and Ru_2(II,III)) were isolated. The activity of some complexes was tested for the hydrogenation of imines and the results are discussed. X-ray structures of [(dppb)ClRu–(μ-Cl)$_3$–RuCl(dppb)] (**5**) and [(η^6-C_6H_6)Ru–(μ-Cl)–RuCl(dppb)] are presented.

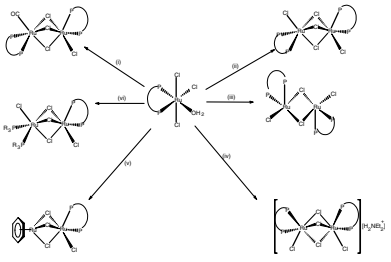

V. Anbalagan, T.S. Srivastava

Polyhedron 23 (2004) 3173

Spectral and photophysical properties of mono and dinuclear Pt(II) and Pd(II) complexes: An unusual emission behaviour

Mononuclear complexes of the formula [M(N-N)(DHB)] and dinuclear complexes of the formula [M_2(BPY)$_2$(THB)] were synthesized and characterized. These complexes were found to show an optically active LLCT band and the platinum complexes of the series were found to show dual emitting states.

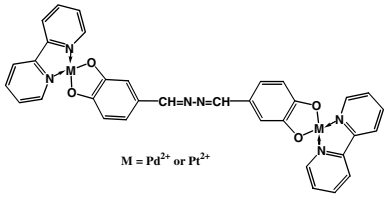

Céline Schneider, Frédéric Doucet, Stanislav Strekopytov, Christopher Exley

Polyhedron 23 (2004) 3185

The solubility of an hydroxyaluminosilicate

Silicic acid, $Si(OH)_4$, reacts with aluminium to form hydroxyaluminosilicates (HAS). When $Si(OH)_4$ is in excess (twofold) an HAS with a Si:Al ratio of 1.0 is formed (HAS_B) which upon its aggregation towards a critical nucleus (the size of which is as yet unknown) is precipitated. Herein, we provide the first estimate of the solubility of HAS_B.

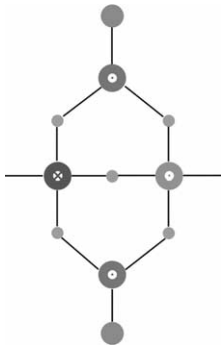

F. Pelascini, Manuel Wesolek, F. Peruch, A. De Cian, N. Kyritsakas, P.J. Lutz, J. Kress

Polyhedron 23 (2004) 3193

Iron complexes of terdentate nitrogen ligands: formation and X-ray structure of three new dicationic complexes

The synthesis and X-ray structure of the iron complexes $(L^1)_2Fe^{2+}(FeCl_4^-)_2$, $(L^2)_2Fe^{2+}FeCl_4^{2-}$ and $(L^2)_2Fe^{2+}(FeCl_4^-)_2(THF)_4$ (L = 6,6″-di(*p*-tolyl)-2,2′:6′,2″-terpyridine and L = 2,6-bis-(3-mesitylpyrazol-1-yl)pyridine) are presented. $(L^1)_2Fe$ was shown to be a high-spin complex, whereas $(L^2)_2Fe^{2+}$ was low-spin.

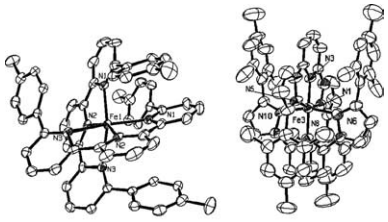

Michelle K. Taylor, John Reglinski, Dawn Wallace

Polyhedron 23 (2004) 3201

Coordination geometry of tetradentate Schiff's base nickel complexes: the effects of donors, backbone length and hydrogenation

The crystal structures of six tetradentate Schiff's base nickel complexes have been determined. These have been used to analyse the effects of backbone length, donor set, hydrogenation and hydrogen bonding on the coordination geometries of the complexes they are capable of forming.

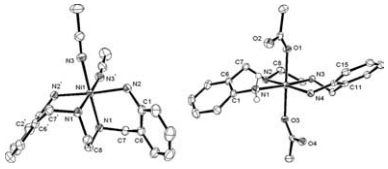

Heather L. Milton, Matthew V. Wheatley, Alexandra M.Z. Slawin, J. Derek Woollins

Polyhedron 23 (2004) 3211

Synthesis and coordination of 2-diphenylphosphinopicolinamide

The new ligand 2-diphenylphosphinopicolinamide behaves as a monodentate *P* or bidentate *P*, *O*; *P*, *N* donor.

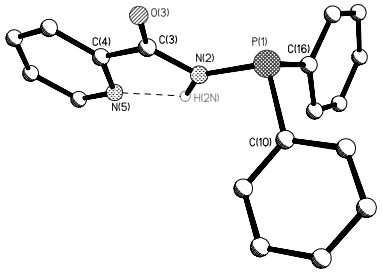

Author Index to Volume 23 3221
Subject Index to Volume 23 3243

The Publisher encourages the submission of articles in electronic form thus saving time and avoiding rekeying errors. For detailed instructions on the preparation of manuscripts and of electronic artwork, consult the Author Gateway for Elsevier at http://authors.elsevier.com

SCIENCE DIRECT™

Full text of this journal is available, on-line from **ScienceDirect**. Visit **www.sciencedirect.com** for more information.

CONTENTS Direct

This journal is part of **ContentsDirect**, the *free* alerting service which sends tables of contents by e-mail for Elsevier books and journals. You can register for **ContentsDirect** online at: **www. elsevier.com/locate/contentsdirect**

Available online at www.sciencedirect.com
SCIENCE DIRECT®
Polyhedron 23, issue 11, 8 July 2004
POLYHEDRON
www.elsevier.com/locate/poly

Contents

Papers

Xiao-Qing Shen, Hong-Jian Zhong, Hao Zheng, Hong-Yun Zhang, Guang-Hua Zhao, Qing-An Wu, Hong-Yan Mao, En-Bo Wang, Yu Zhu

Polyhedron 23 (2004) 1851

Crystal structure, thermal decomposition kinetics and antimicrobial activities of $[Zn(eatz)_2(OAc)_2]$ (eatz=5-ethyl-2-amino-1,3,4-thiadiazole)

A signal crystal of $[Zn(eatz)_2(OAc)_2]$ has been synthesized and determined by X-ray diffraction. The structural unit is a distorted tetrahedron. Thermal analysis reveals that the complex decomposes in three transitions in N_2 atmosphere. The thermal decomposition kinetic analysis and antimicrobial activities assays have also been reported.

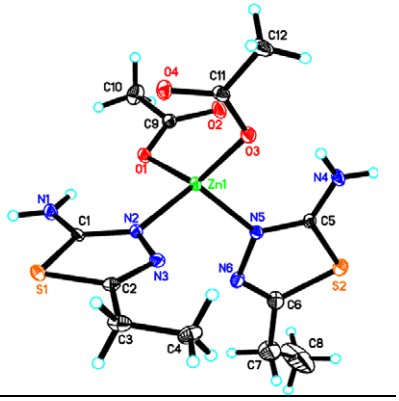

Marina Cindrić, Višnja Vrdoljak, Tanja Kajfež Novak, Neven Strukan, Ana Brbot-Šaranović, Predrag Novak, Boris Kamenar

Polyhedron 23 (2004) 1859

Synthesis, characterization and crystal structures of molybdenum(VI) and (V) complexes with differently N-substituted β′-hydroxy-β-enaminones

Mononuclear molybdenum(VI) $[MoO_2L_2]$ and dinuclear molybdenum(V) $[Mo_2O_4(L^{1b})_2(CH_3OH)_2]$ complexes have been prepared by the reaction of $[MoO_2(acac)_2]$ or $[Mo_2O_3(acac)_4]$ (acac=acetylacetonate ion), respectively, with the appropriate β′-hydroxy-β-enaminones. All compounds have been characterized by means of chemical analyses, IR and one- and two-dimensional NMR spectroscopy, and some of them by X-ray crystallography.

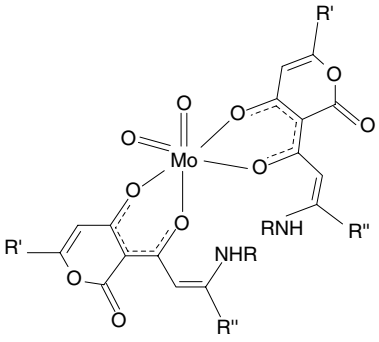

Verónica Paredes-García, Ramón O. Latorre, Evgenia Spodine

Polyhedron 23 (2004) 1869

Electronic and magnetic properties of iron (III) dinuclear complexes with carboxylate bridges

Dinuclear iron (III) complexes with a carboxylate bridges of the type $[Fe_2L_2(H_2O)_4](NO_3)_2(H_2O)_m$, where L=a Schiff base, have been prepared and characterised by different spectroscopic techniques, magnetic susceptibility, and electrochemical measurements. Mössbauer Spectroscopy for dinuclear iron (III) complexes show two inequivalent hexacoordinated atoms in high spin. Temperature dependence of the reciprocal molar susceptibility indicate a weakly antiferromagnetically coupled system.

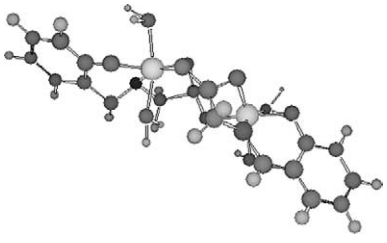

Jian-Xin Chen, Shi-Xiong Liu, En-Qing Gao

Polyhedron 23 (2004) 1877

Syntheses, structures and fluorescence of three novel 3D coordination polymers $[Cd_3(TMA)_2(H\text{-}PRZ)(H_2O)_3(OH)] \cdot H_2O$, $Cd_2Na_2(TMA)_2(H_2O)_4$ and $[Cd_2Co(TMA)_2(H_2O)_4] \cdot 2H_2O$ (TMA=trimesic acid, PRZ=piperazine)

Three novel coordination polymers $[Cd_3(TMA)_2(H\text{-}PRZ)(H_2O)_3(OH)] \cdot H_2O$ (**1**), $Cd_2Na_2(TMA)_2(H_2O)_4$ (**2**) and $[Cd_2Co(TMA)_2(H_2O)_4] \cdot 2H_2O$ (**3**) have been synthesized via a hydrothermal route and characterized. Complex **1** is a sandwich-like 2D coordination polymer with a porous dimension of ca. 7.5×5.5 Å; complex **2** is a 3D polymer based on tetranuclear heterometallic clusters and the complex **3** is the first trimesate complex containing two different transitional metals.

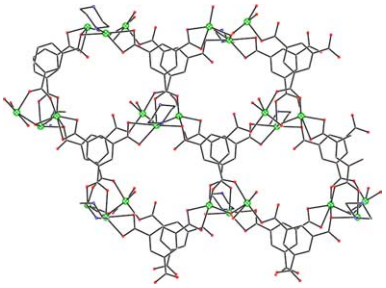

Franco Cataldo

Polyhedron 23 (2004) 1889

Polyynes: a new class of carbon allotropes. About the formation of dicyanopolyynes from an electric arc between graphite electrodes in liquid nitrogen

A mixture of dicyanopolyynes having the general formula $N{\equiv}C{-}(C{\equiv}C)_n{-}C{\equiv}N$ with $n = 2$, 3 and 4 is formed and collected in a simple apparatus when graphite electrodes are arced in liquid nitrogen. As secondary products regular polyynes, i.e. hydrogen-terminated polyynes with the general formula $H{-}(C{\equiv}C)_n{-}H$, are formed. This study has confirmed the key role played by the graphite electrodes as the source of elemental carbon in the form of sp-hybridized carbon chains which are then terminated by atoms derived from the medium where the electric arc is struck. Nitrogen end groups of the cyanopolyynes are derived from the plasmalysis of molecular nitrogen.

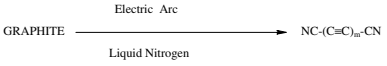

Heilen Arce, Mavis L. Montero, Alejandro Sáenz, Victor M. Castaño

Polyhedron 23 (2004) 1897

Effect of pH and temperature on the formation of hydroxyapatite at low temperatures by decomposition of a Ca–EDTA complex

Hydroxyapatite (HAp) was synthesized through the decomposition of a Ca(EDTA) complex in presence of phosphate ions. Ion concentrations are much higher than previously reported. This route allows the formation of HAp at temperatures below 140 °C and at different pH values.

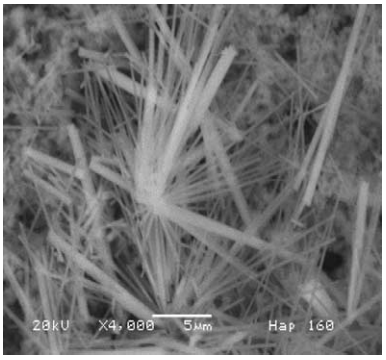

Fouad Bentiss, Michel Lagrenée, Hervé Vezin, Jean-Pierre Wignacourt, Elizabeth M. Holt

Polyhedron 23 (2004) 1903

Syntheses and crystal structures of two mononuclear Zn(II) complexes with the 2,5-bis(2-pyridyl)-1,3,4-thiadiazole ligand

The structures of the monomeric zinc (diaquo-2,5-bis(2-pyridyl)-1,3,4-thiadiazole) cationic complexes with zinc tetrachloride (**II**) and perchlorate (**III**) as counter ions are reported. Comparison of the energy-minimized structure of the solid-state uncoordinated ligand and of the two monomeric zinc(2,5-bis(2-pyridyl)-1,3,4-thiadiazole)$_2$ complexes permits an evaluation of the relative importance of conformation and planarity in complex formation. From this information, the potential of the ligand as a bridging unit may be evaluated.

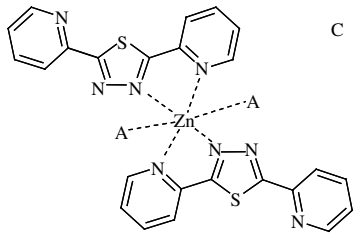

(II) A=HOH, C=$ZnCl_4^{2-}$

(III) A=HOH, C= ClO_4^-

A.D. Garnovskii, Boris I. Kharisov, E.L. Anpilova, A.V. Bicherov, O.Yu. Korshunov, A.S. Burlov, Miguel A. Méndez-Rojas, L.M. Blanco, G.S. Borodkin, I.E. Uflyand, U. Ortiz Méndez

Polyhedron 23 (2004) 1909

New β-aminovinylketonates with annealated 1,2-benzothiazine-1,1-dioxide fragment

New β-aminovinylketones with heterocyclic 1,2-benzothiazine-1,1-dioxide and antipyrine moieties (LH) and their 3d-metal (Co^{II}, Ni^{II}, Cu^{II}, Zn^{II}) chelates have been synthesized via traditional and electrochemical techniques and characterized. It is shown that, depending on the metal nature, the studied ligand system may behave as an ambidentate ligand, forming metal-chelates with both distorted tetrahedral (Cu^{2+} and Zn^{2+}) or octahedral (Co^{2+} and Ni^{+}) geometries around the metal center.

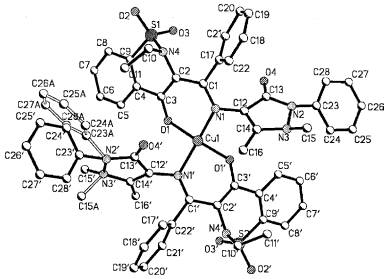

Michael B. Hursthouse, William Levason, Raju Ratnani, Gillian Reid

Polyhedron 23 (2004) 1915

Synthesis and spectroscopic properties of Mo(VI) complexes with phosphine oxide ligands and the crystal structures of $[MoO_2X_2(OPMe_3)_2]$ (X=Cl or Br) and $[MoO_2Br_2\{o\text{-}C_6H_4(P(O)Ph_2)_2\}] \cdot 2CH_2Cl_2$

A series of distorted octahedral Mo(VI) complexes $[MoO_2X_2(OPMe_3)_2]$ and $[MoO_2X_2(L–L)]$ (L–L=$Ph_2P(O)CH_2P(O)Ph_2$, $Ph_2P(O)CH_2CH_2P(O)Ph_2$ and $o\text{-}C_6H_4(P(O)Ph_2)_2$) have been prepared and their spectroscopic properties established, including ^{95}Mo NMR data where possible. Crystal structures of representative examples are also described.

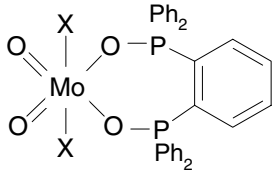

Martin D. Rudd, Matt A. Creighton, Jason A. Kautz

Polyhedron 23 (2004) 1923

Synthesis and characterization of chalcogenoic aminophosphines: X-ray structures of $Bu^t_2P(E)NHPr^n$ (E=Se, Te), $Ph_2P(Se)NHPr^n$ and $\{Et_2P(Se)\}_2NPr^n$

The reaction of $LiNHPr^n$ with chlorodialkyl- or chlorodiaryl-phosphines at low temperatures followed by reaction in refluxing toluene with either elemental selenium or tellurium led to the isolation of the new chalcogenoic aminophosphines of the form $(R_2P)N(E)HPr^n$ [E=Se,Te; R=^{t}Bu, Ph]. Addition of two equivalents of chlorodiethylphosphine to Li_2NPr^n yielded $\{Et_2P(Se)\}_2NPr^n$. They have been characterized by multinuclear NMR spectroscopy and single crystal X-ray diffraction.

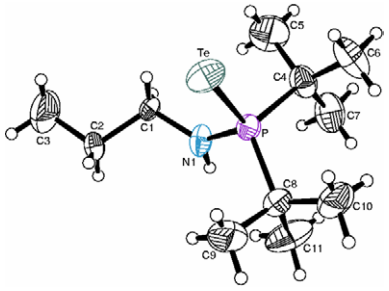

Fatma Ylmaz, Devrim Atilla, Vefa Ahsen

Polyhedron 23 (2004) 1931

Synthesis and liquid-crystalline behaviour of Ni(II) and Zn(II) phthalocyanines with peripheral monoazacrown ethers

Monoazacrown ether substituted Ni(II) and Zn(II) phthalocyanies have been synthesized from the corresponding phthalonitrile derivatives. The Ni(II) phthalocyanine shows a discotic mesophase in a large temperature interval including room temperature.

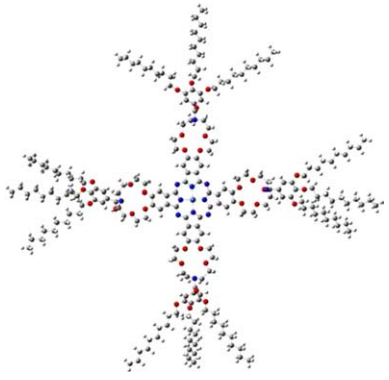

Barbara Kurzak, Agnieszka Woźna, Julia Jezierska, Małgorzata Jeżowska-Bojczuk, Wojciech Szczepanik, Paweł Kafarski

Polyhedron 23 (2004) 1939

Copper(II) complexes of several monophosphono dipeptides: the role of phosphonic oxygen and thioether sulfur in complex stabilization

The coordination in $[CuLH_{-1}]^-$, the major species in the studied systems, is realized by the $\{PO_3^{2-}, NH_2, N^-\}$ donor set but both ligands Gly–(Bz)Cys(P) are more effective chelating agents than other ones. In this case both benzyl ring and thioether group can stabilize this complex by competition with the phosphonic oxygen towards copper ion coordination in an axial position.

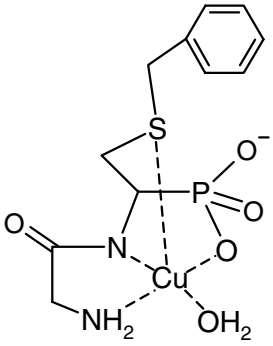

Chun-Wei Yeh, Maw-Cherng Suen, Hui-Ling Hu, Jhy-Der Chen, Ju-Chun Wang

Polyhedron 23 (2004) 1947

Synthesis and structural characterization of two new chiral coordination polymers of Cu(nicotinate)$_2$(H$_2$O) and Co(nicotinate)$_2$

The synthesis and structures of two new chiral coordination polymers, $Cu(nic)_2(H_2O) \cdot CH_3OH$ (nic=nicotinate) (**1**), and $Co(nic)_2 \cdot H_2O$ (**2**), are reported. Single-crystal X-ray crystallography structure determinations show that complexes **1** and **2** crystallize in the chiral space groups $P3_221$ and $C2$, respectively. Complex **1** exhibits open channels, while complex **2** shows planar molecular grids.

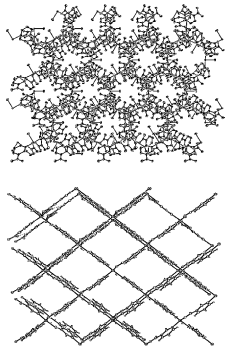

Glaico Chiericato Júnior, Ana Paula Saldanha Silva, Luciana Simionatto Guinesi

Polyhedron 23 (2004) 1953

Synthesis, characterization and electropolymerization of a new polypyrrole iron(II) Schiff-base complex

This work reports the synthesis, characterization and anodic electropolymerization of the pyrrole-substituted monomer complex $[Fe(\mathbf{L})_2](PF_6)_2 \cdot 1H_2O$, where **L** is 2,6-bis[1-(3-pyrrol-1-yl-propylimino)ethyl] pyridine. Characterization was performed through elemental and thermal analyzes, X-ray diffraction and UV–Vis, IR and ^{1}H NMR spectra. Film surface morphology has been characterized by atomic force microscopy.

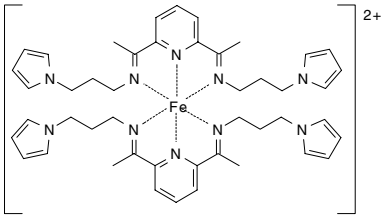

Hong-Yan Mao, Xiao-Qing Shen, Gang Li, Hong-Yun Zhang, Chen Xu, Hong-Lei Liu, En-Bo Wang, Qing-An Wu, Hong-Wei Hou, Yu Zhu

Polyhedron 23 (2004) 1961

Novel hydrogen-bonded and π–π interaction networks generated from the reaction of copper(II) chloride hydrates with heterocyclic diimines (2,2′-bipyridine, 1,10-phenanthroline) and bidentate diamine (ethylenediamine)

Two novel supramolecular complexes containing $Cu^{II}N_4Cl$ chromophores, $[Cu(en)(bipy)Cl][OH] \cdot (H_2O)_3$ (**1**) and $[Cu(phen)_2Cl][OH] \cdot (CH_3OH)_2 \cdot (H_2O)_6$ (**2**) were synthesized and structurally characterized. Complex **1** is the first example of a $Cu^{II}N_4X$ complex generated from mixed ligands. Magnetic behaviors for complex **2** exhibit very weak ferromagnetic interactions.

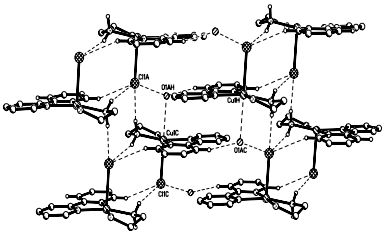

Aminou Mohamadou, Gerard A. van Albada, Willem L. Driessen, René de Gelder, Jan Reedijk

Polyhedron 23 (2004) 1969

Crystal structures, spectroscopy and EPR of two distortion isomers of Cu(II) perchlorate with 2,2′-bi-imidazoline

Two new mononuclear Cu(II) compounds with the ligand 2,2′-bi-imidazoline are reported in this study. The two distortion isomers differ in the (non) coordination of the perchlorate anions and on the hydrogen bonding system.

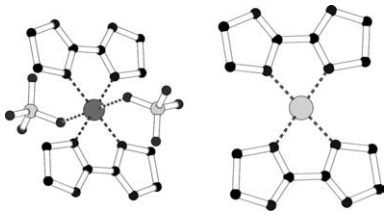

Quanzheng Zhang, Canzhong Lu, Wenbin Yang, Shumei Chen, Yaqin Yu, Xiang He, Ying Yan, Jiuhui Liu, Xinjiang Xu, Changkun Xia, Lijuan Chen, Xiaoyuan Wu

Polyhedron 23 (2004) 1975

Synthesis and characterization of vanadium(IV)–M (M=Mn, Zn) and vanadium(IV)–Ln (Ln=La, Nd) complexes with nitrilotriacetate ligands: $\{(NH_4)_2[(V^{IV}O)_2(\mu_2\text{-}O)(nta)_2M(H_2O)_4]\cdot 2H_2O\}_n$ and $NH_4[Ln(H_2O)_9][(V^{IV}O)_2(\mu_2\text{-}O)(nta)_2]$

Four heterometal complexes, namely $\{(NH_4)_2[(V^{IV}O)_2(\mu_2\text{-}O)(nta)_2Mn(H_2O)_4]\cdot 2H_2O\}_n$ (**1**), $\{(NH_4)_2[(V^{IV}O)_2(\mu_2\text{–}O)(nta)_2Zn(H_2O)_4]\cdot 2H_2O\}_n$ (**2**), $NH_4[La(H_2O)_9][(V^{IV}O)_2(\mu_2\text{–}O)(nta)_2]$ (**3**) and $NH_4[Nd(H_2O)_9][(V^{IV}O)_2(\mu_2\text{–}O)(nta)_2]$ (**4**), where nta=nitrilotriacetate, have been prepared and characterized by single-crystal X-ray diffraction analyses.

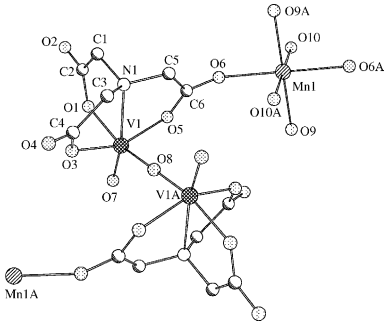

Chunlin Ma, Junhong Zhang, Rufen Zhang

Polyhedron 23 (2004) 1981

Syntheses, characterizations and crystal structures of new triorgano-tin or -germanium complexes with 1H-5-mercapto-1,2,3-triazolato

A series of triorganotin and triorganogermanium (IV) complexes with 1H-5-mercapto-1,2,3-triazolato of the type, $R_3MSC_2H_2N_3$ (M=Sn, R=CH_3, (**1**); C_2H_5, (**2**); *n*-C_4H_9, (**3**); C_6H_5, (**4**); M=Ge, R=CH_3, (**5**); C_2H_5, (**6**); *n*-C_4H_9, (**7**); C_6H_5, (**8**)) have been synthesized. All the complexes **1**–**8** have been characterized by elemental, IR and ^{1}H NMR analyses. Among them complexes **4** and **8** have also been characterized by X-ray crystallography diffraction analyses, which revealed that the Sn and Ge atom environments are distorted tetrahedral coordination polyhedrons, coordinated to three phenyl groups and to one sulfur atom of the ligand. The packing of complexes **4** and **8** are stabilized into a one-dimensional infinite chain by intermolecular N–H···N hydrogen bonds.

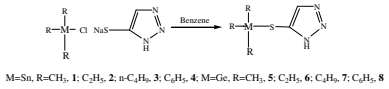

M=Sn, R=CH_3, **1**; C_2H_5, **2**; n-C_4H_9, **3**; C_6H_5, **4**; M=Ge, R=CH_3, **5**; C_2H_5, **6**; C_4H_9, **7**; C_6H_5, **8**

Mehmet Kandaz, Atf Koca, Ali Rza Özkaya

Polyhedron 23 (2004) 1987

A new redox-active multisite ligand: synthesis, spectroscopy and electrochemistry of its mono and dinuclear complexes, and the interaction of (*E*,*E*)M (M=Ni) complex with Pd^{II} and Ag^{I}

A novel redox active (*E*,*E*)-dioxime ligand, *S*,*S*′-bis-[2(2′-ferrocenemethylaminobenzyl)]-dithioglyoxime (LH_2), containing ferrocene and flexible aminobenzenesulfanyl-moieties on the periphery has been synthesized from 2-(2′-ferrocenemethylamino)benzenethiol, which was obtained by the reduction of 2,2′-pyridylbenzothiazolidine with a large excess of $NaBH_4$. The structures of the complexes were characterized by elemental analysis, ^{1}H NMR, IR, MS, UV–Vis spectral and cyclic voltammetry.

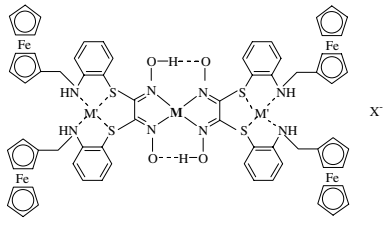

M=Ni	M'=---	**4**	M=Ni	M'=Pd^{2+}	X=4Cl	**10**
M=Cu	M'=---	**5**	M=Ni	M'=Ag^{+}	X=$2NO_3$	**11**
M=Co	M'=---	**6**				
M=Fe	M'=---	**7**				
M=Mn	M'=---	**8**				

Abhik Mukhopadhyay, Samudranil Pal

Polyhedron 23 (2004) 1997

Complexes of nickel with tetradentate ligands formed by ring opening of 1-benzoyl-3,5-dimethyl-5-(1′-benzoylhydrazido)pyrazoline

Treatment of the pyrazoline obtained from acetylacetone and benzoylhydrazine with nickel(II) causes the ring opening and formation of a neutral complex with a trianionic tetradentate ligand, which in the presence of moisture and oxygen produces a square-planar nickel(II) complex wherein the methine fragment is transformed to keto group.

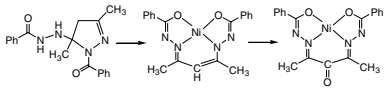

Barbara Machura, M. Jaworska, Rafal Kruszynski

Polyhedron 23 (2004) 2005

DFT calculation and X-ray structure of the $[ReCl_3(pzH)_3]$ complex

The $[ReCl_3(pzH)_3] \cdot H_2O \cdot HCl$ complex has been obtained in the reaction of $[ReOCl_3(PPh_3)_2]$ with an excess of pzH in wet benzene under argon atmosphere. The well-known capacity of PPh_3 to interact with the Re≡O bond in rhenium(V) oxo-complexes explains the course of the reaction. The rhenium atom of $[ReCl_3(pzH)_3]$ is in a distorted octahedral environment and the two groups of ligands (halide ions and pyrazole molecules) are arranged in a *meridional* fashion. The geometric parameters of $[ReCl_3(pzH)_3]$ have been examined using the density functional theory (DFT) method. The UV–Vis spectrum of $[ReCl_3(pzH)_3]$ has been discussed on the basis of the electronic transitions calculated with the time-dependent DFT method (TDDFT).

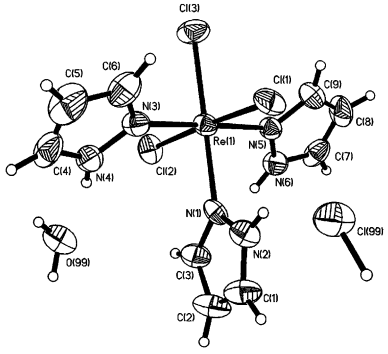

Othman H. Amin, Lamaan J. Al-Hayaly, Subhi A. Al-Jibori, Talal A.K. Al-Allaf

Polyhedron 23 (2004) 2013

Heterobimetallic complexes of palladium(II) and platinum(II) bridged by the ligand 5-phenyl-1,3,4-oxadiazole-2-thione

The complexes $[(ML_2(A_2)or(B)]$ react with various metal ions to give the heterobimetallic complexes, $[(A_2)or(B)M(\mu\text{-}L)_2 M'Cl_2]$, where M=Pd or Pt, L=5-phenyl-1,3,4-oxadiazole-2-thione ion, A=monophosphine, B=diphosphine and M′=Co, Pd or $SnCl_2$. These complexes were characterized physicochemically and spectroscopically.

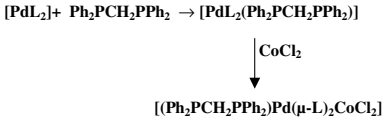

Angeliki Galani, Dimitra Kovala-Demertzi, Nikolaos Kourkoumelis, Aglaia Koutsodimou, Vaso Dokorou, Zbigniew Ciunik, Umberto Russo, Mavroudis A. Demertzis *

Polyhedron 23 (2004) 2021

Organotin adducts of indomethacin: synthesis, crystal structures and spectral characterization of the first organotin complexes of indomethacin

The complexes $[Me_2(Indo)SnOSn(Indo)Me_2]_2$, (**1**) $[Bu_2(Indo)SnOSn(Indo)Bu_2]_2$, (**2**), where Hindo is indomethacin, have been prepared and structurally characterized by means of ^{119}Sn Mössbauer, vibrational, and NMR spectroscopy. The crystal structures of the complexes $[Me_2(Indo)SnOSn(Indo)Me_2]_2 \cdot 2C_4H_8O_2$, **3** and **2** have been determined by X-ray crystallography. Complexes **2** and **3** are self-assembled via π → π, C–H-π and stacking interactions.

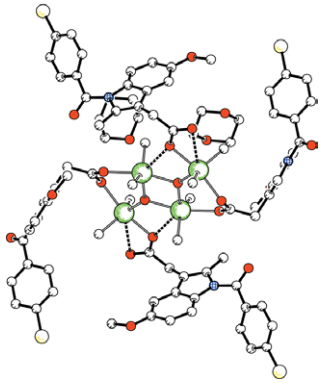

Mohammad Akbar Ali, A.H. Mirza, Thahira B.S.A. Ravoof, Paul V. Bernhardt

Polyhedron 23 (2004) 2031

Synthetic, spectroscopic and X-ray crystallographic structural study of the monomeric [Cu(pysme)(sac)(MeOH)] and dimeric $[Cu(6mptsc)(sac)]_2$ complexes [pysme=anion of the pyridine-2-carboxaldehyde Schiff base of *S*-methyldithiocarbazate, 6mptsc=the anion of the 6-methyl-2-pyridinecarbaldehydethiosemicarbazone and sac=the saccharinate anion]

The complexes [Cu(pysme)(sac)(MeOH)] and $[Cu(6mpptsc)(sac)]_2$ have been prepared and characterized. X-ray structural analysis shows that the former is a monomer whereas the latter is a dimer. In both complexes, the Cu^{II} ions adopt a distorted square-pyramidal geometry with the Schiff bases coordinated as NNS tridentate chelating agents and the sac^- ion as a monodentate ligand in [Cu(pysme)(sac)(MeOH)] and as a bridging bidentate ligand in $[Cu(6mptsc)(sac)]_2$.

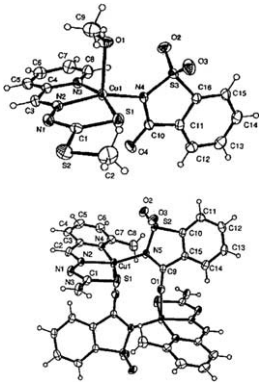

Mohammad Akbar Ali, Aminul Huq Mirza, Ai Ling Tan, Lim Kok Wei, Paul V. Bernhardt

Polyhedron 23 (2004) 2037

The preparation and characterization of seven-coordinate tin(IV) complexes of the 2,6-diacetylpyridine Schiff bases of *S*-alkyl/aryl-dithiocarbazates and the X-ray crystal structure of the $[Sn(dapsme)I_2]$ complex (dapsme=doubly deprotonated form of the 2,6-diacetylpyridine Schiff base of *S*-methyldithiocarbazate)

The complexes, $[Sn(SNNNS)I_2]$ ($SNNNS^{2-}$= doubly deprotonated forms of the 2,6-diacetylpyridine Schiff bases of *S*-methyl- and *S*-benzyldithiocarzates) have been prepared and characterized. An X-ray structure analysis shows that the complex, $[Sn(dapsme)I_2]$ has a seven-coordinate pentagonal-bipyramidal geometry with the Schiff base coordinated to the tin(IV) ion via the pyridine nitrogen atom, the two azomethine nitrogen atoms and the two thiolate sulfur atoms. The iodo ligands are coordinated to the tin(IV) ion at axial positions.

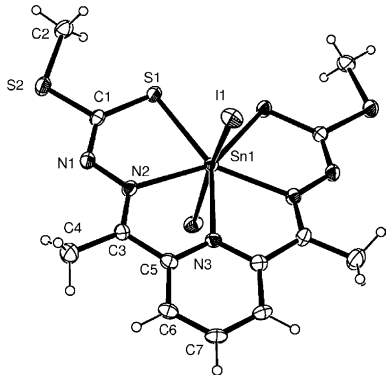

The Publisher encourages the submission of articles in electronic form thus saving time and avoiding rekeying errors. For detailed instructions on the preparation of manuscripts and of electronic artwork, consult the Author Gateway for Elsevier at http://authors.elsevier.com

SCIENCE DIRECT™

Full text of this journal is available, on-line from **ScienceDirect**. Visit **www.sciencedirect.com** for more information.

CONTENTS Direct This journal is part of **ContentsDirect**, the *free* alerting service which sends tables of contents by e-mail for Elsevier books and journals. You can register for **ContentsDirect** online at: **www. elsevier.com/locate/contentsdirect**

Available online at www.sciencedirect.com
SCIENCE DIRECT®
Polyhedron 23, issue 8, 6 May 2004
POLYHEDRON
www.elsevier.com/locate/poly

Contents

Papers

Zora Popović, Vibor Roje, Gordana Pavlović, Dubravka Matković-Čalogović, Maša Rajić, Ivan Leban

Polyhedron 23 (2004) 1293

Complexes of zinc(II) halides with *N*-benzyl- and *N*-*p*-tolyl-2-oxo-1-naphthylideneamine – preparation and characterization

The 1:2 complexes of zinc(II) halides with *N*-benzyl and *N*-*p*-tolyl-2-hydroxy-1-naphthylideneamine Schiff-bases (LH) are prepared and characterized; the crystal structures reveal monodentate (via oxygen) ligation of the neutral Schiff-base, while UV–Vis and ^{1}H NMR spectra show that all complexes are instable in solution.

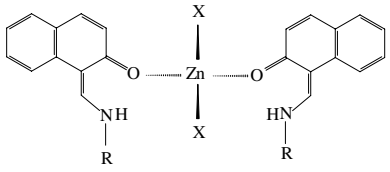

Petra Stachová, Dušan Valigura, Marián Koman, Milan Melník, Maria Korabik, Jerzy Mroziski, Tadeusz Glowiak

Polyhedron 23 (2004) 1303

Crystal structure, magnetic and spectral properties of tetrakis(2-nitrobenzoato)di-(aqua)dicopper(II) dihydrate

The synthesis, characterization and structure of $[Cu_2(2\text{-}NO_2bz)_4(H_2O)_2] \cdot 2H_2O$ are reported. The structure is centrosymmetric and the copper(II) atom has a square–pyramidal coordination by four oxygen atoms of carboxylate groups and the apical position is occupied by a water molecule. The electronic and infrared spectra exhibit typical features consistent with the observed structure. The magnetic susceptibility measurements of a polycrystalline sample proved the dimeric structure.

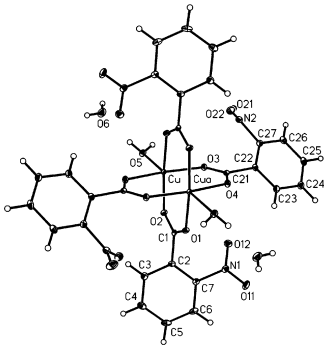

Barbara Barszcz, Tadeusz Głowiak, Julia Jezierska, Alina Tomkiewicz

Polyhedron 23 (2004) 1309

Synthesis of new pyrazole-containing binuclear and mononuclear Cu(II) complexes: crystal structure, EPR, magnetic and spectroscopic properties

Reaction of 1-hydroxymethyl-3,5-dimethylpyrazole (LOH) with copper(II) salts yields new dinuclear $[CuLLONO_3]_2$ (**1**) or mononuclear $CuL_3(NO_3)_2$ (**2**) co-ordination compounds (L – 3,5-dimethylpyrazole; LO – 1-methoxy-3,5-dimethylpyrazole). The type of the obtained complex strongly depends on the solvent used during the preparation. The structural feature of (**1**) is compared with that observed previously for two similar $[CuL(LO)X]_2$ complexes where $X=BF_4^-$(3) or ClO_4^- (**4**) instead of NO_3^- (**1**). Variable-temperature EPR spectra (77–295 K) and magnetic susceptibility measurements (1.9–300 K) indicate the antiferromagnetic exchange interaction dependent on the compensating ligand.

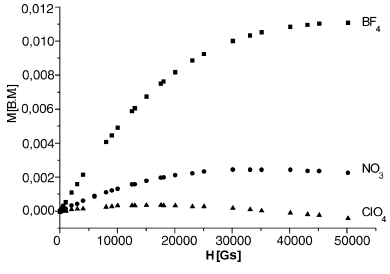

V.E. Marquez, J.R. Anacona, D. Loroño

Polyhedron 23 (2004) 1317

Crystal structure and electrochemistry of copper(II) macrocycles containing terpyridine

The macrocycle L, prepared by template condensation of bis-6,6″-(α-methylhidrazino)-4′-phenyl-2,2′:6″,2′-terpyridine with glyoxal, forms a stable crystalline complex of copper(II) $[Cu(L)(H_2O)_2][PF_6]_2$ which has been used as a starting material to prepare, for electrochemical studies, a series of seven coordinate copper(II) complexes $[Cu(L)X_2][PF_6]_2$ (X=pyridine, 4-cyanopyridine, 4-aminopyridine, 4-dimethylaminopyridine, pyrazine, imidazole, 1-methylimidazole, 2-methylimidazole, and trimethylphosphite).

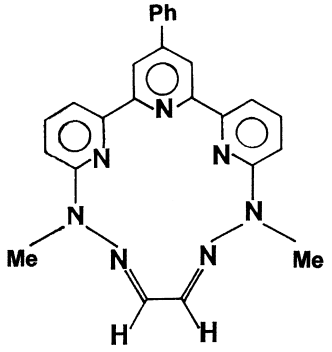

Masoud Salavati-Niasari, Mostafa Rezai-Adaryani

Polyhedron 23 (2004) 1325

Template condensation reactions of formaldehyde with amines and 2,3-butanedihydrazone: preparation and properties of nickel(II) complexes of 18-membered decaaza macrocycles

Six new square planar nickel(II) complexes of 18-membered decaazamacrocyclic ligands 5,6,14,15-tetramethyl-1,3,4,7,8,10,12,13,16,17-decaazacyclooctadecane have been prepared from the one-pot template condensation reaction of formaldehyde,2,3-butanedihydrazone with alkyl and benzyl amine in the pre sence of the nickel(II) ion.

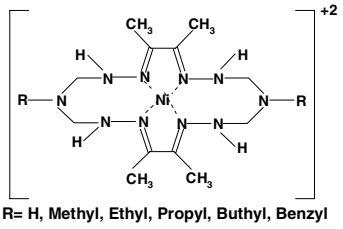

Jinkwon Kim, Sujin Han, In-Ku Cho, Ki Young Choi, Min Heu, Seokwon Yoon, Byoung Jin Suh

Polyhedron 23 (2004) 1333

Synthesis of a cyano-bridged Fe_2Mn linear unit and a Fe_2Mn_2 square unit by using the $[fac\text{-}Fe\{HB(pz)_3\}(CN)_3]^-$ building block

A new linear trinuclear Fe^{III}–Mn^{II}–Fe^{III} complex has been prepared and reacted with 2,2′-bipyridine to form a tetranuclear square $Fe_2^{III}Mn_2^{II}$ complex.

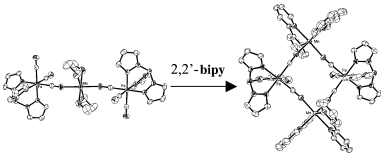

José Parada, Guillermo Larrazábal

Polyhedron 23 (2004) 1341

The origin of optical activity in complexes of the type $[Co(diimine)_2carbohydrate]^{2+}$

Complexes of the type Δ- and Λ-$[Co(diimine)_2carbohydrate]^{2+}$ have been prepared and characterized through their absorption and circular dichroism spectra. All of them showed excitonic effect in the UV region. In the visible region the transitions $^1A_1 \rightarrow {}^1B_2$ and $^1A_1 \rightarrow {}^1B_3$, under D_2 symmetry around Co(III).

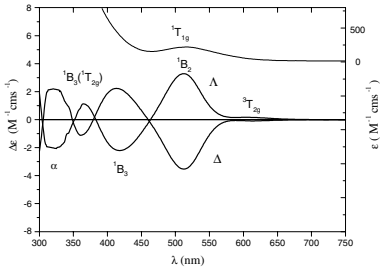

D. Belo, I.C. Santos, M. Almeida

Polyhedron 23 (2004) 1351

5,6-Dicyano-2,3-dithiopyrazine (dcdmp) chemistry: synthesis and crystal structure of Au(III)(dcdmp)$_2$ complexes and 2,3,7,8-tetracyano-1,4,6,9-tetraazothianthrene

As an effort to explore new complexes of the 2,3-dicyano-5,6-dimercaptopyrazyne (dcdmp) ligand with different transition metals, different salts containing both the Au(dcdmp)$_2^-$ complex and the new species 2,3,7,8-tetracyano-1,4,6,9-tetraazothianthrene (tctata), namely *n*-Bu$_4$N[Au(dcdmp)$_2$], *n*-Bu$_4$N AuBr$_2$ (tctata) and *n*-Bu$_4$N[Au(dcdmp)$_2$] (tctata), were obtained and characterized. Crystal structure analysis shows that tctata appears as a planar molecule in the last two compounds.

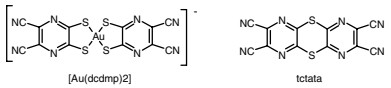

Gregory J. Grant, Ketankumar N. Patel, Monte L. Helm, Larry F. Mehne, David W. Klinger, Donald G. VanDerveer

Polyhedron 23 (2004) 1361

Heteroleptic platinum(II) complexes with crown thioethers and diimine ligands: the crystal structures of [Pt(9S3)(2,2′-bipy)](PF$_6$)$_2$ and [Pt(9S3)(4,4-dimethyl-2,2′-bipy)](PF$_6$)$_2$ · 2.5CH$_3$NO$_2$

A series of heteroleptic Pt(II) complexes with the thiacrown 9S3 and several diimines show a *cis*-PtS$_2$N$_2$ coordination sphere. The third sulfur from the 9S3 forms a long distance interaction with the Pt center, but these distances demonstrate that better π acids, in fact, do not result in shorter Pt–S axial distances as previously proposed.

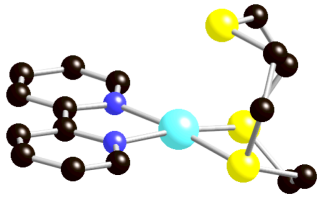

Jungsook Kim, Stephen L. Gipson

Polyhedron 23 (2004) 1371

Oxidatively induced one-electron reductive elimination of pentafluorophenyl from [Mo(C$_6$F$_5$)(CO)$_5$]$^-$

The anionic molybdenum(0) complex [Mo(C$_6$F$_5$)(CO)$_5$]$^-$ has been shown to undergo a one-electron oxidation followed by cleavage of the Mo–C$_6$F$_5$ bond in a one-electron reductive elimination process. Simulated cyclic voltammograms have provided an estimate of the rate constant for the cleavage reaction in the presence of pyridine of approximately 700 M^{-1} s^{-1}.

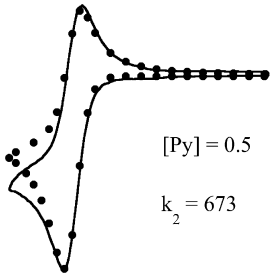

Terence L. Schull, Ray Butcher, Walter J. Dressick, Susan L. Brandow, Laura K. Byington, D. Andrew Knight

Polyhedron 23 (2004) 1375

Cis-[PtCl$_2$(*p*-TPPTP(H)$_7$)$_2$]Cl$_2$ · 4H$_2$O · (CH$_3$-CH(OH) CH$_3$): a platinum phosphine complex exhibiting both inter- and intra-molecular hydrogen bonding

The single-crystal X-ray structure of the water-soluble phosphine complex *cis*-[PtCl$_2$(*p*-TPPTP(H)$_7$)$_2$]Cl$_2$ · 4H$_2$O · (CH$_3$CH-(OH)CH$_3$) has been determined. The complex shows both intra-molecular hydrogen bonding between protonated phosphonic acid moieties, and inter-molecular hydrogen bonding.

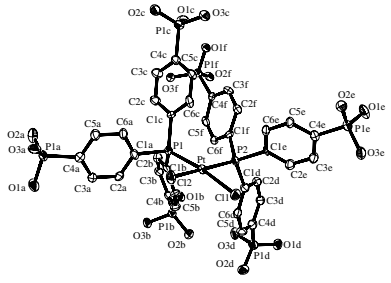

Chang Seop Hong, Young Sin You

Polyhedron 23 (2004) 1379

Synthesis, crystal structures and magnetic studies of terephthalato-bridged binuclear nickel(II) complexes

Two new binuclear compounds $[Ni_2(pmdtn)_2(tp)(H_2O)_2](ClO_4)_2(H_2O)_4$ (**1**) and $[Ni_2(pmdtn)_2(tp)(N_3)_2](H_2O)_4$ (**2**) (tp=terephthalate, pmdtn=*N*,*N*,*N*′,*N*′,*N*″-pentamethyldiethyltriamine) have been prepared and characterized by X-ray crystallography and magnetic measurements. The magnetic results indicate that weak antiferromagnetic interactions are transmitted through the tp bridge, which can be understood by the structural parameters.

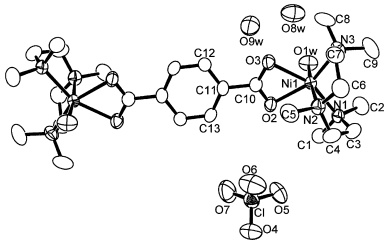

Kar-Beng Chew, M.T.H. Tarafder, Karen A. Crouse, A.M. Ali, B.M. Yamin, H. Fun

Polyhedron 23 (2004) 1385

Synthesis, characterization and bio-activity of metal complexes of bidentate N–S isomeric Schiff bases derived from *S*-methyldithiocarbazate (SMDTC) and the X-ray structure of the bis[*S*-methyl-β-*N*-(2-furylmethylketone)dithiocarbazato]cadmium(II) complex

Condensation of SMDTC with 2-furyl-methylketone and 5-methyl-2-furaldehyde gave isomeric Schiff bases, (NS) and (NS′). Metal complexes of these Schiff bases with cadmium, tin, iron, lead and cobalt were prepared and have been characterized by a variety of physico-chemical techniques. X-ray crystallographic analysis shows that the Cd(II) complex, bis [*S*-methyl-β-*N*-(2-furylmethyl-ketone)dithiocarbazato]Cd(II), consists of two molecules with distorted octahedral structures. The bioactivity of these complexes has been investigated.

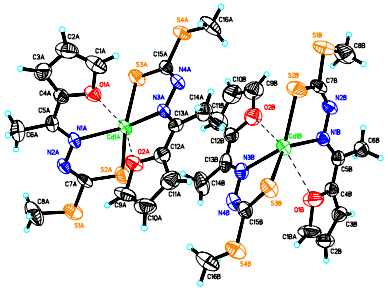

Thomas Höcher, Brian A. Salisbury, Klaus H. Theopold, Evamarie Hey-Hawkins

Polyhedron 23 (2004) 1393

Phosphanylalkylcyclopentadienyl ligands: synthesis, molecular structures and catalytic properties of $[\{(\eta^5\text{-}C_5H_4)CMe_2PHR\}CrCl_2(PMe_2Ph)]$ (R = Ph, ^{t}Bu)

$Li[(C_5H_4)CMe_2PHPh]$ reacted with $[CrCl_3(THF)_3]$ with formation of a mixture of products among which only $[\{(\eta^5\text{-}C_5H_4)CMe_2PPh\}CrCl]_2$ (**1**) could be isolated. However when $[CrCl_3(PMe_2Ph)_3]$ was treated with $Li[(C_5H_4)CMe_2PHR]$ the paramagnetic complexes $[\{(\eta^5\text{-}C_5H_4)CMe_2PHR\}CrCl_2(PMe_2Ph)]$ (R = Ph (**2**), ^{t}Bu (**3**)) were obtained. **2** and **3** were studied in the catalytic polymerisation of ethylene with methylalumoxane as cocatalyst.

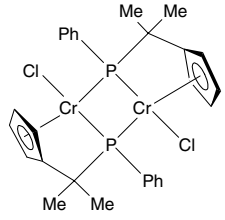

Carla Sousa, Paula Gameiro, Cristina Freire, Baltazar de Castro

Polyhedron 23 (2004) 1401

Nickel(II) and copper(II) complexes with N₂O Schiff base ligands bearing benzo-15-crown-5 functionalities as probes for spectroscopic recognition of lanthanide ions

Nickel(II) and copper(II) complexes with N_2O Schiff base ligands bearing benzo-15-crown-5 functionalities as flexible arms have been successfully used as spectroscopic probes for lanthanide and aluminium ions. Stability constants corresponding to the adduct formation [complex · 2 M^{3+}] have been calculated.

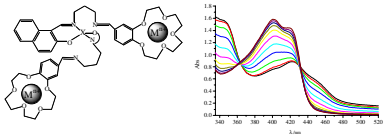

Albert Escuer, Franz A. Mautner, Núria Sanz, Ramon Vicente

Polyhedron 23 (2004) 1409

New examples of the unusual X-phenylcyanamido bridging ligands. Crystal structure and magnetic properties of Mn^{II} derivatives

Several new Mn^{II} compounds with X-phenylcyanamido (Xpcyd) and 1,10-phenantroline (phen) ligands have been characterised. These compounds contain the unusual double end-to-end R-cyanamide bridge and give supramolecular one-dimensional networks by means of H-bonds involving the N-amide atoms of the phenylcyanamide ligands. Susceptibility measurements on these new systems confirm moderate AF coupling mediated by the R–NCN pathway. Coupling constants related with the phenylcyanamido bridges are compared with the superexchange model recently proposed for ligands of this kind.

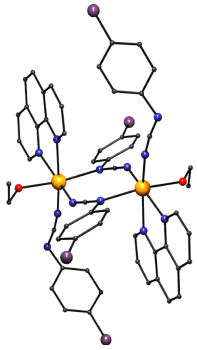

Christiane Fernandes, James L. Wardell, Adolfo Horn Jr., Janet M.S. Skakle, Valderes Drago

Polyhedron 23 (2004) 1419

Reactions of [{bis(2-pyridylmethyl)amine}-trichloroiron(III)] with $(HOCH_2)_3CNHCO(CH_2)_nCONHC(CH_2OH)_3$ $(n = 0 - 2)$: crystal structures of (μ-oxo)bis{(oxalato)-{[bis(pyridylmethyl)amine]iron(III)} and $(HOCH_2)_3CNHCO(CH_2)_2CONHC(CH_2OH)_3$

Crystal structures have been determined for [(oxalato)(BMPA)Fe^{III} (μ-O)Fe^{III}(BMPA)- oxalato)] **4** [BMPA=bis(2-pyridylmethyl)-amine] and *N*,*N*′-bis[tris(hydroxymethyl) methyl] propanediamide **2**. The Mössbauer and IR spectra of **4** are also reported.

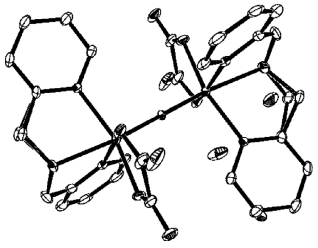

Matthew I.J. Polson, Sarah L. Howell, Amar H. Flood, Anthony K. Burrell, Allan G. Blackman, Keith C. Gordon

Polyhedron 23 (2004) 1427

Synthesis and electronic properties of mononuclear osmium(II) and rhenium(I) complexes containing ligands derived from [2,3-a:3′,2′-c]dipyridophenazine (ppb)

A method for the synthesis of a series of new ligands based on [2,3-a:3′,2′-c]dipyridophenazine (ppb) is reported, and spectroscopic and electrochemical data for mononuclear $[Os(bpy)_2L]^{2+}$, $[Os(phen)_2L]^{2+}$ and $[Re(CO)_3(Cl)L]$ complexes of these and related ligands are detailed.

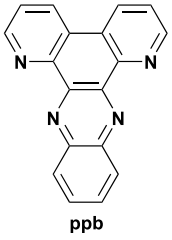

ppb

Konrad Kowalski, Janusz Zakrzewski, Agnieszka Rybarczyk-Pirek

Polyhedron 23 (2004) 1441

$[(\eta^5\text{-}C_5H_5)Fe(CO)_2]$(Fp)-complexes of the parabanic acid mono- and dianion: synthesis, X-ray structures and reactivity of the heterocyclic ligand

$[(\eta^5\text{-}C_5H_5)Fe(CO)_2]$(Fp)-complexes of the parabanic acid mono- and dianion have been synthesised. The former contains a reactive *N(3)*–H bond and can be readily thallated with TlOEt. Reaction of the thallated complex with Ph_3PAuCl, benzyl chloride and ethyl bromoacetate in DMF gave *N(3)*-aurated, *N(3)*-benzyl and *N(3)*-carboethoxymethyl complex, respectively. The structures of these complexes were confirmed by X-ray diffraction.

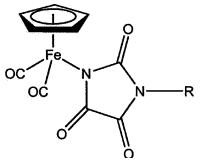

R = $CpFe(CO)_2$, Ph_3PAu, CH_2Ph, CH_2COOEt, CH_2COOH

Jie Dai, Wei Yang, Zhi-Gang Ren, Qin-Yu Zhu, Ding-Xian Jia

Polyhedron 23 (2004) 1447

Copper(I) and palladium(II) complexes of 4,5-bis(methylthio)-1,3-dithiole-2-thione, coordination and S···S contact assembled ribbon structures

Two complexes $C_5H_6S_5CuI$ and $(C_5H_6S_5)_2PdI_2$ have been synthesized and characterized crystallographically. They are assembled into ribbon structures by coordination bonds and S···S contacts. The very short distance of S···S contact is 3.268 Å.

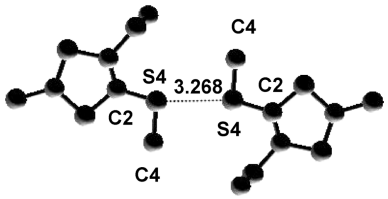

F.J. Barros-García, Alvaro Bernalte-García, Fransisco J. Higes-Rolando, F. Luna-Giles, R. Pedrero-Marín

Polyhedron 23 (2004) 1453

X-ray and spectroscopic characterisation of cobalt(III) and nickel(II) complexes with 2-(2-pyridyl)iminotetrahydro-1,3-thiazine hydrochloride · water (1/2) ($PyTzHCl \cdot 2H_2O$) in the solid state and study of its interaction with cobalt(II) and nickel(II) in aqueous solution

Mononuclear cobalt(III) and nickel(II) complexes have been prepared with 2-(2-pyridyl)iminotetrahydro-1,3-thiazine hydrochloride · water (1/2) ($PyTzHCl \cdot 2H_2O$). Their molecular structures and the physico-chemical properties are presented here. In these complexes, PyTz is a chelating ligand. The nitrogen atom of the thiazine ring and the imino nitrogen atom are donors in the coordinate bonds. The environment around the central ion for both complexes may be described as a distorted octahedral geometry. The stability constants of the Co(II) and Ni(II) complexes with the studied ligand in aqueous solution have been determined by a potentiometric method.

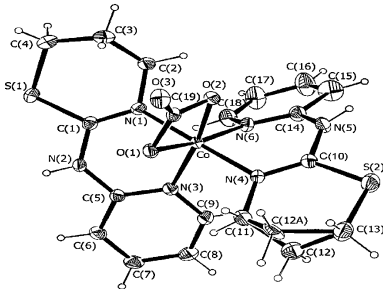

Qian-Ling Guo, Wen-Xiang Zhu, Shu-Lan Ma, Shu-Jing Dong, Miao-Qiong Xu

Polyhedron 23 (2004) 1461

Assembly of superanion capsules of *p*-sulfonatothiacalix[4]arenes with transition metal ions and diaza-crown ether

Assembly of superanion capsules of *p*-sulfonatothia-calix[4]arenes with transition metal ions and diaza-crown ether. The reaction of tetrasodium *p*-sulfonatothiacalix[4]arene and transition metal ions in the presence of 4,13-diaza-18-crown-6 forms ionic capsules and intercalation within the thiacalixarene bilayer system shows that amphiphilic macrocyclic compounds without aromatic rings can span the hydrophobic layers.

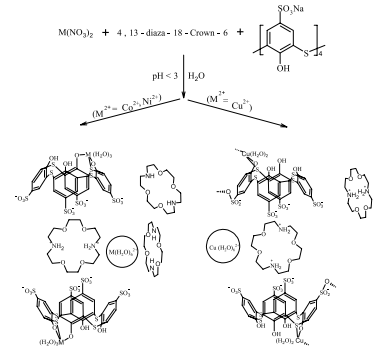

Hervé Guillon, Stéphane Daniele, Liliane G. Hubert-Pfalzgraf, J.M. Letoffe

Polyhedron 23 (2004) 1467

Synthesis, characterisation and thermal decomposition study of cerium(IV) 2-(2′-hydroxyphenyl)-2-oxazoline derivatives

Cerium(IV) oxazoline derivatives $Ce(Me_2oxaz)_4$ (**1**) [Me_2oxazH=2-(2′-hydroxyphenyl)-4-dimethyl)oxazoline] and $Ce(Pr^iHoxaz)_4$ (**2**) [$Pr^iHoxazH$=2-(2′-hydroxyphenyl)-4-isopropyl)oxazoline] were prepared in high yields by ligand exchange reactions between $Ce_2(OPr^i)_8(Pr^iOH)_2$ and the corresponding 2-(2′-hydroxyphenyl)-2-oxazolines. Characterisation was achieved by elemental analysis, FT-IR, ^1H NMR and mass spectroscopy (MS). **2** was also characterized by polarimetric measurement. Their thermal decomposition pathways under nitrogen were studied by TGA and coupled TGA-CG/MS experiments.

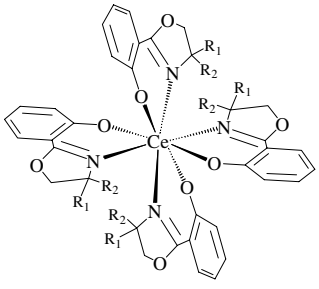

$R_1 = R_2 = Me$ (**1**)

$R_1 = H$, $R_2 = {}^iPr$ (**2**)

Wan-Fei Li, Hong-Mei Sun, Qi Shen, Yong Zhang, Kai-Bei Yu

Polyhedron 23 (2004) 1473

Synthesis, structural characterization and catalysis of ethyl-substituted indenylnickel (II) halides

Neutral 1-ethylindenyl nickel complexes (1-Et-Ind)Ni(PPh_3)X [X=Cl (**1**), Br (**2**), I (**3**)] have been synthesized and characterized by single-crystal X-ray analysis. When combined with $NaBPh_4$ and PPh_3, all of them are able to initiate the polymerization of styrene efficiently to give poly(styrene) with M_n values in the range of 10^4. The nature of the halogen atom has a slight effect on the structures of (1-Et-Ind)Ni(PPh_3)X, and a great effect on the catalytic activity of (1-Et-Ind)Ni(PPh_3)X.

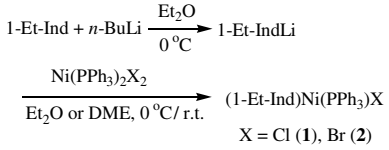

The Publisher encourages the submission of articles in electronic form thus saving time and avoiding rekeying errors. For detailed instructions on the preparation of manuscripts and of electronic artwork, consult the Author Gateway for Elsevier at http://authors.elsevier.com

SCIENCE DIRECT™

Full text of this journal is available, on-line from **ScienceDirect**. Visit **www.sciencedirect.com** for more information.

CONTENTS Direct This journal is part of **ContentsDirect**, the *free* alerting service which sends tables of contents by e-mail for Elsevier books and journals. You can register for **ContentsDirect** online at: **www. elsevier.com/locate/contentsdirect**

http://ChemWeb.com The World Wide Club for the Chemical Community

http://chemweb.com/gateways/elsevier.html

Available online at www.sciencedirect.com
SCIENCE DIRECT®
Polyhedron 23, issue 7, 15 April 2004
POLYHEDRON
www.elsevier.com/locate/poly

Contents

Papers

Swapnalee Sarmah, Diganta Kalita, Pankaj Hazarika, Ruli Borah, Nashreen S. Islam

Polyhedron 23 (2004) 1097

Synthesis of new dinuclear and mononuclear peroxovanadium(V) complexes containing biogenic co-ligands: a comparative study of some of their properties

Dinuclear vanadium compounds with a μ-peroxo moiety, $[V_2O_2(O_2)_3L_3] \cdot H_2O$, L=asn(**1**) and gln(**2**), were found to be distinctly different in nature, stability and reactivity from the monomeric complexes, $Na[VO(O_2)_2L] \cdot H_2O$, L=asn(**3**) and gln(**4**), with side-on bound peroxo groups. The experiments confirm the reactivity of synthetic μ-peroxovanadate dimer in producing bromination competent intermediate at physiological pH.

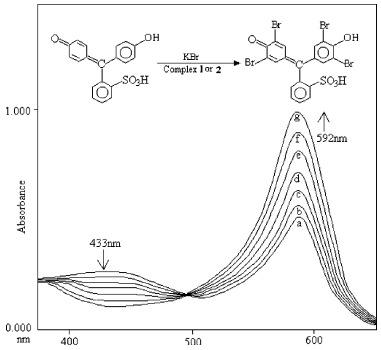

N. Can, S.E. Sözerli Can, A. Ataç, F. Bardak

Polyhedron 23 (2004) 1109

Structural characterization and luminescence properties of an isonicotinic acid N-oxide Mn(II) complex

An isonicotinic acid N-oxide Mn(II) compound was synthesized and characterized on the basis of elemental analysis and X-ray crystallography. In the complex, Mn(II) ions are coordinated by six water molecules, and the coordination number of the Mn(II) ion is six, FTIR spectra of the compound free isonicotinic acid N-oxide (INO) have been recorded in the range 4000–400 cm^{-1}. Cathodoluminescence (CL) spectra from the Mn(II) complex have been recorded.

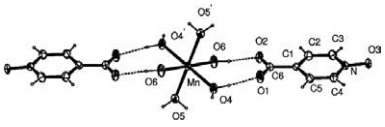

R. Srinivasan, I. Sougandi, K. Velavan, R. Venkatesan, Babu Verghese, P. Sambasiva Rao

Polyhedron 23 (2004) 1115

Synthesis and characterization of $[Cu_2(L)_2(OCOCH_3)(OCH_3)]ClO_4$ {L=2-[(4-methyl-pyridin-2-ylimino)-methyl]-phenol}: EPR and X-ray studies

A dicopper complex of a Schiff's base, 2-[(4-methyl-pyridin-2-ylimino)-methyl]-phenol, with a bridging acetato ligand has been synthesized and characterized by single crystal XRD, EPR, magnetic susceptibility, IR, UV–Vis, CV and elemental analysis. One of the copper atoms in the binuclear complex adopts a square-pyramidal geometry, while the other copper assumes a square-planar geometry. A seven line pattern observed at half-field in the frozen solution EPR spectrum confirms the interaction between the two copper ions.

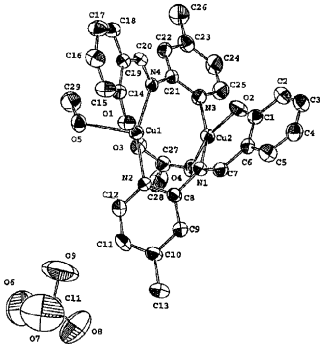

Guangcai Bai, Denis Vidovic, Herbert W. Roesky, Jörg Magull

Polyhedron 23 (2004) 1125

A novel potassium-centered highly symmetrically polynuclear zirconium complex: $K[\{(Cp^*Zr)_3(\mu_3\text{-}N)(\mu_3\text{-}NH)(\mu\text{-}NH_2)_3\}_4(NH_2)_5(NH_3)_7]$

A new synthetic approach is described for the novel highly symmetrical potassium zirconium cluster $K[\{(Cp^*Zr)_3(\mu_3\text{-}N)(\mu_3\text{-}NH)(\mu\text{-}NH_2)_3\}_4(NH_2)_5(NH_3)_7]$, whose crystal structure showed four trinuclear zirconium building blocks arranged around an interstitial potassium cation.

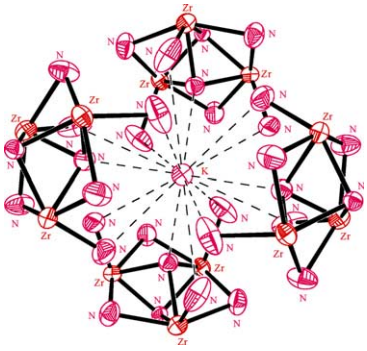

Hai-Bin Zhu, Zhen-Ya Dai, Wei Huang, Kai Cui, Shao-Hua Gou, Cheng-Jian Zhu

Polyhedron 23 (2004) 1131

Chiral copper(II) complexes of optically active Schiff bases: syntheses, crystal structure and asymmetric oxidation of methyl phenyl sulfide with hydrogen peroxide

Chiral copper(II) complexes of optically active Schiff bases with central seven-membered chelate rings for asymmetric oxidation of methyl phenyl sulfide with hydrogen peroxide.

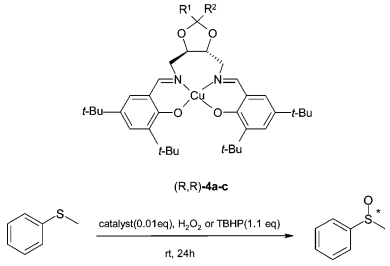

François Baril-Robert, André L. Beauchamp

Polyhedron 23 (2004) 1139

Preparation and crystal structure of (2,2′-bibenzimidazole)dihalobis(triphenylphospine) rhenium(III) halides

The rhenium(III) cationic complexes $[ReX_2(PPh_3)_2(bibzimH_2)]X$ were obtained by reduction of $ReOX_3(PPh_3)_2$ (X=Cl, Br) with excess PPh_3 in the presence of 2,2′-bibenzimidazole. The halide counter-ion is attached to the complex cation via a pair of N–H···X^- hydrogen bonds. The ^1H NMR spectra of these paramagnetic species were fully assigned.

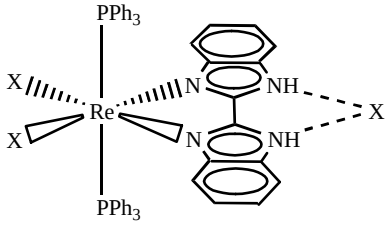

Damian G. Allis, Eric Burkholder, Jon Zubieta

Polyhedron 23 (2004) 1145

A new octamolybdate: observation of the θ-isomer in $[Fe(tpyprz)_2]_2[Mo_8O_{26}] \cdot 3.7H_2O$ (tpyprz=tetra-2-pyridylpyrazine)

The hydrothermal reaction of $Fe(CH_3CO_2)_2$, tetra-2-pyridylpyrazine (tpyprz) and $(NH_4)_6Mo_7O_{24} \cdot 4H_2O$ yields $[Fe(tpyprz)_2]_2[Mo_8O_{26}] \cdot 3.7H_2O$. The discrete octamolybdate anions represent a new isomeric form, θ-$[Mo_8O_{26}]^{4-}$. A computational study of the isomer illustrates the similarities of the θ-isomer and the low energy δ-isomer reported previously.

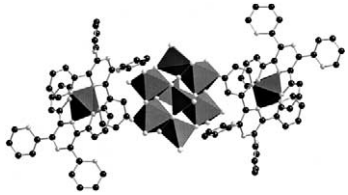

Marcelo R.L. Oliveira, Mayura M.M. Rubinger, Silvana Guilardi, Eduardo de Faria Franca, Javier Ellena, Vito M. De Bellis

Polyhedron 23 (2004) 1153

Preparation, crystal structure and spectroscopic characterization of novel *N*-*R*-sulfonyldithiocarbimate platinum(II) complexes

Two novel platinum(II) dithiocarbimates complexes were described. Their tetra-*n*-butylammonium salts were obtained in crystalline form and were characterized by X-ray diffraction techniques. All complexes present a similarly distorted square-planar configuration due to the asymmetric bidentate chelation by two sulfur atoms.

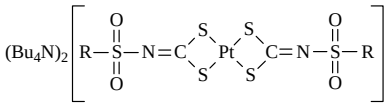

1 (R = C_6H_5), **2** (R = 4-BrC_6H_4)

Eric W. Ainscough, Andrew M. Brodie, Anthony K. Burrell, Andreas Derwahl, Geoffrey B. Jameson, Steven K. Taylor

Polyhedron 23 (2004) 1159

Platinum(II) and palladium(II) complexes containing a mixed donor 'P_2N' multidentate ligand

The 'P_2N' mixed donor ligand 2-(diphenylphosphino)-*N*-[2-(diphenylphosphino)benzylidene]benzeneamine (PNCHP) forms four or five coordinate complexes with Pt or Pd, e.g. $[Pt(PNCHP\text{-}\kappa^3P,N,P)L]^{2+}$ [L=the monodentate ligands: triphenylphosphine, 2-picoline, 3-picoline or the chelate ligands: 1,10-phenanthroline, 2,2′-bipyridine, bis(diphenylphosphino)ethane, 2,2′:6′,2″-terpyridine].

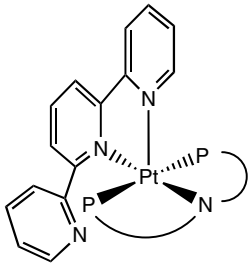

Jingcai Yao, Wei Huang, Haibin Zhu, Jianglin Fang, Shaohua Gou

Polyhedron 23 (2004) 1169

A novel tetranuclear copper(II) complex with 3,5-pyridinedicarboxylate bridges

An unprecedented tetranuclear complex bridged by 3,5-pyridinedicarboxylate (abbreviated as 3,5-PDC) with an empirical formula $[Cu_2(2,2'\text{-bpy})_3(3,5\text{-PDC})]_2(ClO_4)_4 \cdot 2(H_2O)$, has been synthesized and spectrally characterized. X-ray structural analysis reveals that there are two types of copper(II) centers, one is penta-coordinate with a distorted pyramidal geometry, while the other is tetra-coordinate with a distorted square planar geometry. 3,5-PDC serves as a tridentate ligand linking three adjacent metals with its one nitrogen and two monodentate carboxylic donors.

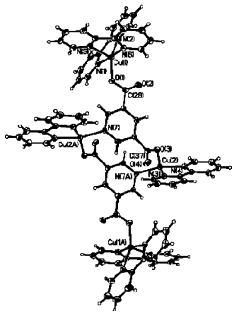

Laurence K. Thompson, Virginie Niel, Hilde Grove, David O. Miller, Michael J. Newlands, Peter H. Bird, Wasantha A. Wickramasinghe, A.B.P. Lever

Polyhedron 23 (2004) 1175

Cobalt and nickel complexes of a tetradentate phthalazine ligand – mononuclear, dinuclear and trinuclear derivatives

The potentially bis-bidentate ligand 1,4-di-2′-pyridylaminophthalazine (pap), forms mononuclear (Ni(II)), dinuclear (Ni(II), Co(III)) and trinuclear (Ni(II)) complexes, with combined N–N diazine and OH (Ni(II), Co(III)), and H_2O (Ni(II)) bridges. The dinuclear and trinuclear Ni(II) complexes exhibit intramolecular antiferromagnetic exchange interactions, from a combination of the exchange effects of both the N–N and 'O' bridge groups.

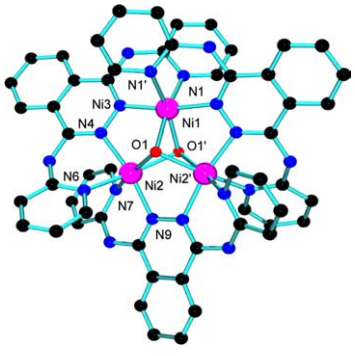

Shi-Xia Liu, Antonia Neels, Helen Stoeckli-Evans, Melanie Pilkington, John D. Wallis, Silvio Decurtins

Polyhedron 23 (2004) 1185

Organosulfur donor with hydroxy groups and its conducting salt: crystal structures and physical properties

The unique crystal structure of a conducting radical salt shows that this donor has potential applications in electrical conductivity systems.

Farba Bouyagui Tamboura, Pepe Marcel Haba, Mohamed Gaye, Abdou Salam Sall, Aliou Hamady Barry, Tahar Jouini

Polyhedron 23 (2004) 1191

Structural studies of bis-(2,6-diacetylpyridine-bis-(phenylhydrazone)) and X-ray structure of its Y(III), Pr(III), Sm(III) and Er(III) complex

The ligand 2,6-diacetylpyridine-bis-(benzoylhydrazone) has been found in solution in three forms which can coordinate with lanthanide ions. Crystal structures of yttrium and erbium complexes where one ligand molecule is coordinated to the metal and crystal structures of praseodymium and samarium complexes where two ligand molecules are present are reported. In the yttrium and the erbium complexes the metal ions have an eight coordination number while the praseodymium and the samarium complexes have a ten coordination number.

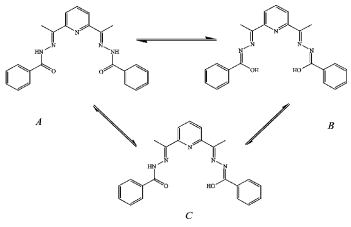

Ondrej Šedo, Zbyněk Voráč, Milan Alberti, Josef Havel

Polyhedron 23 (2004) 1199

Laser ablation synthesis of new phosphorus and phosphorus-sulfur clusters and their TOF mass spectrometric identification

Laser ablation of elemental phosphorus, sulfur, theirs mixtures or some phosphorus sulfides connection with simultaneous TOF mass spectrometry was done. Formation of singly charged P_n^+ ($n = 1$–189) and P_n^- ($n = 1$–225) and S_m^+ ($m = 1$–11) and S_m^- ($m = 1$–15) clusters was proved. Similarly to laser ablation of red phosphorus, P_nS_m clusters generated from P_4S_3 and P_4S_{10} with odd number of phosphorus atoms were much higher than those with even numbers. Various mixed clusters were also obtained via direct laser ablation of a mixture of the elements while higher yield of the mixed clusters was obtained when the mixture was first homogenised using ultrasound. Totally, 68 new P_nS_m clusters were formed and detected. The laser ablation represents a new method to synthesise mixed P_nS_m clusters.

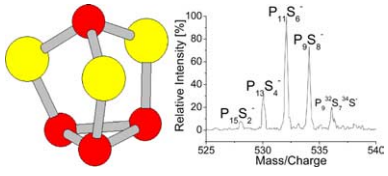

Chunlin Ma, Yinfeng Han, Dacheng Li

Polyhedron 23 (2004) 1207

Synthesis and crystal structures of diorganotin dicyanoethylene-1,2-dithiolate compounds and their derivatives with 4,4′-Bipy or Phen

Six diorganotin(IV) compounds from dicyanoethylene-1,2-dithiolate (mnt) of the type $[R_2Sn(mnt)Cl_nL] \cdot Y$ (when $n = 0$, L=0: R=CH_3, Y=0, **1**; R=*n*-Bu, Y=0, **2**; R=C_6H_6, Y=0.5C_6H_6, **3**; R=CH_3, Y=1.5(4,4′-Bipy), **4**; when $n = 1$, L=0, R=CH_3, Y=4,4′-Bipy, **5**; when $n = 0$, L=phen, R=CH_3, Y=0, **6**; 4,4′-Bipy=4,4′-Bipyridyl; phen=1,10-Phenanthroline) are synthesized by reactions of diorganotin dichloride and disodium maleonitriledithiolate (Na_2mnt) in the presence of 4,4′-Bipy or Phen.

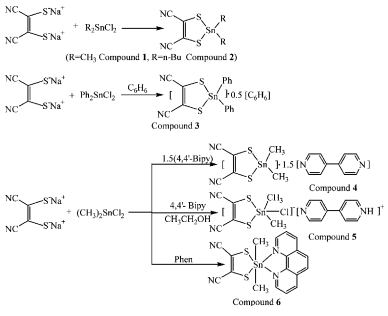

Franz A. Mautner, Christian Gspan, Karl Gatterer, Mohamed A.S. Goher, Morsy A.M. Abu-Youssef, Edith Bucher, Werner Sitte

Polyhedron 23 (2004) 1217

Synthesis and characterization of three 5-(4-pyridyl)tetrazolato complexes obtained by reaction of 4-cyanopyridine with metal azides from aqueous solutions

Two isomorphic mononuclear compounds $[M(4\text{-PTZ})_2(H_2O)_4] \cdot 2H_2O$, [M=Mn, Cd; (4-PTZ=5-(4-pyridyl)tetrazolate)] and the chain system $[Ca_{1.5}((4\text{-PTZ})_2H)(N_3)_2(H_2O)_5](H_2O)_{0.3}$ have been synthesized and characterized by structural, spectral and thermoanalytical methods.

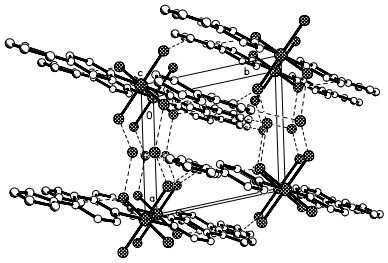

Varughese Philip, V. Suni, Maliyeckal R. Prathapachandra Kurup, Munirathinam Nethaji

Polyhedron 23 (2004) 1225

Structural and spectral studies of nickel(II) complexes of di-2-pyridyl ketone N^4,N^4-(butane-1,4-diyl) thiosemicarbazone

Three Ni(II) complexes with general formula $[NiLX] \cdot \frac{1}{2}H_2O$ (X=Cl, N_3 and NCS) were synthesized using di-2-pyridyl ketone N^4,N^4-(butane-1,4-diyl) thiosemicarbazone (HL). X-ray diffraction studies of compounds NiLCl and $NiL(N_3)$ reveal a square planar geometry where the thiosemicarbazone acts as an NNS donor ligand. Spectral data for compound NiL(NCS) suggest a structure similar to the chloro and azido derivatives.

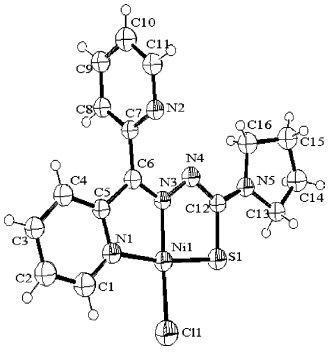

V. Madhu, Samar K. Das

Polyhedron 23 (2004) 1235

Near-IR absorption due to supramolecular electronic interaction in an extended 3D hydrogen-bonding network material: synthesis, crystal structure and properties of [4,4′-H_2bpy][$Cu(mnt)_2$]

Reaction of $[Bu_4N]_2[Cu(mnt)_2]$ with [4,4′-H_2bpy]Cl_2 affords ion-pair complex [4,4′-H_2bpy][$Cu(mnt)_2$] showing three-dimensional supramolecular network in the solid state; the relevant interaction involves bifurcated (bpyN)–H···(NC–mnt) hydrogen bonds and the compound exhibits ion-pair charge transfer transition in the near-IR region.

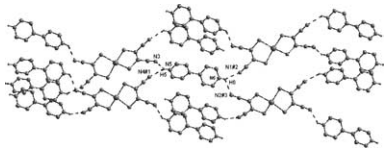

Jun Luo, Xi-Geng Zhou, Song Gao, Lin-Hong Weng, Ze-Huai Shao, Chun-Mei Zhang, Yan-Rong Li, Jie Zhang, Rui-Fang Cai

Polyhedron 23 (2004) 1243

Synthesis and characterization of copper(II) azide complexes containing polyamines as co-ligands

Two new copper(II) azide complexes $Cu_2(pn)_2(N_3)_4$ (**1**) and $Cu_3(dien)_2(N_3)_6$ (**2**) (pn=1,3-diaminopropane and dien=diethylenetriamine) have been synthesized and characterized by single crystal X-ray diffraction. Magnetic susceptibility measurement for complex **2** in the range 2–300 K showed weak antiferromagnetic exchange between the copper(II) ions ($J = -2.09(8)$ cm^{-1}) in the trinuclear unit.

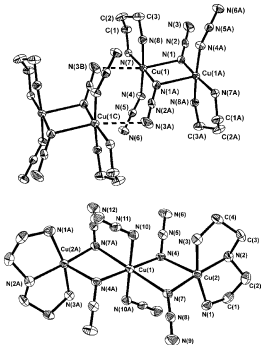

Suaad Abuskhuna, John Briody, Malachy McCann, Michael Devereux, Kevin Kavanagh, Julia Barreira Fontecha, Vickie McKee

Polyhedron 23 (2004) 1249

Synthesis, structure and anti-fungal activity of dimeric Ag(I) complexes containing bis-imidazole ligands

Five Ag(I) complexes containing the ligands bis(imidazol-2-yl)methane (2-BIM) and its derivatives were prepared and $[Ag_2(2\text{-}BIM)_2](ClO_4)_2$ and $[Ag_2(2\text{-}BIM(Bz)OH)_2](ClO_4)_2 \cdot EtOH$ were characterised using X-ray crystallography. In each dimer the two Ag(I) ions are two-coordinate and there are small but definite argentophilic Ag–Ag (d^{10}–d^{10}) interactions. All of the complexes display anti-fungal activity when tested in vitro against the fungal pathogen *Candida albicans*.

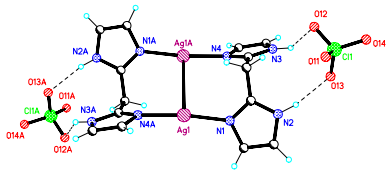

Xiang-Jun Zheng, Li-Cun Li, Song Gao, Lin-Pei Jin

Polyhedron 23 (2004) 1257

Hydrothermal syntheses, structures and magnetic properties of two transition metal coordination polymers with a square grid framework

Coordination polymers $[M(NDA)(4,4'\text{-}bpy)(H_2O)_2] \cdot nH_2O]$ (M=Co, Ni) with a square grid metal-organic framework constructed by M(II), 1,4-naphthalenedicarboxylate and 4,4′-bipyridine shows weak antiferromagnetic and ferromagnetic exchange interaction between the Co^{2+} ions and Ni^{2+} ions, respectively.

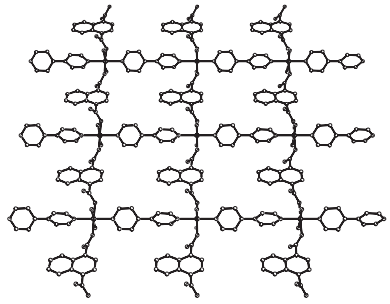

Sofia S.M.C. Godinho, Beatriz Royo, Maria T. Lobato, Eberhardt Herdtweck, Carlos C. Romão

Polyhedron 23 (2004) 1263

Synthesis and structure of diphenylphosphine derivatives of molybdenocene

The phosphino molybdenocene complex $[Cp_2Mo(PPh_2H)_2][BF_4]_2$ **(1)** ($Cp = \eta^5\text{-}C_5H_5$) was prepared by reaction of Cp_2MoI_2 with PPh_2H and excess of $TlBF_4$ in NCMe. The synthesis of the monocation $[Cp_2MoI(PPh_2H)]^+$ **(2)** as the BF_4^- or I^- salt is also reported. The molecular structures of $[Cp_2Mo(PPh_2H)_2][BF_4]_2$ and $[Cp_2MoI(PPh_2H)]^+$ have been determined by single-crystal X-ray diffraction.

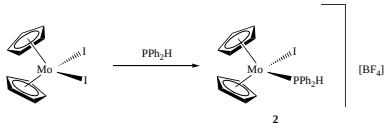

Athanassios K. Boudalis, Catherine P. Raptopoulou, Aris Terzis, Spyros P. Perlepes

Polyhedron 23 (2004) 1271

2,2′-Bipyrimidine (bpym) in iron(III) carboxylate chemistry: preparation and characterization of $[Fe_2O(O_2CMe)_2(bpym)_2(H_2O)_2](ClO_4)_2$, and the influence of weak interactions in the formation of metal clusters

The reaction system $Fe(ClO_4)_3 \cdot 6H_2O/NaO_2CMe/bpym$ (bpym=2,2′-bipyrimidine) in MeCN leads to complex $[Fe_2O(O_2CMe)_2(bpym)_2(H_2O)_2](ClO_4)_2$ **(3)**, which contains the $\{Fe_2(\mu\text{-}O)(\mu\text{-}O_2CMe)_2\}^{2+}$ core. The crystal structure is stabilized by hydrogen bonds and π–π interactions. These aspects of the crystal structure are considered responsible for the failure to isolate larger molecular aggregates.

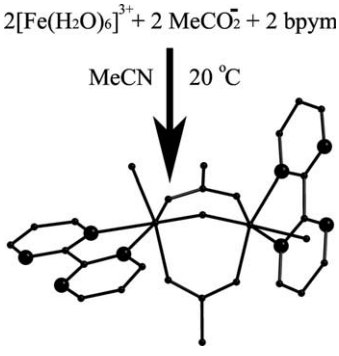

Ismail Yilmaz, Makbule Burkut Koçak

Polyhedron 23 (2004) 1279

Electrochemical, spectroelectrochemical, and pyridine binding properties of tetrathia macrocycle-bridged dimeric cobalt phthalocyanine

Tetrathia macrocycle-bridged dimeric cobalt phthalocyanine, $[(RS)_6CoPc]_2CR$ where R= C_6H_{13}, CR=[1,4,7,10-tetrathia-(12-crown-4)], was investigated electrochemically and spectroelectrochemically. The pyridine-binding properties of the complex were also investigated by spectrophotometric technique in the solution of dichloromethane. A highly aggregated neutral complex resulted in monomeric forms for the mono-and doubly reduced species of the complex in CH_2Cl_2. The pyridine binding properties of the complex confirms the formation of mono-pyridine adduct.

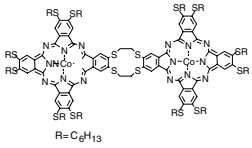

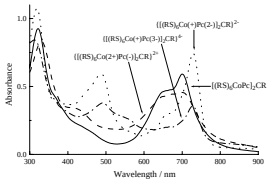

Erratum to: "Synthesis, characterization and crystal structures of (*Z*)-1-(triarylstannyl)-3-phenyl-1-buten-3-ols and their arylhalostannyl derivatives" [Polyhedron 22 (2003) 3523] 1287

Erratum to: "Effect of free and chelating phosphine coordination environments on the NiS_2P_2 chromophore: synthesis, NMR and other spectral studies. Crystal and molecular structures of (*N,N*-dipropyldithiocarbamato)di(triphenylphosphine)nickel(II) perchlorate and (*N,N*-dipropyldithiocarbamato)1,2-bis((diphenylphosphino)ethane)nickel(II) tetraphenylborate" [Polyhedron 23 (2004) 77] 1289

Erratum to: "Synthesis and X-ray crystal structures of hydridotris(3,5-dimethylpyrazolyl)borate (Tp′) molybdenum(VI) bis(imido) complexes" [Polyhedron 23 (2004) 189] 1291

The Publisher encourages the submission of articles in electronic form thus saving time and avoiding rekeying errors. For detailed instructions on the preparation of manuscripts and of electronic artwork, consult the Author Gateway for Elsevier at http://authors.elsevier.com

SCIENCE DIRECT™

Full text of this journal is available, on-line from **ScienceDirect**. Visit **www.sciencedirect.com** for more information.

CONTENTS Direct This journal is part of **ContentsDirect**, the *free* alerting service which sends tables of contents by e-mail for Elsevier books and journals. You can register for **ContentsDirect** online at: **www. elsevier.com/locate/contentsdirect**

http://ChemWeb.com The World Wide Club for the Chemical Community

http://chemweb.com/gateways/elsevier.html

Available online at www.sciencedirect.com
SCIENCE DIRECT®
Polyhedron 23, issue 5, 4 March 2004
POLYHEDRON
www.elsevier.com/locate/poly

Contents

Papers

Daniel L. Reger, Delia M. Ciurtin Smith, Ken D. Shimizu, Mark D. Smith

Polyhedron 23 (2004) 711

Syntheses and solid state structures of europium and terbium complexes of *N*, *N*′-bis(2-pyridylmethyl)urea and *N*, *N*′-bis(3-pyridylmethyl)oxalamide

The synthesis, structural characterization and luminescence properties of three new lanthanide-containing compounds are reported. Two display a molecular structure, while the third is a one-dimensional polymeric chain. Hydrogen bonds assemble the molecular structures in one-dimension and the chain-like structure in three dimensions.

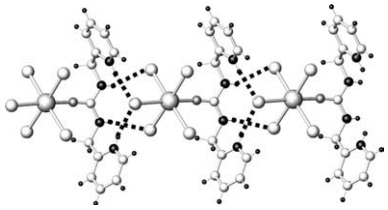

Jose A.A. Sales, Flavia P. Faria, Alexandre G.S. Prado, Claudio Airoldi

Polyhedron 23 (2004) 719

Attachment of 2-aminomethylpyridine molecule onto grafted silica gel surface and its ability in chelating cations

The chelate molecule, 2-aminomethylpyridine (AMP), was attached to previous chemical modified silica, to give a degree of pendant groups of 0.76 mmol per gram of silica. The new synthesized surface has property in cation removal from aqueous solution, as expressed by favorable thermodynamic data.

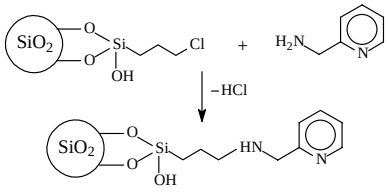

Sk. Jasimuddin, P. Byabartta, G. Mostafa, T. Lu, C. Sinha

Polyhedron 23 (2004) 727

Synthesis, spectral studies, crystal structure and redox properties of homoleptic tris-chelated ruthenium(II)-arylazoimidazoles

The one pot syntheses of tris-chelated [Ru(*o*/*p*-RaaiR′)$_3$]Cl$_2$ (RaaiR′=1-alkyl-(2-arylazo)-imidazole) are described. Solution spectra show a MLCT transition. The complexes show Ru(II)/Ru(III) and three successive ligand reduction couples. The EHMO results support the spectral and electrochemical properties.

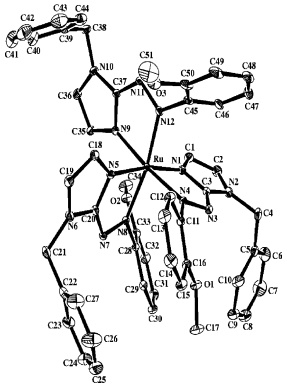

Sergej Pasko, Liliane G. Hubert-Pfalzgraf, Adulfas Abrutis, Jacqueline Vaissermann

Polyhedron 23 (2004) 735

Synthesis and molecular structures of cobalt(II) β-diketonate complexes as new MOCVD precursors for cobalt oxide films

Complexes of cobalt(II) 2,4-pentanedionate (acac) and 2,2,6,6-tetramethyl-3,5-heptanedionate (thd) with TMEDA and 1-dimethylamino-2-propanol (DMAPH) or 2-dimethylaminoethanol (DMAEH), were synthesized. X-ray diffraction showed $Co(acac)_2$(TMEDA) (**1**) to be monomeric and $[Co(acac)_2(DMAPH)]_2$ (**2**) dimeric due to H-bonds. The most stable and volatile adducts **1** and $Co(thd)_2$(TMEDA) (**4**), the first adduct of $Co(thd)_2$ reported, were used for cobalt oxide deposition by liquid injection MOCVD. Films of Co_3O_4 were characterized by XRD and XPS. Epitaxial films can be obtained by using both TMEDA adducts.

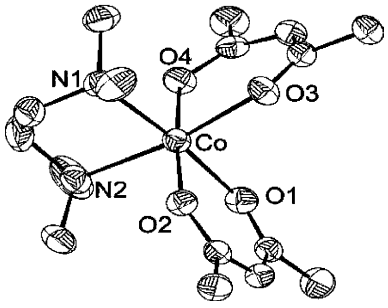

Mohammad Abul-Haj, Miguel Quirós, Juan M. Salas

Polyhedron 23 (2004) 743

Divalent transition metal complexes of the anionic form of 4,7-dihydro-1,2,4-triazolo[1,5-*a*]pyrimidine-7-one: crystal structure of the zinc(II) compound

Divalent metal (Mn, Fe, Co, Ni, Cu, Zn and Cd) complexes of the anion of 4,7-dihydro-1,2,4-triazolo[1,5-*a*]pyrimidine-7-one have been isolated and characterized. The crystal structure of the Zn compound has been solved showing that it is mononuclear and octahedral with the ligand coordinated via N3. Spectroscopic and magnetic data suggest analogous structures for the other compounds except for Cu, which is dinuclear according to magnetic and EPR data.

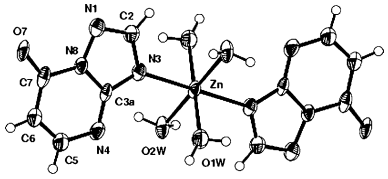

Yao-Cheng Shi, Wen-Bin Shen, Hua-Mei Yang, Hai-Bin Song, Xiao-Ya Hu

Polyhedron 23 (2004) 749

Copper and nickel complexes of the tetradentate ligand derived from the condensation of ferrocenoylacetone with 1,2-diaminoethane

Ferrocenoylacetone reacts with 1,2-diaminoethane to yield three isolated isomers $\mathbf{H_2L}$, $\mathbf{H_2L^1}$ and $\mathbf{H_2L^2}$. Reaction of the tetradentate enaminone ligand $[C_5H_5FeC_5H_4C(O)CH{=}C(CH_3)NHCH_2]_2$($\mathbf{H_2L}$) with copper acetate and nickel acetate affords complexes **I** and **II**. The X-ray crystallography of complexes **I** and **II** reveals that complex **I** exists as a mixture of *anti* and *syn* isomers whereas complex **II** as a single *syn* isomer.

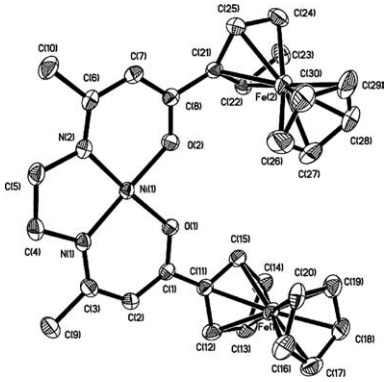

Jing Lu, Chang-Hai Lü, Jie-Hui Yu, Ji-Qing Xu, Yong Li, Xiao Zhang, Tie-Gang Wang, Qing-Xin Yang

Polyhedron 23 (2004) 755

Syntheses, structures and third-order nonlinear optical properties of heterometal and homometal clusters containing iron

The title compound is a hexanuclear $[Mo_2Fe_4O_{10}]$ cluster including two solvent molecules DMF with α-furoic acid and DMF as auxiliary ligands.

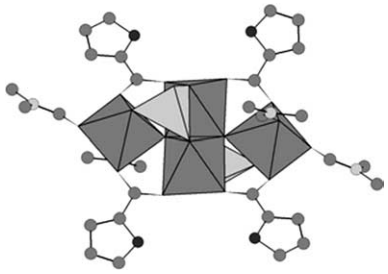

Eugene V. Tretyakov, Olga V. Koreneva, Galina V. Romanenko, Yu G. Shvedenkov, Victor I. Ovcharenko

Polyhedron 23 (2004) 763

Synthesis, structure and magnetism of $M(hfac)_2$ complexes with spin labelled amides

Reactions of $Mn(hfac)_2$, $Cu(hfac)_2$ and $Co(hfac)_2$ with amide derivatives of nitronyl and imino nitroxides lead to heterospin compounds tending to form in solids bi- or tetranuclear complexes due to intermolecular H-bonding between the peripheral NH_2 groups and the coordinated carbonyl oxygen atoms.

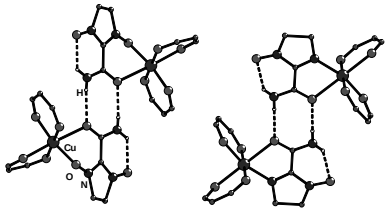

Jing-Yang Niu, Zi-Liang Wang, Jing-Ping Wang

Polyhedron 23 (2004) 773

Hydrothermal synthesis and structure characterization of a Keggin tungstocobaltate $[Co(2,2'\text{-bipy})_3]_2H_2[CoW_{12}O_{40}] \cdot 9.5H_2O$

The Keggin tungstocobaltate $[Co(2,2'\text{-bipy})_3]_2H_2[CoW_{12}O_{40}] \cdot 9.5H_2O$, consisting of a Keggin anion $[CoW_{12}O_{40}]^{6-}$ and two isolated chiral ions $[Co(2,2'\text{-bipy})_2]^{2+}$, was obtained by a hydrothermal synthesis for the first time. EPR spectra reveal two Co^{2+} coordination environments, high spin state ($g = 5.1$, 4.2) and low spin state ($g = 2.0$), exhibited in the title compound. Furthermore, when the temperature increases from 110 K to room temperature, the signal $g = 5.1$ of high spin Co^{2+} disappears, caused by the negative zero-field splitting.

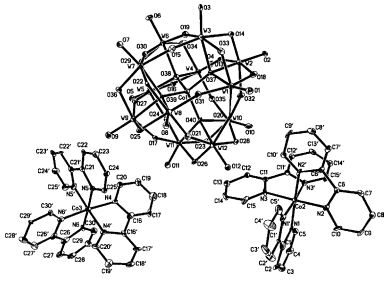

Chunlin Ma, Qin Jiang, Rufen Zhang

Polyhedron 23 (2004) 779

Syntheses, characterizations and crystal structures of new organotin complexes with 2-mercapto-6-nitrobenzothiazole

A series of organotin (IV) complexes with 2-mercapto-6-nitrobenzothiazole (HMNBT) of the type, $[R_nSn(MNBT)_{4-n}]$ ($n = 2$, R = Me, **4**; $n = 3$, R = Me, **5**; *n*-Bu, **6**; Ph–, **7**; $PhCH_2$–, **8**) were synthesized. All the complexes **4**–**8** have been characterized by elemental, IR, ^1H NMR or X-ray diffraction analyses.

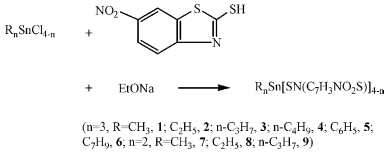

(n=3, R=CH_3, **1**; C_2H_5, **2**; n-C_7H_7, **3**; n-C_4H_9, **4**; C_6H_5, **5**; C_7H_9, **6**; n=2, R=CH_3, **7**; C_2H_5, **8**; n-C_7H_7, **9**)

H. Yasemin Yenilmez, İbrahim Özçeşmeci, Ali İhsan Okur, Ahmet Gül

Polyhedron 23 (2004) 787

Synthesis and characterization of metal-free and metallo phthalocyanines with four pendant naphthoxy-substituents

We have described the synthesis and spectral characterization of four new phthalocyanines with 1-naphthoxy and 2-naphthoxy substituents on the periphery; the distinctive property of these compounds is a second absorption in the ultraviolet region of comparable intensity to the intense B band of phthalocyanines.

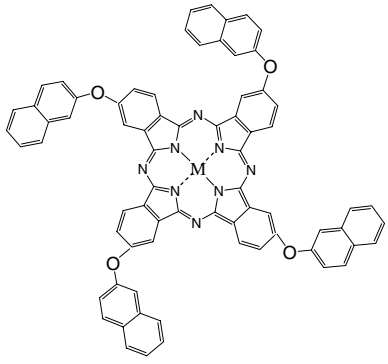

Joydev Dinda, Sk. Jasimuddin, G. Mostafa, C.-H. Hung, Chittaranjan Sinha

Polyhedron 23 (2004) 793

Silver(I) complexes of the naphthyl-azoimine function: single crystal X-ray structure of bis-[1-ethyl-2-(naphthyl-α-azo)imidazole]silver(I) perchlorate

Silver(I) complexes of 1-alkyl-2-(naphthyl-(α/β)-azo)imidazole are described. The single crystal X-ray diffraction study of bis-[1-ethyl-2-(naphthyl-α-azo)imidazole]silver(I) perchlorate confirms the structure of the complexes. The complexes show intra-molecular and intermolecular H-bonding leading to a 1D helical framework.

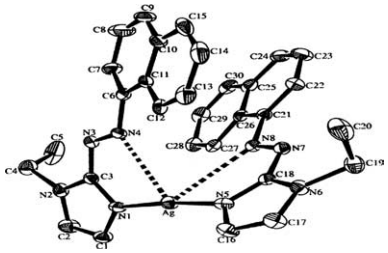

Michael S. Hill, Peter B. Hitchcock, Nikki Smith

Polyhedron 23 (2004) 801

Routes to titanium tetrazole complexes

Potential routes to titanium tetrazole derivatives for use as molecular precursors to TiN are described. Direct reaction of 5-phenyltetrazole and $TiCl_4$ produced a six-coordinate adduct. Attempted reaction of $TiCl_4$ and a tributylstannyl tetrazole derivative, synthesised by cycloaddition of Bu_3SnN_3 and 2-toluinitrile, gave only incomplete elimination of the expected Bu_3SnCl by-product.

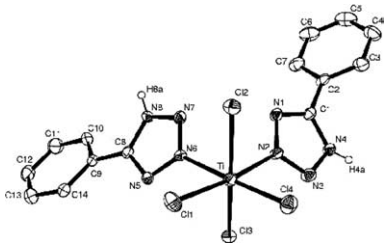

Vladislav V. Krisyuk, Assia E. Turgambaeva, Shi-Woo Rhee

Polyhedron 23 (2004) 809

Homobinuclear copper(I) hexafluoroacetylacetonate complexes with non-cyclic diene ligands

Binuclear copper(I) hexafluoroacetylacetonate complexes with non-cyclic divinyl ligands of $[Cu^I(hfac)]_2L$ composition (**1**) L = 1,5-hexadiene, (**2**) L = allyl ether, (**3**) L = diallyldimethylsilane, (**4**) L = 1,3-divinyltetramethyldisiloxane were prepared as yellow crystalline solids. Complexes **1** and **4** are most stable and can be sublimated at 50–70 °C in a vacuum with good yield. The $[Cu^I(hfac)]_2L$ composition for both complexes is realized by copper(I) ions coordination to a chelate-bound β-diketonate and η^2-coordinated vinyl unit. A possible copper–silicon interaction is postulated for compound **4**.

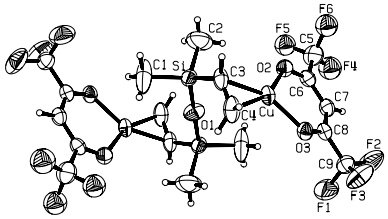

Xian-Lan Hong, Hui Chao, Jun-Hua Yao, Hong Li, Liang-Nian Ji

Polyhedron 23 (2004) 815

Synthesis, characterization, electrochemistry and solvatochromic studies of $[Ru(dppt)(dien)]^{2+}$ and $[Ru(pta)(dien)]^{2+}$

Two novel Ru(II) complexes $[Ru(dppt)(dien)]^{2+}$ (**1**) and $[Ru(pta)(dien)]^{2+}$ (**2**) (dppt, pta and dien stand for 3-(1,10-phenanthrolin-2-yl)-5,6-diphenyl-as-triazine, 3-(1,10-phenanthrolin-2-yl)-5,6-diphenyl-as-triazino-[5,6-f]acenaphthylene and diethylenetriamine, respectively) have been synthesized and characterized. The electrochemical and solvatochromic properties of them were also investigated.

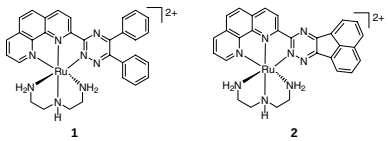

Lin Yu, Yong-Qiang Ma, Run-Chang Liu, Guo-Cang Wang, Jin-Shan Li, Guan-Hua Du, Juan-Juan Hu

Polyhedron 23 (2004) 823

Synthesis, characterization and in vitro antitumor activity of some arylantimony ferrocenylcarboxylate derivatives and the crystal structures of $[C_5H_5FeC_5H_4C(CH_3)=CHCOO]_2Sb(C_6H_4F\text{-}4)_3$ and $[4\text{-}(C_5H_5FeC_5H_4)C_6H_4COO]_2Sb(C_6H_4F\text{-}4)_3$

A series of novel arylantimony ferrocenylcarboxylate derivatives with the formulae $[C_5H_5FeC_5H_4C(CH_3)=CHCOO]_2SbAr_3$ and $[4\text{-}(C_5H_5FeC_5H_4)C_6H_4COO]_2SbAr_3$ (Ar = C_6H_5, 4-$CH_3C_6H_4$, 4-ClC_6H_4, 4-FC_6H_4) were synthesized and characterized by elemental analysis, IR, ^1H NMR. The crystal structures of $[C_5H_5FeC_5H_4C(CH_3)=CHCOO]_2Sb(C_6H_4F\text{-}4)_3$ and $[4\text{-}(C_5H_5FeC_5H_4)C_6H_4COO]_2Sb(C_6H_4F\text{-}4)_3$ were determined by X-ray diffraction.

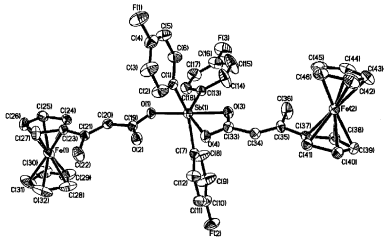

Debabrata Maiti, Himadri Paul, Nripen Chanda, Soma Chakraborty, Biplab Mondal, Vedavati G. Puranik, Goutam Kumar Lahiri

Polyhedron 23 (2004) 831

Synthesis, structure, spectral and electron-transfer properties of octahedral-$[Co^{III}(L)_2]^+$/$[Zn^{II}(L)_2]$ and square planar-$[Cu^{II}(L)\{OC(=O)CH_3\}]$ complexes incorporating anionic form of tridentate bis(8-quinolinyl)amine $[N^1C_9H_6\text{–}N^2\text{–}C_9H_6N^3, L^-]$ ligand

The reactions of bis(8-quinolinyl)amine $[N^1C_9H_6\text{–}N^2H\text{–}C_9H_6N^3, LH]$ with $Co^{II}(ClO_4)_2 \cdot 6H_2O$, $Zn^{II}(ClO_4)_2 \cdot 6H_2O$ and Cu^{II}-acetate result in octahedral-$[Co^{III}(L^-)_2]^+$ and $[Zn^{II}(L^-)_2]$ and square planar-$[Cu^{II}(L^-)\{^-OC(=O)CH_3\}]$ complexes, respectively, incorporating an sp^2-amido nitrogen center (N^2) in the coordinated ligand frame of L. The structural, spectral and electrochemical aspects of the complexes have been described.

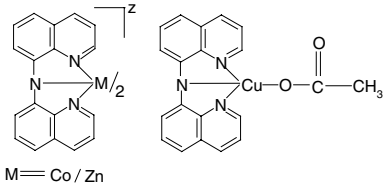

Veysel T. Yilmaz, Sevim Hamamci, Carsten Thöne

Polyhedron 23 (2004) 841

Cobalt(II) complexes of 2-methanol-, 2,6-dimethanol- and 2-ethanolpyridines: syntheses, spectroscopic, thermal and structural characterizations of $[Co_2(\mu\text{-}Cl)_2(mpy)_4]Cl_2 \cdot 2H_2O$, $[Co(dmpy)_2]Cl_2$ and $[Co(Cl)_4](Hpyet)_2$ (mpy = 2-methanolpyridine; dmpy = 2,6-dimethanolpyridine and Hpyet = 2-ethanolpyridinium)

Cobalt(II) complexes of 2-methanol-, 2,6-dimethanol- and 2-ethanolpyridines are reported. The 2-methanolpyridine (mpy) complex $[Co_2(\mu\text{-}Cl)_2(mpy)_4]Cl_2 \cdot 2H_2O$ is dimeric with chloro bridges and each cobalt(II) ion has an octahedral coordination with two chloro and two bidentate (N, O) ligands. In the 2,6-dimethanolpyridine (dmpy) complex $[Co(dmpy)_2]Cl_2$, dmpy exhibits a tripodal chelating coordination mode through the N and two hydroxyl O atoms. The protonated 2-ethanolpyridinium cation Hpyet in $[Co(Cl)_4](Hpyet)_2$ serves as a non-coordinating, but hydrogen bonded counter ion.

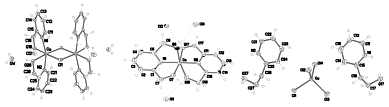

Wen-Long Liu, Yang Zou, Chun-Lin Ni, Zhao-Ping Ni, Yi-Zhi Li, Yuan-Gen Yao, Qing-Jin Meng

Polyhedron 23 (2004) 849

Synthesis and characterization of copper(II) Schiff base complexes derived from salicylaldehyde and glycylglycylglycine

Two new copper(II) tripeptide Schiff base complexes: $[Mg(H_2O)_6][CuL]_2 \cdot 3.5H_2O$ (**1**) and $[Cd(H_2O)_4(CuL)_2] \cdot 3.5H_2O$, (**2**) ($H_3L$ = *N*-salicylideneglycylglycylglycine) have been synthesized and structurally characterized. The UV–Vis, IR, ESR spectra and magnetic properties are reported.

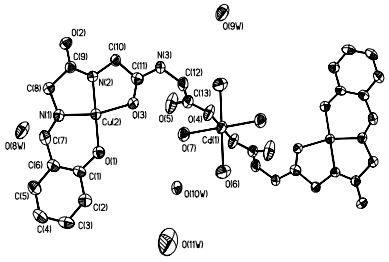

Lin-Ping Zhang, Miao Du, Wen-Jie Lu, Thomas C.W. Mak

Polyhedron 23 (2004) 857

Porous coordination networks generated from lanthanum trifluoromethanesulfonate and single/mixed N-oxide spacer linkers

Porous coordination networks are found in $\{[La(\mu\text{-}L)_2L(H_2O)_2](CF_3SO_3)_3\}_n$ (**1**), $\{[La(\mu\text{-}L')(CF_3SO_3)(H_2O)_2(\mu\text{-}L)_{0.5}L](H_2O)_3(CF_3SO_3)\}_n$ (**2**) and $\{[La(\mu\text{-}L')_2(\mu\text{-}L)](H_2O)_{1.5}(CF_3SO_3)\}_n$ (**3**) prepared by the reaction of $La(CF_3SO_3)_3$ with 1,2-bis(4-pyridyl)ethane-*N*,*N*′-dioxide (L), or with mixed N-oxide ligands L and L′ (HL′ = isonicotinic acid N-oxide) in different molar ratios. Compounds **2** and **3** represent the first metal complexes containing two different N-oxide bridging ligands. Thermogravimetric analysis (TGA) studies revealed that the ligands L and L′ are bound differently in compounds **1**–**3** due to their distinctive coordination modes.

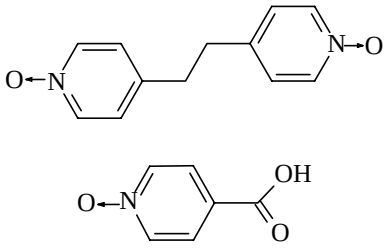

M. Rodriguez i Zubiri, Heather L. Milton, Alexandra M.Z. Slawin, J. Derek Woollins

Polyhedron 23 (2004) 865

The preparation and coordination of 1,3-C_6H_4-$\{C(O)N(PPh_2)CH_2Ph\}_2$ – a new multidentate ligand

The new ligand 1,3-C_6H_4-$\{C(O)N(PPh_2)$-$CH_2Ph\}_2$ gives the P,P',C tridentate [Pt(Cl)l{1,3-C_6H_4-$\{C(O)N(PPh_2)CH_2Ph\}_2$}] which contains two fused six-membered rings and [$\{PdCl(C_3H_5)\}_2${1,3-C_6H_4{C(O)-$N(PPh_2)CH_2Ph\}_2$}] in which the ligand bridges two palladium centres.

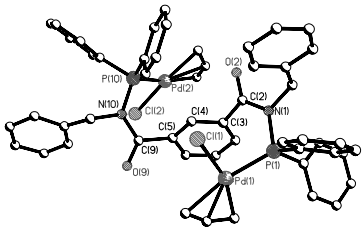

Paul V. Bernhardt, Tri Erny Dyahningtyas, Sang Cheol Han, Jack M. Harrowfield, Il Chool Kim, Yang Kim, George A. Koutsantonis, Elisabeth Rukmini, Pierre Thuéry

Polyhedron 23 (2004) 869

Stereocontrol in complexes of cyclam-like macrocycles – influences of chirality

Cyclam-like ligands with unusual coordination characteristics can be generated by a combination of conventional organic synthesis and a template reaction to provide derivatives of 3,7-diazacycloheptane.

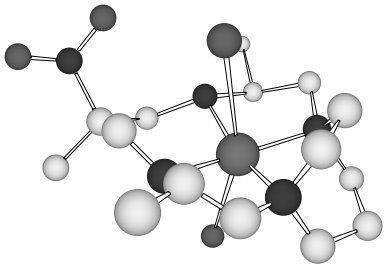

Mikhail Ryazanov, Sergey Troyanov, Marek Baran, Ritta Szymczak, Natalia Kuzmina

Polyhedron 23 (2004) 879

Synthesis, crystal structure and magnetic properties of dinuclear manganese(II) diketonate with cyanopyridine-N-oxide bridging ligands $[Mn(hfac)_2(4\text{-}cpyNO)]_2$

A new manganese(II) hexafluoroacetylacetonate adduct with 4-cyanopyridine N-oxide is described along with its crystal structure and magnetic studies, that revealed the presence of a ferromagnetic intramolecular interaction between the manganese atoms.

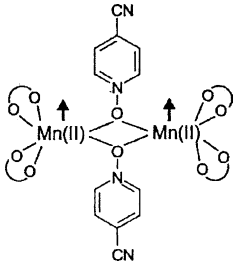

J.G. Małecki, J.O. Dzięgielewski, M. Jaworska, R. Kruszynski, T.J. Bartczak

Polyhedron 23 (2004) 885

Synthesis, molecular, crystal and electronic structures of $[(C_6H_6)RuCl(HPz)_2]Cl$ and $[(C_6H_6)RuCl_2(Me_2HPz)]$

The reactions of $(C_6H_6)RuCl_2]_2$ complex with pyrazole and dimethylpyrazole have been examined. The ruthenium complexes – $[(C_6H_6)RuCl(C_3N_2H_4)_2]Cl$ and $[(C_6H_6)RuCl(C_5N_2H_8)_2]$ have been obtained and characterized by IR, UV–Vis and 1H NMR measurements. Crystal, molecular and electronic structures of the complexes have been determined. The geometries of the complexes were optimized with the DFT method and their UV–Vis spectra were calculated with the TDDFT method.

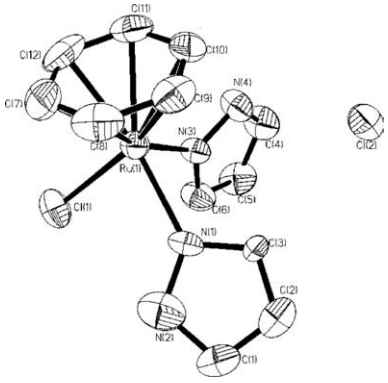

Amit Das, Subrata Mukhopadhyay

Polyhedron 23 (2004) 895

Kinetics of oxidation of glyoxylic acid by [ethylenebis(biguanide)]silver(III) in aqueous media

In aqueous media [ethylenebis(biguanide)]-silver(III) quantitatively oxidises glyoxylic acid to formic acid and carbon dioxide possibly by successive one-electron transfer.

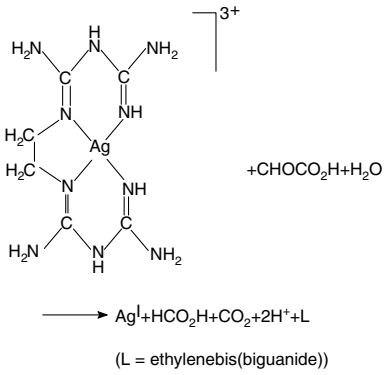

Validation and deposition of crystallographic data I

The Publisher encourages the submission of articles in electronic form thus saving time and avoiding rekeying errors. For detailed instructions on the preparation of manuscripts and of electronic artwork, consult the Author Gateway for Elsevier at http://authors.elsevier.com

SCIENCE DIRECT™

Full text of this journal is available, on-line from **ScienceDirect**. Visit **www.sciencedirect.com** for more information.

CONTENTS Direct This journal is part of **ContentsDirect**, the *free* alerting service which sends tables of contents by e-mail for Elsevier books and journals. You can register for **ContentsDirect** online at: **www. elsevier.com/locate/contentsdirect**

http://ChemWeb.com The World Wide Club for the Chemical Community

http://chemweb.com/gateways/elsevier.html

Available online at www.sciencedirect.com
SCIENCE DIRECT®
Polyhedron 23, issue 13, 19 August 2004
POLYHEDRON
www.elsevier.com/locate/poly

Contents

Papers

Ming Wen, Megumu Munakata, Yusaku Suenaga, Takayoshi Kuroda-Sowa, Masahiko Maekawa, Iwade Kodai

Polyhedron 23 (2004) 2117

Dinuclear silver(I) complexes of *N*, *N*′-dibenzyl-4,13-diaza-18-crown-6-ether and dibenzo-24-crown-8-ether

Three silver(I) coordination complexes of diaza- and dibenzo-crown ethers, [Ag(DDAC)](CF_3SO_3) (**1**), [Ag_2(DDAC)(CF_3SO_3)$_2$]$_2$ (**2**) and Ag_2(DB24C8)(CF_3SO_3)$_2$ (**3**), have been synthesized and characterized structurally. The X-ray structure analyses reveal mononuclear complex **1**, and dinuclear complexes **2** and **3** based on metal-oxygen and metal-nitrogen bonds.

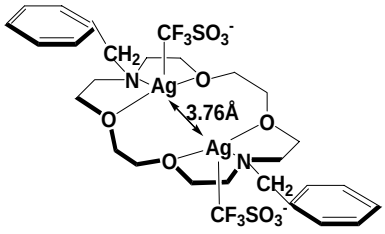

Wen-Long Liu, Yang Zou, Chang-Sheng Lu, Dong-Bin Dang, Yi-Zhi Li, Yuan-Gen Yao, Qing-Jin Meng

Polyhedron 23 (2004) 2125

Self-assembly, structure and magnetic properties of carboxylate-bridged Cu(II)–M(II) (M=Mg, Ca, Sr, Ba) complexes with a new metalloligand as a building block

The carboxylate-bridged Cu(II)–M(II) (M=Mg, Ca, Sr, Ba) mononuclear entity, polynuclear clusters, extended 1D ladder-like and 2D layer coordination polymers were self-assembled and structurally characterized. The UV–Vis, IR spectra and magnetic properties are reported.

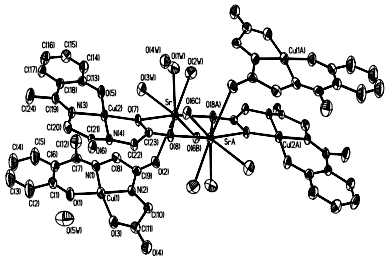

A. Semioshkin, B. Brellochs, V. Bregadze

Polyhedron 23 (2004) 2135

Reactions of *closo*-$[B_{12}H_{12}]^{2-}$ anion with aromatic acylchlorides: synthesis of novel 1,2-disubstituted dodecaborates [1-HO-2-Ar-$COB_{12}H_{10}]^{2-}$

Reaction of $Na_2[B_{12}H_{12}]$ with aromatic acylchlorides in boiling acetone results in novel [1-HO-2-Ar$COB_{12}H_{10}]^{2-}$ dodecaborates: The mechanism of the reaction is studied by NMR techniques and the intermediate **B** is characterized.

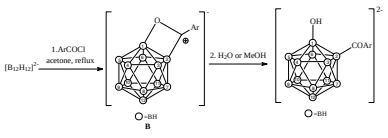

Faye E. Bradford, Lee P. Connor, Colin A. Kilner, Malcolm A. Halcrow

Polyhedron 23 (2004) 2141

Iron complexes of 3-(pyrazinyl)-1,2,4-triazole ligands

Different salts of the homoleptic iron(II) complexes of 3-(pyrazinyl)-1,2,4-triazole and 1-methyl-3-(pyrazinyl)-1,2,4-triazole show varying spin-state regimes, with most of the compounds examined undergoing a spin-state transition upon cooling or warming. Synthesis of these compounds is complicated by autooxidation of the reaction mixtures, yielding in one case an oxo-bridged diiron(III) complex.

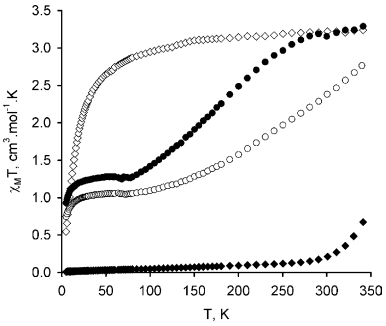

Xin He, Ping Zhang ,Tian-You Song, Zhong-Cheng Mu, Jie-Hui Yu, Yue Wang, Jia-Ning Xu

Polyhedron 23 (2004) 2153

Hydrothermal synthesis and structure of a molybdenum(VI) phosphate cluster and a three dimensional cobalt molybdenum(V) phosphate

Two new molybdenum phosphates $[Co(en)_3][C_4H_{12}N_2]_{0.5}[(Mo_5O_{15})(HOPO_3)_2]\cdot 3H_2O$ (**1**), (en=ethylenediamine) and $(C_4N_2H_{10})_5[Co_3Mo_{12}O_{18}(HOPO_3)_6(PO_4)_2(OH)_{12}(H_2O)_4]\cdot 9H_2O$ (**2**) have been synthesized hydrothermally. It was demonstrated the three-dimensional **2** was synthesized from the zero-dimensional **1** under hydrothermal reaction.

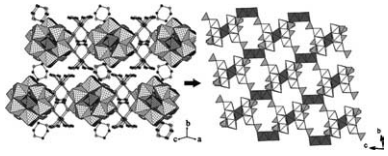

Karen J. Nordell, Kristin N. Schultz, Khadine A. Higgins, Mark D. Smith

Polyhedron 23 (2004) 2161

Hydrothermal synthesis of two new lead-containing coordination polymers: $^2{}_\infty[PbCl_2(4,4'\text{-bipy})]$ and $^2{}_\infty[Pb_2(NO_3)_4(H_2O)_2(4,4'\text{-bipy})_2](4,4'\text{-bipy})_2$

Hydrothermal reaction of $Pb(II)X_2$ ($X=Cl^-$, NO_3^-) and 4,4′-bipyridine in a molar ratio of 1:1 resulted in the formation of two new Pb(II) coordination polymers, $^2{}_\infty[PbCl_2(4,4'\text{-bipy})]$ and $^2{}_\infty[Pb_2(NO_3)_4(H_2O)_2(4,4'\text{-bipy})_2](4,4'\text{-bipy})_2$.

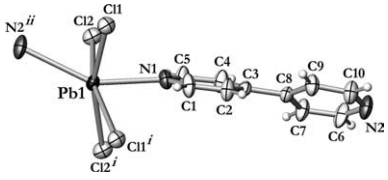

Stephen J. Scales, Haiwen Zhang, Paul A. Chapman, Ciara P. McRory, Eric J. Derrah, Christopher M. Vogels, Mazen T. Saleh, Andreas Decken, Stephen A. Westcott

Polyhedron 23 (2004) 2169

Synthesis, characterization, and cytotoxicities of palladium(II) and platinum(II) complexes containing fluorinated pyridinecarboxaldimines

Sixteen palladium and platinum dichloride pyridinecarboxaldimine complexes containing fluorine have been prepared and characterized fully. Cytotoxicities of the complexes have been investigated against OV2008 (human ovarian carcinoma) and the analogous cisplatin-resistant cell line C13.

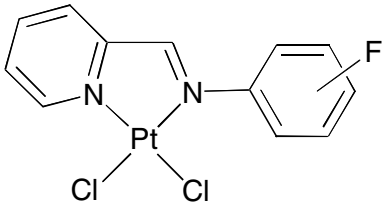

Arindam Mukherjee, Manas K. Saha, Munirathinam Nethaji, Akhil R. Chakravarty

Polyhedron 23 (2004) 2177

Dicopper(II) Schiff base aminobenzoates with discrete molecular and 1D-chain polymeric structures

Discrete dimeric *o*-aminobenzoate and 1D-chain polymeric *p*-aminobenzoate complexes having a $[Cu_2(\mu\text{-}OR)(\mu\text{-}O_2CR)]$ core, with the endogenic alkoxide bridge derived from a trianionic pentadentate Schiff base (L), are prepared and structurally characterized. Magnetic studies show antiferromagnetic properties of the complexes.

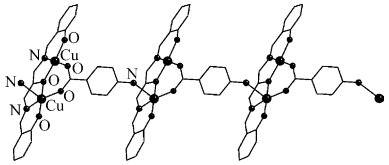

The Publisher encourages the submission of articles in electronic form thus saving time and avoiding rekeying errors. For detailed instructions on the preparation of manuscripts and of electronic artwork, consult the Author Gateway for Elsevier at http://authors.elsevier.com

SCIENCE DIRECT™

Full text of this journal is available, on-line from **ScienceDirect**. Visit **www.sciencedirect.com** for more information.

CONTENTS Direct This journal is part of **ContentsDirect**, the *free* alerting service which sends tables of contents by e-mail for Elsevier books and journals. You can register for **ContentsDirect** online at: **www. elsevier.com/locate/contentsdirect**

Available online at www.sciencedirect.com
SCIENCE DIRECT®
Polyhedron 23, issue 15, 30 September 2004
POLYHEDRON
www.elsevier.com/locate/poly

Contents

Papers

Roman Boča, Miroslav Boča, Milan Gembický, Lothar Jäger, Christoph Wagner, Hartmut Fuess

Polyhedron 23 (2004) 2337

Versatile coordination mode of dicyanamide in nickel(II) complexes containing polyamines as blocking ligands

Triethylenetetramine (L^4) and dipropylenetriamine (L^3) were used as blocking ligands that, after complexation with Ni^{II}, leave two or three sites ready for ligation with $N(CN)_2^-$. The formed complexes are $[Ni(\mathbf{N}CNCN)_2L^4]$ – mononuclear (**1**), $[(NCN\text{-}C\mathbf{N})L^3Ni(\mathbf{N}CNCN)_2NiL^3(\mathbf{N}CNCN)]$ – binuclear (**2**) and $[Ni(\mathbf{N}CNC\mathbf{N})L^4](ClO_4)$ – polymeric (**3**). The magnetic susceptibility measurements for **1** confirm that the Curie law is obeyed at higher temperatures whereas the zero-field splitting is effective below 10 K ($D/hc = -4$ cm^{-1}); **2** shows a weak antiferromagnetic coupling ($J/hc = -0.6$ cm^{-1}); **3** exhibits a negligible exchange coupling ($J/hc \approx 0$).

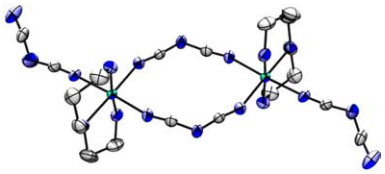

Mohamed A.S. Goher, Afaf K. Hafez, Morsy A.M. Abu-Youssef, Ahmed M.A. Badr, Christian Gspan, Franz A. Mautner

Polyhedron 23 (2004) 2349

New metal(II) complexes containing monodentate and bridging 3-aminopyridine and azido ligands

Three new metal(II)complex: $[Mn(3\text{-ampy})_4(N_3)_2]$, $[Cd(3\text{-ampy})(H_2O)_4]_n(SO_4)_n(H_2O)_n$ and $[Cd(3\text{-ampy})(N_3)_2]_n$ (3-ampy = 3-aminopyridine), have been synthesized and found by X-ray crystallography to contain monodentate, and bridging 3-ampy and azido ligands.

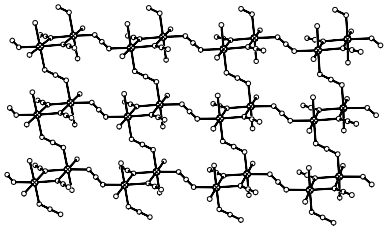

He Meng, Guang-Hua Li, Yan Xing, Yu-Lin Yang, Yan-Jie Cui, Li Liu, Hong Ding, Wen-Qin Pang

Polyhedron 23 (2004) 2357

Hydrothermal synthesis and characterization of a new 3D iron phosphatooxalate templated by organo-amine

A new organically templated iron(II) phosphatooxalate, $(N_2C_4H_{12})[Fe_4(C_2O_4)_3(HPO_4)_2(H_2O)]$, **I** has been synthesized under hydrothermal conditions, in which oxalate groups act as bidentate ligands to Fe and hold the structure together by strong interlayer P–O–H-oxalate hydrogen bonds.

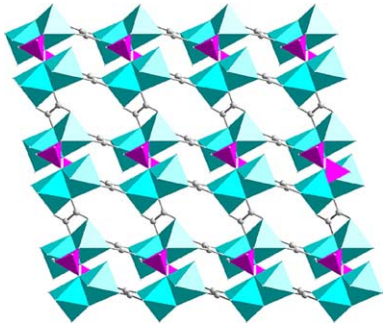

Barbara Machura

Polyhedron 23 (2004) 2363

Electronic structure and UV–Vis spectroscopy of $[Re(NO)Br_3(PPh_3)_2]$ and $[Re(NO)Br_3(OPPh_3)_2]$ complexes

Density functional calculations for $[ReBr_3(NO)(PPh_3)_2]$ (**1**) and $[ReBr_3(NO)(OPPh_3)_2]$ (**2**) complexes have been carried out using the DFT method with the B3LYP functional. The experimentally characterised molecular structures of **1** and **2** have been properly reproduced by the B3LYP method. The UV–Vis spectra of both complexes have been interpreted on the basis of the electronic transitions calculated with the time-dependent DFT method (TDDFT) for **1** and **2**.

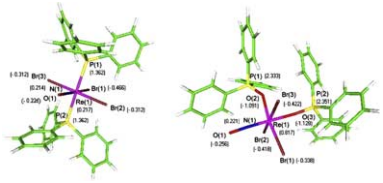

Mohammad Abul-Haj, Miguel Quirós, Juan M. Salas

Polyhedron 23 (2004) 2373

Dinuclear Pd(II) complexes with the anionic form of 4,5-dihydro-1,2,4-triazolo[1,5-a]pyrimidine-5-one

The compounds $[PdCl_2(5HtpO)_2]$, $[Pd_2(5tpO)_4] \cdot 4H_2O$ and $[Pd_2(a–a)_2\ (5tpO)_2] \cdot nH_2O$ with 5HtpO = 4,5-dihydro-1,2,4-triazolo[1,5-a]pyrimidine-5-one and a–a = bipyridine (bpy), phenanthroline (phen) or *trans*-diaminocyclohexane (*t*-dach) have been synthesized. The relative disposition of the ligands is, according to single crystal X-ray analysis, head–tail–head–tail for $[Pd_2(5tpO)_4] \cdot 4H_2O$ and head–tail for the compounds with a–a = phen or *t*-dach. On the contrary, the NMR data for the compound with a–a = bpy indicates a head–head disposition in solution.

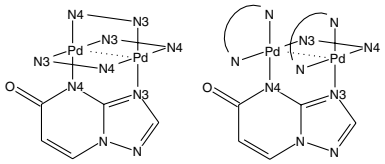

Achim Müller, Bogdan Botar, Samar K. Das, Hartmut Bögge, Marc Schmidtmann, Alice Merca

Polyhedron 23 (2004) 2381

On the complex hedgehog-shaped cluster species containing 368 Mo atoms: simple preparation method, new spectral details and information about the unique formation

The compound $Na_{48}[H_xMo_{368}O_{1032}(H_2O)_{240}(SO_4)_{48}] \cdot$ ca. $1000H_2O \equiv Na_{48}$ **1a** $\cdot$ ca. $1000H_2O$ (**1**) exhibiting an unusual nanosized hedgehog-type cluster anion has been obtained in good yield. **1** was characterized by elemental analysis thermogravimetry and spectroscopic methods. Information about unusual aspects of the formation is reported.

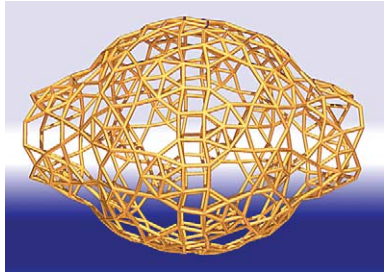

Gerard A. van Albada, Aminou Mohamadou, Willem L. Driessen, René de Gelder, Stefania Tanase, Jan Reedijk

Polyhedron 23 (2004) 2387

A dinuclear Mn(II) chloro-bridged compound with a weak ferromagnetic Mn–Mn interaction

A novel Mn(II) di-chloro-bridged dinuclear compound with the ligand 2,2′-bi-imidazoline has been synthesised and characterised, possessing a weak ferromagnetic interaction of $J = 0.33(1)\ cm^{-1}$ between the cation pairs.

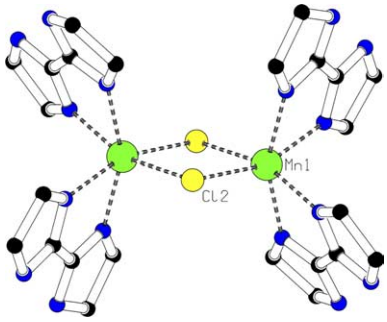

Sébastien Giroux, Sabrina Aury, Patrice Rubini, Stéphane Parant, Jean-Roger Desmurs, Michel Dury

Polyhedron 23 (2004) 2393

A spectroscopic investigation of the complexing ability of catecholate or salicylate derivatives towards aluminium(III)

This paper reports the study of the complexation of the Al(III) ion with four ligands: 2,3-dihydroxybenzoic acid (2,3-dhba), 5-nitrosalicylic acid (5-nsa), 4-nitrocatechol (4-ncat) and 3,5-dinitrocatechol (3,5-dncat) in aqueous solutions as a function of pH. Besides the pH-potentiometric study that allowed us to propose a set of complexes for each Al(III)/ligand system, an extensive spectroscopic investigation was made (IR, UV–visible and especially ^{1}H and ^{13}C NMR) to confirm the potentiometric results and to obtain information on the structure and the dynamics of the complexes. Additionally, the proton exchange kinetics between the OH function and the phenolate form of 5-nsa could be studied.

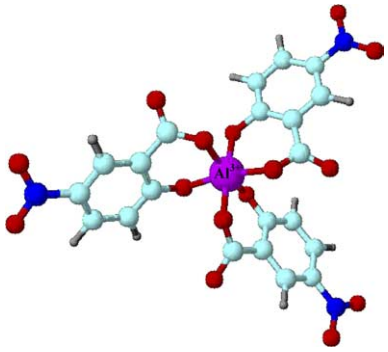

Mohammad Akbar Ali, Aminul H. Mirza, Malai Haniti S.A. Hamid, Fatriah Hj Bujang, Paul V. Bernhardt

Polyhedron 23 (2004) 2405

The preparation and characterization of tin(IV) complexes of 2-quinolinecarboxaldehyde Schiff bases of *S*-methyl- and *S*-benzyldithiocarbazates and the X-ray crystal and molecular structures of the 2-quinolinecarboxaldehyde Schiff base of *S*-benzyldithiocarbazate (Hqaldsbz) and its tin(IV) complex [Sn(qaldsbz)I_3]

The complexes, [Sn(NNS)I_3] (NNS = anionic forms of the 2-quinolinecarboxaldehyde Schiff bases of *S*-methyl- and *S*-benzyldithiocarzates) have been prepared and characterized. The structures of the free ligand, Hqaldsbz and its tin(IV) complex, [Sn(qaldsbz)I_3] have been determined by X-ray diffraction. The complex, [Sn(qaldsbz)I_3] has a distorted octahedral geometry with the Schiff base coordinated to the tin atom via the quinoline nitrogen atom, the azomethine nitrogen atom and the thiolate sulfur atom. The three iodo ligands are coordinated meridionally to the tin atom.

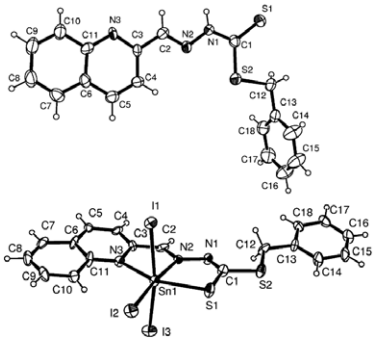

Lin-Ping Zhang, Chi-Keung Lam, Hai-Bin Song, Thomas C.W. Mak

Polyhedron 23 (2004) 2413

Crystalline hydrates and polymeric Ag(I) complexes of isomeric flexible double betaines 1,4-bis(*n*-picolyloxyl)benzene-*N*,*N*′-diacetate (*n* = 2,3,4)

The synthesis and structural characterization of the stoichiometric hydrates and silver (I) complexes of three isomeric double betaines 1,4-bis(2-picolyloxyl)benzene-*N*,*N*′-diacetate (L^1), 1,4-bis(3-picolyloxyl)benzene-*N*,*N*′-diacetate (L^2) and 1,4-bis(4-picolyloxyl)benzene-*N*,*N*′-diacetate (L^3) are reported. The silver complexes exhibit different coordination frameworks, which may be attributed to the varied positions of the betaine moieties in the relevant molecular skeletons.

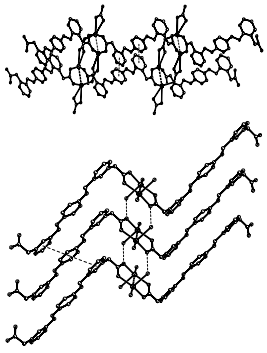

Ali Morsali, Alireza Mahjoub

Polyhedron 23 (2004) 2427

Coordination polymers of lead(II) with 4,4′-bipyridine: syntheses and structures

Some lead(II) complexes with the 4,4′-bipyridine (4,4′-bipy) ligand have been synthesized and characterized by CHN elemental analysis, IR, ^{1}H NMR and ^{13}C NMR spectroscopy.

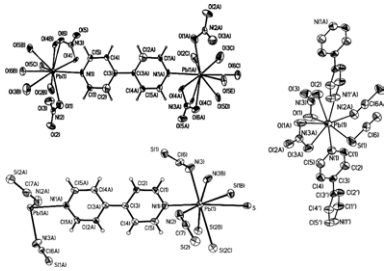

Fábio A. Kunrath, Osvaldo L. Casagrande Jr., Loic Toupet, Jean-François Carpentier

Polyhedron 23 (2004) 2437

Synthesis and reactivity in salt metathesis reactions of trivalent [La(Tp^{Me2})$_2$X] (X = Cl, I) complexes: crystal structures of [La(Tp^{Me2})$_2$Cl] and [La(Tp^{Me2})$_2$(κ^2-pz^{Me2})]

The side-formation of a pyrazolato complex La(Tp^{Me2})$_2$(κ^2-pz^{Me2}) (**2**; see structure below) that results during the preparation by salt metathesis of bis-Tp^{Me2} complexes [La(Tp^{Me2})$_2$X] is reported. An effective synthesis of [Ln(Tp^{Me2})(OC_6H_2-2,6-^{t}Bu-4-Me)$_2$] (Ln = La, Nd) derivatives is described.

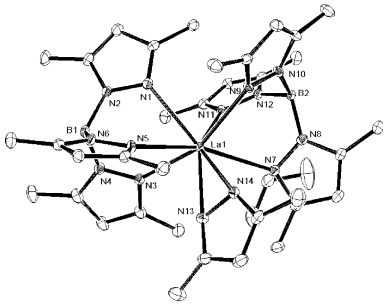

Dušan Valigura, Milan Melník, Marian Koman, Ladislav Martiška, Maria Korabik, Jerzy Mrozińsky, Tadeusz Glowiak

Polyhedron 23 (2004) 2447

Structural confirmation of the 3,5-dinitrosalicylato anion coordination ability to metal ion: crystal structure, spectral and magnetic properties of the [Cu_3{3,5-$(NO_2)_2sal^{2-}$}$_2${3,5-$(NO_2)_2sal^{1-}$}$_2$($H_2O)_4$] · 4H_2O

Reaction 3,5-dinitrosalicylic acid with copper(II) salts gives the compound [Cu_3-{3,5-$(NO_2)_2sal^{2-}$}$_2${3,5-$(NO_2)_2sal^{1-}$}$_2$($H_2O)_4$] · 4H_2O. Structure of the complex consists of linear trimeric complex molecules held together by hydrogen bonds system and van der Waals interactions. The stacked packing of the molecules allows weak antiferromagnetic intermolecular interaction in addition to significant ferromagnetic intramolecular interaction.

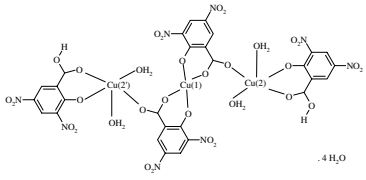

The Publisher encourages the submission of articles in electronic form thus saving time and avoiding rekeying errors. For detailed instructions on the preparation of manuscripts and of electronic artwork, consult the Author Gateway for Elsevier at http://authors.elsevier.com

SCIENCE DIRECT™

Full text of this journal is available, on-line from **ScienceDirect**. Visit **www.sciencedirect.com** for more information.

CONTENTS direct This journal is part of **ContentsDirect**, the *free* alerting service which sends tables of contents by e-mail for Elsevier books and journals. You can register for **ContentsDirect** online at: **www. elsevier.com/locate/contentsdirect**

Available online at www.sciencedirect.com
SCIENCE DIRECT®
Polyhedron 23, issue 12, 29 July 2004
POLYHEDRON
www.elsevier.com/locate/poly

Contents

Papers

Doyel Bose, Jaya Banerjee, Sk Hafijur Rahaman, Golam Mostafa, Hoong-Kun Fun, Rosa D. Bailey Walsh, Michael J. Zaworotko, Barindra Kumar Ghosh

Polyhedron 23 (2004) 2045

Polymeric end-to-end bibridged cadmium-(II)thiocyanates containing monodentate and bidentate N-donor organic blockers: supramolecular synthons based on π–π and/or C–H···π interactions

Synthesis and X-ray structural characterisation of two neutral 1D polymers, $[Cd(imH)_2(NCS)(SCN)]_n$ (**1**) and $[Cd(pfan)(NCS)(SCN)]_n$ (**2**) were carried out. In both polymers **1** and **2**, octahedral Cd^{II} ions occupy centre of symmetry with a CdN_4S_2 chromophore. Supramers **1** and **2** display intraligand $^1(\pi–\pi^*)$ fluorescence and intraligand $^3(\pi–\pi^*)$ phosphorescence in glassy solutions (MeOH at 77 K).

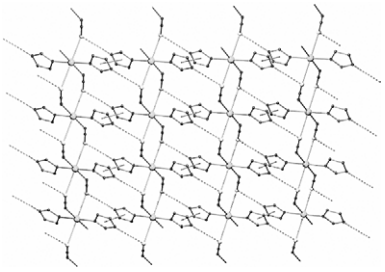

Qian-Ling Guo, Wen-Xiang Zhu, Ying-Chun Liu, Da-Qiang Yuan, Jing Zhang, Shu-Lan Ma

Polyhedron 23 (2004) 2055

Anionic capsules of *p*-sulfonatothiacalix[4]-arene with trivalent lanthanide ions and diaza-crown ether

The reaction of tetrasodium *p*-sulfonatothiacalix[4]arene and trivalent lanthanide ions in the presence of 4,13-diaza-18-crown-6 forms ionic capsules, and the diaza-crown ethers can also insert into the hydrophobic layers so that thiacalixarenes form irregular bi-layer structures.

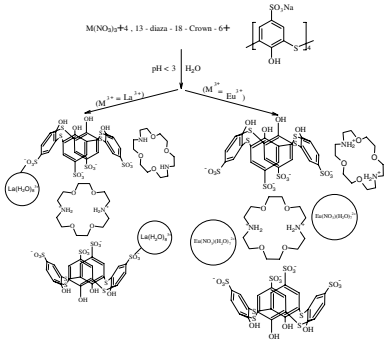

Soo Gyun Roh, Jong Uk Yoon, Jong Hwa Jeong

Polyhedron 23 (2004) 2063

Synthesis and characterization of a chiral Zn(II) complex based on a *trans*-1,2-diaminocyclohexane derivative and catalytic reduction of acetophenone

Reaction of $ZnCl_2$with *R*,*R*-bmbcd (=*N*,*N*′-bis(4-methoxy-benzyl)-cyclohexane-1,2-diamine) yields the chiral $[ZnCl_2(R,R\text{-bmbcd})]$ in which the Zn atom has a distorted tetrahedral geometry involving two nitrogen atoms of *R*,*R*-bmbcd and two chloro ligands. The catalytic enantioselective reduction of acetophenone promoted by *R*,*R*-bmbcd:Zn-$(OTf)_2$=1:1 mole ratio in the presence of catecholborane give (*S*)-(−)-1-phenylethanol in 48% ee with 77% yield.

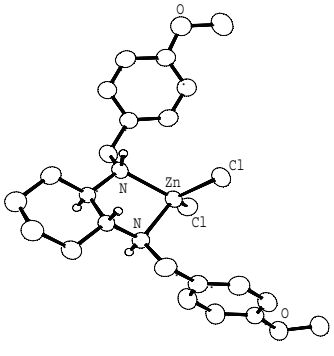

Angela C. Raimondi, Vagner R. de Souza, Henrique E. Toma, Antonio S. Mangrich, Tai Hasegawa, Fábio S. Nunes

Polyhedron 23 (2004) 2069

An unusual vanadium(II) promoted hydrogenation of a magnesium tetraiminediphenolate compound yielding an asymmetric oxovanadium(IV) macrocyclic complex

The $[VO(didadf)(H_2O)](BF_4)_2$(didadf=diiminediaminediphenolate ligand) complex and its characterization are described. This compound was obtained from the reaction between $[V(H_2O)_6]^{2+}$ and the tetraiminediphenolate macrocyclic ligand under severe inert atmosphere conditions through an unusual hydrogenation reaction.

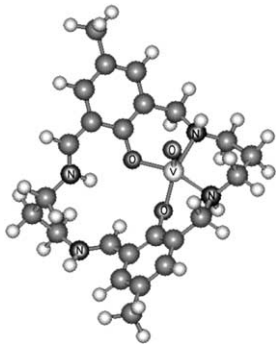

Alexandra L. Pickering, Geoffrey J.T. Cooper, De-Liang Long, Leroy Cronin

Polyhedron 23 (2004) 2075

Facile synthesis and structures of infinite one-dimensional silver(I) coordination polymers

The synthesis and structural characterization of three new silver(I) coordination compounds are reported. Each represents an infinite tubular coordination network that is isolated within a three-dimensional hydrogen-bonded network involving counter ions. Both the silver(I) ions and the two triamino ligands are three-connected nodes, forming a $4^2 \cdot 6$ topological network.

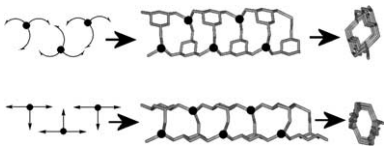

Alan Hazell

Polyhedron 23 (2004) 2081

Is bipyridine planar in metal complexes?

Deviations from planarity of the bipyridine ligand are discussed in terms of bow and twist angles and an S-shaped deformation.

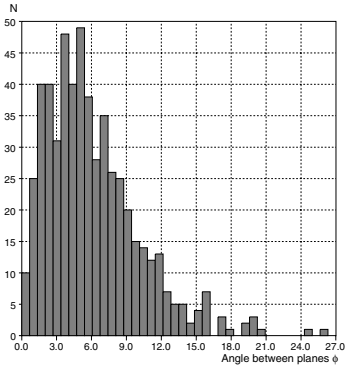

Chang-Yan Sun, Lin-Pei Jin

Polyhedron 23 (2004) 2085

Hydrothermal synthesis and characterization of the first examples of lanthanide(III) isoorotates with a 3D supramolecular network

The structures of the first examples of lanthanide(III) isoorotates are reported. Their 3D supramolecular networks are formed by O–H···O, N–H···O and/or N–H···N hydrogen bonds, and/or π–π stacking interactions.

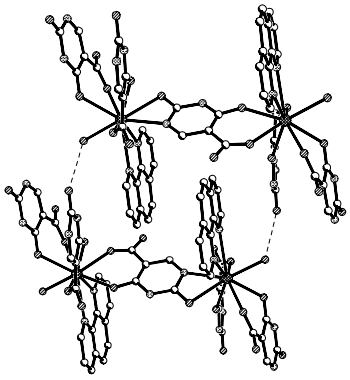

Ivanise Gaubeur, Márcia Guekezian, Lúcia H.S. Ávila Terra, Maria Carolina B. Moraes, Claudimir L. Lago, Jivaldo R. Matos, Maria Encarnación V. Suárez-Iha

Polyhedron 23 (2004) 2095

Synthesis, characterization, thermodynamic and thermal studies of Zn(II) complexes with di-2-pyridyl ketone salicyloylhydrazone

Zinc(II) in aqueous/ethanolic (50% V/V), pH 4.5, solution forms with di-2-pyridyl ketone salicyloylhydrazone (DPKSH) two complexes, $[Zn(C_{18}H_{13}N_4O_2)]^+$ and $[Zn(C_{18}H_{13}N_4O_2)_2]$, which were characterized by electron ionization and electrospray mass spectra, IR, thermogravimetry (TG) and differential scanning calorimetry (DSC). The overall formation constants and the molar absorptivies were obtained for both of the complexes.

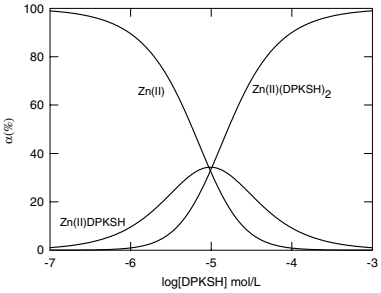

D.C. Menezes, G.M. de Lima, A.O. Porto, C.L. Donnici, J.D. Ardisson, A.C. Doriguetto, J. Ellena

Polyhedron 23 (2004) 2103

Synthesis, characterisation and thermal decomposition of tin(IV) dithiocarbamate derivatives – single source precursors for tin sulfide powders

The reaction of ammonium pyrrolidinedithiocarbamate with $SnPh_2Cl_2$ and $SnPh_3Cl$ produced in good yield the compounds $[Sn\{S_2CN(CH_2)_4\}_2\{C_6H_5\}_2]$·toluene (1) and $Sn\{S_2CN(CH_2)_4\}\{C_6H_5\}_3$ (2). They were fully characterised by multinuclear NMR [^1H,$^{13}C\{^1H\}$ and $^{119}Sn\{^1H\}$] and ^{119}Sn Mössbauer spectroscopies.

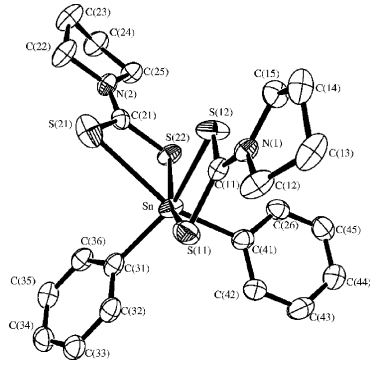

Sung-Nak Choi, Woo-Sung Jung, Min-Joo Lee, Yong-Min Lee, Young-Inn Kim

Polyhedron 23 (2004) 2111

Synthesis and physicochemical properties of charge transfer compounds derived from the reaction of tetrathiafulvalene with copper(II)

The powdered electrical conductivities of some $(TTF)_4CuX_2$ (X=NCS, NO_3, Br and Cl) compounds are in the semiconductor region ($\sigma_{r.t}=10^0$–10^1 S cm^{-1}), whereas the other compounds (X=NCO and NO_2) are in the insulator range ($\sigma_{r.t}<10^{-4}$ S cm^{-1}) at room temperature.

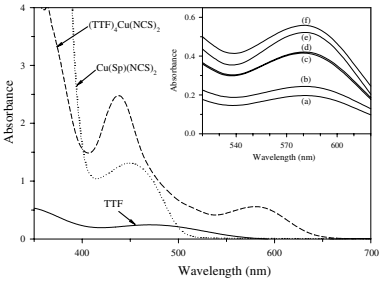

The Publisher encourages the submission of articles in electronic form thus saving time and avoiding rekeying errors. For detailed instructions on the preparation of manuscripts and of electronic artwork, consult the Author Gateway for Elsevier at http://authors.elsevier.com

Full text of this journal is available, on-line from **ScienceDirect**. Visit **www.sciencedirect.com** for more information.

This journal is part of **ContentsDirect**, the *free* alerting service which sends tables of contents by e-mail for Elsevier books and journals. You can register for **ContentsDirect** online at: **www. elsevier.com/locate/contentsdirect**

Available online at www.sciencedirect.com
SCIENCE DIRECT®
Polyhedron 23, issue 16, 20 October 2004
POLYHEDRON
www.elsevier.com/locate/poly

Contents

Papers

Pulak K. Dhara, Sadhan Pramanik, Tian-Huay Lu, Mike.G.B. Drew, Pabitra Chattopadhyay

Polyhedron 23 (2004) 2457

Copper(II) complexes of new tetradentate NSNO pyridylthioazophenol ligands: synthesis, spectral characterization and crystal structure

Three sets of copper(II) complexes of a series of new tetradentate NSNO ligands have been synthesized and characterized spectroscopically, using different copper(II) salts. The geometry about the copper ion of the complexes is dependent on the counter anion (Cl^-, SCN^- and ClO_4^-) in the copper salt used. The five-coordinated copper ion is distorted square pyramidal when SCN^- or Cl^- ligate with the copper(II) ion, occupying the equatorial position, whereas the geometry about the four-coordinated copper ion is square planar when the counter anion is perchlorate in the cationic copper(II)–pyridylthioazophenols complexes.

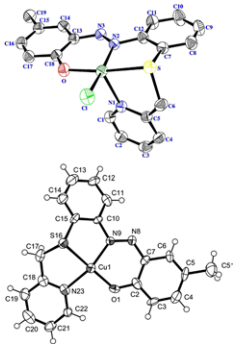

Rajendra N. Jadeja, J.R. Shah, E. Suresh, Parimal Paul

Polyhedron 23 (2004) 2465

Synthesis and structural characterization of some Schiff bases derived from 4-[{(aryl)-imino}ethyl]-3-methyl-1-(4′-methylphenyl)-2-pyrazolin-5-one and spectroscopic studies of their Cu(II) complexes

A series of bidentate ligands have been synthesized by condensation of 4-acetyl-2,4-dihydro-5-methyl-2-(4′-methylphenyl)-3H-pyrazol-3-one with various aromatic amines, X-ray structure determination reveals that these ligands exist in the amine-one tautomeric form. With Cu(II), these ligands form octahedral complexes, $[CuL_2(H_2O)_2]$; TGA, μ_{eff}, electronic and EPR spectral studies of which have been carried out. PM3 calculations have been performed on the ligands.

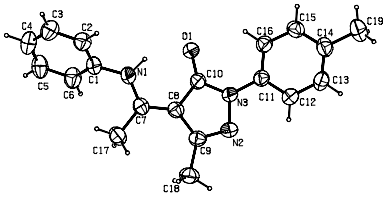

C. Krempner, H. Reinke, K. Weichert, A. Spannenberg

Polyhedron 23 (2004) 2475

Diastereoselective formation of a *meso*-disilane-1,2-diol – a dianionic siloxide ligand for Ti and Zr

The *meso* form of $(RMeSiOH)_2$ [R=Si(SiMe$_3$)$_3$] (**2**) was synthesized exclusively by hydrolysis of $(RMeSiCl)_2$ (**1**). The novel cyclic metal disiloxides (*E*)-$(RMeSiO)_2$-$Ti(OEt)_2$ (**3**) and $[(Z)\text{-}(RMeSiO)_2]_2Zr \cdot HNEt_2$ (**4**) are readily prepared from the reaction of *meso*-**2** with $Ti(OEt)_4$ and $Zr(NEt_2)_4$. The results of X-ray analyses reveal complexes **3** and **4** to be strained five-membered ring compounds which form a dimeric structure and an adduct with diethylamine, respectively.

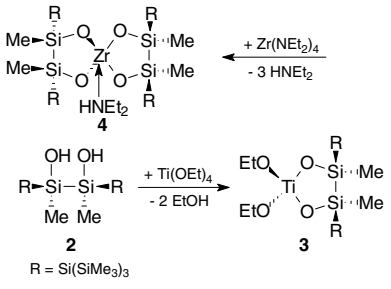

Elsevier Ltd.

Fabiola Téllez, Angelina Flores-Parra, Noráh Barba-Behrens, Rosalinda Contreras

Polyhedron 23 (2004) 2481

Cobalt(II) and zinc(II) compounds with unsaturated ligands derived from 2-aminobenzothiazole

Four zinc(II) (**6**, **8**, **10** and **12**) and four cobalt(II) (**5**, **7**, **9** and **11**) compounds derived from *N*-(benzothiazol-2-yl)-dithiocarbamic methyl ester (**1**) (**5** and **6**), 1-benzothiazol-2-ylid-3-methyl-thio urea (**2**) (**7**, **8**), 1-benzothiazol-2-yl-2,3-dimethyl-*iso* thiourea (**3**) (**9** and **10**) and *N*-(benzothiazol-2-yl)-*S*,*S*′-dimethyl dithio-carboimine (**4**,**11**,**12**) are reported. The complexes were characterized by UV–Vis–NIR diffuse reflectance, IR, mass spectrometry and **5**, **9**–**12** by X-ray diffraction analyses. In all cases two ligand molecules are bonded to a tetracoordinated metal atom. In **5**–**10** the ligand is anionic and bidentate with the metal in the center of spirocyclic structures formed by two planar unsaturated six membered rings. In **7**–**10** the metal is linked to four N and in **5** and **6** to two S and two N atoms. In **11** and **12** the ligand is neutral and monodentate and the metal ion remains coordinated to the chlorine atoms.

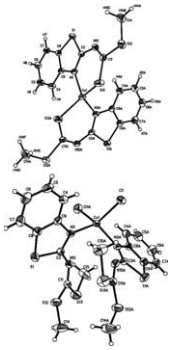

Thahira B.S.A. Ravoof, Karen A. Crouse, M. Ibrahim M. Tahir, Andrew R. Cowley, M. Akbar Ali

Polyhedron 23 (2004) 2491

Synthesis, characterization and bioactivity of mixed-ligand Cu(II) complexes containing *S*-methyldithiocarbazate derivatives and saccharinate ligands and the X-ray crystal structure of the copper–saccharinate complex containing *S*-methyl-β-*N*-(6-methylpyrid-2-yl)methylenedithiocarbazate

Mixed-ligand complexes of general empirical formula, $[Cu(NNS)(sac)(H_2O)]$(NNS′=*S*-methyl-β-*N*-(6-methylpyrid-2-yl)-methylenedithiocarbazate, NNS″=*S*-methyl-β-*N*-(2-acetylpyrid-2-yl)-methylene-dithiocarbazate and NNS‴=*S*-methyl-β-*N*-(2-benzoylpyrid-2-yl) methylene-dithio-carbazate, sac=saccharinate anion) are reported. The complexes were characterized by elemental analyses and various physico-chemical techniques. X-ray structure analysis of $[Cu(NNS')$-$(sac)(H_2O)]$ indicates a distorted square-pyramidal structure where the Schiff base coordinates as a uninegative tridentate NNS ligand, the fourth and fifth coordination positions of the five-co-ordinate copper(II) ion being occupied by the imino nitrogen of the saccharinate anion and oxygen atom of the aqua ligand. The bioactivity of these complexes has been investigated.

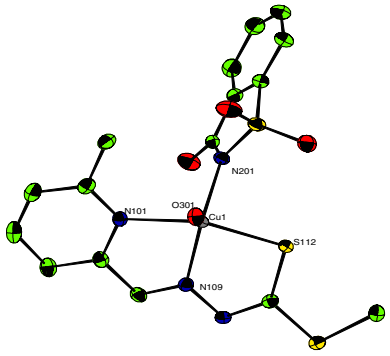

Roger Nassar, Bruce C. Noll, Kenneth W. Henderson

Polyhedron 23 (2004) 2499

Solid-state studies of the Horner–Wittig reagent $[\{\{Ph_2P(O)\}_2CHLi \cdot (THF)\}_2 \cdot THF]$ and its mixed-anion intermediate $[\{\{Ph_2P(O)\}_2$-$CHLi\}_4 \cdot \{Ph_2P(O)_2Li\}_2 \cdot 8C_6H_6]$ formed by reaction with dioxygen

The bis(phosphoryl)-stabilized carbanion $[\{\{Ph_2P(O)\}_2CHLi \cdot (THF)\}_2 \cdot THF]$ (**1**) has been characterized by X-ray crystallography and found to adopt a chelated dimeric structure with a Li_2O_2 ring core. The controlled reaction of **1** with O_2 results in P–C bond cleavage and formation of the mixed-anion complex $[\{\{Ph_2P(O)\}_2CHLi\}_4 \cdot \{Ph_2P(O)_2Li\}_2 \cdot 8C_6H_6]$ (**2**). The crystal structure of **2** shows an unusual hexalithium cage composed of four- and six-membered rings.

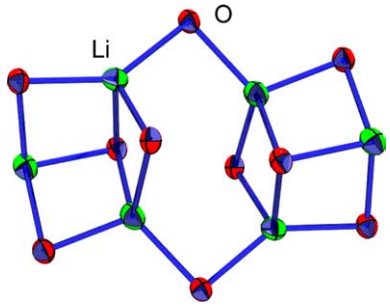

R.M. Mulla, Sharanappa T. Nandibewoor

Polyhedron 23 (2004) 2507

Mechanistic and spectral investigation of the oxidation of 4-hydroxycoumarin by aqueous alkaline permanganate using the stopped flow technique

The title reaction was studied using a spectrophotometer connected to a rapid kinetic accessory. A mechanism involving the formation of a complex between 4-hydroxycoumarin and alkaline permanganate has been proposed. The main product was characterized by IR and NMR.

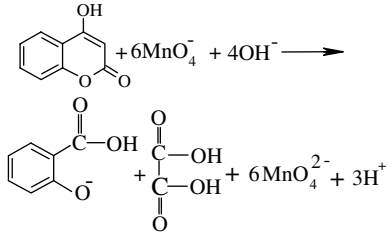

P.S. Subramanian, E. Suresh, P. Dastidar

Polyhedron 23 (2004) 2515

Model for type 2 Cu(II) oxidase: structure reactivity correlation studies on some mononuclear Cu(X–Salmeen)Im complexes, where X=H, Cl and Im=Imidazole: molecular association, electronic spectra and ascorbic oxidation

Two mononuclear Cu(II) complexes containing a Salmeen schiff base ligand were synthesized and characterized. The molecular association and their catalytic properties using ascorbic acid as a model for type 2 copper oxidase are discussed in detail.

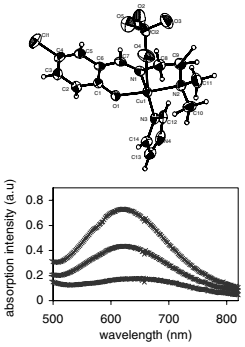

Barbara Machura, M. Jaworska, R. Kruszynski

Polyhedron 23 (2004) 2523

Synthesis, crystal, molecular and electronic structure of the $[ReBr_3(NO)(AsPh_3)(pzH)]$ complex

The $[ReBr_3(NO)(AsPh_3)(pzH)]$ complex has been obtained in high yield in the reaction of $[ReBr_3(NO)(AsPh_3)_2]$ with pyrazole. The rhenium atom is in a distorted octahedral environment with the bromine ligands in *meridional* geometry and the linear N–O group *trans* to the pyrazole molecule and *cis* to the $AsPh_3$ ligand. The geometric parameters of $[ReBr_3(NO)(AsPh_3)(pzH)]$ have been examined using the density functional theory (DFT) method. Considering the molecular orbital composition and positive total charge on the NO group, the character of the nitrosyl ligand in $[ReBr_3(NO)(AsPh_3)(pzH)]$ may be described as NO^+. The UV–Vis spectrum of $[ReBr_3(NO)(AsPh_3)(pzH)]$ has been discussed on the basis of the electronic transitions calculated with the time-dependent DFT method.

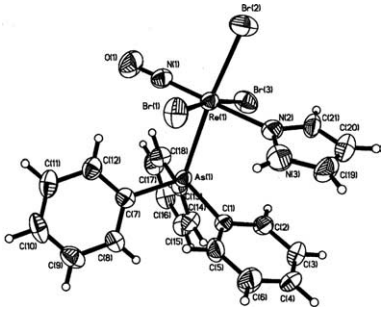

H.V. Rasika Dias, Xiaoyu Wang

Polyhedron 23 (2004) 2533

Sterically demanding methyl tris(pyrazolyl)-borate ligands: synthesis and characterization of thallium(I) complexes supported by $[MeB(3\text{-}(t\text{-}Bu)Pz)_3]^-$ and $[MeB(3\text{-}(Mes)Pz)_3]^-$

Thallium(I) derivatives of the sterically demanding, methyl tris(pyrazolyl)borate ligands $[MeB(3\text{-}(t\text{-}Bu)Pz)_3]^-$ and $[MeB(3\text{-}(Mes)Pz)_3]^-$ have been synthesized using the corresponding pyrazole, $Li[MeBH_3]$ and thallium(I) acetate. $[MeB(3\text{-}(t\text{-}Bu)Pz)_3]Tl$ and $[MeB(3\text{-}(Mes)Pz)_3]Tl$ display monomeric structures. The crystal structure of 3-(Mes)PzH as well as the ^{11}B and ^1H NMR spectra of $Li[MeBH_3]$ are also reported.

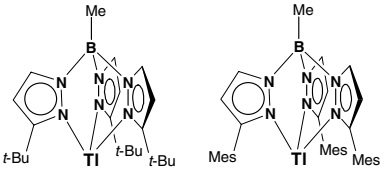

$[MeB(3\text{-}(t\text{-}Bu)Pz)_3]Tl$ **$[MeB(3\text{-}(Mes)Pz)_3]Tl$**

S. Salunke-Gawali, S.Y. Rane, V.G. Puranik, C. Guyard-Duhayon, F. Varret

Polyhedron 23 (2004) 2541

Three dimensional hydrogen-bonding network in a copper complex of 2-hydroxy-1,4-naphthoquinone: structural, spectroscopic and magnetic properties

Three types of intermolecular H-bondings between H_2O and ONQ molecules result in a supramolecular 3D structure of complex **1**, $[Cu(II)(ONQ)_2(H_2O)_2]_n$. The magneto-structural correlation is explained by magnetic chains with antiferromagnetic exchange (J=−3.26 cm^{-1}) between Cu(II)ions in **1** via non-covalent H-bondings together with interchain exchange (zJ'=0.01 cm^{-1}) using the Bonner and Fisher model.

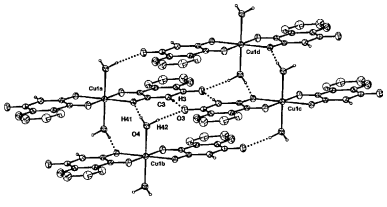

Rohith P. John, A. Sreekanth, V. Rajakannan, T.A. Ajith, M.R. Prathapachandra Kurup

Polyhedron 23 (2004) 2549

New copper(II) complexes of 2-hydroxyacetophenone *N*(4)-substituted thiosemicarbazones and polypyridyl co-ligands: structural, electrochemical and antimicrobial studies

Seven new copper(II) complexes of 2-hydroxyacetophenone *N*(4)-substituted thiosemicarbazones (H_2L) and bidentate polypyridyl compounds 2,2′-bipyridine and 1,10-phenanthroline (B) were prepared and characterized. The thiosemicarbazones bind to the metal as dianionic ONS donors (L^{2-}) and yield compounds of the stochiometry [MLB]. Spin Hamiltonian and bonding parameters of the compounds calculated from the EPR spectra suggest square pyramidal (SPY) structure for the compounds. The cyclic voltammetric study of the complexes shows irreversible redox peaks corresponding to Cu(II/I) couple and quasi-reversible redox peaks corresponding to copper(II/III) oxidation. The thiosemicarbazones and their copper complexes show significant growth inhibitory activity against bacteria *Escherichia coli*, *Staphylococcus aureus*, and fungi *Candida albicans* and *Aspergillus flavus*.

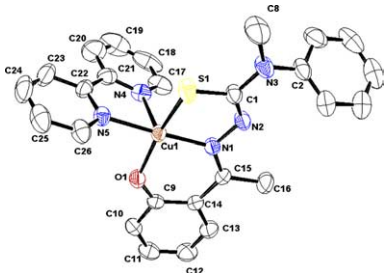

John Fawcett, Andrew W.G. Platt, Steven Vickers, Michael D. Ward

Polyhedron 23 (2004) 2561

Lanthanide halide and nitrate complexes with potentially tridentate bisphosphine dioxide – ether donors

The synthesis and structures of lanthanide nitrate and halide complexes of the potentially tridentate phosphine oxide – ether ligands show differences in coordination geometry as a result of the ligand backbone.

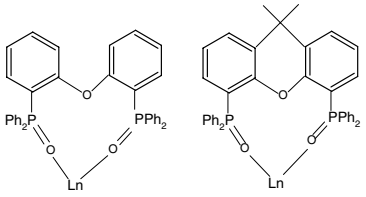

Alexandra M.Z. Slawin, Joanne Wheatley, J. Derek Woollins

Polyhedron 23 (2004) 2569

Preparation and coordination chemistry of *p*-(xylylenediaminodiphenyl) phosphine

The new bridging ligand *p*-(xylylenediaminodiphenyl)phosphine has been prepared and its coordination chemistry studied.

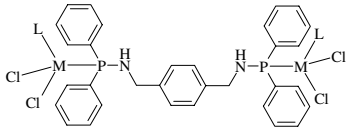

Heather L. Milton, Matthew V. Wheatley, Alexandra M.Z. Slawin, J. Derek Woollins

Polyhedron 23 (2004) 2575

Synthesis and coordination of 2-diphenylphosphinothiophenocarboxamide and bis-(2,5-diphenylphosphinepicolinamide)

Index entry: New phosphines with significant H bonding sites have been prepared.

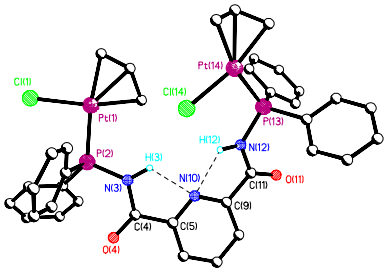

Adonis Michaelides, Christos D. Papadimitriou, John C. Plakatouras, Stavroula Skoulika, Panagiotis G. Veltsistas

Polyhedron 23 (2004) 2587

Synthesis, characterization and crystal structure of *catena*-bis(1,10-phenanthroline)-μ-chloranilatocadmium(II): a zig-zag polymer based on eight-coordinated square antiprismatic units

The synthesis, and the structural and physicochemical characterization of the type I chain polymer $[Cd(CA)(phen)_2]_n$, where phen is 1,10-phenanthroline and CA^{2-} is the dianion of 3,6-dichloro-2,5-dihydroxy-1,4-benzoquinone, is described. A 3D supramolecular architecture is formed through π–π stacking interactions between the phenanthroline moieties.

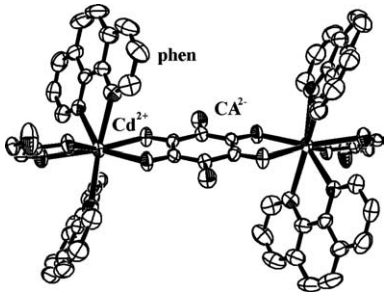

The Publisher encourages the submission of articles in electronic form thus saving time and avoiding rekeying errors. For detailed instructions on the preparation of manuscripts and of electronic artwork, consult the Author Gateway for Elsevier at http://authors.elsevier.com

SCIENCE DIRECT™

Full text of this journal is available, on-line from **ScienceDirect**. Visit **www.sciencedirect.com** for more information.

CONTENTS Direct This journal is part of **ContentsDirect**, the *free* alerting service which sends tables of contents by e-mail for Elsevier books and journals. You can register for **ContentsDirect** online at: **www. elsevier.com/locate/contentsdirect**

Available online at www.sciencedirect.com
SCIENCE DIRECT®
Polyhedron 23, issue 14, 9 September 2004
POLYHEDRON
www.elsevier.com/locate/poly

Contents

Papers

Dušanka D. Radanović, Urszula Rychlewska, Miloš I. Djuran, Beata Warajtis, Nenad S. Drašković, Dejan M. Gurešić

Polyhedron 23 (2004) 2183

Alkaline earth metal complexes of the edta-type with a six-membered diamine chelate ring: crystal structures of $[Mg(H_2O)_6]$-$[Mg(1,3\text{-pdta})] \cdot 2H_2O$ and $[Ca(H_2O)_3$-$Ca(1,3\text{-pdta})(H_2O)] \cdot 2H_2O$: comparative stereochemistry of edta-type complexes

X-ray crystallography, infrared and solid-state ^{13}C NMR have been applied to investigate structural differences in 1,3-pdta complexes of Ca^{2+}, Ba^{2+} and Mg^{2+}.

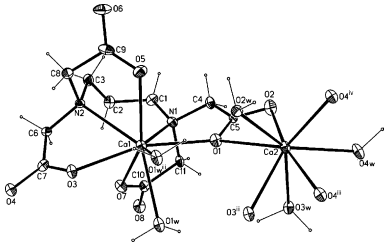

Pavel Kopel, Zdeněk Trávníček, Radek Zbořil, Jaromír Marek

Polyhedron 23 (2004) 2193

Synthesis, X-ray and Mössbauer study of iron(II) complexes with trithiocyanuric acid ($ttcH_3$)

Mixed-ligand Fe(II) complexes involving the trithiocyanurate anion and nitrogen-donor ligands have been prepared and characterized by Mössbauer, IR and UV–Vis spectroscopies. All the complexes are low spin with a deformed octahedral arrangement as was also proved by X-ray analysis, in the case of two complexes. DFT calculations were used for IR bands assignment.

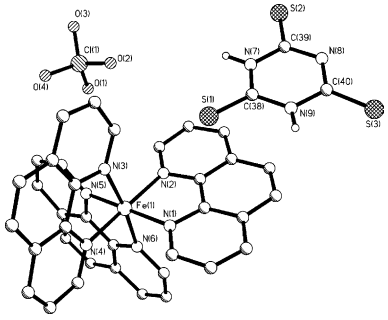

Mao Liang, Qing-Lun Wang, Li-Hua Yu, Dai-Zheng Liao, Zong-Hui Jiang, Shi-Ping Yan, Peng Cheng

Polyhedron 23 (2004) 2203

A novel 3D malonato-bridged compound $Cu(mal)(pz)_2$: synthesis, spectroscopy, crystal structure and magnetism

A novel malonato-bridged copper(II) complex of the formula $Cu(mal)(pz)_2$ (**1**) has been synthesized and characterized by its IR, electronic and EPR spectra and TG analysis. Each copper atom is coordinated by a *syn–anti* carboxylate bridge to form a 3D framework. Magnetic behavior for the title complex exhibits weak ferromagnetic interactions.

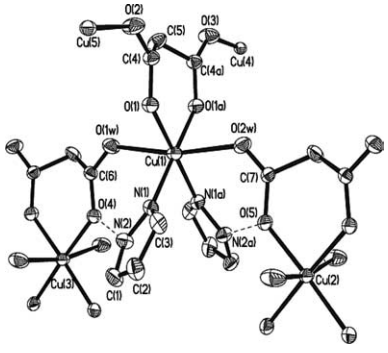

Jian-Kai Cheng, Jian Zhang, Yao Kang, Ye-Yan Qin, Zhao-Ji Li, Yuan-Gen Yao

Polyhedron 23 (2004) 2209

Syntheses, structures and photoluminescent properties of 1D, 2D, 3D silver (I) coordination polymers with flexible long-chain dinitriles and tetranitriles

A four-connected silver (I) coordination polymer with *meso* tetranitriles.

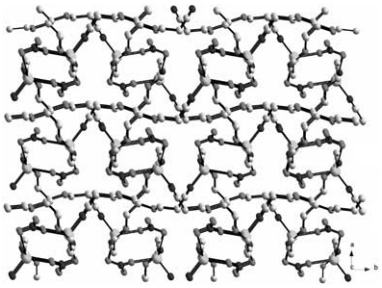

Clint A. Sharrad, Lawrence R. Gahan

Polyhedron 23 (2004) 2217

Synthesis and characterization of cobalt(III) complexes with sinambic amplector ligands

The complex [Co(*rac*-1,2-$Me_2EtN_4S_2$amp)]-$Cl_2(ClO_4) \cdot 2H_2O$, containing the sinambic ligand 5,6-dimethyl-2,2,9,9-tetra(methyleneamine)-4,7-dithiadecane, is employed to explore the relationship between the ^{59}Co magnetogyric ratio (γ_{Co}) and the product of the nephelauxetic ratio and the wavelength of the $^1A_{1g} \rightarrow {}^1T_{1g}$ transition ($\beta(\Delta E)^{-1}$) for complexes of mixed donor nitrogen–thioether ligands.

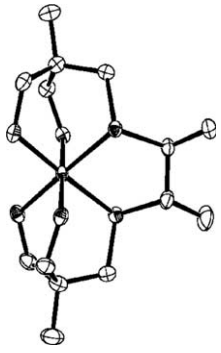

Chang-Yan Sun, Lin-Pei Jin

Polyhedron 23 (2004) 2227

Three-dimensional porous frameworks constructed by transition metal ions and isoorotic acid

Four new coordination polymers of isoorotic acid are reported. They all comprise 1D chains that are further interlinked via hydrogen bonds, resulting in the formation of 3D frameworks with channels.

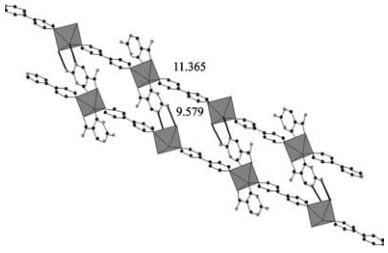

Kateřina Brudíková, Martin Breza

Polyhedron 23 (2004) 2235

MP2 studies of the bis(methoxycarbimido)-amine ligand and its anion

Various conformations of the title ligands have been optimized. The determining role of the central atom for the geometry and electronic structure of their complexes may be concluded. Preferential methoxy group positions may be explained by energy arguments of the free ligands.

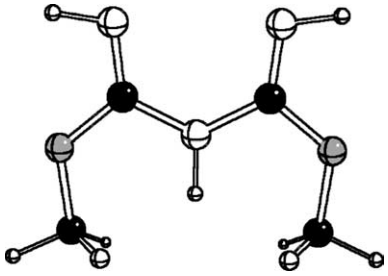

Nail G. Zabirov, Vasiliy V. Brusko, Alexander Y. Verat, Dmitry B. Krivolapov, Igor A. Litvinov, Rafael A. Cherkasov

Polyhedron 23 (2004) 2243

Synthesis and crystal structure of complexes of bipodal thiophosphorylated thioureas with divalent transition metals

According to X-ray crystallography, the title compounds exist as metallomacrocycles in the crystal.

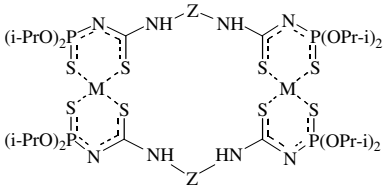

Yang Zou, Wen-Long Liu, Song Gao, Chang-Shen Lu, Dong-Bin Dang, Qing-Jin Meng

Polyhedron 23 (2004) 2253

Synthesis, structure and magnetic properties of carboxylate-bridged polynuclear copper-(II)–lanthanide(III) rings: $[Ln(H_2O)_5(CuL)_2]$-$[CuL]\cdot 8H_2O$ (Ln = La, Ce)

$[Ln(H_2O)_5(CuL)_2][CuL]\cdot 8H_2O$ (Ln = La (**1**) and Ce (**2**)) (H_3L = Schiff base derived from 5-bromosalicylaldehyde and glycylglycine), has been synthesized; complex **1** exhibits ferromagnetic interaction and **2** exhibits antiferromagnetic interaction

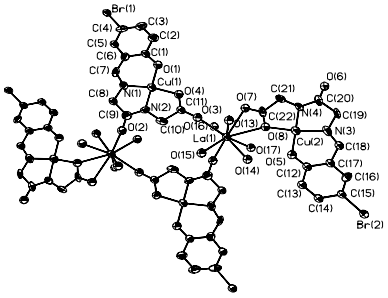

Qin-Yu Zhu, Jie Dai, Ding-Xian Jia, Li-Hui Cao, Hai-Hong Lin

Polyhedron 23 (2004) 2259

$\pi \cdots \pi$ Interaction assembled silver(I) complexes with the ligand 4′,5′-diaza-9′-(4,5-disubstituted-1,3-dithiol-2-ylidene)fluorene

New silver (I) complexes with a linear coordinated planar cation of $[Ag(L^1)_2]^+$ have been characterized. These planar ions are further assembled into columns via inter-ion interactions.

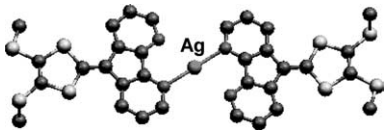

Jian-Jun Zhang, Sheng-Chang Xiang, Sheng-Min Hu, Sheng-Qing Xia, Rui-Biao Fu, Xin-Tao Wu, Ya-Min Li, Hui-Shuang Zhang

Polyhedron 23 (2004) 2265

Syntheses and characterizations of a series of heptanuclear octahedral polyhedra $\{LnNi_6\}$ with different amino acids as ligands in aqueous media

Heptanuclear octahedral clusters $[LnNi_6(AA)_{12}]^{3+}$ (Ln = La, Pr) were obtained through the reaction of Ln^{3+}, Ni^{2+} and amino acid (AA = glycine, L-alanine or L-threonine) in aqueous solution. In the cluster, the Ln^{3+} ion is in the center of the octahedral cage formed by six nickel atoms.

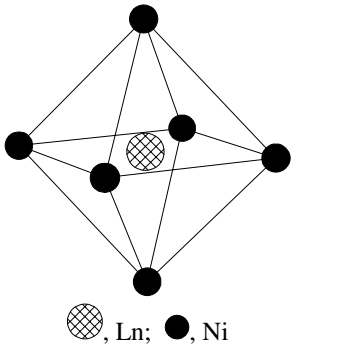

Richard J. Bowen, Judy Caddy, Manuel A. Fernandes, Marcus Layh, Messai A. Mamo

Polyhedron 23 (2004) 2273

Synthesis of phosphine stabilised group 11 1-azaallyl complexes; molecular structure of $bu^i_3PAuCH(R)C(bu^t) = NR$ ($R = SiMe_3$)

The bonding mode (η^1-enamide for Cu; η^1-iminoalkyl for Ag, Au) of the linear, two-coordinate 1-azaallyl complexes $bu^i_3PM[N(R)C(bu^t) = C(H)R]$ (M = Cu, Ag, Au; $R = SiMe_3$), synthesised from bu^i_3PMCl (M = Cu, Ag, Au) and $[Li\{\mu\text{-}N(R)C(bu^t)C(H)R\}]_2$ ($R = SiMe_3$), was determined by NMR spectroscopy and in the case of the Au-derivative by X-ray crystallography.

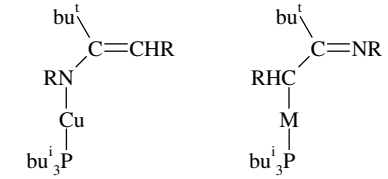

η^1-enamide η^1-iminoalkyl

Mehmet Karakus, Peter Lönnecke, Evamarie Hey-Hawkins

Polyhedron 23 (2004) 2281

Zwitterionic ferrocenyldithiophosphonates: the molecular structure of $[FcP(S)S(OCH_2CH_2NH_2Me)]$ [Fc = $Fe(\eta^5\text{-}C_5H_4)(\eta^5\text{-}C_5H_5)$]

Ferrocenyldithiodiphosphetane $[FcPS(\mu\text{-}S)]_2$ [Fc = $Fe(\eta^5\text{-}C_5H_4)(\eta^5\text{-}C_5H_5)$] reacts with the aminoethanol derivatives $HOCH_2CH_2NHMe$ and $HOCH_2CH_2NEt_2$ to give the first structurally characterised examples of zwitterionic (*O*-ethylammonium)ferrocenyldithiophosphonates, $[FcP(S)S(OCH_2CH_2NHR^1R^2)]$ (R^1 = H, R^2 = Me (**1**); R^1 = R^2 = Et (**2**)). **1** and **2** were characterised by elemental analyses, IR, NMR spectroscopy (^1H, ^{13}C (for **2**) and ^{31}P) and mass spectrometry. A crystal structure determination was carried out on **1**.

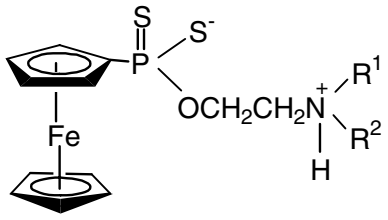

R^1 = H, R^2 = Me (**1**)
R^1 = R^2 = Et (**2**)

Ramu Kannappan, Stefania Tanase, Duncan M. Tooke, Anthony L. Spek, Iipo Mutikainen, Urho Turpeinen, Jan Reedijk

Polyhedron 23 (2004) 2285

Separation of actinides and lanthanides: crystal and molecular structures of *N,N′*-bis(3,5-di-*t*-butylsalicylidene)-4,5-dimethyl-1,2-phenylenediamine and its uranium complex

The preparation of the tetradentate dianionic ligand *N,N′*-bis(3,5-di-*t*-butylsalicylidene)-4,5-dimethyl-1,2-phenylenediamine [H_2L] is described, together with the corresponding uranium complex [$UO_2(L)CH_3OH$]. Both the free ligand and uranyl complex were characterized by elemental analysis, spectroscopic methods and single-crystal X-ray diffraction.

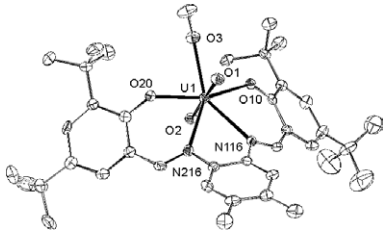

S. Petriček

Polyhedron 23 (2004) 2293

Syntheses of lanthanide bromide complexes from oxides and the crystal structures of $[LnBr_3(DME)_2]$ (Ln = Pr, Nd, Sm, Eu), $[LnBr_3(THF)_4]$ (Ln = Pr, Sm) and $[EuBr_2(THF)_5][EuBr_4(THF)_2]$

Lanthanide oxides were used to prepare lanthanide bromide complexes in very high yields. The reactions take place at room temperature:

$$6(CH_3)_3SiBr + Ln_2O_3 + 4DME \xrightarrow{RT} 2[LnBr_3(DME)_2] + 3(CH_3)_3SiOSi(CH_3)_3$$

All complexes crystallized from DME contain a similar mononuclear molecule $[Ln\text{-}Br_3(DME)_2]$ (Ln = Pr, Nd, Sm, Eu), while crystallization from THF resulted in **A** – neutral $[LnBr_3(THF)_4]$ (Ln = Pr, Sm) or **B** – ionic $[EuBr_2(THF)_5]$-$[EuBr_4(THF)_2]$ compounds.

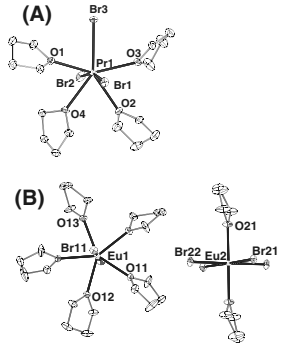

Elena Bermejo, Alfonso Castiñeiras, Larissa M. Fostiak, Isabel García Santos, John K. Swearingen, Douglas X. West

Polyhedron 23 (2004) 2303

Spectral and structural studies of Zn and Cd complexes of 2-pyridineformamide N(4)-ethylthiosemicarbazone

Zn(II) and Cd(II) complexes of 2-pyridineformamide N(4)-ethylthiosemicarbazone have been synthesized and characterized using physical and spectral methods. X-ray structure analysis of the complexes $[Zn(Am4E)(OAc)]_2$, $[Zn(HAm4E)I_2]$, $[Cd(Am4E)_2]$, $[Cd(HAm4E)Br_2] \cdot DMSO$ and $[Cd(HAm4E)I_2] \cdot DMSO$, as representative species, has authenticated that coordination is via the pyridyl nitrogen, imine nitrogen and thione or hiolato sulphur atoms when coordinating as the neutral and anionic ligand, respectively.

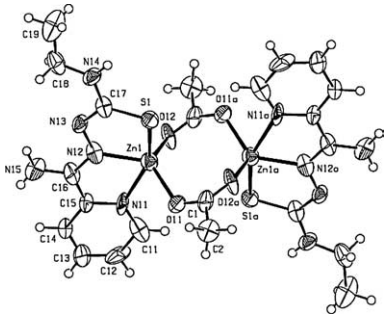

Jacqui Cusack, Michael G.B. Drew, Trevor R. Spalding

Polyhedron 23 (2004) 2315

Syntheses and spectroscopy of diamine complexes of Zn(II) and Cd(II) ethylxanthates and the molecular structures of $[M(S_2COEt)_2TMEDA]$: formation of CdS nanoparticles from $[Cd(S_2COEt)_2]$ and $[Cd(S_2COEt)_2TMEDA]$

The zinc and cadmium ethylxanthate complexes of *N*,*N*,*N*′,*N*′-tetramethyethylenediamine (TMEDA), $[M(S_2COEt)_2TMEDA]$, were synthesized and characterized with infrared, ^1H and ^{13}C NMR spectroscopy, mass spectrometry and X-ray crystallography. The cadmium species $[Cd(S_2COEt)_2(diamine)]$ (where diamine = *N*,*N*-dimethylethylenediamine or *N*,*N*′-diisopropylethylenediamine) were also synthesized. The surfactant-assisted formation of nanoparticles from $[Cd(S_2COEt)_2]$ and $[Cd(S_2COEt)_2TMEDA]$ was studied.

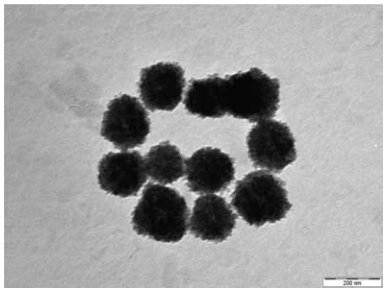

Tushar S. Basu Baul, Antonin Lycka, Ray Butcher, Frank E. Smith

Polyhedron 23 (2004) 2323

Synthesis, X-ray crystal structures and multinuclear NMR characterization of Hg(II) complexes of 2-[(*E*)-2-(aryl)-1-diazenyl]pyridine

Two Hg(II) complexes, viz., dichloro-{2-[(*E*)-2-(4-methylphenyl)-1-diazenyl]pyridine} Hg(II) [**1**] and dichloro-{2-[(*E*)-2-(3-methylphenyl)-1-diazenyl]pyridine}Hg(II) [**2**] were characterized by ^1H, ^{13}C and ^{199}Hg (NMR) and X-ray crystallographic techniques. Complex **2** is polymeric where the ligand coordinate via the pyridyl nitrogen, and all the chlorine atoms serving to bridge mercury atoms. In contrast, complex **1** has a dimeric structure with bidentate ligand chelation via the pyridyl nitrogen and one of the azyl nitrogens, with a terminal chlorine on each Hg and a μ,μ′-dichloro bridge between the mercury atoms.

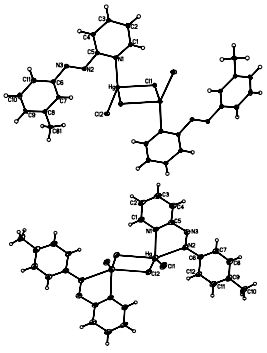

R. Alan Howie, Marcelo V.H. Moura, James L. Wardell, Solange M.S.V. Wardell

Polyhedron 23 (2004) 2331

Further study of tris(cyclohexyl)stannane compounds, Cy_3SnX. Syntheses of the compounds with X = Br, I, N_3 and NCS and redetermination of the crystal structures of Cy_3SnX (X = Br and I)

Compound sythesis and far IR data are presented for various Cy_3SnX compounds. Redeterminations of the crystal structures of tris(cyclohexyl)tin bromide and iodide, Cy_3SnBr and Cy_3SnI, confirm their molecular nature providing, in particular, a revised estimate of the Sn–I bond length, now 2.7463(6) Å. The nature of the solid state structure of Cy_3SnCl is also discussed.

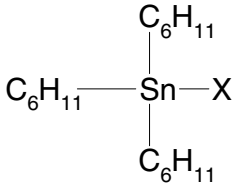

The Publisher encourages the submission of articles in electronic form thus saving time and avoiding rekeying errors. For detailed instructions on the preparation of manuscripts and of electronic artwork, consult the Author Gateway for Elsevier at http://authors.elsevier.com

SCIENCE DIRECT™

Full text of this journal is available, on-line from **ScienceDirect**. Visit **www.sciencedirect.com** for more information.

CONTENTS direct

This journal is part of **ContentsDirect**, the *free* alerting service which sends tables of contents by e-mail for Elsevier books and journals. You can register for **ContentsDirect** online at: **www. elsevier.com/locate/contentsdirect**

Available online at www.sciencedirect.com
SCIENCE DIRECT®
Polyhedron 23, issue 10, 17 June 2004
POLYHEDRON
www.elsevier.com/locate/poly

Contents

Papers

Brojogopal Chand, Umasankar Ray, Golam Mostafa, Tian-Huey Lu, Chittaranjan Sinha

Polyhedron 23 (2004) 1669

2D Extended supramolecular structures via π–π interactions of 1D coordination polymers of cadmium(II) complexes of arylazoimidazole using azido and thiocyanato bridging ligands

In the title complexes, 1-alkyl-2-(arylazo) imidazoles (RaaiR′) act as N,N′ end capping agents and coordination polymers are generated by two double bridging azides (end-on) or thiocyanates (end-to-end) to the Cd centres. The 1D chain structures are confirmed by X-ray diffraction studies.

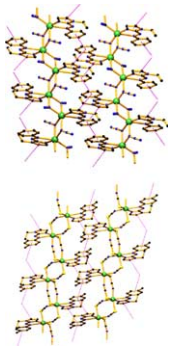

Alvaro J. Pardey, Clementina Longo, Tiziana Funaioli, Giuseppe Fachinetti

Polyhedron 23 (2004) 1677

Hydrocarboxylation and stepwise alternating oligomerization of carbon monoxide and ethylene catalyzed by *cis*-$[Rh(CO)_2(amine)_2](PF_6)$ complexes in a wet liquid tetrabutylammonium hydrogensulfate

Rhodium complexes of the type, *cis*-$[Rh(CO)_2(amine)_2](PF_6)$ where (amine=4-picoline, 3-picoline, 2-picoline, pyridine, or 2,6-lutidine) dissolved in aqueous tetrabutylammonium hydrogensulfate (0.2 M) catalyzed the stepwise co-oligomerization of CO/ethylene to penta-3-one, octane-3,6-dione and undecane-3,6,9-trione. Also the hydrocarboxylation of ethylene to propionic acid was observed.

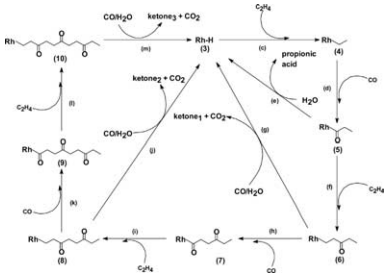

Sujittra Youngme, Pongthipun Phuengphai, Saksit Booncoon, Narongsak Chaichit

Polyhedron 23 (2004) 1685

The crystal structure and electronic properties of a *cis*-distorted octahedral CuN_4O_2 chromophore: $[Cu(dpyam)_2(OXO)]^+$, OXO= ONO^-, O_2CH^- and ONO_2^-

The crystal structures and electronic properties of $[Cu(dpyam)_2(NO_2)](NO_2)$ (**I**) and $[Cu(dpyam)_2(O_2CH)](ClO_4)$ (**II**) and $[Cu(dpyam)_2(ONO_2)](BF_4)$ (**III**) have been examined in the context of fluxional behaviour. In **I**, the copper atom and the asymmetrically bonded nitrito group lie on a crystallographic C_2-axis. The nitrito group is clearly disordered about the C_2-axis giving a square pyramidal *cis*-distorted octahedral $(4 + 1 + 1^*)$ chromophore rather than a pseudo-regular *cis*-distorted octahedral chromophore previously reported. In **II** and **III**, a distortion of the *cis*-distorted CuN_4O_2 chromophore towards a square pyramidal $(4 + 1 + 1^*)$ stereochemistry is also present.

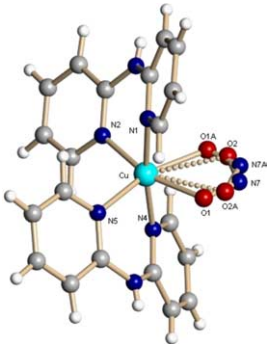

Montserrat Barquín, María J. González Garmendia, Sergio Pacheco, Elena Pinilla, José M. Seco, María R. Torres

Polyhedron 23 (2004) 1695

Synthesis, spectroscopic, magnetic and EPR results and crystal structure of di-μ-(*N*-methyl-*N*-methoxy-2-pyridinamine)bis[(2,2′-bipyridine)copper(II)]hexaflourophosphate

The dinuclear complex $[\{Cu(bipy)\}_2\{\mu\text{-}Me(OCH_2)Npy\}_2](PF_6)_2$ has been synthesized by the reaction of $[\{Cu(bipy)\}_2(\mu\text{-}OH)_2](PF_6)_2$ with MeNHpy. The X-ray crystal structure shows a distorted square-planar pyramidal coordination for Cu(II). The compound is slightly antiferromagnetic ($2J = -3.6$ cm^{-1}). In the Q-band EPR spectrum signals of triplet ($D > hv$) are observed.

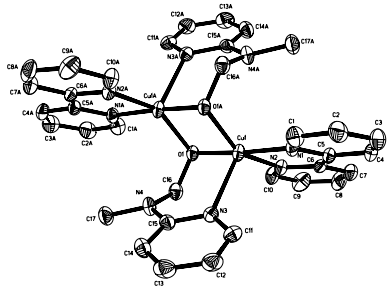

Wenyong Guo, Zhenghe Peng, Daocong Li, Yunhong Zhou

Polyhedron 23 (2004) 1701

Synthesis and structural characterization of zinc(II) and cadmium(II) complexes with 2-oxo-1,3-dithiole-4,5-dithiolate and 1,10-phenanthroline

Complexes Zn(dmid)(phen)$_2$ and Cd(dmid)(phen)$_2$ were synthesized and studied. In the crystal packing, there exists a strong π–π interaction between two parallel 1,10-phenanthrolines of adjacent molecules.

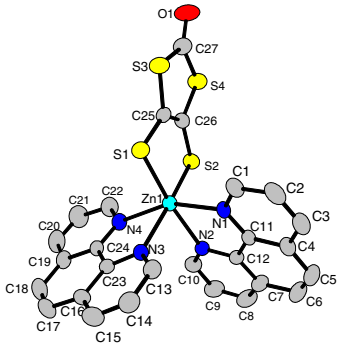

Diane L. Stone, David K. Smith, Adrian C. Whitwood

Polyhedron 23 (2004) 1709

Copper amino-acid complexes – towards encapsulated metal centres

Two new copper complexes have been investigated by electrochemical and electron spin resonance techniques to determine the extent of encapsulation of the copper ions. There were significant differences between the two complexes, indicating that the copper ion in each of these complexes experiences different microenvironments.

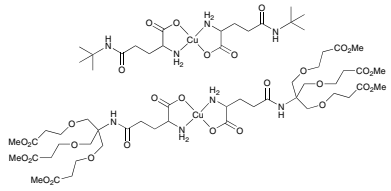

Jennifer M. Butler, Gary M. Gray, Juan Pablo Claude

Polyhedron 23 (2004) 1719

Synthesis, characterization and X-ray crystallography of a metallacrown ether complex containing a $Ru^{II}(bpy)_2^{2+}$ chromophore and its $Mo(CO)_4$ analog

The new metallacrown ether complexes *cis*-$[Ru(bpy)_2((2,2'\text{-}C_{12}H_8O_2)P(CH_2CH_2O)_4P(2,2'\text{-}O_2C_{12}H_8))](O_3SCF_3)_2$ and *cis*-$[Mo(CO)_4((2,2'\text{-}C_{12}H_8O_2)P(CH_2CH_2O)_4P(2,2'\text{-}O_2C_{12}H_8))]$ have been prepared. The effect of interactions of the metallacrown ether complex with selected monoatomic cations on the emissive properties of the $Ru(bpy)_2^{2+}$ chromophore were studied by steady-state and time-dependent emission spectroscopy. The complex interacts weakly with Li^+, Na^+ and Hg^{2+}, and subtle changes are observed in its photophysical properties.

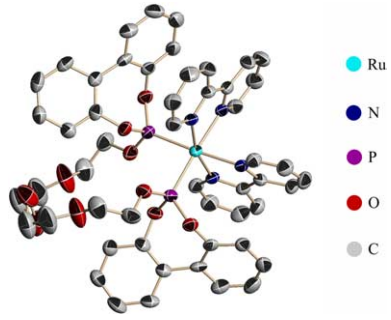

Suaad Abuskhuna, Malachy McCann, John Briody, Michael Devereux, Vickie McKee

Polyhedron 23 (2004) 1731

Synthesis and structure of Mn(II), Cu(II) and Zn(II) complexes containing bis-imidazole ligands

A family of bis-imidazole ligands based on the parent bis(imidazol-2-yl)methane structure, and which can mimic multi-histidine coordination in biological systems, have been complexed to Mn(II), Cu(II) and Zn(II) centres. Five complexes were characterised by X-ray crystallography. A common structural feature of the ligands is that the two imidazole rings, which have a single spacer tetrahedral carbon atom between them, form stable, six-membered *N*,*N*′ chelate rings with the metals.

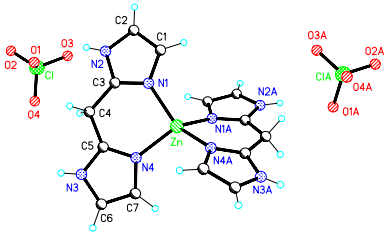

Eric N. Coker, Timothy J. Boyle, Mark A. Rodriguez, Todd M. Alam

Polyhedron 23 (2004) 1739

Structurally characterized magnesium carboxylates with tuned melting points

A series of sterically varied carboxylic acids was used to synthesize meltable magnesium carboxylates, which were structurally and thermophysically characterized. A variety of nuclearities and carboxylate binding modes were observed in the crystal structures. Melting points ranged from 130 to 440 °C, and some compounds were volatile under inert atmosphere.

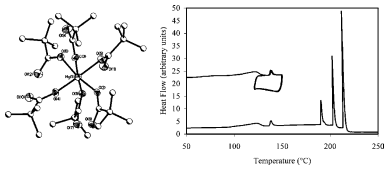

Paul Emseis, Timothy W. Failes, David E. Hibbs, Peter Leverett, Peter A. Williams

Polyhedron 23 (2004) 1749

Intramolecular NH–π and π–π interactions in ternary cobalt(III) complexes of aromatic aminoacids: a structural and NMR study

A structural and NMR study of a series of chiral cobalt(III) diastereomeric complexes containing a tetradentate ligand and a *R*- or *S*-tryptophan bidentate is reported. Non-covalent π–π and NH–π interactions are present in these species in the solid state, and are shown to persist in solution where they serve to influence markedly the molecular conformation.

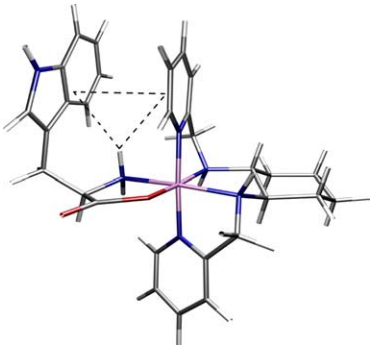

Yufei Song, Iryna A. Koval, Patrick Gamez, Gerard A. van Albada, Ilpo Mutikainen, Urho Turpeinen, Jan Reedijk

Polyhedron 23 (2004) 1769

Solution studies and structure of a dinuclear-based double-stranded helicate of [Cu_2-(*p*-xysal)$_2$] (H_2-*p*-xysal=bis(hydroxylbenzyl) diaminoxylene)

The complex Cu_2(*p*-xysal)$_2$ has been obtained by reaction of H_2-*p*-xysal with copper(II) perchlorate. The compound shows a double-stranded helicate structure, constructed from two slightly different units of dinuclear Cu(II). All the copper(II) ions have distored tetrahedral geometries. Solution studies have been done by different methods (UV/Vis, ESI-MS, EPR, cyclic voltammetry measurement). The intra- and inter-molecular interactions are demonstrated to play important roles in the formation and the stabilization of the molecular architectures of the complex.

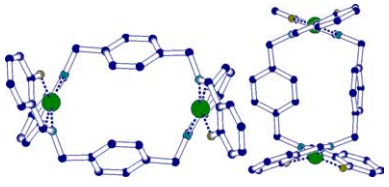

Catherina Raptopoulou, Dimitra Daphnomili, Athanassios Karamalides, Massimo Di Vaira, Aris Terzis, Athanassios G. Coutsolelos

Polyhedron 23 (2004) 1777

Perhalogenated porphyrinic derivatives with indium and thallium: the X-ray structures of (β-Cl_4TPP)Tl(Cl), (β-Cl_4TPP)In(Cl) and (T*p*FTPP)Tl(Cl)

The family of indium and thallium porphyrinic derivatives is completed by new complexes represented by the formula (Porph)M(III)Cl. A variety of porphyrin rings such as T*p*FPP, TPyP, β-Cl_4TPP, β-Cl_8TPP or β-Cl_4TPP were used in order to study their physicochemical behaviour with respect to their ring basicity, by various spectroscopic methods.

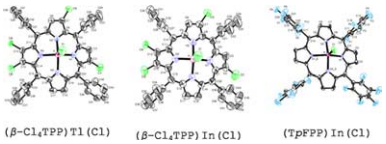

Piotr Drożdżewski, Anna Brożyna, Maria Kubiak

Polyhedron 23 (2004) 1785

Synthesis, X-ray crystal structure and vibrational spectra of a polymeric copper(II) complex with 2-thiopheneacetic acid

A new polymeric complex of Cu(II) and 2-thiopheneacetic acid was synthesized and characterized by X-ray structure determination, together with IR and Raman spectroscopy. The metal ions are arranged into dinuclear [Cu_2O_8] units joined into a polymer chain via direct Cu–O bonds. The FIR bands corresponding to Cu–O vibrations were localized with help of ^{63}Cu–^{65}Cu substitution.

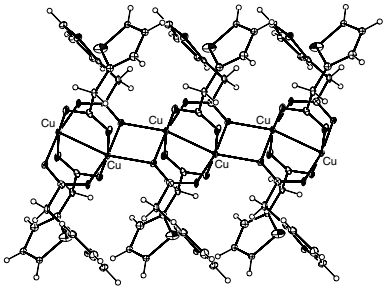

Astrid Koban, Gert Bernhard

Polyhedron 23 (2004) 1793

Complexation of uranium(VI) with glycerol 1-phosphate

Uranium(VI) forms in aqueous solution with glycerol 1-phosphate two complexes, $UO_2(C_3H_7O_3PO_3)$ and $UO_2(C_3H_7O_3PO_3)_2^{2-}$, which were characterized by potentiometric titration and TRLFS. Complex stability constants were calculated for both complexes, main fluorescence emission bands and the fluorescence lifetime were determined for $UO_2(C_3H_7O_3PO_3)$.

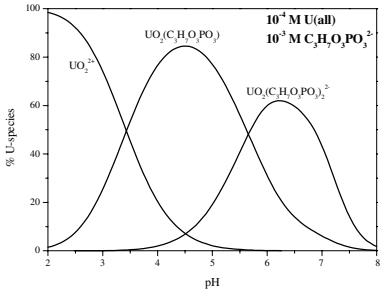

Hong-Lei Liu, Hong-Yan Mao, Chen Xu, Hong-Yun Zhang, Hong-Wei Hou, Qing-an Wu, Yu Zhu, Bao-Xian Ye, Li-Jie Yuan

Polyhedron 23 (2004) 1799

Four novel sulfur-rich complexes: syntheses, crystal structures of three nickel(II) and one cobalt(II) complex with derivatives of Lawesson's Reagent

Reaction of Lawesson's Reagent (LR) with $NiCl_2$ and $Co(CH_3COO)_2$ in methanol or ethanol gives four novel sulfur-rich complexes. These complexes were characterized by IR and X-ray crystallography. We found that the solvent can influence the crystal structure in the reaction of LR with metals.

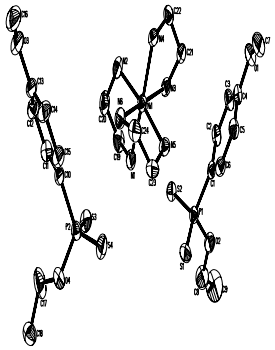

Han-Dong Yin, Chuan-Hua Wang, Qiu-Ju Xing

Polyhedron 23 (2004) 1805

Synthesis and characterization of triphenyltin esters of heteroaromatic carboxylic acids and the crystal structure of $[Ph_3SnO_2CC_5H_4N \cdot 0.5H_2O]_\infty$

Reactions of triphenyltin hydroxide with 2-furanyl, 2-furanvingl, 2-(5-terbutyl)furanyl, 2-(5-benzoyl)furanyl, 2-pyridinyl, 4-pyridinyl, 3-indolyl, 3-indolmethyl, 3-indolethyl and 3-indolpropyl carboxylates yield triphenyltin esters of heteroaromatic carboxylic acids Ph_3SnO_2CR. All compounds are characterized by elemental analysis, IR and ^1H NMR. The crystal structure of the triphenyltin ester of 4-pyridinyl carboxylic acid is determined by single crystal X-ray diffraction.

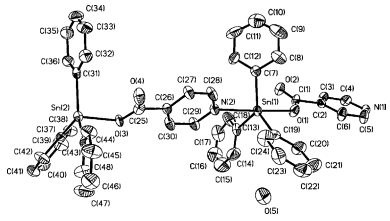

Sandip Saha, Dasarath Mal, Subratanath Koner, Ashis Bhattacherjee, Philipp Gütlich, Swastik Mondal, Monika Mukherjee, Ken-Ichi Okamoto

Polyhedron 23 (2004) 1811

Synthesis, X-ray structure and magnetic properties of the azido adducts of quadridentate Schiff base manganese(III) complexes

Two new azido adducts of Mn(III) schiff base complexes have been synthesized, characterized structurally and magnetically. X-ray structure analysis revealed that both the complexes exist as phenoxo bridged dimmers: one of them is ferromagnetic and other is antiferromagnetic.

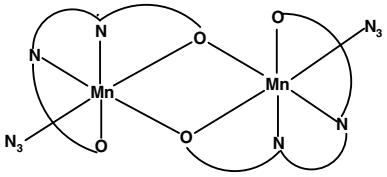

Barbara Machura, M. Jaworska, Rafal Kruszynski

Polyhedron 23 (2004) 1819

X-ray and electronic structure of the $[ReCl_3(pzH)_2(PPh_3)]$ and $[ReCl_3(3,5\text{-}Me_2pzH)_2(PPh_3)]$ complexes

The $[ReCl_3(pzH)_2(PPh_3)]$ and $[ReCl_3(3,5\text{-}Me_2pzH)_2(PPh_3)]$ complexes have been obtained in the reactions of $[ReCl_3(MeCN)(PPh_3)_2]$ with pyrazole and 3,5-dimethylpyrazole, respectively. The rhenium atom of the both complexes is a in distorted octahedral environment with three chlorine ligands in *mer* geometry, two N-donor ligands (pzH or 3,5-Me_2pzH) in *cis* position to each other and one PPh_3 molecule occupying *trans* position to N(3) atom. The geometric parameters of $[ReCl_3(pzH)_2(PPh_3)]$ have been examined using the density functional theory (DFT) method. The UV–Vis spectra of the complexes have been discussed on the basis of the electronic transitions of $[ReCl_3(pzH)_2(PPh_3)]$ calculated with the time-dependent DFT method (TDDFT).

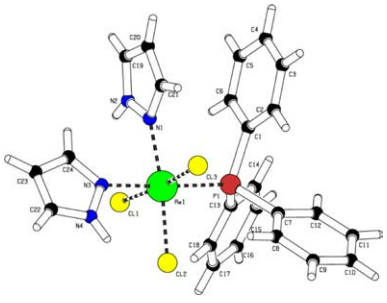

Marcello Gennari, Marco Giannetto, Maurizio Lanfranchi, Luciano Marchiò, Maria Angela Pellinghelli, Matteo Tegoni

Polyhedron 23 (2004) 1829

Synthesis, structure and electrochemical properties of a nickel complex with the hydrotris[thioxotriazolyl-3-(2-pyridyl)]borate podand ligand

The complex $[Ni(Tr^{Me,o\text{-}Py})_2]$ {$Tr^{Me,o\text{-}Py}$= hydrotris[1,4-dihydro-4-methyl-3-(2-pyridyl)-5-thioxo-1,2,4-triazolyl]borate} was synthesized and structurally characterized. Cyclic voltammetry performed on acetonitrile solution of **2** shows that the $Tr^{Me,o\text{-}Py}$ ligand undergoes irreversible oxidation and reduction processes at potential $> +0.7$ and ~ 0 V (Ag/AgCl/KCl 0.1 M as reference electrode).

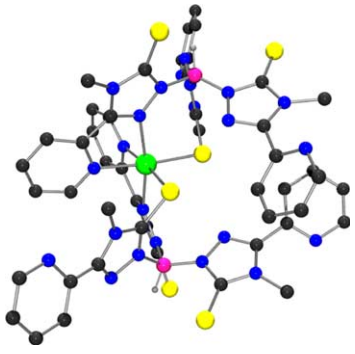

Horacio López-Sandoval, Arlette Richaud, Rosalinda Contreras, G. Jeffery Leigh, Peter B. Hitchcock, Angelina Flores-Parra, Juan Carlos Galvez-Ruíz, Alejandro Cruz, Heinrich Nöth, Noráh Barba-Behrens

Polyhedron 23 (2004) 1837

Triangulo-μ_3-sulfido-trinickel(II) cone-shaped clusters and anion traps: structural characterization

The synthesis and structural characterization of triangular trinuclear $Ni_3S_4N_3$ complexes obtained from an ephedrine derivative (tpmp) and Ni^{II} are reported. Three homochiral ligand molecules together with three Ni^{II} ions give rise to a cone-shaped cluster topped by a μ_3-sulfide ion. The three phenyl groups form the rim of a cage which contains R-OSO_3 (R=C_2H_5, C_3H_7) or nitrate anions.

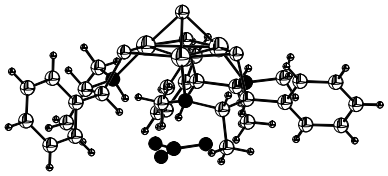

Ergün Gonca, Yüksel Köseoğlu, Bekir Aktaş, Ahmet Gül

Polyhedron 23 (2004) 1845

Octakis(1-naphthylmethylthio) substituted porphyrazine derivatives

New porphyrazines surrounded with eight bulky and electron-rich naphthyl-appended groups have been described; high electron density on the substituents results in a second absorption in the ultraviolet region of comparable intensity as the intensity to B band of porphyrazines.

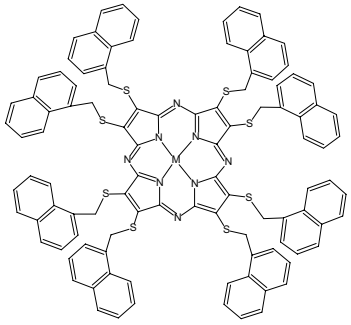

M= Mg, 2H, Cu, Zn, Co.

The Publisher encourages the submission of articles in electronic form thus saving time and avoiding rekeying errors. For detailed instructions on the preparation of manuscripts and of electronic artwork, consult the Author Gateway for Elsevier at http://authors.elsevier.com

SCIENCE DIRECT™

Full text of this journal is available, on-line from **ScienceDirect**. Visit **www.sciencedirect.com** for more information.

CONTENTS Direct This journal is part of **ContentsDirect**, the *free* alerting service which sends tables of contents by e-mail for Elsevier books and journals. You can register for **ContentsDirect** online at: **www. elsevier.com/locate/contentsdirect**

Available online at www.sciencedirect.com
SCIENCE DIRECT®
Polyhedron 23, issue 9, 27 May 2004
POLYHEDRON
www.elsevier.com/locate/poly

Contents

Report

Katharina M. Fromm, Estelle D. Gueneau

Polyhedron 23 (2004) 1479

Structures of alkali and alkaline earth metal clusters with oxygen donor ligands

This review article presents the most representative aggregates of group 1 and 2 metals containing oxygen donor ligands. Apart from their synthesis and possible applications, the compounds were chosen for their fascinating variety of original structures, which lead to high expectations of further new results in this research field.

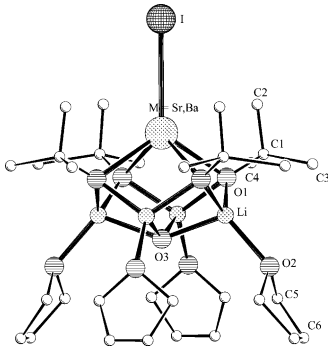

Papers

R. Carballo, A. Castiñeiras, B. Covelo, E. García-Martínez, J. Niclós, E.M. Vázquez-López

Polyhedron 23 (2004) 1505

Solid state coordination chemistry of mononuclear mixed-ligand complexes of Ni(II), Cu(II) and Zn(II) with α-hydroxycarboxylic acids and imidazole

Several metal complexes of α-hydroxycarboxylates (HL′) with imidazole as a coligand have been synthesised and structurally characterized. The octahedral Ni(II) complexes present two formulae: $[Ni(HL')_2(Im)_2]$ and $[Ni(HB')_2(Im)_3]$, HB=benzylate. The Cu(II) complexes of formula [Cu(HL′)(Im)] presents a square pyramidal coordination geometry. The octahedral Zn(II) complexes have two formulae: $[Zn(HL')_2(Im)_2]$ and $[Zn(Im)_6](HB)_2$. Spectroscopic data and the thermal behaviour are presented and discussed.

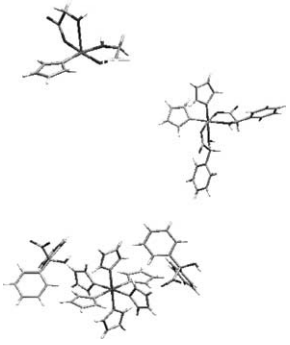

Victor I. Baranovski, Dimitry V. Korolkov

Polyhedron 23 (2004) 1519

Electron density distribution, polarizability and bonding in the octahedral clusters $[Mo_6S_8(CN)_6]^{6-}$, $[Re_6S_8(CN)_6]^{4-}$ and $Rh_6(CO)_{16}$

Geometrical structure, electron density distribution and polarizabilities were calculated for $[Mo_6S_8(CN)_{12}]^{6-}$, $[Re_6S_8(CN)_6]^{4-}$ and $Rh_6(CO)_{16}$. The noticeable electron density in the inner part of the M_6 octahedrons leads to the model of the clusters with octahedral cores, in which the mobile electrons are moving in a potential well of spherical symmetry. The high values of the calculated polarizabilities of the compounds under consideration are in accord with the suggested model.

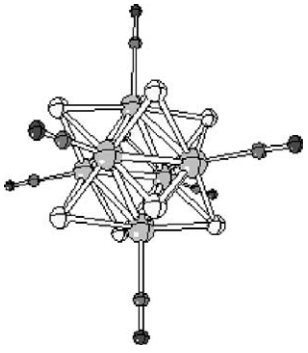

S. Kannan, N. Rajalakshmi, K.V. Chetty, V. Venugopal, M.G.B. Drew

Polyhedron 23 (2004) 1527

Complexes of the uranyl ion with bis(diphenylphosphino)methane dioxide

Bis(diphenylphosphino)methane dioxide compounds of uranyl nitrate and uranyl bis(β-diketonates) show monodentate, bidentate chelate and bridging bidentate modes of coordination for this ligand in its compounds $[UO_2(DBM)_2DPPMO]$, $[UO_2(NO_3)_2DPPMO]$ and $[\{UO_2(DBM)_2\}_2DPPMO]$, respectively.

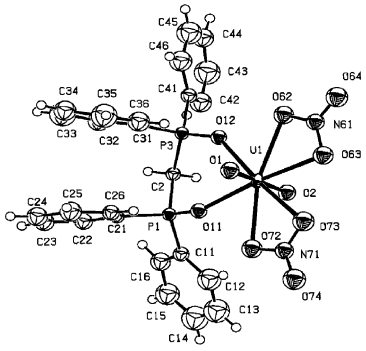

Yulin Yang, Yunlin Liu, Chao Chen, Wei Wang, Zhuo Yi, Wenqin Pang

Polyhedron 23 (2004) 1535

Hydrothermal synthesis and characterization of an organically templated gallophosphate JGP-5

A gallophosphate compound, $[C_6H_{10}(NH_3)_2]$-$Ga_2P_2O_8(OH)_2$ has been synthesized hydrothermally by using *trans*-1,4-diaminocyclohexane as the template, in which the organic amines display a strong templating effect on the inorganic layer.

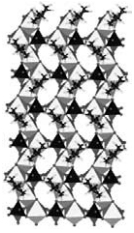

Yao-Cheng Shi, Hua-Mei Yang, Hai-Bin Song, Yong-Hong Liu

Polyhedron 23 (2004) 1541

Syntheses and crystal structures of a ferrocene-containing enaminone and its copper complex

Reaction of ferrocenoylacetone $[C_5H_5FeC_5H_4C(O)CH_2C(O)CH_3]$ and 2-methoxyaniline yields an enaminone $[C_5H_5FeC_5H_4C(O)CH{=}C(NHAr)CH_3]$ (**HL**, Ar=2-$CH_3OC_6H_4$). Reaction of the enaminone **HL** and copper acetate affords complex **I**. Their structures have been determined by X-ray crystallography.

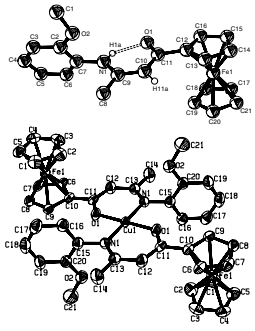

Chunlin Ma, Jiafeng Sun

Polyhedron 23 (2004) 1547

Hydrogen bonding and π–π stacking interaction in the coordination of sulfur and nitrogen donor heterocycle to organotin(IV): syntheses and crystal structures of di- and triorganotin(IV) derivatives with 1-(4-hydroxyphenyl)-1*H*-tetrazole-5-thiol

A series of organotin(IV) complexes with 1-(4-hydroxyphenyl)-1*H*-tetrazole-5-thiol of the type, $R_nSn[S(C_7H_5N_4O)]_{4-n} \cdot L$ ($n = 3$, L=0: R=Me (**1**), *n*-Bu (**2**), Ph (**3**); $n = 3$, L=$0.5C_2H_5OH \cdot 0.5H_2O$, R=$PhCH_2$ (**4**); $n = 2$, L=H_2O, R=Me (**5**); $n = 2$, L=0: R=*n*-Bu (**6**), Ph (**7**), $PhCH_2$ (**8**)) have been synthesized. All the complexes **1**–**8** have been characterized by elemental, IR and ^1H NMR analyses. Among them complexes **3**, **4**, **5** and **6** have also been characterized by X-ray crystallography diffraction.

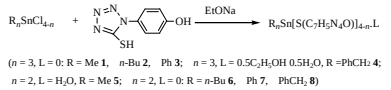

Andrew A. Smith, Robert A. Coxall, Andrew Harrison, Madeleine Helliwell, Simon Parsons, Richard E.P. Winpenny

Polyhedron 23 (2004) 1557

High-temperature synthesis of polynuclear iron oxo-hydroxy complexes

Four iron cage complexes are reported; two have hexanuclear cores and two undecanuclear cores. Magnetic studies show antiferromagnetic exchange between the Fe(III) centres.

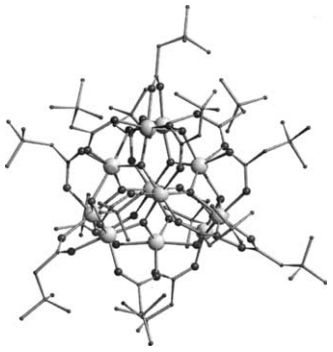

P. Govindaswamy, Yurij A. Mozharivskyj, Mohan Rao Kollipara

Polyhedron 23 (2004) 1567

Synthesis and characterization of cyclopentadienylruthenium(II) complexes containing *N*,*N*′-donor Schiff base ligands: crystal and molecular structure of $[(\eta^5\text{-}C_5H_5)Ru(C_5H_4\text{-}N\text{-}2\text{-}CH{=}N\text{–}C_6H_4\text{–}p\text{-}OCH_3)(PPh_3)]PF_6$

Reaction of the complex $[(\eta^5\text{-}C_5H_5)Ru(PPh_3)_2Cl]$ (**1**) with a series of *N*,*N*′-donor Schiff bases, viz., *para*-substituted *N*-(pyrid-2-ylmethylene)phenylamines in methanol yielded cyclopentadienyl ruthenium(II) complexes of formulation $[(\eta^5\text{-}C_5H_5)Ru(PPh_3)\text{-}(C_5H_5N\text{-}2\text{-}CH{=}N\text{–}C_6H_4\text{–}p\text{-}X)]^+$. Representative complex **2c** has been established by X-ray diffraction study.

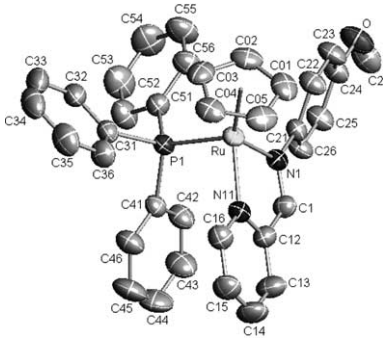

Pavel Kopel, Zdeněk Trávníček, Jaromír Marek, Jerzy Mrozinski

Polyhedron 23 (2004) 1573

Syntheses and study on nickel(II) complexes with thiodiglycolic acid and nitrogen-donor ligands. X-ray structures of $[Ni(bpy)(tdga)(H_2O)] \cdot 4H_2O$ and $[(en)Ni(\mu\text{-}tdga)_2Ni(en)] \cdot 4H_2O$ ($tdgaH_2$=thiodiglycolic acid)

Mononuclear and binuclear mixed-ligand Ni(II) complexes involving thiodiglycolate(2−) anion and nitrogen-donor ligands in the coordination sphere have been prepared and characterized. All the complexes are deformed octahedral as was also proved by X-ray analysis. Temperature dependence of magnetic susceptibility was measured for binuclear complex with carboxylate bridges.

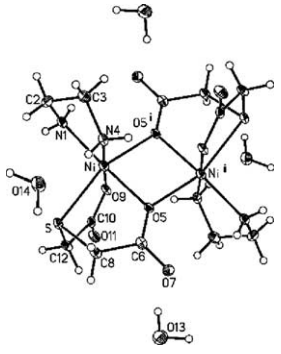

Yu-Wei Lu, Bineta Keita, Louis Nadjo

Polyhedron 23 (2004) 1579

Rational approach of the stoichiometries of lanthanide complexes with $\alpha_2\text{-}[P_2W_{17}O_{61}]^{10-}$ heteropolytungstate in aqueous solution

The reaction constant for this formal dimerization process varies from 3.0 × 104 to 5.5 × 106.

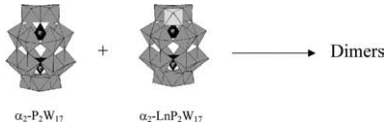

Ui Gab Joung, Tae Ho Kim, Dae June Joe, Bun Yeoul Lee, Dong Mok Shin, Young Keun Chung

Polyhedron 23 (2004) 1587

Pyridineenolato and pyridineenamido complexes of zirconium, titanium and aluminum

Pyridineenolate complexes, $[CH_2{=}C(C_5H_4N)O\text{-}\kappa^2N,O]_2M(NR_2)_2$ (M=Zr, R=Et, **3**; M=Ti, R=Me, **4**) and pyridineenamido complexes, $[ArNC(C_5H_4N)(=CH_2)\text{-}\kappa^2N,N]_2M(NR_2)_2$ (M=Zr, Ar=1,3-$Me_2C_6H_3$, R=Et, **9**; M=Ti, Ar=1,3-$Me_2C_6H_3$, R=Me, **10**; M=Zr, Ar=1,3-*i*$Pr_2C_6H_3$, R=Et, **11**) have been prepared. Addition of excess $AlMe_3$ to **3** or **4** and **11** results in the formation of transmetallated complexes, $[CH_2{=}C(C_5H_4N)(OAlMe_3)\text{-}\kappa^2N,O]AlMe_2$ (**13**) and [(2,6-*i*$Pr_2C_6H_3$)$NC(C_5H_4N)$ (=CH_2)]$AlMe_2$ (**14**). Solid structures of **4, 8, 13** and **14** were determined by X-ray crystallography.

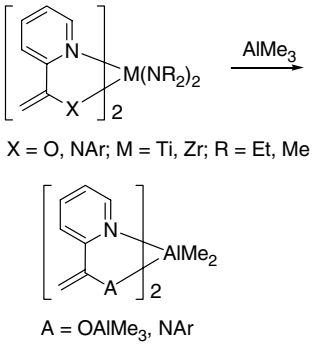

Nikhil Ranjan Pramanik, Saktiprosad Ghosh, Tapas Kumar Raychaudhuri, Sibdas Ray, Ray J. Butcher, Sudhanshu Sekhar Mandal

Polyhedron 23 (2004) 1595

Synthesis, characterization and crystal structure of oxomolybdenum (VI) and (IV) complexes of some tridentate ONS donor ligands

An array of oxomolybdenum (VI) and (IV) complexes of some tridentate ONS donor ligands (H_2L) have been synthesized and structurally characterized. Mo(VI) complexes are pentacoordinated and have a vacant site for substrate binding. All the $Mo^{VI}O_2L$ complexes could be transformed into the corresponding $Mo^{IV}OL$ complexes by oxo-abstraction using PPh_3.

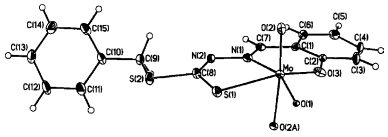

Tetsuo Asaji, Eigo Akiyama, Fukue Tajima, Kazuo Eda, Masao Hashimoto, Yoshihiro Furukawa

Polyhedron 23 (2004) 1605

Salts of tetrachloroauric acid with pyridine *N*-oxide having various base/acid ratios of 1/1, 4/3, 3/2 and 2/1: crystal structures, ^{35}Cl NQR and phase transitions

Due to variety in the aggregation motif of $[AuCl_4]^-$ and that in the structure of the protonic adduct of pyridine *N*-oxide (PyO), various salts having different base-to-acid ratio can be formed. The crystal of [(PyO)-D][$AuCl_4$] is built by alternating stacking of the layers of disordered $[(PyO)D]^+$ and $[AuCl_4]^-$.

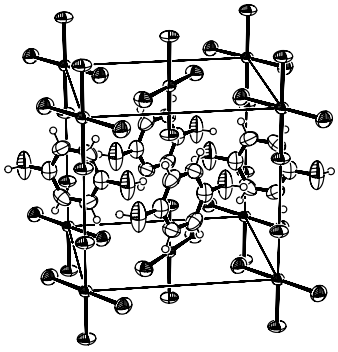

Claude Villiers, Pierre Thuéry, Michel Ephritikhine

Polyhedron 23 (2004) 1613

Crystal structure of first- and second-sphere complexes of uranyl nitrate with 1,2- and 1,4-diols

Whereas pinacol (in a staggered conformation) complexes the uranyl ion in a bidentate fashion, two 1,4-diols are shown to act as second-sphere ligands through hydrogen bonding to coordinated nitrate ions and water molecules. Hydrogen bonded assemblages, either discrete, two- or three-dimensional, are obtained.

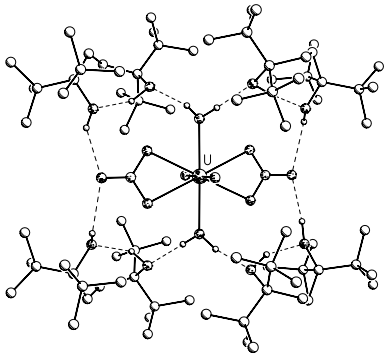

Hua Liang, Jingyu Liu, Xiaofang Li, Yuesheng Li

Polyhedron 23 (2004) 1619

Synthesis, structure and norbornene polymerization behavior of neutral palladium complexes

A new class of palladium complexes bearing non-symmetric bidentate pyrrole-iminato or salicylaldiminato chelate ligands has been synthesized and characterized, and the complexes are shown to be highly active catalysts for vinylic polymerization of norbornene.

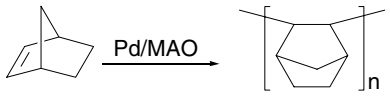

Prakash C. Srivastava, S. Bajpai, R. Lath, S.M. Bajpai, R. Kumar, Raymond J. Butcher

Polyhedron 23 (2004) 1629

Molecular aggregates, zig-zag 2D-stairs, -ribbons and 3D-supramolecular networks of cyclic telluranes assisted by intermolecular Te···Cl and Te···Br secondary bonding

Te···Cl and Te···Br secondary bonds assisted molecular aggregates zig-zig 2D-stairs, -ribbons of cyclic telluranes in **1**–**3** and 3D-supramolecular networks in **4** and are described after **5**. The supramolecular associations of these cyclic telluranes **1**–**5** are compared with the supramolecular associations in their precursors and in acyclic telluranes ($C_4H_8TeCl_2$,$C_4H_8TeBr_2$,C_5H_{10}-$TeBr_2$,$C_8H_8TeCl_2$.$C_8H_8TeBr_2$).

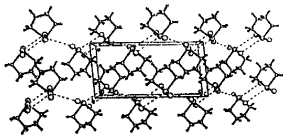

Sujittra Youngme, Chatkaew Chailuecha, Narongsak Chaichit

Polyhedron 23 (2004) 1641

The novel dinuclear doubly and triply bridged copper(II) compound with monoatomic bridges

The novel planar di-μ-hydroxo-bridged copper (II) compound, $[Cu_2(dpyam)_2(\mu\text{-}OH)_2I_2] \cdot 2H_2O$ (**1**), contains a dinuclear $[I(dpyam)Cu(\mu\text{-}OH)_2$-$Cu(dpyam)I]^+$ unit with a strictly planar CuO_2 network. Each copper(II) ion is in a tetrahedrally distorted square pyramidal coordination geometry of the CuN_2O_2I chromophore. The novel dinuclear copper(II) compound containing three monoatomic bridges with homospecies, $[Cu_2(dpyam)_2(\mu\text{-}OH)_3]Cl \cdot 3H_2O$ (**2**) involves the $[(dpyam)Cu(m\text{-}OH)_3Cu(dpyam)]^+$ unit. The triply bridged Cu(II) ions show a distorted square pyramidal coordination. The fifth apical ligand is a longer bonded bridging OH^- group, which joins the basal CuN_2O_2 planes in a roof-shaped configuration.

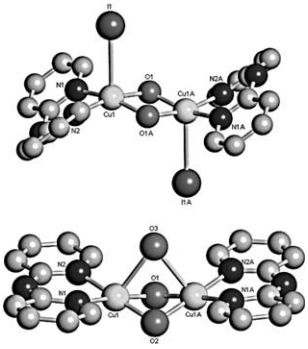

Mika Kettunen, Adnan S. Abu-Surrah, Hamzeh M. Abdel-Halim, Timo Repo, Markku Leskelä, Maarit Laine, Ilpo Mutikainen, Markku Ahlgren

Polyhedron 23 (2004) 1649

Synthesis, spectroscopy and molecular structures of new salicylketiminato nickel(II) complexes

A series of salicylketimines (2-[(2,6-diisopropylphenylimino)ethyl]phenol, 2-[(2,6-diisopropylphenylimino)ethyl]naphthol and 2-[(2,6-diisopropylphenylimino)(phenyl) methyl]-phenol), and their nickel complexes of general forms [(salicylketiminato)-Ni(PPh_3)(Ph)] and [(salicylketiminato)$_2$Ni] were synthesized, characterized and their solid state structures were determined. The formation of monophenyl-nickel(II) complexes versus the corresponding bis(sal)Ni(II) complexes was studied.

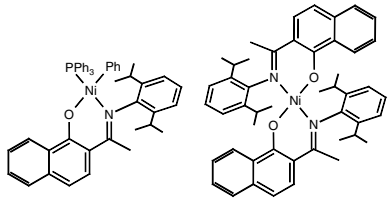

Pratap Chutia, Nandini Kumari, Manab Sharma, J. Derek Woollins, Alexandra M. Z. Slawin, Dipak Kumar Dutta

Polyhedron 23 (2004) 1657

Ruthenium(II) carbonyl complexes containing tertiary phosphine chalcogenide ligands of the type Ph_3PX; X=O, S, Se

The complexes $[Ru(CO)_2Cl_2(Ph_3PX)]$ and $[Ru(CO)_2Cl_2(Ph_3PX)_2]$ are produced on treatment of $[Ru(CO)_2Cl_2]_n$ with 1:1 and 1:2 mol ratio of the ligands Ph_3PX; X=O, S, Se, respectively. The molecular structure of $[Ru(CO)_2Cl_2(Ph_3PS)_2]$ was determined by single X-ray crystallography and Ru atom occupies the center of the slightly distorted octahedral geometry.

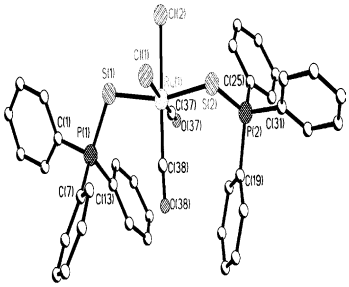

Yao-Cheng Shi

Polyhedron 23 (2004) 1663

Reactions of Mo–Mo singly-bonded complexes $[(\eta^5\text{-}RC_5H_4)_2Mo_2(CO)_6]$ with diphenylditelluride in the presence of $^nBu_4NI$. Crystal structures of complexes $[(\eta^5\text{-}C_5H_5)Mo(CO)_3Te]$ and *cis*/ae-$[(\eta^5\text{-}C_2H_5O_2CC_5H_4)_2Mo_2(\mu\text{-}Te)_2\ (\mu\text{-}TePh)_2]$

Reactions of singly-bonded dimolybdenum complexes $[(\eta^5\text{-}RC_5H_4)_2Mo_2(CO)_6]$ (**I**, R=CH_3CO; **II**, C_6H_5CO; **III**, R=CH_3O_2C; **IV**, R=$C_2H_5O_2C$) with Ph_2Te_2 in the presence of $^nBu_4NI$ afford one mononuclear complex **1** $[(\eta^5\text{-}C_5H_5)Mo(CO)_3Te]$ and four dinuclear complexes *cis*/ae-$[(\eta^5\text{-}RCC_5H_4)_2Mo_2(\mu\text{-}Te)_2(\mu\text{-}TePh)_2]$ (**2**, R=CH_3CO; **3**, R=C_6H_5CO; **4**, R=CH_3O_2C; **5**, R=$C_2H_5O_2C$). Crystal structures of complexes **1** and **5** have been determined by X-ray diffraction analyses.

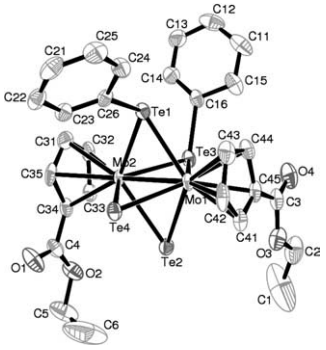

The Publisher encourages the submission of articles in electronic form thus saving time and avoiding rekeying errors. For detailed instructions on the preparation of manuscripts and of electronic artwork, consult the Author Gateway for Elsevier at http://authors.elsevier.com

SCIENCE DIRECT™

Full text of this journal is available, on-line from **ScienceDirect**. Visit **www.sciencedirect.com** for more information.

CONTENTS direct This journal is part of **ContentsDirect**, the *free* alerting service which sends tables of contents by e-mail for Elsevier books and journals. You can register for **ContentsDirect** online at: **www. elsevier.com/locate/contentsdirect**

Available online at www.sciencedirect.com
SCIENCE DIRECT®
Polyhedron 23, issues 6, 25 March 2004
POLYHEDRON
www.elsevier.com/locate/poly

Contents

Papers

Ki-Young Choi, Yong-Man Jeon, Haiil Ryu, Je-Jik Oh, Hae-Hwan Lim, Moon-Won Kim

Polyhedron 23 (2004) 903

Synthesis and characterization of *syn–anti* carboxylate-bridged one-dimensional copper(II) complexes with bis(2-pyridylmethyl)-amino acids

One-dimensional polymeric chain complexes $\{[Cu(\mu\text{-pmea})](ClO_4) \cdot H_2O\}_n$ (**1**), $\{[Cu(\mu\text{-pmpa})](ClO_4) \cdot 2H_2O\}_n$ (**2**) and $\{[Cu(\mu\text{-pmba})(H_2O)](ClO_4) \cdot 3H_2O\}_n$ (**3**) were synthesized and structurally characterized. Each copper atom is coordinated by *syn–anti* carboxylate bridges to form a one-dimensional polymeric chain. Magnetic behaviors for all complexes exhibit very weak ferromagnetic interactions.

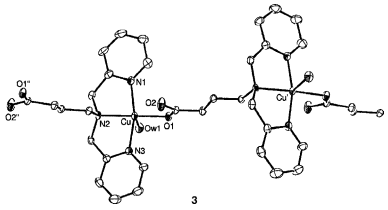

Sujoy Baitalik, Bula Dutta, Kamalaksha Nag

Polyhedron 23 (2004) 913

Spectroscopic and redox properties of $Rh^{III}Ru^{II}$ and $Ru^{II}Ru^{II}$ complexes derived from 2,2′-bipyridine, pyrazole-3,5-bis(benzimidazole) and 1,2,4-triazole-3,5-dicarboxylic acid as bridging ligands

The heterodinuclear complex $[(bpy)_2Ru^{II}(H_2pzbzim)Rh^{III}(bpy)_2](ClO_4)_4 \cdot 3H_2O$ and the homodinuclear complex $[(bpy)_2Ru^{II}(trzdc)Ru^{II}(bpy)_2](ClO_4) \cdot 5H_2O$ have been synthesized and characterized by their IR, UV–Vis, luminescence and ^1H NMR spectra. The redox behavior of the complexes has been studied.

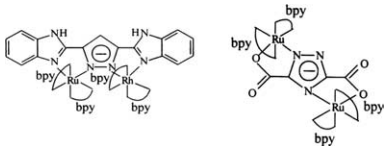

Petr Štěpnička, Martin Lamač, Ivana Císařová

Polyhedron 23 (2004) 921

Preparation, structure and catalytic activity of palladium(II) complexes with a carboxyferrocenylphosphine and an ortho-metallated C,N-ligand

Complexes **3** and **5** (X = ClO_4 (**a**), BF_4, (**b**)) were synthesized by reacting $[\{Pd(\mu\text{-}Cl)(C_6H_4CHNMe_2\text{-}\kappa^2C^1,P)\}_2]$ and $[Pd(C_6H_4CHNMe_2\text{-}\kappa^2C^1,P)(MeCN)_2]X$ (**4**), respectively, with methyl 1′-(diphenylphosphino) ferrocenecarboxylate. Solid-state structures of **4a** and **5a** were determined. Complexes **3** and **5b**, and catalysts based on the related ferrocene phosphines were tested in Suzuki–Miyaura coupling.

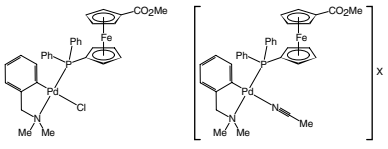

Izaskun Gil de Muro, Luis Lezama, Maite Insausti, Teófilo Rojo

Polyhedron 23 (2004) 929

Layered $[BaMn_{1-x}M_x(C_3H_2O_4)_2(H_2O)_4]$ (M = Fe, Co or Cu) solid solutions: thermal, spectroscopic and magnetic properties

Isostructural metallo-organic complexes $[BaMn_{1-x}M_x(C_3H_2O_4)_2(H_2O)_4]$ (M = Fe, Co and Cu) exhibit two-dimensional arrangements of M–malonate layers. All the iron and cobalt compounds show 2D antiferromagnetic interactions with the presence of a weak ferromagnetism. The copper solid solution also shows 2D antiferromagnetic interactions, unlike the BaCu complex which exhibits ferromagnetic interactions.

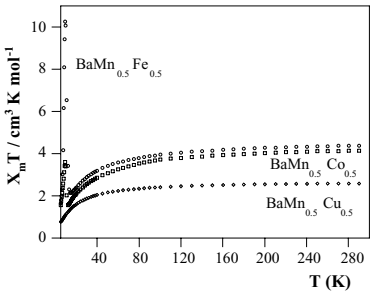

Ding-Xian Jia, Jie Dai, Qin-Yu Zhu, Yong Zhang, Xiao-Mei Gu

Polyhedron 23 (2004) 937

Syntheses, crystal structures and thermoanalyses of thiostannates $[Ni(en)_3]_2Sn_2S_6$ and $[Ni(dien)_2]_2Sn_2S_6$

Two tiostannates $[Ni(en)_3]_2Sn_2S_6$ (**1**) (en = ethylenediamine) and $[Ni(dien)_2]_2Sn_2S_6$ (**2**) (dien = diethylenetriamine) were prepared by the reaction of $SnCl_4 \cdot 5H_2O$, $NiCl_2 \cdot 6H_2O$ and S_8. Both compounds are composed of the discrete $[Sn_2S_6]^{4-}$ anions. The coordinated cations $[Ni(en)_3]^{2+}$ and $[Ni(dien)_2]^{2+}$ act as structure directing agents which lead to different packing of the $[Sn_2S_6]^{4-}$ anions. The hydrogen bonds are considered to be one of the important reasons for their difference in decomposition temperature.

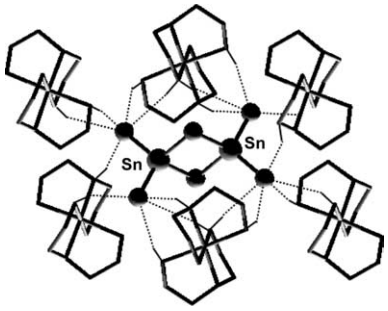

Hong-Lei Liu, Hong-Yan Mao, Hong-Yun Zhang, Chen Xu, Qing-An Wu, Gang Li, Yu Zhu, Hong-Wei Hou

Polyhedron 23 (2004) 943

Two novel heterometallacrowns: syntheses and crystal structures of two copper(II) complexes with malonate and *o*-pthalate

Two copper(II) sodium(I) coordination compounds of the formulae $[C_{16}H_{12}CuNa_2O_{10}]$ (**1**) and $[C_6H_8CuNa_2O_{10}]$ (**2**) were prepared and their structures were characterized by single-crystal X-ray diffraction, IR spectra and thermal analyses.

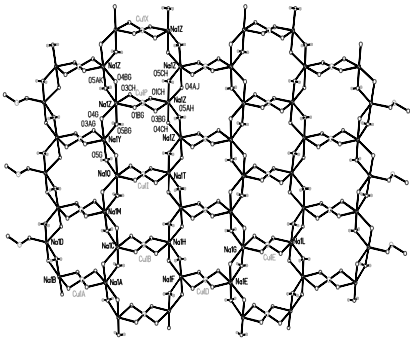

Ruma Karmakar, Chirantan Roy Choudhury, Georges Bravic, Jean-Pascal Sutter, Samiran Mitra

Polyhedron 23 (2004) 949

A novel manganese(III) quadridentate Schiff-base dimeric complex: synthesis, crystal structure and magnetic properties

One new dimeric manganese(III) complex $[MnL(H_2O)]_2(ClO_4)_2 \cdot H_2O$ (**1**) where [L = *N*,*N*′-bis(2-hydroxyacetophenylidene)-1,2-diaminopropane] has been synthesised and characterised by spectroscopic and electrochemical study, and the single crystal structure of the complex was determined.

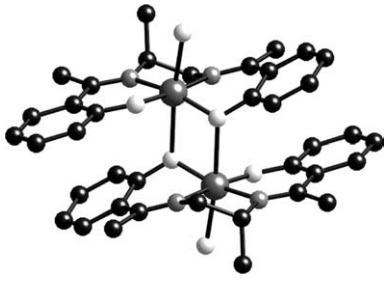

Hidenobu Matsuo, Yoshinobu Miyazaki, Hiroyuki Takemura, Shiro Matsuoka, Hirofumi Sakashita, Kazuhisa Yoshimura

Polyhedron 23 (2004) 955

^{11}B NMR study on the interaction of boric acid with Azomethine H

A ^{11}B NMR study quantitatively clarified the complexation of boric acid with Azomethine H. The interaction between boric acid and Azomethine H yields a 1:1 bischelate complex. The reaction includes two chemical equilibria; one is related to the ligand formation and the other to the complex formation.

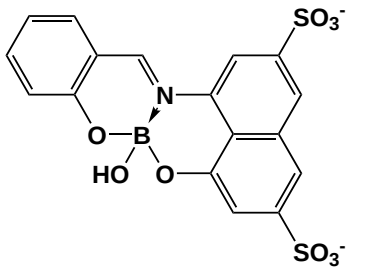

Jesús Sanmartín, Ana M. García-Deibe, Matilde Fondo, Débora Navarro, Manuel R. Bermejo

Polyhedron 23 (2004) 963

Synthesis and crystal structure of a mononuclear iron(III) (η^2-acetato) complex of a β-*cis* folded salen type ligand

Fe(H_2SB)(η^2-O_2CMe) · MeCN [H_4SB: *N*,*N*′-bis(5-hydroxysalicylidene)-1,4-diaminobutane] was synthesised via an electrochemical procedure and its crystal structure was determined.

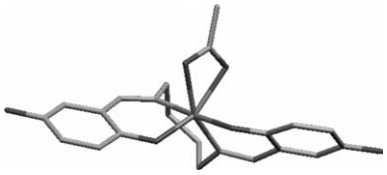

Anandaram Sreekanth, M.R. Prathapachandra Kurup

Polyhedron 23 (2004) 969

Synthesis, EPR and Mössbauer spectral studies of new iron(III) complexes with 2-benzoylpyridine-N(4), N(4)-(butane-1,4-diyl) thiosemicarbazone (HBpypTsc): X-ray structure of [Fe(BpypTsc)$_2$]$FeCl_4$ · $2H_2O$ and the free ligand

Three novel iron(III) complexes of 2-benzoylpyridine N(4), N(4)-(butyl-1,4-diyl) thiosemicarbazone (HBpypTsc), [Fe(BpypTsc)$_2$]ClO_4, [Fe(BpypTsc)$_2$]NO_3 and [Fe(BpypTsc)$_2$]$FeCl_4$ were synthesized and characterized by partial elemental analyses, magnetic measurements, UV–Vis and IR spectroscopies. The spin Hamiltonian parameters were assigned by variable temperature EPR. Isomer shifts and quadrupolar splitting values of the complexes were evaluated from Mössbauer spectra.

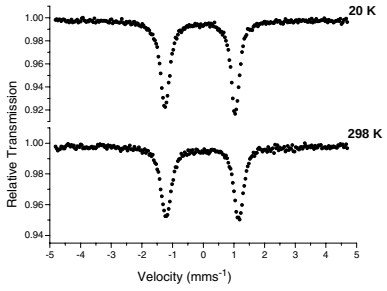

N. Satish Kumar, K.C. Kumara Swamy

Polyhedron 23 (2004) 979

Synthesis and structures of unsymmetrical bis- and tris-cyclotriphosphazenes

Synthesis and structures of an unsymmetrical bis-spirocyclic (**1**) and the first example of an unsymmetrical tris-spirocyclic (**2**) cyclotriphosphazene is reported. In addition, several chiral cyclotriphosphazenes (e.g., **5** and **6**) using 1,1′-bi-2-naphthol have been synthesized.

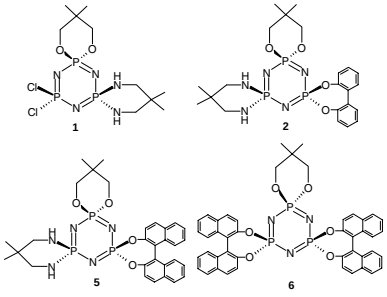

Hong-Bin Chen, Hui Zhang, Jin-Mei Yang, Zhao-Hui Zhou

Polyhedron 23 (2004) 987

Transformation of maleato manganese(II): temperature effect and coordination modes

Reaction of maleato manganese with 2,2′-bipyridine at 0 °C results in the formation of a hepta-coordinated one-dimensional coordination polymer $[Mn(male)(bpy)(H_2O)]_n \cdot 2nH_2O$ (**1**), which undergoes dehydration to form the hexacoordinated two-dimensional polymer $[Mn(male)(bpy)]_n$ (**2**) at ambient temperature.

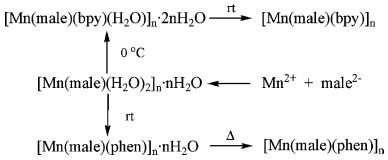

Gerard A. van Albada, Ilpo Mutikainen, Urho Turpeinen, Jan Reedijk

Polyhedron 23 (2004) 993

Synthesis, spectroscopy, crystal structure and magnetism of tetrakis(2-aminopyrimidine) bis(μ-methoxo)bis(perchlorato)dicopper(II): a rare case of distortion isomerism

A new dinuclear methoxo-bridged Cu(II) compound with the ligand 2-aminopyrimidine and a strong antiferromagnetism of $J = -621\ cm^{-1}$ is reported in this study.

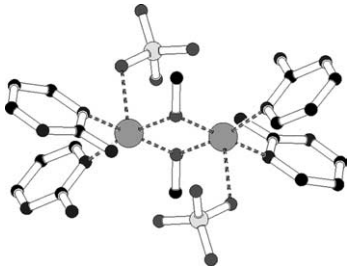

Ting-Wai Lee, Jasmine Po-Kwan Lau, Wing-Tak Wong

Polyhedron 23 (2004) 999

Synthesis and characterization of coordination polymers of Zn(II) with 1,3-bis(4-pyridyl)propane and 4,4′-pyridine ligands

The title complexes $[Zn_2(bpy)(OAc)_4]_n$ (**1**) and $[Zn(bpp)(NO_3)_2]_n$ (**2**) were synthesized by the layering method using Zn(II) ions, bpy and bpp ligands. They are structurally characterized by single-crystal X-ray diffraction analyses. Complexes **1** and **2** were both found to be one-dimensional coordination polymers.

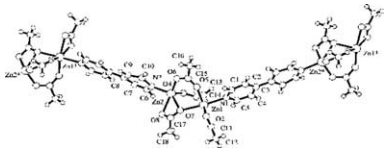

Sheng-Qing Xia, Sheng-Min Hu, Jing-Cao Dai, Xin-Tao Wu, Zhi-Yong Fu, Jian-Jun Zhang, Wen-Xin Du

Polyhedron 23 (2004) 1003

Syntheses and structures of 1D, 2D, 3D cadmium(II) coordination polymers with oxalate and aromatic co-ligands

The use of different co-ligands affects the building units of cadmium oxalate polymers, and infinite 1D, 2D and 3D frameworks can be obtained, which feature dinuclear (for **1** and **2**), trinuclear (for **3**) and tetranuclear (for **4**) units. **TGA** experiments on these polymers show they have relatively high thermal stability.

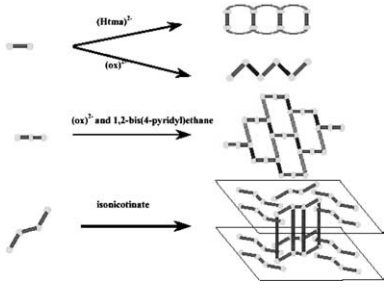

S.I.G. Dias, Fenton Heirtzler, T. Bark, Gael Labat, Antonia Neels

Polyhedron 23 (2004) 1011

Helical zinc complexes of pyrazine–pyridine hybrids

Reaction of the sterically-hindered pyrazine–pyridine hybrid ligands **1a** and **1b** with zinc(II) chloride affords the helically twisted complexes **1a**$ZnCl_2$ and **1b**$ZnCl_2$. The introduction of the nitrile groups into the structure of **1b** appears to cause an incomplete preference for a dimeric structure, as indicated from mass spectroscopic and X-ray crystallographic studies.

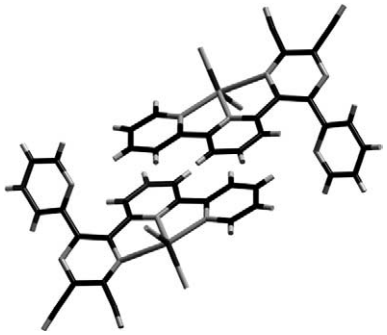

Weijun Niu, Edward H. Wong, Gary R. Weisman, Lev N. Zakharov, Chris D. Incarvito, Arnold L. Rheingold

Polyhedron 23 (2004) 1019

Copper(II) and zinc(II) complexes of amide pendant-armed cross-bridged tetraamine ligands

Copper(II) and zinc(II) complexes of the amide-armed cross-bridged tetraamine ligands **1** and **2** have been synthesized and characterized spectrally and structurally. The cyclam-derived **1** clearly provides a better fit for both metal cations compared to the cyclen-derived **2**. These complexes of **1** also provide the first examples of a [2233]/[2233] cross-bridged cyclam conformation.

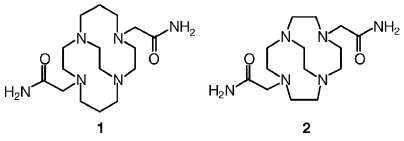

Carlos Díaz, Miguel Barbosa, Zaida Godoy

Polyhedron 23 (2004) 1027

Monobranched and hyperbranched dendrimers based on cyclophosphazene containing nitrile and phosphine donors and their Fe and Ru organometallic derivatives

The series of complexes $[N_3P_3(OC_6H_5)_5X.ML_n]PF_6$, $X=OC_6H_4CH_2CN$, $N(CH_3)(CH_2)_2CN$ or $OC_6H_4PPh_2$, and $[N_3P_3(X)_6 \cdot (ML_n)_6](PF_6)_6$ $X=OC_6H_4CH_2CN$ or $N(CH_3)(CH_2)_2CN$ with ML_n=CpFe(dppe) and $CpRu(PPh_3)_2$ have been synthesized. The new compounds were characterized by elemental analysis and IR, UV–Visible and multinuclear NMR spectroscopy. The hexametallic molecules, one of them is shown in the picture, exhibits non-interaction between the metal centers indicating that the cyclophosphazenes dendrimers act as insulators between the organometallics centers.

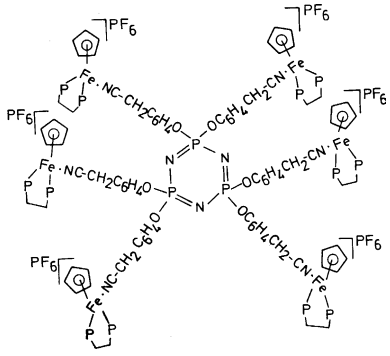

Josie R. Sheets, Franklin A. Schultz

Polyhedron 23 (2004) 1037

Coupled electron-transfer and spin-exchange reactions of metal–bis[tris(pyrazolyl)methane] complexes

Electrochemical M^{2+} to M^{3+} oxidation of bis[tris(pyrazolyl)methane] complexes is accompanied by a change in metal atom spin-state. The influence of metal ion and ligand substituents on the kinetics and thermodynamics of such reactions is described.

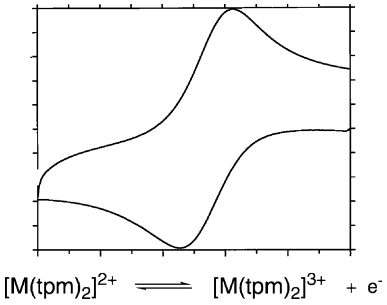

María C. Rodríguez, Jorge Bravo, Eduardo Freijanes, Enrique Oñate, Soledad García-Fontán, Pilar Rodríguez-Seoane

Polyhedron 23 (2004) 1045

Synthesis and reactivity of [Re($ClCH_2Cl$)-($CO)_3$L][A] and [Re(OSO_2CF_3)($CO)_3$L] (L= $Ph_2PO(CH_2)_2OPPh_2$; A=BF_4, [B{3,5-$(CF_3)_2$-C_6H_3}$_4$]): the crystal structure of [Re(OSO_2-CF_3)($CO)_3$L] and [Re($NCCH_3$)($CO)_3$L][BF_4]

The complex [ReBr($CO)_3$L] (L = 1,2-bis[diphenylphosphinite]ethane) was reacted with $AgBF_4$ and with AgOTf in dichloromethane to yield *fac*-[Re($ClCH_2Cl$)($CO)_3$L][BF_4] (**1**) (presumably in equilibrium with [Re-(FBF_3)($CO)_3$L] in solution), and *fac*-[Re-(OTf)($CO)_3$L] (**2**), respectively. Substitution of the loosely held ligands $ClCH_2Cl$ and OTf resulted in the formation of the compounds showed in the scheme. The new complexes were characterized by IR and NMR spectroscopies, and in the case of **2** and [Re-(CH_3CN)($CO)_3$L][BF_4], the crystal structures are reported.

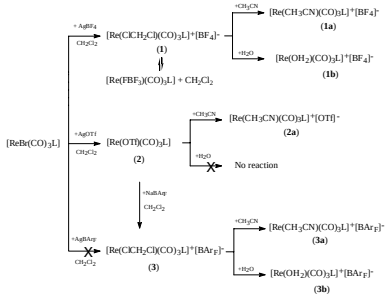

David A. McMorran, Christopher M. Hartshorn, Peter J. Steel

Polyhedron 23 (2004) 1055

Copper(II) complexes of bis- and tetrakis-(2-pyridylsulfanylmethyl)benzenes

Copper(II) salts react with new multi-armed ligands, which contain either two or four 2-pyridylsulfanylmethyl arms appended to a benzene core, to give, in the case of the two-armed ligand, a one-dimensional polymer, while, for the four-armed ligands, discrete bimetallic complexes are observed. Weak Cu–S interactions contribute to the observed structures.

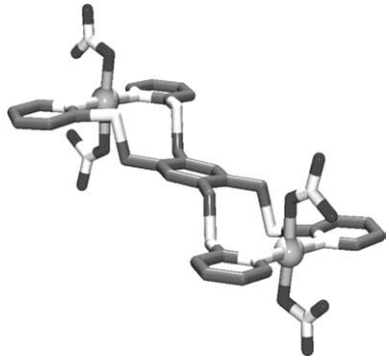

Welter C. Silva, Eduardo E. Castellano, Douglas W. Franco

Polyhedron 23 (2004) 1063

Structural and reactivity changes in ruthenium ammines induced by the NO ligand

The structural, thermodynamic and kinetic data of the [$Ru(NH_3)_5(OH_2)]_2(S_2O_6)_3 \cdot 2H_2O$ and *trans*-$Ru(NH_3)_4NO(OH_2)]Cl_3$ complexes are compared, in order to understand the NO influence on reactivity metal complex.

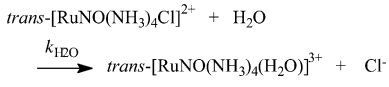

R. Lalrempuia, P. Govindaswamy, Yurij A. Mozharivskyj, Mohan Rao Kollipara

Polyhedron 23 (2004) 1069

Reactivity studies of cyclopentadienyl bis (triphenylphosphine)ruthenium(II) complex towards some polypyridyl ligands

The reaction of some potential bridging polypyridyl ligands with [$CpRu(PPh_3)_2Cl$] in methanol resulted in the dissociation of one of the triphenylphosphines and the chloride ligands from the latter, finally giving cationic monomeric chelate complexes. Alteration of the molar ratios of the reactants fails to give anticipated dimers.

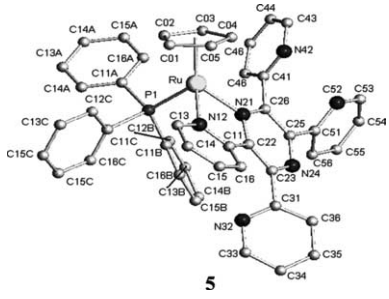

Jianhua Cheng, Dongmei Cui, Wenqi Chen, Tao Tang, Baotong Huang

Polyhedron 23 (2004) 1075

Syntheses and crystal structures of bis(tetrahydrofurfurylindenyl) lanthanocene chlorides $(C_4H_7OCH_2C_9H_6)_2LnCl$ (Ln=La, Lu)

$(C_4H_7OCH_2C_9H_6)_2LnCl$(Ln = La, Lu) were synthesized and characterized. Compared with other lanthanides of these series complexes, the detail relations between the rare earth ionic radii and the structures are described. The changes of the bond length of Ln–C(ring), Ln–Cent, Ln–Cl, and △M–C are consistent with lanthanide contraction.

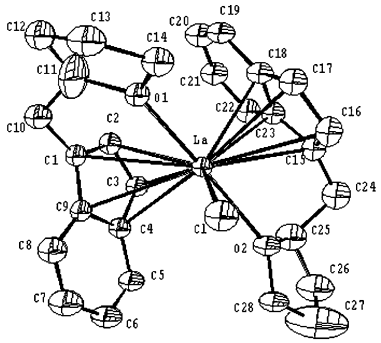

Susmita Bandyopadhyay, Ansuman Das, G.N. Mukherjee, Andrea Cantoni, Gabriele Bocelli, Siddhartha Chaudhuri, Joan Ribas

Polyhedron 23 (2004) 1081

Synthesis, X-ray crystal structures, physicochemical and magnetic studies on copper(II) *N*-(2-carboxyphenyl) iminodiacetate polymers

Crystal lattices of $\{[Cu(Hcpida)] \cdot H_2O\}_n$ (**1**) and $\{[Cu(Hcpida)(H_2O)] \cdot H_2O\}_n$ (**2**) are made up of 1D polymer of ferromagnetically coupled square pyramidal and distorted octahedral Cu(II) units, respectively, linked by carboxylato bridges in *syn–anti* (equatorial–equatorial) bonding mode, stabilized by H-bonding and π–π stacking interactions. Complex **2** forms cylindrical channels that host the lattice H_2O molecules.

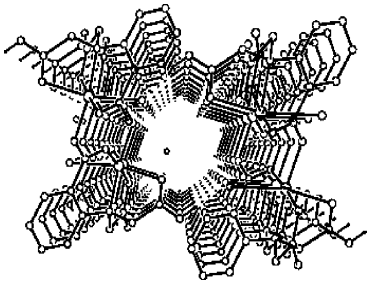

Wen-Jie Lu, Lin-Ping Zhang, Hoi-Shan Chan, Tze-Lock Chan, Thomas C.W. Mak

Polyhedron 23 (2004) 1089

Di-protonated 1,4,8,11-tetramethyl-1,4,8,11-tetraazacyclotetradecane tetra-*N*-oxide, a bulky di-cation that induces the assembly of unusual lanthanide(III) complexes

The new di-cation $[Me_4cyclam(OHO)_2]^{2+}$ takes the *RSSR* configuration and induces the formation of lanthanide(III) complexes $[Ln(NO_3)_6]^{3-}$ (Ln = Ce, La, Nd), $[Er(NO_3)_3(H_2O)_3]$ and *catena*-$[Ce(NO_3)_4(\mu\text{-}NO_3)]_n^{2n-}$, the latter being a novel linear coordination polymer constructed by chelating and μ-*O*, *O*, *O*′, *O*″ nitrate groups.

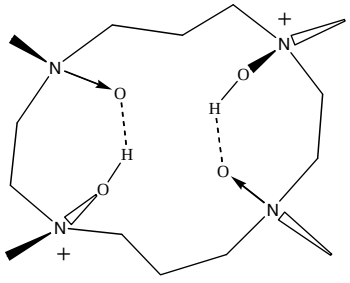

The Publisher encourages the submission of articles in electronic form thus saving time and avoiding rekeying errors. For detailed instructions on the preparation of manuscripts and of electronic artwork, consult the Author Gateway for Elsevier at http://authors.elsevier.com

SCIENCE DIRECT™

Full text of this journal is available, on-line from **ScienceDirect**. Visit **www.sciencedirect.com** for more information.

CONTENTS direct

This journal is part of **ContentsDirect**, the *free* alerting service which sends tables of contents by e-mail for Elsevier books and journals. You can register for **ContentsDirect** online at: **www. elsevier.com/locate/contentsdirect**

http://ChemWeb.com
The World Wide Club for the Chemical Community
http://chemweb.com/gateways/elsevier.html

Available online at www.sciencedirect.com
SCIENCE DIRECT®
Polyhedron 23, issue 4, 12 February 2004
POLYHEDRON
www.elsevier.com/locate/poly

Contents

Papers

Marciela Scarpellini, Ademir Neves, Eduardo E. Castellano, Eduardo F. de Almeida Neves, Douglas W. Franco

Polyhedron 23 (2004) 511

A structural model for oxidized type II copper nitrite reductase with a polyimidazole tripodal ligand

This paper describes a new Cu^{II}–nitrite complex (**2**) with a tripodal ligand, which was characterized by X-ray crystallography, spectroscopic and electrochemical techniques. Some aspects concerning the formation constant of **2** are also discussed. The arrangements of the ligand and nitrite coordination allow considering **2** a potential structural model for type II copper in nitrite reductases.

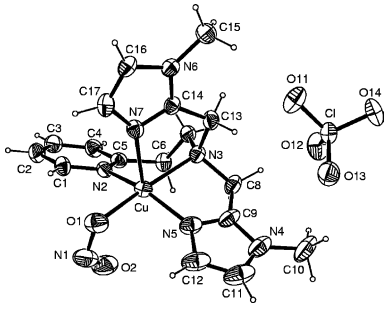

M. Thirumavalavan, P. Akilan, P. Amudha, M. Kandaswamy

Polyhedron 23 (2004) 519

Compartmental unsymmetrical lateral macrobicyclic ligands with an aromatic backbone providing a phenoxo bridge: synthetic, spectral, magnetic, electrochemical and kinetic features of mono and binuclear copper(II) complexes

New types of lateral macrobicyclic compartmental ligands with an aromatic backbone and their mono and binuclear copper(II) complexes were synthesized. Spectral, magnetic, electrochemical and catalytic studies of the complexes were carried out. Magnetic studies rationalize the presence of antiferromagentic coupling in the binuclear complexes. Cyclic voltammetric studies show quasireversible one electron reduction waves in the cathodic region. The catalytic activities of the complexes towards catechol oxidation increase with macrocyclic ring size. Spectral, electrochemical and catalytic studies evidence the distortion in the geometry with the increasing size of the macrocycle.

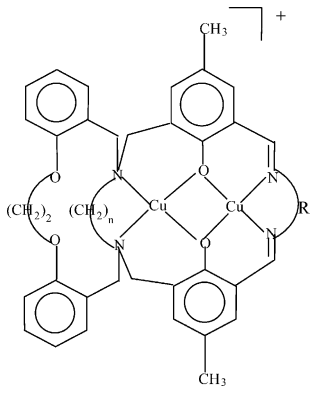

Ming-Cai Yin, Liang-Jie Yuan, Chang-Chun Ai, Chi-Wei Wang, E-Ting Yuan, Ju-Tang Sun

Polyhedron 23 (2004) 529

Synthesis, structure and luminescence properties of europium and zinc ionic complexes

Two europium and zinc ionic complexes $[Eu_2(Hsal)_8][Zn(phen)_3] \cdot (H_2sal)(H_2O)$ (**1**) and $[Eu_2(TPA)_8][Zn(TPA)(Phen)_2]_2 \cdot (H_2O)_2$ (**2**) have been synthesized and structurally characterized. Interestingly, in complex **1**, there are two types of dimeric Eu1 units with inversion centers. These two complexes emit strong red light when irradiated by UV light.

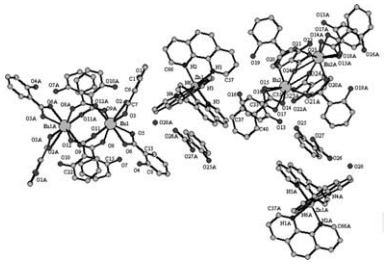

Francisco J. Arnáiz, Rafael Aguado, Mara R. Pedrosa, Miguel A. Maestro

Polyhedron 23 (2004) 537

Dioxomolybdenum(VI) thionates: molecular structure of dioxobis(pyridine-2-thiolate-*N*,*S*)molybdenum(VI)

Dioxomolybdenum(VI) thionates have been prepared in high yield by reacting MoO_2Cl_2 with thallium thionates. They behave as Lewis acids and addition compounds with N-donor ligands have been prepared. The molecular structure of dioxobis(pyridine-2-thiolate-*N*,*S*)molybdenum(VI) has been established by X-ray diffraction analysis.

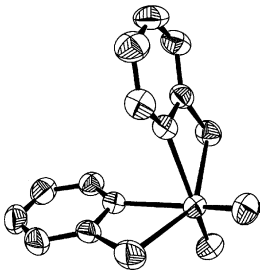

Doyel Bose, Sk Hafijur Rahaman, Golam Mostafa, Rosa D. Bailey Walsh, Michael J. Zaworotko, Barindra K. Ghosh

Polyhedron 23 (2004) 545

Synthesis, structure and properties of $[Zn(dpa)(N_3)_2]$ and $[Zn(dpa)(N_3)(NO_3)]_2$ (dpa=2,2′-dipyridylamine): composition tailored architectures

Two new zinc(II)azido complexes of types $[Zn(dpa)(N_3)]_2$ (**1**) and $[Zn(dpa)(N_3)(NO_3)]_2$ (**2**) containing a tailored diimine, 2,2′-dipyridylamine (dpa), have been synthesized and X-ray crystallographically characterized, of which **1** forms a 2D sheet and **2** shows a 3D continuum through cooperative hydrogen bonds and – interaction; the photoluminescence behaviours are described in the background of their structures.

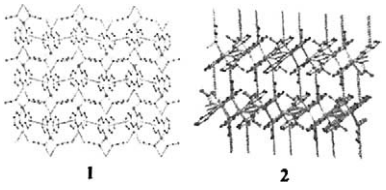

Jian-Fang Ma, Jin Yang, Guo-Li Zheng, Li Li, Yong-Mei Zhang, Fang-Fang Li, Jing-Fu Liu

Polyhedron 23 (2004) 553

Four new coordination polymers of Cu(II) with 1,1′-(1,4-butanediyl)bis(imidazole)

Cu(II) ions are bridged by 1,1′-(1,4-butanediyl)bis(imidazole) to form infinite (4,4) networks, and two (4,4) networks are interpenetrated in parallel mode to form a layer.

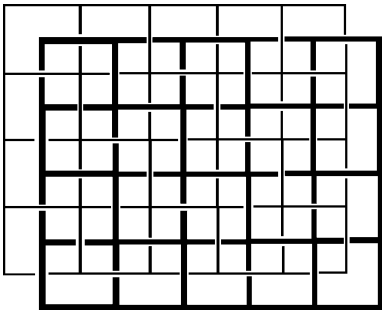

Grigori B. Nikiforov, Herbert W. Roesky, Mathias Noltemeyer, Hans-Georg Schmidt

Polyhedron 23 (2004) 561

Reactivity of $Ti(bipy)_3$ and preparation of the $Li(THF)_4[Al(bipy)_2]$ complex with the dinegative bipy ligand

A ligand transfer in the $Ti(bipy)_3$–$LiAlH_4$ system leads to formation of $[Al(bipy)_2]^-$ with the dinegatively charged bipy ligand.

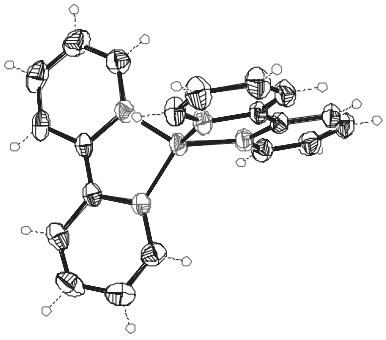

Yao-Cheng Shi, Hua-Mei Yang, Hai-Bin Song, Chao-Guo Yan, Xiao-Ya Hu

Polyhedron 23 (2004) 567

Syntheses and crystal structures of the potential tridentate ligand formed from condensation of ferrocenoylacetone and S-benzyldithiocarbazate and its bivalent metal complexes

Reaction of ferrocenoylacetone and S-benzyldithiocarbazate in refluxing benzene leads to a new potential tridentate ligand ($\mathbf{H_2L}$). Reaction of ($\mathbf{H_2L}$) with a bivalent metal salt ($M(OAc)_2 \cdot xH_2O$, M=Cu, Ni, Mn, Hg, Zn; $SnCl_2 \cdot 2H_2O$) affords the corresponding metal complexes $M(\mathbf{HL})_2$ **(I–VI).** The single-crystal X-ray analysis indicates that the ligand exists as a single iminone isomer in the solid state. The crystallography of complex **VI** shows that the ligand acts as monoanionic tridentate coordinated to the tin atom via the carbonyl oxygen, deprotanated enamine nitrogen and thione sulfur atoms and the coordination geometry of the central metal is a distorted octahedron.

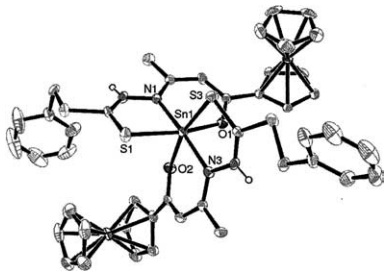

P.B. Sreeja, M.R. Prathapachandra Kurup, Archana Kishore, C. Jasmin

Polyhedron 23 (2004) 575

Spectral characterization, X-ray structure and biological investigations of copper(II) ternary complexes of 2-hydroxyacetophenone 4-hydroxybenzoic acid hydrazone and heterocyclic bases

Two new heterocyclic base adducts of copper(II) complexes of general formula CuLB have been synthesized and characterized by different physicochemical methods. The electronic and IR spectroscopic data indicate that the complexes have square pyramidal geometry with one dibasic tridentate ligand L^{2-}, and one bidentate heterocyclic base. The magnetic susceptibility values at room temperature are consistent with the spin only value for monomeric copper(II) species. EPR studies of all compounds gave axial spectra. The crystal and molecular structure of CuLphen was determined by single crystal X-ray diffraction method. Investigations on antimicrobial activities showed that the compounds are moderately active against *Gram negative* bacteria.

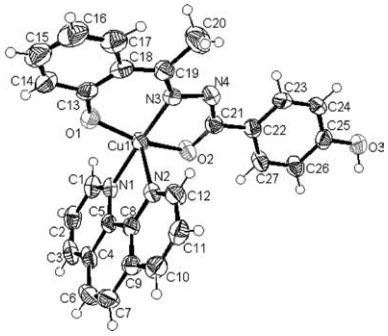

Yousif Sulfab, Fawziyah M. Al-Sogair

Polyhedron 23 (2004) 583

Kinetics and mechanism of reduction of 3, 9-diethyl-4,8-diaza-3,8-undeca-2,10-dionedioximatocopper(III) complex by p-methoxyphenol, 1,2-dihydroxybenzene, 1,4-dihydroxybenzene and some of its derivatives in aqueous acidic solutions

The copper(III)–imine–oxime complex was readily reduced by catechol (H_2Cat), *p*-methoxyphenol (*p*MHP), hydroquinone (H_2Q), 2-methylhydroquinone (MH_2Q), 2-chlorohydroquinone (ClH_2Q) in aqueous weakly acidic solutions. The kinetics were of the second-order; first-order in each reactant. The second-order rate constant showed a complex dependence on $[H^+]$. The experimental rate constants were compared with calculated values using Marcus equation.

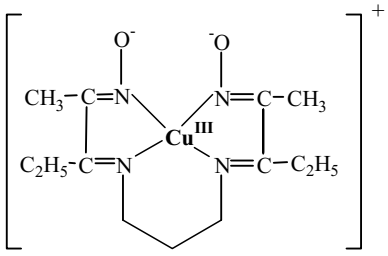

(I)

Viviane Aranyos, Anders Hagfeldt, Helena Grennberg, Egbert Figgemeier

Polyhedron 23 (2004) 589

Electropolymerisable bipyridine ruthenium(II) complexes: synthesis, spectroscopic and electrochemical characterisation of 4-((2-thienyl) ethenyl)- and 4,4′-di((2-thienyl) ethenyl)-2, 2′-bipyridine ruthenium complexes

Four new ruthenium polypyridyl complexes with mono- or di-((2-thienyl) ethenyl) substituted 4,4′-bipyridines have been synthesized and characterized by NMR, elemental analysis, UV–Vis absorption and electrochemistry. Electroactive polymer films of these complexes have been prepared by oxidative electropolymerisation and characterized.

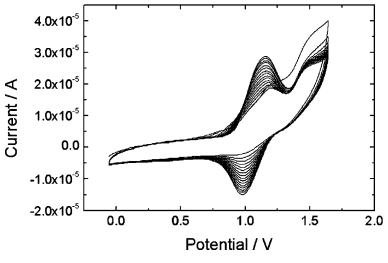

Nikolai G. Naumov, Konstantin A. Brylev, Yuri V. Mironov, Alexander V. Virovets, Dieter Fenske, Vladimir E. Fedorov

Polyhedron 23 (2004) 599

Synthesis and structures of new octahedral water-soluble heterometal rhenium–molybdenum clusters

The interaction of polymeric $Re_3MoS_4Te_4$ with molten KCN at 850 °C results in rearrangement of the tetrahedral $\{Re_3MoS_4\}$ cluster core to an octahedral one, $\{Re_{6-x}Mo_xS_8\}$, and formation of two new molecular octahedral heterometal rhenium–molybdenum thiocyanide cluster complexes, $[Re_5MoS_8(CN)_6]^{5-}$ and $[Re_4Mo_2S_8(CN)_6]^{5-}$, co-existing in the crystals $Cs_5[Re_{4.5}Mo_{1.5}(\mu_3\text{-}S)_8(CN)_6] \cdot 2H_2O$.

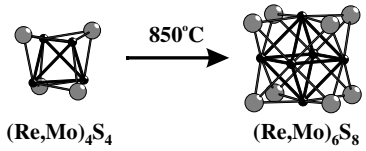

William Levason, Melissa L. Matthews, Bhavesh Patel, Gillian Reid, Michael Webster

Polyhedron 23 (2004) 605

Titanium(IV) iodide complexes with phosphine and arsine donor ligands and the crystal structures of the iron(II)/(III) redox pair $[FeI_2\{o\text{-}C_6H_4(AsMe_2)_2\}_2]^{0/+}$

Rare examples of titanium(IV) iodide complexes, $[TiI_4\{o\text{-}C_6H_4(PMe_2)_2\}]$ and $[TiI_4\{o\text{-}C_6H_4(AsMe_2)_2\}]$ have been prepared and characterised, but reports of 2:1 complexes are shown to be in error. The structures of two iron–diarsine complexes $[FeI_2\{o\text{-}C_6H_4(AsMe_2)_2\}_2]$ and $[FeI_2\{o\text{-}C_6H_4(AsMe_2)_2\}_2]I_3 \cdot 2CH_2Cl_2$ arising from iron iodide impurities in one commercial sample of TiI_4 are reported.

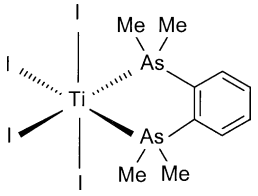

Montserrat Gómez, Eduardo Peris, Helena Teruel, Ingrid Arevalo, José A. Mata, Guillermo Muller

Polyhedron 23 (2004) 611

Novel ferrocenyl-oxazoline ligands: first preparation of non-symmetrical bis(oxazoline)

New ferrocenyl-arenylethenyl-oxazoline derivatives have been prepared (**5**–**10**) from the mono- and (1,1′)-disubstituted (nitrile-ethenylaryl)ferrocene compounds (**1** and **2**) and the appropriated -aminoalcohol (**3** and **4**) in one step synthesis. The X-ray crystal structure of one of the ferrocenyl-ethenylaryl-oxazoline (**5**) is described.

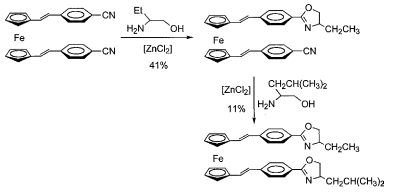

Hamsell M. Alvarez, Patricia A. Gillespie, Cornelius D. Gause, Arnold L. Rheingold, James A. Golen, Daniel Rabinovich

Polyhedron 23 (2004) 617

Thallium(I) bis(mercaptoimidazolyl)borates

The thallium(I) bis(mercaptoimidazolyl)borates $Tl(Bm^R)$ (R=Me, Bz, Bu^t, p-Tol) have been readily prepared by metathesis of thallium(I) acetate and the corresponding sodium derivatives $Na(Bm^R)$. These new compounds, potentially valuable $[Bm^R]^-$ transfer reagents, have been characterized by a combination of analytical and spectroscopic techniques and, in the case of the *tert*-butyl derivative, by X-ray crystallography.

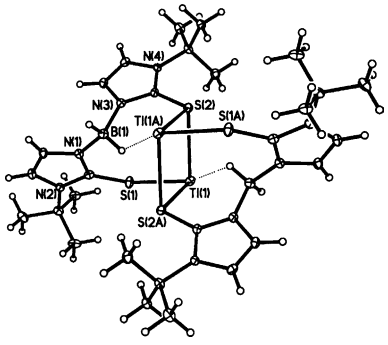

Lionel Salmon, Pierre Thuéry, Michel Ephritikhine

Polyhedron 23 (2004) 623

Crystal structure of the first octanuclear uranium(IV) complex with compartmental Schiff base ligands

The compartmental Schiff base *N*,*N*′-*bis*(3-hydroxysalicylidene)-1,2-phenylenediamine (H_4L) is able to complex uranium(IV) ions both in its inner N_2O_2 and outer O_4 coordination sites. Further phenoxide-, oxo- and chlorine-bridging results in the formation of an octanuclear dianionic $[U_8L_4Cl_{10}O_4]^{2-}$ cluster, in which the eight metal atoms define four edge-sharing tetrahedra with central μ_4-oxo atoms.

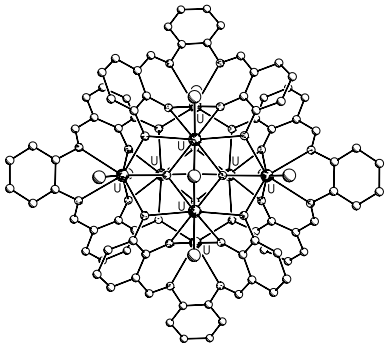

Ulaganathan Venkatasubramanian, David J. Donohoe, David Ellis, Barry T. Giles, Stuart A. Macgregor, Susan Robertson, Georgina M. Rosair, Alan J. Welch, Andrei S. Batsanov, Lynn A. Boyd, Royston C.B. Copley, Mark A. Fox, Judith A.K. Howard, Kenneth Wade

Polyhedron 23 (2004) 629

The synthesis and molecular and crystal structures of 1-methyl-2-carboxy-1,2-dicarba-*closo*-dodecaborane(12), 1-phenyl-2-carboxy-1,2-dicarba-*closo*-dodecaborane(12) and 1-phenyl-2-benzoyl-1,2-dicarba-*closo*-dodecaborane(12)

The structures of 1-Me-2-COOH-1,2-*closo*-$C_2B_{10}H_{10}$ (**1**), 1-Ph-2-COOH-1,2-*closo*-$C_2B_{10}H_{10}$ (**2**) and 1-Ph-2-COPh-1,2-*closo*-$C_2B_{10}H_{10}$ (**3**) have been determined by X-ray crystallography.

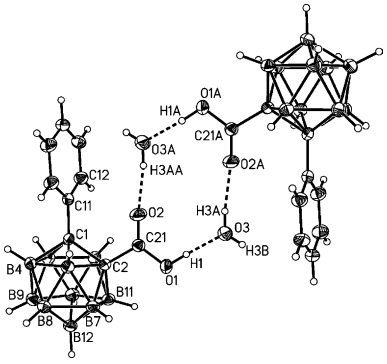

Moayad Hossaini Sadr, William Clegg, Hamid Reza Bijhanzade

Polyhedron 23 (2004) 637

Synthesis and characterization of two pentanuclear complexes $(NEt_4)_2[MS_4(CuBp)_4]$ (M=Mo, W; Bp=H_2B(pyrazolyl)$_2$) and crystal structure determination of $(NEt_4)_2[WS_4(CuBp)_4]$

The pentanuclear mixed-metal complex anions $[MS_4(CuBp)_4]^{2-}$ (M=Mo or W; Bp= bis(pyrazolyl)borate) are readily prepared from $[MS_4]^{2-}$, CuCl and KBp. The tungsten complex has been crystallographically characterized and contains essentially regular tetrahedrally coordinated W and four distorted tetrahedral Cu(I) atoms.

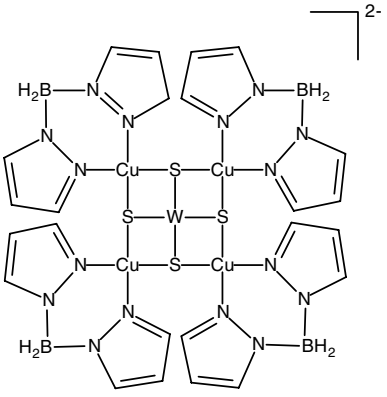

Sunita Gupta, Arindam Mukherjee, Munirathinam Nethaji, Akhil R. Chakravarty

Polyhedron 23 (2004) 643

An angular trinuclear copper(II) complex as a model for the active site of multicopper oxidases

An angular copper(II) complex $[Cu_3L^1L^2(1\text{-MeIm})(H_2O)](ClO_4)$ has been synthesized by reacting type-2 and type-3 mimic precursor complexes, where H_3L^1 and H_2L^2 are penta and tetradentate Schiff base ligands. The complex, characterized by X-ray diffraction, models the active site structural features and magnetic properties of blue copper oxidases.

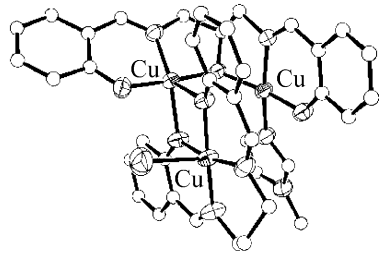

Pierre Thuéry, Bernardo Masci

Polyhedron 23 (2004) 649

Hetero(tri- and tetra-)nuclear complexes of uranyl and alkali metal (Li^+, K^+) ions with *p-tert*-butylhexahomotrioxacalix[6]arene

Heteropolymetallic complexes are obtained when uranyl nitrate is reacted with *p-tert*-butylhexahomotrioxacalix[6]arene in the presence of alkali metal hydroxides. Depending on the size of the alkali cation, a monomeric heterotrinuclear species is obtained in the case of Li^+ and a dimeric tetranuclear one in the case of K^+. In the latter complex, two potassium ions ensure the bridging of two homooxacalixarenes and a K–oxo(uranyl) bond is also observed.

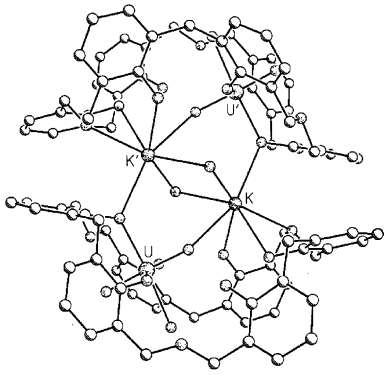

M. Ahmed, P. Schwendt, J. Marek, M. Sivak

Polyhedron 23 (2004) 655

Synthesis, solution and crystal structures of dinuclear vanadium(V) oxo monoperoxo complexes with mandelic acid: $(NR_4)_2[V_2O_2(O_2)_2(mand)_2] \cdot xH_2O$ [R=H, Me, Et; mand=mandelato(2−)=$C_8H_6O_3^{2-}$]

The dinuclear mandelatooxoperoxovanadates are synthesized and characterized. Structure of $(NMe_4)(NH_4)[V_2O_2(O_2)_2(R,S\text{-mand})_2] \cdot 2H_2O$ contains in the unit cell differently coordinated water molecules in two types of dinuclear anions: $[V_2O_2(O_2)_2(R\text{-mand})_2(H_2O)]^{2-}$, with nearly symmetrically bonded bridging water molecule and pentagonal bipyramidal arrangement around both vanadium atoms, and $[V_2O_2(O_2)_2(S\text{-mand})_2(H_2O)]^{2-}$, with the water molecule coordinated only to one vanadium atom. The vanadium atoms thus have different coordination geometries: pentagonal pyramidal and pentagonal bipyramidal.

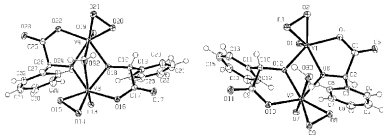

D. Saravanakumar, N. Sengottuvelan, G. Priyadarshni, M. Kandaswamy, H. Okawa

Polyhedron 23 (2004) 665

Synthesis of unsymmetrical end-off phenoxo and oximinato di bridged copper(II) and nickel(II) complexes: spectral, electrochemical and magnetic properties

New mononuclear and unsymmetrical binuclear copper(II) and nickel(II) complexes of the general formula $[ML^1](ClO_4) \cdot H_2O$, $[M_2L^1](ClO_4)_2 \cdot 2H_2O$, $[ML^2](ClO_4) \cdot H_2O$ and $[M_2L^2](ClO_4)_2 \cdot 2H_2O$ have been prepared. The complexes were characterized by elemental and spectral analysis. Magnetic properties were ascertained.

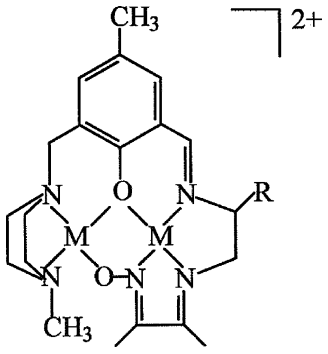

Mirela Pascu, Marius Andruh, Achim Müller, Marc Schmidtmann

Polyhedron 23 (2004) 673

Binuclear coordination compounds as building-blocks in designing polynuclear complexes

A tetranuclear heterometallic rectangle, $[Cu_2Zn_2]$, and a 1D coordination polymer with bimetallic nodes have been obtained by using binuclear [CuZn] and $[Cu_2]$ complexes as starting materials.

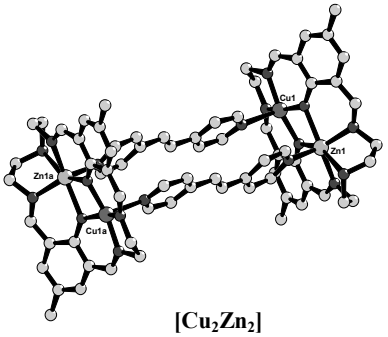

$[Cu_2Zn_2]$

P. Bindu, J.V. Kingston, M.N. Sudheendra Rao

Polyhedron 23 (2004) 679

Dianionic silicate derivatives of transition metals: synthesis by a facile ion exchange route, characterization and thermolysis studies

A new series of transition metal complexes [M = Cr(III) (**1**), Mn(II) (**2**), Co(III) (**3**), Ni(II) (**4a–d**) and Cu(II) (**5a–b**)] of $[Si(C_6H_4O_2)_3]^{2-}$ have been synthesized by an ion exchange reaction between $[(C_2H_5)_3NH]_2[Si(C_6H_4O_2)_3]$ and a cationic (2+ or 3+) transition metal complex, $[ML_n]X$ [L = ethylenediamine (en), diethylenetriamine (dien), ammonia or water and X = Cl^-, SO_4^{2-}]. Their stability depends both on the coordination environment of the metal centre and the bulky tris(catecholato)silicate ion.

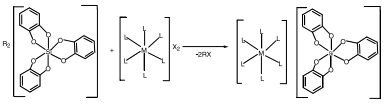

Ludovic Vieille-Petit, Bruno Therrien, Georg Süss-Fink

Polyhedron 23 (2004) 687

2,3,4,7-Tetrahydro-1*H*-inden-2-ol: synthesis, molecular structure and coordination chemistry

2,3,4,7-Tetrahydro-1*H*-inden-2-ol (**1**) has been synthesised by Birch reduction of indan-2-ol. Peptidic coupling with ferrocene carboxylic acid gives 2,3,4,7-tetrahydro-1*H*-inden-2-yl ester (**2**), which reacts with $RuCl_3 \cdot nH_2O$ in refluxing ethanol to afford $[Ru(arene)Cl_2]_2$ (**4**) (arene=ferrocene carboxylic acid indan-2-yl ester) as a mixture of isomers.

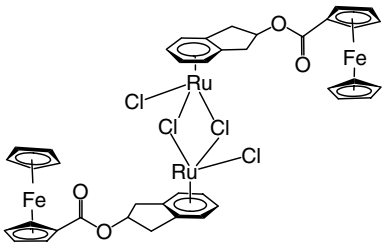

4

Mireia Rodriguez I. Zubiri, Heather L. Milton, David J. Cole-Hamilton, Alexandra M.Z. Slawin, J. Derek Woollins

Polyhedron 23 (2004) 693

Bis(phosphine) derivatives of diamines

The use of organic amines in the formation of bisphosphines allows rapid testing of catalytic properties.

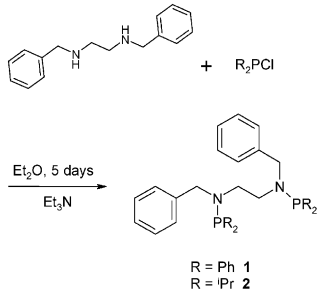

Axel Knödler, Jan Fiedler, Wolfgang Kaim

Polyhedron 23 (2004) 701

Characterization of the mixed-valent intermediate (n=3) of the complex series $\{(\mu,\eta^3{:}\eta^3\text{-L})[(Ru(terpy)]_2\}^{n+}$ with the unsaturated bridging ligand N,N'-bis(-picolinoyl)hydrazido(2−)=L^{2-}

The mixed-valent diruthenium(II,III) complex with a conjugated bis(N,N',O)-coordinated bridge was characterized in comparison to the phenyl-substituted system with (N,O)-coordination. Whereas the electrochemical comproportionation constants are very similar, the EPR- and UV–Vis–NIR-spectroscopic results show significant differences.

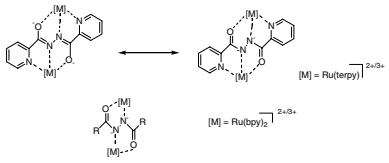

Corringendum to: Silver(I) and mercury (II) complexes of $Me_3N(+)$—$N(-)X$ ylides: synthesis and structure [Polyhedron 22 (2003) 3345–3535] . . 709

The Publisher encourages the submission of articles in electronic form thus saving time and avoiding rekeying errors. For detailed instructions on the preparation of manuscripts and of electronic artwork, consult the Author Gateway for Elsevier at http://authors.elsevier.com

SCIENCE DIRECT™

Full text of this journal is available, on-line from **ScienceDirect**. Visit **www.sciencedirect.com** for more information.

CONTENTS direct

This journal is part of **ContentsDirect**, the *free* alerting service which sends tables of contents by e-mail for Elsevier books and journals. You can register for **ContentsDirect** online at: **www. elsevier.com/locate/contentsdirect**

http://ChemWeb.com
The World Wide Club for the Chemical Community
http://chemweb.com/gateways/elsevier.html

Available online at www.sciencedirect.com
SCIENCE DIRECT®
Polyhedron 23, issues 2–3, 22 January 2004
POLYHEDRON
www.elsevier.com/locate/poly

Contents

Foreword: Symposia-In-Print number 26. Scorpionate and Related Ligands 195

Papers

Swiatoslaw Trofimenko

Polyhedron 23 (2004) 197

Scorpionates: genesis, milestones, prognosis

The development of the polypyrazolylborate/scorpionate ligand system is traced from its inception to the current state, based largely on the authors experiences and contributions.

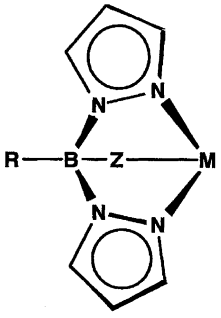

Z = Y or CR_2Y;
Y = pz, H, OR, SR, NR_2.....

Luis F. Soares, Daniele C. Menezes, Rosalice M. Silva, Antonio C. Doriguetto, Javier Ellena, Yvonne P. Mascarenhas, Eduardo E. Castellano

Polyhedron 23 (2004) 205

Potassium tetrakis(2-mercaptothiazolyl)borate; an open-framework material: synthesis and X-ray structure analysis

KMte crystallizes in the non-centrosymmetric space group $F\bar{4}3c$ (No. 219) with two independent molecules in the asymmetric unit. A packing of the structure on plane *ab* is shown. In this unit cell fraction the anion generated by molecule B is in the central position; there is an alternation between molecules A and B. Each anion is octahedrally surrounded by four other anions and two holes. The holes betweeen the anions have a mean diameter of ~9 Å.

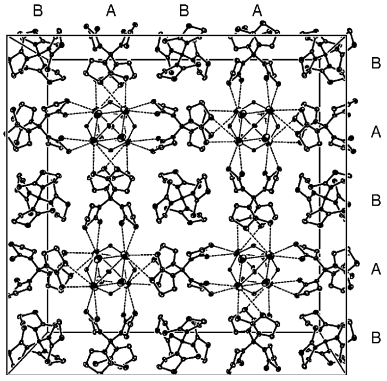

Ying-Ji Sun, Wei-Zheng Shen, Peng Cheng, Shi-Ping Yan, Dai-Zheng Liao, Zong-Hui Jiang, Pan-Wen Shen

Polyhedron 23 (2004) 211

Synthesis, structure and spectroscopic properties of novel half-sandwich nickel(II) complexes with less hindered hydrotris(pyrazolyl)borate ligand

This paper presents the syntheses, crystal structures and spectroscopic properties of a series of half-sandwich nickel(II) complexes with hydrotris(3,5-dimethylpyrazolyl)borate and azide or thiocyanate, $[Tp^*Ni(pz^*)_2(N_3)]$ (**1**), $[Tp^*Ni(pz^*)(SCN)(H_2O)]$ (**2**) and $[Tp^*Ni(SCN)(CH_3OH)_2]$ (**3**) (Tp^*: hydrotris(3,5-dimethylpyrazolyl)borate; pz*: 3,5-dimethylpyrazole). The half-sandwich compound $[Tp^*Ni(\eta_2\text{-}O_2N)(CH_3OH)]_4$ (**4**), which has been previously reported in a short communication, has the nickel(II) center with N_3O_3 coordination environment. The influences of N_3^-, SCN^- and NO_2^- in all these half-sandwich nickel(II) complexes were discussed.

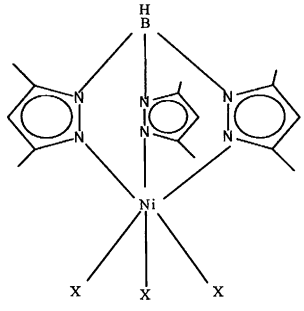

X = N, N, N (**1**) ; N, N, O (**2**) ; N, O, O (**3**) and O, O, O (**4**)

Tomasz Ruman, Zbigniew Ciunik, Stanisław Wołowiec

Polyhedron 23 (2004) 219

Complexes of heteroscorpionate trispyrazolylborate ligands. Part XII. Variable hapticity of hydrobis(3-phenyl-5-isopropylpyrazolyl)(3,5-dimethylpyrazolyl)borate in its rhodium(I) complexes with COD and NBD

Hydrobis(3-phenyl,5-isopropylpyrazolyl)(3,5-dimethylpyrazolyl)borate(Tp) coordinate in κ^3 fashion in TpRh(NBD) complexes, which was characterized crystallographically, while the mode of coordination of Tp is κ^3 in TpRh(COD) aanalogue, as studied by variable-temperature ^{1}H NMR spectroscopy.

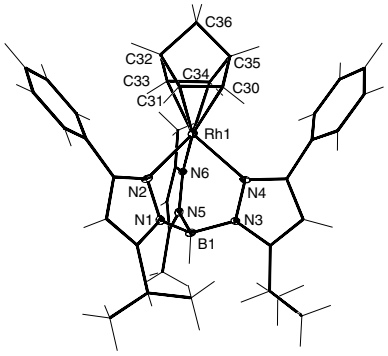

Yoshiaki Takahashi, Shiro Hikichi, Yoshihiko Moro-oka, Munetaka Akita

Polyhedron 23 (2004) 225

Oxygenation of a series of cationic aquoruthenium complexes, $Tp^{iPr2}Ru(OH_2)_n L_{3-n}{\cdot}CF_3SO_3{\cdot}(THF)_x$, leading to mono- and dinuclear aquo-hydroxo complexes supported by unique hydrogen bonding networks

O_2-treatment of the labile cationic aquo-Ru(II) complexes, $Tp^{iPr2}(L)_nRu(OH_2)_{3-n}(OTf)(THF)_x$ (L=bipy,py,THF), results in oxidation of the metal center to give the mononuclear hydroxo-Ru(III) complexes and the dinuclear Ru(II)–Ru(III) and Ru(III)–Ru(III) mixed aquo-hydroxo complexes bridged by the Ru–O···H···O–Ru hydrogen-bonding interactions.

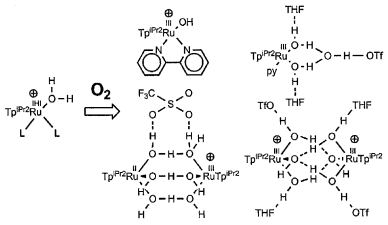

Christopher J. Siemer, Michael J. VanStipdonk, Pawan K. Kahol, David M. Eichhorn

Polyhedron 23 (2004) 235

A coordination polymer from a cyanoscorpionate complex

The reaction of $Bp^{Ph,4CN}{}_2Cu$ with $Rh_2(CF_3COO)_4$ results in the isolation of a polymeric material with coordination of the Rh dimers by the CN substituents on the scorpionate ligands.

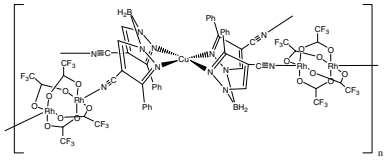

Zahida Shirin, Carl J. Carrano

Polyhedron 23 (2004) 239

New heteroscorpionate ligands with hydrogen bond donor and acceptor groups: synthesis, characterization and reactivity with divalent Co, Zn and Ni ions

Three new N_2O heteroscorpionate ligands designated L6OH, L7OH and L9OH, containing either appended hydrogen bond donating or accepting residues have been synthesized and characterized. Metal complexes of these ligands with Co(II) and Ni(II) have been characterized by X-ray crystallography.

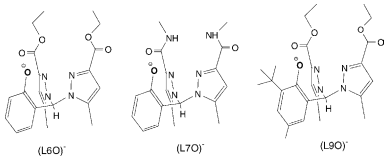

Liv Peters, Nicolai Burzlaff

Polyhedron 23 (2004) 245

Complexes bearing an enantiopure N,N,O scorpionate ligand derived from (−)-menthone

Starting from (−)-menthone an enantiopure chiral tripod ligand is obtained via C_2 symmetric bis(menthylpyrazol-1-yl)methane by introducing a carboxylate donor at the bridging carbon atom. A prochiral centre, but no additional stereo centre is formed at this carbon atom resulting in a homochiral tripod ligand. First examples of ruthenium, manganese and rhenium complexes bearing this enantiopure scorpionate ligand are reported, too.

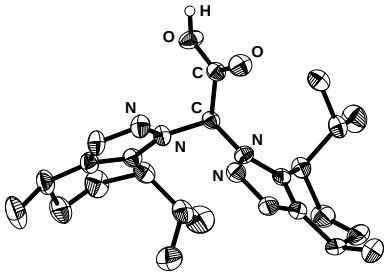

Jennifer L. Galler, Sam Goodchild, James Gould, Robert McDonald, Andrea Sella

Polyhedron 23 (2004) 253

Tris-pyrazolylborate complexes of redox inactive lanthanides – the structures of $[(Tp^{Me2})_2NdX]$ (X=Cl, NPh_2, dpm, H_2BEt_2)

A range of complexes of formula $[Ln(Tp^{Me2})_2X]$ (Ln=Ce, Nd) have been prepared to compare the chemistry of the non-reducible Ce and Nd with that reported previously for the redox-active Sm ion. Seven-coordinate chloride, alkoxide, and amide complexes have been isolated. The eight-coordinate diketonates and a bidentate BH_2Et_2 have been prepared.

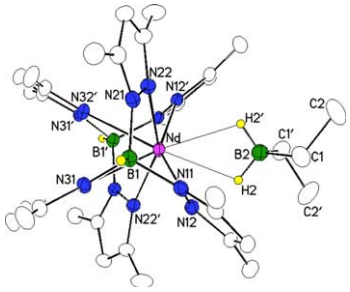

Martin Morissette, Stefan Haufe, Robert McDonald, Gregory M. Ferrence, Josef Takats

Polyhedron 23 (2004) 263

Steric saturation of the ytterbium coordination environment: $(Tp^{tBu,Me})Yb(OMes)$, a four coordinate, monomeric, base-free divalent lanthanide complex, its solvation with tetrahydrofuran, and comparison to the β-diketonate complex, $(Tp^{tBu,Me})Yb(dpm)$

Three hydrotris(3-*tert*-butyl-5-methylpyrazolyl)borate supported, monomeric divalent ytterbium complexes are reported. X-ray crystallographic analysis of the THF solvated and solvent free aryloxide complexes $(Tp^{tBu,Me})Yb(OMes)(THF)$ (**1**) and $(Tp^{tBu,Me})Yb(OMes)$ (**2**), as well as the related β-diketonate complex $(Tp^{tBu,Me})Yb(dpm)$ (**3**), is used to discuss the structural characteristics of these complexes.

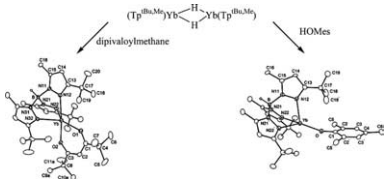

H.V. Rasika Dias, Timothy K.H.H. Goh

Polyhedron 23 (2004) 273

Fluorinated tris(pyrazolyl)borates. Syntheses and characterization of sodium and copper complexes of $[HB(3\text{-}(CF_3),5\text{-}(Ph)Pz)_3]^-$

Sodium salt of the fluorinated tris(pyrazolyl)borate ligand $[HB(3\text{-}(CF_3),5\text{-}(Ph)Pz)_3]^-$ has been synthesized from the corresponding pyrazole and $NaBH_4$ in high yield. It forms stable adducts with oxygen-based donors like THF and water. X-ray crystal structures and IR data have been ascertained.

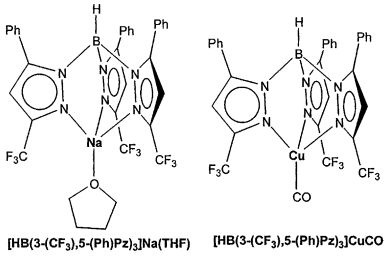

Tsuyoshi Kitano, Yoshiki Sohrin, Yasuo Hata, Hiroshi Mukai, Hiroki Wada, Kazumasa Ueda

Polyhedron 23 (2004) 283

Highly selective extraction of Cu(II) and Zn(II) using $[B(3\text{-iPrpz})_4]^-$ (iPrpz=isopropylpyrazolyl)

Solvent extraction of first-series transition metal ions with $[B(3\text{-iPrpz})_4]^-$ is reported. This ligand quantitatively extracts only Cu(II) and Zn(II). The structures of the extracted species were determined by single-crystal X-ray diffraction. Because the bulky isopropyl groups prevent octahedral geometry, the other metal ions cannot form stable and extractable complexes with $[B(3\text{-iPrpz})_4]^-$.

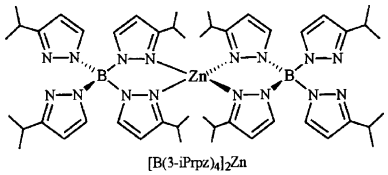

Daniel L. Reger, James R. Gardinier, Mark D. Smith

Polyhedron 23 (2004) 291

Synthesis of *meta*-$C_6H_4[C(1\text{-pyrazolyl})_2(2\text{-pyridyl})]_2$, a fixed geometry bitopic heteroscorpionate and the crystal structure of its unusual square planar silver(I) complex

A ligand with two bis(1-pyrazolyl)(2-pyridyl)methane heteroscorpionate donors positioned 120° from one another about a connecting arene ring has been prepared. This ligand coordinates to silver in a bidentate κ^2-fashion with its pyrazolyl groups and also enforces an atypical square planar coordination geometry for silver(I).

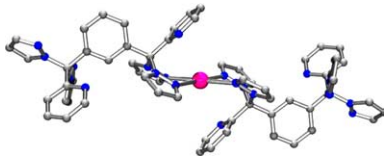

Rosario Criado, Mercedes Cano, José A. Campo, José V. Heras, Elena Pinilla, M. Rosario Torres

Polyhedron 23 (2004) 301

Mono and binuclear rhodium dicarbonyl complexes containing the hydridotris(3-*p*-chlorophenylpyrazol-1-yl)borate ligand (Tp^{PhCl}). X-ray structures of the binuclear complex $[(OC)_2Rh(\mu{:}\kappa^2,\kappa^1\text{-}Tp^{PhCl})Rh(Cl)(CO)_2]$ and of three isomers of $[Rh(\kappa^2\text{-}Tp^{PhCl})(CO)_2]$

Two Rh-dicarbonyl complexes $[Rh(\kappa^2\text{-}Tp^{PhCl})(CO)_2]$ (**1**) and $[(OC)_2Rh(\mu{:}\kappa^2,\kappa^1\text{-}Tp^{PhCl})Rh(Cl)(CO)_2]$ (**2**) have been synthesized and structurally characterized by IR and NMR spectroscopies and X-ray crystallography.

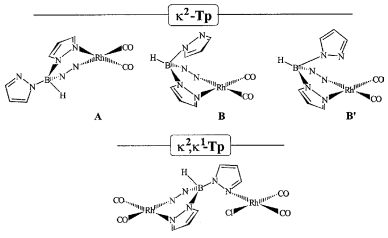

Neil J. Vogeley, Joseph L. Templeton

Polyhedron 23 (2004) 311

Interconversions of simple monodentate nitrogen donor ligands bound to Tp′ tungsten fragments

Nitrogen donor ligands incorporated into $[Tp'(CO)_2W]^+$ and $[Tp'(CO)(PhCCMe)W]^+$ coordination spheres undergo ligand based addition of nucleophiles and electrophiles with different regioselectivity. The effects of metal ligand π bonds are discussed.

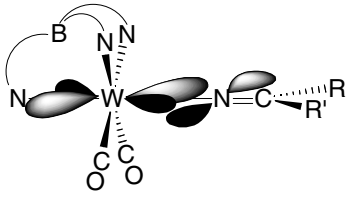

Jake D. Soper, Ian J. Rhile, Antonio G. DiPasquale, James M. Mayer

Polyhedron 23 (2004) 323

Oxidation of $TpOs^{III}(NH_2Ph)Cl_2$ to $TpOs^{IV}(NHPh)Cl_2$ by O_2

The hydrotris(1-pyrazolyl)borate osmium(III) aniline complex $TpOs^{III}(NH_2Ph)Cl_2$ reacts with O_2 to give the Os(IV) anilido complex $TpOs^{IV}(NHPh)Cl_2$. The reaction is catalyzed by bases and proceeds by a stepwise mechanism of initial deprotonation to give $\mathbf{Os^{III}NHPh^-}$, which then reacts with O_2 by outer-sphere electron transfer.

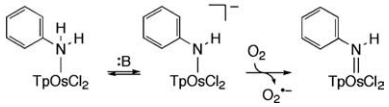

António Paulo, João D.G. Correia, Maria P.C. Campello, Isabel Santos

Polyhedron 23 (2004) 331

A short ride on scorpionates: from d- to f-elements

An overview of progress involving group 7 elements and actinides with scorpionate ligands is given. This includes oxides, polyhydrides and carbonyls of group 7 elements and any type of compounds of actinides (III) and (IV). Synthetic procedures, reactivity and structural data are reviewed.

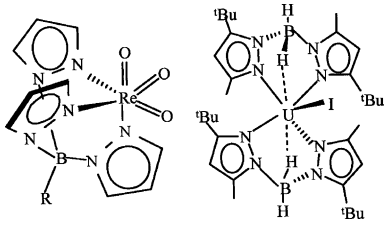

Agustín Caballero, M. Carmen Carrión, Gustavo Espino, Félix A. Jalón, Blanca R. Manzano

Polyhedron 23 (2004) 361

Ruthenium hydride complexes with a heteroscorpionate ligand derived from methane: 2-phenoxy-bis(pyrazol-1-yl)methane. The hemilabile role of the ligand in substitution and proton transfer reactions

The anionic heteroscorpionate 2-phenoxy-bis(pyrazol-1-yl)methane has been coordinated to ruthenium to give the hydride complexes of the figure. These isomers react with phosphines of different size and donor abilities reflecting a hemilabile behavior of the scorpionate ligand. Proton transfer reactions from HBF_4 have also been studied in acetone and methanol.

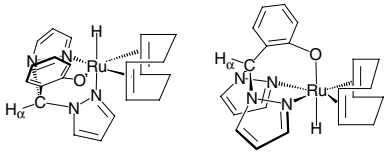

1a **1b**

Luigi Fabbrizzi, Maurizio Licchelli, Antonio Poggi, Donatella Sacchi, Cristina Zampa

Polyhedron 23 (2004) 373

A chromogenic penta-aza scorpionand for nickel(II) and copper(II) ions

The powerful chromophore 4-amino-7-nitrobenzo-2-oxa-1,3-diazole (NBD) has been introduced on the side chain of a novel cyclam derivative. The nickel(II) and copper(II) complexes of the new scorpionand undergo a reversible deprotonation process involving the aniline nitrogen atom of the NBD fragment, with simultaneous coordination of the pendant arm to the metal centre. The resulting pH-dependent complexation/decomplexation process induces drastic modifications of the spectral features of the chromophore and a sharp colour change.

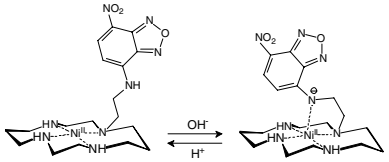

Michel Etienne, Jean-Cyrille Hierso, Paul J. Daff, Bruno Donnadieu, Françoise Dahan

Polyhedron 23 (2004) 379

Mono and dinuclear hydrotris(3,5-dimethylpyrazolyl)borato tantalum complexes

Reaction of KTp^{Me2} with $[TaCl_2(tht)]_2(\mu\text{-}Cl)_2(\mu\text{-tht})$ (**1**) (tht=tetrahydrothiophene) gives the X-ray characterized unsymmetrical $(Tp^{Me2}Ta)(TaCl_3)(\mu\text{-}Cl_2)(\mu\text{-tht})$ (**2**) in fair yield. This doubly bonded Ta=Ta complex [2.6791(5) Å, diamagnetic, 18e per Ta] is a rare example of an unsymmetrical $Ta_2X_6L_3$ complex.

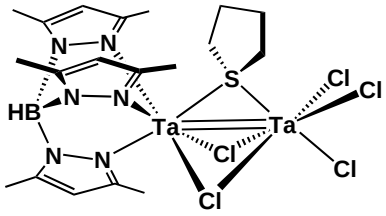

Aston A. Eagle, Robert W. Gable, Simon Thomas, Stephen A. Sproules, Charles G. Young

Polyhedron 23 (2004) 385

Sulfur atom transfer reactions of tungsten (VI) and tungsten(IV) chalcogenide complexes

The sulfur and oxygen atom transfer reactions and X-ray crystal structures of $Tp^*W^{VI}S_2(S_2PPh_2\text{-}S)$ and $Tp^*W^{IV}S(S_2PPh_2\text{-}S,S')$ are reported, along with the sulfur and oxygen atom transfer and catalytic sulfur atom transfer reactions of related Tp* complexes.

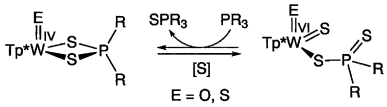

Hamsell M. Alvarez, Joseph M. Tanski, Daniel Rabinovich

Polyhedron 23 (2004) 395

Poly(mercaptoimidazolyl)borate chemistry and the predominance of κ^3-*S*,*S*,*H* over κ^2-*S*,*S* or κ^3-*S*,*S*,*S* coordination modes: unexpected formation of square pyramidal Ni(II) complexes

Paramagnetic square-pyramidal nickel(II) complexes $[(dppe)Ni(L)]X$ ($L=Bm^R$ or Tm^R; X=Cl, Br) have been readily prepared from $Ni(dppe)X_2$ and the thallium(I) poly(mercaptoimidazolyl)borates $Tl(Bm^R)$ or $Tl(Tm^R)$. These compunds have been characterized by a combination of analytical and spectroscopic techniques and, in the case of $[(dppe)Ni(Bm^{Me})]Cl$ and $[(dppe)Ni(Tm^{p\text{-}Tol})]Cl$, by X-ray crystallography

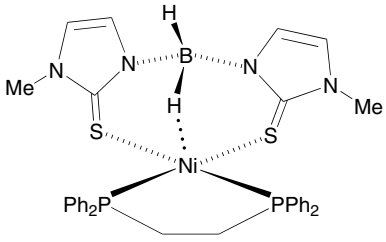

Janis K. Voo, Christopher D. Incarvito, Glenn P.A. Yap, Arnold L. Rheingold, Charles G. Riordan

Polyhedron 23 (2004) 405

Tris(imidazolyl) cadmium and zinc complexes: structural and spectroscopic characterization of $M\text{–}OH_2$ motifs

Monomeric aqua complexes of Cd and Zn coordinated by a tris(imidazolyl) ligand are reported. The molecular structures are characterized by trigonal pyramidal metal ion coordination and hydrogen-bonding between the bound water molecule and the noncoordinating counter ions.

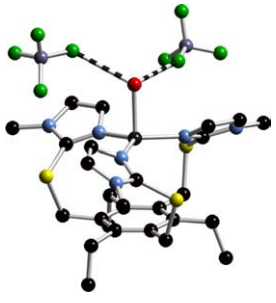

Andrew J. Vetter, William D. Jones

Polyhedron 23 (2004) 413

Carbon–hydrogen bond activation of chloroalkanes by a rhodium trispyrazolylborate complex

C–H activation of chloroalkanes by [Tp*Rh(CNR)] leads to oxidative addition to a methyl C–H bond; but if β-chlorine is present in the functionalized alkyl ligand, β-chloride elimination is observed.

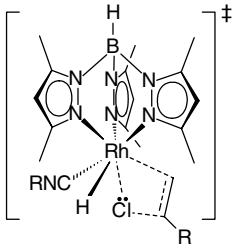

Jian Li, Peter I. Djurovich, Bert D. Alleyne, Irina Tsyba, Nam N. Ho, Robert Bau, Mark E. Thompson

Polyhedron 23 (2004) 419

Synthesis and characterization of cyclometalated Ir(III) complexes with pyrazolyl ancillary ligands

The syntheses and structures of a series of $(N,C^{2'}$-(2-*para*-tolylpyridine))$_2$Ir(LX) [$(tpy)_2$Ir(LX)] and $(N,C^{2'}$-(4′,6′-difluorophenylpyridine))$_2$Ir(LX) [$(dfppy)_2$Ir(LX)] are reported, where LX are pyrazolyl and pyrazolyl-borate ligands. $(tpy)_2$Ir(pz_2H), $(tpy)_2$Ir(pzH)$_2$(CF_3SO_3), $(tpy)_2$Ir(pz_2Bpz_2) and $(tpy)_2$Ir(pz_2BEt_2) have been structurally characterized by X-ray crystallography.

Hemant K. Joshi, Michael E. Arvin, Jason C. Durivage, Nadine E. Gruhn, Michael D. Carducci, Barry L. Westcott, Dennis L. Lichtenberger, John H. Enemark

Polyhedron 23 (2004) 429

Photoelectron spectra of potassium salts of hydrotris(pyrazol-1-yl)borates: electronic structure of the electron withdrawing scorpionates $Tp^{(CF_3)_2}$, Tp^{*Cl} and comparison to Tp* and Tp

The electronic structures of KTp*, KTp^{*Cl} and $KTp^{(CH_3)_2}$ have been investigated by gas-phase photoelectron spectroscopy and compared to KTp using density functional theory. Use of HeI and HeII excitation energies provides distinct experimental assignments of the nitrogen σ-donor orbitals (σ_N) and the σ_{BH} molecular orbitals.

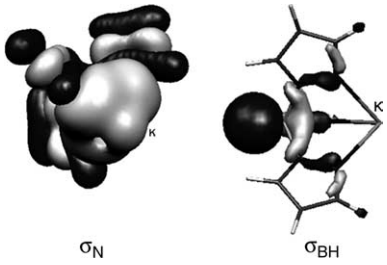

Chandi Pariya, Christopher D. Incarvito, Arnold L. Rheingold, Klaus H. Theopold

Polyhedron 23 (2004) 439

Preparation and ligand substitution reactions of Tp^{Ms}Ru(COD)H including intramolecular ligand metalation

Reaction of $[RuH(COD)(NH_2N(CH_3)_2)_3]BPh_4$ (COD=1,5-cyclooctadiene) with Tp^{Ms}Tl (Tp^{Ms}=hydrotr is(3-mesitylpyrazolyl)borate) yielded Tp^{Ms}Ru(COD)H (**1**). Treatment of **1** with CO afforded acyl complex $Tp^{Ms}Ru(CO)_2$-$C(O)C_8H_{13}$ (**2**). Reaction of **1** with acetonitrile produced $Tp^{Ms@}Ru(NCCH_3)_2$ (**3**). The molecular structures of complexes **1**–**3** have been determined by single crystal X-ray diffraction methods.

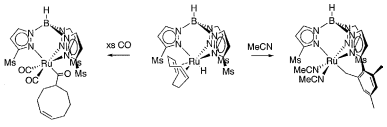

Christopher A. Dodds, Małgorzata Jagoda, John Reglinski, Mark D. Spicer

Polyhedron 23 (2004) 445

Soft scorpionate complexes of the fourth and fifth period elements arsenic and tin

We report the synthesis and structure of arsenic (III) and tin(IV) adducts of the hydrotris(methimazolyl)borate anion (Tm^{Me}). Both species are found to be $[E(\kappa^3Tm^{Me})_2]^{n+}$ anions (E=As, $n = 1$; E=Sn, $n = 2$). Comparisons are made between each of these species and the compounds formed with their heavier and larger group partners bismuth and lead.

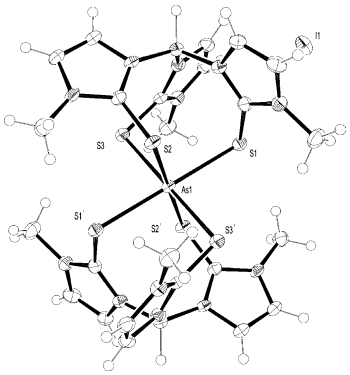

Claudio Pettinari, Augusto Cingolani, Giancarlo Gioia Lobbia, Fabio Marchetti, Domenico Martini, Maura Pellei, Riccardo Pettinari, Carlo Santini

Polyhedron 23 (2004) 451

Copper and silver derivatives of scorpionates and related ligands

A review of the syntheses and of spectroscopic, analytical and structural data of silver(I), copper(I), and copper(II) complexes containing scorpionate and related ligands.

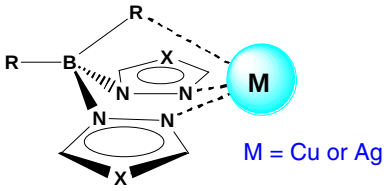

Vivek V. Karambelkar, Robert C. diTargiani, Christopher D. Incarvito, Lev N. Zakharov, Arnold L. Rheingold, Charlotte L. Stern, David P. Goldberg

Polyhedron 23 (2004) 471

Multiple bonding modes exhibited by heteroscorpionate N_2S(alkylthiolate) ligands with Zn(II) and Fe(II)

A related pair of heteroscorpionate N_2S(alkylthiolate) ligands, L^1H and L^2H, have been reacted with Zn(II) and Fe(II) to give monomeric $(L^2)_2Fe$, dimeric $[(L^2)_2Zn_2Br_2]$, and trimeric $[(L^1)_3Zn_3Br_2]Br$ complexes. Structural characterization of these complexes show that the ligands L^1 and L^2 can adopt a wide range of bonding modes. Structural and electronic factors influencing the preferred coordination of L^1 and L^2 are discussed.

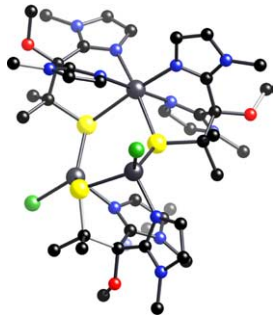

Arefa Docrat, Melissa M. Morlok, Brian M. Bridgewater, David G. Churchill, Gerard Parkin

Polyhedron 23 (2004) 481

N–H···O hydrogen bonding interactions in tetrahedral $[ZnS_4]$ complexes of relevance to zinc enzymes: the synthesis, structures and reactivity of *tris*(2-mercapto-1-arylimidazolyl)hydroborato zinc(2-mercapto-1-arylimidazole) complexes, $\{[Tm^{Ar}]Zn(mim^{Ar})\}[ClO_4]$ (Ar=Ph, *p*-Tol)

The *tris*(2-mercapto-1-arylimidazolyl) hydroborato complexes $\{[Tm^{Ar}]Zn(mim^{Ar})\}[ClO_4]$, which feature tetrahedrally coordinated zinc centers in a sulfur rich environment, may be prepared by the reaction of $[Tm^{Ar}]Li$ with $Zn(ClO_4)_2$ in the presence of 2-mercapto-1-arylimidazole (mim^{Ar}; Ar= Ph, *p*-Tol).

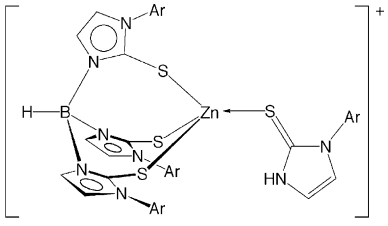

J. Christopher Thomas, Jonas C. Peters

Polyhedron 23 (2004) 489

Platinum-alkyl and hydride complexes supported by a tris(phosphino)borate ligand: structural and spectroscopic studies

The synthesis and characterization of platinum-methyl and hydride complexes containing the ligand $[PhBP_3]$ ($[PhBP_3]$= $[PhB(CH_2PPh_2)_3]^-$) are described. Metallation of $[PhBP_3][TBA]$ (**1[TBA]**, [TBA]= $[^nBu_4N]^+$) with platinum methyl precursors provided the corresponding phosphine methyl platinum species $[PhBP_3]PtMe_3$ (**2**) and $[[\kappa^2\text{-}PhBP_3]PtMe_2][TBA]$ (**3**). The reactivity of octahedral **2** and square planar **3** are discussed, and their X-ray diffraction structures are reported.

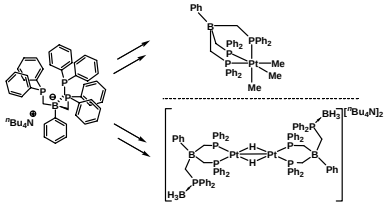

Martin L. Kirk, Katrina Peariso

Polyhedron 23 (2004) 499

Ground and excited state spectral comparisons of models for sulfite oxidase

Ground and excited state spectra have been analyzed and compared for models of the one-electron reduced sulfite oxidase active site. Use of the heteroscorpionate ligand (2-dimethylethanethiol) bis(3,5-dimethylpyrazolyl)methane (L3SH) has provided the framework for an oxo-molybdenum(V) model complex that possesses both thiolate and ene-1,2,-dithiolate donors in the equatorial plane. The complex [(L3S)MoO(bdt)] possesses a constrained O–Mo–$S_{thiolate}$–C torsion angle that is close to the ~90° O–Mo–S_{Cys}–C torsion angle observed in the structure of chicken liver sulfite oxidase. The constrained torsion angle in [(L3S)MoO(bdt)] allows for the examination in how second-coordination sphere effects influence the electronic structure of the Mo site in the enzyme.

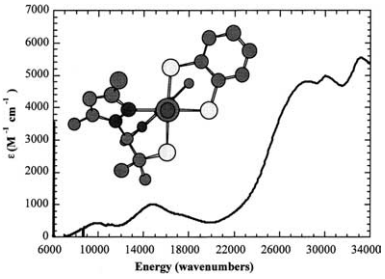

Author Index of Symposia-In-Print number 26 507

The Publisher encourages the submission of articles in electronic form thus saving time and avoiding rekeying errors. For detailed instructions on the preparation of manuscripts and of electronic artwork, consult the Author Gateway for Elsevier at http://authors.elsevier.com

SCIENCE DIRECT™

Full text of this journal is available, on-line from **ScienceDirect**. Visit **www.sciencedirect.com** for more information.

CONTENTS Direct

This journal is part of **ContentsDirect**, the *free* alerting service which sends tables of contents by e-mail for Elsevier books and journals. You can register for **ContentsDirect** online at: **www. elsevier.com/locate/contentsdirect**

http://ChemWeb.com
The World Wide Club for the Chemical Community
http://chemweb.com/gateways/elsevier.html

Available online at www.sciencedirect.com
SCIENCE DIRECT®
Polyhedron 23, issue 17, 11 November 2004
POLYHEDRON
www.elsevier.com/locate/poly

Contents

Preface: Special Issue in Honour of Professor Malcolm L.H. Green 2595

Papers

Alireza Haghiri Ilkhechi, Matthias Scheibitz, Michael Bolte, Hans-Wolfram Lerner, Matthias Wagner

Polyhedron 23 (2004) 2597

On the way to ferrocene-based multiple-decker sandwich complexes

Three ferrocene derivatives, $Li[FcBH_3]$, $Li_2[1,1'\text{-fc}(BMe_3)_2]$ and $Li_2[1,1'\text{-fc}(BMe_2pz)_2]$ [Fc = $(C_5H_5)Fe(C_5H_4)$, fc = $(C_5H_4)_2Fe$, pz = pyrazolyl], have been synthesized and structurally characterized to investigate the interaction of the negatively charged sandwich complex with its Li^+ counterion(s) in the solid state.

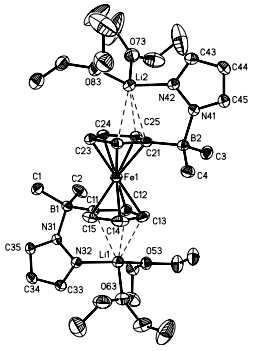

Edmond Collange, Laurent Metteau, Philippe Richard, Rinaldo Poli

Polyhedron 23 (2004) 2605

Synthesis and structure of a new organometallic polyoxomolybdate, $Cp^*_2Mo_6O_{17}$

The new organometallic polyoxomolybdate $Cp^*_2Mo_6O_8$ has been obtained by the straightforward combination of organometallic and inorganic oxomolybdenum(VI) reagents.

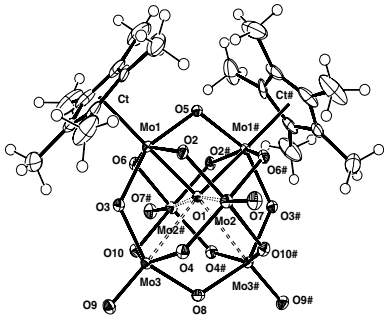

Nobuaki Sakai, Taro Saito

Polyhedron 23 (2004) 2611

Synthesis and structures of tetranuclear rhenium–cobalt mixed metal sulfide clusters $[Re_3CoS_4Cl_6(PMe_2Ph)_4]$

An isomeric pair of rhenium–cobalt sulfide clusters $[Re_3CoS_4Cl_6(PMe_2Ph)_4]$ was synthesized by the reaction of $[(Ph_3P)_2N]$-$[Re_3S_4Cl_6(PMe_2Ph)_3]$ with $CoCl_2$ in the presence of PMe_2Ph and their crystal structures were determined. The isomers differ in the orientation of the dimethylphenylphosphine ligands, which controls the coordination of three μ-S atoms in the starting cluster to the cobalt atom.

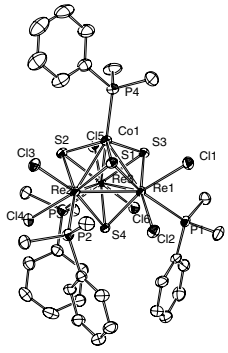

Sergei B. Bushuk, Francis H. Carré, Daniel M.H. Guy, William E. Douglas, Yulia A. Kalvinkovskya, Larissa G. Klapshina, Anatoly N. Rubinov, Alexander P. Stupak, Boris A. Bushuk

Polyhedron 23 (2004) 2615

Hypercoordinate silicon and phosphorus acetylene compounds: crystal structure determinations and fluorescence spectroscopic study

The steady-state fluorescence, fluorescence excitation spectra and fluorescence lifetime of pentacoordinate [8-(dimethylamino-κ*N*)-1-naphthalenyl-κ*C*]diethynylmethylsilicon as a function of excitation and emission wavelengths were investigated in solvents of various polarities at room temperature. The crystal structure of the silicon monomer shows a monocapped tetrahedral geometry in which the N atom is opposite one of the acetylene groups.

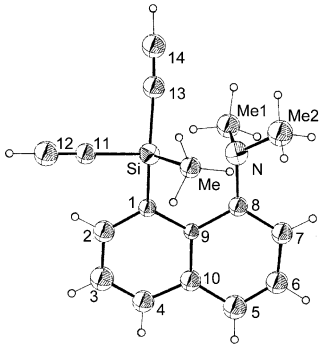

F. Geoffrey N. Cloke, Peter B. Hitchcock, Matthew C. Kuchta, Neil A. Morley-Smith

Polyhedron 23 (2004) 2625

Mononuclear tantalum (V) pentalene complexes: synthesis of $[Ta\{\eta^8\text{-}C_8H_4(1,4\text{-}Si^iPr_3)_2\}X_3]$ (X = CH_3, Cl, I) and the X-ray crystal structures of $[Ta\{\eta^8\text{-}C_8H_4(1,4\text{-}Si^iPr_3)_2\}(CH_3)_3]$, $[Ta\{\eta^8\text{-}C_8H_4(1,4\text{-}Si^iPr_3)_2\}(CH_3)_2Cl]$, $[Ta\{\eta^8\text{-}C_8H_4(1,4\text{-}Si^iPr_3)_2\}(CH_3)Cl_2]$ and $[Ta\{\eta^8\text{-}C_8H_4(1,4\text{-}Si^iPr_3)_2\}I_3]$

The reaction between $[TaMe_3Cl_2]$ and the potassium salt of the silylated pentalene dianion $[K_2\{C_8H_4(1,4\text{-}Si^iPr_3)_2\}]$ gives the η^8-pentalene complex $[Ta\{\eta^8\text{-}C_8H_4(1,4\text{-}Si^iPr_3)_2\}(CH_3)_3]$.

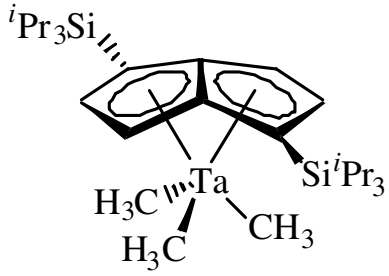

Alan Bailey, William P. Griffith, David W.C. Leung, Andrew J.P. White, David J. Williams

Polyhedron 23 (2004) 2631

Ozonolysis for the preparation of high-oxidation state transition metal complexes, and the X-ray crystal structure of $Co(py)_2(OAc)_2(H_2O)_2$

The use of an environmentally friendly ozone/dioxygen mixture under ambient conditions to synthesise pyridine-carboxylato complexes of silver(II) and manganese(III), and the heteropolyoxocobaltate(III) ion $[CoW_{12}O_{40}]^{5-}$ is described. During attempts to make other cobalt(III) complexes ozonolytically $Co(py)_2(OAc)_2(H_2O)_2$ was obtained and its X-ray structure determined.

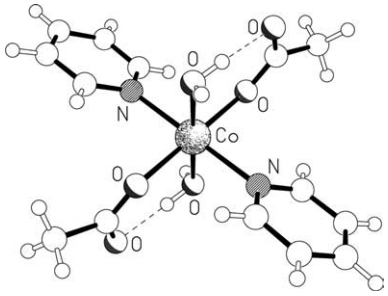

M.C. Barral, R. González-Prieto, S. Herrero, Reyes Jiménez-Aparicio, J.L. Priego, E.C. Royer, M.R. Torres, F.A. Urbanos

Polyhedron 23 (2004) 2637

Synthesis and crystal structure of high and low spin diruthenium complexes with diphenylformamidine and diphenyltriazene ligands

The synthesis and structure of the complexes $Ru_2(CN)(\mu\text{-}DPhF)_4$ (**1**) (DPhF=*N*,*N*′-diphenylformamidinate), $Ru_2(N_3)(\mu\text{-}O_2CMe)(\mu\text{-}DPhF)_3$ (**2**), $Ru_2(NCS)(\mu\text{-}O_2CMe)(\mu\text{-}DPhF)_3$ (**3**) and $Ru_2Cl(\mu\text{-}N_3Ph_2)_4$ (**4**) are reported. The isolation of $Ru_2Cl_2(\mu\text{-}N_3Ph_2)_4$ (**5**) is also described. Complexes **2** and **4** display magnetic moments corresponding to three unpaired electrons whereas compounds **1** and **3** are low spin complexes. Compound **5** is diamagnetic.

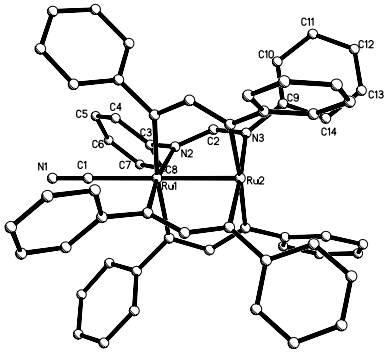

Helmut Werner, Norbert Mahr, Michael E. Schneider, Marco Bosch, Justin Wolf

Polyhedron 23 (2004) 2645

Acetylacetonato, pentachlorophenolato and carboxylato rhodium(I) complexes and their reactivity in the C–C coupling reaction of olefins and diazoalkanes

This work extends the series of chelate rhodium(I) complexes with $Rh(PiPr_3)_2$ as the core unit. The complexes not only react with ethene but also with diazoalkanes.

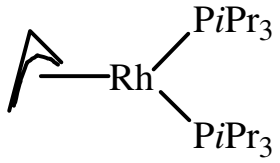

Ronan M. Bellabarba, Graham C. Saunders

Polyhedron 23 (2004) 2659

Intramolecular dehydrofluorinative coupling of pentamethylcyclopentadienyl and phosphine ligands in iridium complexes

Cationic iridium(III) complexes of bifunctional $\eta^5,\kappa P$-Cp–P and trifunctional $\eta^5,\kappa P,\kappa L$-Cp–PL ligands may be conveniently prepared by intramolecular dehydrofluorinative carbon–carbon coupling.

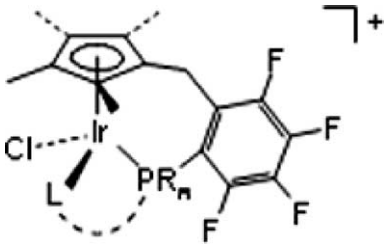

Stephen A. Westcott, Todd B. Marder, R. Thomas Baker, Richard L. Harlow, Joseph C. Calabrese, King Chung Lam, Zhenyang Lin

Polyhedron 23 (2004) 2665

Reactions of hydroborating reagents with phosphinorhodium hydride complexes: molecular structures of a Rh_2B_3 metallaborane cluster, an $L_2Rh(\eta^2\text{-}H_2BR_2)$ complex and a mixed valence Rh dimer containing a semi-bridging Bcat (cat=1,2-$O_2C_6H_4$) group

Reactions of hydroborating reagents with phosphinorhodium complexes have been investigated in detail. While alkylboranes proceed via initial insertion of B–H into a Rh–H bond, reactions with catecholborane show an enhanced tendency towards oxidative addition. Implications for rhodium-catalyzed hydroborations are addressed.

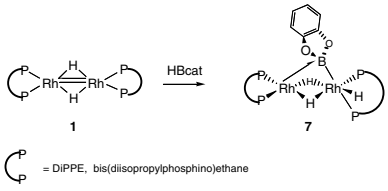

Christian P. Mehnert, Raymond A. Cook, Nicholas C. Dispenziere, Edmund J. Mozeleski

Polyhedron 23 (2004) 2679

Biphasic hydroformylation catalysis in ionic liquid media

A series of ionic liquids have been investigated as reaction media for biphasic hydroformylation catalysis. In the study the rhodium/tppti* (tppi* = tri(*m*-sulfonyl) triphe-nyl phosphine 1,2-dimethyl-3-butyl-imidazolium salt) catalyst system was investigated together with hexene-1 as the substrate. The activity of the biphasic ionic liquid system containing the Rh/tppti* catalyst was approximately one order of magnitude lower than that observed for the conventional Rh/PPh_3 catalyst in toluene.

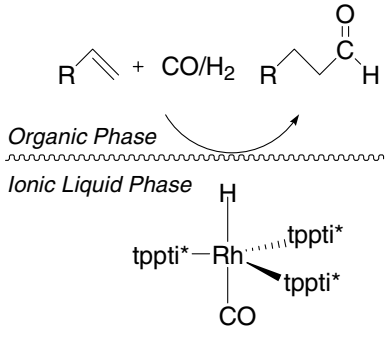

William J. Evans, Stosh A. Kozimor, Joseph W. Ziller

Polyhedron 23 (2004) 2689

Bis(pentamethylcyclopentadienyl) U(III) oxide and U(IV) oxide carbene complexes

Oxidation of the sterically crowded complex $(C_5Me_5)_3U$ provides access to two new classes of uranium compounds that previously were unknown, a U(III) oxide and a U(IV) carbene: $[(C_5Me_5)_2U]_2(\mu\text{-O})$, **1**, and $(C_5Me_5)_2U(O)[C(NMeCMe)_2]$, **2**, respectively. The structure of **1** allows a direct actinide versus lanthanide comparison within the $[(C_5Me_5)_2M]_2(\mu\text{-O})$ class. The structure of **2**, shown here, contains a rare terminal U(IV) oxide as well as a carbene.

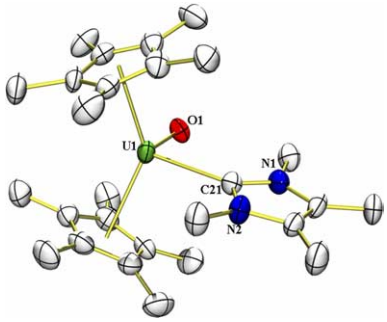

Emma Hodson, Stephen J. Simpson

Polyhedron 23 (2004) 2695

Synthesis and characterisation of $[(\eta^6\text{-cymene})Ru(L)X_2]$ compounds: single crystal X-ray structure of $[(\eta^6\text{-cymene})Ru(P\{OPh\}_3)Cl_2]$ at 203 K

Treatment of the chloro bridged dimer $\{[(\eta^6\text{-cymene})RuCl]_2(\mu\text{-Cl})_2\}$ (**1**) with the donor molecules in hot hexane causes bridge splitting reactions that produce the monomeric compounds $[(\eta^6\text{-cymene})Ru(L)Cl_2]$.

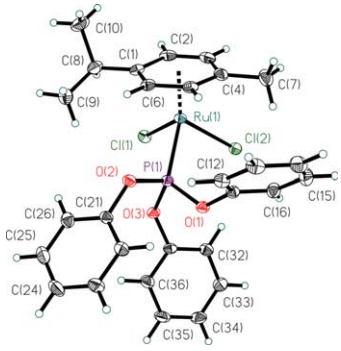

Graham H. Maunder, Maria Rosa Russo, Andrea Sella

Polyhedron 23 (2004) 2709

NO to NO_2^- conversion by divalent lanthanides: synthesis and crystal structure of $[Sm(Tp^{Me2,4\text{-}Et})_2NO_2]$

The reaction of nitric oxide with the divalent lanthanide complex $[Ln(Tp^{Me2})_2]$ and $[Ln(Tp^{Me2,4\text{-}Et})_2]$ (Ln=Sm, Eu, Yb) gives the corresponding seven-coordinate nitrites $[Ln(Tp^{Me2,X})_2NO_2]$.

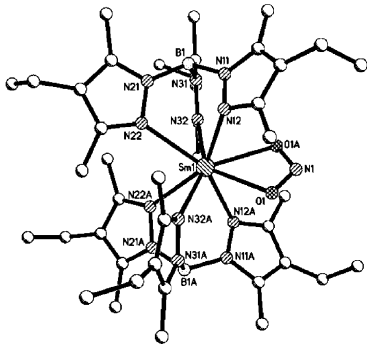

Alejandro F.G. Ribeiro, Pedro T. Gomes, Alberto R. Dias, João L. Ferreira da Silva, M. Teresa Duarte, Rui T. Henriques, Cristina Freire

Polyhedron 23 (2004) 2715

Reactions between isocyanides and a binuclear nickel(II) phosphine complex linked by a bridged bis(cyclopentadienyl) ligand. X-ray molecular structure of $[(CN^tBu)(PPh_3)Ni\{\mu\text{-}(\eta\text{-}C_5H_4)CMe_2(\eta\text{-}C_5H_4)\}Ni(PPh_3)(CN^tBu)][PF_6]_2$

The new binuclear compounds $[(CNR)(PPh_3)Ni\{\mu\text{-}(\eta\text{-}C_5H_4)CMe_2(\eta\text{-}C_5H_4)\}Ni(PPh_3)(CNR)][PF_6]_2$ (R = *S*-(−)-CH(Ph)Me (**2**), cyclohexyl (**3**), *tert*-butyl (**4**) and mesityl (**5**)) were prepared from the reaction of $[(PPh_3)_2Ni\{\mu\text{-}(\eta\text{-}C_5H_4)CMe_2(\eta\text{-}C_5H_4)\}Ni(PPh_3)_2][PF_6]_2$ (**1**) with 2 or 4 equivalents of isocyanides. Addition of an excess of *S*-(−)-CNCH(Ph)Me to **1** led to the catalytic formation of poly(*S*-(−)-1-phenylethyl isocyanide) (**6**).

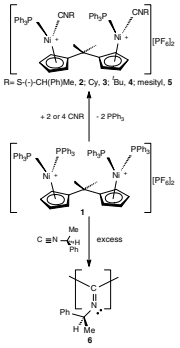

Benjamin G. Harvey, Atta M. Arif, Richard D. Ernst

Polyhedron 23 (2004) 2725

Incorporation of polybasic aromatic amines into ruthenium(II) chloro complexes

The reactions of $RuCl_2[P(C_6H_5)_3]_3$ with excesses of various aromatic amines led to six coordinate, pseudo-octahedral complexes. Reaction with 1,8-naphthyridine led to the incorporation of one bidentate ligand. X-ray structural data were obtained for the pyridazine, phthalazine and 1,8-naphthyridine complexes.

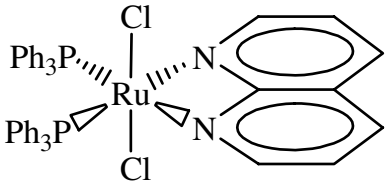

Shu-Yu S. Wang, Khalil A. Abboud, James M. Boncella

Polyhedron 23 (2004) 2733

Synthesis and mechanistic investigations of the decomposition of β-hydrogen containing W(VI) dialkyl complexes: β-H elimination vs. β-H abstraction

Mechanistic studies of the conversion of the 5 coordinate phenylimido W(VI) dialkyls to olefin complexes reveal that the reaction proceeds via β-H abstraction or β-H elimination paths depending upon the nature of the alkyl groups or the presence of absence of PMe_3.

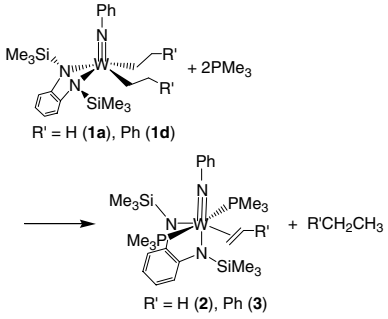

Emma L. Sceats, Joshua S. Figueroa, Christopher C. Cummins, Nikolaus M. Loening, Patrick Van der Wel, Robert G. Griffin

Polyhedron 23 (2004) 2751

Complexes obtained by electrophilic attack on a dinitrogen-derived terminal molybdenum nitride: electronic structure analysis by solid state CP/MAS ^{15}N NMR in combination with DFT calculations

^{15}N Solid state CP/MAS NMR spectroscopy has been used to study a dinitrogen-derived terminal nitride of molybdenum, $^{15}NMo(N[^tBu]Ar)_3$ (Ar = 3,5-$C_6H_3(CH_3)_2$). Several derivatives were prepared by the reaction of $^{15}NMo(N[^tBu]Ar)_3$ with Lewis acids and potent electrophiles (e.g., CH_3I, Me_3Si–OTf, PhC(O)OTf). ^{15}N solid state NMR spectroscopy and density functional calculations were used to probe the electronic structure of $^{15}NMo(N[^tBu]Ar)_3$ and its derivatives.

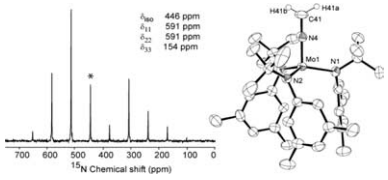

Wendy Leslie, Robert A. Poole, Paul R. Murray, Lesley J. Yellowlees, Andrew Beeby, J.A. Gareth Williams

Polyhedron 23 (2004) 2769

Near infra-red luminescence from bis-terpyridyl iridium(III) complexes incorporating electron-rich pendants

Iridium(III) bis-terpyridine complexes have been prepared which incorporate aminobenzene or pyrene substituents at the 4′-position of the terpyridine. The complexes are weakly luminescent in the near infra-red (λ_{max} 750–800 nm); this short-lived, low-energy emission, whose likely origin is an excited state of primarily ILCT character, is in contrast to the long-lived $^3\pi$–π^* luminescence of previously studied bis-terpyridyl iridium complexes. The electrochemical properties of the pyrene-substituted ligand and complex in solution are also described.

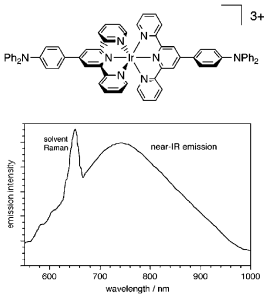

Muralee Murugesu, Khalil A. Abboud, George Christou

Polyhedron 23 (2004) 2779

New hexanuclear and dodecanuclear Fe(III) clusters with carboxylate and alkoxide-based ligands from cluster aggregation reactions

An Fe_3 starting material has been employed in cluster aggregation reactions that have yielded two Fe_6 and one Fe_{12} products. These are constructed of recognizable Fe_3 fragments, and one of the Fe_6 products contains a rare methanediolate ($^{-}OCH_2O^{-}$) group in a quadruply-bridging mode. Magnetic studies establish that all three compounds have $S = 0$ ground states.

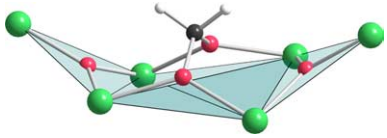

David N. Coventry, Andrei S. Batsanov, Andres E. Goeta, Judith A.K. Howard, Todd B. Marder

Polyhedron 23 (2004) 2789

Synthesis and molecular structures of α-diimines and their zinc and palladium dichloride complexes

Three α-iimines have been prepared and structurally characterised by single-crystal X-ray diffraction. In addition, molecular structures of some of their tetrahedral $ZnCl_2$ and square-planar $PdCl_2$ complexes are reported allowing a comparison as a function of coordination geometry.

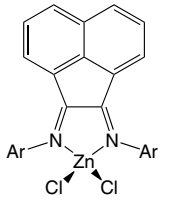

2, Ar = C_4H_4-*p*-OMe
5, Ar = 2,6-$^{i}Pr_2C_6H_3$

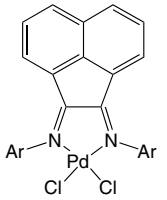

6, Ar = C_4H_4-*p*-OMe
7, Ar = 2,6-$^{i}Pr_2C_6H_3$

Nicholas A. Piro, Jonathan S. Owen, John E. Bercaw

Polyhedron 23 (2004) 2797

Pyridinium-derived *N*-heterocyclic carbene ligands: syntheses, structures and reactivity of *N*-(2′-pyridyl)pyridin-2-ylidene complexes of nickel(II), palladium(II) and platinum(II)

Pyridinium-derived *N*-heterocyclic carbene complexes $[(i\text{-BIPY})M(acac)]^{+}[OTf]^{-}$ (M = Ni (**2a**), Pd (**3a**), Pt (**4a**)) (*i*-BIPY = *N*-(2′-pyridyl)- 4-*tert*-butylpyridin-2′-ylidene) are obtained as insoluble microcrystalline powders by cyclometallation of the ligand precursor $[i\text{-BIPY-H}]^{+}[OTf]^{-}$ (OTf = trifluormethylsulfonate) to $M(acac)_2$ (acac = acetylacetonate) in chlorobenzene at 160 °C. X-ray and reactivity studies were performed.

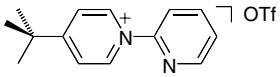

1

Sungho Yoon, Amy E. Kelly, Stephen J. Lippard

Polyhedron 23 (2004) 2805

Di- and tetra-bridged diiron(II) complexes with four terphenyl-derived carboxylates and two water molecules

The water-containing diiron(II) complexes $[Fe_2(\mu\text{-}OH_2)_2(\mu\text{-}O_2CR)_2(O_2CR)_2(THF)_2]$ (**2**) and $[Fe_2(\mu\text{-}OH_2)_2(\mu\text{-}O_2CR)_2(O_2CR)_2(4\text{-}^{t}BuC_5H_4N)_2]$ (**3**) were synthesized and characterized. Two pseudo-octahedral iron(II) centers in **2** and **3** are bridged by terphenyl-derived carboxylate ligands and two water molecules. Loss of the bridging water molecules in **3** to form the dehydrated complex $[Fe_2(\mu\text{-}O_2CR')_4(4\text{-}^{t}BuC_5H_4N)_2]$ is an equilibrium process.

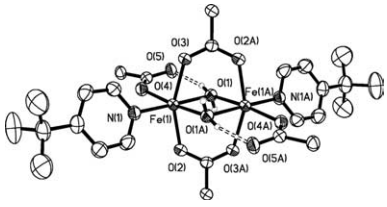

Scott Winston, Neoklis Stylianides, Arran A.D. Tulloch, Joseph A. Wright, Andreas A. Danopoulos

Polyhedron 23 (2004) 2813

Picoline and pyridine functionalised chelate N-heterocyclic carbene complexes of nickel: synthesis and structural studies

The synthesis of pyridine- and picoline-functionalised N-heterocyclic carbene complexes of Ni(II) is described. The complexes adopt tetrahedral, square planar or octahedral geometries, depending on the nature of the ligand and the reaction conditions.

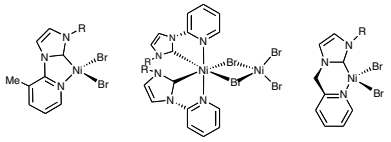

Wallace W.H. Wong, Dale E. Phipps, Paul D. Beer

Polyhedron 23 (2004) 2821

Acyclic and macrocyclic transition metal dithiocarbamate complexes containing imidazolium moieties for anion binding

The synthesis of acyclic and macrocyclic transition metal dithiocarbamate complexes containing positively charged imidazolium moieties is reported. The assemblies have been characterised by a range of spectroscopic techniques and the ability of these compounds to bind various anions was also examined.

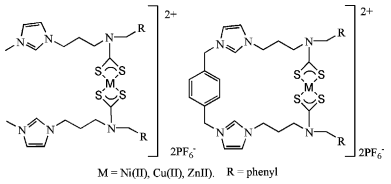

Jeffrey L. Cross, Andrew D. Garrett, Todd W. Crane, Peter S. White, Joseph L. Templeton

Polyhedron 23 (2004) 2831

Coordination and reactivity of acetonitrile in tungsten(IV) complexes: oxidation, methylation and dimerization of coordinated acetonitrile

The reaction of Tp′W(O)(CO)(I) (**1**) with [Ag][SO_3CF_3] generates the triflate complex Tp′W(O)(CO)(OTf) (**2**). Dissolution of **2** in acetonitrile and metathesis of the triflate anion for the [BAr'_4] anion produces the cationic nitrile complex [Tp′W(O)(NCMe)-(CO)][BAr'_4] (**4**). Photolysis of **1** in acetonitrile generates the neutral nitrile complex Tp′W(O)(I)(NCMe) (**5**). Spectroscopic data for the neutral acetonitrile complex **5** is consistent with an η^2-bound nitrile ligand.

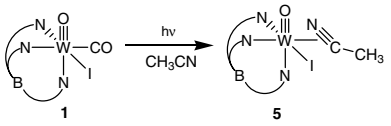

Orson L. Sydora, Jonas I. Goldsmith, Thomas P. Vaid, Abigail E. Miller, Peter T. Wolczanski, Hector D. Abruña

Polyhedron 23 (2004) 2841

Syntheses and electrochemistry of (*p*-$XC_6H_4O)_6W$ (1-X, X = H, CH_3, OCH_3, Cl, Br, OH, OCH_2Ph) and (*p*-$XC_6H_4O)_5W(O-C_6H_4OH)$ (X = H, CH_3, OCH_3, Cl, Br): an approach to electrocatalytic CH bond activation

Hexaphenoxides (*p*-$XC_6H_4O)_6W$ (**1**-X, X = H, CH_3, OCH_3, OCH_2Ph, Cl, Br) serve as starting materials for (*p*-$XC_6H_4O)_5$-$W(OC_6H_4OH)$ (**6**-X, X = OH, OMe, Me, H, Br, Cl), whose electrochemical oxidations were studied in reference to CH bond activation.

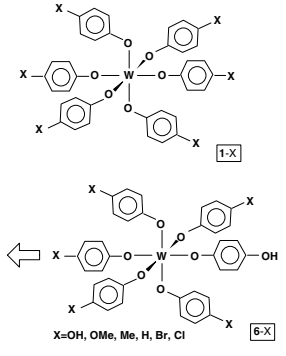

John R. Miecznikowski, Robert H. Crabtree

Polyhedron 23 (2004) 2857

Transfer hydrogenation reduction of ketones, aldehydes and imines using chelated iridium(III) *N*-heterocyclic bis-carbene complexes

We have developed a series of iridium bis-imidazole and bis-triazole precatalysts for the transfer hydrogenation reduction of ketones, aldehydes, and imines in 2-propanol. The choice of linker group is important; the best results were obtained with methylene and neopentanediyl linkers.

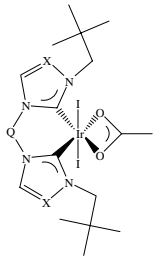

X = CH (Q = *o*-xylene, neopentanediyl, methylene)
X = N (Q = *o*-xylene, neopentanediyl, methylene)

Richard K. Merwin, Allyn C. Ontko, James F. Houlis, Dean M. Roddick

Polyhedron 23 (2004) 2873

Synthesis and characterization of CpMn(dfepe)(L) complexes (dfepe = $(C_2F_5)_2PCH_2$-$CH_2P(C_2F_5)_2$; L = CO, H_2, N_2): an unusual example of a dihydride to dihydrogen photochemical conversion

CpMn(dfepe)(CO) (**1**) was prepared by treatment of $CpMn(CO)_2(thf)$ with excess dfepe. Photolysis of **1** under a H_2 purge produced a 6:1 equilibrium isomeric mixture of the hydride complexes $CpMn(dfepe)(H)_2$ (**2a**) and $CpMn(dfepe)(\eta^2\text{-}H_2)$ (**2b**).

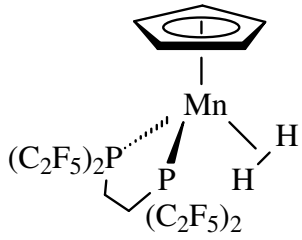

Mu-Hyun Baik, Richard A. Friesner, Gerard Parkin

Polyhedron 23 (2004) 2879

Theoretical investigation of the metal–metal interaction in dimolybdenum complexes with bridging hydride and methyl ligands

DFT calculations on dinuclear molybdenum complexes with bridging hydride and methyl ligands, namely $[CpMo(\mu\text{-}O_2CH)]_2(\mu\text{-}PH_2)$-$(\mu\text{-}H)$ and $[Cp^*Mo(\mu\text{-}O_2CMe)]_2(\mu\text{-}PMe_2)$-$(\mu\text{-}Me)$, indicate that the bonding is best described in terms of: (i) a 2-center-2-electron Mo–Mo single bond and (ii) a 3-center-2-electron Mo–H–Mo or Mo–Me–Mo bond.

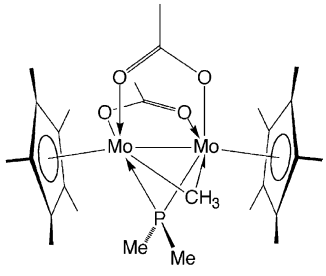

1 3c-2e Mo–Me–Mo bond
1 2c-2e Mo–Mo bond

J. Christopher Thomas, Jonas C. Peters

Polyhedron 23 (2004) 2901

Structural and spectroscopic studies of three-coordinate copper(I) supported by bis(phosphino)borate ligands

Monoanionic and neutral three-coordinate complexes of copper(I) have been prepared using several bis(phosphino)borate ligands. Substitution of a labile acetonitrile ligand in $[(3,5\text{-}Me_2Ph)_2B(CH_2P^tBu_2)_2]Cu(NCCH_3)$ provides access to a variety of $[BP_2]Cu^I\text{-}L$ species that should serve as a useful entry point to future group transfer studies.

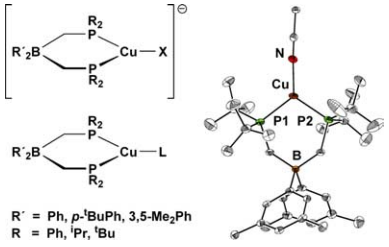

Jennifer C. Green, Claire Burney

Polyhedron 23 (2004) 2915

Open shell metallocenes and exchange splitting of ligand bands: a reassignment of the photoelectron spectra of manganocene

Open shell metallocenes and exchange splitting of ligand bands: a reassignment of the photoelectron spectra of manganocene.

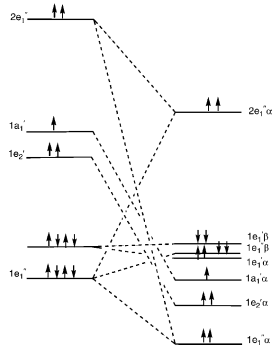

Rachel K. O'Reilly, Vernon C. Gibson, Andrew J.P. White, David J. Williams

Polyhedron 23 (2004) 2921

Five-coordinate iron(II) complexes bearing tridentate nitrogen donor ligands as catalysts for atom transfer radical polymerisation

Five-coordinate iron complexes containing tridentate nitrogen donor ligands have been evaluated for the atom transfer radical polymerisation of styrene. Catalyst activities decrease in the order of donor group: alkyl amine ≈ pyridine > alkyl imine ≫ aryl imine > aryl amine. The trend in polymerisation activity correlates with the redox potential of the corresponding complexes. Complexes derived from aryl-imine or -amine ligands afford catalytic chain transfer rather than ATRP catalysis.

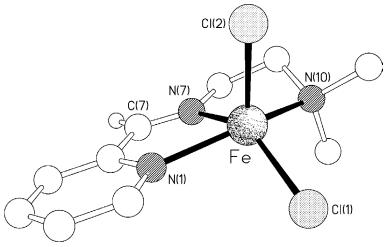

Kenneth D. Camm, Stephen J. Furtado, Andrew L. Gott, Patrick C. McGowan

Polyhedron 23 (2004) 2929

Synthesis and structural studies of bis-amino-functionalised ferrocene salts and ferrocenium salts

New bis-amino-functionalised ferrocene salts and ferrocenium salts have been synthesised and characterised, some of which have N–H···O and N–H···F hydrogen bonds.

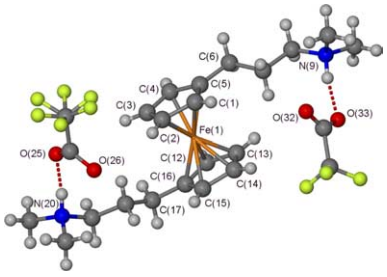

Sviatoslav Inyushin, Alexandr Shafir, John E. Sheats, Michael Minihane, Charles E. Whitten Jr., John Arnold

Polyhedron 23 (2004) 2937

Synthesis and X-ray structures of metallocenium diamines of iron and cobalt

A detailed, reproducible synthesis of 1,1′-diaminocobaltocenium hexafluorophosphate is provided. The X-ray structures of 1,1′-diaminocobaltocenium hexafluorophosphate and a related 1,1′-diaminoferrocenium salt, are described.

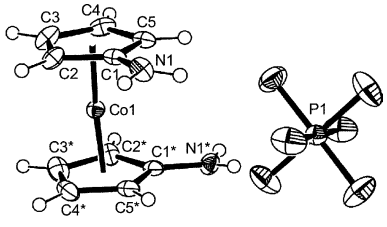

Britton K. Corkey, Felicia L. Taw, Robert G. Bergman, Maurice Brookhart

Polyhedron 23 (2004) 2943

Aromatic and aldehyde carbon–hydrogen bond activation at cationic Rh(III) centers. Evaluation of electronic substituent effects on aldehyde binding and C–H oxidative addition

Cationic rhodium methyl complexes, $[Cp^*(L)Rh(Me)(CH_2Cl_2)]^+$ (L = PMe_3, $P(OMe)_3$) react with benzene to yield the corresponding phenyl complexes, $[Cp^*(L)Rh(Ph)(CH_2Cl_2)]^+$. Reactions of $[Cp^*(L)Rh(Me)(CH_2Cl_2)]^+$ with *p*-X-substituted benzaldehydes (X = $-CF_3$, $-CH_3$, and –OMe) produce acyl aldehyde adducts, $[Cp^*(L)Rh(C(O)C_6H_4X)(p\text{-}XC_6H_4CHO)]^+$. In the case of L = PMe_3, decarbonylation of the aldehyde adducts occurs cleanly to form $[Cp^*(PMe_3)Rh(C_6H_4X)(CO)]^+$. For L = $P(OMe)_3$, decarbonylation is a more complicated process.

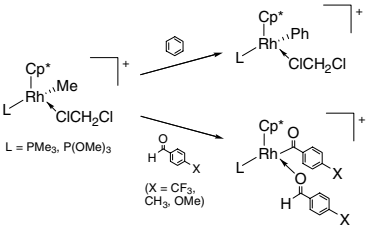

Oliver S. Wenger, Lawrence M. Henling, Michael W. Day, Jay R. Winkler, Harry B. Gray

Polyhedron 23 (2004) 2955

Rhenium(I) tricarbonyl complexes with photoisomerizable ligands

A rhenium(I) complex with a photoisomerizable pyridyl-dithienylperfluorocyclopentene ligand exhibits reversible photoswitchable luminescence. Rhenium(I) tricarbonyls with styryl and azobenzene substituted 2,2′-bipyridines also undergo photoisomerization reactions.

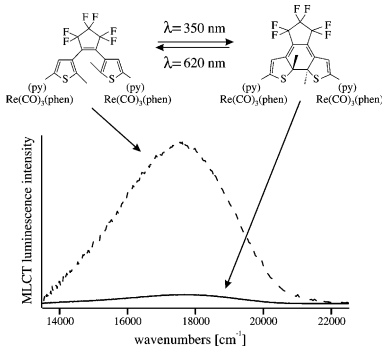

Stephen S. Oster, William D. Jones

Polyhedron 23 (2004) 2959

Synthesis, structure and reactivity of $[Ir(dippe)(\mu\text{-}Cl)]_2$, $[Ir(dippe)_2][Ir(dippe)Cl_2]$ and $[Ir(dippe)_2]Cl$

$[Ir(COD)Cl]_2$ reacts with varying stoichiometries of bis-(diisopropylphosphino)ethane to give either a μ-chloro-dimer, a cation/anion pair or a fully substituted cation. Solvent is also found to affect the species formed.

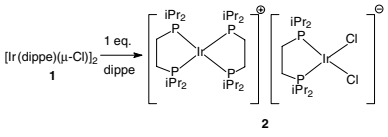

Christopher P. Morley, Susan Ford, Massimo Di Vaira

Polyhedron 23 (2004) 2967

Palladium complexes of novel azo-compounds derived from cycloalkeno-1,2,3-selenadiazoles: X-ray crystal structure of cyclohexeno-1,2,3-selenadiazole

Cycloalkeno-1,2,3-selenadiazoles react with $[Pd_2(dba)_3]/PR_3$ to yield the Pd(II) complexes $[PdL(PR_3)]$, containing a novel Se, N, Se tridentate ligand (L) formed by the coupling of two 1,2,3-selenadiazole molecules; the structures of cyclohexeno-1,2,3-selenadiazole and one of the products have been determined by X-ray crystallography.

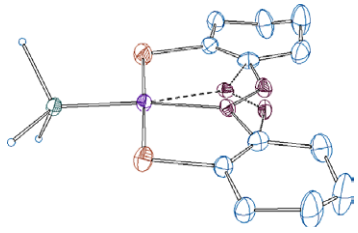

John F.C. Turner, Alan K. Soper

Polyhedron 23 (2004) 2975

On the determination of the structure of ferrocene in solution

The molecular structure of ferrocene in toluene solution is examined for the first time, using neutron scattering with hydrogen isotope substitution on the ferrocene hydrogen atoms. The results are interpreted via a computer-simulated model of ferrocene and toluene molecules at the same concentration and density as the experiment.

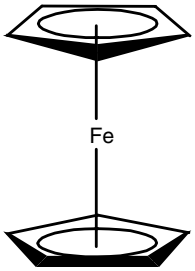

Rosa M. Claramunt, M. Dolores Santa María, José Elguero, Swiatoslaw Trofimenko

Polyhedron 23 (2004) 2985

Isomer distribution in thallium hydrotris(polymethylenepyrazol-1-yl)borates (thallium scorpionates): a multinuclear NMR study

The structure of two thallium scorpionates derived from 3(5),4-trimethylene- and 3(5),4-hexamethylenepyrazole was determined by multinuclear NMR, both in solution and in the solid state. The isomeric distribution is the same in both phases suggesting a kinetic origin. A $^{1}J(^{15}N\text{-}^{205}T1)$ coupling of 862 Hz was measured for $[T1(Tp^{(3,4-(CH_2)_6)})]$ in the solid state.

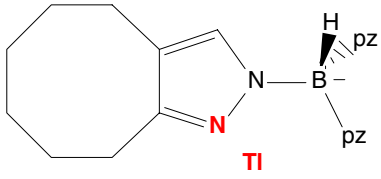

Constance M. Brett, Bruce E. Bursten

Polyhedron 23 (2004) 2993

Theoretical studies of 18-electron $M(C_nH_n)(C_{10-n}H_{10-n})$ (M = Fe, Ru, Os; n = 3, 4, 5) sandwich complexes

DFT has been used to explore the energetics and bonding of the isomeric sandwich complexes $(\eta^5\text{-}C_5H_5)_2M$, $(\eta^4\text{-}C_4H_4)M(\eta^6\text{-}C_6H_6)$, and $(\eta^3\text{-}C_3H_3)M(\eta^7\text{-}C_7H_7)$ (M = Fe, Ru, Os). The symmetric "5–5" metallocenes were the most stable isomers, with the "4–6" and "3–7" isomers ca. 40 and 80 kcal/mol higher in energy, respectively. Orbital analysis is used to explore the dominant bonding in the unsymmetric complexes.

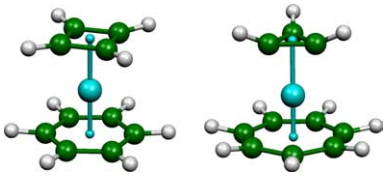

Author Index to Special Issue in Honour of Professor Malcolm L.H. Green 3003

The Publisher encourages the submission of articles in electronic form thus saving time and avoiding rekeying errors. For detailed instructions on the preparation of manuscripts and of electronic artwork, consult the Author Gateway for Elsevier at http://authors.elsevier.com

Full text of this journal is available, on-line from **ScienceDirect**. Visit **www.sciencedirect.com** for more information.

This journal is part of **ContentsDirect**, the *free* alerting service which sends tables of contents by e-mail for Elsevier books and journals. You can register for **ContentsDirect** online at: **www. elsevier.com/locate/contentsdirect**

Polyhedron Reports

REPORTS EDITOR

G. Christou

Polyhedron Reports are specially commissioned critical reports reviewing research of topical importance. Such articles will be commissioned by the Reports Editor of *Polyhedron* from recognised authorities in the appropriate field. Subject to availability, back issues of *Polyhedron* containing *Polyhedron Reports* may be obtained from the Publisher. Please send enquiries to Elsevier B.V., PO Box 211, 1000 AE, Amsterdam, the Netherlands.

Reports published

No. 1
Carbonylhydrido *tris*(triphenylphosphine)rhodium(I)
1982 **1**(7–8) 569–605 by F.H. Jardine

No. 2
The preparation and properties of metallacyclic compounds of the transition elements
1982 **1**(11–12) 739–777 by S. David Chappell and David J. Cole-Hamilton

No. 3
Mechanisms in the racemization of optically active coordination complexes in the solid state. A review
1983 **2**(4) 233–243 by P. O'Brien

No. 4
The reactions of nucleophiles with complexes of chelating heterocyclic imines; a critical survey
1983 **2**(7) 551–572 by Edwin C. Constable

No. 5
Metal–metal bonds and metal–carbon bonds in the chemistry of molybdenum and tungsten alkoxides
1983 **2**(8) 681–721 by Malcolm H. Chisholm

No. 6
Double bonding between the heavier main-group elements: from reactive intermediates to isolable molecules
1984 **3**(4) 389–432 by Alan H. Cowley

No. 7
Cyclometallated complexes incorporating a heterocyclic donor atom: the interface of coordination chemistry and organometallic chemistry
1984 **3**(9/10) 1037–1057 by Edwin C. Constable

No. 8
Reactions of triosmium clusters with organic compounds
1984 **3**(11) 1175–1225 by Kevin Burgess

No. 9
Chromium(III) and the glucose tolerance factor
1985 **4**(1) 1–14 by J. Barrett, P. O'Brien and J. Pedrosa De Jesus

No. 10
Carbon–hydrogen bond activation in early transition metal systems
1985 **4**(2) 177–200 by Ian P. Rothwell

No. 11
Arene–chromium tricarbonyl complexes: bonding and behaviour
1985 **4**(6) 901–927 by A. Solladié–Cavallo

No. 12
Transition–metal thiocarbonyl complexes: preparative methods, reactivity and thiocarbonyl ligand bonding properties
1985 **4**(11) 1801–1846 by Peter V. Broadhurst

No. 13
The synthesis, structures, bonding and unusual reactivity of sulfido osmium carbonyl cluster compounds
1985 **4**(12) 2003–2025 by Richard D. Adams

No. 14
The preparation and structure of complexes containing simple sulphur–nitrogen ligands
1986 **5**(3) 607–632 by Paul F. Kelly and J. Derek Woollins

No. 15
The structural chemistry of metal thiolate complexes
1986 **5**(5) 1037–1104 by Ian G. Dance

Continued from previous page

Reports published

No. 16
Transition-metal complexes of inorganic sulphur-nitrogen ligands
1986 **5**(11) 1661–1699 by Tristram Chivers and Frank Edelmann

No. 17
Transition-metal aluminohydride complexes
1986 **5**(12) 1897–1917 by Andrew R. Barren and Geoffrey Wilkinson

No. 18
The organometallic chemistry of phosphazenes
1987 **6**(2) 119–157 by Harry R. Allcock, James L. Desorcie and Geoffrey H. Riding

No. 19
Naked phosphorus atoms and units in transition-metal compounds
1987 **6**(3) 151–182 by Massimo Di Vaira, Piero Stoppioni and Maurizio Peruzzini

No. 20
The organometallic chemistry of the lanthanide elements in low oxidation states
1987 **6**(5) 803–835 by William J. Evans

No. 21
Organometallic oxides: the example of trioxo (η^5-pentamethylcyclopentadienyl)rhenium(VII)
1987 **6**(6) 1165–1182 by Wolfgang A. Herrmann, Eberhardt Herdtweck, Martina Flöel, Jürgen Kulpe, Ulrich Küsthardt and Jan Okuda

No. 22
From metallaboranes to transition metal borides: the chemistry of metal-rich metallaborane clusters
1997 **6**(11) 1935–1958 by Catherine E. Housecroft

No. 23
Electron counting in clusters: A view of the concepts
1998 **7**(4) 253–283 by Steven M. Owen

No. 24
Advances in vanadium, niobium and tantalum carbonyls
1988 **7**(18) 1639–1665 by S.C. Srivastava and A.K. Shrimal

No. 25
Homonuclear and heteronuclear oxo-bridged compounds of the transition elements
1989 **8**(3) 219–274 by B.O. West

No. 26
Kinetic deuterium isotope effects in transition metal hydride clusters
1989 **8**(4) 383–405 by E. Rosenberg

No. 27
Bi-phasic and phase transfer catalysis
1989 **8**(4) 407–413 by T.G. Southern

No. 28
Phosphorane iminato complexes of transition metals
1989 **8**(6) 707–726 by K. Dehnicke and J. Strähle

No. 29
Structure, bonding and electron counts in cubane-type clusters having M_4S_4, $M_2M'_2S_4$ and MM'_3S_4 cores
1989 **8**(24) 2843–2882 by S. Harris

No. 30
Electrochemical studies on iron, ruthenium and osmium carbonyl clusters
1990 **9**(4) 455–474 by Simon R. Drake

No. 31
New developments in the organometallic chemistry of calcium, strontium and barium
1990 **9**(11) 1345–1362 by Timothy P. Hanusa

No. 32
Kinetics and mechanisms of CO substitution of metal carbonyls
1990 **9**(13) 1503–1535 by Fred Basolo

No. 33
Synthesis, molecular structures, properties and reactions of halo- and carbonyl(amine)copper(I) complexes
1990 **9**(19) 2319–2351 by K.G. Caulton, G. Davies and E.M. Holt

No. 34
Recent developments in the chemistry of mono- and dinuclear complexes of the macrocyclic dianion, 5,7,12,14-teramethyldibenzo[b,i][1,4,8,11]tetraazacyclotetradecine
1990 **9**(21) 2553–2566 by F.A. Cotton and J. Czuchajowska

No. 35
Coordinatively unsaturated tripalladium and triplatinum clusters: models for reactions on metal surfaces
1990 **9**(23) 2767–2802 by R.J. Puddephan, L. Manojlovic-Muir and K.W. Muir

Continued from previous page

Reports published

No. 36
Homoleptic and related aryls of transition metals
1991 **10**(2) 135–173 by S.U. Koschmieder and G. Wilkinson

No. 37
Ruthenium clusters containing N-donor ligands
1991 **10**(3) 277–322 by M.I. Bruce, M.P. Cifuentes and M.G. Humphrey

No. 38
Aluminium alkoxides, β-diketonates and carboxylates
1991 **10**(17) 1967–1994 by R.C. Mehrotra and A.K. Rai

No. 39
Alkyne rotation on a Rh—Rh bond: an entry to diverse chemistry
1991 **10**(17) 1995–2023 by R.S. Dickson

No. 40
The structures of compounds containing selenium nitrogen, and tellurium–nitrogen bonds
1991 **10**(20/21) 2353–2370 by M. Björgvinsson and H.W. Roesky

No. 41
Reactions of L-ascorbic acid with transition metal complexes
1992 **11**(3) 285–321 by Michael B. Davies

No. 42
Halide ion transfer between main group and transition metal halides as a valuable method for the synthesis of new compounds and catalyst precursors
1992 **11**(7) 715–728 by Piotr Sobota

No. 43
Cyclopentadienylmetal oxides
1992 **11**(14) 1707–1731 by F. Bottomleys

No. 44
Relevance of X-ray structural data to kinetic studies: substitution behaviour of transition metal tetracyano complexes containing oxo or nitrido ligands
1992 **11**(18) 2277–2284 by J.G. Leipoldt, S.S. Basson, A. Roodt and W. Purcell

No. 45
Excited-state acid–base properties of inorganic compounds
1992 **11**(18) 2285–2299 by Johannes G. Vos

No. 46
A thermodynamic scale for oxygen atom transfer reactions
1993 **12**(6) 571–589 by R.H. Holm and James P. Donahue

No. 47
The ligand polyhedral model and its application to the binary carbonyls
1993 **12**(9) 977–990 by Brian F.G. Johnson and Yvonne V. Roberts

No. 48
Lewis base adducts of alane and gallane
1993 **12**(15) 1829–1848 by Cameron Jones, George A. Koutsantonis and Colin L. Raston

No. 49
Stable compounds of the heavier group 14 and 15 elements involving pπ–pπ multiple bonding: an overview of the first decade
1993 **12**(20) 2431–2446 by N.C. Norman

No. 50
The influence of catalyst structure on the dehydro-polymerization of phenylsilane
1994 **13**(15/16) 2231–2243 by Toru Immure and T. Don Tilley

No. 51
Structural systematic in nickel carbonyl cluster anions
1995 **14**(3) 339–365 by Anthony F. Masters and Josephine T. Meyer

No. 52
Multidentate ligands bound via alkyne and group 15 or 16 donor sites
1995 **14**(4) 465–481 by Michael J. Went

No. 53
Chemical vapour deposition of copper from (hfac)CuL compounds
1995 **14**(6) 699–732 by Mark J. Hampden-Smith and Toivo T. Kodas

No. 54
Nickel carbonyl cluster complexes
1995 **14**(7) 829–868 by James K. Beattie, Antinony F. Masters and Josephine T. Meyer

Continued from previous page

Reports published

No. 55
Transition metal butadienyl complexes
1995 **14**(10) 1259–1276 by Brian J. Brisdon and Richard A. Walton

No. 56
Bis(diphenylphosphino)amine and related chemistry
1995 **14**(23/24) 3367–3388 by Pravat Bhattacharyya and J. Derek Woollins

No. 57
Stereochemical aspects of phosphor-1,1-dithiolato metal complexes (dithiophosphates, dithiophosphinates): coordination patterns, molecular structures and supramolecular associations – I
1994 **14**(23/24) 3389–3472 by Ionel Haiduc, D. Bryan Sowerby and Shao-Fang Lu

No. 58
Organotellurium precursors for metal organic chemical vapour deposition (MOCVD) of mercury cadmium telluride (MCT)
1996 **15**(5/6) 745–763 by Harkesh B. Singh and Narasimhan Sudha

No. 59
The chemistry of inorganic and organometallic compounds with adamantane-like structures
1996 **15**(10) 1585–1642 by Jagadese J. Vittal

No. 60
Stereochemical aspects of phosphor-1,1-dithiolato metal complexes: coordination patterns, molecular structures and supramolecular associations in dithio- phosphinates and related compounds
1996 **15**(15) 2469–2521 by Ionel Haiduc and D. Bryan Sowerby

No. 61
Toxic and mutagenic effects of chromium(VI). A review
1996 **15**(21) 3667–3689 by Maria Cieślak-Golonka

No. 62
Ring-opened polymerization (ROP) of strained, ring-titled silicon-bridged [l]ferrocenophanes: synthetic methods and mechanisms
1996 **15**(24) 4311–4329 by Ian Manners

No. 63
Metal–metal bond formation in the oxidative addition to dinuclear gold(I) species. Implications from dinuclear and trinuclear gold chemistry for the oxidative additional process generally
1997 **16**(1) 1–17 by John P. Fackler Jr

No. 64
Applications of electrospray mass spectrometry in organometallic chemistry
1998 **17**(25–26) 4291–4313 by William Henderson, Brian K. Nicholson and Louise J. McCaffrey

No. 65
Recent advances in the chemistry of scandium
1999 **18**(12) 1691–1715 by S.A. Cotton

No. 66
Metal-containing dendritic polymers
1999 **18**(27) 3575–3591 by Fiona J. Stoddart and Thomas Welton

No. 67
Primary alanes and alanates: useful synthetic reagents in aluminium chemistry
2000 **19**(14) 1649–1661 by Rudolph J. Wehmschulte and Philip P. Power

No. 68
The Bioinorganic chemistry of chromium (III)
2001 **20**(1–2) 1–26 by John B. Vincent

No. 69
Recent advances in homogenous catalysis using platinum complexes
2001 **20**(3–4) 151–164 by Matthew L. Clarke

No. 70
Structures of alkali and alkaline earth metal clusters with oxygen donor ligands
2004 **23**(9) 1479–1504 by Katharina M. Fromm and Estelle D. Gueneau

Available online at www.sciencedirect.com
SCIENCE DIRECT®
Volume 23, issue 1, 1 January 2004
POLYHEDRON
www.elsevier.com/locate/poly

Contents

Publisher's note xiii

Papers

Mohammed. Fettouhi, Mohamed I. M. Wazeer, Saeed Ahmad, Anvarhusein A. Isab

Polyhedron 23 (2004) 1

X-ray structure and ^{77}Se, ^{31}P and ^{13}C MAS NMR of the dinuclear complex 1,2-*bis*(selenourea)-1\κSe,2\κSe-1,2-*bis*(trimethylphosphine)digold(I) chloride

The single crystal X-ray structure of the compound $[(Me_3P\text{-}Au\text{-}Selenourea)_2^{2+}\ 2Cl^-]$ has been determined. The $[Me_3P\text{-}Au\text{-}(selenourea)]$ units are dimerized and adopt a binuclear structure characterized by a metal–metal interaction (Au–Au:3.0386(5) Å). The principal components of the ^{77}Se, ^{31}P and ^{13}C shielding tensors were determined from solid-state NMR data.

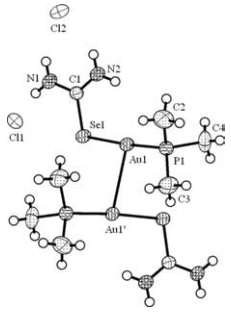

Dhiman Kumar Sau, Ray J. Butcher, Siddhartha Chaudhuri, Nityananda Saha

Polyhedron 23 (2004) 5

Synthesis and spectroscopic characterization of new cobalt(III) complexes with 5-methyl-3-formyl pyrazole 3-hexamethyleneiminyl thiosemicarbazone (HMPz3Hex): X-ray crystallographic identification of HMPz3Hex and $[Co(MPz3Hex)_2]Br \cdot H_2O$ with evidence for unusual rotation about the azomethine double bond of the ligand on complexation with cobalt(III)

The synthesis and spectroscopic characterization of 5-methyl-3-formyl pyrazole 3-hexamethyleneiminyl thiosemicarbazone (HMPz 3Hex) and its cobalt(III) complexes, $[Co(MPz3Hex)_2]X{\cdot}nH_2O$ (X=Cl, Br, NO_3, ClO_4 or BF_4; $n = 1$ to 2) are reported. X-ray structure analysis of the complex $[Co(MPz3Hex)_2]Br{\cdot}H_2O$, as a representative species, has authenticated a CoN_4S_2 octahedral coordination with a monoprotic NNS tridentate function of the primary ligand system with two azomethine nitrogen atoms in *trans* positions and the pyrazolyl nitrogen atoms and thiolato sulfurs in *cis* positions. Comparison with the crystal structure of the free ligand (HMPz3Hex) has shown that there is an unusual rotation about the azomethine double bond during complexation. A plausible reaction mechanism for this observation has been proposed.

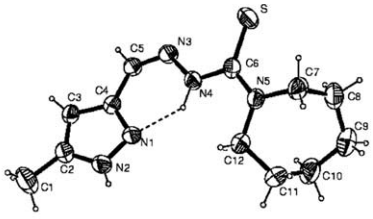

HMPz3Hex

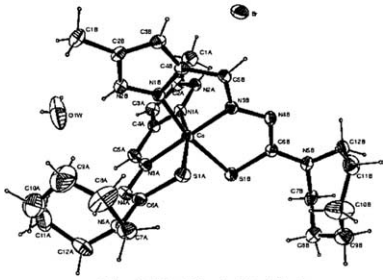

$[Co(MPz3Hex)_2]Br.H_2O$

Yao-Cheng Shi, Hua-Mei Yang, Wen-Bin Shen, Chao-Guo Yan, Xiao-Ya Hu

Polyhedron 23 (2004) 15

Syntheses and crystal structures of ferrocene-containing enaminones and their copper complexes

Reaction of the ferrocene-containing β-diketone $[C_5H_5FeC_5H_4C(O)CH_2C(O)R]$ (**1**, R=CH_3; **2**, R=C_6H_5) and the corresponding aniline $[H_2NAr]$ (Ar=Ph, 2-$CH_3C_6H_4$, 2,6-$(CH_3)_2C_6H_3$) yields a series of enaminones $[C_5H_5FeC_5H_4C(O)CH=C(NHAr)R]$ (**HL^1**–**HL^6**). Reaction of the enaminones (**HL^1**–**HL^5** and copper acetate affords complexes **I**–**V**. Their structures have been determined by the X-ray crystallography of enaminone **HL^6** and complex **I**.

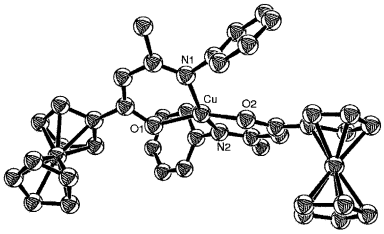

Magdi F. Iskander, Laila El-Sayed, Nahed M.H. Salem, Wolfgang Haase, Hans Jorg Linder, Sabine Foro

Polyhedron 23 (2004) 23

Synthesis, characterization and magnetochemical studies of some copper(II) complexes derived from *n*-salicylidene-*n*-alkanoylhydrazins: X-ray crystal and molecular structure of bis [monochloro(μ-*n*-salicylidenemyristoylhydrazine)ono(−1)] dicopper(II)

Three types of copper(II) complexes, $[Cu(HL)Cl{\cdot}H_2O]{\cdot}xH_2O$, $[\{Cu(HL)Cl\}_2]$ and $[\{Cu(L)\}_2]$, derived from *N*-Salicylidene-*n*-alkanoylhydrazines (H_2L) have been synthesized and characterized by elemental analyses, infrared spectra and field desorption mass spectra as well as variable temperature magnetic susceptibility measurements. The X-ray molecular structure of bis[monochloro(μ-*N*-salicylidene myristoylhydrazine)ONO′(−1)] dicopper(II) showed that this complex is a centrosymmetric dimer in which each copper(II) is in a distorted square pyramidal environment.

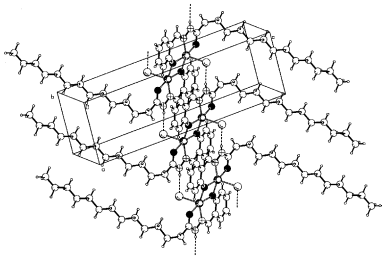

Joanna Borowiec, Irena Trojnar, Stanisław Wołowiec

Polyhedron 23 (2004) 33

Mono- and dizinc complexes of diporphyrins with flexible spacers of variable length

The efficient synthetic route to mono-zinc complexes of diporphyrins with flexible hydrocarbon spacers was described. Monozincdiporphyrin complexes were demonstrated to be useful substrates for heterodimetalodiporphyrins. The discriminating factor in complementary binding of azaheteroaromatic bases: bipyridyl and pyrazine to dizincdiporphyrins was the length of spacer.

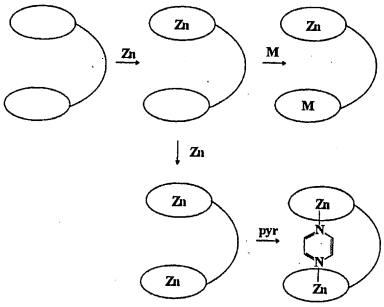

A. Sreekanth, U.L. Kala, Chandini R. Nayar, M.R. Prathapachandra Kurup

Polyhedron 23 (2004) 41

Cobalt(III) complexes of 2-hydroxyacetophenone N(4)-phenyl semicarbazone containing heterocyclic coligands: syntheses, structure and spectral studies

A series of four novel mixed ligand Co(III) complexes of 2-hydroxyacetophenone 4-phenyl semicarbazone (H_2L), heterocyclic base, B [1,10-phenanthroline (phen), piperidine (pip) and pyrrolidine (pyrr)] and azide/thiocyanate (X) with a general formula $[CoLB_xX]$ were prepared and their structures and spectra studied.

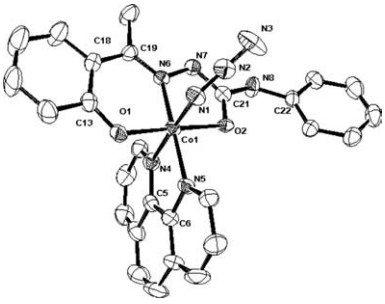

Xue-Lei Hu, Yi-Zhi Li, Qin-Hui Luo

Polyhedron 23 (2004) 49

Characterization and crystal structure of lanthanide cryptates of a ligand derived from 2,6-diformyl-pyridine

Seven lathanide cryptates $[LnL](NO)_3{\cdot}nH_2O$ ($n = 1$–3; Ln=La, Ce, Pr, Sm, Eu, Gd, Tb) were synthesized by the reactions of lanthanide nitrates with free ligand L (L was derived from the (2+3) condensation of 2,6-diformyl-pyridine (*dfp*) with tris-(2-aminoethyl) amine (*tren*)). The crystal structure of Eu(III) cryptate displays a tricapped prismatic coordination geometry

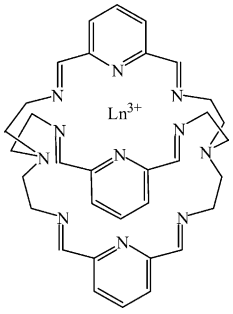

Hui Huang, Shu-Yan Yu, Hong-Bo Liu, Mei Shi

Polyhedron 23 (2004) 55

Neutral coordination frameworks with host–guest properties constructed by dicopper(II) units and 4,7-phenanthroline

Reaction of $[Cu_2(O_2CR)_4]$ [R=Me(**1**), Ph(**2**)] with 4,7-phenanthroline produced neutral coordination frameworks $\{[Cu_2(O_2CR)_4](C_{12}N_2H_8)\}_n$ showing inclusion behavior toward solvent molecules; through variation of the equatorial ligands of the dimetal units, the channels size and host–guest properties of the coordination polymers can be controlled.

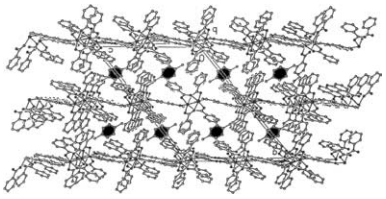

Jian Gao, Ralph A. Zingaro, Ming Z. Gao

Polyhedron 23 (2004) 59

A silica immobilized cobalt complex: absorption of dioxygen and the redox ability in aqueous solution

A new dioxygen carrier has been synthesized through the tethering of a dinuclear chelating ligand to the surface of mesoporous silica. The material is extremely efficient for the selective absorption of dioxygen and displays good catalytic activity for the disproportionation of H_2O_2.

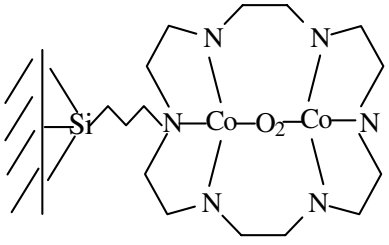

V.D. de Castro, Geraldo M. de Lima, Arilza O. Porto, Helmuth G.L. Siebald, José D. de Souza Filho, J.D. Ardisson, José D. Ayala, Gabriella Bombieri

Polyhedron 23 (2004) 63

Synthesis, structural characterisation and thermal decomposition of [{Pt(dppf)(2-SPy)}{BF_4}] (dppf = 1,1′-bisdiphenylphosfinoferrocene and 2-SPy = 2-mercaptopyridine) – a source for a Fe–Pt containing alloy

The reaction of 2-PySK with [Pt(dppf)Cl_2] [dppf=1,1′-bis(diphenylphosfinoferrocene and 2-PyS=2-mercaptopyridine] produced Pt(dppf)(2-SPy)$_2$ (**1**) and its subsequent reaction with $SnBu_2(BF_4)_2$ or $SnBu_3(BF_4)$ yielded [{Pt(dppf)(2-SPy)}{BF_4}] (**2**). A thermal decomposition study was carried out with **2** in three different atmosphere: oxygen, nitrogen or hydrogen. The residues were characterised by X-ray powder diffraction (XRD), X-ray electron probe microanalysis (EPMA), scanning electron microscopy (SEM) and ^{57}Fe Mossbauer spectroscopy. The results have shown the formation of a disordered $Pt_{1-x}Fe_x$ based alloy when the pyrolysis process was performed in H_2, simultaneously with small amount of Fe(II) and Fe(III) phosphides. Furthermore, in oxygen and nitrogen the thermal decomposition of **2** produced metallic agglomerates of Pt dispersed in a combination of Fe(II) and Fe(III) phosphates in O_2, and an intricate mixture of sulphides and phosphides in N_2.

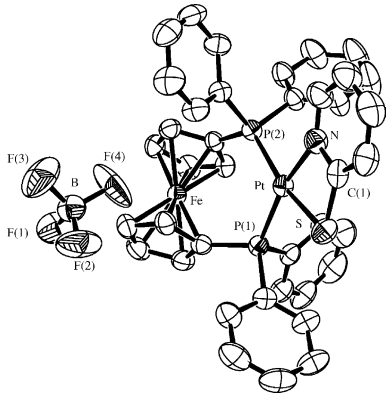

Ravi Shankar, Mukesh Kumar, Raj K. Chadha, Suraj P. Narula

Polyhedron 23 (2004) 71

Reactivity behavior of (hydroxy)diorganotin(IV)methanesulfonates with ionic nucleophiles – synthesis and structural characterization of novel diorganostannate salts, [$R_2Sn(\mu\text{-}OH)(OSO_2Me)(ONO_2)]_2$ $2Bu_4N$

The reaction of $R_2Sn(OH)OSO_2Me$ [R=*n*-Pr (**1a**) or *n*-Bu (**1b**)] with Bu_4NNO_3 proceeds by nucleophilic addition of NO_3^- ion to the Lewis acidic tin center to yield the novel stannates, [$R_2Sn(\mu\text{-}OH)(OSO_2Me)(ONO_2)]_2$ $2Bu_4N$ [R=*n*-Pr (**2a**), *n*-Bu (**2b**)]. The use of strong nucleophiles such as Bu_4NX (X=F^-, OAc^-) or RLi (R=*n*-Bu, Me), however favors ionic metathesis involving the cleavage of Sn–OSO_2Me group.

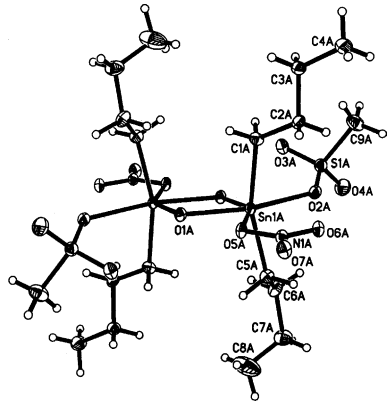

B. Arul Prakasam, Kuppukkannu Ramalingam, M. Saravanan, Gabriele Bocelli, Andrea Cantoni

Polyhedron 23 (2004) 77

Effect of free and chelating phosphine coordination environments on the NiS_2P_2 chromophore: synthesis, NMR and other spectral studies. Crystal and molecular structures of (*N*,*N*-dipropyldithiocarbamato)di(triphenylphosphine)nickel(II) perchlorate and (*N*,*N*-dipropyldithiocarbamato)1,2-bis((diphenylphosphino)ethane)nickel(II) tetraphenylborate

Planar [Ni(dnpdtc)(PPh_3)$_2$]ClO_4·PPh_3 (**1**) and [Ni(dnpdtc)(dppe)]BPh_4 (**2**) complexes were prepared. NMR spectra of the complexes show very large (~20 ppm) ^{31}P chemical shifts in both the compounds. The most important $N^{13}CS_2$ chemical shifts appear at 199.17 and 201.88 ppm for (**1**) and (**2**) respectively. Structural implications are very large for (**2**) compared to (**1**) when free phosphines are replaced by chelating dppe with the P-Ni-P angle shrinking to approximately 12°.

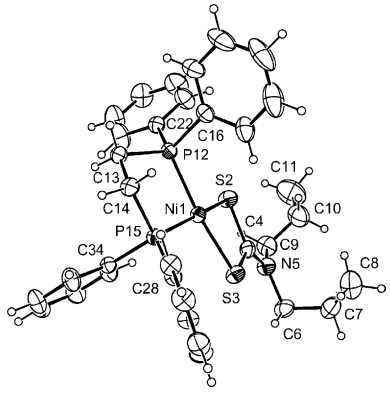

Constantinos J. Milios, Elena Kefalloniti, Catherine P. Raptopoulou, Aris Terzis, Albert Escuer, Ramon Vicente, Spyros P. Perlepes

Polyhedron 23 (2004) 83

2-Pyridinealdoxime [(py)CHNOH] in manganese(II) carboxylate chemistry: mononuclear, dinuclear, tetranuclear and polymeric complexes, and partial transformation of (py)CHNOH to picolinate(−1)

The reactions of 2-pyridinealdoxime, (py)CHNOH, with various manganese(II) sources lead to complexes $[Mn_4(O_2CPh)_6\{(py)CO_2\}_2\{(py)CHNOH\}_2]$ (**1**), $[Mn(O_2CPh)\{(py)CO_2\}\{(py)CHNOH\}]_n$ (**2**), $[Mn_2(O_2CMe)_2\{(py)CO_2\}_2\{(py)CHNOH\}_2]$ (**3**) and $[Mn(O_2CCF_3)_2\{(py)CHNOH\}_2]$ (**4**) which have been structurally characterised. The most interesting feature in the synthesis of **1**–**3** is the in situ formation of the picolinate(−1) ligand, $(py)CO_2^-$, while the $CF_3CO_2^-$ ligand present in **4** is one of the decomposition products of the hexafluoroacetylacetonate(−1), $hfac^-$, ligand.

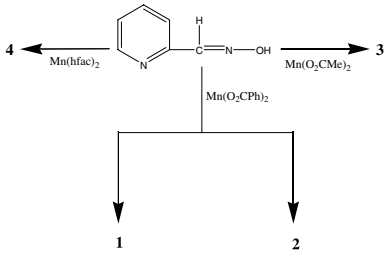

Natasha J. Lundin, Ian G. Hamilton, Allan G. Blackman

Polyhedron 23 (2004) 97

Synthesis and hypodentate Cu(II) complexes of new tripodal tetraamine ligands incorporating a long pendant arm

The tetrahydrochloride salts of the new tripodal ligands apba (*N*-(5-aminopentyl)-*N,N*-bis(2-aminoethyl)amine) and ahba (*N*-(6-aminohexyl)-*N,N*-bis(2-aminoethyl)amine) react with $CuCO_3{\cdot}Cu(OH)_2$ to give complexes in which the ligands are coordinated in a hypodentate fashion, with the longest pendant arm of the ligands remaining protonated and unbound.

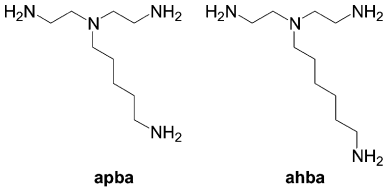

Florian P. Pruchnik, Zbigniew Ciunik, Mirosław Pruchnik

Polyhedron 23 (2004) 103

New one- and two-dimensional rhodium–tin polynuclear complexes, synthesis, properties and structural characterization

New dendritic tin–rhodium complexes $[Sn\{CH_2CH_2CNRhCl(CO)_2\}_4]{\cdot}CH_2Cl_2$ and $[Sn_2\{CH_2CH_2CNRhCl(CO)_2\}_4(CH_2CH_2CN)_2]\cdot CHCl_3$ have been synthesized and described. Owing to the interactions between the rhodium atoms, complexes in the solid state have one-dimensional and two-dimensional structure. Unexpectedly the ditin(III) moiety shows an eclipsed conformation. The latter compound in solutions decomposes giving $[Rh_6(CO)_{16}]$.

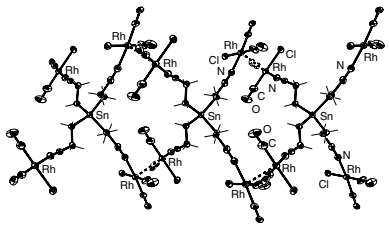

Zoya A. Starikova, Vadim G. Kessler, Nataliya Ya. Turova, Dmitriy E. Tcheboukov, Evgeniya V. Suslova, Gulaim A. Seisenbaeva, Alexandr I. Yanovsky

Polyhedron 23 (2004) 109

New polynuclear aluminium oxoalkoxides: molecular structures of $Al_{11}(\mu_4\text{-}O)_2(\mu_3\text{-}O)_2(\mu\text{-}O)_2(\mu\text{-}OPr^n)_{10}(\mu\text{-}OPr^i)_2(\mu\text{-}ROH)_2(OPr^i)_8(OR)$, $R = Pr^{n,i}$ and $Al_5Mg_4(\mu_4\text{-}O)_2(\mu_3\text{-}O)(\mu\text{-}OH)_3(\mu\text{-}OPr^i)_8(\mu,\eta^2\text{-}acac)_4(\eta^2\text{-}acac)_2$

Two new aluminium oxoisopropoxide complexes, $Al_{11}O_6(OPr^n)_{10}(OPr^i)_{10}(OR)(ROH)_2$ ($R=Pr^i$, Pr^n) (**1**) and $Al_5Mg_4O_3(OH)_3(OPr^i)_8(acac)_6{\cdot}0.5PhMe$ (**2**) have been isolated and structurally characterized. Both molecules contain two pentanuclear cores $[M_5(\mu_4\text{-}O)(\mu_3\text{-}O)(\mu\text{-}OX)_6(Y)_4]$ ($X=H$, Pr^n, $Y=OPr^i$, acac/2) and differ only in the manner in which they are attached to each other. The core structures in the molecules of aluminium and iron oxoalkoxides are discussed.

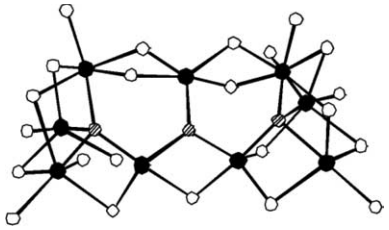

Hye Jin Nam, Ha-Jin Lee, Dong-Youn Noh

Polyhedron 23 (2004) 115

Novel mercury(II) complexes of 1,3-dithiole-2-thiones containing the 2-pyridyl moiety: syntheses, X-ray crystal structures and solution behavior

The reaction of 2PyEDT-DTT (**1**) with HgX_2 (X=Cl, Br, I) leads to the formation of $[Hg(2PyEDT\text{-}DTT)X_2]_2$ (**2**) and $Hg(2PyDT\text{-}DTT)_2$ (**3**). The crystal structures of **1**, **2** (X=Br, I) and **3** have been determined by X-ray structure analysis. It is disclosed that the intermolecular Hg···S and Hg···N interactions in **2** are cleaved by H_2O in the KBr matrix as well as in organic solvents. In complex **3**, the 2PyDT-DTT ligand is reversibly transformed to 2PyEDT-DTT and Hg(II) in the organic solvent, which was evidenced by the time-dependent UV–Vis and ^1H NMR measurements.

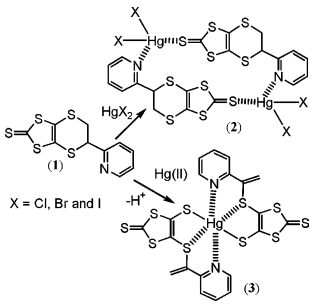

Jason Anagnostis, Mark M. Turnbull

Polyhedron 23 (2004) 125

Rotational barriers in dialkylaminochlorophosphines: methyl-substituted piperidinochlorophenylphosphines

Barriers to rotation about the P–N bond (measured via variable temperature NMR) indicate that the steric requirements of 2- and/or 6-methyl substituents on the piperidine ring in the title compounds are negligible. This is in agreement with cone angle measurements.

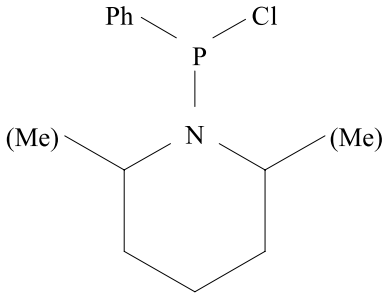

Edwin C. Constable, Robyn Handel, Catherine E. Housecroft, Markus Neuburger, Emma R. Schofield, Margareta Zehnder

Polyhedron 23 (2004) 135

Efficient syntheses of 4′-(2-thienyl)- and 4′-(3-thienyl)-2,2′:6′,2″-terpyridine: preparation and characterization of Fe(II), Ru(II), Os(II) and Co(II) complexes

Efficient and convenient, one-pot syntheses of the isomeric ligands 4′-(2-thienyl)-2,2′:6′,2″-terpyridine and 4′-(3-thienyl)-2,2′:6′,2″-terpyridine are described. The formation and characterization of Fe(II), Ru(II), Os(II) and Co(II) complexes containing these ligands are described.

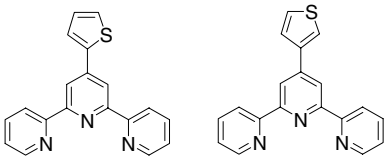

Benjamin P. Hay, Jamal Uddin, Timothy K. Firman

Polyhedron 23 (2004) 145

Eight-coordinate stereochemistries of U(IV) catecholate and aquo complexes

An extended MM3 model has been used to identify all low energy configurations for U(IV) complexes, $[U(catecholate)_n(OH_2)_{8-2n}]^{4-2n}$, $n = 1$–4. The stable stereochemistries are reported for each stoichiometry and, where possible, the results are compared with experimental data and with the predictions from prior repulsion energy calculations.

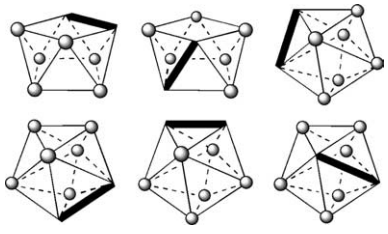

Xiao-Feng He, Christopher M. Vogels, Andreas Decken, Stephen A. Westcott

Polyhedron 23 (2004) 155

Pyridyl benzimidazole, benzoxazole, and benzothiazole platinum complexes

Addition of pyridyl benzimidazole, benzoxazole, and benzothiazole compounds (L_p) to $[PtCl_2(coe)]_2$ (coe=*cis*-cyclooctene) or K_2PtCl_4 gives didentate *cis*-$PtCl_2(L_p)$ or monodentate *cis*-$PtCl_2(L_p)_2$ in moderate to high yields.

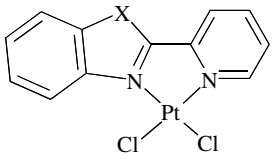

1a : X = NH
1b : X = O
1c : X = S

Karen A. Crouse, Kar-Beng Chew, M.T.H. Tarafder, A. Kasbollah, A.M. Ali, B.M. Yamin, H.-K. Fun

Polyhedron 23 (2004) 161

Synthesis, characterization and bio-activity of *S*-2-picolyldithiocarbazate (S2PDTC), some of its Schiff bases and their Ni(II) complexes and X-ray structure of *S*-2-picolyl-β-*N*-(2-acetylpyrrole)dithiocarbazate

A new dithiocarbazate ligand, *S*-2-picolyldithiocarbazate (S2PDTC) was synthesized using 2-picolylchloride hydrochloride. Tridentate Schiff bases were prepared with pyridine-2-carbox-aldehyde (NNS′), 2-acetylpyrrole (NNS″) and 2-acetylthiophene (NSS), while a bidentate Schiff base (NS) was prepared with 2-acetylfuran. Complexes with Ni(II) salts were synthesized and characterized by elemental analyses and various physico-chemical techniques. The bioactivity of these compounds has been investigated.

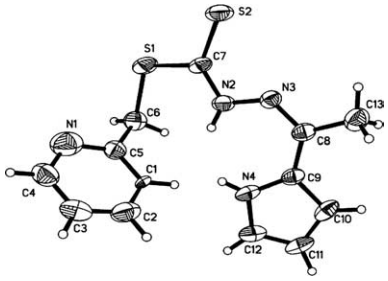

Lin-Ping Zhang, Wen-Jie Lu, Thomas C.W. Mak

Polyhedron 23 (2004) 169

Construction of lanthanide(III) coordination polymers with 1,2-bis(4-pyridyl) ethane-*N*, *N*′-dioxide and *trans*-1,2-bis(4-pyridyl) ethene-*N*,*N*′-dioxide

The flexible 1,2-bis(4-pyridyl)ethane-*N*, *N*′-dioxide (L^1) and rigid *trans*-1,2-bis(4-pyridyl)ethene-*N*, *N*′-dioxide (L^2) ligands have been used to generate lanthanide(III) complexes $\{[Ce(L^1)_{1.5}(NO_3)_3](CH_2Cl_2)_{0.25}(H_2O)_{0.25}\}_\infty$ **1**, $[Ln(L^2)_{1.5}(NO_3)_3]_\infty$ (Ln = Ce, **2**; Gd, **3**) and $[Yb(L^2)(CH_3OH)(NO_3)_3]_\infty$ **4**. Compound **1** shows a three-dimensional network based on binuclear Ce_2O_2 units with triangular and distorted square channels. The isomorphous pair **2** and **3** composed of Ln_2O_2 units exhibit a layered structure of (4,4) topology. In **4**, the mononuclear Yb(III) ions are bridged by L^2 ligands to form a sinuous chain.

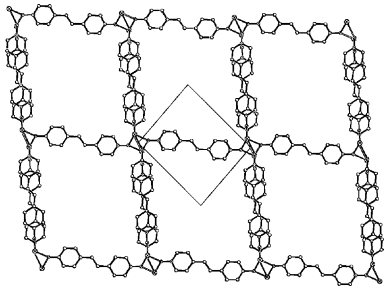

Kunio Mochida, Kiyoko Amada, Hideo Sugimoto, Mitsuo Akiba, Katsuyuki Sato

Polyhedron 23 (2004) 177

Preparation of polystyrene-supported hydrogermanes and their reduction of organic halides

The preparation of polystyrene-supported hydrogermanes (**1–4)** and their reduction of organic halides is reported.

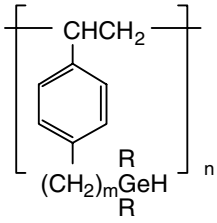

1 (m = 0, R = Et**), 2** (m = 1, R = Et)
3 (m = 1, R = H), **4** (m = 2, R = Et)

Ana Mirela Neculai, Dante Neculai, Herbert W. Roesky, Jorg Magull

Polyhedron 23 (2004) 183

Synthesis and structure of $LLnBr_2$ ($L = Et_2NCH_2CH_2NC(Me)CHC(Me)NCH_2CH_2NEt_2$; Ln = Y, Sm, and Yb)

The reaction of the in situ prepared LLi ($L = Et_2NCH_2CH_2NC(Me)CHC(Me)NCH_2CH_2NEt_2$ with $LnBr_3$ (Ln = Y, Sm, and Yb) led to the solvent and alkali salt free dibromoderivative of type $LLnBr_2$ (Ln = Y, **1**, Sm, **2**, and Yb, **3**). Compounds **1**–**3** were characterized by X-ray crystallography, elemental analysis, and NMR (**1**).

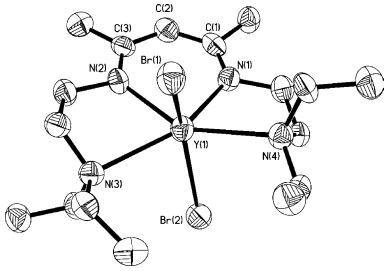

Vernon C. Gibson, Carl Redshaw, William Clegg, Mark R.J. Elsegood, Ulrich Siemeling, Thomas Turk

Polyhedron 23 (2004) 189

Synthesis and X-ray crystal structures of hydridotris(3,5-dimethylpyrazolyl)borate (Tp′) molybdenum(VI) bis(imido) complexes

Three bis(imido) complexes of molybdenum with Tp′ as a tridentate ligand have octahedral coordination geometry with a *cis* arrangement of the two imido ligands; Mo–N bond lengths show the strong *trans* influence of the imido ligands compared with chloro in the sixth coordination site.

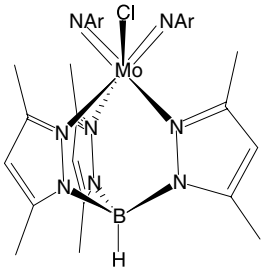

Instructions concerning crystallographic data I

The Publisher encourages the submission of articles in electronic form thus saving time and avoiding rekeying errors. For detailed instructions on the preparation of manuscripts and of electronic artwork, consult the Author Gateway for Elsevier at http://authors.elsevier.com

SCIENCE DIRECT™

Full text of this journal is available, on-line from **ScienceDirect**. Visit **www.sciencedirect.com** for more information.

CONTENTS Direct This journal is part of **ContentsDirect**, the *free* alerting service which sends tables of contents by e-mail for Elsevier books and journals. You can register for **ContentsDirect** online at: **www. elsevier.com/locate/contentsdirect**

http://ChemWeb.com The World Wide Club for the Chemical Community

http://chemweb.com/gateways/elsevier.html